JANUARY/FEBRUARY 2000
Volume 11, Number 1

© Copyright 2000 by the American Chemical Society

Bioconjugate Chemistry

Editorial: What's New

New in 2000, color photographs and artwork, if approved by the editor, may be printed in *Bioconjugate Chemistry* at no cost to the author. Color illustrations should only be submitted if essential for clarity of communication. A surcharge of $100 per 100 reprints will be added to the standard cost of the reprints.

We welcome the new members of the *Bioconjugate Chemistry* Editorial Advisory Board for 2000:

Dr. Edith Dellacherie, Laboratoire de Chimie-Physique Macromoleculaire, ENSIC-INPL, Nancy, France

Dr. Anna Grandas, Departament de Quimica Organica, Facultat de Quimica - Universitat de Barcelona, Spain

Dr. Anne Gruaz-Guyon, INSERM U.339 et Service de Biophysique, Faculte de Medecine Saint Antoine, Paris, France

Dr. Sung Wan Kim, University of Utah, Department of Pharmaceutics and Pharmaceutical Chemistry - CCCD, Salt Lake City, Utah

Dr. Shuang Liu, The DuPont Merck Pharmaceutical Company, North Billerica, MA

Dr. Thomas J. Meade, California Institute of Technology, Division of Biology & Beckman Institute, Pasadena, CA

Dr. Annie C. Roche, Department de Biochimie des Glyconconjugues, CNRS 1 - Universite de'Orleans, France

Dr. Donald A. Tomalia, Center for Biologic Nanotechnology, Michigan Molecular Institute, Midland, MI

Dr. Pamela A. Trail, Bristol-Myers Squibb Pharmaceutical Research Institute, Princeton, NJ

Dr. Eishun Tsuchida, Department of Polymer Chemistry, Advanced Research Center for Science and Engineering, Waseda University, Tokyo, Japan

Dr. Ralph Weissleder, Department of Radiology, MGH-NMR Center, Harvard Medical School, Boston, MA

Dr. John Yates, Department of Molecular Biotechnology, University of Washington, Seattle, WA

Thanks to Our Reviewers

It is a pleasure to acknowledge the contributions of the reviewers of manuscripts submitted in 1999 for publication in *Bioconjugate Chemistry*. Their unselfish service has been essential in the shaping of the 10th volume of the journal. The scientific community is fortunate that its members are willing to share their time and specialized knowledge in this way. The reviewers are on the following page.

Claude F. Meares
Editor-in-Chief

10.1021/bc9901752 CCC: $19.00 © 2000 American Chemical Society
Published on Web 01/17/2000

List of Reviewers

Michael J. Abrams
Maciej Adamczyk
Sudhir Agrawal
Kazunari Akiyoshi
A. I. Alayash
Giuseppe D'Alessio
Trevor George Appleton
Christian Auclair
Alexandre Avrameas
Robert W. Baldwin
James R. Baker
James R. Ballinger
Jan Balzarini
Joel Barrish
Serge Beaucage
Kevin Beam
Craig C. Beeson
Jean-Paul Behr
Donald E. Bergstrom
Purshotam Bhan
Gary Bignami
Alexei A. Bogdanov
Robert C. Brasch
Art D. Broom
Josef Brunner
Philip Burke
Jacek Capala
Paul Carter
Luigi Casella
Anthony Cerami
Chien-Hsing Ken Chang
J. P. Chen
Marco Chinol
Wen-Jang Chu
A. J. Chmura
James P. Collman
John E. T. Corrie
David Curiel
Max Deinzer
Edith Dellacherie
Thierry Delair
Thomas J. Dougherty
Ruth Duncan
P. L. Felgner
Mark A. Findeis
Raymond A. Firestone
Joseph Francisco
Alan D. Frankel
Arthur E. Frankel
Alan R. Fritzberg
Yasuhisa Fujibayashi
Alexander Gall
Kieran F. Geoghegan
C. G. Geraldes
Alexander N. Glazer
David M. Goldenberg
Victor S. Goldmacher
David A. Goodwin
Serengulam V. Govindan
Anna Grandas
David E. Graves
Scott R. Graves
A. G. Greenburg
Marc M. Greenberg
Richard B. Greenwald
Gary L. Griffiths
Paul Grothaus
Jun Haginaka
Ton T. Hai
Michelle M. Hanna
Richard Haugland
Claude Hélène
Ilkka Hemmila
Jacobus D. M. Herscheid
Donald J. Hnatowich
Allan S. Hoffman
Harold P. Hogenkamp
Peter Hoogerhout
Thomas Horn
Leaf Huang
Jeffrey A. Hubbell
Wayne L. Hubbell
Ferenc Hudecz
Jeffrey A. Hughes
Lisbeth Illum
Nebojsa Janjic
David A. Jans
Andres Jäschke
Rudy L. Juliano
Alexander V. Kabanov
Lou-Sing Kan
M. Kashiwayanagi
Kazunori Kataoka
John A. Katzenellenbogen
Randal J. Kaufman
Sung Wan Kim
H. Dalton King
Jindrich Kopecek
Pavia Kopecekova
Robert J. Kreitman
Bengt R. Långström
Patrick Leahy
Bernard Lebleu
Moses Lee
J. Y. Legendre
Robert L. Letsinger
Shuang Liu
Harri Lönnberg
Joseph Loo
Philip S. Low
Matthew H. Lyttle
Hiroshi Maeda
Atsushi Maruyama
Stephen J. Mather
Gary R. Matsueda
Katsumi Matsuzaki
William McBride
Thomas J. McIntosh
Thomas J. Meade
Gary E. Means
F. M. Menger
Damon L. Meyer
Patrick Midoux
Nabuo Monji
Serge Moreau
Veli-Matti Mukkala
Ron Nachman
Peter E. Nielsen
Makiya Nishikawa
David F. O'Brien
Teruo Okano
Wilma K. Olson
Sean O'Malley
Leslie E. Orgel
David Oupicky
Giovanni Paganelli
William M. Pardridge
Kinam Park
Tae Gwan Park
Ira Pastan
Dinshaw Patel
Pradeep Pathare
David E. Pereira
Candice Pert
Wolfgang Pieken
Michael C. Pirrung
Brian Poki
Richard T. Pon
Oliver Press
Glenn D. Prestwich
Michael Przybylski
F. Raffi
Tariq M. Rana
M. P. Reddy
Jennifer Reed
Michael W. Reed
Steven L. Regen
Bob Reife
Mark A. Reynolds
Annie C. Roche
Steven R. Roffler
Keith Rose
T. Saison-Behmoaras
Hideo Saji
Harri Salo
Lauge Schäffer
Peter Schuck
J. Seelig
Alec H. Sehon
Hartmut Seliger
Paul Selvin
Jolanta Sereikaite
Jonathan L. Sessler
L. W. Seymour
Wei Chiang Shen
David Shortle
Clay Siegall
Natan Siemers
Richard D. Smith
John Sommerville
Steven Soper
John D. Spikes
Caroline J. Springer
Larry Stanker
C. A. Stein
Stanley Stein
Dmitry A. Stetsenko
Gohsuke Sugihara
Yasuhiko Tabata
Ewald Terpetschnig
Lou Theodore
David H. Thompson
Vladimir P. Torchilin
C. M. Tsai
Eishun Tsuchida
Ganesan Vaidyanathan
J. E. van Muijlwijk-Koezen
Francesco M. Veronese
Wynn A. Volkert
Wolfgang Voelter
Vivekananda M. Vrudhula
Alan Wahl
E. Sally Ward
Michael J. Waring
David S. Watt
Shulamit Weinstein
Ralph Weissleder
Michael J. Welsh
David E. Wemmer
Ronald Wetzel
D. Scott Wilbur
Meir Wilchek
Itamar Willner
George S. Wilson
Robert W. Woody
Lugi E. Xodo
David J. Yang
Cecil C. Yip
Masayuki Yokoyama
Yong Yu
Nobuhiko Yui
Samuel Zalipsky

BC9901752

COMMUNICATIONS

Synthesis of Bioadhesive Lectin-HPMA Copolymer−Cyclosporin Conjugates

Zheng-Rong Lu,[†] Song-Qi Gao,[†] Pavla Kopečková,[†,‡] and Jindřich Kopeček*[,†,‡]

Departments of Pharmaceutics and Pharmaceutical Chemistry/CCCD, and Bioengineering, University of Utah, Salt Lake City, Utah 84112. Received July 26, 1999

An amino group containing cyclosporin A (CsA) derivative has been synthesized and conjugated to *N*-(2-hydroxypropyl)methacrylamide (HPMA) copolymer via an aromatic azo bond, which can be specifically cleaved by azoreductase activity in colon to release the drug for the treatment of colon diseases. Lectins, peanut (*Arachis hypogea*) agglutinin (PNA) and wheat germ agglutinin (WGA), have been conjugated to HPMA copolymer−CsA derivative conjugates (PCsA), respectively, to give bioadhesive conjugates. The PNA and WGA are the targeting proteins that can bind to diseased colon tissue and healthy tissue, respectively. There were on average four P(CsA) copolymer chains attached on one WGA molecule with a drug content of 16.0 wt % and five P(CsA) copolymer chains attached on one PNA molecule with a drug content of 11.5 wt %. The incubation of a P(CsA) copolymer with the rat cecal contents resulted in the cleavage of the azo bond and release of the cyclosporin derivative. The biological evaluation of the conjugates is under way.

Cyclosporin A (CsA)[1] is a lipophilic cyclic undecapeptide with unique immunosuppressive properties. It is widely used in organ transplantation and was also found to be effective in the treatment of inflammatory bowel diseases (IBD) (ulcerative colitis, Crohn's disease) (*1*−*3*). The oral administration of the drug has shown some success in the treatment of the IBD. However, it has been found that CsA was predominantly absorbed in the small intestine after oral administration (*4*), and significant nephrotoxicity and other toxic side effects were associated with the administration of high doses of CsA (*5*). A placebo-controlled trial showed that CsA enemas for ulcerative colitis were not efficacious because of its poor aqueous solubility and its low absorption via colon (*6*). Therefore, alternative ways are required to increase the aqueous solubility of CsA to deliver it specifically to the disease sites in the colon and enhance its efficacy with concomitant reduction of side effects.

The colon-specific bioadhesive, water-soluble polymeric delivery system may be one of the options to specifically deliver CsA to the colon (*7*). The CsA solubility can be dramatically increased by attachment to water-soluble polymers. The site-specific colon delivery can be achieved by the conjugation of the drug via an aromatic azo linkage and the introduction of biorecognizable moieties such as lectins. The specific azoreductase activities in the colon of many species (*8*) can cleave the azo linkage to release the drug (*7*). Lectins are proteins or glycoproteins of nonimmunological origin, capable of recognizing and binding to the antigens (carbohydrates) expressed in the tissue or on cell surface and have potential in oral colon-specific drug delivery (*9*). The differences in the structure of the carbohydrates result in the selective bioadhesion of lectins. For example, peanut (*Arachis hypogea*) agglutinin (PNA) binds to the Thomson−Friedenreich (TF) antigen, which has an increased expression in the diseased colon tissue (e.g., in ulcerative colitis). The binding of PNA to the diseased tissue is proportional to the severity of ulcerative colitis (*10*), whereas wheat germ agglutinin (WGA) binds to brush border and goblet cell mucins in healthy colon tissue (*11*). Previously, we conjugated lectins, PNA and WGA, to *N*-(2-hydroxypropyl)methacrylamide (HPMA) copolymer, a water-soluble drug carrier, and found that the polymeric conjugates showed different binding patterns in the healthy rat intestinal tissue (*12*). HPMA copolymer−WGA conjugate bound strongly to the intestinal tissue, and the HPMA copolymer−PNA conjugate bound minimally, but specifically. The results suggested that the lectin−HPMA

* To whom correspondence should be addressed. Phone: (+801) 581 4532. Fax: (+801) 581 3674. E-mail: Jindrich.Kopecek@m.cc.utah.edu.

[†] Department of Pharmaceutics and Pharmaceutical Chemistry/CCCD.

[‡] Department of Bioengineering.

[1] Abbreviations: AIBN, 2,2′-azobisisobutyronitrile; CsA, cyclosporin A; DCC, dicyclohexyl carbodiimide; DCU, dicyclohexyl urea; DMSO, dimethyl sulfoxide; HPMA, *N*-(2-hydroxypropyl)-methacrylamide; IBD, inflammatory bowel disease; MA, methacryloyl; MeBmt, 2-*N*-methyl-(*R*)-((*E*)-2-butenyl)-4-methyl-L-threonine; M_n, number average molecular mass; M_w, weight average molecular mass; ONp, *p*-nitrophenoxy; P(CsA), HPMA copolymer-CsA derivative conjugate; PBS, phosphate-buffered saline; PNA, peanut (*Arachis hypogea*) agglutinin; PNA-PCsA, peanut (*Arachis hypogea*) agglutinin-HPMA copolymer-CsA derivative conjugate; SEC, size-exclusion chromatography; THF, tetrahydrofurn; WGA, wheat germ agglutinin; WGA-PCsA, wheat germ agglutinin-HPMA copolymer-CsA derivative conjugate; wt %, weight percentage.

10.1021/bc990098a CCC: $19.00 © 2000 American Chemical Society
Published on Web 12/10/1999

Scheme 1. Synthesis of Amino Group Containing CsA Derivative 3[a]

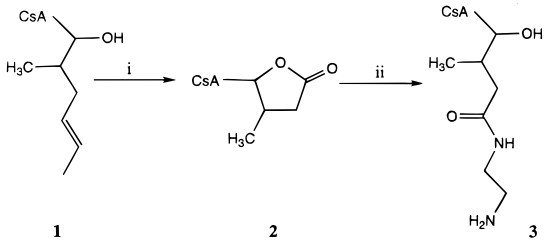

[a] (i) $NaIO_4$, $KMnO_4$, K_2CO_3, H_2O, t-BuOH, 14 h, 92%; (ii) $NH_2CH_2CH_2NH_2$, THF, reflux, 24 h, 60%.

Scheme 2. Synthesis of Monomer 9[a]

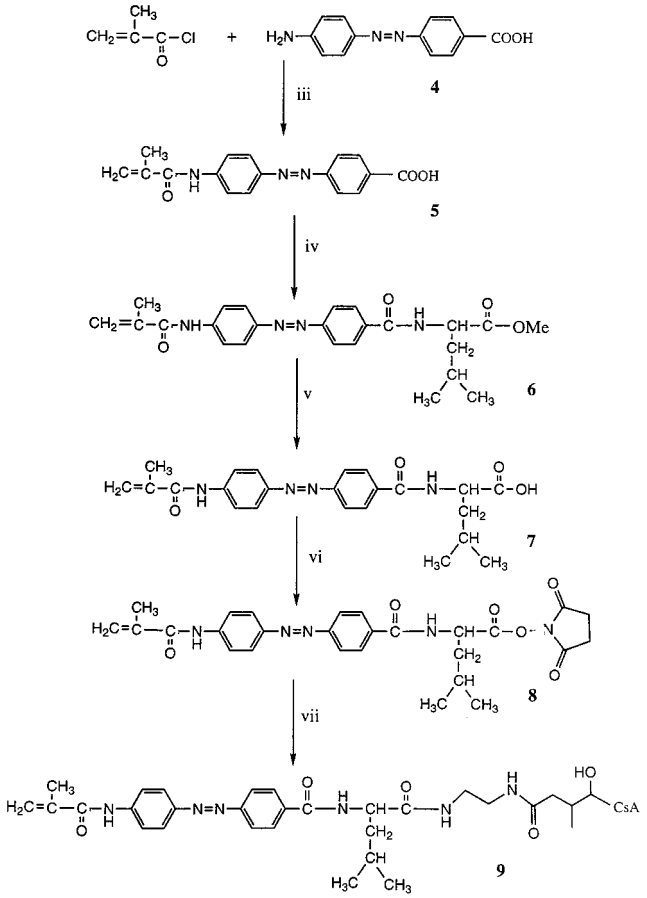

[a] (iii) Diisopropylethylamine, CH_2Cl_2, rt, overnight, 52%; (iv) L-leucine methyl ester hydrochloride, diisopropylethylamine, DCC, CH_2Cl_2, 4 °C, overnight, 57%; (v) NaOH, rt, 6 h, HCl, 81%; (vi) *N*-hydroxysuccinimide, DCC, THF/CH_2Cl_2 (1:1), 4 °C, overnight, 49%; (vii) 3, THF, rt, 24 h, 68%.

copolymer conjugates could be suitable carriers for colon site-specific delivery of CsA.

We report on the synthesis of lectin (PNA or WGA)−HPMA copolymer−CsA derivative conjugates for site-specific colon delivery. An HPMA copolymer precursor containing a CsA derivative and a reactive ester group was first synthesized by free-radical copolymerization of HPMA with a CsA-containing monomer **9** and MA-Gly-Gly-ONp in the presence of AIBN. The lectins (PNA and WGA) were conjugated to the copolymer precursor by reacting their amino groups with the active ester groups in the copolymer, respectively.

The CsA derivative-containing monomer **9** was designed and synthesized according to the procedure described in Schemes 1 and 2. An aromatic azo compound, 4-(4-aminophenylazo)benzoic acid (*13*), and L-leucine were employed as a biodegradable spacer between the polymerizable double bond and the CsA derivative. The aromatic azo bond can be cleaved to release the drug specifically by the azoreductase activity produced by microorganisms commonly present in the colon. The conjugation of CsA via aromatic azo bond might avoid the major side effect—fast absorption in small intestine and subsequent nephrotoxicity. The aromatic azo spacer has been successfully used in colon-specific delivery of 5-aminosalicylic acid, a potent drug for the treatment of ulcerative colitis (*8*, *14*). The L-leucine was introduced between the drug and the aromatic residue in order to free the CsA derivative completely by peptidase and/or aminopeptidase (*15*, *16*) after initial cleavage of the aromatic azo bond by the azoreductase activities.

CsA has a cyclic undecapeptide structure (structure 1)

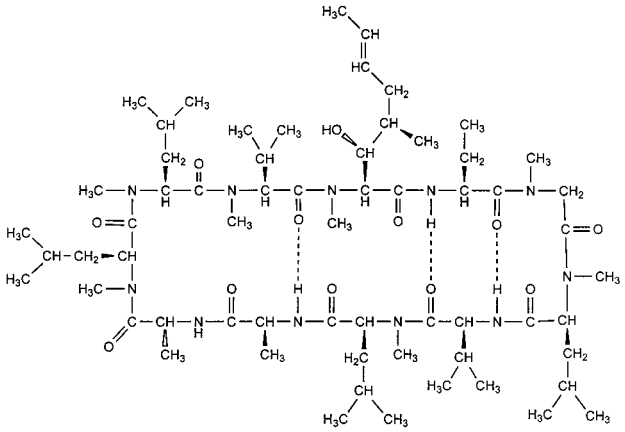

and has one functional group, the hydroxyl group on the 2-*N*-methyl-(*R*)-((*E*)-2-butenyl)-4-methyl-L-threonine (MeBmt) residue, which could be used as an attaching point in monomer synthesis. The attachment of CsA via the hydroxyl group to a polymerizable group would result in a monomer where the intact structure of CsA is maintained. However, the attempt to conjugate CsA to a monomer via the hydroxyl group was not successful because the hydroxyl group shows very low reactivity due to the steric hindrance. A reactive functional group, e.g., amino group, had to be introduced to CsA for the conjugation. The double bond on the MeBmt residue can be chemically modified to introduce an amino group, and it has been reported that the modified CsA maintained its pharmacological effectiveness (*17*−*19*). The conjugation of CsA derivative to HPMA copolymers may decrease the side effects associated with administration of CsA (*20*). Due to the combination of local and systemic actions of CsA releases in the colon (*21*), lower CsA plasma levels should be therapeutically effective when compared to intravenous administration.

A reactive amino group was introduced to MeBmt residue of CsA by the reaction of 1,2-ethylenediamine with a CsA lactone (**2**), Scheme 1. The CsA lactone was prepared by the oxidative cleavage of the double bond of the CsA using $NaIO_4$ and $KMnO_4$ (*22*). The lactone was refluxed with excess 1,2-ethylenediamine for 24 h in methanol. The solvent was removed, and solid residue was dissolved in CH_2Cl_2 and washed with water. The amino-functionalized CsA derivative (**3**) was obtained from the organic phase and was purified by silica gel chromatography. The compound **3** was characterized by proton NMR and electrospray mass spectrometry (m/z = 1248.38 ($M^+ + 1$), and the calculated molecular weight is 1247.73).

Scheme 3. Copolymerization of Monomer 9[a]

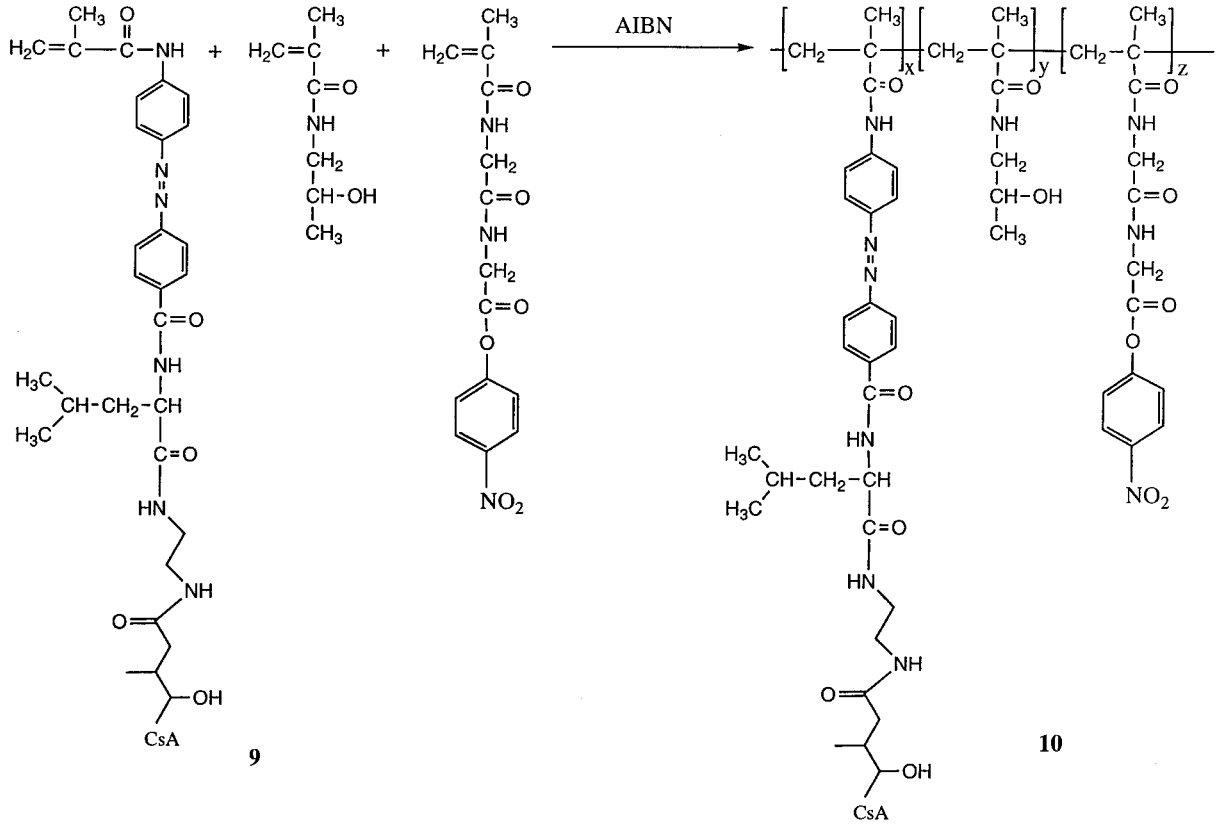

[a] HPMA and MA-Gly-Gly-ONp. AIBN, Acetone, 50 °C, 48 h, 76%.

The synthesis of the monomer **9** is shown in Scheme 2. 4-(4-Aminophenylazo)benzoic acid (**4**) was employed as a degradable spacer (*14*). The polymerizable residue, methacryloyl group, was introduced by reacting methacryloyl chloride with **4** in the presence of diisopropylethylamine to give compound **5**. L-Leucine methyl ester was coupled to compound **5** in the presence of DCC to form compound **7** after the hydrolysis of the ester group with dilute NaOH in methanol. The active ester **8** was synthesized by reacting compound **7** with *N*-hydroxysuccinimide in the presence of DCC. The CsA derivative containing monomer **9** was synthesized by the coupling reaction of compound **8** with **3**. The orange monomer **9** was isolated using silica gel chromatography. The intermediate reaction products and the monomer **9** were characterized by proton NMR and electrospray mass spectrometry. The *m/z* ($M^+ + 1$) of the monomer **9** was 1652.75 (calculated 1652.19).

The monomer **9** (90 mg), HPMA (210 mg), and MA-Gly-Gly-ONp (28 mg) were copolymerized in the presence of AIBN at 50 °C in acetone (Scheme 3).

Copolymer **10** was obtained with a yield of 76%. The number and weight average molecular masses of the copolymer were 17 500 and 25 900 Da, respectively, as determined by size-exclusion chromatography (SEC) using polyHPMA calibration, eluted with 30% acetonitrile containing PBS buffer. The content of the CsA derivative **3** in the copolymer was 0.20 mmol/g as determined spectrophotometrically at 360 nm based on the absorbance of the aromatic azo residue ($\epsilon = 2.5 \times 10^4\ M^{-1}\ cm^{-1}$, methanol). The content of the ONp active ester was 0.2 mmol/g (of copolymer) as determined spectrophotometrically at 400 nm based on the released *p*-nitrophenolate ($\epsilon = 1.8 \times 10^4\ M^{-1}\ cm^{-1}$, water) after hydrolysis of the copolymer in basic condition and separation using a Sephadex G-25 column. Because of the hydrophobicity of CsA derivative, the copolymer aggregated partially in PBS solution as shown by the SEC profile of the copolymer. The hydrophobic aggregation completely disappeared in the 30% (volume) acetonitrile containing PBS solution.

The lectins, WGA (molecular mass = 43 kDa) and PNA (molecular mass = 110 kDa), were bound to the HPMA copolymer−CsA derivative conjugate [P(CsA)] **10**, respectively, by reacting their amino groups with the *p*-nitrophenol ester of the copolymer. A high concentration of lectin or copolymer precursor should be avoided in the conjugation reaction because precipitation occurred due to lectin (especially the PNA) aggregation or cross-linking. However, a too low concentration of reactants might result in low yield of conjugate due to large amount of unreacted protein. The concentrations of lectin and polymer solutions were optimized to give higher yields. A 4 wt % concentration of copolymer solution and 1.7 wt % of WGA (1.5 wt % of PNA) were used in the conjugation. The lectin solution was added dropwise to the copolymer solution. The conjugation reaction was carried out at neutral pH (7.3) for 2 h at room temperature and left at 4 °C overnight after the pH was gradually raised to 8.0 with diluted NaOH. The unreacted *p*-nitrophenol ester was destroyed by raising the pH to 9.0 for a short period. The lectin−copolymer conjugates were separated from unconjugated copolymer and lectins by SEC. The isolated lectin−copolymer conjugates were dialyzed against deionized water, and lyophilized. The weight average molecular masses of the conjugates were determined by using SEC with a laser light scattering detector (Mini-Dawn, Wyatt). The molecular masses of the conjugates were 150 kDa for WGA−P(CsA) conjugate and 250 kDa for PNA−P(CsA) conjugate, respectively. The lectin contents were 36.5 wt % in the WGA−P(CsA) conjugate and 54.5 wt % in the PNA−P(CsA) conjugate, respec-

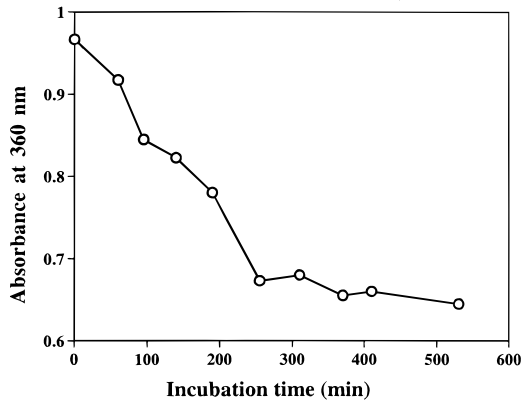

Figure 1. The time-dependent degradation of P(CsA) with rat cecal contents. The P(CsA) was incubated with preincubated cecum contents in N_2 atmosphere at 37 °C. The absorbance of aromatic azo bond at 360 nm was recorded at different time intervals.

tively, as determined by Lowry assay. The CsA derivative content was determined spectrophotometrically at 360 nm based on the aromatic azo residues. The contents of CsA derivative were 16.0 wt % in the WGA−P(CsA) conjugate and 11.5 wt % in the PNA−P(CsA) conjugate, respectively. There were on average four P(CsA) chains attached to one WGA molecule and five P(CsA) chains attached to one PNA molecule.

The lectins, especially PNA, have a tendency to aggregate and precipitate in aqueous solution. However, when the lectins were conjugated to the copolymer, the stability of the lectins was significantly increased. No precipitation was observed in the lectin−copolymer conjugate solution, pH 7.3 (1 wt %), during 1 month storage at 4 °C.

To verify the stability of the amide bond originating in the leucine residue in the GI tract, we incubated the P(CsA) with rat small intestine contents (10 wt %) at 37 °C. No significant release of the CsA derivative was detected after 5 h of incubation. The HPLC analysis of the methylene dichloride extract of the P(CsA) incubation mixture indicated that less than 1% of total CsA derivative was released. However, an 1 h incubation of Z-Ala-Ala-Leu-Nap (1 mM), used as a control, resulted in 50% of *p*-nitroaniline release. This indicates that the amide bond originating in the leucine residue in the P(CsA) side chains is considerably stable in conditions mimicking the small intestine.

The cleavage of the aromatic azo bond and the release of the CsA derivative were investigated by incubation of P(CsA) with rat cecal contents at 37 °C. The degradation of the aromatic azo bond was monitored by UV spectrophotometry at 360 nm, and the degradation kinetics is shown in Figure 1. The absorbance of the azo spacer at 360 nm decreased with increasing the incubation time and appeared to reach a plateau after 6 h. The incubation mixture was extracted with methylene chloride and the extract was analyzed by MALDI-TOF mass spectrometry. The *p*-amino-benzoyl-Leu-ED-CsA residue (m/z = 1519, + K^+) expected after the cleavage of the azo bond and free CsA derivative (m/z = 1248, **3** + H^+; 1287, **3** + K^+) were identified in MALDI-TOF mass spectra. Both compounds were present in a significant amount in the organic extract as determined by HPLC. As demonstrated above that the P(CsA) was stable in the small intestinal contents, however, in cecal contents the free CsA derivative was released in addition to the fragment resulting from the cleavage of the azo bond. This indicates that the CsA containing side chain in P(CsA) was resistant to endopeptidase activities. The ultimate cleavage of the amide bond originating in the leucine residue in the cecal contents suggests that the azo bond was cleaved first, followed by the cleavage of the amide bond by aminopeptidases. The results seem to validate the design of the conjugates and the importance of the colon-specific cleavage of the azo bond. The azoreductase activity of the colonic bacteria is suitable for site-specific delivery of drugs to the large intestine. This is based on the facts that the proteolytic activity in the colon is less than that of the small intestine and that the concentration of microbial flora present in the colon is orders of magnitude higher than in both the stomach and the small intestine (*7*).

In summary, the above results indicated that the HPMA copolymer−CsA derivative conjugate will be stable during the transport via GI tract but will specifically release the drug in the colon after cleavage of the azo bond by the azoreductase activities. The lectins, WGA and PNA, were conjugated to the P(CsA), respectively, to enhance the bioadhesion of the conjugate to the colon tissue (*23*). Further biological evaluation of the nontargeted and the lectin-targeted HPMA copolymer−CsA conjugates is ongoing.

ACKNOWLEDGMENT

The research project was supported in part by NIH Grant DK39544.

Supporting Information Available: Further experimental procedures. This material is available free of charge via the Internet at http://pubs.acs.org.

LITERATURE CITED

(1) Brynskov, J. (1993) Cyclosporin for inflammatory bowel disease: mechanisms and possible actions. *Scand. J. Gastroenterol. 28*, 849−857.
(2) Aiko, S., Conner, E. M., Fuseler, J. A., and Grisham, M. B. (1997) Effects of cyclosporine or FK506 in chronic colitis. *J. Pharmcol. Exp. Ther. 280*, 1075−1084.
(3) Wenzl, H. H., Petritsch, W., Aichbichler, B. W., Hinterleitner, T. A., Fleischmann, G., and Krejs, G. J. (1998) Short-term efficacy and long-term outcome of cyclosporine treatment in patients with severe ulcerative colitis. *Z. Gastroenterol. 36*, 287−293.
(4) Drewe, J., Beglinger, C., and Kissel, T. (1992) The absorption site of cyclosporin in the human gastrointertinal tract. *Br. J. Clin. Pharmacol. 33*, 39−43.
(5) Faulds, D., Goa, K. L., and Benfield, P. (1993) Cyclosporin: a review of its pharmacodynamic and pharmacokinetic properties, and therapeutic use in immunoregulatory disorders. *Drugs 45*, 953−1040.
(6) Sandborn, W. J., Tremaine, W. J., Schroeder, K. W., Batts, K. P., Lawson, G. M., Steiner, B. L., Harrison, J. M., and Zinsmeister, A. R. (1994) A placebo-controlled trial of cyclosporine enemas for mildly to moderately active left-sided ulcerative colitis. *Gastroenterology 106*, 1429−1435.
(7) Kopeček, J., and Kopečková, P. (1992) N-(2-Hydroxypropyl)-methacrylamide copolymers for colon-specific drug delivery. In *Oral Colon-Specific Drug Delivery* (D. R. Friend, Ed.) pp 189−211, CRC Press, Boca Raton, FL.
(8) Kopečková, P., Rathi, R. C., Takada, S., Říhová, B., Berenson M. M., and Kopeček, J. (1994) Bioadhesive N-(2-hydroxypropyl)methacrylamide copolymers for colon-specific drug delivery. *J. Controlled Release 28*, 211−222.
(9) Lehr, C.-M. (1999) Lectin-mediated drug delivery - the second generation of bioadhesives. *Abstracts Ninth Int. Symp. Recent Adv. Drug Delivery Syst.*, p 12, Salt Lake City, UT, February 22, 1999.
(10) Cooper, H. S., Farano, P., and Coapman, R. A. (1987) Peanut lectin binding sites in colon of patients with ulcerative colitis. *Arch. Pathol. Lab. Med. 111*, 270−275.

(11) Philips, T. E., and Frisch, E. B. (1990) Secretory glycoconjugates of a mucin-synthesizing human colonic adenocarcinoma cell line. Analysis using double labeling with lectins. *Histochemistry 93*, 311−317.

(12) Wróblewski, S., Kopečková, P., Říhová, B., and Kopeček, J. (1998) Lectin-HPMA copolymer conjugates: potential oral drug carriers for targeting diseased tissues. *Macromol. Chem. Phys. 199*, 2601−2608.

(13) Jaffe, C. L., Lis, H., and Sharon, N. (1980) New cleavable photoreactive heterobifunctional cross-linking reagents for studying membrane organization. *Biochemistry 19*, 4423−4429.

(14) Grim, Y., and Kopeček, J. (1991) Bioadhesive water-soluble polymeric drug carriers for site-specific oral drug delivery. Synthesis, characterization, and release of 5-aminosalicylic acid by *Streptococcus faecium in vitro*. *New Polym. Mater. 3*, 49−59.

(15) Kopečková, P., Ikesue, K., and Kopeček, J. (1992) Cleavage of oliogopeptide *p*-nitroanilides attached to N-(2-hydroxypropyl)methacrylamide copolymers by guinea pig intestinal enzymes. *Makromol. Chem. 193*, 2605−2619.

(16) Ikesue, K., Kopečková, P., and Kopeček, J. (1993) Degradation of proteins by guinea pig intestinal enzymes. *Intl. J. Pharm. 95*, 171−179.

(17) Říhová, B., Jegorov, A., Strohalm, J., Matha, V., Rossmann, P., Fornůsek, L., and Ulbrich, K. (1992) Antibody-targeted cyclosporin A. *J. Controlled Release 19*, 25−40.

(18) Říhová, B., Strohalm, J., Plocová, D., Šubr, V., Šrogl, J., Jelínková, M., Šírová, M., and Ulbrich, K. (1996) Cytotoxic and cytostatic effects of anti-Thy 1.2 targeted doxorubicin and cyclosporin A. *J. Controlled Release 40*, 303−319.

(19) Šťastný, M., Ulbrich, K., Strohalm, J., Rossmann, P., and Říhová, B. (1997) Abnormal differentiation of thymocytes induced by free cyclosporine is avoided when cyclosporine bound to N-(2-hydroxypropyl)methacrylamide copolymer carrier is used. *Transplantation 63*, 1818−1827.

(20) Von Graffenried B., and Krupp, P. (1986) Side effects of cyclosporin in renal transplant recipients and in patients with autoimmune disease. *Transplant. Proc. 18*, 876−883.

(21) Sandborn, W. J. (1995) A critical review of cyclosporine therapy in inflammatory bowel disease. *Inflam. Bowel Dis. 1*, 48−63.

(22) Paprica, P. A., Margaritis, A., and Petersen, N. O. (1992) Preparation of novel Cyclosporin A derivatives. *Bioconjugate Chem. 3*, 32−36.

(23) Wróblewski, S., Berenson, M., Kopečková, P., and Kopeček, J. (1999) Biorecognition of HPMA copolymer - lectin conjugates as an indicator of differentiation of cell-surface glycoproteins in development, maturation and diseases of human and rodent tissues. *J. Biomed. Mater. Res.* (in preparation).

BC990098A

© 1999 American Chemical Society, Bioconjugate Chem., Lu bc990098a Supporting Info Page 1

Supplementary material of experimental section

Preparation of CsA amine derivative (3). The CsA lactone (**2**) was prepared as described by Paprica et al. (20). The CsA lactone (92 mg, 0.077 mmol) was refluxed with 1,2-ethylenediamine (1.0 ml, excess) in THF for 24 h. The solvent and excess ethylene diamine were removed under vacuum. The solid residue was washed with water and extracted with CH_2Cl_2, and the CH_2Cl_2 solution was dried with anhydrous Na_2SO_4. The solvent was removed to give a slight yellowish crystalline product. The product was further purified by silica gel chromatography, eluted with acetone/hexane (2/1), acetone and methanol. Yield: 58 mg, 60%. The product was characterized with proton NMR and electrospray mass spectrometry. Proton-NMR (δ, ppm, $CDCl_3$): NH protons, 8.44, 8.08, 7.89, 7.52 (all d, each 1H), 6.58 (t, 1H); N-CH_3 protons, 3.47(s, 3H), 3.42(s, 3H), 3.25(s, 3H), 3.15(s, 6H), 2.65(s, 6H). m/z = 1248.38 (M^++1, $C_{62}H_{112}N_{13}O_{13}$).

Preparation of 4-(4-methacryloylaminophenylazo)benzoic acid (5). 4-(4-Aminophenylazo)benzioc acid hydrochloride (**4**) (1.90 g, 6.8 mmol) and diisopropylethylamine (2.0 ml, 11.5 mmol) was dissolved in 150 ml, and a methylene chloride solution (20 ml) of methacryloyl chloride (670 μl, 6.8 mmol) was added dropwise with stirring at room temperature. The reaction mixture was stirred overnight, then diluted HCl (5.0 ml, 6N) was added to neutralize the excess of diisopropylethyl amine. The solvent was removed under vacuum giving an oily residue. The residue

solidified when water was added, and the red solid was washed with water and dried. The solid was recrystallized with THF and ethyl acetate giving an orange crystalline product (1.1 g, 52%). M.p.: > 285 °C (dec.). Rf: 0.45 (hexanes/acetone: 1:2). Proton NMR (δ, ppm, DMSO-d_6): 1.96 (s, 3H, CH_3); 5.58, 5.86 (d, 2H, CH2); 7.92-8.14 (m, 9H, Ph-H); 10.18 (s, 1H, COOH). Electrospray MS ($C_{17}H_{15}N_3O_3$, m/z): 310.22 ($M^+ + 1$).

Preparation of 4-(4-methacryloylaminophenylazo)benzoyl L-leucine methyl ester (6). 4-(4-Methacryloylaminophenylazo)benzoic acid (**5**) (1.0 mg, 3.2 mmol), L-leucine methyl ester hydrochloride (1.2 g, 6.6 mmol) and diisopropylethyl amine (1.0 ml, 5.7 mmol) were dissolved in 40 ml methylene chloride, cooled in an ice bath, and DCC (1.4 g, 6.8 mmol) was added. The reaction mixture was stirred at 4 °C overnight. The precipitate was removed by filtration. The solvent was removed under vacuum, and the solid residue was washed with dilute HCl solutions and water, and dried. The orange solid product was separated on a silica gel column, eluted with hexane, hexane/acetone (2:1, 1:1 and 1:2). The product fraction was collected: a light orange crystalline product was obtained when the solvent was removed. Yield: 800 mg, 57%. M.p.: 196-198 °C. Rf: 0.63 (hexane/acetone: 1:2). Proton NMR (δ, ppm, $CDCl_3$): 0.98 (m, 6H, CH_3); 1.74 (m, 3H, CH-CH_2); 2.07 (s, 3H, CH_3); 3.77 (s, 3H, CH_3); 4.87 (m, 1H, CH); 5.50, 5.82 (d, 2H, CH_2); 6.67 (d, 1H, NH); 7.72-7.96 (m, 8H, Ph-H). Electrospray MS ($C_{24}H_{28}N_4O_4$, m/z): 436.6 (M^+).

Preparation of 4-(4-methacryloylaminophenylazo)benzoyl L-leucine (7). 4-(4-Methacryloylaminophenylazo)benzoyl L-leucine methyl ester (**6**) (700 mg, 1.60 mmol) was dissolved in 20 ml methanol/THF (1:1), and NaOH (300 mg, 7.5 mmol) in 2.0 ml

water was added. The reaction mixture was stirred at r.t. for 6 h, and acidified with diluted HCl to pH 2. The reaction mixture was extracted with ethyl acetate, dried over anhydrous Na_2SO_4. A red crystalline product was isolated by silica gel chromatography, using hexane/acteone(2:1, 1:1, and 1:2) as eleunts. Yield: 550 mg, 81%. M.p.: 168-170 °C. Rf: 0.42 (hexane/acetone: 1:2). Proton-NMR (δ, ppm, DMSO-d_6): 0.90 (m, 6H, CH_3); 1.72 (m, 3H, CH-CH_2); 1.97(s, 3H, CH_3); 4.51 (m, 1H, CH); 5.58, 5.85 (d, 2H, CH_2); 7.90-8.09 (m, 8H, Ph-H); 8.88 (d, 1H, NH); 10.16 (s, 1H, COOH). Electrospray MS ($C_{23}H_{26}N_4O_4$, m/z): 422.6 (M^+).

Preparation of 4-(4-methacryloylaminophenylazo)benzoyl L-leucine N-hydroxysuccinimide ester (8). 4-(4-Methacryloylaminophenylazo)benzoyl L-leucine (7) (500 mg, 1.18 mmol) and N-hydroxysuccinimide (400 mg, 3.5 mmol) were dissolved in 40 ml THF/CH_2Cl_2 (1:1), cooled in an ice bath. DCC (600 mg, 2.9 mmol) was added and the reaction mixture was stirred at 4 °C overnight, and r.t. for 4 h. The precipitate was removed by filtration and the solvent was removed under vacuum to give a red solid residue. An orange crystalline product was isolated by silica gel chromatography, eluted with hexane/acteone(2:1, 1:1, and 1:2). Yield: 300 mg, 49%. M.p.: 207 – 209 °C. Proton NMR (δ, ppm, $CDCl_3$): 1.02 (m, 6H, CH_3); 1.92 (m, 3H, CH-CH_2); 2.07 (s, 3H, CH_3); 2.83 (s, 4H, CH_2CH_2); 5.24 (m, 1H, CH); 5.50, 5.83 (d, 2H, CH_2); 5.59 (d, 2H, NH); 7.71-7.95 (m, 8H, Ph-H).

Preparation of monomer 9. The CsA amine derivative (**3**) (100 mg, 0.08 mmol), 4-(4-methacryloylaminophenylazo)benzoyl L-leucine N-hydroxysuccinimide ester (**8**) (100

mg, excess) and 4-dimethylaminopyridine (20 mg) were dissolved in 10 ml THF and stirred at room temperature for 24 h. The solvent was removed under vacuum, and the solid residue was separated by silica gel chromatography. The column was eluted with hexane, hexane/acetone (2:1, 1:1, and 1:2) and acetone, and the orange colored product fraction was collected. An orange crystalline product was obtained after the solvent was removed. The product was characterized with proton NMR and electrospray mass spectrometry. Yield: 90 mg, 68%. Rf: 0.24 (acetone/hexane: 3/2). Proton-NMR(δ, ppm, $CDCl_3$): NH protons, 8.42, 8.03, 7.43, 7.15, 6.88 (all d, each 1H); N-CH_3 protons, 3.48(s, 3H), 3.41(s, 3H), 3.20(s, 3H), 3.18(s, 3H), 3.15(s, 3H), 2.64(s, 6H); C=CH_2 proton, 5.83(s, 1H), 5.51(s, 1H); MA-CH_3 protons, 2.06 (s, 3H); aromatic protons, 7.75 – 8.00 (m, 8H). Electrospray MS (m/z, $C_{85}H_{136}N_{17}O_{16}$): 1652.75 ($M^+$+1).

Synthesis of copolymer 10. HPMA (210 mg, 1.45 mmol), monomer **9** (90 mg, 54 μmol), MA-Gly-Gly-ONp (28 mg, 90 μmol) and AIBN (20 mg) were dissolved in 5.0 ml acetone, saturated with nitrogen, and sealed in an ampoule. The reaction mixture was stirred at 50 °C for 48 h. Orange copolymer precipitated during the polymerization, and washed collected by filtration. The copolymer was washed with acetone, ether and dried under vacuum. Yield: 250 mg, 76 %. The molecular weights of the copolymer (M_n = 17,500; M_w = 25,900) were determined by SEC on a Superose 6 HR 10/30 column with a light scattering detector (MiniDawn, Wyatt) eluted with 30% acetonitrile containing PBS buffer. The incorporation of the monomer **9** in the copolymer was 0.20 mmol/g as determined spectrometrically (ε = 2.49 x 10^4 at 360 nm). The content of p-nitrophenol active ester in the copolymer was 0.20 mmol/g (of copolymer), which was determined

spectrophotometrically as the content of p-nitrophenolate anion ($\varepsilon = 1.8 \times 10^4\ M^{-1}cm^{-1}$ at 400 nm) released from the copolymer after aminolysis with aminoethanol, and isolation on a Sephadex G-25 column.

Synthesis of Lectin-P(CsA) conjugates. The solution of 50 mg lectin in 3 ml PBS pH 7.3 was added dropwise to the solution of 75 mg polymer **10** (13 μmol ONp) dissolved in 0.4 ml DMSO and 1.5 ml D.I. water. The mixture was gently stirred at room temperature for 2 h. After that the pH of the reaction mixture was gradually raised within 2 h to pH 8.0 by the addition of 0.1 N NaOH and left overnight at 4 °C. The unreacted ONp groups were hydrolyzed by adjusting the pH of reaction mixture to 9.0. Low molecular weight impurities were removed by filtration on Sephadex G-25 column. The conjugates were purified using size exclusion Superose 6 (HR16/60) column in PBS buffer. Fractions corresponding to the conjugate (based on RI, UV detection of polymer) were collected and concentrated by ultrafiltration (Centricon 30, Amicon). The yield of conjugates WGA-P(CsA) and PNA-(CsA) was 58 and 52 mg, respectively, after dialysis and freeze drying. The content of polymer (and CsA) was determined by azo absorbance and the content of lectin by Lowry assay (after subtraction of polymer background; usually less than 5%, relative to protein absorbance response). The content of CsA derivative and protein were 16.0 wt-% and 36.5 wt-%, respectively, in WGA-P(CsA) conjugate and 11.5 wt-% and 54.5 wt-%, respectively, in PNA-P(CsA) conjugate.

Incubation of P(CsA) with rat small intestine content. The small intestine contents were isolated from sacrificed rats and diluted to 10 % with PBS. The suspension was

homogenized and the supernatant was used for enzymatic cleavage study. The enzymatic activity of the supernatant was first evaluated with Z-Ala-Ala-Leu-NAp, and 50 % of p-nitroaniline was released from the substrate after one-hour incubation at 37 °C. P(CsA) (6.9 mg, 0.9 mg of **3**) in 1.0 ml PBS was incubated with 300 μl of the supernatant at 37 °C for 5 hours. The incubation mixture was extracted with methylene dichloride, and the organic extract was analyzed with HPLC (MICROSORB-MV column, eluted with a gradient of acetonitrile and water at 50 °C) pure CsA as an external standard.

Cleavage of aromatic azo bond of HPMA copolymer-CsA derivative conjugate. A suspension of rat cecal contents and D-glucose in PBS buffer (pH = 7.4) was saturated with nitrogen and preincubated for 14 h at 37 °C. An HPMA copolymer-CsA derivative conjugate was added to the suspension. The final concentrations of the conjugate, D-glucose and cecum contents (freeze-dried) were 0.47 mg/ml, 2.94 mg/ml and 1.82 mg/ml, respectively. The reaction mixture was further incubated at 37 °C under anaerobic condition. At time intervals samples (0.6 ml) were withdrawn in nitrogen atmosphere, and 2 M NaOH (40 μl) was added to stop the reaction. Each sample was centrifuged at 7000 g for 20 min, and the absorbance difference at 360 nm and 600 nm of the supernatant was determined. The absorbance at 360 nm, reflecting the concentration of the aromatic azo bond, decreased with increasing incubation time. The reaction mixture was extracted with methylene dichloride, and the extract was analyzed by HPLC (MICROSORB-MV, eluted a gradient of acetonitrile and water at 50 °C), and matrix assisted laser desorption ionization time of flight mass spectrometry.

ARTICLES

Hydrogen Gas Evolution and Carbon Dioxide Fixation with Visible Light by Chlorophyllin Coupled with Polyethylene Glycol

Tetsuji Itoh, Hideharu Asada, Kazunori Tobioka, Yoh Kodera, Ayako Matsushima, Misao Hiroto, Hiroyuki Nishimura, Toshiaki Kamachi,† Ichiro Okura,† and Yuji Inada*

Toin Human Science and Technology Center, Department of Biomedical Engineering, Toin University of Yokohama, Kurogane-cho, Aoba-ku, Yokohama 225-8502 Japan, and Department of Bioengineering, Tokyo Institute of Technology, Nagatsuta, Midori-ku, Yokohama 226-8501, Japan. Received April 21, 1999; Revised Manuscript Received September 20, 1999

Chlorophyllin *a* was conjugated with α-(3-aminopropyl)-ω-methoxypoly(oxyethylene), PEG-NH_2, to form the PEG−chlorophyllin conjugate through acid-amide bonds. The PEG−chlorophyllin conjugate was stable toward light illumination under anaerobic condition in comparison with chlorophyllin *a*. The conjugate catalyzed the reduction of methyl viologen in the presence of 2-mercaptoethanol and the evolution of hydrogen gas in the presence of methyl viologen (an electron carrier), 2-mercaptoethanol (an electron donor) and hydrogenase (Scheme 1). Furthermore, the PEG−chlorophyllin conjugate catalyzed the photoreduction of $NADP^+$ or NAD^+ in the presence of ascorbate as an electron donor and ferredoxin-$NADP^+$ reductase as the coupling enzyme. Utilizing the reducing power of NADPH generated by the PEG−chlorophyllin conjugate under the illumination, CO_2 fixation was accomplished by the synthesis of malate (C_4) from pyruvate (C_3) and CO_2 in the presence of malic enzyme (Scheme 2). These reactions mentioned above did never proceed in dark or without each emzyme.

INTRODUCTION

Chemical modification of proteins with poly(ethylene glycol) (PEG), nontoxic, nonimmunogenic and amphiphathic polymer has been extensively studied for the purpose of applying proteins to biomedical and biotechnological processes (*1*, *2*). Exogenous enzymes such as L-asparaginase with antitumor activity and adenosine deaminase (ADA) were successfully modified with PEG to reduce their immunoreactivity and immunogenicity (*3*, *4*). In the biotechnological field, PEG-modified hydrolases became soluble and active in hydrophobic media and catalyzed the reverse reactions of hydrolysis, ester synthesis, and ester exchange reactions (*5*, *6*). Along this line of investigations, Itoh et al. (*7*) reported that chlorophyllin *a* was conjugated with α-(3-aminopropyl)-ω-methoxypoly(oxyethylene), PEG-NH_2,[1] to form PEG−chlorophyllin through acid−amide bonds. The PEG−chlorophyllin conjugate was soluble not only in aqueous solution but also in organic solvents and possessed a potent photosensitizing activity to produce superoxide anion during the illumination, although chlorophyllin immediately lost its activity by light illumination.

It is well-known that chlorophyll molecules, in vivo, bind to proteins to form chlorophyll−protein conjugates in the layered thylakoid membrane of chloroplast and exhibit physiological functions: the photolysis of water and the reduction of $NADP^+$ and CO_2 fixation under visible light illumination (*8*). Photocatalytic reduction of carbon dioxide was reported using semiconductor photocatalysis such as titanium oxide (TiO_2), silicon carbide (SiC) (*9*), and strontinum titanate ($SrTiO_3$) (*10*) under the illumination of ultraviolet ray. Furthermore, Willner et al. (*11*−*13*, *25*, *26*) reported CO_2 fixation and synthesis of amino acid via photoreduction of $NAD(P)^+$ by ruthenium(II)-tris-bipyridine, $Ru(bpy)_3^{2+}$, or Zn(II)-*meso*-(*N*-tetramethylpyridinium)porphyrin, Zn-$TMPyP^{4+}$, as photosensitizer under visible light. Okura et al. (*14*, *15*) observed the hydrogen evolution using zinc *meso*-tetraphenylporphyrintrisulfonate (Zn-$TPPS_3$) as a photosensitizer in the presence of an electron donor and an electron carrier under visible light illumination.

On the other hand, chlorophylls obtained by extracting with an organic solvent from living leaves have been seldom used as a photocatalyst because they are quite unstable on illumination. Quite recently, we reported a photostable chlorophyll *a*-poly(vinylpyrrolidone)−smectite conjugate, which catalyzes photoreduction and hydrogen gas evolution under visible light (*16*).

The present paper deals with the photostability of the PEG−chlorophyllin conjugate under anaerobic condition and photochemical functions of the PEG−chlorophyllin conjugate: hydrogen gas evolution, photoreduction of

* To whom correspondence should be addressed. Phone: +81-45-974-5060. Fax: +81-45-972-5972.

† Tokyo Institute of Technology.

[1] Abbreviations: PEG-NH_2, α-(3-aminopropyl)-ω-methoxypoly(oxyethylene); PEG, polyethylene glycol; ADA, adenosine deaminase; $Ru(bpy)_3^{2+}$, ruthenium(II)-tris-bipyridine; Zn-$TMPyP^{4+}$, Zn(II)-*meso*-(*N*-tetramethylpyridinium)porphyrin; Zn-$TPPS_3$, *meso*-tetraphenylporphyrintrisulfonate; MV^{2+}, methyl viologen; MV^+, methyl viologen cation radical.

10.1021/bc990045t CCC: $19.00 © 2000 American Chemical Society
Published on Web 12/16/1999

$NADP^+$ or NAD^+, and CO_2 fixation, that is formation of malate (C_4) from pyruvate (C_3) and CO_2.

EXPERIMENTAL PROCEDURES

General. Chlorophyll *a* purified from *Spirulina* and $NADP^+$ were purchased from Wako Pure Chemical Industries, Ltd. (Osaka, Japan). Ferredoxin-$NADP^+$ reductase (EC 1.18.1.2) and malic enzyme, [(*S*)-malate, $NADP^+$ oxidoreductase(oxaloacetate-decarboxylating), EC 1.1.1.40] were obtained from Sigma Chemical Co. (St. Louis, MO). α-(3-Aminopropyl)-ω-methoxypoly(oxyethylene) with an average molecular weight of 5050, PEG-NH_2, was kindly provided by Nippon Oil and Fats Co., Ltd. (Tokyo, Japan). Hydrogenase was isolated from *Desulfovibrio vulgaris* according to Yagi's method (*17*). Other reagents used were of analytical grade.

PEG−Chlorophyllin Conjugate. Purified chlorophyllin *a* was prepared by the method of Oster et al. (*18*) as follows: chlorophyll *a* (50 mg) dissolved in benzene (3 mL) was diluted with 47 mL of *n*-hexane and was saponified to chlorophyllin *a* by adding 1 mL of 7% KOH in methanol. After neutralizing excess alkali by bubbling carbon dioxide, purified chlorophyllin *a* was obtained by filtration, evaporation, and dialysis against water. Chlorophyllin *a* conjugated with PEG-NH_2, the PEG−chlorophyllin conjugate, was prepared as follows (*7*). To chlorophyllin *a* (2.2 μmol) dissolved in 3 mL of 50 mM tris-HCl buffer (pH 7.8) was added 6.6 μmol of PEG-NH_2, followed by adding stepwise 1-ethyl-3-(3-dimethylaminopropyl)carbodiimide (100 mg). The mixture was stirred for 6 h at room temperature to complete the reaction. After adding 50 mL of chloroform to the reaction mixture, the PEG−chlorophyllin conjugate was extracted into the chloroform layer followed by evaporation to obtain the PEG−chlorophyllin conjugate powder. Since the chlorophyllin *a* molecule has three carboxyl groups (*18*), three PEG chains bind to chlorophyllin *a* with acid−amide bonds to form the PEG−chlorophyllin conjugate (*7*). The amino group in tris, tris(hydroxymethyl)aminomethane, did not react with carboxyl groups in chlorophyllin, which is proved by analyzing with NMR and IR analyses. Photostability of chlorophyllin derivative under anaerobic condition was tested as follows: PEG−chlorophyllin conjugate (13 μM) and chlorophyllin *a* (14 μM) in 3 mL of 50 mM phosphate buffer (pH 7.4) were illuminated by a 60 W incandescent lamp at a distance of 10 cm (light intensity = 200 J m^{-2} s^{-1}) at 30 °C.

Photoreduction of Methyl Viologen and Evolution of Hydrogen Gas. Photoreduction of methyl viologen by the PEG−chlorophyllin was tested in the presence of 2-mercaptoethanol. The PEG−chlorophyllin conjugate (13.8 nmol) was dissolved in 3 mL of 25 mM Tris-HCl buffer (pH 7.4) containing 0.6 μmol of methyl viologen (MV^{2+}) and 1 mmol of 2-mercaptoethanol. The sample mixture was deaerated by repeated freeze−pump−thaw cycles and was illuminated with a 60 W incandescent lamp at a distance of 3.5 cm, light-intensity: 1500 J m^{-2} s^{-1}, at 30 °C. The photochemical reduction of methyl viologen was observed by measuring the absorbance increase at 605 nm, using the molar extinction coefficient of 1.65×10^4 M^{-1} cm^{-1}.

Hydrogen gas evolution by the PEG−chlorophyllin conjugate in the presence of methyl viologen (MV^{2+}), 2-mercaptoethanol, and hydrogenase was tested according to the modified method of Okura et al. (*14*, *15*). The reaction system (3 mL) consisted of PEG−chlorophyllin (4.2 or 15 nmol) dissolved in 25 mM Tris-HCl buffer (pH 7.4) in the presence of 0.6 μmol of methyl viologen (MV^{2+}),

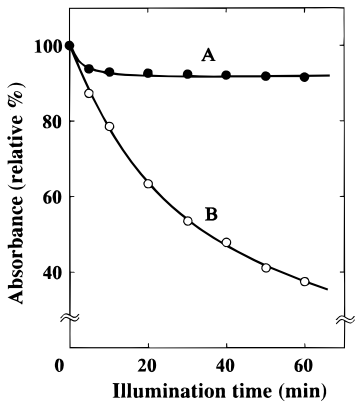

Figure 1. Photostability of chlorophyllin *a* and the PEG−chlorophyllin conjugate under anaerobic condition. (A, B) The PEG−chlorophyllin conjugate (0.13 μM) and chlorophyllin *a* (0.14 μM) in aqueous solution, respectively. Samples were illuminated with a 60 W incandescent lamp at distance of 10 cm (light intensity of 200 J m^{-2} s^{-1}) at 30 °C. The peak positions of the PEG−chlorophyllin conjugate and chlorophyllin a in aqueous solution were 657 and 654 nm, respectively.

Scheme 1

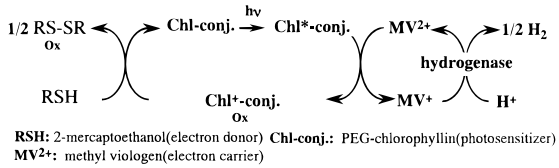

Scheme 2

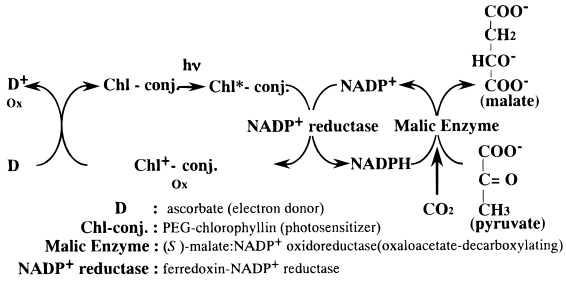

2-mercaptoethanol (1 mmol) and hydrogenase solution (40 μL). The sample mixture in a Pyrex cell (17.5 cm^3) was deaerated by repeated freeze−pump−thaw cycles and the upper space of the cell (14.5 cm^3) was filled up with argon gas. The sample in the cell equipped with a magnetic stirrer bar was illuminated with a 200 W tungsten lamp (light intensity, 200 J m^{-2} s^{-1}). Ultraviolet ray with wavelength shorter than 390 nm was cut off by a Toshiba L-39 filter (Tokyo, Japan). The hydrogen gas evolved in sample cell was taken out through sampling valve and was analyzed by gas chromatography (*14*, *15*).

Photoreduction of $NADP^+$ and NAD^+. Photoreduction of $NADP^+$ or NAD^+ was performed as the method described by Vernon et al. (*19*) with some minor modification. The pH value in the sample mixture was maintained at 7.8 by 33 mM Tris-HCl buffer. The reaction mixture (3 mL) contained the PEG−chlorophyllin (4.5 μM), ascorbate (3.3 mM), $NADP^+$ or NAD^+ (0.33 mM), and ferredoxin-$NADP^+$ reductase (2.5 units). The sample mixture was deaerated by repeated freeze−pump−thaw cycles and was illuminated with a 60 W incandescent lamp at a distance of 3.5 cm, light intensity: 1500 J m^{-2} s^{-1}, at 30 °C. The photochemical

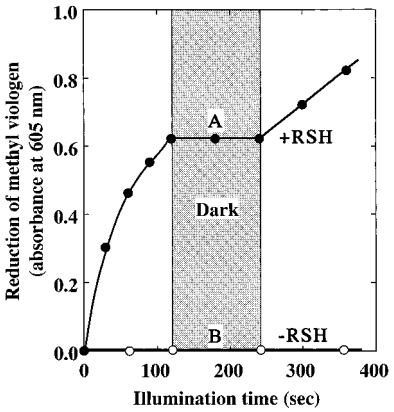

Figure 2. Photoreduction of methyl viologen by the PEG−chlorophyllin conjugate in the presence of 2-mercaptoethanol under illumination with a 60 W incandescent lamp at a distance of 3.5 cm (light intensity = 1500 J m^{-2} s^{-1}) at 30 °C. (A) PEG−chlorophyllin conjugate (13.8 nmol), methyl viologen (0.6 μmol), and 2-mercaptoethanol (1 mmol) in 3 mL of 25 mM Tris-HCl buffer at pH 7.4.(B) In the absence of 2-mercaptoethanol.

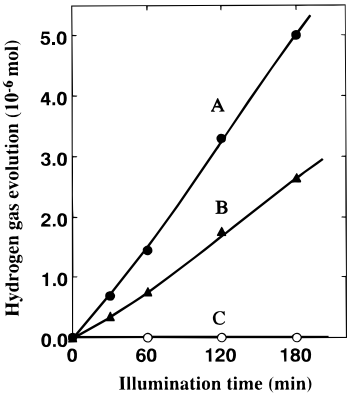

Figure 3. Hydrogen gas evolution by the PEG−chlorophyllin conjugate in the presence of 2-mercaptoethanol, methyl viologen, and hydrogenase under illumination with visible light (light intensity of 200 J m^{-2} s^{-1}) at 30 °C. (A, B) PEG−chlorophyllin conjugates of 15 and 4.2 nmol, respectively, in the presence of 2-mercaptoethanol (1 mmol), methyl viologen (0.6 μmol), and hydrogenase (40 μL) in 3 mL of 25 mM Tris-HCl buffer at pH 7.4. (C) In dark.

reduction of $NADP^+$ or NAD^+ was observed by measuring the absorbance increase at 340 nm, using the molar extinction coefficient of 6.22×10^3 M^{-1} cm^{-1}.

Carbon Dioxide Fixation via Photoreduction of $NADP^+$. To the sample mixture of the PEG−chlorophyllin conjugate (15 μM), $NADP^+$ (3.2 mM), pyruvate (0.8 mM), magnesium chloride (15 mM) and ascorbate (6 mM) dissolved in 10 mL of 50 mM phosphate buffer (pH 7.0) were added ferredoxin-$NADP^+$ reductase (2.5 units) and malic enzyme (5 units). The sample mixture in a three-necked round-bottomed flask was deaerated by repeated freeze−pump−thaw cycles. Then sodium hydrogen carbonate (180 mM) was added to the sample mixture (the pH value shifted to 7.4) and the upper space of the cell was filled with argon gas. The sample solution was stirred with a magnetic stirrer and was illuminated with a 60 W incandescent lamp from a distance of 10 cm (light intensity, 200 J m^{-2} s^{-1}) at 30 °C. The amount of malate formed by the coupling reaction of pyruvate and CO_2 through NADPH (see Scheme 2) was determined by the method described by Ochoa et al. (*20*, *21*).

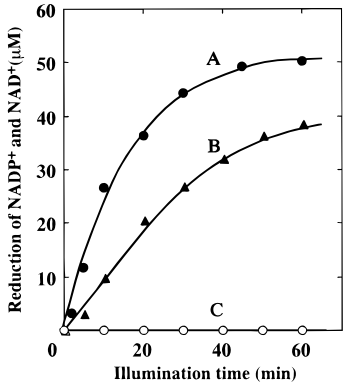

Figure 4. Photoreduction of $NADP^+$ or NAD^+ by the PEG−chlorophyllin conjugate under illumination with a 60 W incandescent lamp at a distance of 3.5 cm (light intensity = 1500 J m^{-2} s^{-1}) at 30 °C. (A) The PEG−chlorophyllin conjugate (4.5 μM), ascorbate (3.3 mM), monosodium $NADP^+$ (0.33 mM), and ferredoxin-$NADP^+$ reductase (2.5 U) in 3 mL of 33 mM Tris-HCl buffer at pH 7.8. (B) Monosodium NAD^+ (0.33 mM) was used instead of monosodium $NADP^+$ in the above reaction system. (C) In dark.

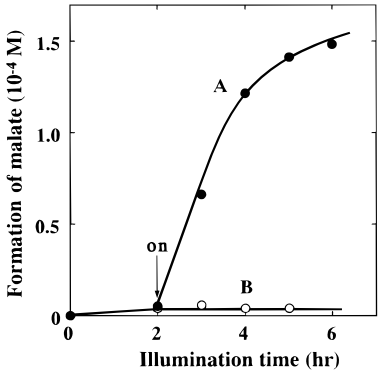

Figure 5. Carbon dioxide fixation by the PEG−chlorophyllin conjugate in the presence of ascorbate, magnesium chloride, CO_2, pyruvate, $NADP^+$, ferredoxin-$NADP^+$ reductase and malic enzyme under illumination with a 60 W incandescent lamp at distance of 10 cm (light intensity of 200 J m^{-2} s^{-1}) at 30 °C. (A) The PEG−chlorophyllin conjugate (15 μM), ascorbate (6 mM), sodium hydrogen carbonate (180 mM), magnesium chloride (15 mM), pyruvate (0.8 mM), $NADP^+$ (3.2 mM), ferredoxin-$NADP^+$ reductase (2.5 U) and malic enzyme (5 U) in 10 mL of 50 mM phosphate buffer at pH 7.4. (B) In dark.

RESULTS AND DISCUSSION

Photostability of PEG−Chlorophyllin Conjugate under Anaerobic Conditions. It is well-known that chlorophylls extracted from living leaves are markedly breached by light illumination. Therefore, the stabilization of chlorophyll and its derivatives toward light illumination is essential to develop the artificial photosynthesis system in the future. In the present study, two kinds of chlorophyll derivatives, chlorophyllin *a* and the PEG−chlorophyllin conjugate, were subjected to photostability test under anaerobic condition. The results are shown in Figure 1; curves A and B show the photostabilization of the PEG−chlorophyllin conjugate and chlorophyllin *a* in aqueous solution under anaerobic conditions, respectively. The PEG−chlorophyllin conjugate (curve A) was more stable than chlorophyllin *a* (curve B). In aerobic conditions, the stability of each pigment was extensively reduced by light illumination in comparison with that in anaerobic conditions.

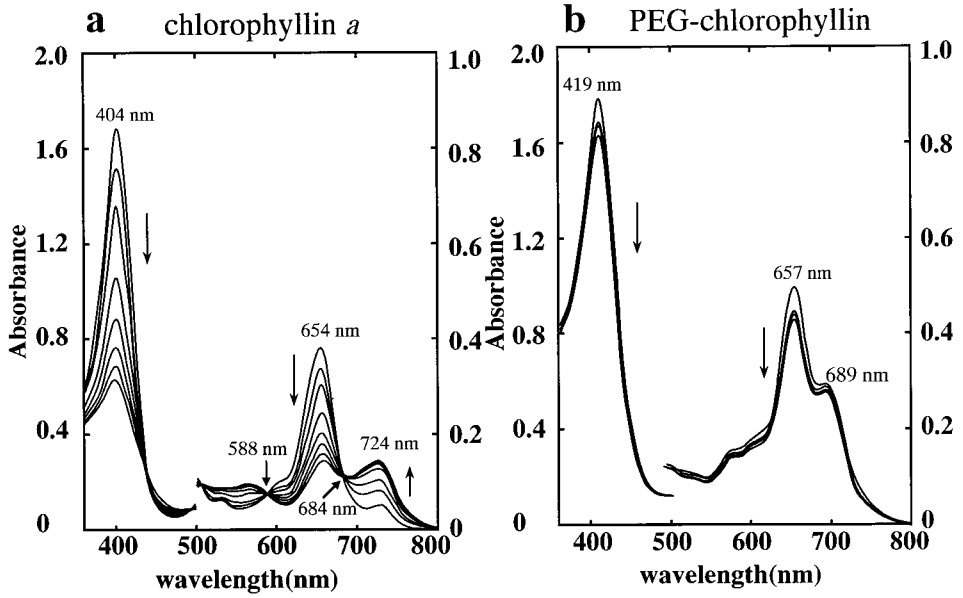

Figure 6. Spectral change of chlorophyllin and the PEG−chlorophyllin conjugate by light illumination under anaerobic condition. (a, b) Chlorophyllin *a* (0.14 μM) and the PEG−chlorophyllin conjugate (0.13 μM) in aqueous solution, respectively. Samples were illuminated with a 60 W incandescent lamp at distance of 10 cm (light intensity of 200 J m^{-2} s^{-1}) at 30 °C. Illumination time: 0, 5, 10, 20, 30, 40, 50, and 60 min.

Photoreduction of Methyl Viologen and Evolution of Hydrogen Gas. Photochemical redox system has been developed for the purpose of solar energy utilization (*16*), which is shown in Scheme 1. The system, including a photosensitizer (the PEG−chlorophyllin conjugate), an electron donor (2-mercaptoethanol), and electron carrier (methyl viologen) in Tris-HCl buffer (pH 7.4), has been able to evolve hydrogen gas when suitable catalyst (hydrogenase) is applied. A first series of experiments was conducted to test whether the PEG−chlorophyllin conjugate induces the reduction of methyl viologen by light illumination. Figure 2 represents the photoreduction of methyl viologen by the PEG−chlorophyllin conjugate. When a sample solution containing the PEG−chlorophyllin conjugate is illuminated in the presence of methyl viologen and 2-mercaptoethanol, the absorbance at 605 nm due to MV^+ was sharply increased with illumination time. The reduction of methyl viologen ceased completely in the dark and the reduction proceeded again on light, which is shown by curve A. Without 2-mercaptoethanol (electron donor) in the reaction system, no photoreduction of methyl viologen took place even by light illumination (curve B).

Since the reduction of methyl viologen proceeds in coupling reaction of the PEG−chlorophyllin conjugate and 2-mercaptoethanol by light illumination, the next experiment was conducted whether hydrogen gas is evolved or not in the presence of hydrogenase as shown in Scheme 1. Figure 3 shows the hydrogen gas evolution by PEG−chlorophyllin conjugate in the presence of 2-mercaptoethanol, methyl viologen and hydrogenase under illumination with visible light. The amount of hydrogen gas was linearly increased with illumination time depending upon the amount of the PEG−chlorophyllin conjugate. Curves A and B were the results obtained by 15 and 4.2 nmol of the PEG−chlorophyllin conjugate, respectively. No evolution of hydrogen gas was observed in the dark (curve C). In curve B, approximately 2.6 μmol of hydrogen gas was evolved for 3 h of illumination. Therefore, the amount of hydrogen ion reduced by the 3 h illumination is 5.2 μmol, which is 1200 times greater than 4.2 nmol of the PEG−chlorophyllin in the reaction system. From the results obtained above, it can be concluded that PEG−chlorophyllin conjugate excited by illumination (Chl*−conj) releases an electron and changes to cationic PEG−chlorophyllin conjugate (Chl^+−conj). The released electron reduces methyl viologen dication (MV^{2+}) to methyl viologen cation radical (MV^+), which reduces hydrogen ion to form hydrogen gas by the catalytic action of hydrogenase. On the other hand, cationic Chl^+−conj is reduced by 2-mercaptoethanol as electron donor to be reproduced as the PEG−chlorophyllin conjugate (Scheme 1).

Carbon Dioxide Fixation via Photoreduction of $NADP^+$. A next series of experiments was conducted to test whether the PEG−chlorophyllin conjugate induces the reduction of $NADP^+$ or NAD^+ followed by the carbon dioxide fixation, which is shown in Scheme 2. CO_2 fixation via photoreduction of NADP by the PEG−chlorophyllin conjugate was conducted, in which the formation of malate (C_4) from pyruvate (C_3) and CO_2 proceeds with the generation of NADPH in the presence of malic enzyme. Figure 4 represents the photoreduction of $NADP^+$ or NAD^+ by the PEG−chlorophyllin in the presence of ascorbate (electron donor). The absorbance at 340 nm due to NADPH or NADH is increased with illumination−time, which is shown by curve A or B, respectively. However, no reduction of $NADP^+$ or NAD^+ was observed in the dark (curve C). In the absence of ascorbate or ferredoxin-$NADP^+$ reductase in the reaction system, no photoreduction of $NADP^+$ or NAD^+ occurs, even by light illumination (data not shown).

Since the reduction of $NADP^+$ proceeds in coupling reaction of the PEG−chlorophyllin conjugate and ascorbate in the presence of ferredoxin-$NADP^+$ reductase by light illumination, a next experiment was conducted to test whether CO_2 fixation proceeds in the presence of pyruvate, carbon dioxide, and malic enzyme. Figure 5 shows the formation of malate (C_4) from pyruvate (C_3) and CO_2 under illumination in the presence of ascorbate, the PEG−chlorophyllin conjugate, $NADP^+$, ferredoxin-$NADP^+$ reductase and malic enzyme. The amount of malate is markedly increased with time after illumination (curve A). During illumination for 4 h, the amount

of malate synthesized from pyruvate and CO_2 was 0.15 mM in which approximately 18.5% of pyruvate (0.8 mM) was converted to malate. No appreciable synthesis of malic acid from pyruvate and CO_2 is observed in dark which is shown by curve B.

The success of the present study is based on the finding of photostable chlorophyllin *a* conjugated with methoxypolyoxyethylene amine with the molecular weight of 5050, the PEG−chlorophyllin conjugate. Generally, chlorophyll derivatives including chlorophyllin and the PEG−chlorophyllin are not photostable in aerobic conditions (*7*, *16*). However, in anaerobic conditions, the PEG−chlorophyllin conjugate is extensively stable in aqueous solution in comparison with chlorophyllin. Figure 6 represents their spectral changes of chlorophyllin and the PEG−chlorophyllin conjugate in aqueous solution under anaerobic conditions by light illumination. The absorption spectra of chlorophyllin and the PEG−chlorophyllin conjugate are shown in Figure 6, panels a and b, respectively. In the case of chlorophyllin, the absorption maximum at 654 nm is lowered with illumination followed by appearing a new band at 724 nm with the isobestic points at 684 and 588 nm. The Soret band at 404 nm is also lowered with illumination. On the other hand, the absorption spectrum of PEG−chlorophyllin conjugate with an absorption maximum at 657 nm with a shoulder at 689 nm is scarcely lowered by illumination. These phenomena are noteworthy facts, although the reason is unclear. A conceivable possibility of the phenomenon may be due to the interaction of tetrapyrrole ring having magnesium with long carbon chain $(CH_2-CH_2-O)_n$ of poly(ethylene glycol). The changes of absorbance at 654 nm (peak position of chlorophyllin *a*) and at 657 nm (peak position of the PEG−chlorophyllin conjugate) with light illumination are shown in Figure 1.

The chemical modification of bioactive substances with low molecular weight by polyethylene glycol derivatives has been extensively studied. Polyethylene glycol-modified hemin(PEG-hemin) with amphipathic properties exhibited peroxidase activity in organic solvents as well as in an aqueous solution (*22*). This technique became a good tool for determining peroxide in unsaturated fatty acids and lipids (*23*). PEG−hematoporphyrin with amphipathic properties acted as a photosensitizer; imidazole and indole were photooxidized in organic solvents, and uric acid was also photooxidized in neutral aqueous solution (*24*).

The PEG−chlorophyllin conjugate, which is photostable in anaerobic conditions, catalyzed the CO_2 fixation though formation of NADPH by light illumination. This finding may lead to not only the prevention of the Greenhouse effect due to accumulation of CO_2 in terrestrial ecosystem but also photosynthesis in vitro.

LITERATURE CITED

(1) Kodera, Y., Matsushima, A., Hiroto, M., Nishimura, H., Ishii, A., Ueno, T., and Inada, Y. (1998) Pegylation of proteins and bioactive substances for medical and technical applications. *Prog. Polym. Sci. 23*, 1233−1271.

(2) Inada, Y., Yoshimoto, T., Matsushima, A., and Saito, Y. (1986) Engineering physicochemical and biological properties of proteins by chemical modification. *Trends Biotechnol. 4*, 68−73.

(3) Yoshimoto, T., Nishimura, H., Saito, Y., Sakurai, K., Kamisaki, Y., Wada, H., Sako, M., Tsujino, G., and Inada, Y. (1986) Characterization of polyethylene glycol-modified L-asparaginase from *Escherichia coli* and its application to therapy of leukemia. *Jpn. J. Cancer Res. Gann. 77*, 1264−1270.

(4) Weinberg, K., Hershfield, M. S., Bastian, J., Kohn, D., Sender, L., Parkman, R., and Lenarsky, C. (1986) T lymphocyte ontogeny in adenosine deaminase-deficient severe combined immune deficiency after treatment with polyethylene glycol-modified adenosine deaminase. *J. Clin. Invest. 92*, 596−602.

(5) Inada, Y., Nishimura, H., Takahashi, K., Yoshimoto, T., Saha, A. R., and Saito, Y. (1984) Ester synthesis catalyzed by polyethylene glycol-modified lipase in benzene. *Biochem. Biophys. Res. Commun. 122*, 845−850.

(6) Matsushima, A., Kodera, Y., Hiroto, M., Nishimura, H., and Inada, Y. (1996) Bioconjugates of proteins and polyethylene glycol: potent tools in biotechhnological processes. *J. Mol. Catal B: Enzym. 2*, 1−17.

(7) Itoh, T., Ishii, A., Kodera, Y., Hiroto, M., Matsushima, A., Nishimura, H., and Inada, Y. (1996) Chlorophyllin coupled with polyethylene glycol: A potent photosensitizer. *Res. Chem. Intermed. 22*, 129−136.

(8) Scheer, H. (1991) In *Chlorophylls* (H. Scheer, Eds.) CRC Press, London.

(9) Inoue, T., Fujishima, A., Konishi, S., and Honda, K. (1979) Photoelectrocatalytic reduction of carbon dioxide in aqueous suspensions of semiconductor powders. *Nature 277*, 637−638.

(10) Aurian-Blajeni, B., Halmann, M., and Manassen, J. (1980) Photoreduction of carbon dioxide and water into formaldehyde and methanol on semiconductor meterials. *Solar Energy 25*, 165−170.

(11) Willner, I., and Mandler, D. (1989) Enzyme-catalysed biotransformations through photochemical regeneration of nicotinamide cofactors. *Enzyme Microb. Technol. 11*, 467−483.

(12) Mandler, D., and Willner, I. (1984) Solar light induced formation of chiral 2-butanol in an enzyme-catalyzed chemical system. *J. Am. Chem. Soc. 106*, 5352−5353.

(13) Mandler, D., and Willner, I. (1986) Photoinduced enzyme-catalysed synthesis of amino acids by visible light. *J. Chem. Soc., Chem. Commun.* 851−853.

(14) Okura, I., Kaji, N., Aono, S., Kita, T., and Yamada, A. (1985) Photoinduced hydrogen evolution using bipyridinium salts as electron carrier. *Inorg. Chem. 24*, 451−453.

(15) Okura, I., Kusunoki, S., and Aono, S. (1984) The complexation of zinc tetraphenylporphyrintrisulfonate by viologen and its role in photoredox processes. *Bull. Chem. Soc. Jpn. 57*, 1184−1188.

(16) Itoh, T., Ishii, A., Kodera, Y., Matsushima, A., Hiroto, M., Nishimura, H., Tsuzuki, T., Kamachi, T., Okura, I., and Inada, Y. (1998) Photostable chlorophyll *a* with poly(vinylpyrrolidone)-smectite catalyzes photoreduction and hydrogen gas evolution by visible light. *Bioconjugate Chem. 9*, 409−412.

(17) Yagi, T. (1970) Solubilization, purification and properties of particulate hydrogenase from *Desulfovibrio vulgaris*. *J. Biochem. 68*, 694.

(18) Oster, G., Broyde, S. B., and Bellin, J. S. (1964) Spectral properties of chlorophyllin *a*. *J. Am. Chem. Soc. 86*, 1309−1313.

(19) Vernon, L. P., San Pietro, A., and Limbach, D. A. (1965) Photoreduction of NAD and NADP by chlorophyllin *a* in the presence of ascorbate: Requirement for NADP reductase. *Arch. Biochem. Biophys. 109*, 92−97.

(20) Ochoa, S., Mehler, A., and Kornberg, A. (1947) Reversible oxidative decarboxylation of malic acid. *J. Biol. Chem. 167*, 871−872.

(21) Ochoa, S., Mehler, A. H., and Kornberg, A. (1948) Biosynthesis of dicarboxylic acids by carbon dioxide fixation. *J. Biol. Chem. 174*, 979−1000.

(22) Takahashi, K., Matsushima, A., Saito, Y., and Inada, Y. (1986) Polyethylene glycol-modified hemin having peroxidase activity in organic solvents. *Biochem. Biophys. Res. Commun. 138*, 283−288.

(23) Ajima, A., Cao, S. G., Takahashi, K., Matsushima, A., Saito, Y., and Inada, Y. (1987) An attempt to determine lipid peroxides with polyethylene glycol-modified hemin *Biotechnol. Appl. Biochem. 9*, 53−57.

(24) Kodera, Y., Ajima, A., Takahashi, K., Matsushima, A., Saito, Y., and Inada, Y. (1988) Polyethylene glycol-modified hematoporphyrin as photosensitizer *Photochem. Photobiol. 47*, 221−223.

(25) Willner, I., Mandler, D., and Riklin, A. (1986) Photoinduced carbon dioxide fixation forming malic and isocitric acid. *J. Chem. Soc. Chem. Commun.* 1022−1024.

(26) Willner, I., and Willner, B. (1991) Artificial photosynthetic model systems using light-induced electron-transfer reactions in catalytic and biocatalytic assemblies. *Top. Curr. Chem. 159*, 153-218.

BC990045T

Synthesis of Polyamide Oligomers Based on 14-Amino-3,6,9,12-tetraoxatetradecanoic Acid

Rajiv Dhawan, Mark G. A. Kadijk, Terry J. Joikinen, Michael Feng, and Steven M. Ansell*

Inex Pharmaceuticals Corp., 100-8900 Glenlyon Parkway, Burnaby, B.C., V5J 5J8, Canada.
Received December 1, 1998; Revised Manuscript Received October 22, 1999

A series of oligomers of polyamides based on 14-amino-3,6,9,12-tetraoxatetradecanoic acid monomers (ATTAn) was synthesized. These materials were designed as monodisperse analogues of poly(ethylene glycol) for use in biomedical applications where reproducible behavior is important. Synthesis of the monomer was evaluated using two routes. For small-scale preparations, tetraethylene glycol (TEG) was monoprotected with dihydropyran, converted to an alkoxide, and alkylated with ethyl bromoacetate. On larger scales, TEG was alkylated directly by treatment with sodium, followed by ethyl bromoacetate. The amine function was introduced by mesylation followed by treatment with sodium azide. Reduction of the azide to amino groups was performed over Pd/C using either hydrogen or formic acid as proton sources. Assembly of the oligomers was accomplished using standard DCC/NHS chemistry and an iterative dimerization sequence after appropriate deprotection of a pair of monomers. The amino group was protected by retaining the azido group as a latent amine. A series of ATTAn oligomers was prepared ($n = 1-8$). A lipid conjugate of the octamer, ATTA8-DSPE, was synthesized.

INTRODUCTION

Poly(ethylene glycol) (PEG)[1] has been widely used for the modification of surfaces in biomedical applications in order to reduce undesirable interactions with the biological milieu (*1*). PEG has many useful properties that make it attractive material for use in these applications, including (a) solubility in organic as well as aqueous environments; (b) low toxicity; (c) low immunogenicity; (d) chemical stability; and (e) low cost. The polymer has been particularly useful in drug delivery systems, for example, by derivatizing drugs, peptides, or proteins to improve water solubility or to reduce clearance rates in vivo. Another important application involves coating the surfaces of particulates, such as polymer beads or liposomes which have been used as drug delivery systems, to increase the clearance half-life in vivo (*2, 3*) or to reduce aggregation of these systems during preparation (*4*).

We have been developing drug delivery systems based on liposomes or lipid-based particulates for the delivery of conventional therapeutic agents or genetic medicines, such as plasmid DNA (*5*) or antisense oligonucleotides.[2] In many of these systems we make extensive use of various PEG−lipids to control particle formation and/or in vivo behavior. PEG functions as a steric barrier on liposome surfaces which inhibits interactions with other surfaces or macromolecules in solution. This property allows us to use these compounds for a variety of purposes, for example, prevention of aggregation reactions during formulation and changing pharmacokinetic behavior in vivo. PEG−lipids are traditionally used in liposomes to reduce clearance rates in vivo (*2*). However, these lipids may also inhibit uptake of liposomes by cells (*6*), reduce extravasation efficiencies in target tissues (*7*), and inhibit fusion events believed to be important in the intracellular delivery of DNA by transfection reagents (*8*). To address these problems, we have been developing PEG−lipids (*9*) which exchange out of the liposomes in vivo at significant rates on pharmacologically relevant time scales. In some cases, such as with our DNA and antisense formulation, we require the presence of steric barrier molecules to prevent aggregation during the formulation process. In other cases, PEG is required to prevent rapid clearance in vivo but must exchange out before the formulation can become active. In these applications, we attempt to keep the liposomes in circulation using PEG−lipids for long enough to allow reasonable accumulation at a disease site, after which the PEG−lipid must exchange out to expose a fusogenic surface which facilitates delivery of the drug to target cells. Obviously, the exchange behavior of the PEG−lipid is critical for optimization of these formulations. This strategy is under development with formulations of conventional therapeutic agents (*10*) and plasmid DNA.[3]

* To whom correspondence should be addressed. E-mail: sansell@inexpharm.com. Phone: (604) 419-3200. Fax: (604) 419-3201.

[1] Abbreviations: PEG, poly(ethylene glycol); TEG, tetraethylene glycol; DCC, *N*,*N*-dicyclohexylcarbodiimide; NHS, *N*-hydroxysuccinimide; ATTA, 14-amino-3,6,9,12-tetraoxatetradecanoic acid; PEG-DSPE, *N*-(2′-*O*-(ω-monomethoxypoly(ethylene glycol)$_{2000}$)-acetoyl)-1,2-distearoyl-*sn*-glycero-3-phosphoethanolamine; DSPE, 1,2-distearoyl-*sn*-glycero-3-phosphoethanolamine; DSPC, 1,2-distearoyl-*sn*-glycero-3-phosphocholine; chol, cholesterol; PPTS, pyridinium *p*-toluenesulfonate.

[2] Semple, S. C., Klimuk, S. K., Harasym, T. O., Dos Santos, N., Ansell, S. M., Wong, K. F., Maurer, N., Stark, H., Cullis, P. R., Hope, M. J., and Scherrer, P. (1999) Efficient encapsulation of antisense oligonucleotides in lipid vesicles using ionizable aminolipids: formation of novel small multilammelar vesicle structures (manuscript in preparation).

[3] Tam, P., Lee, D. K., Joshi, P. B., Clow, K., Cullis, P. R., and Graham, R. W. (1999) Influence of exchangeable poly(ethylene glycol) coatings on the pharmacokinetics, tumor accumulation and tumor transfection properties of stabilized plasma-lipid particles (manuscript in preparation).

10.1021/bc9801427 CCC: $19.00 © 2000 American Chemical Society
Published on Web 12/08/1999

In all of these systems, controlling the rate of exchange is a critical aspect of the formulation design.

Fine-tuning the behavior of these systems presents considerable challenges, in part due to the nature of the PEG which is commercially available. Problems include a limited selection of molecular weights for monofunctional and heterobifunctional derivatives, polydispersity variability, and average molecular weight variability of these compounds, which potentially leads to reproducibility issues with different batches and variable exchange rates associated with different size populations. In addition, the presence of low molecular weight homomers in PEG would result in a small population of PEG−lipid, which would not be rapidly exchanged out of formulations in vivo and potentially could have major implications in systems where immune responses against PEG are an issue. We have therefore sought to develop a series of monodisperse oligomers which behave in much the same way as PEG but which can be tailored to specific sizes. We plan to use these oligomers as reproducible tools for optimizing the formulation and pharmacokinetic behavior of our lipid-based delivery systems.

Studies have suggested that any polymer which is hydrophilic and flexible in aqueous solution can be used in place of PEG in these applications, provided that it is nontoxic and nonimmunogenic (*11*−*13*). Our approach has been to prepare oligomers of poly(14-amino-3,6,9,12-tetraoxatetradecanoic acid) by using a series of dimerization reactions starting from the monomer. These convergent synthetic protocols have allowed us to prepare oligomers up to and including $n = 8$. Molecular modeling showed that the amide bonds of these oligomers are too far apart for rigid secondary structures to form, suggesting that these compounds are unlikely to be immunogenic and would be flexible enough to act as steric barriers when attached to particles. The tetraethylene glycol backbone of the oligomers allowed solubility in both organic and aqueous solutions. This is an important consideration, both for preparation of the oligomer and for conjugation to either an individual lipid or a preformed particle. ATTA8 was deprotected and conjugated to DSPE in preparation for comparative studies of the behavior of the new materials in liposomes.

EXPERIMENTAL PROCEDURES

General. All synthetic reagents were purchased from Sigma-Aldrich. Lipids from purchased from Northern Lipids, Vancouver, Canada. PEG-DSPE was synthesized as previously reported (*14*). ^{1}H NMR spectra were recorded on a Bruker MSL200 spectrometer using the solvent ($CDCl_3$, δ 7.24) as an internal standard. TLC plates were visualized using a 10% ammonium molybdate solution in aqueous sulfuric acid (10%). Elemental analyses were carried out by Quantitative Technologies Inc, NJ. Positive ion electrospray LC/MS was carried out by BRI Biopharmaceutical Research Inc., Vancouver.

Synthesis of Crude Ethyl 14-Hydroxy-3,6,9,12-tetraoxatetradecanoate 3. Method A. Concentrated hydrochloric acid (5 mL) was slowly added to a solution of dihydropyran (215 g) in **1** (600 g). The exothermic reaction was cooled in an ice bath and then stirred overnight at room temperature. The solution was diluted with water (*1l*), neutralized with excess sodium bicarbonate solution, and washed twice with diethyl ether (200 mL). The combined ethereal extracts were washed twice with water (200 mL), which in turn was washed with diethyl ether (100 mL). The combined aqueous fractions were extracted with methylene chloride (four times). The combined methylene chloride fractions were washed with water (200 mL), and the solvent was removed on a rotovap. Residual water was removed by azeotropic distillation with toluene on a rotovap (four times), yielding **2** as a colorless crude oil (390 g). The oil was dissolved in toluene (1 L) and treated with sodium (64 g) in a closed flask vented through a mineral oil bubbler. The mixture was stirred at room temperature for 5 days and then filtered through glass wool to remove unreacted sodium. Ethyl bromoacetate (100 mL) was added and the mixture refluxed for 3 h. The solution was cooled and washed with water (2 × 500 mL). The aqueous phase was washed with methylene chloride (2 × 100 mL). The organic fractions were combined and the solvent removed on a rotovap. The residue was then dissolved in ethanol (1 L) and treated with pyridium *p*-toluenesulfonate (30 g) at 60 °C for 1 h. The solution was diluted with water and washed with ether (2 × 400 mL). The ether fractions were washed with water (100 mL). The combined aqueous fractions were washed with methylene chloride (four times), yielding 180 g of crude **3** after removal of the solvent.

Synthesis of Crude Ethyl 14-Hydroxy-3,6,9,12-tetraoxatetradecanoate 3. Method B. 1 (3 kg) was treated with sodium (180 g) in a 5 L flask under argon vented through a mineral oil bubbler. The mixture was stirred at 120 °C, using a temperature controller to maintain constant temperature, overnight or until all of the sodium had dissolved. Ethyl bromoacetate (1.25 kg) was added slowly, and the mixture heated at 120 °C overnight. The suspension was cooled to room temperature, diluted with water (1:3), and washed with diethyl ether (1 L). The aqueous fractions were extracted with methylene chloride (four times). The combined methylene chloride fractions were washed with water (1 L), which in turn was washed with methylene chloride (three times). The solvent was removed under vacuum, and the residual oil dried azeotropically using toluene, yielding crude **3** as a yellow oil (∼1.4 kg). A sample was isolated by column chromatography over silica gel. ^{1}H NMR ($CDCl_3$) δ 4.15 (q, 2H, $J = 7.1$ Hz), 4.08 (s, 2H), 3.5−3.7 (m, 14H), 2.95 (t, 1H), 1.22 (t, 3H, $J = 7.1$ Hz)

Synthesis of 14-Azido-3,6,9,12-tetraoxatetradecanoic Acid 6a. Triethylamine (81 mL) was slowly added

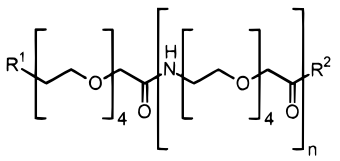

n	$R^1 = N_3$, $R^2 = OCH_2CH_3$	$R^1 = N_3$, $R^2 = OH$	$R^1 = NH_2$, $R^2 = OCH_2CH_3$
0	**4a**	**6a**	**7a**
1	**4b**	**6b**	**7b**
2	**4c**	**6c**	**7c**
3	**4d**	**6d**	**7d**
4	**4e**		
5	**4f**		
6	**4g**		
7	**4h**	**6h**	**7h**

to a stirred solution of crude **3** (110 g) and methane sulfonyl chloride (36 mL) in benzene (600 mL). The solution was stirred at room temperature for 1 h and

filtered, and the solvent removed on a rotovap. Residual methylene chloride was removed by addition of toluene followed by removal of solvent on a rotovap (three times). The residue was dissolved in ethanol (750 mL). Sodium azide (24 g) was added, and the solution refluxed for 4 h. Periodic additions of water were made as a gel-like precipitate formed to keep most of the material in solution. The mixture was then stirred at room-temperature overnight. The mixture was diluted with water and extracted with methylene chloride (six times). The combined methylene chloride fractions were washed with water, which in turn was washed with methylene chloride (four times). The solvent was removed from the combined methylene chloride fractions using a rotovap. The residue was suspended in a solution of sodium hydroxide (32 g) in water (100 mL), stirred at 45 °C for half an hour, and extracted with methylene chloride (4 × 100 mL). The aqueous fraction was acidified with concentrated hydrochloric acid and extracted with methylene chloride (3 × 100 mL). The solvent was removed from the organic fractions using a rotovap, and the residue dried by addition of ethanol followed by removal of the solvent, yielding **6a** as a yellow oil (77 g). A sample was isolated after base hydrolysis of a pure sample of **4a**. ^{1}H NMR ($CDCl_3$) δ 4.12 (s, 2H), 3.5−3.8 (m, 14H), 3.36 (t, J = 4.9 Hz, 2H).

Synthesis of Ethyl 14-Azido-3,6,9,12-tetraoxatetradecanoate 4a. A solution of anhydrous hydrogen chloride in ethanol was prepared by slow addition of acetyl chloride (100 mL) to anhydrous ethanol (500 mL), followed by stirring at room temperature for 1 h. **6a** (44 g) was added, and the solution stirred for a further hour. Water (1 L) was added and the solution extracted with methylene chloride (three times). The solvent was removed on a rotovap, and the residue passed down a silica gel column, yielding **4a** as a colorless oil. ^{1}H NMR ($CDCl_3$) δ 4.14 (q, J = 7.2 Hz, 2H), 4.07 (s, 2H), 3.55−3.7 (m, 14H), 3.31 (t, J = 5 Hz, 2H), 1.20 (t, J = 7.1H, 3H). Anal. ($C_{12}H_{23}O_6N_3$) C, H, N.

Synthesis of ω-Azido-oligo-(14-amino-3,6,9,12-tetraoxatetradecanoic) Acid 6b−d and 6h. A solution of **4b−d** and **6h** in Na_2CO_3)(aq) (4 equiv) was stirred at 50 °C for 1 h. The solution was cooled, washed with methylene chloride (two times), acidified to pH 3−5 with dilute hydrochloric acid, and extracted with methylene chloride (four times). Higher molecular weight oligomers partially extracted from the basic aqueous phase and generally required additional basic washes to separate the acid from the unhydrolizable material. The recovered acid was used in subsequent reactions without further purification.

Synthesis of Ethyl-ω-amino-oligo-(14-amino-3,6,9,12-tetraoxatetradecanoate) 7a−d. A solution of **4a−d** in ethanol was treated with formic acid (2 equiv). The solution was warmed, and palladium (10% on carbon) added slowly until evolution of nitrogen gas was self-sustaining (***Caution***: the reaction is exothermic and may require additional cooling in order to control gas evolution.) The mixture was filtered though Celite and most of the ethanol removed on a rotovap. The residue was dissolved in water, neutralized to pH 7, extracted with methylene chloride, and the water removed under vacuum. The residue was dissolved in methylene chloride and filtered to removed inorganic salts. Removal of the residual solvent yielded the crude amine **7a−d** as a pale yellow oil. The crude amine was used without further purification.

Dimerization Protocol. A solution of the oligo acid **6a−d** (1 equiv) in methylene chloride was treated with NHS (1.5 equiv). A solution of DCC (1.1 equiv) in methylene chloride was slowly added, and the resultant solution stirred at room temperature for 1 h. Oligo amine **7a−d** (1 equiv) was added, followed by triethylamine (2 equiv). The reaction mixture was stirred for a further half hour, filtered, and the solvent removed. The residue was taken up in water, acidified, filtered, and extracted with methylene chloride. The organic fraction was washed with Na_2CO_3 solution (pH 9), dried over anhydrous magnesium sulfate, filtered, and the solvent removed. Isolation of the product **4b−h** was effected by column chromatography using silica gel (2−15% methanol/methylene chloride).

Ethyl-ω-azido-di-(14-amino-3,6,9,12-tetraoxatetradecanoate) 4b. 4b was prepared from **6a** and **7a** using the dimerization protocol. ^{1}H NMR ($CDCl_3$) δ 7.2 (bs), 4.18 (q, J = 7.2 Hz, 2H), 4.10 (s, 2H), 3.97 (s, 2H), 3.4−3.7 (m, 30H), 3.35 (t, J = 5.0 Hz, 2H), 1.94 (s, H_2O), 1.25 (t, 3H, J = 7.1 Hz). Anal. ($C_{22}H_{42}O_{11}N_4$) C, H, N.

Ethyl-ω-azido-tri-(14-amino-3,6,9,12-tetraoxatetradecanoate) 4c. 4c was prepared from **6b** and **7a** using the dimerization protocol. ^{1}H NMR ($CDCl_3$) δ 7.2 (bs), 4.18 (q, J = 7.2 Hz, 2H), 4.10 (s, 2H), 3.97 (s, 4H), 3.65−3.40 (m, 46H), 3.35 (t, J = 4.8 Hz, 2H), 2.16 (bs, H_2O), 1.25 (t, J = 7.1 Hz, 3H). Anal. ($C_{32}H_{61}O_{16}N_5$) C, H, N.

Ethyl-ω-azido-tetra-(14-amino-3,6,9,12-tetraoxatetradecanoate) 4d. 4d was prepared from **6b** and **7b** using the dimerization protocol. ^{1}H NMR ($CDCl_3$) δ 7.1 (bs, 3H), 4.13 (q, J = 7.2 Hz, 2H), 4.06 (s, 2H), 3.92 (s, 6H), 3.35−3.65 (m, 62H), 3.30 (t, J = 5 Hz, 2H), 2.37 (bs, H_2O), 1.20 (t, J = 7.1 Hz, 3H). Anal. calcd ($C_{42}H_{80}O_{21}N_6$): C, 50.19; H; N, 8.36. Found: C, 49.64; H; N, 7.93.

Ethyl-ω-azido-penta-(14-amino-3,6,9,12-tetraoxatetradecanoate) 4e. 4e was repared from **6c** and **7b** using the dimerization protocol. ^{1}H NMR ($CDCl_3$) δ 7.2 (bs), 4.18 (q, J = 7.2 Hz, 2H), 4.11 (s, 2H), 3.97 (s, 8H), 3.65−3.40 (m, 78H), 3.35 (t, J = 4.8 Hz, 2H), 1.96 (s, H_2O), 1.25 (t, J = 7.1 Hz, 3H). Anal. calcd ($C_{52}H_{99}O_{26}N_7$): C, 50.43; H; N, 7.92. Found: C, 49.67; H; N, 7.38.

Ethyl-ω-azido-hexa-(14-amino-3,6,9,12-tetraoxatetradecanoate) 4f. 4f was prepared from **6d** and **7b** using the dimerization protocol. ^{1}H NMR ($CDCl_3$) δ 7.2 (bs), 4.18 (q, J = 7.2 Hz, 2H), 4.11 (s, 2H), 3.97 (s, 10H), 3.65−3.40 (m, 94H), 3.35 (t, J = 4.8 Hz, 2H), 1.95 (s, H_2O), 1.25 (t, J = 7.1 Hz, 3H). Anal. ($C_{62}H_{118}O_{31}N_8$) C, H, N.

Ethyl-ω-azido-hepta-(14-amino-3,6,9,12-tetraoxatetradecanoate) 4g. 4g was prepared from **6d** and **7c** using the dimerization protocol. ^{1}H NMR ($CDCl_3$) δ 7.2 (bs, 6H), 4.18 (q, J = 7.2 Hz, 2H), 4.11 (s, 2H), 3.97 (s, 12H), 3.65−3.40 (m, 110H), 3.35 (t, J = 4.8 Hz, 2H), 1.98 (s, H_2O), 1.25 (t, J = 7.1 Hz, 3H). Anal. ($C_{72}H_{137}O_{36}N_9$) C, H, N.

Ethyl-ω-azido-octa-(14-amino-3,6,9,12-tetraoxatetradecanoate) 4h. 4h was prepared from **6d** and **7d** using the dimerization protocol. ^{1}H NMR ($CDCl_3$) δ 7.2 (bs, 7H), 4.12 (q, J = 7.2 Hz, 2H), 4.05 (s, 2H), 3.91 (s, 14H), 3.35−3.65 (m, 126H), 3.30 (t, J = 5 Hz, 2H), 2.55 (s, H_2O), 1.20 (t, J = 7.1 Hz, 3H). Anal. calcd ($C_{82}H_{156}O_{41}N_{10}$): C, 50.82; H; N, 7.23. Found: C, 47.36; H; N, 7.72.

Synthesis of *N*-(ω-azido-octa-(14′-amino-3′,6′,9′,12′-tetraoxatetradecanoyl))-1,2-distearoyl-*sn*-3-phosphoethanolamine (ATTA8-DSPE) 8. A solution of **6h** in chloroform (50 mL) was treated with NHS (0.66 g) and DCC (0.44 g) at room temperature with stirring for 1 h. The solution was filtered, treated with DSPE (1.35 g), and warmed to 60° until most of the DSPE had dissolved.

Scheme 1[a]

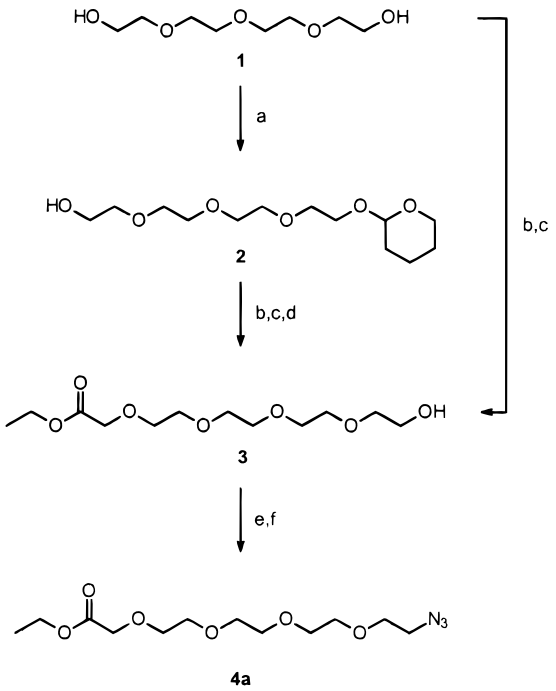

[a] Reagents: (a) dihydropyran, concd HCl, RT; (b) Na, 120 °C; (c) $BrCH_2COOEt$, 100 °C; (d) PPTS, EtOH; (e) methansulfonyl chloride, CH_2Cl_2, Et_3N; (f) NaN_3, EtOH, 60 °C.

Triethylamine (0.5 mL) was added and the solution warmed until all solids had dissolved. The solution was stirred at room temperature for 1 h, diluted with water and carefully acidified to pH 5 with dilute hydrochloric acid. The mixture was extracted with methylene chloride (three times). The solvent was removed on a rotovap. The residue was taken up in water, filtered and extracted with methylene chloride. The solvent was removed on a rotovap. The residue was suspended in methanol, centrifuged at 3000 rpm for 1 h, and the supernatant decanted. The solvent was removed on a rotovap. The residue was then taken up in water, filtered through a 0.22 μm filter, and lyophilized. Column chromatography (100 g of silica gel, 4−100% MeOH/CH_2Cl_2), followed by uptake in water and lyophilization, yielded **8** (1.76 g) as a sticky white powder. ^{1}H NMR ($CDCl_3$) δ 5.2 (bs, 1H), 3.98 (s, 16H), 4.35 (dd, 1H), 4.15 (dd, 1H), 3.2−3.7 (m, 132H), 2.2 (m, 4H), 1.6 (m, 4H), 1.3 (bs, 56H), 0.8 (t, 6H). Anal. ($C_{121}H_{232}O_{48}N_{11}P$) C, H, N.

RESULTS AND DISCUSSION

Three methods for generating the monomer precursor were evaluated in terms of potential for large-scale synthesis. Our primary objective at this point was the development of a protocol capable of generating large amounts of reasonably pure monomers without having to resort to chromatography. The requirement was important since the subsequent dimerization steps are not yet optimized and result in relatively low net yields.

Initially, we monoprotected tetraethylene glycol (TEG) using dihydropyran in a ~1:1 ratio in the presence of an acid catalyst (Scheme 1). Concentrated hydrochloric acid or PPTS in methylene chloride could be used for this purpose although hydrochloric acid was far more convenient. Crude isolation of TEG monoderivatized with hydrophobic moieties, such as azide, acetate, or THP, may be performed convieniently by a series of extractions using polar and apolar organic solvents. Treatment of TEG with the appropriate reactive reagent generally yields a mixture of unreacted TEG and the mono- and diderivatized products. The diderivatized TEG partitions from water into diethyl ether easily, whereas TEG and mono-derivatized TEG remain in the aqueous fraction. The mono-derivatized TEG can then be extracted into methylene chloride or chloroform. Free TEG remains in the aqueous phase, but may also be extracted at high concentrations. Removal of this residual TEG may require additional water/methylene chloride washes. This behavior was observed with azide, acetate, and THP functionalized TEG and probably is true for many other small hydrophobic capping groups.

Alkylation of **2** was achieved by treatment of the alkoxide with ethyl bromoacetate. The alkoxide was generated using either sodium metal or potassium hydride. We found that potassium hydride generally gave unsatisfactory results, apparently due to side reactions driven by excess potassium hydride after addition of the ethyl bromoacetate. Sodium was more useful in generating the alkoxide since unreacted metal could be readily removed before addition of the ethyl bromoacetate. The reaction was performed in toluene in order to maintain reasonably fluid solutions since the viscosity increased considerably as the reaction progressed. Even so, the reaction took a long time to proceed to completion. PPTS in ethanol was used to remove the THP protecting group. The resultant 2-ethoxytetrahydropyran was removed by diluting the ethanol solution with water, washing with diethyl ether and then extracting the aqueous phase with methylene chloride. This process worked well on small scales but presented technical problems at larger scales due to the volumes requiring extraction. Removal of the 2-ethoxytetrahydropyran was critical since it could potentially reprotect **3** on removal of the solvent prior to the next step.

An alternative approach to synthesizing **3** involved generation of the alkoxide directly from TEG without the protecting group (Scheme 1). The reaction was performed using sodium in an excess of TEG, which essentially acts as a solvent. High temperatures were necessary to avoid the viscosity problems mentioned above. We usually tried to keep the reaction temperature in the 100−120 °C range. However, temperature spikes up to 190 °C were observed on occasion due to the exothermic nature of the reaction. Toluene could not be used as a solvent since the alkoxide caused phase separation to occur. This problem was not evident with **2** since the THP group acts to keep the alkoxide in solution. A related procedure using triethylene glycol and bromo acetic acid as the alkylating reagent has previously been reported (*15*). In that instance, excess triethylene glycol was removed under reduced pressure and the carboxyl group reacylated by addition of acetyl chloride to a solution of the product in 2-propanol.

Both approaches gave similar overall yields of **4a** (~10% overall), with the monoprotection route being more convenient on small scales and the direct route more practical on large scales. Introduction of the azido function into **3** was effected by mesylation followed by treatment with sodium azide in ethanol. The crude, fully protected monomer **4a** obtained in this manner still contained substantial impurities. These could be effectively removed by hydrolyzing the ethyl protecting group. The sodium salt of **6a** partitioned into the aqueous phase when the solution was extracted into methylene chloride. Extraction, however, was possible after acidification of the aqueous phase. This behavior facilitated separation of **6a** from most of the other impurities carried

Scheme 2[a]

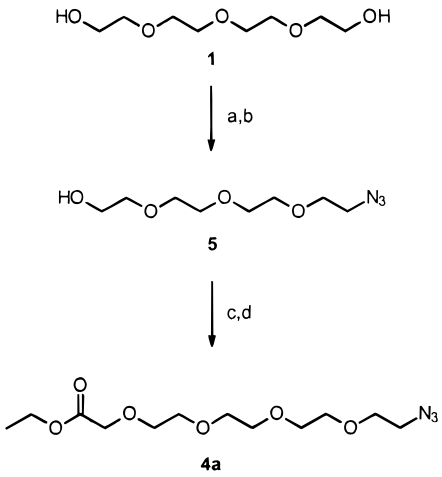

[a] Reagents: (a) methansulfonyl chloride, CH_2Cl_2, Et_3N; (b) NaN_3, EtOH, 60 °C; (c) KOH, $BrCH_2COOH$, DMF, 45°; (d) HCl, EtOH.

through the course of the synthesis. **4a** was then recovered by esterification using anhydrous hydrogen chloride in ethanol.

A recently reported route to **6a** (*16*) (Scheme 2) was also evaluated. This involved the synthesis of 12-azido-3,6,9-trioxaundecanol (*17*) followed by alkylation of a bromoacetate salt in the presence of potassium hydroxide in DMF. A major problem when using alkoxides to alkylate ethyl bromoacetate appears to be transesterification of the ethyl group. This results in low yields and complicates processing since many of the impurities are carried though to the final step of the synthesis. O-Alkylation of 12-azido-3,6,9-trioxaundecanol resolves these problems since side reactions are limited. Isolation of **6a** could be achieved by washing basic aqueous solutions with CH_2Cl_2 or $CHCl_3$ to remove apolar impurities and then extracting the product after reducing the pH to ~3. In our hands, the O-alkylation resulted in yields of ~30%, considerably less than those previously reported (*16*). Even so, this process appears to be more suitable for large-scale preparations than the other two.

The oligomers were assembled by iterative dimerization using standard peptide chemistry (Scheme 3). The azido group of **4a** is essentially a proto-amino function which can be readily converted to the amine **7a** by reduction using palladium/carbon in the presence of formic acid. Base hydrolysis of **4a** produced the complementary deprotected acid **6a**, which was then converted to an active ester using NHS and DCC. Treatment of the active ester with **7a** yielded the dimerized oligomer **4b**, which in turn served as the monomer for the next iterative cycle. Three iterations were required to generate the octamer **4h**, which is roughly the same size as a MW2000 poly(ethylene glycol). All oligomers up to **4h** were synthesized in this way using the appropriate precursor oligomers for the final dimerization step.

The reduction of the azide group presented special problems. The conversion can be readily effected under hydrogen in the presence of palladium, if the azide is pure. However, this was not typically the case with large quantities, especially in the case of the smaller oligomers such as **4a** and **4b**. These impurities cause loss of catalyst function, as a result, it is frequently necessary to add additional catalyst in order to get the reaction to work. This is quite difficult to do under a hydrogen atmosphere, particularly if large quantities are involved. We resolved the problem by using formic acid as a hydrogen source.

Scheme 3[a]

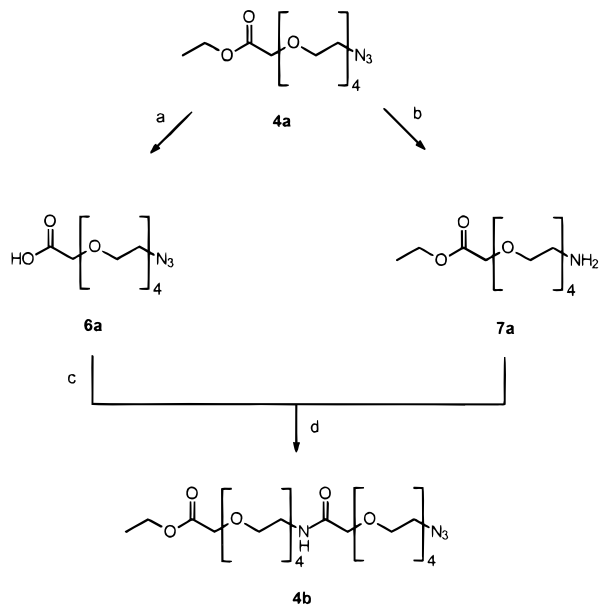

[a] Reagents: (a) Na_2CO_3(aq), 45 °C; (b) Pd/C, HCOOH, EtOH; (c) NHS, DCC, CH_2Cl_2; (d) Et_3N, CH_2Cl_2.

This allowed us to do the reaction in an open vessel. A further advantage in using formic acid rather than hydrogen lies in the nature of the reaction. Reduction of the azide group releases nitrogen; however, this is offset by hydrogen uptake. Under hydrogen this results in a zero volume change in the atmosphere, making it difficult to follow the course of the reaction in the absence of TLC analysis. When using formic acid as the hydrogen source, the reaction is characterized by rapid evolution of gas, which can be used to monitor the reaction (or lack thereof). This is particularly important when it is necessary to add additional catalyst. Recovery of the amine was effected by washing an acidified solution of the reaction mixture with methylene chloride, followed by neutralization of the aqueous fraction and removal of the water. Yields were generally in the 60−70% range, with the remainder of the material being converted to unspecified byproducts, all of which partitioned into the methylene chloride fractions.

Contamination of the ATTAn oligomers by other homomers after dimerization can arise in a number of ways. Activation of the ATTAn-acids (**6*n***) using carbodiimides in the presence of ethanol may result in reformation of the corresponding monomer, which of course would contaminate the dimerized product and have to be removed by chromatography. This side reaction was minimized by removal of any residual alcohol by repeated addition and removal of toluene on a rotovap.

A second source of homomer formation arises from hydrolysis of some of the ethyl protecting group during the reduction of the azide, resulting in some amino-ATTAn-acid being present in the amino monomer. Excess carbodiimide remaining after activation of ATTAn-acid may mediate some activation of this amino-ATTAn-acid, causing formation of higher order homologues of the dimerized product. This side reaction was minimized by ensuring that the activation of the ATTAn-acid precursor was performed with exactly 1 equiv of carbodiimide.

Incomplete deprotection of the monomer precursors may also be a source of homomer contamination. These impurities, however, are readily extracted into the organic phases whereas the desired acid or amine remains in the aqueous phase at the appropriate pH. It was

important to ensure that these aqueous phases are properly washed before recovery of the deprotected monomers to avoid contamination of the reaction.

Removal of unwanted homomers can be effected by chromatography but becomes more difficult as the size of the oligomers increases. It is therefore important to use purified monomers for the dimerization reaction and to observe the simple precautions mentioned above to minimize the problem. Unreacted amines and acids are readily removed from the reaction mixture by acidic or basic washes, allowing recovery of relatively clean dimerized product after workup. The overall yields in the various deprotection and dimerization steps were consistent. Purity was based on TLC analysis using potential homomeric contaminants as controls. The molecular weight of the purified product was confirmed using NMR by comparing the integrals of the peaks due to the ethyl group [δ 4.18 (q, 2H) and 1.25 (t, 3H)] and the *n*(C-2) methylenes [δ 4.10 (s, 2H) and 3.97 (s, 2*n*-2H)]. The oligomeric purity of the samples was established using positive electrospray LC/MS. No evidence of homomeric contamination could be observed in any of the samples (**4b**−**h**) except for the tetramer, **4d**, which contained small amounts of the trimer **4c**.

Generally, reduction of the azide resulted in 60−70% formation of the amine while hydrolysis of the ester function yielded 80−90% of the corresponding acid. Yields in the dimerization step were typically ∼70%. This yield could probably be improved by taking additional precautions to ensure that all of the reagents and solvents used are dry. Most of the unreacted acid monomer could be recovered by acidification of the basic aqueous wash. Recovery of unreacted amine monomer is technically difficult since in most cases it is difficult to extract. Consequently, we usually only recovered the unreacted acid. In most cases, it is necessary to reacylate and repurify this material since some of the dimer is hydrolyzed during workup of the reaction and would be recovered along with the monomer acid. Since a large part of the loss material during the course of successive dimerizations is due to the azide reduction step, a more efficient procedure would involve using monomers with a BOC-protected amine rather than the azide group. Deprotection of the BOC group with TFA followed by recovery should result in an overall synthesis which considerably more efficient than that described here. We used the azide groups as latent amines in this work primarily because they are easier to track by TLC and not because they make for a more efficient synthesis.

We were primarily interested in using these compounds as substitutes for PEG−lipid conjugates in liposome applications; therefore, it was necessary to attach lipid anchors to the oligomers. In the case of PEG, this is done by converting the polymer to an acid, in a number of ways (*14*), and then conjugating the product to a lipid, such as phosphatidylethanolamine (*14*) or ceramide (*9*). The ATTAn oligomers are intrinsically heterobifunctional, so deprotection of the carboxyl group followed by activation with DCC/NHS allowed facile conjugation to amino-lipids. As examples, we prepared the DSPE (**8**, Scheme 4) conjugate of the octamer **6h**. Conjugation to lipids such as ceramide is more problematic. In the case of the PEG analogue, the conjugation is mediated through DCC/DMAP. The polyamide oligomers may undergo imide formation under these conditions; consequently, it was not attempted. A more detailed evaluation of these and other oligomer−lipid conjugates in liposomes, including formulation characteristics, utility, immunogenicity, and toxicity, has been reported elsewhere (*18*).

Scheme 4[a]

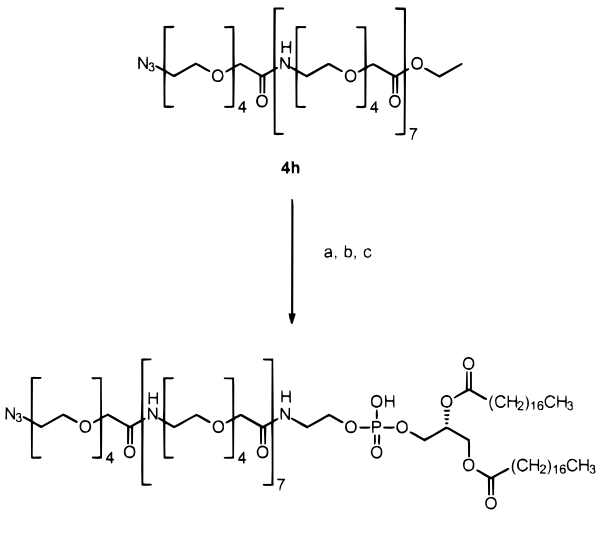

[a] Reagents: (a) Na_2CO_3(aq), 45 °C; (b) NHS, DCC, CH_2Cl_2; (c) DSPE, Et_3N, CH_2Cl_2, 60 °C.

The ATTAn oligomers could potentially be used in any application where PEG currently is employed. The principal applications of the new materials are likely to be those where tight control of the polymer size is important, for example, in rigorous studies of structure−activity relationships. Procedures for the synthesis of monodisperse PEG oligomers have previously been described (*19*, *20*); however, they are likely to present technical difficulties when used to assemble larger heterobifunctional oligomers (∼20−45mer) in quantity. Iterative dimerization of oligo(ethylene glycol) amino acid monomers represents a powerful technique for the assembly of this type of compound, particularly if additional functionality is required in the oligomer chain. This could be accomplished by including other amino acids with acidic, basic, hydrophilic, or hydrophobic substituents, or aliphatic linkers as spacers between the monomer units at various points in the chain.

An important difference between PEG and ATTAn is the fact that PEG is a mixture of a wide range of oligomers. The ATTAn oligomers reported here can be used as monodisperse tools for investigating the role of polymer length in applications where polymers act as cross-linkers or steric barriers. A number of reports have recently appeared which describe the use of related oligomers as components in defined ABA amphiphiles (*21*) or as polyamide linkers in peptide constructs (*22*). The simple chemistry and isolation protocols described here allow the rapid generation of libraries of homomers that can be used to determine structure−activity relationships in these and a variety of other applications involving macromolecules cross-linked to other molecules or surfaces.

An application in which we are particularly interested involves regulated exchange of the polymer−lipid conjugate (*23*). To understand and control this process, we require access to detailed information relating to the effect of lipid anchor, polymer length, colipids, and concentration on the polymer−lipid exchange rates. We have set an arbitrary specification for these studies requiring that 90% of the polymer must be within ±10% of the nominal molecular mass, a specification which we do not believe is unduly narrow for the investigation of structure−activity relationships. Calculations indicate that for a theoretical normal distribution a polymer would

have to have a polydispersity of approximately 1.005 or less to meet the criteria. To the best of our knowledge, the highest grade of commercially available bifunctional PEGs have polydispersities in the range 1.03−1.06. Monomethoxy PEGs are available with polydispersities of 1.01−1.02, but still fall outside of our specifications.

A further specification for these studies was that the polymers used had to have suitable functionality that allowed a label to be readily introduced after assembly of the lipid−polymer conjugate. The labels anticipated included radiolabels and flourescent labels. Radiolabeled PEG−lipids can be produced in a number of ways: (1) using labeled lipid precursors; (2) using labeled PEG; (3) using a labeled cross-linker; or (4) attaching a label to the distal end of a suitably modified PEG−lipid. We have previously synthesized MePEGS−DSPE conjugates using approaches 1−3 (*14*); however, the techniques used are technically complex and time consuming. In addition, many labels, particularly flourescent labels, are not suitable when used as cross-linkers since they may affect the exchange rate through interactions with the bilayer surface. An alternative approach which we recently developed (*24*) involved preparing a cholesterol−PEG amine conjugate which was then acylated with labeled acetic acid. This method is particularly attractive since the label is introduced at the final stage, minimizing the technical complexity of the synthesis. We intend to use this approach to label our ATTAn−lipid conjugates.

However, the synthesis of the *N*-acetylcholesterol-PEG-amine described in ref *24* did expose one of the problems associated with PEG conjugates, namely the effects of polydispersity and batch variability with respect to molecular weight. In that particular case, the final molecular mass of the PEG component of the conjugate was determined by ^{1}H NMR as being approximately 1400 Da, considerably different from the nominal molecular mass of 1000 Da. The oligomers comprising PEG derivatives may be resolvable during workup and chromatographic processes, particularly in the case of lower molecular masses, and this can lead to a selection of a subpopulation of the original polymer. We believe that this was the case with the cholesterol-PEG-amine. Since we intended to use the labeled derivative to describe the exchange behavior of the unlabeled material, the difference in nominal molecular mass limited the significance of the information obtained. The ATTAn derivatives described in this work present considerable advantages over PEG in these applications since the compounds are intrinsically heterobifunctional, are monodisperse with specified molecular masses, and maintain a constant molecular mass during the workup phases of a synthesis.

In conclusion, we have demonstrated that iterative dimerization of 14-amino-3,6,9,12-tetraoxatetradecanoic acid derivatives can be used to generate a wide range of oligomers which are soluble both in water and organic solvents and which can be used as cross-linkers or steric barrier molecules in biotechnology applications. Conjugation of the octamer to DSPE yielded a steric barrier lipid suitable for liposome applications.

Supporting Information Available: Elemental analysis data, ^{1}H NMR spectra, positive ion electrospray mass spectra, and polydispersity calculations. This material is available free of charge via the Internet at http://pubs.acs.org.

LITERATURE CITED

(1) Zalipsky, S. (1995) Functionalized poly(ethylene glycol) for the preparation of biologically relevant conjugates. *Bioconjugate Chem. 6*, 150−165.

(2) Allen, T. M. (1994) The use of glycolipids and hydrophilic polymers in avoiding rapid uptake of liposomes by the mononuclear phagocyte system. *Adv. Drug Deliv. Rev. 13*, 285−309.

(3) Lasic, D. D., and Needham, D. (1995) The "Stealth" liposome: a prototypical biomaterial. *Chem. Rev. 95*, 2601−2628.

(4) Harasym, T. O., Tardi, P., Longman, S. A., Ansell, S. M., Bally, M. B., Cullis, P. R. C., and Choi, L. S. L (1995) Poly(ethylene glycol)-modified phospholipids prevent aggregation during covalent conjugation of proteins to liposomes. *Bioconjugate Chem. 6*, 187−194.

(5) Wheeler, J. J., Palmer, L., Ossanlou, M., MacLachlan, I., Graham, R. W., Zhang, Y. P., Hope, M. J., Scherrer, P., and Cullis, P. R. (1999) Stabilized plasmid-lipid particles: construction and characterization. *Gene Ther. 6*, 271−281.

(6) Klibanov, A. L., Maruyama, K., Beckerleg, A. M., Torchilin, V. P., and Huang, L. (1991) Activity of amphiphatic poly(ethylene glycol) 5000 to prolong the circulation time of liposomes depends on the liposome size and is unfavourable for immunoliposome binding to target. *Biochim. Biophys. Acta 1062*, 142−148.

(7) Mayer, L. D., Cullis, P. R., and Bally, M. B. (1998) Designing therapeutically optimized liposomal anticancer delivery systems: Lessons from conventional liposomes. In *Medical Applications of Liposomes* (D. D. Lasic and D. Papahadjipoulos, Eds.) pp 231−256, Elsevier Press, B. V.

(8) Mori, A., Chonn, A., Choi, L. S., Israels, A., Monck, M. A., and Cullis, P. R. (1998) Stabilization and regulated fusion of liposomes containing a cationic lipid using amphipathic poyethyleneglycol derivatives. *J. Liposome Res. 8*, 195−211.

(9) Webb, M. S., Saxon, D., Wong, F. M. P. Lim, H. J., Wang, Z., Bally, M. B., Choi, L. S. L., and Cullis, P. R., Mayer, L. D. (1998) Comparison of different hydrophobic anchors conjugated to poly(ethylene glycol): effects on the pharmacokinetics of liposomal vincristine. *Biochim. Biophys. Acta 1372*, 272−282.

(10) Adlakha-Hutcheon, G., Bally, M. B., Shew, C. R., and Madden, T. D. (1999) Controlled destabilization of a liposomal drug delivery system enhances mitoxantrone antitumor activity. *Nat. Biotechnol. 17*, 775−779.

(11) Torchilin, V. P. (1996) How do polymers prolong circulation time of liposomes. *J. Liposome Res. 6*, 99−116.

(12) Torchilin, V. P., Omelyanenko, V. G., Papisov, M.I., Bogdanov, A. A., Trubetskoy, V. S., Herron, J. N., and Gentry, C. A. (1994) Poly(ethylene glycol) on the liposome surface: on the mechanism of polymer-coated liposome longevity. *Biochim. Biophys. Acta 1195*, 11−20.

(13) Woodle, M. C., Engbers, C. M., and Zalipsky, S. (1994) New amphipatic polymer−lipid conjugates forming long-circulating reticuloendothelial system-evading liposomes. *Bioconjugate Chem. 6*, 493−496.

(14) Parr, M. J., Ansell, S. M., Choi, L. S., and Cullis, P. R. (1994) Factors influencing the retention and chemical stability of poly(ethylene glycol)-lipid conjugates incorporated into large unilamellar vesicles. *Biochim. Biophys. Acta 1195*, 21−30.

(15) Agback, H., Ahrgren, L., Haraldsson, M., and Akerblom, E. (1991) A conjugate substance, a reagent and novel polyethers. *International patent appl. PCT/SE91/00497* (Publication no. WO92/01474).

(16) Schwabacher, A. W., Lane, J. W., Schiesher, M. W., Leigh, K. M., and Johnson, C. W. (1998) Desymmetrization reactions: efficient preparation of unsymmetrically substituted linker molecules. *J. Org. Chem. 63*, 1727−1729.

(17) Bertozzi, C. R., and Bednarski, M. D. (1991) The synthesis of heterobifunctional linkers for the conjugation of ligands to molecular probes. *J. Org. Chem. 56*, 4326−4329.

(18) Ansell, S. M., Kojic, L. D., Hankins, J. S., Sekirov, L., Boey, A., Lee, D., Klimuk, S. K., Harasym, T. O., Dos Santos, N., and Semple, S. C. (1999) Application of oligo-(14-amino-3, 6, 9, 12-tetroxatetradecanoic acid) lipid conjugates as steric barrier molecules in liposomal formulations. *Bioconjugate Chem. 10*, 653−666.

(19) Keegstra, E. M. D., Zwikker, J. W., Roest, M. R., and Jenneskens, L. W. (1992) A highly selective synthesis of monodisperse oligo(ethylene glycols). *J. Org. Chem. 57*, 6678−6680.
(20) Kinugasa, S., Takatsu, A., Nakanishi, H., Nakahara, H., and Hattori, S. (1992) Preparation and charaterization of pure oligo(ethylene glycol)s. 2. *Macromolecules 25*, 4848−4853.
(21) Chen, Y., and Baker, G. L. (1999) Synthesis and properties of ABA amphiphiles. *J. Org. Chem. 64*, 6870−6873.
(22) Rose, K., and Vizzavona, J. (1999) Stepwise solid-phase synthesis of polyamides as linkers. *J. Am. Chem. Soc. 121*, 7034−7038.
(23) Holland, J. W., Hui, C., Cullis, P. R., and Maddent, T. D. (1996) Poly(ethylene glycol)-lipid conjugates regulate the calcium-induced fusion of liposomes composed of phoshatidylethanolamine and phosphatidylserine. *Biochemistry 35*, 2618−2624.
(24) Bradley, A. J., Devine, D. V., Ansell, S. M., Janzen, J., and Brooks, D. E. (1998) Inhibition of liposome-induced complement activation by incorporated PEG−lipids. *Arch. Biochem. Biophys. 357*, 185.

BC9801427

© 1999 American Chemical Society, Bioconjugate Chem., Dhawan bc9801427 Supporting Info Page 1

Supporting information

Rajiv Dhawan, Mark G.A. Kadijk, Terry J. Joikinen, Michael Feng and Steven M. Ansell*

Synthesis of polyamide oligomers based on 14-amino-3,6,9,12-tetraoxatetradecanoic acid

Elemental analysis

Sample	%C		%H		%N	
	found	calc.	found	calc.	found	calc.
ATTA1	47.45	47.20	7.76	7.59	13.51	13.79
ATTA2	49.03	49.06	7.98	7.86	10.06	10.40
ATTA3	49.76	49.79	7.77	7.97	8.79	9.07
ATTA4	49.64	50.19	8.07	8.02	7.93	8.36
ATTA5	49.67	50.43	8.08	8.06	7.38	7.92
ATTA6	50.49	50.60	8.19	8.08	7.31	7.61
ATTA7	50.69	50.72	8.09	8.10	7.11	7.39
ATTA8	49.85	50.82	7.91	8.11	7.02	7.23
ATTA8-DSPE	53.95	55.05	8.71	8.86	5.57	5.84

^{1}H NMR spectra

Recorded in CDCl3 using a Bruker MSL200 spectrometer.

Page 2. ATTA1, ATTA2, ATTA3, ATTA4
Page 3. ATTA5, ATTA6, ATTA7, ATTA8
Page 4. ATTA8-DSPE

Positive ion electrospray mass spectra

Samples were analysed using using a Hewlett Packard Model 1100 liquid chromatograph interfaced to a Micromass Quattro-LC triple quadrupole mass spectrometer with MassLynx software and computer control. The spectrometer was operated with an ESI source and the column eluant was interfaced directly into the ion source.

Page 5. ATTA2, ATTA3, ATTA4
Page 6. ATTA5, ATTA6, ATTA7
Page 7. ATTA8

© 1999 American Chemical Society, Bioconjugate Chem., Dhawan bc9801427 Supporting Info Page 2

ATTA1

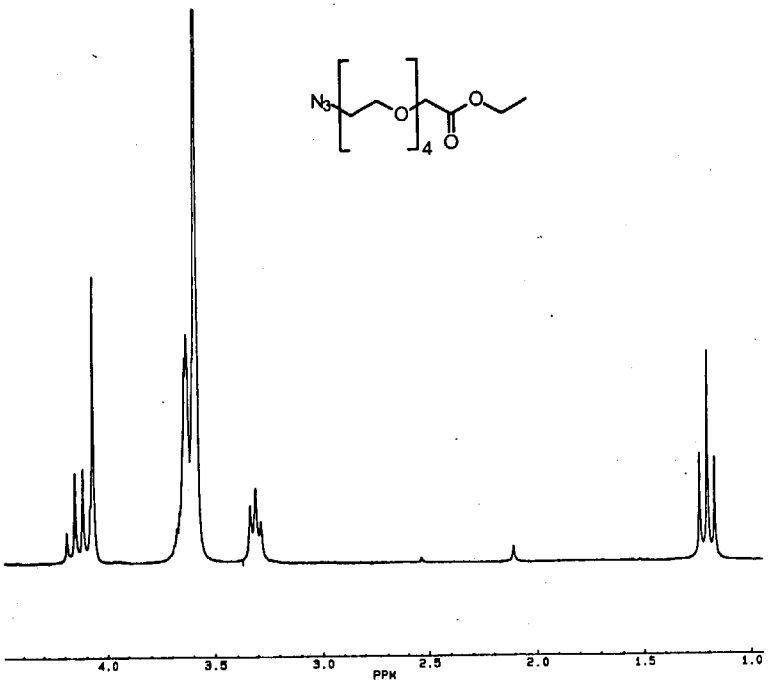


```
SMA.001
PPG:
 QUADCYCL.PC
DATE 18-7-98

SF    200.130
O1   3200.000
SI    16384
TD     8192
SW   2000.000
HZ/PT    .244

RG     18
NE      1
NS     32
TE    323

DW    250.0
FW     2400
O2 100000.000
DP    63L PO

D0     5.000S
D1     2.750U
D2    15.000U
D3    12.000U
D4     1.000U

LB       0.0
GB      .050
NC        2
CX    20.00
CY      0.0
SR   2345.54
```

ATTA2

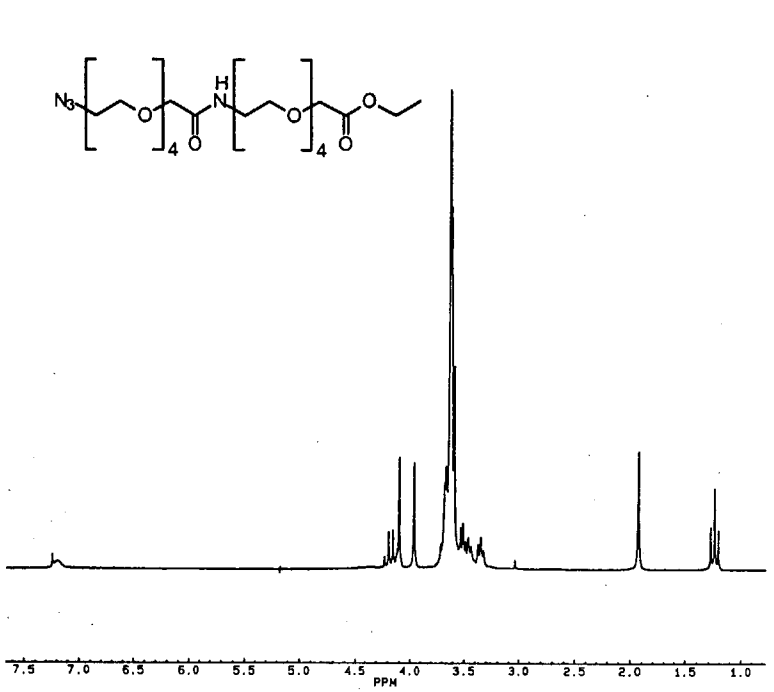


```
SMA.001
PPG:
 QUADCYCL.PC
DATE 5-7-98

SF    200.130
O1   3200.000
SI    16384
TD     8192
SW   2000.000
HZ/PT    .244

RG      8
NE      1
NS    128
TE    323

DW    250.0
FW     2400
O2 100000.000
DP    63L PO

D0     5.000S
D1     2.750U
D2    15.000U
D3    12.000U
D4     1.000U

LB      .100
GB      .050
NC        3
CX    20.00
CY      0.0
SR   2344.56
```

ATTA3

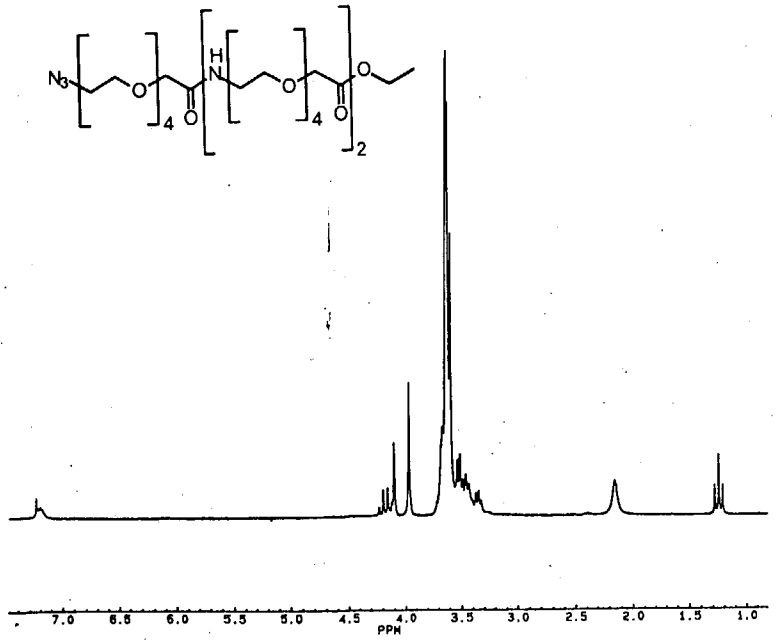


```
SMA.001
PPG:
 QUADCYCL.PC
DATE 5-6-98

SF    200.130
O1   3200.000
SI    16384
TD     8192
SW   2000.000
HZ/PT    .244

RG      8
NE      1
NS     32
TE    323

DW    250.0
FW     2400
O2 100000.000
DP    63L PO

D0     5.000S
D1     2.750U
D2    15.000U
D3    12.000U
D4     1.000U

LB      .100
GB       0.0
NC        1
CX    20.00
CY      0.0
SR   2344.81
```

ATTA4

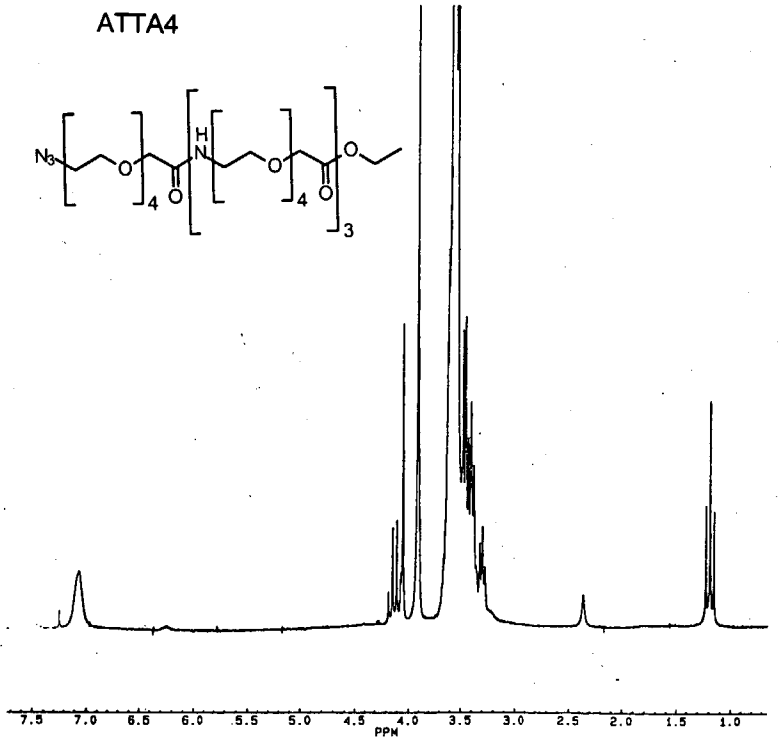


```
SMA.001
PPG:
 QUADCYCL.PC
DATE 18-7-98

SF    200.130
O1   3200.000
SI    16384
TD     8192
SW   2000.000
HZ/PT    .244

RG     18
NE      1
NS     64
TE    323

DW    250.0
FW     2400
O2 100000.000
DP    63L PO

D0     5.000S
D1     2.750U
D2    15.000U
D3    12.000U
D4     1.000U

LB       0.0
GB      .050
NC        2
CX    20.00
CY      0.0
SR   2345.54
```

ATTA5

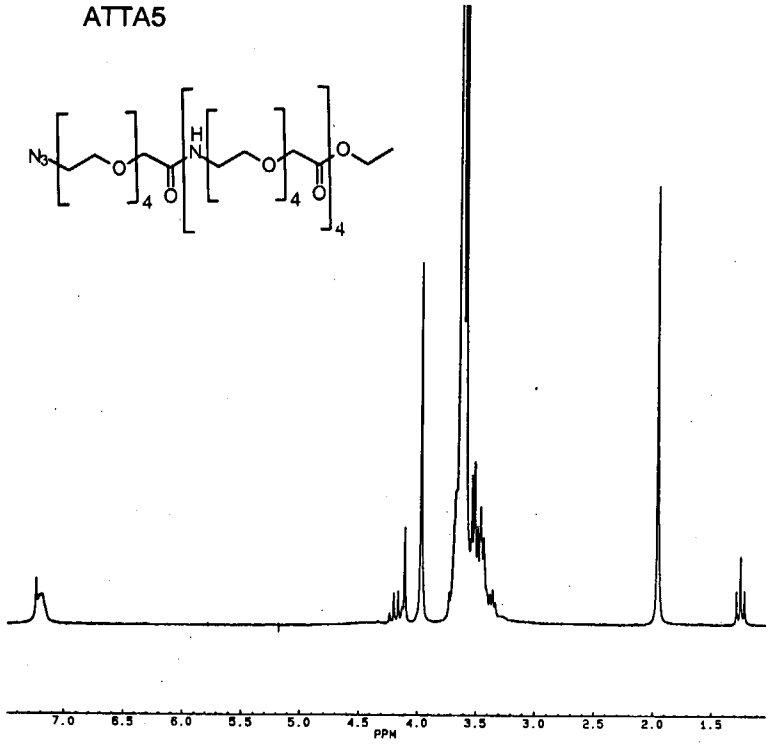

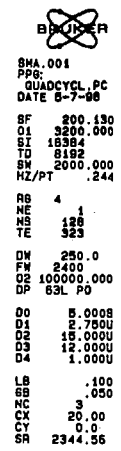

```
SMA.001
PPG:
 QUADCYCL.PC
DATE 8-7-98

SF    200.130
O1   3200.000
SI     16384
TD      8192
SW   2000.000
HZ/PT     .244

RG         4
NE         1
NS       128
TE       323

DW       250.0
FW        2400
O2  100000.000
DP      63L PO

D0       5.000S
D1       2.750U
D2      15.000U
D3      12.000U
D4       1.000U

LB        .100
GB        .050
NC           3
CX       20.00
CY         0.0
SR     2344.56
```

ATTA6

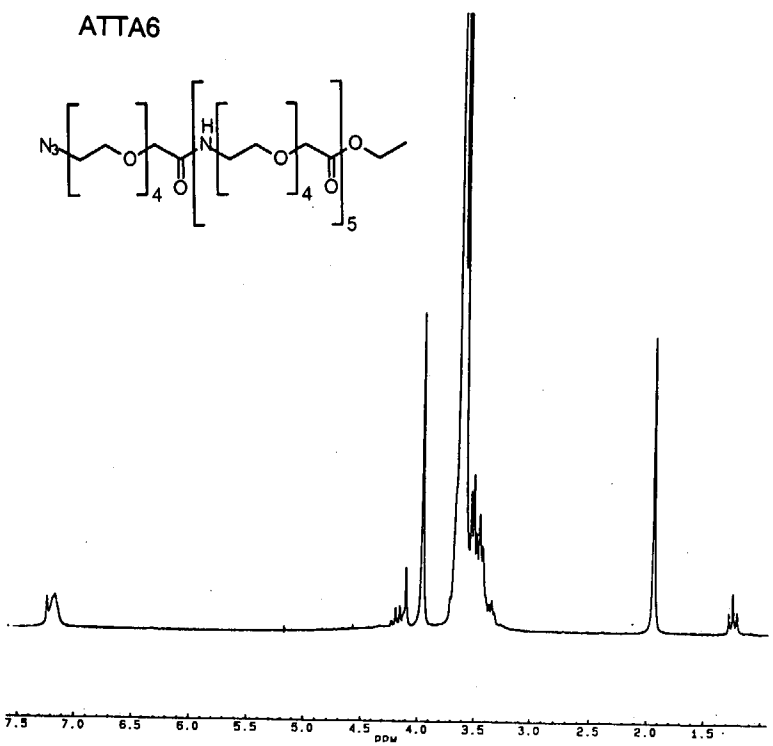

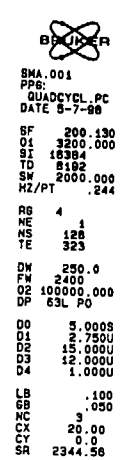

```
SMA.001
PPG:
 QUADCYCL.PC
DATE 8-7-98

SF    200.130
O1   3200.000
SI     16384
TD      8192
SW   2000.000
HZ/PT     .244

RG         4
NE         1
NS       128
TE       323

DW       250.0
FW        2400
O2  100000.000
DP      63L PO

D0       5.000S
D1       2.750U
D2      15.000U
D3      12.000U
D4       1.000U

LB        .100
GB        .050
NC           3
CX       20.00
CY         0.0
SR     2344.56
```

ATTA7

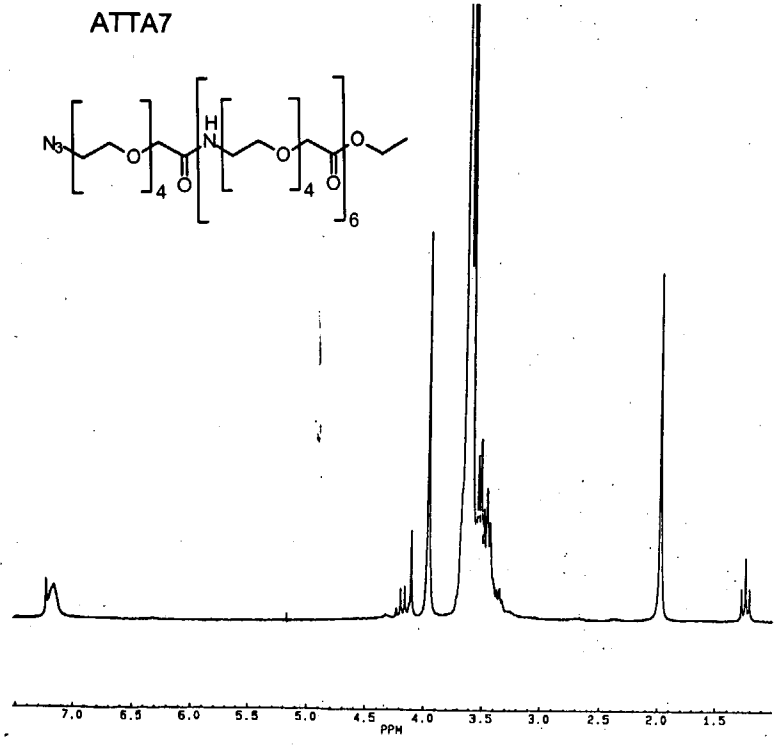

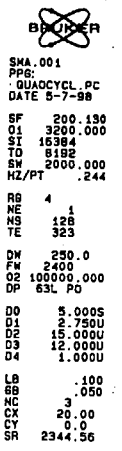

```
SMA.001
PPG:
 QUADCYCL.PC
DATE 8-7-98

SF    200.130
O1   3200.000
SI     16384
TD      8192
SW   2000.000
HZ/PT     .244

RG         4
NE         1
NS       128
TE       323

DW       250.0
FW        2400
O2  100000.000
DP      63L PO

D0       5.000S
D1       2.750U
D2      15.000U
D3      12.000U
D4       1.000U

LB        .100
GB        .050
NC           3
CX       20.00
CY         0.0
SR     2344.56
```

ATTA8

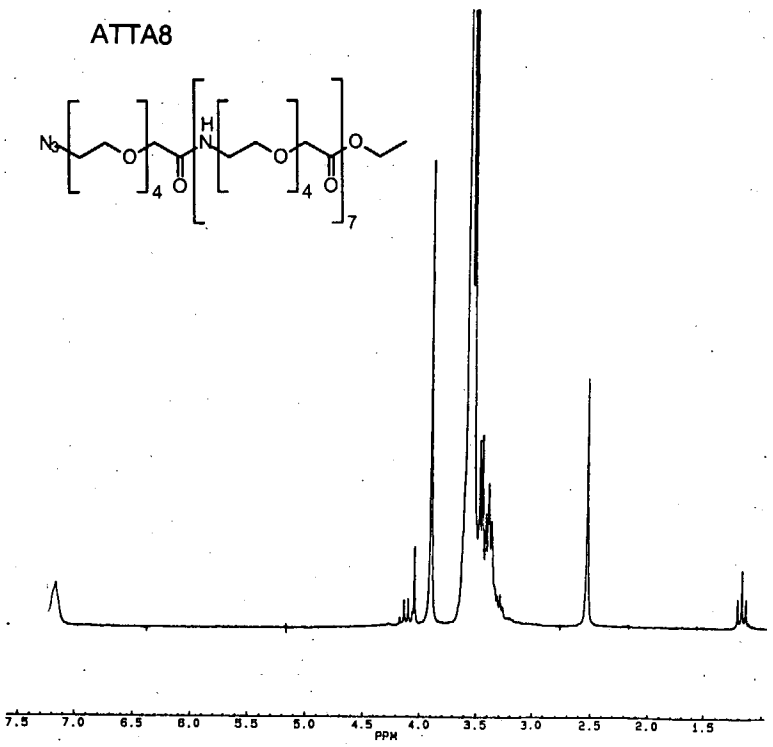

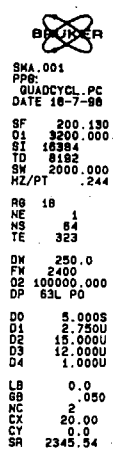

```
SMA.001
PPG:
 QUADCYCL.PC
DATE 16-7-98

SF    200.130
O1   3200.000
SI     16384
TD      8192
SW   2000.000
HZ/PT     .244

RG        18
NE         1
NS        64
TE       323

DW       250.0
FW        2400
O2  100000.000
DP      63L PO

D0       5.000S
D1       2.750U
D2      15.000U
D3      12.000U
D4       1.000U

LB         0.0
GB        .050
NC           2
CX       20.00
CY         0.0
SR     2345.54
```

© 1999 American Chemical Society, Bioconjugate Chem., Dhawan bc9801427 Supporting Info Page 3

© 1999 American Chemical Society, Bioconjugate Chem., Dhawan bc9801427 Supporting Info Page 4

9. ATTA8-DSPE

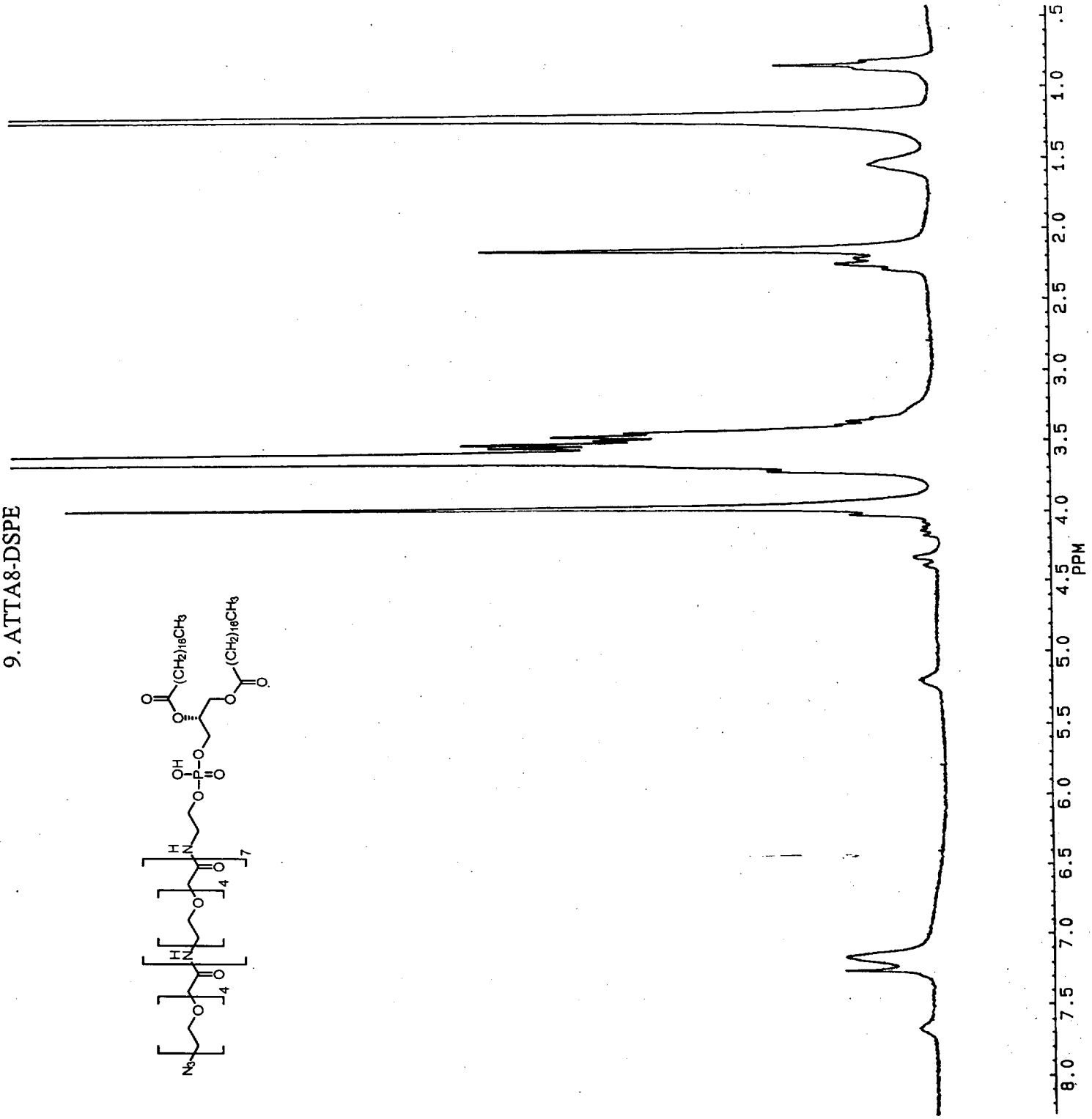

© 1999 American Chemical Society, Bioconjugate Chem., Dhawan bc9801427 Supporting Info Page 5

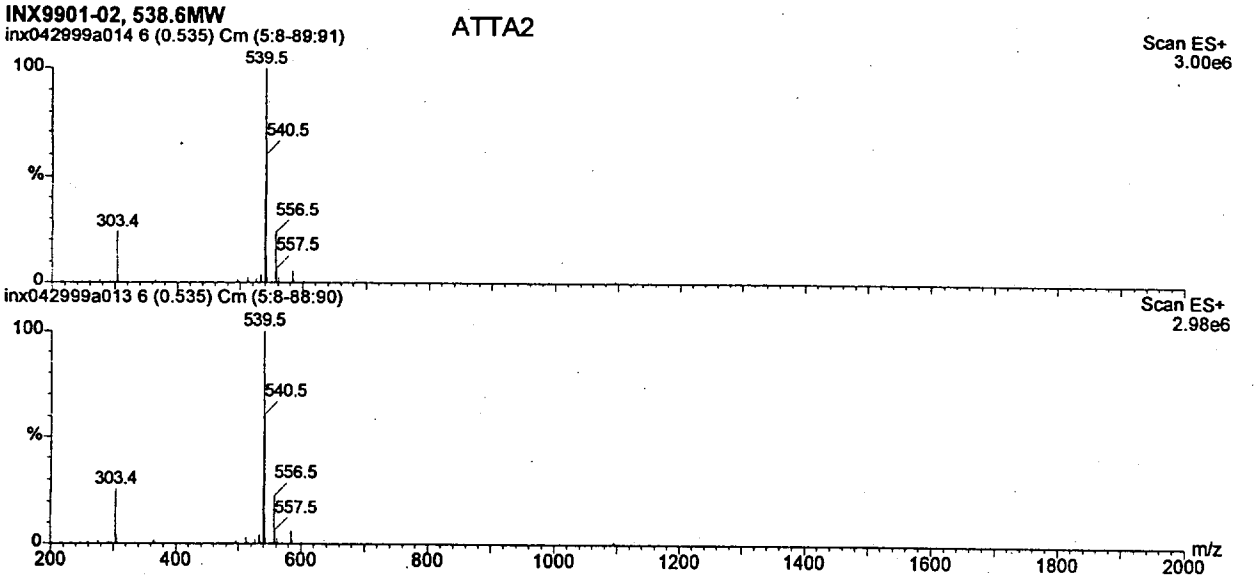

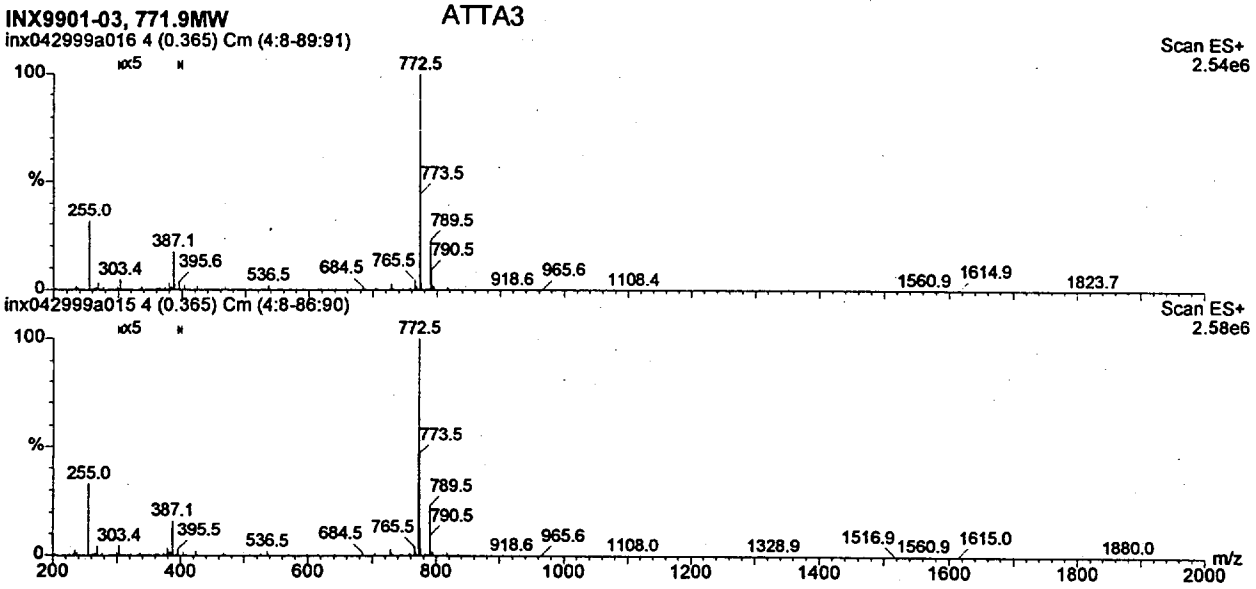

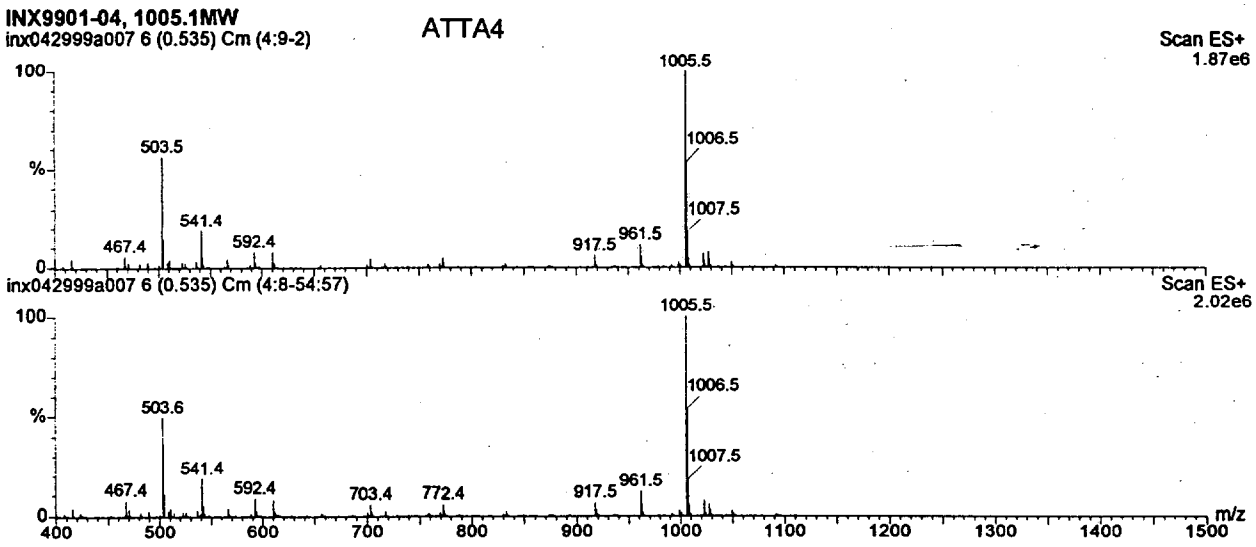

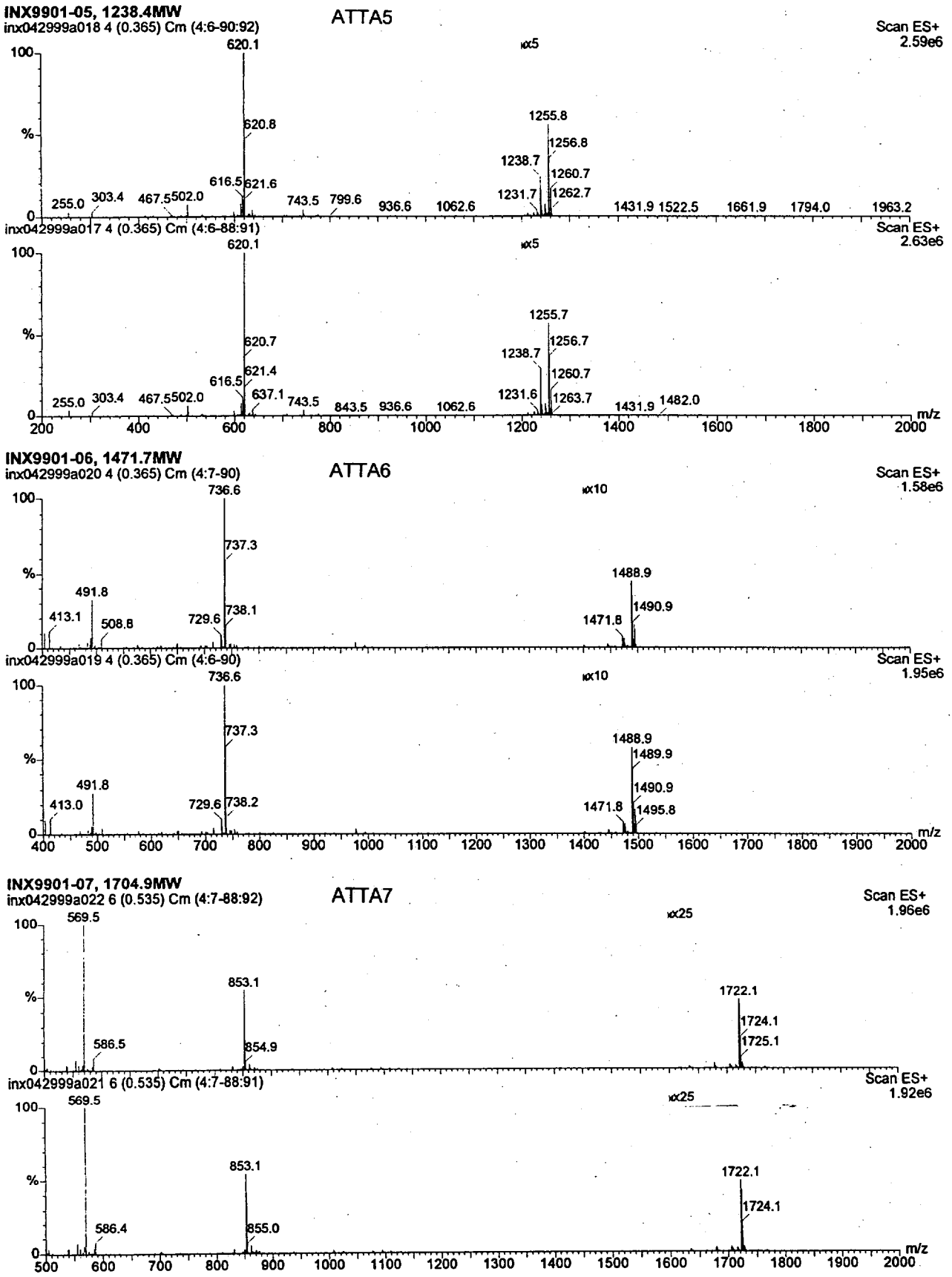
INX9901-05, 1238.4MW
inx042999a018 4 (0.365) Cm (4:6-90:92)
ATTA5
Scan ES+
2.59e6
620.1
620.8
616.5
621.6
255.0
303.4
467.5
502.0
743.5
799.6
936.6
1062.6
1255.8
1256.8
1238.7
1260.7
1231.7
1262.7
1431.9
1522.5
1661.9
1794.0
1963.2
inx042999a017 4 (0.365) Cm (4:6-88:91)
Scan ES+
2.63e6
620.1
620.7
616.5
621.4
637.1
255.0
303.4
467.5
502.0
743.5
843.5
936.6
1062.6
1255.7
1256.7
1238.7
1260.7
1231.6
1263.7
1431.9
1482.0
m/z
INX9901-06, 1471.7MW
inx042999a020 4 (0.365) Cm (4:7-90)
ATTA6
Scan ES+
1.58e6
736.6
737.3
491.8
413.1
508.8
729.6
738.1
1488.9
1490.9
1471.8
inx042999a019 4 (0.365) Cm (4:6-90)
Scan ES+
1.95e6
736.6
737.3
491.8
413.0
729.6
738.2
1488.9
1489.9
1490.9
1471.8
1495.8
m/z
INX9901-07, 1704.9MW
inx042999a022 6 (0.535) Cm (4:7-88:92)
ATTA7
Scan ES+
1.96e6
569.5
853.1
586.5
854.9
1722.1
1724.1
1725.1
inx042999a021 6 (0.535) Cm (4:7-88:91)
Scan ES+
1.92e6
569.5
853.1
586.4
855.0
1722.1
1724.1
m/z

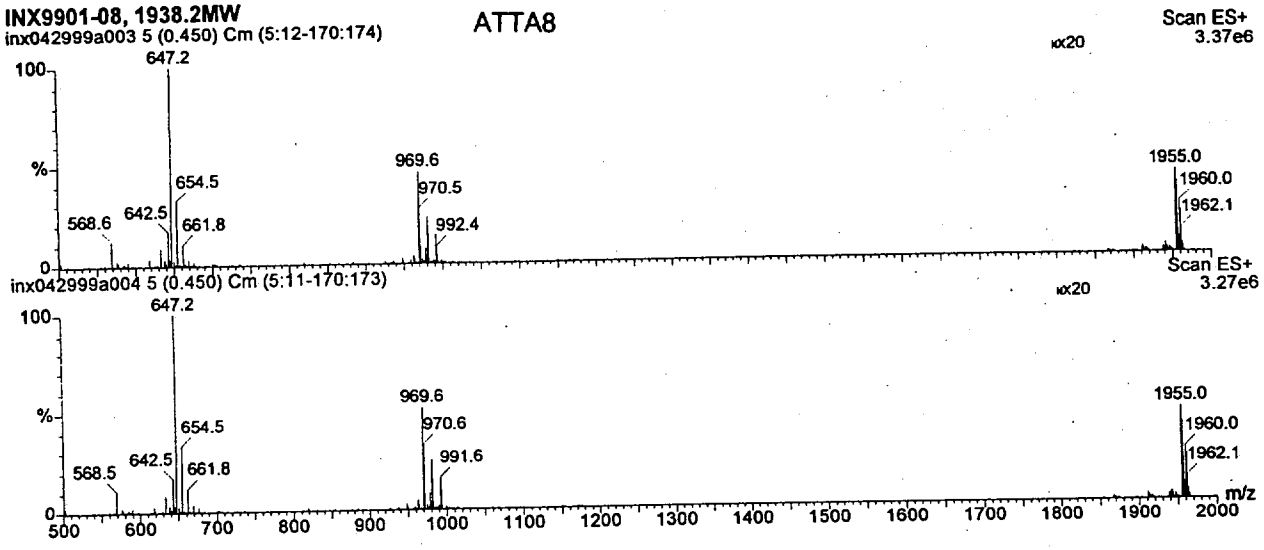
INX9901-08, 1938.2MW
inx042999a003 5 (0.450) Cm (5:12-170:174)
ATTA8
Scan ES+
3.37e6
x20
647.2
969.6
1955.0
654.5
970.5
1960.0
642.5
661.8
992.4
1962.1
568.6
inx042999a004 5 (0.450) Cm (5:11-170:173)
Scan ES+
3.27e6
x20
647.2
969.6
1955.0
654.5
970.6
1960.0
642.5
661.8
991.6
1962.1
568.5
%
100
0
m/z
500
600
700
800
900
1000
1100
1200
1300
1400
1500
1600
1700
1800
1900
2000

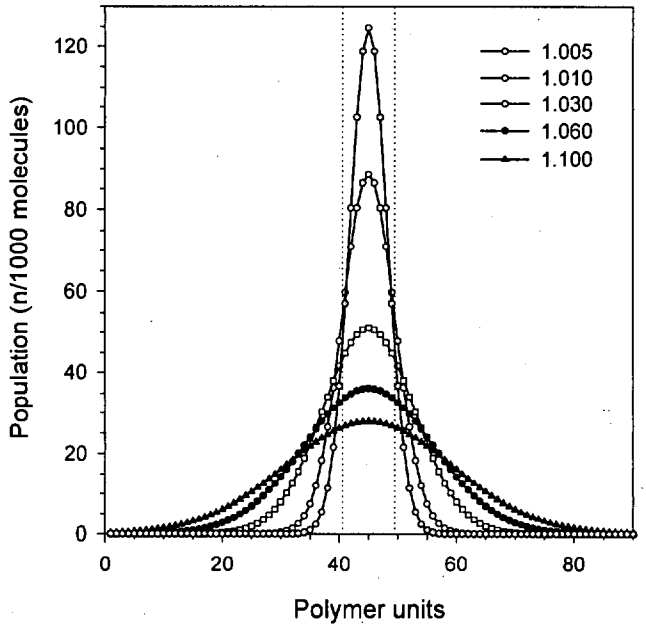

The effect of polydispersity on the theoretical molecular weight distribution of PEG 2000, based on ethoxy monomer units. The normal distribution for a population of 1000 molecules was calculated using the equation:

$$f_1 = \frac{1}{\sigma\sqrt{2\pi}} e^{(x_1-\mu)^2/2\sigma^2}$$

where f_1 is the population of oligomers composed of molecular mass x_1, σ is the standard deviation, and μ is the molecular mass of the oligomer closest to the nominal molecular mass.

Polydispersity was calculated using the ratio *Mw/Mn* where *Mn* is the number average molecular mass and *Mw* is the weight average molecular mass. *Mn* and *Mw* are defined using the equations:

$$Mn = \frac{\sum_i n_i M_i}{n} \qquad Mw = \frac{\sum_i n_i M_i^2}{\sum_i n_i M_i}$$

where n_i is the number of molecules of length i, n is the total number of molecules, and M_i is the molecular mass of a molecule of length i

The distributions for particular polydispersities were calculated with a QuatroPro spreadsheet using ethoxy monomer units to represent molecular mass. The dotted vertical lines represent +/- 10% of the nominal molecular mass. Our specification required greater than 90% of the distribution to be within these limits.

Noncovalent Adducts of Poly(ethylene glycols) with Proteins

Irina N. Topchieva,* Elena M. Sorokina,† Nadezhda V. Efremova,† Alexander L. Ksenofontov,‡ and Boris I. Kurganov†

Lomonosov Moscow State University, Department of Chemistry, Leninskii Gory, 119899, Moscow, Russia, A.N. Bakh Institute of Biochemistry, Russian Academy of Sciences, Leninskii pr., 33, 117071, Moscow, Russia, and Lomonosov Moscow State University, Belozerskii Institute of Physico-Chemical Biology, Leninskii Gory, 119899, Moscow, Russia. Received January 12, 1999; Revised Manuscript Received October 15, 1999

A new method of preparation of noncovalent complexes between poly(ethylene glycol) (PEG) and proteins (α-chymotrypsin (ChT), lysozyme, bovine serum albumine) under high pressure has been developed. The involvement of polymer in the complexes was proved using ^{3}H-labeled PEG. The composition of the complexes (the number of polymer chains per one ChT molecule) depends on the molecular mass of PEG and decreases with the increase in molecular mass from 300 to 4000, whereas the portion of the protein (wt %) in complexes does not depend on the molecular mass of incorporated PEG and corresponds to ∼70 wt %. The kinetic constants for enzymatic hydrolysis of *N*-benzoyl-L-tyrosine ethyl ester and azocasein catalyzed by the PEG−ChT complexes are identical with the corresponding values for the native ChT. According to the data obtained by the method of circular dichroism, the enzyme in the complexes fully retains its secondary structure. The steric availability of PEG polymer chains in the complexes was evaluated by their complexation with α-cyclodextrin (CyD) or polymer derivatives of *β*-CyD modified with PEG (PEG−*β*-CyD). In contrast to free PEG, only part of PEG polymer chains (∼10%) interact with α-CyD. Thus, the complexation of PEG with ChT proceeds by means of multipoint interaction with surface groups of the protein globule located far from the active site and results in the sufficient decrease in the availability of polymer chains. The complexes between PEG chains in PEG−protein adducts and PEG−*β*-CyD may be considered as a novel type of dendritic structures.

INTRODUCTION

It is known that poly(ethylene glycol) (PEG)[1] in aqueous solutions is inert in respect to biomacromolecules (proteins, nucleic acids, and dextrans) (*1*). Surface adsorption or grafting of PEG to sorbents, liposomes, proteases, and detector elements of biosensors is widely used for keeping them from undesirable nonspecific binding (*2*). Due to the incompatibility between proteins and PEG, the crystallization of a variety of proteins may be realized by the addition of PEG to aqueous solutions of proteins (*3*). At the same time, some properties of PEG conflict with the conception of its inertness in respect to proteins. For instance, the addition of PEG favors to the increase in the degree of folding of some proteins and inhibition of the process of aggregation of folding intermediates (*4*, *5*), that is possible only at the direct contact between protein molecules and PEG. In this case, PEG resembles chaperones—specific proteins responsible for the folding of synthesized polypeptide chains to native structures (*6*−*8*). Direct measurements of interaction between monolayers, one of which contains grafted PEG, and the other grafted protein, also demonstrate the existence of attractive forces between PEG and protein (*9*). That is why one may suppose that under certain conditions PEG is able to form noncovalent complexes with proteins. It is known that high pressure (∼400 MPa) induces denaturation of proteins (*10*). Moderate nondenaturing pressures exert reversible conformational changes related to intrinsic compressibility of proteins and hydration density effects (*11*). Besides, it is known that binding of proteins with specific ligands may be accompanied by a significant increase in packing density (*12*). In this case, the increase of pressure would favor the complexation process. Earlier we showed that the increase in pressure favors the formation of the complex between poly(ethylene oxide)−poly(propylene oxide) block copolymers (Proxanols, Pro) and ChT (*13*). In this work we first synthesized and isolated complexes based on PEG and a number of proteins prepared under elevated pressures. Their composition and some functional properties have been studied.

EXPERIMENTAL PROCEDURES

Chemicals. In this work, the following compounds were used: crystalline α-chymotrypsin from bovine pancreas with an activity of 40−60 IU/mg from Sigma (USA), a number of PEGs with number average molecular masses ($\bar{M}_n$) of 300, 750, 1500, 1900, 3000, and 4000 Da from Serva (Germany), monobutyl ether of block copolymers of ethylene oxide and propylene oxide (Pro) with number average molecular mass of 2000 Da containing 40 wt % propylene oxide from Scientific Manufacturing Association NIOPIK (Russia):

* Address correspondence to this author at the Department of Chemistry, Lomonosov Moscow State University. Phone: (7-095) 939-31-27. Fax: (7-095) 939-01-74. E-mail: kurganov@gagarinclub.ru.

† A. N. Bakh Institute of Biochemistry. Fax: (7-095) 954-27-32.

‡ Belozerskii Institute of Physico-Chemical Biology. Fax: (7-095) 939-31-81.

[1] Abbreviations: BTEE, *N*-benzoyl-L-tyrosine ethyl ester; ChT, α-chymotrypsin; BSA, bovine serum albumin; CD, circular dichroism; CyD, cyclodextrin; PEG, poly(ethylene glycol); Pro, proxanol; TLC, thin-layer chromatography.

10.1021/bc990004x CCC: $19.00 © 2000 American Chemical Society
Published on Web 12/23/1999

$$C_4H_9O\text{-}[CH(CH_3)\text{-}CH_2O]_{14}\text{-}(CH_2\text{-}CH_2\text{-}O)_{25}\text{-}H$$

As substrates of α-ChT, the following compounds were used: *N*-benzoyl-L-tyrosine ethyl ether (BTEE) from Serva (Germany) and azocasein (casein, containing covalently bounded *p*-sulfodiazobenzene), kindly presented by Prof. V. V. Mozhaev (Lomonosov Moscow State University, Department of Chemistry, Chair of Chemical Enzymology). To prepare buffer solutions, Tris from Reanal (Hungary) was used.

Synthesis of PEG−*β*-CyD conjugate was performed by the polymerization of ethylene oxide initiated with hydroxyl groups of polyfunctional initiator, *β*-CyD, using the method described in ref *14*. Molecular mass of PEG−CyD derivative was found to be equal to 3500 Da.

As a support for affinity chromatography, Sepharose modified with classical soyabean Bauman-Birk inhibitor of trypsin from Sigma was used. The synthesis of the support was performed by mixing 5.0 g of BrCN−Sepharose (Pharmacia, Sweden) in 20 mL of 0.1 M borate buffer, pH 8.45, with 40 mg of soyabean inhibitor of trypsin. The reaction mixture was gently mixed at 0−4 °C during 24 h. After this, the support was incubated in 0.5 M Tris-HCl buffer, pH 8.9, during 6 h. Then the support was sequentially washed with 3 M KCl and 1 mM HCl (500 mL each solution) and finally repeatedly washed with 0.02 M phosphate buffer, pH 7.8.

Preparation of Isotope-Labeled PEG. The insertion of isotope label (tritium) in PEG 1900 was performed using the apparatus described by Shishkov et al. (*15*). The solution of the polymer in methanol (2 mg/mL) was evenly distributed over the inner surface of the reaction vessel, freezed in liquid nitrogen, and dried in a vacuum. A target was thermostated at the temperature of liquid nitrogen (77 K) in a deep vacuum. A reaction vessel was filled up to the point where pressure will reach 1.5−2.0 Pa. The production of tritium-reactive atoms was achieved due to the heating of tungsten spiral by variable current during 15 s at 2000 K. This procedure was repeated several times. To remove species containing free exchanged tritium incorporated into end groups of the polymer, the sample was dissolved in 50% ethanol solution and dried in a vacuum repeatedly. Then the polymer was purified by repeating precipitation from the saturated solution of the sample in ethanol to diethyl ether. The final product had specific radioactivity of 1.7×10^5 disintegration/min per 1 mg. Radioactivity was measured by liqiuid scintillator based on dioxane at the counter Delta (Tracor Analytic). The amount of [^{3}H]PEG bounded with protein was estimated by the value of specific radioactivity calculated from the ratio of radioactivity to mass of the sample normalized to specific radioactivity of the polymer.

Synthesis of PEG−Protein Complexes. To prepare PEG−protein complexes, the solution of protein (2 mg/mL) in 0.02 M phosphate buffer, pH 7.0, was mixed with 200-fold molar excess of the polymer. A mixture was stirred up to complete dissolution of components. Gauge pressure in the system was created by means of centrifuging during 1 h at 25 °C (37000−142000*g* and r_{av} = 5.1 cm) in a preparative ultracentrifuge MOM-3180. For every meaning of the speed, the corresponding value of maximal pressure in the system (without regard for the gradient from menisk to the bottom of the cell) was calculated:

$$P = \frac{dF}{dS} = \frac{\omega^2\rho}{3r_{max}}(r_{max}^3 - r_{min}^3)$$

where P is the maximal pressure in the system, dF is the centrifugal force, dS is the square under pressure, ρ is density of the solution (g/cm^3), ω is the angle rate (rad s^{-1}), and r_{min} and r_{max} are the minimum and maximum distances from the center of rotation correspondently.

Isolation of Complexes. The isolation of the complexes from the reaction mixture was performed by two methods. According to the first method, an aliquote of the reaction mixture was diluted up to 20 mL with 0.02 M phosphate buffer, pH 7.6−7.8. The preparative separation of the complexes from the excess of the polymer was made using affinity chromatography at the column (0.7 × 10.0 cm) with the support containing soyabean inhibitor of trypsin. Phosphate buffer, 0.02 M and pH 7.8, was used as an eluent. The composition of the eluate was analyzed by UV method at 206 nm. The elution of the complexes was performed using 1 mM HCl. The elution of protein fraction was detected at 280 nm. Complexes were isolated by means of dialysis of eluate and subsequent lyophilization.

According to the second method, the solution containing PEG−protein complex and the excess of the polymer was dialyzed against water during 6 h. The samples were concentrated by pouring the solution into dialyzing tube surrounded by dry PEG with molecular mass of 100 kDa. The complex was isolated by precipitation with cooled acetone.

The absence of free polymer impurity was monitored by the method of thin-layer chromatography (TLC) on Silufol plates (Kevalier, Czechia) in chloroform−ethanol−water (36:12:1 v/v). Iodine vapor was used to reveal the products. After the identification, plates were divided into horizontal strips of equal width and the support from every strip was placed into separate vessel with liquid scintillator based on dioxane. After the incubation of the solution during 12 h at 20 °C, radioactivity was measured at counter Delta (Tracor Analytic).

Characterization of Complexes. The protein content in the complexes was assayed either using UV spectrophotometry at 280 nm or by the biuret reaction using native ChT as a standard. The content of polymer (a number of polymer chains per one protein molecule), n, was calculated according to the following formula:

$$n = \frac{(100 - \text{wt \% ChT})/\bar{M}_n}{\text{wt \% ChT}/M}$$

where $\bar{M}_n$ is number average molecular mass of the polymer and M is molecular mass of the protein.

Enzymatic activity of the complexes was assayed by measuring the initial rate of hydrolysis of BTEE (*16*). Titration of active centers was performed using *trans*-cinnamoylimidazol as a titration agent (*17*).

The kinetics of thermoinactivation of ChT and its complexes with polymers were registered as follows. The solution of the enzyme or adduct with polymer (10^{-5} M) was incubated in thermostat at 45 ± 0.05 °C (0.2 M Tris-HCl buffer, pH 8.0). Aliquots were withdrawn at certain intervals, and their residual activities were assayed at 20 °C by measuring the initial rate of hydrolysis of BTEE.

The α-CyD content in the complexes PEG−ChT−α-CyD was assayed using IR spectrophotometry according to the intensity of the absorption at 1030 cm^{-1}, which corresponds to the valent fluctuations of C−O, O−C bonds in CyD. First, the essential calibration has been made (*18*).

Synthesis of Three-Component Complexes. Synthesis of three-component systems containing PEG, ChT, and PEG−*β*-CyD was performed using two methods.

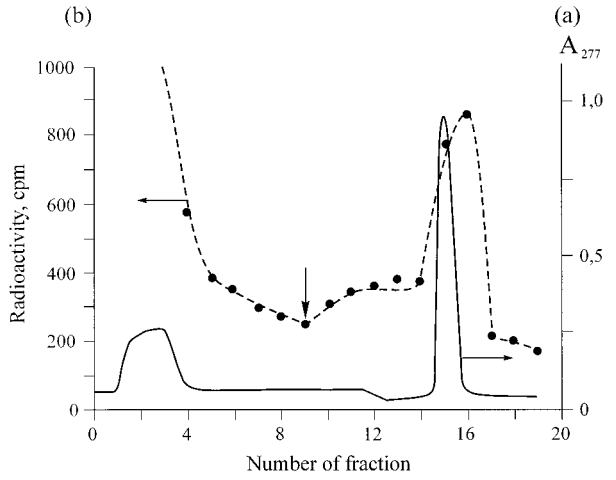

Figure 1. Profiles of elution of the reaction mixture containing complex between ChT and PEG1900. Elution was registered by the adsorption at 277 nm (a) and radioactivity of fractions (b). Vertical arrow points the beginning of elution of PEG−ChT complex with the solution of HCl.

Method 1 is based on the preparation of noncovalent PEG−ChT adducts and subsequent addition of PEG−β-CyD. Method 2 presents an one-step procedure based on the mixing of three components. To the solution of ChT (2 mg/mL) in 0.02 M phosphate buffer, pH 7.0, 200-fold molar excess of PEG and 400-fold molar excess of PEG−β-CyD were added. The mixture was stirred until complete dissolution of components and underwent to the action of elevated pressure in a preparative ultracentrifuge MOM-3180 (r_{av} = 5.1 cm) during 1 h at 25 °C and 37000−142000*g*. The product was isolated by the precipitation with cooled acetone.

RESULTS AND DISCUSSION

Synthesis and Characteristics of Complexes. In the present work, it was shown that the action of elevated pressure in the range 1.1−400 MPa on the systems containing proteins [ChT, lysozyme, and bovine serum albumine (BSA)] and PEG results in the formation of complexes. In control experiments under atmospheric pressure and room temperature, the complexation between PEG and protein does not occur.

Methods of isolation of complexes from the solution are worthy of particular attention. With the help of the affinity sorbent, Sepharose with covalently bound soyabean inhibitor, ChT containing fraction was isolated, and the excess of unreacted polymer was eliminated. Figure 1 shows profiles of elution of the reaction mixture containing ChT-PEG1900 complex. The elution of complexes was monitored by the adsorption at 277 nm (a) and radioactivity of fractions (b). From this figure, it is seen that fractions 14−16 contain both ChT and tritium-labeled PEG1900, whereas an excess of free polymer eluted at early stages (fractions 1−10). Precipitation of complexes with acetone is an alternative effective method of separation from the excess of polymer. In control experiments with [^{3}H]PEG, it was shown that the precipitation of the mixture of the polymer and the protein with acetone allows us to isolate pure protein, which does not contain coprecipitated [^{3}H]PEG.

Figure 2 demonstrates the distribution of radioactive label in the process of TLC of the complex isolated using acetone (curve 1), mixture of ChT and [^{3}H]PEG (curve 2), and initial labeled PEG (curve 3). Each point at the curve corresponds to radioactivity of the separate fraction. As it is seen from the Figure 2, complex of ChT with

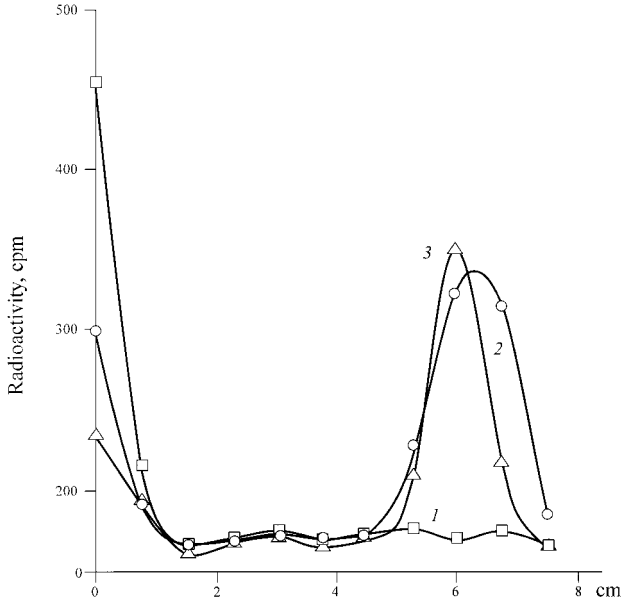

Figure 2. Distribution of radioactive label on TLC plates for [^{3}H]PEG1900-ChT complex isolated by the precipitation in acetone (curve 1), mixture of native ChT and [^{3}H]PEG 1900 (curve 2), and initial [^{3}H]PEG 1900 (curve 3). A total of 10 μL of the solution of the complex (15 mg/mL) was sprayed.

[^{3}H]PEG remained on the start as well as the original protein. R_f of free polymer in this system is equal to ∼0.6−0.65. Essential differences in R_f values between the complex and unbound polymer make possible using TLC as a control of the complex purity.

Data on the composition of complexes obtained from PEG of different molecular masses ($\bar{M}_n$) are presented in Table 1. It was found, that optimal molar ratio of polymer to protein for the synthesis of complexes is 200:1, and the content of polymer in complexes practically does not depend on the value of applied pressure in the above range and temperature 5−25 °C. In control experiments, it was shown that there were no polymer chains in the complexes produced by just mixing PEG and protein at room temperature and atmospheric pressure.

It is seen that the increase of $\bar{M}_n$ from 300 to 4000 Da results in the monotonic decrease in the number of polymer chains in the complex, whereas the content of the protein in all complexes practically does not change and comprises ∼70%. The content of PEG in the complex calculated from the measurement of [^{3}H]PEG1900 coincides with indirect data obtained by the protein assay in complexes. For reference, data on the content of the protein in temperature-induced complexes based on Pro and ChT (*19*) are also presented in this table. It is seen that the composition of complexes 4, 7, and 8 based on PEG and Pro of equal $\bar{M}_n$ but obtained under the action of different physical factors (elevated pressure or elevated temperature) is identical. Analysis of the data presented in Table 2 reveals the dependence between the number of polymer chains in complexes and dimensions of the protein. By the example of complexes based on PEG1900 and three different proteins with decreasing molecular mass (lysozyme < ChT < BSA), it was shown that the greater the radius of the protein, the greater the number of polymer chains in the complexes. The data presented in Tables 1 and 2 testify that the composition of polymer−protein complex primarily depends on the geometric fitness between the surface of protein globule and the length of polymer chain of PEG.

Table 1. Characteristics of Polymer−ChT Complexes

no.	complex	conditions for complex preparation	$\bar{M}_n$ of the polymer	no. of polymer chains in the complex	content of the protein in the complex (%)
	PEG1900 + ChT	atmospheric pressure	1900	0	98 ± 2
1	PEG300-ChT	16.0 MPa	300	31 ± 2	73 ± 4
2	PEG750-ChT	16.0 MPa	750	12 ± 1	74 ± 4
3	PEG1500-ChT	16.0 MPa	1500	7.8 ± 0.4	68 ± 3
4	PEG1900-ChT	16.0 MPa	1900	5.9 ± 0.3	69 ± 3
5	PEG3000-ChT	16.0 MPa	3000	2.9 ± 0.1	74 ± 4
6	PEG4000-ChT	16.0 MPa	4000	1.9 ± 0.1	76 ± 4
7	Pro-ChT	16.0 MPa	2000	6.2 ± 0.3	67 ± 3
8	Pro-ChT	48 °C	2000	7.0 ± 0.4	64 ± 3

Table 2. Characteristics of Complexes of PEG1900 with Different Proteins[a]

protein	molecular mass of protein (Da)	no. of polymer chains in the complex	content of the protein in the complex (%)
lysozyme	11 000	2.7 ± 0.1	68 ± 3
ChT	25 000	5.9 ± 0.3	69 ± 3
BSA	68 000	10 ± 1	77 ± 4

[a] Complexes were synthesized under the pressure 16.0 MPa.

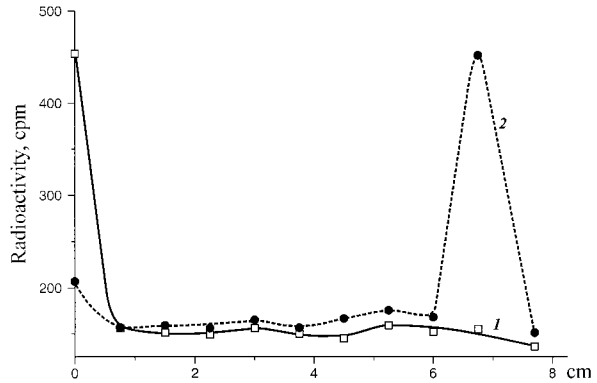

Figure 3. Distribution of radioactive label on TLC plates of [^{3}H]PEG−ChT complex, starting material (1) and incubated in water at 4 °C during 3 days (2). A total of 10 μL of the solution of the complex (15 mg/mL) was sprayed.

To study the stability of PEG−ChT complexes in the solution, [^{3}H]PEG1900-ChT complex was incubated in distilled water at 4 °C during 3 days. Aliquots were withdrawn at certain intervals, and the appearance of free polymer was assayed using TLC. It was shown that free polymer came to view already overnight. Figure 3 shows distribution of radioactive label on TLC plates for [^{3}H]PEG1900-ChT for initial complex (curve 1) and for the complex incubated during 3 days (curve 2). It is seen that after 3 days complex was fully decomposed. At the same time, it appears that the incubation of PEG−ChT complex at 45 °C during 3 h does not result in the appearance of free polymer that testifies its stability at elevated tempertature. These data suggest that the main driving force of complexation is hydrophobic interactions between PEG and protein globule. An analogous conclusion was made by Furness E. L. et al. studying complexes based on lysozyme and PEG (*20*).

Enzymatic Properties of PEG−ChT Complexes. Enzymatic properties of PEG−ChT complexes were assayed by measuring the hydrolysis of low molecular weight substrate, *N*-benzoyl-L-tyrosine ethyl ester (BTEE), and macromolecular substrate, azocaseine.

The values of the Michaelis constant (K_m) and catalytic constant (k_{cat}) of BTEE hydrolysis catalyzed by PEG−ChT complexes [$K_m = (5.6 \pm 0.4) \times 10^{-5}$ M and $k_{cat} = 24 \pm 2$ s^{-1}) in the limits of the experimental error coincide with the corresponding values for native ChT. The same picture was observed for the hydrolysis of the macromolecular substrate catalyzed with PEG−ChT adduct: $K_m = 0.026 \pm 0.003$ M and $k_{cat} = 4.8 \pm 0.4$ s^{-1}. The fact that PEG−ChT complexes retain high enzymatic activity in respect to both subtrates suggests that polymer chains in complexes are placed far from the active site of enzyme.

Earlier (*13*) we showed that noncovalent complexes based on Pro and ChT are characterized by higher thermostability than native ChT. The investigation of the kinetics of thermoinactivation of PEG−ChT complexes at 45 °C shows that their stability does not differ from the stability of ChT. Since, as was shown earlier, complexes are not destroyed under these conditions, one may suppose that noncovalent fixation of PEG in contrast to block copolymers (*13*) does not result in the screening of hydrophobic patches at the surface of the protein globule of ChT, that is necessary for the increase in thermostability of the protein (*21*, *22*).

Complexes Based on PEG−ChT Adducts and Cyclodextrins. The steric availability of polymer chains of PEG incorporating in complexes with proteins was characterized by the investigation of the ability of polymers to form inclusion complexes with α-cyclodextrin (CyD). We used this approach for the localization of polymer chains in conjugates of ChT with Pro (*23*) and PEG (*24*). It is known that PEG forms inclusion complexes, "molecular necklaces", with α-CyD (*25*, *26*). In these structures, dozens of CyD molecules are threaded onto polymer chains of PEG. Polymer chains in covalent PEG−ChT conjugates also form complexes with CyD of the same composition as complexes based on free polymers (*23*). Thus, one-end coupling of PEG at the surface of protein globule exert no sufficient influence on the availability of the second end of polymer chain that is responsible for the recognition of PEG by CyD molecules and subsequent formation of molecular necklaces.

Mixing of CyD with the solution of PEG1900-ChT complex results in the formation of insoluble complex too. The content of CyD in ternary complexes CyD−PEG−ChT is ∼10% from the amount which might be expected if all polymer chains of PEG would participate in the complexation process. In addition, on the basis of the analysis of the composition of the precipitate it was shown that the interaction of PEG−ChT complex with CyD did not accompany by the disruption of noncovalent bonds between PEG and ChT. Thus, most of polymer chains in complexes appears to be spatially inavailable for the interaction with CyD. The structure of ternary complex CyD−PEG−ChT is schematically drawn in Figure 4. Thus, these data suggests the following model of PEG−protein complexes. It is shown that only a part of polymer chains in PEG−ChT complex is saturated with CyD, whereas other chains remain free. This suggestion is based on the data of cooperative character of complexation (*18*, *24*).

Table 3. Constants of the Rate of Thermoinactivation of ChT and Its Complexes with PEG (45.0 °C; pH 8.0)

complex	molar ratio of PEG incorporated in adduct to PEG-β-CyD	A_1	k_1 (s^{-1})	A_2	k_2 (s^{-1})
native ChT		0.33 ± 0.11	0.15 ± 0.07	0.67 ± 0.11	0.0240 ± 0.0040
		PEG−ChT Complexes			
$(PEG300)_{31}$-ChT		0.46 ± 0.10	0.20 ± 0.09	0.54 ± 0.12	0.0230 ± 0.0050
$(PEG300)_{31}$-ChT-PEG-β-CyD	1:2	~0.01		0.99 ± 0.01	0.0059 ± 0.0003
$(PEG750)_{12}$-ChT		0.56 ± 0.10	0.10 ± 0.01	0.44 ± 0.08	0.0240 ± 0.0060
$(PEG750)_{12}$-ChT-PEG-β-CyD	1:2	0.25 ± 0.02	0.13 ± 0.05	0.75 ± 0.05	0.0097 ± 0.0012
$(PEG1500)_8$-ChT		0.54 ± 0.05	0.22 ± 0.01	0.46 ± 0.04	0.0230 ± 0.0030
$(PEG1900)_7$-ChT		0.58 ± 0.06	0.32 ± 0.01	0.42 ± 0.04	0.0230 ± 0.0030
	1:0.25	0.32 ± 0.02	0.20 ± 0.06	0.68 ± 0.05	0.0170 ± 0.0016
	1:0.4	0.29 ± 0.01	0.15 ± 0.04	0.71 ± 0.03	0.0090 ± 0.0009
	1:0.5	0.27 ± 0.01	0.19 ± 0.01	0.73 ± 0.02	0.0070 ± 0.0007
$(PEG1900)_7$-ChT-PEG-β-CyD	1:1	0.38 ± 0.02	0.14 ± 0.03	0.62 ± 0.03	0.0070 ± 0.0009
	1:2	0.35 ± 0.01	0.24 ± 0.04	0.65 ± 0.02	0.0060 ± 0.0005
	1:4	0.36 ± 0.01	0.29 ± 0.06	0.63 ± 0.02	0.0050 ± 0.0005

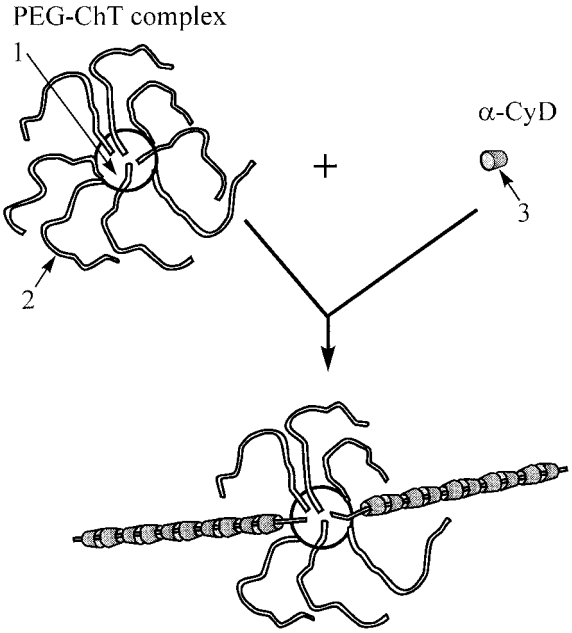

Figure 4. Structures of supramolecular ensemble on the basis of PEG−protein complexes and α-CyD. Abbreviations: *1*, ChT; *2*, PEG; *3*, α-CyD.

Thus, sorbtion of PEG occurs by means of multipoint interaction with the surface of protein globule resulting in sufficient decrease of the mobility of polymer chains. PEG is held on the protein globule by relatively few attached segments and the remaining segments form loops and tails. Polymer chains of PEG of different molecular mass are placed at the same sites of protein globule which are far from the active site. Total occupied surface in all cases is approximately the same.

One may expect that if we shall substitute CyD for its derivatives, the formation of molecular necklaces will be improbable because of inability of CyD derivatives of forming dense packing along the polymer chain. With this aim in mind, a branched polymer derivative of β-CyD, PEG−β-CyD (*14*), was used. Structure of this compound is presented in Figure 5. The choice of polymer derivative of β-CyD is caused by the following considerations. The modification of CyD by PEG chains results in the decrease of effective diameter of inner cavity of CyD. That is why PEG−α-CyD conjugate does not complex with PEG, whereas PEG−β-CyD does. The formation of inclusion complexes between PEG incorporated in PEG−protein complexes and single molecules of PEG−β-CyD seems to be quite probable. An analogous type of complexation was demonstrated by the example of the interaction between PEG-surfactants and PEG−β-CyD (*27*). Besides, using branched hydrophilic derivative of CyD would yield water-soluble inclusion complexes with PEG−protein adducts. One may anticipate that the change in microenvironment of protein globule due to the complexation with PEG−β-CyD would affect the functional properties of the protein.

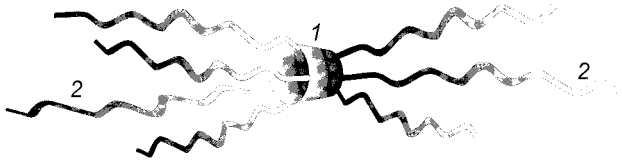

Figure 5. The structure of covalent adducts of β-cyclodextrin with PEG. 1 and 2 are cyclodextrin and PEG, respectively.

Three component complexes PEG−ChT−(PEG−β-CyD) were prepared using two methods: the addition of PEG−β-CyD to the solution of PEG−ChT complexes (stepwise method) and the action of elevated pressure on the mixture of three components with subsequent isolation of the product from the solution (one-step method). As the test for complexation between PEG−ChT complexes and PEG−β-CyD, we used the study of thermostability of ChT in three component complexes. The study of the kinetics of thermoinactivation of PEG−ChT complex shows that the addition of PEG−β-CyD results in the increase of thermal stability of the protein (Figure 6). The kinetic data are treated assuming that they can be described by the sum of two exponential terms:

$$A/A_0 = A_1 e^{-k_1 t} + A_2 e^{-k_2 t}$$

where A/A_0 is the relative enzyme activity, A_1 and A_2 are the relative contributions of each stage of the process, respectively ($A_1 + A_2 = 1$), and k_1 and k_2 are the rate constants of thermal inactivation for each stage. The results of this mathematical treatment of the curves are presented in Table 3.

As is seen from the Table 3, the increase in thermostability of the protein in ternary complexes based on PEG300, PEG750, and PEG1900 produced by stepwise method is first due to the decrease in the constant of the rate of thermoinactivation, k_2 (the change of k_1 is negligible). Figure 7 demonstrates the dependence of the k_2 value on molecular ratio of PEG−β-CyD to PEG incorporated in PEG−ChT complex. This plot looks like a titration curve with a breakpoint. Thus, the complexation between components takes place. The value of the breakpoint corresponds to a molar ratio of PEG−β-CyD to PEG

Table 4. Characteristics of Complexes Including ChT and PEG−β-CyD Prepared under the Pressure 16.0 MPa

no.	complex	content of the protein in complex (%)	number of molecules of branched component in the complex	A_1	k_1 (s^{-1})	A_2	k_2 (s^{-1})
1	ChT- PEG-β-CyD	81 ± 4	2	0.15 ± 0.01	0.12 ± 0.06	0.85 ± 0.04	0.0075 ± 0.0008
2	ChT-PEG-β-CyD-PEG1900[a]		2	0.35 ± 0.05	0.10 ± 0.03	0.65 ± 0.10	0.0078 ± 0.0014
3	ChT-PEG-β-CyD-PEG1900[b]	57 ± 3		0.45 ± 0.03	0.03 ± 0.01	0.55 ± 0.04	0.0062 ±0.0012

[a] Complex was prepared by two stages: (1) by the action of elevated pressure on the mixture of ChT and PEG-β-CyD and (2) by adding of PEG1900 to the two component complex. [b] Complex was synthesized by the action of elevated pressure on the mixture of three compounds: ChT, PEG1900, and PEG-β-CyD (method 2).

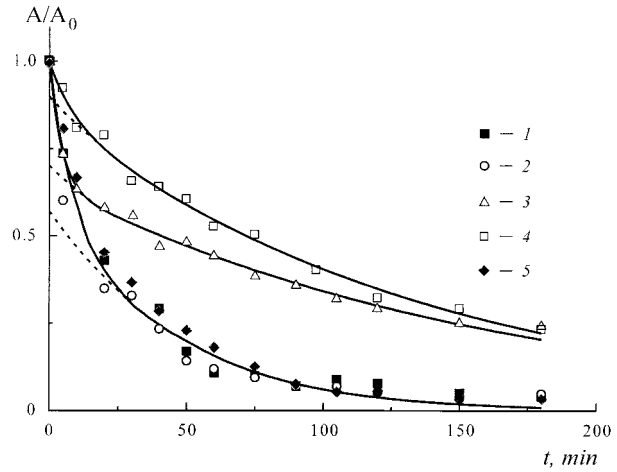

Figure 6. Kinetics of thermal inactivation of ChT (*1*) and its complexes: (*2*) $(PEG1900)_7$−ChT; (*3*) $(PEG1900)_7$−ChT-PEG−β-CyD complex was synthesized according to the method 1 at molar ratio of PEG−β-CyD to PEG incorporated in PEG-ChT complex equal to 1:2; (*4*) $(PEG1900)_7$−ChT-PEG−β-CyD, complex was synthesized according to the method 2; (*5*) a control mixture ChT and β-CyD. Conditions: 0.2 M Tris-HCl buffer, pH 8.0; 45 °C. Dotted lines correspond to the slow phases of thermal inactivation.

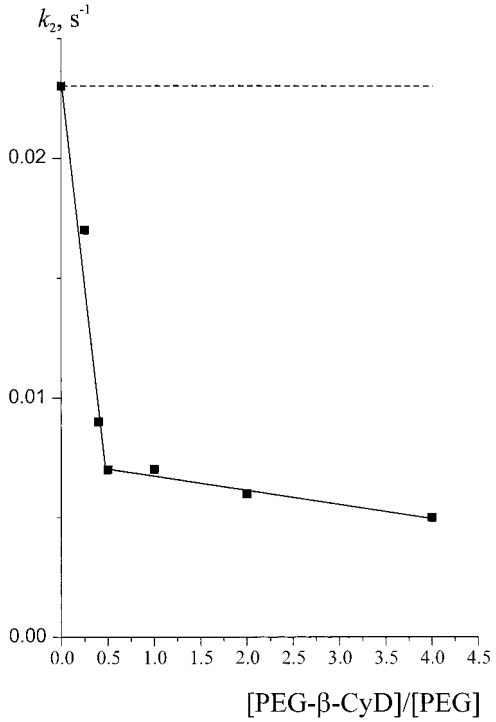

Figure 7. The dependence of the rate constant k_2 for thermoinactivation of ChT in three component complexes [$(PEG1900)_7$−ChT−PEG−β-CyD] on molecular ratio of PEG−β-CyD to PEG incorporated in PEG−ChT complex. Dotted line indicates the value of the k_2 for thermoinactivation of the native ChT and ChT in the presence of PEG−β-CyD.

incorporated in PEG−ChT complex equal to 0.5:1 (or 1:2). It means that only half the chains connected with a protein are available for the complexation with PEG−β-CyD. It should be noted that the same approach used for the study of steric availability of PEG chains incorporated in covalent PEG−ChT conjugates demonstrates that each chain of PEG participates in the complexation with PEG−β-CyD (*28*).

The increase in thermostability of the systems involving PEG−ChT complexes and PEG−β-CyD is probably caused by the fact that the complexation results in the "lengthening" and "branching" of polymer chains in polymer−protein complex. It is known that using polymer reagents with branched structure (e.g., di-PEG-reagents) for modification of proteins results in a sufficient increase in their stability compared with conjugates based on mono-PEG-reagents (*29*). Figure 8 shows the proposed structure of supramolecular ensemble containing all three components. This structure involving highly branched elements of PEG−β-CyD derivative, PEG, and protein is close by its architecture to dendrimers (*30*).

The formation of supramolecular structures based on PEG−protein complexes and PEG−β-CyD is a way for preparation of the protein samples with increased thermostability, which allows us to dispense with time-consuming stage of the chemical modification of the protein. It should be noted that the simplest approach for the formation of such supramolecular structures was realized when the pressure was applied to a mixture of three components (PEG, ChT, and PEG−β-CyD). As is seen from the Table 4 and Figure 6 (curve 3 and 4), constant k_2 for the system obtained by mixing of three components is close to this value for the complex obtained by stepwise synthesis.

When discussing the structure of the resulting ternary complex prepared under the action of elevated pressure on the mixture of three components, it was crucial to find out if PEG−β-CyD may form complexes with protein. A special experiment on the action of elevated pressure on the mixture of ChT and PEG−β-CyD conjugate verified the formation of the adduct containing two molecules of PEG−β-CyD per one molecule of the protein. It is of interest to compare the composition of complexes based on linear and branched PEG with equal length of the polymer chain. As was shown in ref *14*, an average molecular mass of the polymer chain in PEG−β-CyD is equal to 350 Da. Therefore, for comparison, we may use the data on the composition of the complex based on PEG300. As it is seen from the Table 1, the number of polymer chains in PEG300-ChT adducts equals to 31. This value exeeds the number of bound PEG−β-CyD in the complex with ChT in more than 1 order in magnitude. It seems to be quite reasonable from steric point of view and demonstrates that the complexation of linear PEG chains with proteins is favored over branched chains. It is of importance that in contrast to the PEG−ChT adduct,

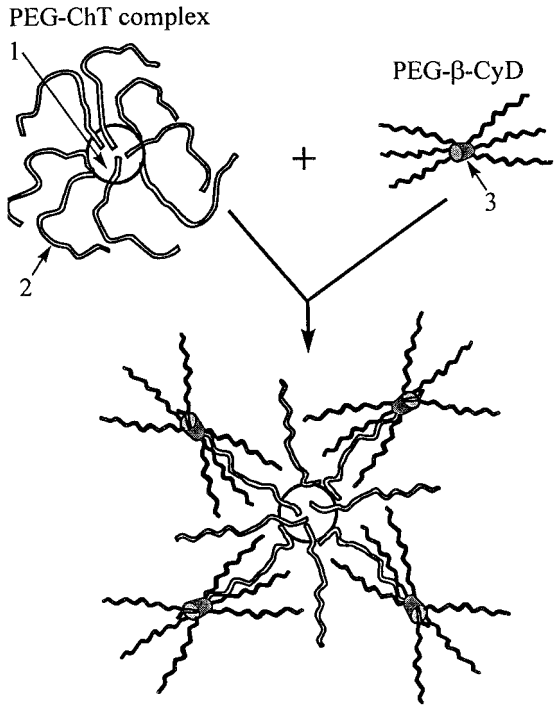

Figure 8. Structures of supramolecular ensemble on the basis of PEG−protein complexes and PEG−β-CyD. Abbreviations: *1*, ChT; *2*, PEG; *3*, PEG−β-CyD.

the adduct based on ChT and PEG−β-CyD is characterized by increased thermostability compared to the native ChT (Table 4). This fact demonstrates that the binding of branched PEG-macromolecules to the protein globule even at their less content produces a stabilizing effect. The addition of PEG to the adduct between PEG−β-CyD and ChT results in even more stabilizing effect (Table 4), which probably is indicative of the inclusion of PEG molecules in the adduct containing ChT and PEG−β-CyD.

Thus, the method of self-assembly which we used earlier for the synthesis of dendritic structures based on PEG-surfactants (*27*) was applied in this work for the preparation of adducts, which contain protein and are characterized by increased thermostability. These structures present unique example of supramolecular ensembles including native and synthetic macromolecules.

ACKNOWLEDGMENT

The study was funded by Grant 96-03-33519a from Russian Foundation for Basic Reasearch.

LITERATURE CITED

(1) Topchieva, I. N. (1980) Biotechnology application of poly(ethylene glycol). *Usp. khim. 49*, 260−271.

(2) Harris, J. M. (1997) Introduction to biomedical application of poly(etylene glycol). *Polym. Preprints 38*, 520−521.

(3) Patel, S., Cudney, B., and Mac Pherson, A. (1995) Polymeric precipitants for the crystallization of macromolecules. *Biochem Biophys. Res. Commun. 207*, 819−828.

(4) Arakawa, T., and Timasheff, S. N. (1985) Mechanism of poly(ethylene glycol) interaction with proteins. *Biochemistry 24*, 6756−6762.

(5) Otamiri, M., Adlercreutz, P., and Mattiasson, B. (1994) A different scanning calorimetric study of chymotrypsin in the presence of added polymers. *Biotechnol. Bioeng. 44*, 73−78.

(6) Hartl, F. U. (1996) Molecular chaperons in cellular protein folding. *Nature 381*, 571−580.

(7) Kurganov, B. I., and Topchieva, I. N. (1998) Artificial chaperon-assisted refolding of proteins. *Biochemistry (Moscow) 63*, 413−419.

(8) Rozema, D., and Gellman, S. H. (1996) Artificial chaperon-assisted refolding of carbonic anhydrase B. *Biol. Chem. 271*, 3478−3487.

(9) Sheth, S. R., and Leckband, D. E. (1997) Investigating the molecular mechanism of protein interactions with poly(ethylene glycol). *Polym. Preprints 38*, 616−617.

(10) Gross, M., and Jaenicke, R. (1994) The influence of high hydrostatic pressure on structure, function and assembly of proteins and protein complexes. *Eur. J. Biochem. 221*, 617−630.

(11) Low, P. S., and Somero, G. N. (1975) Activation volumes in enzymic catalysis: their sources and modification by low-molecular weight solutes. *Proc. Natl. Acad. Sci. U.S.A. 72*, 3014−3018.

(12) Jaenicke, R., Gregory, E., and Laepple, M. (1979) Hydrodynamic and spectral effects upon ligand binding to porcine LDH. *Biophys. Struct. Mech. 6*, 57−65.

(13) Topchieva, I. N., Sorokina, E. M., Kurganov, B. I., Zhulin, V. M., and Makarova, Z. G. (1996) High-pressure-induced complexes of α-chymotrypsin with block copolymers based on ethylene and propylene oxides. *Biochemistry (Moscow) 61*, 746−749.

(14) Topchieva, I. N., Polyakov, V. A., Elezkaya, S. V., Bystryzkiy, G. I., and Karezin, K. I. (1997) One-pot synthesis of cyclodextrins, modified with poly(ethylene oxide). *Polymer Bull. 38*, 359−364.

(15) Goldanskii, V. I., Kashirin, I. A., Shishkov, A. V., Baratova, L. A., and Grebenchikov, N. I. (1988) The use of thermally activated tritium atoms for structural-biological investigations: the topography of the TMV protein-accessible surface of the virus. *J. Mol. Biol. 201*, 567−574.

(16) Efremova, N. V., Mozhaev, V. V., and Topchieva, I. N. (1992) Thermal stability of α-chymotrypsin conjugates with water-soluble poly(alkylene oxides). *Biochemistry (Moscow) 57*, 214−223.

(17) Schonbaum, G. R., Zerner, B., and Bender, M. (1961) The spectrophotometric determination of the operational normality of an α-chymotrypsin solution. *J. Biol. Chem. 236*, 2930−2938.

(18) Topchieva, I. N., Kolomnikova, E. L., Banatskaya, M. I., and Kabanov, V. A. (1993) Complexation between β-cyclodextrins and poly(ethylene oxide)-poly(propylene oxide) block copolymers. *Polym. Sci. 35*, 464−466 (Russ.).

(19) Topchieva, I. N., Efremova, N. V., Snitko, Ya. E., and Chvorov, N. V. (1994) Thermoinduced complex formation between α-chymotrypsin and amphiphilic block copolymer. *Doklady Chem. 339*, 257−260.

(20) Furness, E. L., Ross, A., Davis, T. P., and King, G. C. (1998) A hydrophobic interaction site for lysozyme binding to poly(ethylene glycol) and model contact lens polymers. *Biomaterials 19*, 1361−1369.

(21) Mozhaev, V. V., and Martinek, K. (1984) Structure−stability relationship in proteins: a new approaches to stabilizing enzymes. *Enzyme Microb. Technol. 6*, 50−59.

(22) Mozhaev, V. V., Martinek, K., and Berezin, I. V. (1988) Structure−stability relationship in proteins: fundamental tasks and strategy for the development of stabilized enzyme catalysts for biotechnology. *CRC Crit. Rev. Biochem. 23*, 235−281.

(23) Efremova, N. V., and Topchieva, I. N. (1993) Supramolecular structures based on protein conjugates with polyalkylene oxides. β-Cyclodextrin complexes. *Biochemistry (Moscow) 58*, 753−757 (Russ.).

(24) Topchieva, I. N., Gerasimov, V. I., Panova, I. G., Karezin, K. I., and Efremova, N. V. (1998) Nanostructures based on poly(alkylene oxide)-cyclodextrin complexes. *Polym. Sci. 40*, 171−178 (Russ.).

(25) Harada, A., Li, J., and Kamachi, M. (1993) Preparation and properties of inclusion complexes of poly(ethylene glycol) with α-cyclodextrin. *Macromolecules 26*, 5698−5703.

(26) Harada, A., Li, J., and Kamachi, M.(1990) Complex formation between poly(ethylene glycol) and α-cyclodextrin. *Macromolecules 23*, 2821−2823.

(27) Topchieva, I. N., Mischnick, P., Kûhn, G., Polyakov, V. A., Elezkaya, S. V., Bystryzkiy, G. I., and Karezin, K. I. (1998) Novel derivatives of cyclodextrins, modified with poly(ethylene oxide) and their complexation properties. *Bioconjugate Chem. 9*, 676−682.

(28) Topchieva, I. N., Sorokina, E. M., Medvedeva, E. M., Efremova, N. V., and Kurganov, B. I. (1999) Dendritic supramolecular structures of complexes based on covalent and noncovalent poly(ethylene glycol)-α-chymotrypsin adducts and cyclodextrins, modified by poly(ethylene glycol). *Bioorg. Chem*. (Russ.). *25*, 520−527.

(29) Monfardini, C., Schiavan, O., Caliceti, P., Morpurgo, M., and Harris, J. M. (1995) A branched monometoxypoly(ethylene glycol) for protein modification. *Bioconjugate Chem. 6*, 62−69.

(30) Newkome, G. R., Moorefield, C. N., and Vogtle, F. (1997) Dendritic molecules. Concepts. Syntheses. Perspectives. *VCH Verlagsgesellschaft mbH*, Weinheim.

BC990004X

Phospholipid−Model Membrane Interactions with Branched Polypeptide Conjugates of a Hepatitis a Virus Peptide Epitope

Ildikó B. Nagy,[†] Maria A. Alsina,[‡] Isabel Haro,[§] Francesca Reig,[§] and Ferenc Hudecz*,[†]

Research Group for Peptide Chemistry, Hungarian Academy of Science, Eötvös L. University, P.O. Box 32, Budapest 112, Hungary, H-1518, Physicochemical Unit, Faculty Pharmacy, Pza. Puis XII s/n 08028, Barcelona, Spain, and Department of Peptide and Protein Chemistry, Research Council, CID. CSIC. Jordi Girona 16. 08034, Barcelona, Spain. Received April 2, 1999; Revised Manuscript Received September 8, 1999

To establish correlation between structural properties (charge, composition, and conformation) and membrane penetration capability, the interaction of epitope peptide−carrier constructs with phospholipid model membranes was studied. For this we have conjugated a linear epitope peptide, ^{110}FWRGDLVFDFQV^{121} (110−121), from VP3 capside protein of the Hepatitis A virus with polylysine-based branched polypeptides with different chemical characteristics. The epitope peptide elongated by one Cys residue at the N-terminal [C(110−121)] was attached to poly[Lys-(DL-Ala$_m$-X$_i$)] ($i < 1$, $m \approx 3$), where $x = \varnothing$ (AK), Ser (SAK), or Glu (EAK) by the amide-thiol heterobifunctional reagent, 3-(2-pyridyldithio)propionic acid *N*-hydroxy-succinimide ester. The interaction of these polymer−[C(110−121)] conjugates with phospholipid monolayers and bilayers was studied using DPPC and DPPC/PG (95/5 mol/mol) mixture. Changes in the fluidity of liposomes induced by these conjugates were detected by using two fluorescent probes 1,6-diphenyl-1,3,5-hexatriene (DPH) and sodium anilino naphthalene sulfonate (ANS). The binding of conjugates to the model membranes was compared and the contribution of the polymer component to these interactions were evaluated. We found that conjugates with polyanionic/EAK−[C(110−121)] or polycationic/SAK−[C(110−121)], AK−[C(110−121)]/character were capable to form monomolecular layers at the air/water interface with structure dependent stability in the following order: EAK−[C(110−121)] > SAK−[C(110−121)] > AK−[C(110−121)]. Data obtained from penetration studies into phospholipid monolayers indicated that conjugate insertion is more pronounced for EAK−[C(110−121)] than for AK−[C(110−121)] or SAK−[C(110−121)]. Changes in the fluorescence intensity and in polarization of fluorescent probes either at the polar surface (ANS) or within the hydrophobic core (DPH) of the DPPC/PG liposomes suggested that all three conjugates interact with the outer surface of the bilayer. Marked penetration was documented by a significant increase of the transition temperature only with the polyanionic compound/EAK−[C(110−121)]. Taken together, we found that the binding/penetration of conjugates to phospholipid model membranes is dependent on the charge properties of the constructs. Considering that the orientation and number of VP3 epitope peptides attached to branched polypeptides were almost identical, we can conclude that the structural characteristics (amino acid composition, charge, and surface activity) of the carrier have a pronounced effect on the conjugate−phospholipid membrane interaction. These observations suggest that the selection of polymer carrier for epitope attachment might significantly influence the membrane activity of the conjugate and provide guidelines for adequate presentation of immunogenic peptides to the cells.

INTRODUCTION

New vistas for vaccine production arise with the application of synthetic peptide antigens, although these small molecules induce weaker immune responses than those elicited by intact proteins or viruses (*1*−*3*). To resolve this problem, multiple antigen peptide systems (*4*) or lipid vesicles that can elicit potent immune response against antigens entrapped or covalently linked have been introduced. The efficacy of these constructs has been clearly established for a great variety of antigens such as bacterial toxins (*5*, *6*), parasite proteins (*7*), and tumor antigens (*8*). An alternative approach suggested by Sela (*9*) is the covalent attachment of haptens/epitopes to proteins (KLH, BSA)[1] or synthetic polymers (reviewed in ref *10*) as macromolecular carriers.

To contribute to the rational design of synthetic macromolecular carrier, we have developed a new group of branched polypeptides based on a poly[L-Lys] backbone that contains short side chains composed of about three DL-Ala residues and one different amino acid residue (X) either at the end of the branches (XAK) or at the position next to the polylysine backbone (AXK). The general formula of these biodegradable, water-soluble compounds are poly[Lys(X$_i$-DL-Ala$_m$)] (XAK) or poly[Lys(DL-Ala$_m$-X$_i$)]

* To whom correspondence should be addressed. Fax: 36 1 209 0602. Phone: 36 1 209 0555/1433. E-mail: hudecz@szerves.chem.elte.hu.

[†] Research Group for Peptide Chemistry.

[‡] Physicochemical Unit.

[§] Department of Peptide and Protein Chemistry.

[1] Abbreviations: AK, poly[Lys-(DL-Ala$_m$)]; ANS, sodium anilino naphthalene sulfonate; AXK, poly[Lys-(DL-Ala$_m$-X$_i$)]; BSA, bovine serum albumin; DPH, 1,6-diphenyl-1,3,5-hexatriene; DPPC, dipalmitoyl phosphatidyl choline; EAK, poly[Lys(Glu$_i$-DL-Ala$_m$)]; KLH, keyhole limpet hemocyanin; PBS, phosphate-buffered saline; PG, phosphatidyl glycerol; SAK, poly[Lys(Ser$_i$-DL-Ala$_m$)]; SPDP, 3-(2-pyridyldithio)propionic acid *N*-hydroxy-succinimide ester; XAK, poly[Lys(X$_i$-DL-Ala$_m$)].

10.1021/bc9900385 CCC: $19.00 © 2000 American Chemical Society
Published on Web 12/02/1999

(AXK), where $i < 1$, $m \approx 3$, and X represents an optically active residue (*11*−*14*).

Considering the structural [e.g., solution conformation (*16*)] and functional characteristics [e.g., in vitro cytotoxicity (*15*), immunoreactivity (*14*, *17*), and biodistribution (*18*)] of these polypeptides, various bioconjugates were prepared. In these constructs, a B-cell epitope from *mucin-1* glycoprotein (*19*), peptide fragment from *Herpes simplex* virus glycoprotein D1 (*17*), and T cell epitopes of 16 and 38 kDa proteins of *Mycobacterium tuberculosis* (*20*, *21*) were attached to branched polypeptides.

In the interaction between conjugates and cellular/subcellular membranes, the polymeric polypeptide component might have an important role. Therefore, the aim of present study was to investigate the influence of branched polymeric polypeptide in conjugates on phospholipid mono- and bilayers used as biomembrane models. As first step, we have analyzed the interaction of some branched polypeptides with simple mono- and bilayer membranes composed of DPPC or DPPC/PG mixture (*22*). We found that all three polymers studied were capable of inserting into lipid monolayers, but this interaction was more pronounced for the polycationic poly[Lys(Ser$_i$-DL-Ala$_m$)] (SAK) and poly[Lys(DL-Ala$_m$)] than for the amphoteric poly[Lys(Glu$_i$-DL-Ala$_m$)] (EAK). Using fluorescent reporter molecules, we have also demonstrated that even the most marked penetration of polycationic polypeptide (SAK) did not result in alteration of the ordered state of the alkyl chains of liposomal bilayers composed of DPPC/PG.

For the present experiments, we have prepared conjugates with a linear epitope peptide, ^{110}FWRGDLVFDFQV^{121} (110−121) from VP3 capside protein of the Hepatitis A virus (*23*) with known phospholipid interaction characteristics (*24*). We have previously shown that branched polypeptide conjugates of the elongated and Abu-substituted 20-mer peptide, ^{101}LASI(Abu)QMF(Abu)-FWRGDLVFDFQV^{121} influence the stability of mono- and bilayers composed of DPPC *(25)*. To get insight about the carrier effect on membrane activity a new set of conjugates with AK, SAK, or EAK were prepared and tested on DPPC/PG phospholipid model membranes. These conjugates possess similar relative molecular mass and number of epitope (110−121) copies, but the hydrophobicity and electrical charge of the carrier are different (*22*).

In this paper, we report the preparation of branched polypeptide conjugates of the 12-mer peptide elongated by one cysteine residue at the N-terminal C^{110}FWRGDLVFDFQV^{121} [C(110−121)]. For the disulfide bond formation between the polymer (AK, SAK, and EAK) and the epitope peptide the amide-thiol heterobifunctional coupling reagent, 3-(2-pyridyldithio)propionic acid *N*-hydroxy-succinimide ester (SPDP) (*19*, *26*) was used. The interaction of these polymer−[C(110−121)] conjugates dissolved in aqueous solution with phospholipid monolayers and bilayers was studied using DPPC and DPPC/PG (95/5 mol/mol) mixture mimicking cell membranes containing the smallest percentage of negatively charged lipids (*27*). Changes in the fluidity of liposomes induced by these conjugates were detected by using two fluorescent probes 1,6-diphenyl-1,3,5-hexatriene (DPH) and sodium anilino naphthalene sulfonate (ANS). The binding of conjugates to the model membranes was compared and the contribution of the polymer component to these interactions was evaluated.

EXPERIMENTAL SECTION

Synthesis of Polypeptide-[C(110−121)] Conjugates. Experimental details of the synthetic procedures for branched chain polypeptides were described previously (*12*, *13*). Briefly, the poly[L-Lys] backbone was prepared by the polymerization of N^{α}-carboxy-N^{ϵ}-benzyloxycarbonyl-lysine anhydride under conditions that allowed a number average degree of polymerization approximately 60. After cleavage of benzyloxycarbonyl protecting groups, DL-alanine oligomers were grafted to the ϵ-amino groups of polylysine by polymerization of *N*-carboxy-DL-alanine anhydride to produce poly[Lys-(DL-Ala$_m$)] (AK). The suitably protected Glu/Ser residue was coupled to α-amino groups of branch terminal Ala of AK. The amide bond was formed by HOBt-catalyzed active ester method (*28*). After the removal of protecting groups from Glu (EAK) and Ser (SAK) residues by HBr/AcOH, samples were dialyzed against distilled water and freeze-dried.

Peptide C(110−121) was synthesized by Fmoc/OtBu strategy on solid support (*24*) and after HPLC purification was coupled to the N-terminal amino acid residue of the AK, SAK, and EAK using SPDP (*26*).

Conjugation was performed as described earlier with mucin peptides (*19*). Briefly, polymeric polypeptides (AK, SAK, or EAK) (215 μmol) were dissolved in 7.5 mL of 0.1 M phosphate buffer (pH 7.4, adjusted with 0.1 M NaOH). A total of 20 mg (64.0 μmol) of SPDP dissolved in 2 mL of absolute methanol was added dropwise to the solution. The reaction mixture was stirred for 30 min at room temperature. After dialysis against distilled water for 24 h, the modified polymers were isolated by freeze-drying. To determine the average degree of 2-pyridyl-disulfide group incorporation, 400 μL of (SSP)polymer solution was reacted with 200 μL of DL-dithiotreitol (5 mg/mL PBS), and after 10 min, the absorbance of the released pyridine-2-thione was measured at $\lambda = 343$ nm using $\epsilon = 8080$ M^{-1} cm^{-1} (*29*). In the second step of conjugation, 10 mg of (SSP)polymer samples (containing 5 μmol protected thiol groups) were dissolved in 1 mL in 0.1 M phosphate buffer (pH 7.4) and mixed with 10 μmol of peptide C(110−121) dissolved in the same buffer (1 mL). The reaction mixture was stirred for 30 min at room temperature. Conjugate samples were purified by dialysis and isolated by freeze-drying, and the substitution degree was determined by amino acid analysis.

Abbreviations for Amino Acids and Their Derivatives. Abbreviations for amino acids and their derivatives follow the revised recommendation of the IUPAC-IUB Committee on Biochemical Nomenclature, entitled *Nomenclature and Symbolism for Amino Acids and Peptides* (recommendations of 1983). Nomenclature of branched polypeptides is used in accordance with the recommended nomenclature of graft polymers (*30*). For the sake of brevity, codes of branched polypeptides were constructed by us using the one-letter symbols of amino acids. The abbreviations used in this paper are the following: AK, poly[Lys(DL-Ala$_m$)]; XAK, poly[Lys(X$_i$-DL-Ala$_m$)]; X = Ser (SAK) or Glu (EAK). All amino acids are of L configuration unless otherwise stated. The symbols used for the conjugates are AK−[C(110−121)], SAK−[C(110−121)]. and EAK−[C(110−121)].

Chemicals. 3-(2-Pyridyldithio)propionic acid *N*-hydroxy-succinimide ester (SPDP), 1,6-diphenyl-1,3,5-hexatriene (DPH), sodium anilino naphthalene sulfonate (ANS), dipalmitoyl phosphatidyl choline (DPPC), and phosphatidyl glycerol (PG) of bovine origins were ob-

tained from Merck (Barcelona, Spain). All solvents as well as dithiotreitol were from Reanal (Budapest, Hungary).

MATERIALS AND METHODS

Surface Activity Measurement. Hydrophobic character of conjugate samples was analyzed by Wilhelmy plate method as reported earlier (*31*). All measurements were carried out in a cylindrical Teflon cuvette with capacity of 70 mL (type A). All conjugates were dissolved in 0.1 M sodium acetate buffer (pH 7.4) and were injected under the air−water interface at different final bulk concentration [$(0.2-1.8) \times 10^{-8}$ M]. Pressure increase was recorded as a function of time up to 60 min as detailed in ref *32*.

Compression Isotherms. Surface pressure vs area ($\Pi-A$) isotherms were recorded in the same device using a rectangular Teflon cuvette of 28.5 cm × 17.5 cm (type B). Conjugate samples dissolved in 0.1 M sodium acetate buffer (pH 7.4) were either spread on or injected under the air−water interface. After 10 min, the monolayer was compressed by a Teflon barrier at a speed of 4.2 cm/min. The stability of all conjugate monolayers was assessed by compression till 10 mN/m and after stopping the barrier, changes in pressure were recorded for 1 h. Experiments were carried out in triplicate at 22 °C using 0.1 M sodium phosphate buffer (pH 7.4) as subphase. The reproducibility of the measurements was in the range ±0.02 nm^2/molecule.

Penetration of Polymer−[C(110−121)] Conjugates into Phospholipid Monolayers. For the insertion experiments, phospholipid solutions of DPPC or DPPC/PG (95/5 mol/mol) mixture were spread on the aqueous phase to form a monolayer with a given initial surface pressure in the type A cuvette. Once the monolayer at 5, 10, or 20 mN/m was established, conjugate solutions were injected in the subphase and pressure increases were recorded as a function of time. In addition, phospholipid monolayers were formed on aqueous subphase in the presence or absence of conjugate in type B cuvette, and after 10 min of stabilization period, compression isotherms were recorded.

Preparation of Liposomes. Liposomes were prepared using mixture of DPPC and PG (95/5, mol/mol) as follows. Phospholipids dissolved in chloroform were mixed in a round-bottomed flask and solvent was eliminated by rotary evaporation from the clear solution at 55 °C in a vacuum. The liposome preparation was dried in high vacuum for 2 h. Lipid film was hydrated with 2 mL of 0.1 M sodium acetate buffer (pH 7.4), and multilamellar vesicles thus formed were submitted to sonication in an ultrasound bath until the solution was only slightly turbid. Size of liposomes measured in Malvern Autosizer and as described earlier (*33*) was lower than 80 nm in diameter.

Fluorescence Studies. Fluorescence experiments were performed by detecting changes in fluorescence intensity and polarization of ANS and DPH probes located in the bilayers. For this, a PE-LS50 spectrofluorometer provided with four cuvettes and thermostated bath was used. Liposomes (small unilamellar vesicles) described above were incubated with different concentrations of fluorescent probes in the dark at 55 °C for 60 min. Fluorescence intensity was measured to determine the saturation. Once the optimal phospholipid/probe ratio was selected [ANS/phospholipid = 1/26, DPH/phospholipid = 1/240 (mol/mol)], liposomes were mixed with either conjugate solution or 0.1 M sodium acetate (pH 7.4) and fluorescence intensity as well as polarization were recorded. Temperature was increased step by step, leaving enough time between lectures to allow the system to equilibrate. The suspension was continuously stirred, and the temperature inside the cuvettes monitored before and after the scan. Experiments were carried out in duplicate. Excitation (λ_{ex}) and emission (λ_{em}) wavelengths were 380 and 480 nm for ANS and 365 and 425 nm for DPH, respectively. The degree of fluorescence polarization was calculated according to Shinitzky and Barenholz (*34*),

$$P = (I_{||} - I_{\perp}{}^{*}G)/(I_{||} + I_{\perp}{}^{*}G)$$

where $I_{||}$ and $I_{\perp}$ are the intensities measured with its polarization plane parallel (||) and perpendicular ($\perp$) to that of the exciting beam. G is a factor used to correct polarization of the instrument and is given by the ratio of vertically to horizontally polarized emission components when the excitation light is polarized in the horizontal direction.

RESULTS AND DISCUSSION

Synthesis and Structure of Branched Polypeptide−[C(110−121)] Conjugates. Polymeric branched polypeptides ($DP_n = 61$) with polycationic (AK, SAK) or amphoteric (EAK) charge properties (*13*, *14*) were conjugated with a 12-mer synthetic peptide representing a B-cell epitope of VP3 capside protein of Hepatitis A virus. The schematic structure of branched polymer−peptide conjugates is depicted in Figure 1. To achieve uniform orientation in conjugates, disulfide bridge was introduced between the branches of the polymer and the peptide epitope. For this the native epitope sequence, ^{110}FWRGDLVFDFQV^{121} was elongated at the N-terminal by incorporation of a Cys residue to provide free SH group for conjugation. At the same time, protected thiol function was formed at the end of the branches of polymers using an amine-thiol type heterobifunctional cross-linking reagent, SPDP (*19*, *26*). The polymer-dithio-propionate derivatives prepared (Scheme 1) were purified, isolated, and characterized by UV spectroscopy. After reduction of an aliquot samples, the amount of pyridine-2-thione coupled to the α-amino groups of the branches was determined. The average degree of substitution calculated was between 27 and 37%. In the second step of the synthesis, disulfide bond was formed by thiolysis using free thiol group of peptide C(110−121) (Scheme 1).

The characteristics of conjugates are summarized in Table 1. These data obtained from two independent methods (UV-chromophore content and amino acid composition determination) indicate that the average incorporation of C(110−121) was in the range 27−37%.

Peptide C(110−121) bears net negative charge under physiological pH. Therefore, its coupling to the polymers changes the net electrical charge of the polymers. In case of conjugates with polycations (AK and SAK), 27−37% of the positively charged amino groups was replaced by the epitope peptide. However, these conjugates still had pronounced polycationic character (Figure 1.). In contrast, the amphoteric polymer, EAK, after reaction with C(110−121) had a 31% increase in negatively charged groups. It is due to the blocking of approximately 1/3 of the amino groups of glutamic acid residues of the branches by C(110−121) (Figure 1.). Consequently, this compound can be considered as a polyanionic conjugate in which the ratio of positive and negative charges is 2−3.

Surface Characteristics of Polypeptide−[C(110−121)] Conjugates. The properties of branched polypep-

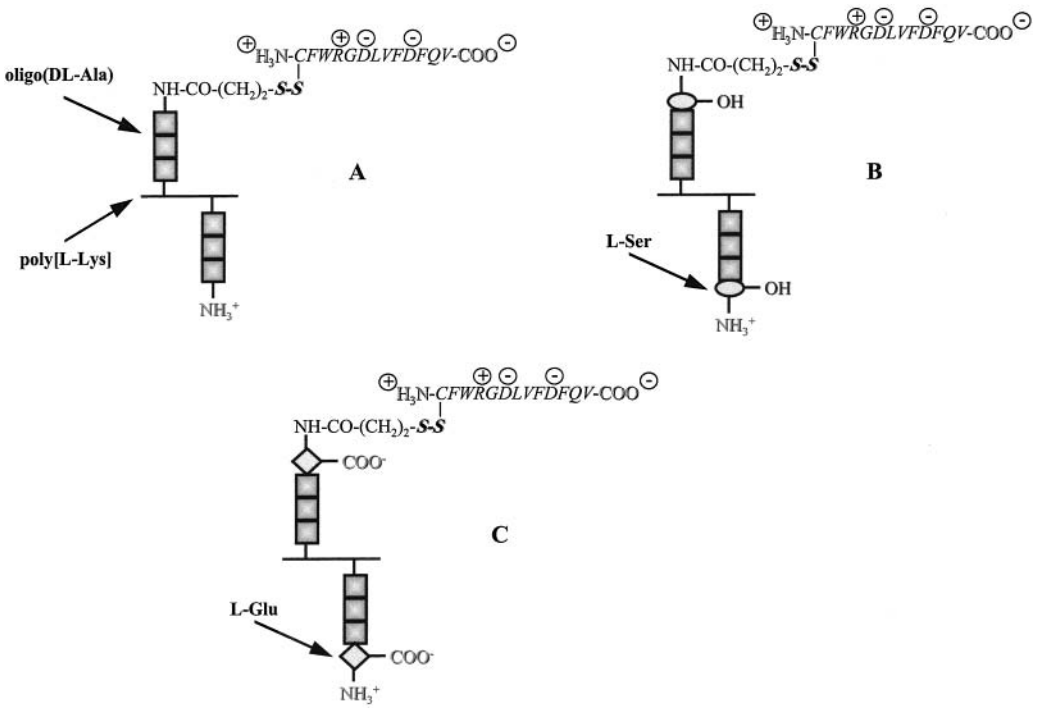

Figure 1. Simplified structure of the branched polypeptide−[C(110−121)] conjugates. (A) AK−[C(110−121)], (B) SAK−[C(110−121)], and (C) EAK−[C(110−121)].

Scheme 1. Schematic Presentation of the Synthesis of AK-[C(110−121)] Conjugate[a]

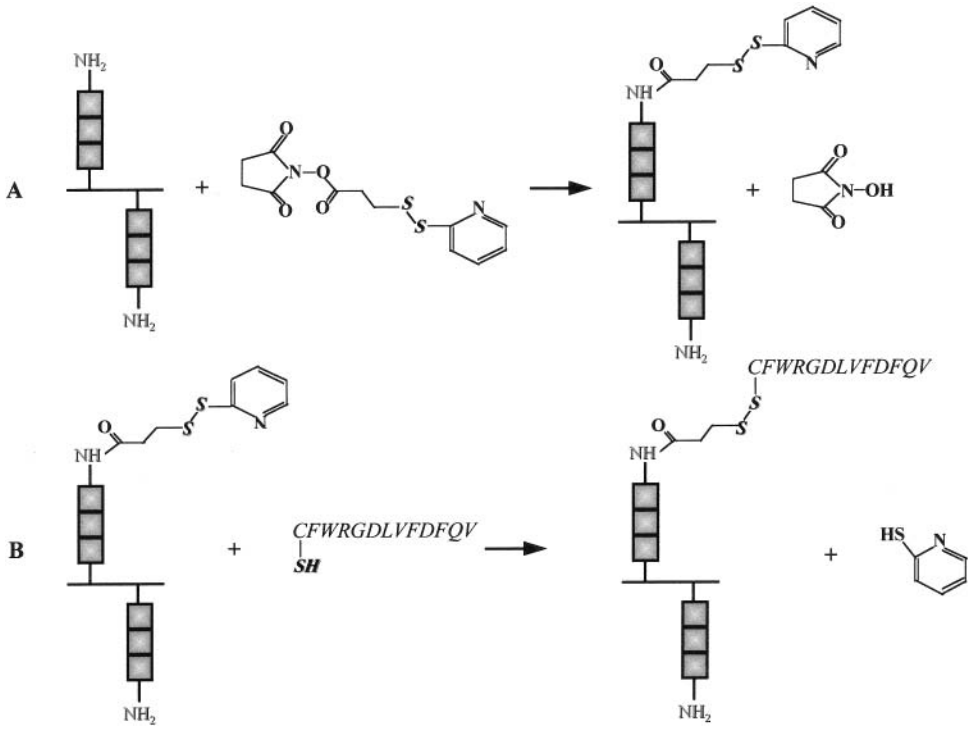

(A) Introduction of the 2-piridyl disulfide groups into a-amino group of the branches. (B) Formation of disulfide bond between the modified branches and [C(110−121)].

tide−epitope conjugates in absence of phospholipids at the air−water interface was studied first. Conjugate solutions at different concentrations were injected to the subphase, and surface pressure vs time curves were recorded. In all three cases, we have observed a certain period of time needed for the conjugate incorporation to the interface. This induction time decreased with sample concentration (data not shown). The kinetics of the process for the conjugates was similar (data not shown). Similar findings were reported for proteins (*35*, *36*) as well as for the free polymeric-branched polypeptides used for conjugate preparation (*22*). This phenomenon could be related to the presence of an ordered/packed structure whose adsorption to the air−water interface required time to reach the equilibrium.

Surface pressure values achieved after 60 min are depicted as a function of conjugate concentration in Figure 2. The pattern of these curves indicates that the maximum pressures achieved were dependent on the macromolecular component of the conjugate. A tendency

Table 1. Characteristics of Branched Polypeptide−[C(110−121)] Conjugates

		amino acid composition[b]					
polypeptide	code[a]	Lys	Ala (m)	Ser/Glu (i)	conjugate code[c]	DS[d]	M_w[e] (±5%)
poly[Lys(DL-Ala$_m$)	AK	1.00	4.20		AK-[C(110−121)]	0.27	51 500
poly[Lys(Ser$_i$-DL-Ala$_m$)	SAK	1.00	4.20	0.75	SAK-[C(110−121)]	0.37	57 000
poly[Lys(Glu$_i$-DL-Ala$_m$)	EAK	1.00	4.20	0.95	EAK-[C(110−121)]	0.31	59 000

[a] Code of branched polypeptides based on one letter symbol of amino acids. [b] Determined by amino acid analysis after hydrolysis in 6 M HCl at 105 °C for 24 h as described in ref *22*. [c] Code of polymer−peptide conjugates based on one letter symbol of amino acids. [d] Average degree of substitution determined from the amino acid analysis after hydrolysis of the conjugate samples in 6 M HCl at 105 °C for 24 h. [e] Calculated from the number average degree of polymerization of polylysine ($DP_n = 61$) and from the amino acid composition of conjugates.

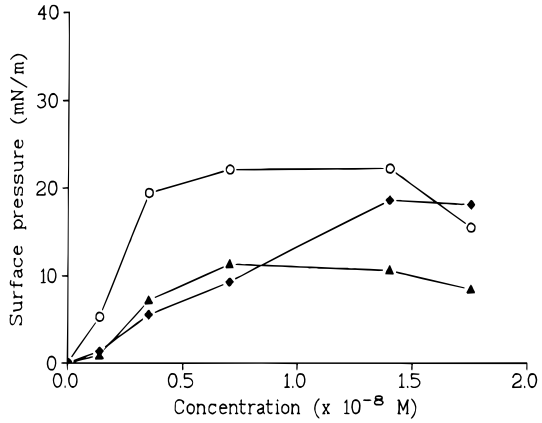

Figure 2. Effect of concentration of branched polypeptide−[C(110−121)] conjugate on the increase of surface pressure. Conjugate samples were dissolved in 0.1 M sodium acetate buffer, (pH 7.4) and injected in the subphase and surface pressure values were determined after 60 min: AK−[C(110−121)] (▲), SAK−[C(110−121)] (◆), and EAK−[C(110−121)] (○).

of surface pressure to increase with concentration was also revealed, up to 0.7×10^{-8} M for AK−[C(110−121)], but at higher concentration (1.4×10^{-8} M) for SAK−[C(110−121)] and EAK -[C(110−121)]. Above these values, there was a soft decrease in surface pressure that could be indicative of formation of aggregates. Similar data were reported for poly(ethyleneglycol)s (*37*). According to the maximum pressure values achieved, EAK−[C(110−121)] conjugate incorporated to the air−water interface most efficiently (22 mN/m).

Formation and stability of monolayers were also investigated by the analysis of surface pressure/area isotherms of conjugates. The monolayers were prepared in two ways. Conjugate solution was either spread on or injected under the aqueous surface. After 10 min, the monolayer was compressed by a movable barrier. The stability of monolayers was determined by compressing them up to 5 mN/m and leaving the system in equilibrium for 1 h. The unchanged surface pressure indicated that monolayers were stable under these conditions (data not shown). The pattern of compression isotherms indicated that all three conjugates formed monomolecular layer independently from the method used (Figure 3). In the case of conjugates with AK and SAK, the pressure vs area curves obtained after spreading samples on the surface displayed a similar pattern (Figure 3, panels A and B). Monolayers were formed in liquid expanded state at low compression pressures and after phase change around 9 mN/m isotherms showed a typical profile of condensed state without collapse. In contrast, no phase change was observed with EAK−[C(110−121)] conjugate compression isotherms (Figure 3C). The monolayer was almost in liquid state during the whole compression process, and no collapse occurred at the end of compression. The monomolecular layer of this conjugate was more

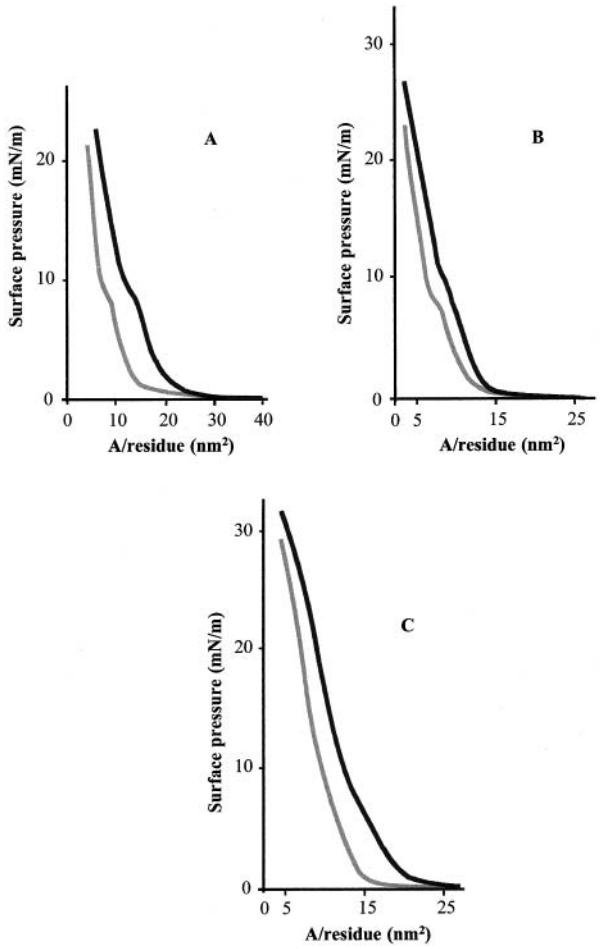

Figure 3. Compression isotherms of monomolecular layers formed by branched polypeptide conjugates AK−[C(110−121)] (A), SAK−[C(110−121)] (B), and EAK−[C(110−121)] (C) spread on the surface (black curve) or injected into (gray curve) the 0.1 M phosphate buffer subphase, (pH 7.4).

expanded than those of AK and SAK. These data are in agreement with the characteristics described in surface activity measurements (Figure 2) where EAK−[C(110−121)] was the most active compound. These differences can be explained by the altered charge properties of the conjugates. Repulsion forces between negatively charged groups characteristic for EAK−[C(110−121)] seems to be more pronounced than that of positively charged groups which predominate the net charge of AK- or SAK-based conjugates. Maximum surface pressure values obtained for EAK−[C(110−121)] conjugate [31.8 mN/m (spreading on the surface) and 29.1 mN/m (injecting under the surface)] indicate that these values are interestingly in the range of those described for hydrophobic proteins (*38*). The area/amino acid residue values at the end of compression and maximal pressures achieved are summarized in Table 2.

Table 2. Area/Amino Acid Residue Values Calculated and Maximum Pressure (Π_{Max}) Values Obtained from the Compression Isotherms of the Polypeptide−[C(110−121)] Conjugates Spread on or Injected under the Air−Water Interface

	spread		injected	
conjugate	area/residue[a] (nm^2/m)	Π_{max} (mN/m)	area/residue[a] (nm^2/m)	Π_{max} (mN/m)
AK-[C(110−121)]	0.031 ± 0.000 32	22.8	0.057 ± 0.000 32	22.2
SAK-[C(110−121)]	0.020 ± 0.000 32	23.0	0.028 ± 0.000 32	17.6
EAK-[C(110−121)]	0.024 ± 0.000 32	31.8	0.030 ± 0.000 32	29.1

[a] The area/residue values were calculated from compression isotherms recorded at 10 mN/m.

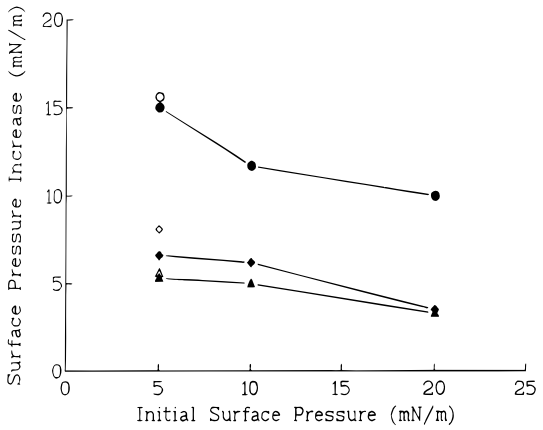

Figure 4. Effect of initial surface pressure on penetration of branched polypeptide−[C(110−121)] conjugates into DPPC (open symbol) and DPPC/PG (95/5, mol/mol) (filled symbol) monolayers. AK−[C(110−121)] (△,▲), SAK−[C(110−121)] (◇,◆) and EAK−[C(110−121)] (○,●).

The method of conjugate sample application had some effect on the properties of monolayers. Films formed after injection to the subphase were qualitatively the same, but maximal pressures achieved were slightly lower and area/amino acid residue values higher than those of calculated for monolayers obtained after spreading of conjugate samples. As monolayers were stable in both cases, these differences can be interpreted by different conformation adopted by conjugates at the air−water interface. Structures formed after spreading were probably more stable/packed than those adopted after conjugate injection into the subphase.

Conjugation of the 12-mer epitope peptide increased the hydrophobicity of all polymeric polypeptides (*22*). This effect was dependent on the polymer structure. The most marked increase was observed for EAK−[C(110−121)] (almost 4-fold), whereas the surface activity of AK−[C(110−121)] and of SAK−[C(110−121)] was elevated by about 50% (*22*).

Interaction of Polypeptide−[C(110−121)] Conjugates with Phospholipid Monolayers. The ability of conjugates to insert in phospholipid monolayers was evaluated using two phospholipid compositions: DPPC and DPPC/PG (95/5, mol/mol). Aqueous solutions of the conjugates were injected into the phosphate buffer subphase under monolayers spread at different initial surface pressures (5, 10, and 20 mN/m). Results summarized in Figure 4. indicate that EAK−[C(110−121)] induced the highest surface pressure increase both for DPPC and for DPPC/PG (95/5, mol/mol) monolayers. No significant differences were observed between the two conjugates possessing polycationic carrier (AK or SAK). These findings are in agreement with results obtained in surface activity measurements and compression isotherms at the air−water interface. Stronger interaction of EAK−[C(110−121)] with these model membranes initiates an expansion/deformation of the phospholipid monolayer. This

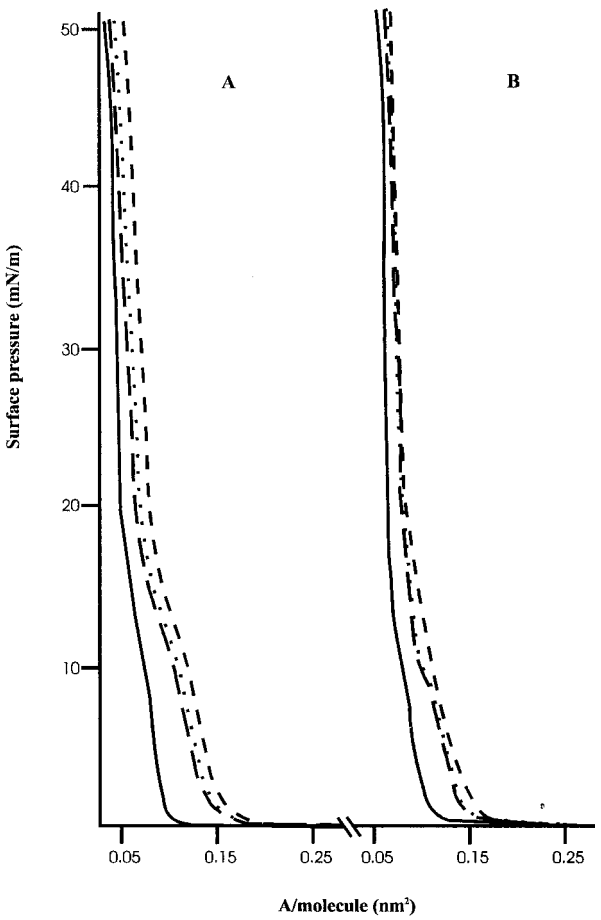

Figure 5. Compression isotherms of monolayers formed by DPPC (A) or DPPC/PG (95/5, mol/mol) (B) spread on 0.1 M phosphate buffer subphase, (pH 7.4) (—). Containing AK−[C(110−121)] (− − −), SAK−[C(110−121)] (- - -), or EAK−[C(110−121)] (···) in the subphase.

results in an elevated surface pressure recorded at all initial surface pressure values studied.

The interactions of all three conjugates with phospholipid monolayers were also investigated in a dynamic model spreading either DPPC or DPPC/PG (95/5, mol/mol) on the air−water interface of the conjugate solutions (Figure 5). Pattern of the compression isotherms of DPPC monolayers (Figure 5A) indicated an expansion due to the presence of conjugates in the subphase at low and medium surface pressures, but at 20 mN/m, curves were indistinguishable. This value was in the range of the collapse pressures for conjugates, suggesting that epitope−polypeptide conjugates are squeezed out from the films under this condition.

In addition, conjugates had also expanding effect on monolayers composed of DPPC and PG (95/5, mol/mol) all over the compression pressures (Figure 5B). This is indicative for a more pronounced interaction compared with neutral monolayers. This finding also suggests that,

though an exclusion of conjugates is evident at high pressures, fractions incorporated initially in the lipid monolayers still remain there during the whole compression process. A similar behavior has been described for multiple antigenic peptides (*39*). Data summarized in Figure 5 show that all three conjugates inserted strongly in charged monolayers. Conjugate EAK−[C(110−121)] proved to be the most active compound; however, differences recorded among conjugates were small.

Taken together, these results document that conjugation of C(110−121) peptide epitope increased the penetration of all three polymers. The most prominent effect was observed in case of EAK−[C(110−121)] conjugate vs EAK polymer where the surface pressure increased to almost 4-fold *(22)*.

Interaction of Polypeptide−[C(110−121)] Conjugates with Phospholipid Bilayers. The interaction of these conjugates with lipid bilayers was further studied using liposomes with DPPC/PG (95/5 mol/mol) phospholipid composition. Bilayers were saturated either with negatively charged ANS or with DPH possessing hydrophobic character. Altered fluorescent properties of the probes (fluorescence intensity and polarization) were recorded and related to the degree of ordered structure of the bilayers. The former compound incorporated into the surface of liposomes was used to analyze the effect of conjugates on the outer part, while the latter one was applied to monitor changes in the hydrophobic core of bilayers.

The presence of conjugate SAK−[C(110−121)] or AK−[C(110−121)] increased the fluorescence of the samples containing ANS. In contrast, conjugate EAK−[C(110−121)] reduced this parameter (data not shown). Fluorescence polarization values obtained with ANS/liposomes are shown in Figure 6. These data indicate that all conjugates gave values higher than the reference thus reflecting the rigidification of the bilayer at the outer polar heads level. The intensity of fluorescence of ANS in conjugates' solution in the absence of liposomes was slightly higher than in water (data not shown). This might indicate the presence of hydrophobic component for ANS provided by conjugate aggregates. It should be noted that these intensity values were low; therefore, the corresponding polarization was not reliable. Consequently, the polarization changes detected in the presence of liposomes are by far reflecting the interaction between liposomes polar heads and conjugates.

The interaction of epitope conjugates with the internal part of the bilayer was studied on liposomes saturated with DPH. Fluorescence polarization changes determined as a function of the temperature are summarized in Figure 7. The transition temperature was also determined (Figure 7, insert). In all three cases, conjugates induce a clear rigidification of bilayers mainly at temperatures above the phase transition (T_c = 40.5 °C), where bilayer is more fluid and insertion is favored. These data demonstrate that the presence of conjugates resulted in an increased temperature range of transition reflecting the reduction in the cooperativity of the process. Conjugates with polycationic polymers, SAK−[C(110−121)] or AK−[C(110−121)] slightly reduced the transition temperature (T_c = 39.5 °C). In contrast, this value was shifted by about 2 °C in case of EAK−[C(110−121)] (T_c = 43.5 °C). These findings are in agreement with those described earlier in the sense that EAK−[C(110−121)] conjugate has more pronounced effect on phospholipid monolayers than SAK−[C(110−121)] or AK−[C(110−121)]. As the PG content of the liposomes was relatively low, it seems that differences in this behavior were more likely due to the higher charge density of EAK−[C(110−121)] conjugate versus the SAK or AK analogues.

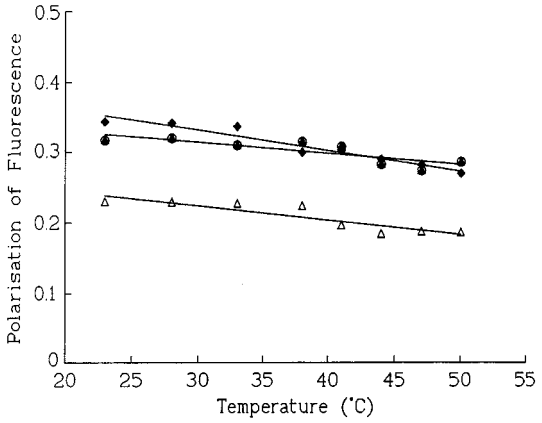

Figure 6. Polarization of ANS/DPPC/PG liposome preparations in the presence or absence of branched polypeptide−[C(110−121)] conjugates: AK−[C-VP3(110−121)] (▲), SAK−[C-VP3-(110−121)] (◆), and EAK−[C-VP3(110−121)] (○), or with 0.1 M sodium acetate buffer, (pH 7.4) (△).

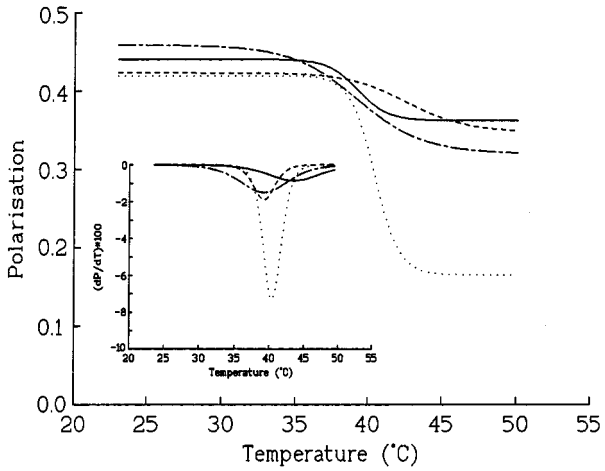

Figure 7. Polarization and its first derivative (insert) of DPH/DPPC/PG (95/5, mol/mol) liposome preparation in the presence or absence of branched polypeptide−[C(110−121)] conjugates: AK−[C(110−121)] (- - -), SAK−[C(110−121)] (-·-), EAK−[C(110−121)] (—). Sodium acetate buffer, 0.1 M (pH 7.4) (···).

Considering that free polymers interact only with the outer surface of the phospholipid bilayer and did not result in alteration of the ordered state of the alkyl chains (*22*), it can be assumed that the presence of peptide C(110−121) in the conjugates has marked effect on the stabilization of both the outer and the inner regions of the bilayer.

CONCLUSIONS

Taken together, these data indicate that branched polypeptide−[C(110−121)] conjugates interact with lipid mono- and bilayers in fluid state, inserting the peptide containing side chains into phospholipid membranes. We found that the binding/penetration of conjugates to phospholipid model membranes composed of dipalmitoylphosphatidyl-choline (DPPC) and phosphatidylglycerol (PG) is dependent on the charge properties of the constructs. Considering that the orientation and number of VP3 epitope peptides attached to branched polypeptide carrier were almost identical, we can conclude that the characteristics (amino acid composition, charge, and surface activity) of the carrier have a pronounced effect on the conjugate−phospholipid membrane interaction.

These observations suggest that the selection of polymer carrier for epitope attachment might significantly influence the membrane activity of the conjugate and provide guidelines for adequate way to present immunogenic peptides to the cells in order to induce biological response.

ACKNOWLEDGMENT

This work was financed by a grants from Hungarian-Spanish Intergovernmental Program (E-13/1997), CICYT SAF-93-0063 and the Hungarian Research Fund (OTKA) no. T 014964 and T 03838.

LITERATURE CITED

(1) Emini, E. A., Hughes, J. V., Perlow, D. S., and Boger, J. (1985) Induction of Hepatitis A virus-neutralizing antibody by a virus-specific synthetic peptide. *J. Virol. 55*, 836−839.
(2) Wheeler, C. M., Robertson, B. H., Van Nest, G., Dina, G., Bradley, D. W., and Fields, H. A. (1986) Structure of the hepatitis A virion: peptide mapping of the capsid region. *J. Virol. 58*, 307−313.
(3) Neurath, A. R., Kent, S. B. H., and Strick, S. (1984) Antibodies to hepatitis B surface antigen (HBsAg) elicited by immunization with synthetic peptide covalently linked to liposomes. *J. Gen. Virol. 65*, 1009−1014.
(4) Tam, J. P. (1988) Synthetic peptide vaccine design: synthesis and properties of a high-density multiple antigenic peptide system. *Proc. Natl. Acad. Sci. U.S.A. 85*, 5409−5413.
(5) Allison, A. C., and Gregoriadis, G. (1974) Liposomes as immunological adjuvants. *Nature 252*, 252−253.
(6) Davis, D., and Gregoriadis, G. (1989) Primary immune response to liposome tetanus toxoid in mice: the effect of mediators. *Immunology 68*, 277−282.
(7) Hui, G. S., Chang, S. P., Gibson, H., Hashimoto, A., Hashiro, C., Barr, P. J., and Kotani, S. (1991) Influence of adjuvants on the antibody specificity to the Plasomdium falciparum major merozoite surface protein, gp195. *J. Immunol. 147*, 3935−3941.
(8) Ullrich, S. E., and Fidler, I. J. (1992) Liposomes containing muramyl tripeptide phosphatidylethanolamine (MTP-PE) are excellent adjuvants for induction of an immune response to protein and tumour antigens. *J. Leukocyte Biol. 52*, 489−494.
(9) Sela, M., and Arnon, R. (1980) In *New Developments with Human and Veterinary Vaccines* (A. Mizrahi, I. Hertman, M. A. Klingberg, and A. Kohn, Eds.) pp 315−323, Liss, New York.
(10) Hudecz, F., and Tóth, G. K. (1994) In *Synthetic peptide constructs to increase the immunogenity of B cell epitopes. Synthetic peptides in the search for B and T cell epitopes* (E. Rajnavölgyi, Ed.) pp 97−119, R. G. Landres Company, Austin.
(11) Hudecz, F., and Szekerke, M. (1980) Investigation of drug−protein interactions and the drug-carrier concept by the use of branched polypeptides as model systems. Synthesis and characterization of the model peptides. *Collect. Czech. Chem. Commun. 45*, 933−940.
(12) Hudecz, F., and Szekerke, M. (1985) Synthesis of new branched polypeptides with poly(lysine) backbone. *Collect. Czech. Chem. Commun. 50*, 103−113.
(13) Mezö, G., Kajtár, J., Nagy, I., Majer, Zs., Szekerke, M., and Hudecz, F. (1997) Carrier design: Synthesis and conformational studies of poly[L-lysine] based branched polypeptides with hydroxyl groups. *Biopolymers 42*, 719−730.
(14) Hudecz, F. (1995) Design of synthetic branched-chain polypeptides as carriers for bioactive molecules. *Anti-Cancer Drugs 6*, 171−193.
(15) Hudecz, F., Gaál, D., Kurucz, I., Lányi, S., Kovács, A. L., Mezö, G., Rajnavölgyi, É., and Szekerke, M. (1992) Carrier design: cytotoxicity and immunogenicity of synthetic branched polypeptides with poly(L-Lys) backbone. *J. Control. Relat. 19*, 231−243.
(16) Hudecz, F., Kutassi-Kovács, S., Mezö, G., and Szekerke, M. (1989) Biodegradability of synthetic branched polypeptide with poly(L-lysine) backbone. *Biol. Chem. Hoppe-Seyler 370*, 1019−1026.
(17) Hudecz, F., Hilbert, Á., Mezö, G., Mucsi, I., Kajtár, J., Bösze, Sz., Kurucz, I., and Rajnavölgyi, É. (1993) Epitope mapping of the 237−284 region of HSV glycoprotein D by synthetic branched polypeptide-carrier conjugates. *Pept. Res. 6*, 263−271.
(18) Clegg, J. A., Hudecz, F., Mezö, G., Pimm, M. V., Szekerke, M., and Baldwin, R. W. (1990) Carrier design: biodistribution of branched polypeptides with poly-(L-lysine) backbone. *Bioconjugate Chem. 2*, 425−430.
(19) Hudecz, F., and Price, M. R. (1992) Monoclonal antibody binding to peptide epitopes conjugated to synthetic branched polypeptide carriers. Influence of the carrier upon antibody recognition. *J. Immunol. Methods. 147*, 201−210.
(20) Hudecz, F., Bogdán, K., Vordermeier, H. M., Jurcevic, S., and Ivanyi, J. (1997) In *Modulation of T cell specific immune responses against 16 kDa protein of M. tuberculosis by alteration of flanks and/or conjugation to synthetic branched polymeric carrier. Peptides 1996*, Proc. 24th European Peptide Symposium (R. Ramage and R. Epton, Eds.) pp 115−118, Mayflower Scientific, Birmingham.
(21) Wilkinson, K. A., Vordermeier, H., Wilkinson, R., Ivanyi, J., and Hudecz, F. (1998) Synthesis and in vitro T-cell immunogenicity of conjugates with dual specificity: attachment of epitope peptides of 16 kDa and 38 kDa proteins from *Mycobacterium tuberculosis* to branched polypeptide. *Bioconjugate Chem. 9*, 539−547.
(22) Nagy, I. B., Alsina, M. A., Haro, I., Reig, F., and Hudecz, F. (1998) Surface and polarisation fluorescence study of branched polymeric polypeptides. *Biopolymers 46*, 169−179.
(23) Perez, J. A., Gonzales-Dankart, J. F., Reig, F., Pintó, R. M., Bosch, A., and Haro, I. (1995) Solid-phase synthesis and immunogenicity of a VP3 peptide from Hepatitis A virus. *Biomed. Pept., Proteins Nucleic Acids 1*, 93−100.
(24) Perez, J. A., Haro, I., Martín, I., Alsina, M. A., and Reig, F. (1995) Surface and polarization fluorescence studies on the interaction of an RGD sequence containing a Hepatitis A virus peptide with phospholipids. *Anal. Chim. Acta 303*, 65−72.
(25) García, M., Nagy, I. B., Alsina, M. A., Mezö, G., Reig, F., Hudecz, F., and Haro, I. (1998) Analysis of the interaction with biomembrane models of the HAV-VP3(101-121) sequence conjugated to synthetic branched chain polypeptide carriers with a poly[L-Lysine] backbone. *Langmuir 14*, 1861−1869.
(26) Carlsson, J., Drevin, H., and Axen, R. (1978) Protein thiolation and reversible protein−protein conjugation. *Biochem. J. 173*, 723−737.
(27) Bretscher, M. (1973) Membrane structure: some general principles. *Science 181*, 622−629.
(28) Mezö, G., Votavová, H., Hudecz, F., Kajtár, J., Sponar, J., and Szekerke, M. (1988) Conformation of branched polypeptides: The influence of DL-alanine oligomer spacers in the side chains. *Collect. Czech. Chem. Commun. 53*, 2843−2853.
(29) Stuchbury, T., Shipton, M., Norris, R., Paul, J., Malthouse, G., and Brocklehurst, K. (1975) A reporter group delivery system with both absolute and selective specificity for thiol groups and an improved fluorescent probe containing the 7-nitrobenzo-2-oxa-1,3-diazole moiety. *Biochem. J. 151*, 417−432.
(30) IUPAC-IUB Joint Commission on Biochemical Nomenclature and Symbolism for amino acids and peptides, Recommendation 1983 (1984) *Eur. J. Biochem. 138*, 9−37.
(31) Verger, R., and De Haas, G. H. (1973) Enzyme reactions in a membrane model. 1. A new technique to study enzyme reactions in monolayers. *Chem. Phys. Lipids 10*, 127−136.
(32) Rubió, N., Pujol, M., Munoz, M., Alsina, M. A., Haro, I., and Reig, F. (1997) Synthesis and physicochemical characterisation of Laminin related peptides. *Supramol. Sci. 4*, 449−453.
(33) Cajal, Y., Alsina, M. A., Rabanal, F., and Reig, F. (1996) A fluorescence and CD study on the interaction of synthetic lipophilic Hepatitis B virus preS(120−145) peptide analogues with phospholipid vesicles. *Biopolymers 38*, 607−618.
(34) Shinitzky, N., and Barenholz, Y. (1978) Fluorescence parameters of lipid regions determined by fluorescence polarisation. *Biochim. Biophys. Acta 515*, 367−394.
(35) Ardite, E., Egea, M. A., Haro, I., Reig, F., and Alsina, M. A. (1994) Conformational changes and physicochemical properties of transferrin upon derivatization with cholesterol. *Anal. Chim. Acta 290*, 75−85.

(36) Egea, M. A., Garcia, M. L., Alsina, M. A., and Reig, F. (1994) Coating of liposomes with transferrin: Physicochemical study of the transferrin-lipid system. *J. Pharm. Sci. 83*, 169−173.
(37) Winterhalter, M., Bürner, H., Marzinka, S., Benz, R., and Kasianowicz, J. J. (1995) Interaction of Poly(etylene-glycols) with air−water interfaces and lipid monolayers: investigations on surface pressure and surface potential. *Biophys. J. 69*, 1372−1381.
(38) Nag, K., Perez-Gil, J., Cruz, A., and Keough, K. M. W. (1996) Fluorescently labeled pulmonary surfactant protein C in spread phospholipid monolayers. *Biophys. J. 71*, 246−256.
(39) Haro, I., Busquets, M. A., Ortiz, A., Reig, F., and Alsina, M. A. (1995) Analysis of the perturbation of phospholipid model membranes by a multiple antigenic peptide. *Anal. Chim. Acta 303*, 57−64.

BC9900385

Structure of a Synthetic Glucose Derived Advanced Glycation End Product That Is Immunologically Cross-Reactive with Its Naturally Occurring Counterparts†

Yousef Al-Abed* and Richard Bucala

The Picower Institute for Medical Research, 350 Community Drive, Manhasset, New York 11030.
Received May 20, 1999; Revised Manuscript Received September 6, 1999

Glucose reacts nonenzymatically with the amino groups of proteins to form stable, cross-linking adducts called advanced glycation end products or AGEs. While several lines of evidence have established that AGEs accumulate in tissues and contribute to the pathological sequelae of diabetes and aging, the identity of the major cross-link(s) that forms in vivo has remained enigmatic. This has been considered to be due to the labile nature and to the low fluorescence properties of this cross-link, despite the fact that fluorescence has been generally associated with AGE formation in vivo. Accordingly, the few AGE adducts that have been isolated thus far from proteins in vivo or from model systems in vitro have been found to account for only a fraction of the glucose-derived cross-links that occur in tissues. This situation has been further underscored by the development of a well-characterized class of antibodies that recognize in vivo AGEs but which fail to react with the structurally defined AGEs that have been identified to date. This particular class of anti-AGE antibodies has proven valuable in the quantification of AGE-modified forms of hemoglobin, low-density lipoprotein (LDL), and β-amyloid peptide, and can provide prognostic information on the course of certain diabetic complications. To obtain insight into the structure of this immunoreactive, AGE adduct, we used an anti-AGE antibody (RU) as a probe to isolate novel AGE(s) that formed within a reaction mixture of glucose and the model glycation substrate, N^{α}-CBZ-Arg-Lys. HPLC purification of an immunoreactive fraction that accumulated in this preparation showed the presence of a compound that was determined by ^{1}H NMR and electrospray ionization mass spectrometry (ESI-MS) to be a stable, imidazole-based cross-link (termed arginine-lysine imidazole or ALI). The properties of ALI, immunoreactivity, acid-lability, nonfluorescence, and inhibition of formation by aminoguanidine, suggest that ALI is likely to typify an important class of the AGE cross-links that form in vivo.

INTRODUCTION

The posttranslational modification process known as advanced glycation begins with the nonenzymatic addition of reducing sugars to the free amino groups of macromolecules. Over time, the initial Schiff base and Amadori products that form undergo rearrangement, dehydration, and fragmentation reactions to produce more complex and irreversibly bound structures that can exhibit varied spectral and covalent cross-linking properties. These later products, termed advanced glycation end products or AGEs,[1] have been shown to adversely affect the functional properties of proteins, lipids, and DNA (*1*−*3*). The significance of AGE formation in biological systems has become increasingly apparent over the last 15 years, and it is now evident that AGEs accumulate in situ in living tissues and play an important role in protein turnover, tissue remodeling, and certain of the pathological sequelae of diabetes, renal insufficiency, and aging (*1*, *3*). AGEs have been identified to form in vivo on basement membrane collagen (*4*), red cell hemoglobin (*5*), the serum protein 2-microglobulin (*6*), and the Alzheimer's disease-amyloid peptide (*7*, *8*). AGEs also have been shown to modify the apolipoprotein and the lipid components of low-density lipoprotein (LDL), and to inhibit the normal, receptor-mediated clearance of LDL from the circulation (*9*, *10*).

While several lines of evidence relying on glucose-dependent increases in protein cross-linking, fluorescence, and amino group modification have established that AGEs exist in living tissue, the identity of the major AGE cross-link(s) that forms in vivo has remained unknown. This situation has been attributed in large part to the chemical complexity of the cross-linking process, which follows the principles of the Maillard reaction 2, and the inherent instability of the cross-links to the hydrolysis procedures that are necessary to liberate the adduct structure from the macromolecular backbone (*1*−*4*). One AGE-cross-link, pentosidine, that has been purified from human dura collagen appears to form as the condensation product of lysine, arginine, and a reducing sugar precursor (*4*, *11*). Nevertheless, measurements of pentosidine content indicate that this product accounts for only a small percentage (1%) of the glucose-

† Portions of this work were presented at the 6th International Symposium on the Maillard Reaction, London, U.K. (July 27−30, 1997), and published in the proceeding volume from that symposium.

* To whom correspondence should be addressed. Phone: (516) 562-9461. Fax: (516) 365-5090. E-mail: yal-abed@picower.edu.

[1] Abbreviations: AFGP, 1-alkyl-2-formyl-3,4-diglycosylpyrrole; AGE, advanced glycation endproduct; AL, N^{α}-CBZ-Arg-Lys; ALAP, N^{α}-CBZ-Arg-Lys-Amadori product; ALI, Arg-Lys-imidazole; AP, Amadori product; BSA, bovine serum albumin; CML, carboxy-methyllysine; CP, cyclic pentosidine; ESI-MS, electrospray ionization mass spectrometry; FFI, 4-furanyl-2-furoyl-1H-imidazole; IA, imidazolium adduct; N^{α}-CBZ-Arg-Lys, *N*-carboxybenzoyloxy-Arg-Lys; P, pentosidine; PA, pyrimidinium adduct; PY, pyrraline; RNase, ribonuclease.

10.1021/bc990061q CCC: $19.00 © 2000 American Chemical Society
Published on Web 12/10/1999

derived cross-links that exist in biological samples (*11*). There is also data to suggest that the pathologically relevant cross-links may not themselves be fluorescent, a property that has been associated historically with AGE formation and used almost universally as an indicator of the Maillard reaction in vivo (*1*, *11*−*14*).

Several years ago, we utilized hyperimmunization techniques against an AGE-cross-linked antigen to produce polyclonal and monoclonal antibodies that recognize in vivo formed AGEs (*15*). These antibodies made possible the development of immunohistochemical and ELISA-based technologies that were free of many of the specificity and sensitivity problems associated with fluorescence-based assays and provided for the first assessment of advanced glycation in living systems (*5*). Remarkably, these anti-AGE antibodies were found to recognize a class of AGEs that formed in vivo, but which were immunochemically distinct from previously characterized adducts such as pentosidine, pyrraline, carboxymethyllysine (CML), or (1-alkyl-2-formyl-3,4-diglycosylpyrrole) AFGP (*15*). Of importance, the specific AGE epitope recognized by these antibodies increased as a consequence of hyperglycemia on various proteins such as collagen, hemoglobin, and LDL (*5*, *10*, *15*−*17*). One particular polyclonal antibody species, designated "RU", has been employed in human clinical studies to examine the efficacy of the pharmacological inhibitor of AGE formation, aminoguanidine (*5*, *10*), and has been shown to provide prognostic information on the course of diabetic renal disease (*17*).

To obtain insight into the chemical structure of this potentially important in vivo cross-link(s), we have used the RU anti-AGE antibody as a molecular probe to isolate the immunoreactive and potentially novel AGEs(s) contained within reaction mixtures prepared by the in vitro reaction of glucose with the model glycation substrate, *N*-CBZ-Arg-Lys. We report herein the isolation and characterization of a novel, imidazole-based arginine-lysine cross-link. This AGE is nonfluorescent, acid-labile, and appears to represent an important class of the AGE cross-links that form in vivo.

EXPERIMENTAL PROCEDURES

Preparation of AGE Reaction Mixtures. To a solution of N^{α}-CBZ-Arg-Lys (1 g, 2.25 mmol, Princeton Biochemical, Cleveland OH) in 500 mL of aqueous 0.2 M phosphate buffer (pH 7.4) was added D-glucose (22.5 mmol). The reaction mixture was stirred at 37 °C for 5 weeks. At intervals, 10 μL of the reaction mixture was analyzed by HPLC using an analytical primesphere column (5C18 MC, 5 micron, 250 × 4.6 mm, Phenomenex, Torrance, CA) and a binary solvent gradient consisting of 0.05% TFA in H_2O (solvent A) and methanol (solvent B). Solvent was delivered at a flow rate of 1.0 mL/min as follows: 0−30 min, a linear gradient from A:B (95:5) to A:B (25:75); 30−45 min, a linear gradient from A:B (25:75) to A:B (0:100). Detection was by monitoring UV absorption at 214, 254, 280, 320, and 350 nm. For preparative HPLC, a 250 × 21.2 mm primesphere column 5C18 MC was employed. Solvent was delivered at a flow rate of 10 mL/min using the same gradient as described above. One milliliter fractions were collected and concentrated 10-fold, and 50 L aliquots subjected to competitive ELISA as described below. A prominent immunoreactive peak was identified and further purified by repetitive HPLC. Spectroscopic analysis of this subfraction revealed the structure of compound ALI, and in a high purity (>95%): ESI-MS *m*/*z* 545 $[M]^+$; ^{1}H NMR (270 MHz, D_2O) 1.27−1.63 (10 H, m, $-CH_2-$), 2.46 (1H, dd, J = 18.3, 1.2 Hz, H_b), 2.89 (2H, m, $-CH_2-N$), 2.91 (1H, d, J = 17.6 Hz, H_b), 3.12 (2H, m, $-CH_2-N$), 4.06 (1H, m, $-NCHCO-$), 4.23 (1H, m, $-NCHCO-$), 4.30 (1H, dd, J = 10.4, 1.0 Hz, H_d), 4.48 (1H, dd, J = 10.4, 4.2 Hz, H_d), 4.66 (1H, m, H_c), 5.07 (2H, s, $-OCH_2Ph$), 7.36 (6H, m, $-Ph$ and H_a).

The ability of aminoguanidine to inhibit ALI formation was tested by including 50 mM aminoguanidine-HCl (Alteon Inc, Ramsey, NJ) in the incubation described above together with N^{α}-CBZ-Arg-Lys and D-glucose. The acid stability of ALI was tested by subjecting a preparation of purified ALI to standard acid hydrolysis conditions (6 N HCl, 110 °C, overnight), removing the acid by lyophilization, and subjecting a neutralized solution of the preparation to ^{1}H NMR and ELISA analysis.

Immunochemical Detection of AGEs. HPLC fractions and purified compounds were analyzed by an AGE-specific ELISA following methods described previously (*15*). This ELISA employed a polyclonal anti-AGE antibody raised by hyperimmunization against an AGE-cross-linked preparation of ribonuclease (AGE-RNase). Total IgG was prepared by protein-G affinity chromatography and the RNase backbone specificities removed by immunoabsorption against an RNase-linked affinity column. For assaying AGE immunoreactivity, 96-well round-bottom microtiter plates (Costar, Cambridge, MA) first were coated with AGE-modified BSA (AGE-BSA, 3 mg/mL, dissolved in 0.1 M sodium bicarbonate, pH 9.6). After washing, the unbound sites were blocked with Super-Block following the manufacturer's recommendations (Pierce, Rockford, IL). Dilutions of test antigen together with anti-AGE IgG then were added and the plates incubated at room temperature for 1 h. The plates were washed again and incubated with a secondary antibody (alkaline phosphatase-conjugated anti-rabbit IgG) at 37 °C for 1 h. The unbound antibodies were removed by extensive washing, and the bound antibodies were detected by incubation with *p*-nitrophenyl phosphate (pNPP) substrate for 30−60 min and recording the optical density at 405 nm by an ELISA reader (EL309, Bio-Tek Instruments Inc., Burlington, VT). Results were expressed as B/B_0, calculated as [experimental OD − background OD (i.e., no antibody)]/[total OD (i.e., no competitor) − background OD] (*15*).

The various test antigens included 4-furanyl-2-furoyl-1H-imidazole (FFI) (*18*), carboxy-methyllysine (CML) (*19*), 1-alkyl-2-formyl-3,4-diglycosylpyrrole (AFGP) (*20*), pyrraline (PY) (*21*), pentosidine (P) (*4*), cyclic pentosidine (CP) (*22*), N^{α}-CBZ-Arg-Lys (AL), N^{α}-CBZ-Arg-Lys-AP (ALAP), a pyrimidinium AGE adduct (PA) (*23*), and an imidazolium AGE adduct (IA) (*13*). Histidine and Lys-His dipeptide were purchased from Bachem (Torrance, CA).

Analytical Methods. NMR spectra were recorded in D_2O on a JEOL (270 MHz) spectrometer. HPLC was performed using a Hewlett-Packard model 1090 and Waters Instruments model 626 pump and 490 E multi-wavelength detector. Electrospray ionization (ESI) samples were run on a Quattro triple quadrupole mass spectrometer. Loop injection samples were performed using an ABI model 140B syringe pump employing H_2O/CH_3CN at a flow of 15 μL/ min, a Rheodyne model 7125 valve with a 10 μL loop, and a Micromass Megaflow ESI probe using nitrogen for the nebulizer/drying gas. LC/MS samples were run employing the ABI pump and Rheodyne valve with a 20 μL loop at a flow of 50 μL/min.

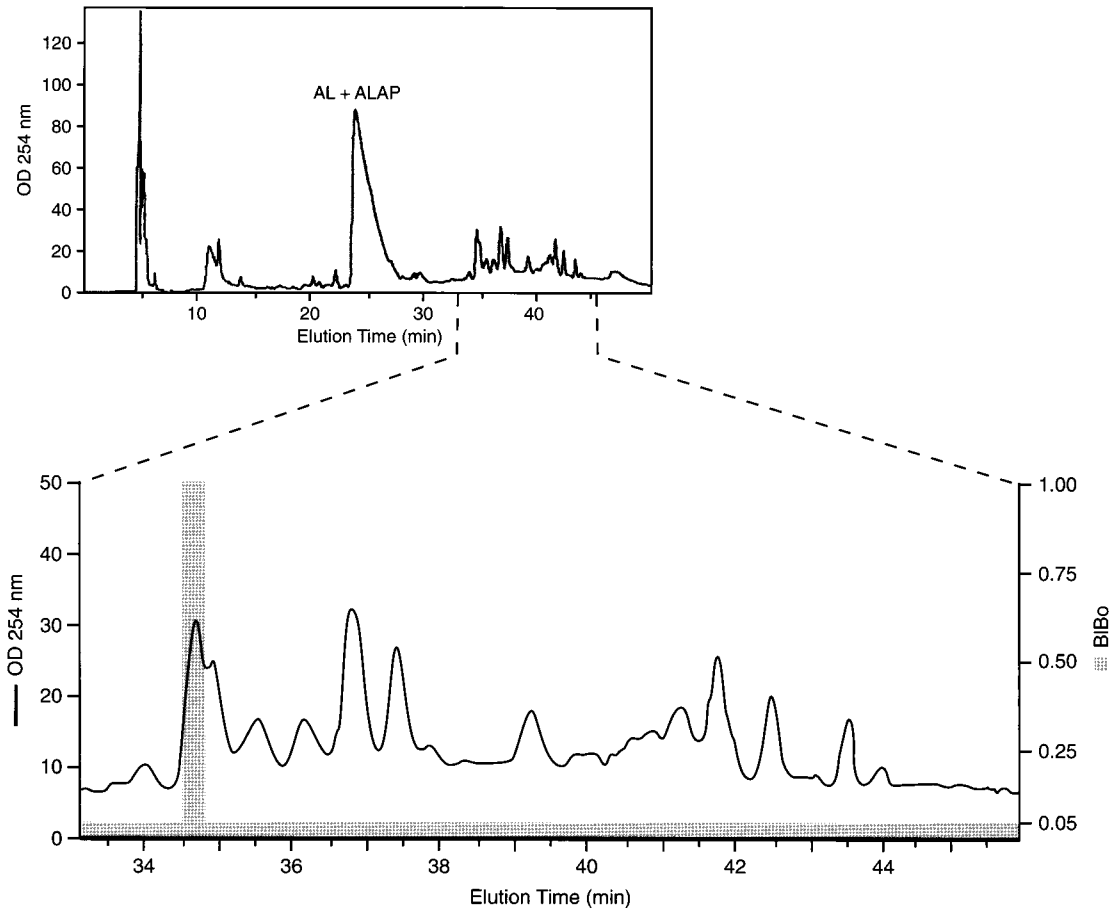

Figure 1. Reversed-phase HPLC profile of the reaction products formed by the incubation of N^{α}-carboxybenzoyloxy-Arg-Lys (N^{α}-CBZ-Arg-Lys) with 10 equivalents of glucose at 37 °C. The elution position of N^{α}-CBZ-Arg-Lys (AL) and the *N*-CBZ-Arg-Lys-Amadori product (ALAP) is indicated. The lower panel shows an expansion of the chromatogram from 33 to 46 min (—) and the reactivity of collected fractions when analyzed by competitive ELISA with the anti-AGE antibody species "RU". The ELISA immunoreactivity is expressed as B/B_o (■). No immunoreactivity was demonstrable elsewhere in the chromatogram.

RESULTS

We selected as a target substrate for AGE formation the model dipeptide N^{α}-carboxybenzoyloxy-Arg-Lys (*N*-CBZ-Arg-Lys). The close, intramolecular association of the arginine and lysine side chains provides for an important proximity effect that promotes cross-link formation, and a synthetic strategy employing an Arg-Lys dipeptide has been used recently to isolate a cyclic pentosidine in high yield (*22*). We incubated N^{α}-CBZ-Arg-Lys together with 10 equiv of glucose in 0.2 M phosphate buffer (pH 7.4) for up to 5 weeks at 37 °C. Analysis of this mixture by reversed-phase HPLC revealed a number of chromatographically distinct reaction products (Figure 1). Each fraction was isolated, concentrated, and analyzed by ^{1}H NMR and for its reactivity with anti-AGE antibody by competitive ELISA. The product(s) contained in fractions corresponding to the 34.5−34.7 min peak (and present in 1.5% yield) were found to completely block antibody binding and showed both dose dependence and a steep inhibition curve (Figure 1, and data not shown). Further purification of this fraction by repetitive HPLC using a semipreparative column showed the presence of a single UV-active compound (0.6% yield). The complete UV spectrum of the purified compound was unremarkable, and similar to that of the starting material. No fluorescence emission properties were noted. A ^{1}H NMR spectrum in D_2O showed, in addition to the N^{α}-CBZ-Arg-Lys protons, five aliphatic protons that resonate between 2.46 and 4.65 ppm (5H), and an olefinic proton that resonates at 7.3 ppm within the CBZ-group (Figure 2). ^{1}H NMR analysis revealed a geminal coupling of ∼18 Hz between the two protons at 2.46 and 2.91 ppm. A geminal coupling of the magnitude 10.4 Hz also was found across the two protons which resonate at 4.30 and 4.48 ppm. Of note, each proton of the methylene sets displayed an additional vicinal coupling to a single methine proton [−CH2−C*H*(OH)−CH2−]. The methine proton resonates at 4.65 ppm as multiplet however, with coupling constants of 1.24, 5.4, and 4.2 Hz. Overall, these data confirmed the presence of a glucose-derived adduct involving the side chain amines of N^{α}-CBZ-Arg-Lys.

The electrospray ionization mass spectrometry of the *N*-CBZ-Arg-Lys adduct displayed a molecular ion of *m*/*z* 545.3 $[MH]^+$, an increase of 108 Da compared to the starting material, N^{α}-CBZ-Arg-Lys (mol. mass: 435 Da) (Figure 3). Taken together, these data are consistent with the structure of a imidazole-derived cross-link in which the guanidino group of the arginine side chain is linked covalently to the Amadori product-derived moiety.

We propose the following mechanism of formation for this imidazole cross-link, which we have assigned the trivial name arginine-lysine imidazole (ALI) (Figure 4). Glucose reacts with N^{α}-CBZ-Arg-Lys to give an Amadori product (AP) at the amino group. The N^{α}-CBZ-Arg-Lys Amadori product (ALAP) forms in 18% yield under the reaction conditions used in these studies, based on HPLC isolation and ^{1}H NMR characterization. Dehydration of the hydroxyl group at the C-4 position then occurs to produce the obligate, 1,4-dideoxy-1-alkylamino-2,3-hexodiulose reactive intermediate (ALAP-dione). The revers-

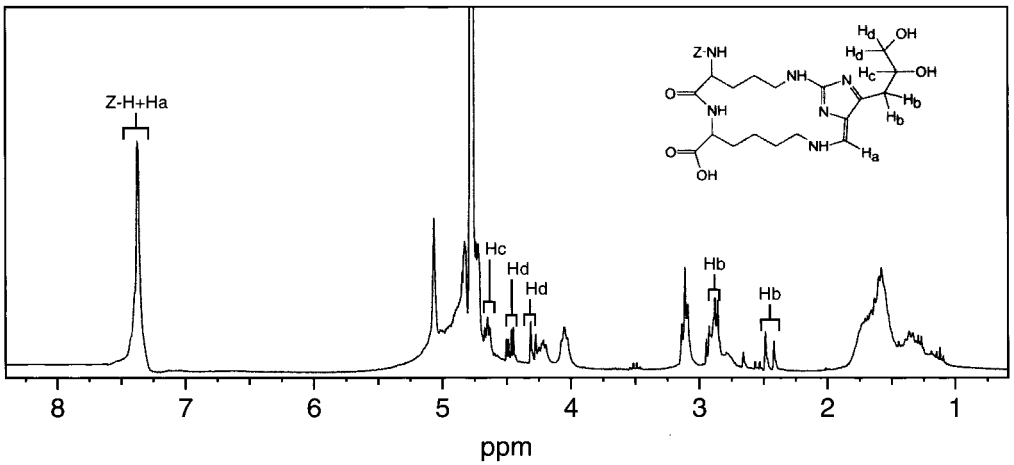

Figure 2. ^{1}H NMR spectrum recorded in D_2O of the purified, immunoreactive adduct ALI.

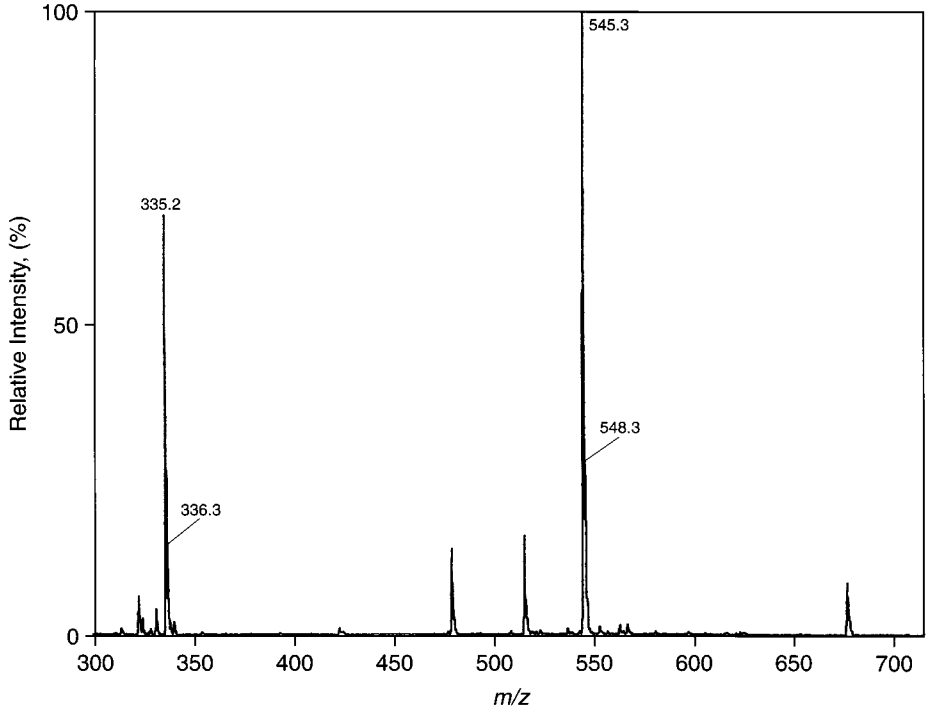

Figure 3. ESI mass spectrum of purifed ALI obtained as described in the Experimental Procedures.

ible addition of the guanidino moiety to the dicarbonyl then yields the 2-amino-4,5-dihydroxyimidazole, which undergoes dehydration to deliver the stable ALI. ALI is nonfluorescent and destroyed by acidification (6 N HCl). ALI also was not identified by HPLC and ^{1}H NMR, or by immunoreactivity, in reaction mixtures supplemented with the glycation inhibitor aminoguanidine (data not shown).

Figure 5 shows the dose-dependent reactivity of pure ALI in a competitive, ELISA utilizing the anti-AGE species "RU". This antibody has been shown previously to recognize a major class of in vivo-formed AGEs which are sensitive to pharmacological inhibition by aminoguanidine (*10*, *13*). The binding curve is steep, shows 50% inhibition at 500 nmol, and is almost coincident with that of AGE-modified BSA, suggesting an immunochemical relationship between ALI and AGE-BSA. For comparison purposes, we also studied the immunochemical reactivity of several structurally defined AGEs [4-furanyl-2-furoyl-1H-imidazole (FFI) (*18*), carboxy-methyllysine (CML) (*19*), 1-alkyl-2-formyl-3,4-diglycosylpyrrole (AFGP) (*20*), pyrraline (PY) (*21*), pentosidine (P) (*4*), cyclic pentosidine (CP) (*22*), a pyrimidinium (non-cross-linking) AGE adduct (PA) (*13*), an imidazolium (non-cross-linking) adduct (IA) (*13*, *23*)], two precursor products [N^{α}-CBZ-Arg-Lys (AL), N^{α}-CBZ-Arg-Lys-AP (ALAP)], and related epitopes [histidine (H), Lys-His (LH)]. With the exception of ALI and consistent with prior studies (*15*), none of these compounds showed detectable crossreactivity with the RU anti-AGE antibody species.

DISCUSSION

AGEs form by chemical principles first described for the Maillard reaction 2. In the case of protein glycation, the initial event is the reaction of a reducing sugar such as glucose with the N-terminus of a protein or the amino group of a lysine to form an aldimine or Schiff base. The Schiff base can hydrolyze back to its reactants or undergo an Amadori rearrangement to form the more stable *N*-(1-deoxy-1-fructosyl)lysine AP. The reaction pathway leading to reactive, cross-linking moieties (i.e., AGE formation) commences by further rearrangement of the AP. Possible routes include loss of the 4-hydroxyl group of the AP by dehydration to give a 1,4-dideoxy-1-alkyl-

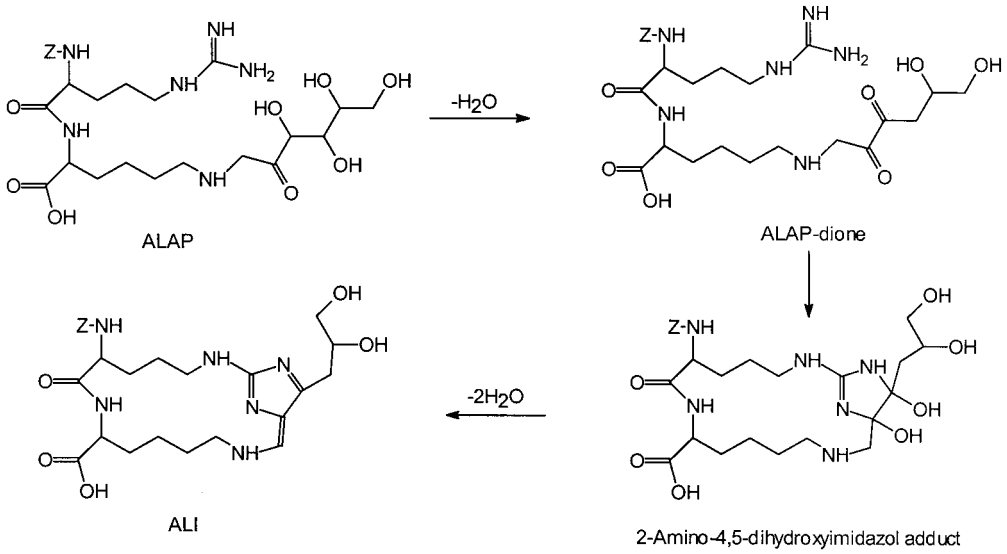

Figure 4. Proposed scheme for the formation of ALI, showing the important role of dehydration in producing the reactive, ALAP−dione intermediate. ALAP, *N*-CBZ-Arg-Lys-Amadori product.

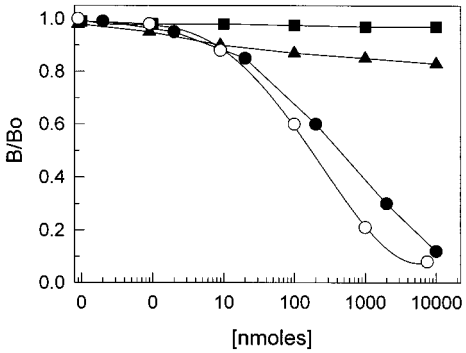

Figure 5. ELISA competition curves for ALI, selected AGEs, precursors, and related compounds utilizing anti-AGE antibody species "RU", shown previously to recognize in vivo formed AGEs (*13*). Assays employed glucose-derived, AGE-albumin (AGE-BSA) as the absorbed antigen and were performed as described in the Experimental Procedures. All points represent the mean of triplicate determinations and each curve is representative of at least two independent experiments. (○) AGE-BSA, (●) ALI, (▲) CML, (■) common line defined by the reactivity of AL, ALAP, AFGP, CP, FFI, IA, H, LH, P, PA, PY. No detectable crossreactivity was observed with acid-treated ALI, or N^a-CBZ-Arg-Lys incubated with glucose in the presence of the advanced glycation inhibitor aminoguanidine.

amino-2,3-hexodiulose (AP-dione) (*2*), and an AP-dione with the structure of an amino-1,4-dideoxyosone has been isolated by trapping model Amadori products with the AGE inhibitor aminoguanidine (*2*, *24*). Among the biological activities of early- and late-forming (i.e., AGE) glycation products, the formation of stable cross-links is considered to be their most important pathological manifestation (*1*, *3*).

In an important study (*4*), Sell and Monnier isolated from human dura collagen the fluorescent cross-link pentosidine, which is a condensation product of lysine, arginine, and a reducing sugar precursor. While the exact mechanism of pentosidine formation in vivo remains uncertain, cross-link formation requires that the sugar-derived intermediate contain a dicarbonyl functionality that can react irreversibly with the guanidinium group of arginine. Short-chain, dicarbonyl-containing compounds such as methylglyoxal and glyoxal are known to participate in condensation reactions with the side chains of arginine and lysine, and the addition of methylglyoxal to the guanidine moiety of arginine in vitro has been shown to produce pyrimidinium (*13*) and imidazol-4-one (*13*, *22*) adducts. Similarly, the dicarbonyls 1- and 3-deoxyglucosone have been implicated in the formation of certain AGE cross-links in vitro (*25*, *26*).

Despite these mechanistic insights, the identification of the major cross-links that form in vivo has been problematic. While pentosidine has been identified to form in collagen (*4*, *11*), circulating serum proteins (*27*), and the central nervous system plaques of Alzheimer's disease plaque (*8*, *28*), it does not appear to account for more than a small percentage of the glucose-derived cross-links that exist in aged or diabetic tissues (*4*, *11*, *27*). Indirect assessments of protein cross-linking based on collagen digestion and fluorescence measurements argue that the major AGE cross-link that forms in vivo is nonfluoresecent and acid labile (*1*, *11*, *12*). This conclusion has been reinforced by the development of a class of anti-AGE antibodies, such as RU, which can identify AGE-modified species of collagen, serum proteins, hemoglobin, and LDL that form in vivo in a glucose- and age-dependent fashion but which does not recognize pentosidine or any of the other model AGE structures that have been elucidated to date (*15*). Moreover, the AGE epitope(s) defined by the RU antibody can be inhibited from forming in human subjects by the pharmacological inhibitor of AGE formation, aminoguanidine (*5*, *10*).

By utilizing the RU anti-AGE antibody as a selection criteria for the identification of immunoreactive AGE structures, we have identified a novel, AGE cross-link, termed ALI, that forms in a synthetic mixture consisting of glucose and the N-blocked dipeptide, N^{α}-CBZ-Arg-Lys. The structure of ALI is that of an imidazole-based cross-link and fulfills the criteria proposed for that of the major, AGE cross-link that forms in vivo: nonfluorescence, acid-lability, and inhibition of formation by aminoguanidine. While we cannot exclude the possibility that additional AGEs, perhaps also bearing an imidazole cross-link structure, may yet be uncovered, the identification of ALI should assist in the further molecular analysis of the glucose-derived, macromolecular damage that occurs in vivo.

When analyzed for immunoreactivity, ALI displayed an antibody inhibition curve that was virtually coincident, on a molar basis, with that of AGE-modified

albumin (AGE-BSA). This suggests a potentially close immunochemical relationship between ALI and AGE-BSA. Interestingly, a major site of AGE-modification within albumin has been proposed to be at an Arg-Lys motif (*22*). This could produce an *intra*molecular, AGE-cross-link within albumin (*22*), and explain the relatively poor *inter*molecular cross-linking activity of albumin when compared to other AGE-substrates such as ribonuclease or collagen (*11, 29*). Of note, ribonuclease can form intramolecular cross-linking via the arginine and lysine side chain residues due to their proximity in the following sequence arginine-serine-lysine (*31*−*33*) and arginine-cysteine-lysine (*39*−*41*).

The structure of ALI further affirms the important role of arginine in effecting glucose-mediated protein cross-linking (*2*). By this pathway, the amino group of lysine or the free amino terminus of a protein acts to initiate AGE formation by generating the Amadori and the subsequent dehydration products that constitute the reactive, cross-linking intermediates. The guanidinium group of arginine then traps the dicarbonyl moiety to produce a stable, covalent cross-link. The AP-dione is thus a critical intermediate in this pathway, supporting prior, pharmacologically based studies that have implicated both the AP-dione and its dehydration product, the AP-ene-dione in the formation of stable protein−protein cross-links (*30*). These dehydration products also have been shown to be involved in the formation of the cyclization product cypentodine (*31*) and to contribute to an additional pathway of protein cross-linking that may occur by the Michael addition of lysine, histidine, or cysteine (*2*).

In conclusion, the identification of the nonfluorescent cross-link ALI fills an important gap in our understanding of the advanced glycation process. Further studies of ALI will facilitate the clinical assessment of pathologically important AGEs and potentially aid in the design of more specific, pharmacological inhibitors of AGE formation.

ACKNOWLEDGMENT

This work was supported by NIH Grant DK19655-15. We are grateful to Dr. Tomoko Mitsuhashi for assistance with the ELISA analysis.

LITERATURE CITED

(1) Njoroge, F. G., and Monnier, V. M. (1989) The chemistry of the Maillard reaction under physiological conditions: a review. *Prog. Clin. Biol. Res. 304*, 85−107.

(2) Ledl, F., and Schleicher, E. (1990) The Maillard reaction in food and in human body-New results in chemistry, biochemistry and medicine. *Angew. Chem., Int. Ed. Engl. 29*, 565−706.

(3) Bucala, R., and Vlassara, H. (1995) Advanced glycosylation end products in diabetic renal and vascular disease. *Am. J. Kidney Dis. 26*, 875−888.

(4) Sell, D. R., and Monnier, V. M. (1989) Structure elucidation of a senescence cross-link from human extracellular matrix. Implication of pentoses in the aging process. *J. Biol. Chem. 264*, 21597−21602.

(5) Makita, Z., Vlassara, H., Rayfield, E., Rodby, R., Cerami, A., and Bucala, R. (1992) Structure elucidation of a senescence cross-link from human extracellular matrix. Implication of pentoses in the aging process. *Science 258*, 651−653.

(6) Miyata, T., Oda, O., Inagi, R., Iida, Y., Araki, N., Yamada, N., Horiuchi, S., Taniguchi, N., Maeda, K., and Kinoshita, T. (1993) β-2-Microglobulin modified with advanced glycation end products is a major component of hemodialysis-associated amyloidosis. *J. Clin. Invest. 92*, 1243−1252.

(7) Vitek M. P., Bhattacharya, K. B., Glendening, J. M., Stopa, E., Vlassara, H., Bucala, R., Manogue, K., and Cerami, A. (1994) Advanced glycation end products contribute to amyloidosis in Alzheimer disease. *Proc. Natl. Acad. Sci. U.S.A. 91*, 4766−4770.

(8) Smith, M. A., Taneda, S., Richey, P. L., Miyata, S., Yan, S.-D., Stern D., Sayre, L. M., Monnier, V. M., and Perry, G. (1994) Advanced Maillard reaction end products are associated with Alzheimer disease pathology. *Proc. Natl. Acad. Sci. U.S.A. 91*, 5710−5714.

(9) Bucala, R., Makita, Z., Koschinsky, T., Cerami, A., and Vlassara, H. (1993) Advanced Maillard reaction end products are associated with Alzheimer disease pathology. *Proc. Natl.* Acad. Sci. *U.S.A. 90*, 6434−6438.

(10) Bucala, R., Makita, Z., Vega, G., Grundy, S., Koschinsky, T., Cerami, A., and Vlassara, H. (1994) Modification of low-density lipoprotein by advanced glycation end products contributes to the dyslipidemia of diabetes and renal insufficiency. *Proc. Natl. Acad. Sci. U.S.A. 91*, 9441−9445.

(11) Dyer, D. G., Blackledge, J. A., Thorpe, S. R., and Baynes, J. W. (1991) Formation of pentosidine during nonenzymatic browning of proteins by glucose. Identification of glucose and other carbohydrates as possible precursors of pentosidine in vivo. *J. Biol. Chem. 266*, 11654−11660.

(12) Monnier, V. M., Glomb, M., Elgawish, A., and Sell, D. R. (1996) The mechanism of collagen cross-linking in diabetes: a puzzle nearing resolution. *Diabetes 45* (Suppl. 3), S67−S72.

(13) Al-Abed, Y., Mitsuhashi, T., Ulrich, P., and Bucala, R. (1996) Novel modifications of N′-Boc-arginine and N′-CBZ-lysine by methylglyoxal. *Bioorg. Med. Chem. Lett. 6*, 1577−1578.

(14) Brinkmann, E., Thorsten, P., Degenhardt, S., Thorpe, S., and Baynes, J. W. (1998) Immunochemical detection of advanced glycosylation end products in vivo. *J. Biol. Chem. 30*, 1874−1879.14.

(15) Makita, Z., Vlassara, H., Cerami, A., and Bucala, R. (1992) Immunochemical detection of advanced glycosylation end products in vivo. *J. Biol. Chem. 267*, 5133−5138.

(16) Wolffenbuttel, B. H. R., Giordano, D., Founds, H. W., and Bucala, R. (1996) Long-term assessment of glucose control by haemoglobin-AGE measurement. *Lancet 347*, 513−515.

(17) Beisswenger, P. J., Makita, Z., Curphey, T. J., Moore, L. L., Jean, S., Brinck-Johnsen, T., Bucala, R., and Vlassara, H. (1995) Formation of immunochemical advanced glycosylation end products precedes and correlates with early manifestations of renal and retinal disease in diabetes. *Diabetes 44*, 824−829.

(18) Pongor, S., Ulrich, P., Bencsath, F. A., and Cerami, A. (1984) Aging of proteins: isolation and identification of a fluorescent chromophore from the reaction of polypeptides with glucose. *Proc. Natl. Acad. Sci. U.S.A. 81*, 2684−2688.

(19) Ahmed, M. U., Thorpe, S. R., and Baynes, J. W. (1986) Identification of N-ϵ-carboxymethyllysine as a degradation product of fructoselysine in glycated protein. *J. Biol. Chem. 261*, 4889−4894.

(20) Farmar, J. G., Ulrich, P. C., and Cerami, A. (1988) *J. Org. Chem. 53*, 2346−2349.

(21) Njoroge F. G., Sayre, L. M., and Monnier, V. (1987) Detection of D-glucose-derived pyrrole compounds during Maillard reaction under physiological conditions. *Carbohydr. Res. 167*, 211−220.

(22) Al-Abed, Y., Ulrich, P., Kapurniotu, A., Lolis, E., and Bucala, R. (1995) Model studies of the Maillard reaction of Arg-Lys with *D*-Ribose. Model studies of the Maillard reaction of Arg-Lys with *D*-Ribose. *Bioorg. Med. Chem. Lett. 5*, 2929−2930.

(23) Brinkmann, E., Wells-Knecht, K. J., Thorpe, S. R., Baynes, J. W. (1995) *J. Chem. Soc., Perkin Trans. 1*, 2817.

(24) Chen, H.-J. C., and Cerami, A. (1993) Mechanism of inhibition of advanced glycosylation by aminoguanidine *in vitro*. *J. Carbohydr. Chem. 12*, 731−742.

(25) Nakamura, K., Hasegawa, T., Fukunaga, Y., and Ienaga, K. (1992) *J. Chem. Soc., Chem. Commun. 14*, 992−994.

(26) Hayase, F., Hinuma, H., Asano, M., Kato, H., and Arai, S. (1994) *Bioscience Biotech. Biochem. 58*, 1936−1937.

(27) Odetti, P., Fogarty, J., Sell, D. R., and Monnier, V. M. (1992) Chromatographic quantitation of plasma and erythrocyte pentosidine in diabetic and uremic subjects. *Diabetes 41*, 153−159.

(28) Horie, K., Miyata, T., Yasuda, T., Takeda, A., Yasuda, Y., Maeda, K., Sobue, G., and Kurokawa, K. (1997) Immunohistochemical localization of advanced glycation end products, pentosidine, and carboxymethyllysine in lipofuscin pigments of Alzheimer's disease and aged neurons. *Biochem. Biophys. Res. Commun. 236*, 327−332.

(29) Watkins, N. G., Thorpe, S. R., and Baynes, J. W. (1985) Glycation of amino groups in protein. Studies on the specificity of modification of RNase by glucose. *J. Biol. Chem. 260*, 10629−10636.

(30) Vasan, S., et al. (1996) An agent cleaving glucose-derived protein cross-links in vitro and in vivo. *Nature 382*, 275−278.

(31) Zhang, X., and Ulrich, P. (1996) Direct approach to reactive Maillard intermediates: Formation of a novel 3-alkylamino-2-hydroxy-4-hydroxymethyl-2-cyclopentene-1-one (Cypentodine) *Tetrahedron Lett. 37*, 4667−4670.

BC990061Q

Exchange Transfusion with Albumin-Heme as an Artificial O_2-Infusion into Anesthetized Rats: Physiological Responses, O_2-Delivery, and Reduction of the Oxidized Hemin Sites by Red Blood Cells

Eishun Tsuchida,*[,†,‡] Teruyuki Komatsu,[‡] Kazuyoshi Hamamatsu,[‡] Yasuko Matsukawa,[‡] Atsushi Tajima,[§] Akira Yoshizu,[§] Yotaro Izumi,[§] and Koichi Kobayashi[§]

Department of Polymer Chemistry, Advanced Research Institute for Science & Engineering, Waseda University, Tokyo 169-8555, Japan, Department of General Thoracic Surgery, School of Medicine, Keio University, Tokyo 160-8582, Japan. Received May 27, 1999; Revised Manuscript Received September 27, 1999

Human serum albumin (HSA) incorporating synthetic hemes, the tetrakis(*o*-pivalamido)phenylporphinatoiron(II) derivative (FeP), is an artificial hemoprotein (HSA-FeP) which is able to reversibly bind and release dioxygen under physiological conditions (in aqueous media, pH 7.4, 37 °C) like hemoglobin and myoglobin. Physiological responses to exchange transfusion with HSA-FeP solution [[HSA], 5 g/dL; FeP/HSA, 4 (mol/mol)] into rats after hemodilution and hemorrhage (Hct, about 10%) has been evaluated. The declined mean arterial pressure (MAP) and blood flow after a 70% exchange with HSA and the further 40% bleeding of blood were significantly recovered up to about 90% of the baseline values by the injection of HSA-FeP. Furthermore, the renal cortical O_2-tensions and skeletal tissue O_2-tensions were also increased, indicating the in vivo O_2-delivery of HSA-FeP. Autoxidation of ferrous Fe(II)P to ferric Fe(III)P was retarded in the blood stream; the half-lifetime of the dioxygenated FeP [$\tau_{1/2}(O_2)$] in vivo was 4.1 h [cf. 1.0 h (in vitro)]. It has been found that autooxidized Fe(III)P was certainly reduced in the whole blood suspension. Physiological concentrations of ascorbic acid continuously provided by red blood cells probably rereduces Fe(III)P, leading to the apparent long lifetime of the dioxygenated species of FeP.

INTRODUCTION

Human serum albumin (HSA) in blood plasma incorporates numerous endogenous and exogenous compounds with noncovalent interactions and transports them to the appropriate places in the body (Peters, 1985, 1996). It has been of great interest over the past several decades to clarify this unusual ligand-binding aspect [for example, Kragh-Hansen (1981)]. Furthermore, the crystal structure of HSA was first discovered in 1989; the HSA molecule showed a unique heart-shaped morphology with sides of 80 Å and a depth of 30 Å (Carter et al., 1989, 1994; He et al., 1992). We have recently found that a synthetic heme, 2-[8-{*N*-(2-methylimidazolyl)}octanoyloxymethyl]-5,10,15,20-tetrakis(α,α,α,α-*o*-pivalamido)-phenylporphinatoiron(II), (FeP), was efficiently incorporated into a certain domain of HSA, providing a new type of hemoprotein (HSA-FeP), which can transport reversibly dioxygen under physiological conditions (in aqueous media, pH 7.3, 37 °C) similar to hemoglobin and myoglobin (Komatsu et al., 1995; Tsuchida et al., 1997). The maximal binding numbers of the FePs are estimated to be eight per one HSA molecule, in which the main binding sites are inferred to be the subdomains IB, IIA, and IIIB (Komatsu et al., 1999). The 5 g/dL (0.75 mM) of HSA-FeP (FeP/HSA, 8) solution should deliver 3.4 mL/dL of dioxygen as a red cell substitute, which corresponds to about 60% of the O_2-delivery of human blood (5.9 mL/dL). The solution properties also satisfied the physiological needs for O_2-infusion; the specific gravity and the viscosity were almost the same as those of HSA itself.

Herein, we report for the first time the physiological responses to exchange transfusion with HSA-FeP [[HSA], 5 g/dL; FeP/HSA, 4 (mol/mol)] into rats after hemodilution and hemorrhage. The decreased mean arterial pressure (MAP) and blood flow after a 70% exchange with HSA and further 40% bleeding of blood were significantly increased by the injection of the HSA-FeP solution. In vivo O_2-delivery to the renal cortex and to the cervical muscle was also observed. Furthermore, it has been found that the autoxidation of the dioxygenated Fe(II)P to Fe(III)P in vivo is longer than that in vitro. We assume that the nonenzymatic reduction process of Fe(III)P by red blood cells is mediated by physiological concentrations of ascorbic acid (AsA).

EXPERIMENTAL PROCEDURES

Preparation of HSA-FeP Solution. HSA-FeP solutions [[HSA], 5 g/dL; FeP/HSA, 4 (mol/mol)] were prepared according to our previous reports (Tsuchida et al., 1997; Komatsu et al., 1999). HSA was purchased from Bayer Co., Ltd. (Albumin Cutter, 5 g/dL).

Exchange Transfusion with HSA-FeP in Anesthetized Rats. The exchange transfusions were carried out according to our previously reported experimental protocols (Izumi et al., 1996; Sakai et al., 1997). Twelve male Wister rats (334 ± 19 g) were anesthetized with an intraperitoneal injection of pentobarbital (50 mg/kg).

* To whom correspondence should be addressed. Phone: +81 3-5286-3120. Fax: +81 3-3205-4740. E-mail:eishun@mn.waseda.ac.jp.
† CREST investigator.
‡ Waseda University.
§ Keio University.

10.1021/bc990065v CCC: $19.00 © 2000 American Chemical Society
Published on Web 12/01/1999

After a ventral incision was made in the neck, a catheter (PE-20 tubing, outer 0.8 mm ϕ, inner 0.5 mm ϕ) was introduced into the right jugular vein for sample infusion. The second catheter was inserted into the right common carotid artery for blood withdrawal and was connected to a pressure transducer (Polygraph System, Nihon Koden, Tokyo, Japan) for continuous monitoring of the mean arterial pressure (MAP). A median abdominal incision was then made, and a pulsed Doppler probe (20 MHz, HDP 20 20R, Crystal Biotech, Hopkinton, MA) was placed around the abdominal aorta to measure the blood flow as an indicator of cardiac output. Needle-type polarographic O_2-electrodes (Intermedical Co., Tokyo, Japan) were placed in the cortex of the left kidney and the cervical muscle to continuously measure the renal cortical O_2-tensions [$(P_{t,O_2(R)}$] and the skeletal tissue O_2-tensions [$P_{t,O_2(M)}$], respectively. Approximately 10 min was allowed to stabilize each parameter.

Seventy percent of the total blood volume was first exchanged with 5 g/dL HSA by withdrawal via the common carotid artery and infusion via the jugular vein (each 1 mL/min/cycle), leading to a decrease of about 14% in the hematocrit value (Hct). The arterial and venous blood samples taken on the first withdrawal were used for determination of the basal values as a baseline for each measurement. After 10 min of 70% exchange transfusion with HSA, 40% of the estimated circulatory volume was further withdrawn at once via the arterial line, producing severe hemorrhagic states. The same volume of HSA-FeP solution was then intravenously injected (HSA-FeP group, $n = 6$). The HSA solution was also applied to the similarly treated rats for reference data (HSA group, $n = 6$). Samples for blood gas analyses were taken from the arterial or venous line (0.5 mL each) (i) before 70% exchange, (ii) after 70% exchange, (iii) 10 min later, (iv) after 40% bleeding, (v) after injection of HSA-FeP (or HSA), and (vi) 30 min after injection. Blood gas measurements were performed by a pH/blood gas analyzer (Corning 170, Corning Medical, Medfield, MA). The rats were sacrified at the end of the experiments by pentobarbital overdose. All animal studies were approved by the Animal Care and Use Committee of Keio University. The care and handling of the animals were in accordance with the NIH guidelines.

Data Analysis. The data are expressed as mean ± standard deviation (SD). All the data are represented as percentages of the basal values, except for arterial pH and base excess (BE), which are shown as differences from the baseline values. The data were evaluated using analysis of variance (ANOVA) followed by Fischer's protected least significant difference (PLSD) test. The level of confidence was placed at 95% for all experiments.

Half-Lifetime of the Dioxygenated HSA-FeP. The half-lifetime of the dioxygenated HSA-FeP [$\tau_{1/2}(O_2)$] was determined from the time-course of the absorption of the O_2-adduct species (λ_{max}, 548 nm) (Yuasa et al., 1987). In the ex vivo experiments, the absorption changes of the HSA-FeP solution ([FeP], 0.1 mM) in a 1 cm quartz cuvette after exposure to 20% O_2 gas were monitored by a UV−vis absorption spectrophotometer (V-570, JASCO, Tokyo, Japan) equipped with a thermocontrolled cell holder. The temperature was always maintained at 37 °C during the measurements. Determination of [$\tau_{1/2}(O_2)$] in the whole blood suspension was carried out by glass capillary procedures (vide infra).

On the other hand, the $\tau_{1/2}(O_2)$ value in vivo was estimated as follows. Anesthetized and catheter inserted Wister rats (male, 330 ± 12 g) were prepared in a manner similar to the transfusion experiments. Forty percent of the total blood volume (56 mL/kg) was withdrawn from the arterial line and the same volume of HSA-FeP [[HSA], 5 g/dL; FeP/HSA, 4 (mol/mol)] was intravenously injected. A blood sample (0.2 mL) taken from the arterial line was put into a glass capillary (0.5 mm ϕ) and centrifuged (12 kG) for 5 min. Since the HSA-FeP molecule was dispersed in the supernatant, spectral measurement of the supernatant using a special cuvette for the glass capillary (Shimadzu, Tokyo, Japan) gave an absorption intensity of the oxy band (548 nm). The FeP concentration in the supernatant was also assayed using a cyano-met hemoglobin kit (Wako Pharm. Co., Tokyo, Japan). On the basis of these results, the concentration of the dioxygenated FeP was calculated each time.

Rereduction of Fe(III)P by Red Blood Cells. The HSA-Fe(III)P (Fe(III)P is abbreviation for the ferric complex, 2-[8-{*N*-(2-methylimidazolyl)}octanoyloxymethyl]-5,10,15,20-tetrakis(α,α,α,α-*o*-pivalamido)phenylporphinatoiron(III)) solution ([Fe(III)P], 0.5 mM) was first mixed with whole blood under nitrogen and incubated at 37 °C (Hct, 27%). After 0.5, 1, 1.5, 2, 3, 4, and 5 h, part of the solution was taken up and exposed to CO gas for 1 min. The sample was then put into a glass capillary and centrifuged (12 kG) for 5 min. The visible absorption spectrum of the supernatant was measured as already described. The reduction yield of the Fe(III)P to carbonyl FeP was calculated by the absorption ratio versus that of 100% carbonyl FeP. In the presence of ascorbic acid (AsA) or plasma, the absorption of the CO-adduct species was measured using a 0.2 mm quartz cuvette each time.

RESULTS AND DISCUSSION

Physiological Responses to Exchange Transfusion with HSA-FeP in Anesthetized Rats and the O_2-Delivery. The characteristics of the HSA-FeP solution used for the exchange transfusions are summarized in Table 1. Even after the incorporation of the FePs, the physicochemical properties of the HSA molecule, e.g., isoelectric point (pI), viscosity, etc., did not change (Komatsu et al., 1999). The O_2-binding affinity [$P_{1/2}(O_2)$] was adjusted to 32 mm Hg (37 °C) by the chemical structure of the FeP, and the O_2-association and -dissociation rate constants (k_{on}, k_{off}) are much higher than those of human blood.

There are no significant differences in the basal values of any measurements between the HSA-FeP and HSA groups (Table 2). For the 70% dilution of the estimated blood volume (56 mL/kg) with HSA, a total of nine cycles of withdrawal (2 mL) and infusion (2 mL) was performed to achieve a decrease in the hematocrit value (Hct) of 11.4% (Figure 1). After further bleeding of 40% blood volume, the Hct became 10.5%. During the injection of the HSA-FeP or HSA solution, no remarkable acute reaction was observed in the appearance of the rats. In the glass capillaries (0.1 mm ϕ) for the Hct measurements, HSA-FeP was homogeneously dispersed in the supernatant after the centrifugation (12 kG, 5 min), exhibiting good compatibility of this artificial hemoprotein with the blood components.

Table 1. Representative Characteristics of HSA-FeP

HSA (g/dL)	5.0
FeP (mM)	3.0
FeP/HSA (mol/mol)	4
isoelectric point (−)[a]	4.8
Viscosity (cP, at 230 s^{-1})[b]	1.1
COP (mm Hg)[a]	18
$P_{1/2}(O_2)$ (mm Hg)[a]	32

[a] 25 °C. [b] 37 °C.

Table 2. Basal Values of HSA and HSA-FeP Group

	HSA	HSA-FeP
Hct (%)	50.5 ± 4.7	46.2 ± 5.5
MAP (mmHg)	93 ± 12	106 ± 11
blood flow (mL/min)	4.9 ± 1.4	5.0 ± 2.1
pH	7.322 ± 0.025	7.343 ± 0.027
BE (mmol/L)	−0.9 ± 2.0	0.9 ± 2.2
P_{a,O_2} (mm Hg)	87.6 ± 15	87.5 ± 3.1
P_{v,O_2} (mm Hg)	42.6 ± 7.8	45.8 ± 2.4
$P_{t,O_2(R)}$ (mm Hg)	19.8 ± 5.1	18.7 ± 5.8
$P_{t,O_2(M)}$ (mm Hg)	22.5 ± 5.2	21.0 ± 5.7

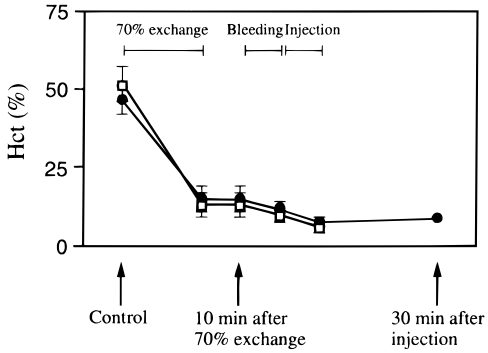

Figure 1. Change of Hct during exchange transfusion experiments; 70% exchange with HSA → 40% exchange with HSA-FeP [(●) HSA-FeP group ($n = 6$)] or with HSA [(□) HSA group ($n = 6$)] → 30 min after 40% exchange.

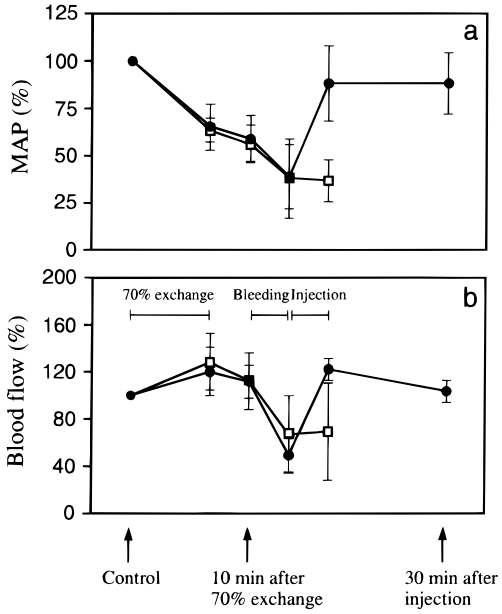

Figure 2. Change of (a) MAP and (b) blood flow of abdominal aorta during exchange transfusion experiments; 70% exchange with HSA → 40% exchange with HSA-FeP [(○) HSA-FeP group ($n = 6$)] or with HSA [(□) HSA group ($n = 6$)] → 30 min after 40% exchange.

Changes in the hemodynamic parameters are summarized as percentages of the basal values in Figure 2. The MAP declined to about 64% of the baseline after a 70% exchange transfusion with HSA and further decreased to about 39% of the baseline after the 40% bleeding (Figure 2a). In the HSA group, the low MAP could not be recovered by injection of the same amount of HSA and all rats died within 30 min. These results suggest that this hemorrhagic state is suitable for judging the lifesaving effect of the O_2-carrying albumin solution, HSA-FeP. As expected, the HSA-FeP group showed a significant increase in MAP up to 88 ± 20% of the

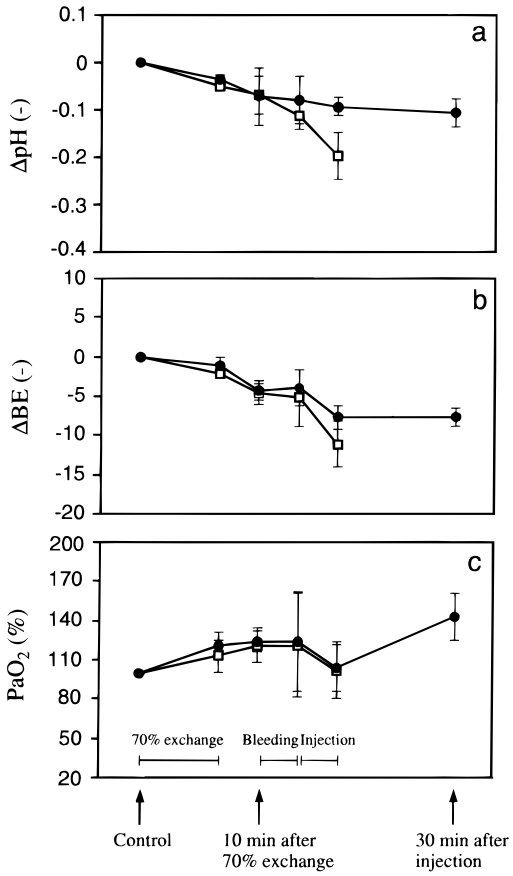

Figure 3. Change of (a) pH, (b) BE, and (c) P_{a,O_2} during exchange transfusion experiments; 70% exchange with HSA → 40% exchange with HSA-FeP [(●) HSA-FeP group ($n = 6$)] or with HSA [(□) HSA group ($n = 6$)] → 30 min after 40% exchange.

baseline which was sustained even after 30 min. All rats injected with HSA-FeP survived for more than 30 min until sacrificed.

The initial 70% exchanging transfusion with HSA led to a slight increase in the aortic blood flow (about 120% of the baseline) (Figure 2b). The low viscosity of the HSA solution presumably promotes blood flow in the capillaries. After 40% bleeding, the aortic blood flow dramatically decreased to about 60% of the baseline. In contrast to the HSA group in which the blood flow still stayed at a low level after the injection, the HSA-FeP group represented a significant efficacy, completely recovering to the value before bleeding.

The changes in pH, base excess (BE), and P_{a,O_2} are summarized in Figure 3. Although the pH slightly decreased in the HSA-FeP group, it was not very complete compared to that of the HSA group (Figure 3a). The BE also showed a profile similar to pH change (Figure 3b), indicating that the metabolic acidosis was more progressive in the HSA group. P_{a,O_2} increased in the HSA-FeP group especially 30 min after the sample injection (maximum 143.0 ± 18% of the baseline), probably due to a hyperventilation induced by the slight acidosis (Figure 3c).

The mixed venous partial O_2-pressure (P_{v,O_2}) is one of the significant parameters for the O_2-supply. The decreased P_{v,O_2} generally indicates a low O_2-saturation of Hb and implies declined O_2-transport. In the HSA-FeP group, the reduced P_{v,O_2} (53.3 ± 11% of the baseline) after 40% bleeding rapidly increased after the HSA-FeP injection to the value before bleeding (80.2 ± 9% of the

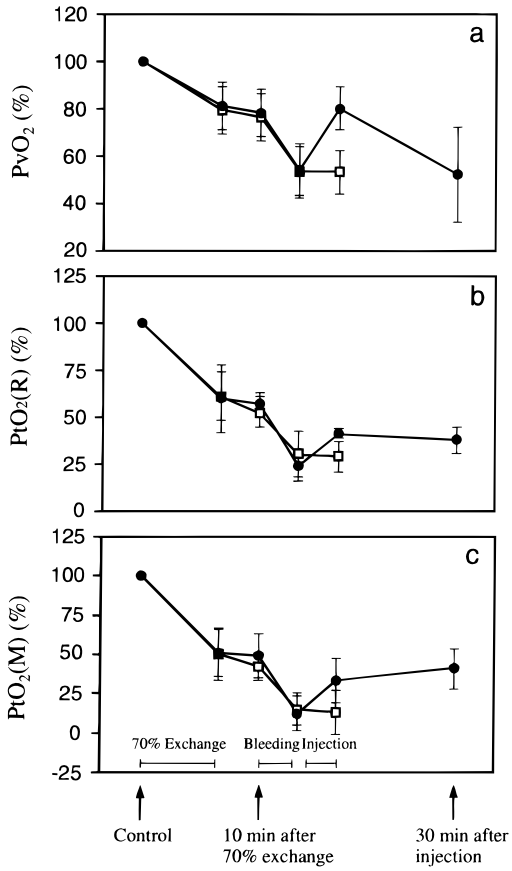

Figure 4. Change of (a) P_{v,O_2}, (b) $P_{t,O_2(R)}$, and (c) $P_{t,O_2(M)}$ during exchange transfusion experiments; 70% exchange with HSA → 40% exchange with HSA-FeP [(●) HSA-FeP group ($n = 6$)] or with HSA [(□) HSA group ($n = 6$)] → 30 min after 40% exchange.

baseline). However, it slowly decreased again to 52.3 ± 20% of the baseline after 30 min (Figure 4a).

An extreme exchange transfusion with HSA normally leads to anemia, which decreases P_{v,O_2} and blood flow by lowering O_2-delivery to the cardiac muscles. As compensation for this decrease in O_2-delivery, peripheral vasoconstriction occurs in order to maintain the blood flow for vital organs, e.g., heart and brain. Among the vital organs, renal perfusion is first impaired under systemic hypoperfusion due to redistribution of the systemic blood flow. Consequently, $P_{t,O_2(R)}$ is sensitive to a subtle change in the systemic circulation and correlates well with the systemic O_2-delivery. The $P_{t,O_2(R)}$ obviously declined to about 27% of the baseline after 40% bleeding, but increased after injection of HSA-FeP to 41.4 ± 6.1% of the baseline (Figure 4b). $P_{t,O_2(M)}$ also showed a similar recovery (from 11.9 ± 11% to 33.4 ± 14% of the baseline, Figure 4c). Although these were significant increases, the recovery ratios were almost 50% of the value before injection. This is probably due to the following two reasons. (i) The first is the relatively low FeP concentration of HSA-FeP, because 5 g/dL HSA-FeP solution contains a total of 3 mM FeP, corresponding to one-third that of whole blood ([heme], 9.2 mM). (ii) The second reason may be vasoconstriction induced by nitric oxide (endothelial derived relaxation factor) binding to the acellular HSA-FeP. It decreases the capillary densities; therefore, the O_2-diffusion from the capillaries to the tissues should be reduced as observed in the cross-linked hemoglobin solution (Schults et al., 1993; Keipert et al., 1993). Moreover, it has been found that an endothelial relaxation factor is generated in response to the shear stress on the vascular wall (Malek et al., 1995). The prompt flow of the HSA-FeP solution with low viscosity compared to the red blood cell may also result in a decrease of the shear stress on the vascular wall and may induce vasoconstruction.

On the basis of these results, we can conclude that the HSA-FeP solution transports dioxygen in rats and shows significant O_2-transport in vivo.

Half-Lifetime of Dioxygenated FeP [$\tau_{1/2}(O_2)$] in HSA. The O_2-binding to HSA-FeP is reversible and the degree of dioxygenation corresponds to the O_2-partial pressure. The dioxygenated species of FeP was, however, slowly autooxidized to the ferric state, which corresponds to a methemoglobin and cannot coordinate molecular dioxygen anymore. The absorption band of the oxy state (548 nm) was gradually breached and almost disappeared after 24 h. It is noteworthy that the $\tau_{1/2}(O_2)$ in vivo (4.1 h) was significantly long compared to that in vitro (1.0 h). Indeed, $\tau_{1/2}(O_2)$ in human plasma at 37 °C (ex vivo) was prolonged to 3.3 h (Figure 5a). These observations clearly show that some plasma contents contribute to the apparent long-lifetime of the O_2-adduct species of FeP in the bloodstream.

Rereduction of Fe(III)P by Red Blood Cells. We then examined the Fe(III)P reduction capability of several systems under anaerobic conditions at 37 °C (Figure 5b). When whole blood is added to the HSA-Fe(III)P solution, Fe(III)P was gradually reduced over a period of 5 h, until it reached a plateau at which 63% had been reduced and 37% remained as Fe(III)P. In contrast, only 38% of Fe(III)P was reduced in plasma. McGown et al. reported a similar reduction behavior of methemoglobin by red blood cells and concluded that this reduction was accompanied by ascorbic acid (AsA) in the blood, which is released and recycled through a transmembrane process across the red blood cell membrane (McGown et al., 1990). It is well-known that red blood cells actively take up dehydroascorbic acid and release AsA (Basu et al., 1979). We also observed that HSA-Fe(III)P could be reduced by AsA itself. Under a physiological ascorbate

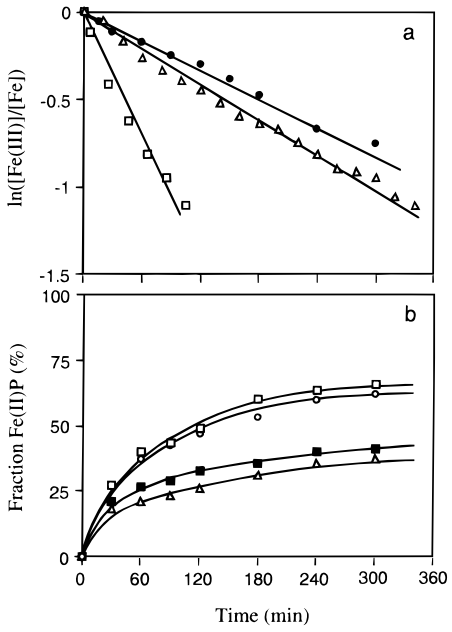

Figure 5. (a) Autoxidation of O_2-coordinated species of FeP incorporated into HSA at 37 °C; (□) in saline solution (pH 7.4, P_{O_2}, 150 mm Hg); (△) in plasma (P_{O_2}, 150 mm Hg); (●) in vivo. (b) Reduction of HSA-Fe(III)P (0.5 mM) by several systems under anaerobic condition at 37 °C; (○) in whole blood (Hct, 27%); (△) in plasma, (□) with AsA (2.5 mM); (■) with AsA (0.1 mM).

concentration (0.1 mM), the reduction proceeded about 40%, and the excess molar AsA (5-fold mole) reduced Fe(III)P up to 66%. The existence of the limiting reduction ratio of about 65% probably indicates that axial imidazolylalkyl groups cannot partially coordinate again to the Fe(II) ion centers of the rereduced FeP molecules in HSA. The reaction obeyed the second-order (k, 13.3 M^{-1} min^{-1}) like the methemoglobin reduction by AsA (Tomoda et al., 1976; Yubisui et al., 1980). The reduction of HSA-FeP by whole blood also showed a second-order reaction with a similar rate constant (k, 10.9 M^{-1} min^{-1}). It is remarkable that the rate constants of the HSA-FeP reduction were much faster than that of the methemoglobin reduction by AsA. On the basis of these results, we have concluded that the red blood cells reduce Fe(III)P by providing a renewable source of AsA.

In conclusion, all physiological responses to the exchange transfusion with the HSA-FeP into rats after hemodilution and hemorrhage reveal the in vivo O_2-transport of this new type of synthetic O_2-infusion. The nonenzymatic reduction of HSA-Fe(III)P is achieved by physiological ascorbate which is continuously recycled by red blood cells. This behavior is similar to that observed for the same kind of acellular-type red cell substitute, namely cross-linked hemoglobin. On the other hand, AsA itself can also promote heme oxidation and degradation, thus the reduction mechanism in the bloodstream is more complicated.

ACKNOWLEDGMENT

This work was partially supported by the Health Science Research Grants (Artificial Blood Project), the Ministry of Health and Welfare, Japan.

LITERATURE CITED

(1) Basu, S., Som, S., Deb, S., Mukherjee, D., and Chatterjee, I. B. (1979) Dehydroascorbic Acid Reduction in Human Erythrocytes. *Biochem. Biophys. Res. Commun. 90*, 1335−1340.

(2) Carter, D. C., He, X.-M., Munson, S. H., Twigg, P. D., Gernert, K. M., Broom, M. B., and Miller, T. Y. (1989) Three-dimensional Structure of Human Serum Albumin. *Science 244*, 1195−1198.

(3) Carter, D. C., and Ho, J. X. (1994) Structure of Serum Albumin. *Adv. Protein Chem. 45*, 153−203.

(4) He, X. M., and Carter, D. C. (1992) Atomic Structure and Chemistry of Human Serum Albumin. *Nature 356*, 209−215.

(5) Izumi, Y., Sakai, H., Hamada, K., Takeoka, S., Yamahata, T., Kato, R., Nishide, H., Tsuchida, E., and Kobayashi, K. (1996) Physiological Responses to Exchange Transfusion with Hemoglobin Vesicles as an Artificial Oxygen Carrier in Anesthetized Rats: Changes in Mean Arterial Pressure and Renal Cortical Tissue Oxygen Tention. *Crit. Care Med. 24*, 1869−1873.

(6) Keipert, P. E., Gonzales, A., Gomez, G. L., Macdonald, V. W., Hess, J. R., and Winslow, R. M. (1993) Acute Changes in Systemic Blood Pressure and Urine Output of Consious Rats Following Exchange Transfusion with Diaspirin-cross-linked Hemoglobin. *Transfusion 33*, 701−708.

(7) Komatsu, T., Ando, K., Kawai, N., Nishide, H., and Tsuchida, E. (1995) O_2-Transport Albumin: A New Hybrid-Haemoprotein Incorporating Tetraphenylporphyrinato- iron(II) Derivative. *Chem. Lett. 1995*, 813−814.

(8) Komatsu, T., Hamamatsu, K., Wu, J., and Tsuchida, E. (1999) Physicochemical Properties and O_2−Coordination Structure of Human Serum Albumin Incorporating Tetrakis-(*o*-pivalamido)phenylporphyrinatoiron(II) Derivatives. *Bioconjugate Chem. 10*, 82−86.

(9) Kragh-Hansen, U. (1981) Molecular Aspect of Ligand Binding to Serum Albumin. *Pharmacol. Rev. 33*, 17−53.

(10) Malek, A. M., and Izumo, S. (1995) Control of Endotherial Cell Gene Expression by Flow. *J. Biomech. 28*, 1515−1528.

(11) McGown, E. L., Lyons, M. F., Marini, M. A., and Zegna, A. (1990) Reduction of Extracellular Methemoglobin by Erythrocytes. *Biochim. Biophys. Acta 1036*, 202−206.

(12) Peters, T., Jr. (1985) Serum Albumin. *Adv. Protein Chem. 37*, 161−245.

(13) Peters, T., Jr. (1996) *All about Albumin, Biochemistry, Genetics, and Medical Applications*, Academic Press, New York.

(14) Sakai, H., Takeoka, S., Park, S. I., Kose, T., Nishide, H., Izumi, Y., Yoshizu, A., Kobayashi, K., and Tsuchida, E. (1997) Surface Modification of Hemoglobin Vesicles with Poly(ethylen glycol) and Effects on Aggregation, Viscosity, and Blood flow during 90% Exchange Transfusion in Anesthetized Rats. *Bioconjugate Chem. 8*, 23−30.

(15) Schults, S. C., Grady, B., Cole, F., Hamilton, F., Burhop, K., and Malcolm, D. S. (1993) A Role for Endotherin and Nitric Oxide in the Pressor Response to Diaspirin Cross-linked Hemoglobin. *J. Lab. Clin. Med. 122*, 301−308.

(16) Tomoda, A., Matsukawa, S., Takeshita, and M., Yoneyama, Y. (1976) Effect of Organic Phosphates on Methemoglobin Reduction by Acorbic Acid. *J. Biol. Chem. 251*, 7494−7498.

(17) Tsuchida, E., Ando, K., Maejima, H., Kawai, N., Komatsu, T., Tekeoka, S., and Nishide, H. (1997) Properties of and Oxygen Binding by Albumin-Tetraphenyl-porphinatoiron(II) Derivative Complexes. *Bioconjugate Chem. 8*, 534−538.

(18) Yuasa, M., Tani, Y., Nishide, H., and Tsuchida, E. (1987) Stabilization Effect of Tocopherol and Catalase on the Lifetime of the Liposome-embedded Heme as an Oxygen-carrier. *Biochim. Biophys. Acta 900*, 160−162.

(19) Yubisui, T., Matsukawa, S., and Yoneyama, Y. (1980) Stopped Flow Studies on the Nonenzymatic Reduction of Methemoglobin by Reduced Flavin Mononmucleotde. *J. Biol. Chem. 255*, 11694−11697.

BC990065V

Novel Method for Covalent Fluorescent Labeling of Plasmid DNA That Maintains Structural Integrity of the Plasmid

Carole Neves, Gerardo Byk,† Virginie Escriou, Florence Bussone, Daniel Scherman,* and Pierre Wils

UMR 133 CNRS/Rhône-Poulenc Rorer, Centre de Recherche de Vitry Alfortville, B.P.14, 13 quai Jules Guesde 94403 Vitry-sur-Seine Cedex France. Received June 8, 1999; Revised Manuscript Received October 11, 1999

We have developed a chemical strategy for covalent coupling of fluorophores to plasmid DNA. A *p*-azido−tetrafluoro-benzyl-lissamine conjugate was synthesized and purified. This conjugate was used to covalently associate fluorescent molecules to plasmid DNA by photoactivation. In contrast to nick-translated plasmid DNA, plasmid−lissamine conjugates appeared on gel as supercoiled DNA. Reporter gene was expressed after transfection of the plasmid−lissamine conjugates in NIH 3T3 cells, although gene transfer efficiency was decreased by 60% as compared with unlabeled DNA. Intracellular traffic of plasmid−lissamine conjugates was studied in transfected cells. After cytoplasmic microinjection, fluorescent plasmid did not diffuse from the site of injection and appeared to be progressively degraded in the cytoplasm.

INTRODUCTION

Complexes of cationic lipid and plasmid DNA (lipoplexes) are widely used for transferring genes into eukaryotic cells in vitro and in vivo (*1*). The mechanism of vector-mediated plasmid DNA entry into cells during lipoplex-mediated gene delivery is not well understood. Labeled plasmids are valuable tools to follow DNA traffic during transfection in cells and to elucidate the mechanism of DNA entry into the cell and transport to the nucleus.

Various noncovalent or covalent techniques have been described so far for direct labeling of plasmid DNA. DNA-intercalating dyes such as ethidium bromide (*2*, *3*) have been used to label DNA, but it may exchange with endogenous nucleic acid, raising questions about the intracellular source of the fluorescent signal. Recently, fluorescent PNA (peptide nucleic acids) were used to label functionally intact plasmid DNA (*4*). Some covalent labeling methods use nucleic acid modifying enzymes in order to incorporate labeled nucleotides into DNA. Thus, polymerase chain reaction and nick transslation were used to incorporate fluorescent nucleotides into plasmid DNA (*5*, *6*). These covalent techniques induce relaxation or linearization of plasmid DNA. This represents a serious drawback since, to properly study intracellular DNA traffic, maintaining plasmid topology supercoiled is preferable.

The use of photoactive molecules leads to an efficient photomodification of DNA (*7*−*9*). For example, tetrafluorophenylazido reagents can modify more chemical groups than their nonfluorinated analogues (*10*). A photoactivable derivative of ethidium bromide was successfully used for following intracellular traffic of lipoplexes (*11*).

In the present work, we developed a new methodology allowing to covalently associate fluorophores to DNA while maintaining plasmid structurally intact. We describe here the synthesis and characterization of photoactivable fluorescent conjugates (*p*-azido−tetrafluorobenzylamido−lissamine), their use for plasmid DNA labeling by photoactivation, as well as intracellular trafficking studies using the labeled plasmids.

EXPERIMENTAL PROCEDURES

Analytical and Semipreparative HPLC. Analytical and semipreparative HPLC were performed on a Merck-Hitachi gradient pump equipped with an AS-2000A autosampler, an L-6200A intelligent pump, and a UV−vis detector L-4000.

Method 1. For analytical separations, we used a column C18 Vydac TP54 (4.6 mm × 250 mm) (Interchim, Montlucon, France) using as solvents A (0.1 M triethylammonium acetate, pH 7.1) and B (90/10 v/v acetonitrile/0.01% triethylammonium acetate). The elution was obtained using an isocratic mixture of 50% A and B with a flow rate of 1 mL/min. Detection was by UV absorbance at 254 nm.

Method 2. For semipreparative purification, we used a Bio-Rad C18 column (1 cm × 25 cm) using the same solvents as for method 1 but at a flow rate of 2.5 mL/min and detection at 250 nm.

Preparation of *p*-Azido-Tetrafluorobenzylamido-Lissamine. *Solution 1.* Lissamine sulfonyl chloride obtained from Aldrich (65.77 mg/0.114 mmol) was dissolved in 1 mL of DMF.

Solution 2. N-(4-Azido-2,3,5,6-tetrafluorobenzylamine obtained from Molecular Probes (25 mg, 0.114 mmol) and TEA (20 microL, 0.15 mmol) were dissolved in 0.5 mL of DMF in a 3 mL rectivial equipped with a micro stirrer. The mixture was left at room temperature, and the reaction was monitored by HPLC using method 1. After 3 h, the reaction was complete (no further modification of HPLC profile). The product was directly purified from the reaction mixture by HPLC method 2. Product was eluted at 12−13 min. Fractions containing the product were collected, pooled, and reanalyzed by analytical HPLC (method 1). Purity was 98% by HPLC analysis (T_r = 16.02 min.).

* To whom correspondence should be addressed. E-mail: daniel.scherman@rp-rorer.fr. Phone: 33 1 55 71 38 47. Fax: 33 1 55 71 37 96.

† Laboratory of Peptidomimetics and Genetic Chemistry, Department of Chemistry, Bar-Ilan University, 52900-Ramat Gan, Israël.

10.1021/bc990070z CCC: $19.00 © 2000 American Chemical Society
Published on Web 12/15/1999

Scheme 1. Synthesis of *p*-Azido-Tetrafluorobenzylamido-Lissamine Conjugate

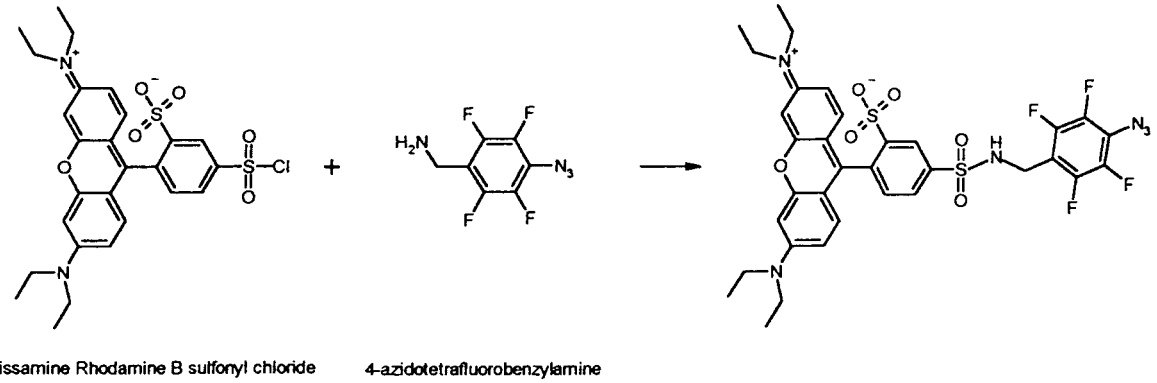

Lissamine Rhodamine B sulfonyl chloride 4-azidotetrafluorobenzylamine

MS: MH^+ theoretical, 761; obtained, 761. ^1H spectrum of NMR [400 MHz, $(CD_3)_2SO$ d6, δ (ppm)]: 1.24 (t, J = 7.5 Hz, 12H, CH_3); 3.66 (q, J = 7.5 Hz, 8H, NCH_2); 4.29 (broad s, 2H, $ArCH_2N$); from 6.90 to 7.05 (m, 6H, H aromatics); 7.46 (d, J = 8 Hz, 1H, H aromatic in meta of SO_3); 7.90 (dd, J = 8 and 1.5 Hz, 1H, H aromatic in para of SO_3); 8.24 (d, J = 1.5 Hz, 1H, H aromatic in ortho of SO_3); 8.78 (broad band, 1H, NH). The IR spectrum was obtained from a KBr pellet, using a Nicolet-510 FT-IR spectrometer. Main characteristics absorption bands were observed at 2155 + 2125 cm^{-1} n_s N=N from azide, 1593 + 1495 cm^{-1} n C=C, and C=N, 1388 cm^{-1} n_s S=O from SO_2N, 1199 + 1180 cm^{-1} n_s S−O from SO_3^-, and n_{as} S=O from SO_2N, 1207 cm^{-1} n_{as} from SO_3^-, 922 cm^{-1} n S−N from SO_2N.

Covalent Coupling of Conjugates to Plasmid DNA. Plasmid pCMVLacZ (6.9 kbp) carries a cassette containing the enhancer-promoter from the immediate-early gene of cytomegalovirus (CMV) and the gene coding β-galactosidase. Plasmid DNA was purified using Wizard Megaprep kit (Promega, Madison, WI). *p*-Azido−tetrafluorobenzylamido−lissamine conjugate was mixed with dsDNA (final concentration, 0.7 μg/μL) using a 2000 M excess of conjugate. The mixture was cooled in an ice−water bath below a sun lamp (Rad Free UV lamp-365 nm, Schleicher and Schuell, Ecquevilly, France) and illuminated for 15 min in the dark. Excess *p*-azido−tetrafluorobenzylamido−lissamine conjugate was removed by ion-exchange chromatography (PCR Purification kit, Qiagen, Hilden, Germany). The average number of fluorophores attached to plasmid DNA was determined with a Titertek Fluoroskan II Spectrofluorimeter with free and illuminated *p*-azido−tetrafluorobenzylamido−lissamine conjugate for calibration curve (excitation, 544 nm; emission, 590 nm).

Plasmid Labeling by Nick Translation. Fluorescently labeled plasmid was prepared by nick translation as described previously (*6*), with the following modifications. DNAse I quantity was 50 pg, and incubation time 3 h at 16 °C. Nonincorporated nucleotides were separated by plasmid ethanol precipitation. Labeled plasmid was resuspended in water at a concentration of 1 μg/μL. Nick translation was optimized to produce plasmid DNA modification at one fluorescent residue for 30 base pairs.

Transient Expression Studies. NIH 3T3 cells were obtained from the American Type Culture Collection (ATCC CRL-1658). The cells were grown in Dulbecco's modified Eagle's medium (DMEM, Gibco) containing 4.5 g/L glucose, supplemented with 2 mM glutamine, 100 units/mL penicillin, 100 μg/mL streptomycin, and 10% Calf Serum. Cells were grown at 37 °C in a 5% CO_2/air incubator. One day before transfection, 24-well culture plates were seeded with 80 000 cells/well. Cationic lipid RPR 120535 (*12*) was used for the transfection assays. Plasmids (20 ng/μL) were diluted in 150 mM NaCl/$NaHCO_3$ 20 mM and mixed with a cationic lipid solution (0.12 mM). The DNA−cationic lipid complex was diluted in supplemented culture medium and then added to the cells (0.5 μg of DNA and 3 nmol of lipid/well). The cells were incubated for 24 h at 37 °C in a 5% CO_2/air incubator. The cells were washed twice with PBS and lysed with 250 μL of cell culture lysis reagent (Promega, Madison, WI). β-Galactosidase expression was measured according to the "Lumigal β-Galactosidase genetic reporter system" (Clontech, Palo Alto, CA). Light emission was measured by integration over 10 s using a Lumat LB9501 luminometer (EG and G, Berthold, Evry, France). Light emission was normalized to the protein concentration determined using the Pierce BCA assay (Pierce, Rockford, IL).

Intracellular Traffic Studies. CV-1 cells were kindly provided by Dr. S. Koutouzov (INSERM U25, Paris, France). Cells were cultured in Minimum Essential Medium (MEM, Gibco, Grand Island, NY) supplemented with 2 mM glutamine, 100 units/mL penicillin, 100 μg/mL streptomycin, and 10% Foetal Bovine Serum. Cells were grown at 37 °C in a 5% CO_2/air incubator. One day before the transfection assay, cells were seeded on glass slides in 24-well culture plates with 50 000 cells/well. Labeled plasmids were diluted in 150 mM NaCl at 20 ng/μL concentration, then mixed with a cationic lipid solution (0.12 mM). The DNA−cationic lipid complex was diluted in culture medium (Minimum Essential Medium) in the absence of serum and then added to the cells (0.5 μg of DNA and 3 nmol of lipid/well). After 2 h at 37 °C in a 5% CO_2/air incubator, 10% Foetal Bovine Serum was added to the cells. After 24 h, cells were washed three times with PBS, fixed for 20 min in 3% *p*-formaldehyde in PBS, and washed three times with PBS. Nuclei were then stained with 4,6-diamidino-2-phenylindole (DAPI), at a concentration of 0.1 μg/mL, for 15 min, and washed with PBS. The cells were mounted in Mowiol for examination. Slides were examined with a Zeiss Axiophot fluorescence microscope, with a 100× objective lens, coupled to a cooled CCD camera (Hamamatsu), and a Samba imaging software (Unilog, Meylan, France).

Microinjection Studies. CV-1 cells were grown at 37 °C in a 5% CO_2/air incubator on CELLocate microgrid coverslips (Eppendorf, Hamburg, Germany). The solution of DNA was injected into the cells via glass micropipets having tip diameters ranging 0.3−0.7 μm (Femtotips, Eppendorf, Hamburg, Germany) at 1 μg/μL concentration. Injections were carried out under visual control on a fixed stage of an inverted phase contrast microscope (Axiovert 135, Zeiss, Le Pecq, France) using a Micromanipulator 5171 and Microinjector 5242 (Eppendorf, Ham-

burg, Germany). The average volume (0.1−0.2 pL) injected into each cell was determined by injecting [^{35}S]-dATPαS (^{35}S-labeled nucleotide) into cells and measuring the radioactive content (*13*). These corresponded to average 6000−12000 plasmid molecules/cell. Following injection, the cells were incubated for 30 min to 6 h at 37 °C in a 5% CO_2/air incubator. The cells were fixed and examined as described above.

RESULTS

Preparation of *p*-Azido-Tetrafluorobenzylamido-Lissamine Conjugates. Scheme 1 illustrates the chemistry used to prepare the *p*-azido−tetrafluorobenzylamido−lissamine conjugate. The coupling step involves reaction of lissamine rhodamine B sulfonyl chloride with 4-azido-tetrafluorobenzylamine. The yield of this reaction was 50%. The final product was analyzed by mass spectroscopy, which confirmed the disappearance of starting reagents and gave an experimental mass similar to the calculated mass. The final product was also analyzed by NMR and infrared, which confirmed the integrity of the azido group (see complete data in the experimental procedures).

Covalent Attachment of *p*-Azido-Tetrafluorobenzylamido-Lissamine to dsDNA. The *p*-azido−tetrafluorobenzylamido−lissamine was used to covalently modify plasmids by photoactivation. *p*-azido−tetrafluorobenzylamido−lissamine conjugate was mixed with dsDNA at conjugate/DNA molar ratios of 2000 and illuminated at 365 nm. After purification on ion-exchange columns, the average number of fluorophores linked to the DNA was determined. Conjugates bearing an average number of 80 ± 20 fluorophores/plasmid molecule (eight experiments) were obtained. *p*-Azido−tetrafluorobenzylamido−lissamine conjugate/DNA molar ratios ranging 1000−10000 were also assayed. Conjugates bearing 20−200 fluorophores/plasmid molecule were thus obtained (data not shown). Plasmids covalently modified with lissamine rhodamine B are referred to as plasmid−lissamine conjugates. No lissamine rhodamine B was coupled to DNA when plasmid DNA was mixed with nonilluminated *p*-azido−tetrafluorobenzylamido−lissamine conjugate (data not shown). This control showed that light was required for conjugation.

Characterization of Plasmid−Lissamine Conjugates. Plasmid−lissamine conjugates were analyzed by agarose gel electrophoresis. With 70 fluorophores/ plasmid DNA molecule, there was no visible modification of plasmid DNA migration and plasmid−lissamine conjugates appeared on gels as supercoiled DNA (Figure 1, lane 2). Another labeling method was used as a comparison. Plasmid DNA enzymatically labeled by nick translation and bearing 250 rhodamine nucleotides/plasmid molecule was linearized or relaxed (Figure 1 − lane 4).

Transgene Expression. Reporter gene expression was studied after transfection of NIH 3T3 cells. Plasmid−lissamine conjugate with 70 fluorophores/plasmid DNA molecule expressed β-galactosidase. The expression was decreased by 60%, as compared to nonmodified plasmid (Figure 2, lane 2). Comparatively, nick-transslated plasmid DNA expression was completely abolished (Figure 2, lane 3). Nick-transslated plasmid DNA, bearing less rhodamine nucleotides per plasmid molecule (100), retained 10% activity, as compared to nonmodified plasmid (data not shown).

Lipofection Studies. CV-1 cells were exposed to plasmid−lissamine conjugate complexed to the cationic lipid RPR 120535 for 24 h. Plasmid DNA was observed

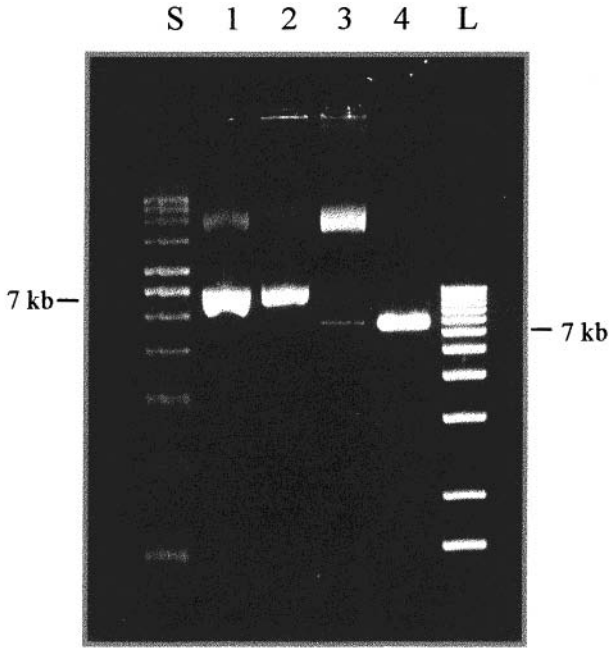

Figure 1. Unmodified plasmid (1), plasmid−lissamine conjugate with 70 fluorophores/plasmid molecule (2), nick-translated plasmid with 250 fluorophores/plasmid molecule (3), and *Hin*dIII-linearized plasmid (4). Plasmids (200 ng) were analyzed by 0.8% agarose gel electrophoresis and ethidium bromide staining. L = molecular weight marker for linear DNA fragments (1 kb ladder). S = molecular weight marker for supercoiled DNA fragments (1 kb ladder).

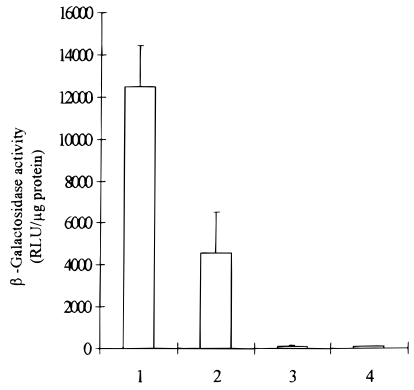

Figure 2. Transgene expression after transfection of plasmid−lissamine conjugate. Nonmodified plasmid (1), plasmid−lissamine conjugate with 70 fluorophores/plasmid molecule (2), and nick-translated plasmid with 250 fluorophores/plasmid molecule (3) were used for transfecting NIH 3T3 cells with cationic lipid RPR 120535. The β-galactosidase expression was evaluated after 24 h of incubation. A control condition, without plasmid, was assayed (4). Values are means ± SD (n = 3).

in 100% of the cells, displaying a punctuate cytoplasmic staining (Figure 3). Vesicles containing plasmid−lissamine conjugates were heterogeneous in size and shape.

Microinjection Studies. Plasmid−lissamine conjugates were microinjected into the cytoplasm of CV-1 cells. Plasmids with 100 fluorophores/plasmid molecule were used. Cells were fixed after 30 min, 2 h (data not shown), or 6 h, and nuclei were stained with DAPI. An intense cytoplasmic fluorescence was observed 30 min after microinjection and DNA could only be detected in the cytoplasm (Figure 4A). The DNA fluorescence pattern evolved 2 h after microinjection into the cytoplasm: half of the stained cells showed the same intense fluorescent pattern observed at 30 min and the other cells exhibited

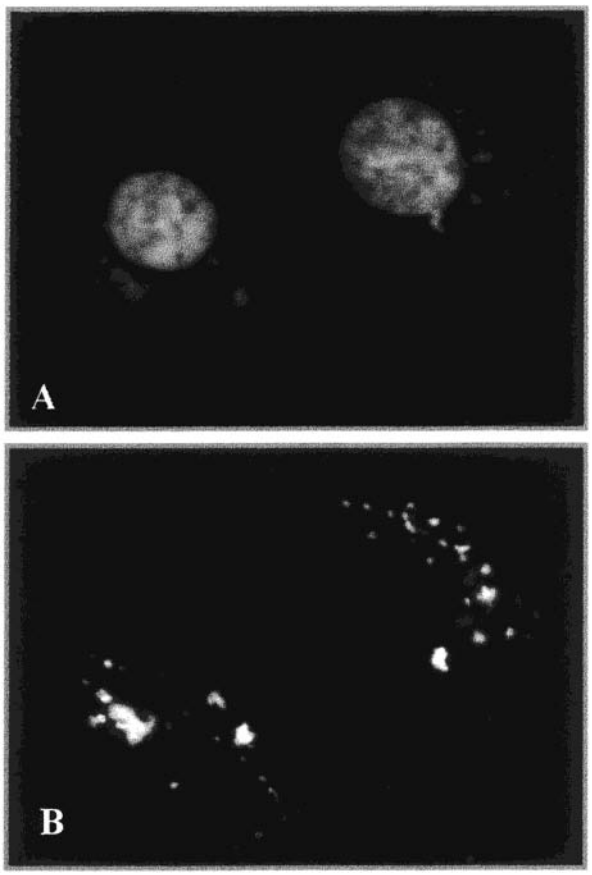

Figure 3. Transfection of plasmid−lissamine conjugate. Plasmid−lissamine conjugates with 100 fluorophores/plasmid molecule were used for transfecting CV-1 cells with cationic lipid RPR 120535. Cells were fixed after 24 h of incubation. Fluorescent microscopy of plasmid−lissamine (B) and nuclei staining with 4,6-diamidino-2-phenylindole (A) are shown.

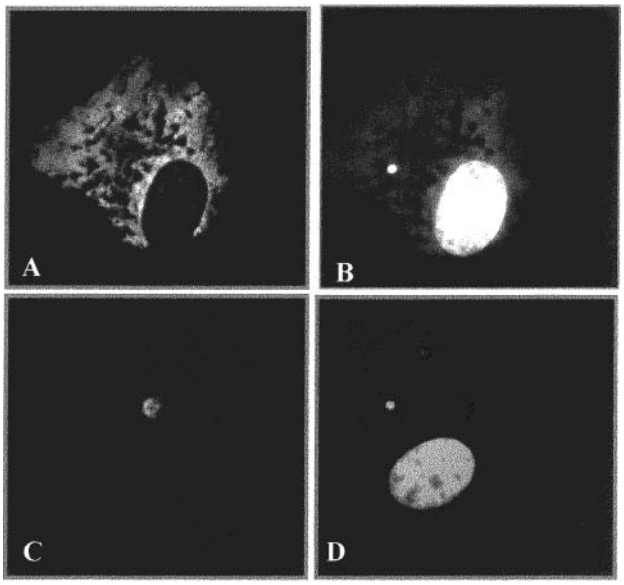

Figure 4. Cytoplasmic microinjection of plasmid−lissamine conjugate. CV-1 cells were cytoplasmically microinjected with plasmid−lissamine (100 fluorophores/plasmid DNA molecule) and fixed after 30 min (A and B) or 6 h (C and D). Fluorescent microscopy of plasmid−lissamine (A and C) and nuclei staining with 4,6-diamidino-2-phenylindole (B and D) are shown.

a single fluorescent spot in the cytoplasm (data not shown). After 6 h, nearly all cells displayed only one residual fluorescent spot in the cytoplasm (Figure 4C).

DISCUSSION

Several methods for covalent attachment of molecules to nucleic acids have been developed and reported so far (*8*, *9*, *14*). Among them, the use of photoactive molecules, such as tetrafluorophenylazido groups, leads to an efficient photomodification of DNA (*7*). A *p*-azido−tetrafluorobenzylamido−lissamine conjugate bearing on one side a fluorophore and on the other a photoactive group was synthesized in one single step. The fluorophore makes it possible to quantify the average number of fluorophores bound to DNA and to study the intracellular fate of transfected or microinjected plasmids. Moreover, we found that molecules labeled with lissamine rhodamine B were easier to purify and more chemically stable than those labeled with another fluorophore such as tetramethylrhodamine.

Having covalently linked fluorophores is very important for studies of plasmid DNA intracellular traffic. The use of plasmid labeled with intercalating dyes or noncovalently associated fluorophores could lead to nonrelevant intracellular labeling since these dyes can dissociate from plasmid DNA inside the cells. It is also important to underline that plasmid−lissamine conjugates appeared on gels as supercoiled DNA. On the contrary, labeling by nick transslation formed relaxed or linearized plasmid DNA molecules. Intracellular traffic studies with intact plasmid is more representative of the original plasmid behavior. Furthermore, linear plasmid is theoretically more sensitive to degradation by DNases, which could generate labeled nucleotides inside the transfected cells.

Ultraviolet light in the range of 320 nm has been shown to induce damage to DNA mostly through indirect photosensitization reactions involving molecular oxygen (*15*). Therefore, it is important to control the properties of the light source to maintain plasmid integrity (*16*). Using *p*-azido−tetrafluorobenzylamido−lissamine conjugates, coupling was obtained using light at 365 nm, thus causing less damage to DNA.

Covalent coupling of ligands to the DNA could cause transcriptional inactivation. According to a study on the expression of a biotinylated plasmid prepared with a similar photomodification chemistry, a plasmid with up to 40 biotins coupled per plasmid retained 40% of its biological activity (*14*). Accordingly, plasmid−lissamine prepared with our photoactive conjugates still showed 40% of the gene expression compared to unmodified plasmid. Transcription apparatus may have difficulty in reading through the gene cassette because of the presence of the tag. On the contrary, enzymatic labeling method (nick translation) led to inactivation of the plasmid. This result could be explained by the high number of fluorescent nucleotides incorporated (250 per plasmid molecule) and by the modification of plasmid DNA structure. We have observed that relaxed or linearized plasmid displayed highly decreased expression functionality.

We studied plasmid−lissamine conjugate fate after lipofection using cationic lipid RPR120535. Plasmid DNA was observed in 100% of the cells, displaying a punctuate cytoplasmic staining. But, plasmids were not detected in the nucleus of transfected cells. Similar results were obtained using nick-translated plasmid (*6*) or plasmid DNA labeled by other covalent methods (*17*). Plasmids labeled by a noncovalent method were observed in the nucleus after lipofection (*3*). The differences could be explained by the noncovalently associated fluorophores leading to nonrelevant intracellular labeling since these dyes could dissociate from plasmid DNA inside the cells.

After microinjection in the cytoplasm, plasmid−lissamine conjugates could be easily detected but remained

in the cytoplasm. Our microscopic studies suggest that microinjected plasmid−lissamine conjugates are progressively degraded in the cytoplasm, since the staining observed gradually decreased with time. After 6 h, only one spot of fluorescent plasmid−lissamine was detected, which probably corresponded to the site of injection. This suggests that the bulk of microinjected plasmid did not readily diffuse from the site of injection. It is possible that plasmid−lissamine molecules could be sequestered or degraded in the cytoplasm as previously observed (*18*−*20*).

In conclusion, we have designed a novel and simple chemistry for covalently coupling fluorophores to plasmid DNA by photoactivation. This technology makes it possible to control the number of fluorophores linked to DNA which is determinant for maintaining plasmid integrity. Large amounts of fluorescent plasmid (100 μg) can be prepared with this method. Fluorescent DNA prepared with this method can be used for following the intracellular traffic of lipoplexes and possibly, the biodistribution of plasmid DNA after in vivo gene transfer. The present strategy could also be used for coupling other markers to plasmid DNA.

ACKNOWLEDGMENT

This work was supported by a grant from the French Ministry of Research. We thank Dr. Marc Vuilhorgne and his staff from the Structural Analysis Department of Rhône-Poulenc Rorer.

LITERATURE CITED

(1) Ledley, F. D. (1995) Non viral gene therapy: the promise of genes as pharmaceutical products. *Hum. Gene Ther. 6*, 1129−1144.

(2) Pecq, J. B. L. (1971) Use of ethidium bromide for separation and determination of nucleic acids of various conformational forms and measurement of their associated enzymes. *Methods Biochem. Anal. 20*, 41−86.

(3) Zhang, F., Andreassen, P., Fender, P., Geissler, E., Hernandez, J. F., and Chroboczek, J. (1999) A transfecting peptide derived from adenovirus fiber protein. *Gene Ther. 6*, 171−181.

(4) Zelphati, O., Liang, X., Hobart, P., and Felgner, P. L. (1999) Gene chemistry: functionnally and conformationally intact fluorescent plasmid DNA. *Hum. Gene Ther. 10*, 15−24.

(5) Hagstrom, J. E., Luddtke, J. J., Bassik, M. C., Sebestyén, M. G., Adam, S. A., and Wolff, J. A. (1997) Nuclear import of DNA in digitonin-permeabilized cells. *J. Cell Sci. 110*, 2323−2331.

(6) Escriou, V., Ciolina, C., Lacroix, F., Byk, G., Scherman, D., and Wils, P. (1998) Cationic lipid-gene transfer: effect of serum on cellular uptake and intracellular fate of polyamine/DNA complexes. *Biochim. Biophys. Acta 1368*, 276−288.

(7) Levina, A. S., Tabatadze, D. R., Dobrikov, M. I., Shishkin, G. V., and Zarytova, V. P. (1996) Sequence-specific photomodification of single-stranded and double-stranded DNA fragments by oligonucleotide perfluoroazide derivative. *Antisense Nucleic Acid Drug Dev. 6*, 127−132.

(8) Forster, A. C., McInnes, J. L., Skingle, D. C., and Symons, R. H. (1985) Nonradioactive hybridization probes prepared by the chemical labeling of DNA and RNA with a novel reagent, photobiotin. *Nucleic Acids Res. 13*, 745−761.

(9) Geselowitz, D. A., and Neumann, R. D. (1995) Quantitation of triple-helix formation using a photocross-linkable aryl azide/biotin/oligonucleotide conjugate. *Bioconjugate Chem. 6*, 502−506.

(10) Levina, A. S., Tabatadze, D. R., Dobrikov, M. I., Shishkin, G. V., Khalimskaya, L. M., and Zarytova, V. P. (1996) Site-specific photomodification of single-stranded DNA targets by aryl azide and perfluoroaryl azide derivatives of oligonucleotides. *Antisense Nucleic Acid Drug Dev. 6*, 119−126.

(11) Tseng, W., Purvis, N. B., Haselton, F. R., and Giorgio, T. D. (1996) Cationic liposomal delivery of plasmid to endothelial cells measured by quantitative flow cytometry. *Biotechnol. Bioeng. 50*, 548−554.

(12) Byk, G., Dubertret, C., Escriou, V., Frederic, M., Jaslin, G., Rangara, R., Pitard, B., Crouzet, J., Wils, P., Schwartz, B., and Scherman, D. (1998) Synthesis, activity, and structure−activity relationship studies of novel cationic lipids for DNA transfer. *J. Med. Chem. 41*, 224−235.

(13) Escriou, V., Ciolina, C., Helbling-Leclerc, A., Wils, P., and Scherman, D. (1998) Cationic lipid-mediated gene transfer: analysis of cellular uptake and nuclear import of plasmid DNA. *Cell Biol. Toxicol. 14*, 95−104.

(14) Leahy, P., Carmichael, G. G., and Rossomando, E. F. (1996) Novel biotinylated plasmid expression vectors retain biological function and can bind streptavidin. *Bioconjugate Chem. 7*, 545−551.

(15) Cadet, J., Berger, M., Decarroz, C., Wagner, J. R., Lier, J. E. V., Ginot, Y. M., and Vigny, P. (1986) Photosensitized reactions of nucleic acids. *Biochim. 68*, 813−834.

(16) Dowty, M. E., Gurevich, V., Berg, R. K., Repetto, G., and Wolff, J. A. (1992) Characterization of biotinylated and gold-labeled plasmid DNA. *Methods Mol. Cell. Biol. 3*, 167−174.

(17) Zabner, J., Fasbender, A. J., Moninger, T., Poellinger, K. A., and Welsh, M. J. (1995) Cellular and molecular barriers to gene transfer by a cationic lipid. *J. Biol. Chem. 270*, 18997−19007.

(18) Dowty, M. E., Williams, P., Zhang, G., Hagstrom, J. E., and Wolff, J. A. (1995) Plasmid DNA entry into postmitotic nuclei of primary rat myotubes. *Proc. Natl. Acad. Sci. U.S.A. 92*, 4572−4576.

(19) Ciolina, C., Byk, G., Blanche, F., Thuillier, V., Scherman, D., and Wils, P. (1998) Coupling of Nuclear Localization Signals to plasmid DNA and specific interaction of the conjugates with importin α. *Bioconjugate Chem. 10*, 49−55.

(20) Lechardeur, D., Sohn, K. J., Haardt, M., Joshi, P. B., Monck, M., Graham, R. W., Beatty, B., Squire, J., O'Brodovich, H., and Lukacs, G. L. (1999) Metabolic instability of plasmid DNA in the cytosol: a potential barrier to gene transfer. *Gene Ther. 6*, 482−497.

BC990070Z

Synthesis and Physicochemical Characterization of a Series of Hemoglobin-Based Oxygen Carriers: Objective Comparison between Cellular and Acellular Types

Hiromi Sakai, Minako Yuasa, Hiroto Onuma, Shinji Takeoka, and Eishun Tsuchida*

Department of Polymer Chemistry, Advanced Research Institute for Science and Engineering, Waseda University, Tokyo 169-8555, Japan. Received June 14, 1999; Revised Manuscript Received September 20, 1999

A series of hemoglobin (Hb)-based O_2 carriers, acellular and cellular types, were synthesized and their physicochemical characteristics were compared. The acellular type includes intramolecularly cross-linked Hb (XLHb), polyoxyethylene (POE)-conjugated pyridoxalated Hb (POE-PLP-Hb), hydroxyethylstarch-conjugated Hb (HES-XLHb), and glutaraldehyde-polymerized XLHb (Poly-XLHb). The cellular type is Hb-vesicles (HbV) of which the surface is modified with POE (POE-HbV). Their particle diameters are 7 ± 2, 22 ± 2, 47 ± 17, 68 ± 24, and 224 ± 76 nm, respectively, thus all the materials penetrate across membrane filters with 0.4 μm pore size, though only the POE-HbV cannot penetrate across the filter with 0.2 μm pore size. These characteristics of permeability are important to consider an optimal particle size in microcirculation in vivo. POE-PLP-Hb ([Hb] = 5 g/dL) showed viscosity of 6.1 cP at 332 s^{-1} and colloid osmotic pressure (COP) of 70.2 Torr, which are beyond the physiological conditions (human blood, viscosity = 3−4 cP, COP = ca. 25 Torr). XLHb and Poly-XLHb showed viscosities of 1.0 and 1.5 cp, respectively, which are significantly lower than that of blood. COP of POE-HbV is regulated to 20 Torr in 5% human serum albumin (HSA). HES-XLHb and POE-HbV/HSA showed comparable viscosity with human blood. Microscopic observation of human red blood cells (RBC) after mixing blood with POE-PLP-Hb or HES-XLHb disclosed aggregates of RBC, a kind of sludge, indicating a strong interaction with RBC, which is anticipated to modify peripheral blood flow in vivo. On the other hand, XLHb and POE-HbV showed no rouleaux or aggregates of RBC. The acellular Hbs (P_{50} = 14−32 Torr) have their specific O_2 affinities determined by their structures, while that of the cellular POE-HbV is regulated by coencapsulating an appropriate amount of an allosteric effector (e.g., P_{50} = 18, 32 Torr). These differences in physicochemical characteristics between the acellular and cellular types indicate the advantages of the cellular type from the physiological points of view.

INTRODUCTION

Acellular chemically modified hemoglobin (Hb) solutions have been developed for use as red blood cell substitutes (O_2 carriers) in surgical procedures and the treatment of trauma patients. The acellular Hbs include intramolecularly cross-linked Hb (Przybelski et al., 1997; Chatterjee et al., 1986), recombinant cross-linked Hb (Murray et al., 1995), polymerized Hb (Gould et al., 1998; Kasper et al., 1996), and polymer-conjugated Hb (Iwashita et al., 1991; Caron et al., 1998). The principal side effect consistently reported in the administration of acellular Hb solutions is a hypertension presumably due to vasoconstriction (Doherty et al., 1998; Abassi et al., 1997; Saxena et al., 1999). Hypertension, a well-defined reaction of the acellular intramolecularly cross-linked Hb with nitric oxide (NO) as an endothelial-derived relaxation factor (Moncada et al., 1991), was proposed to be beneficial in the treatment of hypotension concomitant to hemorrhagic shock (Przybelski et al., 1997). However, vasoconstriction reduces blood flow, lowering functional capillary density, affecting tissue perfusion and oxygenation (Tsai et al., 1995; Sakai et al., 1998b).

Another type of Hb-based O_2 carrier is phospholipid vesicles encapsulating concentrated Hb (Hb vesicles, HbV).[1] Numerous studies have been reported on the HbV since Djordjevici and Miller first reported (1977), and sufficient O_2 transporting ability comparable with blood has been confirmed (Djordjevici et al., 1987; Rudolph, 1998; Tsuchida, 1998). We have improved the physicochemical properties of HbV from the viewpoint of molecular assembly. For example, Hb encapsulation efficiency and size regulation have been improved by regulating the electrostatic and hydrophobic interactions among the components during an extrusion method which is superior to the other groups (Takeoka et al., 1996). Surface modification of HbV with polyoxyethylene (POE) prevents vesicular aggregation both in vitro and in vivo. (Sakai, 1997, 1998). Moreover, coencapsulation of a metHb-reducing system prolongs the oxygen-transporting ability of HbV in vivo (Takeoka, 1997). Even though HbV has not been clinically tested yet, it most closely reproduces the characteristics of natural blood such as the red cell membrane function of physically preventing direct con-

* To whom correspondence should be addressed. Phone: +81-3-5286-3120. Fax: +81-3-3205-4740. E-mail: eishun@mn.waseda.ac.jp.

[1] Abbreviations: HbV, Hb-vesicles; XLHb, intramolecularly cross-linked Hb; POE, polyoxyethylene; PLP, pyridoxal 5′-phosphate; POE-PLP-Hb, POE-conjugated pyridoxalated Hb; HES, hydroxyethylstarch; HES-XLHb, HES-conjugated XLHb; Poly-XLHb, glutaraldehyde-polymerized XLHb; POE-HbV, POE-modified HbV; DBBF, (2,3-dibromosalicyl)fumarate; PBS, phosphate-buffered saline; OTE, O_2 transporting efficiency; COP, colloid osmotic pressure; P_{50}, O_2 affinity; HSA, human serum albumin.

10.1021/bc9900789 CCC: $19.00 © 2000 American Chemical Society
Published on Web 12/14/1999

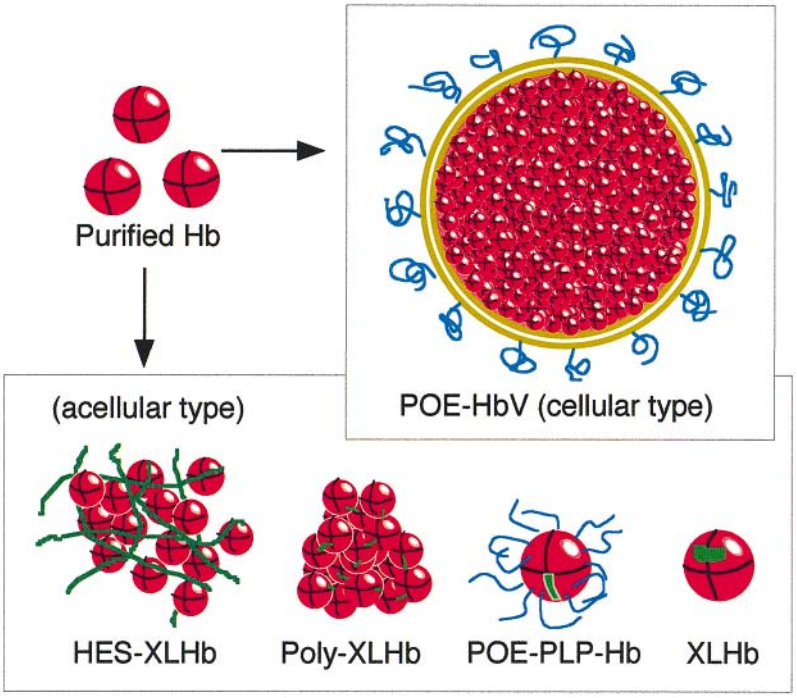

Figure 1. Schematic representation of a series of Hb-based O_2 carriers (cellular vs acellular Hbs). One HbV particle contains $(2 \times 10^4)-(3 \times 10^4)$ Hb molecules.

tact of Hb with the components of blood and vasculature in circulation. The desirability of this barrier function of the cellular structure is evident in considering the side effects found in the use of acellular Hb solutions. Hb encapsulation shields the microcirculation from the biological activity or toxicity of Hb and Hb-related products such as metHb, released heme, and active O_2 species generated during Hb oxidation. Moreover, NO-related vasoconstriction by HbV has not been observed (Nakai et al., 1996; Sakai et al., 1999; Rudolph et al., 1997).

As the results of the clinical trials have been disclosed, there appears to be a general trend in product characteristics and properties whereby solutions based on larger molecules appear to cause a lesser pressor response (Gulati et al., 1999). In this paper, we synthesized a series of acellular modified Hb formulations and cellular HbV and compared them in terms of physicochemical properties such as molecular dimensions, viscosity, colloid osmotic pressure (COP), induction of red blood cell aggregation, and O_2 affinity and considered their physiological impacts.

MATERIALS AND METHODS

Preparation of Chemically Modified Hbs (Figure 1). Hb was purified from outdated donated blood kindly offered from Hokkaido Red Cross Blood Center, Japan, as previously reported in the literature (Sakai et al., 1996).

Intramolecularly cross-linked αα Hb (XLHb) was prepared according to Chatterjee et al. (1986). Deoxygenation of an Hb solution (1 mM, 6.45 g/dL) in the presence of inositolhexaphosphate (5 mM, Sigma) and 100 mM Hepes was performed by N_2 flowing and monitored with a Clark type O_2 electrode (Intermedical Co., Tokyo). The resulting deoxyHb was reacted with (2,3-dibromosalicyl)-fumarate (DBBF, 1.5 mM, Aldrich) at a molar ratio of Hb/DBBF = 1/1.5 and then heated at 75 °C for 1.5 h to denature unreacted Hb and concomitant proteins, and they were removed with ultracentrifugation (19000*g*, 30 min). In XLHb, two 99α Lys are cross-linked at T-state in an anaerobic condition, and sodium dodecyl sulfate−polyacrylamide gel electrophoresis showed the presence of αα dimer (M_w 32 kDa) and β subunits (16 kDa). Dialysis against 10 mM phosphate-buffered saline (PBS, Dulbecco A, Oxoid Ltd., England) using a cellulose tube and filtration through sterilized filters (pore size, 0.2 μm) gave purified XLHb.

Pyridoxalated Hb (PLP-Hb) was prepared by reacting deoxygenated Hb (16 g/dL, 5.3 g) with 2 equiv mol of pyridoxal 5′-phosphate (PLP, Merck) at 4 °C for 1 h, and then the Schiff base of the cross-links was reduced by adding 10 equiv mol of $NaBH_4$ (Kanto Chem. Co.) (Iwashita, 1991). Polyoxyethylene (POE) conjugation of PLP-Hb (POE-PLP-Hb) was performed by reacting PLP-Hb at 4 °C for 12 h with 18 equiv mol of POE (M_w, 5 kDa)-cyanuric chloride (Sigma), which binds amino group of Hb (Jackson et al., 1987). The POE-cyanuric chloride was recrystalized from petroleum ether/benzene prior to use (Abuchowski et al., 1984). The obtained POE-PLP-Hb solution was carbonylated, ultrafiltrated using 200 kDa membrane and then dialyzed to remove unreacted materials, suspended in PBS, and finally filtrated through sterilized filters (pore size, 0.45 μm).

HES-XLHb was prepared using hydroxyethylstarch (HES, M_w, 70 000 kDa, Kyorin Co.) according to Tam et al. (1976) and Baldwin et al. (1981) with some modification. One-fifth of hydroxyl groups of HES chains in a 4%-HES solution (50 mL, 5.4 mol of glucose unit) was activated by the addition 1.5 mL of acetonitrile solution of cyanogen bromide (CNBr, 1.14 mmol, Wako Chem.) with careful regulation of pH at 10.8 with 1 N NaOH. We selected the ratio of [OH group]/[CNBr] = 5/1 by mol, because further addition of CNBr resulted in aggregation of activated HES probably due to the hydrophobic interaction. Conversely, a decrease in the amount of CNBr resulted in a low yield of XLHb conjugation. The activated HES ([OH group]/[CNBr] = 5/1 by mol) was bubbled with nitrogen and mixed with deoxyXLHb (13.1 g/dL, 2.6 g) in an anaerobic condition at 37 °C. Amino

groups on an Hb molecule react with the activated HES to form amide bonds. The unreacted sites in HES chains were inactivated overnight with excess amount of glycine (0.8 g, 11 mmol). The crude Hb product was stabilized by carbonylation and purified twice by salting out using ammonium sulfate (ionic strength, 6 M) to remove unreacted Hb and HES (Green, 1932). The precipitate was redissolved in PBS. The obtained HES-XLHbCO was converted to oxy form (Chung et al., 1995), dialyzed against PBS, and then filtered through sterilized filters (pore size, 0.45 μm).

Polymerization of XLHb in PBS (10 g/dL, 170 mL, 0.26 mmol) was carried out by a stepwise addition of glutaraldehyde (3.4 mmol, 13 equiv mol to Hb) in the presence of 1.5 mmol of lysine in an anaerobic condition for 8 h at 4 °C (Sehgal et al., 1983). The polymerization was monitored by size-exclusion chromatography (Shodex GS-620HQ). The unreacted glutaraldehyde was inactivated by excess amount of lysine (10 equiv mol to glutaraldehyde). After carbonylation, unreacted Hb was removed twice by salting out using ammonium sulfate (ionic strength, 6 M). The precipitate was redissolved in PBS, and the obtained Poly-XLHbCO was converted to oxy form, dialyzed against PBS, and finally filtered through sterilized filters (pore size, 0.45 μm).

Preparation of Polyoxyethylene-Modified Hb-Vesicles (POE-HbV). POE-HbV was prepared as previously reported in the literature (Takeoka et al., 1996; Sakai et al., 1997). The encapsulated Hb (38 g/dL) contained 5.9 mM of pyridoxal 5′-phosphate (PLP) as an allosteric effector at a molar ratio of Hb/PLP = 1. The surface of HbV was modified with POE (M_w, 5 kDa) by mixing an HbV suspension with a saline suspension of 1,2-distearoyl-*sn*-glycero-3-phosphatidylethanolamine-*N*-POE (NOF Co. Tokyo). The resulting POE-HbV was ultracentrifuged to remove unintroduced POE-lipid and redispersed in PBS or 5% human serum albumin (HSA, Bayer Co.). The suspension was then filtered through sterilizable filters (pore size, 0.45 μm).

Physicochemical Characterization of Hb Products. The properties of the five kinds of Hb preparations were characterized in terms of particle size, molecular weight, filter permeability, colloid osmotic pressure (COP), viscosity, RBC-aggregate induction, and O_2-binding properties.

Particle sizes were measured by a light-scattering method (Coulter particle analyzer, model N4SD). The results were confirmed with a size-exclusion chromatography (Shodex GS-620 column) using a phosphate-buffered saline as an eluent (flow rate, 0.5 mL/min). The absorbance at 419 nm corresponding to λ_{max} of Soret band of HbCO was used for detection. The elution profile was calibrated with HbV and size-regulated vesicles containing 5(6)-carboxy fluoresceine (diameter, 210 ± 43 and 105 ± 34 nm) and monomeric XLHb.

Colloid osmotic pressure (COP) was measured with a colloid osmometer (model 4420, Wescor) at room temperature (Vandegriff et al., 1997). Number-average molecular weights (M_n) of Hb samples can be calculated from the COP (π) using the next eq 1

$$\pi = RT(C/M_n + BC^2 + \cdots\cdots\cdots) \quad (1)$$

where C is the solute concentration, R is the gas constant, T is absolute temperature (K), M_n is first virial coefficient, and B is the second virial coefficient. Equation 1 can be rearranged into a linear form as eq 2 by ignoring higher order virial coefficient terms in eq 1

$$\pi/C = RT/M_n + RTBC \quad (2)$$

Therefore, M_n can be determined as

$$M_n = RT/(\pi/C)_{C\to 0} \quad (3)$$

where its value is the intercept obtained from linear least-squares regression of π/C versus C, where C is in units of grams per deciliter.

Absolute weight-average molecular weights (M_w) of acellular Hb samples were determined by a size-exclusion chromatography coupled with a multiangle laser light-scattering detection system. An effluent of a SEC column (Shodex Protein KW-804) at 30 °C was monitored sequentially with a miniDAWN light-scattering detector (Wyatt Technology Co., CA) and a differential refractometer (Shodex RI-71). The flow rate was 0.8 mL/min. The design of the miniDAWN flow cell incorporates a fixed photodiode detector array, capable of measuring scattered light intensity simultaneously at three angles (45, 90, and 135°).

The amount of POE in POE-PLP-Hb and the amount of HES in HES-XLHb were determined by gravinometry after drying up the sample solutions in vacuo at 110 °C overnight. The molecular weight of SFHb was confirmed with the same gravinometric measurement as a reference, and the value was 64.3 kDa which was close to the theoretical value (64.5 kDa). Therefore, the gravinometirc measurement is effective to estimate compositions of modified Hbs.

Viscosity was measured with a capillary viscometer (Oscillatory Capillary Rheometer and Density Meter, OCR-D, Anton Paar) at 37 °C with a shear rate range $1-332\ s^{-1}$ (capillary diameter and length, 0.9948 and 100.2 mm, respectively).

To mimic the blood flow in narrow capillaries and permeabilities across endothelial cell layers, the permeability of Hb samples across membrane filters were observed (Reinhart et al., 1984). Each isopore membrane filter (Nuclepore, Coaster Co.; pore size = 0.4, 0.2, 0.1 μm; diameter = 25 mm) was attached to a high-pressure resistant chamber (Extruder, Lipex Biomembrane, Inc., Canada). Four milliliters of each sample solution ([Hb] = 0.5 g/dL) was poured into the chamber and the initial filtration rate of the outlet volume was measured at a pressure of 1.5 kgf/cm^2 at 37 °C.

Human venous blood (from M.Y.) was drawn into EDTA (1 mg/mL blood)-containing tubes. One hundred microliters of blood was mixed with the same volume of an Hb sample, and the morphology of RBC was observed with an optical microscope (Olympus BH-2) at a magnification of x 150. All of the experiment was performed within 4 h after blood withdrawal.

Oxygen affinity (P_{50}) and Hill number were calculated from an O_2 equilibrium curve obtained with a Hemox Analyzer (TCS Medical Products). A decarbonylated (O_2-bound) Hb solution was diluted with a Hemox solution, and measurement was performed at 37 °C.

RESULTS AND DISCUSSION

Determination of Molecular Size and Molecular Weights and Permeation through Isopore Membrane Filters. The particle size of POE-HbV measured with a light-scattering method (Coulter particle analyzer) was 224 ± 76 nm (Table 1), which was regulated by the extrusion method. The sizes of XLHb and POE-PLP-Hb were 7 ± 2 and 22 ± 2 nm, respectively. Poly-XLHb and HES-XLHb showed 47 ± 17 and 68 ± 24 nm, respectively, with wide distribution. The sizes of the Hb samples

Table 1. Physicochemical Properties of Hb-Based O_2 Carriers and Human Red Blood Cell (RBC)

parameters	XLHb		POE-PLP-Hb	poly-XLHb	HES-XLHb		POE-HbV		blood (RBC)
particle diameter (nm)	7 ± 2		22 ± 2	47 ± 17	68 ± 24		224 ± 76		ca. 8000
M_n (kDa)[a]	72		186 (123)[c]	510	431				
M_w (kDa)[b]	66		189	2154	2782				
P_{50} (Torr)	32		14	20	22		18 (32)[d]		28
Hill number (-)	2.0		1.3	2.2	2.2		2.1		2.7−3.0
OTE (%)[e]	32		17	22	27		20		28
[metHb] (%)	2.2		4.5	8.0	4.5		2.5		<0.5
monomeric Hb (%)[f]	100		4.4	2.7	3.3		not detected		
[Hb] (g/dL)	5	10	5	5	5	10	5	10	12−17
[HES, POE, or lipid] (g/dL)[c]	0	0	4.5	0	3.4	6.8	2.9	5.8	
COP (Torr)	15.8	36.4	70.2	2.5	9.5	32	0(20)[g]	0(20)[g]	ca. 25
viscosity (cP) at 332 s^{-1}	1.0	1.3	6.1	1.5	2.2	7.8	2.6(3)[g]	(4)[g]	3−4

[a] Number-average molecular weight calculated with colloid osmotic pressure (COP). [b] Weight-average molecular weight measured with light scattering analysis. [c] The weights of HES and POE were obtained by gravinometry of dried samples. [d] PLP/Hb = 3 by mol. [e] Oxygen transporting efficiency: difference in oxygen saturation between 40 and 110 Torr pO_2. [f] Monomeric Hb was detected by size-exclusion chromatography (TOSO) TSKgel G3000SW_{XL}) for acelluar Hb. For HbV the monomeric Hb was not detected in the supernatant after ultracentrifugation (50000*g*, 40 min). [g] POE-HbV was suspended in 5% human serum albumin (HSA).

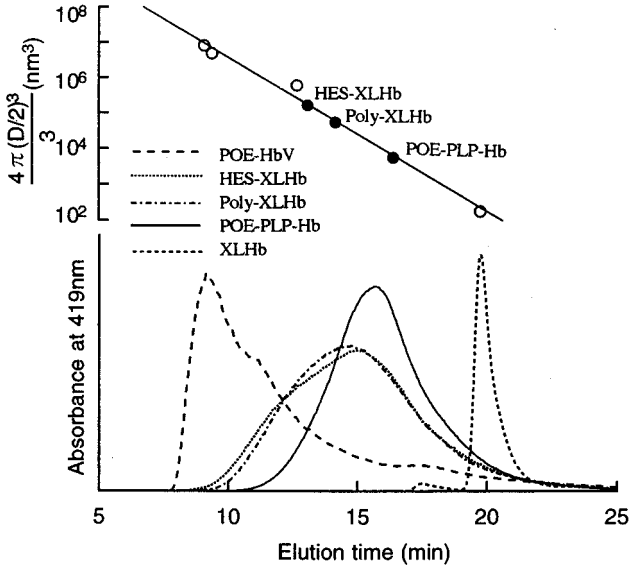

Figure 2. Elution profiles of Hb-based O_2 carriers with a size exclusion chromatography [Shodex GS-620, elution flow rate 0.5 mL/min; eluent, phosphate buffered saline (pH 7.4)] detected with the absorbance at 419 nm. The particle volume was calculated with the mean diameter of the samples obtained with a light scattering method, and the caliburation curve was obtained with white plots (liposomes and XLHb as markers). The positions of black plots which correspond to HES-XLHb, Poly-XLHb and POE-PLP-Hb, correlate with the peaks of these elution profiles. All the peaks are not sharp enough in this method due to the significant size difference and the nature of the separation condition and the column. However, we can tell the dimensional relationship among the five Hb products.

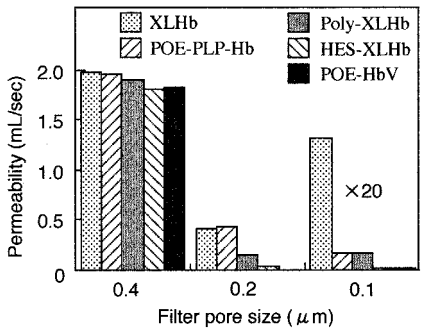

Figure 3. Permeability across isopore membrane filters of Hb-based O_2 carriers ([Hb] = 0.5 g/dL) at a pressure of 1.5 kgf/cm^2 at 37 °C. The permeabilities at 0.1 μm pore size were very small due to the small number of pores in a filter, and the values are 20 times expanded.

were compared by size-exclusion chromatography (Figure 2). HbV was eluted at 8−9 min indicating the largest particle. HES-XLHb, PolyXLHb, then POE-PLP-Hb, and finally XLHb followed. The positions of peaks of HES-XLHb, Poly-XLHb, and POE-PLP-Hb correlate with the volumes calculated with the mean diameters measured with a Coulter particle analyzer.

Number-average molecular weights (M_n) of the obtained Hb samples were determined with colloid osmotic pressure (COP), and weight-average molecular weight (M_w) were obtained by light scattering (Table 1). M_n and M_w of XLHb were 72 and 66 kDa, respectively, which were coincided well with the theoretical molecular weight of XLHb, 64.5 kDa. M_n and M_w of POE-PLP-Hb appeared to be similar values, indicating homogeneous POE modification of Hb. On the other hand, HES-XLHb and Poly-XLHb showed about 5 times larger M_w than M_n, indicating the wider distributions.

Measurement of permeation through isopore membrane filter is conventionally used for the red cell deformability measurement (Reinhart et al., 1984). The capillary and precapillary diameter is usually 5−8 μm, and some narrow during circulatory failure. A biconcave-shaped RBC with a diameter of 8 μm deforms to a parachute-like configuration and penetrates through narrow capillaries. However, RBC cannot penetrate through a pore less than 3 μm. On the other hand, all the Hb-based O_2 carriers, which are much smaller than RBC can penetrate through 0.4 μm pore size (Figure 3). POE-PLP-Hb, which shows higher viscosity than blood, can also penetrate through the filter due to the smaller particle diameter. This result indicates that these Hb materials would be useful for oxygenation of tissues where RBC flow is not sufficient due to thrombosis or infarction. The flow rate of POE-HbV is nearly zero at 0.2 μm pore size, which is the limitation of POE-HbV because the average particle diameter is 224 nm. Poly-XLHb and HES-XLHb showed reduced permeability in comparison with XLHb. The smallest XLHb showed the highest permeability through 0.1 μm pore size.

The size of molecule, however, directly relates to the plasma retention time and permeation across the endothelial cell layer. We measured plasma retention half-time of XLHb, and it was about 1.6 h in Wistar rats at the dose rate of 10% volume of whole blood. The other Hb samples, Poly-XLHb and POE-HbV, showed longer half-lives of 3 and 4 h, respectively. Abbasi et al. (1997) reported that the polymerization of XLHb with a POE-

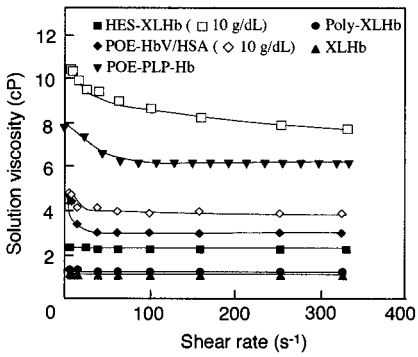

Figure 4. Shear rate dependence of the solution viscosity of Hb-based O_2 carriers ([Hb] = 5 g/dL), measured with a capillary rheometer at 37 °C. POE-HbV was suspended in 5% HSA to regulate colloid osmotic pressure. Viscosities of HES-XLHb and POE-HbV/HSA at [Hb] = 10 g/dL were also measured.

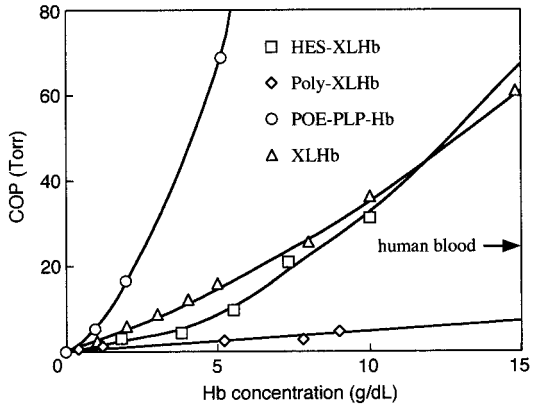

Figure 5. Colloid osmotic pressure (COP) of chemically modified Hbs as a function of Hb concentration. The Hb concentrations of POE-PLP-Hb and HES-XLHb do not include the weights of POE and HES chains, respectively. The COPs at Hb concentration of 5 and 10 g/dL are listed in Table 1. COP of human blood is about 25 Torr.

cross-linker resulted in reduced hypertensive responses in rats. Glutaraldehyde polymerization of XLHb was tested by Nelson et al. (1992) and resulted in longer circulation time and less renal excretion. It was reported that an Hb molecule can diffuse across the fenestrated endothelium into the space of Disse in a perfused liver, and elicited a marked sinusoidal constriction due to the trapping of CO, while the largest HbV cannot enter this space and does not change the vascular tone (Goda et al., 1998). Moreover, Nakai et al. (1998) has indicated that the molecular size of Hb products influences the Hb permeability across the endothelial cell layer and accessibility to the smooth muscle and resulting NO trapping. In this sense, the smallest-sized XLHb is the most permeable across the endothelial cell layer and may show the higher level of vasoconstriction and hypertension than the others. However, polymerized bovine or human Hb, which are currently under clinical trials, are also reported vasoactive to induce hypertension (Rohlfs et al., 1998; Kasper et al., 1998). These physiological results indicate that there should be an optimal particle size of the molecule, thus the largest HbV seems optimal for the present.

Viscosity Measurements. Viscosity of the Hb samples ([Hb] = 5 g/dL) was measured with a capillary rheometer (Figure 4). XLHb showed 1.0 cP without shear rate dependence, indicating that this solution is a Newtonian fluid. Raising the concentration to 10 g/dL increased the viscosity to 1.3 cP at 332 s^{-1}, which is still lower than that of blood. POE modification of Hb increases the viscosity to 6.1 cP, which is significantly higher than that of blood even though the concentration of Hb is one-third of blood (15 g/dL). Poly-XLHb showed viscosity of 1.5 cP with Newtonian characteristics. This value is comparable with the clinically tested Hb polymers (1.3−2.2 cP) (Gould et al., 1992; Kasper et al., 1996). HES-XLHb showed 2.2 cP with Newtonian characteristics at 5 g/dL Hb, though it showed significantly high viscosity (7.8 cP at 332 s^{-1}) when Hb concentration was raised to 10 g/dL with non-Newtonian characteristics indicating the presence of a kind of aggregates. POE-HbV suspended in 5% HSA, on the other hand, showed 3 and 4 cP at Hb concentrations of 5 and 10 g/dL, respectively, the values comparable with that of human blood.

It has been confirmed that increased blood flow in vivo acts as an important signal for the coordination of vasodilation along the arterial tree. The ability of small and large vessels to dilate in response to elevated blood flow has been demonstrated (Pohl et al., 1991). This flow-induced dilation is endothelium-dependent and primarily mediated by NO and, in some cases, by prostacyclin (Frangos et al., 1985). It has been proposed that the viscous drag exerted on the endothelial cells by the flowing blood, wall shear stress, triggers flow- induced dilation. Wall shear stress is expressed as $8 \cdot \eta \cdot V_m/D$, where V_m is the mean red blood cell velocity, η is the viscosity, and D is the vessel diameter. Hemodilution with plasma expanders inevitably reduces blood viscosity, leading to lowered shear stress. To maintain wall shear stress and diameter, viscosity should be increased. Studies from our group and another group tend to confirm the beneficial effect of perfusion with high-molecular-weight-dextran solutions as a viscous plasma expander (Wit et al., 1997; Tsai et al., 1998a). There is an idea that acellular Hb solutions, which have a lower viscosity than blood, may induce vasoconstriction due to a lower shear stress (Tsai et al., 1998b). From the viewpoint of the relationship between the viscosity and blood flow rates, the viscosities of XLHb and polyXLHb are too low in comparison with that of blood, and viscosities of HES-XLHb and POE-HbV/HSA are appropriate.

Colloid Osmotic Pressure. Colloid osmotic pressure (COP) is an important factor to determine a blood volume in a body. XLHb showed the COP of 15.8 Torr at 5 g/dL (Figure 5, Table 1). Polymerization of XLHb resulted in a reduction to 2.5 Torr due to the colligative property. POE-PLP-Hb showed the largest COP of 72.1 Torr, which was about 3 times higher than blood (ca. 25 Torr) due to the highly hydrated POE chains (Vandegriff et al., 1997), even though the Hb concentration, 5 g/dL, was one-third of blood. On the other hand, the POE-HbV showed 0 Torr because of the suspension of large particles: the number of total particles is less than $1/10^4$ of the number of POE-PLP-Hb molecules at the same Hb concentration. HES-XLHb showed higher COP than Poly-XLHb (9.5 vs 2.5 Torr) and larger particle size (68 ± 24 vs 41 ± 17 nm). This is due to the additional effect of highly hydrated HES chains.

COP acts in opposition to hydrostatic pressure to balance the distribution of fluid between blood and interstitial compartments (Vandegriff et al., 1997). COP is a colligative property, depending proportionally on the concentration of protein exerting the force and specifically on the macromolecular properties of that protein. Solutions with high COP cause significant transcapillary filtration of water in the direction from the interstitial space into the vascular lumen. Actually, isovolemic

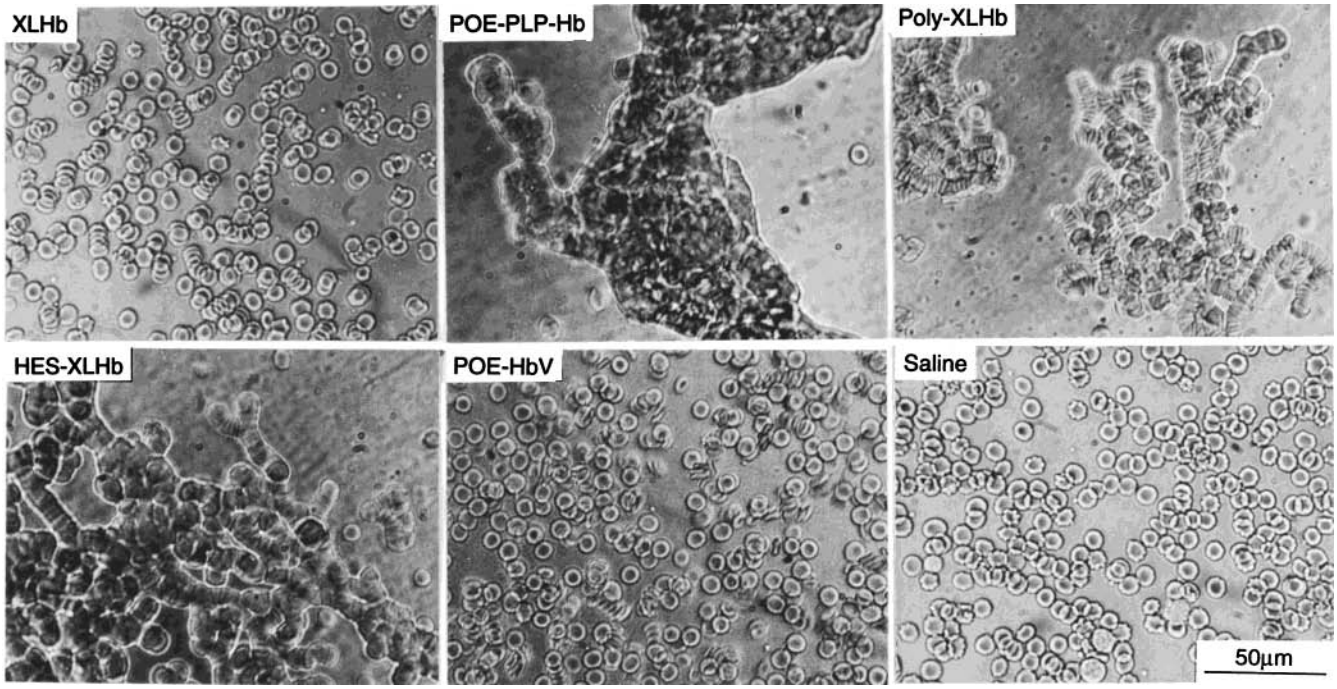

Figure 6. Optical micrographs of mixtures of EDTA-added human blood with each Hb-based O_2 carrier (5 g/dL) at a volume ratio of 1/1. POE-PLP-Hb and HES-XLHb showed a kind of sludge of RBC, and Poly-XLHb showed significant rouleaux. On the other hand, POE-HbV and XLHb does not induce aggregation.

exchange transfusion with POE-modified bovine Hb increases blood volume and mean arterial pressure, and there was not a blood pressure reduction after the succeeding hemorrhage (Migita et al., 1997). On the other hand, Baldwin et al. reported that infusion of POE-Hb enhances extravasation of POE-Hb and plasma proteins and tissue edema and eventually causes intestinal inflammation (Baldwin et al., 1998). An increase in blood volume is advantageous to increase cardiac output for resuscitation, though the composition of other components of blood and tissue will also be compromised by the POE-Hb infusion. Poly-XLHb showed a significantly low COP, and some additional plasma expander, which depends on the molecular weight and Hb concentration, is required to regulate its COP to the blood level for a large amount of infusion. POE-HbV, on the other hand, does not have an oncotic effect, and the particle should be suspended in a plasma expander. The COP of the resulting suspension is identical to that of the suspending medium. When POE-HbV is suspended in 5% human serum albumin (HSA), the suspension shows 20 Torr at any Hb concentration. When suspended in 8% HSA, it shows 39 Torr (Sakai et al., 1999).

RBC Aggregation. EDTA-added human blood was mixed with the same volume of each Hb sample, and the morphology of RBC was observed with an optical microscopy. POE-PLP-Hb and HES-XLHb showed the aggregates of RBC, a kind of sludge, indicating that the interaction between the components is very strong (Figure 6). On the other hand, their precursors, PLP-Hb, XLHb, and activated HES, did not show such strong aggregates. Mixture of blood with Poly-XLHb showed formation of rouleaux, indicating that the interaction of the components is very weak. POE-HbV and XLHb did not show RBC aggregates at all.

There are some proposed mechanisms of RBC aggregation: (1) bridging of RBCs by the added polymers; (2) volume excluded effect by the polymers; (3) negatively charged elements on the surface are removed; and (4) adhesive elements are produced on the surface (Oka, 1983). It is reported that glutaraldehyde-polymerized Hb with molecular mass over 200 kDa (3.4 Hb molecules) accelerates RBC aggregation, which was analyzed by erythrocyte sedimentation rate (Tsai and Wong, 1996), where it was speculated that the minimum distance between RBCs in an aggregate is 19 nm and Hb polymer with diameter larger than 22 nm can theoretically bridge the RBCs. Poly-XLHb and HES-XLHb in our study have much larger diameter, and their induction of RBC aggregation is plausible. All of the polymerized Hbs reported in the literature possess fractions greater than 200 kDa, and they may accelerate RBC aggregation. Since the COP is quite small for the Poly-XLHb, the second proposed mechanism, volume excluded effect is ruled out. On the other hand, POE-PLP-Hb showed quite high COP, and its mechanism should be the excluded volume effect with large amount of associated water molecules.

It has been confirmed that the aggregate formation is reversible in vitro in a viscometric measurement. However, once the aggregate is formed in vivo in venules where blood flow and shear stress are low, it would reduce blood flow rate and shear stress in a vicious circle. It is reported that high-molecular-weight-dextran (1000 kDa)-induced RBC aggregation reduces blood flow rate in a peripheral tissue (Gustafsson et al., 1981). Actually, exchange transfusion with one POE-Hb induced blood flow reduction due to the RBC aggregation and increased peripheral resistance (Alonsozana et al., 1997; Sprung et al., 1995). POE-HbV, on the other hand, does not induce RBC aggregation, indicating that there is no interaction with RBC. POE modification also inhibits intervesicular aggregation by the steric hindrance (Sakai et al., 1997, 1998a). The negatively charged vesicular surface (ζ potential, -21 mV) is repulsive to the RBC surface (ζ potential, -18 mM) (Sakai et al., 1996), and that may also help prevent interaction with RBC.

Oxygen Affinity. Purified stroma-free Hb shows a significantly high O_2 affinity (low P_{50}) of <5 Torr due to the absence of 2,3-diphosphogrycelic acid as an allosteric

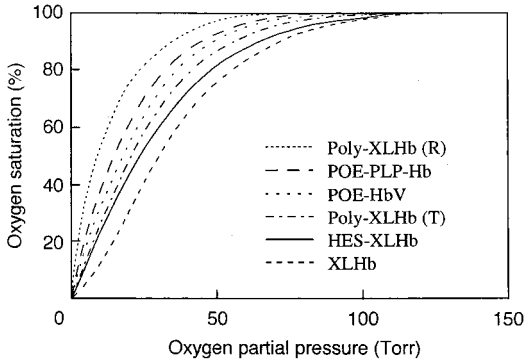

Figure 7. O_2 equilibrium curves of Hb-based O_2 carriers measured with a Hemox Analyzer at 37 °C. Poly-XLHb (R) and (T) were obtained by polymerization with glutaraldehyde at R- and T-state, respectively, and Poly-XLHb (R) showed higher O_2 affinity then Poly-XLHb (T).

effector which is originally present in RBC. The value of P_{50} affects the O_2 transporting efficiency (OTE), which expresses O_2 saturation difference (%) between arterial and venous O_2 partial pressures (40 and 110 Torr, respectively). Human RBC and purified Hb show OTE of 23% and nearly 0%, respectively. Therefore, modification of Hb to increase P_{50} is required for the design of Hb-based O_2 carriers aiming a prompt O_2 unloading in peripheral circulation. The O_2 equilibrium curves of the five Hb products are shown in Figure 7, and P_{50}, Hill number, and OTE are summarized in Table 1. XLHb shows the lowest O_2 affinity (highest P_{50} value, 32 Torr). Pyridoxalation of Hb reduces O_2 affinity to 21 Torr, though POE conjugation increased the affinity to 14 Torr with a reduction of Hill number to 1.3, which is coincided well with the results in the literature (Iwashita, 1991), thus the OTE value is significantly low (17%). The significant reduction of Hill number indicates that the quaternary conformational change from tense (T) to relax (R) state, cooperativity between the 4 subunits, may be distorted by the attachment of POE chains. Glutaraldehyde polymerization of XLHb in an anaerobic condition (T-state) resulted in a reduction of P_{50} from 32 to 22 Torr. On the other hand, polymerization in an aerobic condition (R-state) significantly reduced P_{50} to 8 Torr. Therefore, it is important to polymerize it in a T-state to prevent an increase in O_2 affinity (decrease in P_{50}). HES-conjugation of XLHb, performed in a T-state, could minimize an increase in O_2 affinity of Hb, and the resulting HES-XLHb showed P_{50} of 22 Torr. The P_{50} of HbV can be regulated to 5−150 Torr by coencapsulating the appropriate amount of PLP or inositol hexaphosphate as an allosteric effector (Wang et al., 1992). In this study, equimolar PLP to Hb (PLP/Hb = 1/1 by mol) was coencapsulated, and P_{50} was regulated to 18 Torr. When the molar ratio PLP/Hb was 3/1, P_{50} was regulated to 32 Torr.

O_2 affinity (P_{50}) of blood is a crucial factor in determining O_2 delivery and unloading to tissues. In the case of red blood cells (RBC), shifting the O_2 equilibrium curve to the right (lower O_2 affinity, higher P_{50}) facilitates O_2 unloading to the tissue, reduces cardiac output, and increases vascular resistance in the absence of changes in O_2 consumption or blood pressure. On the other hand, shifting the O_2 equilibrium curve to the left (lower P_{50}) is advantageous only during severe hypoxia. In the case of O_2 carriers, it has been assumed that their O_2 affinity should be the same or lower than that of RBC to increase the OTE value and facilitate O_2 unloading. Stroma-free Hb should be modified at least to have lower O_2 affinity (higher P_{50}). However, the determination of an appropriate P_{50} for Hb-based O_2 carriers is controversial.

O_2 transfer from stroma-free Hb to the vascular wall is faster than that from RBCs as shown by stopped flow in vitro analysis [O_2 dissociation rate constants (k_{off}); Hb, 80 s^{-1}; RBC, 4 s^{-1} (Sakai et al., 1999)], even though O_2 affinity of stroma-free Hb is much higher than RBC. This is due to morphological differences arising from the diffusion of the O_2 molecule from the viscous and concentrated Hb solution in RBC's and the plasma barrier present between RBC's and the vascular wall (Vandegriff et al., 1984), a situation markedly different from the rapid release of O_2 from the homogeneous dispersion of Hb in plasma. Since all of the acellular Hb solutions in our study show lower O_2 affinity, their O_2 release rates are faster than stroma-free Hb. Although the faster release of O_2 could be advantageous (Page et al., 1998), it may possibly lead to the autoregulatory vasoconstriction. Arterial constriction and/or the decreased functional capillary density have been observed in conditions of increased O_2 concentration (Jackson et al., 1983; Pries et al., 1995). HbV has a cell-like structure, and it releases O_2 at a slower rate than XLHb (Kawai et al., 1998), though it releases O_2 still faster than RBC due to their smaller size (224 nm) and consequent greater dispersion homogeneity. One method to retard the O_2 release is to increase O_2 affinity (k_{off}, 27 and 32 s^{-1} at P_{50} = 16 and 30 Torr, respectively), and actually, we confirmed that HbV with P_{50} = 16 Torr showed better microcirculation than HbV with P_{50} = 30 Torr after exchange transfusion (Sakai et al., 1999). Baines et al. (1998) have also shown that an intramolecularly cross-linked Hb with P_{50} = 11 Torr showed better O_2 delivery in perfused kidney than that with P_{50} = 35 Torr.

The O_2 affinities of HbV can be regulated quite easily without changing other physical parameters, whereas in the case of the other modified Hb solutions their chemical structures of themselves determine their O_2 affinities, thus regulation is difficult. The appropriate O_2 affinities for O_2 carriers have not been completely decided yet, however, the easy regulation of O_2 affinity may be useful to meet the requirement of the clinical indications.

Conclusions. The recent trend in the development of Hb-based O_2 carrier is to increase the molecular dimension. Polymerization or polymer conjugation is one method for the enlargement of Hb molecules, and some of the modified Hbs in our study possess physicochemical properties comparable with blood in some parameters. In our recent study of the physiological responses to the infusion of small amount of these Hb samples, the enlargement of molecular size by polymerization or polymer conjugation actually resulted in less vasoconstrictive responses (Sakai et al., 2000). However, RBC aggregation when mixed with equal volume of blood will be a problem because in some cases the presence of aggregation deteriorates microcirculation. Our research indicates difficulties to simultaneously regulate an acellular Hb formulation to possess important physicochemical properties. POE-modified HbV, on the other hand, shows reasonable values of O_2 affinity, viscosity, O_2 release rate, and does not induce RBC aggregation, and no hypertension nor vasoconstriction was reported. Accordingly, cellular HbV seems appropriate as a Hb-based O_2 carrier for the present.

ACKNOWLEDGMENT

The authors thank Prof. K. Kobayashi (Keio University School of Medicine) for the discussion on the plasma retention time measurement, Prof. M. Intaglietta (Uni-

versity of California, San Diego) for the discussion on microcirculatory effects, Mr. K. Tomiyama for the HbV preparation, and Mr. J. Ohno (Shoko Co.) for the help of the averaged molecular weight measurements. H. Sakai is a research fellow of the Japan Health Sciences Foundation. This work has been supported in part by the Health Science Research Grants (Research on Advanced Medical Technology, Artificial Blood Project), the Ministry of Health and Welfare, Japan.

LITERATURE CITED

Abassi, Z., Kotob, S., Pieruzzi, F., Abouassali, M., Keiser, H. R., Fratantoni, J. C., and Alayash, A. I. (1997) Effect of Polymerization on the hypertensive action of diaspirin cross-linked hemoglobin in rats. *J. Lab. Clin. Med. 129*, 603−610.

Abuchouski, A., Kazo, G. M., Verhoest, C. R., Jr., Es, T. V., Kafkewitz, D., Nucci, M. L., Viau, A. T., and Davis, F. K. (1984) Antitumor properties of poly(ethylene glycol) asparaginase conjugates. *Cancer Biochem. Biophys. 7*, 175−186.

Alonsozana, G. L. G., Elfath, M. D., Mackenzie, C., Gregory, L. C., Duh, S. H., Trump, B., and Christenson, R. H. (1997) In vitro interference of the red cell substitute pyridoxalated hemoglobin-polyoxytethylene with blood compatibility, coagulation, and clinical chemistry testing. *J. Cardiothoracic Vasc. Anesth. 11*, 845−850.

Baines, A. D., Adamson, G., Wojciechowski, P., Pliura, D., Ho, P., and Kluger, R. (1998) Effect of modifying O_2 diffusivity and delivery on glomerular and tubular function in hypoxic perfused kidney. *Am. J. Physiol. 274 (Renal Physiol. 43)*, F744−F752.

Baldwin, A. L., Wilson, L. M., and Valeski, J. E. (1998) Ultrastructural effects of intravascularly injected poly-(ethylene glycol)-hemoglobin in intestinal mucosa. *Am. J. Physiol. 275 (Heart Circ. Physiol. 44)*, H615−H625.

Baldwin, J. E., Gill, B., Whitten, J. P., and Taegtmeyer, H. (1981) Synthesis of polymer-bound hemoglobin samples. *Tetrahedron 37*, 1723−1726.

Caron, A., Menu, P., Labrude, P., and Vigneron, C. (1998) Proposition of a technique to assess the vasoactive effects of hemoglobin-based O_2 carrying solutions in vivo: preliminary results in the rabbit aorta. *Artif. Cells, Blood Substitutes, Immobilization Biotechnol. 26*, 293−308.

Frangos, J. A., Eskin, S. G., McIntire, L. V., and Ives, C. L. (1985) Flow effects on prostacyclin production in cultures human endothelial cells. *Science 227*, 1477−1479.

Chatterjee, R., Welty, E. V., Walder, R. Y., Pruitt, S. L., Rogers, S. L., Arnone, A., and Walder, J. A. (1986) Isolation and characterization of a new hemoglobin derivative cross-linked between the a chains (lysine 99α_1 → lysine 99α_2). *J. Biol. Chem. 261*, 9929−9937.

Chung, J. E., Hamada, K., Sakai, H., Takeoka, S., and Tsuchida, E. (1995) Ligand exchange reaction of carbonylhemoglobin to oxyhemoglobin in a hemoglobin liquid membrane. *Nihonkagakukaishi 2*, 123−127.

Djordjevich, L., Mayoral, J., Miller, I. F., and Ivankovich, A. D. (1987) Cardiorespiratory effects of exchange transfusions with synthetic erythrocytes in rats. *Crit. Care Med. 15*, 318−323.

Djordjevich, L., and Miller, I. F. (1977) Lipid encapsulated hemoglobin as a synthetic erythrocyte. *FASEB Proc. 36*, 567.

Doherty, D. H., Doyle, M. P., Curry, S. R., Vali, R. J., Fattor, T. J., Olsen, J. S., and Lemon, D. D. (1998) Rate of reaction with nitric oxide determines the hypertensive effect of cell-free hemoglobin. *Nat. Biotechnol. 1*, 672−676.

Goda, N., Suzuki, K., Naito, M., Takeoka, S., Tsuchida, E., Ishimura, Y., Tamatani, T., and Suematsu, M. (1998) Distribution of heme oxygenase isoforms in rat liver: topographic basis for carbon monoxide-mediated microvascular relaxation. *J. Clin. Invest. 101*, 604−612.

Gould, S. A., Sehgal, L. R., Sehgal, H. L., and Moss, G. S. (1992) Artificial blood: current status of hemoglobin solutions. *Crit. Care Clin. 8*, 293−309.

Gould, S. A., Moore, E. E., Hoyt, D. B., Burch, J. M., Haenel, J. B., Garcia, J., DeWoskin, R., and Moss, G. S. (1998) The first randomized trial of human polymerized hemoglobin as a blood substitute in acute trauma and emergency surgery. *J. Am. Coll. Surg. 187*, 113−122.

Green, A. A. (1932) Studies in the physical chemistry of the proteins. X. The solubility of hemoglobinin solutions of chlorides and sulfates of varying concentration. *J. Biol. Chem. 95*, 47−66.

Gulati, A., Barve, A., and Sen, A. P. (1999) Pharmacology of hemoglobin therapeutics. *J. Lab. Clin. Med. 133*, 112−119.

Gustafsson, L., Appelgren, L., and Myrvold, H. E. (1981) Blood flow and in vivo apparent viscosity in working and nonworking skeletal muscle of the dog after high and low molecular weight dextran. *Circ. Res. 48*, 465−9.

Iwashita, Y. (1991) Pyridoxalated hemoglobin-polyoxyethylene conjugate (PHP) as an O_2 carrier. *Artif. Organs Today 1*, 89−114.

Jackson, C. J., Charlton, J. L., Kuxminski, K., Lang, G. M., and Sehon, A. H. (1987) Synthesis, isolation, and characterization of conjugates of ovalbumin with monomethoxypolyoxyethylene glycol using cyanuric chloride as the coupling agent. *Anal. Biochem. 165*, 114−127.

Jackson, W. F., and Duling, B. R. (1983) The oxygen sensitivity of hamster cheek pouch arterioles. *Circ. Res. 53*, 515−525.

Kasper, S. M., Walter, M., Grune F., Bischoff, A., Erasmi, H., and Buzello, W. (1996) Effect of a hemoglobin-based oxygen carrier (HBOC-201) on hemodynamics and oxygen transport in patients undergoing preoperative hemodilution for elective abdominal aortic surgery. *Cardiovasc. Anesth. 83*, 921−927.

Kawai, N., Ohkawa, H., Maejima, H., Takeoka, S., Nishide, H., and Tsuchida, E. (1998) Oxygen releasing from cellular hemoglobin. *Artif. Cells Blood Substitutes Immobilization Biotechnol. 26*, 507−517.

Migita, R., Gonzales, A., Gonzales, M. L., Vandegriff, K. D., and Winslow, R. M. (1997) Blood volume and cardiac index in rats after exchange transfusion with hemoglobin-based oxygen carriers. *J. Appl. Physiol. 82*, 1995−2002.

Moncada, S., Palmer, R. M. J., and Higgs, E. A. (1991) Nitric oxide: physiology, pathophysiology, and pharmacology. *Pharmacol. Rev. 43*, 109−131.

Murray, J. A., Ledlow, A., Launspach, J., Evans, D., Loveday, M., and Conklin, J. L. (1995) The effects of recombinant human hemoglobin on esophageal motor function in humans. *Gastroenterology 109*, 1241−1248.

Nakai, K, Ohta, T., Sakuma, I., Akama, K., Kobayashi, Y., Tokuyama, S., Kitabatake, A., Nakazato, Y., Takahashi, T. A., and Sekiguchi, S. (1996) Inhibition of endothelium-dependent relaxation by hemoglobin in rabbit aortic strips: comparison between acellular hemoglobin derivatives and cellular hemoglobins. *J. Cardiovasc. Pharmacol. 28*, 115−23.

Nakai, K., Sakuma, I., Ohta, T., Ando, J., Kitabatake, A., Nakazato, Y., and Takahashi, T. A. (1998) Permeability characteristics of hemoglobin derivatives across cultured endothelial cell monolayers. *J. Lab. Clin. Med. 132*, 313−319.

Nelson, D., Hai, T., Srnak, A., Ebeling, A., Kunas, G., Catarello, J., and Burhop, K. (1992) Synthesis and properties of polymerized diaspirin cross-linked hemoglobins. *Biomater. Artif. Cells Immobilization Biotechnol. 20*, 253−258.

Oka, S. (1984) *Biorheology*, Shokabo Publisher, Tokyo.

Page, T. C., Light, W. R., Mckay, C. B., and Hellums, J. D. (1998) Oxygen transport by erythrocyte/hemoglobin solution mixtures in an in vitro capillary as a model of hemoglobin-based oxygen carrier performance. *Microvasc. Res. 55*, 54−64.

Pohl, U., Herlan, K., Huang, A., and Bassenge, E. (1991) EDRF-mediated, shear-induced dilation opposes myogenic vasoconstriction in small rabbit arteries. *Am. J. Physiol. 261 (Heart Circ. Physiol. 29)*, H2016−H2023.

Pries, A. A., Heide, J., Ley, K., Klotz, K.-F., and Gaehtgens, P. (1995) Effect of oxygen tension on regulation of arteriolar diameter in skeletal muscle in situ. *Micovasc. Res. 49*, 289−299.

Przybelski, R. J., Daily, E. K., and Birnbaum, M. L. (1997) The pressor effect of hemoglobin − good or bad? In *Advances in Blood Substitutes: Industrial Opportunities and Medical Challenges* (R. M. Winslow, K. D. Vandegriff, and M. Intaglietta, Eds.) Birkhauser, Boston.

Reinhart, W. H., Usami, S., Schmalzer, E. A., Lee, M. M., and Chien, S. (1984) Evaluation of red blood cell filterability

test: influences of pore size, hematocrit level, and flow rate. *J. Lab. Clin. Med. 104*, 501−516.

Rohlfs, R. J., Bruner, E., Chiu, A., Gonzales, A., Gonzales, M. L., Magde, D., Magde, M. D., Jr., Vandegriff, K. D., and Winslow, R. M. (1998) Arterial blood pressure responses to cell-free hemoglobin solutions and the reaction with nitric oxide. *J. Biol. Chem. 273*, 12128−12134.

Rudolph, A. S., Sulpizio, A., Hieble, P., MacDonald, V., Chavez, M., and Feuerstein, G. (1997) Liposome encapsulation attenuates hemoglobin-induced vasoconstriction in rabbit arterial segments. *J. Appl. Physiol. 82*, 1826−35.

Rudolph, A. S., Rabinovici, R., and Feuerstein, G. Z., Eds. (1998) *Red blood cell substitutes: basic principles and clinical applications*, Marcel Dekker, New York.

Sakai, H., Hara, H., Tsai, A. G., Takeoka, S., Tsuchida, E., and Intaglietta, M. (2000) Molecular Dimensions of Hb-based O_2 Carriers Determine Constriction of Resistance Arteries and Hypertension. *Am. J. Physiol. (Heart Circ. Physiol.)* (submitted for publication).

Sakai, H., Tsai, A. G., Rohlfs, R. J., Hara, H., Tsuchida, E., and Intaglietta, M. (1999) Microvascular responses to hemodilution with Hb vesicles as red blood cell substitutes: influence of O_2 affinity. *Am. J. Physiol. 276 (Heart Circ. Physiol. 45)*, H553−H562.

Sakai, H., Tsai, A. G., Kerger, H., Park, S.-I., Takeoka, S., Nishide, H., Tsuchida, E., and Intaglietta, M. (1998a) Subcutaneous microvascular responses to hemodilution with red cell substitutes consisting of poly(ethylene glycol)-modified vesicles encapsulating hemoglobin. *J. Biomed. Mater. Res. 40*, 66−78.

Sakai, H., Tsai, A. G., Tsuchida, E., and Intaglietta, M. (1998b) Microvascular responses to hemodilution with Hb-vesicles: Importance of resistance arteries and mechanisms of vasoconstriction, In *Present and future perspectives of blood substitutes* (Tsuchida, E., Ed.), pp 185−199, Elsevier Science, Amsterdam.

Sakai, H., Takeoka, S., Park, S.-I., Kose, T., Izumi, Y., Yoshizu, A., Nishide, H., Kobayashi, K., and Tsuchida, E. (1997) Surface-modification of hemoglobin vesicles with poly(ethylene glycol) and effects on aggregation, viscosity, and blood flow during 90%-exchange transfusion in anesthetized rats. *Bioconjugate Chem. 8*, 15−22.

Sakai, H., Hamada, K., Takeoka, S., Nishide, H., and Tsuchida, E. (1996) Physical Properties of Hemoglobin Vesicles as Red Cell Substitutes. *Biotechnol. Prog. 12*, 119−125.

Saxena, R., Wijnhoud, A. D., Carton, H., Hacke, W., Kaste, M., Przybelski, R. J., Stern, K. N., and Koudstaal, P. J. (1999) Controlled safety study of a hemoglobin-based oxygen carrier, DCLHb, in acute ischemic stroke. *Stroke 30*, 993−996.

Sehgal, L. R., Rosen, A. L., Gould, S. A., Sehgal, H. L., and Moss, G. S. (1983) Preparation and in vitro characteristics of polymerized pyridoxylated hemoglobin. *Transfusion 23*, 158−162.

Sprung, J., Mackenzie, C. F., Barnas, G. M., Williams, J. E., Parr, M., Christenson, R. H., Hoff, B. H., Sakamoto, R., Kramer, A., and Lottes, M. (1995) Oxygen transport and cardiovascular effects of resuscitation from severe hemorrhagic shock using hemoglobin solutions. *Crit. Care Med. 23*, 1540−1553.

Takeoka, S., Ohgushi, T., Terase, K., Ohmori, T., and Tsuchida, E. (1996) Layer-controlled hemoglobin vesicles by interaction of hemoglobin with a phospholipid assembly. *Langmuir 12*, 1755−1759.

Takeoka, S., Sakai, H., Kose, T., Mano, Y., Seino, Y., Nishide, H., and Tsuchida, E. (1997) Methenoglobin formation in hemoglobin vesicles and reduction by encapsulated thiols. *Bioconjugate Chem. 8*, 539−544.

Tam, S. C., Blumenstein, J., and Wong, J. T. F. (1976) Soluble dextran-hemoglobin complex as a potential blood substitute. *Proc. Natl. Acad. Sci. U.S.A. 73*, 2128−2131.

Tsai, A. G., Friesenecker, B., McCarthy, M., Sakai, H., and Intaglietta, M. (1998a) Plasma viscosity regulates capillary perfusion during extreme hemodilution in hamster skinfold model. *Am. J. Physiol. 275 (Heart Circ. Physiol. 44)*, H2170−H2180.

Tsai, A. G., Friesenecker, B., Sakai, H., Kerger, H., and M. Intaglietta. (1998b) Biophysical criteria for microcirculatory efficacy of blood substitutes. In *Present and future perspectives of blood substitutes* (E. Tsuchida, Ed.) pp 125−133, Elsevier Science, Amsterdam.

Tsai, A. G., Friensenecker, B., Kerger, H., and Intaglietta, M. (1995) Microcirculatory consequences of blood substitution with αα-hemoglobin. In *Blood Substitutes Physiological Basis of Efficacy* (R. M. Winslow, K. D. Vandegriff, and M. Intaglietta, Eds.), pp 155−174, Birkhauser, Boston.

Tsai, S. P., and Wong, T. F. (1996) Enhancement of erythrocyte sedimentation rate by polymerized hemoglobin. *Artif. Cells Blood Substitutes Immobilization Biotechnol. 24*, 513−523.

Tsuchida, E., Ed. (1998) *Blood substitutes: present and future perspectives*. Elsevier Science, Amsterdam.

Vandegriff, K. D., and Olson, J. S. (1984) Morphological and physiological factors affecting oxygen uptake and release by red blood cell. *J. Biol. Chem. 259*, 12619−12627.

Vandegriff, K. D., McCarthy, M., Rohlfs, R. J., and Winslow, R. M. (1997) Colloid osmotic properteis of modified hemoglobins: chemically cross-linked versus poly(ethylene glycol) surface conjugated. *Biophys. Chem. 69*, 23−30.

Wang, L., Morizawa, K., Tokuyama, S., Satoh, T., and Tsuchida, E. (1992) Modulation of oxygen-carrying capacity of artificial red cells (ARC). *Polym. Adv. Technol. 4*, 8−11.

Wit, C., Schfer, C., Bismarck, P., Bolz, S. S., and Pohl, U. (1997) Elevation of plasma viscosity induces sustained NO-mediated dilation in the hamster cemaster microcirculation in vivo. *Pflugers Arch. Eur. J. Physiol. 434*, 354−361.

BC9900789

Bioluminescence and Secondary Structure Properties of Aequorin Mutants Produced for Site-Specific Conjugation and Immobilization

J. C. Lewis, J. J. López-Moya, and S. Daunert*

Department of Chemistry, University of Kentucky, Lexington, Kentucky 40506-0055

Aequorin is one of several photoproteins that emits visible light upon binding to calcium ions. It has been widely used as a Ca^{2+}-indicator and as an alternative highly sensitive bioluminescent label in binding assays. The apoprotein of aequorin binds an imidazopyrazine compound (coelenterazine) and molecular oxygen to form a stable photoprotein complex. Upon addition of calcium, the photoprotein undergoes a conformational change leading to the oxidation of the chromophore with the release of CO_2 and blue light. To gain more information of structure−function relationships within the photoprotein that will aid in the design of mutants suitable for site-specific conjugation and immobilization, polymerase chain reaction (PCR)-based site-directed mutagenesis was employed to produce five different aequorin mutants. The five mutants included a cysteine-free mutant and four other mutants with single cysteine residues at selected positions within the protein. The aequorin mutants exhibited different bioluminescence emission characteristics with two mutants showing a decrease in relative light production in comparison to the cysteine-free mutant. Additionally, circular dichroism (CD) spectra revealed that the single amino acid substitutions made for two of the aequorin mutants did alter their secondary structures.

INTRODUCTION

Certain jellyfish within the class Hydrozoa produce proteins termed "photoproteins" that emit light in the visible region. One such photoprotein, aequorin, has become a widely used bioluminescent label in a variety of bioanalytical applications. Aequorin was first isolated from the jellyfish *Aequorea victoria* found in the Pacific Northwest. The photoprotein consists of an apoprotein, a chromophoric unit (coelenterazine), and molecular oxygen, which when combined form a stable complex. Binding to Ca^{2+} ions causes the photoprotein to undergo a conformational change, which results in the catalytic oxidation of the noncovalently bound coelenterazine. The coelenterazine is converted to coelenteramide with the release of CO_2 and a flash of light ($\lambda_{max} \cong 469-470$ nm) lasting less than 10 s (*1*).

The cDNA sequence for the apoprotein of aequorin (apoaequorin) has been determined (*2*, *3*), and the recombinant protein is readily produced in the laboratory. Amino acid sequencing of apoaequorin revealed a single polypeptide chain consisting of 189 amino acids (21.4 kDa) containing three EF-hand structures (Ca^{2+}-binding sites consisting of a helix-loop-helix structural motif). These sites contained within the apoaequorin structure were shown to be homologous with the EF-hand structures of other Ca^{2+}-binding proteins such as calmodulin and paralbumin, suggesting a common evolutionary origin (*4*). However, the apoprotein component of aequorin contains an unusually high content of histidine, tryptophan, cysteine, and proline residues in comparison to other Ca^{2+}-binding proteins. It also has an extended carboxy-terminal region, and studies have demonstrated that deletion of the C-terminal proline causes an almost complete loss of luminescence activity. Other site-directed mutagenesis studies have shown that His16, His58, His169, Trp108, and Trp173 are critical to the activity of the photoprotein as well (*1*). Since 2-mercaptoethanol is required for full regeneration of aequorin, site-directed mutagenesis was also performed on the three cysteine residues present within the protein at positions 145, 152, and 180. Interestingly, a mutant in which all three cysteines were replaced with serine (mutant S) had greater bioluminescence activity in comparison to the wild-type aequorin (*5*).

We have employed aequorin as a highly sensitive label in binding assays for small biomolecules (*6*, *7*). Our studies and those from others have demonstrated that fusion to the N-terminus of the protein with a small peptide (*7*) or a large protein (*8*) is possible without a significant decrease in the bioluminescent activity, unlike fusion to the C-terminus (*9*). We selected gene fusion as one method by which site-specific attachment of our desired analyte to the photoprotein could be achieved in the development of a binding assay for a small biomolecule. To further extend the application of aequorin in bioanalytical methods, we have explored the feasibility of producing a mutant of aequorin (i.e., one containing a single cysteine residue) suited for site-specific conjugation of nonpeptidic molecules and site-specific immobilization of the protein onto a surface. Even though crystallization of the protein has been achieved (*10*), the three-dimensional structure of aequorin has yet to be determined. Thus, to achieve our goal and gain more structure−activity information about the photoprotein, we have produced five mutant aequorins, four of which each contain a unique cysteine residue at selected positions within the apoprotein. PCR-based site-directed mutagenesis was employed to initially replace all three cysteine residues with serine and then introduce a single cysteine residue at positions 5, 53, 71, and 84 in the polypeptide chain. All five mutant aequorins were characterized in terms of their bioluminescence emission properties and secondary structure.

* To whom correspondence should be addressed. Phone: (606) 257-7060. Fax: (606) 323-1069. E-mail: daunert@pop.uky.edu.

10.1021/bc9900800 CCC: $19.00 © 2000 American Chemical Society
Published on Web 12/15/1999

Table 1. Synthetic Oligonucleotides Used for Site-Specific Mutagenesis

name	oligonucleotide[a]	amino acid substitution
C1,2S	GAA GAT **TCC** GAG GAA ACA TTC AGA GTG **TCC** GAT ATT GAT GAA AGT	Cys145,152 → Ser
C3S	ATG GAC CCT GCT **TCC** GAA AAG CTC TAC GGT GGA GC	Cys180 → Ser
AQ5	AAG CTT ACA **TGC** GAC TTC GAC TTC GAC AAC CCA AG	Ser5 → Cys
AQ53	GGA GCA ACA CCT **TGC** CAA GCC AAA CGA CAC AAA GAT	Glu53 → Cys
AQ71	GGA GCT GGA **TGC** AAA TAT GGT GTG GAA ACT GAT TGG	Met71 → Cys
AQ84	GCA TAT ATT **TGC** GGA TGG AAA AAA TTG GCT ACT GAT	Glu84 → Cys

[a] Lettering highlighted in bold and underlined indicates nucleotide substitutions.

EXPERIMENTAL PROCEDURES

Reagents. All restriction endonucleases, T4 DNA ligase, Luria Bertani (LB) broth, LB agar, DNA mass ladder, ampicillin, and kanamycin were purchased from Gibco-BRL (Gaithersburg, MD). Tris(hydroxymethyl) amino methane (Tris), ethylenediaminetetraacetic acid (EDTA) disodium salt, sodium chloride, dithiothreitol (DTT), and all other reagents were obtained from Sigma (St. Louis, MO). HQH, quaternized polyethyleneimine anion exchanger, was purchased from Perseptive Biosystems (Cambridge, MA). Coelenterazine was obtained from Biosynth International (Naperville, IL). All oligonucleotides (primers) employed for PCR were provided by Operon Technologies (Alameda, CA). The polymerase selected for PCR was *Pfu* polymerase from Stratagene (La Jolla, CA). All solutions were prepared using deionized (Milli-Q Water Purification system, Millipore, Bedford, MA) distilled water. All chemicals were reagent grade or better and were used as received.

Bacterial Strains and Plasmids. The expression vector pSbt and bacterial strain *Bacillus subtilis* (trpC2, MetB10, npr, apr::cat) was provided by Dr. Philip N. Bryan, University of Maryland. The mammalian expression vector, pMtAEQ, containing the apoaequorin gene was purchased from Molecular Probes (Eugene, OR). The *Escherichia coli* strain, JM109, employed for initial cloning reactions, was from Gibco-BRL (Gaithersburg, MD).

PCR-Based Site-Specific Mutagenesis. The technique of overlap extension PCR was employed to produce the aequorin mutants. Initially, primers C1, 2S, and C3S (see Table 1) were used in order to obtain the apoaequorin gene in which all three cysteine residues were replaced by serine (referred to as mutant S). PCR reactions to amplify DNA fragments used in overlap extension PCR reactions were carried out with 2.5 units of *Pfu* polymerase, 50 ng of DNA template, 250 μM of each dNTP, and 50 pmol of each primer in a total volume of 100 μL. The overlap extension PCR reactions to amplify the entire mutated apoaequorin gene were performed using 30 ng of each previously amplified fragment, 50 pmol of each outside primer, 250 μM of each dNTP, and 5 units of *Pfu* polymerase in a total volume of 100 μL. The cycling parameters for the overlap extension PCR reactions were 94 °C for 1 min, 45 °C for 1 min, and 72 °C for 1 min 30 s for the first 10 cycles, followed by 20 cycles with an annealing temperature of 50 °C. An additional overlap extension PCR reaction was performed to attach the sequence for the "pre"-signal peptide of the protein subtilisin, an alkaline serine protease of *Bacillus subtilis*. This signal peptide facilitates the secretion of a desired protein outside of the bacterial cell and into the culture medium, simplifying the purification process for the protein. All PCR reactions were performed using a Perkin-Elmer GeneAmp PCR System 2400 (Norwalk, CT). The final DNA product containing the cysteine-free mutant apoaequorin (mutant 3) was cloned into the pSbt expression vector as a *Eco*RI−*Sal*I fragment, to yield the pSD110 vector shown in Figure 1. Bacteria (*E. coli* strain JM109) were then transformed with the pSD110 vector. Clones carrying the mutant plasmid were identified through restriction analysis using the restriction enzymes *Eco*RI/*Sal*I and a unique restriction enzyme site introduced as a silent mutation in the apoaequorin gene during the first set of PCR reactions. The apoaequorin mutants containing unique cysteine residues at positions 5, 53, 71, and 84 in the polypeptide chain were prepared in the same manner (see Table 1) as described above using the gene encoding for apoaequorin mutant 3 as a template in the PCR reactions. The site-specific mutations were confirmed through DNA sequencing performed at the Macromolecular Center (University of Kentucky). All molecular biology procedures were conducted using standard protocols (*11*).

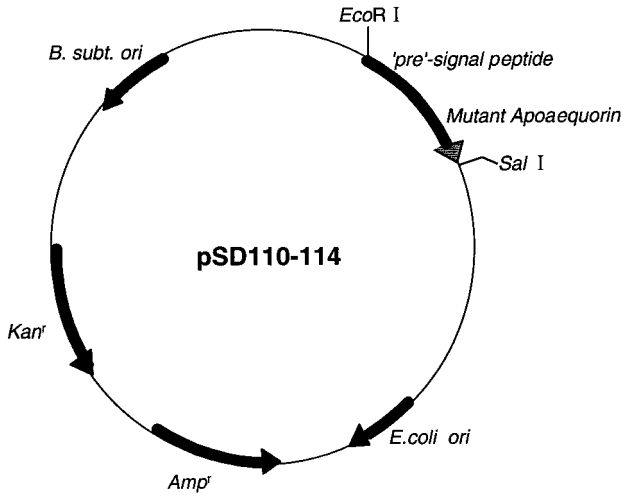

Figure 1. Schematic representation of the plasmids pSD110−114 containing the oligonucleotide sequences of the "pre"-signal peptide and the mutated apoaequorin genes, fused in frame.

Expression and Purification of Mutant Apoaequorins. Plasmids containing the mutant apoaequorin genes were transformed into competent *B. subtilis* cells, and cultured to express the mutant proteins. Specifically, bacteria were grown in 100 mL of LB broth supplemented with 30 μg/mL of kanamycin for 16 h at 37 °C with shaking (250 rpm). The culture was centrifuged at 5930*g* at 10 °C for 40 min to pellet the cells. The culture medium containing the secreted protein was removed and filtered with a 0.2 μM cellulose acetate syringe filter to ensure the complete removal of any remaining cells. The pH of the medium ranged 7.5−7.8 and was decreased to 4.2 with concentrated acetic acid to precipitate the protein. The mixture was incubated at 4 °C for 2 h before centrifugation at 12100*g* at 4 °C for 40 min. The precipitate was dissolved in 40 mM Tris-HCl, pH 8.0, buffer containing 5 mM EDTA and 5 mM DTT. The mixture was incubated at 37 °C for 15 min before it was purified by perfusion chromatography using an HQH anion-exchange column (4.6 mm × 100 mm). The column was preequilibrated with a 40 mM Tris-HCl, pH 7.0,

buffer containing 5 mM EDTA and 5 mM DTT. DTT was not added during the purification process for mutant S. A salt gradient from 0.0 to 4.0 M NaCl was employed to elute the protein. All the apoaequorin mutant proteins eluted between 0.15 and 0.20 M NaCl. The fractions containing the mutant protein were combined and concentrated using a Centriplus 3000 device from Millipore (Bedford, MA). The desired buffer exchange was achieved employing a polyacrylamide 6000 desalting column from Pierce (Rockford, IL). The purity of the mutant proteins was verified by sodium dodecyl sulfate−polyacrylamide gel electrophoresis (SDS−PAGE) using an electrophoresis PhastSystem from Pharmacia Biotech (Uppsala, Sweden). Polyacrylamide (12.5%) gels were developed by the method of silver staining. The protein concentrations were determined by measuring absorbance at 280 nm using the formula $E_{1\%,1cm} = 18.0$.

Conversion of Apoaequorin Mutants to Photoproteins. Generation of the aequorin mutants from the apoproteins was achieved by mixing a set amount of the purified proteins in a glass test tube with a molar excess of coelenterazine (0.2 μg) in Tris-HCl, pH 7.6, buffer containing 2 mM EDTA with or without 5 mM DTT as indicated. The mixture was briefly vortexed and then placed on ice for the required time.

Assay for Mutant Aequorin Activity. The luminescence activity of the mutant aequorins was measured by placing 10 μL of the regeneration mixture described above in a glass test tube, which was then placed in a Optocomp I luminometer from GEM Biomedical (Carrborro, NC). A volume of 100 μL of a 100 mM $CaCl_2$ and 100 mM Tris-HCl, pH 7.6, buffer (luminescence triggering buffer) was injected into the sample solution in order to trigger light emission. The luminescence signal was collected at 0.1 s intervals over a 5 s time period.

CD Spectra of Apoaequorin Mutants. CD spectra were obtained using a Jasco model J-710 (Tokyo) spectropolarimeter with a 0.1 cm path-length cell. The mutant protein concentrations were 0.1−0.2 mg/mL in 10 mM Tris-HCl, pH 7.6, buffer containing 2 mM EDTA. Protein samples were stored on ice, and then placed in a RT bath for 60 min before taking the CD spectra. The CD spectra shown are an average of 16 scans per sample.

Bioluminescence Emission Spectra of Apoaequorin Mutants. Emission spectra were obtained using a Fluorolog-τ2 spectrofluorometer from Spex Industries (Edison, NJ) without turning on the lamp or chopper. Luminescence was triggered by careful addition of 1.5 mL of a 2.5×10^{-6} M solution of mutant aequorin using a constant-rate syringe pump into 0.5 mL of luminescence triggering buffer. The spectra were not corrected for changes in the sensitivity of the photomultiplier tube to the luminescence at different wavelengths.

RESULTS

To produce the aequorin mutants containing unique cysteine residues, PCR-based site-directed mutagenesis was employed to construct expression vectors pSD110-114 (Figure 1) using the oligonucleotides shown in Table 1. Restriction analysis was performed to verify the presence of the mutated apoaequorin genes in the expression vectors followed by DNA sequencing to confirm the desired mutations. Following expression of the apoaequorin mutants in *B. subtilis*, the mutant proteins were successfully secreted into the culture medium by the "pre"-signal peptide of subtilisin. The proteins were purified using perfusion chromatography with a HQH anion-exchange column. All five mutant apoaequorins were eluted from the column at salt concentrations between 0.15 and 0.20 M. The purity of the eluted fractions was determined by SDS−PAGE using the method of silver staining, which indicated a purity of greater than 95% (*11*). The yields for the protein purification ranged 22−43 mg of protein/L of culture.

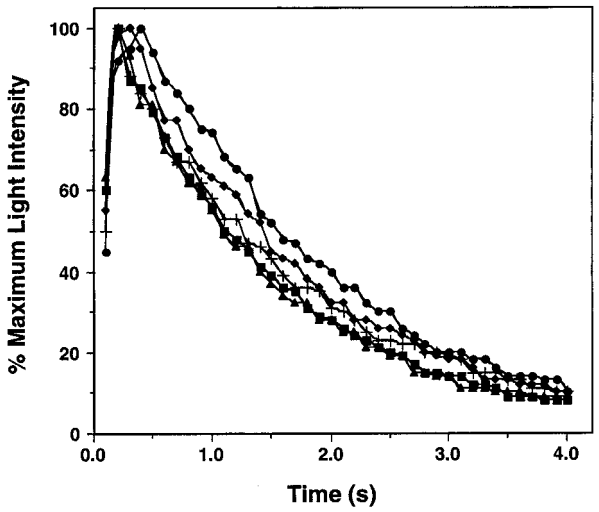

Figure 2. Flash-type bioluminescence emission obtained from each aequorin mutant [mutant S (■), mutant 5 (▲), mutant 53 (●), mutant 71 (◆), mutant 84 (+)]. The bioluminescence signal was measured as light intensity in relative units, and then converted to percent using the maximum signal obtained for each aequorin mutant.

Table 2. Characterization of Aequorin Mutants in Terms of Luminescence Activity and Secondary Structure

Aequorin mutant	luminescence activity (%)[a]	half-life (s)	λ_{max}	α-helix content (%)
mutant S (no Cys)	100	1.00	465	27.2
mutant 5 (Ser5Cys)	102	0.99	463	27.4
mutant 53 (Glu53Cys)	98	1.02	467	26.9
mutant 71 (Met71Cys)	13	1.10	465	19.6
mutant 84 (Glu84Cys)	14	1.13	469	31.0

[a] Composition of regeneration mixtures were 1 μg of purified mutant protein in 350 μL of 30 mM Tris-HCl, 2 mM EDTA, 5 mM DTT, pH 7.6, buffer containing 0.2 μg of coelenterazine (0.1 μg/μL). All measurements were performed in triplicates with 10 μL aliquots of the regeneration mixture. Relative activities are reported as the percentage of maximum activity obtained for mutant S (100%).

The purified apoaequorin mutants were converted to the corresponding photoproteins (regeneration of the photoprotein) by mixing the apoproteins with a molar excess of coelenterazine followed by incubation of these mixtures on ice or at 4 °C. A bioluminescence emission study was performed to determine if the mutant proteins had retained the same flash-type emission characteristics of native aequorin and to compare the mutants containing a specifically placed cysteine residue with mutant S (Figure 2). All five mutants did emit approximately 95% of their total bioluminescence signal within 3 s. The half-lives for the bioluminescence light emission of the mutants are shown in Table 2. The half-lives for the mutants are longer in comparison to the native aequorin with a value of 0.60 s. Also, the values calculated for mutants 71 and 84 are slightly larger than those for mutants 3, 5, and 53. These difference could be attributed to the presence of the mutations within the apoprotein structures.

To compare the luminescence activity of the individual mutants to mutant S, as well as determine the time

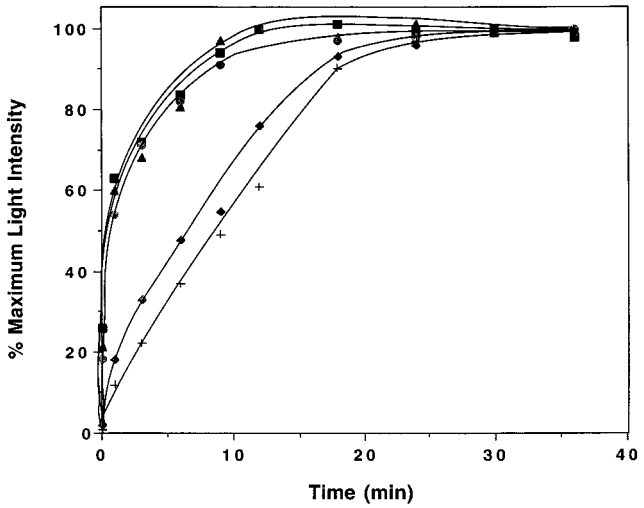

Figure 3. Time course study for conversion of apoaequorin mutants [mutant S (■), mutant 5 (▲), mutant 53 (●), mutant 71 (◆), mutant 84 (+)] to fully regenerated photoproteins. Bioluminescence measurements were taken at various times for up to 36 h using protein solutions containing 1 μg of apoprotein and 0.2 μg of coelenterazine in 30 mM Tris-HCl, 2 mM EDTA, 5 mM DTT, pH 7.6, buffer.

required for full regeneration of the photoproteins, a regeneration time course study was performed using each of the mutant apoaequorins. Due to the possible formation of dimers for the mutants containing a single cysteine residue, the study was conducted using a Tris-HCl/EDTA buffer with 5 mM DTT, the presence of which has been shown not to affect the luminescence activity of mutant S (*5*). Figure 3 shows that mutants S, 5, and 53 have similar regeneration characteristics with each reaching >90% of its maximum signal after 9 h. However, mutants 71 and 84 required 18 h to reach the same point. The luminescence activities of each of the four mutants with unique cysteine residues at positions 5, 53, 71, and 84 in comparison to mutant S with no cysteine residues are shown in Table 2. While mutants 5 and 53 demonstrate no decrease in bioluminescence activity, mutants 71 and 84 have less than 15% of the bioluminescence activity of mutant S.

To further study the affects of the mutagenesis on the photoprotein structures, circular dichroism (CD) spectra were taken with each individual mutant using mutant 3 as a baseline for comparison of secondary structure. The acquired CD spectra are shown in Figure 4 and exhibit typical protein secondary structures of α-helix and β-sheet. As seen from the figure, mutant 84 shows the largest change in secondary structure, while mutant 53 appears almost identical to mutant S. The α-helix content for each apoaequorin mutant (Table 2) was determined by analysis of the data using the program by Yang et al. (*12*). Whereas mutants 5 and 53 have similar values for their α-helix content in comparison to mutant S, both mutants 71 and 84 have either a significant decrease or an increase in the amount of α-helix contained within the apoprotein structure. The bioluminescence activity was measured before and after taking each CD spectra to ensure no denaturation of the proteins had taken place. Interestingly, it would appear that an alteration in the α-helix content of protein, whether positive or negative, could possibly lead to a siginifcant loss in activity.

Previously, it was demonstrated that a single amino acid substitution (Trp86Phe) produced a mutant aequorin with two emission maxima at 400 and 465 nm, unlike the native protein with a single emission maximum at 465 nm (*13*). Therefore, we decided to generate bioluminescence emission spectra for each of the five mutants employed here, as shown in Figure 5. The curves were obtained by following a modification of the method by Shimomura (*14*). Specifically, the aequorin mutants were added to the luminescence triggering buffer using a constant-rate syringe pump. The mutant aequorin solution is assumed to be completely saturated with calcium ions as soon as it is added to the quartz cell, thus, producing a constant luminescence signal over the required time period of 3−4 min. As seen from the figure, certain mutants (S, 53, and 5) appear to have a shoulder in their spectrum between 420 and 440 nm. However, mutants 71 and 84 exhibit no such shoulder. Emission maxima for each of the individual mutants were similar with values ranging 463−469 nm (Table 2).

DISCUSSION

The photoprotein, aequorin, produces a highly sensitive bioluminescent signal allowing for detection of the protein down to subattomol levels (*15*). Therefore, the photoprotein has found application as a label in a variety of bioanalytical methods. Since there is no available crystal structure for the protein, site-directed mutagenesis studies have been performed in order to elucidate information on structure−function relationships within the protein. The protein contains three calcium-binding sites (EF-hand structures) that consist of 12 amino acid residues arranged sequentially in a loop. When a key glycine residue was replaced at position 6 within the EF-hand structures, it was demonstrated that only Ca^{2+}-binding sites I and II are required for full bioluminescence activity (*16*). Another important consideration for the bioluminescence activity of the protein is the O_2-binding site and the hydrophobic regions in which the chromophore becomes noncovalently bound. The hydrophobic regions of the protein are between residue positions 40−50, 55−65, and 100−110 within the polypeptide chain (*16*). The unusually high content of histidine residues within the protein suggested the possibility that one of these residues was part of the O_2-binding site. Modification of the five histidine residues present within the protein (positions 16, 18, 27, 58, and 169) to alanine produced four mutants with decreased bioluminescent activity, and one mutant (169) with a complete loss of activity. Thus, His169, has been suggested as the O_2-binding site (*17*). The six tryptophan residues present within the protein were altered as well; each was replaced with the close analogue phenylalanine. Five of the six mutant aequorins showed a significant decrease in luminescence activity. CD spectra of these mutants demonstrated that complex changes had occurred within the secondary structure of the proteins as a result of the single amino acid substitutions. Only one mutant (Trp79Phe) had retained full activity, and this mutant showed only a small change in secondary structure in comparison to the native aequorin (*16*).

Critical to the work proposed here were site-directed mutagenesis studies on the three cysteine residues present within apoaequorin at positions 145, 152, and 180 (*6*, *16*). The requirement for 2-mercaptoethanol in the regeneration of the photoprotein indicated that these residues played an important role in the bioluminescence activity of aequorin (*16*). Replacement of the individual cysteine residues with serine produced three mutants, all of which had significantly lower activity in comparison to native aequorin. Interestingly, however, was a mutant produced in a later study in which all three cysteine residues were simultaneously replaced with serine (*5*).

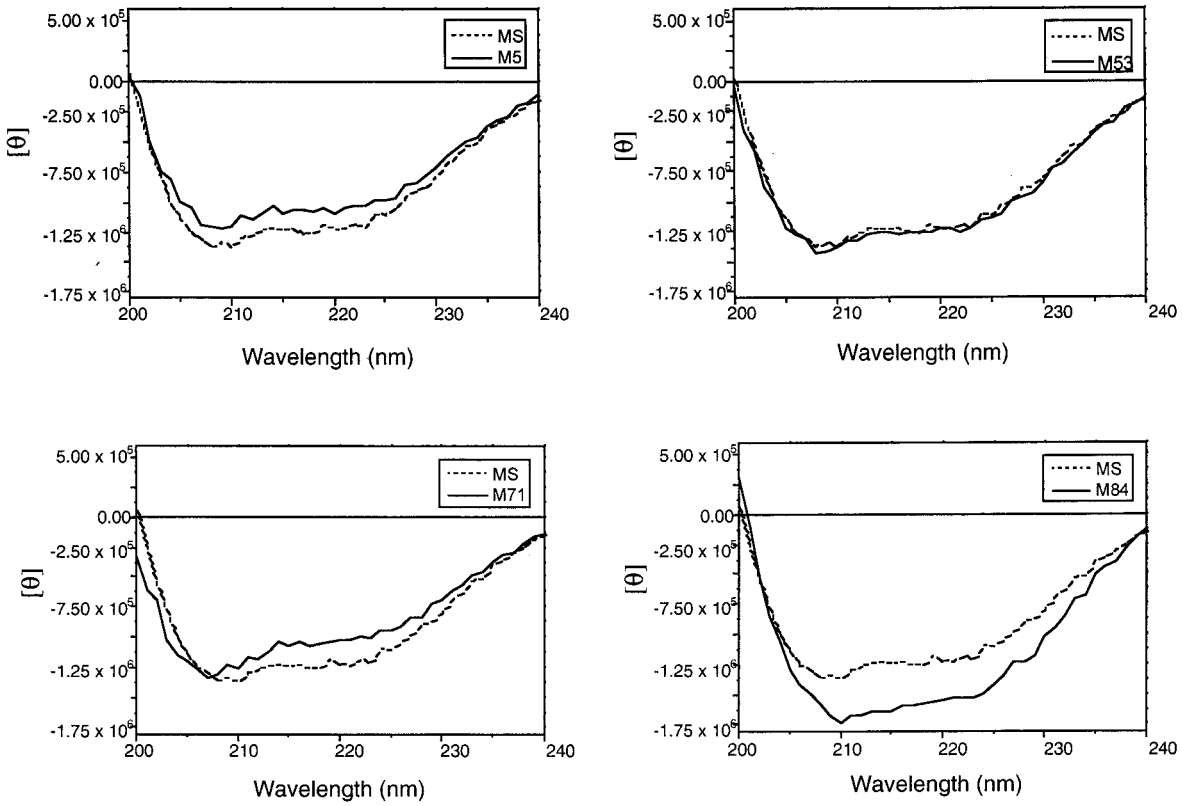

Figure 4. CD spectra for apoaequorin mutants. Each panel shows the spectra for mutant S (dashed lines) in comparison to spectra obtained for one of the apoaequorin with a unique cysteine residue (solid lines).

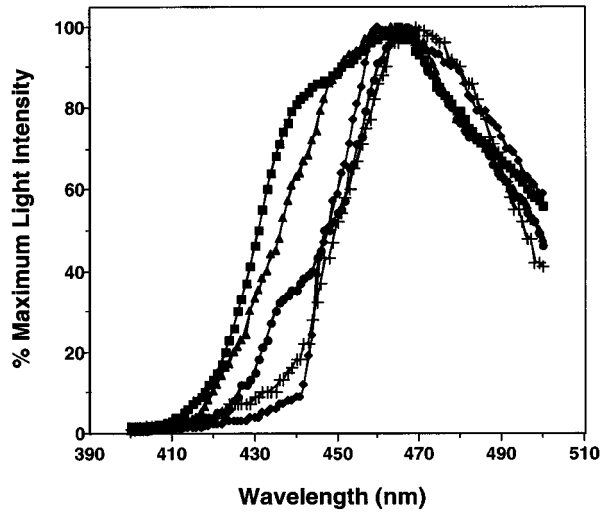

Figure 5. Bioluminescence emission spectra for aequorin mutants [mutant S (■), mutant 5 (▲), mutant 53 (●), mutant 71 (◆), mutant 84 (+)] using spectrofluorometer with lamp and chopper turned off.

This cysteine-free mutant had an increase (124%) in bioluminescence activity in comparison to the wild-type photoprotein without the additional requirement of a reducing agent. These studies suggested that introduction of a unique cysteine residue within apoaequorin for the purpose of site-specific chemistries on the protein, was possible while still retaining the complete light-producing properties of photoprotein. However, without an available three-dimensional structure for the protein, selection of an appropriate site for a unique cysteine residue within the apoprotein required additional studies on structure−function relationships present within aequorin. On the basis of information obtained from the previous studies discussed above, we generated a cysteine-free mutant of aequorin (mutant S), and used this mutant to produce four additional mutants with unique cysteine residues at various positions (5, 53, 71, and 84) within the photoprotein. The positions selected were not part of any of the amino acid sequences previously identified within apoaequorin as being critical to its bioluminescence activity including the three EF-hand structures (Ca^{2+}-binding sites), hydrophobic regions of the protein, and the C-terminal region. Since the apoprotein contains only a single serine residue (position 5 in the polypeptide chain) that is not part of a critical region within the protein, replacement of this serine with cysteine was the only conservative mutation possible. Also, this residue was at the N-terminus of the protein, and studies have demonstrated that N-terminal fusions are possible without significant losses in the luminescence activity of aequorin (*7*, *8*), thus, indicating that amino acid substitution at this position was unlikely to produce an aequorin mutant with significantly decreased luminescence activity. The incorporation of a unique cysteine residue within the protein structure allows for the site-specific attachment of a desired biomolecule or the site-specific immobilization of the photoprotein onto a surface.

The apoaequorin mutant produced in our laboratory containing all three cysteine residues present within the native protein replaced with serines was successfully converted to an active photoprotein as previously reported. This mutant functioned as a baseline for comparison between the four additional mutants generated containing specifically placed unique cysteine residues. The four aequorin mutants containing single cysteine residues were different in terms of their light emission properties and secondary structure features. In particular, two of the mutants (5 and 53) showed similar

secondary structure characteristics and bioluminescence emission properties to mutant S. However, the other two mutants produced (71 and 84) exhibited a large decrease in their light-generating capabilities in comparison to mutant S. CD spectra revealed that the mutagenesis had produced significant changes in the secondary structure of the proteins in comparison to mutant S with either increasing or decreasing α-helix content. These two proteins also required a much longer regeneration time of 18 h versus 9 h for the other mutants. On the other hand, two of the mutants obtained (5 and 53) demonstrated no loss in bioluminescence activity and exhibited similar secondary structures in comparison to mutant S, as well as regeneration time and half-lives. Due to the dramatic decrease in bioluminescence signal observed for mutants 71 and 84, it could be postulated that these amino acid residues are in close proximity to one of the active sites within the photoprotein structure, most presumably the hydrophobic region in which coelenterazine binds. Further studies should reveal whether the decrease in activity is a result of decreased stability, quantum yield, or binding of the chromophore. The properties of the four different mutants produced indicate that mutants 5 and 53 are more suitable for site-specific immobilization of the photoprotein because these mutants retained the same degree of bioluminescence activity as compared to the cysteine-free aequorin mutant. However, while mutants 5 and 53 would also be excellent candidates for site-specific conjugation of desired analytes, mutants 71 and 84 are viable as well. Since these mutants have different bioluminescence and secondary structure characteristics, it is conceivable that they might demonstrate a change in their luminescence signal upon binding to an appropriate binder. Thus, mutants 71 and 84 could function as bioluminescence labels in homogeneous binding assays for desired biomolecules.

ACKNOWLEDGMENT

We would like to thank the Department of Energy (DE-FG05-95ER62010) and the National Institutes of Health (GM47915) for support of this work. S. Daunert is a Cottrell Scholar and a Lilly Faculty Awardee. J. C. Lewis acknowledges support from the National Science Foundation for an IGERT Predoctoral Fellowship. We would also like to thank Dr. Paul Bummer of the Department of Pharmaceutical Sciences of the University of Kentucky for his assistance in aquiring the CD spectra of the apoaequorin mutants.

LITERATURE CITED

(1) Ohmiya, Y., and Hirano, T. (1998) Shining the light: mechanism of the bioluminescence reaction of calcium-binding photoproteins. *Chem. Biol. 3*, 337.

(2) Prasher, D., McCann, R. O., and Cormier, M. J. (1985) Cloning and expression of the cDNA coding for aequorin, a bioluminescent calcium-binding protein. *Biochem. Biophys. Res. Commun. 126*, 1259.

(3) Inouye, S., Noguchi, M., Sakaki, Y., Takagi, Y., Miyata, T., Iwanaga, S., and Tsuji, F. I. (1985) Cloning and sequence analysis for the cDNA for the luminescent protein aequorin. *Proc. Natl. Acad. Sci. U.S.A. 82*, 3154.

(4) Charbonneau, H., Walsh, K. A., McCann, R. O., Prendergast, F. G., Cormier, M. J., and Vanaman T. C. (1985) Amino acid sequence of calcium-dependent photoprotein aequorin. *Biochemistry 24*, 6762.

(5) Kurose, K., Inouye, S., Sakaki, Y., and Tsuji, F. I. (1989) Bioluminescence of the Ca^{2+}-binding photoprotein aequorin after cysteine modification. *Proc. Natl. Acad. Sci. U.S.A. 86*, 80.

(6) Witkowski, A., Ramanathan, S., and Daunert, S. (1994) Bioluminescence binding assay for biotin with attomol detection based on recombinant aequorin. *Anal. Chem. 66*, 1837.

(7) Ramanthan, S., Lewis, J. C., Kindy, M. S., and Daunert, S. (1998) Heterogeneous bioluminescence binding assay for an octapeptide using recombinant aequorin. *Anal. Chim. Acta 369*, 181.

(8) Zenno, S., and Inouye, S. (1990) Bioluminescent immunoassay using a fusion protein of protein A and the photoprotein aequorin. *Biochem. Biophys. Res. Commun. 171*, 169.

(9) Nomura, M., Inouye, S., Ohmiya, Y., and Tsuji, F. I. (1991) A C-terminal proline is required for bioluminescence of the Ca^{2+}-binding protein, aequorin. *FEBS Lett. 295*, 63.

(10) Hannick, L. I., Prasher, D. C., Schultz, L. W., Deschamps, J. R., and Ward, K. B. (1993) Preparation and initial characterization of crystals of the photoprotein aequorin from *Aequorea victoria*. *Proteins 15*, 103.

(11) Sambrook, J., Fritsch, E. F., and Maniatis, T. (1989) *Molecular Cloning: A Laboratory Manual*, 2nd ed., Cold Spring Harbor Laboratory Press, Plainview, NY.

(12) Yang, J. T., Wu, C. C., and Martinez, H. M. (1986) Calculation of protein conformation from circular dichroism. *Methods Enzymol. 130*, 208.

(13) Ohmiya, Y., Ohashi, M., and Tsuji, F. I. (1992) Two excited states in aequorin bioluminescence induced by tryptophan modification. *FEBS Lett. 301*, 197.

(14) Shimomura, O. (1986) Isolation and properties of various molecular forms of aequorin. *Biochem. J. 234*, 271.

(15) Actor, J. K., Kuffner, T., Dezzutti, C. S., Hunter, R. L., and McNichol, J. M. (1998) A flash-type bioluminescent immunoassay that is more sensitive than radioimaging: quantitative detection of cytokine cDNA in activated and resting human cells. *J. Immunol. Methods 211*, 65.

(16) Tsuji, F. I., Inouye, S., Goto, T., and Sakaki, Y. (1986) Site-specific mutagenesis of the calcium-binding photoprotein aequorin. *Proc. Natl. Acad. Sci. U.S.A. 83*, 8107.

(17) Ohmiya, Y., and Tsuji, F. (1993) Bioluminescence of the Ca^{2+}-binding photoprotein, aequorin, after histidine modification. *FEBS Lett. 320*, 267.

BC9900800

Dye-Pair Reporter Systems for Protein−Peptide Molecular Interactions

Kieran F. Geoghegan,* Philip J. Rosner, and Lise R. Hoth

Central Research Division, Pfizer Inc., Eastern Point Road, Groton, Connecticut 06340. Received June 23, 1999; Revised Manuscript Received October 19, 1999

Modifying a linear peptide near each terminus with a fluorescent dye can make it able to signal its own binding to a protein. As originally described, the dye pair is composed of fluorescein and tetramethylrhodamine [Wei, A.-P., Blumenthal, D. K., and Herron, J. N. (1994) *Anal. Chem*. *66*, 1500−1506]. This paper shows that it may also be two molecules of tetramethylrhodamine. In aqueous solution, mutual affinity of the dyes causes fluorescence-quenching contact between them. When the peptide is bound by an antibody or cleaved by a proteinase, or when acetonitrile is added, dye-to-dye contact decreases and fluorescence increases 3−15-fold. When five peptides of 4−20 amino acid residues were doubly modified with tetramethylrhodamine, each product had the absorption spectrum of a tetramethylrhodamine dimer. As the peptides were not known to have special conformational features, self-affinity of the dye appeared to be the main cause of dimerization. Disruption of the dye dimers by acetonitrile suggested that dimerization of the dye(s) in aqueous solution was largely an effect of hydrophobicity. Dye-tagged peptides were used in fluorometric assays for two peptide−protein interactions. First, a peptide from type II collagen recognized by a monoclonal antibody was derivatized with two different dye pairs. The monoclonal bound each modified peptide, disrupting dye-to-dye contact and increasing fluorescence up to 4-fold. Second, a phosphopeptide recognized by an SH2 domain was tagged with fluorescein and tetramethylrhodamine, and its binding to the SH2 domain was detected through fluorescence. Doubly dye-tagged peptides offer a direct, solution-phase assay for protein−peptide binding.

INTRODUCTION

Wei et al. (*1*) described a new optical assay for the binding of a peptide to an antibody. A peptide corresponding to a recognized epitope was tagged at one end with fluorescein and at the other with tetramethylrhodamine. In the free molecule, contact between the dyes caused their fluorescence to be quenched. When the antibody bound the intervening peptide, the dyes were pulled apart, and the relief of fluorescence quenching signaled the binding event. This paper extends known applications of this principle to include a new dye pair and an assay for a peptide−protein binding event in which the protein is not an antibody.

Peptides doubly tagged with tetramethylrhodamine were previously introduced as fluorogenic substrates for proteinases (*2*−*7*). As with the fluorescein−tetramethylrhodamine heteropair (*1*), dye-to-dye contact in the intact species diminished the fluorescence of the participating dyes by more than 90%. On enzymatic cleavage of the intervening peptide, the dye-tagged products dissociated and the contact quenching of their fluorescence was abolished. As a result, the enzyme activity could be measured by following the increase in fluorescence. As double modification with a single dye is easier than placing two different dyes at specific sites, we found it interesting to evaluate the performance of a doubly tetramethylrhodamine-tagged peptide in protein-to-peptide binding assays. Some general properties of these products are also presented and discussed.

* To whom correspondence should be addressed. Phone: (860) 441-3601. Fax: (860) 441-3783. E-mail: kieran_f_geoghegan@groton.pfizer.com.

Finally, other types of protein in addition to antibodies also recognize and bind peptide ligands. Among these are proteins containing SH2 (Src homology type-2) domains, which bind phosphotyrosine-containing regions in many proteins involved in intracellular signal transduction pathways. We used an interaction of this type as a further test case for the “double-dye” binding assay.

EXPERIMENTAL PROCEDURES

Chemicals. Peptides were obtained through custom synthesis performed by AnaSpec Inc., 2149 O'Toole Ave, Suite F, San Jose, CA 95131. Dyes purchased from Molecular Probes Inc., 4849 Pitchford Ave, Eugene, OR 97402, included 5-carboxytetramethylrhodamine succinimidyl ester, tetramethylrhodamine-5-maleimide, and 5-carboxyfluorescein succinimidyl ester. The C-terminal SH2 domain of the p85α subunit of phosphatidylinositol-3-kinase was expressed and purified as described (*8*). Monoclonal antibodies were a gift from Dr. I. G. Otterness, Pfizer Central Research.

Absorbance and Fluorescence Spectroscopy. Absorption spectra were collected using quartz cuvettes of 1 cm path length in a Hewlett-Packard model 8452A diode-array spectrophotometer. Fluorescence spectra were collected using either a Perkin-Elmer model LS-50 fluorimeter or a Spex Instruments FluoroMax-2 fluorimeter.

Derivatization of Peptides with Dyes. Dye-to-peptide coupling reactions were performed in solution on unprotected peptide by minor variations of the methods described (*9*, *10*). As our interest was in the spectral properties of the desired products, syntheses were not optimized for yield. However, products were characterized with respect to purity and structure by direct

10.1021/bc9900845 CCC: $19.00 © 2000 American Chemical Society
Published on Web 12/14/1999

infusion to ES-MS or by LC-MS (spectra supplied with manuscript for review). LC-MS was performed using either a Perkin-Elmer Sciex API 100 single-quadrupole spectrometer or a Finnigan LCQ ion-trap spectrometer. Vydac C4 or C18 reversed-phase columns were used for the HPLC component of these analyses. Accounts of selected coupling reactions follow.

Double Modification with Tetramethylrhodamine at Cysteine. α-*N*-Acetyl-CKPDRSSFVPSLFSKKKKNC−NH_2 was modified at both cysteine residues with tetramethylrhodamine-5-maleimide. Peptide (8.5 mg; 0.003 mmol, if the solid was taken as 80% peptide) and tetramethylrhodamine-5-maleimide (5 mg; 0.010 mmol) were dissolved in 0.6 mL of a 60:40 mixture of 0.05 M sodium phosphate, pH 6.5, with acetonitrile. The reaction was allowed to proceed at 22 °C overnight, during which analysis by LC-MS indicated that the desired product with mass of 3303.7 Da (theoretical value 3303.9 Da) was the dominant component of the reaction mixture. The reaction mixture was then fractionated in two equal portions by HPLC using an acetonitrile gradient in 0.1% TFA on a Vydac C4 column (1 cm × 25 cm, type 214TP1010) operating at 4 mL/min. Solvents were A, 0.1% (v/v) TFA; B, 0.085% (v/v) TFA in 80% acetonitrile. The major peak in 575 nm absorbance gave a mass spectrum consistent with the desired product, with no other species significantly represented. After collection, this product was >95% pure by analytical HPLC. Aliquots of the product peak were dried in a SpeedVac concentrator.

Double Modification with Tetramethylrhodamine at Amino Groups. AGEPGDDAPSGK-d−R was modified at both amino groups with 5-carboxytetramethylrhodamine succinimidyl ester. In 0.5 mL of a 60:40 mixture of 0.1 M $NaHCO_3$, pH 8.8 with acetonitrile, peptide (4.9 mg; 0.003 mmol if the solid was taken as 80% peptide) was combined with 5 mg (0.009 mmol) of 5-carboxytetramethylrhodamine succinimidyl ester. The reaction mixture was incubated at 22 °C, and small samples were occasionally withdrawn for analysis by HPLC. After 2 h, the reaction mixture was fractionated by HPLC as described above, and the desired product was isolated and identified by its mass and by its dye dimer-like absorption spectrum when diluted into PBS (see Results). LC-MS showed that the product was >95% pure and had a mass of 2081.2 Da (theory 2081.3 Da). Aliquots of the product peak were dried in a SpeedVac concentrator.

Modification with Fluorescein at a Sulfhydryl Group and with Tetramethylrhodamine at an Amino Group. AGEPGDDAPSGC-d−R was modified first at its cysteine sulfhydryl with tetramethylrhodamine-5-maleimide, and then at its α-amino group with 5-carboxyfluorescein succinimidyl ester. Peptide (5.5 mg of solid; 0.003 mmol, if the solid was taken as 80% peptide) and tetramethylrhodamine-5-maleimide (2 mg; 0.004 mmol) were dissolved in 0.2 mL of a 60:40 mixture of 0.05 M sodium phosphate, pH 6.0, with acetonitrile. HPLC analysis showed that the reaction was substantially complete in 2 h, and the reaction mixture was fractionated by HPLC on a Poros R1/M 10/100 column operating at 10 mL/min. Identity of the singly modified peptide was confirmed by ES-MS, and the product (5 mg) was dried in a centrifugal concentrator, resuspended in 0.2 mL of a 60:40 mixture of 0.1 M $NaHCO_3$, pH 8.5, with acetonitrile, and combined with 5-carboxyfluorescein succinimidyl ester (2 mg), about a 1.4-fold excess of 5-carboxyfluorescein succinimidyl ester over peptide. The reaction was incubated at room temperature for 4 h, and then fractionated by HPLC on the same Poros column. The doubly dye-tagged product (1.5 mg) was recovered and identified by ES-MS (mass observed for major component of product, 2070.6 Da; theory, 2071.1 Da). An estimated 15−20% of the product had mass of 2089 Da, 18 Da above the theoretical value (see Results).

RESULTS

Preparation of Peptide−Dye Conjugates. Tetramethylrhodamine and fluorescein were coupled to unprotected peptides in solution by standard methods as detailed above. Succinimidyl esters of 5-carboxy-TMR[1] and 5-carboxy-FL were used to acylate peptide amino groups, and 5-maleimido-TMR was used to S-alkylate at cysteine. Commercial dye reagents were used without further purification, and mass spectra of the products usually indicated the presence of impurities with mass 14 Da less than the major, desired products. This was tentatively attributed to low levels (less than 5% in recently purchased batches) of trimethylrhodamine in the tetramethylrhodamine stocks. On reversed-phase HPLC using water/acetonitrile/TFA, des-methyl products were eluted slightly earlier than the major products.

Simultaneous coupling of 5-carboxy-TMR to the α- and ϵ-amino groups of peptides with a free N-terminus and single Lys was performed in 0.1 M $NaHCO_3$ using 5-carboxy-TMR succinimidyl ester and yielded the expected product in all cases. Reaction mixtures were fractionated by HPLC and the desired products were identified by ES-MS of peak fractions (spectra were supplied for review) and by their distinctive absorption spectra in aqueous solution (see below).

In peptides tagged with 5-carboxy-FL at the α-amino group and 5-maleimido-TMR at Cys (e.g., SITEGE-ARGSVC-d−R), varying levels of product had mass 18 Da above the expected value. Wei et al. (*1*) attributed this to an artifact of mass spectrometry, but a more likely explanation is that the succinimidyl group formed when 5-maleimido-TMR reacts with Cys can undergo ring-opening hydrolysis (*11*). LC-MS of the fragments from trypsin-catalyzed cleavage placed the extra 18 Da in the fragment containing TMR-tagged cysteine, while the fragment with 5-carboxy-FL on the α-amino group had the predicted mass (not shown). The amount of +18 Da product was reduced by running the second coupling step, in which 5-carboxy-FL succinimidyl ester reacted with the succinimidyl-TMR derivative in 0.1 M $NaHCO_3$ at pH 8.3, without heating.

Peptides Doubly Modified with TMR. SITEGE-ARGSVK-d−R has two amino groups, one at the N-terminus and one in the single Lys. Following reaction of the peptide with 5-carboxy-TMR succinimidyl ester in 0.1 M $NaHCO_3$, the product was purified by HPLC and dried. The absorption spectrum of monomeric TMR has its maximum near 554 nm (ϵ_{max} = 90 000 M^{-1} cm^{-1}) and a 520 nm shoulder near half the maximal absorptivity. The doubly tagged peptide in PBS had its absorption maximum near 520 nm and a shoulder near 550 nm (Figure 1A, solid line). Similar departures from a monomeric rhodamine line shape occurred in proteins tagged

[1] Abbreviations; 5-carboxy-TMR, 5-carboxytetramethylrhodamine; 5-maleimido-TMR, 5-maleimidotetramethylrhodamine; TMR, tetramethylrhodamine (used generically to include either of the preceding derivatives); 5-carboxy-FL, 5-carboxyfluorescein; PBS, Dulbecco's phosphate-buffered saline solution without $CaCl_2$ or $MgCl_2$ (see Experimental); hCG, human chorionic gonadotropin; the presence of D-arginine in synthetic peptides is indicated by -d−R.

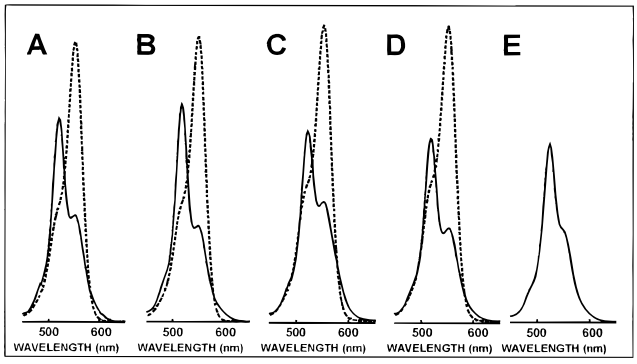

Figure 1. Absorption spectra of peptides doubly modified with TMR. Solid line, intact modified peptide; dashed line (panels A−D), products of tryptic cleavage. Peptides were dissolved in PBS at 1−5 μM. Apart from the peptide in panel B, peptides were acylated at their α- and ϵ-amino groups with 5-carboxy-TMR. (A) SITEGEARGSVK-d−R; (B) α-*N*-acetyl-CKPDRSSFVPSLFSKKKKNC−NH_2, *S*-alkylated with 5-maleimido-TMR at the cysteines; (C) SPGLGLRAK; (D) SRPIEFFRLAK; (E) AHHK.

with multiple dye equivalents (*12*, *13*), indicating an intramolecular interaction between the dye residues.

To study how peptide length and/or sequence influenced this, four additional peptides with 4−20 residues between rhodamines were doubly tagged with TMR. α-*N*-Acetyl-CKPDRSSFVPSLFSKKKKNC−NH_2 was tagged at each of its two cysteines with 5-maleimido-TMR (Figure 1B). Three peptides were tagged with 5-carboxy-TMR at α- and ϵ-amino groups; these were SPGLGLRAK (Figure 1C), SRPIEFFRLAK (Figure 1D), and AHHK (Figure 1E). The products all had similar absorption spectra (Figure 1, solid lines), but with subtle variations of the relative intensity at the peak and shoulder.

Trypsin-catalyzed cleavage shifted the spectrum of (5-carboxy-TMR)-SITEGEARGSVK(5-carboxy-TMR)-d−R (2.5 μM in PBS) to that of monomeric TMR (Figure 1A, dashed line), and had the same effect on the other three trypsin-cleavable peptides (Figure 1, spectra B−D, dashed lines). Therefore, at low micromolar concentration, the anomalous line shape associated with doubly tagged peptides depended on the peptide link. This was reported elsewhere, but with dye-derivatives of a single "relatively rigid, bent" elastase−substrate peptide (*2*−*7*). This implied conformational factor seemed in those papers to be attributed an active role in bringing the dyes into proximity. Therefore, it was useful to show that the effect was also true for unrelated peptides with 9−20 amino acids between the dyes.

Similar spectral changes occurred in doubly TMR-tagged peptides in increasing concentrations of acetonitrile (Figure 2). At 60% acetonitrile, the peptides with 9−20 amino acids between dyes had rhodamine monomer spectra (Figure 2, spectra A−D). The final peptide, Ala-His-His-Lys, retained a significant dimer-like component in its spectrum (Figure 2E).

Fluorescence emission of doubly TMR-tagged peptides was strongly increased by peptide cleavage or acetonitrile. In PBS, tryptic cleavage of (5-carboxy-TMR)-SITEGEARGSVK(5-carboxy-TMR)-d−R caused about a 15-fold fluorescence increase (λ_{ex} = 540 nm) (Figure 3A), in reasonable agreement with the 10-fold increase reported by Packard et al. for a different peptide (*2*, *3*). The presence of 60% acetonitrile with the products caused a further 83% increase in the fluorescence. When the peptide was not cleaved, addition of 60% acetonitrile still increased the fluorescence (Figure 3B), but it reached

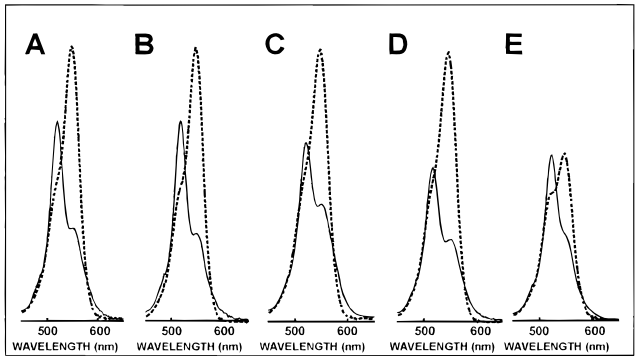

Figure 2. The effect of acetonitrile on the absorption spectra of peptides doubly modified with TMR. Spectra are shown for PBS:water 3:7 (solid line) and for PBS:water:acetonitrile 3:1:6 (dashed line). Identification of peptides as in Figure 1.

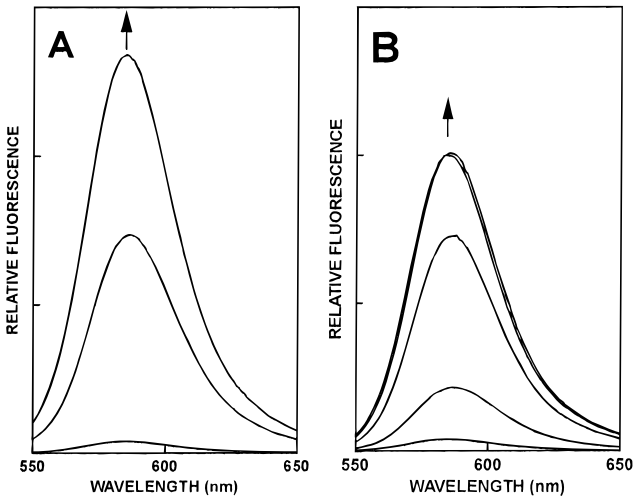

Figure 3. The effects of (A) tryptic cleavage and acetonitrile, and (B) acetonitrile alone on the fluorescence of (5-carboxy-TMR)-SITEGEARGSVK(5-carboxy-TMR)-d−R (λ_{ex} 540 nm). (A) Fluorescence emission spectra of: least intense, (5-carboxy-TMR)-SITEGEARGSVK(5-carboxy-TMR)-d−R, 2 μM in PBS; middle intensity, the same sample after tryptic cleavage; highest intensity, tryptic cleavage products in the presence of 60% acetonitrile. (B) Fluorescence emission spectra of: least intense, (5-carboxy-TMR)-SITEGEARGSVK-(5-carboxy-TMR)-d−R, 2 μM in PBS; and, in order of increasing intensity, in the presence of 20, 40, 60, and 70% acetonitrile. The arrows show the trend of spectral change through the sample list.

only 75% of the intensity from a cleaved sample in the same solvent.

The fluorescence increase upon cleavage in PBS was measured for other doubly TMR-tagged peptides, specifically α-*N*-acetyl-CKPDRSSFVPSLFSKKKKNC−NH_2, SPGLGLRAK, and AGEPGDDAPSGK-d−R. In each case, it was in the range 11−15-fold (data not shown).

Peptides Modified with 5-Carboxy-FL and TMR. The absorption spectrum of (5-carboxy-FL)-SITEGEARGSVC(5-maleimido-TMR)-d−R was similar to that of the peptide used by Wei et al. (*1*) (Figure 4A). Its principal bands were centered near 493 and 560 nm, respectively. Trypsin-catalyzed proteolysis mainly shifted the one at 560 nm, a change very similar to the shift demonstrated by Wei et al. (*1*), consequent to antibody binding of their hCG-derived peptide, and by Packard et al. (*7*), consequent to proteolysis of their 11-residue peptide bearing the same dye pair. Addition of acetonitrile to (5-carboxy-FL)-SITEGEARGSVC(5-maleimido-TMR)-d−R (Figure 4B) led to a very similar spectral change as proteolysis or antibody binding.

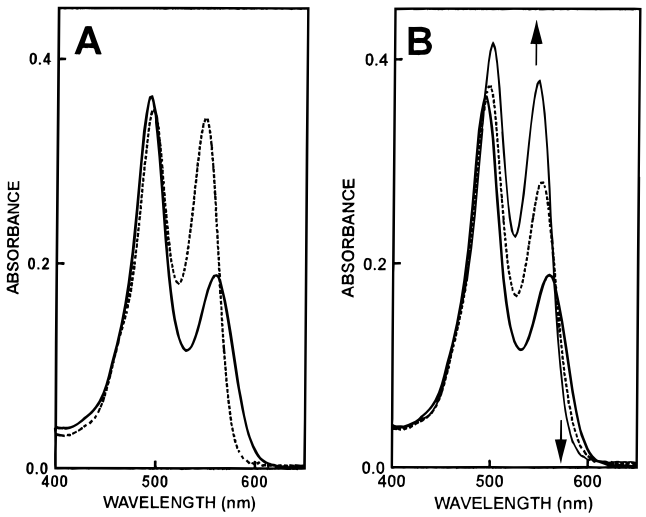

Figure 4. The effects of (A) trypsin and (B) acetonitrile on the absorption spectrum of (5-carboxy-FL)-SITEGEARGSVC-(5-maleimido-TMR)-d−R. (A) Solid line, intact peptide in PBS; dashed line, products of tryptic cleavage in PBS. (B) Spectra of the intact peptide in PBS with 0, 20, and 40% acetonitrile; the spectrum in 60% acetonitrile (not shown) was very close to the one obtained in 40% acetonitrile. Arrows show the trend of spectral change through the sample list.

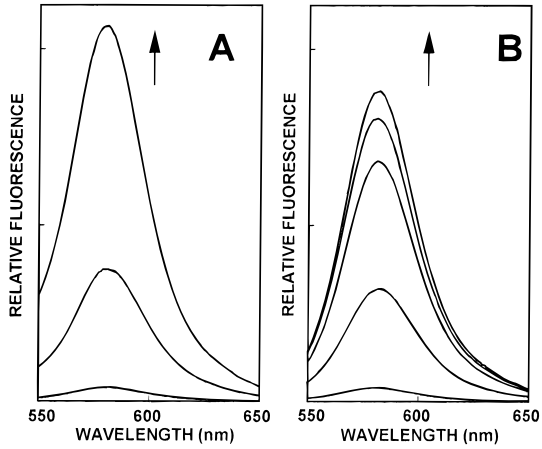

Figure 5. The effects of (A) trypsin and (B) acetonitrile on the fluorescence (λ_{ex} 540 nm) of (5-carboxy-FL)-SITEGEARGSVC-(5-maleimido-TMR)-d−R. Arrows indicate the trend of spectral change through the sample list. (A) Intact peptide in PBS; products of tryptic cleavage in PBS; peptide products of tryptic cleavage, same concentration, in PBS/60% acetonitrile. (B) Intact peptide in PBS and in PBS containing 20, 40, 60, and 70% acetonitrile.

Proteolysis of (5-carboxy-FL)-SITEGEARGSVC(5-maleimido-TMR)-d−R was also signaled by fluorescence changes (Figure 5A). Proteolysis liberated tetramethylrhodamine from a poorly fluorescent condition so that excitation at 540 nm gave 8-fold increased fluorescence over the intact molecule. Fluorescence of the fluorescein could also be detected after cleavage (*7*), as separation from the rhodamine ended intramolecular quenching. This did not occur when the peptide was linearized by antibody binding but not cleaved (*1*). Addition of acetonitrile to (5-carboxy-FL)-SITEGEARGSVC(5-maleimido-TMR)-d−R also caused a similar change in the spectrum (Figure 5B). Overall, the separate effects of cleavage and acetonitrile agreed in the same way as for a peptide doubly tagged with TMR (Figure 2).

Peptide Doubly Modified with 5-Carboxy-FL. Double tagging with 5-carboxy-FL of SITEGEARGSVK-d−R (modification of the amino groups with 5-carboxy-FL succinimidyl ester) gave a product with an absorption spectrum close to that of monomeric fluorescein (not shown). As reported by Packard et al. (*5*) using a different peptide, proteolytic cleavage of the linker gave minimal spectral change.

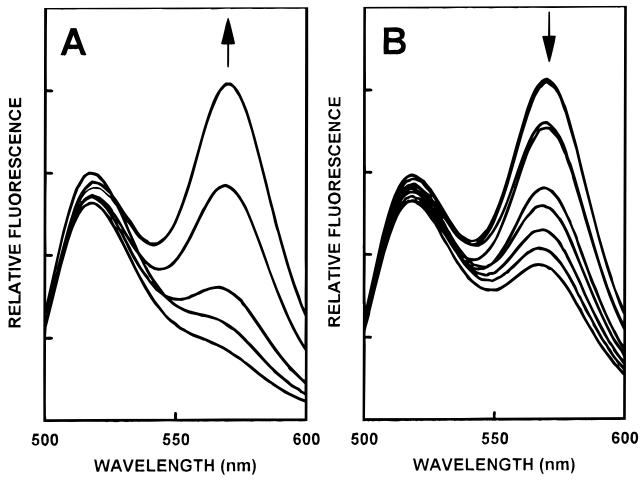

Figure 6. Fluorescence of (5-carboxy-FL)-AGEPGDDAPSGC-(5-maleimido-TMR)-d−R, showing increased fluorescence on binding to an antibody and competition by unmodified peptide (λ_{ex} 493 nm, 6 °C). (A) Spectra in the order indicated by the arrow (least intense to most intense): dye-tagged peptide alone (100 nM); dye-tagged peptide with a MAb (100 nM) that does not bind it specifically; dye-tagged peptide with MAb 5109 (25, 50, 100, and 200 nM; the last two traces are superimposed), which does bind it. Removal and replacement of the cuvette was a source of experimental variation between scans. (B) Spectra in the order indicated by the arrow, i.e., most intense to least intense: dye-tagged peptide (100 nM) with MAb 5109 (100 nM), and the same sample with unmodified AGEPGDDAPSGK-d−R at 25, 50, 100, 200, 400, 600, 800 nM and 1 μM.

Peptide−Antibody Association. Proteolysis of type II collagen is an important deteriorative process in osteoarthritis and other joint diseases. Osteoarthritis proceeds slowly through its early stages without clinical manifestation, but can eventually cause severe pain and disability. Effective assays for circulating or excreted markers of its early stages would create opportunities for therapy to prevent this progression.

Type II collagen contains unique sequence elements, and proteolytic fragments containing these are promising markers for its breakdown. Moreover, the course of proteolytic attack on collagen can guide hypotheses as to which distinctive regions of type II collagen are likely to be released into the circulation and excreted in urine. An especially acidic region of the sequence (see below) is now known to be released and excreted in this way. A monoclonal antibody raised against a corresponding synthetic peptide was designated MAb 5109 and has been used in ELISA and other assays to detect tissue-derived fragments of collagen in human urine (J. T. Downs et al., manuscript in preparation).

The peptide AGEPGDDAPSGC-d−R encompassed the sequence GEPGDDAPSG corresponding to residues 888−897 of human type II procollagen (SWISS−PROT accession number Q14046) apart from a single change of Gly to Ala. It contained the epitope recognized by MAb 5109. This was modified with 5-carboxy-FL and 5-maleimido-TMR, and the fluorescence of the doubly dye-tagged peptide (λ_{ex} = 493 nm) was monitored during addition of MAb 5109 (Figure 6A). There was little change in the fluorescein emission band near 520 nm, but tetramethylrhodamine fluorescence near 575 nm increased more than 4-fold at the limit of the titration. In a control

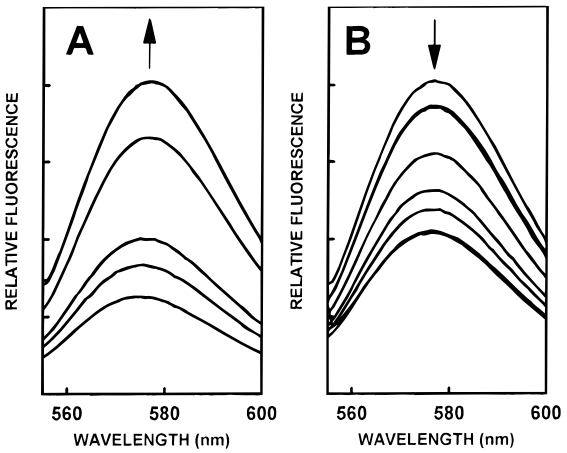

Figure 7. Fluorescence emission spectra of (5-carboxy-TMR)-AGEPGDDAPSGK(5-carboxy-TMR)-d−R showing the increase in fluorescence resulting from binding to an antibody and competition by unmodified peptide (λ_{ex} 540 nm, 6 °C). (A) Spectra in the order indicated by the arrow, i.e., least intense to most intense: doubly TMR-tagged peptide (100 nM) alone; doubly TMR-tagged peptide with addition of a MAb (100 nM) that does not bind it specifically; doubly TMR-tagged peptide with addition of MAb 5109 (25, 50, 100, and 200 nM; the last two traces are superimposed), which does recognize it. Removal and replacement of the cuvette was a source of experimental variation between scans. (B) Spectra in the order indicated by the arrow, i.e., from most intense to least intense: doubly TMR-tagged peptide (100 nM) with MAb 5109 (100 nM), and the same sample with the subsequent additions of unmodified AGEPGD-DAPSGK-d−R at 25, 50, 100, 200, 400, 600, 800 nM and 1 μM.

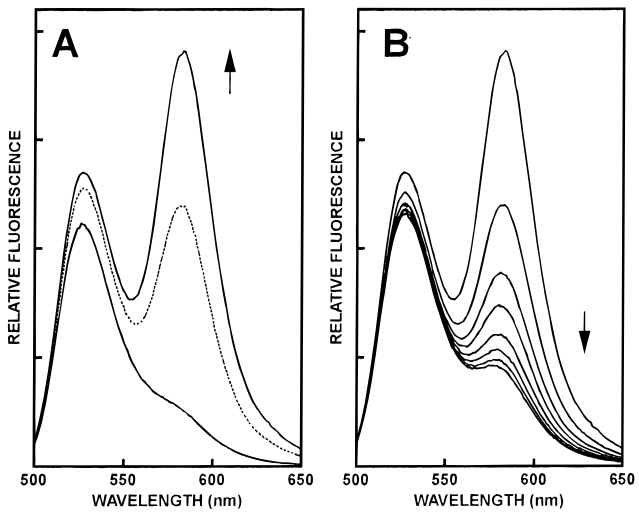

Figure 8. The effect of C-p85 SH2 domain on the fluorescence emission spectrum of (5-carboxy-FL)-EpYMVMQC(-5-maleimido-TMR)-NH_2 (1 μM) at 6 °C. (A) Spectra in the order indicated by the arrow: (5-carboxy-FL-)EpYMVMQC(-5-maleimido-TMR)-NH_2 alone (the least intense spectrum), and with addition of 1 μM and 2 μM C-p85 SH2 domain. (B) Competition by addition of untagged EpYMVMQC−NH_2 to the mixture of 1 μM (5-carboxy-FL-)EpYMVMQC(-5-maleimido-TMR)-NH_2 and 2 μM C-p85 SH2 domain: molar ratios of untagged peptide to tagged peptide were 0:1 (most intense spectrum), 1:1, 2:1, 3:1, 4:1, 5:1, 6:1, and 7:1 (least intense spectrum).

experiment using an antibody with different specificity, there was a small increase possibly due to nonspecific binding between the peptide and protein. When an unmodified peptide, AGEPGDDAPSGK-d−R, was added as a competitive agent, the increase in fluorescence was partly reversed in a concentration-dependent manner (Figure 6B). This presumably was because (5-carboxy-FL)-AGEPGDDAPSGC(5-maleimido-TMR)-d−R was displaced from the antibody. These results confirmed the main finding of Wei et al. (*1*).

An alternative to labeling a peptide with a dye heteropair is to introduce two copies of a single dye that can form an intramolecular dimer. The results in Figure 1 and simple theory (see Discussion) suggest that this is likely to occur with most peptide sequences of about 10−20 amino acid residues. Using the same dye twice simplifies the chemistry and also opens the possibility of using different optical configurations for the assay. The peptide AGEPGDDAPSGK-d−R was doubly modified with 5-carboxy-TMR as described, and fluorometric titrations were performed to determine whether dequenching of TMR in the doubly tagged peptide could be used to follow peptide-to-antibody binding. Addition of MAb 5109 to the peptide gave a more than 4-fold increase in TMR fluorescence (Figure 7A). As in the previous experiment, addition of an antibody with different specificity caused a small increase that may have been due to nonspecific binding effects. Such effects may also cause the failure of fluorescence to return completely to the initial values in the competitive assays with unmodified peptide (Figures 6B and 7B).

When untagged AGEPGDDAPSGK-d−R was added to the complex of antibody and doubly TMR-tagged peptide, fluorescence was diminished in a concentration-dependent manner by addition of the competing peptide (Figure 7B). This confirmed the specificity of the peptide−MAb interaction. As a further control, MAb 5109 was added to a doubly TMR-tagged peptide with a core sequence unrelated to its cognate epitope. No increase of fluorescence was detected (not shown).

Phosphopeptide−SH2 Domain Interaction. SH2 domains are small (about 100 amino acids), autonomously folding units of protein structure. They participate in cellular signal transduction of recognizing specific amino acid sequences that contain phosphotyrosine. A doubly dye-tagged phosphopeptide was prepared from a sequence recognized by the more C-terminal of the two SH2 domains of p85α (called here C-p85), a regulatory subunit of phosphoinositol-3-kinase. The peptide, EpYM-VMQC−NH_2, was modified at its free cysteine thiol using 5-maleimido-TMR and then at its α-amino group using 5-carboxy-FL succinimidyl ester.

The product, termed (5-carboxy-FL)-EpYMVMQC(-5-maleimido-TMR)-NH_2, had a fluorescence emission spectrum (λ_{ex} = 493 nm) similar to the collagen-based doubly dye-tagged peptide in Figure 6. When C-p85 SH2 domain was added to it in small molar excess, there was an increase in fluorescent emission from the TMR residue in the peptide (Figure 8A). This was attributed to separation of the dyes as the intervening peptide was bound by the SH2 domain. When free (i.e., not dye-modified) EpYMVMQCNH_2 was added to the complex, it displaced the dye-tagged peptide from the protein-binding site, and the fluorescence change consequent to binding was reversed (Figure 8B).

As noted by Wei et al. (*1*), disruption of fluorescein-TMR contact still leaves fluorescein liable to intermolecular fluorescence quenching by resonance energy transfer to TMR. In fact, this newly viable energy transfer is the basis of the increased fluorescence from TMR used to follow peptide-antibody binding in Figures 6 and 8. An alternative means of following binding is to direct excitation to TMR. Figure 9 compares the fluorescent changes obtained by these two approaches when (5-carboxy-FL)-EpYMVMQC(-5-maleimido-TMR)-NH_2 binds to the C-p85 SH2 domain.

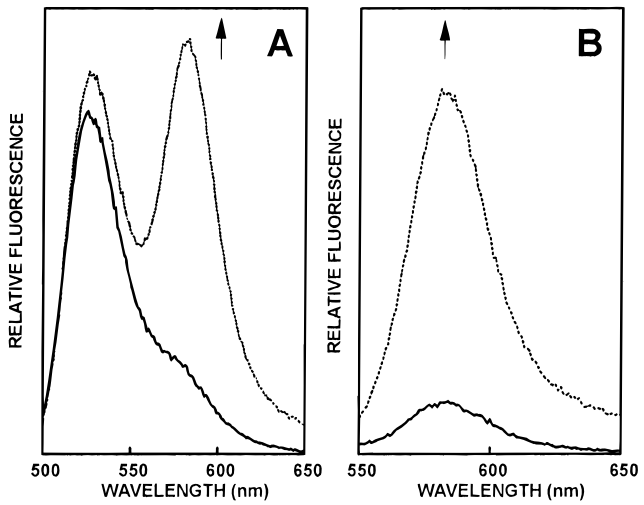

Figure 9. Comparison of the fluorescence changes in (5-carboxy-FL)-EpYMVMQC(-5-maleimido-TMR)-NH_2 (1 μM) consequent to addition of C-p85 SH2 domain (2.5 μM). Solid line, peptide alone; dashed line, peptide with SH2 domain added. (A) $\lambda_{ex} = 493$ nm; (B) $\lambda_{ex} = 540$ nm.

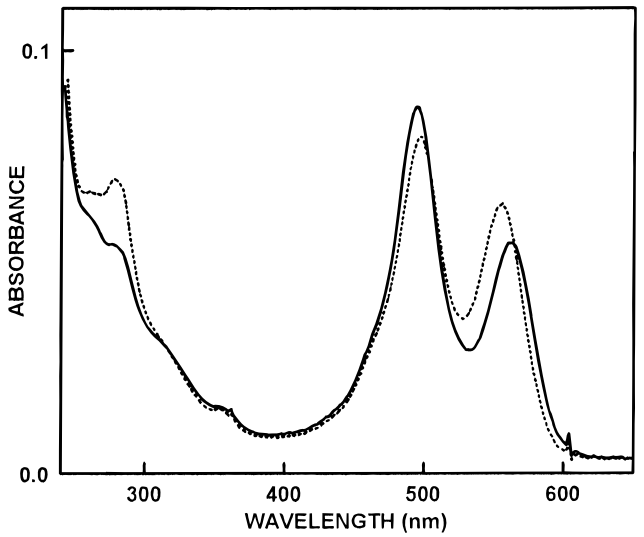

Figure 10. The effect of binding to an SH2 domain on the absorption spectrum of (5-carboxy-FL)-EpYMVMQC(-5-maleimido-TMR)-NH_2. Spectra are those of the dye-tagged phosphopeptide (1 μM) in the absence (solid line) and presence (dashed line) of C-p85 SH2 domain (2 μM). The extra band near 280 nm in the presence of the SH2 domain was due to the protein.

Binding of (5-carboxy-FL)-EpYMVMQC(-5-maleimido-TMR)-NH_2 to the SH2 domain changed its absorption spectrum (Figure 10) in a manner similar to that reported by Wei et al. (*1*) for binding of their hCG-derived peptide to an antibody. Thus, proteolysis, protein binding, and the presence of acetonitrile are three factors that have now been shown to change the spectra of doubly dye-tagged peptides.

DISCUSSION

The ability to switch between optically distinct states is the defining property of fluorescence-based sensors. Switching may be reversible or irreversible and can be achieved in several ways but always requires a change in the physical or chemical environment of a signaling molecule. Although doubly dye-tagged peptides are only a small and new part of this large field (*14*), the biological significance of peptides and proteins adds to their interest. The switch that they undergo is between a weakly fluorescent dye dimer state, and the dye monomer state in which they are more strongly fluorescent. As the system depends on no particular amino acid sequence, it can be applied to many problems.

The innovators of this method (*1*) presented a single example in great detail, while also referring to the broader potential of the system. Disruption of dye-to-dye contact in a peptide tagged with fluorescein and tetramethylrhodamine provided a fluorescence change that reported binding to an immunoglobulin. The driving force for interdye contact was proposed to be the intrinsic mutual affinity of xanthene-type dye molecules (*15*), and the peptide was viewed as a passive linker. A rather different emphasis appeared in papers on a doubly tetramethylrhodamine-tagged peptide, in which conformational features of the peptide linker were sometimes ascribed a principal role (*2*, *6*). Thus, there are two theories about the principle that governs the most useful property of these molecules. Sampling the behavior of several more peptides allowed assessment of the relative importance of dye self-affinity and specific peptide sequence.

All members of a set of five doubly tetramethylrhodamine-tagged peptides ranging 4−20 amino acid residues in length had absorption spectra typical of the rhodamine dimer, with a maximum near 520 nm and a shoulder near 550 nm. The different spectra had subtle variations, suggesting modulation of the dye-to-dye contact by the linking peptide, but their general similarity was obvious. Proteolysis or the presence of acetonitrile gave complete conversion to a rhodamine monomer state in the 9−20 amino acid peptides (Figures 1 and 2), and tetramethylrhodamine in the 4-residue peptide (which lacked a convenient cleavage site) was partly monomerized by acetonitrile.

In the four doubly TMR-tagged peptides tested, the increase in fluorescence upon peptide cleavage was in the range 11−15-fold, suggesting that the efficiency of fluorescence emission from the (mostly) quenched state was roughly equivalent for each product. However, the limited number of cases tested means that this result should be considered preliminary, as it is possible that other compounds with similar absorption spectra may be found to have quite different emission quantum yields. This factor would govern the amount of fluorescence increase that could be obtained as a result of proteolysis or protein binding.

Rhodamine B, a near structural relative of tetramethylrhodamine, dimerizes with K_d near 500 μM in aqueous solution (*16*−*18*). At this concentration, the mean distance between unassociated molecules in solution would be about 150 Å. Linking two copies of the dye with a 20 amino acid peptide, even if extended, brings them to within about 72 Å of each other (*19*). It follows that association of the two dye moieties is to be expected unless the peptide impedes it. This argument suggests that there is no need for "conformation-determining residues" (*5*) to be built into the peptide in order to promote dye-to-dye contact and that the system can be widely applicable rather than being restricted to special types of peptide.

On testing the original system composed of fluorescein and tetramethylrhodamine, we noted that proteolysis and acetonitrile separately disrupted the heterodimer of these dyes (Figures 4 and 5). However, peptides doubly tagged with fluorescein showed little spectral response to these factors (not shown). The presence of tetramethylrhodamine appeared conducive to dye association, whether with itself or fluorescein.

The fluorescein-tetramethylrhodamine and tetramethylrhodamine-tetramethylrhodamine systems were then compared directly. Two variants of a peptide based on an acidic region of type II collagen were modified with the dye pairs, and the binding of each one to a monoclonal antibody was monitored by fluorescent titrations. The fluorescein-tetramethylrhodamine system performed essentially as reported (*1*), with antibody binding giving a more than 4-fold increase in fluorescence at 580 nm (from excitation at 493 nm) (Figure 6A). The tetramethylrhodamine-tetramethylrhodamine system, in which tetramethylrhodamine was directly excited at 540 nm, gave a comparable increase in fluorescence at 580 nm (Figure 7A). In both cases, an unmodified peptide was competitive with the dye-tagged peptide, and monoclonal antibody with no ability to recognize the peptide linker failed to generate a fluorescence increase outside the range of experimental variation due to cuvette replacement.

The exact manner in which tetramethylrhodamine self-associates remains unsettled. Packard et al. (*2*, *6*) have proposed that dimerization occurs in an edge-on rather than stacked fashion. This result was derived from application of exciton theory (*20*), which previously led other authors studying rhodamine dimerization to arrive at a wide range of structures (*17*, *18*, *21*). The problem has also been addressed directly by NMR (*22*) and by crystallography of complexes between Bence-Jones proteins and multiple dye molecules (*23*). The effect of acetonitrile would seem to argue for a hydrophobic component to the forces causing dye dimer formation to be favored. This result may be interpretable in more than one way, but it points most obviously to the dye association being driven by a thermodynamic preference for the hydrophobic dyes to be shielded from the aqueous solvent. With free dyes, this occurs even at the cost of surpassing the entropic barrier associated with bringing them together out of free solution. Making the solvent less polar by adding acetonitrile makes the monomeric state more favored again, and this also occurs with dyes tethered to a peptide.

This paper has confirmed and extended the results of Wei et al. (*1*) by using doubly dye-tagged peptides to assay the binding function of an antibody against a collagen-derived peptide and an SH2 domain against a particular phosphopeptide. The specificity of both interactions was confirmed by experiments with competitive, unlabeled peptides. There are multiple ways to measure binding events of this kind, each providing certain benefits; these include enzyme-linked immunospecific assays, surface plasmon resonance-based biosensors, and the fluorescence polarization method. As noted by Wei et al. (*1*), perhaps the main advantages of the method using doubly tagged peptides is the fact that measurements are made on homogeneous solutions and that simple fluorescence measurements are all that is required.

LITERATURE CITED

(1) Wei, A.-P., Blumenthal, D. K., and Herron, J. N. (1994) Antibody-mediated fluorescence enhancement based on shifting the intramolecular dimer-monomer equilibrium of fluorescent dyes. *Anal. Chem. 66*, 1500−1506.

(2) Packard, B. Z., Toptygin, D. D., Komoriya, A., and Brand, L. (1996) Profluorescent protease substrates: Intramolecular dimers described by the exciton model. *Proc. Natl. Acad. Sci. U.S.A. 93*, 11640−11645.

(3) Packard, B. Z., Toptygin, D. D., Komoriya, A., and Brand, L. (1997) Design of profluorescent protease substrates guided by exciton theory. *Methods Enzymol. 278*, 15−23.

(4) Packard, B. Z., Toptygin, D. D., Komoriya, A., and Brand, L. (1997) Characterization of fluorescence quenching in bifluorophoric protease substrates. *Biophys. Chem. 67*, 167−176.

(5) Packard, B. Z., Komoriya, A., Toptygin, D. D., and Brand, L. (1997) Structural characteristics of fluorophores that form intramolecular H-type dimers in a protease substrate. *J. Phys. Chem. B 101*, 5070−5074.

(6) Packard, B. Z., Komoriya, A., Nanda, V., and Brand, L. (1998) Intramolecular excitonic dimers in protease substrates - modification of the backbone moiety to probe the H-dimer structure. *J. Phys. Chem. B 102*, 1820−1827.

(7) Packard, B. Z., Toptygin, D. D., Komoriya, A., and Brand, L. (1998) Intramolecular resonance dipole−dipole interactions in a profluorescent protease substrate. *J. Phys. Chem. B 102*, 752−758.

(8) Geoghegan, K. F., Dixon, H. B. F., Rosner, P. J., Hoth, L. R., Lanzetti, A. J., Borzilleri, K. A., Marr, E. S., Pezzullo, L. H., Martin, L. B., LeMotte, P. K., McColl, A. S., Kamath, A. V., and Stroh, J. G. (1999) Spontaneous α-*N*-6-phosphogluconoylation of a "His Tag" in *Escherichia coli*: the cause of extra mass of 258 or 178 Da in fusion proteins. *Anal. Biochem. 267*, 169−184.

(9) Geoghegan, K. F., Emery, M. J., Martin, W. H., McColl, A. S., and Daumy, G. O. (1993) Site-directed double fluorescent tagging of human renin and collagenase (MMP-1) substrate peptides using the periodate oxidation of N-terminal serine. An apparently general strategy for provision of energy-transfer substrates for proteases. *Bioconjugate Chem. 4*, 537−544.

(10) Geoghegan, K. F. (1996) Improved method for converting an unmodified peptide to an energy-transfer substrate for a proteinase. *Bioconjugate Chem. 7*, 385−391.

(11) Ishii, Y., and Lehrer, S. S. (1986) Effects of the state of the succinimido-ring on the fluorescence and structural properties of pyrene maleimide-labeled αα-tropomyosin. *Biophys. J. 50*, 75−80.

(12) Ravdin, P., and Axelrod, D. (1977) Fluorescent tetramethyl rhodamine derivatives of α-bungaratoxin: preparation, separation and characterization. *Anal. Biochem. 80*, 585−592.

(13) Meadows, D. L., Shafer, J. S., and Schultz, J. S. (1991) Determining the extent of labeling for tetramethylrhodamine protein conjugates. *J. Immunol. Methods 143*, 263−272.

(14) De Silva, A. P., Gunaratne, H. Q. N., Gunnlaugsson, T., Huxley, A. J. M., McCoy, C. P., Rademacher, J. T., and Rice, T. E. (1997) Signaling recognition events with fluorescent sensors and switches. *Chem. Rev. 97*, 1515−1566.

(15) Valdes-Aguilera, O., and Neckers, D. C. (1989) Aggregation phenomena in xanthene dyes. *Acc. Chem. Res. 22*, 171−177.

(16) Selwyn, J. E., and Steinfeld, J. I. (1972) Aggregation equilibria of xanthene dyes. *J. Phys. Chem. 76*, 762−774.

(17) Gál, M. E., Kelly, G. R., and Kurucsev, T. (1973) Derivation and interpretation of the spectra of aggregates. Part 2.- Dimer of Rhodamine B in aqueous solutions. *J. Chem. Soc., Faraday Trans. 2 69*, 395−402.

(18) Obermueller, G., and Bojarski, C. (1977) Electronic absorption spectra and dimeric properties of rhodamines in solutions. *Acta Phys. Polon. A52*, 431−444.

(19) Creighton, T. E. (1983) *Proteins. Structures and Molecular Properties*, W. H. Freeman, New York.

(20) McRae, E. G., and Kasha, M. (1964) The molecular exciton model. *Physical Processes in Radiation Biology.* (L. Augenstein, R. Mason, and B. Rosenberg, Eds.) pp 23−42, Academic Press, New York.

(21) Arbeloa, I. L., and Ojeda, P. R. (1982) Dimeric states of rhodamine B. *Chem. Phys. Lett. 87*, 556−560.

(22) Ilich, P., Mishra, P. K., Macura, S., and Burghardt, T. P. (1996) Direct observation of rhodamine dimer structures in water. *Spectrochim. Acta, Part A 52*, 1323−1330.

(23) Edmundson, A. B., Ely, K. R., and Herron, J. N. (1984) A search for site-filling ligands in the Mcg Bence-Jones dimer: crystal binding studies of fluorescent compounds. *Mol. Immunol. 21*, 561−576.

BC9900845

Site-Specific Polymer−Streptavidin Bioconjugate for pH-Controlled Binding and Triggered Release of Biotin

Volga Bulmus,† Zhongli Ding, Cynthia J. Long, Patrick S. Stayton,* and Allan S. Hoffman*

Department of Bioengineering, University of Washington, Seattle, Washington 98195. Received July 13, 1999

Low molecular weight copolymers of acrylic acid (AAc) and *N*-isopropylacrylamide (NIPAAm) have been synthesized with reactive OH groups at one end, using a chain transfer polymerization technique. The copolymer displays both pH and temperature sensitivity over a wide and useful range of pHs and temperatures, which permits both pH and temperature control of polymer conformation. This copolymer has been conjugated to a specific cysteine thiol site inserted by genetic engineering near the recognition site of streptavidin (SAv). In this paper, we demonstrate that this bioconjugate can provide pH control of biotin binding to and triggered release from the mutant SAv. These actions are relevant to affinity separations, biosensors, diagnostics, enzyme processes, and targeted delivery of drugs or chemical agents, labels, and other signals.

INTRODUCTION

Random conjugates of stimuli-responsive (or "smart") polymers to proteins have received increasing attention in recent years due to the many potential applications of such interesting hybrid molecular systems in affinity separations, immunoassays, enzyme, and cell processes and drug delivery (*1*−*3*). Site-specific conjugates of polymers to proteins are a special class of such conjugates. In most published examples of site-specific conjugates, the polymer is generally conjugated away from the active site in order to minimize its potential interference on protein activity (*4*−*9*). However, in an earlier study, we conjugated a temperature-sensitive polymer, poly(*N*-isopropylacrylamide) (NIPAAm), to a genetically engineered streptavidin (SAv) at a specific site which was specifically designed to be near the biotin-binding site of SAv (*10*). We found that small changes in temperature, which cause the polymer coil to collapse, simultaneously also caused blockage of biotin binding to SAv. More recently, we have shown that the thermally induced collapse of this conjugated polymer can cause the release of a significant fraction of already-bound biotin from the SAv-binding pocket. (*11*) In the work presented here, we have designed and synthesized a pH-sensitive polymer, which is a copolymer of NIPAAm and acrylic acid (AAc), and conjugated this copolymer to the same specific site on the genetically engineered SAv molecule. We have demonstrated that (a) lowering the pH to cause the polymer to collapse leads to blockage of biotin binding, (b) raising the pH to cause the polymer to fully hydrate permits biotin to bind, and (c) lowering the pH once again to cause the collapse of the polymer causes partial ejection of the already-bound biotin. These actions are relevant to affinity separations, biosensors, diagnostics, enzyme processes, and targeted delivery of drugs or chemical agents, labels and other signals.

† Present address: Bioengineering Division, Hacettepe University, Turkey.

* To whom correspondence should be addressed. (A.S.H.) Box 352255 at the University of Washington. Phone: (206) 543-9423. Fax: (206) 543-6124. E-mail: hoffman@u.washington.edu. (P.S.S.) Box 352125 at the University of Washington. Phone: (206) 685-8148. Fax: (206) 685-8256. E-mail: stayton@u.washington.edu.

MATERIALS

N-Isopropylacrylamide (Eastman Kodak, Rochester, NY) was purified by recrystallization from *n*-hexane. Acrylic acid (AAc, Aldrich, Milwaukee, WI) was redistilled in a vacuum. Dimethylformamide (DMF, J. T. Baker, Phillisburg), and ethylene chloride, anhydrous (Sigma, St. Louis, MO) were used without further purification. 2-Mercapthoethanol (ME, 98%, Aldrich, Milwaukee, WI) was redistilled before used. 2,2′-Azoisobutyronitrile (AIBN, J. T. Baker, Phillisburg, USA) was recrystallized from methanol. Potassium *tert*-butoxide (95%, Aldrich, Milwaukee, WI) and divinyl sulfone (DVS, Sigma, St. Louis, MO) were used as received. Dynabeads M-280 (tosyl-activated) and d-[8,9-^{3}H]biotin (^{3}H-biotin) were purchased from Dynal (Norway) and Amersham Life Science (UK), respectively. All other reagents used were of analytical grade.

METHODS

Synthesis and Characterization of poly(NIPAAm-*co*-AAc). A series of OH-terminated copolymers of NIPAAm and AAc [poly(NIPAAm-*co*-AAc)] was synthesized by chain transfer free-radical copolymerization of NIPAAm and AAc in DMF, using mercaptoethanol as the chain transfer agent and AIBN as the initiator (*12*) (see also Figure 1a). In a typical copolymerization experiment, 100 mmol of NIPAAm, various amounts of AAc, 4 mmol of ME, and 1 mmol of AIBN were dissolved in 40 mL of DMF. Copolymerizations were carried out at 60 °C under nitrogen atmosphere. Table 1 gives the experimental conditions of the NIPAAm and AAc copolymerizations. The final product was obtained by precipitating the reaction solution in diethyl ether, filtering through a sintered glass filter, washing repeatedly with diethyl ether, and drying in a vacuum at 40 °C for 24 h. The phase separation temperature, also called the lower critical solution temperature (LCST), was determined for each of the different copolymers. We chose one of the polymers to conjugate to the genetically engineered SAv in the study reported here. This polymer had a MW of ca. 2800 and a composition of 5.5 mol % AAc and 94.5 mol % NIPAAm.

Molecular weight of the copolymer was determined by vapor pressure osmometry (VPO, model OSV111 from

10.1021/bc9901043 CCC: $19.00 © 2000 American Chemical Society
Published on Web 12/03/1999

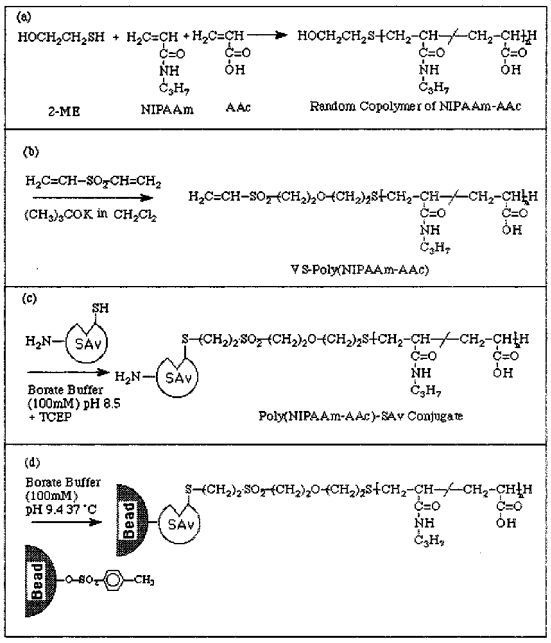

Figure 1. (a) Synthesis of OH-terminated copolymer (b) divinyl sulfone (DVS) derivatization of copolymer OH group (c) conjugation of VS-terminated copolymer to mutant streptavidin (SAv) cysteine SH groups, and (d) immobilization of copolymer−streptavidin conjugate onto tosyl-activated magnetic microbeads via streptavidin lysine amino groups.

Table 1. Copolymerization Recipes and Conditions[a]

experiment	$[M_1]/[M_2]/[CT]/[I]$[b]	time (min)
1	100.0/8.3/4.0/1.0	120
2	100.0/5.6/4.0/1.0	60
3	100.0/4.0/4.0/1.0	15
4	100.0/4.0/4.0/0.5	60
5	100.0/3.0/4.0/1.0	60
6	100.0/1.0/4.0/1.0	60
7	100.0/1.0/4.0/1.0	20

[a] Polymerization was performed at 60 °C; dimethylformamide as solvent, 40 mL. [b] Mol ratio of NIPAAm $[M_1]$, AAc $[M_2]$, ME [CT], and AIBN [I].

Knauer, Germany). The composition of the copolymer was analyzed by dissolving the copolymer in an excess of 5 mM NaOH to neutralize the carboxyl groups, and then back-titrating the excess of NaOH with 5 mM HCl. Lower critical solution temperatures (LCST) at different pHs were obtained spectrophotometrically (UV Spectrophotometer, Bausch & Lomb Spectronic 1001) at 500 nm. Copolymer solutions at 2.0 mg/mL in citric-phosphate buffers (CPB, 50 mM) were used for LCST measurements. The ionic strength of the buffer solutions was adjusted by adding an appropriate amount of NaCl. The temperature at 10% of maximum absorbance of the copolymer solution was defined as the LCST.

Derivatization of poly(NIPAAm-*co*-AAc). Vinyl sulfone (VS)-terminated poly(NIPAAm-*co*-AAc) was prepared by the reaction of the hydroxyl end group of the copolymer (1.9 mmol) with 10 mol % excess of DVS in the presence of potassium-*tert*-butoxide (2.5 mmol) as a base (Figure 1b). The reaction was carried out in anhydrous methylene chloride (100 mL) under nitrogen atmosphere at room temperature for 18 h. After the neutralization of reaction solution with concentrated acetic acid, the product was recovered by precipitation in diethyl ether. The degree of end group conversion was estimated using ^{1}H NMR (in dimethyl sulfoxide-d_6).

Preparation of a Cysteine Mutant of Streptavidin. Streptavidin is a tetramer of identical monomers. The glutamic acid at residue 116 of the streptavidin was selected as the specific site for polymer conjugation, and it was replaced with cysteine to provide a thiol group for reaction with the vinyl sulfone terminal group on the polymer. Thus, each streptavidin tetramer will have four new cysteines, one each per subunit. The E116C streptavidin mutant was constructed via cassette mutagenesis. Synthetic oligonucleotides containing the codon coding for cysteine were substituted for the sequence coding for the native glutamate at position 116. This cassette was cloned directly into a pUC18/SA plasmid between the *Msc*I and *Mlu*I restriction enzyme sites. This plasmid and gene construct has been previously described (*13*) and was designed for bacterial expression with *Escherichia coli*. The DNA sequence of the mutant gene was confirmed using automated dyedeoxy sequencing and subsequently subcloned into pET21a (Novagen, Madison, WI) for expression in *E. coli* strain BL21(DE3). The protein was expressed and refolded using established protocols (*13*). Mass spectrometry was performed to confirm the production of the correct mutant amino acid sequence, and biotin-binding studies confirmed that the biotin-binding affinity was unaltered by mutation (data not shown}.

Site-Specific Conjugation of VS-Derivatized poly-(NIPAAm-co-AAc) to Mutant Streptavidin. Conjugation of the VS-derivatized copolymer to the cysteine SH group of the mutant protein was carried out at pH 8.5 in 100 mM borate buffer containing 100 mM NaCl and 5 mM EDTA at room temperature for 24 h (Figure 1c). The molar ratio of copolymer to the protein was 80:1. Tris-(2-carboxyethyl)phosphine (TCEP) was used as a disulfide reducing agent. After 24 h, the pH of the reaction solution was lowered with dilute HCl to quench the reaction, and then the copolymer−protein conjugate and any unreacted polymer were separated from the unconjugated protein by thermal precipitation at 39 °C, followed by centrifugation at 39 °C and 15 000 rpm for 20 min. The recovered conjugate and unreacted polymer were washed three times by dissolving in 1 mL of borate buffer (100 mM) at pH 8.5 at room temperature and thermally precipitating, using the same procedure. The conjugation efficiency was estimated spectrophotometrically at 280 nm.

Immobilization of the poly(NIPAAm-*co*-AAc)−Streptavidin Conjugate onto the Magnetic Beads. Copolymer−streptavidin conjugates were then immobilized onto tosyl-activated magnetic microbeads (5 mg) in 100 mM borate buffer (3 mL) at pH 9.4 for 24 h (Figure 1d). The temperature for immobilization was 37 °C. After immobilization, the conjugate-immobilized microbeads were magnetically separated from the reaction solution and washed three times with phosphate buffer (100 mM) at pH 7.4. We presumed that this procedure removed any excess, unreacted polymer from the immobilization reaction step. Immobilization efficiency was estimated by calculating the amount of depleted conjugate in the supernatant by means of UV absorption at 280 nm.

Determination of Ligand Blocking and Release Capacity of poly(NIPAAm-*co*-AAc)−Streptavidin Conjugates. To determine the ligand binding and release capacity of the copolymer−streptavidin conjugate, we measured the binding and release of ^{3}H-biotin at four different pHs (pH 4.0, 5.0, 6.0, and 7.4) using a β-counter (Beckman LS 7000) to quantitate the biotin in the different solutions. In a typical three-step assay, an excess amount of a mixture of ^{3}H-biotin and cold biotin was first incubated (at 37 °C for 1 h in CPB at a specific pH) with the polymer−streptavidin conjugate on the

microbeads. After removing samples from the supernatants for β-counting, the temperature was lowered to 4 °C for 1 h and additional samples were taken from the supernatants for β-counting. In the last step, the temperature was raised once again to 37 °C for 1 h and samples for β-counting were taken from the supernatants of the microbead suspensions. As controls, biotin binding, and release capacity of unconjugated mutant streptavidin and wild-type streptavidin that had been similarly immobilized onto the beads were measured under each set of conditions, using the same procedure as described above.

RESULTS AND DISCUSSION

Although the focus of this study is to demonstrate pH control of ligand binding to and triggered release from a polymer−protein bioconjugate, there are several reasons for combining both pH and temperature sensitivity in the copolymer that we have studied. First, the phase transition behavior of these copolymers can be controlled by more than one environmental variable, thus increasing the opportunities for designing polymer compositions with temperature, pH, and ionic strength responses that meet the requirements for a particular application. Second, there is a potential cooperative effect of (lowered) pH and (raised) temperature on the phase transition of these copolymers due to H-bonding between the AAc and NIPAAm components. This mutual influence can be used to design polymer systems with pH-controlled temperature sensitivity or with temperature-controlled pH sensitivity. The chain transfer polymerization technique was employed in order to prepare hydroxyl-terminated poly(NIPAAm-*co*-AAc). 2-Mercaptoethanol (ME) and 2,2′-azoisobutyronitrile (AIBN) was used as a chain transfer agent and a free radical initiator at 60 °C, respectively. Figure 1 shows the synthesis of the copoly(NIPAAm-AAc).

The derivatization of the OH end group of the copolymer with DVS provided single vinyl sulfone end groups, for subsequent reaction with the genetically engineered cysteine SH groups near the biotin-binding site (Figure 1b). DVS modification of the copolymer was confirmed with ^{1}H NMR in dimethyl sulfoxide-d_6. The product showed characteristic vinyl sulfone peaks at 6.21 ppm (two hydrogens) and 6.97 ppm (one hydrogen). The degree of end group conversion was found to be 100% from the ^{1}H NMR results.

As noted above, vinyl sulfone (VS) groups are highly selective for reaction with SH groups. Mutant streptavidin was conjugated in solution at pH 8.5 by reaction of the protein SH group with the VS derivative of the copolymer (Figure 1c). After the conjugation reaction, any remaining unconjugated protein was separated from the reaction solution by thermally induced precipitation of the polymer-conjugated protein and free copolymer at 39 °C. This is one of the advantages of utilizing a pH-sensitive polymer that is also temperature sensitive. The immobilization of the conjugate onto the beads (Figure 1d) via reaction of the protein lysine amino groups with the tosyl groups on the beads then permitted the removal of the excess, unreacted free copolymer from the microbead-immobilized, conjugated streptavidin since the unreacted polymer VS end group should not react with the tosyl groups on the beads. This is one of several conveniences of using magnetic microbeads in the biotin binding and release assays.

One of our aims in this study was to synthesize a random copolymer of NIPAAm and AAc which retains its pH-controlled temperature sensitivity over a wide and useful pH range, especially including physiological conditions. Copolymers of NIPAAm with AAc were expected to have LCSTs above the LCST of homo-PNIPAAm (32 °C) at all pHs, because both the protonated COOH and ionic COO^- states of the AAc monomer units are more hydrophilic than NIPAAm units. For high AAc content in the copolymer, as pH is raised above the pK_a of AAc, the LCST cannot be observed, which means a loss of thermosensitivity (*14, 15*). This occurs simply due to the increased overall polymer hydrophilicity. To avoid the loss of thermosensitivity, a random copolymer which contains a low content of AAc was prepared. Therefore, we worked with high NIPAAm to AAc molar ratios (100/8.3−100/1.0) in the starting mixture for copolymerization. Table 2 gives the results of the copolymerization of NIPAAm with AAc. AAc contents of copolymers were determined by back-titration. The average molecular weight of the copolymers was estimated by vapor pressure osmometry measurements.

Table 2. Results of NIPAAm and AAc Copolymerizations

experiment	conversion (%)[a]	MW	AAc content (mol %)	no. of AAc units[b]	no. of NIPAAm units[b]
1	87	4700	10.0	4.3	33.9
2	62	ND[c]	6.6	ND	ND
3	27	ND	6.1	ND	ND
4	55	2800	5.5	1.4	23.9
5	52	2100	4.9	0.9	18.0
6	58	ND	1.3	ND	ND
7	22	1200	1.6	0.2	10.5

[a] Monomer conversion based on weight %. [b] Number of AAc and NIPAAm units in a copolymer chain. [c] ND = not determined.

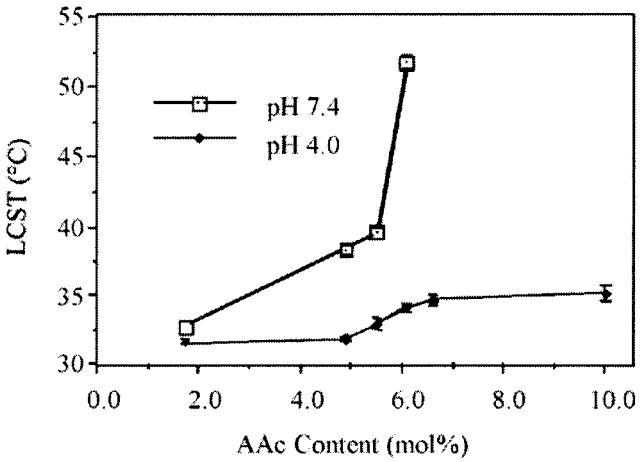

Figure 2. Effect of AAc content on the LCSTs of poly(NIPAAm-*co*-AAc) at pH 4.0 and 7.4. LCSTs were determined by spectrophotometric measurement of the absorbance (at 500 nm) of 0.2 wt % copolymer solutions in citrated phosphate buffer (50 mM). The temperature at 10% of the maximum absorbance was defined as the LCST.

Figure 2 presents the effect of copolymer composition on the LCST. At pH 7.4, as the AAc content in the copolymer increases, and the copolymer chains become more hydrophilic because of the ionization of COOH groups. Increase in the hydrophilicity of the chains leads to the rise in LCST. At pH 4.0 and when the AAc content in the copolymer is lower than 6 mol %, the LCSTs increase with the increase of the AAc content, even though the −COOH groups on the copolymer chain are not ionized at this pH. This is simply due to the greater hydrophilicity of the COOH AAc side group compared to the N-isopropyl side group of NIPAAm. However, for higher AAc contents at pH 4.0, the LCST gradually levels

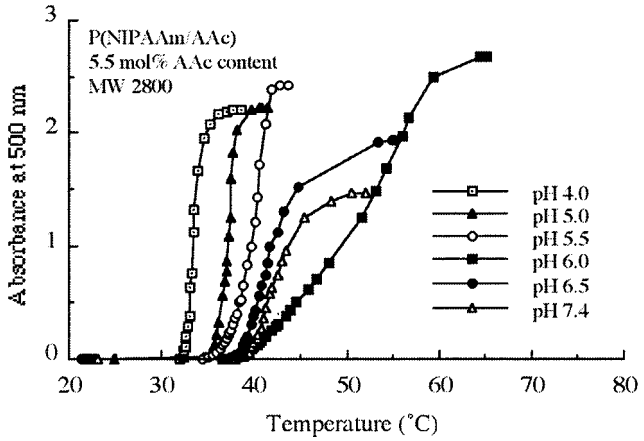

Figure 3. Change in absorbance of 0.2 wt % copolymer solutions at different pHs with temperature. Citric-phosphate buffer (CPB, 50 mM) was used to control the pH of the solutions. An appropriate amount of NaCl was added in order to maintain the same ionic strength of the buffer solutions at different pHs.

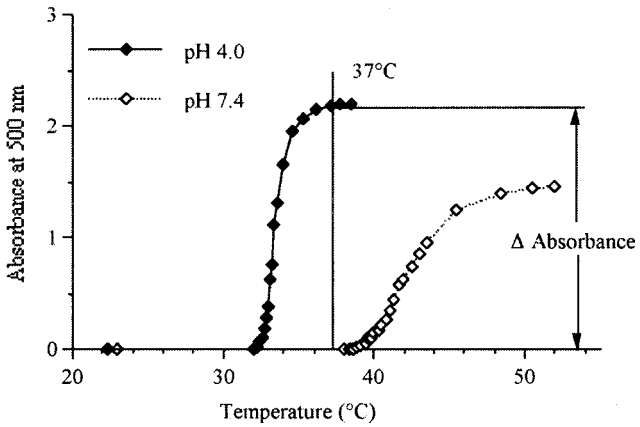

Figure 4. Change in light absorbance vs temperature for 0.2 wt % solutions of the 5.5 mol % AAc and 94.5 mol % NIPAAm copolymer at pH 4.0 and 7.4. Citric-phosphate buffers (CPB, 50 mM) were employed at the two different pHs. Ionic strengths were kept the same for each of the buffer solutions by adding NaCl.

out. This behavior might be explained by compensation for the increased hydrophilicity by an increased possibility of inter or intramolecular hydrogen bonding. That is, when the AAc content increases, it may be possible for hydrogen bonds to form between two COOH or COOH and CONH groups. These possible hydrogen bonds should cause a reduction in the hydrophilicity (or an increase in the hydrophobicity) of the copolymer microenvironment by preventing the access of water molecules to NIPAAm and AAc units.

The temperature-induced change in light absorbance of poly(NIPAAm-*co*-AAc) having a 5.5 mol % AAc content was examined using 0.2 wt % copolymer solutions in CPB (50 mM) at different pHs (see Figure 3). It is clear that with a fixed amount of AAc content in the copolymer, increasing pH leads to the increase in the phase transition temperature of the copolymer solution at constant ionic strength. As the pH of the solution is increased, the $COOH/COO^-$ ratio in the copolymer decreases, which makes the copolymer chains more hydrophilic. The decrease in the maximum absorbance at higher pH might be due to the formation of less condensed aggregates of copolymer chains in the solution because of the more hydrophilic character of the copolymer chains and possible ionic repulsion between chains at higher pHs. In other words, at higher pH, the copolymer chains are in their most soluble state, and therefore, when they precipitate and form aggregates, the copolymer solution becomes less cloudy because the precipitated aggregates leave more open space in the solution for light to pass through. This could be the cause of the observed gradual leveling out of the light absorbance of the solution, as seen in Figure 3. It is worth noting that even though the pH range studied included pHs above and below the pK_a of AAc, the 5.5 mol % copolymer retained its sharp phase transition behavior at all pHs and, in addition, the temperature-induced phase transition occurred over a useful temperature range (between 33 and 40 °C).

We chose the copolymer having 5.5 mol % AAc content for conjugation to SAv because of its pH- and temperature-dependent phase transition behavior (Figure 4). This copolymer is completely soluble in citric-phosphate buffered saline (CPBS) at pH 7.4 and 37 °C and essentially insoluble in CPBS at pH 4.0 and 37 °C. Thus, it afforded an opportunity to test the effect of pH on biotin binding and release from the conjugate at 37 °C.

Figure 5 shows the effect of pH on the relative biotin binding at two temperatures, 4 and 37 °C for the

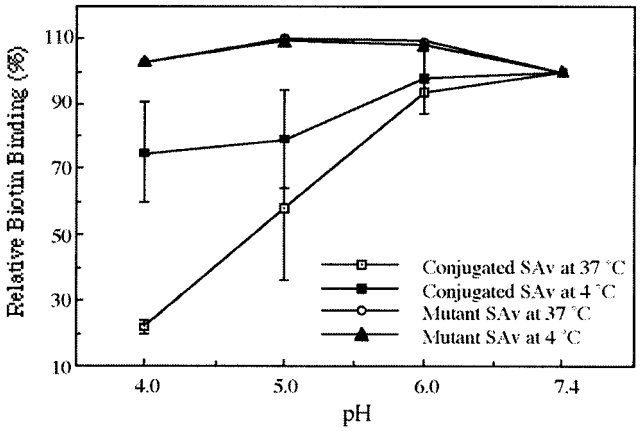

Figure 5. Effect of pH on the relative ^{3}H-biotin binding to poly-[NIPAAm-*co*-AAc]−streptavidin conjugate at 4 and 37 °C compared to the E116C streptavidin mutant control. Relative biotin binding was calculated as [(amount of ^{3}H-biotin binding at pH 4.0) − (binding at 7.4)]/[amount of ^{3}H-biotin binding at pH 7.4] × 100.

polymer−streptavidin conjugate and the unconjugated mutant streptavidin. To understand and interpret the biotin-binding data in Figure 5, it would be useful to try to visualize the effect of pH and temperature on the conformation of the copolymer as it might appear on the streptavidin conjugate. This is shown in Figure 6. It can be expected that the pH- and temperature-sensitive copolymer will be the most collapsed at the lowest pH (4.0) and highest temperature (37 °C) and the most expanded and hydrated at the highest pH (7.4) and lowest temperature (4 °C). Repulsion of the ionized carboxyl groups at the pH 7.4 would be expected to expand the polymer beyond a random coil. Furthermore, since NIPAAm is the major component of the copolymer, the conformation would be expected to be more sensitive to temperature than to pH, leading to more condensed conformations at any particular pH and 37 °C vs the same pH and 4 °C; this can also be noted in Figure 3. Thus, the increases in relative biotin binding with increase in pH seen for the conjugate at 4 or 37 °C in Figure 5 are most likely due to the increase in coil sizes of the copolymer chain as the carboxyl groups ionize, with the greater rise in relative binding with pH seen at 37 °C being due to the temperature sensitivity of PNIPAAm. It can also be seen in Figure 5 that the unconjugated

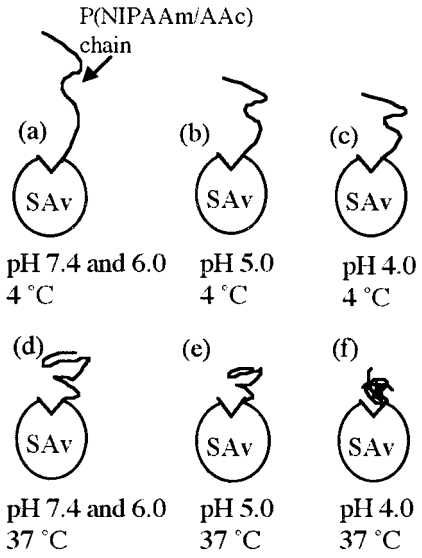

Figure 6. Proposed conformations of the polymer chain coils of poly(NIPAAm-*co*-AAc) conjugated to mutant streptavidin (SAv) at various pHs at 4 and 37 °C.

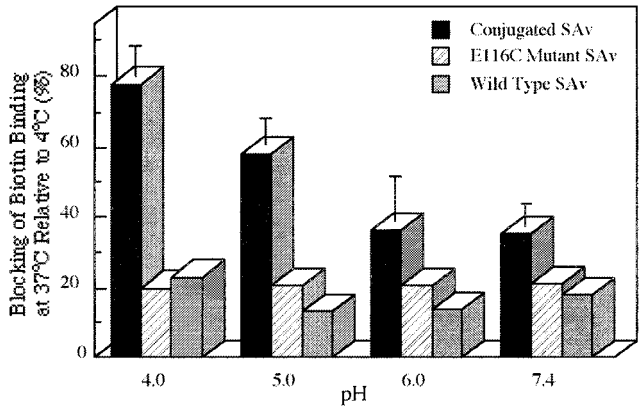

Figure 7. Effect of pH on blocking of ^{3}H-biotin binding to the poly[NIPAAm-*co*-AAc]−streptavidin conjugate at 37 °C relative to 4 °C, compared to the wild-type and E116C streptavidin mutant controls. Blocking at 37 °C relative to 4 °C for each pH value was calculated as [(amount of ^{3}H-biotin binding at 4 °C) − (binding at 37 °C)]/[amount of ^{3}H-biotin binding at 4 °C] × 100.

mutant streptavidin does not exhibit any significant pH and/or temperature-dependent biotin binding over the ranges studied.

The data in Figure 5 are replotted in Figure 7 as percent blocking of biotin binding at 37 °C relative to 4 °C. It is clear from these bar graphs that the ability of the conjugated copolymer chain to prevent the biotin from binding at 37 vs 4 °C is strongly dependent on the pH. Blocking efficiencies at 37 °C relative to 4 °C were 78% at pH 4.0 and 58% at pH 5.0. At pH 6.0 and 7.4, there was less efficient blocking of biotin, e.g., 63 and 65%, respectively. Although the copolymer has an LCST above 37 °C at pH 6.0 and pH 7.4, the copolymer-conjugated streptavidin is still able to show partial biotin-blocking capacities of 37 and 35% at 37 °C relative to 4 °C, respectively. Neither the wild-type nor the mutant streptavidin controls showed a significant effect of pH and/or temperature on biotin binding.

The pH-triggered release of bound biotin from the polymer-conjugated SAv, unconjugated mutant, and wild-type SAv was also measured at four different pHs. This was done for each pH in a three-step sequence by first measuring biotin binding (a) at 37 °C, where conjugated

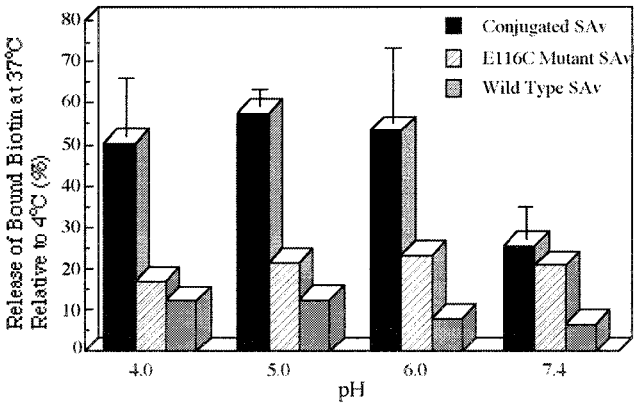

Figure 8. Effect of pH on release of bound ^{3}H-biotin from the poly[NIPAAm-*co*-AAc]-streptavidin (SAv) conjugate at 37 °C relative to 4 °C, compared to the wild type and E116C streptavidin mutant controls. Release at 37 °C relative to 4 °C for each pH value was calculated as [(amount of ^{3}H-biotin bound at 4 °C) − (bound at 37 °C)]/[amount of ^{3}H-biotin bound at 4 °C] × 100.

sites should be blocked, then (b) at 4 °C where the conjugated sites should be unblocked, and finally (c) at 37 °C to assay the triggered release of those biotin molecules previously bound at 4 °C. The pH-triggered release is represented in Figure 8 by the percent release of bound biotin at 37 °C relative to 4 °C. The percentage drop in the amount of biotin bound to the copolymer−streptavidin conjugate as temperature is raised from 4 to 37 °C was found to be 50−58% in the range of pHs between 4.0 and 6.0, while at pH 7.4, 26% of the biotin that is bound at 4 °C is released from the conjugate at 37 °C. Release of bound biotin from the unconjugated mutant SAv control at 37 °C relative to 4 °C was found to be 17−23% and did not show any significant dependence on pH and/or temperature. The wild-type streptavidin control showed only 6−13% release of bound biotin regardless of pH and/or temperature of the medium.

One explanation of these data is that the off-rate of biotin from a copolymer-conjugated streptavidin-binding site may be influenced more by pH and temperature than for the unconjugated mutant or wild-type streptavidin, due to allosteric changes in the streptavidin-binding site conformation caused by the conjugated copolymer coil when it collapses. Perhaps some hydrophobic interactions between the collapsed polymer and the protein-binding site region may be involved. We are looking further into the mechanism of the pH-triggered release of bound biotin induced by the "smart" copolymer conjugated near the biotin-binding site.

CONCLUSIONS

We have synthesized low molecular weight copolymers of AAc and NIPAAm having both pH and temperature sensitivity over a wide and useful range of pHs and temperatures. The copolymers have reactive OH groups at one end, which is used to conjugate to a specific SH site on a genetically engineered streptavidin molecule. By incorporation of as little as 5.5 mol % of AAc in a random copolymer with NIPAAm, we have prepared a copolymer that, at 37 °C, is completely soluble at pH 7.4 and insoluble at pH 4.0. When this copolymer is conjugated to a specific site near the biotin-binding site of streptavidin, biotin binding at 37 °C is significantly reduced at pH 4.0 compared to pH 7.4. This is most likely due to the more compact copolymer coil at pH 4.0, 37 °C compared to pH 7.4, 37 °C. We were also able to trigger the release of bound biotin at 37 °C by lowering the pH

from 7.4 to 4.0. The mechanism of this action is not yet completely understood, but it may be related to an allosteric effect of the collapsing polymer coil on the binding site configuration, leading to a greater off-rate of the biotin. The effect of pH and temperature on the blocking and triggered-release of biotin could be useful in a variety of separations and diagnostic applications and may also be useful for pH-triggered drug delivery at body sites where the pH is significantly below 7.0, such as the stomach, vagina, salivary glands and within intracellular vesicles such as endosomes and lysosomes.

ACKNOWLEDGMENT

One of the authors (V.B.) would like to thank the Scientific and Technical Research Council of Turkey (TUBITAK) for support of her living expenses while at the University of Washington. We would also like to acknowledge support of NIH, NIGMS Grant R01-GM-53771-01, which evolved from NSF Grant BCS-9101716. We are also grateful for the support of the Office of Technology Transfer at the University of Washington, the Washington Technology Center, and the Washington Research Foundation.

LITERATURE CITED

(1) Hoffman, A. S. (1995) Intelligent Polymers in Medicine and Biotechnology. *Macromol. Symp. 98*, 645−664.

(2) Okano, T., Ed. (1998) *Biorelated Functional Polymers: Controlled Release and Applications in Biomedical Engineering,* Academic Press, New York.

(3) Hoffman, A. S. (1998) A Commentary on the Advantages and Limitations of Synthetic Polymer-Biomolecule Conjugates. In *Biorelated Functional Polymers: Controlled Release and Applications in Biomedical Engineering* (T. Okano, Ed.) Academic Press, New York (in press).

(4) Goodson, R. J., and Katre, N. V. (1990) Site-directed PEGylation of Recombinant Interleukin-2 at its Glycosylation Site. *Biotechnology 8*, 343−346.

(5) Slinkin, M. A., Curtet, C., Sai-Maurrrrel, C., Gestin, J. F., Torchilin, V. P., and Chatal, J. F. (1992) Site-specific Conjugation of Chain-terminal Chelating Polymers of Fab' Fragments of Anti-CEA mAb: Effect of Linkage Type and Polymer Size of Conjugate Biodistribution in Nude Mice Bearing Human Colorectal Carcinoma. *Bioconjugate Chem. 3*, 477−483.

(6) Husain, M., and Bieniarz, C. (1994) Fc Site-specific Labeling of Immunoglobulins with Calf Inteestinal Alkaline Phosphatase. *Bioconjugate Chem. 5*, 482−490.

(7) Chilkoti, A., Chen, G., Stayton, P. S., and Hoffman, A. S. (1994) Site-specific Conjugation of a Temperature-sensitive Polymer to a Genetically engineered Protein. *Bioconjugate Chem. 5*, 504−507.

(8) Gaetner, H. F., and Offord, R. E. (1996) Site-specific Attachment of Functional PEG to the Amino Terminus of Proteins. *Bioconjugate Chem. 7*, 38−44.

(9) Baudys, M., Uchio, T., Song, S. C., Mix, D. C., and Kim, S. W. (1996) Physical Stabilization of Insulin Through Chemical Modification: Site-specific Glycosylation or PEGylation. In *Advanced Biomaterials in Biomedicical Engineering and Drug Delivery Systems* (N. Ogata, S. W. Kim, J. Feijen, and T. Okano, Eds.) Springer, Tokyo.

(10) Stayton, P. S., Shimoboji, T., Long, C., Chilkoti, A., Chen, G., Harris, J. M., and Hoffman, A. S. (1995) Control of protein−ligand recognition using a stimuli-responsive polymer. *Nature 378*, 472−474.

(11) Ding, Z. L., Long, C. J., Hayashi, Y., Bulmus, V., Fong, R., Hoffman, A. S., and Stayton, P. S. (1998) Temperature Control of Biotin Binding and Release with a Streptavidin-poly(N-isopropyl acrylamide) Site-Specific Conjugate. *Bioconjugate Chem. 10*, 395−400.

(12) Ding, Z. L., Chen, G. H., and Hoffman, A. S. (1996) Synthesis and purification of thermally sensitive oligomer-enzyme conjugates of poly(N-isopropylacrylamide)-trypsin. *Bioconjugate Chem. 7*, 121−125.

(13) Chilkoti, A., Tan, P. H., and Stayton, P. S. (1996) Site-Directed Mutagenesis Studies of the High Affinity Streptavidin−Biotin Complex: Contributions of Tryptophan Residues 79, 108, and 120. *Proc. Natl. Acad. Sci. U.S.A. 92*, 1754−1758.

(14) Chen, G. H., and Hoffman, A. S. (1995) Graft copolymer compositions that exhibit temperature-induced transitions over a wide range of pH. *Nature 373*, 49−52.

(15) Dong, L. C., and Hoffman, A. S. (1991) A Novel Approach for Preparation of pH- and Temperature-Sensitive Hydrogels for Enteric Drug Delivery. *J. Controlled Release 15*, 141−152.

BC9901043

Reduced Immunogenicity of β-Lactoglobulin by Conjugation with Carboxymethyl Dextran

Makoto Hattori,*,† Koichi Nagasawa,† Koki Ohgata,† Noriko Sone,† Ayumu Fukuda,† Hiroshi Matsuda,‡ and Koji Takahashi†

Department of Applied Biological Science and Department of Veterinary Clinic, Faculty of Agriculture, Tokyo University of Agriculture and Technology, 3-5-8 Saiwai-cho, Fuchu-City, Tokyo 183-8509, Japan.
Received July 19, 1999; Revised Manuscript Received September 27, 1999

We prepared two β-lactoglobulin (β-LG)−carboxymethyl dextran (CMD) conjugates (Conj. 10A and Conj. 10B) by using a water-soluble carbodiimide to decrease the immunogenicity of β-LG. The molar ratios of β-LG to CMD in the conjugates were 5:1 (Conj. 10A) and 2:1 (Conj. 10B). The β-LG−CMD conjugates maintained the retinol-binding activity of native β-LG. Intrinsic fluorescence study indicated that shielding of the surface of β-LG by CMD occurred in each conjugate, which was eminent in Conj. 10B. A local conformational change around ^{125}Thr−^{135}Lys (α-helix) in each conjugate was detected by ELISA with monoclonal antibodies. The denaturation temperature of β-LG evaluated by differential scanning calorimetry was greatly enhanced in each conjugate. The anti-β-LG antibody response was markedly reduced after immunization with the β-LG−CMD conjugates in BALB/c, C57BL/6, and C3H/He mice. We determined the B cell epitopes of β-LG and each conjugate recognized in these mice and found that the linear epitope profiles of the β-LG−CMD conjugates were similar to those of β-LG, while the antibody response for each epitope was dramatically reduced. The reduced immunogenicity of β-LG was most marked in the case of Conj. 10B, which contained more CMD than Conj. 10A, and was effectively shielded by CMD. We concluded that masking of epitopes by CMD is responsible for the decreased immunogenicity of the β-LG in these conjugates.

INTRODUCTION

β-Lactoglobulin (β-LG),[1] a major whey protein found in the milk of mammalian species (*1*), is a globular protein of M_r 18 400, with two disulfide bridges and one free cysteine residue, containing plenty of essential amino acids (*2*). The X-ray crystallography (*3*, *4*) and protein sequence determination (*5*) have shown remarkable similarity between β-LG and plasma retinol-binding protein. Although the function of β-LG still remains unclear, β-LG can bind small hydrophobic ligands such as retinol, fatty acids, and so on and is categorized as a member of the lipocalin superfamily (*6*). β-LG has many useful functional properties such as emulsifying ability (*7*), foaming ability (*8*), and gelling ability (*9*). Although β-LG is considered to be a valuable protein in terms of food science, it is also known as a potent allergen associated with milk allergy; about 82% of milk allergy patients is sensitive to β-LG (10). Hence, it is very desirable to develop a new method to decrease the allergenicity of β-LG. Methods employed to decrease the allergenicity of proteins have involved their digestion and denaturation (*11*−*15*). However, these methods might destroy useful functions of the proteins and bring about problems with their taste. In contrast, the conjugation of proteins with materials having low allergenicity can simultaneously decrease the allergenicity and improve the function of the proteins. To achieve low allergenicity of β-LG, we planned to prepare neoglycoconjugates of β-LG. Neoglycoconjugates have been widely investigated in the last 20 years, and various improvements to the functions of proteins have been reported. In fact, in our previous studies, we improved the emulsifying properties and thermal stability of β-LG while maintaining the retinol-binding activity by conjugating this protein with carboxymethyl dextran (CMD) (*16*−*18*).

Many attempts to decrease the antigenicity and immunogenicity of proteins by conjugation have been reported. Since Lee and Sehon (*19*) found that conjugates of antigens (ovalbumin and ragweed pollen) and polyethylene glycol (PEG) derivatives were nonimmunogenic, immunological studies focusing on conjugates of protein antigens and PEGs were initiated. Some of PEG and polymer conjugated proteins have actually been used as pharmaceuticals for therapy (*20*, *21*). Conjugation of proteins with dextrans also is reported to be effective to reduce immunogenicity. The conjugates of monoclonal and polyclonal antibodies with oxidized dextrans of low molecular weight have been reported to have optimal immunoreactivity, in vivo pharmacokinetics, and tumor-localization properties, as well as low immunogenicity in vivo (*22*). Lipophilization is reported to be effective to suppress production of anti-β-LG IgG and IgE upon modification to a high degree (*23*). The shielding of epitopes by materials having low-antigenicity and immunogenicity is thought to be important to reduce the antigenicity and immunogenicity of the protein, and the

* To whom correspondence should be addressed. Phone: +81-42-367-5879. Fax: +81-42-360-8830. E-mail: makoto@cc.tuat.ac.jp.

† Department of Applied Biological Science.

‡ Department of Veterinary Clinic.

[1] Abbreviations: β-LG, β-lactoglobulin; CMD, carboxymethyl dextran; RCM−β-LG, reduced and carboxymethylated β-lactoglobulin; PBS, phosphate-buffered saline; PBS-Tween, PBS containing 0.05% Tween 20; SEC, size-exclusion chromatography; DSC, differential scanning calorimetry.

10.1021/bc990096q CCC: $19.00 © 2000 American Chemical Society
Published on Web 12/21/1999

use of a modifier with high molecular weight is desirable to achieve effective shielding of epitopes (*24*). Hence, we selected carboxymethyl dextran (CMD) as a modifier which is homogeneous in molecular weight and sequence, with a relatively high molecular weight (M_r 10 000) and low antigenicity and immunogenicity.

Our purpose was to create a novel β-LG−CMD conjugate with high thermal stability and improved functional properties, while maintaining the retinol-binding activity, without allergenicity. In particular, we investigated the structure and function of novel protein conjugates in detail in an effort to develop an effective method to decrease the allergenicity of β-LG and to elucidate the mechanisms involved. Although many studies on protein conjugates have been carried out and functional improvement of proteins has been well described so far, the relationships between structural changes and these functional improvements have not been clearly elucidated and the precise mechanisms responsible for the decrease in antigenicity and immunogenicity of the proteins still remain unclear. Changes in epitope profiles of proteins after conjugation with saccharides have not been clarified. In this study, we prepared covalently bonded β-LG−CMD conjugates. After exploring the structure of these conjugates, we investigated the immunogenicity profiles of β-LG and the conjugates in detail and demonstrated the reduced immunogenicity of β-LG when conjugated with CMD. The results of this study are essentially important to develop designing of novel foods with low allergenicity.

MATERIALS AND METHODS

Materials. Dextran T10 was purchased from Pharmacia LKB (Uppsala, Sweden). Water-soluble carbodiimide, 1-ethyl-3-(3-dimethylaminopropyl) carbodiimide (EDC), was purchased from Dojindo (Kumamoto, Japan).

Carboxymethylation of Dextran. Carboxymethyl dextran was prepared by carboxymethylation with monochloroacetic acid according to the method described previously (*16*−*18*) on a larger experimental scale than that of the previous experiments. In brief, dextran T10 (10 g, Pharmacia LKB, Uppsala, Sweden) was dissolved in 47 mL of a 15% monochloroacetic acid solution containing 7 g of sodium hydroxide (pH 11.5), and then incubated at 40 °C for 48 h. The reaction mixture was neutralized to pH 6.5 with acetic acid after cooling to room temperature. After dialyzing against distilled water and lyophilizing, carboxymethyl dextran (CMD) was obtained. The degree of modification (DM) was determined by hydrochloride-methanol titration (*25*). The DM value for CMD was about 17 carboxyl group residues per dextran molecule, corresponding to 27 residues/100 glucose residues.

Preparation of β-LG and RCM−β-LG. Crude β-LG (genotype AA) was prepared by the method of Armstrong et al. (*26*) and then purified by ion-exchange chromatography, using a DEAE-Sephacel column (2.5 ID x 50 cm; Pharmacia LKB, Uppsala, Sweden) as described previously (*16*−*18*). The purity of β-LG was confirmed by polyacrylamide gel electrophoresis (PAGE) according to the method of Davis (*27*).

RCM−β-LG was prepared as described previously (*31*, *34*, *35*). The disulfide bonds in β-LG were reduced with 2-mercaptoethanol and then the free sulfhydryl groups were carboxymethylated with sodium iodoacetate.

Preparation of the β-LG−CMD Conjugates. The β-LG−CMD conjugates were prepared by referring to the method described previously (*16*−*18*), on a larger experimental scale than in the previous experiments, by the following two methods.

Method 1. β-LG (2.7 g) and CMD (2.7 g) were each dissolved in 324 mL of a 0.9% NaCl solution. An EDC solution (2.7 g/ 54 mL) was added to this CMD solution. After adjusting the solution to pH 5.0 with 1 N HCl, the β-LG solution was added. The reaction was stopped by adding acetic acid (22.7 mL), and the solution was dialyzed against distilled water. The coacervate, the phase separated during dialysis, was recovered by lyophilization as a crude β-LG−CMD conjugate (Conj. 10A).

Method 2. β-LG (2.7 g) and 11.8 g of CMD were dissolved in 338 mL of distilled water, and the solution was adjusted to pH 4.75 with 1 N NaOH. An EDC solution (4.7 g/ 13.5 mL of distilled water) was gradually added over 30 min while maintaining the pH at 4.75. The reaction mixture was then incubated at room temperature for 3 h. The reaction was stopped by adding 22.5 mL of a 2 M acetate buffer (pH 5.5), and the solution was dialyzed against distilled water. The crude β-LG−CMD conjugate (Conj. 10B) was recovered by lyophilization.

Purification of these β-LG−CMD conjugates was then carried out as follows. Free CMD in each crude conjugate was removed by salting out with ammonium sulfate (final concentration, 5 M). After salting out, free β-LG and polymerized β-LG were removed by ion-exchange chromatography, using a DEAE-Sepharose Fast Flow column (2.5 ID x 40 cm, Pharmacia LKB, Uppsala, Sweden) as described previously (*18*).

Size-Exclusion Chromatography (SEC). The molecular weight of each β-LG−CMD conjugate was measured by SEC. A TSKgel G3000SW_{XL} column (7.8 ID × 300 mm, Tosoh, Tokyo, Japan) was equilibrated with a 0.067 M phosphate buffer containing 0.3 M NaCl at pH 7.0. Each β-LG−CMD conjugate (100 μg of protein/50 μL) was applied to the column and eluted at a flow rate of 1.0 mL/min. The absorbance was monitored at 280 nm.

Conformational Analysis of the β-LG−CMD Conjugates by the Spectroscopic Methods. The CD spectrum for each β-LG−CMD conjugate was measured with a J-720 spectropolarimeter (Jasco, Tokyo, Japan), using a cell with a 1.0 mm path length. Samples were dissolved in PBS (phosphate-buffered saline; a 0.11 M phosphate buffer at pH 7.1 containing 0.04 M NaCl and 0.02% NaN_3) at a protein concentration of 0.02%. The intrinsic fluorescence of each β-LG−CMD conjugate dissolved in PBS at 0.001% (as the protein concentration) was measured at an excitation wavelength of 283 nm by means of an RF-510 (Shimadzu, Kyoto, Japan) fluorescence spectrophotometer.

Differential Scanning Calorimetry (DSC). Each sample was dissolved in PBS (pH 7.0) at a protein concentration of 5% (w/ v), and 50 μL of the sample solution was sealed in a silver DSC cell. Distilled water was used as a reference. DSC was performed with an SSC-5020 DSC 100 instrument (Seiko Instruments, Tokyo, Japan) at a heating rate of 2 K/min.

Determination of the Carbohydrate Binding Site in the β-LG−CMD Conjugates. β-LG and the β-LG−CMD conjugates (80 mg) were digested with Dextranase (0.8 mg, EC 3.2.1.11, Sigma, St. Louis, MO) in 0.1 M potassium phosphate buffer (pH 6.0) at 39 °C for 12 h. After digestion, the digested saccharides were removed by salting-out with ammonium sulfate (final concentration, 4 M). The precipitate was recovered by centrifugation (at 12 000 rpm for 10 min at 4 °C), washed with a 0.1 M potassium phosphate buffer (pH 6.0) containing 4

M ammonium sulfate, and redissolved in the 0.1 M potassium phosphate buffer (pH 6.0). After dialysis against distilled water and lyophilization, samples with undigested small saccharide fragments were recovered.

These samples were tagged with 2-aminopyridine by the method of Hase et al. (*28*). In brief, the samples were mixed with 0.7 mL of a reagent made by mixing 2-aminopyridine (1 g), acetic acid (0.47 mL), and methanol (0.6 mL). The solution was heated in a sealed tube at 90 °C for 15 min and dried at 60 °C to remove the nonreacted reagent. Acetic acid (1 mL) containing a borane-dimethylamine complex (59 mg) was added to the sample, and the solution was incubated at 90 °C for 30 min. The solution was mixed with toluene (1.5 mL) and dried at 40 °C to remove the nonreacted reagent. The dried sample was redissolved in 0.067 M phosphate buffer at pH 7.0. The 2-aminopyridine-tagged sample was obtained after dialysis and lyophilization.

The 2-aminopyridine-tagged sample was reduced with 2-mercaptoethanol, carboxymethylated with sodium iodoacetate, and extensively digested with TPCK-trypsin (EC 3.4.21.4, Sigma, St. Louis, MO) at 37 °C for 24 h (S:E = 100:1). TPCK-trypsin and the nondigested protein were removed by ultrafiltration with a USY-1 ultrafilter (Advantec, Tokyo, Japan). The digested fragments were separated by reversed-phase HPLC (ODS-120T column, 7.8 ID x 300 mm, Tosoh, Tokyo, Japan). Peptides were detected by their absorbance at 230 nm, and the 2-aminopyridine-tagged saccharides were detected by fluorescence (excitation at 310 nm and emission at 380 nm). The peaks containing peptide and 2-aminopyridine-tagged saccharide were further purified by reversed-phase HPLC, and the amino acid sequence was determined by means of a 470A peptide sequencer (Perkin-Elmer Applied Biosystems, Foster, CA).

Measurement of the Retinol Binding Activity of the β-LG−CMD Conjugates. The retinol binding activity of the β-LG−CMD conjugates was measured by fluorescence titration as described previously (*16*, *29*−*33*).

Preparation of Antisera. Female BALB/c, C57BL/6, and C3H/He mice were purchased from Charles River Japan (Yokohama, Japan). Five mice of each group at 6 weeks of age were immunized intraperitoneally with 100 μg of protein in Freund's complete adjuvant (Difco Laboratories, Detroit, MI). Fourteen days after the primary immunization the mice were administered, a booster consisting of 100 μg of protein in Freund's incomplete adjuvant (Difco Laboratories). The mice were bled 7 days after the primary and secondary immunization. Blood from five mice of each group was pooled and stored at 4 °C for 24 h to form a clot. Antisera were collected from each blood sample after clot formation.

Enzyme-Linked Immunosorbent Assay (ELISA). A noncompetitive ELISA was carried out as follows. Antigen (β-LG, Conj. 10A, Conj. 10B, or RCM−β-LG) was dissolved in PBS at 0.01% (as protein). One hundred microliters of antigen solution was added to the wells of a polystyrene microtitration plate (Nunc, Roskilde, Denmark) and incubated at 25 °C for 2 h to coat the wells with each antigen. The plate was washed three times with 125 μL of PBS-Tween, and 125 μL of a 1% ovalbumin solution was then added. The plate was again incubated at 25 °C for 2 h and washed. One hundred microliters of antibody solution [the antiserum after the secondary immunization or monoclonal antibody (mAb)] was added. The plate was further incubated at 25 °C for 2 h. After washing, 100 μL of alkaline phosphatase-labeled goat anti-mouse immunoglobulin (Dako A/S, Glostrup, Denmark) diluted with PBS-Tween was added, and the plate was incubated again at 25 °C for 2 h. After washing, 100 μL of 0.1% *p*-nitrophenyl phosphate disodium salt dissolved in 1 M diethanolamine hydrochloride buffer (pH 9.8) was added as a substrate. The plate was incubated at 25 °C, the reaction was stopped by adding 20 μL of 6 M sodium hydroxide, and the absorbance at 405 nm was measured.

A competitive ELISA was carried out to investigate the local conformational changes in β-LG after conjugation with CMD, using anti-β-LG mAbs (mAbs 21B3 and 61B4) as probes and to evaluate the antigenicity of the β-LG−CMD conjugates as described previously (*16*−*18*, *34*, *35*). The equilibrium constant (K_{AS}) of the mAb in binding to β-LG, RCM−β-LG, or β-LG−CMD conjugates was calculated according to the method of Hogg et al. (*36*), from the results of competitive and noncompetitive ELISA.

Peptide Synthesis. Peptides were synthesized (*37*, *38*) using a five-in-one B cell and T cell epitope scanning kit (Chiron Mimotopes, Clayton, Victoria, Australia). A series of overlapping 15-mer peptides moving one amino acid at a time in accordance with the amino acid sequence of β-LG was synthesized on activated polyethylene gears in each pin. Fmoc (9-fluorenylmethoxycarbonyl)-deprotection of the pins was performed by immersing in *N*,*N*-dimethylformamide (DMF) containing 20% piperidine at 25 °C for 20 min. The Fmoc-deprotected pins were successively washed with DMF for 2 min and methanol for 2 min. This washing procedure was conducted three times, before the washed pins were air-dried for 30 min in an acid-free fume. Each Fmoc-activated amino acid was dissolved in DMF containing 1-hydroxybenzotriazole (HOBt). The activated amino acid solutions were added to the wells of the reaction tray. Pins were placed in the wells and coupled with the activated amino acid at 25 °C overnight. After this coupling step, the pins were immersed in methanol for 5 min and air-dried for 2 min, before being immersed in DMF for 5 min. The Fmoc-deprotection step and coupling step were repeated 14 times. After the last coupling step, the Fmoc-deprotection step was performed, and protective groups on amino acid residues were removed by treatment with trifluoroacetic acid (TFA) containing ethanedithiol and anisole. The pins were finally washed and air-dried. The success of the peptide synthesis was confirmed by ELISA using control peptide pins.

Epitope Scanning. B cell epitopes were scanned by ELISA, using a series of overlapping 15-mer peptides on each pin as the antigen on a solid phase. A total of 200 μL of precoat buffer [0.11 M PBS at pH 7.0, containing 2% ovalbumin (w/v), 0.1% Tween 20 (v/v) and 0.1% NaN_3 (w/v)] was added to the wells of the tray for blocking. Pins were put in the wells and incubated at 25 °C for 1 h to block with ovalbumin, before being washed in a bath of 0.01 M PBS (pH 7.2) for 10 min while shaking. Anti-β-LG, anti-Conj. 10A, and anti-Conj. 10B antisera were each diluted with PBS (pH 7.0). Each antiserum (200 μL) prepared from blood after the secondary immunization was added to wells of a microtitration plate (Nunc Roskilde, Denmark). The pins were placed in the wells and incubated at 25 °C for 1.5 h before being removed from the plate and washed four times. A total of 200 μL of alkaline phosphatase-labeled goat anti-mouse immunoglobulin diluted with PBS-Tween was added to wells of a new plate. The pins were put in the wells again and incubated at 25 °C for 1 h. The pins were removed from the plate and washed four times. A total of 200 μL of 0.1% *p*-nitrophenyl phosphate disodium salt dissolved in a 1 M diethanolamine hydrochloride buffer (pH 9.8) was

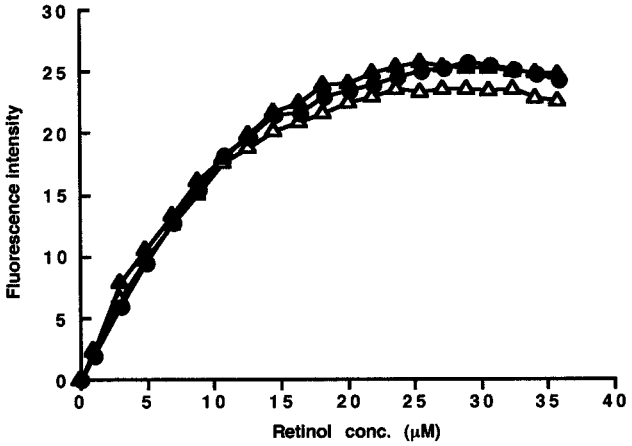

Figure 1. Retinol binding activity of the β-LG−CMD conjugates. β-LG (●), Conj. 10A (▲), Conj. 10B (△).

added to a new plate as a substrate. The pins were placed in the wells and incubated again at 25 °C. The enzyme reaction was stopped by removing the pins from the substrate solution, and the absorbance was determined at 405 nm.

RESULTS AND DISCUSSION

Structural Features of the β-LG−CMD Conjugates. The covalent binding of CMD to β-LG was confirmed by the coincidence of the protein and saccharide stained bands observed upon analysis by SDS−PAGE (data not shown). The molecular weights as determined by SEC were 282 000 for Conj. 10A and 251 000 for Conj. 10B; the respective molar ratios of β-LG to CMD were about 5:1 (Conj. 10A) and 2:1 (Conj. 10B). These results indicate that Conj. 10A and 10B were composed of 14 molecules of β-LG and 3 molecules of CMD and of 10 molecules of β-LG and 5 molecules of CMD, respectively. The thermal denaturation temperatures determined by DSC were 86.5 °C for Conj. 10A and 91.6 °C for Conj. 10B, which are much higher than that of β-LG (72.6 °C).

The retinol-binding activity of the β-LG−CMD conjugates was found to be similar to that of β-LG (Figure 1). The structure involved in retinol binding in the β-LG−CMD conjugates is considered to have been maintained in the native form.

The CD spectra of the β-LG−CMD conjugates are shown in Figure 2a. The CD spectrum of native β-LG showed a negative maximum at 216 nm, indicating that β-LG is rich in β-sheet structure, while that of each β-LG−CMD conjugate showed a broad negative maximum with a blue-shift. The β-sheet regions in β-LG are considered to have been changed by conjugation with CMD.

The intrinsic fluorescence spectra of the β-LG−CMD conjugates were measured to evaluate the conformational changes around the Trp residues (^{19}Trp and ^{61}Trp) of β-LG (Figure 2b). The fluorescence emission maximum wavelength for β-LG was 337 nm, while those for Conj. 10A and 10B were 339 and 338 nm, respectively. It has previously been clarified that the fluorescence intensity increases with the red-shift of the wavelength for maximum emission as the conformation of β-LG changes (*31*, *34*). Although a slight red-shift was observed in the case of each conjugate, the conformation around the Trp residues of the β-LG−CMD conjugates is considered to have retained a nativelike structure. The fluorescence intensity of each β-LG−CMD conjugate was lower than that of native β-LG, which indicates that the CMD polysaccharide chain shielded the area around the Trp residues (*16*). This effect of shielding of the Trp fluorescence was most marked in the case of Conj. 10B.

Local conformational changes in β-LG after conjugation with CMD were evaluated by competitive ELISA with two anti-β-LG mAbs (21B3 and 61B4) as probes. These mAbs can detect the subtle conformational changes in local areas within the β-LG molecule during unfolding and refolding (*31*, *34*, *35*) and after conjugation with saccharides (*16*−*18*, *32*, *33*) by determining the affinity change. The epitope regions for mAbs 21B3 and 61B4 are ^{15}Val−^{29}Ile (β-sheet region) and ^{125}Thr−^{135}Lys (α-helix region), respectively. MAb 61B4 binds preferentially to native β-LG, while mAb 21B3 binds more strongly to RCM−β-LG (the denatured form of β-LG). The equilibrium constants (K_{AS}) for binding of mAb 21B3 to the β-LG−CMD conjugates were similar to that for binding to native β-LG, while the K_{AS} values for binding of mAb 61B4 to the β-LG−CMD conjugates were smaller than

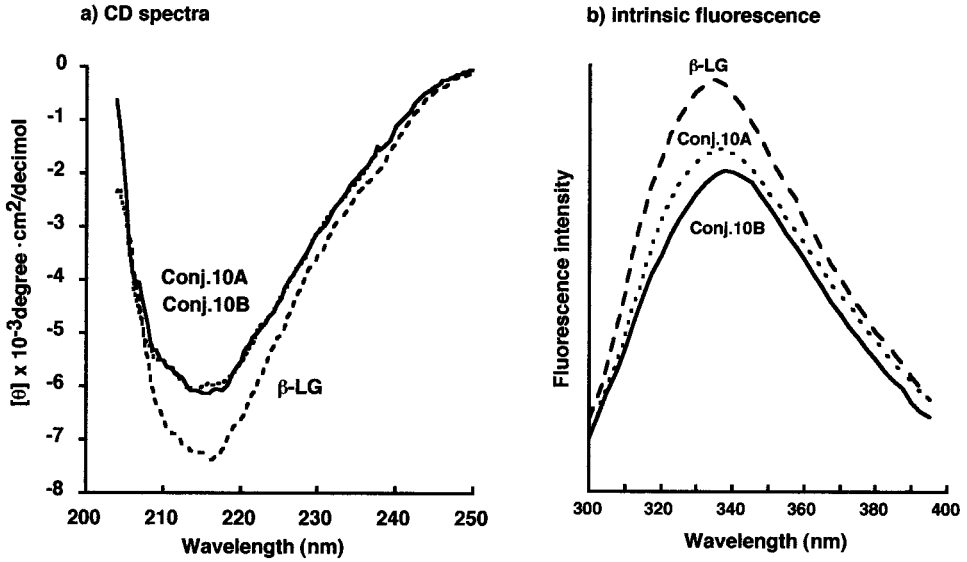

Figure 2. Spectroscopic analysis of the β-LG−CMD conjugates. CD spectra (a), intrinsic fluorescence (b). β-LG (broken line), Conj. 10A (dotted line), Conj. 10B (solid line).

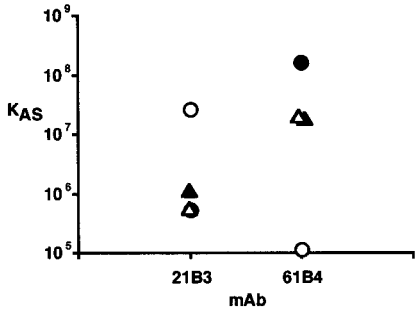

Figure 3. Equilibrium constants (K_{AS}) of the β-LG−CMD conjugates in binding to anti-β-LG mAbs. β-LG (●), RCM−β-LG (○), Conj. 10A (▲), Conj. 10B (△). K_{AS} values were calculated from the results of competitive and noncompetitive ELISA according to the procedure of Hogg et al. (*36*).

that for binding to native β-LG (Figure 3). Hence, the conformation around ^{15}Val−^{29}Ile (β-sheet region) is considered to have maintained its native form, while the conformation around ^{125}Thr−^{135}Lys (α-helix region) is considered to have been changed by conjugation with CMD. These results also raise the possibility that steric hindrance by CMD in the conjugates brought about the weak affinity of mAb 61B4 in binding to the β-LG−CMD conjugates.

Carbohydrate-binding sites in the β-LG−CMD conjugates were partially determined to be ^{47}Lys, ^{60}Lys, and ^{138}Lys for Conj. 10A and ^{101}Lys for Conj. 10B, which are located on the surface of the β-LG molecule (*3*, *4*). The low fluorescence intensity of the β-LG−CMD conjugates can be ascribed to the carbohydrate binding at ^{60}Lys which is adjacent to ^{61}Trp.

Antigenicity of the β-LG−CMD Conjugates. The antigenicity of each β-LG−CMD conjugate in three strains of mice was evaluated by competitive ELISA (Figure 4). β-LG was adsorbed to the solid phase, and β-LG, Conj. 10A, Conj. 10B, and RCM−β-LG were used as competitive antigens. Although anti-β-LG antisera were elicited by immunization with native β-LG, they showed higher affinity to the denatured form of β-LG (RCM−β-LG) than to the native material in the case of all strains. These results are consistent with findings obtained by Takahashi et al. (*39*) that the binding of a trypsin-generated fragment of RCM−β-LG to anti-β-LG antisera of BALB/c mice was as strong as that of native β-LG. In our previous study (*31*) on the unfolding/refolding of β-LG, using mAbs as probes, we found that a region of β-LG within the molecule was easily exposed during the denaturation process and was hard to refold. Such a structural feature of β-LG may be responsible for triggering the production of antibodies that preferentially react with the unfolded molecule although the antibodies were elicited by immunization with native material. CMD showed no reactivity with the anti-β-LG antiserum and was proven to have low antigenicity. Since the reactivity of the anti-β-LG antiserum with each β-LG−CMD conjugate was similar to that with native β-LG, the antigenicity of the β-LG−CMD conjugates is considered to have been similar to that of native β-LG. This nativelike antigenicity is believed to result from the total of an increase in reactivity with anti-β-LG antiserum due to conformational changes in β-LG that occurred as a result of conjugation with CMD and of a decrease in reactivity of the β-LG molecule due to the shielding effect of the CMD.

Immunogenicity of the β-LG−CMD Conjugates. The immunogenicity of each β-LG−CMD conjugate in BALB/c, C57BL/6, and C3H/He mice was evaluated by

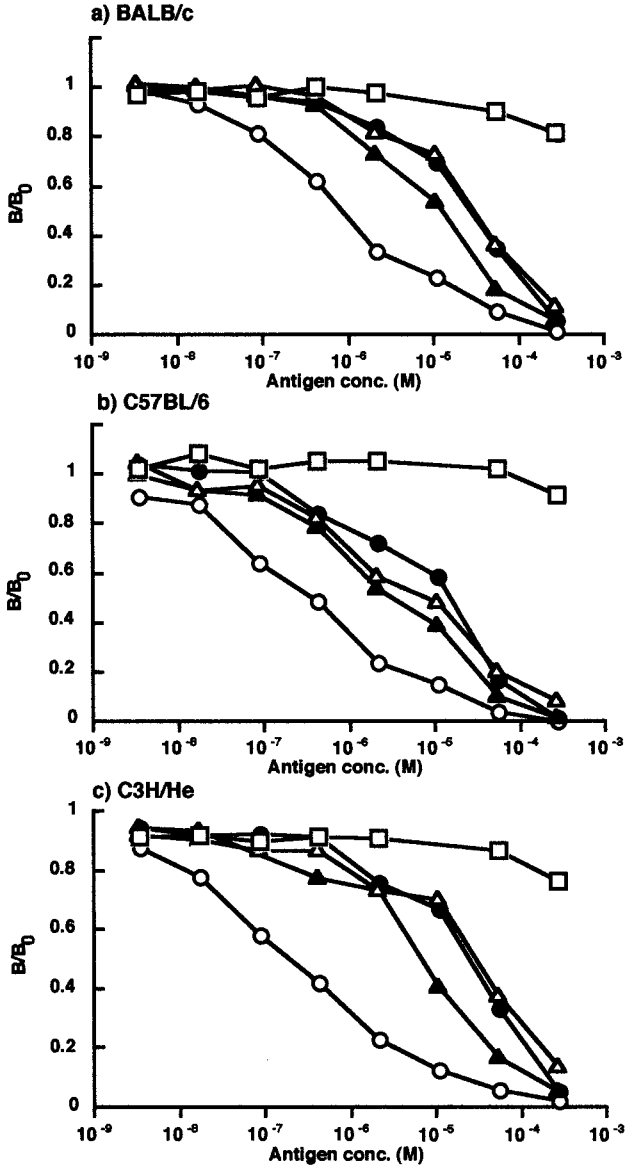

Figure 4. Antigenicity of the β-LG−CMD conjugates. The reactivity of anti-β-LG antisera after the secondary immunization from BALB/c (a), C57BL/6 (b), and C3H/He mice (c) with β-LG (●), RCM−β-LG (○), Conj. 10A (▲), Conj. 10B (△), and CMD (□) was evaluated by competitive ELISA. B/B_0 is the ratio of the absorbance at the last step of ELISA in the presence of various concentrations of a competitive antigen to the absorbance in the absence of the competitive antigen.

measuring the reactivity of 10000-fold diluted antisera with antigen (β-LG, RCM−β-LG, Conj. 10A, and Conj. 10B) adsorbed to the solid phase of a microtitration plate by noncompetitive ELISA (Figure 5). As already described, the anti-β-LG antisera reacted strongly with the denatured form of β-LG, so evaluation of the reactivity of each antiserum with the denatured material (RCM−β-LG) is considered to be required for examining immunogenicity. The anti-β-LG antibody response was markedly low in those three strains of mice immunized with each β-LG−CMD conjugate (Figure 5, panels a, e, and i). Effective reduction in immunogenicity of β-LG was observed with Conj. 10B. The antibody response to denatured β-LG (RCM−β-LG) was also only slightly elicited by immunization with each β-LG−CMD conjugate (Figure 5, panels b, f, and j). When each β-LG−CMD conjugate was used as the coating antigen on the solid

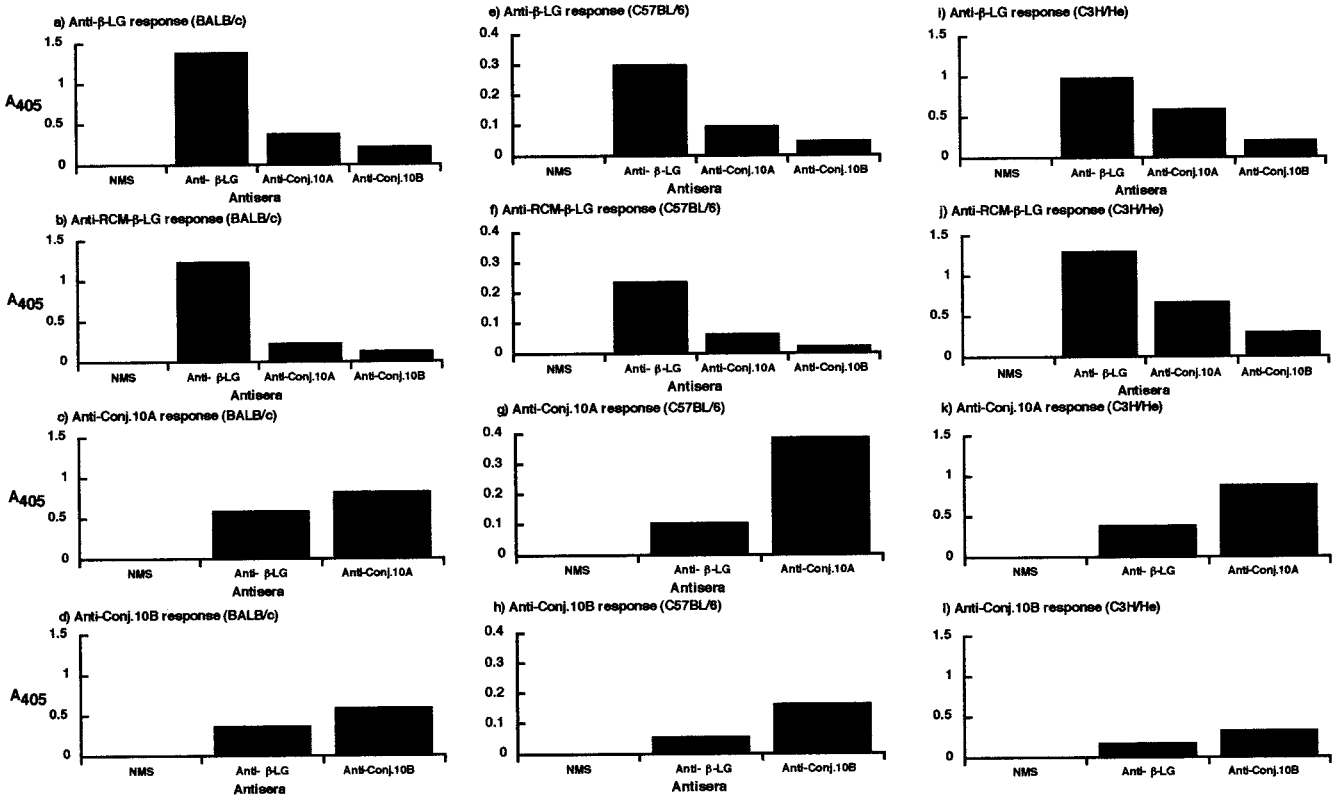

Figure 5. Immunogenicity of the β-LG−CMD conjugates in three strains of mice. The anti-β-LG response, anti-RCM−β-LG response, anti-Conj. 10A response, and anti-Conj. 10B response after the secondary immunization in BALB/c (a−d), C57BL/6 (e−h), and C3H/He mice (i−l) were evaluated by noncompetitive ELISA.

phase to evaluate the productivity of the specific antibody for each conjugate (Figure 5c, d, g, h, k, and l), both anti-Conj. 10A antisera and anti-Conj. 10B antisera showed a higher antibody titer than anti-β-LG antisera. These results indicate the production of antibodies specific not for β-LG but for each conjugate and the emergence of novel immunogenicity in β-LG as a result of conjugation with CMD. The conformational changes in β-LG due to conjugation with CMD may have brought about new epitopes. Berzofsky (*40*) has reported that the hydrophobic region tended to become an epitope. New epitopes may have emerged as a result of exposure of the hydrophobic region, buried in the native state, upon conjugation with CMD. However, the decrease in immunogenicity of β-LG observed upon conjugation with CMD surpassed the emergence of novel immunogenicity. Thus, the conjugation of CMD to β-LG is considered to be effective for decreasing the immunogenicity of β-LG. In particular, immunization with Conj. 10B was more effective than that with Conj. 10A to lower anti-β-LG antibody production. Since shielding of the β-LG molecule by CMD was more marked with Conj. 10B than with Conj. 10A, as described in the section on the structural features of the β-LG−CMD conjugates, it is considered that masking of the epitopes by CMD was more effectively achieved in Conj. 10B than in Conj. 10A.

Scanning of Epitopes in the β-LG−CMD Conjugates. Since the anti-β-LG antiserum reacted more strongly with the denatured form of β-LG (RCM−β-LG) than with native β-LG, determination of the linear epitopes (*41*) is important to clarify the B cell epitope profiles of β-LG and to clarify how conjugation with CMD leads to reduced immunogenicity of β-LG. In this study, the B cell epitopes were scanned by ELISA using overlapping 15-mer multipin peptides.

The results obtained with BALB/c mice are shown in Figure 6, panels a−c. The horizontal axis indicates the number of the N-terminal amino acid residue in each peptide, and the vertical axis shows the reactivity of each 15-mer peptide with each antiserum. In determining the immunogenicity profiles, an A_{405} value above 0.1 was adopted as positive. The epitopes were identified by determining the common amino acid sequence among the immunoreactive peptides by referring to the method of Gammon et al. (*42*) as summarized in Figure 7, in which the horizontal axis indicates the sequence number in β-LG, and the line thickness indicates the response to each epitope.

Anti-β-LG-antiserum reacted to the peptides 1−3, 6−12, 21−31, 46−54, 61−69, 73−79, 92−93, 127−129, 133−137, and 141−143 (the number indicates residue number of N-terminus of the peptides). The linear B cell epitopes of β-LG recognized in BALB/c mice were determined to be ^{3}Val−^{15}Val, ^{12}Ile−^{20}Tyr, ^{31}Leu−^{35}Gln, ^{54}Leu−^{60}Lys, ^{69}Lys−^{75}Lys, ^{79}Pro−^{87}Leu, ^{93}Leu−^{106}Cys, ^{129}Asp−^{141}Lys, ^{137}Asp−^{147}Ile, and ^{143}Leu−^{155}Gln, the dominant epitope being ^{69}Lys−^{75}Lys, which is located in a β-sheet region. Although other B cell epitopes recognized in BALB/c mice were found in various regions, they tended to exist in regions with α-helix or β-sheet secondary structure (Figure 7). As for the anti-conjugates response in BALB/c mice (Figure 6, panels b and c), the epitope distribution did not change, while the decrease in response was marked through the entire amino acid sequence as compared with the anti-β-LG antiserum, which was eminent with Conj. 10B. The B cell epitopes of conjugates recognized in BALB/c mice were determined to be ^{3}Val−^{15}Val, ^{11}Asp−^{20}Tyr, ^{28}Asp−^{42}Tyr, and ^{69}Lys−^{80}Ala for Conj. 10A and ^{3}Val−^{15}Val and ^{11}Asp−^{20}Tyr for Conj. 10B (Figure 7). A decrease in the immunogenicity

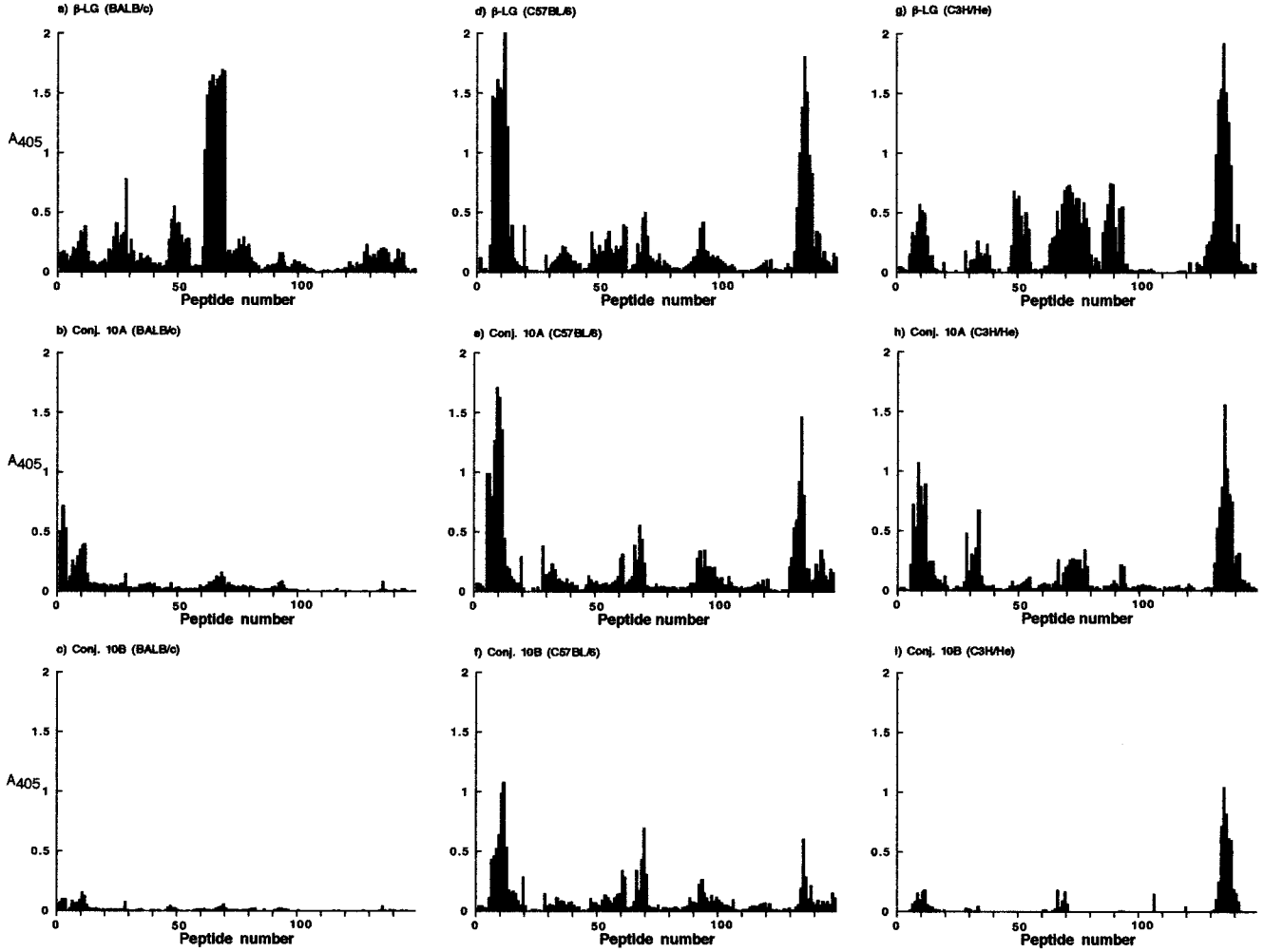

Figure 6. Reactivity of anti-β-LG, anti-Conj. 10A and anti-Conj. 10B antisera with overlapping 15-mer peptides covering the amino acid sequence of β-LG. The reactivity of anti-β-LG (a, d, g), anti-conjugate 10A (b, e, h), and anti-conjugate 10B (c, f, i) antisera after the secondary immunization from BALB/c (a−c), C57BL/6 (d−f), and C3H/He mice (g−i) with multipin peptides was evaluated by ELISA.

of β-LG by conjugation with CMD was achieved in each conjugate as far as the linear B cell epitopes were concerned. In particular, the immunogenicity of β-LG was almost completely nullified in Conj. 10B. However, ^{3}Val−^{15}Val showed a stronger signal with the anti-Conj. 10A antiserum than with the anti-β-LG serum, so this region might be involved in the emergence of novel immunogenicity in Conj. 10A.

The results obtained with C57BL/6 and C3H/He mice are shown in Figure 6, panels d−i, and B cell epitope profiles of β-LG and the conjugates were determined as shown in Figure 7. The B cell epitopes of β-LG recognized in C57BL/6 mice were determined to be ^{12}Ile−^{20}Tyr, ^{19}Trp−^{33}Asp, ^{36}Ser−^{49}Thr, ^{47}Lys−^{61}Trp, ^{54}Leu−^{67}Ala, ^{61}Trp−^{74}Glu, ^{70}Lys−^{82}Phe, ^{93}Leu−^{106}Cys and ^{138}Lys−^{147}Ile, the dominant epitopes being ^{12}Ile−^{20}Tyr and ^{138}Lys−^{147}Ile (Figure 7), most of which contained loop regions of the β-LG molecule. With respect to the anti-conjugates response in C57BL/6 mice, the epitope distribution was similar to that of β-LG, and the response was less throughout the entire amino acid sequence than the anti-β-LG response (Figure 6, panels e and f). In particular, an effective reduction of the immunogenicity of β-LG was achieved by conjugation with CMD in the case of Conj. 10B so far as the linear B cell epitopes were concerned. The B cell epitopes of the conjugates in C57BL/6 mice were determined to be ^{11}Asp−^{19}Trp, ^{19}Trp−^{33}Asp, ^{28}Asp−^{42}Tyr, ^{69}Lys−^{82}Phe, ^{99}Tyr−^{106}Cys, ^{136}Phe−^{146}His, and ^{148}Arg−^{155}Gln for Conj. 10A and ^{12}Ile−^{20}Tyr, ^{19}Trp−^{33}Asp, ^{61}Trp−^{74}Glu, ^{70}Lys−^{80}Ala, ^{93}Leu−^{106}Cys, and ^{138}Lys−^{148}Arg for Conj. 10B (Figure 7). ^{28}Asp−^{42}Tyr and ^{148}Arg−^{155}Gln showed slightly stronger signals with the anti-Conj. 10A antiserum than with the anti-β-LG serum. This region might be involved in the emergence of novel immunogenicity in Conj. 10A.

As for the anti-β-LG antiserum response in C3H/He mice, the linear B cell epitopes of β-LG recognized in C3H/He mice were determined to be ^{12}Ile−^{20}Tyr, ^{38}Pro−^{42}Tyr, ^{54}Leu−^{61}Trp, ^{67}Ala−^{77}Lys, ^{73}Ala−^{82}Phe, ^{79}Pro−^{90}Asn, ^{90}Asn−^{99}Tyr, ^{93}Leu−^{106}Cys, and ^{138}Lys−^{146}His, the dominant epitope being ^{138}Lys−^{146}His (Figure 7), most of which also contained loop regions. Regarding the anti-conjugates response in C3H/He mice, the epitope distribution was also similar to that of β-LG, and for each peptide, the signal obtained with the anti-conjugates sera was weaker than that with the anti-β-LG antiserum (Figure 6, panels h and i). A decrease in the immunogenicity of β-LG in C3H/He mice was achieved in the case of each conjugate as far as the linear B cell epitopes were concerned. In particular, the response of anti-Conj. 10B antisera was almost completely lacking, except for the weak signals obtained with peptides corresponding to the C-terminal region. The B cell epitopes of conjugates recognized in C3H/He mice were determined to be ^{11}Asp−^{20}Tyr, ^{33}Asp−^{42}Tyr, ^{77}Lys−^{80}Ala, ^{93}Leu−^{106}Cys, and ^{138}Lys−^{146}His for Conj. 10A and ^{11}Asp−^{22}Leu, ^{69}Lys−^{80}-

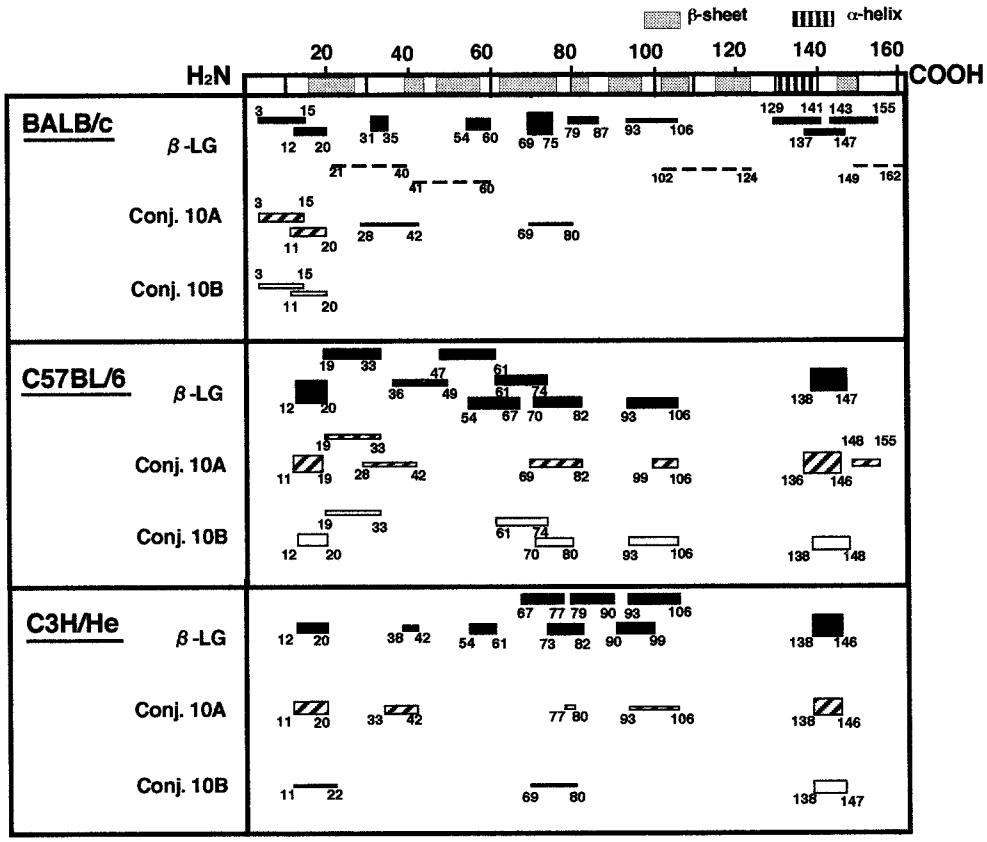

Figure 7. B cell epitope profiles of β-LG and the β-LG−CMD conjugates. The common regions which gave high ELISA values are shown. Hatched lines represent the antigenic peptides obtained from β-LG by tryptic digestion that were previously found to be immunogenic in BALB/c mice by Takahashi et al. (*39*).

Ala, and ^{138}Lys−^{147}Ile for Conj. 10B. (Figure 7). However, the reactivity of ^{11}Asp−^{20}Tyr and ^{33}Asp−^{42}Tyr with the anti-Conj. 10A antiserum was greater than that with the anti-β-LG antiserum, so these regions might be involved in the emergence of novel immunogenicity in Conj. 10A.

The results of the precise analysis with multipin peptides enabled the profiles of the B cell epitopes of β-LG recognized in three strains of mice to be clarified, and reduction of the immunogenicity of β-LG by conjugation with CMD was demonstrated. A reduction of the immunogenicity of β-LG as a result of conjugation with CMD was achieved with each conjugate. Although the precise mechanism responsible for the reduction of the immunogenicity of proteins through conjugation with polysaccharides is still unclear, a plausible one is that shielding of the epitopes in β-LG by CMD brought about its escape from recognition by the immune system. In fact, Conj. 10B, in which the surface of β-LG was effectively shielded by CMD, showed very low immunogenicity. Moreover, after conjugation with CMD, the response to the epitope regions around the carbohydrate-binding sites in the β-LG−CMD conjugates (^{47}Lys, ^{60}Lys, and ^{138}Lys for Conj. 10A and ^{101}Lys for Conj. 10B) was lowered in each strain of mice. For instance, responses to ^{54}Leu−^{60}Lys, ^{129}Asp−^{141}Lys, and ^{137}Asp−^{147}Ile in BALB/c mice, ^{47}Lys−^{61}Trp in C57BL/6 mice, and ^{54}Leu−^{61}Trp in C3H/He mice were dramatically reduced. CMD-conjugation was especially effective in reduction of the immunogenicity of β-LG in the case of BALB/c mice, for which the epitopes recognized were found in various regions. Several studies on the mechanisms responsible for the reduction of immunogenicity of proteins as a result of conjugation with macromolecules have been carried out so far. Among them, the induction of regulatory T cells upon immunization with conjugates has been reported. In the pioneering work of Lee et al. (*43*), they investigated the mechanism of suppression of IgE antibody production upon immunization with ovalbumin−polyethylene glycol conjugate and suggested that the induction of regulatory T cells would bring about the suppressive effect. Kishimoto et al. (*44*) also have reported that regulatory T cells were induced by injection of dinitrophenol (DNP)-tubercle bacillus conjugates and that the production of anti-DNP IgE antibody was suppressed. Takata et al. (*45*) reported that regulatory T cells and a soluble factor derived from these cells suppressed the growth of spleen cells from mice sensitized by treatment with antigen. One of the other reasons for the low immunogenicity of modified proteins is the increased resistance of modified proteins to proteolysis during antigen processing. So et al. (*46*, *47*) have reported that PEG-modified lysozyme showed a level of incorporation by spleen cells similar to that of lysozyme, but it showed low susceptibility to digestion by various proteases.

In the case of the β-LG−CMD conjugates prepared in the present work, there is a possibility that the induction of regulatory T cells upon immunization of the mice with each conjugate and low susceptibility to digestion by endosomal/lysosomal enzymes, as well as masking of epitopes by CMD, may contribute to the diminished anti-β-LG antibody response. Further studies focusing on these aspects should be carried out. Totsuka et al. (*48*) have recently determined the T cell determinants of β-LG recognized in BALB/c, C57BL/6, and C3H/He mice. We intend to clarify the change in T cell response to β-LG after conjugation with CMD.

Concluding Remarks. Although many protein conjugates have been prepared and studied to decrease the antigenicity and immunogenicity so far, changes in the epitope profiles have not been clarified. Our work is the

first study to clarify the changes in the epitope profiles of a protein after conjugation with saccharides. We could show that the immunogenicity of β-LG is dramatically reduced by conjugation with CMD. However, the possibility of the emergence of novel immunogenicity was also indicated. Since the reduction of the immunogenicity of β-LG was most marked in the case of Conj. 10B, which contains a greater amount of polysaccharide than Conj. 10A and in which shielding of the surface of β-LG was effective, it is evident that the problem of the emergence of novel immunogenicity can be overcome by glycoconjugation with a high shielding effect. It would be of interest to evaluate the effects of different amounts of CMD of differing molecular weights conjugated with β-LG in terms of the reduction of immunogenicity. We conclude that the conjugation with CMD performed in this study is an effective method for diminishing the immunogenicity of β-LG. Further studies on the mechanism responsible for the reduction of immunogenicity by this method should be carried out, and it is strongly hoped that such conjugates will contribute to the development of new foods with low allergenicity.

ACKNOWLEDGMENT

This work was supported in part by the grant of The Japan Food Industry Center (JAFIC). We are grateful to Professor Shuichi Kaminogawa of The University of Tokyo for his help in the ELISA experiments. We are grateful to Dr. Akio Ametani of La Jolla Institute for Allergy and Immunology for critical review of the manuscript. We gratefully acknowledge helpful discussions with Drs. Jun-ich Kurisaki and Mamoru Totsuka on several points in this paper. We are very grateful to Takashi Takakuwa of Jasco, Tokyo, Japan for his help in measuring the CD spectra.

LITERATURE CITED

(1) Jennes, R. (1979) Comparative aspects of milk proteins. *J. Dairy Res. 46*, 197−210.

(2) McKenzie, H. A. (1971) β-Lactoglobulins. In *Milk Proteins: Chemistry and Molecular Biology* (H. A. McKenzie, Ed.) pp 257−330, Academic Press, New York.

(3) Papiz, M. Z., Sawyer, L., Eliopoulos, E. E., North, A. C. T., Findlay, J. B. C., Sivaprasadrao, R., Jones, T. A., Newcomer, M. E., and Kraulis, P. J. (1986) The Structure of β-Lactoglobulin and Its Similarity to Plasma Retinol-Binding Protein. *Nature 324*, 383−385.

(4) Brownlow, S., Morais, C. J., Cooper, R., Flower, D. R., Yewdall, S. J., Polikarpov, I., North, A. C., and Sawyer, L. (1997) Bovine β-Lactoglobulin at 1.8 A Resolution−Still an Enigmatic Lipocalin. *Structure 5*, 481−495.

(5) Pervaiz, S., and Brew, K. (1985) Homology of β-Lactoglobulin, Serum Retinol Binding Protein, and Protein HC. *Science 228*, 335−337.

(6) Åkerstrom, B., and Lögdberg, L. (1990) An Intriguing Member of the Lipocalin Protein Family: α_1-Microglobulin. *Trends Biochem. Sci. 15*, 240−243.

(7) Shimizu, M., Saito, M., and Yamauchi, K. (1985) Emulsifying and Structural Properties of β-Lactoglobulin at Different pHs. *Agric. Biol. Chem. 49*, 189−194.

(8) Waniska, R. D., and Kinsella, J. E. (1988) Foaming and Emulsifying Properties of Glycosylated β-Lactoglobulin. *Food Hydrocolloids 2*, 439−449.

(9) Mulvihill, D. M., and Kinsella, J. E. (1987) Gelation Characteristics of Whey Proteins and β-Lactoglobulin. *Food Technol. 41* (*9*), 102−111.

(10) Spies, J. (1973) Milk Allergy. *J. Milk Food Technol. 36*, 225−231.

(11) Kurisaki, J., Nakamura, S., Kaminogawa, S., and Yamauchi, K. (1982) The Antigenic Properties of β-Lactoglobulin Examined with Mouse IgE Antibody. *Agric. Biol. Chem. 46*, 2069−2075.

(12) Watanabe, M., Suzuki, T., Ikezawa, Z., and Arai, S. (1994) Controlled Enzymatic Treatment of Wheat Proteins for Production of Hypoallergenic Flour. *Biosci. Biotech. Biochem. 58*, 288−390.

(13) Patterson, R., Suszko, I. M., Pruzansky, J. J., and Zeiss, R. (1973) Polymerized Ragweed Antigen E. ii. In vivo Elimination Studies and Reactivity with IgE Antibody Systems. *J. Immunol. 110*, 1413−1418.

(14) Takatsu, K., and Ishizaka, K. (1976) Reaginic Antibody Formation in the Mouse. VII. Induction of Suppressor T cells for IgE and IgE Antibody Response. *J. Immunol. 116*, 1257−1264.

(15) Ishizaka, K., Okudaira, H., and King, T. P. (1975) Immunogenic Properties of Modified Antigen E II. Ability of Urea-Denatured Antigen and a-Polypeptide Chain to Prime T cells Specific For Antigen C. *J. Immunol. 114*, 110−115.

(16) Hattori, M., Nagasawa, K., Ametani, A., Kaminogawa, S., and Takahashi, K. (1994) Functional Changes in β-Lactoglobulin by Conjugation with Carboxymethyl Dextran. *J. Agric. Food Chem. 42*, 2120−2125.

(17) Nagasawa, K., Takahashi, K., and Hattori, M. (1996) Improved Emulsifying Properties of β-Lactoglobulin by Conjugating with Carboxymethyl Dextran. *Food Hydrocolloids 10*, 63−67.

(18) Nagasawa, K., Ohgata, K., Takahashi, K., and Hattori, M. (1996) Role of the Polysaccharide Content and Net Charge on the Emulsifying Properties of β-Lactoglobulin-Carboxymethyl Dextran Conjugates. *J. Agric. Food Chem. 44*, 2538−2543.

(19) Lee, W. Y., and Sehon, A. H. (1977) Abrogation of reaginic antibodies with modified allergens. *Nature 267*, 618−619.

(20) Kimoto, A., Konno, T., Kawaguchi, T., Miyauchi, Y., and Maeda, H. (1992) Antitumor effects of SMANCS on Rat Mammary Tumor Induced by 7,12-Dimethylbenz[*a*]anthracene. *Cancer Res. 52*, 1013−1017.

(21) Holle, L. M. (1997) Pegaspargase: An Alternative? *Ann. Pharmacother. 31*, 616−624.

(22) Fagnani, R., Hagan, M. S., and Bartholomew, R. (1990) Reduction of Immunogenicity by Covalent Modification of Murine and Rabbit Immunoglobulins with Oxidized Dextrans of Low Molecular Weight. *Cancer Res. 50*, 3638−3645.

(23) Akita, E. M., and Nakai, S. (1990) Lipophilization of β-lactoglobulin: Effect on Allergenicity and Digestibility. *J. Food Sci. 55*, 718−723.

(24) Sehon, A. H. (1982) Suppression of IgE Antibody Responses with Tolerogenic Conjugates of Allergens and Haptens. *Prog. Allergy 32*, 161−202.

(25) Smith, R. J. (1967) Characterization and Analysis of Starches. In *Starch, Chemistry and Technology* (R. L. Whistler and F. F. Paschall, Eds.) pp 569−635, Academic Press, New York.

(26) Armstrong, J. M., McKenzie, H. A., and Sawyer, W. H. (1967) On the Fractionation of β-Lactoglobulin and α-Lactalbumin. *Biochim. Biophys. Acta 147*, 60−72.

(27) Davis, B. J. (1964) DISC ELECTROPHORESIS − II: Method and Application to Human Serum Proteins. *Ann. N. Y. Acad. Sci. 121*, 404−427.

(28) Hase, S., Ikenaka, T., and Matsushima, Y. (1978) Structure Analyses of Oligosaccharides by Tagging of the Reduced End Sugars with a Fluorescent Compound. *Biochem. Biophys. Res. Commun. 85*, 257−263.

(29) Cogan, U., Kopelman, M., Mokady, S., and Shintzky, M. (1976) Binding Affinities of Retinol and Related Compounds to Retinol Binding Proteins. *Eur. J. Biochem. 65*, 71−78.

(30) Futterman, S., and Heller, J. (1972) The Enhancement of Fluorescence and Decreased Susceptibility to Enzyme Oxidation of Retinol Complexed with Bovine Serum Albumin, β-Lactoglobulin, and the Retinol-Binding Protein of Human Plasma. *J. Biol. Chem. 247*, 5168−5172.

(31) Hattori, M., Ametani, A., Katakura, Y., Shimizu, M., and Kaminogawa, S. (1993) Unfolding/Refolding Studies on Bovine β-Lactoglobulin with Monoclonal Antibodies as Probes: Does a Renatured Protein Completely Refold? *J. Biol. Chem. 268*, 22414−22419.

(32) Hattori, M., Aiba, Y., Nagasawa, K., and Takahashi, K. (1996) Functional Improvements in Alginic Acid by Conjugating with β-Lactoglobulin. *J. Food Sci. 61*, 1171−1176.

(33) Hattori, M., Ogino, A., Nakai, H., and Takahashi, K. (1997) Functional Improvement of β-Lactoglobulin by Conjugating with Alginate Lyase-Lysate. *J. Agric. Food Chem. 45*, 703−708.

(34) Kaminogawa, S., Hattori, M., Ando, O., Kurisaki, J., and Yamauchi, K. (1987) Preparation of Monoclonal Antibody against Bovine β-Lactoglobulin and Its Unique Affinity. *Agric. Biol. Chem. 51*, 797−802.

(35) Kaminogawa, S., Shimizu, M., Ametani, A., Hattori, M., Ando, O., Hachimura, S., Nakamura, Y., Totsuka, M., and Yamauchi, K. (1989) Monoclonal antibodies as probes for monitoring the denaturation process of bovine β-lactoglobulin. *Biochim. Biophys Acta 998*, 50−56.

(36) Hogg, P. J., Johnson, S. C., Bowles, M. R., Pond, S. M., and Winzor, D. J. (1987) Evaluation of Equilibrium Constants for Antigen−Antibody Interaction by Solid-phase immunoassay: the Binding of Paraquant to Its Elicited Mouse Monoclonal Antibody. *Mol. Immunol. 24*, 797−801.

(37) Maeji, N. J., Bray, A. M., and Geysen, H. M. (1990) Multipin peptide synthesis strategy for T cell determinant analysis. *J. Immunol. Methods 134*, 23−33.

(38) Geysen, H. M., Rodda, S. J., Mason, T. J., Tribbick, G., and Schoofs, P. G. (1987) Strategies for epitope analysis using peptide synthesis. *J Immunol. Methods 102*, 259−274.

(39) Takahashi, T., Yamauchi, K., and Kaminogawa, S. (1990) Comparison between the antigenicity of native and unfolded β-lactoglobulin. *Agric. Biol. Chem. 54*, 691−697.

(40) Berzofsky, J. A. (1985) Intrinsic and extrinsic factors in protein antigenic structure. *Science 229*, 932−940.

(41) Atassi, M. Z. (1984) Antigenic Structures of Proteins. Their Determination Has Revealed Important Aspects of Immune Recognition and Generated Strategies for Synthetic Mimicking of Protein Binding Sites. *Eur. J. Biochem. 145*, 1−20.

(42) Gammon, G., Geysen, H. M., Apple, R. J., Pickett, E., Palmer, M., Ametani, A., and Sercarz, E. E. (1991) T Cell Determinant Structure: Cores and Determinant Envelopes in Three Mouse Major Histocompatibility Complex Haplotypes. *J. Exp. Med. 173*, 609−617.

(43) Lee, W. Y., Sehon, A. H., and Åkerblom, E. (1981) Suppression of Reaginic Antibodies with Modified Allergens. IV. Induction of Suppressor T cells by Conjugates of Polyethylene glycol (PEG) and Monomethoxy PEG with Ovalbumin. *Int. Arch. Allergy. Appl. Immunol. 64*, 100−114.

(44) Kishimoto, T., Hirai, Y., Suemura, M., and Yamamura, Y. (1976) Regulation of Antibody Response in Different Immunoglobulin Classes. I. Selective Suppression of Anti-DNP IgE Antibody Response by Preadministration of DNP-coupled Mycobacterium. *J. Immunol. 117*, 396−404.

(45) Takata, M., Maiti, P. K., Kubo, R. T., Chen, Y. H., Holford, S. V., Rector, E. S., and Sehon, A. H. (1990) Cloned Suppressor T Cells Derived from Mice Tolerized with Conjugates of Antigen and Monomethoxypolyethylene glycol. Relationship between Monoclonal T Suppressor Factor and the T Cell Receptor. *J. Immunol. 145*, 2846−2853.

(46) So, T., Ito, H. O., Koga, T., Ueda, T., and Imoto, T. (1996) Reduced Immunogenicity of Monomethoxypolyethylene glycol-Modified Lysozyme for Activation of T Cells. *Immunol. Lett. 49*, 91−97.

(47) So, T., Ito, H. O., Koga, T., Watanabe, S., Ueda, T., and Imoto, T. (1997) Depression of T-cell Epitope Generation by Stabilizing Hen Lysozyme. *J. Biol. Chem. 272*, 32136−32140.

(48) Totsuka, M., Ametani, A., and Kaminogawa, S. (1997) Fine Mapping of T-cell Determinants of Bovine β-Lactoglobulin. *Cytotechnology 25*, 101−113.

BC990096Q

Caged Single and Double Strand Breaks

Phillip Ordoukhanian and John-Stephen Taylor*

Department of Chemistry, Washington University, St. Louis, Missouri 63130. Received July 23, 1999; Revised Manuscript Received October 8, 1999

Ionizing radiation and radiomimetic drugs such as bleomycin, calichieamycin, neocarzinostatin chromophore, and other synthetic agents can produce both single and double strand breaks in DNA. The ability to study the structure−activity relationships of single and double-strand break repair, lethality, and mutagenesis in vivo is complicated by the numerous types and sites of DNA cleavage products that can be induced by such agents. The ability to "cage" such breaks in DNA might help to further such studies and additionally afford a mechanism for activating and deactivating nucleic acid based drugs and probes. The major type of single strand break induced by ionizing radiation is a 3′- and 5′-phosphate terminated single nucleotide gap. Previously, a caged strand break of this type had been developed that was designed to produce the 5′-phosphate directly upon irradiation with 366 nm light, and the 3′-phosphate by a subsequent β-elimination reaction [Ordoukhanian, P., and Taylor, J.-S. (1995) *J. Am. Chem. Soc. 117*, 9570]. Unfortunately, the release of the 3′-phosphate group was quite slow at pH 7. To circumvent this problem, a second caged strand break has been developed that produces the 3′-phosphate directly upon irradiation, and the 5′-phosphate by a subsequent β-elimination reaction. When this caged strand break was used in tandem with the previous caged strand break, 5′- and 3′-phosphate terminated gaps could be directly produced by irradiation with 366 nm light. These caged single strand breaks were also incorporated in tandem into hairpin substrates to demonstrate that they could be used to cage double strand breaks. These caged single strand breaks should be generally useful for generating site-specific DNA single and double strand breaks and gaps, using wavelengths and doses of light that are nondetrimental to biological systems. Because the position of the single strand break can be varied, it should now be possible to examine the effect of the sequence context and cleavage pattern of single and double strand breaks on the lethality and mutagenicity of this important class of DNA damage.

INTRODUCTION

Much of the lethality of ionizing radiation and radiomimetic agents has been attributed to double strand breaks (*1*−*5*). Little is known, however, about the structure−activity relationships in this process because of a lack of methods for producing site-specific double strand breaks with specific cleavage patterns and termini. In most studies of double strand break repair, the double strand breaks are produced by restriction enzyme cleavage (*6*), which results in a directly religatable break (5′-phosphate and 3′-hydroxyl terminated nick) with a limited pattern of cleavage. Ionizing radiation, on the other hand, often produces phosphate-terminated single nucleotide gaps that result from C4′ radical assisted solvolysis of the 5′ and 3′ phosphates (Figure 1), which cannot be directly religated (*1*, *7*). The same phosphate-terminated gap can also be produced by AP lyase activity on an abasic site formed by glycosylases which process ionizing radiation damaged bases in base excision repair (BER) pathway (*8*). Because double strand breaks are inherently unstable, a method for triggering the formation of site-specific double strand breaks of varying termini and sequence context would facilitate their construction and subsequent in vitro or in vivo activation.

Photorelease of "caged" substrates, drugs, and enzymes has been increasingly used as a means of triggering biological events (see articles in ref *9*), since the first reports of caged ATP in the late 1970s (*10*, *11*). Molecules are generally caged by covalent attachment to a photochemically cleavable auxiliary that renders the molecule inactive as a substrate, drug, or enzyme, and allows it to diffuse into the system of interest. The photochemical auxiliary is chosen so that it can be released from the molecule of interest by irradiation under wavelengths and fluences that are not injurious to the system under study. The rate of release can be controlled by the amplitude or the wavelength of light used and structural modifications that increase the quantum yield of cleavage. Caged molecules are typically used for kinetic investigations in biological systems where rapid mixing techniques are impractical, such as, inside cells or tissues. Native and damaged DNA are the substrates for a wide variety of enzymes, most notably those involved in replication, transcription, and repair, and caged substrates could play an important role in studying the mechanisms of such processes. RNA molecules also interact with a wide variety of enzymes, some have their own enzymatic activity, and their study could also be aided by the availability of caged RNA substrates. Though notable advances have been made in caging cofactors, drugs, and proteins, there are only a few examples of site-specifically caged polynucleotide substrates. For DNA, a caged abasic site (*12*), and deoxyribonolactone (*13*) have been reported, and for RNA, a caged ribozyme has been reported (*14*).

A number of years ago, we reported the synthesis of a photocleavable DNA building block based on a cis-syn thymine dimer lacking an internucleotide phosphate (*15*).

* To whom correspondence should be addressed. Phone: (314) 935−6721. Fax: (314) 935-4481. E-mail: taylor@wuchem.wustl.edu.

10.1021/bc9900993 CCC: $19.00 © 2000 American Chemical Society
Published on Web 12/23/1999

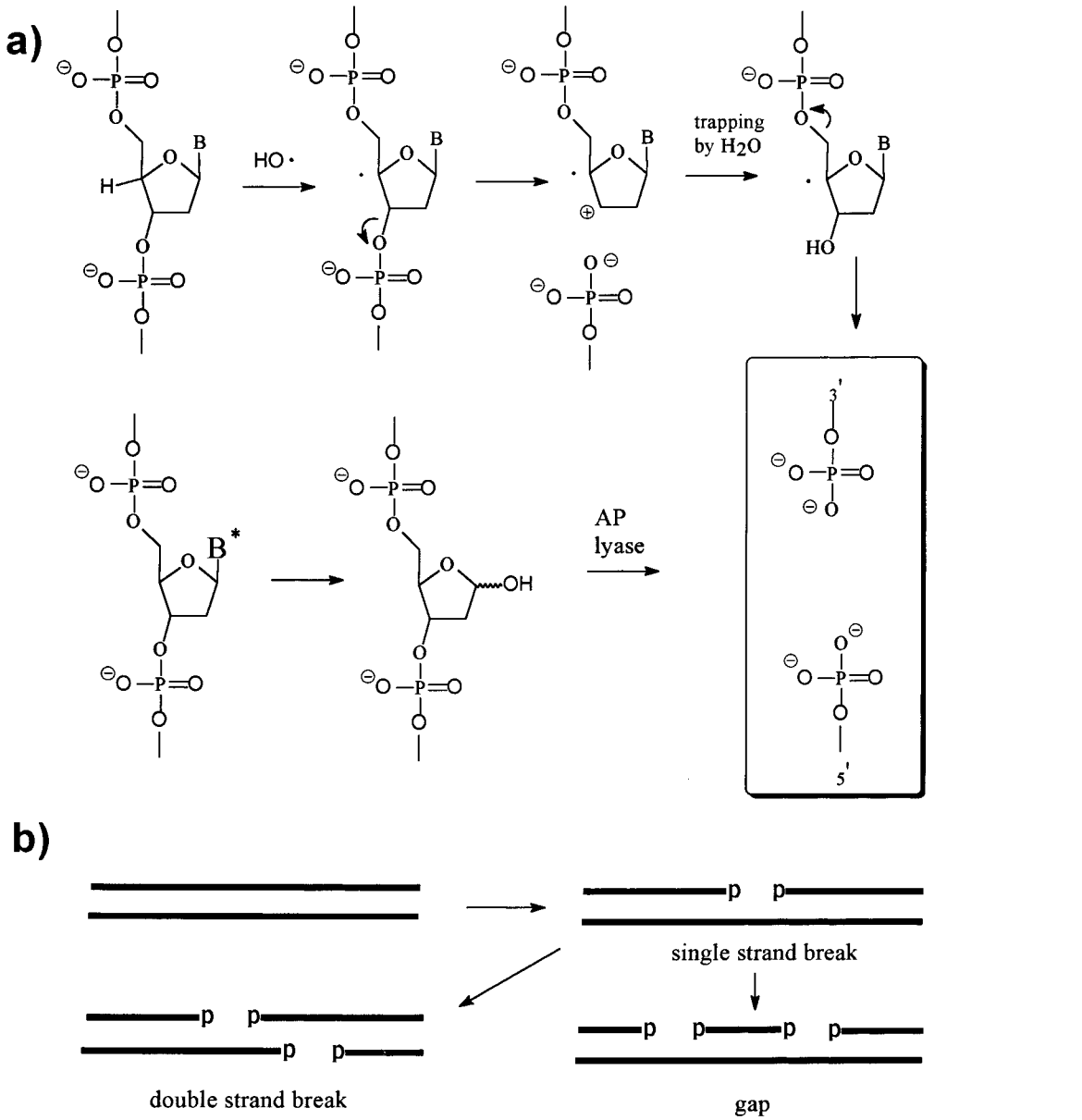

Figure 1. (a) Direct and indirect formation of a single strand break consisting of a one nucleotide gap terminating in a 5′-and 3′-phosphate by ionizing radiation. In the direct pathway, hydrogen abstraction of the H4′ hydrogen by hydroxyl radical causes the stepwise solvolysis of both 5′- and 3′-phosphates. In the indirect pathway, the base portion of a nucleotide becomes damaged which results in spontaneous or enzymatic glycosidic bond hydrolysis to yield an abasic site which releases the phosphates by β-elimination reactions catalyzed by an enzymatic AP lyase activity. (b) Examples of strand breaks that can be produced directly or indirectly by exposure of double strand DNA to ionizing radiation in vivo.

Strand cleavage could be induced by either direct photoreversion of the thymine dimer by irradiation with 254 nm light or by irradiation with 400 nm light in the presence of photolyase. This building block is not generally useful, however, because direct photoreversal with 254 nm light also damages DNA, and because the enzymatic photoreversal reaction was not very efficient and is limited to dithymine sequences in DNA. Subsequently, a C4′-phenyl selenide adenosine derivative was shown to give a phosphate-terminated one nucleotide gap upon photolysis at >320 nm under anaerobic and nonreducing conditions (*7*), but unfortunately, under aerobic or reducing conditions, a number of other side products were also obtained (*16*). To circumvent the drawbacks of the previously reported building blocks, we designed an *o*-nitrobenzyl-based photocleavable building block **1** with the same backbone as in DNA (Figure 2a) (*17*).[1] This building block was designed to introduce a caged strand break **X** that would produce a phosphate-terminated gap by a two step reaction initiated by irradiation with 360 nm light. Photolysis of 2 with 366 nm light was expected to directly release the DNA fragment **4** terminating in a 5′-phosphate and another terminating in the 3′-β-keto-phosphate derivative **3**. The latter product was then expected to release the DNA fragment **5** terminating in a 3′-phosphate by a β-elimination reaction (Figure 2a). When an oligonucleotide containing this building block was irradiated at 366 nm, the DNA fragment **4**, terminating in a 5′-phosphate, was immediately released, but the release of the DNA fragment **5** terminating in a 3′-phosphate did not occur spontaneously at pH 7 and required heating with piperidine.

Herein, we report the design, synthesis, and use of a second *o*-nitrobenzyl building block **11** for introducing a

[1] A similar building block based on 1-(*o*-nitrophenyl)-1,2-ethanediol has been described by M. S. Urdea and T. Horn in U.S. Patent 5,258,506.

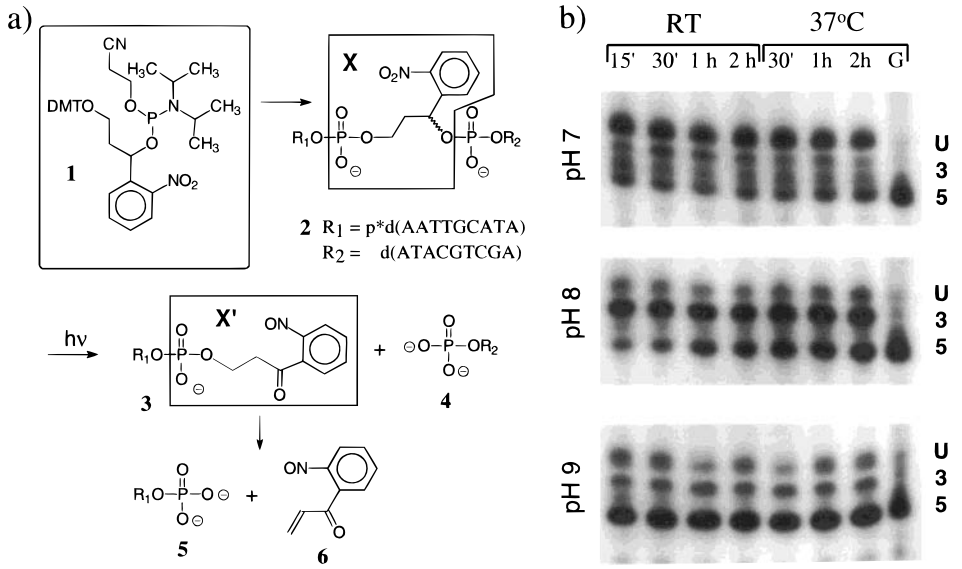

Figure 2. (a) Scheme for the synthesis of building block **1** used to incorporate the caged single strand break **X** into oligodeoxynucleotides, and the expected photolysis products of an oligodeoxynucleotide containing **X**. (b) An autoradiogram of a denaturing polyacrylamide electrophoresis gel of the products from exposing 5′-end labeled oligodeoxynucleotide **2** at pH 7.0, 8.0, and 9.3 (Tris-HCl) to 366 nm light from a hand held UV-lamp for 15 min at room temperature, followed by incubation at the times and temperatures shown prior to gel electrophoresis at pH 7.0. The fastest moving band comigrates with product **5** that was produced by a Maxam−Gilbert G reaction on the oligodeoxynucleotide corresponding to **2** in which **X** was replaced with pdG (Lane G). Only the second slowest moving band appeared to be readily converted to the product and was assigned as intermediate **3**. The slowest migrating band U, which is the major product of irradiation at pH 7, was not readily converted to **5**.

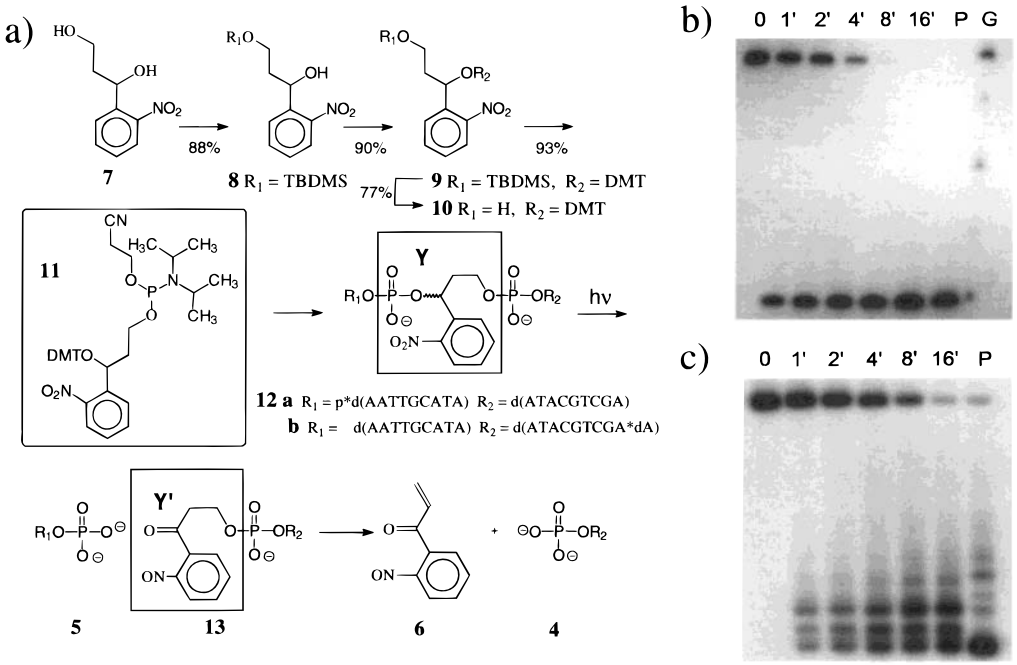

Figure 3. (a) Synthesis of the building block **11** used to incorporate a caged single strand break **Y** into oligodeoxynucleotides, and the expected photolysis products of oligodeoxynucleotides containing **Y**. On the right are autoradiograms of denaturing polyacrylamide electrophoresis gels of the products of exposing (b) 5′-end and (c) 3′-end labeled oligodeoxynucleotides **12a** and **12b** at pH 7.0 and room temperature to 366 nm light from a hand held UV-lamp for the indicated time in min. The products of the 16 min irradiation were also subjected to 1 M piperidine at 90 °C for 30 min (lane P). The fastest moving band in panel b comigrates with the product **5** that was produced by a Maxam−Gilbert G reaction on the oligodeoxynucleotide corresponding to **12a** in which **Y** was replaced with pdG (lane G).

caged strand break **Y** that leads directly to a 3′-phosphate terminated DNA fragment upon irradiation (Figure 3a). We also show that when the caged strand break **Y** is linked in a tandem fashion with the caged strand break **X**, phosphate-terminated gaps can be produced directly by photolysis (Figure 4). In addition, we demonstrate that these building blocks can be used to efficiently induce double strand breaks in DNA.

MATERIALS AND METHODS

All reactions were conducted under anhydrous conditions and an argon atmosphere. Methylene chloride and THF[2] were dried by distillation from the appropriate drying reagents. The 1 M solution of TBAF in THF was obtained from Aldrich. ^{1}H NMR and ^{13}C NMR spectra were acquired on a Varian Gemini-300 spectrometer, ^{31}P NMR spectra were acquired on a Varian XL-300 spec-

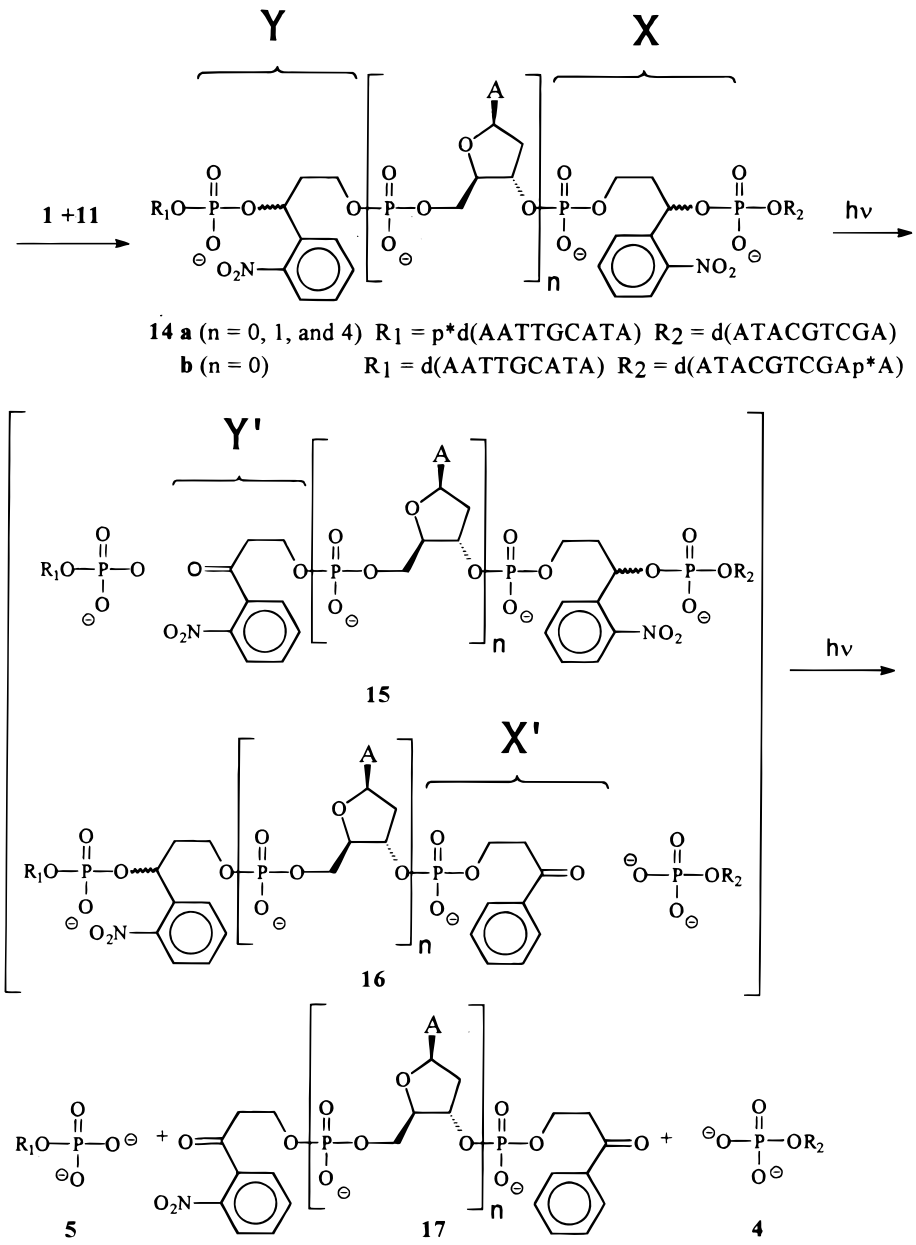

Figure 4. Scheme illustrating how two caged single strand breaks **X** and **Y** can be used to produce 3′- and 5′-phosphate terminated gaps directly upon photolysis.

trometer. Low- and high-resolution mass spectra were obtained from the Washington University Resource for Biomedical and Bio-organic Mass Spectrometry, Department of Chemistry, Washington University. Oligodeoxynucleotides were synthesized on an ABI 380B synthesizer by standard β-cyanoethyl phosphoramidite chemistry and purified on a preparative, 2 mm thick 165 mm long, 7 M urea, 1:19 cross-linked, 19% acrylamide gel at 300 V. The coupling yield for the modified building block **11** was >98%, with a 2 h coupling time. Photosensitive oligodeoxynucleotides were visualized on the preparative gel by doping with 5′-[^{32}P]-end labeled oligonucleotide and autoradiography. Nonphotosensitive oligodeoxynucleotides were visualized by shadowing with 254 nm light against a fluorescent TLC plate. All oligodeoxynucleotide concentrations were determined by UV absorbance measurements (*18*). Oligodeoxynucleotides were 5′-end labeled with [γ-^{32} P]ATP (Amersham) and T4 polynucleotide kinase (New England Biolabs) in 70 mM Tris-HCl, pH 7.6, 10 mM $MgCl_2$, and 5 mM DTT according to standard procedures (*19*). Oligodeoxynucleotides were 3′-end labeled with [α-^{32}P]ddATP (Amersham) and terminal deoxynucleotide transferase in 100 mM sodium cacodylate, pH 7.2, 0.2 mM 2-mercaptoethanol, and 2 mM $CoCl_2 \cdot 6H_2O$. Alternatively, the photocleavable oligodeoxynucleotides were 3′-end labeled by annealing to the complementary 10-mer, d(TTCGACGTAT), and gap filling with [α-^{32}P]dATP and 1 unit of DNA polymerase I large (Klenow) fragment (New England Biolabs) in 10 mM Tris-HCl, pH 7.5, and 5 mM $MgCl_2$. Photolyses were conducted in the lid of a polyethylene microcentrifuge tube with a model UVGL-25 (VWR) hand-held light with an intensity of approximately 0.75 mW/cm^2 (0.21 mW).

[2] Abbreviations: BER, base excision repair; ddATP, dideoxyadenosinetriphosphate; DBU, diazabicycloundecane; DMT, 4, 4′-dimethoxytrityl; DTT, dithiothreitol; NER, nucleotide excision repair; TBAF, tetrabutylammonium fluoride; TBDMS, *tert*-butyldimethylsilyl; TEA, triethylamine; THF, tetrahydrofuran; TMP, trimethyl phosphate; TMS, tetramethylsilane; UVA, 320−400 nm.

Photolysis products were analyzed by electrophoresis on 0.4 mm thick, 31 cm wide, 38.5 cm long, 7 M urea, 1:19 cross-linked, 19% or 15% acrylamide gels. Radiolabeled products were visualized by autoradiography with Kodak XAR-5 film at −70 °C or, for quantitative purposes, with a Molecular Dynamics Phosphoimager.

1-*o*-Nitrophenyl-1-O-*tert*-butyldimethylsilyl-1,3-propanediol (8). To a stirred solution of 1 g (5.06 mmol) of the diol **7** (*17*) in 15 mL methylene chloride was added 517 mg (7.6 mmol) of imidazole. After the imidazole had all dissolved, 1.15 g (7.6 mmol) of TBDMS chloride was added and allowed to stir for an additional 2 h. A saturated Na_2CO_3 solution was added to quench the reaction, and the organic layer was separated. The aqueous layer was further extracted with methylene chloride, the organic layers were combined and dried with $MgSO_4$, and the solvent was removed under reduced pressure. The resulting residue was chromatographed on a silica gel column (8:2 hexane/ethyl acetate) to give the desired compound **8** (1.39 g, 4.5 mmol) in 88% yield: $R_f = 0.54$ (8:2 hexane/ethyl acetate); ^{1}H NMR (300 MHz, CD_3COCD_3, referenced to TMS): δ 7.90 (d, $J = 8$ Hz, 1H, $ArNO_2$), 7.86 (d, $J = 8$ Hz, 1H, $ArNO_2$), 7.71 (t, $J = 8$ Hz, 1H, $ArNO_2$), 7.49 (td, $J = 8$, 1 Hz, 1H, $ArNO_2$), 5.40−5.33 (m, 1H), 4.61 (d, $J = 4$ Hz, 1H), 3.98−3.79 (m, 2H), 2.06−1.92 (m, 1H), 1.89−1.75 (m, 1H), 0.91 (s, 9H), 0.08 (s, 6H); ^{13}C NMR (75 MHz, CD_3COCD_3, referenced to TMS): δ 148.8, 141.7, 133.8, 129.0, 128.6, 124.5, 66.7, 66.6, 61.0, 42.3, 26.2, 18.7, −5.3, −5.2; IR (neat) 3441, 2946, 2857, 1654, 1647, 1636, 1594, 1566, 1560, 1491, 1455, 1437, 1399, 1376, 1313, 1282 cm^{-1}; FAB HRMS *m/z* C_{15} H_{26} O_4 N Si, $[M + H]^+$ calcd, 312.1631; found, 312.1633.

1-*o*-Nitrophenyl-1-*O*-dimethoxytrityl -3-*O*-*tert*-butyldimethylsiyl-1,3-propanediol (9). To a stirred solution of 0.51 g (1.6 mmol) of **8** in 10 mL methylene chloride was added 0.34 mL (2.3 mmol) of DBU, followed by 0.72 g (2.1 mmol) of DMT chloride. The reaction was allowed to stir for 2 days at room temperature, after which a saturated Na_2CO_3 solution was added and the organic layer was separated. The aqueous layer was further extracted with ethyl acetate, the organic layers were combined and dried with $MgSO_4$, and the solvent was removed under reduced pressure. The resulting residue was chromatographed on a silica gel column (8.9:0.9:0.2 hexane/ethyl acetate/TEA) to give **9** (0.91 g, 1.5 mmol) in 90% yield: $R_f = 0.57$ (8.9:0.9:0.2 hexane/ethyl acetate/TEA); ^{1}H NMR (300 MHz, CD_2Cl_2, referenced to TMS) δ 7.58 (d, $J = 8$ Hz, 2H, Ar), 7.46 (d, $J = 8$ Hz, 2H, Ar), 7.37−7.07 (m, 9 H, Ar), 6.66 (d, $J = 9$ Hz, 2 H, Ar), 6.60 (d, $J = 9$ Hz, 2 H, Ar), 5.43−5.26 (m, 1H), 3.74−3.64 (m, 8H), 2.18 (quartet, $J = 7$ Hz, 2 H), 0.82 (s, 9H), −0.03 (s, 6H); ^{13}C NMR (75 MHz, CD_2Cl_2, referenced to TMS) δ 158.9, 158.8, 146.9, 146.2, 140.7, 136.5, 136.2, 132.7, 130.7, 130.6, 130.6, 127.0, 124.0, 113.3, 113.1, 87.6, 69.6, 59.7, 55.5, 41.6, 26.0, 18.4, −5.2; IR (neat) 3853, 3744, 3059, 3035, 3000, 2954, 2930, 2898, 2884, 2855, 2837, 1608, 1525, 1509, 1464, 1445, 1359, 1340, 1302, 1252, 1177, 1092, 1036, 1009 cm^{-1}; FAB HRMS *m/z* C_{36} H_{43} O_6 N Si Na $[M + Na]^+$ calcd, 636.2757; found, 636.2758.

1-*o*-Nitrophenyl-1-*O*-dimethoxytrityl-1,3-propanediol (10). To a stirred solution of 0.9 g (1.5 mmol) of **9** in 8 mL of THF was added 2.3 mL (2.3 mmol) of a 1 M solution of TBAF in THF. The reaction was allowed to stir for 2 h, after which the solvent was removed under reduced pressure. The resulting residue was chromatographed on a silica gel column (7.9:1.9:0.2 hexane/ethyl acetate/TEA) to give **10** (0.56 g, 1.1 mmol) as a white foam in 77% yield: $R_f = 0.17$ (7.9:1.9:0.2 hexane/ethyl acetate/TEA); ^{1}H NMR (300 MHz, CD_3COCD_3, referenced to TMS) δ 7.74−7.61 (m, 2H), 7.54−7.48 (m, 2H, Ar), 7.44 (td, $J = 8$, 1 Hz, 1H, Ar), 7.31 (dd, $J = 9$, 2 Hz, 2H, Ar), 7.27−7.11 (m, 6H), 6.72 (dd, $J = 9$, 2 Hz, 2H), 6.65 (dd, $J = 9$, 2 Hz, 2H), 5.39 (m, 1H), 3.72 (overlapping s, 6H, $ArOCH_3$), 3.69−3.53 (m, 2H), 3.45 (br s, 1H), 2.35−2.10 (m, 2H); ^{13}C NMR (75 MHz, CD_3COCD_3, referenced to TMS) δ 184.7, 159.4, 159.3, 147.4, 146.5, 140.5, 136.7, 136.4, 133.1, 130.9, 130.9, 130.8, 128.6, 128.3, 127.6, 127.3, 124.3, 113.6, 113.5, 88.1, 70.1, 70.0, 58.5, 55.2, 41.6; IR (neat) 3416, 3406, 3241, 3058, 3036, 3001, 2956, 2934, 2908, 2837, 1701, 1607, 1577, 1522, 1509, 1464, 1445, 1357, 1340, 1302, 1251, 1225, 1177, 1153 cm^{-1}; FAB HRMS *m/z* C_{30} H_{29} O_6 N Na $[M + Na]^+$ calcd, 522.1892; found, 522.1893.

Photocleavable DNA Building Block (11). To a stirred solution of 0.18 g (0.37 mmol) of **10** in 5 mL methylene chloride were added 0.2 mL TEA (1.4 mmol) and 0.19 mL (0.85 mmol) of *N*,*N*-diisopropyl-(2-cyanoethyl)-phosphonamidic chloride. The reaction was allowed to stir for and additional 30 min, after which a saturated Na_2CO_3 solution was added. The organic layer was separated, and the aqueous layer further extracted with ethyl acetate. The organic layers were combined and dried with $MgSO_4$. The solvent was removed under reduced pressure, and the resulting residue chromatographed on a silica gel column (7.9:1.9:0.2 hexane/ethyl acetate/TEA) to give **11** (0.24 g, 0.34 mmol) as a white foam in 93% yield: $R_f = 0.37$ (7.9:1.9:0.2 hexane/ethyl acetate/TEA); ^{31}P NMR (121.5 MHz, CD_2Cl_2, referenced to TMP) δ 144.3, 144.3; ^{1}H NMR (300 MHz, CD_2Cl_2, referenced to TMS) δ 7.68−7.57 (m, 2H, Ar), 7.49−7.42 (m, 2H, Ar), 7.34 (t, $J = 8$ Hz, 1H, Ar), 7.30−7.09 (m, 8H), 6.66 (dd, $J = 9$, 2 Hz, 2H), 6.60 (dd, $J = 9$, 2 Hz, 2H), 5.32 (br, s, 1H), 3.84−3.62 (m, 10 H), 3.61−3.43 (m, 2H), 2.53 (t, $J = 3$ Hz, 2H), 2.32 (m, 2H), 1.29−1.02 (m, 13 H); ^{13}C NMR (75 MHz, CD_2Cl_2, referenced to TMS) δ 160.5, 160.4, 148.5, 147.7, 141.9, 137.9, 137.6, 134.4, 132.2, 132.1, 129.7, 129.7, 129.6, 128.7, 128.6, 125.6, 119.8, 114.9, 114.8, 89.3, 71.1, 71.0, 61.5, 61.5, 61.3, 61.3, 60.4, 60.4, 60.2, 60.1, 57.1, 44.9, 44.7, 41.3, 41.2, 41.1, 26.3, 26.2, 26.2, 26.1, 22.3, 22.2; IR (neat) 2965, 2933, 2874, 1680, 1673, 1666, 1660, 1650, 1642, 1631, 1608, 1590, 1563, 1552, 1525, 1509, 1480, 1451, 1426, 1406, 1389, 1364, 1350, 1322, 1275, 1252, 1231, 1210, 1195, 1179, 1163, 1154, 1139, 1121, 1072, 1012, 996 cm^{-1}.

Photolysis of d(AATTGCATAXATACGTCGA) (2), at pH 7.0, 8.0, and 9.3. Three 30 μL solutions, ~0.27 mM in oligodeoxynucleotide **2** (*17*) and 100 mM in Tris-HCl at either pH 7.0, 8.0, or 9.3, were photolyzed with 366 nm light for 15 min at 0 °C. Each solution was divided into two portions, one of which was incubated at room temperature and the other at 37 °C. Aliquots of about 3 μL were taken immediately after photolysis and at 0.5, 1.0, and 2.0 h of incubation. All aliquots were stored at −20 °C until they could be loaded on a pH 7 denaturing 19% polyacrylamide electrophoresis gel. The products were also compared to the products of a Maxam−Gilbert G reaction (*20*) that was carried out on an otherwise identical sequence in which **X** was replaced with pdG.

Photolysis of the 5′-End Labeled d(AATTGCATAYATACGTCGA) (12a) and 3′-End Labeled d(AATTGCATAYATACGTCGAdA) (12b). Two 50 μL solutions of either oligodeoxynucleotide **12a** (24 nM) or oligodeoxynucleotide **12b** (30 nM) in 100 mM in Tris-HCl (pH 7.0) were photolyzed with 366 nm light at room temperature. Aliquots of about 4 mL were taken following 0, 1, 2, 4, 8, and 16 min of irradiation and electrophoresed

on a 19% polyacrylamide gel. An additional final aliquot was taken and diluted up to 50 mL in a 1 M piperidine solution and heated to 90 °C for 30 min. The products were also compared to the products of a Maxam−Gilbert G reaction (*20*) that was carried out on an otherwise identical sequence in which **Y** was replaced with pdG.

Photolysis of 5′-End Labeled d(AATTGCATAY-A_nXATACGTCGA) (14a, n = 0, 1, or 4), and 3′-End Labeled d(AATTGCATAYXATACGTCGAA) (14b, n = 0). Two 60 μL solutions of either oligonucleotide **14a** (20 nM) or oligonucleotide **14b** (20 nM) in 100 mM in Tris-HCl (pH 7.0) were photolyzed at 366 nm and room temperature. Aliquots of about 4 μL were taken at 0, 1, 2, 4, 8, and 16 min of irradiation and electrophoresed on a 19% polyacrylamide gel. An additional final aliquot was taken and diluted up to 50 mL in a 1 M piperidine solution and heated to 90 °C for 30 min. The products were also compared to the products of a Maxam−Gilbert G reaction (*20*) that was carried out on an otherwise identical sequence to **14a** (n = 0) in which **X** and **Y** were replaced by a single pdG.

Preparation of Internally Labeled Hairpins 18 and 19 Containing Opposed Photocleavable Building Blocks X and Y. Two 40 μL solutions of d(TATC-GAATTGTTXGGTACCCTTTCCCAAAAAGGGAAAGG) (3.6 mM) and either the 5′-[^{32}P]-end labeled d(GTAC-CTYACAATTCG) (0.25 mM) or 5′-[^{32}P]-end labeled d(G-TAC̄CTAACYATTCG) (0.25 mM), were combined with 6 Weiss units of T4 DNA Ligase (Promega) and 1.25 mM ATP, 50 mM Tris-HCl (pH 7.8), 10 mM $MgCl_2$, 10 mM DTT, and 50 μg/mL BSA. The mixture was incubated for ∼40 h at 0 °C to give the ligated 54 mer hairpins **18** and **19**, respectively.

Photolysis of the Internally Labeled Hairpins 18 and 19. A 30 μL solution of either oligodeoxynucleotide **18** or **19** (33 nM) in 100 mM Tris-HCl (pH 7.0) and 25 mM NaCl, was annealed by heating to 95 °C for 3 min and allowed to cool to room temperature over ∼2 h. The annealed hairpin oligodeoxynucleotides were photolyzed at 366 nm and room temperature, and 3 μL aliquots taken at 0, 1, 2, 4, 8, and 16 min of irradiation and electrophoresed on a 19% polyacrylamide gel. Photolysis under denaturing conditions was carried out in the same way, except that the solution contained 0.15 N NaOH in place of the Tris-HCl buffer.

RESULTS AND DISCUSSION

Before embarking on the synthesis of a new building block to directly release a DNA fragment terminating in a 3′-phosphate, we first reexamined the photochemistry of the original caged strand break **X** at different pHs, with the expectation that the β-elimination reaction should occur more rapidly at higher pH (Figure 2a). When 5′-end labeled oligodeoxynucleotide **2** was photolyzed at pH 7, three intermediate bands appeared, the slowest moving of which was the major product (Figure 2b). As we had found previously, the major product, which was originally assigned to structure **3,** was stable to incubation at pH 7 for 2 h at 37 °C. When oligodeoxynucleotide **2** was photolyzed at pH 8, however, the major product was now the second most slowly moving band. This second band converted to the 3′-phosphate terminated product **5** slowly at room temperature, and more rapidly at 37 °C. Product **5** was produced independently by conducting a Maxam Gilbert G reaction (*20*) on an oligodeoxynucleotide identical in sequence to **2** except that **X** was replaced by G. When irradiated at pH 9, the 3′-phosphate-terminated product was the major product, even at short incubation times. These results suggest that the major product at pH 7 is not the desired β-ketophosphate intermediate **3**. Furthermore, the results suggest that intermediate **3** is only produced at pH 8 or above, and that it only β-eliminates rapidly at pH 9. We do not know the structure of the pH 7 product at this time.

To directly photogenerate a 3′-phosphate-terminated fragment, we designed a second building block **11** (Figure 3a) that is based on the synthetic route used to prepare the original photocleavable building block **1** (Figure 2a) (*17*). The building block **11** was synthesized in four steps, in an overall yield of ∼60%, starting from the same intermediate **7** used in the synthesis of **1**. The building block **11** was used to incorporate the caged strand break **Y** into a 19-mer oligodeoxynucleotide by automated synthesis, which was then 5′-end labeled with [γ-^{32}P]-dATP and polynucleotide kinase to give **12a**. The 19-mer was also 3′-end labeled either with [α-^{32}P]ddATP and terminal transferase or by end filling with [α-^{32}P]dATP and Klenow fragment in the presence of a complementary strand with a 5′-protruding T to give **12b**. Exposure of the labeled oligodeoxynucleotides to increasing amounts of 366 nm irradiation from a hand-held UV-lamp caused increasing amounts of strand cleavage. With the 5′-end labeled **12a**, only a single cleavage band was produced that comigrated with the expected 3′-phosphate terminated product that was produced by a Maxam−Gilbert G sequencing reaction (*20*) on a substrate with a G in place of **Y** (Lane G, Figure 3b). With the 3′-end labeled substrate **12b**, three major cleavage products were observed (Figure 3c) as expected from the results of the previous study on the photolysis of **2** (Figure 2b) (*17*). When the product mixture resulting from 16 min of photolysis was further treated with hot piperidine, the slower moving bands disappeared and only the band comigrating with the 5′-phosphate-terminated product was observed (Lane P, Figure 3c), also as expected from the results of the prior study.

Now that we had a caged strand break **Y** that could produce a 3′-phosphate directly upon photolysis, we expected that we could directly produce a gap terminating in both 3′- and 5′-phosphates by incorporating caged strand breaks **Y** and **X** in tandem (Figure 4). To investigate this idea, we incorporated the caged strand breaks **Y** and **X** side by side into oligodeoxynucleotide **14** (n = 0). Irradiation of either the 5′- or 3′-end labeled substrates **14a** or **14b** (n = 0) with 366 nm light resulted in strand cleavage, ultimately giving only one band which comigrated with an authentic reference band produced by a Maxam−Gilbert G sequencing reaction (Lane G, Figure 5c). This band was also resistant to further treatment with hot piperidine (Lane P, Figure 5c). Unexpectedly, very little of the expected intermediate band corresponding to **15b** or **16** was observed by visual inspection of the autoradiograms, suggesting that the second photocleavage event might be faster than the first photocleavage event. It was possible that an intermediate *o*-nitroso ketone product from the first photocleavage event, which is known to absorb strongly at 366 nm, or some other product might be sensitizing the second photocleavage event. If true, such a photosensitization mechanism should be distance dependent, and oligodeoxynucleotides were also synthesized in which the caged strand breaks **Y** and **X** were spaced 1 and 4 nucleotides apart (**14**, n = 1 or 4). These substrates were also of interest because they could be used to prepare caged DNA strand gaps when annealed to a complementary strand. Plotting the relative yield of reaction products quantified by Phosphoimager analysis as a function of irradiation time

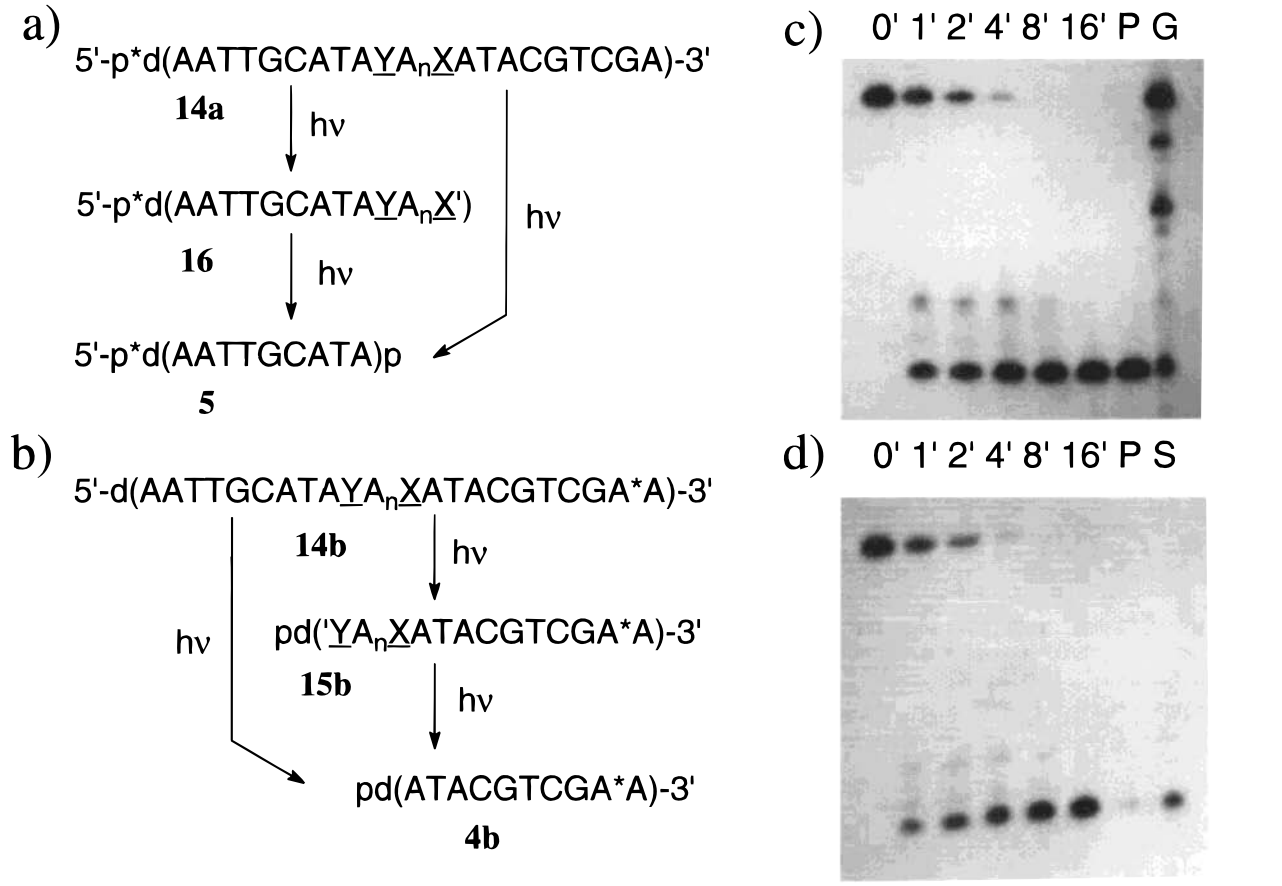

Figure 5. Expected products of the photolysis of (a) 5′- and (b) 3′-end-labeled oligodeoxynucleotides **14a** and **14b** containing two tandem caged single strand breaks **X** and **Y**. To the right are the autoradiograms of denaturing polyacrylamide electrophoresis gels of the products resulting from exposure of the corresponding (c) 5′- and (d) 3′-end labeled oligodeoxynucleotides **14a** and **14b** (n = 0) to the indicated number of minutes of 366 nm light from a hand held UV-lamp. The products of the 16 min irradiation were also subjected to 1 M piperidine at 90 °C for 30 min (lane P). The fastest moving band in panel c corresponds to the product **5** that was produced by a Maxam−Gilbert G reaction that was carried out on an otherwise identical sequence in which **X** and **Y** was replaced with a single pdG (lane G). Lane S corresponds to an authentic sample of 5′-end labeled **4b**.

(Figure 6) revealed that the rate of formation and decay of the intermediate band corresponding to **16** was the same for each spacing, indicating that the photosensitization mechanism was not taking place. The photolysis reactions were also repeated in the presence of 5 mM DTT to react with and eliminate a possible nitroso group (*21*), but once again, the rate of formation and decay of the intermediate band corresponding to **16** was the same as in the previous experiment (data not shown). The maximum value of approximately 25% of the intermediate is consistent with a mechanism in which the rates of cleavage at either site are identical and independent of the order of cleavage, as determined by simulation of the kinetics.

To demonstrate the formation of a double-strand break in which one of the duplex fragments is terminated by 5′- and 3′-phosphates, we took advantage of an internally labeled hairpin substrate used by Stubbe and co-workers to probe double strand break formation induced by bleomycin (*22*). Two 54 mer hairpins **18** and **19** were constructed (Figures 7a and 8a), in which the caged strand breaks were one and three nucleotides apart, respectively, on opposite strands. The internally ^{32}P-labeled hairpins were constructed by ligation of a preformed 34-mer hairpin structure that had the caged strand break **X** 13 nucleotides from the 5′-end to either one of two different 5′-end labeled 15-mers in which the caged strand break **Y** was either 6 or 9 nucleotides from the 3′-end. Single strand cleavage at **X** could be differentiated from single strand cleavage at **Y** and from a double strand break by the length of the radiolabeled oligodeoxynucleotides produced. Irradiation under native (Figure 7b and 8b) and denaturing conditions (Figure 7c and 8c) indicated that photocleavage was sensitive to secondary structure for the more closely spaced strand break substrate but not for the more separated one. For the more closely spaced strand break substrate **18**, cleavage at **Y** was slower in the duplex than in the denatured state. In the more closely opposed arrangement, building block **Y** is stacked between a T and an A, whereas in the more separated arrangement it is stacked between a C and an A. In the denatured state, cleavage at **Y** was faster than cleavage at **X** for both substrates, which may reflect an intrinsic preference for photocleavage at a 3′-phosphate over a 5′-phosphate. In any case, almost complete double strand cleavage was observed without the formation of any side products within 16 min of irradiation, making these caged substrates synthetically useful.

CONCLUSION

We have developed a new building block for caging site-specific and sequence-independent DNA strand breaks leading to the direct production of a 3′-phosphate, with doses of UVA light that cause little or no damage to DNA or protein, and that are not significantly lethal to mammalian cells (*23*). We have also demonstrated that when this building block is linked in tandem with our previously designed building block (17), it can be used to generate a major type of DNA strand break induced

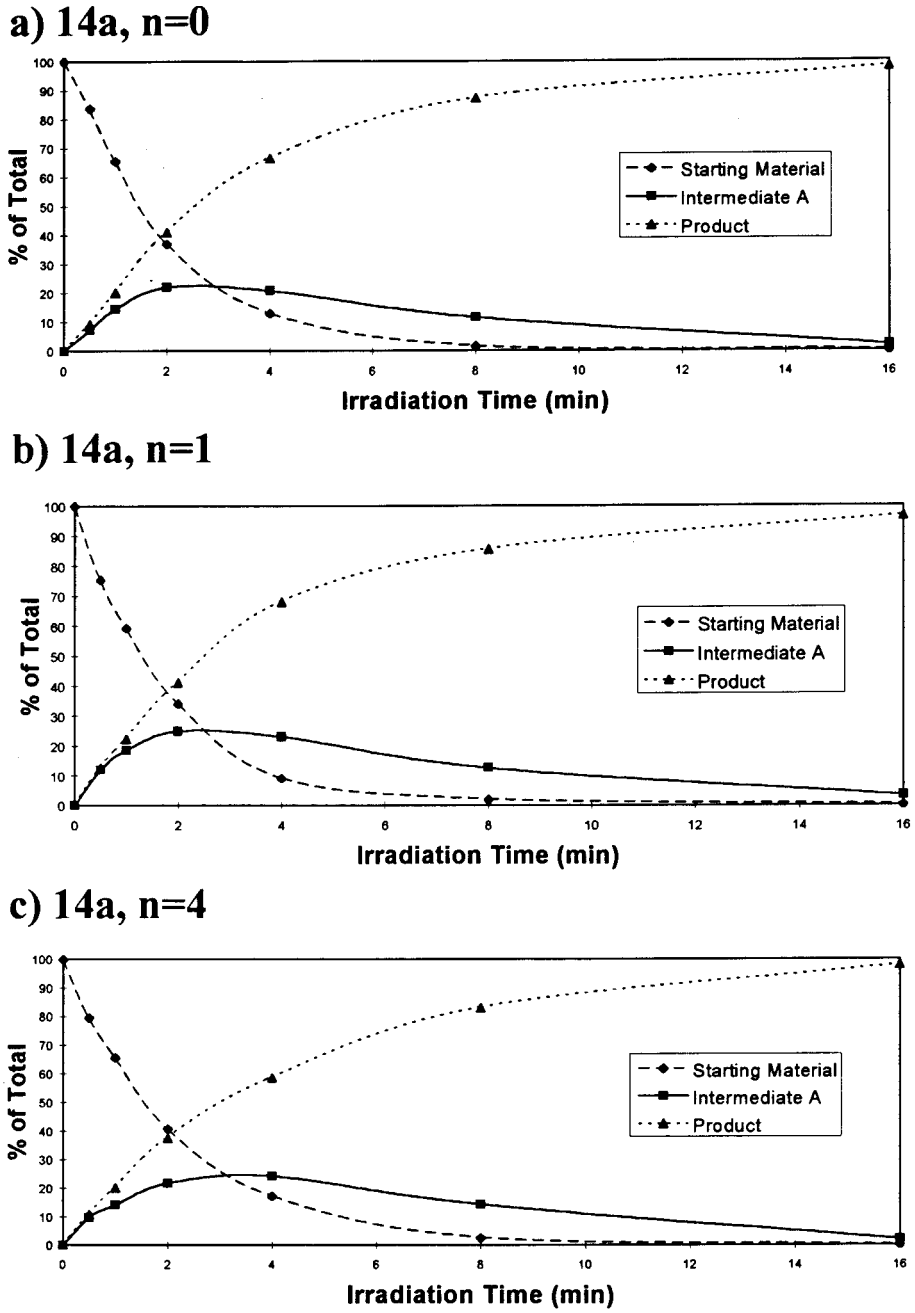

Figure 6. Plots of the photolysis products of 5′-end labeled oligonucleotide **14a** (n = 0, 1, and 4) as a function of irradiation time.

by ionizing radiation, a nucleotide gap terminating in 3′- and 5′-phosphates. These caged single strand breaks should be useful in the construction of DNA fragments and phagemid-based substrates needed to study the structure−activity relationships of single and double strand break repair using reconstituted repair systems or cell free extracts. The caged breaks could be introduced into phagemids by standard methods used to incorporate DNA damage-containing oligodeoxynucleotides into single and double-stranded vectors (*24*, *25*) and then decaged following purification.

To be a useful "caged" substrate for in vivo studies of strand break repair and mutagenesis, the modified oligonucleotides must not be substrates for other repair processes, such as nucleotide excision repair (NER), that might repair them before they can be activated. Although NER is generally attributed to repair of bulky lesions, it has been shown to repair DNA containing synthetic mimics of abasic sites (*26*). If the two caged breaks **Y** and **X** directly follow each other, they may create a highly distorted DNA structure that might be readily detected and repaired by NER. The two building blocks might not be as easily detected and repaired, however, if they were spaced apart. Thus, to form a double strand break terminating in 3′- and 5′-phosphates in vivo, it may be better to space the two building blocks apart in each strand. Irradiation of such a construct would then produce a short duplex fragment in addition to the desired phosphate terminated double strand break. For in vivo studies, it may also be possible to use a single caged break **X** or **Y** in each strand, because endogenous exonucleases may be able to remove the **X′** or **Y′** that remains on the 3′- or 5′-phosphate following photolysis (Figures 2a and 3a). For instance, in *E. coli*, exonuclease III is known to process 3′-phosphate, 3′-phosphoglycolate, and other fragmented sugars groups left on the 3′-end (*8*). Clearly, further studies are required to explore the usefulness of these caged substrates.

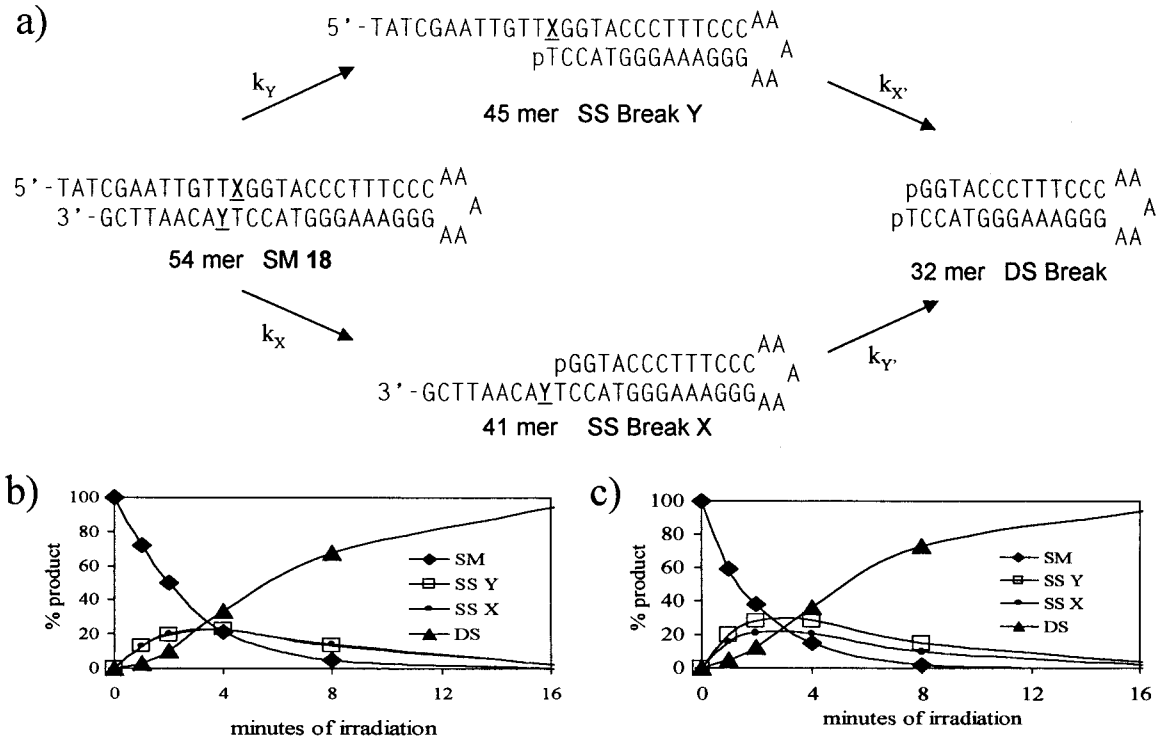

Figure 7. (a) Expected single and double strand cleavage products resulting from the photolysis of the internally labeled hairpin substrate **18** containing caged strand breaks **X** and **Y** that are one nucleotide apart. Below are plots of the product distributions as a function of irradiation time under (b) native and (c) denaturing conditions.

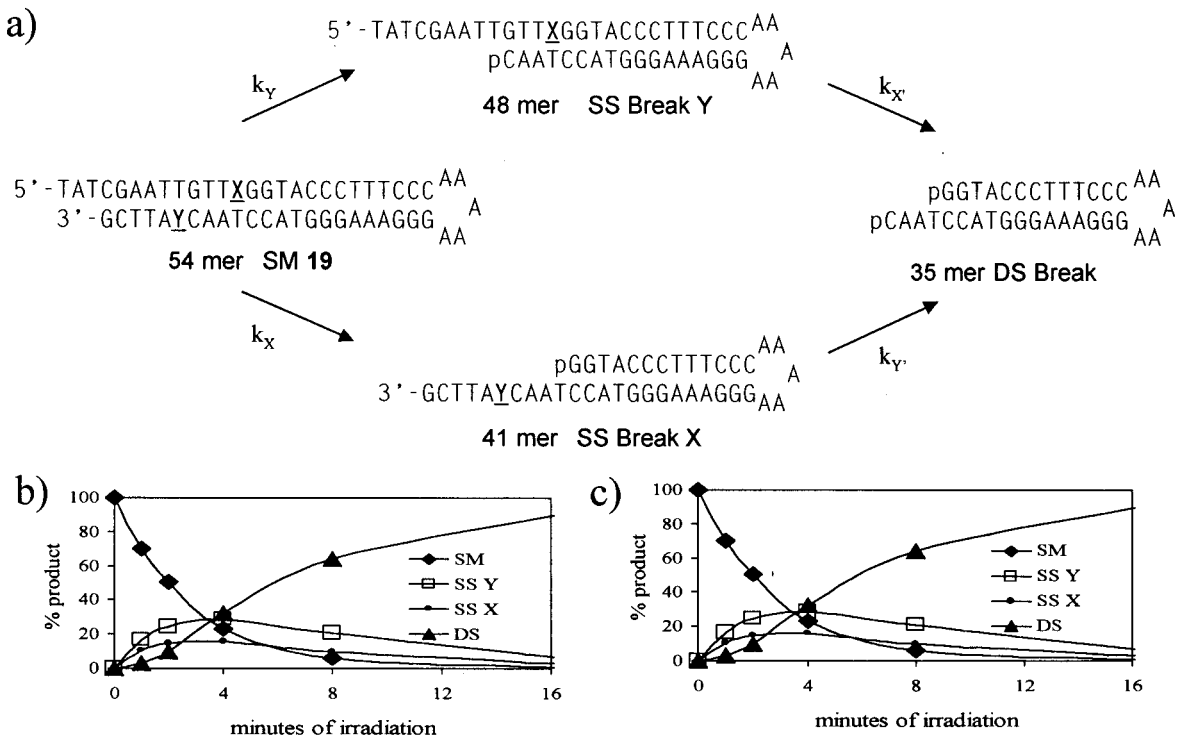

Figure 8. (a) Expected single and double strand cleavage products resulting from the photolysis of the internally labeled hairpin substrate **19** containing caged strand breaks **X** and **Y** that are three nucleotides apart. Below are plots of the product distributions as a function of irradiation time under (b) native conditions and (c) denaturing conditions.

ACKNOWLEDGMENT

This work was partially supported by NIH Grants CA51116 and CA40463 and a GANN fellowship to P.O. (Department of Education Grant P200A20106). The assistance of the Washington University High Resolution NMR Facility, funded in part through NIH Biomedical Research Support Shared Instrument Grants RR-02004, RR-05018, and RR-07155 is gratefully acknowledged, as is the Washington University Mass Spectrometry Resource, an NIH Research Resource (Grant P41RR0954).

LITERATURE CITED

(1) Sonntag, C. v. (1987) *The Chemical Basis of Radiation Biology*, Taylor & Francis, New York.

(2) Obe, G., Johannes, C., and Schulte-Frohlinde, D. (1992) DNA double-strand breaks induced by sparsely ionizing radiation and endonucleases as critical lesions for cell death, chromosomal aberrations, mutations and oncogenic transformation. *Mutagenesis 7*, 3−12.
(3) Ward, J. F. (1995) Radiation mutagenesis: the initial DNA lesions responsible [published erratum appears in *Radiat. Res.* (1995) *143* (3), 355]. *Radiat. Res. 142*, 362−368.
(4) Povirk, L. F. (1996) DNA damage and mutagenesis by radiomimetic DNA-cleaving agents: bleomycin, neocarzinostatin and other enediynes. *Mutat. Res. 355*, 71−89.
(5) Dedon, P. C., and Goldberg, I. H. (1992) Free-radical mechanisms involved in the formation of sequence-dependent bistranded DNA lesions by the antitumor antibiotics bleomycin, neocarzinostatin, and calicheamicin. *Chem. Res. Toxicol. 5*, 311−332.
(6) Thacker, J. (1994) The study of responses to "model" DNA breaks induced by restriction endonucleases in cells and cell-free systems: achievements and difficulties. *Int. J. Radiat. Biol. 66*, 591−596.
(7) Giese, B., Dussy, A., Elie, C., Erdmann, P., and Schwitter, U. (1994) Synthesis and selective radical cleavage of C-4′-modified oligonucleotides. *Angew. Chem., Int. Ed. Engl. 33*, 1861−1863.
(8) Friedberg, E. C., Walker, G. C., and Siede, W. (1995) *DNA Repair and Mutagenesis*, ASM Press, Washington DC.
(9) Marriott, G. (1998) Caged compounds. *Methods in Enzymology*, Academic Press, New York.
(10) Engels, J., and Schlaeger, E. J. (1977) Synthesis, structure, and reactivity of adenosine cyclic 3′,5′-phosphate benzyl triesters. *J. Med. Chem. 20*, 907−911.
(11) Hoffman, J. F., Forbush, B., III, and Kaplan, J. H. (1978) Rapid photolytic release of adenosine 5′-triphosphate from a protected analogue: utilization by the Na:K pump of human red blood ghosts. *Biochemistry 17*, 1929−1935.
(12) Horn, T., Downing, K., Gee, Y., and Urdea, M. S. (1991) Controlled chemical cleavage of synthetic DNA at specific sites. *Nucleosides Nucleotides 10*, 299−302.
(13) Kotera, M., Bourdat, A.-G., Defrancq, E., and Lhomme, J. (1998) A highly efficient synthesis of oligodeoxyribonucleotides containing the 2′-deoxyribonolactone lesion. *J. Am. Chem. Soc. 120*, 11810−11811.
(14) Chaulk, S. G., and MacMillan, A. M. (1998) Caged RNA: photocontrol of a ribozyme reaction. *Nucleic Acids Res. 26*, 3173−3178.
(15) Nadji, S., Wang, C.-I., and Taylor, J.-S. (1992) Photochemically and photoenzymatically cleavable DNA. *J. Am. Chem. Soc. 114*, 9266−9269.
(16) Giese, B., Beyrich-Graf, X., Erdmann, P., Giraud, L., Imwinkelried, P., Muller, S. N., and Schwitter, U. (1995) Cleavage of single-stranded 4′-oligonucleotide radicals in the presence of oxygen. *J. Am. Chem. Soc. 117*, 6146−6147.
(17) Ordoukhanian, P., and Taylor, J.-S. (1995) Design and synthesis of a versatile photocleavable DNA building block. Application to phototriggered hybridization. *J. Am. Chem. Soc. 117*, 9570−9571.
(18) Fasman, G. D. (1975) Nucleic Acids. *Handbook of Biochemistry and Molecular Biology*, Vol. I CRC Press, Cleveland.
(19) Sambrook, J., Fritsch, E. F., and Maniatis, T. (1989) *Molecular Cloning: A Laboratory Manual*, 2nd ed., Vol. 1, Cold Spring Harbor Laboratory Press, Plainview, NY.
(20) Maxam, A. M., and Gilbert, W. (1980) Sequencing end-labeled DNA with base-specific chemical cleavages. *Methods Enzymol. 65*, 499−560.
(21) Trentham, D. R., Corrie, J. E. T., Barth, A., Gradwell, M. J., Maeda, Y., Mantele, W., and Meir, T. (1997) Time-resolved infrared spectroscopy of intermediates and products from photolysis of 1-(2-nitrophenyl)ethyl phosphates: reaction of the 2-nitrosoacetophenone byproduct with thiols. *J. Am. Chem. Soc. 119*, 4149−4159.
(22) Stubbe, J., Absalon, M. J., and Kozarich, J. W. (1995) Sequence-specific double-strand cleavage of DNA by Fe-bleomycin. The detection of sequence-specific double-strand breaks using hairpin oligonucleotides. *Biochemistry 34*, 2065−2075.
(23) Churchill, M. E., Peak, J. G., and Peak, M. (1991) Correlation between cell survival and DNA single-strand break repair proficiency in the chinese hamster ovary cell line AA8 and EM9 irraidated with 365-nm ultraviolet-A radiation. *Photochem. Photobiol. 53*, 229−236.
(24) Basu, A. K., and Essigmann, J. M. (1988) Site-specifically modified oligodeoxynucleotides as probes for the structural and biological effects of DNA-damaging agents. *Chem. Res. Toxicol. 1*, 1−18.
(25) Banerjee, S. K., Christensen, R. B., Lawrence, C. W., and LeClerc, J. E. (1988) Frequency and spectrum of mutations produced by a single cis-syn thymine-thymine cyclobutane dimer in a single-stranded vector. *Proc. Natl. Acad. Sci. U.S.A. 85*, 8141−8145.
(26) Huang, J. C., Hsu, D. S., Kazantsev, A., and Sancar, A. (1994) Substrate spectrum of human excinuclease: repair of abasic sites, methylated bases, mismatches, and bulky adducts. *Proc. Natl. Acad. Sci. U.S.A. 91*, 12213−12217.

BC9900993

Controlled Template-Assisted Assembly of Plasmid DNA into Nanometric Particles with High DNA Concentration

Ming Ouyang,[†] Jean-Serge Remy,[‡] and Francis C. Szoka Jr.*[,†]

Department of Biopharmaceutical Sciences and Pharmaceutical Chemistry, School of Pharmacy, University of California, San Francisco, California 94143-0446, and Laboratoire de Chimie Genetique Associe CNRS, Universite Louis Pasteur, Faculte de Pharmacie de Strasbourg, F-67401 Illkirch, France

A series of novel cationic detergents that contain cleavable hydrophilic isothiuronium headgroups was synthesized, and their utility in controlled assembly of plasmid DNA into small stable particles with high DNA concentration investigated. The detergents have alkyl chains of C_8-C_{12} and contain hydrophilic isothiuronium headgroups that give relatively high critical micelle concentration (CMC) to the detergents (>10 mM). The isothiuronium group masks a sulfhydryl group on the detergent and can be cleaved in a controlled manner under basic conditions to generate a reactive thiol group. The thiol group can undergo a further reaction after the detergents have accumulated on a DNA template to form a disulfide-linked lipid containing two alkyl chains. The pH-dependent kinetics of cleavage of the isothiuronium group, the CMC of the surfactants, the formation of the complexes, and the transfection efficiency of the DNA complexes have been investigated. Using the C_{12} detergent, a ~6 kilo-basepair plasmid DNA was compacted into a small particle with an average diameter of around 40 nm with a ~ −13 mV ζ-potential at high DNA concentration (up to 0.3 mg/mL). The compounds were well tolerated in cell culture and showed no cytotoxicity under their CMCs. Under appropriate conditions, the small particle retained transfection activity.

INTRODUCTION

How to assemble a small diameter DNA complex is a long-standing problem for nonviral gene delivery systems (*1*, *2*). Previous methods either gave large and polydisperse particle complexes (*3*−*5*), typically from 200 nm to many microns, or unstable small particle complexes at low DNA concentration (*6*−*8*). In either case, the complexes formed are not optimal for in vivo use. Recently, Blessing and co-workers (*9*, *10*) and Trubetskoy and colleagues (*11*) used template-directed methods to prepare small particles at the low particle concentration (0.02 mg/mL). In an attempt to increase the DNA concentration at which small particles form, we designed and synthesized a series of novel cationic detergents that are suitable for the template-directed assembly strategy. The detergents contain isothiuronium groups as hydrophilic components (Scheme 1). As a part of the detergent, the isothiuronium group promotes a high CMC. This helps to avoid aggregation of the compact DNA at high DNA concentration because there are no cationic micelles in the solution even at a high detergent concentration. The isothiuronium group also masks the cross-linking group (sulfhydryl group) and eliminates the possibility for premature detergent dimerization leading to larger particles or aggregates of particles. After the detergent associates with DNA, the isothiuronium group can be cleaved by changing the pH or temperature, and thiol groups are generated that can dimerize into lipids with low CMC. This promotes the stability of the particles (Scheme 2). Herein we describe the detailed characterization of the chemical and physical properties of the detergent as well as the DNA complexes that are formed by the procedure.

Scheme 1. Designed Molecule

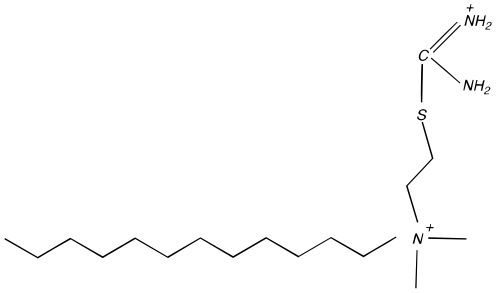

Scheme 2. Controlled Template-Assisted Assembly

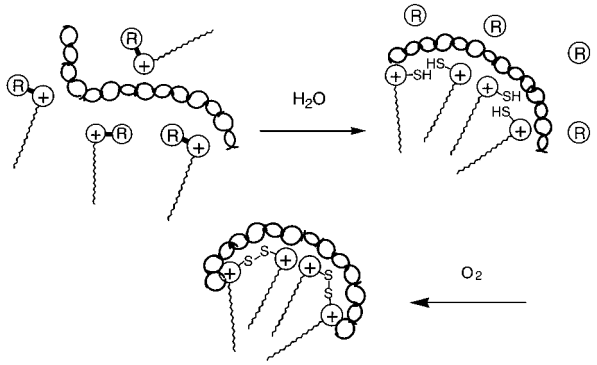

EXPERIMENTAL SECTION

All purchased chemicals were of ACS grade or better and were used without further purification. Melting points are uncorrected. Ultraviolet−visible spectra were carried out on a Hewlett-Packard 8452A diode array

* Address correspondence to this author. Fax: (415) 476-0688. Phone: (415) 476-3895. E-mail: szoka@cgl.ucsf.edu.
[†] University of California.
[‡] Universite Louis Pasteur.

10.1021/bc990101q CCC: $19.00 © 2000 American Chemical Society
Published on Web 12/28/1999

spectrophotometer. Fluorescence measurements were performed on a Perkin-Elmer luminescence spectrometer LS 50B. Elemental microanalytical data were obtained at Microanalytical Laboratory, College of Chemistry, University of California, Berkeley, CA. NMR spectra were recorded on a GE 300 MHz instrument, and chemical shifts are expressed as parts per million using as internal standard, tetramethylsilane ($\delta = 0.0$ ppm) for ^{1}H NMR and $CDCl_3$ ($\delta = 77.0$ ppm) for ^{13}C NMR. Mass spectra were obtained by using a Kratos Tandem MS/MS mass spectrometer.

Bromoethyloctyldimethylammonium Bromide (1a). *N*,*N*-Dimethyloctylamine (3.15 g, 20 mmol) was added dropwise into 1,2-dibromoethane (18.79 g, 100 mmol) at 100 °C over 1 h period. The mixture was stirred at 100 °C for another 3 h. After it was cooled to room temperature, acetone was used for recrystallization and gave the product as white crystals (5.66 g, 16.4 mmol, 82%). $R_f = 40$ ($CHCl_3$/MeOH/H_2O = 65/25/2). Mp 137−138 °C. Anal. calcd for $C_{12}H_{27}NBr_2$ (FW 345.17): C, 41.76; H, 7.88; N, 4.06. Found: C, 41.54; H, 7.68; N, 3.95. ^{1}H NMR (300 MHz, $CDCl_3$): δ 0.89 (3H, t, $J = 6.5$ Hz); δ 1.02−1.51 (10H, m); δ 1.69−1.83 (2H, m); δ 3.52 (6H, s); δ 3.68 (2H, t, $J = 8.4$ Hz); δ 3.93 (2H, t, $J = 7.4$ Hz); δ 4.14 (2H, t, $J = 7.4$ Hz). ^{13}C NMR (75 MHz, $CDCl_3$): δ 13.87, 21.94, 22.23, 22.61, 25.80, 28.75, 28.90, 28.99, 31.45, 51.17, 63.55, 64.81. +LSIMS: *m*/*z* 264 (M − Br$^-$, 100%).

Bromoethylnonyldimethylammonium Bromide (1b). This compound was prepared similarly to bromoethyloctyldimethylammonium bromide (**1a**) with *N*,*N*-dimethylnonylamine to give a white crystals that was recrystallized from acetone (5.46 g, 15.2 mmol, 76%). $R_f = 42$ ($CHCl_3$/MeOH/H_2O = 65/25/2). Mp 145−146 °C. Anal. calcd for $C_{13}H_{29}NBr_2$ (FW 359.20): C, 43.47; H, 8.14; N, 3.90. Found: C, 43.34; H, 8.04; N, 3.90. ^{1}H NMR (300 MHz, $CDCl_3$): δ 0.89 (3H, t, $J = 6.5$ Hz); δ 1.05−1.50 (12H, m); δ 1.66−1.81 (2H, m); δ 3.49 (6H, s); δ 3.66 (2H, t, $J = 8.4$ Hz); δ 3.92 (2H, t, $J = 7.4$ Hz); δ 4.15 (2H, t, $J = 7.4$ Hz). ^{13}C NMR (75 MHz, $CDCl_3$): δ 13.77, 21.97, 22.27, 22.57, 25.82, 28.79, 28.92, 28.98, 31.41, 51.14, 63.49, 64.72. +LSIMS: *m*/*z* 278 (M − Br$^-$, 100%).

Bromoethyldecyldimethylammonium Bromide (1c). This compound was prepared similarly to bromoethyloctyldimethylammonium bromide (**1a**) with *N*,*N*-dimethyldecylamine to give a white crystals that was recrystallized from acetone (6.53 g, 17.5 mmol, 88%). $R_f = 44$ ($CHCl_3$/MeOH/H_2O = 65/25/2). Mp 154−155 °C. Anal. calcd for $C_{14}H_{31}NBr_2$ (FW 373.23): C, 45.05; H, 8.37; N, 3.75. Found: C, 44.57; H, 8.50; N, 3.64. ^{1}H NMR (300 MHz, $CDCl_3$): δ 0.87 (3H, t, $J = 6.5$ Hz); δ 1.02−1.47 (14H, m); δ 1.67−1.83 (2H, m); δ 3.49 (6H, s); δ 3.67 (2H, t, $J = 8.4$ Hz); δ 3.92 (2H, t, $J = 7.4$ Hz); δ 4.20 (2H, t, $J = 7.4$ Hz). ^{13}C NMR (75 MHz, $CDCl_3$): δ 13.96, 22.01, 22.31, 22.62, 25.88,29.13, 29.36, 29.40, 31.56, 51.23, 63.58, 65.00. +LSIMS: *m*/*z* 292 (M − Br$^-$, 100%).

Bromoethylundecyldimethylammonium Bromide (1d). This compound was prepared similarly to bromoethyloctyldimethylammonium bromide (**1a**) with *N*,*N*-dimethylundecylamine to give a white crystals that was recrystallized from acetone (6.04 g, 15.6 mmol, 78%). $R_f = 48$ ($CHCl_3$/MeOH/H_2O = 65/25/2). Mp 160−162 °C. Anal. calcd for $C_{15}H_{33}NBr_2$ (FW 387.25): C, 46.53; H, 8.59; N, 3.62. Found: C, 46.63; H, 8.30; N, 3.43. ^{1}H NMR (300 MHz, $CDCl_3$): δ 0.88 (3H, t, $J = 6.5$ Hz); δ 1.04−1.50 (16H, m); δ 1.66−1.82 (2H, m); δ 3.48 (6H, s); δ 3.66 (2H, t, $J = 8.4$ Hz); δ 3.95 (2H, t, $J = 7.4$ Hz); δ 4.17 (2H, t, $J = 7.4$ Hz). ^{13}C NMR (75 MHz, $CDCl_3$): δ 14.00, 22.21, 22.55, 22.79, 26.07, 29.23, 29.30, 29.41, 29.55, 31.78, 51.41, 63.67, 64.93. +LSIMS: *m*/*z* 306 (M − Br$^-$, 100%).

Bromoethyldodecyldimethylammonium Bromide (1e). This compound was prepared similarly to bromoethyloctyldimethylammonium bromide (**1a**) with *N*,*N*-dimethyldodecylamine to give a white crystals that was recrystallized from acetone (6.42 g, 16.0 mmol, 80%). $R_f = 52$ ($CHCl_3$/MeOH/H_2O = 65/25/2). Mp 167−168 °C. Anal. calcd for $C_{16}H_{35}NBr_2$ (FW 401.28): C, 47.89; H, 8.79; N, 3.49. Found: C, 47.38; H, 8.85; N, 3.40. ^{1}H NMR (300 MHz, $CDCl_3$): δ 0.89 (3H, t, $J = 6.5$ Hz); δ 1.04−1.50 (18H, m); δ 1.66−1.81 (2H, m); δ 3.50 (6H, s); δ 3.70 (2H, t, $J = 8.4$ Hz); δ 3.92 (2H, t, $J = 7.4$ Hz); δ 4.19 (2H, t, $J = 7.4$ Hz). ^{13}C NMR (75 MHz, $CDCl_3$): δ 14.02, 22.01, 22.57, 22.79, 26.05, 29.21, 29.37, 29.47, 31.78, 51.48, 63.70, 65.03. +LSIMS: *m*/*z* 320(M − Br$^-$, 100%).

Isothiuroniumethyloctyldimethylammonium Bromide (2a). The mixture of bromoethyloctyldimethylammonium bromide (**1a**) (1.03 g, 2.98 mmol) and thiourea (1.13 g, 14.8 mmol) prepared at room temperature in 5 mL of DMSO was stirred at 100 °C for 30 min. It was cooled to room temperature, acetone was used to precipitate the product, then the product was dissolved in 1 mL of $CHCl_3$/MeOH (1/1), 2 mL of acetone was added for recrystallization, and the product formed as white crystals (0.65 g, 1.55 mmol, 52%). $R_f = 39$ ($CHCl_3$/MeOH/H_2O/HOAc = 65/25/5/5). Mp 178−179 °C. Anal. calcd for $C_{13}H_{31}N_3Br_2S$ (FW 421.29): C, 37.06; H, 7.42; N, 9.97; S, 7.61. Found: C, 36.97; H, 7.39; N, 10.12; S, 7.55. ^{1}H NMR (300 MHz, d_6-DMSO): δ 0.89 (3H, t, $J = 6.5$ Hz); δ 1.06−1.52 (10H, m); δ 1.64−1.75 (2H, m); δ 3.11 (6H, s); δ 3.69 (2H, t, $J = 8.4$ Hz); δ 3.94 (2H, t, $J = 7.4$ Hz); δ 4.17 (2H, t, $J = 7.4$ Hz); 9.39 (s, 4H, disappeared after D_2O was added). ^{13}C NMR [75 MHz, $CDCl_3$/CD_3OD (4/1)]: δ 14.03, 22.62, 22.77, 24.93, 26.15, 29.19, 29.30, 29.45, 29.60, 31.86, 50.82, 62.10, 65.70, 169.40. +LSIMS: *m*/*z* 260 (M − HBr − Br$^-$, 100%).

Isothiuroniumethylnonyldimethylammonium Bromide (2b). This compound was prepared similarly to Isothiuroniumethyloctyldimethylammonium bromide (**2a**) with bromoethylnonyldimethylammonium bromide (**1b**) and gave the product as white crystals (0.71 g, 1.64 mmol, 55%). $R_f = 39$ ($CHCl_3$/MeOH/H_2O/HOAc = 65/25/5/5). Mp 181−182 °C. Anal. calcd for $C_{14}H_{33}N_3Br_2S$ (FW 435.32): C, 38.63; H, 7.64; N, 9.65; S, 7.37. Found: C, 38.57; H, 7.60; N, 9.45; S, 7.32. ^{1}H NMR (300 MHz, d_6-DMSO): δ 0.86 (3H, t, $J = 6.5$ Hz); δ 1.03−1.45 (12H, m); δ 1.63−1.73 (2H, m); δ 3.08 (6H, s); δ 3.68 (2H, t, $J = 8.4$ Hz); δ 3.93 (2H, t, $J = 7.4$ Hz); δ 4.14 (2H, t, $J = 7.4$ Hz); 9.37 (s, 4H, disappeared after D_2O was added). ^{13}C NMR [75 MHz, $CDCl_3$/CD_3OD (4/1)]: δ 14.06, 22.65, 22.74, 24.95, 26.13, 29.19, 29.31, 29.47, 29.58, 31.84, 50.79, 62.11, 65.73, 169.45. +LSIMS: *m*/*z* 274(M − HBr − Br$^-$, 100%).

Isothiuroniumethyldecyldimethylammonium Bromide (2c). This compound was prepared similarly to Isothiuroniumethyloctyldimethylammonium bromide (**2a**) with bromoethyldecyldimethylammonium bromide (**1c**) and gave the product as white crystals (0.60 g, 1.34 mmol, 45%). $R_f = 39$ ($CHCl_3$/MeOH/H_2O/HOAc = 65/25/5/5). Mp 182−183 °C. Anal. calcd for $C_{15}H_{35}N_3Br_2S$ (FW 449.35): C, 40.10; H, 7.85; N, 9.35; S, 7.14. Found: C, 40.21; H, 8.15; N, 9.40; S, 7.09. ^{1}H NMR (300 MHz, d_6-DMSO): δ 0.86 (3H, t, $J = 6.5$ Hz); δ 1.05−1.45 (14H, m); δ 1.65−1.73 (2H, m); δ 3.09 (6H, s); δ 3.65 (2H, t, $J = 8.4$ Hz); δ 3.96 (2H, t, $J = 7.4$ Hz); δ 4.25 (2H, t, $J = 7.4$ Hz); 9.50 (s, 4H, disappeared after D_2O was added). ^{13}C NMR [75 MHz, $CDCl_3$/CD_3OD (4/1)]: δ 14.05, 22.58, 22.78, 24.88, 26.19, 29.15, 29.33, 29.50, 29.63, 31.91, 50.77, 61.98, 65.55, 168.95. +LSIMS: *m*/*z* 288 (M − HBr − Br$^-$, 100%).

Isothiuroniumethylundecyldimethylammonium Bromide (2d). This compound was prepared similarly to isothiuroniumethyloctyldimethylammonium bromide (**2a**) with bromoethylundecyldimethylammonium bromide (**1d**) and gave the product as white crystals (0.55 g, 1.19 mmol, 40%). $R_f = 40$ ($CHCl_3$/MeOH/H_2O/HOAc = 65/25/5/5). Mp 184−185 °C. Anal. calcd for $C_{16}H_{37}N_3Br_2S$ (FW 463.37): C, 41.47; H, 8.05; N, 9.07; S, 6.92. Found: C, 41.58; H, 8.35; N, 9.00; S, 6.77. ^{1}H NMR (300 MHz, d_6-DMSO): δ 0.88 (3H, t, $J = 6.5$ Hz); δ 1.07−1.47 (16H, m); δ 1.60−1.71 (2H, m); δ 3.07 (6H, s); δ 3.68 (2H, t, $J = 8.4$ Hz); δ 3.95 (2H, t, $J = 7.4$ Hz); δ 4.18 (2H, t, $J = 7.4$ Hz); 9.45 (s, 4H, disappeared after D_2O was added). ^{13}C NMR [75 MHz, $CDCl_3$/CD_3OD (4/1)]: δ 13.99, 22.56, 22.72, 24.89, 26.10, 29.17, 29.27, 29.41, 29.56, 31.82, 50.78, 62.05, 65.66, 168.60. +LSIMS: *m/z* 302 (M − HBr − Br^-, 100%).

Isothiuroniumethyldodecyldimethylammonium Bromide (2e). This compound was prepared similarly to Isothiuroniumethyloctyldimethylammonium bromide (**2a**) with bromoethyldodecyldimethylammonium bromide (**1e**) and gave the product as white crystals (0.65 g, 1.37 mmol, 46%). $R_f = 40$ ($CHCl_3$/MeOH/H_2O/HOAc = 65/25/5/5). Mp 188−189 °C. Anal. calcd for $C_{17}H_{39}N_3Br_2S$ (FW = 477.40): C, 42.77; H, 8.23; N, 8.80; S, 6.72. Found: C, 42.86; H, 8.56; N, 9.02; S, 6.54. ^{1}H NMR (300 MHz, d_6-DMSO): δ 0.87 (3H, t, $J = 6.5$ Hz); δ 1.02−1.46 (18H, m); δ 1.64−1.72 (2H, m); δ 3.10 (6H, s); δ 3.66 (2H, t, $J = 8.4$ Hz); δ 3.92 (2H, t, $J = 7.4$ Hz); δ 4.13 (2H, t, $J = 7.4$ Hz); 9.35 (s, 4H, disappeared after D_2O was added). ^{13}C NMR [75 MHz, $CDCl_3$/CD_3OD (4/1)]: δ 13.97, 22.59, 22.73, 24.89, 26.12, 29.15, 29.27, 29.42, 29.56, 31.83, 50.78, 62.08, 65.67, 169.36. LSIMS: *m/z* 214 [M − HBr − Br^- - $(CH_2)_2SC(NH)NH_2$, 100%], 316 (M − HBr − Br^-, 100%).

Kinetics of Hydrolysis of the Isothiuronium Group. The following buffers were used to determine the hydrolysis rate of the isothiuronium group at various pH at 25 ± 0.1 °C: 20 mM sodium acetate−acetic acid, pH 5.0 buffer; 15 mM sodium phosphate, pH 7.0 buffer; 15 mM Tris·HCl, pH 8.5 buffer; 15 mM Tris·HCl, pH 9.0 buffer; 15 mM Na_2CO_3−$NaHCO_3$, pH 10.0 buffer. The 15 mM Tris·HCl, pH 8.5 buffer was used for testing the hydrolysis rate at various temperature. Each buffer was saturated by argon and contained 10 mM EDTA to protect sulfhydryl group from oxidation catalyzed by heavy metals (*12*). Free thiol concentration was quantitated spectrophotometrically according to Ellman (*13*) and Tarnowski (*12*). The reaction was maintained under argon during the entire procedure to avoid detergent oxidation. For each hydrolysis reaction sample, about 3 mM isothiuronium detergent solution was used, and for each time point, a 125 μL aliquot was removed and mixed with 5 mL of 15 mM Tris·HCl, 10 mM EDTA, pH 7.5 buffer, and 100 μL of 10 mM fresh 5,5′-dithiobis(2-nitrobenzoic acid) solution. For the experiment of hydrolysis rate on DNA template, pLC 0888.143 plasmid DNA containing the luciferase reporter gene was added to a final concentration of 0.25 mg/mL before addition of the detergent. The plasmid was obtained from Valentis, Inc. (The woodlands, TX) and had less than 20 units of endotoxin per mg of DNA (*14*). All of the points were tested in duplicate.

Critical micelle concentrations (CMC) were determinated by a fluorescence enhancement method by using *N*-phenyl-1-naphthylamine (*15*). The CMCs of isothiuronium detergents were tested at pH 6.8, in 20 mM sodium phosphate buffer. Mercaptan detergent solutions for CMC determination were obtained by the following method: 0.2 M argon saturated sodium hydroxide solution was used to dissolve the isothiuronium detergents and to prepare the pH 8.5 stock solutions of the mercaptan detergents. These stock solutions were stored at room temperature for 10 min, and then, a pH 8.5, 20 mM Tris·HCl buffer containing 10 mM DTT was used to dilute the solutions for the CMC determination. Disulfide lipid solutions for CMC determination were obtained in the following way: the mercaptan detergent stock solutions were oxidized by treatment with 10% excess H_2O_2 at room temperature for 2 h, and then, a pH 8.5, 20 mM Tris·HCl buffer containing 10 mM H_2O_2 was used to dilute the solutions for CMC determination. All of the points were tested in triplicate.

DNA−Surfactant Complex Formation. The DNA complexes were formed by mixing a defined concentration of the DNA solution and an appropriate amount of detergent in an oxygen saturated pH 8.5, 20 mM Tris·HCl buffer at room temperature. DNA concentration was confirmed by using absorbance at 260 nm: 1 unit = 50 μg/mL DNA. The charge ratio (±) of detergent to DNA nucleotide phosphate is computed and indicated for each experiment. The mixture was placed at room temperature for 24 h, and then the solution was characterized for the formation of particles and for the ability to transfect cell.

Fluorescence Method (*15*) to Test the Accumulation of Detergent in the Complexes. The fluorescence enhancement of *N*-phenyl-1-naphthylamine (NPN) was used to measure the formation of a hydrophobic environment in the complex. The condition was as follows. Excitation: wavelength 350 nm, slit width 10 mm. Emission: wavelength 410 nm; slit width 10 mm. Integration time: 3 s. A total of 20 μL of 20 μM *N*-phenyl-1-naphthylamine was added to each of the following samples: (1) positive control [400 μL 167 mM isothiuroniumethyldodecyldimethylammonium bromide (**2**) in 15 mM Tris·HCl, pH 8.5 buffer], (2) detergent control [400 μL of 0.76 mM isothiuroniumethyldodecyldimethylammonium bromide (**2**) in 15 mM Tris·HCl, pH 8.5 buffer], (3) DNA control [400 μL 500 μg/mL (1.52 mM nucleotide phosphate) pLC 0888.143 plasmid DNA in 15 mM Tris·HCl, pH 8.5 buffer], (4) DNA complex sample (400 μL of DNA complex solution containing 250 μg/mL (0.76 mM nucleotide phosphate) pLC 0888.143 plasmid DNA and 0.38 mM isothiuroniumethyldodecyldimethylammonium bromide (**2**) in 15 mM Tris·HCl, pH 8.5 buffer], (5) blank sample [400 μL of 15 mM Tris·HCl, pH 8.5 buffer]. The relative fluorescence of NPN in buffer (25 units) was subtracted from the fluorescence of NPN in the presence of the other compounds. All of the points were tested in triplicate.

Light Scattering Measurements of Particle Size and ζ-Potential. Particle size was determined on a Zetasizer 1000 (Malvern Instruments Ltd., Spring Lane South, Malvern, Worcs. WR14 1AT, France) at 25 °C with a 90° angle. ζ-Potential was measured on a Zetasizer 4 (Malvern Instruments) at 25 °C in a buffer of 20 mM Tris·HCl, pH 8.5. The values for the diameter are based upon the intensity average and determined using the programs that are furnished with the zetasizer.

Electron Microscopy. The solution of pLC0888.143 DNA complex compacted by isothiuroniumethyldodecyldimethylammonium bromide (**2**) in 15 mM Tris·HCl, pH 8.5 buffer, at 250 μg/mL DNA with 1:1 charge ratio was used in transmission electron microscopy experiment. Negative stain method (*9*) and freeze−fracture method (*16*) were used to observe the structure of the complex:

(1) Negative Stain Method. Carbon films were prepared

by sublimation on freshly cleaved mica and recovered by flotation on Cu/Rh grids (300 mesh, Touzard & Matignon, Courtaboeuf, France). After drying overnight, grids were kept on blotting paper in a Petri dish. Immediately before sample addition, grids were glow-discharged (110 mV, 25 s, 25−30 μA). A drop (5 μL) of sample solution was left on the grid for 1 min. The complex sample was negatively stained with 35 μL of aqueous uranyl acetate (1−2% w/v) for 20 s, and excess liquid was removed with blotting paper. Observations were performed at 80 kV with a Philips EM 410 transmission electron microscope.

(2) Freeze−Fracture Method. Freeze−fracture electron micrographs were prepared by Dr. Brigitte Sternberg-Papahadjopoulos as previously described (*16*).

Thin-Layer Chromatography Identification of the Lipid in the Complexes. A modified Bligh−Dyer method (*17*, *18*) was used to extract the lipids from the DNA complexes. For each extracted sample, two plates were developed in the same solvent pool at the same time to minimize the error. A solvent of $CHCl_3/MeOH/H_2O$ = 65/35/4 was used to develop the silica gel TLC. After the chromatography was completed, one TLC plate was sprayed by Ellman's reagent [10 mM fresh 5,5′-dithiobis-(2-nitrobenzoic acid) solution in 20 mM Tris, 0.04 M EDTA, pH 8.5 buffer] to develop the color of the mercaptan spot. Iodine was used to develop the other plate to locate the other material. To determine the R_f of the mercaptan detergent, a mercaptoethyldodecyldimethylammonium bromide sample was obtained by the following method: the isothiuroniumethyldodecyldimethylammonium bromide (**2**) was dissolved in an appropriate amount of 0.2 M argon saturated sodium hydroxide solution to obtain a final pH 8.5 solution. This solution was stored at room temperature for 10 min, and then the modified Bligh−Dyer method was used to extract the detergent. A sample from the chloroform phase was applied to TLC to obtain the R_f of the mercaptan detergent. To obtain the R_f of the disulfide lipid, the mercaptan detergent solution was oxidized by treatment with 10% excess H_2O_2 at room temperature for 2 h, and then the Bligh−Dyer method was used to extract the lipid. The lipid in the chloroform phase was applied to the TLC.

Cytotoxicity of isothiuroniumethyldodecyldimethylammonium bromide (2) was assessed using Sulforhodamine-B (SRB) assay (19). CV-1 cells were plated in 96 well plates at 3×10^3 cells/well in 100 μL of growth medium consisting of DME-H21 with 10% fetal calf serum and antibiotics (100 units/mL penicillin and 100 μg/mL streptomycin). The cells were incubated for 24 h at 37 °C in a 95% air, 5% CO_2 atmosphere. The growth medium was then removed, and 225 μL of growth medium was added. Isothiuroniumethyldodecyldimethylammonium bromide (**2**) was dissolved in 15 mM Tris-acetic acid, pH 8.5 buffer, in a concentration serial: 5.0, 2.5, 1.2, 0.6, 0.3, and 0 mM (buffer only). The detergent solutions were added in 25 μL, and the cells were incubated in this medium for 5 h or 24 h. Normally cultured cells provided a blank. All the points were tested in triplicate.

Transfection of Monkey Kidney Fibroblast Cells. CV-1 cells were plated in a 24 well plate at 3×10^4 cells/well in 1 mL of growth medium consisting of DME-H21 with 10% fetal calf serum and antibiotics (100 units/mL penicillin and 100 μg/mL streptomycin). The cells were incubated for 19−24 h at 37 °C in a 95% air, 5% CO_2 atmosphere. The growth medium was then removed, the cells were washed with serum free media, and serum-free medium was added (1 mL). The transfection system was then added in 50 μL in 15 mM Tris·HCl, pH 8.5 buffer, and the cells were incubated in this medium for 3 h. Subsequently, the medium was removed and replaced with complete growth medium, and the cells incubated for a further 21 h. The medium was removed. The cells were lysed and assayed for luciferase activity and total cell protein (Bio-Rad BCA protein assay) performed according to the manufactures' instruction. The positive controls contained of 1 μg of luciferase DNA and 4 μg of functional dendrimer (*4*). The surfactant compacted DNA (1 μg) was also mixed with 4 μg of functional dendrimer and applied to a group of wells to associate the negatively charged detergent complex with the cell surface. Normally cultured cells provided a blank. All the points were tested in triplicate.

Scheme 3. Synthesis of the Isothiuronium Detergent[a]

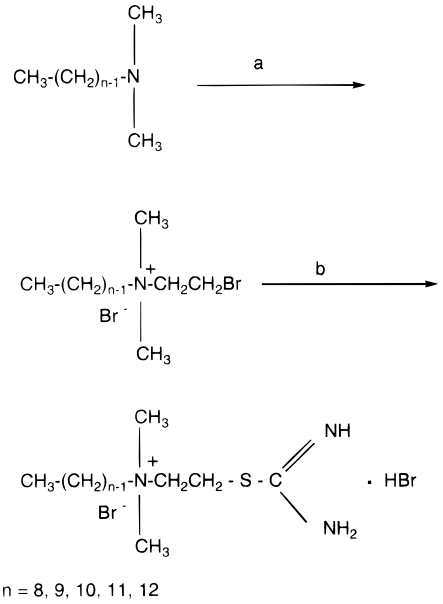

[a] n = 8, 9, 10, 11, 12. (a) Large excess of dibromoethane, 100 °C, ambient, 4 h, 76−88%. (b) Large excess of thiourea, 100 °C, ambient, 30 min, 40−55%.

RESULTS

Synthesis. Our approach to the synthesis of isothiuronium detergents employed tertiary amines with alkyl chain of C_8−C_{12} as the starting lipophilic moiety (Scheme 3). The reaction was straightforward, although in the first step to obtain the bromoethyl derivatives, a large excess of dibromoethane was used as the reaction solvent. The tertiary amine was added dropwise to avoid both of the bromo groups on a dibromoethane molecule to react with the tertiary amine. For the synthesis of the isothiuronium detergents, DMSO was used as the reaction solvent because it is a good solvent for a SN_2 displacement of bromo group by thiourea (*20*). A previous paper (*21*) has used ethanol as the solvent in this kind of reaction; however, we obtained a very poor yield using ethanol. All the products are stable at room temperature when stored as dry powders in a low humidity environment.

Kinetics of Hydrolysis of Isothiuronium Group. Base-catalyzed hydrolysis was employed to generate the reactive sulfhydryl required to obtain a cationic two alkyl chain amphiphile with a low CMC. We used isothiuroniumethyldodecyldimethylammonium bromide (**2**) to determine the kinetics of hydrolysis of the isothiuronium group from the detergent. The preliminary experiments revealed that the hydrolysis was a first-order reaction.

Table 1. Hydrolysis Rate of Isothiuronium Group of Isothiuroniumethyldodecyldimethylammonium Bromide (2) at Various pH Value at 25 ± 0.1 °C[a]

pH (± 0.1)	k (× 10^{-4} s^{-1})	$t_{1/2}$ (min)
5.0	no reaction observed	no reaction observed
7.0	0.078 ± 0.006	1500 ±110
8.5	4.3 ± 0.2	27 ± 1
9.0	7.4 ± 0.5	16 ± 1
10.0	170 ± 10	0.68 ± 0.1

[a] Mean ± SD of three measurements.

Table 2. Hydrolysis Rate of Isothiuronium Group of Isothiuroniumethyldodecyldimethylammonium Bromide (2) at Various Temperatures at pH 8.5 ± 0.1[a]

temp (°C ± 0.1 °C)	k (× 10^{-4} s^{-1})	$t_{1/2}$ (min)
0	0.6 ± 0.02	190 ± 6
15	1.4 ± 0.1	83 ± 5
25	4.3 ± 0.2	27 ± 1
38	28 ± 3	4.1 ± 0.4
60	130 ± 10	0.89 ± 0.06

[a] Mean ± SD of three measurements.

The rate of the cleavage of the isothiuronium group can be controlled as a function of the pH of the solution. Table 1 summarizes the reaction rate constant (k) and half-life ($t_{1/2}$) of the hydrolysis at various pH at room temperature. At pH 5.0, the reaction was very slow and no obvious hydrolysis reaction was observed in our experiments over 1 day. However, as the pH was increased from 7.0 to 10.0, the half-life of the hydrolysis was reduced from more than a day to less than 1 min, indicating the hydrolysis of the isothiuronium group is highly pH dependent. According to the data in Table 1, we fitted a formula for the half-life of the reaction as a function of pH value at 25 °C:

$$\ln(t_{1/2}) = A + B(\text{pH value}) \quad (1)$$

where $A = 25 \pm 1$, $B = -2.6 \pm 0.1$, and correlation coefficient $r > 0.99$. Thus, regulating the pH is an effective way to control the rate of appearance of the mercaptan.

The influence of the reaction temperature on the reaction rate constant (k) and half-life ($t_{1/2}$) of hydrolysis at pH 8.5 is tabulated in Table 2. On the basis of the data in Table 2, we computed the activation energy of the reaction using the Arrhenius equation:

$$\ln k = \ln A - E_a/(RT) \quad (2)$$

the preexponential factor $\ln A = 22 \pm 3$ and the activation energy $E_a = (7.2 \pm 0.7) \times 10^4$ J mol^{-1}, and correlation coefficient $r > 0.99$. Thus, the hydrolysis rate was highly temperature dependent. Regulating the temperature is another practical way to control the cleavage rate of isothiuronium group from the detergent. This should permit the controlled formation of the mercaptan and, in this way, the controlled assembly of the DNA−surfactant complex.

We examined the effect on the hydrolysis of the isothiuronium group in the presence of DNA in the reaction mixture. The reaction rate constant and the half-life of the hydrolysis at pH 8.5 at 25 °C was reduced between 3 and 4-fold when DNA was present in the solution (Table 3).

CMC of the Surfactants. The concept behind the controlled template-directed assembly of plasmid DNA complexes is that the self-assembly of the surfactants can be controlled to permit a stable micelle structure to form only on the DNA template. The control for the assembly is obtained by altering the CMC of the surfactant. Ideally,

Table 3. Hydrolysis Rate of Isothiuronium Group of Isothiuroniumethyldodecyldimethylammonium Bromide (2) on DNA Template at pH 8.5 ± 0.1, 25 ± 0.1 °C[a]

	k (× 10^{-4} s^{-1})	$t_{1/2}$ (min)
without DNA	4.3 ± 0.2	27 ± 1
with DNA	1.3 ± 0.1	89 ± 5

[a] Mean ± SD of three measurements.

Table 4. Critical Micelle Concentration of Surfactants at 25 ± 0.1 °C[a]

n	isothiuronium detergent (mM)	mercaptan detergent (mM)	disulfide lipid (mM)
8	320 (±30)	20 (±2)	7.2 (±0.7)
9	190 (±13)	12 (±1)	4.2 (±0.3)
10	69 (±4)	8.6 (±0.3)	1.3 (±0.2)
11	25 (±2)	3.8 (±0.2)	0.55 (±0.03)
12	10 (±1)	0.21 (±0.03)	0.047(±0.009)

[a] Mean ± SD of three measurements.

each step of the process in forming a stable small particle should be associated with a decrease of the CMC of the detergent. To learn if the compounds fulfilled this criterion, we measured the CMCs of the three forms of the surfactant (Table 4). The CMC of the surfactant is significantly decreased when the isothiuronium group is cleaved from the detergent and can be decreased further by oxidizing the mercaptan detergent into the disulfide lipid. By the appropriate selection of the alkyl chain length, we could identify a structure which had a high enough CMC for the isothiuronium detergent to be added to high concentration of DNA without causing aggregation, yet a low enough CMC to allow the corresponding disulfide lipid to form a stable micelle on the DNA template.

Complex Formation and Properties. The accumulation of detergent on the DNA template could be demonstrated by following the increase in the fluorescence quantum yield of *N*-phenyl-1-naphthylamine (NPN) when the fluorophore partitions into a hydrophobic environment (*15*). The fluorescence quantum yield of NPN increases about 10-fold, and the wavelengths of maximum fluorescence emission is blue-shifted to about 410 nm when NPN partitions into the apolar core of micelle structures from the aqueous phase. The detergent control and the DNA control samples had almost no fluorescence increase over the blank. However, the mixture of the detergent and DNA at the same concentration as the individual components showed a large fluorescence increase as well as a blue-shift of the absorbance spectrum. The fluorescence intensity of the NPN in the complex was about one-half of the fluorescence of NPN in 167 mM detergent solution (where the detergent is in a micelle), although the total concentration of the detergent and the DNA were only <0.3% of the positive control sample (Figure 1). In the absence of NPN, there was no change in the fluorescence signal; therefore, light scattering from the particles formed in the presence of both the DNA and detergent is not responsible for the observed change in NPN fluorescence. Thus, the surfactants had accumulated on the DNA template, providing a hydrophobic environment for the NPN.

The relationship of charge ratio, DNA concentration, and the particle diameter of the complex is summarized in Table 5. At low DNA concentration, 0.02 mg/mL, the light-scattering signal was too low to analyze the diameter of the particles made by mixing **2** with DNA, even when an excess of detergent was used to prepare the complex. At this concentration and charge ratio, the complex of DOTAP/DNA formed aggregates that were

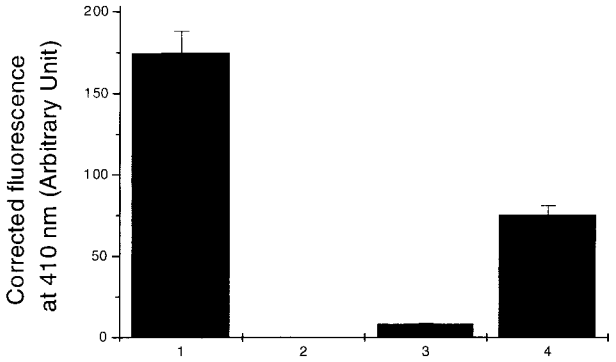

Figure 1. Fluorescence enhancement of *N*-phenyl-1-naphthylamine (NPN) in the DNA−surfactant complex. Excitation wavelength 350 nm, emission wavelength 410 nm. A total of 20 μL of 20 μM *N*-phenyl-l-naphthylamine was added to (1) positive control: 400 μL 167 mM isothiuroniumethyldodecyldimethylammonium bromide (**2**) in 15 mM Tris. HCl, pH 8.5 buffer. (2) Detergent control: 400 μL of 0.76 mM isothiuroniumethyldodecyldimethylammonium bromide (**2**) in 15 mM Tris·HCl, pH 8.5 buffer. (3) DNA control: 400 μL of 500 μg/mL (1.52 mM nucleotide phosphate) pLC 0888.143 plasmid DNA in 15 mM Tris·HCl, pH 8.5 buffer. (4) DNA complex sample: 400 μL of DNA complex solution containing 250 μg/mL (0.76 mM nucleotide phosphate) pLC 0888.143 plasmid DNA and 0.38 mM isothiuroniumethyldodecyldimethylammonium bromide (**2**) in 15 mM Tris·HCl, pH 8.5 buffer. The relative fluorescence of NPN in the blank sample: 400 μL of 15 mM Tris. HCl, pH 8.5 buffer (25 units) was subtracted from the fluorescence of NPN in the presence of the other compounds. All the points were tested in triplicate. The standard deviation is indicated by the vertical bar.

Table 5. Diameter (nm) of DNA−Surfactant Complexes Compacted by Isothiuroniumethyldodecyldimethylammonium Bromide (2) under Various Conditions[a]

DNA concentration (mg/mL)	starting charge ratio (±)			
	1	1.2	1.5	2
0.02	not detected	not detected	not detected	not detected
0.05	not detected	not detected	40 ± 29	50 ± 30
0.1	not detected	52 ± 26	51 ± 10	85 ± 34
0.2	43 ± 16	104 ± 59	129 ± 74	781 ± 654
0.3	42 ± 17	192 ± 118	173 ± 88	precipitate
0.4	238 ± 174	261 ± 179	precipitate	precipitate

[a] Mean ± SD of 10 measurements.

visible by eye. In the high concentration condition, 0.2−0.3 mg/mL DNA, 1/1 charge ratio (+/−), only one ∼40 nm diameter population with a ζ-potential of −13 ± 2 mV was observed. At a higher DNA concentration (0.4 mg/mL), at the 1/1 charge ratio (+/−), large diameter particles were observed. Large particles were also observed at a 0.2 mg/mL DNA concentration when the (+/−) charge ratio was 1.2 (Table 5).

In negative stain transmission electron microscopy of the DNA−surfactant complex at 0.25 mg/mL DNA concentration (Figure 2A), DNA complexes are evident. Most of the complexes are spherical and have a diameter around 25 nm. However, there was evidence of larger particles with diameter between 100 ∼200 nm (Figure 2B). These larger particles appeared to be aggregates of the smaller particles that were connected by strands of material. Freeze−fracture electron micrograph (Figure 2C) revealed small round particles with diameters from 20 to 40 nm that are consistent with the particle diameters observed by negative stain EM and measured by dynamic light scattering.

Thin-layer chromatography was used to identify the surfactant in the complexes after the plasmid DNA particles had been formed. In the solvent of $CHCl_3$/MeOH/H_2O (65/35/4), isothiuroniumethyldodecyldimethylammonium bromide (**2**) had an R_f = 0, while the mecaptoethyldodecyldimethylammonium bromide sample had an R_f = 0.5, and the corresponding disulfide lipid had an R_f = 0.7. Lipid samples extracted from the DNA

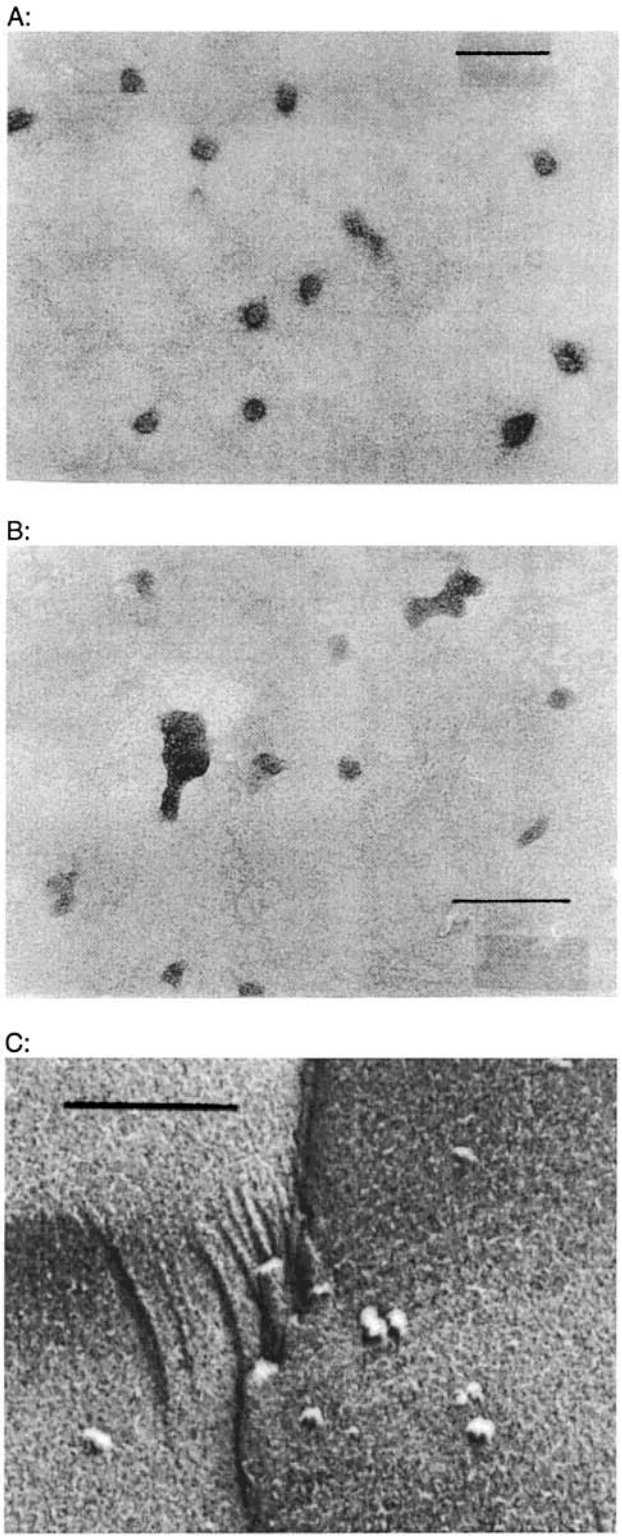

Figure 2. Electron microscopy of DNA−surfactant complex prepared by isothiuroniumethyldodecyldimethylammonium bromide (**2**) at pLC0888.143 DNA concentration of 250 μg/mL in 15 mM Tris·HCl, pH 8.5 buffer. The samples in panel A and B were done by the negative stain method, Bar = 100 nm. The sample in panel C used the freeze-fracture method, Bar = 200 nm.

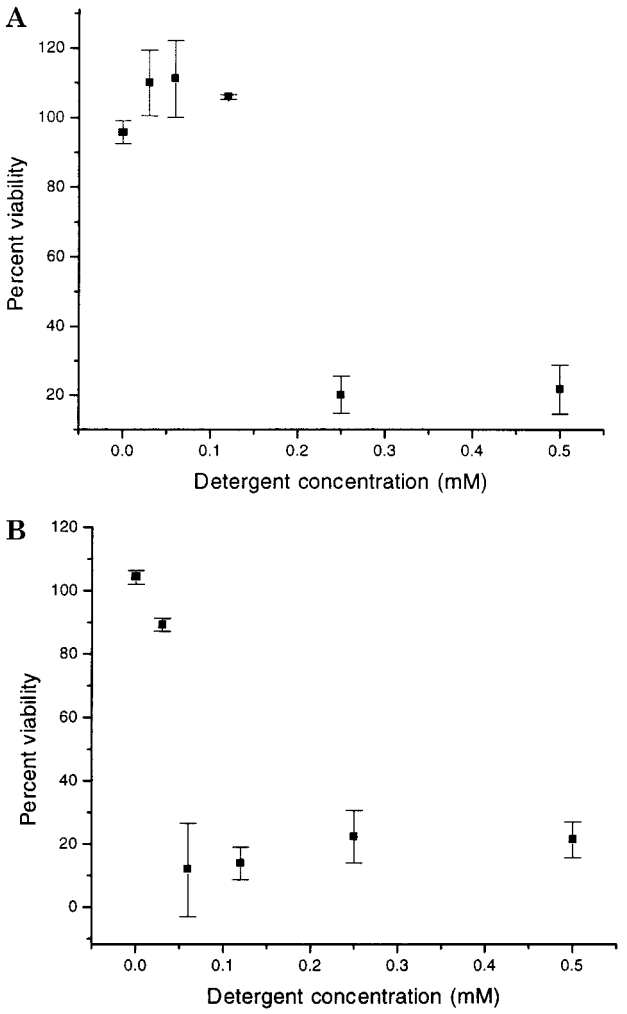

Figure 3. Cytotoxicity of isothiuroniumethyldodecyldimethylammonium bromide (**2**) on the CV-1 cell line. Results were expressed as percent viability of the untreated control cells. Percent viability = [OD_{564}(treated cells) − background]/[OD_{564}(untreated cells) − background] × 100. The cells were treated by (**2**) for 5 h, only cells in the environment with <0.25 mM (**2**) were alive. All the cells in the wells which containing (**2**) >0.25 mM died. (B) Cells treated for 24 hours, the detergent showed higher toxicity. Only cells treated with <0.06 mM (**2**) were alive. Cells treated with concentration >0.06 mM (**2**) died.

complexes showed only a single spot (R_f = 0.7). This suggested that the lipid is primarily in the disulfide form in the DNA complex.

Cytotoxicity Study. Cytotoxicity of isothiuroniumethyldodecyldimethylammonium bromide (**2**) to CV-1 cells is shown in Figure 3. Results were expressed as percent viability. Percent viability = [OD_{564}(treated cells) − background]/[OD_{564}(untreated cells) − background] × 100. Figure 3a showed that, after 5 h exposure, cytotoxicity was observed when the concentration of the detergent was higher than 0.25 mM, which is above the CMC of the mercaptan. At 24 h time point, cytotoxicity was observed at a concentration of 0.06 mM which was just above the CMC of the disulfide.

Transfection Studies. The ability of the condensed DNA−surfactant complexes to transfect CV-1 cells in vitro is shown in Figure 4. The transfection efficiency of the DNA−surfactant complexes was observed to be slightly higher than blank. However, when polyamidoamine fractured dendrimers (*4*) were mixed with the DNA−surfactant complex at a subeffective charge ratio, high transfection was observed. Thus, formation of the

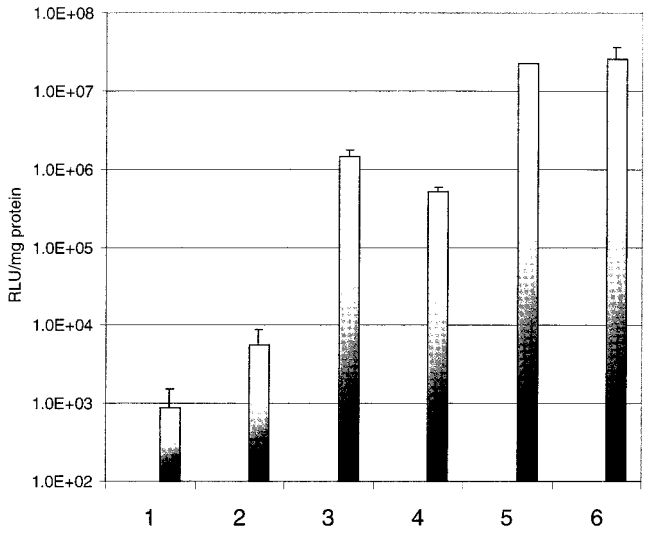

Figure 4. Transfection mediated by luciferase DNA in the presence of various effects. (1) Blank: cells treated with normal media; (2) 1 μg of DNA−isothiuroniumethyldecylammonium bromide (**2**) complex (± = 1/1); (3) 1 μg of pLC0888.143 DNA + fractured dendrimer, charge ratio ± = 1/1; (4) 1 μg of DNA−isothiuroniumethyldodecyldimethylammonium bromide (**2**) complex (± = 1/1) + fractured dendrimer (another 1 fold positive charge); (5) 1 μg of pLC0888.143 DNA + fractured dendrimer, charge ratio ± = 4.5/1; (6) 1 μg of DNA−isothiuroniumethyldodecyldimethylammonium bromide (**2**) complex (± = 1/1) + fractured dendrimer (another 4.5-fold positive charge).

complex did not interfere with the ability of the DNA to transfect cells if a means was found to promote its attachment and entry into the cell.

DISCUSSION

A long-standing problem in the construction of nonviral gene delivery systems is how to assemble the DNA vectors to obtain small diameter complexes at DNA concentrations that can be used for in vivo applications (*5*). Small diameter complexes are conjectured to be better for in vivo gene delivery in many organs because they should circulate for a longer period and pass more readily through fenestrations in the endothelial cells lining blood vessels.

Most previous methods to prepare DNA complexes used a preformed multivalent cationic moiety, such as cationic polymers or cationic liposomes to condense plasmid DNA; however, the procedures of the DNA condensation through these methods are difficult to control, and aggregation is often found so that particle diameters of between 200 and 600 nm are obtained. Template-assisted methods offer another pathway to assemble nonviral vectors. The concept behind the template-assisted method is based upon the physicochemical observations that a polymer template can bring about a cooperative binding of surfactants (*22*, *23*). Template-assisted methods avoid the use of preformed multivalent groups which readily induce aggregation of complex even at modest DNA concentration. Instead, compounds containing reactive groups that can undergo a reaction to form multivalent cationic counterions on the DNA template are used. Through this way, the template-directed methods can prepare small diameter complexes, avoid aggregation, and lead to monomolecular DNA particles (*9*, *11*).

Blessing (*9*) and Trubetskoy (*11*) and their co-workers used polymerizable cationic detergents as the cationic moiety for the template-assisted assembly and got small particles (20−100 nm). This was a clever solution to the

problem of obtaining small complexes and opened the way to further improvement in DNA compaction. However, a limitation to these first template-directed methods was that the starting detergents did not have a high enough CMC, thus small particles could only be formed at low DNA concentration. This was because as the DNA concentration was increased, the amount of detergent needed to compact the DNA exceeded the CMC. Another limitation to the previous template-assisted methods was in the synthesis chemistry. To get the proper monomers, they employed long synthesis routes including protecting and deprotecting procedures. The long chemistry procedures gave low yields of the final compounds.

To use this method with reasonably high DNA concentrations, we designed a series of detergents with high CMC based upon the isothiuronium groups (Scheme 3). In our work, the synthesis procedure is straightforward, and there are only two steps to obtain the final products with a satisfactory yield. Since the isothiuronium group is positively charged, it is highly hydrophilic. When it is attached on the detergent, there is an order of magnitude increase in the CMC of the detergent (Table 4). Thus, the detergent can be used in relatively high concentration while it still remains under its CMC. Aggregation caused by cationic micelles in the solution during the DNA compaction can be avoided. Another very important property of the isothiuronium group is that it masks the sulfhydryl group on the detergent. Before it is cleaved, there is no cross-linking of the detergents in the solution. Thus minimizes the possibility of micelle formation, and the resulting multicationic surface that can nucleate DNA aggregation.

A very practically useful property of isothiuronium group is that it can be cleaved in a controlled manner. Regulating the pH and/or temperature can precisely control the hydrolysis of the isothiuronium group (formulas 1 and 2). The cleavage of the isothiuronium group and the resulting dimerizing reaction can cause the significant increase of the hydrophobic force (Table 4), which is a major contributor to stabilizing the DNA complexes. Although a systematic kinetic study of the rate of complex formation was not undertaken, we observed that the cationic detergent attached to the DNA template quite rapidly. A hydrophobic core on the DNA was observed using NPN fluorescence by 10 min after addition of the detergent to the DNA. Since the hydrolysis of the isothiuronium group under this condition is much slower than the electrostatic neutralization procedure, detergent hydrolysis and dimerization proceeds on the DNA template over a much longer period of time. Thus, the complex must undergo some maturation as the surfactant dimerizes. This dimerization may also be associated with a change of structure of the complex since aggregated morphology depends on the structure of the detergent and so-called gemini surfactant may have a lower spontaneous curvature than monovalent surfactants (*24*, *25*). The TLC experiments demonstrate that the disulfide lipid was the predominant form of surfactant detected in the DNA complex after 24 h.

A variety of physical methods confirm that small diameter complexes are produced by this technique. Transmission electron microscopy of the DNA−surfactant complex demonstrated that the complexes are spherical and have a diameter around 25 nm (Figure 2). However, we also found some bigger particles with diameters around 100 nm (Figure 2b). This may explain why light-scattering measurements detected a slightly larger complex, 40 nm (Table 5). It should be noted that for the microscopic studies the complex was prepared in San Francisco and transferred to Europe where the samples were prepared and examined. This procedure took about a week. This suggests that the complexes are quite stable when stored at 4 °C, even at high concentration.

We found that both charge ratio and DNA concentration are critical for nanometric complex formation at high DNA concentration (Table 5). Slight changes in charge ratio or DNA concentration lead to large particles. This is partially due to the fact that, in the DNA compaction condition, the total detergent concentration is already high, even a 20% excess of detergent in the solution is enough to cause aggregation. If a prehydrolyzed and dimerized isothiuroniumethyldodecyldimethylammonium bromide (**2**) solution was used in compacting DNA instead of a fresh-made isothiuronium detergent solution, only aggregates or complexes with diameters of >200 nm were observed. This demonstrated that using the isothiuronium detergent for controlled template-assisted assembly is required to form small complex particles, especially at high DNA concentration. Although the conditions required to form the small diameter complexes occur over a narrow range, the precise and predictable control of the process by adjusting the temperature and pH makes the isothiuronium detergents a resolution method to form small diameter complexes.

Because the isothiuronium group is positively charged, it provides an additionally electrostatic force to bind DNA. After the isothiuronium group is hydrolyzed, the positive charge on the DNA is decreased, thus negatively charged complexes were expected, and a −13 mV ζ-potential was found. The DNA complex migrated slower than naked DNA on agarose gel electrophoresis but none of the nanometric complexes were fully retarded. This is different from the previous paper (*9*, *11*). We think the reason is that, in all the previous methods, there were an excess of positive charged polymers or detergents in the complex solutions.

Cytotoxicity of the compounds is an important aspect of a gene delivery system. In the template-directed method introduced by Trubetskoy and co-workers (*11*), thermal free radical polymerization initiators were used. The free radical initiators are usually highly toxic. These free radical initiators had to be removed using dialysis before applying the complex to cells. Moreover, the covalent bonds formed during the polymerization were not biodegradable. So the degradation of the polymers formed on the DNA template depended upon the disulfide bonds in the cross-linkers. This limited the type of the cross-linker compounds that was suitable for preparing complexes with this method. The disulfide bond is biodegradable and can be reduced in the cell cytoplasma if it reaches this compartment. Thus, the DNA can be released from the complex for expression. An advantage of using isothiuronium linkers for template-directed DNA compaction is that the degradation product of hydrolysis of the isothiuronium group that forms the reactive sulfhydryl group is urea. Urea does not influence the structure of the complex and is not toxic, so it does not have to be separated from the complex prior to use. Indeed, the isothiuroniumethyldodecyldimethylammonium bromide (**2**) was toxic to the CV-1 cell line when the concentration was higher than its CMC. After a 24 h incubation with the cells, the thiol detergent was oxidized and was cytotoxic at 0.06 mM, which is near the disulfide lipid CMC (0.047 mM). Thus, these experiments suggest that the acute toxicity of the synthesized compounds is due to detergent effects and are otherwise well tolerated by CV-1 cells.

The complexes exhibited detectable but low transfec-

tion when added to cells in culture. The activity was consistently greater than naked plasmid DNA when they were treated with proper transmembrane introducing agent. They provided almost the same activity as the original plasmid DNA when a subeffective concentration of the fractured dendrimer were added to cells with them (*4*) (Figure 4). This finding is consistent with conclusions from results using the original template-directed complex formation methods (*9*, *11*).

Controlled assembly of plasmid DNA into nanometric complexes with template-assisted method has a high potential in assembly nonviral gene delivery systems. With this method, the barriers of aggregation and DNA concentration can be overcome. The negative surface charge can protect the complex from rapid elimination in vivo as compared to cationic lipoplexes (*5*, *14*) and also opens the way for further modification, such as liposome encapsulation of the particle or the addition of a targeting ligand which may give efficient gene delivery in vivo.

CONCLUSION

A systematical method has been established to control the procedure of DNA compaction to form nanometric DNA complex at high DNA concentration. Using the isothiuronium detergents, a 6 kilo-basepair plasmid DNA can be compacted into a 40 nm particle at a DNA concentration of 0.3 mg/mL. This DNA−surfactant complex is well tolerated to CV-1 cells and maintained high transfection activity when combined with a reagent that increased its association with cells.

ACKNOWLEDGMENT

This work was supported by NIH Grant DK 46052 and by State of California Tobacco research Grant 6RT-0109 FS. Mass spectra were obtained by using a Kratos Tandem MS/MS mass spectrometer. It was provided by the UCSF Mass Spectrometry facility (A. L. Burlingame, Director) supported by the Biomedical Research Technology Program of the National Center for Research Resources, NIH NCRR BRTP RR01614 and NSF DIR 8700766. We thank Dr. Brigitte Sternberg-Papahadjopoulos for preparing the freeze−fracture electron micrograph and Lucie Gagne for help in the tissue culture experiments.

LITERATURE CITED

(1) Felgner, P. L., Heller, M. J., Lehn, P., Behr, J. P., and Szoka, F. C., Eds. (1996) *Artificial self-assembling systems for gene delivery*, American Chemical Society, Washington DC.
(2) Friedmann, T. (1997) Overcoming the obstacles to gene therapy. *Sci. Am.* 96−101.
(3) Nishikawa, M., Takemura, S., Takakura, Y., and Hashida, M. (1998) Targeted delivery of plasmid DNA to hepatocytes in vivo: optimization of the pharmacokinetics of plasmid DNA/galactosylated poly(L-lysine) complexes by controlling their physicochemical properties. *J. Pharmacol. Exp. Ther. 287*, 408−415.
(4) Tang, M. X., Redemann, C. T., and Szoka, F. C. (1996) In vitro gene delivery by degraded polyamidoamine dendrimers. *Bioconjugate Chem. 7*, 703−714.
(5) Kabanov, A. V., Felgner, P. L., and Seymour, L. W. Eds. (1998) *Self-assembling complexes for gene delivery - From laboratory to clinical trial*, John Wiley & Sons Ltd., Chichester, England.
(6) Wagner, E., Cotten, M., Foisner, R., and Birnstiel, M. L. (1991) Transferrin-polycation−DNA complexes: The effect of polycations on the structure of the complex and DAN delivery to cells. *Proc. Natl. Acad. Sci. U.S.A. 88*, 4255−4259.
(7) Tang, M. X., and Szoka, F. C. (1997) The influence of polymer structure on the interactions of cationic polymers with DNA and morphology of the resulting complexes. *Gene Ther. 4*, 823−832.
(8) Kaneda, Y., Iwai, K., and Uchida, T. (1989) Increased expression of DNA co-introduced with nuclear protein in adult rat liver. *Science 243*, 375−378.
(9) Blessing, T., Remy, J. S., and Behr, J. P. (1998) Monomolecular collapse of plasmid DNA into stable virus-like particles. *Proc. Natl. Acad. Sci. U.S.A. 95*, 1427−1431.
(10) Blessing, T., Remy, J. S., and Behr, J. P. (1998) Template oligomerization of DNA-bound cations produces calibrated nanometric particles. *J. Am. Chem. Soc. 120*, 8519−8520.
(11) Trubetskoy, V. S., Budker, V. G., Hanson, L. J., Slattum, P. M., Wolff, J. A., and Hagstrom, J. E. (1998) Self-assembly of DNA-polymer complexes using template polymerization. *Nucleic Acids Res. 26*, 4178−4185.
(12) Tarnowski, G. S., Barclay, R. K., Mountain, I. M., Nakamura, M., Satterwhite, H. G., and Solney, E. M. (1965) Determination of acid-soluble thiols and disulfides in transplanted animal tumors. *Arch. Biochem. Biophys. 110*, 210−216.
(13) Ellman, G. L. (1959) Tissue sulfhydryl groups. *Arch. Biochem. Biophys. 82*, 70−77.
(14) Barron, L. G., Meyer, K. B., and Szoka, F. C. (1998) Effects of complement depletion on the pharmacokinetics and gene delivery mediated by cationic lipid-DNA complexes. *Human Gene Ther. 9*, 315−23.
(15) Brito, R. M. M., and Vaz, W. L. C. (1986) Determination of the critical micelle concentration of surfactants using the fluorescent probe N-phenyl-1-naphthylamine. *Analy. Biochem. 152*, 250−255.
(16) Sternberg, B., Hong, K., Zheng, W., and Papahadjopoulos, D. (1998) Ultrastructural characterization of cationic liposome-DNA complexes showing enhanced stability in serum and high transfection activity in vivo. *Biochim. Biophys. Acta 1375*, 23−35.
(17) Felgner, J. H. (1997) Separation and quantitation of cationic liposome components by high performance liquid chromatiography with evaporative light-scattering detection. *Pharm. Res. 14*, 1269−1271.
(18) Bligh, E. G., and Dyer, W. J. (1959) A rapid method of total lipid extraction and purification. *Can. J. Biochem. Physiol. 37*, 911−917.
(19) Skehan, P., Storeng, R., Scudiero, D., Monks, A., McMahon, J., Vistica, D., Warren, J. T., Bokesch, H., Kenney, S., and Boyd, M. R. (1990) New colorimetric cytotoxicity assay for anticancer-drug screening. *J. Natl. Cancer Inst. 82*, 1107−1112.
(20) Pan, H. L. a. F., T. L. (1968) A facile preparation of sulphydryl compounds in dimethyl sulphoxide. *Chem. Ind.* 546.
(21) Koenig, N. H., Sasin, G. S., and Swern, D. (1958) Organic sulfur derivatives. V. preparation and properties of some long-chain mercapto acids and related compounds. *J. Org. Chem. 23*, 1525−1530.
(22) Ruckenstein, E., Huber, G., and Hoffmann, H. (1987) Surfactant aggregation in the presence of polymers. *Langmuir 3*, 382−387.
(23) Melnikov, S. M., Sergeyev, V. G., and Yoshikawa, K. (1995) Transition of Double-Stranded DNA Chains Between Random Coil and Compact Globule States Induced By Cooperative Binding of Cationic Surfactant. *J. Am. Chem. Soc. 117*, 9951−9956.
(24) Zana, R., and Talmon, Y. (1993) Dependence of aggregate morphology on structure of dimeric surfactants. *Nature 362*, 228−230.
(25) Karaborni, S., Esselink, K., Hilbers, P. A. J., Smit, B., Karthauser, J., van Os, N. M., and Zana, R. (1994) Simulating the self-assembly of gemini (dimeric) surfactants. *Science 266*, 254−256.

BC990101Q

Radio-LC-MS for the Characterization of ^{99m}Tc-Labeled Bioconjugates

Shuang Liu,* Marisa C. Ziegler, and D. Scott Edwards

DuPont Pharmaceuticals Company, Medical Imaging Division, 331 Treble Cove Road, North Billerica, Massachusetts 01862. Received August 23, 1999; Revised Manuscript Received October 26, 1999

This report describes the first example of using radio-LC-MS for determining the composition of ^{99m}Tc radiopharmaceuticals at the tracer level. The in-line radiometric detector is a useful addition to a standard LC-MS and provides direct correlation between the MS data and the radioactive species in a radiopharmaceutical kit. Complexes [^{99m}Tc(HYNICtide)(tricine)(L)] (RP444, L = TPPTS; RP445, L = TPPDS; and RP446, L = TPPMS) were prepared using a decayed generator eluant. All the ternary ligand ^{99m}Tc complexes show the expected monoprotonated molecular ions, $(M + 1)^+$, and diprotonated molecular ions, $(M + 2)^{2+}$. The LC-MS spectral data support the proposed structure and are consistent with those obtained for their corresponding ^{99}Tc analogues. Ternary ligand complexes [^{99m}Tc-(HYNICtide)(tricine)(L)] (L = ISONIC-HE and ISONIC-Sorb) are neutral, and the molecular weights are also lower than that of RP444. Using a fresh generator eluant (24 h prior elution), only 1−2 mCi of ^{99m}Tc [(7×10^{-12})−(1.5×10^{-11}) mol of technetium complex] are required to obtain a reasonably clean mass spectrum. Radio-LC-MS is a quick and accurate analytical tool for characterization of ^{99m}Tc radiopharmaceuticals at the tracer level.

INTRODUCTION

Radiopharmaceuticals are drugs containing a radionuclide and are used routinely in nuclear medicine departments for the diagnosis or therapy of various diseases (*1*−*4*). Nearly 80% of all radiopharmaceuticals used in nuclear medicine departments are ^{99m}Tc-labeled compounds. The reasons for such a preeminent position of ^{99m}Tc in clinical practice include its extremely favorable nuclear characteristics ($t_{1/2}$ = 6.02 h, E_{max} = 142 keV), easy availability, and low cost. Because of the high specific radioactivity for ^{99m}Tc radiopharmaceuticals, their concentrations are often very low (10^{-8}−10^{-7} M). While the radioactivity can be monitored using radiometric detectors, the complete molecular characterization of a ^{99m}Tc radiopharmaceutical, using currently available analytical techniques, is not possible at these low concentrations. Therefore, there is a growing need for a quick and accurate method to determine the composition of the radiopharmaceutical in the radiolabeled kit at the tracer (^{99m}Tc) level.

Mass spectrometry has been used for a number of years as a powerful tool for the study of drug metabolism and biodeposition (*5*−*9*). These types of studies have been traditionally carried out by GC-MS techniques. However, the use of LC-MS has been growing in importance, especially since the introduction of the thermospray interface, which works well for compounds of moderate polarity. More recently, with the advent of modern liquid-phase ionization techniques, such as electrospray, it has become possible to use LC-MS methods for the structural characterization of highly polar molecules at very low concentrations. LC-MS has been used for characterization of ^{11}C-labeled small molecules, such as [^{11}C]harmine (*10*, *11*), the molecular masses of which are often less than 300 Da. To our knowledge, there is no prior literature describing the use of LC-MS for direct characterization of ^{99m}Tc radiopharmaceuticals.

In this report, we describe the first example of using LC-MS for determining the composition of several ^{99m}Tc-labeled peptide radiopharmaceuticals (Figure 1). Since ^{99m}Tc radiopharmaceuticals are prepared at very low concentrations, it is very difficult to use the UV profile alone to identify the signals due to the radiopharmaceutical. Therefore, we added an in-line radiometric detector between the LC and MSD. The radiometric detector was used for the identification and the electrospray MS for the composition determination of ^{99m}Tc-labeled peptide radiopharmaceuticals. A minimum amount of 1−2 mCi ($\sim 1.0 \times 10^{-11}$ M for fresh generator eluant with 24 h prior elution time) of low molecular weight and neutral ternary ligand ^{99m}Tc complexes is necessary for their characterization by this method. Radio-LC-MS is a quick and accurate analytical tool for characterization of ^{99m}Tc radiopharmaceuticals at the tracer level.

EXPERIMENTAL SECTION

Materials. TPPTS and *N*-(2-hydroxyethyl)isonicotinamide (ISONIC-HE)[1] was purchased from Aldrich Chemical Co. TPPDS was purchased from STREM Chemicals Co., Newburyport, MA, and was used as received. TPPMS was purchased from TCI America, Portland, OR, and was used without further purification. $Na^{99m}TcO_4$ was obtained from a Technelite ^{99}Mo/^{99m}Tc generator, DuPont Pharmaceuticals Company, North Billerica, MA. Syn-

* To whom correspondence should be addressed. Phone: (978) 671-8696. Fax: (978) 436-7500. E-mail: shuang.liu@dupontpharma.com.

[1] Abbreviations: HYNICtide, cyclo(D-Val-NMeArg-Gly-Asp-Mamb(5-(6-(6-hydrazinonicotinamido)hexanamide))); ISONIC-HE, *N*-(2-hydroxyethyl)-isonicotinamide; ISONIC-Sorb, 1-(*N*-isonicotinamide)-1-deoxy-D-sorbitol; TPPTS, trisodium triphenylphosphine-3,3′,3″-trisulfonate; TPPDS, disodium triphenylphosphine-3,3′-disulfonate; TPPMS, sodium triphenylphosphine-3-monosulfonate.

10.1021/bc990111r CCC: $19.00 © 2000 American Chemical Society
Published on Web 12/22/1999

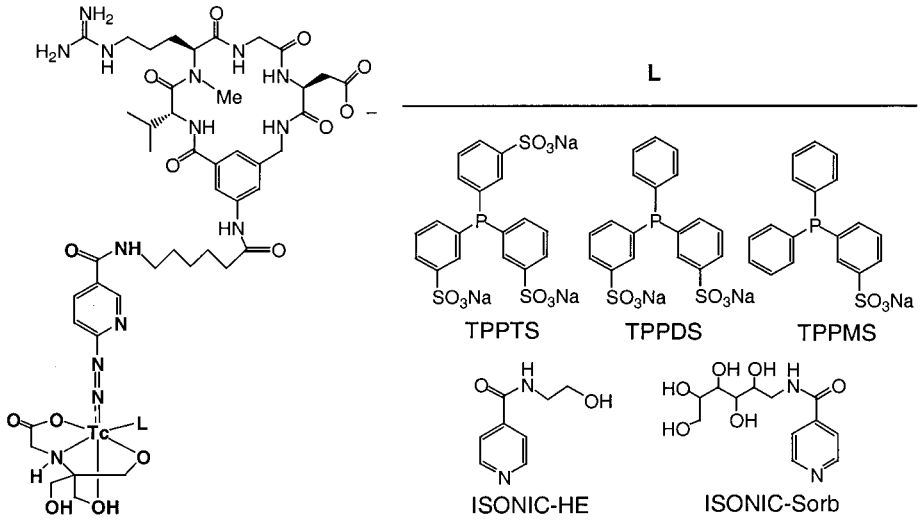

Figure 1. Structures for ^{99m}Tc complexes used in this study.

thesis of 1-(*N*-isonicotinamide)-1-deoxy-D-sorbitol has been described previously (*12*). Complexes [^{99}Tc(HYNICtide)(tricine)(L)] (L = TPPTS, TPPDS, and TPPMS) were prepared according to the published procedure (*13*, *14*).

Instruments and Methods. LC-MS spectra were collected using an HP1100 LC/MSD system with API-electrospray interface. The LC-MS method used a Zorbax C_{18} column (4.6 mm × 150 mm, 3.5 μm particle size) and a gradient mobile phase starting from 92% solvent A (10 mM ammonium acetate buffer, pH 7.0) and 8% solvent B (methanol) to 100% B at 23 min at a flow rate of 1 mL/min. The MSD parameters are as follows:

detection mode	positive	mass range	600−2000
gain	1.0	fragmentor	30 V
gas temperature	350 °C	drying gas flow	13 L/min
nebullizer pressure	60 psig (max)	V capillary	4000 V
radio-detector	NaI	UV detector	230 nm

Synthesis of [^{99m}Tc(HYNICtide)(tricine)(L)] (TPPTS, TPPDS, and TPPDS). A sealed 10 mL vial containing 0.4 mL of tricine solution (100 mg/mL in 0.25 M succinate buffer, pH 5.0), 0.2 mL of HYNICtide solution (100 μg/mL in H_2O), 0.2 mL of the phosphine coligand solution (25 mg/mL in H_2O), and 0.8 mL of decayed $^{99m}TcO_4^-$ solution (25 mCi/mL in saline) was heated in a boiling water bath for 10 min. After cooling at room temperature, the reaction mixture was analyzed by radio-LC-MS.

Synthesis of [^{99m}Tc(HYNICtide)(tricine)(L)] (ISONIC-HE and ISONIC-Sorb). A sealed 10 mL vial containing 0.4 mL of tricine solution (100 mg/mL in 0.25 M succinate buffer, pH 5.0), 0.2 mL of HYNICtide solution (100 μg/mL in H_2O), 0.2 mL of ISONIC-HE or ISONIC-Sorb solution (50 mg/mL in 0.25 M succinate buffer, pH 5.0), 0.25 mL of the fresh $^{99m}TcO_4^-$ eluant (400 mCi/mL in saline), and 25 μL of $SnCl_2 \cdot 2H_2O$ solution (1.0 mg/mL in 0.1 N HCl) was heated at 100 °C for 15 min. After cooling at room temperature, the reaction mixture was analyzed by radio-LC-MS.

RESULTS AND DISCUSSION

Radiolabeled compounds have an important role in the discovery and development of new chemical entities in the pharmaceutical industry. They are often used for early studies of metabolism and pharmacokinetics to determine the fate of newly synthesized chemical leads. The use of a radiotag permits the easy identification and quantification of the material in complex matrixes and systems. Certain radiolabeled compounds, such as those which incorporate ^{99m}Tc are useful as diagnostic agents. Often these compounds are first synthesized in very low concentrations (10^{-6}−10^{-8} M) and their biological distribution and/or activity must be assessed before further development. While the radioactivity of these compounds permits them to be monitored using radiodetectors, complete molecular characterization of these new structures is not possible at these low levels.

Table 1. LC-MS Spectral Data for [^{99}Tc]RP444, [^{99}Tc]RP445, and [^{99}Tc]RP446

compd	formula	formula weight	found $(M+1)^+$	found $(M+2)^{2+}$
[^{99}Tc]RP444	$C_{62}H_{78}N_{14}O_{23}PS_3Tc$	1613.4	1614.6	807.3
peak A	$C_{62}H_{78}N_{14}O_{23}PS_3Tc$	1613.4	1614.4	807.2
peak B	$C_{62}H_{78}N_{14}O_{23}PS_3Tc$	1613.4	1614.7	807.3
[^{99}Tc]RP445	$C_{62}H_{79}N_{14}O_{20}PS_2Tc$	1533.4	1534.5	767.2
[^{99}Tc]RP446	$C_{62}H_{80}N_{14}O_{17}PSTc$	1453.3	1453.2	727.2

Traditionally, characterization of a new ^{99m}Tc radiopharmaceutical involves synthesis of the corresponding ^{99}Tc complex at the macroscopic level. The composition and the structure of ^{99}Tc complexes are determined by IR, NMR, FAB-MS, and X-ray crystallography. An HPLC concordance experiment is performed to demonstrate that the same Tc complex is prepared at both the macroscopic and the tracer levels. For peptide-based technetium radiopharmaceuticals, isolation of the ^{99}Tc−peptide complex usually involves multiple step synthesis and tedious HPLC purification. It is also very difficult to grow single crystals for highly water-soluble ^{99}Tc−peptide complexes. The chemistry of some chelating systems may differ at the macroscopic and tracer levels. Thus, it necessary to determine the composition of the radiopharmaceutical at the tracer level.

LC-MS of [^{99}Tc]RP444, [^{99}Tc]RP445, and [^{99}Tc]-RP446. RP444, RP445, and RP446 are ternary ligand ^{99m}Tc complexes of a HYNIC-conjugated cyclic platelet GPIIb/IIIa receptor antagonist (Figure 1). Both animal and clinical studies have demonstrated the utility of RP444 as a new thrombosis imaging agent. To determine the composition and structure of these ternary ligand complexes, the corresponding ^{99}Tc complexes, [^{99}Tc]-RP444, [^{99}Tc]RP445, and [^{99}Tc]RP446 were prepared. Unlike those of the ^{99m}Tc analogues, the yields for the ternary ligand ^{99}Tc complexes were generally very low (≤10%). These complexes were isolated from the reaction mixture by HPLC. After purification, the ^{99}Tc complexes

Table 2. LC-MS Data for ^{99m}Tc Complexes

complex	formula	exact mass	found $(M + 1)^+$	found $(M + 2)^{2+}$
[^{99m}Tc(HYNICtide)(tricine)(TPPTS)] (RP444)	$C_{62}H_{78}N_{14}O_{23}PS_3Tc$	1613.4	1613.8	807.5
peak A	$C_{62}H_{78}N_{14}O_{23}PS_3Tc$	1613.4	1613.8	807.2
peak B	$C_{62}H_{78}N_{14}O_{23}PS_3Tc$	1613.4	1613.8	807.4
[^{99m}Tc(HYNICtide)(tricine)(TPPDS)] (RP445)	$C_{62}H_{79}N_{14}O_{20}PS_2Tc$	1533.4	1534.5	767.7
[^{99m}Tc(HYNICtide)(tricine)(TPPMS)] (RP446)	$C_{62}H_{80}N_{14}O_{17}PSTc$	1454.5	1454.3	727.8
[^{99m}Tc(HYNICtide)(tricine)(ISONIC-HE)]	$C_{52}H_{73}N_{16}O_{16}Tc$	1277.1	1277.3	639.3
[^{99m}Tc(HYNICtide)(tricine)(ISONIC-Sorb)]	$C_{56}H_{81}N_{16}O_{20}Tc$	1397.2	1398.3	699.2

were obtained only in microgram quantities, which is enough for LC-MS, but not enough for extensive NMR studies.

All three ^{99}Tc complexes were analyzed by LC-MS using both direct flow injection (FIA) MS and LC/MS. For the initial sample run, a number of 1.5−2.0 min isocratic flow injections were made without the use of an HPLC column. The fragmentor voltage, drying gas temperature and drying gas flow were varied until maximum signal strength was obtained for the first sample. Once the MS parameter optimization was completed, a Zorbax C18 reversed-phase column (4.6 mm × 150 mm, 3.5 μm) was installed. The concentration of these complexes was about 10 μM. The injection volume was 5−20 μL. Under these conditions, all three ^{99}Tc complexes yielded sufficiently intense MS peaks. LC-MS results, expressed as mass-to-charge ratios, were compared to the expected molecular weights of these complexes. The results are summarized in Table 1. In general, all three ^{99}Tc complexes show the expected monoprotonated molecular ions, $(M + 1)^+$, and diprotonated molecular ions, $(M + 2)^{2+}$. The molecular ions were detected in their acid forms because the sulfonato groups of the phosphine coligands became protonated when the mobile phase and electrolytes were evaporated in the desolvation chamber. The LC-MS spectral data support the proposed structure (Figure 1) and is completely consistent with the 1:1:1:1 composition for Tc:HYNICtide:tricine:TPPTS, as determined via a series of mixed-ligand experiment on the tracer (^{99m}Tc) level (*13*). [^{99}Tc]RP444 shows two peaks (peak 1 and peak 2) in both the HPLC chromatogram and MSD profile. Both peaks show almost identical fragmentation patterns and the same molecular ions. The observation of the predominant diprotonated molecular ions, $(M + 2)^{2+}$, is characteristic of both labeled and unlabeled HYNICtide. The fact that these three complexes all show the diprotonated molecular ions suggests that they share the same coordination sphere in the technetium chelate. The two proton acceptors are probably from the carboxylate-oxygen and the uncoordinated pyridine-nitrogen atoms.

LC-MS of Complexes [^{99m}Tc(HYNICtide)(tricine)-(L)] (L = TPPTS, TPPDS, TPPMS, ISONIC-HE, and ISONIC-Sorb). RP444, RP445, and RP446 were prepared using a decayed generator eluant. The concentration of the total technetium (^{99m}Tc and ^{99}Tc) was calculated to be approximately 1.5×10^{-6} M. A sample of the reaction solution (200 μL) containing ~3.0×10^{-10} mol of technetium (^{99m}Tc and ^{99}Tc) was injected and a gradient LC method was used for the LC-MS analysis. We used a reversed-phase Zorbax C_{18} column and a mixture of acetonitrile and 10 mM ammonium acetate buffer as the mobile phase. The flow rate for the LC was 1.0 mL/min, which is common for high-flow electrospray interfaces. Under these conditions, RP444 shows two radiometric peaks (peak A and peak B) in the radio-HPLC chromatogram and MSD profile (Figure 2). This method was used for the characterization of several ^{99m}Tc complexes comprised of the same peptide sequence.

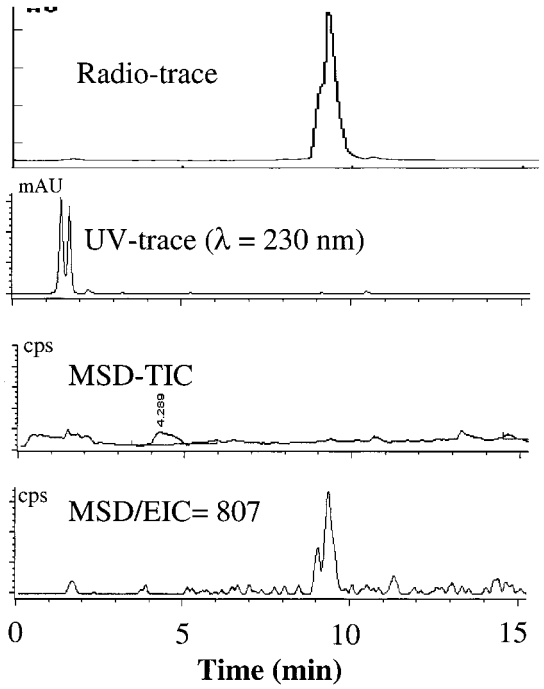

Figure 2. Radio-LC-MS concordance for RP444 (decayed generator eluant, ~1.5×10^{-10} mol injected).

The LC-MS results are summarized in Table 2. All the ternary ligand ^{99m}Tc complexes show the expected monoprotonated molecular ions, $(M + 1)^+$, and diprotonated molecular ions, $(M + 2)^{2+}$. The LC-MS spectral data support the proposed structure (Figure 1) and are consistent with those obtained by FAB-MS for their corresponding ^{99}Tc analogues (*15*). Previously (*14*), we have demonstrated by a chirality experiment that the presence of two radiometric peaks in the HPLC chromatograms of RP444 is due to the resolution of diastereomers, which result from the presence of chiral cyclic peptide and the formation of two enantiomers of the technetium chelate. In this study, both peak A and peak B show identical fragmentation patterns and the same molecular ions, providing direct evidence that the two species are really due to diastereomeric forms of RP444.

RP444, RP445, and RP446 were also prepared using a fresh generator eluant. Since they were prepared at much lower concentrations (~2×10^{-7} M), it is very difficult to determine their retention times based on either the UV (λ = 220 nm) trace or the MS profiles (Figure 2). There are two approaches to solve the problem. In the first approach, we used the corresponding ^{99}Tc analogue to identify the radiopharmaceutical peak in the MSD profile. In the second approach, we installed an in-line radio-detector before the MSD. The retention time of the ^{99m}Tc radiopharmaceutical recorded by the radio-detector is clearly correlated with the location of the tracer level electrospray MS peak (Figure 2). This approach is

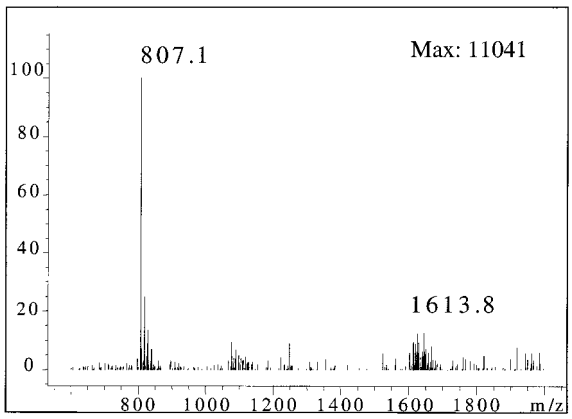

Figure 3. LC-MS spectrum of RP444 (decayed generator eluant, $\sim 3.0 \times 10^{-10}$ mol injected).

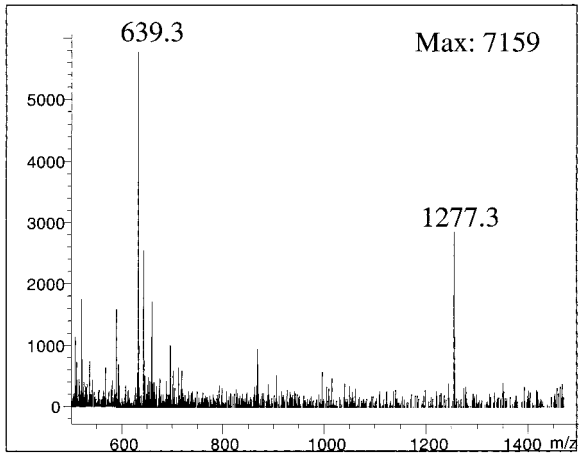

Figure 4. LC-MS spectrum of [^{99m}Tc(HYNICtide)(tricine)-(ISONIC-HE)] (fresh generator eluant, $\sim 5.0 \times 10^{-11}$ mol injected).

particularly useful for ^{99m}Tc complexes with low UV absorption.

It should be noted that the minimum amount of injected activity necessary to obtain interpretable results is very much dependent on the charge and molecular weight of the ^{99m}Tc complex. For example, RP444 is highly charged and usually requires a larger amount of activity to obtain a mass spectrum with signal-to-noise ratio of >3. Thus, the decayed generator eluant is recommended to increase the technetium concentration. The alternative is to use multiple injections to concentrate the radiopharmaceutical on the LC column under isocratic conditions. Figure 3 shows the LC-MS spectrum of RP444 using the decayed generator eluant containing $\sim 3.0 \times 10^{-10}$ mol of technetium complex. Using a fresh generator eluant (24 h prior elution), at least 10 mCi of ^{99m}Tc ($\sim 7 \times 10^{-11}$ mol of technetium complex) is required to obtain an interpretable mass spectrum.

Complexes [^{99m}Tc(HYNICtide)(tricine)(L)] (L = ISONIC-HE and ISONIC-Sorb) are neutral, and the molecular weights are also lower than that of RP444. Using a fresh generator eluant (24 h prior elution), only 1−2 mCi of ^{99m}Tc [(7×10^{-12})−(1.5×10^{-11}) mol of technetium complex] are required to obtain a reasonably clean mass spectrum. Figure 4 shows the LC-MS spectrum of [^{99m}Tc-(HYNICtide)(tricine)(ISONIC-HE)] using a fresh generator eluant containing $\sim 5.0 \times 10^{-11}$ mol of technetium complex.

The radio-LC-MS method used in this study is particularly useful for ^{99m}Tc-radiolabeled bioconjugates, the corresponding ^{99}Tc analogues of which cannot be readily prepared. For example, complexes [^{99}Tc(HYNICtide)-(tricine)(ISONIC-HE)] and [^{99}Tc(HYNICtide)(tricine)-(ISONIC-Sorb)] could not be prepared according to the procedure used for the preparation [^{99}Tc]RP444, [^{99}Tc]-RP445, and [^{99}Tc]RP446 (*15*). This is mainly due to the competition between HYNICtide, which contains a pyridine-N donor, and the corresponding functionalized pyridine coligand. At the tracer level (^{99m}Tc), the molar ratio of ISONIC-HE to HYNICtide is ~2000:1. It is possible for ISONIC-HE to compete with HYNICtide and form the ternary ligand technetium complex. At the macroscopic level (^{99}Tc), this ratio is very difficult to achieve. HYNICtide can compete with ISONIC-HE in bonding to the technetium. Syntheses of [^{99}Tc(HYNIC-tide)(tricine)(ISONIC-HE)] and [^{99}Tc(HYNICtide)(tricine)(ISONIC-HE)] become extremely difficult. Using the LC-MS method, we are able to determine the composition of ternary ligand complexes [^{99m}Tc(HYNICtide)(tricine)-(ISONIC-HE)] and [^{99m}Tc(HYNICtide)(tricine)(ISONIC-HE)] at the tracer level.

In conclusion, this study reported the first example of using LC-MS for the direct characterization of ^{99m}Tc radiopharmaceuticals. Radio-LC-MS is a quick and accurate analytical tool for determining the composition of ^{99m}Tc radiopharmaceuticals at the tracer level. Mass spectrometry by itself cannot determine the structure of compounds. It supplements structural information obtained from other analytical tools such as NMR. Therefore, radio-LC-MS may also be a complimentary technique for structure determination of radiolabeled compounds by analyzing the fragmentation patterns of the mass spectra. Radio-LC-MS has the potential to become a routine analytical tool for new radiopharmaceuticals labeled with ^{99m}Tc or other radioisotopes such as ^{186}Re and ^{177}Lu.

ACKNOWLEDGMENT

Authors would like to thank Dr. Joseph L. Glajch and Neal Williams for their technical assistance.

LITERATURE CITED

(1) Jurisson, S ., and Lydon, J. D. (1999) Potential technetium small molecule radiopharmaceuticals. *Chem. Rev. 99,* 2205−2218.

(2) Anderson, C. J., and Welch, M. J. (1999) Radiometal labeled agents (non-technetium) for diagnostic imaging. *Chem. Rev. 99,* 2219−2234.

(3) Liu, S., and Edwards, D. S. (1999) ^{99m}Tc-labeled small peptides as diagnostic radiopharmaceuticals. *Chem. Rev. 99,* 2235−2268.

(4) Volkert, W. A., and Hoffman, T. J. (1999) Therapeutic radiopharmaceuticals. *Chem. Rev. 99,* 2269−2292.

(5) Lee, M. S., Kerns, E. H., Hail, M. E., Liu, J.-P., and Volk, K. J. (1997) Recent applications of LC-MS techniques for the structure identification of drug metabolites and related compounds. *Liq. Chromatogr. Mass Spectrom. 15,* 542−558.

(6) Niessen, W. M. A., and Tinke, A. P. (1995) Liquid chromatography−mass spectrometry: general principles and instrumentation. *J. Chromatogr. A 703,* 37−57.

(7) Gelpé, E. (1995) Biomedical and biochemical applications of liquid chromatography−mass spectrometry. *J. Chromatogr. 703,* 59−80.

(8) Regnier, F., and Huang, H. (1996) Future potential of targeted component analysis by multidimensional liquid chromatography−mass spectrometry. *J. Chromatogr. 750,* 3−10.

(9) Bruins, A. P. (1991) Liquid chromatography−mass spectrometry with ionspray and electrospray interfaces in pharmaceutical and biomedical research. *J. Chromatogr. 554,* 39−46.

(10) Hyllbrant, B., Tyrefors, N., Markides, K. E., and Längström. (1997) LC-radio-UV coupled to MS for improved sensitivity and selectivity in analysis of PET radiopharmaceuticals. *J. Labeled Compd. Radiopharm. 40*, 197−198.

(11) Hyllbrant, B., Tyrefors, N., Markides, K. E., and Längström. (1995) Improved sensitivity and selectivity in the determination of specific radioactivity by means of radio-HPLC-MS. *J. Labeled Compd. Radiopharm. 37*, 704−705.

(12) Liu, S., Edwards, D. S., Harris, A. R. (1998) Functionalized pyridine analogues as coligands for ^{99m}Tc labeling of HYNIC-conjugated biomolecules. In *Technetium, Rhenium and Other Metals in Chemistry and Nuclear Medicine* (M. Nicolini, G. Banoli, and U. Mazzi, Eds.) Vol. 5, pp 661−668, SGEditoriali, Padova.

(13) Edwards, D. S., Liu, S., Barrett, J. A., Harris, A. R., Looby, R. J., Ziegler, M. C., Heminway, S. J., and Carroll, T. R. (1997) New and versatile ternary ligand system for technetium radiopharmaceuticals: water soluble phosphines and tricine as coligands in labeling a hydrazinonicotinamide-modified cyclic glycoprotein Iib/IIIa receptor antagonist with ^{99m}Tc. *Bioconjugate Chem. 8*, 146−154.

(14) Liu, S., Edwards, D. S., Harris, A. R. (1998) A novel ternary ligand system for ^{99m}Tc-labeling of hydrazino nicotinamide-modified biologically active molecules using imine-N-containing heterocycles as coligands. *Bioconjugate Chem. 9*, 583−595.

(15) Liu, S., Edwards, D. S., Harris, A. R., Hemingway, S. J., and Barrett, J. A. (1999) Technetium complexes of a hydrazinonicotinamide-conjugated cyclic peptide and 2-hydrazinopyridine: synthesis and characterization. *Inorg. Chem. 38*, 1326−1335.

BC990111R

TECHNICAL NOTES

Differential Reactivity of Maleimide and Bromoacetyl Functions with Thiols: Application to the Preparation of Liposomal Diepitope Constructs

Philippe Schelté, Christophe Boeckler, Benoît Frisch,* and Francis Schuber

Laboratoire de Chimie Bioorganique, UMR 7514 CNRS-Université Louis Pasteur, Faculté de Pharmacie, 74 route du Rhin, 67400 Strasbourg-Illkirch, France . Received September 20, 1999; Revised Manuscript Received November 1, 1999

The comparative reactivity of maleimide and bromoacetyl groups with thiols (2-mercaptoethanol, free cysteine, and cysteine residues present at the N-terminus of peptides) was investigated in aqueous media. These studies were performed (i) with water-soluble functionalized model molecules, i.e., polyoxyethylene-based spacer arms that could also be coupled to lipophilic anchors destined to be incorporated into liposomes, and (ii) with small unilamellar liposomes carrying at their surface these thiol-reactive functions. Our results indicate that an important kinetic discrimination (2−3 orders of magnitude in terms of rate constants) can be achieved between the maleimide and bromoacetyl functions when the reactions with thiols are performed at pH 6.5. The bromoacetyl function which reacts at higher pH values (e.g., pH 9.0) retained a high chemoselectivity; i.e., under conditions where it reacted appreciably with the thiols of, e.g., HS-peptides, it did react with other nucleophilic functions such as α- and ϵ-amino groups or imidazole, which could also be present in peptides. This differential reactivity was applied to design chemically defined and highly immunogenic liposomal diepitope constructs as synthetic vaccines, i.e., vesicles carrying at their surface two different peptides conjugated each to a specific amphiphilic anchor. This was realized by coupling sequentially at pH 6.5 and 9.0 two HS-peptides to preformed vesicles containing lipophilic anchors functionalized with maleimide and bromoacetyl groups [Boeckler, C., et al. (1999) *Eur. J. Immunol. 29*, 2297−2308].

INTRODUCTION

Synthetic peptides representative of epitopes are useful for the development of new classes of subunit vaccines in infectious diseases or cancer (*1*−*4*). However, because of their weak immunogenicity, peptide antigens must generally be coupled to carriers such as proteins or synthetic polymers (*5*, *6*) and administered in the presence of adjuvants. Alternatively, peptides can also be associated to particulate systems such as liposomes (*7*, *8*) or immunostimulating complexes, e.g., ISCOMs (*9*). During these last years, our group has elaborated a strategy that elicits very potent and long-lasting immune responses against small peptide epitopes (*10*−*13*). It is based on liposomal constructs combining the peptide antigens and amphipathic adjuvants such as monophosphoryl lipid A (*10*−*12*) or the totally synthetic lipopeptide *S*-[2,3-bis(palmitoyloxy)-(2-*RS*)-propyl]-*N*-palmitoyl-(*R*)-cysteinyl-alanyl-glycine (Pam_3CAG) (*13*). In our approach, the peptides are covalently coupled, via well-defined chemical steps (*14*, *15*), to the surface of preformed small unilamellar vesicles containing the adjuvants. In general, the conjugation step was performed according to the method originally developed by Martin and Papahadjopoulos for the preparation of immunoliposomes (*16*). Thus, the peptide extended at its N-terminus by a CG (i.e., cysteinyl-glycine in single letter code) spacer arm (i.e., HS-peptide) is reacted with a liposome containing a thiol-reactive phospholipid derivative such as phosphatidylethanolamine carrying a maleimide function (*14*, *16*). This methodology presents the advantage to preserve the structural integrity of the peptide epitopes, and because of the lack of intrinsic immunogenicity of liposomes as carrier, it is appealing for the development of totally synthetic vaccination formulations.

We have now designed a second generation of liposome-based carriers in which two different peptides, such as B and Th epitopes, are conjugated to vesicles with the aim to mimic and amplify a natural immune response. Diepitope constructs, which have been for example realized by co-linearization of B and Th epitopes in synthetic polypeptides, are considered to be the minimal built-in subunit vaccines (*17*, *18*). Because of the vastly different role fulfilled by the B and Th epitopes in humoral immune responses, there is no a priori necessity for these epitopes to be covalently linked. We have therefore designed constructs with two structurally independent peptides conjugated to the surface of a same vesicle via different types of lipophilic anchors (*19*). The B epitope was classically conjugated to a phospholipid anchor (see above), whereas the Th epitope was coupled to a functionalized lipopeptide Pam_3CAG (*20*). This latter anchor, which is a synthetic analogue of an *Escherichia coli*

* To whom correspondence should be addressed. Phone: +33 388 67 68 72. Fax: +33 388 67 88 91. E-mail: frisch@pharma.u-strasbg.fr.

10.1021/bc990122k CCC: $19.00 © 2000 American Chemical Society
Published on Web 00/00/0000

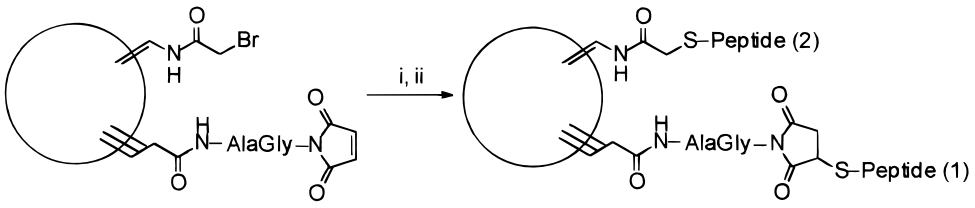

i, HS-Peptide (1), pH 6.5; ii, dialysis pH 9.0, HS-Peptide (2)

Figure 1. Liposome-based construct for immunization with synthetic peptides. The peptide carrying a cysteine residue, e.g., at its N-terminus, is conjugated to the surface of preformed SUV containing thiol-reactive lipophilic anchors. In the present example, the diepitope construct, HS-peptide (1) is conjugated to Pam_3CAG functionalized with a maleimide group, and HS-peptide (2) to a phosphatidylethanolamine functionalized with a bromoacetyl group such as **2**.

lipopeptide, was chosen for its immunoadjuvanticity and its known efficiency to elicit humoral as well as cell-mediated immune responses against peptide antigens that are coupled to it (*21*). To that end, we have developed a chemical strategy that allows a controlled sequential coupling of two different HS-peptides to preformed liposomes containing thiol-reactive derivatives of phosphatidylethanolamine and Pam_3CAG (*19*). On the basis of previous preliminary observations (*14*, *22*) where maleimide and bromoacetyl functions were found to react differently with thiols, in aqueous media, we have used these groups to design our diepitope constructs (Figure 1).

In the present publication, we describe our study on the comparative reactivity of maleimide and bromoacetyl groups with thiols in aqueous media as a function of pH. These studies were performed (i) with water-soluble functionalized model molecules, i.e., spacer arms that could also be coupled to lipophilic anchors incorporated into liposomes and (ii) with liposomes carrying at their surface these thiol-reactive functions. The aim was to define rate constants useful in predicting coupling rates and product distribution. We have also verified, under our most basic experimental conditions, the chemoselectivity of the bromoacetyl function by comparing its reactivity with thiols and other nucleophilic functions such as α- and ϵ-amino groups or imidazole that are present in peptides. Our results indicate that an important kinetic discrimination can be achieved between the maleimide and bromoacetyl functions when the reactions with thiols, e.g., HS-peptides, are performed in aqueous media at pH 6.5 and 9.0, respectively. The present data also validate our strategy used to prepare liposomal diepitope constructs (Figure 1).

EXPERIMENTAL SECTION

General. Reagent-grade solvents were used without further purification. Cholesterol (recrystallized in methanol), phosphatidylcholine (PC; egg yolk), phosphatidylglycerol (PG; transesterified from egg PC), and *N*-α-acetyl-GK were from Sigma-Aldrich (L'Isle D'Abeau Chesnes, France). Fluorescamine (Fluram) and 5,5′-dithiobis(2-nitrobenzoic acid) (DTNB) were from Fluka (L'Isle D'Abeau Chesnes, France). *N*-Benzoyl-GHL was from Calbiochem-Novabiochem AG (Läufelfingen, Switzerland). Silica gel 60 F 254 plates for thin-layer chromatography were purchased from Merck (Darmstadt, Germany). The peptide, CGIRGERA, was a kind gift from Dr. J.-P. Briand (CNRS−IBMC, Strasbourg, France). Compounds **3** and **4** were prepared according to our previously published procedures (*14*). ^{1}H NMR were recorded on Bruker AC-200 (200 MHz) and DPX 300 (300 MHz) spectrometers. Mass spectra were recorded on a VG ZAB-HF mass spectrometer.

2-Bromo-*N*-(2-(2-(2-hydroxyethoxy)ethoxy)ethyl)-acetamide (1). This compound was synthesized in four steps starting from tri(ethylene glycol) with the same procedure as described previously by Frisch et al. (*14*): R_f 0.2 ($CHCl_3$:CH_3OH, 95:5). ^{1}H NMR (200 MHz, $CDCl_3$) δ 7.10 (s, 1H, N*H*), 3.87 (s, 2H, CH_2Br), 3.76−3.44 (m, 12H, HOCH_2, CH_2OCH_2, CH_2N), 2.74 (s, 1H, O*H*). ^{13}C NMR (50 MHz, $CDCl_3$) δ 166.1, 72.4, 70.1 (2C), 69.3, 61.5, 39.7, 28.9. HRMS (FAB^-) found for $C_8H_{16}BrNO_4$, *m*/*z* 270.2 ($M - H^+$); calcd for ($M - H^+$) $C_8H_{16}BrNO_4$, 270.12.

Hexadecanoic Acid 3-((2-(2-(2-(2-(2-bromoacetyl-amino)ethoxy)ethoxy)acetylamino)ethoxy)hydroxy-phosphoryloxy)-2-hexadecanoyloxypropylester (2). Compound **1** was oxidized into its corresponding carboxylic acid, which was then conjugated to DPPE according to procedures described in ref *14*: R_f 0.34 ($CHCl_3$:CH_3OH:H_2O, 60:15:1). ^{1}H NMR (300 MHz, $CDCl_3$:CD_3OD, 1:1) δ 5.28−5.18 (m, 1H, C*H*CH_2OP), 4.41−4.14 (m, 4H, CH_2CHCH_2OP, CHCH_2OP), 4.02 (s, 2H, COCH_2O) 3.99−3.43 (m, 12H, POCH_2CH_2N, POCH_2CH_2N, OCH_2CH_2), 3.87 (s, 2H, NCOCH_2Br), 2.34−2.28 (m, 4H, CH_2CO_2), 1.68−1.52 (m, 4H, CH_2CH_2CO_2), 1.26 (m, 48H, (CH_2)$_{24}$), 0.88 (t, J = 6.0 Hz, 6H, CH_3). ^{13}C NMR (50 MHz, $CDCl_3$) δ 173.7, 173.4, 171.3, 167.2, 70.8, 70.3, 69.9, 69.6, 64.5, 63.8, 62.8, 39.9, 34.3, 34.1, 31.9 (2C), 29.7−29.1 (23C), 25.0, 24.9, 22.7 (2C), 14.1 (2C). HRMS (FAB^-) found for $C_{45}H_{87}N_2O_{12}PBr$, *m*/*z* 958.5 ($M - H^+$); calcd for ($M - H^+$) $C_{45}H_{87}N_2O_{12}PBr$, 959.07.

Rate of Reaction of Thiol-Reactive Derivatives 1 and 3 with Thiols. An aqueous solution of 2-mercaptoethanol or L-cysteine or peptide CGIRGERA (40 μL, 200 nmol) was added to 450 μL of 50 mM sodium phosphate buffers (pH 6.0, 6.5, 7.0 or 7.5) or 50 mM sodium borate buffers (pH 8.0, 8.5 or 9.0) maintained at 25 °C (thermostat). At time zero, an aqueous solution of **1** or **3** (10 μL, 100 nmol) was added and the reaction progress was followed by determining at given times the residual thiols (*23*) on 40 μL aliquots with 1 mL of Ellman's reagent (DTNB 2 mM and EDTA 1 mM in 0.2 M sodium phosphate buffer, pH 7.27). The absorbance was read at 412.5 nm (ϵ = 14 150 M^{-1} cm^{-1}). All the given data have been corrected for the spontaneous dimerization of the thiols, which was estimated in parallel under the same experimental conditions, but in the absence of **1** and **3**.

Reaction of Thiols with Thiol-Reactive Functionalized Phosphatidylethanolamines 2 and 4 Incorporated into Liposomes. Small unilamelar vesicle (SUV) were prepared from PC, PG, **2**, or **4** and cholesterol (molar ratio 65:25:10:50) as previously described (*10*). Briefly, the lipids in chloroform were dried under high

vacuum and resuspended to 5 μmol of lipid/mL in 10 mM Hepes buffer, pH 6.5, containing 145 mM NaCl or 50 mM sodium borate, pH 9.0, containing 105 mM NaCl, vortexed during 5 min and sonicated under argon at room temperature in a sonicator bath for 20 min. Then the suspension was extruded six times on 0.1 μm Nucleopore membranes. The mean diameter of the vesicles was determined by a photon correlation spectroscopy technique, using a Malvern Autosizer. The liposome concentration was determined by assaying the inorganic phosphate (*24*). At time zero, to a liposome suspension (700 μL, 140 nmol of surface-accessible thiol-reactive functions), maintained at 25 °C, was added an aqueous solution of the peptide CGIRGERA (30 μL, 280 nmol). The reaction progress was measured at given times by determining the residual thiols on 50 μL aliquots as described above. The data have been corrected for the spontaneous dimerization of the thiols which was estimated in parallel under the same experimental conditions, but in the absence of **2** and **4**.

Rate of Reaction of 1 with Peptidic Amine Functions. An aqueous solution of *N*-α-acetyl-GK (40 μL, 200 nmol) was added to 450 μL 50 mM sodium borate buffer (pH 9.0). An aqueous solution of **1** (10 μL, 100 nmol) was added at time zero. The reaction was thermostated at 25 °C, and its progress was measured at given times by measuring the residual primary amines with the fluorometric assay using fluorescamine (*25*). Briefly, 5−40 μL of the test solution containing from 0 to 100 nmol of amines was added to 1.5 mL of 50 mM sodium borate buffer, pH 9.0, followed, under rapid stirring, by 500 μL of fluorescamine in dioxane (30 mg/100 mL). The fluorescence was measured at 475 nm (excitation 390 nm). The primary amines were quantified using a standard curve obtained with of *N*-α-acetyl-GK.

Reaction of the Bromoacetyl Function with a Peptidic Imidazole Residue at pH 9.0. To determine the reactivity of an imidazole moiety present in a peptide, SUVs were prepared in 50 mM sodium borate buffer, pH 9.0, from 5 μmol of lipid/mL containing PC, PG, **2**, and cholesterol in the molar ratio of 65:25:10:50. To a suspension of vesicles (800 μL, 200 nmol of bromoacetyl function), an aqueous solution of peptide *N*-benzoyl-GHL (80 μL, 400 nmol) was added. After 90 min at 25 °C, the liposomes were dialyzed 2 × 12 h against 1 L of 50 mM sodium borate buffer, pH 9.0. One hundred microliter aliquots were then added to 100 μL of 12 N HCl and hydrolyzed 12 h at 110 °C followed by neutralization with 6 N NaOH. The conjugation of the peptide to the liposomes was assessed by determining the amines with the fluorescamine fluorometric assay (see above). Liposomes without **2** were used as control and known quantities of *N*-benzoyl-GHL as standard.

Competitive Reaction between Thiol and Amine Functions of CGIRGERA with the Bromoacetyl Function of 1. A solution (40 μL) containing 100 nmol of the peptide CGIRGERA was added to 450 μL 50 mM sodium borate buffer, pH 9.0. At time zero, an aqueous solution of **1** (10 μL, 50 nmol) was added and the progress of the reaction, at 25 °C, was measured by assaying at given times on 40 μL aliquots (i) the residual thiols as described above (Ellman's reagent) and (ii) the residual primary amines with the fluorescamine assay (see above, using CGIRGERA as standard). The given data take into account the dimerization of the thiol that was measured in parallel under the same experimental conditions but in the absence of **1**.

Rate Constants Determination. The apparent rate constants between the thiols and the thiol-reactive functions **1**−**4** were determined using a standard second-order reaction rate expression and linear-regression programs (GraphPad Prism and Microsoft Excel).

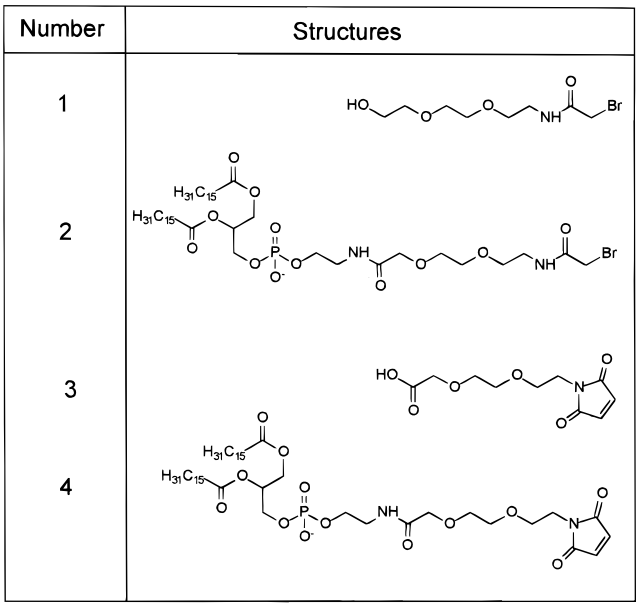

Figure 2. Structure of the thiol-reactive derivatives **1** and **3** and their DPPE derivatives **2** and **4**.

RESULTS AND DISCUSSION

To investigate the comparative reactivity of maleimide and bromoacetyl functions with thiols under conditions that could be exploited for the coupling, in aqueous media, of HS-peptides to preformed liposomes carrying such reactive groups at their surface, we have first prepared the water-soluble model heterobifunctional molecules **1** and **3** (Figure 2). These polyoxyethylene-based flexible molecules could also be used to produce **2** and **4**, i.e., thiol-reactive dipalmitoylphosphatidylethanolamine (DPPE) derivatives that were incorporated into the (phospho)lipid composition of liposomes. The chemistry used to prepare molecules **1**−**4** has been adapted from our previous work in this domain (*14*).

Reactivity of the Thiol-Reactive Moieties in 1 and 3 with Different Thiols as a Function of pH. The aim of our study was to couple two different HS-peptides, each on a specific anchor, to the surface of the same preformed liposome (Figure 1). It was therefore of importance to define experimental conditions (pH, temperature, and time) allowing a sequential conjugation of the peptides on two different thiol-reactive lipophilic anchors, which would be compatible with the integrity of the vesicles used in the immunization experiments. We have therefore first studied the rate of reaction, in aqueous media, of the bromoacetyl derivative **1** and the maleimide derivative **3** with 2-mercaptoethanol, L-cysteine, and CGIRGERA, an antigenic model peptide (*10*, *11*) which carries a cysteine residue at its N-terminus. The reactions were performed at 25 °C and at fixed pH values, at a molar ratio of 2 in favor of the thiol. Reaction progress was determined by measuring residual-free thiols with Ellman's reagent. Controls, under these different reaction conditions, allowed the determination of the spontaneous oxidation of thiols (e.g., dimerization) and accordingly the correction of the experimental data. At pH 9.0 and 25 °C, the spontaneous oxidation [k_{dim} (M^{-1} s^{-1})] was 0.054 ± 0.003 for mercaptoethanol, 0.113 ± 0.01 for cysteine,

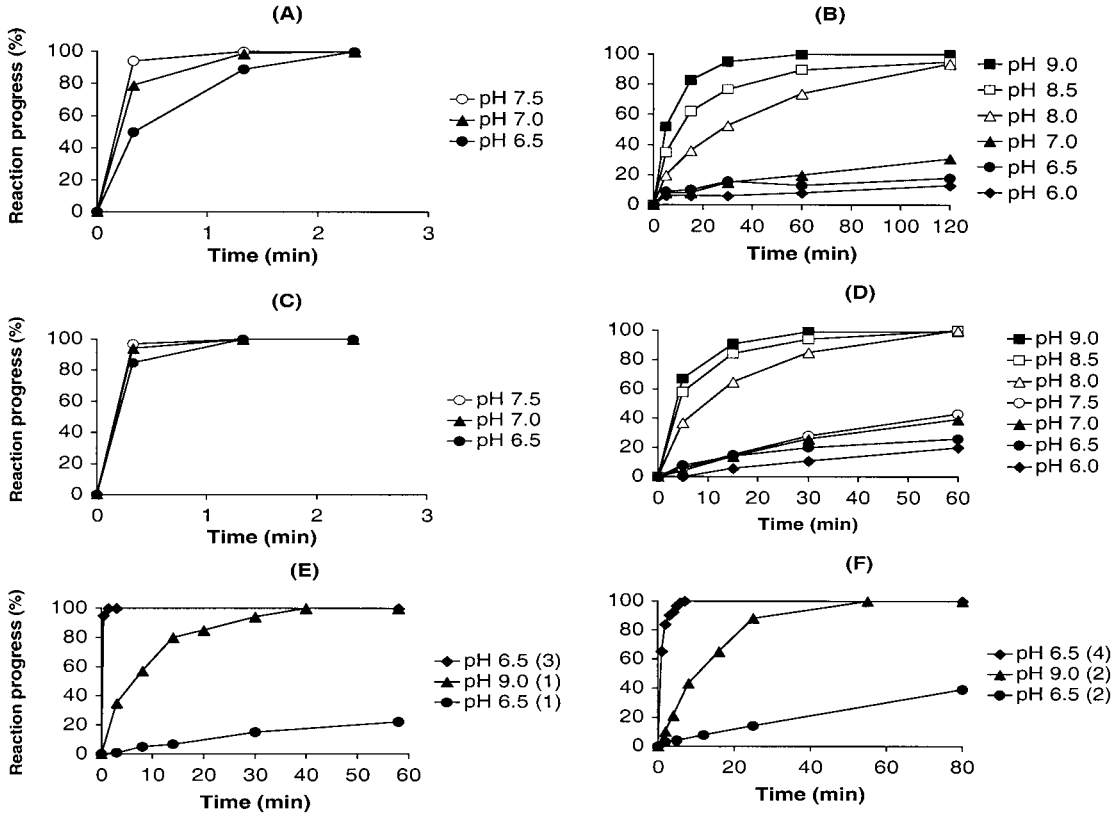

Figure 3. Reaction between the thiol-reactive derivatives **1**−**4** with 2-mercapthoethanol, cysteine, and the peptide CGIRGERA at different pH values. The reactions were performed at 25 °C in the presence of a 2-fold molar excess of thiol (see text) and reaction progress was determined by measuring residual thiols with Ellman's reagent. Reaction of 2-mercapthoethanol with **3** (panel A) and **1** (panel B), of cysteine with **3** (panel C) and **1** (panel D) and of CGIRGERA with **1** and **3** (panel E) and with liposomal **2** and **4** (panel F). (Panels E and F) The numbers in parentheses designate the thiol-reactive reagents **1**−**4** used in these experiments.

and 0.466 ± 0.03 for CGIRGERA. At pH 6.5, k_{dim} was <0.04 for mercaptoethanol, <0.07 for cysteine, and 0.136 ± 0.02 for CGIRGERA. Representative reaction progress curves are given in Figure 3. Another control was the hydrolysis of bromoacetyl function in **1**; under our experimental conditions, no changes were detected at pH 9 within 2 h. As expected, the maleimide moiety of **3** (Figure 3A) reacted very rapidly and quantitatively with the thiol function of 2-mercaptoethanol at pH values near neutrality. In sharp contrast under these conditions, the bromoacetyl derivative **1** reacted very sluggishly, and it was necessary to raise the pH to more basic values to observe appreciable rates and a reaction approaching completion (Figure 3B). Similar observations could be made with L-cysteine (Figure 3, panels C and D) and the peptide CGIRGERA (Figure 3E).

The different progress curves were analyzed, and apparent second-order rate constants were determined; however, because of the fast reactions observed with the maleimide derivative **3** in most cases, only rough estimates of the minimal rates could be obtained. Several conclusions can be drawn from these data: (i) at pH 6.5, the rates of reaction of **1** and **3** are dependent on the nature of the thiol. Thus, the peptide CGIRGERA reacts about 1 order of magnitude faster with **3** than 2-mercaptoethanol (k = >800 and 101 ± 0.3 M^{-1} s^{-1}, respectively). Such differences can be ascribed to the respective nucleophilicity of the thiols involved in these reactions. Indeed, it is known that the nucleophilicity of thiols is most generally correlated to their pK_a and that reactions of thiols with, e.g., **3**, are characterized by high Brønsted coefficients (see, e.g., ref *26*), (ii) at pH 6.5, there exists an important difference of reactivity between **1** and **3** with a given thiol. Thus, the peptide CGIRGERA reacts about 3 orders of magnitude faster with the maleimide **3** than with the bromoacetyl derivative **1** (k = >800 and 0.38 ± 0.02 M^{-1} s^{-1}, respectively). A similar difference was observed in the case of cysteine (k = >330 and 0.21 ± 0.04 M^{-1} s^{-1}, respectively) and 2-mercaptoethanol (k = 101 ± 0.3 and 0.052 ± 0.02 M^{-1} s^{-1}, respectively). These differences of reactivity between the thiol-reactive functions are large enough to perform a preferential coupling, at pH 6.5, of an HS-peptide to a maleimide derivative even in the presence of a bromoacetyl function which reacts much faster at basic pH. Thus, a sequential coupling of two HS-peptides can be envisaged, first on a maleimide derivative at pH 6.5 followed by a coupling to a bromoacetyl derivative at, e.g., pH 9.0 under experimental conditions that respect the integrity of liposomes.

Reaction of the Peptide CGIRGERA with the Thiol-Reactive Functionalized Phosphatidylethanolamines 2 and 4 Incorporated into Liposomes. In solution, we have found an important difference of reactivity, at pH 6.5, between the bromoacetyl **1** and maleimide **3** with the terminal Cys residue of CGIRGERA (Figure 3E). Next, we wanted to assess the extent of the differential reactivity of these functions when present at the surface of liposomes. The functionalized spacer-arms were thus conjugated to DPPE to give, respectively, the thiol-reactive lipophilic anchors **2** and **4** (Figure 2), which could be incorporated into liposomes. SUVs composed of PC, PG, **2** or **4**, and cholesterol (molar ratio 65:25:10:50) were prepared (average diameter 100 nm) and incubated in the presence of 2 equiv of CGIRGERA/reactive group. At pH 6.5, the reaction with **4** was very fast, whereas with **2**, the rate of coupling was much lower (Figure 3F) and the difference in rate constants between the two conjugation reactions was estimated to

be about 2 orders of magnitude ($k = >54 \pm 6$ and 0.28 ± 0.01 M^{-1} s^{-1}, respectively). As expected, the peptide reacted with the bromoacetyl derivative **2** at higher pH (Figure 3F).

The difference of reactivity between the maleimide and bromoacetyl functions with the HS-peptide is affected by their presence on liposomes; thus, we find 2-orders of magnitude difference instead of 3 in solution. Interestingly, only the reactivity of the maleimide moiety is affected when present at the surface of the vesicles, whereas the bromoacetyl function reacts at similar rates in solution or exposed on liposomes. It seems that the reaction of the maleimide with the peptide is so fast that when present at the surface of liposomes the lower diffusion rate of the vesicles could come into play.

This difference of reactivity, at pH 6.5, between the maleimide and bromoacetyl functions, although diminished when present at the surface of liposomes, is still important enough to permit the preparation of the diepitope constructs (Figure 1). In principle, this difference could be optimized further when needed by reacting the maleimide at lower pH values and/or by using in the first step equimolar amounts of HS-peptide and liposomal maleimide derivative such as **4**. We have used this latter strategy which is kinetically more controllable and thus avoids "overshooting" by a slow reaction of the excess peptide with the bromoacetyl derivative (e.g., **2**) (*19*).

Reactivity of the Bromoacetyl Derivative 1 with Other Functions at Basic pH. To be able to use a bromoacetyl functionalized lipophilic anchor to conjugate a HS-peptide to the surface of preformed liposomes, we wanted to make sure that the coupling reaction was still chemoselective, at the basic pH used, for the thiol group present at its N-terminus. We thus controlled the reactivity of **1,** at pH 9.0, with other nucleophilic moieties likely to be present in peptides such as the N-terminal function, ϵ-NH_2 of lysine or imidazole of histidine residue.

The reactivity of the ϵ-NH_2 function of lysine was tested with the dipeptide of *N*-α-acetyl-GK. When **1** was reacted with 2 equiv of this peptide, no disappearance of amine functions was measurable over a period of 60 min, at 25 °C, as assessed by the fluorescamine assay. Under the same conditions, to test the reactivity of a N-terminal function of a peptide, we used 2 equiv of CGIRGERA and measured in parallel the reactivity of the thiol group and of the amine residues, respectively, with the Ellman's reagent and fluorescamine. The results indicated over the same time a complete loss of reactive thiols and no reaction of the N-terminus. To test the reactivity of an imidazole moiety of a peptide with the bromoacetyl group at pH 9, we used the tripeptide *N*-benzoyl-GHL, which contains an imidazole side chain whose N-terminus is protected. This peptide (2 equiv) was added to liposomes containing **2** and after 90 min at 25 °C an extensive dialysis was performed. After complete hydrolysis of the liposomal preparation, analysis revealed no coupling of the peptide to the vesicles.

Altogether, these results indicate that the bromoacetyl function of **1** and **2** presents a high chemoselectivity for peptidyl thiol groups; i.e., under experimental conditions where the reaction of thiols is essentially complete, no reaction with peptidic α- or ϵ-NH_2 and imidazole functions could be detected. This is in excellent agreement with previous reports showing that of the nucleophilic groups present in proteins/peptides thiols are modified most readily by electrophilic reagents, whereas amino groups are less reactive by 2−3 orders of magnitude and imidazole groups of histidine are even less reactive (*27* and references therein). Therefore, it is most likely that, in our constructs, a HS-peptide will be conjugated via the unique formation of a thioether bond between its N-terminal thiol and the bromoacetyl group.

CONCLUSION

We have demonstrated the existence of a great difference of reactivity, in aqueous media, of thiols carried by peptides with maleimide and bromacetyl functions. The reaction with maleimide is much faster at pH 6.5 than with the bromoacetyl group; the conjugation to the latter becomes exploitable only at higher pH values (e.g., pH 9.0) while remaining chemoselective for the thiol functions. We have applied this differential reactivity to conjugate sequentially, to the surface of a same preformed vesicle, two different HS-peptide epitopes on predefined and different thiol-reactive lipophilic anchors. Thus, using a B epitope originating from a *Streptococcus mutans* cell surface adhesin and a "universal" Th epitope from tetanus toxin, we have prepared a liposomal diepitope construct (*19*) and showed that this synthetic formulation when administered i.p. to BALB/c mice induced a highly intense, anamnestic, and long-lasting (over 2 years) immune response. This differential reactivity of maleimide and bromoacetyl functions could be exploitable with any other construct where sequential coupling of different thiol carrying ligands is of importance.

LITERATURE CITED

(1) Arnon, R., and Horwitz, R. J. (1992) Synthetic peptides as vaccines. *Curr. Opin. Immunol. 4*, 449−453.

(2) Arnon, R., and Van Regenmortel, M. H. V. (1992) Structural basis of antigenic specificity and design of new vaccines. *FASEB J. 6*, 3265−3274.

(3) Brown, F. (1994) Synthetic peptides and purified antigens as vaccines. *Int. J. Technol. Assess. Health Care 10*, 161−166.

(4) Ben Yedidia, T., and Arnon, R. (1997) Design of peptide and polypeptide vaccines. *Curr. Opin. Biotechnol. 8*, 442−448.

(5) Jackson, D. C., O'Brien-Simpson, N., Ede, N. J., and Brown, L. E. (1997) Free radical induced polymerization of synthetic peptides into polymeric immunogens. *Vaccine 15*, 1697−1705.

(6) Tam, J. P. (1996) Recent advances in multiple antigen peptides. *J. Immunol. Methods 196*, 17−32.

(7) Alving, C. R., Koulchin, V., Glenn, G. M., and Rao, M. (1995) Liposomes as carriers of peptide antigens: induction of antibodies and cytotoxic T lymphocytes to conjugated and unconjugated peptides. *Immunol. Rev. 145*, 5−31.

(8) Gregoriadis, G., Gursel, I., Gursel, M., and McCormack, B. (1996) Liposomes as immunological adjuvants and vaccine carriers. *J. Controlled Release 41*, 49−56.

(9) Barr, I. G., Sjolander, A., and Cox, J. C. (1998) ISCOMs and other saponin based adjuvants. *Adv. Drug Delivery Rev. 32*, 247−271.

(10) Frisch, B., Muller, S., Briand, J. P., Van Regenmortel, M. H. V., and Schuber, F. (1991) Parameters affecting the immunogenicity of a liposome-associated synthetic hexapeptide antigen. *Eur. J. Immunol. 21*, 185−93.

(11) Friede, M., Muller, S., Briand, J. P., Van Regenmortel, M. H. V., and Schuber, F. (1993) Induction of immune response against a short synthetic peptide antigen coupled to small neutral liposomes containing monophosphoryl lipid A. *Mol. Immunol. 30*, 539−547.

(12) Friede, M., Muller, S., Briand, J. P., Plaue, S., Fernandes, I., Frisch, B., Schuber, F., and Van Regenmortel, M. H. V. (1994) Selective induction of protection against influenza virus infection in mice by a lipid-peptide conjugate delivered in liposomes. *Vaccine 12*, 791−797.

(13) Fernandes, I., Frisch, B., Muller, S., and Schuber, F. (1997) Synthetic lipopeptides incorporated in liposomes: In vitro stimulation of the proliferation of murine splenocytes and in

vivo induction of an immune response against a peptide antigen. *Mol. Immunol. 34*, 569−576.
(14) Frisch, B., Boeckler, C., and Schuber, F. (1996) Synthesis of short polyoxyethylene-based heterobifunctional cross-linking reagents. Application to the coupling of peptides to liposomes. *Bioconjugate Chem. 7*, 180−186.
(15) Boeckler, C., Frisch, B., Muller, S., and Schuber, F. (1996) Immunogenicity of new heterobifunctional cross-linking reagents used in the conjugation of synthetic peptides to liposomes. *J. Immunol. Methods 191*, 1−10.
(16) Martin, F. J., and Papahadjopoulos, D. (1982) Irreversible Coupling of Immunoglobulin Fragments to Preformed Vesicles. *J. Biol. Chem. 257*, 286−288.
(17) Goodman-Snitkoff, G., Eisele, L. E., Heimer, E. P., Felix, A. M., Anderson, T. T., Fuerst, T. R., and Mannino, R. J. (1990) Defining minimal requirements for antibody production to peptide antigen. *Vaccine 8*, 257−262.
(18) Brumeanu, T. D., Casares, S., Bot, A., Bot, S., and Bona, C. A. (1997) Immunogenicity of a contiguous T−B synthetic epitope of the A/PR/8/34 influenza virus. *J. Virol. 71*, 5473−5480.
(19) Boeckler, C., Dautel, D., Schelté, P., Frisch, B., Wachsmann, D., Klein, J. P., and Schuber, F. (1999) Design of highly immunogenic liposomal constructs combining structurally independent B cell and T helper cell peptide epitopes. *Eur. J. Immunol. 29*, 2297−2308.
(20) Boeckler, C., Frisch, B., and Schuber, F. (1998) Design and synthesis of thiol-reactive lipopeptides. *Bioorg. Med. Chem. Lett. 8*, 2055−2058.
(21) Bessler, W. G., Baier, W., van den Esche, U., Hoffmann, P., Heinevetter, L., Wiesmüller, K.-H., and Jung, G. (1997) Bacterial lipopeptides constitute efficient novel immunogens and adjuvants in parenteral and oral immunization. *Behring Inst. Mitt. 98*, 390−399.
(22) Kichler, A., Remy, J. S., Boussif, O., Frisch, B., Boeckler, C., Behr, J. P., and Schuber, F. (1995) Efficient gene delivery with neutral complexes of lipospermine and thiol-reactive phospholipids. *Biochem. Biophys. Res. Commun. 209*, 444−450.
(23) Riddles, P. W., Blakeley, R. L., and Zerner, B. (1979) Ellman's reagent: 5, 5′-dithiobis(2-nitrobenzoïc acid): a reexamination. *Anal. Biochem. 94*, 75−81.
(24) Rouser, G., Fleischer, J., and Yamamoto, A. (1970) Two-dimensional thin layer chromatographic separation of plant lipids and determination of phospholipids by phosphorus analysis of spots. *Lipids 5*, 494−496.
(25) Böhlen, P., Stein, S., Dairman, W., and Udenfriend, S. (1973) Fluorometric assay of proteins in the nanogram range. *Arch. Biochem. Biophys. 155*, 213−220.
(26) Nieslanik, B. S., and Atkins, W. M. (1998) Contribution of linear free energy relationships to isozyme- and pH-dependent substrate selectivity of glutathione S-transferases: comparison of model studies and enzymatic reactions. *J. Am. Chem. Soc. 120*, 6651−6660.
(27) Dienys, G., Sereikaité, J., Gavènas, G., Kvederas, R., and Bumelis, V. A. (1998) Cross-linking of protein subunits by 1,3,5-triacryloyl-hexahydro-*s*-triazine. *Bioconjugate Chem. 9*, 744−748.

BC990122K

Collagen Cross-Links. Synthesis of Immunoreagents for Development of Assays for Deoxypyridinoline, a Marker for Diagnosis of Osteoporosis

Maciej Adamczyk,* Donald D. Johnson, and Rajarathnam E. Reddy

Department of Chemistry (9NM), Building AP20, Diagnostics Division, Abbott Laboratories, 100 Abbott Park Road, Abbott Park, Illinois 60064-6016

(+)-Deoxypyridinoline (Dpd, **2**) is a cross-link of bone collagen, which is released and excreted in urine during process of bone resorption. It has been shown that this bone collagen degradation product, Dpd (**2**) is a useful marker for diagnosis of osteoporosis and other metabolic bone diseases. In this paper, the design and synthesis of two immunogens (**3**, **4**) via of conjugation of succinimidyl ester (**14**) to carrier protein, bovine serum albumin, or keyhole limphet hemocyanin, was presented. Additionally, fluorescent (**5**) and chemiluminescent (**6**) tracers were prepared from (−)-acid (**13**) via in situ activation and subsequent reaction with 6-Fln-CH_2NH_2 (**17**) or Acr-NH_2 (**18**) and hydrolysis. The key hapten (−)-acid (**13**) was prepared by quaternization of 3-hydroxypyridine derivative (*S*,*S*)-(−)-**11** with iodide (*S*)-(−)-**10** followed by selective hydrolysis. These immunreagents (immunogens **3** and **4** and tracers **5** and **6**) are useful for the development of sensitive and high throughput immunoassays, such as FPIA and CLIA for Dpd (**2**).

INTRODUCTION

Osteoporosis is a crippling degenerative bone disease, which affects the aged population, particularly postmenopausal women, and is responsible for 1.5 million fractured bones each year in the United States alone (*1*, *2*). This metabolic disease is the consequence of an inbalance in the bone renewal process, which occurs when the bone resorption exceeds bone formation. Current methods for diagnosis of osteoporosis involve histomorphometry studies and densitometric measurements (*2*−*4*). Efforts for prevention of this disease as well as development of an effective antiresorptive therapy have increased the need for reliable and noninvasive biochemical markers of bone resorption (*5*−*7*). The traditional markers of bone resorption, i.e., urinary calcium (*8*, *9*) and hydroxyproline (*10*, *11*), lack clinical sensitivity and specificity for diagnosis of osteoporosis.

Since bone is densely packed with collagen, a family of structurally related proteins, its strength is mainly governed by the physiological and pathological changes of collagen (*12*). It has been shown that, during the process of maturation of collagen, the cross-links, (+)-pyridinoline (Pyd, **1**) (*13*) and (+)-deoxypyridinoline (Dpd, **2**) (*14*) (Figure 1), are formed from lysine and hydroxylysine by a lysyl oxidase-mediated enzymatic process (*15*−*17*). These pyridinium cross-links (**1**, **2**) play an important role in maintaining the structure of the collagen fibril network. However, in the process of bone resorption, the cross-links (**1**, **2**) are released into serum and excreted in urine either in free form or linked to different peptide fragments of collagen (*5*−*7*, *18*). Therefore, markedly elevated levels of cross-links (**1**, **2**) are present in urine of patients with osteoporosis and other metabolic bone diseases. Subsequently, it was found that the cross-link (+)-Dpd (**2**) shows greater specificity for bone, and consequently, it became a marker of choice for diagnosis of osteoporosis (*19*−*20*). A number of methods were developed for quantification of cross-links (**1**, **2**), i.e., amino acid analysis (*15*−*17*, *21*), HPLC (*22*−*26*), and immunoassays (*27*−*35*). However, there is no report in the literature on preparation of immunogens and tracers (fluorescent/chemiluminescent) from a specific position of optically pure (+)-Dpd (**2**) with full experimental details. This fact might be attributed to the high cost ($2510.40/1.0 mg) and complex structure of Dpd (**2**), which requires multiple steps for its total synthesis or tedious isolation from the natural sources. The need for well-characterized reagents required for development of immunoassays is widely recognized (*36*−*40*). In this endeavor, we recently described the chiral synthesis of (+)-Dpd (**2**) and a variety of its analogues (*41*−*43*). In this report, we present the synthesis of immunoreagents [immunogens (**3**, **4**) and tracers (**5**, **6**)], which are needed for development of fluorescence polarization immunoassay (FPIA), and chemiluminescence immunoassays (CLIA) for diagnosis of osteoporosis.

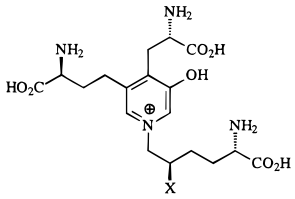

(+)-**1**: X = OH, Pyridinoline
(+)-**2**: X = H, Deoxypyridinoline

Figure 1.

EXPERIMENTAL SECTION

General Methods and Materials. ^1H and ^{13}C NMR spectra were recorded on a Varian Gemini spectrometer (300 MHz), the chemical shifts (δ) were reported in parts

* To whom correspondence should be addressed.

10.1021/bc9900892 CCC: $19.00 © 2000 American Chemical Society
Published on Web 12/16/1999

per million relative to TMS, and coupling constants (*J*) were reported in hertz. Electrospray ionization mass spectrometry (ESI/MS) was carried on a Perkin-Elmer (Norwalk, CT) Sciex API 100 Benchtop system employing Turbo Ionspray ion source, and HRMS were obtained on Nermang 3010 MS-50, JEOL SX102-A mass spectrometers. Thin-layer chromatography was performed on precoated Whatman MK6F silica gel 60 Å plates (layer thickness: 250 μm). Column chromatography was performed on silica gel, Merck grade 60 (230−400 mesh). THF was freshly distilled from a purple solution of sodium and benzophenone. All reagents were purchased from Aldrich Chemical Co. (Milwaukee, WI) or Sigma Chemical Co. (St. Louis, MO) and used without purification, except where noted. All the solvents employed were of HPLC grade purchased from EM Science (Gibbstown, NJ) and used as received. Analytical reversed-phase (RP) HPLC was performed using a Waters, μBondapak RCM C18 10 μm (8 × 100 mm) column (solvents ratio v/v reported) unless otherwise stated. Preparative reversed-phase (RP) HPLC was performed using a Waters μBondapak RCM C18 10 μm (40 × 100 mm) column (solvents ratio v/v reported) unless otherwise stated. Optical rotations were measured on Autopol III polarimeter, Rudolph Research, Flanders, NJ.

(−)-*tert*-Butyl-(2*S*)-4-(4-{(2*S*)-3-(*tert*-butoxy)-2-[(*tert*-butoxycarbonyl)amino]-3-oxopro pyl}-5-hydroxy-3-pyridinyl)-2-[(*tert*-butoxycarbonyl)amino]butanoate (**11**) was prepared from a commercially available *N*-*t*-Boc-L-glutamic acid-α-*tert*-butyl ester (*41*).

(*S*)-(−)-Methyl-2-[(*tert*-butoxycarbonyl)amino]-6-hydroxyhexanoate (9). (*S*)-(−)-6-Amino-2-[(*tert*-butoxycarbonyl)amino]hexanoic acid (**7**, 3.69 g, 15.0 mmol) was dissolved in water (50 mL) and the pH adjusted to 9.5 using 4 M NaOH(aq). The mixture was heated to 60 °C, and sodium nitroprusside (7.07 g, 23.7 mmol, 1.6 equiv) was added portionwise over 30 min period. The reaction mixture was heated for an additional 5 h, while maintaining the pH between 9 and 10 by adding 4 M NaOH(aq) during and after the addition of sodium nitroprusside. The reaction mixture was cooled to room temperature and filtered through Celite powder. The pH of the filtrate was adjusted to 3.5 using 6 M HCl and extracted with EtOAc (3 × 40 mL). The combined organic layers were washed with brine (40 mL) and dried (Na_2SO_4), and the solvent was removed on a rotary evaporator. The resulting crude (*S*)-2-[(*tert*-butoxycarbonyl)amino]-6-hydroxyhexanoic acid (**8**) (2.40 g) was dried and carried to the next reaction without purification.

The above prepared crude hydroxy acid (*S*)-**8** (1.15 g, 4.65 mmol) was dissolved in MeOH (30 mL) and cooled with an ice bath. To this mixture was added a freshly generated ethereal diazomethane solution [generated from *N*-nitroso-*N*-methylurea (4.79 g, 46.5, mmol, 10 equiv), KOH (11.6 g, 207.1 mmol, 4.4 equiv.), ether (30 mL), and water (35 mL)] at 0 °C. After 15 min, the cooling bath was removed, and stirring was continued for an additional 1.5 h. Excess diazomethane was removed by bubbling the nitrogen for 10 min and then concentrated on a rotary evaporator. The crude product was purified by silica gel column chromatography (60% EtOAc in hexanes) to afford 0.624 g of (*S*)-(−)-methyl-2-[(*tert*-butoxycarbonyl)amino]-6-hydroxyhexanoate (**9**) in 41% yield for two steps. R_f: 0.33 (60% EtOAc in hexane). Analytical RP HPLC: MeCN:0.1% acetic acid(aq)/40:60, 1.0 mL/min at 225 nm. R_t: 6.88 min, >99%. $[\alpha]^{20}_D$: −19.4 (c 1.29, MeOH). ^{1}H NMR ($CDCl_3$): δ 5.07 (d, 1 H, J = 7.8 Hz), 4.33−4.26 (m, 1 H), 3.73 (s, 3 H), 3.69−3.58 (m, 2 H), 1.85−1.55 (m, 6 H), 1.43 (s, 9 H). ^{13}C NMR ($CDCl_3$): δ 173.5, 155.6, 79.9, 62.3, 53.2, 52.2, 32.3, 31.9, 28.2, 21.4, 14.0. ESI-MS (*m*/*z*): 262 $(M + H)^+$.

(*S*)-(−)-Methyl-2-[(*tert*-butoxycarbonyl)amino]-6-iodohexanoate (10). Triphenylphos phine (0.792 g, 3.02 mmol, 1.5 equiv), imidazole (0.219 g, 3.22 mmol, 1.6 equiv), and iodine (0.767 g, 3.02 mmol, 1.5 equiv) were added sequentially to a solution of (*S*)-(−)-**9** (0.524 g, 2.01 mmol) dissolved in THF (20 mL) at room temperature under nitrogen. After stirring the mixture for 2 h, the solvent was removed on a rotary evaporator to dryness. The residue was diluted with EtOAc (40 mL) and water (40 mL). The organic layer was separated and extracted with EtOAc (2 × 40 mL). The combined organic layers were dried (Na_2SO_4), and the solvent was removed on a rotary evaporator. The crude product was purified by silica gel column chromatography (20% EtOAc in hexanes) to afford 0.655 g of (*S*)-(−)-**10** in 88% yield as a colorless thick oil. R_f: 0.31 (20% EtOAc in hexanes). Analytical RP HPLC: MeCN:0.1% acetic acid(aq)/80:20, 1.0 mL/min at 225 nm. R_t: 5.91 min, 98%. $[\alpha]^{20}_D$: −8.8 (c 1.51, MeOH). ^{1}H NMR ($CDCl_3$): δ 5.03 (d, 1 H, J = 8.1 Hz), 4.36−4.26 (m, 1 H), 3.74 (s, 3 H), 3.16 (t, 2 H, J = 6.9 Hz), 1.90−1.58 (m, 6 H), 1.43 (s, 9 H). ^{13}C NMR ($CDCl_3$): δ 173.3, 155.4, 79.9, 53.0, 52.3, 32.6, 31.5, 28.2, 26.0, 6.0. ESI-MS (*m*/*z*): 372 $(M + H)^+$.

Pyridinium Compound (12). A mixture of (*S*,*S*)-(−)-**11** (0.369 g, 0.619 mmol) and iodide (*S*)-(−)-**10** (0.461 g, 0.1.24 mmol, 2.0 equiv) were dissolved in anhydrous 1,4-dioxane (10 mL) and gently refluxed for 6.5 h under nitrogen. The solvent was removed on a rotary evaporator to dryness, the crude product was dissolved in MeCN-0.05% acetic acid(aq) (50 mL, ratio, 80:20) and purified by preparative RP HPLC [MeCN:0.05% trifluoroacetic acid(aq)/70:30, 25 mL/min at 225 nm]. The solvent was removed on a rotary evaporator to about 300 mL volume and finally lyophilized. The resulting product (oil) was azeotroped using toluene-MeOH (1:1 ratio, 3 × 20 mL) on a rotary evaporator to afford 0.558 g of **12** as its TFA salt in 94% yield. Analytical RP HPLC: MeCN:0.05% acetic acid(aq)/80:20, 1.0 mL/min at 225 nm, R_t: 5.76 min, 96%. ^{1}H NMR ($CDCl_3$): δ 9.24 (s, 1 H), 7.95 (s, 1 H), 5.45−5.35 (m, 1 H), 5.23 (d, 1 H, J = 7.8 Hz), 5.03 (d, 1 H, J = 7.8 Hz), 4.42−4.22 (m, 4 H, 4.18−4.06 (m, 1 H), 3.75 (s, 3 H), 3.40−3.10 (m, 2 H), 3.10−2.90 (m, 2 H), 2.18−1.22 (m, 8 H), 1.47 (s, 9 H), 1.45 (s, 9 H), 1.44 (s, 9 H), 1.43 (s, 9 H), 1.34 (s, 9 H). ESI-MS (*m*/*z*): 839 $(M)^+$. HRMS (*m*/*z*): calcd for $C_{42}H_{71}N_4O_{13}$, 839.5012; observed, 839.5010.

(−)-Acid (13). Lithium hydroxide monohydrate (0.063 g, 1.5 mmol, 3.0 equiv) and water (8 mL) were added sequentially to a solution of pyridinium compound (**12**, 0.422 g, 0.502 mmol) dissolved in THF (24 mL) at room temperature. After stirring the mixture for 30 min, it was then concentrated on a rotary evaporator. The crude product was purified by preparative RP HPLC (MeCN: 0.05% trifluoroacetic acid(aq)/70:30, 25 mL/min at 225 nm). The solvent was removed on a rotary evaporator to about 300 mL volume and finally lyophilized to afford 0.165 g of (−)-acid (**13**) as its TFA salt in 40% yield. Analytical RP HPLC: MeCN:0.05% trifluoroacetic acid-(aq)/70:30, 1.0 mL/min at 225 nm. R_t: 6.57 min, 98%. $[\alpha]^{20}_D$: −20.0 (c 1.29, MeOH). ^{1}H NMR (CD_3OD): δ 8.37 (s, 1 H), 8.13 (s, 1 H), 4.58−4.42 (m, 2 H), 4.18−3.90 (m, 3 H), 3.40−2.82 (m, 4 H), 2.20−1.20 (m, 8 H), 1.46 (s, 9 H), 1.45 (s, 9 H), 1.44 (s, 9 H), 1.43 (s, 9 H), 1.36 (s, 9 H). ESI-MS (*m*/*z*): 839 $(M)^+$.

Succinimidyl Ester (14). *N*-Hydroxysuccinimide (HOSu, 0.034 g, 0.296 mmol, 2.0 equiv) and 1-(3-dimethylaminopropyl)-3-ethylcarbodiimide (EDAC, 0.057 g,

0.296 mmol, 2.0 equiv) were added sequentially to solution of (−)-acid (**13**, 0.122 g, 0.148 mmol) and dissolved in anhydrous DMF (8 mL) at room temperature under nitrogen. The mixture was stirred for 16 h, and solvent removed on a rotary evaporator under vacuum. The crude product was dissolved in MeCN−0.1% aqueous trifluoroacetic acid (70:30 ratio, 15 mL) and purified by preparative RP HPLC [MeCN:0.05% trifluoroacetic acid-(aq)/70:30, 25 mL/min at 225 nm]. The solvent was removed on a rotary evaporator (<40 °C bath temperature) to about 200 mL volume and finally lyophilized to afford 0.090 g of succinimidyl ester (**14**) as its TFA salt in 66% yield. Analytical RP HPLC: MeCN:0.05% trifluoroacetic acid(aq)/70:30, 1.0 mL/min at 225 nm. R_t: 8.4 min, 91%. ^{1}H NMR ($CDCl_3$): δ 9.19 (s, 1 H), 7.92 (s, 1 H), 5.50−5.30 (m, 3 H), 4.70−4.60 (m, 1 H), 4.45−4.30 (m, 2 H), 4.18−4.06 (m, 2 H), 3.20−3.18 (m, 2 H), 3.00−2.80 (m, 2 H), 2.85 (s, 4 H), 2.18−1.20 (m, 8 H), 1.46 (s, 9 H), 1.45 (s, 18 H), 1.44 (s, 9 H), 1.36 (s, 9 H). ESI-MS (m/z): 924 $(M)^+$.

BSA-Immunogen (3). A solution of succinimidyl ester (**14**, 0.042 g, 0.045 mmol, 15.0 equiv) dissolved in DMF (2 mL) was added to a solution of BSA (0.200 g, 0.003 03 mmol) dissolved in buffer (pH 8.00, 10 mL) at room temperature. The mixture was stirred for 16 h and dialyzed in a mixture of 0.05 N phosphate buffer (1.8 L) and EtOH (200 mL) for 4 h. The mixture was further dialyzed in deionized (DI) water (2.0 L) for four times by changing to the fresh DI water for every 5 h. Lyophilization of the mixture afforded 0.202 g of an intermediate immunogen (**15**) with Boc protective groups as white powder. Analysis of this immunogen precursor (**15**) by gel electrophoresis showed a single narrow band and the absence of free and polymeric BSA. MALDI mass spectrum: 72 093 [BSA with 6 haptens (**14**)]. A mixture of TFA (9.5 mL) and water (0.5 mL) was added to this immunogen precursor (**15**, 103 g) at room temperature and stirred for 2 h. The solvent was removed on a rotary evaporator to dryness, the resulting residue was diluted with water (10 mL), and the pH adjusted to 9.0 using 6 N NaOH(aq). The mixture was dialyzed in a mixture of 0.05 N phosphate buffer (1.8 L) and EtOH (200 mL) for 16 h. The mixture was further dialyzed in deionized (DI) water (2.0 L) for four times by changing to the fresh DI water for every 5 h. Lyophilization of the mixture afforded 0.067 g of immunogen (**3**) as a white powder. Analysis of immunogen (**3**) by gel electrophoresis showed a single narrow band and the absence of free and polymeric BSA. MALDI mass spectrum: 68 618 [BSA with six haptens (Dpd, **2**)].

KLH-Immunogen (4). A solution of succinimidyl ester (**14**, 0.021 g, 0.023 mmol) dissolved in DMF (1 mL) was added to a solution of KLH (0.100 g) dissolved in buffer (pH 8.00, 5 mL) at room temperature. The mixture was stirred for 16 h and then dialyzed in a mixture of 0.05 N phosphate buffer (2.0 L) and EtOH (200 mL) for 4 h. The mixture was further dialyzed in deionized (DI) water (1.8 L) for four times by changing to the fresh DI water for every 5 h. Lyophilization of the mixture afforded 0.129 g of an immunogen precursor (**16**). A mixture of TFA (9.5 mL) and water (0.5 mL) was added to this immunogen precursor (**16**, 0.063 g) at room temperature and stirred for 2 h. The solvent was removed on a rotary evaporator to dryness, the resulting residue was diluted with water (10 mL) and the pH adjusted to 9.0 using 6 N NaOH-(aq). The mixture was stirred at room temperature for 16 h and centrifuged. The solid material was washed with water and centrifuged. The washing and centrifuge process was repeated two more times, and finally, the solid was washed into a flask and lyophilized to afford 0.041 g of KLH-immunogen (**4**) as a pale gray powder.

Fluorescein-Conjugate (19). *N*-Hydroxysuccinimide (HOSu, 0.021 g, 0.185 mmol, 5.0 equiv) and 1-(3-dimethylaminopropyl)-3-ethylcarbodiimide (EDAC, 0.025 g, 0.133 mmol, 3.6 equiv) were added sequentially to a solution of (−)-acid (**13**, 0.035 g, 0.037 mmol) and dissolved in anhydrous DMF (1.0 mL) at room temperature under nitrogen. The reaction mixture was stirred at room temperature for 5 h to form the corresponding succinimidyl ester (**14**). 6-Fln-CH_2NH_2HBr (**17**, 0.016 g, 0.037 mmol, 1.0 equiv) and triethylamine (0.052 mL, 0.37 mmol, 10.0 equiv) were added sequentially to the reaction mixture containing the succinimidyl ester (**14**) at room temperature and stirred for 2 h. The solvent was removed on a rotary evaporator under vacuum and the residue was dissolved in MeCN:0.1% aqueous trifluoroacetic acid (6.0 mL, 1:1 ratio). The crude product was purified by preparative RP HPLC (MeCN: 0.1% trifluoroacetic acid-(aq)/50:50, 45.0 mL/min at 215 nm). The product was collected and concentrated on a rotary evaporator to about 100 mL volume, and finally lyophilized to afford 0.018 g of fluorescein-conjugate (**19**) in 38% yield as a yellow powder. Analytical RP HPLC: MeCN:0.1% trifluoroacetic acid(aq)/60:40, 2.0 mL/min at 215 nm. R_t: 5.79 min, 98.9%; ^{1}H NMR (CD_3OD): δ 8.33 (s, 1 H), 8.13 (s, 1 H), 7.93 (d, 1 H, J = 7.8 Hz), 7.62 (d, 1 H, J = 8.1 Hz), 7.13 (s, 1 H), 6.68−6.55 (m, 6 H), 4.54−4.35 (m, 5 H), 4.02−3.90 (m, 2 H), 3.42−3.12 (m, 2 H), 3.00−2,84 (m, 2 H), 2.20−1.40 (m, 8 H), 1.45 (s, 27 H), 1.35 (s, 18 H). ESI-MS (m/z): 1169 $(M)^+$.

Fluorescent Tracer (6-Fln tracer, 5). A mixture of trifluoroacetic acid and water (4.0 mL, ratio, 9.5:0.5) was added to the fluorescein-conjugate (**19**, 0.017 g, 0.013 mmol) at room temperature and stirred for 2 h. The solvent was removed on rotary evaporator and the residue was dissolved in MeCN−0.1% trifluoroacetic acid-(aq) (4.0 mL, ratio, 20:80). The crude product was purified by preparative RP HPLC [MeCN:0.1% trifluoroacetic acid(aq)/20:80, 45.0 mL/min at 215 nm]. The product was collected, concentrated on rotary evaporator to about 175 mL volume, and finally lyophilized to afford 0.011 g of fluorescent tracer (**5**) in 70% yield as a yellow powder. Analytical RP HPLC: MeCN:0.1% trifluoroacetic acid-(aq)/20:80, 2.0 mL/min at 215 nm. R_t: 4.63 min, 94%. ^{1}H NMR (CD_3OD): δ 8.32 (s, 1 H), 8.26 (s, 1 H), 7.97 (d, 1 H, J = 8.1 Hz), 7.64 (d, 1 H, J = 7.8 Hz), 7.12 (s, 1 H), 6.67 (d, 2 H, J = 2.1 Hz), 6.60−6.50 (m, 4 H), 4.54−4.50 (m, 2 H), 4.42−4.32 (m, 2 H), 4.18 (t, 1 H, J = 7.5 Hz), 3.91 (t, 1 H, J = 6.0 Hz), 3.83 (t, 1 H, J = 6.3 Hz), 3.42−3.36 (m, 2 H), 3.10−2.93 (m, 2 H), 2.36−2.16 (m, 2 H), 2.94−1.82 (m, 2 H), 1.80−1.70 (m, 2 H), 1.40−1.26 (m, 2 H). ESI-MS (m/z): 756 $(M)^+$.

Acridinium-Conjugate (20). Acr-NH_2 TFA (**18**, 0.020 g, 0.027 mmol, 1.1 equiv) and triethylamine (0.026 mL, 0.19 mmol, 8.0 equiv) were added sequentially to a solution of succinimidyl ester (**14**, 0.034 g, 0.024 mmol) dissolved in anhydrous DMF (2.0 mL) at room temperature under nitrogen. The flask was covered with aluminum foil, and the mixture stirred for 22 h. The solvent was removed on a rotary evaporator under vacuum, and the residue was dissolved in MeCN:0.1% trifluoroacetic acid(aq) (4.0 mL, ratio 55:45). The crude product was purified by preparative RP HPLC (MeCN:0.1% trifluoroacetic acid(aq)/55:45, 25.0 mL/min at 215 nm). The product was collected, concentrated on rotary evaporator to about 125 mL volume, and finally lyophilized to afford 0.019 g of acridinium-conjugate (**20**) in 51% yield as yellow powder. Analytical RP HPLC: MeCN:0.1% trif-

luoroacetic acid(aq)/60:40, 1.0 mL/min at 215 nm. R_t: 9.18 min, 98.4%. ^{1}H NMR (CD_3OD): δ 9.02−8.92 (m, 2 H), 8.48−7.78 (m, 8 H), 7.63 (d, 2 H, J = 7.8 Hz), 7.15 (s, 2 H), 5.80−5.50 (m, 2 H), 4.56−4.40 (m, 4 H), 4.30−4.24 (m, 1 H), 4.04−4.12 (m, 2 H), 3.44−3.04 (m, 6 H), 3.02−2.84 (m, 2 H), 2.82−2.02 (m, 8 H), 2,58 and 2.37 (two s, 3 H), 2.18−1.24 (m, 8 H), 1.45 (s, 18 H), 1.43 (s, 9 H), 1.37 (s, 9 H), 1.35 (s, 9 H). ESI-MS (m/z): 1434 $(M)^+$.

Chemiluminiscent Tracer (Acr-Tracer, 6). A mixture of trifluoroacetic acid−water (4.0 mL, ratio, 9.5:0.5) was added to **20** (0.018 g, 0.012 mmol) at room temperature and stirred for 2 h. The solvent was removed on rotary evaporator and residue was dissolved in MeCN: 0.1% trifluoroacetic acid(aq) (4.0 mL, ratio, 18:82). The crude product was purified by preparative RP HPLC (Waters, RCM, C18, Novapak, 40 × 100 mm, 6.0 μm; MeCN:0.1% trifluoroacetic acid(aq)/18:82, 45.0 mL/min at 215 nm). The product was collected, concentrated on rotary evaporator to about 40 mL volume, and finally lyophilized to afford 0.016 g of chemiluminiscent tracer (Acr-tracer, **6**) in 90% yield as a yellow powder. Analytical RP HPLC (Waters, RCM, C18, Novapak, 8 × 100 mm, 6.0 μm): MeCN:0.1% trifluoroacetic acid(aq)/22:78, 2.0 mL/min at 215 nm. R_t: 4.98 min, 98.6%. ^{1}H NMR (CD_3-OD): δ 8.95−8.90 (m, 2 H), 8.48−8.36 (m, 2 H), 8.19 (d, 2 H, J = 8.4 Hz), 8.02−7.96 (2 H), 7.90−7.81 (m, 2 H), 7.63 (d, 2 H, J = 8.4 Hz), 7.14 (s, 2 H), 5.80−5.70 (m, 2 H), 4.60−4.44 (m, 4 H), 4.32−4.24 (m, 1 H), 3.90−3.82 (m, 2 H), 3.50−3.20 (m, 6 H), 2.82−2.02 (m, 10 H), 2,58 and 2.37 (two s, 3 H), 2.18−1.24 (m, 8 H). ESI-MS (m/z): 1022 $(M)^+$.

RESULTS AND DISCUSSION

In recent years, there has been a tremendous surge in the development of new immunoassay technologies and innovative automated analyzers to meet the numerous challenges faced by the clinical laboratories (*44*). The automated immunoassay analyzers developed by Abbott Laboratories, i.e., *TDx* and *AxSYM* utilize FPIA (*45*), and the recently launched *ARCHITECT* instrument is based on CLIA (*46*) technology. Both FPIA and CLIA methods require two key reagents, antibodies for binding and a signal producing material (tracer) for detection. Since the low molecular weight analytes (e.g., Dpd, **2**) do not as such induce the formation of antibodies, they need to be conjugated to a carrier protein, thus forming an immunogen (*47*). These immunogens are then used for inoculation of an animal (i.e., mice, hamster, rabbit, and sheep) for production of antibodies. Thus, first phase in the development of immunoassay is the design and synthesis of immunogen and tracers.

There are number of important issues which need to be considered when preparing the immunogen. For example, site of the analyte modification, selection of carrier protein, method of conjugation, and the hapten density. More importantly, for optically active analytes (e.g., Dpd, **2**), preservation of their chirality in preparing the immunogen is also critical. Bovine serum albumin (BSA, molecular mass 66 430 Da) and keyhole limphet hemocyanin (KLH, molecular mass 450−13000 kDa) are two commonly used carrier proteins for the preparation of immunogens. Among these, BSA is well suited as carrier protein because of its solubility in various aqueous buffers and high content of primary amines (59 lysines and a terminal amine) available for conjugation with hapten. Although, the immunogens prepared using KLH as carrier protein are difficult to characterize due to poor solubility and variable mass, they are also frequently

Scheme 1

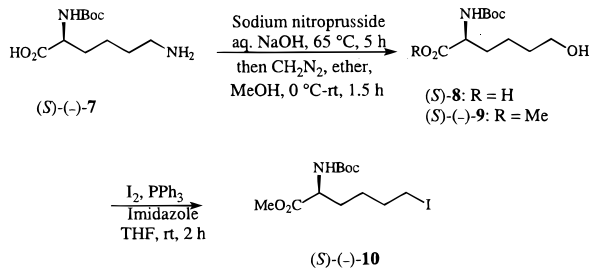

used for production of antibodies. Since the antibodies produced for carrier protein are also present in the host animal bleeds, an alternative hapten-carrier protein conjugate such as KLH-immunogen, is required to select the *anti*-analyte antibodies. Therefore, the acid functionality on the lysine chain of (+)-Dpd (**2**) was differentiated in the form of methyl ester, which can be selectively hydrolyzed and conjugated to the carrier protein. Thus, (−)-acid (**13**), a key hapten was prepared from (*S*,*S*)-(−)-**11** (*41*) via quaternization with (*S*)-(−)-iodide (**10**) followed by selective hydrolysis of the methyl ester.

The (*S*)-(−)-methyl-2-[(*tert*-butoxycarbonyl)amino]-6-iodohexanoate (**10**) required for quaternization of pyridine derivative (*S*,*S*)(−)-**11** was prepared (Scheme 1) from a commercially available L-lysine derivative (*S*)-(−)-**7** in three steps. Thus, (*S*)-6-amino-2-[(*tert*-butoxy carbonyl) amino]hexanoic acid (**7**) upon heating with sodium nitroprusside (*41*) in aqueous NaOH for 6 h at pH. 9.5 afforded the corresponding hydroxy compound (*S*)-**8**. Treatment of crude (*S*)-**8** with ethereal diazomethane and purification by silica gel column chromatography afforded the corresponding methyl ester (*S*)-(−)-**9** in 41% yield for two steps. The ester (*S*)-(−)-**9** was converted to the iodo compound (*S*)-(−)-**11** by treatment with iodine and triphenylphosphine in THF in 88% yield. Quaternization of (*S*,*S*)-(−)-**11** with (*S*)-(−)-iodide (**10**) was (Scheme 2) carried out in refluxing 1,4-dioxane to afford the (−)-pyridinium compound (**12**) in excellent yield (94%). Hydrolysis of **12** using LiOH in THF-water gave (−)-acid (**13**), the hapten required for preparation of immunoreagents (**3**, **4** and **5**, **6**). Since the in situ activation and coupling of acid hapten [i.e., (−)-**13**] to the carrier protein using reagents such as EDAC can lead to the undesired modification of carrier protein, we found that it is critical to use pure activated ester [i.e., succinimidyl ester (**14**)] for preparation of immunogen. Therefore, the (−)-acid (**13**) was activated with HOSu and EDAC in DMF to afford the corresponding succinimidyl ester **14** in 66% yield. Conjugation of active ester **14** with carrier protein, BSA, was carried out in DMF and buffer (pH 8.0) at room temperature. After 16 h, the crude reaction mixture was purified by dialysis to remove the hydrolyzed hapten (**13**) and other low molecular weight impurities. Lyophilization of the product gave an immunogen precursor (**15**) in which the Boc-protected amino groups of the hapten were unmasked using trifluoroacetic acid. Immunogen (**3**) was purified by dialysis and isolated as a white powder after lyphilyzation. Analysis of immunogen (**3**) by gel electrophoresis (*48*) showed a single narrow band and the absence of free or polymeric BSA. The resolution of gel electrophoresis is inadequate to determine the hapten density. Therefore, the molecular weight of the immunogen (**3**) was determined by MALDI (*38*) and found to be 68 618 Da, which represents an average of six haptens incorporated per BSA. The KLH-

Scheme 2

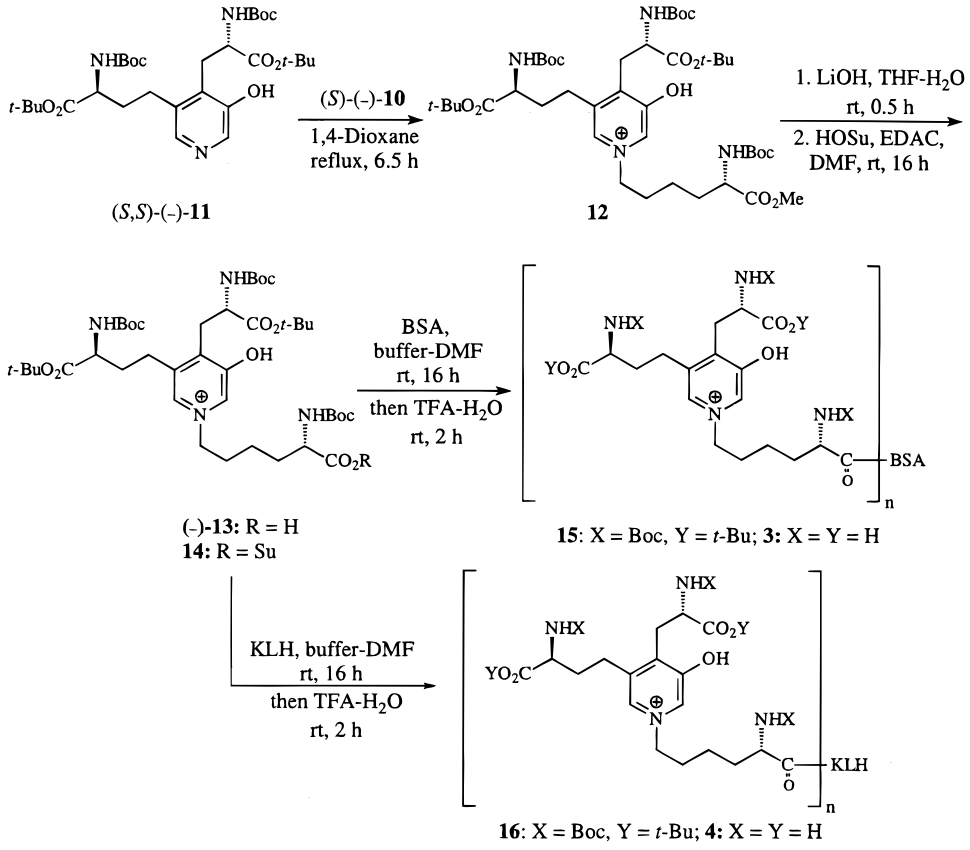

Scheme 3

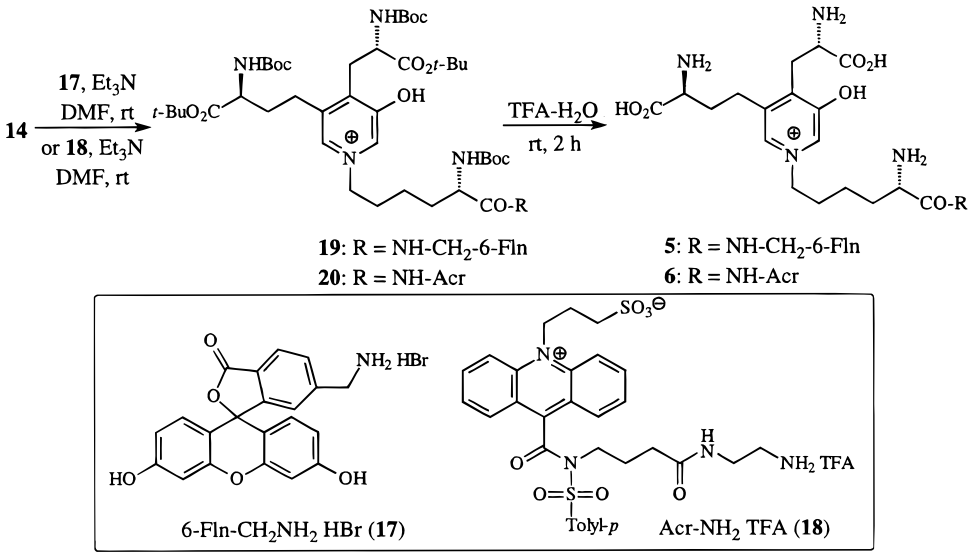

immunogen (**4**) was prepared from active ester (**14**) and KLH by following the procedure developed for BSA-immunogen (**3**).

To allow the tracer to mimic overall topology of the hapten, which was used to prepare the immunogen, the fluorescent and chemilumimescent labels were directly attached to hapten (−)-**13**. Thus, active ester **14** was treated (Scheme 3) with 6-aminomethyl fluorescein hydrobromide (6-Fln-CH_2NH_2, **17**) in DMF in the presence of triethylamine at room temperature to afford **19** in 38% yield. Hydrolysis of the Boc groups in **19** using trifluoroacetic acid and water and purification by HPLC afforded the fluorescent tracer [6-Fln-tracer (**5**)] in 70% yield and >99% purity as a pale yellow powder. Similarly, the active ester (**14**) was treated with acridinium derivative (Acr-NH_2 TFA, **18**) (*49*) and triethylamine in DMF at room temperature to afford **20** in 72% yield after purification by preparative HPLC. Finally, hydrolysis of **20** using trifluoroacetic acid and water followed by HPLC purification afforded the chemiluminescent tracer (Acr-tracer, **6**) in 77% yield and >99% purity as a pale yellow powder.

In summary, two immunogens [BSA-immunogen (**3**) and KLH-immunogen (**4**)] and two tracers [fluorescent (**5**) and chemiluminescent (**6**)] were prepared from succinimidyl ester (**14**). These immunoreagents (**3**,**4** and **5**,**6**)

are needed for generation of *anti*-Dpd antibodies and for development assays for diagnosis of osteoporosis.

LITERATURE CITED

(1) Sato, M., Grese, T. A., Dodge, J. A., Bryant, H. U., and Turner, C. H. (1999) Emerging therapies for the prevention or treatment of postmenopausal osteoporosis. *J. Med. Chem. 42*, 1−24.

(2) Bilezikian, J. P., Raisz, L. G., and Rodan, G. A. (1996) *Principles of Bone Biology*, Academic Press, New York.

(3) Hagiwara, S., Yang, S. O., Gluer, C. C., Bendavid, E., and Genant, H. K. (1994) Noninvasive bone mineral density measurement in the evaluation of osteoporosis. *Rheum. Dis. Clin. North. Am. 20*, 651−669.

(4) Genant, H. K., Lang, T. F., Engelke, K., Fuerst, T., Glüer, C., Majumdar, S., and Jergas, M. (1996) Advances in the noninvasive assessment of bone density, quality, and structure. *Calcif. Tissue Int. 59* (Suppl. 1), S10−S15.

(5) Eyre, D. R. (1996) Biochemical basis of collagen metabolites as bone turnover markers. *Principles of Bone Biology*, pp 143−153, Academic Press, New York.

(6) James, I. T., Walne, A. J., and Perrett, D. (1996) The measurement of pyridinium cross-links: A methodological overview. *Ann. Clin. Biochem. 33*, 397−420.

(7) Knott, L., and Bailey, A. J. (1998) Collagen cross-links in mineralizing tissues: a review of their chemistry, function, and clinical relevance. *Bone 22*, 181−187.

(8) Raisz, L. G. (1963) Stimulation of bone resorption by parathyroid hormone in tissue culture. *Nature 197*, 1015−1016.

(9) Raisz, L. G. (1965) Bone resorption in tissue culture. Factors influencing the response to parathyroid hormone. *J. Clin. Inv. 44*, 103−116.

(10) Weiss, P. H., and Klein, L. (1969) The quantitative relationship of urinary peptide hydroxyproline excretion to collagen degradation. *J. Clin. Inv. 48*, 1−10.

(11) Lippincott, S., Chesney, R. W., Friedman, A., Pityer, R., Barden, H., and Mazess, R. B. (1989) Rapid determination of total hydroxyproline (HYP) in human urine by HPLC analysis of the phenylisothiocyonate (PITC)-derivative. *Bone 10*, 265−268.

(12) Kadler, K. (1995) Extracellur matrix 1: Fibril-forming collagen. *Protein Profile 2*, 491−619.

(13) Fujimoto, D., Moriguchi, T., Ishida, T., and Hayashi, H. (1978) The structure of pyridinoline, A collgen cross-link. *Biochem. Biophys. Res. Commun. 84*, 52−57.

(14) Ogawa, T., Ono, T., Tsuda, M., and Kawanishi, Y. (1982) A novel fluor in insoluble collagen: A cross-linking moiety in collgen molecule. *Biochem. Biophys. Res. Commun. 107*, 1252−1257.

(15) Eyre, D. R., and Oguchi, H. (1980) The hydroxypyridinium cross-links of skeletal collagens: their measurement, properties and a proposed pathway of formation. *Biochem. Biophys. Res. Commun.* 92, 403−410.

(16) Gunja-Smith, Z., and Boucek, R. J. (1981) Collagen cross-linking compounds in urine. *Biochem. J. 197*, 759−762.

(17) Robins, S. P. (1983) Cross-linking of Collagen. Isolation, structural Characterization and glycosylation of pyridinoline *Biochem. J. 215*, 167−173.

(18) Hanson, D. A., and Eyre, D. R. (1996) Molecular site specificity of pyridinoline and pyrrole cross-links in type I collagen of human bone. *J. Biol. Chem. 271*, 26508−26516.

(19) Eyre, D. R., Paz, M. A., and Gallop, P. M. (1984) Cross-linking in collagen and elastin. *Annu. Rev. Biochem. 53*, 717−748.

(20) Siebel, M. J., Robins, S. P., and Bilezikian, J. P. (1992) Urinary pyridinium cross-links of collagen. Specific markers of bone resorption in metabolic bone disease. *Trends Endocrinol. Metab. 3*, 263−270.

(21) Fugimoto, D., Suziki, M., Uchiyama, A., Miyamoto, S., and Inoue, T. (1983) Analysis of pyridinoline, a cross-linking compound of collagen fibers in human urine. *J. Biochem. 94*, 1133−1136.

(22) Eyre, D. R., Koob, T. J., and Van Ness, K. P. (1984) Quantitation of hydroxypyridinium cross-links in collagen by high-performance liquid chromatography. *Anal. Biochem. 137*, 380−388.

(23) Black, D., Duncan, A., and Robins, S. A. (1988) Quantitative analysis of the pyridinium cross-links of collagen in urine using ion-paired reversed-phase high-performance liquid chromatography. *Anal. Biochem. 169*, 197−203.

(24) James, I. T., Perrett, D., and Thompson, P. W. (1990) Rapid assay for hard tissue collagen cross-links using isocratic ion-pair reversed-phase liquid chromatography. *J. Chromatogr. 525*, 43−57.

(25) Takahashi, M., Hoshino, H., Kushida, K., and Inoue, T. (1995) Direct measurement of cross-links, pyridinoline, deoxypyridinoline, and pentosidine, in the hydrolysate of tissues using high-performance liquid chromatography. *Anal. Biochem. 232*, 158−162.

(26) Pratt, D. A., Daniloff, Y., Duncan, A., and Robins, S. P. (1992) Automated analysis of the pyridinium cross-links of collagen in tissue and urine using solid-phase extraction and reversed-phase high-performance liquid chromatography. *Anal. Biochem. 207*, 168−175.

(27) Robins, S. P. (1982) An enzyme-linked immunoassay for the collagen cross-link pyridinoline. *Biochem. J. 207*, 617−620.

(28) Delmas, P. D., Gineyts, E., Bertholin, A., Garnero, P., and Marchand, F. (1993) Immunoassay of pyridinoline cross-link excretion in normal adults and in Paget's disease. *J. Bone Miner. Res. 8*, 643−648.

(29) Seyedin, S. M., Kung, V. T., Daniloff, Y. N., Hesley, R. P., Gomez, B., Nielsen, L. A., Rosen, H. N., and Zuk, R. F. (1993) Immunoassay for urinary pyridinoline: the new marker of bone resorption.. *J. Bone Miner. Res. 8*, 635−641.

(30) Gomez, B., Jr., Ardakani, S., Evans, B. J., Merrell, L. D., Jenkins, D. K., and Kung, V. T. (1996) Monoclonal antibody assay for free urinary pyridinium cross-links. *Clin. Chem. 42*, 1168−1175.

(31) Ureña, P., Ferreira, A., Kung, V. T., Morieux, C., Simon, P., Ang, K. S., Souberbielle, J. C., Segre, G. V., Drüeke, T. B., and De Vernejoul, M. C. (1995) Serum pyridinoline as a specific marker of collagen breakdown and bone metabolism in hemodialysis patients. *J. Bone Miner. Res. 10*, 932−939.

(32) Robins, S. P., Woitge, H., Hesley, R., Ju, J., Seyedin, S., and Seibel, M. J. (1994) Direct, enzyme-linked immunoassay for urinary deoxypyridinoline as a specific marker for measuring bone resorption.. *J. Bone Miner. Res. 9*, 1643−1649.

(33) Rosano, T. G., Peaston, R. T., Bone, H. G., Woitge, H. W., Francis, R. M., and Seibel, M. J. (1998) Urinary free deoxypyridinoline by chemiluminescence immunoassay: analytical and clinical evaluation. *Clin. Chem. 44*, 2126−2132.

(34) Sarno, M, Powel, H., Tjersland, G., Schoendorfer, D., Harris, H., Adams, K., Ogata, P., and Warnick, G. R. (1999) A collection method and high-sensitivity enzyme immunoassay for sweat pyridinoline and deoxypyridinoline cross-links. *Clin. Chem. 45*, 1501−1509.

(35) Waelchli, R., Beerli, Ch., Meigel, H., and Revesz, L. (1997) First total synthesis of the bone resorption markers deoxypyridinoline and hydroxypyridinoline. *Bioorg. Med. Chem. Lett. 7*, 2831−2836.

(36) Henry, C. (1996) FDA, reform, and the well characterized biologics. *Anal. Chem. 68*, 674A−677A.

(37) Van Weemen, K. K., and Schuurs, A. H. W. M. (1975) The influence heterologous combinations of antiserum and enzyme labeled estrogen on the characteristics of estrogen enzyme-immoassays. *Immunochemistry 12*, 667−670.

(38) Adamczyk, M., Buko, A., Chen, Y. Y., Fishpaugh, J. R., Gebler, J. C., and Johnson, D. D. (1994) Characterization of protein-hapten conjugates. 1. Matrix-assisted laser desorption ionization mass spectrometry of immuno BSA-hapten conjugates and comparison with other characterization methods. *Bioconjugate Chem. 5*, 631−635.

(39) Adamczyk, M., Fino, L., Fishpaugh, J. R., Johnson, and D. D. Mattingly, P. G. (1994) Immunoreagents for thyroid testing. 1. Synthesis of thyroxine conjugates. *Bioconjugate Chem. 5*, 459−462.

(40) Adamczyk, M., Fishpaugh, J. R., Heuser, K. J., Ramp, J. M., Reddy, R. E., and Wong, M. (1998) Synthesis of immunocomponents for the measurement of lead (Pb) by fluorescence polarization immunoassay. *Tetrahedron 54*, 3093−3112.

(41) Adamczyk, M., Johnson, D. D., and Reddy, R. E. (1999) Collagen cross-links: Synthesis of pyridinoline, deoxypyridinoline and their analogues. *Tetrahedron 55*, 63−88.

(42) Adamczyk, M., Johnson, D. D., and Reddy, R. E. (1999) Collagen cross-links: a convenient synthesis of *tert*-butyl-(2*S*)-2-[(*tert*-butoxycarbonyl)amino]-4-(2-oxiranyl)butanoate. *Tetrahedron: Asymmetry 10*, 775−781.

(43) Adamczyk, M., Akireddy, S. R, and Reddy, R. E. (1999) Versatile synthesis of (+)-deoxypyridinoline, a biochemical marker for diagnosis of osteoporosis. *Tetrahedron: Asymmetry 10*, 3107−3110.

(44) Sokoll, L. J., and Chan, D. W. (1999) Clinical analyzers. Immunoassays. *Anal. Chem. 71*, 356R−362R.

(45) Dandliker, W. B., Hsu, M.-L., and Vanderlaan, W. P. (1980) *Immunoassays: Clinical laboratory Techniques for the 1980* (Nakamura, R. M., Dito, W. R., and Tucker, E. S., Eds.) pp 89−126, Alan R. Liss, New York.

(46) Jandreski, M. A. (1998) Chemiluminescence Technology in immunoassays. *Lab. Med. 29*, 555−560.

(47) Wild, D. (1994) *The Immunoassay Handbook*, Stocton Press, New York.

(48) Kamps-Holtzapple, C., Carlin, R. J., Sheffield, C., Kubena, L., Stanker, L., and DeLoach, J. R. (1993) Analysis of hapten-carrier protein conjugates by nondenaturing gel electrophoresis. *J. Immunol. Meth*ods *164*, 245−253.

(49) Mattingly, P. G. (1991) Chemiluminescent 10-methylacridinium-9-(*N*-sulfonyl carboxamide)salts. Synthesis and kinetics of light emission. *J. Biolumin. Chemilumin. 6*, 107−114.

BC9900892

MARCH/APRIL 2000
Volume 11, Number 2

© *Copyright 2000 by the American Chemical Society*

Bioconjugate Chemistry

ARTICLES

Poly(ethylene glycol) Multiblock Copolymer as a Carrier of Anti-Cancer Drug Doxorubicin

Michal Pechar,* Karel Ulbrich, and Vladimír Šubr

Institute of Macromolecular Chemistry, Academy of Sciences of the Czech Republic, Heyrovský Square 2, 162 06 Prague 6, Czech Republic

Leonard W. Seymour

CRC Institute for Cancer Studies, University of Birmingham, B15 2TA, United Kingdom

Etienne H. Schacht

Laboratory of Organic Chemistry, State University of Ghent, Krijgslaan 281, B-9000, Belgium. Received June 28, 1999; Revised Manuscript Received November 1, 1999

The synthesis of a novel water-soluble polymer drug carrier system based on biodegradable poly(ethylene glycol) block copolymer is described in this paper. The copolymer consisting of PEG blocks of molecular weight 2000 linked by means of an oligopeptide with amino end groups was prepared by interfacial polycondensation of the diamine and PEG bis(succinimidyl carbonate). The structure of the oligopeptide diamine consisting of glutamic acid and lysine residues was designed as a substrate for cathepsin B, a lysosomal enzyme, which was assumed to be one of the enzymes responsible for the degradation of the polymer carrier in vivo. Each of the oligopeptide blocks incorporated in the carrier contained three carboxylic groups of which some were used for attachment of an anti-cancer drug, doxorubicin (Dox), via a tetrapeptide spacer Gly-Phe-Leu-Gly. This tetrapeptide spacer is susceptible to enzymatic hydrolysis. In vitro release of Dox and the degradation of the polymer chain by cathepsin B as well as preliminary evaluation of in vivo anti-cancer activity of the conjugate are also demonstrated.

INTRODUCTION

Water-soluble synthetic polymers conjugated with a desirable targeting moiety (e.g., an antibody) provide a drug delivery system capable of site-specific delivery. In recent years, such conjugates based on copolymers of *N*-(2-hydroxypropyl)methacrylamide (HPMA)[1] have been extensively studied as drug carriers facilitating site-specific delivery of immunosuppressants and anti-cancer drugs (*1*−*3*). In these conjugates, the nondegradable poly(HPMA) backbone is modified by biodegradable oligopeptide side chains that are terminated with targeting and/

* To whom correspondence should be addressed. E-mail: pechar@imc.cas.cz. Fax: +420 (2)367981.

10.1021/bc990092l CCC: $19.00 © 2000 American Chemical Society
Published on Web 02/15/2000

Scheme 1

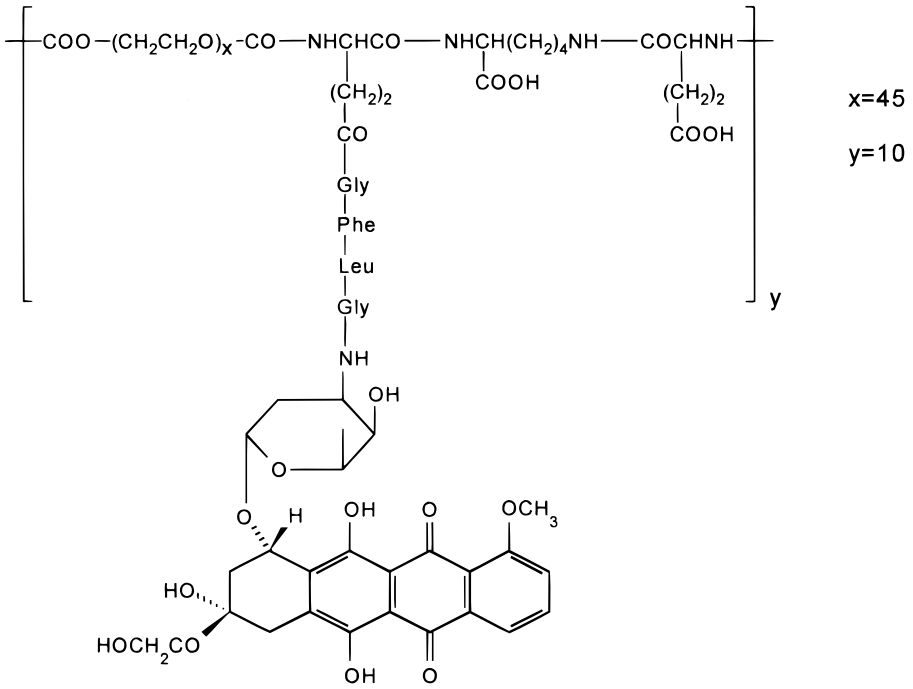

or drug moieties. The oligopeptide side chains are randomly distributed along the polymer chain and render controlled drug release.

Poly(ethylene glycol) has been the most frequently used hydrophilic polymer for protein modification. It has been found that "pegylated" proteins (enzymes, antibodies, etc.) are more resistant to proteolytic degradation than unmodified ones. They also exhibit much longer circulating times in blood and lower immunogenicity. In some cases, such a modification is necessary for their therapeutic application. Although there were many attempts to use PEG as a drug carrier, its application is rather limited as the molecule of PEG has only two potential binding sites situated at the ends of the polymer chain enabling attachment of only two drug molecules or one drug molecule and one targeting moiety per macromolecule. The molecular weight of some anti-cancer drugs (5-fluorouracil, doxorubicin) (*4*, *5*) modified with single PEG chain was probably still too low to slow their excretion from body and enhance their accumulation in tumors (EPR effect) (*6*), thus improving their therapeutic activity. Zalipsky et al. prepared (*7*) a high-molecular-weight multiblock copolymer PEG-lysine which they also used as a carrier of doxorubicin. Although they reported synthesis of a copolymer with M_w up to 100 000, the nondegradability of the urethane bonds between PEG and Lys residues by proteolytic enzymes still persists as a major drawback of the system.

To overcome this problem, we suggested a high-molecular-weight multiblock PEG-based drug carrier system where PEG blocks are connected by diamine oligopeptide linkages enabling attachment of two or three drug molecules to each repeating block. In our previous studies (*8*, *9*), we have described a model diblock copolymer consisting only of two PEG chains connected by one diamine linkage bearing 4-nitroaniline as a drug model. Using such a model system, we have verified both the degradability of the oligopeptide linkages between the PEG blocks and the possibility to release the drug model from the polymer incubated with lysosomal enzymes. The results of a drug model, 4-nitroaniline, release from polymer carriers based on PEG incubated in cathepsin B solutions, have shown that the relationship between the rate of release and the structure of the oligopeptide spacer is very similar to that found for the poly(HPMA)-based systems (*10*). The conjugates of poly(HPMA) containing doxorubicin linked to the polymer carrier with the oligopeptide spacer Gly-Phe-Leu-Gly exhibit high anti-cancer activity in vivo and are currently being clinically tested. The major drawback of poly(HPMA)-based drug carriers is their nondegradability under physiological conditions. That limits the use of such carriers only to molecular weights lower than renal threshold of the living body (50 000) ensuring safe elimination of the polymer from the organism after releasing the active compound from the carrier. On the contrary, only high-molecular-weight conjugates can be efficiently accumulated in many solid tumors due to the EPR (enhanced permeation and retention) effect (*6*). To obtain a high-molecular-weight carrier facilitating accumulation of drug in a tumor and elimination of the polymer after releasing the cytostatic drug, we have prepared anti-cancer polymer drug based on biodegradable block copolymers of PEG, analogous to poly(HPMA) conjugates, with cytostatic drug doxorubicin (Dox) attached via enzymatically degradable Gly-Phe-Leu-Gly spacer. (For structure, see Scheme 1.)

[1] Abbreviations: aq., aqueous; Boc, *tert*-butoxycarbonyl; Boc_2O, di-*tert*-butyl dicarbonate; Bz, benzyl; DCC, *N*,*N*′-dicyclohexylcarbodiimide; DCU, *N*,*N*′-dicyclohexylurea; DMAP, 4-(dimethylamino)pyridine; DMF, dimethylformamide; Dox, doxorubicin; FPLC, fast protein liquid chromatography; HOBt, 1-hydroxybenzotriazole; HOSu, *N*-hydroxysuccinimide; HPMA, *N*-(2-hydroxypropyl)methacrylamide; Me, methyl; M_n, number-average molecular weight; M_w, weight-average molecular weight; NAp, 4-nitroanilide group; NDA, naphthalene-2,3-dicarbaldehyde; Np, 4-nitrophenyl; OPA, phthaldialdehyde; OSu, *N*-succinimidyl; PEG, α-hydro-ω-hydroxypoly(oxyethylene); PEG-BSC, PEG bis-(*N*-succinimidyl) carbonate; TFA, trifluoroacetic acid; THF, tetrahydrofuran; Z, benzyloxycarbonyl.

EXPERIMENTAL SECTION

Doxorubicin hydrochloride was a kind gift from Dr. Suarato (Pharmitalia). PEG 2000, L-amino acids (if not stated otherwise), palladium catalyst, cathepsin B, and reagents for peptide synthesis were commercial products (Fluka AG, Switzerland). All other chemicals and solvents were of analytical grade. Solvents were purified and dried by standard procedures. The reagents were used without further purification. NMR spectra were recorded on a Bruker spectrometer (300 MHz, Switzerland). The block copolymers were characterized by size-exclusion chromatography on TSK columns 3000 and 4000 using 50% methanol as an eluent on FPLC system (Pharmacia, Sweden) calibrated with PEG standards. Amino acid analysis was performed by an amino acid analyzer (LDC Analytical) on a reversed-phase column Nucleosil 120-3 C_{18} (125 × 4 mm) (Macherey Nagel) with precolumn derivatization by NDA with 3-sulfanylpropanoic acid (excitation at 229 nm, emission at 490 nm) or OPA with 1-thio-β-D-glucose for determination of the optical purity of amino acids (λ_{exc} = 330 nm, λ_{em} = 420 nm) and using gradient elution from 35% to 100% of solvent B within 65 min and flow rate 0.5 mL/min (solvent A, 0.05 M sodium acetate buffer, pH 6.5; solvent B, 300 mL of 0.17 M sodium acetate and 700 mL of methanol) (*11*, *12*). Doxorubicin derivatives were analyzed by HPLC using Watrex reversed-phase column, Nucleosil C18, 250 × 4 mm, gradient MeOH-H_2O, 40−90% MeOH during 50 min, UV detector at 484 nm, fluorescence detector FluoroMonitor 4100, LDC Analytical (λ_{exc} = 490 nm, λ_{em} = 560 nm). Concentration of doxorubicin in the samples was determined by UV spectrophotometry at 484 nm (ϵ = 11 500 L mol^{-1} cm^{-1} in H_2O, 13 500 L mol^{-1} cm^{-1} in MeOH).

Preparation of Multiblock Copolymer poly[PEG-Glu-Lys-(-Glu)]. *PEG Bis(N-succinimidyl carbonate) (PEG-BSC) (**1**): Method A.* PEG 2000 (3.6 g, 1.8 mmol) azeotropically dried with toluene was dissolved in pyridine (20 mL) together with DMAP (88 mg, 0.72 mmol) and mixed with a solution of di-*N*-succinimidyl carbonate (1.8 g, 7.2 mmol) in acetonitrile (15 mL). The reaction mixture was protected from light at 25 °C for 12 h. The solvents were removed on a rotary evaporator, the residue was dissolved in ethyl acetate (50 mL, dried and distilled), at 50 °C, and the product was isolated by precipitation and filtration after addition of diethyl ether (50 mL) to the cooled ethyl acetate solution. This operation was repeated three times yielding 3.1 g of the active carbonate **1**.

Method B. PEG was activated by phosgene solution (20% in toluene) and the resulting chlorocarbonate derivative reacted with HOSu according to the literature (*13*).

*Poly[PEG-GluLysGlu(OBz)]—Interfacial Polycondensation (**2**).* Solution of PEG-BSC (1.3 g, 0.572 mmol) in dichloromethane (20 mL) was added to the mixture of tripeptide derivative **19** (0.516 g, 0.572 mmol) and sodium hydrogencarbonate (230 mg, 2.73 mmol) in water (20 mL) under vigorous stirring at 25 °C. The reaction mixture was acidified with 0.1 M HCl to pH 3 after 5 h of stirring. The organic layer was separated, washed with NaCl(aq) and dried over anhydrous Na_2SO_4. The drying agent was filtered, and the filtrate was concentrated to volume 10 mL. The precipitation of the polymer in diethyl ether failed (resulting in an oil layer). The solvent was removed under vacuum, and the residue was suspended in water (white emulsion) and freeze-dried. Yield: 1.1 g of polymer **2**.

Molecular weight of polymer strongly depends on reaction conditions (stirring speed, ratio of reactants, etc.). Usually M_w = 15000−30000.

*Poly[PEG-GluLysGlu(OH)]—Hydrogenation (**3**).* The polymer benzyl ester **2** (800 mg) was dissolved in ethanol (10 mL) with a drop of acetic acid and hydrogenated on a palladium catalyst (Pd/C, 10%) 3 h. The reaction mixture was bubbled with nitrogen, the catalyst was filtered, and ethanol was removed under vacuum. The residue was dissolved in water and freeze-dried yielding over 700 mg of hygroscopic polymer **3**.

Poly[PEG-GluLysGlu(ONp)] (**4**). The polymeric acid **3** (200 mg), 4-nitrophenol (100 mg), and DCC (140 mg) were dissolved in dichloromethane (2 mL) at 0 °C. A gel was formed almost immediately (probably due to the formation of acid anhydride linkages between COOH groups belonging to different polymer chains) but dissolved within 5 min. The reaction mixture was kept at 4 °C over the weekend. A drop of acetic acid was added and the precipitated DCU was filtered off 20 min later. The precipitation of the polymer in diethyl ether was unsuccessful (forming an oil). The solvents were evaporated and the polymer was purified (removal of 4-nitrophenol) by gel filtration (Sephadex LH20, dichloromethane). The polymer was isolated by freeze-drying from benzene resulting in a yellowish powder which "melts" when not kept under vacuum. Yield: 200 mg (90%) of the active ester **4**.

Preparation of Oligopeptide Derivatives. *HCl.Leu-Gly-OMe (**5**); HCl.Gly-Phe-OMe (**6**).* H-Leu-Gly-OH or H-Gly-Phe-OH were converted to the corresponding methyl esters by refluxing in dry MeOH with thionyl chloride (*14*). HCl·Gly-Phe-OMe was recrystallized from methanol-diethyl ether. HCl·Leu-Gly-OMe was obtained in crystalline form by trituration of an oily crude product with diethyl ether.

*Tr-Gly-Phe-OMe (**7**).* H-Gly-Phe-OMe·HCl (3.0 g, 11 mmol) was suspended in dry $CHCl_3$ (25 mL). Triethylamine (2.3 g, 22.7 mmol) was added, and the solid dissolved. Trityl chloride (3.1 g, 11.1 mmol) was added, and reaction mixture was left standing at 25 °C for 2 h. Chloroform was evaporated, and the oily residue was diluted with ethyl acetate (60 mL). Triethylamine hydrochloride precipitate was filtered off, and the filtrate was washed with water (2 × 20 mL) and dried over $MgSO_4$. Ethyl acetate was taken off, and the product was recrystallized from isopropyl alcohol-hexane. Yield was 4.5 g (9.4 mmol, 85%) of white crystalline product, mp 154−156 °C. TLC: R_f = 0.92 (silica gel, ethyl acetate).

*Tr-Gly-Phe-OH (**8**).* Tr-Gly-Phe-OMe (3.0 g, 6.27 mmol) was dissolved in dioxane (25 mL) and KOH(aq) (6.3 mL, 1 mol L^{-1}) was added. The reaction mixture was stirred at 45 °C for 1 h and then evaporated to dryness under reduced pressure. The crude product was dissolved in water (20 mL) and ethyl acetate was added followed by dilute acetic acid (20%). The free acid dipeptide derivative was taken up to ethyl acetate (3 × 20 mL), and collected organic extracts were dried over $MgSO_4$. White crystalline solid (2.8 g, 6.03 mmol, 96%) was obtained after filtration, concentration under vacuum, and trituration with hexane. TLC: R_f = 0.75 (silica gel, ethyl acetate).

*Tr-Gly-DL-Phe-Leu-Gly-OMe (diastereomeric mixture, **9a**, **b**).* A solution of Tr-Gly-Phe-OH (2.8 g, 6.03 mmol) in THF (20 mL) was mixed with HCl·Leu-Gly-OMe (1.44 g, 6.08 mmol) and triethylamine (0.61 g, 6.03 mmol). A solution of DCC (1.5 g, 7.27 mmol) in THF (10 mL) was added with stirring at −5 °C. After 48 h at 4 °C, the

precipitated DCU was filtered off and the solution was concentrated under vacuum to give a viscous oily residue. The crude product was redissolved in ethyl acetate (30 mL), washed with water (3 × 20 mL), dried over $MgSO_4$ and finally purified by column chromatography (silica gel, ethyl acetate). The unreacted Tr-Gly-Phe-OMe was eluted first followed by the desired product. Yield after crystallization from ethyl acetate−hexane 2.65 g (4.08 mmol, 68%) of white crystalline solid, mp >90 °C (decomp.). TLC: R_f = 0.55 (silica gel, ethyl acetate) (L-Phe/D-Phe, 1:1).

*Tr-Gly-L-Phe-L-Leu-Gly-OMe (**9a**).* A solution of Tr-Gly-Phe-OH (0.89 g, 1.92 mmol), HCl·Leu-Gly-OMe (0.46 g, 1.93 mmol), HOBt (0.30 g, 1.93 mmol) in DMF (8 mL) was mixed with a solution of DCC (0.40 g, 1.93 mmol) in DMF (1 mL) at 0 °C followed by triethylamine (0.27 mL, 1.93 mmol). After 48 h at 4 °C, the precipitated DCU was filtered off and the solution was concentrated under vacuum to give a viscous oily residue. The crude product was redissolved in ethyl acetate (30 mL). The solution was washed with aq. solutions of $NaHCO_3$ and NaCl, dried over Na_2SO_4, filtered, and concentrated under vacuum. Yield after crystallization from ethyl acetate−hexane was 0.40 g (0.62 mmol, 33%) of pure L-Phe isomer, mp 172−175 °C. TLC: R_f = 0.55 (silica gel, ethyl acetate).

*Tr-Gly-D-Phe-L-Leu-Gly-OMe (**9b**).* was synthesized in the same way as the L-Phe isomer starting with D-phenylalanine.

*Tr-Gly-DL-Phe-Leu-Gly-OH (diastereomeric mixture, **10a**−**b**).* Tr-Gly-DL-Phe-Leu-Gly-OMe (2.65 g, 4.08 mmol) was dissolved in dioxane (20 mL) and mixed with a KOH solution in dry methanol (4.2 mL, 1 mol L^{-1}). After 1 h at 50 °C, the solvent was taken off under reduced pressure, and the residue was redissolved in water (20 mL). The solution was covered with an ethyl acetate layer and acidified with dilute acetic acid (5%). The free acid was extracted with ethyl acetate (3 × 20 mL). The collected organic layers were washed with NaCl(aq), dried over $MgSO_4$, and filtered. The tetrapeptide derivative was crystallized from ethyl acetate-diethyl ether yielding 2.4 g (3.78 mmol, 93%) of white crystalline solid, mp 194−196 °C. (L-Phe/D-Phe, 1:1).

Tr-Gly-D-Phe-L-Leu-Gly-OH (**10b**) was obtained by repeated crystallization of the diastereomeric mixture from ethyl acetate- diethyl ether−hexane (D-isomer/L-isomer 95:5 after two crystallizations) as the less soluble isomer.

Tr-Gly-L-Phe-L-Leu-Gly-OH (**10a**) was isolated from the mother liquid of the above-described crystallization by precipitation with hexane (L/D, 90:10). The other method of the preparation of the tritylated tetrapeptide acids is based on the hydrolysis of the corresponding optically pure methyl esters as described for the diastereomeric mixture.

Tr-Gly-L-Phe-Leu-Gly-OSu (**11a**); *Tr-Gly-D-Phe-Leu-Gly-OSu* (**11b**). Tr-Gly-Phe-Leu-Gly-OH (0.5 g, 0.788 mmol), HOSu (0.1 g, 0.869 mmol), and DCC (0.2 g, 0.969 mmol) were dissolved in THF (8 mL) at 0 °C and kept at 4 °C overnight. Acetic acid (10 μL) was added and the precipitated DCU was filtered 30 min later. The solvent was removed under reduced pressure, and the crude product was crystallized from isopropyl alcohol-ether yielding 0.32 g (0.437 mmol, 55%) of the active ester. Mp 109−113 °C for L-Phe, 118−120 °C for D-Phe.

Tr-Gly-L-Phe-Leu-Gly-Dox (**12a**); *Tr-Gly-D-Phe-Leu-Gly-Dox* (**12b**). Dox·HCl (95 mg, 0.164 mmol) was dissolved in DMF (1.5 mL, freshly distilled from P_2O_5), and active ester **11a** or **11b** (120 mg, 0.164 mmol) in DMF (1.3 mL) was added followed by triethylamine (23 μL, 0.164 mmol) with stirring at 25 °C. The progress of the reaction was monitored by TLC (silica gel, chloroform−methanol−water, 120:20:1). Two diastereoisomers containing L-Phe and D-Phe residues (R_f = 0.66 and R_f = 0.63, respectively) were detected as red spots in visible light. After 24 h at room temperature, the solvent was evaporated to dryness, and the crude product was chromatographed on silica gel using chloroform−methanol (95:5) as an eluent. The fraction containing the diastereomeric mixture was evaporated to dryness and triturated with ether to yield 144 mg (0.124 mmol, 76%) of a red solid.

*H-Gly-L-Phe-Leu-Gly-DOX·CH_3COOH (**13a**); H-Gly-D-Phe-Leu-Gly-DOX·CH_3COOH (**13b**).* Trityl derivative **12a** or **12b** (140 mg, 0.121 mmol) was suspended in 75% acetic acid (2.8 mL, 35 mmol) and stirred at room temperature for 1 h. Any solid part was removed by centrifugation, and the supernatant was evaporated to dryness. The product was redissolved in water and freeze-dried yielding 65 mg (0.068 mmol, 57%) of the title acetate salt. The purity of the title compounds was determined by HPLC, indicating less than 5% of the undesired diastereoisomer, in accord with the amino acid analysis. The configuration of the amino acid residues was determined by HPLC of the hydrolyzed product.

Boc-Gly-Phe-OH (**14**) was prepared as described previously (*9*).

*Boc-Gly-Phe-Leu-Gly-OMe (**15**).* Boc-Gly-Phe-OH (2.92 g, 9.05 mmol), HCl·H-Leu-Gly-OMe (2.14 g, 9.05 mmol), HOBt (1.67 g, 10.9 mmol), and triethylamine (1.38 mL, 9.9 mmol) were dissolved in DMF (30 mL), and DCC (2.25 g, 10.9 mmol) was added with stirring at 0 °C. The progress of the reaction was checked by TLC (silica gel, ethyl acetate, R_f = 0.52). After 2 h at 0 °C and 20 h at 25 °C, the precipitated DCU was filtered off, the solvent was evaporated under vacuum and the oily residue was dissolved in ethyl acetate. The solution was filtered again and washed with $NaHCO_3$(aq), citric acid(aq), again $NaHCO_3$(aq), and NaCl(aq), and dried over Na_2SO_4. Then it was filtered and concentrated on rotavapor yielding 2.56 g (5.07 mmol, 56%) of white crystalline solid melting at 172−174 °C. Anal. ($C_{25}H_{38}N_4O_7$) C, H, N.

^{1}H NMR [$(CD_3)_2SO$]: δ 0.80 two d, 6H (CH_3-Leu); 1.31 s, 9H (Boc); 1.35−1.70 m, 3H ($CHCH_2$-Leu); 2.70 dd, 1H (CH_2-Phe); 2.95 dd, 1H (CH_2-Phe); 3.35−3.45 m, 2H (CH_2-N-Boc-Gly); 3.55 s, 3H (OCH_3); 3.75 t, 2H (Gly-OCH_3); 4.25 m, 1H (α-Leu); 4.50 m, 1H (α-Phe); 6.85 t, 1H (NH-Boc); 7.15 m, 5H (arom.); 7.80 d, 1H (NH); 8.10 d, 1H (NH); 8.20 t, 1H (NH).

^{13}C NMR [$(CD_3)_2SO$]: δ 19.71 (CH_3-Leu); 20.92 (CH_3-Leu); 22.04 (CH-Leu); 22.45 (CH_2-Leu); 26.16 (Boc); 31.35 (CH_2-Phe); 35.58 (CH_2-N-Boc-Gly); 41.19 (Gly-OCH_3); 48.82 (α-Leu); 49.64 (OCH_3); 51.52 (α-Phe); 76.07 (C-Boc); 124.19 (arom.); 125.97 (arom.); 127.27 (arom.); 135.55 (C-quart. arom.); 153.72 (OCONH); 167.12 (CO); 168.11 (CO); 168.60 (CO); 170.32 (CO).

H-Gly-L-Phe-Leu-Gly-OMe·TFA (**16a**). The corresponding N-Boc derivative **15** (0.5 g) was dissolved in neat TFA (5 mL). TFA was evaporated under vacuum after 1 h at 25 °C and a white crystalline product was obtained by trituration with diethyl ether in almost quantitative yield. Mp 160−162 °C.

Z-Gly-D-Phe-$NHNH_2$ (**17**) was prepared by hydrazinolysis of the corresponding methyl ester in methanol according to literature (*15*). The protected dipeptide hydrazide was recrystalized from methanol. Mp 104−105 °C. Anal. ($C_{19}H_{22}N_4O_4$·CH_3OH) calcd: C, 59.69; H, 6.52; N, 13.93. Found: C, 60.70; H, 6.36; N, 14.09.

*Z-Gly-D-Phe-Leu-Gly-OMe (**18**).* *Z*-Gly-D-Phe-$NHNH_2$ (1.7 g, 4.59 mmol) was dissolved in freshly distilled DMF (15 mL), the solution was cooled to −10 °C, and HCl (aq) (4 mol L^{-1}, 4.6 mL, 18.4 mmol) was added followed by $NaNO_2$ (aq) (397 mg in 0.7 mL, 5.75 mmol). Triethylamine (1.77 mL, 12.65 mmol) was added 5 min later, the reaction mixture was briefly dried with Na_2SO_4 and filtered directly to a solution of H-Leu-Gly-OCH_3·HCl (1.1 g, 4.59 mmol) and triethylamine (1.28 mL, 9.2 mmol) in 25 mL of DMF at −10 °C. The reaction was stirred for 2 h under cooling and then let warm to room temperature. The precipitated triethylamine hydrochloride was filtered off, the solvent was evaporated under vacuum, and the residue was dissolved in ethyl acetate (50 mL). The solution was washed with $NaHCO_3$(aq), $KHSO_4$, again $NaHCO_3$ (aq) and NaCl (aq). Then it was filtered and concentrated to crystallization to yield 1.19 g (2.2 mmol, 48%) of white crystalline solid, mp 138−139 °C. The content of the L-Phe isomer was <1% (by amino acid analysis). Anal. ($C_{28}H_{36}N_4O_7$) calcd: C, 62.21; H, 6.72; N, 10.37. Found: C, 61.78; H, 6.76; N, 9.99. TLC (silica gel, ethyl acetate, $R_f = 0.39$).

^{1}H NMR [$(CD_3)_2SO$]: δ 0.68 d, 3H (CH_3-Leu); 0.74 d, 3H (CH_3-Leu); 1.20−1.40 m, 3H ($CHCH_2$-Leu); 2.78 dd, 1H (CH_2-Phe); 2.87 dd, 1H (CH_2-Phe); 3.54 m, 2H (CH_2-N-Boc-Gly); 3.55 s, 3H (OCH_3); 3.75 d, 2H (CH_2-Gly-OMe); 4.18 m, 1H (α-Leu); 4.51 m, 1H (α-Phe); 4.96 s, 2H (CH_2-Ph); 7.17 m, 5H (arom.); 7.28 m, 5H (arom.); 7.30 t, 1H (NH-Gly-OMe); 8.05 d, 1H (NH-Phe); 8.22 d, 1H (NH-Leu); 8.23 t, 1H (OCONH).

^{13}C NMR [$(CD_3)_2SO$]: δ 19.32 (CH_3-Leu); 21.07 (CH_3-Leu); 21.79 (CH-Leu); 35.84 (CH_2-Phe); 38.50 (Gly-OCH_3); 38.60 (CH_2-Leu); 41.29 (CH_2-N-Boc-Gly); 48.72 (α-Leu); 49.63 (OCH_3); 52.12 (α-Phe); 63.45 (OCH_2Ph); 124.25 (arom., Phe-4); 125.66 (arom.); 125.76 (arom., Z-4); 126.00 (arom.); 126.32 (arom.); 127.19 (arom.); 135.01 (arom., Phe-1); 135.26 (arom., Z-1); 154.47 (OCONH); 166.95 (CO-Boc-Gly); 168.10 (COOMe); 168.66 (CO-Leu); 170.48 (CO-Phe).

*H-Gly-D-Phe-Leu-Gly-OMe (**16b**).* *Z*-Gly-D-Phe-Leu-Gly-OMe (270 mg, 0.5 mmol) was dissolved in ethanol (3 mL) with cyclohexa-1,4-diene (0.5 mL, 5 mmol). The solution was bubbled with nitrogen, palladium catalyst (10% on active carbon) was added, and the reaction mixture was stirred under nitrogen overnight. The catalyst was filtered off, and the filtrate was evaporated to dryness. The amorphous residue was triturated with diethyl ether to yield 110 mg (0.27 mmol, 54%) of white crystalline product with mp 98−102 °C. Anal. ($C_{20}H_{30}N_4O_5$) calcd: C, 59.09; H, 7.45; N, 13.78. Found: C, 57.91; H, 7.32; N, 13.15.

^{1}H NMR [$(CD_3)_2SO$]: δ 0.68 d, 3H (CH_3-Leu); 0.74 d, 3H (CH_3-Leu); 1.20−1.40 m, 3H ($CHCH_2$-Leu); 2.83 m, 2H (CH_2-Phe); 3.35 m, 2H (CH_2-Gly); 3.55 s, 3H (OCH_3); 3.75 m, 2H (CH_2-Gly-OMe); 4.17 m, 1H (α-Leu); 4.54 m, 1H (α-Phe); 7.16 m, 5H (arom.); 8.01 br, 1H (NH-Leu); 8.24 d, 1H (NH-Phe); 8.29 t, 1H (NH-Gly-OMe).

Preparation of Diamine Linker "GluLysGlu". *N,N′-Bis(-benzyl glutamyl)lysine benzyl ester bis(trifluoroacetate)* (**19**) was prepared as described previously (*8*).

Preparation of Polymer Conjugates of DOX. *Poly[PEG-GluLysGlu(Gly-Phe-Leu-Gly-OMe)] (**20a** and **20b**; L-Phe and D-Phe derivatives, respectively).* Polymer acid **3** (0.5 g, 6×10^{-4} mol of COOH groups), tetrapeptide derivative **16a** (100 mg, 2×10^{-4} mol) or **16b** (81 mg, 2×10^{-4} mol), HOBt (153 mg, 1 mmol), triethylamine (140 μL, 1 mmol), and DCC (206 mg, 1 mmol) were dissolved in DMF (3 mL) at 0 °C and left at 4 °C over weekend. Dilute acetic acid (50%, 0.2 mL) was added to the reaction, and the precipitated DCU was filtered off 20 min later. DMF was removed under reduced pressure, and the residue was dissolved in chloroform. The organic solution was washed with NaCl (pH 2 adjusted with HCl), dried over Na_2SO_4, filtered, evaporated to dryness and the residue was chromatographed on Sephadex LH 60 in methanol (RI detector). The high-molecular-weight fraction was collected and used for the subsequent reaction. Yield: 254 mg of white polymer methyl ester **20a** or **20b**. Coupling efficacy calculated from the results of amino acid analysis was 75% of the starting tetrapeptide derivative.

*Poly[PEG-GluLysGlu(Gly-Phe-Leu-Gly-$NHNH_2$)] (**21a** and **21b**; L-Phe and D-Phe derivatives, respectively).* The polymer methyl ester **20a** or **20b** (0.25 g, 86×10^{-6} mol of COOMe) and hydrazine hydrate (0.1 mL, 2.86×10^{-3} mol) were dissolved in absolute methanol (2.5 mL). After 2 days at 25 °C, the solvent was taken off under reduced pressure, and the residue was freeze-dried from water solution yielding 240 mg of the polymer hydrazide **21a** or **21b**.

*Poly[PEG-GluLysGlu(Gly-Phe-Leu-Gly-DOX)] (**22a** and **22b**; L-Phe and D-Phe derivatives, respectively; polymer **22** prepared from 1:1 diastereomeric mixture of **13a** and **13b**). Method A.* Polymer hydrazide **21a** or **21b** (0.1 g, 36×10^{-6} mol of $-NHNH_2$) and diluted HCl (4 M, 60 μL) were dissolved in DMF (0.7 mL), and $NaNO_2$ (aq) (5 M, 40 μL) with 0.2 mL of DMF was added at 0 °C with stirring. Triethylamine (50 μL, 0.36 mmol) and anhydrous Na_2SO_4 (200 mg) were added about 5 min later followed by Dox·HCl (20 mg, 35 μmol) again after 5 min. The reaction mixture was kept 30 min at 0 °C with stirring, then placed to 4 °C overnight. Any insoluble material was removed by filtration, the solvent was evaporated under reduced pressure, and the residue was purified by gel filtration. After chromatography on PD10 columns (Pharmacia, Sephadex G25) in water, some low-molecular-weight derivatives of doxorubicin were found by analytical HPLC in MeOH, which were completely removed by chromatography on Sephadex LH20 in MeOH. Yield: 98 mg of very hygroscopic red polymer **22a** or **22b**. Content of polymer-bound doxorubicin was 6.0%w/w (10 μmol, 30% of starting Dox).

Method B. Polymeric acid **3** (80 mg, 87×10^{-6} mol of COOH groups), tetrapeptide derivative of Dox **13a** or **13b** (28 mg, 29×10^{-6} mol), HOBt (44 mg, 0.29 mmol), triethylamine (4 μL, 29×10^{-6} mol), and DCC (60 mg, 0.29 mmol) were dissolved in DMF (2.5 mL) at 0 °C and left at 4 °C overnight. Dilute acetic acid (50%, 0.1 mL) was added to the reaction and the precipitated DCU was filtered off 2 h later. DMF was removed under reduced pressure, the residue was dissolved in MeOH (5 mL), and the remaining DCU was filtered off. The residue was chromatographed on Sephadex LH20 in MeOH. The high-molecular-weight fraction was collected and freeze-dried yielding 82 mg of the polymer **22a**, **22b**, or **22** with 6.5% w/w of Dox. $M_w = 29\,000$ and $M_w/M_n = 3.3$ were determined by FPLC. The amino acid analysis of the hydrolyzed product **22** found molar ratio Gly:L-Phe:D-Phe:L-Leu = 2:0.5:0.5:1. Polymer **22** was used for the in vitro and in vivo experiments described below.

Enzymatic Hydrolysis of the Polymer Substrate (Figure 1). Enzymatic degradation of the polymer **22** (prepared by method B) by cathepsin B was performed according to the previously published procedure (*9*) (0.05 M phosphate buffer, 0.001 M EDTA, pH 6.0, 37 °C, 0.005 M glutathione), increasing the concentration of the active sites of cathepsin B to 4×10^{-7} M due to the slow rate of the enzymatic reaction. Both the release of Dox and the

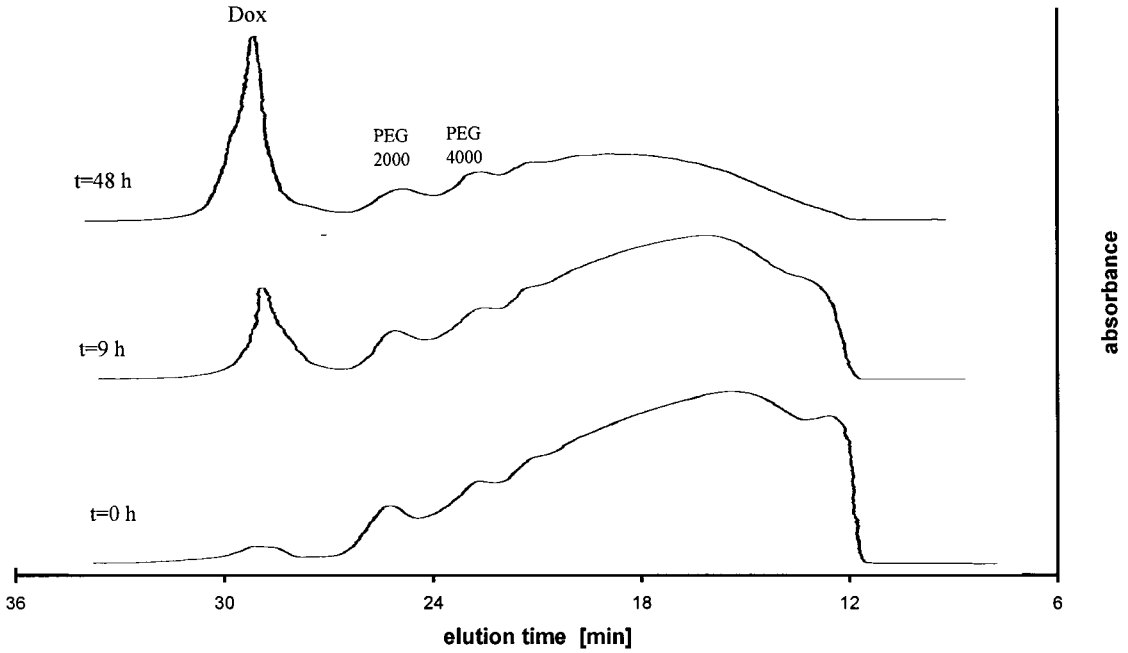

Figure 1. GPC records of degradation products of polymer **22** incubated with cathepsin B (0, 9, and 48 h after the addition of the enzyme) [E] = 4×10^{-7} M, [Dox] = 0.001 M, [polymer] = 21 mg/mL, 0.05 M phosphate buffer, pH 6.0, 37 °C, column TSK 3000, 50% MeOH, 0.1% TFA, UV 480 nm.

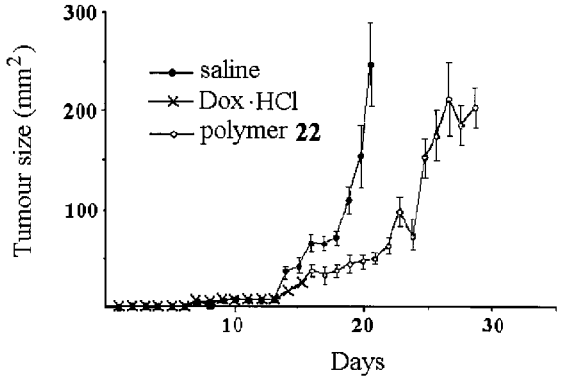

Figure 2. Anti-cancer activity of free and polymer-bound doxorubicin 5 BALB/C female mice were injected i.v. on 3 consecutive days (9, 10, and 11). One dose was 100 μL of a drug solution in saline of concentration 1 mg/mL, i.e., 5 mg/kg calculated for content of Dox·HCl. The mice were bearing s.c. murine colorectal carcinoma C26 injected 8 days earlier.

degradation of the block copolymer were monitored by FPLC (column TSK 3000, 50% MeOH, 0.1% TFA, UV detector, 484 nm, RI detector).

In Vivo Evaluation (Figure 2). Polymer **22** (prepared by method B), Dox·HCl, and physiological saline were injected each to groups of five BALB/C female mice i.v. on three consecutive days (9, 10, and 11). One dose was 100 μL of the drug solution in saline of concentration 1 mg/mL, i.e., equivalent to 5 mg/kg of Dox·HCl. The mice were bearing s.c. murine colorectal carcinoma C26 injected 8 days earlier. Solid tumors were just palpable at the start of the drug administration.

RESULTS AND DISCUSSION

Synthesis of the Block Copolymer. The alternating copolymer of PEG and the oligopeptide-based diamine linker Glu-Lys(-Glu) was prepared by interfacial polycondensation (dichloromethane-water) of the activated bifunctional PEG 2000 (PEG-BSC) **1** and oligopeptide **19** protected by benzyl ester moieties (Scheme 2). The polycondensation was carried out according to the method of Zalipsky and co-workers (*7*, *16*) who described synthesis of analogous copolymer based on ethyl lysinate and PEG. Nevertheless, the molecular weight of the resulting copolymers (M_w = 50 000) prepared with our tripeptide diamine linker was lower than the molecular weight of those described in the literature (M_w = 100 000). That is quite obvious if all the many factors influencing the course of the polycondensation reaction are taken into account. The most important of them are the solubility of reacting components in both phases, the yield of substitution of PEG derivative, and its hydrolytic stability, reactivity of the functional groups, presence of impurities, etc. For GPC, see Figure 1 (t = 0); no significant change was observed before and after drug attachment.

The block copolymer **2** was hydrogenated on palladium catalyst to remove the protecting benzyl ester groups, and the resulting copolymer with three carboxyls in each repeating block was used for the attachment of the oligopeptide spacer and doxorubicin. FPLC of the polymers confirmed that there were no changes in molecular weight and its distribution during the modification reactions (deprotection, binding of spacer and drug, etc.). The polycarboxylic acid **3** can be further converted to the corresponding active 4-nitrophenyl ester **4**. This reaction step is not necessary for subsequent coupling with spacer and drug but results in a convenient precursor for further modification with a targeting moiety (antibody or its fragments, lectins, etc.) in aq. media.

Attachment of the Drug to the Polymer Carrier. The covalent attachment of doxorubicin to the polymer carrier was performed by two different synthetic routes, both leading to the same final structure with the amide bond between the drug moiety and the tetrapeptide spacer. The first method involves quite elaborate and expensive synthesis of the Gly-Phe-Leu-Gly-Dox derivative and its conjugation with the polymer carrier, the other is based on the azide procedure commonly used in peptide synthesis. In the latter case, free doxorubicin can

Scheme 2

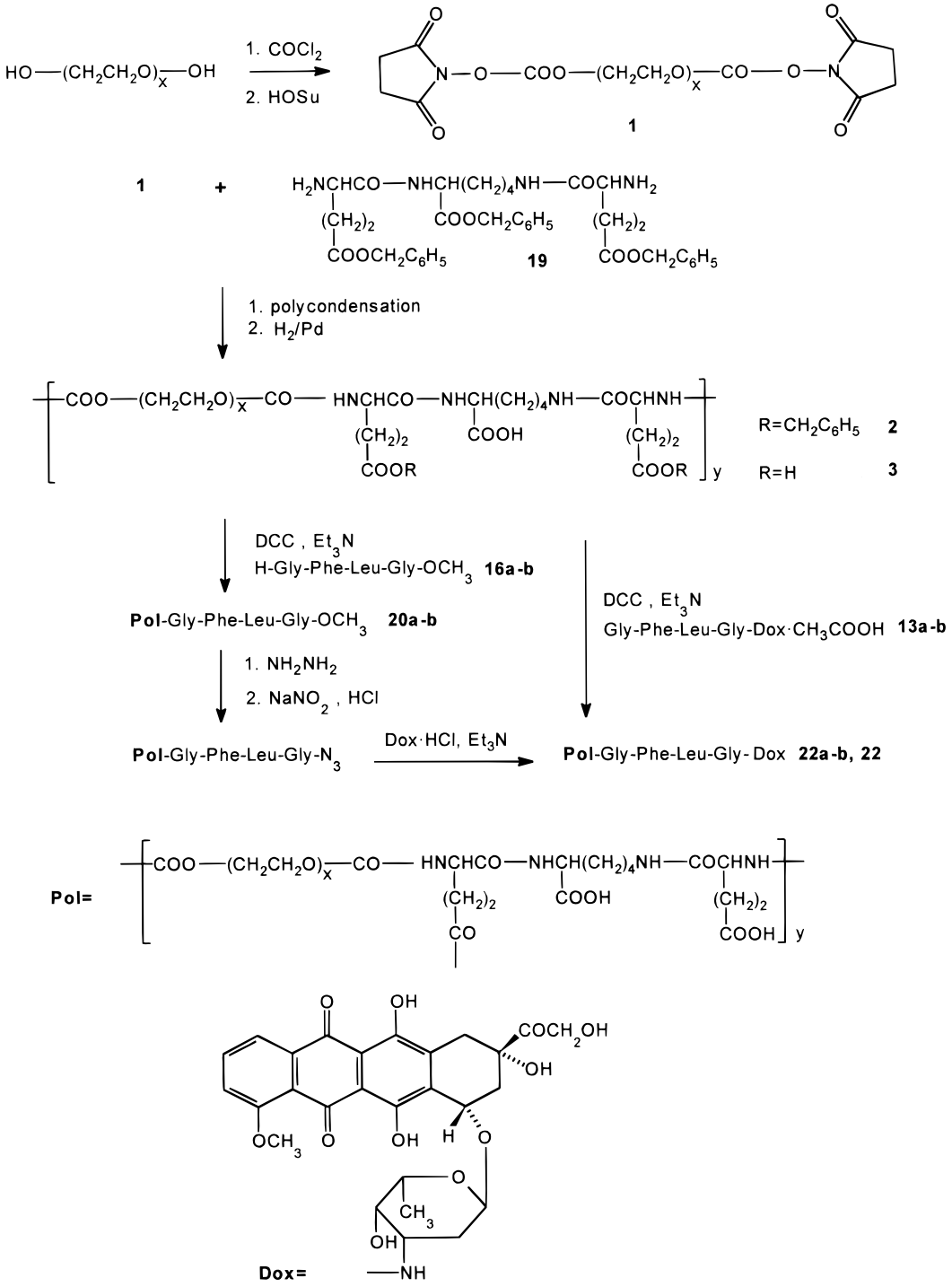

be directly coupled with the reactive copolymer-tetrapeptide precursor.

The first route leading to the suggested polymer drug consists of synthesis of the tetrapeptide derivative H-Gly-Phe-Leu-Gly-Dox and its covalent binding to the carboxylic groups of the polymer carrier via amide bond. The synthesis started from the methyl esters H-Leu-Gly-OMe and H-Gly-Phe-OMe. The latter reacted with triphenylmethyl (trityl) chloride yielding the corresponding N-trityl derivative, which was converted to the free acid by alkaline hydrolysis. Tr-Gly-Phe-OH was coupled with H-Leu-Gly-OMe in the presence of DCC to yield protected tetrapeptide Tr-Gly-Phe-Leu-Gly-OMe. Most probably, racemization of the phenylalanine residue occurred in this step if no HOBt was added to the reaction as determined by amino acid analysis. The methyl ester was hydrolyzed to the free carboxylic acid, which was converted to the active succinimidyl ester used for the acylation of the primary amino group of doxorubicin. The resulting tetrapeptide derivative Tr-Gly-Phe-Leu-Gly-DOX gave two spots on TLC plate when a diastereomeric mixture was used for the acylation. The two diastereoisomers of the tritylated tetrapeptide-Dox derivative could be partially separated by column chromatography on silica gel. The protecting trityl group was removed by reaction with dilute acetic acid, and the desired H-Gly-Phe-Leu-Gly-Dox was bound to the pendant carboxylic groups (Glu and Lys residues) of the polymer carrier.

The described synthetic route requires a quite difficult and time-consuming preparation of the tetrapeptide

derivative of doxorubicin. Therefore, we have tried another strategy based on the well-known azide procedure. Methyl ester of the tetrapeptide was prepared and coupled with the free carboxylic groups of the block copolymer precursor. The resulting polymer methyl ester was converted to hydrazide by reaction with hydrazine, and the hydrazide was transformed to the active polymer azide by reaction of the hydrazide moiety with nitrous acid. The azide was then used in the reaction of the polymer with the primary amino group of doxorubicin. The major advantage of this synthetic pathway is that we work with the expensive drug only in the last reaction step compared with the three steps of the other method.

Biological evaluation of poly(HPMA)-Dox conjugates have shown the highest anti-tumor activity (both in vitro and in vivo experiments) when the D/L ratio of Phe residues in the tetrapeptide spacer was 1:1. (Diastereomeric mixture of the tetrapeptide precursor was used in the synthesis.) Although this interesting effect has not been yet fully explained, the use of the diastereomeric mixture in the synthesis of doxorubicin conjugates with PEG block copolymers is quite acceptable. The influence of the Phe configuration on the biological activity of the PEG-based polymer anticancer drug is being investigated at present and the corresponding polymer conjugates with doxorubicin are under biological evaluation. We have found that the biodegradability of the spacer and the drug release is a prerequisite for the biological activity in vivo, but the higher rate of enzymatic release (L-Phe > DL-Phe > D-Phe in the tetrapeptide spacer) of the drug from the polymer carrier in vitro does not necessarily mean a better anti-cancer activity in vivo as we discovered (*17*) using the poly(HPMA)-based doxorubicin conjugates.

Enzymatic Degradation of the Polymer Drug. It was reported (*6*) that high-molecular weight polymers are predominantly accumulated in solid tumors (EPR effect). The degradability of the polymer drug carrier is a prerequisite for its therapeutic application if the polymer molecular weight exceeds the renal threshold (approx. 50 000). The incubation of the polymer substrate **22** with lysosomal enzyme cathepsin B (Figure 1) resulted both in the splitting of the diamine linkages between the PEG blocks and in the release of doxorubicin. Both RI and UV detectors gave almost the same GPC profiles after injection of the polymer **22** incubated with cathepsin B. The chromatograms obtained from both detectors were completely superimposable except for the low-molecular-weight region where only UV detector at 484 nm indicated the amount of the drug (or its low-molecular-weight derivatives) released by the enzymatic reaction. (The response of the RI detector in this region is overlapped by solvent signal, so-called "buffer peak"). No degradation was observed in the case of a control sample incubated in physiological saline under the same conditions. About 30% of the total amount of the drug was released within 48 h of incubation with the enzyme. Only about 10% of the starting PEG 2000 was detected after that time, but the molecular weight of the polymer changed dramatically, indicating the degradation of the block copolymer both from the ends and in the middle of the chain.

Cathepsin B was chosen as a representative of lysosomal enzymes, the specificity of which is very close to that one of tritosomes (mixture of rat-liver lysosomal enzymes). As we found in our previous studies (*18*), glycine derivative of doxorubicin (60%) was released together with the free drug (40%) during the incubation with cathepsin B, but it was further degraded to free doxorubicin when tritosomes were used instead of cathepsin B. The rate of the drug release seems to be higher than the rate of the polymer carrier degradation. That is an important requirement for the anti-tumor activity of the whole system in vivo. The polymer drug−conjugate suggested in our work meets that well.

In Vivo Evaluation of Anti-Cancer Activity. Preliminary results of anti-cancer efficacy of our new polymer drug **22** (administered i.v.) in murine colorectal carcinoma C26 have shown quite significant inhibition of the tumor growth compared with the control group treated only with physiological solution (Figure 2). Unmodified doxorubicin hydrochloride was administered to another group of animals at the same dose as in the group treated with the polymer−Dox conjugate (dose converted to Dox·HCl). The mice treated with the free cytostatic drug had to be put down about 5 days after the drug administration due to the severe acute toxicity. A significant loss of body weight was observed in that group. On the other hand, the polymer-bound doxorubicin has shown no signs of toxicity at all (no decrease of body weight, good performance of the animals). The colorectal carcinoma chosen for the experiment generally exhibits a very low sensitivity to any common chemotherapy. Although we are aware of the fact that we are presenting only preliminary data obtained with a limited amount of the target compound **22**, which must be repeated in a more detailed study, the absence of toxicity of the polymer drug in particular and the inhibition of the tumor growth encouraged us to publish these promising results.

The polymer system described in this work consists only of the nontargeted polymer carrier and the drug moiety. We know that analogous nontargeted poly(HPMA)-based conjugates with doxorubicin exhibit much lower anti-tumor activity both in vitro and in vivo compared with the antibody-targeted ones (*19*, *20*). Therefore, we recently tried to prepare corresponding conjugates with antibody starting with the active ester **4**. Biological activity of the resulting biodegradable PEG block copolymers targeted with antibodies specifically interacting with receptors of the target cancer cells is being tested at present. On the basis of the results obtained with the HPMA-based polymer drugs, we expect the anti-cancer activity of such targeted biodegradable copolymers to be significantly higher than that of polymer **22**.

CONCLUSIONS

Two different synthetic routes for preparation of a water-soluble high-molecular-weight polymer drug carrier based on PEG block copolymer have been developed. The first method involves a quite elaborate and expensive synthesis of the Gly-Phe-Leu-Gly-Dox derivative and its conjugation with the polymer carrier, the other is based on the azide procedure used in peptide synthesis. In the latter case, free doxorubicin can be directly coupled with the active copolymer−tetrapeptide precursor. The degradability of the proposed polymer carrier is a prerequisite for successful excretion by glomerular filtration of high-molecular-weight polymer drugs after release of the active substance. Preliminary results of biological evaluation of the polymer−Dox in vivo have shown a lower toxicity and higher anti-tumor activity compared with free Dox using murine C26 colorectal carcinoma as a model tumor (this paper). Full assessment of advantages of the biodegradable carrier system compared with the nondegradable poly(HPMA) carriers would require de-

tailed evaluation of their activity with various tumor models. Our latest results show significantly improved anti-cancer efficacy compared with poly(HPMA)−Dox conjugate in mice bearing murine EL-4 lymphoma.

ACKNOWLEDGMENT

The authors thank the Grant Agency of the Czech Republic for supporting the project by Grants 307/96/K226 and 203/98/P096.

LITERATURE CITED

(1) Ulbrich, K. (1991) Water-soluble polymeric carriers of drugs. *J. Bioact. Compat. Polym. 6*, 348−357.
(2) Duncan, R. (1992) Drug-polymer conjugates: potential for improved chemotherapy. *Anti-Cancer Drugs 3*, 175−210.
(3) Říhová, B., Strohalm, J., Plocová, D., Šubr, V., Šrogl, J., Jelínková, M., Šírová, M., and Ulbrich, K. (1996) Cytotoxic and cytostatic effects of anti-Thy 1.2 targeted doxorubicin and cyclosporin A. *J. Controlled Release 40*, 303−319.
(4) Ouchi, T., Kuroda, H., and Ohya, Y. (1997) Design of Antitumor Agent-Terminated Poly(Ethylene Glycol) Conjugate as Macromolecular Prodrug. *Polym. Prepr. 38*, 582−583.
(5) Caliceti, P., Monfardini, C., Sartore, L., Schiavon, O., Baccichetti, F., Carlassare, F., and F. M. Veronese (1993) Preparation and Properties of Monomethoxy Poly(Ethylene Glycol) Doxorubicin Conjugates Linked by an Amino Acid or A Peptide As Spacer. *Farmaco 48*, 919−932.
(6) Seymour, L. W., Miyamoto, Y., Maeda, H., Brereton, M., Strohalm, J., Ulbrich, K., and Duncan, R. (1995) Influence of molecular weight on passive tumour accumulation of a soluble macromolecular drug carrier. *Eur. J. Cancer 31A*, 766−770.
(7) Nathan, A., Zalipsky, S., and Kohn, J. (1994) Strategies for covalent attachment of doxorubicin to poly(PEG-Lys), a new water-soluble poly(ether urethane). *J. Bioact. Compat. Polym. 9*, 239−251.
(8) Pechar, M., Strohalm, J., and Ulbrich, K. (1995) Synthesis of poly(ethylene glycol) block copolymers as potential water-soluble drug carriers. *Collect. Czech. Chem. Commun. 60*, 1765−1780.
(9) Pechar, M., Strohalm, J., and Ulbrich, K. (1997) Biodegradable drug carriers based on poly(ethyleneglycol) block copolymers. *Macromol. Chem. Phys. 198*, 1009−1020.
(10) Rejmanová, P., Pohl, J., Baudyš, M., Kostka, V., and Kopeček, J. (1983) Polymers containing enzymatically degradable bonds. 8. *Makromol. Chem. 184*, 2009−2020.
(11) Jegorov, A., Tříska, J., and Trnka, T. (1994) 1-Thio-β-D-galactose as a chiral derivatization agent for the resolution of D, L-amino acid enantiomers. *J. Chromatogr. A 673*, 286−290.
(12) Jegorov, A., Tříska, J., Trnka T., and Černý, M. (1988) Separation of α-amino acid enantiomers by reversed-phase high-performance liquid chromatography after derivatization with *o*-phthaldialdehyde and a sodium salt of 1-thio-β-D-glucose. *J. Chromatogr. 434*, 417−434.
(13) Zalipsky, S., and Lee, C. (1992) In *Poly(Ethylene Glycol) Chemistry: Biotechnical and Biomedical Applications* (J. M. Harris, Ed.) pp 347−370, Plenum Press, New York.
(14) Bodanszky, M., and Bodanszky, A. (1985) *The Practice of Peptide Synthesis*, Akademie-Verlag, Berlin.
(15) Kenner, G. W., and Stedman, R. J. (1952) Peptides. Part I. The synthesis of peptides through anhydrides of sulphuric acid. *J. Chem. Soc.* 2069−2076.
(16) Nathan, A., Bolikal, D., Vyavahare, N., Zalipsky, S., and Kohn, J. (1992) Hydrogels based on water-soluble poly(ether urethanes) derived from l-lysine and poly(ethylene glycol). *Macromolecules 25*, 4476−4484.
(17) Ulbrich, K., Strohalm, J., Šubr, V., and Plocová, D. (1996) Polymeric conjugates of drugs and antibodies for site-specific drug delivery. *Macromol. Symp. 103*, 177−192.
(18) Ulbrich, K., Pechar, M., Strohalm, J., Šubr, V., and Říhová, B. (1997) Synthesis of biodegradable polymers for controlled drug release. *Ann. N. Y. Acad. Sci. 831*, 47−56.
(19) Jelínková, M., Strohalm, J., Plocová, D., Šubr , V., Šťastný, M., Ulbrich, K., and Říhová, B. (1998) Targeting of human and mouse T-lymphocytes by monoclonal antibody-HPMA copolymer-doxorubicin conjugates directed against different T-cell surface antigens. *J. Controlled Release 52*, 253−270.
(20) Říhová, B., Jelínková, M., Strohalm, J., Šubr, V., Plocová, D., Hovorka, O., Novák, M., Plundrová, D., Germano, Y., and Ulbrich, K. Polymeric drugs based on conjugates of synthetic and natural macromolecules II. Anticancer activity of antibody or $(Fab')_2$-targeted conjugates and combined therapy with immunomodulators. *J. Controlled Release* (in press).

BC990092L

Site-Specifically Labeled Photoprotein-Thyroxine Conjugates Using Aequorin Mutants Containing Unique Cysteine Residues: Applications for Binding Assays (Part II)

J. C. Lewis, L. C. Cullen, and S. Daunert*

Department of Chemistry, University of Kentucky, Lexington, Kentucky 40506-0055. Received June 21, 1999; Revised Manuscript Received November 29, 1999

The jellyfish *Aequorea victoria* produces a protein, aequorin, which belongs to the class of Ca^{2+}-dependent photoproteins known for their ability to emit visible light. This property of aequorin has allowed for its as a bioluminescent label in binding assays for a variety of analytes. Due to the excellent detection limits we demonstrated in assays for small peptides using a fusion protein between the peptide of interest and the photoprotein, our next goal was to expand the range of possible analytes for producing homogeneous populations of conjugates with the aequorin label to those that were nonpeptidic in nature. Recently, we prepared and characterized four aequorin mutants containing unique cysteine residues at various positions in the polypeptide chain. In the work reported here, the four aequorin mutants were each conjugated with a maleimide-activated methyl ester derivative of thyroxine, a hormone frequently determined to evaluate thyroid function. The thyroxine−aequorin mutant conjugates were characterized in terms of the bioluminescence activities and binding properties with an anti-thyroxine monoclonal antibody for possible future employment in either heterogeneous or homogeneous binding assays for thyroxine and/or other desired analytes.

INTRODUCTION

The photoprotein aequorin was originally isolated from the jellyfish *Aequorea victoria* located in Friday Harbor, Washington, by Shimomura and co-workers (*1*). The photoprotein was shown to emit blue light with the requirement of a single cofactor, calcium. Due to its calcium-dependent, nontoxic nature, aequorin has found widespread application as an intracellular calcium indicator (*2*, *3*). Aequorin is a photoprotein complex consisting of an apoprotein, a luciferin (coelenterazine), and molecular oxygen. The binding of calcium ions triggers the protein to undergo a conformational change, which leads to the oxidation of the noncovalently bound coelenterazine. The products of the reaction are the blue fluorescent protein, CO_2, and light ($\lambda_{max} \cong 469$ nm) (*4*).

The bioluminescent signal produced by the photoprotein has virtually no background signal and a quantum yield of 15%, allowing the photoprotein to be detected down to attomol levels (*5*). The lack of need to irradiate the sample eliminates problems associated with light scattering, unselective excitation, and source stability (*6*). Bioluminescence can have a linear dynamic range up to 6 orders of magnitude and can be measured readily using inexpensive luminometers. Additionally, employing luminometry offers the advantage that while many biological samples contain a variety of fluorescent molecules, bioluminescence occurs relatively rarely in the biological kingdom, thus, furthering decreasing possible background problems in the sample (*7*). Because of all these advantages of bioluminescence detection, aequorin has not only been used as a calcium indicator but also as a highly sensitive bioluminescent label in binding assays as well (*8*−*10*).

The photoprotein has been employed indirectly as a label through biotinylation of aequorin, and subsequent use in conjunction with avidin or streptavidin. In one such assay to detect *Salmonella* antigen, the bioluminescent immunoassay demonstrated 50 times better sensitivity in comparison to the corresponding enzyme assay (*11*). The photoprotein has also been used directly through chemical conjugation to either the antigen (*12*) or antibody (*13*). A particular advantage of using a relatively small protein as a quantitative label is that the gene encoding for the protein can be fused to another desired protein or peptide. Thus, one-to-one homogeneous populations of conjugates can be produced employing genetic engineering techniques (*14*). Such conjugates yield better assay performance, by overcoming many problems associated with conventional chemical conjugation methods. Our group and others have successfully fused peptides (*15*) and proteins (*16*) to the N-terminus of aequorin to yield homogeneous populations of aequorin-labeled conjugates for assay development.

Recently, we reported the preparation and characterization of four aequorin mutants containing unique cysteine residues for site-specific conjugation and immobilization [part I (*17*)]. The four aequorin mutants obtained were based on a previously described cysteine-free mutant that demonstrated increased bioluminescence activity in comparison to the native photoprotein (*18*). The four mutants contained single cysteine residues at positions 5, 53, 71, and 84 in the polypeptide chain. To produce homogeneous populations of aequorin conjugates for assay development using nonpeptidic analytes, the photoprotein mutants were conjugated to a maleimide-activated methyl ester derivative of thyroxine synthesized in our laboratory. Thyroxine was chosen as a model analyte because it is one of two hormones assayed routinely in clinical laboratories along with triiodothyronine. These two hormones are typically determined

* To whom correspondence should be addressed. Phone: (606) 257-7060. Fax: (606) 323-1069. E-mail: daunert@pop.uky.edu.

10.1021/bc990081s CCC: $19.00 © 2000 American Chemical Society
Published on Web 02/04/2000

using radioimmunoassays (*19*). The four thyroxine−aequorin conjugates were evaluated in terms of their bioluminescence activities and binding properties to a anti-thyroxine monoclonal antibody. The ability to site-specifically label aequorin to desired nonpeptidic analytes has possible applications in the development of highly sensitive heterogeneous or homogeneous binding assays for important small biomolecules such as drugs, vitamins, or hormones. To the best of our knowledge, this is the first time that aequorin has been genetically modified and then site-specifically conjugated to a desired analyte for the development of an immunoassay.

EXPERIMENTAL PROCEDURES

Reagents. All restriction endonucleases, T4 DNA ligase, Luria Bertani (LB) broth, LB agar, DNA mass ladder, ampicillin, and kanamycin were purchased from Gibco-BRL (Gaithersburg, MD). Tris(hydroxymethyl) amino methane (Tris), ethylenediaminetetraacetic acid (EDTA) disodium salt, sodium chloride, dithiothreitol (DTT), thyroxine, and all other reagents were obtained from Sigma (St. Louis, MO). HQH, quaternized polyethyleneimine anion exchanger, was purchased from Perseptive Biosystems (Cambridge, MA). Coelenterazine was obtained from Biosynth International (Naperville, IL). All oligonucleotides (primers) employed for PCR were provided by Operon Technologies (Alameda, CA). The polymerase selected for PCR was *Pfu* polymerase from Stratagene (La Jolla, CA). The bicinchoninic acid (BCA) protein assay kit, Sulfo-GMBS, and Ellman's Reagent were purchased from Pierce (Rockford, IL). The anti-human thyroxine monoclonal antibody was obtained from Cortex Biochem (San Leandro, CA). The goat anti-mouse IgG (Fc) particles were from Bangs Laboratories (Fishers, IN). All solutions were prepared using deionized (Milli-Q Water Purification system, Millipore, Bedford, MA) distilled water. All chemicals were of reagent grade or better and were used as received.

Bacterial Strains and Plasmids. The expression vector pSbt and bacterial strain *Bacillus subtilis* (trpC2, MetB10, npr, apr::cat) was provided by Dr. Philip N. Bryan, University of Maryland. The mammalian expression vector, pMtAEQ, containing the apoaequorin gene was purchased from Molecular Probes (Eugene, OR). The *Escherichia coli* strain, JM109, employed for initial cloning reactions was from Gibco-BRL (Gaithersburg, MD).

Apparatus. Bioluminescence measurements were made on an Optocomp I luminometer from GEM Biomedical (Carrboro, NC) using a 100 μL fixed-volume injector. Absorbance measurements were conducted on a HP Diode-Array Spectrophotometer from Hewlett-Packard (Palo Alto, CA). All luminescence measurements are the average of a minimum of three replicates and have been corrected for the blank. All PCR reactions were performed using a Perkin-Elmer GeneAmp PCR System 2400 (Norwalk, CT).

PCR-Based Site-Specific Mutagenesis. The five mutant aequorins including one mutant in which the cysteine residues at positions 145, 152, and 180 were replaced with serine (mutant S), and four additional mutants containing unique cysteine residues at positions 5, 53, 71, and 84 in the polypeptide chain were prepared as previously described [part I (*17*)]. The site-specific mutations were confirmed through DNA sequencing performed at the Macromolecular Center (University of Kentucky). The final DNA products containing the apoaequorin mutants were cloned into the pSbt expression vector as *Eco*RI−*Sal*I fragments to yield the pSD110−114 vectors shown in Figure 1. All molecular biology procedures were conducted using standard protocols (*20*).

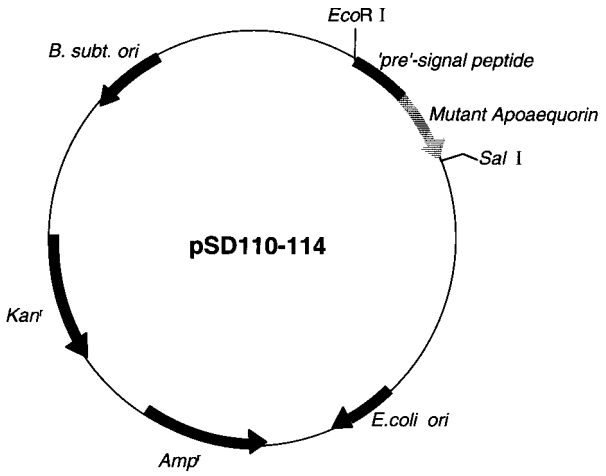

Figure 1. Schematic representation of the pSD110−114 expression vectors using PCR-based site-directed mutagenesis to obtain the desired mutations.

Expression and Purification of Mutant Apoaequorins. The five apoaequorin mutants were expressed and purified as described [part I (*17*)]. The fractions containing the mutant protein were combined and concentrated using a Centriplus 3000 device from Millipore (Bedford, MA). The desired buffer exchange was achieved employing a polyacrylamide 6000 desalting column from Pierce (Rockford, IL). The purity of the mutant proteins was verified by sodium dodecyl sulfate−polyacrylamide gel electrophoresis (SDS−PAGE) using an electrophoresis PhastSystem from Pharmacia Biotech (Uppsala, Sweden). Polyacrylamide (12.5%) gels were developed by the method of silver staining. The protein concentrations were estimated by using the BCA protein assay, with BSA as the standard.

Conversion of Apoaequorin to Aequorin. The mutant aequorins were generated from the apoproteins by mixing a set amount of the purified proteins in a glass test tube with a molar excess of coelenterazine in 10 mM Tris-HCl, 0.15 M NaCl, 2.0 mM EDTA, 5 mM DTT, pH 7.4, (TBS/EDTA/DTT) buffer. The mixture was briefly vortexed, and then placed on ice for a minimum of 4 h.

Calibration Plots of Aequorin Mutants. To compare the bioluminescence activities of the mutant aequorins containing unique cysteine residues with mutant S, calibration plots were constructed by serially diluting stock solutions of the aequorin mutants in TBS/EDTA buffer containing 1% BSA. Luminescence was triggered by injecting 100 μL of a 100 mM $CaCl_2$, 100 mM Tris-HCl, pH 7.5, buffer (activation buffer) to a volume of 100 μL of the different concentrations of the aequorin mutants. The bioluminescence signal was integrated over a 3-s time period.

Synthesis of Methyl L-Thyroxyl-(γ-maleimido)-butanamide (maleimide-activated thyroxine). The free acid of thyroxine was methylated by placing 1 g of the acid in the bottom of a test tube followed by the immediate addition of 10 mL of methanol. HCl gas was then bubbled through the suspension producing a yellow solid that was cooled with an ice bath. After allowing the mixture to reach RT, the above step was repeated. Since treatment with HCl/methanol produces the salt of the amino acid, the mixture was reacted with base (KOH) to yield the free amino acid. The solid was isolated by filtration, and washed with cold absolute ethanol and cold

ether. The product was subjected to high vacuum overnight in a P_2O_5 desiccator to dry the solid. To synthesize the maleimide-activated thyroxine suitable for conjugation to the photoproteins, 75 mg of the methylated L-thyroxine was placed in a round-bottom flask with 5 mL of dry dimethyl sulfoxide (DMSO). The mixture was stirred for 10 min before 36.25 mg of *N*-[γ-maleimidobutyryloxy]sulfosuccinimide ester (Sulfo-GMBS) was added, and the mixture was allowed to further stir overnight at RT under argon. The solvent was removed from the product in a rotavaporator under high vacuum. ^{1}H NMR was performed to verify the desired structure in (DMSO-d_6): δ 1.27 (triplet, $J = 5.66$ Hz, CH_2), 1.64 (multiplet, $J = 5.66$ Hz, 7.51 Hz, CH_2), 2.06 (triplet, $J = 7.51$ Hz, CH_2), 2.90 (quartet, $J = 4.36$ Hz, CH_2), 3.60 (singlet, OCH_3), 4.45 ($J = 4.36$ Hz, CH), 6.98 (singlet, CH olefinic), 7.03 (singlet, CH aromatic), 7.78 (singlet, CH aromatic), 8.33 (doublet, $J = 8.06$ Hz, NH), 9.20 (broad OH).

Site-Specific Conjugation of Aequorin Mutants with Maleimide-Activated Methyl Ester Derivative of Thyroxine. A volume of 2 mL of each of the purified apoaequorin mutants was incubated with fresh DTT at a final concentration of 5 mM for 1 h at RT. The mixtures were concentrated to 0.5 mL using a Centriplus 3000 device and then desalted with a polyacrylamide 6000 desalting column into a phosphate-buffered saline solution (PBS) with a pH of 7.0. A 20-fold molar excess of the maleimide-activated methyl ester derivative of thyroxine in dimethyl formamide (DMF) was added to the protein solution, and the mixture was allowed to stir overnight at 4 °C in the dark. The excess thyroxine was removed through desalting as described above. The thyroxine:aequorin molar ratio was calculated before addition of the chromophore (coelenterazine) using an extinction coefficient for thyroxine of $E_{1\%,1cm} = 73.7$ (*21*). A 5-fold molar excess of coelenterazine was then added to the mixture, which was left at 4 °C in the dark for an additional 24 h to form the photoprotein. The excess coelenterazine was removed through dialysis for 12 h at 4 °C against TBS/EDTA buffer. Care was taken at each step not to expose the labile thyroxine to light.

Calibration Plots of Thyroxine−Aequorin Mutant Conjugates. Stock solutions of the thyroxine−aequorin mutant conjugates were serially diluted in TBS/EDTA buffer containing 1% gelatin (assay buffer). Luminescence was triggered by injecting 100 μL of a 100 mM $CaCl_2$, 100 mM Tris-HCl, pH 7.5, buffer (activation buffer) to a volume of 100 μL of the different concentrations of the thyroxine−aequorin mutant conjugates. The bioluminescence signal was integrated over a 3 s time period.

Homogeneous Association Study. The anti-thyroxine antibody was diluted from a stock solution of 500 μg/mL in assay buffer to various concentrations ranging from 5 μg/mL to 150 μg/mL. Next, a fixed concentration of the thyroxine−aequorin mutant in a volume of 100 μL was added to the same volume of the various antibody concentrations followed by an incubation step of 2 h at 4 °C with shaking (150 rpm). To determine whether an increase or decrease in the bioluminescence signal occurred upon binding of the conjugate to the antibody, a blank containing 100 μL of the assay buffer in place of the antibody plus the thyroxine−aequorin mutant was used. The luminescence signal was measured as described above.

Heterogeneous Association Study. The anti-thyroxine antibody was diluted from a stock solution of 500 ng/mL in assay buffer to various concentrations ranging from 10 to 200 ng/mL. Goat anti-mouse IgG (Fc specific) magnetic particles (10 mg/mL) were diluted with assay buffer to 1 mg/mL. A volume of 100 μL of the antibody dilutions was added to 100 μL of the diluted anti-mouse magnetic particles followed by an incubation step of 1 h at 4 °C with shaking (150 rpm). Following a wash step to remove unbound antibody, a volume of 100 μL of a fixed concentration of the thyroxine−aequorin mutant was added and incubated with magnetic particles for 2 h at 4 °C with shaking (150 rpm). The particles were washed three times with assay buffer before measuring the bioluminescence signal.

RESULTS AND DISCUSSION

The photoprotein aequorin has been successfully employed by us and others as a highly sensitive bioluminescent label in binding assays for important biomolecules. The bioluminescence signal produced requires only the addition of a single cofactor and calcium and occurs as a rapid flash of light lasting less than 10 s. The characteristics of the bioluminescence reaction allow the photoprotein to be detected down to attomol levels. Aequorin has been used to assay a diverse array of analytes such as hormones (*22*, *23*), serum antibodies (*7*), cytokines (*24*), proteins and nucleic acids in Western and Southern blots (*25*), and vitamins (*26*). In most of these assays aequorin has been covalently attached to either the antigen or antibody being used by employing chemical conjugation methods that produce multi-labeled heterogeneous populations of conjugates. Such conjugation techniques often result in a large decrease in the bioluminescence activity of the photoprotein (*22*, *27*). Also, it has been demonstrated that it is advantageous in the development of binding assays to use one-to-one homogeneous populations because such populations result in more sensitive assays (*14*).

Recently, we have developed both homogeneous and heterogeneous binding assays for small biomolecules using aequorin as a label (*15*, *26*). In the case of the homogeneous assay, we employed a biotinylated-aequorin in a competitive assay format that produced detections limits for biotin of 1×10^{-14} M (4 attomoles). For the heterogeneous assay, we used the technique of gene fusion to produce a one-to-one population of octapeptide−aequorin conjugates that retained the full bioluminescence activity of the photoprotein. Even with a relatively low association constant between the octapeptide and the corresponding antibody of $\cong 10^{-7}$ M^{-1}, detection limits for the octapeptide were on the order of 1×10^{-9} M. To further expand the range of assays to nonpeptidic analytes while still producing homogeneous population of conjugates, we prepared four different aequorin mutants. The mutants produced were based on a previous study in which all three cysteine residues present within the native protein had been replaced with serine producing a mutant aequorin that demonstrated increased bioluminescence activity (*16*). On the basis of this information, it was foreseable that aequorin mutants could be genetically engineered to contain unique cysteine residues at various positions for site-specific conjugation of a desired biomolecule. In part I (*17*) of this study, we produced four such mutants with single cysteine residues at positions 5, 53, 71, and 84. In the current study, we have chosen the thyroid hormone, thyroxine, as a model analyte for the site-specific conjugation to the photoprotein mutants in order to demonstrate the feasibility of using these conjugates in binding assays.

To produce the aequorin mutants with unique cysteine residues, we chose the technique of PCR-based site-directed mutagenesis [see part I (*17*)]. Table 1 lists the

Table 1. Characterization of Aequorin Mutants Containing Unique Cysteine Residues

aequorin mutants	amino acid substitution	% relative bioluminescence[a]	no. of free sulfhydryl groups[b]
5	Ser5 → Cys	102	1.3
53	Glu53 → Cys	98	0.98
71	Met71 → Cys	13	0.90
84	Glu84 → Cys	14	0.93

[a] Relative bioluminescence activities are reported as the percentage of the maximum signal obtained for mutant S using 1 μg of each purified mutant aequorin in 350 μL of TBS/EDTA/DTT, pH 7.6, buffer containing 0.2 μg of coelenterazine. All measurements were performed in triplicate with 10 μL aliquots of the mutant aequorin mixtures. [b] The number of free sulfhydryl groups was determined using Ellman's reagent according to the manufacturer's instructions.

apoaequorin mutants prepared and the amino acid substitutions that were made by introducing the single cysteine residues into the apoprotein. Overlap extension PCR was used in the final step of the genetic manipulation of the apoaequorin gene to fuse the "pre"-signal peptide of the protein subtilisin to the N-terminus of the photoprotein. The peptide facilitates the secretion of a desired protein outside the cell into the culture medium, thus, simplifying the purifcation procedure. The final PCR product containing the DNA sequence encoding for the "pre"-signal peptide and the mutant apoaequorin was cloned into the pSbt expression vector as an *Eco*RI−*Sal*I fragment (see Figure 1). The newly constructed expression vectors, pSD110−114, were used to express and purify the mutant apoaequorin proteins as previously described in part I (*17*). Typical yields for the purification procedure ranged from 22 to 43 mg of protein/L of culture. The protein concentrations were estimated using standard BCA assays.

The purified apoaequorin mutants were converted to their corresponding photoproteins by mixing the apoproteins with a molar excess of coelenterazine. All five mutant proteins exhibited flash-type emission characteristics with the resulting luminescence signal rising sharply after injection with the activation buffer followed by an exponential decay of the light intensity [data shown in part I (*17*)]. The bioluminescence activities of the mutants were characterized by generating calibration curves for the mutants including mutant S, which contained no cysteine residues (Figure 2). The bioluminescence signal emitted by all five mutant aequorins extended over 5−6 orders of magnitude. Mutants S, 5, and 53 yielded detection limits on the order of 1×10^{-14} M, corresponding to 1×10^{-18} mol of photoprotein. The detection limits for mutants 71 and 84 were 1 order of magnitude higher at 1×10^{-13} M (1×10^{-17} mol of photoprotein). Further comparison can be made by determining the percent relative bioluminescence activity in of the mutants as shown in Table 1. Mutants 71 and 84 showed a substantial decrease in luminescence activity; however, both of these mutants were still detected down to very low levels. On the other hand, mutants 5 and 53 retained the full bioluminescence activity of the unmodified mutant S.

Before conjugating the activated-thyroxine analogue with the photoprotein, it was verified that a single sulfhydryl group had been introduced into each mutant protein. This was accomplished by first reducing each mutant protein with DTT and then employing Ellman's reagent [5,5′-dithio-bis-(2-nitrobenzoic acid (DTNB)], which reacts with free thiol groups to release TNB ($\epsilon_{412} = 14\,150$ M^{-1} cm^{-1} at 412 nm). Reaction of each of the mutant apoaequorins with Ellman's reagent indicated the presence of one available thiol group for conjugation (see Table 1). The purified apoproteins were incubated for 1 h with fresh DTT to prevent any disulfide bond formation before buffer exchange into a PBS buffer at pH 7.0 was performed using polyacrylamide desalting columns. A 20-fold molar excess of the maleimide-activated methyl ester derivative of thryoxine was used for the conjugation with protein concentrations ranging between 1.0×10^{-6} and 1.5×10^{-6} M. The reaction was carried out overnight at 4 °C in the dark to protect the thyroxine from exposure to light. After removing the excess conjugation reagent, the degree of conjugation of thyroxine to the apoaequorin mutants was determined using the extinction coefficient for thyroxine at 326 nm (*21*). The thyroxine:aequorin molar ratio for each of the mutants was determined to be approximately 1. Because the chromophoric unit for the photoprotein, coelenterazine, absorbs at 326 nm, conversion of the thyroxine−apoaequorin conjugates to photoproteins was not performed until after the excess thyroxine had been removed. At this time, a 5-fold molar excess of coelenterazine in methanol was added followed by an incubation step of 24 h at 4 °C.

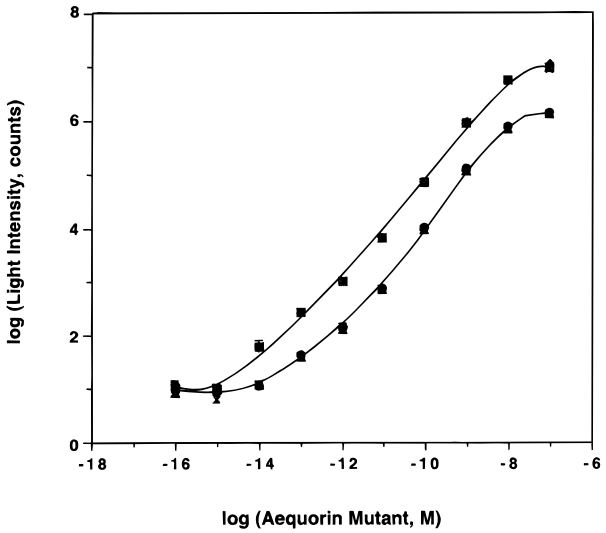

Figure 2. Calibration plots of aequorin mutants including mutant S (+) with no cysteine residues, and mutants with unique cysteine residues at positions 5 (◆), 53 (■), 71 (▲), and 84 (●) in the polypeptide chain. Light intensity is measured in counts and integrated over a 3 s time period.

To study the effect of conjugation on the bioluminescence activity of the individual aequorin mutants, as well as to select appropriate conjugate concentrations for the remainder of the experiments, calibration plots were constructed for the each of the thyroxine−aequorin conjugates (Figure 3). By comparing the calibration curves generated before and after conjugation, it is evident that mutants 5 and 53 demonstrated little, if any, loss in their bioluminescence activity. However, the calibration curves generated for the thyroxine−aequorin conjugates using mutants 71 and 84 produced detection limits on the order of 1×10^{-11} M for the conjugates, which is 2 orders of magnitude higher than the above detection limits for the unconjugated mutant aequorins.

The calibration curves were then used to select the appropriate concentration of the thyroxine−aequorin conjugates for association studies with the anti-thyroxine monoclonal antibody. Homogeneous binding curves were generated using fixed concentrations of the thyroxine−aequorin conjugates with various dilutions of the antibody followed by an incubation step. To determine if a change in signal had occurred, blanks were used in which

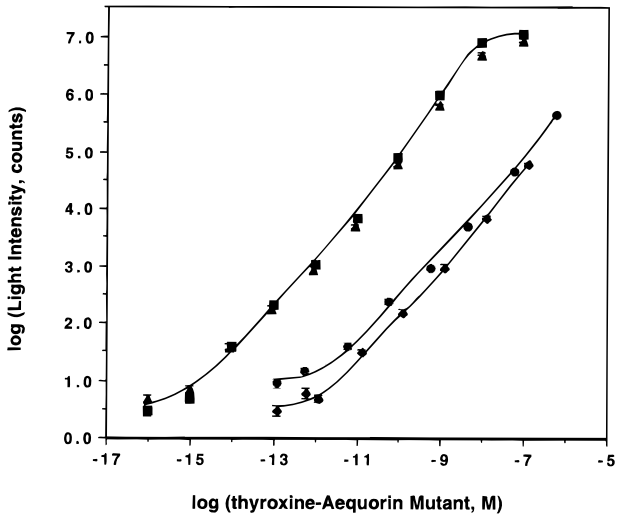

Figure 3. Calibration plots of thyroxine−aequorin mutant conjugates including maleimide-activated thyroxine conjugated to mutants 5 (■), 53 (▲), 71 (●), and 84 (◆).

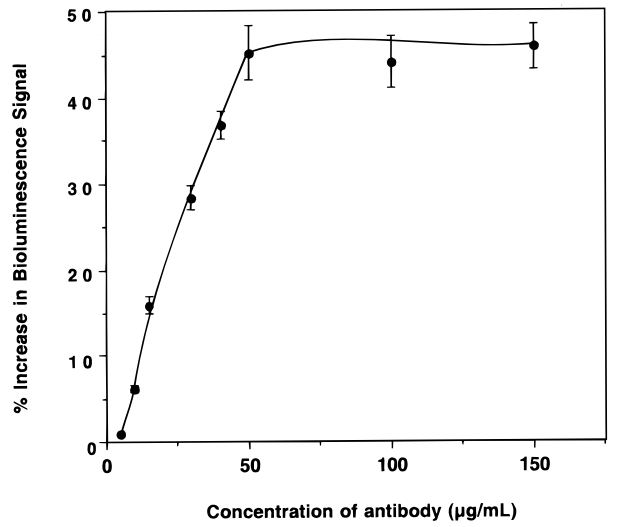

Figure 4. Homogeneous association curve employing thyroxine−aequorin mutant 71. The curve was obtained by incubating various concentrations of the anti-thyroxine monoclonal antibody with a set amount of the conjugate. Data are the average of ± one standard deviation ($n = 3$).

an equal volume of buffer was substituted for the antibody. Of the four thyroxine−aequorin conjugates studied, one conjugate (mutant 71) produced an increase in signal upon binding with the anti-thyroxine antibody (Figure 4). Since this particular conjugate exhibited a loss in bioluminescence activity upon conjugation with thyroxine, it may be postulated that upon binding with the antibody the thyroxine moiety is somehow displaced from a position at which it interacts with certain amino acid residues within the protein structure causing an interference in the production of the luminescence signal by the photoprotein. This position may be in the hydrophobic region of the photoprotein that interacts with the chromophoric unit coelenterazine. Because of the lack of a three-dimensional structure of the protein, the explanation for of this observation cannot be verified. A maximum signal increase of 45% was observed at antibody concentrations of 50 μg/mL and greater using a final concentration of the conjugate of 5×10^{-9} M.

Heterogeneous association curves were also generated employing the thyroxine−aequorin conjugates that demonstrated no loss in bioluminescence activity, namely mutants 5 and 53, and therefore would be more suitable for development of heterogeneous assays for thyroxine. The curves were produced employing a secondary antibody approach using magnetic particles coated with Goat anti-mouse IgG (Fc specific) antibody. This method allows for less consumption of the primary antibody, as well as specific orientation of the antibody on the solid phase. Figure 5 shows both curves generated for the two thyroxine−aequorin conjugates (mutants 5 and 53). It is apparent from the figure that both conjugates did successfully bind to the anti-thyroxine monoclonal antibody. Also, using a final concentration of 8.5×10^{-12} M for the conjugates, the luminescence signal was observed to remain constant at antibody concentrations greater than 125 ng/mL, thus, indicating the presence of an excess amount of antibody.

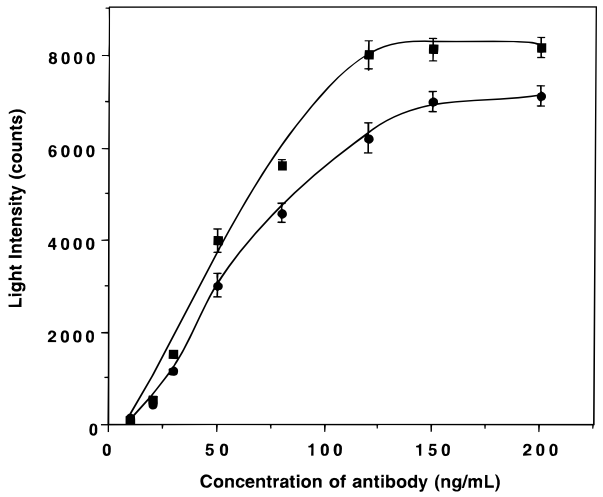

Figure 5. Heterogeneous association curve employing thyroxine−aequorin mutants 5 (■) and 53 (●). A secondary antibody approach was used to obtain the curve employing magnetic particles coated with goat anti-mouse IgG (Fc specific) antibodies, and then varying the amount of anti-thyroxine antibody with a set amount of the conjugates.

As described in part I (*17*), we determined that positions 5, 53, 71, and 84 in apoaequorin were viable for introduction of a unique cysteine residue. Here, we have demonstrated that site-specific conjugation to these unique cysteine residues is possible for all four mutants produced and that the four thyroxine−aequorin conjugates exhibit varying bioluminescence and binding properties. Of the four aequorin mutants conjugated to thyroxine, two of the mutants, 71 and 84, that previously showed a dramatic change in their bioluminescence activities, also produced interesting binding properties. The conjugate prepared with mutant 84 did not appear to bind with the anti-thyroxine monoclonal antibody to any degree (data not shown). However, the thyroxine−aequorin mutant 71 conjugate produced a homogeneous change (the bioluminescence signal increased following binding to the antibody) in the bioluminescence signal upon binding with the anti-thyroxine antibody (the bioluminescence signal was observed to increase). This mutant has the potential to be employed in the development of homogeneous assays for small biomolecules; these assays require fewer steps to complete and present a number of advantages, for example, when automation of the assay is desired. We also demonstrated that generation of one-to-one homogeneous populations of thyroxine−aequorin conjugates in a site-specific manner enables the production of conjugates that have not been

compromised in terms of the bioluminescence activity of the photoprotein label, as in the case of mutants 5 and 53. This may be especially critical for developing assays for analytes such as thyroxine, which contains four iodine atoms that may quench the luminescence signal (*28*). It is also essential to retain the full bioluminescence activity of the photoprotein following conjugation in order to achieve current and future requirements for the low detection limits needed for commonly assayed drugs, vitamins, hormones, etc. Finally, this is the first time that a bioluminescent photoprotein label has been genetically manipulated to produce homogeneous conjugates with nonpeptidic analytes for the purpose of developing immunoassays with superior performance.

ACKNOWLEDGMENT

We would like to thank the Department of Energy (DE-FG05-95ER62010), the National Institutes of Health (GM47915) for support of this work. J. C. Lewis acknowledges the National Science Foundation for an IGERT Predoctoral Fellowship. S. Daunert is a Cottrell Scholar and a Lilly Faculty Awardee.

LITERATURE CITED

(1) Shimomura, O., Johnson, F. H., and Saiga, Y. (1962) Extraction, purification and properties of aequorin, a bioluminescent protein from luminous hydromedusan, Aequorea. *J. Cell. Comput. Physiol. 59*, 223.

(2) Rizzuto, R., Simpson, A. W. M., Brini, M., and Pozzan, T. (1992) Rapid changes of mitochondrial Ca^{2+} revealed by specifically targeted recombinant aequorin. *Nature 358*, 325.

(3) Brini, M., Marsault, R., Bastianutto, C., Alvarez, J., Pozzan, T., and Rizzuto, R. (1995) Transfected aequorin in the measurement of cytosolic Ca^{2+} concentration *J. Biol. Chem. 17*, 9896−9903.

(4) Ohmiya, Y., and Hirano, T. (1998) Shining the light: mechanism of the bioluminescence reaction of calcium-binding photoproteins. *Chem. Biol. 3*, 337−347.

(5) Campbell, A. K., and Sala-Newby, G. (1993) In *Fluorescent and Luminescent Probes for Biological Activity* (W. T. Mason, Ed.) pp 58−82, Academic Press, New York.

(6) Rongen, H. A. H., Hoetelmans, R. M. W., Bult, A., and Van Bennekom, W. P. (1994) Chemiluminescence and immunoassays. *J. Pharm. Biomed. Anal. 12*, 433.

(7) Jackson, R. J., Fujihashi, K., Kiyono, H., and McGhee, J. R. (1996) Luminometry: a novel bioluminescent immunoassay enhances the quantitation of mucosal and systemic antibody responses. *J. Immunol. Methods 190*, 189.

(8) Actor, J. K., Kuffner, T., Dezzutti, C. S., Hunter, R. L., and McNichol, J. M. (1998) A flash-type bioluminescent immunoassay that is more sensitive than radioimaging: quantitative detection of cytokine cDNA in activated and resting human cells. *J. Immunol. Methods 211*, 65.

(9) Rigl, C. T., Rivera, H. N., Patel, M. T., Ball, R. T., Stults, N. L., and Smith, D. F. (1995) Bioluminescence immunoassays for human endocrine hormones based on aqualite, a calcium-activated photoprotein. *Clin. Chem. 41*, 1363.

(10) Kricka, L. (1993) Ultrasensitive Immunoassay Techniques. *Clin. Biochem. 26*, 325.

(11) Stults, N. L., Stocks, N. A., Cummings, R. D., Cormier, M. J., and Smith, D. F. (1991) Applications of recombinant bioluminescent proteins as probes for proteins and nucleic acids. In *Bioluminescence and chemiluminescence: Current Status* (P. E. Stanley, and L. J. Kricka, Eds.) pp 529−32, Wiley, Chichester.

(12) Galvan, B., and Christopoulos, T. K. (1996) Bioluminescence hybridization assays using recombinant aequorin. Application to the detection of prostate-specific antigen mRNA. *Anal. Chem. 68*, 3545.

(13) Rigl, C. T., Rivera, H. N., Patel, R. T., Ball, R. T., Stults, N. L., and Smith, D. F. (1995) Bioluminescence immunoassays for human endocrine hormones based on aqualite, a calcium-activated photoprotein. *Clin. Chem. 41*, 1363.

(14) Witkowski, A., Kindy, M. S., Daunert, S., and Bachas, L. G. (1993) Enzyme-linked immunosorbet assay for an octapeptide based on a genetically engineered fusion protein. *Anal. Chem. 65*, 1147.

(15) Ramanthan, S., Lewis, J. C., Kindy, M. S., and Daunert, S. (1998) Heterogeneous bioluminescence binding assay for an octapeptide using recombinant aequorin. *Anal. Chim. Acta 369*, 181.

(16) Zenno, S., and Inouye, S. (1990) Bioluminescent immunoassay using a fusion protein of protein A and the photoprotein aequorin. *Biochem. Biophys. Res. Commun. 171*, 169.

(17) Lewis, J. C., López-Moya, J. J., and Daunert, S. (1999) Bioluminescence and secondary structure properties of aequorin mutants produced for site-specific conjugation and immobilization, Part I. *Bioconjate Chem. 11*, 65−70.

(18) Tsuji, F. I., Inouye, S., Goto, T., and Sakaki, Y. (1986) Site-specific mutagenesis of the calcium-binding photoprotein aequorin. *Proc. Natl. Acad. Sci. U.S.A. 83*, 8107.

(19) Christofides, N. D., and Sheehan, C. P. (1995) Multicenter evaluation of enhanced chemiluminescence labeled-antibody immunoassay for free thyroxine. *Clin. Chem. 41*, 24.

(20) Sambrook, J., Fritsch, E. F., and Maniatis, T. (1989) *Molecular Cloning: A Laboratory Manual*, 2nd ed., Cold Spring Harbor Laboratory Press, Plainview, NY.

(21) Ferrua, B., Genetet, F., Savaron, M. L., Moulin, C., Salard, J. L., and Masseyeff, R. (1986) A novel enzyme immunoassay for total thyroxine using immobilized antibodies and hydrophobic chromatography purified thyroxine-peroxidase conjugate. *J. Immunol. Methods 87*, 137.

(22) Rigl, C. T., Patel, M. T., Rivera, H. N., Stults, N. L., and Smith, D. F. (1994) A bioluminescent immunoassay for testosterone based on recombinant photoprotein, aequorin. In *Biolumin. Chemilumin., Proc. Int. Symp.* (A. K. Campbell, L. J. Kricka, and P. E. Stanley, Eds.) pp 345−348, Wiley, Chichester.

(23) Rivera, H. N., Patel, M. T., Stults, N. L., Rigl, C. T., and Smith, D. F. (1994) A single-addition bioluminescence immunoassay for HCG that features recombinant aequorin as a dried reagent. *Biolumin. Chemilumin., Proc. Int. Symp.* (A. K. Campbell, L. J. Kricka, and P. E. Stanley, Eds.) pp 349−352, Wiley, Chichester.

(24) Actor, J. K., Kuffner, T., Dezzutti, C. S., Hunter, R. L., and McNichol, J. M. (1998) A flash-type bioluminescent immunoassay that is more sensitive than radioimaging: quantitative detection of cytokine cDNA in activated and resting human cells. *J. Immunol. Methods 211*, 65.

(25) Stults, N. L., Stocks, N. F., Rivera, H., Gray, J., McCann, R. O., O'Kane, D., Cummings, R. D., Cormier, M. J., and Smith, D. F. (1992) Use of Recombinant biotinylated aequorin in microtiter and membrane-based assays: purification of recombinant apoaequorin from *Escherichia coli*. *Biochemistry 31*, 1433.

(26) Witkowski, A., Ramanathan, S., and Daunert, S. (1994) Bioluminescence binding assay for biotin with attomol detection based on recombinant aequorin. *Anal. Chem. 66*, 1837.

(27) Erikaku, E., Zenno, S., and Inouye, S. (1991) Bioluminescent immunoassay using a monomeric Fab-photoprotein aequorin conjugate. *Biochem. Biophys. Res. Commun. 174*, 1331.

(28) Schroeder, H. R., and Yeager, F. M. (1978) Chemiluminescence yields and detection limits of some isoluminol derivatives in various oxidation systems. *Anal. Chem. 50*, 1114.

BC990081S

Electrostatically Driven Immobilization of Peptides onto (Maleic Anhydride-*alt*-methyl Vinyl Ether) Copolymers in Aqueous Media

Catherine Ladavière, Carmen Lorenzo, Abdelhamid Elaïssari, Bernard Mandrand, and Thierry Delair*

Unité Mixte UMR-103, CNRS-bioMérieux, ENS-Lyon, 46, allée d'Italie, 69364 Lyon, France.
Received July 9, 1999; Revised Manuscript Received December 3, 1999

The covalent immobilization of a model peptide onto the MAMVE copolymer, via the formation of amide bonds, occurred in moderate yields in aqueous conditions. The improvement of the grafting reaction was achieved by adding at the amino terminus of the model peptide a sequence (tag) of three positively charged amino acids, lysine or arginine, and by taking profit of electrostatic attractive interactions between the negatively charged copolymer and the tagged peptides. The arginine tag was more efficient than the lysine tag for enhancing the immobilization reaction, proving that the effect was due to an electrostic driving force. On the basis of these results, a tentative mechanism is discussed, and Scatchard plots pointed out two regimes of binding. With the first, at low polymer load (up to 50% of saturation for a lysine tag and 60−70% for an arginine tag), the binding occurred with a positive cooperative effect, the already bound peptide participating to the binding of others. A second one for higher coverages, for which the binding occurred with a negative cooperativity, and saturation was reached in the presence of a large excess of peptide.

INTRODUCTION

Binding biomolecules to polymers is essential for biomedical applications either in diagnostics to improve the test sensitivity (*1*), in therapy for targeted drug (*2*), or in nucleic acid (*3*) delivery. Chemical conjugation is often achieved by reaction of aminogroups of the biomolecules with reactive moieties of the polymer, aldehydes, or esters. This type of chemistry is well adapted as most biomolecules bear amines, but, in some cases, conjugation can result in a loss of the specific properties of the bound molecule, due to the alteration of its chemical integrity. To avoid this denaturation, other grafting methods were developped using chemical groups only found at a particular site of the biomolecules, not involved in the biological properties of the biomolecule. For instance, sulfydryl groups of Fab (*4*) fragments or carbohydrates on immunoglobulines (*5*) allow the direction of the covalent-binding reaction to a position different from the active site.

Our latest approach toward a directed immobilization of biomolecules consisted in adding a site enriched with reactive groups at the COOH terminus of a recombinant protein in order to enhance the immobilization, relying on a statistical orientation of the protein and taking profit of attrative electrostatic interactions (*6*).

Here, we report on a similar approach involving peptides, for which directed coupling is of paramount importance as they are smaller molecules than proteins, only representing the active domaine of the protein they are derived from. The investigation of the mechanism of binding by an analysis of the binding isotherms using Scatchard plots is also described.

EXPERIMENTAL PROCEDURES

Materials. The maleic anhydride-*alt*-methyl vinyl ether copolymer [P(MAMVE)], $\overline{M}_n$ = 67 000 g/mol, 1:1 ratio, approximately 430 anhydride groups per chain, was from Polysciences Inc. (Warrington) and used as such. Other chemicals were from Aldrich (L'Isle d'Abeau, France) and used as received. Milli-Q grade (Millipore SA, France) deionized water was used for all buffers.

Peptides were obtained from Eurogentec (Seraing, Belgium) and were used after dissolution in deionized water. S23G sequence, H_2N−SPPVSAPAKAAAPPAAAR-SAEPHVG-COOH, corresponds to an antigenic domain of TC 40 protein of *Trypanosoma cruzi*, a parasite responsible for Chagas' disease. Peptide 1 corresponded to the S23G sequence and peptide 2 to the S23G sequence plus three lysine residues at the amino terminus of S23G.

Coupling of Peptides to the Copolymer. In Figure 1 are recalled the coupling reaction and the hydrolysis reaction. The appropriate amounts of polymer were disolved in anhydrous dimethyl sulfoxide (DMSO) at 37 °C. To a peptide buffer solution at the appropriate concentrations was added the required volume of polymer solution in DMSO. The reaction mixture was stirred 3 h at 37 °C. The pH of the buffers were measured and monitored using an Ingold HA405-DXK-58/120 electrode and a Minisis 8000 pH-meter (Taccussel-Radiometer, Villeurbanne, France). As stated by the supplier, the electrode was Tris compatible.

Kinetics of the Coupling Reaction. To monitor the course of the coupling of peptide onto polymers, 20 μL of the reaction mixture was pipetted off and the reaction was quenched by addition of 10 μL of 15% ammonium hydroxide solution.

Peptide Interaction with the Hydrolyzed Copolymer. The copolymer sample was hydrolyzed at the same concentration as for coupling (stock concentration, 1 g/L), during 15 h at 67 °C in various buffers (pH 5.5, 6.8, and 9.2). Then, the coupling reactions with the various investigated peptides were performed as described above. The eventual presence of conjugate would be detected by SEC analysis, as described below.

* To whom correspondence should be addressed.

10.1021/bc990093d CCC: $19.00 © 2000 American Chemical Society
Published on Web 02/19/2000

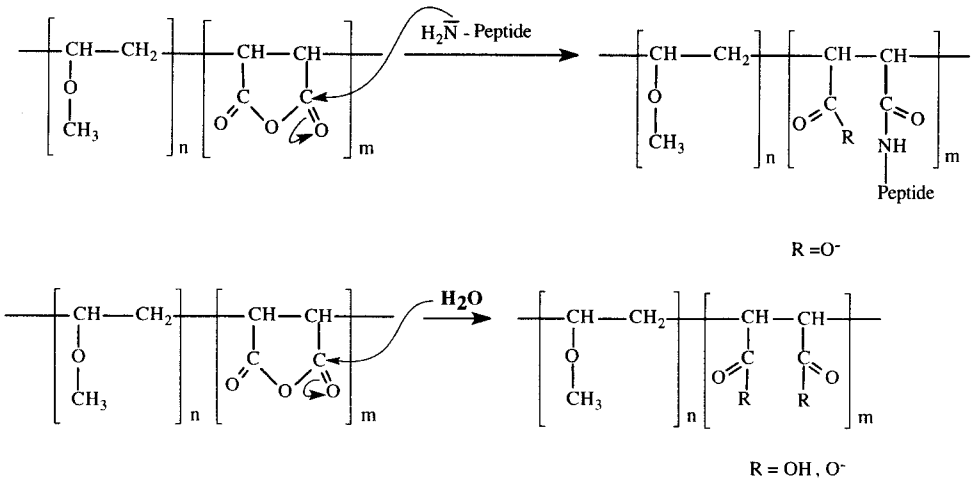

Figure 1. Reaction scheme for the coupling reaction above and for the hydrolysis reaction below.

Stability of Peptides and Conjugates. This study was carried out for peptides 1 and 2 and for the conjugates in the coupling medium (DMSO/0.1 M phosphate buffer, pH 6.8, 5/95, [peptide] = 74 μM, [MAMVE] = 0.72 μM) at 37 °C, for 30 days. Prior to use, the buffer was filtered on a 0.22 μm membrane.

Analyses of the Coupling Reactions. The crude coupling mixture was analyzed by size-exclusion chromatography (SEC) using an Ultra-Hydrogel column, UH 500 (Waters Corporation, Milford), a Kontron HPLC 422 pump, a Kontron HPLC autosampler 465 and a Kontron UV Diode Array detector (Kontron Instrument, Saint Quentin en Yvelines, France). Purifications were run in a 0.1 M phosphate buffer, pH 6.8, at a flow rate of 0.5 mL/min. Detection was achieved by measuring the absorbance at 220 nm corresponding to the peptide [at the concentrations used, the polymer had a weak absorption, the value of the optical density (OD) read for the polymer was subtracted in each sample]. The ratio of the peak area corresponding to the polymer-bound peptide versus the sum of the two peaks corresponding to the unbound and to the bound peptide (i.e., the total amount of peptide involved in the reaction) gave the coupling yield (Y%). The extinction coefficients of the bound and unbound peptides were checked by measuring the OD at 220 nm of crude conjugates compared to the reference free peptide. Furthermore, for each HPLC analysis, the sum of the areas of the bound and unbound peptide were routinely compared to that of a reference sample recorded in the absence of polymer. The average amount of peptide molecules per polymer chain was calculated according to $\bar{N} = nY/n'$ where n and n', respectively, correspond to the number of peptide molecules and the number of polymer chains in the reaction mixture. As a first approximation, we assumed that each polymer chain reacted according to the same pattern [which is the case for oligonucleotide immobilization (*1*)]. To calculate $\bar{N}$, which gives access to the level of loading of the polymer, we assumed that no cross-linking had occurred. This assumption seems realistic given that, in most conditions, the peptide to polymer molar ratio is 100:1.

RESULTS

Determination of the Conjugation Conditions. On the basis of results obtained with proteins (*6*), the conjugation media consisted in a mixture of DMSO, to allow polymer disolution and a buffer at a relative volume ratio of 5/95. In Figure 2 are reported the results of the coupling efficiency (expressed as the coupling yield, Y%) as a function of the chemical composition of the buffer for peptides 1 and 2 (Table 1). For both peptides, only a slight buffer composition effect was observed, the least favorable reaction mixture being the carbonate buffer, pH 10.8. Worth noting is that the immobilization reactions were less efficient in carbonate buffers than in borate or Tris buffers, at similar pH values, for peptides but as well for oligonucleotides (*7*) and proteins (*6*, *8*). This can be attributed to either a slower hydrolysis of the anhydride moieties in borate and tris buffers or to a difference in conformation of the polymer in solution, less favorable to the reaction in the carbonate buffers.

There is a slight increase in coupling yields from acidic phophate buffers to moderately alkaline phosphate buffers, corresponding to increased deprotonation of the peptide amino groups. When the medium got too alkaline, hydrolysis of the reactive anhydride moieties of the polymer was favored (*9*), resulting in a decrease in coupling efficiency. The hydrolysis reaction is a competing process, whose impact on the grafting reaction can prove very important. To illustrate this last statement, a coupling reaction was carried out in a reaction mixture consisting of 91% DMSO and 9% (v/v) 0.1 M phosphate buffer, pH 6.8. For peptide 1, a coupling yield of 83% was obtained in this medium as compared to 14% in the standard condition (DMSO/buffer, 5/95, identical polymer and peptide amounts in both experiments).

The kinetics of the conjugation reactions were investigated for peptides 1 and 2 in the 0.1 M phosphate buffer pH 6.8 (Figure 3). Ten minutes was required to obtain a couling yield of 80% for peptide 2 and 15 min for peptide 1 to react at only a 20% yield. The kinetics of the reaction depend on the nature of the biomolecule to be grafted, as, according to results previously published by our group, oligodeoxynucleotides were covalently bonded to the polymer within 5 min (*7*) whereas 40 min was required to immobilize bovine serum albumin (*8*). So, in the view of the preceding results, the fact that the immobilization of peptides stopped after 20 min can be attributed to steric factors (saturation of the polymer chain by peptide molecules) and not to the exhaustion of the anhydride groups of the polymer chain by water molecules.

A major physicochemical factor to take into account was the salt concentration of the buffer. The salt effect can be observed in Figure 4, in which is reported the variation of the grafting yields of peptide molecules versus the salt concentration in the immobilization medium. A decrease in the salt concentration resulted

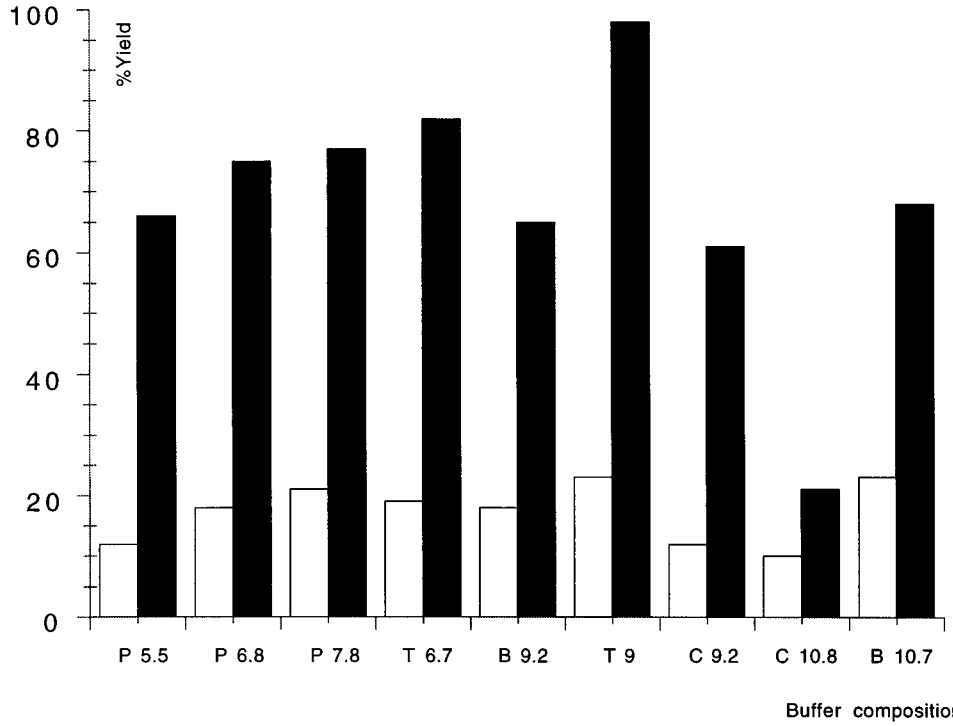

Figure 2. Coupling yield of peptide 1 (empty bar) and peptide 2 (filled bar) to MAMVE copolymer at 37 °C, 3 h. [peptide] = 75 μM, [P(MAMVE)] = 0.72 μM. P, 0.1 M phosphate buffer; T, 0.05 M Tris buffer; C, 0.1 M carbonate buffer; B, 0.1 M borate buffer, 0.01 M borate, pH 10.7.

Table 1. Peptides Sequences and Their Corresponding Coupling Yields to the MAMVE Copolymer in a 5% (v/v) DMSO, 95% 100 mM Sodium Phosphate Buffer, pH 6.8, 3 h, 37 °C[a]

peptide	amino acid sequence	coupling yield (%)
1	H_2N-SPPVSAPAKAAAPPAAARSAEPHVG-COOH (S23G sequence)	17
2	H_2N-**KKK**-S23G	89
3	H_2N-**KKK**-S23G, $K_9 \rightarrow R_9$	89
4	H_2N-**RRR**-S23G, $K_9 \rightarrow R_9$	84
5	CH_3CO-HN-**RRR**-S23G, $K_9 \rightarrow R_9$	9
6	CH_3CO-HN-**RRR**-S23G	45
7	H_2N-**RRR**-S23G	98

[a] Final peptide concentration: 74 μM. Final polymer concentration 0.048 g/L, 0.72 μM.

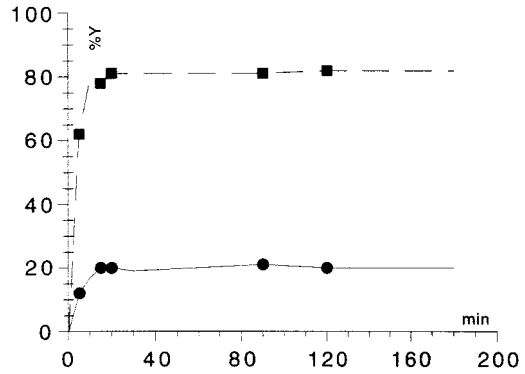

Figure 3. Coupling reaction kinetics for peptide 1 (circles) and peptide 2 (squares). 0.1 M phosphate buffer, pH 6.8, at 37 °C, [peptide] = 75 μM, [P(MAMVE)] = 0.72 μM.

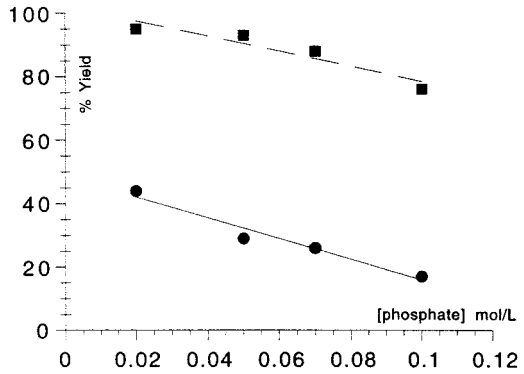

Figure 4. Effect of the salt concentration on the coupling yield. Phosphate buffer pH 6.8, 3 h. at 37 °C, [peptide] = 75 μM, [P(MAMVE)] = 0.72 μM.

in an increase in coupling yields, suggesting that, for both peptides 1 and 2, electrostatic attractive interactions could help improve the grafting yields.

As can be seen from Figure 2, peptide 2 reacted with the polymer, for each of the nine buffers tested, more efficiently than peptide 1. This could be attributed to the sole effect of the added lysines on the peptide which increased the amount of reactive groups available for coupling. Therefore, to address this issue, a more comprehensive study on the role of the tag on the course of the immobilization reaction was undertaken.

Assessment of the Orientation of the Immobilization. As reported in Table 1, seven different peptides were studied in order to help understand the role of the added amino acids at the N-terminus of the original S23G sequence. The coupling yields of peptides 1−7 are re-

ported in Table 1. Replacement in peptide 3 of the lysine by an arginine at position 9 of the S23G sequence resulted in no modification of the immobilization yield, proving that K_9 was not essential for the immobilization to occur for peptides 2 and 3. Very interestingly, peptide 4 was conjugated to the MAMVE copolymer with a similar efficiency as peptides 2 and 3, though only one primary amine goup was available, at the N-terminus of a three arginine sequence, in replacement of the lysines. This result demonstrated that the efficiency of the grafting reaction actually depended on the presence of a positively charged tag, allowing attractive electrostatic forces to develop between the polymer and the peptide. To confirm this observation, the primary amine of peptide 4 was acetylated in peptide 5, and the immobilization yield dropped from 84% for peptide 4 to 9% for peptide 5. The remaining grafting could be due either to reaction of the hydroxyl moiety of the three serine residues (S of the S23G sequence) or of the amino groups of arginine, or, else, to the formation of a polyelectrolyte complexe between the MAMVE copolymer, a polyanion, and the positively charged peptide. This last hypothesis was evaluated by running conjugation reactions of the peptides with the hydrolyzed MAMVE whose anhydride moieties were inactivated under the form of dicarboxylates. In fact, very little (4% for peptide 2 and 2% for peptides 3 and 4) to no (peptides 1 and 5) conjugate was detected by SEC, proving that covalent binding was the predominating process for the formation of polymer−peptide conjugates.

In peptide 6, the only available aminogroup is the lysine corresponding to position 9 in the S23G sequence. The observed coupling yield (45%) was 2.5 times that of peptide 1 (17%), bearing two reactive primary amines, at the N-terminus and at K_9, but no tag.

The immobilization yield observed for peptide 7 (98%) suggests that, out of the two tags tested, the arginine one is the more efficient at enhancing the grafting reaction.

DISCUSSION

Chemical Coupling. The immobilization of S23G model peptide onto the MAMVE copolymer can moderately take place in an aqueous buffer. To improve the grafting efficiency, a three lysine tag was added at the amino terminus of the S23G sequence (peptide 2) and the immobilization yield increased from 17% to 89%. This improvement was not solely due to an increase in the number of reactive moieties on the peptide, since arginine-tagged peptides 4 and 7 were conjugated to the polymer with identical yields as for peptide 2. These results demonstrate the determining role of favorable attractive electrostatic interactions on the course of the reaction. Moreover, an unreactive tag (N-acetylated arginine in peptide 6) allowed approximately a 3-fold increase in grafting efficiency, compared to the nontagged counterpart peptide 1.

With peptide 4, whose only available amino group is at the N-terminus of the arginine tag, the grafting yield was similar to peptides bearing either 2, 4, or 5 primary amines (respectively peptides 7, 3, and 2). This fact pointed out the preferential reaction of the primary amine at the N-terminus of the peptides, close to the positive charges of the tag, as in peptide 4.

The comparison of the grafting yields of peptides 4 and 6 demonstrates an increased reactivity by a 2-fold factor for an amine close to positively charged tag versus an amine in the core of the peptide bearing an unreactive tag.

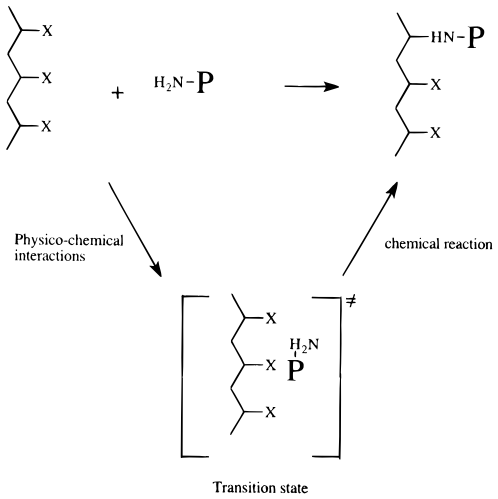

Figure 5. Schematic representation of the chemical pathway.

Analyzing the kinetics results obtained for peptides 1 and 2 in view of other results already reported by our group (*7*, *8*) suggested that the reaction was limited by steric factors. Hence, since more tagged peptide can be bound to the polymer, one can envision that each molecule generates less steric hindrance on the polymer than nontagged one. Therefore, we may think that the amidation reaction takes place at the N-terminus of the peptide leading to an end-on grafting (*6*), whereas, without a tag, a side-on attachment of the peptide would predominantly occur.

All these results emphasize the capabilities of our approach to perform a regioselective coupling reaction between the tagged peptides and the MAMVE copolymer.

Mechanism of Interactions. As depicted in Figure 1, the chemical grafting results from the formation of an amide bond between an amino group of the peptides and an anhydride moiety of the polymer. As we have demonstrated so far, the efficiency of this reaction is controlled by external factors such as ionic strength. Therefore, our results need to be discussed, not only in chemical terms, but as well by taking into account the parameters controlling the interactions of the macromolecules.

The formation of the amide bond that links a peptide molecule to the polymer requires both counterparts to be close to one another, at a distance in the order of the length of a chemical bond. So, the grafting process can be divided into two steps: (i) the formation of an intermediate, the transition state, in which the macromolecules are in close interactions, and (ii) the formation of the chemical bond (Figure 5).

If the chemical reaction is an irreversible process, the formation of the transition state can be regarded as reversible and this step can be investigated via the analysis of the binding isotherms, i.e., the variations of the amounts of bound peptide molecules per polymer chain versus the concentration of free peptides in the coupling mixture. From these isotherms, Figure 6, one can see that more tagged peptides could be bound per polymer chain in comparison with peptide 1, and that their affinities for the polymer were much greater, the slope of the linear part being more pronounced for each tagged peptide than for peptide S23G. These results confirm the important role of electrostatic interactions in the formation of the transition state, hence in the efficiency of the coupling reaction. Moreover, the isotherms show that more arginine-tagged peptides could

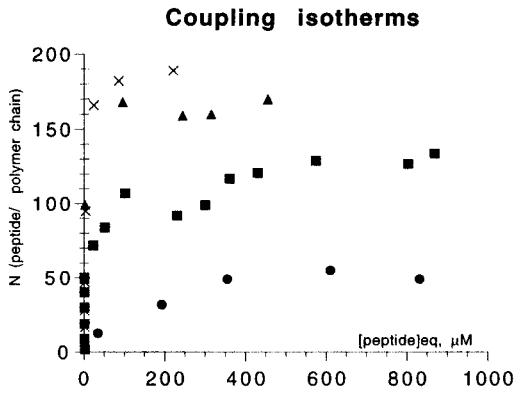

Figure 6. Coupling isotherms for peptide 1 (circles), peptide 2 (squares), peptide 7 (triangles), and peptide 4 (crosses). Phosphate buffer, 0.1 M, pH 6.8, 3 h at 37 °C.

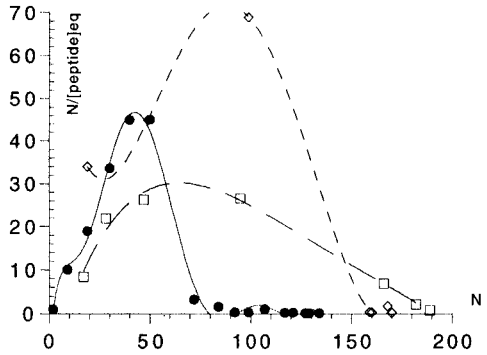

Figure 7. Scatchard plots for peptides 2 (circles), 4 (squares), and 7 (diamonds).

be immobilized on the MAMVE copolymer than the lysine-tagged counterpart (respectively, peptides 4, 7, and 2).

To have a better insight of the mechanism of the coupling reaction, the common method used in the literature is to analyze the coupling isotherms using Scatchard plots. Dubin et al. used this approach to characterize formation of complexes of various proteins with polyelectrolytes (*10*, *11*) and so did Jennisen for the adsorption of proteins on hydrophobized agaroses (*12*, *13*). In Figure 7 is reported the analysis of the coupling isotherms, obtained for the covalent immobilization of peptides 2, 4, and 7, by plotting the ratio N/L vs N (Scatchard plots) where N is the number of peptide molecules bound per polymer chain and L the free peptide concentration, or $[\text{peptide}]_{eq}$. All the curves in Figure 7 display a similar curvature profile as described by Jennisen (*13*) for the adsorption of proteins with positive cooperativity, suggesting a similar process for the binding of tagged proteins to MAMVE copolymers. Several authors have already reported positive cooperativity for the formation of protein−polyelectrolyte complexes (*14*, *15*), but, to our knowledge, this is the first report in which positive cooperativity is observed in the covalent immobilization of peptides to copolymers.

It is worth noting that the Scatchard plots increase and plateau over a range of N values, which correspond to the sharp slope of the immobilization isotherms. In otherwords, in this regime, the amounts of bound peptides depend mainly on the ability of the polymer to accommodate the peptide molecules. The positions of the maxima of the Scatchard plot depend on the nature of the tag. For peptide 2, up to 55 peptides can be efficiently bound to the polymer and 100 molecules for peptides 4 and 7. The decrease in the Scatchard plot is observed at approximately 60−70% of the total peptide loading of the polymer (saturation of the polymer). Further increase in N, up to the saturation of the polymer molecules, could be obtained by increasing the amount of peptide involved in the reaction, but at the expense of the efficiency of the binding reaction.

Interestingly, Gao and Dubin (*11*) investigated, in phosphate buffers, the interaction of proteins, among which bovine serum albumine (BSA) and β-lactoglobuline (BLG), with maleic anhydride-vinyl alkyl ether under the hydrolyzed form (dicarboxylate) of increasing alkyl chain length. MAMVE copolymers and the proteins, at pH 6.3, displayed weak interactions, mainly of electrostatic nature. The curvature of the reported Scatchard plots suggest a negative cooperativity in the formation of the polyelectrolyte complexes, which is quite different from our results, for the formation of covalent conjugates. As stated in the Results, only negligible amounts of peptide−MAMVE complexes were observed under our experimental conditions with the hydrolyzed form of the polymer.

On a practical standpoint, Scatchard plots are very useful as they describe the efficacy of the binding process as a function of the number of bound peptides per polymer chain. For the end-user, this plot can be a tool for predicting the amount of peptide required to bind a selected amount of biomolecules on the polymer. This plot can, as well, be used to define the range of peptide concentration for which binding is most efficient (high N/[L] values).

Further development of a model should take into account (i) that the amount of reactive sites is not constant due to the partial hydrolysis of the anhydride moieties in the reaction mixture (i.e., n is not a constant); (ii) the observed positive cooperativity; (iii) the lateral repulsive interactions between peptide molecule on the polymer chain; (iv) steric and/or electrosteric hindrance due to the presence of bound peptide preventing the approach of free molecules at high polymer loadings; (v) that some of the examined peptides have more than one reactive site (peptides 2 and 7); and (vi) that at the lowest N values, other interactions should be considered, as we will discuss later.

Anyhow, the obtained results point out the presence of at least two regimes depending on the peptide concentration. At low peptide concentration, the binding occurred with positive cooperativity until a limit value beyond which steric hindrance and repulsive electrostatic interactions disfavor the immobilization reaction. In this second domain, increased binding, up to saturation of the grafting capacity of the polymer, was obtained by using high peptide concentrations.

Electrostatic interactions appear to be the major factor controling the course of the coupling reaction of peptides to polymer molecules. But, at the onset of the reaction, prior to hydrolysis of any anhydride moieties, the polymer is neutral. Furthermore, in a previous work (*9*), we showed that hydrolysis was a slow process under acidic conditions. Since the covalent immobilization is a fast process at pH 6.8, how can the very first peptide molecules bind to the polymer?

Two answers are plausible. First hypothesis: some of the polymer functional groups were hydrolyzed in DMSO while preparing the polymer solution, which cannot be excluded even with anhydrous DMSO, or the polymer itself is partially hydrolyzed, but neither FTIR nor TGA (thermogravimetric analysis) experiments have been able to evidence that fact (*16*). Second hypothesis: the polymer, which is in a good solvent in DMSO (*16*), when poured into the aqueous buffer is suddenly in a bad

solvent (unhydrolyzed MAMVE is insoluble in water, dissolution takes place when enough anhydride groups are hydrolyzed to carboxylate moieties). In this medium, the polymer macromolecules aggregated in compact coils and can be coated (via an adsorption process) by a certain amount of peptide molecules. Thus, these adsorbed peptides are in close vicinity to anhydride moieties and they can react to form the peptide bonds with a concomitant formation of carboxylate groups. These carboxylate groups and the first grafted peptides enhance the solubility in water of the polymer and so the availablility of the reactive groups. As a consequence, more peptide molecules can be attracted close to the polymer via increasing electrostatic interactions, which can explain the strong positive cooperativity observed at low peptide concentration in the reaction mixture. All these interactions take place at the very early stage of the immobilization process.

The maximum amount of preadsorbed peptide onto the polymer can be roughly assessed as representing 21 peptides/chain, corresponding to the experiment in Figure 3 with untagged peptide 1. This last statement assumes that, at 0.1 M sodium phosphate, electrostatic attractive interactions are low enough to be neglected, and so the amount of grafted peptide arose from what was previously adsorbed. Only the development of favorable electrostatic interactions can allow higher amounts of peptide 1 bound to the copolymer, like for instance reducing the ionic strength (Figure 4).

Our results lead us to formulate that the immobilization of peptides onto the MAMVE copolymer could be a three step process: (i) onset—adsorption of a limited amount of peptide molecules onto coiled polymer chains; (ii) development of negative charges onto the polymer by reaction of the bound peptides with anhydride moieties; and (iii) enhancement of the grafting efficiency by attractive electrostatic interactions between positively tagged peptides and the negatively charged polymer.

Of paramount importance is that, if the binding reaction relies on attractive electrostatic interactions between the polymer and the peptides, the presence of pure polyelectrolyte complexes between the peptide and the polymer was only evidenced by HPLC, in some cases in minute amounts for the series of experiments run with the fully hydrolyzed polymer. It means that, in the investigated experimental conditions, electrostatic interactions yielded complexes of weak stability, which could be disrupted under HPLC experimental conditions. Nevertheless, this low stabilization energy was enough to generate a transition state with a sufficient half-life to allow the formation of the covalent bond, irreversibly linking the peptide molecule to the polymer.

CONCLUSION

The binding of peptides to MAMVE copolymers in an aqueous buffer suffers from the competing hydrolysis reaction, due to the presence of water in the immobilization mixture. We demonstrated in this work that, to increase the grafting efficiency, electrostatic interactions could be used to favor the approach of the polymer by the peptide molecules. These interactions were increased by adding, at one terminus of the peptide, a sequence (tag) of three positively charged amino acids, either lysine or arginine. We demonstrated that the primary amine at the N-terminus of the peptide was twice as more reactive as a primary amine isolated in the peptide sequence, suggesting a potential orientation of the peptide on coupling.

The isotherms of the coupling reaction showed that tagged peptides had a greater affinity for the polymer and that it was possible to immobilize greater amounts of peptides molecules as compared to their untagged counterparts. Furthermore, the isotherms showed that an arginine tag was more efficient at enhancing the grafting reaction than a lysine tag. Since our data suggest that the reaction to be limited by steric factors, the end-on grafting of tagged peptide on the polymer is likely to be favored.

Using the Scatchard plots, we showed that binding occurred with positive cooperativity at loadings up to 50−60% of the total binding capacity, depending on the nature of the tag. On a practical standpoint, Scatchard plots are a convenient means for defining the peptide concentration range to achieve the most effective immobilization, i.e., with lowest amount of unreacted peptide in the coupling mixture.

It is a goal of our future work to use the optimal coupling conditions to efficiently synthesize polymer−peptide conjugates, for diagnostics applications, and to improve our knowledge of the grafting reaction, in particular devoting efforts toward the understanding of the initial step of the immobilization process and the developement of an appropriate model.

LITERATURE CITED

(1) Erout, M. N., Troesch, A., Kurfurst, R., Pichot, C., and Cros, P. (1996) Preparation of conjugates between oligonucleotides and *N*-vinylpyrrolidone/*N*-acryloxysuccinimide copolymers and applications in nucleic acid assays to improve sensitivity. *Bioconjugate Chem. 5*, 568−575.

(2) Langer, R. (1990) New Methods of drug delivery. *Science 249*, 1527−1553.

(3) Zauner W., Ogris, M., and Wagner, E. (1998) Polylysine-based transfection systems utilizing receptor-mediated delivery. *Adv. Drug Delivery Rev. 30*, 97−113.

(4) Delair, Th., Pichot, C., and Mandrand, B. (1994) Synthesis and characterization of cationic latexes particles bearing sulfhydryl groups and their use in the immobilization of Fab antibody fragments. *Colloid Polym. Sci. 272*, 72−81.

(5) Hermanson, G. T., Krisna Mallia, A., and Smith P. K. (1992) *Immobilized affinity ligand techniques*, Academic Press Inc.: San Diego, CA.

(6) Ladavière, C., Delair, Th., Domard, A., Novelli-Rousseau, A., Mandrand B., and Mallet, F. (1998) Covalent immobilization of proteins onto (maleic anhydride-*alt*-methyl vinyl ether) copolymers: Enhanced immobilization of recombinant proteins. *Bioconjugate Chem. 9*, 655−661.

(7) Ladavière, C., Delair, Th., Domard, A., Pichot, C., and Mandrand, B. (1999) Reactive polymers in diagnostics: syntheses and characterization of nucleic acid probes and (maleic anhydride-*co*-methyl vinyl ether) polymers. *J. Appl. Polym. Sci. 71*, 927−936.

(8) Ladavière, C., Véron, L., Delair, Th., Domard, A., Pichot, C., and Mandrand, B. (1997) Covalent immobilization of Bovine Serum Albumin onto (maleic anhydride-*alt*-methyl vinyl ether) copolymers. *J. Appl. Polym. Sci. 65*, 2567−2577.

(9) Ladavière, C., Delair, Th., Domard, A., Pichot, C., and Mandrand, B. (1999) Covalent immobilization of biological molecules to maleic anhydride and methyl vinyl ether copolymers. A physicochemical approach. *J. Appl. Polym. Sci. 71*, 927−936.

(10) Gao, J. Y., Dubin, P. L., and Muhoberac, B. B. (1997) Measurement of the binding of proteins to polyelectrolytes by frontal analysis continuous capillary electrophoresis. *Anal. Chem. 69*, 2945−2951.

(11) Gao, J. Y., and Dubin, P. L. (1999) Binding of proteins to copolymers of varying hydrophobicity. *Biopolymers. 49*, 185−193.

(12) Jennissen H. P. (1976) Evidence for negative cooperativity in the adsorption of phosphorylase b on hydrophobic agaroses. *Biochemistry 15*, 5683−5692.
(13) Jennissen H. P. (1976) Multivalent adsorption of proteins on hydrophobic agaroses. *Hoppe-Seyler's Z. Physiol. Chem. 357*, 1201−1203.
(14) Mattison K. W., Wang Y., Crymonpé K., and Dubin P. L. (1999) Micro- and macrophase behavior in protein-polyelectrolyte complexes. *Macromol. Symp. 140*, 53−76.
(15) Kabanov, V. A., Evdakov, V. P., Mustafaev, M. I., and Antipina, A. D. (1977) Cooperative bonding of serum albumin by quaternized poly-4-vinylpyridines and structure of the complexes formed. *Mol. Biol. 11*, 582−597.
(16) Ladavière, C. (1997) Ph.D. Thesis, C. Bernard University-Lyon-I.

BC990093D

3′-End Conjugates of Minimally Phosphorothioate-Protected Oligonucleotides with 1-*O*-Hexadecylglycerol: Synthesis and Anti-*ras* Activity in Radiation-Resistant Cells

Antonina Rait,[†] Kathleen Pirollo,[†] David W. Will,[‡] Anush Peyman,[‡] Vladimir Rait,[†] Eugen Uhlmann,[‡] and Esther H. Chang*[,†]

Georgetown University Medical Center, Departments of Oncology and Otolaryngology, NRB/E420, 3970 Reservoir Road, NW, Washington, D.C. 20007, and Hoechst Marion Roussel Deutschland GmbH, Chemical Research G 838, D-65926 Frankfurt am Main, Germany. Received August 10, 1999; Revised Manuscript Received November 2, 1999

Activation of the *ras* oncogene has been implicated in many types of human tumors. It has been shown that downmodulation of *ras* expression can lead to the reversion of the transformed phenotype of these tumor cells. Antisense oligodeoxyribonucleotides (ODNs) can inhibit gene expression by hybridization to complementary mRNA sequences. To minimize toxicity associated with all-phosphorothioated ODNs and improve cellular uptake, we used partially phosphorothioate (PPS)-modified ODNs having an additional hydrophobic tail at the 3′-end (PPS−C_{16}). The PPS ODNs are protected against degradation by PS internucleotide linkages at both the 3′- and 5′-ends and additionally stabilized at internal pyrimidine sites, which are the major sites of endonuclease cleavage. Here we show that anti-*ras* PPS−C_{16} ODN retains the high sequence-specificity of PPS ODNs and provides maximal inhibition of Ras p21 synthesis with minimal toxicity even without the use of a cellular uptake enhancer. Moreover, treatment of T24, a radiation-resistant human tumor cell line that carries a mutant *ras* gene, with anti-*ras* PPS−C_{16} ODN resulted in a reduction in the radiation resistance of the cells in vitro. We also demonstrate that the growth of RS504 (a human c-Ha-*ras* transformed NIH/3T3 cell line) mouse tumors was significantly inhibited by the combination of intratumoral injection of anti-*ras* PPS−C_{16} ODN and radiation treatment. These findings indicate the potential of this combination of antisense and conventional radiation therapy as a highly effective cancer treatment modality.

INTRODUCTION

Sequence-specificity, nuclease resistance, and efficient cellular uptake are the major determinants of oligonucleotides intended for use as antisense therapeutics (*1, 2*). Phosphorothioate oligodeoxyribonucleotides (PS ODNs) are the most studied antisense agents and are currently under evaluation in human clinical trials. While these PS ODNs show appropriate serum and intracellular stability, they suffer from poor cellular uptake, and moreover, they demonstrate nonantisense, nonsequence-specific effects (for reviews, see refs *3* and *4*). The nonantisense effects, originating primarily from the negative charge on sulfur and a high sulfur polarization, can be decreased by reducing the number of PS internucleoside linkages per ODN, using them only for 3′- and 5′-end-capping (*5, 6*) and for the protection of linkages adjoining internal pyrimidine nucleosides (*7*). In serum or medium with cultured cells, such partially phosphorothioated (PPS) ODNs demonstrate a stability which is comparable to uniformly phosphorothioate modified ODNs (*7*) and, in cell-free and cell-based assays, show fewer nonantisense effects than uniformly PS modified ODN (Rait et al., manuscript in preparation).

As summarized by Stein (*8*), ODNs enter cells via fluid phase endocytosis (pinocytosis) and adsorptive endocytosis. The former mechanism markedly contributes to cellular uptake only with a high extracellular ODN concentration. The latter mechanism, mediated by the interaction of negatively charged ODNs with receptor-like cell-surface proteins, seems to be a much more efficient pathway. However, it reaches its limit of capacity at an ODN concentration of around 1 μM. In total, less than 10% of naturally internalized ODNs are released into the cytoplasm with the remainder captured in endosomes and lysosomes (*8*).

Cationic surfactants (called also cationic "lipids") form supramolecular complexes with ODNs, intensify adsorptive endocytosis by bypassing cellular receptors, and assist the escape of ODNs from endosomes (*9*−*11*). However, the cationic lipids were also found to be cytotoxic by damaging the outer and inner cell membranes. Together with the observed instability of the complexes in serum, this may restrict their therapeutic application (*12, 13*).

Another approach for increasing cellular uptake relies on covalent conjugates of ODNs with lipophilic compounds, such as cholesterol, vitamin E, or aliphatic alkyl chains which interact with cellular membranes (*14*−*17*). For example, a 3′-ω-hydroxydodecyl-modified nonadeoxyribonucleotide was taken up by T24 human bladder carcinoma cells four times more efficiently than the unmodified oligomer (*18*). Furthermore, a 5′ undecyl-modified antisense undecamer effectively suppressed influenza virus reproduction in MDCK cells, while non-modified antisense or nonsense oligomers did not (*19*).

* To whom correspondence should be addressed. Phone: (202) 687-8418. Fax: (202) 687-8434. E-mail: change@gunet.georgetown.edu.

[†] Georgetown University Medical Center.

[‡] Hoechst Marion Roussel Deutschland GmbH.

10.1021/bc990106n CCC: $19.00 © 2000 American Chemical Society
Published on Web 01/08/2000

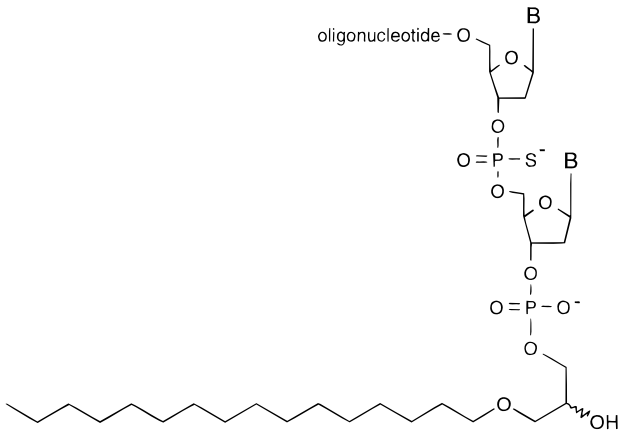

Figure 1. General structure of a hexadecylglycerol-derivatized oligonucleotide.

The conjugation of 1,2-di-*O*-hexadecyl-*rac*-glycerol to the 5′-end of otherwise unmodified ODN resulted in compounds which inhibited viral proliferation in cell culture, however, with poor sequence specificity (*20*).

To compare a PPS ODN and its 3′-end conjugate with 1-*O*-hexadecylglycerol (PPS−C_{16} ODN; Figure 1) for the first time directly, we synthesized the corresponding undecamers complementary to the initiation codon region of human Ha-*ras* along with a variety of noncomplementary control sequences and tested these compounds in lipofectin-mediated and lipofectin-free cell treatment. In contrast to the 5′-conjugates of bis-hexadecyl ether of glycerol with phosphodiester ODNs reported earlier (*20*), we used ODN-3′-conjugates of the mono-hexadecyl ether of glycerol, which are more stable to endo- and 3′-exonucleases present in serum. Interestingly, we found that our 1-*O*-hexadecylglycerol undecamer conjugate no longer required a cationic uptake enhancer for optimal sequence-specific biological activity in cell culture. We also demonstrated that the antisense PPS−C_{16} ODN could reduce the radiation resistance of T24 tumor cells that carry a mutant Ha-*ras* gene. More significantly, when combined with radiation treatment, intratumorally injected PPS−C_{16} effectively inhibited the growth of Ha-*ras*-transformed mouse tumors.

MATERIALS AND METHODS

Reagents and solvents were obtained from Sigma (St. Louis, MO), Aldrich Chemical Co. (Milwaukee, WI), or Fluka Chemical Corp. (Milwaukee, WI). Three radiation-resistant, Ha-*ras*-transformed cell lines were used in this study. RS485 is a NIH/3T3-derived cell line, transformed by multiple copies of normal human c-Ha-*ras* activated by a viral long terminal repeat (*21*). RS504 is an NIH/3T3-derived cell line transformed by mutated (at 12th codon) human c-Ha-*ras* (*22*). The human bladder carcinoma cell line T24 has the Ha-*ras* gene activated by a G → T transversion in the 12th codon (*23*). All cells were grown in Dulbecco's modified Eagle's minimal essential medium (DMEM; Flow Laboratories, McLean, VA) supplemented with 10% heat inactivated fetal calf serum (FCS), antibiotics (50 μg/mL each of penicillin, streptomycin, and neomycin), and 2 mM of L-glutamine.

Synthesis of a Hexadecylglycerol-Derivatized Solid Support. 1-*O*-Hexadecyl-*rac*-glycerol (**1**) (1 mmol; Sigma) was dried by coevaporation with and dissolved in anhydrous pyridine (3 mL). The solution was cooled to 0 °C, and 4,4′-dimethoxytrityl chloride (1.15 mmol; Fluka) was added. The mixture was stirred overnight, the reaction was quenched by the addition of water (100 μL), and the mixture was evaporated to dryness. The residue was suspended in dichloromethane (20 mL) and extracted three times with 10 mL of 0.1 M phosphate buffer, pH 7. The organic phase was dried over sodium sulfate, filtered, and evaporated. The residue was dried by coevaporation with and dissolved in anhydrous pyridine (2 mL). 4,4-(Dimethylamino)pyridine (1.4 mmol; Aldrich) and succinic anhydride (2.1 mmol; Fluka) were added. The mixture was stirred overnight, evaporated to dryness, and coevaporated twice with toluene/dichloromethane (1:1, v:v). The residue was dissolved in dichloromethane (20 mL), extracted with 10% citric acid (11 mL) and washed three times with water (11 mL). Two drops of triethylamine were added to the organic phase that was then dried over sodium sulfate, filtered, and evaporated. The product was purified by silica gel chromatography using a gradient of methanol (1−4%) in dichloromethane containing 1% triethylamine. Succinic acid mono-(1-*O*-dimethoxytrityl-3-*O*-hexadecyl-*rac*-glycerol)-ester (**2**) was obtained as a clear oil in 510 mg yield (62%). The succinic acid mono-ester (0.056 mmol), *N*-ethylmorpholine (0.07 mmol; Aldrich) and *N*,*N*,*N*′,*N*′-tetramethyl-*O*-(benzotriazol-1-yl)uronium tetrafluoroborate (TBTU; 0.056 mmol; Sigma) were dissolved in DMF (2 mL) and added to a 550 Å aminopropyl controlled-pore glass (CPG; 500 mg; Fluka). The mixture was shaken for 4 h, and the resulting C_{16}-derivatized CPG **3** (Scheme 1) was recovered by filtration and washed with methanol and dichloromethane. Finally, the solid support was capped for 1 h using acetic anhydride/*N*-methyl imidazole in THF, filtered, and washed with methanol, dichloromethane, THF, and diethyl ether. After drying in vacuo, the loading of dimethoxytrityl groups was determined to be 80 μmol/g.

Scheme 1. Reagents: (a) 4,4′-dimethoxytrityl Chloride, Anhydrous Pyridine; (b) Succinic Anhydride, 4,4-(dimethylamino)pyridine, Pyridine; (c) CPG, *N*-ethylmorpholine, TBTU, DMF

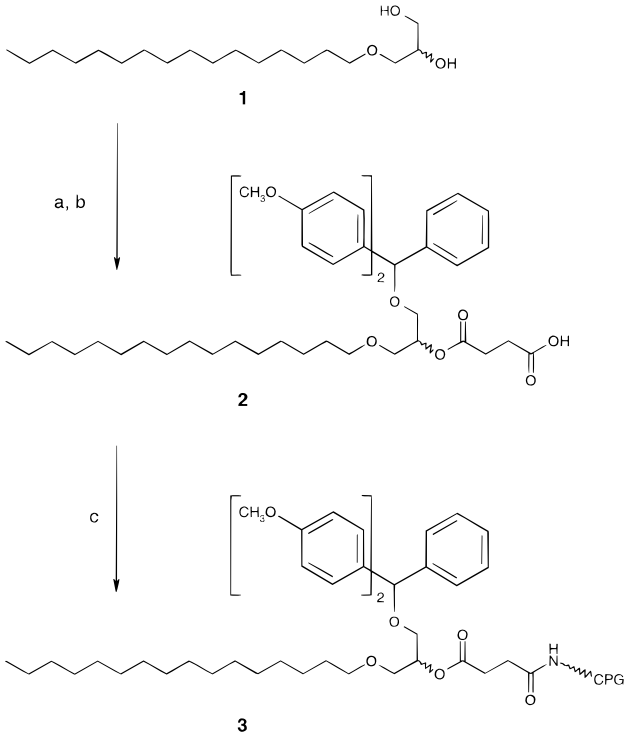

Oligodeoxynucleotide Synthesis. The ODNs listed in Table 1 were synthesized using standard phosphoramidite chemistry on a 394 DNA synthesizer (Applied

Table 1. Oligonucleotides Used In Study[a]

sequence, 5′ → 3′	description, abbreviation	T_m (°C)[b]	molecular weight calcd	molecular weight measured
partially phosphorothioated ODNs	PPS			
TsAsToToCsCoGoTsCsAsT	antisense, AS PPS	36.9	3378.58	3378.1 ± 0.03
AsTsGoAoCsGoGoAsAsTsA	sense, S PPS		3485.68	3484.9 ± 0.53
partially phosphorothioated, 3′ C16-modified ODNs	PPS−C_{16}			
TsAsToToCsCoGoTsCsAsT-C_{16}	antisense, AS PPS−C_{16}	37.2	3757.05	3756.47 ± 0.15
AsTsGoAoCsGoGoAsAsTsA-C_{16}	sense, S PPS−C_{16}		3864.14	3863.51 ± 0.14
TsTsAoToAsCoGoTsCsCsT-C_{16}	mismatch		3757.05	3756.24 ± 0.16
AsTsCoToTsAoCoGsTsTsC-C_{16}	scrambled		3757.05	3778.17 ± 0.24[c]

[a] s = phosphorothioate internucleoside linkage, o = phosphodiester internucleoside linkage. [b] T_m of duplex formed with r(AUGACGGAAUA). [c] M + Na^+.

Biosystems, Foster City, CA). The PPS−C_{16} ODNs were prepared starting with the C_{16}-derivatized CPG support **3**. Where the introduction of phosphorothioate linkages was required, sulfurization was performed immediately after coupling using 0.075 M Beaucage reagent (Aldrich) in acetonitrile (*24*), followed by capping with 10% acetic anhydride, 10% 2,6-lutidine, and 16% *N*-methylimidazole in THF. All ODNs were deprotected by treatment with concentrated ammonia at 55 °C for 16 h and then purified by electrophoresis through a denaturing 19% polyacrylamide gel. After elution with 2% SDS, 75 mM EDTA, 0.3 M NaCl in 0.2 M Tris-HCl buffer, pH 7.6, and ethanol precipitation, the ODNs were dissolved in deionized water. The purity and integrity of all ODNs were found to be greater than 95% by HPLC on Waters Gen-Pak FAX column using a 0.1−1.5 M NaCl gradient in 20% acetonitrile containing 10 mM NaH_2PO_4. The ODNs were further analyzed by negative ion electrospray mass spectroscopy (Fisons Bio-Q, U.K.) that, in all cases, confirmed the correct mass (Table 1).

Thermal Denaturation of Oligomer Heteroduplexes. ODNs were mixed with the complementary oligoribonucleotides at 1 μM of each strand in 10 mM sodium phosphate buffer, pH 7.4, containing 140 mM KCl and 0.1 mM EDTA. Absorbance vs temperature profiles (15−85 °C, heating rate 0.5 °C/min) were recorded at 260 nm using a 8452A diode array spectrophotometer (Hewlett-Packard). All samples were premelted at 85−90 °C and then allowed to thermally equilibrate. In Table 1, the T_m values are the mean values of at least three measurements.

Preparation of ODN−Lipofectin Complexes and ODN Treatment of Cells. ODN−lipofectin complexes were prepared as recommended by the manufacturer using Lipofectin Reagent (1 mg/mL; Life Technologies, Gaithersburg, MD), a 1:1 (w/w) mixture of *N*-[1-(2,3-dioleyloxy)propyl]-*N*,*N*,*N*-trimethylammonium chloride and dioleyl phosphatidylethanolamine. Briefly, 7 μL of lipofectin was diluted into 100 μL of DMEM and allowed to stand at room temperature for 30 min. The diluted lipofectin was gently mixed with 100 μL of 0−50 μM ODN solution in DMEM and incubated for an additional 15 min. Finally, the mixture was combined with 800 μL of DMEM.

RS485 or RS504 cells were seeded in 6-well plates (10^5 cells/well) and, 18−24 h later at 40−60% confluence, treated with ODNs. The medium was removed, 1 mL of fresh, serum-supplemented DMEM containing ODNs at various concentrations was added to each well, and the plates were incubated at 37 °C in a humidified atmosphere containing 5% CO_2 for 48 h.

In lipofectin-mediated treatment, the RS485 cells were washed twice with serum-free medium and then overlayed with 1 mL of DMEM containing an ODN−lipofectin complex. After 6 h, 1 mL of DMEM supplemented with 4 mM L-glutamine and 20% FCS was added, and incubation was continued for an additional 42 h.

Postincubational 5′-End ^{32}P-Labeling of Oligonucleotides. The unlabeled ODNs were incubated in media with RS504 cells for 24 h. After incubation, the media with ODNs was removed from the cell monolayer, heated to 95 °C for 5 min, and immediately cooled on ice. The 5′-end ^{32}P-labeling was performed with [γ-^{32}P]ATP, 6000 Ci/mmol, (NEN, Boston, MA) and T4 polynucleotide kinase in a reaction buffer provided by New England Biolabs (Beverly, MA) as recommended (*25*). The reaction mixtures were separated on 19% polyacrylamide/urea gels and bands visualized via autoradiograhpy using Biomax MS film (Kodak).

Preparation of Cell Lysates and Western Blot Analysis of Ras Protein. For total cellular protein determination, the cells were washed twice with phosphate-buffered saline (PBS), overlayed with 0.5 mL of RIPA buffer (PBS, 1% nonidet P-40, 0.5% sodium deoxycholate, and 0.1% SDS), and agitated gently for 60 min at room temperature. Total protein in the lysate was determined using the Pierce Micro BCA protein assay reagent kit (Pierce, Rockford, IL).

For Western analysis, the cells were washed with PBS, harvested with trypsin, collected by centrifugation at 1000*g* for 7 min at 4 °C, and washed once more with cold PBS. The cells were resuspended in 50−100 μL of cold RIPA buffer, containing 0.1 mg/mL PMSF, 30 μg/mL aprotinin, and 1 mM sodium orthovanadate, and lysed for 20 min in an ice bath. The lysates were passed through a 21 gauge needle, incubated on ice an additional 30 min, and then centrifuged at 15000*g* for 20 min at 4 °C. Protein concentrations of the cleared lysates were measured and the lysates aliquoted and stored at −80 °C.

Lysate samples, containing 40 μg of total protein, were denatured, separated on a 12.5% SDS−PAGE, and electroblotted onto Protran BA 85 nitrocellulose transfer membrane (Schleicher and Schuell, Keene, NH). To block nonspecific binding, the membrane was incubated at room temperature for 1 h with 5% nonfat dry milk in 10 mM Tris-HCI buffer, pH 8.0, containing 150 mM NaCl and 0.05% Tween 20 (TBST). The blot was probed for 4 h with 0.1 μg/mL human Ras p21-directed primary antibody (C-20, rabbit polyclonal IgG; Santa Cruz Biotechnology, Santa Cruz, CA) and washed three times with TBST. Proteins were detected using 1:1000 diluted horseradish peroxidase-conjugated goat anti-rabbit IgG (Santa Cruz Biotechnology), ECL Western blotting detection reagent, and Hyperfilm ECL (Amersham). Films were scanned and quantified using a PDI scanner, model DNA 35 (Huntington Station, NY), and the Quantity One PDI analysis software.

In Vitro Radiobiology. The in vitro response of anti-*ras* ODN-treated T24 cells to radiation was evaluated by

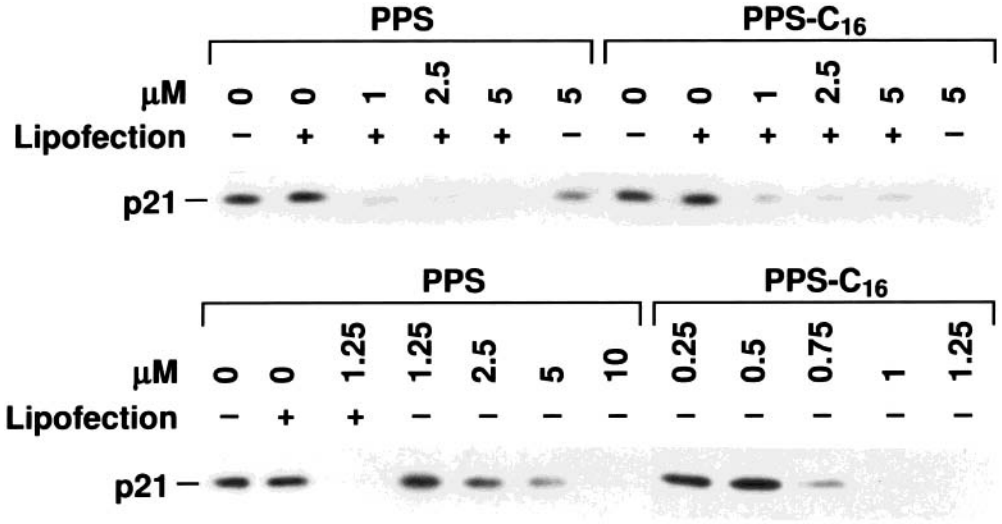

Figure 2. Representative Western blot analysis of human Ras p21 levels in RS485 cells treated with free (−) or lipofectin-bound (+) antisense PPS or PPS-C_{16} ODNs. RS485 cells were incubated with ODNs for 48 h. Cell lysates were fractionated by discontinuous gel electrophoresis. Ras p21 was detected using human Ras p21-directed rabbit primary antibody, peroxidase-conjugated goat anti-rabbit IgG, and ECL Western blotting reagents.

the cell survival assay (*26*). Briefly, T24 cells were seeded at 3×10^4 cells/well of a 6-well tissue culture plate. Twenty-four hours later, the cells were treated with antisense (or sense) PPS−C_{16} ODNs at 1 μM concentration in 1 mL of medium (DMEM plus 10% FCS, glutamine, and antibiotics) per well. After 48 h at 37 °C, the cells were harvested, suspended in fresh medium, and irradiated with graded doses of ^{137}Cs γ-rays at a dose rate of 36 Gy/min in a Mark I irradiator (J. L. Shepard and Associates, San Fernando, CA) at room temperature. Irradiated cells were plated at 300−5000 cells/well and incubated in 3 mL of medium per well at 37 °C.

Two days after plating, the wells were supplemented with 0.5 mL of FCS plus 5 μg/mL hydrocortisone. Ten to fourteen days later, the plates were stained with 1% crystal violet and colonies of 50 cells or more of normal appearance were scored. D_{10} (the dose required to reduce survival to 10%) values were calculated from the initial survival data.

In Vivo Studies. To evaluate the ability of antisense ODNs to sensitize tumors to radiation in vivo, female athymic nude mice were subcutaneously injected with 5×10^6 radiation-resistant RS504 cells in 50 μL of PBS. Tumors were treated with ODNs when the size of the tumors was between 2 and 6 mm^3. A total of 50 μL/tumor of a 5 μM solution of antisense (or sense) PPS−C_{16} ODN (250 pmol) was injected directly into the tumors. After 24 h, the tumor area only was irradiated with 2.0−2.5 Gy. The irradiation was repeated every 48 h until an accumulated dose of 20 Gy had been delivered. ODN injections were repeated at 48 h (50 μL), 192 h (50 μL), and 240 h (100 μL) following the initial injection. Tumor volume was recorded in mm^3. For comparison, some tumors received only the antisense PPS−C_{16} or only radiation, while one group of tumors was left completely untreated.

RESULTS

Synthesis of 1-*O*-Hexadecylglycerol ODN Conjugates. In the antisense PPS ODN (see Table 1) that targets the initiation codon region 5′ AUG ACG GAA UA 3′ of human Ha-*ras* mRNA (*27*), the phosphorothioate pattern was designed according to the "minimal protection" strategy (*7*). To render the ODN stable against 3′- and 5′-exonucleases, it was capped by three and two phosphorothioate residues at the 3′- and 5′-ends, respectively. An additional phosphorothioate linkage was also placed between internal pyrimidine nucleosides, major sites of degradation by endonucleases. The position of the phosphorothioate linkages was retained in the structure of the control ODNs (Table 1).

Figure 1 shows that PPS−C_{16} ODNs contain an extra phosphodiester linkage joining the 3′-terminal nucleoside with the 1-O-hexadecylglycerol residue, intended to facilitate permeation of the cell membrane. The 3′-end 1-*O*-hexadecylglycerol residue might also provide additional resistance to 3′-exonucleases. In the solid-phase synthesis of PPS−C_{16} ODNs, the general strategy of MacKellar et al. (*28*) for alcohol end-attachment was adopted. Thus, [1-(4,4′-dimethoxytrityl)-2-succinyl-3-hexadecyl]glycerol (**2**) was first synthesized starting from commercially available 1-*O*-hexadecyl-*rac*-glycerol (**1**), which was regioselectively dimethoxytritylated at the primary hydroxy group and then converted to the corresponding succinate **2** in 62% overall yield (Scheme 1). The succinic acid mono-(1-*O*-dimethoxytrityl-3-hexadecyl-*rac*-glycerol)-ester **2** was then coupled with TBTU/*N*-ethylmorpholine to a 550 Å aminopropyl-CPG to yield the functionalized solid support **3** (Scheme 1) with a loading of 80 μmol/g.

Purified by denaturing PAGE, antisense PPS or PPS−C_{16} undecamers and complementary oligoribonucleotide r(AUGACGGAAUA) formed heteroduplexes with almost identical T_ms of 36.9 and 37.2 °C, respectively (Table 1). These values are approximately 4 °C higher than the T_m measured for the corresponding heteroduplex with uniformly phosphorothioated ODN (data not shown).

Inhibition of Ras p21 Expression by PPS−C_{16} ODN Conjugates in RS485 and RS504 Cells. To evaluate the in vitro anti-*ras* activity of the PPS and PPS−C_{16} ODNs, the human Ras p21 level was determined in RS485 cells by Western blot analysis after cell treatment with ODNs alone or in combination with lipofectin. The concentration of the ODNs was varied in the 0.25−5 μM range, while the concentration of lipofectin, where included, was kept constant at 7 μg/mL. Representative results of the Western analysis and relating quantitative data are shown in Figures 2−4. The comparison of the dose effect obtained without lipofectin (Figures 3 and 4) shows that, while 5 μM antisense PPS

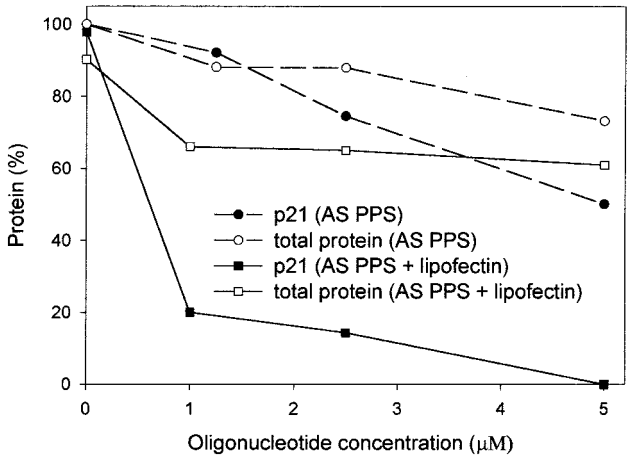

Figure 3. Ras p21 and total protein levels in RS485 cells versus concentration of free or lipofectin-bound antisense (AS) PPS ODNs. RS485 cells were incubated with ODNs for 48 h. At a fixed ODN concentration, three experiments were run in parallel in three separate wells. Before quantifying, lysates from the wells were combined to obtain an average value. The level of Ras p21 was determined by Western blot analysis.

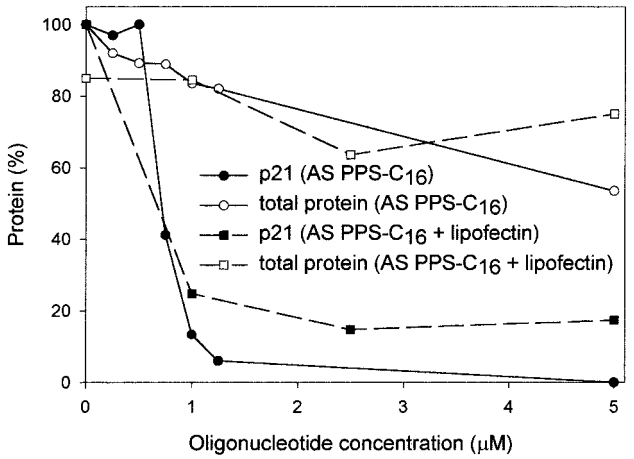

Figure 4. Ras p21 and total protein levels in RS485 cells versus concentration of free or lipofectin-bound antisense (AS) PPS−C_{16} ODNs. RS485 cells were incubated with ODNs for 48 h. At a fixed ODN concentration, three experiments were run in parallel in three separate wells. Before quantifying, lysates from the wells were combined to obtain an average value. The level of Ras p21 was determined by Western blot analysis.

ODN was required to reach 50% inhibition of Ras p21, the same level of inhibition was achieved with the PPS−C_{16} at a concentration less than 0.75 μM. Additionally, PPS−C_{16} ODN exerted its major effect (up to 94% inhibition) in a narrow range of concentrations, 0.5−1.25 μM, although a 5 μM concentration was required to completely supress the human Ha-*ras* expression in RS485 cells (Figure 4). Interestingly, within the 0.75−5 μM interval, the PPS−C_{16} ODN without lipofectin was even slightly more efficient in inhibiting Ha-*ras* expression than either the lipofectin-PPS ODN complex or the lipofectin-PPS−C_{16} ODN complex (Figures 3 and 4).

At 7 μg/mL, a concentration considered to be nontoxic (*11*), lipofectin alone did not affect Ras p21 synthesis (Figures 3 and 4). In contrast, total cellular protein appeared to be more sensitive to lipofectin treatment, decreasing by 15% in the absence of ODNs. The same decline in total protein synthesis was observed with antisense PPS−C_{16} ODN treatment at a concentration of 1−1.25 μM, where Ras p21 synthesis was already 89−95% inhibited.

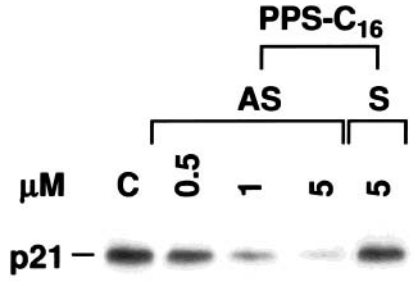

Figure 5. Western blot analysis of Ras p21 levels in RS504 cells treated by antisense (AS) or sense (S) PPS−C_{16} ODNs. Lane C corresponds to untreated RS504 cells. RS504 cells were incubated with ODNs for 48 h. Cellular lysates were fractionated by discontinuous gel electrophoresis. Ras p21 was detected using human Ras p21-directed rabbit primary antibody, peroxidase-conugated goat anti-rabbit IgG, and ECL Western blotting reagents.

To estimate the sequence specificity of the inhibition, three control PPS−C_{16} ODNs were tested at a concentration of 1.25 μM. The relative levels of Ras p21 were 87, 97, and 124% for the sense, mismatched, and scrambled PPS−C_{16} ODNs, respectively. None of the controls decreased total protein synthesis by more than 6%.

The antisense efficacy and sequence specificity of the PPS−C_{16} ODN were also tested using RS504 cells, another murine transformant expressing mutated human c-Ha-ras (*22*). Scanning of the bands in Figure 5, we found 16, 73, and 92% inhibition of p21 synthesis at 0.5, 1, and 5 μM, respectively. At the highest tested concentration (5 μM), the control sense PPS−C_{16} ODN caused only minimal (13%) inhibition of Ras p21 and total protein syntheses.

To evaluate serum stability, C_{16}-conjugated and nonconjugated ODNs were incubated for 24 h in complete medium with RS504 cells and then postlabeled with [γ-^{32}P]ATP (Figure 6). No degradation was seen in the case of the antisense PPS−C_{16} ODN (lane 4 in Figure 6), while the nonconjugated PPS ODN showed at least some cleavage products (lane 3). The bands shown in lane 3 represent degradation products less than 6 nucleotides in length (*25*).

Reversal of Radiation Resistant Phenotype by Antisense PPS−C_{16} ODN in Vitro and in Vivo. *Ras* genes are known to be involved in signal-transduction of various factors for growth, differentiation, and oncogenesis (*29, 30*). Moreover, a strong association has been made between the presence of either a mutated form of, or overexpression of the normal, Ha-*ras* gene and cellular radiation resistance (*26*). Treatment of cells with an abnormal Ha-*ras* gene (RS485 and RS504) with antisense PPS−C_{16} was able to downregulate Ras expression. Since the failure to respond to radiotherapy is a significant problem in the treatment of human cancer, we wished to determine if the downmodulation could revert a radiation-resistant phenotype, such as the radiation-resistant T24 human bladder carcinoma cell line. As shown in Figure 7, there was a decrease in the radiation resistance level of the cells treated with 1 μM antisense PPS−C_{16} ODN, reducing the D_{10} level from 5.4 ± 0.2 Gy to 4.5 ± 0.4 Gy, a value in the range considered to be radiosensitive.

To examine the possible therapeutic potential of antisense PPS−C_{16} ODN in treating human cancer, we wished to determine if the radiosensitization observed in vitro translated to the in vivo radiation-induced inhibition of tumor growth in a mouse model. Since T24 cells are poorly tumorigenic, the radiation-resistant NIH/

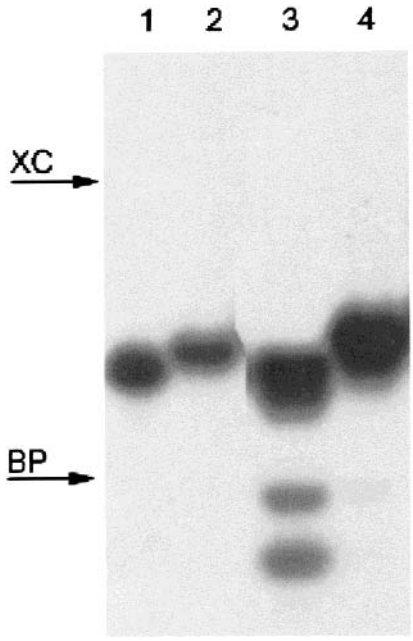

Figure 6. Autoradiograph of antisense PPS and PPS−C_{16} ODNs (lanes 3 and 4, respectively), incubated 24 h with RS504 cells in serum-supplemented medium and then 5′-end ^{32}P-labeled in withdrawn heat-denatured medium. Control antisense PPS and PPS−C_{16} ODNs are shown in lanes 1 and 2, respectively. ODNs were separated by electrophoresis on 19% polyacrylamide/urea gel. XC, xylene cyanol, and BP, bromophenol blue. These dyes comigrate with ODNs of 22 and 6 nucleotides, respectively (*25*).

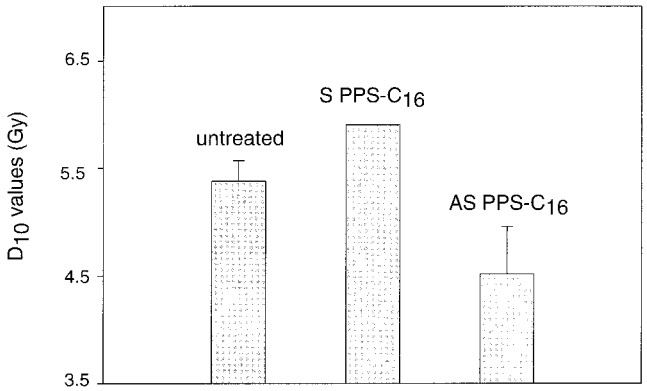

Figure 7. Effect of sense (S) or antisense (AS) PPS−C_{16} ODNs on the radiation resistance level of T24 bladder carcinoma cells in vitro. T24 cells were incubated with antisense or control sense PPS−C_{16} ODNs at 1 μM for 48 h, and then irradiated with graded doses of ^{137}Cs γ-rays. Radioresistance levels are given as D_{10} values. Error bars represent SEM of 1−3 values.

3T3 transformant cell line RS504 was used in this experiment. RS504 was obtained by transfection of NIH/3T3 with genomic DNA from T24 cells and consequently carries the point mutated human Ha-*ras* gene (*22*). As shown in Figure 5, treatment of RS504 with antisense PPS−C_{16} ODN in vitro was able to decrease synthesis of Ras p21.

Subcutaneous RS504 tumors were induced in female nude mice. Once the tumors were palpable, they were intratumorially injected with 250 pmol of the antisense PPS−C_{16} ODN or, as control, sense PPS−C_{16} ODNs. Radiation treatment was started 24 h later. Radiation was administered every other day. A total of four injections of the ODN (days 0, 2, 8, and 10) and a total of 20 Gy (days 1, 3, 5, 7, 9, 11, 13, 15, and 17) were administered over the course of 18 days. The results of this

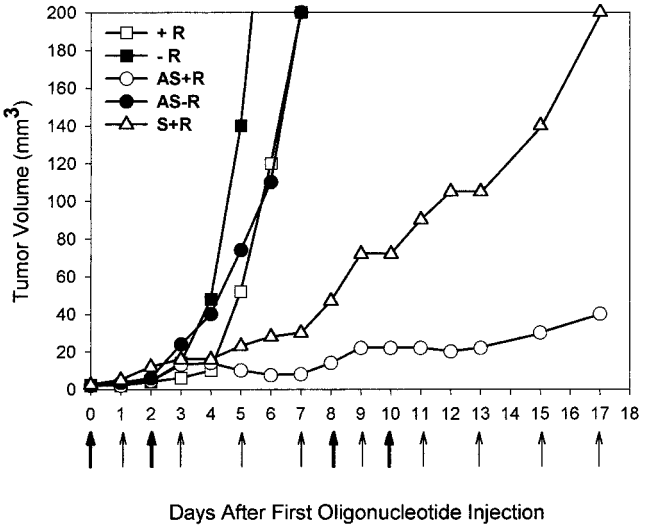

Figure 8. Effect of combination of sense (S) or antisense (AS) PPS−C_{16} ODNs and radiation on tumor growth in a xenograft mouse model. RS504 cells were subcutaneously injected on the back of female athymic nude mice. The antisense or sense PPS−C_{16} ODNs (250 pmol in 50 μL) were injected directly into the tumors. Beginning 24 h after the first ODN injection, the tumor area only was exposed to 2−2.5 Gy doses of ionizing radiation (X-rays), as indicated by the arrows, to a total of 20 Gy. (−R) Control untreated tumor; (+R) tumor received only radiation; (AS+R) tumor treated with AS PPS−C_{16} ODN and radiation; (AS-R) tumor treated with AS PPS−C_{16} ODN only; (S+R) tumors treated with control S PPS−C_{16} ODN and radiation. Bold arrows indicate ODN injections; thin arrows indicate doses of irradiation.

experiment are shown in Figure 8. Neither the antisense PPS−C_{16} ODN nor radiation alone had much effect on tumor growth. Although some nonspecific radiosensitizing effect was observed with the control sense ODN, only the combination of the antisense treatment and radiation was able to significantly inhibit the growth of these tumors. These results demonstrate the considerable potential of the PPS−C_{16} modified anti-*ras* ODNs in future clinical studies of radiation resistance reversal.

DISCUSSION

The antisense efficacy and sequence-specificity of ODNs, bearing 3′-terminally attached acyclic hydrocarbons, has been the subject of only a few studies. Encouraging results were obtained with an antisense nonamer carrying a dodecandiol tail at the 3′-end which was directed against codon 12 point mutated Ha-*ras* (18). This derivative, designed as a control for a more sophisticated 3′,5′-disubstituted construct with acridine at the 5′-end, was used in both cell-free and cell-based translation assays. The former assay showed that the concentration needed for 50% inhibition of targeted mRNA translation was 1.5 μM, i.e., 15 times lower than was the case with the nonmodified parent ODN and 3 times higher than the double terminally modified construct. Although no data was shown, it was mentioned that the dodecandiol tail caused a 4-fold increase in the uptake of the nonamer by T24 cells (*18*).

Quantitative, and even qualitative, results of cellular uptake and biological activity of lipophilic conjugates may vary significantly depending on the cells employed, the antisense ODN backbones, and/or the lipophilic group position in a conjugate structure. This has been demonstrated by a recent comparison of methylphosphonate chimeric ODNs, all 3′-labeled with fluorescein and 5′-modified with lipophilic groups, such as dodecanol,

cholesterol, or vitamin E (*31*). None of the conjugated substances, as well as lipofectin, improved delivery of the chimeric 18-mer or displayed molecular effects in human leukemic KYO1 cells. Moreover, the ODN, when conjugated to cholesterol or vitamin E, caused lysis of the target cells if its concentration exceeded 2 μM.

The remainder of the currently available data was obtained using viral assays where the host cell survival was not the principal issue. A 5′ undecyl-modified antisense undecamer was used to inhibit synthesis of the influenza virus polymerase 3 (and, consequently, virus reproduction) in infected MDCK cells (*19*). It has been shown semiquantitatively that the obtained suppression was sequence specific and modification dependent. However, suppression of virus reproduction was achieved at conjugate concentrations of 50−200 μM.

A more comprehensive study, including evaluation of cellular uptake and cellular toxicity, was carried out with phosphodiester ODNs, 5′-end conjugated to 1,2-di-O-hexadecyl-*rac*-glycerol, complementary to the initiation codon regions of the N, NS, and G protein mRNAs of vesicular stomatitis virus (*20*). In comparison to the PPS−ODN-3′-glycerol-hexadecyl-mono-ether conjugate of this work, the 5′-glycerol-bis-hexadecylesters phosphodiester ODN conjugates of Shea et al. (*20*) should be even more lipophilic, but metabolically much less stable, since they are neither protected against 3′-exonucleases nor against endonucleases present in serum. These glycerol-bis-hexadecyl ether conjugated ODNs associated 8−10 times more efficiently with uninfected L929 cells than either phosphodiester or phosphorothioate ODNs. Although these conjugates showed enhanced antiviral activity, they suffered from poor sequence discrimination (*20*), an observation also made with lipophilic antisense conjugates in other viral assay systems (*32*). Furthermore, no adequate solution to the proof of antisense mechanism in viral replication studies is available (*33*).

In our study, the "minimal protection strategy" (*7*) was applied to minimize the number of PS bonds to render the ODN resistant to nuclease degradation and at the same time retain sequence specificity. In addition, a 1-*O*-hexadecylglycerol was attached to the 3′-terminal phosphate group of the antisense and control ODNs, which confers additional stability against 3′-exonucleases, rendering them practically indigestible in complete medium with RS504 cells. In principle, antisense oligonucleotides with a free 3′-hydroxy group could serve as primers for DNA polymerases and reverse transcriptases in vivo. Clearly, a 3′-modification fully deprives the conjugates of priming properties.

Due to the decreased content of PS groups, both antisense PPS and PPS−C_{16} ODNs formed more thermostable hybrids with complementary RNA than the uniformly PS-modified ODN ($\Delta T_m = +4.2$ °C). Moreover, the attached lipophilic fragment did not affect the duplex stability. In preliminary studies, we have also investigated the uptake of the PPS−ODN-3′-glycerol-hexadecyl-monoether with a fluorescence label at its 5′-end by fluorescence microscopy. A 1 μM ODN concentration was used for incubation of NIH/3T3 cells in the absence of uptake enhancers. After 4 h, strong fluorescence could be observed inside the cells, concentrated mostly in the nucleus. No punctate distribution was observed as is frequently reported. The same FITC-labeled ODN without the 3′-glycerol-hexadecyl-monoether did not show any significant uptake under the same conditions (E. Unger, G. Gothe, M. Schwerdel, and E. Uhlmann, unpublished results). In summary, the fluorescence microscopy study showed us that the lipophilic 3′-end modification does not only enhance cell uptake of the ODN, but appears also to influence the intracellular distribution in favor of nuclear localization.

Comparison of the effect of antisense PPS and PPS−C_{16} ODNs on target human Ras p21 synthesis in RS485 or RS504 cells clearly demonstrated a dramatic increase in anti-Ras activity caused by the 3′-end hexadecylglyceryl group. The dose of PPS−C_{16} ODN necessary to decrease p21 expression by 50% in these *ras*-transformed cells in culture was 8- to 10-times lower than that of PPS−ODN. The addition of lipofectin had no significant effect on the delivery and inhibitory effect of the PPS−C_{16} ODN. More than 90% inhibition was reached at a concentration of 1 μM. This ability to reach high levels of specific inhibition at low concentrations of oligonucleotide in the absence of lipofectin has the benefit of reducing the toxic side effects sometimes seen with lipofectin treatment. In our studies, the PPS−C_{16} oligonucleotide at concentrations ranging from 0.25 to 1.0 μM inhibits cell growth by only 6 to 16%.

Of particular importance to future applications of antisense oligonucleotide treatment of tumors is the efficacy of the PPS−C_{16} anti-*ras* oligonucleotide in reversing the radiation resistance associated with tumors that arise through activation of the *ras* oncogene. Our experiments show that *ras*-transformed T24 cells in culture and RS504-induced tumors in nude mice (which contain an activated *ras*) are more sensitive to ^{137}Cs γ-rays following introduction of PPS−C_{16} oligonucleotides into the cells and injection into the tumors.

CONCLUSION

In conclusion, (i) a synthetic route for obtaining 3′-end conjugates of minimally phosphorothioate-protected oligonucleotides with 1-*O*-hexadecylglycerol was designed; the route is compatible with standard phosphoramidite chemistry and the solid-phase strategy; (ii) 3′-end C_{16} modification does not alter the hybridization properties of ODNs and increases nuclease resistance and antisense potency of partially phosphorothioated oligonucleotides without affecting their sequence specificity; (iii) in *ras*-transformed cells in culture, the addition of a C_{16} alkyl group provides the ODN with the ability to exert high inhibitory activity without the need of uptake enhancers; (iv) treatment of T24 tumor cells with partially phosphorothioated C_{16}-modified anti-*ras* undecamer reverts the radiation resistant phenotype of the cells in vitro; (v) the combination of intratumorial injection of C_{16}-modified anti-*ras* undecamer and radiation treatment inhibits the growth of RS504 xenograft tumors in a synergistic manner due to reversal of radio-resistance.

ACKNOWLEDGMENT

This work was supported in part by National Foundation for Cancer Research, Grant HU0001 (E.H.C). We are indebted to S. Hein, L. Hornung, and C. Weiser for excellent technical assistance and to Dr. A. Schaefer and M. Girg for measuring the ESI mass spectra.

LITERATURE CITED

(1) Cook, P. D. (1993) Medicinal Chemistry Strategies for Antisense Research. In *Antisense Research and Applications* (S. T. Crooke and B. Lebleu, Eds.) pp 149−187, CRC Press, Boca Raton, FL.

(2) Uhlmann, E., and Peyman, A. (1990) Antisense Oligonucleotides: A New Therapeutic Principle. *Chem. Rev. 90,* 543−584.

(3) Agrawal, S., and Zhao, Q. (1998) Antisense Therapeutics. *Curr. Opin. Chem. Biol. 2,* 519−528.

(4) Neckers, L. M., and Iyer, K. (1997) Non-Antisense Effects of Antisense Oligonucleotides. In *Antisense Oligodeoxynucleotides and Antisense RNA* (B. Weiss, Ed.) pp 79−89, CRC Press, Boca Raton, FL.
(5) Stein, C. A., Subasinghe, C., Shinozuka, K., and Cohen, J. S. (1988) Physicochemical Properties of Phosphorothioate Oligodeoxynucleotides. *Nucleic Acids Res. 16*, 3209−3221.
(6) Hoke, G. D., Draper, K., Freier, S. M., Gonzalez, C., Driver, V. B., Zounes, M. C., and Ecker, D. J. (1991) Effects of Phosphorothioate Capping on Antisense Oligonucleotide Stability, Hybridization and Antiviral Efficacy Versus Herpes Simplex Virus Infection. *Nucleic Acid Res. 19*, 5743−5748.
(7) Peyman, A., and Uhlmann, E. (1996) Minimally Modified Oligonucleotides - Combination of End-Capping and Pyrimidine-Protection. *Biol. Chem. Hoppe-Seyler 377*, 67−70.
(8) Stein, C. A. (1997) Controversies in the Cellular Pharmacology of Oligodeoxynucleotides. *Oligonucleotides as therapeutic agents* (Ciba Foundation Symposium 209), pp 79−93, Wiley, Chichester.
(9) Chiang, M.-Y., Chan, H., Zounes, M. A., Freier, S. M., Lima, W. F., and Bennett, C. F. (1991) Antisense Oligonucleotides Inhibit Intercellular Adhesion Molecule-1 Expression by Two Distinct Mechanisms. *J. Biol. Chem. 266*, 18162−18171.
(10) Bennett, C. F., Chiang, M., Chan, H., Shoemaker, J. E. E., and Mirabelli, C. K. (1992) Cationic Lipids Enhance Cellular Uptake and Activity of Phosphorothioate Antisense Oligonucleotides. *Mol. Pharmacol. 41*, 1023−1033.
(11) Marcusson, E. G., Balkrishen, B., Manoharan, M., Bennett, C. F., and Dean, N. M. (1998) Phosphorothioate Oligodeoxyribonucleotides Dissociate from Cationic Lipids Before Entering the Nucleus. *Nucleic Acids Res. 26*, 2016−2023.
(12) Senior, J. H., Trimble, K. R., and Maskiewicz, R. (1991) Interaction of Positively-Charged Liposomes with Blood: Implication for Their Application In Vivo. *Biochim. Biophys. Acta 1070*, 173−179.
(13) Gao, X., and Huang, L. (1995) Cationic Liposome-Mediated Gene Transfer. *Gene Ther. 2*, 710−722.
(14) Letsinger, R. L., Zhang, G., Sun, D. K., Ikeuchi, T., and Sarin, P. S. (1989) Cholesterol-Conjugated Oligonucleotides: Synthesis, Properties, and Activity as Inhibitors of Replication of Human Immunodeficiency Virus in Cell Culture. *Proc. Natl. Acad. Sci. U.S.A. 86*, 6553−6556.
(15) Boutorin, A. S., Gus'kova, L. V., Ivanova, E. M., Kobetz, N. D., Zarytova, V. F., Ryte, A. S., Yurchenko, L. V., and Vlassov, V. V. (1989) Synthesis of Alkylating Oligonucleotide Derivatives Containing Cholesterol or Phenazinium Residues at Their 3′-Terminus and Their Interaction with DNA within Mammalian Cells. *FEBS Lett. 254*, 129−132.
(16) Ryte, A. S., Karamyshev, M. V., Nechaeva, M. V., Guskova, Z. V., Ivanova, E. M., Zarytova, V. F., and Vlassov, V. V. (1992) Interaction of Cholesterol-Conjugated Alkylating Oligonucleotide Derivatives with Cellular Biopolymers. *FEBS Lett. 299*, 124−126.
(17) Will, D. W., and Brown, T. (1992) Attachment of Vitamin E Derivatives to Oligonucleotides During Solid-Phase Synthesis. *Tetrahedron Lett. 33*, 2729−2732.
(18) Saison-Behmoaras, T., Tocquo, B., Rey, I., Chassignol, M., Thuong, N. T., and Hilone, C. (1991) Short Modified Antisense Oligonucleotides Directed Against Ha-*ras* Point Mutation Induce Selective Cleavage of the mRNA and Inhibit T24 Cells Proliferation. *EMBO J. 10*, 1111−1118.
(19) Kabanov, A. V., Vinogradov, S. V., Ovcharenko, A. V., Krivonos, A. V., Melik-Nubarov, N. S., Kiselev, V. I., and Severin, E. S. (1990) A New Class of Antivirals: Antisense Oligonucleotides Combined with a Hydrophobic Substituent Effectively Inhibit Influenza Virus Reproduction and Synthesis of Virus-Specific Proteins in MDCK Cells. *FEBS Lett. 259*, 327−330.
(20) Shea, R. G., Marsters, J. C., and Bischofberger, N. (1990) Synthesis, Hybridization Properties and Antiviral Activity of Lipid-Oligodeoxynucleotide Conjugates. *Nucleic Acids Res. 18*, 3777−3783.
(21) Chang, E. H., Furth, M. A., Scolnick, E. M., and Lowy, D. R. (1982) Tumorigenic Transformation of Mammalian Cells Induced by a Normal Human Gene Homologous to the Oncogene of Harvey Murine Sarcoma Virus. *Nature 297*, 479−483.
(22) Tabin, C. J., Bradley, S. M., Bargmann, C. I., Weinberg, R. A., Papageorge, A. G., Scolnick, E. M., Dhar, R., Lowy, D. R., and Chang, E. H. (1982) Mechanism of Activation of a Human Oncogene. *Nature 300*, 143−149.
(23) Reddy, E. P., Reynolds, R. K., Santos, E., and Barbacid M. (1982) A Point Mutation Is Responsible for the Acquisition of Transforming Properties by the T24 Human Bladder Carcinoma Oncogene. *Nature 300*, 149−152.
(24) Iyer, R. P., Egan, W., Regan, J. B., and Beaucage, S. L. (1990) 3H-1,2-Benzodithiole-3-one 1,1-Dioxide as an Improved Sulfurizing Reagent in the Solid-Phase Synthesis of Oligodeoxyribonucleoside Phosphorothioates. *J. Am. Chem. Soc. 112*, 1253−1254.
(25) Sambrook, J., Fritsch, E. F., and Maniatis, T. (1989) *Molecular Cloning*, Cold Spring Harbor Laboratory Press, Plainview, NY.
(26) Pirollo, K. F., Tong, Y. A., Villegas, Z., Chen, Y., and Chang, E. H. (1993) Oncogene-Transformed NIH 3T3 Cells Display Radiation Resistance Levels Indicative of a Signal Transduction Pathway Leading to the Radiation-Resistant Phenotype. *Radiation Res. 135*, 234−243.
(27) Chang, E. H., Yu, Z., Shinozuka, K., Zon, G., Wilson, W. D., and Strekowska, A. (1989) Comparative Inhibition of *ras* p21 Protein Synthesis with Phosphorus-Modified Antisense Oligonucleotides. *Anti-Cancer Drug Des. 4*, 221−232.
(28) MacKellar, C., Graham, D., Will, D. W., Burgess, S., and Brown, T. (1992) Synthesis and Physical Properties of *Anti*-HIV Antisense Oligonucleotides Bearing Terminal Lipophilic Groups. *Nucleic Acids Res. 20*, 3411−3417.
(29) Marshall, C. J. (1996) Ras Effectors. *Curr. Opin. Cell Biol. 8*, 197−204.
(30) Khosravi-Far, R., Campbell, S., Rossman, K. L., and Der, C. J. (1998) Increasing Complexity of Ras Signal Transduction: Involvement of Rho Family Proteins. *Adv. Cancer Res. 72*, 57−107.
(31) Spiller, D. G., Giles, R. V., Grzybowski, J., Tidd, D. M., and Clark, R. E. (1998) Improving the Intracellular Delivery and Molecular Efficacy of Antisense Oligonucleotides in Chronic Myeloid Leukemia Cells: a Comparison of Streptolysin-O Permeabilization, Electroporation, and Lipophilic Conjugation. *Blood 91*, 4738−4746.
(32) Stein, C. A., Pal, R., Devico, A. L., Hoke, G., Mumbauer, S., Kinstler, O., Sarngadharan, M. G., and Letsinger, R. L. (1991) Mode of Action of 5′-Linked Cholesteryl Phosphorothioate Oligodeoxynucleotides in Inhibiting Syncytia Formation and Infection by HIV-1 and HIV-2 In Vitro. *Biochemistry 30*, 2439−2444.
(33) Crooke, S. T. (1996) Proof of Mechanism of Antisense Drugs. *Antisense Nucleic Acid Drug Dev. 6*, 145−147.

BC990106N

Preparation of Thiol-Reactive Cy5 Derivatives from Commercial Cy5 Succinimidyl Ester†

Hermann J. Gruber,* Gerald Kada, Bernt Pragl, Christian Riener, Christoph D. Hahn, Gregory S. Harms, Werner Ahrer,‡ Thomas G. Dax,‡ Karin Hohenthanner,‡ and Hans-Günther Knaus§

Institute of Biophysics and Institute of Chemistry, J. Kepler University, Altenberger Strasse 69, A-4040 LINZ, Austria, and Institute of Biochemical Pharmacology, University of Innsbruck, Peter Mayr Strasse 1, A-6020 Innsbruck, Austria. Received August 13, 1999; Revised Manuscript Received December 2, 1999

The present study offers reliable protocols for the preparation of new thiol-reactive Cy5 derivatives which are urgently needed for single molecule fluorescence microscopy. In a systematic approach, two alternate strategies were found for the extension of commercial amine-reactive Cy5 with thiol-reactive end groups. In the two-step method, Cy5 succinimidyl ester was first reacted with ethylenediamine under conditions which gave ~99% asymmetric "Cy5-amine" and only ~1% symmetric product with two Cy5 residues. Subsequently, "Cy5-amine" was derivatized with commercial heterobifunctional cross-linkers to introduce thiol-reactive end groups (maleimide or pyridyldithio). Alternatively, commercial Cy5 succinimidyl ester was reacted with a primary amine (MTSEA, methanethiosulfonylethylamine, or PDEA, pyridyldithioethylamine) or a secondary amine (PEM, piperazinylethylmaleimide) to give the corresponding thiol-reactive derivatives in a single step. Results were good for MTSEA, moderate for PEM, and poor for PDEA. An additional drawback of the one-step method was the need for rigorous removal of unreacted Cy5 succinimidyl ester, which would label lysine residues on probe molecules. It is concluded that, except for the Cy5-MTSEA conjugate, the two-step method is much more general, reliable, and easier to follow by the typical biophysicist, biologist, etc., for whose benefit, these procedures are being published. All thiol-reactive Cy5 derivatives showed similar absorption and fluorescence properties as Cy5 succinimidyl ester, and fluorescence was fully retained after binding to thiols on proteins. The kinetics of protein labeling was also examined in order to get an idea of proper labeling conditions.

INTRODUCTION

Single molecule fluorescence microscopy (SMFM)[1] depends on fluorochrome labels with a high extinction coefficient, high fluorescence quantum yield, and high resistance to photobleaching. TMR, Cy3, Cy5, and Cy7 have been found to fulfill these requirements (Funatsu et al., 1995; Schmidt et al., 1995; Schütz et al., 1997; La Jolly Blue has not been tested yet). So far SMFM has been used in cell-free systems (Schmidt et al., 1996; Schütz et al., 1998; Trabesinger et al., 1998; Vale et al., 1996). However, the present challenge of SMFM is the imaging of single molecules in live cells, the main obstacle being high autofluorescence background. Fortunately, autofluorescence is very low at excitation wavelengths of >600 nm (Aubin, 1979; Benson et al., 1979; Marelius, 1995; Wolfbeis and Leiner, 1985). Thus, Cy5 (λ_{ex} = 630−650 nm) is the most promising label for SMFM on cells by one-photon excitation and, as a matter of fact, a Cy5-labeled phospholipid was the first single molecule visualized in live cells (Schütz et al., 1999). Further SMFM studies on cells will require other Cy5-labeled probe molecules, but this is limited by the fact that commercial Cy5 dye can only be used for statistical labeling of proteins on lysine residues. Although statistically labeled antibodies (and other probes) may be good for high-sensitivity detection, the single molecule information is lost because the number of Cy5 per individual antibody molecule greatly varies and multiple Cy5 labels on one antibody exhibit strong quenching (e.g., by 75% at an average number of 4 Cy5 labels/IgG, unpublished observation). In addition, many probe molecules lose function when labeled with amine-reactive reagents (see Discussion); in these cases, expression and SH-specific labeling of cysteine mutants is imperative.

As the popularity of SMFM increases (see special issue in *Science*, March 12, 1999), it is obvious that thiol-

† This article is dedicated to Prof. Heinz Falk on occasion of his 60th birthday.

* To whom correspondence should be addressed. Phone: +43 (732) 2468-9271. Fax: +43 (732) 2468-822. E-mail: hermann.gruber@jk.uni-linz.ac.at.

‡ J. Kepler University.

§ University of Innsbruck.

[1] Abbreviations: BSA, bovine serum albumine; BSA-SH, BSA with ≥2 mercaptopropionyl residues on lysine residues; Cy5-monofunctional dye (or Cy5-mono-*O*-Su), sodium 1-[5-(*N*-succinimidyloxycarbonyl)-pent-1-yl]-2-[5-(3,3-dimethyl-1-ethyl-5-sulfonato-indolin-2-ylidene)-1,3-pentadien-1-yl]-3,3-dimethyl-3*H*-indolium-5-sulfonate; Cy5 derivatives were abbreviated as shown in Schemes 1-3; DIEA, *N*,*N*-diisopropyl-*N*-ethylamine; DMF, dimethylformamide; DTDP, 4, 4′-dithiodipyridine; 2-ME, 2-mercaptoethanol; MS, mass spectroscopy; MTS, methanethiosulfonyl group; MTSEA, methanethiosulfonylethylamine; NHS, *N*-hydroxysuccinimide; PDEA, 2-(2-pyridyldithio)ethylamine; PEM, *N*-[2-(1-piperazinyl)-ethyl]maleimide; PDP, 3-(2-pyridyldithio)-propionyl group; SMCC, *O*-(*N*-succinimidyl)-4-(maleimidomethyl)-cyclohexane-1-carboxylate; SPDP, *O*-(*N*-succinimidyl)-3-(2-pyridyldithio)-propionate; SbTMU, *O*-(*N*-succinimidyl)-*N*,*N*,*N*′,*N*′-bis-(tetramethylene)-uronium hexafluorophosphate.

10.1021/bc990107f CCC: $19.00 © 2000 American Chemical Society
Published on Web 02/16/2000

Table 1. R_f Values[a] and Spectral Properties[b] of Cy5 Derivatives

Cy5 derivative	R_f^{I}	R_f^{II}	R_f^{III}	absorption maximum (nm)	fluorescence yield[c]
Cy5-COOH	0.09	0.17	0.27	647	nd
Cy5-CO-NHS	0.30	0.37	0.40	647	≡1.0
Cy5-MTSEA	0.25	0.28	0.31	648	1.4
Cy5-amine	0.11	0.10	0.08	648	1.1
Cy5-PDP	0.35	0.25	0.36	648	1.7
Cy5-mal	0.31	0.24	0.25	648	0.7
Cy5-mal-BSA[d]				653	1.7

[a] R_f values were determined after spotting from the reaction mixture, i.e., from DMF solution. To some degree these R_f values depended on the time between spotting and TLC plate development. [b] In comparison to Cy5-monofunctional dye. Determined in buffer A, except for Cy5-MTSEA which was measured in buffer C. [c] Cy5 was excited at 630 nm (5 nm slit) and emission was measured at 670 nm (5 nm slit). [d] Cy5-mal-BSA refers to a ratio of 0.097 ± 0.03 Cy5 labels per BSA molecule.

reactive Cy5 derivatives will be in great demand soon. Since the presentation of the Cy5-phospholipid study (Schütz et al., 1999), we have received many requests of how to synthesize the thiol-reactive Cy5 labels because they cannot be purchased. It is the goal of this report to present our methods of preparation of thiol-reactive Cy5.

EXPERIMENTAL PROCEDURES[2]

Materials. Analytical-grade materials were used as long as they were commercially available. Cy5-monofunctional dye and PD-10 columns were obtained from Amersham Pharmacia Biotech. MTSEA·HBr was purchased from Toronto Research Chemicals. DTDP, DTT, 2-ME, SMCC, and SPDP were obtained from Sigma. SbTMU was supplied by Fluka. Purified BSA (fatty acid-free) was obtained from Behring Werke AG, Germany. PDEA was purchased from BIAcore. PEM was supplied by Dojindo Laboratories.

Buffers. Buffer A contained 100 mM NaCl, 50 mM NaH_2PO_4, and 1 mM EDTA (pH 7.5 adjusted with NaOH). Buffer B contained 150 mM NaCl, 5 mM citric acid, and 1 mM EDTA (pH 5.5 adjusted with NaOH). Buffer C contained 100 mM NaCl and 20 mM sodium acetate (pH 4.5 adjusted with HCl).

Methods. General Comments. All operations were performed under dim light, and flasks containing Cy5 dye were wrapped with aluminum foil. Oxidation of primary amines (ethylenediamine, Cy5-amine, MTSEA) was suppressed by performing experiments in an argon atmosphere, especially when deprotonating with DIEA. Unless specified otherwise, all operations were at room temperature (20−25 °C).

The molar amounts of all Cy5 derivatives were determined by diluting defined aliquots from the reaction mixtures or from the dissolved products to about 1−4 μM in buffer A and recording the UV−vis absorption spectrum. Molar concentrations were calculated from absorbance at λ_{max} (Table 1), assuming the same molar extinction coefficient ($\epsilon = 250\,000\ M^{-1}\,cm^{-1}$) as published for Cy5-monofunctional dye (Mujumdar et al., 1993). No significant difference in absorption was seen whether buffer or methanol was used as solvent.

[2] The Experimental Procedures in this article describe the synthesis of Cy5-mal by the two-step procedure (Scheme 2) and the synthesis of Cy5-MTSEA by the one-step procedure (Scheme 3). More detailed descriptions of all syntheses and of covalent labeling of BSA-SH with thiol-reactive Cy5 derivatives can be found in the Supporting Information.

Scheme 1. Conversion of the Cy5-COOH Impurity in Cy5-Monofunctional Dye into the Corresponding Succinimidyl Ester

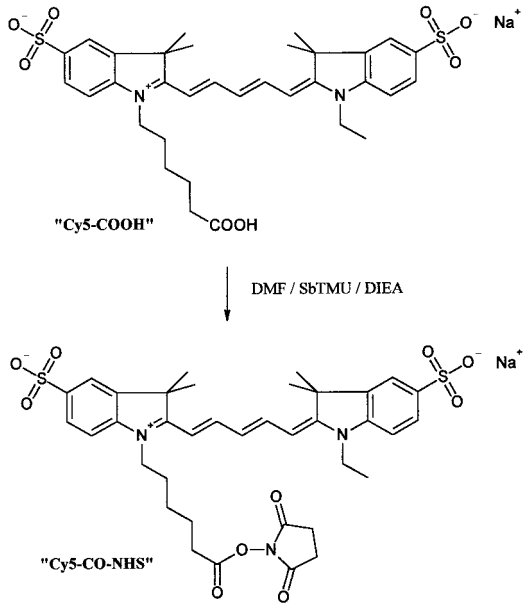

Scheme 2. Two-Step Procedure for the Synthesis of Thiol-Reactive Cy5 Derivatives

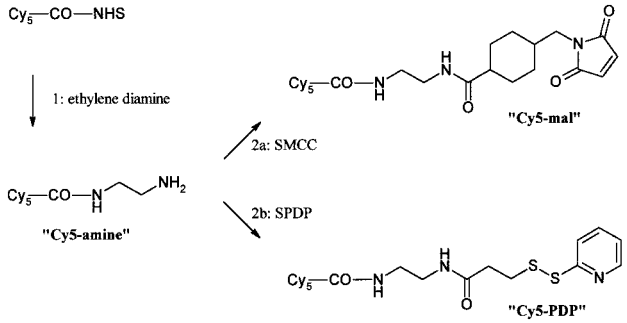

TLC. Merck plastic sheets (silica gel 60) without fluorescent indicator were used. Eluents I, II, and III contained 70 parts of chloroform, 30 parts of methanol, and 4 parts of concentrated ammonia or water or acetic acid, respectively. Cy5 derivatives were visible without staining, and other components were stained with iodine vapor.

Complete Conversion of Cy5-Monofunctional Dye into Succinimidyl Ester (Scheme 1). Commercial Cy5-monofunctional dye (4.3 μmol, a mixture of Cy5-CO-NHS with 10−50% Cy5-COOH) was dissolved in DMF (2 mL), and SbTMU (7.2 mg, 18 μmol) was added at once with stirring (Bannwarth and Knorr, 1991). DIEA (50 μL of a 5% solution in DMF, 15 μmol) was added, and the mixture was stirred for 25 min. TLC indicated quantitative conversion of Cy5-COOH into Cy5-CO-NHS (see Table 1).

Synthesis of Cy5-Amine (Scheme 2). Ethylenediamine dihydrochloride (62 mg, 470 μmol) was dissolved in water (0.8 mL), and 4 mL of DMF was added (pH ∼6−6.5). Cy5-CO-NHS (4.3 μmol, see above) was subsequently added dropwise (pH ∼7−7.5). The coupling reaction was started by dropwise addition of DIEA (400 μL of a 5% solution in DMF, 240 μmol). After 30 min of stirring, the reaction mixture was taken to dryness.

Cy5-amine was purified by low-pressure reversed-phase chromatography on Merck LiChroprep RP-18 gel (bed size 1.5 × 3.5 cm, flow 2 mL/min). Solvent A

consisted of water containing 0.1% acetic acid, and solvent B was a 5/2 mixture (v/v) of ethanol and 1-propanol (Feldhoff, 1991). The crude Cy5-amine was loaded in 2.5% solvent B. After washing with 12 mL quantities each of 5, 10, and 15 solvent B, the product was eluted with 20% solvent B. Removal of solvent gave 4.2 μmol of Cy5-amine, which was pure by TLC (see Table 1). MS (electrospray, negative mode, 80% methanol in water) *m/z* (%) = 697 (21, M), 375 (16), 348 (100, M/2), 255 (*19*). MS (electrospray, positive mode, 80% methanol in water) *m/z* (%) = 699 (27, M), 487 (13), 369 (100), 329 (20), 257 (16).

Synthesis of Cy5-mal (Scheme 2). Cy5-amine (4.2 μmol) was dissolved in DMF (1 mL) and added to dry SMCC (27 mg, 80 μmol) with stirring. Another 0.5 mL portion of DMF was used to transfer all Cy5-amine into the reaction mixture. After addition of DIEA (5 μL neat phase, 57 μmol) the mixture was stirred for 50 min, and the solvent was removed. The dry residue was dissolved in 0.4 mL of methanol and 1 mL of chloroform and diluted with 8 mL of chloroform. This solution was extracted with 2 × 20 mL of water containing 0.1% acetic acid and 6 × 20 mL of water. Residual dissolved chloroform in the combined aqueous layer was expelled with nitrogen bubbling, and after addition of solvent B (final contents 2.5%), the solution was loaded on the same LiChroprep column as used for Cy5-amine (see above). After washing with 5, 10, 15, 20, and 25% solvent B, the product was eluted at 30% solvent B. Evaporation yielded 3.3 μmol of Cy5-mal, which was pure by TLC. MS (electrospray, negative mode, 80% methanol in water) *m/z* (%) = 917 (11, M), 488 (21), 458 (100, M/2), 255 (18), 227 (11).

Cy5-mal was further purified by HPLC on a Vydac C-18 column (no. 218TP510, 250 × 10 mm, 2 mL/min, 0.1% acetic acid instead of trifluoroacetic acid in all eluents). When applying a 30 min gradient from 5 to 50%, acetonitrile pure Cy5-mal was eluted at 20−20.5 min after the start of the gradient. The solvent was removed, and the structure of Cy5-mal was confirmed by ^{1}H NMR (see below). In parallel, a small aliquot was purified on an analytical Vydac C-18 column (no,. 218TP54, 250 × 4 mm, 1 mL/min), using the same elution protocol as above. Pure Cy5-mal was eluted 16.5 min after the start of the gradient, as detected by UV−vis absorption and by direct analysis of the eluent with electrospray MS. Only two *m/e* peaks were detected which exactly met expectation for the monoanion (917) and dianion (458) of Cy5-mal.

^{1}H NMR (CD_3OD, 500 MHz): δ 8.34 (2H, m, β,β' protons of the methin bridge) 7.91−7.93 (4H, m, positions 4 and 6 of the indolin residues), 7.37 (2H, t, $J_{ortho} = J_{para}$ = 7.5 Hz, position 7 of the indolin residue), 6.81 (2H, s, C*H*=C*H* of maleimid), 6.70 (1H, m, γ proton of the methin bridge), 6.37 (2H, t, J = 13.2 Hz, α and α′ protons of the methin bridge), 4.19 (2H, q, J = 6.8 Hz, CH_2 of the *N*-ethyl group), 4.15 (2H, t, J = 7.1 Hz, N-C*H*$_2$-CH$_2$-CH$_2$-CH$_2$-CH$_2$-CO), 3.27−3.33 (d, $J \approx$ 8 Hz, CH_2 between cyclohexane and maleimide, seen in ^{1}H-^{1}H-COSY, hidden under CHD_2-OD in the 1-d-spectrum), 3.24 (4H, s, CO-NH-C*H*$_2$-C*H*$_2$-NH-CO), 2.21 (2H, t, 7.2 Hz, N-CH$_2$-CH$_2$-CH$_2$-CH$_2$-C*H*$_2$-CO), 2.12 (1H, t, $J \approx$ 11 Hz from axial−axial coupling with two axial neighbors, the coupling to the two equatorial neighbors is not well resolved, position 1 of cyclohexane in 100% axial conformation), 2.05 (∼10 H, s, acetic acid from reversed-phase chromatography), 1.80−1.88 (4H, m, N-CH$_2$-C*H*$_2$-CH$_2$-CH$_2$-CH$_2$-CO and equatorial protons in position 2 and 6 of cyclohexane), 1.78 (12 H, s, four methyl groups of Cy5 residue), 1.60−1.75 (5H, m, N-CH$_2$-CH$_2$-CH$_2$-*CH*$_2$-CH$_2$-CO, one axial proton in position 4 of cyclohexane, two equatorial protons in position 3 and 5 of cyclohexane), 1.35−1.51 (7H, m, N-CH$_2$-CH$_2$-C*H*$_2$-CH$_2$-CH$_2$-CO, C*H*$_3$ of the *N*-ethyl group, two axial protons in position 2 and 6 of cyclohexane), 1.01 (2H, q, $J_{gem} \approx J_{axial-axial} \approx$ 12 Hz, one geminal and two axial neighbors, the coupling to the one equatorial neighbor is not well resolved, axial protons in position 3 and 5 of cyclohexane). All NMR signal assignments were confirmed by COSY spectra of Cy5-mal, of commercial Cy5-NHS (in D_2O, slightly different ppm values but the same patterns were observed) and of SMCC (in $CDCl_3$).

Scheme 3. Single-Step Conversions of Cy5-Monofunctional Dye into Thiol-Reactive Derivatives

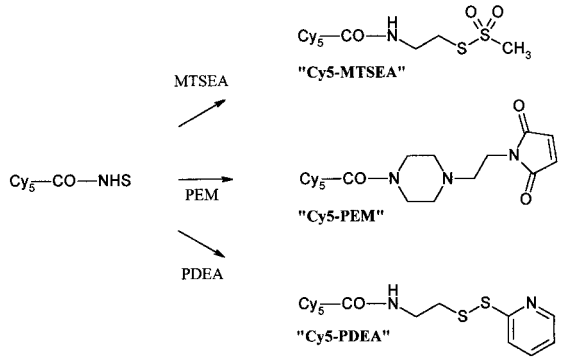

Synthesis of Cy5-MTSEA (Schemes 1 and 3). A modified activation protocol was used to maintain a high Cy5 dye concentration despite working on a small scale. Cy5-monofunctional dye (1.9 μmol) was dissolved in DMF (1 mL) containing SbTMU (8.4 mg/mL). Neat DIEA (5 μL, 29 μmol) was added with a Hamilton syringe. After 20 min of stirring in the dark, the TLC showed quantitative conversion of the Cy5-COOH fraction into Cy5-CO-NHS (see Table 1). Then, MTSEA·HBr (25 mg, 150 μmol) was added at once, more neat DIEA (20 μL, 110 μmol) was injected, and the mixture was stirred for exactly 5 min. TLC indicated ∼100% conversion of Cy-CO-NHS into Cy5-MTSEA. The reaction mixture was frozen in liquid nitrogen, and the solvent removed at 1−10 Pa. The dry residue was dissolved in 15% solvent B and quickly loaded on the LiChroprep column (see above). After washing with 20 and 25% solvent B, the product was eluted with 30% solvent B. Removal of solvent gave 1.3 μmol of Cy5-MTSEA, which was pure by TLC (see Table 1). MS (electrospray, negative mode, 80% methanol in water): *m/z* (%) = 792 (100, M), 396 (91, M/2), 388 (82), 265 (20).

Cy5-MTSEA was further purified by HPLC either on a semipreparative or an analytical Vydac C-18 column, as described for Cy5-mal (see above). Only two peaks were detected in electrospray MS after HPLC, corresponding to the monoanion (792) and the dianion (396) of Cy5-MTSEA.

^{1}H NMR (CD_3OD, 500 MHz): δ 8.32 (2H, m, β,β' protons of the methin bridge), 7.86−7.93 (4H, m, positions 4 and 6 of the indolin residues), 7.34 (2H, t, $J_{ortho} \approx J_{para} \approx$ 7 Hz, position 7 of the indolin residues), 6.69 (1H, t, J = 12.4 Hz, γ proton of the methin bridge), 6.34 (2H, t, J = 14.6 Hz, α and α′ protons of the methin bridge), 4.18 (2H, q, J = 7.2 Hz, CH_2 of the *N*-ethyl group), 4.13 (2H, t, J = 7.3 Hz, N-C*H*$_2$-CH$_2$-CH$_2$-CH$_2$-CH$_2$-CO), 3.51 (2H, t, J = 6.5 Hz, CO-NH-C*H*$_2$-CH$_2$-SO$_2$), 3.43 (3H, s, SO$_2$-C*H*$_3$), 3.32 (t, $J \approx$ 7 Hz, CO-NH-CH$_2$-C*H*$_2$-SO$_2$, seen in ^{1}H-^{1}H-COSY, hidden under CHD_2-OD in the 1-d-spectrum), 2.22 (2H, t, 7.2 Hz, N-CH$_2$-CH$_2$-CH$_2$-CH$_2$-C*H*$_2$-CO), 2.02 (∼1H, s, acetic acid from reversed-phase chromatography), 1.99 (∼1H, s, acetonitrile from reversed-phase chromatography), 1.84 (2H, quintet, J = 7.4 Hz, N-CH$_2$-

C*H*$_2$-CH$_2$-CH$_2$-CH$_2$-CO), 1.76 (12 H, s, four methyl groups of Cy5 residue), 1.71 (2H, quintet, J = 7.5 Hz, N-CH$_2$-CH$_2$-CH$_2$-*CH*$_2$-CH$_2$-CO), 1.46 (2H, quintet, J = 7.7 Hz, N-CH$_2$-CH$_2$-C*H*$_2$-CH$_2$-CH$_2$-CO), 1.40 (3H, t, J = 7.2 Hz, C*H*$_3$ of the *N*-ethyl group).

RESULTS

Complete Activation of Cy5-Monofunctional Dye. The fraction of Cy5 succinimidyl ester in commercial Cy5-monofunctional dye has improved from ~50% in the past (Gruber et al., 1997) to >90% during the past year. Nevertheless, complete conversion of the residual Cy5-COOH contents into Cy5-CO-NHS (Scheme 1) was advantageous for the purpose of this study because unreacted Cy5-COOH would have coeluted with Cy5-amine (Scheme 2) or with Cy5-MTSEA (Scheme 3) from the preparative RP-18 column and many small-scale HPLC runs would have been necessary to remove Cy5-COOH from the products. In situ activation of Cy5-COOH (Scheme 1) with SbTMU (Bannwarth and Knorr, 1991) was ideal because (i) 100% activation was easily achieved, (ii) the reaction conditions (DMF/DIEA) were the same as in all subsequent steps, and (iii) excess of SbTMU did not interfere with all further reactions, thus activation could be done in situ.

Synthesis of Cy5-mal and Cy5-PDP by the Two-Step Protocol. Cy5 is supplied as amine-reactive NHS-ester only, whereas numerous heterobifunctional cross-linkers with a thiol-reactive function on one end and with a NHS-ester on the other are commercially available. Therefore, it was an obvious idea to use a simple diamine (like NH$_2$-CH$_2$-CH$_2$-NH$_2$) for the linking of Cy5 with a heterobifunctional cross-linker, as shown in Scheme 2.

The first requirement was the synthesis of Cy5-amine, in pure form and high yield. Addition of Cy5-CO-NHS to a DMF solution of ethylenediamine, however, resulted in a 70:30 mixture of Cy5-amine and Cy5 dimer, even if a 10^3-fold excess of ethylenediamine in DMF was vigorously stirred and dilute Cy5-CO-NHS was added very slowly (results not shown). The identity of the Cy5 dimer was not rigorously proven, but from very tight binding to the reversed-phase column (elution at 50% "organic solvent"), as well as to an anion-exchange column [as described in Gruber et al. (1997); not shown], it was concluded that it must be the ethylenediamine derivative with two Cy5 residues. Formation of this undesired byproduct was effectively suppressed by complete mixing of Cy5-CO-NHS with the dihydrochloride of ethylenediamine, followed by gradual deprotonation with DIEA. With this improvement >99% of Cy5-CO-NHS were converted into asymmetric Cy5-amine and <1% of the symmetric byproduct was obtained. The 20% water content necessary for solubility of the dihydrochloride did not cause hydrolysis of Cy5-CO-NHS because both before and during addition of DIEA the concentration of [OH$^-$] was orders of magnitude below the concentration of deprotonated NH$_2$-groups. Purification of Cy5-amine by preparative RP-18 chromatography was easy, due to much tighter binding of the fluorochrome as compared to the reagents.

In the second step, Cy5-amine was reacted with SMCC or SPDP to obtain Cy5-mal or Cy5-PDP (Scheme 2). Longer reaction times were needed with SMCC than with SPDP.[2] Fortunately, Cy5-amine was well-separated from Cy5-mal (or Cy5-PDP), even on the low pressure RP-18 column, due to the additional hydrophobicity of the thiol-reactive moieties. It should be mentioned that trifluoroacetic acid was omitted in RP-18 chromatography because prolonged exposure of Cy5 to strong acid (like 0.1 % TFA) was observed to greatly reduce fluorescence (measured after return to neutral pH) while causing little change in the absorption spectrum (not shown). Acetic acid, however, was included to minimize hydrolysis of thiol-reactive groups by OH$^-$.

Before loading on the RP-18 column, unreacted SMCC or SPDP had to be removed by an extraction step because they were insoluble in RP-18 solvents. SMCC and SPDP remained in the chloroform phase while, surprisingly, the Cy5 derivatives could be extracted into water, due to multiple charges in the fluorophore molecule (see Scheme 1).

Synthesis of Cy5-MTSEA by the One-Step Procedure. At first sight, Scheme 3 looked simple because products should be formed in single steps from commercial educts. In practice, however, two basic problems were encountered, and it was difficult (Cy5-PEM) or impossible (Cy5-PDEA) to solve both at a time.

The first requirement was to find reaction conditions under which all Cy5-CO-NHS was consumed by product formation because even on HPLC RP-18 columns the resolution between Cy5-CO-NHS (second peak) and Cy5-MTSEA or Cy5-PEM (always first peak) was poor unless very low amounts were loaded.[2] Contamination of the products with Cy5-CO-NHS is unacceptable for applications in which selective labeling of a single cysteine in a protein is desired. Even a small fraction of Cy5-CO-NHS would lead to significant lysine labeling, given the abundance of lysine residues, the fast kinetic of lysine labeling by NHS esters, and the large excess of thiol-reactive Cy5 needed for efficient thiol labeling (see Figure 1B).

The second problem was an inherent conflict between the amine function that was to be reacted with Cy5 succinimidyl ester and the thiol-reactive terminus in the same molecule (see Scheme 3). It is well-known that maleimides are not fully selective for thiols as compared to primary amines (Keller and Rudinger, 1973). Consequently NH$_2$-CH$_2$-CH$_2$-maleimide would immediately polymerize in the deprotonated state. Dojindo Laboratories found an elegant solution to this problem by linking a secondary amine (piperazine) to a maleimide function (PEM, see Scheme 3). PEM had already been used by others to convert Cy5-bifunctional dye into a thiol-reactive derivative (Funatsu et al., 1995), but neither the procedure nor the yield have been reported. We observed sluggish reaction of the secondary amine (PEM) with the NHS ester of Cy5[2], and no further attempts were made after successful synthesis of Cy5-mal (Scheme 2).

Reaction of Cy5-CO-NHS with PDEA looked promising according to TLC, yet subsequent chromatography by RP-18 HPLC gave only a tiny product fraction that was thiol-reactive.[2] Obviously, the pyridyldithio group in PDEA and in transiently formed Cy5-PDEA was destroyed during the reaction by the high concentration of NH$_2$-groups. This agreed with our previous observation that in buffer (pH 8.6), pyridyldithio groups also decomposed in the presence, but not in absence of 10 mM ethanolamine (Haselgrübler et al., 1995).

Unexpectedly, Cy5-MTSEA was easily synthesized by quantitative reaction of Cy5-CO-NHS with MTSEA (Scheme 3). MTS groups are known for exceptionally high reactivity toward thiols [10 times faster than shown for Cy5-mal in Figure 1B; Stauffer and Karlin (1994)] and for hydrolysis at neutral pH [45 min half-life at pH 7.5, Stauffer and Karlin (1994)], thus we were surprised not to see any decomposition of MTSEA (and of the newly formed Cy5-MTSEA) during reaction. Stability was

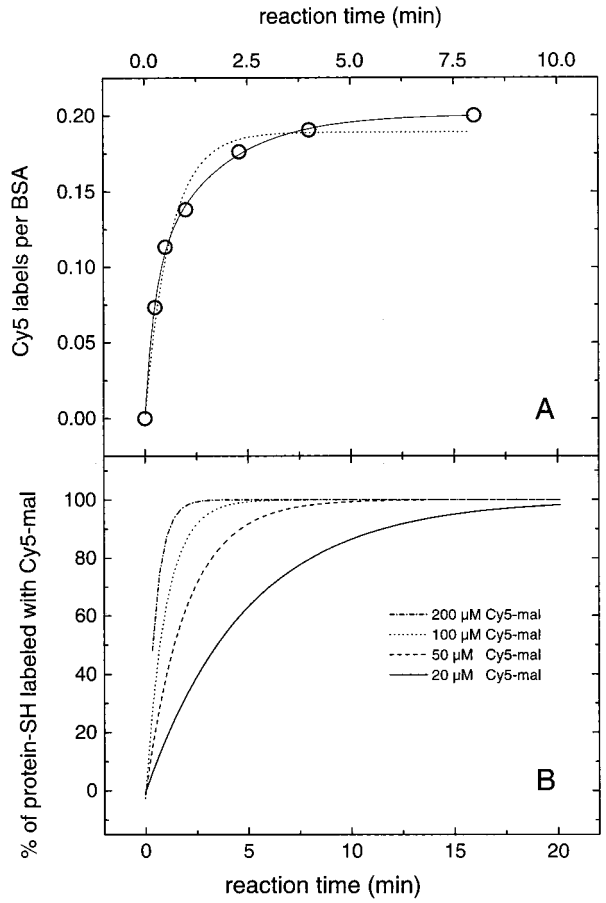

Figure 1. Kinetics of BSA-SH labeling with Cy5-mal[2]. (A) Reaction of BSA-SH (56 μM SH groups) with Cy5-mal (9.1 μM) at pH 7.0 and 20 ± 1 °C (circles). The monoexponential fit (---) gave a half time of 0.43 min, from which the bimolecular kinetic constant k_{bi} = 32 000 M^{-1} min^{-1} was calculated. The biexponential fit (—) gave the half times 0.17 and 1.13 min, corresponding to the bimolecular kinetic constants k_{bi} = 83 000 M^{-1} min^{-1} and k'_{bi} = 12 000 M^{-1} min^{-1}. (B) Prediction for the time course of protein-SH labeling with Cy5-mal. On the basis of the data in panel A the kinetic constant k_{bi} was assumed to be 10^4 M^{-1} min^{-1}. [Protein-SH] was assumed to be negligible in comparison to [Cy5-mal].

checked in parallel by treating MTSEA alone with DMF/DIEA and analyzing the ^{1}H NMR spectrum before and after this treatment (Stauffer and Karlin, 1994). It is concluded that MTSEA is uniquely suited to convert succinimidyl esters into thiol-reactive MTS derivatives in a single reaction step.

Characterization of the New Cy5 Derivatives. TLC helped to monitor and optimize the syntheses. The R_f values of all thiol-reactive derivatives were usually lower than the R_f of Cy5-CO-NHS in any of the three solvent systems (Table 1); thus, product formation could well be monitored in the single-step method. The TLC effects were even more pronounced in the two-step procedure because the R_f of intermediate Cy5-amine was much lower than of educt and of final products (see Table 1).

The identity of the products and the absence of other Cy5 derivatives was confirmed by NMR and electrospray MS (see Experimental Procedures). Not unexpectedly, the double-zwitterionic Cy5-amine gave a strong signal for the dianion while no dication was observed in the positive measuring mode.

The reactivity of all Cy5 products toward protein thiols was tested by reacting 2 nmol of fluorophore with a large excess of thiols (37 nmol, in 220 μL, pH 7.0) offered in the form of BSA-SH.[2] Cy5-labeled BSA was separated from unbound Cy5 by gel filtration on a PD-10 column. With a few percent uncertainty (due to the PD-10 column), it was observed that almost 100% of each Cy5 product was covalently bound to BSA, while in the presence of 2-ME, only a few percent of the Cy5 labels comigrated with BSA on the PD-10 column.[2] The latter was not surprising since fatty acid-free BSA had been used the hydrophobic binding sites of which may have some affinity for Cy5 labels. As expected, all the disulfidic conjugates between BSA-SH and Cy5-PDP, Cy5-MTSEA, and Cy5-PDEA were cleaved by 2-ME which further corroborated thiol-specific coupling.[2]

Some absorption and fluorescence data of the new Cy5 derivatives are summarized in Table 1. Only for BSA-bound Cy5 residues the absorption maximum shifted to 653 nm while in all free Cy5 derivatives it was almost the same as in Cy5 succinimidyl ester. Furthermore, the Cy5 derivatives showed similar fluorescence yields as Cy5-monofunctional dye (Cy5-CO-NHS in Table 1). Most importantly, fluorescence was retained after binding to proteins with SH groups. When Cy5-PDP was coupled to a cysteine mutant of hongotoxin, the Cy5−hongotoxin conjugate showed the same fluorescence per Cy5 label as commercial Cy5−monofunctional dye (unpublished data). The increase in fluorescence observed after linking of Cy5-mal to BSA-SH (Table 1) may be a BSA-specific effect.

Finally, the kinetics of BSA-SH labeling with Cy5-mal was also examined (Figure 1A) in order to give the practical user an idea of the time course of protein labeling (Figure 1B). The predictions in Figure 1B apply to a situation where [protein-SH] ≪ [Cy5-mal] so that [Cy5-mal] changes little during reaction; thus, the time course should be monoexponential, and the *relative* turnover of protein-SH should be independent of [protein-SH] itself.[2] If higher protein-SH concentrations are used, then the initial kinetics will be much faster, but turnover of the last few units of micromolarity of SH groups will follow the time course shown in Figure 1B when relating [Cy5-mal] to *unreacted* Cy5-mal. The labeling kinetics of Cy5-PDP was not measured, but from comparable unpublished data, it is concluded that it should be ~20-fold slower than shown in Figure 1B.

Please note that the model reaction of BSA-SH with Cy5-mal is not fully comparable to the labeling of native cysteines. The lysine-bound mercaptopropionyl residues in BSA-SH may be more accessible than cysteine side chains in proteins. The main need for roughly knowing the time course of cysteine labeling derives from the fact that no thiol-specific coupling function has perfect selectivity for SH over NH_2-groups; therefore, unnecessary long incubation times will cause some undesired labeling of lysine residues.

DISCUSSION

In a systematic approach, two alternate routes were found for conversion of commercial Cy5 succinimidyl ester into thiol-reactive derivatives. The single-step procedure (Scheme 3) appeared of limited use since applicability was problem dependent. Successful synthesis of Cy5-MTSEA by this method was particularly fortunate since there was little alternative to introduce the MTS group in another way.

The two-step procedure was preferred for three reasons: (i) Cy5-mal and Cy5-PDP were synthesized in good yield (in contrast to Cy5-PEM and Cy5-PDEA). (ii) There was no possibility that the final Cy5-products were

contaminated with unreacted Cy5-CO-NHS, which would preclude application for selective labeling of thiol groups in proteins. (iii) If desired, Cy5-amine can be derivatized with many other heterobifunctionals to introduce other useful end groups (photoreactive, etc.).

Availability of SH-reactive Cy5 derivatives will be of particular interest for fluorescence microscopy on single ion channels, for two reasons: (i) Typical ion channel densities in biomembranes (few per squared micrometer) are too low for conventional microscopy whereas such rare occurrence is ideal for study by far-field SMFM. (ii) The derivatization of most ion channel-blocking toxins through lysine chemistry is precluded since they are essential for high-affinity interaction with the respective channels (Stampe et al., 1992; Stampe et al., 1994). In particular, a cysteine mutant of hongotoxin (Koschak et al., 1998) has successfully been derivatized with Cy5-PDP, the resulting Cy5−hongotoxin conjugate retaining high fluorescence and affinity for Kv1 channels (unpublished data). Moreover, single Kv1 channels on Jurkat cells were indeed visualized by SMFM using Cy5-hongotoxin as the biospecific probe (unpublished data).

The present study exclusively focused on Cy5 because, at present, Cy5 is a most promising label for single molecule fluorescence detection in live cells (Schütz et al., 1999). Clearly the same protocol should work for Cy3-monofunctional dye, as well. The one-step method should also be applicable to derivatize the bifunctional forms of Cy3, Cy5, and Cy7, as mentioned in an earlier study (Funatsu et al., 1995). Finally, it is expected that the procedures and purification methods of this study should be useful for the conversion of many other amine-reactive labels into thiol-reactive derivatives.

ACKNOWLEDGMENT

We are indebted to Prof. H. Falk and Prof. K. Grubmayr for helpful advice, to Prof. Wolfgang Buchberger and Prof. Norbert Müller for use of HPLC and spectrometer facilities, and to Dr. Heino Prinz, Max Planck Institute Dortmund, Germany, for part of the MS data. This work was supported by the Austrian Research Funds (project P-12803).

Supporting Information Available: Detailed descriptions of all syntheses and of covalent labeling of BSA-SH with thiol-reactive Cy5 derivatives. This information is available free of charge via the Internet at http://pubs.acs.org.

LITERATURE CITED

Aubin, J. E. (1979) Autofluorescence of viable cultured mammalian cells. *J. Histochem. Cytochem. 27*, 36−43.

Bannwarth, W., and Knorr, R. (1991) Formation of carboxamides with N,N,N′,N′-tetramethyl (succinimido) uronium tetrafluoroborate. *Tetrahedron Lett. 9*, 1157−1160.

Benson, R. C., Mayer, R. A., Zaruba, M. E., and McKhann, G. M. (1979) Cellular autofluorescence−is it due to flavins? *J. Histochem. Cytochem. 27*, 44−48.

Feldhoff R. (1991) Why not ethanol-based solvents for RP-HPLC of peptides and proteins? *Tech. Protein Chem. 17*, 55−63.

Funatsu, T., Harada, Y., Tokunaga, M., Salto, K., and Yanagida, T. (1995) Imaging of single fluorescent molecules and individual ATP turnovers by single myosin molecules in aqueous solution. *Nature 374*, 555−559.

Gruber, H. J., Marek, M., Schindler, H., and Kaiser, K. (1997) Biotin-Fluorophore Conjugates with Poly(ethylene glycol) Spacers Retain Intense Fluorescence after Binding to Avidin and Streptavidin. *Bioconjugate Chem. 8*, 552−559

Haselgrübler, Th., Amerstorfer, A., Schindler, H., and Gruber, H. J. (1995) Synthesis and applications of a new poly(ethylene glycol) derivative for the cross-linking of amines with thiols. *Bioconjugate Chem. 6*, 242−248.

Keller, O., and Rudinger, J. (1973) Preparation and some properties of maleimido acids and maleoyl derivatives of peptides. *Helv. Chim. Acta 58*, 531−541.

Koschak, A., Bugianesi, R. M., Mitterdorfer, J., Kaczorowsky, G. J., Garcia, M. L., and Knaus, H.-G. (1998) Subunit composition of brain voltage-gated potassium channels determined by hongotoxin-1, a novel peptide derived from *Centruroides limbatus* venom. *J. Biol. Chem. 273*, 2639−2644.

Marelius, J. (1995) *Autofluorescence imaging of living cells*, MSc Thesis, Uppsala University, School of Engineering.

Mujumdar. R. B., Ernst, L. A., Mujumdar, S. R., Lewis, C. J., and Waggoner, A. S. (1993) Cyanine dye labeling reagents: sulfoindocyanine succinimidyl esters. *Bioconjugate Chem. 4*, 105−111.

Schmidt, Th., Schütz, G. J., Baumgartner, W., Gruber, H. J., and Schindler, H. (1995) Characterization of photophysics and mobility of single molecules in a fluid lipid membrane. *J. Phys. Chem. 99*, 17662−17668.

Schmidt, Th., Schütz, G. J., Gruber, H. J., and Schindler, H. (1996) Local stoichiometries determined by counting individual molecules. *Anal. Chem. 68*, 4397−4401.

Schütz, G. J., Gruber, H. J., Schindler, H., and Schmidt, Th. (1997) Fluorophores for single molecule microscopy. *J. Lumin. 72−74*, 18−21.

Schütz, G. J., Trabesinger, W., and Schmidt, Th. (1998) Direct observation of ligand colocalization on individual receptor molecules. *Biophys. J. 74*, 2223−2226.

Schütz, G. J., Schindler, H., and Schmidt, Th. (1999) Diffusion of single lipid molecules in cell membranes. *Biophys. J. 76*, A57.

Stampe, P., Kolmakova-Partensky, L., and Miller, C. (1992) Mapping hydrophobic residues of the interaction surface of charybdotoxin. *Biophys. J. 62*, 8−9.

Stampe, P., Kolmakova-Partensky, L., and Miller, C. (1994) Intimations of K^+ channel structure from a complete functional map of the molecular surface of charybdotoxin. *Biochemistry 33*, 443−450.

Stauffer, D. A., and Karlin, A. (1994) Electrostatic potential of acetylcholine binding sites in the nicotinic receptor probed by reaction of binding-site cysteines with charged methanethiosulfonates. *Biochemistry 33*, 6840−6849.

Trabesinger, W., Schütz, G. J., Gruber, H. J., Schindler, H. J., and Schmidt, Th. (1998) Detection of individual oligonucleotide pairing by single molecule microscopy. *Anal. Chem. 71*, 279−283

Vale, R. D., Funatsu, T., Pierce, D. W., Romberg, L., Harada, Y., and Yanagida, T. (1996) Direct observation of single kinesin molecules moving along microtubules. *Nature 380*, 451−453.

Wolfbeis, O. S., and Leiner, M. (1985) Mapping of the total fluorescence of human blood serum as a new method for its characterization. *Anal. Chim. Acta 167*, 203-215.

BC990107F

EXPERIMENTAL PROCEDURES

General Comments. When repeating these syntheses it is critical to use similar reagent concentrations and reaction times, except that the Cy5 component may be much more dilute than described below. When working with higher amounts of Cy5, however, it is advisable to scale up all other components (including solvent and DIEA) accordingly. As an exception, the amount of SbTMU is noncritical, full activation (Scheme 1) was also seen at smaller SbTMU concentrations. Moreover insufficient activation was easily detected by TLC (see Table 1) and more SbTMU could be added in that case, due to high stability of the product (Cy5-CO-NHS) in DMF/DIEA.

All operations were performed under dim light, and flasks were wrapped with aluminum foil. Oxidation of primary amines (ethylene diamine, Cy5-amine, MTSEA) was suppressed by performing experiments in an argon atmosphere, especially when deprotonating with DIEA. Unless specified otherwise, all operations were at room temperature (20 to 25 °C, preferably at 24-25 °C).

All products were purified by low pressure reversed phase chromatography on Merck LiChroprep gel (see Cy5-amine). At this stage Cy5-mal, Cy5-PDP, and Cy5-MTSEA were well suited for specific labeling of thiol groups on proteins because no other protein-reactive component (with or without a Cy5 residue) was present. HPLC reversed phase chromatography (see main article) was solely used to achieve high enough purity of Cy5-mal and Cy5-MTSEA for NMR spectroscopy and electrospray MS (see main article). It is important to note that HPLC chromatography failed when directly applied to the crude reaction mixtures, except when loading very small aliquots. Only low pressure chromatography was able to separate the high excess of reagents (such as SbTMU, ethylene diamine, SMCC, MTSEA, *etc.*) in a single column run.

Splitting of a large Cy5 batch into aliquots. One batch of commercial Cy5-monofunctional dye (nominally 5 mg or 6.4 µmoles, dry powder) was dissolved in DMF (e.g. at 2.5 mg/mL) and the desired aliquots were pipetted into 5 mL flasks, each containing a stir bar. While the other flasks were stored at -70 °C one flask was frozen in liquid nitrogen and attached to a strong vacuum source (1-10 Pa, vapor trap cooled in liquid nitrogen). The flask was wrapped with aluminum foil and kept in ambient air (no water bath). Magnetic stirring was applied as soon as DMF became liquid. In this way DMF was pulled off at low temperature and without splashing. The same procedure was used after all synthetic steps since DMF was used in all reactions. The dried portions were stored at -25 °C.

Complete Conversion of Commercial Cy5-monofunctional Dye into Succinimidyl Ester (Scheme 1). Cy5-monofunctional dye (4.3 µmol) was dissolved in DMF (2 mL) and SbTMU (7.2 mg, 18 µmol) was added at once with stirring (Bannwarth and Knorr, 1991). DIEA (50 µL of a 5% solution in DMF, 15 µmol) was added and the mixture was stirred for 20 min. TLC proved quantitative conversion of Cy5-COOH into Cy5-CO-NHS (see Table 1). This mixture was immediately used in the next step (see below).

Synthesis of Cy5-amine (Scheme 2). Ethylene diamine dihydrochloride (62 mg, 470 µmol) was dissolved in water (0.8 mL), then 4 mL of DMF was added (pH ~6 to 6.5). Fully activated Cy5-CO-NHS (4.3 µmol, see above) was subsequently added dropwise with stirring (pH ~7 to 7.5). The coupling reaction was started by dropwise addition of DIEA (400 µL of a 5 % solution in DMF, 240 µmol). After 30 min of stirring the reaction mixture was taken to dryness (see above, "Splitting of a large Cy5 batch").

Cy5-amine was purified by low-pressure reversed phase chromatography. Merck LiChroprep RP-18 gel (7 mL dry material, 1.5 x 3.5 cm bed) was suspended in ethanol, degassed by vacuum and packed into a BioRad Econo

column which was equipped with a flow adaptor and connected to a peristaltic pump with silicon tubing. Solvent A contained 0.1 % acetic acid in water. Solvent B was a 5/2 mixture (v/v) of ethanol and 1-propanol (Feldhoff, 1991).The column was always operated at 2 mL/min. The crude Cy5 derivative was dissolved in 5 % solvent B and loaded on the column which had been equilibrated with 5 % solvent B. After washing with 12 ml quantities each of 5 %, 10 %, and 15 % solvent B the product was eluted with 20 % solvent B. 50 % solvent B was necessary to elute the blue-colored by-product. The column was regenerated at 0.2 mL/min with 80 % solvent B containing 0.1 % trifluoroacetic acid (instead of acetic acid) at 0.2 mL/min overnight to remove the last traces of blue color.

The simple column equipment described here was fully sufficient, except for slow but inevitable appearance of air underneath the flow adaptor. The problem was completely solved by placing the flow adaptor ~1 cm above the gel so that the air could not enter the column bed. When switching from 80 % solvent B (low density) to 5 % solvent B (high density) it was necessary to slightly shake the column for several minutes, thereby using the air bubble for constant mixing of dense and light solution above the column bed.

The eluted product fraction (i.e. the 20 % solvent B fraction) was transferred into a 500 ml round bottomed flask and the alcohol content was reduced on the rotavap (aspirator vacuum, 10 min, water bath at 20 °C). The remaining solution was cooled by swirling the flask in liquid nitrogen until a small fraction of the solvent started to freeze. The flask was attached to a rotavap which was connected to a strong vacuum source (1-10 Pa, nitrogen-cooled vapor trap) via 1.5 m vacuum tubing (8 mm inner diameter). After removal of residual alcohol content (~30 min) the flask was slightly dipped into the water bath (20 °C) until all water was removed. This procedure was faster and safer than speed vac drying or lyophilization. During lyophilization more

than half of the product would usually fly into the cold trap, and in the typical speed vac setup the vacuum source was too weak and/or the vacuum connection was too narrow to maintain the solution at ~0°C during evaporation, resulting in decomposition, especially of Cy5-mal and Cy5-PDP. An even more rigorous protocol was used to prevent hydrolysis of Cy5-MTSEA during drying (see below).

The blue residue was dissolved in methanol (at this point a defined aliquot was removed for measurement of the Cy5 dye content) and taken to dryness in a small flask. The product (4.2 µmol) was pure by TLC (see Table 1). MS (electrospray, negative mode, 80 % methanol in water) m/z (%) = 697 (21, M), 375 (16), 348 (100, M/2), 255 (19). MS (electrospray, positive mode, 80 % methanol in water) m/z (%) = 699 (27, M), 487 (13), 369 (100), 329 (20), 257 (16).

Synthesis of Cy5-mal (Scheme 2). Cy5-amine (4.2 µmol) was dissolved in DMF (1 mL) and added to dry SMCC (27 mg, 81 µmol) with stirring. Another 0.5 mL portion of DMF was used to transfer all Cy5-amine into the reaction mixture. After addition of DIEA (5 µL neat phase, 57 µmol) the mixture was stirred for 50 min, and the solvent was removed as described above (see "splitting of a large Cy5 batch").

The dry residue was dissolved in 0.4 mL methanol and 1 mL chloroform, and subsequently diluted with 8 mL of chloroform. This solution was extracted with 2 x 20 mL of water containing 0.1 % acetic acid and 6 x 20 mL of water, resulting in almost complete decoloration of the chloroform phase (which contains the water-insoluble SMCC). Each aqueous layer was harvested separately, and any contaminating chloroform droplets were allowed to settle before the aqueous phase was combined with the previous aqueous layers (the chloroform droplets were returned to the chloroform phase). The pooled

aqueous layer was bubbled with nitrogen gas in a ventilator hood until dissolved chloroform was expelled (~10 min).

After addition of solvent B (final contents 2.5 %) the solution was loaded on the same LiChroprep column as used for Cy5-amine (see above). The column was washed with 12 mL portions each of 5 %, 10 %, 15 %, 20 %, and 25 % solvent B, elution of product was with 30 % solvent B. Evaporation (see Cy5-amine) yielded 3.3 µmol Cy5-mal. The product was pure by TLC (see Table 1). MS (electrospray, negative mode, 80 % methanol in water) m/z (%) = 917 (11, M), 488 (21), 458 (100, M/2), 255 (18), 227 (11). Complete purity was achieved by HPLC and the structure was confirmed by NMR spectroscopy and electrospray MS (see main article).

Synthesis of Cy5-PDP (Scheme 2). Cy5-amine (0.50 µmol) was dissolved in DMF (1 mL) and added to dry SPDP (21 mg, 66 µmol) with stirring. Another 0.5 mL of DMF was used to transfer residual Cy5-amine into the reaction mixture. After addition of DIEA (75 µL of a 5 % solution in DMF, 22 µmol) the mixture was stirred for 30 min. All further steps (extraction for removal of unreacted SPDP and low-pressure reversed phase chromatography) were analogous to those described for Cy5-mal. Evaporation of the 30 % solvent B fraction (as described for Cy5-amine) gave 0.26 µmol of Cy5-PDP. The product was pure by TLC (see Table 1). MS (electrospray, negative mode, 80 % methanol in water) m/z (%) = 894.3 (5.8 M), 446.6 (100, M/2), 255 (14), 227 (9), 142 (37), 89 (37).

Synthesis of Cy5-MTSEA (Schemes 1 and 3). A modified activation protocol was used to maintain a high Cy5 dye concentration in spite of working on a small scale. Cy5-monofunctional dye (1.9 µmol, dry film) was dissolved in DMF (1 mL) containing SbTMU (8.4 mg/mL). Neat DIEA (5 µL, 29 µmol) was added with a Hamilton syringe. After 20 min of stirring in the dark the TLC showed quantitative conversion of the Cy5-COOH fraction into pure Cy5-CO-

NHS (see Table 1). Then MTSEA·HBr (24 mg, 150 µmol) was added at once, more neat DIEA (20 µL, 110 µmol) was injected, and the mixture was stirred for exactly 5 min at 24-25 °C. After freezing in liquid nitrogen the solvent was removed (see "Splitting of a large Cy5 batch"). TLC from an aliquot removed before freezing indicated ~100 % conversion of Cy-CO-NHS into Cy5-MTSEA. The dry residue was immediately dissolved in 15 % solvent B and quickly loaded on a LiChroprep column (as described for "Cy5-amine"). After washing with 12 mL portions each of 20 % and 25 % solvent B the product was eluted with 30 % solvent B. The product fraction was immediately frozen as a thin film in a 250 mL flask, the flask was wrapped with aluminum foil and attached to a rotavap which was connected to a strong vacuum source (1-10 Pa, nitrogen-cooled vapor trap) via 1.5 m vacuum tubing (8 mm inner diameter). Overnight rotation in ambient air (no water bath) gave completely dry product which was re-dissolved in 5 mL methanol (plus 0.1 % acetic acid for suppression of decomposition) and taken to dryness on the rotavap. The product (1.3 µmol) was pure by TLC (see Table 1). MS (electrospray, negative mode, 80 % methanol in water) m/z (%) = 792 (100, M), 396 (91, M/2), 388 (82), 265 (20). Complete purity was achieved by HPLC and the structure was confirmed by NMR spectroscopy and electrospray MS (see main article).

Synthesis of Cy5-PEM (Schemes 1 and 3). Fully activated Cy5-CO-NHS (2.3 µmol in 0.3 mL DMF) was reacted with PEM (~1 mg, ~3.5 µmol), and DIEA (100 µL 1.2 % in DMF, 7 µmol) was added. After 10 min of stirring at RT the mixture was frozen in liquid nitrogen, taken to dryness at 1-10 Pa with stirring (see "splitting of a large Cy5 batch"), redissolved in 300 µL 5 % solvent B, and 100 µL aliquots were immediately stored frozen at -70 °C.

Purification of Cy5-PEM was by RP-18 HPLC (250 x 8 mm column, Grom-Sil 300 ODS-3CP). The same low-toxicity solvent system was used as for the LiChroprep column (see Cy5-amine). The flow was 2.5 mL/min. In one

column run a 100 µL aliquot of the product mixture was loaded and washed with 5 % solvent B for 5 min. Within the next 5 min the solvent B content was raised to 20 %, followed by another linear gradient (20 min) from 20 % to 27 % solvent B. The first major blue peak (~1 mL, 90 µM Cy5) was collected and quickly frozen in liquid nitrogen. The pooled product fractions were taken to dryness and the product characterized by UV-vis absorption and thiol-specific coupling to BSA-SH (see below).

Synthesis of Cy5-PDEA (Schemes 1 and 3). Fully activated Cy5-CO-NHS (2.6 µmol, see above) was stirred at RT under argon, and PDEA (4 mg, 18 µmol) was added. After 20 min of stirring the solvent was removed at 1-10 Pa (see "splitting of a large Cy5 batch") and the dry solid was dissolved in 2 mM NaH_2PO_4 (pH adjusted to 6.5 with NaOH). Chromatography on QAE Sephadex A-25 (Gruber et al., 1997) was used to separate the colored components from the reagents. The Cy5 derivatives were further purified by RP-18 HPLC as described above (see Cy5-PEM). The Cy5-PDEA peak was identified by covalent (and reversible coupling) to BSA-SH (see below).

Preparation of BSA-SH. Lysine residues were derivatized with mercaptopropionyl residues as described (Carlsson et al., 1978). BSA (200 mg) was dissolved in 3 mL buffer A with stirring. SPDP (4.7 mg) was dissolved in DMSO (150 µL) and added to the stirred BSA solution. After 60 min of stirring the mixture was acidified to pH 5.5 by gradual addition of 0.5 M acetic acid (~350 µL), and then to pH 4.5 by addition of 1 M HCl (~85 µL). Slight turbidity was removed by centrifugation. After 5 min of stirring under argon DTT (300 µL 500 mM, in water) was added and stirring was continued. Selective cleavage of PDP groups (but not of endogeneous disulfides (Carlsson et al., 1978) was monitored by diluting small aliquots 100-fold with buffer B and measuring released 2-thiopyridone (ε_{343} = 8080 M^{-1} cm^{-1}; Leserman et al., 1984). The reaction was complete within 20 min at room temperature. The mixture was

loaded on a Sephadex G-25 M column (1.5 x 48 cm, equilibrated in argon-bubbled buffer B) and eluted at 1 mL/min while collecting fractions (5 mL) under argon. For detection of BSA-SH (void peak) and of small thiols, >50 µL fractions were collected separately before each large 5 mL fraction, 50 µL thereof were diluted with 1150 µL of buffer C and mixed with 50 µL of 4 mM DTDP (in 12 mM HCl). After 2 min at RT released 4-thiopyridone was measured at 324 nm (Grassetti and Murray, 1967). The fractions containing BSA-SH were pooled and aliquots were stored at -25 °C. The BSA concentration was determined as 179 µM and the SH group content as 370 µM.

Covalent coupling of thiol-reactive Cy5 derivatives to BSA-SH. Polystyrene tubes (4 mL) were capped with rubber septa (Aldrich Z10,073-0) and the air content was exchanged for argon via hypodermic needles. All solutions were deoxygenated with argon before use (to avoid foaming, the BSA-SH stock solution was not bubbled but vortexed in a septum-covered tube while exchanging air for argon). 100 µL of buffer B containing ~18 nmol BSA with ~37 nmol SH groups (prepared as described above) was injected into each argon-filled tube (Hamilton syringes were used for all injection steps, 3-fold lower concentrations of BSA-SH were used in kinetc experiments, see Figure 1A). Second, 80 µL of water were injected. Only in the case of control experiments, the next injection was with 10 µL of 500 mM 2-ME. After injection of 20 µL water (or aqueous elutants from RP-18 columns) typically containing 2 nmol of Cy5 derivative the reaction was accelerated by injection of 20 µL 50 mM Na_2HPO_4 which raised the pH to 7.0 (in kinetic experiments the pH was raised to 7.0 before the addition of Cy5-mal). The coupling reaction was allowed to proceed for 60 min (room temperature, exclusion of light). Then the mixture was diluted with 300 µL buffer A and loaded on a PD-10 column (equilibrated in buffer A, outlet initially closed). After washing with 2 x 1 mL buffer A the Cy5-labeled BSA was eluted with 1.5 mL of buffer A. A very dilute "tail" of labeled BSA was further eluted with 1 mL of water.

Subsequently the unbound Cy5 dye was eluted with 10 mL of water (better desorption of Cy5 than with buffer), and the column was regenerated with 15 mL of buffer A. PD-10 columns were discarded if 2-ME had been loaded. BSA and Cy5 labels were measured as described below. When labeling BSA-SH with Cy5-MTS, Cy5-PDEA, and Cy5-PDP, the disulfide linkage between BSA and the Cy5 label was also tested for reductive cleavage by 2-ME. The PD-10 column peak containing the BSA-Cy5 conjugate was mixed with 0.2 volumes of 500 mM 2-ME, incubated for 40 min at RT, and re-chromatographed on a PD-10 column.

BSA concentrations were calculated from A_{280} (ε_{280} = 44300 M^{-1} cm^{-1}; Elgersma et al., 1990), taking into account the small absorbance of the Cy5 labels at 280 nm (A_{280} of Cy5 was about 0.057 % of its absorbance at λ_{max}). Bound Cy5 label concentrations were calculated from absorbance at λ_{max} (Table I), assuming the same molar extinction coefficient (ε = 250000 M^{-1} cm^{-1}) as published for Cy5-monofunctional dye (Mujumdar et al., 1993).

Kinetic analysis of Cy5-mal coupling to BSA-SH. The coupling reaction is denoted as

$$\text{BSA-SH} + \text{Cy5-mal} \rightarrow \text{BSA-S-mal-Cy5} \qquad (1)$$

The kinetics of Cy5-mal coupling to BSA-SH is described by equation (2)

$$d/dt\,[\text{Cy5-mal}] = k_{bi}\,[\text{BSA-}\mathbf{SH}]\,[\text{Cy5-mal}] \qquad (2)$$

When testing for the reactivity of Cy5-mal to the model protein BSA-SH the latter obviously had to be used in excess, i.e. [Cy5-mal] << [BSA-**SH**]. Typically 37 nmol of **SH** groups were used to "trap" 2 nmol of Cy5-mal (or other Cy5 derivatives). Consequently [BSA-**SH**] remained approximately constant and the time course of Cy5-mal consumption was pseudo-monoexponential:

$$k = k_{bi}\,[\text{BSA-}\mathbf{SH}] \approx \text{constant} \qquad (3)$$

$$[\text{Cy5-mal}]_t \;/\; [\text{Cy5-mal}]_{t=0} = e^{-kt} \tag{4}$$

$$t_{1/2} = \ln 2 / k \tag{5}$$

In a typical labeling experiment (e.g. of a cysteine mutant) quantitative and rapid labeling of SH-groups is desired, thus [Cy5-mal] should be >> [protein-SH]. Consequently only a minor fraction of Cy5-mal will be consumed and the reaction will follow a pseudo-monoexponential time course:

$$d/dt\,[\text{protein-SH}] = k_{bi}\,[\text{Cy5-mal}]\,[\text{protein-SH}] \tag{6}$$

$$k' = k_{bi}\,[\text{Cy5-mal}] \approx \text{constant} \tag{7}$$

$$[\text{protein-SH}]_t \;/\; [\text{protein-SH}]_{t=0} = e^{-k't} \tag{8}$$

$$t'_{1/2} = \ln 2 / k' \tag{9}$$

LITERATURE CITED IN THE SUPPLEMENTS ONLY

Carlsson, J., Drevin, H., and Axen, R. (1978) Protein thiolation and reversible protein-protein conjugation: *N*-Succinimidyl 3-(2-pyridyldithio)propionate, a new heterobifunctional reagent. *Biochem. J. 173,* 723-737.

Elgersma, A.V., Zsom, R.L.J., Norde, W., and Lyklema, J. (1990) The adsorption of bovine serum albumin on positively and negatively charged polystyrene latices. *J. Coll. Int. Sci. 138*, 145-156

Grassetti, D. R. and Murray, J. F. Jr. (1967) Determination of sulfhydryl groups with 2,2'- or 4,4'-dithiodipyridine. *Archives Biochem. Biophys. 119,* 41-49.

Leserman, L.D., Machy, P., and Barbet, J. (1984) Covalent coupling of monoclonal antibodies and protein A to liposomes: Specific interaction with cells in vitro and in vivo. *Liposome Technology* (Gregoriadis, G., ed.), vol III, pp 29-40.

Structural Characterization, Kinetic Studies, and in Vitro Biological Activity of New *cis*-Diamminebis-cholylglycinate(*O,O′*) Pt(II) and *cis*-Diamminebis-ursodeoxycholate(*O,O′*) Pt(II) Complexes

Julio J. Criado,*[,†] María F. Domínguez,[‡] Manuel Medarde,[§] Emilio R. Fernández,[†] Rocío I. R. Macías,[‡] and José J. G. Marín[‡]

Departamento de Química Inorgánica, Departamento de Fisiología y Farmacología, and Departamento de Química Orgánica, Campus Miguel de Unamuno, Universidad de Salamanca, 37007-Salamanca, Spain. Received August 20, 1999; Revised Manuscript Received November 25, 1999

The complexes *cis*-diamminebis-cholylglycinate (*O,O′*) [Pt(II) $C_{52}H_{90}N_4O_{12}Pt$, for convenience referred to as Bamet-R1] and *cis*-diamminebis-ursodeoxycholate (*O,O′*) Pt(II) ($C_{48}H_{84}N_2O_8Pt$, Bamet-UD2) were prepared. The structural integrity of the compounds was confirmed by elemental analysis, FT-IR, NMR, FAB-MS, and UV spectroscopies. The kinetic study of both compounds was accomplished by combining the conductivity measurement and those of the analysis of the electronic spectra in aqueous solution for NaCl concentrations of 4 mM (similar to cytoplasmatic concentration), 150 mM (similar to plasmatic concentration), and 500 mM. In water, the compound Bamet-R1 showed a half-life, $t_{1/2}$, of 3.0 h. This compound forms the chelate species through loss of a ligand, and the other one acts as a bidentate ligand. Ring opening in the presence of chloride ion was produced with a $k_{Cl^-}$of 0.25 M^{-1} h^{-1}. The half-life of Bamet-UD2 in aqueous solution was 3.2 h. However, since this species is not able to chelate and has a lower degree of solubility in the presence of chloride ion, its kinetic behavior was very different from that of the other compound. We consider this to be of great interest with regards to its cytostatic activity. All kinetic measurements were performed under pseudo-first-order conditions, and a pseudo-first-order behavior was found. The antitumoral effect of Bamet-UD2 on several cell lines derived from rat hepatoma, human hepatoma, mouse leukemia, and human colon carcinoma was found to be, in general, similar to that of cisplatin, but higher than that observed for Bamet-R1.

INTRODUCTION

Since its introduction in clinical essays in 1972, the wide success of *cis*-diamminedichloroplatinum(II) (cisplatin) and its analogues in the treatment of a variety of solid tumors (*1*) has encouraged the search for new cisplatin derivatives in order to improve the therapeutic index of this compound, which is reduced by dose-limiting toxicity, namely, nephrotoxicity, myelotoxicity, neurotoxicity, nausea, and vomiting (*2*). Despite many different cisplatin analogues that have been synthesized to date, few of them are actually used in clinical practice. This is probably due to the fact that circumvention of side effects is only partial and is often accompanied by loss of tumoricidal activity.

The ability to interact with DNA and to inhibit tumor growth (*3*, *4*) as well as the liver organotropic characteristics (*5*, *6*) of several platinum-containing bile acid derivatives such as Bamet-R2 [[$Pt(NH_3)_2CGCl$], *cis*-diammineplatinum(II)chlorocholylglycinate] and Bamet-H2 [Na[Pt(CG-*O*,*N*) (CG-*O*)Cl], sodium platinum(II)-chloro-bischolylglycinate], which were synthesized by our group (*7*, *8*), have been reported previously. These compounds were obtained by using cholylglycinate as the bile acid moiety. In later studies, several alternatives to this choice have been explored. One of them is described in the present paper, in which two molecules of ursodeoxycholic (UDCA, 3α,7*β*-dihydroxy-5*β*-cholanoic acid) were bound to cisplatin to obtain the new complex named Bamet-UD2. The structural characterization of the compound, kinetic studies of hydrolysis, and determination of its cytostatic activity "in vitro" were performed, comparing the results to those obtained with another new complex named Bamet-R1, similar to Bamet-UD2, except that, in the former, two UDCA moieties were replaced by two cholylglycinate moieties.

Because of its peculiar physical-chemical and biological characteristics (*9*), much work has been devoted to investigating UDCA during the past decade. Owing to the *β* position of the hydroxyl group located on C7, the behavior of UDCA differs from that of most 7α-hydroxylated bile acids, such as cholic acid and chenodeoxycholic acids, with regards to detergent activity (*10*, *11*) and the $pK_{a'}$ value of the carboxylate on the side chain (*12*). These differences are probably related to the very low toxicity of this bile acid as well as in its biological effects, among them its ability to induce hypercholeresis (*13*), to stimulate bile bicarbonate output (*14*), and to have a beneficial effect in several pathological conditions characterized by hypercholanemia (*15*). Accordingly, Bamet-UD2 was synthesized with the aim of maintaining or improving the cytostatic effect of previously described members of Bamet's family using a complex whose leaving groups (UDCA) present hepatoprotective activity (*16*).

EXPERIMENTAL SECTION

Chemicals. *cis*-diammineplatinum(II)dichloride Pt-$(NH_3)_2Cl_2$ was purchased from Fluka AG. Sodium cholylglycinate (NaCG; >95%, "glycocholic acid sodium salt")

* To whom correspondence should be addressed. Fax: 34-923 29 45 15. E-mail: jjct@gugu.usal.es.
† Departamento de Química Inorgánica.
‡ Departamento de Fisiología y Farmacología.
§ Departamento de Química Orgánica.

10.1021/bc9901088 CCC: $19.00 © 2000 American Chemical Society
Published on Web 02/24/2000

and ursodeoxycholic acid (UDCA; 99%) were obtained from Sigma. All other reagents were of high purity and were used as purchased without any further purification.

Analytical Methods. Chemical analysis for C, H, and N were performed on a Perkin-Elmer 2400 elemental analyzer. Platinum was determined by atomic absorption on a Hitachi Z-8100 flameless graphite furnace spectrophotometer set at a wavelength of 265.9 nm, using the following temperature program: 90 °C (20 s), 100 °C (20 s), 800 °C (20 s), 1600 °C (30 s), 2800 °C (5 s), and 3000 °C (4 s). Infrared (IR) spectra were recorded in the 4000−200 cm^{-1} range on a Perkin-Elmer FT-IR 1730 instrument coupled to a Perkin-Elmer Data Station. KBr pellets and spectrophotometric-grade Nujol (Fluka AG) or polyethylene disks were used to record the spectra above and below 400 cm^{-1}, respectively. Mass spectrometry studies were carried out on a VG-Autospec (Universidad Autonoma, Madrid, Spain), using L-SIMS ionization in the FAB^+ mode (Cs ion emission) and *m*-nitrobenzyl alcohol (m-NBA) as matrix. Electrical conductivity in solution was measured using a CDM2e conductimetry Radiometer, with a CDC104 immersion cell. Temperature was controlled in a Unitherm water bath with a precision of ±0.01 °C. ^1H (400 MHz), ^{13}C (102.6 MHz), and ^{195}Pt (64.5 MHz) NMR spectra were obtained in methanol-d_4 and DMSO-d_6 solutions on a Bruker DX400 instrument. Carbon resonances were distinguished in DEPT-90 and DEPT-135 experiments. TMS was used as an internal standard for ^1H and ^{13}C spectra. Using K_2PtCl_6 ($\delta = 0$ ppm) as external standard, 300 000 scans, 2 s relaxation delay, and 48 h acquisition time were used to obtain the ^{195}Pt spectra.

Synthesis and Purification. The platinum complex, named Bamet-R1 $Pt(NH_3)_2(CG)_2$, was obtained (*8*) by the following procedure: a 1.5 mM $Pt(NH_3)_2Cl_2$ solution in water (250 mL) was prepared at 40 °C and filtered onto paper. Then, an aqueous solution of NaCG, sodium cholylglycinate (0.75 mM, 250 mL), was added. To prevent physicochemical effects due to the presence of bile acid micelles in the reaction mixture, attempts were made to keep the concentrations of free NaCG in the reaction mixture below the critical micellar concentration (CMC) for this bile acid (*17*). Thus, the NaCG solution was added dropwise (1 mL/min) by means of a peristaltic pump, to the continuously stirred $Pt(NH_3)_2Cl_2$ solution, which was maintained in the dark at 40 °C. This procedure took about 3 h. The final pH was 5.6. The reaction mixture was allowed to reach room temperature for approximately 3 h, before undergoing solid−liquid extraction. The reaction products were separated from the excess of unreacted platinum by solid−liquid extraction in octadecylsilane cartridges (C18, Sep-Pak, Waters) following a classical procedure (*18*). The compounds retained were recovered from the cartridges with methanol. Yield was 40% from the starting NaCG.

The extract was then concentrated for thin-layer chromatography (TLC) on silica gel plates (60 F254) using butyl acetate/methanol 30/70 (v/v) as the solvent system. Two major bands, one of them corresponding to unreacted CG ($R_f = 0.71$) and the other corresponding to Bamet-R1 ($R_f = 0.27$), were obtained. The latter was scraped off and extracted with methanol. The resulting solution was further purified by semipreparative high-performance liquid chromatography (HPLC) in reversed-phase, using a Waters C18 RCM column (5 μm, 10 mm × 25 cm) with a gradient pump module and a photodiode-array detector set simultaneously at 205 and 250 nm. The system was controlled by an IBM computer using System Gold software from Beckman. The column was equilibrated with 10 mM KH_2PO_4/methanol 25/75 (v/v), pH 7.02 (solvent A), and eluted with an isocratic system with solvent A for 10 min and then with a linear gradient from 100% A to 20% A and 80% methanol in 15 min. The solvent rate was 10 mL/min. In this HPLC system, the retention time for CG was 4.8 min, and that for Bamet-R1 was 17.5 min. During the semipreparative HPLC, 0.5 min fractions were collected automatically. Those corresponding to the Bamet-R1 elution time, taking into account 1-min time lapse between the detector and the fraction collector, were pooled together and dried. The resulting powder was desalted by methanolic extraction in C18 cartridges and dried again.

To obtain the platinum complex named Bamet-UD2 $Pt(NH_3)_2(UDC)_2$, it was necessary to change the synthesis procedure due to the difficulty of purification by chromatographic techniques. AgUDC was synthesized (*19*) by adding 0.50 mmol of $AgNO_3$ to a stirring solution of 0.50 mmol of UDCA with 0.50 mmol of Na_2CO_3 in 50 mL of water. The reaction was carried out at room temperature over 30 min. Then, the solid AgUDC was filtered onto paper and washed with water. The white precipitate was desiccated at 50 °C to give AgUDC in 54% yield. The platinum reagent $Pt(NH_3)_2I_2$ was synthesized (*20*) as follows: 2 mmol of KI was added under a N_2 atmosphere to a stirred 16.5 mM cisplatin aqueous solution at 60 °C. The reaction was carried out at 60 °C for 2 h. The yellow solid was filtered, washed with water, and desiccated at 50 °C to produce $Pt(NH_3)_2I_2$ (49% yield). Finally, 0.13 mmol of $Pt(NH_3)_2I_2$ was added to 0.27 mmol of AgUDC in 45 mL of water at 65 °C. The reaction was kept at 65 °C for 3 days, stirring for 8 h/day, up to a final pH 6. When the reaction had reached room temperature, the AgI formed was filtered and washed with water. It was then washed with MeOH and dried to produce crude product. Following this, liquid−liquid extraction was carried out, the solvents being benzene and water at pH 8. The supernatant was dissolved in MeOH and was then evaporated to afford Bamet-UD2 in 38% yield. All processes were carried out in the dark.

Bamet-R1 was obtained as a slightly yellowish solid in a 6% yield. mp: 165 ± 2 °C. Solubility in water: 352 mM. EA $C_{52}H_{90}N_4O_{12}Pt$: %C, 53.26 (53.90 theor.); %H, 7.75 (7.84 theor.); %N, 4.70 (4.84 theor.); %Pt, 16.21 (16.84 theor.). IR (ν, cm^{-1}): 1636, 1378, 532. ^1H NMR (δ, ppm): 0.69 (s, 3H, Me18), 0.89 (s, 3H, Me19), 1.01 (d, 3H, Me21), 3.38 (m, 1H, H3), 3.76 (bs, 1H, H7), 3.95 (bs, 1H, H12), 3.82 (s, 2H, H25). ^{13}C NMR (ppm): C3 (72.9), C7 (69.1), C12 (74.0), C17 (48.1), C18 (13.0), C19 (23.2), C20 (36.9), C21 (17.6), C22 (33.9), C23 (33.1), C24 (177.0), C25 (42.5), C26 (182.7). ^{195}Pt NMR: −2100 ppm. MS: *m/z* 1180.8 $[M + Na]^+$, 1158.8 $[M + 1]^+$, 693.3 $[M - L]^+$.

Bamet-UD2 a yellowish solid, mp: 175 ± 2 °C. Solubility in water: 288 mM. EA. $C_{48}H_{84}N_2O_8Pt$: %C, 56.37 (56.94 theor.); %H, 8.16 (8.37 theor.); %N, 2.34 (2.77 theor.); %Pt, 18.96 (19.27 theor.). IR (ν, cm^{-1}): 1617, 1378, 536. ^1H NMR (δ, ppm): 0.60 (s, 3H, Me18), 0.86 (s, 3H, Me19), 0.83 (d, 3H, Me21), 3.30 (m, 1H, H3), 3.30 (bs, 1H, H7). ^{13}C NMR (ppm): C3 (69.7), C7 (69.4), C17 (54.6), C18 (12.6), C19 (23.9), C20 (35.0), C21 (18.6), C22 (32.6), C23 (32.0), C24 (180.6). ^{195}Pt NMR: −1554 ppm. MS: *m/z* 1034.4 $[M + Na]^+$, 1012.4, $[M + 1]^+$), 620.2 $[M - L]^+$.

In Vitro Cytostatic Studies. The complexes were evaluated for in vitro cytostatic activity against rat hepatoma McA-RH 7777, human hepatoma HepG2, and murine lymphocytic leukemia L1210, and human colon adenocarcinoma LS174T cells were obtained and cultured as recommended by the American Type Culture Collec-

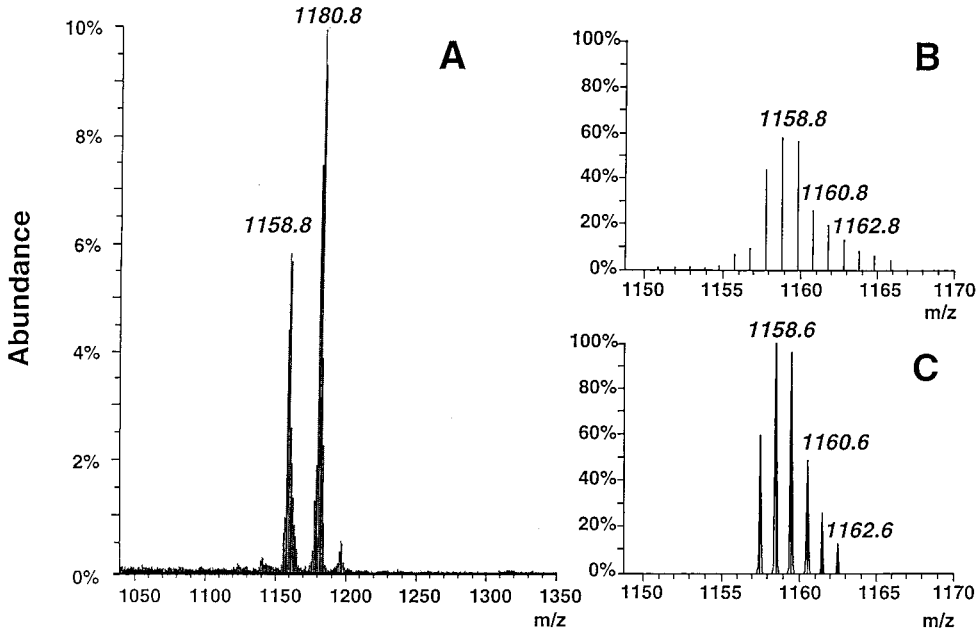

Figure 1. (A) FAB^+/MS spectrum of a freshly prepared sample of Bamet-R1. (B) Zoom region corresponding to the $[M + 1]^+$ ion. (C) Calculated isotopic mass distribution for the $[M + 1]^+$ ion.

tion (ATCC, Rockville, MD). Cells were grown in a humidified atmosphere of 95% air/5% CO_2 at 37 °C. As culture media, the following were used: minimum essential medium Eagle (MEM, Sigma, for LS174T cells) or Dubelcco's modified Eagle's medium (DMEM, Sigma, for McA-RH 7777 and L1210 cells) supplemented with 2 mM glutamine, 26.2 mM $NaHCO_3$, 25 mM Hepes, and 10% horse (L1210 cells), fetal bovine (LS174T cells) serum, or 4 mM glutamine, 26.2 mM $NaHCO_3$, 25 mM Hepes, with 20% horse and 5% fetal bovine serum (McA-RH 7777). F-12 Coon's modification with L-glutamine and zinc sulfate supplemented with 26 mM $NaHCO_3$ and 5% fetal bovine serum (HepG2). On the basis of preliminary studies on the time course of cell growth, the following protocols were carried out for testing purposes. McA-RH 7777, HepG2, L1210, and LS174T cells were harvested during the exponential growth phase, diluted with culture medium, seeded at a cell density of 5700 cells/well into 96-well plates, and incubated with the tested compound for 72 h. Studies comparing the cytostatic activity of cisplatin, Bamet-R1, and Bamet-UD2 were carried out using seven different concentrations (from 0 to 100 μM) of the desired compound in the culture medium and 3 wells/concentration. Similar experiments were carried out in three different cultures. At the end of the culture period, tetrazonium was added to the culture and after incubation for 2 h at 37 °C the absorbance at 490 nm due to formazan was measured.

Statistical Analysis. The equations for kinetic studies were adjusted to the experimental data by means of a nonlinear regression program available in the SIMFIT in the statitics package (Bardsley 1992 SIMFIT package 3.2., Department of Obstretics and Gynecology at St. Mary's Hospital, University of Manchester, U.K.).

The results from biological activity measurements are expressed as means ± SE. To calculate the statistical significance of differences among the groups, the Bonferroni method of multiple-range testing was used. IC_{50} values were calculated from nonlinear regression analysis using Ultrafit software (Biosoft, Cambridge, U.K.). Statistical analysis was performed on a Macintosh LC-III computer (Apple Computer, Inc., Cupertino, CA) with programs supplied by Apple Computer, Inc.

RESULTS AND DISCUSSION

Chemistry. The synthesis and purification of the Platinum complexes were carried out as described in the Experimental Section, by reaction of a solution of the starting platinum complex with sodium cholylglycinate (NaCG) or silver ursodeoxycholate (AgUDC) solutions, followed by chromatographic separations, according to slightly modified previously described procedures (*7*, *8*).

The products isolated were named Bamet-R1 (from NaCG) and Bamet-UD2 (from AgUDC), indicating their origin (Ba-bile acid, met-metal complex; R1 or UD2-from NaCG or AgUDC). The elemental chemical analysis of these complexes are in agreement with the molecular formulas $C_{52}H_{90}N_4O_{12}Pt$ for Bamet-R1 and $C_{48}H_{84}N_2O_8$-Pt for Bamet-UD2. Platinum concentrations were measured in the same solution by flameless atomic absorption. From these data, the depicted structures can be proposed for Bamet-R1 and Bamet-UD2.

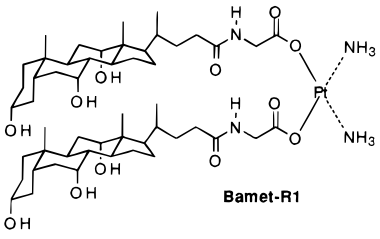

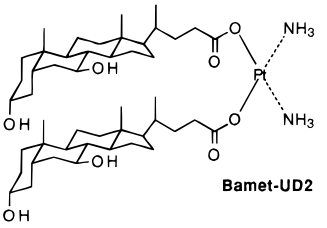

The complexes were characterized by a combination of spectroscopic techniques, which allowed the confirmation of the proposed structures in the absence of X-ray diffraction studies. The latter were not carried out because it was not possible to crystallize the compounds under any of a large list of assayed conditions.

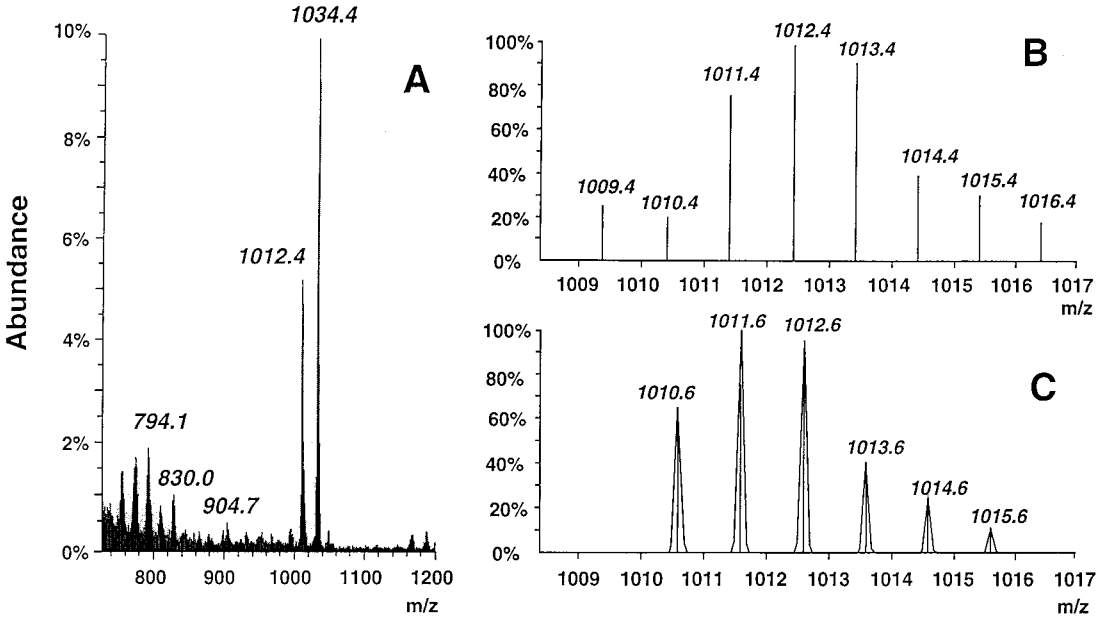

Figure 2. (A) FAB$^+$/MS spectrum of a freshly prepared sample of Bamet-UD2. (B) Zoom region corresponding to the $[M + 1]^+$ ion. (C) Calculated isotopic mass distribution for the $[M + 1]^+$ ion.

The MS of Bamet-R1, Figure 1, shows representative peaks at *m/z* 1180.8, 1158.8, and 693.3 (25% real abundance), which can be respectively assigned to Na^+ addition $[M + Na]^+$ (theor. 1180.6), molecular ion $[M + 1]^+$ (calculated 1158.6), and loss of a cholylglycinate ligand $[M\text{-}CG]^+$ (calculated 693.3). Similarly, in the MS of Bamet-UD2, Figure 2, related representative peaks appear at *m/z* 1034.4, 1012.4, and 620.2 (30% real abundance), which can be respectively assigned to Na^+ addition $[M + Na]^+$ (calculated 1034.5), molecular ion $[M + 1]^+$ (calculated 1012.6), and loss of a ursodeoxycholate ligand $[M - UDC]^+$ (calculated 620.3). The remaining signals in both spectra, with lower *m/z* values, correspond to fragmentations of the bile acid moieties (*21*, *22*).

Owing to the existence of six different isotopic masses for the metal (190, 192, 194, 195, 196, and 198), it was possible to recognize the presence of the metal in the fragmentation peaks of the MS. An identical isotopic distribution was observed in both cases when the experimental data and previously calculated distribution for high *m/z* peaks were compared (Figure 1, panels B and C, and Figure 2, panels B and C).

Small differences between the IR spectra of the complexes and the ligands (NaCG and AgUDC) were also observed for Bamet-R1 and Bamet-UD2 in their IR spectra. The most significant are ν_{as} and ν_s of the COO^- group, which appear at 1602 and 1399 cm^{-1} in the NaCG ligand and 1636 and 1378 cm^{-1} in the Bamet-R1 complex, respectively, and are observed at 1593 and 1380 cm^{-1} in the AgUDC ligand and 1617 and 1387 cm^{-1} in the Bamet-UD2 complex (*23*, *24*). These data point to a monodentate union of these ligands in both complexes. An additional absorption band ν(Pt−N) at 532 cm^{-1} in Bamet-R1 and 536 cm^{-1} in Bamet-UD2 appears in both complexes (*25*, *26*).

The ^{1}H NMR and ^{13}C NMR data confirm the presence of unaltered bile acid moieties in the complexes, and only small differences are observed in comparison with the free ligands. The greatest, though still small, differences were observed in the signals of the C17 chain, in agreement with their close proximity to the metal, mainly affecting C22−C26 in Bamet-R1 and C20−C24 in Bamet-UD2.

The ^{1}H NMR spectrum of the cholylglycinate complex was recorded in methanol-d_4. Comparison with the NaCG spectrum only revealed a minor deshielding of the H25 in the complex. The same deshielding effect was observed in the ^{13}C NMR, because shifts of 6.2 ppm for C26 and 2.1 ppm for C25 were detected for the signals of these carbon atoms in the complex. The spectra of Bamet-UD2 were obtained in DMSO-d_6 because of solubility problems with this complex. The differences between the complex and the free lignad in this solvent were not appreciable in their ^{1}H NMR spectra (<0.03 ppm). A deshielding effect was observed for C22−C24 in ^{13}C NMR, with a shift of ca. 6 ppm for the carboxylate C24, similar to that of the carboxylate C26 in the Bamet-R1 complex. All these data are in agreement with the monodentate union of cholylglycinate and ursodeoxycholate to the metal in both Bamet-R1 and Bamet-UD2 complexes (*27*−*29*).

The NMR analysis of these complexes was completed with the ^{195}Pt NMR spectra. In 48 h, Bamet-R1 produced a well-defined signal at −2100 ppm and Bamet-UD2 afforded a signal at −1554 ppm for the same acquisition time. Comparison of these data with those of related complexes (about −2000 ppm described for two diammine and one bidentate aminocarboxylate) suggest a bidentate union of one of the cholylglycinate ligands and two ammine ligands in the Bamet-R1, due to loss of the other colylglycinate ligands in the NMR solution (*30*−*32*). The process producing the bidentate complex is also in agreement with the kinetic studies described below, which gave $t_{1/2} = 3.0$ h, much shorter than the long time required for the acquisition ^{195}Pt NMR spectrum. Essays aimed at acquiring this spectrum in ca. 3 h failed to produce any distinguishable signal. It is not possible for Bamet-UD2 complex to be transformed by a similar process, because no bidentate union can be formed. Therefore, the complex observed in the ^{195}Pt NMR must keep the original structure with two ursodeoxycholate ligands. The shift of the platinum signal in this case is in agreement with the data described in the literature (*27*, *33*, *34*) (about −1400 ppm) for similar situations with two monodentate carboxylate and two ammine ligands. With the previously above given, we can conclude that the solvent (DMSO) does not substitute the ligands, as,

Scheme 1

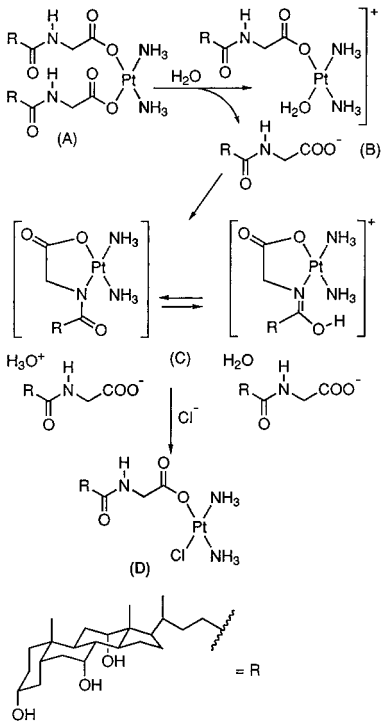

in such a case, the peak corresponding to the ^{195}Pt NMR should move to the −3100 to −3200 ppm, and this has not been observed (*35*).

Kinetic Studies. By combining the condutivity measurements and the study of the variations with time of the electronic spectra in water, the hydrolysis process of Bamet-R1 can be envisaged as depicted in Scheme 1. This proposal is based on kinetic studies of other similar glycinate Pt complexes.

This scheme is based on earlier studies described by Appleton et al. (*30, 31*) for related complexes carrying glycine as ligand. The proposed mechanism is supported by the evolution of UV−vis spectra along time, obtained from water and NaCl solutions of increasing concentrations (4, 150, and 500 mM), as depicted in Scheme 1. These studies address the effect of chloride ion on the biological activity of this class of antineoplastic compounds (*36, 37*). The initial equivalent conductivity of Bamet-R1 in aqueous medium was 112 Ω^{-1} cm^2 mol^{-1}, corresponding to a 1:1 electrolyte, and persisted without variation for 10 days. This conductivity can be explained in terms of a process (A → B) of rapid loss of a cholylglycinate ligand, followed by a slow conversion (B → C) into the bidentate cholylglycinate complex, which maintains the electrolytic character. This second process can be explained as a first-order reaction in B because the experimental data can be fitted to a first-order rate equation, in this case of type $A = A_o(1 - e^{-kt})$, where A is the absorbance corresponding to the reaction product, A_o is the absorbance at time zero, and k is the first-order reaction constant in (hours)$^{-1}$. The values obtained for the rate constant and half-life, respectively, were $k = (2.3 \pm 0.1) \times 10^{-1}$ h^{-1} and $t_{1/2} = 3.0$ h.

When complex A was dissolved in a 4 mM solution of NaCl (similar to cytoplasmatic concentration), the results were similar to those described above, and the ascending curve was fitted with $k = (4.67 \pm 0.1) \times 10^{-1}$ h^{-1} and $t_{1/2} = 1.5$ h. When the concentration of NaCl was 150 mM (similar to plasmatic concentration) an inversion was observed, obtaining a decaying curve that could be fitted

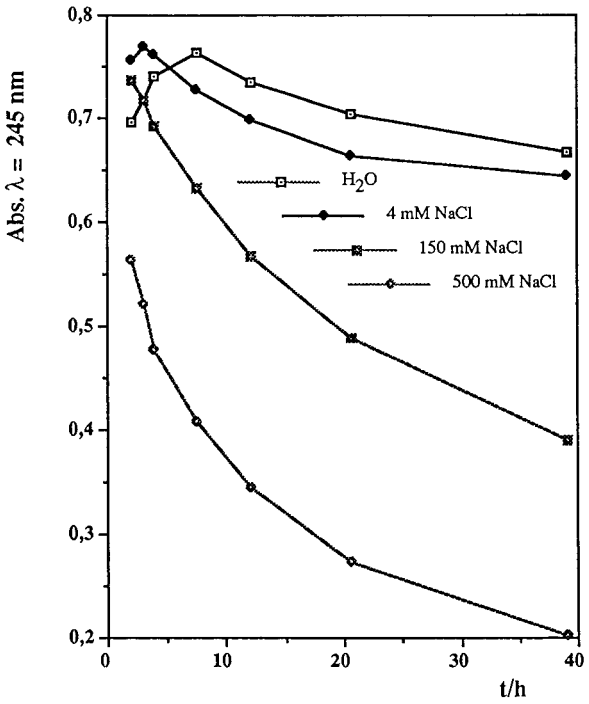

Figure 3. Experimental kinetic curves (absorbance at $\lambda = 245$ nm vs time/hours) for Bamet-R1 in H_2O and different chloride concentrations.

Scheme 2

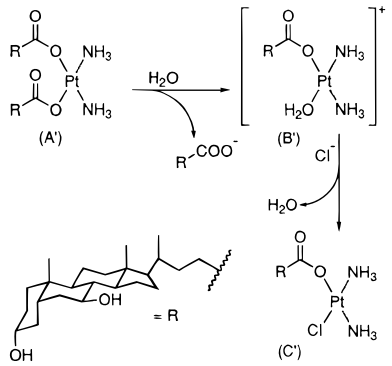

to a pseudo first order of the type $A = A_o e^{-kt}$, where A corresponds to the absorbance of species C at time t and A_o is the absorbance at time zero, thus affording a rate constant and half-life values of $k = (3.96 \pm 0.1) \times 10^{-2}$ h^{-1} and $t_{1/2} = 17.5$ h. This is also in agreement with the results obtained at higher concentration of NaCl (500 mM NaCl). For this concentration, the behavior was similar, with values of $k = (1.19 \pm 0.1) \times 10^{-1}$ h^{-1} and $t_{1/2} = 5.8$ h, and an increase in the rate constant and a decrease of the half-life in comparison to the results obtained for 150 mM. Accordingly, the opening of the bidentate ring is favored by the presence of chloride ion and the rate equation for the C → D step could be expressed by $v = k_{Cl^-}[Cl^-][C]$; taking $k_{Cl^-}[Cl^-]$ as an experimental constant k', a pseudo first-order equation of type $v = k'[C]$ can be deduced. Thus, the rate constants at these two concentration allowed us to calculate the value of k_{Cl^-}, which revealed strong agreement between $k_{Cl^-(150)} = 0.26$ M^{-1} h^{-1} and $k_{Cl^-(500)} = 0.25$ M^{-1} h^{-1}.Taking into account similar considerations, the process proposed for Bamet-UD2 complex is shown in Scheme 2.

In this case, all the observed processes show ascending curves. When (A′) evolves in water, the values obtained for the step (A′ → B'), taking into account pseudo first-

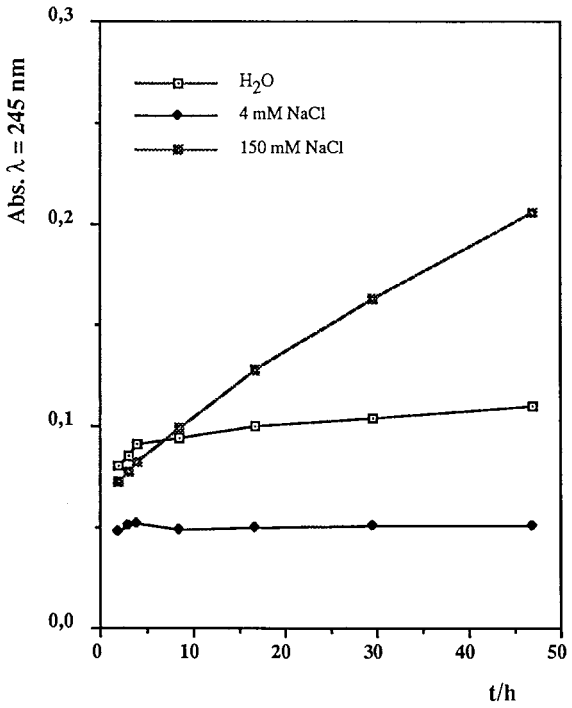

Figure 4. Experimental kinetic curves (absorbance at $\lambda = 245$ nm vs time/hours) for Bamet-UD2 in H_2O and different chloride concentrations.

order kinetics, were $k = (2.17 \pm 0.1) \times 10^{-1}$ h^{-1} and $t_{1/2} = 3.2$ h. No variations were observed for the kinetic followed in 4 mM solution of NaCl, the values of k and $t_{1/2}$ being very close to those obtained in water. At a higher NaCl concentration (150 mM), the variation in absorbance with time becomes more evident and the process (B′ → C′) can be proposed, with $k = (1.33 \pm 0.1) \times 10^{-2}$ h^{-1} and $t_{1/2} = 52$ h. At higher concentrations of NaCl, solubility was so low that it was not possible to obtain the kinetic parameter.

Cytostatic Activity. The cytostatic activities of cisplatin, Bamet-UD2, and Bamet-R1 were determinated in vitro by cell survival after 72 h of exposure to the desired concentration of the indicated compound. The inhibitory concentration 50 (IC_{50}), defined as the concentration required to reduce the size of the cell population by 50%, revealed that the sensitivity to cisplatin was much higher (LS 174T, $IC_{50} = 10$ μM; L1210, $IC_{50} = 13.7$ μM; McA-RH 7777, $IC_{50} = 17.5$ μM; HepG2, $IC_{50} = 17.5$ μM) than to Bamet-R1 (LS 174T, $IC_{50} = 80$ μM; L1210, $IC_{50} = 68.7$ μM; McA-RH 7777, $IC_{50} = >100$ μM; HepG2, $IC_{50} = 61.2$ μM) and higher, although in the same order, than that measured for Bamet-UD2 (LS 174T, $IC_{50} = 23.7$ μM; L1210, $IC_{50} = 33.7$ μM; McA-RH 7777, $IC_{50} = 42.5$ μM; HepG2, $IC_{50} = 50$ μM).

The higher cytostatic activity observed for Bamet-UD2 as compared with Bamet-R1 in certain cell lines is probably related to differences in the dissociation kinetic of this compound. However, these results reveal clearly cell line-dependent effects for both Bamet-UD2 and Bamet-R1. This suggests that factors others than just disociation rate are involved in determining the cytostatic activity of these compounds. Moreover, differences in the ability of these cells lines to repair Bamet-DNA adducts or to neutralize or extrude the complexes cannot be ruled out.

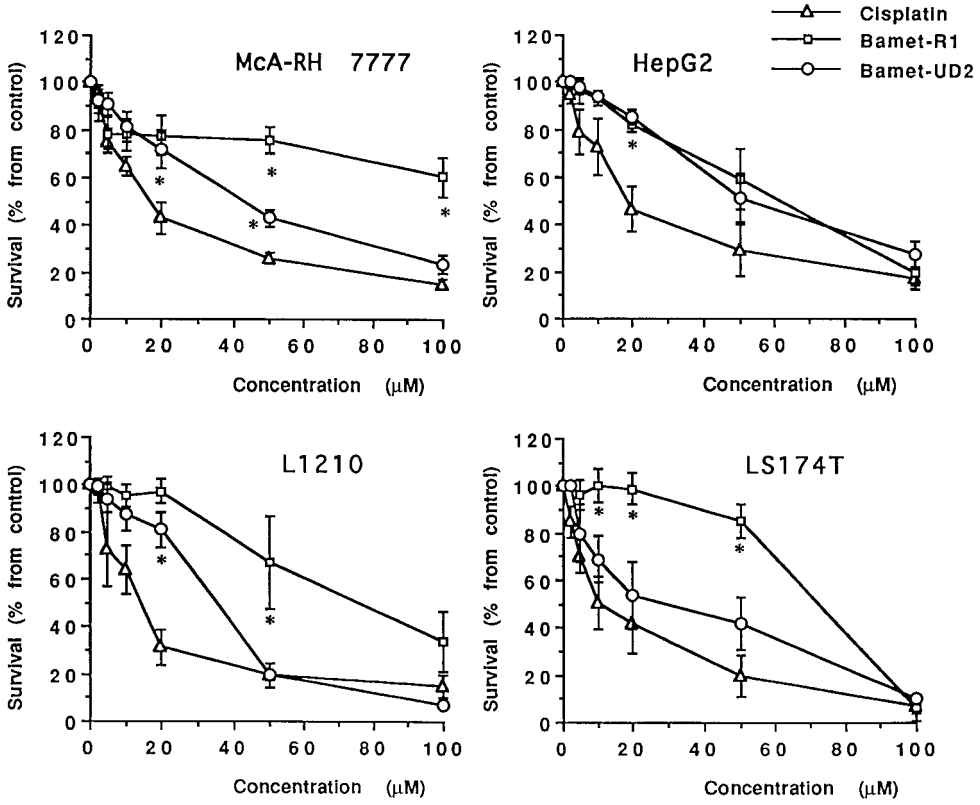

Figure 5. Effect of cisplatin (open triangles), Bamet-R1 (open squares) and Bamet-UD2 (open circles), on cell viability as measured by mitochondrial capacity of metabolize the tretazolium salt to formazan. (Rat hepatoma McA-RH 7777, human hepatoma HepG2, murine lymphocytic leucemia L1210 and human colon adenocarcinoma LS 174T cells). Values are means ± SE of three different cultures. Carried out using three differents wells per concentration point. (*) $p < 0.05$ as compared with cultures incubated with cisplatin by the Bonferroni method of multiple-range testing.

CONCLUSION

The application of synthetic methodology for the preparation of bile acids derivatives of *cis*-diammine platinum-(II) gave two new agents endowed with interesting cytostatic activity. The higher cytostatic activity observed for Bamet-UD2 as compared with that seen for Bamet-R1 in certain cell lines is probably related to differences in the dissociation kinetics of this compound.

ACKNOWLEDGMENT

This study was supported in part by the Junta de Castilla y Leon (Grant SA36/99) and the CICYT (Grants SAL9410693 and SAF9610146). The authors thank Dr. F. J. Burguillo for his assistance in the kinetic studies, Prof. J. Casado and Prof. V. Rives for fruitful discussions and Dr. M. A. Serrano for her valuable help with cell culture.

LITERATURE CITED

(1) Loeher, P. J., and Einhorn, L. H. (1984) Cisplatin. *Ann. Int. Med. 100*, 704−713.

(2) Kelland, L. R. (1999) In *Cisplatin-based anticancer agents* (N. P. Farrell, Ed.) pp 113−120, Royal Society of Chemistry, Cambridge, U.K.

(3) Marin, J. J. G., Palomero, M. F., Herrera, M. C., Macias, R. I. R., Criado, J. J., and Serrano, M. A. (1998) In vitro cytostatic activity and DNA-interaction of the new liver organotropic complex chloro-bis-cholylglicinate-platinum(II). *Anticancer Res. 18*, 1641−1648.

(4) Marin, J. J. G., Macias, R. I. R., Criado, J. J., Bueno, A., Monte, M. J., and Serrano, M. A. (1998) DNA interaction and cytostatic activity of the new liver organotropic complex of cisplatin with glycocholic acid: Bamet-R2. *Int. J. Cancer. 78*, 346−352.

(5) Marin, J. J. G., Herrera, M. C., Palomero, M. R., Macias, R. I. R., Monte, M. J., Elmir, M. Y., and Villanueva, G. R. (1998) Rat liver transport and biotransformation of cytostatic complex of bis-cholylglycinate and platinum (II). *J. Hepatol. 28*, 417−425.

(6) Macias, R. I. R., Monte, M. J., El-Mir, M. Y., Villanueva, G. R., and Marin, J. J. G. (1998) Transport and biotransformation of the new cytostatic complex *cis*-diammineplatinum(II)-chlorocholylglycinate (Bamet-R2) by the rat liver. *J. Lipid Res. 39*, 1792−1798.

(7) Criado, J. J., Herrea, M. C., Palomero, M. F., Medarde, M., Rodriguez, E., and Marin, J. J. G. (1997) Synthesis and characterization of a new bile acid and platinum(II) complex with cytostatic activity. *J. Lipid Res. 38*, 1022−1032.

(8) Criado, J. J., Macias, R. I. R., Medarde, M., Monte, M. J., Serrano, M. A., and Marin, J. J. G. (1997) Synthesis and characterization of the new cytostatic complex *cis*-diammine-platinum(II) chlorocholylglycinate. *Bioconjugate Chem. 8*, 453- 458.

(9) Erlinger, S. (1985) Ursodeoxycholic acid: a very special bile acid. *Hepatology*, 311−317.

(10) Gildutuna, S., Deisinger, B., Weiss, A., Freisleben, H. J., Zimmer, G., Sipos, P., and Leuschner, U. (1997) Ursodeoxycholate stabilizes phospholipid rich membranes and mimics the effect of cholesterol: investigations on large unilamellar vesicles. *Biochim. Biophys. Acta Biomembr. 1326*, 265−274.

(11) Heuman, D. M., and Bajaj, R. (1994) Ursodeoxycholate conjugates protect against disruption of cholesterol-rich membranes by bile salts. *Gastroenterology 106*, 1333−1341.

(12) Carey, M. C. (1984) Bile acids and bile salts: ionization and solubility properties. *Hepatology 4*, 66S−71S.

(13) Dumont, M., Erlinger, S., and Uchman, S. (1980) Hypercholeresis induced by ursodeoxycholic acid and 7-ketolitocholic acid in rat: possible role of bicarbonate transport. *Gastroenterology 79*, 82−89.

(14) Marin, J. J. G., Corbic, M., Dumont, M., De Couet, G., and Erlinger, S. (1985) Role of H^+ transport in ursodeoxycholate-induced biliary HCO_3^- secretion in the rat. *Am. J. Physiol. Gastroent. Liver Physiol. 249*, G-335−341.

(15) Calmus, Y., and Poupon, R. (1991) Ursodeoxycholic acid (UDCA) in the treatment of the chronic cholestatic diseases. *Biochimie 73*, 1335−1338.

(16) Botla, R., Spivey, J. R., Aguilar, H., Bronk, S. F., and Gores, G. J. (1995) Ursodeoxycholate (UDCA) inhibits the mitochondrial membrane permeability transition induced by glycochenodeoxycholate: A mechanism of UDCA cytoprotection. *J. Pharmcol. Exp. Ther. 272*, 930−938.

(17) Roda, A., Hofmann, A. F., and Mysels, K. J. (1983) The influence of bile salt structure on self-association in aqueous solutions. *J. Biol. Chem. 258*, 6362−6370.

(18) Setchell, K. D. R., and Worthington, J. (1982) A rapid method for the quantitative extraction of bile acids and their conjugates from serum using commercially available reverse phase octadecylsilane-bonded silica cartridges. *Clin. Chim. Acta 125*, 135−144.

(19) Al-Baker, S., Perez-Soler, R., and Khokhar, A. R. (1992) Synthesis and biological studies of new lipid-soluble cisplatin analogues entrapped in liposomes. *J. Inorg. Biochem. 47*, 99−108.

(20) Khokhar, A. R., Deng, Y., Al-Baker, S., Yoshida, M., and Siddik, Z. H. (1993) Synthasis and antitumor activity of amine/amine platinum(II) and platinum(IV) complexes. *J. Inorg. Biochem. 50*, 9−20.

(21) Wood, K. V., Sun, Y., and Elkin, R. G. (1991) Differentiation of isomeric conjugated bile acids using positive-ion B/E linked scans. *Anal. Chem. 63*, 247−250.

(22) Mingrone, G., Greco, A. V., Boniforti, L., and Passi, S. (1983) Analysis of conjugate bile acids by high performance liquid chromatography and mass spectrometry. *Lipids 18*, 90−95.

(23) Kieft, J. A., and Nakamoto, K. (1967) Infrared spectra of some Platinum(II) glycine complexes. *J. Inorg.-Nucl. Chem. 29*, 2561−2568.

(24) Paul, A. K., Mansuri-Torshizi, H., Srivastava, T. S., Chavan, S. J., and Chitnis, M. P. (1993) Some potencial antitumor 2,2′-dipyridylamine Pt(II)/Pd(II) complexes with amino acids: Their synthesis, spectroscopy, DNA binding, and cytotoxic studies. *J. Inorg. Biochem. 50*, 9−20.

(25) Hanessian, S., and Wang, J. (1993) Design and synthesis of a cephalosporin- carboplatinum prodrug activatable by a β-lactamase. *Can. J. Chem. 71*, 896−906.

(26) Khokhar, A. R., Xu, Q., and al-Baker, S. (1991) Synthesis and characterization of highly lipophilic antitumor Platinum-(II) complexes. *J. Coord. Chem. 24*, 77−82.

(27) Watabe, M., Takayama, T., Kuwahara, A., Kawahashi, T., Koike, Y., Horiuchi, A., Suzuki, M., Watanabe, T., Mikami, K., Matsumoto, T., and Narusawa, Y. (1995) Preparation and ^{13}C and ^{195}Pt spectra of Platinum(II) peptide complexes and their growth-inhibitory activity against mouse meth A solid tumor in vivo. *Bull. Chem. Soc. Jpn. 68*, 2559−2565.

(28) Lee, Y. A., Jung, O. S., Lee, C. O., Choi, S. U., Jun, M. J., and Sohn, Y. S. (1995) Cationic diamineplatinum (II) complexes of nalidixic acid. *Inorg. Chim. Acta 239*, 133−138.

(29) Lee, Y. A., Jung, O. S., and Sohn, Y. S. (1995) Synthesis and properties of diamine(isopropylidemalonato) platinum-(II): Crystal structure of $O(CH_2CH_2)_2C(CH_2NH_2)_2Pt(OOC)_2$-$C{=}C(CH_3)_2$. *Polyhedron 14*, 2099−2106.

(30) Appleton, T. G., Hall, J. R., and Ralph, S. F. (1985) Reactions of Platinum(II) aquo complexes. 3. Multinuclear (^{15}N, ^{195}Pt, ^{13}C and ^{1}H) NMR. Study of reactions of aqua and hydroxo complexes with glycine and (Methylimino)diacetic acid. *Inorg. Chem. 24*, 673−677.

(31) Appleton, T. G. (1997) Donor atom preferences in complexes of platinum and palladium with amino acids and related molecules. *Coord. Chem. Rev. 166*, 313−359.

(32) Hegmans, A., Sabat, M., Baxter, I., Freisinger, E., and Lippert, B. (1998) Synthetic ways to tris(nucleobase) complexes derived from *cis*-diammineplatinum(II) and a platinum(II) complex containing four different ligands, three of which are nucleobases. *Inorg. Chem. 37*, 4921−4928.

(33) Lin, F. T., and Shepherd, R. E. (1998) Substitution of inosine for chloride in $[Pt_2(hdta)Cl_2]^{2-}$ ($hdta^{4-}$=1,6-hexanediamine-N,N,N′,N′-tetraacetate). *Inorg. Chim. Acta 271*, 124−128.
(34) Gibson, D., Rosenfeld, A., Apfelbaum, H., and Blum, J. (1990) Multinuclear (^{195}Pt, ^{15}N, ^{13}C) NMR studies of the reactions between cis-diaminediaquaplatinum(II) complexes and aminomalonate. *Inorg. Chem. 29*, 5125−5129.
(35) Pregrosin, P. S. (1986) Platinum NMR spectroscopy. *Annu. NMR Spectrosc. 17*, 285−349.
(36) Fekl, U., and Eldik, R. van. (1998) Specfic chelate tuning of the substitution kinetic of Platinum(II) complexes in aqueous solution. *Eur. J. Inorg. Chem*. 389−396.
(37) Chen, Y., Guo, Z., Parsons, S., and Sadler, P. J. (1998) Stereospecific and kinetic control over the hydrolysis of the sterically hindered Platinum picoline anticancer complex. *Chem. Eur. J. 4*, 672−676.

BC9901088

Single Isomer Technetium-99m Tamoxifen Conjugates

Duncan H. Hunter* and Leonard G. Luyt

Department of Chemistry, University of Western Ontario, London, Ontario, Canada N6A 5B7. Received August 20, 1999; Revised Manuscript Received December 3, 1999

To produce an imaging agent for breast cancer using a technetium-99m-labeled agent specific for estrogen receptors, an N_2S_2 bifunctional chelator was conjugated to *Z*- and *E*-aminotamoxifens through an amide linker. These bioconjugates have been chelated with both technetium-99m and rhenium. For the *Z*-isomer, chelation with rhenium in the presence of sodium acetate yields a mixture of two isomers, anti and syn, in a 1:1 ratio and in the presence of hydroxide results in only the anti isomer. Both the *Z*- and *E*-tamoxifen conjugates have been chelated with technetium-99m at the tracer level yielding a single isomer product, which is assigned as anti based on chromatographic comparison to the rhenium complexes. Radiochemical yields were consistently greater than 80%, with Sep-Pak column purification yielding a final product with >99% radiochemical purity and no residual starting material. Both in vitro and in vivo biological evaluation of the tamoxifen chelates indicated very limited estrogen receptor binding.

INTRODUCTION

Breast cancer is the leading form of cancer in females, with one out of every eight women in North America developing the disease in their lifetime (*1*). The proper diagnosis and therapy of breast cancer is continuing to evolve with an ever increasing number of diagnostic procedures and therapeutic agents including nuclear medicine techniques (*2*). Estrogen receptor (ER) status of the tumor is used as a guide for the selection of appropriate tumor therapy, with the drug tamoxifen (**1**) playing a leading role in the therapy of ER positive carcinomas (*3*). Since over 60% of breast cancer tumors contains estrogen receptors, the discovery of an estrogen receptor specific radiopharmaceutical is desirable. Not surprisingly, tamoxifen has been the target of several radiolabeling studies including ^{3}H (*4*, *5*), ^{18}F (*6*), ^{111}In (*7*), ^{123}I (*8*), ^{125}I (*9*), and ^{131}I (*10*), but labeling with ^{99m}Tc has not been reported. Given the widespread use of technetium-99m for radiopharmaceuticals, our previous experience with a radiolabeled tamoxifen, and our recent preparation of an N_2S_2 bifunctional chelator, the attachment of ^{99m}Tc via a linker from tamoxifen to an N_2S_2 bifunctional chelator was attempted.

In determining the location for attachment of a chelator to tamoxifen, the potential metabolism of the radiopharmaceutical was considered. The metabolism of tamoxifen in vivo has been extensively studied (*11*, *12*), with the primary active metabolites in humans being 4-hydroxytamoxifen with the OH on ring-2 and N-demethylated compounds**.** No metabolites have been found involving modification of phenyl ring-3. Placing a metal chelator on phenyl ring-3 may be advantageous, as the resultant metal complex will be able to undergo in vivo metabolism congruous to what occurs for tamoxifen.

The large size of a technetium chelator makes it important to attach the chelator at a region of tamoxifen that can manage steric bulk without sacrificing receptor binding affinity. Table 1 presents the relative binding affinity (estradiol = 100) for tamoxifen derivatives modified at the 4-position of ring-3 (*10*). Compared to tamoxifen, the relative binding affinities of the 4-amino (**2**) and 4-iodo (**3**) tamoxifens show that ring-3 accommodates additional steric bulk with some improvement in estrogen receptor binding. However, a recently published X-ray crystal structure of tamoxifen bound in the estrogen receptor binding site suggests that only limited steric bulk can be accommodated at this position (*13*).

Table 1. Relative Binding Affinities of Tamoxifen Analogues Modified at Ring 3, for Rat Uterine Estrogen Receptors (*10*)

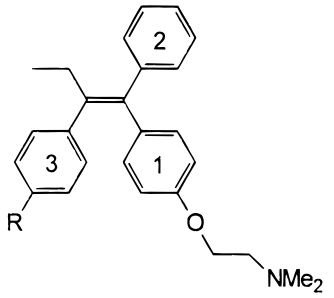

	relative binding affinity (estradiol = 100)	
R	*Z* isomer	*E* isomer
NH_2 (**2**)	1	0.9
I (**3**)	3.3	0.1
H (tamoxifen, **1**)	0.2	~0.02

On the basis of the metabolism studies and on the relative binding affinity of tamoxifen derivatives, it was decided that the preferred location for a technetium chelator would be ring-3 of tamoxifen. The bifunctional chelator chosen for conjugation to tamoxifen is the symmetrical N_2S_2 ligand **4** (*14*). This chelator forms conjugates with amine containing compounds, which upon chelation can produce a single isomer metal complex without the need for HPLC separation. This will greatly ease the purification and characterization of both technetium-99m and rhenium bioconjugates. Using this

* To whom correspondence should be directed. Phone: (519) 661-3122. Fax: (519) 661-3022. Email: dhunter@julian.uwo.ca.

10.1021/bc990110z CCC: $19.00 © 2000 American Chemical Society
Published on Web 02/19/2000

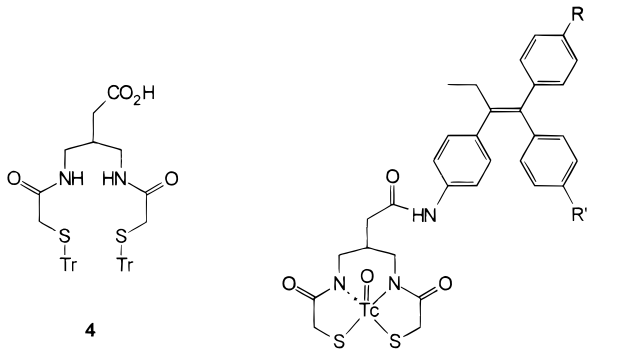

Figure 1. Bifunctional chelator and the proposed [^{99m}Tc]-tamoxifen analogues.

N_2S_2 bifunctional chelator, the [^{99m}Tc]tamoxifen analogues *Z*-**5** and *E*-**5** shown in Figure 1 are proposed as potential estrogen receptor imaging agents.

EXPERIMENTAL SECTION

Chemicals were purchased from commercial sources (Sigma-Aldrich Canada Ltd., Mississauga, Ontario, and Lancaster, Georgetown, Ontario) as reagent grade and were used as received with the following exceptions: 3,3-bis(triphenylmethylthio-acetamidomethyl)propanoic acid **4** (*14*), *trans*-bis(ethylenediamine)dioxorhenium(V) chloride (*15*), and the aminotamoxifens *Z*-**2** and *E*-**2** (*10*) were all prepared according to literature procedures and had physical and spectroscopic properties consistent with those reported previously. ^{1}H, ^{13}C, and two-dimensional NMR spectra were collected on a Varian Gemini-300 or Varian Gemini-200 spectrometer with TMS as an internal reference. Infrared spectra were recorded in the range 4000−600 cm^{-1} on a Bruker IFS 5500 FT-IR with a Spectra-Tech diffuse reflectance accessory (DRIFT); UV spectra were recorded on a Hewlett-Packard 8451A Diode Array spectrophotometer. Routine mass spectra (MS) and negative ion fast-atom bombardment mass spectra (FABMS) were measured on a Finnigan MAT 8200 spectrometer. HPLC was performed using a Dionex DX 300 HPLC with a Waters μBondpak C_{18}-RP column under an eluent gradient (44% acetonitrile/56% 10 mM KH_2PO_4 ramped to 53% acetonitrile/47% 10 mM KH_2PO_4 over 20 min). The UV detector was set at 249 nm, and the γ counter window was at 140 ± 30 keV. Elemental analyses were performed by Guelph Chemical Laboratories Ltd. (Guelph, Ontario). Na[^{99m}Tc]TcO_4^- was obtained from a commercial ^{99}Mo/^{99m}Tc generator as supplied by Dupont. The receptor binding affinity was performed in the laboratories of J. A. Katzenellenbogen, Department of Chemistry, University of Illinois, Champagne-Urbana, IL. Mice were used with approval of the University of Western Ontario University Council on Animal Care and were cared for in accordance with the Canadian Council on Animal Care and the Animals for Research Act of the Province of Ontario.

2-(4-(3,3-Bis(triphenylmethylthio-acetamidomethylene)propanamido)phenyl)-1-(4-[2-(*N*,*N*-dimethylamino)ethoxy]phenyl)-1-phenyl-1(*Z*)-butene (*Z*-6). The amine *Z*-**2** (112 mg, 0.291 mmol), **4** (210 mg, 0.275 mmol), dicyclohexylcarbodiimide (63.5 mg, 0.308 mmol), 1-hydroxybenzotriazole (49.6 mg, 0.324 mmol), and 40 μL of collidine (0.36 mmol) were added to 20 mL of CH_2Cl_2. The mixture was stirred under argon for 1 day at which time the white precipitate (dicyclohexylurea, 56 mg) was filtered. The filtrate, with additional CH_2Cl_2, was transferred to a separatory funnel and washed with 1 M HCl (three times), 0.5 M Na_2CO_3 (two times), and saturated NaCl. The organic layer was dried over $MgSO_4$ and filtered, and the solvent was removed by rotary evaporation. The crude product was then dried under vacuum (0.1 mmHg, RT) yielding 334 mg. A ^{1}H NMR spectrum of the crude product indicated a mixture of *Z*-**6**, dicyclohexylurea, and a small quantity of starting material. Purification was carried out by flash chromatography (silica, column 23 × 80 mm), with ethyl acetate as the first eluent and 20% methanol/80% ethyl acetate to elute the product. This second eluent was placed in a flask and the solvent was removed by rotary evaporation, followed by drying under vacuum (0.05 mmHg, RT) to give a pale yellow solid. This was recrystallized from chloroform/hexanes yielding 203 mg (65% yield) of *Z*-**6** as fine buff white crystals: mp 187−189 °C; ^{1}H NMR spectrum (δ, $CDCl_3$, RT) 0.89 ppm (t, 3H, CH_3, J = 7.4 Hz), 1.78 (m, 1H, CH), 1.90 (d, 2H, CH_2), 2.29 (s, 6H, NCH_3 × 2), 2.42 (q, 2H, CH_2NMe_2, J = 7.4 Hz), 2.52 (m, 2H, CH_2N), 2.65 (t, 2H, CH_2N, J = 5.8 Hz), 3.09 (s, 4H, CH_2−S × 2), 3.18 (m, 2 H, CH_2N), 3.92 (t, 2H, CH_2O, J = 5.8 Hz), 6.55 (ar, 2H), 6.77 (ar, 2H), 6.83 (m, 2H, NH × 2), 7.03 (ar, 2H), 7.20−7.40 (ar, 37 H), 9.76 (s, 1H, NH); ^{13}C NMR spectrum (δ, $CDCl_3$, RT) 13.61 ppm (CH_3), 28.80 (CH_2 of ethyl), 36.03 (SCH_2 × 2), 37.90 (CH_2), 38.34 (CH), 40.01 (NCH_2 × 2), 45.73 (NCH_3 × 2), 58.14 (CH_2NMe_2), 65.30 (OCH_2), 67.79 (CPh_3), 113.35 (C=C), 118.98 (C=C), 126.35 (ar), 126.97 (ar), 127.08 (ar), 127.98 (ar), 128.10 (ar), 129.27 (ar), 129.41 (ar), 130.07 (ar), 131.79 (ar), 135.57 (ar), 136.48 (ar), 137.70 (ar), 137.97 (ar), 140.74 (ar), 143.84 (ar), 156.57 (ar), 169.50 (C=O), 170.06 (C=O); UV (95% ethanol) 296 nm (14 300 M^{-1} cm^{-1}), 251 nm (25 000 M^{-1} cm^{-1}), 202 nm (151 400 M^{-1} cm^{-1}); Anal. calcd for $C_{73}H_{72}N_4O_4S_2$: C, 77.35; H, 6.40; N, 4.94; O, 5.65; S, 5.66. Found: C, 77.80; H, 6.53; N, 5.22; O, 6.09; S, 5.30.

2-(4-(3,3-Bis(triphenylmethylthio-acetamidomethylene)propanamido)phenyl)-1-(4-[2-(*N*,*N*-dimethylamino)ethoxy)phenyl)-1-phenyl-1(*E*)-butene (*E*-6). The preparation of *E*-**6** followed the procedure for *Z*-**6** using 69 mg of *E*-**2** (0.178 mmol) and 136 mg **4** (0.178 mmol). After column chromatography, *E*-**6** was recrystallized from chloroform/hexanes yielding 139 mg (0.123 mmol, 69% yield) of fine buff white crystals: mp 200−201.5 °C; ^{1}H NMR spectrum (δ, $CDCl_3$, RT) 0.92 ppm (t, 3H, CH_3), 1.78 (m, 1H, CH), 1.89 (d, 2H, CH_2), 2.38 (s, 6H, NCH_3 x2), 2.48 (m, 4H, CH−N × 2 and CH_2), 2.79 (t, 2H, CH_2NMe_2, J = 5.7 Hz), 3.08 (s, 4H, CH_2−S × 2), 3.16 (m, 2 H, CH−N × 2), 4.09 (t, 2H, CH_2O, J = 5.7 Hz), 6.85 (m, 2H, NH × 2), 6.86−7.43 (ar, 43 H), 9.75 (s, 1H, NH); ^{13}C NMR spectrum (δ, $CDCl_3$, RT) 13.60 ppm (CH_3), 28.81 (CH_2 of ethyl), 36.04 (SCH_2 × 2), 37.90 (CH_2), 38.29 (CH), 39.98 (NCH_2 × 2), 45.56 (NCH_3 × 2), 58.01 (CH_2NMe_2), 65.46 (OCH_2), 67.74 (CPh_3), 113.95 (C=C), 118.90 (C=C), 125.55 (ar), 126.94 (ar), 127.29 (ar), 128.07 (ar), 129.39 (ar), 130.04 (ar), 130.47 (ar), 130.74 (ar), 136.25 (ar), 136.48 (ar), 137.64 (ar), 138.06 (ar), 141.29 (ar), 143.29 (ar), 143.83 (ar), 157.25 (ar), 169.51 (C=O), 170.02 (C=O); Anal. calcd for $C_{73}H_{72}N_4O_4S_2$: C, 77.35; H, 6.40; N, 4.94; O, 5.65; S, 5.66. Found: C, 77.60; H, 6.08; N, 4.94; O, 6.00; S, 5.32.

2-(4-(3,3-Bis(thioacetamidomethylene)propanamido)phenyl)-1-(4-(2-(*N*,*N*-dimethylamino)ethoxy)-phenyl)-1-phenyl-1(*Z*)-butene (*Z*-7). Z-**6** (149 mg, 0.131 mmol) was dissolved in 4 mL of methylene chloride and was cooled to 0 °C on an ice bath. To the clear and

colorless stirred solution was added 4 mL of cold (0 °C) trifluoroacetic acid resulting in an immediate yellow color. Triethylsilane (50.2 μL, 0.30 mmol) was then added with the mixture slowly turning to a clear colorless solution. After 30 min the reaction was warmed to RT and was transferred to a separatory funnel with an additional 20 mL of methylene chloride. The mixture was washed with H_2O and 1 M Na_2CO_3. The organic layer was placed in a flask and the solvent was removed by rotary evaporation. The resulting solid was repeatedly triturated with hexane to remove the triphenylmethane, leaving behind *Z*-**7** as a pale yellow solid: HPLC, t_r = 25.0 min, area = 99.1%.

2-(4-(3,3-Bis(thioacetamidomethylene)propanamido)phenyl)-1-(4-(2-(*N*,*N*-dimethylamino)ethoxy)phenyl)-1-phenyl-1(*E*)-butene (*E*-7). The preparation of *E*-**7** followed the identical procedure as used for *Z*-**7**. The dithiol *E*-**7** was recovered as a white solid: HPLC *E*-**7** (21.1 min, 90.6%), *Z*-**7** (24.5 min, 9.4%).

***anti*- and *syn*-2-(4-(3,3-Bis(thioacetamidomethylene)propanamido)phenyl)-1-(4-(2-(*N*,*N*-dimethylamino)ethoxy)phenyl)-1-phenyl-1(*Z*)-butene Oxorhenium (V) [*anti*- and *syn*-(*Z*)-8].** A flask was charged with *Z*-**7** (85 mg, 0.131 mmol), $ReOCl_3(PPh_3)_2$ (111 mg, 0.133 mmol), and 5 mL of 1 M sodium acetate in methanol (degassed by bubbling argon through the solvent). The reaction was heated at reflux under an argon blanket for 5 h. After cooling to room temperature, the solvent was removed by a rotary evaporator and dried under 0.3 mmHg overnight. The resulting pale orange powder was washed well with water leaving 72 mg as a mixture of *anti*-(*Z*)-**8** and *syn*-(*Z*)-**8** (63% crude yield): HPLC (UV at 249 nm) 16.00 min (46.1% area), 16.75 min (42.0%); HRMS FAB (negative ion, thioglycine and oxalic acid matrix) *m*/*z* calcd for $C_{35}H_{40}N_4O_5S_2{}^{187}Re$ 847.1998; found 847.1998 (100%); calcd for $C_{35}H_{40}N_4O_5S_2{}^{185}Re$ 845.1970; found 845.1970 (59%).

***anti*-2-(4-(3,3-Bis(thioacetamidomethylene)propanamido)phenyl)-1-(4-(2-(*N*,*N*-dimethylamino)ethoxy)phenyl)-1-phenyl-1(*Z*)-butene Oxorhenium (V) [*anti*-(*Z*)-8].** Z-**6** (222 mg, 0.196 mmol) was deprotected as previously described. The crude **Z-7** was dissolved in 25 mL of methanol, to which was added *trans*-bis-(ethylenediamine)dioxorhenium (V) chloride (84 mg, 0.208 mmol) and 8 mL of 10% tetraethylammonium hydroxide aqueous solution. The reaction mixture was heated at reflux for 1 h and cooled to RT, and 10 mL of water was added. The methanol volume was reduced by a rotary evaporator, resulting in precipitation of *anti*-(*Z*)-**8** as a pale orange powder (108 mg, 56% yield): mp 129−132 °C; ^{1}H NMR spectrum (δ, $CDCl_3$, RT) 0.87 ppm (t, 3H, J = 7.4 Hz, CH_3), 1.20 (t, 12H, J = 7.1 Hz, CH_3 of NEt_4), 2.25 (s, 6H, $NCH_3 \times 2$), 2.39 (q, 2H, J = 7.4 Hz, CH_2 of ethyl), 2.50 (m, 1H, CH), 2.62 (m, 4H, CH_2NMe_2 and CH_2CO), 2.89 (m, 2H, $CHN \times 2$ axial), 3.17 (q, 8H, J = 7.1 Hz, CH_2 of NEt_4), 3.80/3.88 (AB, 4H, $CH_2S \times 2$, J = 17.1 Hz), 3.92 (t, 2H, OCH_2), 4.01 (m, 2H, $CHN \times 2$ equatorial), 6.54 (ar, 2H), 6.75 (ar, 2H), 7.01 (ar, 2H), 7.07−7.33 (ar, 5H), 7.40 (ar, 2H), 9.10 (s, 1H, NH); ^{13}C NMR spectrum (δ, $CDCl_3$, RT) 7.53 (CH_3 of NEt_4), 13.67 ppm (CH_3), 28.85 (CH_2 of ethyl), 38.79 ($SCH_2 \times 2$), 40.33 (CH_2CO), 41.19 (CH), 45.80 ($NCH_3 \times 2$), 52.36 (CH_2 of NEt_4), 55.35 ($NCH_2 \times 2$), 58.21 (CH_2NMe_2), 65.63 (OCH_2), 113.49 (C═C), 119.13 (C═C), 126.45 (ar), 128.04 (ar), 128.22 (ar), 129.35 (ar), 129.97 (ar), 131.88 (ar), 135.65 (ar), 136.75 (ar), 137.67 (ar), 140.60 (ar), 143.78 (ar), 156.61 (ar), 170.03 (NHC═O), 196.04 (NC═O); IR 969 cm^{-1} (Re═O); HPLC *anti*-**(*Z*)-8** 16.4 min; HRMS FAB (negative ion, thioglycine and oxalic acid matrix) *m*/*z* calcd for $C_{35}H_{40}N_4O_5S_2187Re$ 847.1998, found 847.2005 (100%).

2-(4-(3,3-Bis(thioacetamidomethylene)propanamido)phenyl)-1-(4-(2-(*N*,*N*-dimethylamino)ethoxy)phenyl)-1-phenyl-1(*Z*)-butene Oxotechnetium-99m (V) (*Z*-5). A 3 mL conical vial was charged with 28.1 mCi freshly eluted [^{99m}Tc]TcO_4^- in 500 μL of normal saline, 400 μL of 0.5 mM *Z*-**7** (50% ethanol/water solution), 40 μL of 1 M NaOH and 80 μg of $SnCl_2$ in 40 μL of 0.1 M HCl. The vial was sealed with a Teflon-lined cap and heated at 90 °C for 30 min. After cooling to room temperature, a 29.7 μCi aliquot (2.5 μL) was checked by HPLC and found to contain 16.6% [^{99m}Tc]TcO_4^- and 83.4% product. The remaining 26.1 mCi was placed onto a Sep-Pak (Waters C_{18} 1 cm^3) and was eluted with 3 mL of distilled water removing 3.22 mCi. No additional radioactivity was being eluted with additional water. The Sep-Pak was then flushed with 1 mL of ethanol removing 18.9 mCi. An additional ethanol flush removed only 0.06 mCi and was not used. An aliquot of the ethanol eluent was checked by HPLC, with one γ peak appearing at a retention time of 16.6 min (area = 100.00%). The ethanol eluent was placed into a small test tube in a warm water bath, and air was bubbled through it until the volume was reduced to less than 0.1 mL. To this was added 9.0 mL of saline solution (2% ethanol, 0.1% Tween), and the solution was filtered through a sterile 0.22 μm Millex GS filter yielding 15.2 mCi of dissolved product. Purity of the radiopharmaceutical was checked by HPLC analysis of a 53 μCi aliquot (30 μL) resulting in a single peak on the γ trace, eluting at 16.6 min with 100.00% purity. The UV chromatogram shows very little UV absorbable impurities, indicating that the dithiol starting material has been removed. Radiochemical yield corrected for decay is 71%.

2-(4-(3,3-Bis(thioacetamidomethylene)propanamido)phenyl)-1-(4-(2-(*N*,*N*-dimethylamino)ethoxy)phenyl)-1-phenyl-1(*E*)-butene Oxotechnetium-99m (V) (*E*-5). A 3 mL conical vial was charged with 517 μCi freshly eluted [^{99m}Tc]TcO_4^- in saline, 160 μL of 0.5 mM *E*-**7** (50% ethanol/water solution filtered through a 0.22 μm syringe tip filter), 20 μL of 1 M NaOH and 0.04 mg $SnCl_2$ in 20 μL of 0.1 M HCl. The vial was sealed with a Teflon lined cap and heated at 90 °C for 30 min. After cooling to room temperature an 75.0 μCi aliquot (40 μL) was checked by HPLC and found to contain 35.8% [^{99m}Tc]TcO_4^- (RT = 3.0 min.), 58.4% *anti*-(*E*)-**5** (RT = 11.9 min) and 5.8% *anti*-(*Z*)-**5** (RT = 16.1 min). The remaining 349 μCi was placed onto a Sep-Pak (Waters C_{18}, 1 cm^3) and was flushed with 2 mL of distilled water removing 127 μCi. No additional radioactivity was being eluted with additional water. The Sep-Pak was then eluted with 1 mL of ethanol removing 213 μCi. The Sep-Pak was found to contain only 7 μCi of residual radioactivity. An 31 μCi aliquot of the ethanol eluent was checked by HPLC and was found to contain 0.3% [^{99m}Tc]TcO_4^- (RT = 2.5 min), 93.9% *anti*-(*E*)-**5** (RT = 10.8 min) and 5.8% *anti*-(*Z*)-**5** (RT = 16.0 min). The radiochemical yield is 61%, with a radiochemical purity of 99.7%, and an *E*:*Z* ratio of 16:1.

Biodistribution of *anti*-(*Z*)-5. An in vivo biodistribution study was carried out using female C3H mice (18.5−22.0 g; 20−25 weeks of age). The [^{99m}Tc]-*anti*-(*Z*)-tamoxifen [*anti*-(*Z*)-**5**] was dissolved in a solution of saline containing 2% ethanol and 0.1% Tween (pH 5−5.5). A total of 100 μL of this solution was injected into the tail vein of the mouse with the syringe being counted pre- and postinjection. The mice were sacrificed at 1, 3, 24,

Table 2. Selected ^{1}H NMR ($CDCl_3$, 300 MHz) Chemical Shifts (ppm) for *Z*- and *E*-6

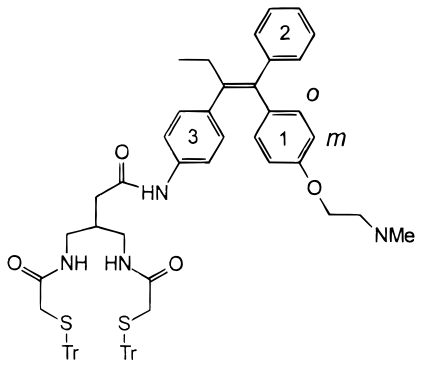

protons	*Z*-6	*E*-6
OCH_2 (of ethoxy)	3.92	4.09
NCH_2 (of ethoxy)	2.52	2.79
ortho of Ar-1	6.77	>6.86
meta of Ar-1	6.55	>6.86

Table 3. Comparison of ^{1}H NMR (300 MHz, δ ppm) Spectroscopy for Protons near the Rhenium Chelation Site

	(*Z*)-**8**	**9**		**10**	
	anti	anti	syn	anti	syn
NCH_2 (axial)	2.96	2.63	3.31	2.87	3.42
(equatorial)	3.92	3.78	3.88	3.92	3.86
SCH_2	3.65/3.76	3.57/3.64	3.48/3.79	3.62/3.74	3.76/3.84
				3.62/3.76	4.04/4.09

Table 4. In Vivo Biodistribution of (*anti*)-*Z*-5 in Mice at Various Time Points (4 or 5 mice/time point)

	% injected dose/gram of tissue at four time points			
tissue	1 h	3 h	24 h	48 h
blood	0.88 ± 0.20	0.47 ± 0.18	0.15 ± 0.12	0.10 ± 0.05
lung	0.54 ± 0.17	0.28 ± 0.10	0.49 ± 0.39	0.28 ± 0.19
liver	7.78 ± 2.39	4.00 ± 0.75	1.24 ± 0.51	0.66 ± 0.26
kidney	1.43 ± 0.69	0.27 ± 0.05	0.19 ± 0.16	0.23 ± 0.10
uterus	0.30 ± 0.10	0.16 ± 0.07	0.18 ± 0.16	0.33 ± 0.23
muscle	0.15 ± 0.12	0.10 ± 0.10	0.26 ± 0.32	0.31 ± 0.19

or 48 h postinjection with four or five mice at each time point. A blood sample was immediately removed followed by dissection of the lungs, liver, kidneys, uterus, muscle, and tail. The tissues were weighed and then stored in a freezer until all the dissections were complete. The tissues were then counted in a γ well counter along with standards with a total count time per sample of 10 min. The radioactivity uptake, as presented in Table 4, is expressed as the percentage of the injected dose per gram of tissue.

Estrogen Receptor Binding Affinity. The relative binding affinity (RBA) value for *anti*-(*Z*)-**5** was determined by a previously reported competitive radiometric binding assay (*16*). Lamb uterine cytosol, diluted to approximately 1.3 nM of receptor, was incubated with 10 nM [^{3}H]estradiol for19 h at 0 °C. Free ligand was removed by absorption onto dextran-coated charcoal. The ligand concentration was altered from 10^{-4} to 10^{-9} M. Estradiol was run as a control with 50% inhibition occurring at 10 nM. The binding affinity of *anti*-(*Z*)-**5** relative to estradiol (=100) was too low to measure, with a RBA of <0.009%.

RESULTS AND DISCUSSION

The preparation of the target tamoxifen analogue was carried out using the amino-tamoxifen derivatives *Z*- and *E*-**2** and the N_2S_2 bifunctional chelator **4** as starting materials. This section first discusses the preparation and characterization of both *Z*- and *E*-tamoxifen analogues **6** and then discusses the chelation of the complex with rhenium and technetium-99m. Finally, the results of an in vivo biodistribution study of *anti*-(*Z*)-**5** in mice and a relative binding assay of the rhenium complex *anti*-(*Z*)-**8** are presented.

Preparation of *Z*- and *E*-6. As shown in Scheme 1, coupling of **2** to the chelator **4** was accomplished using DCC as the coupling reagent with 1-hydroxybenzotriazole as an activating agent. Purification was carried out by flash chromatography, first with ethyl acetate as the eluent in order to remove the dicyclohexyl urea and then with 20% methanol/80% ethyl acetate to recover the product **6**. The purified yields after recrystallization were 65 and 69% for the Z- and E-isomers, respectively.

Characterization of both isomers was carried out by NMR spectroscopy, including ^{1}H, ^{13}C, and two-dimensional NMR spectra. It is reported that the OCH_2 protons of the ethoxy chain allows for identification of the E- and Z-isomers, with the Z-isomer shift appearing upfield of 4.0 ppm and the E-isomer downfield of 4.0 ppm (*17*). As shown in Table 2, this is indeed the case, with the Z-isomer OCH_2 protons appearing at 3.92 ppm and the Z-isomer at 4.08 ppm. Differences in the ^{1}H spectra of the two isomers is also expected in the aromatic region (*18*). The most substantial difference is the ortho and meta protons of ring 1, where the Z-isomer protons have an upfield shift of around 0.3 ppm. The ^{13}C NMR spectra of *Z* and *E*-**6** showed very slight (<1.0 ppm) differences in chemical shifts, with peaks being assigned based on HETCOR and APT analysis. The UV spectrum of *Z*-**6** indicates absorptions at 251 nm (ϵ = 25 000 M^{-1} cm^{-1}) and 296 nm (ϵ = 14 300 M^{-1} cm^{-1}), which is very similar to other amide containing tamoxifen analogues (*19*).

Rhenium Chelation. Deprotection of the thiol groups was carried out as shown in Scheme 1, using trifluoroacetic acid in dichloromethane, with triethylsilane as the cation scavenger. The dithiols *Z* and *E*-**7** were purified by trituration, which removed all of the triphenylmethane. As shown in Figure 2, product purity was checked by HPLC with the Z-isomer (Figure 2a) showing >99% purity and the E-isomer (Figure 2b) being contaminated with approximately 9% of the Z-dithiol. The presence of the Z-isomer contaminant was confirmed by a co-injection of the two products, as shown in Figure 2c.

Chelation of *Z*-**7** with rhenium was achieved using $ReOCl_3(PPh_3)_2$ in the presence of sodium acetate, with methanol as the solvent. The rhenium-tamoxifen product **8** is poorly soluble and precipitates out of solution, presumably as the sodium salt. As shown in Figure 3a, HPLC analysis of this crude product showed two peaks near 16 min retention time, which indicated that two isomers *anti*- and *syn*-(*Z*)-**8** had formed in a near 1:1 ratio. The small peak at approximately 11 min retention time is attributed to (*E*)-**8.** If a solution of these two isomers in ethanol was subjected to 1 M NaOH solution at room temperature, isomerization to the earlier eluting isomer occurred with an equilibrium ratio of 9:1 as indicated by the HPLC trace in Figure 3b. Coinjection of the single isomer (Figure 3c) with the mixture confirmed that isomerization was occurring and not the formation of a new product. This epimerization is consistent with previously reported metal complexes **9**, **10**, and **11**, all of which, as shown in Figure 4, contain the identical N_2S_2 core (*14, 20*). These complexes were found to chelate in a near 1:1 mixture of anti:syn isomers and converted

Scheme 1

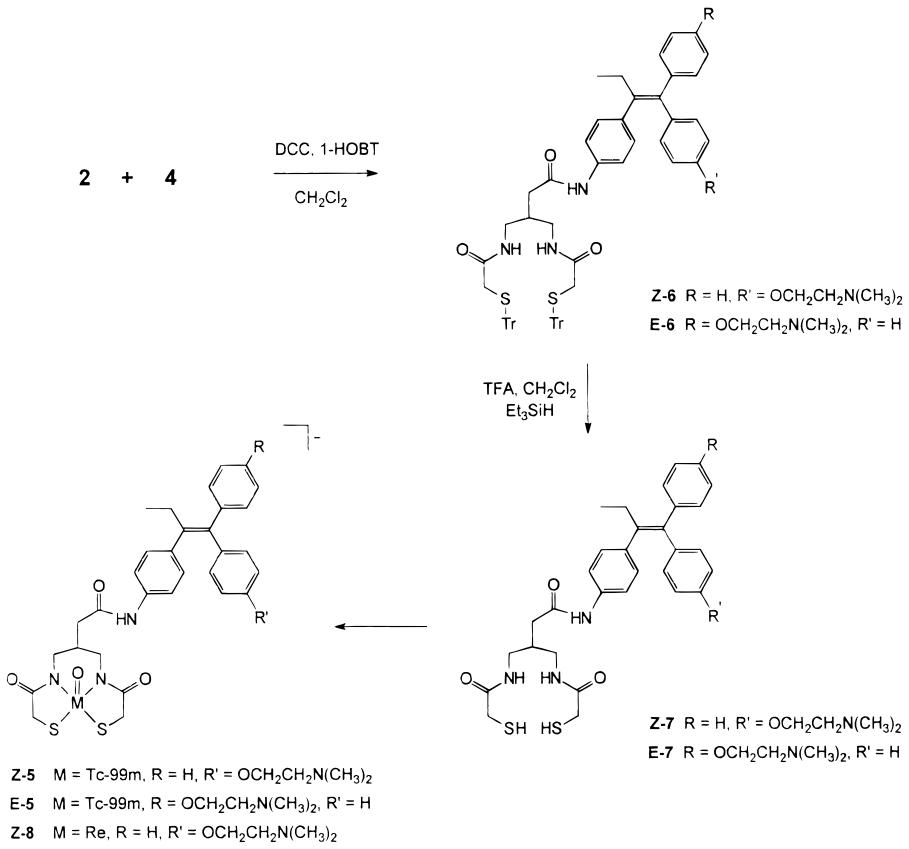

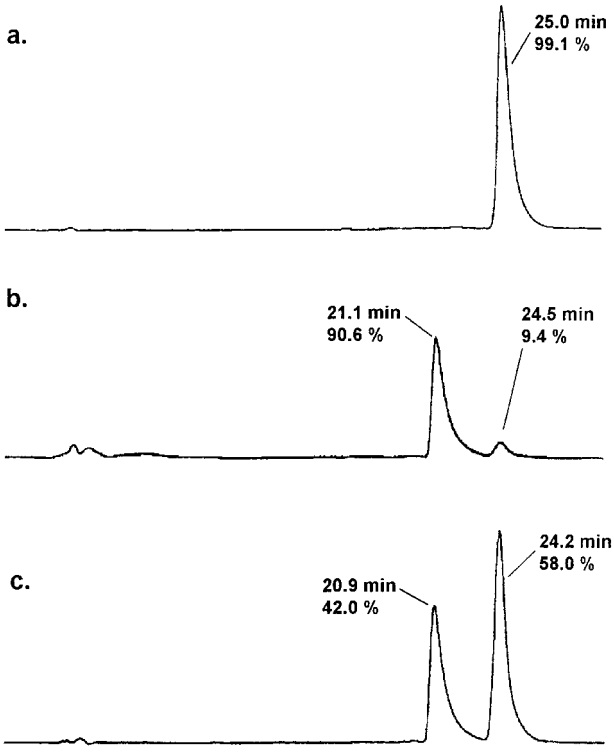

Figure 2. HPLC chromatograms (UV detector) of **7**: (a) *Z*-**7**; (b) *E*-**7**; (c) co-injection.

entirely to the less lipophilic anti isomer when exposed to basic (aqueous) conditions.

High-resolution FAB mass spectrometry was used to identify the mass of the complex, with 100% signal for the ^{187}Re complex at 847.1998 *m/z* and 59% signal for the ^{185}Re complex at 845.1970.

The poor solubility of the sodium salt of **8** precluded additional characterization, and instead, the reaction was repeated with an quaternary ammonium cation being present instead of sodium. Rhenium chelation of *Z*-**7** was successfully achieved using *trans*-bis(ethylenediamine)-dioxorhenium(V) chloride as the rhenium source, with a reaction solvent consisting of methanol and 10% tetraethylammonium hydroxide (aqueous) solution, giving *anti*-(*Z*)-**8** in a 56% yield. The product purity was >95%, with the sole contaminant, as discovered by HPLC analysis, being (*E*)-**8**. In this reaction, the anionic product remained in solution, allowing for it to be precipitated as a tetraethylammonium salt by the removal of methanol. This single isomer product was characterized by ^{1}H and ^{13}C NMR spectroscopy, which allowed for its assignment as *anti*-(*Z*)-**8**. Table 3 presents a comparison of the chemical shifts of *anti*-(*Z*)-**8** to two other *anti*-rhenium products (*14*). The chemical shifts and coupling constants for the protons of the chelate core are consistent with this isomer being the anti-epimer. This is especially apparent for the NCH_2 axial protons, where the anti-epimers invariably appear between 2.6 and 3.0 ppm, with two large coupling constants. The chromatographic behavior of this isomer is also consistent with it being the anti-isomer, in that it elutes as the first product as seen in Figure 3d. The product was further characterized by high-resolution FAB mass spectrometry with the parent signal for the ^{187}Re complex at 847.2005 *m/z* and by FT-IR spectroscopy with the Re═O absorption occurring at 969 cm^{-1}.

Radiolabeling and Biological Evaluation. Radiolabeling of the dithiol tamoxifen analogue **7** was performed using $Na[^{99m}Tc]TcO_4$ with tin(II) chloride as the reducing agent. Under mildly basic conditions (0.1 M sodium acetate) and D-gluconate, very little chelation occurred with low radiochemical yields. When 1 M NaOH

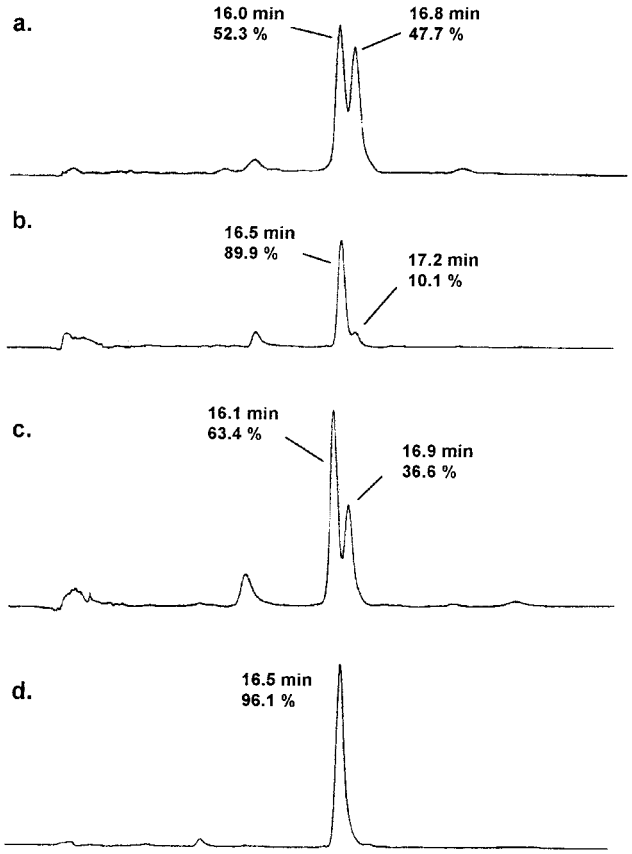

Figure 3. HPLC chromatograms (UV detector) of *Z*-**8**: (a) rhenium chelation yielding both *anti-Z*-**8** and *syn-Z*-**8**; (b) after mixture is exposed to 1 M NaOH; (c) co-injection; (d) rhenium chelation under basic conditions yielding only *anti-Z*-**8**.

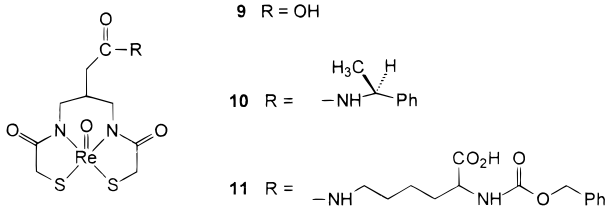

Figure 4. Previously reported anionic rhenium complexes (*13*, *20*).

was added to the reaction medium, radiochemical yields of over 80% were achieved. The addition of D-gluconate for ligand exchange, did not improve the yield or product purity and was, therefore, not further employed. As seen in Figure 5a, the chelation for the Z-isomer is very clean, yielding essentially a single product with an HPLC retention time of 16.6 min and a small trailing peak. The crude chelation reaction mixture typically contained traces of residual [^{99m}Tc]TcO_4^- eluting just after the solvent front. For the E-isomer, the crude reaction mixture was also checked by HPLC analysis with the γ trace, indicating that pertechnetate, *E*-**5**, and *Z*-**5** are all present with the desired E-isomer being obtained in 79% radiopurity.

Purification was carried out for both isomers using a C_{18} Sep-Pak column. The aqueous solution was passed through the column, with the pertechnetate being washed out with water. Elution with ethanol yielded the [^{99m}Tc]-tamoxifen product **5**. HPLC analysis of these eluents (Figure 5b for *Z*-**5** and Figure 5c for *E*-**5**) indicates the product is >99% radiochemically pure, although the E-isomer is contaminated with 5.8% of *Z*-**5**.

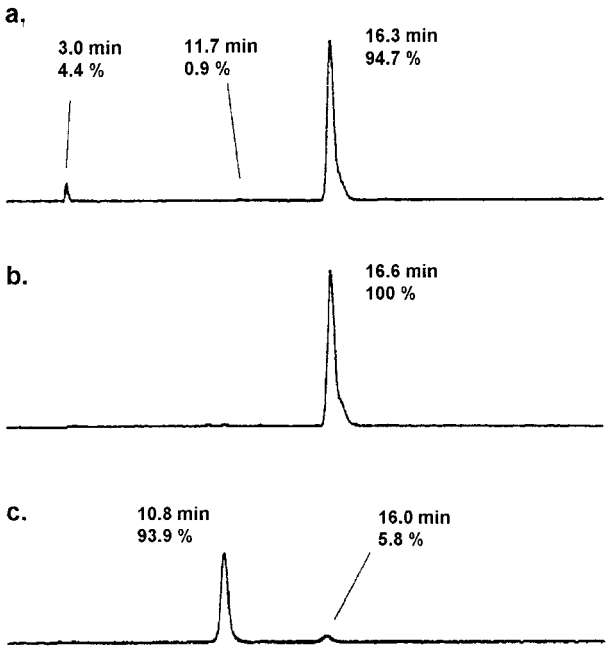

Figure 5. HPLC chromatograms (radiometric γ detector) of [^{99m}Tc]tamoxifen analogues: (a) crude reaction yielding *anti-Z*-**5**; (b) *anti-Z*-**5** after C_{18} Sep-Pak purification; (c) *anti-E*-**5** after C_{18} Sep-Pak purification.

For biodistribution experiments, the ethanol eluent volume was reduced and a saline solution containing 2% ethanol and 0.1% Tween-80 was added. The solution was then filtered through a sterile 0.22 μm filter yielding the final pure product with a radiochemical yield (decay corrected) of 71%. HPLC analysis again indicated a radiochemical purity of >99%. It should be mentioned that *Z*-**5** is not soluble in saline, but is soluble in saline with 10% ethanol. It was necessary to introduce the surfactant Tween-80 in order to keep the concentration of ethanol to an appropriate level (2%) for injection into mice.

One requirement for a radiopharmaceutical to be suitable for a biodistribution study is that it be free of any nonradioactive tamoxifen dithiol (**7**), as this would potentially bind to the estrogen receptors, thereby competing with the radiopharmaceutical. HPLC analysis of the ^{99m}Tc reaction product indicated that there existed very little residual dithiol, as deduced by the lack of UV absorbance at 25 or 21 min (for *Z*-**7** and *E*-**7,** respectively). Since the dithiol is being used in a very large excess as compared to the pertechnetate, it was presumed that the dithiol is being oxidized during the reaction. To validate this hypothesis, a study of the oxidation of *Z*-**7** was carried out by HPLC monitoring. It was determined that oxidation is occurring when the dithiol is heated in the presence of sodium hydroxide solution, presumably with oxygen as the oxidant. Oxidation also occurs at room temperature, but at a much slower rate. All oxidation products elute with or shortly after the solvent front and are removed by the Sep-Pak purification.

The biodistribution results of *anti*-(*Z*)-**5** in C3H female mice are summarized in Table 4 as percentage of the injected dose per gram of tissue. C3H mice were chosen for this study to allow for comparison of the results to a previous study of radioiodinated tamoxifen derivatives (*10*). Four time points for sacrificing were used, including 24 and 48 h time points in order to allow for comparison to a previous study of [^{131}I]tamoxifen, where the maximal uterus uptake occurred between 12 and 48 h (*10*). The overall radioactivity found in the tissues was very low,

with an average 9.5% of the injected dose being recovered at the 1 h time point. This suggests very rapid clearance of the radiopharmaceutical. Since the uterus is a major target organ for estrogens, it was expected that significant uptake would be observed in that tissue. Selective uterine uptake was not observed in this biodistribution study, with the percent injected dose per gram of uterine tissue remaining below 0.4% throughout all of the time points. A blocking study was not performed due to this low uterine uptake.

An estrogen receptor binding study of the rhenium analogue *anti*-(*Z*)-**8** using lamb uterine tissue gave a relative binding affinity of <0.009% compared to estradiol. This lack of specific receptor binding is consistent with the biodistribution results in mice using *anti*-(*Z*)-**5**, where very low uptake was observed in estrogen receptor abundant regions.

It is interesting to compare the binding of **1**, **2**, and **3** with *anti*-(*Z*)-**8,** which represent different substituents on the 4-position of ring-3. Changing from H (**1**) to NH_2 (**2**) to I (**3**) resulted in increased receptor binding but the introduction of the N_2S_2 rhenium chelate [*anti*-(*Z*)-**8**] has resulted in loss of binding affinity. This ligand brings with it both a significant increase in size but also a negative charge. It is feasible that either or both of these may be responsible for the lack of binding.

ACKNOWLEDGMENT

This work is jointly supported by an IOR grant of the Natural Sciences and Engineering Research Council of Canada and Merck-Frosst, Canada, Inc. We wish to thank John Katzenellenbogen, Rick Cesati, and Kathryn Carlson of the Department of Chemistry, University of Illinois, for the in vitro estrogen receptor binding assay and Pam Zabel and Leslie Gray of the Nuclear Medicine Department of the London Health Sciences Centre for assistance with the in vivo binding study.

LITERATURE CITED

(1) Feuer, E. J., Wun, L. M., Boring, C. C., Flanders, W. D., Timmel, M. J., and Tong, T. (1993) The Lifetime Risk of Developing Breast Cancer. *J. Natl. Cancer Inst. 85* (11), 892−897.

(2) Bombardieri, E., Crippa, F., Maffioli, L., and Greco, M. (1997) Nuclear Medicine Techniques for the Study of Breast Cancer. *Eur. J. Nucl. Med. 24*, 809−824.

(3) Buckley, M., and Goa, K. L. (1989) Tamoxifen: A Reappraisal of its Pharmacodynamic and Pharmacokinetic Properties, and Therapeutic Use. *Drugs 37*, 451−490.

(4) Seitz, D. E., Milius, R. A., and El-Wakil, H. (1981) Tritiodestannylation. Synthesis of a Specifically Labeled [^{3}H]Tamoxifen. *Synth. Commun. 11* (4), 281−286.

(5) Robertson, D. W., and Katzenellenbogen, J. A. (1982) Synthesis of the E and Z Isomers of the Antiestrogen Tamoxifen and Its Metabolite, Hydroxytamoxifen, in Tritium-Labeled Form. *J. Org. Chem. 47*, 2387−2393.

(6) Yang, D., Kuang, L., Cherif, A., Tansey, W., Li, C., Lin, W. J., Liu, C., Kim, E., and Wallace, S. (1993) Synthesis of [^{18}F]-Fluoroalanine and [^{18}F]Fluorotamoxifen for Imaging Breast Tumors. *J. Drug Targeting 1*, 259−267.

(7) Delpassand, E. S., Yang, D. J., Wallace, S., Cherif, A., Quadri, S. M., Price, J., Joubert, A., Inoue, T., and Podoloff, D. A. (1996) Synthesis, Biodistribution, and Estrogen Receptor Scintigraphy of Indium-111-Diethylenetriaminepentaacetic acid-Tamoxifen Analogue. *J. Pharm. Sci. 85* (6), 553−559.

(8) Kruijer, P. S., Klok, R. P., van den Koedijk, C. D., Blackenstein, M. A., Voskuil, J.-H., Verzeijlbergen, J. F., Ensing, G. J., and Herscheid, J. D. (1997) Biodistribution of ^{123}I-Labeled 4-Hydroxytamoxifen Derivatives in Rats with Dimethylbenzanthracene-Induced Mammary Carcinomas. *Nucl. Med. Biol. 24*, 719−722.

(9) Bloomer, W. D., McLaughlin, W. H., Weichselbaum, R. R., Tonnesen, G. L., Hellman, S., Seitz, D. E., Hanson, N., Adelstein, S. J., Rosner, A. L., Burstein, N. A., Nove, J. J., Little, J. B. (1980) Iodine-125-Labeled Tamoxifen is Differentially Cytoxic to Cells Containing Oestrogen Receptors. *Int. J. Radiat. Biol. 38*(2), 197−202.

(10) Strickland, L. A., Ponce, Y. Z., Hunter, D. H., Zabel, P. L., Powe, J. E., Morrissey, G., Driedger, A. A., Chamberlain, M. J. (1990) Amino and Iodotamoxifens: Synthesis, Estrogen Receptor Affinity and Biodistribution. *Drug Design and Delivery 6*, 195−212.

(11) Fromson, J. M., Pearson, S., Bramah, S. (1973) The Metabolism of Tamoxifen (I. C. I. 46, 474) Part II: In Female Patients. *Xenobiotica 3*(11), 711−714.

(12) Adam, H. K., Douglas, E. J., Kemp, J. V. (1979) The Metabolism of Tamoxifen in Humans. *Biochem. Pharm. 27*, 145−147.

(13) Shiau, A. K., Barstad, D., Loria, P. M., Cheng, L., Kushner, P. J., Agard, D. A., and Greene, G. L. (1998) The Structural Basis of Estrogen Receptor/Coactivator Recognition and the Antagonism of This Interaction by Tamoxifen. *Cell 95*, 927−937.

(14) Luyt, L. G., Jenkins, H. A., and Hunter D. H. (1999) An N_2S_2 Bifunctional Chelator for Technetium-99m and Rhenium: Complexation, Conjugation and Epimerization to a Single Isomer. *Bioconjugate Chem. 10*(3), 470−479.

(15) Johnson, N. P., Lock, C. J. L., and Wolkinson, G. (1964) Amine, Phosphine, and Stibine Complexes of Rhenium-(III), -(IV), and -(V). *J. Chem. Soc.* 1054−1066.

(16) Katzenellenbogen, J. A., Johnson, H. J., and Myers, H. N. (1973) Photoaffinity labels for estrogen binding proteins of rat uterus. *Biochemistry 12*, 4085−4092.

(17) Collins, D. J., Hobbs, J. J., and Emmens, C. W. (1971) Antiestrogenic and Antifertility Compounds. 4. 1,1,2-Triarylalkan-1-ols and 1,1,2-Triarylalk-1-enes Containing Basic Ether Groups. *J. Med. Chem. 14*, 952−957.

(18) Hunter, D. H., Payne, N. C., Rahman, A., Richardson, J. F., and Ponce, Y. Z. (1983) The Iodo-Tamoxifens: Molecular Structures and Syntheses of Estrogens for External Imaging of Carcinoma. *Can. J. Chem. 61* (3), 421−426.

(19) Shani, J., Gazit, A., Livshitz, T., and Biran, S. (1985) Synthesis and Receptor-Binding Affinity of Fluorotamoxifen, a Possible Estrogen-Receptor Imaging Agent. *J. Med. Chem. 28*, 1504−1511.

(20) Hunter, D. H., and Luyt, L. G. (1999) Lysine Conjugates for the Labeling of Peptides with Technetium-99m and Rhenium. *J. Labelled Compd. Radiopharm.*, in press.

BC990110Z

Bioconjugation of Ribonuclease A: A Detailed Chromatographic and Mass Spectrometric Analysis of Chemical Modification by a Cross-Linking Reagent

T. Joy Méndez, Jodie V. Johnson, Linda S. Nichols, G. H. Lisa Lang, John R. Eyler, David H. Powell, and David E. Richardson*

Department of Chemistry, University of Florida, P.O. Box 117200, Gainesville, Florida 32611. Received September 8, 1999; Revised Manuscript Received November 7, 1999

The modification of ribonuclease A with the heterobifunctional cross-linker, 4-succinimdyloxycarbonyl-methyl-α-[2-pyridyldithio]-toluene (SMPT) is described. RNase A has 11 potential sites of modification by the SMPT reagent. Tracking the two-dimensional separation and proteolytic digestion of SMPT-modified RNase A with ESI/FTICR-MS and HPLC/ESI/QIT-MS demonstrates the detailed information about number of SMPT modifications and sites of modification that can be obtained by application of these techniques. Analysis of native and modified RNase A tryptic digests by ESI/FTICR-MS resulted in the identification of the sites of modification. Semiquantitative results of the reactivity of certain lysine residues toward the coupling reagent SMPT are presented. Two sites (lysines 1 and 37) are highly reactive, while three sites (lysines 41, 61, and 104) appear to be unreactive toward SMPT under the conditions used. Experimental results demonstrate that quantitative comparison of relative intensities of peptide sequences of different charge states is not possible. No correlation was found between number of basic residues and sensitivity to detection. Digestion of the modified and unmodified RNase A by subtilisin followed by examination by HPLC/ESI/QIT-MS and MS^n enabled further investigation of modification on lysines 1 and 7, including modification at the ϵ- and α-amino positions on lysine 1.

INTRODUCTION

Electrospray ionization mass spectrometry (ESI-MS)[1] and tandem mass spectrometry (MS^n)[1] have become powerful techniques for characterization and analysis of proteins and bioconjugates, especially when coupled to high-performance liquid chromatography (HPLC)[1] (*1*−*5*). Proteolytic digestion with MS determination of peptide masses (peptide mapping) and MS^n determination of partial peptide sequences (peptide sequence tags) have proven especially valuable for protein identification via database searching (*6*−*8*). These techniques are also useful for de novo sequencing and identification of posttranslational modifications (*9*−*12*). HPLC/ESI/QIT-MS^1 and MS^n and ESI/FTICR-MS^1 for mapping of conjugation are useful methods for tracking and guiding an amino acid chemical modification process.

The ability of these analytical tools to examine the propensity of a given residue to be modified under a given set of conditions has been demonstrated (*13*−*16*). For example, Glocker et al. (*16*) reported the acetylation and succinylation of bovine pancreatic Ribonuclease A (RNase A).[1] HPLC and mass spectrometry were used to identify sites of modification and to quantify the reactivity of those sites.

RNase A is a well-characterized enzyme that hydrolytically cleaves the phosphodiester backbone of RNA.[1] The protein contains 10 lysine residues, which can be chemically modified by exploiting the nucleophilicity of their ϵ-amino groups and the terminal α-amino group. Characterization of RNase A by MS has included studies on protein conformation and the differences between RNase A and Ribonuclease B (RNase B), which is a glycosylated form of RNase A (*11*, *17*). Noncovalent interactions of substrates, inhibitors and adducts with RNase A and variants of RNase A have also been studied by ESI (*18*−*20*). ESI-MS was used to study noncovalent interactions, thermal denaturation and entropy changes of RNase S (*21*−*23*).

We report here on the chemical modification of RNase A by 4-succinimdyloxycarbonyl-methyl-α-[2-pyridyldithio]-toluene (SMPT).[1] SMPT is a heterobifunctional coupling reagent that has been used for the preparation of immunotoxins, linking a cell-binding component to a potent toxin to target Hodgkin's lymphoma (*24*−*26*). SMPT has also been used in a similar manner for the development of thrombolytic and antiplatelet agents (*27*). The N-hydroxy-succinimide group of SMPT reacts with nucleophilic amino groups on proteins (Scheme 1). The covalently linked SMPT provides a dithio group that can be exchanged with a thiol compound to further derivatize the protein (Scheme 2).

At the outset, certain lysine residues were considered more appropriate for modification due to their proximity to the active site. Thus, various synthetic cofactors would

* To whom correspondence should be addressed. Phone: (352) 392-6736. Fax: (352) 392-3255. E-mail: der@chem.ufl.edu.

[1] Abbreviations: RNase A, bovine pancreatic ribonuclease A; SMPT, 4-succinimdyloxycarbonyl-methyl-α-[2-pyridyldithio]-toluene; ESI, electrospray ionization; FTICR, Fourier transform ion cyclotron resonance; HPLC, high-performance liquid chromatography; QIT, quadropole ion trap; MS, mass spectrometry; MS^n, tandem mass spectrometry; RNA, ribonucleic acid; DTT, dithiothreitol; cCMP, cytidine 2′,3′-cylic monophosphate; EPPS, *N*-[2-hydroxyethyl] piperazine-*N*′-[3-propane-sulfonic acid]; Tris, tris(hydroxymethyl)-aminoethane; SCID, source collision induced dissociation; CID, collision induced dissociation; ACN, acetonitrile; TFA, trifluoroacetic acid.

10.1021/bc990117g CCC: $19.00 © 2000 American Chemical Society
Published on Web 03/20/2000

Scheme 1

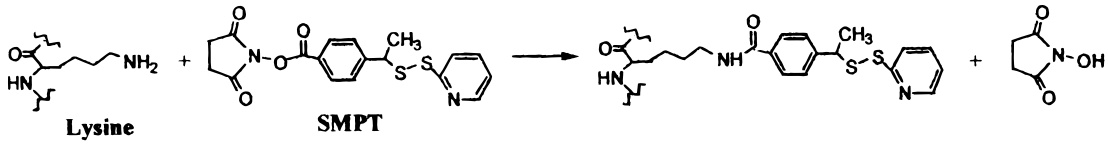

Scheme 2

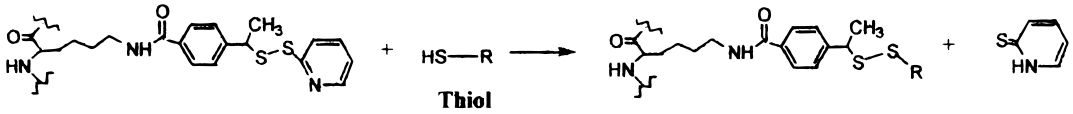

be incorporated at these residues and alter the active-site chemistry. Single modification of RNase A by SMPT at a specific lysine is impossible with simple reagents such as SMPT given the similar pK_as of the lysine residues and the number of locations, 11, where modification can occur (*28*). In the present study, the process of modification of RNase A by SMPT is followed by ESI/FTICR-MS, HPLC/ESI/QIT-MS, and MS^n, which allows for the optimization of conditions for SMPT bioconjugation. When coupled with proteolytic digestions of modified RNase A, these mass spectrometric techniques allow for identification and quantification of modified lysine residues as well as providing detailed information regarding the location of SMPT modification.

EXPERIMENTAL PROCEDURES

General Reagents. All reagents were of reagent grade unless otherwise specified. All buffers were purchased from Sigma (St. Louis, MO). Water was purified by a Sybron/Barnsted Module Deionization System.

Ribonuclease A Purification. Ribonuclease A, type 1-AS from bovine pancreas, was purchased from Sigma. It was purified using a Bio-Rex 70[2] cationic exchange resin from Bio-Rad (Hercules, CA). The column (0.7 × 70 cm) was eluted with an exponential gradient from 10−160 mM ammonium phosphate, pH 7.2. The last eluted peak (RNase A) was collected and desalted by using a Sephadex G50 (Sigma) column with 0.2 mM Tris[1] buffer (Acros, New Jersey), pH 8.0. The protein was dialyzed into H_2O and lyophilized for long-term storage.

Enzyme activity was determined by the methods of Crook et al. (*29*) and Eftink et al. (*30*). Briefly, the RNase A-catalyzed hydrolysis of 2,3-cCMP[1] at 25 °C was monitored by following the increasing concentration of the reaction product, 3-CMP,[1] at 295 nm. The pseudo-first-order rate constant, k_{obs}, was determined. Under the assay conditions, native RNase A had a rate constant (k_{obs}/[E]) of (1.2 ± 0.5) × 10^3 M^{-1} s^{-1}. Eftink et al. have reported a rate constant of 2.57 × 10^3 M^{-1} s^{-1} (*30*).

Modification of RNase A by SMPT. Purified RNase A was dissolved in 50 mM EPPS[1] buffer (Sigma) at pH 7.0 or 8.0. RNase A was modified at nucleophilic lysine residues with SMPT (Pierce). The reaction was run in 20% acetonitrile (Fisher)/80% 50 mM EPPS buffer at pH 7.0 or 8.0 with a final reaction volume of 1.5 mL. With a molar ratio of 2:1 at pH 8.0 (4:1 at pH 7.0) for SMPT to RNase A, an incubation time of 6.5 h at room temperature was sufficient for maximum conversion of native RNase A to singly modified RNase A.

Separation of SMPT-Modified Ribonuclease A Products. The reaction solution was applied directly to a Bio-Rex 70 column (0.7 × 70 cm) and was eluted overnight with an exponential gradient of 10−160 mM ammonium phosphate at a flow rate of 0.3 mL/min. The elution was monitored at 229 nm, and the fractions were collected, concentrated, and either lyophilized and reconstituted in 49% methanol/49% H_2O/2% acetic acid for electrospray or prepared for proteolytic digestion. If the fractions were to be further separated by HPLC, they were collected and concentrated to 250 μL by Amicon filtration, MW cutoff = 3500.

HPLC of SMPT Modified RNase A. Some Bio-Rex 70 separated SMPT modified RNase A fractions were further separated on a Phenomenex Jupiter 5 μm C18 column (Torrance, CA) (4.6 mm i.d. × 250 mm; guard column, 4.6 mm i.d. × 30 mm, 300 Å pore). Buffer A consisted of 1% stock buffer (below), 10% acetonitrile (HPLC grade, Fisher), 89% H_2O and buffer B was 1% stock buffer, 75% acetonitrile, and 24% H_2O. The stock buffer consisted of 7.5% trifluoroacetic acid (Fisher), 50% triethanolamine (Fisher), 25% acetonitrile, and 62.5% H_2O. The column was equilibrated with 5% buffer B at 1 mL/min. The elution was as follows: 0 min (A:B = 95:5), 5 min (A:B = 95:5), 20 min (A:B = 70:30), 30 min (A:B = 65:35), 40 min (A:B = 25:75), 50 min (A:B = 95:5). The various forms of modified RNase A were detected by their absorbance at 229 nm. The peak fractions were collected, concentrated, lyophilized, and reconstituted in 49% methanol/49% H_2O/2% acetic acid for HPLC/ESI/QIT-MS.

Trypsin Proteolytic Digest. All reagents were purchased from Sigma unless otherwise specified. The modified RNase A was dissolved in 1 mL of 0.1 M NH_4HCO_3 at pH 8.0, and guanidine hydrochloride was added to a final concentration of 6 M. A 100:1 molar excess of dithiothreitol (DTT)[1] (Acros) to protein was then added, and the solution was incubated at 57 °C for 1 h. After cooling to room temperature, 4-vinyl pyridine was added in a 2.2:1 molar excess of 4-vinyl pyridine to DTT. The solution was then incubated at room temperature for 30 min. Acetic acid was added until pH <3, which stopped the alkylation. The solution was then dialyzed exhaustively against 0.1% trifluoroacetic acid (Fisher) followed by lyophilization.

The denatured protein solution was reconstituted in 1 mL of 0.1 M NH_4HCO_3, pH 8.0. Trypsin stock solution was prepared in 0.1 M NH_4HCO_3 buffer that had been acidified to pH <3 with 3 N HCl. Five milligrams of trypsin was dissolved in 1 mL of the acidic buffer. A 100:1 molar ratio of RNase A to trypsin was used by adding an aliquot of trypsin stock solution to the denatured RNase A solution. The reaction mixture was allowed to incubate at 37 °C for 24 h. The digestion was stopped by lyophilization. The digested protein was reconstituted in 2-propanol or 49% methanol/49% H_2O/2% acetic acid for examination by ESI/FTICR-MS.

[2] Bio-Rex is a registered trademark of Bio-Rad Laboratories, Hercules, CA.

Subtilisin Proteolytic Digest. Modified RNase A fractions were dialyzed into 0.1 M NH_4HCO_3 at pH 8.0 to a volume of 500 μL. A stock solution of subtilisin (Carlsberg, Sigma) was prepared by dissolving 5 mg of the protease in 100 mL of 0.1 M NH_4HCO_3 at pH 8.0. Ten microliters of subtilisin stock was added to each 500 μL modified RNase A solution. The mixtures were allowed to incubate for 24 h at 4 °C. Digestion was stopped by lyophilization. Samples were reconstituted in 49% methanol/49% H_2O/2% acetic acid for mass spectrometric analysis.

Electrospray Fourier Transform Ion Cyclotron Resonance Mass Spectrometer. All ESI/FTICR mass spectrometric experiments were performed with a Bruker BioAPEX external source shielded 4.7-Tesla FT-ICR mass spectrometer (Bruker Analytical Systems, Inc., Billerica, MA) equipped with a Bruker Xmass 4.0.3 data system. A detailed description of the instrument can be found elsewhere. (*31*, *32*) The electrospray source was a modified Analytica electrospray source (Analytica of Branford, Branford, CT). The stainless steel desolvation capillary was held at ground potential and 120 °C. The FTICR cell pressure was 1×10^{-9} Torr. The samples were sprayed at a rate of 1 mL/min. The electrospray needle (2950 V) was located at a distance ca. 1 cm from the capillary. The capillary and skimmer voltage were adjusted to values which maximized the signal intensities for the ions of interest, and typical values were 100 and 10 V for the capillary and skimmer, respectively.

Calculations for ESI/FTICR-MS Tryptic Digest. Absolute intensities of ions were generated by using the program Xmass 4.0.3. Calculations were done using ion abundances that had been normalized by dividing the intensities by the charge of the ions (I/z)(*33*).

The percentage of observed ions in the ESI/FTICR-MS spectra of a tryptic digest sample (native or modified RNase A) that could be assigned was calculated by summing all assigned charge-normalized ion abundances and dividing by the total sum of all normalized ion abundances, assigned and unassigned (eq 1). In eq 1,

$$\frac{\sum_{i}^{N}\left(\frac{I}{z}\right)_i}{\sum_{j}^{M}\left(\frac{I}{z}\right)_j} \times 100 = \%\ \text{peaks assigned} \qquad (1)$$

I = intensity of an ion peak, z = charge state of ion, N = total number of assigned peaks, and M = total number of peaks, assigned and unassigned.

The estimated percent contribution of each peptide segment in the native RNase A digest was calculated according to eq 2, where I = intensity, z = charge state, P_n = peptide segment n, resulting from complete cleavage by trypsin, n = indices of sequence peptide (n = 1, 2, 3, ..., 14, see Figure 4), f = fragment of linked peptide segments resulting from complete or incomplete cleavage by trypsin, and L = number of peptides linked in a fragment. The factor L results in the inclusion of the moles of each peptide segment being represented in the total mole sum for the spectrum, which is correlated to the total ion abundance. The first summation in the numerator of eq 2 includes every fragment f that contains peptide segment n. The first summation in the denominator of eq 2 includes every fragment f that is assigned

$$\frac{\sum_{f}^{\text{cont } P_n}\left(\sum_{z=1}^{z_{\max}}\left(\frac{I_f}{z}\right)\right)}{\sum_{f}^{\text{all assign}} L\left(\sum_{z=1}^{z_{\max}}\left(\frac{I_f}{z}\right)\right)} \times 100 = \begin{array}{c}\%\ \text{peptide } n \\ \text{in total ion population}\end{array} \qquad (2)$$

in the spectrum, including fragments containing peptide segment n. The summations over z sum over intensities for all charge states observed for fragment f. This calculation was repeated for each digested peptide segment.

The estimated percentage of modification at a given lysine residue was calculated according to eq 3 where the

$$\frac{\sum_{f}^{\text{cont } P_{n^*}}\left(\sum_{z=1}^{z_{\max}}\left(\frac{I_f}{z}\right)\right)}{\sum_{f}^{\text{cont } P_{n^*}}\left(\sum_{z=1}^{z_{\max}}\left(\frac{I_f}{z}\right)\right) + \sum_{f}^{\text{cont } P_n}\left(\sum_{z=1}^{z_{\max}}\left(\frac{I_f}{z}\right)\right)} \times 100 = \begin{array}{c}\%\ \text{modification at} \\ \text{lysine contained in} \\ \text{peptide } n\end{array} \qquad (3)$$

definitions of all variables are the same as in eq 2 and where P_n* = peptide segment n containing a modification on its lysine residue. The first summation in the numerator and denominator over P_n* includes every fragment that contains modified peptide segment n*. The summations over z and over P_n are the same as in eq 2. Equation 3 was used for every peptide that contains a lysine residue.

HPLC/Quadrupole Ion Trap Mass Spectrometry. High-performance liquid chromatography/electrospray ionization mass spectrometry (HPLC/ESI/QIT-MS) data were acquired on a Finnigan MAT LCQ quadrupole ion trap mass spectrometer (San Jose, CA) operated in the electrospray ionization (ESI) mode. Typical operating parameters were nitrogen sheath and auxiliary gases of 70 and 10 (unitless), respectively, heated capillary temperature of 235 °C, and ion spray voltage of 3.5 kV. The source collision-induced dissociation (SCID)[1] was set between 10 and 20% maximum for declustering. MS and MS^n data were acquired with the normal m/z 50−2000 range, as well as with the extended m/z range (up to m/z 4000) offered with the LCQ's advanced scan function software. Parent ion isolation was typically 5 μm wide with the CID[1] energy set to 35 or 50% maximum for z = +2 ions and 65% for z = +1 ions. A higher resolution scan (Zoom scan) was obtained only in the normal m/z 50−2000 range.

The mobile phase was introduced by a Beckman Instruments (Fullerton, CA) System Gold model 126 pump. A binary HPLC mobile phase system used is the same as described above for offline HPLC. Chromatographic separation was achieved with either a Phenomenex Jupiter 5 μm C18 column size as described above or a Waters (Milford, MA) Symmetry C18 (2.1 mm i.d. x 150 mm, 5 mm particles, 100 Å pore). The gradient for the Phenomenex column is the same as described above. A typical gradient at 0.2 mL/min for the Waters column was 0 min (A:B = 95:5), 1 min (95:5), 41 min (5:95), and 45 min (5:95). The column effluent was split prior to the ESI source with approximately 70−80% of the effluent going to waste.

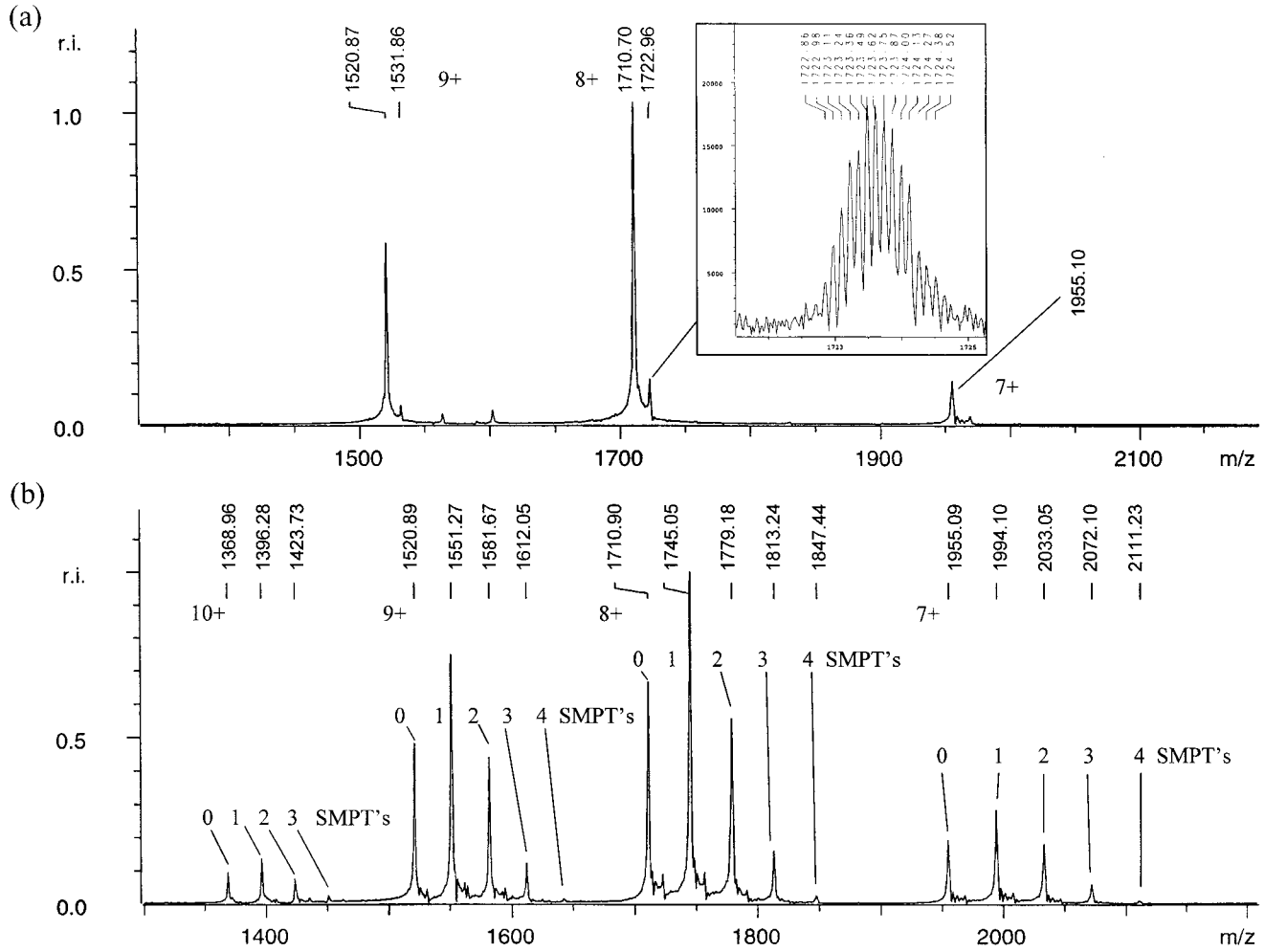

Figure 1. (a) ESI/FTICR-MS of native RNase A at $[M + 7H]^{7+}$, $[M + 8H]^{8+}$, and $[M + 9H]^{9+}$ with phosphate adducts. (Inset) Isotopic resolution of native RNase A with one phosphate adduct, *m/z* 1723-$[M + 8H]^{8+}$. (b) ESI/FTICR-MS multiply modified RNase A (molar ratio 1:2 RNase A to SMPT) at $[M + 7H]^{7+}$, $[M + 8H]^{8+}$ $[M + 9H]^{9+}$ and $[M + 10H]^{10+}$. Peaks corresponding to 0, 1, 2, 3, and 4 SMPT modifications are indicated for each charge state. *m/z* values for modification at $[M + 8H]^{8+}$: Modification, expected *m/z* $[M + 8H]^{8+}$, measured *m/z* $[M + 8H]^{8+}$; 1 SMPT 1745.07, 1745.05; 2 SMPT, 1779.24, 1779.18; 3 SMPT, 1813.14, 1813.24; 4 SMPT, 1847.57, 1847.44.

RESULTS AND DISCUSSION

Modification and Separation of Ribonuclease A. RNase A contains 10 lysine residues, for a total of 11 amino groups, including the α-amino terminus that can be modified by reaction with the N-hydroxy-succinimide (NHS) group of SMPT (Scheme 1). Lysine residues 1, 7, and 41 have a higher propensity for modification by reagents previously investigated as a result of surface accessibility and reduced pK_as (*16, 34*−*36*). One goal of the present study was to examine the selectivity of modifications by SMPT compared to others such as acetic and succinic anhydride (*16*).

RNase A was modified with SMPT and examined by ESI/FTICR-MS. These preliminary data showed series of multiply protonated $[M + zH]^{z+}$ molecular ions. The mass change for one SMPT modification is 273.34 Da. Native and multiply SMPT-modified RNase A ions were identified (Figure 1), as well as phosphate adducts to the native (*11*, *18*) and SMPT-modified RNase A.

Liquid chromatography was used to separate SMPT-modified RNase A that had been modified with different numbers of SMPT. The first separation of the modification reaction solution was performed by cationic exchange chromatography using Bio-Rex 70 resin. The positively charged lysine residues are neutralized upon modification with SMPT. Elution on the Bio-Rex column results in separation of protein modified at different locations with different numbers of SMPT, as well as separation from any unmodified RNase A. The protein modified with the greatest number of SMPT groups tends to elute first as a result of the neutralization of several lysines, and RNase A modified to a lesser extent tends to elute later. Unmodified RNase A eluted last as the most highly charged species. A typical Bio-Rex 70 separation of SMPT-modified RNase A as a result of optimized reaction and separation conditions is shown in Figure 2.

Highly purified RNase A was mostly singly modified with few multiple modifications at molar ratios of 1:1 to 2:1 SMPT to RNase A. Higher concentrations of SMPT were needed with less highly purified RNase A (where the Sephadex G-50 column step was not used). It was also found that a molar concentration that was too high (e.g., 10:1 SMPT to RNase A) would overmodify highly purified RNase A, resulting rapid elution of the entire sample from the Bio-Rex 70 column with little or no separation (data not shown).

Separated peaks were seen during Bio-Rex 70 chromatography when the reaction buffer was at pH 8.0, as in Figure 2. With the goal of isolating increasing quanti-

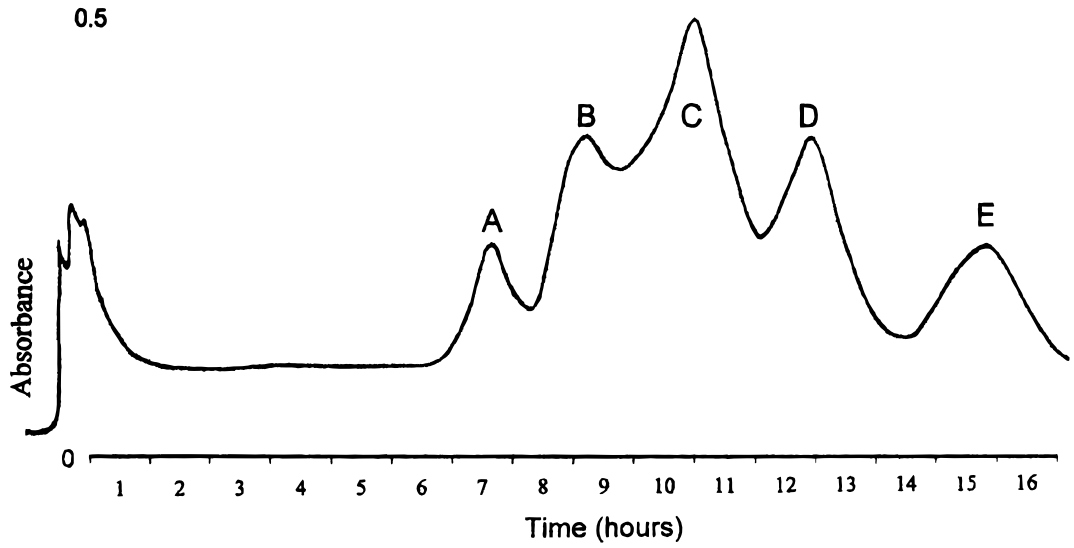

Figure 2. Bio-Rex 70, weakly cationic exchange column chromatogram. RNase A modified with SMPT (molar ratio 1:2) at pH 8.0 then applied to column and eluted with an exponential gradient of ammonium phosphate 10−160 mM at pH 7.2, 4 °C. Multiply modified RNase proteins elute early followed by singly modified RNase A. Unmodified RNase A elutes last.

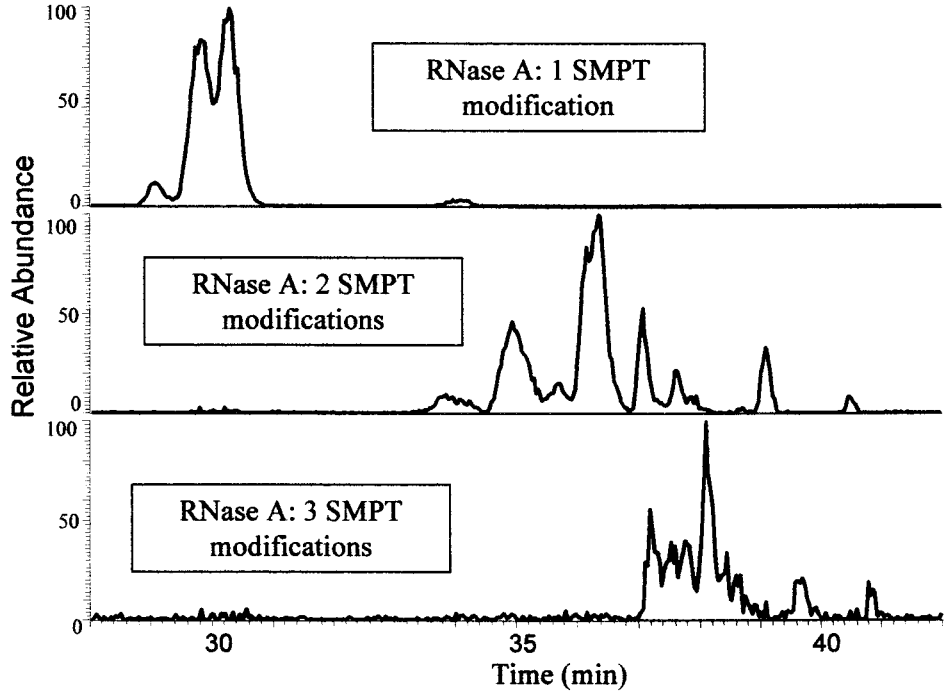

Figure 3. HPLC/ESI/QIT-MS analysis of modified RNase A from peak D in Bio-Rex 70 column in Figure 2. Mass chromatograms of ions corresponding to one to three modifications of RNase are shown.

ties of singly modified RNase A at a known site for further bioconjugation, a modification reaction at pH 7.0 was attempted to direct modification to the α-amino group on Lys-1, as Lys-1 is near the active-site cleft. The pK_a of the α-amino terminus group has been reported as 6.6, whereas the pK_a of the ϵ-amino group for lysine-41 has been as reported as 8.6 and pK_as of the other lysine ϵ-amino groups range from 10.6 to 11.2 (*37*). Lowering the pH of the reaction buffer would theoretically increase the probability of modification at α-Lys-1. With a pH 7.0 reaction, fewer resolved peaks were seen on the Bio-Rex 70 column using the same elution method (data not shown). Therefore, the buffer EPPS at pH 8.0 was considered optimum for the modification reaction.

HPLC/ESI/QIT-MS of Peaks Following Bio-Rex 70 Chromatography. The extent of homogeneity and number of SMPT modifications for each Bio-Rex 70 peak in Figure 2 was examined by C-18 HPLC/ESI/QIT-MS. These results enabled semiquantitative determination of the number of SMPT modifications in a given Bio-Rex 70 peak.

Table 1. Relative Abundances (%) of RNase A Modified to Various Degrees in Bio-Rex 70 Peaks[a]

peak	0 SMPT	1 SMPT	2 SMPT	3 SMPT	4 SMPT
A	0.0	0.0	53.1	42.4	4.5
B	0.2	4.6	75.8	17.9	1.5
C	1.1	67.9	27.3	4.2	0.4
D	1.2	82.9	13.6	2.0	0.4
E	99.0	1.0	0.0	0.0	0.0

[a] Corresponds to peaks A−E in Figure 2.

Separation on a C-18 HPLC column online with ESI-MS of peaks A−E shown in Figure 2 indicated that proteins with various numbers of SMPT modifications

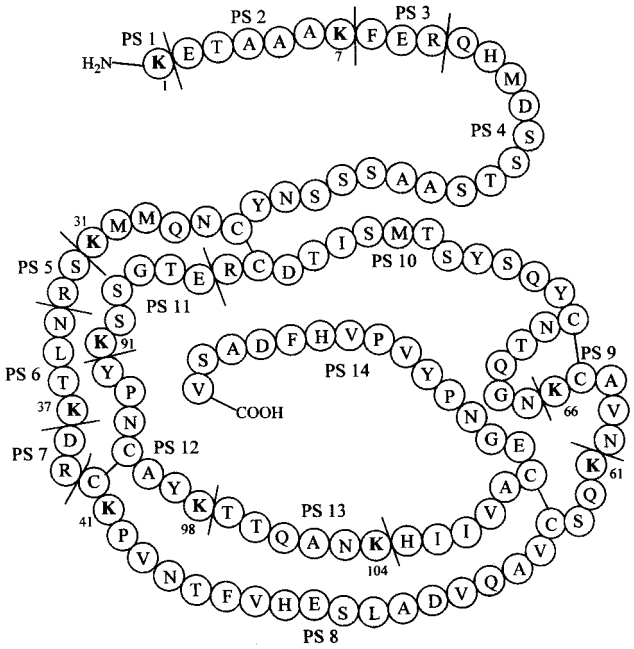

Figure 4. RNase A primary sequence. Cleavage sites by trypsin shown along with peptide segment (PS n) assignments.

are in each Bio-Rex 70 peak. One example of the HPLC/ESI/QIT-MS data (for peak D from Figure 2) is shown in Figure 3. The percentages of RNase A modified with different numbers of SMPT groups in a given peak were based on the relative abundances of certain ions seen under these ESI conditions. The detection sensitivities of the ions were assumed to be equal. The percentages of RNase A modified singly, doubly, etc., in each peak are summarized in Table 1. As expected, percentages of decreasingly modified RNase A increased with elution time, showing peak D (Figure 2) having the highest percentage of singly modified RNase A. Peak E (Figure 2) was almost 100% unmodified RNase A. The change in number of modifications by SMPT seen in each Bio-Rex 70 fraction demonstrates the heterogeneity of each peak. The various peaks seen for each number of SMPT modification (Figure 3) indicate lack of selectivity of SMPT with respect to location of modification. For example, in Figure 3, chromatogram 2, the separation of doubly modified RNase A into many peaks indicates that the SMPT modifications are at several different lysine residues. On the other hand, the singly modified protein appears to predominate in 2 peaks eluting at $t \approx 30$ (Figure 3).

Tryptic Digestion of SMPT-Modified RNase A. Digestion of SMPT-modified RNase A with the specific protease trypsin provides peptide segments and fragments that can be examined by ESI/FTICR-MS. Trypsin cleaves peptide bonds at the C-side of lysine and arginine residues based on recognition of those positively charged residues in the substrate-binding domain of trypsin. Derivatization of a lysine residue by SMPT neutralizes the positive charge and should eliminate the ability of trypsin to cleave at that site, and this hypothesis has been supported by our experimental data. Experimental data also indicates that SMPT modification at a given lysine residue does not inhibit cleavage at the next

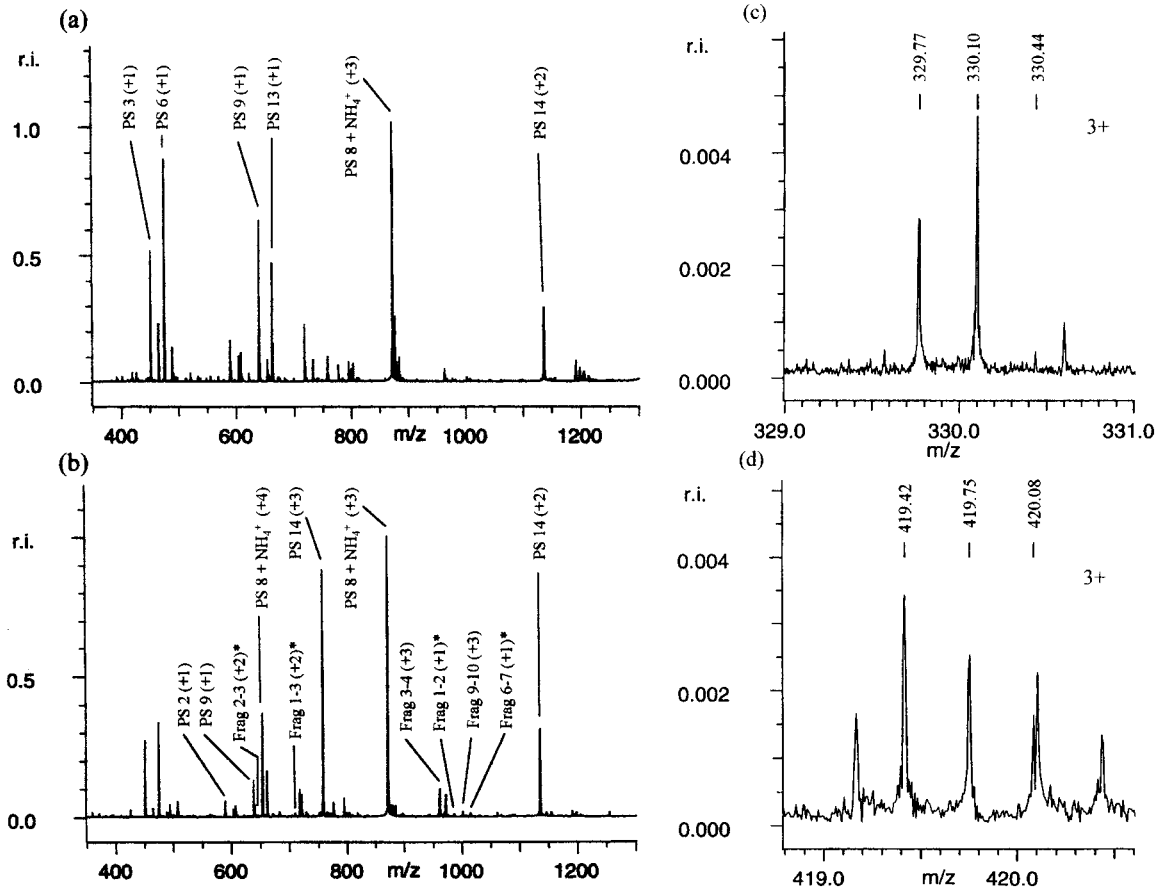

Figure 5. ESI/FTICR-mass spectrum of tryptic digests of (a) native RNase (b) SMPT-modified RNase A. (c) Unmodified peptide fragment 5-7 (residues 32-39), *m*/*z* 329-$[M + 3H]^{3+}$. (d) Peptide fragment 5-7 (residues 32-39) with modification at lysine 37, *m*/*z* 419 $[M + 3H]^{3+}$.

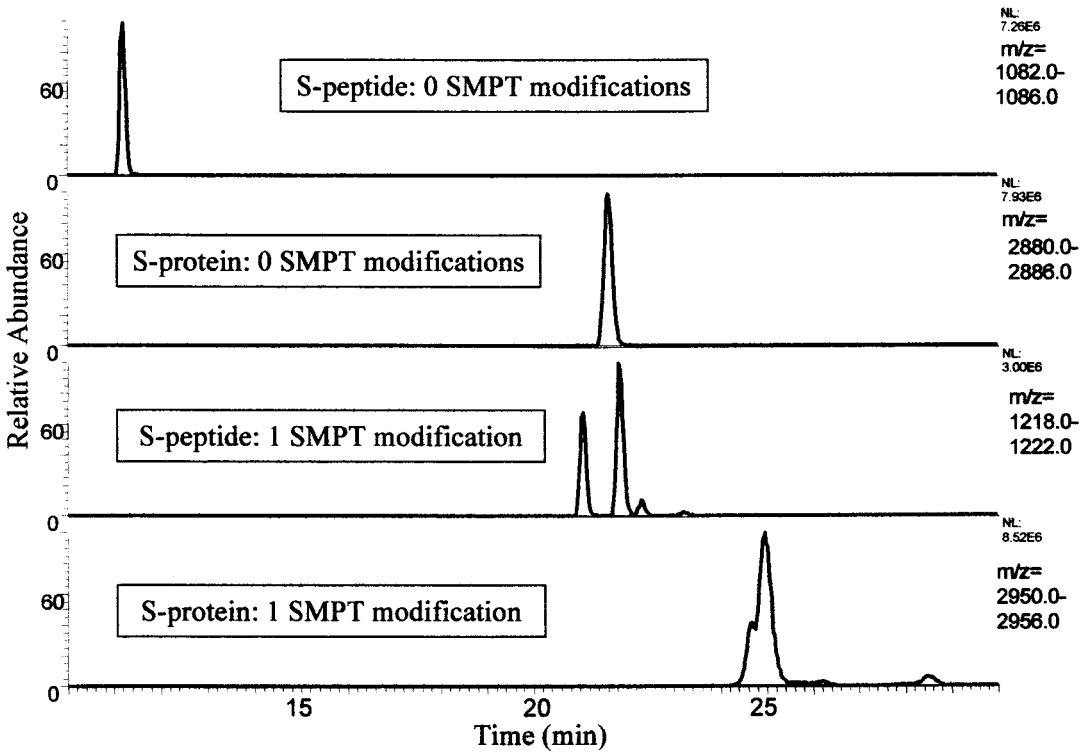

Figure 6. HPLC/ESI/QIT-mass chromatogram of peak D from Bio-Rex 70 chromatogram (Figure 2) that has been digested by subtilisin. Mass chromatograms are indicative of unmodified S-peptide, *m/z* 1083-$[M + 2H]^{2+}$, singly modified S-peptide, *m/z* 1220-$[M + 2H]^{2+}$, unmodified S-protein, *m/z* 2883-$[M + 2H]^{4+}$, singly modified S-protein, and *m/z* 2954-$[M + 2H]^{4+}$. Multiply modified peptides were also detected (not shown).

possible site, some as few as two residues away from the SMPT modification. The changes in peptide masses and digestion pattern between native and SMPT-modified RNase A allow for modification site identification and at least partial quantification of the propensity of those sites to be modified.

Tryptic digests were performed on native and SMPT-modified RNase A. The primary sequence of RNase A is shown in Figure 4, noting the usual cleavage sites by trypsin and the resulting 14 peptide segments. (*Peptide segment* refers to one of the 14 peptides that results from complete digestion by trypsin, *fragment* refers to oligopeptides resulting from complete or incomplete digestion by trypsin and is any single peptide segment or linked peptide segments that might be observed by MS.) Each digested protein sample was examined by ESI/FTICR-MS (Figure 5, panels a and b). Experimental data indicated the incomplete digestion of both native and SMPT-modified RNase A. The result of incomplete digestion by trypsin was many combinations of internal peptide segments (i.e., fragments). An example of this incomplete digestion was the identification of fragments 5−7 (residues 32−39), which was seen as a linked fragment and as cleaved individual peptide segments of 5, 6, and 7 in the observed spectrum. Because of the incomplete digestion of native and modified RNase A, all possible combinations of peptide segments were calculated at all possible charge states including possible cationic adducts (H^+, Na^+, K^+, and NH_4^+) to aid in peak identification in the ESI/FTICR-MS spectra. Using this method (eq 1), approximately 75% of the total ion charge-normalized intensity in the native RNase A and 65% of the ion the total ion charge-normalized intensity in the SMPT-modified RNase A were assigned as known peptide segments or fragments. The mass change for one SMPT modification including alkylation by 4-vinyl pyridine is 268.28 Da. Spectra for the fragment containing unmodified and modified lysine 37 are shown in Figure 5, panels c and d.

Quantification of the absolute abundances of ions corresponding to modified peptides was attempted in order to determine the propensity of a given residue to be modified. It has been shown by Marshall et al. (*33*) that ICR signal increases linearly with ion charge but is independent of mass, such that ICR is increasingly sensitive for multiply charged ions. Therefore, ion intensities were normalized by dividing by their charge states. Summation of the absolute intensities for ions of interest that had been normalized according to their charge state was used as a method for the correlation of absolute abundance (peak area) of an ion to the ion concentration (ion population) and, thus, SMPT modification on that peptide segment (*33*, *38*, *39*). To make such a correlation, assigned ions in the native RNase A tryptic digest were normalized and summed to verify their percent in the overall assigned ion population (see eq 2 in the Experimental Procedures). It was found that certain assigned ions (corresponding to certain peptide segments) represented different percentages of the total assigned ion population. Considering that the number of moles of each peptide segment (1, 2, 3, ..., 14) is the same in the sample, the different percentages of ions (corresponding to certain peptide segments) indicated that peptide segments were being detected with varying sensitivities (Table 2). If the MS method were nondiscriminating, each segment would have a percent abundance of 1/14 × 100 (7.1%). Conditions that occur in the electrospray source, either in the solution droplets or in the gas phase, may lead to chemical reactions that result in variable detection of peptide segments. Chemical reactions may include neutralization of charge by charge transfer from one peptide segment or fragment to an acceptor, resulting in a

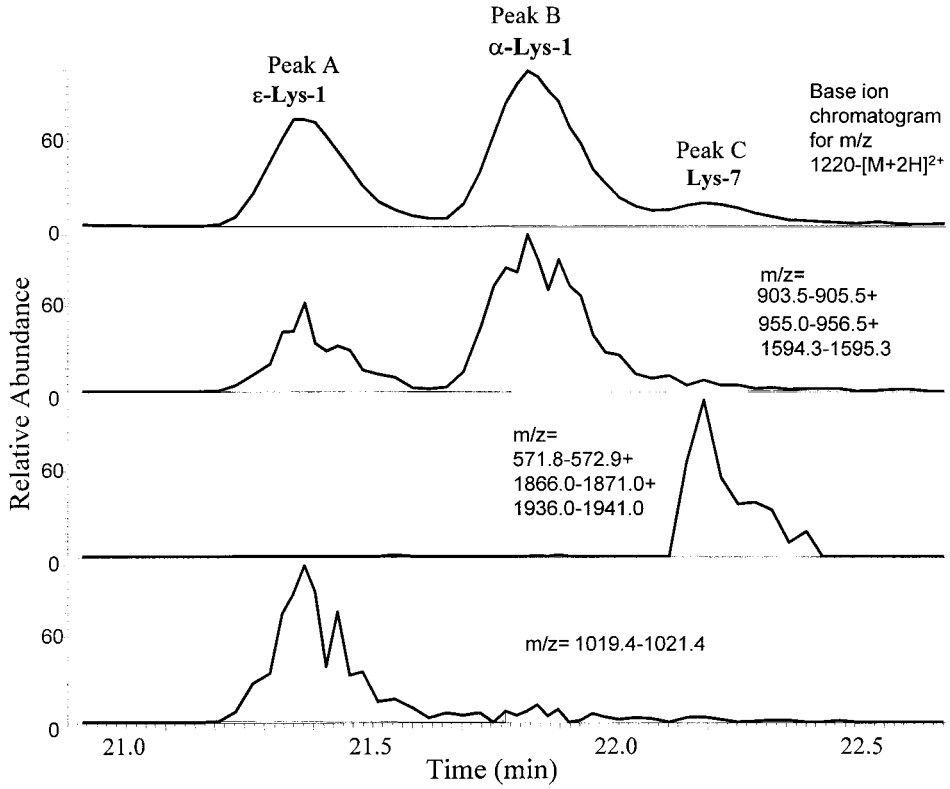

Figure 7. HPLC/ESI/QIT-mass chromatograms of ions that indicate site of modification on singly modified S-peptides in Figure 7. (Top) Base peak chromatogram, retention time 21.0−22.6 minutes with modification site assignments labeled. (Top-middle) Mass selection for ions that indicate modification at lysine 1. (Bottom-middle) Mass selection for ions that indicate modification at lysine 7. (Bottom) Mass selection for y_{19}^{2+} ion, *m/z* 1020-$[M + 2H]^{2+}$, corresponds to retention time 21.2−21.7 minutes in base peak indicating potential modification at ϵ-Lys-1.

Table 2. Percentage of Ion Abundance of Each Peptide Segment (PS) Contribution to the Total Ion Abundance of Tryptic Digested Sample of Native RNase A

PS	%	PS	%
1	2	8	16
2	8	9	11
3	13	10	6
4	1.5	11	4.5
5	2.5	12	2
6	16	13	8
7	1	14	8.5

decreased overall charge of some ions and possibly neutralization, which leads to decreased detection of a peptide segment. Such charge reduction is favored by high charge repulsion in small, multiply charged peptide segments or fragments. Detection sensitivity may also be related to the chemical nature of the residues on each peptide segment (*40*−*42*). These factors could influence the detection sensitivity of a peptide segment ion and, thus, its ion population in the protein digest spectrum. The results shown in Table 2 also indicated no clear correlation between the number of basic residues in a peptide segment and its sensitivity to detection as has been previously suggested (*43*, *44*).

Peptide segment 8 (residues 40−61) has the highest number of basic residues, 5, and was also found to have the highest percentage of ion abundance in the total assigned ion population. The basic residues, lysine, arginine, pyridylethylcysteine and histidine (ES conditions) provide sites for positive charge on the ion. The increased number of basic residues, as in peptide segment 8, may increase the propensity of the ion to maintain positive charge and be detected. Therefore, it is presumed that the peptide segments with lower ion intensities have decreased percentage of the total assigned ion abundance because they either are part of the unassigned ion population or were chemically neutralized in the source.

The lack of an unbiased distribution for assigned ions in the native RNase A sample illustrates the care that should be taken when extracting quantitative data from gas-phase ion populations and using them to deduce the composition of the solution phase.

The propensity of each lysine residue to be modified by SMPT was calculated based on the information presented above. Ion abundances used to identify sites of modification or lack thereof were compared to their unmodified counterparts in the native digest spectrum (see eq 3 in the Experimental Procedures). Such ion abundances were used in calculations if intensities were similar in both modified and unmodified spectra. As an example, peptide segment 8 contains lysine 41 and was found to be detected with greater intensity in the native digest spectrum than other peptide segments. It was concluded that SMPT modification does not occur significantly at lysine 41 because unmodified peptide segment 8 was found to be highly sensitive to detection in the SMPT-modified digest spectrum, yet no modified fragment with peptide segment 8 was found. If there was little detection of unmodified peptide segment 8 in the SMPT-modified digest spectrum, it could not be concluded that modification had not occurred at lysine 41 because the SMPT-modified peptide segment 8 may have been neutralized as described above. This exercise of comparison of sensitivities in the native and modified digest spectra was performed for each assigned peptide segment. The percent of a given assigned ion (corresponding to a modified peptide segment) in the total population of assigned ions containing that same peptide

Table 3. Percentage of SMPT-Modification at Lysine Residues[a]

lysine	<1%	0−10%	10−50%
1			×
7		×	
31		×	
37			×
41	×		
61	×		
66		×	
91		×	
98		×	
104	×		

[a] In the digested modified RNase A, ×% of lysine listed has been shown to be modified with SMPT.

segment (modified and unmodified) was calculated. The results are shown in Table 3.

Apparent selectivity of SMPT for lysine residues differed from the acetic and succinic anhydride modifications reported in the literature (*16*, *34*−*36*). Glocker et al. has shown the lysines 1 and 7 to have a propensity for modification by acetic and succinic anhydride, as well as active-site lysine 41 (*16*). Our experimental data suggest that no significant modification of lysine 41 by SMPT occurs under our reaction conditions. Modification at lysine 7 did not differ in selectivity by SMPT from other lysines such as 31, 66, 91, and 98. Predominant modification by SMPT occurs at lysines 1 and 37. In the three-dimensional structure of RNase A, all lysines are accessible to the solvent, and lysines 1 and 37 are on the same side of the protein. Their similar location in the tertiary structure may be related to their increased propensity for modification. It is likely that modification at either residue would result in a similar change in the dipole moment of the protein, making its separation by cationic exchange chromatography difficult.

ESI/FTICR-MS has been used to detect directly the extent of modification, and when coupled with tryptic digestion, information regarding site of modification is obtained. However, without prepared standards of peptide segments and potential combinations of peptide segments (both modified and unmodified), deduced propensities of modification at a given site will only be semiquantitative.

Subtilisin Digests Post Bio-Rex 70 Chromatography. Digestion of modified RNase A with a nonspecific protease, subtilisin, was used as a complement to the modification site information obtained from tryptic digestion. A detailed examination of modifications at the ϵ- and α-amino positions on lysine-1 was accomplished.

Subtilisin cleaves bovine pancreatic RNase A predominantly between residues 20 and 21. Peptide bond cleavage between residues 20 and 21 results in two polypeptides known as the S-peptide (residues 1−20) and S-protein (residues 21−124). Cleavage also occurs to a lesser extent between other nearby residues. Cleavage by subtilisin at the various cleavage sites was previously quantified by HPLC/ESI/QIT-MS by Mendez et al.[3] All CID on the S-peptide were collected through fragmentation of the predominant S-peptide, *m/z* 1220-$[M + 2H]^{2+}$ (residues 1−20).

Fractions of SMPT-modified protein from the Bio-Rex 70 column were digested by subtilisin followed by separation and examination by HPLC/ESI/QIT-MS. A variety of combinations of unmodified S-peptide, *m/z* 1083-$[M + 2H]^{2+}$, singly modified S-peptide, *m/z* 1220-$[M + 2H]^{2+}$, unmodified S-protein, *m/z* 2882-$[M + 4H]^{4+}$, singly modified S-protein, *m/z* 2954-$[M + 4H]^{4+}$, as well as multiply modified peptides were found in Bio-Rex 70 fractions (see an example in Figure 6). The presence of these various ions demonstrates the heterogeneity in a given Bio-Rex 70 peak in terms of number of SMPT modifications and site of modification. Charge states were obtained under high-resolution detection for ions of interest to confirm peptide assignment.

[3] Unpublished results.

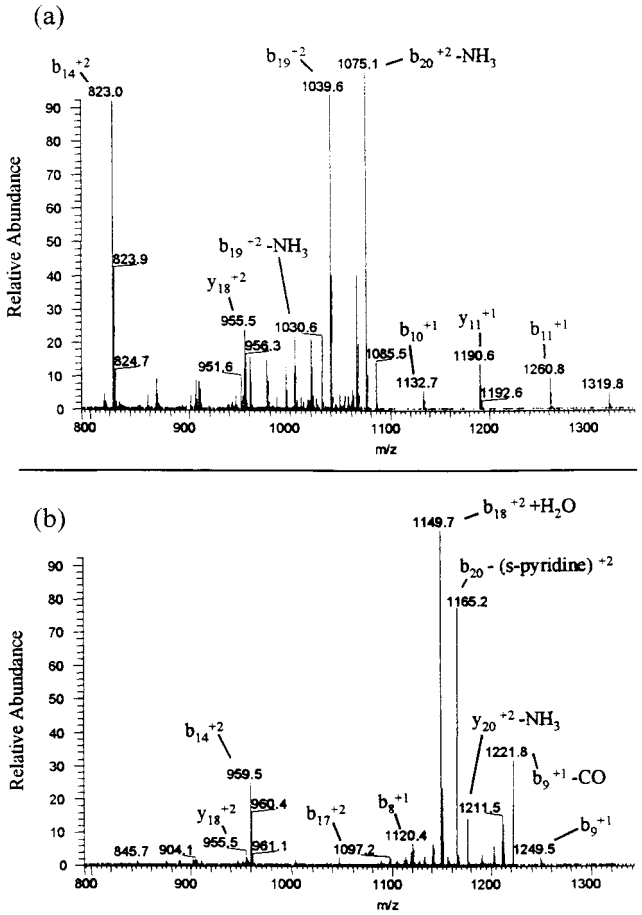

Figure 8. MS/MS CID spectra of (A) Unmodified S-peptide, *m/z* 1083-$[M + 2H]^{2+}$ (B) Modified S-peptide, *m/z* 1220-$[M + 2H]^{2+}$ of Figure 7, peak A with modification at Lys-1.

A characteristic pattern of elution was seen from the HPLC/ESI/QIT-MS, showing three peaks with the same *m/z* that correspond to singly modified S-peptide, *m/z* 1220-$[M + 2H]^{2+}$ [Figure 7 (top); the isotopic pattern confirms the 2^+ charge state.

The reproducible pattern of singly modified S-peptide *m/z* 1220-$[M + 2H]^{2+}$ peaks would logically correspond to the three possible sites of modification on the S-peptide: α-Lys-1, ϵ-Lys-1, and Lys-7. The technique of MS^n was used to determine the collision induced dissociation (CID) patterns of the unmodified S-peptide ion *m/z* 1083-$[M + 2H]^{2+}$ and modified S-peptide ions at *m/z* 1220-$[M + 2H]^{2+}$ to obtain sequence information about the SMPT modification site (see Figure 8).

A characteristic CID pattern was seen for the unmodified S-peptide, *m/z* 1083-$[M + 2H]^{2+}$. CID of the singly modified S-peptide ions at *m/z* 1220-$[M + 2H]^{2+}$ resulted in daughter ions (Table 4), which are indicative of the modification site in each *m/z* 1220-$[M + 2H]^{2+}$ HPLC/ESI mass chromatogram peak (see Figure 7). Peaks A and B of Figure 7 correspond to modification at Lys-1, and peak C corresponds to modification at Lys-7.

Table 4

m/z	b-ions[a]	*m/z*	y ions[b]
	(A) Unmodified S-Peptide Fragment Ions, MS^n of *m/z* 1083.50-$[M + 2H]^{2+}$		
572.6	b_6^{+1}	434.5	y_5^{+1}
700.7	b_7^{+1} or b_{12}^{+2}	523.5	y_6^{+1}
765.6	b_{13}^{+2}	824.7	y_{15}^{+2}
823.1	b_{14}^{+2}	906.7	y_9^{+1}
866.4	b_{15}^{+2}	955.5	y_{18}^{+2}
910.1	b_{16}^{+2}	1019.5	y_{19}^{+2}
951.6	b_{17}^{+2}-NH_3	1190.6	y_{11}^{+1}
961.4	b_{17}^{+2}	1319.8	y_{12}^{+1}
976.8	b_9^{+1}	1466.8	y_{13}^{+1}
995.1	b_{18}^{+2}-NH_3	1594.8	y_{14}^{+1}
1004.1	b_{16}^{+2}	1666.1	y_{15}^{+1}
1030.6	b_{19}^{+2}-NH_3	1737.1	y_{16}^{+1}
1039.6	b_{19}^{+2}	1909.3	y_{18}^{+1}
1075.1	b_{20}^{+2}-NH_3		
1132.8	b_{10}^{+1}		
1260.8	b_{11}^{+1}		
1397.8	b_{12}^{+1}		
1528.9	b_{13}^{+1}		
1643.9	b_{14}^{+1}		
	(B) Singly Modified S-Peptide, Peak A, MS^n of *m/z* 1220.00-$[M + 2H]^{2+}$ [c]		
703.4	b_4^{+1} or b_{10}^{+2}	**823.3**	y_{15}^{+2}
973.7	b_7^{+1}	**904.3**	y_{17}^{+2}
901.4	b_{13}^{+2}	906.7	y_9^{+1}
959.5	b_{14}^{+2}	**955.5**	y_{18}^{+2}
1002.9	b_{15}^{+2}	**1019.5**	y_{19}^{+2}
1045.9	b_{16}^{+2}	1190.6	y_{11}^{+1}
1097.4	b_{17}^{+2}	1319.7	y_{12}^{+1}
1120.4	b_8^{+1}	1466.8	y_{13}^{+1}
1141.3	b_{18}^{+2}	**1594.8**	y_{14}^{+1}
1149.8	b_{18}^{+2}+H_2O	**1665.8**	y_{16}^{+1}
1165.1	b_{20}^{+2}-(s-pyr)	**1720.1**	y_{16}^{+1}-NH_3
1176.1	b_{19}^{+2}	**1736.9**	y_{16}^{+1}
1211.5	b_{20}^{+2}-NH_3	**1909.9**	y_{18}^{+1}
1221.5	b_9^{+1}-CO		
1249.5	b_9^{+1}		
1406.5	b_{10}^{+1}		
1533.8	b_{11}^{+1}		
1670.8	b_{12}^{+1}		
1801.7	b_{13}^{+1}		
1917.8	b_{14}^{+1}		
	(C) Singly Modified S-Peptide, Peak B, MS^n of *m/z* 1220.00-$[M + 2H]^{2+}$ [c]		
513.6	b_2^{+1}-NH_3	523.5	y_6^{+1}
531.6	b_2^{+1}	638.4	y_7^{+1}
549.4	b_2^{+1}+H_2O	751.8	y_8^{+1}-NH_3
616.7	b_3^{+1}-NH_3	769.5	y_8^{+1}
631.9	b_3^{+1}	**904.3**	y_{17}^{+2}
703.4	b_4^{+1} or b_{10}^{+2}	906.6	y_9^{+1}
722	b_4^{+1}+H_2O	**947**	y_{18}^{+2}-NH_3
774.6	b_6^{+1}	**955.5**	y_{18}^{+2}
845.7	b_6^{+1}	1034.9	y_{10}^{+1}
902.1	b_{13}^{+2}	1211.5	y_{20}^{+2}-NH_3
959.5	b_{14}^{+2}	1303.6	y_{12}^{+1}-NH_3
1003.2	b_{15}^{+2}	1319.7	y_{12}^{+1}
1046.7	b_{16}^{+2}	1466.8	y_{13}^{+1}
1088.2	b_{17}^{+2}-NH_3	**1594.8**	y_{14}^{+1}
1097.2	b_{17}^{+2}	**1665.8**	y_{16}^{+1}
1120.4	b_8^{+1}	**1736.9**	y_{16}^{+1}
1141.3	b_{18}^{+2}	**1909.9**	y_{18}^{+1}
1149.8	b_{18}^{+2}+H_2O		
1165.1	b_{20}^{+2}-(s-pyr)		
1176.1	b_{19}^{+2}		
1211.5	b_{20}^{+2}-NH_3		
1221.5	b_3^{+1}-CO		
1249.5	b_9^{+1}		
1405.7	b_{10}^{+1}		
1533.8	b_{11}^{+1}		
1670.8	b_{12}^{+1}		
1801.7	b_{13}^{+1}		
1917.8	b_{14}^{+1}		
	(D) Singly Modified S-Peptide, Peak C, MS^n of *m/z* 1220.00-$[M + 2H]^{2+}$ [d]		
572.4	b_6^{+1}	523.5	y_6^{+1}
902.1	b_{13}^{+2}	638.4	y_7^{+1}
959.5	b_{14}^{+2}	751.8	y_8^{+1}-NH_3
1003.2	b_{15}^{+2}	769.5	y_8^{+1}
1046.7	b_{16}^{+2}	888.5	y_9^{+1}-NH_3
1097.2	b_{17}^{+2}	906.7	y_9^{+1}
1120.4	b_8^{+1}	**1004.1**	y_{16}^{+2}
1140.8	b_{18}^{+2}	**1091.4**	y_{19}^{+2}
1149.8	b_{18}^{+2}+H_2O	1211.5	y_{20}^{+2}-NH_3
1165.1	b_{20}^{+2}-(s-pyr)	1319.8	y_{12}^{+1}
1176	b_{19}^{+2}	1467.8	y_{13}^{+1}
1211.5	b_{20}^{+2}-NH_3	**1868.7**	y_{14}^{+1}
1221.5	b_9^{+1}-CO	**1938.8**	y_{16}^{+1}
1249.5	b_9^{+1}		
1405.9	b_{10}^{+1}		
1533.8	b_{11}^{+1}		
1670.8	b_{12}^{+1}		
1802.9	b_{13}^{+1}		
1916.8	b_{14}^{+1}		

[a] b-ions are fragment ions generated from cleavage at the amide bonds with the charge retained on the N-terminal end of the peptide. The subscript indicates the amide bond where fragmentation occurred, counted from the C-terminal. [b] y-ions are fragment ions generated from cleavage at the amide bonds with the charge retained on the C-terminal end of the peptide. The subscript indicates the amide bond where fragmentation occurred, counted from the N-terminal. [c] Bold *m/z* values indicate those which pinpoint site of modification. In this case ions indicate modification at lysine 1. [d] Modification at lysine 7.

It would be difficult to determine which peak (A or B) corresponds to modification at α-Lys-1 or ϵ-Lys-1, because the CID fragmentation pattern could possibly be identical. One clue, however, to the site of Lys-1 modification was found. CID fragmentation appears to be negligible at peptide bonds connected to the modified residue in peak B. If the close proximity of the modification to the peptide bond inhibits CID fragmentation, then modification at α-Lys-1 would result in a slightly different CID fragmentation pattern from that of modification at ϵ-Lys-1. Fragment ion y_{19}^{2+}, *m/z* 1020-$[M + 2H]^{2+}$, corresponds to loss of the Lys-1 if the modification occurred at Lys-1. This y_{19}^{2+} ion was only seen in the CID fragmentation pattern of HPLC/ESI-mass chromatogram elution peak A but not in B or C.

The formation of the y_{19}^{2+} ion from peak A and not from peak B may indicate that peak A contains S-peptide modified on ϵ-Lys-1 and peak B contains S-peptide modified on α-Lys-1. Modification on ϵ-Lys-1 is far enough away from the peptide backbone to allow Lys-1 to be lost. Modification on α-Lys-1 is closer to the peptide backbone, preventing loss of Lys-1, and thus, ion *m/z* 1020-$[M + 2H]^{2+}$ is absent from CID fragmentation for HPLC peak B. To corroborate this theory, the modification found at Lys-7 in peak C did not inhibit CID fragmentation at the adjacent peptide bond, as seen by the presence of the y_{13}^{1+} in peak C. The experimental data demonstrate the information that may be obtained from careful examination of the CID fragmentation patterns for each S-peptide ion. However, Edman sequencing of separated S-peptides

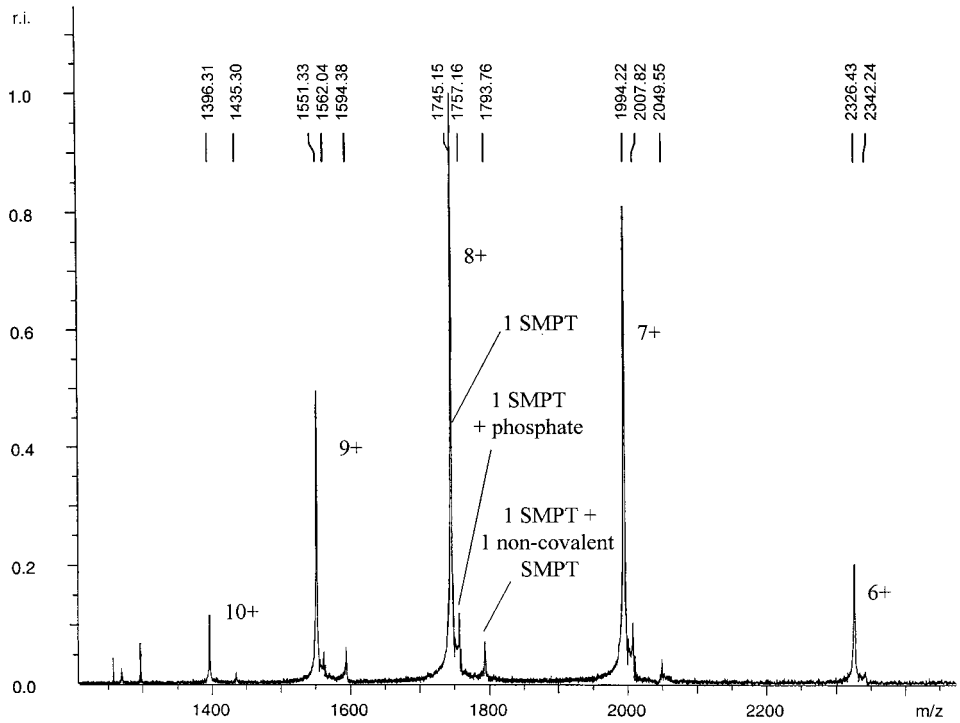

Figure 9. ESI/FTICR-mass spectrum of HPLC separated SMPT-modified RNase A (molar ratio 1:2 RNase A to SMPT). The predominant charge state is 8+, with *m/z* 1745.15-$[M + 8H]^{8+}$ corresponding to RNase A + 1 SMPT (expected *m/z* 1745.07-$[M + 8H]^{8+}$). *m/z* 1757.16-$[M + 8H]^{8+}$ indicates 1 SMPT modification and 1 phosphate adduct. The peak at *m/z* 1793.76-$[M + 8H]^{8+}$ corresponds to a noncovalent SMPT adduct with singly-modified protein. Subsequent preparation of the sample for digestion by trypsin resulted in the removal of the non-covalently bound SMPT.

is required for the conclusive assignment of modification at either the ϵ- or α-amino on Lys-1.

Offline HPLC. This work has been done with the goal of isolating singly modified RNase A for the purposes of introducing enhanced functionality into the protein via subsequent modification (Scheme 2). Such a method could be used as a complement to site-directed mutagenesis, for example. To illustrate the possibility of obtaining protein that has been singly modified at a single, specific site for bioconjugation purposes, offline HPLC was added as a second dimension of separation after Bio-Rex 70. Offline HPLC peaks with retention times consistent with singly modified RNase A (data not shown) were collected and examined by ESI/FTICR-MS. ESI/FTICR-MS of the sample indicated that there was only singly modified RNase A present with and without phosphate adducts (see Figure 9). Tryptic digestion of the two-dimensionally separated, singly SMPT-modified RNase A was performed. Experimental results were consistent with the heterogeneity of modification site in each fraction despite the increased chromatographic separation inherent in a two-dimensional method. Such an example demonstrates the difficulty of targeting single specific residues in a protein containing many reactive sites with a nonspecific modification reagent.

CONCLUSION

Tracking the separation and proteolytic digestion of SMPT-modified RNase A with ESI/FTICR-MS and HPLC/ESI/QIT-MS demonstrates the detailed information on extent of modification and modification sites that can be obtained by application of these techniques. Analysis of native and modified RNase A tryptic digests by ESI/FTICR-MS resulted in the identification of the sites of modification. Semiquantitative results of the reactivity of certain lysine residues toward the coupling reagent SMPT are possible but must be examined with caution as sensitivities of different peptide sequences to detection changes based on chemical nature of the peptide and reactions in the electrospray source. Two sites (lysines 1 and 37) are highly reactive, while three sites (lysines 41, 61, and 104) appear to be unreactive under the conditions used. Quantitative results would require the use of internal standards of each peptide segment and fragment, both modified and unmodified. Digestion of the modified and unmodified RNase A by subtilisin followed by examination by HPLC/ESI/QIT-MS and MS^n enabled further investigation of modification on lysines 1 and 7. MS^n on singly modified S-peptide indicated modification at the ϵ- and α-amine positions on lysine 1. In principle, isolation of singly modified homogeneous protein is possible when the above techniques are applied, even though separation of substantial quantities of RNase A that had been singly modified by SMPT at a known site was not achieved.

ACKNOWLEDGMENT

Authors thank S. Benner of the Department of Chemistry at the University of Florida for the use of lyophilization equipment, P. Borum of the Food Science and Human Nutrition department at the University of Florida for the use of the online HPLC equipment, and Waters Corporation for the donation of the Symmetry C18 HPLC column. Funding for T.J.M., G.H.L.L., and L.S.N. was provided by the National Science Foundation (CHE9727571) and the Army Research Office (37580-CH-2). Funding for J.V.J. was provided by the Interdisciplinary Center for Biotechnology Research (ICBR) at the University of Florida.

LITERATURE CITED

(1) Krell, T., Chackrewarthy, S, Pitt, A. R., Elwell, A., and Coggins, J. R. (1998) Chemical Modification Monitored by Electrospray Mass Spectrometry: A Rapid and Simple Method

for Identifying and Studying Functional Residues in Enzymes. *J. Pept. Res. 51*, 201−209.

(2) Mehlis, B., and Kertscher, U. (1997) Liquid Chromatography Mass Spectrometry of Peptides of Biological Molecules. *Anal. Chim. Acta 352*, 71−83.

(3) Loo, J. A. (1995) Bioanalytical Mass Spectrometry: Many Flavors to Choose. *Bioconjugate Chem. 6*, 644−665.

(4) Black, G. E., and Fox, A. (1996) Liquid Chromatography with Electrospray Ionization Tandem Mass Spectrometry − Profiling Carbohydrates in Whole Bacterial Cells Hydrolysates. *Biochem. Biotechnol. Appl. Electrospray Ionization Mass Spectrom. 619*, 81−105.

(5) Gelpi, E. (1995) Biomedical and Biochemical Applications of Liquid-Chromatography Mass-Spectrometry. *J. Chromatogr. A 703*, 59−80.

(6) Fligge, T. A., Kast, J., Bruns, K., and Przybylski, M. (1999) Direct Monitoring of Protein-Chemical Reactions Utilising Nanoelectrospray Mass Spectrometry. *J. Am. Soc. Mass. Spectrom. 10*, 112−118.

(7) Raida, M., Schulz-Knappe, P., Heine, G., and Forssmann, W. (1999) Liquid Chromatography and Electrospray Mass Spectrometric Mapping of Peptides from Human Plasma Filtrate. *J. Am. Soc. Mass. Spectrom. 10*, 45−54.

(8) Dage, J. L, Sun, H. J., and Halsall, H. B. (1998) Determination of Diethylpyrocarbonate-modified Amino Acid Residues in Alpha (1)-acid Glycoprotein by High-Performance Liquid Chromatography Electrospray Ionization Mass Spectrometry and Matrix-Assisted Laser Desorption/Ionization Time-of-Flight Mass Spectrometry. *Anal. Biochem. 257*, 176−185.

(9) Akashi, S., Shirouzu, M., Terada, T., Ito, Y., Yokoyama, S., and Takio, K. (1997) Characterization of the Structural Difference between Active and Inactive Forms of the Ras Protein by Chemical Modification Followed by Mass Spectrometric Peptide Mapping. *Anal. Biochem. 248*, 15−25.

(10) Ball, L. E., Oatis, J. E., Dharmasiri, K., Busman, M., Wang, J. Y., Cowden, L. B., Galijatovic, A., Chen, N., Crouch, R. K., and Knapp, D. R. (1999) Mass Spectrometric Analysis of Integral Membrane Proteins: Application to Complete Mapping of Bacteriorhodopsins and Rhodopsin. *Protein Sci. 7*, 758−764.

(11) Camilleri, P., Haskins, N. J., Rudd, P. M., and Saunders, M. R. (1993) Applications of Electrospray Mass Spectrometry to Studies on the Structrual Properties of Ribonuclease A and Ribonuclease B. *Rapid Commun. Mass Spectrom. 7*, 332−335.

(12) Kouach, M., Belaiche, D., Jaquinod, M., Couppez, M., Kmiecik, D., Ricart, G., Vandorsselaer, A., Sautiere, P., and Briand, G. (1994) Application of Electrospray and Fast-Atom-Bombardment Mass-Spectrometry to the Identification of Posttranslational and Other Chemical Modifications of Proteins and Peptides. *Biol. Mass S. 23*, 283−294.

(13) Zappacosta, F., Ingallinells, P., Scaloni, A., Pessi, A., Bianchi, E., Sollazzo, M., Tramontano, A., Marino, G., and Pucci, P. (1997) Surface Topology of Minibody by Selective Chemical Modifications and Mass Spectrometry. *Protein Sci. 6*, 1901−1909.

(14) Suckau, D., Mak, M., and Przybylski, M. (1992) Protein Surface Topology-Probing by Selective Chemical Modification and Mass-Spectrometric Peptide-Mapping. *Proc. Natl. Acad. Sci. U.S.A. 89*, 5630−5634.

(15) Glocker, M. O., Nock, S., Sprinzl, M., and Przybylski, M. (1998) Characterization of Surface Topology and Binding Area in Complexes of the Elongation Factor Proteins EF-Ts and EF-Tu Center Dot GDP from *Thermus Thermophilus*: A Study by Protein Chemical Modification and Mass Spectrometry. *Chem.—Eur. J. 4*, 707−715.

(16) Glocker, M. O., Borchers, C., Fiedler, W., Suckau, D., and Przybylski, M. (1994) Molecular Characterization of Surface Topology in Protein Tertiary Structures by Amino-Acylation and Mass Spectrometric Peptide Mapping. *Bioconjugate Chem. 5*, 583−590.

(17) Raverdino, V., Lapolla, A., Fedele, D., Baldo, L., Aronica, R., Catinella, S., Seraglia, R., and Traldi, P. (1996) An Electrospray Investigation on *in vitro* Glycation of Ribonuclease. *Rapid Commun. Mass Spectrom. 10*, 178−182.

(18) Bruce, J. E., Hofstadler, S. A., Winger, B. E., and Smith, R. D. (1994) Characterization of Ribonuclease B Heterogeneity and the Identification and Removal of Phosphate Adducts by High-Resolution Electrospray Ionization Fourier Transform Ion Cyclotron Resonance Mass Spectrometry. *Int. J. Mass Spectrom. Ion Processes 132*, 97−107.

(19) Camilleri, P., and Haskins, N. J. (1993) Investigating the Noncovalent Interaction of Cytidylic Acids with Ribonuclease A by Electrospray Mass Spectrometry. *Rapid Commun. Mass Spectrom. 7*, 603−604.

(20) Neumann, U., and Hofsteenge, J. (1994) Interaction of Semisynthetic Variants of RNase A with Ribonuclease Inhibitor. *Protein Sci. 3*, 248−256.

(21) Goodlett, D. R., Ogorzalek Loo, R. R., Loo, J. A., Wahl, J. H., Udseth, H. R., and Smith, R. D. (1994) A Study of the Thermal Denaturation of Ribonuclease S by Electrospray Ionization Mass Spectrometry. *J. Am. Soc. Mass. Spectrom. 5*, 614−622.

(22) Alexandrescu, A. T., Rathgeb-Szabo, K., Rumpel, K., Jahnke, W., Schulthess, T., and Kammerer, R. A. (1998) ^{15}N Backbone Dynamics of the S−Peptide from Ribonuclease A in its Free and S−Protein Bound Forms: Toward a Site-Specific Analysis of Entropy Changes Upon Folding. *Protein Sci. 7*, 389−402.

(23) Ogorzalek Loo, R. R., Goodlett, D. R., Smith, R. D., and Loo, J. A. (1993) Observation of a Noncovalent Ribonuclease S−Protein/S−Peptide Complex by Electrospray Ionization Mass Spectrometry. *J. Am. Chem. Soc. 115*, 4391−4392.

(24) Schnell, R., Vietta, E., Schindler, J., Barth, S., Winkler, U., Borchmann, P., Hansmann, M. L., Diehl, V., Ghetie, V., and Engert, A. (1998) Clinical Trials with an Anti-CD25 Ricin A-Chain Experimental and Immunotoxin (RFT5-SMPT-dgA) in Hodgkin's Lymphoma. *Leuk. Lymphoma 30*, 525.

(25) Engert, A., Schnell, R., Radszuhn, A., Hatwig, M. T., Drillich, S, Schon, G., Tesch, H., Hansmann, M. L, Barth, S., Schindler, J., Ghetie, V., Uhr, J., and Vietta, E. (1997) A Phase-I Study of an Anti-CD25 Ricin A-Chain Immunotoxin (RFT5-SMPT-dgA) in Patients with Refractory Hodgkin's Lymphoma. *Blood 89*, 403−410.

(26) Ghetie, V., Thorpe, P., Ghetie, M. A., Knowles, P., Uhr, J., and Vietta, E. (1991) The GLP Large-Scale Preparation of Immunotoxins Containing Deglycosylated Ricin-A Chain and a Hindered Disulfide Bond. *J. Immunol. 142*, 223−230.

(27) Sanchez, E. F., Bush, L. R., Swenson, S., and Markland, F. S. (1997) Covalent Attachment of an RGD-Like Peptide to Create a Potentially More Effective Thrombol. S. Chimeric Fibrolase: Covalent Attachment of an RGD-Like Peptide to Create a Potentially More Effective Thrombolytic Agent. *Thromb. Res. 87*, 289−302.

(28) Sigman, D. S., Bruice, T. C., Mazumder, A., and Sutton, C. L. (1993) Targeted Chemical Nucleases. *Acc. Chem. Res. 26*, 98−104.

(29) Crook, E. M., Mathias, A. P., and Rabin, B. R. (1960) Spectrophotometric Assay of Bovine Pancreatic Ribonuclease by the use of Cytidine 2′,3′-phosphate. *Biochem. J. 74*, 234−238.

(30) Eftink, M. R., and Biltonen, R. L. (1983) Energetics of RNase A Catalysis. 3. Temperature Dependence of the Hydrolysis of Cytidine Cyclic 2′,3′-Phosphate. *Biochemistry 22*, 5140−5150.

(31) Wigger, M., Nawrocki, C. H., Watson, J. R., Eyler, J. R., and Benner, S. A. (1997) *Rapid Commun. Mass Spectrom. 11*, 1749−1752.

(32) Lang, G. H. L. (1998) *Studies of Organometallic and Biological Systems with Fourier Transform Ion Cyclotron Resonance Mass Spectrometry*, Ph. D. Dissertation, University of Florida, Gainesville, FL.

(33) Marshall, A. G., Hendrickson, C. L., and Jackson, G. S. (1998) Fourier Transform Ion Cyclotron Resonance Mass Spectrometry: A Primer. *Mass Spectrom. Rev. 17*, 1−35.

(34) Watkins, N. G., Thorpe, S. R., and Baynes, J. W. (1985) Glycation of Amino Groups in Protein. *J. Biol. Chem. 260*, 10629−10636.

(35) Pares, X., Llorens, R., Arus, C., and Cuchillo, C. M. (1980) The reaction of Bovine Pancreatic Ribonuclease A with 6-Chloropurineriboside 5′-Monophosphate. *Eur. J. Biochem. 105*, 571−579.
(36) Alonso, J., Nogues, V., and Cuchillo, C. M. (1986) Modification of Bovine Pancreatic Ribonuclease A with 6-chloropurine Riboside. *Arch. Biochem. Biophys. 246*, 681−689.
(37) Brown, L. R., and Bradbury, J. H. (1975) Proton-Magnetic-Resonance Structures of the Lysine Residues of Ribonuclease A. *Eur. J. Biochem. 54*, 219−227.
(38) Liang, Z., and Marshall, A. G. (1990) Precise Relative Ion Abundances from Fourier Transform Ion Cyclotron Resonance Magnitude-Mode Mass Spectra. *Anal. Chem. 62*, 70−75.
(39) Marshall, A. G., and Verdun, F. R. (1989) *Fourier Transforms in Optical, NMR, and Mass Spectroscopy*, Amsterdam, Elsevier.
(40) Gordon, E. F., and Muddiman, D. C. (1999) *Relative Ion Abundance Measurements of Electrosprayed Biological Molecules from FTICR Mass Spectra*, 47th ASMS Conference on Mass Spectrometry and Allied Topics.
(41) Fenn, J. B. (1993) Ion Formation from Charged Droplets: Roles of Geometry, Energy, and Time. *J. Am. Soc. Mass. Spectrom. 4*, 524−535.
(42) Bruins, A. P. (1998) Mechanistic Aspects of Electrospray Ionization. *J. Chromatogr. A 794*, 345−357.
(43) Ashton, D. S., Beddell, C. R., Cooper, D. J., Green, B. N., and Oliver, R. W. A. (1993) Mechanism and Production of Ions in Electrospray Mass Spectrometry. *Org. Mass Spectrom. 28*, 721−728.
(44) Bleicher, K., and Bayer, E. (1994) Various Factors Influencing the Signal Intensity of Oligonucleotides in Electrospray Mass-Spectrometry. *Biol. Mass S. 23*, 320−322.

BC990117G

Synthesis and Characterization of Poly(ethylene glycol)−Insulin Conjugates

Ken Hinds, Jae Joon Koh, Lisa Joss,† Feng Liu, Miroslav Baudyš, and Sung Wan Kim*

Department of Pharmaceutics and Pharmaceutical Chemistry/Center for Controlled Chemical Delivery, University of Utah, Biomedical Polymers Research Building, Room 205, Salt Lake City, Utah 84112. Received September 8, 1999; Revised Manuscript Received December 23, 1999

Human insulin was modified by covalent attachment of short-chain (750 and 2000 Da) methoxypoly (ethylene glycol) (mPEG) to the amino groups of either residue PheB1 or LysB29, resulting in four distinct conjugates: mPEG(750)-PheB1-insulin, mPEG(2000)-PheB1-insulin, mPEG(750)-LysB29-insulin, and mPEG(2000)-LysB29-insulin. Characterization of the conjugates by MALDI-TOF mass spectrometry and N-terminal protein sequence analyses verified that only a single polymer chain (750 or 2000 Da) was attached to the selected residue of interest (PheB1 or LysB29). Equilibrium sedimentation experiments were performed using analytical ultracentrifugation to quantitatively determine the association state(s) of insulin derivatives. In the concentration range studied, all four of the conjugates and Zn-free insulin exist as stable dimers while Zn^{2+}-insulin was exclusively hexameric and Lispro was monomeric. In addition, insulin (conjugate) self-association was evaluated by circular dichroism in the near-ultraviolet wavelength range (320−250 nm). This independent method qualitatively suggests that mPEG−insulin conjugates behave similarly to Zn-free insulin in the concentration range studied and complements results from ultracentrifugation studies. The physical stability/resistance to fibrillation of mPEG−insulin conjugates in aqueous solution were assessed. The data proves that mPEG(750 and 2000)−PheB1-insulin conjugates are substantially more stable than controls but the mPEG(750 and 2000)−LysB29-insulin conjugates were only slightly more stable than commercially available preparations. Circular dichroism studies done in the far ultraviolet region confirm insulin's tertiary structure in aqueous solution is essentially conserved after mPEG conjugation. In vivo pharmacodynamic assays reveal that there is no loss in biological activity after conjugation of mPEG(750) to either position on the insulin B-chain. However, attachment of mPEG(2000) decreased the bioactivity of the conjugates to about 85% of Lilly's HumulinR formulation. The characterization presented in this paper provides strong testimony to the fact that attachment of mPEG to specific amino acid residues of insulin's B-chain improves the conjugates' physical stability without appreciable perturbations to its tertiary structure, self-association behavior, or in vivo biological activity.

INTRODUCTION

Parenteral administration of insulin formulations has been the primary therapy utilized for the treatment of insulin-dependent diabetes mellitus (IDDM) since insulin's discovery over 75 years ago (*1*). Countless attempts have been made to improve the physicochemical characteristics of insulin preparations through site-directed mutagenesis using recombinant DNA technology or by adjusting the formulation conditions, with varying amounts of success. A recent review by Brange and Volund (*2*) gives detailed physicochemical and pharmacological characterization of numerous insulin formulations/analogues, either used in the last half-century or currently under development.

Physical self-association of insulin substantially affects its pharmacological disposition (*2*−*7*). Aqueous solutions of insulin contain mixtures of monomeric, dimeric, and hexameric association states that coexist under a dynamic equilibrium. The average association state(s) in insulin preparations depend on protein concentration, temperature, ionic strength, and the presence of stabilizing molecules such as Zn^{2+}, phenol, chloride, or *m*-cresol (*4*, *6*, *8*−*10*). Insulin monomers have two nonpolar surfaces that are directly involved in the reversible self-association process (*8*). Dimerization proceeds through intermonomer interactions involving residues ValB12, TyrB16, PheB24, TyrB26, and ProB28. The burial of hydrophobic side chains and creation of four intermonomer hydrogen bonds from PheB24 to ProB28 results in an antiparallel β-sheet conformation between the monomers. Insulin hexamers are formed through both hydrogen bonding and hydrophobic interactions between surfaces formed by residues LeuA13, TyrA14, PheB1, ValB2, LeuB6, AlaB14, LeuB17, and ValB18. Addition of Zn^{2+}-ions further stabilizes the insulin hexamer through complexation of a single Zn^{2+}-ion with an imidazole group from each of three dimers that constitute the insulin hexamer (*8*, *11*). It is important to note that the hexameric form of insulin is not bioactive and is only partly absorbed across the capillary endothelium into the systemic circulation (*6*). In addition, the dissociation of insulin hexamers into dimers and monomers is seen as the rate-limiting barrier to subcutaneous absorption that directly affects the preparation's pharmacological response.

The physical stability of insulin also has a tremendous impact on the ability to design suitable insulin dosing regimes for diabetic patients. Insoluble insulin fibrils

* To whom correspondence should be addressed. Phone: (801) 581-6654. Fax: (801) 581-7848. E-mail: rburns@pharm.utah.edu.
† Department of Oncological Sciences, University of Utah.

10.1021/bc9901189 CCC: $19.00 © 2000 American Chemical Society
Published on Web 02/15/2000

have been shown to illicit increased immunogenic responses and are not biologically active. As a result of fibril formation, many undesirable properties may be introduced into an insulin preparation and the inhibition of fibrillation is necessary for a preparation to generate desirable and reproducible pharmacological effects. Interfacial and shear forces, temperature, pH, and insulin concentration affect insulin stability and its fibrillation (*12*, *13*). Fibrillation is thought to result from the aggregation/burial of hydrophobic residues that are exposed when the insulin monomer has partially unfolded. Previously, the N-terminus of the B-chain (specifically PheB1) was shown to participate in the fibrillation process.

It is well documented that poly(ethylene glycol) (PEG)−protein conjugates exhibit increased plasma half-lives, reduced immunogenecity and antigenecity, improved resistance to proteolysis, and increased aqueous/organic solubilities as compared to parental proteins (*14*−*21*). In certain cases, PEG−protein conjugates also possess a decreased ability to self-aggregate than parental proteins (*17*). We anticipate that the attachment of mPEG to insulin will introduce similar beneficial properties to this important protein drug.

The conjugation of methoxypoly(ethylene glycol) (mPEG) via covalent attachment to the PheB1 ($N^{\alpha B1}$) or LysB29 ($N^{\epsilon B29}$) amino groups of insulin should not have a negative impact on the protein's bioactivity since it has been previously determined that these residues do not directly participate in receptor binding (*22*−*24*). Previously, our group synthesized glucosyl-PEG-PheB1-insulin derivatives that were bound to concavalin-A (conA) for glucose exchange and determined that the conjugation significantly retarded insulin's ability to aggregate without negatively affecting its biological activity (*25*). In another study where only mPEG was attached to the PheB1 amino group of insulin, the conjugate (mPEG-PheB1-insulin) was found to be less immunogenic than native insulin (*26*). These experimental findings support the concept of improving insulin's physicochemical and pharmacological properties through the attachment of mPEG.

Few fragmentary reports have appeared in the literature on PEG-PheB1-insulin conjugates that fail to provide comprehensive physicochemical and biological characterizations (*25*, *27*−*30*). This paper provides a detailed description of the synthesis, physicochemical characterization, physical stability, and bioactivity of four individual mPEG−insulin conjugates. Reversed-phase high-performance liquid chromatography (RP-HPLC)/ion-exchange fast-protein liquid chromatography (IEX-FPLC), matrix-assisted laser desorption mass spectrometry (MALDI-MS), and N-terminal protein sequencing were used to assess the conjugates' purity, extent of conjugation, and site-of-substitution, respectively. The self-association behaviors of mPEG−insulin conjugates were examined using analytical ultracentrifugation and near-ultraviolet circular dichroism. The physical stability of each conjugate was evaluated using an accelerated shake-test (*5*, *31*). Biological activities (blood glucose depression in rats) of the conjugates were determined and compared to the fast-acting insulin formulation HumulinR. All of the studies described in this paper were performed with the purpose of determining if different characteristics exist between conjugates that vary in polymer molecular mass (750 and 2000 Da) and/or site-of-substitution ($N^{\alpha B1}$ and $N^{\epsilon B29}$). Relationships between the conjugate's composition, structure, and bioactivity will be discussed in light of producing a bioactive, neutral, soluble, physically stable, and long-acting parenteral insulin preparation.

EXPERIMENTAL PROCEDURES

Materials. Human crystalline zinc-insulin (Zn^{2+}-insulin, lot no. 506) was purchased from Bayer Corp. (Kankakee, IL) and used without purification. HumulinR and Humalog (Lispro) insulin preparations were purchased from Eli Lilly and Company (Indianapolis, IN). Methoxypoly(ethylene glycol)-succinimidyl propionate (mPEG-SPA, 750 and 2000 Da) was purchased from Shearwater Polymers (Huntsville, AL). All reagents and organic solvents used were at least ACS grade. Urea, ammonium bicarbonate (NH_4HCO_3), diethyl ether (Et_2O), ethanol (EtOH), and acetone (AcO) were purchased from Mallinckrodt Chemical (Paris, KY). Sodium chloride, sodium hydroxide, hydrochloric acid, acetic acid (AcOH), sodium phosphate monobasic, and sodium phosphate dibasic were purchased from Fisher Chemical (Fair Lawn, NJ). Triethylamine (TEA), triflouroacetic acid (TFA), anisole, dimethyl sulfoxide (DMSO), *N*,*N*-dimethylformamide (DMF), and di-*tert*-butyl dicarbonate (*t*-boc) were purchased from Aldrich Chemical Co. (St. Louis, MO). Spercta/Por 7 dialysis tubing (MWCO 3500) was purchased from Spectrum Medical Industries (Houston, TX). Acrodisc LC−PVDF (0.2 μm) syringe filters and Supor-200 (0.2 μm) membrane filters were purchased from Gelman Sciences (Ann Arbor, MI).

***N*$^{\alpha B1}$-Methoxypoly(ethylene glycol)-insulins (mPEG-PheB1-insulins).** Di- $N^{\alpha A1}$,$N^{\epsilon B29}$-*t*-boc-insulin (diboc-insulin) was synthesized as described previously (*25*). Newly synthesized diboc-insulin (200 mg) was purified on a SP Sepharose preparative ion-exchange column (Pharmacia AB) equilibrated with 1 M AcOH/7 M urea containing 0.01 M NaCl at a flow rate of 2.25 mL/min. The bound protein was eluted using a NaCl gradient (0.01 to 0.3M) over 180 min. The eluate corresponding to the major peak detected at 280 nm was collected and dialyzed against 0.01% NH_4HCO_3 to remove any low molecular weight impurities, then lyophilized and stored at −20 °C prior to use.

Both mPEG(750)-PheB1-insulin and mPEG(2000)-PheB1-insulin conjugates were prepared by reacting a 10× molar excess (75 μmol) of 750 or 2000 Da mPEG-SPA with diboc-insulin (7.5μmol) in 5.0 mL of anhydrous DMSO containing 0.5 mL of TEA under a nitrogen atmosphere at room temperature for 4 h. The mPEG-(750 or 2000)-PheB1-diboc-insulin solution was then diluted with 25 mL of H_2O before extensive dialysis against 0.01% NH_4HCO_3 and lyophilization. Deprotection of the lyophilized mPEG-PheB1-diboc-insulin (50 mg) was achieved by reaction with 5 mL of TFA containing 10% anisole (0 °C, under a nitrogen atmosphere) for 1 h to remove both of the *t*-boc-groups. The TFA/mPEG-PheB1-insulin solution was diluted in 15 mL of EtOH and 25 mL of H_2O before being dialyzed against 0.01% NH_4HCO_3 for 4 days and lyophilized. The mPEG-PheB1-insulin conjugates were purified using the same method described above for diboc-insulin. Each conjugate's purity was assessed by reversed-phase HPLC using a Shimadzu Model SCL-10A (Japan) chromatograph fitted with a photodiode-array (PDA) detector to continuously measure the absorbance of the eluent at 280 nm. A Vydac C4 (Hisperia, CA) reversed-phase HPLC column (4.6 mm × 25 cm, 5 μm particle diameter) was equilibrated with 0.1% TFA (solvent A) in 30% acetonitrile at a flow rate of 1.0 mL/min. Following sample injection (50 μL), a linear gradient of 2.0%/min solvent B (0.1% TFA in 95% acetonitrile) was applied for 20 min.

***N*$^{\epsilon B29}$-Methoxypoly(ethylene glycol)-insulin (LysB29-insulin).** This conjugate was synthesized according to a

modified version of a method used for the acetylation of insulin with fatty acids (*32*). Briefly, 20 μmol Zn^{2+}-insulin was dissolved in 10 mL of 60% DMF/40% H_2O (pH 9.5) at room temperature. A 1.5× molar excess of mPEG-SPA (750 or 2000 Da) was dissolved in 1.5 mL of dry DMF and added by immediate injection to the Zn^{2+}-insulin solution, keeping the apparent pH of the reaction solution constant by periodic addition of 1 N NaOH. After 30 min, the reaction was quenched by dilution with 25 mL of H_2O, and the mixture was dialyzed against 0.01% NH_4HCO_3 for 4 days and lyophilized. The same methods were used to isolate and assess the purity of both mPEG-PheB1-insulin and mPEG-LysB29-insulin derivatives.

MALDI-MS Analyses. All samples were run on a Perceptive Biosystems model DERP MALDI/TOF mass spectrometer operated in the linear mode, and positive ions were monitored. The matrix for all samples was α-cyano-4-hydroxycinnamic acid, and the 337 nm line of a nitrogen laser was used with at least 64 shots averaged for the final spectrum.

N-Terminal Protein Sequence Analyses. All samples were analyzed using an Applied Biosystems 477A Protein Sequencer (Pasadena, CA) through three Edman-degradation cycles.

Sedimentation Equilibrium. Sedimentation equilibrium experiments were used to gain insight into the solution states of various insulin preparations including the four mPEG–insulin derivatives. Experiments were conducted at 20 °C using a Beckman Optima XL-A analytical ultracentrifuge fitted with an AnTi60 rotor and 6-channel, 12 mm thick charcoal-epon centerpieces. The three sample channels in each cell contained three different loading concentrations of protein, while reference channels contained the dialysate. Initial loading concentrations of protein, in 50 mM Tris, pH 7.5, with 10 mM EDTA (lacking in the Zn^{2+}-insulin samples) ranged from 0.1 to 0.75 mg/mL. All samples were centrifuged at speeds ranging from 25 000 to 30 000 rpm until sedimentation equilibrium was attained. Cells were scanned radially in continuous mode, with data resulting from 10 absorbance readings taken at 0.001 cm intervals and 280 nm. Equilibrium was confirmed by the lack of differences between scans taken at 4 hourly intervals. Large concentration gradients at the base of the cell can give rise to refractive index gradients that may result in anomalous light redirection. To avoid this problem, a baseline scan at a nonabsorbing wavelength (360 nm) was taken once equilibrium was attained. Significant deviations from zero absorbance occur as a result of light redirection, and thus, these scans can be used to indicate the radial position above which the absorbance data become unreliable.

Data analysis describing the concentration distribution was achieved by fitting the final absorbance versus radius data to various models of insulin self-association using nonlinear least-squares techniques and the analysis program NONLIN (*33, 34*). NONLIN performs simultaneous nonlinear least-squares fits to one or more sets of ultracentrifuge data. This program can be used to determine molecular weights, association constants, and virial coefficients.

In each case, the final fit resulted from the simultaneous fitting of three to six different concentration distributions. To avoid the problem of relative local minima in the variance space, the fitting procedure was begun at many different initial points spanning the range of the parameters. A baseline-offset term was incorporated to account for the zero offset of the optical system or the presence of any absorbing, nonsedimenting components. It is necessary that parameters being estimated by the fitting function be reasonably well-defined before the inclusion of this term. Initial estimates of the baseline-offset term were determined experimentally by overspeeding the sample at the completion of the run in order to deplete the meniscus of solute. In each case the partial specific volume ($\bar{\nu}$) was fixed at 0.72 mL/g, representing the measured value for insulin (*35*).

Circular Dichroism Studies. Six samples, Zn^{2+}-ins, Zn-free-ins, mPEG(750)-PheB1-ins, mPEG(2000)-PheB1-ins, mPEG(750)-LysB29-ins, and mPEG(2000)-LysB29-ins, were prepared in PBS buffer (38 mM, pH 7.4) at three different concentrations (1, 0.1, and 0.001 mM) and filtered through an Acrodisc 0.2 μm syringe filter. Sample protein concentrations were determined by UV spectrometry, both before and after CD measurements, using an extinction coefficient of 6.2×10^3 M^{-1} cm^{-1} at 276 nm on a Hewlett-Packard UV–vis spectrophotometer (Palo Alto, CA) with the optional photodiode-array-detector attachment. Corrections to the extinction coefficient were made for differences in conjugate molecular weight. A Jasco J-720 Spectropolarimeter (Tokyo, Japan) was used without any attempt at noise reduction and three to five scans were averaged before the final spectrum was acquired. The data (ellipticity in mdeg) was then transformed to mean residue ellipticity (θ_m) using the expression (*35*)

$$(\theta_m) = (\theta M)/(Cl)$$

where θ is the observed ellipticity (mdeg), M is the mean residue molecular weight (g/mol), l is the optical path length (cm), and C is the protein concentration (g/mL).

Fibrillation Studies. Separate solutions of the four mPEG–insulin conjugates were prepared by dissolution in PBS (pH 7.4, 38 mM) with 0.01% sodium azide to a final protein concentration of 0.5 mg/mL. Similar solutions of Zn^{2+}-insulin and Zn-free insulin were prepared for use as control samples. The fibrillation kinetics were studied in 5 mL glass HPLC vials (1.5 mL filling volume) using a horizontal shaker at 37 °C and 100 strokes/min. At prescribed time points, individual vials were withdrawn (in triplicate) and their contents filtered through a 0.2 μm syringe filter. Filtered samples were analyzed for residual insulin derivatives' content using the same method described above for purity assessment. Sample concentrations were determined by preparation of a standard curve measuring peak areas of samples with specific concentrations previously determined by UV spectrophotometry. The time elapsed until 50% of the initial protein concentrations remained ($T_{50\%}$) was taken as a relative measure of the samples' physical stabilities.

Blood Glucose Depression Assays. Male Sprague-Dawley (SD) rats were kept under specific pathogen-free conditions in the animal facility. All procedures in handling animals adhered to the Principles of Laboratory Animal Care (NIH Publication 85-23, revised 1985). After the SD rats were fasted overnight, anesthesia was induced by intramuscular injection of a Ketamin (20 mg/kg) and Xylazine (2 mg/kg) mixture. HumulinR (100 IU/mL) or conjugate preparations (1 IU/mL, 0.01 M PBS) were injected at a dose of 0.3 IU/kg ($n = 4–5$) into the jugular vein of fasted nondiabetic rats. Blood samples (300 μL) were obtained at $t = 0$, 15, 20, 30, 45, 60, 90, 120, and 180 min postadministration to determine blood glucose levels. The blood samples obtained from SD rats were assayed for glucose concentration using an Accucheck-Instant glucometer (Boehringer Mannheim, Indianapolis, IN). The blood glucose level (BGL) versus time area-under-curve (AUC_G) was calculated by the trapezoi-

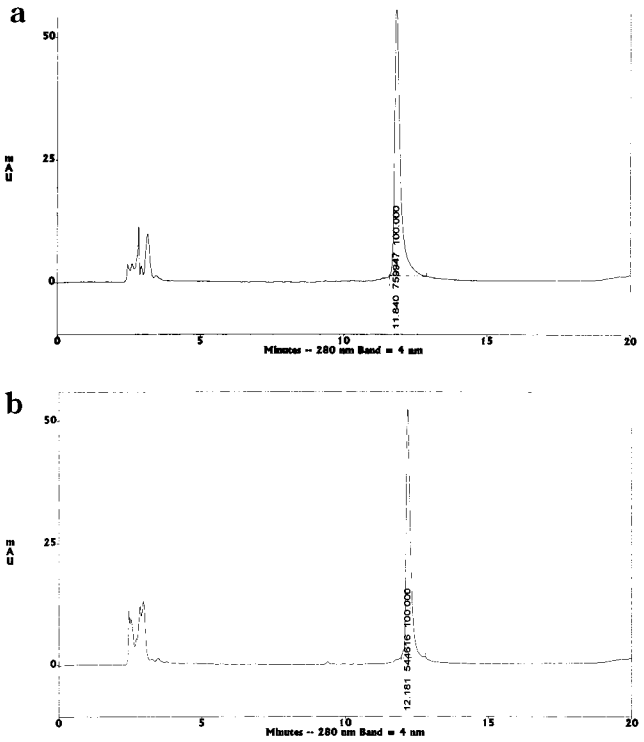

Figure 1. Reversed-phase HPLC chromatograms: (a) PheB1-(750)-insulin, (b) LysB29(750)-insulin. HPLC traces for mPEG-(2000)-insulins were nearly identical to those of the mPEG(750)-insulins except for an increase in retention time of around 0.3 min. Native insulin had a retention time of 11.07 min.

dal method. The nadir BGL (C_{nadir}, % of basal value) and the time to C_{nadir} (T_{nadir}) were determined from the experimental data. For assessment of the statistical significance of the differences, the Student *t*-test was employed and *p*-values for significance were set to 0.05.

RESULTS AND DISCUSSION

The succinimidyl ester of methoxypoly(ethylene glycol)-propionic acid (mPEG-SPA) was used for conjugation to either the α-amino group of PheB1 or to the ϵ-amino group of LysB29. Under the alkaline conditions used for mPEG-SPA conjugation, PheB1 (pK_a < 7.0) is far less reactive than GlyA1 ($pK_a \approx 8.0$) and LysB29 ($pK_a \approx 10.5$) (*26*). To obtain an adequate yield of mPEG-PheB1-insulin, *t*-boc-protection of GlyA1 and LysB29 was necessary to prevent these two residues from out-competing PheB1 during the conjugation (aminolysis) reaction. An adequate degree of selectivity was achieved in synthesizing Di- $N^{\alpha A1}$,$N^{\epsilon B29}$-*t*-boc-insulin (diboc-ins) with a yield of 23% and >95% mPEG-conjugation led to an overall yield of 20−25%. Additionally, mPEG-LysB29-insulin conjugates were synthesized in a basic 60% DMF solution ($pH_{app} \approx 10$), where the $N^{\epsilon B29}$-amino groups are most reactive, with an overall yield of 65−73%. In all cases, the reversed-phase HPLC chromatographs were analyzed to establish the conjugates' purity by the presence of a single peak (Figure 1). In addition, the results from far-ultraviolet circular dichroism studies suggest that the conjugates maintained the native tertiary structure of insulin to a large extent (Figure 3a).

MALDI-TOF analysis was used to determine the number of mPEG chains attached and the conjugate's molecular weight polydispersity (Figure 2). Monomeric insulin has a calculated molecular mass of 5807.2 Da, and the number-average molecular masses of mPEG-(750)-SPA and mPEG(2000)-SPA used in the conjugation

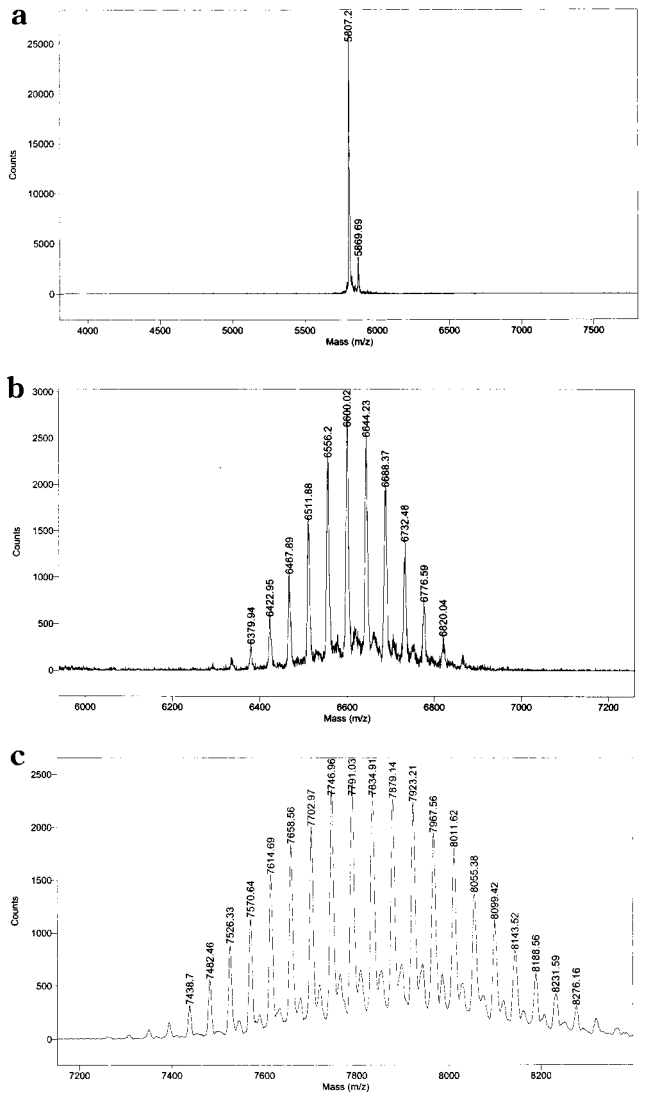

Figure 2. MALDI-TOF mass spectra: (a) Zn^{2+}-insulin, (b) mPEG(750)-LysB29-insulin, and (c) mPEG(2000)-PheB1-insulin. Because derivatives with the same molecular weight mPEG had identical spectra, only three representative spectra were included.

reactions were 827 and 2006 Da, respectively. The mass spectra of mPEG(750)-insulin and mPEG(2000)-insulin conjugates clearly demonstrate that only one mPEG chain was attached to insulin and the individual peaks differed by 44 Da (the molecular mass of an ethylene oxide monomer unit). N-Terminal sequencing was used to evaluate the site-of-substitution by analyzing the N-terminal amino acid molar ratio [GlyA1/PheB1]. A ratio of [GlyA1/PheB1] ≈ 1 is indicative of conjugation to residue LysB29 (or none at all), and [GlyA1/PheB1] ≈ ∞ is indicative of conjugation to residue PheB1 only. We found that the mPEG-PheB1-insulin conjugates had a [GlyA1/PheB1] molar ratio that was at least 3 orders of magnitude larger than either Zn^{2+}-insulin or the mPEG-LysB29-insulin conjugates. Thus, the combined MALDI-TOF mass spectrometry and Edman degradation results provide conclusive evidence that only one mPEG chain was attached to each insulin molecule and the appropriate site-of-substitution was achieved with a high degree of purity (>95% by RP-HPLC).

The solution states of the individual oligomers of insulin and its derivatives were examined using sedimentation equilibrium. Table 1 gives the apparent molecular weights and the calculated average association

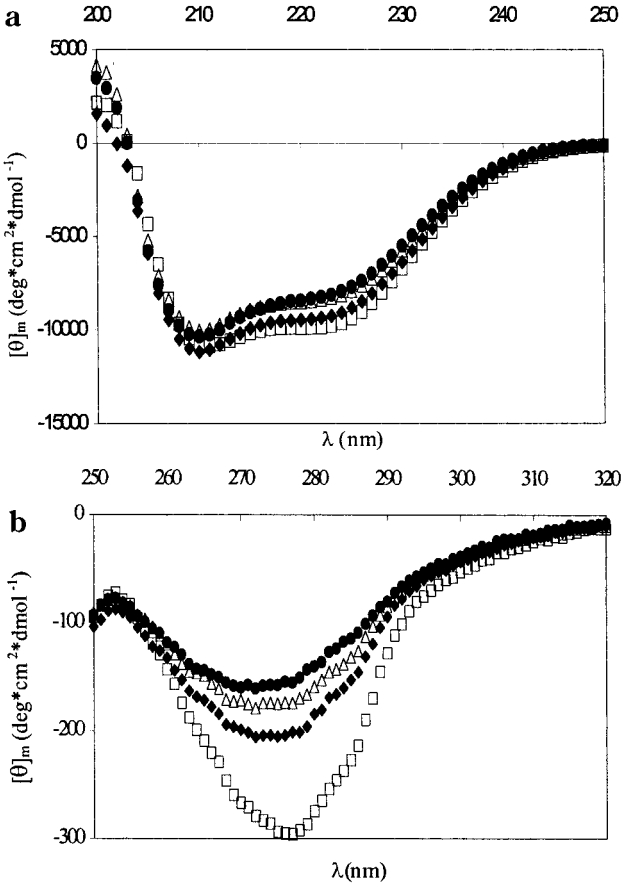

Figure 3. Far (a) and near (b) UV-CD spectra of: Zn2+-insulin (□); Zn-free insulin (◆); mPEG(750)-PheB1-insulin (△); mPEG-(750)-LysB29-insulin (●) samples in PBS (38 mM, pH 7.4) at a protein concentration of 0.1 mM. The mPEG(2000)-insulins did not differ significantly from mPEG(750)-insulins and were not included in the figures for the sake of clarity.

Table 1. Results from Sedimentation Equilibrium Experiments

sample[a]	$MW_{app} \pm SD$ (Da)	$(MW_{app}/MW_m)^b \pm SD$
Zn^{2+}-insulin	30 000 ± 9000	5.17 ± 1.55
Zn-free insulin	10 400 ± 2000	1.79 ± 0.34
Lispro[c]	5700 ± 600	0.98 ± 0.10
Phe750-insulin	13 300 ± 3000	2.0 ± 0.45
Phe2000-insulin	13 324 ± 3000	1.71 ± 0.38
Lys750-insulin	14 410 ± 2000	2.17 ± 0.30
Lys2000-insulin	15 980 ± 3000	2.05 ± 0.38

[a] All samples prepared in Tris/EDTA buffer (50 mM Tris and 5 mM EDTA, pH 7.4) except Zn^{2+}-insulin, which was prepared in Tris buffer only. [b] MW_m is the calculated molecular weight of the derivatives' monomeric species. [c] Monomeric Lispro was prepared after extensive dialysis against distilled water to remove any stabilizing substances (phenol, glycerol, and Zn^{2+}) from the commercial formulation.

states for the samples described in the experimental procedures. In the presence of zinc, insulin appears to be primarily hexameric in solution at the concentration range studied. The Zn^{2+}-insulin data were best described by a single-species model where the final fit was comprised of three separate data files with varying speeds and concentrations. The data from Zn-free insulin was also best described by a single species model in which the association state appears to be dimeric. As expected, Lispro was monomeric in solution at the concentration range studied. This can be explained by the presence of many reports, indicating Lispro is predominantly monomeric at high concentrations without the addition of stabilizers such as phenol, Zn^{2+}, and glycerol.

Table 2. Summary of Results from Circular Dichroism Experiments

sample	$[\theta]_{273}$[a]	$[\theta]_{273}$[b]	$[\theta]_{273}$[c]	$[\theta]_{208}/[\theta]_{223}$[c]
Zn^{2+}-insulin	−305.1	−283.6	−163.3	0.99
Zn-free insulin	−215.8	−204.9	−143.3	1.13
Phe750-insulin	−186.4	−174.7	−127.5	1.13
Phe2000-insulin	−198.4	−158.5	−110.8	1.21
Lys750-insulin	−201.3	−183.5	−136.9	1.12
Lys2000-insulin	−235.8	−190.5	−114.3	1.19

[a] Solutions prepared in PBS (38 mM, pH 7.4) to a protein concentration of 1.0 mM. [b] Solutions prepared in PBS (38 mM, pH 7.4) to a protein concentration of 0.1 mM. [c] Solutions prepared in PBS (38 mM, pH 7.4) to a protein concentration of 0.01 mM.

All of the mPEG−insulin derivatives appear to be dimeric in solution and were best described by a single species model. The fits and residuals from three different concentration distributions were used in the final calculation of the values in Table 1. The residuals were observed to be small and randomly distributed around zero, which indicates that the model was able to describe the data accurately (data not shown). The presence of the PEG made it difficult to assign an accurate $\bar{\nu}$ value to the PEG derivatives. It is likely that the mPEG behaves as a random-coil attachment on the protein and would not change $\bar{\nu}$ significantly. Because the molecular weights obtained for the control samples were analogous to previously published reports and the weights of the conjugates were reasonable, the use of native insulin's $\bar{\nu}$ value seems justified in the realm of calculating an average association-state.

Circular dichroism spectroscopy has been used to examine the conformation and self-association of insulin (*11*, *35*−*40*). The conditions that affect insulin self-association include ionic strength, pH, divalent metal cation (Zn^{2+}, Co^{2+}, Fe^{2+}, etc.) concentration, addition of phenol or other adjuvants, and protein concentration. Usually the magnitudes of three negative minima are evaluated: 208 nm (α-helix), 223 nm (*β*-sheet), and 273 nm (aromatic side-chains) in the analysis of insulin's self-association behavior in aqueous environments. The far-ultraviolet CD-band at 208 nm primarily arises from α-helicies formed from residues between B10−B19, A2-A6, and A13−19. *β*-Structure is the primary component of the far ultraviolet CD-band at 223 nm, and the ratio between these numbers ($[\Theta]_{208}/[\Theta]_{223}$) can be used to provide a qualitative measure of the amount of insulin (conjugate) self-association (*39*). Although both CD-bands (208 and 223 nm) decrease in intensity with decreased concentration/association, the ratio $[\Theta]_{208}/[\Theta]_{223}$ increases. This is because an antiparallel *β*-structure is formed when two monomers dimerize resulting in an increase of $[\Theta]_{223}$ without an increase of $[\Theta]_{208}$ (*39*). The values in Table 2 and spectra depicted in Figure 3a parallel this finding, with Zn^{2+}-insulin having a ratio of unity (insulin hexamer prevails), the mPEG(750)-insulin conjugates and Zn-free insulin having a $[\Theta]_{208}/[\Theta]_{223}$ ratio of 1.13 ± 0.01 and mPEG(2000)-insulin conjugates having a $[\Theta]_{208}/[\Theta]_{223}$ ratio of 1.20 ± 0.01. The spectral characteristics of the samples provided evidence that attachment of mPEG to insulin does not alter the overall conformation (tertiary structure) of the conjugates as compared to Zn^{2+}-insulin and Zn-free insulin.

The near-ultraviolet CD-band at 273 nm primarily results from restriction of rotation of the aromatic side-chains, TyrB16, TyrB26, PheB24, and PheB25, between

Table 3. Results of Long Term Physical Stability Experiments[a]

sample[b]	$T_{50\%}$ (days)[c]
Zn^{2+}-insulin	0.5 ± 0.3
Zn-free insulin	0.4 ± 0.2
Phe750-insulin	18.4 ± 2.8
Phe2000-insulin	20.7 ± 4.1
Lys750-insulin	4.3 ± 1.1
Lys2000-insulin	8.6 ± 1.7

[a] Accelerated shake-test done at 100 strokes/min and 37 °C. [b] Protein solutions prepared in PBS (38 mM, pH 7.4) containing 0.01% sodium-azide. [c] Elapsed time to 50% of the initial protein concentration remaining (mean ± standard deviation).

two insulin monomers in the dimer and between PheB1, PheB16, and TyrA14 in the insulin hexamer (*8*, *9*, *40*). Reduction of the 273 nm CD-band is observed when conditions favor oligomer dissociation such as dilution and alkaline pH. Conversely, strengthening of the 273 nm CD-band is associated with conditions that promote insulin self-association including metal ion concentration, increased protein concentration, and acidic pH. We found that conjugation of mPEG to insulin results in dichroic intensities at 273 nm that are much weaker than Zn^{2+}-insulin, but only slightly weaker than Zn-free insulin at equivalent concentrations (Table 2, Figure 3b). Thus, we conclude that the four mPEG−insulin conjugates and Zn-free insulin have similar self-association tendencies and qualitative estimates of a conjugate's average association state can be made by direct comparison to previously obtained data found in the literature (*4*, *10*, *11*, *35*, *37*, *41*). Because it has been shown that Zn-free insulin exists mostly as a dimer at the concentrations studied here (0.1−1.0 mM), the mPEG−insulin conjugates are believed to also be in a dimeric state.

The physical stability of each conjugate (a tendency to undergo fibrillation) was examined in an accelerated shaking test and compared to that of Zn-free and Zn^{2+}-insulin. The results are summarized in Table 3 and corroborate previous results from our lab for both glucosyl- and glucosyl-PEG−insulin conjugates (*25*, *31*). The PheB1-insulin conjugates possess substantially higher (36−40×) physical stabilities, and the LysB29-insulins were somewhat more stable (4-8×) than control samples. The increased physical stability is due to two complementary effects. One is the specific hydrophilization of the N-terminus in the B-chain by mPEG conjugation resulting in the specific prevention of this surface from participating in the hydrophobic interactions that drive insulin fibril growth (*12*, *13*). The second contributing effect to PheB1-insulin's increased physical stability is nonspecific and steric in nature and increases with an increase in mPEG molecular weight (Table 3). The LysB29-insulin conjugates exhibited increased physical stability (resistance to fibrillation), but not to the same extent as the mPEG-PheB1-insulin conjugates. This can be explained by the lack of LysB29's participation in fibrillation with any stabilizing effects caused by nonspecific steric hindrance of the intermolecular interactions that are involved in fibrillation.

Table 4 compares the bioactivities (AUC_G) of each of the four mPEG−insulin conjugates to that of HumulinR (Lilly's regular insulin formulation) control samples. We found that mPEG(750)-PheB1-insulin and mPEG(750)-LysB29-insulin conjugates had equivalent bioactivities to HumulinR after iv administration. However, the mPEG(2000)-PheB1-insulin and mPEG(2000)-LysB29-insulin conjugates possessed bioactivities that were about 15% lower than HumulinR. The attenuated glucose

Table 4. In Vivo Pharmacodynamic Parameters

sample	T_{nadir} (min)	C_{nadir} ± SD (mg/dL)	AUC_G (mg min/dL)	%bioactivity[a]
HumulinR	45	43 ± 1.38	11 700	100
Phe750-insulin	45	41 ± 3.52	11 250	104
Phe2000-insulin	30	60.5 ± 5.67	14 090	83
Lys750-insulin	45	39 ± 4.97	10 448	112
Lys2000-insulin	30	57 ± 4.96	13 770	85

[a] Calculated relative to HumulinR.

depression of the mPEG(2000)-insulin conjugates is probably due to steric hindrance of the insulin-receptor interactions. As expected, no differences in bioactivity were observed between conjugates with different sites-of-substitution because neither PheB1 nor LysB29 are directly involved in receptor binding (*22*).

CONCLUSIONS

The conjugation of methoxypoly(ethylene glycol) to specific residues on the insulin B-chain was achieved and the derivatives were purified by IEX-FPLC to a point where only a single-peak was observed using RP-HPLC analysis. Native insulin's tertiary structure and self-association patterns were conserved after conjugation of mPEG, as determined by ultraviolet circular dichroism. Over the concentration ranges used in the equilibrium sedimentation experiments, all of the mPEG−insulin derivatives and Zn-free insulin were in a dimeric state, Lispro was monomeric, and Zn^{2+}-insulin was predominantly in a hexameric state. Significant stabilization against aggregation/fibrillation was observed after attachment of mPEG(750 or 2000) to residue PheB1 of insulin that can be attributed to both specific and nonspecific effects. The in vivo potencies were not diminished by attachment of mPEG(750) but the attachment of mPEG(2000) to insulin did decrease the potency of the conjugate preparations by approximately 15%.

By itself, increasing the physical stability of insulin by mPEG-conjugation is a beneficial property of pharmaceutical relevance. Initial pharmacokinetic studies in dogs indicate that these conjugates are retained in the plasma longer than native insulin (K. Hinds, unpublished results) after intravenous administration. However, further work must be done to fully characterize the conjugate's immunological properties and pharmacokinetic (intravenous and subcutaneous) dispositions before their clinical relevance may be established. After careful consideration of the properties that each mPEG−insulin conjugate possesses, we believe mPEG-PheB1-insulins are the best candidates for use as physically stable, soluble, neutral, and fully bioactive insulin replacements.

ACKNOWLEDGMENT

This research was supported by funding from NIH Grant DK50557.

LITERATURE CITED

(1) Banting, F. G., and Best, C. M. (1922) Pancreatic extracts. *J. Lab. Clin. Med. 7*, 464−472.
(2) Brange, J., and Volund, A. (1999) Insulin analogues with improved pharmacokinetic profiles. *Adv. Drug Delivery Rev. 35*, 307−335.
(3) Binder, C. (1969) Absorption of injected insulin. *Acta Pharmacol. Toxicol. 2* (Suppl.), 1−87.
(4) Brange, J. (1987) *Galenics of Insulin*, Springer-Verlag, New York.
(5) Brange, J., Owens, D. R., Kang, S., and Volund, A. (1990) Monomeric insulins and their experimental and clinical implications. *Diabetes Care 13*, 923−954.

(6) Kang, S., Brange, J., Burch, A., Volund, A., and Owens, D. R. (1991) Subcutaneous insulin absorption explained by insulin's physicochemical properties. Evidence from absorption studies of soluble human insulin and insulin analogues in humans. *Diabetes Care 14*, 942−948.
(7) Ribel, U., Jorgensen, K., Brange, J., and Henriksen, U. (1986) The pig as a model for subcutaneous insulin absorption in man in *Diabetes* (M. Serrano-Rios and P. Lefebvre, Eds.), pp 891−896, Elsevier, Amsterdam.
(8) Blundell, T., Dodson, G., Hodgkin, D., and Mercola, D. (1972) Insulin: the structure in the crystal and its reflection in chemistry and biology. *Adv. Protein Chem. 26*, 279−402.
(9) Derwenda, U., Derwenda, Z., Dodson, G. G., Hubbard, R. E., and Korber, F. (1989) Molecular structure of insulin: the insulin monomer and its assembly. *Br. Med. Bull. 45*, 4−18.
(10) Mark, A. E., and Jeffrey, P. D. (1990) The self-association of zinc-free bovine insulin. *Biol. Chem. Hoppe-Seyler 371*, 1165−1174.
(11) Brems, D. N., Alter, A. A., Beckage, M. J., Chance, R. E., DiMarchi, R. D., Green, L. K., Long, H. B., Pekar, A. H., Shields, J. E., and Frank, B. H. (1992) Altering the association properties of insulin by amino acid replacement. *Protein Eng. 5*, 527−533.
(12) Brange, J., Dodson, G. G., Edwards, D. J., Holden, P. H., and Whittingham, J. L. (1997) A model of insulin fibrils derived from the X-ray crystal structure of monomeric insulin (despentapeptide insulin). *Proteins: Struct., Funct., Genet. 27*, 507−516.
(13) Brange, J., Anderson, L., Laursen, E. D., Meyn, G., and Rasmussen, E. (1997) Toward understanding insulin fibrillation. *J. Pharm. Sci. 86*, 517−525.
(14) Abuchowski, A., McCoy, J. R., Palczuk, N. C., van Es, T., and Davis, F. F. (1977) Effect of covalent attachment of poly(ethylene glycol) on immunogenicity and circulating life of bovine liver catalase. *J. Biol. Chem. 252*, 3582−3586.
(15) Beauchamp, C. O., Gonias, S. L., Menapace, D. P., and Pizzo, S. V. (1983) A new proceedure for the synthesis of poly(ethylene glycol)-protein adducts; effects on function, receptor recognition, and clearance of superoxide dismutase, lactoferrin, and alpha 2-macroglobulin. *Anal. Biochem. 131*, 25−33.
(16) Davis, S., Abuchowski, A., Park, Y. K., and Davis, F. F. (1981) Alteration of the circulating life and antigenic properties of bovine adenosine deamidase in mice by attachment of poly(ethylene glycol). *Clin. Exp. Immunol. 46*, 649−652.
(17) Delgado, C., Francis, G. M., and Fisher, D. (1992) The uses and properties of PEG-linked proteins. *CRC Crit. Rev. Ther. Drug Carrier Sys. 9*, 249−304.
(18) Nucci, M. L., and Abuchowski, A. (1991) The therapeutic value of poly(ethylene glycol)-modified proteins. *Adv. Drug Delivery Rev. 6*, 133−151.
(19) Wieder, K. J., Palczuk, N. C., van Es, T., and Davis, F. F. (1979) Some properties of poly(ethylene glycol): phenylalanine ammonia-lyase adducts *J. Biol. Chem. 254*, 12579−12587.
(20) Zalipsky, S., and Lee, C. (1992) Use of functionalized poly(ethylene glycol)s for modification of polypeptides. In *Poly (ethylene glycol) Chemistry: Biotechnical and Biomedical Applications* (J. M. Harris, Ed.), Plenum Press, New York.
(21) Monfardini, C., and Veronese, F. M. (1998) Stabilization of substances in circulation. *Bioconjugate Chem. 9*, 418−450.
(22) Gliemann, J., and Gammeltoft, S. (1974) The biological activity and the binding affinity of modified insulins determined on isolated rat fat cells. *Diabetologia 10*, 105−113.
(23) Hashimoto, M., Takada, K., Kiso, Y., and Muranishi, S. (1989) Synthesis of palmitoyl derivatives of insulin and their biological activities. *Pharm. Res. 6*, 171−176.
(24) Murray-Rust, J., McLeod, A. N., Blundell, T. L., and Wood, S. P. (1992) Structure and evolution of insulins: implications for receptor binding. *BioEssays 14*, 325−331.
(25) Liu, F., Song, S. C., Mix, D., Baudyš, M., and Kim, S. W. (1997) Glucose-induced release of glycosylpoly(ethylene glycol) insulin bound to a soluble conjugate of concavalin A. *Bioconjugate Chem. 8*, 664−672.
(26) Uchio, T., Baudyš, M., Liu, F., and Kim, S. W. (1999) Novel site-specific insulin conjugates with enhanced stability and extended action profile for parenteral delivery. *Adv. Drug Delivery Rev. 35*, 289−306.
(27) Ehrat, M., and Luisi, P. L. (1983) Synthesis and spectroscopic characterization of insulin derivatives containing one or two poly(ethylene glycol) chains at specific positions. *Biopolymers 22*, 569−573.
(28) Hinds, K. D., Liu, F., Koh, J. J., Baudyš, M., and Kim, S. W. (1999) Poly(ethylene glycol) conjugation to improve the physical and biological properties of insulin. *Proc. Int. Symp. Controlled Release Bioactive Mater. 26*, 6424−6425.
(29) Caliceti, P., and Veronese, F. M. (1998) Successful insulin delivery by PEG conjugation. *Proc. Int. Symp. Controlled Release Bioactive Mater. 25*, 263−264.
(30) Neubauer, H. P., Obermeier, R., and Schone, H. H. (1983) Influence of poly(ethylene glycol) insulin on the lipid tissues of experimental animals. *Diabetes 32*, 953−958.
(31) Baudyš, M., Uchio, T., Mix, D., Wilson, D., and Kim, S. W. (1995) Physical stabilization of insulin by glycosylation. *J. Pharm. Sci. 84*, 28−33.
(32) Myers, S. R., Yakubu-Madus, F. E., Johnson, W. T., Baker, J. E., Cusick, T. S., Williams, V. K., Tinsley, F. C., Kriauciunas, A., Manetta, J., and Chen, V. J. (1997) Acylation of human insulin with palmitic acid extends the time action of human insulin in diabetic dogs. *Diabetes 46*, 637−642.
(33) Johnson, M. L., Correia, J. J., Yphantis, D. A., and Halvorson, H. R. (1981) Analysis of data from the analytical ultracentrifuge by nonlinear least squares techniques. *Biophys. J. 36*, 575−588.
(34) Yphantis, D. A. (1964) Equilibrium ultracentrifugation of dilute solutions. *Biochemistry 3*, 297−317.
(35) Goldman, J., and Carpenter, F. H. (1974) Zinc binding, circular dichroism, and equilibrium sedimentation studies in insulin (bovine) and several of its derivatives. *Biochemistry 13*, 4566−4574.
(36) Melberg, S. G., and Johnson, W. C. (1990) Changes in secondary structure follow the dissociation of human insulin hexamers: A circular dichroism study. *Proteins: Struct., Funct., Genet. 8*, 280−286.
(37) Mercola, D. A., Morris, J. W. S., Arquilla, E. R., and Bromer, W. W. (1967) The ultraviolet circular dichroism of bovine insulin and desoctapeptide insulin. *Biochim. Biophys. Acta 133*, 224−232.
(38) Morris, J. W. S., Mercola, D., and Arquilla, E. R. (1968) An analysis of the near-ultraviolet circular dichroism of insulin. *Biochim. Biophys. Acta 160*, 145−150.
(39) Pocker, Y., and Biswas, S. B. (1980) Conformational dynamics of insulin in solution. Circular dichroic studies. *Biochemistry 19*, 5043−5049.
(40) Wood, S. P., Blundell, T. L., Wollmer, A., and Lazarus, N. R. (1975) The relation of conformation and association of insulin to receptor binding; X-ray and circular-dichroism studies on bovine and hystricomorph insulins. *Eur. J. Biochem. 55*, 531−542.
(41) Bakaysa, D. L., Radziuk, J., Havel, H. A., Brader, M. L., Li, S., Dodd, S. W., Beals, J. M., Pekar, A. H., and Brems, D. N. (1996) Physicochemical basis for the rapid time-action of LysB28ProB29-insulin: dissociation of a protein−ligand complex. *Protein Sci. 5*, 2521−2531.

BC9901189

Facile Synthesis of Stable and Lectin-Recognizable DNA-Carbohydrate Conjugates via Diazo Coupling

Kazunori Matsuura, Tsukasa Akasaka, Miki Hibino, and Kazukiyo Kobayashi*

Department of Molecular Design and Department of Biotechnology, Graduate School of Engineering, Nagoya University, Chikusa, Nagoya 464-8603, Japan. Received September 13, 1999; Revised Manuscript Received November 23, 1999

Stable and lectin-recognizable DNA−carbohydrate conjugates were prepared by diazo coupling of lactose and cellobiose derivatives to fragmented salmon testes DNA. The diazo coupling is suggested to take place selectively to guanine bases since the amount of lactose moiety introduced was directly proportional to the G content of various DNAs with different G contents. According to the CD spectra, the conjugates bearing carbohydrate less than 25% content kept a typical B-type conformation similar to native DNA. The conjugates possessed higher melting temperature and stronger nuclease resistance both to exo- and endonucleases than native DNA. Gel shift assay and fluorescence binding assay showed that the DNA-lactose conjugates were specifically bound to galactose-specific lectin RCA_{120} with strong binding affinity ($K_a = 10^4-10^5\ M^{-1}$) due to glycoside cluster effect. This facile method will be a useful protocol of molecular design for cell-targeted gene therapy.

INTRODUCTION

Biological functions of carbohydrate chains of glycolipids and glycoproteins have attracted much attention (*1*, *2*). The carbohydrate chains participate in various biological molecular recognition phenomena, such as fertilization, cell adhesion, tissue formation, antigen−antibody reaction, cancer metastasis, and infection of viruses and bacteria. The importance of multivalency of the carbohydrate chains in carbohydrate−protein interaction has been well cited as the glycoside cluster effect (*3*−*5*). Recently, various kinds of glycosylated polymers (*6*−*18*), dendrimers, (*19*−*21*) and calixarenes (*22*−*24*) have been developed to enhance the cluster effect as useful biorecognizable materials such as culture substrata of cells and trapping materials of viruses.

DNAs bearing glycosylated bases were discovered in T-even phages (*25*, *26*), bacteriophage RL38JI (*27*), bacteriophage SP-15 (*28*), *Trypanosoma brucei* (*29*), and RNA bearing glycosylated bases in rabbit and rat livers (*30*−*32*). In DNA of T-even phages, the cytosine is entirely replaced with 5-hydroxymethylcytosine, to which one or more glucose residues are attached via O-glycoside bond. One hypothetical function of the glycosylated DNAs is to protect T-even DNA from nucleases in infected host cells (*33*), although the other biological roles have not yet been sufficiently elucidated. If carbohydrates can be conjugated to DNA without affecting the structure and stability of DNA, the artificial DNA−carbohydrate conjugates will be useful as a mimic of the glycosylated DNAs in nature. The conjugates will be also of interest as a new class of artificial glycoconjugate materials applicable to cell-targeted gene therapy technique (*34*−*40*) using the strong recognition via carbohydrate-binding proteins due to the cluster effect. However, no facile method to introduce multiple carbohydrates to one DNA chain has been reported so far. Chemical modification of 5′ end group of DNA is widely used, but the method can introduce only one saccharide chain in one DNA chain (*41*). Solid-phase synthesis of oligo DNA bearing glycosylated bases is also useful, but it requires troublesome synthetic routes (*42*). DNA−complex formation strategy through noncovalent bonds such as electrostatic interaction (*34*−*40*) and intercalation (*43*) is simple, but the complexes are readily dissociated in a dilute solution.

We have paid attention to the diazo coupling method which was reported by J. M. Rothenberg et al. to modify DNA with a biotin derivative selectively at 8-position of guanine base (*44*−*46*). The modification is assumed to affect little the complementary hydrogen bonds and the secondary structure of DNA, since the 8-position of guanine base faces at the major groove side in the DNA duplex. The advantage of this modification is its quite simple synthetic procedure, although guanine bases along a DNA chain are modified randomly. The present paper has applied the diazocoupling method to introduce multiple oligosaccharide chains into DNA (*47*). Benzenediazonium derivatives bearing lactose and cellobiose were synthesized and subjected to the diazo coupling to naturally occurring DNAs. The resulting DNA−carbohydrate conjugates were characterized by UV and CD spectra, melting temperature, resistance to nucleases, binding of a intercalater, and a groove binder. Their high recognition ability to lectins was demonstrated by gel shift assay and fluorescence spectroscopy.

EXPERIMENTAL PROCEDURES

Instruments. ^{1}H NMR spectra were recorded on a Varian Gemini 200 spectrometer operating at 200 MHz with TMS as the internal standard. Absorption spectra were taken on a JASCO V-530 spectrophotometer. CD spectra were taken in a 0.05 cm quartz cell with a JASCO J-720 L spectrophotometer. Fluorescence spectra were recorded on a JASCO FP-777 spectrophotometer equipped with a thermal controller. Mass spectra were obtained on a JEOL JMS-AX505HA mass spectrometer using the electron impact method operating in the positive mode.

* To whom correspondence should be addressed. Phone: +81 52 789 2488. Fax: +81 52 789 2528. E-mail: kobayash@mol.nagoya-u.ac.jp.

10.1021/bc9901191 CCC: $19.00 © 2000 American Chemical Society
Published on Web 02/17/2000

IR spectra were recorded with a JASCO Fourier transform IR-230 spectrophotometer. Optical rotations were determined with a JASCO DIP-1000 digital polarimeter using a water-jacketed 1 dm cell at 25 °C.

Materials. DNAs (from salmon testes, *Micrococcus lysodeikiticus*, and *Closteridium perfringens*) and synthetic RNAs (polyA-polyU and polyG-polyC) were purchased from Sigma Co., Ltd. The DNA and RNA fragments were prepared by sonication (70 W, 20 kHz) and fractionation on Sepharose 4B (Pharmacia). The fractions containing 150−300 bp DNA and RNA were collected and used in this work. The length of DNA relative to the *Hinf* I restriction enzyme digest of ϕX174 was determined by electrophoresis on agarose gel.

D-Galactose oxidase (from *Dactylium dendroides*, EC 1.1.3.9), peroxidase (from horseradish, EC 1.11.1.7), DNase I (from bovine pancreas, EC 3.1.21.1), RCA_{120} (from *Ricinus communis*), and concanavalin A (Con A, from Jack bean, *Canavalia ensiformis*) were purchased from Sigma Co., Ltd. Exonuclease III (from *Escherichia coli* BE257/pSGR3) was purchased from Toyobo Co., Ltd. Poly(*N*-vinylbenzyl lactonolactonamido) (PVLA) (*13*) and poly(*p*-vinylbenzamido-β-lactose) (PNLac) (*14*) were prepared in our laboratory previously.

***N*-(*p*-Nitrobenzoyl)-4-*O*-(β-D-galactopyranosyl)-β-D-glucopyranosylamine (2).** Ammonium hydrogen carbonate was added to a solution of lactose (1.00 g, 2.78 mmol) in water (20 mL) until a portion of the solid salt remained undissolved. The mixture was stirred in an open vessel at 40 °C for 6 h. Ammonium hydrogen carbonate (total 40.0 g) was added at intervals to ensure saturation. TLC (chloroform:methanol:water = 4:7:3 in volume): R_f of lactose = 0.68 and of β-lactosylamine (**1**) = 0.43. When TLC indicated no more conversion, the mixture was diluted with water (150 mL) and concentrated to 5 mL in vacuo. The residue was diluted to 150 mL with water and concentrated in vacuo to dryness. This procedure was repeated until excess ammonia gas was removed to afford crude white solid of β-lactosylamine.

To the crude solution of β-lactosylamine in water (10 mL) were added sodium carbonate (1.00 g) and methanol (10 mL). The mixture was stirred at room temperature for 1 h, and *p*-nitrobenzoyl chloride (2.10 g, 11.1 mmol) in tetrahydrofuran (10 mL) was added. TLC (chloroform:methanol:water = 4:7:3 in volume): R_f of the product = 0.87. After 10 h, the reaction mixture was washed with chloroform (50 mL × 3) to remove unreacted *p*-nitrobenzoyl chloride. The solution was concentrated to 5−10 mL, chromatographed on TSKgel HW-40S column (eluent: water), and concentrated in vacuo to dryness to afford pure **2** as a white powder (0.85 g, 62% yield). mp: 165−168 °C. $[\alpha]_D^{25} = -8.2°$ (*c* 0.1 in H_2O). FAB-MS: *m/z* 461 ($M^+ + H$). ^1H NMR (D_2O): δ 7.67 and 6.82 (d, 4H, J = 8.2 Hz, C_6H_4), 5.16 (d, 1H, $J_{1,2}$ = 9.2 Hz, H-1), 4.45 (d, 1H, $J_{1',2'}$ = 7.8 Hz, H′-1), 3.91−3.62 (m, 12H, from sugar). IR (KBr): 3390, 2890, 1620, 1580, 1520, 1350 cm^{-1}. Anal. calcd for $C_{19}H_{26}O_{13}N_2$: C, 46.54; H, 5.34; N, 5.71. Found: C, 46.43; H, 5.52; N, 5.60.

***N*-(*p*-Aminobenzoyl)-4-*O*-(β-D-galactopyranosyl)-β-D-glucopyranosylamine (3).** To a solution of **2** (1.00 g, 2.04 mmol) in water:methanol (1/1 v/v) (50 mL) was added palladium carbon (0.03 g). The mixture was stirred under a hydrogen atmosphere at a room temperature for 3 h. TLC (chloroform:methanol:water = 4:7:3 in volume): R_f of the product = 0.78. Palladium carbon was removed by filtration through Celite. The filtrate was chromatographed on a TSKgel HW-40S column (eluent: water) and concentrated in vacuo to afford pure **3** as a white powder (0.78 g, 84% yield). mp: 283−285 °C. $[\alpha]_D^{25} = -6.2°$ (*c* 0.1 in H_2O). FAB-MS: *m/z* 492 ($M^+ + H$). ^1H NMR (D_2O): δ 8.32 and 7.97 (d, 4H, J = 8.8 Hz, C_6H_4), 5.14 (d, 1H, $J_{1,2}$ = 9.0 Hz, H-1), 4.45 (d, 1H, $J_{1',2'}$ = 7.4 Hz, H′-1), 3.90−3.53 (m, 12H, from sugar). IR (KBr): 3400, 2910, 1650, 1520, 1350 cm^{-1}. Anal. calcd for $C_{19}H_{28}O_{11}N_2$: C, 49.57; H, 6.13; N, 6.08. Found: C, 46.96; H, 6.19; N, 5.88.

***ω*-(*N*-(*p*-Nitrobenzoyl)amino)hexanoic acid.** *p*-Nitrobenzoyl chloride (2.67 g, 14.4 mmol) in tetrahydrofuran (5 mL) was added to a solution of ω-aminohexanoic acid (0.68 g, 4.8 mmol) and sodium carbonate (4.00 g, 28.9 mmol) in water:methanol (1/1 v/v) (40 mL) at 0 °C and stirred magnetically at room temperature for 5 h. TLC (methanol:chloroform = 1:4 in volume): R_f of the product = 0.5. The solution was concentrated in vacuo, chromatographed on a silica gel column (eluent, methanol:chloroform 1:4 in volume), and concentrated in vacuo to afford ω-(*N*-(*p*-nitrobenzoyl)amino)hexanoic acid as a yellow solid (0.74 g, 55% yield). ^1H NMR (CD_3OD): δ 8.32 and 8.02 (m, 4H, C_6H_4), 3.42 (t, 2H, J = 7.0 Hz, H-ω), 2.64 (t, 2H, J = 7.0 Hz, H-α), 1.68−1.24 (m, 6H, CH_2).

***N*-(*ω*-(*N*-(*p*-Nitrobenzoyl)amino)hexanoyl)-4-*O*-(*β*-D-galactopyranosyl)-*β*-D-glucopyranosylamine (5).** ω-(*N*-(*p*-Nitrobenzoyl)amino) hexanoic acid (0.50 g, 1.8 mmol), benzotriazol-1-yloxy-tris(dimethylamino)phosphonium hexafluorophosphate (BOP) (2.43 g, 5.36 mmol), and 1-hydroxybenzotriazole (HOBt) (0.27 g, 1.8 mmol) were dissolved in DMSO (10 mL), and β-lactosylamine (1.83 g, 5.36 mmol) was added and stirred at a room temperature for 48 h. TLC (ethyl acetate:acetic acid: methanol:water = 4:3:3:2 in volume): R_f of the product = 0.77. Chloroform was added to precipitate the product. The precipitate was filtered, rinsed with chloroform, chromatographed on TSKgel HW-40S column (eluent: water), and dried in vacuo to afford the crude **5** as a yellow solid. The crude product was used for the next step without further purification. mp: 220−222 °C. $[\alpha]_D^{25}$ = +3.8° (*c* 0.1 in H_2O). FAB-MS: *m/z* 604 ($M^+ + H$). ^1H NMR (D_2O): δ 8.28 and 7.86 (d, 4H, J = 8.8 Hz, C_6H_4), 4.91 (d, 1H, $J_{1,2}$ = 9.2 Hz, H-1), 4.39 (d, 1H, $J_{1',2'}$ = 7.4 Hz, H′-1), 3.87−3.35 (m, 12H, from sugar), 3.36 (t, 2H, J = 7.0 Hz, H-ω), 2.27 (t, 2H, J = 7.0 Hz, H-α), 1.68−1.24 (m, 6H, CH_2). IR (KBr): 3360, 2940, 1650, 1570, 1520, 1350 cm^{-1}. Anal. calcd for $C_{25}H_{37}O_{14}N_3$: C, 49.75; H, 6.18; N, 6.96. Found: C, 49.18; H, 6.37; N, 7.08.

***N*-(*ω*-(*N*-(*p*-Aminobenzoyl)amino)hexanoyl)-4-*O*-(*β*-D-galactopyranosyl)-*β*-D-glucopyranosylamine (6).** Palladium carbon (0.03 g) was added to a solution of crude **5** in water:methanol (1:2 in volume) (18 mL). The mixture was stirred under a hydrogen atmosphere at a room temperature for 6 h. TLC (ethyl acetate:acetic acid: methanol:water = 4:3:3:2 in volume): R_f of the product = 0.67. Palladium carbon was removed by filtration on Celite. The filtrate was chromatographed on a TSKgel HW-40S column (eluent: water) and concentrated in vacuo to afford pure **6** as a white powder (0.60 g, 58% yield from **5**). mp: 137−140 °C. $[\alpha]_D^{25}$ = +5.3° (*c* 0.1 in H_2O). FAB-MS: *m/z* 574 ($M^+ + H$). ^1H NMR (D_2O): δ 7.54 and 6.79 (d, 4H, J = 7.8 Hz, C_6H_4), 4.89 (d, 1H, $J_{1,2}$ = 9.2 Hz, H-1), 4.38 (d, 1H, $J_{1',2'}$ = 7.6 Hz, H′-1), 3.87−3.35 (m, 12H, from sugar), 3.28 (t, 2H, J = 7.0 Hz, H-ω), 2.27 (t, 2H, J = 7.0 Hz, H-α), 1.68−1.24 (m, 6H, CH_2). IR (KBr): 3350, 2920, 1610, 1540, 1380 cm^{-1}. Anal. calcd for $C_{25}H_{39}O_{12}N_3$: C, 52.35; H, 6.85; N, 7.33. Found: C, 52.08; H, 6.97; N, 7.43.

Typical Procedure of Preparation of DNA−Lactose Conjugates. *p*-Aminobenzoylated lactose derivative **3** (0.35 g, 0.75 mmol) was dissolved in an ice-

cold 1 N HCl solution (8.14 mL). An equivalent volume of an ice-cold aqueous solution of sodium nitrite (7.7 mg/mL) was added, and the solution was kept at 0 °C for 5 min. The reaction was terminated on addition of 1 N NaOH (7.00 mL) to afford the corresponding diazonium salt.

To the solution (23.3 mL) of the diazonium salt was added fragmented salmon testes DNA (150−300 bp, 2.00 mg, 6.38 μmol base), borate buffer (pH 8.4, 20.0 mL), and then 1 N NaOH until the pH of the solution was adjusted to 9.0. The solution was stirred at 25 °C for 15 min. The reaction was terminated on addition of 3 M acetate buffer (pH 5.2, 2.3 mL). The DNA was precipitated into ethanol (60 mL), collected by centrifugation at 12000*g* for 20 min (four times), and purified by anion-exchange chromatography (Cellulofine, Seikagaku Kougyo Co., Ltd.) eluted with water and then with 1 M NaCl(aq) to afford pure DNA-B-Lac (1.34 mg).

A similar procedure was applied to prepare DNA-BH-Lac (salmon testes) conjugate from **6**, the other DNA−lactose conjugates originated from *Micrococcus lysodeikiticus* and *Closteridium perfringens* from **3**, and synthetic RNA (polyA-polyU and polyG-polyC)-lactose conjugates from **3**.

Determination of Lactose Contents in DNA−Lac Conjugates. D-Galactose oxidase from *Dactylium dendroides* (2.80 mg, 45 unit) was dissolved in 10 mL of 0.01 M KH_2PO_4(aq) solution (solution A). Horseradish peroxidase (1.20 mg, 72 unit) and *o*-dianisidine (0.3 mL of 10 mg/mL in methanol) were dissolved in 50 mL of 0.01 M KH_2PO_4(aq) solution (solution B). Aliquots (133 μL) of solution A and solution B were added to aqueous solutions (133 μL of 0.01 M KH_2PO_4) in Eppendorf tubes containing about 80 μg of DNA−Lac conjugates as analytical samples. The enzymatic reaction was carried out at 30 °C for 48 h. The absorbance at 400 nm of the reaction mixture was immediately determined and corrected by subtracting the absorbance of the control experiment using native DNA. Lactose contents in the DNA−Lac conjugates were determined by the calibration curve made for 10, 20, 30, 40, 50, and 60 μg of PNLac.

Melting Temperature. The absorbance at 260 nm of DNA−Lac conjugate and native DNA in water was recorded as a function of rising temperature at 3.0 °C/5min on a spectrophotometer equipped with a thermal controller. The concentration of the nucleic base was 60 μM.

Digestion with DNase I. DNase I (from bovine pancreas, 80 units) was added to DNA solutions in a Tris-HCl buffer (pH 5.0, 50 mM Tris-HCl, 25 mM NaCl, 4 mM $MgSO_4$) and the absorbance at 260 nm was recorded on a spectrophotometer at 25 °C.

Digestion with Exonuclease III. Exonuclease III (from *E. coli*, 150 units) was added to DNA solutions in acetate buffer (pH 7.6, 8.3 mM AcONa, 1.0 mM $MgSO_4$, 1 mM 2-mercaptoethanol), and the absorbance at 260 nm was recorded on a spectrophotometer at 37 °C.

Binding of Ethidium Bromide. A portion of each stock solution of DNA-BH-Lac-14 and native DNA [36 mM bases in 0.1 mM Tris-HCl buffer with 0.1 M NaCl (pH 8.0)] was added to a solution of ethidium bromide (25.4 μM in the same buffer). The decrease in absorption at 480 nm due to intercalation was recorded with a spectrophotometer, converted into the Scatchard form using 5630 M^{-1} cm^{-1} as the molar extinction coefficient of ethidium bromide and treated with the DeltaGraph curve fitting routine using the McGee and von Hippel equation.

Scheme 1. Synthesis of the Diazonium Salts Starting from Lactose and Cellobiose[a]

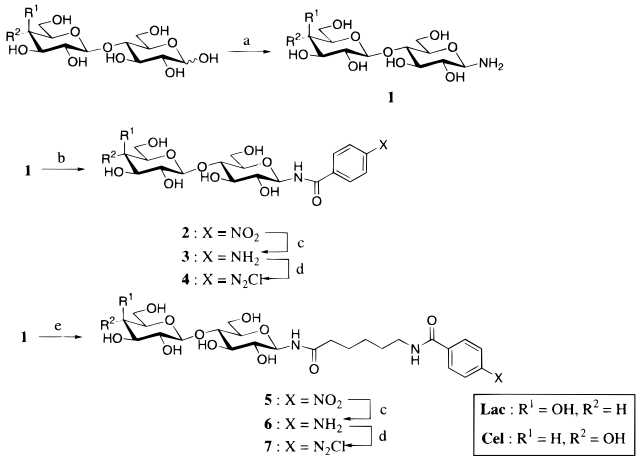

[a] Reagents and conditions: (a) NH_4HCO_3, water, 40 °C, 6 h. (b) *p*-Nitrobenzoyl chloride, Na_2CO_3, water/methanol/THF, 0 °C. (c) H_2 gas, Pd/C, water/methanol (1/2 v/v), rt. (d) $NaNO_2$, 1 N HCl, 0 °C, 5 min. (e) ω-(*N*-(*p*-Nitrobenzoyl)amino)hexanoic acid, BOP, HOBt, DMSO, rt, 48 h.

Binding of Distamycin A. A portion of each stock solution of DNA-BH-Lac-14 and native DNA [36 mM bases in 10 mM Tris-HCl buffer (pH 7.0)] was added to a solution of distamycin A (25.0 μM in the same buffer). The decrease in adsorption at 303 nm due to intercalation was recorded with a spectrophotometer, converted into the Scatchard form using 30 960 M^{-1} cm^{-1} as the molar extinction coefficient of distamycin A, and treated with the DeltaGraph curve fitting routine using the McGee and von Hippel equation.

Gel Shift Assay of the Binding to Lectins. Solutions of native DNA and DNA-BH-Lac-14 (4.2 μM bases) were incubated with various concentrations of lectins in PBS (pH 7.4) at 25 °C for 30 min. Electrophoresis of the solutions and a marker (ϕx174 DNA-*Hin*fI digest) was carried out on 2% agarose gel in TBE buffer at 25 °C at 100 V. The gels were stained with ethidium bromide and imaged with a transilluminator (Atto AB-1500 transilluminator) equipped with 1D Image Analysis Software Mac ver. 2.0 (Kodak Digital Science).

Fluorescence Assay for the Binding to Lectins. To a solution of RCA_{120} lectin (0.103 μM, 3.0 mL) in PBS (pH 7.4) were added 1 μL aliquots of a stock solution of 1.75 μM base DNA−Lac conjugate and native DNA in PBS every 10 min at 25 °C. Fluorescence spectra (300−450 nm) excited at 295 nm were recorded at 25 °C.

RESULTS AND DISCUSSION

Preparation of DNA−Carbohydrate Conjugates. Scheme 1 shows the synthesis of diazo compounds bearing lactose and cellobiose through two different spacer groups. Lactose and cellobiose were treated with an excess amount of ammonium hydrogen carbonate in water, and the resulting β-glycosylamines **1** were amidated with the carboxylate derivatives bearing a nitrophenyl function at the terminal to provide **2** and **5**. The nitro group was hydrogenated and treated with $NaNO_2$ and HCl to provide the diazo compounds **4** and **7**.

Salmon testes DNA was fragmented by sonication to 150−300 base pairs and allowed to react with an excess amount of freshly prepared diazo compounds **4** and **7** in borate buffer (pH 9.0) at 25 °C (Scheme 2). The crude DNA conjugates were purified several times by precipitation into ethanol and ion-exchange column

Scheme 2. Preparation of DNA−carbohydrate Conjugates

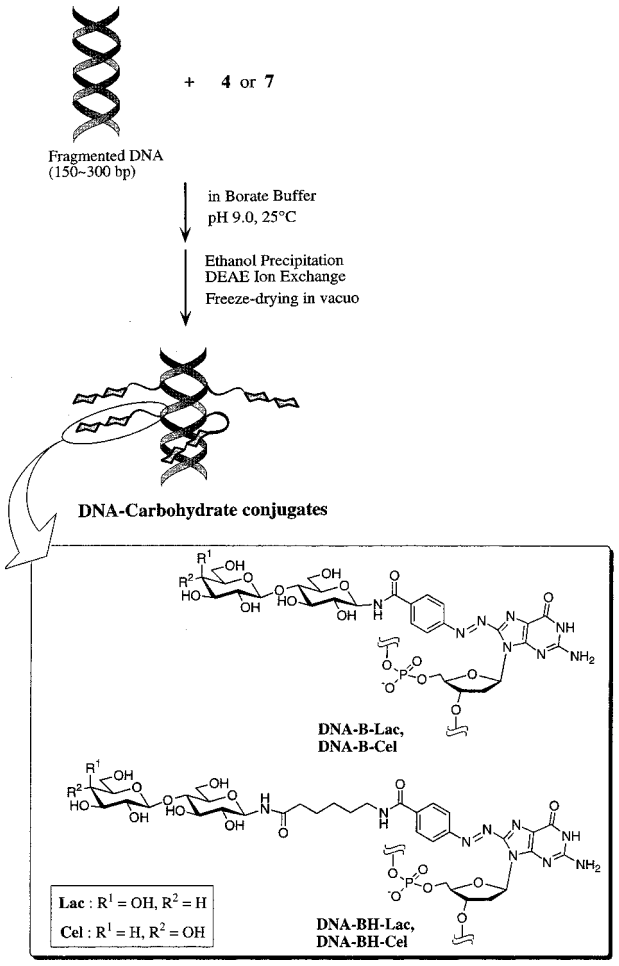

Table 1. Diazocoupling of Lactose Derivatives to Salmon Testes DNA

entry	DNA (mg)	lactose derivative [mg (mmol)]	time (min)	DNA-Lac conjugate yield (mg)	DNA-Lac conjugate Lac/base (mol %)
1	2.00	**4** 175 (0.38)	15	1.34	17
2	2.00	**4** 175 (0.38)	30	0.96	25
3	2.00	**4** 350 (0.75)	30	2.31	38
4	2.00	**7** 433 (0.75)	30	1.87	14
5	2.00	**7** 865 (1.51)	100	1.71	21

[a] Diazocoupling was carried out in 0.2 M borate buffer (pH 9.0, 20 mL) at 25 °C.

chromatography to provide yellowish fibers. The lactose contents in the conjugates were determined by colorimetry using galactoseoxidase and peroxidase as enzymes, *o*-dianisidine as a substrate dye, and poly(*p*-vinylbenzamido-*β*-lactose) (PNLac) as a standard (*48*). The results of diazo coupling of lactose derivatives to fragmented salmon testes DNA are summarized in Table 1. Increasing amount of lactose derivatives and elongation of the reaction time increased the lactose contents in the conjugates. Under the same reaction condition (entry 3 and 4), the diazo compound **4** with the benzoyl spacer was introduced in larger quantities than **7** with the benzoylaminohexanoyl spacer. DNA−cellobiose conjugates were obtained similarly. These DNA−carbohydrate conjugates are coded as DNA-B-Lac-n, DNA-BH-Lac-n, and DNA-B-Cel-n, where B and BH stand for the benzoyl and benzoylaminohexanoyl spacer respectively, and n stands for the disaccharide content in a nucleobase.

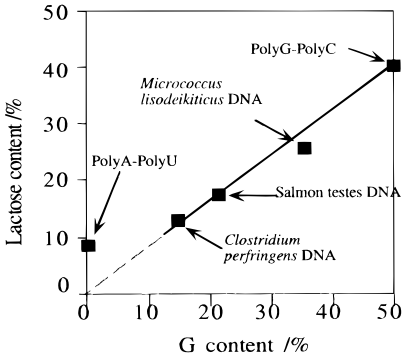

Figure 1. Relationship between the guanine content of nucleic acids and the lactose content introduced. The reaction condition was the same as entry 1 in Table 1.

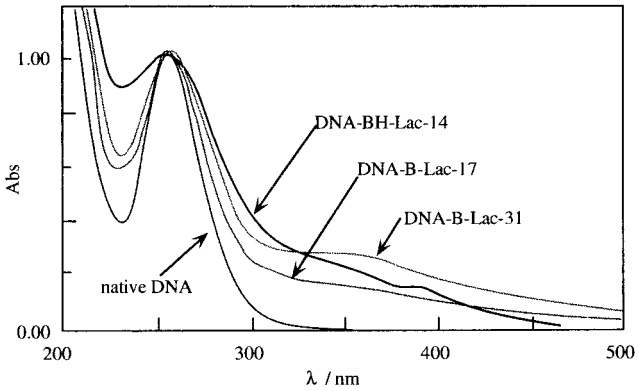

Figure 2. UV−vis spectra of DNA−carbohydrate conjugates at a concentration of 1.2×10^{-4} M base in water, pH 7.0.

To speculate the position of the reaction, the diazo coupling of lactose derivative **4** was carried out under the same reaction condition using native DNA duplexes bearing various G contents [salmon testes (G content = 20.5%), *Closteridium perfringens* (G content = 15.5%), and *Micrococcus lisodeikiticus* (G content = 36.0%)] and synthetic RNA duplexes (polyG-polyC and polyA-polyU). The lactose contents introduced were determined and are plotted against the G content in Figure 1. The lactose contents were directly proportional to the guanine contents in the nucleic acids, except polyA-polyU. We assume that the diazo coupling of the lactose derivative **4** to these DNAs, except polyA-polyU, proceeded selectively at guanine bases, as reported in the literature (*44*−*46*). It was also reported that diazo compounds could attack adenine bases much more slowly than guanine bases (*45*, *46*). We speculate that the repeating adenine bases in polyA-polyU might have higher reactivity than the isolated adenine bases along the other DNA chains and, hence, an amount of lactose derivatives were substituted to polyA-polyU.

The conjugates from salmon testes DNA were used in the following characterizations.

UV−Vis and CD Spectra. Figure 2 compares the UV−vis spectra of DNA-B-Lac and DNA-BH-Lac with the native DNA. There appeared an absorption band at 260 nm attributable to the nucleobase and also a broad absorption band above 300 nm attributable to the azophenyl group. The conjugates with the higher lactose content gave the larger absorbance of the broad band. The cellobiose content in DNA−cellobioses conjugate could not be determined by the colorimetry using galactoseoxidase, but the UV−vis spectra were similar to those of the DNA−lactose conjugate prepared in the same reaction condition.

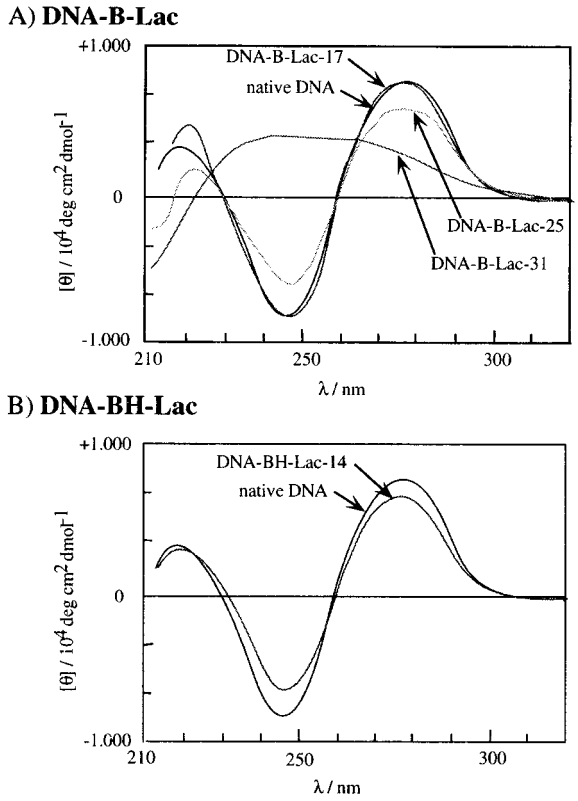

Figure 3. CD spectra of (A) DNA-B-Lac and (B) DNA-BH-Lac at a concentration of 7.3×10^{-5} M base in 0.25 mM NaCl at 25 °C.

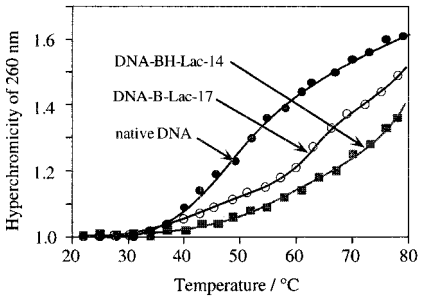

Figure 4. Melting behaviors of DNA−carbohydrate conjugates. Temperature dependency of hyperchromicity at 260 nm was recorded at a heating rate of 3.0 °C/5 min at a concentration of 67 μM nucleobase in H_2O (3.0 mL), pH 7.0.

The conjugate of the lower lactose content (DNA-B-Lac-17, DNA-B-Lac-25, and DNA-BH-Lac-14) showed the typical CD pattern of B-type DNA duplex (Figure 3). The modification little affected the DNA conformation. In addition, none of ellipticity was detected above 300 nm, suggesting that the introduced azophenyl groups are placed outside of the DNA duplex and in random directions. However, the CD spectrum of DNA-B-Lac-31 showed a positive peak around 220−300 nm, indicating that the higher lactose substitution transformed the DNA conformation partly to A-type duplex.

Melting Behavior. The melting curves of DNA-B-Lac-17 and DNA-BH-Lac-14 in water were broaden and shifted to higher temperature (about 15 and 20 °C, respectively) than that of native DNA (Figure 4). Since the DNA conjugates (DNA-B and DNA-BH) modified with azophenyl groups bearing no carbohydrate moiety gave similar melting curves, respectively, to DNA-B-Lac-17 and DNA-BH-Lac-14 (the data not shown), the stabilization of the conjugates may be caused largely by the azophenyl groups. DNA-B-Lac-17 was less stable

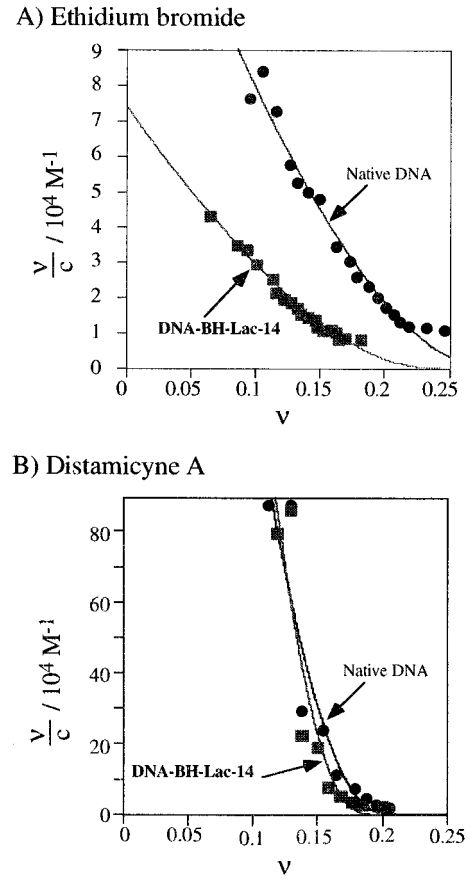

Figure 5. Scatchard plots for binding of (A) ethidium bromide and (B) distamycin A to native DNA and DNA-BH-Lac-14. (A) Changes of absorption at 480 nm were recorded by adding DNA to a solution of ethidium bromide (25.4 μM) in 0.1 mM Tris-HCl buffer with 0.1 M NaCl (pH 8.0). (B) Changes of absorption at 303 nm were recorded by adding DNA to a solution of distamycin A (12.5 μM) in 10 mM Tris-HCl buffer (pH 7.0). The solid curves were theoretically derived from the curve fitting according to eq 1.

Table 2. Association Constants (K_a) and Binding-Site Sizes (n) in Binding of Ethidium Bromide and Distamycin A to Native DNA and DNA−Lactose Conjugate

	ethidium bromide		Distamycin A	
	K_a (M^{-1})	n	K_a (M^{-1})	n
native DNA	1.7×10^5	3.3	4.1×10^4	4.6
DNA-BH−Lac-14	7.4×10^4	3.9	5.8×10^4	5.0

than DNA-BH-Lac-14 of a similar lactose content, suggesting that the lactose moiety linked through no spacer group may cause the larger steric hindrance to the DNA duplex.

Binding of Intercalator and Groove Binder. Binding of an intercalator ethidium bromide and a groove binder distamicyn A to the conjugates was investigated to identify the location of the introduced carbohydrate in DNA duplex. Figure 5 compares the Scatchard plots for the binding of (A) ethidium bromide and (B) distamicyn A to DNA-BH-Lac-14 and native DNA. Ethidium bromide exhibited quite different curves upon binding to the conjugated DNA and to native DNA, whereas distamycin A exhibited almost the same curves to the conjugated DNA and to native DNA. The association constants (K_a) and the binding site sizes (n) in Table 2 were calculated by curve fitting according to the McGhee and von Hippel eq 1 (*49*),

$$\frac{\nu}{c} = K_a(1 - n\nu)\left[\frac{1 - n\nu}{1 - (n - 1)\nu}\right]^{n-1} \quad (1)$$

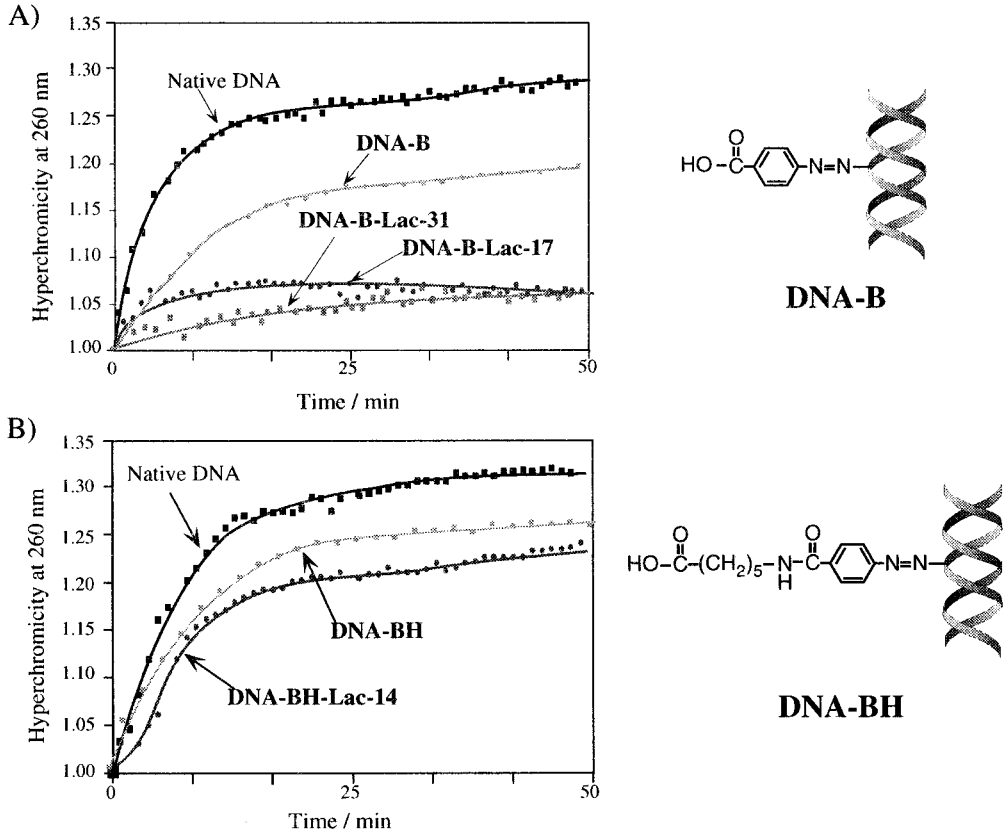

Figure 6. (A) Nuclease digestion of native DNA, DNA-B-Lac-17, DNA-B-Lac-31, and DNA-B by DNase I. (B) Nuclease digestion of native DNA, DNA-BH-Lac-14, and DNA-BH by DNase I. Each sample (64 μM base) was incubated at 25 °C with DNase I from bovine pancreas (27 units/mL) in 3.0 mL of 83 mM AcONa buffer, pH 5.0, containing 25 mM NaCl and 4 mM $MgSO_4$.

where v is the concentration ratio of the bound ligand in the total nucleobase and c is the concentration of the free ligand. The association constant of ethidium bromide to DNA-BH-Lac-14 was about half that of native DNA, whereas the association constant of distamycin A to the conjugate was comparable to that of native DNA. Since ethidium bromide is known to be intercalated from the major groove side, it is suggested that the lactose residues are located along the major groove of DNA duplex with little affecting the minor groove.

Resistance to Nucleases. Digestion of DNA−Lac conjugates with an endonuclease DNase I and an exonuclease III was monitored with the hyperchromicity at 260 nm, as diagramed in Figures 6 and 7, respectively. The DNA conjugates (DNA-B and DNA-BH) carrying no carbohydrate moiety but the two different spacer groups were used together with native DNA for comparison. Significant resistance against DNase I was acquired by the DNA-B-Lac conjugates, and about two-thirds of digestion of native DNA was observed even for DNA-B conjugate (Figure 6A). When the spacer group became longer (DNA-BH-Lac and DNA-BH) (Figure 6B), the resistance was suppressed to some extent in a whole range of the courses. It suggests that the lactose moiety locating apart from DNA through the longer spacer gave less effect to the digestion with DNase I.

The digestion of DNA-B-Lac with exonuclease III was resisted to larger extent (Figure 7A): almost no digestion was observed for DNA-B-Lac and about a half of digestion of native DNA for DNA-B conjugate. While DNA-BH conjugate showed little resistance against exonuclease III, DNA-BH-Lac-14 exhibited effective resistance (Figure 7B). The digestion of DNA-BH-Lac conjugate was significantly suppressed with exonuclease III than with DNase I. We assume that exonuclease III is more sensitive to the steric hindrance than DNase I, since exonuclease III digests the DNA duplex from 5′ end whereas DNase I digests the duplex randomly.

Binding Affinity to Lectins. Gel shift assay of the DNA-BH-Lac-14 conjugate in the presence of β-galactose specific RCA_{120} lectin and α-mannose/α-glucose specific concanavalin A (Con A) was carried out (Figure 8). The electrophoretic mobility of the DNA-Lac conjugate was almost the same as that of native DNA, indicating that the modification of DNA with sugars affected little the character of DNA as an anionic polymer. When DNA-BH-Lac-14 was incubated with RCA_{120} at the concentrations higher than 5 μM (Figure 8A), there appeared a less-mobile band, indicating that the DNA-Lac conjugate was bound to RCA_{120} at the concentration to conceal minus charges on DNA. Such a band was not observed when native DNA was mixed with 56 μM of RCA_{120} (Figure 8B) and also when DNA-BH-Lac-14 was mixed even with much higher concentration (500 μM) of Con A (Figure 8C). The DNA-BH-Lac-14 was specifically bound to the β-galactose-binding lectin.

Binding affinity of the conjugates to RCA_{120} has been estimated quantitatively by the fluorometry using tryptophan chromophore of the lectin. As shown in Figure 9A, addition of an increasing amount of DNA-BH-Lac-14 decreased the fluorescence intensity of the tryptophan at 332 nm with an excitation at 295 nm and evolved a new fluorescence band at 410 nm. The fluorescence spectra of DNA-BH-Lac-14 itself induced a fluorescence band at 410 nm when excited at 295 nm, and the band was shifted to 440 nm when excited at 332 nm, which is the emission wavelength of RCA_{120}. It is reasonable to assume that the decrease in intensity at

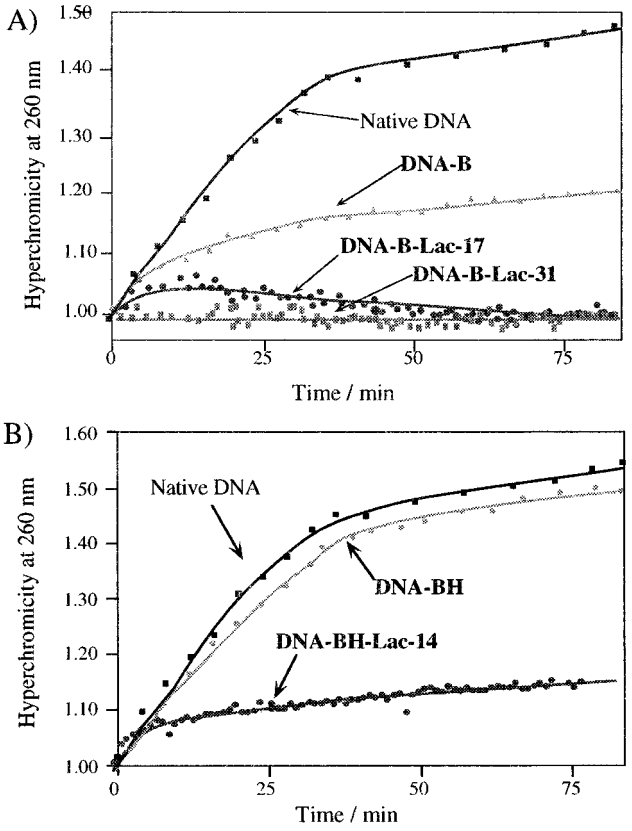

Figure 7. (A) Nuclease digestion of native DNA, DNA-B-Lac-17, DNA-B-Lac-31, and DNA-B by exonuclease III. (B) Nuclease digestion of native DNA, DNA-BH-Lac-14, and DNA-BH by exonuclease III. Each sample (64 μM base) was incubated at 37 °C with exonuclease III from *Escherichia coli* (50 units/mL) in 3.0 mL of 50 mM Tris-HCl buffer, pH 7.6, containing 1 mM $MgCl_2$ and 1 mM 2-mercaptoethanol.

332 nm in Figure 9A is caused by the energy transfer from the tryptophan of the lectin to the conjugate and that the new fluorescence at 410 nm is the superposition of the energy transfer and emission by the direct excitation of the conjugate at 295 nm.

Table 3. Association Constants (K_a) and Maximum Quenching ($-\Delta F_{max}/F_0$) in Binding of DNA-Carbohydrate Conjugate to RCA_{120}

compd	K_a (M^{-1})	$-\Delta F_{max}/F_0$
DNA-B-Lac-17	3.8×10^4	0.67
DNA-B-Lac-31	6.2×10^4	0.97
DNA-BH-Lac-14	2.4×10^5	0.56
DNA-BH-Lac-21	6.2×10^4	0.72
DNA-B-Cel[a]	$<10^2$	
DNA-BH-Cel[a]	$<10^2$	
PVLA	3.2×10^4	0.27
lactose	$<10^2$	

[a] Content of cellobiose is about 14% from UV spectra.

The decrement of fluorescence intensity ($\Delta F/F_0$) at 332 nm was plotted against the concentration of nucleobase. Since a small amount of quenching was induced by native DNA itself, the fluorescence decrement of the conjugate was normalized by subtracting the nonspecific quenching to provide a saturation curve against the lactose concentration (Figure 9B). The binding between the conjugate and Con A obtained by the same treatment was quite small. Thus, the conjugate was bound specifically to RCA_{120}. The saturation curve was treated with eq 2

$$\frac{F_0}{\Delta F}[\text{sugar}] = \frac{F_0}{\Delta F_{max} K_a} + \frac{F_0}{\Delta F_{max}}[\text{sugar}] \qquad (2)$$

to give a linear relationship (Figure 9C). Apparent affinity constant K_a and maximum quenching ratio $-\Delta F_{max}/F_0$ were calculated from the intercept and slope as summarized in Table 3.

DNA-Lac conjugates were bound to RCA_{120} lectin with relatively high affinities $K_a = 10^4 - 10^5$ M^{-1}, which are comparable to those of lactose-carrying polystyrene (PVLA) (*13*). On the other hand, lactose itself, DNA-B-Cel, and DNA-BH-Cel were little bound to RCA_{120}. Thus, RCA_{120} recognized the clustered or multivalent β-galactoside residues along the DNA backbone. The DNA-BH-Lac-14 conjugate had the highest apparent affinity constant $K_a = 2.4 \times 10^5$ M^{-1} among these DNA-Lac conjugates. The appropriate spacer and lactose content are required for the strong binding of the conjugate to the lectin.

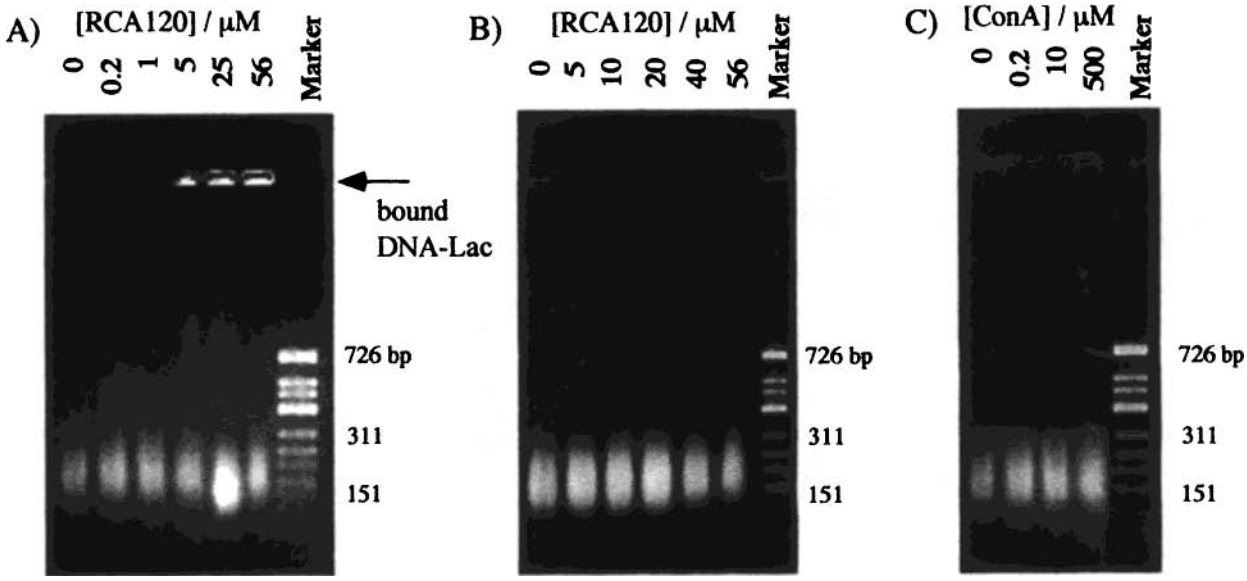

Figure 8. Gel shift assay of (A) DNA-BH-Lac-14 in the presence of RCA_{120}, (B) native DNA in the presence of RCA_{120}, (C) DNA-BH-Lac-14 in the presence of Con A. Interaction with the lectins was carried out in PBS ([nucleobase] = 4.2 μM) at 25 °C for 30 min, followed by electrophoresis on 2% agarose gel in TBE buffer at 100 V at 25 °C. The gels were stained with ethidium bromide.

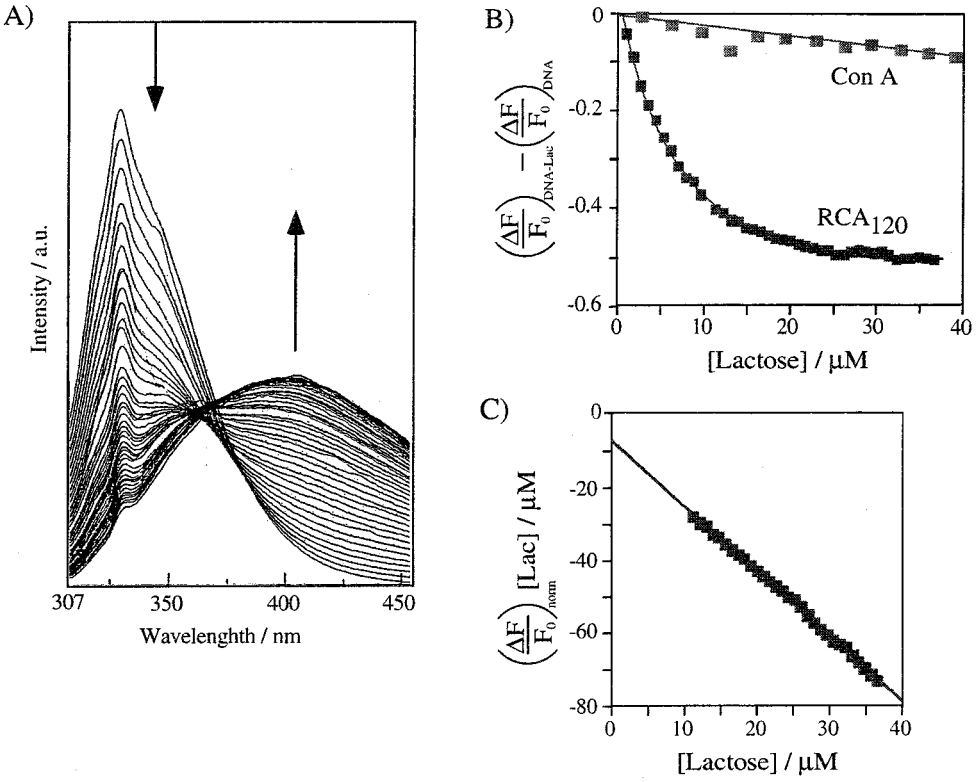

Figure 9. (A) Changes in fluorescence spectra of RCA_{120} (initial concentration = 0.103 μM in 3.0 mL of phosphate buffer saline solution, pH 7.4, 25 °C, excitation at 295 nm) with addition of 0.5 μL aliquots of DNA-BH-Lac-14 (0.87 μM lactose residue). (B) Dependence of the normalized fluorescence intensity $[(\Delta F/F_0)_{DNA-Lac}-(\Delta F/F_0)_{DNA}]$ of RCA_{120} and Con A on the concentration of sugar moiety of DNA-BH-Lac-14. (C) Linearlized plot according to eq 2 for interaction between DNA-BH-Lac-14 and RCA_{120}.

CONCLUSION

We have developed a facile chemical method to modify DNA with oligosaccharide derivatives. The degree of substitution by diazocoupling was directly proportional to the G contents of DNAs of different origins, and a typical B-type conformation was kept in the conjugates of the lower lactose content (<25%). It is suggested that the diazocoupling took place selectively to guanine bases without affecting the higher-order structure of DNA. The conjugate showed higher melting temperature and stronger nuclease resistance than native DNA. Biological recognition ability also could be endowed to DNA, as evidenced by the specific binding to the galactose-specific RCA_{120} lectin ($K_a = 10^4-10^5\ M^{-1}$). These functions of oligosaccharide substituents as physicochemical modifiers and as biological recognition markers in DNA–oligosaccharides conjugates are comparable to those in naturally occurring glycoproteins.

We also expect that the modification of DNA with cell-recognizable oligosaccharide ligands will find a wide variety of clinical applications for gene therapy. Enhancement of structural stability and nuclease resistance of DNAs in cells is essential to develop long-term gene therapy. The present DNA–oligosaccharide conjugates have been found not only to enhance the structural stability and nuclease resistance but also to acquire lectin recognition ability. We have recently reported that plasmid DNAs could be modified randomly with a lactose derivative via diazocoupling and the resulting plasmid DNA–lactose conjugates could be transformed to mRNA and translated to the corresponding protein (*50*). Therefore, the present simple modification of DNA with oligosaccharides via diazo coupling will be a useful and interesting protocol of molecular design for cell-targeted gene therapy.

ACKNOWLEDGMENT

This work was supported by Grant-in-Aid for Scientific Research on Priority Areas, “Biomolecular Design for Biotargeting” (296/10145223), from the Ministry of Science, Education, Sports, and Culture, Japan.

LITERATURE CITED

(1) Mountreuil, J., Vliegenthart, J. F. G., and Schachter, H. (1995) *Glycoproteins*, Elsevier.
(2) Fukuda, M., and Hindsgaul, O. (1994) *Molecular Glycobiology*, IRL, Oxford.
(3) Lee, Y. C., and Lee, R. T. (1995) Carbohydrate-protein interactions: basis of glycobiology. *Acc. Chem. Res. 28*, 321–327.
(4) Kiessling, L. L., and Pohl, N. L. (1996) Strength in numbers: nonnatural polyvalent carbohydrate derivatives. *Chem. Biol. 3*, 71–77.
(5) Mammen, M., Choi, S.-K., and Whitesides, G. M. (1998) Polyvalent interactions in biological systems: implications for design and use of multivalent ligands and inhibitors. *Angew. Chem., Int. Ed. 37*, 2754–2794.
(6) Lee, Y. C., and Lee, R. T., Eds. (1994) *Neoglycoconjugates: Preparation and Applications*, Academic Press, San Diego, CA.
(7) Bovine, N. V. (1998) Polyacrylamide-based glycoconjugates as tools in glycobiology. *Glycoconjugate J. 15*, 431–446.
(8) Nishimura, S., and Lee, Y. C. (1998) Synthetic glycopolymers: new tools for glycobiology. In *Polysaccharides* (S. M. Dekker, Ed.) pp 523–538, Dumitriu.
(9) Furuike, T., Nishi, N., Tokura, S., and Nishimura, S. (1995) Synthetic glycoconjugates. 6. Preparation and biochemical evaluation of novel cluster-type glycopolymers containing Galβ(1–4)GlcNAc residue. *Macromolecules 28*, 7241–7147.
(10) Sigal, G. B., Mammem, M., Dahmann, G., and Whitesides, G. M. (1996) Polyacrylamides bearing pendant α-sialoside groups strongly inhibit agglutination of erythrocytes by influenza virus: the strong inhibition reflects enhanced

binding through cooperative polyvalent interactions. *J. Am. Chem. Soc. 118*, 3789−3800.
(11) Manning, D. D., Hu, X., Beck, P., and Kiessling, L. L. (1997) Synthesis of sulfated neoglycopolymers: selective P-selectin inhibitors. *J. Am. Chem. Soc. 119*, 3161−3162.
(12) Kamitakahara, H.; Suzuki, T., Nishigori, N., Suzuki, Y., Kanie, O., and Wong, C.-H. (1998) Lyso GM3 ganglioside-poly-L-glutamic acid conjugate as inhibitor of influenza hemagglutinin. *Angew. Chem., Int. Ed. 37*, 1524−1528.
(13) Kobayashi, K., Sumitomo, H., and Ina, Y. (1985) Synthesis and functions of polystyrene derivatives having pendant oligosaccharides. *Polymer J. 17*, 567−575.
(14) Kobayashi, K., Tsuchida, A., Usui, T., and Akaike, T. (1997) A new type of artificial glycoconjugate polymers: a convenient synthesis and their interaction with lectins. *Macromolecules 30*, 2016−2020.
(15) Kobayashi, K., Tawada, E., Akaike, T., and Usui, T. (1997) Artificial glycopolypeptide conjugates: simple synthesis of lactose- and N,N′-diacetylchitobiose-substituted poly(glutamic acid)s through N-β-Glycoside linkage and their interaction with lectins. *Biochim. Biophys. Acta 1336*, 117−122.
(16) Matsuura, K., Tsuchida, A., Okahata, Y., Akaike, T., and Kobayashi, K. (1998) A quartz-crystal microbalance study of adsorption behaviors of artificial glycoconjugate polymers onto chemically modified gold surfaces and their interactions with lectins. *Bull. Chem. Soc. Jpn. 71*, 2973−2977.
(17) Suzuki, N., Quesenberry, M. S., Wang, J. W., Lee, R. T., Kobayashi, K., and Lee, Y. C. (1997) Effecient immobilization of proteins by modification of plate surfaces with polystyrene derivatives. *Anal. Biochem. 247*, 412−416.
(18) Oubihi, M., Kitajima, K., Kobayashi, K., Adachi, T., Aoki, N., and Matsuda, T. (1998) Development of an enzyme-linked immunosorbent assay-based method for measuring galactosyltransferase activity using a synthetic glycopolymer acceptor substrate. *Anal. Biochem. 257*, 169−175.
(19) Zanini, D., and Roy, R. (1997) Synthesis of new α-thiosialodendrimers and their binding properties to the sialic acid specific lectin from limax flavus. *J. Am. Chem. Soc. 119*, 2088−2095.
(20) Hansen, H. C., Haataja, S., Finne, J., and Magnusson, G. (1997) Di-, tri-, and tetravalent dendritic galabiosides that inhibit hemagglutination by streptococcus suis at nanomolar concentration. *J. Am. Chem. Soc. 119*, 6974−6979.
(21) Aoi, K., Ito, K., and Okada, M. (1995) Globular carbohydrate macromolecule "sugar balls". 1. synthesis of novel sugar-persubstituted poly(amido amine) dendrimers. *Macromolecules 28*, 5391−5393.
(22) Fujimoto, T., Shimizu, C., Hayashida, O., and Aoyama, Y. (1997) Solution-to-surface molecular-delivery system using a macrocyclic sugar cluster. Sugar-directed adsorption of guest in water on polar solid surfaces. *J. Am. Chem. Soc. 119*, 6676−6677.
(23) Fujimoto, T., Shimizu, C., Hayashida, O., and Aoyama, Y. (1998) Ternary complexation involving protein. Molecular transport to saccharide-binding proteins using macrocyclic saccharide cluster as specific transporter. *J. Am. Chem. Soc. 120*, 601−602.
(24) Roy, R., and Kim, J. M. (1999) Amphiphilic *p-tert*-butylcalix[4]arene scaffolds containing exposed carbohydrate dendrons. *Angew. Chem., Int. Ed. 38*, 369−372.
(25) Lichtenstein, J., and Cohen, S. S. (1960) Nucleotides derived from enzymatic digests of nucleic acids of T2, T4, and T6 bacteriophages. *J. Biol. Chem. 235*, 1134−1141.
(26) Lehman, I. R., and Pratt, E. A. (1960) On the structure of the glucosylated hydroxymethylcytosine nucleotides of coliphages T2, T4, and T6. *J. Biol. Chem. 235*, 3254−3259.
(27) Hsu, F. F., Crain, P. F., McCloskey, J. A., Swinton, D. L., and Hattman, S. (1989) Characterization of glycosylated hydroxydeoxycytidine derivatives from bacteriophage RL38JI DNA. *Adv. Mass Spectrom 11B*, 1450−1451.
(28) Ehrlich, M., and Ehrlich, K. C. (1981) A novel, highly modified, bacteriophage DNA in which thymine is partly replaced by a phosphoglucuronate moiety covalently bound to 5-(4′,5′-dihydroxypentyl)uracil. *J. Biol. Chem. 256*, 9966−9972.
(29) Gommers-Ampt, J., Leeuwen, F. V., De Beer, A. L. J., Viliegenthart, J. F. G., Dizdarouglu, M., Kowalak, J. A., Crain, P. F., and Borst, P. (1993) β-D-glucosyl-hydroxymethyluracil: A novel modified base present in the DNA of the parasitic protozoan T. brucei. *Cell 75*, 1129−1136.
(30) McClosky, J. A., and Nishimura, S. (1977) Modified nucleosides in transfer RNA. *Acc. Chem. Res. 10*, 403−410.
(31) Kasai, H., Nakanishi, K., Macfarlane, R. D., Torgerson, D. F., Ohashi, Z., McClosky, J. A., Gross, H. J., and Nishimura, S. (1976) The structure of Q* nucleoside isolated from rabbit liver transfer ribonucleic acid. *J. Am. Chem. Soc. 98*, 5044−5046.
(32) Okada, N., Shindo-Okada, N., and Nishimura, S. (1977) Isolation of mammalian $tRNA^{Asp}$ and $tRNA^{Tyr}$ by lectin-Sepharose affinity column chromatography. *Nucleic Acids Res. 4*, 415−423.
(33) Wiberg, J. S. (1967) Amber mutants of bacteriophage T4 defective in deoxycytidine diphosphatase and deoxycytidine triphosphatase. *J. Biol. Chem. 242*, 5824−5829.
(34) Wadhwa, M. S., and Rice, K. G. (1995) Receptor mediated glycotargeting. *J. Drug Target. 3*, 111−127.
(35) Midoux, P., Mendes, C., Legrand, A., Raimond, J., Mayer, R., Monsigny, M., and Roche, A. C. (1993) Specific gene transfer mediated by lactosylated poly-L-lysine into hapatoma cells. *Nucleic Acids Res. 21*, 871−878.
(36) Erbacher, P., Bousser, M.-T., Raimond, J., Monsigny, M., Midoux, P., and Roche, A. C. (1996) Gene transfer by DNA/glycosylated polylysine complexes into human blood monocyto-derived macrophages. *Hum. Gene Ther. 7*, 721−729.
(37) Erbacher, P., Roche, A. C., Monsigny, M., and Midoux, P. (1996) Putative role of chloroquine in gene transfer into a human hepatoma cell line by DNA/lactosylated polylysine complexes. *Exp. Cell Res. 225*, 186−194.
(38) Kollen, W. J. W., Midoux, P., Erbacher, P., Yip, A., Roche, A. C., Monsigny, M., Glick, M. C., and Scanlin, T. F. (1996) Gluconoylated and glycosylated polylysine as vectors for gene transfer into cystic fibrosis airway epithelial cells. *Hum. Gene Ther. 7*, 1577−1586.
(39) Perales, J. C., Grossmann, G. A., Molas, M., Liu, G., Ferkol, T., Harpst, J., Oda, H., and Hanson, R. W. (1997) Biochemical and functional characterization of DNA complexes capable of targeting genes to hepatocytes via the asialoglycoprotein receptor. *J. Biol. Chem. 272*, 7398−7407.
(40) Erbacher, P., Roche, A. C., Monsigny, M., and Midoux, P. (1997) The reduction of the positive charges of polylysine by partial gluconoylation increases the transfection efficiency of polylysine/DNA complexes. *Biochim. Biophys. Acta 1324*, 27−36.
(41) Akhtar, S., Routledge, A., Patel, R., and Gardiner, J. M. (1995) Synthesis of mono- and dimannoside phosphoramidite derivatives for solid-phase conjugation to oligonucleotides. *Tetrahedron Lett. 36*, 7333−7336.
(42) Gao, Y., Robinson, H., Wijsman, E. R., van der Marel, G. A., van Boom, J. H., and Wang, A. H.-J. (1997) Binding of daunorubicin to β-D-glucosylated DNA found in protozoa *Trypanosoma brucei* studied by X-ray crystallography. *J. Am. Chem. Soc. 119*, 1496−1497.
(43) Haensler, J., and Szoka, F. C. (1993) Synthesis and characterization of a trigalactosylated bisacridine compound to target DNA to hepatocytes. *Bioconjugate Chem. 4*, 85−93.
(44) (a) Moudrianakis, E. N., and Beer, M. (1965) Base sequence determination in nucleic acids with the electron microscope, III. chemistry and microscopy of guanine-labeled DNA. *Biochemistry 53*, 564−571.
(45) Moudrianakis, E. N., and Beer, M. (1965) Determination of base sequence in nucleic acids with the electron microscope, II. the reaction of a guanine-selective marker with the mononucleotides. *Biochim. Biophys. Acta 95*, 23−39.
(46) Rothenberg, J. M., and Wilchek, M. (1988) *p*-Diazobenzoylbiocytin: a new biotinylating reagent for DNA. *Nucleic Acids Res. 16*, 7197.
(47) Preliminary report: Matsuura, K., Akasaka, T., Hibino, M., and Kobayashi, K. (1999) Synthesis of DNA-carbohydrate conjugate via diazocoupling: a new class of modified DNA with enhanced stability and lectin-recognition ability. *Chem. Lett.*, 247−248.

(48) Avigard, G., Amaral, D., Asensio, C., and Horecker, B. C. (1962) The D-galactose oxidase of Polyporus circinatus. *J. Biol. Chem. 237*, 2736−2743.
(49) McGhee, J. D., and von Hippel, P. H. (1974) Theoretical aspects of DNA-protein interactions: cooperative and non-cooperative binding of large ligands to a one-dimensional homogeneous lattice. *J. Mol. Biol. 86*, 469−489.
(50) Akasaka, T., Matsuura, K., Emi, N., and Kobayashi, K. (1999) Conjugation of plasmid DNAs with lactose via diazo coupling enhances resistance to restriction enzymes and acquires binding affinity to galactose specific lectin. *Biochem. Biophys. Res. Commun. 260*, 323−328.

BC9901191

Application to a Cartilage Targeting Strategy: Synthesis and in Vivo Biodistribution of ^{14}C-Labeled Quaternary Ammonium−Glucosamine Conjugates

Isabelle Giraud, Maryse Rapp, Jean-Claude Maurizis, and Jean-Claude Madelmont*

INSERM Unité 484, Rue Montalembert, BP 184, 63005 Clermont-Ferrand Cedex, France. Received October 1, 1999; Revised Manuscript Received November 29, 1999

As part of a cartilage targeting program based on the affinity of the quaternary ammonium (QA) moiety for cartilage, QA derivatives of D-glucosamine (DG), an antirheumatic drug exhibiting a natural tropism for cartilaginous tissues, were designed and evaluated by pharmacokinetic studies. Two QA−DG conjugates were synthesized and labeled with ^{14}C by cross-linking the QA entity (trimethylammonium or pyridinium) to [^{14}C]DG via an amide bond in a two-step procedure. After intravenous injection to male Sprague−Dawley rats, the two ^{14}C-labeled conjugates exhibited similar pharmacokinetic profiles, but their behavior clearly differed from that of unconjugated DG in several ways. (i) The tissue distribution for the conjugates was more restricted, with a decreased radioactivity level for whole tissues except for kidney, cartilage, and skin. (ii) The radioactivity concentrated more rapidly and strongly in cartilage for the conjugates than for DG for the short times after injection; on the other hand, 1 h after administration, the radioactivity level in cartilage was higher for DG, this result being consistent with the tropism already observed for this compound. (iii) Both conjugates were eliminated predominantly by the urinary route (85%); the radioactivity level in urine for DG was lower (45% of the injected dose), and significant $^{14}CO_2$ was found in expired air, indicating metabolization and utilization of DG for energy-consuming processes. (iv) Blood and plasma kinetics studies displayed an enterohepatic cycle for DG, whereas for the QA conjugates, a rapid disappearance was observed. (v) HPLC analyses of plasma and urine indicated a low degree of metabolization for the conjugates, most of the radioactivity recovered in urine and plasma corresponding to the unchanged molecule. This study demonstrates that the introduction of the QA moiety on DG modifies its biodistribution and lends it a greater specificity for cartilage, at least for short times after injection. These findings justify further work on QA derivatives of other antirheumatic agents.

INTRODUCTION

Current antirheumatic drugs including nonsteroidal antiinflammatory drugs (NSAIDs), corticosteroids, and disease-modifying antirheumatic drugs (DMARDs) often have severe adverse effects: gastrointestinal damage for NSAIDs, osteoporosis, and muscle weakness for corticosteroids and gastrointestinal distress, hepatic lesions, and lung injury for DMARDs (*1*−*3*). Safer agents are therefore being actively sought.

An alternative way to reduce the adverse reactions is to carry the drugs selectively to their target tissue. On this basis, we are currently conducting research on the targeting of cartilage. This project has been undertaken following previous pharmacokinetic work on ^{14}C-labeled acetylcholinesterase reactivators containing a quaternary ammonium (QA) moiety. This study clearly demonstrated a rapid and intensive concentration of these compounds in cartilaginous tissues after intramuscular injection (*4*, *5*). We next demonstrated on cultured chondrocytes that the high specificity for cartilage resulted from ionic interactions between the QA entity of the reactivators and the anionic sites (carboxylate and ester sulfate groups) of proteoglycans, a major component of cartilage (*6*). This result was consistent with earlier findings concerning the binding of cations to cartilage (*7*−*12*). We therefore hypothesized that the conjugation of the QA moiety with antirheumatic agents might strengthen their selectivity for cartilage, consequently minimizing their efficient doses and so reducing their side effects. To test this hypothesis, we developed a program to study several QA-antirheumatic drug conjugates (*13*). D-Glucosamine (DG) is one of the therapeutic agents we selected.

DG has recently emerged as an alternative treatment for patients with osteoarthritis (*14*−*17*). It is an aminomonosaccharide occurring naturally in almost all human tissues, largely in proteoglycans of articular cartilage, as it is an intermediate substrate used in the synthesis of these macromolecules (*18*). The normal source of DG is endogenous biosynthesis from glucose, but exogenous DG, if available, becomes the preferential source for the proteoglycan biosynthesis (*18*). DG is consequently readily incorporated into proteoglycan molecules and shows a special tropism for cartilaginous tissues (*18*−*20*). Beneficial pharmacologic properties reported for DG include antiarthritic and antiinflammatory activities and an ability to stimulate proteoglycan synthesis through chondrocyte activation (*21*−*24*). DG was of particular interest for us, not owing to its toxicity, DG having a favorable safety profile, but because of its naturally high tropism for cartilage. Enhanced cartilage specificity of the QA−DG derivatives compared with the parent drug would support our cartilage targeting strategy.

Here, we describe the preparation of two ^{14}C-labeled QA−DG conjugates and the comparative pharmacokinetic studies in rats of [^{14}C]DG and both ^{14}C-conjugates.

* To whom correspondence should be addressed. Phone: 33 4 73 15 08 00. Fax: 33 4 73 15 08 01. E-mail: madelmont@inserm484.u-clermont1.fr.

10.1021/bc990128+ CCC: $19.00 © 2000 American Chemical Society
Published on Web 02/17/2000

EXPERIMENTAL PROCEDURES

Syntheses. *General.* All chemicals were from commercial suppliers and used as received. The radiolabeled starting material, D-[1-^{14}C]glucosamine hydrochloride ([^{14}C]DG hydrochloride), was purchased from NEN Life Science Products (Boston, MA). Proton nuclear magnetic resonance (^{1}H NMR) and carbon nuclear magnetic resonance (^{13}C NMR) spectra were recorded at, respectively, 200.1 and 50.3 MHz on a Bruker AM 200 (4.5 T) spectrometer. Chemical shifts are reported in parts per million relative to the internal tetramethylsilane standard for ^{1}H NMR and the solvent for ^{13}C NMR (DMSO-d_6, $\delta = 39.5$ ppm). Coupling constants (J values) are given in hertz. Infrared (IR) spectra were recorded on a Bruker Vector 22 FTIR system. Electrospray ionization mass spectra (ESI-MS) and elemental analyses were performed by the CNRS Service Central d'Analyse (Vernaison, France). Elemental analyses for carbon, hydrogen, and nitrogen were within ±0.4% of theory for the formulas given. Melting points (mp) were determined on an Electrothermal digital apparatus and are uncorrected. Thin-layer chromatography (TLC) was conducted on precoated silica gel plates (Merck, 60 F254, 0.25 mm thick). Radiochemical purity was evaluated by scanning the TLC plates with an Ambis 4000 detector (B. Braun Sciencetec) and by high-performance liquid chromatography (HPLC) studies for final compounds. HPLC analyses were performed on an HP 100 system (Hewlet Packard, D76337 Waldbronn, Germany) equipped with a Partisil SCX analytical column (10 μm, 250 × 4.6 mm; Whatman, Clifton) and coupled with a 500TR flow scintillation analyzer (Packard Instrument S. A., Rungis, France). A solution of 0.2 M KH_2PO_4 acidified to pH 2.8 with H_3PO_4 was used as the mobile phase, with a flow rate of 1 mL/min. Specific activity of synthesized compounds was measured in a Wallac Winspectral 1414 liquid scintillation spectrometer (EGG Instruments, Evry, France), using Packard Ultima Gold liquid scintillation cocktail.

N-Chloroacetyl-α,β-D-[1-^{14}C]glucosamine. To a solution of [^{14}C]DG hydrochloride [1.95 g, 9.02 mmol, 1502 MBq (40.6 mCi), specific activity: 167 MBq/mmol (4.5 mCi/mmol)] and potassium carbonate (1.87 g, 13.53 mmol) in water (10 mL) was added chloroethanoyl choride (1.43 mL, 18 mmol) with stirring at 0 °C. After 1 h, the solution was evaporated under reduced pressure. The residue was washed with ethanol (3 × 50 mL). The ethanol solutions were then concentrated under reduced pressure until a white precipitate appeared. Filtration and recrystallization in ethanol afforded the *N*-chloroacetyl intermediate [1.31 g, 855 MBq (23.1 mCi), 57%] as a white solid. Specific activity: 167 MBq/mmol (4.5 mCi/mmol). Radiochemical purity was 97% as determined by TLC analysis (R_f = 0.54, dichloromethane/methanol/ammonium hydroxide 50/48/2). Analytical data for the unlabeled compound: mp 183−185 °C (dec); ^{1}H NMR (DMSO-d_6) δ 3.06−3.18 (m, 1H, H-4), 3.43−3.62 (m, 5H, H-2, H-3, H-5, H-6), 4.05 [s, 0.1H, CH_2(β)Cl], 4.11 [s, 1.9H, CH_2(α)Cl], 4.42−4.48 (m, 1.05H, H-1β, OH-6; after exchange with D_2O, d, J = 7.6, 0.05H, H-1β), 4.78 (d, J = 5.1, 0.95H, OH-3α), 4.92−4.98 (m, 2H, H-1α, OH-3β, OH-4; after exchange with D_2O, d, J = 3.1, 0.95H, H-1α), 6.57 (d, J = 4.4, 1H, OH-1), 7.98 (d, J = 7.7, 1H, NH); ^{13}C NMR (DMSO-d_6) δ 42.77 [CH_2(α)Cl], 43.10 [CH_2(β)Cl], 54.77 (C-2α), 57.54 (C-2β), 61.07 (C-6αβ), 70.47, 70.98 (C-3α C-4α), 70.79 (C-4β), 72.16 (C-5α), 74.03 (C-3β), 76.80 (C-5β), 90.37 (C-1α), 95.03 (C-1β), 165.79 (C=Oβ), 165.92 (C=Oα); ESI-MS m/z 257 and 259 [M(^{35}Cl,^{37}Cl) + H]$^+$; IR (KBr) ν (cm^{-1}) 1645 (C=O).

N-(Trimethylammonio)acetyl-α,β-D-[1-^{14}C]glucosamine Chloride ([^{14}C]TMG). A solution of the *N*-chloroacetyl derivative (639 mg, 2.35 mmol) and trimethylamine (5 mL of a 4.2 M solution in ethanol) under argon was warmed to 40 °C. A white precipitate appeared in a few hours. The reaction was complete after 3 days. The solution was then evaporated under reduced pressure. The resulting solid was washed with ethanol and then ether and dried to give [^{14}C]TMG [651 mg, 340 MBq (9.2 mCi), 87%] as a white solid. Specific activity: 167 MBq/mmol (4.5 mCi/mmol). Radiochemical purity was 96% as determined by HPLC analysis (retention time = 5.3 min). Analytical data for the unlabeled compound: mp 240−242 °C (dec); ^{1}H NMR (DMSO-d_6) δ 3.05−3.75 [m, 15H, H-2, H-3, H-4, H-5, H-6, N$^+$(CH_3)$_3$], 4.06 [s, 0.3H, CH_2-(β)N$^+$], 4.09 [s, 1.7H CH_2(α)N$^+$], 4.46−4.61 (m, 1.15H, H-1β, OH-6; after exchange with D_2O, d, J = 7.8, 0.15H, H-1β), 4.94−5.07 (m, 2.85H, H-1α, OH-3, OH-4; after exchange with D_2O, d, J = 3.1, 0.85H, H-1α), 6.66 (d, J = 4.0, 0.85H, OH-1α), 6.77 (d, J = 6.0, 0.15H, OH-1β), 8.51 (d, J = 8.0, 0.85H, NHα), 8.71 (d, J = 8.4 Hz, 0.15H, NHβ); ^{13}C NMR (DMSO-d_6) δ 53.35 [N$^+$(CH_3)$_3$], 54.56 (C-2α), 57.05 (C-2β), 60.90 (C-6αβ), 64.47 [CH_2(α)N$^+$], 64.88 [CH_2(β)N$^+$], 70.37, 70.80 (C-3α, C-4α), 70.63 (C-4β), 72.14 (C-5α), 73.94 (C-3β), 76.89 (C-5β), 90.14 (C-1α), 94.90 (C-1β), 162.80 (C=Oβ), 163.04 (C=Oα); IR (KBr) ν (cm^{-1}) 1660 (C=O); ESI-MS m/z 279 (M)$^+$; Anal. ($C_{11}H_{23}ClN_2O_6$·0.2H_2O) C, H, N.

N-Pyridinioacetyl-α,β-D-[1-^{14}C]glucosamine Chloride ([^{14}C]PG). A solution of the *N*-chloroacetyl derivative (600 mg, 2.35 mmol) in pyridine (30 mL) under argon was warmed to 40 °C. A white precipitate appeared in a few hours. The reaction was complete after 3 days. Pyridine was then evaporated under reduced pressure. The resulting solid was washed with ethanol and then ether and dried to give [^{14}C]PG [583 mg, 285 MBq (7.7 mCi), 73%] as a white solid. Specific activity: 167 MBq/mmol (4.5 mCi/mmol). Radiochemical purity was 96% as determined by HPLC analysis (retention time = 7.2 min). Analytical data for the unlabeled compound: mp 223−225 °C (dec); ^{1}H NMR (DMSO-d_6) δ 3.08−3.72 (m, 6H, H-2, H-3, H-4, H-5, H-6), 4.47−4.59 (m, 1.95H, H-1β, OH-6; after exchange with D_2O, d, J = 7.6, 0.95H, H-1β), 5.04−5.09 (m, 2.05H, H-1α, OH-3, OH-4; after exchange with D_2O, d, J = 2.9, 0.05H, H-1α), 5.45 (s, 2H, CH_2N$^+$), 6.71 (d, J = 6.0, 1H, OH-1), 8.18 (t, J = 7.6, 2H, aromatic protons), 8.61−8.69 (m, 2H, aromatic protons, NH; after exchange with D_2O, t, J = 7.7, 1H, aromatic proton), 8.97 (d, J = 6.0, 2H, aromatic protons); ^{13}C NMR (DMSO-d_6) δ 55.21 (C-2α), 58.02 (C-2β), 61.01 (C-6αβ), 61.78 (CH_2N$^+$), 70.31 (C-4β), 70.44 70.65 (C-3α C-4α), 72.12 (C-5α), 74.05 (C-3β), 76.86 (C-5β), 90.34 (C-1α), 94.83 (C-1β), 127.45, 146.00, 146.13 (aromatic carbons), 164.11 (C=Oβ), 164.33 (C=Oα); ESI-MS m/z 299 (M)$^+$; IR (KBr) ν (cm^{-1}) 1675 (C=O); Anal. ($C_{13}H_{19}ClN_2O_6$·0.3H_2O) C, H, N.

Pharmacokinetic Studies. *Tissue Distribution Study.* Tissue distribution analyses were performed in 4-week-old male Sprague−Dawley rats weighing 80−100 g (Iffa-Credo, L'Arbresle, France) by injection via the tail vein of each ^{14}C-labeled test compound [75 μmol g/kg, 1110 kBq (30 μCi) in 200 μL of physiological saline]. Animals were sacrified by ether inhalation 5, 15, and 30 min and 1, 2, 6, and 24 h after injection. Carcasses rapidly frozen by immersion in liquid nitrogen were then embedded in a 2% gel of carboxymethyl cellulose. The resulting carboxyl methylcellulose block was sagittally sectioned at −22 °C with a Reichert-Jung Cryopolycut cryomicrotome (Heidelberg, Germany). When section surfaces of interest appeared, the corresponding 40-μm-thick slices

Scheme 1[a]

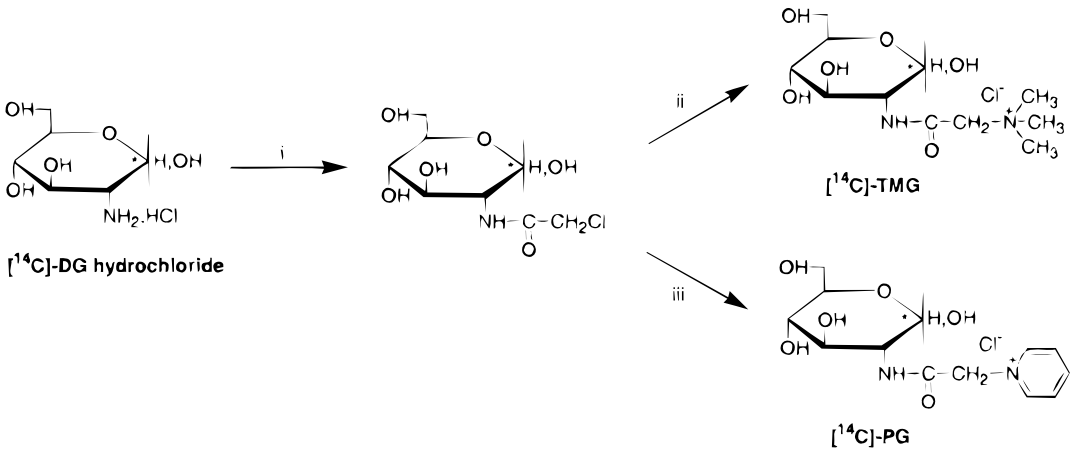

[a] (i) $ClCOCH_2Cl$, K_2CO_3, H_2O, 0 °C; (ii) trimethylamine (4.2 M solution in ethanol), 40 °C; (iii) pyridine, 40 °C.

were taken using no. 810 Scotch band tape (3 M, Saint Paul, MN) and dried for 48 h at −22 °C. These selected slices (n = 8 for each time studied) were subsequently analyzed with the Ambis 4000 detector (described in the chemical part), which allows visualization and quantification of the radioactivity distribution in whole-body sections (*25*). The results of these tissue distribution analyses were expressed as the percentage of the injected dose of radioactivity per gram of tissue (*25*).

Blood and Plasma Kinetics Study. Blood and plasma kinetics experiments were performed as decribed above for tissue distribution studies. Rats were exsanguinated by a cardiac puncture (n = 3 for each time studied). Plasma and red cells were separated by centrifugation (Rotanta RP, Hettish, Tuttlingen, Germany). The radioactivity in blood and plasma samples was counted in a Wallac Winspectral 1414 liquid scintillation spectrometer. The results were expressed as the percentage of the injected dose of radioactivity per gram of blood or plasma.

Excretion Study. The excretion study was conducted in 6-week-old male Sprague−Dawley rats weighing 180−200 g by intravenous injection of each ^{14}C-labeled test compound [75 μmol g/kg, 555 kBq (15 μCi) in 200 μL of physiological saline]. Urine and feces were collected by housing animals (n = 5 for each test compound) in a metabolic cage (Iffa-Credo, L'Arbresle, France) for 24, 48, and 72 h after administration. For the collection of expired [^{14}C]CO_2, animals (n = 1 for each test compound) were housed in an apparatus designed by us to trap [^{14}C]-CO_2 with a flask containing a solution of ethanolamine/methanol (20:80 v/v). Radioactivity of urine and ethanolamine/methanol samples was directly measured after addition of Packard Ultima Gold scintillation cocktail in the Wallac Winspectral 1414 liquid scintillation spectrometer. Radioactivity of feces was counted after combustion in a Packard 306 Oxidizer (Packard Instrument SA, Rungis, France). The results are given as percentages of the injected dose.

Metabolism Study. Plasma samples were deproteinized by treatment with methanol (1:7 v/v). After stirring and centrifugation, the supernatant was evaporated under reduced pressure. The resulting dry residue was dissolved in the HPLC eluent and analyzed by HPLC (conditions described in the chemical part). The urine samples were also analyzed by HPLC after filtration through Dynagard syringe filters (Spectrum Microgon, Laguna Hills, CA).

Determination of Pharmacokinetic Parameters. The elimination half-life ($t_{1/2}$) was calculated on an Apple Macintosh computer with the pharmacokinetic data treatment software SIPHAR (Simed, Créteil, France), using the formula $t_{1/2} = \ln 2/K$, where K is the slope of the elimination phase.

RESULTS

^{14}C-Synthesis of the QA−DG Conjugates. The [^{14}C]-QA−DG conjugates were prepared according to the sequence described in Scheme 1. The linkage between DG and the QA carrier was achieved via an amide bond by a two-step procedure. First, condensation of [^{14}C]DG hydrochloride [specific activity: 167 MBq/mmol (4.5 mCi/mmol)] with chloroethanoyl chloride in the presence of potassium bicarbonate in aqueous medium at 0 °C provided the *N*-chloroacetyl ^{14}C-derivative in 57% yield. Subsequent reaction of this intermediate with pyridine (reactant and solvant) or with trimethylamine (4.2 M solution in ethanol) at 40 °C for 3 days gave, respectively, the trimethylammonium ([^{14}C]TMG) and the pyridinium ([^{14}C]PG) conjugates with overall yields of 50% and 42%. The two final quaternary ammonium compounds were found by NMR and TLC to be identical to the unlabeled reference compounds. They were obtained with a specific activity of 167 MBq/mmol (4.5 mCi/mmol) and a radiochemical purity of 96% as determined by HPLC analysis. Their physical data and spectral characterizations are presented in the Experimental Procedures.

Pharmacokinetic Studies. *Tissue Distribution.* Results of the in vivo biodistribution experiments with the two [^{14}C]QA−DG conjugates and the parent molecule in male Sprague−Dawley rats are summarized in Table 1. These data were determined by the method of whole-body autoradiography coupled with Ambis 4000 counting (*25*). Representative two-dimensional images of whole-body sections obtained by this method are shown in Figure 1.

Following intravenous administration of [^{14}C]DG, a fast distribution of the radioactivity was observed in a great number of tissues and specifically in kidney, brain, liver, skin, and cartilaginous tissues (Table 1). In the first 2 h, the radioactivity was highly concentrated in liver and kidney. For the liver, a specific kinetic law was observed, with a first increase in the radioactivity level until 15 min after injection, followed by a slow decrease.

The radioactivity distribution pattern obtained with [^{14}C]TMG was similar to that found with [^{14}C]PG. At the short times, a marked radioactivity retention was detected in kidney. Until 30 min after administration, the highest levels of radioactivity were observed in cartilaginous tissues, skin, and kidney. In contrast, low concen-

Table 1. Comparative Biodistribution of [^{14}C]DG, [^{14}C]TMG, and [^{14}C]PG in Male Sprague−Dawley Rats Following Intravenous Injection[a]

tissue/organ		5 min	15 min	30 min	1 h	2 h	6 h	24 h
liver	DG	3.36 ± 0.56	5.46 ± 0.85	4.94 ± 1.27	4.91 ± 0.33	2.59 ± 0.35	1.89 ± 0.20	0.74 ± 0.01
	TMG	1.23 ± 0.03	0.83 ± 0.04	0.38 ± 0.04	0.19 ± 0.04	0.12 ± 0.02	0.15 ± 0.02	*b*
	PG	0.76 ± 0.15	0.88 ± 0.19	0.49 ± 0.09	0.30 ± 0.10	0.15 ± 0.02	0.14 ± 0.02	*b*
kidney	DG	4.76 ± 0.11	4.44 ± 0.16	2.51 ± 0.38	1.99 ± 0.26	1.79 ± 0.06	0.98 ± 0.08	*b*
	TMG	8.06 ± 0.76	9.54 ± 1.41	2.83 ± 1.56	1.24 ± 0.30	0.66 ± 0.12	0.27 ± 0.11	*b*
	PG	9.57 ± 6.55	5.40 ± 2.66	2.52 ± 0.71	1.43 ± 0.45	0.70 ± 0.10	*b*	*b*
brain	DG	0.58 ± 0.16	1.08 ± 0.11	0.95 ± 0.09	0.92 ± 0.18	0.77 ± 0.11	0.66 ± 0.07	0.44 ± 0.03
	TMG	0.07 ± 0.04	0.07 ± 0.07	0.04 ± 0.01	0.02 ± 0.01	0.02 ± 0.01	0.01 ± 0.01	*b*
	PG	0.07 ± 0.11	0.15 ± 0.08	0.10 ± 0.08	0.07 ± 0.06	0.03 ± 0.01	*b*	*b*
bone	DG	0.96 ± 0.01	0.29 ± 0.01	0.33 ± 0.08	0.36 ± 0.04	*b*	*b*	*b*
marrow	TMG	0.83 ± 0.04	0.59 ± 0.02	0.21 ± 0.01	*b*	*b*	*b*	*b*
	PG	0.64 ± 0.02	0.64 ± 0.03	0.19 ± 0.09	*b*	*b*	*b*	*b*
cartilage	DG	1.77 ± 0.14	1.56 ± 0.14	0.95 ± 0.20	0.88 ± 0.25	0.88 ± 0.20	1.17 ± 0.17	0.76 ± 0.30
	TMG	3.28 ± 0.31	2.68 ± 0.27	1.08 ± 0.16	0.37 ± 0.08	*b*	*b*	*b*
	PG	2.51 ± 0.20	2.30 ± 0.40	1.49 ± 0.09	0.53 ± 0.05	*b*	*b*	*b*
skin	DG	1.47 ± 0.44	1.17 ± 0.16	0.49 ± 0.11	0.32 ± 0.04	0.45 ± 0.17	0.48 ± 0.03	0.51 ± 0.13
	TMG	2.37 ± 0.25	2.00 ± 0.28	0.65 ± 0.16	0.19 ± 0.06	0.12 ± 0.06	0.12 ± 0.08	*b*
	PG	2.75 ± 0.29	1.97 ± 0.52	0.87 ± 0.14	0.26 ± 0.03	0.20 ± 0.06	0.19 ± 0.07	*b*

[a] Results are expressed as the percentage of the injected dose per gram of tissue and correspond to the mean ± standard deviation for the quantification of eight whole-body sections of one animal for each point. [b] Could not be quantified.

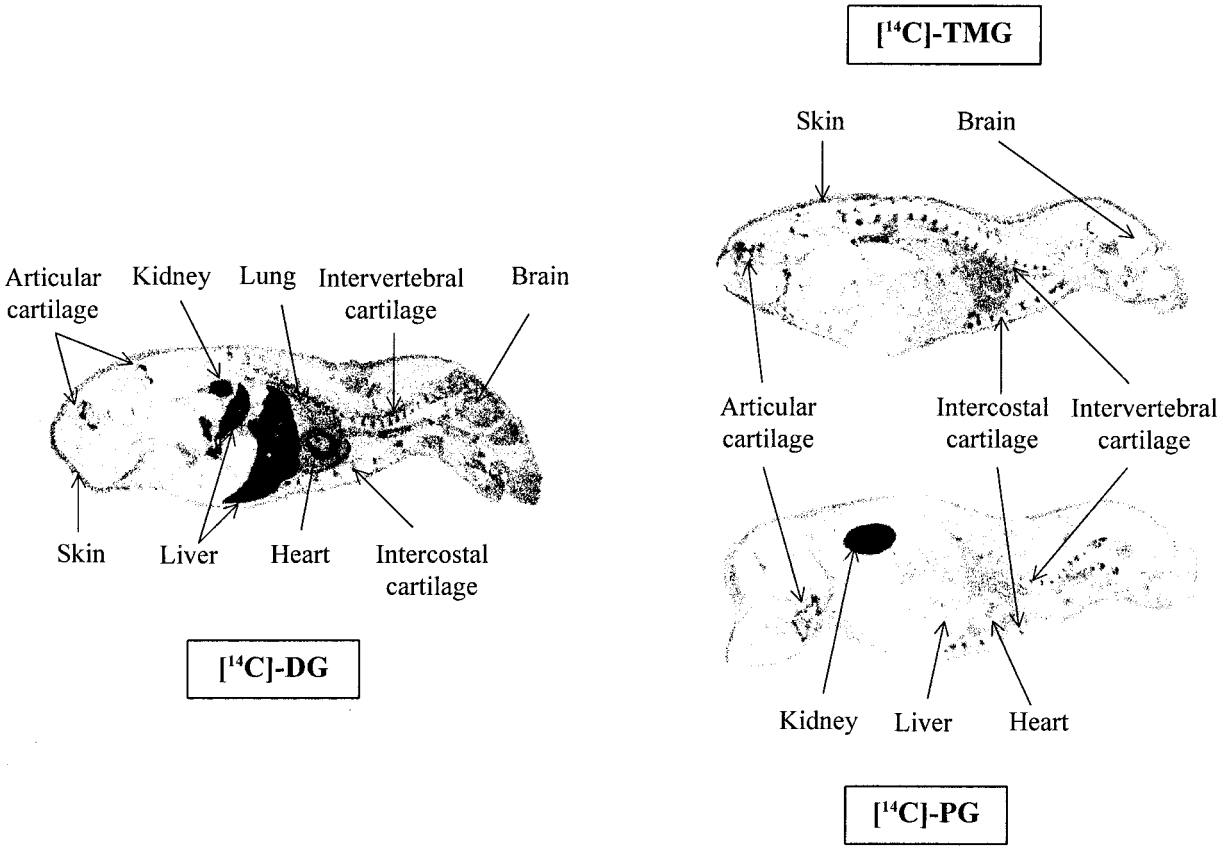

Figure 1. Representative two-dimensional images obtained with Ambis 4000 detector of rat whole-body sections showing the tissue distribution of radioactivity 15 min following intravenous administration of each ^{14}C-labeled test compound: [^{14}C]DG, [^{14}C]TMG, and [^{14}C]PG. The radioactivity distribution pattern obtained with both congugates was more restricted than that found with DG, with a decreased radioactivity distribution for whole tissues except for kidney, cartilage and skin.

trations were found in brain and liver. The radioactivity levels quantified in cartilaginous tissues for both conjugates were higher than those detected with [^{14}C]DG until 30 min after administration. From 1 h after injection, the cartilaginous radioactivity concentration became greater for [^{14}C]DG, and the elimination rate was slower than that observed for TMG and PG.

Blood and Plasma Kinetics. The radioactivity levels found in blood and plasma of animals after intravenous injection of [^{14}C]DG, [^{14}C]TMG, and [^{14}C]PG are presented in Figure 2. For each test compound, the plasma kinetics followed the blood kinetics. As observed for tissue distribution analyses, DG exhibited a different plasma behavior from its two conjugates. For DG, a fast decrease in the radioactivity was first detected, reaching a minimal value 15 min after injection. An increase until 2 h after administration followed by a slow disappearance phase were then observed. In contrast, for the QA−DG derivatives, a rapid plasma clearance was detected.

Radioactivity Excretion. Table 2 presents the radioactivity excreted in urine, feces and in expired air ($^{14}CO_2$) after injection to rats of [^{14}C]DG, [^{14}C]TMG, and [^{14}C]PG.

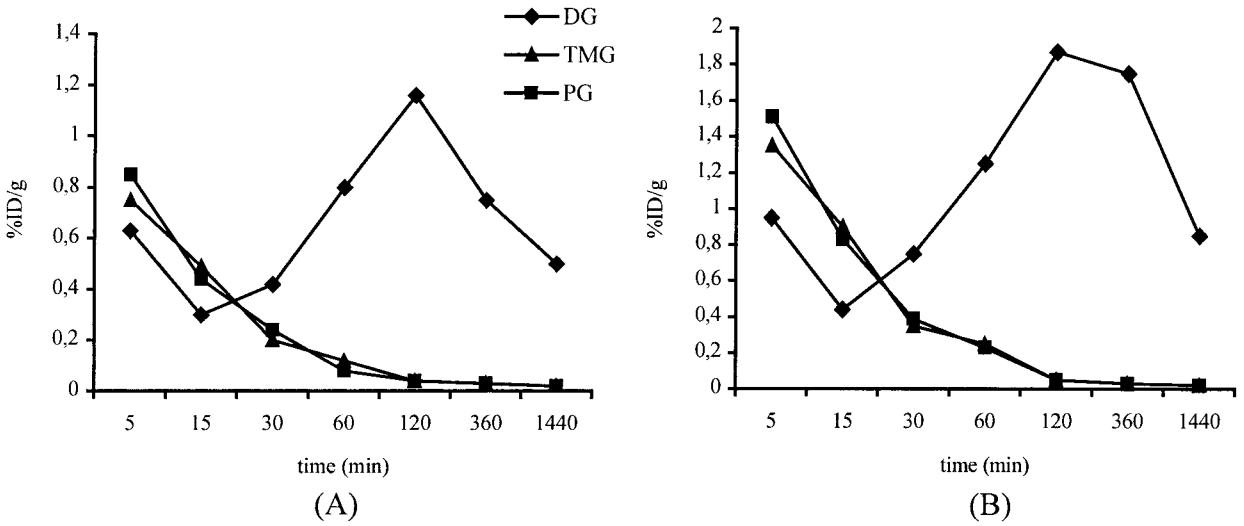

Figure 2. A comparison of the blood (A) and plasma (B) kinetics of [^{14}C]DG, [^{14}C]TMG and [^{14}C]PG in male Sprague−Dawley rats following intravenous administration. Results are expressed as the percentage of the injected dose per gram of blood or plasma and correspond to the mean ± standard deviation for three animals for each point.

Table 2. Radioactivity Excreted in Urine Feces and Expired Air after Intravenous Administration of [^{14}C]DG, [^{14}C]TMG, and [^{14}C]PG in Male Sprague−Dawley Rats[a]

	time (h)	urine	feces	$^{14}CO_2$
DG	0−24	41.7 ± 1.2	4.5 ± 0.4	18.9
	24−78	1.3 ± 0.1	3.1 ± 0.2	4.5
	48−72	0.8 ± 0.2	0.8 ± 0.1	1.5
TMG	0−24	85.3 ± 3.4	7.8 ± 0.7	4.2
	24−78	1.5 ± 0.5	2.7 ± 0.3	0.6
	48−72	0.3 ± 0.1	0.9 ± 0.1	0.2
PG	0−24	84.6 ± 4.9	7.1 ± 0.4	6.3
	24−78	1.4 ± 0.9	1.6 ± 0.1	0.9
	48−72	0.4 ± 0.1	0.4 ± 0.1	0.6

[a] Results are expressed as the percentage of the injected dose and correspond to the mean ± standard deviation for five animals for each point, except for $^{14}CO_2$ excretion (one rat studied).

Whereas for the two conjugates more than 85% of the radioactivity was excreted by the urine route, only 44% of the injected dose was recovered in the urine for DG, and a significant level of radioactivity was detected in the expired air (25% of the injected dose was found in the expired CO_2 72 h after injection).

Metabolism Study. Plasma and urine samples were analyzed by HPLC to determine the percentage of unchanged molecule and to find potential metabolites. In our HPLC conditions, the retention times were 3.7, 5.3, and 7.2 min for [^{14}C]DG, [^{14}C]TMG, and [^{14}C]PG, respectively.

Chromatographic analyses of plasma samples were performed on deproteinized plasma. For [^{14}C]DG, the radioactive concentration found in deproteinized plasma represented 93% of the radioactivity of whole plasma 5 min after injection. The percentage then decreased to 6% after 1 h. Simultaneously, the radioactivity incorporated into plasma proteins increased (from about 10% 5 min after administration to 91% after 1 h). The HPLC profiles of initial deproteinized plasmas showed that the radioactivity was mainly due to DG (more than 90%). For the [^{14}C]QA−DG derivatives, the radioactivity measured in deproteinized plasmas represented more than 90% of the radioactivity of whole plasma, whatever the time studied. The HPLC analyses of this radioactivity indicated that 1 h after injection, for both conjugates, more than 90% of the radioactivity corresponded to the unchanged molecule. This percentage was still 83% after 2 h. From 6 h following administration, the plasma radioactivity became too low to permit HPLC analysis. Thus, for the two QA−DG derivatives, the radioactivity found in plasma was identified as the unchanged molecule. This result enabled us to calculate the half-life time in the plasma of compounds, which was determined to be 15 min for TMG and 14 min for PG.

HPLC study of urine samples for the study of [^{14}C]DG indicated that, while only 42% of the injected dose was recovered in urine 24 h after injection, 87% of this radioactivity corresponded to the parent molecule. For both QA conjugates, more than 85% of the radioactivity detected in urine until 24 h after administration was identified as the unchanged compound.

DISCUSSION

The objective of this work was to determine whether the DG−QA conjugates exhibited a higher tropism for cartilaginous tissues than DG. This involved conducting pharmacokinetic studies in animals of the QA derivatives, which consequently had to be radiolabeled. The preferred isotope for such experiments was ^{14}C because of its long half-life time and convenient energy of decay. As [^{14}C]DG was a commercially available compound, the radiolabeling of the conjugates was performed by functionalization of this ^{14}C-labeled precursor. The QA moiety was attached on the amino group of the carbohydrate. We chose this position because (i) chemically, the amino group reacts more selectively and rapidly in condensation reactions than the hydroxyl groups, and (ii) biologically, DG is incorporated into proteoglycans with an N-acetylated form involving OH-1 and OH-3 or OH-4 groups. Accordingly, we thought a N-functionalization would reproduce this biological form. A trimethylammonium conjugate and a pyridinium derivative ([^{14}C]TMG and [^{14}C]PG) were synthesized to assess the possible influence of the QA structure on the biodistribution of these compounds. The conjugates were prepared from [^{14}C]DG by a two-step procedure via *N*-chloroacetyl-DG as intermediate.

Biodistribution patterns of the radioactivity in rats after intravenous injection of [^{14}C]TMG and [^{14}C]PG were compared with that of [^{14}C]DG. Whatever the parameter studied, both conjugates were found to have similar behavior, while DG exhibited a completely different profile.

From the point of view of tissue distribution, a marked diminution of the affinity of the QA derivatives compared with DG was observed for whole tissues except for kidney, cartilage, and skin. The radioactivity accumulation observed in kidney reflected the major urinary excretion of these compounds. The radioactivity levels found in skin could be explained by the fact that skin is also a proteoglycan-containing tissue. Contrary to DG, low hepatic and cerebral radioactivity concentrations were detected, indicating that the conjugates do not cross the blood brain barrier and are not extensively metabolized. Consequently, this tissue distribution study of the conjugates suggested, through a more restricted distribution profile, a higher specificity for cartilage than DG. In the case of [^{14}C]TMG or [^{14}C]PG, cartilaginous tissues concentrated the radioactivity more rapidly and strongly than [^{14}C]DG (until 30 min after administration). Such high radioactivity levels in cartilage for the short times following the injection were already observed in previous results obtained by us with other QA derivatives (*4*, *5*, *10*). From 1 h after injection, the radioactivity level became higher for DG. This last result is consistent with the literature: exogenous DG has a special tropism for cartilage as it constitutes the preferential substrate for the proteoglycan biosynthesis (*18*−*20*).

The pattern of the radioactivity excretion after administration of the conjugates revealed a predominant urinary excretion. Moreover, these compounds were found to be eliminated unchanged with little metabolic degradation. For DG, the excretion profile was quite different: the radioactivity level detected in urine was lower and a significant amount was found in expired air, suggesting a substantial part of the administered DG was completely broken down and utilized for energy-consuming processes (*19*).

The investigation of blood and plasma kinetics indicated a faster disappearance for the QA derivatives than for the parent drug. For DG, the plasma radioactivity decreased rapidly during the first 15 min. During this phase, DG was taken up in large amounts in the liver, where it was metabolized and incorporated into plasma proteins (*17*−*19*, *26*, *27*). After 15 min, the radioactivity increased in plasma, reaching a peak at 2 h. In this phase, the radioactivity originated from plasma proteins, in which the exogenous DG or fragments were incorporated (*17*−*19*, *26*). Thus, this study provides evidence for the existence of an enterohepatic cycle for DG, which was also confirmed by the radioactivity pattern obtained for liver in the tissue distribution experiment. On the contrary, the conjugates exhibited a rapid clearance from the blood with a monoexponential elimination. Furthermore, they were found to be not hardly metabolized, most of the radioactivity detected in urine and plasma being identified as the unchanged molecule.

To conclude, the work reported here demonstrates a striking difference in the pharmacokinetic profiles of DG and its two QA conjugates. On the other hand, the nature of the QA moiety does not seem to have a significant influence, as both conjugates exhibited similar behavior. Finally, in the context of our cartilage targeting strategy, two points must be underlined: the QA derivatives showed a more restricted tissue distribution than the parent DG and a higher cartilaginous concentration in the short times following intravenous administration. Therefore, this study shows that the introduction of a QA moiety on DG, a compound which already exhibits a special tropism for cartilage, allows the molecule to be carried more selectively and intensively to cartilaginous tissues soon after injection. These results clearly argue in favor of cartilage targeting. Following this encouraging work, we now intend to study the synthesis and evaluation of the QA derivatives of other antirheumatic agents.

ACKNOWLEDGMENT

This work was supported by ADIR, Servier (France).

LITERATURE CITED

(1) Blackburn, W. D. (1996) Management of osteoarthritis and rheumatoid arthritis: prospects and possibilities. *Am. J. Med. 100* (Suppl. 2A), 24S−30S.

(2) Schiff, M. (1997) Emerging treatments for rheumatoid arthritis. *Am. J. Med. 102* (Suppl. 1A), 11S−15S.

(3) Brooks, P. M. (1998) Treatment of rheumatoid arthritis: from symptomatic relief to potential cure. *Br. J. Rheumatol. 37*, 1265−1271.

(4) Garrigue, H., Maurizis, J. C., Nicolas, C., Madelmont, J. C., Godeneche, D., Hulot, T., Morge, X., Demerseman, P., Sentenac-Roumanou, H., and Veyre, A. (1990) Disposition and metabolism of two acetylcholinesterase reactivators Pyrimidoxime and HI6 in rats submitted to organophosphate poisoning. *Xenobiotica 20*, 699−709.

(5) Garrigue, H., Maurizis, J. C., Madelmont, J. C., Nicolas, C., Meyniel, J. M., Louvel, A., Demerseman, P., Sentenac-Roumanou, H., and Veyre, A. (1991) Disposition and metabolism of acetylcholinesterase reactivators 2PAM-I, TMB4 and R665 in rats submitted to organophosphate poisoning. *Xenobiotica 21*, 583−595.

(6) Maurizis, J. C., Ollier, M., Nicolas, C., Madelmont, J. C., Garrigue, H., and Veyre, A. (1992) In vitro binding of oxime acetylcholinesterase reactivators to proteoglycans synthesized by cultured chondrocytes and fibroblasts. *Biochem. Pharmacol. 44*, 1927−1933.

(7) Asghar, K., and Roth, L. J. (1971) Distribution of hexamethonium and other quaternary ammonium compounds in cartilage. *J. Pharmacol. Exp. Ther. 176*, 83−92.

(8) Olsen, G. D., Chan, E. M., and Riker, W. K. (1975) Binding of d-tubocurarine di(methyl-^{14}C)ether iodide and other amines to cartilage, chondroitin sulfate and human plasma proteins. *J. Pharmacol. Exp. Ther. 195*, 242−250.

(9) Van Ootegham, S. P., Smith, R. G., Daves, G. D., El-Matazi, A., Chan, E. M., Olsen, G. D., and Riker, W. K. (1976) Iodobis(quaternary ammonium) Salts. Potential Cartilage−Selective X-ray Contrast Agents. *J. Med. Chem. 19*, 1349−1352.

(10) Larsson, B., Nilsson, M., and Tjälve, H. (1981) The binding of inorganic and organic cations and H^+ to cartilage in vitro. *Biochem. Pharmacol. 30*, 2963−2970.

(11) Yu, W. K. S., Bartlett, J. M., Van Sickle, D. C., and Mock, B. H. (1988) Biodistribution of bis-[β-(*N*,*N*,*N*-trimethylamino)-ethyl]selenide-^{75}Se diiodide, a potential articular imaging agent. *Nucl. Med. Biol. 15*, 229−230.

(12) Yu, W. K. S., Shaw, S. M., Bartlett, J. M., Van Sickle, D. C., and Mock, B. H. (1989) The biodistribution of bis-[β-(*N*,*N*,*N*-trimethylamino)ethyl]selenide-^{75}Se diiodide in adult guinea pigs. *Nucl. Med. Biol. 16*, 255−259.

(13) Madelmont, J.-C., Giraud, I., Nicolas, C., Maurizis, J.-C., Rapp, M., Ollier, M., Renard, P., and Caignard, D.-H. French Patent 99,08020, June 23, 1999, 29 pp.

(14) MacCarthy, M. F. (1994) The neglect of Glucosamine as a treatment for osteoarthritis−a personal perspective. *Med. Hypotheses 42*, 323−327.

(15) Barclay, T. S., Tsourounis, C., and McCart, G. M. (1998) Glucosamine. *Ann. Pharmacother. 32*, 574−579.

(16) da Camara, C. C., and Dowless, G. V. (1998) Glucosamine sulfate for osteoarthritis. *Ann. Pharmacother. 32*, 580−587.

(17) Kelly, G. S. (1998) The role of glucosamine sulfate and chondroitine sulfate in the treatment of degenerative joint disease. *Altern. Med. Rev. 3* (1), 27−39.

(18) Rodén, L. (1956) Effect of hexosamines on the synthesis of chondroitin sulphuric acid in vitro. *Ark. Kemi. 10*, 345−352.

(19) Setnikar, I., Giachetti, C., and Zanolo, G. (1984) Absorption, distribution and excretion of radioactivity after a single intravenous or oral administration of ^{14}Cglucosamine in the rat. *Pharmatherapeutica 3*, 538−550.

(20) Setnikar, I., Giacchetti, C. and Zanolo, G. (1986) Pharmacokinetics of glucosamine in the dog and in man. *Arzneim. Forsch./Drug Res. 36* (I), 729−735.
(21) Bassleer, C., Henrotin, Y., and Franchimont, P. (1992) In vitro evaluation of drugs proposed as chondroprotective agents. *Int. J. Tissue React. 14*, 231−241.
(22) Setnikar, I. (1992) Antireactive properties of "chondroprotective" drugs. *Int. J. Tissue React. 14*, 253−261.
(23) Karzel, K., and Domenjoz, R. (1971) Effects of hexosamine derivatives and uronic derivatives on glycosaminoglycan metabolism of fibroblast cultures. *Pharmacology 5*, 337.
(24) Vidal, Y., Plana, R. R., Bizarri, D., and Rovati, A. L. (1978) Articular cartilage pharmacology. I. In vitro studies on glucosamine and non steroidal antiinflammatory drugs. *Pharmacol. Res. Commun. 10*, 557.
(25) Labarre, P., Papon, J., Moreau, M.-F., Madelmont, J.-C., and Veyre, A. (1998) A new quantitative method to evaluate the biodistribution of a radiolabeled tracer for melanoma using whole-body cryosectioning and a gaseous detector: comparison with conventional tissue combustion technology. *Eur. J. Nucl. Med. 25*, 109−114.
(26) Akamastsu, N., Nakajima, H., and Miyata, S. (1976) Glucosamine metabolism in regenerating rat liver. *Biochem. J. 158*, 589−592.
(27) Lo, C.-H., and Marsh, J. B. (1970) Biosynthesis of plasma lipoproteins. *J. Biol. Chem. 245*, 5001−5006.

BC990128+

Sequence-Recognition and Cleavage of DNA by a Netropsin-phenazine-di-*N*-oxide Conjugate

Philippe Helissey,[†] Sylviane Giorgi-Renault,*[,†] Pierre Colson,[‡] Claude Houssier,[‡] and Christian Bailly*[,§]

Laboratoire de Chimie Thérapeutique, Faculté des Sciences Pharmaceutiques et Biologiques, UMR CNRS-Université René Descartes no. 8638, 4, Avenue de l'Observatoire, 75270 Paris Cedex 06, France, Laboratoire de Chimie Macromoléculaire et Chimie Physique, Université de Liège au Sart-Tilman 4000 Liège, Belgium, and INSERM U-524 et Laboratoire de Pharmacologie Antitumorale du Centre Oscar Lambret, Place de Verdun, 59045 Lille, France. Received October 6, 1999; Revised Manuscript Received December 2, 1999

We report the synthesis, DNA-binding and cleaving properties, and cytotoxic activities of **R-128**, a hybrid molecule in which a bis-pyrrolecarboxamide-amidine element related to the antibiotic netropsin is covalently tethered to a phenazine-di-*N*-oxide chromophore. The affinity and mode of interaction of the conjugate with DNA were investigated by a combination of absorption spectroscopy, circular dichroism, and electric linear dichroism. This hybrid molecule binds to AT-rich sequences of DNA via a bimodal process involving minor groove binding of the netropsin moiety and intercalation of the phenazine moiety. The bidentate mode of binding was evidenced by linear dichroism using calf thymus DNA and poly(dA-dT)•(dA-dT). In contrast, the drug fails to bind to poly(dG-dC)•poly(dG-dC), because of the obstructive effect of the guanine 2-amino group exposed in the minor groove of this polynucleotide. DNase I footprinting studies indicated that the conjugate interacts preferentially with AT-rich sequences, but the cleavage of DNA in the presence of a reducing agent can occur at different sequences not restricted to the AT sites. The main cleavage sites were detected with a periodicity of about 10 base pairs corresponding to approximately one turn of the double helix. This suggests that the cleavage may be dictated by the structure of the double helix rather than the primary nucleotide sequence. The conjugate which is moderately toxic to cancer cells complements the tool box of reagents which can be utilized to produce DNA strand scission. The DNA cleaving properties of **R-128** entreat further exploration into the use of phenazine-di-*N*-oxides as tools for investigating DNA structure.

INTRODUCTION

The antibiotics netropsin and distamycin bind with a high selectivity to AT-rich sequences of DNA (*1*). The crescent-shaped conformation of these two oligopyrrolecarboxamide-amidine antibiotics is ideally suited for fitting into the minor groove of the DNA double helix (*2*). They have long been used as prototypes for the design of sequence-specific drugs (*3*, *4*). A large variety of conjugates containing pyrrole-amidine moieties attached to a polyamine, an alkylating agent, a metal complex, a enediyne structure, or intercalating chromophore have been synthesized and studied for their capacity to recognize and/or cleave specific DNA sequences (*5*). Some of these conjugates, such as the nitrogen mustard-distamycin conjugate FCE24517 (tallimustine), demonstrate significant anticancer activity (*6*, *7*). These compounds provide an improved understanding of the mechanisms whereby small molecules can recognize and bind to specific nucleotide sequences in DNA (see ref *8* for a recent review).

Netropsin and distamycin have also been coupled with photosensitive groups, including psoralen and coumarin derivatives, to induce light-dependent sequence-specific reaction with DNA. In the same vein, minor groove binding oligopeptides have been attached to pyrene, cationic porphyrins or isoalloxazine photosensitizers (*9*). Upon photoactivation flavin-netropsin hybrids can generate oxy radicals capable of causing DNA breaks, preferentially at AT-rich sites (*10*, *11*). We have also previously reported the DNA-binding properties of hybrids composed of a minor-groove binder covalently linked to anthraquinone derivatives. The conjugates were found to catalyze DNA cleavage after activation by irradiation (*12*). We have now extended our synthetic program with the design of oligopyrrolecarboxamide-phenazine-di-*N*-oxide hybrid ligands.

Phenazine-di-*N*-oxide derivative can produce diffusible oxygen radicals responsible for DNA strand scission under physiological conditions (*13*). The proposed mechanism of action involves reductive activation of the phenazine moiety to produce $O_2^{-\bullet}$ or •OH-mediated DNA cleavage depending on aerobic or anaerobic conditions, in the absence of light or metal ions. Hecht and coworkers have also demonstrated that the cleavage activity of phenazine-di-*N*-oxide can be directed to specific sites in DNA via the tethering of oligonucleotides. Antisense oligonucleotides covalently linked to the phenazine-di-*N*-oxide prosthetic group via an aminopropyl chain can provoke DNA strand scission at the target DNA sequence (*14*). By analogy, we reasoned that the linkage of a phenazine-di-*N*-oxide group to a DNA minor groove binding element might plausibly lead to a synthetic endonuclease capable of inducing efficient DNA cleavage.

* To whom correspondence should be addressed. (S.G.-R.) Fax: (+33)143291403. E-mail: S.Giorgi-Renault@pharmacie.univ-paris5.fr. (C.B.) Fax: (+33)320169229. E-mail: bailly@lille.inserm.fr.

[†] UMR 8638 CNRS.

[‡] Université de Liège.

[§] INSERM U-524.

10.1021/bc990131t CCC: $19.00 © 2000 American Chemical Society
Published on Web 02/23/2000

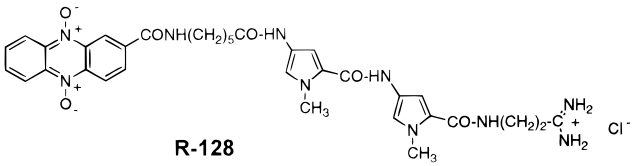

R-128

Figure 1. Structure of the netropsin-phenazine-di-*N*-oxide conjugate **R-128**.

Here, we describe the synthesis, DNA-binding and strand cleaving properties, and cytotoxic activities of the netropsin-phenazine-di-*N*-oxide hybrid ligand **R-128**, the structure of which is shown in Figure 1.

EXPERIMENTAL PROCEDURES

Chemistry. Melting points were determined on a Maquenne apparatus and are uncorrected. The IR spectra were recorded on a Perkin-Elmer 1600 spectrophotometer, and only the principal sharply defined peaks are reported. The ^{1}H NMR spectra were recorded on a Bruker AC-300 (300.13 MHz) MHz spectrometer. Mass spectra were determined by FAB (fast atom bombardment) on a VG 70-SEQ (VG Analytical Ldt, G. B.) apparatus, source FAB (positive ions) with direct introduction using glycerol-thioglycerol (1:1) as a matrix. Thin-layer chromatography was carried out on Merck GF 254 silica gel plates. Flash chromatography was performed on silica gel (Silice 60 A C. C., SDS).

Methyl 6-(Phenazine-2-carboxamido)hexanoate (3). A solution of phenazine-2-carboxylic acid (**2**) (*15*) (0.863 g, 3.85 mmol), EDC (0.886 g, 4.62 mmol), HOBT (0.520 g, 3.85 mmol), triethylamine (1.60 mL, 11.55 mmol), and methyl 6-aminohexanoate (0.840 g, 4.62 mmol) in dry DMF (60 mL) was stirred for 24 h at 20 °C and then further amounts of amine (0.086 g, 0.38 mmol) and EDC (0.089 g, 0.46 mmol) were added. One day later, after evaporation to dryness, the residue was dissolved in MeOH and precipitated by the addition of Et_2O. The resulting solid was filtered off and purified by flash chromatography [solvents: CH_2Cl_2-MeOH (10:0) to (8.5:1.5)] to give 0.660 g (49%) of pure compound **3**: mp 144 °C; IR (KBr) 1638, 1733 [ν (CO)], 3302 [ν (NH)] cm^{-1}; NMR (Me_2SO-d_6) δ 1.41 (m, 2, $CH_2CH_2CH_2CH_2CH_2$), 1.62 (m, 4, $CH_2CH_2CH_2CH_2CH_2$), 2.36 (t, 2, CH_2CO), 3.38 (m, 2, $NHCH_2$), 3.62 (s, 3, OCH_3), 8.07 (m, 2, ArH), 8.34 (m, 4, ArH), 8.81 (m, 1, ArH), 8.96 (t, 1, $NHCH_2$). Anal. ($C_{20}H_{21}N_3O_3$), C, H, N.

Methyl 6-(5,10-Dioxyphenazine-2-carboxamido)-hexanoate (4). An aqueous solution of 30% H_2O_2 (2 mL) was added to a solution of compound **3** (0.200 g, 0.57 mmol) in glacial acetic acid (20 mL). The mixture was stirred at 50 °C for 48 h. After elimination of the solvant in vacuo, the residue was purified by flash-chromatography [solvents CH_2Cl_2−AcOEt (10:0) to (4:6)] to afford 0.141 g (64%) of pure orange compound **4**: mp 165 °C; IR (KBr) 1632, 1719 [ν (CO)], 3313 [ν (NH)] cm^{-1}; NMR (Me_2SO-d_6) δ 1.34 (m, 2, $CH_2CH_2CH_2CH_2CH_2$), 1.60 (m, 4, $CH_2CH_2CH_2CH_2CH_2$), 2.34 (t, 2, CH_2CO), 3.35 (m, 2, $NHCH_2$), 3.59 (s, 3, OCH_3), 7.99 (m, 2, ArH), 8.30 (m, 1, ArH), 8.69 (m, 3, ArH), 9.07 (m, 2, ArH and $NHCH_2$). Anal. ($C_{20}H_{21}N_3O_5$), C, H, N.

6-(5,10-Dioxyphenazine-2-carboxamido)hexanoic acid (5). To a suspension of ester **4** (0.200 g, 0.52 mmol) in EtOH (5 mL) was added a solution of NaOH (0.104 g, 2.61 mmol) in H_2O (5 mL). After refluxing for 5 min, the reaction mixture was acidified with dilute HCl until a pH of 2 was reached. The resulting precipitate was filtered off and recrystallized from MeOH to give 0.152 g (78%) of pure compound **5**: mp 216 °C; IR (KBr) 1630, 1698 [ν (CO)], 3276 [ν (NH) and ν (OH)] cm^{-1}; NMR (Me_2SO-d_6) δ 1.38 (m, 2, $CH_2CH_2CH_2CH_2CH_2$), 1.59 (m, 4, $CH_2CH_2CH_2CH_2CH_2$), 2.26 (t, 2, CH_2CO), 3.38 (m, 2, $NHCH_2$), 8.00 (m, 2, ArH), 8.34 (m, 1, ArH), 8.65 (m, 3, ArH), 9.12 (m, 2, ArH and $NHCH_2$), 12.07 (s, 1, CO_2H). Anal. ($C_{19}H_{19}N_3O_5$), C, H, N.

3-[1-Methyl-4-[1-methyl-4-[5-[(5,10-dioxyphenazine-2-carboxamido)]pentylcarboxamido]pyrrole-2-carboxamido] pyrrole-2-carboxamido]propionamidinium Chloride (R-128). A solution of acid **5** (0.111 g, 0.30 mmol), EDC (0.075 g, 0.39 mmol), HOBT (0.045 g, 0.33 mmol), and amine **6** (0.132 g, 0.36 mmol) in dry DMF (60 mL) was stirred for 24 h at 20 °C, and then further amounts of **6** (0.037 g, 0.10 mmol), EDC (0.019 g, 0.10 mmol), and HOBT (0.014 g, 0.10 mmol) were added. After 24 h, the solvent was removed under reduced pressure, the resulting residue was dissolved in MeOH and precipited by the addition of Et_2O. The precipitate was filtered off and purified by flash chromatography [solvents CH_2Cl_2-MeOH (9.5:0.5) to (5:5)] to afford 0.108 g (50%) of pure **R-128**: mp 212−215 °C; IR (KBr) 1648, 1684 [ν (CO)], 3313 [ν (NH) and (NH_2)] cm^{-1}; NMR (Me_2SO-d_6) δ 1.38 (m, 2, $CH_2CH_2CH_2CH_2CH_2$), 1.64 (m, 4, $CH_2CH_2CH_2CH_2CH_2$), 2.28 (t, 2, CH_2CO), 2.66 (m, 2, $CH_2C(=^+NH_2)NH_2$), 3.38 (m, 2, $NHCH_2$), 3.52 (m, 2, $CH_2CH_2C(=^+NH_2)NH_2$), 3.82 (s, 6, $2NCH_3$), 6.90, 6.94, 7.18, 7.21 (4s, 4 × 1, pyrrolic H), 7.98 (m, 2, ArH), 8.32 (m, 2, ArH and $NHCH_2$), 8.62 (m, 3, ArH), 8.86 (broad s, 2, NH_2), 9.13 (m, 4, ArH, $NHCH_2$ and NH_2), 9.94 (s, 2, 2NH). MS (FAB) *m*/*z* 683 [(M − Cl)$^+$], 667.6 [(M − Cl−O)$^+$], 651.3 [(M − Cl-2O)$^+$].

Chemicals and Biochemicals. Ammonium persulfate, tris base, acrylamide, bis-acrylamide, ultrapure urea, boric acid, tetramethylethylenediamine, formic acid, piperidine, and formamide were from Sigma. The nucleoside triphosphate labeled with ^{32}P (α-dATP) was obtained from Amersham. Unlabeled dATP, avian myeloblastosis virus reverse transcriptase, and restriction endonucleases *Eco*RI and *Pvu*II were from Boehringer Mannheim (Germany). Bovine pancreatic deoxyribonuclease I (DNase I, Sigma Chemical Co.) was stored as a 7200 units/mL solution in 20 mM NaCl, 2 mM $MgCl_2$, and 2 mM $MnCl_2$, pH 8.0. The stock solution of DNase I was kept at −20 °C and freshly diluted to the desired concentration immediately prior to use. All other chemicals were analytical grade reagents, and all solutions were prepared using doubly deionized, Millipore filtered water.

Absorption Spectra and Melting Temperature Studies. Melting curves were measured using an Uvikon 943 spectrophotometer coupled to a Neslab RTE111 cryostat. For each series of measurements, 12 samples were placed in a thermostatically controlled cell-holder, and the quartz cuvettes (10 mm path length) were heated by circulating water. The measurements were performed in BPE buffer pH 7.1 (6 mM Na_2HPO_4, 2 mM NaH_2PO_4, 1 mM EDTA). The temperature inside the cuvette was measured with a platinum probe; it was increased over the range 20−100 °C with a heating rate of 1 °C/min. The "melting" temperature T_m was taken as the midpoint of the hyperchromic transition. The Uvikon 943 spectrophotometer was also used to record the absorption spectra. Titrations of the drug with DNA, covering a large range of DNA phosphate/drug ratios (*P*/*D*), were performed by adding aliquots of a concentrated DNA solution to a drug solution at constant ligand concentration (20 μM). DNA blanks at the same nucleotide concentrations were prepared concomitantly and used as a reference in the recording of absorption spectra.

Circular Dichroism (CD). CD spectra were recorded from 250 to 500 nm on a Roussel-Jouan dichrograph Mark IV. Samples were placed in a quartz cell (3 mL, 1 cm path length) thermostated at 25 °C. The DNA (typically 70 μM) was dissolved in 10 mM sodium cacodylate buffer, pH 7, containing 100 mM NaCl. Concentrations of the ligands were in the range from 1 to 7 μM in a water-DMSO solution (0.1% maximum final DMSO concentration). Baseline corrected spectra were stored in an IBM/AT computer.

Electric Linear Dichroism (ELD). ELD measurements were performed using a computerized optical measurement system built by C. Houssier and the procedures outlined previously were followed (*16*). All experiments were conducted at 20 °C with a 10 mm pathlength Kerr cell having 1.5 mm electrode separation, in 1 mM sodium cacodylate buffer, pH 7.0. The DNA samples were oriented under an electric field strength of 13 kV/cm, and the drug under test was present at 10 μM together with the DNA or polynucleotide at 100 μM unless otherwise stated. This electrooptical method senses only the orientation of the polymer-bound ligand: free ligand is isotropic and does not contribute to the signal (*17*).

Purification and Radiolabeling of the DNA Substrates. The 265-mer fragment was rendered radioactive by 3′-^{32}P-end labeling of the *Eco*RI−*Pvu*II double digest of the plasmid pBS (Stratagene, La Jolla, CA) using [α-^{32}P]dATP (6000 Ci/mmol) and avian myeloblastosis virus reverse transcriptase. The labeled digestion products were separated on a 6% polyacrylamide gel under nondenaturing conditions in TBE buffer (89 mM Tris-borate, pH 8.3, 1 mM EDTA). After autoradiography, the requisite band of DNA was excised, crushed, and soaked in elution buffer (500 mM ammonium acetate and 10 mM magnesium acetate) overnight at 37 °C. This suspension was filtered through a Millipore 0.22 μm filter and the DNA was precipitated with ethanol. Following washing with 70% ethanol and vacuum-drying of the precipitate, the labeled DNA was resuspended in 10 mM Tris adjusted to pH 7.0 containing 10 mM NaCl.

Footprinting Experiments. Cleavage reactions by DNase I were performed essentially according to the protocol previously described (*18*). Reactions were conducted in a total volume of 10 μL. Samples (3 μL) of the labeled DNA fragment were incubated with 5 μL of the buffer solution supplemented with the drug under test. After 30 min of incubation at 37 °C to ensure equilibration of the binding reaction, digestion was initiated by the addition of 2 μL of the endonuclease solution whose concentration had been adjusted to limit the enzyme attack to less than 30% of the starting material so as to minimize the incidence of multiple cuts in any strand ("single-hit" kinetic conditions). Optimal enzyme dilutions were established in preliminary calibration experiments. Typically, DNase I experiments included 0.01 unit/mL enzyme, 20 mM NaCl, 2 mM $MgCl_2$, and 2 mM $MnCl_2$, pH 7.3. At the end of the reaction time (routinely 4 min at room temperature), the digestion was stopped by freeze-drying. After lyophilization, each sample was washed once with deionized water and then lyophilized again prior to resuspending in 3 μL of an 80% formamide solution containing tracking dyes (purchased from Sigma).

Cleavage of Plasmid DNA. Each reaction mixture contained 4 μL of supercoiled pUC12 DNA ($\sim$0.5 μg), 5 μL of **R-128** at concentrations varying from 1 to 500 μM, and 1 μL of 10 mM dithiothreitol. After 14 h of incubation at room temperature in the dark, 3 μL of loading buffer (0.25% bromophenol blue, 0.25% xylene cyanol, and 30% glycerol in H_2O) was added to each tube and the solution was applied to a 1% agarose gel. The electrophoresis was carried out for about 2 h at 100 V in TBE buffer. Gels were stained with ethidium bromide (1 μg/mL) then destained for 30 min in water prior to being photographed under UV light.

Cleavage of Radiolabeled DNA. The reaction mixture contained 4 μL of 3′-end-labeled 265-mer DNA ($\sim$500 cps), 5 μL of R-128 at concentrations varying from 1 to 500 μM, and 1 μL of 10 mM dithiothreitol. After 14 h of incubation at room temperature in the dark, the drug−DNA samples were precipitated with 100 μL of cold ethanol and then resuspended in 4 μL of an 80% formamide solution containing tracking dyes. Samples were heated at 90 °C for 4 min and chilled in ice for 4 min prior to electrophoresis.

Electrophoresis and Quantitation. DNase I- and DTT-mediated DNA cleavage products were resolved by polyacrylamide gel electrophoresis under denaturing conditions (0.3 mm thick, 8% acrylamide containing 8 M urea). Electrophoresis was continued until the bromophenol blue marker had run out of the gel (about 2.5 h at 60 W, 1600 V in TBE buffer, BRL sequencer model S2). Gels were soaked in 10% acetic acid for 15 min, transferred to Whatman 3MM paper, dried under vacuum at 80 °C, and subjected to the phosphorimager. A Molecular Dynamics 425E PhosphorImager was used to collect data from storage screens exposed to the dried gels overnight at room temperature. Baseline-corrected scans were analyzed by integrating all the densities between two selected boundaries using ImageQuant version 3.3 software. Each resolved band was assigned to a particular bond within the DNA fragment by comparison of its position relative to sequencing standards generated by treatment of the DNA with formic acid (G+A) followed by piperidine-induced cleavage at the modified bases.

Cell Cultures and Survival Assay. Human HL-60 promyelocytic leukemia and Raji mammary carcinoma cells were obtained from the European Collection of Cell Cultures. Cells were grown at 37 °C in a humidified atmosphere containing 5% CO_2 in RPMI 1664 medium, supplemented with 10% fetal bovine serum, glutamine (2 mM), penicillin (100 IU/mL), and streptomycin (100 μg/mL). The cytotoxicity of the drug was assessed using a cell proliferation assay developed by Promega (CellTiter 96 AQ_{ueous} one solution cell proliferation assay, Promega). Briefly, 2×10^4 exponentially growing cells were seeded in 96-well microculture plates with various drug concentrations in a volume of 100 μL. After 72 h of incubation at 37 °C, 20 μL of MTS (*19*) was added to each well and the samples were incubated for a further 2 h at 37 °C. Plates were analyzed on a Labsystems Multiskan MS (type 352) reader at 492 nm.

RESULTS

Chemistry. The 2-aminophenazine-di-*N*-oxide derivatives which have been conjugated to oligonucleotides (*13*, *14*) were not optimized for reductive generation of oxygen free radicals. In our case, we decided to substitute the phenazine-5,10-dioxide nucleus at position 2 by a carboxamido function to facilitate its reduction and the radical formation. The hybrid molecule **R-128** contains a phenazine-5,10-dioxide heterocycle linked to the pyrrolecarboxamide moiety via a pentamethylenic chain (Figure 1). The synthesis of the hybrid **R-128** required the preparation of the 2-carboxamidophenazine-5,10-dioxide moiety substituted at position 2 with a pentamethylenic carboxylic acid linker **5** and the aminooligopy-

Scheme 1

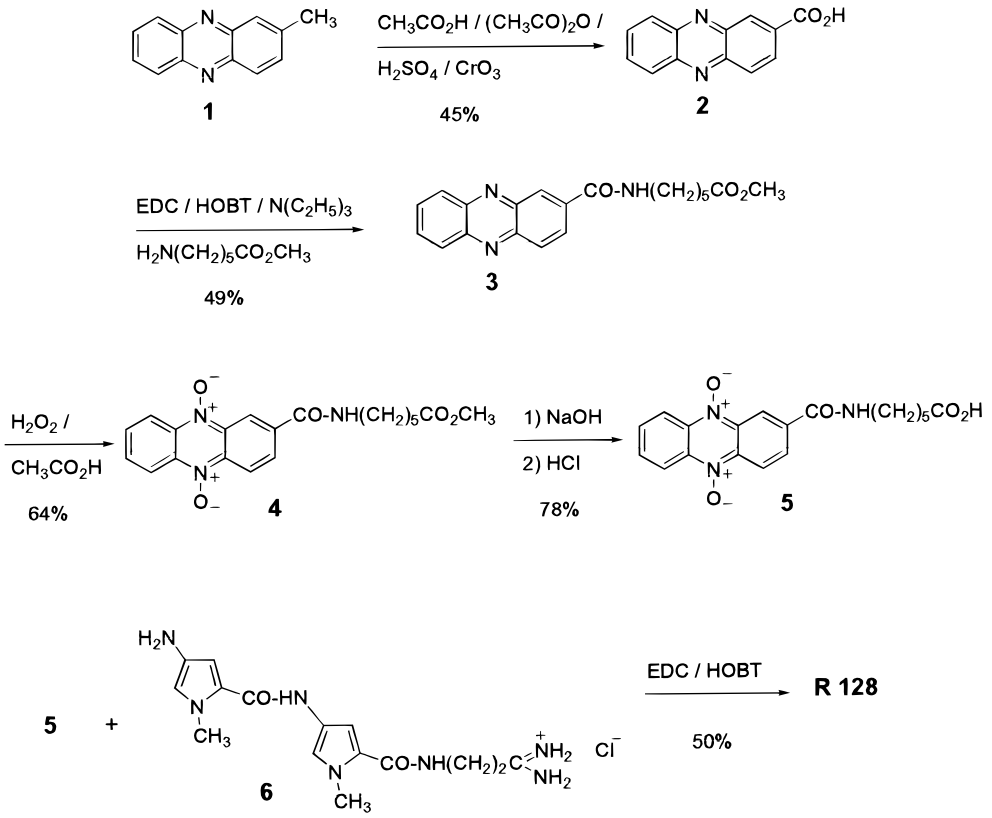

rrole derivative bearing an amidinium function **6** (Scheme 1). Compound **6** was prepared from 1-methyl-4-nitropyrrole-2-carboxylic acid according to a procedure previously described (*12*). Three synthetic routes have been described in the literature for the preparation of phenazine-2-carboxylic acid (**2**) (*15*, *20*, *21*). The method reported by Kidani (*15*) was found to be the most efficient although we have not be able to reproduce the 75% yield claimed for the chromic oxidation of 2-methylphenazine (**1**) (*22*). Our first attempted route to oxidize the acid **2** into 5,10-dioxyphenazine-2-carboxylic acid by hydrogen peroxide in acetic medium according to ref *23* was unsuccessful whatever the experimental conditions. Therefore, the amide **3** was prepared by condensation of **2** with methyl 6-aminohexanoate. The highest yield (49%) was obtained using EDC, HOBT, and triethylamine as peptide coupling agents. Treatment of **3** with hydrogen peroxide in acetic medium at 50 °C afforded **4** in a 64% yield. After saponification of **4**, a final peptide coupling between acid **5** and amine **6** gave the hybrid **R-128** in 50% yield.

DNA Affinity. The absorption spectrum of conjugate is largely modified in the presence of DNA (Figure 2). The two absorption bands centered at 288 and 477 nm, corresponding to the netropsin and phenazine moieties, respectively, are shifted by about 15 nm when the ligand is fully bound to DNA. The interaction of the drug with DNA also causes a marked hypochromism in the 290 nm band. The UV spectra suggested that the two moieties of the hybrid drug are engaged in the complex with DNA. The equilibrium constant measured for the binding of **R-128** to calf thymus DNA is 1.2×10^6 (M^{-1}, per nucleotide; $n = 3.5$), i.e., about four times higher than that measured with netropsin ($K_a = 2.9 \times 10^5$ M^{-1}, per nucleotide) under identical conditions. Therefore, we can

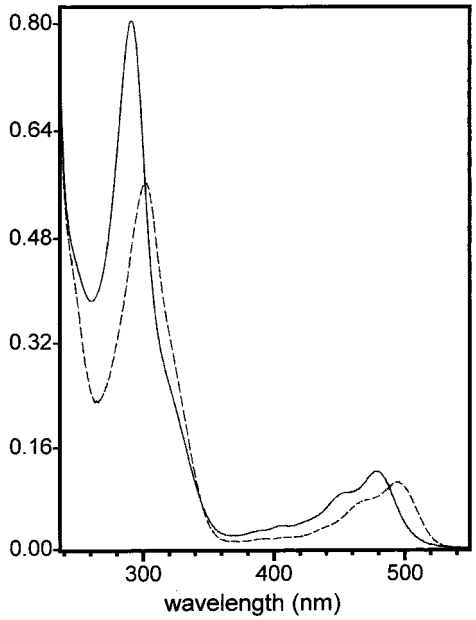

Figure 2. Absorption spectra of **R-128** (15 μM) in the absence (full line) and presence (dashed line) of calf thymus DNA (500 μM) in 1 mM sodium cacodylate buffer, pH 7.0. The spectrum corresponding to the drug bound to DNA was referenced against a DNA solution of exactly the same concentration and was adjusted to a common baseline.

conclude that the linkage of the phenazine moiety reinforces significantly the interaction of the drug with DNA.

We examined the ability of **R-128** to affect the thermal denaturation profile of nucleic acids using three natural DNAs of different base pair composition [DNAs from calf thymus (42% GC), *Clostridium perfringens* (26% GC), and *Micrococcus lysodeikticus* (72% GC)] and two synthetic

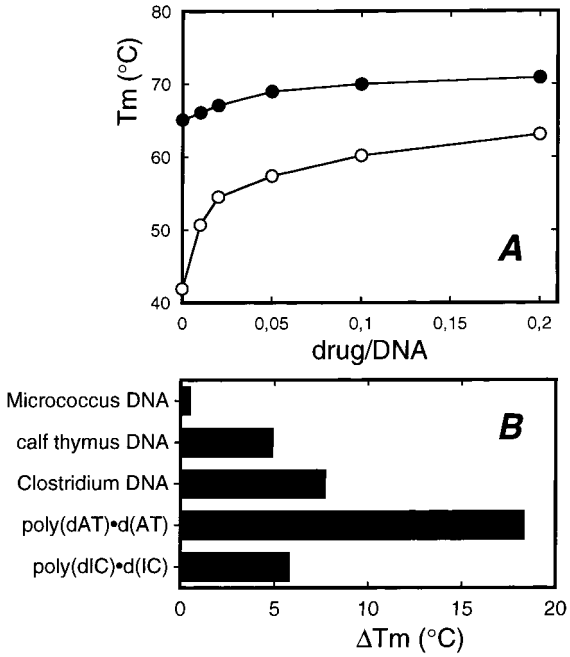

Figure 3. (A) Variation in melting temperature (ΔT_m in BPE buffer) of poly(dA-dT)·(dA-dT) (open circles) and calf thymus DNA (filled circles) induced by the binding of **R-128**. The DNA concentration was fixed at 100 μM while the drug concentration varied from 1 to 20 μM. (B) Stabilizing effect of **R-128** measured with various DNA and polynucleotides. In this case, the DNA and drug concentrations were 100 and 10 μM, respectively.

polynucleotides with different base pair arrangements poly(dA-dT)·poly(dA-dT) and poly(dI-dC)·poly(dI-dC). The stabilization of poly(dA-dT)·poly(dA-dT) by **R-128** against thermal denaturation is much higher than that observed with calf thymus DNA, which contains roughly equal proportions of AT and GC base pairs (Figure 3A). With the natural DNA, the measured ΔT_m values indicate that the extent of stabilization is related to the AT content of the DNA (Figure 3B). The thermal protection of the double helix induced by **R-128** is much higher with the DNA from *Clostridium* than with the DNA from *Micrococcus*. It was not possible to study the thermal stability with poly(dG-dC)·poly(dG-dC) due to the very high stability of this polynucleotide, under the ionic conditions used in these experiments (T_m > 90 °C in BPE buffer), but we used the polynucleotide poly(dI-dC)·poly(dI-dC), which contains inosine residues in place of guanosines. The effects observed with poly(dA-dT)·poly(dA-dT) and poly(dI-dC)·poly(dI-dC) can be compared because the two polynucleotides melt at about the same temperature (T_m = 40 °C in BPE buffer). The stabilizing effect of R-128 was much higher with the AT polymer than with the IC polymer.

DNA Binding Mode. Circular dichroism (CD) and electric linear dichroism (ELD) experiments were performed to define the orientation of the hybrid ligand with respect to the DNA helix. With the DNAs from *Micrococcus* and *Clostridium*, the CD signal monitored at 300−320 nm increased with increasing DNA/drug ratios until a *D*/*P* value of 0.1 was reached (spectra not shown). Such an intense positive CD is characteristic of netropsin and is commonly observed with netropsin and distamycin conjugates. No CD signal was detected at 500 nm in the phenazine band, and therefore, it was not possible to define the orientation of the photosensitive group by this optical technique. In contrast, the electric linear dichroism (ELD) measurements provided very useful information. In the past, we have employed extensively this

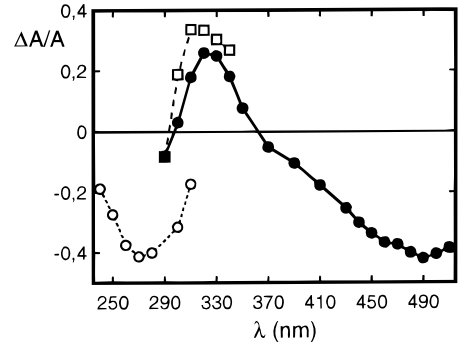

Figure 4. Reduced electric linear dichroism ($\Delta A/A$) spectra of (○) calf thymus DNA alone or in interaction with (□) netropsin or (●) **R-128**. ELD data were recorded in the presence of 100 μM DNA and 10 μM drug, in 1 mM sodium cacodylate buffer pH 7.0, under a field strength of 13 kV/cm.

electrooptical method to determine the orientation of drugs bound to DNA, including both minor groove binders and intercalators as well as a variety of hybrid molecules *(17)*.

The ELD spectrum of **R-128** bound to calf thymus DNA (Figure 4) provides direct evidence that both linked functionalities of the hybrid are engaged in the binding reaction. Such an ELD spectrum is characteristic of a bimodal binding process, with the 400−500 nm negative band due exclusively to the phenazine moiety of the hybrid and the 300−330 nm positive band due to the bis-pyrrole moiety, with little or no contribution from the phenazine moiety. Two essential facts can be obtained from these ELD data. First, the positive dichroism at 320 nm is similar for the hybrid **R-128** and its parent compound netropsin. Second, the reduced dichroism of the DNA bases at 260 nm in the absence of ligand ($\Delta A/A$ = −0.41 at 13 kV/cm) is the same as the reduced dichroism measured at 490 nm with the hybrid ligand−DNA complex. This implies that (i) the bis-pyrrole moiety of **R-128** is inserted into the minor groove of DNA, as is known to be the case with netropsin and (ii) the phenazine portion of the conjugate is oriented parallel to the DNA base pair, and this is perfectly consistent with an intercalation binding mode. It seems therefore that the linkage of the phenazine moiety does not impede minor groove binding of the attached bis-pyrrole unit, and conversely, the minor groove entity does not hinder intercalation of the attached planar chromophore. Thus, the ELD experiments strongly suggest that the hybrid molecule interacts with DNA in a geometrically well-defined fashion, placing its netropsin moiety in the minor groove and with the phenazine chromophore inserted between the base pairs.

ELD was used further to compare the binding mode of **R-128** to poly(dA-dT)·poly(dA-dT) and poly(dG-dC)·poly(dG-dC) (Figure 5). The ELD spectrum of **R-128** bound to the AT polymer is almost the same as the one obtained with calf thymus DNA. It shows a positive band at 320 nm and a negative band at 480 nm, in agreement with a bidentate mode of binding involving minor groove binding of the netropsin moiety and intercalation of the phenazine ring. In sharp contrast, the ELD measurements performed in the presence of the GC polymer and **R-128** showed no specific signal, be it at 320 or 480 nm. Both the netropsin moiety and the appended phenazine ring apparently fail to bind to the GC sites. The removal of the 2-amino group of guanine protruding into the minor groove of DNA restored the dual binding mode. Indeed, with poly(dI-dC)·poly(dI-dC), the ELD spectrum was again totally similar with those obtained with calf

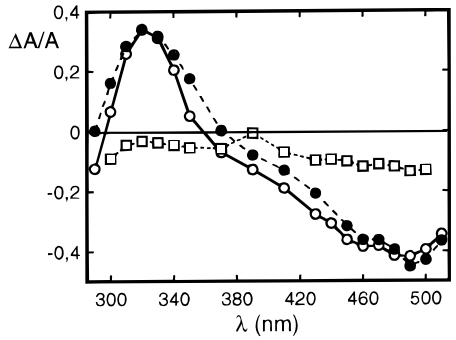

Figure 5. Reduced electric linear dichroism (Δ*A*/*A*) spectra of **R-128** bound to (○) poly(dA-dT)·poly(dA-dT), (□) poly(dG-dC)·poly(dG-dC), or (●) poly(dI-dC)·poly(dI-dC). ELD data were recorded in the presence of 100 μM polynucleotide and 10 μM drug, in 1mM sodium cacodylate buffer, pH 7.0, under a field strength of 13 kV/cm.

thymus DNA or poly(dA-dT)·poly(dA-dT) (Figure 5). It is known that the guanine 2-amino group obstructs the insertion of netropsin into the minor groove (*24*), but it is surprising to observe that the intercalation of the phenazine ring is also directly dependent on the absence of that group.

Sequence selectivity. The classical DNase I footprinting methodology was used to determine if the hybrid molecule can recognize preferentially certain sequences in DNA. Netropsin is reputed to be capable of selectively recognizing AT-rich sequences (*25*). The footprinting gel presented in Figure 6 shows that **R-128** exhibits a moderate sequence selectivity. The radiolabeled 265 base pair fragment from plasmid pBS was incubated with graded concentrations of **R-128** prior to limited cleavage by DNase I. Two marked footprints can be discerned around nucleotide positions 77 and 125, which both correspond to AT-rich sequences. The densitometric analysis of the gel revealed other weaker **R-128** binding sites around positions 26, 55, 64, and 94 as presented in Figure 7. Apart from the binding site at position 24−28 (3′-GAGAT), all the other sites coincide with sequences composed of at least four contiguous A·T base pairs. The hybrid has thus retained, at least partially, the AT selectivity of netropsin, but the footprints are less frequent and less pronounced than those obtained with the antibiotic on the same DNA fragment (*26*).

DNA Cleavage. Prior to investigating the sequence specificity of the cleavage reaction with **R-128**, we optimized the procedure using a plasmid DNA analyzed on agarose gel. A typical gel obtained after treatment of a supercoiled plasmid for 12 h with increasing concentrations of **R-128** is presented in Figure 8. The cleavage of DNA is relatively limited. Supercoiled DNA (form I) is gradually converted to nicked DNA (form II) in the presence of concentrations of **R-128** ranging from 2 to 75 μM. At the highest drug concentration, about 80% of the DNA is under a nicked form but no linear DNA (form III) was detected. Therefore, the drug only produces single-stranded cleavage of DNA. Next, we repeated the cleavage experiments using the radiolabeled 265 bp substrate as used in the footprinting experiments. A typical gel is presented in Figure 9, and the positions of the most intense cleavage sites are represented by arrows in Figure 7. In the control lane with no drug present, the DNA remained intact after the incubation with DTT. With **R-128**, the cleavage of DNA is very clear. At the lowest drug concentration (1 μM), the cutting is almost uniform; all nucleotide positions are cleaved. When the drug concentration is raised, the patterns of cleavage

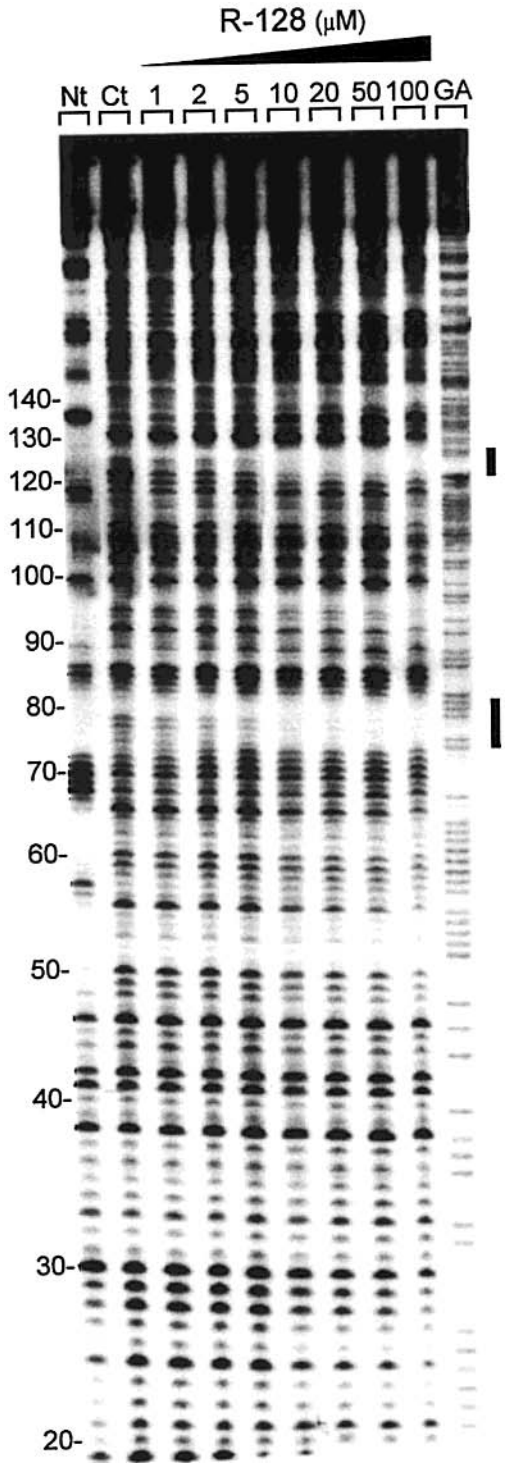

Figure 6. DNase I footprinting of **R-128** bound to the 265-mer *Eco*RI−*Pvu*II restriction fragment cut out from plasmid pBS. The DNA was 3′-end labeled with [α-^{32}P]dATP in the presence of AMV reverse transcriptase. The drug concentration (μM) is shown at the top of the appropriate gel lanes. The tracks labeled "Ct" contained no drug. The tracks labeled "GA" represent formic acid−piperidine markers specific for purines. Numbers on the left side of the gels refer to the numbering scheme of the fragment as indicated in Figure 7.

changed markedly. Certain sequences become poorly cut, whereas the extent of cleavage at other sites has increased considerably. The gel was analyzed by densitometry, and the positions of the most pronounced cleavage sites were mapped and compared with the positions of the drug-binding sites, inferred from the footprinting experiments (Figure 7). No obvious correlation can be

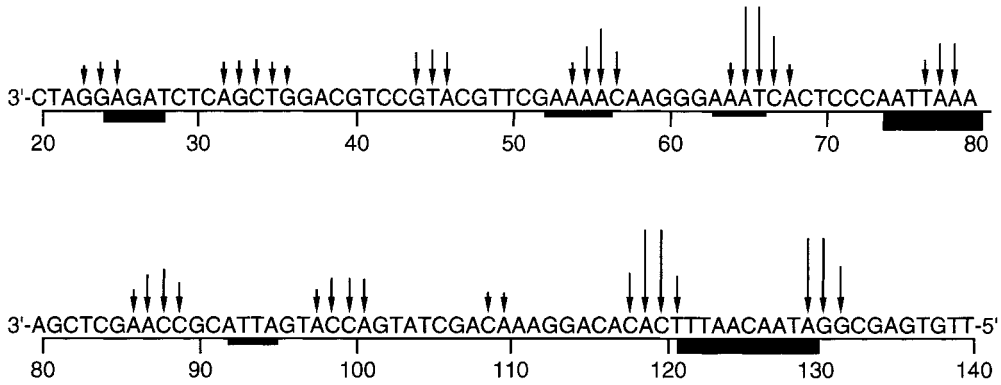

Figure 7. Summary map representing the DNase I footprints and DNA strand cleavage sites produced by **R-128** on the lower strand of the 265-mer DNA fragment. Only the region of the restriction fragment which was analyzed by densitometry is shown. The sequences underlined by black boxes represent the measured footprints, i.e., positions of inhibition of DNase I cutting by R-128 and, therefore, the putative reversible binding sites. The thickness of each box is roughly proportional to the relative intensity of the footprint at the indicated sequence. Arrows pointing toward the lettered sequence refer to the main sites of **R-128**-mediated cleavage, with small and large arrows denoting moderate and large variations in the amplitude of the cleavage, respectively.

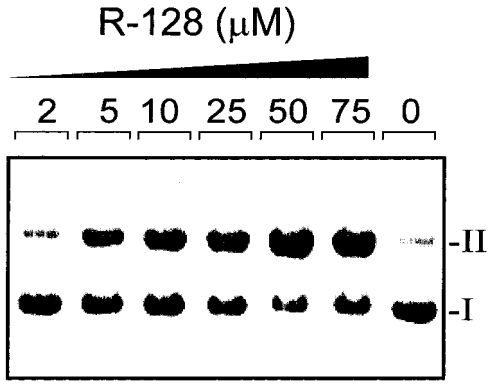

Figure 8. Cleavage of closed circular DNA. Supercoiled DNA (0.5 μg) was incubated overnight at 20 °C with the drug at the indicated concentration in the presence of 1 mM dithiothreitol (DTT). The control lane (marked 0) refers to the plasmid DNA incubated without drug but in the presence of DTT. Forms I and II refer to the supercoiled and nicked DNA forms, respectively.

discerned. The cleavage can occur at sequences adjacent to the AT-binding sites (such as around positions 66 and 78) as well as at sequences distal from the binding sites (such as around positions 45 and 99 for examples). Therefore, it was not possible to correlate the cleavage experiments with the binding data.

Cytotoxicity. The cytotoxic activities of the hybrid ligand **R-128** were evaluated using human HL-60 leukemia cells and human Raji mammary carcinoma cells. After a 72 h incubation period, IC50 values of 0.75 and 0.08 μM were calculated with HL-60 and Raji cells, respectively. In the same cytotoxicity assay, netropsin proved totally nontoxic to both cell lines.

DISCUSSION

The conjugate described here was designed to contain a bispyrrolecarboxamide moiety covalently linked to a 2-carboxamidophenazine-di-*N*-oxide chromophore capable of triggering reductive cleavage of DNA. The complementary biophysical and footprinting data show that substituting the phenazine chromophore for the guanidinium terminal residue of netropsin does not impede the AT sequence preference of the parent antibiotic. The conjugate can still recognize AT-rich sequences in DNA selectively. Conversely, the cleavage experiments concur that the introduction of the minor groove binding element does not abolish the capacity of the prosthetic DNA-cleaving group to induce strand scission in the presence of a reducing agent such as dithiothreitol. The relative geometrical requirements of the two moieties of the hybrids were satisfied. The linker between the two drug moieties seems to present the correct length and/or flexibility to ensure the proper binding to DNA of the two parts of the molecules. It is interesting to observe that the oligopyrrolecarboxamide moiety is located in the minor groove of the double helix while the appended phenazine chromophore behaves as a typical intercalating agent. Our study confirms that double-stranded DNA is highly adaptable and can accommodate a minor groove binding process in close proximity to a more invasive type of binding such as intercalation. Interestingly, we noticed that our previously synthesized anthraquinone-netropsin hybrid $AQ_{(CN)}$-Net (*12*), which differs from **R-128** only by the nature of the heterocyclic nucleus (replacement of the 2-carboxamidophenazine-di-*N*-oxide by a 2-carboxamidoanthraquinone), was found not to present such a bimodal interaction with DNA. In this case, the netropsin element prevented intercalation of the anthraquinone nucleus.

At first sight, we were surprised to find the phenoxazine-di-*N*-oxide moiety intercalated into DNA. Intercalation was not reported in the previous cleavage studies (*13, 14*). Recently, 2-aminophenazine−oligonucleotide conjugates have been synthesized (*27, 28*). The fluorescence studies suggested that the phenazine moiety could not intercalate or bind to the minor groove of DNA but interact with the outside of the double helix. However, we found in the literature evidences that structurally related phenazine derivatives (3-hydroxyethylamino-5-phenazinium and a phenazine annelated to an imidazoglycoside) can intercalate into DNA (*29*). Nevertheless, it was proposed that the phenazines intercalate preferentially between G·C base pairs compared to A·T base pairs. Here, we observe that the tethered phenoxazine-di-*N*-oxide element intercalates into poly(dA-dT)·poly(dA-dT), but not into poly(dG-dC)·poly(dG-dC). The sequence selectivity and the binding geometry are most likely imposed by the netropsin element. A similar molecular arrangement has been previously observed with oligopyrrolecarboxamide−anilinoacridine conjugates (*30*).

It is manifest that the hybrid ligand **R-128** binds preferentially to AT-rich tracts and cleaves DNA in the presence of a reducing agent. However, it does seem clear that there is no simple correlation between the binding data and the cutting profile for the drug. Sequence

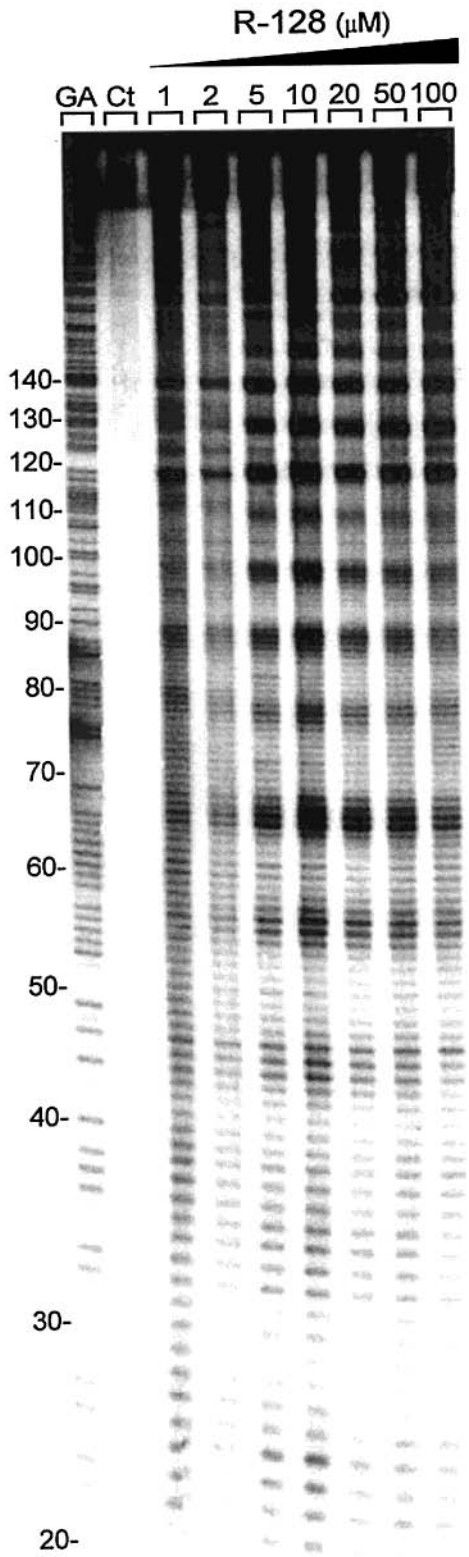

Figure 9. Cleavage of the DNA restriction fragment. The 265-mer DNA fragment labeled at the 3′-end of the *Eco*RI site was reacted with graded concentrations of **R-128** (μM as indicated) in the presence of 1 mM dithiothreitol overnight at 20 °C. The DNA was subsequently precipitated with cold ethanol and then electrophoresed on an 8% denaturating polyacrylamide gel. Lane marked control corresponds to the DNA subjected to the same treatment in the absence of drug but in the presence of DTT. Purine-specific sequence markers obtained by treatment of the DNA with formic acid−piperidine were run in the lane marked G+A. Numbers between on the left side of the gel refer to the nucleotide sequence of the DNA fragment as indicated in Figure 7.

recognition of DNA by **R-128** and cleavage of DNA likely correspond to two unrelated events. The cleavage of DNA proved to be nonspecific at low drug concentrations (e.g., 1 μM). At higher concentrations ($\geq$5 μM) the cleavage profile becomes clearly nonuniform, with regions of attenuated cleavage separated by sequences where the scission is much more pronounced. Interestingly, the most pronounced cleavage sites are separated one from another by approximately 10 base pairs (Figure 7). The cutting is more pronounced at certain sites, such as 3′-ATC (positions 65−67) and 3′-ACT (positions 119−121), but on average a peak of cleavage appears every 9−10 base pairs. The reason for such a periodic cleavage remains obscure at present, but it is plausible to envisage that it is related to the helical periodicity of B-DNA. Perhaps the cleavage process is dictated by the structure of the double helix rather than the primary nucleotide sequence. Further experiments will be needed to verify this hypothesis. The conjugate which is moderately toxic to cancer cells complements the tool box of reagents which can be utilized to produce DNA strand scission.

ACKNOWLEDGMENT

This work was supported by grants (to C. B.) from the Association pour la Recherche sur le Cancer and the Ligue Nationale Française Contre le Cancer and (to C. H. and P. C.) from the Actions de Recherches Concertées Contract 95/00-93. Support by the “convention INSERM-CFB” is acknowledged. S. G. R. thanks Dr. S. Fermandjian for the use of the CD equipment and Dr. A. Deroussent for mass spectra recording.

LITERATURE CITED

(1) Zimmer, C., and Wähnert, U. (1986) Nonintercalating DNA-binding ligands: specificity of the interaction and their use as tools in biophysical, biochemical and biological investigations of the genetic material. *Prog. Biophys. Mol. Biol. 47*, 31−112.

(2) Kopka, M. L., and Larsen, T. A. (1992) Netropsin and the lexitropsins. The search for sequence-specific minor-groove-binding ligands. In *Nucleic Acid Targeted Drug Design* (C. L. Propst and T. J. Perun, Eds.) pp 303−374. Marcel Dekker, Inc., New York.

(3) Zunino, F., Animati, F., and Capranico, G. (1995) DNA minor groove binding drugs. *Curr. Pharm. Des. 1*, 83−94.

(4) Geierstanger, B. H., and Wemmer, D. E. (1995) Complexes of the minor groove of DNA. *Annu. Rev. Biophys. Biomol. Struct. 24*, 463−493.

(5) Bailly, C. (1998) Sequence-specific recognition and modification of double-helical DNA by minor groove binding conjugates structurally related to netropsin and distamycin. In *Advances in DNA Sequence Specific Agents* (M. Palumbo, Ed.) Vol. 3, pp 97−156, JAI Press. Inc.

(6) Broggini, M., Erba, E., Ponti, M., Ballinari, D., Geroni, C., Spreafico, F., and D'Incalci, M. (1991) Selective DNA interaction of the novel distamycin derivative FCE 24517. *Cancer Res. 51*, 199−204.

(7) Pezzoni, G., Grandi, M., Biasoli, G., Capolongo, L., Ballinari, D., Giuliani, F. C., Barbieri, B., Pastori, A., Pesenti, E., and Mongelli, N. (1991) Biological profile of FCE 24517, a novel benzoyl mustard analogue of distamycin A. *Br. J. Cancer 64*, 1047−1050.

(8) Bailly, C., and Chaires, J. B. (1998) Design of sequence-specific DNA minor groove binders. Netropsin and distamycin analogues. *Bioconjugate Chem. 9*, 513−538.

(9) Herfeld, P., Helissey, P., Giorgi-Renault, S., Goulaouic, H., Pager, J., and Auclair, C. (1994) Poly(pyrrolecarboxamides) linked to photoactivable chromophore isoalloxazine. Synthesis, selective binding, and DNA cleaving properties. *Bioconjugate Chem. 5*, 67−76.

(10) Bouziane, M., Ketterlé, C., Helissey, P., Herfeld, P., Le Bret, M., Giorgi-Renault, S., and Auclair, C. (1995) Sequence-

directed single-strand cleavage of DNA by a netropsin-flavin hybrid molecule. *Biochemistry 34*, 14051−14058.

(11) Ketterlé, C., Gabarro-Arpa, J., Ouali, M., Bouziane, M., Auclair, C., Helissey, P., Giorgi-Renault, S., and Le Bret, M. (1996) Binding of Net-Fla, a netropsin-flavin hybrid molecule, to DNA: Molecular mechanics and dynamics studies in vacuo and in water solution. *J. Biomol. Struct. Dyn. 13*, 963−977.

(12) Helissey, P., Bailly, C., Vishwakarma, J. N., Auclair, C., Waring, M. J., and Giorgi-Renault, S. (1996) DNA minor groove cleaving agents: synthesis, DNA binding and DNA cleaving properties of anthraquinone-oligopyrrolecarboxamide hybrids. *Anti-Cancer Drug Des. 11*, 527−551.

(13) Nagai, K., Carter, B. J., Xu, J., and Hecht, S. M. (1991) DNA cleavage by oxygen radicals produced in the absence of metal ions or light. *J. Am. Chem. Soc. 113*, 5099−5100.

(14) Nagai, K., and Hecht, S. M. (1991) Site-specific DNA cleavage by antisense oligonucleotides covalently linked to phenazine di-*N*-oxide. *J. Biol. Chem. 266*, 23994−24002.

(15) Kidani, Y. (1959) Studies on phenazines. Synthesis of phenazine-carboxylic acids. *Chem. Pharm. Bull. 7*, 88−90.

(16) Houssier, C. (1981) Investigating nucleic acids, nucleoproteins, polynucleotides, and their interactions with small ligands by electrooptical systems. In *Molecular Electrooptics* (S. Krause, Ed.) pp 363−398, Plenum Publishing Corporation, New York.

(17) Colson, P., Bailly, C., and Houssier, C. (1996) Electric linear dichroism as a new tool to study sequence preference in drug binding to DNA. *Biophys. Chem. 58*, 125−140.

(18) Bailly, C., and Waring, M. J. (1995) Comparison of different footprinting methodologies for detecting binding sites for a small ligand on DNA. *J. Biomol. Struct. Dyn. 12*, 869−898.

(19) Cory, A. H., Owen, T. C., Barltrop, J. A., and Cory, J. G. (1991) Use of an aqueous soluble tetrazolium/formazan assay for cell growth assays. *Cancer Commun. 3*, 207−212.

(20) Kögl, F., and Tönnis, B. (1932) Uber Chlororaphin und Xanthoraphin, ein Beitrag zur Chemie der Chinhydrone. *Liebigs Ann. 497*, 265−289.

(21) Vivian, D. L., Hartwell, J. L., and Waterman H. C. (1955) Phenazine syntheses. IV. Nitriles. *J. Org. Chem. 20*, 797−802.

(22) Rozum, Y. S. (1955) Some carbonyl derivatives of phenazine. *J. Gen. Chem. 25*, 583−587.

(23) Maffei, S., and Pietra, S. (1952) La sintesi dell'acido 2-fenazincarbonico. *Ann. Chim. 42*, 519−525.

(24) Bailly, C., and Waring, M. J. (1995) Transferring the purine 2-amino group from guanines to adenines in DNA changes the sequence-specific binding of antibiotics. *Nucleic Acids Res. 23*, 885−892.

(25) Portugal, J., and Waring, M. J. (1987) Comparison of binding sites in DNA for berenil, netropsin and distamycin. A footprinting study. *Eur. J. Biochem. 167*, 281−289.

(26) Plouvier, B., Bailly, C., Houssin, R., Rao, K. E., Lown, J. W., Hénichart, J.-P., and Waring, M. J. (1991) DNA-sequence specific recognition by a thiazole analogue of netropsin: a comparative footprinting study. *Nucleic Acids Res. 19*, 5821−5829.

(27) Zamaratski, E., and Chattopadhyaya, J. (1998) Synthesis of phenazine-tethered arabino and xylofuranosyl oligonucleotide conjugates: the thermal stability and fluorescence properties of their duplexes (DNA-DNA & DNA-RNA) and triplexes. *Tetrahedron 54*, 8183−8206.

(28) Ossipov, D., and Chattopadhyaya, J. (1998) Synthesis of 1′-phenazine-tethered psicofuranosyl oligonucleotide conjugates: the thermal stability and fluorescence properties of their duplexes and triplexes. *Tetrahedron 54*, 5667−5682.

(29) Zozulya, V., Blagoi, Y., Löber, G., Voloshin, I., Winter, S., Makitruk, V., and Shalamay, A. (1997) Fluorescence and binding properties of phenazine derivatives in complexes with polynucleotides of various base compositions and secondary structures. *Biophys. Chem. 65*, 55−63.

(30) Bourdouxhe-Housiaux, C., Colson, P., Houssier, C., Waring, M. J., and Bailly, C. (1996) Interaction of a DNA-threading netropsin-amsacrine combilexin with DNA and chromatin. *Biochemistry 35*, 4251−4264.

BC990131T

Solution Structure of an LNA Hybridized to DNA: NMR Study of the d(CT^{L}GCT^{L}T^{L}CT^{L}GC):d(GCAGAAGCAG) Duplex Containing Four Locked Nucleotides

Katrine E. Nielsen,[†] Sanjay K. Singh,[‡] Jesper Wengel,[‡] and Jens Peter Jacobsen*,[†]

Department of Chemistry, University of Southern Denmark, Odense University, DK-5230 Odense M, Denmark, Center for Synthetic Bioorganic Chemistry, Department of Chemistry, University of Copenhagen, Universitetsparken 5, DK-2100 Copenhagen, Denmark. Received September 15, 1999; Revised Manuscript Received December 3, 1999

We have used two-dimensional ^{1}H NMR spectroscopy at 750 MHz to determine a high-resolution solution structure of an oligonucleotide containing restricted nucleotides with a 2′-*O*, 4′-*C*-methylene bridge (LNA) hybridized to the complementary DNA strand. The LNA:DNA duplex examined contained four thymidine LNA modifications (**T^{L}**), d(C1**T^{L}**2G3C4**T^{L}**5**T^{L}**6C7**T^{L}**8G9C10):d(G11C12A13G14A15-A16G17C18A19G20). A total relaxation matrix approach was used to obtain interproton distance bounds from NOESY cross-peak intensities. These distance bounds were used as restraints in molecular dynamics (rMD) calculations. Forty final structures were generated for the duplex from A-form and B-form DNA starting structures. The root-mean-square deviation (RMSD) of the coordinates for the 40 structures of the complex was 0.6 Å. The sugar puckerings are averaged values of a dynamic interchange between N- and S-type conformation except in case of the locked nucleotides that were found to be fixed in the C3′-endo conformation. Among the other nucleotides in the modified strand, the furanose ring of C7 and G9 is predominatly in the N-type conformation whereas that of G3 is in a mixed conformation. The furanose rings of the nucleotides in the unmodified complementary strand are almost exclusively in the S-type conformation. Due to these different conformations of the sugars in the two strands, there is a structural strain between the A-type modified strand and the B-type unmodified complementary strand. This strain is relaxed by decreasing the value of rise and compensating with tip, buckle, and propeller twist. The values of twist vary along the strand but for a majority of the base pairs a value even lower than that of A-DNA is observed. The average twist over the sequence is 32 ± 1°. On the basis of the structure, we conclude that the high stability of LNA:DNA duplexes is caused by a local change of the phosphate backbone geometry that favors a higher degree of stacking.

INTRODUCTION

A potential nucleotide-based gene inhibitor must possess an enhanced stability toward cellular nucleases, the ability to penetrate the cell membrane, and an efficient hybridization to the target RNA/DNA[1] (Hélène and Toulmé, 1990; Uhlmann and Peyman, 1990). Several chemically modified DNA and RNA oligonucleotides have been synthesized, but only a few of them fulfill the requirements (Hélène and Toulmé, 1990; Uhlmann and Peyman, 1990; Nielsen, 1991; Hélène, 1991; Thuong and Hélène, 1993; De Mesmaeker et al., 1995). The LNA nucleotide monomer (Scheme 1) is a conformational restricted nucleotide analogue containing a 2′-*O*, 4′-*C*-methylene bridge locked in an 3′-endo conformation (Singh et al., 1998; Singh and Wengel, 1998; Obika et al., 1997; Wengel, 1998; Koshkin et al., 1998ab,c). Ther-

Scheme 1

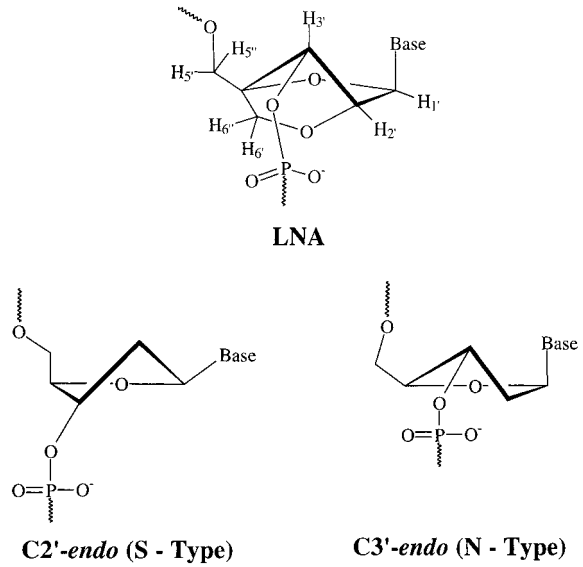

* To whom correspondence should be addressed. E-mail: jpj@chem.sdu.dk.
[†] University of Southern Denmark.
[‡] University of Copenhagen.

[1] Abbreviations: AMBER, assisted model building with energy refinement; DQF-COSY, double quantum filtered correlation spectroscopy; dsDNA, double-stranded DNA; ssDNA, single-stranded DNA; DSS, 2,2-dimethyl-2-silapentane-5-sulfonate; E-BURP, excitation band-selective pulse with uniform response and pure phase; EDTA, ethylenediaminetetraacetic acid; LNA, locked nucleic acid; MARDIGRAS, matrix analysis of relaxation for discerning the geometry of an aqueous structure; NOE, nuclear Overhauser effect; NOESY, nuclear Overhauser effect spectroscopy; RANDMARDI, randomized MARDIGRAS; rMD, restrained molecular dynamics; RMSD, root-mean-square deviation; TOCSY, total correlation spectroscopy.

10.1021/bc990121s CCC: $19.00 © 2000 American Chemical Society
Published on Web 02/23/2000

mal denaturation studies of duplexes formed between oligonucleotides containing the LNA modification and complementary DNA and RNA show that LNA recognizes both complementary DNA and RNA with remarkable thermal affinities. Thus, compared to the corresponding unmodified reference duplexes, the duplexes involving LNA (hybridized toward DNA or RNA) display unprecedented melting temperatures with increases between +4.0 and +9.3 °C obtained per modification (Singh et al., 1998; Singh and Wengel, 1998; Wengel, 1998; Koshkin et al., 1998a), and incorporation of a given number of LNA monomers into an oligonucleotide appears to be a very convenient and predictable way of upgrading the stability of duplexes toward complementary DNA or RNA. The LNA:LNA base pairing constitutes the most stable modified nucleic acid type duplex system hitherto discovered. Thus, melting temperatures greater than 93 °C have been observed for duplexes between two all-modified complementary LNAs (Koshkin et al., 1998c). Preliminary experiments (Wengel et al., 1999) suggest the LNA molecule so far to be the most promising candidate for efficient recognition of a given mixed sequence in a nucleic acid duplex. These results, togther with the demonstration that LNA is stable toward 3′-exonucleolytic degradation (Singh et al., 1998) and that fluorescein-labeled LNA can be transferred into living MCF-7 breast cancer cells (Wengel et al., 1999), have stimulated the evaluation of LNA as antisense and/or antigene molecule.

To obtain a detailed understanding of the foundation for the unprecedented enhanced thermal stability of LNA modified duplexes, we are currently investigating a series of LNA:DNA and LNA:RNA oligonucleotides using NMR spectroscopy. Recently, we reported the sugar conformations of a partly modified 9-mer single-stranded LNA as well as three 9- and 10-mer partly modified LNAs hybridized to unmodified DNA (Petersen et al., 1999). By use of selective DQF-COSY NMR spectra, we determined the ratio between the N-type (C3′-endo) and S-type (C2′-endo) sugar conformations of the nucleotides. We found that the locked conformation of the LNA nucleotides both in ssLNA and in the duplexes organize the phosphate backbone in such a way as to introduce higher population of the N-type conformation of the neighboring unmodified nucleotides on the same strand.

In general, the conformations of the flexible deoxyribose rings determine the overall structure of a (deoxy)-ribo nucleic acid duplex. Duplexes in A-type conformation contain nucleotides with an N-type sugar conformations, while B-type duplexes contain nucleotides with an S-type sugar conformations (Dickerson et al., 1989; Saenger, 1984). In the attempt to investigate these structural properties of LNA:DNA duplexes, we have used 2D ^{1}H NMR spectroscopy to determine the solution structure of the d(C**T^L**GC**T^{L}T^L**C**T^L**GC): d(GCAGAAGCAG) duplex (called the "LNA duplex" in the following) containing four thymidine LNA modifications as indicated by **T^L**. A total relaxation matrix approach was used to obtain interproton distance bounds from NOESY cross-peak intensities (Borgias and James, 1990; Borgias et al., 1990; Liu et al., 1995). These distance bounds were used as restraints in molecular dynamics (rMD) calculations. Since many NOE contacts were observed, the resulting structure has high resolution and allowed the determination of local conformational features in the LNA duplex.

EXPERIMENTAL PROCEDURES

Sample Preparation. The d(C**T^L**GC**T^{L}T^L**C**T^L**GC) oligonucleotide was synthesized as described elsewhere (Singh et al., 1998; Petersen et al., 1999; Koshkin et al., 1998a). The unmodified oligonucleotides were purchased from DNA Technology, Århus, Denmark. The oligonucleotides were purified by site exclusion on a Sephadex G15 column. The duplex was obtained by dissolving an equimolar amount of the two single strands in 0.5 mL of 10 mM sodium phosphate buffer (pH 7.0), 0.05 mM NaEDTA, 0.01 mM NaN_3, and 0.1 mM DSS. The mixture was heated to 80 °C and slowly cooled to achieve hybridization. The numbering scheme used for the duplex was as follows:

		1	*2*	*3*	*4*	*5*	*6*	*7*	*8*	*9*	*10*		
5'	**-**	**C**	***T^L***	**G**	**C**	***T^L***	***T^L***	**C**	***T^L***	**G**	**C**	**-**	**3'**
3'	**-**	**G**	**A**	**C**	**G**	**A**	**A**	**G**	**A**	**C**	**G**	**-**	**5'**
		20	*19*	*18*	*17*	*16*	*15*	*14*	*13*	*12*	*11*		

For experiments carried out in D_2O, the solid duplex was lyophilized three times from D_2O and redissolved in 99.96% D_2O (Cambridge Isotope Laboratories). A mixture of 90% H_2O and 10% D_2O (0.5 mL) was used for experiments examining exchangeable protons. The final concentration of the duplex was 2 mM. A similar sample was made of the unmodified duplex.

NMR Experiments. NMR experiments were performed on a Varian UNITY 500 spectrometer or a Varian INOVA 750 spectrometer at 27 °C unless otherwise stated. NOESY spectra of the duplex at 500 MHz were acquired in D_2O using 1024 complex points in t_2 and a spectral width of 5000 Hz. NOESY spectra at 750 MHz were acquired using 2048 complex points in t_2 and a spectral width of 7500 Hz. A total of 512 t_1 experiments were recorded using the States phase cycling scheme. The residual signal from HOD was removed by low-power presaturation. The NOESY spectra in H_2O at 750 MHz were acquired with a spectral width of 15.000 Hz using 4096 complex points and the WATERGATE pulse sequence (Stein et al., 1995). TOCSY spectra with mixing times of 90 ms were obtained in the TPPI mode at 500 MHz. An inversion recovery experiment to estimate the T_1 relaxation rates was also obtained at 750 MHz.

The NOE buildups were obtained at 750 MHz. These NOESY spectra were acquired in D_2O using 2048 complex points in t_2 and a spectral width of 7500 Hz. A total of 512 t_1 experiments of 64 scan each was recorded using the States phase cycling scheme. NOESY spectra with mixing times of 50, 100, 150, and 200 ms were obtained sequentially without removing the sample from the magnet. 64 scans were acquired for each t_1 value with a repetition delay of 4.0 s between each scan. The residual signal from HOD was removed by low-power presaturation.

The acquired data were processed using FELIX (version 97.2, MSI, San Diego, Ca). All spectra were apodized by a skewed sine bell squared in F_1 and F_2. The four spectra used in the NOE buildups were zero-filled in F_1 to 2K points and baseline corrected by a second-order polynomial fit in F_2 and F_1. The NOESY spectrum recorded in H_2O was zero-filled in F_1 to 4K points and baseline corrected by a second-order polynomial fit in F_2 and F_1.

Distance Restraints. The upper and lower diagonal part of each of the four NOESY buildup spectra were integrated separately with FELIX, yielding a total of eight peak intensity sets that were corrected for minor saturation effects. The RANDMARDI procedure (Liu et al., 1995) of the complete relaxation matrix analysis method MARDIGRAS (Borgias and James, 1990; Borgias et al., 1990) was used to calculate interproton distance

bounds from the eight intensity sets. In the calculations, an absolute noise level of the same order of magnitude as the smallest integrated cross-peak was used. A relative noise level for each integrated peak was set at 5% of the integrated peak intensity. The dynamic range of observed cross-peak intensities at a given mixing time was 1000. In the RANDMARDI procedure, 30 different intensity sets were generated from each experimental data set based on the given noise levels, and MARDIGRAS calculations were performed on all of them. Resulting distances from all 8 × 30 intensity sets were combined into a single bounds file from which the rMD restraint file was generated. Upper and lower bounds in the bounds file were average interproton distances ± one standard deviation calculated from all of the MARDIGRAS runs. An additional 0.2 Å was added to the upper bounds.

Restrained Molecular Dynamics. The obtained distance restraints were incorporated into an rMD procedure using DISCOVER (version 3.0, MSI, San Diego, CA) with the AMBER force field. The two starting models for structure refinement were either A-form or B-form DNA built in INSIGHTII (version 97, MSI, San Diego, CA), modified to include the LNA modification and followed by minimization using DISCOVER.

All the distance restraints were incorporated into an rMD procedure for structure refinement. An initial energy minimization was followed by 28 ps of restrained molecular dynamics at 600 K for 4 ps, followed by cooling to 200 K in 50 K steps of 3 ps each. The final structure was then energy minimized to a maximum derivative of 0.01 Å. A distance-dependent dielectric constant ($\epsilon = r$) was employed to account for solvent effects.

The pseudo-energy term used to enforce the distance restraints was

$$E_{NOE} = \begin{cases} k_1 (r - r_1)^2 & \text{when } r_1 > r \\ 0 & \text{when } r_2 \geq r \geq r_1 \\ k_2 (r - r_2)^2 & \text{when } r > r_2 \end{cases}$$

where r_1 and r_2 are the lower and upper distance bounds determined from cross-peak intensities and k_1 and k_2 are the force constants. A force constant of 50 kcal mol^{-1} Å^{-2} for lower and upper bounds was assigned to all distance restraints. DISCOVER uses a limit on the magnitude a distance restraint can contribute to the force field. This limit was set to 1000 kcal mol^{-1} Å^{-1}.

Helix parameters were calculated with the program CURVES 5.1 (Lavery and Sklenar, 1988; Lavery and Sklenar, 1989).

RESULTS

Spectral Analysis. The 1D ^{1}H NMR spectrum of the sample of the modified LNA:DNA duplex exhibits only lines from the expected LNA:DNA duplex. No signs of alternative hybridization were observed. The NOESY spectra of the LNA duplex exhibit the characteristic features of dsDNA sequential connectivities. The assignment of the nonexchangeable protons in the modified duplex was performed using standard methods (Wüthrich, 1986; Hare et al., 1983; Scheek et al., 1983; Feigon et al., 1983). Aromatic (H6, H5, H8, and H2) and sugar protons (H1′,H2′, H2″,H3′, H4′, and H5′,H5″) were assigned. The chemical shift values and the NOE connectivity pattern of the imino protons were observed to be in accordance with normal Watson−Crick base pairing. The NOESY spectrum with short mixing time (50 ms) allowed unambiguous assignments of the H2′ and H2″ resonances. The assignment of the exchangeable protons was obtained from the NOESY spectrum in H_2O (Boelens et al., 1985). The chemical shift values are given in Table 1 and compared to the corresponding values of the unmodified duplex.

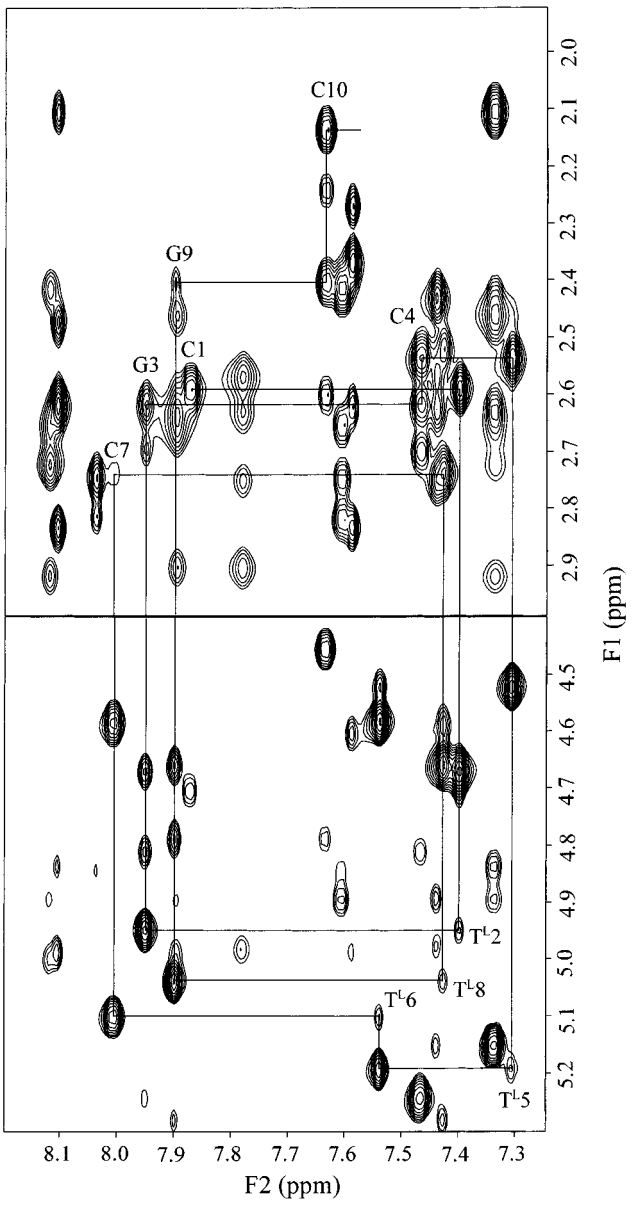

Figure 1. Parts of the 200 ms NOESY spectrum of the d(C**T^L**-GC**T^{L}T^L**C**T^L**GC):d(GCAGAAGCAG) duplex showing the sequential connectivity pattern H6/8 and H2′ on the modified strand. Some of the strong cross-peaks in the lower region are between H3′ and H6/8 indicative of the C3′-endo conformations.

Structure Calculations. More than 800 NOE cross-peaks were observed in the NOESY spectrum obtained with a mixing time of 200 ms. The accuracy of the integration of some cross-peaks was hampered by spectral overlap. These cross-peaks were therefore not included in the MARDIGRAS calculations. Integrations of the cross-peaks in the four NOESY spectra used were done separately for each side of the diagonal. This resulted in four sets of 325 NOE cross-peak intensities and four sets of 310 NOE cross-peak intensities, giving a total of 2540 integrated cross-peak intensities used in the RANDMARDI calculations. Some of the cross-peaks used in the structure calculations resulted predominantly from spin diffusion. This is taken into account during the statistical analysis of the results generated by the

Table 1. Chemical Shift Values (ppm) in the d(CT^{L}GCT^{L}T^{L}CT^{L}GC):d(GCAGAAGCAG) Duplex[a]

	H1′	H2′	H2″	H3′	H4′	H5′	H5″	H6/H8	H5/H2/CH$_3$	H1/H3	H4	H4
C1	5.97	2.59	2.59	4.71	4.13	3.80	3.83	7.86	5.93		8.05	7.08
	(5.95)	(2.14)	(2.56)	(4.69)	(4.12)	(3.80)	(3.80)	(7.83)	(5.93)		(−)	(−)
T^{L}2	5.43	4.95	−	4.67	−	4.36	4.31	7.39	1.70	13.81		
	(5.84)	(2.19)	(2.53)	(4.88)	(4.20)	(−)	(−)	(7.48)	(1.70)	(−)		
G3	6.08	2.62	2.70	4.81	4.37	4.33	4.15	7.94		12.66		
	(5.92)	(2.53)	(2.73)	(5.01)	(4.40)	(4.16)	(4.09)	(7.93)		(12.73)		
C4	5.96	2.54	2.54	4.76	4.26	4.14	4.19	7.43	5.25		8.35	6.73
	(5.96)	(2.16)	(2.55)	(4.72)	(4.27)	(−)	(−)	(7.44)	(5.34)		(8.09)	(6.50)
T^{L}5	5.35	5.19	−	4.52	−	4.27	4.27	7.31	1.56	14.26		
	(6.04)	(2.17)	(2.60)	(4.86)	(4.20)	(−)	(−)	(7.48)	(1.62)	(14.12)		
T^{L}6	5.52	5.09	−	4.58	−	4.29	4.23	7.54	1.64	13.91		
	(6.08)	(2.43)	(2.57)	(4.90)	(4.21)	(−)	(−)	(7.47)	(1.68)	(13.74)		
C7	5.69	2.73	2.52	4.59	4.21	4.30	4.11	8.00	5.63		8.31	6.81
	(5.97)	(2.11)	(2.48)	(4.81)	(4.20)	(−)	(−)	(7.60)	(5.65)		(8.39)	(6.93)
T^{L}8	5.28	5.03	−	4.66	−	4.31	4.21	7.42	1.61	13.54		
	(5.71)	(2.07)	(2.41)	(4.87)	(4.14)	(−)	(−)	(7.33)	(1.69)	(13.90)		
G9	6.04	2.40	2.60	4.79	4.21	4.11	4.31	7.89		12.73		
	(5.95)	(2.65)	(2.73)	(4.99)	(4.37)	(4.12)	(4.09)	(7.92)		(12.91)		
C10	6.15	2.14	2.24	4.45	4.02	4.15	4.15	7.63	5.43	−	8.23	6.90
	(6.20)	(2.19)	(2.19)	(4.49)	(4.06)	(−)	(−)	(7.48)	(5.52)	(−)	(8.15)	(6.70)
G11	6.04	2.74	2.81	4.84	4.26	3.81	3.81	8.03		−		
	(5.97)	(2.60)	(2.78)	(4.84)	(4.23)	(3.71)	(3.71)	(7.95)		(−)		
C12	6.02	2.42	2.65	4.89	4.32	4.23	4.23	7.61	5.42		8.65	6.75
	(5.55)	(2.04)	(2.36)	(4.86)	(4.16)	(−)	(−)	(7.45)	(5.45)		(8.50)	(6.52)
A13	6.20	2.73	2.92	5.00	4.41	4.22	4.25	8.12	7.12			
	(5.95)	(2.71)	(2.86)	(5.05)	(4.38)	(4.15)	(4.00)	(8.18)	(7.63)			
G14	5.72	2.46	2.67	4.90	4.35	4.23	4.23	7.33		12.46		
	(5.38)	(2.54)	(2.66)	(4.99)	(4.34)	(4.16)	(4.16)	(7.69)		(12.51)		
A15	6.13	2.64	2.90	4.98	4.43	4.24	4.24	7.89	7.07			
	(5.92)	(2.60)	(2.86)	(5.03)	(4.42)	(4.19)	(4.19)	(8.04)	(7.24)			
A16	6.02	2.57	2.75	4.97	4.40	4.24	4.24	7.77	7.30			
	(5.94)	(2.56)	(2.80)	(5.02)	(4.40)	(4.20)	(4.20)	(7.98)	(7.48)			
G17	5.84	2.43	2.63	4.89	4.37	4.21	4.21	7.43		12.73		
	(5.68)	(2.40)	(2.58)	(4.91)	(4.34)	(4.18)	(4.18)	(7.53)		(12.77)		
C18	5.83	2.10	2.47	4.83	4.21	4.09	4.09	7.34	5.15		8.40	6.38
	(5.50)	(1.85)	(2.24)	(4.78)	(4.09)	(−)	(−)	(7.26)	(5.25)		(8.26)	(6.26)
A19	6.08	2.62	2.83	4.98	4.37	4.09	4.17	8.10	7.43			
	(6.04)	(2.68)	(2.85)	(5.00)	(4.38)	(4.00)	(4.10)	(8.16)	(7.81)			
G20	6.07	2.37	2.27	4.61	4.18	4.13	4.22	7.58		−		
	(6.04)	(2.45)	(2.29)	(4.63)	(4.18)	(4.24)	(4.12)	(7.71)		(−)		

[a] The value of the unmodified duplex are given in parentheses. The values are given at 25 °C relative to DSS. The protons in the C2′,C4′ linker have the following chemical shift values: **T^L**2 H6′/H6″, 4.00/4.15; **T^L**5 H6′/H6″, 4.00/4.10; **T^L**6 H6′/H6″, 4.02/4.10; **T^L**8 H6′/H6″, 3.93/4.09.

RANDMARDI procedure (Liu et al., 1995). Cross-peak integrals that corresponded to fixed distances in the dsDNA were used for internal calibrations in MARDIGRAS and, therefore, not converted into distance restraints for use in the rMD simulations. The MARDIGRAS calculations were performed by using a value of the correlation time of $\tau_c = 2.5$ ns. This value was justified from earlier work (Spielmann et al., 1995; Gotfredsen et al., 1996; Petersen and Jacobsen, 1998; Johansen and Jacobsen, 1998). Furthermore, it turns out that the results of the calculations are rather insensitive to the exact values of τ_c used. Calculation with $\tau_c = 1.0$ ns and $\tau_c = 3.75$ ns yielded exactly the same structure but with slightly larger RMSD deviations This is similar to what was found earlier (Mujeeb et al., 1993; Gotfredsen et al., 1996).

The RANDMARDI calculations returned 339 interproton distances that are not covalently fixed in the modified DNA. The distance bounds used in RMD simulations were determined by combining the results from all of the individual MARDIGRAS calculations performed during the RANDMARDI procedure into one set. They were calculated individually for each proton pair corresponding to a NOESY cross-peak included in the RANDMARDI calculations. Each individual restraint was generated from the MARDIGRAS calculations. Table 2 gives a summary of the distance restraints used in the RMD calculations. The range of differences between the upper and lower bounds for the 339 NOE-derived restraint bounds used (Table 2) was between 0.24 and 2.64 Å with an average flat well potential width of 0.77 Å. This range between the upper and lower bounds represents the precision of the restraint calculated from the NOESY data. Weak NOESY cross-peaks that are primarily from spin diffusion had the largest distance between the upper and lower distance bounds.

Evaluation of the spectra obtained in H_2O shows normal Watson−Crick hydrogen bonding, justifying the inclusion of 26 hydrogen bond distance restraints. Three hydrogen bonds were included for each of the six GC base pairs, and two hydrogen bonds were included for each of the four AT base pairs with upper and lower bounds of 1.74 and 2.10 Å, respectively. An additional 24 restraints with loose bounds involving labile protons were derived using the isolated spin pair approximation on the NOESY spectra recorded of the sample in H_2O. Thus, a total of 389 interproton restraints was used in the RMD calculations.

Twenty final structures for each of the two starting structures were generated. All the structures converged to one family of conformations. The average all atom root-mean-square (RMS) deviation of the coordinates of the 40 structures was 0.6 Å. The average sum of violations was 10.48 Å for the A-form starting structures and 10.09 Å for the B-form starting structures. We observed only six to eight violations greater than 0.2 Å and none greater

Table 2. Number of Distance Restraints Used in the rMD Calculations of the d(CT^{L}GCT^{L}T^{L}CT^{L}GC):d(GCAGAAGCAG) Duplex[a]

intraresidue		interresidue		intraresidue		interresidue		interstrand	
C1	7	C1−T^{L}2	7	G11	10	G11−C12	7	T^{L}2−A19	1
T^{L}2	16	T^{L}2−G3	6	C12	9	C12−A13	5	T^{L}6−A15	2
G3	10	G3−C4	10	A13	11	A13−G14	9	T^{L}6−A16	2
C4	3	C4−T^{L}5	6	G14	5	G14−A15	5	T^L 8−A13	2
T^{L}5	13	T^{L}5−T^{L}6	10	A15	10	A15−A16	6	T^{L}8−A15	1
T^{L}6	14	T^{L}6−C7	10	A16	8	A16−G17	3	C7−A15	3
C7	12	C7−T^{L}8	13	G17	7	G17−C18	3	G9−A13	3
T^{L}8	16	T^{L}8−G9	6	C18	10	C18−A19	5		
G9	5	G9−C10	9	A19	9	A19−G20	6		
C10	13			G20	11				
total	109		77		90		49		14

[a] The restraints were derived from MARDIGRAS calculations unless otherwise stated. The NOESY spectrum in H_2O gave rise to 24 loose distance restraint of which 14 were interstrand distance restraints. The Watson−Crick base pairing were ensured by further including 26 distance restraints in the rMD calculations.

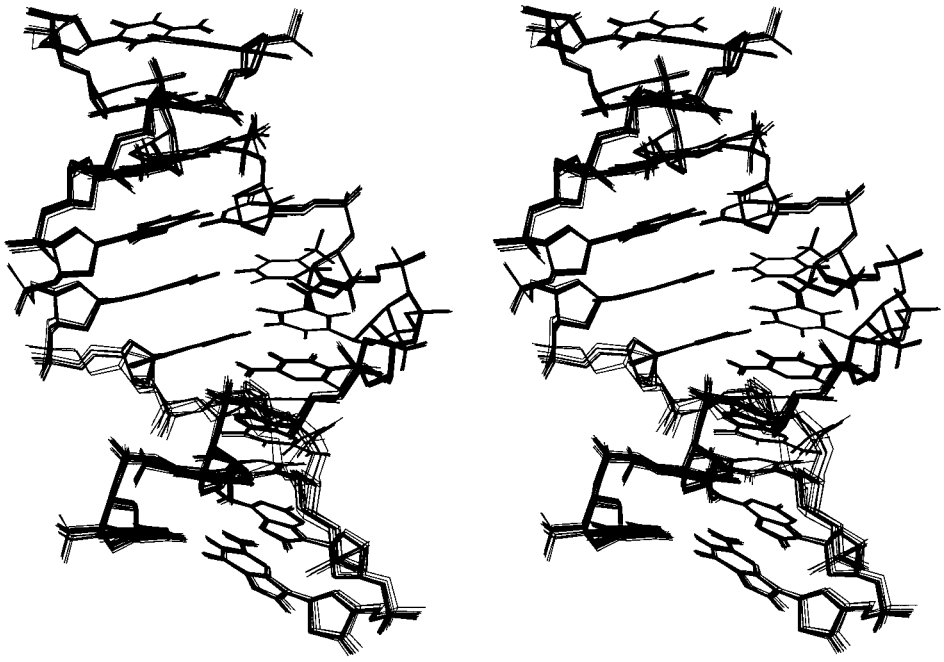

Figure 2. Stereoview of a superposition of stick plots of 20 calculated structures of the d(C**T^L**GC**T^{L}T^L**C**T^L**GC):d(GCAGAAGCAG) duplex. Deoxyribose protons have been omitted for clarity. Ten structure were randomly picked from each of the two sets of structures obtained from A- and B-DNA starting structures, respectively.

than 0.26 Å. Different views of the structure are presented in Figures 2 and 3.

The reliability of the structure calculations was carefully evaluated. rMD calculations were performed where the force constants of the distance restraints changed to 25 and 100 kcal mol^{-1} Å^{-2}, respectively. All the calculations generated structures that converged to the same family of structures as with the force constants of 50 kcal mol^{-1} Å^{-2}. A lower force constant resulted in a higher RMSD and more violations. The structure obtained is not strongly dependent on the exclusion of any of the restraints. In particular, calculations performed without the Watson−Crick restraints yielded exactly the same structure but with slightly larger RMSD.

Helix Parameters. Helical parameters for the 40 final structures were analyzed with the program CURVES 5.1 (Lavery and Sklenar, 1988; Lavery and Sklenar, 1989). Plots of some global helical parameters for the LNA duplex are shown in Figure 4.

DISCUSSION

Spectral Data. The chemical shift values given in Table 1 demonstrate close agreement between the modified and unmodified duplex except for the protons near the modification sites. As expected from the sugar conformation, the protons in the LNA nucleotides differ from those in the unmodified nucleotide. The protons on the other nucleotides show differences in chemical shift values between the modified and the unmodified duplex primarily at the A13, A19, C7, and G14 nucleotides. The largest effect is observed for the adenine H2 protons, especially those of A13 and A19 with downfield shifts of 0.51 and 0.38 ppm, respectively. A large effect is also observed at some of the other aromatic protons, e.g., C7H6 and G14H8, with an upfield shift of 0.40 ppm and a downfield shift of 0.36, respectively. The chemical shift values of the other aromatic proton are changed more moderately. The pronounced shifts of the resonances of the aromatic protons are most probably related to an enhanced stacking of the nucleobases. It is noteworthy that this effect is observed both on the base paired to the LNA nucleotide as well as the base neighboring the LNA nucleotide on the same strand.

The changes of the chemical shift of the sugar protons of the modified nucleotides are clearly related to the chemical modification introduced whereas those of the unmodified nucleotides may, at least partly, be related to conformational changes of the deoxyribose ring.

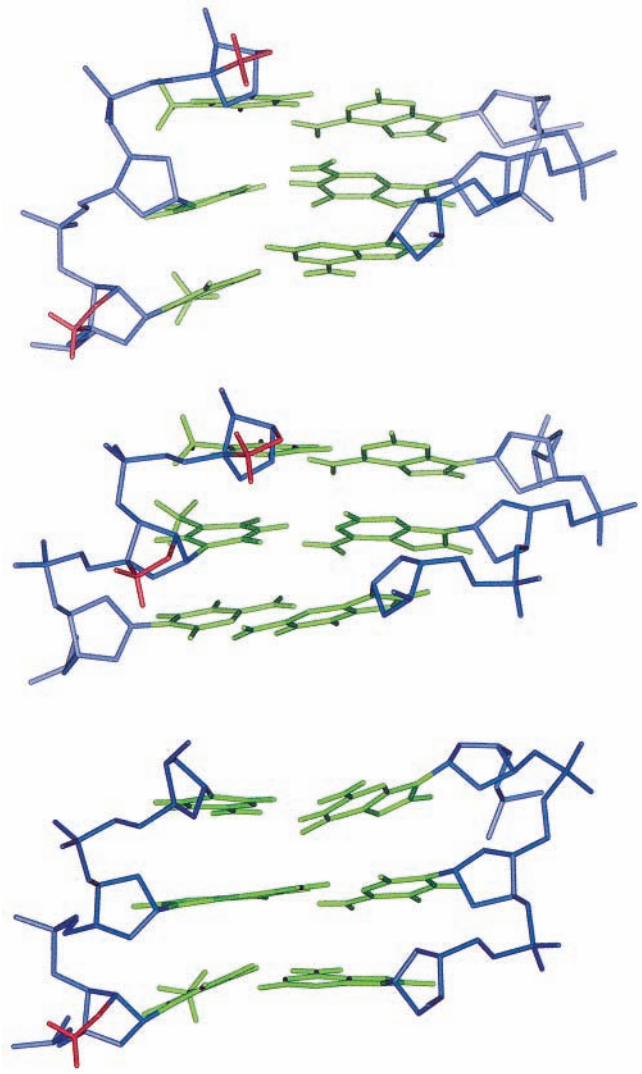

Figure 3. Basepair stacking in the d(C**T**^{L}GC**T**^{L}**T**^{L}C**T**^{L}GC): d(GCAGAAGCAG) duplex viewed from the minor groove side. The bases are shown in green and the sugar backbone in blue. The 2′-*O*,4′-*C* bridge is indicated in red. The (**T**^{L}2-G3-C4):(G17-C18-A19) step are shown at the *bottom*, the (C4-**T**^{L}5-**T**^{L}6):(G14-A15-A16) in the *middle* and the (**T**^{L}6-C7-**T**^{L}8):(A13-G14-A15) at the *top*.

Description of the Structure. Qualitatively, the NOESY spectra of the LNA duplex indicate that it adopts a right-handed helix conformation. All bases are in the anti conformation and they all form normal Watson−Crick base pairs. Recently, we reported the use of a selective DQF-COSY spectrum to determine the sugar conformations (Petersen et al., 1999). The LNA nucleotides are locked in a C3′-endo (N-type) conformation. The unmodified nucleotide C7 is also exclusively in the N-type conformation whereas G3 and G9 are in mixed conformations with substantial N-type contributions. The nucleotides in the complementary strand are predominantly in the normal S-type configuration. This mixed situation forced us not to include any dihedral angle restraints in the rMD calculations. Doing that, it would have been necessary to include a description of the dynamic ring puckering motions of the sugars. Such a description is not available.

Experimentally derived NMR distance restraints are distributed anisotropically and are short range in nature. This largely establishes local structures with some helical parameters better defined by the experimental data than others. We have used a number of NMR derived interstrand restraints in the center of the helix originating from AH2 protons to H1′ protons and a number of loose bounds interstrand distance restraints that improved the ability to define the overall structure of the oligonucleotide (Weisz et al., 1994).

We have shown representations of the structure of the duplex in Figures 2 and 3. Figure 2 demonstrates the high accuracy of this structure determination. The colored graphic representation in Figure 3 shows a picture of the base pairing and stacking of the bases close to the modification.

Helical Parameters. There are three major categories of helical parameters: axis−base pair, intra−base pair, and inter−base pair parameters (Dickerson et al., 1989). These parameters for the duplex are shown in Figure 4. However, the parameters reported for the terminal base pairs of the complex are probably less reliable because of dynamic processes and a lower density of restraints and are only included for completeness.

The global helix axis is slightly bent as shown in Figure 5. The width of the minor groove measured as the shortest interstrand phosphorus distance across the groove is included in Figure 6. Although local narrowing of the minor groove occurs, the width of the minor groove does not deviate much from what is observed in unmodified DNA duplexes.

Values of the pseudorotational angles obtained from CURVES are averaged values of a dynamic interchange between N- and S-type conformation. The values for T^{L}2, T^{L}5, T^{L}6, and T^{L}8 were found by CURVES to be very close to 17° as reported earlier (Obika et al., 1997). The values obtained for the other nucleotides on the modified strand indicate that C7 and G9 are predominantly in the N-type conformation, whereas G3 is in a mixed conformation. The unmodified complementary strand was found to be almost exclusively in the S-type conformation. As mentioned earlier, structure calculation using NOE restraints do not include the necessary description of the dynamic ring puckering motion of the sugar. This implies that it is not expected that the values for the pseudorotation angle obtained from the CURVES analysis agree completely with the values obtained from the conformational study reported earlier (Petersen et al., 1999). However, we do find from the CURVES analysis that the obtained structure reproduces very well the values for the pseudorotation angles obtained earlier (Petersen et al., 1999).

Axis−Base Pair Parameters. The helix parameters Xdisp, Ydisp, tip, and inclination deviate significantly from the values in B-DNA (Baleja et al., 1990; Mujeeb et al., 1993; Schmitz et al., 1992; Weisz et al., 1994). The values of Xdisp and tip show that the duplex is between B-type and an A-type DNA. There is a significant trend in the variation of the values of Ydisp and inclination along the strand. This is related to the slightly bended helix axis.

Intra-Base Pair Parameters. The calculated values for shear, stretch, stagger, and opening do not show much deviation from B-type DNA. The buckle changes significantly along the strand. Large changes from −25 to 20° occur. This is connected to the change in sugar conformation of the nucleotides on the modified strand. The structural strain between the modified strand, having sugar conformations partly of the N-type, and the complementary strand, having almost exclusively S-type sugar conformations, is relaxed by large variation of values of the buckle. In conjunction with that, the values of propeller twist do also deviate from both A-type and B-type DNA. Especially, the large value of the propeller twist for the base pair T^{L}5:A16 is noteworthy.

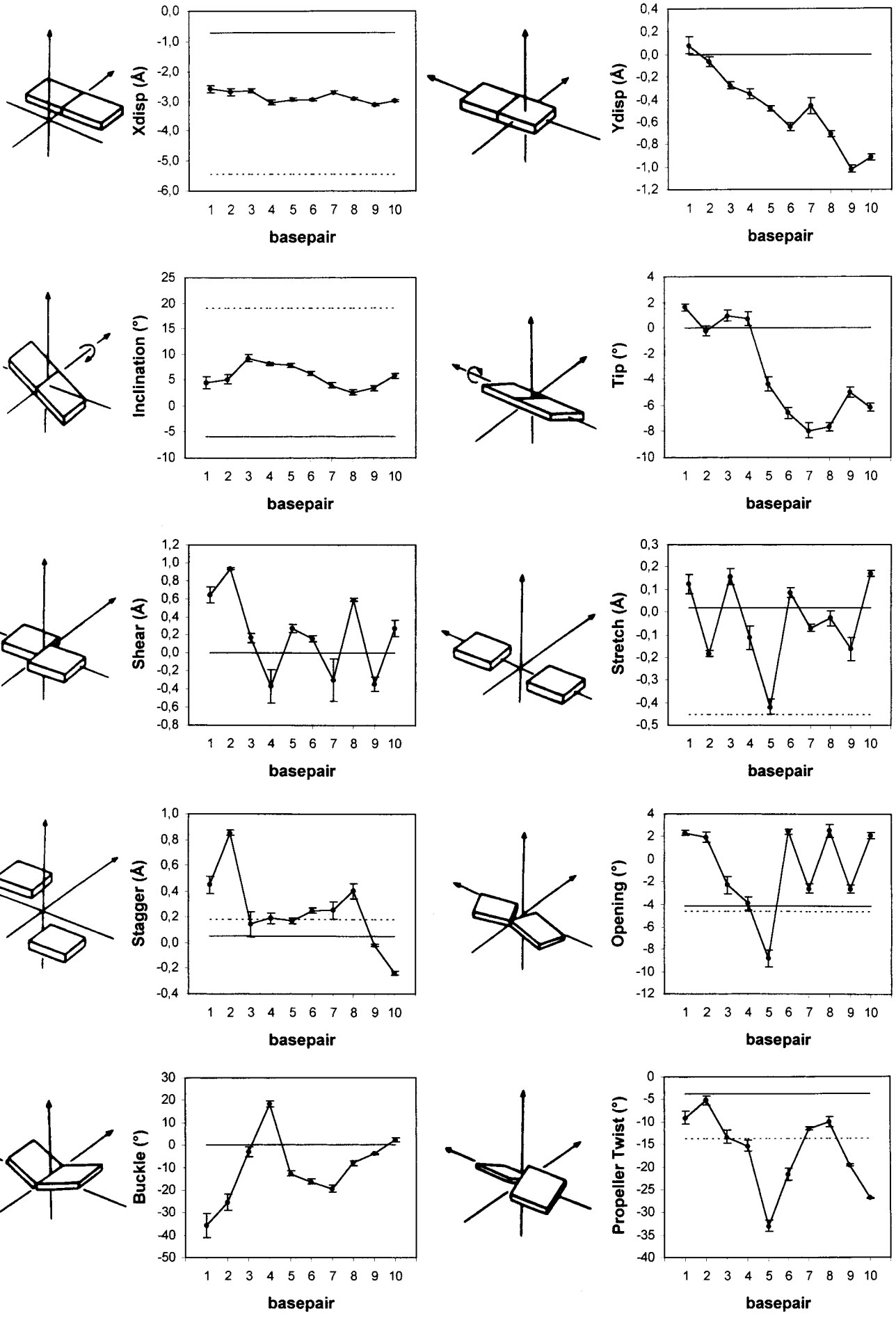
Xdisp (Å)
Ydisp (Å)
Inclination (°)
Tip (°)
Shear (Å)
Stretch (Å)
Stagger (Å)
Opening (°)
Buckle (°)
Propeller Twist (°)
basepair

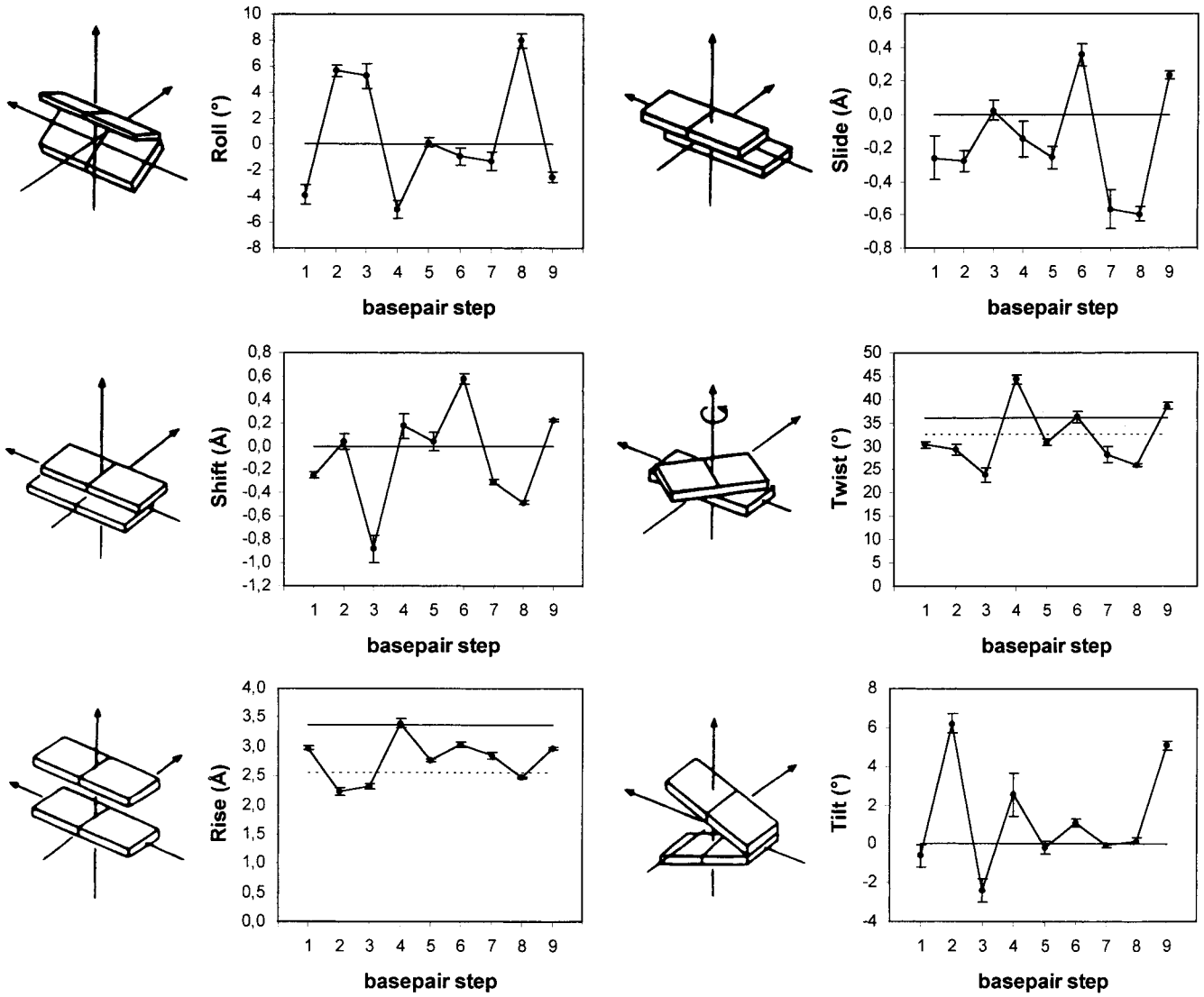

Figure 4. Helical parameters for the d(C**T**^{L}GC**T**^{L}**T**^{L}C**T**^{L}GC):d(GCAGAAGCAG) duplex (●) calculated using CURVES and compared with canonical A-DNA (- - -) and canonical B-DNA (——).

Inter−Base Pair Parameters. The values for rise are markedly different in canonical B-DNA (3.4 Å) and A-DNA (2.6 Å). The values of rise in the LNA duplex vary from below 2.6 to 3.4 Å, but the average rise is below 2.8 Å, which is closer to the canonical A-type than to the canonical B-type DNA. This indicates increased base stacking and is connected to the sugar conformations of the modified strand that has much more N-type conformation than in normal B-DNA. However, since the sugar conformations on the base-paired nucleotides at the complementary strand are kept in the S-type conformation, the resulting strain is relaxed by decreasing the value of rise and compensated with tip, buckle, and propeller twist as described. The values of twist differ along the strand, but for a majority of the base pairs, a value even lower than that of A-DNA is observed. The average twist over the sequence is 32 ± 1°. This value is close to the one in the canonical A-type DNA. This shows in particular that the modification does not cause the helix to unwind. The roll, tilt, slide, and shift parameters do not deviate much from neither B- nor A-DNA and are within values normally observed in both A-type and B-type DNA (Mujeeb et al., 1993).

Comparison with Related Structures. An impressive number of modified nucleotides for use in antisense or antigene strategy has appeared. Some of them have been studied by structural techniques, but only a few high-resolution structures have been obtained of sugar-modified oligonucleotides, among these are the 2′-*O*-methylated RNA analogues. The substitution of one 2′-*O*-CH_3-modified ribose nucleotide into a DNA duplex has been studied by X-ray crystallography (Lubini et al., 1994). It shows that the presence of one 2′-*O*-CH_3 ribonucleotide is sufficient to induce local transition from B-type DNA to A-type DNA with the 2′-*O*-CH_3 group pointing into the minor groove. Blommers and co-workers used a fully modified 2′-*O*-CH_3 ribonucleotide strand instead of an RNA strand to evaluate the effect of a single amide backbone modification in a complementary DNA strand (Blommers et al., 1994). Recently, a high-resolution structure of an all 2′-*O*-CH_3-modified duplex 2′-*O*-Me$(CGCGCG)_2$ was published (Propenda et al., 1997; Adamiak et al., 1997). In this structure all residues have N-type sugar pucker with a very small rise and a high helical twist and inclination. Although, it may be somewhat difficult to justify a comparison between 2′-*O*-CH_3-modified oligonucleotides and the LNA duplex reported here, there is definitely the same trend of the structures in shifting from a B-type toward an A-type.

Recently, we reported (Nielsen et al., 1999) the NMR structure of the modified d(CCGC**T**^{L}AGCG): d(CGCTAGCGG) containing one modified LNA nucleotide. This

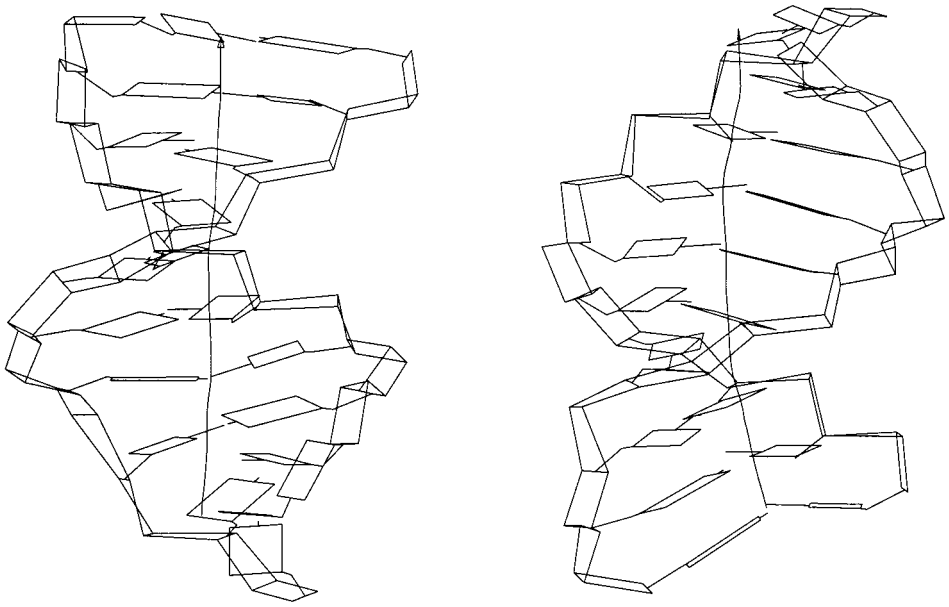

Figure 5. A schematic representation of the structure of the d(C**T**^{L}GC**T**^{L}**T**^{L}C**T**^{L}GC):d(GCAGAAGCAG) duplex showing the position of the helix axis as calculated by CURVES. To the *left*, the structure is viewed from the direction at which the helix axis is most straight. To the *right*, the structure has been turned 90°.

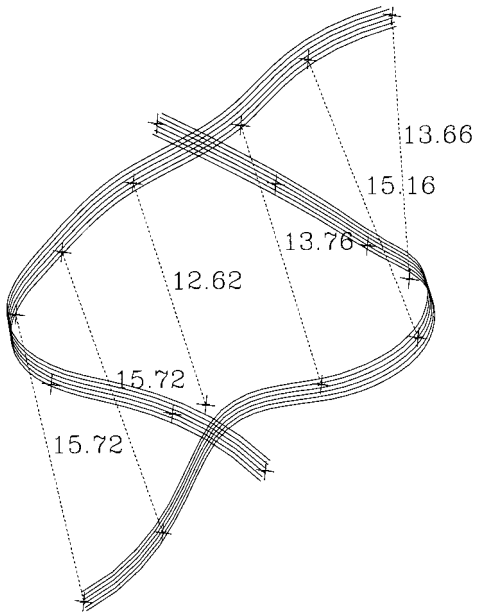

Figure 6. The structure of the d(C**T**^{L}GC**T**^{L}**T**^{L}C**T**^{L}GC):d(GCAGAAGCAG) duplex presented as a ribbon along the sugar backbone. The distances between the phosphate groups perpendicular to the two strand are indicated. The width of the minor groove is traditionally give by this distance reduced by 5.8 Å to account for the van der Waals' radius.

structure was found to be close to a B-type helix, but shows some deviation from canonical B-DNA in the vicinity of the modification. These changes were most pronounced for the opening, buckle, tip rise, and twist completely in analogy to the one observed in the present study, but to a much lesser extent. The average twist observed for the d(CCGC**T**^{L}AGCG): d(CGCTAGCGG) oligonucleotide was 35.0 ± 0.3°, which is close to the value in the canonical B-type DNA. A comparison between the d(CCGC**T**^{L}AGCG):d(CGCTAGCGG) and d(C**T**^{L}GC**T**^{L}**T**^{L}C**T**^{L}GC):d(GCAGAAGCAG) duplexes shows that the small structural changes from B-type DNA toward A-type DNA in the former oligonucleotide containing one modification have further increased in the latter oligonucleotide containing four modifications.

Stability of LNA:DNA Duplexes. The stability of a DNA duplex can thermodynamically be described by use of Gibbs, free energy for duplex formation: $\Delta G = \Delta H - T\Delta S$. Searle and Williams (Searle and Williams, 1993) have in relation to that discussed the stability of nucleic acid structures in solution in terms of enthalpy−entropy compensations. Following their outline the effect of introducing a modification can be explained in terms of a change of the free energy of the "internal rotors" of the phosphate backbone (ΔG_r) and the free energy related to the base stacking (ΔG_s). The change of the free energy of the base stacking is dominated by an enthalpy change ($\Delta G_s \approx \Delta H_s$) whereas the change of the free energy of the internal rotors of the backbone is dominated by entropy ($\Delta G_r \approx \Delta S_r$) (Searle and Williams, 1993). Earlier, we found that the conformations of the nucleotides in the ssLNA d(C**T**^{L}GA**T**^{L}A**T**^{L}GC) had larger amounts of N-type conformation than in the unmodified ssDNA and that this ssLNA oligonucleotide was preorganized for the formation of the d(C**T**^{L}GA**T**^{L}A**T**^{L}GC):d(GCATATCAG) duplex (Nielsen et al., 1999). This implies that a smaller change of backbone entropy (ΔS_r) has to be paid in the duplex formation. In this paper, we show that the organization of the backbone and the sugar rings into a C3′-endo fashion favors a more efficient stacking. This is equivalent to the structural changes from B-DNA (C2′-endo conformation) to A-DNA (C3′-endo conformation) (Saenger, 1984). Thus, in LNA modified duplexes there is a local change of the phosphate backbone geometry that favors a higher degree of stacking and hence an increased value of $-\Delta H_s$.

A straightforward consequence of the explanation given above is that the increase in the stability of LNA modified LNA:DNA duplexes should saturate as the number of modifications increase. This is exactly the observation. In the d(G**T**^{L}GA**T**^{L}A**T**^{L}GC):d(GCATATCAC) duplex the melting temperature is increased by 5.3 °C per modification compared to the unmodified DNA duplex whereas in the fully modified d(**G**^{L}**T**^{L}**G**^{L}**A**^{L}**T**^{L}**A**^{L}**T**^{L}**G**^{Lme}**C**^{L}):d(GCATATCAC) duplex the increase in the melting

temperature was 4.5 °C per modification (Singh et al., 1998; Koshkin et al., 1998a). Thus, the largest effect per modification is observed in duplexes that are not fully modified.

The combined contribution to the stability of the LNA:DNA duplexes from both preorganization and improved stacking was further investigated by the synthesis of an abasic LNA nucleotide and the inclusion of this abasic modified nucleotide in an oligonucleotide (Kværnø and Wengel, 1999). From melting temperature measurement, it was concluded that the base stacking are of crucial importance for the stability of LNA:DNA and LNA:RNA duplexes.

It seems difficult to specify the amount of stabilization that arises from the ordering of the phosphate backbone and the part caused by increased stacking. Breslauer et al. (1986) have determined the nearest neighbor thermodynamic parameters related to the base pairing in DNA duplex formation and used these values to predict duplex stability. They found very convincing agreement between calculated values and experimentally determined ones. The values of $\Delta G°$, $\Delta H°$, and $\Delta S°$ for duplex formation of two nearest neighboring base pairs are very sequence specific with value of $-\Delta G°$ between 4 and 15 kJ/mol, $-\Delta H°$ between 23 and 50 kJ/mol, and $-\Delta S°$ between 54 and 116 J/mol. Within these limits, the stability of LNA:DNA duplexes is easily explained by a slightly increased value of $-\Delta H°$ and a slightly decreased value of $-\Delta S°$.

ACKNOWLEDGMENT

This work was supported by grants from The Danish Natural Science Research Council and The Danish Technical Research Council. We thank The Instrument Center for NMR-Spectroscopy of Biological Macromolecules at The Carlsberg Laboratory, Copenhagen for providing spectrometer time at the 750 MHz spectrometer. Ms Britta M. Dahl is thanked for synthesis of the LNA oligonucleotides.

LITERATURE CITED

Adamiak, D. A., Milecki, J., Propenda, M., Adamiak, R. W., Dauter, Z., and Rypniewski, W. R. (1997) Crystal Structure of 2′-*O*-Me(CGCGCG)$_2$, an RNA duplex at 1.30 Å Resolution. Hydration Pattern of 2′-*O*-methylated RNA. *Nucleic Acids Res. 25*, 4599−4607.

Baleja, J. D., pon, R. T., and Sykes, B. D. (1990) Solution Structure of Phage Lamda Half-Operator DNA by Useof NMR, Restrained Molecular Dynamics, and NOE-Based Refinement. *Biochemistry 29*, 4828−4839.

Blommers, M. J. J., Pieles, U., and De Mesmaeker, A. (1994) An Approach to the Structure Determination of Nucleic Acid Analogues Hybridized to RNA. NMR Studies of a Duplex Between 2′-*O*-Me RNA and an Oligonucleotide Containing a Single Backbone Modification. *Nucleic Acids Res. 22*, 4187−4194.

Boelens, R., Scheek, R. M., Dijkstra, K., and Kaptein, R. (1985) Sequential Assigment of Imino- and Amino-Proton Resonances in ^{1}H NMR Spectra of Oligonucleotides by Two-Dimensional NMR Spectroscopy. Application to *lac* Operator Fragment. *J. Magn. Reson. 62*, 378−386.

Borgias, B. A., and James, T. L. (1990) MARDIGRAS-A Procedure for Matrix Analysis of Relaxation for Discerning Geometry of an Aqueous Structure. *J. Magn. Reson. 87*, 475−487.

Borgias, B. A., Gochin, M., Kerwood, D., and James, T. L. (1990) Relaxation Matrix Analysis of 2D NMR Data. *Prog. NMR Spectrosc. 22*, 83−100.

Breslauer, Frank, R., Blücker, H., and Marky, L. (1986) Predicting DNA Duplex Stability from Base Sequence. *Proc. Natl. Acad. Sci. 83*, 3746−3750.

De Mesmaeker, A., Häner, R., Martin, P., and Moser, H. E. (1995) Antisense Oligonucleotides. *Acc. Chem. Res. 28*, 366−374.

Dickerson, R. E., Bansal, M., Calladine, C. R., Diekmann, S., Hunter, W. N., Kennard, O., von Kitzing, E., Nelson, H. C. M., Lavery, R., Olson, W. K., Saenger, W., Shakked, Z., Soumpasis, D. M., Tung, C.-S., Sklenar, H., Wang, A. H. J., and Zhurkin, V. B. (1989) Definitions and Nomenclature of Nucleic Acid Structure Parameters. *EMBO J. 8*, 1−4.

Feigon, J., Leupin, W., Denny, W. A., and Kearns, D. R. (1983) Two-Dimensional Proton Nuclear Magnetic Resonance Investigation of the Synthetic Deoxyribonucleic Acid Decamer d(ATATCGATAT)$_2$. *Biochemistry 22*, 5943−5951.

Gotfredsen, C. H., Spielmann, H. P., Wengel, J., and Jacobsen, J. P. (1996) Structure of a DNA duplex Containing a Single 2′-O-Methyl-beta-D-araT: Combined Use of NMR, Restrained Molecular Dynamics and Full Relaxation Matrix Refinement. *Bioconjugate Chem. 7*, 680−688.

Hare, D. R., Wemmer, D. E., Chou, S.-H., Drobny, G., and Reid, B. R. (1983) Assignment of the Non-Exchangeable Proton Resonances of d(C−G-C−G-A−A-T−T-C−G-C−G) Using Two-Dimensional Nuclear Magnetic Resonance Methods. *J. Mol. Biol. 171*, 319−336.

Hélène, C. (1991) The Anti-Gene Strategy: Control of Gene Expression by Triplex-Forming-Oligonucleotides. *Anti-Cancer Drug Des. 6*, 569−584.

Hélène, C., and Toulmé, J.-J. (1990) Specific Regulation of Gene Expression by Antisense, Sense and Antigene Nucleic Acids. *Biochim. Biophys. Acta 1049*, 99−125.

Johansen, F., and Jacobsen, J. P. (1998) Site Selective Bis-Intercalation of a Homodimeric Oxazole Yellow dye in DNA Oligonucleotides. *J. Biomol. Struct. Dyn. 16*, 205−222.

Koshkin, A. A., Singh, S. K., Nielsen, P., Rajwanshi, V. K., Kumar, R., Meldgaard, M., Olsen, C. E., and Wengel, J. (1998a) LNA (Locked Nucleic Acids): Synthesis of the Adenine, Cytosine, Guanine, 5-Methylcytosine, Thymine and Uracil Bicyclonucleoside Monomers, Oligomerisation, and Unprecedented Nuclei Acid Recognition. *Tetrahedron 54*, 3607−3630.

Koshkin, A. A., Rajwanshi, V. K., and Wengel, J. (1998b) Novel Convinient Syntheses of LNA [2.2.1]Bicyclo Nucleosides. *Tetrahedron Lett. 39*, 4381−4384.

Koshkin, A. A., Nielsen, P., Meldgaard, M., Rajwanshi, V. K., Singh, S. K., and Wengel, J. (1998c) LNA (Locked Nucleic Acid): An RNA Mimic Forming Exceedingly Stable LNA:LNA Duplexes. *J. Am. Chem. Soc. 120*, 13252−13253.

Kværnø, l., and Wengel, J. (1999) Investigation of Restricted Backbone Conformations as an Explanation for the Exceptional Thermal Stabilities of Duplexes Involving LNA (Locked Nucleic Acid): Synthesis and Evaluation of Abasic LNA. *Chem. Commun. 1999*, 657−658.

Lavery, R., and Sklenar, H. (1988) The Definition of Generalized Helicoidal Parameters and of Axis Curvature of Irregular Nucleic Acids. *J. Biomol. Struct. Dyn. 6*, 63−91.

Lavery, R., and Sklenar, H. (1989) Defining the Structure of Irregular Nucleic Acids: Conventions and Principles. *J. Biomol. Struct. Dyn. 7*, 655−667.

Liu, H., Spielmann, H. P., Ulyanov, N. A., Wemmer, D. E., and James, T. L. (1995) Interproton Distances Bounds from 2D-NOE Intensities: Effect of Experimental Noise and Peak Integrations Errors. *J. Biol. NMR 6*, 390−402.

Lubini, P., Zürcher, W., and Egli, M. (1994) Stabilizing Effects of the RNA 2′-Substituent: Crystal Structure of an Oligodeoxynucleotide Duplex Containing 2′-*O*-Methylated Adenosines. *Chem. Biol. 1*, 39−45.

Mujeeb, A., Kerwin, S. M., Kenyon, G. L., and James, T. L. (1993) Solution Structure of a Conserved DNA Sequence from the HIV-1 Genome: Restrained Molecular Dynamics Simulation with Distance and Torsion Angle Restraints Derived from Two-Dimensional NMR Spectra. *Biochemistry 32*, 13419−13431.

Nielsen, C. B., Singh, S. K., Wengel, J., and Jacobsen, J. P. (1999) The Solution Structure of a Locked Nucleic Acid (LNA) Hybridized to DNA. *J. Biomol. Struct. Dyn. 17*, 175−191.

Nielsen, P. E. (1991) Sequence-Selective DNA Recognition by Synthetic Ligands. *Bioconjugate Chem. 2*, 1−12.

Obika, S., Nanbu, D., Hari, Y., Mori, K., In, Y., Ishida, T., and Imanishi, T. (1997) Synthesis of 2′-*O*, 4′-*C*-Methyleneuridine and -Cytidine. Novel Bicyclic Nucleosides Having a Fixed C3′-*endo* Sugar Puckering. *Tetrahedron Lett. 38*, 8735

Petersen, M., and Jacobsen, J. P. (1998) Solution Structure of a DNA Complex with the Fluorescent Bis-Intercalator TOTO Modified in the Major Groove. *Bioconjugate Chem. 9*, 331−340.

Petersen, M., Nielsen, C. B., Nielsen, K. E., Jensen, G. A., Bondensgaard, K., Singh, S. K., Rajwanshi, V. K., Koshkin, A. A., Dahl, B. M., Wengel, J., and Jacobsen, J. P. (2000) Conformation of Locked Nucleic Acid (LNA) Hybridized to DNA. *J. Mol. Recognit. 13*, 44−53.

Propenda, M., Biala, E., Milecki, J., and Adamiak, R. W. (1997) Solution Structure of RNA Duplexes containing Alternating CG Base Pairs: NMR Study of r(CGCGCG)$_2$ and 2′-*O*-Me-(CGCGCG)$_2$ under Low Salts Conditions. *Nucleic Acids Res. 25*, 4589−4598.

Saenger, W. (1984) *Principles of Nucleic Acid Structure*, Springer-Verlag, New York.

Scheek, R. M., Russo, N., Boelens, R., and Kaptein, R. (1983) Sequential Resonance Assigments in DNA ^{1}H NMR Spectra by Two-Dimensional NOE Spectroscopy. *J. Am. Chem. Soc. 105*, 2914−2916.

Schmitz, U., Sethson, I., Egan, W. M., and James, T. L. (1992) Solution Structure of a DNA Octamer Containing the Pribnow Box via Restrained Molecular Dynamics Simulation with Distance and Torsional Angle Constraints Derived from Two-Dimensional Nuclear Magnetic Resonance Spectral Fitting. *J. Mol. Biol. 227*, 510−531.

Searle, M. S., and Williams, D. H. (1993) On the Stability of Nucelic Acid Structures in Solution: Enthalpy − Entropy Compensations, Internal Rotations and Reversability. *Nucleic Acid Res. 21*, 2051−2056.

Singh, S. K., and Wengel, J. (1998) Universality of LNA-Mediated High-Affinity Acid Recognition. *Chem. Commun.* 1247−1248.

Singh, S. K., Nielsen, P., Koshkin, A. A., and Wengel, J. (1998) LNA (Locked Nucleic Acids): Synthesis and High-Affinity Acid Recognition. *Chem. Commun. 1998*, 455−456.

Spielmann, H. P., Wemmer, D. E., and Jacobsen, J. P. (1995) The Solution Structure of a DNA Complex with the Fluorescent TOTO Determined by NMR Spectroscopy. *Biochemistry 34*, 8542−8553.

Stein, P. C., Jacobsen, J. P., and Spielmann, H. P. (1995) Design and Implementation of a Simple Shaped Notch Filter. *J. Magn. Res., Ser. B 109*, 93−96.

Thuong, N. T., and Hélène, C. (1993) Sequence-Specific Recognition and Modification of Double-Helical DNA by Oligonucleotides. *Angew. Chem., Int. Ed. Engl. 32*, 666−690.

Uhlmann, E., and Peyman, A. (1990) Antisense Oligonucleotides: A New Therapeutic Principle. *Chem. Rev. 90*, 543−584.

Weisz, K., Shafer, R. H., Egan, W., and James, T. L. (1994) Solution Structure of the Octamer Motif in Immunoglobulin Genes via Restrained Molecular Dynamics Calculations. *Biochemistry 33*, 354−366.

Wengel, J. (1998) Synthesis of 3′-*C*- and 4′-*C*-Branched Oligonucleotides and the Development of Locked Nucleic Acid (LNA). *Acc. Chem. Res. 32*, 301−310.

Wengel, J., Koshkin, A., Singh, S. K., Nielsen, P., Meldgaard, M., Rajwanshi, V. K., Kumar, R., Skouv, J., Nielsen, C. B., Jacobsen, J. P., Jacobsen, N., and Olsen, C. E. (1999) LNA (Locked Nucleic Acids). *Nucleosides Nucleotides 18*, 1365−1370.

Wüthrich, K. (1986) *NMR of Proteins and Nucleic Acids*, John Wiley & Sons, New York.

BC990121S

Concepts for the Syntheses of Biotinylated Steroids. Part I: Testosterone Derivatives as Immunochemical Probes

Hagen Hauptmann,[†] Birgit Paulus,[†] Thomas Kaiser,[‡] Eberhardt Herdtweck,[§] Erasmus Huber,[||] and Peter B. Luppa*[,‡]

Institute for Organic Chemistry, Universität Regensburg, D-93053 Regensburg, Germany, Institute for Clinical Chemistry and Pathobiochemistry, Klinikum rechts der Isar, Technische Universität München, D-81675 München, Germany, Institute for Anorganic Chemistry, Technische Universität München, D-85747 Garching, Germany, and Roche Diagnostics GmbH, Werk Penzberg, D-82377 Penzberg, Germany.
Received October 18, 1999; Revised Manuscript Received December 20, 1999

We describe synthetic strategies for the biotinylation of testosterone (T) at positions 3, 7α, 17α, and 19. These T probes are able to mimic ligand binding and may provide for a better understanding of the biospecific interaction with steroid-binding proteins such as the androgen receptor, anti-steroid antibodies, or steroid-binding serum globulins. For the 7α- and 17α-derivatives, biotinyl-*N*-hydroxysuccinimide esters with different types of spacer chains were used. The 3-biotin hydrazone derivative was produced using *N*-(ϵ-biotinyl)-caproyl hydrazide, whereas for the 19-biotinylation, a biotinyl-1-*N*-diamino-3,6-dioxaoctane-amide was applied. Key reaction for the biotinylation at position 3 is the oximation of the 3-oxo function. The 17α-position is accessible by the reaction of the 3-protected 4-androsten-17-epoxide with oxygen in the β-position, followed by nucleophilic ring opening with cyanide which provides the 17α-cyanomethyl derivative. The key step is the regioselective ketal protection of the 3-oxo function of androst-4-ene-3,17-dione using a stannoxane catalyst. An alternative pathway for the insertion of biotin at the 19-position was established by the synthesis of 17β-hydroxy-androst-4-en-3-one-19-yl carboxymethyl ether. After activation by the carbodiimide method, the compound reacts with aminoterminal biotin derivatives. The copper(I)-catalyzed 1,6 Michael addition of 17-acetoxy-6,7-dehydro-T leads to 7α-derivatives by use of ω-silyl protected hydroxylalkyl-modified Grignard reagents. A functional group interconversion using the Staudinger reaction transforms the azide function into a primary ω-amino group. The absolute configurations of the different biotinylated derivatives were investigated by ^{1}H NMR studies. For the 7α-biotinylated T series, additionally, an X-ray analysis proved the axial position of the spacer group. This results in a vertical orientation of the biotin moiety toward the α-face of the planar tetracyclic backbone. Thus, a negligible alteration of the original structure of the upper β-face offers the feasibility of applying the 7α-derivatives as optimal immunochemical tracers in competitive immunoassays. Biotinylated T derivatives should be also suitable for ligand-binding studies to the androgen receptor or to sex hormone-binding globulin.

INTRODUCTION

To mimic ligand binding, the design and synthesis of steroid derivatives is still a field of major interest. The tools of organic chemistry for the synthesis of modified testosterone (T)[1] probes can help for a better understanding of the biospecific interaction with steroid-binding proteins such as the androgen receptor (AR), anti-T antibodies, or sex hormone-binding globulin (SHBG). Important application is the analysis of T in human serum or urine by use of immunoassay methods for a series of endocrine disorders (Brooks, 1984; Lindzey et al., 1994; Wheeler, 1995). Also, the determination of the AR in tumor tissues is of interest as a prognostic factor in oncology. AR mutations associated with prostatic cancer commonly alter the ligand-binding specificity of the receptor (Veldscholte et al., 1990, 1992; Lindzey et al., 1994; Quigley, 1998). Additionally, the study of ligand-binding properties of various T derivatives to the AR can provide insights in the molecular mechanism of the receptor physiology and yields hints for the pharmaceutical construction of novel antineoplastic agents (Waller et al., 1996).

Synthetic Approaches for the Derivatization of T at Different Ring Positions. The aim of this presentation is to summarize in detail the different organic

* To whom correspondence should be addressed. Phone: +49 89 4140 4751. Fax: +49 89 4140 4875: E-mail: luppa@klinchem.med.tu-muenchen.de.

[†] Institute for Organic Chemistry.

[‡] Institute for Clinical Chemistry and Pathobiochemistry.

[§] Institute for Anorganic Chemistry.

[||] Roche Diagnostics GmbH.

[1] Abbreviations: AR, androgen receptor; biotin-NHS, d-(+)-biotinyl-*N*-hydroxysuccinimide ester; CBG, corticoid-binding globulin; DMF, dimethylformamide; E2, 17β-estradiol; DCC, *N*,*N*′-dicyclohexylcarbodiimide; DHT, 17β-hydroxy-5α-dihydroandrostan-3-one; DADOO-biotin, d-(+)-biotinyl-1-*N*-diamino-3,6-dioxaoctane-amide; DDS-biotin, d-(+)-biotinyl-amino-3,6-dioxaoctanyl-aminocarbonyl-heptanoic acid-*N*-hydroxysuccinimide ester; HMPT, hexamethyl phosphoric acid triamide; LC-biotin, d-(+)-biotinyl-ϵ-aminocaproic acid-*N*-hydroxysuccinimide ester; LSC, liquid-solid chromatography; mp, melting point; MTBE, methyl-*t*-butyl ether; NHS, *N*-hydroxy-succinimide; PE, petroleum ether; RBA, relative binding activities; PPTS, pyridinium-*p*-toluenesulfonate; t_r, retention time; SHBG, sex hormone-binding globulin; stannoxane, 1-hydroxy-3-(isothiocyanato)-tetrabutyl-stannoxane; T, testosterone; THF, tetrahydrofuran; TBAF, tetrabutylammonium fluoride; TBDMS, *t*-butyl-dimethylsilyl; THP, tetrahydropyran.

10.1021/bc9901402 CCC: $19.00 © 2000 American Chemical Society
Published on Web 03/20/2000

chemical pathways for the biotinylation of T at the following positions: 3, 7α, 17α, and 19. The insertion of biotin in the T molecule was chosen due to the enormous advantages of the high binding affinity of the noncovalent interaction between biotin and (strept)avidin, which allows the application in many analytical assays that require the formation of an nearly irreversible and specific linkage between macromolecules (Wilchek and Bayer, 1990; Diamandis and Christopoulos, 1991).

Concerning the ring position, the following considerations must be made: for the production of immunochemical tracers, which are used in combination with different poly- and monoclonal antibodies in immunoassays, the T molecule can be biotinylated primarily at the 3, 7α, and 19 positions. SHBG accepts only T derivatives with alterations at the 17α, 18, and 19 positions, whereas 17β derivatives do not bind to this transport protein (Pugeat et al., 1981). Hydrogenation of the 4-ene bondage, resulting in 5α-androstane steroids [like 5α-dihydro-T (DHT)], improves the binding affinity considerably. Whether 7α/β substituents lead to altered binding conditions is unknown to our knowledge.

Additional considerations have to be entitled for the chemical structure of the spacer group linking the biotin residue to the steroid ring system: this spacer group has to minimize steric hindrances between the biotin moiety and the binding protein. Moreover, when applying biotinylated steroids as tracers in immunoassays, the chemical structure of the spacer has a relevant influence on the process of antibody recognition: the structure must be similar to the linkage used in the immunization procedure. Care must be taken that the spacer should not be too long, however, as this might result in considerable loss in antibody binding through the diminished hydrophilic character of the tracer. This fact is supported by investigations of Tiefenauer and Andres (1990), who also discussed structural requirements of biotinylated 17β-estradiol (E2) derivatives for optimal antibody binding. Our own results using a 7α-biotinylated T derivative for a chemiluminescence immunoassay for the determination of total T in serum point out that high specificity can be achieved when combining this tracer with an anti-T antibody, which was raised using a 7α-T derivative as the immunogen (Luppa et al., 1997).

An additional topic in this context is the functionality of the derivatization point at the ring-core (Adamczyk et al., 1997a). It depends on the special issue for which these steroidal derivatives are used. For the most commonly used carboxymethyloxime derivatives the altered hybridization (sp^2 vs sp^3) is unfavorable, since the double bond in the chemical bridge denies free rotation, flattens the B-ring and gives rise to a mixture of syn- and anti-isomers (Rao et al., 1998). Additionally, it should be noticed that the native electronic environment might be altered in case of amide bondages at the ring system (Adamczyk et al., 1998). By use of polyether or pure aliphatic spacer groups the hydrophilicity should also be considered. Thus, chemical approaches to these structural demands for spacer groups can be on one hand the synthesis of appropriate steroidal precursors and on the other hand the appropriate choice of the biotinylation reagent.

EXPERIMENTAL PROCEDURES

General Methods. *Apparatus*. Melting points (uncorrected) were determined on a Reichert Thermovar and on a Büchi 510. ^{1}H NMR spectra were recorded in $CDCl_3$ on a Bruker WM 250 (250 MHz), an ARX 400 (400 MHz), and on an Avance DPX 300 (300 MHz), using Me_4Si (TMS) for reference signal (δ 0.00 ppm). Data are reported in the following form: chemical shift (multiplicity, coupling constant in Hz if available, number of protons, position of proton). IR spectra were obtained from KBr or neat on a Mattson Genesis Series FT-IR spectrophotometer and a Shimadzu IR-43 5, and only characteristic IR bands are reported as wavenumbers (cm^{-1}). UV spectra were measured in MeOH on a Hitachi U-2000 and on a Perkin-Elmer Lambda 5 UV/VIS spectrophotometer. Optical rotation values were gained from a Perkin-Elmer 241 polarimeter, *c* is given in g/100 cm^{-3}. MS analyses were performed on Finigan MAT 90 (FAB) and MAT SSQ 700 (EI) as well as on Varian MAT 112S and 311 A (both for EI). Elementary analyses were performed using a Heraeus CHN Rapid. The X-ray analysis was carried out on a four-circle diffractometer Nonius MACH3 (Nonius BV, Delft, The Netherlands) equipped with rotating anode (Nonius FR591) and graphite monochromated MoKα radiation. All X-ray calculations were performed on a DEC 3000 AXP workstation with the *STRUX-V* system, including the programs *PLATON-92*, *PLUTON-92*, *SIR-92*, and *SHELXL-93*. Crystallographic data (excluding structure factors) for the structure reported in this paper have been deposited with the Cambridge Crystallographic Data Centre as supplementary publication no. CCDC-135481. Copies of the data can be obtained free of charge on application to CCDC, 12 Union Road, Cambridge CB2 1EZ, U.K. [fax, (+44)1223−336−033; e-mail, deposit@ccdc.cam.ac.uk]. The preparative HPLC system for the syntheses of the 3-, 7α, and 17α-biotinylated T derivatives consisted of a Knauer 64 pump (Knauer, Bad Homburg, Germany) and an UV detector ERC 7210 (ERC, Alteglofsheim, Germany). Columns were purchased from Bischoff Analysentechnik, Leonberg, Germany (Kromasil SC 100/7 μm/20 × 250 mm) and Knauer (Eurospher 100 C_{18}). For the 19-Bio-T synthesis, a preparative HPLC from Gynkotec (Germering, Germany) was used (HPLC pumps 11480P and M300 CSP; detector Soma S-3710, software Chromeleon 4.20). Here, the column used (Vydac C_{18}/300 Å/15α20 μm/50 × 250 mm) was purchased from MZ Analysentechnik (Mainz, Germany) with a guard cartridge (Bischoff Polygosil C_{18}/60 Å/10 μm/20 × 50 mm).

Chemicals. For column chromatography, silica gel (grain 0.063−0.200) from E. Merck (Darmstadt, Germany) and neutral Al_2O_3 (aluminia N Super I, W 200) and basic Al_2O_3 (aluminia B Super I, W 200) from Woelm Pharma (Bad Honnef, Germany) were used. Thin-layer chromatography was performed using silica gel 60 F_{254} (0.2 mm) and neutral Al_2O_3 60 F254 type E (0.2 mm), both materials from Merck. T and androst-4-ene-3,17-dione were from Sigma (Deisenhofen, Germany); 19-hydroxy-androst-4-ene-3,17-dione and d-(+)-biotinyl-*N*-hydroxysuccinimide ester (biotin-NHS) were from Fluka Chemie (Buchs, Switzerland); *N*-(ε-biotinyl)-caproyl hydrazide was from Pierce Europe BV (Oud Beijerland, The Netherlands); d-(+)-biotinyl-ε-aminocaproic acid-*N*-hydroxysuccinimide ester (LC-biotin), d-(+)-biotinyl-1-*N*-diamino-3,6-dioxaoctane-amide (DADOO-biotin), and d-(+)-biotin-yl-amino-3,6-dioxa-octanyl-aminocarbonyl-heptanoic acid-*N*-hydroxysuccinimide ester (DDS-biotin) were from Roche Molecular Biochemicals, Penzberg, Germany. All other laboratory chemicals were from Fluka.

Preparation of 17β-Hydroxy-androst-4-ene-3-(biotinylaminocaproyl-hydrazone) (3-Bio-T) (2) (Janoski et al., 1974; Kohler et al., 1997). A total of 1 equiv of *N*-(ε-biotinyl)-caproyl hydrazide and 1 equiv of T (**1**)

were dissolved in MeOH. After addition of acetic acid, the clear solution was stirred for 3 days at room temperature (rt). After removal of the solvent, the residue was freeze-dried with benzene. The liquid-solid chromatography (LSC) at silica gel (SiO_2) using MeOH:CH_2Cl_2 (1:9, v/v) as the eluent gave a colorless solid substance, yield 92%. Final purification of **2** by preparative HPLC [flow 7.8 mL/min, retention time (t_r) 16.1 min]. IR (KBr): $\bar{\nu}$ 3384, 3288 (−OH, NH), 2933, 2866 ($CH_{aliphat}$), 1690, 1658 (C═O−biotin), 1535 (CO−NH). ^{1}H NMR (400 MHz, CD_3OD): δ 0.77 (s, 3 H, 18-CH_3), 1.08 (s, 3 H, 19-CH_3), 3.61 (t, 1 H, 17-CH), 4.42 (m, 1 H, biotin), 4.51 (m, 1 H, biotin), 5.82 (s, 1 H, 4-CH). MS (FAB, *m*/*z*): 642.6 (MH^+, 100%).

Preparation of 17*β*-hydroxyandrost-4-en-3-one 7α-(biotinyl-*N*-*n*′-alkylamide) (7α-Cn′-Bio-T). Spectroscopic data of the compounds **5c**−**12c** and **5e**−**12e** (except for **9c, e** and **10c, e**) are given representatively in Table 1 for all synthesized 7α-Cn′-Bio-T derivatives.

***n*-(Dimethyl-*t*-butylsilyloxy)-*n*-alkyl bromide precursors** 3-(dimethyl-*t*-butylsilyloxy)-propyl bromide **4a**, 6-(dimethyl-*t*-butyl-silyloxy)-hexyl bromide **4b**, 11-(dimethyl-*t*-butylsilyloxy)-undecyl bromide **4c**, 9-dimethyl-*t*-butylsilyloxy-5-oxa-nonyl bromide **4d**, and 13-dimethyl-*t*-butylsilyloxy-7-oxa-tridecyl bromide **4e** were synthesized according prescriptions given in Corey and Venkateswarlu (1972), Bowler et al. (1989), Poppe et al. (1993), and Luppa et al. (1996).

17*β*-Acetoxy-7α/*β*-(*n*′-dimethyl-*t*-butylsilyloxyalkyl)-androst-4-en-3-one. According to Bowler et al. (1989), the Grignard reagents were prepared by dripping a solution of 3.5 equiv of *n*-alkyl-*tert*-butyl-di-methylsilyloxy bromide in THF to 4.0 equiv of Mg in THF under N_2. The resulting clear solution was diluted with further solvent and after 1 h cooled to −40 to −30 °C in an 2-propanol/dry ice bath. A total of 2 equiv of freshly prepared CuI was added, 15 min later, 1 equiv of 17α-hydroxyandrost-4,6-dien-3-one 17*β*-acetate [6-dehydro-T-17*β*-acetate **3**, preparation according to the prescription given in (Luppa et al., 1996)] in THF was dripped to the solution within 50 min at −45 to −35 °C, giving a reddish suspension. After being stirred for further 40 min, the reaction mixture was quenched with glacial acetic acid at −30 °C, then subsequently basified with a saturated NH_4Cl solution. The solvent was removed, and the residue treated with methyl-*t*-butyl ether (MTBE) and an aqueous saturated $NaHCO_3$ solution. The crude oily extract was chromatographed to purify and separate the stereoisomers on SiO_2, using an appropriate eluent system.

17α-Acetoxy-7α/β-(3′-dimethyl-t-butyl-silyloxy-propyl)-androst-4-en-3-one, ***5a***. The resulting yellow oil was chromatographed using CH_2Cl_2:ethyl acetate, 9:1 (v/v) as the eluent. The main product as yellow oil was the 7α-isomer, yield 49%, second yellow product was the 7*β*-isomer, yield 39%.

17β-Acetoxy-7α/β-(6′-dimethyl-t-butylsilyloxy-hexyl)-androst-4-en-3-one, ***5b***. The synthesis is already described in Luppa et al., (1996).

17β-Acetoxy-7α/β-(11′-dimethyl-t-butylsilyloxy-undecyl)-androst-4-en-3-one, ***5c***. The resulting yellow oil was chromatographed using CH_2Cl_2:ethyl acetate, (19:1, v/v) as the eluent. The main product as colorless oil was the 7α isomer, yield 58%, second colorless product was the 7*β*-isomer, yield 34%.

17β-Acetoxy-7α-(9′-dimethyl-t-butylsilyloxy-5′-oxa-nonyl)-androst-4-en-3-one, ***5d***. After LSC on SiO_2 using MTBE:PE (1:2, v/v) as eluent, a yellowish oil was isolated, yield 80%. The stereoisomers were not separable from the isomeric mixture by use of LSC alone.

17β-Acetoxy-7α-(13′-dimethyl-t-butylsilyloxy-7′-oxa-tridecyl)-androst-4-en-3-one, ***5e***. after LSC on SiO_2 using CH_2Cl_2:ethyl acetate (9:1, v/v) as eluent a colorless oil was isolated, yield 88%. The stereoisomers were also not separable from the isomeric mixture by use of LSC alone.

17*β*-Acetoxy-7α-(*n*′-alkanol)-androst-4-en-3-one (Corey and Venkateswarlu, 1972a; Corey and Snider, 1972b). A total of 1 equiv of the respective T 7-silyl ether was dissolved under N_2 in THF, 2 equiv of 1 mol/L tetrabutylammonium fluoride solution (TBAF) in THF was added, and the mixture was stirred at room temperature. Then, a saturated NaCl solution was added, and the product extracted three times with MTBE. The remaining oil was further purified by LSC after removal of the solvent using MTBE as the eluent.

7β-Acetoxy-7α-(3′-propanol)-androst-4-en-3-one, ***6a***. After LSC colorless needles were separated, yield 83%, mp 89−91 °C.

17β-Acetoxy-7α-(6′-hexanol)-androst-4-en-3-one, ***6b***. The synthesis is already described in Luppa et al. (1996).

17β-Acetoxy-7α-(11′-undecanol)-androst-4-en-3-one, ***6c***. After LSC, a colorless oil was separated, yield 97%.

17β-Acetoxy-7α-(9′-hydroxy-5′-oxa-nonyl)-androst-4-en-3-one, ***6d***. After LSC, a colorless oil was separated, yield 83%.

17β-Acetoxy-7α-(13′-hydroxy-7′-oxa-tridecyl)-androst-4-en-3-one, ***6e***. After LSC, a colorless oil was separated, yield 89%.

17*β*-Acetoxy-7α-(*n*′-alkylmesylate)-androst-4-en-3-one. A total of 1 equiv of the respective T 7-alcohol was dissolved in CH_2Cl_2, and 3 equiv of freshly prepared NEt_3 was added. Through a dropping funnel, mesyl chloride, dissolved in CH_2Cl_2, was added slowly. After being stirred at room temperature, a saturated $NaHCO_3$ solution was added and the yellow reaction mixture was extracted three times with CH_2Cl_2. The remaining yellow oil was further purified by LSC.

17β-Acetoxy-7α-(3′-propylmesylate)-androst-4-en-3-one, ***7a***. The oil was purified by LSC using SiO_2 as the stationary and MTBE as the mobile phase, resulting in colorless crystals, yield 93%, mp 135−138 °C. X-ray data concerning this compound are presented in Results.

17β-Acetoxy-7α-(6′-hexylmesylate)-androst-4-en-3-one, ***7b***. The oil was purified by LSC using SiO_2 as the stationary and Et_2O:ethyl acetate (9:1, v/v) as the mobile phase, resulting in a colorless oil, yield 93%.

17β-Acetoxy-7α-(11′-undecylmesylate)-androst-4-en-3-one, ***7c***. The oil was purified by LSC using SiO_2 as the stationary and MTBE as the mobile phase, resulting in a yellow oil, yield 95%.

17β-Acetoxy-7α-(9′-mesyl-5′-oxa-nonyl)-androst-4-en-3-one, ***7d***. The oil was purified by LSC using SiO_2 as the stationary and MTBE as the mobile phase, resulting in a yellowish oil, yield 80%.

17β-Acetoxy-7α-(13′-mesyl-7′-oxa-tridecyl)-androst-4-en-3-one, ***7e***. The oil was purified by LSC using SiO_2 as the stationary and Et_2O:ethyl acetate (9:1, v/v) as the mobile phase, resulting in a yellow oil, yield 89%.

17*β*-Acetoxy-7α-(*n*′-alkyl azide)-androst-4-en-3-one (Gololobov and Kasukhin, 1992). A total of 1 equiv of the respective T 7-mesylate was dissolved in hexamethyl phosphoric acid triamide (HMPT). A total of 2 equiv of NaN_3 was added, and the mixture stirred at room temperature. The yellow reaction mixture was diluted with H_2O and extracted three times with MTBE. The remaining yellow oil was further purified by LSC.

Table 1. Spectroscopic Data for the Synthesis of 7α-Biotinylated Ts

code	IR (cm^{-1})	^1H NMR δ (ppm) (400 MHz, $CDCl_3$)	MS	elementary analysis	UV (λ, lgϵ)	$[\alpha]_D^{20}$
5c (α)	(neat): 2962, 2856 ($CH_{aliphat}$), 1730 (17-OAc), 1670 (3-C=O), 1611 (C=C_{conj}), 1102, 836, 770 (Si−R)	0.03 [s, 6 H, $Si(CH_3)_2$], 0.83 (s, 3H, 18-CH_3), 0.88 (s, 9H, Si^{t}butyl), 1.19 (s, 3H, 19-CH_3), 2.03 (s, 3H, COAc), 2.31 (dd, $J_{6\alpha6\beta}$ = 14.2, $J_{6\alpha7\beta}$ = 2.4, 1H, 6α-H), 2.39 (dd, $J_{6\alpha6\beta}$ = 14.2, $J_{6\alpha7\beta}$ = 4.9, 1H, 6β-H), 3.58 (t, 2H, R−CH_2−OSi), 5.71 (s, 1H, 4-CH)	(70 eV EI, *m/z*) 614 (M^+, 0.8%), 557 ($M^+ - C_4H_9$, 100%)	$C_{38}H_{68}O_4Si$ (614.01) calcd: C, 74.27; H, 11.16 found: C, 74.02 H, 11.34	242, 4.14	+25° (MeOH, *c* = 3.11)
5c (β)	(neat): 2981, 2880 ($CH_{aliphat}$), 1730 (17-OAc), 1665 (3-C=O), 1610 (C=C_{conj}), 1090, 842, 771 (Si−R)	0.05 [s, 6 H, $Si(CH_3)_2$], 0.85 (s, 3H, 18-CH_3), 0.89 (s, 9H, Si^{t}butyl), 1.16 (s, 3H, 19-CH_3), 2.05 (s, 3H, COAc), 2.17 (dd, $J_{6\alpha6\beta}$ = 14.6; $J_{6\beta7\alpha}$ = 12.6, 1H, 6β-H), 2.29 (dd, $J_{6\alpha6\beta}$ = 14.6, $J_{6\alpha7\alpha}$ = 4.8, 1H, 6α-H), 3.60 (t, 2H, R−CH_2−OSi), 5.72 (s, 1H, 4-CH)	(70 eV EI, *m/z*) 614 (M^+, 1.5%), 487 ($M^+ - C_4H_9$, 100%)	$C_{38}H_{68}O_4Si$ (614.01) calcd: C, 74.27 H, 11.16 found: C, 73.99 H, 11.02	241, 4.14	+32° (MeOH, *c* = 3.35)
5e	(neat): 2934, 2856 ($CH_{aliphat}$), 1739 (17-OAc), 1677 (3-C=O), 1619 (C=C_{conj}), 1111 (C−O−C), 1101, 837, 777 (Si−R)	0.04 [s, 6 H, $Si(CH_3)_2$], 0.84 (s, 3H, 18-CH_3), 0.88 (s, 9H, Si^{t}butyl), 1.15 (s, 3H, 19-CH_3), 2.04 (s, 3H, COAc), 2.30 (dd, $J_{6\alpha6\beta}$ = 14.2, $J_{6\alpha7\beta}$ = 2.5, 1H, 6α-H), 2.44 (dd, $J_{6\alpha6\beta}$ = 14.2, $J_{6\beta7\beta}$ = 5.0, 1H, 6β-H), 3.38 (m, 4 H, CH_2−O-), 4.56 (m, 1H, 17-CH), 3.59 (m, 2H, R−CH_2−OSi), 5.71 (s, 1H, 4-CH)	(FAB, *m/z*) 145.2 (MH^+, 100%)	$C_{39}H_{68}O_5Si$ (645.04) calcd: C, 72.62 H, 10.63 found: C, 72.19 H, 10.50	241, 4.00	
6c	(neat): 3390 (OH), 2980, 2889 ($CH_{aliphat}$), 1730 (17-OAc), 1666 (3-C=O), 1610 (C=C_{conj})	(TMS): 0.84 (s, 3H, 18-CH_3), 1.21 (s, 3H, 19-CH_3), 2.05 (s, 3H, COAc), 2.32 (dd, $J_{6\alpha6\beta}$ = 14.2; $J_{6\alpha7\beta}$ = 2.5, 1H, 6α-H), 2.40 (dd, $J_{6\alpha6\beta}$ = 14.2, $J_{6\beta7\beta}$ = 4.6, 1H, 6β-H), 3.62 (t, 2H, R−CH_2−OH), 5.73 (s, 1H, 4-CH)	(70 eV EI, *m/z*) 430 (M^+, 23%), 329 ($M^+ - C_6H_{12}OH$, 100%)	$C_{33}H_{52}O_4$ (500.79) calcd: C, 79.07 H, 10.47 found: C, 78.86 H, 10.66	241, 4.12	+21° (MeOH, *c* = 2.33)
6e	(neat): 3444 (OH), 2935, 2858 ($CH_{aliphat}$), 1732 (17-OAc), 1669 (3-C=O), 1615 (C=C_{conj}), 1115 (C−O−C)	(TMS): 0.84 (s, 3H, 18-CH_3), 1.20 (s, 3H, 19-CH_3), 2.05 (s, 3H, COAc), 2.31 (dd, $J_{6\alpha6\beta}$ = 14.4, $J_{6\alpha7\beta}$ = 2.4, 1H, 6α-H), 2.41 (dd, $J_{6\alpha6\beta}$ = 14.3, $J_{6\beta7\beta}$ = 5.0, 1H, 6β-H), 3.40 (m, 4 H, CH_2−O-), 3.64 (t, 2H, R−CH_2−OH), 4.61 (t, 1H, 17.CH), 5.73 (s, 1H, 4-CH)	(FAB, *m/z*) 531.6 (MH^+, 100%), 329.4 ($M^+ - C_{12}H_{25}O_2$, 38%)	$C_{33}H_{54}O_5$ (530.79) calcd: C, 74.67 H, 10.25 found: C, 74.34 H, 9.99	241, 3.93	+22° (MeOH, *c* = 3.11)
7c	(neat): 2980, 2899 ($CH_{aliphat}$), 1730 (17-OAc), 1660 (3-C=O), 1605 (C=C_{conj}), 1350, 1250, 1170 (−SO_2)	(TMS): 0.84 (s, 3H, 18-CH_3), 1.21 (s, 3H, 19-CH_3), 2.05 (s, 3H, COAc), 2.32 (dd, $J_{6\alpha6\beta}$ = 14.2; $J_{6\alpha7\beta}$ = 2.4, 1H, 6α-H), 2.40 (dd, $J_{6\alpha6\beta}$ = 14.2, $J_{6\beta7\beta}$ = 4.8, 1H, 6β-H), 3.01 (s, 3H, SO_2−CH_3), 4.22 (t, 2H, R−CH_2−OSO_2), 5.72 (s, 1H, 4-CH)	(70 eV EI, *m/z*) 578 (M^+, 9%), 329 ($M^+ - C_{11}H_{22}O-SO_2CH_3$, 100%)	$C_{33}H_{56}O_6S$ (578.85) calcd: C, 68.47 H, 9.75 found: C, 67.93 H, 9.64	241, 3.71	+19° (MeOH, *c* = 1.21)
7e	(neat): 2937, 2848 ($CH_{aliphat}$), 1737 (17-OAc), 1672 (3-C=O), 1616 (C=C_{conj}), 1358, 1245, 1175 (−SO_2), 1115 (C−O−C)	(TMS): 0.84 (s, 3H, 18-CH_3), 1.21 (s, 3H, 19-CH_3), 2.05 (s, 3H, COAc), 2.29 (dd, $J_{6\alpha6\beta}$ = 14.4; $J_{6\alpha7\beta}$ = 2.2, 1H, 6α-H), 2.40 (dd, $J_{6\alpha6\beta}$ = 14.4, $J_{6\beta7\beta}$ = 4.9, 1H, 6β-H), 3.01 (s, 3H, SO_2−CH_3), 3.39 (m, 4 H, CH_2−O-), 4.23 (t, 2H, R−CH_2−OSO_2), 4.60 (t, 1H, 17-CH), 5.72 (s, 1H, 4-CH)	(FAB, *m/z*) 609.6 (MH^+, 100%), 329.4 ($M^+ - C_{12}H_{24}O-SO_2CH_3$, 12%)	$C_{34}H_{56}O_7S$ (608.88) calcd: C, 67.07 H, 9.27 found: C, 66.88 H, 8.99	241, 3.93	+27° (MeOH, *c* = 2.88)
8c	(neat): 2960, 2860 ($CH_{aliphat}$), 2099 (−N_3), 1730 (17-OAc), 1665 (3-C=O), 1600 (C=C_{conj})	(TMS): 0.84 (s, 3H, 18-CH_3), 1.20 (s, 3H, 19-CH_3), 2.05 (s, 3H, COAc), 2.36 (dd, $J_{6\alpha6\beta}$ = 14.2, $J_{6\alpha7\beta}$ = 2.5, 1H, 6α-H), 2.40 (dd, $J_{6\alpha6\beta}$ = 14.2, $J_{6\beta7\beta}$ = 4.8, 1H, 6β-H), 3.26 (m, 2H, R−CH_2−N_3), 5.72 (s, 1H, 4-CH)	(70 eV EI, *m/z*) 527 (M^+, 2%), 499 ($M^+ - N_2$, 69%), 329 ($M^+ - C_{11}H_{22}N_3$, 100%)	$C_{32}H_{53}O_3N_3$ (526.97) calcd: C, 72.81 H, 10.13 N, 7.97 found: C, 72.91 H, 9.84 N, 7.73	241, 4.36	+42° (MeOH, *c* = 1.10)
8e	(neat): 2934, 2858, 2802 ($CH_{aliphat}$), 2096 (−N_3), 1735 (17-OAc), 1674 (3-C=O), 1617 (C=C_{conj}), 1118 (C−O−C)	(TMS): 0.84 (s, 3H, 18-CH_3), 1.20 (s, 3H, 19-CH_3), 2.05 (s, 3H, COAc), 2.29 (dd, $J_{6\alpha6\beta}$ = 14.2, $J_{6\alpha7\beta}$ = 2.5, 1H, 6α-H), 2.41 (dd, $J_{6\alpha6\beta}$ = 14.2, $J_{6\beta7\beta}$ = 4.9, 1H, 6β-H), 3.27 (m, 2H, R−CH_2−N_3), 3.38 (m, 4 H, CH_2−O-), 4.61 (t, 1H, 17-CH), 5.73 (s, 1H, 4-CH)	(FAB, *m/z*) 556.7 (MH^+, 100%), 528.7 ($MH^+ - N_2$, 11%), 329.4 ($M^+ - C_{12}H_{24}N_3O$, 11%)	$C_{33}H_{53}O_4N_3$ (555.80) calcd: C, 71.31 H, 9.61 N, 7.56 found: C, 70.98 H, 9.70 N, 7.22	241, 3.87	+31° (MeOH, *c* = 2.95)

Table 1 (Continued)

code	IR (cm^{-1})	^1H NMR δ (ppm) (400 MHz, $CDCl_3$)	MS	elementary analysis	UV (λ, lgϵ)	$[\alpha]_D^{20}$
11c		(TMS): 0.80 (s, 3H, 18-CH_3), 1.21 (s, 3H, 19-CH_3), 2.36 (dd, $J_{6\alpha6\beta}$ = 14.2; $J_{6\alpha7\beta}$ = 2.3, 1H, 6α-H), 2.40 (dd, $J_{6\alpha6\beta}$ = 14.2, $J_{6\beta7\beta}$ = 4.9, 1H, 6β-H), 3.21 (m, 2H, R−CH_2−NH_2), 4.36 (m, 1H, biotin), 4.52 (m, 1H, biotin), 5.61 (s, 1H, biotin-NH), 5.71 (s, 1H, 4-CH), 6.18 (t, 1H, amide-NH), 6.35 (s, 1H, biotin-NH)	(FAB, *m/z*) 686 ($M^+ - H$, 100%), 702 ($MNa^+ - H$, 29%)	$C_{40}H_{67}O_4N_3S$ (686.06) calcd: C, 70.01 H, 9.85 N, 6.13 found: C, 68.91 H, 9.52; N, 5.92	241, 4.14	+20° (MeOH, *c* = 0.85)
11e		(TMS): 0.78 (s, 3H, 18-CH_3), 1.21 (s, 3H, 19-CH_3), 2.30 (dd, $J_{6\alpha6\beta}$ = 14.4; $J_{6\alpha7\beta}$ = 2.0, 1H, 6α-H), 2.41 (dd, $J_{6\alpha6\beta}$ = 14.4, $J_{6\beta7\beta}$ = 4.8, 1H, 6β-H), 4.33 (m, 1H, biotin), 4.51 (m, 1H, biotin), 5.46 (s, 1H, biotin-NH), 5.73 (s, 1H, 4-CH), 6.09 (t, 1H, amide-NH), 6.35 (s 1H, biotin-NH)	(FAB, *m/z*) 715 (MH^+, 100%)		241, 3.88	+21° (MeOH, *c* = 1.68)
12c	(neat): 2985, 2938, 2868 ($CH_{aliphat}$), 1710, 1662 (C═O DDS-biotin-chain), 1521 (−CO−NH−)	(TMS): 0.79 (s, 3H, 18-CH_3), 1.21 (s, 3H, 19-CH_3), 2.30 (dd, $J_{6\alpha6\beta}$ = 14.3, $J_{6\alpha7\beta}$ = 2.2, 1H, 6α-H), 2.40 (dd, $J_{6\alpha6\beta}$ = 14.3, $J_{6\beta7\beta}$ = 4.9, 1H, 6β-H), 4.32 (m, 1H, biotin), 4.51 (m, 1H, biotin), 5.71 (s, 1H, 4-CH), 6.56 (m, 1H, amide-NH), 6.68 (t, 1H, amide-NH), 6.81 (s, 1H, amide-NH)	(FAB, *m/z*) 970.6 (MH^+, 100%)		241, 4.08	+23° (MeOH, *c* = 1.85)
12e		(TMS): 0.79 (s, 3H, 18-CH_3), 1.21 (s, 3H, 19-CH_3), 2.30 (dd, $J_{6\alpha6\beta}$ = 14.4, $J_{6\alpha7\beta}$ = 4.8, 1H, 6α-H), 2.41 (dd, $J_{6\alpha6\beta}$ = 14.4, $J_{6\beta7\beta}$ = 4.8, 1H, 6β-H), 4.32 (m, 1H, biotin), 4.51 (m, 1H, biotin), 5.63 (s, 1H, biotin-NH), 5.71 (s broad, 1H, 4-CH), 6.70 (t, 1H, amide-NH), 6.77 (s, 1H, amide-NH), 6.88 (t, 1H, amide-NH)	(FAB, *m/z*) 1000.7 (MH^+, 100%)		241, 4.03	+23° (MeOH, *c* = 1.88)

17β-Acetoxy-7α-(3′-propyl azide)-androst-4-en-3-one, ***8a***. The oil was purified by LSC using SiO_2 as the stationary and Et_2O:ethyl acetate (9:1, v/v) as the mobile phase, resulting in colorless crystal needles, yield 91%, mp 93−96 °C.

17β-Acetoxy-7α-(6′-hexyl azide)-androst-4-en-3-one, ***8b***. The oil was purified by LSC using SiO_2 as the stationary phase and MTBE as the mobile phase, resulting in a colorless oil, yield 94%.

17β-Acetoxy-7α-(11′-undecyl azide)-androst-4-en-3-one, ***8c***. The oil was purified by LSC using SiO_2 as the stationary phase and MTBE:petroleum ether (PE), 4:1 (v/v), as the mobile phase, resulting in a colorless oil, yield 95%.

17β-Acetoxy-7α-(9′-azido-5′-oxa-nonyl)-androst-4-en-3-one, ***8d***. The oil was purified by LSC using SiO_2 as the stationary and MTBE as the mobile phase, resulting in a colorless oil, yield 80%.

17β-Acetoxy-7α-(13′-azido-7′-oxa-tridecyl)-androst-4-en-3-one, ***8e***. The oil was purified by LSC using SiO_2 as the stationary phase and Et_2O:ethyl acetate, 9:1 (v/v), as the mobile phase, resulting in a colorless oil, yield 89%.

17*β*-Acetoxy-7α-(*n*′-alkylamine)-androst-4-en-3-one (Pilard and Vaultier, 1984; Afonso, 1995). A total of 1 equiv of the respective T 7-*n*′-alkyl azide was dissolved under N_2 in a wet THF solution. (n-Bu)$_3$P or Ph_3P were added, and the reaction mixture was stirred at room temperature, then the solvent was removed. The oily product was processed without further purification.

17β-Acetoxy-7α-(3′-propylamine)-androst-4-en-3-one, ***9a***. A total of 1.2 equiv of (n-Bu)$_3$P was added, and the mixture was stirred for 1 h. A brown oil was isolated.

17β-Acetoxy-7α-(6′-hexylamine)-androst-4-en-3-one, ***9b***. A total of 1.1 equiv of Ph_3P was added, and the mixture was stirred for 12 h. A yellow solid was isolated.

17β-Acetoxy-7α-(11′-undecylamine)-androst-4-en-3-one, ***9c***. A total of 1.5 equiv of (n-Bu)$_3$P was added, and the mixture was stirred for 2.5 h. A yellow oil was isolated. IR (neat): 2980, 2880 ($CH_{aliphat}$), 1730 (17-OAc), 1670 (3-C═O), 1610 (C═C_{conj}), 1190, 1160 [(n-Bu)$_3$P, (n-Bu)$_3$PO].

17β-Acetoxy-7α-(9′-amino-5′-oxa-nonyl)-androst-4-en-3-one, ***9d***. A total of 1.1 equiv of Ph_3P was added, and the mixture was stirred for 18 h. A yellow solid was isolated.

17β-Acetoxy-7α-(13′-amino-7′-oxa-tridecyl)-androst-4-en-3-one, ***9e***. A total of 1.1 equiv of Ph_3P was added, and the mixture was stirred for 15 h. A yellow solid was isolated. IR (neat): 3600 (−OH), 2970, 2884 ($CH_{aliphat}$), 1670 (3-C═O), 1610 (C═C_{conj}), 1190. 1160 [(n-Bu)$_3$PO].

17*β*-Hydroxy-7α-(*n*′-alkylamine)-androst-4-en-3-one. The respective 17β-acetoxy-T 7-*n*′-alkyl-amine product was dissolved in a H_2O:MeOH solution (1:25, v/v, adjusted to pH 11−12 with NaOH) and stirred for 15 h at room temperature. A total of 2 mol/L NaOH was added to the yellow solution. The reaction mixture was extracted three times with CH_2Cl_2. The crude product was adsorbed to basic Al_2O_3 and chromatographed. Remnants of phosphines were eluted with Et_2O, and the product was eluted subsequently with MeOH. This procedure reduced the portion of phosphine remnants to 5−10%.

17β-Hydroxy-7α-(3′-propylamine)-androst-4-en-3-one, ***10a***, *17β-Hydroxy-7α-(6′-hexylamine)-androst-4-en-3-one,*

10b**, 17β-Hydroxy-7α-(11′-undecylamine)-androst-4-en-3-one, **10c**, 17β-Hydroxy-7α-(9′-amino-5′-oxa-nonyl)-androst-4-en-3-one, **10d,** 17β-Hydroxy-7α-(13′-amino-7′-oxa-tridecyl)-androst-4-en-3-one, **10e. All products were yellow oils. IR (neat): $\bar{\nu}$ (10c) 3600 (−OH), 2970, 2884 ($CH_{aliphat}$), 1670 (3-C═O), 1610 (C═C_{conj}), 1190, 1160 [$(n\text{-}Bu)_3PO$]; (10e) 3579 (−OH), 2959, 2849 ($CH_{aliphat}$), 1674 (3-C═O), 1616 (C═C_{conj}), 1430 (Ph_3P), 1260 (P═O).

17β-Hydroxy-7α-(biotinyl-*n*′-alkylamine)-androst-4-en-3-one (Bodmer and Tiefenauer, 1990). The respective T 7α-*n*′-alkyl-amine product was dissolved under N_2 in DMF. A total of 3 equiv of NEt_3 and 1 equiv of biotin-NHS were added, and the solution was stirred for 18 h at room temperature. The solvent was removed and the residue chromatographed on SiO_2 [eluent MeOH: CH_2Cl_2, 1:4 (v/v)]. The final purification was achieved by preparative HPLC (column, Kromasil SC 100; eluent, MeOH:CH_2Cl_2, 1:6.14, v/v).

*17β-Hydroxy-7α-(biotinyl-3′-propylamine)-androst-4-en-3-one, **11a***. The LSC gave a yellowish solid, yield 88%. Final purification by preparative HPLC: flow 10 mL/min, t_r of the product 9.9 min.

*17β-Hydroxy-7α-(biotinyl-11′-undecylamine)-androst-4-en-3-one, **11c***. The LSC gave a colorless oil, yield 88%. Final purification by preparative HPLC: flow 9.3 mL/min, t_r 9.3 min.

*17β-Hydroxy-7α-(13′-biotinyl-7′-oxa-tridecylamine)-androst-4-en-3-one, **11e***. The LSC gave a colorless oil, yield 86%. Final purification by preparative HPLC: flow 9.3 mL/min, t_r 9.3 min.

17β-Hydroxy-7α-(biotinyl-amino-3,6-dioxa-octanyl-aminocarbonylheptyl-*n*′-alkylamine)-androst-4-en-3-one (Bodmer and Tiefenauer, 1990). The syntheses were performed analoguously to **8**.

*17β-Hydroxy-7α-(biotinyl-amino-3,6-dioxa-octanyl-aminocarbonylheptyl-6′-hexylamine)-androst-4-en-3-one, **12b***. A total of 1 equiv of **10b** was dissolved together with 3 equiv of NEt_3 and 1.1 equiv of DDS-biotin. After LSC, a yellow solid was isolated, yield 75%. The product was further purified by HPLC (flow 8.0 mL/min, t_r 21.0 min).

*17β-Hydroxy-7α-(biotinyl-amino-3,6-dioxaoctanyl-aminocarbonyl-heptyl-11′-undecylamine)-androst-4-en-3-one, **12c***. A total of 1 equiv of **10c** was converted. After LSC, a colorless oil was isolated, yield 79%. The product was further purified by HPLC (flow 7.8 mL/min, t_r 13.5 min).

*17β-Hydroxy-7α-(13′-biotinyl-amino-3,6-dioxaoctanyl-aminocarbonylheptyl-7′-oxatridecylamine)-androst-4-en-3-one, **12e***. A total of 1 equiv of **10e** was converted. After LSC, a colorless oil was isolated, yield 81%. The product was further purified by HPLC (flow 7.8 mL/min, t_r 13.5 min).

17β-Hydroxy-7α-(9′-biotinyl-aminocaproyl-5′-oxa-nonylamine)-androst-4-en-3-one) (13d). The synthesis was performed analogously to **8**. A total of 1 equiv of **10d** was converted. The LSC of the product gave a yellowish solid, yield 80%. Final purification by preparative HPLC: flow 7.8 mL/min, t_r 13.3 min.

Preparation of 3,17β-Dihydroxy-17α-(2′-biotinyl-amino-3,6-dioxa-octanylaminocarbonylheptyl-2′-ethylamide)-androst-4-ene (17α-Bio-T) (18). *3,3-(Dioxymethylen)-androst-4-en-17-one, **14***. The synthesis by applying a stannoxane catalyst was performed according to Otera et al. (1992).

*17β-(2′-Oxiran)-3,3-(dioxymethylen)-androst-4-ene, **15** (Trost and Melwin, 1975).* A total of 1.1 equiv of *n*-BuLi (1.6 mol/L in hexane) was added dropwise at −10 °C to a suspension of 1.1 equiv of trimethylsulfonium iodide in THF abs. and stirred for 30 min at −10 °C. After dropwise addition of 1.0 equiv of 3,3-(dioxy-methylen)-androst-4-en-17-one **14** in dry THF, the mixture was stirred for further 2 h without cooling. Then, the mixture was hydrolyzed with H_2O and extracted three times with Et_2O. After removal of the solvent, the residue was chromatographed on SiO_2, mobile phase: Et_2O:PE (2:1, v/v). The product was recrystallized from acetone:PE (1:2, v/v), yield 82%, mp 138−141 °C. IR (KBr): $\bar{\nu}$ 2946, 2871 ($CH_{aliphat}$), 1660 (C═C), 1089 (C−O−C). ^1H NMR (400 MHz, $CDCl_3$): δ 0.90 (s, 3 H, 18-CH_3), 1.04 (s, 3 H, 19-CH_3), 2.60 (d, ^2J = 5.0 Hz, 3′-CH), 2.89 (d, ^2J = 5.0 Hz, 3′-CH), 3.83−4.04 (m, 4 H, −O−CH_2CH_2−O), 5.24 (s, 1 H, 4-CH). MS (EI 70 eV, *m*/*z*): 344 (M^+, 100%). Anal. calcd ($C_{22}H_{32}O_3$): C, 76.76; H, 9.30. Found: C, 74.33; H, 9.32.

*17β-Hydroxy-17α-(cyanomethyl)-3,3-(dioxymethylen)-androst-4-ene, **16** (Ponsold et al., 1974, Hörhold et al., 1975).* A total of 1 equiv of **15** was dissolved with 12 equiv of NaCN in ethylene glycol and heated for 2 h at 100 °C. After adding ice-cold H_2O, the mixture was extracted three times with Et_2O. The extract was chromatographed at SiO_2 with Et_2O as the eluent and recrystallized from acetone:PE (1:3, v/v). **16** was isolated in a yield of 74%, mp 193−196 °C. IR (KBr): $\bar{\nu}$ 3475 (OH), 2255 (CN), 2948, 2865 ($CH_{aliphat}$), 1657 (C═C), 1090 (C−O−C). ^1H NMR (400 MHz, $CDCl_3$): δ 0.93 (s, 3 H, 18-CH_3), 1.05 (s, 3 H, 19-CH_3), 2.52 (AB−Signal, J = 16.3 Hz, −CH_2−CN), 3.85−4.03 (m, 4 H, −O−CH_2CH_2−O), 5.24 (s, 1 H, 4-CH). MS (EI 70 eV, *m*/*z*): 371 (M^+, 26%). Anal. calcd ($C_{23}H_{33}O_3N$): C, 74.41; H, 8.89; N, 3.77. Found: C, 72.39; H, 8.79; N, 3.27.

*17β-Hydroxy-17α-(aminoethyl)-3,3-(dioxymethylen)-androst-4-ene, **17** (Ray et al., 1991; Roy and Ray, 1995).* A total of 1 equiv of **16** in dry Et_2O was added dropwise to a suspension of 10 equiv of $LiAlH_4$ in Et_2O and stirred for 12 h under reflux. After addition of a saturated $NaHCO_3$ solution, the mixture was stirred for 1 h at 0 °C. Then, the product **17** was continuously extracted with Et_2O overnight. After removal of the solvent and evaporation in the high vacuum (on a diffusion pump), a colorless resin was obtained, yield 99%. IR (KBr): $\bar{\nu}$ 3356, 3274 (NH), 3214 (OH), 2862, 2843 ($CH_{aliphat}$), 1660 (C═C), 1097 (C−O−C). ^1H NMR (400 MHz, $CDCl_3$): δ 0.87 (s, 3 H, 18-CH_3), 1.06 (s, 3 H, 19-CH_3), 2.81−2.94 (m, 2 H, −CH_2−NH_2), 3.83−3.98 (m, 4 H, −O−CH_2−CH_2−O-), 5.18 (s, 1 H, 4-CH). MS (70 eV CI, *m*/*z*): 375 (M^+, 20%).

*3,17β-Dihydroxy-17α-(2′-biotinyl-amino-3,6-dioxa-octanyl-aminocarbonylheptyl-2′-ethylamine)-androst-4-ene, **18***. A total of 1 equiv of **17** and 1.2 equiv of DDS-biotin were dissolved with 2 equiv (d = 0.74) of NEt_3 in DMF and stirred for 20 h at room temperature. After removal of the solvent, the residue was chromatographed on SiO_2 using CH_2Cl_2:MeOH (4:1, v/v) as the eluent. The product was dissolved in MeOH:CH_2Cl_2 (1:1, v/v) and added to a stirred suspension of SiO_2 in EtOH 90%:CH_2Cl_2 (1:2, v/v). After 15 min, the solvent was removed, and the residue was left overnight. The steroid-coated SiO_2 was mounted on a SiO_2 chromatographic column and eluted with CH_2Cl_2:MeOH (4:1, v/v), yielding 70% of the 17α-Bio-T product **18**, which was further purified by HPLC (eluent, MeOH:CH_2Cl_2, 1:4, v/v, flow 8.0 mL/min, t_r 13.5 min). IR (KBr): $\bar{\nu}$ 3340, 3310 (NH, OH), 2869, 2847 ($CH_{aliphat}$), 1698, 1656, 1548 (C═O), 1127, 1097 (C−O−C). ^1H NMR (400 MHz, CD_3OD): δ 0.85 (s, 3 H, 18-CH_3), 1.15 (s, 3 H, 19-CH_3), 4.25 (m, 1 H, biotin), 4.45 (m, 1 H, biotin), 5.68 (s, 1 H, 4-CH). MS (FAB, *m*/*z*): 844 (MH^+, 100%). UV: 241 nm, lgϵ = 4.14; $[\alpha]_D^{20}$ = +19° (MeOH, c = 1.75).

Preparation of 17β-hydroxyandrost-4-en-3-one-19-yl-oxymethylenecarbonyl-DADOO-biotin (19-Bio-T) (21). *17β-Hydroxyandrost-4-en-3-one-19-yl-carboxymethyl ether*, **19**, was prepared starting from 19-hydroxy-androst-4-ene-3,17-dione according to a method of Rao et al. (1978). Protection of the hydroxyl group at position 19 was performed by reacting with dihydropyran/*p*-toluenesulfonic acid to give the tetrahydropyranyl (THP) ether. The 17-carbonyl group was then site-selectively reduced with diiso-butyl-aluminum hydride to the β-isomer of the secondary alcohol, which was subsequently acetylated with acetic anhydride in pyridine. Removal of the THP group at position 19 by mild acetic treatment was followed by alkylation of the primary alcohol with diazoacetate on rhodium(II)-acetate catalysis in toluene. The carboxymethyl ether **19** was obtained after alkaline deprotection with sodium methoxide in methanol.

17β-Hydroxyandrost-4-en-3-one-19-yl-oxymethylenecarbonyl-N-oxy-succinimide, ***20.*** A total of 1 equiv of **19** was dissolved in dry THF. A total of 1.2 equiv of *N*-hydroxysuccinimide and 1.2 equiv of *N,N′*-dicyclohexylcarbodiimide was added at room temperature under N_2. The solution was stirred for 16 h, while a crystalline precipitate of *N,N′*-dicyclohexyl urea started to form after some minutes. The solid was filtered off, and the solution evaporated to dryness. The crude product was dissolved in ethyl acetate, allowed to stand at room temperature for 2 h, and then the solution was filtered again. After removing the solvent, the crude product was dissolved in DMF and purified by gradient HPLC: eluent A, water (0.1% trifluoroacetic acid, v/v); B, 80% acetonitrile (0.1% trifluoroacetic acid, v/v), flow 15 mL/min, gradient $t = 0$ min (0% B), 120 min (60% B), 130 min (100% B), 150 min (100% B); $t_r = 131$ min. A total of 71% yield of the pure solid product **20** was obtained after lyophilization. MS (pos. ESI): *m/z* calcd for $C_{37}H_{58}N_4O_8S$: 459.5. Found: 459.3. IR (KBr): $\bar{\nu}$ 3414, 2931, 1734. ^{1}H NMR: 0.79 (s, 3H, 18-CH_3), 2.88 (s, 4H, −CO−CH_2−CH_2−CO−), 3.67 (t, 1H, 17-CH), 3.90 (AB signal, $J = 8.5$ Hz, 2H, 19-CH_2−O), 4.42 (s, 2H, O−CH_2COO), 5.94 (s, 1H, 4-CH). UV: 239 nm, lg$\epsilon = 7.097$.

17β-Hydroxyandrost-4-en-3-one-19-yl-oxymethylenecarbonyl-DADOO-biotin, ***21.*** A total of 1 equiv of **20** was dissolved in freshly distilled DMF. A total of 1.2 equiv of DADOO-biotin and 1.0 equiv NEt_3 were added under N_2. The solution was stirred at room temperature for 20 h and then injected directly into the preparative HPLC system for isolation of the pure product (same system as applied to **20**, gradient: $t = 0$ min (0% B), 150 min (50% B), 160 min (100% B), 180 min (100% B); $t_r = 157$ min). 47% yield of the pure solid product **21** was obtained after lyophilization. MS (pos. ESI): *m/z* calcd for $C_{25}H_{33}NO_7$: 719.0 Found: 718.6. IR (KBr): $\bar{\nu}$ 3402, 3092, 1658, ^{1}H NMR: 0.79 (s, 3H, 18-CH_3), 3.65 (t, 1H, 17-CH), 3.82 (AB signal, $J = 8.9$ Hz, 2H, 19-CH_2−O), 3.97 (AB signal, $J = 15.0$ Hz, 2H, O−CH_2−CON), 5.96 (s, 1 H, 4-CH). UV: 240 nm, lg$\epsilon = 9.966$.

RESULTS

3-Biotinylated T (Scheme 1). Among the wide range of different reaction types applicable for derivatizing the 3-position of T, we chose the hydrazone formation to insert the biotin moiety. Reaction of T with *N*-(ε-biotinyl)-caproyl hydrazide in methanol with catalytic amounts of acetic acid for 3 days at 25 °C (Janoski et al., 1974; Kohler et al., 1997) gave the hydrazone **2** as one reaction compound. The ^{1}H NMR data do not distinguish between the possible syn- or anti-configuration.

Scheme 1. Synthetic Strategies for the 3-Biotinylation of T

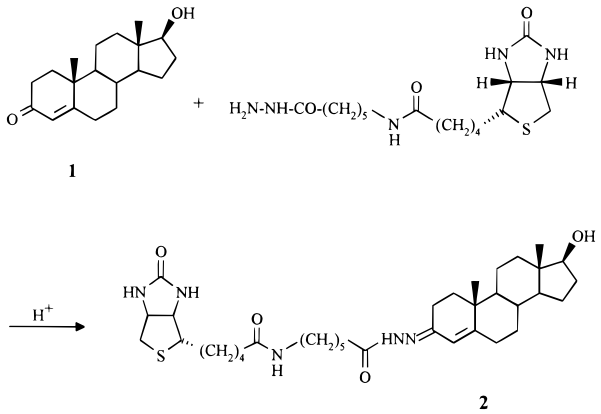

7α-Biotinylated Ts (Scheme 2). Many copper-catalyzed 1,6-additions of alkyl Grignard reagents to Δ^6-T and Δ^6-nor-T derivatives are known. We added ω-silyl protected hydroxylalkyl-modified Grignard reagents (ω-*t*-BuMe_2OSi−$(CH_2)_n$MgBr [$n = 3$, 6, and 11]) in the presence of copper(I) iodide to Δ^6-T following the protocol of Bowler et al. (1989). The 17-acetoxy-6,7-dehydro-T precursor **3** was prepared according to the literature (Bucourt et al., 1978), also the synthesis of the Grignard precursors was given (Kim et al., 1990). The Michael addition provided the *n′*-alkyl linked steroids **5a**−**5c** as α/β-mixtures which were separated by LSC into the epimers (de-values see Scheme 2). In contrast to the nonstereoselective reaction of these pure aliphatic Grignard compounds, the 1,6-addition of the 9-*t*-butyldimethylsilyloxy-5-oxa-nonyl- and 13-*t*-butyldimethylsilyloxy-7-oxa-tridecyl-magnesium bromides (**4d** and **4e**), respectively, provided the ether chain-linked steroids **5d** and **5e** with high α-stereoselectivity. These novel Grignard reagents are described in Scheme 3. There were no β-epimers detectable by NMR spectroscopy of the HPLC-separated products. All α-products were desilylated with TBAF. Mesylation and substitution with sodium azide in HMPT proceeded smoothly to give the azides **8a**−**e**. Conversion to the respective amines **9a**−**e** was achieved by the Staudinger reaction with triphenylphosphine in boiling wet THF. The synthesis was completed after hydrolysis of the 17-acetoxy group with diluted sodium hydroxide in methanol (pH=13) by amidation with the reagents biotin-NHS, LC-biotin and DDS-biotin, to give the products **11a**, **c**, **e**, **13d**, and **12b**, **c**, and **e**, respectively.

The stereochemistry of the 7α-C-linked epimers was established on the basis of ^{1}H and ^{13}C-experiments (DEPT, COSY, NOE, and decoupling experiments). The results are in accordance to spectroscopic data of other reported 7-substituted testosterone derivatives (Luppa et al., 1997). A characteristic proton-coupling pattern for the 6α,6β,7β-ABX system exhibited the α-stereochemistry of 7α-biotinylated T compounds. As an example, the ABX pattern of **11c** was as follows: δ 2.36 ppm; $J_{6\alpha6\beta}$ =14.2 Hz, $J_{6\alpha7\beta} = 2.3$ Hz (6α-H); $\delta = 2.40$ ppm; $J_{6\alpha6\beta} = 14.2$ Hz, $J_{6\beta7\beta} = 4.9$ Hz (6β-H).

The 7α-T configuration of the precursor **7a** could be determined independently to the NMR experiments by X-ray crystallography as shown in Figure 1. The data are as follows: $C_{25}H_{38}O_6S$, $M = 466.64$, orthorhombic, $P2_12_12_1$, $a = 581.89(3)$, $b = 1403.0(1)$, $c = 2976.1(2)$ pm, $V = 2429.7(3) \times 10^6$ pm^3; $Z = 4$; $\rho_{calcd} = 1.276$ gcm^{-3}, $F_{000} = 1008$, $\mu = 0.171$ mm^{-1}. Data collections were performed at 163 K within the Θ-range of $2.51° < \Theta < 30.04°$. A

Scheme 2. Synthetic Strategies for the 7α-Biotinylation of T

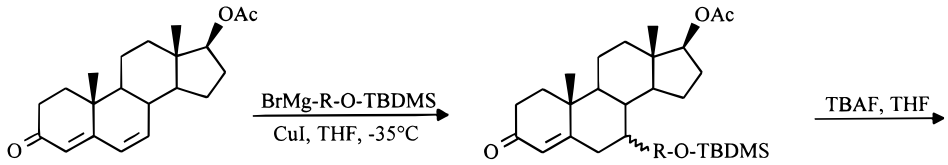

3

Grignard reagents (**4**):

4a	R = $(CH_2)_3$, (88%, α:β ~ 5:3)	**5a**	R = $(CH_2)_3$, (83%)
4b	R = $(CH_2)_6$, (84%, α:β ~ 2:1)	**5b**	R = $(CH_2)_6$, (94%)
4c	R = $(CH_2)_{11}$, (92%, α:β ~ 5:3)	**5c**	R = $(CH_2)_{11}$, (94%)
4d	R = $(CH_2)_4$-O-$(CH_2)_4$, (80%)	**5d**	R = $(CH_2)_4$-O-$(CH_2)_4$, (58%)
4e	R = $(CH_2)_6$-O-$(CH_2)_6$, (80%)	**5e**	R = $(CH_2)_6$-O-$(CH_2)_6$, (58%)

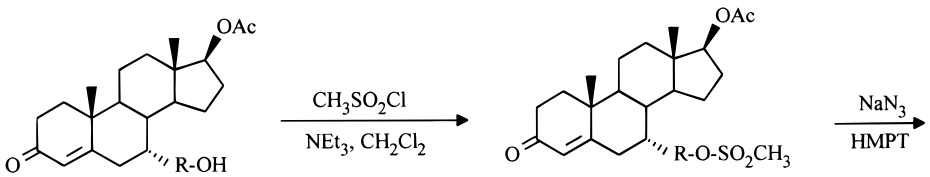

6a	R = $(CH_2)_3$, (93%)	**7a**	R = $(CH_2)_3$, (91%)
6b	R = $(CH_2)_6$, (93%)	**7b**	R = $(CH_2)_6$, (94%)
6c	R = $(CH_2)_{11}$, (95%)	**7c**	R = $(CH_2)_{11}$, (95%)
6d	R = $(CH_2)_4$-O-$(CH_2)_4$, (80%)	**7d**	R = $(CH_2)_4$-O-$(CH_2)_4$, (80%)
6e	R = $(CH_2)_6$-O-$(CH_2)_6$, (89%)	**7e**	R = $(CH_2)_6$-O-$(CH_2)_6$, (89%)

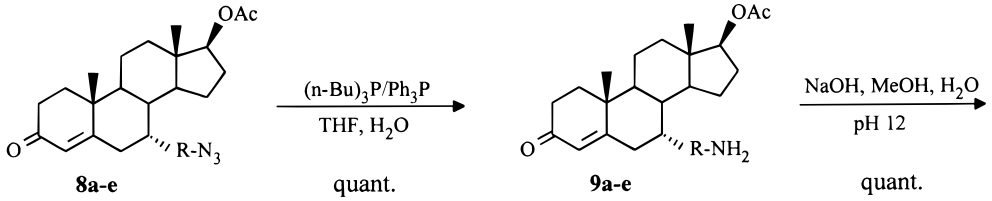

8a-e quant. **9a-e** quant.

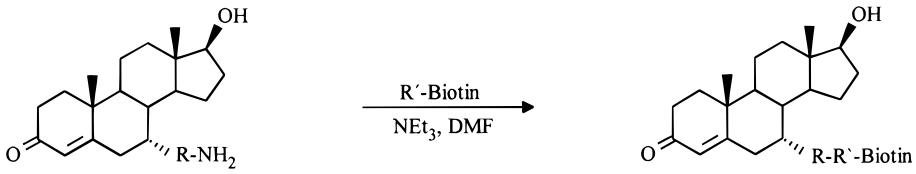

10a-e

Biotin-NHS:

R = $(CH_2)_6$-O-$(CH_2)_6$, (86%)	**11e**
R = $(CH_2)_3$, (88%)	**11a**
R = $(CH_2)_{11}$, (88%)	**11c**
LC-Biotin:	
R = $(CH_2)_4$-O-$(CH_2)_4$, (80%)	**13d**
DDS-Biotin:	
R = $(CH_2)_6$-O-$(CH_2)_6$, (81%)	**12e**
R = $(CH_2)_6$, (88%)	**12b**
R = $(CH_2)_{11}$, (79%)	**12c**

total number of 8146 reflections was collected. A total of 826 negative intensities, 52 systematically absent reflections together with 2553 very weak high order reflections (Θ > 25.00°) were rejected from the original data set. After merging (R_{int} = 0.0270), a sum of 4059 independent reflections remained and were used for all calculations. Data were corrected for Lorentz and polarization effects. The structure was solved by a combination of direct methods and difference Fourier syntheses. All "heavy atoms" of the asymmetric unit were refined anisotropically. All H atoms were located and refined with individual isotropic displacement parameters. For the H atoms at C24 and C25, which where influenced by the disordered O4 atom, a riding model was applied. Full-matrix least-squares refinements were carried out by minimizing $\sum w(F_o^2 - F_c^2)^2$ with *SHELXL-93* weighting scheme and stopped at R_1 = 0.0443, wR_2 = 0.1058, GOF = 1.133, and shift/err < 0.001. The correct enantiomer was confirmed by Flack's parameter ϵ = −0.07(10). Neutral atom scattering factors for all atoms and anoma-

Scheme 3. Synthesis of the Grignard Reagents 9-*t*-Butyl-dimethylsilyloxy-5-oxa-nonyl- and 13-*t*-Butyl-dimethylsilyoxy-7-oxa-tridecyl-magnesium Bromide from the Well-Known Monoprotected Diols (*n* = 4,6) (Corey and Venkateswarlu, 1972; Bowler et al., 1989; Poppe et al., 1993; Luppa et al., 1996) to 4d and 4e Using Conventional Methods

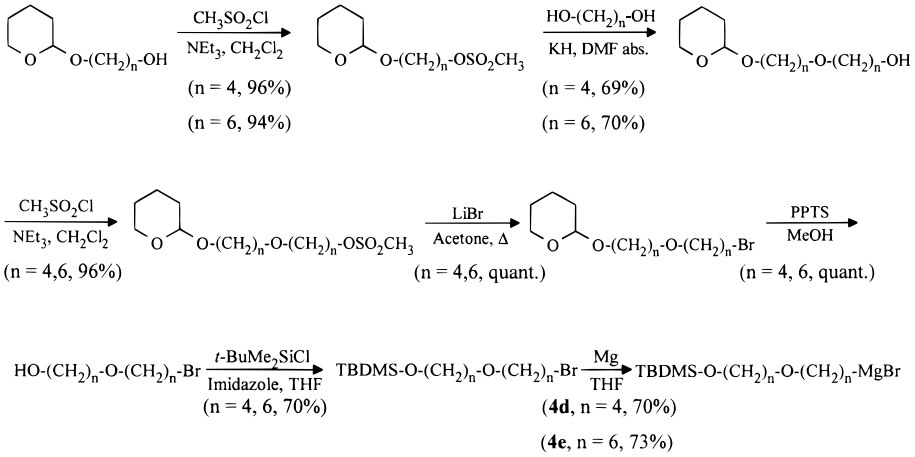

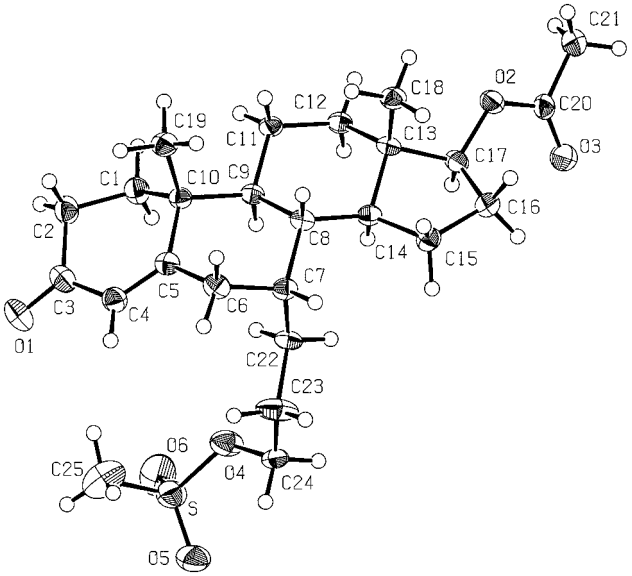

Figure 1. ORTEP drawing of the molecular structure of the 7α-T precursor 17*β*-acetoxy-7α-(3-propylmesylate)-androst-4-en-3-one **7a**. Thermal ellipsoids are at the 50% probability level. Selected bond lengths (pm) and angles (deg): O1−C3 122.1(3), C2−C3 150.1(4), C3−C4 146.5(4), C4−C5 134.3(4), all other carbon−carbon bonds the 7α-T skeleton ranges from 150.5(4) to 156.6(4); O1−C3−C4 122.1(3), C3−C4−C5 123.4(2), C4−C5−C6 120.5(2).

lous dispersion corrections for the non-hydrogen atoms were taken from *International Tables for X-ray Crystallography*.

We isolated the 7β-$(CH_2)_{11}$-Bio-T from a mixture of 17*β*-acetoxy-7α/*β*-(11′-*t*-butyl-dimethylsilyloxy-undecyl) T **5c** after treatment with TBAF cleaved by HPLC and subsequent desilylation, amine transformation, saponification of the 17-acetoxy group, and biotinylation. The ^{1}H NMR data [400 MHz, $CDCl_3$, δ (ppm)] for this compound are as follows: 0.80 (s, 3 H, 18-CH_3), 1.17 (s, 3 H, 19-H_3), 2.18 (dd, $J_{6\alpha6\beta}$ = 14.4 Hz; $J_{6\beta7\alpha}$ = 12.1 Hz, 1 H, 6*β*-H), 2.29 (dd, $J_{6\alpha6\beta}$ = 14.4 Hz, $J_{6\alpha7\alpha}$ = 4.9 Hz, 1 H, 6α-H), 3.21 (m, 2 H, R−CH_2−NH_2), 4.32 (m, 1 H, biotin), 4.52 (m, 1 H, biotin), 5.40 (s, 1 H, biotin-NH), 5.71 (s broad, 1H, 4-CH), 5.93 (t, 1 H, amide-NH), 6.35 (s, 1 H, biotin-NH). We have hints that 7*β*-biotinylated Ts in contrast to the 7α derivatives are of interest as ligands for SHBG. A detailed description of the syntheses of different 7*β*-derivatives will be presented elsewhere.

17α-Biotinylated T (Scheme 4). The synthesis commenced with the regioselective ketal protection of the 3-oxo function of androst-4-ene-3,17-dione using a stannoxane complex as catalyst (Otera et al., 1992). Treatment of the 3-protected steroid **14** with dimethylsulfonium methylide, generated from trimethylsulfoniumiodide with 1 equiv *n*-buLi in THF at −20 °C yielded the epoxide **15** with the oxygen in *β*-position (Gella et al., 1994a,b). Nucleophilic ring opening with cyanide in ethylene glycol at 100 °C gave the 17α-cyanomethyl derivative **16**. The stereochemistry results from an α-face attack of the nucleophile. Reduction with $LiAlH_4$ led to the amine **17** which was biotinylated with DDS-biotin. Deprotection with wet SiO_2 at 24 °C afforded the target molecule **18**.

19-Biotinylated T (Scheme 5). The biotinylation of the 19-position started from 17*β*-hydroxy-androst-4-en-3-one-19-yl carboxymethyl ether **19**, a precursor not easily accessible. This carboxymethyl ether was prepared from 19-hydroxy-androst-4-en-3,17-dione after protecting the 19-OH-group and selectively reducing the 17-oxo function. Removal of the protecting group at position 19 and subsequent alkylation gave the ether derivative which was finally deprotected in alkaline medium. The carboxylic acid was then activated with *N*-hydroxysuccinimide/*N*,*N*′-dicyclohexylcarbodiimide to give **20**. This compound reacted then by aminolysis with biotin-DADOO to the 19-biotinylated T product **21**.

DISCUSSION

Chemical modifications of the androgenic steroid T can easily be planned at the functional groups at position 3, 17, and 19. But these groups define in a high degree the identity of the androgenic steroid. Therefore, for different ligand-binding applications ring core-based modifications are advisable in order to preserve the epitope structure of the hapten. To guarantee high affinities to the respective ligand-binding domains of the AR and also SHBG, the site of substitution, structure, stereochemistry, and functionality of the modification are important.

Chemical Properties of 17*β*-Hydroxy-androst-4-en-3-one (testosterone, T). T, like all androgenic steroids, is a relatively lipophilic compound with a rigid and planar tetracyclic backbone. X-ray studies (Thakkar et al., 1970) show that for T the A ring is in a conformation between envelope at C1 and half chair, whereas both B and C rings are in a chair conformation. The D ring is in an envelope conformation at C13. We conclude from

Scheme 4. Synthetic Strategies for the 17α-Biotinylation of T

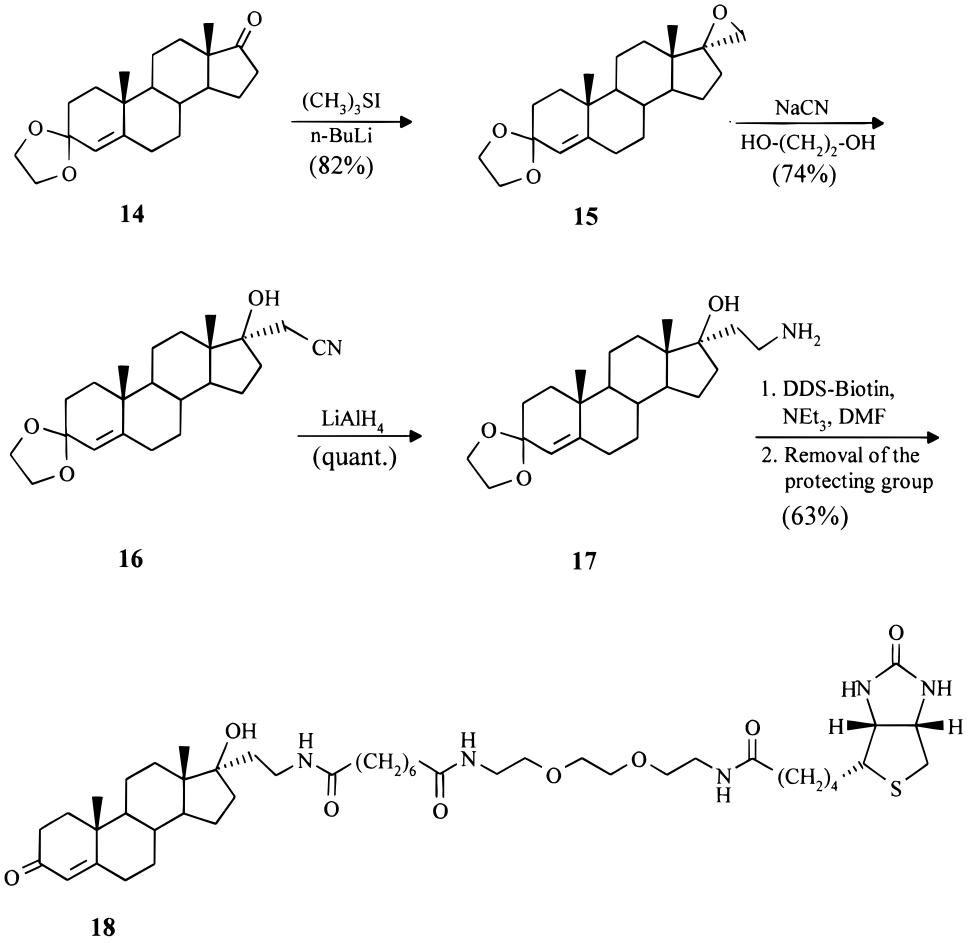

14 15 16 17 18

Scheme 5. Synthetic Strategies for the 19-Biotinylation of T

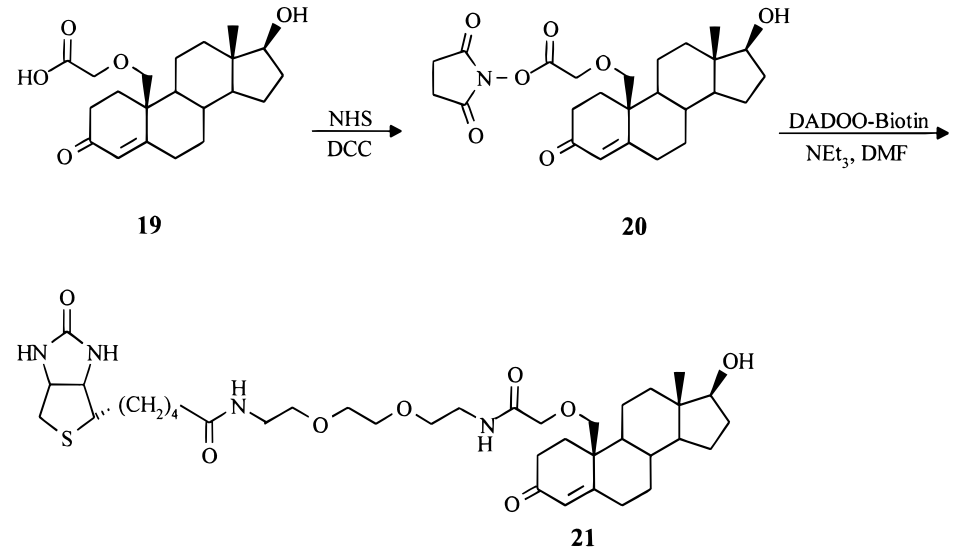

19 20 21

these X-ray data that T has a molecular thickness in the *z*-axis of 4.42 Å [derived from the distance of C3 to C19 (3.02 Å) plus 1.40 Å for the hydrogen distances]. The molecular volume is 250 Å^3 in the *xy*-plane (derived from the distance of O3 to O17 of 10.73 Å multiplied by the distance of the C6, C7−C11, and C12 distance of 3.87 Å plus 1.40 Å for the hydrogen distances multiplied by 4.42 Å).

Synthetic Strategies. This presentation describes synthetic approaches for the biotinylation of T at the following positions: 3, 7α, 17α, and 19. Besides the synthetic pathways for the *aliphatic 7α-biotinylated derivatives* using the 1,6 Michael addition of hydroxyl-alkyl-modified Grignard compounds to 17-acetoxy-6,7-dehydro-T [already described by our group (Luppa et al., 1996)], which represents a nonstereoselective reaction, the 1,6-addition of the 9-*t*-butyldimethyl-silyloxy-5-oxa-nonyl- and 13-*t*-butyldimethylsilyoxy-7-oxa-tridecyl-magnesium bromides provides *ether chain-linked 7α-derivatives* with high α-stereoselectivity. *3-Biotinylated T* derivatives are available by the well-known hydrazone formation procedures at the 3-oxo position in an one pot

reaction. Novel syntheses for the 17α- and 19-biotinylation complete our synthetic repertoire. In contrast to 17α-alkylated E2 derivatives, rather little is known about 17α-alkylated Ts (Li et al., 1994). The novel 17α-*biotinylated T* was derived from the key intermediate 3-protected 4-androsten-17-epoxide **15** with oxygen in the *β*-position (Otera et al., 1992; Gella et al., 1994a,b). Nucleophilic attack of cyanide from the α-face opened the epoxide ring to give the 17α-cyanomethyl derivative **16**. The reduction to amine and the biotinylation were performed as usual. We used an alternative way to insert biotin at the T 19 position for the synthesis of *19-biotinylated T*. The steroidal carboxymethyl ether precursor **19** was prepared starting from 19-hydroxy-androst-4-en-3-one-3,17-dione. The carboxylic acid was then activated by the carbodiimide method and reacted directly by aminolysis with DADOO-biotin to give the 19-biotinylated T **21**.

Different biotinylation reagents together with various spacers with different lengths and functionalities provide methods for tailoring immunochemical T probes for a series of different purposes. The critical issue for all syntheses is the choice of the protecting groups. Concerning the allylic ethylene glycol protected androst-4-ene-3,17-dione, e.g., it is of interest that the allylic dioxolan group is easily deprotected in comparison to the Δ^5-isomer which prevents a E1 elimination of the 17*β*-hydroxy group of the target.

The series of different spacer groups connecting T derivatives to the biotin moiety is accessible by different biotinylation reagents and the functional group interconversion concept using the Staudinger reaction to elongate C−C coupled spacer precursors at the steroid core. This approach converts the azide function into a primary *ω*-amino group. The use of *ω*-hydroxyl-n-oxaalkyl-modified Grignard reagents additionally enables a better hydrophilicity for immunochemical applications of the biotinylated T probes.

Immunoassay Applications for Biotinylated T Derivatives. T compounds labeled with prosthetic groups such as biotin can be used as immunochemical probes for the determination of T in serum or other body fluids. The knowledge of the molecular chemistry of the antigen/antibody reaction has led to the development of immunoassays with enhanced specificity and reaction times (Gosling, 1990). But for steroids, the major concern is still the degree of subtlety in structural variability of the similar steroid families such as estrogens, androgens, gestagens, and corticoids (Price, 1998). Additionally, the precision of an assay, which is closely related to sensitivity, can only be improved when automation can be achieved. An assumption for this is the availability of chemically stable and easy-to-handle steroid tracers, linked to a reporter group. In the last years, a series of different nonisotopic T immunoassays with labeled tracers were developed (Ali et al., 1992; Rassaie et al., 1992a,b; Sengupta et al., 1992; Mikola et al., 1993; Wheeler et al., 1996; Adamczyk et al., 1997b; Tschöp et al., 1998).

For the antibody production in a host animal, steroids have to be coupled to immunogenic proteins. The specificity of the resulting anti-steroid antibody depends on the position of coupling to the carrier protein, which determines the cross-reactivity of the antibody. When applying isotope or enzyme-labeled steroids as tracers in competitive immunoassays, analytical sensitivity and specificity is affected by a limited competitiveness when the tracer has been derivatized at ring positions 3 or 17, which has been shown for the estrogens estrone (E1) and E2 (Kim et al., 1982; DeBoever et al., 1986; Folan et al., 1988; Barnard et al., 1989; Elder et al., 1990). High specificity is achievable only if the tracer resembles in structure to the native steroid (Chames and Baty, 1998). Recently, we showed that the introduction of a biotin label to E1 at the ring position 6α and to T at the position 7α leads to negligible alterations in comparison to the structure of the respective steroidal hapten (Luppa et al., 1994, 1996). These characteristics allow sensitive and reproducible determinations of E1 and T over large dynamic ranges (Luppa et al., 1995, 1997). In addition, the 7α-C_{11}−Bio-T tracer, which we applied in the chemiluminescence immunoassay, provided higher specificity through a better availability of the critical antigen sites which is in accordance with suggestions made by Fránek (1987). For the 7α-biotinylated T series, the X-ray analysis of **7a** proved the axial position of the spacer group. This results in a vertical orientation of the biotin moiety toward the α-face of the planar tetracyclic backbone. Also Landsteiner's principle (1962) is confirmed that antibody specificity is directed primarily at that portion of the hapten furthest from the group linking it to the carrier protein. Other authors also use biotinylated steroids as tracers in immunoassays. Bodmer et al. (1989) presented a sp^3-hybridized 6α-biotinylated E2 conjugate as key component in antigen- and antibody-immobilized enzyme-linked immunosorbent assay techniques for E2. But in most described applications, the oximation of steroid 3-CMO-derivatives was applied for biotinylation (Kanazaki and Iwasawa, 1995; Mares et al., 1995; Dressendörfer et al., 1998; Tschöp et al., 1998).

Ligand-Binding Studies of Biotinylated Steroid Derivatives to SHBG. A possible application of these immunochemical probes is the determination of ligand-binding properties of androgen derivatives to steroid-binding globulins. Natural steroid hormones circulate in human plasma bound to the three major transport proteins: albumin, corticoid-binding globulin (CBG) and SHBG (Rosner, 1990). SHBG forms a specific 1:1-complex as homodimer with T, DHT, or E2, while the 1:1-CBG-complex was found to be monomeric (Hammond, 1995; Hammond and Bocchinfuso, 1995). Up to now, SHBG-binding studies have been performed for many steroids. Especially, Pugeat et al. (1981) and Dunn et al.. (1981) described a method for the determination of association constants in detail, derived from relative binding activities (RBA). The RBA were measured under equilibrium conditions using tritiated T as tracer and a solid matrix of Con A-sepharose, which adsorbs SHBG. Alternatively, biotinylated steroid derivatives can be used for online SHBG-binding studies when being immobilized in a continuous-flow biosensor system (Kaiser et al., 1998).

Ligand-Binding Studies of Biotinylated Steroid Derivatives to the AR. Steroid hormones control a wide spectrum of intracellular metabolic processes in target tissues by interacting first with their respective receptors, members of the nuclear receptor superfamily of transcription factors (Weigel, 1996; Quigley, 1998). These receptor proteins are characterized by a high affinity for the corresponding hormones and an ability to discriminate between structurally closely related ligands. The receptors exist in inactive complexes with chaperone proteins (e.g., hsp9, hsp70, hsp56, immunophilins) in the absence of hormones. The complexes are cytoplasmatic or weakly associated within the nucleus. Ligand binding displaces them from the chaperone proteins and alters the conformation of the receptors leading to homodimerization, so that they can function as transcription factors. Subsequently, the receptors modulate transcription by

virtue of their binding to a specific sequence in the DNA of target gene promoters known as hormone response elements. The DNA-binding area of a steroid receptor is structurally characterized by a zinc finger. Hormone-binding activity alone, however, does not determine whether a ligand will have positive or negative effects on the action of the receptor. X-ray studies of the 3D-structure of the ligand-binding domain of the AR and the ER-α demonstrate a consensus structure comprising 12 α_l-helices arranged in a three-layer sandwich-like configuration with minor regions of variation (Quigley, 1998; Wurtz et al., 1998). The site at which the steroidal ligand binds is buried in a hydrophobic pocket arranged by 24 residues in different helices (1, 3, 5, 11, and 12) and loops (6, 7, 11, and 12). The receptor surrounds the steroidal ligand involving all four rings in the binding pocket (Anstead et al., 1997).

The binding of androgens and structurally related analogues to the androgen receptor is often studied by competition experiments using cytosolic preparations of AR containing tissues using [^{3}H]R1881 (methyltrienolone) as the radioligand. Many potent ligands in the T-, 19-nor-T, and DHT-family were found with 7α-, 11*β*-, and 17α-substituents. ^{18}F or ^{125}I labels of these compounds allow excellent receptor-mediated tumor imaging or are useful in assaying low levels of AR in small tissue specimens (Schilling and Liao, 1984; Stobaugh and Blickenstaff, 1990; Salman and Chamness, 1991; Choe and Katzenellenbogen, 1995; Choe et al., 1995; Labaree et al., 1999). However, the application of biotinylated T compounds for the oncological relevant determination of the AR in tumors is still a future project.

ACKNOWLEDGMENT

The authors thank the Fond der Deutschen Chemischen Industrie and the Bundesministerium für Bildung, Wissenschaft, Forschung und Technologie (Project 0311392) for financial grants.

Supporting Information Available: Tables giving details of the single-crystal X-ray experiment: data collection and refinement, atomic coordinates, displacement parameters, and bond lengths and angles. This material is available free of charge via the Internet at http://pubs.acs.org.

LITERATURE CITED

(1) Adamczyk, M., Mattingly, P. G., and Reddy, R. E. (1997a) An efficient stereoselective synthesis of 6-alpha-aminoestradiol: preparation of estradiol fluorescent probes. *Steroids 62*, 462−467.

(2) Adamczyk, M., Chen, Y, Johnson, D. D., and Reddy, R. E. (1997b) A stereoselective synthesis of 1α-(3′-carboxypropyl)-4-androsten-17*β*-ol-3-one: preparation of immunoreagents for quantification of testosterone by fluorescence polarization immunoassay. *Tetrahedron 53*, 12855−12866.

(3) Adamczyk, M., Johnson, D. D., and Reddy, R. E. (1998) Synthesis of 6*β*-[(2′-aminoethyl)-carboxamidomethyl]estradiol and preparation of estradiol probes. *Bioconjugate Chem. 9*, 403−408.

(4) Afonso, C. A. M. (1995) Transformation of azidogroup to *N*-(*tert*-butoxycarbonyl)amino group under mild conditions via Staudinger reaction. *Tetrahedron Lett. 36*, 8857−8858.

(5) Ali, E., Sengupta, J., and Dhar, T. K. (1992) Sandwich immunoassay of small molecules. I. Investigation with testosterone as model hapten. *J. Immunol. Methods 147*, 173−179.

(6) Anstead, G. M., Carlson, K. E., and Katzenellenbogen, J. A. (1997) The estradiol pharmacophore: ligand structure-estrogen receptor binding affinity relationships and a model for the receptor binding site. *Steroids 62*, 268−303.

(7) Barnard, G., Kohen, F., Mikola, H., and Lövgren, T. (1989) Measurement of estrone-3-glucu-ronide in urine by rapid, homogeneous time-resolved fluoroimmunoassay. *Clin. Chem. 35*, 555−559.

(8) Bodmer, D. M., Tiefenauer, L. X., and Andres, R. Y. (1989) Antigen- versus antibody-immobilized ELISA procedures based on a biotinyl-estradiol conjugate. *J. Steroid Biochem. 33*, 1161−1166.

(9) Bodmer, D. M., and Tiefenauer, L. X. (1990) Treatment of antibodies to reduce nonspecific binding in immunoassays using the avidin−biotin complex. *J. Immunoassays 11*, 139−145.

(10) Bowler, J., Lilley, T. J., Pittam, J. D., and Wakeling, A. E. (1989) Novel steroidal pure antiestrogens. *Steroids 54*, 71−99.

(11) Brooks, R. V. (1984) Androgens: physiology and pathology. In *Biochemistry of steroid hormones* (H. L. J. Makin, Ed.) pp 565−594, Blackwell, Oxford.

(12) Bucourt, R., Wignau, M., Torelli, V., Richard-Foyh, H., Geynet, C., Secco-Millet, C., Redeuilh, G., and Baulieu, E. (1978) New biospecific adsorbants for the purification of estradiol receptor. *J. Biol. Chem. 253*, 8221−8228.

(13) Chames, P., and Baty, D. (1998) Engineering of an anti-steroid antibody: amino acid substitutions change antibody fine specificitiy from cortisol to estradiol. *Clin. Chem. Lab. Med. 36*, 355−359.

(14) Choe, Y. S., and Katzenellenbogen, J. A. (1995) Synthesis of C-6 fluoroandrogens: evaluation of ligands for tumor receptor imaging. *Steroids 60*, 414−422.

(15) Choe, Y. S., Lidstrom, P. J., Chi, D. Y., Bonasera, T. A., Welch, M. J., and Katzenellenbogen, J. A. (1995) Synthesis of 11 beta-[18F]fluoro-5alpha-dihydrotestosterone and 11beta-[18F]fluoro-19-nor-5alpha-dihydrotestosterone: preparation via halofluorination-reduction, receptor binding, and tissue distribution. *J. Med. Chem. 38*, 816−825.

(16) Corey, E. J., and Venkateswarlu, A. (1972a) Protection of hydroxyl groups as *tert*-butyl-dimethylsilyl derivates. *J. Am. Chem. Soc. 94*, 6190−6191.

(17) Corey, E. J., and Snider, B. B. (1972b) A total synthesis of (±)-fumagillin. *J. Am. Chem. Soc. 94*, 2549−2550.

(18) De Boever, J., Kohen, F., Usanachitt, C., Vandekerckhove, D., Leyseele. D., and Vandewalle, L. (1986) Direct chemiluminescence immunoassay for estradiol in serum. *Clin. Chem. 32*, 1895−1900.

(19) Diamandis, E. P., and Christopoulos, T. K. (1991) The biotin-(stept)avidin system: principles and applications in biotechnology. *Clin. Chem. 37*, 625−636.

(20) Dressendörfer, R. A., Strasburger, C. J., Bidlingmaier, F., Klug, I., Kistner, A., Siebler, T., and Kiess, W. (1998) Development of a highly sensitive nonisotopic immunoassay for the determination of salivary 17-hydroxyprogesterone: reference ranges throughout childhood and adolescence. *Pediatr. Res. 44*, 1−6.

(21) Dunn, J. F., Nisula, B. C., and Rodbard, D. (1981) Transport of steroid hormones: binding of 21 endogenous steroids to both testosterone-binding globulin and corticosteroid-binding globulin in human plasma. *J. Clin. Endocrinol. Metab. 53*, 58−68.

(22) Elder, P. A., Manley, L., and Lewis, J. G. (1990) Use of a monoclonal antibody to estrone-3-glucuronide in an enzyme-linked immunosorbent assay (ELISA). *J. Steroid Biochem. 36*, 439−443.

(23) Folan, J., Gosling, J. P., and Fottrell, P. F. (1988) Solid-phase enzymoimmunoassay of estrone in serum. *Clin. Chem. 34*, 1843−1846.

(24) Fránek, M. (1987) Structural aspects of steroid-antibody specificity. *J. Steroid Biochem. 28*, 95−108.

(25) Gella, I. M., Bryzgalova, G. A., and Sergienko, J. Y. (1994) Steroidal oxetanes. 2. Introduction of oxirane and oxetane rings into Δ^4-3-ketosteroids using an enamine protecting group. *Pharm. Chem. J. 28*, 650−653.

(26) Gella, I. M., Sergienko, L. Y., and Cherevko, A. N. (1994) Steroidal spirooxetanes. I. Synthesis and antiandrogenic

properties of some 17-spirooxetanoandrostanes. *Pharm. Chem. J. 28*, 561−565.
(27) Gololobov, Y. G., and Kasukhin, L. F. (1992) Recent advances in the Staudinger reaction. *Tetrahedron 48*, 1353−1406.
(28) Gosling, J. P. (1990) A decade of development in immunoassay methodology [Review]. *Clin. Chem. 36*, 1408−1427.
(29) Hammond, G. L. (1995) Potential functions of plasma steroid-binding proteins. *Trends Endocrinol. Metab. 6*, 298−304.
(30) Hammond, G. L., and Bocchinfuso, W. P. (1995) Sex hormone-binding globulin/androgen-binding protein: steroid-binding and dimerization domains. *J. Steroid Biochem. Mol. Biol. 53*, 543−552.
(31) Hörhold, C., Hübner, M., Ponsold, K., Schnabel, R., and Schubert, K. (1975) Structure-metabolism-activity relationship in 17alpha-CH_2X-substituted estra-1,3,5,(10)-trienen. *Pharmazie 30*, 35−41.
(32) Janoski, A. H., Shulman, F. C., and Wright, G. E. (1974) Selective 3-(O-carboxymethyl)-oxime formation in steroidal 3,20-diones for hapten immunospecificity. *Steroids 23*, 49−64
(33) Kaiser, T., Pappert, G., and Luppa, P. (1998) Establishment of a novel continuous-flow biosensor system for online ligand-binding studies of sex hormone-binding globulin using immobilized steroid derivatives. *Xth Int. Congr. Hormonal Steroids*, Québec City, p 219.
(34) Kanzaki, M., and Iwasawa, A. (1995) A sensitive, nonisotopic immunoassay for progesterone using the avidin−biotin system. *Biomed. Res. 16*, 381−386.
(35) Kim, J. B., Barnard, G. J., Collins, W. P., Kohen, F., Lindner, H. R., and Eshhar, Z. (1982) Measurement of plasma estradiol-17β by solid-phase chemiluminescence immunoassay. *Clin. Chem. 28*, 1120−1124.
(36) Kim, S., and Kee, I. S. (1990) A novel method for direct conversion of tetrahydropyranyl ethers into *tert*-butyldimethylsilyl ethers with *t*-butyldimethylsilyl triflate and dimethyl sulfide. *Tetrahedron Lett. 31*, 2899−2900.
(37) Kohler, A. D., Beale, M. H., Rollason, R., Barratt, D. H. P., Lewis, M. J., Van der Meulen, R. M., and Wang, M. (1997) A radio-iodinated abscisic photoaffinity probe, *J. Chem. Soc., Perkin Trans. 1*, 1543−1548.
(38) Labaree, D. C., Hoyte, R. M., Nazareth, L. V., Weigel, N. L., Hochberg, R. B. (1999) 7alpha-Iodo and 7alpha-fluoro steroids as androgen receptor-mediated imaging agents. *J. Med. Chem. 42*, 2021−2034.
(39) Landsteiner, K. (1962) *The specificity of serological reactions*, pp 240−266, Dover Publications, New York.
(40) Li, X., Singh, S. M., and Labrie, F. (1994) Highly efficient nucleophilic addition of alkyl Grignard reagents to 17-ketosteroids in the presence of cerium(III) chloride: synthesis of 17β-propyl-17β-hydroxy-4-androsten-3-one, an androgen receptor antagonist. *Tetrahedron Lett. 35*, 1157−1160.
(41) Lindzey, J., Kumar, M. V., Grossman, M., Young, C., and Tindall, D. J. (1994) Molecular mechanisms of androgen action. *Vitam. Horm. 49*, 383−432.
(42) Luppa, P., Birkmayer, C., and Hauptmann, H. (1994) Synthesis of 3-hydroxyestra-1,3,5(10)-trien-17-one and 3,17β-dihydroxyestra-1,3,5(10)triene 6α-*N*-(ϵ-biotinyl)caproamide, tracer substances for developing immunoassays for estrone and estradiol. *Bioconjugate Chem. 5*, 167−171.
(43) Luppa, P., Hauck, S., Schwab, I., Birkmayer, C., and Hauptmann, H. (1995) 6α-Biotinylated estrone: novel tracer in competitive chemiluminescence immunoassay of estrone in serum. *Clin. Chem. 41*, 564−570.
(44) Luppa, P., Hauck, S., Schwab, I., Birkmayer, C., and Hauptmann, H. (1996) Synthesis of 17β-hydroxy-androst-4-en-3-one-7α-(biotinyl-6-*N*-hexylamide), a conjugate useful for affinity chromatography and for testosterone immunoassays. *Bioconjugate Chem. 7*, 332−337.
(45) Luppa, P., Hauck, S., Schmidmayr, S., Schwab, I., Birkmayer, C., Hauptmann, H., and Neu-meier, D. (1997) Different 7α-biotinylated testosterone derivatives as tracers for competitive chemiluminescence immunoassays for testosterone in serum. *Clin. Chem. 43*, 2345−2352.
(46) Mares, A., DeBoever, J., Stans, G., Bosmans, E., and Kohen, F. (1995) Synthesis of a novel biotin-estradiol conjugate and its use for the development of a direct, broad range enzyme immunoassay for plasma estradiol. *J. Immunol. Methods 183*, 211−219.
(47) Mikola, H., Sundell, A., and Hänninen, E. (1993) Labeling of estradiol and testosterone alkyloxime derivatives with a europium chelate for time-resolved fluoroimmunassays. *Steroids 58*, 330−334.
(48) Otera, J., Dan-oh, N., and Nozaki, H. (1992) Distannoxane-catalyzed acetalizaton of carbonyls. *Tetrahedron 48*, 1449−1456.
(49) Pilard S., and Vaultier, M. (1984) A stereospecific synthesis of (±)-α-conhydrine and (±)-β-conhydrine. *Tetrahedron Lett. 25*, 1555−1556.
(50) Ponsold, K., Hübner, M., Schnabel, R., and Strecke, J. (1974) Synthesis and uterotrophic effect of new delayed-action estrogens of the type 17alpha substituted derivatives of estradiol-3-methyl ether. *Arzneim. Forsch./Drug Res. 24*, 896−900.
(51) Poppe, L., Hull, W. E., and Rétey, J. (1993) Synthesis and characterization of (5′-deoxy-adenosin-5′-yl)cobalamin (adenosylcobalamin) analogues mimicking the transition-state geometry of coenzyme-B_{12}-dependent rearrangements. *Helv. Chim. Acta 76*, 2367−2383.
(52) Price, C. P. (1998) Progress in immunoassay technology. *Clin. Chem. Lab. Med. 36*, 341−347.
(53) Pugeat, M. M., Dunn, J. F., and Nisula, B. C. (1981) Transport of steroid hormones: inter-action of 70 drugs with testosterone-binding globulin and corticosteroid-binding globulin in human plasma. *J. Clin. Endocrinol. Metab. 53*, 69−75.
(54) Quigley, C. A. (1998) The androgen receptor: physiology and pathophysiology. In *Testosterone−Action, deficiency, substitution* (E. Nieschlag, and H. M. Behre, Eds.) pp 33−106, Springer-Verlag, Berlin.
(55) Rao, P. N., Moore, P. H., Peterson, D. M., and Tcholakian, R. K. (1978) Synthesis of new steroid haptens for radioimmunoassay − part V. 19-*O*-carboxymethyl ether derivative of testosterone. A highly specific antiserum for immunoassay of testosterone from both male and female plasma without chromatography. *J. Steroid Biochem. 9*, 539−545.
(56) Rao, P. N., Wang, Z., Cessac, J. W., and Moore, O. H. (1998) Synthesis of new immunogens for estrone and estradiol-17β and antisera evaluation. *Steroids 63*, 141−145.
(57) Rassaie, M. J., Kumari, G. L., Rao, P. N., Shrivastav, T. G., and Pandey, H. P. (1992a) Influence of different combinations of antibodies and penicillinase-labeled testosterone derivatives on sensitivity and specificity of immunoassays. *Steroids 57*, 112−118
(58) Rassaie, M. J., Kumari, L. G., Pandey, P. K., Gupta, N., Kochupillai, N., and Grover, P. K. (1992b) A highly specific heterologous enzyme-linked immunosorbent assay for measuring testosterone in plasma using antibody-coated immunoassay plates or polypropylene tubes. *Steroids 57*, 288−294.
(59) Ray, R., Bouillon, R., Van Baelen, H., and Holick, M. F. (1991) Photoaffinity labeling of human serum vitamin D binding protein and chemical cleavages of the labeled protein: identification of an 11.5-kDa peptide containing the putative 25-hydroxyvitamin D3 binding site. *Biochemistry 30*, 7638−7642.
(60) Rosner, W. (1990) The functions of corticosteroid-binding globulin and sex hormone-binding globulin: recent advances. *Endocr. Rev. 11*, 80−91.
(61) Roy, A., and Ray, R. (1995) Aminopropylation of vitamin D hormone (1α,25-dihydroxy-vitamin D3), its biological precursors, and other steroidal alcohols: an anchoring moiety for affinity studies of sterols. *Steroids 60*, 530−533.
(62) Salman, M., and Chamness, G. C. (1991) A potential radioiodinated ligand for androgen receptor: 7alpha-methyl-17alpha-(2′-(E)-iodovinyl)-19-nortestosterone. *J. Med. Chem. 34*, 1019−1024.
(63) Schilling, K., and Liao, S. (1984) The use of radioactive 7alpha, 17alpha-dimethyl-19-nor-testosterone (mibolerone) in the assay of androgen receptors. *Prostate 5*, 581−588.
(64) Sengupta, J., Dhar, T. K., Ali, E. (1992) Sandwich immunoassay of small molecules. II. Effects of heterology and

development of a highly sensitive and specific enzyme immunassay for testosterone. *J. Immunol. Methods 147*, 181−188.

(65) Stobaugh, M. E., and Blickenstaff, R. T. (1990) Synthesis and androgen receptor binding of dihydrotestosterone hemisuccinate homologues. *Steroids 55*, 259−262.

(66) Thakkar, A. L., Jones, N. D., Rose, H. A., Tensmeyer, L. G., and Hall, N. A. (1970) Crystallographic data for testosterone hydrate and anhydrate. *Acta Crystallogr., Sect. B 26*, 1184.

(67) Tiefenauer, L. X., and Andres, R. Y. (1990) Biotinylestradiol derivatives in enzyme immunoassays: structural requirements for optimal antibody binding. *J. Steroid Biochem. 35*, 633−639.

(68) Trost, B. M., and Melwin, L. S. (1975) *Sulfur ylides, emerging synthetic intermediates*, Academic Press, New York.

(69) Tschöp, M., Behre, H. M., Nieschlag, E., Dressendörfer, R. A., and Strasburger, C. J. (1998) A time-resolved fluorescence immunoassay for the measurement of testosterone in saliva: monitoring of testosterone replacement therapy with testosterone buciclate. *Clin. Chem. Lab. Med. 36*, 223−230.

(70) Veldscholte, J., Ris-Stalpers, C., Kuiper, G. G., Jenster, G., Berrevoets, C., Claassen, E., van Rooij, H. C., Trapman, J., Brinkmann, A. O., and Mulder, E. (1990) A mutation in the ligand binding domain of the androgen receptor of human LNCaP cells affects steroid binding characteristics and response to anti-androgens. *Biochem. Biophys. Res. Commun. 173*, 534−540.

(71) Veldscholte, J., Berrevoets, C. A., Ris-Stalpers, C., Kuiper, G. G., Jenster, G., Trapman, J., Brinkmann, A. O., and Mulder, E. (1992) The androgen receptor in LNCaP cells contains a mutation in the ligand binding domain which affects steroid binding characteristics and response to antiandrogens. *J. Steroid Biochem. Mol. Biol. 41*, 665−669.

(72) Waller C. L., Juma, B. W., Gray, L. E., and Kelce, W. R. (1996) Three-dimensional quantitative structure−activity relationships for androgen receptor ligands. *Toxicol. Appl. Pharmacol. 137*, 219−227.

(73) Weigel, N. L. (1996) Steroid hormone receptors and their regulation by phosphorylation. *Biochem. J. 319*, 657−667.

(74) Wheeler, M. J. (1995) The determination of bio-available testosterone. *Ann. Clin. Biochem. 32*, 345−357.

(75) Wheeler, M. J., d'Souza, A., Matadeen, J., and Croos, P. (1996) Ciba Corning ACS:180 testosterone assay evaluated. *Clin. Chem. 42*, 1445−1449.

(76) Wilchek, M., and Bayer, E. A. (1990) Biotin-containing reagents. *Methods Enzymol. 184*, 123−138.

(77) Wurtz, J. M., Egner, U., Heinrich, N., Moras, D., and Mueller-Fahrnow, A. (1998) Three-dimensional models of estrogen receptor ligand binding domain complexes, based on related crystal structures and mutational and structure−activity relationship data. *J. Med. Chem. 41*, 1803−1814.

BC9901402

Synthesis of [^{99m}Tc]DTPA-Folate and Its Evaluation as a Folate-Receptor-Targeted Radiopharmaceutical

Carla J. Mathias, David Hubers, Philip S. Low,† and Mark A. Green*

Department of Medicinal Chemistry and Molecular Pharmacology, 1333 Pharmacy Building, and Department of Chemistry, Purdue University, West Lafayette, Indiana 47907-1333. Received October 22, 1999; Revised Manuscript Received December 22, 1999

A DTPA−folate conjugate was radiolabeled with ^{99m}Tc by stannous chloride reduction of [^{99m}Tc]sodium pertechnetate in an aqueous solution of DTPA−folate. The radiochemical purity of the product consistently exceeded 97%, as assessed by thin-layer chromatography employing conditions analogous to those for radiochemical quality control of the radiopharmaceutical [^{99m}Tc]DTPA. HPLC demonstrated that the radiolabeled product resulted from the intact DTPA−folate conjugate and not unconjugated DTPA. The ability of [^{99m}Tc]DTPA−folate to target folate receptors in vivo was assessed in biodistribution studies with athymic mice bearing subcutaneous folate-receptor-positive human KB cell tumors. As an internal control, previously studied [^{111}In]DTPA−folate was coinjected with the [^{99m}Tc]DTPA−folate, along with varying amounts of DTPA−folate (0.38 mg/kg, 1.6 mg/kg, or 14 mg/kg). At each DTPA−folate dose, [^{99m}Tc]DTPA−folate exhibited tumor uptake comparable to that of the coadministered [^{111}In]DTPA−folate, with radiotracer levels declining at the higher DTPA−folate doses due to competitive receptor binding of the unlabeled conjugate. Tumor uptake of both tracers was also competitively blocked by preadministered folic acid dihydrate (2.9 mg/kg). Tumor-to-background tissue contrast obtained with [^{99m}Tc]DTPA−folate was generally similar to that obtained with [^{111}In]DTPA−folate. The ^{99m}Tc-labeled DTPA−folate conjugate may have utility as a targeted radiopharmaceutical for imaging neoplastic tissues known to overexpress the folate receptor.

INTRODUCTION

A tumor-cell-membrane-associated receptor for the vitamin folic acid appears viable as a molecular target for tumor-selective delivery of drugs and radiopharmaceuticals (*1*−*9*). The folate receptor (or folate binding protein, FBP) is overexpressed by a variety of neoplastic tissues, including breast, cervical, ovarian, colorectal, renal, and nasopharyngeal tumors, while being highly restricted in most normal tissues (*10*−*17*). It has been previously shown that this receptor system can be targeted with low-molecular-weight folate−chelate conjugates, such as [^{67}Ga]deferoxamine-folate and [^{111}In]-DTPA−folate (*5*−*9*). The biokinetics of [^{111}In]DTPA−folate suggest that selective folate-receptor-mediated tumor targeting might be feasible with shorter-lived, and less expensive, Tc-99m. We report here conditions for the preparation of [^{99m}Tc]DTPA−folate and evaluation of this agent in an athymic mouse tumor model (*18*).

EXPERIMENTAL PROCEDURES

General. A radionuclide dose calibrator was used for assays of radioactivity in the microcurie to millicurie range, while low level (<0.01 μCi) samples of radioactivity were counted in an automatic gamma scintillation counter with a 3-in. large-bore NaI(Tl) crystal. Counting windows of 160−300 and 120−160 keV were employed for simultaneous measurement of ^{111}In and ^{99m}Tc, respectively, in samples containing both nuclides; all such samples were recounted after ^{99m}Tc decay to define the extent of ^{111}In crossover into the ^{99m}Tc counting window and appropriate corrections made. Folate-deficient rodent chow was obtained from ICN Biomedicals (Costa Mesa, CA) and UV irradiated prior to use. The DTPA−folate conjugate (Figure 1) and [^{111}In]DTPA-folate were prepared as described previously (*8*, *9*). [^{99m}Tc]DTPA was prepared from a commercial cold kit (Mallinckrodt Medical, Inc., St. Louis, MO) according to the package insert instructions. The growth and preparation of KB cells, a human oral epidermoid carcinoma cell line that overexpresses the folate binding protein, has been detailed elsewhere (*9*). All animal experiments were performed in accordance with protocols approved by the Purdue University Animal Care and Use Committee. Statistical analysis of variations in tracer biodistribution between experimental groups employed the Wilcoxon test (*19*).

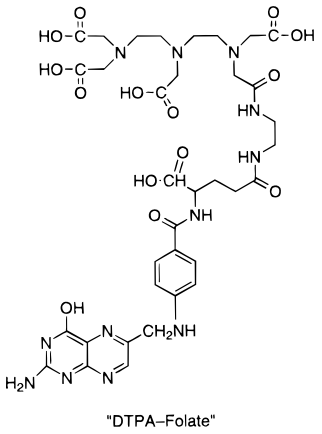

Figure 1. Structural formula of the DTPA−folate conjugate. An amide-linked ethylenediamine spacer is employed for connecting the DTPA chelator to the gamma-carboxylate of the folate fragment.

* To whom correspondence should be addressed. Phone: (765) 494-1445. Fax: (765) 494-1414: E-mail: magreen@purdue.edu.
† Department of Chemistry.

10.1021/bc9901447 CCC: $19.00 © 2000 American Chemical Society
Published on Web 02/19/2000

[^{99m}Tc]DTPA-Folate. In a "kit-like" method, 2 mg of DTPA−folate was dissolved in 0.2 mL of helium-purged water and immediately transferred to a multidose serum vial previously purged with nitrogen. Freshly eluted (<2 h old) [^{99m}Tc]sodium pertechnetate (30−50 mCi in 5 mL of saline) was added to the shielded vial containing the DTPA−folate solution, followed ca. 30 s later by 23−35 μg of stannous chloride dissolved in helium-purged water (0.3 mg/mL). The reaction vial was purged with nitrogen, shaken to mix, and allowed to stand for 1−2 min at room temperature before analysis. The final [^{99m}Tc]DTPA-folate reaction mixture, as well as control solutions of $^{99m}TcO_4^-$ and [^{99m}Tc]DTPA, was analyzed by chromatography on both ITLC SG strips eluted with normal saline and on Whatman 1 paper strips eluted with acetone. After development, the chromatography strips were either cut into 2 cm sections, beginning at the origin and continuing to the solvent front, and the ^{99m}Tc activity associated with each section quantified or scanned on an automatic TLC linear analyzer. TLCs were performed at 20 min, 2, 4, 6, 18, and 24 h after preparation to assess the radiochemical stability of the [^{99m}Tc]DTPA−folate product. Because these TLC methods would not distinguish [^{99m}Tc]DTPA−folate from [^{99m}Tc]DTPA, complementary HPLC analyses of the [^{99m}Tc]DTPA−folate, $^{99m}TcO_4^-$, and [^{99m}Tc]DTPA were also performed with a C18 (4.6 mm × 25 cm) column eluted with 5 mM tetrabutylammoniumphosphate dihydrate:methanol (7:3) at a flow rate of 1 mL/min. HPLC analyses were performed in duplicate at both 10−15 min and 6 h after compounding.

Athymic Mouse Tumor Model. Three to four week old male athymic mice (Nu/Nu strain) were obtained from Harlan Sprague Dawley, Inc. (Indianapolis, IN). All food, water, and bedding were sterilized prior to use. Mice were housed under conditions of controlled temperature (72 ± 2 °F) and humidity with daily light cycles of 12 h light, 12 h dark. After a 7 day acclimation period, the mice were inoculated subcutaneously with 0.1 mL of tumor cell suspension (2.5×10^5 KB cells) into the interscapular region using a 25 gauge needle. All inoculations were performed in a laminar flow cabinet using aseptic technique. Radiotracer distribution studies were performed 14 days after tumor cell inoculation. Animals used in the reported biodistribution experiments were exclusively fed folate-free rodent chow ad libitum for 21−23 days prior to radiopharmaceutical administration to reduce their serum folate to near the normal levels of human serum (*6*, *9*).

Radiotracer Biodistribution Studies. The general procedure for the animal biodistribution studies has been described previously (*6*, *7*, *9*). Animals were anesthetized by inhalation of diethyl ether during radiotracer injections via the exposed femoral vein, as well as at the time of sacrifice. Syringes used for radiotracer injections were weighed on an analytical balance before and after injection to quantitate the dose received by each animal. The biodistribution of tracer in each animal was calculated as both a percentage of the injected dose per organ (% ID/organ) and as a percentage of the injected dose per gram of tissue wet weight (% ID/g), using reference counts from a weighed and accurately diluted sample of the original injectate. Tumor/nontarget tissue ratios were calculated from the corresponding % ID/g values. As an internal control, [^{111}In]DTPA-folate was coinjected with the [^{99m}Tc]DTPA-folate complex, along with varying amounts of unlabeled DTPA-folate (0.38, 1.6, or 14 mg/kg) or folic acid dihydrate (2.9 mg/kg).

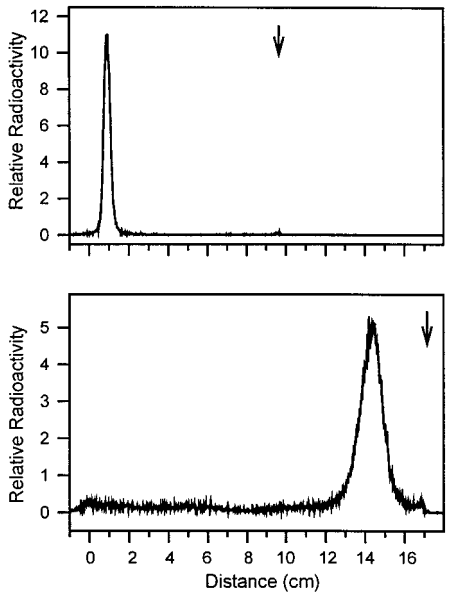

Figure 2. Thin layer chromatograms for [^{99m}Tc]DTPA−folate. (Top) Whatman 1 paper eluted with acetone. (Bottom) ITLC−SG eluted with saline. In both cases, the origin is at 0.0 cm. The arrows designate the solvent fronts.

RESULTS AND DISCUSSION

Radiochemistry. The [^{99m}Tc]DTPA−folate radiopharmaceutical was successfully prepared by stannous chloride reduction of [^{99m}Tc]sodium pertechnetate in an aqueous solution of the DTPA−folate conjugate (pH 7). The radiochemical purity of the [^{99m}Tc]DTPA−folate was established by radio-TLC and HPLC. The TLC conditions separate hydrolyzed-reduced ^{99m}Tc, $^{99m}TcO_4^-$, and conjugated [^{99m}Tc]DTPA−folate (Figure 2). However, these TLC conditions do not provide sufficient resolution to distinguish [^{99m}Tc]DTPA−folate from [^{99m}Tc]DTPA; therefore, HPLC analysis of the [^{99m}Tc]DTPA−folate product was performed to confirm the identity of the radiolabeled product, employing control solutions of $^{99m}TcO_4^-$ and [^{99m}Tc]DTPA. Retention times of 21, 29, and 50 min were observed for $^{99m}TcO_4^-$, [^{99m}Tc]DTPA, and [^{99m}Tc]DTPA−folate, respectively, allowing these radiochemical species to be readily distinguished (Figure 3). The radiochemical purity of the [^{99m}Tc]DTPA−folate product consistently exceeded 97% (n = 10). No [^{99m}Tc]DTPA contamination was observed in the [^{99m}Tc]DTPA−folate product. No decomposition of the compounded [^{99m}Tc]DTPA−folate product was observed over 6 h at room temperature, although by 18 h the TLC showed impurities of $^{99m}TcO_4^-$ and hydrolyzed-reduced ^{99m}Tc at 26% and 2%, respectively.

Biological Assessment. The ability of [^{99m}Tc]DTPA−folate to target folate-receptor positive tumors was evaluated by examining tracer biodistribution in athymic mice with human KB cell tumor xenografts. As an internal reference, previously studied [^{111}In]DTPA−folate was coinjected with the [^{99m}Tc]DTPA−folate radiopharmaceutical. The behavior of these two radiopharmaceuticals was similar in vivo, with the agents exhibiting identical tumor uptake at 4 h postinjection (Figure 4 and Table 1). The blood was the only sampled tissue that exhibited significant differences between the levels of ^{99m}Tc and ^{111}In at 4 h, with somewhat higher blood radioactivity found for the ^{99m}Tc radiolabel (Figure 4 and Table 1). Preadministration of excess folic acid dihydrate (2.9 mg/kg, i.v.) 1−2 min prior to the [^{99m}Tc]DTPA−folate/[^{111}In]-DTPA−folate injection resulted in competitive blocking

Table 1. Biodistribution of Coinjected [^{99m}Tc]DTPA−Folate and [^{111}In]DTPA−Folate in Athymic Male Mice with KB Xenografts

	percentage of injected dose per gram (tissue) ca. 4 h following intravenous administration[a]			
	^{99m}Tc-99m	^{111}In-111	^{99m}Tc-99m + folic acid[b]	^{111}In-111 + folic acid[b]
blood	0.19 ± 0.05	0.026 ± 0.018	0.17 ± 0.04	0.0077 ± 0.0057
heart	0.51 ± 0.07	0.43 ± 0.11	0.076 ± 0.007	0.013 ± 0.002
lungs	0.36 ± 0.07	0.23 ± 0.01	0.15 ± 0.02	0.030 ± 0.010
liver and gall bladder	1.05 ± 0.30	0.64 ± 0.23	0.27 ± 0.04	0.062 ± 0.014
spleen	0.15 ± 0.01	0.12 ± 0.01	0.082 ± 0.011	0.027 ± 0.005
kidney (one)	21 ± 3	25 ± 6	2.3 ± 0.7	2.1 ± 0.9
intestines and contents	0.83 ± 0.30	0.70 ± 0.29	0.064 ± 0.008	0.47 ± 0.11
muscle	0.70 ± 0.14	0.71 ± 0.26	0.62 ± 0.07	0.0090 ± 0.0062
tumor	2.9 ± 0.8	2.9 ± 0.9	0.32 ± 0.10	0.19 ± 0.07
tumor/blood	15.2 ± 0.1	136 ± 56	2.0 ± 0.8	26 ± 11
tumor/liver	3.8 ± 2.2	5.7 ± 4.4	1.2 ± 0.4	3.1 ± 1.2
tumor/kidney	0.15 ± 0.06	0.13 ± 0.06	0.14 ± 0.05	0.10 ± 0.05
tumor/muscle	4.2 ± 1.1	4.4 ± 1.6	5.1 ± 1.5	40 ± 24
animal mass (g)	31 ± 1	31 ± 1	26 ± 2	26 ± 2
tumor mass (g)	0.45 ± 0.07	0.45 ± 0.07	0.37 ± 0.12	0.37 ± 0.12

[a] Values shown represent the mean ± standard deviation of data from three animals. Total DTPA−folate dose of 187 ± 29 μg/kg. [b] Preadministered 2.9 mg/kg folic acid dihydrate (i.v.) 1−2 min prior to [^{111}In]DTPA−folate and [^{99m}Tc]DTPA−folate injection.

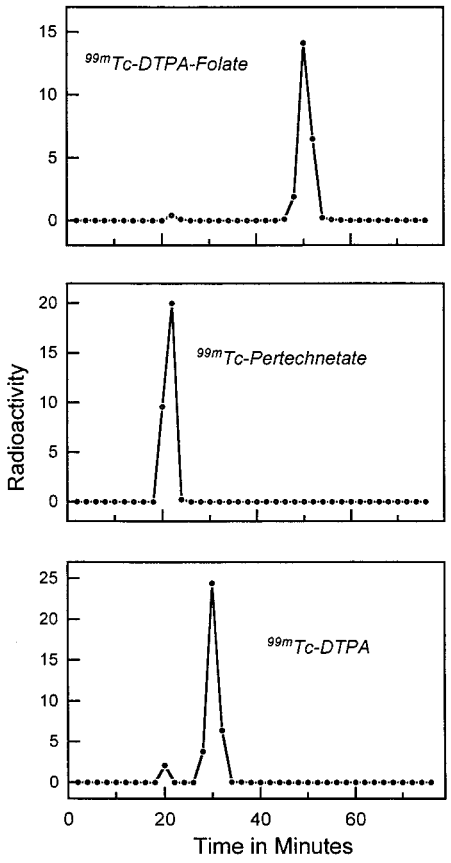

Figure 3. RadioHPLC results for [^{99m}Tc]DTPA−folate (top), [^{99m}Tc]Sodium-pertechnetate (center), and [^{99m}Tc]DTPA (bottom).

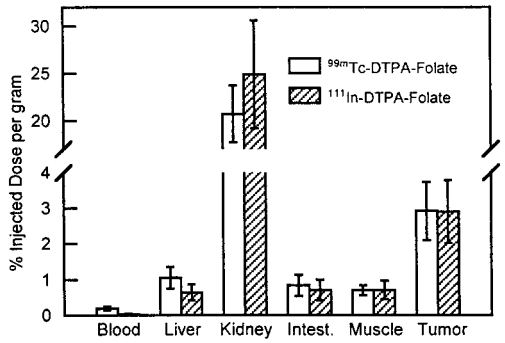

Figure 4. Biodistribution of coinjected [^{99m}Tc]DTPA−folate and [^{111}In]DTPA−folate in athymic male mice with human KB tumor xenografts. Data were acquired 4 h following i.v. administration of the radiotracers (n = 3; DTPA−folate dose = 187 ± 29 μg/kg).

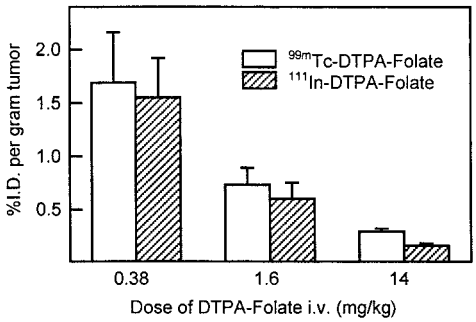

Figure 5. Effect of DTPA−folate dose on the tumor uptake of co-injected [^{99m}Tc]DTPA−folate and [^{111}In]DTPA−folate using the athymic mouse KB tumor xenograft model. All animals were sacrificed at 4 h postinjection (n = 4).

of the tumor uptake of both radiotracers (Table 1), as would be expected with a folate-receptor-mediated pathway for localization in tumor. Kidney uptake of both radiotracers was similarly reduced by preadministration of folic acid, consistent with the known presence of folate receptors in the proximal tubules of the kidneys (*20*−*24*).

The biodistribution of [^{99m}Tc]DTPA-folate and [^{111}In]-DTPA−folate was also evaluated following co-injection with varying quantities of the DTPA−folate conjugate (0.38, 1.6, or 14 mg/kg, respectively) (Table 2). At 4 h postinjection, the tumor uptake of [^{99m}Tc]DTPA−folate was 1.69 ± 0.47, 0.73 ± 0.16, and 0.29 ± 0.03% ID/g (n = 4) with DTPA−folate doses of 0.38, 1.6, and 14 mg/kg, respectively, compared to [^{111}In]DTPA−folate uptake of 1.55 ± 0.37, 0.60 ± 0.15, and 0.16 ± 0.02% ID/g (Figure 5). The tumor uptake of both agents progressively declined with increasing doses of DTPA−folate, due to competitive receptor binding by the unlabeled folate−ligand conjugate. Notably, no significant differences were observed between the behavior of the coadministered ^{99m}Tc and ^{111}In radiolabels (Table 2 and Figure 5).

Table 2. Biodistribution of Coinjected [^{99m}Tc]DTPA−Folate and [^{111}In]DTPA−Folate with Various Doses of Folic Acid Dihydrate in Athymic Male Mice with KB Xenografts

	percentage of injected dose per gram (tissue) ca. 4 h after intravenous administration[a]					
	^{99m}Tc-99m	^{111}In-111	^{99m}Tc-99m	^{111}In-111	^{99m}Tc-99m	^{111}In-111
DTPA−folate dose (mg/kg)	0.38 ± 0.05	0.38 ± 0.05	1.6 ± 0.2	1.6 ± 0.2	14.5 ± 1.2	14.5 ± 1.2
animal mass (g)	30 ± 3	30 ± 3	29 ± 2	29 ± 2	29 ± 2	29 ± 2
tumor mass (g)	0.54 ± 0.09	0.54 ± 0.09	0.42 ± 0.19	0.42 ± 0.19	0.51 ± 0.21	0.51 ± 0.21
blood	0.10 ± 0.02	0.029 ± 0.008	0.067 ± 0.015	0.017 ± 0.004	0.16 ± 0.04	0.044 ± 0.035
heart	0.25 ± 0.06	0.23 ± 0.03	0.12 ± 0.05	0.095 ± 0.043	0.072 ± 0.006	0.039 ± 0.006
lungs	0.21 ± 0.04	0.17 ± 0.04	0.12 ± 0.03	0.081 ± 0.025	0.15 ± 0.03	0.061 ± 0.018
liver and gall bladder	0.57 ± 0.01	0.32 ± 0.01	0.49 ± 0.14	0.22 ± 0.12	0.47 ± 0.23	0.28 ± 0.29
spleen	0.10 ± 0.01	0.08 ± 0.01	0.09 ± 0.01	0.055 ± 0.006	0.49 ± 0.60	0.64 ± 0.86
kidney (one)	11 ± 1	13 ± 2	4.4 ± 0.8	4.2 ± 0.8	1.4 ± 0.1	1.3 ± 0.1
intestines & contents	1.7 ± 1.8	0.72 ± 0.20	1.1 ± 0.6	1.0 ± 0.6	0.69 ± 0.18	0.52 ± 0.19
muscle	0.3 ± 0.1	0.4 ± 0.0	0.63 ± 1.0	0.21 ± 0.11[b]	0.049 ± 0.005	0.049 ± 0.009
tumor	1.7 ± 0.5	1.6 ± 0.4	0.73 ± 0.16	0.60 ± 0.15	0.29 ± 0.03	0.16 ± 0.02
tumor/blood	17 ± 5	59 ± 22	11 ± 1	35 ± 2	1.9 ± 0.5	6 ± 4
tumor/liver	3 ± 1	4.8 ± 1.1	1.6 ± 0.5	3.2 ± 1.4	0.71 ± 0.28	1.1 ± 0.8
tumor/kidney	0.16 ± 0.04	0.12 ± 0.03	0.16 ± 0.02	0.14 ± 0.02	0.20 ± 0.01	0.12 ± 0.01
tumor/muscle	5 ± 2	4 ± 1	12 ± 19	2.8 ± 0.6	5.9 ± 0.6	3.2 ± 0.4

[a] Values shown represent the mean ± standard deviation of data from four animals. [b] $n = 3$.

Table 3. Biodistribution of [^{99m}Tc]DTPA−Folate in Athymic Mice with KB Cell Tumors

	percentage of injected ^{99m}Tc dose per gram following intravenous administration[a]		
	5 min	1 h	4 h
[^{99m}Tc]DTPA−folate dose (μg/kg)	51 ± 3	53 ± 3	47 ± 4
animal mass (g)	28.7± 1.4	27.8 ± 0.7	27.6 ± 2.7
tumor mass (g)	0.17 ± 0.10	0.20 ± 0.10	0.26 ± 0.14
blood	7.9 ± 1.7	1.5 ± 0.04	0.76 ± 0.03
heart	3.4 ± 0.8	1.0 ± 0.1	0.72 ± 0.06
lungs	6.0 ± 1.2	1.4 ± 0.06	0.95 ± 0.14
liver and gall bladder	8.4 ± 2.0	6.3 ± 0.7	4.9 ± 0.3
spleen	2.5 ± 0.2	2.2 ± 0.7	1. 4 ± 0.3
kidney (one)	20.5 ± 3.4	24.5 ± 2.0	26.1 ± 2.6
stomach, intestines, and contents	1.3 ± 0.2	1.02 ± 0.2	1.1 ± 0.2
muscle	2.1 ± 0.2	0.92 ± 0.2	0.88 ± 0.20
tumor	2.2 ± 0.9	3.06 ± 0.32	3.65 ± 0.23
tumor/blood[b]	0.31 ± 0.17	2.1 ± 0.2	4.8 ± 0.27
tumor/liver[b]	0.29 ± 0.15	0.49 ± 0.05	0.74 ± 0.03
tumor/kidney[b]	0.12 ± 0.06	0.12 ± 0.01	0.14 ± 0.01
tumor/muscle[b]	1.1 ± 0.5	3.4 ± 0.7	4.3 ± 0.8

[a] Values shown represent the mean ± standard deviation of data from four animals. [b] Tumor/background tissue ratios based on corresponding %injected dose per gram data.

Pharmacokinetics. To better define the pharmacokinetics of [^{99m}Tc]DTPA−folate, tracer biodistribution was evaluated in the KB tumor xenograft model at three time points following intravenous administration: 5 min, 1 h, and 4 h (Table 3). At 4 h, the observed tumor uptake of ^{99m}Tc increased significantly ($p \leq 0.05$) over the uptake at 5 min, while tracer levels in the kidneys did not significantly vary over this time frame. The differences in the kinetics of ^{99m}Tc accumulation for these two folate-receptor-positive tissues presumably arise from the kidneys behaving both as a clearance organ and as a tissue capable of receptor-specific tracer accumulation. The slight variations in 4 h tissue uptake in this experiment (Table 3) compared to the prior distribution study (Table 1) are presumed to arise from the 3-fold difference in the total injected dose of DTPA−folate, which will compete with [^{99m}Tc]DTPA−folate for receptor binding sites. Similar variations in radiopharmaceutical biodistribution with total folate loading have been observed with [^{111}In]-DTPA−folate (*8*, *9*).

CONCLUSIONS

[^{99m}Tc]DTPA-folate was obtained with high radiochemical purity and yield. The [^{99m}Tc]DTPA−folate radiopharmaceutical behaved in a fashion similar to [^{111}In]DTPA−folate in an athymic mouse model, where both agents exhibited folate-receptor-mediated localization in receptor-positive tumor xenografts. These results indicate that [^{99m}Tc]DTPA−folate may be suitable for use as a radiopharmaceutical for imaging folate-receptor-positive tumors.

The kidneys are expected to be the "critical organ" receiving the highest radiation exposure from [^{99m}Tc]-DTPA-folate. However, due to the more favorable nuclear properties of ^{99m}Tc, [^{99m}Tc]DTPA-folate dosimetry will be significantly more favorable than that of [^{111}In]DTPA-folate, which is already in clinical trials for imaging ovarian cancers (*25*).

ACKNOWLEDGMENT

This work was supported in part by NIH Grant RO1-CA70845. The Purdue Athymic Mouse Facility is partially supported by Cancer Center (Core) Support Grant P30-CA23168.

Supporting Information Available: Tabulation of biodistribution results calculated as the percent injected

dose per organ. This material is available free of charge via the Internet at http://pubs.acs.org.

LITERATURE CITED

(1) Anderson, R. G. W., Kamen, B. A., and Rothberg, K. G. et al. (1992) Potocytosis: Sequestration and transport of small molecules by caveolae. *Science 255*, 410−411.

(2) Leamon, C. P., and Low, P. S. (1992) Cytotoxicity of momordin-folate conjugates in cultured human cells. *J. Biol. Chem. 267*, 24966−24971.

(3) Leamon, C. P., and Low, P. S. (1991) Delivery of macromolecules into living cells: a method that exploits folate receptor endocytosis. *Proc. Natl. Acad. Sci. U.S.A. 88*, 5572−5576.

(4) Leamon, C. P., and Low, P. S. (1993) Membrane folate binding proteins are responsible for the folate-protein conjugate endocytosis into cultured cells. *Biochem. J. 291*, 855−860.

(5) Wang, S., Lee, R. J., Mathias, C. J., Green, M. A., Low, P. S. (1996) Synthesis, Purification, and Tumor Cell Uptake of ^{67}Ga-Deferoxamine-Folate, a Potential Radiopharmaceutical for Tumor Imaging. *Bioconjugate Chem.* 7, 56−62.

(6) Mathias, C. J., Lee, R. J., Wang, S., Waters, D. J., Low, P. S., M. A. Green. (1996) Tumor-selective radiopharmaceutical targeting via receptor-mediated endocytosis: Evaluation of a gallium-67 labeled deferoxamine-folate conjugate. *J. Nucl. Med.* 37, 1003−1008.

(7) Mathias, C. J., Wang, S., Low, P. S. Waters, D. J., and Green, M. A. (1999) Receptor-Mediated Targeting of ^{67}Ga-Deferoxamine-Folate to Folate-Receptor-Positive Human KB Tumor Xenografts. *Nucl. Med. Biol. 26*, 23−25.

(8) Wang, S., Luo, J., Lantrip, D. A., Waters, D. J., Mathias, C. J., Green, M. A., Fuchs, P. L., and Low, P. S. (1997) Design and Synthesis of ^{111}In-DTPA-Folate for Use as a Tumor-Targeted Radiopharmaceutical. *Bioconjugate Chem. 8*, 673−679.

(9) Mathias, C. J., Wang, S., Waters, D. J., Turek, J. J., Low, P. S., and Green, M. A. (1998) Evaluation of ^{111}In-DTPA-Folate as a Potential Folate-Receptor-Targeted Radiopharmaceutical, *J. Nucl. Med. 39*, 1579−1585.

(10) Weitman, S. D., Lark, R. H., and Coney, L. R., et al. (1992) Distribution of the folate receptor GP38 in normal and malignant cell lines and tissues. *Cancer Res. 52*, 3396−3401.

(11) Li, P. Y., DelVecchio, S., Fonti, R., Carriero, M. V., Potena, M. I., and Botti, G., et al. (1996) Local concentration of folate binding protein GP38 in sections of human ovarian carcinoma by in vitro quantitative autoradiography. *J. Nucl. Med. 37*, 665−672.

(12) Miotti, S., Canevari, S., and Menard, S., et al. (1987) Characterization of human ovarian carcinoma-associated antigens defined by novel monoclonal antibodies with tumor-restricted specificity. *Int. J. Cancer 39*, 297−303.

(13) Rothenberg, S. P., and daCosta, M. (1971) Further observations on the folate-binding factor in some leukemic cells. *J. Clin. Invest. 50*, 719−726.

(14) Campbell, I. G., Jones, T. A., and Foulkes, W. D., et al. (1991) Folate-binding protein is a marker for ovarian cancer. *Cancer Res. 51*, 5329−5338.

(15) Garin-Chesa, P., Campbell, I., and Saigo, P. E., et al. (1993) Trophoblast and ovarian cancer antigen LK26: Sensitivity and specificity in immunopathology and molecular identification as a folate-binding protein. *Am. J. Pathol. 142*, 557−567.

(16) Toffoli, G., Cernigoi, C., Russo, A., Gallo, A., Bagnoli, M., and Boiocchi, M. (1997) Overexpression of folate binding protein in ovarian cancers. *Int. J. Cancer (Pred. Oncol.) 74*, 193−198.

(17) Wu, M., Gunning, W., and Ratnam, M. (1999) Expression of folate receptor type α in relation to cell type, malignancy, and differentiation in ovary, uterus, and cervix. *Cancer Epidemiol. Biomarkers Prev. 8*, 775−782.

(18) A portion of this work was presented in abstract form: Mathias, C. J., Hubers, D., Trump, D. P., Wang, S., Luo, J., Waters, D. J., Fuchs, P. L., Low, P. S., and Green, M. A. (1997) Synthesis of Tc-99m-DTPA-Folate and Preliminary Evaluation as a Folate-Receptor-Targeted Radiopharmaceutical. *J. Nucl. Med. 38*, 87P.

(19) Swinscow, T. D. V. (1980) *Statistics at Square One*, 6th ed.; British Medicial Association, London.

(20) Selhub, J., and Franklin, W. A. (1984) The folate binding protein of rat kidney. *J. Biol. Chem. 259*, 6601−6606.

(21) Selhub, J., Emmanouel, D., Stavropoulos, T., and Arnold, R. (1987) Renal folate adsorption and the kidney folate binding protein. I. Urinary Clearance studies. *Am. J. Physiol. 252*, F750−F756.

(22) Selhub, J., Nakamura, S., and Carone, F. A. (1987) Renal folate adsorption and the kidney folate binding protein. II. Microinfusion studies. *Am. J. Physiol. 252*, F757−F760.

(23) Williams, W. M., and Huang, K. C. (1982) Renal tubular transport of folic acid and methotrexate in the monkey. *Am. J. Physiol. 272*, F757−F760.

(24) Birn, J., Nielsen, S., and Christensen, E. I. (1997) Internalization and apical-to-basolateral transport of folate in rat kidney proximal tubule. *Am. J. Physiol. 272*, F70−F78.

(25) Green, M. A., Mathias, C. J., Low, P. S., Ellis, P. R., Stabin, M. G., Wendt, R. E., III, McCullough, S. P., Broussard, W. F., Gershenson, D. M., and Podoloff, D. A. (1998) Initial experience with In-111-DTPA-Folate (FolateScan) in humans: Assessment of tracer excretion kinetics and radiation dosimetry. *J. Nucl. Med. 39*, 191P.

BC9901447

Supporting Table 1 . Biodistribution of Co-injected ^{99m}Tc-DTPA-Folate and ^{111}In-DTPA-folate in Athymic Male Mice with KB Xenografts

	Percentage of Injected Dose per Organ ca. 4 Hours Following Intravenous Administration*			
	Tc-99m	*In-111*	*Tc-99m + folic acid†*	*In-111 + folic acid†*
Blood:	0.41 ± 0.11	0.043 ± 0.030	0.31 ± 0.05	0.011 ± 0.002
Heart:	0.074 ± 0.015	0.064 ± 0.019	0.0102 ± 0.0002	0.0017 ± 0.0004
Lungs:	0.076 ± 0.006	0.099 ± 0.012	0.028 ± 0.004	0.016 ± 0.002
Liver & Gall Bladder:	1.3 ± 0.1	0.94 ± 0.23	0.36 ± 0.04	0.081 ± 0.015
Spleen:	0.036 ± 0.006	0.030 ± 0.008	0.014 ± 0.003	0.0048 ± 0.0014
Kidney (one):	5.7 ± 0.3	6.8 ± 0.6	0.57 ± 0.15	0.47 ± 0.08
Intestines & Contents:	1.9 ± 0.7	1.6 ± 0.7	1.2 ± 0.2	0.90 ± 0.24
Muscle:	9.0 ± 1.4	9.0 ± 3.0	0.71 ± 0.05	0.10 ± 0.06
Tumor:	1.3 ± 0.2	1.3 ± 0.2	0.12 ± 0.04	0.067 ± 0.024
Tumor / Blood:	*15.2 ± 0.1*	*136 ± 56*	*2.0 ± 0.8*	*26 ± 11*
Tumor / Liver:	*3.8 ± 2.2*	*5.7 ± 4.4*	*1.2 ± 0.4*	*3.1 ± 1.2*
Tumor / Kidney:	*0.15 ± 0.06*	*0.13 ± 0.06*	*0.14 ± 0.05*	*0.10 ± 0.05*
Tumor / Muscle:	*4.2 ± 1.1*	*4.4 ± 1.6*	*5.1 ± 1.5*	*40 ± 24*
Animal Mass (g):	*31 ± 1*	*31 ± 1*	*26 ± 2*	*26 ± 2*
Tumor Mass (g):	*0.45 ± 0.07*	*0.45 ± 0.07*	*0.37 ± 0.12*	*0.37 ± 0.12*

* Values shown represent the mean ± standard deviation of data from three animals. Total DTPA-Folate dose of 187 ± 29 µg/kg.

© 2000 American Chemical Society, Bioconjugate Chem., Mathias bc9901447 Supporting Info Page 1

Supporting Table 2. Biodistribution of Co-injected ^{99m}Tc-DTPA-Folate and ^{111}In-DTPA-Folate with Various Doses of Folic Acid Dihydrate in Athymic Male Mice with KB Xenografts

	Percentage of Injected Dose per Organ ca. 4 Hours After Intravenous Administration†					
	Tc-99m	*In-111*	*Tc-99m*	*In-111*	*Tc-99m*	*In-111*
DTPA-Folate dose (mg/kg)	***0.38 ± 0.05***		***1.6 ± 0.2***		***14.5 ± 1.2***	
Animal Mass (g):	*30 ± 3*	*30 ± 3*	*29 ± 2*	*29 ± 2*	*29 ± 2*	*29 ± 2*
Tumor Mass (g):	*0.54 ± 0.09*	*0.54 ± 0.09*	*0.42 ± 0.19*	*0.42 ± 0.19*	*0.51 ± 0.21*	*0.51 ± 0.21*
Blood:	0.16 ± 0.02	0.047 ± 0.015	0.10 ± 0.02	0.026 ± 0.005	0.25 ± 0.06	0.072 ± 0.057
Heart:	0.036 ± 0.010	0.033 ± 0.008	0.015 ± 0.006	0.013 ± 0.004	0.011 ± 0.002	0.0057 ± 0.0010
Lungs:	0.082 ± 0.007	0.63 ± 0.01	0.047 ± 0.006	0.030 ± 0.005	0.071 ± 0.011	0.029 ± 0.006
Liver & Gall Bladder:	0.77 ± 0.09	0.43 ± 0.05	0.62 ± 0.25	0.29 ± 0.18	0.63 ± 0.34	0.38 ± 0.42
Spleen:	0.026 ± 0.004	0.020 ± 0.001	0.023 ± 0.007	0.015 ± 0.004	0.15 ± 0.19	0.19 ± 0.27
Kidney (one):	2.6 ± 0.1	3.2 ± 0.2	1.0 ± 0.2	0.94 ± 0.15	0.34 ± 0.00	0.31 ± 0.01
Intestines & Contents:	3.4 ± 3.5	1.5 ± 0.50	2.1 ± 1.3	2.0 ± 1.3	1.5 ± 0.6	1.1 ± 0.4
Muscle:	4.3 ± 1.0	4.9 ± 0.6	1.8 ± 1.2	2.5 ± 0.9	0.59 ± 0.06	0.59 ± 0.08
Tumor:	0.93 ± 0.35	0.85 ± 0.28	0.31 ± 0.19	0.60 ± 0.15	0.14 ± 0.05	0.077 ± 0.021
Tumor / Blood:	*17 ± 5*	*59 ± 22*	*11 ± 1*	*35 ± 2*	*1.9 ± 0.5*	*6 ± 4*
Tumor / Liver:	*3 ± 1*	*4.8 ± 1.1*	*1.6 ± 0.5*	*3.2 ± 1.4*	*0.71 ± 0.28*	*1.1 ± 0.8*
Tumor / Kidney:	*0.16 ± 0.04*	*0.12 ± 0.03*	*0.16 ± 0.02*	*0.14 ± 0.02*	*0.20 ± 0.01*	*0.12 ± 0.01*
Tumor / Muscle:	*5 ± 2*	*4 ± 1*	*13 ± 18*	*2.9 ± 0.5*	*5.9 ± 0.6*	*3.2 ± 0.4*

* n=3

†Values shown represent the mean ± standard deviation of data from four animals.

© 2000 American Chemical Society, Bioconjugate Chem., Mathias bc990144 7 Supporting Info Page 2

© 2000 American Chemical Society, Bioconjugate Chem., Mathias bc9901447 Supporting Info Page 3

Supporting Table 3. Biodistribution of ^{99m}Tc-DTPA-Folate in Athymic Mice with KB Cell Tumors

	Percentage of Injected ^{99m}Tc Dose per Organ Following Intravenous Administration*		
	5 minutes	**1 hour**	**4 hours**
Folic Acid Dihydrate Dose (μg/kg)	*0.0 ± 0.0*	*0.0 ± 0.0*	*0.0 ± 0.0*
Tc-99m-DTPA-Folate Dose (μg/kg):	*51 ± 3*	*53 ± 3*	*47 ± 4*
Animal mass (g):	*28.7± 1.4*	*27.8 ± 0.7*	*27.6 ± 2.7*
Tumor mass (g):	*0.17 ± 0.10*	*0.20 ± 0.10*	*0.26 ± 0.14*
Blood:	12 ± 3	2.3 ± 0.09	1.1 ± 0.08
Heart:	0.46 ± 0.12	0.14 ± 0.02	0.095 ± 0.010
Lungs:	2.4 ± 0.4	0.53 ± 0.06	0.41 ± 0.04
Liver&Gall Bladder:	11.2± 2.7	8.4 ± 0.9	5.9 ± 0.2
Spleen:	0.52 ± 0.06	0.47 ± 0.16	0.26 ± 0.03
Kidney (one):	4.8 ± 0.8	5.6 ± 0.5	5.4 ± 0.3
Stomach,Intestines & Contents:	2.9 ± 0.4	2.1 ± 0.3	2.4 ± 0.5
Muscle	25 ± 2	10.7 ± 2.0	10 ± 1
Tumor	0.37 ± 0.21	0.59 ± 0.29	0.96 ± 0.50
Tumor/Blood‡:	*0.31 ± 0.17*	*2.1 ± 0.2*	*4.8 ± 0.27*
Tumor/Liver‡:	*0.29 ± 0.15*	*0.49 ± 0.05*	*0.74 ± 0.03*
Tumor/Kidney‡:	*0.12 ± 0.06*	*0.12 ± 0.01*	*0.14 ± 0.01*
Tumor/Muscle‡:	*1.1 ± 0.5*	*3.4 ± 0.7*	*4.3 ± 0.8*

*Values shown represent the mean ± standard deviation of data from four animals.

‡Tumor/Backgound Tissue ratios based on corresponding %Injected Dose per Gram data.

Efficient Clearance of Poly(ethylene glycol)-Modified Immunoenzyme with Anti-PEG Monoclonal Antibody for Prodrug Cancer Therapy

Tian-Lu Cheng,[†] Bing-Mae Chen,[†] Ji-Wang Chern,[‡] Ming-Fang Wu,[§] and Steve R. Roffler*[,†]

Institute of Biomedical Sciences, Academia Sinica; School of Pharmacy, National Taiwan University; College of Medicine, National Taiwan University, Taipei, Taiwan. Received October 28, 1999; Revised Manuscript Received December 17, 1999

The F(ab′)$_2$ fragment of the anti-TAG-72 antibody, B72.3, was covalently linked to *Escherichia coli*-derived β-glucuronidase that was modified with methoxypoly(ethylene glycol). The conjugate (B72.3-βG-PEG) localized to a peak concentration in LS174T xenografts within 48 h after injection, but enzyme activity persisted in plasma such that prodrug administration had to be delayed for at least 4 days to avoid systemic prodrug activation and associated toxicity. Conjugate levels in tumors decreased to 36% of peak levels at this time. Intravenous administration of AGP3, an IgM mAb against methoxypoly(ethylene glycol), accelerated clearance of conjugate from serum and increased the tumor/blood ratio of B72.3-βG-PEG from 3.9 to 29.6 without significantly decreasing the accumulation of conjugate in tumors. Treatment of nude mice bearing established human colon adenocarcinoma xenografts with B72.3-βG-PEG followed 48 h later with AGP3 and a glucuronide prodrug of *p*-hydroxyaniline mustard significantly ($p \leq 0.0005$) delayed tumor growth with minimal toxicity compared to therapy with a control conjugate or conventional chemotherapy.

INTRODUCTION

A major goal of antitumor drug development is to increase the therapeutic index of chemotherapy, thereby improving treatment efficacy. One approach to increase the therapeutic index of chemotherapy is to preferentially activate antineoplastic prodrugs at cancer cells but not normal tissues. Tumor selectivity may be achieved by enzymatically converting prodrugs possessing low toxicity to highly toxic anti-neoplastic agents by previously administered antibody-enzyme conjugates (immunoenzymes) that have been allowed to accumulate at tumor cells (Bagshawe et al., 1988; Senter et al., 1988). Even though maximum accumulation of immunoenzymes in tumors occurs around 24 h after administration (Bosslet et al., 1994; Wallace et al., 1994), prodrugs are generally administered from 3 to 7 days (Bosslet et al., 1994; Svensson et al., 1998) to up to 2 weeks (Eccles et al., 1994) later to allow adequate time for conjugate to clear from the blood, thereby minimizing systemic prodrug activation and associated toxicity to normal tissues. Although exceptions have been reported for rapidly clearing immunoenzymes (Siemers et al., 1997), the requisite of low circulating levels of immunoenzyme often precludes prodrug administration when maximum localization has been achieved.

Prodrugs can be administered during the period of maximum tumor accumulation of immunoenzymes if circulating conjugates are removed or deactivated. Several methods have been devised to accelerate the clearance of radioimmunoconjugates and immunoenzymes from the circulation including the administration of polyclonal (Stewart et al., 1990) and anti-idiotypic antibodies (Ullen et al., 1995) against the antibody portion of the immunoconjugate, injection of avidin to clear biotinylated antibodies (Paganelli et al., 1991), use of monoclonal antibodies against enzymes to clear (Kerr et al., 1993; Haisma et al., 1995) or deactivate (Sharma et al., 1990) immunoenzymes, and extracorporeal immunoadsorption (Tennvall et al., 1997) to remove immunoconjugates from plasma.

We have recently developed a mAb[1] (AGP3) that binds to poly(ethylene glycol) (PEG) and accelerates the clearance of immunoconjugates that have been modified with PEG (Cheng et al., 1999b). PEG-modified proteins often exhibit extended serum half-lives, reduced immunogenicity, and decreased susceptibility to proteolytic degradation (Delgado et al., 1992). Antibody fragments and immunoconjugates that have been modified with PEG also display reduced normal tissue uptake and enhanced tumor accumulation (Pedley et al., 1994; Delgado et al., 1996; Cheng et al., 1997). Clearance of PEG-modified immunoconjugates with AGP3 may, therefore, be generally useful. In the present study, we examined whether AGP3 could improve tumor-blood ratios and allow earlier administration of prodrug in a preclinical model of human colorectal carcinoma. PEG-modified βG was covalently linked to the F(ab′)$_2$ fragment of mAb B72.3, an

* To whom correspondence should be addressed. Phone: 886-22-652-3079. Fax: 886-22-782-9142. E-mail: sroff@ibms.sinica.edu.tw.

[†] Institute of Biomedical Sciences.

[‡] School of Pharmacy.

[§] College of Medicine.

[1] Abbreviations: βG, β-glucuronidase derived from *E. coli*; βG-PEG, β-glucuronidase modified with methoxypoly(ethylene)-glycol; pHAM, *p*-hydroxyaniline mustard; BHAMG, tetra *n*-butylammonium salt of the glucuronide of p-hydroxyaniline mustard; mAb, monoclonal antibody; B72.3-βG-PEG, conjugate of the F(ab′)$_2$ fragment of mAb B72.3 with βG-PEG; H25-βG-PEG, conjugate of the F(ab′)$_2$ fragment of mAb H25B10 with βG-PEG; TAG-72, tumor-associated glycoprotein; PNPG, *p*-nitrophenol β-D-glucuronide; IC_{50}, drug concentration causing 50% inhibition of cellular protein synthesis.

10.1021/bc990147j CCC: $19.00 © 2000 American Chemical Society
Published on Web 02/24/2000

IgG_1 antibody that binds to TAG-72 antigen expressed on the majority of colon adenocarcinomas, invasive ductal carcinomas of the breast, nonsmall cell lung carcinomas, common epithelial ovarian carcinomas, and gastric, pancreatic, and esophageal cancers with limited reactivity to normal adult tissues (Thor et al., 1986). mAb B72.3 is approved for clinical use as an imaging agent (Oncoscint CR/OV) for colorectal and ovarian carcinoma (Divgi, 1996). We show that clearance of a PEG-modified B72.3 immunoenzyme with AGP3 produced higher tumor-blood ratios without sacrificing tumor accumulation, allowing earlier prodrug administration with minimal toxicity.

MATERIALS AND METHODS

Reagents. The syntheses of pHAM and BHAMG have been described (Roffler et al., 1991). Bolton−Hunter reagent (^{125}I) was purchased from Amersham (Buckinghamshire, England). Succinimidyl succinate poly(ethylene glycol), MW = 5000, *p*-nitrophenyl-β-D-glucuronide, and Sepharose CL-4B protein A were purchased from Sigma Chemical Company, St. Louis, MO. Succinimidyl-4-(*N*-maleimidomethyl)cyclohexane 1-carboxylate (SMCC) was from Pierce Chemical Company, Rockford, IL. Sephadex G-25 and Sephacryl S-300 HR gels were purchased from Pharmacia Biotech Far East Ltd., Taipei, Taiwan. Recombinant βG was produced as described (Cheng et al., 1997).

Cells. LS174T colon adenocarcinoma cells were obtained from the American Type Culture Collection (Manassas, VA). Cells were cultured in Dulbecco's modified Eagle's medium (Gibco BRL, Grand Island, NY) supplemented with 10% heat-inactivated bovine serum, 100 units/mL penicillin and 100 μg/mL streptomycin. Cells were routinely tested for mycoplasma with the Rapid Detection Kit according to the manufacturer's instructions (Gene Probe).

Animals. BALB/c mice were obtained from the animal room of the Institute of Biomedical Sciences, Academia Sinica. BALB/c *nu/nu* mice were from the Cancer Research Laboratory, Tri-Service General Hospital, Taipei. Animal experiments were performed in accordance with institute guidelines.

Antibodies. Hybridomas secreting mAb B72.3, an IgG_1 mAb specific for TAG-72 antigen (Johnson et al., 1986), and H25B10, a control IgG_1 mAb against the surface antigen of hepatitis B virus, were obtained from the American Type Culture Collection. mAbs were purified from ascites by affinity chromatography on Sepharose CL-4B protein A in high-salt buffer (Ey et al., 1978). $F(ab')_2$ fragments were generated by proteolytic digestion of whole antibodies (2−5 mg/mL) with 2% bromelain in 50 mM Tris-HCl, pH 7.0, containing 2 mM EDTA and 0.1 mM cysteine for 4 h at 37 °C (Milenic et al., 1989). After stopping the reaction by addition of *N*-ethylmaleimide to 10 mM, the mixture was passed in series through Sephadex G-50 and DE 52 columns equilibrated with 5 mM Tris-HCl, pH 7.5, to remove IgG and Fc fragments. The flow through fraction was concentrated to 5 mg/mL and purified by gel filtration on Sephacryl S-200HR (100 × 2.5 cm) equilibrated with PBS. AGP3, an IgM mAb that binds to PEG (Cheng et al., 1999b), was purified from ascites by gel filtration on Sephacryl S-400HR (2.5 × 100 cm) equilibrated with PBS.

Antibody-βG-PEG Conjugates. $F(ab')_2$ fragments of mAb B72.3 and H25B10 were passed through a 2.6 × 30 cm Sephadex G-25 column equilibrated with coupling buffer (deoxygenated PBS containing 1 mM EDTA, pH 8.0) and concentrated by ultrafiltration to 3.0 mg/mL. A 3-fold molar excess of SMCC (1 mg/mL in dioxane) was slowly added to the antibodies and allowed to react at room temperature for 50 min. Unreacted SMCC was removed by gel filtration on a 2.6 × 30 cm Sephadex G-25 column equilibrated with coupling buffer. The average number of maleidido groups introduced into antibodies (0.8−1.4) was assessed as described (Ishikawa et al., 1987). Succinimidyl succinate poly(ethylene glycol) was added to recombinant βG derived from *Escherichia coli* (2 mg/mL) at a weight ratio of 3.3:1 in coupling buffer at room temperature for 2 h. One-tenth volume of a saturated solution of glycine in coupling buffer was added to stop the reaction. βG-PEG was concentrated by ultrafiltration to 1.5 mg/mL and partially reduced by adding dithiothreitol to a final concentration of 20 mM for 30 min at room temperature. βG-PEG was desalted on a 2.6 × 30 cm Sephadex G-25 column equilibrated with coupling buffer and concentrated to 1.5 mg/mL. Freshly derivatized antibody and βG-PEG were immediately mixed at equal molar ratios, concentrated to 1.5 mg/mL by ultrafiltration, and incubated at room temperature for 2 h. Cysteine was added to a final concentration of 2 mM to stop the reaction, and the mixture was concentrated by ultrafiltration to 5−8 mg/mL. Conjugates (B72.3-βG-PEG and H25-βG-PEG) were purified by gel filtration on a 2.6 × 100 cm Sephacryl S-300 HR column equilibrated with PBS at a flow rate of 15 mL/h. Fractions containing conjugate monomers (antibody/enzyme = 1:1) were pooled and concentrated by ultrafiltration to 2.0 mg/mL for storage at −80 °C. The yield of conjugates averaged around 31% based on the weight of purified conjugate divided by the total starting weights of antibody and enzyme. The antigen-binding activity of conjugates was measured by ELISA in 96-well microtiter plates coated with bovine submaxillary gland mucin (King et al., 1994). βG activity was measured as described (Chen et al., 1997).

Drug Sensitivity. LS174T cells were plated overnight in 96 well microtiter plates at 40 000 cells/well. Serial dilutions of pHAM or BHAMG in medium containing 10% fetal calf serum were added to cells in triplicate for 24 h at 37 °C. Cells were subsequently washed once with sterile PBS, incubated until hour 48 in fresh medium, and then pulsed for 12 h with [^{3}H]leucine (1 μCi/well) in fresh leucine-free medium. Cells were harvested with a Filter-mate apparatus (Packard) and incorporated radioactivity was determined on a Top-Count scintillation counter (Packard). Results are expressed as percentage inhibition of [^{3}H]leucine incorporation compared with untreated cells by the following formula:

$$\% \text{ inhibition} = 100 \times \frac{\text{cpm sample} - \text{cpm background}}{\text{cpm control} - \text{cpm background}}$$

Radiolabeling of Conjugates. B72.3-βG-PEG and H25-βG-PEG were labeled with [^{125}I]Bolton−Hunter reagent to specific activities of 0.3−0.7 μCi/μg according to the manufacturer's instructions. Conjugates retained antigen-binding activity and specificity as determined by radioimmunoassay against bovine submaxillary gland mucin in 96-well microtiter plates. βG activity was unaffected and conjugates were not degraded as determined by autoradiography of gels after sodium dodecyl sulfate−polyacrylamide electrophoresis.

Tumor Localization of B72.3-βG-PEG. A total of 5 × 10^6 LS174T cells were injected s.c. in 6−8 week old BALB/c *nu/nu* mice. After tumors reached 100−200 mm^3, 200 μg (60 μCi) of [^{125}I]B72.3-βG-PEG or [^{125}I]H25-

βG-PEG were i.v. injected into the lateral tail vein of mice. Groups of 3 mice were sacrificed after 24, 48, 72, and 96 h. Tumors, blood, and organs were weighed on an analytical balance and assayed for radioactivity in a multichannel γ-counter. Results are expressed as uptake of conjugate in tumor or tissues (% injected dose/gram).

In Vivo Clearance of Conjugates. Groups of two to three BALB/c *nu/nu* mice were i.v. injected with 250 μg of B72.3-βG-PEG or H25-βG-PEG at time zero. Blood samples were periodically removed before two sequential i.v. injection of 300 and 200 μg of AGP3 or PBS at 48 and 50 h. Additional blood samples were taken at subsequent times and the βG activity in duplicate samples was measured using *p*-nitrophenol β-D-glucuronide as substrate (Wang et al., 1992). Sample concentrations were calculated by comparison of absorbance values with a standard curve constructed from known concentrations of B72.3-βG-PEG or H25-βG-PEG.

Tumor Localization of B72.3-βG-PEG after Clearance. Groups of six to seven BALB/c *nu/nu* mice bearing 100−200 mm^3 LS174T tumor xenografts were i.v. injected at time 0 with 200 μg (140 μCi) [^{125}I]B72.3-βG-PEG or [^{125}I]-H25-βG-PEG. One-half of the mice was i.v. injected 48 and 50 h later with two sequential doses of 300 and 200 μg of AGP3. Mice were sacrificed after 6 h, and tumor, blood, and organs were weighed on an analytical balance and assayed for radioactivity in a multichannel γ-counter. Urine sample were electrophoresed on a 3−12.5% SDS−PAGE under reducing conditions. Dried gels were exposed to X-ray film to visualize radioactive proteins.

Therapy of LS174T Tumor Xenografts. Groups of nine BALB/c *nu/nu* mice were s.c. injected on the right flank with 5×10^6 LS174T cells on day 1. On day 10, the mice were i.v. injected via the lateral tail vein with PBS, 250 μg of B72.3-βG-PEG or H25-βG-PEG. Forty-eight and 50 h later, mice were i.v. injected with two sequential doses of 300 and 200 μg of AGP3. Mice were i.v. injected 6 h later with three fractionated doses of 7.5 mg/kg BHAMG at 1 h intervals. Control groups of tumor-bearing mice were treated with BHAMG (7.5 mg/kg × 3), pHAM (2 mg/kg × 3) or PBS alone. Therapy was repeated starting on days 16, 26, and 41. All mice received two to four rounds of therapy. Tumor volumes (length × width × height × 0.5) were estimated twice a week. Mean weight loss was normalized to the weight of control mice by weight loss % $= 100 - [(T_i/T_0)(C_0/C_i)] \times 100$ where T_i and C_i are the mean weights of treated and control groups at time *i*, respectively, and T_0 and C_0 are the mean weights of treated and control groups before initiation of treatment, respectively. Mice were killed when they displayed signs of morbidity or when the tumor size exceeded 2.5 cm^3. Groups of 8 BALB/c *nu/nu* mice bearing larger 200−250 mm^3 tumors were also treated as above with two rounds of therapy starting on days 11 and 23.

Statistical Analysis. Statistical significance of differences between mean values was estimated with the shareware program Schoolstat (White Ant Occasional Publishing, West Melbourne, Australia) using the independent *t*-test for unequal variances.

RESULTS

Characterization of the LS174T Tumor Model. LS174T colon adenocarcinoma cells were used as a human tumor model to examine the effect of clearance on the localization and therapeutic efficacy of glucuronide prodrug activation by B72.3-βG-PEG, a conjugate formed by covalently linking F(ab′)$_2$ fragments of mAb B72.3 to PEG-modified βG. Antigen-binding activity of B72.3-βG-PEG was assessed against bovine submaxillary gland mucin due to the low expression of TAG-72 antigen on cultured tumor cells (Horan Hand et al., 1985). B72.3-βG-PEG retained 75% of the mucin binding activity of mAb B72.3 (Figure 1A) and 100% of the enzyme activity of unmodified βG (Figure 1B). Control conjugate H25-βG-PEG did not bind mucin (Figure 1A) but retained 92.4% of native βG activity (Figure 1B). Immunohistochemical analysis of antibody binding confirmed that mAb B72.3 (Figure 2A) but not mAb H25B10 (Figure 2B) bound to LS174T xenografts. mAb B72.3 binding to LS174T sections was heterogeneous (Figure 2A). The sensitivity of LS174T tumor cells to pHAM and BHAMG was determined by measuring [^{3}H]leucine incorporation into cellular proteins after exposure to drugs for 24 h. Comparison of IC_{50} values showed that BHAMG was 800 times less toxic than pHAM to LS174T cells (Figure 3). The simultaneous addition of βG and BHAMG to tumor cells resulted in a cytotoxic effect equal to pHAM alone, indicating efficient cleavage of the glucuronide functional group of BHAMG.

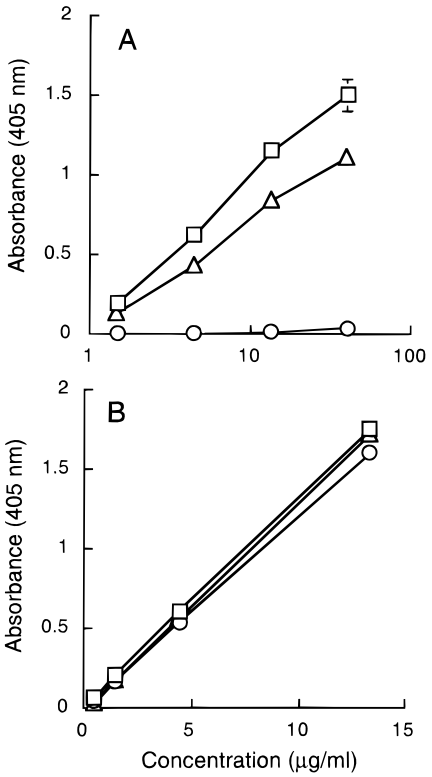

Figure 1. Immunoenzyme activity. (A) mAb B72.3 (□), B72.3-βG-PEG (△), and H25-βG-PEG (○) were assayed by ELISA for binding to bovine submaxillary gland mucin. Absorbance (405 nm) of wells was measured 30 min after addition of ABTS substrate. (B) The absorbance (405 nm) of wells containing the indicated concentrations of βG (□), B72.3-βG-PEG (△), and H25-βG-PEG (○) was measured 15 min after addition of PNPG substrate. Mean values of duplicate determinations are shown. Bars, SE.

Tumor Localization of B72.3-βG-PEG. Figure 4 shows that [^{125}I]B72.3-βG-PEG preferentially localized in LS174T xenografts. Maximum accumulation of [^{125}I]B72.3-βG-PEG in LS174T xenografts (3.11 ± 0.8% injected dose/g) was achieved within 48 h after injection. However, the tumor-to-blood ratio at 48 h was only 1.9. The tumor/blood ratio of B72.3-βG-PEG increased to 4.8 at 96 h, but immunoenzyme in tumors decreased about 3-fold from levels achieved at 48 h. [^{125}I]H25-βG-PEG did not specifically localize in LS174T xenografts (Figure 4).

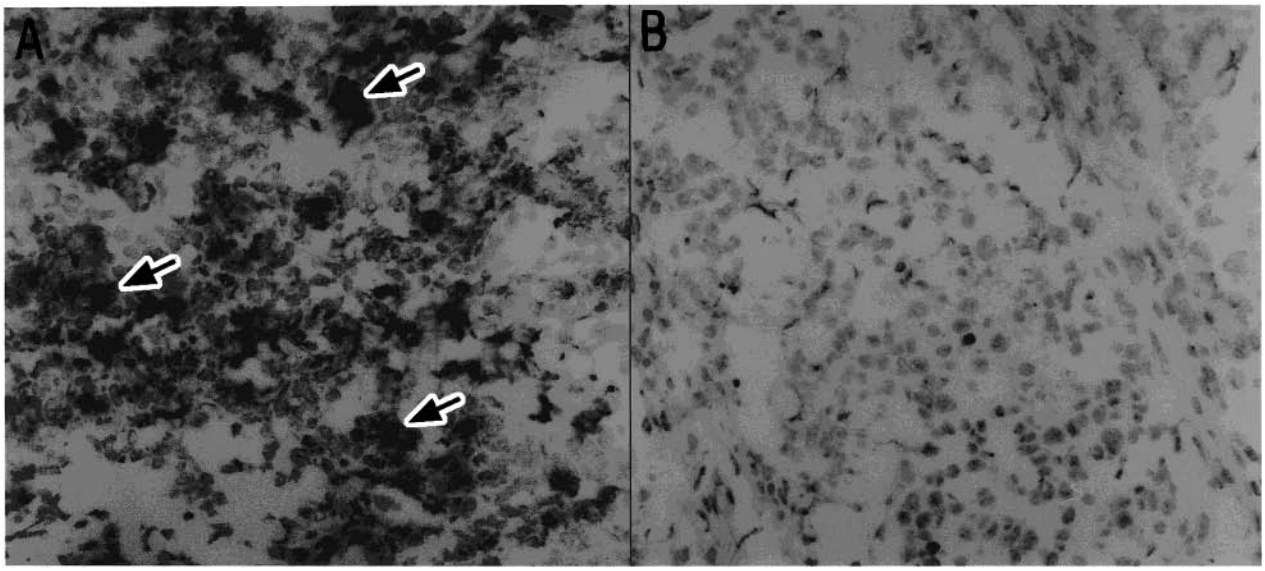

Figure 2. Specificity of B72.3 for LS174T xenografts. Frozen section of LS174T tumors were incubated with mAb B72.3 (A) or H25B10 (B) followed by biotin-labeled goat anti-mouse Ig and streptavidin-conjugated horseradish peroxidase before addition of substrate. Magnification: 200×. The sections were counterstained with hematoxylin. Examples of positive immunostaining are indicated with arrows.

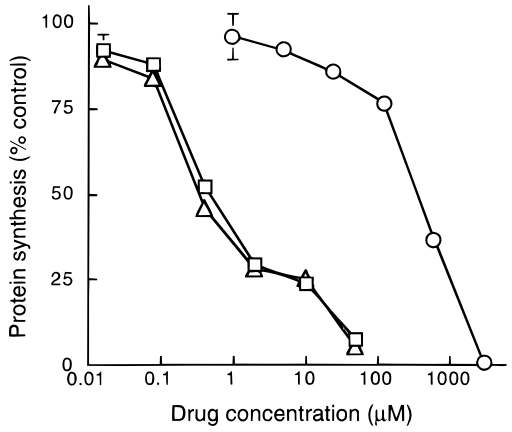

Figure 3. Sensitivity of tumor cells to pHAM and BHAMG. LS174T colon adenocarcinoma cells were expose to pHAM (□), BHAMG (○), or BHAMG plus 1 μg/well βG (△) for 24 h, washed with PBS and incubated in fresh medium for 24 h before [^{3}H]-leucine incorporation was determined. The cellular protein synthesis rate of drug-treated cells is compared to untreated control cells. Bars, SE of triplicate determinations.

In Vivo Clearance of Conjugates. The ability of AGP3, an anti-PEG mAb, to clear B72.3-βG-PEG and H25-βG-PEG from the circulation was examined by i.v. injecting BALB/c mice with 250 μg conjugates followed 48 and 50 h later by two i.v. injections of AGP3. Figure 5 shows that AGP3 reduced the concentration of B72.3-βG-PEG in blood by 33-fold (13.4 to 0.41 μg/mL) and H25-βG-PEG by 65-fold (16.8 to 0.26 μg/mL) in 6 h.

Tumor Localization of B72.3-βG-PEG with AGP3 Clearance. The effect of clearance on tumor localization was determined in BALB/c *nu/nu* mice bearing 100−200 mm^3 LS174T xenografts. Mice were injected with radiolabeled conjugates followed 48 and 50 h later by two i.v. injections of AGP3. After 6 h, tumors, blood, urine, and normal tissues were removed and counted for radioactivity. Figure 6A shows that [^{125}I]B72.3-βG-PEG specifically localized in LS174T tumors. Tumor localization of B72.3-βG-PEG after AGP3 clearance did not significantly ($p > 0.1$) differ from tumor uptake without clearance (2.35 ± 0.18 versus 2.14 ± 0.23% injected dose/g). In contrast, the radioactivity in serum and all tissues except for the colon was lower with AGP3 clearance. This resulted in improved tumor/tissue ratios of B72.3-βG-PEG for most tissues (Table 1). For example, the tumor/blood ratio increased from 3.9 ± 0.2 to 29.6 ± 3.1. Although the control conjugate did not specifically accumulate in LS174T xenografts, clearance with AGP3 further decreased the concentration of H25-βG-PEG in the blood and most tissues (Figure 6B). The radioactivity in urine after clearance of both B72.3-βG-PEG and H25-βG-PEG with AGP3 was significantly ($p < 0.005$) greater than without clearance (results not shown). Autoradiographic analysis of urine samples after electrophoresis on SDS−PAGE revealed the presence of low-molecular-weight ^{125}I-labeled peptides but no intact conjugates (data not shown), indicating that AGP3 clearance resulted in the rapid metabolism of conjugates.

Therapy of LS174T Xenografts. The antitumor activity of BHAMG in combination with B72.3-βG-PEG after clearance of free conjugate with AGP3 was examined. BALB/c *nu/nu* mice bearing 50−100 mm^3 xenografts received two i.v. injections of AGP3 48 and 50 h after i.v administration of B72.3-βG-PEG or H25-βG-PEG. Mice then received three i.v. injections of BHAMG. Control groups of tumor-bearing mice were treated with BHAMG alone, pHAM alone, or PBS. All mice received two to four rounds of therapy. Figure 7A shows that mean tumor size in mice treated with B72.3-βG-PEG, AGP3, and BHAMG was significantly ($p \leq 0.0005$) smaller than mice receiving other forms of treatment. Control conjugate in combination with AGP3 and BHAMG as well as prodrug or pHAM alone did not significantly ($p > 0.1$) delay tumor growth compared to untreated controls. Table 2 shows that treatment toxicity was minimal with a maximum weight loss of 6% over four rounds of therapy. In contrast, pHAM treatment caused a maximum weight loss of 13% over two rounds of therapy even though it did not provide antitumor activity. Treatment of mice bearing larger LS174T xenografts with a combination of B72.3-βG-PEG, AGP3, and BHAMG also produced significant antitumor activity (Figure 7B).

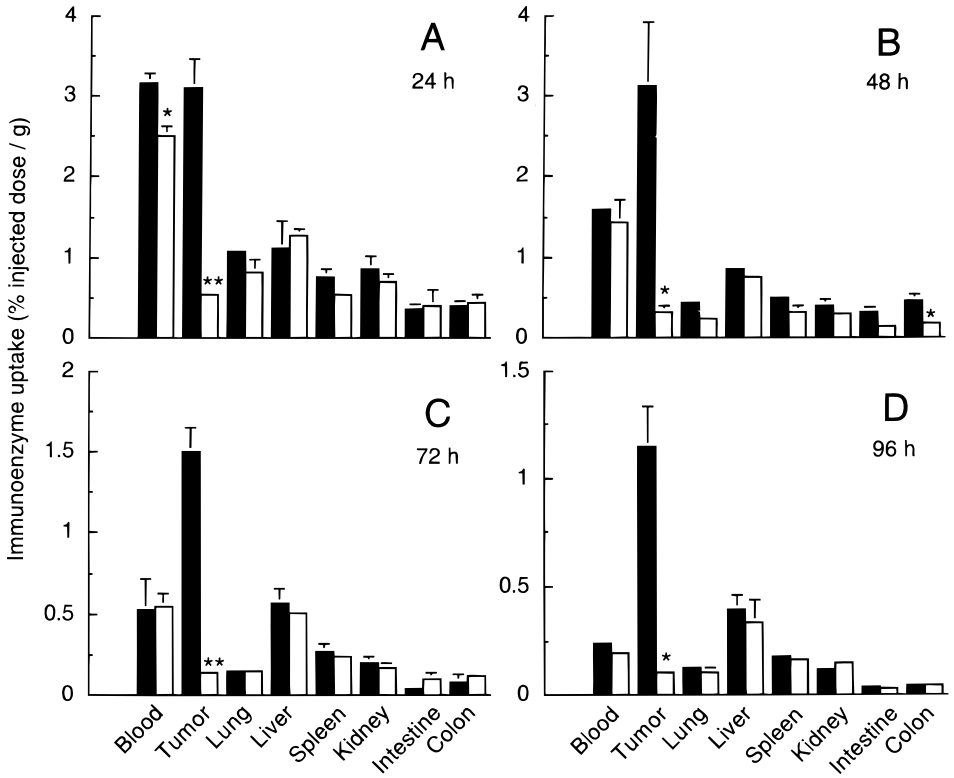

Figure 4. Biodistribution of ^{125}I-labeled immunoenzymes in LS174T tumor-bearing mice. Radioactivity of tumors and tissues was determined (A) 24, (B) 48, (C) 72, and (D) 96 h after nude mice bearing 100−200 mm^3 LS174T tumors were i.v. injected with 200 μg (140 μCi) B72.3-βG-PEG (solid bars) or H25-βG-PEG (open bars). Results represent the mean values of three mice. Significant differences between B72.3-βG-PEG and H25-βG-PEG are indicated; (*) $p \leq 0.05$; (**) $p \leq 0.005$. Bars, SE.

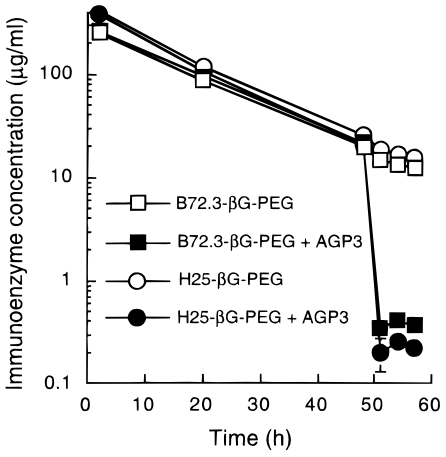

Figure 5. In vivo clearance of immunoenzymes by AGP3 antibody. BALB/c mice were i.v. injected at time 0 with 250 μg B72.3-βG-PEG or H25-βG-PEG. Two i.v. injections of AGP3 (300, 200 μg) or PBS were given at 48 and 50 h. Mean serum concentrations from two to three mice are shown. Bars, SE.

DISCUSSION

mAb B72.3 has been utilized for diagnostic imaging in more than 1000 carcinoma patients with specific tumor localization demonstrated in 70−80% of carcinomas. Cyt-103, ^{111}In-labeled B72.3, is also approved for the detection of extrahepatic intraabdominal metastases from colorectal or ovarian cancer (Divgi, 1996). Preclinical and clinical imaging studies have demonstrated that B72.3 does not internalize after binding to TAG-72 but remains at the tumor site for a number of days following localization (Colcher et al., 1984). Lack of antigen modulation after antibody binding is required to allow efficient activation of BHAMG because this prodrug must be enzymatically activated outside of tumor cells for maximum cytotoxicity (Cheng et al., 1999a). Although cultured tumor cells express low levels of TAG-72, tumor xenografts display up to a 100-fold increase in antigen expression (Horan Hand et al., 1985). TAG-72 distribution, however, is heterogeneous in both LS174T xenografts (this work) and mucinous adenocarcinoma of the human colon (Schlom, 1986).

βG-PEG was covalently linked to the F(ab′)$_2$ fragment of mAb B72.3 to reduce the size of B72.3-βG-PEG and prevent binding to Fc receptors on hematopoietic cells. We have previously shown that PEG modification of βG allows increased serum half-life and tumor uptake with decreased normal tissues binding (Cheng et al., 1997). In the present study, maximum uptake of [^{125}I]B72.3-βG-PEG in LS174T xenografts was achieved within 48 h. BHAMG could not be administered at this time, however, because serum concentrations of conjugate exceeded 1 μg/mL, the maximum concentration of βG in serum that produced acceptable toxicity from systematically activated prodrug (unpublished results). Without AGP3-mediated clearance, attainment of safe levels of B72.3-βG-PEG in plasma required at least 4 days, at which time the conjugate level in tumor had decreased to 36% of the peak levels at 48 h. Similar or longer intervals are required for other antibody-enzyme conjugates (Bosslet et al., 1994; Svensson et al., 1998), prompting the interest (Sharma et al., 1990; Rogers et al., 1995) in accelerating the clearance of immunoenzymes after maximum tumor uptake has been achieved.

mAb AGP3 has previously been demonstrated to efficiently remove PEG-modified proteins from the circulation (Cheng et al., 1999b). In the present study, we found that AGP3 not only reduced the serum concentration of conjugates by 33−65-fold in 6 h but also accelerated the clearance of immunoenzyme from most normal tissues.

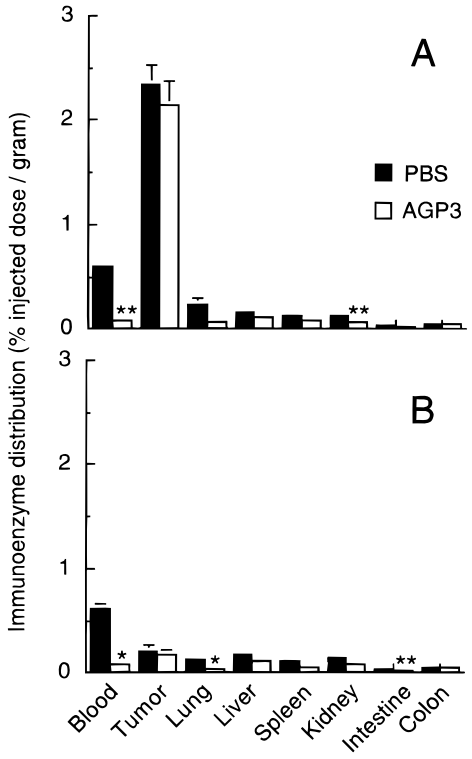

Figure 6. The effect of AGP3 clearance on tumor localization of immunoenzyme. Groups of 6−7 BALB/c *nu/nu* mice bearing 100−200 mm^3 LS174T tumor xenografts were i.v. injected at time 0 with 200 μg (140 μCi) [^{125}I]B72.3-βG-PEG (A) or [^{125}I]-H25-βG-PEG (B). At 48 and 50 h, half the mice were i.v. injected with two fractionated doses of AGP3 (300 and 200 μg) whereas the other half received PBS. Mice were sacrificed after 6 h and tumors, blood and organs were assayed for radioactivity. Results represent the mean values of 3−4 mice. Significant differences between immunoenzyme uptake with and without AGP3 clearance are indicated; (*) $p \leq 0.05$; (**) $p \leq 0.005$. Bars, SE.

Table 1: Tumor/Tissue Ratio of Conjugates after Clearance with AGP3[a]

	tumor/tissue ratio			
	B72.3-βG-PEG		H25-βG-PEG	
tissue	no clearance	AGP3 clearance	no clearance	AGP3 clearance
tumor	1	1	1	1
blood	3.9 ± 0.2	29.6 ± 3.1	0.3 ± 0.1	2.2 ± 0.8
lung	12.5 ± 3.3	33.5 ± 3.0	1.4 ± 0.4	5.5 ± 2.1
liver	15.9 ± 2.9	19.2 ± 0.8	1.1 ± 0.2	1.5 ± 0.6
spleen	19.0 ± 2.6	27.7 ± 5.2	1.8 ± 0.5	3.5 ± 1.5
kidney	18.1 ± 1.3	31.0 ± 2.0	1.4 ± 0.5	2.2 ± 0.2
intestine	6.4 ± 1.7	165 ± 56	4.8 ± 1.3	10.1 ± 2.9
colon	54.3 ± 7.4	50.2 ± 8.3	3.6 ± 0.5	3.1 ± 0.33
urine	1.1 ± 0.1	0.6 ± 0.1	0.1 ± 0.02	0.03 ± 0.001

[a] Groups of three or four mice bearing 100−200 mm^3 solid LS174T tumors were injected with radiolabeled conjugates followed 48 and 50 h later by two i.v. injections of AGP3 or PBS. After 6 h, tumors, blood, urine, and normal tissues were removed and counted in a gamma counter.

Importantly, AGP3 did not significantly reduce tumor accumulation of B72.3-βG-PEG, in contrast to some other clearance systems (Pedley et al., 1989; Sharkey et al., 1992; Kerr et al., 1993). The large size of AGP3 (IgM) may hinder passage of the mAb into the tumor interstitial space, minimizing interactions between localized immunoconjugate and AGP3. The tumor/blood ratios of B72.3-βG-PEG increased from 3.9 to 29.6 at 48 h with AGP3 clearance. This can be contrasted with a tumor/blood ratio of 4.8 at 96 h without clearance. The low tumor/blood ratio without clearance can be attributed to the loss of immunoenzyme from the tumor during the prolonged period required for immunoenzyme to reach safe levels in serum. Clearance of immunoenzyme with AGP3 thus allowed earlier administration of prodrug when immunoenzyme localization at tumor cells was maximal.

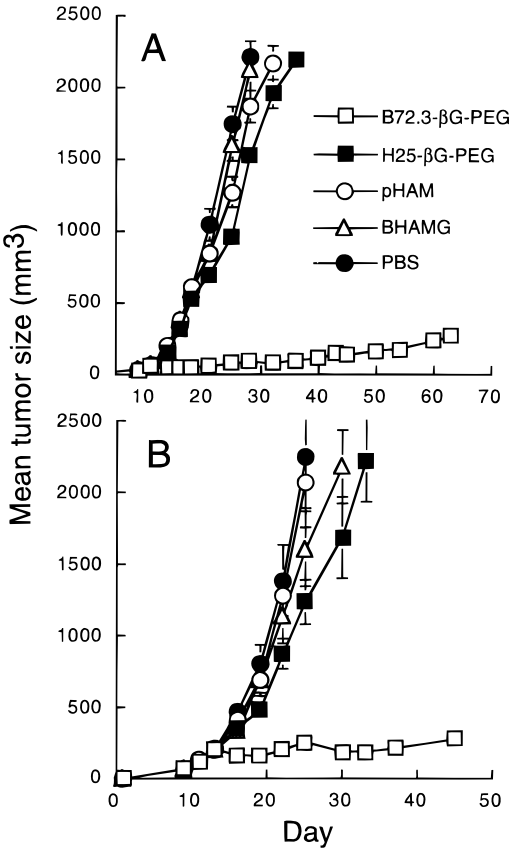

Figure 7. In vivo antitumor activity of prodrug treatment. (A) Groups of 9 BALB/c *nu/nu* mice bearing 50−100 mm^3 LS174T tumors were i.v. injected with B72.3-βG-PEG (□) or H25-βG-PEG (■) on day 9 followed by two i.v. injections of AGP3 on day 11. After 6 h, mice were i.v. injected with BHAMG (7.5 mg/kg × 3). Control groups of tumor-bearing mice were treated with BHAMG (△), pHAM (○), or PBS (●) alone. Therapy was repeated starting on days 16, 26, and 41. The mean size of tumors in mice sequentially treated with B72.3-βG-PEG, AGP3, and BHAMG was significantly ($p \leq 0.0005$) smaller than control tumors after day 14. B, Groups of eight nude mice bearing 200−250 mm^3 LS174T tumors were treated with two round of therapy as above starting on days 11 and 23. The mean size of tumors in mice sequentially treated with B72.3-βG-PEG, AGP3 and BHAMG were significantly ($p \leq 0.005$) smaller than control tumors after day 16. Bars, SE.

Table 2: Toxicity of Therapy[a]

	round of therapy			
	1	2	3	4
	weight loss %			
PBS	0	0	0	NM
pHAM	6.8	13.0	NM	NM
BHAMG	1.7	4.0	1.7	
B72.3-βG-PEG/AP3/BHAMG	3.5	5.0	3.8	6.0
H25-βG-PEG/AGP3/BHAMG	3.9	6.6	4.6	NM

[a] Groups of 9 BALB/c *nu/nu* mice bearing 50−100 mm^3 solid tumors were i.v. injected with PBS, 250 μg of B72.3-βG-PEG or H25-βG-PEG follow 48 h later by two i.v. injections of AGP3 or PBS. After 6 h, mice were i.v. injected with BHAMG (7.5 mg/kg × 3). Control groups of mice were treated with BHAMG (7.5 mg/kg × 3), pHAM (2 mg/kg × 3) or PBS alone. Mice received 2−4 rounds of therapy. [b] NM, not meaningful due to mouse deaths.

Significant antitumor activity with minimal toxicity was demonstrated against LS174T xenografts treated with B72.3-βG-PEG and AGP3 followed by BHAMG administration. The degree of tumor suppression achieved with minimal toxicity by prodrug therapy compares favorably with conventional drugs such as 5-fluorouracil (Blumenthal et al., 1994) and doxorubicin (Meyer et al., 1995) in the LS174T xenograft model. B72.3-βG-PEG appeared to be rapidly catabolized into small peptides that were eliminated in the urine and possibly bile. Soluble IgM immune complexes are primarily removed from the circulation and catabolized by the mononuclear phagocyte system in the liver, spleen, and lungs by receptor-mediated binding of high mannose oligosaccharides exposed upon conformational changes in IgM induced by antigen binding (Day et al., 1980). The low toxicity of BHAMG treatment observed after clearance of B72.3-βG-PEG with AGP3 indicates that cleared conjugate was unavailable for prodrug activation, consistent with rapid degradation of the immunoenzyme after clearance.

mAb B72.3 possesses modest affinity for TAG-72 ($K_a = 2.54 \times 10^9$ M^{-1}) (Muraro et al., 1988). High antibody affinity, however, may be critical for the success of immunoconjugate therapy. For example, a β-lactamase immunoenzyme constructed from a high-affinity antibody against melanotransferrin showed greater tumor uptake and produced tumor regressions and cures in mice, whereas a low affinity L6 immunoenzyme was ineffective, even though the expression of L6 antigen was 2-fold higher than that of melanotransferrin (Svensson et al., 1998). Similarly, a high-affinity mAb against ovarian cancer accumulated to higher levels in tumor xenografts compared to a lower affinity mAb (Kievit et al., 1996). Second generation mAbs against TAG-72 with higher affinities [CC49, $K_a = 16.2 \times 10^{-9}$ M^{-1} and CC83, $K_a = 27.7 \times 10^{-9}$ (Muraro et al., 1989)] display improved tumor uptake (O'Boyle et al., 1994) and therapeutic efficacy as radioimmunoconjugates (Schlom et al., 1992) compared with B72.3. Immunoenzymes employing CC49 or CC83 may, therefore, improve the therapeutic efficacy of prodrug treatment.

Most of the enzymes currently under investigation for the targeted activation of anti-neoplastic prodrugs are of microbial origin such as β-lactamase from *Enterobacter cloacae* (Kerr et al., 1995), carboxypeptidase G2 from *Pseudomonas* species (Blakey et al., 1996), β-glucuronidase (Chen et al., 1997), nitroreductase (Anlezark et al., 1995), and penicillin-G amidase (Vrudhula et al., 1993) from *E. coli*, and cytosine deaminase from bakers yeast (Wallace et al., 1994). These enzymes are expected to induce a strong immune response as has been found for carboxypeptidase G2 in a pilot clinical trial (Sharma et al., 1996), thereby limiting the number of times that immunoenzymes can be administered to patients. The utilization of human enzymes to activate antineoplastic prodrugs may not completely prevent this problem since recombinant human proteins can also induce immune responses in patients (Atkins et al., 1986; Gribben et al., 1990). Immunosuppressive drugs such as cyclosporin A, cyclophosphamide, and deoxyspergualin can decrease or delay the immune response against antibodies (Ledermann et al., 1991), immunotoxins (Pai et al., 1990) and antibody-enzyme conjugates (Sharma et al., 1996). Immunosupression, in addition to producing toxicity in some patients (Sharma et al., 1996), may hinder the development of antitumor immunity generated by prodrug therapy (Chen et al., 1997).

Immune responses against proteins are attenuated by attachment of PEG (Abuchowski et al., 1977). PEG, in contrast to immunosuppressive drugs, is not toxic and does not affect systemic immunity. PEG modification has been shown to reduce the immunogenicity of enzymes (Abuchowski et al., 1977), antibodies (Kitamura et al., 1991), toxins (Wang et al., 1993), and recombinant human proteins (Katre, 1990). PEG modification of bacterial enzymes may allow repeated administration of immunoenzymes for ADEPT without the need to employ toxic immunosuppressive drugs. PEG-modified enzymes of the proper molecular size can also preferentially accumulate in tumors and are under investigation for tumor selective prodrug activation (Bagshawe et al., 1999). AGP3 binds to the backbone of PEG (Cheng et al., 1997 and unpublished results) independent of the linker or protein employed. AGP3 should therefore be generally applicable to the accelerated clearance of PEG-modified immunoenzymes, radioimmunoconjugates and imaging agents as well as for the analysis of PEG-modified proteins.

ACKNOWLEDGMENT

This work was supported by Academia Sinica and Grant DOH88-HR-716 from the National Health Research Institutes, Taipei, Taiwan.

LITERATURE CITED

Abuchowski, A., McCoy, J. R., Palczuk, N. C., van Es, T., and Davis, F. F. (1977) Effect of covalent attachment of polyethylene glycol on immunogenicity and circulating life of bovine liver catalase. *J. Biol. Chem. 252*, 3582−3586.

Anlezark, G. M., Melton, R. G., Sherwood, R. F., Wilson, W. R., Denny, W. A., Palmer, B. D., Knox, R. J., Friedlos, F., and Williams, A. (1995) Bioactivation of dinitrobenzamide mustards by an E. coli B nitroreductase. *Biochem. Pharmacol. 50*, 609−618.

Atkins, M. B., Gould, J. A., Allegretta, M., Li, J. J., Dempsey, R. A., Rudders, R. A., Parkinson, D. R., Reichlin, S., and Mier, J. W. (1986) Phase I evaluation of recombinant interleukin-2 in patients with advanced malignant disease. *J. Clin. Oncol. 4*, 1380−1391.

Bagshawe, K. D., Sharma, S. K., Know, R., and Amooquaye, E. (1999) Studies with polymer enzyme conjugates and AMIRACS. *Advances in the Application of Monoclonal Antibodies in Clinical Oncology*, Vol. 28, Samos, Greece.

Bagshawe, K. D., Springer, C. J., Searle, F., Antoniw, P., Sharma, S. K., Melton, R. G., and Sherwood, R. F. (1988) A cytotoxic agent can be generated selectively at cancer sites. *Br. J. Cancer 58*, 700−703.

Blakey, D. C., Burke, P. J., Davies, D. H., Dowell, R. I., East, S. J., Eckersley, K. P., Fitton, J. E., McDaid, J., Melton, R. G., Niculescu Duvaz, I. A., Pinder, P. E., Sharma, S. K., Wright, A. F., and Springer, C. J. (1996) ZD2767, an improved system for antibody-directed enzyme prodrug therapy that results in tumor regressions in colorectal tumor xenografts. *Cancer Res. 56*, 3287−3292.

Blumenthal, R. D., Sharkey, R. M., Natale, A. M., Kashi, R., Wong, G., and Goldenberg, D. M. (1994) Comparison of equitoxic radioimmunotherapy and chemotherapy in the treatment of human colonic cancer xenografts. *Cancer Res. 54*, 142−151.

Bosslet, K., Czech, J., and Hoffmann, D. (1994) Tumor-selective prodrug activation by fusion protein-mediated catalysis. *Cancer Res. 54*, 2151−2159.

Chen, B. M., Chan, L. Y., Wang, S. M., Wu, M. F., Chern, J. W., and Roffler, S. R. (1997) Cure of malignant ascites and generation of protective immunity by monoclonal antibody-targeted activation of a glucuronide prodrug in rats. *Int. J. Cancer 73*, 392−402.

Cheng, T. L., Chen, B. M., Chan, L. Y., Wu, P. Y., Chern, J. W., and Roffler, S. R. (1997) Poly(ethylene glycol) modification

of beta-glucuronidase-antibody conjugates for solid-tumor therapy by targeted activation of glucuronide prodrugs. *Cancer Immunol. Immunother. 44*, 305−315.

Cheng, T. L., Chou, W. C., Chen, B. M., Chern, J. W., and Roffler, S. R. (1999a) Characterization of an antineoplastic glucuronide prodrug. *Biochem. Pharmacol. 58*, 325−328.

Cheng, T. L., Wu, P. Y., Wu, M. F., Chern, J. W., and Roffler, S. R. (1999b) Accelerated clearance of polyethylene glycol-modified proteins by anti-polyethylene glycol IgM. *Bioconjugate Chem. 10*, 520−528.

Colcher, D., Keenan, A. M., Larson, S. M., and Schlom, J. (1984) Prolonged binding of a radiolabeled monoclonal antibody (B72.3) used for the in situ radioimmunodetection of human colon carcinoma xenografts. *Cancer Res. 44*, 5744−5751.

Day, J. F., Thornburg, R. W., Thorpe, S. R., and Baynes, J. W. (1980) Carbohydrate-mediated clearance of antibody·antigen complexes from the circulation. The role of high mannose oligosaccharides in the hepatic uptake of IgM·antigen complexes. *J. Biol. Chem. 255*, 2360−2365.

Delgado, C., Francis, G. E., and Fisher, D. (1992) The uses and properties of PEG-linked proteins. *Crit. Rev. Ther. Drug Carrier Sys. 9*, 249−304.

Delgado, C., Pedley, R. B., Herraez, A., Boden, R., Boden, J. A., Keep, P. A., Chester, K. A., Fisher, D., Begent, R. H., and Francis, G. E. (1996) Enhanced tumour specificity of an anti-carcinoembrionic antigen Fab′ fragment by poly(ethylene glycol) (PEG) modification. *Br. J. Cancer 73*, 175−182.

Divgi, C. R. (1996) Status of radiolabeled monoclonal antibodies for diagnosis and therapy of cancer. *Oncology (Huntingt) 10*, 939−953.

Eccles, S. A., Court, W. J., Box, G. A., Dean, C. J., Melton, R. G., and Springer, C. J. (1994) Regression of established breast carcinoma xenografts with antibody-directed enzyme prodrug therapy against c-erbB2 p185. *Cancer Res 54*, 5171−5177.

Ey, P. L., Prowse, S. J., and Jenkin, C. R. (1978) Isolation of pure IgG1, IgG2a and IgG2b immunoglobulins from mouse serum using protein A-Sepharose. *Immunochemistry 15*, 429−436.

Gribben, J. G., Devereux, S., Thomas, N. S., Keim, M., Jones, H. M., Goldstone, A. H., and Linch, D. C. (1990) Development of antibodies to unprotected glycosylation sites on recombinant human GM-CSF. *Lancet 335*, 434−437.

Haisma, H. J., Van Muijen, M., Scheffer, G., Scheper, R. J., Pinedo, H. M., and Boven, E. (1995) A monoclonal antibody against human beta-glucuronidase for application in antibody-directed enzyme prodrug therapy. *Hybridoma 14*, 377−382.

Horan Hand, P., Colcher, D., Salomon, D., Ridge, J., Noguchi, P., and Schlom, J. (1985) Influence of spatial configuration of carcinoma cell populations on the expression of a tumor-associated glycoprotein. *Cancer Res. 45*, 833−840.

Johnson, V. G., Schlom, J., Paterson, A. J., Bennett, J., Magnani, J. L., and Colcher, D. (1986) Analysis of a human tumor-associated glycoprotein (TAG-72) identified by monoclonal antibody B72.3. *Cancer Res. 46*, 850−857.

Katre, N. V. (1990) Immunogenicity of recombinant IL-2 modified by covalent attachment of polyethylene glycol. *J. Immunol. 144*, 209−213.

Kerr, D. E., Garrigues, U. S., Wallace, P. M., Hellstrom, K. E., Hellstrom, I., and Senter, P. D. (1993) Application of monoclonal antibodies against cytosine deaminase for the in vivo clearance of a cytosine deaminase immunoconjugate. *Bioconjugate Chem. 4*, 353−357.

Kerr, D. E., Schreiber, G. J., Vrudhula, V. M., Svensson, H. P., Hellstrom, I., Hellstrom, K. E., and Senter, P. D. (1995) Regressions and cures of melanoma xenografts following treatment with monoclonal antibody beta-lactamase conjugates in combination with anticancer prodrugs. *Cancer Res. 55*, 3558−3563.

Kievit, E., Pinedo, H. M., Schluper, H. M., Haisma, H. J., and Boven, E. (1996) Comparison of monoclonal antibodies 17−1A and 323/A3: the influence of the affinity on tumour uptake and efficacy of radioimmunotherapy in human ovarian cancer xenografts. *Br. J. Cancer 73*, 457−464.

King, D. J., Turner, A., Farnsworth, A. P., Adair, J. R., Owens, R. J., Pedley, R. B., Baldock, D., Proudfoot, K. A., Lawson, A. D., and Beeley, N. R., et al. (1994) Improved tumor targeting with chemically cross-linked recombinant antibody fragments. *Cancer Res. 54*, 6176−6185.

Kitamura, K., Takahashi, T., Yamaguchi, T., Noguchi, A., Takashina, K., Tsurumi, H., Inagake, M., Toyokuni, T., and Hakomori, S. (1991) Chemical engineering of the monoclonal antibody A7 by polyethylene glycol for targeting cancer chemotherapy. *Cancer Res. 51*, 4310−4315.

Ledermann, J. A., Begent, R. H., Massof, C., Kelly, A. M., Adam, T., and Bagshawe, K. D. (1991) A phase-I study of repeated therapy with radiolabelled antibody to carcinoembryonic antigen using intermittent or continuous administration of cyclosporin A to suppress the immune response. *Int. J. Cancer 47*, 659−664.

Meyer, D. L., Law, K. L., Payne, J. K., Mikolajczyk, S. D., Zarrinmayeh, H., Jungheim, L. N., Kling, J. K., Shepherd, T. A., and Starling, J. J. (1995) Site-specific prodrug activation by antibody-beta-lactamase conjugates: preclinical investigation of the efficacy and toxicity of doxorubicin delivered by antibody directed catalysis. *Bioconjugate Chem. 6*, 440−446.

Milenic, D. E., Esteban, J. M., and Colcher, D. (1989) Comparison of methods for the generation of immunoreactive fragments of a monoclonal antibody (B72.3) reactive with human carcinomas. *J. Immunol. Methods 120*, 71−83.

Muraro, R., Kuroki, M., Wunderlich, D., Poole, D. J., Colcher, D., Thor, A., Greiner, J. W., Simpson, J. F., Molinolo, A., and Noguchi, P., et al. (1988) Generation and characterization of B72.3 second generation monoclonal antibodies reactive with the tumor-associated glycoprotein 72 antigen. *Cancer Res. 48*, 4588−4596.

Muraro, R., Nuti, M., Natali, P. G., Bigotti, A., Simpson, J. F., Primus, F. J., Colcher, D., Greiner, J. W., and Schlom, J. (1989) A monoclonal antibody (D612) with selective reactivity for malignant and normal gastro-intestinal epithelium. *Int. J. Cancer 43*, 598−607.

O'Boyle, K. P., Goya, V., Zuckier, L. S., Chun, S., and Bhargava, K. (1994) Expression of human tumor mucin-associated carbohydrate epitopes, including sialylated Tn, and localization of murine monoclonal antibodies CC49 and B72.3 in a syngeneic rat colon carcinoma model. *J. Immunother. Emphasis Tumor Immunol. 16*, 251−261.

Paganelli, G., Stella, M., De Nardi, P., Magnani, P., Zito, F., Siccardi, A. G., Di Carlo, V., and Fazio, F. (1991) A new method for faster blood clearance in radioimmuno-guided surgery. *J. Nucl. Biol. Med. 35*, 88−89.

Pai, L. H., FitzGerald, D. J., Tepper, M., Schacter, B., Spitalny, G., and Pastan, I. (1990) Inhibition of antibody response to Pseudomonas exotoxin and an immunotoxin containing Pseudomonas exotoxin by 15-deoxyspergualin in mice. *Cancer Res. 50*, 7750−7753.

Pedley, R. B., Boden, J. A., Boden, R., Begent, R. H., Turner, A., Haines, A. M., and King, D. J. (1994) The potential for enhanced tumour localisation by poly(ethylene glycol) modification of anti-CEA antibody. *Br. J. Cancer 70*, 1126−1130.

Pedley, R. B., Dale, R., Boden, J. A., Begent, R. H., Keep, P. A., and Green, A. J. (1989) The effect of second antibody clearance on the distribution and dosimetry of radiolabelled anti-CEA antibody in a human colonic tumor xenograft model. *Int. J. Cancer 43*, 713−718.

Roffler, S. R., Wang, S. M., Chern, J. W., Yeh, M. Y., and Tung, E. (1991) Anti-neoplastic glucuronide prodrug treatment of human tumor cells targeted with a monoclonal antibody-enzyme conjugate. *Biochem. Pharmacol. 42*, 2062−2065.

Rogers, G. T., Burke, P. J., Sharma, S. K., Koodie, R., and Boden, J. A. (1995) Plasma clearance of an antibody−enzyme conjugate in ADEPT by monoclonal anti-enzyme: its effect on prodrug activation in vivo. *Br. J. Cancer 72*, 1357−1363.

Schlom, J. (1986) Basic principles and applications of monoclonal antibodies in the management of carcinomas: the Richard and Hinda Rosenthal Foundation award lecture. *Cancer Res. 46*, 3225−3238.

Schlom, J., Eggensperger, D., Colcher, D., Molinolo, A., Houchens, D., Miller, L. S., Hinkle, G., and Siler, K. (1992) Therapeutic advantage of high-affinity anticarcinoma radioimmunoconjugates. *Cancer Res. 52*, 1067−1072.

Senter, P. D., Saulnier, M. G., Schreiber, G. J., Hirschberg, D. L., Brown, J. P., Hellstrom, I., and Hellstrom, K. E. (1988)

Anti-tumor effects of antibody-alkaline phosphatase conjugates in combination with etoposide phosphate. *Proc. Natl. Acad. Sci. U.S.A. 85*, 4842−4846.

Sharkey, R. M., Boerman, O. C., Natale, A., Pawlyk, D., Monestier, M., Losman, M. J., and Goldenberg, D. M. (1992) Enhanced clearance of radiolabeled murine monoclonal antibody by a syngeneic anti-idiotype antibody in tumor-bearing nude mice. *Int. J. Cancer 51*, 266−273.

Sharma, S. K., Bagshawe, K. D., Burke, P. J., Boden, R. W., and Rogers, G. T. (1990) Inactivation and clearance of an anti-CEA carboxypeptidase G2 conjugate in blood after localisation in a xenograft model. *Br. J. Cancer 61*, 659−662.

Sharma, S. K., Bagshawe, K. D., Melton, R. G., and Begent, R. H. (1996) Effect of cyclosporine on immunogenicity of a bacterial enzyme carboxypeptidase G2 in ADEPT. *Transplant Proc. 28*, 3154−3155.

Siemers, N. O., Kerr, D. E., Yarnold, S., Stebbins, M. R., Vrudhula, V. M., Hellstrom, I., Hellstrom, K. E., and Senter, P. D. (1997) Construction, expression, and activities of L49-sFv-beta-lactamase, a single-chain antibody fusion protein for anticancer prodrug activation. *Bioconjugate Chem. 8*, 510−519.

Stewart, J. S., Sivolapenko, G. B., Hird, V., Davies, K. A., Walport, M., Ritter, M. A., and Epenetos, A. A. (1990) Clearance of 131I-labeled murine monoclonal antibody from patients' blood by intravenous human anti-murine immunoglobulin antibody. *Cancer Res. 50*, 563−567.

Svensson, H. P., Frank, I. S., Berry, K. K., and Senter, P. D. (1998) Therapeutic effects of monoclonal antibody-beta-lactamase conjugates in combination with a nitrogen mustard anticancer prodrug in models of human renal cell carcinoma. *J. Med. Chem. 41*, 1507−1512.

Tennvall, J., Garkavij, M., Chen, J., Sjogren, H. O., and Strand, S. E. (1997) Improving tumor-to-normal-tissue ratios of antibodies by extracorporeal immunoadsorption based on the avidin−biotin concept: development of a new treatment strategy applied to monoclonal antibodies murine L6 and chimeric BR96. *Cancer 80*, 2411−2418.

Thor, A., Ohuchi, N., Szpak, C. A., Johnston, W. W., and Schlom, J. (1986) Distribution of oncofetal antigen tumor-associated glycoprotein-72 defined by monoclonal antibody B72.3. *Cancer Res. 46*, 3118−3124.

Ullen, A., Sandstrom, P., Ahlstrom, K. R., Sundstrom, B., Nilsson, B., Arlestig, L., and Stigbrand, T. (1995) Use of anticytokeratin monoclonal anti-idiotypic antibodies to improve tumor: nontumor ratio in experimental radioimmunolocalization. *Cancer Res. 55*, 5868s−5873s.

Vrudhula, V. M., Senter, P. D., Fischer, K. J., and Wallace, P. M. (1993) Prodrugs of doxorubicin and melphalan and their activation by a monoclonal antibody-penicillin-G amidase conjugate. *J. Med. Chem. 36*, 919−923.

Wallace, P. M., MacMaster, J. F., Smith, V. F., Kerr, D. E., Senter, P. D., and Cosand, W. L. (1994) Intratumoral generation of 5-fluorouracil mediated by an antibody-cytosine deaminase conjugate in combination with 5-fluorocytosine. *Cancer Res. 54*, 2719−2723.

Wang, Q. C., Pai, L. H., Debinski, W., FitzGerald, D. J., and Pastan, I. (1993) Polyethylene glycol-modified chimeric toxin composed of transforming growth factor alpha and Pseudomonas exotoxin. *Cancer Res. 53*, 4588−4594.

Wang, S. M., Chern, J. W., Yeh, M. Y., Ng, J. C., Tung, E., and Roffler, S. R. (1992) Specific activation of glucuronide prodrugs by antibody-targeted enzyme conjugates for cancer therapy. *Cancer Res. 52*, 4484−4491.

BC990147J

Binding Properties of a Monoclonal Antibody Directed toward Lead−Chelate Complexes

Mehraban Khosraviani,[†,‡] Robert C. Blake II,[§,⊥] Andrey R. Pavlov,[†] Stanley C. Lorbach,[§] Haini Yu,[†] James B. Delehanty,[†] Martin W. Brechbiel,[∥] and Diane A. Blake*[,†,⊥]

Department of Ophthalmology, Tulane University School of Medicine, 1430 Tulane Avenue, New Orleans, Louisiana 70112, Department of Basic Pharmaceutical Sciences, Xavier University of Louisiana, New Orleans, Louisiana 70125, Radioimmune and Inorganic Chemistry Section, NCI/NIH, Bethesda, Maryland 20892, Tulane/Xavier Center for Bioenvironmental Research, New Orleans, Louisiana 70112. Received November 2, 1999; Revised Manuscript Received January 19, 2000

A monoclonal antibody (2C12) that recognizes a Pb(II)−cyclohexyldiethylenetriamine pentaacetic acid complex was produced by the injection of BALB/c mice with a Pb(II)−chelate complex covalently coupled to a carrier protein. The ability of purified antibody to interact with a variety of metal-free chelators and metal−chelate complexes was assessed by measuring equilibrium dissociation constants. The antibody bound to metal-free *trans*-cyclohexyldiethylenetriamine pentaacetic acid (CHXDTPA) with an equilibrium dissociation constant of 2.3×10^{-7} M. Addition of Pb(II) increased the affinity of the antibody for the complex by 25-fold; Pb(II) was the only metal cation (of 15 different di-, tri-, and hexavalent metals tested) that increased the affinity of the antibody for CHXDTPA. The increased affinity was due primarily to an increase in the association rate constant. The antibody also had the ability to interact with ethylenediamine tetraacetic acid (EDTA), diethylenetriamine pentaacetic acid (DTPA), and structurally related derivatives, but with affinities from 50- to 10000-fold less than that determined for CHXDTPA. Addition of metals to EDTA-based chelators reduced the affinity of the antibody for these ligands. However, when DTPA was used as the chelator, addition of Pb(II) increased the affinity of the antibody for the complex by 200-fold. The sensitivity of prototype immunoassays for Pb(II) could be modulated by changing the structure of the immobilized metal−chelate complex and/or the soluble chelator used to complex Pb(II) in the test solution.

INTRODUCTION

Lead is a persistent, ubiquitous toxin in the environment, and the consequences of lead contamination are a subject of both ancient interest and great contemporary concern (*1*−*3*). Humans are exposed to lead primarily by inhalation of lead-containing dusts and via ingestion of lead-contaminated food, dust, soil, and paint (*4*−*6*). In small children engaged in hand-to-mouth behavior, lead-contaminated soil is a greater risk factor than lead-based paints (*7*). Simple, rapid techniques for the determination of lead contamination in environmental samples could ultimately reduce the incidence of lead intoxication in the human population. Antibody-based analytical methods are being widely adapted for other environmental applications (*8*−*10*). The availability of an antibody that could distinguish the cationic form of lead from a variety of other metals could provide the basis for a rapid, sensitive immunoassay to assess lead contamination in the environment.

Heavy metals, under appropriate conditions, can induce specific antibody responses. Reardan et al. first demonstrated the use of an EDTA-chelate[1] immunogen to generate a monoclonal antibody, CHA255, that bound with subnanomolar affinity to an In(III)-L-benzyl-EDTA complex and with between 10- and 8000-fold lesser affinity to 12 other tri- and bivalent metals complexed with L-benzyl-EDTA (*11*). This antibody did not bind significantly to metal-free EDTA at concentrations as high as 5 mM. The basis for the metal ion specificity was explained when the crystal structure of the CHA255·benzyl-EDTA-In(III) and CHA255·benzyl-EDTA-Fe(III) complexes were solved to 2.2 and 2.8 Å resolution (*12*). The most significant feature of the interaction of CHA255 with hapten was the coordination of histidine 99 of the heavy chain to the hapten's indium ion. This coordination did not occur with the benzyl-EDTA-Fe(III) ligand, apparently because the imidazole could not approach the Fe(III) without contacting the relatively more enveloping carboxylate chelating groups of the EDTA moiety. The participation of histidine in metal ion binding has also

* To whom correspondence should be addressed at Tulane University School of Medicine. Phone: (504) 584-2478. Fax: (504) 584-2684. E-mail: dblake@tmcpop.tmc.tulane.edu.

† Tulane University School of Medicine.

‡ Present address, LINCO Research, Inc., 14 Research Park Dr., St. Charles, MO 63304.

§ Xavier University of Louisiana.

∥ Radioimmune and Inorganic Chemistry Section.

⊥ Tulane/Xavier Center for Bioenvironmental Research.

[1] Abbreviations: BSA, bovine serum albumin; CHX-A, *N*-[2-amino-3-*p*-isothiocyanatophenyl)propyl]-*trans*-cyclohexane-1,2-diamine-*N*,*N*′,*N*′,*N*″,*N*″-diethylenetriamine pentaacetic acid (A isomer); CHXEDTA, *trans*-1,2-diaminocyclohexane-*N*,*N*,*N*′,*N*-tetraacetic acid; CHXDTPA, *trans*-cyclohexyldiethylenetriamine pentaacetic acid; EDTA, ethylenediamine tetraacetic acid; DOTA, 1,4,7,10-tetraazacyclododecane-*N*,*N*′,*N*″,*N*‴-tetraacetic acid; HBS, Hepes-buffered saline; KLH, keyhole limpet hemocyanin; PBS, phosphate-buffered saline, Pb(II)-CHXDTPA-benzyl-BSA, bovine serum albumin-thioureido-L-benzyl-*trans*-cyclohexyldiethylenetriamine pentaacetic acid-Pb(II) conjugate; PCR, polymerase chain reaction; TETA, 1,4,8,11-tetraazacyclotetradecane-*N*,*N*′,*N*″,*N*‴-tetraacetic acid.

10.1021/bc9901548 CCC: $19.00 © 2000 American Chemical Society
Published on Web 03/20/2000

been suggested for the interaction of another monoclonal antibody, mAb 734, with a DTPA-In(III) hapten (*13*, *14*). Our laboratory has also isolated and characterized an antibody, 2A81G5, that had certain similarities to these anti-indium antibodies (*15*). The 2A81G5 antibody preferentially recognized EDTA complexes of two metals, Cd(II) and Hg(II). However, 2A81G5 also recognized a wide variety of other di- and trivalent metal−EDTA complexes with affinities that varied over several orders of magnitude. Molecular modeling implicated a histidine in the heavy chain in metal ion coordination. As with CHA255, metal-free EDTA was not recognized by the 2A81G5 antibody. Other groups have reported antibodies that recognized other chelators, including DTPA and DOTA (*16*, *17*). However, these monoclonal antibodies were not able to distinguish among different metals bound to the chelator. Feng et al. (*18*) have reported a monoclonal antibody that bound with some selectively to DOTA complexes of yttrium and gadolinium; the affinity of the antibody for metal-free DOTA was not reported in this study.

In the present study, we report the isolation and characterization of a Pb(II)-specific monoclonal antibody that has the ability to recognize structural features of both the metal-free chelator and the Pb(II)−chelate complex. Equilibrium binding and kinetic studies revealed that this antibody, in contrast to CHA255 and 2A81G5, had an absolute specificity for Pb(II) when the immunizing chelator was used to complex soluble Pb(II). This new antibody was also much less promiscuous in its ability to bind other di- and trivalent metal ions when these ions were complexed to chelators structurally related to the immunizing chelator.

EXPERIMENTAL PROCEDURES

Materials. BALB/c inbred mice were purchased from Charles River Laboratories (Wilmington, MA). SP 2/0-Ag14 myeloma cells were from the American Type Culture Collection (Rockville, MD). Ultrapure bovine serum albumin (BSA) and an IsoStrip mouse monoclonal antibody isotyping kit were purchased from Boehringer-Mannheim Biochemicals (Indianapolis, IN). Keyhole limpet hemocyanin (KLH) was a product of Calbiochem (La Jolla, CA). *trans*-Cyclohexyldiethylenetriamine pentaacetic acid (CHXDTPA), the A isomer of the bifunctional derivative, *N*-[2-amino-3-*p*-isothiocyanatophenyl)-propyl]-*trans*-cyclohexane-1,2-diamine-*N*,*N*′,*N*′,*N*″,*N*″-diethylenetriamine pentaacetic acid (CHX-A), and *p*-nitrobenzyl-diethylenetriamine pentaacetic acid were available from previous studies (*19*,*20*). *trans*-1,2-Diaminocyclohexane-*N*,*N*,*N*′,*N*′-tetraacetic acid (CHXEDTA) was purchased from Aldrich (Milwaukee, WI). Atomic absorption grade metals were obtained from Perkin-Elmer Corp. (Norwalk, CT). Diethyl-Pb(IV) dichloride and phenyl-Pb(IV) trichloride were custom-synthesized by All-Chemie, Ltd. (Mt. Pleasant, SC). Ethylenediamine tetraacetic acid (EDTA), diethylenetriamine pentaacetic acid (DTPA), tissue culture medium, L-glutamine, HAT medium supplement, antibiotics, pristane, antibodies specific to mouse IgG1, IgG2a, IgG2b, IgG3, IgM, and IgA, and goat anti-mouse IgG coupled to horseradish peroxidase were purchased from Sigma Chemical Co. (St. Louis, MO). Fetal bovine serum was the product of Hyclone Laboratories (Logan, UT) or Gibco/BRL (Gaithersburg, MD). Microwell plates for ELISA (flat bottom, high binding) and tissue culture plates were products of Coring/Costar (Cambridge, MA). 3,3′,5,5′-Tetramethylbenzidine peroxidase substrate (TMB Microwell Substrate) was from Kirkegaard-Perry Laboratories (Gaithersburg, MD). Immobilized protein G resin and BCA protein assay kit were purchased from Pierce Chemical Co. (Rockford, IL) and used according to the manufacturer's directions. Poly(methyl methacrylate) beads (98 ± 8 μm diameter) were obtained from Bangs Laboratories (Carmel, IN) or Sapidyne Instruments (Boise, ID). The Cy3 and fluorescein conjugates of affinity purified goat anti-mouse IgG were products of Jackson ImmunoResearch Laboratories (West Grove, PA). Primers for PCR amplification of mouse IgG light- and heavy-chain variable regions were purchased from Pharmacia, Inc. (Piscataway, NJ). Glassware was mixed-acid washed (*21*) and plasticware was soaked overnight in 3 N HCL and rinsed liberally with purified water before use.

Preparation of Protein−Chelate Conjugates. Protein−chelator conjugates were prepared by a modification of a previously described method (*20*), in a final volume of 500 μL which contained 5 mg of protein (BSA or KLH), 2.6 mM CHX-A, 2.9 mM $Pb(NO_3)_2$, and 46 mM triethylamine in 50 mM Hepes buffer, pH 9.0. The pH of the reaction mixture was maintained at 9.0 by the addition of KOH. A metal-free BSA conjugate was prepared by omitting the $Pb(NO_3)_2$ from the reaction mixture. The reactions were stirred at 25 °C for 3 h, then unreacted low molecular weight components were removed by buffer exchange using a Centricon-30 filter (Amicon, Inc., Beverly, MA). The protein conjugates were characterized as described previously (*22*). Extent of substitution of free lysine groups was 17.1% for the KLH conjugate and 5.5% for the BSA conjugates.

Mouse Immunization, Hybridoma Production, and Purification of Monoclonal Antibody. Five 6-week old female BALB/c mice were injected intraperitoneally with 50 μg of the KLH conjugate emulsified in Ribi adjuvant (Ribi Immunochemicals, Hamilton, MT) at days 0, 21, and then 2-week intervals. Antibody response of each mouse was determined by indirect ELISA using both metal-free CHXDTPA-benzyl-BSA and lead-loaded conjugate (*15*). After correction for dilution of the antiserum, the mouse with the highest antibody response to the lead-loaded chelate was given a final intraperitoneal boost of 50 μg of the KLH conjugate in phosphate-buffered saline (PBS, 137 mM NaCl, 3 mM KCl, 10 mM sodium phosphate buffer, pH 7.4) 72 h prior to fusion. Mouse spleen cells were harvested, washed twice in RPMI 1640 medium, and fused with SP 2/0-Ag14 myeloma cells as described previously (*15*). The fused cells were suspended in RPMI medium containing 20% fetal bovine serum and HAT supplementation and then distributed into 96-well tissue culture plates at 200 μL (10^4 cells)/well. Each well contained a feeder layer of normal splenocytes to support the hybridoma cell growth. The plates were incubated at 37 °C in a humidified atmosphere supplemented with 5% CO_2. Supernatants from viable, replicating hybridoma clones were collected and screened for antibodies to Pb(II)-CHXDTPA-benzyl-BSA by competitive ELISA (described below). Positive hybridoma clones were subcultured and frozen. Those hybridomas synthesizing and secreting metal-specific antibodies were subcloned two times by limiting dilution.

Ascites fluid was produced in pristane-primed BALB/c mice by intraperitoneal injection of 3×10^6 hybridoma cells. Ascites fluid was collected 7−10 days after the hybridoma injection, and the immunoglobulin G fraction of ascites was isolated by affinity chromatography on immobilized protein G. The immunoglobulin subclass of the 2C12 monoclonal antibody was determined and quantified by sandwich ELISA using antibodies specific to IgG1, IgG2a, IgG2b, IgG3, IgM, and IgA. Protein

concentration of the purified antibody was determined using the BCA protein assay kit, and the light-chain isotype was determined using an IsoStrip antibody isotyping kit according to the manufacturers' instructions.

Competitive ELISA. Microwell plates were coated overnight with 0.5 μg/mL of Pb(II)-CHXDTPA-benzyl-BSA, washed three times with PBS containing 0.05% Tween 20, and blocked with 3% BSA in PBS. After an additional wash step, the immobilized antigen was incubated with hybridoma supernatant diluted with an equivalent volume of Hepes-buffered saline (HBS, 137 mM NaCl, 3 mM KCl, and 10 mM Hepes buffer, pH 7.4) containing 10 mM DTPA or HBS containing 10 mM DTPA and 200 ppm of one of the following metals: Pb(II), Hg(II), Au(I), Cd(II), Zn(II), Fe(III), Ag(I), or Ca(II). Hybridoma supernatant diluted with an equivalent volume of HBS was used as a control. After 1 h at room temperature, the plates were washed again and incubated sequentially with goat anti-mouse IgG-horseradish peroxidase conjugate and TMB Microwell Substrate as previously described (*15*). Plates were read in the dual wavelength mode (450−650 nm) using a Vmax Kinetic Microplate Reader from Molecular Devices (Sunnyvale, CA).

Determination of Equilibrium Dissociation Constants and Association Rate Constants. Equilibrium and kinetic measurements of the interactions of metal-free chelators and chelated metals with the 2C12 monoclonal antibody were performed with a KinExA automated immunoassay system (Sapidyne Instruments, Inc., Boise, ID). The method was essentially as described previously (*15*, *23*, *24*); however, a modified procedure was used to prepare antigen-coated beads for use in the instrument. Poly(methyl methacrylate) beads (200 mg) were incubated in 1 mL of HBS containing 100 μg of Pb-CHXDTPA-benzyl-BSA conjugate. After 1 h of gentle agitation at 37° C, the beads were centrifuged and the supernatant was decanted. Any nonspecific protein-binding sites remaining on the beads were blocked by subsequent incubation with 1 mL of 1% BSA in HBS containing 1 μM $Pb(NO_3)_2$ for 1 h at 37° C. The blocked beads could be stored for up to a week at 4° C in the blocking solution. The beads were diluted to a concentration of 6.7 mg/mL in HBS containing 1 μM $Pb(NO_3)_2$ before use in the immunoassay instrument.

A bead pack approximately 4 mm high was created in the observation cell by drawing 675 μL of a suspension of the blocked beads (6.7 mg beads/mL) over the screen at a flow rate of 1.5 mL/min and washing the retained beads with sufficient HBS buffer (1.0 mL) to remove the excess $Pb(NO_3)_2$ and BSA. The beads were then gently disrupted with a brief backflush of HBS (50 μL at 300 μL/min), followed by a 20 s settling period to create a uniform and reproducible pack.

For equilibrium measurements of antibody−antigen binding, the purified 2C12 monoclonal antibody (final concentration of 0.1 μg/mL) was combined with metal-free chelators in HBS or individual metal ions in HBS amended with chelator. Once equilibrium was achieved (less than 20 min in all cases), 500 μL of the mixture was drawn past the beads, followed by 166 μL of the HBS buffer to wash out unbound primary antibody and excess ligand. One milliliter of fluorescently labeled goat anti-mouse antibody (1.0 μg/mL) was then drawn past the beads. All solution transfers up to this point were accomplished with a flow rate of 500 μL/min. Unbound labeled secondary antibody was subsequently removed by drawing 3.0 mL of HBS through the bead pack over a period of 2 min. For equilibrium binding of the CHXDTPA complexes of diethyl-Pb(IV) and phenyl-Pb(IV), antibody (1.5 nM in binding sites) and organolead-CHXDTPA complexes were incubated for ≥20 min before separation of the antibody into bound and free fractions. The concentration of total CHXDTPA was 125 nM in all experiments.

For kinetic measurements, equal volumes (250 μL) of the primary antibody (0.2 μg/mL) and metal−chelate solutions were mixed at rates of 250 μL/min each. The binding reaction proceeded for the 7 s it took the mixture to transverse the distance from the point of mixing to the point where the bead pack was first encountered. One milliliter of labeled secondary antibody was then drawn past the beads (at 500 μL/min), followed by 1.5 mL (at 750 μL/min) of HBS. Data acquisition (initiated in both cases at the introduction of primary antibody to the beads) and instrument control were accomplished via an PC-based computer interfaced to the KinExA using software provided by Sapidyne, Inc. Dissociation constants were obtained from nonlinear regression analyses of the equilibrium binding data using a one-site homogeneous binding model and software contained in SlideWrite (version 4.1, Advanced Graphics, Inc., Carlsbad, CA). Association rate constants were obtained from nonlinear regression fits of the kinetic data to single-exponential functions of time and ligand concentration also using SlideWrite.

cDNA Synthesis, Cloning, and Nucleotide Sequencing of Antibody Variable Region Genes. Total RNA was prepared from 5×10^6 hybridoma cells grown in tissue culture flasks using an RNA isolation and purification kit from Qiagen (Santa Clarita, CA) according to the manufacturer's protocol. First-strand cDNA was prepared from total RNA using poly A primers in the First-Strand cDNA Synthesis Kit from GIBCO/BRL (Gaithersburg, MD). The cDNA encoding the light- and heavy-chain variable regions of the 2C12 monoclonal antibody were specifically amplified by polymerase chain reaction (PCR) using the primer sets in the Mouse single-chain variable fragment (ScFv) Module/Recombinant Phage Antibody System (Pharmacia Biotech, Piscataway, NJ) and Taq DNA polymerase (Promega, Madison, WI). The PCR products were visualized by electrophoresis on 1.5% agarose gels containing 0.5 μg/mL ethidium bromide. The PCR products were ligated into the pCR 2.1 plasmid vector from TA Cloning Kit (Invitrogen, San Diego, CA). *Escherichia coli* INVαF′ cells were transformed with either light- or heavy-chain plasmid. Blue/white screening method was used to select possible transformants. Plasmids were isolated after alkaline lysis of bacterial cells and the presence of appropriately sized insert was confirmed by EcoR1 restriction endonuclease digestion. Plasmid DNA was sequenced in an institutional facility using a model 373A Automated Sequencer from Applied Biosystems (Foster City, CA). The variable light- and heavy-chain sequences were aligned to the Kabat numbering scheme and scanned against the Kabat sequence database using the software interface developed by Martin (*25*).

RESULTS

Design of Antigen and Animal Response. The Pb(II)−chelate complexes of interest in this study were of insufficient size to elicit an immune response; therefore, a Pb(II)-loaded chelate covalently linked to a carrier protein was used as an immunogen. To increase the likelihood of inducing Pb(II)-specific antibodies, a hapten-

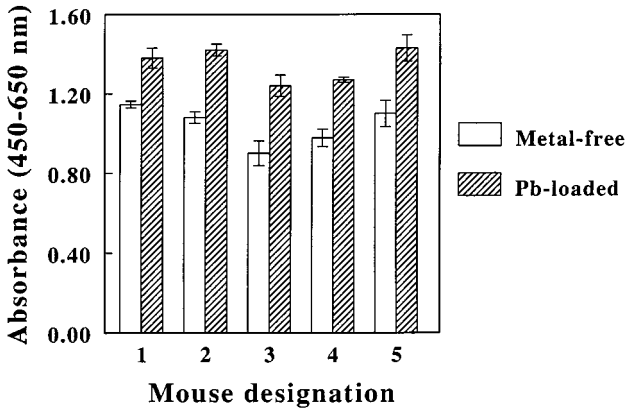

Figure 1. Serum reactivity of BALB/c mice injected with Pb(II)-CHXDTPA-benzyl-KLH. Blood was collected from the tail vein of each mouse, and the resulting serum was serially diluted into PBS + 1% BSA. The polyclonal antibody response to immobilized metal-free CHXDTPA-benzyl-BSA and Pb(II)-CHXDTPA-benzyl-BSA was determined at a point in the serial dilution series approximately halfway between the maximum and minimum absorbance as determined by indirect ELISA (*22*). Serum dilutions used for mouse 1, 2, 3, 4, and 5 were 1/40000, 1/40000, 1/64000, 1/20000, and 1/20000, respectively.

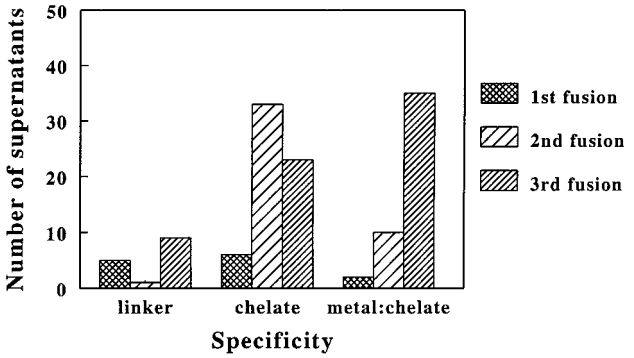

Figure 2. Screening of culture supernatants for antibodies to metal−chelate complexes. Tissue culture supernatants that had passed a preliminary screen were assessed by competitive ELISA to determine the binding characteristics of the antibodies contained therein. Of the 124 culture supernatants subjected to this screening assay, 15 contained linker-specific antibodies, 62 had antibodies directed toward the chelator, and 47 showed some preferential binding for metal-DTPA complexes.

carrier conjugate was sought that would retain Pb(II) in the chelate complex during antigen processing and presentation in vivo. The choice of the CHXDTPA-benzyl-protein conjugate employed in this study was based on the superior ability of this chelate−protein conjugate to retain its metal ion upon intravenous injection into nude mice (*26*). The conjugate was used to immunize the BALB/c mice and the presence of antibodies in the sera directed toward the Pb(II)−chelator complex was assessed by indirect ELISA, as shown in Figure 1. Sera from all five mice showed preferential reactivity toward the Pb(II)-loaded conjugate; mouse 3 was given an additional intraperitoneal injection with Pb(II)-CHXDTPA-KLH in PBS and the spleen was used 72 h later in the preparation of hybridoma cells.

Hybridoma Screening. The hybridomas generated after fusion with myeloma cells were initially screened by indirect ELISA for their ability to bind to Pb(II)-CHXDTPA-benzyl-BSA. Culture supernatants from hybridomas that passed the initial screen were subsequently tested for antibody specificity. Although antibodies with specificity for the metal−chelate complex were detected in the first fusion, the cells secreting these antibodies did not survive subsequent subculture; in total, three fusions were performed to generate the stable hybridoma (2C12) reported in these studies.

The preliminary screen of 1015 tissue culture supernantants from the three fusions yielded 124 clones which bound to immobilized Pb(II)-CHXDTPA-benzyl-BSA. The supernatants were subsequently screened by competitive ELISA to determine antibody specificity, as shown in Figure 2. Culture supernatants whose binding could not be competed with either metal-free DTPA or metal−DTPA complexes were assumed to contain antibodies with a primary specificity for the benzyl group in the linker region of the conjugate. Supernatants whose binding was inhibited equally by metal-free DTPA and metal DTPA complexes were assumed to contain chelate-specific antibodies. Those antibodies whose binding was more strongly inhibited by a metal−chelate complex than by metal-free DTPA were assumed to have preferential affinity for the metal−chelate complex. Of the 124 culture supernatants tested by competitive ELISA, 15 contained linker-specific antibodies, 62 had antibodies directed toward the chelator, and 47 showed some preferential binding for metal−DTPA complexes. Very few of these 47 clones, however, showed any specificity for Pb(II)-chelate complexes. Upon limiting dilution of a clone that did exhibit preferential binding for Pb(II), a hybridoma (2C12) was established. The 2C12 hybridoma synthesized a monoclonal antibody of the IgG1 subtype with a κ light chain. Ascites from this clone was produced and purified to obtain large amounts of antibody for subsequent characterization. The purified protein had an IgG1 content of 1.56 mg/mL and a protein content of 1.58 mg/mL.

Binding Specificity. The binding specificity of the 2C12 monoclonal antibody was investigated by conducting equilibrium binding measurements on a KinExA immunoassay instrument. Briefly, the KinExA is a flow spectrofluorimeter designed to achieve the rapid separation and quantification of free, unbound antibody present in reaction mixtures of antibody, antigen, and antibody−antigen complexes (*15*, *23*, *24*). Uniform particles were absorption-coated with Pb(II)-CHXDTPA-benzyl-BSA and deposited in the flow/observation cell. This immobilized Pb(II)-CHXDTPA-benzyl-BSA was exploited to capture those 2C12 antibodies with unoccupied binding sites in a reaction mixture. After percolation of each equilibrium reaction mixture through the packed bed of coated beads under negative pressure, quantification of the 2C12 antibody thus captured was achieved by exposure of the particles to a Cy3-labeled goat anti-mouse secondary antibody, followed by measurement of the resulting fluorescence from the particles after the removal of excess unbound secondary antibody. Thus, the binding characteristics determined using this instrument were those of the soluble reactants in homogeneous solution, and the immobilized antigen was simply a tool to affect the capture and subsequent quantification of unbound antibody remaining in solution mixtures.

The structure of the chelator had an influence on the affinity of the 2C12 monoclonal antibody. Figure 3 shows the structures and corresponding equilibrium dissociation constants determined for the binding of six different metal-free chelators to the antibody. The structure of the original immunogen in its metal-free state, also given in Figure 3, can be arbitrarily divided into three regions: a benzyl portion that links the chelator to the protein, a cyclohexyl portion, and the DTPA portion. The positive influence of each of these three regions on the binding of the metal-free chelator to the antibody is evident. The

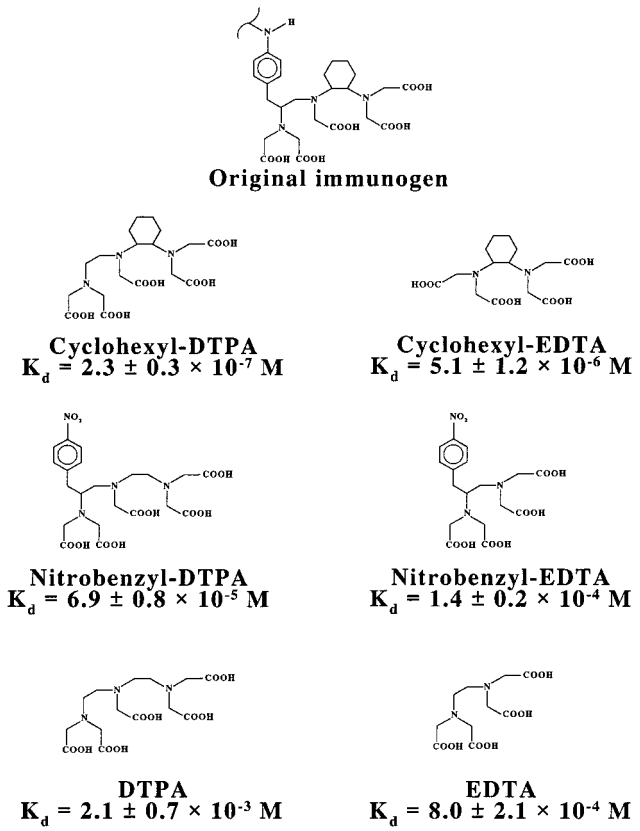

Figure 3. Effect of chelator structure on the binding of the metal-free chelator to monoclonal antibody 2C12. Equilibrium dissociation constants were determined with a KinExA immunoassay system. The value of each dissociation constant represents binding measurements conducted with a minimum of eight different concentrations of the metal-free chelator distributed over a range that spanned the binding isotherm from 10 to 90% saturation.

antibody bound with lowest affinity to metal-free DTPA and EDTA, with K_d's of 2.1×10^{-3} and 8.0×10^{-4} M, respectively. Addition of a *p*-nitrobenzyl group to the chelate structure of DTPA increased the binding affinity 30-fold over that for DTPA alone; addition of the same group to EDTA increased the affinity 5.7-fold over that for EDTA alone. Addition of a cyclohexyl group to each chelator had an even greater effect: CHXDTPA bound to the 2C12 antibody 9100-fold more tightly than did DTPA, while CHXDTPA bound 160-fold better than EDTA.

The structure of the chelator also had an influence on the metal ion specificity exhibited by the 2C12 antibody. When Pb(II) was added to EDTA, the affinity of the antibody for the resulting complex actually decreased to the point where a reliable value for the K_d of the Pb(II)−EDTA complex could not be determined (data not shown). Similarly, the antibody's affinity for the Pb(II)−CHXEDTA complex (2.1×10^{-5} M) was approximately 4-fold lower than that determined for metal-free CHXEDTA (as shown in Table 1). In contrast, the affinity of 2C12 for DTPA increased by several orders of magnitude in the presence of Pb(II) and Ca(II). The equilibrium binding data shown in Figure 4 were obtained by amending reaction mixtures of the antibody and 500 μM metal-free DTPA with varying concentrations of either Ca(II) or Pb(II). Binding of either metal ion to the antibody in the absence of DTPA could not be detected with the KinExA system at concentrations of divalent metal ion up to 500 μM. The binding curves shown in Figure 4 were thus considered to represent the interaction of the

Table 1. Binding of Chelators and Chelated Metals to 2C12 Antibody[a]

ligand	equilibrium dissociation constant (M)
CHXEDTA complexes	
metal-free	$(5.1 \pm 1.2) \times 10^{-6}$
Pb(II)	$(2.1 \pm 0.2) \times 10^{-5}$
DTPA complexes	
metal-free	$(2.1 \pm 0.7) \times 10^{-3}$
Ca(II)	$(2.8 \pm 0.3) \times 10^{-6}$
Pb(II)	$(1.0 \pm 0.1) \times 10^{-5}$
Hg(II)	$(4.8 \pm 0.5) \times 10^{-5}$
Cd(II)	$(1.3 \pm 0.2) \times 10^{-4}$
CHXDTPA complexes	
metal-free	$(2.1 \pm 0.7) \times 10^{-7}$
Pb(II)	$(8.4 \pm 0.5) \times 10^{-9}$
phenyl-Pb(IV)	$(1.3 \pm 0.1) \times 10^{-8}$
diethyl-Pb(IV)	$(1.6 \pm 0.1) \times 10^{-8}$
CHXDTPA-benzyl-BSA complex	
Pb(II)	$(1.7 \pm 0.1) \times 10^{-9}$

[a] Equilibrium dissociation constants were determined as described in the Experimental Procedures. Refer to Figure 3 for structures of the chelators.

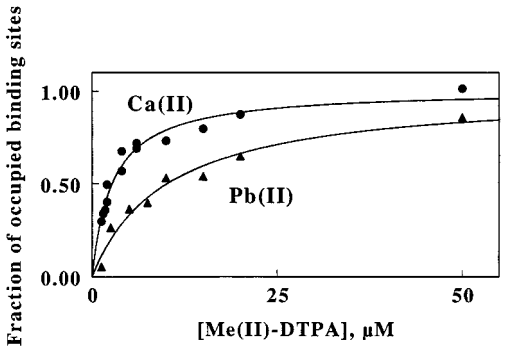

Figure 4. Effect of ionic calcium (circles) and lead (triangles) on the equilibrium binding of DTPA to the 2C12 monoclonal antibody. Antibody (1.5 nM in binding sites) and metal-DTPA complexes were incubated for ≥20 min before separation of the antibody into bound and free fractions. The concentration of total DTPA was 500 μM in all experiments. The curves drawn through the data points were generated using a one-site homogeneous binding model and the corresponding values for the dissociation constants are given in Table 1.

antibody with the corresponding metal−DTPA complexes. The value of the equilibrium dissociation constant, K_d, for each metal−DTPA complex was obtained from a nonlinear regression fit of the data to the following rectangular hyperbole:

$$\text{fraction of occupied binding sites} = [L]/(K_d + [L]) \quad (1)$$

where [L] represents the free ligand concentration. Values for the dissociation constants thus obtained are given in Table 1. The DTPA complexes of Cd(II) and Hg(II) also bound to the 2C12 antibody with greater affinity than that of the metal-free DTPA; values for the dissociation constants for these latter two complexes are also included in Table 1. The DTPA complexes of Mg(II), Ni(II), and Cu(II) bound to the 2C12 antibody with affinities equal to or less than that of the metal-free DTPA. The same trend in relative metal ion reactivity was observed in corresponding competitive ELISAs conducted with metal−DTPA complexes in the soluble phase and Pb(II)-CHXDTPA-benzyl-BSA as the immobilized ligand (data not shown).

When CHXDTPA was substituted for DTPA in solution, Pb(II) was the only cation tested that increased the

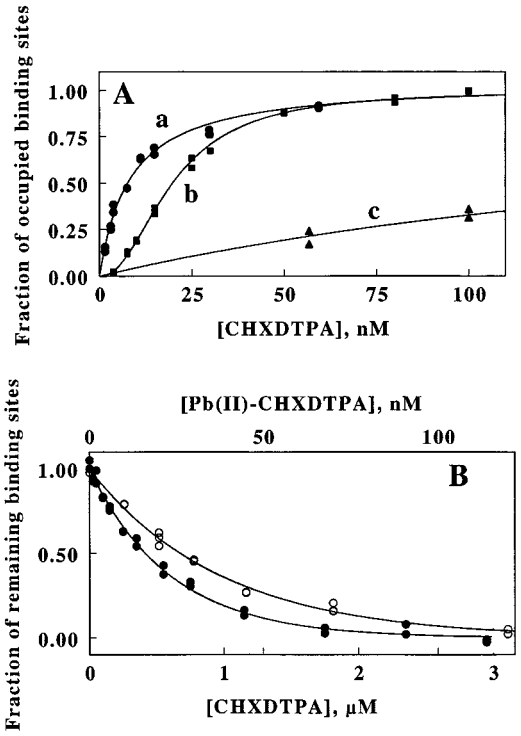

Figure 5. Effect of ionic lead on the binding of CHXDTPA to monoclonal antibody 2C12. (A) Equilibrium data for the binding of CHXDTPA to 2C12 when the concentration of ionic lead was in molar excess (1.0 μM) to that of CHXDTPA (a, circles), equimolar to that of CHXDTPA (b, squares), or zero (c, triangles). The parameters for the curves drawn through the data points were determined by nonlinear regression fits of the data to eq 1 (curves a and c) or 2 (curve b) in the text. (B) Determination of association rate constants for the bimolecular combination of Pb(II)-CHXDTPA (open circles, upper *x*-axis) and metal-free CHXDTPA (closed circles, lower *x*-axis) with the 2C12 monoclonal antibody. Antibody (2.0 nM in binding sites) and CHXDTPA ± 1.0 μM Pb(II) were incubated for 7 s before separation of the antibody into bound and free fractions. The curves drawn through the data points were generated using a single-exponential function of time and ligand concentration and values for the association rate constants given in Table 2. Data in the two sets were normalized to facilitate a comparison of the curves. Each determination in *A* and *B* was performed in duplicate or triplicate; in some cases the error in the data was less than the diameter of the plotted points.

affinity of the 2C12 antibody for the chelator. Equilibrium binding data are shown in Figure 5A for the interaction of CHXDTPA with antibody 2C12 in the absence (curve c) and the presence of equimolar (curve b) or excess (curve a) Pb(II). The parameters for the sigmoidal curve drawn through the data points obtained in the presence of equimolar Pb(II) and CHXDTPA were obtained from a nonlinear regression fit of the data to the following equation:

$$\text{fraction of occupied binding sites} = \frac{[\text{L}]^n}{(K_{0.5})^n + [\text{L}]^n} \quad (2)$$

where n is a number greater than 1.0 and $K_{0.5}$ is the concentration of CHXDTPA that resulted in occupancy of half of the available antibody-binding sites. A value of $K_{0.5}$ equal to 19.8 ± 0.3 nM and of n equal to 2.1 ± 0.1 produced the best fit of the regression line to the data. This nonhyperbolic dependence of the binding site occupancy as a function of ligand concentration was consistent with the hypotheses that (i) only the Pb(II)−CHXDTPA complex bound with the highest affinity to the antibody and (ii) dissociation of the Pb(II) from the Pb(II)−CHXDTPA complex occurred over the same concentration range as that employed in the antibody-binding study. If that were the case, the ligand concentration term in eq 1 would be replaced with [CHXDTPA]-[Pb(II)]/K_{chel}, where K_{chel} is the dissociation constant for the Pb(II)−CHXDTPA complex. Under the experimental conditions that existed for curve b in Figure 5A, where [CHXDTPA] = [Pb(II)], this model predicts the value of n to be 2; the value determined experimentally was 2.1 ± 0.1. To further test this hypothesis, the binding of CHXDTPA to the 2C12 antibody was determined in the presence of a 10−1000-fold molar excess of Pb(II) (curve a). Control experiments conducted in the absence of CHXDTPA established that high concentrations of Pb(II) did not compete with immobilized ligand for the 2C12 antibody (data not shown). The excess of Pb(II) ensured that all of the CHXDTPA would be present as the lead complex. Under these conditions, one would predict that the sigmoidal curve described by eq 2 would revert to the hyperbolic curve described by eq 1, with a value for K_d less than that of $K_{0.5}$. The data in Figure 5A were consistent with this prediction. The value of 8.4×10^{-9} M for the concentration of half-maximal occupancy extracted from curve a in Figure 5*A* is thus the true K_d for dissociation of the Pb(II)−CHXDTPA complex from the antibody. The value of $K_{0.5}$ extracted from curve b is simply equal to the product of $K_d \times K_{chel}$; a value of $K_{chel} = 2.4 \times 10^{-9}$ M was calculated from the experimental data for the dissociation of Pb(II) from its complex with DTPA.

The CHXDTPA complexes of a variety of other metal cations bound to the 2C12 antibody with affinities indistinguishable from that of the metal-free CHXDTPA. The metal cations investigated were as follows: Ca(II), Mg(II), Mn(II), Cd(II), Hg(II), Ni(II), Cu(II), Zn(II), U(VI), Au(III), Sn(IV), Ag(I), Ga(III), In(III), and Fe(III). For all practical purposes, the 2C12 antibody exhibited an absolute specificity for Pb(II) when the soluble chelator was CHXDTPA.

Organolead compounds also bound to the 2C12 antibody with high affinities when the chelator was CHXDTPA. Values for the equilibrium dissociation constants were obtained as described and are summarized in Table 1. The CHXDTPA complex of each organolead compound bound to the antibody with an affinity that was only slightly less than that of the CHXDTPA−Pb(II) complex. The organic portion of the lead compound (diethyl versus phenyl) had a negligible influence on the value of the equilibrium dissociation constant.

Rate constants for the interaction of CHXDTPA with 2C12 in the presence and absence of Pb(II) were also obtained with the KinExA instrument. Instead of exposing an equilibrium mixture of the binding partners to the immobilized antigen on the beads, the unbound antibody remaining in reaction mixtures far from equilibrium was separated and quantified to achieve a kinetic analysis of the binding reaction. A solution of the monoclonal antibody was injected into and mixed with a stream of ligand that reacted for 7 s before the mixture encountered the packed beads. The extent of reaction was controlled by varying the concentration of the reagent in excess, the chelator in the absence or presence of Pb(II). Figure 5B shows the dependence of the fraction of antibody binding sites remaining at 7 s after mixing on the concentration of either metal-free CHXDTPA or Pb(II)−CHXDTPA. A single-exponential function of time and ligand concentration was fit to each set of data:

$$A = A_0 e^{-k_{obs}t} \quad (3)$$

where A is the concentration of remaining antibody binding sites at ligand concentration [L], A_0 is the concentration of binding sites when no ligand is present, t is 7 s, and k_{obs} is the observed pseudo-first-order rate constant for the concentration-dependent change. The value of k_{obs} equals $k_1[L] + k_2$ for the reversible bimolecular combination of an antibody with a molar excess of antigen, where k_1 and k_2 are the bimolecular association and unimolecular dissociation rate constants, respectively. Since time was fixed in these experiments at 7 s, the k_2t term in the argument of the exponent became a constant that could be separated mathematically, and the k_{obs} term in eq 3 reduced to $k_1[L]t$. A value for each association rate constant was thus obtained from the nonlinear regression fit of an exponential curve to each data set in Figure 5B. Values for the corresponding unimolecular dissociation rate constants were subsequently obtained for each binding reaction from the identity $K_d = k_2/k_1$. Kinetic constants for the binding of metal-free CHXDTPA and Pb(II)−CHXDTPA to the 2C12 monoclonal antibody are summarized in Table 2. The Pb(II)−CHXDTPA complex bound approximately 10-fold more rapidly to the antibody than did the metal-free complex, while the respective rates of dissociation from the antibody were minimally affected by the presence of Pb(II). The apparent increase in the affinity of the antibody for Pb(II)-CHXDTPA over that for the metal-free chelator is thus due primarily to an increase in the bimolecular association rate constant for binding of the Pb(II)-laden chelator.

Prototype Immunoassays for Pb(II). The wide range of equilibrium dissociation constants exhibited by the antibody for Pb(II)−chelator complexes with different structures suggested that immunoassays with differing sensitivities for ionic lead could be assembled that would be capable of spanning a broad range of analyte concentrations. Three examples of such immunoassays purposefully constructed to modulate the sensitivity of the assay are shown in Figure 6. Curve a in Figure 6A represents an antigen inhibition ELISA for Pb(II) conducted with DTPA as the soluble chelator and a Pb(II)−CHXDTPA-benzyl-BSA conjugate as the immobilized ligand. Since the immobilized ligand bound to the 2C12 antibody with approximately 4 orders of magnitude greater affinity than did the soluble Pb(II)−DTPA, this immunoassay was expected to be the least sensitive to soluble Pb(II). As anticipated, the effective range of this immunoassay was from approximately 10 μM to 1.0 mM. The sensitivity of the immunoassay could be increased either (i) by decreasing the competitiveness of the ligand on the solid phase or (ii) by increasing the competitiveness of the ligand in the soluble phase. Curve b in Figure 6A is an example of the former strategy. Curve b shows another antigen inhibition ELISA where the weaker binding Pb(II)-DTPA-BSA conjugate was substituted for Pb(II)−CHXDTPA on the solid phase. Removal of the cyclohexyl portion of the ligand on the solid phase increased the sensitivity of the immunoassay by approximately an order of magnitude. Figure 6B shows an example of the latter strategy, wherein CHXDTPA is utilized as the chelator for soluble Pb(II). The standard curve in Figure 6B represents a competitive immunoassay conducted on the KinExA where the high-affinity Pb(II)−CHXDTPA was substituted for the low affinity Pb(II)−DTPA in the soluble phase. The standard curve gave a linear response over the range 1.0 to 10 nM (approximately 0.2 to 2.0 ppb) in ionic lead, an assay sensitivity sufficient for measurement of relevant Pb(II) concentrations in drinking water samples (*27*).

Table 2. Effect of Pb(II) on Interaction of 2C12 Antibody with CHXDTPA[a]

CHXDTPA complex	association rate constant ($M^{-1}s^{-1}$)	dissociation rate constant (s^{-1})
metal-free	$(2.4 \pm 0.1) \times 10^5$	$(5.5 \pm 0.6) \times 10^{-2}$
Pb(II)	$(3.8 \pm 0.2) \times 10^6$	$(3.2 \pm 0.3) \times 10^{-2}$

[a] Association rate constants were determined as described in the Experimental Procedures. Values for the dissociation rate constants were obtained by calculation from the association rate constant and the K_d. Refer to Figure 3 for the structure of CHXDTPA.

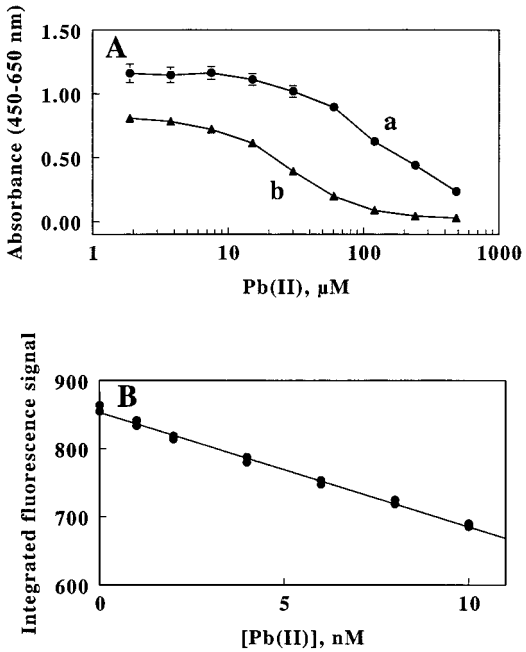

Figure 6. Effect of assay format on the sensitivity of immunoassays for ionic lead using monoclonal antibody 2C12. (A) Competitive ELISA with covalent conjugates of Pb(II)-CHXDTPA-benzyl-BSA (a, circles) or Pb(II)-DTPA-BSA (b, triangles) as the immobilized ligand. The final antibody concentration was 0.1 μg/mL and the soluble phase was DTPA (1.0 mM in HBS + 1% BSA) in the presence of the indicated concentrations of Pb(II). (B) Competitive immunoassay performed on the KinExA. The immobilized ligand was a covalent conjugate of Pb(II)-CHXDTPA-benzyl-BSA. Different concentrations of Pb(II) were diluted into 125 nM CHXDTPA and incubated with the 2C12 antibody (1.5 nM final concentration in binding sites). Unliganded 2C12 antibody subsequently captured by the immobilized ligand was quantified with a goat anti-mouse polyclonal antibody conjugated with Cy3.

Cloning and Nucleotide Sequencing. A histidine residue in the third complementarity-determining region of the heavy chain has been implicated in metal ion coordination of three different monoclonal antibodies directed toward metal−chelate complexes (*12*, *13*, *15*). It was of interest, therefore, to determine if a similar histidine coordination was possible in the binding of Pb(II)−chelate complexes by the 2C12 antibody. Primers for the light- and heavy-chain variable regions of mouse IgG were utilized with cDNA from the 2C12 hybridoma to obtain PCR products of the correct molecular size, which were subsequently cloned and sequenced. The nucleic acid sequences and deduced amino acid sequences of the variable regions of the light- and heavy-chain are shown in Figures 7 and 8, respectively. Numbering of the amino acids is according to the Kabat system (*28*), and complementarity-determining regions (CDRs) are shown

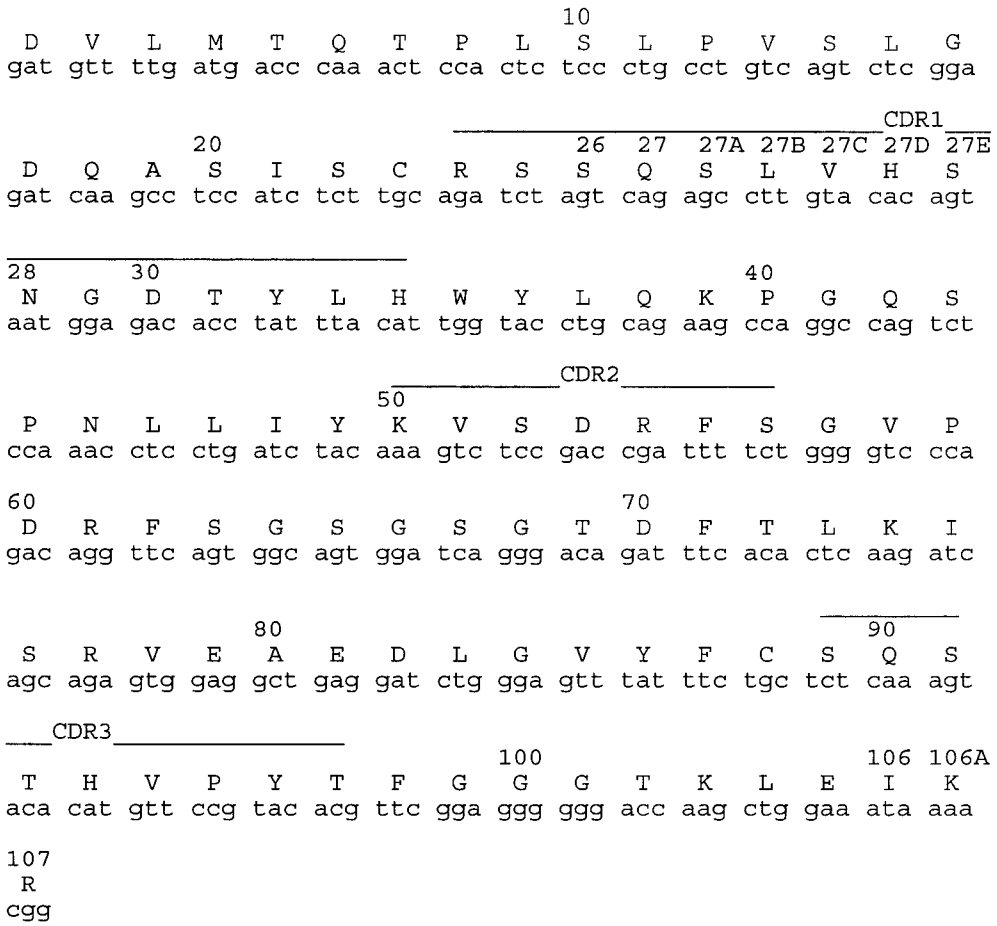

Figure 7. Nucleotide and deduced amino acid sequence of 2C12 light chain variable region. The numbering scheme is according to Kabat (*28*), and the CDR regions are indicated by a line over the one-letter amino acid code.

as a line over the appropriate amino acid sequences. The light chain of the 2C12 antibody utilized a V segment of the V_κ Group II subgroup and a $J_\kappa 2$ gene segment; the heavy chain utilized a member of the $V_H 2$ gene family and a $J_H 1$ gene segment. The heavy-chain D segment DFL16.1 was used in reading frame 1.

DISCUSSION

These studies describe the isolation and binding properties of 2C12, the first monoclonal antibody reported to show a preferential affinity for chelated complexes of Pb(II). In contrast to previously reported antibodies (CHA255 and 2A81G5) that showed little or no recognition of metal-free chelator (*11*, *15*, *22*), the 2C12 antibody had the ability to recognize features of several structurally related chelators, both in their metal-loaded and metal-free forms. The immunizing ligand used in the present study contains two different hydrophobic regions, a benzyl group in the linking region and a rigid, cyclohexylene bridge that holds the two $N(CH_2CO_2H)_2$ chelate groups in a mutually cis arrangement (*29*). A comparison of antibody affinity for metal-free DTPA, *p*-nitrobenzyl-DTPA and CHXDTPA indicates that the cyclohexylene bridge is much more important for antibody recognition than is the benzyl group in the linking region; addition of a benzyl group to the DTPA structure increased antibody affinity by 30-fold while addition of the cyclohexylene bridge increased affinity by 9100-fold. A similar, albeit less dramatic trend was seen for EDTA-based chelators.

In the metal-free state, both EDTA and DTPA exhibit a great deal of flexibility, and it is not surprising that the 2C12 antibody does not discriminate between them (*30*). Once metal is bound to these chelators, however, they exhibit quite different geometries. EDTA forms hexacoordinate complexes with most metal cations (*30*) while DTPA and CHXDTPA appear to form octacoordinate complexes (*29*, *31*). Complexation of Pb(II) with EDTA-based chelators decreased the equilibrium-binding affinity of the antibody for the complexes, while complexation of Pb(II) to the DTPA-based chelators increased affinity. In addition, the kinetic data presented herein demonstrated that the enhanced recognition of the Pb(II)−CHXDTPA complex over the metal-free chelator was due to an increased association rate constant with little effect on the dissociation rate constant. If the antibody interacted directly with the metal ion in the chelate complex, the observed dissociation rate constant would be expected to decrease, assuming that other recognition elements in the chelator were unperturbed. Instead, the Pb(II)-dependent increase in the association rate constant implies that the antibody may recognize a specific conformation of the chelator induced by the metal ion. This specific conformation may be a small subset of the total conformations available to metal-free CHXDTPA. Thus, the differential effect of Pb(II) on the binding affinity may reflect the antibody's preference for those metal−chelate complexes that show a particular octacoordinate geometry. Unfortunately, no crystal structures or NMR data exist for Pb(II)−DTPA or Pb(II)−CHXDTPA complexes, and such studies will be required to determine if the coordinate geometry of the metal−chelate complex is responsible for the differential affinity

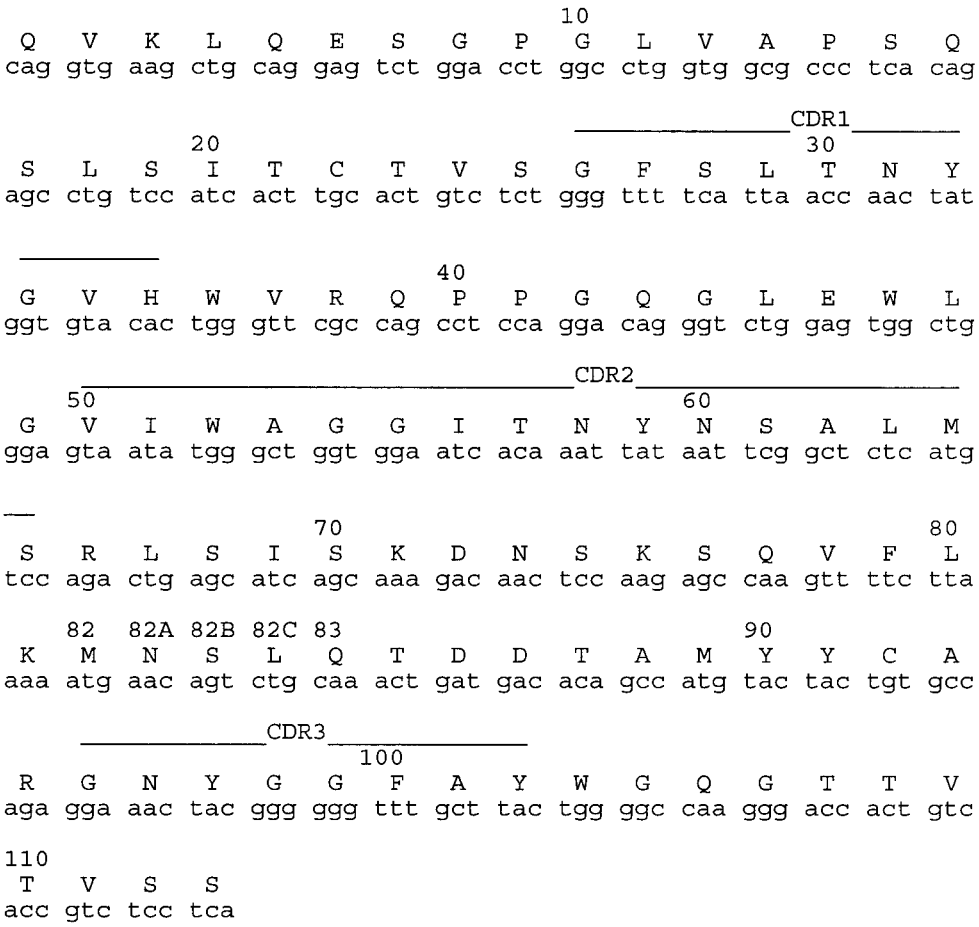

Figure 8. Nucleotide and deduced amino acid sequence of the 2C12 heavy-chain variable region. The numbering scheme is according to Kabat (*28*) and the complementarity determining regions (CDR) are indicated by a line over the one-letter amino acid code.

the 2C12 antibody shows for Pb(II)-loaded versus Pb(II)-free chelators.

In previous studies with antibodies directed toward metal−chelate complexes, a histidine in the third complementarity determining region (CDR3) of the heavy chain was implicated in metal ion recognition (*12*, *15*). However, cloning and sequencing of 2C12 showed that there are no histidine residues in the heavy-chain CDR3 of this antibody; therefore, amino acid side chains other than a histidine in this position must be participating in recognition of the Pb(II)−chelate complexes. Almost half of the 20 commonly occurring amino acids have been shown to participate in metal ion ligation in proteins, and there is an abundant literature on protein interactions with metals that participate in catalytic cycles (for reviews, see refs *32*−*34*). However, much less is known about how proteins may interact with Pb(II). Barbas et al. isolated antibody fragments that recognized metals [including Pb(II)] in complex with iminodiacetic acid by screening a recombinant library with randomized amino acids in the third CDR of the heavy chain (*35*, *36*). Sequence analysis of the selected CDRs revealed that histidine in CDR3 appeared to confer binding selectivity for Cu(II), Ni(II), or Zn(II); one Cu(II)-specific clone was enriched for tryptophan. These authors also reported antibodies with some selectivity for Pb(II). Although they could not identify specific amino acids residues in the CDR that were responsible for Pb(II) ligation, they did note that the CDRs of Pb(II) selective antibodies were slightly enriched in glutamate and aspartate (10% of total amino acids compared to 4−7% in Cu(II), Ce(II), and Fe(III) selective clones), and in serine, threonine, and tyrosine [18% in Pb(II) and Ce(III) selective clones, 11−9% in other clones]. In the 2C12 monoclonal antibody reported herein, serine, threonine, and tryosine were found abundantly in the CDRs of both the light and heavy chain (40.6 and 27.3% of CDR amino acids, respectively), and it is highly likely that some of these hydroxyl-containing ligands are participating in antigen recognition. In contrast to the data reported by Barbas (*35*, *36*), aspartate and glutamate were not abundant in the light- and heavy-chain CDRs of 2C12 (6.25 and 0%, of CDR amino acids, respectively), and it seems less likely that the carboxylate functional groups of these residues are participating in the recognition of the Pb(II)−chelate complex.

Structural studies with catalytic metalloantibodies have identified specific resides in the light chain CDRs with the proper orientation for metal ion ligation (L32, L34, L89, and L91) and site-directed mutagenesis to insert histidine at these residues increased the affinity of the antibodies for zinc ions (*37*). In the metalloantibodies under investigation in the previous report, the protein provided all the coordination sites for the metal; this is in contrast to the 2C12 monoclonal reported herein, where the chelator provides most, if not all, of the coordinating ligands. It is interesting to note, however, the presence of a histidine at the L34 position in CDR1 of the 2C12 monoclonal antibody. Future studies are ongoing in the laboratory to ascertain whether this histidine residue and the abundant hydroxylated amino acids in the light- and heavy-chain contribute to the Pb(II) selectivity of the 2C12 antibody.

The 2C12 antibody may provide both the sensitivity and selectivity required for a antibody-based methods for Pb(II) determination, and knowledge of the antibody's binding characteristics have permitted us to construct prototype immunoassays with a wide range of sensitivities. The prototype competitive immunoassays described herein had the ability to quantify Pb(II) over concentrations from 2 nM to 100 μM (0.4 ppb to 20 ppm), depending upon the assay format. Because the antibody exhibits an almost absolute specificity for Pb(II) when the soluble chelator is CHXDTPA, a competitive immunoassay using this chelator would be highly selective for Pb(II). Even though the addition of Pb(II) to the CHXDTPA chelator increased antibody affinity by only 25-fold, careful control of chelator concentration (at its K_d) permitted the construction of a highly sensitive Pb(II) assay (see Figure 6B). When a less sensitive test is desired, it may be advantageous to use commercially available DTPA as the chelator. In assays that utilize DTPA as the soluble complexing agent, there is the potential for interference from calcium ions, because the 2C12 antibody binds to Ca(II)−DTPA complexes with an affinity approximately 3.5-fold greater than that determined for Pb(II)−DTPA. Under conditions when Ca(II) may be present in an environmental sample, reagents that selectively remove Ca(II) from the DTPA-binding equilibrium have proven useful in masking Ca(II) interference.[2] Studies are in progress to further develop 2C12 for antibody-based determinations of lead.

ACKNOWLEDGMENT

This work was supported by grants from Department of Energy (DE-FG01-93EW53023) and the Department of Defense (DSWA01-98-1-0012) to the Tulane-Xavier Center for Bioenvironmental Research.

LITERATURE CITED

(1) Tong, S. (1998) Lead exposure and cognitive development: persistence and a dynamic pattern. *J. Pediatr. Child Health 34*, 114−118.

(2) Rice, D. C. (1996) Behavioral effects of lead: commonalities between experimental and epidemiologic data. *Environ. Health Perspect. 104* (Suppl.) *2*, 337−351.

(3) Winneke, G., Lilienthal, H., and Kramer U. (1996) The neurobehavioural toxicology and teratology of lead. *Arch. Toxicol. Suppl. 18*, 57−70.

(4) Silbergeld, E. K. (1997) Preventing lead poisoning in children. *Annu. Rev. Public Health 18*, 187−210.

(5) Flegal, A. R., and Smith, D. R. (1995) Measurements of environmental lead contamination and human exposure. *Rev. Environ. Contamin. Toxicol. 143*, 1−45.

(6) Sedman, R. M. (1989) The development of applied action levels for soil contact: a scenario for the exposure of humans to soil in a residential setting. *Environ. Health Perspect. 79*, 291−313.

(7) Mielke, H. W., and Reagan, P. L. (1998) Soil is an important pathway of human lead exposure. *Environ. Health Perspect. 106* (Suppl.) *1*, 217−229.

(8) Ballesteros, B., Barcelo, D., Sanchez-Baeza, F., Camps, F., and Marco, M. P. (1998) Influence of the hapten design on the development of a competitive ELISA for the determination of the antifouling agent Irgarol 1051 at trace levels. *Anal. Chem. 70*, 4004−4014.

(9) Fischer, J. B., and Michael, J. L. (1997) Use of ELISA immunoassay kits as a complement to HPLC analysis of imazapyr and triclopyr in water samples from forest watersheds. *Bull. Environ. Contam. Toxicol. 59*, 611−618.

(10) Torres, C. M., Pico, Y., and Manes J. (1996) Determination of pesticide residues in fruit and vegetables. *J. Chromatogr. A 754*, 301−331.

(11) Reardan, D. T., Meares, C. F., Goodwin, D. A., McTigue, M., David, G. S., Stone, M. R., Leung, J. P., Bartholomew, R. M., and Frincke, J. M. (1985) Antibodies against metal chelates. *Nature 316*, 265−268.

(12) Love, R. A., Villafranca, J. E., Aust, R. M., Nakamura, K. K., Jue, R. A., Major, J. G. J., Radhakrishnan, R., and Butler, W. F. (1993) How the anti-(metal chelate) antibody CHA255 is specific for the metal ion of its antigen: X-ray structures for two Fab′/hapten complexes with different metals in the chelate. *Biochemistry 32*, 10950.

(13) Boden, V., Colin, C., Barbet, J., Le Doussal, J. M., and Vijayalakshmi, M. (1995) Complementary approach for the determination of histidine in the metal-binding site of an anti-DTPA-indium monoclonal antibody. *Annals New York Acad. Sci. 750*, 284−287.

(14) Boden, V., Colin, C., Barbet, J., Le Doussal, J. M., and Vijayalakshmi, M. (1995) Preliminary study of the metal binding site of an anti-DTPA-indium antibody by equilibrium binding immunoassays and immobilized metal ion affinity chromatography. *Bioconjugate Chem. 6*, 373−379.

(15) Blake, D. A., Chakrabarti, P., Khosraviani, M., Hatcher, F. M., Westhoff, C. M., Goebel, P., Wylie, D. E., and Blake, R. C., II (1996) Metal binding properties of a monoclonal antibody directed toward metal-chelate complexes. *J. Biol. Chem. 271*, 27677−27685.

(16) Anderson, W. H. K., Reed, J. A., and Pollock, D. K. (1993) Elicitation of a predominantly lambda light chain-bearing antibody response in BALB/c mice to a novel bifunctional aminocarboxylate chelating agent. *Hybridoma 17*, 677−688.

(17) Gillette, R. W., Singleton, J., Janowicz, A., and Gilman, S. C. (1989) Development and characterization of monoclonal antibodies with specificity for metallic radioisotope chelators linked to antibodies and other proteins. *J. Immunol. Methods 124*, 277−282.

(18) Feng, X., Pak, R. H., Kroger, L. A., Moran, J. K., DeNardo, D. G., Meares, CF, DeNardo, G. L., and DeNardo, S. J. (1998) New anti-Cu-TETA and anti-Y-DOTA monoclonal antibodies for potential use in the pre-targeted delivery of radiopharmaceuticals to tumor. *Hybridoma 17*, 125−132.

(19) Brechbiel, M. W., and Gansow, O. A. (1992) Synthesis of C-functionalized *trans*-cyclohexyldiethylenetriaminepentaacetic acids for labeling of monoclonal antibodies with the bismuth-212-particle emitter. *J. Chem. Soc., Perkin Trans. 1*, 1173−1178.

(20) Brechbiel, M. W., Gansow, O. A., Atcher, R. W., Schlom, J., Esteban, J., Simpson, D. E., and Colcher, D. (1986) Synthesis of 1-(*p*-isocyanotobenzyl) derivatives of DTPA and EDTA: Antibody labeling and tumor-imaging studies. *Inorg. Chem. 25*, 2772−2781.

(21) Thiers, R. E. (1957) Contamination in trace element analysis and its control. *Methods Biochem. Anal. 5*, 273−335.

(22) Chakrabarti, P., Hatcher, F. M., Blake, R. C., II, Ladd, P. A., and Blake, D. A. (1994) Enzyme immunoassay to determine heavy metals using antibodies to specific metal-EDTA complexes: optimization and validation of an immunoassay for soluble indium. *Anal. Biochem. 217*, 70−75.

(23) Blake, D. A., Khosraviani, M., Pavlov, A. R., Blake, R. C., II (1997) in *Immunochemical Technology for Environmental Applications* (Aga, D. S., and Thurman, E. M., Eds.) pp 49−60, American Chemical Society, Washington DC.

(24) Blake, R. C., II, Pavlov, A. R., and Blake, D. A. (1999) Kinetic exclusion assays for protein−ligand interactions. *Anal. Biochem. 292*, 123−134.

(25) Martin, A. C. R. (1996) Accessing the Kabat Antibody Sequence Database by Computer. *Proteins: Struct., Funct., Genet. 25*, 130−133.

(26) Camera, L., Kinuya, S., Garmestani, K., Wu, C., Brechbiel, M. W., Pai, L. H., McMurry, T. J., Gansow, O. A., Pastan, I., and Paik, C. H. (1994) Evaluation of the serum stability and in vivo biodistribution of CHX-DTPA and other ligands for yttrium labeling of monoclonal antibodies. *J. Nucl. Med. 35*, 882−889.

[2] Pavlov, A. R., et al. manuscript in preparation.

(27) United States Environmental Protection Agency (1976) *Quality Criteria for Water*, Washington DC.

(28) Kabat, E. A., Wu, T. T., Reid-Miller, M., Perry, H. M., Gottesman, K. S., and Foeller, C. (1991) *Sequences of Proteins of Immunological Interest*, National Institutues of Health, Bethesda, MD.

(29) Brechbiel, M. W., Gansow, O. A., Pippin, C. G., Rogers, R. D., and Planap, R. P. (1996) Preparation of the novel chelating agent N−(2-aminoethyl)-*trans*-1,2-diaminocyclohexane-N,N′, N″-pentaacetic acid (H5CyDTPA), a preorganized analogue of diethylenetriaminepentaacetic acid (H5DTPA), and the structure of Bi(III)(CyDTPA)2 and Bi(III)(H2DTPA) complexes. *Inorg. Chem. 35*, 6343−648.

(30) Margerum, D. W., Cayley, G. R., Weatherburn, D. C., and Pagenkopf, G. K. (1978) in *Coordination Chemistry Monograph 174* (A. E., Martell, Ed.) American Chemical Society, Washington DC.

(31) Maecke, H. R., Riesen, A., and Ritter, W. (1989) The molecular structure of indium-DTPA. *J. Nucl. Med. 30*, 1235−1239.

(32) Glusker, J. P. (1991) in *Advances in Protein Chemistry*, pp 1−76, Academic Press, NY.

(33) Tainer, J. A., Roberts, V. A., and Getzoff, E. D. (1992) Protein metal-binding sites. *Curr. Opin. Biotechnol. 3*, 378−3827

(34) Hellinga, H. W. (1998) The construction of metal centers in proteins by rational design. *Folding Des. 3*, R1−R8.

(35) Barbas, C. F., Bain, J. D., Hoekstra, D. M., and Lerner, R. A. (1992) Semisynthetic combinatorial antibody libraries: a chemical solution to the diversity problem. *Proc. Natl. Acad. Sci. U.S.A. 89*, 4457−4461.

(36) Barbas, C. F., Rosenblum, J. S., and Lerner, R. A. (1993) Direct selection of antibodies that coordinate metals from semisynthetic combinatorial libraries. *Proc. Nat. Acad. Sci U.S.A. 90*, 6385−6389.

(37) Roberts, V. A., Iverson, B. L., Iverson, S. A., Benkovic, S. J., Lerner, R. A., Getzoff, E. D., and Tainer, J. A. (1990) Antibody remodeling: a general solution to the design of a metal-coordination site in an antibody binding pocket. *Proc. Nat. Acad. Sci. 87*, 6654−6658.

BC9901548

TECHNICAL NOTES

Synthesis of Biotinylated Glyfoline for Immunoelectron Microscopic Localization

Tsann-Long Su,*,† Chin-Tarng Lin,‡ Ching-Huang Chen,† and Hue-Ming Huang‡

Institute of Biomedical Sciences, Academia Sinica, Taipei 115, Taiwan, and Institute of Pathology, College of Medicine, National Taiwan University, Taipei 100, Taiwan

Antineoplastic glyfoline (**1**) has potent antitumor efficacy against various murine and human solid tumors. To elucidate the actual mechanism of action, we synthesized biotinylated glyfoline (B-Gly) and used it for the visualization of glyfoline-binding sites in nasopharyngeal carcinoma (NPC) cells. Under the electron microscope (EM), after cells were incubated for 6−36 h, the reaction products of anti-B-Gly were seen on some areas of the external cell surface and on the outer and inner membranes of the mitochondria. Pure EM morphology of NPC cells after glyfoline treatment revealed the similar morphological change of mitochondria. These findings indicate that the binding site of glyfoline in NPC is the inner membrane of the mitochondria, suggesting that B-Gly can be used as a marker for glyfoline localization.

The natural antineoplastic glyfoline (**1**, Figure 1), a 9-acridone alkaloid isolated from *Glycosmis citrifolia*, was previously revealed to have significant antitumor activity both in vitro and in vivo against several murine solid tumors (*1*). Glyfoline does not interact with DNA or with topoisomerases I and II, but is capable of partially inhibiting nucleoside transport across the cell membrane (*2*). Recently, we found most human tumor cells such as leukemia K-256 and nasopharyngeal carcinoma (NPC) tumor cells showed apoptotic change when they were treated with glyfoline (*3*). Moreover, we found that glyfoline may damage tumor cells at the G2/M phase. Hence, the action mechanism of glyfoline is novel and is quite different from other antitumor drugs currently being used in clinical settings.

It is, therefore, of great interest to study the possible action mechanism of glyfoline and its binding site(s) in the glyfoline-treated tumor cells. NPC cell lines developed in our laboratory were used for identification of glyfoline cytotoxic effect and action mechanism. NPC cells showed apoptosis after treatment with 8.8 μM (2 × IC_{50}) glyfoline (*3*). Apoptotic changes were judged by DNA fragmentation, TUNEL, and cytofluorometric analyses. However, no apoptotic gene expression, including ICE-α,β, Bcl-2, Bax, or c-myc genes, were involved, nor did cytokines such as TNF-α appear to induce abnormal expression. Although G2/M phase arrest was identified by FACScan analysis and cytochrome *c* was found to be released from the mitochondria into the cytosol in NPC cells (*4*), the actual target site for glyfoline action remained undetermined.

Glyfoline is a fluorescent compound. When NPC cells were treated with glyfoline, the fluorescent glyfoline was observed surrounding the cell membrane at first and then penetrating into the cytoplasm of the cell under light fluorescent microscope. However, the fluorescence of the agent disappeared within a few minutes. Therefore, in the present experiment, we synthesize biotinylated glyfoline (B-Gly, **2**, Figure 1) and use it for the localization of the glyfoline target site in NPC cells using light and immunoelectron microscopes.

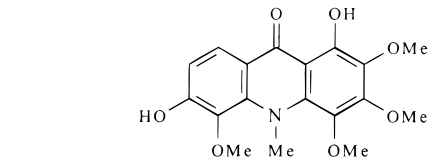

1 Glyfoline

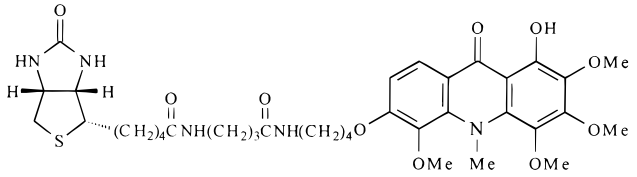

2 Biotinylated Glyfoline (B-Gly)

Figure 1. Chemical structure of glyfoline and biotinylated glyfoline.

The synthetic route to B-Gly (**2**) with a spacer between biotin and glyfoline is illustrated in Scheme 1 (*5*, *6*). By following the procedure developed by Mouton et al. (*7*), the known hydroxysuccinimido biotinate (**3**) (*7*) was treated with 4-aminobutyric acid in dry DMSO containing triethylamine to give 4-(biotinylamido)butyric acid (**4**), which was then reacted with *N*-hydroxysuccinimide and DCC in dry DMSO at room temperature for 2 days to yield *N*-hydroxysuccinimido 4-biotinylamido-butyrate (**5**). Treatment of potassium phthalimide (**6**) with 1,4-

* To whom correspondence should be addressed. Phone: 886-2-2789-9045. Fax: 886-2-2782-7685. E-mail: tlsu@ibms.sinica.edu.tw).

† Institute of Biomedical Sciences.

‡ Institute of Pathology.

10.1021/bc990105v CCC: $19.00 © 2000 American Chemical Society
Published on Web 12/28/1999

Scheme 1 Chemical Synthesis of Biotinylated Glyfoline (2)

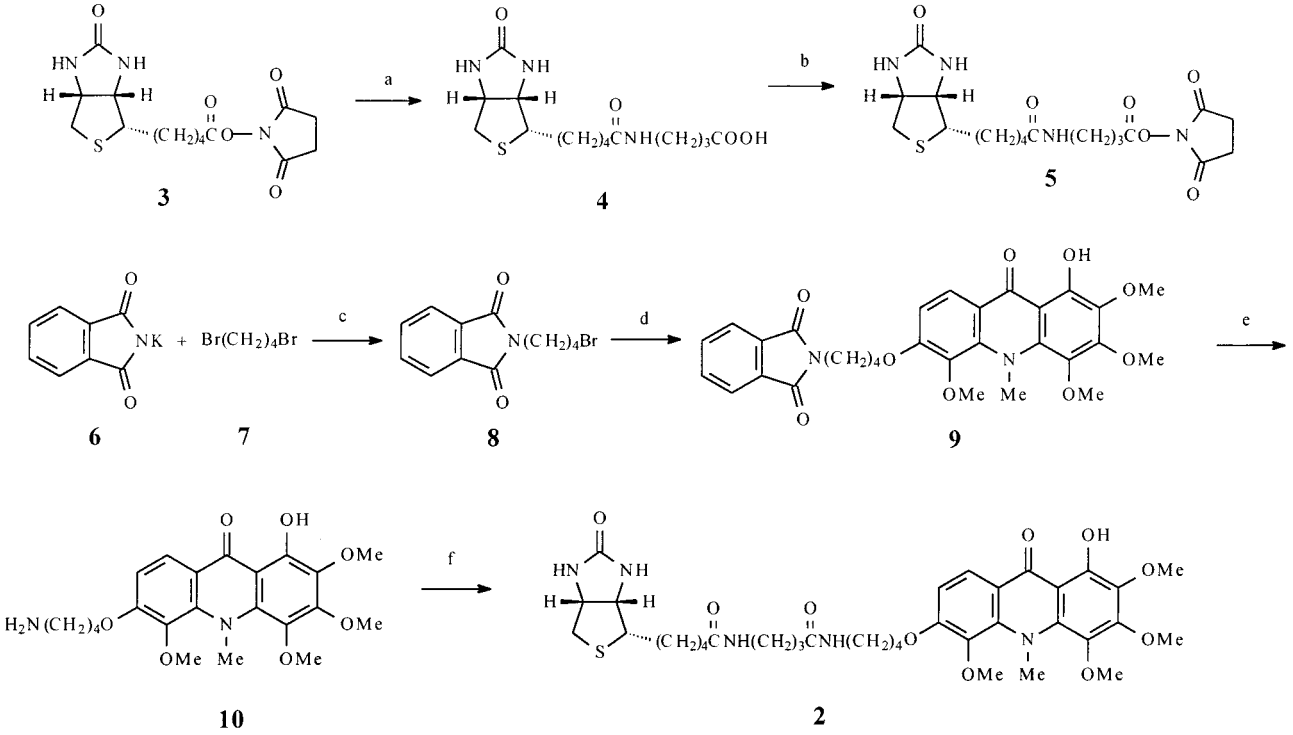

a: 4-aminobutyric acid, Et_3N/DMSO/rt, 6h. 75%; b: DCC/DMSO/rt, 2 days, 50%; c: DMF/reflux, 6h, 57%; d: glyfoline, K_2CO_3/MeCN/reflux, 6h, 84%; e: hydrazine/0 °C, 2h, 65%; f: Et_3N/DMF/rt, 2h, 68%.

dibromobutane (**7**) in dry DMF (30 mL) afforded *N*-(4-bromobutyl)phthalimide (**8**), which was reacted with glyfoline (**1**) in MeCN/K_2CO_3 to give 6-*O*-4-(phthalimido-*N*-yl)butylglyfoline (**9**). The N-protecting function of **9** was removed by treating with hydrazine in an ice-bath to afford 6-*O*-(4-aminobutyl)glyfoline (**10**), which was then condensed with compound **5** to give the desired B-gly (**2**) in good yield.

The chemical properties of the highly specific and very strong binding of biotin to avidin (*9*) provided a technology for the identification of drug's target site(s) in cells even when the compound is present at very low concentrations. Biotin−peptide conjugates were widely used as tools for detecting monoclonal antibody receptors. For example, a polypeptide hormone covalently linked with biotin was incubated with cells and later retrieved by adsorption on immobilized avidin for studies of hormone catabolism and for isolation of hormone−receptor complexes (*10*). However, conjugation of biotin to the chemical agent may change or inhibit the activity of this chemical agent at certain degree. Hoffman et al. (*11*) reported that there is a dramatic effect on the ability of succinylavidin to bind biotinylated insulin. The attachment of the bulky insulin molecule to biotin appears to exert a steric impediment to avidin binding. This suggests that avidin weakens the ability of biotinylinsulin to interact with insulin receptors and that the interference is inversely proportional to the distance between the biotin and insulin. During the course of our study, we also found that there is also an effect of avidin binding to the B-Gly after the B-Gly binds to the cytoplasm of NPC cells. Therefore, we used antibody against biotin to replace the avidin.

NPC cells were treated with B-Gly and used antibody to detect biotin under the light microscope. We observed that the conjugate was found to bind to the cell surface membrane and bind diffusely in the cytoplasm after the first hour of incubation. Within 6 h, the conjugate gradually concentrated in many vesicles. These findings indicate that B-Gly binds to the cell membrane, then enters into the cytoplasm, probably by passive diffusion. After 6−24 h, this phenomenon became more prominent, indicating that a certain specific organelle in the cytoplasm is the target site for glyfoline binding. However, the light microscopic observation cannot clarify the definite target organelle.

The fact that under the electron microscope, in certain tumor cells, electron dense reaction product of anti-B-Gly was seen concentrated in the mitochondria (Figure 2), especially in certain cristae and in the inner membrane, suggests that B-Gly may first bind to the mitochondrial outer membrane and then move to the inner membrane. The inner membranes of the mitochondria, especially the cristae, were bound by B-Gly. Gradual degeneration and formation of myelinated bodies with local disappearance of cristae and loss of the dense granule (calcium apatite) in the matrix of the mitochondria were apparent, suggesting that B-Gly not only binds to the inner membrane of mitochondria, but also causes membrane disintegration that may result in leakage of cytochrome *c* and matrix substance into the cytosol. This increase in the cytosolic fraction then results in activation of the caspase system to induce apoptosis (*13*−*16*). Additionally, the increase of calcium ion concentration in the cytoplasm may help to activate endonuclease, causing DNA condensation and fragmentation and cellular apoptosis. Furthermore, since B-Gly binds to the inner membrane and causes degeneration of the mitochondrial inner membrane, it may induce a decrease in ATP production and activate reactive oxygen species production (*17*), resulting in a hypoxic state of treated cells and subsequent membrane damage. However, it is

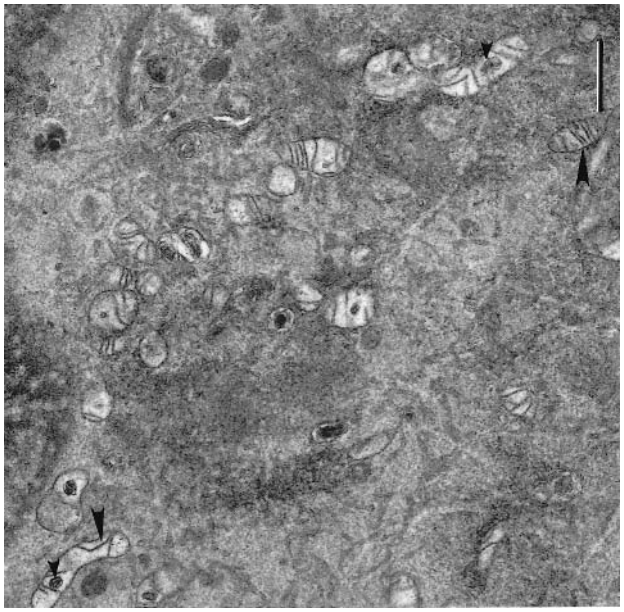

Figure 2. Immunoelectron microscopic localization of B-Gly in NPC cells. NPC-TW06 cells (*12*) were incubated with B-Gly for 48 h and subjected to tissue preparation. Briefly, the NPCs were grown on the Teflon-coated coverslips and fixed in 3% formaldehyde and 1% glutaraldehyde mixture for 15 min and incubated with peroxidase labeled goat antibodies against biotin and then with peroxidase substrate (diaminobenzidine), followed by fixation in 1% OsO_4 and routine electron microscopic procedure. Reaction product of anti-B-Gly is seen on the inner, some outer and cristal membranes of many mitochondria (large arrowheads). Many mitochondria reveal focal degeneration of cristae with dilatation of matrix chambers, which contain some myelinated bodies stained with or without reaction product (small arrowheads). The ground substance and other organelles in the cytoplasm show no specific reaction product.

not known what enzyme or protein at the inner membrane is the major target site for B-Gly. Apparently, the main target site of B-Gly is the mitochondria. This phenomenon is similar to that seen in fluorescent Rhodamine 123 (*18*). For comparison, NPC cells were treated with glyfoline and prepared for routine electron microscopic observation. Results also showed marked alternation of mitochondrial cristal and inner membrane (data not shown) similar to the B-Gly-treated cells. This finding suggested that B-Gly can be used as a marker for glyfoline localization.

In summary, the above new findings suggest that the target site of glyfoline may be the mitochondrial inner membrane. The binding of B-Gly to the mitochondria may be resulted in the release of cytochrome *c* into the cytosol. The damaged mitochondria may also release calcium into the cytosol, produce free radicals, and deprive tumor cell from ATP, any of which would accelerate cellular apoptosis. The mode of action of this agent is quite different from currently available anticancer drugs for chemotherapy, indicating that glyfoline may be a good candidate for antitumor chemotherapy. Currently, we are studying whether glyfoline itself also targets to the mitochondria in NPC cells and releases cytochrome *c* that may induce apoptosis in the tumor cells. The present studies will facilitate to understand a clear action mechanism of glyfoline.

ACKNOWLEDGMENT

This work was supported in part by a program project grant (1997) from the Institute of Biomedical Sciences, Academia Sinica, Taipei, to T.L.S. and C.T.L. and research grants (NSC 86-2314-B-001 to T.L.S.; NSC 86-2314-002-281 to C.T.L.) from National Science Council, Taipei, Taiwan.

LITERATURE CITED

(1) Su, T.-L., Kohler, B., Chou, T. C., Chun, M. W., and Watanabe, K. A. (1992) Synthesis of the Acridone Alkaloids Glyfoline and Congeners. Structure−Activity Relationship Studies of Cytotoxicity Acridones. *J. Med. Chem. 35*, 2703−2710.

(2) Su, T.-L., and Chou, T.-C. (1994) Experimental Antitumor Activity of Acridone Alkaloids, Acronycine and Glyfoline. *Chin. Pharm. 46*, 371−391.

(3) Su, T.-L., Yang, D.-M., Huang, H.-M., Yang, W.-K., Lin, C.-T., and Whang-Peng, J. (1997) Effects of antitumor agent, glyfoline on human cancer cells in vitro. *Proc. Am. Assoc. Cancer Res. 38*, 219.

(4) Huang, H.-M., Su, T.-L., Wu, H.-C., and Lin, C.-T. Unpublished data.

(5) Melting points were determined on a Fargo Melting Apparatus and were uncorrected. Column chromatography was carried out on silica gel G60 (70-230 mesh, ASTM, Merck). Thin-layer chromatography was performed on silica gel $60F_{254}$ (Merck) with short-wavelength UV light for visualization. Element analyses were determined on a Heraeus NCH-Rapid Apparatus. ^{1}H NMR spectra were recorded on a Brucker AMX-400 spectrometer with Me_4Si as the internal standard. Chemical shifts are reported in parts per million (δ), and the signals are described as s (singlet), d (doublet), t (triplet), q (quartet), m (multiplet), br (broad), and brs (broad singlet). Values reported for coupling constants are first order.

(6) Melting point, ^{1}H NMR spectra and elemental analysis of compounds described in the text are follows. Compound **4**: mp 220−221 °C. ^{1}H NMR (DMSO-d_6): δ 1.31, 1.50, 2.06, 2.35 (each 2H, brs, 4 × CH_2), 1.62 (4H, brs, 2 × CH_2), 2.52, 2.60, and 2.82 (each 1H, s, CH), 3.05 (2H, brs, CH_2), 3.10 (1H, s, CH), 4.32, and 12.1 (1H, br exchangeable, COOH). Anal. calcd for $C_{14}H_{23}N_3O_4S$: C, 51.04; H, 7.04; N, 12.76. Found: C, 51.23; H, 6.95; N, 12.65. C. Compound **5**: mp 119−121 °C. ^{1}H NMR (DMSO-d_6): δ 1.29 (2H, br CH_2), 1.49 and 1.58 (4H, m, 2 × CH_2), 1.73 and 2.05 (each 2H, br, 2 × CH_2), 2.57 (1H, s, CH), 2.80 (4H, s, 2 × CH_2), 2.81 (1H, s, CH), 3.02 (4H, br, 2 × CH_2), 4.12 and 4.29 (each 1H, s, CH), 6.34, 6.42, and 7.85 (each 1H, br, exchangeable, 3 × NH). Anal. calcd for $C_{18}H_{26}N_4O_6S$: C, 50.69; H, 6.14; N, 13.14. Found: C, 50.75; H, 6.08; N, 13.26. Compound **8**: mp 73−74 °C. ^{1}H NMR (DMSO-d_6): δ 1.86 (4H, brs 2 × CH_2), 3.45 and 3.78 (each 2H, brs, NCH_2 and $BrCH_2$), 7.71 and 7.85 (each 2H, brs, 4 × ArH). Anal. calcd for $C_{12}H_{12}BrNO_2$: C, 51.08; H, 4.29; N, 4.96. Found: C, 51.20; H, 4.35; N, 5.05. Compound **9**: mp 135−136 °C. ^{1}H NMR (DMSO-d_6): δ 1.98 (4H, brs, 2 × CH_2), 3.46, 3.80 (6H, s, 2 × OMe), 3.87 and 3.90 (each 3H, s, 2 × Me), 4.16 (3H, s, N.-Me), 4.22 (2H, brs, N.-CH_2), 6.96 and 8.08 (each 1H, d, J = 8.0 Hz), 7.74 and 7.78 (each 2H, brs, 4 × ArH), 14.0 (1H, s, OH). Anal. calcd for $C_{30}H_{30}N_2O_9$: C, 64.05; H, 5.38; N, 4.98. Found: C, 64.17; H, 5.43; N, 5.06. Compound **10**: mp 175−176 °C. ^{1}H NMR (DMSO-d_6): δ 1.82 and 1.89 (each 2H, m, 2 × CH_2), 2.89 (2 H, brs, OMe), 3.69, 3.78, 3.81 and 3.84 (each 3H, s, 3 × OMe), 4.22 (3H, s, NMe), 4.40 (2H, s, J = 4.8 Hz, NCH_2), 7.22 and 7.95 (each 1H, d, J = 8.0 Hz, Ar−H), 8.12 (2H, br, exchangeable, NH_2), 14.11 (1H, s, exchangeable, OH). Anal. calcd for $C_{22}H_{28}N_2O_7$: C, 61.10; H, 6.53; N, 6.48. Found: C, 6.21; H, 6.48; N, 6.53. Compound **2**: mp 127−128 6 °C. ^{1}H NMR (DMSO-d_6): δ 1.30 (2H, m, CH_2) 1.5−1.52 (4H, m, 2 × CH_2), 1.65 (6H, m, 3 × CH_2), 1.82 (2H, m, CH_2), 2.07 (4H, m, 2 × CH_2), 2.57 (1H, d, J = 12.3 Hz, CH), 2.81 (1H, dd, J = 5.91 Hz, CH_2) 3.69, 3.75, 3.81, and 3.82 (each 3H, s, 4 × OMe), 4.11 (3H, s, NMe), 4.18 (1H, m, CH), 4.19 (2H, t, J = 5.82 Hz, CH_2), 4.29 (1H, t, J = 4.80 Hz, CH), 7.19 and 7.94 (each 1H, J = 8.0 Hz, 2 × ArH), 7.77 and 7.78 (each 1H, exchangeable 2 × NH), 14.0 (1H, s, exchangeable, OH). Anal. calcd for $C_{39}H_{49}N_5O_{10}S$: C, 56.09; H, 6.80; N, 9.09. Found: C, 56.15; H, 6.94; N, 8.91.

(7) Mouton, C. A., Pang, D., Natraj, C. D., and Shafer, J. A. (1982) A Reagent for Covalently Attaching Biotin to Proteins via a Cleavable Connector Arm. *Arch. Biochem. Biophys. 218*, 101−108.
(8) Lin, C.-T., Chen, C.-C., How, S.-W., Huang, W.-M., and Peck, K. (1992) Localization of HPV-16 DNA Sequence in CaSKi Cells by Electron Microscopic Hybridocytochemistry. *J. Histochem. Cytochem. 40*, 467−478.
(9) Green, N. M. (1975) Avidin. *Adv. Protein Chem. 29*, 85−133.
(10) Hoffman, K., Finn, F. M., Friccsn, H. J. Diaconesou, C., and Zahn, H. (1997) Biotinylinsulins as Potential Tools for Receptor Studies. *Proc. Natl. Acad. Sci. U.S.A. 74*, 2697−2700.
(11) Hofmann, K., Judith, A., Montibeller, J. A., and Finn, F. M. (1982) Avidin Binding of Carboxysubstituted Biotin and Analogues. *Biochemistry 21*, 978−984.
(12) Lin, C. T., Chen, W. Y., Chen, W., Huang, H. W., Wu, H. C., Hsu, M. M., Chuang, S. M., and Wang, C. C (1993) Charaterization of seven newly established nasopharyngeal carcinoma cell lines. *Lab. Invest. 68*, 716−723.
(13) Cai, J., Yang, J., and Jones, D. P. (1998) Mitochondrial Control of Apoptosis: the Role of Cytochrome C. *Biochim. Biophys. Acta 1366*, 139−149.
(14) Allen, R. T., Cluck, M. W., and Agrawal, D. K. (1998) Mechanisms Controlling Cellular Suicide: Role of Bcl-2 and Caspases. *Cell. Mol. Life Sci. 54*, 427−445.
(15) Kroemer, G., Dalloprta B., and Resche-Rigon M. (1998) The Mitochondrial Death/Life Regulator in Apoptosis and Necrosis. *Annu. Rev. Physiol. 60*, 619−642.
(16) Cecconi, F., Alvarez-Bolado, G., Meyer, B. I., Roth, K. A., and Gruss, P. (1998) Apaf1 (CED-4 homolog) Regulates Programmed Cell Death in Mammalian Development. *Cell 94*, 727−737.
(17) Skulachev V. P. (1998) Cytochrome C in the Apoptotic and Antioxidant Cascades. *FEBS Lett. 423*, 275−280.
(18) Bernal, S. D., Lampidis, T. J., Summerhayes, I. C., and Chen, L. B. (1982) Rhodamine-123 Selectively Reduces Clonal Growth of Carcinoma Cells In Vitro. *Science 218*, 117−119.

BC990105V

Solid-Phase Oligonucleotide Synthesis and Flow Cytometric Analysis with Microspheres Encoded with Covalently Attached Fluorophores

Alaganandan Nanthakumar,[†] Richard T. Pon,[‡] Abhijit Mazumder,*[,†] Shuyuan Yu,[‡] and Andrew Watson[†,§]

Axys Pharmaceuticals, 11099 North Torrey Pines Road, Suite 160, La Jolla, California 92037, Department of Biochemistry and Molecular Biology, University of Calgary, Health Sciences Center, 3330 Hospital Drive NW, Calgary, Alberta, Canada T2N 4N1. Received October 25, 1999; Revised Manuscript Received January 12, 2000

A novel combinatorial approach to synthesize oligonucleotides on fluorescently encoded microspheres based on flow sorting and segmental solid-phase synthesis is described. BODIPY dyes were covalently attached to polystyrene (8.8 μm, 55% DVB) microsphere particles to generate four fluorescently encoded sets. 20-mer oligonucleotide sequences can be synthesized on these microspheres with yields comparable to conventional CPG supports (80% overall yield, average stepwise yield = 99%). The concept of segmental solid-phase synthesis by flow sorting was demonstrated by synthesizing unique 20-mer oligonucleotide sequences on each of four fluorescently encoded microsphere sets by including a flow sorting step (after first eight base additions) and flow cytometric detection of sequences synthesized on each microsphere set by hybridization with fluorescently labeled complementary sequence.

INTRODUCTION

Solid-phase methods for the synthesis of oligonucleotides has evolved into a high-throughput automated system and is based on phosphoramidite coupling chemistry (*1*−*4*). Current synthesizers can be programmed to routinely synthesize in the nanomole to micromole scale using porous polystyrene or controlled pore glass (CPG) supports. However, the amount of oligonucleotide synthesized is generally larger than required for most biochemical hybridization assays. The scale of synthesis could be dramatically reduced (to attomoles) by performing oligonucleotide synthesis on a single microsphere (micrometer-sized particles). Typical loading of nonporous microsphere solid supports is ∼1 μmol/g or 100 amol/microsphere. Our approach couples in situ synthesis on microspheres with a combinatorial segmental solid-phase method which was first used with individual paper filter disks as supports (*5*−*8*). However, to synthesize large numbers of oligonucleotide sequences, a rapid method of sorting is required. Efficient sorting of fluorescently encoded microspheres or cells can be achieved using flow cytometric methods. State-of-the-art flow sorters can perform sorting with yields exceeding 90% and purity >99% for a sort rate of 25 000 events/s.

Solid supports having covalently anchored oligonucleotide sequences have been of interest due to potential applications involving multiplexed hybridization assays (*9*, *10*). In situ synthesis of oligonucleotides and hybridization studies have also been performed on glass plates (*11*) derivatized with spacers containing ethylene glycol linkages. Automated in situ oligonucleotide synthesis and hybridization on uniformly sized polymeric microparticles (50 μm) have been previously demonstrated by Lonnberg et al. (*12*−*14*) on linkers stable to ammonolysis deprotection conditions. Another study has reported on synthesis of oligonucleotide combinatorial libraries using a split−pool−combine technique with tentagel (*15*) or polystyrene (*8*) microspheres. We have adopted a similar approach by covalently immobilizing a bifunctional (DMTO/COOH), hydrocarbon linker (**I**) to amino functionalized 8.8 μm, 55% divinylbenzene cross-linked polystyrene microspheres and performing flow sorting to separate mixture of fluorescently encoded microspheres.

Methods to synthesize uniform fluorescent latex particles are well documented in the literature (*16*). However, the methods used are exclusively devoted to applications which are limited to aqueous medium due to the means by which the microspheres are noncovalently labeled with dye. Labeling polymeric microspheres depends on the ability of microspheres to swell in organic solvents, thus allowing incorporation of dye into the interior of particles. Removal of the solvent then allows entrapment of the dye within the microparticles. However, this approach is not feasible for oligo synthesis applications, since nonswelling, rigid polymeric supports (macroporous high cross-linked polystyrene) are required to perform efficient synthesis (*17*). This manuscript also describes an alternate encoding approach by covalently binding functionalized dye molecules to reactive functional groups on the microsphere surface thus allowing nonswelling high cross-linked polystyrene microparticles to be used as fluorescently encoded oligonucleotide synthesis supports. These encoded microspheres are then used in segmental solid phase synthesis with flow sorting to rapidly generate oligonucleotide sequences on a subnanomole scale.

EXPERIMENTAL PROCEDURES

Derivatization of Microspheres. Scheme 1 shows the method adopted to synthesize microspheres with

* To whom correspondence should be addressed. Present address: Motorola Biochip Systems, 4088 Commercial Ave., Northbrook, IL 60062.

[†] Axys Pharmaceuticals.

[‡] University of Calgary.

[§] Present address: Quantum Dot Corporation, 4030 Fabian Way, Palo Alto, CA 94303.

10.1021/bc990145z CCC: $19.00 © 2000 American Chemical Society
Published on Web 02/25/2000

Scheme 1. Synthetic Scheme to Generate Fluorescently Encoded Microspheres Suited for Oligonucleotide Synthesis[a]

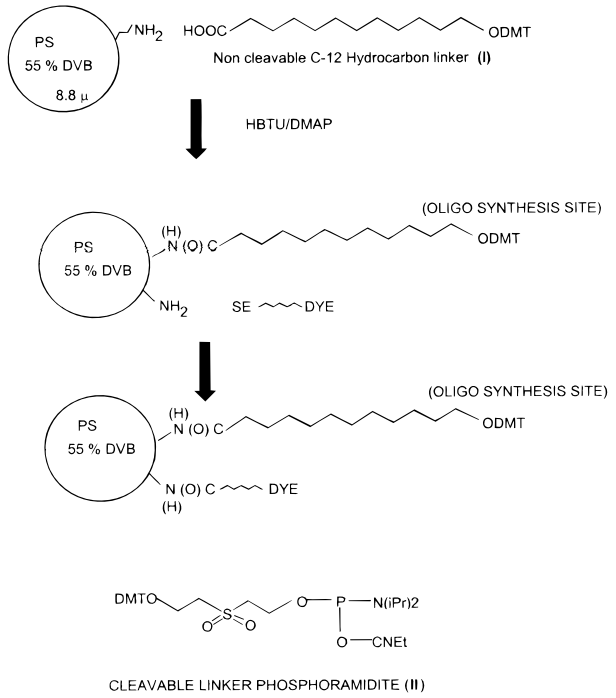

[a] SE = succinimidyl ester functional group.

bifunctionality, separating oligonucleotide synthesis sites from sites to be used for coupling of dye molecules. Compact (nonporous) polystyrene (55% DVB/20%GMA, 8.8 μm) microspheres with $-NH_2$ functional groups were purchased from Bangs Laboratories. Dry microspheres were recovered from the suspension by filtering through a Whatman type 42 (2−5 μm pore) filter paper followed by washes with water, methanol, acetonitrile, and dichloromethane. Bifunctional DMTO/carboxyl derivatized hydrocarbon linker (**1**) [DMTO-$(CH_2)_{11}$COOH] was synthesized by coupling dimethoxytrityl chloride with 12-hydroxydodecanoic acid and was purified by silica gel column chromatography. Hydrocarbon linker (**I**) [DMTO-$(CH_2)_{11}$COOH] was initially attached to amino functionalized to 8.8 μm 55% DVB cross-linked polystyrene microsphere surface to separate the oligonucleotide synthesis sites from amino sites to be used for covalent attachment of fluorescent dye. The linker was attached to the surface amine of microparticles by direct coupling of carboxyl group on linker with aliphatic amine sites on particles using HBTU (O-benzotriazol-1-yl-*N*,*N*,*N*′,*N*′-tetramethyluronium hexafluorophosphate) as the coupling reagent. [DMTO-$(CH_2)_{11}$COOH] linker disolved in acetonitrile was mixed with dried polystyrene microparticles to form a suspension in a 1 mL glass vial. The linker was added in more than 10-fold M excess relative to the amino sites on microspheres. Equal moles of HBTU and (dimethylamino)pyridine were disolved in acetonitrile in a separate glass vial and added to microsphere suspension (moles of HBTU per DMAP added was equal to amount of linker). After 30 min of reaction, the microspheres were filtered (Whatman grade 42 filter) and washed with several portions of acetonitrile and dichloromethane and allowed to air-dry. The derivatized microspheres were stored in a vacuum desiccator. The DMT loading of the derivatized microspheres was estimated to be ∼1.5 μmol/g by measuring the absorbance of the released trityl ions at 503 nm (the amount of linker on microspheres can be controlled by varying the amount of linker and time of reaction). A loading of 1 μmol/g is equivalent to $\sim 2 \times 10^{-16}$ mol/microsphere for 8.8 μm polystyrene beads. The total surface loading of amino functional groups was determined to be ∼4 μmol/g by reaction with dimethoxytrityl chloride and tetrabutylammonium perchlorate (*18*, *19*) and subsequent analysis of released DMT group upon detritylation. Hence, a large fraction of reactive surface amino sites is still available for subsequent conjugation with fluorescent dye molecules. Total coverage of surface sites with linker and dye molecules is not possible due to steric constraints associated with close proximity of reactive sites. The amino groups remaining after attachment of hydrocarbon linker and dye molecules were blocked prior to oligonucleotide synthesis, using standard capping reagents (*N*-methylimidazole/acetic anhydride). Capping of underivatized surface sites on fluorescently encoded microspheres was done manually on the synthesizer by exposing microspheres in synthesis columns to capping solution for ∼30−45 min. The microspheres were then washed by acetonitrile flow through the column. As an alternate, multiple capping/washing steps were performed in the synthesizer prior to synthesis, to achieve more efficient capping. A cleavable linker (**II**) was used when quality of oligonucleotide product was interrogated.

Column Preparation. Microsphere support derivatized with linker (**I**) was weighed directly in to an empty synthesis column (1 μmol empty columns from PE Biosystems). A Zitex 5−10 μm membrane filter disk (Norton Plastics) was used to hold the microparticles. The top and bottom column fittings were sealed in place with aluminum caps using a crimper tool. A TWIST type column, custom-made to include 5 μm frits (Glen Research) was also used with similar results. Microsphere suspensions were transferred into the column via plastic syringe attached to column body.

Oligo Synthesis/Deprotection. PE Biosystems model 394 (4 column) automated DNA synthesizer was used for all oligonucleotide synthesis. The 0.2 μmol scale oligonucleotide synthesis cycle was modified by increasing washing and reagent contact times appropriately to compensate for lower flow rates through column (due to impeded flow through smaller pores of membrane filters). The flow rate through TWIST type (5 μm frit) columns was not significantly affected despite smaller pore size, and product quality was not affected by unmodified cycles.

The microspheres, after oligo synthesis, were dried by argon flow-through column. The dried particles were transferred into a screw-capped microcentrifuge tube (1.5 mL) and treated with concentrated ammonia for 16 h at room temperature or for 4 h at 55° C. The excess ammonia was decanted off and the microspheres washed with water. Deprotection of sorted beads were performed directly on synthesizer (ammonia, 18 h room temperature). The beads were recovered from synthesis column by extraction with TE (PH 8. SDS 0.4%) buffer. We note that the synthesis process could be increased additionally by using UltraFAST chemistry (for cleavage and deprotection using methylamine).

Reagents. Standard PE Biosystems reagents were used for synthesis of oligonucleotides. Protected phosphoramidites used were dA^{bz}, dG^{DMF}, and dC^{bz} (PE Biosystems). The cleavable phosphoramidite linker (**II**) [2[2-(4,4′-dimethoxy trityloxy)ethylsulfonyl]ethyl-(2-cyanoethyl)−(*N*,*N*-diisopropyl)phosphoramidite)] was purchased from Glen Research. BODIPY dyes were obtained

from Molecular Probes. Fluorescein-labeled oligonucleotide probe sequences were purchased from Operon Technologies.

Flow Cytometric Analysis/Sorting. Two-way sorting was performed using BD FACStar at the VA Hospital in San Diego. Flow cytometric analysis for 488 nm excitation was done using FACScan (Becton Dickinson). The filter for FL1 (green) channel transmits 530 nm light (bandwidth = 30 nm) and FL2 (orange) filter transmits at 585 nm (bandwidth = 40 nm). Four-way sorting and analysis using He−Ne 630 nm laser excitation was performed using MOFLO (cytomation) instrument (FL1; 670 nm, 40 nm band-pass; FL2; 700 nm and above). Analysis and sorting were performed in TE (10 mM Tris and 1 mM EDTA, pH 8) or PBS (phosphate-buffered saline) buffers.

Trityl Assays/Product Analysis. The coupling efficiency was measured by monitoring the absorbance (503 nm) of released dimethoxytrityl ions following the detritylation step. The trityl output was collected in glass test tubes by fraction collector (Bio-Rad model 2110). The solution was allowed to evaporate to dryness by placing tubes in fume hood for 48 h. A total of 1.5 mL of trichloroacetic acid/dichloromethane solution was added to each tube, and the weight of solution was measured. The absorbance was measured using a spectrophotometer (Pharmacia Biotech, Uptrospec 4000). The absorbance readings were corrected for discrepancy in volumes due to solvent evaporation. Oligonucleotide products were analyzed by capillary electrophoresis at the University of Calgary, DNA synthesis core facility. MALDI (matrix-assisted laser desorption ionization) mass spectroscopy analysis was performed at the Mass Consortium in San Diego.

Covalent Attachment of BODIPY-TMR and Generation of 4 Microsphere Set. All BODIPY (4,4-difluoro-4-bora-3a,4a-diaza-*s*-indacene) dyes were purchased from Molecular Probes with succinimidyl ester functionality. The succinimidyl ester functional group of the dye (Bodipy TMR SE, BODIPY substitute for tetramethylrhodamine, Abs/Em = 542/574 nm) was coupled directly to the free (unreacted) surface aliphatic amine sites of hydrocarbon (**I**)-linked microparticles in acetonitrile to form a carboxamide bond. The amount of dye attached to the surface of microparticles was controlled by varying the concentration of the dye. Four microsphere sets could be generated by reacting with four solutions of dye prepared by serial dilution (10-fold dilution) of stock solution (~1 mM). The dye-loaded microspheres were filtered through a 2.5 μm (Whatman grade 42) filter paper and washed with several portions of acetonitrile. As an alternate, the background fluorescence emission from unlabeled hydrocarbon (**I**)-linked microspheres could also be used as a fluorescently addressable microsphere set. The amount of hydrocarbon linker (oligo synthesis sites) on the microparticles corresponds to ~40% of total available sites, thus leaving about 60% of the sites available for dye binding. However, steric crowding would prevent occupation of all available sites. Steric factors associated with close proximity of oligonucleotides on surface of microspheres is known to prevent hybridization reactions (*20*). Optimum hybridizations have been observed for support surfaces occupied by less than 50% of available sites.

Synthesis/Two-Way Sorting. The sorted microsphere suspensions were transferred via plastic syringe attached to the open end of a synthesis column. The suspension was filtered through membrane filter (5−10 μm, sealed on other end of column) by mild pressure on the plunger. The microsphere support was washed by flowing acetonitrile through synthesis column for at least 5 min.

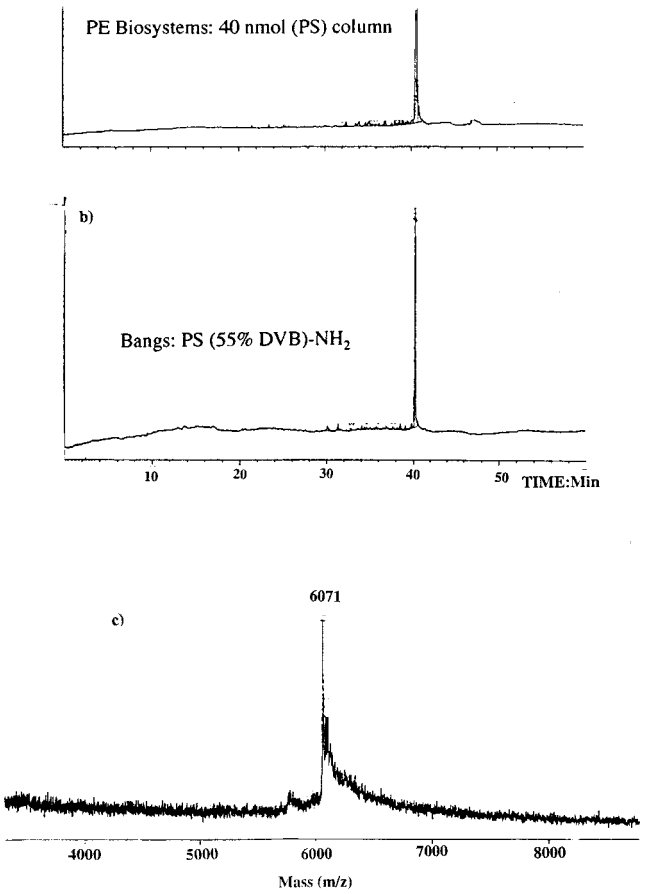

Figure 1. (a) Capillary electrophorograms of 20-mer sequence synthesized on 8.8 μm polystyrene (55% DVB cross-linked) microspheres; Sequence synthesized; 5′-d(AGCT AGCT TTTT AGCT AGCT)-3′. (b) CE data for same sequence synthesized on 40 nmol polystyrene column (PE Biosystems). The products were simultaneously cleaved from support and deprotected in ammonium hydroxide (55 °C, 16 h). Cleavable linker 2[2-(4,4′-dimethoxytrityl-oxy)ethylsulfonyl]ethyl-(2-cyanoethyl)-(*N*,*N*-diisopropyl)-phosphoramidite) was linked to surface amino sites of polystyrene microspheres before synthesis of sequence. (c) Mass spectroscopy (MALDI) data for 20-mer synthesized on 8.8 μm 55% DVB polystyrene support. Expected mass = 6072; observed mass = 6071 (mass includes 3′ phosphorylation from cleavable chemical phosphorylating reagent). Sequence synthesized: 5′-d(ATCCCCAACAGACCACTGCTC)-3′ DMT off.

RESULTS AND DISCUSSION

In Situ Synthesis on Microspheres. The cleavable linker (**II**) was used for cleavage and analysis by capillary electrophoresis. 20-mer synthesized on 8.8 μm, 55% DVB polystyrene microsphere supports gave comparable results as the same 20-mer sequence synthesized on standard 40 nmol (PE Biosystems) columns (Figure 1, panels a and b). Average stepwise yields of 99 and 98.3% were calculated for 20-mer synthesis on 8.8 μm polystyrene microspheres derivatized with linker (**1**) and 40 nmol PE Biosystems polystyrene columns, respectively. Spectrophotometric trityl (DMT) assays also confirmed the high coupling efficiencies observed when synthesis was performed on polystyrene microsphere supports with ~1 μmol/g DMT loadings. Supports with higher loadings showed low-coupling efficiencies for initial coupling steps but proceeded with high coupling efficiencies after DMT

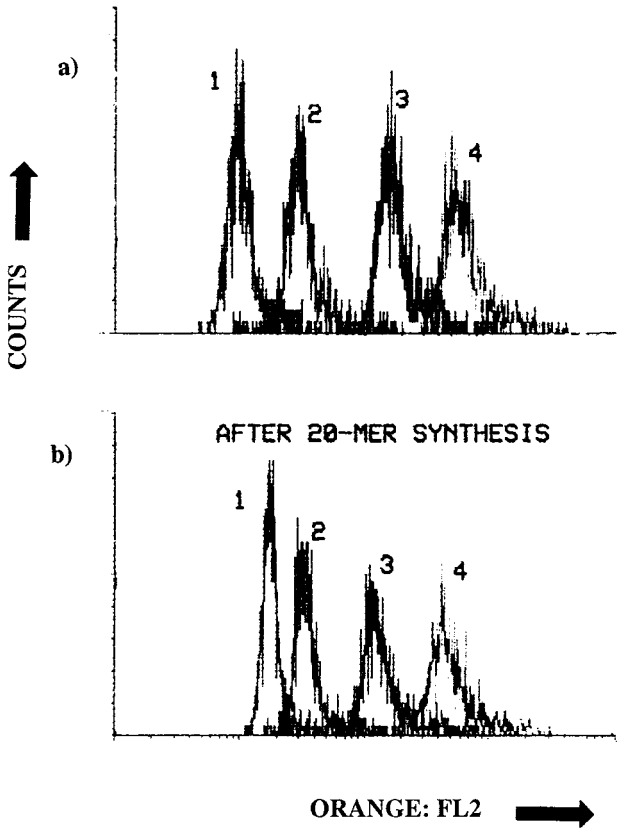

Figure 2. Effect of oligo synthesis conditions on mixture of microsphere sets 1, 2, 3, and 4; FL2 (orange) histograms of (a) mixture, before oligo synthesis treatment, (b) after subjecting microspheres with 20-mer synthesis using modified synthesis cycle and deprotection with ammonium hydroxide. Analysis performed in TE, pH 8 buffer. All intensities were recorded in logarithmic scale.

loading of ~1 μmol/g was achieved. The exclusion of the hydrocarbon linker (**I**) did not significantly effect overall yield of product.

The 20-mer oligonucleotide synthesized on polystyrene (8.8 μ, 55% DVB) microspheres was also analyzed by mass spectroscopy (MALDI) after cleavage and deprotection by ammonia (product was not purified). The mass spectrum shows the presence of only the mass peak of the complete 20-mer sequence (Figure 1c).

Encoded, Organotolerant Microsphere Sets. To demonstrate stability of covalently attached BODIPY-TMR dye to oligo synthesis conditions, histograms (FL2, orange) were recorded before and after oligonucleotide synthesis/deprotection (Figure 2). Intensities for microspheres 2−4 remain unchanged. Increase in intensity on microsphere 1 is due to added background emission from the synthetic process (reagents). However, intensities are not changed sufficiently as to hinder the subsequent sorting.

Flow Sorting-Directed Segmental Solid-phase Synthesis. A synthetic strategy was devised to include (a) initial synthesis of common 8-mer 5′-d(TCGA TCGA)-3′ on all four sets; (b) sorting of microsphere sets; (c) transfer to four separate synthesis columns; (d) synthesis of unique 4-mer sequence on each microsphere set followed by common 8-mer to complete 20-mer sequences which differ by only four bases in the middle of sequence (Table 1).

The sequence 5′-d(TCGA TCGA)-3′ was synthesized (DMT removed after last base addition) on microsphere sets 1, 2, 3, and 4. The microspheres were combined and

Table 1. Complete Sequences Synthesized on Fluorescently Encoded Microspheres 1, 2, 3, and 4

microsphere 1, seq 1: 5′-d(TCGA TCGA AAAA TCGA TCGA)-3′
microsphere 2, seq 2: 5′-d(TCGA TCGA GGGG TCGA TCGA)-3′
microsphere 3, seq 3: 5′-(TCGA TCGA CCCC TCGA TCGA)-3′
microsphere 4, seq 4: 5′-d(TCGA TCGA TTTT TCGA TCGA)-3′

Table 2. Probe Sequences Used[a]

probe 1: 5′-d(TCGA TCGA TTTT TCGA TCGA F)-3′
probe 2: 5′-d(TCGA TCGA CCCC TCGA TCGA F)-3′
probe 3: 5′-d(TCGA TCGA GGGG TCGA TCGA F)-3′
probe 4: 5′-d(TCGA TCGA AAAA TCGA TCGA F)-3′

[a] F = fluorescein amidite. Hybridization was performed in TE, pH 8, 1 M NaCl, 0.5 % SDS solution at 50 °C for 30 min.

suspended in TE (pH 8) buffer and divided into two portions. Microsphere sets 1 and 2 were sorted from the first portion and microspheres 3 and 4 were sorted from the second portion. The sorted microspheres were collected in PBS buffer. Sorts 1, 2, 3, and 4 were transferred into four different synthesis columns and subjected to 12-mer synthesis to complete unique 20-mer sequences on each microsphere set.

The histogram of mixed microspheres (before sorting) and histograms for each sort (sort 1, 2, 3, and 4) are shown in Figure 3. Visual inspection of the figure indicates efficient sorting of mixture with minor amounts of impurities. Overlap of intensities due to broad nature of histograms results in loss or improper sorting of beads found between defined gate regions selected for sorting. Exposure of micropheres with dye solutions (BODIPY TMR in acetonitrile) for shorter periods (less than 1 min) resulted in sharper and better resolved histograms. Aggregation of microspheres was evident from forward and side scatter (FSC vs SSC) two-dimensional dot plots (not shown). Loss of yield due to aggregation could be minimized by adding small amounts of surfactants (~0.5% SDS) to microsphere suspension.

Detection of Microsphere Type (sequence) by Hybridization. Microspheres 1, 2, 3, and 4 were mixed together and divided into five portions. Probes 1−4 (complementary sequences labeled with green fluorescein dye, ~7 pmol) were added to each tube (probe 1 to tube 1, probe 2 to tube 2, probe 3 to tube 3, and probe 4 to tube 4). The fifth tube contained no added probe. The probe sequences used for hybridization are summarized in Table 2.

Results of the above experiment are shown in Figure 4. The increase in FL1 intensity (green probe channel) is observed only for microspheres containing a perfectly matched complementary sequence. Although the microsphere set affected by hybridization is clearly evident from the plots, a small fraction of the population from that set remains unaffected. This may be as a result of inefficient sorting due to poorly resolved fluorescence emission histograms as explained above.

Effect of Transfer to Aqueous Medium. To determine the effect on nucleotide-coupling efficiency from the transfer of beads to and from the synthesis column, a necessary maneuver involved in moving from the aqueous flow sorting environment to the anhydrous oligonucleotide synthesis environment, the following experiments were performed. Two microsphere sets were generated by reacting BODIPY 630/650 and BODIPY 650/665 succinimidyl ester-linked dyes with the amino-functionalized, 55% DVB polystyrene microspheres derivatized with hydrocarbon linker (**I**). Cleavable chemical phosphorylating reagent (**II**) was attached initially for subsequent cleavage of synthesized oligonucleotide from

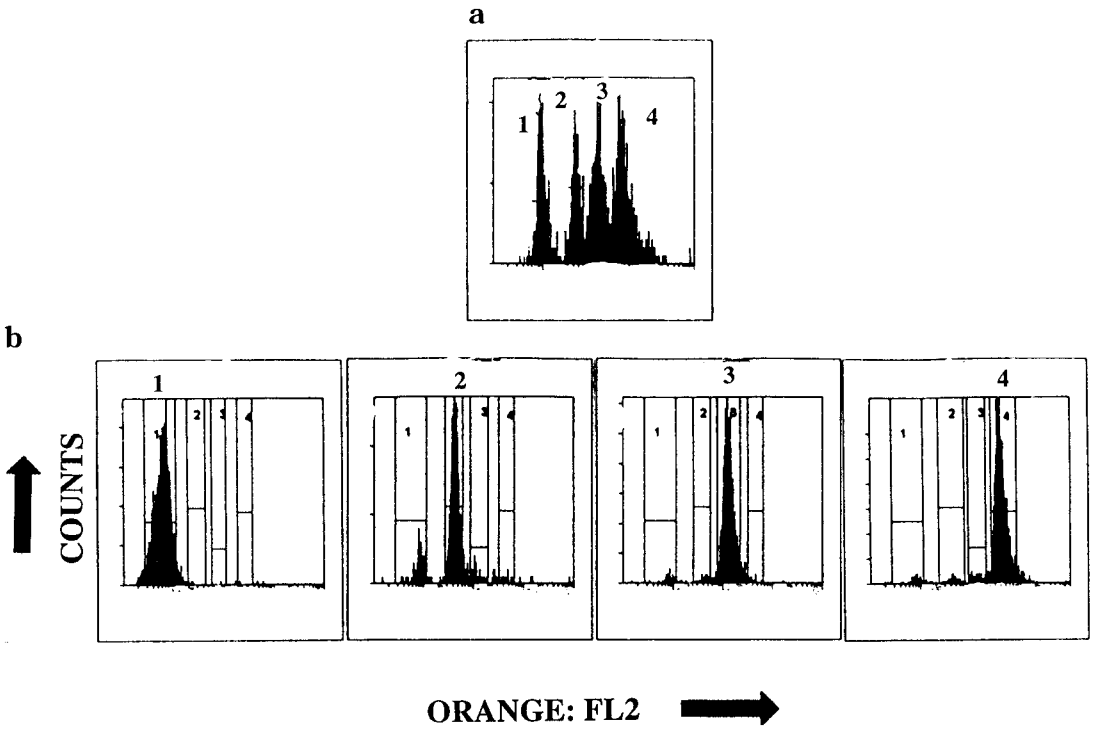

Figure 3. Sorting mixture of microspheres: FL2 (orange) histograms of (a) mixture of microspheres (1, 2, 3, 4) before sorting, (b) after sorting each component of mixture based on intensity of FL2 (orange) emission (sort 1, sort 2, sort 3, sort 4). TE, pH 8 buffer. All intensities were recorded in logarithmic scale.

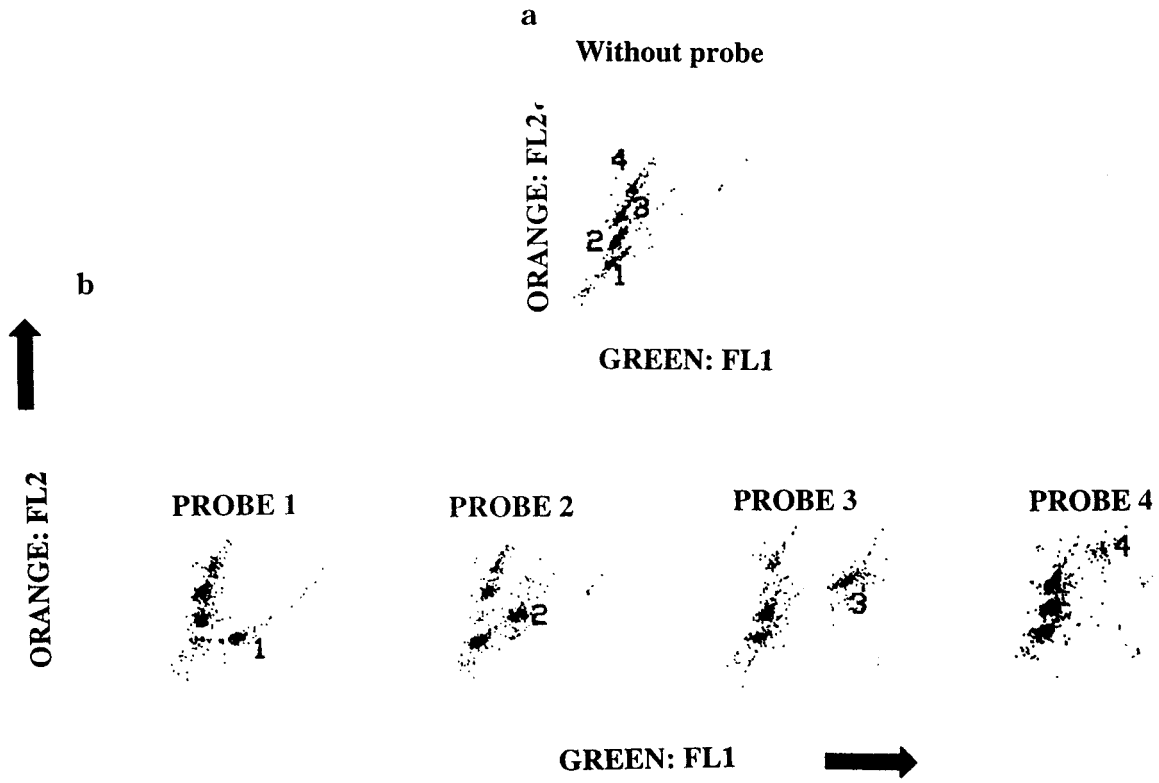

Figure 4. Two-dimensional dot plot (orange FL2 vs green FL1) of mixture of microspheres 1, 2, 3, and 4 with oligo sequences 1, 2, 3, and 4, respectively, and intensity changes observed upon adding fluorescently labeled (green FL1) probes 1, 2, 3, and 4. Analysis were performed in TE (pH 8) buffer with 50% FL2-FL1 compensation. Probes 1, 2, 3, and 4 have sequences which are complementary to sequences 1, 2, 3, and 4, respectively. Histograms were recorded with FL2-FL1 50% compensation. All intensities were recorded in logarithmic scale.

support. The beads were extracted from column using PBS buffer (after each nucleotide base addition) and transferred back into synthesis column (TWIST type) via syringe attached to column body. The emission intensities of the beads were monitored using the flow cytometer (He−Ne laser excitation). Extensive acetonitrile-washing steps were performed before each synthesis cycle to remove traces of water from support. The emission intensities of the microsphere sets remained unchanged throughout the synthesis/transfer process (data not

shown), thus confirming the suitability of using BODIPY dyes to encode microspheres for oligonucleotide synthesis.

After completion of T_{10} synthesis, the oligonucleotide was cleaved and deprotected by ammonia. The cleaved product was analyzed by capillary electrophoresis (CE) and mass spectroscopy. MALDI spectrum indicated the presence of only mass peaks indicative of full-length T_{10} sequence (split peaks were observed due to association of cations from PBS buffer). However, CE data showed the presence of shorter sequences presumably due to lower coupling efficiencies during the first coupling steps. Loss of capping and/or generation of new reactive sites on microsphere surface due to transfer/washing process may also account for the presence of shorter sequences.

Optimization of Sorting, Synthesis, and Transfer. The above manipulations are a simulation study for synthesis by sorting protocols. Loss of beads are expected due to inefficient extraction from synthesis column as a result of beads sticking to column walls and frits. The TWIST type column is easier to manipulate since the top fitting can be removed with ease and sorting could be performed directly into columns. The flow of reagents through this column is also not impeded, thus allowing shorter reagent flow times compared with membrane filters. BODIPY dyes are available in a wide spectrum of excitation, and emission wavelengths, hence, are easily adaptable to varying excitation sources (wavelengths). The number of microsphere sets generated by covalent attachment of dye is limited by the number of available reactive sites, background emission from particles, and broad nature of histogram profiles. Supports with higher loading such as poly(ethylene glycol) grafted polystyrene polymers (tentagel) should allow generation of more fluorescently encoded microsphere sets.

Problems and Limitations. Although we have successfully demonstrated sorting-directed synthesis with the four microsphere set, increasing the complexity (i.e., the size of the library) will generate new issues. For example, the sorting rate, purity, and yield will dictate the total sorting time and initial number of microspheres needed for synthesis of an oligonucleotide. Optimizing these parameters is critical to enable execution of the combinatorial approach in a meaningful time frame and with final yields appropriate for subsequent assays. Furthermore, the availability of dyes which produce little or no spectral overlap and quenching will determine the size of the library. Finally, the success of the combinatorial method of oligonucleotide synthesis ultimately would depend on finding methods to efficiently transfer beads to and from the synthesis column and flow sorter as well as minimizing losses due to aggregation of particles. Preliminary studies performed with a four-way flow sorter indicate efficient sorting is possible using 630 nm He−Ne laser excitation and a four microsphere set generated by reacting succinimidyl ester functionalized BODIPY 630/650 dye with amino functionalized polystyrene (55% DVB) microspheres (sorting purity >98%). For these studies, a custom designed curved charge plate (Cytomation, Inc.) was used to sort microspheres directly into DNA synthesis columns.

In summary, we have shown efficient oligonucleotide synthesis on fluorescently encoded microspheres generated by covalent attachment of linkers and dye and demonstrated feasibility of using flow sorting to identify and separate microphere sets. Sequences synthesized on each microsphere set were identified by performing hybridization with fluorescently labeled complementary sequences.

ACKNOWLEDGMENT

This work was supported by a grant from the National Institute of Science and Technology, Advanced Technology Program (70NANB8H4003).

LITERATURE CITED

(1) Mattecui, M. D., and Caruthers, M. H. (1981) Synthesis of deoxyoligonucleotides on a polymer support. *J. Am. Chem. Soc. 103*, 3185−3191.

(2) Beaucage, S. L., and Iyer, R. P. (1992) Advances in the synthesis of oligonucleotides by the phosphoramidite approach. *Tetrahedron 48*, 2223−2311.

(3) Beaucage, S. L., and Iyer, R. P. (1993) The functionalization of oligonucleotides via phosphoramidite derivatives. *Tetrahedron 49*, 1925−1963.

(4) Gait, M. J., Ed. (1984) Oligonucleotide synthesis. In *A Practical Approach*, IRL Press, New Edition, Oxford.

(5) Frank, R., Heikens, W., Heisterberg-Moutsis, G., and Blocker, H. (1983) A new general approach for the simultaneous synthesis of large numbers of oligonucleotides: segmental solid supports. *Nucleic Acids Res. 13*, 4365−4377.

(6) Ott, J., and Eckstein, F. (1984) Filter disc supported oligonucleotide synthesis by the phosphite method. *Nucleic Acids Res. 12*, 9137−9142.

(7) Matthes, H. W. D., Zenke, W. M., Grundstrom, T., Staub, A., Wintzerith, M., and Chambon, P. (1984) Simultaneous rapid chemical synthesis of over one hundred oligonucleotides on a microscale. *EMBO J. 3*, 801−805.

(8) Markiewicz, W. T., Adrych-Rozek, K., Markiewicz, M., Zebrowska, A., and Astriab, A. (1994) Synthesis of oligonucleotides permanently linked with solid supports for use as synthetic oligonucleotide combinatorial libraries. In *Innovation and Perspectives in Solid-Phase Synthesis: Peptides, Proteins and Nucleic Acids: Biological and Biomedical Applications* (Epton, R., Ed.) pp 339−346, Mayflower Worldwide, Birmingham.

(9) Watson, A., Mazumder, A., Stewart, M., and Balasubramanian, S. (1998) Technology for microarray analysis of gene expression. *Curr. Opin. Biotechnol. 9*, 609−614.

(10) Southern, E., Mir, K., and Shchepinov, M. (1999) Molecular interactions on microarrays. *Nat. Genet. 21* (Suppl), 5−9.

(11) Maskos, U., and Southern, E. M. (1992) Oligonucleotide hybridisations on glass supports: a novel linker for oligonucleotide synthesis and hubridisation properties of oligonucleotides synthesised in situ. *Nucleic Acids Res. 20*, 1679−1684.

(12) Hakala, H., Heinonen, P., Iitia, A and Lonnberg, H. (1997) Detection of oligonucleotide hybridization on a single microparticle by time-resolved fluorometry: Hybridization assays on polymer particles obtained by direct solid phase assembly of the oligonucleotide probes. *Bioconjugate Chem. 8*, 378−384.

(13) Hovinen, J., Guzaev, A., Azhayev, A., and Lonnberg, H. (1994) Novel solid supports for the preparation of 3′-alkyl phosphate tether groups bearing amino, carboxy, carboxamido and mercapto functionalities. *Tetrahedron 50*, 7203−7218.

(14) Hakala, H., and Lonnberg, H. (1997) Time-resolved fluorescence detection of oligonucleotide hybridization on a single microparticle: Covalent immobilization of oligonucleotides and quantitation of a model system. *Bioconjugate Chem. 8*, 232−237.

(15) Seliger, H., Bader, R., Hinz, M., Rotte, B., Astriab, A., Makiewicz, M., and Markiewicz, W. T. (1997) Synthetic oligonucleotide combinatorial libraries-tools for studying nucleic acid interactions. *Nucleosides Nucleotides 16*, 703−710.

(16) Fluorescent labeling using microparticles with controllable Stokes shift. Singer, V. L. and Haugland, R. P. U.S. patent 5,573,909, Nov 1996.

(17) McCollum, C., and Andrus, A. (1991) An optimized polystyrene support for rapid efficient oligonucleotide synthesis. *Tetrahedron Lett. 32*, 4069−4072.

(18) Reddy, M. P., and Voelker, P. J. (1988) Novel method for monitoring coupling efficiency in solid-phase peptide synthesis. *J. Pept. Protein Res. 31,* 345−348.
(19) Reddy, M. P., Rampal, J. B., and Beaucage, S. L. (1987) An efficient procedure for the solid-phase tritylation of nucleosides and nucleotides. *Tetrahedron Lett. 28,* 23−26.
(20) Shchepinov, M. S., Case-Green, S. C., and Southern, E. M. (1997) Steric factors influencing hybridisation of nucleic acids to oligonucleotide arrays. *Nucleic Acids Res. 25,* 1155−1161.

BC990145Z

Use of a Steroid Cyclic Disulfide Anchor in Constructing Gold Nanoparticle–Oligonucleotide Conjugates

R. L. Letsinger,* R. Elghanian, G. Viswanadham, and C. A. Mirkin*

Department of Chemistry, Northwestern University, 2145 Sheridan Road, Evanston, Illinois 60208.
Received November 8, 1999; Revised Manuscript Received December 23, 1999

A new anchoring group is described for binding oligonucleotides to gold surfaces. On the basis of a ketal derived from 4,5-dihydroxy-1,2 dithiane and epiandrosterone, it is easy to prepare and to link to oligonucleotides. Gold nanoparticle–oligonucleotide conjugates made using this cyclic disulfide linker serve as effective probes for detecting specific oligonucleotide sequences, and they exhibit much greater stability toward dithiothreitol than corresponding conjugates prepared with the conventional mercaptohexyl group or an acyclic disulfide unit. The high stability toward thiol deactivation likely results, in part at least, from anchoring each oligonucleotide to gold through two sulfur atoms.

INTRODUCTION

Pairs of oligonucleotide–gold nanoparticle conjugates serve as unique probes for recognizing specific sequences in DNA segments (*1*, *2*) and as building blocks for assembling novel structures and materials (*3*, *4*). These applications depend on the reversible association of complexes formed by hybridization of the oligonucleotides attached to the nanoparticles with target oligonucleotides in solution. A simple test for a given oligonucleotide is to add appropriate nanoparticle probes to the sample and spot a few microliters of the solution on a TLC plate. A blue spot signifies the presence of the target oligonucleotide; in absence of the target, the spot is red. The oligonucleotide–gold probes used in previous studies were prepared by the reaction of oligonucleotides bearing terminal mercaptoalkyl groups with gold nanoparticles in an aqueous buffer. They proved to be surprisingly robust, functioning well even after heating to 100 °C or after storing for 3 years at 5 °C. We have found, however, that these conjugates lose activity as hybridization probes when soaked in solutions containing thiols, which act by displacing the derivatized oligonucleotides from the gold surface. This feature poses a problem when the nanoparticle probes are to be used in a solution containing a thiol, as for example, a PCR solution that contains dithiothreitol (DTT) as a stabilizer for the polymerase enzyme. We describe here a new anchoring group, based on steroid disulfide **1** (Figure 1), that is simple to prepare, is broadly useful, and affords gold–oligonucleotide conjugates exhibiting greater stability toward DTT than those prepared using mercaptohexyl linkers.

EXPERIMENTAL PROCEDURES

General. NMR spectra were recorded on 500 MHz (^{1}H) and 400 MHz (^{31}P; acquisition at 161.9 MHz) Varian spectrometers using $CDCl_3$ as a solvent and TMS as an internal (^{1}H) and H_3PO_4 as an external (^{31}P) standard; chemical shifts are expressed in δ units. MS data were obtained on a Quattro II triple quadrupole mass spectrometer. Automated oligonucleotide synthesis was carried out on a Milligene Expedite DNA synthesizer. The analysis for S was made by Oneida Research Services.

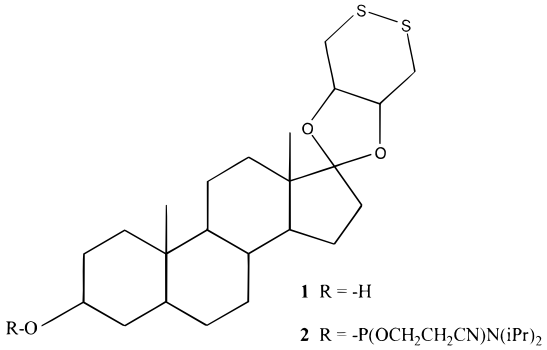

Figure 1. Formula for the "steroid-disulfide" unit obtained by condensation of 4,5-dihydroxy-1,2-dithiane with epiandrosterone.

Compound 1 (Steroid-Disulfide). A solution of epiandrosterone (0.5 g), 1,2-dithiane-4,5-diol (0.28 g), and *p*-toluenesulfonic acid (15 mg) in toluene (30 mL) was refluxed for 7 h under conditions for removal of water (Dean Stark apparatus); then the toluene was removed under reduced pressure and the residue taken up in ethyl acetate. This solution was washed with water, dried over sodium sulfate, and concentrated to a syrupy residue, which on standing overnight in pentane/ether afforded compound **1** as a white solid (400 mg); R_f (TLC, silica plate, ether as eluent) 0.5; for comparison, R_f values for epiandrosterone and 1,2-dithiane-4,5-diol obtained under the same conditions are 0.4 and 0.3, respectively. Recrystallization from pentane/ether afforded a white powder, mp 110–112 °C; ^{1}H NMR δ 3.6 (1H, C^{3}O*H*), 3.54–3.39 (2H, m 2OC*H* of the dithiane ring), 3.2–3.0 (4H, m 2CH_2S), 2.1–0.7 (29H, m steroid *H*); mass spectrum (ES$^+$) calcd for $C_{23}H_{37}O_3S_2$ (M + H), 425.2179; found, 425.2151. Anal. ($C_{23}H_{36}O_3S_2$) S: calcd, 15.12; found,15.26.

Phosphoramidite Derivative, Compound 2. Compound **1** (100 mg) was dissolved in THF (3 mL) and cooled in a dry ice alcohol bath. *N*,*N*-Diisopropylethylamine (80 μL) and β-cyanoethyl chlorodiisopropylphosphoramidite (80 μL) were added successively; then the mixture was warmed to room temperature, stirred for 2 h, mixed with ethyl acetate (100 mL), washed with 5% $NaHCO_3$(aq) and

* To whom correspondence should be addressed. E-mail: (R.L.L.) r-letsinger@chem.nwu.edu, (C.A.M.) camirkin@chem.nwu.edu.

10.1021/bc990152n CCC: $19.00 © 2000 American Chemical Society
Published on Web 03/02/2000

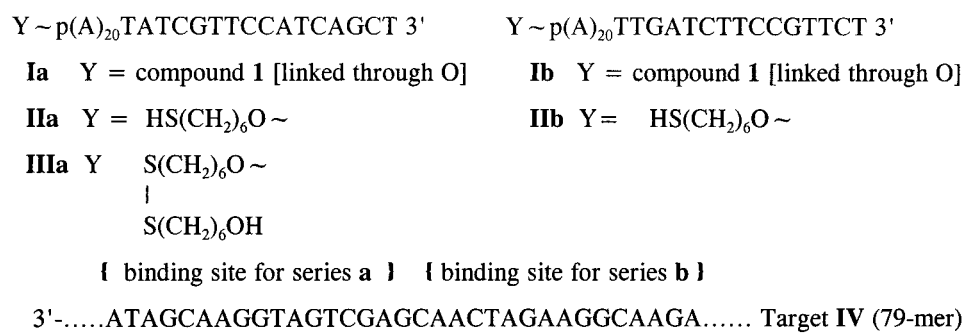

Figure 2. Probe and target oligonucleotides (note that the corresponding gold nanoparticle−oligonucleotide conjugates are designated as **Ia′**, **Ib′**, **IIa′**, etc.).

with water, dried over sodium sulfate, and concentrated to dryness. The residue was taken up in the minium amount of dichloromethane, precipitated at −70 °C by addition of hexane, and dried under vacuum; yield 100 mg; ^{31}P NMR 146.02.

Preparation of Modified Oligonucleotides and Nanoparticle Conjugates. Modified oligonucleotides **Ia** and **Ib** were constructed on CPG supports using conventional phosphoramidite chemistry, except that reagent **2** was employed in the final phosphitilation step. Products were cleaved from the support by treatment with concentrated NH_4OH for 16 h at 55 °C. The oligonucleotides were purified by reversed-phase HPLC on a Dionex DX500 system equipped with a Hewlett-Packard ODS Hypersil column (4.6 × 200 nm, 5 μm particle size) using TEAA buffer (pH 7.0) and a 1%/min gradient of 95% CH_3CN/5% 0.03 TEAA at a flow rate of 1 mL/min. A nice feature of the hydrophobic steroid group is that the capped derivatives separate cleanly from uncapped oligomers. Sulfur-derivatized oligonucleotides **IIa** and **IIb** were prepared similarly using the commercially available "5′-Thiol-Modifier reagent" (C6 Glen Research) and cleavage of the trityl protecting group with silver nitrate as previously described (*1*). For preparation of disulfide conjugate **IIIa**, "Thiol-Modifier C6 S-S" (Glen Research) was used in the final phosphitilation and the terminal dimethoxytrityl group was cleaved with aqueous 80% acetic acid. Each of the modified oligonucleotides was immobilized on ~13 nm gold nanoparticles by the procedure used for anchoring oligonucleotides through a mercaptohexyl headgroup (*1*). This involved soaking citrate stabilized nanoparticles (~13 nm in diameter) for 56 h in a buffer-salt solution containing an oligonucleotide bearing a terminal sulfur substituent (HS− or acyclic or cyclic disulfide). The nanoparticles were then thrown down by centrifugation, the supernatant solution was removed, and the nanoparticles were washed, resuspended in buffer, recentrifuged, and then suspended in 0.1 M NaCl, 10 mM phosphate. This procedure afforded the nanoparticle oligonucleotide conjugates free from the excess sulfurized oligonucleotides employed in the loading process.

RESULTS AND DISCUSSION

A cyclic disulfide was selected as the reactive site of the anchor unit since ester derivatives of 1,2-dithiane-4,5-diol were known to form monolayers on gold surfaces (*5*) and a cyclic disulfide would plausibly bind to the surface through both sulfur atoms (*6*) to give a chelate structure that could exhibit enhanced stability. Epiandrosterone was selected as a linking element since it is a readily available, easily derivatized keto alcohol and, as a substituent with a large hydrophobic surface, might be expected to help screen the approach of water soluble molecules to the gold surface (*7*).

To evaluate the utility of nanoparticle−oligonucleotide probes containing the disulfide-steroid anchor, we prepared probes **Ia′**, **Ib′**, **IIa′**, **IIb′**, and **IIIa′** by immobilizing modified oligonucleotides **Ia**, **Ib**, **IIa**, **IIb**, and **IIIa**, respectively, on gold nanoparticles (Figure 2). The oligomers in a given series have the same nucleotide sequence but differ in structure of the 5′-headgroup Y. Conjugates **Ia** and **Ib** have steroid-disulfide headgroups; **IIa** and **IIb**, mercaptohexyl headgroups; and **IIIa′**, acylic disulfide headgroups. The $(dA)_{20}$ chains serve as spacers between the gold and the oligonucleotide recognition regions to facilitate hybridization. Many of the sulfur-derivatized oligomers bind to each nanoparticle. Hybridization of pairs of nanoparticle probes with target oligonucleotides leads to formation of three-dimensional networks and a change in color from red to blue-gray (*1*).

Hybridization Assays. Hybridization of the probes was examined using a 79-mer oligonucleotide target, **IV**, containing sequences complementary to the probes. The reactions were carried out at room temperature by adding 1 μL of the target solution (10 pmol of **IV**) to colloidal solutions of **Ia′** + **Ib′**, **IIa′** + **IIb′**, **IIIa′** + **Ib′**, and **IIIa′** + **IIb′** (50 μL and 1.0 A_{520} unit of each nanoparticle probe) in 0.5 M NaCl and 10 mM phosphate (pH 7.0). At times 10 s, 5 min, and 10 min, aliquots (3 μL) were removed and spotted on a C-18 reversed-phase TLC plate. The various probe pairs all behaved the same: the spots for the 10 s reactions were red, indicative of free nanoparticles; those for the 10 min reactions were deep blue-gray, characteristic of aggregates of nanoparticles, and the 5 min reactions afforded spots with a reddish blue color, indicative of a mixture of nonassociated and associated nanoparticles. In agreement with previous observations for aggregation of nanoparticles effected by hybridization of oligonucleotides (*1*−*4*), the reactions were reversible. Thus, warming the aggregate mixture derived from **Ia′** + **Ib′** to 90 °C (above the dissociation temperature for the oligomers linking the nanoparticles together) and spotting while hot afforded a red spot. For control experiments in which the oligonucleotide target was omitted or was not complementary to the probes, the color was red under all conditions.

We conclude that the nanoparticle conjugates generated via the steroid-disufide anchor function effectively as hybridization probes. Moreover, as judged by the spot test, the conjugates with the various anchor units react with the target oligonucleotides at comparable rates. This feature is consistent with expectations for probes having comparable densities of oligonucleotides on the surface

Table 1. Colors from Reactions of Gold Nanoparticle Probes with DTT

	0	20 s	5 min	40 min	100 min
Ia′ + Ib′	red	red	red	red	red-blue
IIa′ + IIb′	red	red-blue	blue	blue	(black prec.)
III′	red	red-blue	blue	blue	(black prec.)

of the nanoparticles and nucleotide recognition regions relatively far removed from the 5′-headgroups.

Reaction of Nanoparticle Probes with Dithiothreitol. Addition of thiols to colloidal solutions of gold nanoparticles or gold nanoparticles loaded with mercaptohexyl-oligonucleotides leads to aggregation of the nanoparticles. The color changes from red to deep blue, and when the solution is undisturbed, a dark precipitate settles out. As demonstrated with experiments with nanoparticles bearing fluorescently labeled oligonucleotides, the thiol displaces the mercaptoalkyl-oligonucleotides bound at the gold surface (*8*). In contrast to aggregation induced by hybridization of oligonucleotide−nanoparticle conjugates, these reactions are irreversible; neither heating nor addition of NaOH disassembles the aggregates.

We have used this color change to monitor the reaction of DTT with probes prepared with the steroid cyclic disulfide, the mercaptohexyl, and the acyclic disulfide headgroups. The experiments were carried out by adding 1 μL of 1 M DTT in water to 100 μL of the nanoparticle-oligonucleotide probe solution (2 A_{520} units of nanoparticles) in 0.5 M NaCl and 10 mM phosphate (pH 7.0), then spotting 3 μL aliquots on a TLC plate at various times and observing the color. As shown in Table 1, colloidal probes derived from oligonucleotides with the mercaptohexyl (**IIa′** + **IIb′**) and acyclic oligonucleotide headgroups (**IIIa′**) reacted rapidly. A red-blue spot was obtained in 20 s and a strong blue spot within 5 min. By 100 min, most of the gold had precipitated. In contrast, no color change was observed for the reaction of the probes prepared with the steroid-cyclic disulfide headgroup (**Ia′** + **Ib′**) within 40 min. It took 100 min to reach the same color obtained with **IIa′** + **IIb′** or **IIIa′** in 20 s. On this basis, we estimate that the rate of reaction of **Ia′** + **Ib′** with DTT is of the order of 1/300th that of the other probes. **IIIa′** reacts at about the same rate as the probes prepared with the mercaptohexyl anchor. The latter result is not surprising in view of evidence that the reaction of an acyclic disulfide with gold probably involves cleavage of the S−S bond (*9*). Accordingly, an oligonucleotide with an acyclic headgroup would likely be linked to gold through a single sulfur atom, as in the case of mercaptohexyl-oligonucleotide derivatives.

To see if **Ia′** and **Ib′** in fact still serve as hybridization probes after standing in the presence of DTT, we treated two samples of mixtures of the probes with DTT under the conditions used for the reactions in Table 1. After 30 min, 1 μL of a solution of target oligonucleotide **IV** (10 pmol) was added to one. Both samples were frozen quickly, allowed to thaw, and assayed by the spot test. The spot for the sample containing **IV** was blue and that for the control lacking the target was red, demonstrating that conjugates **Ia′** + **Ib′** were not only stable but also effective as probes after exposure to DTT under conditions causing aggregation of **IIa′** + **IIb′** and **IIIa**.

CONCLUSION

Oligonucleotides containing a steroid-cyclic disulfide headgroup (**1**) bind readily to gold nanoparticles in an aqueous medium. As shown by color changes accompanying aggregation of the colloids, the resulting nanoparticle conjugates function well as hybridization probes and are much more resistant to attack by a thiol than conventional gold conjugates containing an alkyl mono-thiol or an acyclic disulfide linker. These features have practical implications and also raise interesting questions concerning the chemistry involved in the immobilization process. Studies designed to shed further light on the reaction of the cyclic disulfide with gold and the influence of hydrophobic linkers on stability of the nanoparticle probes are in progress.

ACKNOWLEDGMENT

This work was supported by the National Institute of General Medical Sciences (GM 57356), Nanosphere LLC., the National Science Foundation (CHE-999871903), and an ARO-MURI Award (DAAG55-97-1-0133).

LITERATURE CITED

(1) Storhoff, J. J., Elghanian, R., Mucic, R. C., Mirkin, C. A., and Letsinger, R. L. (1998) One-Pot Colorimetric Differentiation of Polynucleotides with Single Base Imperfections Using Gold Nanoparticle Probes. *J. Am. Chem. Soc. 120,* 1959−1964.

(2) Elghanian, R., Storhoff, J. J., Mucic, R. C., Letsinger, R. L., and Mirkin, C. A. (1997) Selective Colorimetric Detection of Polynucleotides Based on the Distance-Dependent Optical Properties of Gold Nanoparticles. *Science 277,* 1078−1081.

(3) Mucic, R. C., Storhoff, J. J., Mirkin, C. A., and Letsinger, R. L. (1998) DNA-Directed Synthesis of Binary Nanoparticle Network Materials. *J. Am. Chem. Soc. 120,* 12674−12675.

(4) Mitchell, G. P., Mirkin, C. A., and Letsinger, R. L. (1999) The Programmed Assembly of DNA Functionalized Quantum Dots. *J. Am. Chem. Soc. 121,* 8122−8123.

(5) Nuzzo, R. G., and Allara, D. L. (1983) Adsorption of Bifunctional Organic Disulfides on Gold Surfaces. *J. Am. Chem. Soc. 105,* 4481−4483.

(6) Ulman, A. (1995) Surface Absorption of Monolayers. *MRS Bulletin,* June 46−51.

(7) For examples of hydrophobic interactions in steroid-oligonucleotide conjugates, see (a) Letsinger, R. L, Chaturvedi, S. K., Farooqui, F., and Salunkhe, M. (1993) Use of Hydrophobic Substituents in Controlling Self-Assembly of Oligonucleotides. *J. Am. Chem. Soc. 115,* 7535−7536; (b) Letsinger, R. L., and Chaturvedi, S. (1998) Tailored Hydrophobic Cavities in Oligonucleotide-Steroid Conjugates. *Bioconjugate Chem. 9,* 826−830.

(8) Mucic, R. C. (1999) *Synthetic Programmable Nanoparticle Assembly Using DNA,* Ph.D. Thesis, Northwestern University.

(9) Zhong, C.-J., Brush, R. C., Anderegg, J., Porter, M. D. (1999) *Langmuir 15,* 518−525.

BC990152N

Efficient Multigram Synthesis of the Bifunctional Chelating Agent (*S*)-1-*p*-Isothiocyanatobenzyl-diethylenetetraminepentaacetic Acid

Donald T. Corson and Claude F. Meares*

Department of Chemistry, University of California Davis, One Shields Avenue, Davis, California 95616-5295.
Received September 22, 1999; Revised Manuscript Received December 22, 1999

We have developed and optimized the synthesis of the title compound, eliminating all HPLC purifications prior to the final product. The yield (and scale) of the synthesis was increased from 19% (200 mg) to 75% (26 g).

INTRODUCTION

Approximately 26 700 women are diagnosed with ovarian cancer annually in the United States; of these, 14 800 will die from their disease (*1*). Ovarian cancer is generally diagnosed at an advanced stage. Current standard health care consists of surgery followed by platinum-based chemotherapy. Advances in treatment have produced response rates of 65−80%, but only a small improvement in long-term survival (*2*). Progressions and relapses following treatment are common, and in most cases, the second line of treatment is of limited use. The majority of the these patients die from the disease, suggesting that benefits from surgery and chemotherapy, whether from new drugs or new combinations of old drugs, have reached a plateau (*3*).

Targeted strategies offer a promising alternative, because the cancer cells can be selectively treated while normal tissue is spared. Radioimmunotherapy (RIT)[1] employs the use of a monoclonal antibody (mAb) that binds to antigen sites on cancer cells. A short-lived radionuclide such as ^{90}Y is attached to the mAb via a bifunctional chelating agent, which is covalently bound to the antibody (*4*). The tumor-targeted radioisotope emits cytotoxic radiation.

Polymorphic epithelial mucin (PEM), the secreted product of the MUC1 gene, is highly expressed by ovarian cancer cells. Over 90% of epithelial ovarian tumors express PEM at levels much higher than background levels present on normal cells (*5*). HMFG1, a monoclonal antibody against PEM, binds to ovarian cancer cells (*6*, *7*). An adjuvant RIT for ovarian cancer has been developed using the mAb HMFG1 conjugated with the bifunctional chelator CITC-DTPA (Figure 1) and carrying chelated ^{90}Y (*8*).

The CITC-DTPA-HMFG1 immunoconjugate is radiolabeled with ^{90}Y to produce the radiopharmaceutical

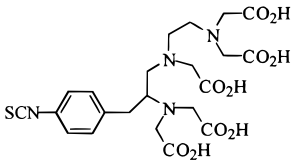

Figure 1. CITC-DTPA.

^{90}Y-CITC-DTPA-HMFG1 (Theragyn) (*9*−*11*). ^{90}Y has favorable properties for radioimmunotherapy: it is a high-energy β-emitter (E_{max} = 2.28 MeV) with a physical half-life of 2.7 days (*12*). ^{90}Y-CITC-DTPA-HMFG1 is administered as a one-time intraperitoneal injection to patients who have already received standard care. In phase I-II trials, patients receiving the Theragyn adjuvant treatment have shown a 5-year survival rate of over 80%, versus 55% for those receiving standard care alone (*13*). For the Theragyn adjuvant therapy to enter phase III trials, the development of an efficient large-scale synthesis of CITC-DTPA was required. The procedure described below (Scheme 1) was designed to provide for a minimum of a 10-g scale preparation of CITC-DTPA with >50% overall yield (in practice 2−4 times this amount of product was realized).

EXPERIMENTAL PROCEDURES

All reagents and solvents were the purest commercially available and used without further purification. (*S*)-*p*-Nitrophenylalanine was purchased from BACHEM. Borane-THF (1 M) was purchased from Aldrich. The HPLC solvents were purchased from Fisher. Precautions were taken to minimize contamination with adventitious metal ions. All the laboratory glassware was washed with mixed acid solution and rinsed copiously with 18 MΩ cm H_2O. Trace-metal grade HCl was used for acid washing and as a reagent. All plasticware was washed in 3 M HCl overnight and thoroughly rinsed. Glassware was oven dried overnight and cooled under an argon atmosphere.

Thin-layer chromatography was run on plastic-backed silica gel plates with 0.2-mm-thick silica gel 60 F254 (E. Merck, Germany). Three solvent systems were used to develop the TLC plates. System 1 was 15% (w/v) ammonium hydroxide/ethanol (1:4 v/v); system 2 was hexanes/EtOAc (2:1 v/v); system 3 was 10% ammonium acetate/CH_3OH (w/v).

High-performance liquid chromatography was carried out on a Rainin HPXL system (Rainin Instrument, Woburn, MA) equipped with titanium self-washing

* To whom correspondence should be addressed. Phone: (530) 752-0936. Fax: (530) 752-8938. E-mail: cfmeares@ucdavis.edu.

[1]Abbreviations: CH_3CN, acetonitrile; CH_3OH, methanol; $CHCl_3$, chloroform; CITC-DTPA, (*S*)-1-*p*-isothiocyanatobenzyl-diethylenetetraminepentaacetic acid; DIEA, diisopropylethylamine; DMF, *N*,*N*-dimethylformamide; EtOAc, ethyl acetate; EtOH, ethanol; Et_2O, ethyl ether; HMFG1, Human Milk Fat Globule 1 antibody; HPLC, high-performance liquid chromatography; mAb, monoclonal antibody; NH_2-Bn-DTPA, 1-(*S*)-*p*-aminobenzyl-diethylenetetraminepentaacetic acid; PEM, polymorphic epithelial mucin; RIT, radioimmunotherapy; TFA, trifluoroacetic acid; THF, tetrahydrofuran; TMAP, tetramethylammonium phosphate.

10.1021/bc990125x CCC: $19.00 © 2000 American Chemical Society
Published on Web 02/11/2000

Scheme 1. Synthetic Scheme for CITC-DTPA

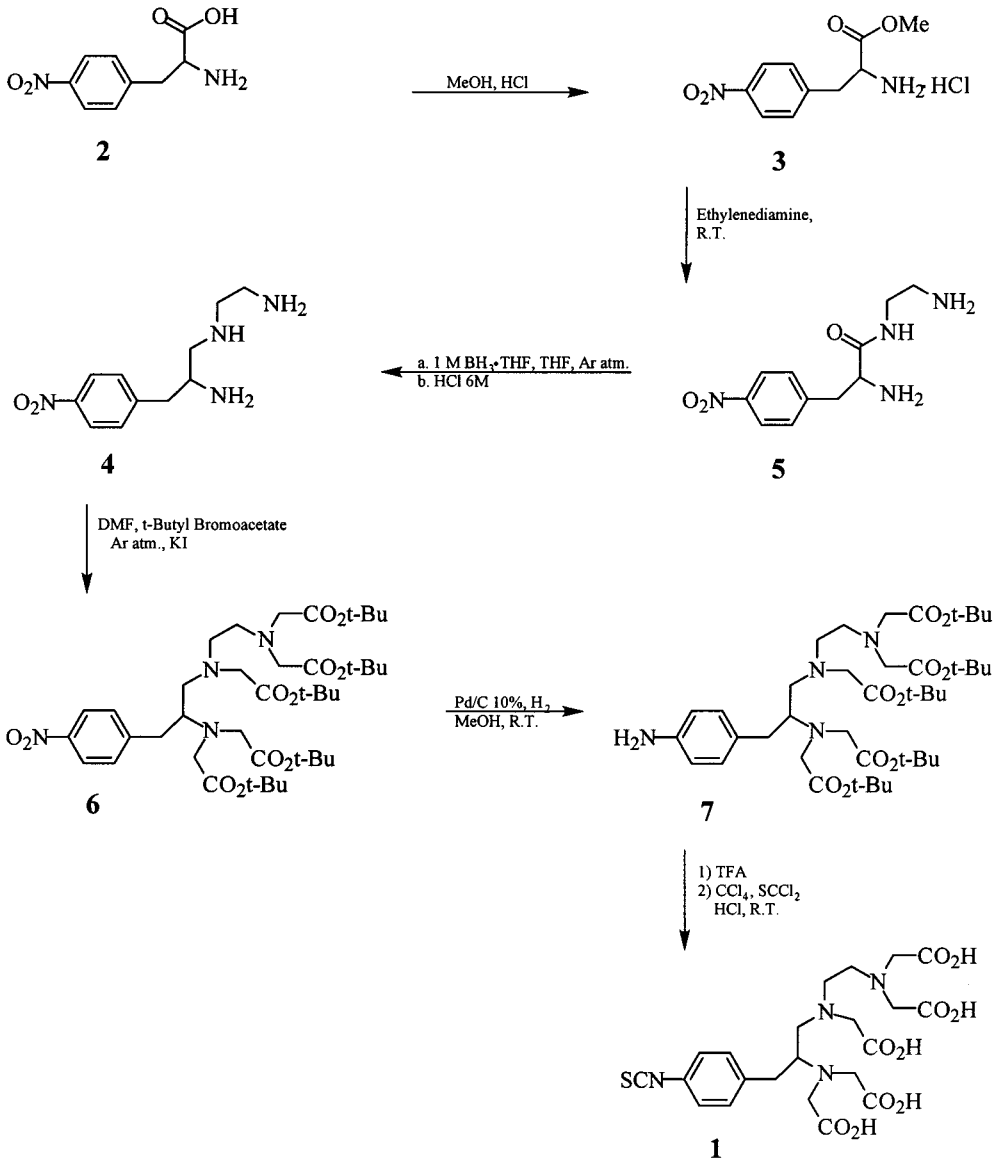

pump heads. Solvents were mixed using a Dynamax titanium dual-chamber mixer. UV absorbance was measured at 254 or 280 nm. The HPLC system was controlled by Dynamax software on a Macintosh Plus computer. Analytical reversed-phased HPLC was performed at room temperature at 1 mL/min with an Alltima 4.6 × 250 mm column and 4.6 × 7.5 mm guard column (Alltech Associates, Inc, Deerfield, IL). The running solvents were CH_3-CN containing 0.1% TFA and H_2O containing 0.1% TFA.

Ultraviolet spectra were generated on a HP 8450A diode array spectrophotometer after blanking the instrument against the sample diluent. The absorbance was measured at 280 nm in a 1-cm path-length cell. Samples were diluted to give absorbance readings of 0.1−1.2.

Radiation counting was done in a Beckman model 310 counter with the energy windows set for ^{57}Co emissions at 136 122, and 14 keV. TLC plates containing radiolabeled materials were visualized with an AMBIS radioanalytical imaging system.

NMR Spectroscopy. ^{1}H and ^{13}C spectra were obtained at 300 and 75.5 MHz, respectively. For samples containing D_2O (plus CF_3COOD), a value of 4.67 ppm was assigned for the HDO peak for the proton spectra and a value of 116.6 ppm was assigned for the aliphatic carbon in CF_3COOD for the ^{13}C spectra. For samples in $CDCl_3$, values of 7.26 and 77.0 ppm were assigned for the ^{1}H and ^{13}C spectra, respectively.

Mass Spectrometry. The samples were analyzed on a Micromass Bio-Q mass spectrometer using the electrospray technique. Immediately before analysis, the samples were diluted in CH_3OH. Results reported for *m*/*z* are for $[M + H^+]^+$.

FTIR Spectroscopy. Samples were prepared as KBr pellets or applied to NaCl plates. A Mattson Galaxy 3000 FTIR spectrophotometer was used in collecting and analyzing spectra.

Preparation of CITC-DTPA (1). *Methyl (S)-p-Nitrophenylalanate (**3**).* (*S*)-*p*-Nitrophenylalanine (**2**, 80.0 g, 0.381 mol) was added into a 2 L three-neck flask equipped with a thermometer, a gas inlet, and a rubber septum. The flask was purged with dry argon. Anhydrous CH_3OH (1 L) was transferred into the 2 L flask via a cannula. The (*S*)-*p*-nitrophenylalanine clumped at the bottom upon addition of the CH_3OH. Anhydrous $HCl_{(g)}$ was bubbled into the stirring CH_3OH through a glass wool plug in a pipet, to dissolve the (*S*)-nitrophenylalanine. An ice bath was used to keep the temperature below 10 °C. Thirty minutes after beginning the bubbling of the

HCl(g), the reaction solution became clear. It then turned light yellow and became cloudy after an hour of stirring. After saturating the solution with HCl(g), the tubing for the HCl was replaced with a drierite drying tube. The solution stirred at 10 °C for another 45 min. The flask was wrapped with aluminum foil to protect it from light and left in a cold room at 4 °C overnight to crystallize the methyl ester product. The pale yellow crystals were filtered on a coarse-fritted funnel under an Ar atmosphere. The collected crystals were washed with cold CH_3OH (two 50 mL portions) and dried under reduced pressure, yielding 68.5 g of the methyl ester. The clear yellow supernatant was concentrated to one-third of the original volume under reduced pressure and placed in a 4 °C cold room overnight (some crystals formed); the flask was moved to a −20 °C refrigerator for another 24 h. After filtration and washing the crystals, a second crop of the crystalline methyl ester (19.17 g) was obtained and dried under reduced pressure. TLC showed the two crops to be equivalent, so they were combined. The total yield of **3** was 87.67 g, 0.337 mol (88.5%): FTIR ν_{max} 2983, 1747, 1600, 1509, 1347, 1240 cm^{-1}; ^1H NMR δ 3.29 (dd, 1H, J = 14.5, 7.5 Hz), 3.39 (dd, 1H, J = 14.7, 6.3 Hz), 3.74 (s, 3H), 4.44 (t, 1H, J = 7.2 Hz), 7.44 (d, 2H, J = 8.7 Hz), and 8.16 (d, 2H, J = 8.7 Hz). FAB-MS *m/e* calcd (M + H^+): 225.08. Found: 225.09.

*(S)-p-Nitrophenylalanine N-(2-Aminoethyl) Amide (**4**).* Ethylenediamine (240 mL, 3.59 mol) was cannulated into a three-neck, 1 L round-bottom flask that had been oven dried, flushed with Argon, and equipped with a magnetic stirrer. The three openings of the flask were equipped with a gas inlet, a gas outlet, and a glass stopper. (*S*)-*p*-Nitrophenylalanine methyl ester (80.0 g, 0.306 mol) was added in 6 equal portions over a 2 h period via a powder funnel. The ester was added to the ethylenediamine to prevent the formation of polymer. The ester readily dissolved to give a dark red solution. After 24 h, the reaction solution was concentrated under reduced pressure to a red-brown viscous oil. NH_4OH, 7 M (550 mL), was added to this oil, and the pH was adjusted from 10.5 to 11.5 with a 50% NaOH solution. The aqueous phase was extracted with CH_2Cl_2 (10 portions of 550 mL). The organic extracts were pooled, dried with Na_2SO_4, filtered, concentrated, and dried under reduced pressure. The amide product **4** was an amorphous, hygroscopic, brown solid with a yield of 73.10 g (95.0%). FTIR ν_{max} 3361, 3293, 3072, 2933, 2867, 1656, 1604, 1515, 1347, and 1108 cm^{-1}; ^1H NMR δ 2.73 (t, 2H, J = 6.0 Hz), 2.86 (dd, 1H, J = 8.4, 13.7 Hz), 3.21 (t, 2H, J = 6.0 Hz), 3.24−3.28 (m, 1H), 3.60 (dd, 1H, J = 4.5, 8.4 Hz), 7.40 (d, 2H, J = 8.7 Hz), 7.55 (br s, 1H), 8.18 (d, 2H, J = 8.7 Hz); ^{13}C NMR ($CDCl_3$) δ 147.3, 147.6, 129.9, 123.5, 55.7, 52.4, 52.3, 42.4, 41.6. FAB-MS *m/e* calcd (M + H^+): 253.12. Found: 253.13.

*Reduction of (S)-p-Nitrophenylalanine N-(2-Aminoethyl) Amide (**4**).* ***Caution: explosion hazard.*** *p*-Nitrophenylalanine 2-aminoethylamide (23.9 g, 100 mmol) was placed in a 5 L three-neck flask in a heating/cooling oil bath. The apparatus included a 1 L addition funnel, a reflux condenser with Teflon sleeves on the ground glass joints, a thermometer, and a large Teflon stirbar. After purging with argon, anhydrous THF (800 mL) was added via the addition funnel rapidly in one portion to the reaction flask with stirring. The amide only partially dissolved in the THF. The reaction was cooled to 5−10 °C. The 1 M BH_3/THF (800 mL) solution was cannulated into the addition funnel. The BH_3/THF solution was added dropwise with stirring to the amide solution. Initially, one drop was added to see if bubbles formed; no more was added until the bubbling ceased. If the solution contained traces of water, the first few drops of BH_3/THF caused vigorous bubbling. After the addition of BH_3/THF was complete, the reaction was gradually warmed and brought to reflux for 15 h.

The solution was cooled to 9 °C. The septum was removed from the top of the condenser before adding H_2O. Excess borane was quenched by the slow, cautious dropwise addition of H_2O until the evolution of gas ceased. The reaction solution was then concentrated in situ under reduced pressure to a crusty yellow residue. HCl (560 mL, 6 M) was added to the residue, and the resulting solution was refluxed for 3 h followed by stirring at room temperature for 24 h. The solution was concentrated to dryness under reduced pressure. The residue was dissolved in 400 mL of H_2O and 400 mL of concentrated NH_4OH. The pH was adjusted to 11.5 with 5 M KOH. The aqueous solution was extracted with six 800 mL portions of $CHCl_3$. The pooled $CHCl_3$ extracts were dried over Na_2SO_4, filtered, concentrated, and dried at ∼50 mTorr to yield 22.0 g (96.0%) of an amorphous, hygroscopic solid product **5**. FTIR ν_{max} 3357, 3276, 2923, 2846, 1596, 1515, 1346, and 1108 cm^{-1}; ^1H NMR δ 2.48 (dd, 1H, J = 8.4, 11.7 Hz), 2.60−2.86 (m, 6H, J = 6.0 Hz), 2.89 (dd, 1H, J = 4.8, 11.4 Hz), 3.10−3.18 (m, 1H), 7.37 (d, 2H, J = 8.7 Hz), 8.16 (d, 2H, 8.7 Hz); ^{13}C NMR ($CDCl_3$) δ 173.6, 147.0, 145.8, 130.1, 123.7, 56.2, 41.8, 41.3, and 41.0. FAB-MS: *m/e* calcd (M + H^+): 2239.14. Found: 239.15.

*1-(S)-(p-Nitrobenzyl)diethylenetriaminepentaacetic Acid Penta-t-butyl ester (**6**).* A 2 L three-neck round-bottom flask was equipped with a 500 mL addition funnel and a stir bar. Compound **5** (38.8 g, 163 mmol) was added to the flask under an argon atmosphere. Anhydrous DMF (1.30 L) was cannulated into the addition funnel and then added in one portion. After all the **5** dissolved, DIEA (340 mL, 1.95 mol) was cannulated into the addition funnel and added in one portion to the reaction mixture. *t*-Butyl bromoacetate (217 mL, 1.47 mol) was syringed into the reaction in one portion. The reaction was a golden brown color. KI (29.7 g, 179 mmol) was added in one portion to the reaction. The solution immediately turned yellow and cloudy and became warm to the touch. The reaction was stirred under an argon atmosphere for 12 h at room temperature. After 12 h, a 100 μL aliquot was removed via syringe and concentrated on a rotary evaporator. The dried aliquot was dissolved in CH_3OH (1.25 mL) to a 10 mM concentration. TLC showed only one spot corresponding to product and the complete disappearance of the triamine starting material. The reaction lane was negative to ninhydrin. The reaction was stirred for an additional hour, for a total reaction time of 16 h. The reaction was a cloudy yellow color with no change in appearance from time zero. The reaction was concentrated in a rotary evaporator at ∼50 mTorr and using a water bath temperature no higher than 35 °C. The reaction mixture was taken to complete dryness, until only an amorphous solid remained in the flask.

Et_2O (2 L) and H_2O (1 L) were added to the reaction residue and swirled until everything dissolved. The solution was poured into a separatory funnel (4 L) and shaken. The aqueous layer was removed, and the ether layer was washed with H_2O (1 L). The aqueous layer was removed and the Et_2O phase washed with a saturated NaCl(aq) solution (500 mL). The Et_2O solution was dried with Na_2SO_4, filtered on a coarse frit, concentrated in situ, and dried under reduced pressure. A yellow-brown oil remained in the flask.

The crude *t*-Butyl-NO_2-Bn-DTPA **6** was purified via a

3-in. SiO_2 plug with a hexane/EtOAc (2:1) eluent. After 2 L of solvent was collected, the TLC showed all of **6** had eluted from the column. The eluent was concentrated under reduced pressure and dried at ~50 mTorr to yield 138.9 g (94%) of the penta-alkylated product: FTIR ν_{max} 3448, 2977, 2933, 1739, 1598, 1519, 1456, 1392, 1367, 1344, 1255, 1218, and 1151 cm^{-1}; ^1H NMR δ 1.41 (s, 27H), 1.43 (s, 18H), 2.45 (dd, 1H, J = 8.4, 12.9 Hz), 2.70−3.10 (m, 8H), 3.30 (s, 2H), 3.39 (s, 2H), 3.40 (s, 2H), 3.42 (s, 4H), 7.48 (d, 2H, J = 8.4 Hz), 8.10 (d, 2H, J = 8.4 Hz). FAB-MS *m/e* calcd ($M + H^+$): 809.48. Found: 809.49.

*Penta-t-Butyl 1-(S)-(p-Aminobenzyl)-diethylenetriaminepentaacetate (**7**).* All glassware was washed in mixed acids (1:1 mixture of concentrated H_2SO_4 and concentrated HNO_3) for a minimum of 12 h and rinsed with pure H_2O. In a fume hood, Pd/C 10% (6.2 g) was added to a 250 mL round-bottom flask under an Ar atmosphere. CH_3OH was slowly added until all the Pd/C was wet (reduces fire hazard). CH_3OH (100 mL) was added and the slurry poured into an 8 L three-neck flask under an argon atmosphere. Compound **6** (124.0 g, 71.4 mmol) and CH_3OH (5 L) were added to the 8 L round-bottom flask (under Ar to avoid fire) equipped with a stir bar. The reaction was stirred at room temperature until all of the **6** dissolved, at which point it was cooled to 0 °C in an ice bath. H_2 gas was bubbled continuously into the reaction solution through a fritted bubbler. The ice bath was allowed to melt and the reaction gradually warmed to room temperature. After 24 h, TLC showed the hydrogenation to be complete (solvent hexane/EtOAc 1:2). Celite (20 g) was added to the reaction mixture and stirred for 15 min. The reaction solution was filtered through Celite packed on a 600 mL coarse glass frit. The Celite plug was washed with CH_3OH (five 100 mL portions). The clear yellow filtrate was concentrated under reduced pressure to a yellow oil, which was dried at ~50 mTorr to a final mass of 120.2 g (99%): FTIR ν_{max} 2978, 2931, 1737, 1520, 1367, 1344, 1249, 1219, and 1149 cm^{-1}; ^1H NMR δ 1.40 (s 9H), 1.44 (s, 36H), 2.47−2.53 (m, 2H), 2.75−2.80 (m, 6H), 2.95−3.05 (m, 1H), 3.20−3.52 (m 10H), 6.60 (d, J = 8.1 Hz, 2H), 6.99 (d, J = 8.1 Hz, 2H).

1-(S)-(p-Aminobenzyl)diethylenetriaminepentaacetic Acid. To remove adventitious metals, all glassware was soaked in mixed acids overnight and rinsed with double-deionized H_2O. TFA (1.05 L) was added to compound **7** (77.0 g, 75.4 mmol) at room temperature. The reaction mixture was stirred for 15 h at room temperature. The TFA was removed under reduced pressure. The resulting brown-yellow crusty solid was dried at ~50 mTorr and stored at −70 °C. The yield was quantitative (122 g): FTIR ν_{max} 3428, 2992, 1733, 1666, 1515, 1425, and 1193 cm^{-1}; ^1H NMR δ 2.56 (dd, J = 9.2, 13.6 Hz, 1H), 2.89 (m, 3H), 3.13−3.29 (m, 2H), 3.52−3.65 (m, 9H), 3.78 (br s, 4H), 7.16 (d, J = 8.0 Hz, 2H), 7.21 (d, J = 8.0 Hz, 2H). FAB-MS *m/e* calcd ($M + H^+$): 541.15. Found: 541.15.

*CITC-DTPA (**1**).* All glassware was soaked in mixed acidsfor a minimum of 12 h and rinsed with pure H_2O. HCl (3 M, 832 mL), CCl_4 (487 mL), and Cl_2CS (229 mL, 3.02 mol) were added to NH_2-Bn-DTPA (122 g, 75.4 mmol) in a 3 L round-bottom flask equipped with a magnetic stir bar. The reaction was protected from light by wrapping the reaction flask with Al foil. The reaction was complete after 6 h, as shown by both ninhydrin and the fluorescamine tests as follows: 1 μL of the aqueous layer (top layer) and 1 μL of starting material were spotted on filter paper, which was sprayed with ninhydrin (200 mg of ninhydrin:100 mL of acetone) and gently warmed on an oven top. The starting NH_2-Bn-DTPA was positive (brown spot) and the reaction solution negative to ninhydrin (*14*). For the fluorescamine test, 1 μL of NH_2-Bn-DTPA and 1 μL of the reaction's aqueous layer were each spotted separately on a filter paper (*15*). The paper was sprayed with borate buffer, dried, sprayed with fluorescamine, and visualized under UV light (254 nm). The NH_2-Bn-DTPA was positive (green fluorescence) and the reaction mixture was negative to fluorescamine. The reaction mixture was concentrated to a crusty solid and dried at ~50 mTorr to yield 97.6 g, quantitative by ninhydrin and fluorescamine: FTIR ν_{max} 3447, 3011, 2540, 2182, 2120, 1733, 1652, 1419, 1362, 1194, and 1147 cm^{-1}. ^1H NMR δ 2.01 (dd, J = 9.2, 13.6 Hz, 1H), 2.38−2.50 (m, 3H), 2.67−2.78 (m, 2H), 2.95−3.21 (m, 9H), 3.52 (s, 4H), 6.45 (d, J = 8.0 Hz, 2H), 6.52 (d, J = 8.0 Hz, 2H). FAB-MS *m/e* calcd ($M + H^+$): 541.15. Found: 541.15.

HPLC Purification of CITC-DTPA (1). Sample Preparation. Crude **1** (97.6 g) was dissolved in the following manner: a 2% TFA in 9:1 H_2O:CH_3CN solution was prepared by adding TFA (2.2 mL) to a 9:1 solution of H_2O (99 mL) and CH_3CN (11 mL), which was added to the crude **1**. A clear reddish-brown solution resulted after stirring for 2 min. Approximately 40−60% of the mass of the crude **1** is salt; the solution was approximately 36.4 mg/mL **1**, after correction for the presence of salt. The solution was diluted by adding a 9:1 H_2O:CH_3CN solution in 100 mL aliquots. After the addition of each aliquot, the mixture was stirred vigorously to ensure complete mixing and prevent **1** from precipitating. The solution was diluted to a final volume of 1.1 L of 9:1 H_2O:CH_3CN solution containing 0.2% TFA, and filtered through a 0.2 μm filter. The solution was stored frozen at −70 °C and not thawed until immediately before use.

The **1** solution was purified by reversed-phase HPLC using a 7.7 × 29 cm Alltima 5 μm C18 (Alltech Associates) column. The HPLC system consisted of 3 pumps, each with a self-washing titanium pump head. Precautions were taken to keep the system metal-free. The plumbing was peek tubing or stainless steel passivated overnight with 6 N HNO_3. All plumbing fittings were titanium or peek. Pump A pumped the aqueous solvent, 0.2% TFA in H_2O. Pump B pumped the organic solvent, 0.2% TFA in CH_3CN. Pump C was used to inject the sample. The detector was a Dynamax UV-1 detector equipped with a preparatory flow cell. The detector wavelength was set at 254 nm. The flow rate was 155 mL/min. Approximately 2 g of crude **1** was applied to the column. The HPLC method used was as follows: 25% solvent B, 0−2 min; 25−26% solvent B, 2−7 min; 26% solvent B, 7−43 min; 26−34% solvent B, 43−48 min; 34% solvent B, 48−58 min; 34−100% solvent B, 58−63 min.

The frozen **1** solution was removed from the −70 °C freezer and thawed and filtered through a 0.2 μm filter. The solution was kept on ice. The pump C intake line was placed directly into the crude **1** solution. The injection volume (55 mL) contained approximately 2 g of **1**/injection. Between six and eight fractions were collected into glass flasks for each run (A−G in Figure 2). All glassware was acid washed in 6 N HCl for 24 h and rinsed with pure H_2O. Several fractions were collected based on the peak shape and elution profile of the chromatogram. Each peak was analyzed by HPLC for purity and stored at −70 °C, if not concentrated immediately. Fractions with >97.5% purity were pooled and concentrated to one-fourth to one-third of their original volume under reduced pressure, then frozen in a dry ice/acetone bath and lyophilized to dryness (constant weight)

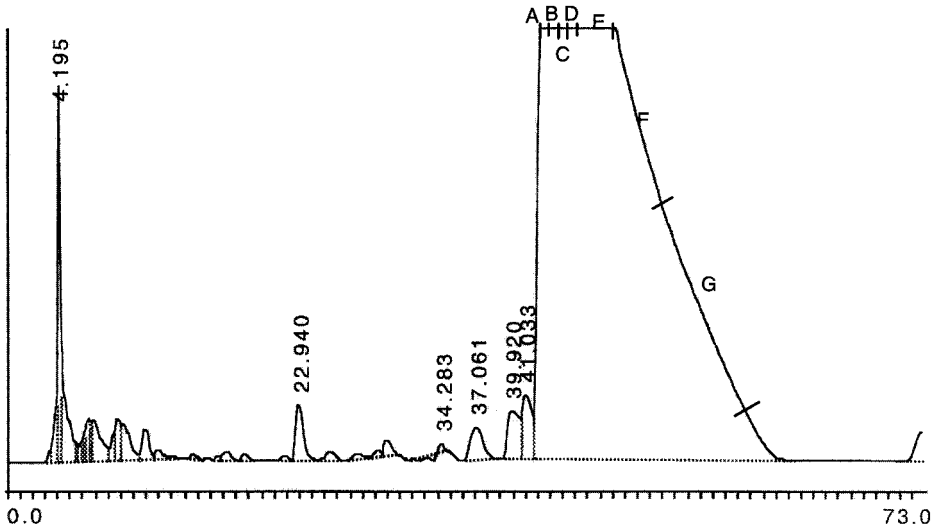

Figure 2. Reversed-phased HPLC purification of CITC-DTPA with typical fraction cutoffs. A−G indicates where fractions were collected.

overnight. The resulting fluffy white powder was transferred to an acid-washed plastic container and stored at −70 °C.

HMFG1 Conjugation with CITC-DTPA (1). To test the labeling ability of the CITC-DTPA, a few small-scale conjugations of CITC-DTPA with the mAb HMFG1 were carried out. Conjugations to prepare immunoconjugates with approximately two, three, or four chelates per mAb were performed in the following manner:

2 CITC-DTPA/HMFG1. HMFG1 was supplied at 5.5 mg/mL in 0.1 M ammonium acetate, pH 6.0, by the Imperial Cancer Research Fund. The HMFG1 (27 mL, 148.5 mg) was buffer exchanged and concentrated into 0.2 M TMAP, pH 8.5, using an Amicon Centriprep 50. A total of 6 mL of HMFG1 was recovered at 20.4 mg/mL in 0.2 M TMAP, pH 8.5. HMFG1 in 0.2 M TMAP, pH 8.5 (189 μL, 3.85 mg) was added to 0.2 M TMAP and 5 mM DTPA, pH 8.5 (136.3 μL), in a metal-free 500 μL eppendorf tube. Compound **1** (19.1 mM, 2.66 μL) was added to the eppendorf and vortex mixed. The pH was adjusted to 9.5−10 with 2 μL of 25% tetramethylammonium hydroxide. The reaction was kept at room temperature for 2 h. The excess CITC-DTPA and DTPA were removed and the 0.2 M TMAP buffer exchanged in one step by Penefsky gel filtration columns (*16*) into 0.1 M ammonium acetate, pH 5.5.

3 CITC-DTPA/HMFG1. TMAP (0.2 M) and 5 mM DTPA, pH 8.5 (135 μL), and HMFG1 in 0.2 M TMAP, pH 8.5 (189 μL, 3.85 mg), were added to a metal-free eppendorf tube. CITC-DTPA (19.1 mM) (4.02 μL) was added to the reaction and vortex mixed. The reaction proceeded as above for the 2 CITC-DTPA/HMFG1 conjugate.

4 CITC-DTPA/HMFG1. TMAP (0.2 M) and 5 mM DTPA, pH 8.5 (133.3 μL), and HMFG1 in 0.2 M TMAP, pH 8.5 (189 μL, 3.85 mg), were added to a metal-free eppendorf tube. CITC-DTPA (19.1 mM) (5.33 μL) was added to the reaction and vortex mixed. The reaction proceeded as above for the 2 CITC-DTPA/HMFG1 conjugate.

Determination of the Number of Chelates/Antibody. The average number of CITC-DTPA chelating groups/antibody was determined by using the method developed by Meares et al. (*17*).

RESULTS AND DISCUSSION

Previously published syntheses of CITC-DTPA did not provide the simplicity, purity, or scale required for a large clinical trial (17, 18). The new synthesis (Scheme 2) successfully avoids metal contamination, requires no chromatographic purification of intermediates, and increases the reaction scale severalfold. The procedure also generates easily handled, organic-soluble intermediates. It was required to reproduce this procedure three times exactly for regulatory purposes. A minimum of 10 g of CITC-DTPA per lot was needed for the phase III clinical trial. We successfully produced several times this amount using this synthetic procedure, which gave equivalent results with each lot. The overall yield was improved from 19% to 78% with the only purification coming after the final transformation.

The *p*-nitrophenylalanine methyl ester was prepared by dissolving *p*-nitrophenylalanine in anhydrous CH_3OH and saturating the solution with HCl(g); after crystallization, the yield was 89%. The methyl ester was converted to the aminoethylamide by adding it gradually in six equal aliquots with vigorous stirring (to prevent polymerization) to a large excess (12 eq) of neat ethylenediamine. Dimers, trimers, tetramers, etc. were not produced at detectable levels according to HPLC or mass spectrometry of the final product.

For purification of the amide, several different extraction techniques, pH values, and solvents were examined—including $CHCl_3$, EtOAc, high salt concentrations, and continuous extraction. $CHCl_3$ extraction of the aqueous phase at pH 11.5 was the most effective method for recovering the amide cleanly as a hygroscopic solid with a 97% yield. This material was used in the next step without further purification. After extensive practice and safety precautions, the borane reduction of the amide to the triamine produced a clean product with a yield of ≥95%.

The penta-alkylation of the triamine was the least successful reaction in the earlier synthesis of CITC-DTPA (Scheme 2) and the biggest yield problem. Earlier alkylation methods involved treating the triamine in aqueous solution with bromoacetate at pH 10.5 under metal-free conditions, for 48−72 h. The best reported yield was 36% after a lengthy HPLC purification of the penta-alkylated product. Using *t*-butyl bromoacetate as the alkylating agent in a nonaqueous solvent provided several advan-

Scheme 2. Comparison of New versus Previous CITC-DTPA Methodology[a]

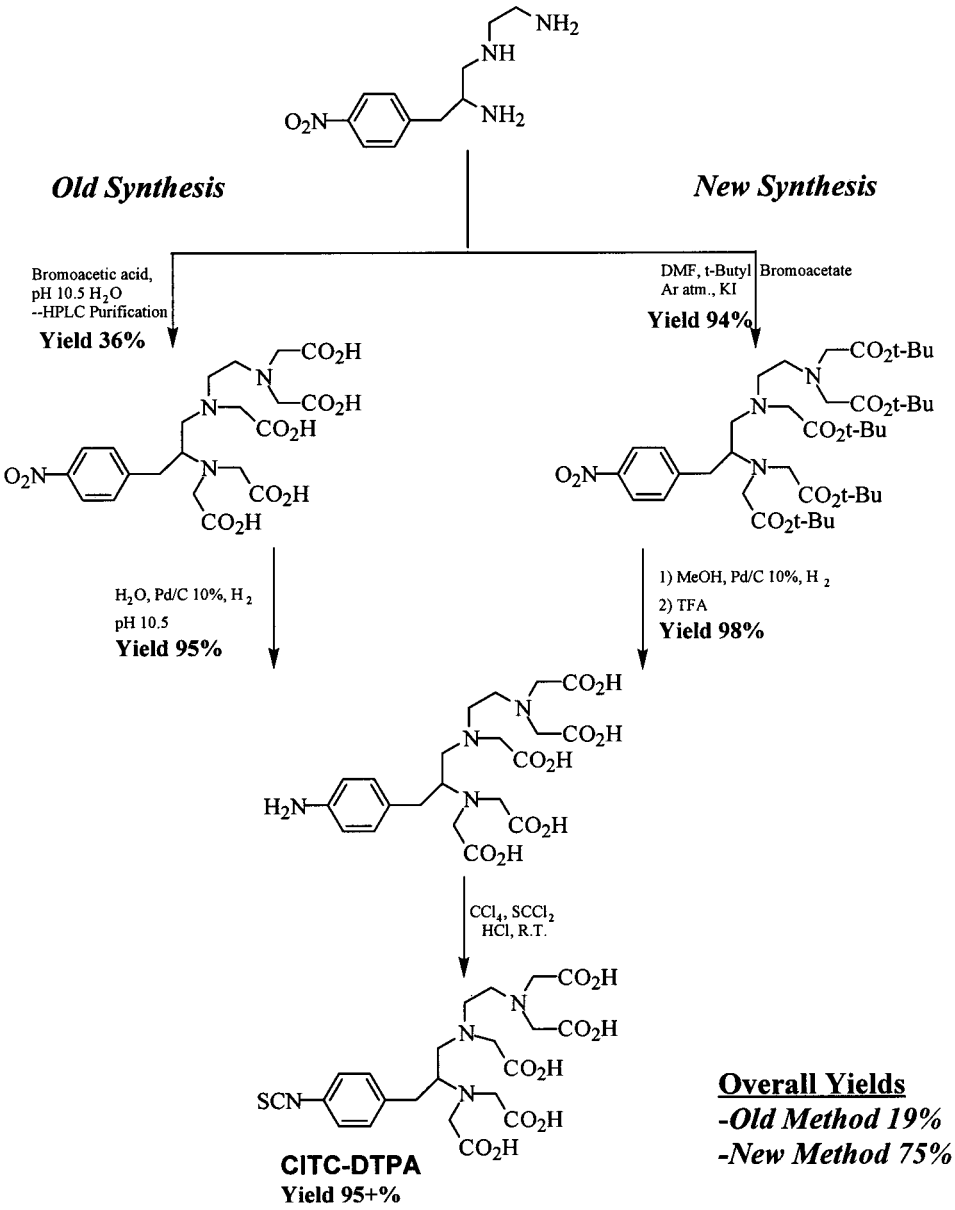

[a] The overall yield is for the entire synthesis and includes yield improvements in previous steps that were primarily due to changes in the work-up procedures, not the reaction conditions.

tages (*19*). S_N2 reactions work best in polar aprotic solvents such as CH_3CN or DMF, not polar protic solvents such as H_2O. The alkylation reactions in CH_3CN did not go to completion, even when refluxed for 72 h in the presence of catalytic NaI. The NaI served to generate the more reactive *t*-butyl iodoacetate, an in situ Finkelstein reaction. The reactions run in DMF were complete (by TLC) in less than 18 h at room temperature with or without NaI, and provided no significant side products. The penta-alkylated *t*-butyl product **6** was also soluble in organic media, allowing the substitution of silica gel plug filtration for HPLC purification. The hindered base DIEA was chosen as the proton scavenger for the reactions run under these conditions. In our hands, it gave higher yields than K_2CO_3. The experimental yields of the penta-alkylation product were best using DMF, NaI, DIEA, argon atmosphere, and room temperature, with yields up to 96% after SiO_2 plug filtration.

The hydrogenation worked best in CH_3OH with Pd/C and hydrogen, smoothly transforming the *p*-nitrobenzyl-DTPA penta-*t*-butyl ester to the *p*-amino-benzyl-DTPA penta-*t*-butyl ester. Several solvents and conditions for the hydrogenation were examined, including ethanol, ethanol with $NaHCO_3$, ethanol with Na_2CO_3, CH_3OH, and EtOAc. The substitution of CH_3OH for H_2O allowed for easier concentration of the reaction when complete. A typical reaction yield was 99%.

Deprotection of with 3 M HCl and CCl_4 had been attempted with the hope of consolidating the deprotection reaction with the isothiocyanate preparation. The *t*-butyl esters were not quantitatively cleaved by this method, so it was abandoned. The penta-*t*-butyl *p*-amino-benzyl-DTPA ester **7** was deprotected with TFA at room temperature for 15 h with a quantitative yield of the *p*-aminobenzyl-DTPA. The isothiocyanate **1** was prepared using standard two-phase methodology. The *p*-aminobenzyl-DTPA was dissolved in 3 M HCl and thiophosgene dissolved in a CCl_4 solution. The CCl_4 organic phase was combined with the aqueous HCl phase and vigorously stirred to mix the two phases. The reaction was complete after 6 h. Completeness of the reaction was tested by spotting 2 μL aliquots onto two different filter papers and

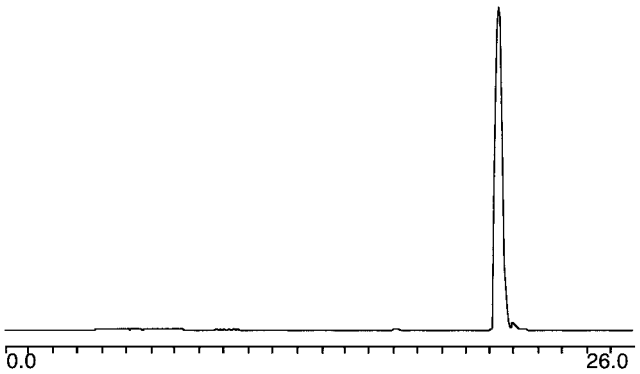

Figure 3. Reversed-phase HPLC analysis of CITC-DTPA, >95% pure after 7 synthetic transformations and no column purification steps.

spraying one with ninhydrin and the other with borate buffer followed by fluorescamine. The reaction solution was concentrated in situ to a crusty solid.

Figure 3 shows the HPLC chromatogram of the crude CITC-DTPA with a >95% purity after seven synthetic steps and no chromatography purification steps. The major impurities in the crude CITC-DTPA were nonchromogenic salts. The preparative reversed-phase C18 HPLC step served to desalt the CITC-DTPA and remove trace amounts of chromogenic impurities (less than 1.5%). The first fraction from the HPLC purification contained the majority of the impurities and was discarded. The major metal-containing contaminant we saw by HPLC was the iron chelate, which eluted 6 min before the CITC-DTPA peak. Experience has shown that the majority of metal contamination comes from the syringe used for injecting the analytical HPLC. After sonicating our HPLC injection syringes with 3 M HNO_3 and installing new needles, we were unable to detect any metal contamination of the crude CITC-DTPA or the final product by HPLC. The HPLC method used to purify the CITC-DTPA used 0.2% TFA in H_2O as the aqueous phase and 0.2% TFA in CH_3CN as the organic phase. The acidic pH of the 0.2% TFA solution increased the solubility and stability of the isothiocyanate during purification, concentration, and lyophilization. We were able to use the low pH provided by the 0.2% TFA due to the stability of the multiply bonded C18 stationary phase. Singly bonded C18 would bleed off the column at a noticeable rate at this pH. The crude CITC-DTPA was prepared for purification by dissolving in a 9:1 H_2O:CH_3CN solution with 2% TFA. The concentrated solution was diluted 10-fold with 9:1 H_2O:CH_3CN. The crude CITC-DTPA solution and purified fractions were stored on ice during and after purification to prevent hydrolysis of the isothiocyanate group. All CITC-DTPA-containing fractions were stored at −70 °C if not concentrated immediately. The fractions containing CITC-DTPA with purity greater than 97.5% by analytical HPLC were combined, concentrated, and lyophilized; yielding a total of 26 g of a fluffy white powder with a final purity of 98%. The mass spectrum and HPLC showed no metal contamination of any sort.

CITC-DTPA (2.00 g) was formulated with sterile H_2O for injection. The initial pH 1.2 was raised with triethylamine in 0.3-eq aliquots and vigorously vortexed until all the CITC-DTPA went into solution, final pH 3.29. This solution was sterile-filtered and dispensed into acid-washed vials in 2 mL aliquots (total of 30). The absolute concentration was determined by a Co-57 assay to be 19.1 mM. The CITC-DTPA solution was analyzed by HPLC and UV.

A CITC-DTPA-HMFG1 conjugate standard was prepared for use in radiolabeling experiments with ^{90}Y. As described above, three 3.85 mg trial reactions and a final large-scale (50 mg) conjugation were performed. Three trial conjugates with a desired chelate-to-antibody ratio of 2:1, 3:1, and 4:1 were planned. After reacting CITC-DTPA with HMFG1, the conjugates were analyzed by Co-57 assay and determined to have 2:1, 3:1, and 3.6:1 chelates/antibody, respectively. The large-scale conjugation was planned for 2 chelates/antibody. The actual reaction gave 1.7 chelates/antibody.

The scale-up of the synthesis of CITC-DTPA was improved in several ways. The alkylation yield of the triamine was greatly improved by the use of *t*-butyl bromoacetate in place of bromoacetic acid. An intermediate preparative HPLC step was also eliminated from the reaction scheme. Using the new procedure, the synthetic yield was increased from a reported literature high of 36% to over 75% (starting from *p*-nitrophenylalanine). Both yields are calculated for the synthesis of aminobenzyl-DTPA. The yield of CITC-DTPA was not included, as it was affected by the high purity requirements imposed for the final product.

ACKNOWLEDGMENT

This work was supported by Antisoma Ltd., London, UK. The authors thank Dr. Leslie Anderson and David Qu for excellent technical assistance. We also thank Brian Schmidt for his assistance in the final purification.

LITERATURE CITED

(1) Boring, C. C., Squires, T. S., and Tong, T. (1995) *Cancer statistics. CA Cancer J. Clin. 45*, 12−13.

(2) Nejit, J. P., Ten Bokkel Huinik, W. W., Van Der Burg, M. E. L., Van Oosterom, A. T., Vriesdendorp, R., Kooyman, C. D., Van Lindert, A. C. M., Hamerlynek, J. V. T. H., Van Houwelingen, J. C., and Pinedo, H. M. (1984) Randomised trial comparing two combination chemotherapy regimes (Hexa-CAF vs CHAP-5) in advanced ovarian carcinoma. *Lancet 2*, 594−600.

(3) Marsoni, S., Torri, V., Valsecchi, M. G., Beloni, C., Bianchi, V., Bolis, G., Bonazzi, C., Colombo, N., Epis, A., Faralli, G., Gambino, A., Landoni, F., Maggi, R., Pecorelli, S., Presti, S., Vassena, L., Zanaboni, F., and Mangoni, C. (1990) Prognostic factors in advanced epithelial ovarian cancer. *Br. J. Cancer, 62*, 21−26.

(4) Sundberg, M. W., Meares, C. F., Goodwin, D. A., and Diamanti, C. T. (1974) Chelating agents for the binding of metal ions to macromolecules. *Nature 250*, 587−588.

(5) Gendler, S. J., Burchell, J. M., Duhig, T., Lamport, D., White, R., Parker, M., and Taylor-Papadimitriou, J. (1987) Cloning the cDNA coding coding for the differentiation and tumor associated mucing glycoproteins expressed by human mammary epithelium. *Proc. Natl. Acad. Sci. U.S.A. 84*, 6060−6063.

(6) Burchell, J., Gendler, S., Taylor-Papadimitriou, J., Girling, A., Lewis, A., and Millis, R. (1987) Development and characterization of breast cancer reactive monoclonal antibodies directed to the core protein of the human milk mucin. *Cancer Res. 47*, 5476−5782.

(7) Taylor-Papadimitriou, J., and Epenetos, A. A. (1994) Exploiting altered glycosylation patterns in cancer: progress and challenges in diagnosis and therapy. *Trends Biotechnol, 12* (6), 227−233.

(8) Hird, V., Maraveyas, A., Snook, D., Dhokia, B., Soutter, W. P., Meares, C. F., Stewart, J. S. W., Mason, P., Lambert, H. E., and Epenetos, A. A. (1993) Adjuvant therapy of ovarian cancer with a radioactive monoclonal antibody. *Br. J. Cancer 68*, 403−406.

(9) Epenetos, A. A., Munro, A. J., Stewart, S., Rampling, R., Lambert, H. E., McKenzie, C. G., Soutter, P., Rahemtulla, A., Hooker, G., Sivolapenko, G. B., Snook, D., Courtenay-

Luck, N., Dhokia, B., Krausz, T., Taylor-Papadimitriou, J., Durbin, H., and Bodmer, W. F. (1987) Antibody-guided radiation of advanced ovarian cancer with intraperitoneally administered radiolabeled monoclonal antibodies. *J. Clin. Oncol. 5*, 1890−1899.

(10) Stewart, J. S. W., Hird, V., Snook, D., Dhokia, B., Sivolapenko, G., Hooker, G., Taylor-Papadimitriou, J., Rowlinson, G., Sullivan, M., Lambert, H. E., Coulter, C., Mason, W. P., and Epenetos, A. A. (1990) Intraperitoneal Yttrium-90-labeled monoclonal antibody in ovarian cancer. *J. Clin. Oncol. 8*, 1941−1950.

(11) Maraveyas, A., Snook, D., Hird, V., Kosmas, C., Meares, C. F., Lambert, H., and Epenetos, A. A. (1994) Pharmacokinetics and toxicity of an yttrium-90-CITC-DTPA-HMFG1 radioimmunoconjugate for intraperitoneal radioimmunotherapy of ovarian cancer. *Cancer 73*, 1067−1075.

(12) Wessels, B. W., and Rogus R. D. (1988) Radionuclide selection and model absorbed dose calculations for radiolabeled tumor associated antibodies. *Med. Phys. 11*, 638−645.

(13) Nicholson, S., Gooden, C. S. R., Hird, V., Maraveyas, A., Mason, P., Lambert, H. E., Meares, C. F., and Epenetos, A. A. (1998) Radioimmunotherapy after chemotherapy compared to chemotherapy alone in the treatment of advanced ovarian cancer: a matched analysis. *Oncol. Rep. 5*, 223−226.

(14) Moore, S., and Stein, W. H. (1948) Photometric ninhydrin method for use in the chromatography of amino acids. *J. Biol. Chem. 176*, 367.

(15) Udenfriend, S., Stein, S., Bohlen, P., Wallace, D., Leimgruber, W., and Weigle, M. (1972) Fluorescamine: A reagent for assay of amino acids, peptides, proteins, and primary amino acids in the picomolar range. *Science 178*, 871−872.

(16) Penefsky, H. S. (1979) A centrifuged-column procedure for the measurement of ligand binding by beef heart F1. *Methods Enzymol. 56*, 527−530.

(17) Meares, C. F., McCall, M. J., Reardan, D. T., Goodwin, D. A., Diamanti, C. I., and McTigue, M. (1984) Conjugation of antibodies with bifunctional chelating agents: isothiocyanate and bromoacetamide reagents, methods of analysis, and subsequent addition of metal ions. *Anal. Biochem. 142*, 68−78.

(18) Brechbiel, M. W., Gansow, O. A., Atcher, R. W., Schlom, J., Esteban, J., Simpson, D. E., and Colcher, D. (1986) Synthesis of 1-(p-isothiocyanatobenzyl) derivatives of DTPA and EDTA: Antibody labelingand tumor imaging studies. *Inorg. Chem. 25*, 2272−2281.

(19) Sergheraert, C., Maes, P., and Tartar, A. (1986) Specific covalent fixation of chelating agents on peptides. *J. Chem. Soc., Perk. Trans. 1*, 1061−1064.

BC990125X

CORRECTIONS

Volume 11, Number 2, March/April

Donald T. Corson and Claude F. Meares*

EFFICIENT MULTIGRAM SYNTHESIS OF THE BIFUNCTIONAL CHELATING AGENT (*S*)-1-*p*-ISOTHIOCYANATOBENZYL-DIETHYLENE-TETRAMINE PENTAACETIC ACID

There is a consistent misspelling in the manuscript. The compound name (*S*)-1-*p*-isothiocyanatobenzyl-diethylenetetraminepentaacetic acid should be spelled (*S*)-1-*p*-isothiocyanatobenzyl-diethylenetriaminepentaacetic acid.

BC000020Q

10.1021/bc000020q
Published on Web 03/20/2000

CORRECTIONS

Volume 11, Number 2, March/April 1999.

Donald T. Corson and Claude F. Meares*

EFFICIENT MULTIGRAM SYNTHESIS OF THE BIFUNCTIONAL CHELATING AGENT (*S*)-1-*p*-ISOTHIOCYANATOBENZYL-DIETHYLENE-TETRAMINE PENTAACETIC ACID

There is a consistent misspelling in the manuscript. The compound name (*S*)-1-*p*-isothiocyanatobenzyl-diethylenetetraminepentaacetic acid should be spelled (*S*)-1-*p*-isothiocyanatobenzyl-diethylenetriaminepentaacetic acid.

BC000020Q

10.1021/bc000020q
Published on Web 03/20/2000

MAY/JUNE 2000
Volume 11, Number 3

© *Copyright 2000 by the American Chemical Society*

Bioconjugate Chemistry

COMMUNICATIONS

Macrocyclic Chelators with Paramagnetic Cations Are Internalized into Mammalian Cells via a HIV-Tat Derived Membrane Translocation Peptide

Rajeev Bhorade, Ralph Weissleder, Tsunenori Nakakoshi, Anna Moore, and Ching-Hsuan Tung*

Center for Molecular Imaging Research, Massachusetts General Hospital, Harvard Medical School, 149 13th St., #5406, Charlestown, Massachusetts 02129. Received December 7, 1999

A major obstacle to using paramagnetic MR contrast agents for in vivo cell tracking or molecular sensing is their generally low cellular uptake. In this study, we show that a paramagnetically labeled DOTA chelator derivatized with a 13-mer HIV-tat peptide is efficiently internalized into mammalian cells. Intracellular concentrations were attained that were readily detectable by MR imaging using both gadolinium and dysprosium chelates. Using this paradigm, it should be feasible to internalize a variety of chemically different agents into mammalian cells.

INTRODUCTION

The cellular plasma membrane represents a natural barrier to many exogeneously administered molecules. To overcome this delivery barrier for therapeutic and diagnostic drugs, a variety of strategies have been proposed to ferry agents through cellular membranes. These strategies include receptor mediated uptake (*1*, *2*), fluid phase endocytosis (pinocytosis) (*3*), direct fusion with the membrane lipid bilayer (*4*), and use of peptide/protein mediated translocation signals (*5*, *6*). Several membrane translocation signal (MTS) peptides have recently been reported, including the HIV-tat (*7*, *8*), the third helix of the homeodomain of Antennapedia (*9*), a peptide derived from anti-DNA monoclonal antibody (*10*), VP22 herpes virus protein (*11*, *12*), and other synthetic peptides (*13*, *14*). Although the mechanism of entry into the cells often remains unknown, MTS have been used to internalize proteins (*7*, *15*−*20*), peptides (*8*, *21*, *22*), antisense oligonucleotides (*23*, *24*), peptide nucleic acid (*25*), and plasmid DNA (*26*−*28*).

Recently, we demonstrated the MTS peptide from the HIV-tat peptide can be used to induce nonphagocytic cells to internalize a diagnostic label often used in MR imaging, superparamagnetic iron oxide particles (29). When attached to the HIV tat peptide, nanometer-sized superparamagnetic iron oxide crystals were internalized by HeLa cells, murine lymphocytes, and human NK cells to levels that made the cells detectable by MR imaging. However, superparamagnetic labels can potentially produce susceptibility artifacts and in their intracellular form have little effect on T1 weighted MR images. In addition, a variety of "smart" paramagnetic MR contrast agents are recently under development that alter their T1 relaxivity when conformational changes occur, thus allowing molecular sensing (*30*, *31*). However, to date one of the main problems of using these reporters is their

* To whom correspondence should be addressed. Phone: (617) 726−5788. Fax: (617) 726-5708. E-mail: tung@helix.mgh.harvard.edu.

10.1021/bc990168d CCC: $19.00 © 2000 American Chemical Society
Published on Web 04/29/2000

poor cell permeability. We hypothesized that macrocyclic chelators could be conjugated to an HIV-tat peptide and thus synthesized a peptide and 1,4,7,10-tetraazacyclododecane-*N*,*N*′,*N*″,*N*‴-tetraacetic acid (DOTA) conjugate. By attaching paramagnetic chelates to the HIV-tat peptide, we show for the first time highly efficient cell uptake and demonstrate these effects by MR imaging of cells. These results suggest a variety of diagnostic agents could be synthesized that will readily cross cell membranes.

RESULTS AND DISCUSSION

The translocating properties of the tat peptide (GRKKRRQRRR) representing residues 48−58 of the HIV tat protein has been demonstrated by several groups (*15*, *17*, *32*). The peptide efficiently localizes to cytoplasmic and nuclear compartments in a time-dependent fashion and seems to have also a high propensity for nucleosomes in several cell types. In one prior study, we have shown that 40 nm particles could be internalized into the nuclear compartment when conjugated to the tat peptide (*29*). In the current study, we conjugated a macrocyclic chelator, DOTA, to the C-terminus of the tat peptide and then complexed with different metal ions. The peptide, GRKKRRQRRRGYK(DOTA)-NH_2 (tat-DOTA), was synthesized using solid-phase synthesis on an automatic peptide synthesizer, as illustrated in Figure 1. An orthogonal approach was applied to result in monodeprotection of the C-terminal lysine side chain. A protected DOTA analogue, 1,4,7,10-tetraazacyclododecane-1,4,7-tris(acetic acid *tert*-butyl ester)-10-acetic acid (DOTA-3tBu) (Macrocyclics, Richardson, TX), was activated by 2-(1H-benzotriazole-1-yl)-1,1,3,3-tetramethyluronium hexafluorophosphate (HBTU)/*N*-hydroxybenzotriazole (HOBt) and coupled to the designated position. The subsequent trifluoroacetic acid treatment not only cleaved the peptide off the resin but also removed all protecting groups from the peptide as well as DOTA-3tBu. The peptide was purified by reversed-phase high-pressure liquid chromatography (HPLC) and characterized by mass spectrum, MALDI-MS; $(M + H)^+$: 2131.4 (calcd), 2131.3 (found). The chelation of gadolinium (Gd) and dysprosium (Dy) was performed by incubating tat-DOTA with $GdCl_3$ and $DyCl_3$, respectively, in glycine/HCl buffer 50 mM, pH 3.5 at 80 °C for 3 h. The conjugates were further purified by reversed-phase HPLC. MALDI-MS $(M + H)^+$: tat-DOTA-Gd, 2285.7 (calcd), 2285.6 (found); tat-DOTA-Dy 2290.9 (calcd), 2291.3 (found). To monitor the cellular distribution of the peptide, a modified peptide was prepared using the same synthetic approach, except that DOTA-3tBu coupling was replaced with fluorescein isothiocyanate (FITC). The sequence of the latter peptide was GRKKRRQRRRGYK(FITC)-NH_2, and its translocation properties were studied in human epithelial HeLa cells. At 37 °C, a pronounced nuclear accumulation was observed within 30 min (Figure 1). A similar distribution has also been described by several other investigators (*7*, *8*, *29*). The precise mechanism of uptake has so far not been elucidated but adsorptive endocytosis has been proposed (*33*).

Cellular uptake of the tat-DOTA conjugate was quantitated using the ^{111}In-labeled tat-DOTA conjugate. Tat-DOTA labeling was performed by adding 50 μCi of $^{111}InCl_3$ to 5 μmol of tat-DOTA in 1 mL of 50 mM glycine/HCl buffer, pH 3.5 at 80 °C for 3 h. The chelation efficiency, determined by analytic reversed-phase HPLC with an ratioactivity detector, was greater than 99%. Fresh lymphocytes (1×10^6 cells) were then obtained from mouse spleen (*34*) and were incubated with various amounts of tat-DOTA-^{111}In (25, 50, 100, 150, or 200 nmol) in 1 mL of RPMI 1620 medium at 37 °C for 60 min. After incubation, cells were washed three times with Hanks-buffered saline solution and then resuspended in RPMI 1620 medium. In parallel, DOTA-^{111}In without tat peptide was used as a control. As shown in Figure 2A, uptake increased with increasing amounts of tat-DOTA conjugate without reaching saturation at 200 nmol of peptide per million cells. In contrast, uptake of DOTA-^{111}In was negligible at all concentrations. Splenocytes, previously labeled with 100 nmol of $InCl_3$, were kept in RPMI 1620 medium for 2 days while the medium was replaced daily. The intracellular tat-DOTA retention was determined by radioactivity counting, and adjusted for cell numbers. At 0, 24, and 48 h, 2.6, 2.2, and 2.5 fmol/cell were found, respectively. This result suggests that the tat peptide is required for translocation, and once the compound is internalized, it will stay inside for several days.

In another experiment, cells were incubated with 40 nmol of tat-DOTA-^{111}In (20 μCi) for 15, 30, 45, or 60 min. The time curve of cellular uptake is shown in Figure 2B. Uptake was relatively rapid with 75% of maximum cell uptake occurring within 15 min of incubation. Additional experiments were also performed at different temperatures (4 and 37 °C), which showed similar uptake kinetics, suggesting that the mechanism of uptake is not receptor mediated as reported by other groups (*7*, *8*).

A cytotoxicity assay was used to determine whether tat-DOTA analogues would be toxic to lymphocytes. Cells (1×10^6) were incubated with 10 or 200 nmol of tat-DOTA-Gd for a period of 5 days, and the cell viability was determined daily by cell counts. About 80% of cells remained alive at all concentrations tested, and similar viability figures were found in the control groups.

To determine whether cell internalized paramagnetic tat-DOTA conjugates would be detectable by MR imaging, we performed the following experiment. Freshly isolated murine lymphocytes (10^6 cells) were labeled with either 100 nmol of tat-DOTA-Gd or tat-DOTA-Dy for a period of 1 h in RPM1 medium. After incubation, cells were washed three times with Hanks buffered saline solution as described previously. The labeled cells were embedded in agar cylinders to minimize air interface artifacts. MR imaging was performed with a 1.5 T superconducting magnet (Signa 5.0; GE Medical Systems, Milwaukee, WI) using a 5-in. surface coil. The time between labeling of cells and imaging was approximately 12 h. The imaging protocol consisted of coronal T1 weighted spin−echo (SE 300/11 where the first number represents the repetition time, TR, and the second number represents the echo time, TE), T2 weighted SE (SE 2000/102) or T2* gradient echo sequence (Steady-State Free Precession pulse sequence with TR/TE 50/20 and a flip angle of 20°) representative of commonly used pulse sequences in clinical imaging. Slice thickness was 1−3 mm. The field of view (FOV) was 10−12 cm^2, using an 256 × 192 imaging matrix and 2−4 acquisition averages.

Figure 3 shows that tat-DOTA-Gd-labeled lymphocytes had significantly higher signal intensity compared to unlabeled cells, whose signal intensity was similar to that of agar. Conversely, the signal of tat-DOTA-Dy labeled cells was lower because of the predominant T2/T2* effect of the latter, which may be desirable for certain imaging studies. The R1 relaxivity of the gadolinium-labeled tat-DOTA conjugate was 4.1 mM^{-1} s^{-1} in aqueous solution (20 °C, 1.5 T), similar to that reported for other Gd chelates (*35*). Tat-DOTA internalized in cells had a lower R1 relaxivity (2.2 mM^{-1} s^{-1}) as predicted by theory of

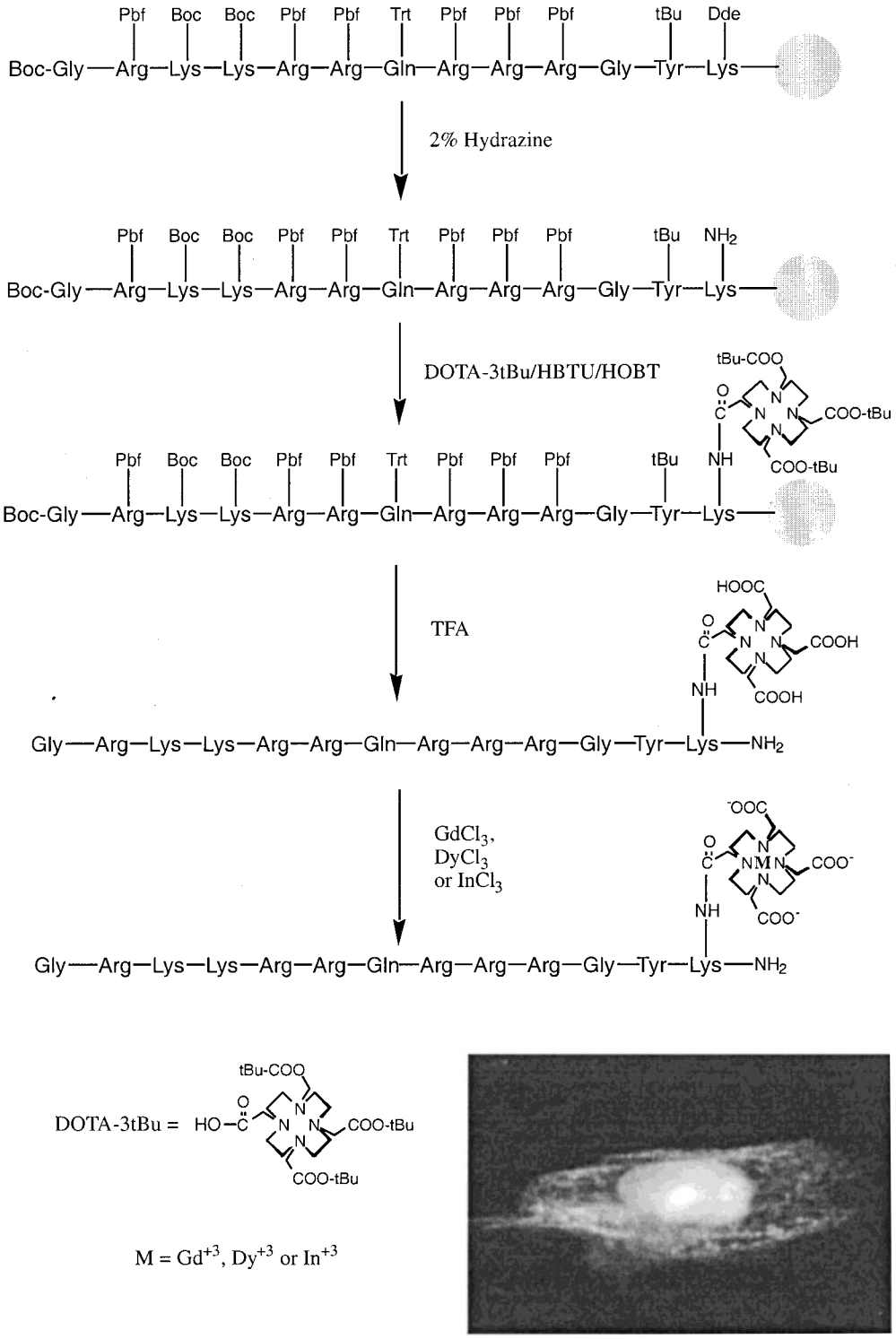

Figure 1. Synthesis. Tat-DOTA was labeled with either Gd, Dy, or ^{111}In for cell uptake experiments. The typical intracellular distribution of tat peptide which is labeled with FITC is shown at the bottom right in a HeLa cell. Note the prominent intracellular and nuclear uptake.

limited water diffusion (*35*). Additional preliminary data indicates that cells other than murine lymphocytes (e.g., mouse neural progenitor cells C17.2; data not shown) can also be labeled by this approach.

Our studies attaching paramagnetic labels to HIV-tat peptides have two major applications for in vivo MR imaging research. First, a variety of immune and other cells could be labeled ex vivo and cell trafficking could be studied noninvasively and repeatedly in recipient animals using MR imaging. Such cell tracking could be performed at high spatial resolutions (~20 μm resolution) and without significant image artifacts as frequently observed with superparamagnetic iron oxide labeled cells. Second, it now seems possible to synthesize membrane impermeable diagnostic probes and deliver them intercellularly through coupling to MTS peptides. Functionalized imaging reporters have recently been described that change their physical properties following interaction with a specific target including molecular beacons (*36*), molecular probes (*37*), and paramagnetic MR contrast agents (*30, 31*). The latter have been shown to alter their T1 relaxivity when conformational changes occur

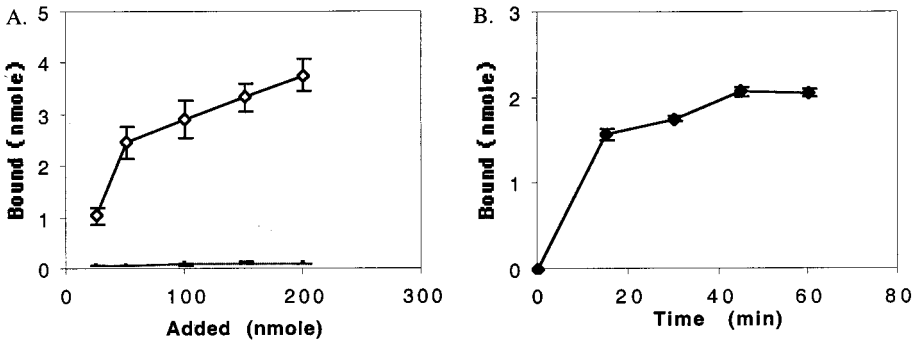

Figure 2. Uptake of tat-DOTA into mouse lymphocytes. One million murine lymphocytes were used to quantitate cellular uptake for each data point shown. Following incubation with tat-DOTA-^{111}In, cells were washed extensively to remove any noninternalized compound. (A) Effect of increasing tat-DOTA-^{111}In concentrations on cellular uptake (60 min incubation, 37°, top curve). Negligible uptake was observed with DOTA-^{111}In at same condition (bottom curve). (B) Effect of time of incubation cellular uptake (at 40 nmol, 37 °C).

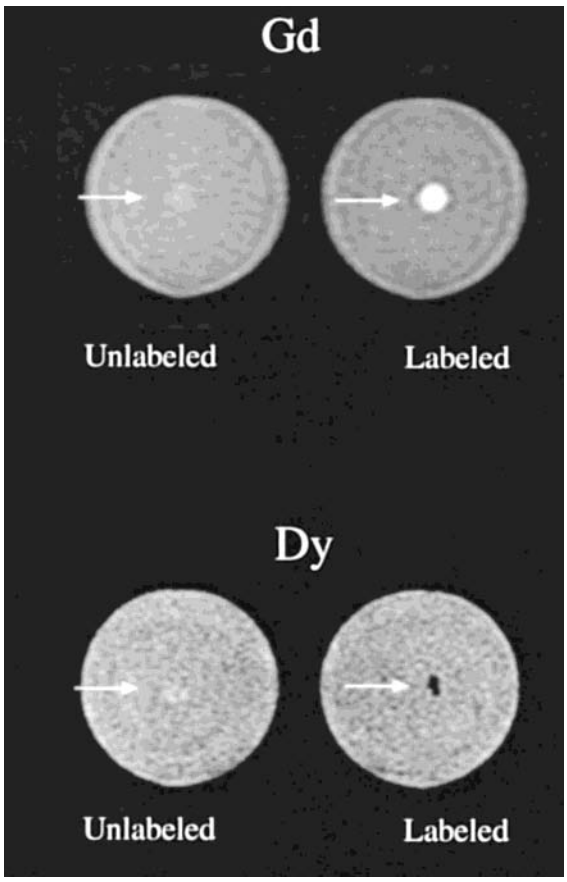

Figure 3. MR images of murine lymphocytes. Unlabeled (left) and labeled (right) murine lymphocytes (10^6 cells) were embedded as central pellets in agar cylinders and subjected to MR imaging [T1 weighted spin−echo (TR/TE) 300/11 for the tat-DOTA-Gd compound, top; T2* weighted gradient echo (TR/TE/angle) 50/20/20° for tat-DOTA-Dy, bottom]. As expected, Gd labeled cells appeared bright while Dy-labeled cells appeared dark, indicating that internalization of the paramagnetic labels occurred at sufficiently high quantities for MR imaging.

such as cleavage of galactose groups after galactosidase interaction (*30*) or interaction with calcium (*31*). These agents, as well as a myriad of other functional agents under development have potential applications for noninvasive in vivo imaging. However, to date one of the problems of some of these new reporters is their poor cell permeability and/or inability to attain intracellular concentrations required for imaging. The intracellular delivery of compounds designed to interact with specific intracellular targets by attachment to MTS peptides could have far reaching implications for both in vitro and in vivo applications of molecular imaging.

ACKNOWLEDGMENT

The authors acknowledge the valuable help of Dr. U. Mahmood in performing the MR imaging experiments, and Dr. L. Josephson for many fruitful discussions and review of the manuscript. Supported by NIH Grants RO1 AI-CA46973 and R21DK55713.

LITERATURE CITED

(1) Dubowchik, G. M., and Walker, M. A. (1999) Receptor-mediated and enzyme-dependent targeting of cytotoxic anticancer drugs. *Pharmacol. Ther. 83*, 67−123.
(2) Reddy, J. A., and Low, P. S. (1998) Folate-mediated targeting of therapeutic and imaging agents to cancers. *Crit. Rev. Ther. Drug Carrier Syst. 15*, 587−627.
(3) Marecos, E., Weissleder, R., and Bogdanov, A., Jr. (1998) Antibody-mediated versus nontargeted delivery in a human small cell lung carcinoma model. *Bioconjugate Chem. 9*, 184−91.
(4) Rojas, M., Donahue, J. P., Tan, Z., and Lin, Y. Z. (1998) Genetic engineering of proteins with cell membrane permeability. *Nat. Biotechnol. 16*, 370−5.
(5) Fernandez, T., and Bayley, H. (1998) Ferrying proteins to the other side. *Nat. Biotechnol. 16*, 418−20.
(6) Cleves, A. E. (1997) Protein transports: the nonclassical ins and outs. *Curr. Biol. 7*, R318−20.
(7) Fawell, S., Seery, J., Daikh, Y., Moore, C., Chen, L. L., Pepinsky, B., and Barsoum, J. (1994) Tat-mediated delivery of heterologous proteins into cells. *Proc. Natl. Acad. Sci. U.S.A. 91*, 664−8.
(8) Vives, E., Brodin, P., and Lebleu, B. (1997) A truncated HIV-1 Tat protein basic domain rapidly translocates through the plasma membrane and accumulates in the cell nucleus. *J. Biol. Chem. 272*, 16010−7.
(9) Derossi, D., Calvet, S., Trembleau, A., Brunissen, A., Chassaing, G., and Prochiantz, A. (1996) Cell internalization of the third helix of the Antennapedia homeodomain is receptor-independent. *J. Biol. Chem. 271*, 18188−93.
(10) Avrameas, A., Ternynck, T., Nato, F., Buttin, G., and Avrameas, S. (1998) Polyreactive anti-DNA monoclonal antibodies and a derived peptide as vectors for the intracytoplasmic and intranuclear translocation of macromolecules. *Proc. Natl. Acad. Sci. U.S.A. 95*, 5601−6.
(11) Phelan, A., Elliott, G., and O'Hare, P. (1998) Intercellular delivery of functional p53 by the herpesvirus protein VP22. *Nat. Biotechnol. 16*, 440−3.
(12) Elliott, G., and O'Hare, P. (1997) Intercellular trafficking and protein delivery by a herpesvirus structural protein. *Cell 88*, 223−33.
(13) Sheldon, K., Liu, D., Ferguson, J., and Gariepy, J. (1995) Loligomers: design of de novo peptide-based intracellular vehicles. *Proc. Natl. Acad. Sci. U.S.A. 92*, 2056−60.

(14) Zhang, L., Torgerson, T. R., Liu, X. Y., Timmons, S., Colosia, A. D., Hawiger, J., and Tam, J. P. (1998) Preparation of functionally active cell-permeable peptides by single-step ligation of two peptide modules. *Proc. Natl. Acad. Sci. U.S.A. 95*, 9184−9.

(15) Efthymiadis, A., Briggs, L. J., and Jans, D. A. (1998) The HIV-1 Tat nuclear localization sequence confers novel nuclear import properties. *J. Biol. Chem. 273*, 1623−8.

(16) Pepinsky, R. B., Androphy, E. J., Corina, K., Brown, R., and Barsoum, J. (1994) Specific inhibition of a human papillomavirus E2 trans-activator by intracellular delivery of its repressor. *DNA Cell Biol. 13*, 1011−9.

(17) Anderson, D. C., Nichols, E., Manger, R., Woodle, D., Barry, M., and Fritzberg, A. R. (1993) Tumor cell retention of antibody Fab fragments is enhanced by an attached HIV TAT protein-derived peptide. *Biochem. Biophys. Res. Commun. 194*, 876−84.

(18) Bayley, H. (1999) Protein therapy-delivery guaranteed. *Nat. Biotechnol. 17*, 1066−1067.

(19) Nagahara, H., Vocero-Akbani, A. M., Snyder, E. L., Ho, A., Latham, D. G., Lissy, N. A., and Becker-Hapak, M., et al. (1998) Transduction of full-length TAT fusion proteins into mammalian cells: TAT-p27Kip1 induces cell migration. *Nat. Med. 4*, 1449−52.

(20) Vocero-Akbani, A. M., Heyden, N. V., Lissy, N. A., Ratner, L., and Dowdy, S. F. (1999) Killing HIV-infected cells by transduction with an HIV protease- activated caspase-3 protein. *Nat Med. 5*, 29−33.

(21) Lin, Y. Z., Yao, S. Y., Veach, R. A., Torgerson, T. R., and Hawiger, J. (1995) Inhibition of nuclear translocation of transcription factor NF-kappa B by a synthetic peptide containing a cell membrane-permeable motif and nuclear localization sequence. *J. Biol. Chem. 270*, 14255−8.

(22) Schluesener, H. J. (1996) Protection against experimental nervous system autoimmune diseases by a human immunodeficiency virus-1 Tat peptide-based polyvalent vaccine. *J. Neurosci. Res. 46*, 258−62.

(23) Morris, M. C., Vidal, P., Chaloin, L., Heitz, F., and Divita, G. (1997) A new peptide vector for efficient delivery of oligonucleotides into mammalian cells. *Nucleic Acids Res. 25*, 2730−6.

(24) Antopolsky, M., Azhayeva, E., Tengvall, U., Auriola, S., Jaaskelainen, I., Ronkko, S., and Honkakoski, P., et al. (1999) Peptide−oligonucleotide phosphorothioate conjugates with membrane translocation and nuclear localization properties. *Bioconjugate Chem. 10*, 598−606.

(25) Pooga, M., Soomets, U., Hallbrink, M., Valkna, A., Saar, K., Rezaei, K., and Kahl, U., et al. (1998) Cell penetrating PNA constructs regulate galanin receptor levels and modify pain transmission in vivo. *Nat. Biotechnol. 16*, 857−61.

(26) Elliott, G., and O'Hare, P. (1999) Intercellular trafficking of VP22-GFP fusion proteins. *Gene Ther. 6*, 149−51.

(27) Zhang, F., Andreassen, P., Fender, P., Geissler, E., Hernandez, J. F., and Chroboczek, J. (1999) A transfecting peptide derived from adenovirus fiber protein. *Gene Ther. 6*, 171−81.

(28) Singh, D., Bisland, S. K., Kawamura, K., and Gariepy, J. (1999) Peptide-based intracellular shuttle able to facilitate gene transfer in mammalian cells. *Bioconjugate Chem. 10*, 745−54.

(29) Josephson, L., Tung, C. H., Moore, A., and Weissleder, R. (1999) High-efficiency intracellular magnetic labeling with novel superparamagnetic-Tat peptide conjugates. *Bioconjugate Chem. 10*, 186−91.

(30) Moats, R. A., Fraser, S. E., and Meade, T. J. (1997) A "smart" magnetic resonance imaging agent that reports on specific enzymatic activity. *Angew. Chem., Int. Ed. Engl. 36*, 726−8.

(31) Li, W. H., Fraser, S. E., and Meade, T. J. (1999) A calcium-sensitive magnetic resonance imaging contrast agent. *J. Am. Chem. Soc. 121*, 1413−4.

(32) Vives, E., Granier, C., Prevot, P., and Lebleu, B. (1997) Structure−activity relationship study of the plasma membrane translocating protential of a short peptide from HIV-1 Tat protein. *Lett. Pept. Sci. 4*, 429−36.

(33) Mann, D. A., and Frankel, A. D. (1991) Endocytosis and targeting of exogenous HIV-1 Tat protein. *EMBO J. 10*, 1733−9.

(34) Schoepf, U., Marecos, E., Melder, R., Jain, R., and Weissleder, R. (1998) Intracellular magnetic labeling of lymphocytes for in vivo trafficking studies. *BioTechniques 24*, 642−651.

(35) Lauffer, R. (1996) MRI contrast agents: basic principles. In *Clinical magnetic resonance imaging* (R. R. Edelman, J. R. Hesselink, and M. B. Zlatkin, Eds.) pp 177−191, WB Sauders, Philadelphia.

(36) Tyagi, S., and Kramer, F. R. (1998) Molecular beacons: probes that fluoresce upon hybridization. *Nat. Biotechnol. 14*, 303−8.

(37) Weissleder, R., Tung, C. H., Mahmood, U., and Bogdanov, A., Jr. (1999) In vivo imaging of tumors with protease-activated near-infrared fluorescent probes. *Nat. Biotechnol. 17*, 375−8.

BC990168D

O-Alkyl dioleoylphosphatidylcholinium Compounds: The Effect of Varying Alkyl Chain Length on Their Physical Properties and in Vitro DNA Transfection Activity

Howard S. Rosenzweig,[†] Vera A. Rakhmanova, Thomas J. McIntosh,[‡] and Robert C. MacDonald*

Department of Biochemistry, Molecular Biology and Cell Biology, Northwestern University, Evanston, Illinois 60208, and The Department of Cell Biology, Duke University, Durham, North Carolina 27710. Received September 1, 1999; Revised Manuscript Received January 3, 2000

1,2-Dioleoyl-*sn*-3-ethylphosphocholine (EDOPC) has been previously shown be a highly effective DNA transfection reagent in vitro. To assess the effect of alkyl chain length on transfection efficiency, the *O*-methyl, *O*-propyl, *O*-hexyl, *O*-decyl, and *O*-octadecyl derivatives have been prepared from dioleoylphosphatidylcholine using the corresponding alkyl trifluoromethylsulfonate. The methyl, ethyl, and propyl derivatives formed liposomes which were very large and unilamellar. The ethyl and propyl derivatives were equally efficient at mediating transfection (even in the presence of serum) of BHK cells, but the chemically labile methyl derivative was a much weaker transfection agent. The *O*-decyl and *O*-octadecyl compounds, which assume the inverted hexagonal phase in excess water (as determined by X-ray diffraction), were almost inactive after manual agitation in both water and in saline; however, after sonication, these compounds exhibited good transfection activity. The *O*-hexyl derivative displayed novel behavior, assuming the lamellar phase at low and a cubic phase at high ionic strength. All compounds, whether lamellar or not, formed lamellar structures when complexed with DNA. In water, where the hexyl compound dispersed well, sonication diminished transfection activity, whereas at physiological ionic strength, which led to poor manual dispersion, sonication was essential for good transfection. These results emphasize the importance of optimal dispersion of a cationic lipid: too little, and interaction with DNA is handicapped, too much, and the resultant particle transfects poorly. Lipid dispersibility is thus an important variable in assessing lipid transfection agents, and caution is advised in attributing too much significance to chemical structure until interaction with DNA has been optimized.

INTRODUCTION

Transfection, the introduction of plasmid DNA into cultured mammalian cells for the transient expression of a desired protein, has become a standard technique in molecular biology. Earlier methods have involved the use of DNA coprecipitation with calcium phosphate, soluble DEAE, or Polybrene resins (*1*), as well as electroporation (*2*). Following the demonstration by Felgner et al. that the cationic amphipath, DOTMA (dioleoloxypropyl-trimethylammonium bromide), is a simple and generally effective method to transfect DNA into cultured cells (*3*), use of "cationic lipids" has become widespread. A number of other cationic lipids with transfection activity have been developed in recent years, e.g., refs *4*−*12*.

One of the potentially most important applications of cationic lipids is as DNA delivery agents for gene therapy (*13*). Another potential clinical application is administration of antisense oligonucleotides (*14*). Other molecules can be delivered to cells as cationic complexes, such as proteins (*15, 16*), and small pharmacological agents (*17*). It is likely that additional applications will be developed soon.

Although with few exceptions (e.g., refs *5* and *12*), most of the compounds described in the literature as "cationic lipids" differ chemically from lipid natural products, it is readily possible to modify phospholipids to convert them into cationic derivatives. We have previously described the reaction which involves the alkylation of the phosphate oxygen of phosphatidylcholine such as to generate *O*-alkyl phosphatidylcholinium compounds (*18*). The ethyl ester has been shown to be an effective transfection agent both in vitro (*19*) and in vivo (*20*). These compounds consist of an essentially unperturbed phospholipid scaffold linked with metabolizable ester linkages. Since they exhibit low toxicity against cells in culture, they could be well suited for clinical applications involving gene and drug therapy. To explore the possibility that other alkyl derivates besides the ethyl esters are also potent transfection agents, we have synthesized a series of *O*-alkyl cationic analogues ranging from methyl to octadecyl, tested them for transfection activity, and examined the nature of their lyotropic phases.

EXPERIMENTAL PROCEDURES

Materials. Lipids were obtained from Avanti Polar Lipids (Alabaster, AL) except for the cationic lipids, which were synthesized according to procedures described below. Most other biochemicals were purchased from Sigma (St. Louis, MO). Organic reagents were purchased from Aldrich (Milwaukee, WI). When commercially available methyl and ethyl triflates were used in synthesis,

* To whom correspondence should be addressed. Phone: (847) 491-5062. Fax: (847) 467-1380. E-mail: macd@northwestern.edu.
[†] Current address: Wesley Jessen, Inc., Des Plaines, IL 60018.
[‡] Duke University.

10.1021/bc9901144 CCC: $19.00 © 2000 American Chemical Society
Published on Web 03/24/2000

as much as possible, they were used very soon after opening the ampule; however, they could be stored for over a month at a time with negligible degradation in a desiccator at −20 °C. Triflic anhydride could be successfully stored after opening for over a month in a desiccator kept at room temperature. Tissue culture reagents were obtained from Life Technologies (Grand Island, NY). A plasmid with the β-galactosidase gene driven by the cytomegalovirus promoter (pCMV-β-gal) was purchased from Life Technologies (Grand Island, NY). It was propagated in DH5 cells and purified with a Plasmid Mega Kit from Qiagen (Valencia, CA).

Synthetic Methods. *Higher Homologues of O-Alkylated DOPC Triflates.* In a 50 mL, one-necked round-bottom flask was placed anhydrous CH_2Cl_2 (3 mL), followed by 250 mmol of the required anhydrous alcohol (e.g., propyl, hexyl, decyl or octadecyl alcohol), and 250 mmol of triethylamine. The reaction flask was sealed with a rubber septum, placed under a positive argon atmosphere, and then cooled in an ice−water bath. A solution of triflic anhydride (250 mmol in 2 mL of anhydrous CH_2Cl_2) was slowly (ca. 5 min) added through a syringe into the cooled reaction solution. The reaction mixture was stirred for 1−2 h at 0 °C under a positive argon atmosphere, after which it was transferred (within 2−3 min) with a Pasteur pipet to a 20 mL screwcap vial containing 5 mL of ice-cold 10% HCl and the mixture was extracted. The lower organic layer was removed and transferred to another 20 mL screwcap vial containing 5 mL of ice-cold H_2O and extracted again. The organic layer was then filtered twice through anhydrous granular sodium sulfate. The dried organic solution was then placed into a 100-mL round-bottom flask, which was sealed with a rubber septum and then placed under a positive argon atmosphere. To this triflate solution, 10 mL of a room-temperature phosphatidylcholine $CHCl_3$ solution (20 mg/mL, 250 mmol) was added through a syringe, and the reaction mixture was allowed to stir at room temperature under argon for at least 2 h. The reaction was monitored by analytical silica gel TLC ($CHCl_3$:MeOH:H_2O; 65:25:4, v:v). When the reaction appeared to be over, the crude product was purified on a dry silica gel column, using at least 10 times the mass of DOPC contained in the reaction (>2 mL of silica). After adding the reaction mixture to the column, the column was washed with several volumes of $CHCl_3$ and then with solvents containing increasing amounts of methanol in chloroform. The product began eluting with 9:1 $CHCl_3$:MeOH and was completely removed from the column with 5:1 or 4:1 $CHCl_3$:MeOH. Slight positive pressure with argon gas ("flash" conditions) accelerated the purification. Yields ranged from 20 to 70%.

O-Methyl and O-Ethyl DOPC. These compounds were synthesized using commercially available ethyl and methyl triflate, following the procedure above from the point where the triflate was synthesized.

Product Characterization. Liquid secondary ion mass spectra were obtained on a VG70 mass spectrometer (V. G. Analytical) with Cs ion as a primary source. Proton NMR spectra were obtained on a Varian Gemini 300 MHz spectrometer. The ^{1}H NMR spectra and mass spectra obtained were all consistent with the structure of the expected product. All lipids gave a single spot by thin-layer chromatography with an R_f of 0.5 when developed in chloroform:methanol:water, 65:25:1.

Lipid Dispersions. Lipids were stored at −20 °C in chloroform. When needed, aliquots were transferred to vials where the bulk of the solvent was evaporated with a gentle stream of argon gas. The vial was then placed under a high vacuum for at least 30 min to remove residual chloroform. Next, water or Dulbecco's phosphate-buffered saline (D-PBS; with calcium and magnesium) was added to obtain a 1 mg/mL concentration, and the vial was either gently vortexed or sonicated for 2 min in an 80 kHz bath sonicator (Laboratory Supply Co., Inc, Hicksville, NY). The bath was tuned by adjusting the height of the water so as to obtain maximum agitation of the surface.

X-ray Diffraction of Cationic Lipids and Their Complexes with DNA. Cationic lipids were hydrated in 10-fold excess water or D-PBS for several hours at room temperature. When the lipids dispersed readily, a portion of the suspension was simply concentrated by centrifugation and a portion of the pellet transferred to thin-walled X-ray capillary tubes. In the case of those lipids that dispersed less well, a portion of the hydrated lipid was scraped from its container and transferred to a capillary tube with a spatula. The capillary tubes were then sealed and mounted in a point-collimation X-ray camera or a mirror-mirror X-ray camera.

Complexes of lipid and DNA were prepared from salmon sperm DNA which had been sonicated to reduce the length of the strands and reduce the solution viscosity. Gel electrophoresis on preparations such as this revealed a broad band corresponding to 400−700 base pairs. Dispersed lipid was mixed with DNA in the same proportions as used for cell transfection (see below), namely 3 parts lipid with 1 part by weight of DNA to generate a near-neutral particle. The complex was collected, by centrifugation if necessary, and transferred to X-ray tubes as described above.

X-ray diffraction patterns were recorded on Kodak DEF X-ray film at ambient temperature. X-ray films were processed by standard techniques and densitometered with a Joyce-Loebl microdensitometer as described previously (*21*, *22*).

Cell Transfection. BHK cells (CCL-10) were obtained from American Type Culture Collection (Rockville, MD) and were cultured according to the recommended conditions. BHK cells were seeded in 96-well microplates at 48 h before transfection at densities to give approximately 80% confluence at the time of transfection. Complete medium was replaced with serum-free medium or medium containing 10% fetal bovine serum immediately prior to transfection. The complex for transfection was prepared by mixing a cationic lipid dispersion (1 mg/mL, normally in D-PBS, but sometimes in water) and β-galactosidase plasmid DNA solution (0.1 mg/mL) at a lipid:DNA mass ratio of 3:1. The lipid−DNA mixture was incubated for 20 min at room temperature. Cells in each well of the 96-well plate were treated with lipid−DNA complexes and then incubated for 4 h, at which time a 1/10 volume of fetal bovine serum was added to the cells. The total volume of medium was 100 μL/well. Replicates of three were used in each experiment.

Cells were tested for β-galactosidase activity 20 h after transfection using a microplate fluorimetric assay that employed the substrate fluorescein digalactoside (*23*).

RESULTS

***O*-Alkylation of Phospholipids Proceeds Readily with Alkyl Trifluoromethylsulfonates (Triflates).** Triflates are among the most potent alkylating agents available for preparative organic chemistry, and they have proven to be very useful reagents for preparing *O*-alkyl derivatives of phospholipids. The reaction, for the

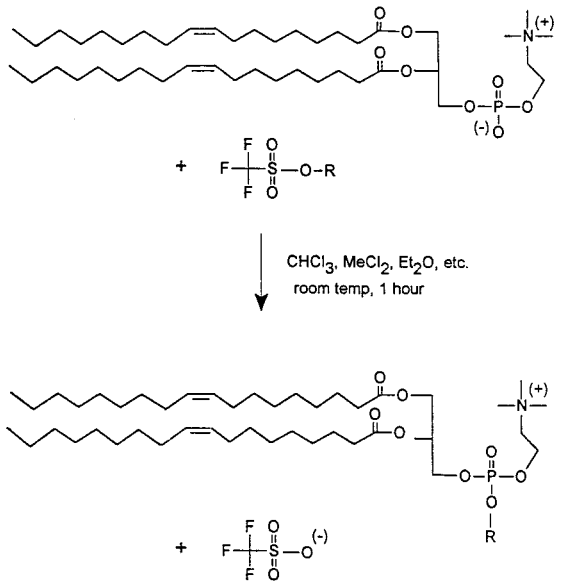

Figure 1. Reaction for preparation of alkyl esters of phosphatidylcholine.

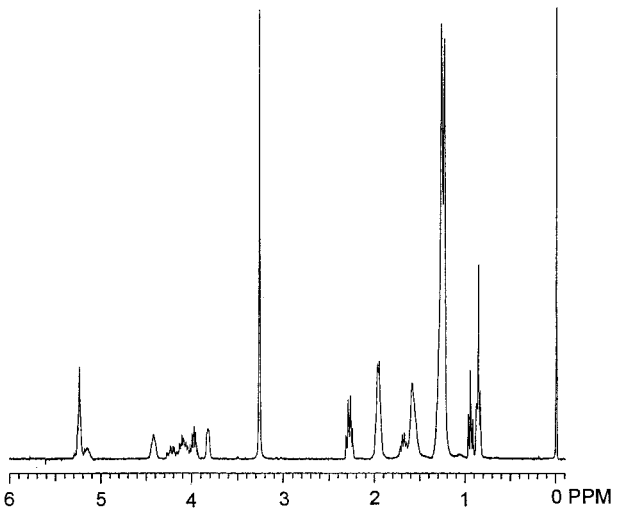

Figure 2. NMR spectrum of *O*-propylDOPC triflate. The 300 MHz proton NMR spectrum shows that the alkylation of DOPC with propyl triflate has been achieved. The quintet centered at 5.34 ppm (4H, from integration) corresponds to the vinyl protons of the oleoyl ester groups, while the broad signal at 5.26 ppm (1H) corresponds to the single proton of the central carbon of the glycerol backbone. The broad signals found at 4.51 ppm (2H) and 3.89 ppm (2H) correspond to the protons of the two methylene carbons of the choline group (the more downfield resonance, 4.51 ppm, derives from the protons of the carbon connected to the phosphate ester group, while the other protons belong to the carbon adjacent to the trimethylammonium group, respectively). The multiplet between 4.37 and 4.00 ppm (6H) results from the overlap of the double triplet arising from the diastereomeric α-methylene protons of the propyl group attached to the third phosphate oxygen (the site of alkylation with propyl triflate) plus the two triplets arising from the two remaining methylene carbon protons of the glycerol backbone. The sharp singlet at 3.32 ppm (9H) represents the protons of the trimethylammonium group. The pseudo quartet centered at 2.33 ppm (4H) corresponds to the α-methylene protons of the oleoyl ester carbonyl groups. The broad doublet centered at ca. 2.00 ppm (8H) is due to the allylic protons, while the slightly obscured hextet centered at ca. 1.72 ppm (2H) represents the β-methylene protons of the appended propyl group. Finally, the triplets centered at 0.97 ppm (3H) and 0.87 ppm (6H) correspond to the terminal methyl group protons of the propyl and both oleoyl ester groups, respectively. The solvent was deuteriochloroform, with tetramethylsilane as the internal standard.

case of dioleoylphosphatidylcholine, is shown in Figure 1. The alkyl triflate was produced in anhydrous methylene chloride, and then the reaction mixture was extracted with cold 10% HCl solution to remove both the triethylamine and triflic acid byproduct, as well as any unreacted triflic anhydride. No attempt was made to isolate the intermediate, due to the thermal instability of long-chain alkyl triflates. Instead, the alkyl triflate solution was dried with anhydrous sodium sulfate, after which it was reacted with DOPC added as a chloroform solution. The appearance of the product was easily monitored by analytical silica gel thin-layer chromatography using either general staining procedures such as charring or standard lipid detection reagents such as those used for visualizing compounds containing phosphate or choline (ref *24*, pp 119−121).

The structure of the product was verified by proton NMR and mass spectral analysis. Mass spectra of all these compounds synthesized to date have been unambiguous; for essentially all of the *O*-alkylated lipids, the parent ion has been by far the most intense peak in the spectrum.

A representative example of a ^{1}H NMR spectrum is shown in Figure 2 for the *O*-propyl derivative**.** The key diagnostic features of it are (a) the slightly obscured hextet centered at ca. 1.72 ppm, which corresponds to the β-methylene carbon protons of the appended propyl group, and especially (b) the triplet centered at 0.97 ppm, which corresponds to the terminal methyl group protons of the appended propyl group. These two features verify that the propyl group is bonded to the DOPC as proposed. Further interpretation of the spectrum is provided in the legend to Figure 2.

Cationic Phospholipids with Short Alkyl Groups Hydrate Well and Disperse Readily as Liposomes. Longer Chain Homologues Disperse Poorly in Aqueous Phases. As observed previously (*18*), *O*-ethyl-DOPC readily hydrates at room temperature and forms large, usually unilamellar vesicles, easily visible under the light microscope. The same behavior was observed with both *O*-methyl- and *O*-propyl-DOPC. In contrast, neither the *O*-decyl- nor *O*-octadecyl-DOPC formed liposomes, in either water or salt solutions, based on light microscopy. The *O*-hexyl compound exhibited unusual and unexpected behavior. In water, it hydrated as a bilayer phase to form liposomes, whereas in salt solution, it remained as a viscous, nonbirefringent liquid.

X-ray Diffraction of Hydrated Lipid Phases and of Their Complexes with DNA. According to X-ray diffraction, both *O*-decyl-DOPC and *O*-octadecyl-DOPC definitely formed hexagonal phases in excess water. Both compounds gave broad, wide-angle bands centered at 4.5 Å. The C10 compound gave spacings of 59.6, 34.4, 29.8, and 22.5 Å, which index as orders of a hexagonal phase with a spacing of $d = 59.6$ Å. The C18 compound gave spacings of 61.4, 35.4, and 30.7, which index as orders of a hexagonal phase with $d = 61.4$ Å. Essentially the same structure was observed when the lipid was dispersed in D-PBS.

In excess D-PBS, the hexyl compound behaved quite differently than in excess water. During preparation of this compound for X-ray analysis, the hydrated material clung to the vessel wall. After scraping it away, a very viscous, clear mass was obtained. This material was not birefringent. It gave an X-ray pattern with a broad wide-angle band at 4.5 Å (consistent with a liquid crystalline phase) and six strong, sharp low-angle reflections at

spacings of 60.6, 49.8, 43.1, 35.3, 30.3, and 29.4 Å. These six reflections index quite closely to orders (110), (111), (200), (211), (220), and (300) of a cubic phase with a fundamental repeat period of 85.7 Å. The only reflections that are missing for the expected first eight reflections of a 85.7 Å cubic phase are the (100) and (210) reflections. Moreover, no observed reflections are unaccounted for by this cubic phase. Cubic phases are viscous and nonbirefringent. So, at least under the ionic strength conditions for phosphate basic saline and at moderately high concentration of lipid (10%), *O*-hexylphosphatidylcholine forms a cubic phase. This conclusion was verified by the observation of a bicontinuous cubic array by freeze-fracture electron microscopy (Y. Tarahovsky et al., unpublished material).

The complexes formed by some of the lipids with DNA were examined by X-ray diffraction. As previously found, the complex of DNA with the ethyl compound was lamellar in both water with salmon sperm DNA and D-PBS with plasmid DNA (R.C.M. and Ashley et al., unpublished material). HexylDOPC, dispersed in water and combined with DNA was not highly ordered, giving two reflections that indexed as d and $d/2$ of a repeating unit of 59 Å. Since there was no indication of a reflection at $d/\sqrt{3}$, which would indicate a hexagonal phase or at any repeats expected for cubic phases, this complex was evidently lamellar.

Octadecyl-DOPC, although it formed a hexagonal complex by itself, gave a lamellar complex with salmon sperm DNA at a 4:1 ratio of lipid to DNA. The initial complex, diffracted immediately after formation, revealed a mixture of lamellar and hexagonal phases, but after standing overnight, the hexagonal reflections disappeared, leaving only the lamellar reflections for a repeating unit of 70 Å.

Cationic Phospholipids Efficiently Mediate DNA Transfection, even in the Presence of Serum. To establish the effect of varying the alkyl chain length on transfection efficiency, we assessed the ability of the *O*-alkyl derivatives, namely, *O*-methyl, *O*-propyl, *O*-hexyl, *O*-decyl, and *O*-octadecyl-DOPC, to mediate DNA transfection in BHK cells. Unlike most cationic lipids available commercially, these cationic phospholipids do *not* require any DOPE co-lipid in order to mediate transfection. Consequently, the transfection complexes were typically prepared simply by combining DNA with the cationic phospholipid, since, from prior experience with the ethyl derivative (*25*), we expected that these cationic phospholipids might also mediate transfection efficiently in the presence of serum proteins, and therefore tested transfection both in the presence and absence of 10% serum.

As shown in Figure 3, the *O*-ethyl (Figure 3B) and *O*-propyl (Figure 3C) compounds were the most active compounds in the series with alkyl chains of 1, 2, 3, and 6 carbons, and essentially equivalent in transfection mediation efficiency. The methyl derivative exhibited significantly lower activity (Figure 3A). The *O*-hexyl derivative mediated transfection—at least at one lipid: DNA ratio—with nearly the same efficiency as the *O*-ethyl and *O*-propyl compounds, but only if the lipid had been dispersed in water (Figure 3D).

Although *O*-hexyl-PC was virtually devoid of transfection activity when prepared according to the standard hydration procedure involving vigorous vortexing in saline, it exhibited good activity when it was sonicated before complex formation (Figure 4A). The long-chain *O*-alkyl derivatives, *O*-decyl-PC and *O*-octadecyl-PC, exhibited little transfection activity when prepared in either water or in saline by manual agitation (Figure 4,

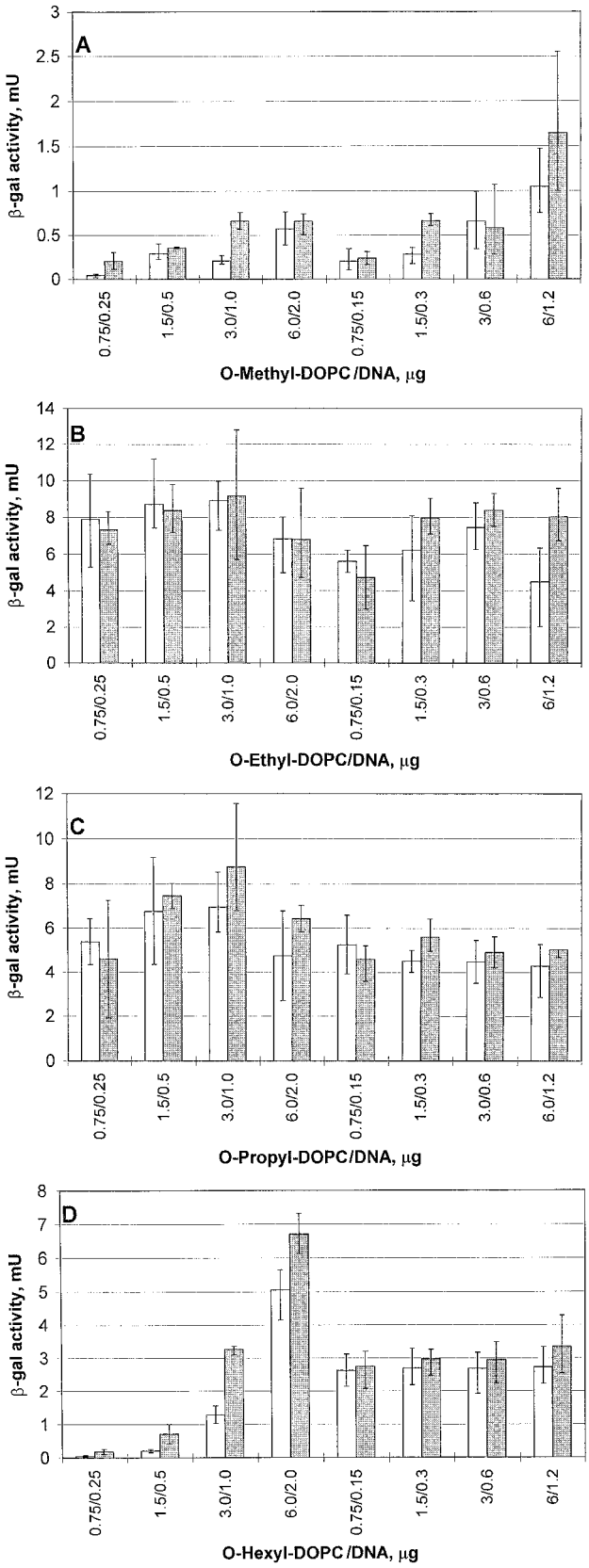

Figure 3. Transfection efficiency of *O*-alkyl compounds in presence of serum. BHK cells were transfected with (A) *O*-methyDOPC/DNA complex, (B) *O*-ethylDOPC/DNA complex, (C) *O*-propylDOPC/DNA complex, and (D) *O*-hexylDOPC/DNA complex. Transfection was performed in medium without supplements (white bars) and in medium containing 10% FBS (gray bars). All lipids were dispersed in D-PBS with the exception of *O*-hexyl-DOPC, which was dispersed in water. Error ranges indicate the highest and the lowest values of replicates.

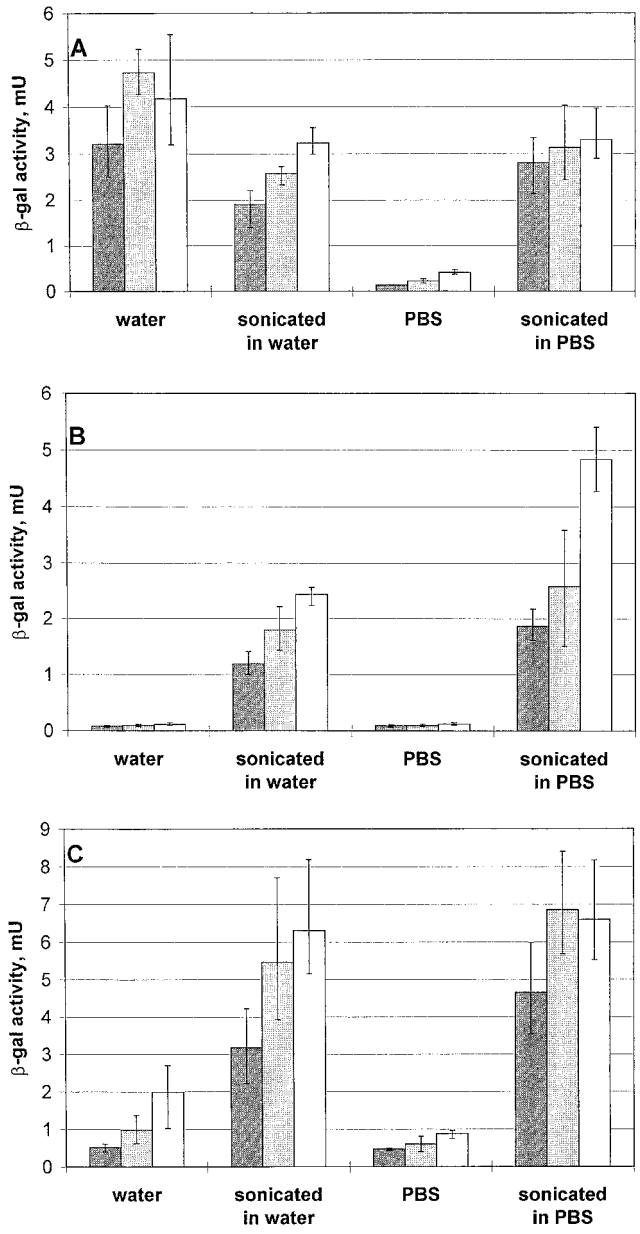

Figure 4. Effect of solvent and dispersion on transfection activity of medium and long chain *O*-alkyl derivatives. BHK cells were transfected with (A) *O*-Hexyl-DOPC/DNA complex, (B) *O*-decyl-DOPC/DNA complex; (C) *O*-Octadecyl-DOPC/DNA complex. *O*-alkyl compounds were dispersed in water or in PBS with or without sonication. Lipid−DNA complexes were used in amounts 1.5/0.5 μg/well (black bars), 3.0/1.0 μg/well (gray bars), 6.0/2.0 μg/well (white bars). Error ranges indicate the highest and the lowest values of replicates.

panels B and C). As mentioned earlier, the long-chain derivatives are very difficult to disperse in aqueous media compared to *O*-methyl, ethyl, or propyl versions, and even when they are first solubilized in ethanol and injected into the aqueous phase, they do not give efficient transfection. After sonication, however, *O*-decyl- and *O*-octadecyl-DOPC exhibit significant transfection activity (Figure 4, panels B and C), although typically less than the other *O*-alkyl compounds mentioned above (except *O*-methyl). The decyl and octadecyl compounds have also been tested for transfection at ratios of lipid to DNA of 4:1 and 5:1, with no marked difference in transfection efficiency from those found for the 3:1 ratio.

The sonication time for the lipids used for the transfection assays of Figure 4 was 2 min. At this duration of sonication, the *O*-hexyl-PC loses activity if dispersed in water. Loss of transfection activity was also seen with the two longer derivatives, but it required longer exposures; at sonication times of 10 min or more, the tranfection efficiency dropped by 90% or more. Thus, in D-PBS, these three compounds require sonication for proper dispersion, but excessive sonication clearly leads to a loss of activity. In general, it appears that the more easily dispersed the lipid, the more quickly sonication reduces transfection activity. In the case of the ethyl compound, which generates liposomes spontaneously without agitation, only a few tens of seconds of sonication eliminated activity. In that case, there was no chemical decomposition of the lipid detectable by thin-layer chromatography even after minutes of sonication (*26*). A related test has been done on octadecyl-PC; it was sonicated to produce a uniform dispersion in water and then allowed to stand at room temperature for a week. By thin-layer chromatography there was no detectable degradation (A. Hashimoto, unpublished). It is thus clear that the effect of sonication is physical. Our preliminary evidence suggests that small lipid particles give rise to small transfection complexes (E. Pozharski, V.A.R., and R.C.M., unpublished material) and that these, probably because they remain in suspension longer than larger complexes, are less effective at transfection. Others have observed that multilamellar dispersions of lipids are more effective transfection agents, at least under some conditions, than sonicated preparations (*11*, *27*−*29*).

DISCUSSION

Alkylation of Zwitterionic Phospholipids Provides a Facile Route to Cationic Phospholipids. Amphipathic molecules have a multitude of important medical, technical, and cosmetic applications. In some cases, the properties of natural compounds are an advantage, either because of diminished toxicity or because of the characteristic required for the natural function. Aside from modifying the fatty acid substituents and derivatizing the headgroup to incorporate markers such as fluorophores, there has been relatively little research involving basic changes in the structure of natural phospholipids. We found that it is straightforward to change zwitterionic phospholipids to their cationic counterparts. It is clear from the present work that such modifications of the structure of phosphatidylcholine can produce molecules with some very unusual properties that were not anticipated. Furthermore, because cationic phospholipids are very rare and those of the alkyl triester type described here are unknown in nature, they are anticipated to have unusual interactions with cells.

Physical Properties of Cationic Phospholipids. The conversion of a phosphatidylcholine to an *O*-alkyl phosphatidylcholinium ion not only eliminates the negative charge but also drastically reduces the hydrogen bond accepting potential of the molecule. In addition, the size and polarity of the headgroup may be altered, depending upon the length of the alkyl chain appended and the size and hydrophobicity of the resulting headgroup. The alkyl group may be varied from the minimum, a methyl group, to a chain as long or potentially longer than the fatty acid groups already present in the molecule. The methyl, ethyl, and propyl derivatives are evidently only modestly affected with respect to size and hydrophobicity, whereas the longer chain compounds are sufficiently changed that they prefer to assume the cubic or hexagonal phase than to reside in the lamellar phase.

The methyl phosphatidylcholinium is, as expected of methyl phosphate esters, somewhat unstable due to

susceptibility to S_N2 nucleophilic attack. However, the ethyl and, it may be presumed, the longer chain members of the family are quite stable. The ethyl compound is susceptible to hydrolysis by some purified lipases and in cells, although loss of the ethyl group was not observed (*25*). The rate of hydrolysis appears to decrease the closer the *O*-alkyl group is to the bond attacked by the lipase. This susceptibility to hydrolysis may contribute to the relatively low toxicity that these compounds exhibit toward mammalian cells. They may also be able to integrate into the various cellular membranes and coexist peacefully with their zwitterionic neighbors. These characteristics, in addition to their ability to mediate transfection efficiently in the presence of serum proteins, make them attractive candidates for agents to deliver nucleic acids and other pharmacological and physiological agents (*17*) to cells, both in the laboratory and the clinic.

The *O*-methyl, *O*-ethyl, and *O*-propyl derivatives hydrate very well, forming a lamellar phase with large spacings, whereas the *O*-decyl and *O*-octadecyl derivatives do not. The latter compounds assume a hexagonal phase (*30*) presumably because the alkyl chains are so long that they must fold back among the acyl chains, where they increase the tail cross-sectional area to the point where lamellar phase packing is not possible. As is typical of inverted hexagonal phases, because they do not exhibit extended hydrophilic surfaces with which to make low-energy interfaces with water, the long-chain *O*-alkyl phosphatidylcholine derivatives are very difficult to disperse in aqueous phases, especially at higher ionic strength where ionization and hence hydration would be repressed.

While the *O*-hexyl derivative can assume a lamellar phase in water, it seems to be on the edge of stability such that it prefers to reside in a cubic phase upon hydration in saline. This behavior is not surprising, though, since cubic phases are typically found in phase diagrams between lamellar and hexagonal phases (*31*) and, structurally, the hexyl derivative stands between shorter chain lamellar phase-forming compounds and longer chain hexagonal phase-forming compounds. Presumably, this behavior of the hexyl compound can be attributed to a folding back of the hexyl group into the region of the acyl chains, which generates enough tail-to-head asymmetry in the molecule for it to favor a cubic phase, but not enough for preference of the inverted hexagonal phase.

Structure and Transfection Efficiency of *O*-Alkyl Derivatives. The newly synthesized *O*-alkyl derivatives were examined for their capacity to mediate transfection in mammalian cells. The first compound in this set, *O*-methyl, hydrated and dispersed well, but its reduced chemical stability, perhaps even after uptake into cells, may explain why it exhibited much less activity compared to the next short-chain compounds. The short-chain derivatives, *O*-ethyl-PC and *O*-propyl-PC, which formed a lamellar phase after hydration, were the most effective in DNA transfection. The former compound is known to form a sandwich-type complex with DNA in which the nucleic acid binds together bilayers of lipid (*26*), as occurs with some other cationic lipid transfection agents (*32*−*35*).

The intermediate chain compound, *O*-hexyl, which is also lamellar in water, had approximately the same transfection efficiency as *O*-ethyl and *O*-propyl. However, in saline, *O*-hexyl assumed a cubic phase and became capable of mediating transfection only when vigorously dispersed by sonication. When combined with DNA, this compound gave a lamellar phase complex, presumably because, topologically, a bicontinuous cubic phase would be incompatible with maximal interaction of lipid and DNA. Transformation to a hexagonal phase complex, while possible, is evidently not energetically favorable with compounds of this type, as evidenced by the behavior of the octadecyl derivative (see next paragraph). As particularly well illustrated by the hexyl derivative, there are critical aspects of formulation with plasmids that impose clear limits on the efficiency of transfection mediated by cationic amphipaths. In water, where *O*-hexyl-PC dispersed fairly well, sonication was detrimental, presumably because the small vesicles so generated give rise to small DNA complexes which transfected poorly, either because of poor uptake or reduced contact with cells (*29*, *36*). In contrast, in D-PBS—in which the compound assumed a cubic phase and dispersed much less well than in water—the lipid had to be sonicated in order to disperse it well enough to form productive interactions with DNA.

The transfection complex that *O*-hexyl-PC forms with DNA at high ionic strength is lamellar, suggesting that there is a smaller structural penalty involved in the transition from a cubic array to a lamellar complex than to a hexagonal complex. Since there is no obvious way in which DNA−lipid surface electrostatic interactions could be maximized given the limited structural parameters of the cubic phase, we would not expect to see a stable cubic array of DNA and lipid. It should be appreciated, however, that the mode of formation of transfection complexes can influence their size, transfection activity, and possibly structure (*37*).

The longest chain compounds in the series, *O*-decyl-PC and *O*-octadecyl-PC, assumed the inverted hexagonal phase in water (and presumably also in saline) and were also essentially inert as transfection agents when prepared according to the standard hydration procedure. These compounds only exhibited significant activity if they were dispersed by sonication. The structure of the complex they formed with DNA was lamellar (*26*). DNA can form hexagonal complexes with cationic lipid mixtures (*38*), and although we were initially surprised that a hexagonal phase cationic phospholipid formed a lamellar phase complex with DNA, theoretical analyses have affirmed that, unless the intrinsic curvature of the lipid is very high, lamellar phases are more stable than hexagonal arrays (*39*−*41*). Consistent with these analyses, we have found that when the long-chain cationic phospholipids are formulated with an equal amount of DOPE, the resulting lipid mixture does indeed generate a hexagonal phase complex with DNA (*19*). In contrast to other investigators (*38*), we found that there hexagonal phase complexes had no advantages over lamellar phase complexes and, indeed, were generally less effective than lamellar phase complexes (*19*).

Implications for Assessment of New Cationic Transfection Mediators. Transfection mediators of the cationic lipid type may exist in a variety of different phase states which have intrinsically much different abilities to be uniformly dispersed in an aqueous phase. It is therefore essential that surveys of new compounds be constructed such as to ensure that the lipid is present in the aqueous phase in a form allowing near-complete exposure to DNA in solution. Otherwise, there is the risk that potentially valuable compounds will be overlooked and that conclusions about particular chemical classes could be erroneous. Our results suggest that with a given chemical type of transfection agent, there is no inherent advantage in either lamellar or hexagonal phases, but

that optimal conditions for DNA complex formation may well differ greatly.

ACKNOWLEDGMENT

We are grateful to Joseph Tucker, Jaime Stearns, and Akihiro Hashimoto for contributions to optimization of reaction conditions and to Jaime Stearns and Akihiro Hashimoto for the synthesis of some of the lipids used here. We are also grateful to Ruby MacDonald for carefully reading and commenting on the manuscript and for support in the laboratory. Funded by grants from the NIH: GM52329 and GM57305 to R.C.M. and GM27278 to T.J.M. We are also grateful to Avanti Polar Lipids for lipid starting materials.

LITERATURE CITED

(1) Keown, W. A., Campbell, C. R., and Kucherlapati R. S. (1990) Methods for introducing DNA into mammalian cells. *Methods Enzymol. 185*, 527−537.

(2) Forster W., and Neumann E. (1989) Gene Transfer by Electroporation- -A Practical Guide. In *Electroporation and Electrofusion in Cell Biology* (E. Neumann, A. E. Sowers, and C. A. Jordan, Eds.) pp 299−318, Plenum Press, New York.

(3) Felgner, P. L., Gadek, T. R., Holm, M., Roman, R., Chan, H. W., Wenz, M., Northrop, J. P., Ringold, G. M., and Danielsen, M. (1987) Lipofection: highly efficient, lipid-mediated DNA-transfection procedure. *Proc. Natl. Acad. Sci. U.S.A. 84*, 7413−7417.

(4) Leventis, R., and Silvius, J. R. (1990) Interactions of mammalian cells with lipid dispersions containing novel metabolizable cationic amphiphiles. *Biochim. Biophys. Acta 1023*, 124−132.

(5) Gao X., and Huang L. (1991) A novel cationic liposome reagent for efficient transfection of mammalian cells. *Biochem. Biophys. Res. Commun. 179*, 280−285.

(6) Rose, J. K., Buonocore, L., and Whitt, M. A. (1991) A new cationic liposome reagent mediating nearly quantitative transfection of animal cells. *Biotechniques 10*, 520−525.

(7) Barthel, F., Remy, J. S., Loeffler, J. P., and Behr, J. P. (1993) Gene transfer optimization with lipospermine-coated DNA. *DNA Cell Biol. 12*, 553−560.

(8) Solodin, I., Brown, C. S., Bruno, M. S., Chow, C. Y., Jang, E. H., Debs, R. J., and Heath, T. D. (1995) A novel series of amphiphilic imidazolinium compounds for in vitro and in vivo gene delivery. *Biochemistry 34*, 13537−13544.

(9) Akao, T., Nakayama, T., Takeshia, K., and Ito, A. (1994) Design of a new cationic amphiphile with efficient DNA-transfection ability. *Biochem. Mol. Biol. Int. 34*, 915−920.

(10) Bichko, V., Netter, H. J., and Taylor, J. (1994) Introduction of hepatitis delta virus into animal cell lines via cationic liposomes. *J. Virol. 68*, 5247−5252.

(11) Felgner, J. H., Kumar, R., Sridhar, C. N., Wheeler, C. J., Tsai, Y. J., Border, R., Ramsey, P., Martin, M., and Felgner, P. L. (1994) Enhanced gene delivery and mechanism studies with a novel series of cationic lipid formulations. *J. Biol. Chem. 269*, 2550−2561.

(12) Wang, J., Guo, X., Xu, Y., Barron, L., and Szoka, F. C. Jr. (1998) Synthesis and characterization of long chain alkyl acyl carnitine esters. Potentially biodegradable cationic lipids for use in gene delivery. *J. Med. Chem. 41*, 2207−2215.

(13) Morgan, R. A., and Anderson, W. F. (1993) Human gene therapy. *Annu. Rev. Biochem. 62*, 191−217.

(14) Bennett, C. F., Chiang, M. Y., Chan, H., Shoemaker, J. E., and Mirabelli, C. K. (1992) Cationic lipids enhance cellular uptake and activity of phosphorothioate antisense oligonucleotides. *Mol. Pharmacol. 41*, 1023−1033.

(15) Debs, R. J., Freedman, L. P., Edmunds, S., Gaensler, K. L., Düzgüneş N., and Yamamoto, K. R. (1990) Regulation of gene expression in vivo by liposome-mediated delivery of a purified transcription factor. *J. Biol. Chem. 265*, 10189−10192.

(16) Huang, L., Farhood, H., Serbina, N., Teepe, A. G., and Barsoum, J. (1995) Endosomolytic activity of cationic liposomes enhances the delivery of human immunodeficiency virus-1 trans-activator protein (TAT) to mammalian cells. *Biochem. Biophys. Res. Commun. 217*, 761−768.

(17) Barber, K., Mala, R. R., Lambert, M. P., Qiu, R., MacDonald, R. C., and Klein, W. L. (1996) Delivery of membrane-impermeant fluorescent probes into living neural cell populations by lipotransfer. *Neurosci. Lett. 207*, 17−20.

(18) Ashley, G. W., Shida, M. M., Qiu, R., Lahiri, M. K., Levisay, P. C., Jones, R. D., Baker, K. A., and MacDonald, R. C. (1996) Phosphatidylcholinium compounds: A new class of phospholipids with transfection activity and unusual physical properties. *Biophys. J. 70*, A88.

(19) Rakhmanova, V. A., McIntosh, T. J., and MacDonald, R. C. (2000) Effects of dioleoylphosphatidylethanolamine on the activity and structure of *O*-alkylphosphatidylcholine-DNA transfection complexes. *Cell Mol. Biol. Lett.* (in press).

(20) Gorman, C. M., Aikawa, M., Fox, B., Fox, E., Lapuz, C., Michaud, B., Nguyen, H., Roche, E., Sawa, T., and Wiener-Kronish, J. P. (1997) Efficient in vivo delivery of DNA to pulmonary cells using the novel lipid EDMPC. *Gene Ther. 4*, 983−992.

(21) McIntosh, T. J., Magid, A. D., and Simon, S. A. (1987) Steric repulsion between phosphatidylcholine bilayers. *Biochemistry 26*, 7325−7332.

(22) McIntosh, T. J., Magid, A. D., and Simon, S. A. (1989) Cholesterol modifies the short-range repulsive interactions between phosphatidylcholine membranes. *Biochemistry 28*, 17−25.

(23) Rakhmanova, V. A., and MacDonald, R. C. (1998) A microplate fluorimetric assay for transfection of the β-galactosidase reporter gene. *Anal. Biochem. 257*, 234−237.

(24) Christie, W. W. (1982) *Lipid Analysis*, pp 161−166, Pergammon, Oxford.

(25) MacDonald, R. C., Rakhmanova, V. A., Choi, K. L., Rosenzweig, H. S., and Lahiri, M. K. (1999) *O*-ethylphosphatidylcholine: A metabolizable cationic phospholipid which is a serum-compatible DNA transfection agent. *J. Pharm. Sci. 88*, 896−904.

(26) MacDonald, R. C., Ashley, G. W., Shida, M. M., Rakhmanova, V. A., Tarahovsky, Y. S., Pantazatos, D. P., Kennedy, M. T., Pozharski, E. V., Baker, K. A., Jones, R. D., Rosenzweig, H. S., Choi, K. L., Qiu, R., and McIntosh, T. J. (1999) Physical and biological properties of cationic triesters of phosphatidylcholine. *Biophys. J. 77*, 2612−2629.

(27) Kojima, H., Ohishi, N., Takamori, M., and Yagi, K. (1995) Cationic multilamellar liposome-mediated gene transfer into primary myoblasts. *Biochem. Biophys. Res. Commun. 207*, 8−12.

(28) Holmen, S. L., Vanbrocklin, M. W., Eversole, R. R., Stapleton, S. R., and Ginsberg, L. C. (1995) Efficient lipid-mediated transfection of DNA into primary rat hepatocytes. *In Vitro Cell. Dev. Biol. 31*, 347−351.

(29) Ross, P. C., and Hui, S. W. (1999) Lipoplex size is a major determinant of *in vitro* lipofection efficiency. *Gene Ther. 6*, 651−659.

(30) Seddon, J. M. (1990) Structure of the inverted hexagonal (H_{II}) phase, and non-lamellar phase transitions of lipids. *Biochim. Biophys. Acta 1031*, 1−69.

(31) Larsson, K. (1994) *Lipids−Molecular Organization, Physical Functions and Technical Applications*, The Oily Press, Dundee.

(32) Xu, Y., Hui, S. W., Frederik, P., and Szoka, F. C., Jr. (1999) Physicochemical characterization and purification of cationic lipoplexes. *Biophys. J. 77*, 341−353.

(33) Rädler, J. O., Koltover, I., Salditt, T., and Safinya, C. R. (1997) Structure of DNA-cationic liposome complexes: DNA intercalation in multilamellar membranes in distinct interhelical packing regimes. *Science 275*, 810−814.

(34) Lasic, D. D., Strey, H., Stuart, M. C. A., Podgornik, R., and Frederik, P. M. (1997) The structure of DNA-liposome complexes. *J. Am. Chem. Soc. 119*, 832−833.

(35) Boukhnikachvili, T., Aguerre-Chariol, O., Airiau, M., Lesieur, S., Ollivon, M., and Vacus, J. (1997) Structure of in-serum transfecting DNA-cationic lipid complexes. *FEBS Lett. 409*, 188−194.

(36) Zuidam, N. J., Hirsch-Lerner, D., Margulies, S., and Barenholz, Y. (1999) Lamellarity of cationic liposomes and

mode of preparation of lipoplexes affect transfection. *Biochim. Biophys. Acta 1419*, 207−220.
(37) Kennedy, M. T., Pozharski, E. V., Rakhmanova, V. A., and MacDonald, R. C. (2000) Factors governing the assembly of cationic phospholipid-DNA complexes. *Biophys. J. 78*, 1620−1633.
(38) Koltover, I., Salditt, T., Rädler, J. O., and Safinya, C. R. (1998) An inverted hexagonal phase of cationic liposome-DNA complexes related to DNA release and delivery. *Science 281*, 78−81.
(39) Dan, N. (1998) The structure of DNA complexes with cationic liposomes-cylindrical or flat bilayers? *Biochim. Biophys. Acta 1369*, 34−38.
(40) Harries, D., May, S., Gelbart, W. M., and Ben Shaul, A. (1998) Structure, stability, and thermodynamics of lamellar DNA-lipid complexes. *Biophys. J. 75*, 159−173.
(41) Bruinsma, R. (1998) Electrostatics of DNA cationic lipid complexes: Isoelectric instability. *Eur. Phys. J. B4*, 75−88.

BC9901144

Synthesis of Cholesteryl Polyamine Carbamates: pK_a Studies and Condensation of Calf Thymus DNA

Andrew J. Geall,[†] Richard J. Taylor,[‡] Mark E. Earll,[‡] Michael A. W. Eaton,[‡] and Ian S. Blagbrough*[,†]

Department of Pharmacy and Pharmacology, University of Bath, Bath BA2 7AY, U.K., and Celltech Chiroscience, 216 Bath Road, Slough SL1 4EN, U.K. Received September 10, 1999; Revised Manuscript Received December 15, 1999

Novel polyamine carbamates have been designed and prepared from cholesterol. Our synthesis uses an orthogonal protection strategy based upon trifluoroacetyl and Boc-protecting groups. These unsymmetrical polyamine carbamates have been prepared from symmetrical (e.g., spermine and thermine) polyamines. Detailed interpretations of ^{1}H and ^{13}C NMR spectroscopic data led to the unambiguous assignment of these polyamine carbamates. These target conjugates contain a variety of positive charges distributed along methylene chains. Their pK_as have been determined potentiometrically for conjugates substituted with up to five amino functional groups. Condensation of calf thymus DNA into particles was monitored using light scattering at 320 nm. Salt-dependent binding affinity for calf thymus DNA was determined using an ethidium bromide fluorescence quenching assay. These cholesteryl polyamine carbamates are models for lipoplex formation with respect to gene delivery (lipofection), a key first step in gene therapy.

INTRODUCTION

Polyamines such as tetraamine spermine **1** are widely distributed in nature and display a variety of important biological activities (*1*−*4*). Polyamines affect DNA replication and translation, protein synthesis, membrane stabilization, and the activity of certain kinases and topoisomerases. Charge neutralization of intracellular polyanions (e.g., DNA and RNA) may be among the most important physiological roles of these compounds. Stabilization of specific DNA conformations may be important for nucleosome formation, chromatin condensation, and gene expression. The binding of polyamines has a profound effect on DNA structure, causing transitions from B to both A and Z forms and, at higher concentrations, conformational changes, e.g., aggregation and condensation (*3*−*7*). Condensation is caused by alleviation of charge repulsion between neighboring phosphates on the DNA helix allowing collapse into a more compact structure (*3*). Polyamine-mediated condensation is a rapidly expanding area of research for nonviral vectors in gene therapy (lipoplexes in lipofection) (*8*).

The application of synthetic lipo-polyamines constitutes safer and more efficient gene transfer strategies which, unlike viral vectors, do not elicit immune responses (*9*−*13*). Within the prerequisites for delivery of DNA across an intact cytoplasmic membrane are condensation and masking the negative charge of the phosphate backbone. Structure−activity relationships (SAR) for the binding of polyamines to DNA and the subsequent condensation of DNA indicate that polyammonium ions are suitable for use as gene delivery systems (*4*−*7*, *14*−*18*). Covalent attachment of a lipid moiety, such as one or two long aliphatic chains (*6*, *15*) or a steroid (*14*, *16*−*20*), further enhances polyamine-mediated DNA condensation. The mechanism by which these compounds cause lipofection is poorly understood. Knowledge about the pK_as, especially accurate prediction along a polyamine (polyammonium) chain, will allow protonation states at physiological pH to be determined, and therefore, DNA-binding affinities can be predicted with greater confidence. Such physicochemical properties are important in the design of lipoplexes for efficient lipofection.

In this paper, we report the synthesis of a series of cholesteryl polyamine carbamates. Using an ethidium bromide (Eth Br) displacement assay, we have investigated the SAR of their binding to, and condensation of, calf thymus (CT) DNA (*20*−*25*). Changes in binding affinity for DNA with respect to variations in the total number of positive charges and the differences in the distribution of these charges along the lipopolyamine were investigated. Salt-concentration dependent binding of these cholesteryl polyamine carbamates to CT DNA was also studied. Condensation was verified using a light scattering (λ = 320 nm) assay.

Using our orthogonal protection strategy for efficient syntheses of unsymmetrical polyamine amides (*21*), six carbamates of cholesterol (at position 3) were designed and synthesized (**13**−**16** see Figure 1 and **23** and **24** see Figure 2) (*22*, *25*). Cholesteryl was our lipid moiety of choice for lipoplex formation (*14*, *16*, *17*, *26*, *27*), it is readily available as the required chloroformate. Six commercially available polyamines were used as the cationic headgroups: 1,12-diamino-4,9-diazadodecane **1** (spermine, 3.4.3, Figure 1), 1,11-diamino-4,8-diazaundecane **2** (thermine, norspermine, 3.3.3, Figure 1), 1,10-diamino-4,7-diazadecane **3** (3.2.3, Figure 1), 1,9-diamino-3,7-diazanonane **4** (2.3.2, Figure 1), 1,11-diamino-3,6,9-triazaundecane **17** (tetraethylenepentamine, 2.2.2.2, Figure 2), and 1,14-diamino-3,6,9,12-tetraazatetradecane **18** (pentaethylenehexamine, 2.2.2.2.2, Figure 2) affording **13**−**16** (Figure 1) and **23** and **24** (Figure 2), respectively. Condensation of CT DNA was monitored using a refined Eth Br displacement assay (*19*, *28*). The pK_as were

* To whom correspondence should be addressed. Phone: 44-1225-826795. Fax: 44-1225-826114. E-mail: prsisb@bath.ac.uk.
[†] University of Bath.
[‡] Celltech Chiroscience.

10.1021/bc990115w CCC: $19.00 © 2000 American Chemical Society
Published on Web 04/13/2000

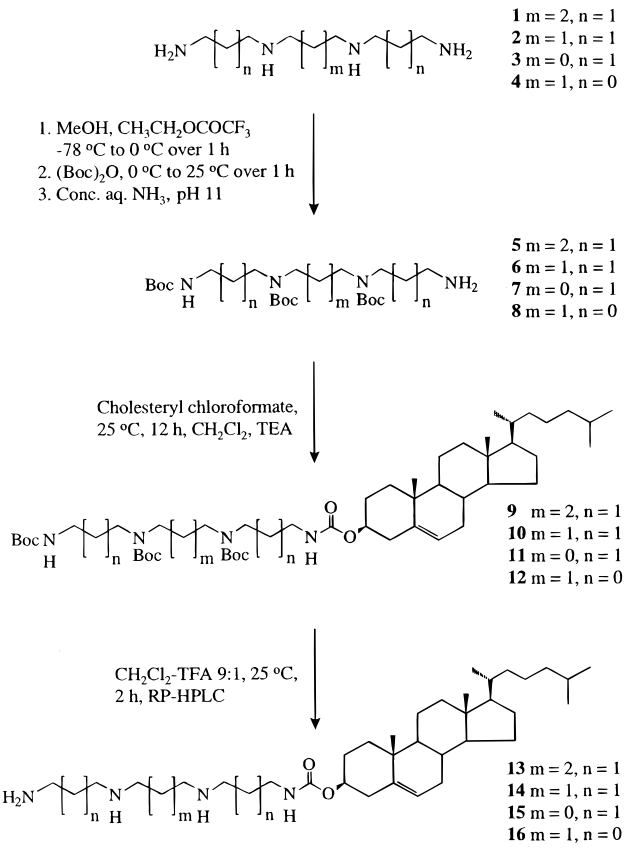

1 m = 2, n = 1
2 m = 1, n = 1
3 m = 0, n = 1
4 m = 1, n = 0

5 m = 2, n = 1
6 m = 1, n = 1
7 m = 0, n = 1
8 m = 1, n = 0

9 m = 2, n = 1
10 m = 1, n = 1
11 m = 0, n = 1
12 m = 1, n = 0

13 m = 2, n = 1
14 m = 1, n = 1
15 m = 0, n = 1
16 m = 1, n = 0

Figure 1. Structure and synthesis of target cholesteryl polyamine carbamates **13**−**16**.

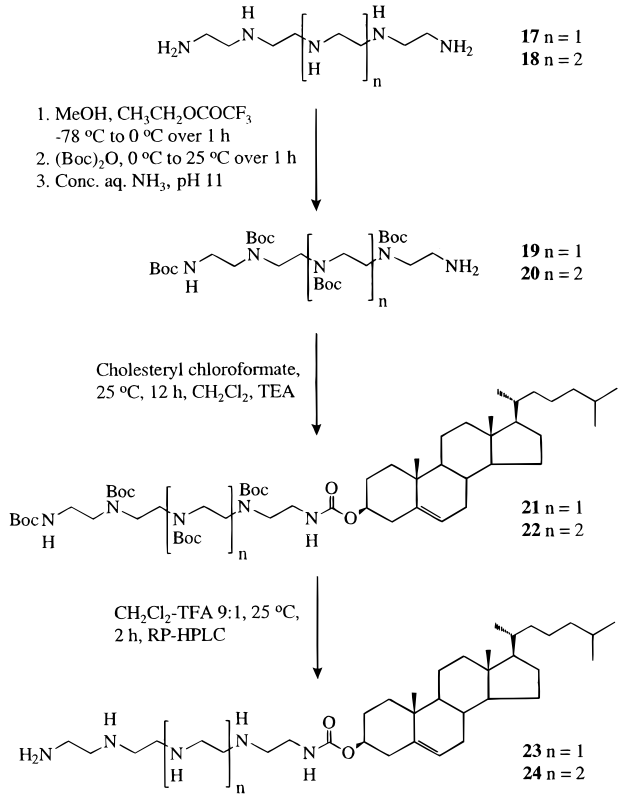

17 n = 1
18 n = 2

19 n = 1
20 n = 2

21 n = 1
22 n = 2

23 n = 1
24 n = 2

Figure 2. Structure and synthesis of target cholesteryl polyamine carbamates **23** and **24**.

measured potentiometrically and their values used in the Henderson−Hasselbach equation to determine the charge carried on the polyamine at physiological pH (7.4) (*22*).

EXPERIMENTAL SECTION PROCEDURES

General Details. Column chromatography was performed over silica gel 60 (35−75 μm) purchased from Prolabo-Merck. Analytical TLC was performed using aluminum-backed plates coated with Kieselgel 60 F_{254}, purchased from Merck. The chromatograms were visualized with either potassium permanganate (basic aqueous) or ninhydrin (acidic butanolic). Analytical and semipreparative RP-HPLC were performed with a Jasco PU-980 pump equipped with a Jasco UV-975 detector (λ = 220 nm). The column stationary phase was Supelcosil ABZ+Plus, 5 μm (15 cm × 4.6 mm for the analytical and 25 cm × 10 mm for the semipreparative columns, respectively). The mobile phases were isocratic mixtures of acetonitrile (MeCN) and 0.1% aqueous trifluoroacetic acid, with 1.5 and 4.0 mL/min flow rates for the analytical and semipreparative columns, respectively. Removal of solvents in vacuo means using a Büchi Rotavapor R-114 at water aspirator pressure. ^{1}H NMR and ^{13}C NMR spectra were recorded using JEOL 270 (operating at 270 MHz for ^{1}H and 67.8 MHz for ^{13}C) or JEOL EX 400 (operating at 400 MHz for ^{1}H and 100.8 MHz for ^{13}C) spectrometers. Chemical shifts values are recorded in parts per million on the δ scale. Spectra were referenced internally using either the residual solvent resonance for ^{13}C or to TMS for ^{1}H. Coupling constants (J values) are expressed in Hertz, and multiplicities are recorded as s (singlet), d (doublet), t (triplet), q (quartet), quin (quintet), m (multiplet), and br (broad). ^{13}C multiplicity determinations were aided by 90° and 135° DEPT pulse sequences. HETCOR spectra were obtained, when required, to confirm the ^{1}H or ^{13}C assignments and were recorded using a JEOL GX400 spectrometer. All mass spectra were recorded on a VG AutoSpec Q instrument. Electron impact (EI) ionization was performed at 70 eV and <70 eV while chemical ionization (CI) used isobutane. High- and low-resolution fast-atom bombardment (FAB) used *m*-nitrobenzyl alcohol (mNBA) as the matrix. Microanalyses were performed by the Microanalysis Laboratory at the University of Bath using a Carla Erba 1106 elemental analyzer, but elemental analysis is inadequate as a criterion of purity if polyamines are present in cationic lipids (*29*). Polyamines, their polytrifluoroacetic acid salts, and other salts were highly hygroscopic, and therefore, their melting points were not determined.

Reagents. Anhydrous methanol was prepared by distillation from magnesium turnings and iodine and was stored over 3 Å molecular sieves under anhydrous nitrogen. Anhydrous CH_2Cl_2 and DMSO were prepared by distillation from calcium hydride (5% w/v) and were stored over 4 Å molecular sieves. Reagents and chemicals were purchased from SAF, solvents (HPLC grade) were purchased from Fisons.

Ethidium Bromide Displacement Assay. CT DNA, polylysine (average RMM 9600 Da, degree of polymerization 38 by viscosity), and Eth Br were obtained from SAF. Polyamine conjugates were used as their TFA salts, weighed, and dissolved in MilliQ water. Eth Br was weighed, and a stock solution (0.5 mg/mL) made up in MilliQ water. The buffer solutions (20 mM NaCl, 2 mM Hepes, 10 μM EDTA, pH 7.4, and 150 mM NaCl, 2 mM Hepes, 10 μM EDTA, pH 7.4) were also made up in MilliQ water, pH adjusted to 7.4 with NaOH. A stock solution of CT DNA of approximately 20 μg/mL (3 mL) was made in buffer (20 mM NaCl, 2 mM Hepes, and 10 μM EDTA, pH 7.4), and the concentration determined spectroscopically (*8*). DNA (6 μg) was diluted to 3 mL with buffer (20 mM NaCl, 2 mM Hepes, and 10 μM EDTA, pH 7.4) in a glass cuvette with a micro-flea. Immediately prior to

analysis, Eth Br (3 μL, 0.5 mg/mL) was added to the stirring solution and allowed to equilibrate for 1 min. Aliquots (5 μL) of the cholesteryl carbamate (0.25 mg/mL) were then added to the stirring solution and the fluorescence measured after 1 min of equilibration. The fluorescence was expressed as a percentage of the maximum fluorescence signal when Eth Br was bound to DNA in the absence of polyamine conjugate and corrected for background fluorescence of free Eth Br in solution. High-salt experiments were conducted with the 150 mM NaCl buffer solution. Fluorescence studies were carried out with a Perkin-Elmer LS50B luminescence spectrometer ($\lambda_{excit} = 260$ nm, $\lambda_{emiss} = 600$ nm; 1 cm path length, 3 mL glass cuvette: slit width 5 nm [20 mM NaCl] and 10 nm [150 mM NaCl]). An IBM-compatible personal computer was used for data collection, using FL WinLab (Perkin-Elmer) software.

DNA Condensation (light scattering) Assay. The polyamine compounds were used as their TFA salts, weighed, and dissolved in MilliQ water. The buffer solutions (20 mM NaCl, 2 mM Hepes, 10 μM EDTA, pH 7.4, and 150 mM NaCl, 2 mM Hepes, 10 μM EDTA, pH 7.4) were also made up in MilliQ water and were pH adjusted to 7.4 with NaOH. A stock solution of CT DNA of approximately 1 mg/mL (3 mL) was made in buffer (20 mM NaCl, 2 mM Hepes, 10 μM EDTA, pH 7.4), and the concentration determined spectroscopically (*8*). DNA (60 μg) was diluted to 3 mL with buffer (20 mM NaCl, 2 mM Hepes, and 10 μM EDTA, pH 7.4) in a glass cuvette with a micro-flea, and the concentration determined spectroscopically. Aliquots (5 μL) of the cholesteryl carbamate (0.25 mg/mL) were then added to the stirring solution and the absorbance (light scattering) measured after 1 min stirring to reach equilibrium. The absorbance at 320 nm was then measured. High-salt concentration experiments were conducted with the 150 mM NaCl buffer solution. UV absorbance studies were carried out with a Milton Roy Spectronic 601 spectrometer (1 cm path length, 3 mL glass cuvette).

General Procedure A: Poly-Boc Protection of Polyamines. To a solution of the polyamine (5 mmol) in methanol (70 mL) at −78 °C under anhydrous nitrogen was added ethyl trifluoroacetate (1 equiv) dropwise over 30 min. Stirring was continued for a further 30 min, then the temperature was increased to 0 °C to afford predominantly the mono-trifluoroacetamide. Using the above protocol and without isolation, the remaining amino functional groups were quantitatively protected by dropwise addition of an excess of di-*tert*-butyl dicarbonate in methanol (10 mL) over 3 min. The reaction was then warmed to 25 °C and stirred for a further 15 h to afford the fully protected polyamine. The trifluoroacetyl protecting group was then removed (in situ) by increasing the pH of the solution above 11 with concentrated aqueous ammonia and stirring at 25 °C for 15 h. The solution was then concentrated in vacuo, and the residue purified over silica gel to afford the title compound as a colorless homogeneous oil by TLC analysis.

General Procedure B: Carbamate Formation. To a solution of the poly-Boc protected polyamine in CH_2Cl_2 (8 mL) and triethylamine (3.0 equiv) at 0 °C under nitrogen was added cholesteryl chloroformate (1.2 equiv) dropwise in CH_2Cl_2 (3 mL) over 30 min. Stirring was continued for a further 10 min, then the temperature was increased to 25 °C, and the solution was stirred for a further 12 h. The solution was then concentrated in vacuo, and the residue purified over silica gel to afford the title compound as a white foam.

General Procedure C: Boc Removal. To a stirring solution of lipo-polyamine dissolved in CH_2Cl_2 (180 mL), under nitrogen, at 25 °C was added TFA (20 mL). After 2 h, the solution was concentrated in vacuo, lyophilized, and the residue purified by semipreparative RP-HPLC over Supelcosil ABZ+Plus [5 μm, 25 cm × 10 mm, MeCN-0.1% TFA(aq)], to yield the title compound as a white solid (poly-TFA salt).

(N^1,N^4,N^9-Tri-*tert*-butoxycarbonyl)-1,12-diamino-4,9-diazadodecane, 5. 1,12-Diamino-4,9-diazadodecane **1** (spermine, 3.4.3) (1.0 g, 4.95 mmol) was reacted according to general procedure A to afford the title compound **5** as a colorless oil (1.24 g, 50%). Purified over silica gel (CH_2Cl_2-MeOH-concentrated NH_3(aq) 70:10:1 to 50:10:1 v/v/v), R_f 0.5 (CH_2Cl_2-MeOH-concentrated NH_3-(aq) 50:10:1 v/v/v). ^{1}H NMR, 400 MHz, $CDCl_3$: 1.42−1.55 [m, 31 H, 6-CH_2, 7-CH_2, OC$(CH_3)_3$ × 3]; 1.60−1.72 (m, 6 H, 2-CH_2, 11-CH_2, NH_2); 2.70 (t, 2 H, J = 7, 12-CH_2); 3.05−3.38 (m, 10 H, 1-CH_2, 3-CH_2, 5-CH_2, 8-CH_2, 10-CH_2); 5.29−5.44 (br s, 1 H, CON*H*-CH_2). ^{13}C NMR, 100 MHz, $CDCl_3$: 25.4, 25.8, 25.9, 26.3 (6-CH_2, 7-CH_2); 28.35, 28.5, 28.7 [2-CH_2, OC(CH_3)$_3$ × 3, overlapping]; 31.3, 32.5 (11-CH_2); 37.3, 37.6 (1-CH_2); 38.8, 39.3 (12-CH_2); 43.7, 44.1, 44.2, 44.4 (3-CH_2, 10-CH_2); 46.3, 46.7 (5-CH_2, 8-CH_2, overlapping); 78.8, 78.9, 79.1, 79.3 (quaternary OC × 3, overlapping); 155.3, 155.5, 155.6, 156.0 (NCOO × 3, overlapping). MS, FAB$^+$ found 503, 21% (M^+ + 1), $C_{25}H_{50}N_4O_6$ requires M^+ = 502. High-resolution MS *m*/*z*, FAB$^+$ found 503.3823, (M^+ + 1), $C_{25}H_{51}N_4O_6$ requires M^+ + 1 = 503.3808.

(N^1,N^4,N^8-Tri-*tert*-butoxycarbonyl)-1,11-diamino-4,8-diazaundecane, 6. 1,11-Diamino-4,8-diazaundecane **2** (thermine, norspermine, 3.3.3) (3.0 g, 16.0 mmol) was reacted according to general procedure A to afford the title compound **6** as a colorless oil (3.16 g, 41%). Purified over silica gel [CH_2Cl_2-MeOH-concentrated NH_3(aq) 100:10:1 v/v/v], R_f 0.18 [CH_2Cl_2-MeOH-concentrated NH_3(aq) 100:10:1 v/v/v]. ^{1}H NMR, 400 MHz, $CDCl_3$: 1.35−1.43 [m, 27 H, OC$(CH_3)_3$ × 3]; 1.48−1.70 (m, 4 H, 2-CH_2, 6-CH_2); 1.70−1.78 (m, 2 H, 10-CH_2); 1.95−2.00 (br s, 2 H, NH_2); 2.63 (t, 2 H, J = 7, 11-CH_2); 2.96−3.30 (m, 10 H, 1-CH_2, 3-CH_2, 5-CH_2, 7-CH_2, 9-CH_2). ^{13}C NMR, 100 MHz, $CDCl_3$: 27.3, 27.7, 27.8, 28.1, 28.4, 28.8, 28.9, 29.5 [2-CH_2, 6-CH_2, OC(CH_3)$_3$ × 3, overlapping]; 31.4, 31.8 (10-CH_2); 37.3, 37.5 (1-CH_2); 38.8, 39.2 (11-CH_2); 43.1, 43.3, 43.8, 44.5 (3-CH_2, 5-CH_2, 7-CH_2, 9-CH_2, overlapping); 79.3, 79.5, 79.6 (quaternary OC × 3, overlapping); 155.5, 156.0 (NCOO × 3, overlapping). MS, FAB$^+$ found 489, 100% (M^+ + 1), $C_{24}H_{48}N_4O_6$ requires M^+ = 488. High-resolution MS *m*/*z*, FAB$^+$ found 489.3645, (M^+ + 1), $C_{24}H_{49}N_4O_6$ requires M^+ + 1 = 489.3652.

(N^1,N^4,N^7-Tri-*tert*-butoxycarbonyl)-1,10-diamino-4,7-diazadecane, 7. 1,10-Diamino-4,7-diazadecane **3** (3.2.3) (3.0 g, 17.2 mmol) was reacted according to general procedure A to afford the title compound **7** as a colorless oil (3.315 g, 41%). Purified over silica gel [CH_2Cl_2-MeOH-concentrated NH_3(aq) 100:10:1 v/v/v], R_f 0.10 [CH_2Cl_2-MeOH-concentrated NH_3(aq) 100:10:1 v/v/v]. ^{1}H NMR, 400 MHz, $CDCl_3$: 1.35−1.50 [m, 27 H, OC$(CH_3)_3$ × 3]; 1.50−1.85 (m, 6 H, 2-CH_2, 9-CH_2, NH_2); 2.57−2.68 (m, 2 H, 10-CH_2); 2.96−3.10 (m, 2 H, 1-CH_2); 3.10−3.34 (m, 8 H, 3-CH_2, 5-CH_2, 6-CH_2, 8-CH_2). ^{13}C NMR, 100 MHz, $CDCl_3$: 26.9, 27.1, 27.9, 28.3, 28.9 [2-CH_2, OC(CH_3)$_3$ × 3, overlapping]; 31.7, 32.6 (9-CH_2); 37.2, 37.5 (1-CH_2); 38.9, 39.3 (10-CH_2); 43.5, 44.3, 44.9, 45.2, 45.3 (3-CH_2, 5-CH_2, 6-CH_2, 8-CH_2, overlapping); 79.6, 79.7, 79.8 (quaternary OC × 3, overlapping); 155.4, 155.8, 156.0 (NCOO × 3, overlapping). MS, FAB$^+$ found 475, 100% (M^+ + 1), $C_{23}H_{46}N_4O_6$ requires M^+ = 474. High-resolution

MS *m/z*, FAB$^+$ found 475.3496, ($M^+ + 1$), $C_{23}H_{47}N_4O_6$ requires $M^+ + 1 = 475.3495$.

(N^1,N^3,N^7-Tri-*tert*-butoxycarbonyl)-1,9-diamino-3,7-diazanonane, 8. 1,9-Diamino-3,7-diazanonane **4** (2.3.2) (2.0 g, 12.5 mmol) was reacted according to general procedure A to afford the title compound **8** as a colorless oil (2.681 g, 47%). Purified over silica gel (CH_2Cl_2-MeOH-concentrated NH_3(aq) 100:10:1 to 75:10:1 v/v/v), R_f 0.18 [CH_2Cl_2-MeOH-concentrated NH_3(aq) 100:10:1 v/v/v]. ^{1}H NMR, 400 MHz, $CDCl_3$: 1.43−1.49 [m, 29 H, $OC(CH_3)_3 \times 3$, NH_2]; 1.50−1.62 (m, 2 H, 5-CH_2); 2.83−2.87 (t, 2 H, $J = 7$, 9-CH_2); 3.16−3.38 (m, 10 H, 1-CH_2, 2-CH_2, 4-CH_2, 6-CH_2, 8-CH_2); 5.00−5.30 (br s, 1 H, CON*H*-CH_2). ^{13}C NMR, 100 MHz, $CDCl_3$: 27.5, 27.7, 28.2, 28.3, 28.4 [5-CH_2, $OC(CH_3)_3 \times 3$, overlapping]; 39.5, 40.5 (1-CH_2); 40.6, 40.7 (9-CH_2); 45.3, 45.5, 46.4, 46.7 (2-CH_2, 8-CH_2); 50.1, 50.1, 50.2 (4-CH_2, 6-CH_2, overlapping); 79.1, 79.5, 79.8 (quaternary OC × 3, overlapping); 155.6, 155.9, 156.0 (NCOO × 3, overlapping). MS, FAB$^+$ found 461, 100% ($M^+ + 1$), $C_{22}H_{44}N_4O_6$ requires $M^+ = 460$. High-resolution MS *m/z*, FAB$^+$ found 461.3345, ($M^+ + 1$), $C_{22}H_{45}N_4O_6$ requires $M^+ + 1 = 461.3339$.

(N^1,N^3,N^6,N^9-Tetra-*tert*-butoxycarbonyl)-1,11-diamino-3,6,9-triazaundecane, 19. 1,11-Diamino-3,6,9-triazaundecane **17** (2.2.2.2) (3.0 g, 15.8 mmol) was reacted according to general procedure A to afford the title compound **19** as a colorless oil (1.364 g, 14%). Purified over silica gel (CH_2Cl_2-MeOH-concentrated NH_3(aq) 200:10:1 to 150:10:1 v/v/v), R_f 0.07 [CH_2Cl_2-MeOH-concentrated NH_3(aq) 100:10:1 v/v/v]. ^{1}H NMR, 400 MHz, $CDCl_3$: 1.44−1.54 [m, 36 H, $OC(CH_3)_3 \times 4$]; 1.96 (s, 2 H, NH_2); 2.75−2.92 (m, 2 H, 11-CH_2); 3.16−3.35 (m, 14 H, 1-CH_2, 2-CH_2, 4-CH_2, 5-CH_2, 7-CH_2, 8-CH_2, 10-CH_2). ^{13}C NMR, 100 MHz, $CDCl_3$: 28.1, 28.3, 28.6, [$OC(CH_3)_3 \times 4$, overlapping]; 39.3, 39.5 (1-CH_2); 40.3, 40.8 (11-CH_2); 45.0, 45.2, 45.3, 45.6, 45.8, 46.5, 47.6, 50.1, 50.8, 50.9 (2-CH_2, 4-CH_2, 5-CH_2, 7-CH_2, 8-CH_2, 10-CH_2, overlapping); 79.0, 79.9, 80.1 (quaternary OC × 4, overlapping); 155.3, 155.4, 155.6, 156.0 (NCOO × 4, overlapping). MS, FAB$^+$ found 590, 90% ($M^+ + 1$), $C_{28}H_{55}N_5O_8$ requires $M^+ = 589$. High-resolution MS *m/z*, FAB$^+$ found 590.4144, ($M^+ + 1$), $C_{28}H_{56}N_5O_8$ requires $M^+ + 1 = 590.4128$.

(N^1,N^3,N^6,N^9,N^{12}-Penta-*tert*-butoxycarbonyl)-1,14-diamino-3,6,9,12-tetraazatetradecane, 20. 1,14-Diamino-3,6,9,12-tetraazatetradecane **18** (2.2.2.2.2) (3.0 g, 12.9 mmol) was reacted according to general procedure A to afford the title compound **20** as a colorless oil (0.899 g, 10%). Purified over silica gel [CH_2Cl_2-MeOH-concentrated NH_3(aq) 200:10:1 to 150:10:1 v/v/v], R_f 0.18 [CH_2Cl_2-MeOH-concentrated NH_3(aq) 100:10:1 v/v/v]. ^{1}H NMR, 400 MHz, $CDCl_3$: 1.43−1.53 [m, 45 H, $OC(CH_3)_3 \times 5$]; 2.53−2.64 (br s, 2 H, NH_2); 2.75−2.92 (m, 2 H, 14-CH_2); 3.20−3.38 (m, 18 H, 1-CH_2, 2-CH_2, 4-CH_2, 5-CH_2, 7-CH_2, 8-CH_2, 10-CH_2, 11-CH_2, 13-CH_2). ^{13}C NMR, 100 MHz, $CDCl_3$: 28.4 [$OC(CH_3)_3 \times 5$, overlapping]; 39.3, 39.5 (1-CH_2); 40.4, 40.7 (14-CH_2); 44.9, 45.3, 45.5, 45.6, 49.8 (2-CH_2, 4-CH_2, 5-CH_2, 7-CH_2, 8-CH_2, 10-CH_2, 11-CH_2, 13-CH_2, overlapping); 79.0, 79.1, 79.6, 79.9 (quaternary OC × 5, overlapping); 155.2, 155.4, 155.8, 155.9, 156.0 (NCOO × 5, overlapping). MS, FAB$^+$ found 733, 90% ($M^+ + 1$), $C_{35}H_{68}N_6O_{10}$ requires $M^+ = 732$. High-resolution MS *m/z*, FAB$^+$ found 733.5083, ($M^+ + 1$), $C_{35}H_{69}N_6O_{10}$ requires $M^+ + 1 = 733.5075$.

N^1-Cholesteryloxy-3-carbonyl-(N^4,N^9,N^{12}-tri-*tert*-butoxycarbonyl)-1,12-diamino-4,9-diazadodecane, 9. Amine **5** (500 mg, 1.0 mmol) was reacted with cholesteryl chloroformate according to general procedure B to afford, after purification over silica gel (EtOAc−hexane; 1:9 to 3:7 v/v), the title compound **9** as a white foam (699 mg, 77%). R_f 0.52 (EtOAc−hexane; 4:6 v/v). ^{1}H NMR, 400 MHz, $CDCl_3$: 0.68 (s, 3 H, 18′-CH_3); 0.84, 0.85 (2 × d, 6 H, $J = 7$, overlapping 2 Hz, 26′-CH_3, 27′-CH_3); 0.91 (d, 3 H, $J = 7$, 21′-CH_3); 1.01 (s, 3 H, 19′-CH_3); 0.94−2.00 [m, 61 H, 3 × $OC(CH_3)_3$, 2-CH_2, 6-CH_2, 7-CH_2, 11-CH_2, 1′-CH_2, 2′-CH_2, 4′-CH_2, 7′-CH_2, 8′-CH, 9′-CH, 11′-CH_2, 12′-CH_2, 14′-CH, 15′-CH_2, 16′-CH_2, 17′-CH, 20′-CH, 22′-CH_2, 23′-CH_2, 25′-CH]; 2.20−2.38 (m, 2 H, 24′-CH_2); 3.05−3.38 (m, 12 H, 1-CH_2, 3-CH_2, 5-CH_2, 8-CH_2, 10-CH_2, 12-CH_2); 4.40−4.55 (m, 1 H, 3′-CH); 5.35−5.40 (m, 1 H, 6′-CH); 5.45−5.60 (br s, 1 H, CH_2−N*H*CO). ^{13}C NMR, 100 MHz, $CDCl_3$: 11.9 (18′-CH_3); 18.7 (21′-CH_3); 19.3 (19′-CH_3); 21.0 (11′-CH_2); 22.6 (27′-CH_3); 22.8 (26′-CH_3); 23.8 (23′-CH_2); 24.3 (15′-CH_2); 25.4, 25.6, 26.0, 26.0 (6-CH_2, 7-CH_2); 28.0, 28.2, 28.4, 28.5, 28.9 [2-CH_2, 11-CH_2, 2′-CH_2, 16′-CH_2, 25′-CH, 3 × $OC(CH_3)_3$, overlapping]; 31.9 (7′-CH_2, 8′-CH, overlapping); 35.8 (20′-CH); 36.2 (22′-CH_2); 36.6 (10′-C); 37.0 (1′-CH_2); 37.5 (1-CH_2, 12-CH_2); 38.6 (24′-CH_2); 39.5, 39.7 (4′-CH_2, 12′-CH_2); 42.3 (13′-C); 43.7, 44.2 (3-CH_2, 10-CH_2, overlapping); 46.3, 46.8 (5-CH_2, 8-CH_2, overlapping); 50.0 (9′-CH); 56.1 (17′-CH); 56.7 (14′-CH); 74.1 (3′-CH); 79.6, 79.7 (quaternary OC × 3, overlapping); 122.3 (6′-CH); 140.0 (5′-C); 156.2 [3 × N*C*OO−$C(CH_3)_3$, N*C*OO−CH, overlapping]. MS, FAB$^+$ found 915, 20% ($M^+ + 1$), $C_{53}H_{94}N_4O_8$ requires $M^+ = 914$. High-resolution MS *m/z*, FAB$^+$ found 915.7128, ($M^+ + 1$), $C_{53}H_{95}N_4O_8$ requires $M^+ + 1 = 915.7151$.

N^1-Cholesteryloxy-3-carbonyl-(N^4,N^8,N^{11}-tri-*tert*-butoxycarbonyl)-1,11-diamino-4,8-diazaundecane, 10. Amine **6** (500 mg, 1.0 mmol) was reacted with cholesteryl chloroformate according to general procedure B to afford, after purification over silica gel (EtOAc−hexane; 2:8 to 4:6 v/v), the title compound **10** as a white foam (788 mg, 85%). R_f 0.33 (EtOAc−hexane; 4:6 v/v). ^{1}H NMR, 400 MHz, $CDCl_3$: 0.66 (s, 3 H, 18′-CH_3); 0.84, 0.85 (2 × d, 6 H, $J = 7$, overlapping 2 Hz, 26′-CH_3, 27′-CH_3); 0.89 (d, 3 H, $J = 7$, 21′-CH_3); 0.99 (s, 3 H, 19′-CH_3); 0.94−2.10 [m, 59 H, 3 × $OC(CH_3)_3$, 2-CH_2, 6-CH_2, 10-CH_2, 1′-CH_2, 2′-CH_2, 4′-CH_2, 7′-CH_2, 8′-CH, 9′-CH, 11′-CH_2, 12′-CH_2, 14′-CH, 15′-CH_2, 16′-CH_2, 17′-CH, 20′-CH, 22′-CH_2, 23′-CH_2, 25′-CH]; 2.25−2.42 (m, 2 H, 24′-CH_2); 3.08−3.40 (m, 12 H, 1-CH_2, 3-CH_2, 5-CH_2, 7-CH_2, 9-CH_2, 11-CH_2); 4.45−4.58 (m, 1 H, 3′-CH); 5.37−5.42 (m, 1 H, 6′-CH); 5.50−5.62 (br s, 1 H, CH_2−N*H*CO). ^{13}C NMR, 100 MHz, $CDCl_3$: 11.8 (18′-CH_3); 18.7 (21′-CH_3); 19.3 (19′-CH_3); 21.0 (11′-CH_2); 22.5 (27′-CH_3); 22.8 (26′-CH_3); 23.8 (23′-CH_2); 24.2 (15′-CH_2); 28.0, 28.1, 28.2, 28.4, 28.8 [2-CH_2, 6-CH_2, 10-CH_2, 2′-CH_2, 16′-CH_2, 25′-CH, $OC(CH_3)_3 \times 3$, overlapping]; 31.8, 31.9 (7′-CH_2, C8′-CH, overlapping); 35.7 (20′-CH); 36.1 (22′-CH_2); 36.5 (10′-C); 37.0 (1′-CH_2); 37.5 (1-CH_2, 11-CH_2); 38.5 (24′-CH_2); 39.5, 39.7 (4′-CH_2, 12′-CH_2); 42.3 (13′-C); 43.7, 44.2, 44.3, 44.4, 44.5, 44.7 (3-CH_2, 5-CH_2, 7-CH_2, 9-CH_2, overlapping); 50.0 (9′-CH); 56.1 (17′-CH); 56.6 (14′-CH); 74.1 (3′-CH); 79.7 (quaternary OC × 3, overlapping); 122.3 (6′-CH); 139.9 (5′-C); 156.0, 156.2 [3 × N*C*OO−$C(CH_3)_3$, N*C*OO−CH, overlapping]. MS, FAB$^+$ found 901, 30% ($M^+ + 1$), $C_{52}H_{92}N_4O_8$ requires $M^+ = 900$.

N^1-Cholesteryloxy-3-carbonyl-(N^4,N^7,N^{10}-tri-*tert*-butoxycarbonyl)-1,10-diamino-4,7-diazadecane, 11. Amine **7** (500 mg, 1.1 mmol) was reacted with cholesteryl chloroformate according to general procedure B to afford, after purification over silica gel (EtOAc−hexane; 2:8 to 4:6 v/v), the title compound **11** as a white foam (713 mg, 76%). R_f 0.33 (EtOAc−hexane; 4:6 v/v). ^{1}H NMR, 400 MHz, $CDCl_3$: 0.70 (s, 3 H, 18′-CH_3); 0.89, 0.90 (2 × d, 6 H, $J = 7$, overlapping 2 Hz, 26′-CH_3, 27′-CH_3); 0.95 (d, 3 H, $J = 7$, 21′-CH_3); 1.04 (s, 3 H, 19′-CH_3); 0.94−2.00 [m, 57 H, 3 × $OC(CH_3)_3$, 2-CH_2, 9-CH_2, 1′-CH_2, 2′-CH_2, 4′-

CH_2, 7′-CH_2, 8′-CH, 9′-CH, 11′-CH_2, 12′-CH_2, 14′-CH, 15′-CH_2, 16′-CH_2, 17′-CH, 20′-CH, 22′-CH_2, 23′-CH_2, 25′-CH]; 2.25−2.43 (m, 2 H, 24′-CH_2); 3.08−3.24 (m, 4 H, 1-CH_2, 10-CH_2); 3.24−3.45 (m, 8 H, 3-CH_2, 5-CH_2, 6-CH_2, 8-CH_2); 4.45−4.58 (m, 1 H, 3′-CH); 5.37−5.42 (m, 1 H, 6′-CH); 5.58−5.62 (br s, 1 H, CH_2−N*H*CO). ^{13}C NMR, 100 MHz, $CDCl_3$: 11.8 (18′-CH_3); 18.6 (21′-CH_3); 19.3 (19′-CH_3); 21.0 (11′-CH_2); 22.5 (27′-CH_3); 22.8 (26′-CH_3); 23.8 (23′-CH_2); 24.2 (15′-CH_2); 28.0, 28.1, 28.2, 28.4, 28.9 [2-CH_2, 9-CH_2, 2′-CH_2, 16′-CH_2, 25′-CH, 3 × O−C−(*C*H_3)$_3$, overlapping]; 31.8 (7′-CH_2, 8′-CH, overlapping); 35.7 (20′-CH); 36.1 (22′-CH_2); 36.5 (10′-C); 36.9 (1′-CH_2); 37.2, 37.4, 37.5 (1-CH_2, 10-CH_2); 38.5 (24′-CH_2); 39.5, 39.7 (4′-CH_2, 12′-CH_2); 42.2 (13′-C); 44.1, 44.2, 44.8, 45.1 (3-CH_2, 5-CH_2, 6-CH_2, 8-CH_2, overlapping); 49.9 (9′-CH); 56.1 (17′-CH); 56.6 (14′-CH); 74.1 (3′-CH); 80.1 (quaternary OC × 3, overlapping); 122.3 (6′-CH); 139.9 (5′-C); 155.9, 156.1, 156.2 [3 × N*C*OO−C(CH_3)$_3$, N*C*OO−CH, overlapping]. MS, FAB$^+$ found 887, 50% ($M^+ + 1$), $C_{51}H_{90}N_4O_8$ requires $M^+ = 886$.

***N*^{1}-Cholesteryloxy-3-carbonyl-(*N*^{3},*N*^{7},*N*^{9}-tri-*tert*-butoxycarbonyl)-1,9-diamino-3,7-diazanonane, 12.** Amine **8** (500 mg, 1.1 mmol) was reacted with cholesteryl chloroformate according to general procedure B to afford, after purification over silica gel (EtOAc−hexane; 2:8 to 4:6 v/v), the title compound **12** as a white foam (788 mg, 83%). R_f 0.20 (EtOAc−hexane; 4:6 v/v). ^{1}H NMR, 400 MHz, $CDCl_3$: 0.65 (s, 3 H, 18′-CH_3); 0.84, 0.85 (2 × d, 6 H, $J = 7$, overlapping 2 Hz, 26′-CH_3, 27′-CH_3); 0.89 (d, 3 H, $J = 7$, 21′-CH_3); 0.98 (s, 3 H, 19′-CH_3); 0.93−2.00 [m, 55 H, 3 × OC(CH_3)$_3$, 5-CH_2, 1′-CH_2, 2′-CH_2, 4′-CH_2, 7′-CH_2, 8′-CH, 9′-CH, 11′-CH_2, 12′-CH_2, 14′-CH, 15′-CH_2, 16′-CH_2, 17′-CH, 20′-CH, 22′-CH_2, 23′-CH_2, 25′-CH]; 2.14−2.30 (m, 2 H, 24′-CH_2); 3.02−3.34 (m, 12 H, 1-CH_2, 2-CH_2 4-CH_2, 6-CH_2, 8-CH_2, 9-CH_2); 4.30−4.50 (m, 1 H, 3′-CH); 5.20−5.35 (m, 1 H, 6′-CH). ^{13}C NMR, 100 MHz, $CDCl_3$: 11.8 (18′-CH_3); 18.6 (21′-CH_3); 19.3 (19′-CH_3); 21.0 (11′-CH_2); 22.5 (27′-CH_3); 22.8 (26′-CH_3); 23.7 (23′-CH_2); 24.2 (15′-CH_2); 27.5, 27.7, 28.0, 28.1, 28.2, 28.4 [5-CH_2, C2′-CH_2, 16′-CH_2, 25′-CH, 3 × OC(*C*H_3)$_3$, overlapping]; 31.8 (7′-CH_2, 8′-CH, overlapping); 35.7 (20′-CH); 36.1 (22′-CH_2); 36.5 (10′-C); 36.9 (1′-CH_2); 38.5 (24′-CH_2); 39.4, 39.7, 39.9 (1-CH_2, 9-CH_2, 4′-CH_2, 12′-CH_2, overlapping); 42.2 (13′-C); 45.1, 45.5, 45.6, 46.3, 46.4, 46.6, 46.7, 46.8 (2-CH_2, 4-CH_2, 6-CH_2, 8-CH_2, overlapping); 49.9 (9′-CH); 56.0 (17′-CH); 56.6 (14′-CH); 74.1 (3′-CH); 79.1, 79.9 (quaternary OC × 3, overlapping); 122.4 (6′-CH); 139.8 (5′-C); 156.1, 156.3 [3 × N*C*OO−C(CH_3)$_3$, N*C*OO−CH, overlapping]. MS, FAB$^+$ found 873, 10% ($M^+ + 1$), $C_{50}H_{88}N_4O_8$ requires $M^+ = 872$.

***N*^{1}-Cholesteryloxy-3-carbonyl-(*N*^{3},*N*^{6},*N*^{9},*N*^{11}-tetra-*tert*-butoxycarbonyl)-1,11-diamino-3,6,9-triazaundecane, 21.** Amine **19** (500 mg, 0.85 mmol) was reacted with cholesteryl chloroformate according to general procedure B to afford, after purification over silica gel (EtOAc−hexane; 2:8 to 4:6 v/v), the title compound **21** as a white foam (322 mg, 38%). R_f 0.24 (EtOAc−hexane; 4:6 v/v). ^{1}H NMR, 400 MHz, $CDCl_3$: 0.67 (s, 3 H, 18′-CH_3); 0.86, 0.87 (2 × d, 6 H, $J = 7$, overlapping 2 Hz, 26′-CH_3, 27′-CH_3); 0.91 (d, 3 H, $J = 7$, 21′-CH_3); 1.00 (s, 3 H, 19′-CH_3); 0.95−2.03 [m, 62 H, 4 × OC(CH_3)$_3$, 1′-CH_2, 2′-CH_2, 4′-CH_2, 7′-CH_2, 8′-CH, 9′-CH, 11′-CH_2, 12′-CH_2, 14′-CH, 15′-CH_2, 16′-CH_2, 17′-CH, 20′-CH, 22′-CH_2, 23′-CH_2, 25′-CH]; 2.18−2.38 (m, 2 H, 24′-CH_2); 3.20−3.40 (m, 16 H, 1-CH_2, 2-CH_2, 4-CH_2, 5-CH_2, 7-CH_2, 8-CH_2, 10-CH_2, 11-CH_2); 4.40−4.53 (m, 1 H, 3′-CH); 5.33−5.40 (m, 1 H, 6′-CH). ^{13}C NMR, 100 MHz, $CDCl_3$: 11.9 (18′-CH_3); 18.7 (21′-CH_3); 19.3 (19′-CH_3); 21.0 (11′-CH_2); 22.6 (27′-CH_3); 22.8 (26′-CH_3); 23.8 (23′-CH_2); 24.3 (15′-CH_2); 28.0, 28.2, 28.4 [2′-CH_2, 16′-CH_2, 25′-CH, 4 × OC(*C*H_3)$_3$, overlapping]; 31.9 (7′-CH_2, 8′-CH, overlapping); 35.8 (20′-CH); 36.2 (22′-CH_2); 36.5 (10′-C); 37.0 (1′-CH_2); 38.6 (24′-CH_2); 39.5, 39.7 (1-CH_2, 11-CH_2, 4′-CH_2, 12′-CH_2, overlapping); 42.3 (13′-C); 45.2, 45.4, 45.7, 46.6, 46.7, 47.9 (2-CH_2, 4-CH_2, 5-CH_2, 7-CH_2, 8-CH_2, 10-CH_2, overlapping); 50.0 (9′-CH); 56.1 (17′-CH); 56.7 (14′-CH); 74.2 (3′-CH); 80.0, 80.2 (quaternary OC × 4, overlapping); 122.4 (6′-CH); 139.8 (5′-C); 155.2, 155.5, 155.8, 156.1, 156.3 [4 × N*C*OO−C(CH_3)$_3$, N*C*OO−CH, overlapping]. MS, FAB$^+$ found 1002, 10% ($M^+ + 1$), $C_{56}H_{99}N_5O_{10}$ requires $M^+ = 1001$.

***N*^{1}-Cholesteryloxy-3-carbonyl-(*N*^{3},*N*^{6},*N*^{9},*N*^{12},*N*^{14}-penta-*tert*-butoxycarbonyl)-1,14-diamino-3,6,9,12-tetraazatetradecane, 22.** Amine **20** (500 mg, 0.70 mmol) was reacted with cholesteryl chloroformate according to general procedure B to afford, after purification over silica gel (EtOAc−hexane; 2:8 to 4:6 v/v), the title compound **22** as a white foam (430 mg, 55%). R_f 0.23 (EtOAc−hexane 4:6 v/v). ^{1}H NMR, 400 MHz, $CDCl_3$: 0.60 (s, 3 H, 18′-CH_3); 0.78, 0.79 (2 × d, 6 H, $J = 7$, overlapping 2 Hz, 26′-CH_3, 27′-CH_3); 0.84 (d, 3 H, $J = 7$, 21′-CH_3); 0.93 (s, 3 H, 19′-CH_3); 0.88−2.00 [m, 71 H, 5 × OC(CH_3)$_3$, 1′-CH_2, 2′-CH_2, 4′-CH_2, 7′-CH_2, 8′-CH, 9′-CH, 11′-CH_2, 12′-CH_2, 14′-CH, 15′-CH_2, 16′-CH_2, 17′-CH, 20′-CH, 22′-CH_2, 23′-CH_2, 25′-CH]; 2.15−2.30 (m, 2 H, 24′-CH_2); 3.10−3.33 (m, 20 H, 1-CH_2, 2-CH_2, 4-CH_2, 5-CH_2, 7-CH_2, 8-CH_2, 10-CH_2, 11-CH_2, 13-CH_2, 14-CH_2); 4.34−4.48 (m, 1 H, 3′-CH); 5.25−5.32 (m, 1 H, 6′-CH). ^{13}C NMR, 100 MHz, $CDCl_3$: 11.8 (18′-CH_3); 18.6 (21′-CH_3); 19.3 (19′-CH_3); 21.0 (11′-CH_2); 22.5 (27′-CH_3); 22.8 (26′-CH_3); 23.7 (23′-CH_2); 24.2 (15′-CH_2); 28.0, 28.1, 28.2, 28.3 [2′-CH_2, 16′-CH_2, 25′-CH, 5 × OC(*C*H_3)$_3$, overlapping]; 31.8 (7′-CH_2, 8′-CH, overlapping); 35.7 (20′-CH); 36.1 (22′-CH_2); 36.5 (10′-CH_2); 36.9 (1′-CH_2); 38.5 (24′-CH_2); 38.5, 39.4, 39.7, 39.8 (1-CH_2, 14-CH_2, 4′-CH_2, 12′-CH_2, overlapping); 42.2 (13′-C); 44.9, 45.2, 45.3, 46.4, 46.8 (2-CH_2, 4-CH_2, 5-CH_2, 7-CH_2, 8-CH_2, 10-C, 11-CH_2, 13-CH_2, overlapping); 49.9 (9′-CH); 56.0 (17′-CH); 56.6 (14′-CH); 74.1 (3′-CH); 79.9, 80.1 (quaternary OC × 5, overlapping); 122.3 (6′-CH); 139.8 (5′-C); 155.1, 156.1 [5 × N*C*OO−C(CH_3)$_3$, N*C*OO−CH, overlapping]. MS, FAB$^+$ found 1145, 10% ($M^+ + 1$), $C_{63}H_{112}N_6O_{12}$ requires $M^+ = 1144$.

(*N*^{1}-Cholesteryloxy-3-carbonyl)-1,12-diamino-4,9-diazadodecane, 13. Carbamate **9** (432 mg, 0.47 mmol) was deprotected according to general procedure C and purified by semi-prep. RP-HPLC [Supelcosil ABZ+Plus, 5 μm, 25 cm × 10 mm, MeCN-0.1% TFA(aq) 50:50 v/v] to afford the title compound **13** as a white solid (polytrifluoroacetate salt, 158 mg, 35%), t_R 9.0 min by RP-HPLC [Supelcosil ABZ+Plus, 5 μm, 15 cm × 4.6 mm, MeCN-0.1% TFA(aq); 50:50 v/v]. ^{1}H NMR, 400 MHz, D_6-DMSO: 0.67 (s, 3 H, 18′-CH_3); 0.86 (d, 6 H, $J = 7$, 26′-CH_3, 27′-CH_3); 0.91 (d, 3 H, $J = 6$, 21′-CH_3); 0.99 (s, 3 H, 19′-CH_3); 0.94−2.00 (m, 34 H, 2-CH_2, 6-CH_2, 7-CH_2, 11-CH_2, 1′-CH_2, 2′-CH_2, 4′-CH_2, 7′-CH_2, 8′-CH, 9′-CH, 11′-CH_2, 12′-CH_2, 14′-CH, 15′-CH_2, 16′-CH_2, 17′-CH, 20′-CH, 22′-CH_2, 23′-CH_2, 25′-CH); 2.15−2.32 (m, 2 H, 24′-CH_2); 2.84−3.08 (m, 12 H, 1-CH_2, 3-CH_2, 5-CH_2, 8-CH_2, 10-CH_2, 12-CH_2); 4.27−4.39 (m, 1 H, 3′-CH); 5.35−5.42 (m, 1 H, 6′-CH); 7.24, 8.03, 8.70, 8.91 (4 × br s, ammonium signals). ^{13}C NMR, 100 MHz, D_6-DMSO: 11.7 (18′-CH_3); 18.6 (21′-CH_3); 19.0 (19′-CH_3); 20.6 (11′-CH_2); 22.4 (26′-CH_3); 22.6 (6-CH_2, 7-CH_2, overlapping); 22.7 (27′-CH_3); 23.2 (23′-CH_2); 23.8, 23.9 (2-CH_2, 15′-CH_2); 26.2 (11-CH_2); 27.4 (16′-CH_2); 27.8, 27.9 (2′-CH_2, 25′-CH); 31.3, 31.4 (7′-CH_2, 8′-CH); 35.2 (20′-CH); 35.7 (22′-CH_2); 36.1, 36.2 (10′-C, 1-CH_2); 36.6 (1′-CH_2); 37.4 (12-CH_2); 38.3 (24′-CH_2); 38.9, 39.0 (4′-CH_2, 12′-CH_2); 41.9 (13′-C); 43.9 (3-CH); 44.6 (10-CH_2); 46.0 (5-CH_2, 8-CH_2, overlapping); 49.5 (9′-CH);

55.6 (17′-CH); 56.1 (14′-CH); 73.0 (3′-CH); 121.9 (6′-CH); 139.7 (5′-C); 155.8 (NCOO). MS, FAB$^+$ found 615, 100% ($M^+ + 1$), $C_{38}H_{70}N_4O_2$ requires $M^+ = 614$. High-resolution MS *m/z*, FAB$^+$ found 615.5577, ($M^+ + 1$), $C_{38}H_{71}N_4O_2$ requires $M^+ + 1 = 615.5577$.

(N^1-Cholesteryloxy-3-carbonyl)-1,11-diamino-4,8-diazaundecane, 14. Carbamate **10** (300 mg, 0.24 mmol) was deprotected according to general procedure C and purified by semi-prep. RP-HPLC [Supelcosil ABZ+Plus, 5 μm, 25 cm × 10 mm, MeCN-0.1% TFA(aq), 49:51 v/v] to afford the title compound **14** as a white solid (polytrifluoroacetate salt, 218 mg, 69%), t_R 8.3 min by RP-HPLC [Supelcosil ABZ+Plus, 5 μm, 15 cm × 4.6 mm, MeCN-0.1% TFA(aq), 49:51 v/v]. ^{1}H NMR, 400 MHz, D_6-DMSO: 0.64 (s, 3 H, 18′-CH_3); 0.83 (d, 6 H, $J = 7$, 26′-CH_3, 27′-CH_3); 0.88 (d, 3 H, $J = 6$, 21′-CH_3); 0.96 (s, 3 H, 19′-CH_3); 0.94−2.00 (m, 32 H, 2-CH_2, 6-CH_2, 10-CH_2, 1′-CH_2, 2′-CH_2, 4′-CH_2, 7′-CH_2, 8′-CH, 9′-CH, 11′-CH_2, 12′-CH_2, 14′-CH, 15′-CH_2, 16′-CH_2, 17′-CH, 20′-CH, 22′-CH_2, 23′-CH_2, 25′-CH); 2.15−2.32 (m, 2 H, 24′-CH_2); 2.80−3.08 (m, 12 H, 1-CH_2, 3-CH_2, 5-CH_2, 7-CH_2, 9-CH_2, 11-CH_2); 4.22−4.35 (m, 1 H, 3′-CH); 5.29−5.32 (m, 1 H, 6′-CH); 77.20, 8.05, 8.93 (3 × br s, ammonium signals, overlapping). ^{13}C NMR, 100 MHz, D_6-DMSO: 11.7 (18′−H_3); 18.6 (21′-CH_3); 19.1 (19′-CH_3); 20.6 (11′-CH_2); 22.5 (26′-CH_3); 22.7 (27′-CH_3); 23.2 (23′-CH_2); 23.8, 23.9 (2-CH_2, 6-CH_2, 15′-CH_2, overlapping); 26.2 (10-CH_2); 27.5 (16′-CH_2); 27.8, 27.9 (2′-CH_2, 25′-CH); 31.4, 31.5 (7′-CH_2, 8′-CH); 35.3 (20′-CH); 35.7 (22′-CH_2); 36.1, 36.2 (10′-C, 1-CH_2); 36.6 (1′-CH_2); 37.4 (11-CH_2); 38.4 (24′-CH_2); 39.1, 39.3 (4′-CH_2, 12′-CH_2); 41.9 (13′-C); 44.0 (3-CH_2, 9-CH_2, overlapping); 44.8 (5-CH_2, 7-CH_2, overlapping); 49.5 (9′-CH); 55.6 (17′-CH); 56.2 (14′-CH); 73.1 (3′-CH); 122.0 (6′-CH); 139.8 (5′-C); 155.9 (NCOO). MS, FAB$^+$ found 601, 100% ($M^+ + 1$), $C_{37}H_{68}N_4O_2$ requires $M^+ = 600$. High-resolution MS *m/z*, FAB$^+$ found 601.5428, ($M^+ + 1$), $C_{37}H_{69}N_4O_2$ requires $M^+ + 1 = 601.5421$.

(N^1-Cholesteryloxy-3-carbonyl)-1,10-diamino-4,7-diazadecane, 15. Carbamate **11** (300 mg, 0.34 mmol) was deprotected according to general procedure C and purified by semi-prep. RP-HPLC [Supelcosil ABZ+Plus, 5 μm, 25 cm × 10 mm, MeCN-0.1% TFA(aq), 50:50 v/v] to afford the title compound **15** as a white solid (polytrifluoroacetate salt, 181 mg, 58%), t_R 8.6 min by RP-HPLC [Supelcosil ABZ+Plus, 5 μm, 15 cm × 4.6 mm, MeCN-0.1% TFA(aq); 50:50 v/v]. ^{1}H NMR, 400 MHz, D_6-DMSO: 0.64 (s, 3 H, 18′-CH_3); 0.83 (d, 6 H, $J = 7$, 26′-CH_3, 27′-CH_3); 0.88 (d, 3 H, $J = 6$, 21′-CH_3); 0.96 (s, 3 H, 19′-CH_3); 0.94−2.40 (m, 30 H, 2-CH_2, 9-CH_2, 1′-CH_2, 2′-CH_2, 4′-CH_2, 7′-CH_2, 8′-CH, 9′-CH, 11′-CH_2, 12′-CH_2, 14′-CH, 15′-CH_2, 16′-CH_2, 17′-CH, 20′-CH, 22′-CH_2, 23′-CH_2, 25′-CH); 2.15−2.32 (m, 2 H, 24′-CH_2); 2.84−3.08 (m, 12 H, 1-CH_2, 3-CH_2, 5-CH_2, 6-CH_2, 8-CH_2, 10-CH_2); 4.27−4.39 (m, 1 H, 3′-CH); 5.35−5.42 (m, 1 H, 6′-CH); 7.22, 8.03, 9.04, 9.23 (4 × br s, ammonium signals). ^{13}C NMR, 100 MHz, D_6-DMSO: 11.9 (18′-CH_3); 18.7 (21′-CH_3); 19.2 (19′-CH_3); 20.8 (11′-CH_2); 22.6 (26′-CH_3); 22.9 (27′-CH_3); 23.4 (23′-CH_2); 24.1 (15′-CH_2); 26.5 (2-CH_2, 9-CH_2, overlapping); 27.6 (16′-CH_2); 28.0, 28.1 (2′-CH_2, 25′-CH); 31.6 (7′-CH_2, 8′-CH, overlapping); 35.5 (20′-CH); 35.9 (22′-CH_2); 36.3 (10′-C, 1-CH_2, overlapping); 36.8 (1′-CH_2); 37.5 (10-CH_2); 38.5 (24′-CH_2); 39.2, 39.4 (4′-CH_2, 12′-CH_2); 42.1 (13′-C); 42.8, 42.9 (3-CH_2, 8-CH_2); 44.5 (5-CH_2); 45.20 (6-CH_2); 49.7 (9′-CH); 55.8 (17′-CH); 56.4 (14′-CH); 73.3 (3′-CH); 122.1 (6′-CH); 139.9 (5′-C); 156.0 (NCOO). MS, FAB$^+$ found 587, 100% ($M^+ + 1$), $C_{36}H_{66}N_4O_2$ requires $M^+ = 586$. High-resolution MS *m/z*, FAB$^+$ found 587.5272, ($M^+ + 1$), $C_{36}H_{67}N_4O_2$ requires $M^+ + 1 = 587.5264$.

(N^1-Cholesteryloxy-3-carbonyl)-1,9-diamino-3,7-diazanonane, 16. Carbamate **12** (300 mg, 0.34 mmol) was deprotected according to general procedure C and purified by semi-prep. RP-HPLC [Supelcosil ABZ+Plus, 5 μm, 25 cm × 10 mm, MeCN-0.1% TFA(aq), 50:50 v/v] to afford the title compound **16** as a white solid (polytrifluoroacetate salt, 133 mg, 42%), t_R 5.7 min by RP-HPLC [Supelcosil ABZ+Plus, 5 μm, 15 cm × 4.6 mm, MeCN-0.1% TFA(aq), 50:50 v/v]. ^{1}H NMR, 400 MHz, D_6-DMSO: 0.65 (s, 3 H, 18′-CH_3); 0.83, 0.84 (2 × d, 6 H, $J = 7$, overlapping 2 Hz, 26′-CH_3, 27′-CH_3); 0.88 (d, 3 H, $J = 6$, 21′-CH_3); 0.96 (s, 3 H, 19′-CH_3); 0.94−2.00 (m, 28 H, 5-CH_2, 1′-CH_2, 2′-CH_2, 4′-CH_2, 7′-CH_2, 8′-CH, 9′-CH, 11′-CH_2, 12′-CH_2, 14′-CH, 15′-CH_2, 16′-CH_2, 17′-CH, 20′-CH, 22′-CH_2, 23′-CH_2, 25′-CH); 2.18−2.33 (m, 2 H, 24′-CH_2); 2.95−3.30 (m, 12 H, 1-CH_2, 2-CH_2, 4-CH_2, 6-CH_2, 8-CH_2, 9-CH_2); 4.28−4.39 (m, 1 H, 3′-CH); 5.30−5.38 (m, 1 H, 6′-CH); 7.27, 8.21, 8.85, 9.21 (4 × br s, ammonium signals). ^{13}C NMR, 100 MHz, D_6-DMSO: 11.7 (18′-CH_3); 18.6 (21′-CH_3); 19.0 (19′-CH_3); 20.6 (11′-CH_2); 22.4, 22.7 (5-CH_2, 26′-CH_3, 27′-CH_3); 23.2 (23′-CH_2); 23.9 (15′-CH_2); 27.4 (16′-CH_2); 27.8 (2′-CH_2, 25′-CH, overlapping); 31.4 (7′-CH_2, 8′-CH, overlapping); 35.1 (1-CH_2); 35.2 (20′-CH); 35.7 (22′-CH_2); 36.1 (10′-C); 36.6 (1′-CH_2); 36.7 (9-CH_2); 38.1 (24′-CH_2); 38.6, 38.9 (4′-CH_2, 12′-CH_2); 41.9 (13′-C); 43.9, 44.2 (4-CH_2, 6-CH_2); 46.5 (2-CH_2, 8-CH_2, overlapping); 49.5 (9′-CH); 55.6 (17′-CH); 56.1 (14′-CH); 73.5 (3′-CH); 122.0 (6′-CH); 139.7 (5′-C); 155.9 (NCOO). MS, FAB$^+$ found 573, 15% ($M^+ + 1$), $C_{35}H_{64}N_4O_2$ requires $M^+ = 572$. High-resolution MS *m/z*, FAB$^+$ found 573.5106, ($M^+ + 1$), $C_{35}H_{65}N_4O_2$ requires $M^+ + 1 = 573.5108$.

(N^1-Cholesteryloxy-3-carbonyl)-1,11-diamino-3,6,9-triazaundecane, 23. Carbamate **21** (298 mg, 0.28 mmol) was deprotected according to general procedure C and purified by semi-prep. RP-HPLC [Supelcosil ABZ+Plus, 5 μm, 25 cm × 10 mm, MeCN-0.1% TFA(aq) 47:55 v/v] to afford the title compound **23** as a white solid (polytrifluoroacetate salt, 95 mg, 30%), t_R 6.2 min by RP-HPLC [Supelcosil ABZ+Plus, 5 μm, 15 cm × 4.6 mm, MeCN-0.1% TFA(aq); 45:55 v/v]. ^{1}H NMR, 400 MHz, D_6-DMSO: 0.65 (s, 3 H, 18′-CH_3); 0.84 (d, 6 H, $J = 7$, 26′-CH_3, 27′-CH_3); 0.89 (d, 3 H, $J = 6$, 21′-CH_3); 0.97 (s, 3 H, 19′-CH_3); 0.94−2.00 (m, 26 H, 1′-CH_2, 2′-CH_2, 4′-CH_2, 7′-CH_2, 8′-CH, 9′-CH, 11′-CH_2, 12′-CH_2, 14′-CH, 15′-CH_2, 16′-CH_2, 17′-CH, 20′-CH, 22′-CH_2, 23′-CH_2, 25′-CH); 2.18−2.35 (m, 2 H, 24′-CH_2); 3.00−3.08 (m, 2 H, 2-CH_2); 3.08−3.17 (m, 2 H, 1-CH_2); 3.17−3.30 (m, 12 H, 4-CH_2, 5-CH_2, 7-CH_2, 8-CH_2, 10-CH_2, 11-CH_2); 4.30−4.40 (m, 1 H, 3′-CH); 5.30−5.38 (m, 1 H, 6′-CH); 7.29, 8.49 (2 × br s, ammonium signals, overlapping). ^{13}C NMR, 100 MHz, D_6-DMSO: 11.7 (18′-CH_3); 18.6 (21′-CH_3); 19.0 (19′-CH_3); 20.6 (11′-CH_2); 22.4, 22.7 (26′-CH_3, 27′-CH_3); 23.2 (23′-CH_2); 23.9 (15′-CH_2); 27.4 (16′-CH_2); 27.8 (2′-CH_2, 25′-CH, overlapping); 31.4 (7′-CH_2, 8′-CH, overlapping); 35.2 (20′-CH); 35.4 (1-CH_2); 35.7 (22′-CH_2); 36.1 (10′-C); 36.6 (1′-CH_2); 36.7 (11-CH_2); 38.2 (24′-CH_2); 38.6, 38.9 (4′-CH_2, 12′-CH_2); 41.9 (13′-C); 42.8, 43.1, 43.3 (4-CH_2, 5-CH_2, 7-CH_2, 8-CH_2, overlapping); 44.2 (10-CH_2); 46.7 (2-CH_2); 49.5 (9′-CH); 55.6 (17′-CH); 56.1 (14′-CH); 73.5 (3′-CH); 122.0 (6′-CH); 139.7 (5′-C); 156.0 (NCOO). MS, FAB$^+$ found 602, 100% ($M^+ + 1$), $C_{36}H_{67}N_5O_2$ requires $M^+ = 601$. High-resolution MS *m/z*, FAB$^+$ found 602.5380, ($M^+ + 1$), $C_{36}H_{68}N_5O_2$ requires $M^+ + 1 = 602.5373$.

(N^1-Cholesteryloxy-3-carbonyl)-1,14-diamino-3,6,9,-12-tetraazatetradecane, 24. Carbamate **22** (300 mg, 0.26 mmol) was deprotected according to general procedure C and purified by semi-prep. RP-HPLC [Supelcosil ABZ+Plus, 5 μm, 25 cm × 10 mm, MeCN-0.1% TFA(aq), 49:51 v/v] to afford the title compound **24** as a white solid

(polytrifluoroacetate salt, 128 mg, 40%), t_R 10.4 min by RP-HPLC [Supelcosil ABZ+Plus, 5 μm, 15 cm × 4.6 mm, MeCN-0.1% TFA(aq), 47:53 v/v]. ^{1}H NMR, 400 MHz, D_6-DMSO: 0.65 (s, 3 H, 18′-CH_3); 0.84, 0.85 (2 × d, 6 H, J = 7, overlapping 2 Hz, 26′-CH_3, 27′-CH_3); 0.89 (d, 3 H, J = 6, 21′-CH_3); 0.97 (s, 3 H, 19′-CH_3); 0.94−2.00 (m, 26 H, 1′-CH_2, 2′-CH_2, 4′-CH_2, 7′-CH_2, 8′-CH, 9′-CH, 11′-CH_2, 12′-CH_2, 14′-CH, 15′-CH_2, 16′-CH_2, 17′-CH, 20′-CH, 22′-CH_2, 23′-CH_2, 25′-CH); 2.18−2.35 (m, 2 H, 24′-CH_2); 3.02−3.10 (m, 2 H, 2-CH_2); 3.10−3.18 (m, 2 H, 1-CH_2); 3.17−3.30 (m, 16 H, 4-CH_2, 5-CH_2, 7-CH_2, 8-CH_2, 10-CH_2, 11-CH_2, 13-CH_2, 14-CH_2); 4.30−4.42 (m, 1 H, 3′-CH); 5.30−5.40 (m, 1 H, 6′-CH); 7.29, 8.50, 9.13 (3 × br s, ammonium signals, overlapping). ^{13}C NMR, 100 MHz, D_6-DMSO: 11.7 (18′-CH_3); 18.6 (21′-CH_3); 19.0 (19′-CH_3); 20.6 (11′-CH_2); 22.4, 22.7 (26′-CH_3, 27′-CH_3); 23.2 (23′-CH_2); 23.9 (15′-CH_2); 27.4 (16′-CH_2); 27.8 (2′-CH_2, 25′-CH, overlapping); 31.4 (7′-CH_2, 8′-CH, overlapping); 35.2 (1-CH_2, 20′-CH, overlapping); 35.7 (22′-CH_2); 36.1 (10′-C); 36.6 (14-CH_2); 36.8 (1′-CH_2); 38.3 (24′-CH_2); 38.9, 40.0 (4′-CH_2, 12′-CH_2); 41.9 (13′-C); 42.8, 43.0 (4-CH_2, 5-CH_2, 7-CH_2, 8-CH_2, 10-CH_2, 11-CH_2, overlapping); 44.2 (13-CH_2); 46.7 (2-CH_2); 49.5 (9′-CH); 55.6 (17′-CH); 56.1 (14′-CH); 73.5 (3′-CH); 122.0 (6′-CH); 139.7 (5′-C); 156.0 (NCOO). MS, FAB$^+$ found 645, 100% ($M^+ + 1$), $C_{38}H_{72}N_6O_2$ requires $M^+ = 644$. High-resolution MS m/z, FAB$^+$ found 645.5802, ($M^+ + 1$), $C_{38}H_{73}N_6O_2$ requires $M^+ + 1 = 645.5795$.

***N*^{1}-*tert*-Butoxycarbonyl-4,9-diazadodecane-1,12-diamine, 25.** A solution of di-*tert*-butyl dicarbonate (900 mg, 4.1 mmol) in THF (10 mL) was added dropwise (over 3 min) to a vigorously stirred solution of spermine (2.5 g, 12.4 mmol, 3 equiv) in THF (15 mL) at 0 °C under an atmosphere of nitrogen. The reaction mixture was stirred for 1 h at 0 °C, warmed to 25 °C and then stirred for a further 23 h. Water (10 mL) was added to the reaction mixture which was then evaporated in vacuo. The resulting yellow oil was purified by column chromatography over silica gel [CH_2Cl_2-MeOH-concentrated NH_3(aq) 20:5:1 to 4:2:1 v/v/v] to afford the title compound **25**, after lyophilization, as a pale yellow, viscous oil (930 mg, 74%); R_f 0.37 [CH_2Cl_2-MeOH-concentrated NH_3(aq) 4:2:1 v/v/v]. ^{1}H NMR, 400 MHz, $CDCl_3$: 1.43 (m, 9 H, CH_3 × 3); 1.50−1.56 (m, 4 H, 6-CH_2, 7-CH_2); 1.60−1.70 (m, 4 H, 2-CH_2, 11-CH_2); 2.54−2.72 (m, 8 H, 3-CH_2, 5-CH_2, 8-CH_2, 10-CH_2); 2.72−2.82 (m, 2 H, 12-CH_2); 2.82−3.24 (m, 4 H, CH_2−NH_2 and 2 × CH_2−N*H*-CH_2); 3.38−3.44 (m, 2 H, 1-CH_2); 5.20−5.40 (br s, 1 H, CH_2−N*H*CO). ^{13}C NMR, 100 MHz, $CDCl_3$: 27.7 (6-CH_2, 7-CH_2, overlapping); 28.5 (CH_3 × 3); 29.9 (2-CH_2); 33.3 (11-CH_2); 39.1 (1-CH_2); 40.4 (12-CH_2); 47.6, 47.8 (3-CH_2, 10-CH_2); 49.7, 49.8 (5-CH_2, 8-CH_2); 78.9 (quaternary OC); 156.2 (NCOO). MS, EI, found 302 (M^+); CI, found 303 (M^++1), $C_{15}H_{34}N_4O_2$ requires $M^+ = 302$.

RESULTS AND DISCUSSION

Spermine **1** (Figure 1) was unsymmetrically protected with di-*tert*-butyl dicarbonate using our orthogonal protection strategy (*21*). Selective protection of one primary amino functional group was achieved by reaction with ethyl trifluoroacetate, at −78 °C, to form the trifluoroacetamide. Immediately, in this methanolic solution, the remaining three amino functional groups were Boc protected, with an excess of di-*tert*-butyl dicarbonate, to afford the fully protected polyamine. The trifluoroacetyl protecting group was then cleaved by increasing the pH to 11 with concentrated aqueous ammonia, to afford the poly-Boc protected polyamine **5**; any excess of di-*tert*-butyl dicarbonate was quenched with the ammonia.

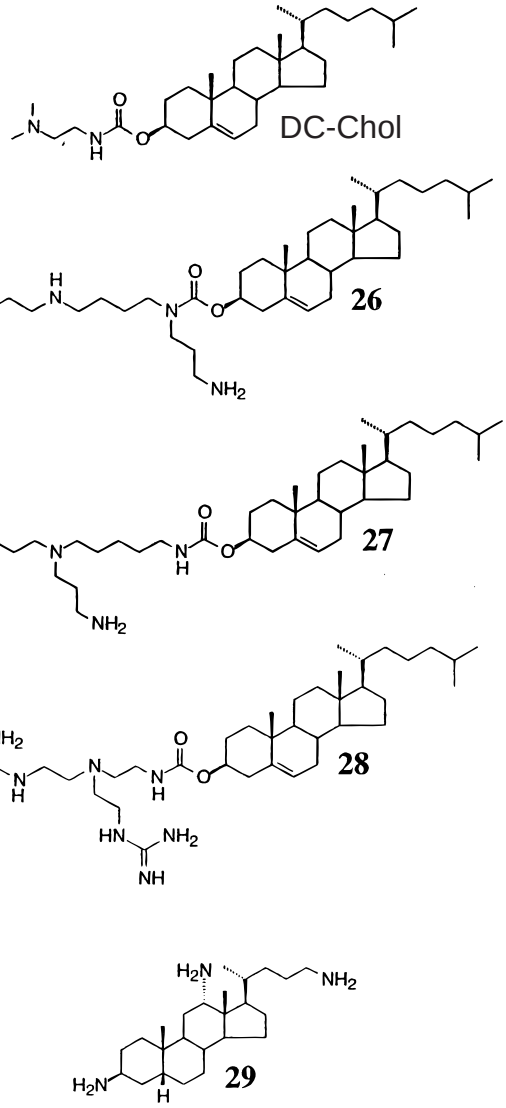

Reaction of the free primary amine of this unsymmetrically protected polyamine **5** with cholesteryl chloroformate afforded the fully protected carbamate **9** (see Figure 1). Deprotection with trifluoroacetic acid in CH_2Cl_2 (1:9) and purification by RP-HPLC afforded the target carbamate **13**, as its polytrifluoroacetate salt. Microanalysis (C, H, and N, Celltech Chiroscience, Slough) was not within ±0.4%. However, elemental analysis is an inadequate method of measuring the purity of polyamines that are highly hygroscopic (*29*). Thus, the proposed structure was unambiguously assigned using accurate MS, ^{1}H, ^{13}C, and HETCOR NMR spectroscopy after RP-HPLC purification to homogeneity. Polyamines **2**, **3**, and **4** (Figure 1) were also unsymmetrically protected using our orthogonal protection strategy to afford poly-Boc protected polyamines **6**, **7**, and **8**, respectively. Carbamoylation with cholesteryl chloroformate afforded carbamates **10**, **11**, and **12**. Deprotection and purification by RP-HPLC afforded the target carbamates **14**, **15**, and **16**, respectively, as their polytrifluoroacetate salts.

The utility of this protection strategy was further demonstrated by the successful preparation of the poly-protected species **19** and **20** (Figure 2) from technical grade pentaamine **17** (2.2.2.2, 80% purity) and hexaamine **18** (2.2.2.2.2, 85% purity) in modest overall yields (14 and 10% respectively). Carbamoylation with cholesteryl chloroformate afforded carbamates **21** and **22**. Deprotection and purification by RP-HPLC afforded the target car-

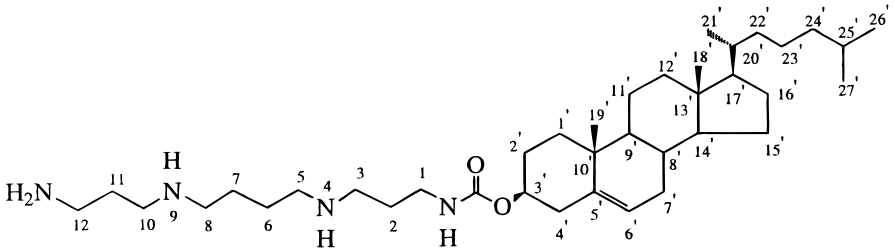

Figure 3. Structure and numbering system of (N^1-cholesteryloxy-3-carbonyl)-1,12-diamino-4,9-diazadodecane **13**.

Table 1. Measured pK_a Values of Cholesteryl Polyamine Carbamates and Their Net Positive Charges at pH 7.4 Calculated Using the Henderson−Hasselbach Equation

polyamine	measured pK_as	net charge
3.4.3 (spermine) **1**	10.9 ± 0.01	3.8
	10.1 ± 0.01	
	8.9 ± 0.01	
	8.1 ± 0.01	
3.4.3-cholesteryl-3-carbamate **13**	10.1 ± 0.06	2.4
	8.6 ± 0.06	
	7.3 ± 0.05	
3.3.3-cholesteryl-3-carbamate **14**	10.7 ± 0.04	2.3
	8.8 ± 0.02	
	7.2 ± 0.02	
3.2.3-cholesteryl-3-carbamate **15**	10.0 ± 0.02	1.8
	8.0 ± 0.02	
	5.5 ± 0.02	
2.3.2-cholesteryl-3-carbamate **16**	9.3 ± 0.01	1.6
	7.6 ± 0.01	
	5.7 ± 0.01	
2.2.2.2-cholesteryl-3-carbamate **23**	9.9 ± 0.20	2.0
	8.4 ± 0.20	
	6.3 ± 0.21	
	3.9 ± 0.21	
2.2.2.2.2-cholesteryl-3-carbamate **24**	10.2 ± 0.10	2.3
	8.6 ± 0.08	
	7.2 ± 0.09	
	4.4 ± 0.09	
	2.5 ± 0.28	

bamates **23** and **24**, respectively, as their polytrifluoroacetate salts. The target compounds are named as polyamine derivatives. In Figure 3, we outline the numbering system used in our NMR assignment of (N^1-cholesteryloxy-3-carbonyl)-1,12-diamino-4,9-diazadodecane **13**.

We have designed and synthesized a series of polyamine cholesteryl carbamates **13**−**16**, **23**, and **24** where both the positive charge and its regiochemical distribution have been varied along the polyamine moiety. The charge on these molecules has been characterized by measuring the pK_as (Table 1) of these molecules potentiometrically, using a Sirius PCA101 automated titrator in 0.15 M KCl ionic strength adjusted water (*22*). The net positive charge carried by these molecules at physiological pH (7.4) has then been calculated using the Henderson−Hasselbach equation (Table 1). The pK_as of polyamines are a function of the interamine distance as well as their substituents. It is important to recognize that any charge is shared across several of the basic centers and that it cannot be attributed to a single point. Even when the first charge is introduced principally on the primary amine, it is also distributed on to the secondary amines. This has been demonstrated using unsymmetrical triamine, spermidine (*30*, *31*), and illustrates that not all amines are protonated at physiological pH. Furthermore, there exists a series of complex equilibria between the ammonium ions and their corresponding amines. This series of molecules carries different numbers of positive charges at pH 7.4 (Table 1), which are distributed on varying lengths of methylene chains and could, therefore, be reasonably expected to impart differences in biological activity.

Table 2. ^{13}C NMR Assignment for Spermine 1[a]

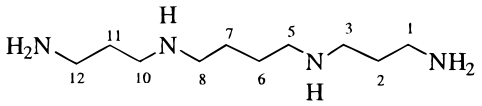

1

assignment	Frassineti et al.	obsd	calcd
5 and 8	51.2	49.8	49.5
3 and 10	49.0	47.6	46.6
1 and 12	41.5	40.3	39.7
2 and 11	34.5	33.7	36.3
6 and 7	29.2	27.7	28.7

[a] Literature values (*33*) are in D_2O at 40 °C for the free base; observed values are measured in $CDCl_3$ at 22 °C for the free base; calculated values are based on additivity rule calculations of ^{13}C chemical shifts in aliphatic compounds (*32*).

Table 3. ^{1}H NMR Assignment for Spermine 1[a]

assignment	Frassineti et al.	obsd	calcd
1 and 12	2.63	2.76, t	2.47
3 and 10	2.56	2.66, t	2.43
5 and 8	2.58	2.61, m	2.43
2 and 11	1.60	1.63, quin	1.65
6 and 7	1.48	1.52, quin	1.45

[a] Literature values (*33*) are in D_2O at 40 °C for the free base; observed values are measured in $CDCl_3$ at 22 °C for the free base; calculated values are based on additivity rule calculations of ^{1}H chemical shifts in aliphatic compounds (*32*).

The assignment of the polyamine headgroups in this series of polyamine carbamates **13**−**16**, **23**, and **24** is based upon HETCOR NMR spectroscopy and calculations using additivity rules (*32*). The key assignments of cholesteryl carbamate **13** are discussed in detail as a representative example. Conformational isomers (populations interconverted by σ-bond rotation) are observed for the poly-Boc protected polyamines, and typically two signals for each carbon on the methylene backbone of the polyamine and of the Boc groups were observed (full data are given in the Experimental procedures, vide supra). Generally, ^{14}N-^{1}H couplings are not observed, but in the case of ammonium compounds, the combination of quadrupolar relaxation and exchange of NH protons is not sufficiently large to eliminate completely the coupling across one bond (*32*). Therefore, carbamates **13**−**16**, **23**, and **24** display broad ammonium signals above δ 7.0 ppm.

As the literature contains conflicting reports in this area (*26*, *27*), accurate, unambiguous spectroscopic ^{1}H and ^{13}C assignments of our lipo-polyamines are essential. Therefore, we investigated the NMR of spermine **1**, and compared our data to the literature values and also to those calculated using additivity rules (*32*, *33*). Our measurements of the ^{13}C NMR (Table 2) and ^{1}H NMR (Table 3) chemical shifts of spermine **1** compare favorably with those found in the literature (*33*), allowing for the

Table 4. ^{13}C NMR Assignments for N^1-*tert*-butoxycarbonyl-4,9-diazadodecane-1,12-diamine 25 Measured in $CDCl_3$ at 22 °C for the Free Base[a]

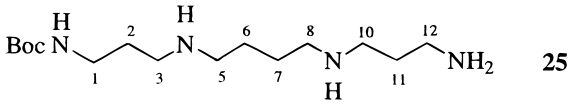

25

assignment	obsd	calcd
5 and 8	49.7, 49.8	50.2
3 and 10	47.6, 47.8	46.6
12	40.4	39.7
1	39.1	42.0
11	33.3	36.3
2	29.9	33.5
6 and 7	27.7	28.7

[a] Calculated values are based on additivity rule calculations of ^{13}C chemical shifts in aliphatic compounds (*32*).

differences in solvent and temperature. The chemical shifts calculated for spermine **1** in Table 2 differ in general by about 5 ppm from the experimental values, within the acceptable error (*32*). Predicted values also agree with the peak order assignments, with C6 and C7 (δ 27.7 ppm) resonating nearest to TMS. Assignments were confirmed by ^{1}H, ^{13}C correlation spectra. ^{1}H NMR chemical shift predictions for spermine free base (Table 3) are in agreement with the measured values, except that C3 and C10 are magnetically distinct from C5 and C8 and resonate further downfield. This can be accounted for by the slight deshielding effect of a γ-primary amine, not allowed for in the calculations.

To investigate the effect of desymmetrization of spermine **1** on N-acylation as a carbamate, N^1-*tert*-butoxycarbonyl-4,9-diazadodecane-1,12-diamine (N^1-Boc-spermine) **25** was prepared. The assignment of the polyamine methylene backbone (Table 4) shows how a primary amine is fractionally more electron withdrawing than a carbamate, so the nuclei at C12 (δ 40.4 ppm) are a little more deshielded relative to those at C1, and therefore, they come into resonance downfield of C1 (δ 39.1 ppm) (assignments were confirmed by 2D NMR spectroscopic experiments). The long-range effect of N^1-carbamoylation (β-effect) brings C2 (δ 29.9 ppm) into resonance further upfield relative to C11 (δ 33.3 ppm). The resonances of C3 and C5 are influenced by the long-range effects of a carbamate to a much lesser extent (cf. C8 and C10) while C6 and C7 are magnetically comparable. The calculated ^{13}C chemical shifts are again within 5 ppm (*32*). However, using the additivity rules, we calculated that C1 will come into resonance downfield of C12 (by 2 ppm), which is clearly not the case.

N-Acylation of one of the primary amines of spermine **1** leads to an unsymmetrical polyamine **13** and, therefore, loss of symmetry of the ^{13}C chemical shifts in the propylene chains of the spermine headgroup (Table 5). Consequently C1, C2, and C3 are under the influence of a carbamate rather than a (protonated) primary amine, are relatively less deshielded, and therefore, come into resonance further upfield than their respective counterparts C12, C11, and C10 on the other propylene chain. During these studies, two other research groups have independently synthesized and published NMR assignments of this carbamate **13** (Table 5) as its free base in $CDCl_3$, but their assignments disagree with each other (*26*, *27*). Our assignments compare favorably with those of Bischoff et al. (*26*), with the differences in chemical shifts being attributable to a change in solvent and the protonation state of the polyamine. Protonation of amines causes a slight decrease in deshielding of the carbon

Table 5. ^{13}C NMR Assignment of Carbamate 13 in D_6-DMSO for the Fully Protonated Species as the Poly-TFA Salt[a]

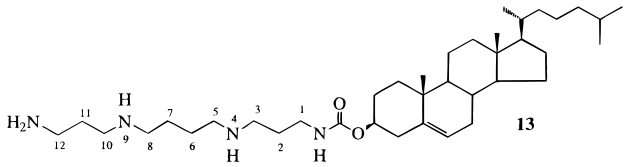

13

assignment	obsd	Bischoff et al.	Cooper et al.
5 and 8	46.0	49.6 and 49.8	36.9 (5), 38.6 (8) only)
10	44.6	47.9	47.4
3	43.9	47.6	49.5
12	37.4	40.6	
1	36.1	38.7	49.9
11	26.2	32.0	
2	23.8	29.7	27.5
6 and 7	22.6	27.7 and 27.8	

[a] Literature values [Bischoff et al. (*26*) and Cooper et al. (*27*)] are in $CDCl_3$ as the free base.

atoms in the vicinity of the ammonium ion, with the chemical shifts lowered by 2 ppm for the α-carbon, 3−4 ppm for the β-carbon, and 0.5−1.0 ppm for the γ-carbon (*32*). However, our assignments for carbamate **13** do not agree with those of Cooper et al. (*27*), who have also published ^{13}C assignments for carbamates **14** and **16** and our unambiguous assignments of these two conjugates (vide supra) also do not agree with their published data. Our assignments of the polyamine headgroups in this carbamate series **13**−**16**, **23**, and **24** are, therefore, based upon comparisons of data from model compounds, literature data (*26*, *33*), chemical shift calculations (*32*), and by ^{1}H, ^{13}C NMR correlation spectroscopy.

Ethidium Bromide Displacement Assay. DNA-binding affinities of polyamine conjugates were measured using an Eth Br fluorescence assay based upon the displacement of Eth Br (1.3 μM) from its intercalation sites in CT DNA (6 μg, [DNA base pair] = 3.0 μM). The assay is an adaptation of the work of Cain et al. (*28*). This rapid method involves the addition of microliter aliquots of polyamine conjugate to a 3 mL solution of Eth Br (1.3 μM) and CT DNA (6 μg, [DNA base pair] = 3.0 μM) in buffer (20 mM NaCl and 2 mM Hepes, pH 7.4) with the decrease in fluorescence monitored (λ_{excit} = 260 nm, λ_{emiss} = 600 nm; 1 cm path-length glass cuvette) after each addition (1 min equilibration time).

The decrease in fluorescence was critically compared against polylysine (PL, average RMM 9600 Da) and spermine **1** (Figure 4) for compound **13** at 20 mM NaCl as a function of charge ratio. At physiological pH, spermine **1** carries a net positive charge of 3.8 (Table 1), whereas that of PL 9600 is in excess of 30 and carbamate **13** is 2.4. In Figure 4, we show that the covalent attachment of cholesterol to spermine makes this carbamate **13** as potent a binder of DNA as the multivalent polylysine. In Figure 5, we compare the relative DNA-binding affinities of all six carbamates **13**−**16**, **23**, and **24** as a function of charge ratio at 20 mM NaCl (low) salt concentration. These data show differences in the binding affinities for DNA of carbamates **13**−**16**, **23**, and **24**. The only structural differences in these molecules are in the polyamine moieties. The changes in methylene spacing and number of nitrogens impart a different net positive charge and distribution to the molecules, which has been shown to have a profound effect on the molecules' ability to induce DNA conformational changes (*34*). These results give support to our hypothesis that binding is a

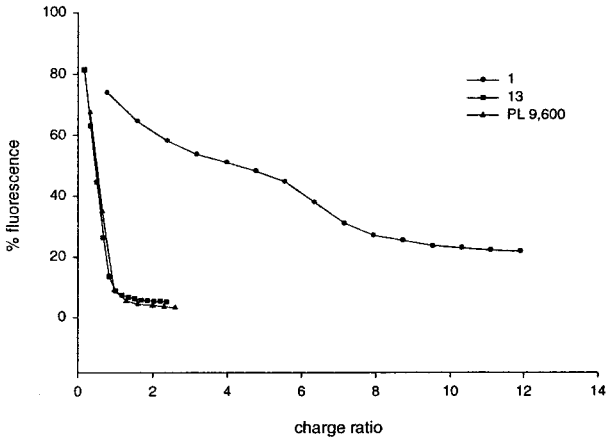

Figure 4. Eth Br displacement assay of carbamate **13**, spermine **1**, and polylysine at low salt (20 mM NaCl). CT DNA (6 μg in buffer, 3 mL, 20 mM NaCl, 2 mM Hepes, and 10 μM EDTA, pH 7.4) was mixed with Eth Br (3 μL of 0.5 mg/mL) and aliquots of polyamine (5 μL of 0.25 mg/mL, 1 min equilibration time) were added and the fluorescence (%) determined.

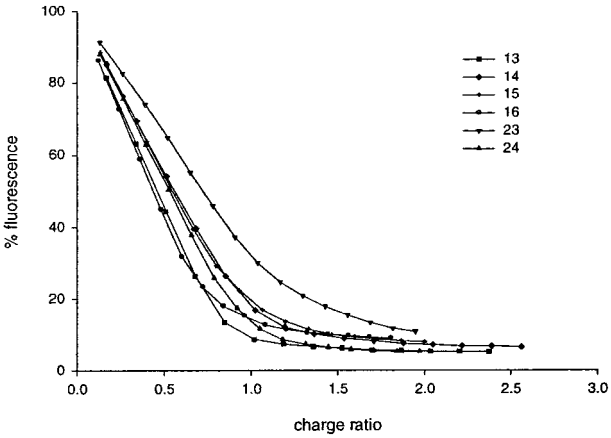

Figure 5. Eth Br displacement assay of carbamates **13**−**16**, **23**, and **24** at low salt (20 mM NaCl). CT DNA (6 μg in buffer, 3 mL, 20 mM NaCl, 2 mM Hepes, and 10 μM EDTA, pH 7.4) was mixed with Eth Br (3 μL of 0.5 mg/mL) and aliquots of carbamate (5 μL of 0.25 mg/mL, 1 min equilibration time) were added and the fluorescence (%) determined.

function of charge and that the regiochemical distribution of such charges is also significant for DNA affinity (*22*). While these data do not prove that the DNA has condensed, they do provide additional evidence that there has been a gross morphological change in the tertiary structure of the DNA, as the binding affinity of Eth Br for duplex DNA is high (*35*).

Salt dependence of the binding affinities of the conjugates has also been investigated using this assay at physiological salt concentrations (150 mM NaCl and 2 mM Hepes, pH 7.4) (Figure 6). The decrease in fluorescence is critically compared as a function of charge ratio for carbamate **13**, against PL 9600 and spermine **1** (Figure 6). These data show that spermine's DNA-binding affinity is salt dependent (*34*, *36*), that PL 9600 is essentially unaffected, and that cholesteryl carbamate **13** is unable to displace completely the Eth Br. Basu and Marton have previously shown a similar inability of pentamines to displace completely Eth Br from DNA at elevated salt concentrations (*37*). This phenomenon was explained by aggregation of the polyamine−DNA complex before complete exclusion of the Eth Br had occurred. With carbamates **14**−**16**, **23**, and **24**, we obtained closely comparable results (data not shown).

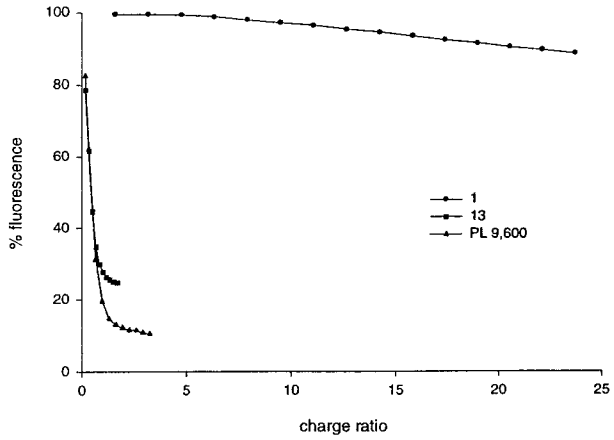

Figure 6. Eth Br displacement assay of carbamate **13**, spermine **1**, and polylysine at high salt (150 mM NaCl). CT DNA (6 μg in buffer, 3 mL, 150 mM NaCl, 2 mM Hepes, and 10 μM EDTA, pH 7.4) was mixed with Eth Br (3 μL of 0.5 mg/mL) and aliquots of polyamine (5 μL of 0.25 mg/mL, 1 min equilibration time) were added and the fluorescence (%) determined.

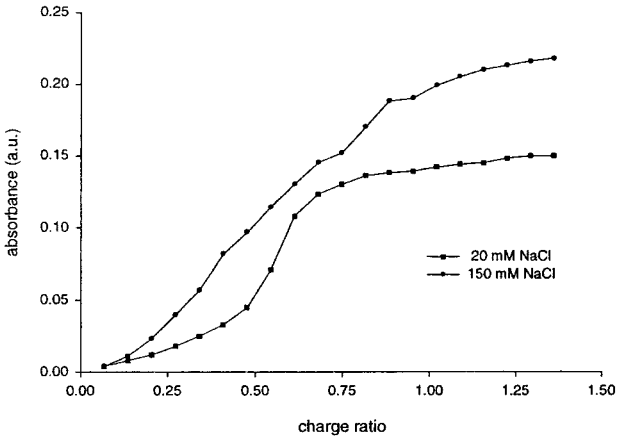

Figure 7. Light-scattering assay of carbamate **13** at low salt (20 mM NaCl) and high salt (150 mM NaCl). CT DNA (60 μg in buffer, 3 mL, 20 mM NaCl, 2 mM Hepes, and 10 μM EDTA, pH 7.4) was stirred and aliquots of carbamate **13** (5 μL of 1.0 mg/mL, 1 min equilibration time) were added and the absorbance (320 nm) measured.

DNA Condensation Assay. To follow the condensation of DNA, UV absorbance at 320 nm has also been measured. As polyamines bind to the double helix and cause condensation (*3*, *38*−*40*) an increase in absorbance is observed above 300 nm (*36*−*38*). Light scattering is being measured rather than UV absorption. Any precipitation of the DNA might be apparent to the naked eye (as a function of the gross amount), but DNA precipitation does not lead to an increase in the absorption above 300 nm and, therefore, cannot explain this phenomenon. In Figure 7, we show the apparent increase in UV absorption (320 nm) of carbamate **13** at both low and high salt concentrations (20 mM and 150 mM NaCl, respectively). At low salt concentrations, these data are consistent with particle formation and similar results were obtained with carbamates **14**−**16**, **23**, and **24** (data not shown). Furthermore, light scattering reaches a plateau at the same charge ratio (approximately 0.9) at which we previously observed maximal Eth Br displacement (Figure 4). However, it should be noted that, due to the lack of sensitivity of this assay, the DNA concentration was in a 10-fold excess compared to that used in the Eth Br assay (Figure 4), and no intercalator Eth Br was present. At high salt concentrations, these data are also

consistent with particle formation. The light scattering reaches a plateau at the same charge ratio (approximately 1.1) as the plateau observed in the Eth Br displacement experiment at high salt (Figure 6). From the elevated absorbances, we observed at 150 mM NaCl (Figure 7), compared to those found in the low-salt experiment (20 mM NaCl), we conclude that the increase in light scattering is due to the formation of larger particles, giving weight to the argument that aggregation has occurred between polyamine−DNA complexes (*34*, *37*). Thus, CT DNA has been condensed into particles, and aggregation of these particles has occurred during this process.

Herein we report the design and synthesis of six polyamine carbamates of cholesterol (at position 3) **13**−**16**, **23**, and **24**, using our orthogonal protection strategy for efficient syntheses of unsymmetrical polyamine amides (*21*). The pK_a values of these compounds were measured and their DNA-binding affinities were determined using CT DNA and a fluorescence quenching assay based upon Eth Br displacement. The data from the light-scattering experiments are consistent with condensation of CT DNA and particle formation. The pK_a values are comparable with those determined for 3.4.3 (spermine **1**) both potentiometrically and spectroscopically (*41*−*44*). The Eth Br displacement data give support to our hypothesis that binding is a function of charge and that the regiochemical distribution of such charges is also significant for DNA affinity. These subtle differences in DNA condensation as a function of charge distribution are clearly important for lipoplex formation (*8*, *29*).

In a recent, comprehensive paper on the role of charge in polyamine analogue recognition, Bergeron and co-workers demonstrated that small structural alterations resulted in substantial differences in biological activities (*44*). The four methylene central spacer (butylene) found in spermine **1** has also been shown to be important for binding affinity, confirming that both the number of positive charges and their distribution have profound effects on the polyamine's ability to induce DNA conformational changes (*29*). Additionally, recently reported results obtained with nonviral gene delivery agents that are based upon this lipopolyamine motif, designed and prepared by other independent research groups, clearly demonstrate that there is great potential within the general class of lipopolyamines for further enhancement of DNA-binding affinity and efficient DNA condensation. Representative nonviral gene delivery agents, where the lipid moiety is cholesterol, may be viewed as having evolved from DC-Chol first reported by Gao and Huang (*45*), though this reagent is typically used to form cationic liposomes in order to achieve efficient transfection of mammalian cells (*45*). Genzyme's GL #67 **26** (*14*), where spermine **1** has been carbamoylated on one secondary amine, and the spermidine incorporating analogue **27** (*16*) also produce efficient gene transfer into mammalian cells. That the cationic charge does not have to be due to an ammonium functional group has been exemplified by the work of Lehn and co-workers in their bis-guanidinium **28** containing cationic lipids, though these are still cholesterol carbamates that achieve supramolecular assemblies and efficiently transfect eukaryotic cells (*46*, *47*). There may be distinct advantages in the use of guanidines, over simple ammonium ions, as the regiochemical distribution of the positive charge might be more readily optimized within such a functional group for phosphate neutralization. The DNA-binding properties of other polyamino-steroids, e.g., **29**, has been reported inter alia by Burrows and co-workers (*19*, *48*) and independently by Walker and co-workers (*18*). It is not an essential requirement to have a steroid as the lipid moiety, as has been elegantly demonstrated by Behr and co-workers with their di-polymethylene chain glycyl amide derivatives of spermine, e.g., DOGS (Transfectam) **30**, and its

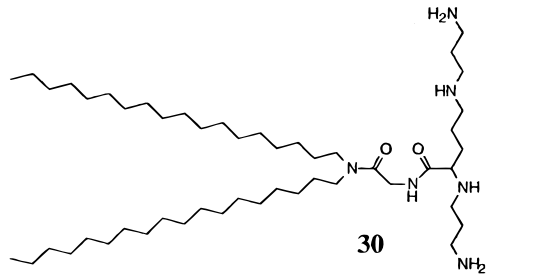

30

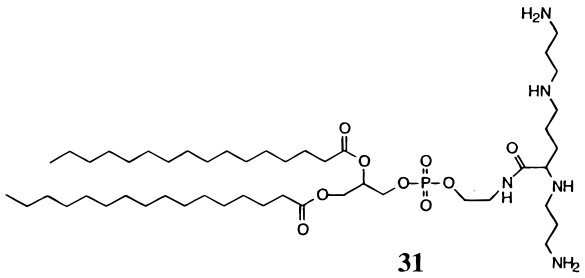

31

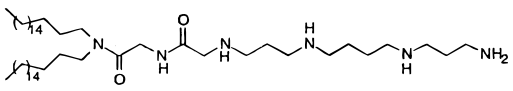

32

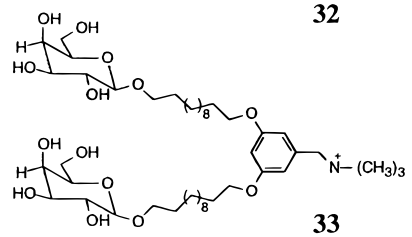

33

diacylglyceryl phosphate analogue **31** (*5*−*7*, *15*, *49*). Similarly, Byk and co-workers have reported their dialkyl spermine containing lipopolyamines, e.g., RPR-120535 **32** (*29*). The possibility of incorporating targeting moieties has also recently been reported with sugar-lipopolyamine conjugate **33**, a cationic amphiphile (*50*). The monosaccharides galactose and mannose were bound to dialkyl chains on a 3,5-dihydroxybenzylammonium template **33** (*50*).

Wilson and Bloomfield predicted (*38*), using the polyelectrolyte theory of Manning (*51*), that ∼90% of the negative charge (phosphate anions) must be neutralized for efficient DNA condensation (*3*). We have achieved this using our cholesteryl polyamine carbamates. These results will be of use in gene therapy studies and should find ready application in the design of lipoplexes with particular reference to spermidine and spermine class alkaloids (*52*−*54*). Thus, our evaluation of pK_a data, the number, and regiochemical distribution of positive charges along the polyamine backbone may lead to a clearer understanding of lipoplex modes of action (*54*).

ACKNOWLEDGMENT

We thank EPSRC and Celltech Chiroscience for a CASE studentship (to A.J.G.). We acknowledge some preliminary experimental work of Ms. Dima Al-Hadithi

(University of Bath) and useful discussions with Dr. Ian S. Haworth (University of Southern California). I.S.B. and I.S.H. are recipients of a NATO grant (CRG 970290).

LITERATURE CITED

(1) Ganem, B. (1982) New chemistry of naturally occurring polyamines. *Acc. Chem. Res. 15*, 290−298.
(2) Bergeron, R. J. (1986) Methods for selective modification of spermidine and its homologues. *Acc. Chem. Res. 19*, 105−113.
(3) Bloomfield, V. A. (1996) DNA condensation. *Curr. Opin. Struct. Biol. 6*, 334−341.
(4) Blagbrough, I. S., Carrington, S., and Geall, A. J. (1997) Polyamines and polyamine amides as potent selective receptor probes, novel therapeutic lead compounds, and synthetic vectors in gene therapy. *Pharm. Sci. 3*, 223−233.
(5) Behr, J.-P. (1986) DNA strongly binds to micelles and vesicles containing lipopolyamines or lipointercalants. *Tetrahedron Lett. 27*, 5861−5864.
(6) Behr, J.-P. (1993) Synthetic gene-transfer vectors. *Acc. Chem. Res. 26*, 274−278.
(7) Behr, J.-P. (1994) Gene transfer with synthetic cationic amphiphiles: prospects for gene therapy. *Bioconjugate Chem. 5*, 382−389.
(8) Felgner, P. L., Barenholz, Y., Behr, J.-P., Cheng, S. H., Cullis, P., Huang, L., Jessee, J. A., Seymour, L., Szoka, F., Thierry, A. R., Wagner, E., and Wu, G. (1997) Nomenclature for synthetic gene delivery systems. *Hum. Gene Ther. 8*, 511−512.
(9) Crystal, R. G. (1995) Transfer of genes to humans. Early lessons and obstacles to success. *Science 270*, 404−410.
(10) Felgner, P. L. (1997) Nonviral strategies for gene therapy. *Sci. Am. 276*, 86−90.
(11) O'Driscoll, C. (1997) Gene geniuses. *Chem. Br. 33*, 66−69.
(12) Mahato, R. I., Rolland, A., and Tomlinson, E. (1997) Cationic lipid-based gene delivery systems: pharmaceutical perspectives. *Pharm. Res. 14*, 853−859.
(13) Verma, I. M., and Somia, N. (1997) Gene therapy − promises, problems and prospects. *Nature 389*, 239−242.
(14) Lee, E. R., Marshall, J., Siegel, C. S., Jiang, C., Yew, N. S., Nichols, M. R., Nietupski, J. B., Ziegler, R. J., Lane, M. B., Wang, K. X., Wan, N. C., Scheule, R. K., Harris, D. J., Smith, A. E., and Cheng, S. H. (1996) Detailed analysis of structures and formulations of cationic lipids for efficient gene transfer to the lung. *Hum. Gene Ther. 7*, 1701−1717.
(15) Behr, J.-P., Demeneix, B., Loeffler, J.-P., and Perez-Mutul, J. (1989) Efficient gene transfer into mammalian primary endocrine cells with lipopolyamine-coated DNA. *Proc. Natl. Acad. Sci. U.S.A. 86*, 6982−6986.
(16) Moradpour, D., Schauer, J. I., Zurawski, V. R., Jr., Wands, J. R., and Boutin, R. H. (1996) Efficient gene transfer into mammalian cells with cholesteryl-spermidine. *Biochem. Biophys. Res. Commun. 221*, 82−88.
(17) Guy-Caffey, J. K., Bodepudi, V., Bishop, J. S., Jayaraman, K., and Chaudhary, N. (1995) Novel polyaminolipids enhance the cellular uptake of oligonucleotides. *J. Biol. Chem. 270*, 31391−31396.
(18) Walker, S., Sofia, M. J., Kakarla, R., Kogan, N. A., Wierichs, L., Longley, C. B., Bruker, K., Axelrod, H. R., Midha, S., Babu, S., and Kahne, D. (1996) Cationic facial amphiphiles: a promising class of transfection agents. *Proc. Natl. Acad. Sci. U.S.A. 93*, 1585−1590.
(19) Hsieh, H.-P., Muller, J. G., and Burrows, C. J. (1994) Structural effects in novel steroidal polyamine-DNA binding. *J. Am. Chem. Soc. 116*, 12077−12078.
(20) Geall, A. J., and Blagbrough, I. S. (1998) Homologation of polyamines in the synthesis of lipo-spermine conjugates and related lipoplexes. *Tetrahedron Lett. 39*, 443−446.
(21) Blagbrough, I. S., and Geall, A. J. (1998) Practical synthesis of unsymmetrical polyamine amides. *Tetrahedron Lett. 39*, 439−442.
(22) Geall, A. J., Taylor, R. J., Earll, M. E., Eaton, M. A. W., and Blagbrough, I. S. (1998) Synthesis of cholesterol-polyamine carbamates: pK_a studies and condensation of calf thymus DNA. *Chem. Commun.* 1403−1404 and 1607.
(23) Geall, A. J., Al-Hadithi, D., and Blagbrough, I. S. (1998) Spermine and thermine conjugates of cholic acid condense DNA, but lithocholic acid polyamine conjugates do so more efficiently. *Chem. Commun.* 2035−2036.
(24) Blagbrough, I. S., Al-Hadithi, D., and Geall, A. J. (1999) DNA condensation by bile acid conjugates of thermine and spermine. *Pharm. Pharmacol. Commun. 5*, 139−144.
(25) Geall, A. J., and Blagbrough, I. S. (1999) DNA condensation by cholesterol polyamine carbamates. *Pharm. Pharmacol. Commun. 5*, 145−150.
(26) Bischoff, R., Cordier, Y., Perraud, F., Thioudellet, C., Braun, S., and Pavirani, A. (1997) Transfection of myoblasts in primary culture with isomeric cationic cholesterol derivatives. *Anal. Biochem. 254*, 69−81.
(27) Cooper, R. G., Etheridge, C. J., Stewart, L., Marshall, J., Rudginsky, S., Cheng, S. H., and Miller, A. D. (1998) Polyamine analogues of 3β-[*N*-(*N*′,*N*′-dimethylaminoethane)-carbamoyl]cholesterol (DC-Chol) as agents for gene delivery. *Chem. Eur. J. 4*, 137−153.
(28) Cain, B. F., Baguley, B. C., and Denny, W. A. (1978) Potential antitumor agents. 28. Deoxyribonucleic acid polyintercalating agents. *J. Med. Chem. 21*, 658−668.
(29) Byk, G., Dubertret, C., Escriou, V., Frederic, M., Jaslin, G., Rangara, R., Pitard, B., Crouzet, J., Wils, P., Schwartz, B., and Scherman, D. (1998) Synthesis, activity, and structure−activity relationship studies of novel cationic lipids for DNA transfer. *J. Med. Chem. 41*, 224−235.
(30) Kimberly, M. M., and Goldstein, J. H. (1981) Determination of pK_a values and total proton distribution pattern of spermidine by carbon-13 nuclear magnetic resonance titrations. *Anal. Chem. 53*, 789−793.
(31) Aikens, D. A., Bunce, S. C., Onasch, O. F., Schwartz, H. M., and Hurwitz, C. (1983) Two-dimensional N. M. R. investigation of the protonation sequence in spermidine. *J. Chem. Soc., Chem. Commun.* 43−45.
(32) *Tables of Spectral Data for Structure Determination of Organic Compounds* (1989) 2nd ed., pp C5−C177 and H15−H80, Springer-Verlag, Berlin.
(33) Frassineti, C., Ghelli, S., Gans, P., Sabatini, A., Moruzzi, M. S., and Vacca, A. (1995) Nuclear magnetic resonance as a tool for determining protonation constants of natural polyprotic bases in solution. *Anal. Biochem. 231*, 374−382.
(34) Basu, H. S., Schwietert, H. C. A., Feuerstein, B. G., and Marton, L. J. (1990) Effects of variation in the structure of spermine on the association with DNA and the induction of DNA conformational changes. *Biochem. J. 269*, 329−334.
(35) Pouton, C. W., Lucas, P., Thomas, B. J., Uduehi, A. N., Milroy, D. A., and Moss, S. H. (1998) Polycation−DNA complexes for gene delivery: a comparison of the biopharmaceutical properties of cationic polypeptides and cationic lipids. *J. Controlled Release 53*, 289−299.
(36) Tikchonenko, T. I., Glushakova, S. E., Kislina, O. S., Grodnitskaya, N. A., Manykin, A. A., and Naroditsky, B. S. (1988) Transfer of condensed viral DNA into eukaryotic cells using proteoliposomes. *Gene 63*, 321−330.
(37) Basu, H. S., and Marton, L. J. (1987) The interaction of spermine and pentamines with DNA. *Biochem. J. 144*, 243−246.
(38) Wilson, R. W., and Bloomfield, V. A. (1979) Counterion-induced condensation of deoxyribonucleic acid. A light-scattering study. *Biochemistry 18*, 2192−2196.
(39) Widom, J., and Baldwin, R. L. (1980) Cation-induced toroidal condensation of DNA. Studies with $Co^{3+}(NH_3)_6$. *J. Mol. Biol. 144*, 431−453.
(40) Böttcher, C., Endisch, C., Fuhrhop, J.-H., Catterall, C., and Eaton, M. (1998) High-yield preparation of oligomeric C-type DNA toroids and their characterization by cryoelectron microscopy. *J. Am. Chem. Soc. 120*, 12−17.
(41) Anderegg, G., and Bläuenstein, P. (1982) Polyamines XIV. Protonation equilibria of linear tetramines containing two ethylenediamines residues. *Helv. Chim. Acta 65*, 162−169.
(42) Takeda, Y., Samejima, K., Nagano, K., Watanabe, M., Sugeta, H., and Kyogoku, Y. (1983) Determination of protonation sites in thermospermine and in some other polyamines by ^{15}N and ^{13}C nuclear magnetic resonance spectroscopy. *Eur. J. Biochem. 130*, 383−389.

(43) Aikens, D., Bunce, S., Onasch, F., Parker, R., Hurwitz, C., and Clemans, S. (1983) The interaction between nucleic acids and polyamines. *Biophys. Chem. 17*, 67−74.

(44) Bergeron, R. J., McManis, J. S., Weimar, W. R., Schreier, K. M., Gao, F., Wu, Q., Ortiz-Ocasio, J., Luchetta, G. R., Porter, C., and Vinson J. R. T. (1995) The role of charge in polyamine analogue recognition. *J. Med. Chem. 38*, 2278−2285.

(45) Gao, X., and Huang, L. (1991) A novel cationic liposome reagent for efficient transfection of mammalian cells. *Biochem. Biophys. Res. Commun. 179*, 280−285.

(46) Vigneron, J.-P., Oudrhiri, N., Fauquet, M., Vergely, L., Bradley, J.-C., Basseville, M., Lehn, P., and Lehn, J.-M. (1996) Guanidinium-cholesterol cationic lipids: efficient vectors for the transfection of eukaryotic cells. *Proc. Natl. Acad. Sci. U.S.A. 93*, 9682−9686.

(47) Pitard, B., Oudrhiri, N., Vigneron, J.-P., Huachecorne, M., Aguerre, O., Toury, R., Airiau, M., Ramasawmy, R., Scherman, D., Crouzet, J., Lehn, J.-M., and Lehn, P. (1999) Structural characteristics of supramolecular assemblies formed by guanidinium-cholesterol for gene transfection. *Proc. Natl. Acad. Sci U.S.A. 96*, 2621−2626.

(48) Hsieh, H.-P., Muller, J. G., and Burrows, C. J. (1995) Synthesis and DNA binding properties of C3-, C12-, and C24-substituted amino-steroids derived from bile acids. *Bioorg. Med. Chem. 3*, 823−835.

(49) Remy, J.-S., Sirlin, C., Vierling, P., and Behr, J.-P. (1994) Gene transfer with a series of lipophilic DNA-binding molecules. *Bioconjugate Chem. 5*, 647−654.

(50) Ren, T., and Liu, D. (1999) Synthesis of targetable cationic amphiphiles. *Tetrahedron Lett. 40*, 7621−7625.

(51) Manning, G. S. (1978) The molecular theory of polyelectrolyte solutions with applications to the electrostatic properties of polynucleotides. *Q. Rev. Biophys. 11*, 179−246.

(52) Labat-Moleur, F., Steffan, A.-M., Brisson, C., Perron, H., Feugeas, O., Furstenberger, P., Oberling, F., Brambilla., and Behr, J.-P. (1996) An electron microcopy study into the mechanism of gene transfer with lipopolyamines. *Gene Ther. 3*, 1010−1017.

(53) Hebling-Leclerc, A., Scherman, D., and Wils, P. (1999) Cellular uptake of cationic lipid/DNA complexes by cultured myoblasts and myotubes. *Biochim. Biophys. Acta 1418*, 165−175.

(54) Geall, A. J., Eaton, M. A. W., Baker, T., Catterall, C., and Blagbrough, I. S. (1999) The regiochemical distribution of positive charges along cholesterol polyamine carbamates plays significant roles in modulating DNA binding affinity and lipofection. *FEBS Lett. 459*, 337−342.

BC990115W

Biodistribution and Radioimmunotherapy of Human Breast Cancer Xenografts with Radiometal-Labeled DOTA Conjugated Anti-HER2/neu Antibody 4D5

S. W. Tsai,[†] YY. Sun,[‡] L. E. Williams,[§] A. A. Raubitschek,[||] A. M. Wu,[⊥] and J. E. Shively*,[†]

Division of Immunology, Beckman Research Institute of the City of Hope, Duarte, California 91010, Department of Anatomic Pathology, City of Hope National Medical Center, Duarte, California 91010, Division of Diagnostic Radiology, City of Hope National Medical Center, Duarte, California 91010, Department of Radioimmunotherapy, City of Hope National Medical Center, Duarte, California 91010, and Department of Molecular Biology, Beckman Research Institute of the City of Hope, 1450 East Duarte Road, Duarte, California 91010. Received October 1, 1999; Revised Manuscript Received January 19, 2000

HER2/neu oncogene encodes a 185 kDa trans-membrane protein which is overexpressed in 20−30% of breast and ovarian cancers and portends a poor prognosis. We have studied the targeting and therapy of this oncoprotein with 4D5, a murine monoclonal antibody which recognizes a distinct epitope on the extracelluar domain of HER2/neu. We conjugated the antibody with an active ester of the macrocyclic chelating agent DOTA, radiolabeled the conjugate with either ^{111}In or ^{90}Y, and studied the antibody distribution and therapy, respectively, in athymic mice bearing xenografts of MCF7/HER2/neu, a human breast cancer cell line transfected with the HER2/neu oncogene. For the biodistribution of ^{111}In-labeled DOTA-4D5, a high specificity of tumor localization (30% ID/g) was seen with a tumor-to-blood ratio of greater than 2 at 48 h postinjection. Compared to a previously published study with ^{125}I-labeled 4D5 in beige nude mice bearing NIH3T3/HER2/neu xenografts [De Santes et al. (1992) *Cancer Res. 52*, 1916−1923], ^{111}In-labeled 4D5 antibody gave superior antibody uptake in tumor (30% ID/g vs 17% ID/g at 48h). In the therapy study, treatment of the nude mice bearing MCF7/HER2/neu xenografts with 100 μCi (3 μg) of ^{90}Y-labeled DOTA-4D5 caused a 3-fold reduction of tumor growth compared to untreated controls (injected with human serum albumin) in 40 days. Treatment of animals with 100 μCi of nonspecific antibody ^{90}Y-labeled DOTA-Leu16 (3 μg) had no tumor growth inhibition. Treatment with unlabeled DOTA-4D5 (3 μg) had a slight effect on tumor growth compared to untreated controls. When analyzed at the level of single animals, no effect was seen in seven of nine animals; however, in two of the animals, tumor growth inhibition was observed. Although a cold antibody therapeutic effect was unexpected at this dose level (3 μg), it may be possible that in some animals that 3 μg of antibody of ^{90}Y-labeled DOTA-4D5 augmented tumor growth reduction. To further explore the effects of cold antibody treatment alone, animals were treated with 100 or 400 μg of unlabeled 4D5 administered in two doses. These animals showed a 1.7−1.8-fold reduction in tumor growth over 28 days, a result less than that obtained with RIT only.

INTRODUCTION

The HER2/neu receptor, the product of the c-erbB2 oncogene, has been the target of monoclonal antibody clinical therapeutic trials (*1*−*3*). The oncogene encodes a 185 000 transmembrane phosphoglycoprotein (*4*−*6*), is amplified in 20−30% of breast carcinoma (*7*−*9*), and is linked to poor prognosis (*10*). Several studies have suggested that reducing expression of HER2/neu gene product may convey a growth disadvantage on the tumor (*11*, *12*). Many preclinical trials have shown that certain anti-HER2/neu antibodies can inhibit the growth of HER2/neu-overexpressing tumors (*12*−*16*). In particular, the anti-HER2/neu monoclonal antibody 4D5, when used with cisplatin, has been shown to promote drug-induced killing in target cells (*17*, *18*). Recently, Herceptin, the humanized version of the murine 4D5 monoclonal antibody (*19*), was approved by the FDA for the treatment of HER2/neu positive tumors. The approach utilizes a combination of Herceptin and chemotherapeutic agents. In a phase II study in which 37 patients received Herceptin and cisplatin, a 24.3% partial response rate was observed (*2*).

In addition to any biological effects resulting from the direct interaction of anti-HER2/neu antibody with the HER2/neu receptor, anti-HER2/neu antibody can also be used to deliver drugs, toxins, or radioisotopes directly to HER2/neu positive malignant cells. In the case of radioimmunotherapy (RIT),[1] the use of β-emitter radiolabeled antibody is appealing because tumor cells inaccessible to antibody may still be killed by radioimmunoconjugates bound to neighboring cells. DeSantes et al. (*20*) demon-

* To whom correspondence should be addressed. Phone: (626) 301-8301. FAX: (626) 301-8186. E-mail: jshively@coh.org.
[†] Division of Immunology.
[‡] Department of Anatomic Pathology.
[§] Division of Diagnostic Radiology.
[||] Department of Radioimmunotherapy.
[⊥] Department of Molecular Biology.

[1] Abbreviations: DOTA, 1,4,7, 10-tetraazacyclododecane-*N*,*N*′,*N*″,*N*‴-tetraacetic acid; DTPA, diethylenetriaminepentaacetic acid; FITC, fluorescein isothiocyanate; HSA, human serum albumin; BSA, bovine serum albumin; RIT, radioimmunotherapy; RTV, relative tumor volume; MTD, maximum tolerated dose; ABC, avidin−biotin complex.

10.1021/bc9901292 CCC: $19.00 © 2000 American Chemical Society
Published on Web 03/24/2000

strated that animals treated with 400−700 μCi of ^{131}I-labeled anti-HER2/neu 4D5 monoclonal antibody showed marked inhibition of tumor growth; however, the choice of ^{131}I-labeled antibody requires a higher activity level due to dehalogenation in normal and malignant tissues.

Radiometals that are conjugated to antibody via chelates may be a better choice as exemplified by RIT studies with radiometal labeled anti-lymphoma (*21*), anti-colon cancer (*22*), and anti-breast cancer (*23*) antibodies. Bifunctional chelates such as DTPA (*24*) or DOTA (*25*, *26*) derivatives have been successfully conjugated to antibodies giving products with high retention of immunoreactivities and radiolabeled to high specific activities with either ^{111}In, a γ-emitter with a half-life of 67.9 h, or ^{90}Y, a pure β-emitter with a 64.0 h half-life. In the case of HER2/neu positive tumors, Horak et al. (*27*) have demonstrated good tumor specificity, pharmacokinetics, and radioimmunotherapy with ^{212}Pb-labeled, DOTA-conjugated AE1 anti-HER2/neu antibody in an ovarian tumor model; however, their reagent did not provide effective therapy for large established tumors. In addition, ^{212}Pb may not be suitable for treatment of bulky solid tumors due to its short half-life of 10.6 h and the low tissue penetration of α-rays. Our recent studies have focused on the therapeutic effect of ^{90}Y-labeled, DOTA-conjugated anti-CEA antibodies (*22*). In this report, we have studied the feasibility of targeting the HER2/neu protein with DOTA-conjugated anti-HER2/neu antibody 4D5. Biodistributions of the ^{111}In-labeled and therapy efficacy with the ^{90}Y-labeled antibodies were determined in a nude mouse model bearing the MCF7/HER2/neu xenograft.

EXPERIMENTAL PROCEDURES

Cell Line. MCF7/HER2/neu is a human breast tumor cell line expressing HER2/neu and was obtained from Dr. Dennis Slamon (UCLA). Cells were maintained in RPMI 1640, supplemented with 10% FBS, 100 units/mL penicillin, 100 units/mL streptomycin, and 2 mM L-glutamine. To establish tumor growth in nude mice, subconfluent monolayer cells were trypsinized in EDTA, washed in PBS, and resuspended in RPMI1640.

Antibody. 4D5 is a murine IgG_1 monoclonal directed against the extracellular domains of p185 (HER2/neu) and was a gift from Dr. Paul Carter, Genentech, Inc. The antibody was conjugated with DOTA, using active ester carbodiimide chemistry, with a DOTA-ester-to-antibody ratio of 100:1 (*25*). The antibody was then radiolabeled at 43° C for 1 h with ^{111}In or ^{90}Y, at pH 5. The labeling efficiency was greater than 80% for both radionuclides. The number of chelates per antibody was 5.0 as determined by a modification of a ^{57}Co(II) binding assay (*28*), except $^{111}InCl_3$ was used. The binding affinity of [^{111}In]-DOTA 4D5 to MCF7/HER2/neu cells was 1.25×10^8 M^{-1}, as determined by Scatchard analysis (data not shown). The immunoreactivity of [^{111}In]DOTA 4D5 as determined by binding to MCF7/HER2/neu cells was 96% by linear extrapolation to binding at infinite antigen excess (*29*). The anti-CD20 murine antibody Leu16 (Becton Dickinson) was conjugated with DOTA active ester as described above.

Flow Cytometry Analysis. Specific binding of 4D5 to HER2/neu gene product on MCF7/HER2/neu cells was assessed by indirect immunofluorescence. Untransfected MCF7 cells which do not express HER2/neu were used as a negative control. MCF7/HER2/neu was used as a HER2/neu positive cell line, and Leu16 a nonspecific antibody control. One million cells in 0.5 mL of PBS/1%BSA were incubated with 0.1 μg of antibody for 1 h on ice. The mixtures were then washed two times, incubated with 1 μg of FITC-conjugated goat anti mouse IgG Fab'_2 fragment (Jackson Immuno Research Labs) for 40 min, washed once with PBS/1% BSA, and then analyzed on a MoFlo flow cytometer (Cytomation, Fort Collins, CO).

Immunohistochemistry. Fresh tumor tissues were excised from the untreated and from the 100 μCi-4D5 treated group 40 days after therapy. Tissues were embedded in O. C. T. (Miles Inc.) and were quick frozen in isopentane. Tissue sections were cut in 4 um thickness and were mounted on Probe-on slides (Vantana Medical System Inc.). Frozen section slides were fixed in cold acetone for 10 min, then washed with PBS three times, 5 min each. All slides were loaded into a Techmate slide holder and stained using the Biotech Techmate 1000 Immunostainer. Sections were incubated 25 min with 5 μg/mL of 4D5, or with 5 μg/mL of Leu16 as a negative control. The antibody−antigen complex was detected by a modified ABC method (30) (Vantana Medical System Inc.) per manufacturer's direction with the Chromagen 3′3-diaminobenzidine.

Animal Model. Three days prior to injection of tumor cells, 2 month old female mice (NCI) weighing 13-21 g were implanted s.c. with 1.7 mg, 60 day release 17 β-estradiol pellets (Innovative Research of America) on the shoulder pads to promote tumor growth. The mice were inoculated s.c. in the flanks with 10 million MCF7/HER2/neu cells resuspended in 0.15 mL of RPMI1640. Solid tumors measuring approximately 100 mm^3 were visible at 12 days postinoculation. The mice were then randomized according to tumor size to prevent any bias in the biodistribution and radioimmunotherapy studies.

Antibody Biodistribution. Groups of five mice per time point bearing MCF7/HER2/neu xenografts were injected with 3.6 μCi of ^{111}In-labeled DOTA-4D5 via tail vein. Animals were sacrificed at 0, 5, 24, 48, 72, and 96 h postinjection. The average tumor weights were 0.13, 0.25, 0.22, 0.29, 0.35, and 0.41 g, respectively. Tumors were dissected and the major organs and blood weighed and the activity measured. The activity expressed in percentage injected dose per gram of tissue was then calculated. The mean values were used to construct biodistribution curves for tumors and normal organs.

Radioimmunotherapy. DOTA-4D5 and DOTA-Leu 16 were labeled with ^{90}Y to specific activities of 33.3 μCi/μg. Groups of nine tumor-bearing mice (average volume 100 mm^3) were injected via tail vein with 50 μCi or 100 μCi DOTA-4D5, 100 μCi DOTA-Leu16, DOTA-4D5, or 1% HSA/saline. Each mouse received equal amounts of protein (3 μg). Tumors were measured twice a week (after antibody injection) for 37 days. Tumor volume was calculated as Length $\times$ $Width^2/2$, where length was the longer of the two measurements. The relative tumor volume was calculated as the ratio of tumor volume on that day to its value at the start of therapy. The growth curve was plotted as the average of the relative tumor volume within a group vs time.

To assess the effect of unlabeled 4D5 on tumor growth, groups of eight tumor-bearing mice (average tumor volume 200 mm^3) were also given 100 μg or 400 μg of 4D5 in two doses by i.p. injection on day zero and on day eight. Leu16 (400 μg) in two doses was used as a negative control. Tumor volumes were measured for 28 days, and the growth curves were constructed as above.

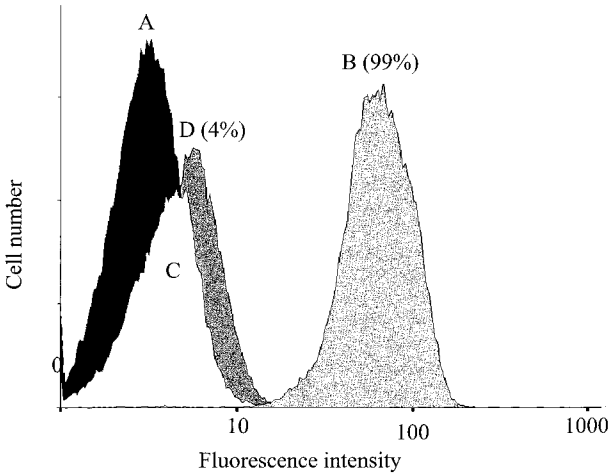

Figure 1. Fluorescent-activated cell sorter analysis of binding of 4D5 to MCF7/HER2/neu and to MCF7 cells. (A) MCF7/HER2/neu control, stained with Leu16, (B) MCF7/HER2/neu stained with 4D5, (C) MCF7 control stained with no primary antibody, (D) MCF7 stained with 4D5. The percent positive cells (vs control) are shown for B and D.

RESULTS

Antibody and Cell Analysis. Indirect immunofluorescence with flow cytometry demonstrated intense, specific binding of the DOTA-4D5 antibody to MCF7/HER2/neu cells (99% positive vs control), but low binding to the parent MCF7cell line (4% vs control), a cell line with limited expression of the HER-2/neu gene product (Figure 1). The 4D5 antibody was conjugated to DOTA, a macrocyclic chelator, using an active ester chemical method (*25*). The DOTA-4D5 conjugate was shown to have a DOTA/antibody ratio of 5/1, radiolabeled with either ^{111}In or ^{90}Y to high efficiency (>90%), and retained high immunoreactivity (>90%) when tested in a cell-binding assay. Nude mice bearing MCF7/HER2/neu xenografts were used as a model for tumor targeting with radiolabeled DOTA-4D5. Immunohistochemical analysis of HER2/neu expression in both treated and nontreated tumors showed membrane staining in approximately 99% of the tumor cells, while staining with the control Leu16 antibody showed only background staining (Figure 2). These results demonstrate that the HER2/neu xenografts continue to produce HER2/neu on the cell surface while growing in nude mice, including after treatment with [^{90}Y]DOTA-4D5.

Antibody Biodistribution. The biodistribution of [^{111}In]DOTA-4D5 was evaluated in nude mice bearing MCF7/HER2/neu xenografts. Groups of five mice per time point were injected with 3.6 μCi of [^{111}In]DOTA-4D5 via the tail vein. Biodistribution studies performed with [^{111}In]DOTA-4D5 showed progressive accumulation of the antibody in MCF7/HER2/neu tumors ranging from 8% ID/g at 5 h to 24% ID/g at 96 h postinjection, as shown in Figure 3 and Table 1 of the Supporting Information. At the same time points, the activity present in blood decreased from 23% to 10% ID/g. The tumor-to-blood ratio increased from 0.36 at 5 h to 2.4 at 96 h postinjection. Organs with significant nonspecific accumulations of antibody included the liver, kidneys, and lung, which ranged from 6 to 11% ID/g at 5 h; however, the accumulations decreased to less than 5% ID/g at 96 h. The results demonstrated specific accumulation of antibody in tumors compared to other major organs.

Radioimmunotherapy. To assess the therapeutic efficacy of DOTA-4D5 in athymic mice bearing MCF7/HER2/neu xenografts, we injected 50 or 100 μCi of ^{90}Y-labeled DOTA-4D5 (3 μg) into groups of nine mice. Control groups were injected with 100 μCi of ^{90}Y-labeled DOTA-Leu16 (3 μg), unlabeled DOTA-4D5 (3 μg), or 1% human serum albumin in saline. With the exception of the HSA control group, all groups received a single injection of 3 μg of antibody. Tumor volumes were measured twice weekly. The average relative tumor volume (RTV) was calculated as the ratio of tumor volume on that day to the volume at the start of therapy. The average relative tumor volume within each group was compared over 37 days (Figure 4). Mice injected with 50 μCi ^{90}Y-labeled DOTA-4D5 showed a 2-fold reduction in tumor growth at day 37, as compared to mice injected with serum albumin/saline [RTV 4.69 vs 9.30, $p < 0.04$, *t*-test; Table 2 (Supporting Information)]. When the

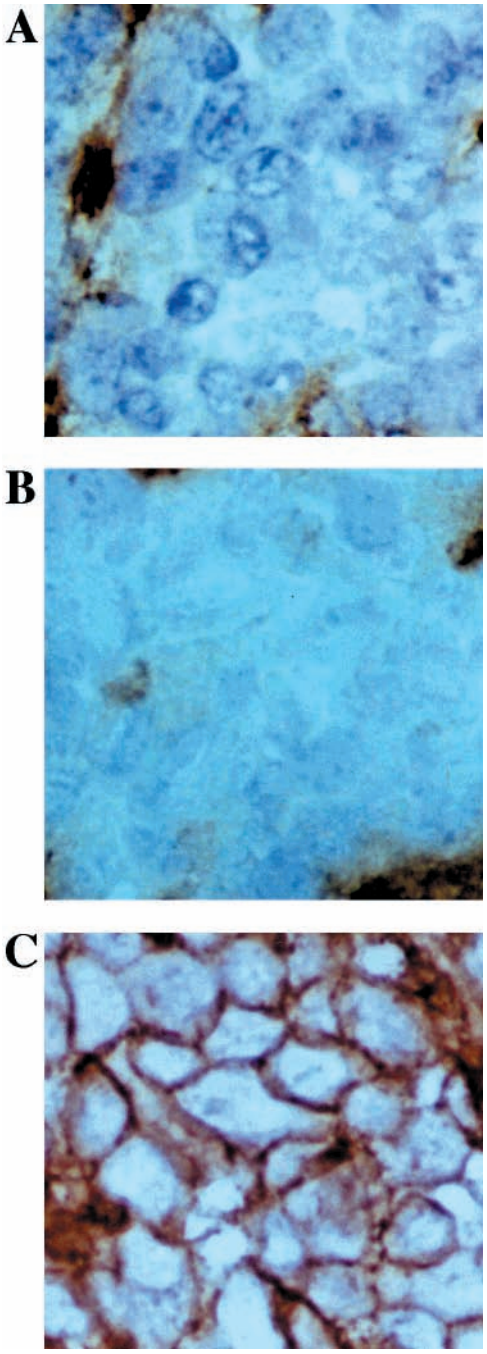

Figure 2. Immunohistochemical frozen sections of MCF7/HER2/neu tumor excised from untreated mice 40 days after therapy. Tumor frozen sections probed with (A) no primary antibody, (B) Leu16 (control), and (C) 4D5.

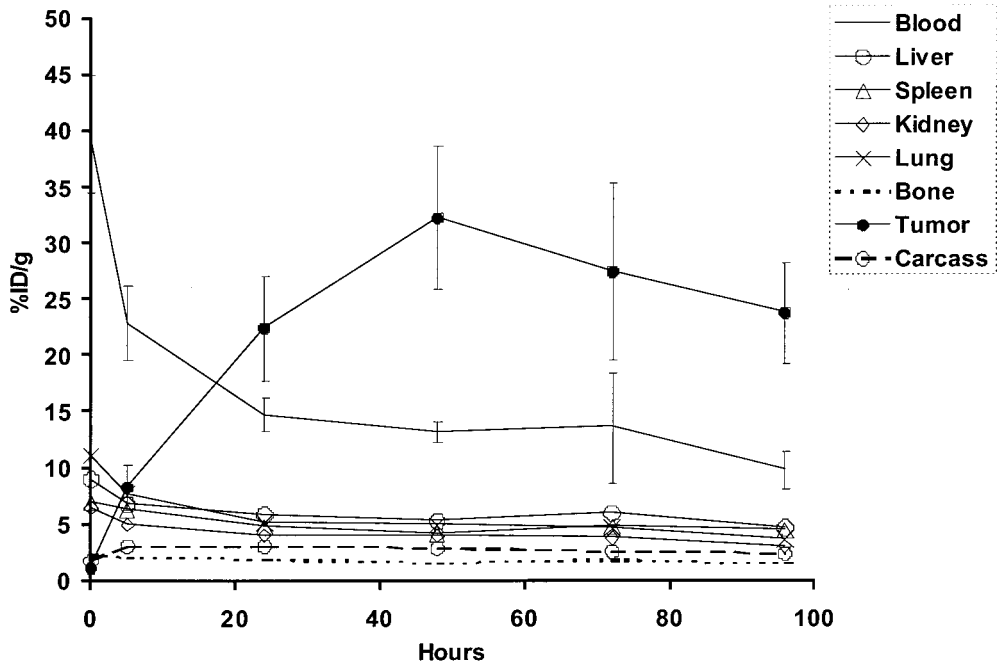

Figure 3. Biodistribution of ^{111}In-labeled DOTA-4D5 in nude mice bearing MCF7/HER2/neu xenografts. Groups of five mice were injected with 3.6 μCi (2.4 μg) of ^{111}In-labeled DOTA-4D5. At 0, 5, 24, 48, 72, and 96 h postinjection the tumors and normal organs were excised, weighed and the ^{111}In activity measured. The mean %ID/g (±std dev) at each time point are shown for blood, liver, spleen, kidney, lung, bone, tumor, and carcass.

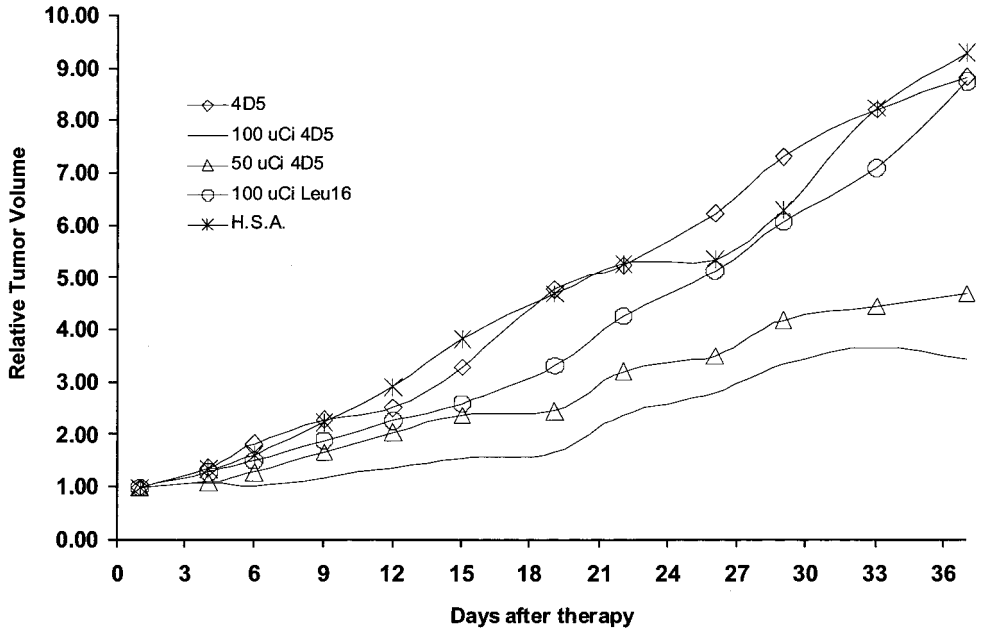

Figure 4. Radioimmunotherapy of established MCF7/HER2/neu tumors in nude mice with ^{90}Y-labeled DOTA-4D5. Groups of nine mice were injected i.v. with (◇) 3 μg of unlabeled DOTA-4D5, (—) 100 μCi (3 μg) of ^{90}Y-labeled DOTA-4D5, (△) 50 μCi (3 μg) of ^{90}Y-labeled DOTA-4D5, (○) 100 μCi (3 μg) of ^{90}Y-labeled DOTA-Leu16, or (*) 1% HSA/saline. The tumor volume for each mouse at the time indicated was normalized to the tumor volume at the start of treatment. Mean values (±std dev) for all animals in each group are shown in Table 2 (Supporting Information).

amount of activity was increased to 100 μCi, the retardation of tumor growth reached 2.7-fold (RTV 3.42 vs 9.30, $p < 0.02$, *t*-test). Treatment with ^{90}Y-labeled control antibody, DOTA-Leu16, however, did not slow tumor growth over the course of study (RTV 8.77 vs 9.30). Similarly, treatment with unlabeled DOTA-4D5 did not result in significant tumor growth retardation compared to the RIT-treated animals (RTV 8.83 vs 9.30). However, if the data is analyzed at the level of single animals, we noted that two of nine animals treated with unlabeled DOTA-4D5 showed tumor growth inhibition (Table 2, Supporting Information). If a single animal had shown this result, we might have dismissed it; however, the finding occurred in two animals and the effect was not seen in the serum/albumin/saline-treated controls.

To assess the effect of cold antibody alone on tumor growth, we treated mice with higher levels of unlabeled 4D5 (Figure 5). Mice injected with 100 μg of 4D5 showed a 1.65-fold reduction in tumor growth at day 28, as compared to mice injected with 400 μg of Leu16 (RTV 4.09 vs 6.75, $p = 0.15$, *t*-test; Table 1). Mice injected with 400 μg of 4D5 showed a 1.80-fold reduction (RTV 3.74 vs

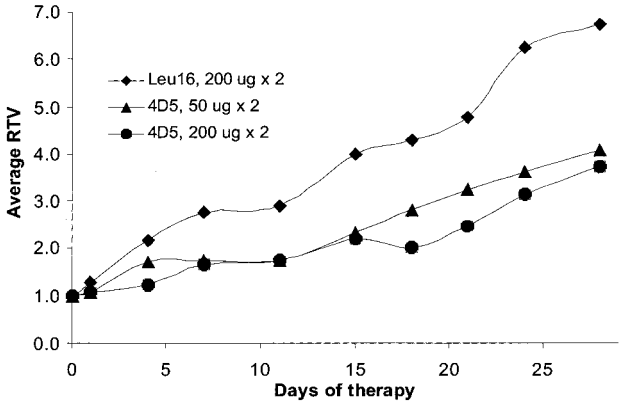

Figure 5. Immunotherapy of established MCF7/HER2/neu tumors in nude mice with 4D5. Groups of eight mice were injected i.p. on day zero and on day eight with (▲) 50 μg of 4D5, (●) 200 μg of 4D5, or (◆) 200 μg of Leu16. The tumor volume for each mouse at the time indicated was normalized to the tumor volume at the start of treatment. Mean values (±std dev) for all animals in each group are shown in Table 1.

6.75, $p = 0.11$, *t*-test). On the basis of these observations, we concluded that even at the level of 3 μg of antibody treatment, the majority of the RIT effect is due to radiation but not to the cytotoxic effects of antibody alone. Thus, despite the unexpected effect of cold antibody, our conclusions remain the same, i.e., that RIT treatment with the HER2/neu specific antibody has a statistically significant effect on tumor growth compared to the unlabeled antibody-treated group. Finally, it should be noted that while [^{90}Y]DOTA-4D5 slowed tumor growth, tumor regrowth occurred after about 19 days after therapy, as shown in Figure 4. Statistical analysis (ANOVA single factor) showed that there was no statistically significant difference among the five groups after 19 days.

DISCUSSION

To use HER2/neu as a target for radioimmunotherapy, it is necessary to show that an anti-HER2/neu antibody can be successfully radiolabeled without loss of immunoreactivity, that the radiolabeled antibody can target to HER2/neu positive tumors with good tumor to normal tissue ratios, and that RIT shows a positive effect compared to appropriate controls in a preclinical model. In this study, we utilized the previously described MCF7/HER2/neu cell line (*31*) as a model system. This cell line is derived from MCF7, a commonly used estrogen-sensitive cell line in tumor models of breast cancer. The cell line grows well in nude mice bearing slow estrogen release implants and, as shown in Figure 1, reacts strongly with the anti-HER2/neu antibody 4D5. In addition, HER2/neu expression was demonstrated in both treated and untreated tumors in the nude mouse xenograft model (Figure 2). We chose the monoclonal antibody 4D5 because its reactivity with HER2/neu is well established (*18*, *20*, *31*−*33*) and its humanized counterpart, Herceptin, is approved for clinical use. Furthermore, we were able to conjugate 4D5 with the macrocylic chelator DOTA and radiolabel it with ^{111}In to high specific activity (>30 μCi/μg, 90% labeling efficiency) while retaining high immunoreactivity (>90%) and good targeting to the MCF7/HER2/neu xenografts in nude mice (Figure 3, Table 1 of the Supporting Information). In comparing our results to those of De Santes et al. (*20*) who used the HER2/neu-transfected cell line NIH3T3/HER2/neu in beige/nude mice and ^{125}I-labeled 4D5, we obtained a higher maximum tumor uptake (30% ID/g vs 17% ID/g) and similar tumor to normal tissue ratios at 48h (e.g., tumor/liver uptake for ^{125}I-labeled 4D5 was 6.3, and for ^{111}In-labeled 4D5, the ratio was 6.1). The better tumor uptake may have been due to either dehalogenation of the ^{125}I-labeled antibody in tumor or to the better expression of HER2/neu in the MCF7/HER2/neu xenograft model. The former effect is more likely and has been shown to be a major advantage of radiometal labeled antibodies over radioiodine labeled antibodies (*34*−*37*). The favorable biodistibutions prompted us to perform RIT in the same model with ^{90}Y-labeled DOTA-4D5.

RIT with ^{90}Y-labeled DOTA-4D5 showed a significant tumor growth inhibitory effect compared to untreated (serum albumin/saline) controls, antibody only controls, or ^{90}Y-labeled DOTA-Leu16 controls (Figure 4 and Table 2 of the Supporting Information). The growth inhibitory effect was seen over a period of 19 days, after which tumor regrowth occurred and there was no further significant difference in growth rates among the four groups. In this model, where a single dose of RIT was given, positive effects of the treatment lasted over 6 half-lives of the isotope used (^{90}Y, 64 h). It is possible that a stronger effect would have been obtained if the animals were retreated or if a larger dose of radioactivity were administered. In this respect, we found a stronger effect for 100 μCi/animal compared to 50 μCi/animal (RTV 3.42 vs 4.69). Since no animals died with the 100 μCi dose of RIT, it may be possible to administer even higher doses. In previous studies using ^{90}Y-labeled anti-CEA antibodies in a colon cancer model with anti-CEA antibodies, we found an MTD of 120−130 μCi, which could be increased to 200 μCi if the animals were supported with bone marrow stem cells (*38*). Since the major toxicity in studies of this kind are hematologic and due to circulating radiolabeled antibody, the calculation of the appropriate highest dose depends on blood levels of the antibody (which differ depending on the tumor antigen and antibody system). In this study, several of the animals in the control (^{90}Y-labeled Leu16) RIT group died, since the circulating levels of ^{90}Y-labeled DOTA-Leu16 were higher than for ^{90}Y-labeled DOTA-4D5. The difference in circulating levels between the two antibodies is due to tumor uptake and possibly antigen−antibody clearance to the liver in the one case, but not in the other. The latter possibility cannot be verified, since soluble HER2/neu levels weren't measured.

In the RIT studies, we included an unlabeled antibody control group in which antibody was administered at the same protein dose (3 μg, 0.1 mg/kg) as in the RIT-treated animals. Since this dose was well below what is considered to be a therapeutic level in other studies with this cell line (*31*), we expected no antitumor effects. However, two of nine animals showed significant tumor growth inhibition. In one animal, the tumor was very small (34 mm^3), while the tumor was larger (75 mm^3) in the second animal. Even with these animals included, there was a significant difference between this control group and the RIT-treated groups until 19 days ($p < 0.02$, ANOVA single factor). If these two animals are excluded from this control group, the difference among the RIT groups is even greater ($p < 0.01$ at 19 days and $p < 0.04$ at 37 days, ANOVA single factor). Since the effect was seen for two animals, we doubt that the effect represents a random biological variance. In fact, in a separate experiment, we found that antibody doses 30 times higher (100 μg) had definite antitumor effects (Figure 5 and Table 1). Furthermore, in a slightly different model system, Baselga et al. (*39*) observed antitumor effects at multiple

Table 1. Average Relative Tumor Volumes vs Days after Therapy[a]

	days of therapy									
treatment	0	1	4	7	11	15	18	21	24	28
4D5,	1.00	1.06	1.71	1.75	1.74	2.32	2.82	3.24	3.62	4.09
50 μg × 2		(0.25)	(0.44)	(0.47)	(0.82)	(1.23)	(1.68)	(2.03)	(2.36)	(2.86)
4D5,	1.00	1.08	1.24	1.65	1.73	2.20	2.02	2.47	3.13	3.74
200 μg × 2		(0.36)	(0.52)	(0.61)	(0.63)	(0.60)	(0.50)	(0.86)	(1.22)	(1.66)
Leu16,	1.00	1.28	2.16	2.76	2.89	4.01	4.29	4.77	6.25	6.75
200 μg ×2		(0.25)	(1.43)	(1.62)	(1.80)	(2.90)	(2.89)	(3.36)	(5.75)	(6.10)

[a] Groups of eight mice bearing MCF7/HER2/neu xenografts were injected on day zero and on day 8 with 50 μg of 4D5, 200 μg of 4D5, or 200 μg of Leu16. Mean value (±std dev) for all animals in each group are shown.

antibody doses in the 0.1 mg/kg range. However, using the same cell line as in our study (MCF7/HER2/neu) and the same antibody (4D5), Pietras et al. (*31*) found that antibody doses 100 times higher were required to produce some antitumor effects. Overall, we believe that a small single dose of antibody was not responsible for the antitumor effect in our model RIT system.

In the RIT studies reported by De Santes and coworkers (*20*), ^{131}I-labeled 4D5 was used to treat NIH 3T3/HER2/neu xenografts in beige/nude mice. Significant tumor growth inhibition was observed out to 28 days with regrowth beginning after day 20. The activity required for maximum effect was 400 μCi, compared to 100 μCi in our study. Significant growth inhibition was also observed for the ^{131}I-labeled irrelevant antibody control, probably due to the high nonspecific doses characteristic of ^{131}I. It is also known that ^{131}I-labeled 4D5 is rapidly internalized in HER2/neu positive cells, followed by dehalogenation and excretion of the radioiodine (*20*). Metabolism of radiometal-labeled antibodies is much slower, allowing accumulation of radiomental within the cell and thus exposure of the cell to higher doses of radiation (*35*, *40*−*41*). Other differences between the two studies can be ascribed to the differences in growth rates of the two cell lines in the xenograft model. In untreated controls, the NIH3T3/HER2/neu tumor reached 10 cm^3 in 15 days compared to only 1.0 cm^3 in 40 days for the MCF7/HER2/neu model. It is likely that the slower growing tumors represent a more realistic model for human breast cancer and that their response to therapy is accordingly lower.

In the RIT studies reported by Horak et al. (*27*), ^{212}Pb-labeled DOTA-conjugated anti-HER2/neu antibody AE1 was used to treat nude mice bearing HER2/neu positive SK-OV3 xenografts. When small tumors (average mean size 15 mm^3) were treated, significant growth inhibition out to 60 days was observed with 10 or 20 μCi of radiolabeled antibody compared to untreated controls or ^{212}Pb-labeled DOTA-anti-TAC (irrelevant antibody control). In their study, tumor regrowth occurred at 60−70 days. When larger tumors were studied (average mean size 146 mm^3), tumor growth inhibition was not observed, suggesting that α-emitters are more effective against smaller tumors, a result in keeping with the short path length of α-emitters (several cell diameters). On the other hand, α-emitters deposit more energy per μCi (6−9 vs 1−2 MeV for ^{90}Y) thus allowing one to use less activity than ^{90}Y for a given experiment. In our study, the mean tumor sizes were approximately 100 mm^3 at the beginning of RIT and a tumor inhibitory effect was observed for ^{90}Y-labeled mAb.

Our preliminary study showed promising results in favor of using radiometal-labeled-anti HER2/neu antibody for treating breast carcinoma. We have shown that the antibody is readily conjugated to DOTA and radiolabeled without loss of immunoreactivity, and that the radiolabeled antibody targets to HER2/neu positive tumors with good tumor to normal tissue ratios, and that RIT shows tumor growth reduction compared to appropriate controls in a preclinical model. However, several issues need to be addressed in order to increase the therapeutic potential. First, although in our therapy groups the tumor growth is significantly reduced, tumor regrowth occurs after 19 days, and few mice were cured. Increasing radiation dose level or giving multiple doses may increase the therapeutic efficacy of the radiometal-labeled antibody. Second, given that even a small amount of cold antibody treatment alone may slow tumor growth, a combination therapy of radiometal-labeled antibody and unlabeled antibody may have additive or synergistic effects on tumor growth reduction. We are currently investigating these possibilities.

ACKNOWLEDGMENT

We thank Anne-Line Anderson and Randall Woo for their technical assistance, Stephanie Wright and Jianyi Yuan for their assistance in animal work. This work was funded by the Army Medical Research and Materiel Command Grant DAMD17-98-1-8031.

Supporting Information Available: Tables showing biodistribution of ^{111}In-labeled DOTA-4D5 in nude mice bearing MCF7/HER2/neu xenografts and average relative tumor volume vs days after therapy. This material is available free of charge via the Internet at http://pubs.acs.org.

LITERATURE CITED

(1) Baselga, J., Tripathy, D., Mendelsohn, J., Baughman, S., Benz, C. C., Dantis, l., Sklarin, N. T., Seidman, A. D., Hudis, C. A., Moore, J., Rosen, P. P., Twaddell, T., Henderson, I. C., and Norton, L. (1996). Phase II study of weekly intravenous recombinant humanized anti-p185^{HER2} monoclonal antibody in patients with HER2/neu-overexpressing metastatic breast cancer. *J. Clin. Oncol. 14*, 737−744.

(2) Pegram, M. D., Lipton, A., Hayes, D. F., Weber, B. L., Baselga, J. M., Tripathy, D., Baly, D., Baughman, S. A., Twaddell, T., Glaspy, J. A., and Slamon, D. J. (1998) Phase II study of receptor-enhanced chemosensitivity using recombinant humanized anti-p185$^{HER2/neu}$ monoclonal antibody plus cisplatin in patients with HER2/*neu*-overexpressing metastic breast cancer refractory to chemotherapy treatment. *J. Clin. Oncol. 16*, 2659−2671.

(3) Valone, F. H., Kaufman, P. A., Guyre, P. M., Lewis, L. D., Memoli, V., Deo, Y., Graziano, R., Fisher, J. L., Meyer, L., and Mrozek-Orlowski, M. (1995) Phase Ia/Ib trial of bispecific antibody MDX-210 in patients with advanced breast or ovarian cancer that overexpresses the proto-oncogene HER-2/neu. *J. Clin. Oncol. 13*, 2281−2292.

(4) Bargmann, C. I., Hung, M.-C., and Weinberg, R. A. (1986) The neu oncogene encodes an epidermal growth factor receptor-related protein. *Nature 319*, 226−230.

(5) Coussens, L., Yang-Feng, T. L., Liao, Y.-C., Chen, E., Gray, A., McGrath, J., Seeberg, P. H., Libermann, T. A., Schlessing-

er, J., Francke, U., Levison, A., and Ulrich, A. (1985) Tyrosine kinase receptor with extensive homology to EGF receptor shares chromosomal location with neu oncogene. *Science 230*, 1132−1139.

(6) Schechter, A. L., Stern, D. F., Vaidyanathan, L., Decker, S. J., Drebin, J. A., Greene, M. I., and Weinberg, R. A. (1984) The neu oncogene: an erb-B related gene encoding a 185,-000 Mr tumor antigen. *Nature 312*, 513−516.

(7) Iglehart, J. D., Kraus, M. H., Langton, B. C., Huper, G., Kerns, B. J., and Marks, J. R. (1990) Increased erb B-2 gene copies and expression in mulitple stages of breast cancer. *Cancer Res. 50*, 6701−6707.

(8) King, C. R., Kraus, M. H., and Aaronson, S. A. (1985) Amplification of a novel v-erb B-related gene in a human mammary carcinoma. *Science 229*, 974−976.

(9) Slamon, D. J., Godolphin, W., Jones, L. A., Holt, J. A., Wong, S. G., Keith, D. E., Levin, W. J., Stuart, S. G., Udove, J., Ulrich, A., and Press, M. F. (1989) Studies of the HER-2/neu proto-oncogene in human breast and ovarian cancer. *Science 244*, 707−712.

(10) Slamon, D. J., Clark, G. M., Wong, S. G., Levin, W. J., Ulrich, A., and McGuire, W. L. (1987) Human breast cancer: correlation of relapse and survival with amplification of the HER-2/neu oncogene. *Science 235*, 177−182.

(11) Drebin, J. A., Link, V. C., Stern, D. F., Weinberg, R. A., and Greene, M. I. (1985) Down-modulation of an oncogene protein product and reversion of the transformed phenotype by monoclonal antibodies. *Cell 41*, 695−706.

(12) Drebin, J. A., Link, V. C., Weinberg, R. A., and Greene, M. I. (1986) Inhibition of tumor growth by a monoclonal antibody reactive with an oncogene-encoded tumor antigen. *Proc. Natl. Acad. Sci. U.S.A. 83*, 9129−9133.

(13) Hancock, M. C., Langton, B. C., Chan, T., Toy, P., Monahan, J. J., Mischak, R. P., and Shawver, L. K. (1991) A monoclonal antibody against the c-erb B-2 protein enhances the cytotoxicity of cis-diamminedichloroplatinum against human breast and ovarian cell lines. *Cancer Res. 51*, 4575−4580.

(14) Hudziak, R. M., Lewis, G. D., Winget, M., Fendly, B. M., Shepard, H. M., and Ulrich, A. (1989) p185HER2 monoclonal antibody has antiproliferative effects in vitro, and sensitizes human breast tumor cells to tumor necrosis factor. *Mol. Cell Biol. 9*, 1165−1172.

(15) Lewis, G. D., Figari, I., Fendly, B., Wong, W. L., Carter, P., Gorman, C., and Shepard, H. M. (1993) Differential responses of human tumor cell lines to anti-p185^{HER2} monoclonal antibodies. *Cancer Immunol. Immunother. 37*, 255−263.

(16) Stancovski, I., Hurwitz, E., Leitner, O., Ulrich, A., Yarden, Y., and Sela, M. (1991) Mechanistic aspects of the opposing effects of monoclonal antibodies to the erbB-2 receptor on tumor growth. *Proc. Natl. Acad. Sci. U.S.A. 88*, 8691−8695.

(17) Arteaga, C. L., Winnier, A. R., Poirier, M. C., Lopez-Larraza, D. M., Shawver, L. K., Hurd, S. D., and Stewart, S. J. (1994) p185c-erbB-2 signal enhances cisplatin induced cytoxicity in human breast carcinoma cells: association between an oncogenic tyrosine kinase and drug-induced DNA repair. *Cancer Res. 54*, 3758−3765.

(18) Pietras, R. J., Fendly, B. M., Chazin, V. R., Pegram, M. D., Howell, S. B., and Slamon, D. J. (1994) Antibody to HER-2/neu receptor blocks DNA repair after cisplatin in human breast and ovarian cancer cells. *Oncogene 9*, 1829−1838.

(19) Carter, P., Presta, L., Groman, C. M., Ridgway, J. B. B., Henner, D., Wong, W. L. T., Rowland, A. M., Kotts, C., Carver, M. E., and Shepard, H. M. (1992) Humanization of an anti-p185^{HER2} antibody for human cancer therapy. *Proc. Natl. Acad. Sci. U.S.A. 89*, 4285−4289.

(20) De Santes, K., Slamon, D., Anderson, S. K., Shepard, M., Fendly, B., Maneval, D., and Press, O. (1992) Radiolabeled antibody targeting of the HER-2/*neu* oncoprotein. *Cancer Res. 52*, 1916−1923.

(21) DeNardo, S. J., DeNardo, G. L., Kukis, D. L., Shen, S., Kroger, L. A., DeNardo, D. A., Goldstein, D. S., Mirick, G. R., Salako, Q., Mausner, L. F., Srivastava, S. C., and Meares, C. F. (1999) 67Cu-2IT-BAT-Lym-1 pharmacokinetics, radiation dosimetry, toxicity, and tumor regression in patients with lymphoma. *J. Nucl. Med. 40*, 302−310.

(22) Wong, J. Y., Williams, L. E., Yamauchi, D. M., Odom-Maryon, L., Esteban, J. M., Neumaier, M., Wu, A. M., Johnson, D. K., Primus, F. J., Shively, J. E., and Raubitschek, A. A. (1995) Initial experience evaluating 90-yttrium radiolabeled anti-CEA chimeric T84.66 in a phase I radioimmunotherapy trial. *Cancer Res. 55*, 5929s−5934s.

(23) DeNardo, S. J., Kramer, E. L., O'Donnell, R. T., Richman, C. M., Salako, Q. A., Shen, S., Noz, M., Glenn, S. D., Ceriani, R. L., and DeNardo, G. L. (1997) Radioimmunotherapy for breast cancer using indium-111/yttrium-90 BrE-3: results of a phase I clinical trial. *J. Nucl. Med. 38*, 1180−1185.

(24) Brechbiel, M. W., Gransow, O. A., Atcher, R. W., Schlom, J., Esteban, J., Simpson, D. E., and Colcher, D. (1986) Synthesis of 1-(p-Isothiocyanatobenzyl) derivatives of DTPA and EDTA. antibody labeling and tumor-imaging studies. *Inorg. Chem. 25*, 2772−2781.

(25) Lewis, M. R., Raubitschek, A., and Shively, J. E. (1994) A facile, water-soluble method for modification of proteins with DOTA. Use of elevated temperature and optimized pH to achieve high specific activity and high chelate stability in radiolabeled immunoconjugates. *Bioconjugate Chem. 5*, 565−576.

(26) Li, M., Meares, C. F., Zhong, G.-R., Miers, L., Xiong, C.-Y., and DeNardo, S. J. (1994) Labeling of monoclonal antibodies with ^{90}Yttrium- and ^{111}Indium-DOTA chelates: A simple and efficient method. *Bioconjugate Chem. 5*, 101−104.

(27) Horak, E., Hartmann, F., Garmestani, K., Wu, C., Brechbiel, M., Gansow, O. A., Landolfi, N. F., and Waldmann, T. A. (1997) Radioimmunotherapy targeting of HER2/neu oncoprotein on ovarian tumor using Lead-212-DOTA-AE1. *J. Nuclear Med. 38*, 1944−1950.

(28) Meares, C. F., McCall, M. J., Reardan, D. T., Goodwin, D. A., Diamanti, C. I., and McTigue, M. (1984) Conjugation of antibodies with bifunctional chelating agents: Isothiocyanate and bromoacetamide reagents, Methods of Analysis, and Subsequent Addition of Metal Ions. *Anal. Biochem. 142*, 68−78.

(29) Lindmo, T., Boven, E., Cuttitta, F., Fedorko, J., and Bunn, P. A., Jr. (1984) Determination of the immunoreactive fraction of radiolabeled monoclonal antibodies by linear extrapolation to binding at infinite antigen excess. *J. Immun. Methods 72*, 77−89.

(30) Hsu, S. M., Raine, L., and Fanger, H. (1981) Use of avidin−biotin-peroxidase complex (ABC) in immunoperoxidase techniques: a comparison between ABC and unlabeled antibody (PAP) procedures. *J. Histochem. Cytochem. 29*, 577−580.

(31) Pietras, R. J., Poen, J. C., Gallardo, D., Wongvipat, P. N., Lee, H. J., and Slamon, D. J. (1999) Monoclonal antibody to HER-2/neureceptor modulates repair of radiation-induced DNA damage and enhances radiosensitivity of human breast cancer cells overexpressing this oncogene. *Cancer Res. 15*, 1347−1355.

(32) Fendly, B. M., Winget, M., Hudziak, R. M., Lipari, M. T., Napier, M. A., and Ulrich, A. (1990) Characterization of murine monoclonal antibodies reactive to either the human epidermal growth factor receptor or HER2/neu gene product. *Cancer Res. 50*, 1550−1558.

(33) Pietras, R. J., Pegram, M. D., Finn, R. S., Maneval, D. A., and Slamon, D. J. (1998) Remission of human breast cancer xenografts on therapy with humanized monoclonal antibody to HER-2 receptor and DNA-reactive drugs. *Oncogene 17*, 2235−2249.

(34) Brown, B. A., Comeau, R. D., Jones, P. L., Liberatore, F. A., Neacy, W. P., Sands, H., and Gallagher, B. M. (1987) Pharmacokinetics of the monoclonal antibody B72.3 and its fragments labeled with either ^{125}I or ^{111}In. *Cancer Res. 47*, 1149−1154.

(35) Schott, M. E., Milenic, D. E., Yakota, T., Whitlow, M., Wood, J. F., Fordyce, W. A., Cheng, R. C., and Schlom, J. (1992) Differential metabolic patterns of iodinated versus radiometal chelated anticarcinoma single-chain Fv molecules. *Cancer Res. 52*, 6413−6417.

(36) Sharkey, R. M., Blumenthal, R. D., Behr, T. M., Wong, G. Y., Haywood, L., Forman, D., Griffiths, G. L., and Goldenberg,

D. M. (1997) Selection of radioimmunoconjugates for the therapy of well established or micrometastatic colon carcinoma. *Int. J. Cancer 72*, 477−485.

(37) Stein, R., Chen, S., Haim, S., and Goldenberg, D. M. (1997) Advantage of yttrium-90-labeled over iodine-131-labeled monoclonal antibodies in the treatment of a human lung carcinoma xenograft. *Cancer 80*, 2636−2641.

(38) Morton, B. A., Beatty, B. G., Mison, A. P., Wanek, P. M., and Beatty, J. D. (1990) Role of bone marrow transplantation in ^{90}Y antibody therapy of colon cancer xenografts in nude mice. *Cancer Res.* (Suppl.) *50*, 1008s−1010s.

(39) Baselga, J., Norton, L., Albanell, J., Kim, Y., and Mendelsohn, J. (1998) Recombinant humanized anti-HER2 antibody (Herceptin^{TM}) enhances the antitumor activity of Paclitaxel and Doxorubicin against HER2/*neu* overexpressing human breast cancer xenografts. *Cancer Res. 58*, 2825−2831.

(40) Novak-Hofer, I., Amstutz, H. P., Macke, H. R., Schwartzbach, R., Zimmermann, K., Morgenthaler, J., and Schubiger, P. A. (1995) Cellular processing of copper-67-labeled monoclonal antibody chCE7 by human neuroblastoma cells. *Cancer Res. 55*, 46−50.

(41) Press, O. W., Shan, D., Howell-Clark, J., Eary, J., Appelbaum, F. R., Matthews, D., King, D. J., Haines, A., Hamann, P., Hinman, L., Shochat, D., and Bernstein, I. D. (1996) Comparative metabolism and retention of Iodine-125, Yttrium-90, and Indium-111 radioimmunoconjugates by cancer cells. *Cancer Res. 56*, 2123−2129.

BC9901292

© 2000 American Chemical Society, Bioconjugate Chem., Tsai bc9901292 Supporting Info Page 1

Table 1. Biodistribution of ^{111}In-labeled DOTA-4D5 in nude mice bearing MCF7/HER2/neu xenografts. *

Organ	Time (h)					
	0 &	5	24	48	72	96
Blood	39.6 (5.20)	22.8 (3.30)	14.7 (1.53)	13.1 (0.89)	13.5 (4.82)	9.77 (1.71)
Liver	8.99 (2.01)	6.75 (1.08)	5.84 (0.69)	5.27 (0.67)	6.01 (1.70)	4.71 (1.24)
Spleen	7.00 (1.53)	6.27 (1.52)	4.80 (0.71)	4.20 (0.56)	4.80 (1.72)	4.52 (0.75)
Kidney	6.51 (0.92)	5.03 (0.53)	4.06 (0.68)	3.94 (0.34)	3.77 (0.70)	3.06 (0.58)
Lung	11.1 (2.49)	7.69 (1.41)	5.13 (0.44)	4.96 (0.75)	4.64 (1.41)	3.70 (1.10)
Bone	2.27 (0.45)	2.13 (0.37)	1.85 (0.23)	1.63 (0.17)	1.79 (0.47)	1.47 (0.29)
Tumor	1.13 (0.43)	8.23 (1.98)	22.4 (4.60)	32.2 (6.32)	27.4 (7.84)	23.7 (4.52)
Carcass	1.83 (0.15)	3.10 (0.25)	3.04 (0.05)	2.86 (0.19)	2.64 (0.48)	.36 (0.33)

* Groups of 5 mice bearing MCF7/HER2/neu were injected with 3.6 μCi of ^{111}In-labeled DOTA-4D5 into nude mice bearing MCF7/Her2/neu xenografts. Mean values (+/- std. dev.) are % ID/g for each organ at each time point.

& Approximately 20 minutes after injection.

© 2000 American Chemical Society, Bioconjugate Chem., Tsai bc9901292 Supporting Info Page 2

Table 2. Average relative tumor volume vs. days after therapy.[1]

	Days of Therapy											
Treatment	1	4	6	9	12	15	19	22	26	29	33	37
4D5	1.00	1.37 (0.36)	1.83 (0.67)	2.31 (0.91)	2.51 (1.46)	3.30 (2.16)	4.79 (3.70)	5.24 (4.22)	6.25 (4.88)	7.32 (5.90)	8.23 (7.09)	8.83 (8.74)
50 uCi 4D5	1.00	1.10 (0.25)	1.30 (0.57)	1.68 (0.79)	2.05 (0.77)	2.38 (0.95)	2.46 (1.46)	3.22 (1.93)	3.51 (2.19)	4.19 (2.76)	4.45 (3.24)	4.69 (3.56)
100 uCi 4D5	1.00	1.09 (0.34)	1.02 (0.37)	1.18 (0.46)	1.38 (0.46)	1.55 (0.77)	1.68 (0.90)	2.39 (2.01)	2.82 (2.39)	3.35 (3.40)	3.67 (4.05)	3.42 (3.64)
100uCi Leu16	1.00	1.29 (0.45)	1.50 (0.35)	1.90 (0.30)	2.26 (0.62)	2.60 (0.79)	3.34 (1.10)	4.27 (1.17)	5.12 (1.30)	6.09 (1.43)	7.10 (2.03)	8.77 (2.98)
H.S.A.	1.00	1.35 (0.30)	1.62 (0.54)	2.25 (0.67)	2.91 (0.73)	3.84 (1.03)	4.70 (1.47)	5.26 (1.87)	5.36 (1.54)	6.30 (2.34)	8.24 (4.25)	9.30 (4.25)

1. Groups of 9 mice bearing MCF7/HER2/neu xenografts were injected with 3 ug unlabeled DOTA-4D5, 50 uCi (3ug) of ^{90}Y-labeled DOTA-4D5, 100 uCi (3ug) of ^{90}Y-labeled DOTA-4D5, 100 uCi (3ug) of ^{90}Y-labeled DOTA-Leu16, or 1% HSA/saline. Mean value (+/- std.dev.) for all animals in each group are shown.

Molecular Characterization of a Tetramolecular Complex between dsDNA and a DNA-Binding Leucine Zipper Peptide Dimer by Mass Spectrometry

Leesa J. Deterding,*,† Juergen Kast,‡ Michael Przybylski,‡ and Kenneth B. Tomer†

Laboratory of Structural Biology, National Institute of Environmental Health Sciences, National Institutes of Health, P.O. Box 12233, Research Triangle Park, North Carolina 27709, and University of Konstanz, Faculty of Chemistry, P.O. Box 5560M732, D-78434 Konstanz, Germany. Received September 22, 1999; Revised Manuscript Received December 10, 1999

The characterization of sequence-specific noncovalent complexes of the GCN4 peptides and dsDNA using mass spectrometry is reported. The GCN4 peptides belong to a class of proteins which bind to sequence-specific dsDNA and are important in the regulation of gene transcription in yeast. These proteins contain a bZIP structural motif which consists of a basic DNA-binding domain and a leucine zipper dimerization domain. The protein dimers specifically bind double-stranded DNA containing the binding element 5′-ATGA(C/G)TCAT-3′ to form a tetramolecular noncovalent complex. Using electrospray ionization, we report the detection of such a specific tetramolecular complex using mass spectrometry. Under conditions necessary for observation of the tetramolecular complex, no ions were detected for the GCN4 peptide dimer or the GCN4 monomer with dsDNA. These observations indicate that the specific interaction of the dsDNA with the protein dimer stabilizes the biologically significant noncovalent complex in the gas phase. Complexes were observed for various lengths of both blunt-ended and cohesive-ended double-stranded DNA containing the specific recognition sequence. The binding specificity of the complex was verified with the use of control DNA not containing the recognition sequence and control peptides not known to bind DNA specifically. Additionally, combining limited proteolysis of GCN4 peptide−DNA complexes with mass spectrometric determination of the products compared to identical experiments with noncomplexed peptides was used to probe interactions of specific amino acids with the DNA. The ability to observe these complexes by mass spectrometry and to probe the specific interactions involved opens the door for utilizing this analytical technique to other structural biological problems including the study of transcription processes and determining the specific binding regions between dsDNA and proteins.

INTRODUCTION

The study of noncovalent complexes formed in biological systems has been the target of much research. These interactions play a critical role in the functions and regulation of biomolecules. Some examples of noncovalent interactions which are of biological relevance include protein−DNA, receptor−ligand, DNA−drug, protein−drug, and antibody−antigen complexes. Understanding these interactions is key to understanding biological functions such as gene regulation, antibody recognition, pharmacological response, and anti-viral applications.

In the present study, we are investigating the applicability of MS-based techniques to the characterization of GCN4:DNA complexes. GCN4 is a sequence-specific DNA-binding protein containing a bZIP structural motif (Landschulz et al., 1988; Abel and Maniatis, 1989). GCN4 is important in the regulation of gene transcription and is responsible for the general control of amino acid synthesis in yeast (Penn et al., 1983; Thireos et al., 1984; Hinnebusch, 1984). The "bZIP" motif consists of a "basic" DNA-binding domain and a "leucine zipper" dimerization domain. The leucine zipper consists of about 30 amino acids containing a heptad repeat of leucine residues (Hope and Struhl, 1986; Hope and Struhl, 1987; Hurst, 1996; Struhl, 1987). The coiled leucine zipper from two proteins interact through parallel coiled coils and form protein dimers (O'Shea et al., 1989a,b; Rasmussen et al., 1991; Oas et al., 1990), while the basic DNA-binding region is thought to be disordered in the absence of DNA and to form α helices when bound to DNA. While alterations of the leucine residues in the zipper region lead to loss of dimerization and DNA binding (Vogt and Bos, 1989; Landshulz et al., 1989, Turner and Tjian, 1989; Gentz et al., 1989; Schuermann et al., 1989), alterations in the basic region prevent DNA binding, but do not inhibit dimerization (Vogt and Bos, 1989; Landshulz et al., 1989; Turner and Tjian, 1989; Gentz et al., 1989).

DNA recognition by GCN4 and related proteins was first proposed as a scissors grip model (Vinson et al., 1989) followed by the proposal of an induced helical fork model (O'Neill et al., 1990). Subsequent X-ray crystallographic studies, using smaller peptide models of the whole protein, GCN4-p1 (residues 249−281), showed a parallel, two-stranded coiled coil of α helices (O'Shea et al., 1991). The crystal structure for a GCN4 bZIP peptide (residues 226−281) complexed with a specific DNA site showed a pair of continuous α helices which diverge toward the N termini, allowing them to scissor grip the major groove of the DNA (Ellenberger et al., 1992).

* To whom correspondence should be addressed. Phone: (919) 541-3009. Fax: (919) 541-0220. E-mail: deterding@niehs.nih.gov.
† National Institute of Environmental Health Sciences.
‡ University of Konstanz.

10.1021/bc990123c CCC: $19.00 © 2000 American Chemical Society
Published on Web 04/29/2000

Mass spectrometry is increasingly being applied to the characterization of tertiary structures and noncovalent complexes. Since the first report in 1991 (Ganem et al., 1991), numerous noncovalent complexes, including protein−protein, protein−ligand, and oligonucleotide dimers and duplexes, have been observed using ESI in combination with mass spectrometry (Przybylski et al., 1996; Loo, 1997). Recent papers have reported the mass spectrometric analyses of nonspecific DNA duplexes (Gale et al., 1994; Bayer et al., 1994; Ding and Anderegg; 1995; Przybylski et al., 1995; Gale and Smith, 1995; Triolo et al., 1997) and trimeric and tetrameric complexes (Gale et al., 1994; Przybylski et al., 1995; Gale and Smith, 1995; Triolo et al., 1997; Baca and Kent, 1992; Schwartz et al., 1994; Siuzdak et al., 1994; Wendt et al., 1995; Miranker et al., 1996; Cheng et al., 1996a; Pócsfalvi et al., 1997), and one report showed the analysis of a sequence-specific trimeric complex between DNA and a protein (Cheng et al., 1996b). There have been very few reports of a successful mass spectrometric analysis of a sequence-specific noncovalent tetramolecular complex not involving four identical subunits or metal ions. A tetrameric noncovalent complex of two molecules of the vitamin D receptor DNA binding domain (VDR DBD) with dsDNA containing two vitamin D response elements in which the two VDR DBDs bound to the dsDNA independently was reported by Veenstra et al. (Veenstra et al., 1998). Potier et al. reported the MS observation of a 1:1 complex of the *trp* apo-repressor (TrpR) homodimer and dsDNA containing the TrpR recognition site, and complexes of this complex with tryptophan (Potier et al., 1998), while a preliminary report of this study of the noncovalent complexes of the GCN4 family of peptides with double-stranded DNA using electrospray ionization was also reported (Deterding et al., 1998).

For direct characterization of the interactions involved in specific complex formation, however, mass spectrometric methods alone are not applicable. MS analysis, however, has been combined with protein-specific reactions, such as covalent modification of individual amino acid residues or enzymatic cleavage (Suckau et al., 1990) for probing protein tertiary structures (Brockerhoff et al., 1992, Polverino de Laureto et al., 1995, Zappacosta et al., 1996, Kriwacki et al., 1997) and protein−nucleic acid complexes (Cohen et al., 1995). In these studies, the identification of proteolytic peptides generated from "limited proteolysis" based on a time course provides additional information. Thus, either exposed regions of tertiary structures or structural differences of a protein in two forms, e.g., a nonbound and a receptor-bound state, can be monitored. In this paper, we report our results of the characterization of protein−DNA complexes using direct MS analyses and MS analysis combined with limited proteolysis of the GCN4:DNA complex.

EXPERIMENTAL PROCEDURES

DNA Samples. The oligonucleotides (desalted) were purchased from Genosys Biotechnologies, Inc. (The Woodlands, TX) and were used without further purification. Sequences of the synthetic oligonucleotides are shown in Table 1. All of the oligonucleotides contain, as duplexes, the GCN4 DNA-binding element 5′-ATGA(C/G)TCAT-3′ (underlined nucleic acids) (Hope and Struhl, 1985; Hill et al., 1986) except for the blunt-ended 24-bp (control DNA) which was used as a control. Ammonium acetate was obtained from Mallinckrodt, Inc. (Paris, KY). All solutions were prepared using 18-MΩ water (Hydro Service and Supplies, Research Triangle Park, NC).

Table 1. Oligonucleotide Sequences

DNA	Sequence
13-bp (blunt)	5′-GG ATGACTCAT TT-3′ 3′-CC TACTGAGTA AA-5′
24-bp (blunt)	5′-CGCAGCGG ATGACTCAT TTTTCGG-3′ 3′-GCGTCGCC TACTGAGTA AAAAGCC-5′
24-bp (cohesive)	5′-TCCACCTAGCGG ATGACTCAT TCT-3′ 3′-GGATCGCC TACTGAGTA AGAATCG-5′
24-bp[§] (blunt)	5′-ACTACTACTACTGATGATGATGAT-3′ 3′-TGATGATGATGACTACTACTACTA-5′
30-bp (cohesive)	5′-TCCACCTAGCGG ATGACTCAT TTTTTTTCT-3′ 3′-GGATCGCC TACTGAGTA AAAAAAAGAATCG-5′

[§] Control DNA.

Oligonucleotide stock solutions (2 nmol/μL) were prepared using 50 mM ammonium acetate buffer, pH 8.0. Equal molar concentrations of the complementary strands of oligonucleotides were combined, heated to 70 °C, and cooled slowly to room temperature over 2.5 h to facilitate double-stranded annealing. Prior to mass spectrometric analysis, 1 μL of the double-stranded DNA (dsDNA) solution (2 nmol/μL) was added to 49 μL of 50:50 water: acetonitrile for negative ion ESI or 49 μL of 90:10 water: methanol for positive ion ESI resulting in 40 pmol/μL solution.

Proteins. The GCN4 proteins, GCN4-bR and GCN4−61, were prepared on an Applied Biosystems-430A or a semi-automated ABIMED synthesizer using Fmoc protection strategy as described previously (Wendt et al., 1995). Stock solutions of the proteins (1 nmol/μL) were prepared in 50 mM ammonium acetate buffer, pH 8.

Complex Preparation. The trimolecular and tetramolecular complexes were formed by first diluting 1 μL of the dsDNA solution (2 nmol/μL) to 2 μL with 50 mM ammonium acetate buffer. This 2 μL solution of dsDNA (1 nmol/μL) was then incubated with 2 μL of the protein solution (1 nmol/μL) at room temperature for approximately 5 min. For mass spectrometric analysis, 2 μL of the noncovalent complex solution was diluted to 50 μL with 90:10 water:methanol resulting in a 20 pmol/μL solution.

Limited Proteolysis Experiments of GCN4-bR and GCN4-bR-13-bp dsDNA Complex. For both nonbound GCN4-bR and GCN4-bR complexed with a 1.25-fold excess of 13-bp dsDNA, endoproteases Lys-C, Glu-C, and Asp-N (Boehringer Mannheim, Mannheim, Germany) were used. All digests were performed in ammonium acetate (0.1 M, pH 6.5) at 20 °C using an enzyme:substrate ratio of 1:30. Because of the dynamics of the complex, quantitative formation of the complex prior to digestion has to be ensured. Cohen proposed the use of an initial excess of DNA high enough to shift the equilibrium in solution toward the side of the complex (Cohen et al., 1995). On the basis of their calculations, a 1.25-fold excess of the previously formed DNA double strand over the peptide subject to this study was chosen to ensure that most of the GCN4-bR was initially bound to the DNA. The 100 mM salt concentration was chosen because it is sufficient to enable specific interactions to occur while excluding nonspecific interactions. Aliquots of the reaction mixtures were taken at different digestion
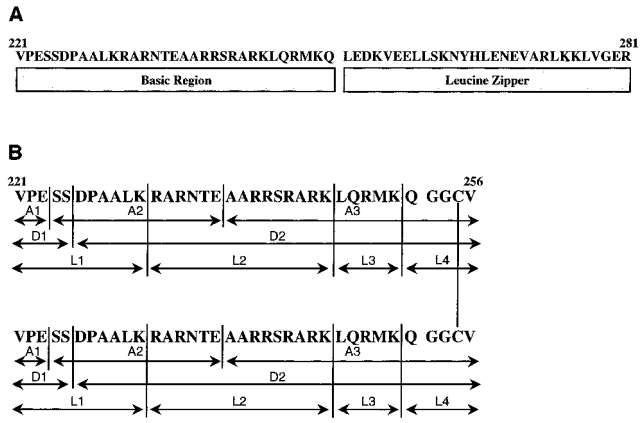
Figure 1. Amino acid sequences of the (A) GCN4−61 peptide and (B) GCN4-bR peptide. Cleavage points for the various enzymes studied in the limited proteolysis experiments are indicated in panel B. The A, D, and L peptide fragments correspond to enzymatic cleavages involving endoprotease Glu-C, Asp-N, and Lys-C, respectively.

times ranging from 1 min to 48 h, and reactions were stopped by diluting with a 4-fold excess of 0.1% TFA. Diluted aliquots of the reaction mixtures were analyzed by MALDI-MS without further purification.

Electrospray Ionization Mass Spectrometry. A Micromass Platform II (Altrincham, U.K.) single-quadrupole mass spectrometer equipped with an ESI interface and an extended mass range quadrupole (4000 Da) was used for all analyses of the noncovalent complexes. The temperature of the ESI source of the mass spectrometer was maintained at 35 °C. Spraying was achieved using nitrogen as the nebulizing and drying gas. Samples were infused into the mass spectrometer at 5 μL/min using a pressure injection vessel (Tomer et al., 1994). The ESI probe voltage was operated at −3 kV for the analysis of the oligonucleotide dimers and at +3 kV for the analysis of the DNA−protein complexes. To obtain spectra of the noncovalent complexes, a cone voltage potential of ±75 to ±125 V was necessary. Full scan mass spectra were acquired in the continuum-data acquisition mode. For all analyses, a mass range of 300−4000 Da was scanned at 3.9 s/scan.

Matrix-Assisted Laser Desorption Mass Spectrometry. All MALDI-MS analyses were carried out on a Bruker Biflex (Bruker-Franzen, Bremen, Germany) linear time-of-flight mass spectrometer using a UV nitrogen laser (337 nm), a dual microchannel plate detector, and the X-MASS data processing system. An accelerator voltage of 20 kV was applied, and spectra were calibrated with insulin as external standard. Previously identified fragments derived from GCN4 peptides were used for additional internal recalibration, if necessary. Samples were diluted with 0.1% trifluoroacetic acid (TFA) to a final concentration of about 10^{-5} M. For mass analyses, 1 μL of this solution was mixed with 1 μL of a saturated solution of α-cyano-4-hydroxy cinnamic acid (HCCA) in 25% formic acid/2-propanol (2:1, v/v).

RESULTS

For the study of sequence-specific noncovalent complexes between proteins and DNA, the GCN4 peptides GCN4-bR, a peptide model of GCN4 similar to the peptide model GCN4-bR1 (Talanian et al., 1990), and the carboxy-terminus peptide GCN4−61, which contains both the basic DNA-binding region and the leucine zipper of GCN4, complexed with dsDNA were used. Figure 1 shows the amino acid sequence of the GCN4 peptides. The sequence of GCN4-bR contains the basic DNA-binding region and a disulfide bond in place of the leucine zipper. A Gly-Gly-Cys-Val linker is added at the carboxyl terminus to provide a flexible linker in the disulfide-bonded dimer. It has been shown that the GCN4-bR1 peptide retains sequence-specific DNA-binding activity (Talanian et al., 1990). GCN4−61, amino acid residues 221−281 of GCN4, corresponds to the entire bZIP structural motif of GCN4 and has been reported to be capable of dimerization and sequence-specific DNA binding (Hope and Struhl, 1986).

The positive ion ESI deconvoluted spectra of the GCN4 peptides are shown in Figure 2. For both GCN4-bR (Figure 2A) and GCN4−61 (Figure 2B), the deconvoluted spectra show primarily the molecular ion of the respective peptides. For GCN4−61, additional ions (ions labeled with an asterisk) are observed which are due to truncated synthetic peptides in the sample. It should be noted that, under these conditions, no ions corresponding to the GCN4−61 dimer are observed. Only monomeric GCN4−61 is observed.

The electrospray ionization mass spectra of the dsDNA samples revealed that the complementary strands of the oligonucleotides were successfully annealed. For example, the positive ion and negative ion ESI mass spectra of the blunt-ended 24-bp dsDNA are shown in Figure 2, panels C and D, respectively. Specific odd-charge 7 and/or 9 ions of the duplex oligonucleotides (D ions) could be detected verifying the formation of the dsDNA from the single-stranded oligonucleotides (S ions). The broadness of the ions in these spectra is most likely due to counterion association with the oligonucleotides (Saenger, 1984; Light-Wahl et al., 1993; Bayer et al., 1994). To obtain the ESI spectra of the DNA duplexes, a cone voltage potential of ca. 75−100 V was necessary. For cone voltages less than 75 V, only ions from the single oligonucleotides were observed. This phenomenon is in agreement with several literature reports for the analysis of duplex oligonucleotides (Bayer et al., 1994; Ding and Anderegg, 1995; Triolo et al., 1997). The higher cone voltages may be necessary to efficiently desolvate the duplex. Triolo and co-workers (Triolo et al., 1997) have suggested that this finding indicates good gas-phase stability of the duplex ions.

The positive ion ESI mass spectrum of the trimolecular complex of the blunt-ended 13-bp dsDNA and GCN4-bR (M_r = 15896.4) is shown in Figure 3A. Molecular ions for the noncovalent complex are observed at ca. *m*/*z* 2000 and 2300 as well as molecular ions due to GCN4-bR peptide in the lower *m*/*z* range of 700−1400. The noncovalent complex ions correspond to the +7 and +8 charge state. No ions corresponding to a complex of GCN4-bR with single-stranded DNA or to the DNA dimer alone were observed. A cone voltage of 80 V was necessary to observe the molecular ions of the trimeric complex in the mass spectrum. The relatively broad peaks of the noncovalent complex are most likely due to incomplete desolvation and/or salt adducts of the molecular ions as observed by others (Huang et al., 1993; Cheng et al., 1996b). The broadness of the peptide ions in the low mass/charge region is due to fragmentation induced by the high cone voltage as well as oxidation of the peptide as a result of the incorporation of the disulfide linker which can be readily oxidized.

The ESI mass spectrum of the tetramolecular complex of the blunt-ended 13-bp dsDNA with the GCN4−61 noncovalent dimer (M_r = 22135.6) is shown in Figure 3B. The ions observed at *m*/*z* 2461, 2213, 2015, and 1848 correspond to the +9, +10, +11, and +12 charge states

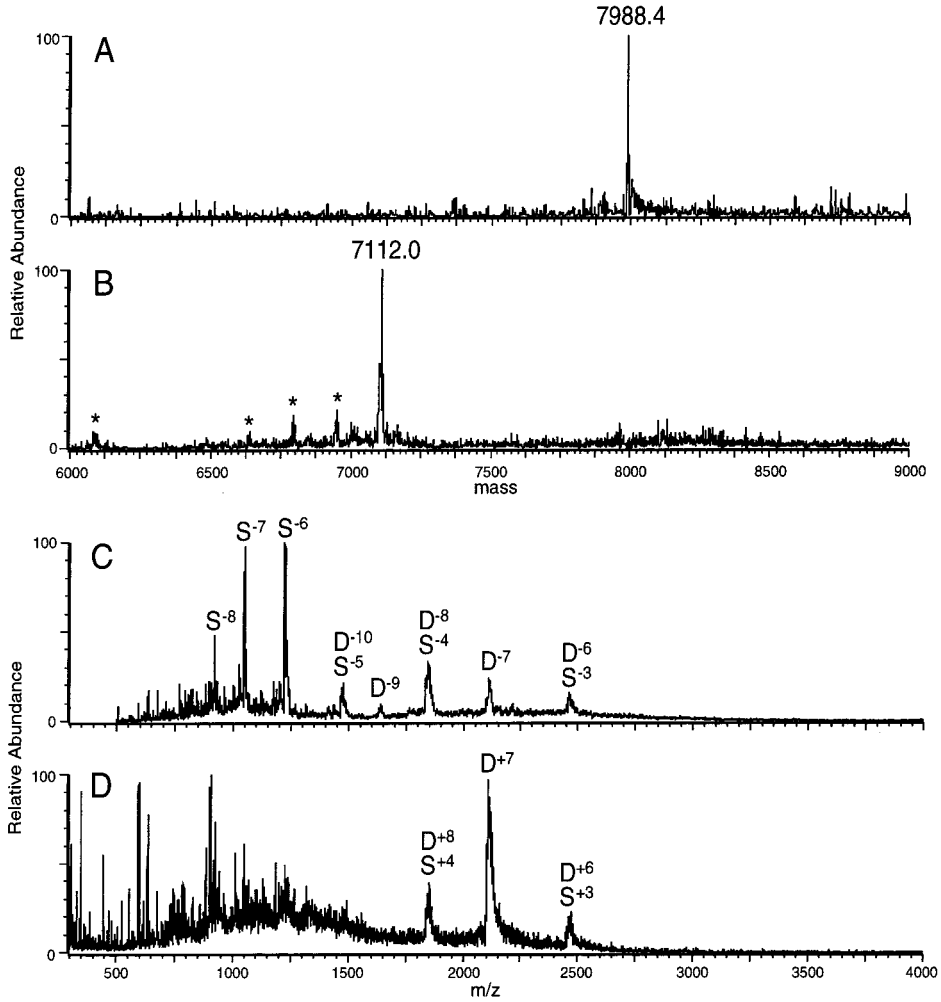

Figure 2. (A) Positive ion ESI deconvoluted mass spectrum of GCN4-bR (average of 28 scans) and (B) positive ion ESI deconvoluted mass spectrum of GCN4−61 (average of five scans). Ions designated with an asterisk (*) are due to truncated synthetic peptides. ESI mass spectra of annealed blunt-ended 24-bp dsDNA acquired under (C) negative ion conditions (average of 12 scans) and (D) positive ion conditions (average of 95 scans). Ions designated as D are due to the dsDNA and ions designated as S are due to the single stranded oligonucleotides.

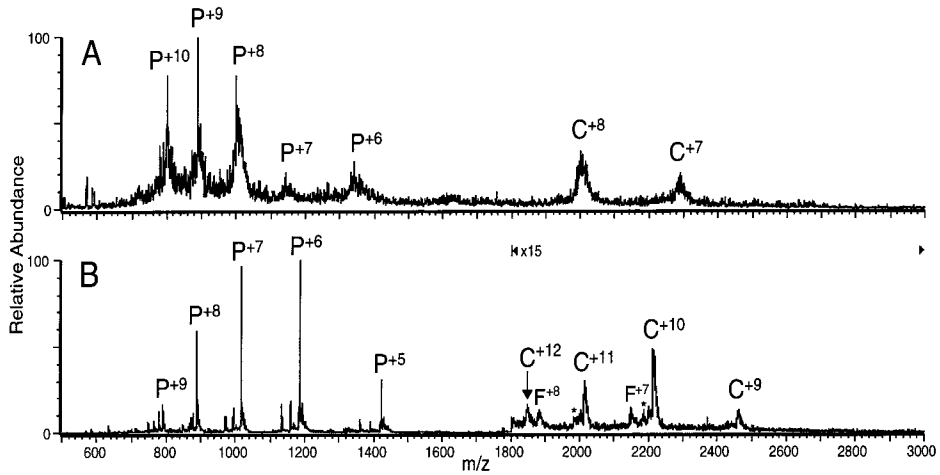

Figure 3. Positive ion ESI mass spectra of the noncovalent complex of the 13-bp dsDNA with (A) GCN4-bR (average of 40 scans) and (B) GCN4−61 dimer (average of 94 scans). Ions designated as P are due to the peptides while ions designated as C are due to the trimolecular and tetramolecular noncovalent complexes. The fragment ions designated as F are due to the loss of one peptide chain from the tetramolecular complex, while the ions designated with an asterisk (*) are due to complexes involving the truncated synthetic peptides.

of the noncovalent complex (C series ions). In addition, ions are observed in the low *m*/*z* range which correspond to the GCN4−61 monomer peptide (P series ions). Additional molecular ion species are observed which correspond to the truncated synthetic peptides noted in Figure 2B. A cone voltage of 85 V was necessary to detect the ions for the tetramolecular complex. The low relative abundance fragment ions at ca. *m*/*z* 1880 and 2145

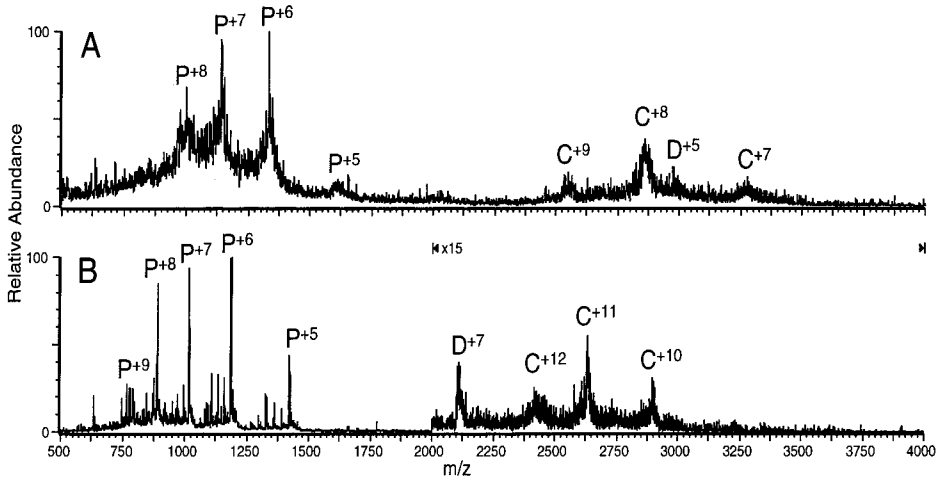

Figure 4. Positive ion ESI mass spectra of the noncovalent complex of the blunt-ended 24-bp dsDNA with (A) GCN4-bR (average of 54 scans) and (B) GCN4−61 dimer (average of 52 scans). Ions designated as P are due to the peptides, ions designated as C are due to the trimolecular and tetramolecular noncovalent complexes, and ions designated as D are due to the dsDNA.

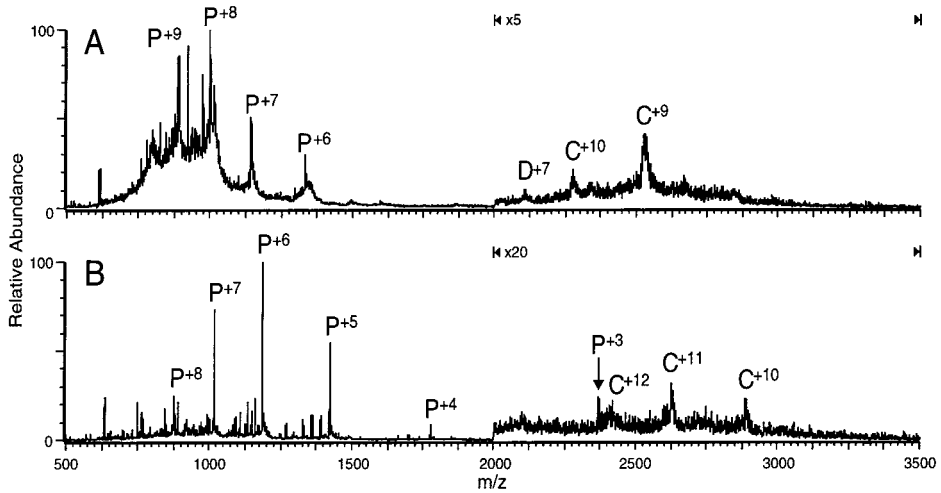

Figure 5. Positive ion ESI mass spectra of the noncovalent complex of the cohesive-ended 24-bp dsDNA with (A) GCN4-bR (average of 86 scans) and (B) GCN4−61 dimer (average of 70 scans). Ions designated as P are due to the peptides, ions designated as C are due to the trimolecular and tetramolecular noncovalent complexes, and the ion designated as D is due to the dsDNA.

correspond to the loss of one peptide chain from the tetramolecular complex due to the high cone voltage (F ions). Similar to the electrospray mass spectrum of the GCN4−61 peptide alone (Figure 2B), only GCN4−61 monomeric ions were detected. No ions were observed for the GCN4−61 dimer.

A slightly longer strand of dsDNA complexed with the GCN4 peptides was evaluated in Figure 4. The positive ion ESI mass spectrum of blunt-ended 24-bp dsDNA and GCN4-bR (M_r = 22695.8) was acquired using a cone voltage of 125 V and is shown in Figure 4A. Molecular ions for the trimolecular complex (C series ions) are observed in the *m*/*z* range 2500−3300 and correspond to the +7, +8, and +9 charge state of the complex. Ions due to the GCN4-bR peptide alone (P series ions) are observed in the low *m*/*z* range region. The low relative abundance ion of *m*/*z* 2980 corresponds to the +5 charge state of the 24-bp dsDNA (D^{+5} ion). This spectrum is similar to that observed for the 13-bp dsDNA complex (Figure 3A) in that no ions were observed for the 24-bp DNA dimer alone or for the GCN4-bR with a 24-bp single strand. In addition, the peaks are relatively broad due to incomplete desolvation and/or salt adducts. The positive ion ESI spectrum for the tetramolecular complex of the blunt-ended 24-bp dsDNA and the GCN4−61 dimer (M_r= 28935) is shown in Figure 4B. A cone voltage of 85 V was necessary to observe the tetramolecular complex ions. The ions of *m*/*z* 2895, 2634, and 2424 correspond to the +10, +11, and +12 charge states, respectively, of the noncovalent complex (C series ions). An additional ion in the higher *m*/*z* range region of *m*/*z* 2110 is also observed and corresponds to the +7 ion of the 24-bp dsDNA dimer (D^{+7} ion). Ions of the GCN4−61 monomer are observed in the lower *m*/*z* range region with the +6 charge state ion being the highest in relative abundance (P series ions). No ions were observed for the GCN4−61 dimer, the GCN4−61 monomer complexed with dsDNA, or any other nonspecific complex.

To determine if the end of the double-stranded DNA has any effect on the stability of the noncovalent complexes during electrospray ionization, cohesive-ended dsDNAs complexed with the GCN4 peptides were analyzed. Cohesive-ended DNA is DNA which has short single-stranded sequences at the ends. The positive ion ESI spectra of the noncovalent complex of the cohesive-ended 24-bp dsDNA (Figure 5) and 30-bp dsDNA (Figure 6) with GCN4-bR and with GCN4−61 show data very similar to that for the previous complexes using blunt-ended dsDNAs. Ions due to the noncovalent complexes with cohesive-ended dsDNA (C series ions) are observed in the mass spectra acquired at a cone voltage of 95 V.

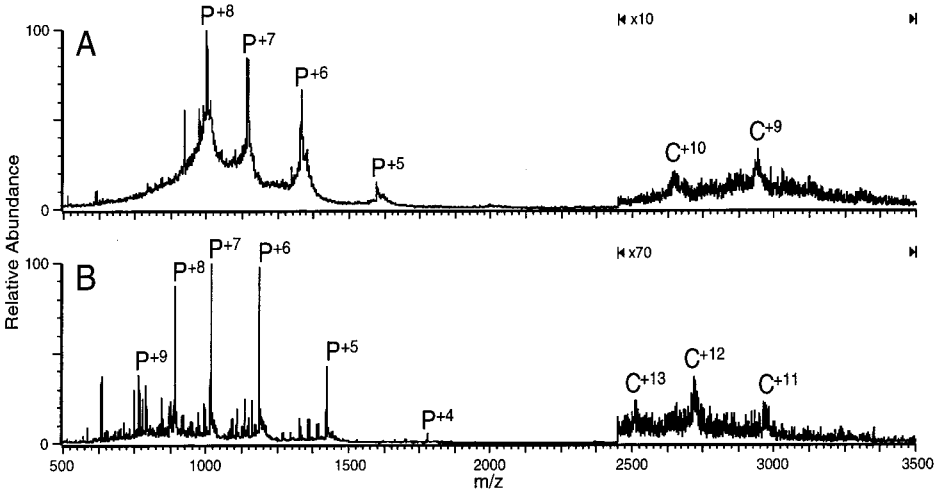

Figure 6. Positive ion ESI mass spectra of the noncovalent complex of the cohesive-ended 30-bp dsDNA with (A) GCN4-bR (average of 64 scans) and (B) GCN4−61 dimer (average of 114 scans). Ions designated as P are due to the peptides, ions designated as C are due to the trimolecular and tetramolecular noncovalent complexes.

Specificity of ESI Mass Spectrometric Detection of Complexes. A variety of control experiments was conducted to verify that the observations in these spectra are due to specific interactions between the GCN4 peptides and the dsDNA. A non-DNA-binding protein, bovine pancreatic trypsin inhibitor (BPTI), was mixed with the dsDNAs to see if a nonspecific trimolecular complex could be detected. Low relative abundance ions (<4%) were observed which may correspond to a noncovalent complex between one of the oligonucleotide strands and BPTI (data not shown). No ions corresponding to a BPTI:dsDNA complex were observed. Similarly, single-stranded 24-bp oligonucleotides which did not contain the GCN4-binding region were mixed individually with the GCN4 peptides and analyzed under the same electrospray ionization conditions necessary for observation of the trimolecular and tetramolecular noncovalent complexes. No ions were observed in any of the mass spectra which correspond to formation of a nonspecific complex between the control ssDNA (control DNA) and the GCN4 peptides (data not shown). In the final control experiment, the complementary 24-bp oligonucleotides which did not contain the GCN4-binding region were annealed and mixed with the GCN4 peptides. Low abundance ions (<1.5%) which may correspond to the +9 and +10 charge state of the molecular ion of the nonspecific complex were observed (data not shown). Nonspecific interactions are known to be characteristic of essentially all DNA-binding proteins and are typically weak interactions.

Limited Proteolysis. To further characterize individual amino acid residues involved in DNA binding of GCN4, a differential limited proteolysis study was performed (Cohen et al., 1995). Proteolytic digestions of the preformed complex of GCN4-bR and 13-bp dsDNA were carried out using different endoproteases. The time courses of all enzymatic cleavage reactions were monitored by sampling the reaction mixtures at different times, stopping the reactions, and analyzing the resulting mixtures by MALDI/MS without further purification. By identifying the cleavage products from their masses, the specific cleavage sites were assigned. These results were then compared to those obtained from proteolysis of nonbound GCN4-bR.

Proteolytic digestion with endoprotease Lys-C was used to characterize the reactivities of the lysine residues Lys231, Lys246, and Lys251. In the first set of experiments, unbound GCN4-bR was digested, while, in a second set, the previously formed complex of GCN4-bR and 13-bp dsDNA was subjected to proteolysis. The positive ion MALDI spectra of both sets, stopped after 5 min reaction time, are shown in Figure 7. For GCN4-bR (Figure 7A), protonated molecules of the proteolytic peptides L2−3 (*m/z* 2457), L1−2 (*m/z* 2900), L2−4 + L4 (*m/z* 3360), and L2−4 + L2−4 (*m/z* 5798) were identified based on their individual masses. (The nomenclature of the proteolytic peptides is summarized in Figure 1.) The proteolytic peptides whose observance corresponds to cleavage at specific residues are summarized in Table 2. By identifying these peptides, proteolytic cleavage at all three lysine residues was observed within 5 min. On the basis of the results of the 1 min endoprotease Lys-C digestion (see Table 2), rapid cleavage at all lysine residues was observed.

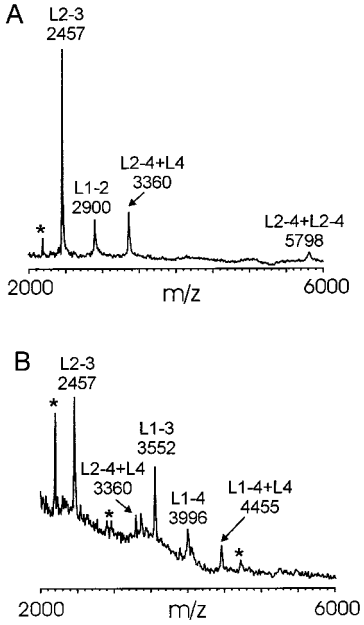

Figure 7. Positive ion MALDI mass spectra of the Lys-C reaction mixture after 5 min time. (A) GCN4-bR. (B) complex of GCN4-bR and 13-bp dsDNA. Molecular ions due to unspecific hydrolytic cleavage are labeled with an asterisk (*).

In comparison to the above, the MALDI/MS obtained from the Lys-C digestion of the complex of GCN4-bR and 13-bp dsDNA after 5 min reaction time is shown in Figure 7B. Singly charged molecule ions of the proteolytic

Table 2. Summary of the Time Course of the Differential Limited Proteolysis

enzyme	peptide bond[a]	identified proteolytic peptides[b]	reaction time for peptide bond cleavage[c]	
			GCN4-bR	GCN4-bR-13bp dsDNA
Lys-C	$K^{231}-R^{232}$	L1, L2, L2−3, L2−4 + L4, L2−4 + L2−4	1 min	1 min
	$K^{246}-L^{247}$	L2, L1−2	1 min	1 hr
	$K^{251}-Q^{252}$	L2−3, L2−4 + L4, L1−3, L1−4 + L4	1 min	2 min
Glu-C	$E^{223}-S^{224}$	A2	1 min	2 hr
	$E^{237}-A^{238}$	A2, A1−2, A3[d], A3 + A3, A1−3 + A3	1 min	1 min
Asp-N	$S^{225}-D^{226}$	D2[d], D2 + D2, D1−2 + D2	1 min	5 min

[a] Amino acid numbers refer to entire GCN4 peptide. [b] Digest fragment nomenclature refers to GCN4-bR peptide. [c] First identification of any peptide originating from cleavage of particular peptide bond. [d] Peptide from photolytic cleavage of disulfide bond.

peptides L2−3, L2−4 + L4, L1−3, and L1−4 + L4 at *m*/*z* 2457, 3360, 3552, and 4455 can be observed. Additionally, a peptide comprising an uncleaved peptide halfsite L1−4 was detected at *m*/*z* 3996. For the formation of this peptide, reduction of the disulfide bond must have taken place (Patterson and Katta, 1994). No peptides arising from cleavage of the Lys246−Leu247 peptide bond could be identified, leaving Lys231 and Lys251 as the only Lys-C sites cleaved in the complex. Additional peptides (labeled with an asterisk) were detected that were observed in a control experiment in which the enzyme was omitted.

All time-dependent differential limited proteolysis results are summarized in Table 2. The reaction time necessary to observe at least one peptide originating from the cleavage of a specific bond is given for both GCN4-bR and GCN4-bR complexed with 13-bp dsDNA. For Lys231, mapping by the peptides L1, L2, L2−3, L2−4 + L4, and L2−4 + L2−4 revealed rapid cleavage after 1 min for both sets of experiments, while for Lys251, characterized by peptides L2−3, L2−4 + L4, L1−3, and L1−4 + L4, a slight increase of the reaction from 1 min for GCN4-bR to 2 min for the peptide−DNA complex was determined. For Lys246, an increased reaction time from 1 min to 1 h upon complexing the peptide with dsDNA was observed based on the detection of peptide L2 (*m*/*z* 1799) at this time (data not shown).

Using Glu-C proteolysis, cleavage sites at Glu223 and Glu237 were characterized, and their reaction times determined by differential limited proteolysis. Reaction rates C-terminal to Glu223 were found to increase from 1 min for GCN4-bR to 2 h for the complex of GCN4-bR and 13-bp dsDNA. Rapid cleavage of the Glu237−Ala238 peptide bond within 1 min was observed for both the free and complexed GCN4-bR. The single cleavage site Ser225−Asp226 was characterized by endoprotease Asp-N digestion. For the nonbound peptide, rapid cleavage after 1 min was observed, while, for the peptide−DNA complex, the reaction time increased to 5 min.

Further experiments using proteolytic enzymes such as endoprotease Arg-C and trypsin were not successful because either peptides arising from specific enzymatic digestion and nonspecific hydrolytic cleavage were indistinguishable or peptides with different sequences had the same molecular weight, thus making their unambiguous identification impossible.

DISCUSSION

Electrospray ionization has recently allowed the detection of noncovalent complexes by mass spectrometry. In this report, we have investigated the noncovalent complexes formed between GCN4 peptides, GCN4-bR and GCN4−61, and dsDNA using ESI/MS. Under ionization conditions necessary for the observation of the tetramolecular complex between the GCN4−61 dimer and dsDNA, the absence of ions corresponding to the GCN4 peptide dimer or the GCN4 monomer with dsDNA indicates that the specific interaction of the dsDNA with the protein dimer stabilizes the noncovalent complex in the gas phase. These data are in agreement with circular dichroism (CD) studies (Weiss et al., 1990), which showed a significant increase in the α helical content for GNC4-p (58-residue DNA-binding domain of GNC4) bound to DNA relative to GCN4-p alone, although NMR data indicated that the lifetimes of the dimers were between 10 ms and 1 s. The helical content increased from ∼70% for the GCN4-p dimer to 95−100% for the DNA-bound conformation of GCN4-p. These authors suggest that the increase in helical content implies that the basic region adjacent to the leucine zipper in the GCN4-p dimer is largely unstructured in the absence of DNA. Upon DNA-binding, the protein undergoes a structural transition to a more stabilized conformation.

Weiss and co-workers (Weiss et al., 1990) also reported that the helical content of the complex saturated at a stoichiometry of two GCN4-p monomers per DNA site. From our mass spectral studies, the stoichiometry of the noncovalent complex can be easily determined from the measured mass of the complex. For the tetramolecular complexes, the ions in the mass spectra due to the noncovalent complexes correspond to a GCN4−61 dimer plus dsDNA. For the mass spectra of the noncovalent complexes of GCN4-bR and dsDNA, the ions correspond to monomeric GCN4-bR and dsDNA.

From the circular dichroism studies (Weiss et al., 1990), it was also reported that additional control experiments demonstrated that the folding transition of GCN4-p required formation of a specific complex. Likewise, the results of our control MS experiments addressing the specificity of the noncovalent interactions verify that the GCN4−DNA trimolecular and tetramolecular complexes reported in this paper are due to sequence-specific interactions between the dsDNA and the protein monomer or dimer.

The amount of charging that a biomolecule exhibits in an ESI mass spectrum has been correlated to a global solution structure. For example, disulfide-containing proteins show less average charging than their disulfide-reduced counterparts (Katta and Chait 1993; Loo et al., 1990a,b). This phenomenon is presumably due to either fewer charge sites exposed in the more-tightly bound configurations or that Coulombic restraints restrict charging for a more compact structure. It has been shown that the distribution of charge states in noncovalent complexes is typically low, e.g., 3−5 charge states (Loo, 1997). The ESI mass spectra of the GCN4−DNA complexes (Figures 3−6) show narrow charge envelopes for all combinations of the GCN4 peptides and the dsDNA. The narrow charge

distribution is consistent with the higher order structure of the noncovalent complex. These results in combination with the results of the stoichiometry of the noncovalent complexes suggest that, under the ionization conditions employed here, the interactions of the complexes in solution are reflected in the gas-phase electrospray mass spectra.

Chait and co-workers have shown that differential limited proteolysis with subsequent MS product idenfication can be used to characterize the role of individual amino acids in protein−DNA interactions (Cohen et al., 1995). We have applied this approach to the GCN4−dsDNA complex using the disulfide-linked GCN4-bR peptide as a model. The results of the differential limited proteolysis of the GCN4-bR-13-bp dsDNA showed that Lys231 and Glu237 underwent rapid cleavage after 1 min reaction time in both noncomplexed and 13-bp dsDNA-bound state. Thus, these amino acid residues must not only be highly susceptible to enzymatic digestion but are not affected by bound DNA. On the basis of these results, the Lys231 and Glu237 can be classified as not being involved in DNA binding by GCN4-bR. Furthermore, the digestion rates of the amino acid residues Lys251 and Asp226 increased from 1 min for the noncomplexed peptide to 2 and 5 min for the complex, respectively, indicating a minor change in protease susceptibility upon DNA interaction. In both cases, the signals of the peptide molecular ions used to characterize these residues were not very abundant. Thus, these two residues have to remain unclassified in terms of their role in DNA binding of GCN4-bR.

In contrast, reduced reactivities of the amino acid residues Lys246 and Glu223 from 1 min each to 1 and 2 h, respectively, were determined upon complexing GCN4-bR with the 13-bp dsDNA. On the basis of these results, it can be concluded that both amino acid residues are affected by DNA binding. There are, however, two possible explanations for these reduced reactivities: (i) the residues under investigation directly interact with the DNA, or (ii) they are not involved in binding but undergo conformational changes upon DNA complexation.

Thus, the results obtained by the differential limited proteolysis approach need to be evaluated by comparing them to those of other studies. For GCN4, several methods for the determination of the putative DNA-binding region have been published. In 1992, Asn235 in the GCN4 protein (Asn15 in GCN4-bR) was characterized as interacting with the specific DNA by mutagenesis (Tzamarias et al., 1992), whereas a similar role was determined for Ala239 (Ala19 in GCN4-bR) by photocross-linking (Blatter et al., 1992). One year later, additional mutagenesis results revealed the importance of the four amino acid residues Thr236−Ala239 (Thr16−Ala19 in GCN4-bR) in DNA binding (Suckow et al., 1993). Upon the basis of the X-ray structure of the specific protein−DNA complex they had solved, Ellenberger et al. supposed that the following amino acid residues may interact with the DNA: Lys246; Arg232, 234, 240, 241, 243, 245, and 249; Ala238 and 239; Asn235; Thr236; and Ser242 (Ellenberger et al., 1992). The identification of these residues, however, as a part of the DNA-binding site of GCN4 was solely based on the atomic distances determined from an X-ray structure.

Comparing these previously identified or supposed interacting amino acid residues with the results obtained in this study, the role of Lys246 for DNA binding was confirmed, while that of Glu223 was not. For the positively charged Lys246, an ionic interaction with a negatively charged phosphate group on the DNA is likely, whereas there is no interaction known between a negatively charged glutamate and the phosphate backbone. Furthermore, the highly susceptible amino acid residue Lys231 was not found to interact with DNA in agreement with our results. The residues which remained unclassified in this study due to their slightly decreased reactivity in the DNA complex, Asp226 and Lys251, have also not been related to any DNA-binding function. These results are in accordance with those already published. In contrast, Glu223 is the only amino acid residue which has not been characterized as part of the GCN4 DNA-binding site that showed reduced reactivity upon DNA binding in our studies. However, its position is some distance from the first residue of the supposed DNA-binding site, Arg232. Therefore, changes in reactivity may be due to conformational changes induced by DNA binding. The previously reported circular dichroism study (Weiss et al., 1990) does, in fact, indicate a significant increase in the α helical content of the peptide upon DNA binding. Additionally, our direct MS characterization of the complex further supports a highly ordered conformation of the peptide when bound to DNA. It should also be noted that the complex whose crystal structure was reported by Ellenberger did not include Glu223 as part of the peptide sequence (Ellenberger et al., 1992). In summary, the decrease in reactivity of Glu223 can thus be explained as due to a conformational change upon DNA binding.

CONCLUSIONS

In conclusion, ESI mass spectra of sequence-specific noncovalent complexes between dsDNA and GCN4 protein monomers and dimers are reported. The results presented here support conclusions that interaction of GCN4 with dsDNA stabilizes the protein conformation to a more ordered state. In addition, the stoichiometry of the noncovalent complex can be easily determined from the observed masses of the complexes. These data show that mass spectrometry can provide extremely useful information for the study of noncovalent complexes.

The ability to observe these supramolecular complexes by mass spectrometry with high mass accuracy and high sensitivity (picomoles per microliter are more than adequate) opens the door for utilizing this analytical technique for other structural biological problems, including determining the specific binding regions between dsDNA and proteins. Determination of the specific amino acids involved in DNA binding may provide key information to further understanding the mechanisms of transcription processes, the functional significance of the DNA−protein interactions, and requirements for specific DNA binding.

In general, the applicability of the differential limited proteolysis approach has been shown. Additionally, relating these results to those obtained by applying molecular biology techniques is important, especially when additional conformational changes need to be taken into consideration. We believe that, because of its ease and ruggedness, this mass spectrometric approach of characterizing amino acid residues involved in DNA binding will gain more importance in the future.

ACKNOWLEDGMENT

This work has been partially supported by grants from the Deutsche Forschungsgemeinschaft, Bonn, Germany (T.M.P.), and the Fonds der Chemischen Industrie.

LITERATURE CITED

(1) Abel, T., and Maniatis, T. (1989) Action of leucine zippers. *Nature 341*, 24−25.

(2) Baca, M., and Kent, S. B. H. (1992) Direct observation of a ternary complex between the dimeric enzyme HIV-1 protease and a substrate-based inhibitor. *J. Am. Chem. Soc. 114*, 3992−3993.

(3) Bayer, E., Bauer, T., Schmeer, K., Bleicher, K., Maier, M., and Gaus, H.-J. (1994) Analysis of double-stranded oligonucleotides by electrospray mass spectrometry. *Anal. Chem. 66*, 3858−3863.

(4) Blatter, E. E., Ebright, Y. W., Ebright, R. H. (1992) Identification of an amino acid−base contact in the GCN4-DNA complex by bromouracil-mediated photo-cross-linking. *Nature 359*, 650−652.

(5) Brockerhoff, S. E., Edmonds, C. G., and Davis, T. N. (1992) Structural analysis of wild-type and mutant yeast proteolysis and electrospray ionization mass spectrometry. *Protein Sci. 1*, 504−516.

(6) Cheng, X., Harms, A. C., Goudreau, P. N., Terwilliger, T. C., and Smith, R. D. (1996a) Direct measurement of oligonucleotide binding stoichiometry of gene V protein by mass spectrometry. *Proc. Natl. Acad. Sci. U.S.A. 93*, 7022−7027.

(7) Cheng, X., Morin, P. E., Harms, A. C., Bruce, J. E., Ben-David, Y., and Smith, R. D. (1996b) Mass spectrometric characterization of sequence-specific complexes of DNA and transcription factor PU.1 DNA binding domain. *Anal. Biochem. 239*, 35−40.

(8) Cohen, S. L., Ferré, D., Amaré, A. R., Burley, S. K., and Chait, B. T. (1995) Probing the solution structure of the DNA-binding protein Max by a combination of proteolysis and mass spectrometry. *Protein Sci. 4*, 1088−1099.

(9) Deterding, L. J., Kast, J., Przybylski, M., and Tomer, K. B. (1998) Mass spectrometric characterization of a tetramolecular complex between dsDNA and a DNA-binding leucine zipper peptide dimer. *Proceedings of the 46th ASMS Conference on Mass Spectrometry and Allied Topics*, Orlando, Florida, May 31−June 4, 274.

(10) Ding, J., and Anderegg, R. J. (1995) Specific and nonspecific dimer formation in the electrospray ionization mass spectrometry of oligonucleotides. *J. Am. Soc. Mass Spectrom. 6*, 159−164.

(11) Ellenberger, T. E., Brandl, C. J., Struhl, K., and Harrison, S. C. (1992) The GCN4 basic region leucine zipper binds DNA as a dimer of uninterrupted α helices: Crystal structure of the protein-DNA complex. *Cell 71*, 1223−1237.

(12) Gale, D. C., Goodlett, D. R., Light-Wahl, K. J., and Smith, R. D. (1994) Observation of duplex DNA-drug noncovalent complexes by electrospray ionization mass spectrometry. *J. Am. Chem. Soc. 116*, 6027−6028.

(13) Gale, D. C., and Smith, R. D. (1995) Characterization of noncovalent complexes formed between minor groove binding molecules and duplex DNA by electrospray ionization-mass spectrometry. *J. Am. Soc. Mass Spectrom. 6*, 1154−1164.

(14) Gentz, R., Rauscher, F. J., Abate, C., and Curran, T. (1989) Parallel association of fos and jun leucine zippers juxtaposes DNA binding domains. *Science 243*, 1695−1699.

(15) Hill, D. E., Hope, I. A., Macke, J. P., and Struhl, K. (1986) Saturation mutagenesis of the yeast his3 regulatory site: Requirements for transcriptional induction and for binding by GCN4 activator protein. *Science 234*, 451−457.

(16) Hinnebusch, A. G. (1984) Evidence for translational regulation of the activator of general amino acid control in yeast. *Proc. Natl. Acad. Sci. U.S.A. 81*, 6442−6446.

(17) Hope, I. A., and Struhl, K. (1985) GCN4 protein, synthesized in vitro, binds HIS3 regulatory sequences: Implications for general control of amino acid biosynthetic genes in yeast. *Cell 43*, 177−188.

(18) Hope, I. A., and Struhl, K. (1986) Functional dissection of a eukaryotic transcriptional activator protein, GCN4 of yeast. *Cell 46*, 885−894.

(19) Hope, I. A., and Struhl, K. (1987) GNC4, a eukaryotic transcriptional activator protein, binds as a dimer to target DNA. *EMBO J. 6* (9), 2781−2784.

(20) Huang, E. C., Pramanik, B. N., Tsarbopoulos, A., Richert, P., Ganguly, A. K., Trotta, P. P., and Nagabhushan, T. L. (1993) Application of electrospray mass spectrometry in probing protein-protein and protein-ligand noncovalent interactions. *J. Am. Soc. Mass Spectrom. 4*, 624−630.

(21) Hurst, H. (1996) *Leucine Zippers Transcription Factors*, Academic Press Inc., San Diego.

(22) Katta, V., and Chait, B. T. (1993) Hydrogen/deuterium exchange electrospray ionization mass spectrometry−A method for probing protein conformational changes in solution. *J. Am. Chem. Soc. 115*, 6317−6321.

(23) Kriwacki, R. W., Wu, J., Tennant, L., Wright, P. E., and Siuzdak, G. (1997) Probing protein structure using biochemical and biophysical methods. Proteolysis, matrix-assisted laser desorption/ionization mass spectrometry, high-performance liquid chromatography and size-exclusion chromatography of p21Waf1/Cip1/Sdi1. *J. Chromatogr. A 777*, 23−30.

(24) Landschulz, W. H., Johnson, P. F., and McKnight, S. L. (1988) The leucine zipper: A hypothetical structure common to a new class of DNA binding proteins. *Science 240*, 1759−1764.

(25) Landschulz, W. H., Johnson, P. F., McKnight, S. L. (1989) The DNA binding domain of the rat liver nuclear protein C/EBP is dipartite. *Science 243*, 1681−1688.

(26) Light-Wahl, K. J., Springer, D. L., Winger, B. E., Edmonds, C. F., Camp, D. G., II, Thrall, B. D., and Smith, R. D. (1993) Observation of a small oligonucleotide duplex by electrospray ionization mass spectrometry. *J. Am. Chem. Soc. 115*, 803−804.

(27) Loo, J. A., Edmonds, C. G., and Smith, R. D. (1990a) Primary sequence information from intact proteins by electrospray ionization tandem mass spectrometry. *Science 248*, 201−204.

(28) Loo, J. A., Edmonds, C. G., Udseth, H. R., and Smith, R. D. (1990b) Effect of reducing disulfide-containing proteins on electrospray mass spectra. *Anal. Chem. 62*, 693−698.

(29) Loo, J. A. (1997) Studying noncovalent protein complexes by electrospray ionization mass spectrometry. *Mass Spectrom. Rev. 16*, 1−23.

(30) Miranker, A., Robinson, C. V., Radford, S. E., and Dobson, C. M. (1996) Investigation of protein folding by mass spectrometry. *FASEB J. 10*, 93−101.

(31) O'Neill, K. T., Hoess, R. H., and DeGrado, W. F. (1990) Design of DNA-binding peptides based on the leucine zipper motif. *Science 249*, 774−778.

(32) O'Shea, E. K., Rutkowski, R., and Kim, P. S. (1989a) Evidence that the leucine zipper is a coiled coil. *Science 243*, 538−542.

(33) O'Shea, E. K., Rutkowski, R., Stafford, W. F., III, and Kim, P. S. (1989b) Preferential heterodimer formation by isolated leucine zippers from fos and jun. *Science 245*, 646−648.

(34) O'Shea, E. K., Klemm, J. D., Kim, P. S., and Alber, T. (1991) X-ray structure of the GCN4 leucine zipper, a two-stranded, parallel coiled coil. *Science 254*, 539−544.

(35) Oas, T. F., McIntosh, L. P., O'Shea, E. K., Dahlquist, F. W., and Kim, P. S. (1990) Secondary structure of a leucine zipper determined by nuclear magnetic resonance spectroscopy. *Biochemistry 29*, 2891−2894.

(36) Patterson, S. D., and Katta, V. (1994) Prompt fragmentation of disulfide-linked peptides during matrix-assisted laser desorption ionization mass spectrometry. *Anal. Chem. 66*, 3727−32.

(37) Penn, M. D., Galgoci, B., and Greer, H. (1983) Identification of *AAS* genes and their regulatory role in general control of amino acid biosynthesis in yeast. *Proc. Natl. Acad. Sci. U.S.A. 80*, 2704−2706.

(38) Pócsfalvi, G., Di Landa, G., Ferranti, P., Ritieni, A., Randazzo, G., and Malorni, A. (1997) Observation of noncovalent interactions between beauvericin and oligonucleotides using electrospray ionization mass spectrometry. *Rapid Commun. Mass Spectrom. 11*, 265−272.

(39) Polverino de Laureto, P., De Filippis, V., Di Bello, M., Zambonin, M., and Fontana, A. (1995) Probing the molten globule state of alpha-lactalbumin by limited proteolysis. *Biochemistry 34*, 12596−12604.

(40) Potier, N., Donald, L. J., Chernushevich, I., Ayed, A., Ens, W., Arrowsmith, C. H., Standing, K. G., and Duckworth, H. W. (1998) Study of a noncovalent trp repressor:DNA operator complex by electrospray ionization time-of-flight mass spectrometry. *Protein Sci. 7*, 1388−1395.
(41) Przybylski, M., Kast, J., Glocker, M. O., Dürr, E., Bosshard, H. R., Nock, S., and Sprinzl, M. (1995) Mass spectrometry approaches to molecular characterization of protein-nucleic acid interactions. *Toxicol. Lett. 82/83*, 567−575.
(42) Przybylski, M., and Glocker, M.O. (1996) Electrospray mass spectrometry of noncovalent complexes of biomacromolecules-New analytical perspectives for supramolecular chemistry and molecular recognition processes. *Angew. Chem. 35*, 807−826.
(43) Rasmussen, R., Benvegnu, D., O'Shea, E. K., Kim, P. S., and Alber, T. (1991) X-ray scattering indicates that the leucine zipper is a coiled coil. *Proc. Natl. Acad. Sci. U.S.A. 88*, 561−564.
(44) Saenger, W. (1984) *Principles of Nucleic Acid Structure*, Springer-Verlag, New York.
(45) Schuermann, M., Neuberg, M., Hunter, J. B., Jenuwein, T., Ryseck, R. P., Bravo, R., and Muller, R. (1989) The leucine repeat motif in Fos protein mediates complex formation with Jun/AP-1 and is required for transformation. *Cell 56*, 507−516.
(46) Schwartz, B. L., Light-Wahl, K. J., and Smith, R. D. (1994) Observation of noncovalent complexes to the avidin tetramer by electrospray ionization mass spectrometry. *J. Am. Soc. Mass Spectrom. 5*, 201−204.
(47) Siuzdak, G., Krebs, J. F., Benkovic, S. J., and Dyson, H. J. (1994) Binding of hapten to a single-chain catalytic antibody demonstrated by electrospray mass spectrometry. *J. Am. Chem. Soc. 116*, 7937−7938.
(48) Struhl, K. (1987) The DNA-binding domains of the jun oncoprotein and the yeast GCN4 transcriptional activator protein are functionally homologous. *Cell 50*, 841−846.
(49) Suckau, D., Kohl, J., Karwath, G., Schneider, K., Casaretto, M., Bitter-Suermann, D., and Przybylski, M. (1990) Molecular epitope identification by limited proteolysis of an immobilized antigen−antibody complex and mass spectrometric peptide mapping. *Proc. Natl. Acad. Sci. U.S.A. 87*, 9848−9852.
(50) Suckow, M., von Wilcken-Bergmann, B., and Müller-Hill, B. (1993) Identification of three residues in the basic regions of the bZIP proteins GCN4, C/EBP and TAF-1 that are involved in specific DNA binding. *EMBO J. 12*, 1193−1200.
(51) Talanian, R. V., McKnight, C. J., and Kim, P. S. (1990) Sequence-specific DNA binding by a short peptide dimer. *Science 249*, 769−771.
(52) Thireos, G., Penn, M. D., and Greer, H. (1984) 5′ untranslated sequences are required for the translational control of a yeast regulatory gene. *Proc. Natl. Acad. Sci. U.S.A. 81*, 5096−5100.
(53) Tomer, K. B., Moseley, M. A., Deterding, L. J., and Parker, C. E. (1994) Capillary liquid chromatography/mass spectrometry. *Mass Spectrom. Rev. 13*, 431−457.
(54) Triolo, A., Arcamone, F. M., Raffaelli, A., and Salvadori, P. (1997) Noncovalent complexes between DNA-binding drugs and double-stranded deoxyoligonucleotides: A study by ionspray mass spectrometry. *J. Mass Spectrom. 32*, 1186−1194.
(55) Turner, R., and Tjian, R. (1989) Leucine repeats and an adjacent DNA binding domain mediate the formation of functional cFos-cJun heterodimers. *Science 243*, 1689−1694.
(56) Tzamarias, D., Pu, W. T., and Struhl, K. (1992) Mutations in the bZIP domain of yeast GCN4 that alter DNA-binding specificity. *Proc. Natl. Acad. Sci. U.S.A. 89*, 2007−2011.
(57) Veenstra, T., Benson, L. M., Craig, T. A., Tomlinson, A. J., Kumar, R., and Naylor, S. (1998) Metal mediated sterol receptor-DNA complex association and dissociation determined by electrospray ionization mass spectrometry. *Nat. Biotechnol. 16*, 262−266.
(58) Vinson, C. R., Sigler, P. B., and McKnight, S. L. (1989) Scissors-grip model for DNA recognition by a family of leucine zipper proteins. *Science 246*, 911−916.
(59) Vogt, P. K., and Bos, T. J. (1989) The oncogen jun and nuclear signaling. *Trends Biochem. Sci. 14*, 172−175.
(60) Weiss, M. A., Ellenberger, T., Wobbe, C. R., Lee, J. P., Harrison, S. C., and Struhl, K. (1990) Folding transition in the DNA-binding domain of GCN4 on specific binding to DNA. *Nature 347*, 575−578.
(61) Wendt, H., Dürr, E., Thomas, R. M., Przybylski, M., and Bosshard, H. R. (1995) Characterization of leucine zipper complexes by electrospray ionization mass spectrometry. *Protein Sci. 4*, 1563−70.
(62) Zappacosta, F., Pessi, A., Bianchi, E., Venturini, S., Sollazzo, M., Tramontano, A., Marino, G., and Pucci, P. (1996) Probing the tertiary structure of proteins by limited proteolysis and mass spectrometry: the case of Minibody. *Protein Sci. 5*, 802−813.

BC990123C

Influence of the Denticity of Ligand Systems on the in Vitro and in Vivo Behavior of ^{99m}Tc(I)−Tricarbonyl Complexes: A Hint for the Future Functionalization of Biomolecules

Roger Schibli,[†] Roberto La Bella,[†] Roger Alberto,[‡] Elisa Garcia-Garayoa,[†] Kirstin Ortner,[‡] Ulrich Abram,[§] and P. A. Schubiger*[,†]

Center for Radiopharmaceutical Science of the ETH Zürich, Paul Scherrer Institute, CH-5232 Villigen, Switzerland, Department of Inorganic Chemistry, University of Zürich, CH-8057 Zürich, Switzerland, Forschungszentrum Rossendorf, Institut für Radiochemie, D-01062 Dresden, Germany. Received October 1, 1999; Revised Manuscript Received January 20, 2000

Functionalization of biologically relevant molecules for the labeling with the novel *fac*-[^{99m}Tc(OH$_2$)$_3$(CO)$_3$]$^+$ precursor has gained considerable attention recently. Therefore, we tested seven different tridentate (histidine **L^1**, iminodiacetic acid **L^2**, *N*-2-picolylamineacetic acid **L^3**, *N*,*N*-2-picolylaminediacetic acid **L^4**) and bidentate (histamine **L^5**, 2-picolinic acid **L^6**, 2,4-dipicolinic acid **L^7**) ligand systems, with the potential to be bifunctionalized and attached to a biomolecule. The ligands allowed mild radiolabeling conditions with *fac*-[^{99m}Tc(OH$_2$)$_3$(CO)$_3$]$^+$ (30 min, 75 °C). The ligand concentrations necessary to obtain yields of >95% of the corresponding organometallic complexes **1**-**7** ranged from 10^{-6} to 10^{-4} M. Complexes of the general formula "*fac*-[^{99m}TcL(CO)$_3$]" (L = tridentate ligand) and "*fac*-[^{99m}Tc(OH$_2$)L′(CO)$_3$]" (L′ = bidentate ligand), respectively, were produced. Challenge studies with cysteine and histidine revealed significant displacement of the ligands in complexes **5**−**7** but only little exchange with complexes **1**−**4** after 24 h at 37 °C in PBS buffer. However, no decomposition to ^{99m}TcO$_4^-$ was observed under these conditions. All complexes showed a hydrophilic character (log $P_{o/w}$ values ranging from −2.12 to 0.32). Time-dependent FPLC analyses of compounds **1**−**7** incubated in human plasma at 37 °C showed again no decomposition to ^{99m}TcO$_4^-$ after 24 h at 37 °C. However, the complexes with bidentate ligands (**5**−**7**) became almost completely protein bound after 60 min, whereas the complexes with tridentate coordinated ligands (**1**−**4**) showed no reaction with serum proteins. The compounds were tested for their in vivo stability and the biodistribution characteristics in BALB/c mice. The complexes with tridentate coordinated ligand systems (**1**−**4**) revealed generally a good and fast clearance from all organs and tissues. On the other hand, the complexes with only bidentate coordinated ligands (**5**−**7**) showed a significantly higher retention of activity in the liver, the kidneys, and the blood pool. Detailed radiometric analyses of murine plasma samples, 30 min p.i. of complex *fac*-[^{99m}TcL^1(CO)$_3$], **1**, revealed almost no reaction of the radioactive complex with the plasma proteins. By contrast, in plasma samples of mice, which were injected with complex *fac*-[^{99m}Tc(OH$_2$)L^5(CO)$_3$]$^+$, **5**, the entire radioactivity coeluded with the proteins. On the basis of these in vitro and in vivo experiments, it appears that functionalization of biomolecules with tridentate-chelating ligand systems is preferable for the labeling with *fac*-[^{99m}Tc(OH$_2$)$_3$(CO)$_3$]$^+$, since this will presumably result in radioactive bioconjugates with better pharmacokinetic profiles.

INTRODUCTION

Beside the established techniques and strategies for the functionalization and radiolabeling of target specific biomolecules with ^{99m}Tc or $^{186/188}$Re, using tetradentate N, S containing bifunctional chelating agents (*1*−*3*) or the HYNIC system (*4*, *5*), the "organometallic approach" pioneered by Jaouen and co-workers (*6*, *7*) is still in its infancy. Nevertheless, organometallic technetium and rhenium complexes in low oxidation states have gained considerable attention in the development of novel, target-specific radiopharmaceuticals in the recent years (*8*−*10*). The reasons are primarily the outstanding features of the corresponding compounds in terms of reduced size and kinetic inertness of the complexes. In particular, Tc(I)− and Re(I)−tricarbonyl complexes seem to be ideal candidates for the labeling of receptor avid biomolecules. The Tc/Re-tricarbonyl core allows the labeling of even smallest biomolecules with high specific activities under retention of the biological activity and specificity (*9*). However, especially the early approaches to produce ^{99m}Tc/^{188}Re−tricarbonyl complexes suffer from the feasibility to be performed in a routine clinical environment due to high pressure and multistep syntheses (*10*, *11*). This drawback can now be circumvented by a convenient and fully aqueous-based kit preparation of the organometallic precursor *fac*-[M(OH$_2$)$_3$(CO)$_3$]$^+$, M = ^{99m}Tc, $^{186/188}$Re, developed in our laboratories (*12*). This precursor is not only readily water-soluble but reveals good stability in aqueous solutions over a broad pH range (pH 2−12) for several hours. The three water molecules coordinated to the highly inert *fac*-[M(CO)$_3$]-core are readily substituted by a variety of functional groups such as amines, thioethers, thiols, and phosphines. This could be representatively shown by numerous substitution reactions with mono-, bi-, and tridentate ligand systems

* To whom correspondence should be addressed. Telephone: ++41-56-310-2813. Fax: ++41-56-310-2849. E-mail: schubiger@psi.ch.

[†] Center for Radiopharmaceutical Science.

[‡] Department of Inorganic Chemistry.

[§] Forschungszentrum Rossendorf.

10.1021/bc990127h CCC: $19.00 © 2000 American Chemical Society
Published on Web 04/07/2000

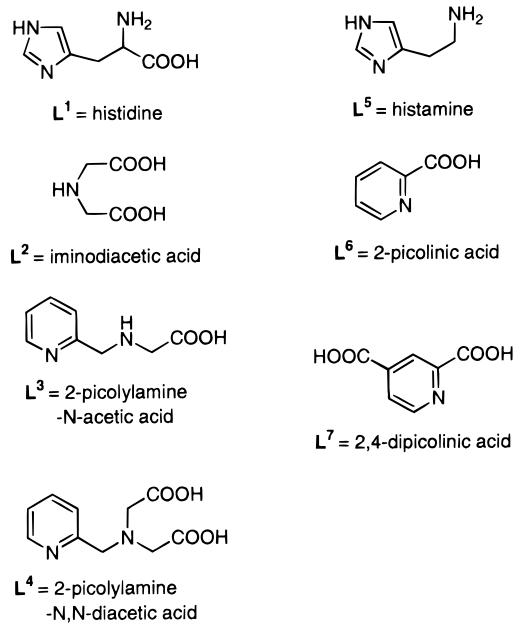

Figure 1. Structures of tridentate and bidentate ligand systems used for the present studies.

on the macroscopic level (*13*−*16*). However, organometallic complexes have an almost unknown in vitro and in vivo behavior. Therefore, a fundamental study of the in vitro and in vivo characteristics of *fac*-$M(CO)_3^+$ complexes is essential for the systematic development of appropriate derivatization and functionalization strategies of biomolecules.

Previous in vitro studies on the macroscopic and nca level suggested that ideal chelating systems for the precursor *fac*-$[^{99m}Tc(OH_2)_3(CO)_3]^+$ (**1**) in respect of a potential radiopharmaceutical application should contain one or more amine (preferentially aromatic N-heterocycles) functionalities in combination with a carboxylic acid function (*12*, *17*). Ligands with a corresponding motif are not only easy to synthesize but are actually occurring in many biological systems (e.g., histidine in proteins and peptides). This will be one of the decisive advantages of the labeling technique using the ^{99m}Tc-carbonyl approach.

To evaluate potential chelating systems for the formation of in vitro and in vivo stable *fac*-$^{99m}Tc(CO)_3^+$ complexes, we choose several bi- and tridentate model ligands containing amines and carboxylic acid functionalities (Figure 1). The selection of the chelating systems was governed by the criteria for use in radiopharmacy: (a) potential to be readily bifunctionalized; (b) efficient complex formation (low ligand concentration, formation of single species), (c) fast complex formation (reaction time max. 30 min) under mild reaction conditions for the complex formation.

Since pharmacokinetics and biodistribution of ^{99m}Tc(I)−tricarbonyl complexes have not yet been systematically investigated, no information about the correlation between in vivo behavior of corresponding complexes and their size, denticity, and lipophilicity/hydrophilicity is available. The ligand systems, which satisfy the abovementioned basic prerequisites (a−c), were tested in vitro and in vivo in order to get a general insight in the (i) in vivo stability of corresponding organometallic complexes, (ii) biodistribution, route, and rate of clearance of these compounds.

EXPERIMENTAL PROCEDURES

Materials and Methods. All chemicals were purchased from Aldrich Chemical Co. or Fluka, Buchs, Switzerland. The chemicals and solvents were of reagent grade and used without further purification. The precursors $(NEt_4)_2[^{99}TcCl_3(CO)_3]$ and $(NEt_4)_2[ReBr_3(CO)_3]$ are synthesized according to the previously published procedure (*13*). $Na[^{99m}TcO_4]$ was eluted from a $^{99}Mo/^{99m}Tc$ generator (Mallinckrodt, Petten, The Netherlands) using 0.9% saline. Female, adult BALB/c mice were purchased from RCC Ltd., Fuellinsdorf, Switzerland. HPLC analyses were performed on a Merck-Hitachi L-7000-system equipped with an L-7400 tunable absorption detector, a Berthold LB 506 B radiometric detector. HPLC solvents consisted of aqueous 0.05 M TEAP (triethylammonium phosphate) buffer, pH 2.25 (solvent A) and methanol (solvent B). For the radiochemical analyses, a Macherey-Nagel C-18 reversed-phase column (10 μm, 150 × 4.1 mm) was used. The HPLC system started with 100% of A from 0 to 3 min. The eluent switched at 3 min to 75% A and 25% B and at 9 min to 66% A and 34% B followed by a linear gradient 66% A/34% B to 100% B from 9 to 20 min. The gradient remained at 100% B for 2 min before switching back to 100% A. The flow rate was 1 mL/min. For the plasma stability studies, a Pharmacia Superdex 200 size-exclusion column (250 mm, 10 μm) and a Pharmacia Superose 12 size-exclusion column (300 mm, 10 μm) were used. The eluent used was PBS buffer (0.1 M NaCl/0.05 M sodium phosphate buffered, pH 7.4) with 0.05% Tween 20. The thin-layer chromatography (TLC) system was performed using glass-backed silica gel (Merck $60F_{254}$) plates and a mobile phase of 99%/1% concentrated HCl. The plates were scanned with a Burkard RAYTEST RITA-3200 radioanalyzer. Nuclear magnetic resonance spectra were recorded on a 300 MHz Varian Gemini 2000 spectrometer. The ^{1}H and ^{13}C chemical shifts are reported relative to residual solvent protons as a reference. IR spectra were recorded on a Perkin-Elmer FT-IR 16PC using KBr pellets.

Preparation of *fac*-$[^{99m}Tc(OH_2)_3(CO)_3]^+$. The organometallic precursor was prepared according to the literature procedure (*12*). Briefly, Na/K-tartrate (15 mg), Na_2CO_3 (4 mg), and $NaBH_4$ (5.5 mg) were placed in a 10 mL glass vial or a 10 mL serum vial. The vial was sealed and flushed with CO for 20 min. The generator eluate (3 mL, 5−8 GBq/mL) was added. The vial was incubated at 75 °C for 30 min. Pressure from the evolving H_2 gas was balanced with a 20 mL syringe. After cooling on an ice bath, 300 μL of a solution of 1 M phosphate buffer, pH 7.4/1 N HCl (1:2) was added to adjust the pH to approximately 7. Yield: >98% determined by means of HPLC and TLC.

Preparation of the Complexes 1−7. The complexes **1**−**7** were prepared according to the following general procedure: 900 μL of a solution of *fac*-$[^{99m}Tc(OH_2)_3(CO)_3]^+$ and 100 μL of a 10^{-3}, 10^{-4}, and 10^{-5} M solution of the corresponding ligand in PBS buffer (0.1 M NaCl/0.05 M sodium phosphate buffered, pH 7.4) were placed in a 10 mL glass vial under nitrogen. The vial was sealed, and the reaction heated to 75 °C for 30 min and cooled on an ice bath. The complex formation was checked by HPLC.

Preparation of the ^{99}Tc/Re Analogues of the Complexes 1−7. The complex *fac*-$[^{99}Tc(L^4)(CO)_3]$ was prepared according to the previously published procedure (*12*). Synthesis of the complex *fac*-$[Re(OH_2)(L^5)(CO)_3]^+$ will be published elsewhere (*17*). The complexes *fac*-$[Re(L^1)(CO)_3]$, *fac*-$[Re(L^3)(CO)_3]$, *fac*-$[Re(OH_2)(L^6)(CO)_3]$, and *fac*-$[Re(OH_2)(L^7)(CO)_3]$ were synthesized according to the following protocol. To 5 mL of a 25 mM aqueous

solution of $(NEt_4)_2[ReBr_3(CO)_3]$ was added 2 equivalents of the corresponding ligand, and the reaction was stirred for 3 h at 70 °C. Then, the volume of the reaction solution was reduced to 1.5 mL under vacuum. After 12 h at 5 °C, the analytically pure products precipitated either as white (*fac*-$[Re(L^1)(CO)_3]$ and *fac*-$[Re(L^3)(CO)_3]$) or bright yellow (*fac*-$[Re(OH_2)(L^6)(CO)_3]$ and *fac*-$[Re(OH_2)(L^7)(CO)_3]$) powders in yields between 68 and 87%. Crystals of complex *fac*-$[Re(L^1)(CO)_3]$ suitable for X-ray analyses were grown from a hot, saturated aqueous solution upon cooling to room temperature. Crystals of compound *fac*-$[Re(OH_2)(L^6)(CO)_3]$ were grown from D_2O in a NMR tube upon cooling at 5 °C for 2 days.

Analytical Data for Complex fac-[Re(L¹)(CO)₃]. ^{1}H NMR (DMSO-d_6): δ 8.26 (m, 1 H), 7.21 (m, 1 H), 5.88 (broad s, 1 H), 5.19 (broad s, 2 H), 3.84 (dd, 1 H), 3.16 (t, 2 H). ^{13}C NMR (DMSO-d_6): δ 199.3, 197.5, 180.8, 140.1, 133.8, 115.6, 51.2, 27.3. IR (KBr, cm^{-1}): 3334 (m), 3150 (m), 3112 (m), 2022 (vs), 1894 (vs), 1856 (vs), 1642 (m), 1618 (s), 1492 (w), 1380 (m), 1318 (w), 1220 (w), 1160 (w), 1086 (w), 894 (w), 776 (w), 626 (w), 534 (w).

Analytical Data for Complex fac-[Re(L³)(CO)₃]. ^{1}H NMR (DMSO-d_6): δ 8.86 (m, 1 H), 8.22 (m, 1 H), 7.84 (m, 1 H), 7.65 (m, 1 H), 4.69 (dd, 1 H), 4.56 (dd, 1 H), 3.68 (dd, 1 H), 3.50 (dd, 1 H). ^{13}C NMR: δ 192.8, 192.7, 182.3, 168.2, 161.5, 156.2, 142.6, 126.1, 124.8, 65.1, 62.4. IR (KBr, cm^{-1}): 3904 (w), 3424 (m), 2022 (vs), 1912 (vs), 1874 (vs), 1614 (s), 1442 (m), 1380 (m), 1298 (w), 1092 (w), 942 (w), 770 (w), 550 (w).

Analytical Data for Complex fac-[Re(OH₂)(L⁶)(CO)₃]. ^{1}H NMR (MeOH-d_4): δ 9.07 (m, 1 H), 8.45 (m, 2 H), 8.00 (m, 1 H). ^{13}C NMR (MeOH-d_4): δ 198.8, 197.8, 194.8, 191.9, 154.0, 141.5, 141.2, 130.5, 128.8. IR (KBr, cm^{-1}): 3100 (w), 2028 (vs), 1912 (vs), 1874 (vs), 1684 (s), 1602 (m), 1360 (m), 1170 (w), 768 (m), 692 (w).

Analytical Data for Complex fac-[Re(OH₂)(L⁷)(CO)₃]. ^{1}H NMR (MeOH-d_4): δ 9.03 (m, 1 H), 8.62 (m, 1 H), 8.27 (m, 1 H). IR (KBr, cm^{-1}): 3210 (m), 3064 (w), 2038 (vs), 1919 (vs), 1734 (s), 1672 (s), 1612 (m), 1560 (m), 1438 (w), 1240 (m), 1172 (m), 964 (w), 770 (w), 714 (w), 632 (w). ^{13}C NMR (MeOH-d_4): δ 192.8, 192,5, 191.4, 185.8, 160.2, 148.4, 146.5, 136.8, 123.0, 121.1.

Preparation of Complexes $[NEt_4][Re(L^2)(CO)_3]$. To a methanolic solution (5 mL) of disodium iminodiacetate (17 mg, 0.1 mmol) was added $(NEt_4)_2[ReBr_3(CO)_3]$ (71 mg, 0.1 mmol), and the reaction was heated for 3 h at 50 °C. After removal of the solvent, the product was extracted into THF. The solvent was evaporated, and white product was dried in vacuum. Yield: 33 mg (67%). ^{1}H NMR (D_2O): δ 3.78 (d, 2H), 3.37 (d, 2H), 3.14 (q, 8 H), 1.15 (tt, 12 H). ^{13}C NMR (D_2O): δ 192.1, 179.8, 50.9, 47.4, 2.0. IR (KBr, cm^{-1}): 3340 (w), 2770 (w) 2028 (vs), 1916 (vs) 1610 (s), 1488 (m), 1442 (m), 1380 (m), 1094 (w), 872 (w), 773 (w), 596 (w).

Cysteine and Histidine Challenge. To 900 μL of a 10^{-3} M cysteine solution and 900 μL of a 10^{-3} M histidine solution in PBS (pH 7.4), were added 100 μL aliquots of the ^{99m}Tc complex (final ligand concentration 10^{-5} M). The samples were incubated at 37 °C and analyzed by means of HPLC after 1, 4, and 24 h.

Octanol−Water Partition Coefficient. The log $P_{o/w}$ values of the complexes **1**−**7** were determined applying the multiple back extraction method described by Troutner et al. (*18*).

In Vitro Plasma Stability. The solutions of the complexes **1**−**7** were adjusted with physiological saline to a concentration of 37 MBq/mL. Aliquots of 25 μL of these solutions were added to 475 μL human plasma and incubated at 37 °C. In case of complexes **1**−**4**, aliquots were taken and analyzed after 1, 4, and 24 h. In case of complexes **5**−**7**, aliquots of 80 μL were taken and analyzed by size-exclusion FPLC (Superdex 200 column) after 5, 15, 30, 60, min and 24 h of incubation.

Table 1. HPLC Retention Times (RT) and log $P_{o/w}$ Values of Complexes 1−7; (RT of Corresponding ^{99}Tc and Re Complexes Monitored at 254 nm)

complex	RT (min)	log $P_{o/w}$
1	12.5 (12.7)	−0.04 ± 0.01
2	12.9 (13.4)	−2.12 ± 0.01
3	17.7 (18.0)	−0.01 ± 0.00
4	18.1 (18.7)	−2.10 ± 0.02
5	14.3 (13.8)	−0.74 ± 0.06
6	18.6 (18.4)	0.32 ± 0.07
7	17.9 (17.3)	−1.51 ± 0.04

Table 2. Stability of Complexes 1−7 (%[a]) against Ligand Exchange in 1 mM Histidine and Cysteine in PBS Buffer at 37°C

	ex. histidine			ex. cysteine		
complex	1 h	4 h	24 h	1 h	4 h	24 h
1				98 ± 1	97 ± 1	95 ± 2
2	95 ± 1	85 ± 6	80 ± 5	96 ± 1	90 ± 2	85 ± 2
3	94 ± 2	92 ± 2	87 ± 5	95 ± 3	93 ± 4	90 ± 5
4	98 ± 2	97 ± 3	93 ± 3	98 ± 2	98 ± 1	96 ± 3
5	85 ± 5	80 ± 7	58 ± 4	90 ± 4	82 ± 2	70 ± 4
6	80 ± 2	68 ± 4	50 ± 7	83 ± 2	80 ± 2	65 ± 6
7	75 ± 6	62 ± 7	52 ± 2	78 ± 4	70 ± 2	60 ± 3

[a] Values represent the means ±SD (n = 3).

In Vivo Plasma Stability of the Complexes 1 and 5. To evaluate the in vivo plasma stability of the complexes **1** and **5**, aliquots of 500 μL of the blood of sacrificed BALB/c mice (30 min p.i.) were collected. The blood was centrifuged at 10 000 rpm for 4 min. The plasma was separated and analyzed by size-exclusion FPLC (Superose 12 column).

Biodistribution of ^{99m}Tc-Carbonyl Complexes. Female, adult BALB/c mice (average weight, 25 g) were used for the biodistribution studies. The complex solutions were diluted and their pH adjusted to physiological conditions with PBS buffer. Aliquots of 100 μL of the complex solution (3−4 MBq) were injected in each animal via the tail vein. Tissues and organs were excised from the sacrificed animals at 24 h (Table 2). Additional time points (at 15 min, 30 min, and 1 h p.i.) were analyzed for complexes **1** and **5** (Tables 4 and 5). The organs and tissues were weighed, the activity counted in a Packard NaI γ counter and the percent injected dose per gram (% ID/g) calculated.

RESULTS AND DISCUSSION

All ligand systems formed well-defined complexes with a metal-to-ligand ratio of 1:1 (Scheme 1). The corresponding ^{99}Tc(I)/Re(I) complexes on the macroscopic level were analyzed by ^{1}H and ^{13}C NMR and IR spectroscopic techniques (see Experimental Section). All compounds, except complex **2**, exist in two enantiomeric forms. The X-ray structures of the complexes *fac*-$[Re(L^1)(CO)_3]$, *fac*-$[Re(L^6)(CO)_3]$ (Figures 2 and 3) and *fac*-$[Tc(L^4)(CO)_3]$ (*12*) could be elucidated, confirming the proposed composition. In all three cases, only one enantiomer crystallized. The complexes on the nca level were characterized by comparing their radioactive traces on the HPLC with the UV traces (monitored at 254 nm) of the analytically pure ^{99}Tc or Re analogues (Table 1). The HPLC profiles of all reactions on the nca level showed the formation of the same product as characterized on the macroscopic level. The applied HPLC system did not allow distinguishing

Scheme 1. Synthesis of Complexes 1−7

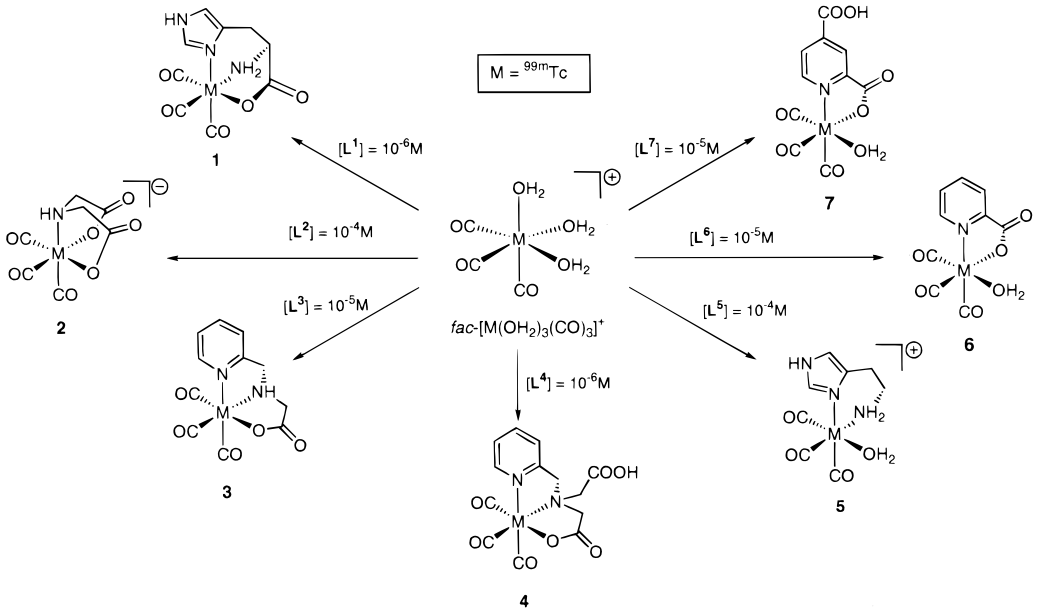

Table 3. Biodistribution (% ID/g)[a] of ^{99m}Tc-Tricarbonyl Complexes 1−7 in BALB/c Mice, 24 h after Intravenous Administration

organ	1	2	3	4	5	6	7
blood	0.02 ± 0.01	0.12 ± 0.01	0.15 ± 0.04	0.05 ± 0.06	3.03 ± 0.87	0.62 ± 0.15	1.36 ± 0.05
heart	0.01 ± 0.01	0.14 ± 0.03	0.27 ± 0.05	0.07 ± 0.10	2.03 ± 0.32	0.69 ± 0.38	0.52 ± 0.04
lung	0.92 ± 0.20	0.20 ± 0.02	0.66 ± 0.06	0.29 ± 0.44	2.21 ± 0.54	1.56 ± 0.24	1.14 ± 0.02
spleen	0.36 ± 0.20	0.21 ± 0.02	0.41 ± 0.09	0.22 ± 0.33	2.23 ± 0.38	0.66 ± 0.08	0.69 ± 0.05
kidneys	0.22 ± 0.07	1.20 ± 0.09	2.32 ± 0.42	0.57 ± 0.74	7.58 ± 3.57	13.73 ± 0.39	30.59 ± 2.61
stomach	0.19 ± 0.10	0.50 ± 0.10	0.45 ± 0.13	0.35 ± 0.43	4.20 ± 5.04	0.83 ± 0.07	0.98 ± 0.47
intestines	0.06 ± 0.02	0.22 ± 0.03	0.60 ± 0.06	0.10 ± 0.09	2.60 ± 0.29	1.37 ± 0.12	2.18 ± 2.44
liver	0.16 ± 0.10	1.57 ± 0.04	9.61 ± 2.74	1.19 ± 1.63	20.56 ± 2.84	5.94 ± 0.43	16.86 ± 2.31

[a] Values represent the means ±SD (n = 3) of the percent injected dose/gram.

Table 4. Biodistribution (% ID/g)[a] of Complex 1 in BALB/c Mice, as a Function of Time after Intravenous Administration

organ	15 min	30 min	1 h
blood	10.64 ± 0.81	2.77 ± 2.15	1.22 ± 0.80
heart	4.26 ± 0.12	1.09 ± 0.81	0.45 ± 0.28
lung	10.77 ± 1.00	3.55 ± 3.47	1.39 ± 0.86
spleen	3.48 ± 0.78	1.04 ± 0.76	0.72 ± 0.47
kidneys	20.60 ± 6.99	4.50 ± 3.47	2.04 ± 1.15
stomach	8.82 ± 0.69	4.29 ± 2.91	3.13 ± 2.08
intestines	9.76 ± 1.09	2.33 ± 1.72	1.23 ± 0.95
liver	15.03 ± 1.95	3.50 ± 2.66	2.02 ± 1.57
muscle	1.99 ± 0.18	0.46 ± 0.32	0.21 ± 0.12
bone	2.25 ± 0.52	0.58 ± 0.44	0.81 ± 0.73

[a] Values represent the means ±SD (n = 3) of the percent injected dose/gram

Table 5. Biodistribution (% ID/g)[a] of Complex 5 in BALB/c Mice, as a Function of Time after Intravenous Administration

organ	15 min	30 min	1 h
blood	7.40 ± 1.34	6.60 ± 2.46	4.97 ± 0.67
heart	8.14 ± 1.89	6.22 ± 1.56	5.75 ± 0.68
lung	10.74 ± 2.48	8.48 ± 1.83	7.43 ± 0.51
spleen	4.69 ± 0.90	4.30 ± 0.89	3.79 ± 0.22
kidneys	48.78 ± 16.97	31.10 ± 2.89	22.57 ± 2.55
stomach	9.14 ± 0.61	10.77 ± 2.68	9.80 ± 0.95
intestines	27.16 ± 1.46	26.66 ± 3.47	24.84 ± 2.97
liver	29.43 ± 1.34	38.01 ± 5.10	36.82 ± 9.01
muscle	2.58 ± 0.67	1.89 ± 0.29	2.04 ± 0.32
bone	2.49 ± 0.59	1.98 ± 0.51	1.96 ± 0.14

[a] Values represent the means ±SD (n = 3) of the percent injected dose/gram.

between the possible enantiomers. The ligand concentrations on the nca level, necessary to achieve a radiochemical purity of >95% (30 min at 75 °C) varied between 10^{-4} and 10^{-6} M (Scheme 1).

Cysteine and Histidine Challenge. All complexes were challenged in 1 mM cysteine (complexes **1**−**7**) and histidine (complexes **2**−**7**) in PBS buffer (pH 7.4) for 24 h at 37 °C to determine their stability against ligand exchange and/or decomposition. The samples were analyzed by means of HPLC at 1, 4, and 24 h. The results are summarized in Table 2. Only insignificant reoxidation (<1%) of the complexes to $^{99m}TcO_4^-$ was detected after 24 h at 37 °C. Besides this, two trends could be observed. (i) With excess histidine, the ligand of complexes **2**−**7** was more efficiently displaced than in the presence of excess cysteine. This is consistent with the coordination efficiency of different amino acid toward *fac*-[^{99m}Tc(OH$_2$)$_3$(CO)$_3$]$^+$ (*8*). (ii) Complexes **5**−**7** revealed significant higher exchange rates than complexes **1**−**4**. Substitution of the coordinated water molecule in the complexes **5**−**7** by the functional groups of histidine and cysteine via a dissociative or dissociative interchange mechanism and subsequent displacement of the ligands L^5-L^7 is probably the reason for the lower (thermodynamic) stability of compounds **5**−**7**. On the other hand, complexes **1**−**4** have a stable, "closed", octahedral coordination sphere, where substitution reaction via a dissociative or an associative mechanism is unlikely.

Comparison of the log $P_{o/w}$ Values. Despite the aromatic backbones of most of the tested ligands, the neutral overall charge of some complexes, and the organometallic nature of the compounds **1**−**7**, they revealed only a low

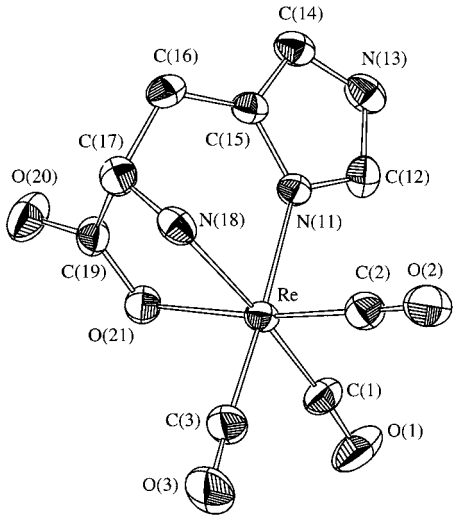

Figure 2. ORTEP of the neutral complex *fac*-[Re(L^1)$(CO)_3$]. Re−O(21), 2.147(4) Å; Re−N(18), 2.188(5) Å; Re−N(11), 2.192(4) Å; Re−C(1), 1.900(6) Å; Re−C(2), 1.9103(6) Å; Re−C(3), 1.909(6) Å; O(21)−Re−N(18), 75.1(2)°; N(18)−Re−N(11), 81.2(2)°; O(21)−Re−N(11), 82.1(2)°; C(1)−Re−C(2), 88.9(3)°; C(1)−Re−C(3), 85.3(3)°; C(3)−Re−C(2), 88.8(3)°.

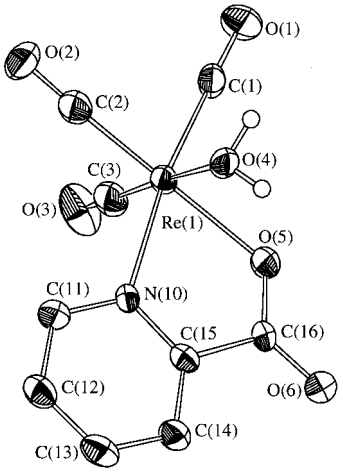

Figure 3. ORTEP of the neutral complex *fac*-[Re(OH_2)-(L^6)$(CO)_3$]. Re−O(5), 2.136(4) Å; Re−N(10), 2.187(5) Å; Re−O(4), 2.191(5) Å; Re−C(1), 1.899(7) Å; Re−C(2), 1.914(6) Å; Re−C(3), 1.904(7) Å; O(5)−Re−N(10), 74.32(16)°; O(4)−Re−N(10), 81.10(16)°; O(5)−Re−O(4), 81.92(16)°; C(1)−Re−C(2), 85.4(4)°; C(1)−Re−C(3), 89.0(3)°; C(3)−Re−C(2), 86.7(3)°.

lipophilicity. The log $P_{o/w}$ values range from −2.12 to 0.34 (Table 1). This is astonishing, since neutral ^{99m}Tc(V) complexes and complexes with aromatic side chains or aromatic backbones are usually characterized by high log $P_{o/w}$ (*19*, *20*).

Plasma Stability and Behavior. All complexes revealed no significant reoxidation to $^{99m}TcO_4^-$ when incubated in human plasma for 24 h at 37 °C, as determined by FPLC. However, while the complexes **1**−**4** displayed only weak aggregation with human plasma (<1% of initial activity) in vitro at 37 °C (Figure 4), the complexes **5**−**7** reacted completely with the plasma proteins after 1 h (Figure 4). Furthermore, we found that the kinetic of binding is almost independent of the nature of the coordinated ligand and the overall charge of the corresponding complex. If the coordination would be unspecific via lipophilic or hydrophilic interactions, an aggregation could be expected for most of the complexes, because the ligands possess similar structural features. This is obviously not the case, since only complexes **5**−**7**

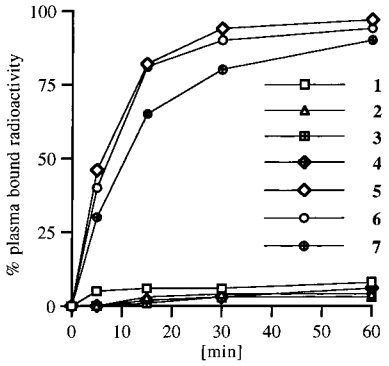

Figure 4. Coordination of complexes **1**−**7** to human plasma in vitro at 37 °C as a function of time determined by radiometric FPLC analyses on a size-exclusion column (Pharmacia Superdex 200; 250 mm, 10 μm).

coelude with the plasma. A complete transchelation of the $^{99m}Tc(CO)_3$-core to the plasma proteins after this short time is unlikely, since the complexes **5**−**7** were stable between 75−85% in the presence of strong tridentate ligand system like cysteine and histidine after 1 h at 37 °C in PBS (Table 2). The characteristic behavior of the "*fac*-[^{99m}Tc(OH_2)L′$(CO)_3$]"-type complexes **5**−**7** (L′ = bidentate ligands) is presumably due to exchange of the substitution labile water molecule by functional groups of the proteins and, thus, formation of a complex-protein conjugate and eventually a transchelation of the whole $^{99m}Tc(CO)_3$-core to the plasma proteins.

Biodistribution of Complexes 1−7, 24 h postinjection. For an initial in vivo evaluation of the seven ^{99m}Tc−tricarbonyl complexes (Scheme 1), the time point of the in vivo experiments was fixed at 24 h postinjection (p.i.). The results of the biodistribution (24 h p.i.) are summarized in Table 3. The data show a clear trend: the complexes **1**, **2**, and **4** (tridentate coordinated ligands) revealed a good clearance from all organs and tissues 24 h p.i. The amounts of activity generally retained in the liver range from 0.16 ± 0.10% ID/g to 1.57 ± 0.04% ID/g, and those in the kidneys from 0.22 ± 0.07% ID/g to 1.20 ± 0.09% ID/g, 24 h p.i. Only complex **3** revealed a considerable uptake in the liver (9.61 ± 2.74% ID/g, 24 h p.i.).

Contrary to these findings, a significant higher retention of activity in all organs and tissues was observed for complexes **5**−**7** with the bidentate coordinated ligands (Table 3). Particularly, the kidneys and the liver were targeted. The three complexes revealed retention in the liver ranging from 5.94 ± 0.43% ID/g to 16.86 ± 2.31% ID/g and in the kidneys from 4.08 ± 0.62% ID/g to 30.59 ± 2.61% ID/g. Compared with the low log $P_{o/w}$ values of the complexes, there is a weak coincidence between the lipophilicity/hydrophilicity and the liver or kidney retention of the corresponding complexes, e.g., compound **5** is less lipophilic than compound **1** but shows a much higher liver retention (Table 3). This physicochemical parameter alone is obviously not sufficient to explain the observed in vivo behavior. The radioactivity found in the blood pool was also by a factor of 4−100 higher (0.62 ± 0.15 to 3.03 ± 0.87% ID/g) than for the complexes **1**−**4**, 24 h p.i.

Detailed Biodistribution Data of Complexes 1 and 5. More detailed studies about the biodistribution and pharmacokinetics of $^{99m}Tc(CO)_3$ complexes with bidentate and tridentate systems were performed with one representative complex (**1** and **5**) of each group at 15 min, 30 min, and 1 h p.i. in order to follow the time course of disappearance from the blood, kidney, and liver. The data of the biodistribution are summarized in Tables 4 and 5. The tridentate coordinated complex **1** is ef-

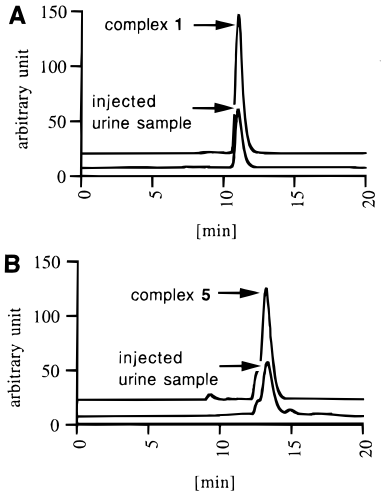

Figure 5. Radioactive HPLC traces of mouse urine samples (30 min p.i.). The mice were injected with complex **1** (A) and complex **5 (**B). The corresponding reference HPLC trace displayed the identity and stability complex in vivo. Experiments were performed using a reversed-phase column (Machery-Nagel C-18; 10 μm, 150 × 4.1 mm).

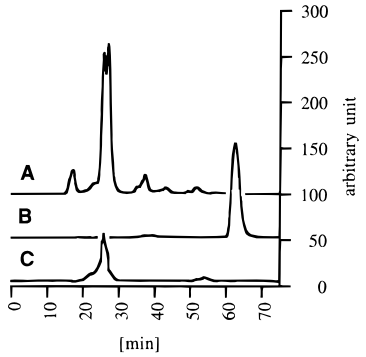

Figure 6. (A) UV trace (240 nm) and radioactive trace of murine plasma sample, 30 min p.i. of complexes **1** (B) and **5** (C). Experiments were performed using a size-exclusion column (Pharmacia Superose 12; 300 mm, 10 μm).

ficiently excreted from all organs and tissues through both the urinary and the hepatobiliary pathways. The activity found in the kidneys and liver 1 h p.i. was 2.04 ± 1.15 and 2.02 ± 1.57% ID/g, respectively. The complex **1** also cleared rapidly from the blood pool (1.22 ± 0.80% ID/g, 1 h p.i.).

The clearance of the bidentate coordinated complex **5** from the blood pool is slower and correlates with a generally higher retention of activity in all organs and tissues by a factor of 10−20 compared to complex **1** (Table 5). Complex **5** is significantly accumulated and retained in the liver and slowly excreted into the intestines (36.82 ± 9.01 and 24.84 ± 2.97% ID/g, respectively, 1 h p.i.).

Parallel to the biodistribution studies, the urine and the blood of the mice were analyzed by radiometric HPLC and FPLC for both complexes to verify the in vivo stability of the compounds. The radioactive HPLC traces of the reinjection of the urine sample (30 min p.i.) on the reversed-phase column proved the identity with compounds **1** and **5** respectively (Figure 5). No traces of pertechnetate could be found, proving the high in vivo stability of the ^{99m}Tc-tricarbonyl core. FPLC analyses of murine plasma samples (30 min p.i.) showed only minor binding of complex **1** to serum proteins (<1%). On the other hand, the entire radioactivity in plasma samples of mice, injected with complex **5,** eluded simultaneously with plasma proteins (Figure 6). Binding to serum proteins could, thus, explain the relatively high activity in the blood pool found for compound **5** even 24 h p.i (3.03 ± 0.87% ID/g). These results are consistent with those made in vitro in human plasma.

CONCLUSION

The first systematic in vitro and in vivo experiments of $^{99m}Tc(CO)_3$ model complexes with various bi- and tridentate ligand systems are presented. All tested ligand systems formed well-defined complexes with a metal-to-ligand ratio of 1:1, at low ligand concentrations and short reaction times. The complexes with tridentate ligands revealed mostly a good and fast clearance from all organs and tissues. On the other hand, the complexes with bidentate-coordinated ligands were characterized by a high retention of activity in the liver and the kidneys. A slightly lower thermodynamic stability of bidentate coordinated complexes and the potential substitution of the water molecule in these compounds by functional groups of proteins might be the reason for the high retention of these compounds in vivo. Further experiments and studies have to be carried out to fully understand this discrepancy in the in vivo distribution. The results so far suggest that, for the radiolabeling with *fac*-$[^{99m}Tc(OH_2)_3(CO)_3]^+$ or *fac*-$[^{186/188}Re(OH_2)_3(CO)_3]^+$, tridentate chelating systems are preferable for the functionalization of biomolecules, since they form organometallic compounds with more favorable pharmacokinetics.

ACKNOWLEDGMENT

We would like to thank Judith Stahel, Martine Willman, René Bugmann, and Yvonne Eichholzer for their assistance in preparing the samples and performing the animal studies. This work was supported by Mallinckrodt Inc.

Supporting Information Available: Tables of crystal data, structure solution and refinement, atomic coordinates, bond lengths and angles, and anisotropic thermal parameters for **1** and **6**. This material is available free of charge via the Internet at http://pubs.acs.org.

LITERATURE CITED

(1) Johannsen, B., and Spiess, H. (1996) Technetium(V) Chemistry as Relevant to Nuclear Medicine. In *Technetium and Rhenium* (Yoshihara, K., and Omori, T., Eds.) Vol. 176, pp 77−122, Springer-Verlag, Berlin, Heidelberg, New York.

(2) Lister-James, J., Moyen, B. R., and Dean, T. (1996) Small peptides radiolabeled with 99mTc. *Q. J. Nucl. Med. 40*, 221−233.

(3) Costello, C. E., Brodack, J. W., Jones, A. G., Davison, A., Johnson, D. L., Kasina, S., and Fritzberg, A. R. (1983) The Investigation of radiopharmaceutical components by fast atom bombardment mass-spectrometry − the identification of Tc−HIDA and the epimers of Tc−CO_2DADS. *J. Nucl. Med. 24*, 353−355.

(4) Decristoforo, C., and Mather, S. J. (1999) 99m-technetium-labeled peptide-HYNIC conjugates: Effects of lipophilicity and stability on biodistribution. *J. Nucl. Biol. Med. 26*, 389−396.

(5) Edwards, D. S., and Liu, S. (1997) Tc-99m-labeling of hydrazinonicotinamide (HYNIC) modified highly potent small molecules: problems and solutions. *Transition Met. Chem. 22*, 425−426.

(6) Salmain, M., Gunn, M., Gorfi, A., Top, S., and Jaouen, G. (1993) Labeling of Proteins by Organometallic Complexes of Rhenium(I). Synthesis and Biological Activity of the Conjugates. *Bioconjugate Chem. 4*, 425−433.

(7) Top, S., Hafa, E. H., Vessières, A., Quivy, J., Vaissermann, J., Hughes, D. W., McGlinchey, M. J., Mornon, J.-P., Thoreau, E., and Jaouen, G. (1995) Rhenium Carbonyl Complexes of β-Estradiol Derivatives with High Affinity for the Estradiol Receptor: An Approach to Selective Organometallic Radiopharmaceuticals. *J. Am. Chem. Soc. 117*, 8372−8380.

(8) Egli, A., Alberto, R., Tannahill, L., Schibli, R., Abram, U., Schaffland, A., Waibel, R., Tourwé, D., Jeannin, L., Iterbeke, K., and Schubiger, P. A. (1999) Organometallic ^{99m}Tc-Aquaion labels peptide to unprecedented High specific activity. *J. Nucl. Med., 40*, 1913−1917.

(9) Alberto, R., Schibli, R., Schubiger, A. P., Abram, U., Pietzsch, H.-J., and Johannsen, B. (1999) First Application of *fac*-$[^{99m}Tc(OH_2)(CO)_3]^+$ in Bioorganometallic Chemistry: Design, Structure and in vitro Affinity of a 5-HT_{1A} Receptor Ligand Labeled with 99mTc. *J. Am. Chem. Soc., 121*, 6076−6077.

(10) Spradau, T. W., Edwards, W. B., Anderson, C. J., Welch, M. J., and Katzenellenbogen, J. A. (1999) Synthesis and Biological Evaluation of Tc-99m-Cyclopentadienyltricarbonyltechnetium-Labeled Octreotide. *Nucl. Med. Biol. 26*, 1−7.

(11) Wenzel, M., and Saidi, M. (1993) Esters of Tc-99m labeled cytectrencarboxylic acid with alcohols of cyclic amines as cerebral radiodiagnostic agents. *J. Labelled Compd. Radiopharm. 33*, 77−80.

(12) Alberto, R., Schibli, R., Egli, A., Schubiger, P. A., Abram, U., and Kaden, T. A. (1998) A Novel Organometallic Aqua-complex of Technetium for the Labeling of Biomolecules: Synthesis of $[^{99m}Tc(OH_2)(CO)_3]^+$ from $[^{99m}TcO_4]^-$ in Aqueous Solution and its Reaction with Bifunctional Ligands. *J. Am. Chem. Soc. 120*, 7987−7988.

(13) Alberto, R., Schibli, R., Schubiger, P. A., Abram, U., and Kaden, T. A. (1996) Reactions with the Technetium and Rhenium Carbonyl Complexes $[NEt_4]_2[MX_3(CO)_3]$. Synthesis and Structure of $[Tc(CN\text{-}^tBu)_3(CO)_3][NO_3]$ and $[NEt_4][Tc_2(\mu\text{-}SCH_2CH_2OH)_3(CO)_6]$. *Polyhedron 15*, 1079−1089.

(14) Schibli, R., Alberto, R., Abram, U., Abram, S., Egli, A., Schubiger, P. A., and Kaden, T. A. (1998) Structural and ^{99}Tc-NMR Investigations of Complexes with *fac*-$[Tc(CO)_3]^+$ Moieties and Macrocyclic Thioethers of Various Ring Size: Synthesis and X-ray Structure of the Complexes *fac*-$[Tc(9\text{-ane-}S_3)(CO)_3]Br$, *fac*-$[Tc_2(tosylate)_2(18\text{-ane-}S_6)(CO)_6]$, and *fac*-$[Tc_2(20\text{-ane-}S_6{-}OH)(CO)_6][tosylate]_2$. *Inorg. Chem. 37*, 3509−3516.

(15) Schibli, R., Katti, K. V., Volkert, W. A., and Barnes, C. L. (1998) Novel Coordination Behavior of *fac*-$[ReBr_3(CO)_3]^{2-}$ with 1,3,5-Triaza-7-Phosphaadamantane (PTA). Systematic Investigation on Stepwise Replacement of the Halides by PTA Ligand. Phase Transfer Studies and X-ray Crystal Structure of $[NEt_4][ReBr_2(PTA)(CO)_3]$, $[ReBr(PTA)_2(CO)_3]$ and $[Re(PTA)_3(CO)_3]PF_6$. *Inorg. Chem. 37*, 5306−5312.

(16) Alberto, R., Schibli, R., Abram, U., Angst, D., and Schubiger, P. A. (1997) Application of Technetium and Rhenium Carbonyl Chemistry to Nuclear-Medicine- Preparation of $[NEt_4][TcCl_3(CO)_3]$ from $[NBu_4][TcO_4]$ and Structure of $[NEt_4]$-$[Tc_2(\mu\text{-}Cl)_3(CO)_6]$-Structures of the Model Complexes $[NEt_4]$-$[Re_2(\mu\text{-}OEt)_2(\mu\text{-}OAc)(CO)_6]$ and $[ReBr((CH_2S(CH_2)_2Cl)_2)(CO)_3]$. *Transition Met. Chem. 22*, 597−601.

(17) Alberto, R., Schibli, R., Abram, U., Kaden, T. A., and Schubiger, P. A. (1999) Substitution Reactions of 2-Picolinic Acid, Histamin and 2-Picolinamine with $[NEt_4]_2[ReBr_3(CO)_3]$ in DMSO. 1H NMR Investigation of Product Formation and Crystal Structure of $[NEt_4][ReBr(pic)(CO)_3]$, $[ReBr(hist)(CO)_3]$ and $[Re(picamin)_2(CO)_3]Br$. *Inorg. Chim. Acta* (in preparation)

(18) Troutner, D. E., Volkert, W. A., Hoffman, T. J., and Holmes, R. A. (1984) A Neutral Lipophilic Complex of ^{99m}Tc with a Multidentate Amine Oxime. *Int. J. Appl. Radiat. Isot. 35*, 467−470.

(19) Mang'era, K. O., Ballande, E., Vanbilloen, H., Boonen, C., Pasqualini, R., and Verbruggen, A. M. (1994) Comparative Evaluation of the Biological Behavior of ^{99m}Tc-Nitrido and ^{99m}Tc-Oxo Complexes of L, L-EC and L,L-EDC. In *Technetium and Rhenium in Chemistry and Nuclear Medicine* (Nicolini, M., Bandoli, G., and Mazzi, U., Eds.) Vol. 4, pp 405−407, SGE, Verona.

(20) Baldwin, R. M., McBride, B. J., Wu, J.-L., Kerr, J. M., Schulze, L. M., MacWhorter, S. E., and Byrne, E. F. (1994) Synthesis and Biodistribution of 99mTc Aromatic Amine-Amide-Thiol-Thioether N_2S_2 Complexes. In *Technetium and Rhenium in Chemistry and Nuclear Medicine* (Nicolini, M., Bandoli, G., and Mazzi, U., Eds.) Vol. 4, pp 329−332, SGE, Verona.

BC990127H

© 2000 American Chemical Society, Bioconjugate Chem., Schibli bc990127h Supporting Info Page 1

Details of X-ray crystallographic analyses of complex Tricarbonyl(histidinato-O,N,N')rhenium(I) • mono aqua.(*fac*-[Re(L1)(CO)3] • H2O).

© 2000 American Chemical Society, Bioconjugate Chem., Schibli bc990127h Supporting Info Page 2

Table 1 : Crystal data and structure refinement for [Re(CO)3(hist)] x H2O.

Name	Tricarbonyl(histidinato-O,N,N)rhenium(I)
Compound	[Re(CO)3(hist)] x H2O
Empirical formula	C9 H10 N3 O6 Re
Formula weight	442.40
Temperature	293(2) K
Wavelength / Radiation	.71073 A / MoKa
Crystal system / Spacegroup	Orthorhombic/ P212121
Unit cell dimensions	a = 9.106(1)A alpha = 90 deg. b = 10.266(3)A beta = 90 deg. c = 12.953(3)A gamma = 90 deg.
Volume	1210.8(4) A^3
Z	4
Density (calculated)	2.427 Mg/m^3
Absorption coefficient	10.064 mm^-1
F(000)	832
Crystal description	colourless needle
Crystal size	0.5 x 0.1 x 0.1 mm
No. of reflns. (lattice)	25
Theta range (lattice)	9.41 to 13.87 deg.
Theta range for data collection	3.15 to 30.96 deg.
Index ranges	-1<=h<=13, 0<=k<=14, -18<=l<=18
Reflections collected	4839
Independent reflections	3839 [R(int) = 0.0268]
Reflections observed	3579
Criterion for observation	>2sigma(I)
Absorption correction	Psi scan
Max. and min. transmission	0.9991 and 0.9044
Measurement method	omega scans
No. of standard reflections	3
Interval count/time	200/3600
Decay	0.1 %
Structure solution	SHELXS-86 (Sheldrick, 1990)
Structure refinement	SHELXL-93 (Sheldrick, 1993)
Molecular graphics	SCHAKAL (Keller, 1992), ZORTEP (Zsolnai, 1994)
Publication material	SHELXL-93 (Sheldrick, 1993)
Refinement method	Full-matrix least-squares on F^2
Weighting scheme	calc w=1/[s^2^(Fo^2^)+(0.0285P)^2^+1.9282P] where P=(Fo^2^+2Fc^2^)/3
Solution primary	Patterson
Hydrogen treatment	refined
Data / restraints / parameters	3839 / 3 / 212
Final R indices [I>2sigma(I)]	R1 = 0.0270, wR2 = 0.0603
Goodness-of-fit on F^2	1.076
Final R indices (all) R1 / wR2	0.0338 / 0.0651
Absolute structure parameter	-.003(14)
Largest diff. peak and hole	.593 and -1.133 e.A^-3

© 2000 American Chemical Society, Bioconjugate Chem., Schibli bc990127h Supporting Info Page 3

Table 2: Atomic coordinates and equivalent isotropic displacement parameters (A^2 x 10^3) for [Re(CO)3(hist)] x H2O. (U(eq) is defined as one third of the trace of the orthogonalized Uij tensor).

	x	y	z	U(eq)
Re	.8593(1)	.2086(1)	.2317(1)	26(1)
C(1)	.9975(6)	.3120(6)	.1585(5)	34(1)
C(2)	.8378(7)	.3468(6)	.3284(5)	36(1)
C(3)	1.0249(7)	.1484(6)	.3085(6)	42(1)
O(1)	1.0889(6)	.3703(6)	.1172(5)	58(2)
O(2)	.8225(6)	.4328(6)	.3852(5)	55(1)
O(3)	1.1264(7)	.1185(6)	.3544(6)	75(2)
N(11)	.6629(5)	.2667(4)	.1454(3)	26(1)
C(12)	.6485(8)	.3765(6)	.0912(4)	33(1)
N(13)	.5189(6)	.3845(6)	.0471(4)	36(1)
C(14)	.4422(6)	.2740(6)	.0728(4)	33(1)
C(15)	.5313(5)	.2004(6)	.1323(4)	28(1)
C(16)	.4977(6)	.0697(6)	.1770(6)	36(1)
C(17)	.6325(7)	-.0042(5)	.2159(4)	34(1)
N(18)	.7028(6)	.0710(5)	.2991(4)	32(1)
C(19)	.7411(7)	-.0277(6)	.1283(5)	31(1)
O(20)	.7178(6)	-.1128(5)	.0647(4)	51(1)
O(21)	.8535(5)	.0480(4)	.1256(3)	32(1)
O(30)	.4827(7)	.7087(8)	.0633(5)	65(2)

© 2000 American Chemical Society, Bioconjugate Chem., Schibli bc990127h Supporting Info Page 4

Table 3: Full bond lengths [A] and angles [deg] for [Re(CO)3(hist)] x H2O.

Re-C(1)	1.900(6)
Re-C(2)	1.903(6)
Re-C(3)	1.909(6)
Re-O(21)	2.147(4)
Re-N(18)	2.188(5)
Re-N(11)	2.192(4)
C(1)-O(1)	1.156(7)
C(2)-O(2)	1.157(8)
C(3)-O(3)	1.141(8)
N(11)-C(12)	1.334(7)
N(11)-C(15)	1.388(7)
C(12)-N(13)	1.314(8)
N(13)-C(14)	1.373(9)
C(14)-C(15)	1.351(8)
C(15)-C(16)	1.493(9)
C(16)-C(17)	1.529(9)
C(17)-N(18)	1.472(8)
C(17)-C(19)	1.525(8)
C(19)-O(20)	1.219(8)
C(19)-O(21)	1.285(7)
C(1)-Re-C(2)	88.9(3)
C(1)-Re-C(3)	85.3(3)
C(2)-Re-C(3)	88.8(3)
C(1)-Re-O(21)	97.3(2)
C(2)-Re-O(21)	172.5(2)
C(3)-Re-O(21)	96.0(2)
C(1)-Re-N(18)	172.4(2)
C(2)-Re-N(18)	98.7(2)
C(3)-Re-N(18)	95.6(3)
O(21)-Re-N(18)	75.1(2)
C(1)-Re-N(11)	97.7(2)
C(2)-Re-N(11)	92.8(2)
C(3)-Re-N(11)	176.6(2)
O(21)-Re-N(11)	82.1(2)
N(18)-Re-N(11)	81.2(2)
O(1)-C(1)-Re	175.5(6)
O(2)-C(2)-Re	178.1(6)
O(3)-C(3)-Re	176.6(7)
C(12)-N(11)-C(15)	105.4(5)
C(12)-N(11)-Re	125.3(4)
C(15)-N(11)-Re	129.2(4)
N(13)-C(12)-N(11)	111.7(6)
C(12)-N(13)-C(14)	107.5(5)
C(15)-C(14)-N(13)	107.1(5)
C(14)-C(15)-N(11)	108.2(5)
C(14)-C(15)-C(16)	127.0(5)
N(11)-C(15)-C(16)	124.8(5)
C(15)-C(16)-C(17)	114.2(5)
N(18)-C(17)-C(19)	110.2(5)
N(18)-C(17)-C(16)	109.3(5)
C(19)-C(17)-C(16)	110.7(5)
C(17)-N(18)-Re	109.3(3)
O(20)-C(19)-O(21)	123.6(6)
O(20)-C(19)-C(17)	120.2(5)
O(21)-C(19)-C(17)	116.2(5)
C(19)-O(21)-Re	117.8(4)

Symmetry transformations used to generate equivalent atoms:

© 2000 American Chemical Society, Bioconjugate Chem., Schibli bc990127h Supporting Info Page 5

Table 4. Anisotropic displacement parameters (A^2 x 10^3) for [Re(CO)3(hist)] x H2O.
The anisotropic displacement factor exponent takes the form:
-2 pi^2 [h^2 a*^2 U11 + ... + 2 h k a* b* U12]

	U11	U22	U33	U23	U13	U12
Re	21(1)	28(1)	29(1)	0(1)	-3(1)	2(1)
C(1)	31(3)	36(3)	34(3)	-8(2)	2(2)	-7(2)
C(2)	31(3)	42(3)	36(3)	-4(2)	-6(2)	0(2)
C(3)	38(3)	39(3)	49(3)	-5(3)	-15(3)	6(3)
O(1)	46(3)	62(3)	67(3)	-13(3)	14(3)	-29(3)
O(2)	39(3)	60(3)	65(3)	-32(3)	-7(2)	6(2)
O(3)	58(4)	57(3)	108(5)	-5(3)	-50(4)	18(3)
N(11)	25(2)	26(2)	29(2)	1(2)	-5(2)	2(2)
C(12)	39(3)	28(2)	32(2)	-1(2)	-4(3)	0(3)
N(13)	37(3)	39(3)	32(2)	2(2)	-6(2)	11(2)
C(14)	28(2)	39(3)	31(2)	-4(2)	-4(2)	5(2)
C(15)	22(2)	34(3)	29(2)	-2(2)	1(2)	2(2)
C(16)	25(3)	36(3)	49(4)	5(3)	2(2)	-5(2)
C(17)	32(2)	30(2)	39(3)	6(2)	12(3)	-1(2)
N(18)	33(2)	33(2)	30(2)	7(2)	5(2)	7(2)
C(19)	33(3)	24(2)	38(3)	1(2)	5(2)	-1(2)
O(20)	49(3)	45(3)	60(3)	-21(2)	20(2)	-18(2)
O(21)	28(2)	29(2)	37(2)	-2(2)	10(2)	-2(2)
O(30)	55(3)	86(4)	54(3)	15(4)	2(3)	-24(4)

© 2000 American Chemical Society, Bioconjugate Chem., Schibli bc990127h Supporting Info Page 6

Table 5. Hydrogen coordinates (x 10^4) and isotropic displacement parameters (A^2 x 10^3) for [Re(CO)3(hist)] x H2O.

	x	y	z	U(eq)
H(12)	7216(88)	4396(77)	941(60)	44(22)
H(13)	4852(81)	4517(75)	89(63)	48(23)
H(14)	3650(69)	2484(98)	364(66)	87(33)
H(16A)	4409(93)	129(79)	1292(63)	45(22)
H(16B)	4242(98)	740(81)	2311(71)	66(26)
H(17)	6088(70)	-824(64)	2466(53)	35(18)
H(18A)	7414(84)	146(74)	3355(59)	35(19)
H(18B)	6498(79)	1108(69)	3394(52)	31(17)
H(30A)	5350(122)	7925(65)	565(100)	127(47)
H(30B)	4016(119)	7116(167)	118(93)	181(69)

© 2000 American Chemical Society, Bioconjugate Chem., Schibli bc990127h Supporting Info Page 7

Figure 1. ORTEP of complex Tricarbonyl(histidinato-O,N,N')rhenium(I) • mono aqua.

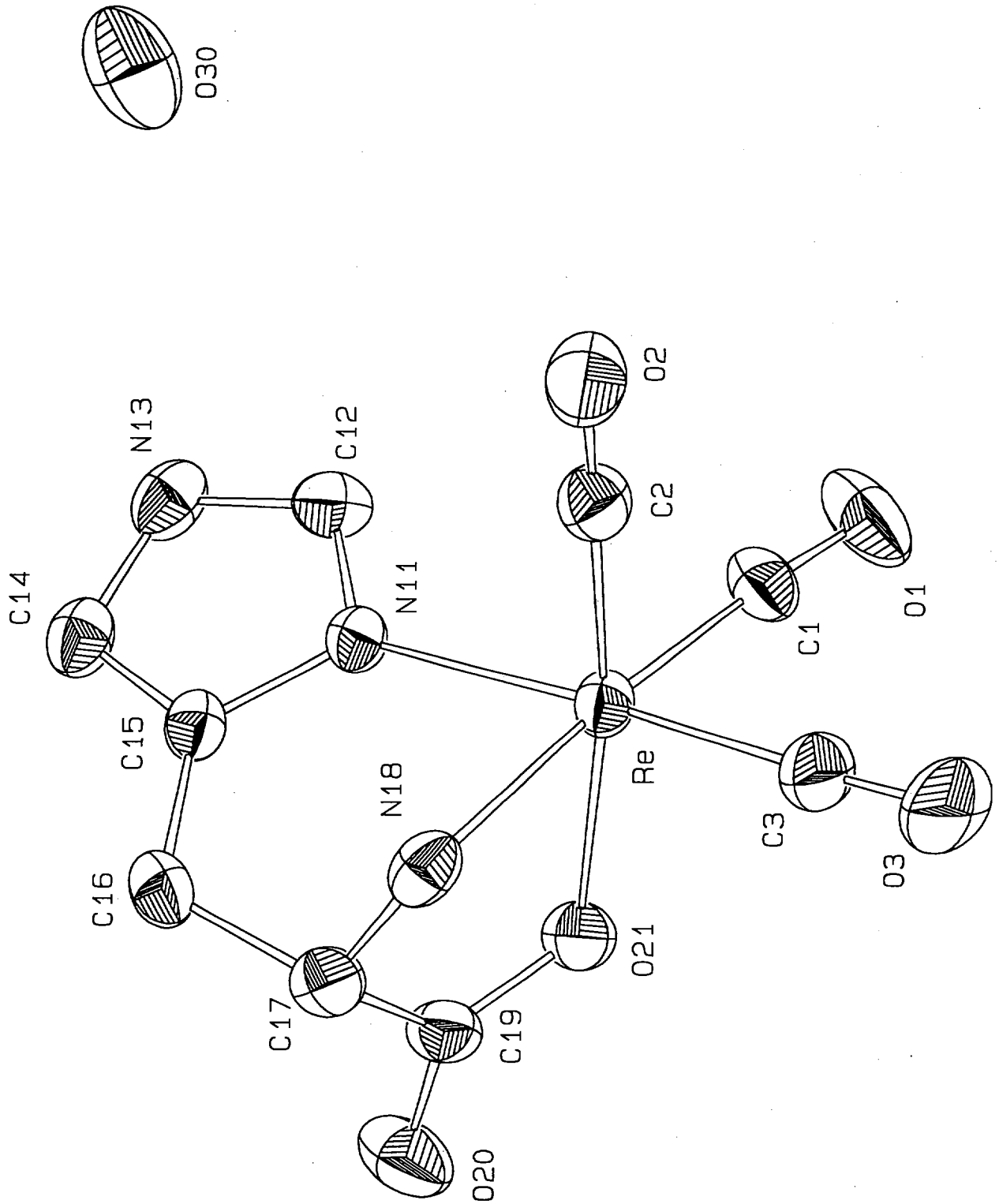

© 2000 American Chemical Society, Bioconjugate Chem., Schibli bc990127h Supporting Info Page 8

Figure 2. Crystallographic cell content of compound Tricarbonyl(histidinato-O,N,N')rhenium(I) • mono aqua.

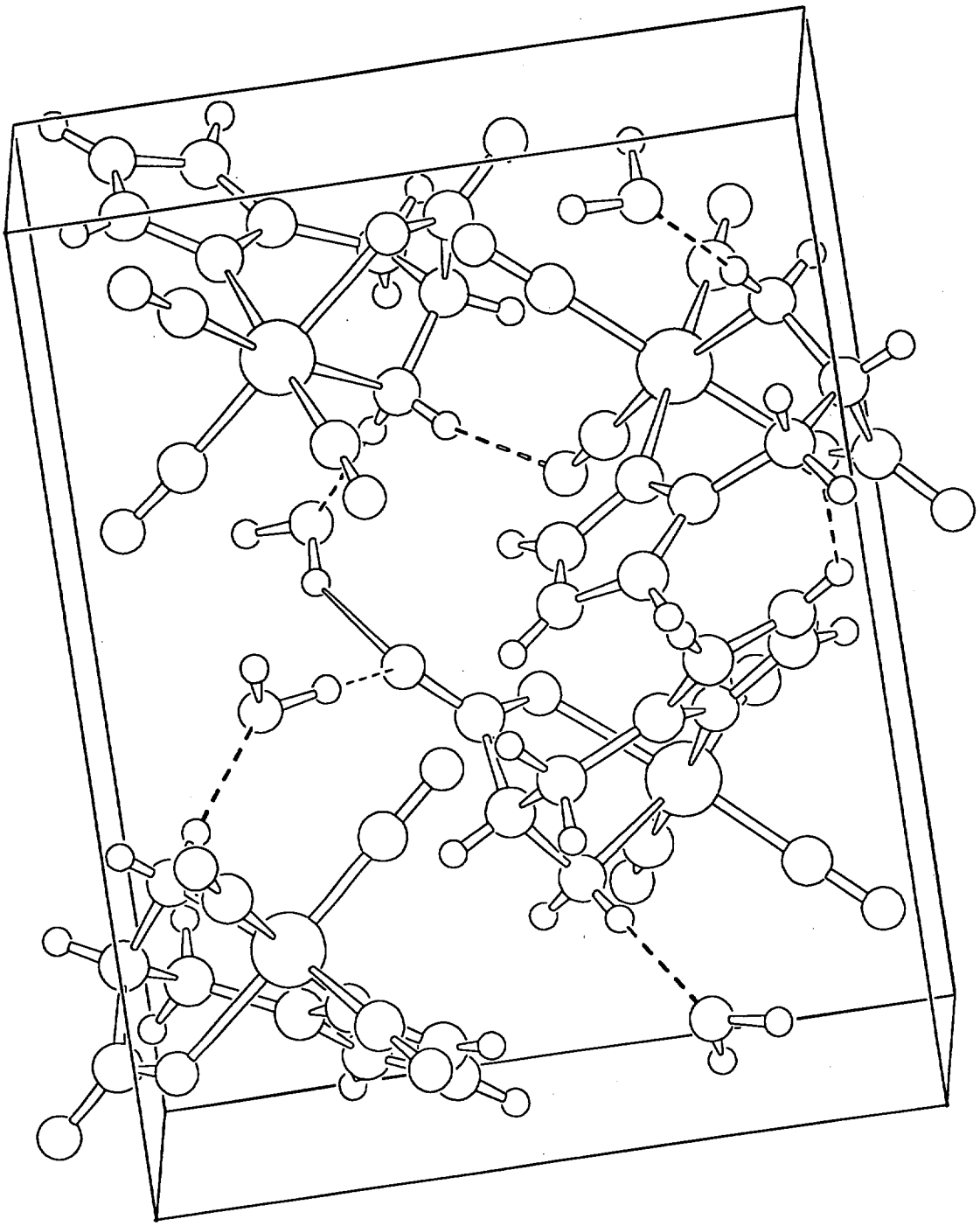

© 2000 American Chemical Society, Bioconjugate Chem., Schibli bc990127h Supporting Info Page 9

Details of X-ray crystallographic analyses of complex Tricarbonyl(deuteriumoxid-2-picolinato-O,N)rhenium(I) • mono deuteriumoxid.(*fac*-[Re(L^6)(CO)3] • D2O).

Table 1 : Crystal data and structure refinement for [Re(CO)3(Pic)(D2O)]D2O.

Name	[Re(CO)3(2-Picolinacetat)(D2O)]*D2O
Compound	[Re(CO)3(Pic)(D2O)]D2O
Empirical formula	C9 H4 D4 N O7 Re
Formula weight	432.39
Temperature	208(2) K
Wavelength / Radiation	0.71073 A / MoK\a
Crystal system / Spacegroup	Monoclinic/ C2/c
Unit cell dimensions	a = 24.244(4)A alpha = 90 deg. b = 11.3233(13)A beta 100.913(17) deg. c = 8.7338(8)A gamma = 90 deg.
Volume	2354.3(5) A^3
Z	8
Density (calculated)	2.440 Mg/m^3
Absorption coefficient	10.349 mm^-1
F(000)	1600
Crystal description	yellow plate
Crystal size	0.30 x 0.20 x 0.03 mm
No. of reflns. (lattice)	25
Theta range (lattice)	8.24 to 15.15 deg.
Theta range for data collect.	3.13 to 26.98 deg.
Index ranges	-30<=h<=30, 0<=k<=14, -1<=l<=11
Reflections collected	3068
Independent reflections	2567 [R(int) = 0.0192]
Reflections observed	2159
Criterion for observation	>2sigma(I)
Absorption correction	Psi scans
Max. and min. transmission	0.9748 and 0.3386
Measurement method	omega scans

© 2000 American Chemical Society, Bioconjugate Chem., Schibli bc990127h Supporting Info Page 11

No. of standard reflections	3
Interval count/time	400/3600
Decay	4.5 %
Structure solution	SHELXS-97 (Sheldrick, 1997)
Structure refinement	SHELXL-97 (Sheldrick, 1997)
Molecular graphics	SCHAKAL, ZORTEP
Publication material	SHELXL-97 (Sheldrick, 1997)
Refinement method	Full-matrix least-squares on F^2
Weighting scheme	calc w=1/[\s^2^(Fo^2^)+(0.0604P)^2^+0.0000P] where P=(Fo^2^+2Fc^2^)/3
Solution primary	Patterson
Hydrogen treatment	mixed
Data / restraints / parameters	2567 / 0 / 195
Final R indices [I>2sigma(I)]	R1 = 0.0293, wR2 = 0.0757
Goodness-of-fit on F^2	0.999
Final R indices (all) R1/wR2	0.0389 / 0.0804
Extinction coefficient	0.00039(6)
Largest diff. peak and hole	1.427 and -1.181 e.A^-3

© 2000 American Chemical Society, Bioconjugate Chem., Schibli bc990127h Supporting Info Page 12

Table 2: Atomic coordinates and equivalent isotropic displacement parameters (A^2 x 10^3) for [Re(CO)3(Pic)(D2O)]D2O.
(U(eq) is defined as one third of the trace of the orthogonalized Uij tensor).

	x	y	z	U(eq)
Re(1)	0.1384(1)	0.8276(1)	0.2236(1)	23(1)
C(1)	0.1926(3)	0.8455(5)	0.0942(9)	35(2)
O(1)	0.2249(2)	0.8598(5)	0.0133(7)	52(1)
C(2)	0.1308(2)	0.9957(5)	0.2081(7)	28(1)
O(2)	0.1256(2)	1.0962(4)	0.1987(6)	44(1)
C(3)	0.1960(3)	0.8548(5)	0.4009(9)	36(1)
O(3)	0.2301(2)	0.8733(4)	0.5071(7)	52(1)
O(4)	0.0714(2)	0.7886(4)	0.0240(5)	27(1)
O(5)	0.0724(2)	0.7954(4)	0.3493(5)	28(1)
O(6)	0.0191(2)	0.6618(4)	0.4379(5)	32(1)
O(7)	0.4686(2)	0.5110(4)	0.1085(6)	33(1)
N(10)	0.1349(2)	0.6358(4)	0.2496(5)	21(1)
C(11)	0.1688(3)	0.5558(5)	0.1982(7)	28(1)
C(12)	0.1598(3)	0.4349(5)	0.2115(7)	30(1)
C(13)	0.1173(3)	0.3962(6)	0.2782(8)	35(2)
C(14)	0.0827(3)	0.4773(6)	0.3331(8)	30(1)
C(15)	0.0936(2)	0.5954(5)	0.3165(6)	23(1)
C(16)	0.0581(2)	0.6898(5)	0.3739(7)	24(1)
D(4A)	0.057(3)	0.845(6)	-0.029(8)	23(17)
D(4B)	0.043(3)	0.768(6)	0.036(7)	22(18)
D(7A)	0.487(4)	0.502(8)	0.065(9)	40
D(7B)	0.446(3)	0.444(7)	0.098(7)	28(18)

© 2000 American Chemical Society, Bioconjugate Chem., Schibli bc990127h Supporting Info Page 13

Table 3: Full bond lengths [A] and angles [deg] for [Re(CO)3(Pic)(D2O)]D2O.

Re(1)-C(1)	1.899(7)
Re(1)-C(3)	1.904(7)
Re(1)-C(2)	1.914(6)
Re(1)-O(5)	2.136(4)
Re(1)-N(10)	2.187(5)
Re(1)-O(4)	2.191(5)
C(1)-O(1)	1.161(9)
C(2)-O(2)	1.146(8)
C(3)-O(3)	1.139(9)
O(5)-C(16)	1.273(7)
O(6)-C(16)	1.228(8)
N(10)-C(15)	1.332(7)
N(10)-C(11)	1.356(8)
C(11)-H(11)	0.90(7)
C(11)-C(12)	1.395(9)
C(12)-H(12)	1.08(8)
C(12)-C(13)	1.349(10)
C(13)-H(13)	0.82(6)
C(13)-C(14)	1.389(9)
C(14)-H(14)	0.68(8)
C(14)-C(15)	1.377(8)
C(15)-C(16)	1.516(7)

C(1)-Re(1)-C(3)	89.0(3)
C(1)-Re(1)-C(2)	85.4(2)
C(3)-Re(1)-C(2)	86.7(3)
C(1)-Re(1)-O(5)	173.6(2)
C(3)-Re(1)-O(5)	96.6(2)
C(2)-Re(1)-O(5)	97.7(2)
C(1)-Re(1)-N(10)	102.3(2)
C(3)-Re(1)-N(10)	96.5(2)
C(2)-Re(1)-N(10)	171.7(2)
O(5)-Re(1)-N(10)	74.32(16)
C(1)-Re(1)-O(4)	92.3(3)
C(3)-Re(1)-O(4)	177.4(2)
C(2)-Re(1)-O(4)	95.6(2)
O(5)-Re(1)-O(4)	81.92(16)
N(10)-Re(1)-O(4)	81.10(16)
O(1)-C(1)-Re(1)	177.8(6)
O(2)-C(2)-Re(1)	179.3(5)
O(3)-C(3)-Re(1)	178.6(6)
C(16)-O(5)-Re(1)	120.0(4)
C(15)-N(10)-C(11)	118.0(5)
C(15)-N(10)-Re(1)	115.7(3)
C(11)-N(10)-Re(1)	126.3(4)
H(11)-C(11)-N(10)	112(4)
H(11)-C(11)-C(12)	126(4)
N(10)-C(11)-C(12)	120.9(6)
H(12)-C(12)-C(13)	120(4)
H(12)-C(12)-C(11)	120(4)
C(13)-C(12)-C(11)	120.0(6)
H(13)-C(13)-C(12)	112(6)
H(13)-C(13)-C(14)	128(6)

© 2000 American Chemical Society, Bioconjugate Chem., Schibli bc990127h Supporting Info Page 14

C(12)-C(13)-C(14)	119.7(6)
H(14)-C(14)-C(15)	122(7)
H(14)-C(14)-C(13)	121(7)
C(15)-C(14)-C(13)	117.6(7)
N(10)-C(15)-C(14)	123.8(5)
N(10)-C(15)-C(16)	115.1(5)
C(14)-C(15)-C(16)	121.1(6)
O(6)-C(16)-O(5)	125.2(5)
O(6)-C(16)-C(15)	120.2(5)
O(5)-C(16)-C(15)	114.6(5)

Hydrogen bonds

D H A	D-H	H...A	D...A	<(DHA)
OD(4AO(7)#1	0.82(7)	1.84(7)	2.646(6)	168(7)
OD(4BO(6)#2	0.75(7)	1.98(7)	2.695(6)	160(7)
OD(7AO(7)#3	0.64(7)	2.03(7)	2.659(9)	167(10)
OD(7BO(5)#4	0.93(8)	1.82(8)	2.687(6)	154(6)

Symmetry transformations used to generate equivalent atoms:
#1 -x+1/2,-y+3/2,-z #2 -x,y,-z+1/2
#3 -x+1,-y+1,-z #4 -x+1/2,y-1/2,-z+1/2

© 2000 American Chemical Society, Bioconjugate Chem., Schibli bc990127h Supporting Info Page 15

Table 4. Anisotropic displacement parameters (A^2 x 10^3) for [Re(CO)3(Pic)(D2O)]D2O.
The anisotropic displacement factor exponent takes the form:
-2 pi^2 [h^2 a*^2 U11 + ... + 2 h k a* b* U12]

	U11	U22	U33	U23	U13	U12
Re(1)	21(1)	15(1)	35(1)	-1(1)	8(1)	1(1)
C(1)	34(3)	20(3)	54(4)	3(3)	12(3)	2(2)
O(1)	48(3)	39(2)	82(4)	8(3)	43(3)	3(2)
C(2)	21(3)	24(3)	42(3)	-3(2)	9(3)	0(2)
O(2)	54(3)	18(2)	63(3)	-1(2)	18(3)	1(2)
C(3)	35(4)	20(2)	53(4)	-1(3)	10(3)	2(2)
O(3)	41(3)	42(3)	63(3)	-16(3)	-14(3)	5(2)
O(4)	25(2)	20(2)	40(2)	0(2)	12(2)	-2(2)
O(5)	29(2)	20(2)	36(2)	-1(2)	11(2)	3(2)
O(6)	31(2)	31(2)	36(2)	7(2)	11(2)	4(2)
O(7)	35(3)	23(2)	43(3)	6(2)	16(2)	-2(2)
N(10)	16(2)	21(2)	25(2)	1(2)	4(2)	3(2)
C(11)	30(3)	22(3)	33(3)	2(2)	8(3)	1(2)
C(12)	36(4)	22(3)	33(3)	-1(2)	7(3)	7(2)
C(13)	43(4)	20(3)	42(4)	3(2)	4(3)	3(3)
C(14)	35(3)	23(3)	34(3)	3(3)	11(3)	5(3)
C(15)	27(3)	19(2)	21(3)	0(2)	4(2)	4(2)
C(16)	21(3)	22(2)	31(3)	2(2)	9(2)	6(2)

© 2000 American Chemical Society, Bioconjugate Chem., Schibli bc990127h Supporting Info Page 16

Table 5. Hydrogen coordinates (x 10^4) and isotropic displacement parameters (A^2 x 10^3) for [Re(CO)3(Pic)(D2O)]D2O.

	x	y	z	U(eq)
H(11)	1930(3)	5890(6)	1440(8)	29(18)
H(12)	1860(4)	3720(7)	1680(9)	50(2)
H(13)	1180(3)	3250(6)	2910(9)	29(19)
H(14)	610(3)	4590(7)	3670(9)	30(2)

© 2000 American Chemical Society, Bioconjugate Chem., Schibli bc990127h Supporting Info Page 17

Figure 3. ORTEP of complex Tricarbonyl(deuteriumoxid-2-picolinato-O,N)rhenium(I) • mono deuteriumoxid.

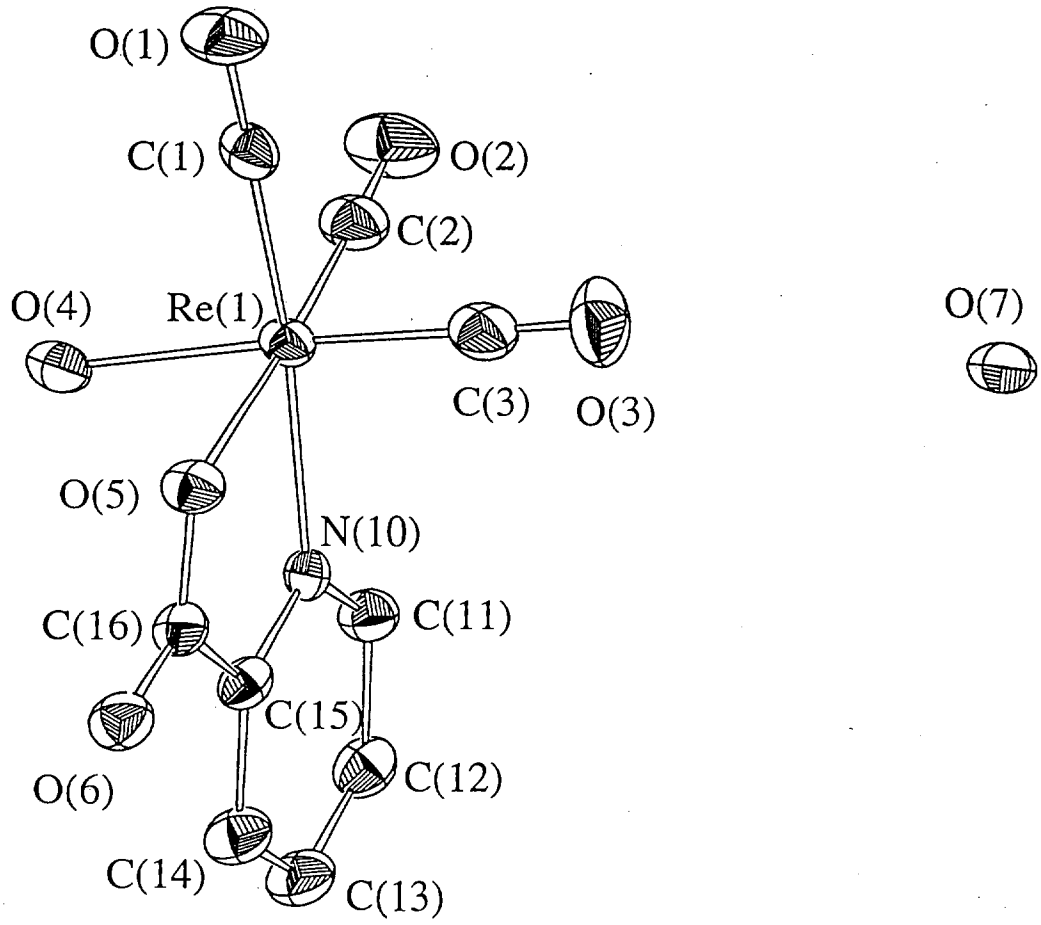

© 2000 American Chemical Society, Bioconjugate Chem., Schibli bc990127h Supporting Info Page 18

Figure 4. Crystallographic cell content of complex Tricarbonyl(deuteriumoxid-2-picolinato-O,N)rhenium(I) • mono deuteriumoxid.

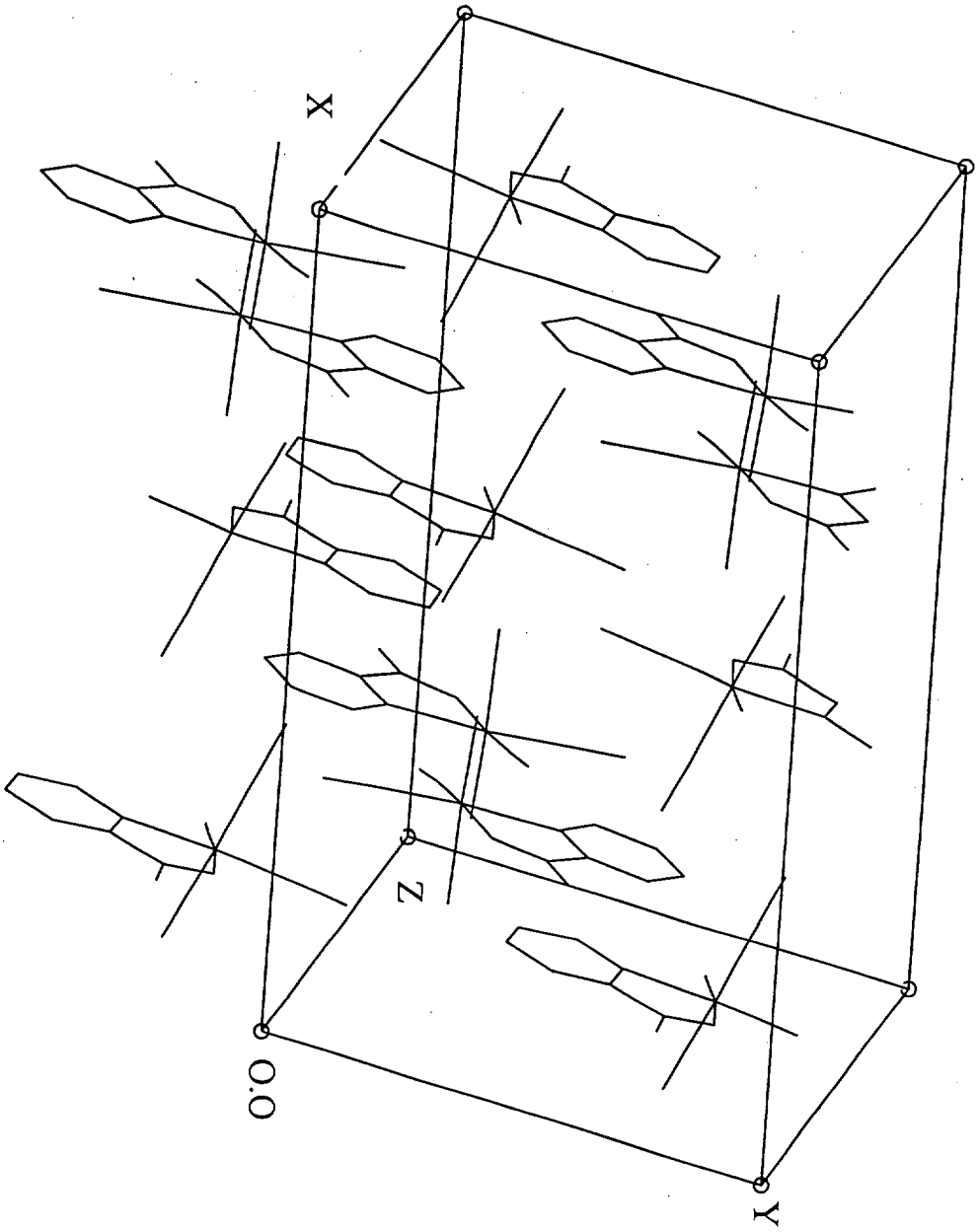

Design Consideration and Probes for Fluorescence Resonance Energy Transfer Studies

Michael Sinev,† Pavel Landsmann, Elena Sineva,† Varda Ittah, and Elisha Haas*

Faculty of Life Sciences, Bar-Ilan University, Ramat Gan 52900, Israel. Received October 6, 1999; Revised Manuscript Received February 29, 2000

Spectroscopic properties of two newly synthesized water-soluble thiol-reactive fluorescent probes, 7-(iodoacetamido)-coumarin-4-carboxylic acid (I-Cca) and *N*-iodoacetyl-*β*-(2-naphthyl)alanine (I-Nal), were characterized using single cysteine mutants of *Escherichia coli* adenylate kinase. Together with two known water-soluble thiol-reactive dyes (Lucifer yellow iodoacetamide and 5-iodoacetamidosalicylic acid) and as well, tryptophan residues (either native or inserted into a protein by site directed mutagenesis), these probes can be arranged pairwise in a molecular tool set for studies of structural transitions in proteins by means of fluorescence resonance energy-transfer (FRET) experiments. A set of seven donor/acceptor pairs which allow determination of intramolecular distances and their distributions over the range 10−40 Å in labeled protein derivatives is described. The charged groups present in the probes facilitate the conjugation reaction and improve postlabeling purification. General considerations for design of charged probes and site-directed labeling for applications of FRET methods in studies of protein structure and dynamics are presented.

INTRODUCTION

The experimental approach, based on the phenomenon of fluorescence resonance energy transfer (FRET),[1] enables evaluation of distances between relatively remote (10−100 Å) parts of macromolecules, thus extending the scope of spectroscopic determination to the monitoring of large-scale structural transitions and dynamics (Cheung, 1991; Van Der Meer et al., 1994). As such, FRET spectroscopy, primarily in the time-resolved mode, proves to be a valuable tool for the investigation of the role of structural flexibility in enzyme action, functioning of macromolecular assemblies and protein folding (Cheung, 1991; Haas, 1996). Yet, the application of the FRET method for studies of structure and dynamics of proteins (and other biological macromolecules) might be hindered by practical problems (e.g., the absence of suitable fluorescent probes and involved preparative procedures).

In general, a protein sample for use in FRET experiment should have a pair of fluorescent probes (donor and acceptor) covalently attached to predetermined sites in the molecule. Preliminary design of a corresponding protein derivative thus first includes selection of the two sites in the protein molecule to be labeled and then selection of the donor/acceptor (D/A) pair to be attached to these sites. The pair of probes should have spectroscopic characteristics optimized for the range of distances between the two selected sites and the time scale of the process to be studied. It should be noted that the spectroscopic characteristics of a given D/A pair (i.e., the Förster distance, R_0, and the donor fluorescence lifetime, τ_d) determine the detection limits for measurements of the distances between the two attached probes. The range for reliable distance determination is evaluated as $R_0 \pm R_0/2$. The time interval available for monitoring protein structural dynamics in FRET experiments may range from subnanoseconds up to milliseconds, depending on the τ_d values and the mode of measurements (Haas 1996, Van Der Meer et al., 1994, Haas and Steinberg 1984). A single D/A pair attached to a protein derivative can yield a limited amount of data, allowing partial description of intramolecular motions in the protein under study. A set of D/A pairs with adequate spectroscopic characteristics (i.e., R_0 and τ_d) should enable a more detailed characterization of large-scale protein dynamics by the FRET method. The current selection of commercially available fluorescent probes suitable for these FRET experiments is still limited. Recent research activities [(see, e.g.,

* To whom correspondence should be addressed. Phone: (972)-3-5318210. Fax: (972)-3-5351824. E-mail: haas@mail.biu.ac.il.

† Current address: Department of Biochemistry and Molecular Biology, The Pennsilvania State University, 201 Alhouse Laboratory, University Park, PA 16802.

[1] Abbreveations: Ac_2O, acetic anhydride; AcOH, acetic acid; AK, adenylate kinase from *Escherichia coli* or, within all abbreviated names of mutant AK derivatives, cysteine-free (Cys77Ser)-AK mutant with additional Cys and/or Trp mutations; AR, analytical reagent; C_i-AK, single-cysteine AK mutant containing Cys-substitution at position i; AQ4CA, 7-acetamidocoumarin-4-carboxylic acid; Cca_i-AK, C_i-AK labeled with I-Cca; CP, chemically pure; D/A pair, donor/acceptor pair of fluorescent probes; DEOA, diethyloxalacetate; DDW, double distilled water; DTT, dithiothreitol; EDTA, ethylenediaminetetraacetic acid; ET, energy transfer; Et_2O, diethyl ether; EtOAc, ethyl acetate; EtOH, ethanol; I-Cca, 7-iodoacetamidocoumarin-4-carboxylic acid; Iac_2O, iodoacetic anhydride; I-LY, Lucifer Yellow iodoacetamide; I-Nal, *N*-iodoacetyl-*β*-(2-naphthyl)-alanine; I-Sa, 5-iodoacetamidosalicylic acid; IDD, intramolecular distance distribution; FRET, fluorescence resonance energy transfer; LY_i-AK, C_i-AK labeled with I-LY; 2-ME, 2-mercaptoethanol; MeCN, acetonitrile; MEK, methylethyl ketone; MeOH, methanol; Nal_i-AK, C_i-AK labeled with I-Nal; Py, pyridine; Q4CA, 7-aminocoumarin-4-carboxylic acid; Q4CE, 7-aminocoumarin-4-carboxylic acid, ethyl ester; r.t., room temperature; S_{77}-AK, cysteine-free (Cys77Ser)-AK mutant; Sa_i-AK, C_i-AK labeled with I-Sa; TFA, trifluoroacetic acid; Tris, tris(hydroxymethyl)aminomethane; TR-FRET, time-resolved FRET, W_i-AK, single-tryptophan AK mutant containing Trp-substitution at position *i*; W_iC_j-AK, single-tryptophan/single-cysteine AK mutant containing Trp- and Cys-substitution at positions *i* and *j*, respectively.

10.1021/bc990132l CCC: $19.00 © 2000 American Chemical Society
Published on Web 04/21/2000

Terpetschnig et al. (1995), Selvin and Hearst (1994), and Chen and Selvin (1999)] are thus focused on synthesis of novel fluorescent probes with modified spectroscopic characteristics designed for investigation of specific research objectives.

Besides spectroscopic properties of fluorescent probes, the properties of the modified protein derivatives and the efficiency of postlabeling purification procedures should be also considered when designing sets of D/A pairs for protein structural studies. The main points to be taken into account are as follows. (a) Site specificity of the chemical modifications, ensuring selective site-directed attachment of fluorescent probes to the desired residues of a protein molecule. Specificity can be achieved by engineering of specific cysteine protein mutants combined with the application of thiol-reactive fluorescent reagents. (Haran et al., 1992; Sinev et al., 1996b; Haas, 1996; Lillo et al., 1997a). (b) Minimal perturbation of the native structure by mutations and by chemical modifications. This implies careful selection of sites to be mutated and design of probes having minimal potential for noncovalent interactions with protein's side chains or backbone. (c) Maximal rotational freedom of the attached probes. This is of primary importance for correct interpretation of results obtained in an energy-transfer experiment (Cheung, 1991; Van Der Meer et al., 1994; Haas, 1996). (d) The postlabeling purification scheme for double-labeled protein derivatives. No general procedure is available, and specific schemes should be developed for each set of derivatives. However, the choice of charged probe molecules for protein labeling may essentially simplify postlabeling purification, by means of ion-exchange chromatographic isolation of labeled derivative-(s) from the unlabeled protein [see, e.g., Sinev et al. (1996a,b) and Lillo et al. (1997a)]. In some cases when a charged probe was used for labeling, ion-exchange chromatography was effective for separation of two single-labeled derivatives of a two-cysteine protein mutant (these two differed in the site of probe attachment yet had equal total charge). Thereby, individual preparation of these two species and, subsequently, the corresponding site-specific double-labeled derivatives was enabled (Sinev et al., 1996b; Lillo et al., 1997a). Besides that, the presence of a charged/polar group(s) in a probe might diminish undesirable hydrophobic interactions of the attached reagent with a protein. Thus, the use of charged probes provide important practical advantages to be considered in the design of labeling strategies for spectroscopic studies of site-specifically labeled protein derivatives.

The present report describes a practical application of the above design considerations, including preparation of two newly synthesized thiol-reactive probes. These reagents were spectroscopically characterized in their conjugates with cysteine residues inserted in mutant protein derivatives. The new probes were used, together with two known fluorescent iodoacetamide reagents and tryptophan residues (native or inserted in the mutant protein), to design a set of seven D/A pairs with R_0 values in the range from 15 to 30 Å. Charged groups present in these thiol-reactive probes enabled their efficient conjugation to engineered cysteine residues and facilitated subsequent chromatographic purification of labeled derivatives. The applicability of the newly synthesized dye, 7-iodoacetamidocoumarin-4-carboxylic acid (I-Cca), as an acceptor for tryptophan donor for distance determination in proteins, was verified by distance determination in two Cca-labeled single cysteine/single tryptophan mutants of a model protein of known X-ray structure (*Escherichia coli* adenylate kinase).

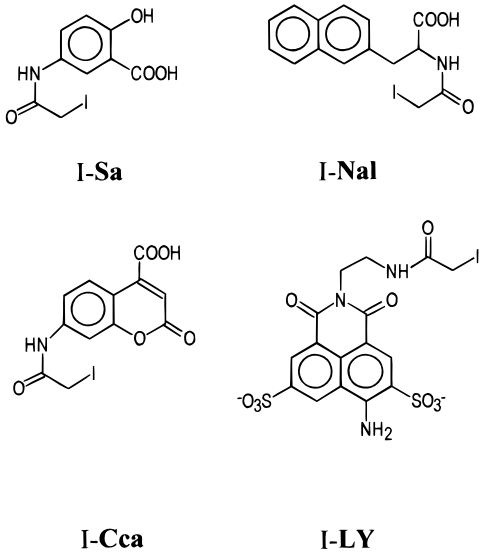

Figure 1. Thiol-reactive fluorescent probes used in the present study. I-LY**,** the commercial Lucifer Yellow iodoacetamide, was purchased from Molecular Probes. I-Sa (5-iodoacetamidosalicylic acid), I-Nal [*N*-iodoacetyl-β-(2-naphthyl)-alanine], and I-Cca (7-iodoacetamidocoumarin-4-carboxylic acid) were prepared by iodoacetylation of the corresponding amines (see Experimental Procedures).

EXPERIMENTAL PROCEDURES

Materials. Unless specified otherwise, inorganic reagents and organic solvents used for synthetic preparations were of CP grade and were purchased from BioLab. Synthetic reagents were from Sigma (Aldrich or Fluka). Double-distilled water (DDW), acetonitrile (MeCN), and trifluoroacetic acid (TFA) for HPLC were from Baker. Lucifer yellow iodoacetamide (I-LY) was purchased from Molecular Probes (Eugene, OR). Iodoacetic anhydride (Iac2O) was obtained as a powder (AR) from Aldrich, Sigma. Immediately after opening, it was aliquoted in freshly opened anhydrous dioxane (Aldrich, Sigma) and stored frozen at −20 °C as recommended by Wetzel et al. (1990).

Verification of Identity and Purity of Synthetic Preparations. The novel thiol-reactive probes for FRET studies, i.e., I-Nal and I-Cca**,** were obtained on the base of known chromofores, i.e., commercially available β-(2-naphthyl)-(*L*) alanine (Bachem, California), and 7-acetamidocoumarin-4-carboxylic acid (AQ4CA*),* which was earlier synthesized and spectroscopically characterized by Besson et al. (1991) from 7-aminocoumarin-4-carboxylic acid (Q4CA). Here, the latter was prepared and iodoacetylated in order to obtain a new iodoacetamide probe, 7-iodoacetamidocoumarin-4-carboxylic acid (I-Cca), which is spectroscopically similar to AQ4CA. Thereby, the identity of all synthetic preparations was verified by comparing their spectroscopic characteristics (^{1}H NMR, UV, fluorescent spectra, quantum yields) to the known ones. The purity of all prepared iodoacetamides was additionally confirmed by estimating their thiol reactivity (Ellmann test, see below) and by examining HPLC purity of their conjugates with thiolic compounds (cysteine, 2-mercaptoethanol). The above verification of purity of synthesized iodoacetamide probes was sufficient for adequate spectroscopic and FRET studies with corresponding protein conjugates presented herein.

Synthesis of Thiol-Reactive Fluorescent Probes (see Figures 1 and 2). *7-Aminocoumarin-4-carboxylic acid, ethyl ester* (Q4CE) (MW 233.2) was prepared ac-

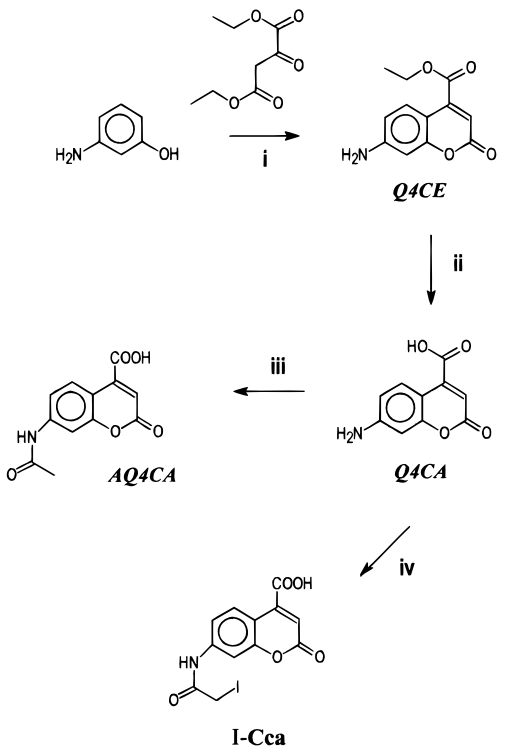

Figure 2. Synthesis of a new thiol-reactive probe I-Cca (7-iodoacetamidocoumarin-4-carboxylic acid) and the reference compound AQ4CA (7-acetamidocoumarin-4-carboxylic acid). (i) Pechmann condensation of 3-aminophenol with diethyloxalacetate (1 h, 110 °C); (ii) 2 N KOH, MeOH, reflux 3 h; (iii) Ac_2O, Py, 5 °C, then 24 h, r.t.; (iv) Iac_2O, dioxane-water, $NaHCO_3$, 5 °C, 3 h. Synthetic intermediates are 7-aminocoumarin-4-carboxylic acid (Q4CA) and 7-aminocoumarin-4-carboxylic acid, ethyl ester (Q4CE).

cording to procedures (Kanaoka et al., 1984; Besson et al., 1991), with modifications, by Pechmann cyclization of 3-aminophenol (Fluka) with diethyloxalacetate (DEOA). The latter was prepared from its commercially available sodium salt, following the earlier procedure (Riegel et al., 1946). Samples of thus prepared Q4CE for analytical purposes was washed with methanol (MeOH) and vacuum-dried. The bulk of the product was used in the next stage without further purification. *7-Aminocoumarin-4-carboxylic acid* (Q4CA) (MW 205.2) was prepared from Q4CE by 3 h reflux in methanolic KOH, according to a procedure modified from (Besson et al., 1991). Recrystallization in MeOH/DDW, followed by dissolving in minimal amount of MeOH, dilution with DDW and lyophilizing, yielded the pure Q4CA. The overall yield of the preparations after the above two synthetic steps constituted 60−70%, as related to the amount of 3-aminophenol taken. TLC, performed in EtOAc−$CHCl_3$ 1:1, neat methylethyl ketone (MEK), and MEK-AcOH-water 18:1:1 systems, confirmed essential purity of both products thus obtained. ^{1}H NMR, UV, and fluorescence spectra of these intermediate products essentially represented the published data (Kanaoka et al., 1984; Besson et al., 1991). An analytical sample (15 mg) of *7-acetamidocoumarin-4-carboxylic acid* (AQ4CA) was prepared according to a procedure modified from (Besson et al., 1991), by acetylation of 20 mg of the crude Q4CA (by ∼5 M excess of Ac_2O in dry pyridine, 0−20 °C, 16 h). This AQ4CA served as a stable reference compound representing essential spectroscopic characteristics of the Cca fluorofore to be synthesized (see next paragraph). The ^{1}H NMR, UV (λ_{max} = 338 nm, in EtOH) and fluorescence spectra of this preparation, as well as its estimated quantum yield (∼0.02, in EtOH), essentially represented the published data (Besson et al., 1991).

7-Iodoacetamidocoumarin-4-carboxylic acid (I-Cca). Example iodoacetylation procedure. All iodoacetylations (final products are depicted in Figure 1), including the following one, were performed according to a procedure modified from (Wetzel et al., 1990; Wood and Wetzel, 1992). A total of 290 mg (1.19 mmol) of previously obtained Q4CA was dissolved in 10 mL of 90% aqueous dioxane (BioLab, AR) and then mixed with 2 mL of 5% $NaHCO_3$ to form clear solution at pH 6−7 (determined upon 1:10 v/v water dilution by indicator paper). The solution was ice-chilled on a magnetic stirrer. To this, 1.2 g of prealiquoted Iac_2O (in 14 mL of dry dioxane) was added by 1 mL portions for 20 min, with intensive stirring. The pH of the mixture (determined as above, immediately after adding the next portion of the reagent), was kept at 6−7 during the reagent addition. It was adjusted at need by 1 mL portions of 5% $NaHCO_3$, followed by 2−3 mL portions of dioxane, so that the water content of the mixture would not exceed 30−40%. Afterward, the mixture was stirred an additional 90 min on the ice, with pH continuous monitoring (checked each 10−15 min). It was then diluted with cold water (1:10 v/v), supplied with 10 mL of 1 M NaI, and carefully acidified with 3 M HCl to final pH ∼1 and left overnight in the dark at 4 °C. The yellow precipitate formed was filtered, washed 2 × 50 mL water, dried in air, and then washed with dry Et_2O (3 × 2 mL). Subsequent vacuum desiccating (1 Torr, 3 h) left 140 mg of light yellow powder (yield 32%). Its ^{1}H NMR spectra was essentially similar to that of AQ4CA obtained above, differing only in a slight shift of the band corresponding to the amide ^{1}H (δ = 9.97, instead of 9.67 ppm, broad), and the appeared peak 3.97 ppm (referred to ^{1}H of ICH_2CO group). UV spectra (λ_{max} = 332 nm, in EtOH) were identical to that of AQ4CA (see above). Thiol reactivity of this preparation (as determined by Ellman test for unreacted thiol groups, see corresponding section below) was ∼85%. The purity of thus prepared I-Cca was checked by HPLC, with sample preparations (from 5 mg of I-Cca each) of corresponding thio-conjugates with L-cysteine and with 2-mercaptoethanol (2-ME), as described below for other iodoacetamides. Both Cys- and 2-ME-conjugates of this product were at least 90% HPLC-pure (a single peak). No further purification of the above I-Cca preparations was thus required, though it might be attained with MeOH/water.

N-Iodoacetyl-β-(2-naphthyl)-alanine (I-Nal) (MW 383.18) was prepared by iodoacetylation of *β*-(2-naphthyl)-(*L*) alanine purchased from Bachem, California. The procedure identical to the above was employed; however, 50 mM sodium phosphate buffer was used instead of 5% $NaHCO_3$. After extensive washings of HCl-precipitated product with water and vacuum-drying performed as above, the crude preparations (average iodoacetylation yield ≈ 50%) were recrystallized from MeOH/DDW. The purity of the recrystallization fractions was checked in sample preparations (5 mg from each recrystallization fraction) of corresponding thio-conjugates with L-cysteine and with 2-mercaptoethanol (2-ME), prepared according to the reaction procedure described below, with cysteine or 2-ME taken at 2:1 molar excess. The conjugate solutions thus obtained were acidified by 1% TFA to quench the reaction and immediately analyzed by reversed-phase HPLC (DDW/0.1% TFA-80% MeCN/0.1% TFA gradient monitored at 280 nm, Waters HPLC binary pump system, 0.5 mL/min flow rate, Protean RP-18 column). Two main recrystallization fractions, that provided essentially HPLC-pure conjugates both with 2-ME

and with cysteine (a single peak, > 90% purity), were combined, dissolved in minimal amount of MeOH, then diluted with excess DDW and lyophilized to leave snow-white crystalline powder, with overall postpurification yield of ~20%. The ^{1}H NMR and UV spectra of this preparation essentially corresponded to those of the starting β-(2-naphthyl)-(*L*) alanine. A quadruplet peak 3.78 in ^{1}H NMR (^{1}H of ICH_2CO-group) appeared in both of the main recrystallization fractions. Thiol-reactivity of this preparation determined as above was ~70% (see the respective section below).

5-Iodoacetamidosalicylic acid (I-Sa) (MW 321.07), which is not commercially available currently (production was discontinued in 1986 by Molecular Probes), was synthesized starting from 5-aminosalicylic acid and purified by recrystallization from MeOH/DDW, with HPLC characterization of sample 2-ME- and *L*-cysteyl-S-conjugates prepared from recrystallization fractions, in the same way as described above for I-Nal. Combining fractions that yielded HPLC-pure (>90%) thiol-conjugates resulted in a white (yellowish) crystalline powder (overall post-purification yield ≈ 20%). The ^{1}H NMR spectra of this preparation essentially corresponded to those of the starting 5-aminosalicylic acid. UV spectra were identical to those described in the catalog of Molecular Probes (1986). A singlet peak 3.90 in ^{1}H NMR (^{1}H of ICH_2CO group) appeared in the main recrystallization fraction. Thiol reactivity of this preparation determined as above approached 100%.

Preparation and Analysis of Protein Mutants. Recombinant plasmid pEAK91, containing the intact gene coding for *E. coli* adenylate kinase (AK) (Reinstain et al., 1988), was gifted by Prof. A. Wittinghofer. The plasmid coding for cysteine-free (C77S)-adenylate kinase mutant (S_{77}-AK) was prepared previously (Sinev et al., 1996a). This plasmid was employed for preparations of mutant plasmids by site-directed mutagenesis method described by Kunkel et al. (1987). Thus, all mutant proteins contained the extra C77S mutation. To confirm the introduced mutations, the full-length AK gene was sequenced for each mutant plasmid. The *E. coli* strain HB101, transformed by the appropriate plasmid, was used for production of wild-type and mutant AKs. Proteins were purified as previously described (Sinev et al., 1996a) and checked for the presence (or the absence, in the case of cysteine-free mutants) of cysteine residues by the Ellman reaction (Riddles et al., 1979).

Reactivity and Specificity of Thiol-Reactive Fluorescent Probes. Reactivity of the used iodoacetamide probes I-Nal, I-Cca, I-Sa, and I-LY (see Figure 1) toward thiol groups was tested with low molecular weight thiols, in 0.1 M Tris-HCl (pH 8.0) containing 1 mM EDTA (the labeling buffer, B_l), each at equivalent ratio of a probe (0.3 mM) and a thiol, L-cysteine (0.3 mM), or DTT (0.15 mM), correspondingly. The reagents were mixed by vortexing and then left for 1 h in the dark at room temperature. The amount of unreacted thiols was determined by the Ellman test (Riddles et al., 1979). The synthesized iodoacetamide fluorescent probes I-Sa, I-Cca, and I-Nal showed almost quantitative SH-reactivity. Both with L-cystein and DTT, the yield was about 100, 85, and 70% for I-Sa, I-Cca, and I-Nal, respectively. Relatively low labeling yield with the commercial I-LY, 40%, might be caused by its known lability under standard SH-labeling conditions (Haugland, 1992).

Possible side reactivity of the probes toward nonthiolic groups in a protein was checked using cysteine-free S_{77}-AK mutant. The latter was incubated for 1 h in buffer B_l (at 100−130 μM), in the presence of high molar excess of an iodoacetamide-containing probe (0.5−2 mM). The incubation was stopped by addition of DTT up to 20 mM final concentration. The content was then transferred to 20 mM Tris-HCl (pH 8.0) (the buffer A), by extensive dialysis. An aliquot of the resulting solution was loaded on an ion-exchange (Mono Q HR 5/5) column equilibrated with buffer A and analyzed [Pharmacia FPLC chromatographic system, linear gradient of NaCl concentration (0−0.3 M), 0.5 mL/min], to detect side covalent attachment of charged species (i.e., the tested iodoacetamide probes). None of the four probes was found to have noticeable reactivity toward nonthiolic residues in the protein used.

Labeling of Cystein Mutants and Purification of the Labeled Protein Derivatives. Prior to labeling, single-cysteine AK mutants were preincubated for 1 h with 10−20 mM DTT as a reducing agent. The DTT was then removed by gel-filtration using a 10 mL Bio-Gel P-6DG column (Bio-Rad), equilibrated with the buffer B_l. Labeling was performed in the buffer B_l, at 50−80 μM protein concentration using a 10−20 M excess of the thiol-reactive probe. Upon mixing, reagents were incubated for 1−1.5 h in the dark at room temperature; the reaction was then stopped by DTT addition (up to 20 mM final concentration). Further, the labeled derivatives were separated from the unreacted protein according to the procedure modified from (Sinev et al., 1996a,b). In brief, the protein solution was first dialyzed against buffer A, containing 1 mM DTT and 1 mM EDTA, to remove the bulk of the unreacted dye. It was then passed through the 10 mL gel-filtration column (Bio-Gel P-6DG) equilibrated in buffer A (containing 1 mM DTT) to remove the residual dye. (DTT and EDTA were added to the buffers in order to prevent oxidation of the unreacted thiol of cysteine mutants. Without these additives, side elution peaks of charged species derived by oxidation/dimerization of thiol groups in unlabeled protein were observed to interfere with the collected peak of the purified product.) The following anion-exchange separation was performed with Mono Q HR 5/5 column [Pharmacia FPLC chromatographic system, linear gradient of NaCl concentration (0 to 0.3 M), 0.5 mL/min], with total protein amount not exceeding 1 mg. In all separation runs, the difference in charge between the unlabeled mutants and their labeled derivatives (bearing an extra negative charge) was large enough for efficient separation (see Figures 3 and 4).

Activity Measurements. Specific enzymatic activities of AK derivatives were determined toward ADP formation (MgATP + AMP ↔ MgADP + ADP) by a spectrophotometric assay employing pyruvate kinase-lactate dehydrogenase coupling system (Rhoads and Lowenstein, 1968). The reaction mixture contained 0.1 M Tris-HCl (pH 7.5), 0.1 M KCl, 10 mM $MgCl_2$, 0.2 mM NADH, 1 mM of phosphoenolpyruvate, the coupling enzymes (3 units/mL for each enzyme), 0.2 mM AMP, and 1 mM ATP (Sinev et al., 1996a). Activity measurements were performed at 25 °C. The values of specific activity were expressed in international units (IU) of enzyme activity per milligram of the protein. One IU defines an amount of enzyme catalyzing the conversion of 1 μmol of substrate/min under the assay conditions.

Spectroscopic Characterization of Fluorescent Probes. Absorption spectra were measured on an Aviv model 17DS UV−vis spectrophotometer (AVIV Assoc., Lakewood, NJ). Fluorescence spectra were recorded on an AVIV ATF-105 spectrofluorimeter, using slit band width of 1 and 3 nm at the excitation and emission monochromators, respectively. All measurements were

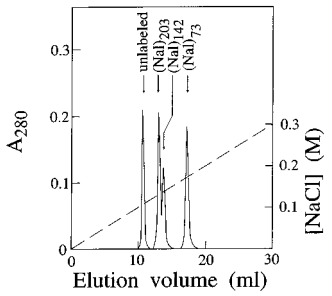

Figure 3. Typical separation of a mixture containing single-cysteine AK mutants labeled with *N*-iodoacetyl-*β*-(2-naphthyl)-alanine (I-Nal) and unlabeled cysteine mutants, by anion-exchange chromatography on a Mono Q column. A total of 720 μL of protein solution in 20 mM Tris-HCl (pH 8), containing unlabeled C_{73}-AK (250 μg), NaI_{73}-AK (200 μg), NaI_{142}-AK (150 μg), and NaI_{203}-AK (200 μg) were applied on the Mono Q column (0.5 × 4.5 cm) equilibrated with the same buffer. The column was washed by 5 mL of the buffer and the proteins were eluted with the linear gradient (0−0.3 M) of NaCl concentration (plotted as the dashed line) at flow rate 0.5 mL/min. Positions of peaks related to the unlabeled C_{73}-AK and Nal-labeled AK derivatives listed above were reproducible from the preceding analytical runs of individual compounds. In separate runs under the same conditions, peak position of NaI_{55}-AK was identical to that of NaI_{203}-AK, whereas those of single-cysteine AK mutants C_{55}- and C_{142}-AK were approximately the same as that of C_{73}-AK. The position of the peak for C_{203}-AK was shifted by ∼0.5 mL toward higher NaCl concentration as compared to that of C_{73}-AK (not shown).

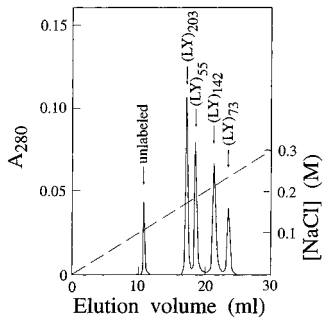

Figure 4. Typical separation of a mixture containing single-cysteine AK mutants labeled with Lucifer yellow iodoacetamide (I-LY) and unlabeled cysteine mutants, by anion exchange chromatography on a Mono Q column. A total of 580 μL of protein solution in 20 mM Tris-HCl (pH 8), containing C_{73}-AK (37 μg), LY_{55}-AK (37 μg), LY_{73}-AK (26 μg), LY_{142}-AK (37 μg), and LY_{203}-AK (37 μg), were applied on the Mono Q column (0.5 × 4.5 cm) equilibrated with the same buffer. The column was washed by 5 mL of the buffer and the proteins were eluted with the linear gradient (0−0.3 M) of NaCl concentration (plotted as the dashed line) at flow rate 0.5 mL/min. Positions of peaks related to the unlabeled C_{73}-AK and LY-labeled AK derivatives listed above were reproducible from the preceding analytical runs of individual compounds. In separate runs under the same conditions, peak positions of C_{55}- and C_{142}-AK were approximately the same as that of C_{73}-AK, whereas the position of the peak for C_{203}-AK was shifted by ∼0.5 mL toward higher NaCl concentration (not shown).

performed at 25 °C with protein solutions prepared in 0.1 M Tris-HCl (pH 7.5) by size-exclusion chromatography using Superose 12 HR 10/30 column (Pharmacia).

Absorption spectra were expressed in the units of molar extinction (M^{-1} cm^{-1}): $\epsilon(\lambda) = [OD(\lambda) \times M_p]/(lc)$, where OD is the optical density of the protein solution; M_p is the protein molecular mass [evaluated as 23 600 Da, which corresponds to the value of molecular mass for the wild-type AK (Brune et al., 1985)]; l is the optical path length (cm); and c is the protein concentration (g/L). Concentrations of protein solutions of the labeled derivatives and cysteine-free tryptophan AK mutants were determined by the method of Lowry et al. (1951) using wild-type AK as a calibration standard. The protein concentration for wild-type AK was determined by using the absorption coefficient $A_{277nm} = 0.5$ $(mg/mL)^{-1}$ cm^{-1} (Girons et al., 1987).

The Förster distance (R_0) and the average fluorescence lifetime of the donor are the basic spectroscopic parameters of a D/A pair of fluorescent probes, which determine the limits of applicability of a given pair for structural studies by FRET techniques. The Förster distance corresponds to the interprobe distance at which the rate of energy transfer (from the excited donor molecule to the acceptor) equals the rate of depopulation of the excited state of the donor, in the absence of the acceptor. (In this case, efficiency of energy transfer equals 50%.) The Förster distance of the donor−acceptor pairs of the fluorescent probes was calculated (in angstroms) using the spectroscopic properties of the probes (Van Der Meer et al., 1994):

$$R_0 = 0.211(\kappa^2 n^{-4} Q_d J_{da})^{1/6} \quad (1)$$

where Q_d is the quantum yield of the donor; κ^2 is the orientation factor (taken as $^2/_3$); n is the refractive index of the medium between the probes (taken as 1.34); J_{da} is the normalized spectral overlap integral (M^{-1} cm^{-1} nm^4). The overlap integral was calculated as $J_{da} = [\sum f_d(\lambda)\epsilon_a(\lambda)\lambda^4\Delta\lambda]/[\sum f_d(\lambda)\Delta\lambda]$, using the corrected fluorescence emission spectrum of the donor, $f_d(\lambda)$, and the absorption spectrum of the acceptor, $\epsilon_a(\lambda)$, respectively. The quantum yield of the donor fluorescent probes, Nal and tryptophan, was determined by the reference method, using solution of degassed naphthalene in cyclohexane [$Q = 0.23$ (Berlman, 1971)] and solution of L-tryptophan in water [$Q = 0.144$ (Wiget and Luisi, 1978)]. Quantum yields of Sa and Cca were determined using a solution of quinine sulfate in 0.05 M H_2SO_4 as a reference [$Q = 0.51$ (Velapoldi and Mielenz, 1980)].

Measurements of fluorescence lifetimes were performed using the time-correlated single-photon counting system described previously (Haas, 1996). Fluorescence emission was collected through a polarizer oriented at the magic angle relative to the polarization of the exciting beam. Decay of fluorescence emission, $I(t)$, was analyzed by a nonlinear list-squares multiexponential fitting (Grinvald and Steinberg, 1974): $I(t) = \sum I_{0i} \exp(-t/\tau_i)$. The average fluorescence lifetime was calculated from the parametrized emission decay: $\langle\tau\rangle = \sum\alpha_i\tau_i$, where α_i and τ_i are the relative amplitude ($\alpha_i = I_{0i}/\sum I_{0i}$) and the lifetime of the ith decay component, respectively.

Energy-Transfer (ET) Experiments. Applicability of the Cca as an acceptor for tryptophan donor for distance determination in proteins was tested by time-resolved ET measurements of two single-tryptophan/single-cysteine AK mutants labeled with I-Cca. Each experiment included measurement of decay of the tryptophan emission in two samples [e.g., W_{169}-AK (the donor without the acceptor) and $W_{169}Cca_{55}$-AK (the donor in the presence of the acceptor)] prepared in 0.1 M Tris-HCl (pH 7.5) at the same protein concentration (0.5 mg/mL). Tryptophan emission was excited at 297 nm and monitored at 360 nm (band width, 8 nm). Efficiency of ET (E) was calculated from the average lifetime of the donor, $\langle\tau_d\rangle$ and $\langle\tau_{da}\rangle$, in the absence and in the presence of the acceptor: $E = 1 - \langle\tau_{da}\rangle/\langle\tau_d\rangle$. An average interprobe distance, R, corresponding to the measured E-value was calculated [$R = R_0 (1/E - 1)^{1/6}$] and was compared with the respective $C_\alpha-C_\alpha$ distance in the crystal structure of the ligand-free AK (Müller et al., 1996).

RESULTS

Purification of the Labeled Derivatives. To ensure the high yield of the labeled derivatives, single-cysteine AK mutants were reacted for 1−1.5 h with 10−20 M excess of thiol-reactive probes. The Ellman test showed that the extent of the labeling reaction was at least 90% for C_{55}-, C_{142}- and C_{203}-AK mutants. However, with C_{73}- and C_{188}-AK, the labeling yields were lower (in several cases ∼50%). In the labeling of C_{73}-AK with LY-I, the yield was as low as 20%. On the other hand, nearly 100% yield with all of the thiol-reactive labels was achieved with C_{203}-AK. Accordingly, in the Mono Q chromatographic profile, the position of the peak corresponding to the unlabeled C_{203}-AK mutant was shifted by ∼0.5 mL toward higher salt concentration, as compared to peak positions corresponding to the unlabeled C_{55}-, C_{73}-, and C_{142}-AK single-cysteine mutants. This shift of the peak position of C_{203}-AK might be related to a larger extent of ionization of the C_{203}-thiol, which is consistent with enhanced reactivity of this mutant.

The difference in charge between the labeled and unlabeled protein species was the basis for postlabeling purification of the conjugates by anion-exchange chromatography. A typical chromatogram demonstrating the separation of single-cysteine AK mutants labeled with a single-charged dye (I-Nal), from the corresponding unlabeled mutants, is shown in Figure 3. The lowest (yet quite satisfactory) resolution was accomplished with the labeled derivatives of C_{203}-AK. The position of the peak corresponding to the C_{142}-AK mutant labeled with I-Nal (i.e., Nal_{142}-AK), was slightly shifted toward higher salt concentration, as compared to that of Nal_{203}-AK or Nal_{55}-AK. The peak position relating to Nal_{73}-AK was even further shifted. A very similar separation pattern was found with the cysteine AK mutants labeled by the other single-charge reactive dyes I-Sa and I-Cca (Sinev et al., 1996a,b). In the case of the cysteine AK mutants labeled with the double-charged I-LY, the separation pattern was essentially similar to those of the corresponding derivatives conjugated with single-charged probes (see Figure 4). In agreement with the difference in charge, the resolution between the peaks of the LY-labeled derivatives and those of the unlabeled mutants was significantly better. Distinctive feature of the chromatographic pattern of the LY-labeled derivatives was good resolution between the peaks related to LY_{203}- and LY_{55}-AK. On the contrary, in the case of the single-charged probes, the peaks corresponding to the labeled derivatives of C_{55}- and C_{203}-AK mutants were not resolved under the same conditions.

Superose 12 size-exclusion chromatography of the labeled AK derivatives did not show any diversity in their elution characteristics. None of the derivatives had elution volume different from that of the wild-type protein.

Spectral Properties of the Labeled Derivatives. Conjugates of single cysteine AK mutants with thiol-reactive labels were used to determine spectroscopic properties of corresponding fluorescent probes, and further, to match possible donor/acceptor pairs of the probes for FRET studies. Absorption spectra and molar extinction coefficients of the protein conjugates were marginally dependent on the location of the probe attachment. Thus, extinction coefficients determined for cysteine AK mutants labeled with I-Nal were 17 100, 17 100, 17 000, 17 200, and 16 800 M^{-1} cm^{-1} for the Nal-AK derivatives labeled at positions 55, 73, 142, 188 and 203, respectively (each value, corresponding to the absorption maximum at 278 nm, represents the average of triplicate determinations). Extinction coefficients determined for Sa-AK derivatives were 3230, 3220, 3170, and 3180 M^{-1} cm^{-1} (the values correspond to absorption maximum at 310 nm) for the Sa-probe at Cys-55, 73, 142, and 203, correspondingly. For each probe, extinction variations depending on the cysteine mutants selected, did not exceed error limits of individual extinction determinations (estimated as 3%). Emission spectra of the fluorescent probes were, in general, slightly dependent on the probe location. Thus, the emission spectrum of Nal in Nal_{142}-, Nal_{188}-, and Nal_{203}-AK derivatives were practically identical to that of Nal conjugate with free L-cysteine. The spectra of Nal in Nal_{55}- and Nal_{73}-AK were 1.5−2 nm red-shifted relative to the spectrum of the Nal-L-cysteine. Small variations in emission spectra of the protein conjugates were also observed with the other fluorescent probes. Examples of absorption and fluorescence emission spectra of fluorescent probes, measured for their protein conjugates, are shown in Figure 5.

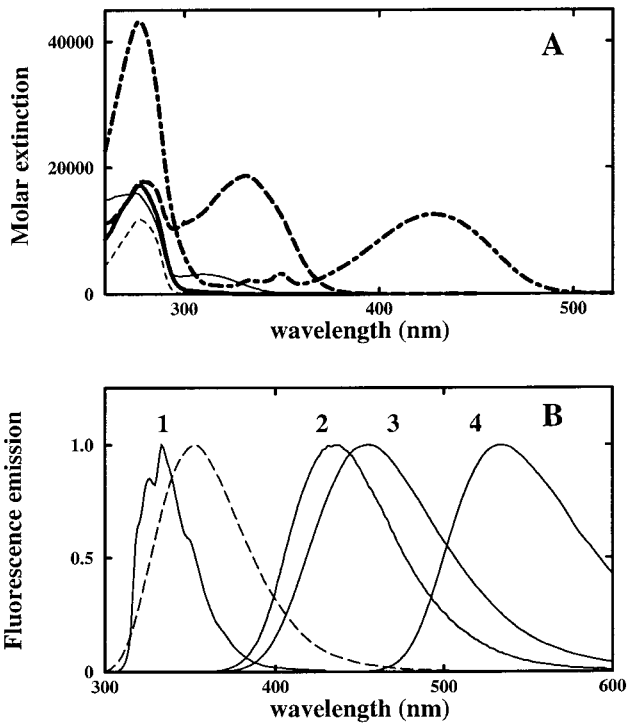

Figure 5. Spectral properties of fluorescent probes in conjugates with single cysteine AK mutants. (A) Absorption spectra of unlabeled C_{203}-AK mutant (dashed line) and its conjugates with Nal (bold solid line), Sa (solid line), Cca (bold dashed line), and LY (bold dotted-dashed line). Absorption spectra are expressed in units of molar extinction (M^{-1} cm^{-1}). (B) Emission spectra of fluorescent probes in conjugates with C_{142}-AK mutant: Nal (1), Sa (2), Cca (3), and LY (4). Emission spectrum of the tryptophan residue in W_{142}-AK is presented by the dashed line. The spectra are corrected for the spectral sensitivity and normalized. Fluorescence emission of tryptophan and Nal was excited at 297 nm. Emission of the other probes was exited at their absorption maximum.

Donor/Acceptor Pairs of Fluorescent Probes. A primary criterion for matching D/A probe pairs for FRET studies is the existence of an essential overlap between fluorescence emission spectrum of one probe (a donor) with absorption spectrum of a second probe (an acceptor). Figure 6 shows overlap of the donor emission spectra (e.g., Nal or tryptophan) and acceptor absorption spectra (e.g., Sa, Cca or LY) of possible D/A pairs. Thus, the excited Nal or tryptophan molecule might be used as an energy donor for nonradiative excitation of Sa, Cca, and

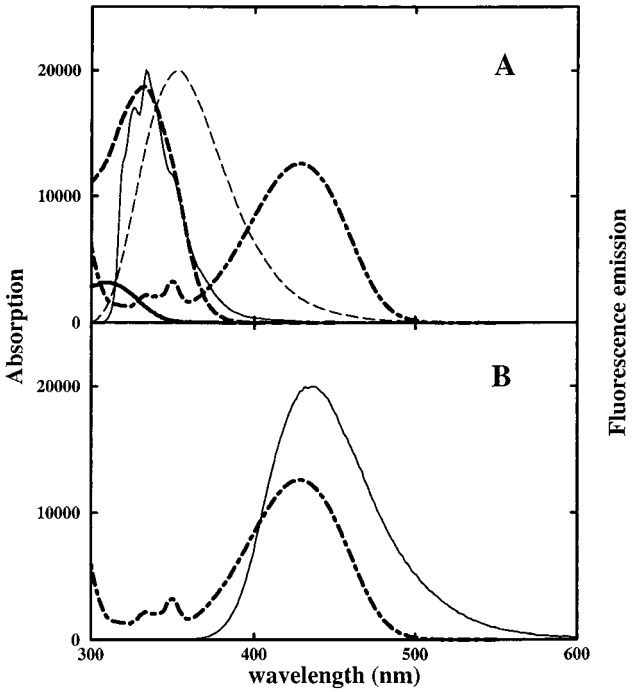

Figure 6. Spectral overlap of fluorescence emission spectra of donor probes and absorption spectra of acceptor probes. (A) The emission spectrum of Nal, conjugate with C_{142}-AK (solid line) and tryptophan, in W_{142}-AK (dashed line), respectively; the absorption spectrum of C_{203}-AK conjugates with Sa (bold line), Cca (bold dashed line) and LY (bold dotted-dashed line), respectively. (B) The emission spectrum of Sa, conjugate with C_{142}-AK (solid line) and the absorption spectrum of C_{203}-AK conjugate with LY. The emission spectra are corrected for the spectral sensitivity and normalized. Absorption spectra are expressed in units of molar extinction ($M^{-1}cm^{-1}$).

LY. Hence, seven possible D/A pairs for FRET studies might be considered, three pairs of probes with Nal as a donor (with Sa, Cca, and LY as acceptors), three corresponding pairs with tryptophan as a donor, and the Sa/LY D/A pair. For each of the above pairs, the quantum yield of donor emission (Q_d), the average fluorescence lifetime of the donor, and the Förster distances (R_0) of the D/A pair were determined (see Table 1). It should be noted that Q_d-values were somewhat dependent on the probe's location [for Nal donor, $Q_d = 0.12$, 0.16, 0.16, 0.17, and 0.23 at Cys-188, 203, 55, 142, and 73, respectively; for Sa donor (see reference *j* in Table 1), $Q_d = 0.26$, 0.28, 0.31, and 0.33 at Cys-203, 142, 55, and 73, respectively]. Due to the weak dependence of R_0 on Q_d, since $R_0 \approx (Q_d)^{1/6}$, the above variations in Q_d-values have minor effect on the calculated R_0-values. Thus, R_0-values calculated for the Sa/LY D/A pair ranged between 31 and 32 Å, depending on variations of Q_d-values and absorption/emission spectra corresponding to different probe location.

When choosing an appropriate fluorescent probe for labeling of a protein, it is strongly desirable to avoid structural alterations caused by the modification. In the case of enzymes, high level of catalytic activity of a labeled protein can provides strong evidence that the original tertiary structure remained essentially intact after the labeling. Thus, specific enzymatic activities of cysteine AK mutants labeled with the thiol-reactive probes studied here were compared with activities of unlabeled mutants. Most of the present derivatives were highly active (see Table 2). Only two out of 23 assayed derivatives (Nal_{55}- and Nal_{73}-AK) showed a major drop in specific activity.

The efficiency of FRET was measured for two labeled derivatives, ($W_{142}Cca_{203}$)-AK and ($W_{169}Cca_{55}$)-AK, and the apparent mean distances were calculated (Table 3). The values of transfer efficiencies found from these measurements (26.7% and 21.2%) were high enough for reliable determination of the corresponding interprobe distances (30.6 and 29.7 Å, for $W_{142}Cca_{203}$-AK and $W_{169}Cca_{55}$-AK, respectively). The apparent mean interprobe distances determined by the ET experiments were in a good agreement with the values between the respective C_α-atoms (30.8 and 29.3 Å) calculated from the recently published crystal structure of the ligand-free enzyme (Müller et al., 1996).

DISCUSSION

The present study was motivated by the need for multiple D/A pairs of probes which can extend the range of time scales and of intramolecular distances, available for determination when characterizing structural processes in proteins. The set of seven D/A pairs presented here allows probing intramolecular distances in proteins in the range 10−40 Å (Table 1). Thus, the R_0 value of the Nal/Sa D/A pair (~17 Å) enables determination of distances from 10 to 26 Å, whereas the R_0 value of the Sa/LY pair (~31 Å) is suitable for probing a range of larger intramolecular distances, from 20 to 40 Å.

Figure 5 shows that for each of the D/A pairs included in the present study, the emission spectra of the corresponding donor and acceptor probes are distinctly resolved (see Figure 5B). This spectral feature allows determination of the contribution of the donor or the acceptor to the emission intensity separately from the contribution of the other probe. The above opportunity, in turn, largely facilitates the separate use of donor and acceptor emission signals for independent evaluation of energy transfer in the double-labeled derivative. Subsequently, this considerably simplifies global analysis of time-resolved ET experiments and, further, simultaneous determination of intramolecular distance distributions (IDDs) and diffusion coefficients (representing rates of structural fluctuations) (Beechem and Haas, 1989; Haas, 1996).

Multiple Measurements Using Sets of Donor/Acceptor Pairs. Three of the four probes studied (Sa, Cca, and LY) can be employed as acceptors when tryptophan or Nal are used as a donor. Both donor probes have similar R_0 with each of the three acceptors and thus the donors seem to be interchangeable when probing similar intramolecular distances in proteins. This opens few practical experimental advantages, as follows.

(a) The use of the tryptophan donor (either naturally present in a protein or specially introduced by site-directed mutagenesis) for structural studies of proteins by FRET spectroscopy extensively simplifies the preparation of the "double labeled" protein derivatives. When a Trp/Cys mutant is used, only one chemical modification is needed. This makes the use of derivatives with Trp-donor useful in preliminary FRET studies of major structural transitions associated with protein functioning (e.g., ligand binding) or folding.

(b) The fluorescence lifetime of the Nal donor is 10-fold larger than that of Trp and offers a time window for more reliable detection of segmental motions in the nanosecond time scales (which are difficult to detect using Trp as a donor). Specifically, as shown in Table 1, substitution of Nal for Trp in each of the present D/A pairs does not lead to a significant shift in R_0 values. The Trp-containing D/A pairs, with τ_d of Trp (3−5 ns), are to be preferred for monitoring faster structural fluctuations

Table 1. Spectroscopic Properties of Donor−Acceptor Pairs of Fluorescent Probes[a]

donor properties[b]					acceptor properties[c]						R_0 (Å)[i]	
	λ_{max} (nm)	Q_d[d]	τ_d (ns)[e,f]			ϵ_a[g]	λ_{max} (nm)		τ_a (ns)[e,h]		donor	
donor	EM	(± 0.01)	τ_i (α_i)	$\langle\tau_d\rangle$ (χ^2)	acceptor	(M^{-1} cm^{-1})	ABS	EM	τ_i (α_i)	$\langle\tau_a\rangle$ (χ^2)	Nal	W
Nal	333	0.17	33.0 (0.62) 40.3 (0.38)	35.8 (1.1)	Sa[j]	3200	310	437	9.15 (0.25) 4.51 (0.75)	5.67 (1.3)	17.0	15.6
W	353	0.24	7.6 (0.06) 5.0 (0.87) 0.5 (0.07)	4.84 (1.2)	Cca[k]	18 700	332	455	1.27 (0.62) 0.65 (0.38)	1.03 (1.0)	26.5	25.9
					LY	12 600	428	534	8.14 (0.87) 5.01 (0.13)	7.73 (1.1)	20.4	24.9

[a] All spectroscopic measurements were performed in 0.1 M Tris-HCl (pH 7.5) at 25 °C. [b] The data refer to spectroscopic properties of *β*-(2-naphthyl)alanine (Nal) and tryptophan (W) donor in single cysteine C_{142}-AK mutant labeled with *N*-iodoacetyl-*β*-(2-naphthyl)alanine (I-Nal) and in single tryptophan W_{142}-AK mutant, respectively. [c] Measurements were performed using C_{203}-AK single cysteine mutant labeled with 5-iodoacetamidosalicylic acid (I-Sa**)**, 7-iodoacetamidocoumarine-4-carboxylic acid (I-Cca) and lucifer yellow iodoacetamide (I-LY), respectively. [d] Q_d is the quantum yield of the donor. [e] Multiexponential analysis of the time-resolved fluorescence emission. Decay parameters of the fluorescence emission τ_i and α_i are the lifetime and the relative amplitude of the *i*th decay component, respectively; $\langle\tau\rangle$ is the average (amplitude-weighted) lifetime (χ^2-values are presented in parentheses). Errors for the average lifetimes are ± 1% of the presented values. [f] Fluorescence emission of the donors (excited at 297 nm) was recorded at 350 and 360 nm for Nal and W, respectively. [g] Molar extinction of the acceptor corresponding to the last absorption maximum (λ_{max}). [h] Acceptor fluorescence was excited at 310 nm for Sa and Cca, and at 400 nm for LY. Fluorescence emission was recorded at the wavelength corresponding to the acceptor emission maximum. [i] The Förster distances of the donor−acceptor pairs. [j] Sa can be as well considered as a donor for LY acceptor; see data given in Results. [k] Quantum yield of the newly synthesized Cca as measured with the Cca-203-AK was 0.11 ± 0.01.

Table 2. Enzymatic Activities of AK Mutants and Their Derivatives Labeled with Thiol-Reactive Fluorescent Probes[a]

	specific activity (IU/mg)[b]										
			single cysteine mutants[e]					tryptophan-containing mutants[e]			
probe	wt[c]	S_{77}[d]	C_{55}	C_{73}	C_{142}	C_{188}	C_{203}	W_{142}	$W_{142}C_{203}$	W_{169}	$W_{169}C_{55}$
none	960	930	920	960	920	940	950	840	940	1190	1100
Nal			360	130	750	820	900				
Sa			710	550	780		960				
Cca			750				980		890		900
LY			650	810	710		940		830		700

[a] Enzymatic activities were determined toward ADP formation (MgATP + AMP ↔ MgADP + ADP). Measurements were performed at 25 °C in 0.1 M Tris-HCl (pH 7.5) containing 0.1 M KCl, 10 mM $MgCl_2$, 0.2 mM AMP, and 1 mM ATP. [b] Specific activities are expressed in international units of enzyme activity (IU) per milligrams of the protein. The values presented are the means of experiments done in triplicates. (As tested separately, reproducibility of the measurements was within 5% of the presented values.) [c] Wild-type enzyme. [d] Cysteine-free (C77S)-AK mutant. [e] All mutant proteins contained the extra C77S mutation. Mutant cysteine and tryptophan positions in AK are denoted with indexed symbols C_i or W_i, correspondingly.

Table 3. Determination of Interprobe Distances in ($W_{142}C_{203}$-Cca)-AK and ($W_{169}C_{55}$-Cca)-AK Derivatives by Time-Resolved Energy Transfer Measurements[a]

	multiexponential analysis of time-resolved fluorescence of the tryptophan donor						
	τ_d (ns)[b]		τ_{da} (ns)[c]				
protein	τ_i (α_i)	$\langle\tau_d\rangle$ (χ^2)	τ_i (α_i)	$\langle\tau_{da}\rangle$ (χ^2)	E[d] (%)	R[e] (Å)	R_{cryst}[f] (Å)
	W_{142}-AK		$W_{142}Cca_{203}$-AK				
$W_{142}Cca_{203}$-AK	7.58 (0.06) 4.97 (0.87) 0.26 (0.07)	4.84 (1.20)	5.22 (0.39) 3.57 (0.38) 0.71 (0.23)	3.55 (1.30)	26.7 (±1.0)	30.6 (±0.3)	30.8
	W_{169}-AK		$W_{169}Cca_{55}$-AK				
$W_{169}Cca_{55}$-AK	6.65 (0.10) 2.35 (0.90)	2.78 (1.22)	4.74 (0.12) 1.84 (0.88)	2.19 (1.24)	21.2 (±1.1)	29.7 (±0.4)	29.3

[a] Each set of energy transfer (ET) experiments included measurements of the time-resolved fluorescence of the tryptophan donor in two protein samples (e.g., W_{142}-AK and $W_{142}Cca_{203}$-AK) prepared in 0.1 M Tris-HCl (pH 7.5) at equal protein concentration (~0.5 mg/mL). Tryptophan fluorescence was excited at 297 nm and detected at 360 nm, with 8 nm slit bandwidth of the emission monochromator. [b] Decay parameters of tryptophan donor emission τ_i and α_i are the lifetime and the relative amplitude of the *i*th decay component, respectively; $\langle\tau_d\rangle$ and $\langle\tau_{da}\rangle$ are the average (amplitude-weighted) lifetimes of the donor in the absence of the Cca-acceptor (χ^2-values are presented in parentheses). Errors for the average lifetimes are ±1% of the presented values. [c] Decay parameters of tryptophan donor emission τ_i and α_i are the lifetime and the relative amplitude of the *i*th decay component, respectively; $\langle\tau_d\rangle$ and $\langle\tau_{da}\rangle$ are the average (amplitude-weighted) lifetimes of the donor in the presence of the Cca-acceptor (χ^2-values are presented in parentheses). Errors for the average lifetimes are ±1% of the presented values. [d] Efficiencies of ET were calculated from the average lifetimes of the donor: $E = 1 - \langle\tau_{da}\rangle/\langle\tau_d\rangle$. [e] Interprobe distances were calculated using the values of the Förster distance (R_0) determined for each derivative: $R = R_0(1/E - 1)^{1/6}$. R_0 values were 25.9 and 23.9 Å for $W_{142}Cca_{203}$-AK and $W_{169}Cca_{55}$-AK, respectively. [f] The average distance between the respective C_α-atoms calculated from the crystal structure of the ligand-free AK from *Escherichia coli* (Müller et al., 1996).

in a protein, whereas Nal-containing pairs (τ_d = 30−50 ns) would be more appropriate when turning to slower fluctuations in the same protein. The synthetic Nal-probe is thereby complementary to Trp as a donor, enabling selection of the proper time scale for studying different structural fluctuations in proteins.

(c) The accuracy of global analysis of time-resolved ET experiments for characterization of protein structural

fluctuations in each of its equilibrium states is enhanced in the case of D/A pairs with increased ratio of the lifetimes of the donor and the acceptor, τ_d/τ_a (Beechem and Haas, 1989). A high τ_d/τ_a ratio enables improved resolution of the ET-induced acceptor emission (excited through energy transfer) and the intrinsic acceptor emission (induced by direct excitation of acceptor probes). This allows improved accuracy in the simultaneous determination of distribution (IDD) parameters and rates of fluctuations related to intramolecular distances, by means of global analysis of the time-resolved fluorescence of both the donor and the acceptor.

(d) Further enhancement of statistical significance in determinations of IDD parameters (particularly in case of wide IDDs) and rates of fluctuations is made possible by series of measurements of each intramolecular distance, using derivatives with different donor and/or acceptor component of the D/A pair. In this way, variation of the optimal time and distance ranges (according to the R_0 and τ_d values) over the range of interest is achieved. This allows additional overdetermination and enhanced statistical significance of the global analysis (Beechem and Haas, 1989). The present series of probes enable either variation of time scale with the distance range fixed (by selecting either Nal or Trp) or variation of distance scales (by using one donor with each one of the three acceptors, i.e., Cca, LY, and Sa).

Thiol-Reactive Charged Probes. So far, the most general and versatile methodology allowing site-specific attachment of various external probes to selected sites on protein's surface is based on the combination of site-directed insertion of cysteine residues (by mutagenesis) and alkylation reaction (thiol-directed labeling) (Mchaourab et al., 1996; Haas, 1996; Sinev et al., 1996a,b; Lillo et al., 1997a,b). This implies the use of probes containing a reliable thiol-reactive linker (that would ensure selective and stable probe conjugation to the cysteine residues in the protein), e.g., iodoacetamide (Haugland, 1992).

All the thiol-reactive probes included in the set presented here are negatively charged at pH >5 and have reactive iodoacetamide linkers. The charged substituents make them water-soluble (at pH >5) and that enables large molar excess of the probe to be used in homogeneous reaction, resulting in high conjugation yields (see Results). The charged groups also diminish undesirable interactions with hydrophobic parts of the protein and thereby reduce the probability for perturbations in the native protein's structure. In the present study, a model protein with enzymatic properties (AK from *E. coli*) was used for tests of the conjugation reactions. This provided a convenient test for overall structural integrity of the labeled protein derivatives, by measurements of the enzymatic activity and comparison with that of the native protein (Table 2). Furthermore, hydrophobic interactions of a covalently linked probe with neighboring protein environment may hinder rotational dynamics of the probe and increase uncertainty in interpretation of the FRET data due to the effect of the dipole orientations (Dale et al., 1979; Van Der Meer et al., 1994). The presence of a polar/charged groups in the probes can enhance the orientation averaging of a D/A pair.

Another advantage of the design and use of charged probes is the enhanced resolution of chromatographic separation of labeled products. High purity of double-labeled protein derivatives is of special concern in applications of FRET spectroscopy for determinations of intramolecular distances and their distributions, where contamination of the double labeled derivatives with single-labeled species might cause problems in processing the experimental data (Lakowicz et al., 1991).

Preparation of Double-Labeled Derivatives. The use of two-cysteine mutants of a protein to be studied provides flexible and efficient means for selection of pairs of sites on the protein surface for attachment of the two probes and for preparation of derivatives labeled by different D/A pairs. This warrants the predominant use of two-cysteine double-labeled derivatives in FRET studies, though labeling of two-cysteine mutants appears to be much more involved as compared to that of the corresponding Trp/Cys mutants.

The practice of double-labeling procedure includes several steps. The first step, labeling of a two-cysteine mutant with one of the probes (either donor or acceptor, depending on separation efficiency of the mono-labeled derivatives obtained), yields a mixture of four products: (1) two single-labeled derivatives which differ in the labeling sites (C−X and X−C), (2) unlabeled protein mutant (C−C), and (3) protein labeled with the first probe in both sites (X−X) (where X is the conjugated probe and C is the free thiol). In general, subsequent separation of such a mixture might be a formidable task, which often requires a multistep purification scheme. However, for charged probes (X), ion-exchange chromatography of this mixture may yield three separate fractions: C−C ("unlabeled"), a still unresolved mixture of C−X and X−C ("single-labeled"), and X−X ("twice labeled"). The second separation step (i.e., the separation of single-labeled species) can be bypassed by labeling a nonseparated C−X/X−C mixture with a second label (denoted as Y). This would yield a mixture Y−X/X−Y (which might contain residual C−X and X−C). The mixture Y−X/X−Y could be useful for FRET experiments by using the original C−X/X−C mixture as a reference, provided that either the extent of labeling of both single-labeled derivatives by the Y probe is close to 100% or at least the rate of labeling for the both of them is essentially the same (and hence the two mixtures have exactly the same molar ratio of the two components, correspondingly). Yet in many cases, neither of these two conditions is fulfilled. The latter thus requires separate use of Y−X and X−Y derivatives in FRET experiments. Site-dependent variations of spectroscopic properties of the X and Y probes commonly suggest that either C−X (in case of Y−X) or X−C (in case of X−Y) derivative should be used as a spectroscopic reference when evaluating energy transfer in the corresponding double-labeled derivative. Apparently, the above could be essentially easier to attain if the corresponding single-labeled species C−X and X−C were available as individual compounds, following efficient separation of the C−X/X−C mixture after the first labeling step.

At first glance, the use of a charged fluorescent probe X for the first labeling of a two-cysteine mutant, though allowing efficient ion-exchange purification of the C−X/X−C mixture from the differently charged postlabeling components (that is C−C and X−X), could hardly assist to the separation between the equally charged C−X and X−C species. However, the electrostatic interaction of a charged protein derivative with an ion-exchange matrix is effected not only by the protein's total charge but also by spatial charge distribution over the protein molecule. The latter, in case of the charged probe attached to the protein, depends on the location of the probe. Indeed, in certain cases, single-labeling of a two-cysteine mutant with a charged probe allowed subsequent separation of

the resulting C−X/X−C mixture by means of ion-exchange chromatography (Sinev et al., 1996b; Lillo et al., 1997a).

In the present study, the effect of the labeling site, in case of a charged probe, on the elution volume of the corresponding single-labeled derivative of the protein in ion-exchange chromatography, was observed with single-cysteine AK mutants. Thus, anion-exchange chromatography of a mixture of cysteine AK mutants, C_{55}-, C_{73}-, C_{142}-, and C_{203}-AK, labeled with the single-charged NaI-probe, yielded three peaks, the first corresponding to coeluted NaI_{203}- and NaI_{55}-AK, the second to NaI_{142}-AK, and the third to NaI_{73}-AK, respectively (Figure 3). When the same cysteine mutants were labeled with the LY probe, which has an extra negative charge as compared to the Cca, NaI, or Sa probes, complete separation of the corresponding derivatives was attained under the same conditions (Figure 4). The latter suggests that the resolution between single-labeled species tends to improve when the charge on the label is increased. The observed effect might be thus practically employed in separating a mixture of single-labeled species C−X and X−C, by choosing, if possible, charged probes for the first labeling of double mutants.

Thereby, the use of charged probes is apparently of advantage when preparing samples of double-labeled protein derivatives suitable for FRET experiments. However, the available probes having the desired spectroscopic characteristics may lack the charged group(s) required for the efficient chromatographic separations of the corresponding protein conjugates. Design of a special charged thiol-reactive reagent ("molecular handle"), which could be reversibly attached to free cysteine residues in the protein, could be of use in the case, e.g., a sulfhydryl similar to the known Ellmann reagent, capable of forming mixed disulfide bonds and charged under chromatographic conditions, could be thus employed for treatment of the corresponding C−X/X−C mixture (where X is an uncharged probe). The resulting mixture of the correspondingly modified (cysteyl-disulfide) protein species, bearing extra charge(s), could be then chromatographically separated and afterward reduced by a thiolic agent (e.g., 2-mercaptoethanole or DTT) in order to detach the handle, thus enabling the subsequent labeling with a second probe.

To summarize, spectroscopic methods that employ labeled protein derivatives, such as time-resolved FRET spectroscopy, fluorescence anisotropy measurements, or electron spin resonance spectroscopy, complement the structure determination methods (X-ray crystallography and NMR) in elucidation of protein structural dynamics (Haas, 1996; Sinev et al., 1996a,b; Lillo et al., 1997a,b; Mchaourab et al., 1996). A preferred set of experimental molecular tools allowing efficient applications of FRET techniques in complex protein studies appears to comprise two major components: first, an appropriately selected set of D/A pairs having both proper spectroscopic characteristics and molecular properties (polarity, charge); second, a corresponding, properly designed set of Cys/Cys (Trp/Cys) mutants. The methodology based on the new FRET probes described above and the procedures of site-specific labeling applied in the present study allows facile site-specific conjugate preparations and wide range of distance determinations. This forms a basis for systematic study of structural transitions in proteins over a wide range of distances. Finally, the Trp/Cca donor/acceptor pair of fluorescent probes, involving newly synthesized cysteinyl-S-linked Cca fluorophore, was successfully used in trial energy transfer experiments for interprobe distance determination, with two Cca-labeled Trp/Cys mutants of *E. coli* AK, $W_{142}C_{203}$ and $W_{169}C_{55}$ (Table 3). Agreement of the distance data obtained here, with the corresponding X-ray parameters (Müller et al., 1996) provides a good practical illustration verifying the suggested design approach.

ACKNOWLEDGMENT

We are thankful to Prof. A. Wittinghoher (Max-Planck Institute für Molekulare Physiologie, Dortmund, Germany) for his gift of the plasmid pEAK91, and to Dr. H. Gottlieb (Bar-Ilan University) for NMR analysis of synthetic preparations. This research was supported by grants from the Israel Science Foundation and the National Institute of Health (USA) RO1-GM39372. The Eshkol fellowship to P. L. is gratefully acknowledged.

LITERATURE CITED

Beechem, J. M., and Haas, E. (1989) Simultaneous determination of intramolecular distance distributions and conformational dynamics by global analysis of energy transfer measurements. *Biophys. J. 55*, 1225−1236.

Berlman, I. D. (1971) *Handbook of Fluorescence Spectra of Aromatic Molecules*, 2nd ed., p 473, Academic Press, New York.

Besson, T., Coudert, G., and Guillaumet, G. (1991) Synthesis and fluorescent properties of some heterobifunctional and rigidized 7-aminocoumarins. *J. Heterocycl. Chem. 28*, 1517−1523.

Brune, M., Schumann, R., and Wittinghofer, A. (1985) Cloning and sequencing of the adenylate kinase gene (*adk*) of *Escherichia coli*. *Nucleic Acids Res. 13*, 7139−7151.

Chen, J., and Selvin, P. R. (1999) Thiol-reactive luminescent chelates of terbium and europium. *Bioconjugate Chem. 10*, 311−315.

Cheung, H. C. (1991) Resonance energy transfer. *Topics in Fluorescence Spectroscopy, Vol. 2, Principles* (J. R. Lakowicz, Ed.) pp 127−176, Plenum Press, New York.

Dale, R. E., Eisinger, J., and Blumberg, W. E. (1979) The orientational freedom of molecular probes. The orientation factor in intramolecular energy transfer. *Biophys. J. 26*, 161−194.

Girons, I. S., Gilles, A.-M., Margarita, D., Michelson, S., Monot, M., Fermandjian, S., *Biophys. J. 26*, 161−194; Danchin, A., and B?rzu, O. (1987) Structural and catalytic characteristics of *Escherichia coli* adenylate kinase. *J. Biol. Chem. 262*, 622−629.

Grinvald, A., and Steinberg, I. Z. (1974) On the analysis of fluorescence decay kinetics by the method of least-squares. *Anal. Biochem. 59*, 583−598.

Haas, E. (1996) The problem of protein folding and dynamics: time-resolved dynamic nonradiative excitation energy transfer measurements. *IEEE J. Sel. Top. Quantum Electron. 2*, 1088−1106.

Haran, G., Haas, E., Szpikowska, B. K., and Mas, M. T. (1992) Domain motions in phosphoglycerate kinase: determination of interdomain distance distributions by site-specific labeling and time-resolved fluorescence energy transfer. *Proc. Natl. Acad. Sci. U.S.A. 89*, 11764−11768.

Haas, E., and Steinberg, I. Z. (1984) Intramolecular Dynamics of Chain Molecules Monitored by Fluctuations in Efficiency of Excitation Energy Transfer. A Theoretical Study. *Biophys. J. 46*, 429−437.

Haugland, R. P. (1992) Molecular Probes. Handbook of fluorescent probes and research chemicals, 5th ed. (1992−1994), Molecular Probes, Inc., Eugene, OR.

Kanaoka, Y., Kobayashi, A., Sato, E., Nakayama, H., Ueno, T., Muno, D., and Sekine, T. (1984) Multifunctional cross-linking reagents. I. Synthesis and properties of novel photoactivable, thiol-directed fluorescent reagents. *Chem. Pharm. Bull. 32*, 3926−3933.

Kunkel, T. A., Roberts, J. D., and Zakour, R. A. (1987) Rapid and efficient site-specific mutagenesis without phenotypic selection. *Methods Enzymol. 154*, 367−382.

Lakowicz, J. R., Gryczynski, I., Wiczk, W., Kusba, J., and Johnson, M. L. (1991) Correction for incomplete labeling in the measurement of distance distributions by frequency-domain fluorometry. *Anal. Biochem. 195*, 243−254.

Lillo, M. P., Beechem, J. M., Szpikowska, B. K., Sherman, M. A., and Mas, M. T. (1997a) Design and characterization of a multisite fluorescence energy-transfer system for protein folding studies: a steady-state and time-resolved study of yeast phosphoglycerate kinase. *Biochemistry 36*, 11261−11272.

Lillo, M. P., Szpikowska, B. K., Mas, M. T., Sutin, J. D., and Beechem, J. M. (1997b) Real-time measurement of multiple intramolecular distances during protein folding reactions: a multisite stopped-flow fluorescence energy-transfer study of yeast phosphoglycerate kinase. *Biochemistry 36*, 11273−11281.

Lowry, O. H., Rosebrough, N. J., Farr, A. L., and Randall, R. J. (1951) Protein measurement with the Folin phenol reagent. *J. Biol. Chem. 193*, 265−275.

Mchaourab, H. S., Lietzow, M. A., Hideg, K., and Hubbell, W. L. (1996) Motion of spin-labeled side chains in T4 lysozyme. Correlation with protein structure and dynamics. *Biochemistry 35*, 7692−7704.

Müller, C. W., Schlauderer, G. J., Reinstein, J., and Schulz, G. E. (1996) Adenylate kinase motions during catalysis: an energetic counterweight balancing substrate binding. *Structure 4*, 147−156.

Reinstein, J., Brune, M., and Wittinghofer, A. (1988) Mutations in the nucleotide binding loop of adenylate kinase of *Escherichia coli*. *Biochemistry 27*, 4712−4720.

Rhoads, D. G., and Lowenstein, J. M. (1968) Initial velocity and equilibrium kinetics of myokinase. *J. Biol. Chem. 243*, 3963−3972.

Riddles, P. W., Blakely, R. L., and Zerner, B. (1979) Ellman's reagent: 5,5′-dithiobis (2-nitrobenzoic acid) − a reexamination. *Anal. Biochem. 94*, 75−81.

Riegel, B., Albisetti, J. C., Jr., Lappin, G. R., and Baker, R. H. (1946) Preparation of 4-qinolinols by the ethyl ethoxalyl acetate method. *J. Am. Chem. Soc. 68*, 2685−2688.

Selvin, P. R., and Hearst, J. E. (1994) Luminescence energy transfer using a terbium chelate: improvements on fluorescence energy transfer. *Proc. Natl. Acad. Sci. U.S.A. 91*, 10024−10028.

Sinev, M. A., Sineva, E. V., Ittah, V., and Haas, E. (1996a) Domain closure in adenylate kinase. *Biochemistry 35*, 6425−6437.

Sinev, M. A., Sineva, E. V., Ittah, V., and Haas, E. (1996b) Towards a mechanism of AMP-substrate inhibition in adenylate kinase from *Escherichia coli*. *FEBS Lett. 397*, 273−276.

Terpetschnig, E., Szmacinski, H., Malak, H., and Lakowicz, J. R. (1995) Metal−ligand complexes as a new class of long-lived fluorophores for protein hydrodynamics. *Biophys. J. 68*, 342−350.

Van der Meer, B. W., Cooker, G., III, and Chen, S. Y. (1994) *Resonance energy transfer. Theory and data*, p 150, VCH Publishers, Inc., New York.

Velapoldi, R. A., and Mielenz, K. D. (1980) *Standard Reference Materials. A Fluorescence Standard Reference Material: Quinine Sulfate Dihydrate*, National Bureu of Standards Special Publication 260-64, p 139, U.S. Government Printing Office, Washington DC.

Wetzel, R., Halualani, R., Stults, J. T., and Quan, C. (1990) A general method for highly selective cross-linking of unprotected polypeptides via pH-controlled modification of *N*-terminal á-amino groups. *Bioconjugate Chem. 1*, 114−122.

Wiget, P., and Luisi, P. L. (1978) Cooligopeptides containing aromatic residues spaced by glycyl residues. IX. Fluorescence Properties of tryptophan-containing peptides. *Biopolymers 17*, 167−180.

Wood, S. J., and Wetzel, R. (1992) Novel cyclization chemistry especially suited for biologically derived, unprotected peptides. *Int. J. Pept. Protein Res. 39*, 533−539.

BC990132L

Self-Assembled Peptides Exposing Epitopes Recognizable by Human Lymphoma Cells

Aijun Tang,[†] Chun Wang,[‡] Russell Stewart,[‡] and Jindřich Kopeček*[,†,‡]

Departments of Pharmaceutics and Pharmaceutical Chemistry/CCCD and of Bioengineering, University of Utah, Salt Lake City, Utah 84112. Received October 11, 1999; Revised Manuscript Received January 19, 2000

A bifunctional *N*-(2-hydroxypropyl)methacrylamide (HPMA) copolymer containing nitrilotriacetic acid (NTA) and benzophenone (BP) groups was synthesized by free-radical copolymerization of HPMA, 2-methacrylamidobutyl nitrilotriacetic acid (MABNTA), and 4-methacrylamido benzophenone (MABP) using 2,2′-azobisisobutyronitrile (AIBN) as initiator. A His-tagged coiled coil stem loop peptide containing a tridecapeptide (TDP) epitope (GFLGEDPGFFNVE) in the loop region (CCSL-TDP) was designed and synthesized genetically by expressing an artificial gene in *Escherichia coli* BL21 (DE3). The peptide was characterized by matrix-assisted laser desorption/ionization time-of-flight mass spectrometry (MALDI-TOF MS), size-exclusion chromatography (SEC), and circular dichroism (CD) spectroscopy. Surfaces containing self-assembled CCSL-TDP peptide were prepared by first covalently grafting poly(HPMA-*co*-MABNTA-*co*-MABP) onto polystyrene (PS) surface by UV irradiation, then charging the surface with nickel through NTA groups, and finally attaching the CCSL-TDP peptide through Ni-histidine chelation. The modified PS surfaces with and without self-assembled CCSL-TDP peptide were characterized by X-ray photoelectron spectroscopy (XPS) and time-of-flight secondary ion mass spectrometry (TOF−SIMS). Cell attachment studies with human Burkitt's lymphoma Raji B cells showed that the cells selectively bound to the self-assembled CCSL-TDP peptide surfaces, but not to the surfaces of PS, PS with grafted copolymer, and PS with grafted copolymer and self-assembled coiled coil peptide with similar structure but without the epitope. This indicates that the cell attachment was mediated by the CCSL-TDP peptide, most probably by the TDP epitope region. The CCSL peptide self-assembly presented here may represent a feasible model of exposing epitopes for biorecognition studies.

INTRODUCTION

In recent years, it has been well accepted that the use of polymeric drug delivery systems is an efficient approach for improving cancer chemotherapy. The covalent binding of anticancer drugs to water soluble polymer carriers can enhance the tumor accumulation and specificity of drug action by the enhanced permeation and retention (EPR) effect (*1*, *2*). *N*-(2-Hydroxypropyl)-methacrylamide (HPMA)[1] copolymers are water soluble and nonimmunogenic and have been frequently used as anticancer drug carriers (reviewed in ref *1*). Clinical data demonstrated that the maximum tolerated dose of HPMA copolymer−doxorubicin (DOX) conjugates was 3−4 times higher than that of free DOX (*3*). In addition, HPMA copolymer-bound DOX has the potential to overcome the P-glycoprotein type of multidrug resistance (*4*), inhibit DNA repair, replication, and biosynthesis and most significantly, to induce apoptosis and lipid peroxidation when compared to free DOX (*5*, *6*). To further increase the specificity and therapeutic efficacy of the HPMA−drug conjugates, our group and collaborators have investigated various compounds such as carbohydrates (*7*) and antibodies (*8*, *9*) for use as targeting moieties to achieve biorecognizability of the conjugates. In addition to antibodies and carbohydrates, receptor-binding epitopes are another type of targeting moiety we are trying to utilize in targetable HPMA copolymer-based drug delivery systems.

Polyvalent interactions are important in biological systems. Such interactions can be collectively much stronger than corresponding monovalent interactions (*10*). Similar polyvalency effects were found in synthetic systems as well. The biorecognition of HPMA copolymers containing side chains terminated in N-acylated galactosamine by the asialoglycoprotein receptor was reported to depend on bound ligand amount (*7*). Polyvalent interactions (cooperative binding) were also observed in the inhibition of virus-mediated agglutination of erythrocytes by polyacrylamides containing pendent sialoside groups (*11*), the recognition of HPMA copolymers containing fucosylamine residues by lectin (*12*), and mouse lymphoma binding of short peptides fused with coiled coil assembly domains into a multivalent binding molecule

* To whom correspondence should be addressed. Phone: (801) 581-4532. Fax: (801) 581-3674. E-mail: Jindrich.Kopecek@m.cc.utah.edu.

[†] Department of Pharmaceutics and Pharmaceutical Chemistry/CCCD.

[‡] Department of Bioengineering.

[1] Abbreviations: AIBN, 2,2′-azobisisobutyronitrile; BP, benzophenone; BSA, bovine serum albumin; CCSL, coiled coil stem loop; CD, circular dichroism; DOX, doxorubicin (adriamycin); HBS, Hepes-buffered saline; HPMA, *N*-(2-hydroxypropyl)-methacrylamide; IMAC, immobilized metal affinity chromatography; MABNTA, 2-methacrylamidobutyl nitrilotriacetic acid; MABP, 4-methacrylamido benzophenone; MALDI-TOF MS, matrix-assisted laser desorption/ionization time-of-flight mass spectrometry; NP, nonapeptide, EDPGFFNVE; NTA, nitrilotriacetic acid; PS, polystyrene; SEC, size-exclusion chromatography; SSIMS, static secondary ion mass spectrometry; TDP, tridecapeptide, GFLGEDPGFFNVE; TOF-SIMS, time-of-flight secondary ion mass spectrometry; XPS, X-ray photoelectron spectroscopy.

10.1021/bc990133d CCC: $19.00 © 2000 American Chemical Society
Published on Web 04/04/2000

(*13*). A main advantage of using small epitopes as targeting moieties is the possibility of incorporating multiple epitope molecules into one macromolecule, which contributes to cooperative interactions. In addition, the use of relatively small epitopes may facilitate the transcompartmental transport compared to that of the large antibody-containing conjugates.

A nonapeptide sequence (NP) EDPGFFNVE is located close to the N terminus of the Epstein−Barr virus (EBV) main envelope protein gp350/220. This NP epitope was demonstrated to be involved in the EBV attachment to CD21 receptor on human B lymphocytes (*14*). CD21/EBV receptor is also expressed on T cells (*15*, *16*). It was found that the amount of CD21 receptor on Raji lymphoblastoid cells is 10−20-fold higher than on normal B cells (*17*). It also appears that EBV receptor is overexpressed on malignant T cells (such as Molt-4) than on normal T cells (*18*). Our group and collaborators investigated the possibility of using the NP epitope as targeting moiety in HPMA copolymer−DOX conjugates for potential treatment of human lymphoma (*19*−*21*). It was found that the apparent binding constants of the NP epitope-containing conjugates to T cells were about two times higher compared to B cells. This modified biorecognition may be explained by the structure of the spacers, i.e, their composition and length. More importantly, the HPMA copolymer(GFLG)-NP-DOX conjugates showed a significantly increased cytotoxicity to the experimental lymphoma cell line when compared to nontargeted conjugates, and the polyvalency effect was also observed. In addition, the targeted conjugate was not toxic to peripheral blood lymphocytes (PBL) at a concentration lethal to T lymphoblastic cells (*19*). Studies of the in vivo targeted delivery of HPMA copolymer-DOX conjugates to HSB-2 human leukemia T cells on a *scid* mouse model showed that the targeted conjugates selectively killed T cells while the nontargeted conjugate did not (*20*). Similar data were obtained on CCRF−CEM human T-cell leukemia model in *scid* mice (*21*). It appears that small synthetic epitopes represent a new category of targeting moieties for polymer-based targetable drug delivery systems.

A coiled coil is a slightly left-handed super-helix formed from two or more right-handed α-helices wound around each other (*22*). The ability of coiled coils to form stable, specific oligomers has been frequently used to engineer novel proteins. Coiled coil structures taken from native proteins or designed de novo have been used to construct highly avid antibodies (*13*, *23*), epitope-displaying scaffolds (*24*−*26*), and other novel chimeric proteins with biological and therapeutic importance (*27*−*30*).

Myszka and Chaiken have applied the basic principle of forming stable coiled coils to design a coiled coil stem loop (CCSL) peptide that has an antiparallel intramolecular coiled coil structure. Their study showed that the RGD sequence incorporated in the loop region is recognizable by the fibrinogen receptor GPIIbIIIa (*24*).

Our long-term goal is to study the structure−biorecognition relationship of motifs including the NP epitope so as to select the optimal oligopeptide(s) for use as targeting moieties in HPMA copolymer−anticancer drug conjugates for the treatment of human lymphoma. To this end, we designed, on one hand, a His-tagged coiled coil stem loop peptide containing a tridecapeptide (TDP) epitope (GFLGEDPGFFNVE) in the loop region (CCSL-TDP) and synthesized the peptide by genetic engineering methods. On the other hand, we designed and prepared a complexed Ni^{2+}-containing surface by covalently grafting onto polystyrene substrate a HPMA copolymer containing nitrilotriacetic acid (NTA) group through which the Ni^{2+} was charged. Upon applying to this surface, the CCSL-TDP peptide would, theoretically, self-assemble through His-Ni chelation in a well-organized manner to expose the receptor-binding epitope moieties on the surface. The biorecognizability of the TDP epitope by human lymphoma cells was studied using Raji B cell line.

EXPERIMENTAL PROCEDURES

Materials. *Chemicals.* N^{ϵ}-*Z*−L-lysine, bromoacetic acid, 5% Pd/C (Fluka, Milwaukee, WI), and 4-aminobenzophenone (Aldrich, Milwaukee, WI) were used without purification. Methacryloyl chloride (Aldrich, Milwaukee, WI) was purified by distillation, and 2,2′-azobisisobutyronitrile (AIBN) (Alfa, Danvers, MA) was purified by recrystallization from ethanol. HPMA was prepared as previously described (*31*).

*Enzymes. Eco*RI, *Nde*I, *Apa*I, T4 polynucleotide kinase, and T4 DNA ligase were obtained from New England Biolabs (Beverly, MA).

Cell Lines. Raji B cell line (Burkitt's lymphoma, human) was obtained from the American Type Culture Collection (ATCC, Rockville, Maryland). Raji cells were cultured in RPMI 1640 medium (Sigma, St. Louis, MO) supplemented with 10% fetal bovine serum (FBS) (Hyclone, Logan, UT). Cells were grown at 37 °C in a humidified atmosphere of 5% (v/v) CO_2 in air.

Falcon 1008 polystyrene dishes (35 × 10 mm, Becton Dickinson, Oxnard, CA) were used as the substrates for the surface modifications and the containers for cell-binding studies.

Synthesis of Poly(HPMA-*co*-MABNTA-*co*-MABP). *Synthesis of 2-Methacrylamidobutyl Nitrilotriacetic Acid (MABNTA).* As described by Schmitt et al. (*32*), N^{α},N^{α}-bis[carboxymethyl]-N^{ϵ}-[benzyloxycarbonyl]-L-lysine (N^{ϵ}-*Z*-NTA derivative) was prepared from bromoacetic acid and N^{ϵ}-benzyloxycarbonyl-L-lysine, and this N^{ϵ}-*Z*-NTA derivative was then hydrogenated using 5% Pd/C to obtain N^{α},N^{α}-bis[carboxymethyl]-L-lysine (NTA derivative). This NTA derivative (2.62 g, 10 mmol) was dissolved in 15 mL of 2 N NaOH and a small amount of the polymerization inhibitor *t*-octylpyrocatechine was added. The solution was cooled to 0 °C. A solution of methacryloyl chloride (1.1 mL, 11.3 mmol) in 10 mL of methylene chloride was added dropwise to this solution while stirring, and with a slight delay, 10 mL of 1 N NaOH was added. The temperature was kept between −10 and 0 °C during the reaction. After addition, the reaction mixture was stirred at room temperature for an additional 2 h. The organic layer was removed, and the aqueous solution was washed with diethyl ether. The aqueous solution was acidified with 6 M HCl to pH 2, and the product was extracted with ethyl acetate (15 × 15 mL). The organic layers were combined and dried over anhydrous magnesium sulfate overnight. The drying agent was filtered off and the solvent was removed by rotary evaporation. The crude product was recrystallized from tetrahydrofuran and dried in vacuo: yield 70%; mp 105−107 °C; TLC R_f 0.78 in methanol/water (4/1). Anal. ($C_{14}H_{22}N_2O_7$) C, H, N. ^{1}H NMR (DMSO-d_6, 200 MHz): δ 1.3−1.6 [m, 6H, (CH_2)$_3$], δ 1.8 (s, 1H, CH_3), δ 3.1 (m, 2H, CONH−CH_2), δ 3.3 [t, 3H, CH_2−CH(COOH)-], δ 3.5 [s, 4H, N(CH_2COOH)$_2$], δ 5.3 and 5.6 (s and s, 2H, CH_2=), δ 7.6 (t, 1H, CON*H*), δ 12.4 (s, 3H, 3COO*H*).

Synthesis of 4-Methacrylamido benzophenone (MABP). 4-Aminobenzophenone (ABP) (0.60 g, 3 mmol) was dissolved in 10 mL of methylene chloride and cooled to 0 °C. Na_2CO_3 (0.32 g, 3 mmol) and a small amount of

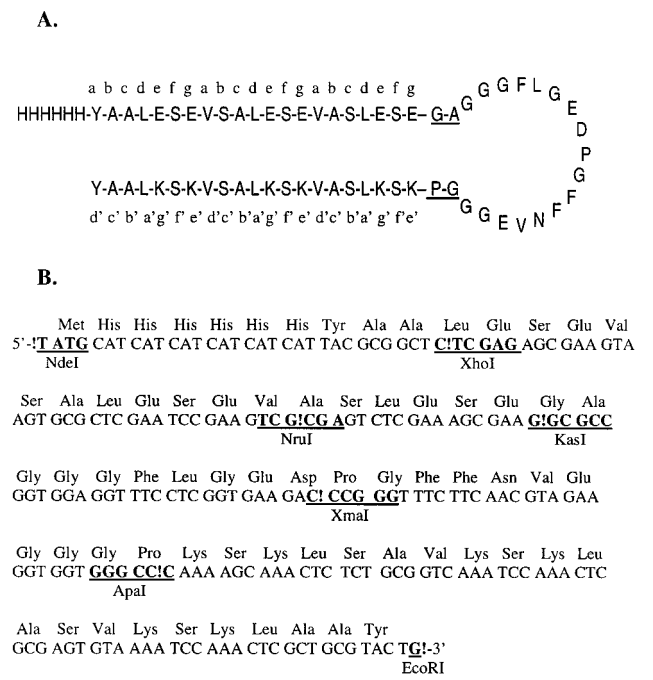

Figure 1. (A) amino acid sequence of the CCSL-TDP peptide containing the tridecapeptide (TDP) epitope in the loop region. (B) cDNA sequence encoding the CCSL-TDP peptide.

polymerization inhibitor were added. A solution of methacryloyl chloride (0.29 mL, 3 mmol) in 5 mL of methylene chloride was added dropwise to the above mixture while stirring, and the reaction temperature was kept between −10 and 0 °C during the reaction. After addition was completed, the reaction mixture was stirred at room temperature for an additional 2 h. The inorganic salt formed was filtered off, and the filtrate was kept at 4 °C overnight. The small amount of solid formed was again filtered off and the filtrate was evaporated to remove most solvent. The residual oily liquid crystallized at 4 °C. The crude product was recrystallized from 2-propanol to obtain white crystals. Molecular weight calculated, 265.33; observed in electrospray ionization mass spectrometry, 265.31; mp 120−122 °C; TLC R_f 0.38 in ethyl acetate/hexane (4/6). ^{1}H NMR (DMSO-d_6): δ 1.98 (s, 3H, CH_3), δ 5.58 and 5.85 (s and s, 2H, CH_2=), δ 7.50−7.90 (m, 9H, C_6H_5−CO−C_6H_4-), δ 10.15 (s, 1H, −CON*H*).

Copolymerization of HPMA, MABNTA, and MABP. Poly(HPMA-*co*-MABNTA-*co*-MABP) was prepared by radical precipitation polymerization in acetone as previously described (*33*). Briefly, HPMA (75 mol %), MABNTA (20 mol %), and MABP (5 mol %) were dissolved in acetone at a total monomer concentration of 12.5 wt %, and the polymerization initiator AIBN was added at a concentration of 0.6 wt %. The copolymerization was allowed to proceed at 50 °C for 24 h, and the copolymer precipitated out as white solid. The copolymer was purified by dissolving it in methanol and reprecipitating it into acetone. The content of NTA group determined by titration was 1.02 μmol/mg copolymer.

Design and Expression of a Coiled Coil Stem Loop (CCSL) Peptide CCSL-TDP. The peptide (Figure 1A) was designed based on the structure proposed by Myszka et al. (*24*). The double-stranded cDNA (Figure 1B), which encods the CCSL-TDP peptide, was chemically synthesized as six single-stranded oligonucleotides of 64−75 nucleotides long. The complementary strands were annealed to form three duplexes (1−3). Duplex 2 was phosphorylated using T4 polynucleotide kinase. A modified expression vector pRSETB (*34*) was digested with *Nde*I and *Eco*RI and purified, and to the two restriction enzyme sites the three duplexes were ligated. The construct was identified by digestion with *Apa*I, and the correctness was verified by direct sequencing. *Escherichia coli* BL21 (DE3) competent cells (Novagen, Madison, WI) were transformed with the recombinant vector, and the target peptide expression was induced by isopropyl β-thiogalactoside (IPTG). The peptide was purified by immobilized metal affinity chromatography (IMAC) using Ni-NTA resin (Qiagen, Santa Clarita, CA) and analyzed by SDS−PAGE for purity.

Characterization of the CCSL-TDP Peptide. *Matrix-Assisted Laser Desorption/Ionization Time-of-Flight Mass Spectrometry (MALDI-TOF MS).* MALDI-TOF MS analysis was performed on a MALDI-TOF mass spectrometer (Voyager-DE STR Biospectrometry Workstation, PerSpective Biosystems, Inc., Framingham, MA).

Circular Dichroism (CD) Spectroscopy. CD spectra were measured in PBS (pH 7.4) or PBS containing 50% trifluoroethanol (TFE) at 4 °C on an AVIV 62DS CD spectrometer equipped with a thermoelectric temperature control system. The wavelength scans were performed using a 0.1-cm cell, a 1-nm bandwidth, and a 5-s averaging time and were repeated three times, averaged, and corrected for buffer contribution. For temperature-induced denaturation−renaturation experiments, the CD signal at 222 nm was monitored over a temperature range of −4 to 70 °C. The temperature was varied in 2 °C increments, and the sample was equilibrated for 5 min before the 60-s data point averaging.

Size-Exclusion Chromatography (SEC). The CCSL-TDP peptide was analyzed on a Pharmacia FPLC system, using an HR10/30 Superdex 75 column and PBS (pH 7.4) as elution buffer. The peptide was dissolved in PBS (pH 7.4) buffer at a concentration of 0.17 and 0.14 mg/mL (or 23.4 and 18.8 μM), and the solutions were filtered through a 0.2 μm filter. The elution of the protein was monitored by UV absorbance at 280 nm and the refractive index.

Construction of a Self-Assembled CCSL-TDP Surface. A poly(HPMA-*co*-MABNTA-*co*-MABP) solution in PBS (1 mL of 0.1 mg/mL) was added to a Falcon 1008 polystyrene dish and it was exposed to 366 nm UV irradiation (1.9 mW/cm^2) for 1 h. The dish was washed with water and ethanol and again with water to remove unbound copolymer. The dish with grafted copolymer was treated with 1 mM NaOH to neutralize the carboxylic groups followed by 40 mM $NiSO_4$ to charge the nickel. After washing, a CCSL-TDP solution (1 mL of 50 μg/mL) in HBS (pH 7.4) was added to the dish and incubation was allowed to proceed for 1 h at room temperature.

Characterization of the Surfaces. *Static Contact Angles.* Static contact angle measurements were performed on polystyrene (PS) before and after copolymer grafting with an NRL C. A. Goniometer (Mountain Lakes, NJ) equipped with a video camera imaging system.

X-ray Photoelectron Spectroscopy (XPS). XPS measurements were performed on a VG Scientific 220i surface analysis system (East Grinstead, U.K.). The XPS spectra and surface composition were determined for PS, PS with grafted copolymer (PS-cop), PS with grafted copolymer and complexed Ni (PS-cop-Ni), and PS with grafted copolymer and self-assembled CCSL-TDP peptide (PS-cop-Ni−CCSLTDP).

Time-of-Flight Secondary Ion Mass Spectrometry (TOF-SIMS). Static SIMS analyses were performed on a CAMECA/IONTOF model TOF-SIMS IV system (Muenster, Germany) with a 3-pA, 25-keV Ga^+ ion beam.

Charge compensation was achieved with a low-energy flood gun. The signal acquisition time was 2 min for all samples.

Cell-Binding Study. Cell-binding study was performed on PS dish without surface modification and on the dishes with modified surfaces, including PS with grafted copolymer, PS with grafted copolymer and self-assembled coiled coil peptide TagEK42 (*34*), and PS with grafted copolymer and self-assembled CCSL-TDP peptide. All dishes were incubated with HBS-2% BSA for 1 h at room temperature to block nonspecific interactions. Raji B lymphoblastoid cells (5×10^5 cells suspended in 1 mL of HBS-2% BSA) were added to the CCSL-TDP-coated dish and control dishes and incubated at 4 °C for 1 h. After washing five times with HBS, cells were fixed by 3% *p*-formaldehyde. Cell attachment was observed by microscopy using a Nikon ECLIPSE E800 Microscope (S&M Microscopes, Colorado Springs, CO) and an image/analysis system Image-Pro Plus (Media Cybernetics, Silver Spring, MD).

The effect of cell density in the suspension on the surface attachment of Raji cells was investigated by using three different cell densities, i.e., 2×10^5, 5×10^5, and 1×10^6 cells/mL.

Cell attachment experiments were also performed with Raji cells at the same density (5×10^5 cells/mL) on different surfaces with adsorbed peptide: PS with adsorbed peptide (PS-CCSLTDP), PS with grafted copolymer and adsorbed peptide (PS-cop-CCSLTDP), PS with grafted and NaOH neutralized copolymer and adsorbed peptide (PS-cop-Na-CCSLTDP), and PS with grafted copolymer and self-assembled CCSL-TDP peptide (PS-cop-Ni-CCSLTDP).

RESULTS

Characterization of the CCSL-TDP peptide. The molecular weight of the CCSL-TDP peptide determined by MALDI-TOF MS was 7277.0, which agrees very well with the theoretical value of 7277.1.

The secondary structure of the CCSL-TDP peptide was characterized by CD spectroscopy. The CD spectra (Figure 2A) indicated that the CCSL-TDP peptide possessed a certain degree of α-helical content and a fairly large amount of random coil structure at 4 °C in PBS buffer. Upon adding the helix-inducing solvent TFE, the ellipticity minimum at 222 nm increased about 2-fold, indicating that the α-helical content was twice of that seen in the absence of TFE. The thermal unfolding of the peptide suggested a largely cooperative structural transition (Figure 2B), yet the broad range of transition and the low midpoint transition temperature ($T_m \approx 20$ °C) are indicative of the presence of loose structures and a relatively low overall stability.

Two peptide concentrations were used in the SEC analysis. A single peptide peak was observed for both concentrations. Using a calibration curve based on elution times of four globular proteins (GCSF 18.8 kDa, carbonate anhydrase 29 kDa, ovalbumin 45 kDa, and albumin 66 kDa), the molecular mass was estimated as 13.1 kDa.

Surface Characterization. The static water contact angles were 82.8 ± 0.4° for PS substrate and 50.4 ± 0.7° for PS with grafted copolymer, indicating a large increase in surface wettability upon modification.

XPS measurements were performed on a control PS surface and on surfaces after subsequent modifications. The spectra are shown in Figure 3 (PS spectrum not shown). The presence of the N1s peak in the spectrum of the PS-cop clearly indicates the attachment of the

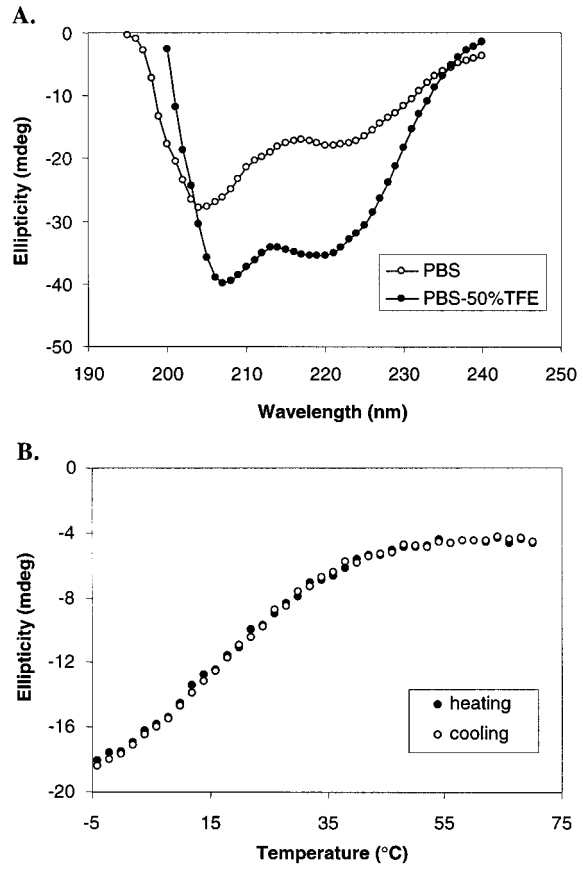

Figure 2. (A) CD spectra of 28 μM CCSL-TDP peptide in PBS (pH 7.4) (open circles) and PBS containing 50% TFE (filled circles) at 4 °C. (B) Temperature dependence of the secondary structure of CCSL-TDP peptide: heating (filled circles), cooling (open circles).

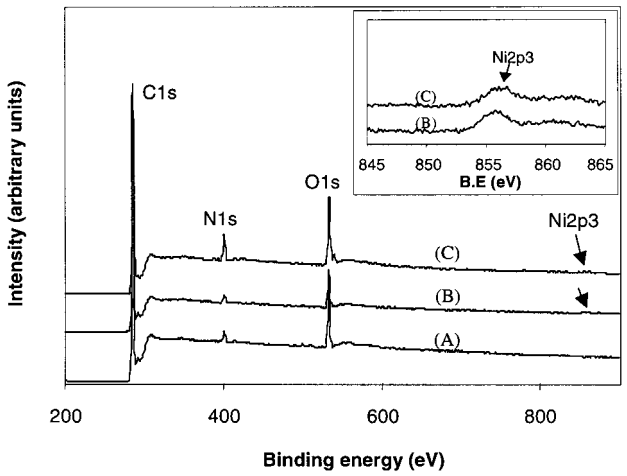

Figure 3. XPS spectra of three surfaces: PS-cop (A), PS-cop-Ni (B), and PS-cop-Ni-CCSLTDP (C).

copolymer to the surface since no N peak was observed for the PS control. The appearance of the Ni2p3 peak in the PS-cop-Ni implies that the Ni^{2+} was charged to the surface.

SSIMS measurements were performed on three surfaces: PS, PS-cop-Ni, and PS-cop-Ni-CCSLTDP, and the spectra of them were compared. Shown in Figure 4A are the positive ion spectra of the PS-cop-Ni (panel I) and PS-cop-Ni-CCSLTDP (panel II). All characteristic peaks listed in the literature for polystyrene (*35*) were observed here for the PS surface (spectra not shown) with correct relative magnitudes. The presence of the peaks with

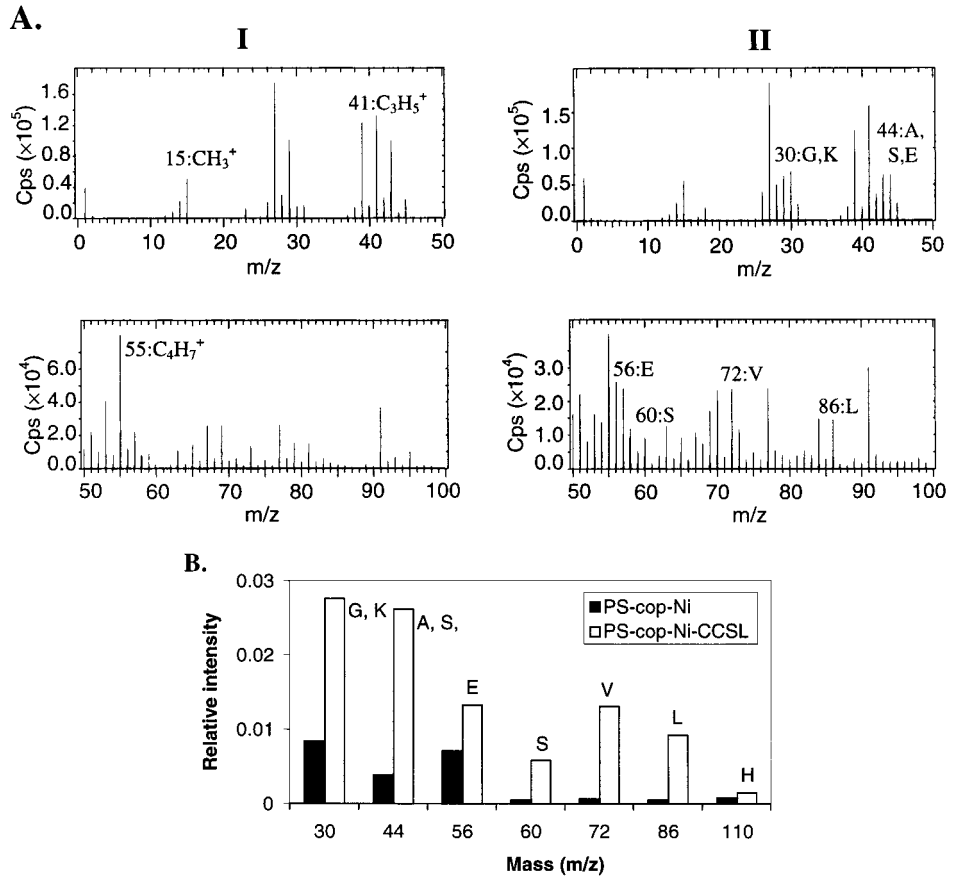

Figure 4. (A) SIMS spectra of two surfaces: PS-cop-Ni (panel I), and PS-cop-Ni-CCSLTDP (panel II). Peaks indicative of some ions from the copolymer are labeled with chemical formulas, and peaks indicative of some of the amino acids are labeled with one-letter abbreviations. (B) Column chart: the relative intensities of relevant peaks in the spectra from the two surfaces, PS-cop-Ni (filled column) and PS-cop-Ni-CCSLTDP (open column).

increased relative intensities in panel I, such as CH_3^+ (*m*/*z* 15), $C_3H_5^+$ (*m*/*z* 41), and $C_4H_7^+$ (*m*/*z* 55), further verified the attachment of copolymer. As is seen from the spectra shown in panel II, some peaks indicative of amino acid residues (*36*) are present with increased relative intensities. Those peaks include the peak at *m*/*z* 30 contributed by glycine, lysine, etc., the peak at *m*/*z* 44 contributed by alanine, serine, and glutamic acid, the peak at *m*/*z* 72 contributed by valine, and the peak at *m*/*z* 86 contributed by leucine, etc. To more clearly present the differences in relative intensities of the relevant peaks for modified PS with and without self-assembled CCSL-TDP peptide, a column chart was graphed in Figure 4B.

Biorecognition of the Self-Assembled Peptide by Lymphoma Cells. Figure 5A shows the pictures of Raji cell attachment to different surfaces. Raji cells attached significantly to the self-assembled CCSL-TDP peptide surface, whereas no cell attachment occurred on the control surfaces of PS, PS-cop, and PS-cop-Ni-TagEK42, where TagEK42 is a coiled coil peptide with similar structure [RGHHHHHHGMASMTGGQQMGRDLYDDDDKDP(VSSLESK)$_6$] to CCSL-TDP but without the epitope (*34*). Figure 5B shows the pictures of cell attachment with increasing cell densities. The higher the cell density in the incubation suspension, the greater the number of cells attached. Shown in Figure 5C are pictures of cell attachment on different surfaces with adsorbed CCSL-TDP peptide. Cells attached to the self-assembled CCSL-TDP peptide surface in a similar manner as before, but attached to the two PS surfaces modified with grafted copolymer and adsorbed peptide in smaller numbers. There was almost no cell attachment to the PS with adsorbed peptide.

DISCUSSION

The combination of receptor-binding epitopes with synthetic water-soluble polymer−drug conjugates to produce targetable polymeric anticancer drugs recognizable by a subset of lymphocytes may yield new potent macromolecular therapeutics effective in the treatment of human lymphomas. The targeting potential of the NP epitope has been evaluated (*19*−*21*); however, detailed studies are needed to find the optimal epitope−receptor pair for the best targeting. While phage display appears to be the most suitable technique for screening a large amount of peptide sequences (*37*), a simplified coiled coil stem loop (CCSL) scaffold may be a better choice as a conformational constraining matrix to present a known epitope sequence to immunocompetent cells for structure-biorecognition studies. The purpose of the current work was to demonstrate the feasibility of preparing a CCSL peptide that would assemble on the surface of a solid substrate and expose an epitope recognizable by lymphoma cells. The rationale of the epitope display and receptor recognition is schematically shown in Figure 6. Figure 6A shows the overall research design, and Figure 6B shows our current approach to assembling the peptide.

The synthetic copolymer poly(HPMA-*co*-MABNTA-*co*-MABP) was designed to contain two types of functional groups, nitrilotriacetic acid (NTA) group and benzophenone (BP) group. NTA is a tetradentate ligand that forms stable bonds with hexacoordinate Ni^{2+}. In fact, Ni-

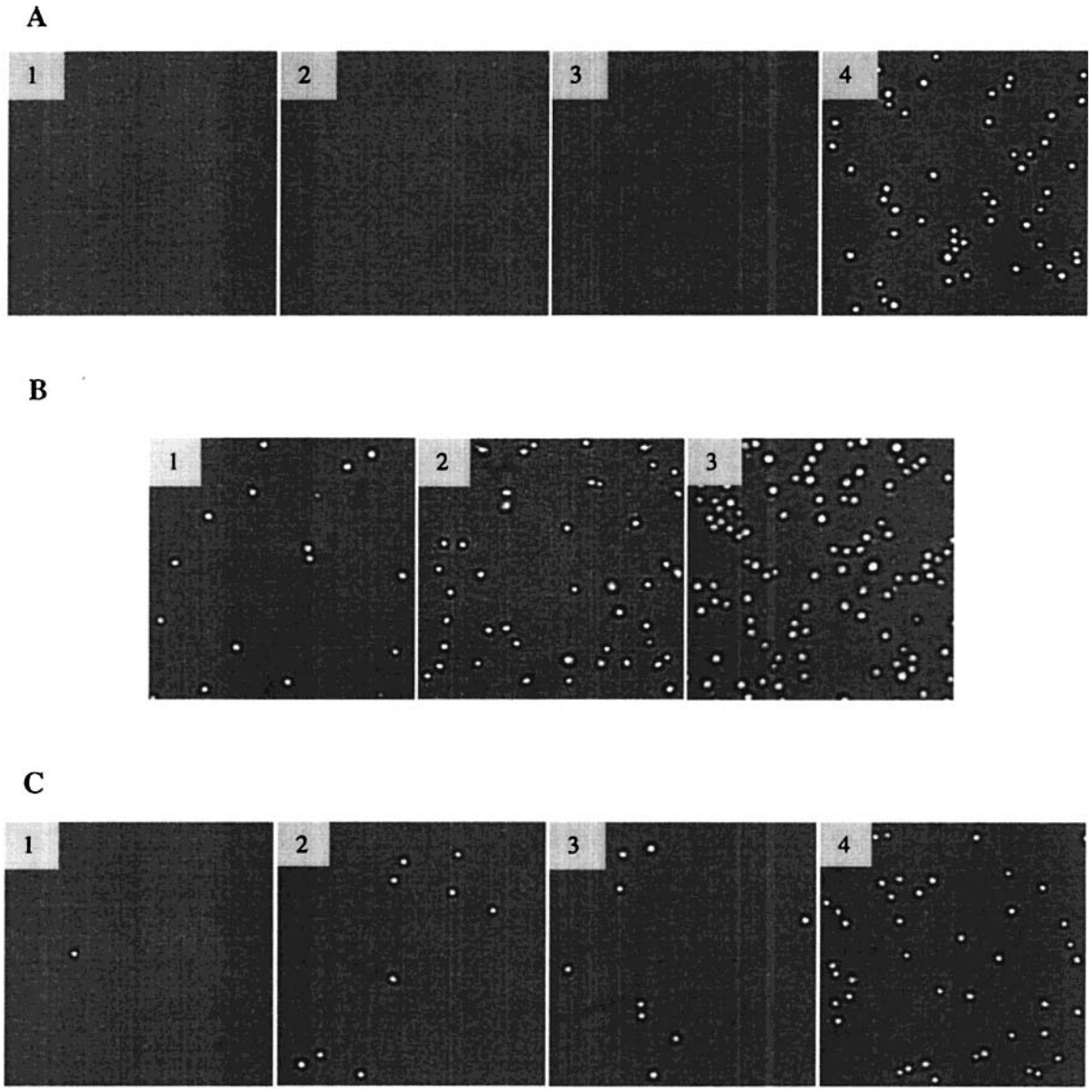

Figure 5. (A) Raji cell attachment to different surfaces: (1) unmodified polystyrene (PS), (2) PS with grafted copolymer (PS-cop), (3) PS with grafted copolymer and self-assembled coiled coil peptide (TagEK42) without the epitope (PS-cop-Ni−TagEK42), (4) PS with grafted copolymer and self-assembled CCSL-TDP peptide displaying the tridecapeptide (TDP) epitope (PS-cop-Ni−CCSLTDP). (B) Raji cell attachment to surfaces containing self-assembled CCSL-TDP peptide at different cell densities: (1) 2×10^5, (2) 5×10^5, (3) 1×10^6 cells/mL. (C) Raji cell attachment to different surfaces containing adsorbed CCSL-TDP peptide: (1) PS with adsorbed peptide (PS-CCSLTDP), (2) PS with grafted copolymer and adsorbed peptide (PS-cop-CCSLTDP), (3) PS with grafted and NaOH neutralized copolymer and adsorbed peptide (PS-cop-Na-CCSLTDP), (4) PS with grafted copolymer and self-assembled CCSL-TDP peptide (PS-cop-Ni-CCSLTDP).

NTA resin has been commercially used in IMAC to purify proteins containing a hexahistidine tag. The BP group is photoreactive (*38*) and serve to covalently attach the copolymer onto a polystyrene substrate. The grafting of the copolymer was visualized by a significant increase in the water wetability of the surface (the static water contact angle changed from 83° before grafting to 50° after grafting). The NTA group, on the other hand, was used to chelate Ni^{2+}. The Ni^{2+} here serves as the bridge between the synthetic polymer and the CCSL-TDP peptide. We hypothesized that if the peptide interacts specifically with the copolymer-modified surface, i.e., through Ni-histidine chelation, a well organized peptide monolayer should form which exposes the biorecognizable epitope.

In our design, we chose a coiled coil peptide to present the receptor-binding epitope. The coiled coil structure is a commonly found folding motif in many native proteins. The most prominent feature of the coiled coil is the heptad repeats $[(abcdefg)_x]$. One heptad constitutes two turns, each covering three and a half residues. Among them, residues "a" and "d" are hydrophobic, while others are usually polar or ionic residues. The coiled coil structure is mainly stabilized by the hydrophobic interactions between helices. Interactions between the ionic residues "e" and "g" are important in specific association among helices. Even though they make only a relatively small contribution to the stabilization of the coiled coil structure, the ion pairs are thought to be important in dictating parallel or antiparallel packing (*24*−*26*, *39*).

Myszka and Chaiken (*24*) designed a 56-residue polypeptide which folded into a stable intramolecular antiparallel coiled coil, referred to as coiled coil stem loop (CCSL). Leucines and valines were used as hydrophobic residues, and glutamic acids and lysines as the ionic ones. Expanding their concept, we designed a 70-residue CCSL

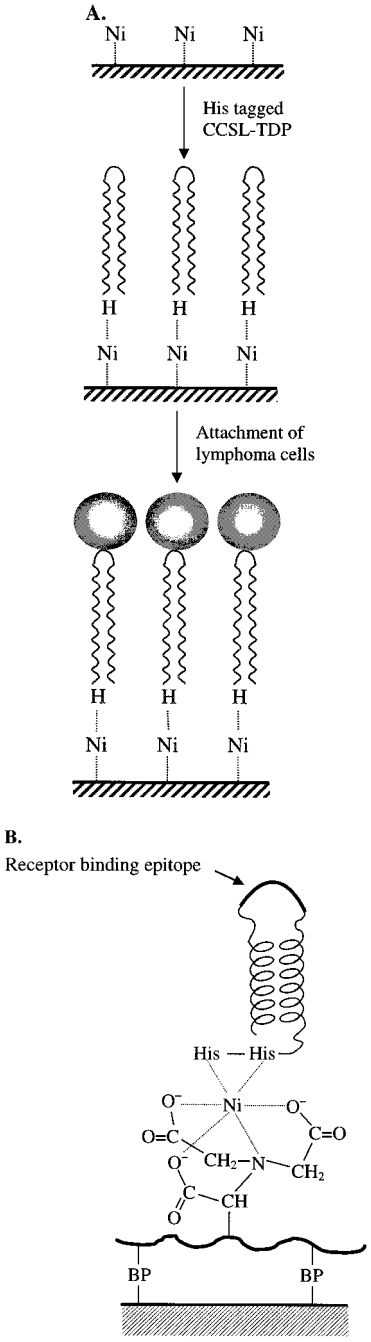

Figure 6. (A) Schematic representation of the general approach to studying the biorecognition of displayed epitopes by lymphoma cells; (B) Current approach to our research design.

peptide (CCSL-TDP) (Figure 1A). The modifications include a 3-heptad stem, a 21-residue loop containing a tridecapeptide (TDP) sequence, a 6-His tag at the N-terminus, and tyrosines at both ends of the stems. The His-tag served to provide means for peptide purification and chelation during self-assembling. Tyrosines were used as chromophores for determining peptide concentration and may be used for radiolabeling. We synthesized the CCSL-TDP peptide by genetic engineering methods. In the design of the cDNA, we incorporated restriction enzyme sites of *Nde*I and *Eco*RI at 5′ and 3′ ends of the coding strand, respectively, so that the DNA segment could be easily inserted into a plasmid vector digested with these two enzymes. Sites of restriction enzymes such as *Apa*I served to detect the insertion of the DNA segment. The *Kas*I and *Apa*I sites corresponding to the hinge regions of the stem loop peptide were specially designed for easy modification of the loop region (Figure 1B).

The CD analyses showed a low α-helical content and a low midpoint transition temperature of the peptide. This may be due to the insufficient ability of the three heptad repeats in each of the stem regions to form a stable coiled coil structure. The length of the coiled coil stem is a major factor in determining the overall stability of the peptide, and it was reported that the helicity of the peptides increased with increasing chain length in a cooperative manner (*40*). The relatively long and randomly structured loop is a significant contributing factor as well. Moreover, the presence of ionic residues (E and K) at the stem-loop junctions as well as the terminal tyrosines may impair the overall stability of the secondary structure. On the other hand, despite the lower content of ordered secondary structure, the thermal unfolding/folding process of this peptide was completely reversible as demonstrated by the overlapping temperature profiles (Figure 2B), which seems to suggest a high specificity for forming such a structure. In addition, the α-helical content in the presence of 50% TFE increased to about 44% as estimated from the observed ellipticity at 222 nm, which is close to the theoretical value of about 60% (42 helix-forming residues and 28 others). This indicates that the designed sequence of the CCSL-TDP stem region has the potential of forming an α-helical structure.

Our approach to the establishment of the peptide self-assembly includes the photografting of a copolymer containing Ni^{2+}-chelating groups and subsequent immobilization of the His-tagged CCSL-TDP peptide in the presence of Ni^{2+}. This peptide immobilization method was similar to the approach of Sigal et al. (*41*) that NTA-Ni-His chelation was employed. However, instead of using a self-assembled monolayer (SAM) formed from alkanethiols on gold surface, we used a polystyrene substrate and a bifunctional HPMA copolymer to constitute the intermediate layer. The generation of the copolymer layer was based on the photoactivity of the benzophenone group. This surface grafting can be conveniently performed on PS Petri dishes, which can be used as such for subsequent modifications and biorecognition studies. The HPMA copolymer chains attached to the substrate surface here may be representative of the environment seen by the target cells during conjugate−cell biorecognition with HPMA copolymer conjugates. The use of a coiled coil scaffold for presenting the biorecognition sequence may be beneficial in providing a constrained conformation mimicking protein domain for the relatively long TDP epitope. The extent of the conformational constraint on the epitope can be modified by varying the structure of the spacers between the stems and the epitope. This model system may be useful for the optimization of peptides that would be most suitable as targeting moieties in HPMA copolymer conjugates.

The surface containing a self-assembled CCSL-TDP peptide and control surfaces were analyzed by both X-ray photoelectron spectroscopy (XPS) and static secondary ion mass spectrometry (SSIMS). XPS and SSIMS are the dominant techniques among others for the surface analysis of real-world polymer systems because they can probe surface chemistry with a high degree of discrimination. They are also highly complementary and are increasingly used together in surface analysis (*42*).

XPS is a surface sensitive technique that provides a quantitative elemental analysis. For each surface, the atomic percentage (at. %) for each element was calculated

Table 1. Comparison of the Atomic Ratios of Selected Elements on Different Surfaces in XPS Analyses

surfaces	*N*/*C*	π^*/C
PS-cop	0.0235	0.0358
PS-cop-Ni	0.0274	0.0368
PS-cop-Ni−CCSLTDP	0.0739	0.0189

from the integrated areas of corresponding peaks after correcting for the different photoelectric cross sections of the orbitals. While the absolute at. % may vary among different measurements for the same sample due to experimental variations, the atomic ratios are always comparable among different samples. Table 1 lists the *N*/*C* and π^*/C (π^* is attributed to the benzene shake-up satellite) ratios of the three surfaces. The *N*/*C* and π^*/C ratios are similar for PS-cop and PS-cop-Ni, which may indicate that the surface copolymer layer is quite uniform in thickness. If this is true, the significant increase in *N*/*C* and decrease in π^*/C ratios can be explained by attachment of CCSL-TDP peptide.

SSIMS is used to probe a material's chemical structure through the mass spectral analysis of its molecular fragments. It is more surface sensitive (~20 Å sampling depth) and more chemically selective than XPS because it can provide detailed molecular information. Mantus et al. (*36*) used SSIMS to analyze proteins adsorbed to biomaterial surfaces and established a spectral interpretation protocol by examining homopolymers of 16 amino acids, which allows for the assignment of peaks unique to various amino acids. Figure 4A, panel II, and Figure 4B showed the presence of some amino acid peaks for the surface containing self-assembled CCSL-TDP peptide. These ions are dominantly immonium ions which have the generic structure of $H_2N^+{=}CH{-}R$. These data suggested the attachment of the peptide on the surface.

In the cell attachment study, the Raji cells selectively bound to the surface containing self-assembled CCSL-TDP peptide but not to control surfaces (Figure 5A). This indicates that there are no specific interactions between the cells and the polystyrene substrate, the copolymer, or a coiled coil peptide that does not contain the epitope. Therefore, the cell attachment was mediated by the CCSL-TDP peptide, most probably by the TDP epitope in the loop region. Not surprisingly, when the cell density was increased, more cells were available to interact with the exposed surface ligands, thus more cells attached to the self-assembled CCSL-TDP surface (Figure 5B).

To test the role of the TDP loop region and the specificity of cell interaction with the CCSL-TDP peptide, a cell attachment study was also performed on different surfaces with adsorbed CCSL-TDP peptide (Figure 5C). In the absence of nickel, the CCSL-TDP peptide probably interacts with the copolymer surfaces mainly through nonspecific interactions rather than Ni-His chelation involving the His-tag. Since the peptide was not well oriented to expose the loop region on the surface, fewer cells attached. The absence of cells on the PS-CCSL surface may indicate that the nonspecific interaction between the peptide and polystyrene results in the TDP region being buried rather than being exposed on the surface. This is not unreasonable considering that the loop region is slightly more hydrophobic than the stem regions where the hydrophobic residues tend to be located in the interface of the α-helices.

In summary, the current data seem to suggest that the CCSL peptide self-assembly on a solid substrate may represent a feasible model for displaying epitopes for biorecognition studies.

ACKNOWLEDGMENT

This work was supported in part by NIH Grants CA51578 and DK39544, and the University of Utah Research Foundation. We thank Dr. David Myszka for valuable discussions, and Mr. Paul Dryden for his assistance with the XPS and SSIMS analyses.

LITERATURE CITED

(1) Putnam, D., and Kopeček, J. (1995) Polymer conjugates with anticancer activity. *Adv. Polym. Sci. 122*, 55−123.

(2) Maeda, H., Seymour, L. W., and Miyamoto, Y. (1992) Conjugates of anticancer agents and polymers: Advantages of macromolecular therapeutics in vivo. *Bioconjugate Chem. 3*, 351−362.

(3) Vasey, P. A., Kaye, S. B., Morrison, R., Twelves, C., Wilson, P., Duncan, R., Thomson, A. H., Murray, L. S., Hilditch, T. E., Murray, T., Burtles, S., Fraier, D., Frigerio, E., and Cassidy, J. (1999) Phase I clinical and pharmacokinetic study of PK1 [N-(2-hydroxypropyl)methacrylamide copolymer doxorubicin]: First member of a new class of chemotherapeutic agents − drug-polymer conjugates. *Clin. Cancer Res. 5*, 83−94.

(4) Minko, T., Kopečková, P., Pozharov, V., and Kopeček, J. (1998) HPMA copolymer bound adriamycin overcomes *MDR1* gene encoded resistance in a human ovarian carcinoma cell line. *J. Controlled Release 54*, 223−233.

(5) Minko, T., Kopečková, P., and Kopeček, J. (1999) Comparison of the anticancer effect of free and HPMA copolymer-bound adriamycin in human ovarian carcinoma cells. *Pharm. Res. 16*, 986−996.

(6) Minko, T., Kopečková, P., and Kopeček, J. (2000) Efficacy of the chemotherapeutic action of HPMA copolymer-bound adriamycin in a solid tumor model of ovarian carcinoma, *Int. J. Cancer 86*, 108−117.

(7) Duncan, R., Seymour, L. C. W., Scarlett, L., Lloyd, J. B., Rejmanová, P., and Kopeček, J. (1986) Fate of N-(2-hydroxypropyl)methacrylamide copolymers with pendent galactosamine residues after intravenous administration to rats. *Biochim. Biophys. Acta 880*, 62−71.

(8) Říhová, B., Kopečková, P., Strohalm, J., Rossmann, P., Větvička, V., and Kopeček, J. (1988) Antibody-directed affinity therapy applied to the immune system: in vivo effectiveness and limited toxicity of daunomycin conjugated to HPMA copolymers and targeting antibody. *Clin. Immunol. Immunopathol. 46*, 100−114.

(9) Omelyanenko, V., Kopečková, P., Gentry, C., Shiah, J.-G., and Kopeček, J. (1996) HPMA copolymer-anticancer drug-OV-TL16 antibody conjugates. 1. Influence of the method of synthesis on the binding affinity to OVCAR-3 ovarian carcinoma cells in vitro. *J. Drug Targeting 3*, 357−373.

(10) Mammen, M., Choi, S.-K., and Whitesides, G. M. (1998) Polyvalent interactions in biological systems: Implications for design and use of multivalent ligands and inhibitors. *Angew. Chem., Int. Ed. 37*, 2754−2794.

(11) Sigal, G. B., Mammen, M., Dahmann, G., and Whitesides, G. M. (1996) Polyacrylamides bearing pendent α-sialoside groups strongly inhibit agglutination of erythrocytes by influenza virus: The strong inhibition reflects enhanced binding through cooperative polyvalent interactions. *J. Am. Chem. Soc. 118*, 3789−3800.

(12) Rathi, R. C., Kopečková, P., and Kopeček, J. (1997) Biorecognition of sugar containing N-(2-hydroxypropyl)-methacrylamide copolymers by immobilized lectin. *Macromol. Chem. Phys. 198*, 1165−1180.

(13) Terskikh, A. V., Le Doussal, J.-M., Crameri, R., Fisch, I., Mach, J.-P., and Kajava, A. V. (1997) "Peptabody": A new type of high avidity binding protein. *Proc. Natl. Acad. Sci. U.S.A. 94*, 1663−1668.

(14) Nemerow, G. R., Houghten, R. A., Moore, M. D., and Cooper, N. R. (1989) Identification of an epitope in the major envelope protein of Epstein−Barr virus that mediates viral binding to the B lymphocyte EBV receptor (CR2). *Cell 56*, 369−377.

(15) Fingeroth, J. D., Clabby, M. L., and Strominger, J. D. (1988) Characterization of a T-lymphocyte Epstein-Barr virus/C3d receptor (CD21). *J. Virol. 62*, 1442−1447.
(16) Hedrick, J. A., Lao, Z., Lipps, S. G., Wang, Y., Todd, S. C., Lambris, J. D., and Tsoukas, C. D. (1994) Characterization of a 70-kDa, EBV gp350/220-binding protein on HSB-2 T cells. *J. Immunol. 153*, 4418−4426.
(17) Rask, R., Rasmussen, J. M., Hansen, H. V., Bysted, P., and Svehag, S.-E. (1988) Complement C3d,g/Epstein-Barr virus receptor density on human B-lymphocytes estimated by immunoenzymatic assay and immunocytochemistry. *J. Clin. Lab. Immunol. 25*, 153−156.
(18) Sauvageau, G., Stocco, R., Kasparian, S., and Menezes, J. (1990) Epstein−Barr virus (EBV) receptor expression on human $CD8^+$ (cytotoxic/suppressor) T lymphocytes. *J. Gen. Virol. 71*, 379−386.
(19) Omelyanenko, V., Kopečková, P., Prakash, R. K., Ebert, C. D., and Kopeček, J. (1999) Biorecognition of HPMA copolymer-adriamycin conjugates by lymphocytes mediated by synthetic receptor binding epitopes. *Pharm. Res. 16*, 1010−1019.
(20) Weis, J. H., et al. (unpublished data).
(21) Prakash, R. K., Clemens, C. M., Ebert, C. D., Omelyanenko, V., Kopečková, P., and Kopeček, J. (1997) Targeting of macromolecular prodrugs to T-lymphocytes. *Proc. Intl. Symp. Controlled Release Bioact. Mater. 24*, 859−860.
(22) Lupas, A. (1996) Coiled coils: new structures and new functions. *Trends Biochem. Sci. 21*, 375−382.
(23) Pack, P., Müller, K., Zahn, R., and Plückthun, A. (1995) Tetravalent miniantibodies with high avidity assembling in *Escherichia coli*. *J. Mol. Biol. 246*, 28−34.
(24) Myszka, D. G., and Chaiken, I. M. (1994) Design and characterization of an intramolecular antiparallel coiled coil peptide. *Biochemistry 33*, 2363−2372.
(25) Miceli, R., Myszka, D., Mao, J., Sathe, G., and Chaiken, I. (1996) The coiled coil stem loop miniprotein as a presentation scaffold. *Drug Des. Discovery 13*, 95−105.
(26) Miceli, R. M., Myszka, D. G., Peishoff, C. E., and Chaiken, I. M. (1996) Phage expression of a de novo designed coiled coil stem loop miniprotein scaffold for constrained peptide library display. In *Molecular Diversity and Combinatorial Chemistry: Libraries and Drug Discovery* (I. M. Chaiken and K. D. Janda, Eds.) pp 172−185, American Chemical Society, Washington, DC.
(27) Waterman, M. J. F., Waterman, J. L. F., and Halazonetis, T. D. (1996) An engineered four-stranded coiled coil substitutes for the tetramerization domain of wild-type p53 and alleviates transdominant inhibition by tumor-derived p53 mutants. *Cancer Res. 56*, 158−163.
(28) Tripet, B., Yu, L., Bautista, D. L., Wong, W. Y., Irvin, R. T., and Hodges, R. S. (1996) Engineering of a *de novo*-designed coiled-coil heterodimerization domain for the rapid detection, purification and characterization of recombinantly expressed peptides and proteins. *Protein Eng. 9*, 1029−1042.
(29) Gonzalez, L., Jr., Plecs, J. J., and Alber, T. (1996) An engineered allosteric switch in leucin-zipper oligomerization. *Nat. Struct. Biol. 3*, 510−515.
(30) Lee, D. H., Granja, J. R., Martinez, J. A., Severin, K., and Ghadiri, M. R. (1996) A self-replicating peptide. *Nature 382*, 525−528.
(31) Kopeček J., and Bažilová, H. (1973) Poly[N-(2-hydroxypropyl)methacrylamide] − I. Radical polymerization and copolymerization. *Eur. Polym. J. 9*, 7−14.
(32) Schmitt, L., Dietrich, C., and Tampé, R. (1994) Synthesis and characterization of chelator-lipids for reversible immobilization of engineered proteins at self-assembled lipid interfaces. *J. Am. Chem. Soc. 116*, 8485−8491.
(33) Kopeček, J., Rejmanová, P., and Chytrý, V. (1981) Polymers containing enzymatically degradable bonds, 1. Chymotrypsin catalyzed hydrolysis of *p*-nitroanilides of phenylalanine and tyrosine attached to side-chains of copolymers of N-(2-hydroxypropyl)methacrylamide. *Macromol. Chem. 182*, 799−809.
(34) Wang, C., Stewart, R. J., and Kopeček, J. (1999) Hybrid hydrogels assembled from synthetic polymers and coiled-coil protein domains. *Nature 397*, 417−420.
(35) Briggs, D., Brown, A., and Vickerman, J. C. (1989) *Handbook of Static Secondary Ion Mass Spectrometry*, John Wiley & Sons, Inc.
(36) Mantus, D. S., Ratner, B. D., Carlson, B. A., and Moulder, J. F. (1993) Static secondary ion mass spectrometry of adsorbed proteins. *Anal. Chem. 65*, 1431−1438.
(37) O'Neil, K. T., and Hoess, R. H. (1995) Phage display: protein engineering by directed evolution. *Curr. Opin. Struct. Biol. 5*, 443−449.
(38) Sigrist, H., Collioud, A., Clémence, J.-F., Gao, H., Luginbühl, R., Sänger, M., and Sundarabaru, G. (1995) Surface immobilization of biomolecules by light. *Opt. Eng. 34*, 2239−2348.
(39) O'Shea, E. K., Klemm, J. D., Kim, P. S., and Alber, T. (1991) X-ray structure of the GCN4 leucine zipper, a two-stranded, parallel coiled coil. *Science 254*, 539−544.
(40) Su, J. Y., Hodges, R. S., and Kay, C. M. (1994) Effect of chain length on the formation and stability of synthetic α-helical coiled coils. *Biochemistry 33*, 15501−15510.
(41) Sigal, G. B., Bamdad, C., Barberis, A., Strominger, J., and Whitesides, G. M. (1996) A self-assembled monolayer for the binding and study of histidine-tagged proteins by surface plasmon resonance. *Anal. Chem. 68*, 490−497.
(42) Brigs, D. (1998) *Surface analysis of polymers by XPS and static SIMS*, Cambridge University Press, Cambridge, U.K.

BC990133D

Poly(ethylene glycol)-Modification of the Phospholipid Vesicles by Using the Spontaneous Incorporation of Poly(ethylene glycol)-Lipid into the Vesicles

Keitaro Sou, Taro Endo, Shinji Takeoka, and Eishun Tsuchida*

Department of Polymer Chemistry, Advanced Research Institute for Science and Engineering, Waseda University, Tokyo 169-8555, Japan. Received October 12, 1999; Revised Manuscript Received January 14, 2000

The critical micelle concentrations of 1,2-dipalmitoyl-*sn*-glycero-3-phosphoethanolamine-*N*-[monomethoxy poly(ethylene glycol) (5000)] (PEG-DPPE) and its distearoyl analogue (PEG-DSPE) were 70 and 9 μM, respectively, in buffer solutions ([Tris] = 20 mM, [NaCl] = 140 mM, pH 7.4) at 37 °C. When these PEG-lipid micelle dispersions were mixed with the dispersions of phospholipid vesicles comprised of a C16 membrane, of which the carbon number is 16, or a C18 membrane, the PEG-lipid micelles were dissociated into monomers and then spontaneously incorporated into the surface of the preformed vesicles. The incorporation rates and the enthalpy changes during incorporation were measured with an isothermal titration microcalorimeter. The incorporation rate of PEG-DPPE was faster than that of PEG-DSPE, because the dissociation rate of the PEG-DPPE micelles was faster than that of PEG-DSPE micelles. The incorporation equilibrium constant of PEG-DSPE was larger than that of PEG-DPPE due to its slow dissociation rate from the membrane, caused by the stronger hydrophobic interaction. The combination of PEG-DSPE and the C18 membrane was the most thermodynamically stabilized pair. Furthermore, the dispersion stability of the surface-modified vesicles prepared by this spontaneous incorporation was analyzed by using the critical molecular weight of the polymer for the aggregation of vesicles. The aggregation of the vesicles was successfully supressed with an increase in the molecular weight of the PEG in the PEG-lipid and its incorporation ratio.

INTRODUCTION

It is well-known that phospholipids spontaneously assemble to form vesicles (or liposomes) in aqueous dispersions. The degree of interaction force has been measured as experimental values such as phase transition temperature, flip-flop rate, the magnitude of fusion between vesicles, and fluorescence anisotropy representing segmental motion (*1*). The findings provided the possibility that some amphiphiles with an appropriate hydrophilic−hydrophobic balance could be incorporated into the vesicles by simple mixing as a result of coassembly.

Poly(ethylene glycol) (PEG) is a physiologically stable water-soluble polymer and prevents the access of plasma proteins by its steric hindrance; it has been extensively used to modify not only the surface of phospholipid vesicles but also proteins, drugs, or immobilized materials such as an artificial blood vessel (*2*, *3*). The vesicles of which the surface was modified with PEG chains are used to prevent aggregation and fusion and to prolong blood circulation (*4*, *5*). The PEG modification and physical properties of PEG-lipid/phospholipid mixed systems have been extensively studied (*6*−*11*). We have studied vesicles encapsulating concentrated hemoglobin as artificial red cells and applied the PEG-modification in order to stabilize the dispersion state and prolong their life in blood circulation (*12*).

The PEG-lipid is generally incorporated into the surface of vesicles by mixing it with components in common organic solvents before dispersing them into an aqueous solution. In this case, both sides of the bilayer membrane are modified. The PEG chains extending from the inner surface should reduce the interior volume for encapsulation because of their exclusion volume effect. Furthermore, they do not take part in the steric stabilization of the vesicle dispersion even if they are important from the standpoint of the thermodynamic stabilization (*13*). Modification only to the outer surface was therefore carried out to couple PEG with the phosphatidylethanolamine incorporated into preformed vesicles (*14*) or to mix the PEG-lipid with a vesicle dispersion, followed by the insertion of PEG-lipids into the preformed vesicles (*15*, *16*). However, the detailed study about the incorporation kinetics and equilibrium states has not been reported yet.

In this paper, we observed the spontaneous incorporation of 1,2-dipalmitoyl-*sn*-glycero-3-phosphoethanolamine-*N*-[monomethoxy poly(ethylene glycol)] or 1,2-distearoyl-*sn*-glycero-3-phosphatidylethanolamine-*N*-[monomethoxy poly(ethylene glycol)] into vesicles using an isothermal titration calorimeter and ^{1}H NMR. The kinetics and thermodynamics of the coassembling phenomenon were discussed relating to the hydrophobic interaction force. Furthermore, we clarified the effect of the molecular weight of the PEG on preventing the vesicle aggregation.

EXPERIMENTAL PROCEDURES

Materials. The poly(ethylene glycol) (standard) [PEG (M_w 640, 1040, 1530, 2060, 3070, 9450, 11 000, and 21 230)] was a gift from NOF Co., and PEG (M_w 2560, 3410, 5050, and 6250) was purchased from Sowa Science Co. The M_w/M_n of each PEG was within 1.04. 1,2-Dipalmitoyl-*sn*-glycero-3-phosphoethanolamine-*N*-[monomethoxy poly(ethylene glycol) (5000)] (PEG-DPPE) and 1,2-distearoyl-*sn*-glycero-3-phosphatidylethanolamine-*N*-[monomethoxy poly(ethylene glycol) (2000 or 5000)]

* To whom all correspondence should be addressed.

10.1021/bc990135y CCC: $19.00 © 2000 American Chemical Society
Published on Web 04/14/2000

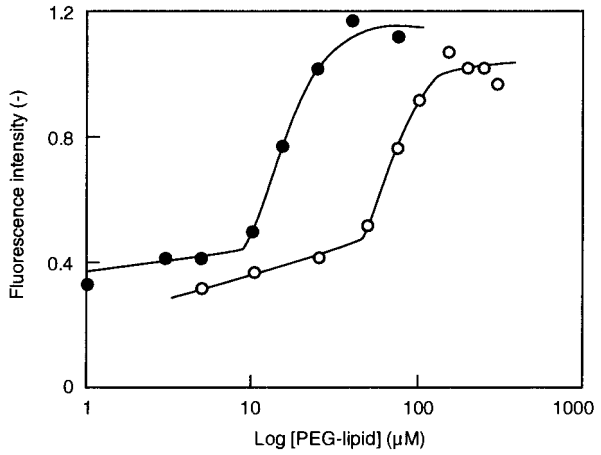

Figure 1. Determination of the critical micelle concentration of PEG-lipids by the fluorescence intensity change of DPH incorporated into PEG-lipid micelles. (○) PEG-DPPE and (●) PEG-DSPE.

(PEG-DSPE) were purchased from NOF Co. The mixed lipid powders of 1,2-dipalmitoyl-*sn*-glycero-3-phosphatidylcholine (DPPC), cholesterol, and 1,2-dipalmitoyl-*sn*-glycero-3-phosphatidylglycerol (DPPG) at 5:5:1 in molar ratio (Presome PPG-I) were used for a C16 membrane. 1,2-Distearoyl-*sn*-glycero-3-phosphatidylcholine (DSPC), cholesterol, and 1,2-distearoyl-*sn*-glycero-3-phosphatidylglycerol (DSPG) purchased from Nippon Fine Chemical Co. were mixed in the same ratio as for the C18 membrane.

Vesicle Preparation. Mixed lipids were dissolved in chloroform and dried in vacuo. to form a film on the wall of a flask. After the film was dispersed into a Tris-HCl buffer solution ([Tris] = 20 mM, [NaCl] = 140 mM, pH 7.4) with glass beads, it was extruded through a polycarbonate membrane filter (the final pore size of the filter was 0.2 μm). The diameter of the resulting vesicles was determined to be 250 ± 40 nm with a Coulter submicron analyzer (model N4SD). The total surface area of the vesicle was measured using 6-*p*-toluidino-2-naphthalenesulfonic acid (Tns) (*17*), and the number of bilayers of the vesicle was measured to be 2.0 and 1.5 for vesicles with a C16 membrane and a C18 membrane, respectively.

Critical Micelle Concentration (CMC). A 1,6-diphenyl-1,3,5-hexatriene (DPH) solution (2 μL, [DPH] = 30 μM, in THF) was added to various concentrations of PEG-DPPE or PEG-DSPE dispersions (2 mL) and incubated at 37 °C for 2 h. We measured the fluorescence intensity of the dispersions and defined the concentration where the intensity increased abruptly as the CMC (*18*). These concentrations were determined to be 70 and 9 μM for PEG-DPPE and PEG-DSPE, respectively, as shown in Figure 1.

Dissociation of the Micelle. The PEG-lipid dispersion ([PEG-lipid] = 0.83 mM, [DPH] = 4.14 μM, 20 μL) was injected into the Tris-HCl buffer (2.7 mL) at 37 °C, and the change in the fluorescent intensity (λ_{ex} = 357 nm, λ_{em} = 430 nm) was recorded with a spectrofluorometer (JASCO FP-770). The initial fluorescence intensity (I_0) decreased gradually to reach the infinite intensity (I_i), and I_t is the fluorescent intensity at t seconds. The intensity ratios, I_t/I_0 or I_i/I_0, show the dynamic change in the DPH environment or an equilibrated state after dilution of PEG-lipid micelles. The concentration of PEG-lipid as micelles at t seconds after diluting them below the CMC is

$$[\text{PEG-lipid}]_{\text{micelle}} = \{(I_t - I_i)/(I_0 - I_i)\}[\text{PEG-lipid}] \quad (1)$$

The rate of demicellization was obtained from the initial change in the $[\text{PEG-lipid}]_{\text{micelle}}$.

Segmental Motion of Acyl Chains of Micelles and Vesicles. A DPH solution (5 μL, [DPH] = 1.4 mM, in THF) was added to a PEG-lipid dispersion (3 mL, [PEG-lipid] = 1 mM). A THF solution in the absence of DPH was added to the PEG-lipid dispersion as a blank. These samples were incubated at 37 °C for 2 h. Fluorescence spectroscopy was carried out with a JASCO FP-770 spectrofluorometer equipped with polarizers and connected to a thermo-controller. DPH was excited at 357 nm, and its fluorescence was detected at 430 nm. The anisotropy of the vesicles with a C16 membrane or C18 membrane was measured by the same method.

Incorporation Rates. The PEG-lipid dispersion (10 μL, [PEG-lipid] = 0.83 mM) was injected by a computer-controlled microsyringe into the vesicle dispersion ([lipid] = 9.9 ≈ 26.0 mM, 1.35 mL) and stirred at 400 rpm, within 2 s. Temperature was strictly controlled to 37 °C. Changes in the calorific values and the total calorific values were measured using an OMEGA titration microcalorimeter (MCS ITC, Microcal, Inc.) (*19*). Identical injection of the PEG-lipid dispersions into buffer solutions in the absence of vesicles or the injection of buffer into vesicle dispersions were performed as control experiments.

The initial rate was analyzed as a second-order reaction, relating to the concentrations of PEG-lipid and the incorporation site from eq 2:

$$\text{d}[\text{PEG-lipid}]/\text{d}t = k_{\text{on}}[\text{PEG-lipid}]_t[\text{incorporation site}]_t \quad (2)$$

where t (seconds) is time passed after injection and $[\text{PEG-lipid}]_t$ and $[\text{incorporation site}]_t$ are concentrations of PEG-lipid and the incorporation site at t (seconds), respectively. The parameter k_{on} was a rate constant for PEG-lipid incorporation. The incorporation site was calculated as described below.

Equilibrium Constants. The PEG-lipid dispersion (19 mL, [PEG-lipid] = 17.5 μM) was added to the vesicle dispersion (25 mL, [lipids] = 17.3 mM) and stirred at 37 °C (final concentration; [PEG-lipid] = 7.6 μM, [lipids] = 9.8 mM). The mixture was intermittently sampled and was used to measure the incorporated amount of PEG-lipid. The sample was centrifuged (100000*g*, 60 min) at 37 °C to remove the unincorporated PEG-lipid as a supernatant. The precipitated vesicles were freeze-dried and dissolved in $CDCl_3$. The peak area ratio of the choline methyl proton of DPPC or DSPC (3.39 ppm) to the methylene proton of PEG (3.63 ppm) was measured by ^{1}H NMR spectroscopy (JEOL JNM-LA500) to obtain the incorporated amount of the PEG-lipid (*9*). The same measurement was carried out for the control sample where unincorporated PEG-lipid was not removed to determine the total amount of PEG-lipid and then free PEG-lipid. The equilibrium constant (K) was calculated from eq 3:

$$K = [\text{incorporated PEG-lipid}]/([\text{incorporation site}][\text{free PEG-lipid}]) \quad (3)$$

where [incorporation site] is the initial concentration of the incorporation site for PEG-lipid in the surface of the mixed lipid vesicles. We estimate it to be the same as the saturated amount of PEG-lipid incorporation, which

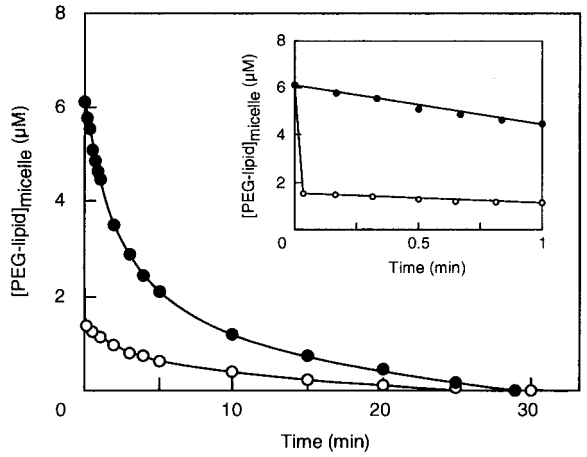

Figure 2. Observation of the PEG-lipid micelle dissociation by dilution below the CMCs at 37 °C from the fluorescence intensity change of DPH. The PEG-lipid dispersions (20 μL, 0.83 mM) were injected into buffer solution (2.7 mL). The final concentration was 6.1 μM (the CMCs of PEG-DPPE and PEG-DSPE were 70 and 9 μM, respectively). The concentration of the PEG-lipids forming micelles was calculated from the fluorescence intensity of DPH. (○) PEG-DPPE and (●) PEG-DSPE.

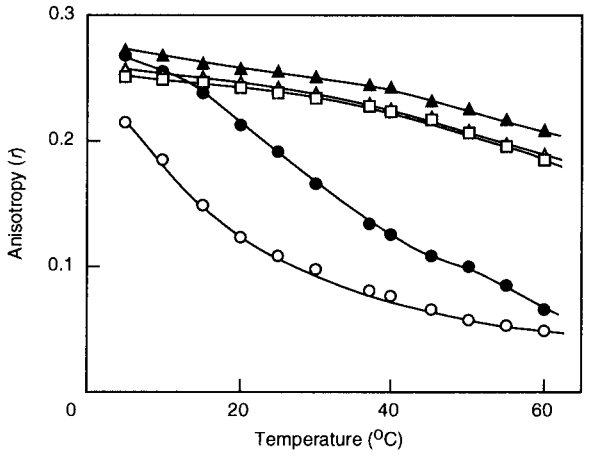

Figure 3. Temperature dependence of the fluorescence anisotropy of the DHP incorporated into micelles or vesicles. (○) PEG-DPPE, (△) C16 vesicle, (●) PEG-DSPE, and (▲) C18 vesicle, (□) C16 vesicles with 5 mol % of PEG-DPPE.

can be obtained from the time course of the PEG-lipid incorporation.

Turbidimetry. The PEG solution (500 μL, 0.12 kg/dm^3) was added to the vesicle dispersion (2 mL, 1.39 mM) in a cuvette (l = 1 cm) at 37 °C. The turbidity change (ΔOD) at 600 nm was monitored for 15 min after the addition of PEG by a UV−vis spectrophotometer (Shimadzu, MPS-2000). The minimum molecular weight of added PEG for the aggregation of the vesicles was defined as a critical molecular weight (M_c) (*20*).

Incorporation of the PEG-Lipid into Unmodified Vesicles by Mixing with Modified Vesicles. The dispersion of vesicles having 1.0 mol % of PEG-lipid (15 mL, [lipids] = 1.39 mM) was mixed with a vesicle dispersion (45 mL, [lipids] = 1.39 mM). The mixed dispersion was incubated at 37 °C, and the time course of M_c was measured by turbidimetry as described above. The PEG-lipid amount incorporated into the unmodified vesicles was calculated from the relationship between M_c and the incorporation ratio of PEG-lipid, because we can monitor only the M_c change. The incorporation rate of the PEG-lipid into unmodified vesicles was calculated from the slope of the straight line in Figure 7.

RESULTS AND DISCUSSION

PEG-Lipid Micelles. As shown in Figure 1, the CMC of the PEG-DSPE is lower than that of PEG-DPPE because of the stronger hydrophobic interaction. However, these values were significantly higher (more than 10^6 times) than diacyl phospholipids (e.g., DPPC < 10^{-10} M), indicating the increase in hydrophilicity by PEG-conjugation. When the PEG-lipid micelle dispersions are diluted below the CMC, the micelles are dissociated into monomers. The concentration of PEG-lipids assembling as micelles was calculated from the fluorescent intensity of DPH. As shown in Figure 2, the rate constant of dissociation for the PEG-DPPE micelles was estimated to be above 3.0 s^{-1} at 37 °C. On the other hand, that for the PEG-DSPE micelles was more than 5×10^{-3} s^{-1} at the same temperature. This also indicates the stronger hydrophobic interaction of PEG-DSPE than that of PEG-DPPE.

PEG-lipid micelles have a lower anisotropy of DPH compared with 250 nm phospholipid vesicles as shown in Figure 3. The lower anisotropy indicates a higher segmental motion of the acyl chains (*21*). The high anisotropy and low temperature dependence of phospholipid vesicles should be due to the cholesterol effect (45 mol % mixture), because cholesterol enhances the membrane packing and alleviates the large change in the segmental motion of acyl chains at the phase transition temperature (*22*). The PEG-lipid micelles have a larger temperature dependence and a larger effect of acyl chain length, attributed to the lower order of the acyl chain packing in the micelles. The PEG-DPPE micelles have a higher segmental motion of the acyl chains than those of PEG-DSPE because of the lower interaction force. The anisotropy of DPH in the phospholipid bilayer having 5 mol % PEG-DPPE in the outer layer is almost the same as that without PEG-DPPE, indicating that the incorporation of PEG-DPPE does not disturb the acyl chain packing in the bilayer membrane. Therefore, when the PEG-lipid micelles, which are not stable assemblies compared with phospholipid vesicles, are mixed with vesicles, the PEG-lipids should be spontaneously incorporated into the highly packed bilayer membrane.

Incorporation of the PEG-lipid into Vesicles. When the PEG-lipid dispersions below the CMC were injected into vesicle dispersions, a heat response could not be detected because of the lower limit of detection (0.2 μcal/s). Therefore, we carried out this experiment above the CMC. When the PEG-lipid dispersion was injected into the vesicle dispersion, an exothermic peak was observed with each addition of titrant as shown in Figure 4, panels a and b. In this figure, the positive and negative values of the y-axis mean the endothermic and exothermic rates, respectively. The first steep increase in the exothermic rate should be caused by the late response of the heat detection after one shot, because the half-response time of this apparatus is around 10 s. If the exothermic rate after baseline compensation with a blank titration were regarded to show the enthalpy change during the incorporation of PEG-lipid, a gradual subsequent return to the baseline would be due to the reduction of the amount of PEG-lipid remaining in the solution. Therefore, we could determine the amount of PEG-lipid in the vesicle from the integration of the exothermic rate and the compensation using molar enthalpy.

Figure 4c represents the incorporation profiles of PEG-DPPE and -DSPE into a C16 membrane. When the concentration of the vesicles was increased twice, the

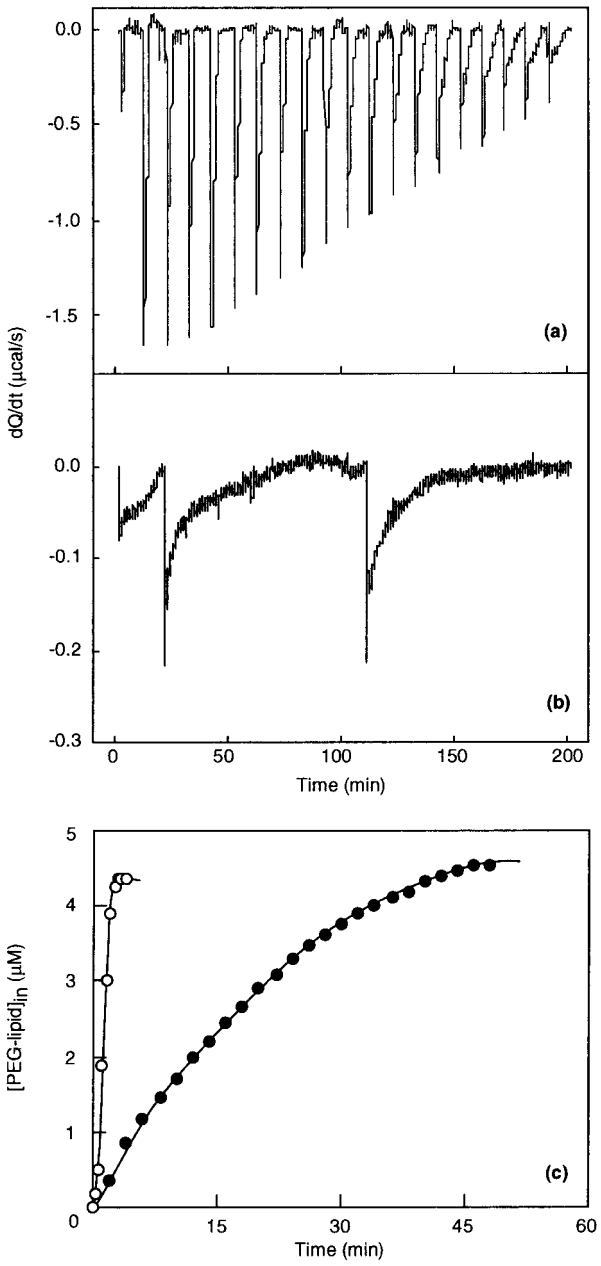

Figure 4. Detection of the PEG-DPPE and PEG-DSPE incorporated into the preformed C16 vesicles by an isothermal titration calorimeter. (a, b) Raw data from the isothermal titration calorimeter ([lipids] = 9.9 mM) for PEG-DPPE and PEG-DSPE, respectively, and (c) the incorporation rate calculated from the equation ($[\text{PEG-lipid}]_{in} = \Delta H_t/\Delta H[\text{PEG-lipid}]_0$). (○) PEG-DPPE, (●) PEG-DSPE.

incorporation rate of the PEG-lipid also increased twice, indicating the validation of eq 2. The k_{on} values of PEG-DPPE and -DSPE being incorporated into the C16 membrane were 41.0 and 5.5 M^{-1} s^{-1} (37 °C), respectively, and those for the C18 membrane were 42.8 and 5.5 M^{-1} s^{-1} (37 °C), respectively. They are summarized in Table 1.

Though the k_{on} values do not show a significant difference between C16 and C18 membranes, the k_{on} values of PEG-DPPE were eight times higher than those of PEG-DSPE. This seems strange because the stronger hydrophobicity of PEG-DSPE should lead to a faster incorporation rate. Two explanations are considered for the incorporation mechanism; one is incorporation as monomers, and the other is incorporation as micelles. The former accompanies the dissociation of micelles, because the PEG-lipids were added in a micelle state, and their concentrations after addition were below the CMC. We consider that the PEG-lipid should incorporate as a monomer after dissociation of the micelles, because the rates of dissociation of the PEG-lipid micelles were faster than the rates of PEG-lipid incorporation. Namely, more than 70% of the PEG-DPPE micelles dissociated within 2 s as shown in Figure 2, and it took more than 2 min for about 70% of the PEG-lipid to incorporate into the C16 membrane. In the case of PEG-DSPE, 70% of the micelles dissociated within 8 min, whereas less than 30% of the PEG-lipid incorporated into the C16 membrane. Therefore, the incorporation of the PEG-lipid would occur as monomer after dissociation of the micelles.

As shown in Table 1, the k_{on}s of PEG-lipids into the C18 membrane were almost the same as those into the C16 membrane. This supports the conclusion that PEG-lipid incorporation was influenced more by the size of the hydrophobic parts of the PEG-lipids than by the nature of the host bilayer membrane.

The calorific values (ΔH) in Table 1 were calculated from the total peak area, which is seen in Figure 4, panels a and b. The enthalpy changes (ΔH) during the incorporation of PEG-lipids into the C16 membrane were small in comparison with those of PEG-lipids into the C18 membrane as depicted in Table 1. The higher ΔH for the C18 membrane would be due to the stronger stabilizing effect of the PEG-lipids after incorporation into the membrane having stronger hydrophobic interaction.

Incorporation Stability of PEG-Lipids. A dispersion of C16 membrane vesicles was diluted into an excess amount of PEG-lipid dispersion, and the incorporated amount of the PEG-lipid was measured using ^{1}H NMR after complete separation of the unincorporated PEG-lipid. Because PEG-lipid incorporates into only the outer layer of the bilayer membranes, we expressed the molar ratio of the PEG-lipid to the total lipids consisting of the outer layer of the bilayer membrane. This was calculated from the number of bilayer membranes of the vesicles, the average size of the vesicles, and the lipid concentration of the dispersion (*17*). The average number of the bilayer membrane was calculated to 2.0 for vesicles with the C16 membrane and 1.5 for vesicles with the C18 membrane. The ratio of the lipids in the outer layer to the total lipids was approximated to be 0.25 and 0.33, respectively. As summarized in Table 1, PEG-DPPE and -DSPE were incorporated into the vesicles to around 9 and 5.5 mol %, respectively. There was no significant difference between the C16 and C18 membranes. We estimated that these were maximun values for incorpora-

Table 1. Thermodynamic Parameters of Incorporation and Dissociation of the PEG-Lipid on Vesicles at 37 °C

	membrane	max ratio (mol %)	$^{app}k_{on}$ (s^{-1} M^{-1})	$^{app}k_{off} \times 10^5$ (s^{-1})	incorporation ratio[a] (%)	$K \times 10^{-4}$ (M^{-1})	ΔG^b (kcal/mol)	ΔH (kcal/mol)
PEG-DPPE	C16	9.2	41.0	2.3	72	1.1	−5.7	−16
	C18	8.9	42.8	1.5	83	1.7	−6.0	−21
PEG-DSPE	C16	5.7	5.5	0.24	74	2.0	−6.1	−13
	C18	5.6	5.5	0.057	93	7.1	−6.9	−23

[a] 0.3 mol % of PEG-lipids were added to the vesicle dispersion ([lipids] = 9.9 mM). [b] $\Delta G = -RT \ln K$.

tion because there was no further change with time and we used them for calculation of k_{on} and K.

In general, the incorporation of amphiphilic molecules having a micelle-forming property into the bilayer membrane accompanies the transition from vesicles to micelles, if their concentrations were beyond the critical values (*23*). From the theoretical analysis of the phase behavior of the PEG-lipid and phospholipid mixture in aqueous media, the maximum amount of PEG-lipid being incorporated into the mixed vesicles could be determined from the membrane elasticity, e.g., the cholesterol content in the bilayer and the PEG chain length (*6*). The maximum concentration of PEG (M_w 5000)-lipid in phospholipid/cholesterol (1/1 mol/mol) was calculated to be ca. 15 mol %. Above this concentration, the thermodynamically favorable structure would be a micelle rather than a vesicle (*7*). This theoretical speculation was also experimentally confirmed elsewhere (*7*−*9*). In those experiments, the PEG-lipids were mixed with phospholipids before preparation of vesicles. In our experimental procedure, the PEG-lipid was incorporated into the vesicles to 9 mol %, not 15 mol %. It is considered that the steric hindrance of the PEG chains extending from the vesicular surface becomes more significant and tends to restrict the further incorporation of the PEG-lipid. Therefore, the steric effect of the PEG chains, which had already been incorporated, and the molecular size of the PEG-lipid should determine the amount of PEG-lipid incorporated into the preformed vesicles. The incorporation behavior in this region (maximum concentration) should not be in an equilibrium state, but in a kinetically limited state.

The maximum incorporation does not depend on the acyl chain length of the phospholipids comprising the host membrane but on the acyl chain length of the guest PEG-lipids. Theoretically, the entire surface of the vesicle should be covered with 1.5 mol % of PEG (5000) fixed onto the surface (*15*). The conformation of the PEG chain in this state is considered a mushroom (*24*). Further PEG incorporation results in a brush conformation, where PEG chains are extended and become compressed with increasing density of the PEG chains. The PEG-lipids have to shove the PEG brush in order to incorporate into the membrane. The size of the PEG-lipids, namely the length of the acyl chains, should influence this process because of the molecular sieving effect of the dense PEG brush.

Figure 5a is the time course of PEG-lipid incorporation for all combinations. There are significant differences in the incorporation rates between PEG-DPPE and PEG-DSPE. Namely, PEG-DPPE was incorporated very fast in the membrane as predicted from the incorporation rates and reached constant values. The constant values represent equilibrium constants (K) of PEG-lipid incorporation, and the C18 membrane always shows the higher values than the C16 membrane. The saturated incorporation ratios and K values for all combinations are summarized in Table 1.

The K value of PEG-DSPE incorporation into the C16 membrane at 37 °C was 2.0×10^4 M^{-1}, which was about twice that (1.1×10^4 M^{-1}) of PEG-DPPE incorporation. However, similar incorporation ratios were obtained for PEG-DPPE and PEG-DSPE. The difference in incorporation sites (maximum incorporation ratio) would explain this result. The incorporation ratio should be dependent on the concentrations of the PEG-lipid and vesicles, in relation to the K values. The constancy of the K values

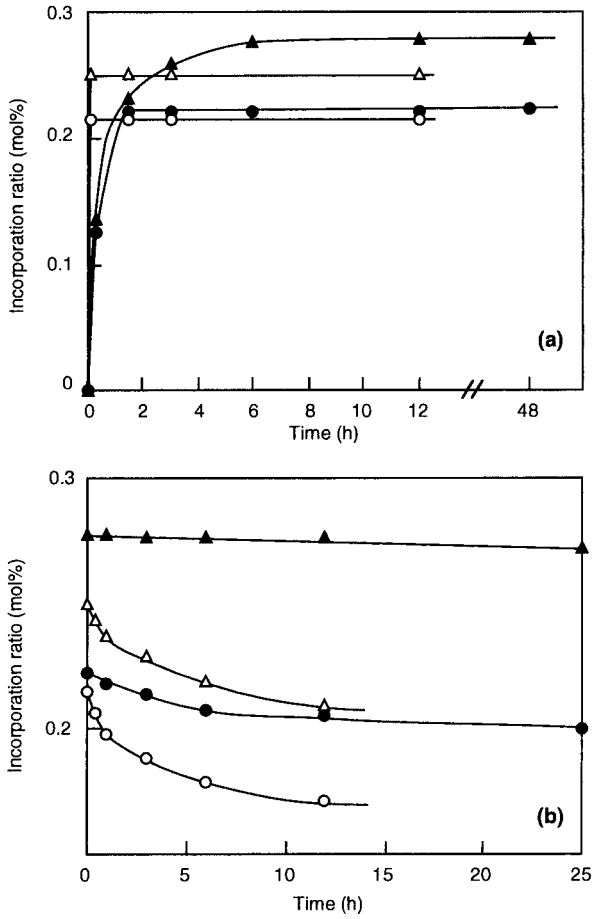

Figure 5. Determination of the incorporated PEG-lipids on preformed vesicles by ^{1}H NMR. Incorporated PEG-lipid was determined by the peak area ratio of the choline methyl proton of DPPC or DSPC (3.39 ppm) to the methylene proton of PEG (3.63 ppm). (a) Incorporation into vesicles and (b) dissociation from vesicles by dilution. The combinations of the PEG-lipids and vesicles were (○) PEG-DPPE and C16, (△) PEG-DPPE and C18, (●) PEG-DSPE and C16, and (▲) PEG-DSPE and C18.

in different concentrations of PEG-lipids and vesicles confirms the appropriateness of the eq 3 (data not shown here).

As depicted in Table 1, despite the smaller k_{on} value of PEG-DSPE than that of PEG-DPPE, the K value of PEG-DSPE was larger than that of PEG-DPPE. This would be explained based on the small dissociation rate (k_{off}) of PEG-DSPE from the C16 membrane. As estimated from the equilibrium constant of PEG-lipid incorporation, the removal of the PEG-lipid from the bilayer membrane should occur after the unincorporated PEG-lipid is removed or the mixture dispersion is diluted. The decrease in the incorporation ratio of PEG-lipids by dilution was measured and is shown in Figure 5b. We confirmed the dissociation of PEG-DPPE to be faster than that of PEG-DSPE as predicted from K and k_{on}. The apparent dissociation rate constants ($^{app}k_{off}$) of PEG-lipids calculated from the pseudo-first-order of the first stage are summarized in Table 1. The combination of PEG-DSPE and the C18 membrane shows the lowest $^{app}k_{off}$ value of the four combinations.

As shown in Table 1, the combination of PEG-DSPE and the C16 membrane is the lowest ΔH of the four combinations, while the combination of PEG-DPPE and the C18 membrane has a relatively high ΔH. It is suggested that the guest PEG-lipid having longer acyl chains than the host phospholipid would not take highly

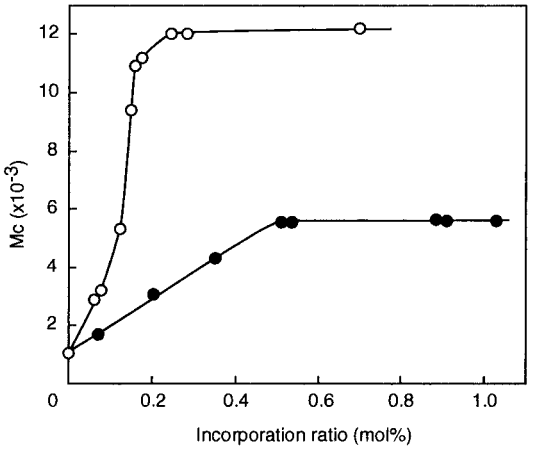

Figure 6. Relationship between incorporation ratio of PEG-lipids into C16 vesicles and M_c. (○) PEG(5,000)-DSPE, (●) PEG-(2000)-DSPE at 37 °C. The incorporation ratio was determined by ^{1}H NMR (see Experimental Procedures) and represented against the outer layer of the vesicles.

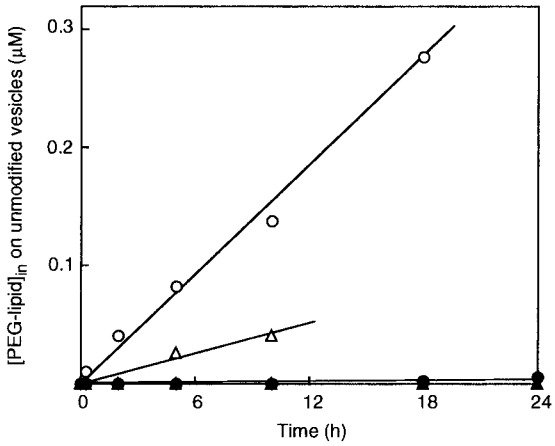

Figure 7. Interbilayer transfer of PEG-lipds from PEG-modified vesicles to unmodified ones at 37 °C. PEG-modified vesicles ([lipids] = 1.39 mM, 1.0 mol % of PEG-lipid) were added to the unmodified C16 vesicles ([lipids] = 1.39 mM) in volume ratios of 1 to 3. The combinations of the PEG-lipids and vesicles were (○) PEG-DPPE and C16, (△) PEG-DPPE and C18, (●) PEG-DSPE and C16, and (▲) PEG-DSPE and C18.

ordered packing after incorporation, because the guest lipid should oblige to take more number of kink conformation in order to adjust itself to the thickness of the outer layer of the bilayer membrane. The guest PEG-lipid having shorter acyl chains than the host phospholipid could order in the bilayer membrane.

Stability of the Vesicle Dispersions. To clarify the relationship between the dispersion stability of the PEG-modified vesicles and the incorporation amount or molecular weight of the PEG-lipid, we prepared PEG-modified vesicles incorporating various amounts of the PEG-lipid. The incorporated amount of PEG-lipids was easily controlled by varying the added amount of PEG-lipids. Phospholipid vesicles tend to aggregate in the presence of water-soluble polymers by molecular interaction (*20*). Because the dissociation process of the absorbed polymer from the surface of the vesicle is dominant in this interaction, the molecular weight of the polymers should represent the degree of interaction between the polymer and the surface of the vesicle. We defined the smallest molecular weight of the polymers for aggregation of the vesicles as a critical molecular weight (M_c) (*10*). The higher M_c of a polymer indicates a smaller degree of interaction. Therefore, it can be influenced by the kinds of polymers, vesicle compositions, and solution composition such as pH and ionic strength.

Figure 6 shows the M_c obtained in the vesicles incorporating PEG-DSPE with different PEG lengths. M_c increases with PEG-lipid concentration and reaches a constant value at a certain PEG-lipid concentration. The PEG-lipid concentration was expressed against lipids only in the outer layer of the vesicle. The increase in the M_c indicates the decrease in the interaction force and the restraint of vesicle aggregation by PEG-surface modification. We have already reported that the M_c was decreased after modification with oligosaccharide chains because of the induced interaction between the oligosaccharide chains and PEG (*20*). Therefore, the PEG chains extending from the surface of the vesicles have the function of excluding the added polymer from the surface. In the case of the PEG(5000)-DSPE, the relationship between the incorporation ratio of the PEG-lipid and M_c could be separated into three regions. The M_c linearly increased below 0.12 mol %, steeply increased from 0.12 to 0.18 mol %, and then became a constant value above 0.18 mol %. Whereas, in the case of PEG(2000)-DSPE, the M_c increased to 0.5 mol % and became a constant value above this ratio. These critical points should be related to the surface property of the vesicles. To clarify the relationship between M_c and the surface condition, we took a theoretical approach. The average M_ws of PEG (2000) and PEG (5000) determined by gel permeation chromatography were 2070 (M_w/M_n = 1.04) and 5340 (M_w/M_n = 1.02), respectively. The areas per PEG (2000) and PEG (5000) chain were calculated to be 9.84 and 30.47 nm^2, respectively (*9*). The critical incorporation ratios to reach the constant M_c values were 0.5 and 0.18 mol % for PEG (2000)-DSPE and PEG (5000)-DSPE, respectively. The ratios of surface coverage calculated from the area per PEG chains at these incorporation ratios were 10 and 11% for PEG (2000)-DSPE and PEG (5000)-DSPE, respectively. These values were similar, indicating that the effect of the PEG modification on the prevention of the vesicle aggregation induced by the addition of polymer was sufficient when 10% of the surface was covered with PEG chains.

Table 2. Incorporation Rates of the PEG-Lipid into Unmofified Vesicles by Mixing with Modified Ones (PEG-Lipid: 1.0 mol %) at 37 °C

PEG-lipid	membrane	$d[\text{PEG-lipid}]_{in}/dt \times 10^3$ (μM/h)
PEG-DPPE	C16	14.9
	C18	4.1
PEG-DSPE	C16	0.2
	C18	0

Incorporation of the PEG-Lipid into Unmodified Vesicles by Mixing with Modified Vesicles. When the vesicles modified with 1.0 mol % of PEG-DPPE or PEG-DSPE were mixed with unmodified ones, the M_c gradually increased. The M_c of vesicles with 1.0 mol % of incorporated PEG-lipids and unmodified vesicles were 12 200 and 1050, respectively. The M_c of the mixture of vesicles with different M_c corresponded to the lower value. The M_c measured immediately after mixing (t = 0) was 1050, which was identified as that of unmodified vesicles. Therefore, the M_c increase was caused by the incorporation of PEG-lipid into the unmodified ones. We could convert the M_c into the concentration of incorporated PEG-lipid using the relationship between the incorporation ratio of PEG-lipid and M_c as shown in Figure 6. As shown in Figure 7 and Table 2, the incorporation rate of PEG-DSPE was slower than that

of PEG-DPPE. The rate of PEG-DPPE was 70 times higher than that of PEG-DSPE, and no incorporation was observed in the combination of PEG-DSPE and the C18 membrane. As shown in Figure 4, the incorporation rate of the free PEG-lipid was significantly faster than that of incorporated one. Therefore, it is suggested that the incorporation rate of the PEG-lipid into unmodified vesicles would be related to the dissociation step of the PEG-lipid from the vesicles because the incorporation rate decreased with the decrease of dissociation rate from the vesicles. In practice, the incorporation rates of each combination measured by M_c were slower compared with the dissociation rate determined by ^{1}H NMR as shown in Tables 1. This would be caused by the difference in the targeted PEG-lipids. The dissociation rate was calculated against the dissociated total PEG-lipids, while the transfer rate was done against only PEG-lipids incorporated into the unmodified vesicles. All of the dissociated PEG-lipids are not always incorporated into the unmodified vesicles following the equilibrium condition, and some part of the dissociated PEG-lipids should return to the modified vesicles. Therefore, the incorporation rate should reflect the dissociation rate and depend on the molecular weight of PEG and the acyl chain length. The increase in the M_w of PEG chains and the decrease in the acyl chain length resulted in an increase in the incorporation rate. Silvius and Zuckermann also reported that the rate of PEG-lipid transfer between vesicles decreased with the increasing acyl chain length of PEG-lipid (*25*).

CONCLUSION

We studied the PEG-lipid incorporation into the phospholipid vesicles from the kinetics of PEG-lipid micelle dissociation, the incorporation, and dissociation of the PEG-lipid into the bilayer membrane of vesicles for the combinations of PEG-DPPE, PEG-DSPE, vesicles with a C16 membrane and a C18 membrane. The k_{on} values of PEG-DPPE were larger than those of PEG-DSPE; however, the K value of PEG-DPSE was larger than that of PEG-DPPE. This was due to the considerably small k_{off} values of PEG-DSPE. The stability of the incorporation would be determined primarily from the hydrophobicity of the guest molecule and secondarily from the relation of the acyl chains of the host−guest molecules. The increase in the hydrophobic interaction force of the PEG-lipids and the vesicles resulted in a decrease in the dissociation rate. The most stable combination was concluded to be PEG-DSPE and the C18 membrane, though the incorporation rate was small. In the design of the PEG-lipid derivatives with large hydrophilic headgroup, one should consider the hydrophobic interaction not to dissociate from the vesicle and to incorporate the preformed vesicles.

The blood circulation time is the most important factor to discuss the effect of PEG-modification to phospholipid vesicles because this is the end to apply this technique for drug delivery systems. If the PEG-lipids were escaped from the surface of the vesicles intravenously injected, this should determine the blood circulation time. We are now studying this effect from blood circulation of PEG-modified vesicles.

ACKNOWLEDGMENT

This work was supported in part by a project of the Material Research Laboratory for Bioscience and Photonics in Waseda University and by Health Science Research Grants (Artificial Blood Project) from the Ministry of Health and Welfare, Japan. We thank to NOF. Co. for the offer of poly (ethylene glycol) (standard).

LITERATURE CITED

(1) Gregoriadis, G. (1984) *Liposome Technology*, Vol. I, II, III, CRC Press, Boca Raton.

(2) Harris, J. M. (1990) Introduction to Biotechnical and Biomedical Appricationsof Poly(Ethylene Glycol). In *Poly-(Ethylene Glycol) Chemistry: Biotechnical and Biomedical Apprications* (J. M. Harris, Ed.) pp 1−14, Plenum Press, New York.

(3) Zalipsky, S. (1995) Functionalized Poly(ethylene glycol) for Preparation of Biologically Relevant Conjugates. *Bioconjugate Chem. 6*, 150−165.

(4) Klibanov, A. L., Maruyama, K., Torchilin, V. P., and Huang L. (1990) Amphipatic poly(ethylene glycol)s effectively prolong the circulation time of liposome. *FEBS Lett. 268*, 235−237.

(5) Woodle, M. C., and Lasic, D. D. (1992) Sterically stabilized liposome. *Biochim. Biophys. Acta 1113*, 171−199.

(6) Hristova, K., and Needham, D. (1995) Phase behavior of a lipid/polymer−lipid mixture in aqueous medium. *Macromolecules 28*, 991−1002.

(7) Hristova, K., Kenworthy, A., and McIntosh, T. J. (1995) Effect of bilayer composition on the phase behavior of liposomal suspensions containing poly(ethylene glycol)-lipids. *Macromolecules 28*, 7693−7699.

(8) Kenworthy, A. K., Simon, S. A., and McIntosh, T. J. (1995) Structure and phase behavior of lipid suspensions containing phospholipid with covalently attached poly(ethylene glycol). *Biophys. J. 68*, 1903−1920.

(9) Kenworthy, A. K., Hristova, K., Needham, D., and Mcintosh, T. J. (1995) Range and magnitude of the steric pressure between bilayers containing phospholipids with covalently attached poly(ethylene glycol). *Biophys. J. 68*, 1921−1936.

(10) Warriner, H. E., Keller, Idziak, S. H. J., Slack, N. L., Davidson, P., and Safinya, C. R. (1996) Lamellar biogels: fluid-membrane based hydrogels containing polymer−lipids. *Science. 271*, 969−973.

(11) Polo, D., Haro, I., Alsina, M. A., and Reig, F. (1997) Physicochemical Characterization of Poly(ethylene glycol)-Coated liposomes loaded with doxorubicin. *Langmuir 13*, 3953−3958.

(12) Sakai, H., Takeoka, S., Park, S. I., Kose, T., Nishide, H., Izumi, Y., Yoshizu, A., Kobayashi, K., and Tsuchida, E. (1997) Surface Modification of Hemoglobin Vesicles with Poly-(ethylene glycol) and Effects on Aggregation, Viscosity, and Blood Flow during 90% Exchange Transfusion in Anesthetized Rats. *Bioconjugate Chem. 8*, 23−30.

(13) Szleifer I., Gerasimov, O. V., and Thompson, D. H. (1998) Spontaneous liposome formation induced by grafted poly-(ethylene oxide) layers: Theoretical prediction and experimental verification. *Proc. Natl. Acad. Sci. 95*, 1032−1037.

(14) Senior, J., Delgado, C., Fisher, D., Tilcock, C., and Gregoriadis, G. (1991) Influence of surface hydrophilicity of liposomes on their interaction with plasma protein and clearance from the circulation: studied with poly(ethylene glycol)-coated vesicles. *Biochim. Biophys. Acta 1062*, 77−82.

(15) Yoshioka, H. (1991) Surface modification of hemoglobin-containing liposomes with polyethylene glycol prevents liposome aggregation in blood plasma. *Biomaterials 12*, 861−864.

(16) Uster, P. S., Allen, T. M., Daniel, B. E., Mendez, C. J., Newman, M. S., and Zhu, G. Z. (1996) Insertion of poly-(ethylene glycol) derivatized phospholipid into pre-formed liposomes results in prolonged in vivo circulation time. *FEBS Lett. 386*, 243−246.

(17) Takeoka, S., Ohgushi, T., Terase, K., Ohmori, T., and Tsuchida, E. (1996) Layer-controlled hemoglobin vesicles by interaction of hemoglobin with a phospholipid assembly. *Langmuir 12*, 1775−1759.

(18) Chattopadhyay, A., and London, E. (1984) Fluorimetric determination of critical micelle concentration avoiding interference from detergent charge. *Anal. Biochem. 139*, 408−412.
(19) Wiseman, T., Williston, S., Brandts, J. F., and Lin, L. N. (1989) Rapid measurement of binding constants and heats of binding using a new titration calorimeter. *Anal. Biochem. 179*, 131−137.
(20) Takeoka, S., Sou, K., Arase, S., Ohguhsi, T., and Tsuchida, E. (1996) Critical molecular weight effects in the aggregation of phospholipid vesicles triggered by water-soluble polymers and an integrated glycolipid. *Macromolecules 29*, 8132−8136.
(21) Shinitzky, M., and Barenholz, Y. (1974) Dynamics of the hydrocarbon layer in liposomes of lecithin and sphingomyelin containing dicetyl phosphate. *J. Biol. Chem. 249*, 2652−2657.
(22) Ladbrooke, B. D., Williams, R. M., and Chapman, D. (1968) Studies on lecithin-cholesterol-water interactions by differential scanning calorimetry and X-ray diffraction. *Biochim. Biophys. Acta 150*, 333−340.
(23) Fattal, D. R., Andelman, D., and Ben-Shaul, A. (1995) The vesicle-micelle transition in mixed lipid-surfactant system: a molecular model. *Langmuir 11*, 1154−1161.
(24) deGennes, P. G. (1987) Polymer at an interface: a simplified view. *Adv. Colloid Interface Sci. 27*, 189−209.
(25) Silvius, J. R., and Zuckermann, M. J. (1993) Interbilayer transfer of phospholipid-anchored macromolecules via monomer diffusion. *Biochemistry 32*, 3153−3161.

BC990135Y

$A\beta^{1-40}$ Peptide Radiopharmaceuticals for Brain Amyloid Imaging: ^{111}In Chelation, Conjugation to Poly(ethylene glycol)-Biotin Linkers, and Autoradiography with Alzheimer's Disease Brain Sections

Atsushi Kurihara and William M. Pardridge*

Department of Medicine, UCLA School of Medicine, Los Angeles, California 90095-1682. Received October 13, 1999; Revised Manuscript Received December 23, 1999

The amyloid plaques of Alzheimer's disease (AD) are formed by the neuropeptide $A\beta^{1-42/43}$, and carboxyl terminal truncated forms of this neuropeptide, designated $A\beta^{1-40}$, bind to amyloid plaques of AD autopsy tissue sections. Therefore, $A\beta^{1-40}$ is a potential peptide radiopharmaceutical that could be used for imaging brain amyloid in living subjects with AD, should this neuropeptide be made transportable through the blood-brain barrier (BBB). To accomplish this, the neuropeptide must be modified to enable (i) attachment to a BBB drug targeting system and (ii) labeling with a radionuclide, e.g., 111-indium, suitable for brain imaging by external detection modalities such as single photon emission computed tomography (SPECT). The present studies describe the synthesis of an $A\beta^{1-40}$ analogue that contains a biotin at the amino terminus and a diethylenetriaminepentaacetic acid (DTPA) moiety conjugated to one of the internal lysine residues. The DTPA-[*N*-biotin]-$A\beta^{1-40}$ was purified by gel filtration fast-protein liquid chromatography (FPLC) using two Superose 12HR columns in series, and the structure of the purified peptide was confirmed by matrix-assisted laser desorption ionization (MALDI) mass spectrometry. The binding of the [^{111}In]DTPA-[*N*-biotin]-$A\beta^{1-40}$ to amyloid plaques of AD autopsy tissue sections was demonstrated by film and emulsion autoradiography. A poly(ethylene glycol) (PEG) linker of 3400 Da molecular mass, designated PEG^{3400}, was inserted between the $A\beta^{1-40}$ and the biotin moiety, but this modification diminishes binding of $A\beta^{1-40}$ to the AD amyloid plaques. In summary, these studies describe a novel formulation of biotinylated $A\beta^{1-40}$ that allows radiolabeling with 111-indium. The peptide radiopharmaceutical may be conjugated to an avidin-based BBB drug targeting system to enable transport through the BBB and imaging of brain amyloid in vivo.

INTRODUCTION

Alzheimer's disease (AD) is a chronic neurodegenerative condition that leads to progressive dementia. The dementia of AD correlates with the deposition in brain of amyloid (*1*, *2*), which is formed by a 42−43 amino acid peptide designated $A\beta^{1-42/43}$ (*3*). There are three forms of brain extracellular amyloid in AD, meningeal vascular amyloid (*4*), cortical microvascular amyloid (*5*), and neuritic plaques (*6*). Presently, there is no premortem diagnostic test for AD. In addition, it is not possible to scan the brain of subjects living with AD to determine the level of the $A\beta$ amyloid burden in brain, which can occupy up to 15% of the brain volume in subjects with AD (*7*). The availability of such an amyloid imaging brain scan would not only provide a diagnostic test specific for AD but also allow for assessing the effects in brain of drugs that inhibit the formation of $A\beta$ amyloid.

An amyloid imaging brain scan could be developed with $A\beta^{1-40/42}$ peptide radiopharmaceuticals because radiolabeled forms of these molecules promptly deposit at preexisting amyloid plaques in tissues sections of autopsy AD brain (*8*). The autoradiographic detection of AD amyloid (*8*) using radiolabeled $A\beta$ analogues can be more sensitive than classical immunocytochemical techniques using monoclonal antibodies (MAb) against $A\beta$. Radiolabeled forms of either $A\beta^{1-40}$ (*9*) or anti-$A\beta$ Mabs (*10*) have been administered to aging primates in an attempt to develop amyloid imaging brain scans. In either case, only amyloid at the meninges was imaged because meningeal vessels lack a blood-brain barrier (BBB). Although [^{125}I]$A\beta^{1-40}$ does bind to brain vessels in vivo following systemic administration, there is no measurable transcytosis of this peptide radiopharmaceutical through the BBB in vivo (*11*). The BBB is intact in AD (*12*), and the $A\beta$ amyloid is deposited beyond the BBB in brain (*13*). Therefore, if $A\beta$ peptide radiopharmaceuticals are to be used as in vivo amyloid imaging agents in AD, it may be necessary to conjugate the peptide to BBB drug targeting systems (*14*).

Peptide radiopharmaceuticals such as $A\beta^{1-40/42}$ may be targeted through the BBB by conjugating the peptide to BBB drug-targeting vectors such as peptidomimetic MAbs that undergo receptor-mediated transcytosis through the BBB on endogenous brain capillary endothelial peptide transport systems (*14*). The OX26 murine MAb to the rat transferrin receptor (TfR) undergoes transport through the rat BBB (*15*). However, rats do not develop brain amyloid and the OX26 MAb is specific for rats and cannot be used in other species such as transgenic mouse models (*16*), which develop $A\beta$ amyloid (*17*). However, $A\beta$ amyloid in transgenic mice could be imaged with either the 8D3 or the RI7 rat MAb to the mouse TfR, as these antibodies have been recently shown to cross the mouse BBB via the TfR (*16*). Alternatively, aged (>30 year old) Rhesus monkeys develop $A\beta$ amyloid plaques and represent a potential animal model for imaging brain amyloid (*18*, *19*). The 83-14 MAb to the human insulin receptor (HIR) is an effective BBB drug-

* To whom correspondence should be addressed. Phone: (310) 825-8858. Fax: (310) 206-5163. E-mail: wpardridge@mednet.ucla.edu.

10.1021/bc9901393 CCC: $19.00 © 2000 American Chemical Society
Published on Web 03/16/2000

targeting vector in Old World primates such as rhesus monkeys, but not New World primates such as squirrel monkeys (*20*).

In an effort to develop an amyloid brain scan that might be effective in mice, monkeys, or humans, previous studies described the synthesis of Aβ^{1-40} radiolabeled with 125-iodine at the Tyr^{10} residue and monobiotinylated at the amino terminus (*14*). This peptide was bound to a conjugate of streptavidin (SA) and the 83-14 HIRMAb and injected intravenously in young rhesus monkeys (*14*). The Aβ peptide radiopharmaceutical labeled with 125-iodine and conjugated to the HIRMAb drug-targeting system was rapidly transported across the BBB in vivo in primates after intravenous administration, and the brain uptake was visualized by quantitative autoradiography (QAR) of frozen tissue sections of brain (*14*). However, the formulation of Aβ^{1-40} labeled with 125-iodine is not ideal for brain imaging for several reasons. First, peptide radiopharmaceuticals labeled with 125-iodine are rapidly converted by peripheral tissues to radiolabeled small molecules, e.g., iodotryosine, that cross the BBB and yield an artifactually high background of brain uptake (*21*). The high "noise" of the brain-imaging signal is virtually eliminated using peptide radiopharmaceuticals labeled with 111-indium (*21*, *22*). Another reason for developing an Aβ^{1-40} peptide radiopharmaceutical labeled with 111-indium is that ^{125}I is not suitable for external brain imaging with either single photon emission computed tomography (SPECT) or positron emission tomography (PET). The ^{125}I could be substituted with ^{124}I for PET studies, but the availability of the ^{124}I radionuclide is severely limited. Therefore, it would be advantageous to develop Aβ peptide radiopharmaceuticals that are amenable to external brain imaging with SPECT using suitable radionuclides such as 111-indium (In).

The present studies describe a formulation of Aβ^{1-40} that is monobiotinylated at the amino terminus and is radiolabeled with ^{111}In via a chelator moiety, diethylenetriaminenpentaacetic acid (DTPA), which is conjugated to one of the two internal lysine residues, Lys^{16} or Lys^{28}. This form of Aβ is designated [^{111}In]DTPA-[*N*-biotin]-Aβ^{1-40}. The present studies also examine the formulation of an Aβ peptide radiopharmaceutical wherein the biotin moiety is attached to the tip of a single polymeric tail of poly(ethylene glycol) (PEG) of 3400 Da molecular mass, designated PEG^{3400}. In this formulation, the PEG^{3400}-biotin is conjugated to one of the two internal lysine residues. Previous studies have shown that receptor binding of neuropeptides that are conjugated to BBB drug-targeting MAbs is enhanced by placing a PEG linker between the peptide and the BBB drug targeting system (*23*). The insertion of the extended PEG linker releases any mutual steric hindrance between the peptide radiopharmaceutical and the BBB-targeting MAb. This form of Aβ was radiolabeled with ^{125}I and is designated [^{125}I]Aβ^{1-40}−PEG^{3400}-biotin.

EXPERIMENTAL PROCEDURES

Materials. Human Aβ^{1-40} was purchased from Bachem Inc. (Torrance, CA). Biotinylated Aβ ([*N*-biotin]-Aβ^{1-40}), which is monobiotinylated at the amino terminus, was obtained from Quality Controlled Biochemicals Inc. (Hopkinton, MA). [^{125}I]Na was supplied by Amersham (Arlington Heights, IL). [^{111}In]Cl_3 was obtained from NEN Life Science Products Inc. (Boston, MA). NHS-PEG^{3400}-biotin was obtained from Shearwater Polymers (Huntsville, AL), where NHS = N-hydroxysuccinimide and PEG^{3400} = poly(ethylene glycol) of 3400 Da molecular mass. Diethylenetriaminepentaacetic (DTPA) dianhydride was obtained from Aldrich Chemical Co., Inc. (Milwaukee, WI). Chloramine-T was purchased from MCB Reagents (Cincinnati, OH). All other chemicals were obtained from Sigma Chemical Co. (St. Louis, MO). Superose 12 HR 10/30 FPLC columns were obtained from Pharmacia Biotech (Piscataway, NJ). Centricon-3 microconcentrators were obtained from Amicon Corp. (Bevery, MA). Snap-frozen human autopsy Alzheimer's disease brain, used for preparation of frozen sections, was provided by Prof. Harry Vinters (UCLA Department of Pathology/Neuropathology).

Iodination of [*N*-Biotin]-Aβ^{1-40}. [*N*-Biotin]-Aβ^{1-40} (10 μg, 2.1 nmol) was iodinated with ^{125}I (2 mCi, 1.1 nmol) and chloramine T (44 nmol) in 95 μL of 0.05 M phosphate-buffered saline (pH 7.4) at room temperature for 2 min (*14*). After addition of sodium metabisulfite to quench the iodination, 50 μL of 0.05 M phosphate buffer (pH 7.4)/1 mM EDTA was added to the reaction solution. [^{125}I][*N*-biotin]-Aβ^{1-40} was purified by Sephadex G25 size-exclusion chromatography with an elution buffer of 0.01 M phosphate-buffered saline (pH 7.4) containing 0.05% Tween-20. The [^{125}I][*N*-biotin]-Aβ^{1-40} had a trichloroacetic acid (TCA) precipitability of >97% and a specific activity of 159 μCi/μg.

Synthesis and Iodination of Aβ^{1-40}-PEG^{3400}-Biotin. NHS-PEG^{3400}-biotin (230 nmol in 50 μL of 0.1 M $NaHCO_3$) was added in a 2:1 molar ratio to 500 μg of Aβ^{1-40} (115 nmol) in 0.033 M $NaHCO_3$, pH 8.3, followed by incubation at room temperature for 60 min. The entire mixture was then applied to two Superose 12 HR 10/30 fast-protein liquid chromatography (FPLC) columns in series, followed by elution in 0.01 M phosphate-buffered saline (pH 7.4) at a flow rate of 0.5 mL/min for 90 min (*21*). For detection of conjugates, UV absorption of 205 nm was used. Aβ^{1-40} containing a single PEG^{3400}-biotin moiety and designated Aβ^{1-40}-PEG^{3400}-biotin, eluted at 58 min from the column, as demonstrated by mass spectrometry analysis (below). Aβ^{1-40}-PEG^{3400}-biotin (1.3 mL from FPLC) was applied to a Centricon-3 microconcentrator and the volume was reduced to 0.3 mL by centrifugation at 7500*g* for 60 min at room temperature. Aβ^{1-40}-PEG^{3400}-biotin (2.3 nmol) was iodinated with ^{125}I (2.6 mCi, 1.4 nmol) and chloramine T (44 nmol) in 95 μL of 0.05 M phosphate-buffered saline (pH 7.4) at room temperature for 2 min (*1*). After addition of sodium metabisulfite to quench the iodination, 50 μL of 0.05 M phosphate buffer (pH 7.4)/1 mM EDTA was added to the reaction solution. [^{125}I]Aβ^{1-40}-PEG^{3400}-biotin was purified by Sephadex G25 size-exclusion chromatography with a elution buffer of 0.01 M phosphate-buffered saline (pH 7.4) containing 0.05% Tween-20. [^{125}I]Aβ^{1-40}-PEG^{3400}-biotin had a TCA precipitation of >98% and a specific activity of 135 μCi/μg.

Synthesis and ^{111}In-Labeling of DTPA-[*N*-Biotin]-Aβ^{1-40}. DTPA dianhydride [2.7 μmol in 20 μL of dimethyl sulfoxide (DMSO)] was added in a 50:1 molar ratio to 250 μg of [*N*-biotin]-Aβ^{1-40} (54 nmol) in 200 μL of 0.05 M $NaHCO_3$, pH 8, followed by incubation at room temperature for 30 min. The entire mixture was then applied to two Superose 12 HR 10/30 FPLC columns in series, followed by elution in 0.01 M phosphate-buffered saline (pH 7.4) at a flow rate of 0.5 mL/min for 90 min. For detection of conjugates, UV absorption of 205 nm was used. [*N*-Biotin]-Aβ^{1-40} containing a single DTPA moiety conjugated to one of two internal lysine residues on Aβ^{1-40} (Lys^{16},Lys^{28}) and designated DTPA-[*N*-biotin]-Aβ^{1-40}, eluted at 64 min from the columns, as demonstrated by mass

spectrometry analysis (below). Two millicurie of ^{111}In (0.4 nmol) in 38 μL of 0.05 N HCl was added to 1.0 nmol of DTPA-[*N*-biotin]-Aβ^{1-40} in 0.1 mL of phosphate-buffered saline (pH 7.4). After 30 min at room temperature, [^{111}In]-DTPA-[*N*-biotin]-Aβ^{1-40} was separated from unreacted free ^{111}In by Sephadex G25 size-exclusion chromatography with an elution buffer of 0.01 M phosphate-buffered saline (pH 7.4) containing 0.05% Tween-20. The specific activity of the [^{111}In]DTPA-[*N*-biotin]-Aβ^{1-40} was 388 μCi/μg.

Matrix-Assisted Laser Desorption Ionization (MALDI) Mass Spectrometry. Mass spectra of Aβ^{1-40}-PEG^{3400}-biotin and DTPA-[*N*-biotin]-Aβ^{1-40} eluted from the two Superose 12 HR 10/30 columns in series were recorded with a reflector time-of-flight instrument (PerSeptive Biosystems Voyager RP) used in the linear mode with stainless steel targets (*21*). An aliquot of sample solution (0.5 μL) was overlaid on top of matrix (α-cyano-4-hydroxycinnamic acid), and after drying, the target was inserted into the mass spectrometer, and time/intensity data from 50 to 100 scans was averaged and converted to mass/intensity data.

Film and Emulsion Autoradiography. Snap-frozen Alzheimer's disease cortex was provided by the UCLA Department of Pathology/Neuropathology, and 15 μm sections were cut on a Bright cryostat and thaw-mounted to glass slides for autoradiography of tissue sections, where the BBB is nonexistent (*11*). The slides were warmed to room temperature, air-dried, and incubated for 30 min with TBM buffer (0.05 M Tris-HCl, 0.1% BSA, 10 mM $MnCl_2$, pH 7.4) (*8*). Then the slides were incubated with 250 μL of TBM buffer containing 0.5 μCi/mL of either [^{125}I][*N*-biotin]-Aβ^{1-40} or [^{125}I]Aβ^{1-40}-PEG^{3400}-biotin. After 2 h at room temperature, the slides were washed four times with 2 min wash in Tris/BSA buffer (0.05 M Tris-HCl, 0.1% BSA, pH 7.4) at 4 °C followed by two 5 s washes in H_2O at 4 °C.

For autoradiography with the ^{111}In, it was necessary to omit the $MnCl_2$ from the mixture, as this divalent cation competed with the ^{111}In for chelation to DTPA; these slides were preincubated in Tris/BSA buffer for 30 min at room temperature, then incubated for 2 h in Tris/BSA buffer containing 1.0 μCi/mL of [^{111}In]DTPA-[*N*-biotin]-Aβ^{1-40}, and washed as for [^{125}I]labeled conjugates.

After drying, half of the slides were dipped with emulsion (NTB3; Eastman Kodak Co., Rochester, NY) in the dark room for 5 s followed by air-drying at room temperature for 30 min, and then exposed at −20 °C in the dark for up to 2 weeks (*11*). Only the ^{125}I reacted with the emulsion, as the ^{111}In provided no reaction in the emulsion autoradiography, perhaps due to dissociation of the ^{111}In by components of the emulsion. The other half of slides were placed in apposition to Kodak Biomax MS X-ray film and exposed for up to 2 weeks at room temperature. The film was scanned with a Hewlett-Packard ScanJet IIcx/T flatbed scanner and transferred to Adobe Photoshop on a Power Macintosh 7100/66 microcomputer, and prints were generated with a Kodak printer.

RESULTS

Three different forms of Aβ^{1-40} peptide radiopharmaceutical were synthesized (Figure 1). All three had the dual modifications of (i) attachment of a radionuclide and (ii) attachment of a biotin group. The monobiotinylation enables conjugation to a BBB drug targeting vector comprised of a transporting MAb and streptavidin or avidin. In the first formulation (Figure 1A), the Aβ^{1-40} is radiolabeled by attachment of 125-iodine to the single Tyr residue at position 10, and the biotin is attached at the amino terminus with a short (<15 atom) linker between the biotin and the amino terminus. In the second formulation (Figure 1B), the Aβ^{1-40} is radiolabeled at Tyr^{10} with ^{125}I, and is biotinylated at one of the two internal lysine residues via an extended PEG^{3400} linker. In the third formulation (Figure 1C), the Aβ^{1-40} is biotinylated at the amino terminus with a short linker and is radiolabeled with ^{111}In via a DTPA chelator moiety conjugated to one of the two internal lysine residues (Figure 1C).

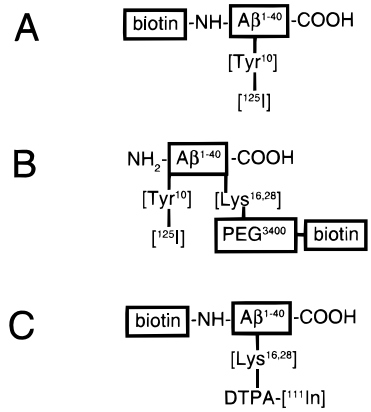

Figure 1. Structures of [^{125}I][*N*-biotin]-Aβ^{1-40} (A), [^{125}I]Aβ^{1-40}-PEG^{3400}-biotin (B), and [^{111}In]DTPA-[*N*-biotin]-Aβ^{1-40} (C). The ^{125}I was attached to Tyr^{10}, and the -PEG^{3400}-biotin or the DTPA was conjugated to the epsilon amino group of one of the two internal lysine residues at position 16 or 28.

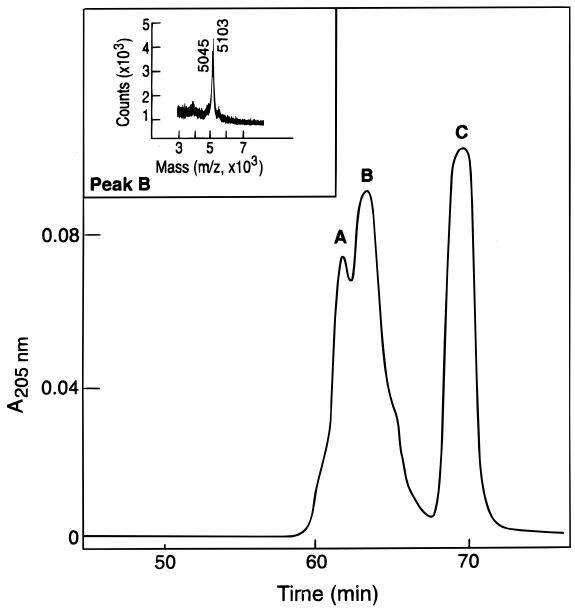

Figure 2. Purification of DTPA-[*N*-biotin]-Aβ^{1-40} by FPLC. Reaction mixture of [*N*-biotin]-Aβ^{1-40} and DTPA dianhydride was applied to two Superose 12 HR 10/30 columns in series, followed by elution in 0.01 M phosphate-buffered saline (pH 7.4) at a flow rate of 0.5 mL/min for 90 min. Peak A, (DTPA)$_2$-[*N*-biotin]-Aβ^{1-40}; peak B, DTPA-[*N*-biotin]-Aβ^{1-40}; peak C, DTPA. (Insert) MALDI mass spectra shows molecular mass of 5045 Da for peak B, the DTPA-[*N*-biotin]-Aβ^{1-40} (theoretical M_r, 5045 Da). Peak A, (DTPA)$_2$-[*N*-biotin]-Aβ^{1-40} showed molecular mass of 5420 Da (theoretical M_r, 5420) with the MALDI analysis.

The DTPA-[*N*-biotin]-Aβ^{1-40} (peak B, Figure 2) was separated from unreacted *N*-biotin-Aβ^{1-40} (peak C, Figure 2) and DTPA$_2$-[*N*-biotin]-Aβ^{1-40} (peak A, Figure 2) by gel filtration FPLC using two Superose 12HR columns in

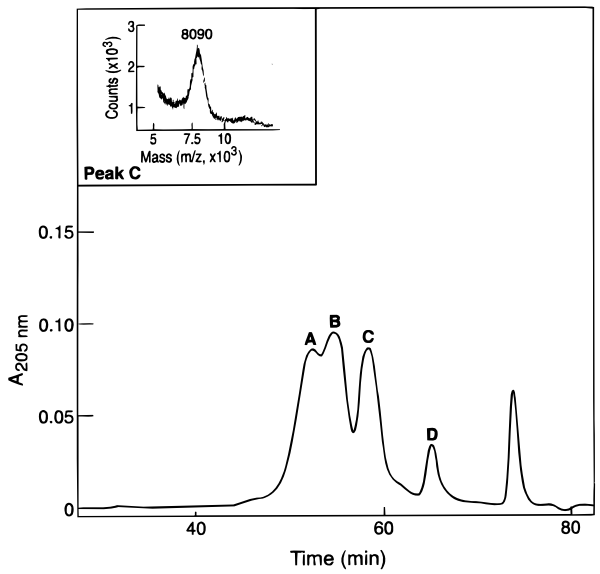

Figure 3. Purification of Aβ1−40-PEG3400-biotin by FPLC. Reaction mixture of Aβ1−40 and NHS-PEG3400-biotin was applied to two Superose 12 HR 10/30 columns in series, followed by elution in 0.01 M phosphate-buffered saline (pH 7.4) at a flow rate of 0.5 mL/min for 90 min. Peak A, Aβ1−40-(PEG3400-biotin)3; peak B, Aβ1−40-(PEG3400-biotin)2; peak C, Aβ1−40-PEG3400-biotin; peak D, Aβ1−40. (Insert) MALDI mass spectra shows mean molecular mass of 8090 Da for peak C, Aβ1−40-PEG3400-biotin (theoretical M_r, 7981 Da). Peak A, Aβ1−40-(PEG3400-biotin)3 and peak B, Aβ1−40-(PEG3400-biotin)2 showed mean molecular masses of 15 356 Da (theoretical M_r, 15283 Da) and 11 676 Da (theoretical M_r, 11 632), respectively, with the MALDI analysis. The (PEG3400-biotin)$_n$ nomenclature, where $n = 1$, 2, or 3, refers to the number of PEG3400 strands conjugated to the Aβ1−40, which can attach to Lys16, Lys28, or the amino terminus. The theroretical M_rs are approximations owing to the uncertainty of the exact M_r of the PEG3400.

series. MALDI mass spectrometry analysis (inset, Figure 2) demonstrated the observed molecular mass of the DTPA-[*N*-biotin]-Aβ1−40 was 5103−5045 Da, with a theoretical molecular mass (M_r) of 5045 Da. MALDI mass spectrometry showed the observed molecular mass of the Aβ conjugate in peak A was 5420 Da, which correlates with the theoretical molecular mass (5420 Daltons) for the [*N*-biotin]-Aβ1−40 that contains DTPA moieties conjugated to both internal lysine residues, designated (DTPA)2-[*N*-biotin]-Aβ1−40. The purity of the peptide following gel filtration FPLC through two columns in series was demonstrated by the absence of peaks of contaminating peptides in the MALDI mass spectrometry analysis.

The Aβ1−40-PEG3400 biotin was purified by gel filtration FPLC using two Superose 12HR columns in series, which allowed for separation of unconjugated Aβ1−40 (peak D, Figure 3) from Aβ conjugates containing 3, 2, or 1 PEG3400-biotin moieties (peaks A, B, and C of Figure 3, respectively). The MALDI mass spectrometry analysis of peak C revealed a molecular mass of 8090 Da (inset, Figure 3), which correlates with the predicted theoretical M_r of 7981 Da. The precise theoretical M_r is an approximation owing to uncertainties regarding the length and M_r of the PEG3400. The M_r of peak A was 15 356 Da as opposed to the theoretical M_r of 15 283 Da for the Aβ conjugate with three PEG3400-biotin residues attached to both internal Lys residues and to the free amino terminus. The MALDI mass spectrometry analysis of peak B indicated the mass of this peptide was 11 676 Da, which correlates with the theoretical M_r of 11 632 Da for the Aβ1−40 containing two PEG3400-biotin resides (peak B, Figure 4).

Film autoradiography examined the binding of the three different Aβ1−40 peptide radiopharmaceuticals to amyloid plaques in frozen sections of autopsy AD brain (Figure 3). All three formulations of the Aβ peptide radiopharmaceutical bound to the amyloid plaques with a predilection for gray matter and sparing of the central white matter track. The binding of the [111In]DTPA-[*N*-biotin]-Aβ1−40 to the amyloid plaques (Figure 4B) was comparable to the binding of [125I][*N*-biotin]-Aβ1−40 (Figure 4A). Although there was still extensive binding of the [125I]Aβ1−40−PEG3400-biotin to the amyloid plaques, this was diminished compared to the other two formulations (Figure 4C).

Emulsion autoradiography studies were also performed and these showed that the 111In formulation did not react with the emulsion. The two Aβ peptide radiopharmaceutical formulations containing the 125I radionuclide did react with the emulsion, and these studies are shown in Figure 5. There was extensive binding to amyloid plaques at both the meningeal surface and internally in the brain

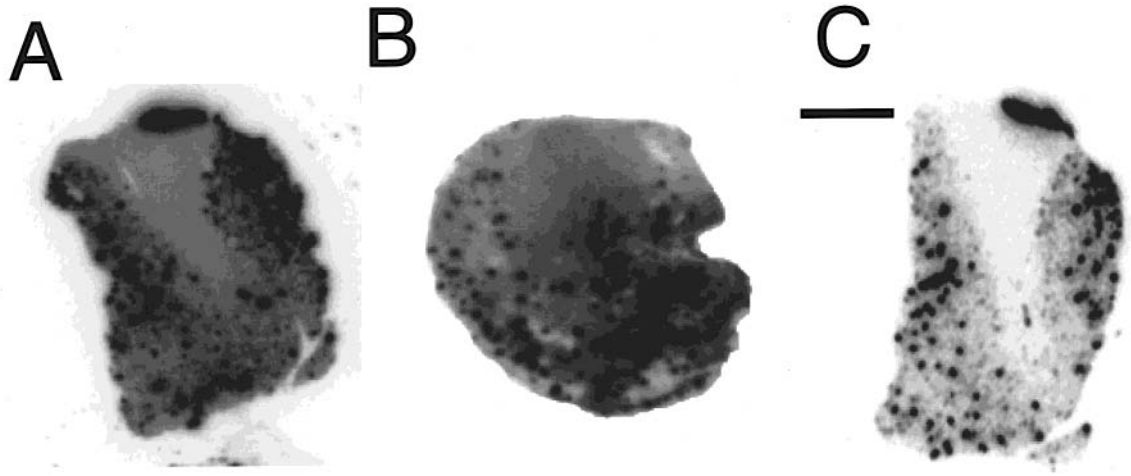

Figure 4. Film autoradiography showing binding of [125I][*N*-biotin]-Aβ1−40 (A), [111In]DTPA-[*N*-biotin]-Aβ1−40 (B), and [125I]Aβ1−40-PEG3400-biotin (C), and to amyloid plaques of frozen sections of human Alzheimer's disease brain. Magnification bar = 4 mm. The central white matter track is spared of amyloid. The amyloid plaques are small structures with a diameter less than 100 μm, as viewed by emulsion autoradiography (*11*). However, when the amyloid plaques are viewed with film autoradiography, such as that shown in Figures 4 and 5, there is a coalescence of the plaque signals (*11*) to yield the large plaque structures of a diameter >1 mm, as shown in the figure.

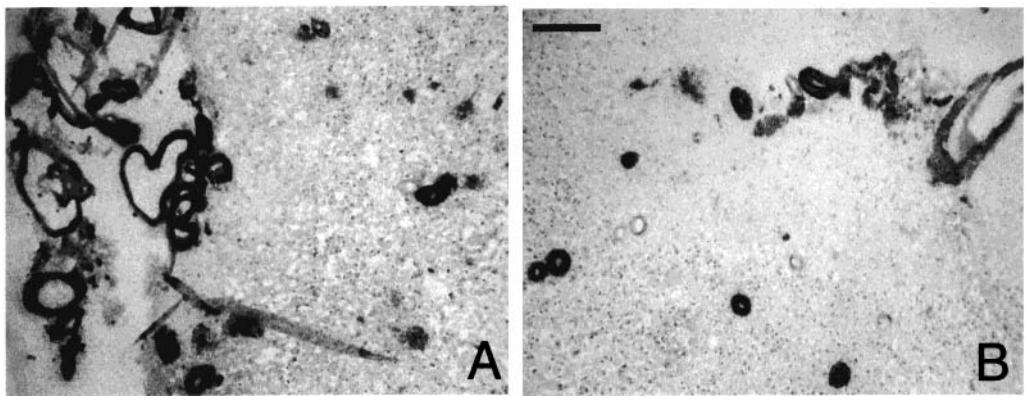

Figure 5. Emulsion autoradiography showing binding of [^{125}I][*N*-biotin]-Aβ^{1-40} (A) and [^{125}I]Aβ^{1-40}-PEG^{3400}-biotin (B) to amyloid plaques of frozen sections of human Alzheimer's disease brain, as viewed under bright field microscopy. Magnification bar = 200 μm.

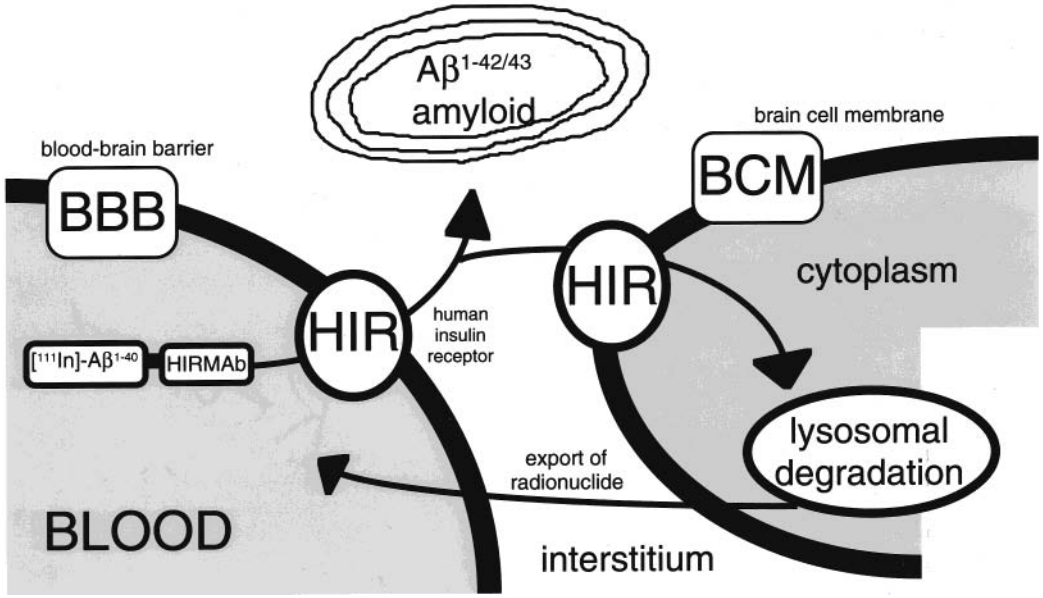

Figure 6. Pathways of metabolism of Aβ^{1-40} conjugates in brain. The mono-biotinylated Aβ^{1-40} (Figure 1) is bound to a conjugate of streptavidin or avidin and a peptidomimetic monoclonal antibody (MAb) that undergoes receptor mediated transcytosis through the blood-brain barrier (BBB). In the case of humans or rhesus monkeys, the MAb is directed against the human insulin receptor (HIR), which is also localized to brain cell membranes (BCM) (*24*) and mediates the endocytosis of the conjugate into brain cells. Once inside brain cells, the conjugate is degraded in the lysosome with export of the radionuclide to blood, which occurs with a $t_{1/2}$ of 16 h in the young rhesus monkey lacking brain A$\beta^{1-42/43}$ amyloid (*14*). In subjects with A$\beta^{1-42/43}$ brain amyloid, the plaques in the brain interstitial space enable deposition of the Aβ^{1-40} peptide radiopharmaceutical on to the surface of the extracellular amyloid plaque. This deposition is hypothesized to delay the metabolic degradation and prolong the residence time in brain of the Aβ^{1-40} peptide radiopharmaceutical, such that at delayed imaging times (e.g., 48−72 h after isotope administration) the brain radioactivity persists at the regions of high plaque content. Conversely, in subjects without brain amyloid, the brain radioactivity returns to background levels at the 48−72 h images (*14*).

parenchyma using the [^{125}I, *N*-biotin] Aβ^{1-40} (Figure 5). Similar to the results with the film autoradiography (Figure 4), there was a diminished binding to the amyloid plaques in the emulsion autoradiography using the [^{125}I]Aβ^{1-40}−PEG^{3400}-biotin formulation as shown in Figure 5B.

DISCUSSION

The results of the present studies are consistent with the following conclusions. First, it is possible to prepare a formulation of Aβ (Figure 1C) that has the dual modifications of (i) attachment to a radionuclide, ^{111}In, suitable for SPECT external imaging of brain, and (ii) attachment of a biotin moiety to enable conjugation to a BBB drug targeting system. This formulation of the Aβ peptide radiopharmaceutical still avidly binds to the amyloid plaques of AD brain (Figure 4). Second, the insertion of a PEG^{3400} linker to spatially separate the Aβ peptide radiopharmaceutical from the biotin linker does not confer any enhanced binding of the Aβ peptide radiopharmaceutical at the amyloid plaques and may inhibit binding (Figures 4 and 5).

The pathways involved in imaging the Aβ amyloid of AD brain in vivo are outlined in Figure 6. The Aβ peptide radiopharmaceutical must be formulated with dual modifications that enable (a) attachment of a radionuclide, e.g., 111-indium, suitable for SPECT imaging, or 124-iodine, suitable for PET imaging, and (b) conjugation to a BBB drug targeting system. The latter is a peptidomimetic MAb that undergoes receptor-mediated transcytosis through the BBB (*15*) and may be the 83-14 MAb that targets the BBB insulin receptor in rhesus monkeys (*18*), or the 8D3 or RI7 MAb that targets the BBB TfR in mice (*16*). The insulin receptor or the TfR are widely expressed on brain cells (*24*, *26*), and binding of the peptidomimetic MAb to the brain cell insulin receptor or TfR will enable

receptor-mediated endocytosis into brain cells behind the BBB (Figure 6). Following entry into the lysosomal system of brain cells, the amyloid imaging agent is degraded, and the radionuclide is exported to the systemic circulation. This has been demonstrated previously in young primates lacking brain amyloid and the half time of conjugate degradation and ^{125}I-radionuclide clearance from brain is 16 h in the living rhesus monkey (*14*). Consequently, >90% of the peptide radiopharmaceutical initially taken up by the primate brain lacking amyloid is cleared by 48 h after single intravenous administration of the conjugate (*14*). In subjects with significant quantities of amyloid plaque in brain, and in patients with AD, this can form up to 15% of the brain volume (*7*), it is hypothesized that the Aβ peptide radiopharmaceutical will be selectively sequestered by the extracellular amyloid in brain (*14*), as depicted in Figure 6. Although $A\beta^{1-40}$ is rapidly degraded, its degradation is markedly delayed upon binding to preexisting amyloid plaques (*26*). Therefore, the brain scan at 48 h after intravenous administration of the Aβ peptide radiopharmaceutical conjugated to a BBB drug targeting system may show persistent radioactivity at regions containing extensive amyloid compared to the minimal radioactivity in regions with no amyloid. The hypothesis that the brain ^{111}In radioactivity will be selectively exported from brain in nonamyloid-bearing regions cannot be verified until these studies are actually executed in mouse or primate animal models of Aβ brain amyloid. However, the ability of the brain to rapidly export ^{111}In following brain uptake of a ^{111}In-peptide radiopharmaceutical conjugated to a BBB drug targeting system has been recently demonstrated in an experimental brain tumor model (*22*). The export of ^{111}In from the brain in vivo contrasts with cultured cells, where ^{111}In is sequestered within the cell (*27*, *28*).

The administration of Aβ amyloid imaging agents to humans for brain scanning by SPECT will require the radiolabeling of Aβ analogues with a SPECT-compatible radionuclide such as 111-indium. The present studies show that one of the internal lysine residues may be conjugated with DTPA to enable chelation of 111-indium. The conjugation of the DTPA chelator moiety to one of the internal lysine residues at Lys^{16} or Lys^{28} does not inhibit the binding to amyloid plaques (Figure 4B). The Lys^{16} is contiguous with the sequence of Aβ that runs from Leu^{17} to Asp^{22}, and which plays an important role in binding of Aβ analogues to amyloid plaques (*29*−*31*). Other active sites in the Aβ molecule that are critical to binding to amyloid plaques must also be in the carboxyl terminus of the peptide, because $A\beta^{1-28}$ does not bind to amyloid plaques, whereas $A\beta^{10-35}$ does bind to plaques (*32*). The conjugation of PEG^{3400}-biotin to one of the two internal lysine residues results in a decreased binding of the peptide to amyloid plaques as shown by the film and emulsion autoradiography studies (Figures 4 and 5). Conjugation of DTPA to one of the internal lysine residues does not affect amyloid binding (Figure 4C). Therefore, the conjugation of an internal lysine residue, per se, would not be expected to inhibit amyloid binding. In previous studies with an epidermal growth factor (EGF) peptide radiopharmaceutical developed for imaging brain tumors expressing the EGF receptor, the insertion of a PEG^{3400} linker between the neuropeptide and the biotin actually enhanced binding of the EGF to its cognate receptor (*23*). The PEG^{3400} linker eliminates steric hindrance of peptide binding to the EGF receptor caused by conjugation of the peptide to the BBB drug targeting MAb. However, in the case of the $A\beta^{1-40}$ peptide analogues, the conjugation of the >200 atom long PEG^{3400} linker may interfere with $A\beta^{1-40}$ binding to amyloid plaques, although this is only a partial inhibition (Figures 4 and 5).

In summary, these studies describe a novel formulation of $A\beta^{1-40}$ that involves conjugation of DTPA to an internal lysine residue of $A\beta^{1-40}$ that contains a biotin residue at the amino terminus. This allows for the dual conjugation of the amyloid imaging peptide to (a) 111-indium, and (b) a BBB drug targeting system, which is comprised of a peptidomimetic MAb and an avidin or streptavidin moiety. Genetically engineered MAb/avidin genes and fusion proteins have been prepared (*33*, *34*), and a chimeric form of the 83-14 HIRMAb has been genetically engineered (*35*). These advances, in conjunction with progress in the synthesis of multifunctional amyloid-imaging agents (Figure 1), may enable the administration of these conjugates in humans for brain imaging of amyloid in subjects living with AD.

ACKNOWLEDGMENT

The manuscript was prepared by Daniel Jeong. This work was supported by a grant from the U.S. Department of Energy.

LITERATURE CITED

(1) Tomlinson, B. E., Blessed, G., and Roth, M. (1970) Observations on the brains of demented old people. *J. Neurol. Sci. 22*, 205−242.

(2) Cummings, B. J., and Cotman, C. W. Image Analysis of β-amyloid load in Alzheimer's disease and relation to demential severity. *Lancet 436*, 1524−1528.

(3) Kang, J., Lemaire, H. G., Unterbeck, A., Salbaum, J., Masters, C., Grzeschik, K., Multhaup, G., Beyreuther, K., and Muller-Hill, B. (1997) The precursor of Alzheimer's disease amyloid A_4 protein resembles a cell-surface receptor. *Nature 325*, 733−736.

(4) Glenner, G., and Wong, C. (1984) Alzheimer's disease: initial report of the purification and characterization of a novel cerebrovascular amyloid protien. *Biochem. Biophys. Res. Commun. 3*, 885−890.

(5) Pardridge, W. M., Vinters, H. V., Yang, J., Eisenberg, J., Choi, T., Tourtellote, W. W., Huebner, V., and Shively, J. E. (1987) Amyloid angiopathy of Alzheimer's disease: amino acid composition and partial sequence of a 4200 dalton peptide isolated from cortical microvessels. *J. Neurochem. 49*, 1394−1401.

(6) Masters, C., Simms, G., Weinman, N., Multhaup, G., McDonald, B., and Beyreuther, K. (1985) Amyloid plaque core protein in Alzheimer's disease and Down's syndrome. *Proc. Natl. Acad. Sci. 82*, 4252−4249.

(7) Kuo, Y. M., Emmerlings, M. R., Vigo-Pelfrey, C., Kasunic, T. M., Kirkpatrick, J. B., Murdoch, G. H., Ball, M. J., and Roher, A. E. (1996) Water-soluble Aβ (N-40, N-42) oligomers in normal and Alsheimer disease brains. *J. Biol. Chem 271*, 4077−4081.

(8) Maggio, J. E., Stimson, E. R., Ghilard, J. R., Allen, C. J., Dahl, C. E., Whitcomb, D. C., Vigna, S. R., Vinters, H. V., Labenski, M. E., and Mantyh, P. W. (1992) Reversible in vitro growth of Alzheimer disease β-amyloid plaques by deposition of labeled amyloid peptide. *Proc. Natl. Acad. Sci. 89*, 5462−5466.

(9) Ghilardi, J. R., Catton, M., Stimson, E. R., Rogers, S., Walker, L. C., Maggio, J. E., and Mantyh, P. W. (1996) Intra-arterial infusion of [^{125}I]Aβ1−40 labels amyloid deposits in the aged primate brain in vivo. *NeuroReport 7*, 2607−2611.

(10) Walker, L. C., Price, D. L., Voytko, M. L., and Schenk, D. B. (1994) Labeling of cerebral amyloid in vivo with a monoclonal antibody. *J. Neuropath. Exp. Neurol. 53*, 377−383.

(11) Saito, Y., Buciak, J., Yang, J., and Pardridge, W. M. (1995) Vector-mediated delivery of [^{125}I]-labeled β-amyloid peptide Aβ^{1-40} through the blood-brain barrier and binding to Alzheimer's disease amyloid of the Aβ^{1-40}/vector complex. *Proc. Natl. Acad. Sci. 92,* 10227−10231.

(12) Vorbrodt, A. W., Dobrogowska, D. H., Tarnawski, M., Meeker, H. C., and Carp, R. I. (1997) Immunocytochemical evaluation of blood-brain barrier to endogenous albumin in scrapie-infected mice. *Acta Neuropathol. 93,* 341−348.

(13) Yamaguchi, H., Yamazaki, T., Lemere, C. A., Frosch, M. P., and Selkoe, D. J. (1992) Beta amyloid is focally deposited within the outer basement membrane in the amyloid angiopathy of Alzheimer's disease. An immunoelectron microscopic study. *Am. J. Pathol. 141,* 249−259.

(14) Wu, D., Yang, J., and Pardridge, W. M. (1997) Drug targeting of a peptide radiopharmaceutical through the primate blood-brain barrier in vivo with a monoclonal antibody to the human insulin receptor. *J. Clin. Invest. 100,* 1804−1812.

(15) Pardridge, W. M. (1997) Drug delivery to the brain. *J. Cereb. Blood Flow Metabol. 17,* 713−731.

(16) Lee, H. J., Engelhardt, B., Lesley, J., Bickel, U., and Pardridge, W. M. (2000) Targeting rat anti-mouse transferrin receptor monoclonal antibodies through the blood-brain barrier in the mouse. *J. Pharmacol. Exp. Ther. 292,* 1048−1052.

(17) Hsaio, K., Chapman, P, Nilsen, S., Eckman, C., Harigaya, Y, Younkin, S., Yang, F., and Cole, G. (1996) Correlative memory deficits, Aβ elevation, and amyloid plaques in transgenic mice. *Science 274,* 99−102.

(18) Walker, L., Masters, C., Beyreuther, K., and Price, D. (1990) Amyloid in the brains of aged squirrel monkeys. *Acta Neuropathol. 80,* 381−387.

(19) Martin, L., Sisodia, S., Koo, E., Cork, L., Dellovade, T., Weidimann, A., Beyreuther, K., Masters, C., and Price, D. (1991) Amyloid precursor protein in aged nonhuman primates. *Proc. Natl. Acad. Sci. 88,* 1461−1465.

(20) Pardridge, W. M., Kang, Y., Buciak, J., and Yang, J. (1995) Human insulin receptor monoclonal antibody undergoes high affinity binding to human brain capillaries in vitro and rapid transcytosis through the blood-brain barrier in vivo. *Pharm. Res. 683,* 164−171.

(21) Kurihara, A., Deguchi, Y., and Pardridge, W. M. (1999) Epidermal growth factor radiopharmaceuticals: ^{111}In chelation, conjugation to a blood-brain barrier delivery vector via a biotin-polyethylene linker, pharmacokinetics, and in vivo imaging of experimental brain tumors. *Bioconjugae Chem. 10,* 502−511.

(22) Kurihara, A., and Pardridge, W. M. (1999) Imaging brain tumors by targeting peptide radiopharmaceuticals throught the blood-brain barrier. *Cancer Res. 54,* 6159−6163.

(23) Deguchi, Y., Kurihara, A., and Pardridge, W. M. (1999) Retention of biologic activity of human epidermal growth factor following conjugation to a blood-brain barrier drug delivery vector via an extended poly(ethylene glycol) linker. *Bioconjugate Chem. 10,* 32−37.

(24) Pardridge, W. M., Eisenberg, J., and Yang, J. (1985) Human blood-brain barrier insulin receptor. *J. Neurochem. 44,* 1541−1550.

(25) Mash, D. C., Pablo, J., Flynn, D. D., Efange, S. M. N., and Weiner, W. J. (1990) Characterization and Distribution of Transferrin Receptors in Rat Brain. *J. Neurochem. 55,* 1972−1979.

(26) Nordstedt, C., Naslund, J., Tjernberg, L. O., Karlstrom, A. R., Thyberg, J., and Terenius, L. (1994) The Alzheimer Aβ peptide develops protease resistance in association with its polymerization into fibrils. *J. Biol. Chem. 269,* 30772−30776.

(27) Shih, L. B., Thorpe, S. R., Griffiths, G. L., Diril, H. D., Ong, G. L., Hansen, H. J., Goldenburg, D. M., and Mattes, M. J. (1994) The processing and fate of antibodies and their radiolabels bound to the surface of tumor cells in vitro: a comparison of nine radiolabels. *J. Nucl. Med. 35,* 899−908.

(28) Press, O. W., Shan, D., Howell-Clark, J., Eary, J., Appelbaum, F. R., Matthews, D., King, D. J., Haines, A. M. R., Hamann, P., Himnan, L., Shochat, D., and Bernstein, I. D. (1996) Comparative metabolism and retention of iodine-125, yttrium-90, and indium-111 radioimmunoconjugates by cancer cells. *Cancer Res. 56,* 2123−2129.

(29) Hilbich, C., Kisters-Woike, B., Reed, J., Masters, C. L., and Beyreuther, K. (1992) Substitutions of hydrophobic amino acids reduce the amyloidogenicity of Alzheimer's disease βA4 peptides. *J. Mol. Biol. 228,* 460−473.

(30) Wood, S. J., Wetzel, R., Martin, J. D., and Hurle, M. R. (1995) Prolines and amyloidogenicity in fragments of the Alzheimer's peptide β/A4. *Biochemistry 34,* 724−730.

(31) Esler, W. P., Stimson, E., Ghilardi, J. R., Lu, Y. A., Felix, A. M., Vinters, H. V., Mantyh, P. W., Lee, J. P., and Maggio, J. E. (1996) Point substitution in the central hydrophobic cluster of a human β-amyloid congener disrupts peptide folding and abolishes plaque competence. *Biochemistry 35,* 13914−13921.

(32) Lee, J. P., Stimson, E. R., Ghilardi, J. R., Mantyh, P. W., Lu, Y. A., Felix, A. M., Llanos, W., Behbin, A., Cummings, M., Van Criekinge, M., Timms, W., and Maggio, J. E. (1995) ^{1}H NMR of Aβ Amyloid peptide congeners in water solution. Conformational changes correlate with plaque competence. *Biochemistry 34,* 5191−5200.

(33) Li, J. Y., Sugimura, K., Boado, R. J., Lee, H. J., Zhang, C., Dubel, S., and Pardridge, W. M. (1999) Genetically engineered brain drug delivery vectors- cloning, expression, and in vivo application of an anti-transferrin receptor single-chain antibody-streptavidin fusion gene and protein. *Protein Eng. 12,* 787−796.

(34) Penichet, M. L., Kang, Y. S., Pardridge, W. M., Morrison, S. L., and Shin, S. U. (1999) An anti-transferrin receptor antibody-avidin fusion protein serves as a delivery vehicle for effective brain targeting in an animal model. Initial applications in antisense drug delivery to the brain. *J. Immunol. 163,* 4421−4426.

(35) Coloma, M. J., Lee, H. J., Kurihara, A., Landaw, E. M., Boado, R. J., Morrison, S. L., and Pardridge, W. M. (1999) Transport across the primate blood-brain barrier of a genetically engineered chimeric monoclonal antibody to the human insulin receptor. *Pharm. Res. 17,* 266−274.

BC9901393

B-Domain Deleted Recombinant Coagulation Factor VIII Modified with Monomethoxy Polyethylene Glycol

Johanna Röstin,[†] Anna-Lisa Smeds,[‡] and Eva Åkerblom*[,§]

Recombinant Factor VIII, R&D, Pharmacia & Upjohn, S-112 87 Stockholm, Sweden. Received October 18, 1999

Recombinant coagulation factor VIII (r-VIII SQ) was chemically modified with monomethoxy poly(ethylene glycol) (mPEG). Three mPEG derivatives were used for coupling to the r-VIII SQ lysines, a mixed anhydride of monomethoxy poly(ethylene glycol) succinic acid (mPEG-SAH), monomethoxy poly(ethylene glycol) succinimidyl succinate (mPEG-SS), and monomethoxy poly(ethylene glycol) tresylate (mPEG-TRES). A consequence of the modification with all derivatives was a substantial reduction in coagulant activity, even at very low degrees of modification. A method was developed with the purpose of avoiding conjugation at certain important biological sites on the factor VIII and thereby producing conjugates with better retained activity. This was achieved by immobilizing the protein onto a solid matrix during the modification reaction. Characterization of conjugates by SDS−PAGE, western blots, interaction with von Willebrand factor (vWf), and thrombin activation/inactivation analyses was undertaken. The SDS−PAGE and western blots revealed coupling heterogeneity regarding degree of modification. The amount of factor VIII able to bind to vWf decreased with the conjugation. Thrombin activated the modified factor VIII to essentially the same extent as the reference preparation of r-VIII SQ. Inactivation of the modified factor VIII was, however, slower than inactivation of the unmodified protein. Finally, an in vitro study was performed to evaluate the influence of the mPEG modification on the protein stability in extract of porcine tissue. Despite that conjugates with low degrees of modification were included in the study, the coagulant activity was preserved to a significantly higher extent in all incubation mixtures containing conjugates compared to that with unmodified protein.

INTRODUCTION

Factor VIII is a protein, which plays a significant role as a cofactor in the blood coagulation process. Deficiency of or defects in this protein results in the bleeding disorder Hemophilia A. Hemophilia A patients are presently treated by intravenous administration of factor VIII, given on demand or preferably as prophylactic treatment several times a week (*1*). It would be more convenient for the patients if the stability of the substance in vivo could be increased to achieve a longer circulation time and a consequent reduction in frequency of administration. About 10−20% of hemophilia patients develop inhibiting antibodies to factor VIII (*1*), and a reduction of immunogenicity would greatly improve the efficacy of the medicine in these patients.

A well-known technique for improving pharmacokinetic properties of therapeutic proteins in vivo is covalent attachment of monomethoxy poly(ethylene glycol) (mPEG)[1] to the proteins. Increased in vivo half-life, increased bioavailability after subcutaneous administration, and reduced immunogenicity are properties that have been enhanced by pegylation of polypeptides for use in a number of therapeutic areas (*2*, *3*). However, an impaired function may also be a result of the modification, an effect that has been reported to increase with the degree of modification (*4*). A number of coupling reagents is described, most of them with reactivity toward the ϵ-amino groups of lysines (for a review, see ref *5*). As polypeptides often contain several lysines, attempts to derivatize more selectively to avoid the loss of activity have been made. Site-directed mutagenesis of recombinant interleukin-2 (rIL-2) is one example where a unique modification site was introduced by conversion of a Thr to a Cys (*6*). Another approach was used by Caliceti et al. (*7*). To protect functional sites of trypsin, the enzyme was reversibly bound to an inhibitor immobilized on a solid matrix during the procedure of mPEG conjugation.

Factor VIII functions in the blood coagulation system as an essential cofactor for activation of factor X to factor Xa. The molecule circulates in plasma as a heterodimer with structural domains A1−A2−B and A3−C1−C2 (*8*) as shown in Figure 1. The heavy chain consists of the A1−A2−B domains with a molecular mass ranging from 90 to 200 kDa due to variability of the B domain (*8*, *9*). The 80 kDa light chain consists of the A3−C1−C2 domains. The two chains are held together by a divalent

* To whom correspondence should be addressed. Telephone: +46 18 471 4337. Fax: +46 18 471 4474. E-mail: eva.akerblom@orgf3.bmc.uu.se.

[†] Recombinant Factor VIII.

[‡] Present address: Medical Product Agency, Box 26, S-751 03 Uppsala, Sweden.

[§] Present address: Department of Organic Pharmaceutical Chemistry, Uppsala Biomedical Center, Box 574, S-751 23 Uppsala, Sweden.

[1] Abbreviations: APC, activated protein C; CHO, Chinese hamster ovary; FF, fast flow; FPLC, fast-protein liquid chromatography; GPC, gel permeation chromatography; HIC, hydrophobic interaction chromatography; HR, high resolution; IU, international unit; kDa, kilodalton; mAb, monoclonal antibody; mPEG, monomethoxy poly(ethylene glycol); mPEG-SA, mPEG succinic acid; mPEG-SAH, mixed anhydride of mPEG succinic acid; mPEG-SS, mPEG succinimidyl succinate; mPEG-TRES, mPEG tresylate; NMR, nuclear magnetic resonance; PAGE, polyacrylamide gel electrophoresis; PG, prep grade; rIL-2, recombinant interleukin 2; r-VIII SQ, recombinant factor VIII SQ; SDS, sodium dodecyl sulfate; SQ, Ser Gln; std, standard deviation; VIII:C, factor VIII activity; vWf, von Willebrand factor.

10.1021/bc990137i CCC: $19.00 © 2000 American Chemical Society
Published on Web 04/04/2000

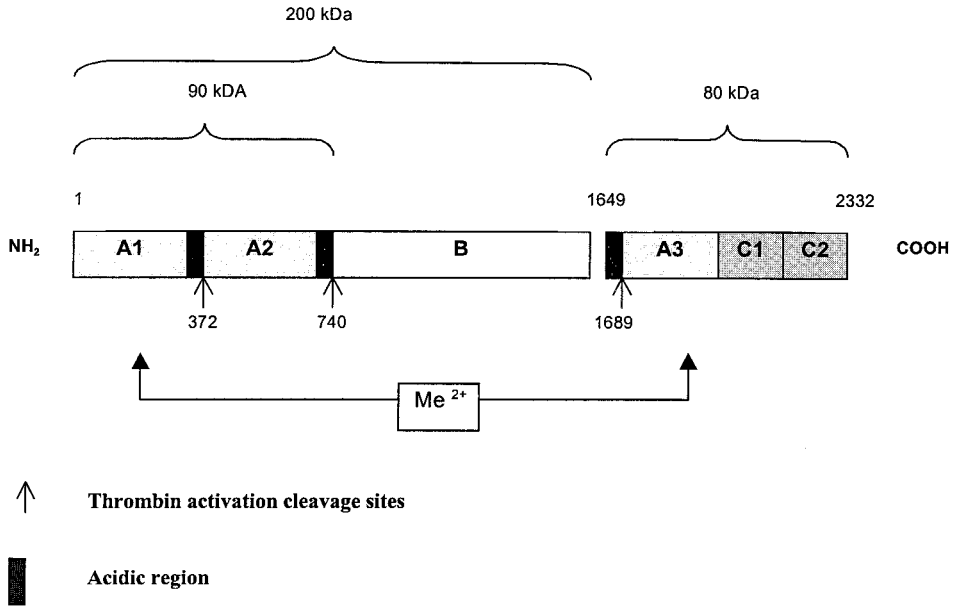

Figure 1. Structural domains of the heavy (90−200 kDa) and the light (80 kDa) chains of factor VIII, acidic regions, and the thrombin activation cleavage sites.

metal ion bridge (*9*). Factor VIII has several sites important for its function. Activation of factor VIII starts by thrombin cleavage at Arg 372 and Arg 740 in the heavy chain and at Arg 1689 in the light chain (*8, 10, 11*). The cleavage sites are located after acidic spacer regions in the polypeptide. Factor VIII is also susceptible to proteolytic cleavage at Arg 336 by activated protein C, APC (*12*), factor Xa, and thrombin (*10*), and this results in inactivation. This is important for the down-regulation of the coagulation cascade. Factor VIII circulates in human plasma noncovalently linked to von Willebrand factor (vWf) (*13*). vWf has an important stabilizing effect on factor VIII by protecting it from proteolytic degradation. The human in vivo half-life of factor VIII is 10−15 h (*1*), and it has been suggested that the half-life is highly dependent on the factor VIII−vWf complex formation (*14−16*). The vWf-binding site is located on the factor VIII light chain, at the A3 domain (*17*). Cleavage of factor VIII by thrombin at Arg 1689 releases the vWf together with the interacting sequence during activation of factor VIII.

The function of the B domain is not known, and it is not required for cofactor activity (*9, 18*). Pharmacia & Upjohn has constructed a recombinant factor VIII lacking this region for treatment of Hemophilia A. The deletion derivative, r-VIII SQ, was produced from a single gene construct encoding for an amino acid sequence, where the Ser 743 of the heavy-chain C-terminal was fused to the Gln 1638 of the light-chain N-terminal (*19*).

In this study, the pegylation technique was applied to r-VIII SQ. Coupling was performed by using three mPEG derivatives with reactivity toward the ϵ-amino groups of lysines. The factor VIII function was easily disturbed, and the coagulant activity decreased rapidly with degree of modification. The stability of modified factor VIII was investigated in in vitro experiments using porcine extracts representing the subcutaneous environment. The mPEG modification protected the r-VIII SQ from rapid inactivation in the incubation mixtures, even at low degrees of modification. These results prompted us to investigate whether this effect was applicable to in vivo conditions, and a pharmacokinetic study was performed in cynomolgus monkeys. A 4-fold higher bioavailability was obtained of the conjugates compared to the unmodified protein after subcutaneous injection (*20*).

MATERIALS AND METHODS

mPEG tresylate (mPEG-TRES) and mPEG succinimidyl succinate (mPEG-SS) of molecular weight 5000 were purchased from Shearwater Polymers, Inc., Huntsville, AL. mPEG was obtained from Hoechst and Union Carbide. Hepes and plasma contact activator kaolin (hydrated aluminum silicate) were purchased from Sigma; boric acid and Tween 80 were from Merck; and deuterium oxide was from Aldrich. Diagen (phospholipid) was obtained from Diagnostic Reagents Ltd., U.K., and triethylamine and *N-tert*-butylurea from Fluka. Human thrombin was purchased from Enzyme Research Laboratories Inc., IN, and antithrombin was produced by Pharmacia & Upjohn. vWf was prepared from a high-purity therapeutic concentrate (Octonativ-M from Pharmacia & Upjohn) by purification on a Sepharose CL-2B, to which polyclonal goat anti-human vWf antibodies were covalently coupled. The following chromatography equipment and media from Amersham Pharmacia Biotech, Sweden, were used: a fast-protein liquid chromatography (FPLC) system, Superose 12 bulk gel, Q Sepharose FF bulk gel, a prepacked Superdex 200 PG XK 16/60 column, and a prepacked Superdex 200 HR 10/30 column. The IR spectra was recorded on a 5% 1,2-dichloroethane solution in a barium fluoride liquid cell with a Perkin-Elmer model 580 infrared spectrophotometer.

Preparation of r-VIII SQ. Briefly, the r-VIII SQ was produced by a cell culture process using Chinese Hamster Ovary (CHO) cells (*19*) in a serum-free medium. The conditioned medium was continuously harvested, and the factor VIII was purified by four chromatography steps (*21*): cationic exchange, immunoaffinity using monoclonal antibodies (mAb), anionic exchange, and hydrophic interaction chromatography (HIC). Virus inactivation was performed after the cationic exchange step using the solvent/detergent method according to Horowitz et al. (*22*). The factor VIII was eluted from the HIC column in a buffer containing 50 mM L-histidine, 0.5 M ammonium acetate, 50 mM calcium chloride, and 0.02% Tween 80,

pH 6.8. The purity was very high, resulting in a mean specific activity of 15 000 IU/mg of protein.

Synthesis of mPEG-SA. mPEG (MW 3000, 120 g, 45 mmol) was added to succinic anhydride (8 g, 80 mmol) in 240 mL of dichloromethane. The solution was refluxed for 20 h. Excess succinic anhydride was then converted to monoethyl succinate by addition of 33 mL of ethanol, and the reaction mixture was refluxed for another 6 h. After evaporation in a vacuum, the residue was repeatedly washed with ether, subsequently dissolved in acetone, and precipitated in petroleum ether. The mPEG-SA was analyzed by titration and shown to contain 0.32 mmol of COOH/g. ^{1}H NMR ($CDCl_3$): δ 2.57−2.66 (m, 4H, CH_2CH_2CO), 3.35 (s, 3H, CH_3O), 3.44 (t, 2H, CH_2OCO), 2.52 (t, 2H, CH_3OCH_2), 3.55−4.00 [br, $(CH_2CH_2O)_n$], 3.79 (t, 2H, $CH_3OCH_2CH_2$), 4.23 (t, 2H, CH_2CH_2OCO). ^{13}C NMR ($CDCl_3$): δ 29.0, 29.5 (CH_2CH_2CO), 59.1 (CH_3O), 63.9 (CH_2OCO), 69.1 (CH_3OCH_2), 70.7 [$(CH_2CH_2O)_n$], 72.0 ($CH_3OCH_2CH_2$), 77.4 (CH_2CH_2OCO), 172.2 (OCO), 173.7 (COOH). The peaks were identified by comparing with ^{1}H and ^{13}C NMR spectra of PEG and mPEG. IR ($ClCH_2CH_2Cl$): ν 1740 cm^{-1} (ester and carboxylic acid carbonyl).

Activation of mPEG-SA (mPEG-SAH). mPEG-SA (77.3 g, 27.7 mmol) was dissolved in 700 mL of dichloromethane. Triethylamine (7.8 mL, 55.3 mmol) and isobutyl chloroformate (7.7 mL, 55.3 mmol) were subsequently added. The reaction solution was stirred for 30 min at room temperature and evaporated in a vacuum. The solid residue was washed seven times with 350 mL of petroleum ether by shaking the flask. After the last wash, the petroleum ether was decanted and the rest of the solvent was removed by evaporation in a vacuum. The mPEG-SAH was stored in a freezer. ^{1}H NMR ($CDCl_3$): δ 0.92 [d, 6H, $CH(CH_3)_2$], 1.93−2.03 [m, 1H, $CH(CH_3)_2$], 2.67 (t, 2H, CH_2CH_2CO), 2.77 (t, 2H, CH_2CH_2CO), 3.34 (s, 3H, OCH_3), 3.42 (t, 2H, CH_2OCO), 3.51 (t, 2H, CH_3OCH_2), 3.55−3.75 [br, $(OCH_2CH_2)_n$], 3.78 (t, 2H, $CH_3OCH_2CH_2$), 4.00 [d, 2H, $OCH_2CH(CH_3)_2$], 4.22 (t, 2H, CH_2CH_2OCO). ^{13}C NMR: δ 18.9 [$CH(CH_3)_2$], 27.7, 28.5, 29.3 [$CH(CH_3)_2$; CH_2CH_2CO], 59.1 (CH_3O), 64.2 (CH_2OCO), 69.0 (CH_3OCH_2), 70.6 [$(CH_2CH_2O)_n$], 72.0 ($CH_3OCH_2CH_2$), 75.6 (CH_2CH_2OCO), 166.9 (COOCO), 171.6 (OCO). In the ^{1}H and ^{13}C NMR spectra, there were peaks indicating an impurity of triethylamine HCl in mPEG-SAH. IR ($ClCH_2CH_2Cl$): ν 1825 cm^{-1} (anhydride carbonyl), 1740 cm^{-1} (ester carbonyl). The ratio between the heights of the peak at 1825 and the peak at 1740 cm^{-1} was used for studying the stability of mPEG-SAH. mPEG-SAH was stable for at least one year in a freezer.

Random Coupling of Activated mPEG Derivatives to Factor VIII. A buffer exchange of the r-VIII SQ HIC eluate was performed by gel permeation chromatography on a Superose 12 column, previously equilibrated with the coupling buffer: 0.25 M Hepes, 3.7 mM calcium chloride, pH 7.8. As a control experiment to determine the influence of mPEG on factor VIII, nonreactive mPEG was first added to aliquots of the factor VIII solution at a molar ratio of mPEG to protein as indicated in Table 1. Factor VIII activity (VIII:C) was determined by the chromogenic assay.

Three mPEG reagents were used to modify the r-VIII SQ lysines randomly (Figure 2). Activated mPEG was added in a solid state to the factor VIII solution (containing 0.4−0.7 mg/mL protein), and the mixture was incubated under rotation for 1.5 h at room temperature. The degree of modification was controlled by the molar excess of the mPEG added. To remove the excess of the activated mPEG and to separate the fractions of modified factor VIII according to size, gel permeation chromatography

Table 1. Factor VIII Activity in an mPEG Containing Environment

molar excess mPEG (mol of mPEG/mol of r-VIII SQ)	VIII:C IU/mL	remaining activity %
0	860	100
100	880	>100
200	960	>100
400	890	>100
2000	960	>100
2800	990	>100

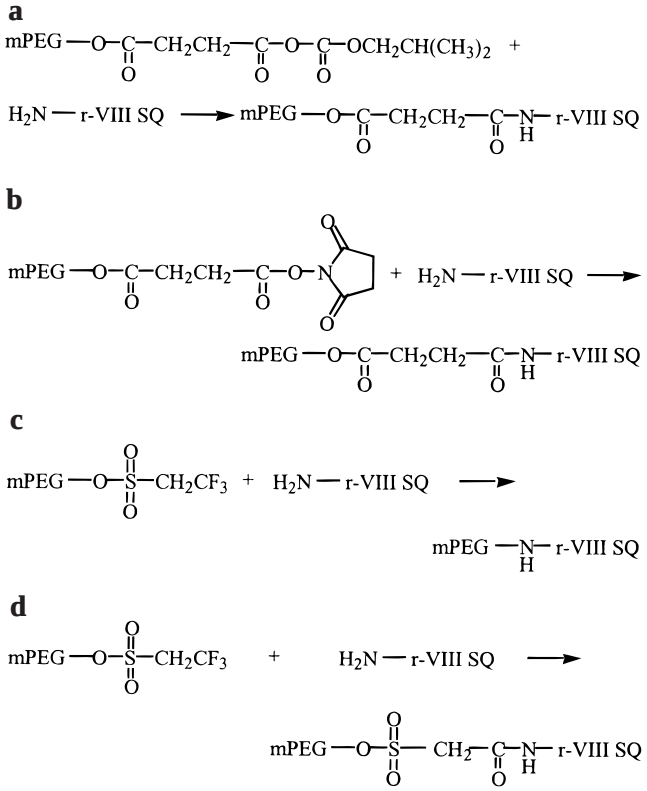

Figure 2. (a) Attachment of mPEG(3000)SAH to r-VIII SQ. (b) Attachment of mPEG(5000)SS to r-VIII SQ. (c) Attachment of mPEG(5000)TRES to r-VIII SQ by alkylation. (d) Attachment of mPEG(5000)TRES to r-VIII SQ by acylation.

was performed. A Superdex 200 PG column equilibrated with a buffer of 14.7 mM L-histidine, 0.4 M sodium chloride, and 3.7 mM calcium chloride, pH 6.9, was used. The conjugates included in Table 2 a refer to protein fractions corresponding to the first and second half of the protein peaks from each coupling reaction. The fractions were analyzed separately and denoted pool 1 and pool 2. The specific activities were calculated from VIII:C determined by the chromogenic assay and the protein content determined by amino acid analysis.

Coupling of Activated mPEG to Factor VIII Immobilized on a Solid Phase. The factor VIII was adsorbed on an anionic exchange gel (approximately 2 mg of protein/g of dry gel) during the modification reaction. A C-10 column packed with Q Sepharose FF, equilibrated with a buffer of the composition 50 mM L-histidine, 0.15 M sodium chloride, and 4 mM calcium chloride, pH 6.5, was used to adsorb the factor VIII. Prior to loading the protein onto the column, the HIC eluate of r-VIII SQ was conformed to the ionic strength and pH of the equilibration buffer by a 3-fold dilution using a buffer of 50 mM L-histidine and 50 mM calcium chloride, pH 6.4. The factor VIII was then loaded onto the column at a linear flow rate of 15 cm/h, and the column was subsequently equilibrated with the coupling buffer (0.25

Table 2. Determination of Specific Activities and Degrees of Modification of Factor VIII

(a) Modified with mPEG Reagents Randomly

conjugate	mPEG reagent	pool	molar excess mPEG added (mol of mPEG/ mol of r-VIII SQ)	degree of modification (mol of mPEG/ mol of r-VIII SQ)	specific activity (kIU/mg)	specific activity (% of r-VIII SQ)
	r-VIII SQ		0	0	15.0	100
	blank[a]		0	0	14.0	93
1	mPEG(3000)SAH	1	35	2.5	4.2	28
2		2	35	1.2	6.8	45
3	mPEG(3000)SAH	1	70	2.4	2.0	13
4		2	70	na	4.7	31
5	mPEG(3000)SAH	1	110	4.8	1.3	9
6		2	110	3.8	2.7	18
7	mPEG(5000)SS	1	30	3.2	3.9	26
8		2	30	2.7	7.3	49
9	mPEG(5000)SS	1	60	6.6	0.5	3
10		2	60	5.8	1.2	8
11	mPEG(5000)TRES	1	50	3.6	7.1	47
12		2	50	2.4	10.3	69
13	mPEG(5000)TRES	1	100	3.6	9.6	64
14		2	100	2.0	10.3	69
15	mPEG(5000)TRES	1	200	5.4	2.9	19
16		2	200	4.2	5.8	39

(b) Modified with mPEG(3000)SAH under Immobilization

conjugate	molar excess mPEG added (mol of mPEG/ mol of r-VIII SQ)	degree of modification (mol of mPEG/ mol of r-VIII SQ)	specific activity (kIU/mg)	specific activity (% of r-VIII SQ)
17	160	3.5	11.4	76
18	170	1.2	12.6	84
19	200	2.6	8.3	55
20	240	3.4	8.2	55
21	250	0.8	13.3	89
22	260	4.2	7.5	50
23	260	2.1	10.6	71
24	310	5.0	5.5	37
25	330	2.4	8.5	57
26	400	5.9	4.3	29
27	480	na	5.2	35
28[b]	370	4.4	7.8	52
29[b]	530	9.5	2.8	19

[a] The r-VIII SQ was subjected to the coupling procedure without addition of mPEG. [b] pH of the protein load was not adjusted prior to adsorption onto the solid phase. The conjugates are not included in Figure 5.

M Hepes and 3.7 mM calcium chloride, pH 7.8). The gel was transferred to a reaction vessel, and the activated mPEG was added in a solid state to the slurry at a molar ratio to factor VIII as indicated in Table 2b. The mixture was incubated under rotation for 1.5 h at room temperature. The gel was then repacked in the column and was extensively washed, and the modified factor VIII was eluted with a buffer of 50 mM L-histidine, 0.6 M sodium chloride, 4 mM calcium chloride, and pH 6.8 at 15 cm/h. The specific activities of the fractions were calculated from VIII:C determined by the chromogenic assay and the protein content was determined spectrophotometrically.

Fractionation of mPEG Modified Factor VIII. Prior to SDS−PAGE, western blots, vWf interaction, and thrombin activation analyses, the material produced by the coupling procedures above was further fractionated by gel permeation chromatography. A Superdex 200 HR 10/30 column equilibrated with 14.7 mM L-histidine, 0.4 M sodium chloride, 3.7 mM calcium chloride, and 0.02% Tween 80, pH 6.9, was used.

Protein Concentration and Amino Acid Content. Approximate factor VIII concentrations were determined spectrophotometrically with a Hitachi U-3200 spectrophotometer at 280 nm; the calculations were based on $\epsilon = 306 \times 10^3$ (M^{-1} cm^{-1}) and a molecular mass of 165 306 Da for the r-VIII SQ, respectively. The amino acid content was determined by first hydrolyzing the protein in 6 M HCl at 155 °C for 45 min and then analyzing the sample on an ion-exchange chromatography column where the amino acids were detected with ninhydrin. A Beckman 6300 amino acid analyzer equipped with a System Gold data handling system (Beckman) was used.

Determination of Degree of Modification. The mPEG content was determined by NMR, and the protein content by amino acid analysis. From these analyses, the degree of modification was calculated as moles of mPEG per moles of protein. The NMR determinations were performed either on a Varian Unity 500 or a Bruker 500 DRX instrument. Prior to the NMR analysis, a buffer exchange of the pegylated protein was performed by gel permeation chromatography using a Superose 12 column equilibrated with a buffer of the following composition: 0.1 M boric acid and 0.2 M sodium chloride, pH 7.8. The samples were repeatedly lyophilized and redissolved in deuterium oxide to remove traces of water before the NMR analysis. A standard curve using mPEG(3000) with concentrations ranging from 0.003 to 0.250 mg/mL was prepared. *N-tert*-Butylurea (0.0125 mg/mL) was used as an internal standard.

SDS−PAGE. SDS−PAGE was performed according to Laemmli (*23*). The gel thickness was 0.75 mm. The total

polyacrylamide concentration was 4% in the stacking gel and 7.5% in the separating gel and the cross-linkage was 3.3%. Samples of 0.7 μg were reduced by 5% (vol) 2-mercaptoethanol in 2% (mass/vol) SDS. The mixtures were heated for 5 min at 90 °C. The PAGE was run at 20 mA/gel for 4 h and the electrophoresis was followed by silver staining.

Western Blot Analysis. Western blot analysis was performed using polyclonal antibodies against plasma factor VIII as described previously (*9*). Two primary anti-(factor VIII) antibodies, produced as described in ref *19*, were used. The antibodies were directed against the C-terminus of the 90 kDa chain (Tyr 729 to Arg 740) and the C-terminus of the 80 kDa chain (Ala 2318 to Tyr 2332), respectively.

Factor VIII Activity. The factor VIII activity, VIII:C, was determined by a chromogenic substrate method (*24*), using the Coatest factor VIII kit (Chromogenix AB, Mölndal) and by a one-stage clotting method (*25*) where the VIII:C was determined using diagen platelet substitute diluted 1:50, containing 5 mg/mL kaolin. The definition of 1 IU corresponds to the coagulant activity of 1 mL of normal plasma as determined using a reference standard calibrated against the current international standard.

Interaction with Thrombin. The VIII:C was determined by the one-stage clotting method. mPEG-modified factor VIII conjugates were diluted to 1 and 10 IU/mL, respectively, in 50 mM Tris buffer, pH 7.4, containing 0.15 M sodium chloride and 4 mM calcium chloride. Thrombin was added to 1 and 10^{-1} NIH U/IU factor VIII, respectively. The changes in factor VIII activity were followed for 20 min by immediate assay of samples from the incubation mixture using the one-stage clotting method.

Interaction with vWf. Determination of the concentration of factor VIII able to bind to vWf was performed by using a BIAcore instrument (BIAcore Amersham, Uppsala, Sweden) (*26*, *27*). The binding of factor VIII to surface immobilized vWf was continuously monitored. Three different dilutions of each sample were analyzed against a reference preparation of r-VIII SQ. The content of factor VIII able to bind to vWf was calculated by dividing the concentration of interacting factor VIII with the total protein concentration.

In Vitro Test of Protein Stability in Extract of Porcine Tissue. After anestethizing the animal, skin samples were taken from its back or side immediately before it was sacrificed. A buffer of the following composition was made: 14.7 mM L-histidine, 0.4 M sodium chloride, 4 mM calcium chloride, 0.02% Tween 80, 13 mM *tri*-sodium-citrate, and 17 units of antithrombin/mL and pH was adjusted to 6.8 with 5 M hydrochloric acid. The buffer was added to the porcine tissue in a volume of 0.6 mL/g tissue. The mixture was incubated on ice for 2 h and stirred. The tissue was then removed. Different mPEG conjugates of factor VIII were incubated in the extract at 37 °C, and aliquots were taken at 0, 2, 4, 6, and 24 h and subsequently analyzed for coagulant activity by chromogenic assay.

RESULTS

Prior to the mPEG modification experiments, the stability of factor VIII was assessed in the buffer compositions applied. It was found that the VIII:C did not decrease during 50 h in the buffers used, at room temperature (data not shown). Control experiments were also made to verify that factor VIII was stable in an mPEG-containing environment. According to the results in Table 1 the activity was not hampered by the presence of mPEG.

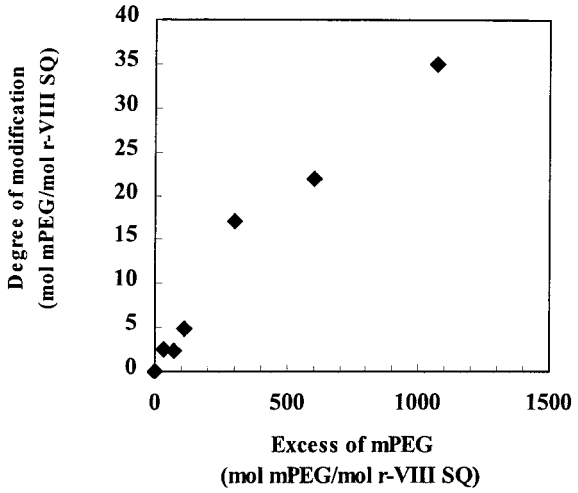

Figure 3. Relation between excess of reagent and degree of modification during random coupling with mPEG-SAH. The lower values of degree of modification, below 5 mPEG/r-VIII SQ, are "pool 1" values reported in Table 2a.

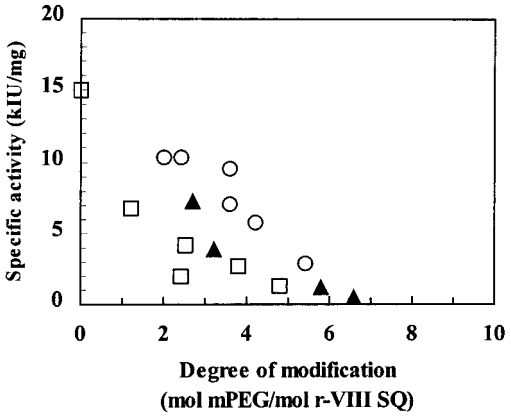

Figure 4. Specific activity as a function of degree of modification; modification at random sites with mPEG(3000)SAH (□), mPEG(5000)SS (▲), and mPEG(5000)TRES (○).

Random Coupling of Activated mPEG to Factor VIII. Three mPEG reagents with reactivity to lysines were chosen for coupling to r-VIII SQ (Figure 2). Previous control experiments performed by using refractometer showed that uncoupled mPEG was separated from the conjugate fractions by the type of chromatographic media used in the GPC step (data not shown). A protein yield of 60−80% was obtained in the chromatography step. First, by use of mPEG-SAH reagent, the degree of modification in relation to excess of mPEG added was studied. The degree of modification increased as the amount of excess mPEG added to the protein solutions increased, showing a correlation between these parameters (Figure 3). The specific activity of the conjugates derivatized above 15 mPEG/r-VIII SQ was, however, eliminated, and the proceeding work was performed by derivatizing r-VIII SQ with very low degrees of modification. Those latter conjugates were found to be heterogenic shown in Figures 6 and 7 by the electrophoresis and western blots (below). The GPC fractions of the first and second half of the protein peaks from these coupling reactions, respectively, were therefore analyzed separately (denoted pool 1 and pool 2 in Table 2a; conjugates 1−16, where the mean values of derivatization are reported). As a consequence of the fractionation by size,

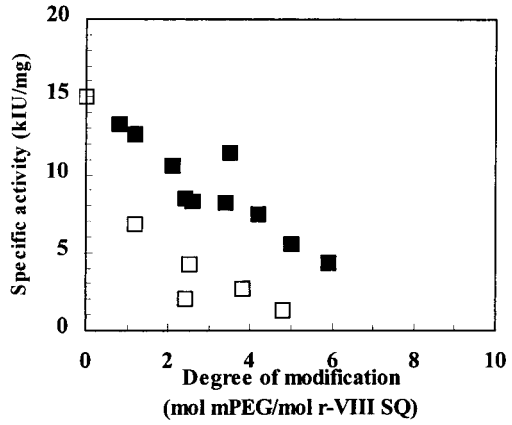

Figure 5. Specific activity as a function of degree of modification after acylation with mPEG(3000)SAH. Coupling was performed randomly (□) or during site protection (■).

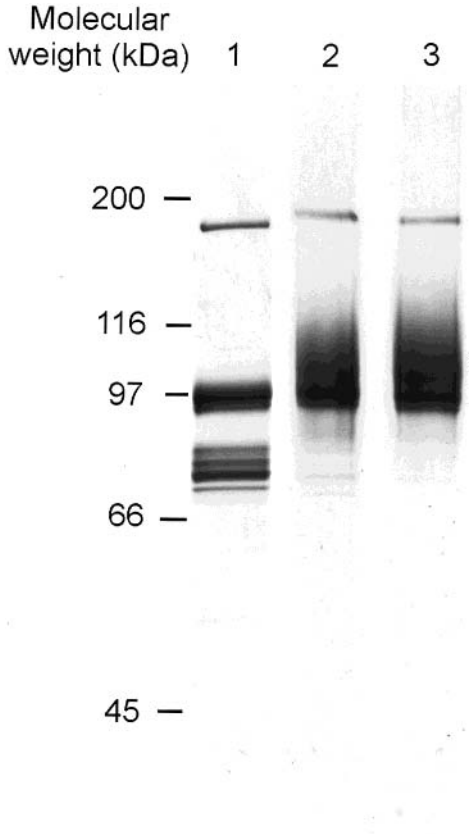

Figure 6. Reduced SDS−PAGE analyses of r-VIII SQ (HIC eluate) and mPEG modified r-VIII SQ. Lane 1, r-VIII SQ HIC eluate; lane 2, conjugate no. 17; lane 3, conjugate no. 22.

the amount of mPEG determined in pool 1 consistently exceeded the amount of mPEG in pool 2. Due to the low content of mPEG in the conjugate fractions, however, the responses in the NMR analysis were in the lower range of the standard curve. To evaluate the influence of the chromatographic procedure on protein activity, a control experiment, "blank", was performed, subjecting the r-VIII SQ HIC-eluate to the buffers and chromatography steps used. The specific activity of the blank was essentially the same as the starting material (Table 2a).

Coupling with mPEG(3000)SAH and mPEG(5000)SS, respectively, resulted in conjugates with a succinic linker (Figure 2, panels a and b). Table 2a (conjugates no 1−10) and Figure 4 show that the specific activity of factor VIII was reduced dramatically, even at low degrees of modification; approximately 1 mPEG/r-VIII SQ reduced the specific activity to 50%. The degree of activity retention was not influenced by the molecular weight of the mPEG.

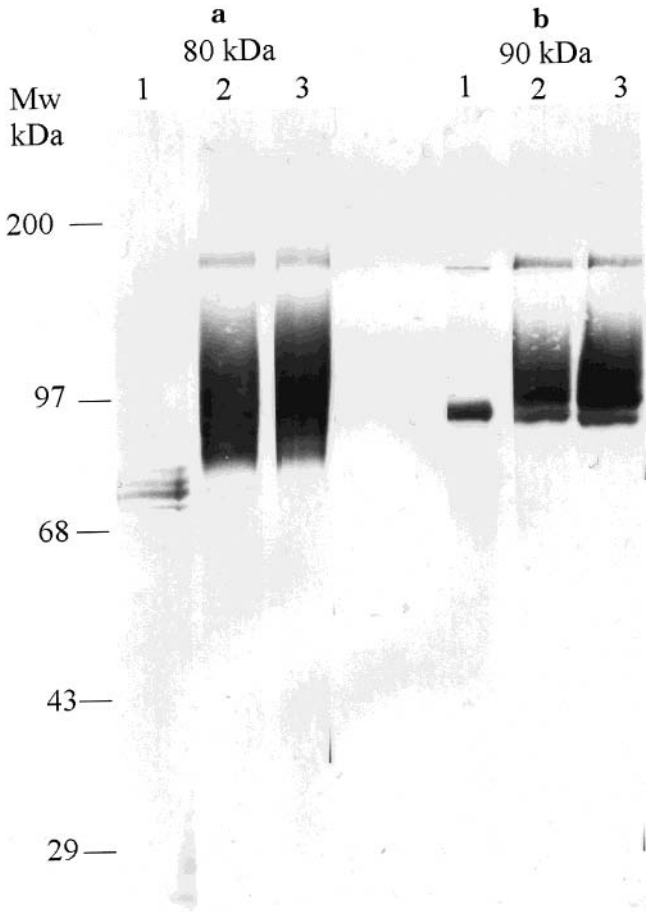

Figure 7. (a) Western blot using polyclonal antibodies raised against the 80 kDa chain of r-VIII SQ. Lane 1, r-VIII SQ; lane 2, conjugate no. 17; lane 3, conjugate no. 22. (b) Western blot using polyclonal antibodies raised against the 90 kDa chain of r-VIII SQ. Lane 1, r-VIII SQ; lane 2, conjugate no. 17; lane 3, conjugate no. 22.

Coupling with the mPEG(5000)TRES reagent was earlier believed to give alkylation on amino groups (*28*) (Figure 2c), but later findings have shown that this reagent also reacts by acylation giving a sulfoacetamide linkage to the protein (*29*, *30*) (Figure 2d). A higher specific activity was retained compared to modification by mPEG-SAH and mPEG-SS; at a mean degree of modification of approximately 3 mPEG/r-VIII SQ, 50% of the activity remained (Table 2a; conjugates 11−16 and Figure 4).

Coupling of Activated mPEG to Factor VIII Immobilized on a Solid Support. By adsorbing the factor VIII to an anionic exchange resin during acylation with the mPEG(3000)SAH, lysines at sites interacting with the solid phase were protected from derivatization. A Q Sepharose FF gel was used as the solid support during the coupling reaction. At 4 mPEG/r-VIII SQ, 50% activity still remained after modification. As shown in Table 2b and Figure 5, the specific activity of the mPEG(3000)-SAH-modified factor VIII was better retained using this solid-phase technique compared to the random acylation. The correlation between excess of mPEG added and the degree of modification obtained was however low.

Characterization of the mPEG-Modified Factor VIII. Reduced SDS−PAGE performed on mPEG-modified factor VIII and a reference preparation of r-VIII SQ (HIC

Table 3. Interaction of Factor VIII Conjugates with vWf

conjugate	specific activity (kIU/mg)	content of protein able to bind to vWf (% of total protein content)
r-VIII SQ	15.0	98 ± 4[a]
17[b]	7.0	43
22[b]	5.3	26

[a] Mean of 12 samples ± std. [b] Fractionated twice by GPC.

eluate) is shown in Figure 6. The bands of the reference r-VIII SQ appeared at 90 kDa (doublet) and 80 kDa (quartet), and trace amounts of the uncleaved single chain appeared at 170 kDa (lane 1). Electrophoretic bands of the conjugates were seen in positions corresponding to a molecular mass of 90 kDa and above (conjugates 17 and 22 in lanes 2 and 3, respectively). The conjugate preparations were prior to the SDS−PAGE analysis fractionated twice by GPC, and minor amounts of protein were seen in positions below 90 kDa, indicating a successful removal of unmodified protein. The blurred bands visualized the heterogeneity of the conjugates, and the separation of the protein bands was too poor for quantification of the degree of modification.

To investigate if modification occurred selectively on any of the two factor VIII chains, western blot analyses were performed on conjugates 17 and 22, using polyclonal antibodies directed against the 80 and 90 kDa chains, respectively. In the blots against both 80 and 90 kDa chains (Figure 7), blurred protein bands appeared in positions corresponding to a molecular mass above that of the unmodified protein. It was therefore concluded that the modification sites were located on both factor VIII chains.

A BIAcore analysis was used for studies on the binding of factor VIII to vWf. The results in Table 3 show that the content of conjugated factor VIII able to bind to vWf was reduced compared to the reference r-VIII SQ. Thus, the vWf interaction site was disturbed by the pegylation.

The one-stage clotting assay was used to analyze the activation and the subsequent inactivation of factor VIII by thrombin. First, the activity response obtained by the one-stage clotting method was compared to the response obtained by the chromogenic assay for each sample. For the conjugates, a discrepancy between the results obtained by the two methods was found; the activities determined by the one-stage clotting method were significantly lower than the activities determined by the chromogenic assay. For the reference r-VIII SQ, however, the results obtained by the two methods coincided. Figure 8 shows the thrombin activation patterns at two levels of VIII:C as determined by the one-stage clotting assay. The conjugates and the reference r-VIII SQ of dilution 1 IU/mL, incubated with 1 NIH U/IU thrombin, were activated at essentially the same rate (Figure 8a). A higher fold of activation was, however, observed for the conjugates of the concentration 10 IU/mL and 10^{-1} NIH U/IU thrombin, compared to the reference r-VIII SQ (Figure 8b). During the decline phase, the activity of the conjugates decreased at a slower rate than the reference, and complete inactivation did not occur during the time of the analysis. This effect was more pronounced when the samples were monitored at the lower thrombin to factor VIII ratio. The amounts of conjugated protein exceeded the amount of reference r-VIII SQ by approximately 5- and 20-fold for conjugates 17 and 22, respectively.

In Vitro Test of Protein Stability in Extract of Porcine Tissue. To investigate the influence of the pegylation on protein stability, an in vitro test was undertaken by incubating conjugates in extract of porcine tissue representative of the subcutaneous environment. In this crude test system, where the amount of factor VIII as well as the conjugates constituted a negligible amount of protein, the activity of the blank sample was markedly reduced during the first 6 h while the activity was preserved to a high extent in all incubation mixtures containing conjugates (Figure 9). In a further experiment, a preparation of a reference r-VIII SQ (HIC eluate) was incubated in the extract and the activity was reduced to the same extent as the blank (data not shown). The results show that the mPEG modification protected factor VIII from inactivation and that the coagulant activity was preserved significantly longer compared to the unmodified protein.

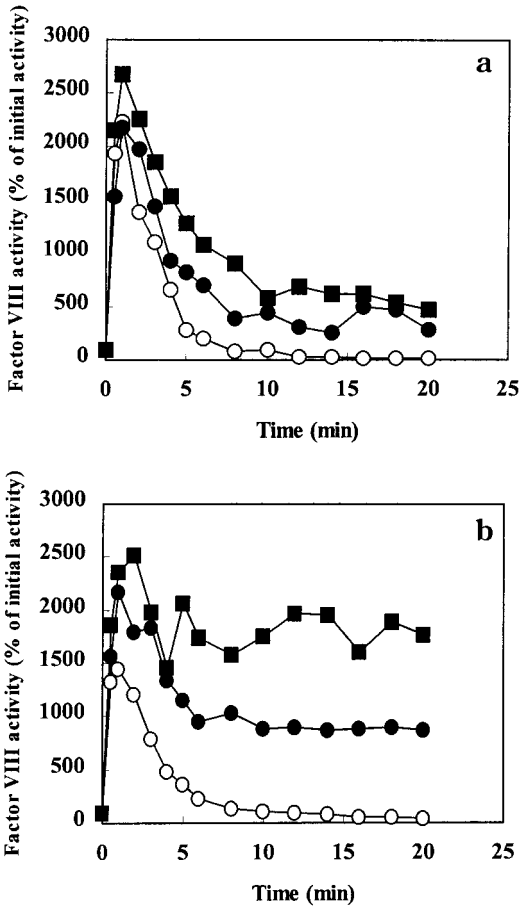

Figure 8. (a) Thrombin activation assay. The concentration of modified factor VIII conjugates no. 17 (●) and 22 (■) was 1 IU/mL and the ratio of thrombin to factor VIII was 1 NIH U/IU. r-VIII SQ (○) of concentration 1 IU/mL was assayed as reference. (b) Thrombin activation assay. The concentration of modified factor VIII conjugates no. 17 (●) and 22 (■) was 10 IU/mL and the ratio of thrombin to factor VIII was 10^{-1} NIH U/IU. r-VIII SQ (○) of concentration 10 IU/mL was assayed as reference.

DISCUSSION

A common problem associated with conjugation of proteins with mPEG is a disturbed biological function and decreased specific activity of the protein. It is not surprising that this problem has also appeared during modification of factor VIII, which is a protein with several biologically functional sites. Reaction products obtained by coupling with the mPEG-SAH and mPEG-SS reagents contain a succinic linker between the mPEG chain and the protein amino groups, the positive charges of which

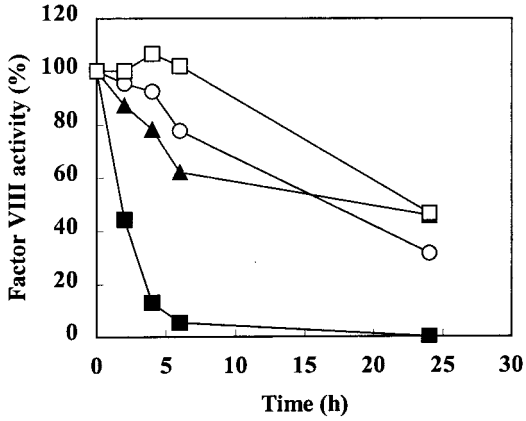

Figure 9. Stability of r-VIII SQ; blank (■) and mPEG modified factor VIII; conjugate no. 1 (▲), conjugate no. 28 (○), and conjugate no. 29 (□), in extract of porcine tissue.

are eliminated after the formation of an amide bond (*5*, *31*). Until recently, coupling with mPEG-TRES was thought to give a stable secondary amine (*28*). Others (*29*, *30*) have, however, showed that the mPEG can attach to the protein lysines through a sulfoacetamide linkage. This linker contains a sulfonic ester instead of a carboxylic ester as compared to the other conjugates. Also, by this coupling route, the lysine charge is eliminated. The specific activity of the conjugates obtained by random modification with all reagents was reduced, probably due to steric effects in combination with the changes of charge. A difference in reactivity between the reagents was observed. The mPEG-TRES reagent was less reactive than the other mPEG derivatives, and a larger excess was needed to modify the protein to the same extent (Table 2). Less reactivity often correlates to higher selectivity (*32*), which may account for the moderately higher specific activity of conjugates obtained with mPEG-TRES. With the aim of introducing the mPEG chains more selectively, factor VIII was immobilized on an anionic solid support during the coupling reaction. Reactive lysines, protected by the solid surface, were brought to be inaccessible, and the targets for mPEG conjugation were confined to other sites. As shown in Figure 5, the retained coagulant activity after directed modification by solid phase adsorption was higher than that retained after random modification using the mPEG-(3000)SAH. Presumably, the acidic regions, important for activation of factor VIII, were protected from conjugation.

All coupling reactions were performed at pH 7.8 due to reduced stability of factor VIII above pH 8 (data not shown). The pH used is considered low for lysine modification as the ϵ-amino groups of the lysines are mainly protonated at this pH [the pK_a of lysine is in free form 10.8 and in a model peptide 10.0−10.2 (*33*)]. Relatively large molar excess of mPEG was therefore added (Table 2). Heterogeneity in respect of the degree of modification is a well-known problem when modifying proteins chemically (*34*). r-VIII SQ contains 79 lysines to which activated mPEG may react. At high degrees of modification (>15 mPEG/r-VIII SQ), a large fraction of reactive lysines located on the protein surface was presumably modified. The degree of modification correlated to the amount of excess reagent added to the protein solutions. At lower degrees of modification, however, only a small fraction of the available lysines was derivatized. Although there was a correlation between amount of reagent added and the degree of modification, these coupling reactions were harder to control. Furthermore, the amounts of mPEG were in the lower range of the standard curve of the NMR analysis. By introducing a solid phase, during derivatization of r-VIII SQ in the immobilized state, the correlation was substantially reduced as more factors affected the coupling, e.g., the diffusion into the solid-phase particles and the masking of sites on the protein by adsorption. A considerable heterogeneity regarding molecular mass of the low derivatized conjugates was seen. This was revealed by the electrophoresis and western blots and by the fact that the mPEG content in two pools of gel permeation chromatography fractions obtained from one reaction mixture clearly differed. Separation techniques of higher resolution are necessary to further fractionate the different conjugates.

The human half-life of factor VIII is 10−15 h for the full-length as well as the B-domain-deleted recombinant variant in the presence of vWf (*35*). In the absence of vWf, the clearance rate is substantially higher and half-lives of 1−2 h have been reported (*14*, *16*). Therefore, the interaction of the modified factor VIII with vWf was considered a key issue, when characterizing the conjugates in the present study. According to the results obtained by the BIAcore assay, the interaction was hampered by the mPEG conjugation. This could of course influence the in vivo function and should be studied further.

Proteolytic cleavage by thrombin activates and subsequently inactivates factor VIII. The activation and inactivation of pegylated factor VIII diluted to 1 IU/mL showed essentially the same kinetics as obtained with the reference r-VIII SQ. The activation of the pegylated factor VIII diluted to 10 IU/mL and incubated with thrombin at 10^{-1} NIHU/IU factor VIII also showed a qualitatively similar pattern during activation as the reference. Inactivation of the conjugates, at this concentration and thrombin to factor VIII ratio, was however slower. The discrepancies between the two methods of determining VIII:C made the interpretation of the results of this study difficult. The one stage clotting method gave a lower response for modified factor VIII per mole of protein compared with the chromogenic assay. Consequently, a higher protein molar concentration of the modified molecule compared with the reference r-VIII SQ was required for a given activity response. Accordingly, the higher activation fold and the slower decline of activity could be an effect of lower thrombin to modified protein ratio than in the case of the reference protein.

The protecting effect of the mPEG often depends on the degree of modification (*36*). A surprisingly good retention of coagulant activity of the conjugates was achieved at incubation in the tissue extract even at these low degrees of modification. Since coagulant activity was maintained for 24 h in the incubation mixtures containing conjugates obtained from both random and directed modification with the mPEG(3000)SAH, the procedure of directing the mPEG coupling from the acid regions did not seem to influence the conjugates to withstand the process of inactivation in this particular environment. Neither was any correlation between the degree of modification and preservation of activity found, since the conjugate with 2.5 mPEG/r-VIII SQ was equally active as compared to the conjugates with higher degrees of modification, after 24 h.

CONCLUSION

In conclusion, r-VIII SQ was chemically modified by covalent attachment of mPEG with a concomitant reduction of coagulant activity. By immobilizing the factor VIII onto a solid matrix, at least one functional site was

shielded from modification, and the specific activity was retained to a higher extent as compared with random modification after acylation. The support chosen was an anionic-exchange chromatography gel, normally used for protein purification. In the field of immobilization techniques and in the context of pegylation, protection of functional sites by immobilization of the target protein onto a specific affinity support has previously been described (*7*). From the standpoint of the pharmaceutical industry, however, adsorbents with ligands manufactured by chemical synthesis is preferable. The use of complex biological substances in the manufacturing process is hereby increasingly avoided. This is important both due to the safety of the patients, which is a major concern, and the regulatory documentation which is a matter of significant cost. Despite the low degrees of modification applied, for the purpose of a satisfactory retention of coagulant activity, the mPEG markedly protected the factor VIII from inactivation in an in vitro environment representative of the subcutaneous space. In the pharmacokinetic study performed in cynomolgus monkeys (*20*), conjugates 17 and 22 were administered subcutaneously. The bioavailability was equal for both conjugates and exceeded that of the unmodified protein by approximately 4-fold. This implies a high potential of the modification technique as applied on this protein.

ACKNOWLEDGMENT

We thank Åke Ljungquist and collaborators for providing the r-VIII SQ HIC eluate. Ulla Oswaldsson and collaborators are acknowledged for skillful analyses of factor VIII activity. Helena Sandberg, Annelie Almstedt, and collaborators are acknowledged for contribution to the biochemical part of the work. We also thank Sven-Olof Larsson for performing the NMR analyses and Kristina Zachrisson for performing the amino acid analyses. Prof. Karl Hult is acknowledged for valuable discussions and advice on the manuscript.

LITERATURE CITED

(1) Nilsson, I. M. (1994) Replacement therapy. *Hemophilia*, Pharmacia Plasma Products, Sweden.

(2) Davis, F. F., Kazo, G. M., Nucci, M. L., and Abuchowski, A. (1991) Reduction of immunogenicity and extension of circulating half-life of peptides and proteins. In *Peptide and Protein Drug Delivery* (V. H. L. Lee, Ed.) pp 831−864, Marcel Dekker, Inc., New York.

(3) Katre, N. (1993) The conjugation of proteins with poly-(ethylene glycol) and other polymers. *Adv. Drug Deliv. Rev. 10*, 91−114.

(4) Inada, Y., Furukawa, M., Sasaki, H., Kodera, Y., Hiroto, M., Nishimura, H., and Matsushima, A. (1995) Biomedical and biotechnological applications of PEG- and PM-modified proteins. *Trends Biotechnol. 13*, 86−91.

(5) Zalipsky, Z. (1995) Functionalized poly(ethylene glycol) for preparation of biologically relevant conjugates. *Bioconjugate Chem. 6*, 150−165.

(6) Goodson, R., and Katre, N. (1990) Site-directed pegylation of recombinant interleukin-2 at its glycosylation site. *Bio/Technology 8*, 343−346.

(7) Caliceti, P., Schiavon, O., Sartore, L., Monfardini, C., and Veronese, F. (1993) Active site protection of proteolytic enzymes by poly(ethylene glycol) surface modification. *J. Bioact. Compat. Polym. 8*, 41−50.

(8) Vehar, G. A., Keyt, B., Eaton, D., Rodriguez, H., O'Brien D. P., Rotblat, F., Oppermann, H., Keck, R., Wood, W. I., Harkins, R. N., Tuddenham E. G. D., Lawn, R. M., and Capon, D. J. (1984) Structure of human factor VIII. *Nature 312*, 337−342.

(9) Andersson, L.-O., Forsman, N., Huang, K., Larsen, K., Lundin, A., Pavlu, B., Sandberg, H., Sewerin, K., and Smart, J. (1986) Isolation and characterization of human factor VIII: Molecular forms in commercial factor VIII concentrate, cryoprecipitate, and plasma. *Proc. Natl. Acad. Sci. U.S.A. 83*, 2979−2983.

(10) Eaton, D., Rodriguez, H., and Vehar, G. A. (1986) Proteolytic processing of human factor VIII. Correlation of specific cleavages by thrombin, factor Xa, and activated protein C with activation and inactivation of factor VIII coagulant activity. *Biochemistry 25*, 505−512.

(11) Pittman, D., and Kaufman, R. (1988) Proteolytic requirements for thrombin activation of anti-hemophilic factor (factor VIII). *Proc. Natl. Acad. Sci. U.S.A. 85*, 2429−2433.

(12) Fay, P. J., Smudzin, T. M., and Walker, F. J. (1991) Activated protein C-catalyzed inactivation of human factor VIII and factor $VIII_a$. *J. Biol. Chem. 266*, 20139−20145.

(13) Lollar, P. (1991) The association of factor VIII with von Willebrand factor. *Mayo Clin. Proc. 66*, 524−534.

(14) Morfini, M., Mannucci, P. M., Tenconi, P. M., Longo, G., Mazzucconi, M. G., Rodeghiero, F., Ciavarella, N., De Rosa, V., and Arter A. (1993) Pharmacokinetics of monoclonally purified and recombinant factor VIII in patients with severe von Willebrand disease. *Thromb. Haemost. 70*, 270−272.

(15) Fijnvandraat, K., Peters, M., and ten Cate, J. W. (1995) Inter-individual variation in half-life of infused recombinant factor VIII is related to pre-infusion von Willebrand factor antigen levels. *Br. J. Haematol. 91*, 474−476.

(16) Tuddenham, E., Lane, R., Rotblat, F., Johanson, A., Snape, T., Middleton, S., and Kernoff, P. (1982) Response to infusions of polyelectrolyte fractionated human factor VIII concentrate in human haemophilia A and von Willebrand's disease. *Br. J. Haematol. 52*, 259−267.

(17) Lollar, P., Hill-Eubanks, D. C., and Parker, C. G. (1988) Association of the factor VIII light chain with von Willebrand factor. *J. Biol. Chem. 263*, 10451−10455.

(18) Pittman, D., Alderman, E., Tomkinson, K., Wang, J., Giles, A., and Kaufaman, R. (1993) Biochemical, immunological, and in vivo functional characterization of B-domain-deleted factor VIII. *Blood 81*, 2925−2935.

(19) Lind, P., Larsson, K., Spira, J., Sydow-Bäckman, M., Almstedt, A., Gray, E., and Sandberg, H. (1995) Novel forms of B-domain-deleted recombinant factor VIII molecules: Construction and biochemical characterization. *Eur. J. Biochem. 232*, 19−27.

(20) Röstin, J., Smeds, A.-L., and Mikaelsson, M. (2000) Bioavailability of B-domain deleted recombinant factor VIII conjugated with monomethoxy poly(ethylene glycol) (manuscript submitted for publication).

(21) Smeds, A.-L., Ljungqvist, A., Ostlin, A., Ljungquist, C., Gaal, A., Sandberg, H., Rosenquist, J., and Mikaelsson, M. (1995) The purification process for recombinant factor VIII SQ. *Thromb. Haemost. 73* (abstract no. 442).

(22) Horowitz, B., Wiebe, M. E., Lippin, A., and Stryker, M. H. (1985) Inactivation of viruses in labile blood derivatives. I. Disruption of lipid-enveloped viruses by tri (n-butyl)-phosphate detergent combinations. *Transfusion 25*, 516−522.

(23) Laemmli, U. K. (1970) Cleavage of structural proteins during assembly of the head of bacteriophage T4. *Nature 227*, 680−685.

(24) Rosén, S. (1984) Assay of factor VIII:C with a chromogenic substrate. *Scand. J. Haematol. 33* (Suppl. 40), 139−145.

(25) Mikaelsson, M., and Oswaldsson, U. (1984) Standardization of VIII:C assays: a manufacturers view. *Scand. J. Haematol. 33* (Suppl. 41), 79−86.

(26) Jönsson, U., and Malmqvist, M. (1992) Real Time Biospecific Interaction Analysis. The Integration of Surface Plasmon Resonance Detection, General Biospecific Interface Chemistry and Microfluidics into One Analytical System. *Adv. Biosensors 2*, 291−336.

(27) Karlsson, R., Fägerstam, L., Nilshans, H., and Persson, B. (1993) Analysis of active antibody concentration. Separation of affinity and concentration parameters. *J. Immunol. Methods 166*, 75−84.

(28) Nilsson, K., and Mosbach, K. (1984) Immobilization of ligands with organic sulfonyl chlorides. *Methods Enzymol. 104*, 56−69.

(29) Gais., H.-J., and Ruppert, S. (1995) Modification and immobilization of proteins with poly(ethylene glycol) tresylates and polysaccharide tresylates: Evidence suggesting a revision of the coupling mechanism and the structure of the polymer−polymer linkage. *Tetrahedron Lett. 36*, 3837−3838.
(30) King, J., and Gill., M. (1996) Alkyl 2,2,2-trifluoroethanesulfonates (tresylates): Elimination-addition vs bimolecular nucleophilic substitution in reactions with nucleophiles in aqueous media. *J. Org. Chem. 61*, 7250−7255.
(31) Wie, S. I., Wie, C. W., Lee, W. Y., Filion, L. G., Sehon, A. H., and Åkerblom, E. (1981) Suppression of reagenic antibodies with modified allergens. *Int. Arch. Allergy Immunol. 64*, 84−99.
(32) Zalipsky, Z., Seltzer, R., and Menon-Rudolph, S. (1992) Evaluation of a new reagent for covalent attachment of poly(ethylene glycol) to proteins. *Biotechnol. Appl. Biochem. 15*, 100−114.
(33) Wong, S. S. (1991) Chemistry of protein conjugation and cross-linking, p 15, CRC Press, Inc., Boca Raton, FL.
(34) Kunitani, M., Dollinger, G., Johnson, D., and Kresin, L. (1991) On-line characterization of poly(ethylene glycol)-modified proteins. *J. Chromatogr. 588*, 125−137.
(35) Fijnvandraat, K., Berntorp, E., ten Cate, J. W., Johnsson, H., Peters, M., Savidge, G., Tengborn, L., Spira, J., and Stahl, C. (1997) Recombinant, B-domain deleted factor VIII (r-VIII SQ): Pharmacokinetics and initial safety aspects in hemophilia A patients. *Thromb. Haemost. 77*, 298−302.
(36) Hooftman, G., Herman, S., and Schacht, E. (1996) Review: Poly(ethylene glycol)s with reactive endgroups. II. Practical consideration for the preparation of protein-PEG conjugates. *J. Bioact. Compat. Polym. 11*, 135−159.

BC990137I

Enhancing the "Stickiness" of Bile Acids to Cross-Linked Polymers: A Bioconjugate Approach to the Design of Bile Acid Sequestrants

Lan-hui Zhang, Vaclav Janout, Jodi L. Renner, Maki Uragami, and Steven L. Regen*

Department of Chemistry and Zettlemoyer Center for Surface Studies, Lehigh University, Bethlehem, Pennsylvania 18015. Received November 2, 1999; Revised Manuscript Received January 6, 2000

A series of cross-linked polymers have been synthesized by reaction of 2% cross-linked, chloromethylated polystyrene with a tertiary amine derivative (**7**) of cholic acid (prepared by reaction of cholic acid methyl ester with *N,N*-dimethyl-ethylenediamine), followed by exhaustive quaternization with trimethylamine. Increased loadings of **7** result in enhanced binding of taurocholate ion and a decrease in its rate of release upon exposure to 50 mM aqueous NaCl. Examination of particle-size effects indicates that film diffusion and particle diffusion both contribute to the observed kinetics. Interruption tests that were carried out confirmed that particle diffusion is kinetically important. The relevance of this bioconjugate approach to the design of bile acid sequestrants for the treatment of hypercholesterolemia is briefly discussed.

INTRODUCTION

Conventional anion-exchange resins such as Dowex 1-X2 (Cholestyramine) serve as important therapeutic agents for the treatment of hypercholesterolemia (*1*). Although their mechanism of action is reasonably well-understood (i.e., they bind and remove bile acids from the intestines, thereby upregulating the conversion of cholesterol to bile acids in the liver), extensive efforts that have been made to improve resin efficiency have led to only modest advances. In an in-depth review of this area, Stedronsky has raised the intriguing possibility that *the rate of release* of bile acids from cross-linked polymers may be as important a factor in defining resin efficiency as its strength of binding, i.e., slow off-rates should help to avoid competitive removal of bile acids from the lumen through the wall of the ileum via active transport (*2*). It is noteworthy, in this regard, that nearly all studies involving bile acid sequestrants have focused on the thermodynamics of binding; only one investigation to date has examined the kinetics of release of bile acids (*3*, *4*).

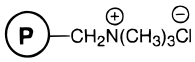

Dowex 1-X2 (Cholestyramine®)

cross-linked polystyrene; 2% divinylbenzene; >90% ring substitution

In this paper, we describe a bioconjugate approach to the synthesis of novel polymers that improves, for the first time, the kinetics as well as the thermodynamics of bile acid sequestration. Specifically, we show that the *conjugation* of a cholic acid derivative to an anion-exchange resin increases the resin's affinity toward taurocholate (*T*), and slows down its rate of release. This work was based on the hypothesis that "cloistering" of an ionically bound bile acid next to ones that are covalently attached should result in enhanced affinity due to van der Waals attraction and/or hydrogen bonding between nearest-neighbors (Scheme 1).

Scheme 1

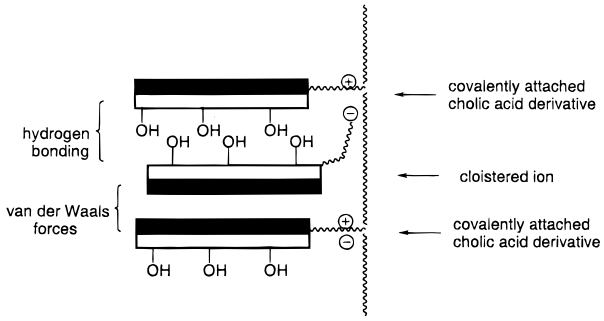

EXPERIMENTAL PROCEDURES

Materials and Methods. Unless stated otherwise, all chemicals were purchased from commercial sources and used without further purification. Cross-linked polystyrene was chloromethylated using experimental procedures similar to those previously described (*5*). Specific protocols, which were used to load quaternized ion-exchange resins with taurocholate have previously been reported (*4*). Typically, a taurocholate-loaded resin was prepared by suspending 1.0 g of a given resin in 400 mL of 1 mM sodium taurocholate solution. After equilibrating the resin for 72 h at room temperature, the concentration of sodium taurocholate that remained in the aqueous phase was determined by UV (205 nm), using an appropriate calibration curve. The resin was then separated from the free taurocholate in solution by filtration, and the resin rinsed with deionized water until no significant absorbance could be detected at 205 nm. The amount of resin-bound taurocholate was then calculated by subtracting the amount of residual sodium taurocholate in solution from the initial quantity that was present in the aqueous phase. Combining this data, with the total exchange capacity of the resin (see below), afforded the initial fraction of pendant ammonium groups (θ_o) having taurocholate as a counterion. The water used in these experiments was purified using a Millipore Milli-Q-filtering system containing one carbon and two ion-exchange stages. All kinetics experiments were carried

* To whom correspondence should be addressed. Phone: (610) 758-4842. Fax: (610) 758-6560. E-mail: slr0@lehigh.edu.

10.1021/bc990151v CCC: $19.00 © 2000 American Chemical Society
Published on Web 04/18/2000

Scheme 2

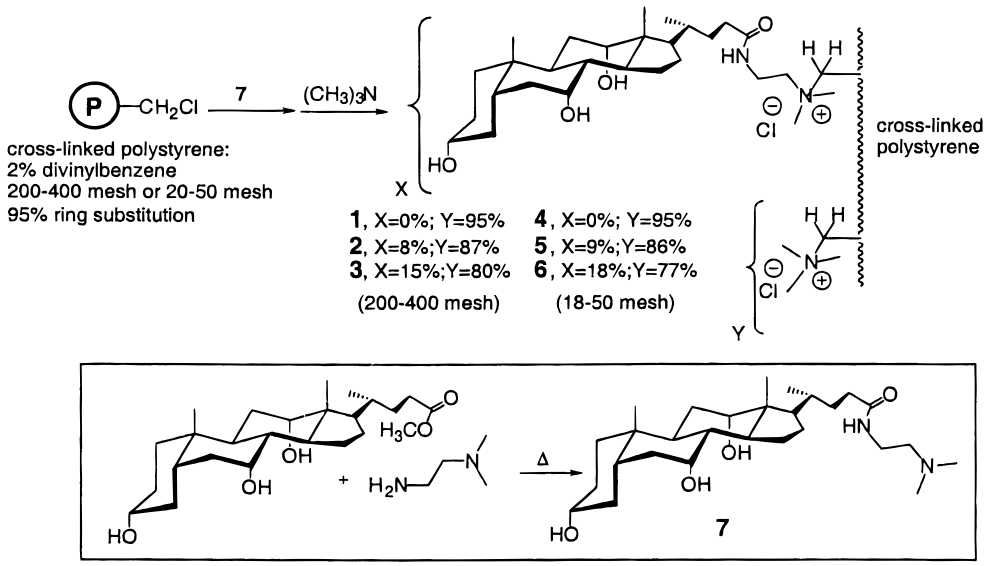

Table 1. Influence of Covalently-Attached 7 on Equilibrium Binding Constants and Initial Release Rates

resin	percent ring substitution	diameter (mm)	θ_o	K	$[-d(\theta/\theta_o)/dt]_o$
1	0	0.13 ± 0.03	0.275 ± 0.005	18 ± 1	0.145 ± 0.010
2	8		0.314 ± 0.005	19 ± 2	0.081 ± 0.005
3	15		0.300 ± 0.005	28 ± 2	0.066 ± 0.005
4	0	0.87 ± 0.13	0.265 ± 0.005		0.0109 ± 0.0005
5	9	0.87 ± 0.09	0.270 ± 0.005		0.0064 ± 0.0008
6	18	0.84 ± 0.11	0.215 ± 0.005		0.0013 ± 0.0002
A[a]	8	0.87			0.0069 ± 0.0005
B[a]	15	0.87			0.0031 ± 0.0003

[a] Initial rates estimated by interpolation of the data from **4**, **5**, and **6**.

out at 22 ± 1 °C, and UV measurements were made using a Milton Roy Spectronic 1201 spectrometer.

***N*$_2$,*N*$_2$-Dimethylamino-*N*$_1$-2-ethyl-choleamide.** A mixture of methylcholeate (2.70 g, 6.3 mmol) and *N*,*N*-dimethylamino ethylamine (2.4 g, 27 mmol) was stirred at 110 °C under a nitrogen atmosphere for 16 h, and the excess of amine then removed under reduced pressure to give crude product. The desired N_2,N_2-(dimethylamino)-N_1-2-ethyl-choleamide (**7**) was recrystallized (two times) from H_2O/CH_3OH (10:1, v/v) to give 2.91 g (90.6%) of product having a mp 192−3 °C. ^{1}H NMR (CD_3OD, 360 MHz): δ 3.93 (s, 1H), 3.79 (s, 1 H), 3.36 (m, 1H), 3.20 (m, 2 H), 2.45 (t, 2 H), 2.27 (s, 6 H), 0.9−2.25 (m, 30 H), 0.69 (s, 3 H). Anal. calcd ($C_{28}H_{50}N_2O_4$): C, 70.24; H, 10.53; N, 5.85. Found: C, 70.14; H, 10.47; N, 5.79.

Quaternization of Chloromethyl-poly(styren-98-*co*-divinylbenzene-2) with *N*$_2$,*N*$_2$-Dimethylamino-*N*$_1$-2-ethyl-choleamide and trimethylamine (Polymer 5). To a suspension of fully swollen chloromethylated polystyrene [3.116 g, 19.6 mmol Cl (95% ring substitution), 2% DVB] in 20 mL of anhydrous THF and 6.0 mL of anhydrous *N*,*N*-dimethylacetamide (DMAA) was added a solution of N_2,N_2-(dimethylamino)-N_1-2-ethyl-choleamide (0.924 g, 1.96 mmol) in 8 mL of anhydrous THF plus 3 mL of DMAA. After the suspension was heated (70 °C) for 64 h in a sealed flask, the polymer was separated, washed with 5 × 20 mL of THF. A small sample (ca. 20 mg) was then dried (23 °C, 0.5 Torr, 48 h) and subjected to elemental analysis. The resulting analysis (N, 1.31; Cl, 15.75) indicated that 9% of the chloromethylene groups were quaternized by the sterol.

The main portion of the polymer was then introduced into 44 mL of a 25% aqueous solution of trimethylamine (196 mmol) containing 12 mL of THF. After the mixture was heated (50 °C) in sealed flask for 5 days, the polymer was separated, washed with 600 mL of water, and dried (23 °C, 0.5 Torr, 48 h) to constant weight. Analysis of the resulting resin by use of a modified Volhard titration indicated that the remaining 85% of the chloromethylene groups was quaternized with trimethylamine to give **5**, i.e., the chloride ion content was 2.47 mmol/g of dry resin (*6*). Similar procedures were used to synthesize the other target polymers.

RESULTS AND DISCUSSION

Polymer-Bioconjugates. Three resins that were designed to test our "cloistering" hypothesis were **1**, **2**, and **3** (Scheme 2). Analogous resins having a larger bead diameter (**4**, **5**, and **6**) were also chosen as synthetic targets, to examine the influence of particle diffusion on the kinetics of exchange of a resin-bound bile acid. Thus, chloromethylation of 2% cross-linked polystyrene, followed by quaternization with excess trimethylamine, afforded **1** and **4**. Alternatively, quaternization with limited quantities of **7**, followed by exhaustive quaternization with trimethylamine yielded **2**, **3**, **5**, and **6**; actual loadings of **7** for each resin are shown in Scheme 2. Each of these resins was then subjected to ion exchange with sodium taurocholate. The fraction of pendant ammonium groups (θ_o) having taurocholate (*T*) as a counterion for each polymer is listed in Table 1.

Kinetics and Thermodynamics of Bile Acid Release. To measure the rate of release of *T* from each target resin, 0.1 g samples were gently agitated in 100

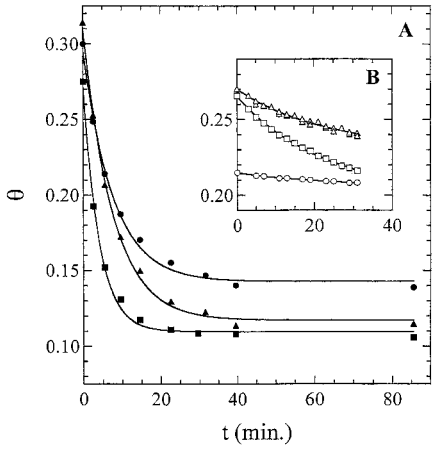

Figure 1. Fraction of pendant ammonium groups (θ) that maintain taurocholate as a counterion as a function of time of exposure to 50 mM NaCl at 23 °C. (A) (■) **1**, (▲) **2**, and (●) **3**. (B) (inset) (□) **4**, (△) **5**, and (○) **6**; values of θ that were measured after 10 days for **4**, **5**, and **6** were 0.120, 0.150, and 0.168.

mL of 50 mM NaCl via "hand rocking". Aliquots (1 mL) of the aqueous phase were then withdrawn over a period of 30 min and analyzed directly by UV (205 nm) using appropriate calibration curves. Specific experimental protocols that were followed were similar to those reported elsewhere (*4*). For the smaller beads, rocking was carried out in chromatography column (25 × 530 mm), equipped with a fine filter and 150 mL of solution. Mild agitation was specifically used in order to simulate physiologically relevant flow conditions. The fraction of pendant ammonium groups that maintain taurocholate as a counterion, θ, was determined as function of time by use of the following equation:

$$\theta = \theta_0 - CV/FW$$

Here, θ_0 is the fraction of pendant ammonium groups having taurocholate as a counterion at the start of the exchange, C is the concentration of taurocholate ion that has been released into the solution, V is the volume of the solution, F is the initial moles of ammonium groups per gram of resin, and W is the initial weight of the resin. The overall relative error of a single measurement of θ is estimated to be less than 2%.

Specific release profiles of T that were observed using resins **1**, **2**, and **3** are shown in Figure 1A. As is readily apparent, increased loadings of **7** resulted in stronger binding of T, i.e., final equilibrium values of θ were higher. Equilibrium binding constants (K) for T, which were calculated by use of eq 1, were listed in Table 1; here X_{Cl} and X_T are the mole fractions of the resin that are in the chloride

$$K = \frac{X_T[Cl^-]}{X_{Cl}[T^-]} \qquad (1)$$

and taurocholate forms, respectively, and $[Cl^-]$ and $[T^-]$ are the concentrations of chloride and taurochlolate anions in the bulk aqueous phase. An analysis of the initial rate of ion exchange $[-d(\theta/\theta_o)/dt]_o$ showed a steady decrease on going from **1** to **2** to **3** (Table 1). Initial rates were estimated by fitting the rate data (first 30 min) according to the following equation: $\theta = ae^{-bt} + C$, where ab/θ_o is taken as the initial rate of ion exchange. Such a decline strongly suggests that diffusion of ions within the polymer (particle diffusion) is at least partly rate limiting,

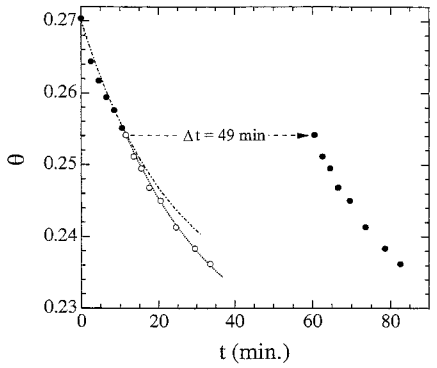

Figure 2. Plot of θ as a function of time of exposure to 50 mM NaCl at 23 °C for (●) the first 10 min as well as a 20 min period immediately following a 49-min interruption, and for (– · –) an uninterrupted 30-min period for **5**. The open circles represent data obtained after the interruption, which have been "moved to the left" by 49 min.

since the rate of processes controlled by film diffusion (diffusion of ions through a thin quiet liquid layer surrounding the polymer beads) are independent of resin composition.

To confirm kinetic contributions from particle diffusion, similar release profiles were obtained using larger-sized particles, i.e., **4**, **5**, and **6** (Figure 1B). For a particle diffusion-controlled exchange, the observed rate is known to be inversely proportional to the square of the radius of the bead. Thus, a ca. 7-fold increase in radius, on going from **1**–**3** to **4**–**6** should lead to a ca. 49-fold reduction in rate. For film diffusion, where the rate is inversely proportional to the radius, the observed rate should decrease by a factor of 7. Comparison of the initial rates of release of T from **1** and **4**, which are devoid of **7**, showed a 13-fold reduction with the larger beads. Similarly, a 12-fold reduction in rate can be estimated on going from **2** to a resin that is ca. 7 times larger, having the *identical* loading of **7** (see **2** and **A** in Table 1). When the loading of **7** reaches 15% ring substitution, the larger beads (see **3** and **B** in Table 1) now show a ca. 21-fold reduction in rate. These results imply that *both* film and particle diffusion are rate limiting and that particle diffusion increases in importance when the loading of **7** along the polymer backbone becomes sufficiently high.

Further evidence that particle diffusion contributes to the observed kinetics was obtained by carrying out an "interruption test" with **4** and **5** (*7*, *8*). Thus, after the ion exchange was allowed to proceed for 10 min, the resin was quickly removed from the aqueous phase. Reimmersion after ca. 50 min resulted in a small but distinct increase in rate, indicating that concentration gradients within the beads are leveling out during the interruption period (Figure 2). Such a finding indicates that particle diffusion is kinetically important in these systems.

The increase in the equilibrium binding constant for T, which accompanies the introduction of **7**, provides compelling evidence for the existence of cloistering. The extent to which cloistering contributes to the observed kinetics, however, is less certain. In principle, three factors could influence the contributions made from particle diffusion: (i) cloistering, (ii) deswelling of the resin, leading to a more compact state, and/or (iii) steric hindrance to diffusion, i.e., filling up the solvent-swollen channels with permanently attached bile acids. Since an examination of water-swollen **4**, **5**, and **6** by optical microscopy revealed bead diameters were the same, within experimental error, swelling changes cannot account for these observed differences. Although we believe

that *both* cloistering and steric hindrance to diffusion are important factors, we are unable to separate their kinetic contributions at the present time.

The modulation of the kinetics and the thermodynamics of bile acid sequestration, via the conjugation of **7** reported herein, represents a fundamentally new approach to a problem that has taunted a large number of polymer/medicinal chemists over the past 40 years. Whether or not such a strategy can lead to improved therapeutic agents, however, remains to be established. Efforts aimed at addressing this question are currently in progress.

ACKNOWLEDGMENT

We thank the National Science Foundation (Grant CHE-9612702) for support of this research. We are also grateful to Dr. Ken Foster (Dow Chemical Co., Midland, MI) for a sample of cross-linked polystyrene, which was used as starting material.

LITERATURE CITED

(1) Ast, M., and Frishman, W. H. (1990) Bile Acid Sequestrants. *J. Clin. Pharmacol. 30*, 99−106.

(2) Stedronsky, E. R. (1994) Interaction of bile acids and cholesterol with nonsystemic agents having hypocholesterolemic properties. *Biochim. Biophys. Acta 210*, 255−287.

(3) Johns, W. H., and Bates, T. R. (1970) Quantification of the Binding Tendencies of Cholestyramine II: Mechanism of Interaction with Bile Salt and Fatty Acid Salt Anions. *J. Pharm. Sci. 59*, 329−333.

(4) Regen, S. L., Stedronsky, E. R., Zhang, L. H., and Janout, V. (1998) Kinetics of exchange of a resin-bound bile acid by chloride ion under mild flow conditions. *Macromolecules 31*, 5542−5545.

(5) Hodge, P., and Sherrington, D. C. (1980) Chloromethylation of cross-linked polystyrene. *Polymer-Supported Reactions in Organic Synthesis*, p 477, John Wiley & Sons, New York.

(6) Stewart, J. M., and Young, J. D. (1969) Chloride analysis by the modified Volhard method. *Solid-Phase Peptide Synthesis*, pp 55−56, W. H. Freeman, San Francisco.

(7) Hellferich, F. (1962) Kinetcs. *Ion Exchange*, pp 250−322, McGraw−Hill, New York.

(8) Kressman, T. R. E., and Kitchener, J. A. (1949) Cation exchange with a synthetic phenolsulphonate resin. *Discuss. Faraday Soc. 7*, 90−104.

BC990151V

Targeting Hypoxia in Tumors Using 2-Nitroimidazoles with Peptidic Chelators for Technetium-99m: Effect of Lipophilicity

Xiuguo Zhang,[†,‡] Zi-Fen Su,[†,‡] James R. Ballinger,[†,§,||] A. M. Rauth,*[,†,‡] Alfred Pollak,[⊥] and John R. Thornback[⊥]

Division of Experimental Therapeutics, Ontario Cancer Institute, 610 University Avenue, Toronto, Ontario M5G 2M9, Canada, Departments of Medical Biophysics and Pharmaceutical Sciences, University of Toronto, 610 University Avenue, Toronto, Ontario M5G 2M9, Canada, Division of Nuclear Medicine, University Medical Imaging Centre, 600 University Avenue, Toronto, Ontario, M5G 1X5, Canada, and Resolution Pharmaceuticals Inc., 6850 Goreway Drive, Mississauga, Ontario L4V 1V7, Canada. Received November 12, 1999; Revised Manuscript Received February 14, 2000

Tumor hypoxia is an important prognostic factor for response to therapy. Radiolabeled 2-nitroimidazoles have been used for imaging hypoxia, and the octanol/water partition coefficient (*P*) of these compounds appears to play a crucial role in their suitability for imaging. A series of 11 2-nitroimidazoles coupled to peptidic chelators for ^{99m}Tc with divergent *P* was developed and evaluated in an in vitro system. Two classes of N_3S chelators were used: dialkyl-Gly-Ser-Cys-linker-2-nitroimidazole (Class I) and dialkyl-Gly-Lys(2-nitroimidazole)-Cys (Class II). The chelators were prepared by automated solid-phase peptide synthesis. Xanthine oxidase was able to reduce the 2-nitroimidiazole moiety on the ligands, but the rate of reduction varied 5-fold among the different chelators. The chelators were labeled by transchelation from [^{99m}Tc]gluconate at temperatures between 22 and 100 °C. The reaction mixtures were analyzed by HPLC and their *P* values determined. The accumulation of each complex in suspension cultures of Chinese hamster ovary cells incubated under aerobic or extremely hypoxic conditions was determined. Radiochemical yields ranged from 5 to 80% for the 11 compounds. HPLC showed that some of the compounds formed two complexes with ^{99m}Tc, possibly syn and anti conformations with respect to the Tc=O bond. In general, the Class I chelators labeled more readily than the class II chelators. The *P* values of the ^{99m}Tc complexes varied from 0.0002 to 5 and were generally in accordance with predictions based on structure. There were also differences in *P* as a function of pH; the free acids had a lower *P* at pH 7.4 than at pH 2.0 due to ionization, whereas the amides did not show this effect. Accumulation levels in aerobic cells were related to *P* but varied over a narrow range. Four of the 11 compounds showed selective accumulation in hypoxic cells. The peptidic class of 2-nitroimidazoles, with flexible design and convenient solid-phase synthesis, deserves further study as agents for imaging hypoxia in tumors.

INTRODUCTION

For a number of years it has been recognized that hypoxia in tumors is a factor in poor response to radiotherapy (*1*, *2*), because the presence of oxygen is required for fixation of radiation-induced damage in DNA. More recently, it has become evident that hypoxia may also be a predictive factor for poor response to chemotherapy, metastatic spread of a tumor, and generally aggressive disease (*3*, *4*). However, assessment of hypoxia in tumors is difficult. Tumors which seem to be identical in their type, size, stage, and radiographic appearance can vary widely in their extent of hypoxia. At present, the "gold standard" for measurement of hypoxia in tumors involves a polarographic electrode which is inserted directly into a tumor (*2*, *3*). This procedure is invasive, expensive, operator-dependent, not readily repeated, and limited to accessible tumors. These limitations have led to the exploration of nuclear imaging techniques for noninvasive detection of tumor hypoxia (*5*, *6*).

The radiopharmaceutical approach generally involves labeled 2-nitroimidazoles (2-NI), a class of compounds which can undergo an enzymatic one-electron reduction to a radical anion. In the presence of normal physiological levels of oxygen, the radical anion is immediately back-oxidized to the starting compound in a futile cycle. However, at low levels of oxygen, the radical anion undergoes further reduction to products which bind to macromolecules, and thus the associated radiolabel is selectively retained in hypoxic cells. Halogenated 2-NI, such as [^{18}F]fluoromisonidazole (FMISO) and [^{123}I]iodoazomycin arabinoside (IAZA), have been used clinically to detect hypoxia in tumors and other conditions (*7*−*12*). However, their use is limited by the choice of radiolabel. This has led to great interest in the development of ^{99m}Tc-labeled analogues which would be less expensive and more convenient to use.

Two such ^{99m}Tc-labeled compounds have been investigated by Bracco Research USA: BMS181321 and BRU59−21, both of which are 2-NI coupled to PnAO-type chelators (Figure 1). The octanol/water partition coefficients (*P*) of the two agents are 40 and 12, respectively. These

* To whom correspondence should be addressed. Phone: (416) 946-2977. Fax: (416) 946-2984. E-Mail: rauth@oci.utoronto.ca.
[†] Division of Experimental Therapeutics.
[‡] Department of Medical Biophysics.
[§] Division of Nuclear Medicine.
[||] Department of Pharmaceutical Sciences
[⊥] Resolution Pharmaceuticals Inc.

10.1021/bc9901595 CCC: $19.00 © 2000 American Chemical Society
Published on Web 04/15/2000

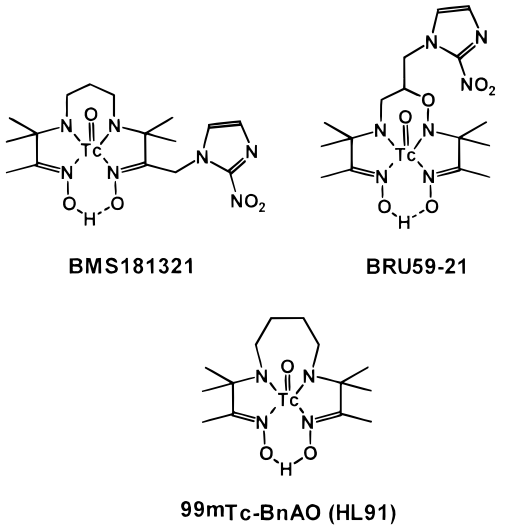

Figure 1. Structures of three previously studied technetium-99m labeled hypoxic cell markers.

complexes show selective accumulation in hypoxic cells in vitro and localization in animal tumor models, but their utility is limited by high blood levels and extensive hepatobiliary excretion related to their high *P* values (*13*−*18*). A drug development program at Nycomed-Amersham produced [^{99m}Tc]HL91 or butylene amine oxime (Figure 1), a nonnitro complex which shows hypoxic-specific localization via an undetermined mechanism (*19*−*21*). There is some uncertainty whether the ^{99m}Tc in [^{99m}Tc]HL91 is in the mono-oxo form, as drawn, or the di-oxo form (*22*).

In the development of radiolabeled 2-nitroimidazoles as diagnostic agents, just as in the therapeutic use of 2-nitroimidazoles, *P* appears to play a crucial role. With therapeutic agents, it was necessary to move to compounds with lower *P* in order to minimize penetration of nerve tissue and reduce the incidence of peripheral neuropathy; however, at extremely low *P*, inadequate levels of drug reached the tumor due to inability to penetrate membranes (*23*). The PnAO-type chelator in BMS181321 and BRU59-21 offers only limited scope for modification of *P*, although Wiebe and colleagues made a glucuronide conjugate of a PnAO-2-NI to decrease *P* (*24*).

The present work explores the use of the hypoxia-targeted 2-NI coupled to peptidic N_3S chelators for ^{99m}Tc, which have been shown to form strong, stable complexes (*25*). These chelators can be conveniently prepared by automated solid-phase peptide synthesis, and *P* can be varied widely by the choice of amino acids and pendant groups. Eleven compounds, comprising two classes of structures (Figure 2, Table 1), have been designed and synthesized. Following labeling with ^{99m}Tc, each complex was purified by HPLC, its *P* was measured, and its behavior in an in vitro model of hypoxic tumor cells was investigated. With this approach, *P* was varied over a range of 4 orders of magnitude, and several complexes which show hypoxia-specific localization in vitro were identified. Studies with one of these compounds (RP435, compound **4** in Table 1) have been reported previously (*26*).

EXPERIMENTAL PROCEDURES

General Synthesis. The peptide backbones of the two classes (Figure 2), consisting of a total of 11 compounds

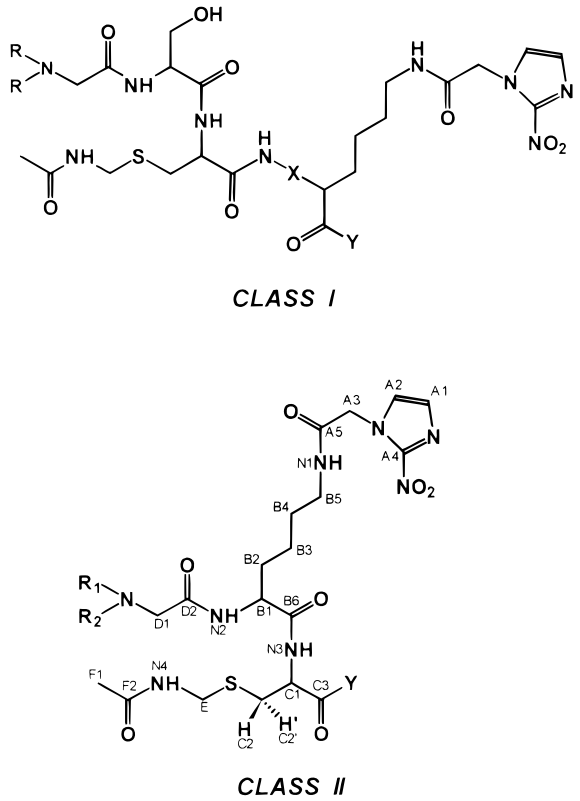

Figure 2. Chemical structures of class I and class II 2-nitroimidazole-linked peptidic chelators. R_1, R_2, X, and Y are defined in Table 1. Nuclear magnetic resonance assignment numbers are included for the class II structure.

Table 1. Chemical Structures and Mass Spectroscopic Analyses of Peptidic 2-Nitroimidazoles

compound code	r_1,r_2	X	Y	MW	M + H$^+$
class I					
1	dimethyl	Gly	Gly acid	759.4	760.0
2	dibenzyl	Gly	Gly acid	911.7	912.4
3	dibenzyl	Val	Gly acid	653.6	654.4
4	dimethyl	none	none (acid)	645.3	646.0
5	dimethyl	none	dibenzylamide	824.7	825.4
class II					
6	dimethyl		acid	558.0	558.8
7	dimethyl		amide	557.3	558.2
8	dimethyl		dibenzylamide	737.4	738.0
9	-$(CH_2)_5$- (i.e., piperidino)		acid	598.2	599.0
10	dibenzyl		acid	710.3	711.0
11	dibenzyl		amide	709.4	710.2

listed in Table 1, were synthesized on an automatic peptide synthesizer (model 433A, Applied Biosystems Inc., Foster City, CA) using standard 9-fluorenylmethoxycarbonyl (Fmoc) chemistry starting with the carboxy-terminal amino acid preloaded on Sasrin resin (Bachem Biosciences Inc., Philadelphia, PA). The α-amino groups were protected with Fmoc, the ϵ-amine on Lys with 1-(4,4-dimethyl-2,6-dioxocyclohexidine)ethyl (Dde), and the thiol of Cys with acetamidomethyl (Acm). When the backbone was complete, the Dde on Lys was cleaved with 2% hydrazine and the free amine was coupled with 2-nitroimidazole acetic acid [synthesized from 2-nitroimidazole and bromoethyl acetate as described previously (*26*)]. Products were cleaved from the resin with trifluoroacetic acid (TFA), precipitated with *tert*-butyl methyl ether, dissolved in water, and lyophilized. Dibenzylamides were prepared by reacting the crude product with

1.1 equiv of dibenzylamine in dry dichloromethane containing 1-hydroxybenzotriazole (HOBT). Condensation was initiated by the addition of 1-[(3-dimethylamino)propyl]-3-ethylcarbodiimide hydrochloride. All products were purified using an HPLC system which consisted of a pump (System Gold model 125, Beckman Instruments Inc., Fullerton, CA), reversed-phase C-18 column (Zorbax Stable Bond, 9.4 mm × 25 cm, Agilent Technologies Inc., Newport, DE), and UV absorbance detector (model 166, Beckman). The mobile phase was a gradient of water and acetonitrile, each containing 0.1% TFA. The eluate was monitored at 214 nm for total UV absorbance and at 325 nm for 2-nitroimidazole absorbance. The desired peak was collected and lyophilized to produce a white powder.

Each compound was characterized by electrospray mass spectroscopy on a Sciex API#3 spectrometer in positive ion mode (Table 1). One compound, **4**, from the class I group and one compound, **9**, from the class II group were further characterized by 500-MHz NMR spectroscopy on a Varian Unity plus-500 spectrometer with TMS as external standard. The results for **4** were presented previously (*26*). The results for **9** were as follows (see Figure 2 for assignment). $\delta_{\mathbf{H}}$ (DMSO): 9.55 (s, 1H, O**H**, **Y**), 8.73 (d, J = 8, 1H, N2), 8.53 (t, J = 6.4, 1H, N4), 8.47 (d, J = 8, 1H, N3), 8.30 (t, J = 5.7, 1H, N1), 7.59 (d, J = 1, 1H, A2), 7.28 (d, J = 1, 1H, A1), 5.05 (s, 2H, A3), 4.36−4.42 (m, 2H, C1 and B1), 4.22 (d, J = 5.4, 2H, E), 3.83−3.93 (broad q, 2H, D1), 3.30−3.43 (broad, 4H, H2 on piperidino group), 3.05 (q, J_1 = 7, J_2 = 6.8, 2H, B5), 2.99 (dd, J1=4.6, J2=13.9, 1H, C2 or C2′), 2.93 (broad, 4H, H3 on piperidino group), 2.82 (dd, J_1 = 9.3, J_2 = 13.7, 1H, C2 or C2′), 1.83 (s, 3H, F1), 1.64−1.74 (m, 2H, H4 on piperidino group), 1.48−1.58 (m, 2H, B2), 1.34−1.46 (m, 2H, B4), and 1.22−1.34 (m, 2H, B3). $\delta_{\mathbf{C}}$ (DMSO): 181.81 (C3), 181.03 (B6), 179.53 (F2), 175.32 (A5), 173.85 (D2), 154.93 (A4), 138.77 (A2), 137.42 (A1), 66.48 (D1), 62.90 (C2 on piperidino group), 62.38 (C1 or B1), 62.32 (C1 or B1), 61.54 (A3), 50.53 (E), 48.71 (B5), 41.80 (B2), 41.61 (C2), 38.68 (B4), 32.56 (B3), 32.42 (C3 on piperidino group), 32.11 (F1), 31.03 (C4 on piperidino group).

Reduction of Ligands by Xanthine Oxidase. The ability of the 2-nitroimidazole group of the peptide chelators to be reduced by xanthine oxidase was assessed for 10 of the 11 peptidic ligands. The procedures used were based on previous work concerning reduction of nitroimidazoles by xanthine oxidase (*27*, *28*). Briefly, samples of each ligand (28−36 μM) dissolved in phosphate buffer (0.1 M) containing 160 μM xanthine (Sigma Chemical Co., St. Louis, MO) were placed in a quartz spectrophotometer cell in a 37 °C water-jacketed cell holder in a UV−vis spectrophotometer (Perkin-Elmer, Lambda 3B, Oak Bank, IL). After bubbling for 15 min with argon (Praxair Products Inc., Mississauga, ON, Canada) to remove oxygen, xanthine oxidase (EC 1.1.3.22, Sigma Chemical Co., St. Louis, MO, Type X4500 from buttermilk, specific activity 1−2 units/mg protein) was added to the vial at a final concentration of 0.45 units/mL. Absorption of the sample was monitored at 325 nm as a function of time. The initial slope for the loss of absorbance was calculated and expressed as percent absorbance lost per minute per unit enzyme. Misonidazole, 1-(2-nitro-1-imidazolyl)-3-methoxy-2-propanol, a gift from the Division of Cancer Treatment, National Institutes of Health, Bethesda, MD, was used as a standard substrate. In addition, BRU59, a gift from Drs. K. Linder and A. Nunn, Bracco Research USA, Princeton, NJ, was also tested for comparison.

Labeling and Purification. For labeling, each ligand was dissolved at 1−2 mg/mL in water, except for compounds **5**, **8**, **10**, and **11**, which were dissolved in acetonitrile:water 1:1 because of limited solubility in water. Labeling was performed by transchelation from [^{99m}Tc]-gluconate under the following conditions: 100 μg of ligand, 100 μL of ^{99m}Tc-pertechnetate (∼200 MBq), and 100 μL of stannous gluconate solution, which contained 25 μg of stannous chloride and 2 mg of sodium gluconate. The pH of the mixture was adjusted to values between 3.5 and 6.0 by addition of 0.1 N HCl or 0.1 N NaOH, and the reaction was carried out at various temperatures between 22 and 100 °C using a water bath, with reaction times generally being 20 min. The reaction mixture was then analyzed with the HPLC system described above, except that an analytical C-18 column was used (Ultrasphere, 4.6 mm × 25 cm, Beckman) and a radiometric detector (model 171, Beckman) was connected in series after the UV detector. The standard linear gradient used was 90% water to 10% water (balance acetonitrile, both containing 0.1% TFA) over 40 min. The major radioactive peaks were collected for measurement of P and for in vitro studies. The purity and stability of the collected peaks was determined by repeated HPLC analysis. By varying pH, temperature, and time the optimal labeling conditions were determined for each compound.

Measurement of Partition Coefficient. The P of each complex was measured at both pH 7.4 and pH 2. Ten microliters (∼1 MBq) of each HPLC-purified compound was added to a tube containing 2 mL of *n*-octanol and 2 mL of phosphate-buffered saline (pH 7.4) or 2 mL of 0.1% TFA (pH 2). Each phase had been presaturated with the opposite phase. The phases were mixed by vortexing for 2 min, then separated by centrifugation at 12000*g* for 5 min. Aliquots of both phases were transferred in triplicate to counting tubes and assayed in a γ well counter. Each measurement was performed at least twice.

Cellular Accumulation in an in Vitro Model. Each complex was evaluated in an in vitro system which has been used in the study of other tracers of hypoxia (*14*, *15*, *18*, *21*). Suspensions of Chinese hamster ovary (CHO) cells or human Hela cells were incubated under an atmosphere of air or nitrogen to generate aerobic or hypoxic conditions, respectively. The tracer was added, and aliquots were removed over the course of 4 h and centrifuged, and the radioactivity associated with the cell pellet was measured in a γ well counter. The results were expressed as the ratio of concentration of radioactivity in the cell pellet to that in an equivalent volume of supernatant medium (C_{in}/C_{out}) as a function of time, as described previously (*14*).

RESULTS

The 11 compounds were conveniently synthesized by automated solid-phase techniques, purified by HPLC, and their structures were confirmed by mass spectroscopy and limited NMR data on one lead compound, compound **4** and compound **9**, from each class (Experimental Procedures and Table 1). In the class I series, the 2-NI-derivatized Lys was a pendant group on the chelator, while in class II, the Lys was integral to the chelation site.

The nitro groups in all of the ligands were capable of reduction by xanthine oxidase, although the rates of reduction, expressed as initial slopes, varied among the compounds. Compound **11** was reduced at a similar rate to misonidazole, while the remainder were reduced more slowly, at 17−60% of the rate of misonidazole (Table 2).

Table 2. Reduction of 2-Nitroimidazole Moiety of Peptidic Chelators by Xanthine Oxidase

compound code	initial slope[a] (% abs/min/unit)	% of misonidazole rate
class I		
1	−2.38	51
2	−1.46	31
3	−1.57	34
4	−0.80	17
5	−1.18	25
class II		
6	−1.14	25
7	−0.77	17
8	n/a[b]	n/a
9	−1.02	22
10	−2.77	60
11	−4.71	102
BRU59	−0.94	20
misonidazole	−4.64	100

[a] Initial concentration: 28−36 μM. [b]Not available.

Table 3. Peak Number, HPLC Retention Time, Radiochemical Yield, and Partition Coefficient for 11 ^{99m}Tc-Labeled Peptidic 2-Nitroimidazoles

compound code	peak no.	retention time (min)	yield (%)	octanol/water partition coefficient pH 2	pH 7.4
class I					
1	SP[a]	10.8	68−80	0.002	0.0002
2	A	17.2	8	n/a[b]	0.004
	B	18.1	20	1.0	0.001
3	A	17.5	8	0.4	0.06
	B	19.6	30	0.8	0.07
4	A	11.0	15−17	0.03	0.001
	B	12.1	26	0.03	0.002
5	SP	29.4	5−10	n/a	3
class II					
6	A	13.0	16−25	0.07	0.006
	B	14.3	20−43	0.29	0.01
7	A	12.0	7−13	0.05	0.02
	B	12.8	8−12	0.05	0.03
8	SP	27.4	5	3.8	4.4
9	A	15.3	21	1.0	0.01
	B	16.0	19	1.9	0.005
10	SP	20.0	6	n/a	0.2
11	SP	21.6	8	n/a	5

[a] Single peaks. [b]Not available.

Labeling with ^{99m}Tc was performed by transchelation from [^{99m}Tc]gluconate, but the optimal pH and temperature varied among compounds, and radiochemical yields ranged from 5 to 80% (Table 3). HPLC analysis showed that some compounds formed a single peak (SP) and others two complexes (A and B) with ^{99m}Tc. Representative labeling data is shown in Figure 3 for compound **6**, demonstrating the formation of two complexes (peaks A and B) in a total of 82% yield, with 14% free pertechnetate remaining.

In the class I series, compound **1**, which contained the dimethylGly-Ser-Cys chelator, formed a single product in up to 80% yield at room temperature (Table 3). Compound **2**, the dibenzylGly analogue, required heating at 50 °C and formed two peaks in a 1:2 ratio and a total yield of 30%. On the basis of studies with the chelator alone, and the chelator linked to 2-nitroimidazole, the two peaks are believed to be syn and anti conformations (*25*, *26*). The remaining class I compounds (**3**−**5**) required at least 70 °C for the labeling reaction to take place. Substitution of Gly by Val (compound **3**) or eliminating two Gly residues (compound **4**) resulted in two peaks again in an approximate 1:2 ratio but at a slightly higher

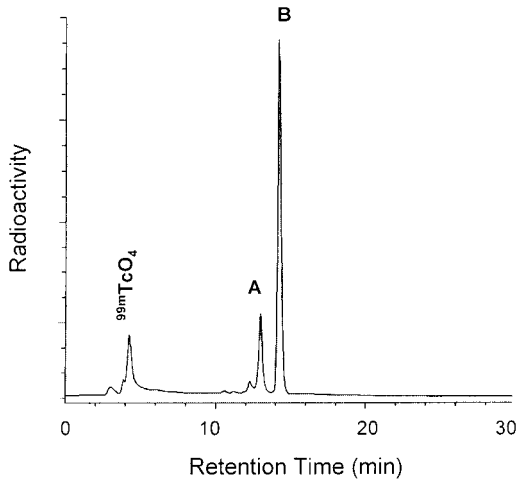

Figure 3. Representative HPLC radioactivity trace for compound **6** labeled with technetium-99m by transchelation from [^{99m}Tc]gluconate. Peaks A and B are thought to be interconvertable syn and anti forms of the Tc=O group.

total yield of 40%. Capping the free acid on the C-terminus of compound **4** with dibenzyl amide (compound **5**) resulted in one peak with lower yield (5−10%). In general, the optimal pH for labeling was 3.5 for the free acids and 6.0 for the amides.

In the class II series, the Lys linker to the 2-NI targeting group was incorporated into the chelator, replacing Ser, rather than being attached to the end of the chelator. The first compound in the series, **6**, produced two peaks in an approximate 1:2 ratio and up to 70% yield. Capping the free acid on the C-terminus of compound **6** with an amide (compound **7**) resulted in a much lower total yield (maximally 25%) of two peaks of equal size. The dibenzylamide of compound **6** (compound **8**) produced an extremely low yield of ^{99m}Tc-labeled compound. The piperidino analogue of compound **6** (compound **9**) resulted in two equal peaks in 40% yield. Substitution of the dimethyl group on Gly in compound **6** with dibenzyl (compound **10**) resulted in a longer retention time with one peak at lower yield (Table 3). Capping the free acid on the C-terminus of compound **10** with an amide (compound **11**) did not increase the yield of ^{99m}Tc-labeled compound.

The *P* of the 11 complexes varied over a wide range (0.0002−5) but generally were in accordance with predictions based on structure (Table 3). There were also differences in *P* as a function of pH. In general, the free acids, which would be neutral at pH 2.0, had much lower *P* at pH 7.4 where they would be ionized, while the amides showed little effect of pH. The *P* values measured at pH 2.0 showed a significant correlation with HPLC retention times when run in 0.1% TFA (Table 3).

Representative data for compound **6** is shown in Figure 4 for its accumulation in CHO cells under aerobic and hypoxic conditions. Under aerobic conditions, this compound showed a ratio of activity inside of the cells (C_{in}) to that outside the cells (C_{out}) of 0.3 in the first 5 min, which increased 2-fold over the next 4 h. In contrast, hypoxic cells, although showing the same initial C_{in}/C_{out} ratio at the first 5 min, steadily accumulated activity inside the cells, so at 4 h there was a 5-fold increase in activity over the 5 min value. Similar experiments were done for all 11 compounds and C_{in}/C_{out} values at 4 h for aerobic and hypoxic incubations are plotted in Figure 5 as a function of *P*.

In the in vitro tracer accumulation studies, the tracers varied in their levels of partitioning into aerobic CHO

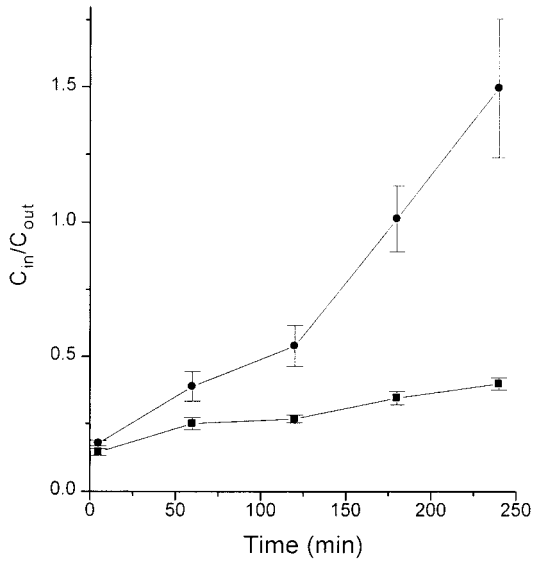

Figure 4. Accumulation of compound **6** in CHO cells measured at 37 °C under aerobic (closed squares) versus hypoxic (closed circles) incubation conditions. The C_{in}/C_{out} values for peaks A and B have been averaged together for each time point. Representative data from four experiments are shown. Error bars are standard error of the mean for $n = 4$ experiments.

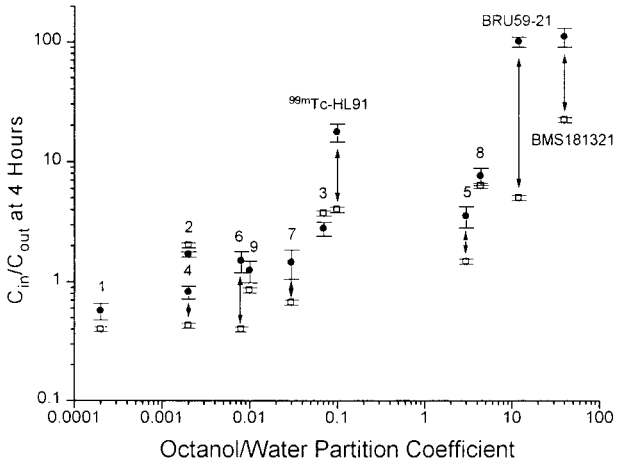

Figure 5. Relationship between lipophilicity (partition coefficient) of nine compounds from Table 1 and 4-h accumulation (C_{in}/C_{out}) in aerobic (open squares) and hypoxic (closed circles) cells. Error bars are standard error of the mean for $n = 3$ or more experiments. Included for comparison are previous results obtained in the same system for BMS181321 (*14*), BRU59−21 (*18*), and [^{99m}Tc]HL91 (*21*). Double-headed arrows indicate compounds with significant hypoxic-aerobic differentials (≥1.5). Numbers indicate compounds as listed in Table 1.

cells (Figure 5). These levels showed some correlation with *P*, but, whereas *P* varied by 4 orders of magnitude, accumulation varied only 30-fold. Although a number of the ^{99m}Tc complexes did not show selective accumulation in hypoxic cells, others showed 1.8−3.8-fold greater accumulation under hypoxia after 4 h. Two compounds of class I showed this differential (compounds **4** and **5**) and two compounds from class II were selectively taken up in hypoxic cells (compounds **6** and **7**). Two of the compounds, **10** and **11**, were not tested in the in vitro assay with CHO cells because of difficulties in labeling. Single experiments in Hela cells showed no significant hypoxic versus aerobic differential for these compounds (data not shown). For compounds which formed two ^{99m}Tc-labeled complexes, both complexes tended to behave similarly, consistent with the suggestion they are interconvertable syn and anti conformations with respect to Tc═O (*25*, *26*). Therefore, the data in Figure 5 is the average accumulation for both peaks; similarly, the *P* values at pH 7.4 for both peaks in Table 3 have been averaged. Also shown in Figure 5 are previous results obtained in the same in vitro system for BMS181321 (*14*), BRU59-21 (*18*) and [^{99m}Tc]HL91 (*21*) for comparison. It was noted that when a plot was made of the hypoxic differential at 4 h of $(C_{in}/C_{out})_{hypoxic}/(C_{in}/C_{out})_{aerobic}$ versus molecular weight there was a tendency for the ratio to increase with decreasing molecular weight (Figure 6).

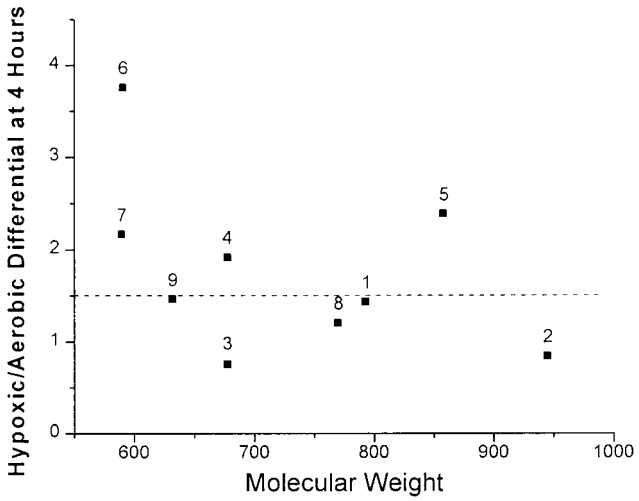

Figure 6. Relationship between the molecular weight of nine of the ^{99m}Tc-labeled ligands from Table 1 and the hypoxic/aerobic differential in CHO cells after 4 h of incubation. Numbers indicate compounds as listed in Table 1. The dotted line indicates a hypoxic/aerobic differential of 1.5.

DISCUSSION

In the search for a radiolabeled 2-NI with optimal properties for imaging hypoxia in tumors, *P* is felt to be an important factor (*6*). Nuclear imaging involves a compromise between two factors: signal and signal-to-noise [or target-to-background (*T*/*B*)] ratio. In other words, there needs to be an adequate signal but there also needs to be sufficient contrast in order for an agent to be useful. *P* plays a role in distribution of drugs within the body, penetration of drugs through membranes, and routes of metabolism and excretion. High *P* is often associated with retention in background tissues, including blood. This is certainly the case with BMS181321, 2-NI with a PnAO chelator, which exhibits a *P* of 40, extensive hepatobiliary excretion, prolonged clearance from blood and muscle, and achieves only modest *T*/*B* ratios (*14*). The second-generation compound BRU59-21 has a *P* of 12 which contributes to more rapid blood clearance and modestly improved *T*/*B* ratios but excretion is still primarily into the GI tract (*18*). Studies in the radioiodinated sugar 2-NI derivatives have shown that a *P* of ∼1 is optimal for achieving renal excretion and high *T*/*B* ratios (*6*). The objective of the present work was to prepare a series of ^{99m}Tc-labeled 2-NI with a wide range in *P* and to evaluate them in an in vitro model of tumor hypoxia.

This range in *P* was achieved using the peptidic ^{99m}Tc chelation sequence dialkylGly-Ser-Cys, which contains one sulfur atom, one amine nitrogen, and two amide nitrogens as an N_3S class chelator and was developed by Resolution Pharmaceuticals (*25*). By varying the amino acids, dialkyl groups, and pendant groups, *P* was varied over 4 orders of magnitude. The class I compounds use

the dialkylGly-Ser-Cys chelator with the 2-NI attached through Lys at the end of the chelator. To reduce molecular weight, the class II compounds were designed with the 2-NI-derivatized Lys as part of the chelator in place of Ser. However, it became apparent that these modifications were not innocuous. While the dimethylGly-Ser-Cys chelator binds ^{99m}Tc in extremely high yield at room temperature (*25*), changing the dialkyl group or substituting Lys for Ser results in a compound which requires harsher labeling conditions and which does not achieve high yields.

With most of the complexes, two peaks were evident on HPLC analysis. Ongoing work in this laboratory suggests that these are syn and anti conformations as described by Wong et al. for the dimethylGly-Ser-Cys chelator (*25*) and that these conformations interconvert after isolation (*26*, unpublished results). This is supported by the observations that the peaks do not differ greatly in their *P* values (Table 3) and that both peaks tend to behave similarly in the in vitro test system.

The xanthine oxidase results show that attachment of a peptidic chelator to 2-nitroimidazole does not prevent the nitro group from being reduced enzymatically; however, it may alter the rate of reduction (Table 2). One of the ligands, **11**, was reduced at a rate similar to misonidazole, while the remainder were reduced more slowly, at 17−60% of that rate. Linder et al. have shown that BMS181321 is reduced at 41% of the rate of misonidazole, which is in the same range as these ligands (*13*). The results for BRU59 showed that it was reduced somewhat more slowly, 20% of the misonidazole rate, than BMS181321.

The accumulation of the tracers in CHO cells in vitro was related to *P* but did not vary over as wide a range as *P*. It has been shown recently by Oya et al. that *P* is not the sole determinant of brain uptake of ^{99m}Tc chelates but that the nature of the chelator plays a role; in particular, amides (such as the peptidic series in the present work) are not taken up as efficiently as amines (e.g., BMS181321 and BRU59-21) (*29*). Several of the compounds showed selective uptake in hypoxic cells, although the magnitude of this selective uptake was not as great as has been obtained with BMS181321, BRU59-21, and [^{99m}Tc]HL91 (refs *14*, *18*, and *21* and Figure 5). The explanation of why only 4 of the present 11 compounds showed a significant hypoxic/aerobic differential (=1.5) is not known at this time. It is clearly not a strict function of *P*. However, as shown in Figure 6 for this limited series, it does appear that the lower molecular weight compounds tended to show a differential while the higher molecular weight compounds did not.

In conclusion, the present studies indicated the usefulness of the automated solid-phase synthetic system in the design of peptidic chelators for ^{99m}Tc covering a broad range of *P* values. Four of the 11 compounds, all containing a 2-nitroimidazole targeting group, were selectively accumulated in hypoxic compared to aerobic cells. Though the degree of selectivity of the present compounds was not as great as that seen previously for several other ^{99m}Tc-labeled hypoxic markers, the present compounds represent a novel approach to the design of hypoxic markers that warrant further investigation.

ACKNOWLEDGMENT

We thank Tam Nguyen and Dr Susan Peers of Resolution Pharmaceuticals Inc. for their assistance. Funding was provided by the Medical Research Council of Canada and Resolution Pharmaceuticals Inc. through the University/Industry grant program (Grant UI-13558).

LITERATURE CITED

(1) Bush, R. S., Jenkin, R. D. T., Allt, W. E. C., Beale, F. A., Bean, H., Dembo, A. J., and Pringle, J. F. (1978) Definitive evidence for hypoxic cells influencing cure in cancer therapy. *Br. J. Cancer 37* (Suppl.), S302−S306.

(2) Hockel, M., Knoop, C., Schlenger, K., Vorndran, B., Baussmann, E., Mitze, M., Knapstein, P. G., and Vaupel, P. (1993) Intratumoral pO_2 predicts survival in advanced cancer of the uterine cervix. *Radiother. Oncol. 26*, 45−50.

(3) Brizel, D. M., Scully, S. P., Harrelson, J. M., Layfield, L. J., Bean, J. M., Prosnitz, L. R., and Dewhirst, M. W. (1996) Tumor oxygenation predicts for likelihood of distant metastases in human soft tissue sarcoma. *Cancer Res. 56*, 941−943.

(4) Graeber, T. G., Osmanian, C., Jacks, T., Housman, D. E., Koch, C. J., Lowe, S. W., and Giaccia, A. J. (1996) Hypoxia mediated selection of cells with diminished apoptotic potential in solid tumours. *Nature 379*, 88−91.

(5) Nunn, A., Linder, K., and Strauss, H. W. (1995) Nitroimidazoles and imaging hypoxia. *Eur. J. Nucl. Med. 22*, 265−280.

(6) Chapman, J. D., Engelhardt, E. L., Stobbe, C. C., Schneider, R. F., and Hanks, G. E. (1998) Measuring hypoxia and predicting tumor radioresistance with nuclear medicine assays. *Radiother. Oncol. 46*, 229−237.

(7) Koh, W.-J., Rasey, J. S., Evans, M. L., Grierson, J. R., Lewellen, T. K., Graham, M. M., Krohn, K. A., and Griffin, T. W. (1992) Imaging of hypoxia in human tumors with [^{18}F]-fluoromisonidazole. *Int. J. Radiat. Oncol. Biol. Phys. 22*, 199−212.

(8) Koh, W.-J., Bergman, K. S., Rasey, J. S., Peterson, L. M., Evans, M. L., Graham, M. M., Grierson, J. R., Lindsley, K. L., Lewellen, T. K., Krohn, K. A., and Griffin, T. W. (1995) Evaluation of oxygenation status during fractionated radiotherapy in human nonsmall cell lung cancers using [F-18]-fluoromisonidazole positron emission tomography. *Int. J. Radiat. Oncol. Biol. Phys. 33*, 391−398.

(9) Yeh, S.-H., Liu, R.-S., Wu, L.-C., Yang, D. J., Yen, S.-H., Chang, C.-W., Yu, T.-W., Chou, K.-L., and Chen K. Y. (1996) Fluorine-18 fluoromisonidazole tumour to muscle retention ratio for the detection of hypoxia in nasopharyngeal carcinoma. *Eur. J. Nucl. Med. 23*, 1378−1383.

(10) Mannan, R. H., Somayaji, V. V., Lee, J., Mercer, J. R., Chapman, J. D., and Wiebe, L. I. (1991) Radioiodinated 1-(5-iodo-5-deoxy-beta-D-arabinofuranosyl)-2-nitroimidazole (Iodoazomycin arabinoside: IAZA): a novel marker of tissue hypoxia. *J. Nucl. Med. 32*, 1764−1770.

(11) Parliament, M. B., Chapman, J. D., Urtasun, R. C., McEwan, A. J., Golberg, L., Mercer, J. R., Mannan, R. H., and Wiebe, L. I. (1992) Non-invasive assessment of human tumor hypoxia with ^{123}I-iodoazomycin arabinoside: preliminary report of a clinical study. *Br. J. Cancer 65*, 90−95.

(12) Urtasun, R. C., Parliament, M. B., McEwan, A. J., Mercer, J. R., Mannan, R. H., Wiebe, L. I., Morin, C., and Chapman, J. D. (1996) Measurement of hypoxia in human tumours by non-invasive SPECT imaging of iodoazomycin arabinoside. *Br. J. Cancer 74* (Suppl.), S209−S212.

(13) Linder, K. E., Chan, Y.-W., Cyr, J. E., Malley, M. F., Nowotnik, D. P., and Nunn, A. D. (1994) TcO(PnAO-1-(2-nitroimidazole)) [BMS-181321], a new technetium-containing nitroimidazole complex for imaging hypoxia: synthesis, characterization, and xanthine oxidase-catalyzed reduction. *J. Med. Chem. 37*, 9−17.

(14) Ballinger, J. R., Wan Min Kee, J., and Rauth, A. M. (1996) In vitro and in vivo evaluation of a technetium-99m-labeled 2-nitroimidazole (BMS181321) as a marker of tumor hypoxia. *J. Nucl. Med. 37*, 1023−1031.

(15) Melo, T., Hua, H. A., Ballinger, J. R., and Rauth, A. M. (1997) Modifying the in vitro accumulation of BMS181321, a technetium-99m-nitroimidazole, with unlabelled nitroaromatics. *Biochem. Pharmacol. 54*, 685−693.

(16) Wedeking, P., Yost, F., Wen, M., Patel, B., Eaton, S., Romero, V., Linder, K. E., Rumsey, W., and Nunn, A. D. (1995) Comparison of the biologic activity of the isomers of Tc-99m-nitroimidazole complex BMS-194796. *J. Nucl. Med. 36*, 17P.

(17) Johnson, L. L., Schofield, L., Mastrofrancesco, P., Donahay, T., and Nott, L. (1998) Technetium-99m-nitroimidazole uptake in a swine model of demand ischemia. *J. Nucl. Med. 39*, 1468−1475.

(18) Melo, T., Duncan, J., Ballinger, J. R., and Rauth, A. M. (2000) BRU59−21, A second-generation technetium-99m-labelled 2-nitroimidazole for imaging hypoxia in tumors. *J. Nucl. Med. 41*, 169−176.

(19) Archer, C. M., Edwards, B., Kelly, J. D., King, A. C., Burke, J. F., and Riley, A. L. M. (1995) Technetium labelled agents for imaging tissue hypoxia in vivo. In *Technetium and Rhenium in Chemistry and Nuclear Medicine* (M. Nicolini, G. Bandoli, and U. Mazzi, Eds.) pp 535−539, S G Editoriali, Padova.

(20) Cook, G. J., Houston, S., Barrington, S. F., and Fogelman, I. (1998) Technetium-99m-labeled HL91 to identify tumor hypoxia: Correlation with fluorine-18-FDG. *J. Nucl. Med. 39*, 99−103.

(21) Zhang, X., Melo, T., Ballinger, J. R., and Rauth, A. M. (1998) Studies of ^{99m}Tc-BnAO (HL91): A non-nitroaromatic compound for hypoxic cell detection. *Int. J. Radiat. Oncol. Biol. Phys. 42*, 737−740.

(22) Brauers, G., Archer, C. M., and Burke, J. F. (1997) The chemical characterization of tumor imaging agent ^{99m}Tc-HL91. *Eur. J. Nucl. Med. 24*, 943.

(23) Brown, J. M., and Workman, P. (1980) Partition coefficient as a guide to the development of radiosensitizers which are less toxic than misonidazole. *Radiat. Res. 82*, 171−190.

(24) Kumar, P., Mannan, R., Zhang, Z., McEwan, A. J. B., and Wiebe, L. I. (1995) ^{99m}Tc-PAO-Azomycin glucuronide (^{99m}Tc-PAO-AZG): synthesis and biological evaluation as a marker of hypoxic tissues. *Q. J. Nucl. Med. 39*, 65−66.

(25) Wong, E., Fauconnier, T., Bennett, S., Valliant, J., Nguyen, T., Lau, F., Lu, L. F. L., Pollak, A., Bell, R. A., and Thornback, J. R. (1997) Rhenium(V) and technetium(V) oxo complexes of an $N_2N'S$ peptidic chelator: evidence of interconversion between the *syn* and *anti* conformations. *Inorg. Chem. 36*, 5799−5808.

(26) Su, Z. F., Zhang, X., Ballinger, J. R., Rauth, A. M., Pollak, A., and Thornback, J. R. (1999) Synthesis and evaluation of two technetium-99m-labeled peptidic 2-nitroimidazoles for imaging hypoxia. *Bioconjugate Chem. 10*, 897−904.

(27) Clarke, E. D., Wardman, P., and Goulding, K. H. (1980) Anaerobic reduction of nitroimidazoles by reduced flavin mononucletide and by xanthine oxidase. *Biochem. Pharmacol. 29*, 2684−2687.

(28) Josephy, P. D., Palcic, B., and Skarsgard, L. D. (1981) Reduction of misonidazole and its derivatives by xanthine oxidase. *Biochem. Pharmacol. 30*, 849−853.

(29) Oya, S., Plossl, K., Kung, M. P., Stevenson, D. A., and Kung, H. F. (1998) Small and neutral Tc(V)O BAT, bisaminoethanethiol (N2S2) complexes for developing new brain agents. *Nucl. Med. Biol. 25*, 135−140.

BC9901595

Sulfur Shuffle: Modulating Enzymatic Activity by Thiol-Disulfide Interchange

June M. Messmore,[†,‡] Steven K. Holmgren,[†,§] Juneko E. Grilley,[†] and Ronald T. Raines*[,†,||]

Department of Biochemistry and Department of Chemistry, University of Wisconsin—Madison, Madison, Wisconsin 53706. Received October 19, 1999; Revised Manuscript Received February 2, 2000

The facile modulation of biological processes is an important goal of biological chemists. Here, a general strategy is presented for controlling the catalytic activity of an enzyme. This strategy is demonstrated with ribonuclease A (RNase A), which catalyzes the cleavage of RNA. The side-chain amino group of Lys41 donates a hydrogen bond to a nonbridging oxygen in the transition state for RNA cleavage. Replacing Lys41 with a cysteine residue is known to decrease the value of k_{cat}/K_m by 10^5-fold. Forming a mixed disulfide between the side chain of Cys41 of K41C RNase A and cysteamine replaces the amino group and increases k_{cat}/K_m by 10^3-fold. This enzyme, which contains a mixed disulfide, is readily deactivated by dithiothreitol. Forming a mixed disulfide between the side chain of Cys41 and mercaptopropyl phosphate, which is designed to place a phosphoryl group in the active site, decreases activity by an additional 25-fold. This enzyme, which also contains a mixed disulfide, is reactivated in the presence of dithiothreitol and inorganic phosphate (which displaces the pendant phosphoryl group from the active site). An analogous control mechanism could be installed into the active site of virtually any enzyme by replacing an essential residue with a cysteine and elaborating the side chain of that cysteine into appropriate mixed disulfides.

INTRODUCTION

The activities of enzymes in vivo are exquisitely controlled by layers of regulatory mechanisms. These modalities are lost in vitro. Yet, the technological and commercial roles of enzymatic processes in vitro are of greater significance than ever before, with applications ranging from synthetic chemistry (Wong and Whitesides, 1994) to biotechnology (Eun, 1996) to food science (Suckling, 1990). Many practical uses of enzymes are likely to benefit from added degrees of control.

Ribonucleases are enzymes that act at a crossroads of transcription and translation by catalyzing the cleavage of RNA (D'Alessio and Riordan, 1997). Controlling ribonucleolytic activity in vitro is especially important in manipulations in which the activity is required in some steps but detrimental in others. The ribonuclease protection assay (RPA),[1] a method for detecting and quantitating RNA transcripts, is a prime example of this sort of manipulation (Zinn et al., 1983; Ausubel et al., 1994).[2] Available methods for controlling ribonucleolytic activity tend to suffer from a lack of specificity, efficacy, or permanence. For example, diethyl pyrocarbonate effectively acylates the active-site histidine residues of ribonuclease A [RNase A; EC 3.1.27.5 (Raines, 1998)], destroying its enzymatic activity, but also covalently modifies nucleic acids and other proteins. Ribonucleoside complexes with vanadium(IV) and technetium(V) are rather weak inhibitors of catalysis by RNase A (Lindquist et al., 1973; Chen and Janda, 1992), and the vanadium(IV) complex is prone to air oxidation. In contrast, the complexes of RNase A with 3′,5′-pyrophosphate-linked deoxynucleotides have K_d values as low as 27 nM, but are likewise noncovalent (Leonidas et al., 1999; Russo and Shapiro, 1999). Although we and others have synthesized affinity labels and mechanism-based inactivators, the affinity labels bind weakly (Hummel et al., 1987) and the mechanism-based inactivators apparently modify nonessential residues (Stowell et al., 1995). Both types of compounds leave uninhibited a significant proportion of the ribonucleolytic activity.

We have engineered a mechanism of in vitro control into RNase A. This method of modulating activity is similar to many natural regulatory mechanisms in that it employs reversible covalent modification. Specifically,

* To whom correspondence should be addressed. Phone: (608) 262-8588. Fax: (608) 262-3453. E-mail: raines@biochem.wisc.edu.

[†] Department of Biochemistry.

[‡] Present address: Department of Biochemistry, Medical College of Wisconsin, Milwaukee, WI 53226.

[§] Present address: Department of Chemistry and Biochemistry, Montana State University—Bozeman, Bozeman, MT 59717.

[||] Department of Chemistry.

[1] Abbreviations: CSA, cysteamine; DEAE, diethylaminoethyl; DTNB, 5,5′-dithiobis(2-nitrobenzoic acid); DTT, dithiothreitol; FAB, fast-atom bombardment; Hepes, *N*-(2-hydroxyethyl)piperazine-*N*′-2-ethanesulfonic acid; Mes, 2-(*N*-morpholino)-ethanesulfonic acid; MPP, 3-mercaptopropyl-1-phosphate; MS, mass spectrometry; NTB, 2-nitro-5-thiobenzoic acid; NMR, nuclear magnetic resonance; poly(C), poly(cytidylic acid); RNase A, bovine pancreatic ribonuclease A; RPA, ribonuclease protection assay; TEA, triethylamine; TLC, thin-layer chromatography; Tris, tris(hydroxymethyl)aminomethane.

[2] In an RPA, a labeled piece of anti-sense RNA is used to probe for an RNA transcript of interest. First, the labeled probe is added to a sample solution and allowed to hybridize with its cognate target RNA. Then, excess single-stranded probe is degraded by treatment with a ribonuclease, such as RNase A. Probe that has hybridized to target RNA is protected from degradation by the ribonuclease by virtue of being in a double-stranded complex with its cognate target RNA. The protected probe is then separated by electrophoresis in a polyacrylamide gel and visualized by autoradiography. If ribonucleolytic activity is not adequately controlled after the degradation step, both prior to and during electrophoresis, the signal resulting from the protected probe will be lost.

10.1021/bc990142m CCC: $19.00 © 2000 American Chemical Society
Published on Web 04/09/2000

we have replaced a Lys41 with a cysteine. Lys41 is known to donate a hydrogen bond to a nonbridging oxygen in the transition state for RNA cleavage (Messmore et al., 1995). The cysteine residue can be used as a "hook" on which to hang activating or deactivating entities. The K41C RNase A variant can be activated by chemical modification with cysteamine (2-aminoethanethiol), thus replacing the primary amine of the wild-type enzyme. Cysteamine can be removed later by gentle treatment with dithiothreitol (DTT) or another reducing agent. An inhibitory phosphoryl group at the end of a thiol-reactive linker can be added to achieve more complete inactivation. A few other enzymes (Pease et al., 1987; Gloss and Kirsch, 1995) and a lectin (Hollenbaugh et al., 1995) have been activated and deactivated by reversible modification of a newly introduced cysteine residue, but further inactivation via additional covalent changes to the cysteine residue is a feature unique to the present work. Similar regimens of transient activation and inactivation may be applicable to other enzymes with critical active-site lysine residues, including other nucleases and phosphotransferases.

EXPERIMENTAL PROCEDURES

Materials. The oligonucleotide used for site-directed mutagenesis was synthesized bearing a trityl group and was purified using an Oligo Purification Cartridge from Applied Biosysytems (Foster City, CA). The *Escherichia coli* strain used for protein production, BL21(DE3), was from Novagen (Madison, WI). Ellman's reagent, DTT, Hepes-free acid, Mes-free acid, and cysteamine·HCl were from Sigma Chemical (St. Louis, MO). Poly(cytidylic acid) [poly(C)] was from either Midland Certified Reagents (Austin, TX) or Sigma Chemical. All starting materials for the synthesis of 2,4-dinitrophenyl 3-phosphoryl disulfide were from Aldrich Chemical (Milwaukee, WI), and the purity of these reagents was assessed by ^{1}H NMR spectroscopy or thin-layer chromatography (TLC) (or both) prior to use.

Spectroscopy and Protein Quantitation. Measurements of ultraviolet and visible absorption were made with a Cary model 3 spectrophotometer from Varian (Sugar Land, TX). Protein concentrations were determined based on the wild-type value of $\epsilon = 0.72$ mL mg^{-1} cm^{-1} at 277.5 nm (Sela et al., 1957). This relationship was assumed to be valid for all forms of K41C RNase A studied herein. The veracity of this assumption was supported by DTT treatment of K41C-ntb RNase A (vide infra) yielding the expected value of 1.0 ± 0.2 equiv of 2-nitro-5-thiobenzoic acid (NTB).

Preparation of K41C-(2-nitro-5-thiobenzoic acid) RNase A. A cDNA encoding K41C RNase A (Messmore et al., 1995) was expressed in *E. coli* strain BL21(DE3) under the control of the T7 RNA polymerase promoter. The resulting protein was purified as described previously (delCardayré et al., 1995; Messmore et al., 1995). After purification, the new sulfhydryl group at position 41 was protected from inadvertent reaction by treatment with 5,5′-dithiobis(2-nitrobenzoic acid), Ellman's reagent or DTNB (Ellman, 1959). The protected protein, K41C-ntb RNase A, was separated from any unprotected protein by cation exchange FPLC (MonoS column; Pharmacia, Piscataway, NJ) using a linear gradient of NaCl (0 to 200 mM) in 50 mM Hepes−NaOH buffer (pH 7.7). The protected protein eluted from the column at 60 mM NaCl, and the unprotected K41C protein eluted at 80 mM. The protected protein was stable for several months when stored at 4 °C.

Preparation of K41C−Cysteamine RNase A. The thiol-disulfide interchange reaction between K41C-ntb RNase A and cysteamine (CSA) was initiated by adding cysteamine·HCl (2−10 μL of a 0.010 M solution in 0.10 M Tris-HCl buffer, pH 7.7) to a solution (1.0 mL) of 50 mM Hepes−NaOH buffer (pH 7.7) containing K41C-ntb RNase A (0.3−0.7 mg/mL). The reaction mixture was incubated at 25 °C, and its progress was monitored by following the increase in absorbance at 412 nm, resulting from the release of a stoichiometric quantity of NTB [$\epsilon = 13\,600$ M^{-1} cm^{-1} (Ellman, 1959)]. Excess cysteamine and released NTB were removed by subsequent dialysis.

Assay of Poly(cytidylic acid) Cleavage. Ribonucleolytic activity was assessed by using poly(C) as a substrate. Prior to an assay, poly(C) was precipitated from aqueous ethanol (70% v/v), solubilized in assay buffer, and quantitated for total cytidyl concentration by absorbance at 268 nm using $\epsilon = 6200$ M^{-1} cm^{-1} (Yakovlev et al., 1992). Assays of poly(C) cleavage were performed at 25 °C in 0.10 M MES-NaOH buffer (pH 6.0) containing NaCl (0.10 M). Cleavage of poly(C) was monitored by the increase in absorbance at 250 nm using $\Delta\epsilon = 2380$ M^{-1} cm^{-1} (delCardayré and Raines, 1994). Concentrations of poly(C) in assays ranged from 0.02 to 1.2 mM, in terms of individual cytidyl units. Initial rates of cleavage were fitted to the Michaelis−Menten equation with the program HYPERO (Cleland, 1979).

Deactivation of K41C−Cysteamine RNase A with Dithiothreitol. The reduction of the mixed disulfide in K41C-csa RNase A (20 μM) by DTT (20 μM or 0.32 mM) was performed in 50 mM Hepes−NaOH buffer (pH 7.7). The reaction was allowed to proceed at 25 °C, and aliquots were removed periodically to assay for ribonucleolytic activity.

Synthesis of 2,4-Dinitrophenyl 3-Phosphopropyl Disulfide (7). Disulfide **7** was synthesized by the route shown in Scheme 1.

*p-Methoxybenzylmercaptan (**1**).* *p*-Methoxybenzylmercaptan was prepared from *p*-methoxybenzyl chloride and thiourea. A 1:1 ratio of the reactants was boiled under reflux and N_2(g) in acetonitrile for 1 h, and then stirred at room temperature. After 12 h, the reaction mixture was concentrated under reduced pressure to give a white solid. To hydrolyze the amidine groups, the solid was then dissolved in an aqueous solution of potassium carbonate and sodium bisulfite, and this solution was heated to 80 °C. The solution was subsequently acidified, and the product was extracted into chloroform, dried over $MgSO_4$, and evaporated to give a slightly yellow oil. ^{1}H NMR ($CDCl_3$, ppm): 7.22−7.25 and 6.86−6.83 (two m, 2H each, $-C_6\mathbf{H}_4-$), 3.79 (s, 3H, $-OC\mathbf{H}_3$), 3.70 (d, $J = 7.4$ Hz, 2H, $-C\mathbf{H}_2SH$), 1.73 (t, $J = 7.4$ Hz, 1H, $-S\mathbf{H}$).

*3-Hydroxypropyl p-Methoxybenzyl Thioether (**2**).* Equimolar amounts of *p*-methoxybenzylmercaptan and 3-bromo-1-propanol in acetonitrile were stirred under N_2(g) in the presence of potassium carbonate. The reaction was allowed to proceed, with stirring, overnight at room temperature. Compound **3** was isolated by silica chromatography, with 1:1 ethyl acetate:hexane as the mobile phase, and then evaporated under reduced pressure to give a colorless oil. ^{1}H NMR ($CDCl_3$, ppm): 7.21−7.26 and 6.84−6.87 (two m, 2H each, $MeOC_6\mathbf{H}_4-$), 3.80 (s, 3H, $-OC\mathbf{H}_3$), 3.71 (t, $J = 6.1$ Hz, 2H, $-C\mathbf{H}_2OH$), 3.68 (s, 2H, $-C_6H_4C\mathbf{H}_2S-$), 2.53 (t, $J = 7.0$ Hz, 2H, $-SC\mathbf{H}_2CH_2-$), 1.81 (m, 2H, $-CH_2C\mathbf{H}_2CH_2-$), 1.61 (br s, 1H, $CH_2O\mathbf{H}$).

*3-Phosphopropyl p-Methoxybenzyl Thioether (**6**).* Compound **6** was synthesized by a method analogous to that of (Kraszewski and Stawinski, 1980). Bis-triazole *p*-nitrophenyl phosphate (**3**) was generated by the reaction

Scheme 1

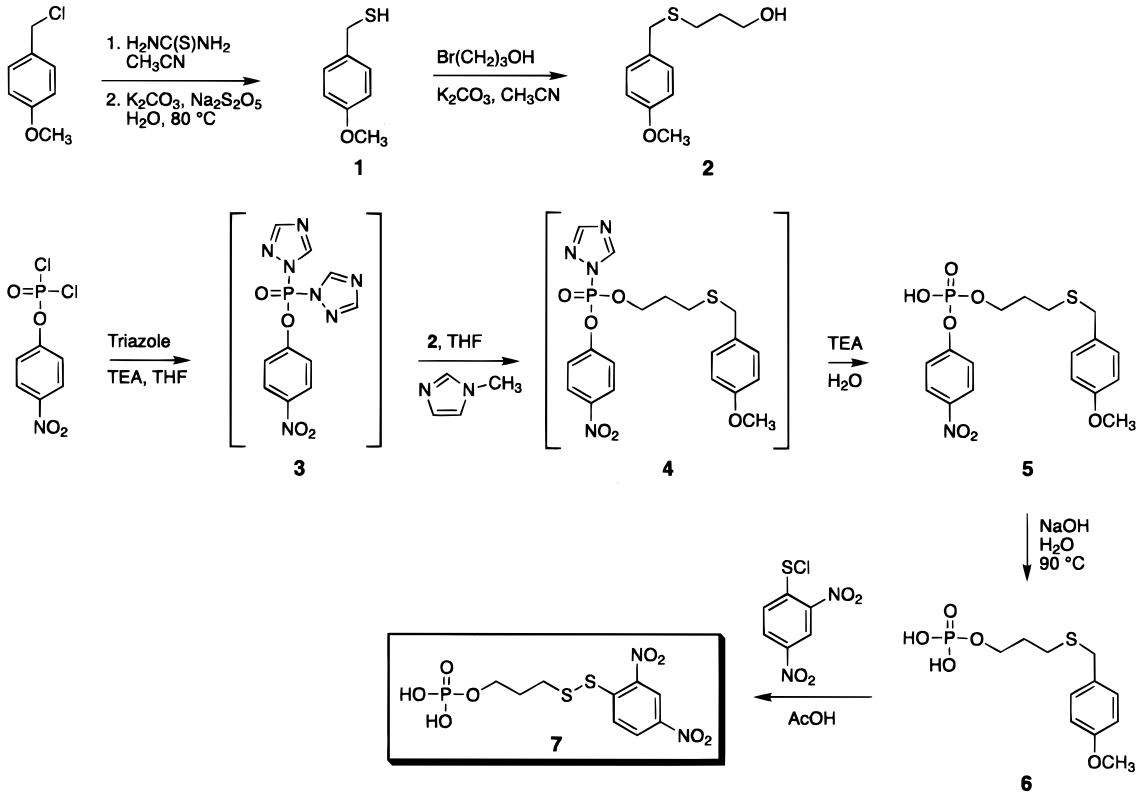

of *p*-nitrophenyl-phosphorodichloridate plus triazole and triethylamine (TEA) in tetrahydrofuran under N_2(g), first at 0 °C and then at room temperature, for a total of 30 min. Compound **2** (500 mg; 2.36 mmol) was then added in a 1:3 molar ratio relative to the dichloridate, along with 1.3 equiv of 1-methylimidazole relative to **3**. The reaction was allowed to proceed, still under N_2(g), for another 30 min. H_2O and TEA were then added to hydrolyze the triazole groups. After 2 h, the reaction mixture was concentrated under reduced pressure to give a yellow solid. The yellow solid was dissolved in chloroform and washed with aqueous $NaHCO_3$, then concentrated to give a yellow oil. The yellow oil was dissolved in H_2O and purified by two chromatographic steps, ion exchange (Sephadex SP C-25) and RP-C18 (isocratic; 1:1 MeOH: H_2O mobile phase), to give the phosphodiester **5** in 62% yield from alcohol **2**. MS of **5** (FAB, *m/e*): 412.1 (calcd for $C_{17}H_{19}NO_7PS$, 412.06). Phosphodiester **5** was hydrolyzed in 1 N NaOH at 90 °C for 16 h, and the resulting phosphomonoester (**6**) was neutralized and purified by anion-exchange chromatographically on DEAE Sephadex resin. Elution from the resin was effected by a linear gradient (0.1 to 1.0 M) of TEA-H_2CO_3, which was removed as the product, was dried under reduced pressure, yielding **6** in 75% yield from **5**. ^{1}H NMR (D_2O, ppm): 7.06−7.10 and 6.72−6.76 (two m, 2H each, $MeOC_6\mathbf{H}_4-$), 3.73 (quartet, J = 6.4 Hz, 2H, $-C\mathbf{H}_2OPO_3H_2$), 3.61 (s, 3H, $-OC\mathbf{H}_3$), 3.50 (s, 2H, $-C_6H_4C\mathbf{H}_2S-$), 2.37 (t, J = 7.5 Hz, 2H, $-SC\mathbf{H}_2CH_2-$), 1.70 (quintet, J = 6.6 Hz, 2H, $-CH_2C\mathbf{H}_2CH_2-$). ^{31}P NMR (D_2O, ppm relative to 85% w/v phosphoric acid): 1.36 (s, decoupled).

*Dinitrophenyl 3-Phosphopropyl Disulfide (**7**).* The simultaneous removal of the *p*-methoxybenzyl group from the sulfur and creation of the disulfide was accomplished by the method of (Johnson et al., 1994). Thioether **6** was stirred at room temperature for 30 min with an equimolar amount of 2,4-dinitrophenylsulfenyl chloride in acetic acid. The reaction mixture was then concentrated by evaporation and dissolved in methanol. The product was crystallized with the addition of diethyl ether and isolated by filtration to yield disulfide **7** as the free acid in 35% yield from **6**. ^{1}H NMR (CD_3OD, ppm): 9.04 and 8.58−8.62 [s and m, respectively, 1H and 2H, respectively, $(NO_2)_2C_6\mathbf{H}_3-$], 4.06 (quartet, J = 6.2 Hz, 2H, $-CH_2C\mathbf{H}_2OPO_3H_2$), 2.96 (t, J = 7.2 Hz, 2H, $-SC\mathbf{H}_2CH_2-$), 2.05 (quintet, J = 6.5 Hz, 2H, $-CH_2C\mathbf{H}_2CH_2-$). ^{31}P NMR (D_2O, ppm relative to phosphoric acid): 0.8 (s, decoupled).

K41C−(3-Mercaptopropyl-1-phosphate) RNase A. K41C RNase A was isolated freshly from K41C-ntb RNase A by DTT treatment and cation-exchange chromatography on a mono S column (vide supra). The protein (at 6 μM) was then reacted with a 10-fold molar excess of **7,** and then reisolated by cation-exchange chromatography. The addition of the MPP moiety caused the protein to elute from the Mono S column at 45 mM NaCl, rather than at 80 mM NaCl.

Zymogram Assay. Extremely small amounts of ribonucleolytic activity can be detected in Laemmli gels impregnated with RNA or poly(C) (Blank et al., 1982; Kim and Raines, 1993; Bravo et al., 1994). Here, such zymogram assays were performed in an polyacrylamide (18% w/v) gel containing poly(C) (0.5 mg/mL). K41C RNase A (0.4 μg) or K41C-mpp RNase A (0.4 μg) were loaded onto the gel in a nonreducing glycerol loading buffer (<20 μL). The gel was run at 50 mV until the sample had entered the resolving gel, and then the voltage was increased to 200 mV. After electrophoresis, the gel was washed for 5 min per wash, twice with 20% (v/v) 2-propanol, and twice with 0.050 M Tris-HCl buffer (pH 7.0). The gel was then incubated for an additional 30 min in the 0.050 M Tris-HCl buffer. Poly(C) remaining within the gel was stained with Toluidine Blue O (0.2% w/v), which binds only to polymeric nucleic acid, and destained with H_2O. Bands from ribonucleolytic activity where poly(C) is absent show up as clear against a deep blue background.

Scheme 2

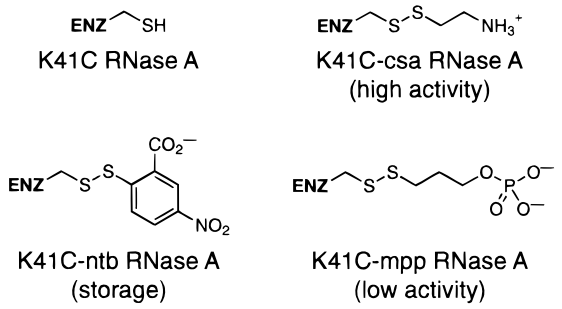

RESULTS AND DISCUSSION

RNase A has eight cysteine residues in its amino acid sequence, which produce four disulfide bonds in the native protein. Site-directed mutagenesis has introduced a ninth cysteine at several different positions, including residues 1, 19, and 88 (R.T.R. and co-workers, unpublished results) as well as residue 41 (Messmore et al., 1995). These protein variants all fold properly and in high yield to proteins with a single free sulfhydryl group at the desired position along with the eight native disulfides. The new cysteine residues are available to react with a variety of sulfhydryl-specific reagents. We had shown previously that the replacing Lys41 of RNase A with a cysteine residue reduces k_{cat} by 2×10^4-fold and k_{cat}/K_m by nearly 10^5-fold (Messmore et al., 1995). We had also shown that alkylation of Cys41 with haloalkylamines can compensate for much of the lost catalytic activity.

Another type of reaction in which a newly introduced cysteine can participate is thiol-disulfide interchange, which leaves the protein involved in an intermolecular disulfide bond (Faulstich and Heintz, 1995). Thiol-disulfide interchange reactions are among the most facile chemical reactions in biology (Raines, 1997). We have exploited this versatility, vis-à-vis position 41, to modulate the ribonucleolytic ability of RNase A. The various forms of K41C RNase A that have been prepared and studied herein are shown in Scheme 2.

K41C RNase A is unstable if stored for long periods of time, presumably due to oxidation of the Cys41 sulfhydryl group by air. Consequently, we stored the K41C variant only after protecting the Cys41 sulfhydryl group by reaction with DTNB. The resultant NTB-protected protein (K41C-ntb RNase A) contains the first disulfide in which Cys41 will participate. This protein reacts rapidly with cysteamine, releasing 1 equiv of NTB and creating K41C-csa RNase A. This reaction can be monitored by the accompanying increase in absorbance at 412 nm. The reaction of enzyme (25 μM) and a 2.5-fold molar excess of cysteamine was more than half complete after 2 min and more than 80% complete after 6 min. The value of k_{cat}/K_m for poly(C) cleavage for K41C-csa RNase A is 1100-fold greater than that of K41C RNase A. Because all steps prior to cleavage of the P−O$^{5'}$ bond are reversible, the increase in k_{cat}/K_m corresponds to an increase of 4.2 kcal/mol in the free energy of binding to the rate-limiting transition state (Table 1) (Cleland and Northrop, 1999). This rate increase is almost identical to that obtained upon alkylation of Cys41 to form K41[*S*-(aminopropyl)cysteine] RNase A (Messmore et al., 1995), which has a side chain at position 41 isologous to that of K41C-csa RNase A.

The stability of the intermolecular disulfide bond with cysteamine contrasts sharply with that of the native, intramolecular ones. Approximately 80% of RNase A molecules retain their native disulfide bonds after exposure to 0.10 M DTT (1200-fold molar excess) for 4 h at pH 8.0 and 25 °C (Li et al., 1995). We have observed that exposure to ≤10 mM DTT (700-fold molar excess) for 45 min at pH 7.8 and 25 °C has little or no effect on the intramolecular disulfide bonds of K41C RNase A, as monitored by enzymatic activity. In contrast, the disulfide bond to cysteamine can be reduced completely with as little as 20 μM DTT (1 M equiv) in less than 30 min. At higher levels of DTT, deactivation is even faster (Figure 2).

The unique reactivity of the sulfhydryl group at position 41 of K41C RNase A can be used as a target for additional modifications leading to more complete inactivation. We took advantage of this reactivity by synthesizing a modification reagent that creates another mixed

Table 1. Steady-State Kinetic Parameters for Catalysis of Poly(cytidylic acid) Cleavage by Wild-Type Ribonuclease A and the K41C and K41C-Cysteamine Variants[a]

RNase A	k_{cat} (s^{-1})	K_m (mM)	k_{cat}/K_m (M^{-1} s^{-1})	$\Delta\Delta G^{\ddagger}$ (kcal/mol)[b]
wild-type	604 ± 47	0.091 ± 0.022	(6.5 ± 1.2) × 10^6	0.0
K41C	0.026 ± 0.004	0.36 ± 0.12	(7.3 ± 1.5) × 10	6.8
K41C-csa	3.6 ± 0.1	0.043 ± 0.009	(8.5 ± 1.5) × 10^4	2.6

[a] Data were obtained at 25 °C in 0.10 M Mes−NaOH buffer (pH 6.0) containing NaCl (0.10 M). Data for wild-type RNase A and the K41C variant are from Messmore et al. (1995). [b] $\Delta\Delta G^{\ddagger} = RT \ln[(k_{cat}/K_m)_{wild-type}/(k_{cat}/K_m)_{variant}]$.

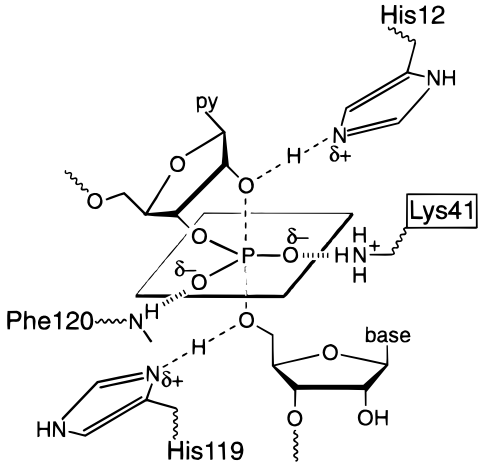

Figure 1. Putative structure of the transition state for catalysis of RNA cleavage by ribonuclease A (Raines, 1998).

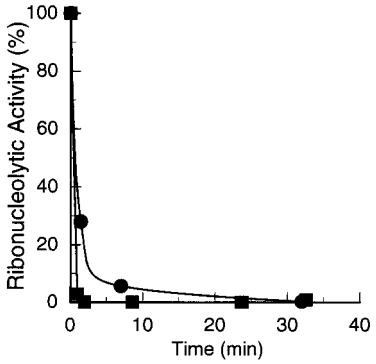

Figure 2. Deactivation of K41C-csa ribonuclease A by dithiothreitol. The reaction was performed at 25 °C in 50 mM Hepes−NaOH buffer (pH 7.7) containing K41C-csa RNase A (20 μM) and DTT [20 mM (●) or 0.32 M (■)].

Figure 3. Zymogram assay of K41C ribonuclease A and K41C−(3-mercaptopropyl-1-phosphate) ribonuclease A. Lane 1: K41C RNase A (0.4 μg). Lane 2: 10 μL of eluent from a Mono S column (negative control). Lane 3: K41C-mpp RNase A (0.4 μg). Samples were subjected to electrophoresis in a nonreducing SDS−polyacrylamide gel containing poly(C). Ribonucleolytic activity is indicated by a clear band after staining with Toluidine Blue O.

disulfide, altering the protein again in a reversible fashion. [Irreversible alkylation of the cysteine residue comprises another useful option (Lundblad, 1991; Viola and Wright, 1999), which was not explored here.] We chose to investigate the attachment of 3-mercaptopropyl-1-phosphate (MPP) to the sulfur of Cys41. We selected MPP because the propyl linkage would allow the phosphoryl group of MPP to assume a position similar to that of inorganic phosphate or inorganic sulfate observed in crystallographic studies (Wlodawer, 1985) and of the pentavalent phosphoryl group in the transition state for RNA cleavage (Figure 1). To attach MPP, we synthesized 2,4-dinitrophenyl 3-phosphopropyl disulfide (**7**). The synthesis of **7** proceeded in three phases (Scheme 1). In the first two phases, the MPP moiety was made by modifying 3-bromo-1-propanol, first with an appropriately protected thiol and then with a triazolephosphate. After the triazole groups had been removed, the desired disulfide was created by using 2,4-dintrophenyl-sulfenyl chloride to replace the protecting group on the sulfur of MPP.

Compound **7** reacts readily with Cys41 of K41C RNase A. Reaction with a 10-fold M excess of **7** was 90% complete within 25 min. K41C-mpp RNase A was isolated from any traces of unreacted protein by additional cation-exchange chromatography. Zymogram analysis of K41C-mpp RNase A indicates that this protein has significantly less ribonucleolytic activity than does K41C RNase A (Figure 3).

Spectrophotometric assays of poly(C) cleavage were used in an attempt to quantify the residual catalytic activity. Changes in absorbance were followed over 5 h. The measured rates averaged (4 ± 1)% of the rates for the K41C enzyme under identical conditions and were too slow to obtain the values of steady-state kinetic parameters. Still, if the effect of adding MPP to K41C RNase A is assumed to be only on K_m, the effective molarity of inorganic phosphate can be computed by the equation describing competitive inhibition. Specifically,

$$v = \frac{k_{cat}[E][S]}{K_m(1 + [I]/K_{P_i})} \quad (1)$$

can be rearranged to give

$$[I] = K_{P_i}\left[\left(\frac{k_{cat}[E]}{v}\right)\left(\frac{[S]}{K_m}\right) - 1\right] \quad (2)$$

where K_{P_i} is the inhibition constant of inorganic phosphate and [I] is the effective molarity of inorganic phosphate at the active site. If the value of K_{P_i} is taken to be 4.6 mM (Anderson et al., 1968) and the K41C RNase A kinetic parameters are used (Table 1), the average effective molarity associated with the measured rates of poly(C) cleavage is 0.3 M. This value is $>10^5$-fold greater than the actual molarity of the phosphoryl group of MPP in our assays ([K41C-mpp RNase A] ≤ 3.5 μM).

Once K41C RNase A has been modified with MPP, noncovalent interactions with the pendant phosphoryl group increased markedly the stability of the intermolecular disulfide bond. DTT and β-mercaptoethanol were used over a range of conditions that are benign to the K41C enzyme in attempts to remove the MPP group from K41C-mpp RNase A. At low and moderate ionic strengths, no increase in activity was observed by zymogram analysis after incubation with up to 2 mM DTT for up to 24 h. Even in the presence of 1 M inorganic phosphate and 0.10 mM DTT, no measurable gain in activity was observable. At 2.5 M inorganic phosphate and 2 mM DTT, a gain of activity indicative of a 20% reversal to K41C RNase A was observed after 90 min.

Conclusion. The unique reactivity of the sulfhydryl group allows for rapid and specific control of enzymatic activity. The activity of K41C RNase A has been increased 1100-fold by modification with cysteamine, and decreased 25-fold by modification with 3-mercaptopropyl-1-phosphate. Enzymatic activity can thus be readily modulated over a range spanning a factor of $10^{4.4}$-fold. An analogous control mechanism could conceivably be installed into the active site of any enzyme if an essential functional group is available for replacement with a cysteine.

ACKNOWLEDGMENT

We are grateful to C. L. Dantzman for advice on the synthesis of dinitrophenyl 3-phosphopropyl disulfide (**7**) and K. J. Woycechowsky and C. L. Jenkins for comments on the manuscript. This work was supported by Grants GM44783 (NIH) and BES 9604563 (NSF). S.K.H. was an Arthritis Foundation postdoctoral fellow.

LITERATURE CITED

Anderson, D. G., Hammes, G. C., and Walz, F. G. J. (1968) Binding of Phosphate Ligands to Ribonuclease A. *Biochemistry 7*, 1637−1645.

Ausubel, F. M., Brent, R., Kingston, R. E., Moore, D. D., Seidman, J. G., Smith, J. A., and Struhl, K., Eds. (1994) *Current Protocols in Molecular Biology*, John Wiley & Sons, Boston.

Blank, A., Sugiyama, R. H., and Dekker, C. A. (1982) Activity staining of nucleolytic enzymes after SDS−PAGE: use of aqueous isopropanol to remove detergent from gels. *Anal. Biochem. 120*, 267−275.

Bravo, J., Fernández, E., Ribó, M., de Llorens, R., and Cuchillo, C. M. (1994) A versatile negative-staining ribonuclease zymogram. *Anal. Biochem. 219*, 82−86.

Chen, Y.-C. J., and Janda, K. D. (1992) A new approach toward the inhibition of ribonucleases: a water-stable ribonucleoside-technetium chelate. *J. Am. Chem. Soc. 114*, 1488−1489.

Cleland, W. W. (1979) Statistical analysis of enzyme kinetic data. *Methods Enzymol. 63*, 103−138.

Cleland, W. W., and Northrop, D. B. (1999) Energetics of substrate binding, catalysis, and product release. *Methods Enzymol. 308*, 3−27.

D'Alessio, G., and Riordan, J. F., Eds. (1997) *Ribonucleases: Structures and Functions*, Academic Press, New York.

delCardayré, S. B., and Raines, R. T. (1994) Structural Determinants of Enzymatic Processivity. *Biochemistry 33*, 6032−6037.

delCardayré, S. B., Ribó, M., Yokel, E. M., Quirk, D. J., Rutter, W. J., and Raines, R. T. (1995) Engineering ribonuclease A: production, purification, and characterization of wild-type enzyme and mutants at Gln11. *Protein Eng. 8*, 261−273.

Ellman, G. L. (1959) Tissue sulfhydryl groups. *Arch. Biochem. Biophys. 82*, 70−77.

Eun, H.-M. (1996) *Enzymology Primer for Recombinant DNA Technology*, Academic Press, San Diego.

Faulstich, H., and Heintz, D. (1995) Reversible introduction of thiol compounds into proteins by use of activated mixed disulfides. *Methods Enzymol. 251*, 357−366.

Gloss, L. M., and Kirsch, J. F. (1995) Examining the structural and chemical flexibility of the active site base, Lys-258, of *Eschericia coli* aspartate aminotransferase by replacement with unnatural amino acids. *Biochemistry 34*, 12323−12332.

Hollenbaugh, D., Aruffo, A., and Senter, P. D. (1995) Effects of Chemical Modification on the Binding Activities of P-Selectin Mutants. *Biochemistry 34*, 5678−5684.

Hummel, C. F., Pincus, M. R., Brandt-Rauf, P. W., Frei, G. M., and Carty, R. P. (1987) Reaction of (Bromoacetamido)-nucleoside Affinity Labels with Ribonuclease A: Evidence for Steric Control of Reaction Specificity and Alkylation Rate. *Biochemistry 26*, 135−146.

Johnson, R., Joshi, B. V., and Reese, C. B. (1994) Synthesis of 2′,3′-dithiouridine. *J. Chem. Soc., Chem. Commun.*, 133−134.

Kim, J.-S., and Raines, R. T. (1993) Ribonuclease S-peptide as a carrier in fusion proteins. *Protein Sci. 2*, 248−356.

Kraszewski, A., and Stawinski, J. (1980) Phosphoryl tris-triazole−a new phosphorylating reagent. *Tetrahedron Lett. 21*, 2935−2936.

Leonidas, D. D., Shapiro, R., Irons, L. I., Russo, N., and Acharya, K. R. (1999) Toward Rational Design of Ribonuclease Inhibitors: High-Resolution Crystal Strcuture of a Ribonuclease A Complex with a Potent 3′,5′-Pyrophosphate-Linked Dinucleotide Inhibitor. *Biochemistry 38*, 10287−10297.

Li, Y.-J., Rothwarf, D. M., and Scheraga, H. A. (1995) Mechanism of reductive protein unfolding. *Nat. Struct. Biol. 2*, 489−494.

Lindquist, R. N., Lynn, J. L., Jr., and Lienhard, G. E. (1973) Possible Transition-State Analogs for Ribonuclease. The Complexes of Uridine with Oxovanadium(IV) Ion and Vanadium(V) Ion. *J. Am. Chem. Soc. 95*, 8762−8768.

Lundblad, R. L. (1991) *Chemical Reagents for Protein Modification*, CRC Press, Boca Raton, FL.

Messmore, J. M., Fuchs, D. N., and Raines, R. T. (1995) Ribonuclease A: Revealing Structure−Function Relationships with Semisynthesis. *J. Am. Chem. Soc. 117*, 8057−8060.

Pease, M. D., Serpersu, E. H., and Mildvan, A. S. (1987) Chemical modification and spin-labelling studies of the Arg 87 to Cys (R87C) mutant of Staphylococcal nuclease. *Fed. Proc. 46*, 1932.

Raines, R. T. (1997) Nature's transitory covalent bond. *Nat. Struct. Biol. 4*, 424−427.

Raines, R. T. (1998) Ribonuclease A. *Chem. Rev. 98*, 1045−1065.

Russo, N., and Shapiro, R. (1999) Potent inhibition of mammalian ribonucleases by 3′,5′-pyrophosphate-linked nucleotides. *J. Biol. Chem. 274*, 14902−14908.

Sela, M., Anfinsen, C. B., and Harrington, W. F. (1957) The correlation of ribonuclease activity with specific aspects of tertiary structure. *Biochim. Biophys. Acta 26*, 502−512.

Stowell, J. K., Widlanski, T. S., Kutateladze, T. G., and Raines, R. T. (1995) Mechanism-Based Inactivation of Ribonuclease A. *J. Org. Chem. 60*, 6930−6936.

Suckling, C. J., Ed. (1990) *Enzyme Chemistry: Impact and Applications*, Chapman and Hall, London.

Viola, R. E., and Wright, S. K. (1999) New enzymes from old. In *Enzymatic Mechanisms* (P. A. Frey and D. B. Northrop, Eds.) pp 116−130, IOS Press, Washington DC.

Wlodawer, A. (1985) Structure of bovine pancreatic ribonuclease by X-ray and neutron diffraction. In *Biological Macromolecules and Assemblies, Vol. II, Nucleic Acids and Interactive Proteins* (F. A. Jurnak and A. McPherson, Eds.) pp 395−439, Wiley, New York.

Wong, C.-H., and Whitesides, G. M. (1994) *Enzymes in Synthetic Organic Chemistry*, Elsevier Science, Tarrytown, NY.

Yakovlev, G. I., Moiseyev, G. P., Bezborodova, S. I., Both, V., and Sevcik, J. (1992) A comparative study on the catalytic properies of guanylyl-specific ribonucleases. *Eur. J. Biochem. 204*, 187−190.

Zinn, K., DiMaio, D., and Maniatis, T. (1983) Identification of two distinct regulatory regions adjacent to the human β-interferon gene. *Cell 34*, 865−879.

BC990142M

Chemical and Biological Characterization of Technetium(I) and Rhenium(I) Tricarbonyl Complexes with Dithioether Ligands Serving as Linkers for Coupling the $Tc(CO)_3$ and $Re(CO)_3$ Moieties to Biologically Active Molecules

H.-J. Pietzsch,*[,†] A. Gupta,[†] M. Reisgys,[†] A. Drews,[†] S. Seifert,[†] R. Syhre,[†] H. Spies,[†] R. Alberto,[‡] U. Abram,[§] P. A. Schubiger,[‡] and B. Johannsen[†]

Forschungszentrum Rossendorf, Institut für Bioanorganische und Radiopharmazeutische Chemie, PF 510119, D-01314 Dresden, Germany, Paul-Scherrer-Institut Villigen, Abteilung für Radiopharmazie, CH-5232 Villigen, Switzerland, and Forschungszentrum Rossendorf, Institut für Radiochemie, PF 510119, D-01314 Dresden, Germany. Received November 22, 1999

The organometallic precursor $(NEt_4)_2[ReBr_3(CO)_3]$ was reacted with bidendate dithioethers (L) of the general formula $H_3C-S-CH_2CH_2-S-R$ ($R = -CH_2CH_2COOH$, $CH_2-C\equiv CH$) and $R'-S-CH_2CH_2-S-R'$ ($R' = CH_3CH_2-$, CH_3CH_2-OH, and CH_2COOH) in methanol to form stable rhenium(I) tricarbonyl complexes of the general composition $[ReBr(CO)_3L]$. Under these conditions, the functional groups do not participate in the coordination. As a prototypic representative of this type of Re compounds, the propargylic group bearing complex $[ReBr(CO_3)(H_3C-S-CH_2CH_2-S-CH_2C\equiv CH)]$ **Re2** was studied by X-ray diffraction analysis. Its molecular structure exhibits a slightly distorted octahedron with facial coordination of the carbonyl ligands. The potentially tetradentate ligand $HO-CH_2CH_2-S-CH_2CH_2-S-CH_2CH_2-OH$ was reacted with the trinitrato precursor $[Re(NO_3)_3(CO)_3]^{2-}$ to yield a cationic complex $[Re(CO)_3(HO-CH_2CH_2-S-CH_2CH_2-S-CH_2CH_2-OH)]NO_3$ **Re8** which shows the coordination of one hydroxy group. **Re8** has been characterized by correct elemental analysis, infrared spectroscopy, capillary electrophoresis, and X-ray diffraction analysis. Ligand exchange reaction of the carboxylic group bearing ligands $H_3C-S-CH_2CH_2-S-CH_2CH_2-COOH$ and $HOOC-CH_2-S-CH_2-CH_2-S-CH_2-COOH$ with $(NEt_4)_2[ReBr_3(CO)_3]$ in water and with equimolar amounts of NaOH led to complexes in which the bromide is replaced by the carboxylic group. The X-ray structure analysis of the complex $[Re(CO)_3(OOC-CH_2-S-CH_2CH_2-S-CH_2-COOH)]$ **Re6** shows the second carboxylic group noncoordinated offering an ideal site for functionalization or coupling a biomolecule. The no-carrier-added preparation of the analogous $^{99m}Tc(I)$ carbonyl thioether complexes could be performed using the precursor fac-$[^{99m}Tc(H_2O)_3(CO)_3]^+$, with yields up to 90%. The behavior of the chlorine containing ^{99m}Tc complex $[^{99m}TcCl(CO)_3(CH_3CH_2-S-CH_2CH_2-S-CH_2CH_3)]$ **Tc1** in aqueous solution at physiological pH value was investigated. In saline, the chromatographically separated compound was stable for at least 120 min. However, in chloride-free aqueous solution, a water-coordinated cationic species **Tc1a** of the proposed composition $[^{99m}Tc(H_2O)(CO)_3(CH_3CH_2-S-CH_2CH_2-S-CH_2CH_3)]^+$ occurred. The cationic charge of the conversion product was confirmed by capillary electrophoresis. By the introduction of a carboxylic group into the thioether ligand as a third donor group, the conversion could be suppressed and thus the neutrality of the complex preserved. Biodistribution studies in the rat demonstrated for the neutral complexes $[^{99m}TcCl(CO)_3(CH_3CH_2-S-CH_2CH_2-S-CH_2CH_3)]$ **Tc1** and $[^{99m}TcCl(CO)_3(CH_2-S-CH_2CH_2-S-CH_2-C\equiv CH)]$ **Tc2** a significant initial brain uptake ($1.03 \pm 0.25\%$ and $0.78 \pm 0.08\%$ ID/organ at 5 min. p.i.). Challenge experiments with glutathione clearly indicated that no transchelation reaction occurs in vivo.

INTRODUCTION

The γ-emitting nuclide technetium-99m plays the dominating role in diagnostic nuclear medicine because of its optimal nuclide properties. Either as nonradioactive surrogate of technetium or because of the favorable properties of rhenium-186 and rhenium-188 for therapy, the congener rhenium is usually included in the consideration of the radiopharmaceutical chemistry of technetium. A number of reviews covering this field have appeared recently (*1*−*3*). Current development of Tc-99m radiopharmaceuticals considers the present needs for new and broadly applicable tracers for metabolism and receptor studies. The strategy to design such technetium-based compounds involves incorporation of the radionuclide into biologically active molecules, which requires chelating of the technetium at an appropriate oxidation state and linking the chelate to the biomolecule. Advances in this field depend on the availability of chelating systems that are well-suited to be combined with the biological "anchor group". In this sense, the chelates should distinguish themselves by high stability, small size, adoptable lipophilicity, and the possibly absence of isomers (*4*−*6*).

* To whom correspondence should be addressed. Fax: (0351) 260 3232. E-mail: h.j.pietzsch@fz-rossendorf.de.

† Forschungszentrum Rossendorf, Institut für Bioanorganische und Radiopharmazeutische Chemie.

‡ Paul-Scherrer-Institut Villigen.

§ Forschungszentrum Rossendorf, Institut für Radiochemie.

10.1021/bc990162o CCC: $19.00 © 2000 American Chemical Society
Published on Web 03/31/2000

In the past years, various concepts for chelating ligands have been outlined. The most successful of them are focused on oxotechnetium(V) complexes (*7*) containing the $[Tc{=}O]^{3+}$ moiety, which is readily accessible by reduction of pertechnetate in the presence of suitable chelators such as tetradentate N_2S_2 ligands (*8*−*12*) or mixtures of ligands according to the so-called "3+1" concept (*13*−*18*). However, the oxo core, usually square-pyramidal coordinated and with a free position trans to the oxo ligand, is a quite polar unit. The stricter that the requirements are for specific agents, the more important the question as to whether such a polarity is beneficial or not. Alternatives are the oxo-free, lower oxidation states, namely, +3 and preferably +1.

The rarely exploited oxidation state +1 came into the limelight by the discovery of myocardium affine hexakis isonitriles of technetium(I) and the successful clinical application of ^{99m}Tc methoxy-isobutyl isonitrile (*19*). Despite this progress, the oxidation state +1 has been addressed only in a minor way (*20*−*24*) before a new most promising approach to low valent, inert technetium compounds on basis of Tc(I) carbonyl complexes has been elaborated (*25*−*27*). Intensive investigations in the Tc carbonyl chemistry made available an organometallic Tc(I) aqua ion, $[Tc(H_2O)_3(CO)_3]^+$, from TcO_4^- under normal pressure, the prerequisite to exploit the small $[Tc(CO)_3]^+$ moiety for the labeling of biomolecules is given (*28*, *29*). It could be shown that isonitriles (*30*), thiourea and its derivatives (*31*), thiophosphoryl amides (*32*), cyclopentadiene (*33*), various N-containing ligands, such as histamine, imidazole, histidine, and Schiff bases (*34*, *35*), and water-soluble phosphines (*36*) are able to easily react with the $[Tc(H_2O)_3(CO)_3]^+$ to yield stable complexes.

Double ligand-transfer reactions developed by Spradau et al. give access to derivatized cyclopentadienyltricarbonyl technetium and rhenium complexes for labeling steroids (*37*, *38*).

Thioether ligands may serve in an alternative approach to fully exploit the potential of the $[M(CO)_3]^+$ moiety (M = Tc, Re) for the design of radiotracers. Thioethers with the π-acceptor properties of the sulfur show a great potency to coordinate at the metal(I) carbonyl center and a couple of Re carbonyl complexes with thioether ligands are known (*29*, *39*−*42*).

Recently, we have published the synthesis of Tc and Re dithioether carbonyl complexes bearing steroids as biologically active anchor group (*43*, *44*) as well as tropanol-functionalized Tc thioether carbonyls to label the dopamine transporter (*45*).

In the present paper, we describe the basic chemistry of the Tc(I)/Re(I) carbonyl thioethers as relevant for the radiotracer design. This involves the synthesis and structural analysis of rhenium complexes with functionalized bidentate thioether ligands derived from $(NEt_4)_2[ReBr_3(CO)_3]$ and $(NEt_4)_2[Re(NO_3)_3(CO)_3]$. The preparation of the analogous ^{99m}Tc complexes is described as well as their stability in aqueous solution and in plasma, and their biodistribution in rats.

EXPERIMENTAL PROCEDURES

General. All chemicals and solvents were of reagent grade and used without further purification. The thioether ligands L^1-L^5 were synthesized according to standard procedures and to Beger et al. (*46*).

$(NEt_4)_2[ReBr_3(CO)_3]$ was prepared as published elsewhere (*47*). $(NEt_4)_2[Re(NO_3)_3(CO)_3]$ was obtained by reaction of $(NEt_4)_2[ReBr_3(CO)_3]$ with a 3-fold equiv of silver nitrate in water (*27*).

Elemental analyses were performed on a LECO Elemental Analyzer CHNS-932. Melting points were obtained on a BOËTIUS-Mikroheiztisch and are uncorrected.

IR spectra were measured as KBr pellets on a Perkin-Elmer FTIR-spectrometer SPECTRUM 2000.

^{1}H NMR spectra (400 MHz) were recorded on a Varian spectrometer INOVA-400.

The Re complexes and the analogous ^{99m}Tc compounds were identified and characterized by gradient HPLC (Hypersil column, Knauer, 10 μm, 250 mm × 4 mm), methanol/phosphate buffer (0.01 M, pH 7.4) from 50% methanol to 100% within 5 min, 1 mL/min.

Cationic ^{99m}Tc and Re species were additionally characterized by paper electrophoresis (400 V, 20 V/cm, 50 min; FN 4 paper (Niederschlag), acetonitrile/0.1 M phosphate buffer (50/50 v/v), pH 7.4.

Further ^{99m}Tc species were characterized by capillary electrophoresis using a ^{3D}CE device (Hewlett-Packard) equipped with a diode array detection (DAD) system and radioactivity detection as published by Jankowsky et al. (*48*). A fused silica capillary with inner diameter of 50 μm and an effective length of 64 cm was employed. For running electrolyte, phosphate buffer 50 mM mixed with 50% of acetonitrile was used. During runs, voltages of 25 kV were applied, and for investigations at a pH of 9.3, an additional external air pressure of 50 mbar was applied.

X-ray Data Collection and Processing. The intensities for the X-ray structure determination were collected on an automated single-crystal diffractometer of the type CAD4 (Enraf-Nonius) MoKα (**Re2**) or CuKα (**Re6**, **Re8**) radiation, respectively, with ω scans. The cell dimensions were determined by the angular setting of 25 high-angle reflections. The structures were solved by heavy-atom Patterson synthesis using SHELXS-86 (*49*). Refinement was performed with SHELXL-93 (*50*). All non-hydrogen atoms were located from successive Fourier maps and refined with anisotropic thermal parameters. In the case of complex **Re8**, the hydrogen atoms were fully refined, whereas for **Re2** and **Re6** the hydrogen atoms were placed in calculated positions and refined using the "riding model" option of SHELXL-93. A summary of the crystallographic data is given in Table 1. More details of the structure determination have been deposited with the Cambridge Crystallographic Data Centre under the deposit numbers CCDC 134865 (RE2), CCDC 134866 (**Re6**), and CCDC 134867 (**Re8**).

General Synthesis Procedure for the Complexes [ReBr(CO$_3$)L] (Re1) − (Re5, Re7). A total of 130 μmol of the appropriate ligand L^1−L^5, dissolved in 1 mL of methanol was added to a stirred solution of 100 mg (130 μmol) $(NEt_4)_2[ReBr_3(CO)_3]$, dissolved in 1 mL of methanol. After stirring the reaction mixture at ambient temperature for 1 h, the solvent was removed to dryness in a vacuum. The remaining residue was taken up in dry THF and the white precipitate (NEt_4Br) was filtered off. The filtrate was dried and washed three times with water and diethyl ether until a white solid was formed. After each washing procedure, the residue was dried in a vacuum.

Bromo(3,6-dithiaoctane-*S*,*S*)tricarbonylrhenium-(I)] (Re1). Yield: 57 mg (88%). HPLC: R_t = 7.6 min. mp = 90−92 °C. IR (KBr) (cm^{-1}): 2024 (CO), 1932 (CO), 1900 (CO). Anal. ($C_9H_{14}BrO_3ReS_2$) calcd: C, 21.60; H, 2.82; S, 12.81; Br, 15.97%. Found: C, 21.68; H, 2.66; S, 12.97; Br, 15.43%.

[Bromo(4,7-dithia-1-octyne-*S*,*S*)tricarbonylrhenium(I)] (Re2). Colorless crystals of **Re2** suitable for X-ray diffraction were obtained from acetone/*n*-hexane.

Table 1. Crystallographic Data for X-ray Diffraction Studies of Re Complexes Re2, Re6, and Re8

	Re2	Re6	Re8
formula	$C_9H_{10}BrO_3ReS_2$	$C_9H_9O_7ReS_2$	$C_9H_{14}NO_8ReS_2$
fw	496.40	479.48	514.53
crystal system	monoclinic	monoclinic	triclinic
space group	*C*2/*c*	*P*2(1)/*cP*	$P\bar{1}$
a (Å)	26.995 (5)	8.615 (1)	8.870 (1)
b (Å)	7.892 (1)	10.630 (1)	11.323 (2)
c (Å)	13.460 (3)	13.899 (1)	16.565 (3)
α (deg)	90	90	105.78 (1)
β (deg)	108.69 (1)	100.17(1)	98.47 (1)
γ (deg)	90	90	102.66 (1)
V (Å^3)	2716.4 (9)	1252.8(2)	1523.7 (4)
	8	4	4
temp (K)	293(2)	213(2)	293(2)
d (g/cm^3)	2.428	2.542	2.243
μ (mm^{-1})	12.184	22.376	18.524
absorbance correction	*ψ* scans	*ψ* scans	*ψ* scans
T_{min}/T_{max}	0.7532/0.9716	0.3808/0.9632	8.8367/0.9985
F(000)	1840	904	984
λ (Å), radiation	0.710 73 MoKα	1.541 84, CuKα	1.541 84, CuKα
crystal size (mm^3)	0.30 × 0.15 × 0.15	0.2 × 0.2 × 0.1	0.30 × 0.05 × 0.05
2*θ*-range	3.01−24.99	5.22 to 64.95	5.24−64.95
hkl	$0 \le h \le 34$	$-1 \le h \le 10$	$-1 \le h \le 10$
	$0 \le k \le 10$	$0 \le k \le 12$	$-13 \le k \le 13$
	$-17 \le l \le 16$	$-16 \le l \le 16$	$-19 \le l \le 19$
no. of coll. reflns	2453	2594	6071
no. of indep. reflns/R_{int}	2401/0.0393	2129/0.0296	4969/0.0445
no. of obsd reflns	1793	2082	4368
no. of parameters	145	208	380
GOF	1.073	1.104	1.079
R [*I* > 2*s*(*I*)]			
R_1	0.0467	0.0355	0.0381
wR_2	0.1014	0.0984	0.1023
R (all data)			
R_1	0.0760	0.0365	0.0446
wR_2	0.1185	0.1030	0.1076

Yield: 49 mg (80%). HPLC: R_t = 7.2 min. mp = 95−96 °C. IR (KBr) (cm^{-1}): 2032 (CO), 1940 (CO), 1900 (CO). Anal. ($C_9H_{10}BrO_3ReS_2$) calcd: C, 21.78; H, 2.03; S, 12.92; Br, 16.10%. Found: C, 21.85; H, 2.09; S, 12.94; Br, 15.10%.

[Bromo(1-carboxy-3,6-dithiaheptane-*S*,*S*)tricarbonylrhenium(I)] (Re3). Yield: 56 mg (81%). HPLC: R_t = 3.2 min. mp = 157−158 °C. IR (KBr) (cm^{-1}): 2032 (CO), 1916 (CO), 1712 (C=O). Anal. ($C_9H_{12}BrO_5ReS_2$) calcd: C, 20.38; H, 2.27; S, 12.09; Br, 15.06%. Found: C, 20.60; H, 2.56; S, 11.97; Br, 14.17%.

[Bromo(1,6-dicarboxy-2,5-dithiahexane-*S*,*S*)tricarbonylrhenium(I)] (Re4). Yield: 57 mg (88%). mp = 90−92 °C. IR (KBr) (cm^{-1}): 2024 (CO), 1932 (CO), 1900 (CO). Anal. ($C_9H_{10}BrO_7ReS_2$) calcd: C, 19.29; H, 1.78; S, 11.43; Br, 14.28%. Found: C, 19.48; H, 1.87; S, 11.28; Br, 14.51%.

[1-Carboxylato-3,6-dithiaheptane-*O*,*S*,*S*)tricarbonylrhenium(I) (Re5). A total of 59 mg (130 *μ*mol) of 1-carboxy-3,6-dithiaheptan (L^3) was added to 130 *μ*L NaOH (1 N) in 1 mL of water. The reaction mixture was stirred until the ligand was dissolved completely. To this solution was added 100 mg (130 *μ*mol) of $(NEt_4)_2[ReBr_3(CO)_3]$ in 1 mL of water. After a reaction time of 1 h, the water was removed by vacuum and the residue was washed with a small amount of water and filtrated. The white powder was washed with diethyl ether to yield 31 mg (53%). HPLC: R_t = 6.5 min. mp = 85 °C. IR (KBr) (cm^{-1}): 2032 (CO), 1940 (CO), 1900 (CO), 1632 (C=O). Anal. ($C_9H_{11}O_5ReS_2$) calcd: C, 24.05; S, 2.47; H, 14.26%. Found: C, 24.13; H, 3.00; S, 14.69%.

[(1-Carboxylato-6-carboxy-2,5-dithiahexane-*O*,*S*,-*S*)tricarbonylrhenium(I)] (Re6). A total of 81 mg (390 *μ*mol) of 2,5-dithiahexane-1,6-dicarboxylic acid was dissolved in 5 mL of water. A total of 300 mg (390 *μ*mol) $(NEt_4)_2[ReBr_3(CO)_3]$ and 1 equiv of 1 N NaOH was added to the clear solution, which became turbid after 15 min. A white precipitate formed over a further hour of stirring. The precipitate was filtered to yield 150 mg (83%) of analytically pure compound **Re6**. IR (KBr) (cm^{-1}): 2032 (CO), 1934 (CO), 1892 (CO). Anal. ($C_9H_9O_7ReS_2$) calcd: C: 22.54, H: 1.89%. Found: C, 22.33; H, 1.92%.

[Bromo(1,8-dihydroxy-3,6-dithiaoctane-*S*,*S*)tricarbonylrhenium(I)] Re7. Yield: 57 mg (83%). mp = 90−92 °C. IR (KBr) (cm^{-1}): 2024 (CO), 1932 (CO), 1900 (CO). Anal. ($C_9H_{14}BrO_5ReS_2$) calcd: C, 20.30; H, 2.63; S, 12.03; Br, 15.04%. Found: C, 20.18; H, 2.47; S, 12.28; Br, 15.33%.

[(1,8-Dihydroxy-3,6-dithiaoctane-*O*,*S*,*S*)tricarbonylrhenium(I)]nitrate (Re8). A total of 24 mg (130 *μ*mol) of 1,8-dihydroxy-3,6-dithiaoctane (L^5), dissolved in 1 mL of methanol, was added to a stirred solution of 93 mg (130 *μ*mol) $(NEt_4)_2[Re(NO_3)_3(CO)_3]$ in 1 mL of water. After 10 min, the solvent was removed and the residue dissolved in dry THF. The precipitate was filtered off. Removing the solvent from the filtrate yields 59 mg (88%) of a white precipitate. Colorless needles for X-ray analysis were obtained from chloroform/*n*-hexane. mp = 119−122 °C. IR (KBr) (cm^{-1}): 2032 (CO), 1936 (CO), 1384 (NO_3). Anal. ($C_9H_{14}NO_8ReS_2$) calcd: C, 21.01; H, 2.74 N 2.72; S, 12.46%. Found: C, 21.36; H, 3.01 N 2.90; S, 12.40%.

General Synthesis Procedure for the Preparation of $[^{99m}Tc(H_2O)_3(CO)_3]^+$ According to Ref *34*. Na_2CO_3 (0.038 mmol) and $NaBH_4$ (0.26 mmol) were added to a 10 mL vial, which was closed and flushed for 10 min with CO. A 1.5 mL sample of a ^{99m}Tc generator eluate mixed with 0.25 mL of propylene glycol (containing up to 200 MBq $Na[^{99m}TcO_4]$ in saline) was added, and the solution heated to 75 °C for 40 min. Quality control was performed by gradient HPLC or TLC (silica gel, methanol/HCl (95/5 v/v, R_f 0.4). Yield: 90−95%.

[Chloro(3,6-dithiaoctane-S,S)tricarbonyltechnetium(I)] (Tc1). A total of 400 μL of 1 N HCl for adjusting the pH to 1, 0.25 mL of propylene glycol, 0.25 mL of methanol, and 30 mg of NaCl were added to the solution of the $[^{99m}Tc(H_2O)_3(CO)_3]^+$ precursor. 3,6-Dithiaoctane (L^1) (1.0 μmol), dissolved in methanol, was added, and the reaction mixture was heated to 70 °C for 15 min. Finally, the reaction mixture was neutralized with 0.1 N NaOH. HPLC: $R_t = 7.6$ min (yield, 70%).

For separation of by-products and ligand excess, the reaction solution was given onto a semipreparative Hypersil column (250 × 8 mm, 10 μm, flow rate 2.0 mL/min) and eluted using a linear gradient system [*t* (min)/% A]: 5/50, 10/100, and 15/100 of methanol (A)/0.01 M phosphate buffer of pH 7.4 (B).

Immediately after separation, the complexes were diluted 1:1 with 0.9% NaCl containing 25% propylene glycol, and the methanol was removed by evaporation to yield a stable solution for biodistribution studies. For stability studies, the complexes were alternatively diluted after separation in PBS, in H_2O, or in a solution of 10 mM GSH in water.

[Chloro(4,7-dithia-1-octyne-S,S)tricarbonyltechnetium(I)] (Tc2). A total of 400 μL of 1 N HCl for adjusting the pH to 1, 0.25 mL of propylene glycol, 0.25 mL of methanol, and a further 30 mg of NaCl were added to the solution of the $[^{99m}Tc(H_2O)_3(CO)_3]^+$ precursor. 4,7-Dithia-1-octyne (L^2) (3.3 μmol), dissolved in methanol, was added, and the reaction mixture was heated to 70 °C for 15 min. Finally the reaction mixture was neutralized with 0.1 N NaOH. HPLC: $R_t = 7.2$ min (yield, 70%).

The separation of **Tc2** followed the procedure as described for **Tc1**.

[Chloro(1-carboxy-3,6-dithiaheptane-S,S)tricarbonyltechnetium(I)] (Tc3). The preparation was carried out as described for **Tc1**, but after preparation, the solution was not neutralized. The separation of complex **Tc3** was carried out with a semipreparative Hypersil column (250 × 8 mm, 10 μm, flow rate 2.0 mL/min) and eluted using a linear gradient system [*t* (min)/% A]: 5/20, 6/100, and 10/100 of methanol (A)/0.01 M phosphate buffer of pH 7.4 (B). To avoid the conversion of complex **Tc3** to **Tc5**, the eluate was given into a saturated solution of NaCl at pH 2 immediately after separation.

[Chloro(1,6-dicarboxy-2,5-dithiahexane-*S,S*)tricarbonyltechnetium(I)] (Tc4). The preparation was carried out as described for **Tc3**, but the gradient system used for purification was modified as follows [*t* (min)/% A]: 5/0, 5/100, and 10/100 of methanol (A)/0.01 M phosphate buffer of pH 7.4 (B).

[1-Carboxylato-3,6-dithiaheptane-*O,S,S*)tricarbonyltechnetium(I) (Tc 5). The preparation was carried out as described for **Tc1**, but after preparation, the pH of the solution was adjusted to pH 8. After standing for about 30 min at room temperature, **Tc5** was separated using the HPLC conditions as described for complex **Tc3**.

[(1-Carboxylato-6-carboxy-2,5-dithiahexane-*O,S,S*)tricarbonyltechnetium(I)] (Tc6). The preparation was carried out as described for **Tc1** but after preparation, the pH of the solution was adjusted to pH 8. After standing for about 30 min at room temperature, **Tc6** was separated using the HPLC conditions as described for complex **Tc4**.

Determination of Partition Coefficients. Partition coefficients of the ^{99m}Tc complexes were determined by shake-flask method by mixing 0.5 mL of the complex solution (0.9% NaCl solution and 20% propylene glycol) and 0.5 mL of octanol and shaking for 5 min. After centrifugation, aliquots of both phases were counted and the partition coefficient calculated.

Stability Studies in Solution. ^{99m}Tc complexes dissolved in MeOH were diluted with an equivalent volume of phosphate buffer 0.1 M, 0.9% NaCl, or H_2O containing 25% propylene glycol immediately after HPLC separation. At various incubation time, the samples were analyzed by HPLC with a Hypersil ODS column (250 × 4 mm) using a linear gradient system [*t* (min)/% A]: 5/50, 5/100, and 10/100 of methanol (A)/0.01 M phosphate buffer of pH 7.4 (B).

Ligand Exchange (Challenge) Experiments with Glutathione (GSH). ^{99m}Tc complexes dissolved in MeOH were diluted with an equivalent volume of an aqueous solution of 20 mM GSH containing 25% of propylene glycol immediately after HPLC separation, resulting in a final glutathione concentration of 10 mM. The analyses were performed by HPLC as described above.

Stability Studies in Plasma. A total of 50 μL of the appropriate ^{99m}Tc complex solution (0.9% NaCl, 12% propylene glycol) was incubated in 200 μL of rat plasma at 37 °C. After an incubation time of 30 min, the samples were analyzed by HPLC with a Supelguard column (20 × 4.6 mm, 10 μm, flow rate 1.0 mL/min) using a linear gradient 95% A to 40% A in 15 min [A, 2-propanol/0.1% trifluoroacetic acid (TFA) (10/90); B, 2-propanol/0.1% TFA (90/10)].

Alternatively, the HPLC analyses were carried out with a PRP-3 column (Hamilton, 150 × 4 mm, 10 μm, flow rate 1.0 mL/min) using a linear gradient system [*t* (min)/% B]: 5/0, 10/70, and 5/70 of 10 mM phosphate buffer (PBS) of pH 7.4 (A) and acetonitrile (B).

Biodistribution Studies. The animal studies in male Wistar rats (5−6 weeks old) were carried out according to the relevant national regulations. A total of 500 μL of ^{99m}Tc complex solution (saline, propylene glycol 25%) was injected into the tail vein of rats. After the injection, the rats were sacrificed by heart puncture under ether anaesthesia 5 and 120 min p.i.. Selected organs were isolated for weighing and counting. The accumulated radioactivity in the tissue of organs were calculated in terms of percentage of injected dose per organ as well as percent injected dose per gram blood.

RESULTS AND DISCUSSION

Rhenium Chemistry. The dithioether ligands L^1 to L^5 listed in Scheme 1 are able to bind to the Re(I) core. Except for L^1, the ligands are equipped with functional groups such as hydroxy, carboxylic, and propargylic groups to bind a biomolecule.

Scheme 1

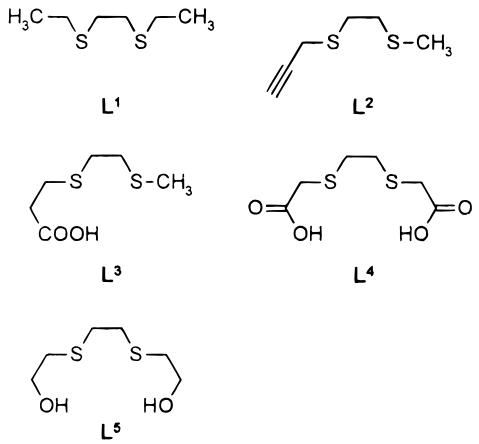

Scheme 2

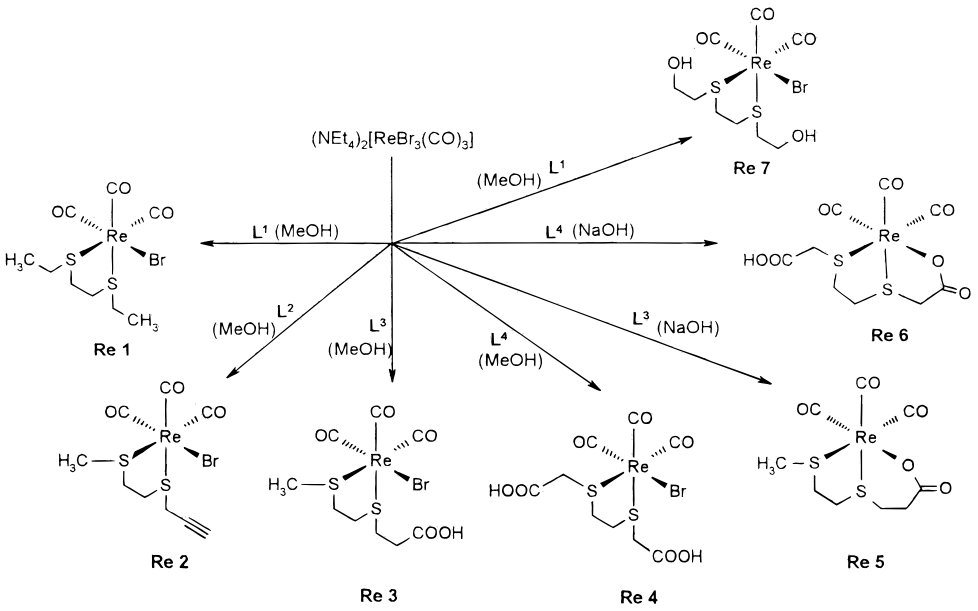

The rhenium complexes have been synthesized as fully characterized surrogates for the analogous ^{99m}Tc complexes prepared at the no-carrier-added level. Coinjections of couples of Re and ^{99m}Tc compounds into HPLC under various elution conditions should confirm the structural similarity of both substances.

The mixed halide/carbonyl complex $(NEt_4)_2[ReBr_3(CO)_3]$ proved to be a very useful starting material and was used as the most convenient source of the "fac-Re$(CO)_3$" fragment in the reaction with thioether ligands. In solution, a complete exchange of the three bromine ligands by solvent molecules was observed (*25*−*27*). The reaction of the resulting species $[Re(CO)_3(solv)_3]^+$ with different thioether ligands leads to complexes **Re1**−**Re5** and **Re7** of the general formula $[ReBr(CO_3)L_2]$ (Scheme 2). The compounds precipitated from the reaction mixtures as white powders and elemental analyses are in good agreement with the proposed formulations.

As can be seen from Scheme 2, in methanol the functional groups do not participate in the coordination. Consequently, only the two sulfur atoms and the three carbonyl ligands are involved beside the remaining bromo ligand.

The attachment of the bromotricarbonyl rhenium(I) core through the dithioether sulfur leads to a rhenium(I) chelate in which the metal is a stereogenic center. Furthermore, the coordination of the prochiral thioether sulfur also results in the formation of stereogenic sulfur donor atoms. The formation of stereoisomers during the complexation reflects a general feature of the dithioether-carbonyl design when a nonsymmetrical dithioether is used. So the complexes **Re2**, **Re3**, **Re5**, and **Re6** occur as isomeric mixtures.

The infrared spectra of **Re1**−**Re4** and **Re7** show strong absorption bands at 2032, 1940, and 1900 cm^{-1}, indicating an approximate C_S symmetry of the complexes (*51*).

^{1}H NMR spectra are negligible because of the overlap of methylene protons leading to complicated signal patterns.

Table 2. Selected Bond Length (Å) and Angles (deg) of Complexes Re2, Re6, and Re8

Re2	Re6	Re8[a]
Re−C1 1.92(2)	Re−C(1) 1.932(8)	Re−C1 1.889(10)
Re−C2 1.903(13)	Re−C(2) 1.914(7)	Re−C2 1.942(10)
Re−C3 1.903(13)	Re−C(3) 1.912(7)	Re−C3 1.922(10)
Re−S12 2.474(3)	Re−S(15) 2.458(2)	Re−S14 2.456(2)
Re−S15 2.463(3)	Re−S(18) 2.507(2)	Re−S17 2.483(2)
Re−Br 2.641(2)	Re−O(11) 2.149(5)	Re−O11 2.193(5)
C1−Re−C2 89.3(6)	C(3)−Re−C(2) 90.1(3)	C1−Re−C2 88.6(4)
C1−Re−C3 90.0(6)	C(3)−Re−C(1) 88.5(3)	C1−Re−C3 88.3(4)
C1−Re−S12 174.7(4)	C(2)−Re−C(1) 89.6(3)	C1−Re−S14 97.8(3)
C1−Re−S15 90.7(5)	C(3)−Re−O(11) 96.7(2)	C1−Re−S17 95.5(2)
C1−Re−Br 95.9(4)	C(2)−Re−O(11) 171.9(2)	C1−Re−O11 176.4(3)
C2−Re−C3 91.2(5)	C(1)−Re−O(11) 94.9(2)	C2−Re−C3 89.9(4)
C2−Re−S12 95.2(4)	C(3)−Re−S(15) 92.1(2)	C2−Re−S14 173.4(3)
C2−Re−S15 179.4(4)	C(2)−Re−S(15) 95.0(2)	C2−Re−S17 93.4(2)
C2−Re−Br 86.5(4)	C(1)−Re−S(15) 175.4(2)	C2−Re−O11 94.7(3)
C3−Re−S12 92.7(4)	O(11)−Re−S(15) 80.5(13)	C3−Re−S14 91.8(3)
C3−Re−S15 89.4(4)	C(3)−Re−S(18) 175.7(2)	C3−Re−S17 175.1(3)
C3−Re−Br 173.7(4)	C(2)−Re−S(18) 93.2(2)	C6−Re−O21 93.5(3)
S12−Re−S15 84.69(11)	C(1)−Re−S(18) 94.3(2)	S24−Re−S27 84.97(7)
S12−Re−Br 81.61(9)	O(11)−Re−S(18) 79.8(13)	S24−Re−O21 78.7(2)
S15−Re−Br 92.89(8)	S(15)−Re−S(18) 84.79(5)	S27−Re−O21 84.3(2)

[a] Two crystallographically independent molecules are contained in the asymmetric unit of the triclinic unit cell. Since there are no significant differences in the observed bond lengths and angles, only the values of one arbitrarily chosen individuum is discussed

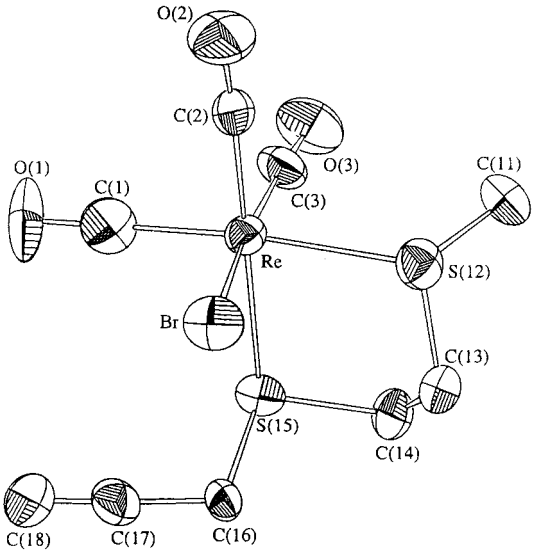

Figure 1. Moleculare structure of complex **Re2**.

As a prototypic representative of this type of Re compound, complex **Re2** was studied by X-ray diffraction analysis. Selected bond lengths and angles are listed in Table 2.

As illustrated in Figure 1, the molecular structure of **Re2** exhibits a slightly distorted octahedron with facial coordination of the carbonyl ligands. The Re−C distances [Re−C(1) = 1.92 Å, Re−C(2) = 1.90 Å, Re−C(3) = 1.90 Å] are found in the range normal for this type of complexes (1.89−1.91 Å) (*29*, *52*). Likewise, the Re−Br bond length is normal with 2.64 Å. The Re−S distances of 2.46 and 2.47 Å are comparable with other thioether-containing rhenium complexes (*54*, *55*). An alternative coordination of the C−C triple bond (*53*, *54*) is not observed.

A rather unexpected coordination behavior of the potentially tetradentate ligand 3,6-dithia-1,6-octanediol (L^5) was observed with the trinitrato precursor complex $[Re(NO_3)_3(CO)_3]^{2-}$. It is available by treatment of $(NEt_4)_2[ReBr_3(CO)_3]$ with an aqueous $AgNO_3$ solution and subsequent precipitation of the halogen atoms as AgBr (see Scheme 3). Here, the ligand exchange reaction of L^5 with $[Re(NO_3)_3(CO)_3]^{2-}$ in THF led to the cationic complex **Re8**, showing the coordination of one hydroxy group.

Scheme 3

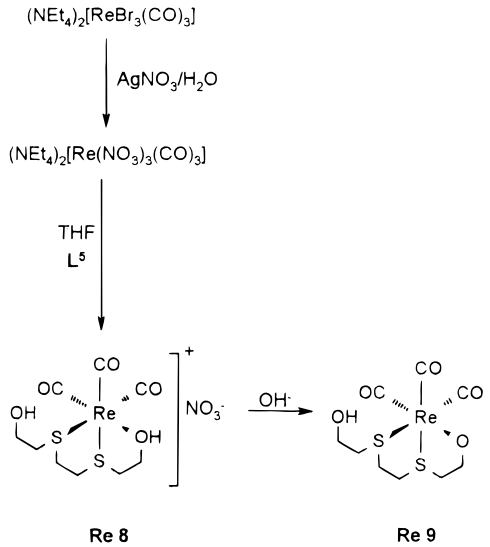

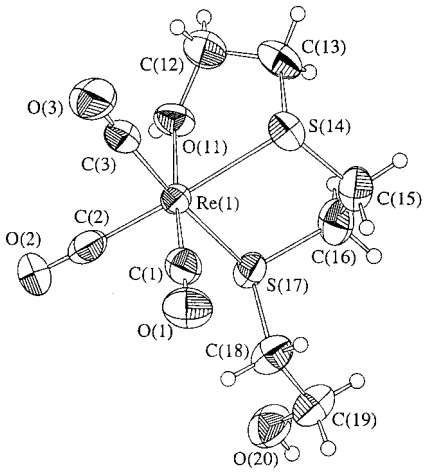

Figure 2. Moleculare structure of complex **Re8**.

Re8 of the formula $[Re(CO)_3(OHSSOH)]NO_3$ has been characterized by correct elemental analysis, infrared spectroscopy, capillary electrophoresis, and X-ray diffraction.

The infrared spectrum of **Re8** is very similar to those of complexes **Re1** and **Re2** but has an additional band at 1384 cm^{-1}, indicating the N−O vibration of the nitrate counterion.

Capillary electrophoretic investigations in aqueous solution confirm the cationic charge of **Re8** in neutral solution. In alkaline medium (pH > 9), the hydroxy group deprotonates resulting in the formation of a neutral species of the proposed structure **Re9**.

The molecular structure of **Re8** shows the coordination of a hydroxy group at the rhenium center (Figure 2). Despite considering the lengthening of the Re−O(11) bond by the trans influence of the CO ligand, the distance of 2.19 Å is too long to be an alcoholato coordination, which is expected to be between 1.91 and 1.95 Å for a chelating OSS ligand in an oxorhenium(V) complex (*55*). With 2.161 Å, it is comparable with the ethanol coordination observed in $(NEt_4)[Re(NO)Br_4(EtOH)]$ (*56*). All the other distances are similar to those found in complex **Re1** described above (Table 2).

Ligand exchange reaction of the carboxylic group bearing ligands L^3 and L^4 with $(NEt_4)_2[ReBr_3(CO)_3]$ in water and with equimolar amounts of NaOH led to the complexes **Re5** and **Re6** in which the original bromide is replaced by the carboxylic group. The compounds precipitate from water and are practically unsoluble in all common organic solvents except DMSO. The elemental analyses show the absence of bromine.

In the infrared spectra the absorption of the coordinating carbonyls is positioned at 2032, 1930, and 1900 cm^{-1}. The vibration band of the carboxylic group is found at 1632 cm^{-1}, i.e., 55 cm^{-1} lower than for the CO moiety of the ligands. This indicates the coordination of the deprotonated carboxylic group at the metal center completing the octahedral structure. The X-ray structure analysis of complex **Re6** confirms this interpretation.

As illustrated in Figure 3, the rhenium atom is centered in a distorted octahedron with facial coordination of the carbonyl ligands. The oxygen of one of the terminal carboxylic groups coordinates in trans position to the third carbonyl ligand. The second carboxylic group remains noncoordinated and offers an ideal site for functionalization or coupling a biomolecule.

Technetium-99m Chemistry. *No-Carrier-Added Preparation of the ^{99m}Tc Complexes.* The no-carrier-added

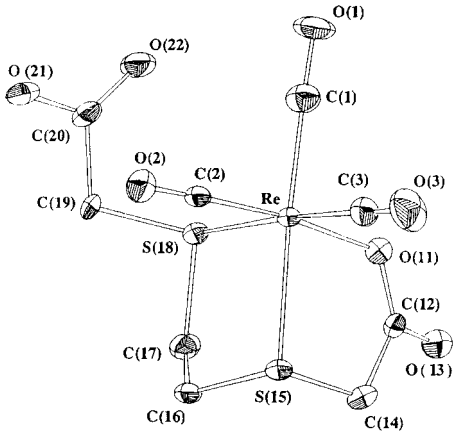

Figure 3. Moleculare structure of complex **Re6**.

preparation of the neutral ^{99m}Tc(I) carbonyl thioether complexes **Tc1**−**Tc4** could be performed with yields up to 90% using optimized preparation conditions (Scheme 4).

To establish the structure of the ^{99m}Tc complexes prepared at tracer level, comparison by HPLC with the respective rhenium complexes prepared in macroscopic amounts was pursued applying parallel radiometric and photometric detection.

Thus, after coinjection of complexes **Tc1** and **Re1**, practically identical retention times were observed, while the recovery through the column was quantitative. Similarly, coinjections of the complex couples **Tc2**/**Re2**−**Tc6**/**Re6** led to identical R_t values for the respective compounds, revealing their structural analogy. R_t values of HPLC and partition coefficients (*P*) in the system octanol/saline are given in Table 3.

As described above for the analogous rhenium complexes **Re3**−**Re6**, ligand exchange reaction of the carboxylic group bearing ligands L^3 and L^4 with $[^{99m}Tc(H_2O)_3(CO)_3]^+$ led to the formation of two ^{99m}Tc complex species in dependence on the reaction conditions. In acidic aqueous solution, complexes **Tc3** and **Tc4** containing a noncoordinated carboxylic group were formed. After neutralization of the reaction mixtures, ligand exchange reactions could be observed leading to the species **Tc5** and **Tc6** both with a coordinated carboxylic group.

In contrast to the tridentate-coordinated compounds **Tc5** and **Tc6**, which are stable during HPLC separation, ligand exchange reaction of the chlorine containing species **Tc3** and **Tc4** has to be suppressed by adding a saturated NaCl solution to the HPLC eluates.

Table 3. HPLC Data of Re and ^{99m}Tc Complexes; Hypersil ODS: MeOH/0.01 M PBS pH 7.4, Linear Gradient 50 to 100 % A in 5 min

complex	R_t (min)	log *P* (octanol/saline)
Re1	7.6	
Tc1	7.7	0.86
Re2	6.7	
Tc2	6.7	0.75
Re3	3.3	
Tc3	3.2	nd
***Re4**	10.5	
***Tc4**	10.6	nd
Re5	6.5	
Tc5	6.5	0.41
***Re6**	11.4	
***Tc6**	11.5	−1.8

* For complex couples **Tc4/Re4** and **Tc6/Re6**, the following gradient was used: (1) 5 min 0% A; (2) linear gradient 0 to 100% A in 5 min.

*Stability of the Chlorine Containing ^{99m}Tc Complex **Tc1** in Aqueous Solution.* The behavior of the chlorine containing ^{99m}Tc complex **Tc1** in aqueous neutral solutions such as 0.1 M phosphate buffer and saline at physiological pH value was investigated. Here, **Tc1** serves as prototypical representative of Tc carbonyl complexes with bidentately coordinated thioethers without additional donor atom in the chelating unit.

In saline, the chromatographically separated compound is stable for at least 120 min. However, in chloride-free aqueous solution, a water-coordinated cationic species of the proposed composition $[^{99m}Tc(H_2O)(CO)_3L_1]^+$ **Tc1a** occurs (Scheme 5). Thus, for biodistribution and plasma-binding studies, the complexes were used in a solution of 0.9% sodium chloride containing 25% propylene glycol for better solubility of the lipophilic products.

Since **Tc1a** was not eluable from the Hypersil column, a Supelguard column with the elution conditions of protein binding studies was used (see Experimental Section). So, it was possible to eluate also the cationic complex **Tc1a** and to observe the time course of the conversion (Figure 4).

The cationic charge of the conversion product was confirmed by paper electrophoresis (Figure 5) as well as by capillary electrophoresis.

The ligand-exchange reaction leading to the cationic complex **Tc1a** proved to be reversible. After complete

Scheme 4

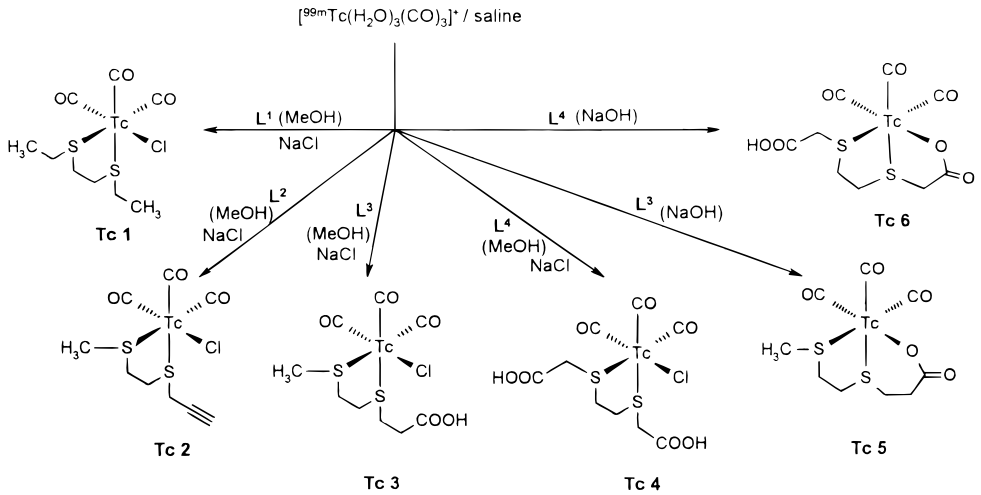

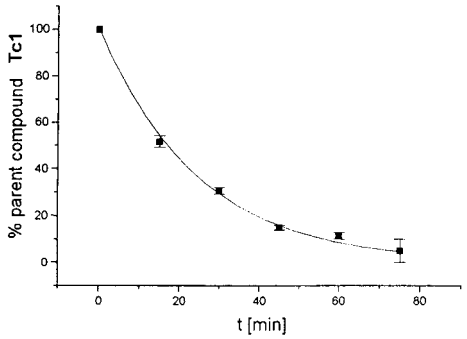

Figure 4. Time course of conversion of the complex **Tc1** into the complex **Tc1a** in a solution of 45% H_2O/45%MeOH/10% propylene glycol.

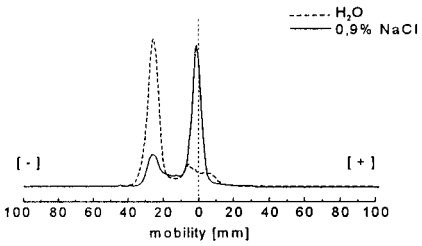

Figure 5. Mobility of **Tc1a** in the electrical field (paper electrophoresis).

Scheme 5

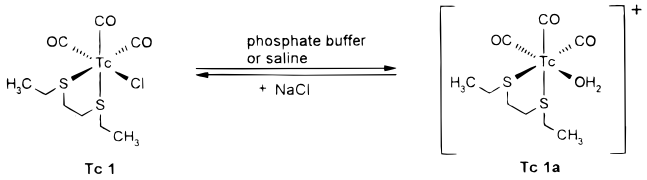

turnover of the parent compound into the cationic species, the parent compound can be reconstituted by an excess of sodium chloride (Figure 6). Obviously, the ligand exchange occurs only on the position of the chlorine atom, and the cationic species is the complex which does exist in an aqueous solution without excess of chloride ions.

In phosphate buffer, the conversion of complex **Tc1** is reversible, too, and the parent compound can be reconstituted by an excess of sodium chloride. The reversibility of the reaction was also confirmed by paper electrophoresis. Obviously, in phosphate buffer, the chlorine atom can be replaced not only by the water molecule but also by the phosphate ions of the buffer (Figure 7).

*Stability of the Carboxylic Group Bearing ^{99m}Tc Complexes **Tc3**−**Tc6** in Aqueous Solution.* The strong tendency of the carboxylic groups to coordinate the technetium core gives rise to conversion of the initially formed complexes **Tc3** and **Tc4**, which still have the carboxylic group noncoordinated. So, these complexes were converted into the compounds **Tc5** and **Tc6** immediately after HPLC purification. Even in saturated solution of sodium chloride at pH 2.0, this conversion cannot be suppressed completely. It was not possible to obtain the **Tc3** and **Tc4** completely pure and stable for a longer period of time, and therefore, no biodistribution and plasma binding studies were performed.

In contrast, **Tc5** and **Tc6** with a coordinated carboxylic group were stable in all investigated solutions at least for 120 min. Capillary electrophoretical studies of the complex couple **Tc3**/**Tc5** support the assumption that the chloride ligand in the above described complexes of the general formula [^{99m}TcCl(CO)$_3$L] is responsible for their

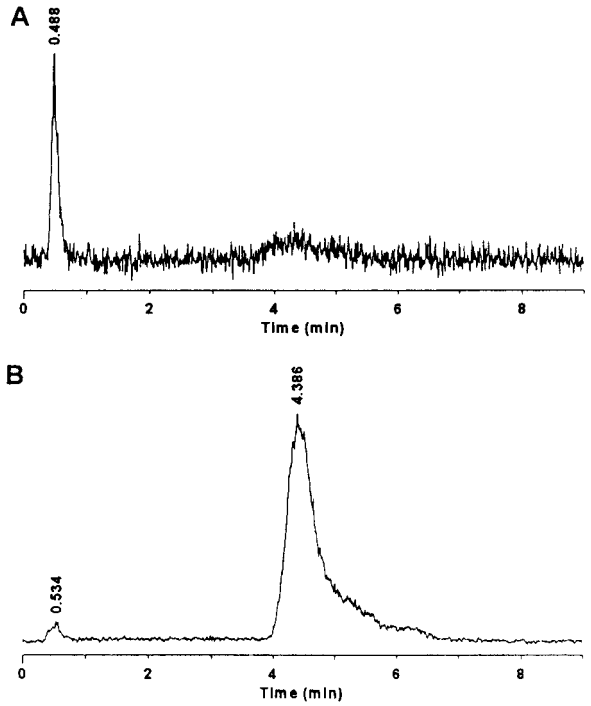

Figure 6. HPLC pattern (radioactivity trace) of complex **Tc1** (Supelguard column). (A) After 120 min incubation in water; (B) parent compound **Tc1** reconstituted with NaCl after incubation in water for 120 min.

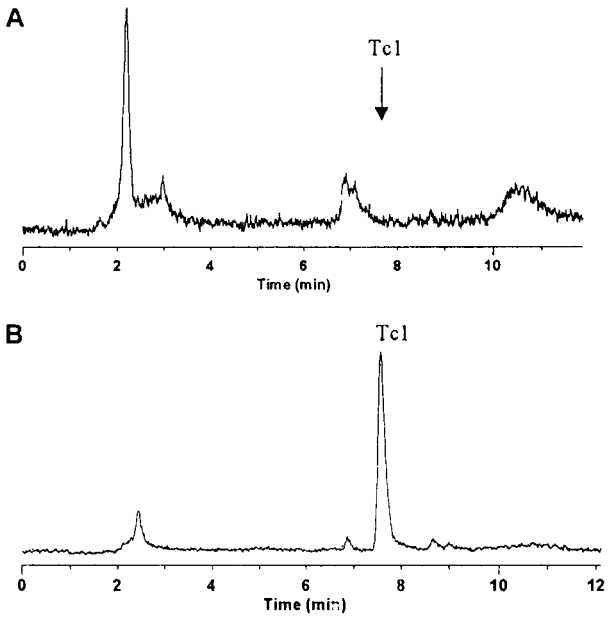

Figure 7. HPLC pattern (radioactivity trace) of complex **Tc1** (Hypersil column). (A) After 120 min incubation in phosphate buffer 0.1 M, pH 7.4; (B) parent compound **Tc1** reconstituted with NaCl after incubation in phosphate buffer for 120 min.

Table 4. HPCE Migration Times of ^{99m}Tc Complexes Tc3 and Tc5 at Various pH values

	acetone mt (min)	complex **Tc3** mt (min)	complex **Tc5** mt (min)
pH 2.5	8.4	8.5	8.3
pH 7.0	8.5	9.7	8.5
pH 9.3	5.3	6.1	5.5

reactivity in aqueous solution (Table 4). **Tc3** was found to be an anionic species in the pH range 9.3−7.0 and a neutral one at pH 2.5, indicating the protonation of the free carboxylic group. **Tc5** is a neutral species over the

Table 5. HPLC Data of ^{99m}Tc Tricarbonyl Complexes Incubated in Rat Plasma 30 min at 37 °C[a]

complex	Supelguard R_t (min) of the parent compound	% protein bound activity after 30 min incubation in rat plasma ($n = 2$)	% parent compound after 30 min incubation in rat plasma ($n = 2$)	complex	Supelguard R_t (min) of the parent compound	% protein bound activity after 30 min incubation in rat plasma ($n = 2$)	% parent compound after 30 min incubation in rat plasma ($n = 2$)
Tc1	4.4	71 ± 2	5 ± 2	**Tc5**	0.5	56 ± 2	44 ± 2
Tc1a	0.5	94 ± 6	6 ± 6	**Tc6**	0.8	31 ± 2	69 ± 2
Tc2	2.9	70 ± 5	7 ± 2				

[a] Supelguard: linear gradient 95% A to 40% A in 15 min [A, isopropanol/0.1% trifluoroacetic acid (TFA) (10/90); B, isopropanol/0.1% TFA (90/10)].

Table 6. Biodistribution Data of Complexes Tc1, Tc2, Tc5, and Tc6 in Male Wistar Rats

complex	time p.i. min	blood % ID/g	brain	heart	lungs % ID	kidneys	liver
Tc1	5	1.01 ± 0.30	1.03 ± 0.25	0.65 ± 0.09	9.19 ± 1.82	5.58 ± 0.57	23.44 ± 3.82
	120	0.71 ± 0.14	0.55 ± 0.08	0.45 ± 0.03	12.12 ± 1.41	5.06 ± 0.55	29.54 ± 3.24
Tc2	5	0.92 ± 0.03	0.78 ± 0.08	0.53 ± 0.05	21.57 ± 3.01	4.83 ± 0.30	24.35 ± 2.13
	120	0.63 ± 0.06	0.55 ± 0.07	0.40 ± 0.03	24.97 ± 1.69	4.66 ± 0.54	27.18 ± 2.58
Tc5	5	1.09 ± 0.25	0.07 ± 0.01	0.56 ± 0.10	1.46 ± 0.26	6.19 ± 0.53	25.01 ± 2.32
	120	0.62 ± 0.06	0.05 ± 0.01	0.30 ± 0.04	0.97 ± 0.07	4.56 ± 0.64	32.37 ± 1.04
Tc6	5	0.91 ± 0.07	0.09 ± 0.01	0.15 ± 0.02	0.70 ± 0.17	8.50 ± 1.09	15.58 ± 1.30
	120	0.25 ± 0.02	<0.05	<0.05	0.14 ± 0.01	1.39 ± 0.06	4.72 ± 0.35

whole pH range showing the same migration time as the neutral marker acetone.

Glutathione Challenge Experiments. Glutathione (GSH), the most abundant thiol compound in tissues, is present in almost all animal cells in relatively high concentrations (0.5−12 mM) (*57*, *58*). Therefore, it has to be considered as a potential agent for transchelating reactions in vivo. In fact, Neirinckx et al. (*59*) pointed out that the intracellular reaction of the brain perfusion agent ^{99m}Tc(V)-HMPAO with GSH is responsible for the trapping of the radiopharmaceutical in the brain. GSH is also responsible for the in vivo reactivity of so-called "3+1" mixed-ligand ^{99m}Tc(V) complexes which consist of a monodentate thiol ligand and a tridentate dithiol (*15*−*18*). Here, a ligand exchange in terms of the replacement of the monodentate ligand by GSH occurs in vivo and in vitro as recently shown (*60*−*62*). In view of these experiences, it would be useful to explore also the behavior of ^{99m}Tc(I) thioether carbonyl complexes against GSH ligand exchange reactions although the difference in the oxidation state (+1 versus +5) does not predispose these complexes for such a ligand exchange.

Saline-containing preparations of the ^{99m}Tc compounds were diluted with a 10 mM GSH solution immediately after HPLC purification. In all cases, no additional peaks, indicating Tc-GSH mixed ligand species, were observed in HPLC studies. In contrast, addition of a 10 mM GSH solution to chlorine-free preparations of **Tc1** and **Tc2** led to the cationic species characterized above.

These results clearly indicate that glutathione has no negative effect on the stability of ^{99m}Tc thioether carbonyl complexes in solutions. Obviously, no transchelation reaction by GSH occurs in vivo. This behavior is considered to be an advantage of the ^{99m}Tc thioether carbonyl complexes over mixed-ligand ^{99m}Tc oxocomplexes in the oxidation state +5.

Biological Evaluation of the ^{99m}Tc Thioether Carbonyl Complexes Tc1, Tc2, Tc5, and Tc6. *In Vitro Plasma Binding.* The neutral complexes **Tc1**, **Tc2**, and **Tc5** exhibit moderate protein binding between 56 and 71%, as determined by HPLC (Table 5). The hydrophilic complex **Tc6** with its ionized carboxylic group has a protein binding of 31% only. Surprisingly, the cationic compound **Tc1a** exhibits the highest protein binding (94%) found among our complexes.

Biodistribution Studies in Rats. All four complexes show similar radioactivity in blood at 5 min p.i., which thereafter decreases within 120 min to a similar extent, except for anionic **Tc6** with its fast clearance (Table 6).

Complexes **Tc1** and **Tc2** showed significant initial brain uptake (1.03 ± 0.25 and 0.78 ± 0.08% ID/organ at 5 min p.i.). This is consistent with the absence of charge of the complexes and their low molecular weight, but astonishing insofar as the octanol/water partition coefficients are as low as log $P = 0.9$ for **Tc1** and log $P = 0.7$ for **Tc2**. The complex **Tc5**, which is also neutral but more hydrophilic (log $P = 0.4$), and the anionic complex **Tc6** (log $P = -1.8$) exhibit only low brain uptake.

Tc1, **Tc2**, and **Tc5** distributed predominantly to the liver with slightly increased retention after 120 min p.i.. It seems that the free carboxylic group in complex **Tc6** leads to significantly lower uptake in heart, lung, and liver with respect to **Tc5**. It also causes a faster clearance and hepatobiliary excretion of the compound.

CONCLUSIONS

Dithioethers containing the small chelating unit −S−CH_2−CH_2−S− are able to form stable technetium(I) and rhenium(I) tricarbonyl complexes. The two residues at the sulfur atoms enable easy functionalization in order to tune physicochemical properties of the complexes or to link the chelate unit to biomolecules. Therefore, we believe that the thioether metallo tricarbonyl complexes may be useful in designing ^{99m}Tc or ^{186}Re/^{188}Re radiopharmaceuticals.

^{99m}Tc complexes can easily be prepared at no-carrier-added level in high radiochemical yield. If neutral complexes are to design, e.g., for CNS receptor imaging, coordinated halide may be an unfavorable characteristic of this class of complexes because possible replacement by water will lead to cationic species. By the introduction of a carboxylic group as third donor group in the chelating ligand molecule, the conversion can be suppressed and thus the neutrality of the complexes preserved. Challenge experiments with glutathione clearly indicate that no transchelation reaction occurs in vivo. This behavior is considered to be an advantage of the ^{99m}Tc thioether carbonyl complexes over mixed-ligand ^{99m}Tc oxocomplexes in the oxidation state +5.

ACKNOWLEDGMENT

Financial support for H.J.P. of the Deutsche Forschungsgemeinschaft is gratefully acknowledged.

LITERATURE CITED

(1) Jurisson, S., Berning, D., Wei, J., and Dangshe, M. (1993) Coordination Compounds in Nuclear Medicine. *Chem. Rev. 93*, 1137−1156.

(2) Reichert, D. E., Lewis, J. S., and Anderson, C. J. (1999) Metal complexes as diagnostic tools. *Coord. Chem. Rev. 184*, 3−66.

(3) Volkert, W. A., and Jurisson, S. (1996) Technetium-99m Chelates as Radiopharmaceuticals. *Topics in Current Chemistry*, Vol. 176, pp 123−148, Springer-Verlag Berlin, Heidelberg..

(4) Schubiger, P. A., Alberto, R., and Smith, A. (1996) Vehicles, Chelators, and Radionuclides: Choosing the "Building Blocks" of an Effective Therapeutic Radioimmunoconjugate. *Bioconjugate Chem. 7* (2), 165−179.

(5) Hom, R., and Katzenellenbogen, J. (1997) Technetium-99m labeled receptor-specific small-molecule radiopharmaceuticals: recent developments and encouraging results. *Nucl. Med. Biol. 24*, 485−498.

(6) Dilworth, J. R., and Parrott, S. (1998) The biomedical chemistry of technetium and rhenium. *Chem. Soc. Rev. 27* (Suppl.), 43−55.

(7) Johannsen, B., and Spies, H. (1996) Tc(V) Chemistry as relevant to Nuclear Medicine. *Topics in Current Chemistry*, Vol. 176, pp 77−121, Springer-Verlag Berlin, Heidelberg.

(8) Zhuang, Z. P., Plossl, K., Kung, M. P., Mu, M., and Kung, H. F. (1999) Neutral and stereospecific Tc-99m complexes: [Tc-99m]N-benzyl-3,4-di-(N-2-mercaptoethyl)-amino-pyrrolidines (P−BAT) *Nucl. Med. Biol. 262*, 217−224.

(9) Chi, D. Y., Neil, J. P. O., Anderson, C. J., Welch, M. J., and Katzenellenbogen, J. A. (1994) homodimeric and heterodimeric bis(amino thiol) oxometal complexes with rhenium(V) and technetium (V). Control of heterodimeric complex formation and an approach to metal complexes that mimic steroid hormones. *J. Med. Chem. 37*, 928−937

(10) O'Neil, J. P., Carlson, K. E., Anderson, C. J., Welch, M. J., and Katzenellenbogen, J. A. (1994) Progestin Radiopharmaceuticals Labeled with Technetium and Rhenium: Synthesis, Binding Affinity, and in Vivo Distribution of a New Progestin N_2S_2-Metal Conjugate. *Bioconjugate Chem. 5*, 182−193.

(11) Meegalla, S., Ploessl, K., Kung, M.-P., Stevenson, D. A., Liable-Sands, L. M., Rheingold, A. L., and Kung, H. F. (1995) First example of a ^{99m}Tc complex as a dopamine transporter imaging Agent. *J. Am. Chem. Soc. 117*, 11037.

(12) Kung, H. F., Kim, H.-J. L., Kung, M.-P., Meegalla, S., Ploessl, K., and Lee, H. K. (1996) Imaging of dopamine transporters in humans with technetium-99m TRODAT-1. *Eur. J. Nucl. Med. 23*, 1527−1530.

(13) Pietzsch, H.-J., Spies, H., and Hoffmann, S. (1989) Lipophilic Technetium Complexes. VI. Neutral Tc(V) complexes with tridentate dithiole/monothiole ligand coordination. *Inorg. Chim. Acta 165*, 163−166.

(14) Pietzsch, H.-J., and Spies, H. (1990) Lipophilic Tc Complexes. VII. Neutral Oxotechnetium(V) Complexes of Tridentate Schiff Bases Containing Monothiols as Co-ligands. *Int. J. Appl. Radiat. Isot. 41*, 185−188.

(15) Spies, H., Fietz, T., Pietzsch, H.-J., Johannsen, B., Leibnitz, P., Reck, G., Scheller D., Klostermann K. (1995) Neutral Oxorhenium(V) Complexes with Tridentate Dithiol Ligands and Monodentate Alkyl/Aryl Thiols as Co-ligands. *J. Chem. Soc., Dalton Trans.* 2277−2280.

(16) Spyriounis, D. M., Pelecanou, M., Stassinopoulou, C. I., Raptopoulou, C. P., Terzis, A., and Chiotellis, E. (1995) Synthesis and characterization of oxotechnetium(V) complexes with aza-substituted 2,6-dimethyl-4-azaheptane-2,6-dithiol ligands and benzyl mercaptan as coligand. *Inorg. Chem. 34*, 1077−1082.

(17) Pirmettis, I. C., Papadopoulos, M. S., and Chiotellis, E. (1997) Novel ^{99m}Tc aminobisthiolato/-monothiolato "3+1" mixed ligand complexes: Structure−activity relationships and preliminary *in vivo* validation as brain blood flow imaging agents. *J. Med. Chem. 40*, 2539−2546.

(18) Seifert, S., Pietzsch, H.-J., Scheunemann, M., Spies, H., Syhre, R., and Johannsen, B. (1998) No carrier added preparations of "3+1" mixed-ligand ^{99m}Tc complexes. *Appl. Rad. Isot. 49*, 5−11.

(19) Wackers, F. J., Berman, D. S., Maddahi, J., Watson, D. D., Beller, G. A., Strauss, H. W., Boucher, C. A., Picard, M., Holman, B. L., and Fridrich, R. (1989) Technetium-99m hexakis 2-methoxyisobutyl isonitrile: human biodistribution, dosimetry, safety, and preliminary comparison to thallium-201 for myocardial perfusion imaging. *J. Nucl. Med., 30*, 301−311.

(20) Wenzel, M., and Saidi, M. (1992) Ester der 99m-Tc markierten Cytectren-Carbonsäure mit Alkoho- len cyclischer Amine als gehirnaffine Radiodiagnostika. *J. Labelled Compd. Radiopharm. 33*, 77−80.

(21) Wenzel, M., Klinge, C., and Saidi, M. (1993) Tc-99m und deuteriummarkierte gehirnaffine Radiodiagnostika. Vergleich von HMPAO mit Cytectren-Derivaten cyclischer Amine *J. Labelled Compd. Radiopharm. 33*, 1040−1051.

(22) Salmain, M., Gunn, M., Gorfti, A., Top, S., and Jaouen, G. (1993) Labeling of proteins by organometallic complexes of rhenium(I). Synthesis and biological activity of the conjugates *Bioconjugate Chem. 4*, 425−433.

(23) Top, S., El Hafa, H., Vessieres, A., Quivy, J., Vaissermann, J., Hughes, D. W., McGlinchey, M. J., Mornon, J. P., Thoreau, E., and Jaouen, G. (1995) Rhenium carbonyl complexes of β-estradiol derivatives with high-affinity for the estradiol receptor: An approach to selective organometallic radiopharmaceuticals. *J. Am. Chem. Soc. 117*, 8372−8380.

(24) Kuntschke, D., Wenzel, M., and Schulze, P. (1995) New [^{99m}Tc]-Cytectrene Amine Compounds as Specific Brain Imaging Agents *J. Labelled Compd. Radiopharm. 36*, 193−203.

(25) Alberto, R., Schibli, R., Egli, A., Schubiger, P. A., Herrmann, W. A., Artus, G., Abram, U., and Kaden, T. A. (1995) Metal carbonyl syntheses XXII. Low-pressure carbonylation of $[MOCl_4]^-$ and $[MO_4]^-$: The Tc(I) and Re(I) compexes $[NEt_4]_2[MCl_3(CO)_3]$. *J. Organomet. Chem. 493*, 119−127.

(26) Alberto, R. (1996) High- and low-valency organometallic compounds of technetium and rhenium. *Topics in Current Chemistry*, Vol. 176, pp 149−187, Springer-Verl., Berlin, Heidelberg.

(27) Egli, A., Hegetschweiler, K., Alberto, R., Abram, U., Schibli, R., Hedinger, R., Gramlich, V., Kissner, R., and Schubiger, P. A. (1997) Hydrolysis of the organometallic aqua ion factriaquatricarbonylrhenium(I). Mechanism, pK(a), and formation constants of the polynuclear hydrolysis products. *Organometallics 16*, 1833−1840.

(28) Alberto, R., Schibli, R., Abram, U., Egli, A., Knapp, F. F., and Schubiger, P. A. (1997) Potential of the "$[M(CO)_3]^{+}$" (M = Re, Tc) moiety for the labeling of biomolecules. *Radiochim. Acta 7*, 999−103.

(29) Alberto, R., Schibli, R., Angst, D., Schubiger, P. A., Abram, U., Abram, S., and Kaden, T. A. (1997) Application of technetium and rhenium carbonyl chemistry to nuclear medicine. *Trans. Met. Chem. 22*, 597−601.

(30) Alberto, R., Schibli, R., Schubiger, P. A., Abram, U., and Kaden, T. A. (1996) Reactions with the technetium and rhenium carbonyl complexes $(NEt_4)_2[MX_3(CO)_3]$. Synthesis and structure of $[Tc(CN-Bu^t)_3(CO)_3](NO_3)$ and $(NEt_4)[Tc_2(\mu\text{-}SCH_2CH_2OH)_3(CO)_6]$. *Polyhedron 15*, 1079−1089.

(31) Abram, U., Abram, S., Alberto, R., and Schibli, R. (1996) Ligand exchange reactions starting from $[Re(CO)_3Br_3]^{2-}$. Synthesis, characterization and structures of rhenium(I) tricarbonyl complexes with thiourea and thiourea derivatives. *Inorg Chim Acta 248*, 193−202.

(32) Abram, U., Abram, S., Schibli, R., Alberto, R., and Dilworth, J. R. (1998) Synthesis and structures of technetium-(I) and rhenium(I) tricarbonyl complexes with bis(diphenylthiophosphoryl)amide, $\{M(CO)_3[(Ph_2PS)_2N](CH_3CN)\}$ (M = Tc, Re). *Polyhedron 17*, 1303−1309.

(33) Alberto, R., Schibli, R., Egli, A., Abram, U., Abram, S., Kaden, T. A., and Schubiger, P. A. (1998) Steps towards $[(C_5Me_5)TcO_3]$: Novel synthesis of $[(C_5Me_5)Tc(CO)_3]$ from [{Tc-

(μ_3-OH)$(CO)_3\}_4$] and oxidation of [$(C_5Me_5)M(CO)_3$] (M = Tc, Re) with Br_2. *Polyhedron 17*, 1133−1140.
(34) Alberto, R., Schibli, R., Egli, A., Schubiger, A. P., Abram, U., and Kaden, T. A. (1998) A novel organometallic aqua complex of technetium for the labeling of biomolecules: Synthesis of [Tc-99m$(OH_2)_3(CO)_3]^+$ from [(TcO_4)-Tc-99m]$^-$ in aqueous solution and its reaction with a bifunctional ligand. *J. Am. Chem. Soc. 120* (31), 7987−7988.
(35) Alberto, R., Schibli, R., Schubiger, A. P., Abram, U., Pietzsch, H. J., and Johannsen, B. (1999) First application of fac-[Tc-99m$(OH_2)_3(CO)_3]^+$ in bioorganometallic chemistry: Design, structure, and *in vitro* affinity of a 5-HT_{1A} receptor ligand labeled with Tc-99m. *J. Am. Chem. Soc. 121* (25), 6076−6077.
(36) Schibli, R., Katti, K. V., Higginbotham, C., Volkert, W. A., and Alberto, R. (1999) In vitro and in vivo evaluation of bidendate, water-soluble phosphine ligands as anchor groups for the organometallic fac-[$^{99m}Tc(CO)_3]^+$-core. *Nucl. Med. Biol. 26*, 711−716.
(37) Spradau, T. W., and Katzenellenbogen, J. A. (1998) Protein and peptide labeling with (Cyclopentadienyl)tricarbonyl rhenium and technetium. *Bioconjugate Chem. 96*, 765−772.
(38) Spradau, T. W., and Katzenellenbogen, J. A. (1998) Ligands for the estrogen receptor, containing cyclopentadienyltricarbonylrhenium units. *Bioorg. Med. Chem. Lett. 822*, 3235−3240.
(39) Murray, S. G., and Hartley, F. R. (1981) Coordination chemistry of thioethers, selenoethers and telluroethers in transition-metal complexes. *Chem. Rev. 81*, 365−414.
(40) Abel, E. W., Corben, E., Moss, I., Orrell, K. G. N., Richardson, R., and Sik, V. (1998) The synthesis and dynamic behaviour of halogenotricarbonylrhenium(I) complexes of some sterically hindered dithioethers. *J. Organomet. Chem. 344*, 343−350.
(41) Abel, E. W., Orrell, K. G., Poole, M. C., and Sik, V. (1995) Conformational studies of transition metal carbonyl Complexes of 1,5-dithiacyclooctane. *Polyhedron 14*, 585−597.
(42) Schibli, R., Alberto, R., Abram, U., Abram, S., Egli, A., Schubiger, P. A., and Kaden, T. A. (1998) Structural and Tc-99 NMR investigations of complexes with fac-[$Tc(CO)_3]^+$ moieties and macrocyclic thioethers of various ring sizes: Synthesis and X-ray structure of the complexes fac-[Tc(9-ane-S-3)$(CO)_3$]Br, fac-[Tc_2(tosylate)$_2$(18-ane-S-6)$(CO)_6$], and fac-[Tc_2(20-ane-S-6-OH)$(CO)_6$][tosylate]$_2$. *Inorg. Chem. 37* (14), 3509−3516.
(43) Reisgys, M., Wüst, F., Alberto, R., Schibli, R., Schubiger, P. A., Pietzsch, H.-J., Spies, H., and Johannsen, B. (1997) Synthesis of rhenium(I) and technetium(I) carbonyl/dithioether ligand complexes bearing 3, 17β-estradiol. *Bioorg. Med. Chem. Lett. 17*, 2243−2246.
(44) Wüst, F., Carlson, K. E., Katzenellenbogen, J. A., Spies, H., and Johannsen, B. (1998) Synthesis and binding affinities of new 17α-substituted estradiol rhenium n+1 mixed-ligand and thioether-carbonyl complexes. *Steroids 63* (12), 665−671.
(45) Hoepping, A., Reisgys, M., Brust, P., Seifert, S., Spies, H., Alberto, R., and Johannsen, B. (1998) TROTEC-1, a new high-affinity ligand for labeling of the dopamine transporter. *J. Med. Chem. 41*, 4429−4432.
(46) Beger, J., and Neumann, R. (1989) Mehrfunktionelle neutrale Komplex-Liganden mit Oximend gruppen. *J. Prakt. Chem. 331*, 354−360.
(47) Hawkes, M. J., and Ginsberg, A. P. (1969) Dianionic rhenium carbonyl halides. *Inorg. Chem. 10*, 2189−2195
(48) Jankowsky, R., Friebe, M., Noll, B., and Johannsen, B. (1999) Determination of dissociation constants of ^{99m}Technetium radiopharmaceuticals by capillary electrophoresis. *J. Chromatogr. A 833*, 83−96.
(49) Sheldrick, G. (1986) SHELXS-86 − A program for the solution of crystal structures, University of Göttingen, Germany.
(50) Sheldrick, G. (1993) SHELXL-93 − A program for the refinement of crystal structures, University of Göttingen, Germany.
(51) Hieber, W., and Rohm, W. (1969) Reaktionsweisen von Rheniumpentacarbonylchlorid mit zweizähligen schwefelorganischen *Liganden Chem. Ber. 102*, 2787−2803.
(52) Adams, R. D., and Falloon, S. B. (1995) Catalytic cyclooligomerization of thietane by dirhenium carbonyl complexes. *Organometallics 14*, 1748−1755.
(53) Casey, C. P., Carino, R. S., and Sakaba, H. (1997) Reaction of Cp*$(CO)_2$Re═Re$(CO)_2$Cp* with Alkynes Produces Dimetallacyclopentenones Cp*$(CO)_2$Re(−1,3-CR═CR′CO)Re(CO)-Cp* Which React with Acid To Form Cationic Bridging Vinyl Complexes, *Organometallics 16* (3), 419−426.
(54) Casey, C. P., Carino, R. S., Sakaba, H., and Hayashi, R. K. (1996) Ligand Additions to Cp*$(CO)_2$Re═Re$(CO)_2$Cp* and Fragmentation and Rearrangement Reactions of Cp*$(CO)_2$Re-(−CO)Re(CO)(L)Cp*, *Organometallics 15* (11), 2640−2649.
(55) Refosco, F., Tisato, F., Bandoli, G., Bolzati, C., Dolmella, A., Moresco, A., and Nicolini, M. (1993) Coordination of (o-Aminophenyl)diphenylphosphine in complexes containing the $[M(V)═O]^{3+}$ (M═Tc or Re) core *J. Chem. Soc., Dalton Trans.* 605−618.
(56) Ciani, G., Giusto, D., Manassero, M., and Sansoni, M. J. (1975) Nitrosyl complexes of rhenium. Crystal and molecular structures of the tetraethylammonium salts of tetrabromoethanol-(nitrosyl)rhenate(II) and acetonitriletetrabromo(nitrosyl)rhenate(II). *J. Chem. Soc., Dalton Trans.* 2156−2161.
(57) Kosower, E. M. (1976) Chemical properties of glutathione. In *Glutathione: Metabolism and Function* (Arias, J. M., and Jakoby, W. B. Eds.) Raven Press, New York.
(58) Sies, H. (1989) Zur Biochemie der Thiolgruppe: Bedeutung des Glutathions. *Naturwissenschaften 76*, 57−64.
(59) Neirinckx, R. D., Burke, J. F., Harrison, R. C., Forster, A. M., Andersen, A. R., and Lassen, N. (1998) The retention mechanism of technetium-99m HMPAO: intracellular reaction with glutathione. *J. Cereb. Blood Flow Metab. 8*, 4−12.
(60) Syhre, R., Seifert, S., Spies, H., Gupta, A., and Johannsen, B. (1998) Stability versus reactivity of "3+1" mixed-ligand technetium-99m complexes *in vitro* and *in vivo*. *Eur. J. Nucl. Med.* 793−796.
(61) Pelecanou, M., Pirmettis, I. C., Nock, B. A., Papadopoulos, M., Chiotellis, E., and Stassinopoulou, C. I. (1998) Interaction of [ReO(SNS)(S)] and [^{99m}Tc(SNS)(S) mixed ligand complexes with glutathione: isolation and characterization of the product. *Inorg. Chim. Acta 281*, 148−152.
(62) Nock, B. A., Maina, T., Yannoukakos, D., Ioannis, C., Papadopoulos, M., and Chiotellis, E. (1999) Glutathione-mediated metabolism of technetium-99m SNS/S mixed ligand complexes: a proposed mechanism of brain retention. *J. Med. Chem. 42*, 1066−1075.

BC990162O

Poly(ethylene glycol)-Conjugation and Deoxygenation Enable Long-Term Preservation of Hemoglobin-Vesicles as Oxygen Carriers in a Liquid State

Hiromi Sakai, Ken-ichi Tomiyama, Keitaro Sou, Shinji Takeoka, and Eishun Tsuchida*,†

Department of Polymer Chemistry, Advanced Research Institute for Science and Engineering, Waseda University, Tokyo 169-8555, Japan. Received December 7, 1999; Revised Manuscript Received February 11, 2000

The stability of hemoglobin vesicles (HbV) as an oxygen infusion was tested during the storage for 1 year at 4, 23, and 40 °C. The surface of the HbV was modified with poly(ethylene glycol) (PEG), and the suspension was deoxygenated with nitrogen bubbling. The samples stored at 4 and 23 °C showed a stable dispersion state for 1 year, though the sample stored at 40 °C showed the precipitation and decomposition of vesicular components, a decrease in pH, and 4% leakage of total Hb after 1 year. The PEG chains on the vesicular surface stabilize the dispersion state and prevent the aggregation and fusion due to their steric hindrance. The original metHb content (ca. 3%) before the preservation gradually decreased to less than 1% in all the samples after 1 month due to the presence of homocysteine inside the vesicles which consumed the residual oxygen and gradually reduced the trace amount of metHb. The rate of metHb formation was strongly dependent on the partial pressure of oxygen, and no increase in metHb formation was observed due to the intrinsic stability of the deoxygenated Hb. Preservation at 4 and 23 °C slightly reduced P_{50} (increased the oxygen affinity) from 38 Torr to 32 and 31 Torr, respectively. These results indicate the possibility that HbV suspension can be stored at room temperature for at least 1 year.

INTRODUCTION

The advantages and/or requirements of hemoglobin (Hb)[1]-based oxygen carriers are the absence of a blood type antigen and infectious virus, and stability for long-term storage. These characteristics will make it possible to use the oxygen carriers in emergency situations without blood type matching and virus tests. In this sense, infusion of oxygen carriers becomes superior to the conventional blood transfusion which still has the potential of mismatching, infection such as HIV, and hepatitis, and graft versus host disease, and the problems of only a few weeks of preservation period.

Phospholipid vesicles encapsulating concentrated Hb (Hb-vesicles, HbV) have been studied as an oxygen carrier (Tsuchida, 1998), and their sufficient oxygen-transporting ability comparable with blood has been clarified (Djordjevici et al., 1987; Rudolph, 1997; Izumi et al., 1996). Even though HbV has not yet been clinically tested, it most closely reproduces some characteristics of natural red blood cells such as the cell membrane function of physically preventing direct contact of Hb with the components of blood and vasculature during circulation (Sakai et al., 2000a). Particularly, in the clinical trials of acellular modified Hbs, they have shown dose-dependent hypertension as a consequence of vasoconstriction, a well-known mechanism of trapping of endothelium-derived relaxation factor (NO) by Hb due to its intrinsic high affinity. On the other hand, Hb encapsulation suppresses NO binding, thus hypertension is not observed (Sakai et al., 2000b).

Since Hb autoxidizes to form metHb and loses its oxygen-binding ability during storage as well as in blood circulation, the prevention of metHb formation is required (Takeoka et al., 1997a,b; Sakai et al., 1994; D'Agnillo and Chang, 1998). The conventional long-term preservation methods are to store modified Hbs in a frozen state or to store them as a freeze-dried powder with some cryoprotective or lyoprotective agents such as saccharides or polyols (Matsumura et al., 1992; Kerwin et al., 1998). Some groups have recently reported the method to preserve deoxygenated Hbs in a liquid state (Kerwin et al., 1999; Gawryl et al., 1997; Kander et al., 1997), using the well-known intrinsic characteristic of Hb that the Hb oxidation rate in a solution is dependent on the oxygen partial pressure and deoxyHb essentially is not autoxidized at ambient temperature (Levy et al., 1988; Balagopalakrishna, 1996; Sakai et al., 1994; Takeoka et al., 1997a).

In the case of Hb-vesicles, not only the inside Hb but also the cellular structure has to be physically stabilized in order to prevent intervesicular aggregation, fusion, and leakage of encapsulated Hb and other reagents. Phospholipid vesicles are molecular assemblies and generally regarded as unstable capsules which require some reinforcement. We studied the γ-ray polymerization in the bilayer membranes of phospholipids bearing dienoyl groups, and the resulting polymerized phospholipid membrane significantly stabilized the Hb-vesicles (Tsuchida et al., 1992; Hosoi et al., 1997; Satoh et al., 1992). The polymerized vesicles preserved the particle diameter and function of the inside Hb even after 10 repeated freeze−thawings and freeze−dryings and rehydrations (Wang et

* To whom correspondence should be addressed. Phone: +81-3-5286-3120. Fax: +81-3-3205-4740. E-mail: eishun@mn.waseda.ac.jp.

† CREST investigator, JSTC.

[1] Abbreviations: Hb, hemoglobin; HbV, Hb-vesicles; PEG, poly(ethylene glycol); PEG-HbV, PEG-modified HbV; PLP, pyridoxal 5′-phosphate; Hcy, homocysteine; PBS, phosphate-buffered saline; P_{50}, O_2 affinity; TLC, thin-layer chromatography; LC-MS, liquid chromatography−mass spectroscopy.

10.1021/bc990173h CCC: $19.00 © 2000 American Chemical Society
Published on Web 04/21/2000

al., 1992a; Sakai et al., 1992). However, the relatively slow rate of metabolism of the polyphospholipid in the reticuloendothelial systems is considered to be a problem. Cryoprotection and lyoprotection of the Hb-vesicles were performed by the addition of saccharides such as trehalose (Rudolph and Cliff, 1990) or glycolipid (Sakai et al., 1995). However, preservation of the oxygen carriers in a liquid state may be more useful for infusion in emergency situations than the time-consuming procedures such as redissolving the Hb powder or thawing several hundreds milliliters of the frozen Hb solution stored in a freezer.

Surface modification of phospholipid vesicles with the poly(ethylene glycol) (PEG)-conjugated lipid is a well-known method to prolong the circulation time of the vesicles in vivo for drug delivery systems (Woodle and Lasic, 1992; Klibanov et al., 1990). For HbV, the surface of HbV was also modified with PEG chains to improve its dispersion state of the vesicles when mixed with blood components (Yoshioka, 1991). The PEG-modified HbV has shown an improved blood circulation and tissue oxygenation due to the absence of HbV aggregate formation and viscosity elevation (Sakai et al., 1997, 1998) and prolonged circulation persistence in vivo (Phillips et al., 1999). However, little attention has been paid to the ability of PEG modification for the long-term preservation of vesicles or liposomes in the liquid state (Singh et al., 1999; Meyer et al., 1998). In this report, we studied the possibility of the long-term preservation of Hb-vesicles by the combination of two technologies, e.g., surface modification of HbV with PEG chains and deoxygenation.

MATERIALS AND METHODS

Preparation of Poly(ethylene glycol) (PEG)-Modified Hb-Vesicles (HbV). PEG-modified HbV was prepared as previously reported in the literature (Takeoka et al., 1996; Sakai et al., 1997). Hb was purified from outdated donated blood provided by the Hokkaido Red Cross Blood Center, Japan (Sakai et al., 1996). The encapsulated carbonylhemoglobin (HbCO, 38 g/dL) contained 5.9 mM of pyridoxal 5′-phosphate (PLP, Merck, NJ) as an allosteric effector at a molar ratio of PLP/Hb = 3, and homocysteine (Hcy, 5 mM, Aldrich) as a reductant. The lipid bilayer was composed of Presome PPG-I [a mixture of 1,2-dipalmitoyl-*sn*-glycero-3-phosphatidylcholine (DPPC), cholesterol, and 1,2-dipalmitoyl-*sn*-glycero-3-phosphatidylglycerol (DPPG) at a molar ratio of 5/5/1 (Nippon Fine Chem. Co., Osaka)]. The HbCO solution and the lipids were mixed and stirred for 12 h at 4 °C. The resulting multilamellar vesicles were extruded through membrane filters using Remolino (Millipore, MA) with the pore size of the final membrane filter being 0.22 μm (Fuji Film Co., Tokyo). After washing with saline, the surface of the HbV was modified with PEG (M_r 5 kDa, 0.3 mol % of the lipids in the outer surface of vesicles) using 1,2-distearoyl-*sn*-glycero-3-phosphatidylethanolamine-*N*-PEG (Sunbright DSPE-50H, H-form, NOF Co., Tokyo), where succinic acid cross-links PEG and DSPE. The acyl chains of PEG-DSPE are inserted into the lipid bilayer of HbV by mixing an HbV suspension with a saline solution of PEG-DSPE at 37 °C for 2 h. After decarbonylation (HbCO → HbO2) (Chung et al., 1995), the resulting PEG-modified HbV was ultracentrifuged to remove any unintroduced PEG-lipid and redispersed in a 20 mM phosphate buffered saline (PBS) at the Hb concentration of 10 g/dL. The suspension was then filtered through sterilizable filters (pore size, 0.45 μm; DISMIC-25, Toyo Roshi Co., Tokyo).

Deoxygenation and Storage. One milliliter of the HbV suspension (oxy form) was sealed in a 10 mL volume of a glass vial with a butyl rubber stopper and an aluminum cap. Deoxygenation was performed by a N_2 bubbling (13 mL/min for 120 min) and the oxygen partial pressure (P_{O_2}) was reduced to less than 1 Torr which was monitored with a Clark-type O_2 electrode (needle type, 0.2 mm in diameter, Intermedical Co., Tokyo). Eighteen vials were separated into three groups and stored either in a refrigerator (4 °C), in a room (23 ± 2 °C), or in an incubator (40 °C). The time points were 1 week, 1, 2, 3, and 6 months, and 1 year of preservation. Each indivisual temperature/time point was evaluated with one vial. After opening the vials, the samples were stored in a freezer (−80 °C) until the lipid analyses. The other analyses described below were carried out soon after completion of the preservation.

Dispersion State, Turbidity, UV−Vis Spectroscopy, Particle Size, and pH. The bottom of the vials was carefully observed visually to confirm whether the HbV was precipitated. A sample solution (30 μL) was diluted 10 times with saline, and the turbidity was measured at 900 nm using an UV−vis spectrophotometer (V-560, Jasco, Tokyo). A sample was diluted 100 times, and the absorption spectrum (300−900 nm) was measured to confirm whether the spectrum had changed. Particle sizes were measured by a light-scattering method (Coulter particle analyzer, model N4SD, Coulter Corporate Communications, FL). PEG-unmodified vesicles, which did not encapsulate Hb (plain empty vesicles), were prepared, and their dispersion state was also measured for 3 months for comparison with the PEG-modified HbV. For the pH measurements, a pH electrode (SE1700GC, Toyo Rika Co., Tokyo) was dipped in a sample suspension of about 0.1 mL in a plastic tube.

Leakage of Hb. An HbV sample of 0.2 mL was diluted 200 times with PBS and ultracentrifuged (100000*g*, 15 min). The Hb concentration in the supernatant was calculated from the absorption at $\lambda_{max} = 415$ nm and its molar absorption coefficient of Hb ($\epsilon = 125\,000\ M^{-1}\,cm^{-1}$).

Oxygen Affinity. Oxygen affinity (P_{50}), Hill number, and oxygen transporting efficiency (oxygen saturation difference of Hb between $P_{O_2} = 40$ and 110 Torr) were calculated from an O_2 equilibrium curve obtained with a Hemox Analyzer (TCS Medical Products, PA). An HbV sample was diluted with a Hemox solution, and a measurement was performed at 37 °C.

MetHb Content. About 5 μL of each HbV sample was diluted with 3 mL of PBS in an UV cuvette. Deoxygenation of the sample using N_2 bubbling resulted in the presence of only deoxyHb and metHb. The percentage of metHb was calculated from the calibration curve which was obtained from the ratio of absorbance at 405 nm (metHb) and 430 nm (deoxyHb) in the Soret band and the mixing ratio of deoxyHbV and metHbV (Hamada et al., 1995). This method does not need to destroy the HbV particles.

Amount of PEG Attached to the HbV. Each HbV sample solution of 0.2 mL was freeze-dried and redissolved into $CDCl_3$ to extract the lipid components and measure the ^{1}H NMR (JNM-LA500, JEOL, Tokyo). The PEG content in the suspension was calculated from the intensity ratio of the PEG methylene proton peak (δ 3.63 ppm) to that of the choline methyl protons in DPPC (δ 3.39 ppm) (Yoshioka, 1991; Hamada et al., 1995). To estimate the dissociated PEG from the surface, the HbV suspension was ultracentrifuged (100000*g*, 15 min) to remove the dissociated PEG, and the precipitate was treated in the same manner.

Qualitative Analysis of Lipids by Two-Dimensional Thin-Layer Chromatography. The freeze-dried HbV samples were dissolved in chloroform and spotted on a corner of a silica gel plate (Silica 60, Merck, 10 × 10 cm). A mixed solvent of chloroform/methanol/28% aqueous ammonia = 13/7/1 by volume was used as the first eluent, and a mixed solvent of chloroform/acetone/methanol/acetic acid/water = 10/4/2/2/1 by volume was used as the second eluent. After drying the plate, it was stained with iodine. To identify the positions of the lipid components, solutions of DPPC, DPPG, cholesterol, dipalmitoylglycerol, and palmitic acid were also tested.

Liquid Chromatography−Mass Spectrometry of Lipids. The decomposition of the lipid components was analyzed with the liquid chromatography−mass spectrometry system (LCMS-QP8000α, Shimadzu Co., Kyoto), which was equipped with atmospheric pressure chemical ionization (APCI) and a gel permeation chromatographic column (Asahipak GF-310HQ, 7.6 mm i.d. × 300 mm, Shodex, Tokyo). The HbV sample solutions of about 0.2 mL were freeze-dried, and the resulting powder was dispersed in chloroform and then filtered. Two microliters of the samples solutions was injected and developed with methanol as the eluent. The flow rate was 0.5 mL/min, and the temperature was maintained at 40 °C with a column oven. In the mass spectroscopic system, the gas flow rate was 2.5 L/min, the applied voltage was 3.5 kV, and the CDL temperature was 250 °C. The range of molecular mass for the detection was *m*/*z* 200−1200. The scan speed was 2.0 s/scan. To identify the elution times of the components, solutions of DPPC, DPPG, cholesterol, and PEG-DSPE were also tested.

Chemical Stability of Pyridoxal 5′-Phosphate (PLP) and DL-Homocysteine (Hcy) and PLP Leakage from Vesicles. PLP was dissolved in PBS (pH 7.4) at a concentration of 4.65 mM. The solution was sealed in three vials and bubbled with N_2 for deoxygenation, and then preserved at 60, 67, and 82 °C to accelerate the decomposition. Periodically, for 2 days 200 μL of the sample solution was diluted with 2.5 mL of PBS and UV−vis spectral changes were monitored. PLP has been reported to decompose to pyridoxal and phosphate anion (Peterson and Sober, 1954; Middleton, 1986). Using the molar coefficients of PLP and pyridoxal at $\lambda_{max} = 388$ nm, ($\epsilon = 4900$ and 200 M^{-1} cm^{-1}, respectively), the rates of decomposition at the three temperatures were obtained, and from the Arrhenius plots, the decomposition rates at 4, 23, and 40 °C were estimated.

A phospholipid vesicle suspension encapsulating only PLP (without Hb) was prepared in the same manner as described above with a PLP solution (18.6 mM in PBS, pH 7.4) and the same lipid components. The unencapsulated PLP was removed by ultracentrifugation (300000*g*, 30 min), and then the surface of the vesicles was modified with PEG. No presence of PLP in the outer aqueous phase was confirmed by the UV−vis spectrum of the supernatant solution. The suspensions (lipid concentration = 1 g/dL) were separated and sealed in two vials and bubbled with N_2 for deoxygenation, and then preserved at 40 and 60 °C to accelerate the PLP leakage across the bilayer membrane. Periodically, for 3 days a portion of each suspension was ultracentrifuged, and the concentration of PLP in the supernatant was measured with absorption at $\lambda_{max} = 388$ nm ($\epsilon = 4900$ M^{-1} cm^{-1}). The initial rates of PLP leakage at the two temperatures were obtained, and the rates at 4 and 23 °C were estimated from the Arrhenius plots.

Hcy was dissolved in saline at a concentration of ca. 10 mM with a pH regulation to 7.0 with 0.1 N NaOH. The solution was sealed in a vial and bubbled with N_2, and then preserved at 40 °C to accelerate decomposition. After 3 days and 1, 2, 3, and 4 weeks, the thiol group in Hcy was quantitatively measured using an *N*-ethylmaleimide method (Morell et al., 1964).

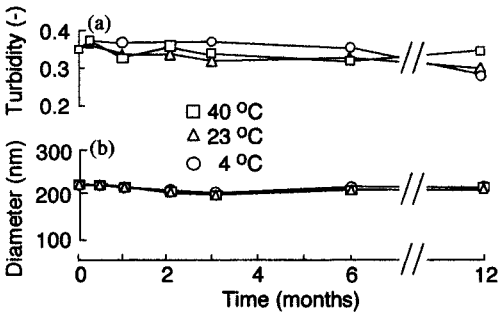

Figure 1. Changes in dispersion state of PEG-modified HbV during preservation at 4, 23, and 40 °C for 1 year. (a) Turbidity of 10 times diluted samples at 900 nm. (b) Mean diameter changes measured with a Coulter particle analyzer.

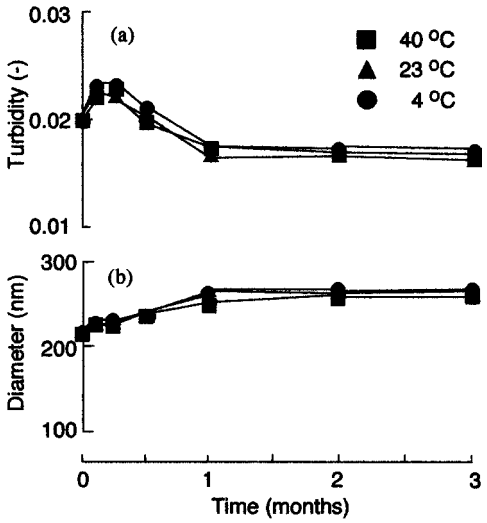

Figure 2. Changes in dispersion state of empty vesicles which were not modified with PEG chains during preservation at 4, 23, and 40 °C for 3 months. (a) Turbidity of 10 times diluted samples at 900 nm. (b) Mean diameter changes measured with a Coulter particle analyzer.

RESULTS

Dispersion State. The diameter of the PEG-modified HbV was originally 222 ± 62 nm, and there was no significant mean diameter changes throughout the preservation period in all the samples (Figure 1). The turbidity change was minimal, and no precipitate was observed for the samples of every storage period and temperature. Conversely, the unmodified plain empty vesicles stored at all temperatures started to aggregate after 3 days, which was confirmed with the increase in mean diameter to 265 nm after 1 month (Figure 2), with precipitates at the bottom of the vials, and with a turbidity increase. The initial turbidity increase is due to the increase in the diameter by aggregation or fusion, and the succeeding decrease is due to the precipitation of the aggregates. The vesicles stored at 4 °C showed slightly lager changes in diameter and turbidity because aggregation was enhanced at lower temperature.

UV−Vis Spectrum and Oxygen Affinities. The results of the absorption spectra before and after preservation as the absorption maximum in the Soret and Q-bands are summarized in Table 1. There are no

Table 1. Spectrophotometric Properties, P_{50}, pH, and Hb Leakage of HbV after Preservation

preservation condition		Q-band (nm) α	Q-band (nm) β	Soret band (nm) γ	P_{50} (Torr)	pH	leaked Hb (%)
4 °C	6 months	575	539	415	36		0
	12 months	575	539	415	32	7.20	0
23 °C	6 months	574	539	416	34		0
	12 months	575	539	415	31	7.01	0
40 °C	6 months	574	537	416	33		0
	12 months	575	536	415	43	6.01	4
before preservation		575	538	415	38	7.38	0

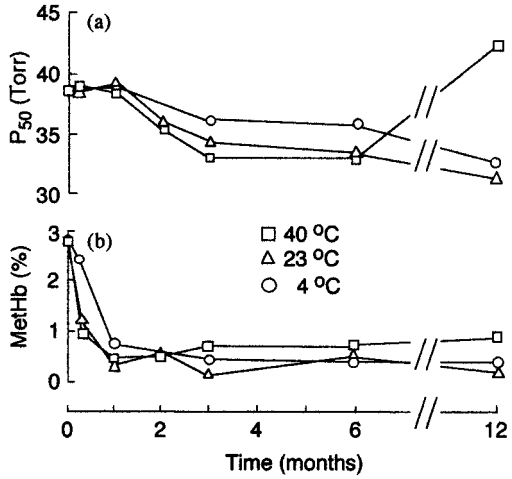

Figure 3. Changes in the parameter of oxygen-binding properties of HbV during preservation at 4, 23, and 40 °C for 1 year. (a) oxygen affinity, P_{50}, and (b) metHb content.

significant differences after preservation under all conditions. All the samples showed the typical spectrum of HbO_2 with turbidity due to the nature of the vesicle suspension.

The original oxygen affinity (P_{50}) of HbV just after preparation was 38 Torr at 37 °C, which was regulated by coencapsulation of pyridoxal 5′-phosphate (PLP) at a molar ratio of 3 to 1 Hb molecule. The P_{50} value gradually decreased with the preservation period depending on the temperature as shown in Figure 3a. The HbV stored at 40 °C showed a larger decrease in P_{50} to 33 Torr at 3 months. The HbV stored at 4 °C showed a slight decrease to 36 Torr. From 3 months until 6 months, the change was not significant. As for the HbV stored at 23 °C, P_{50} decreased to 35 Torr after 3 months and then gradually to 33 Torr. After 1 year, only the HbV stored at 40 °C reversely showed a significant increase in P_{50} to 43 Torr.

pH of the HbV Suspensions. The pH of the HbV suspension was originally 7.38 at 37 °C, which was regulated with PBS (Table 1). After the storage at 4 and 23 °C for 1 year, the pH value slightly decreased to 7.20 and 7.07, respectively. On the other hand, the sample stored at 40 °C for 1 year had a pH decrease to 6.01.

Leakage of Hb. The supernatant obtained after ultracentrifugation of the HbV suspension stored at 4 and 23 °C for 1 year did not show absorption attributed to Hb. On the other hand, HbV stored at 40 °C for 1 year showed 4% Hb leakage (Table 1).

MetHb Content. The metHb content was originally 2.9%. The metHb of all the preservation temperatures had decreased to less than 1% after 1 month (Figure 3b). Preservation at higher temperature showed faster decrease in metHb content; therefore, the reduction of metHb by Hcy would be temperature dependent.

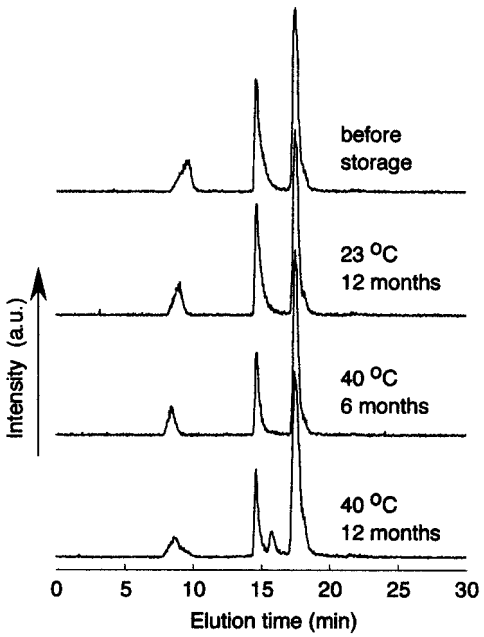

Figure 4. The LC-MS elution profiles of the lipid components of the HbV before and after the preservation. The peaks at around 9.0, 14.5, and 17.5 min correspond to DPPG, DPPC, and cholesterol, respectively. The HbV stored at 40 °C for 1 year showed another peak at 15.8 min indicating lipid decomposition.

Amount of PEG Attached to the HbV. Six percent of the PEG chains on the surface was detached from the surface after 6 months of preservation at 40 °C. On the other hand, the samples stored at 4 and 23 °C did not show any detectable detachment of PEG chains.

Two-Dimensional Thin-Layer Chromatography of Lipids. Cholesterol appeared on a silica gel plate at roughly R_{f1} (R_f of the first dimension) = 0.9 and R_{f2} (R_f of the second dimension) = 0.8−0.9. DPPC and DPPG appeared at (R_{f1}, R_{f2}) = (0.6−0.7, 0.4−0.6). The generation of hydrolytic fragments of phospholipids, dipalmitoyl glycerol and palmitic acid, which should appear at (R_{f1}, R_{f2}) = (0.3, 0.9−1.0) and (0.6−0.8, 0.8−0.9), respectively, were qualitatively detected in the samples stored at 40 °C for 1 year. However, other samples stored at 4 °C and 23 °C did not show any fragments of these lipids.

Liquid Chromatography−Mass Spectrometry (LC-MS) of Lipids. In Figure 4 are shown the elution profiles detected by mass spectroscopy of the lipid components extracted from the freeze-dried HbV samples. In the elution curve of the HbV before preservation (top), the peaks at around 9.0, 14.5, and 17.5 min correspond to DPPG, DPPC, and cholesterol, respectively. The samples stored at 23 °C for 1 year and at 40 °C for 6 months showed identical elution curves with that of before preservation, indicating that the lipid decomposition was minimal. Only the sample stored at 40 °C for 1 year showed the generation of a new peak at 15.8 min, and an increased shoulder at 18.0 min.

In the mass spectrum, DPPG (MW = 723) decomposes during the ionization, and shows *m*/*z* 551, which might be the result of the removal of the phosphoglycerol group (e.g., dipalmitoylglycerol − OH), and *m*/*z* 313 and 314, which would correspond to monopalmitoylglycerol. The LC-MS peak of DPPC (MW = 735) showed fragments of *m*/*z* = 721 (M − CH_3 + H), the peak *m*/*z* = 551, which might be the result of the removal of the phosphocholine group as seen in DPPG, *m*/*z* = 464 for lysophosphocho-

line, and $m/z = 313$ and 314 which would correspond to monopalmitoylglycerol. The peak of cholesterol (MW = 386) mainly showed m/z 369 (M − HO), 370 (M − HO + H, or M − CH_3 − H), and 383 (M − 3H). We have confirmed that the elution time of PEG-DSPE was almost identical to that of DPPG. Due to the significantly small amount of PEG-DSPE (less than 5 wt % of total lipid), the mass spectrum did not indicate the typical periodic fragments of the PEG chains. The mass spectrum of the new peak at 15.8 min for HbV stored at 40 °C for 1 year (Figure 4, bottom) showed m/z 313, 551, etc., the fragments present in the peak of DPPG and DPPC. Therefore, the new peak may correspond to dipalmitoyglycerol as a result of cleavage of phosphate ester bond of DPPC and/or DPPG during preservation. A shoulder on the right side of the peak of cholesterol, at the elution time of 18.0 min, did not show m/z 383 (M) but only 367 and 368. Therefore, this component may correspond to derivatives of cholesterol deprived of a hydroxyl or methyl group. The shoulder at 18 min increased slightly, indicating that a small portion of cholesterol was modified.

Chemical Stabilities of PLP and Hcy, and PLP Leakage from Phospholipid Vesicles. During the incubation of PLP solution at high temperatures, the UV−vis spectrum of PLP slightly changed: a decrease in the absorption at $\lambda_{max} = 388$ nm, and the emergence of a new peak at $\lambda_{max} = 318$ nm. This is due to the generation of pyridoxal as a result of hydrolysis of the phosphate ester bond of PLP. The decomposition rate constants (k_d) of PLP at 60, 67, and 82 °C were clarified to be 8.7×10^{-4}, 1.9×10^{-3}, and 1.2×10^{-2} h^{-1}, respectively. From the Arrhenius plots of these rate constants, the relationship between temperature and decomposition rate was obtained as $\ln k_d = -1.44 \times 10^4 (1/T) + 36.2$. From this equation, the k_d values at 4, 23, and 40 °C were estimated as 1.3×10^{-7}, 3.7×10^{-6}, and 5.2×10^{-5} h^{-1}, respectively, and the amounts of hydrolyzed PLP after 1 year can be estimated as 0.1, 2.3, and 33.7%, respectively.

The leakage of PLP from phospholipid vesicles was temperature dependent. The initial rate constants (k_l) of the PLP leakage from the vesicles at 40 and 60 °C were 2.6×10^{-4} and 6.7×10^{-3} h^{-1}, respectively. From the Arrhenius plots of these rate constants, the relationship between temperature and rate of PLP leakage was obtained as $\ln k_l = -1.7 \times 10^4 (1/T) + 45.5$. From this equation, the k_l values at 4 and 23 °C were estimated as 2.4×10^{-7} and 1.2×10^{-5} h^{-1}, respectively. The percentages of PLP leakage from vesicles (without Hb) after 1 year at 4, 23, and 40 °C can be estimated as 0.2, 10.2, and nearly 100%, respectively.

The initial content of the SH group in Hcy was 98%, which slightly decreased to 95% after 4 weeks of preservation at 40 °C in an anaerobic condition. This is significantly slower than that in an aerobic condition which showed about 10% of Hcy oxidation at 37 °C in 1 h (Takeoka et al., 1997a).

DISCUSSION

Our principal finding is that a phospholipid vesicle suspension, which had been regarded to be very unstable, can be stored for more than 1 year at ambient temperature without a significant diameter change and leakage of the encapsulated Hb. This stability was obtained by surface modification of the vesicles with PEG by inserting a PEG-conjugated phospholipid. Plain vesicles (without PEG modification) are negatively charged [ζ potential = −21 mV (Sakai et al., 1996)] due to the presence of DPPG and repulse each other, thus there seems to be no aggregation originally. However, the plain vesicles started to aggregate after 3 days, which was confirmed by the diameter and turbidity changes as shown in Figure 2. Aggregation and fusion are triggers to release the encapsulated solutes. PEG chains on the vesicular surface should suppress intervesicular aggregation and then fusion due to the steric hindrance, thus the stable dispersion state is preserved, and Hb leakage was not detected.

The PEG modification on the surface of the phospholipid vesicles has been widely studied clinically as the stealth liposomes for the carriers of antitumor drugs (Coukell and Spencer, 1997; Uziely et al., 1995) with the aim to prolonged circulation time in the blood stream by evading the reticuloendothelial system (mononuclear phagocytic system) and to increase the opportunities of contact with tumors. In these studies, the dose rates are generally low. On the other hand, infusion of the HbV suspension results in replacing a large volume of blood with the HbV suspension which influences the hemorheological property. We have reported the importance of PEG modification to improve the peripheral blood flow by suppressing the intervesicular aggregation of the HbV and by reducing the solution viscosity (Sakai et al., 1997, 1998). In this study, we have confirmed another advantage of the PEG modification, namely, the effectiveness of the PEG modification for the preservation of the phospholipid vesicles at ambient temperature. Two groups have quite recently shown that the PEG modification of liposomes is effective for stabilization during storage, though they evaluated the stability only for several weeks at low temperature such as 4 °C (Meyer et al., 1998; Singh et al., 1999). Conversely, we clarified the stability of the PEG-modified vesicles even at 40 °C for 6 months and at 4 and 23 °C for 1 year.

We have studied the influence of the acyl chain length of the PEG-lipids on its incorporation ratio into the outer surface of the vesicles. PEG-DSPE showed a higher incorporation ratio than PEG-DPPE, and it remained in the bilayer membrane longer (Sou et al., 2000). PEG-chain is conjugated to phosphatidylethanolamine via an amide and an ester bonds with succinic acid, which are susceptible to hydrolysis. Actually, 6% of the total amount of PEG on the vesicular surface was dissociated after 6 months of preservation at 40 °C. However, this level of PEG loss does not affect the dispersion state of the vesicles. It has been reported that PEG does not show immunogenicity, and it is finally excreted in urine through kidneys (Yamaoka et al., 1994). Another kind of PEG-DSPE, where PEG and DSPE are bound through a urethane bond, is more resistant to hydrolysis and would show better results. A confirmation study is underway.

Generally, the decomposition of the lipid components may be caused by lipid peroxidation and the hydrolysis of ester bonds (Szebeni et al., 1985; Grit and Crommelin, 1993). Deoxygenation of the suspension may be effective to prevent the oxidation of the lipid components in the case of unsaturated phospholipids (Szebeni et al., 1985). Lipid peroxidation may not be a serious problem in our system because we use saturated phospholipids. However, the hydrolysis of the components is inevitable, primarily at the ester bonds in DPPC and DPPG. The hydrolysis is significantly dependent on the solution pH and temperature, and the conditions of lower temperature and neutral pH (around 6−7) show the lowest rate of hydrolysis. The two-dimensional TLC and LC-MS in our study revealed the phospholipid decomposition after

1 year storage at 40 °C, which should be the cause of the significant decrease in pH from 7.38 to 6.01. On the other hand, we could not detect phospholipid decomposition in the samples stored at 4 and 23 °C for 1 year, and the pH changes were minimal. A small portion of cholesterol might be deprived of hydroxyl or methyl groups according to the mass spectroscopy of HbV stored at 40 °C for 1 year. Even though the mechanism of this reaction is not known, this is not the product of peroxidation.

Szebeni et al. (1988) reported that cholesterol effectively reduces Hb denaturation (unfolding) caused by electrostatic and hydrophobic interactions with the phospholipid membrane. This effect may partly contribute to the Hb stabilization. We suppose the main cause of the Hb stabilization is deoxygenation. The rate of autoxidation of ferrous Hb (Fe^{2+}) to form ferric Hb (Fe^{3+}) is dependent on the partial pressure of oxygen (Levy et al. 1988, Brantrey et al., 1993; Balagopalakrishna, 1996; Takeoka et al., 1997a), and deoxyHb is essentially not autoxidized in the absence of oxygen. MetHb formation initiates further denaturation of the globin moiety. The deoxygenation makes it possible to preserve the ferrous state and Hb function for a long time. The metHb content, which was originally 2.9% (Fe^{3+}, 0.7 mM inside HbV), was decreased to less than 1% after 1 month. This is due to the reduction of metHb by Hcy coencapsulated at the concentration of 5 mM inside HbV. In our previous paper, Hcy was selected among a series of thiols for the reduction of metHb in HbV in vivo (Takeoka et al., 1997a). Under aerobic conditions, thiols and ascorbic acid react with oxygen to produce active oxygen species which sometimes adversely promote metHb formation (Sampath and Caugey, 1985; Sakai et al., 1994). Kerwin et al. (1999) have used ascorbic acid to preserve the deoxygenated recombinant Hb. However, ascorbic acid is such a strong reductant which promotes metHb formation in the presence of oxygen due to the production of active oxygen species. Hcy, on the other hand, reacts with oxygen relatively slower than cysteine, glutathione, and ascorbic acid, thus Hcy does not produce a large amount of active oxygen species. Under anaerobic conditions, thiols act not only as a reductant for metHb but also as an oxygen-removing agent. This is an additional advantage of coencapsulation of Hcy which we found in this study. We have confirmed the significant stability of the thiol group of Hcy in water at 40 °C for more than 4 weeks in the absence of oxygen. After deoxygenation to less than $P_{O_2} = 1$ Torr, the original contents of Hcy, metHb (heme), and oxygen were about 1.3×10^{-3} M (5×10^{-3}M in HbV), 1.9×10^{-4} M (7.0×10^{-4} M in HbV), and 2×10^{-4} M, respectively. The metHb reduction and oxygen removal should be 99% completed in 1 and 2 days at 37 °C, respectively, or longer at lower temperatures according to a computer simulation (Runge−Kutta method) of the time course of the concentration of each component using the apparent rate constants of Hcy at 37 °C for metHb reduction (0.78 M^{-1} min^{-1}) and thiol oxidation (1.7 M^{-1} min^{-1}) (Takeoka et al., 1997a). The initial rates of metHb reduction (2.1×10^{-4} M/day) and oxygen removal (6.4×10^{-4} M/day) are apparently comparable with the initial contents.

The oxygen affinity (P_{50}) of HbV is regulated by coencapsulation of PLP as an allosteric effector (Wang et al., 1992b). In our study, P_{50} was regulated to 38 Torr by coencapsulating PLP at a molar ratio of 3 to 1 Hb molecule. This was maintained for 1 month at all the temperatures, though after 1 month, it started to decrease and reached 31 Torr. The reduction of the oxygen transporting efficiency (difference in oxygen saturation between $P_{O_2} = 40$ and 110 Torr) was from 46% to about 40%. It was reported that PLP was hydrolyzed to form pyridoxal and the phosphate anion (Peterson and Sober, 1954; Middleton, 1986), and we estimated that the amounts of hydrolyzed PLP at 4, 23, and 40 °C after 1 year should be 0.08, 2.3, and 33.7%, respectively. These calculations indicate that the significantly slow PLP hydrolysis cannot solely explain the reduction of P_{50}, especially at 4 and 23 °C. Another possibility will be the leakage of PLP from vesicles. However, we have clarified that the PLP leakage from vesicles containing only PLP (without Hb) at 4 and 23 °C after 1 year will be 0.2 and 10.2%, respectively, which are significantly slow, and they cannot explain the reduction of the P_{50}. Moreover, in the presence of Hb, PLP is bound to Hb via a Schiff base which contributes to stopping the PLP leakage. Even though Hb and PLP show a significantly slow leakage, the concentrations of the smaller Cl^- or H^+, which affect the oxygen affinity of Hb, may have gradually changed after 6 months by permeation across the bilayer membrane due to the transmembrane differences in crystalloid and colloid osmotic pressures after the HbV preparation (inside vs outside; crystalloid, ca. 50 vs 300 mOsm; colloid, >100 vs 0 Torr). Another possibility will be the reduction of the aldehyde group in PLP in the presence of Hcy to form pyridoxine 5′-phosphate, which does not form a Schiff base resulting in the reduced allosteric effect. Even though the mechanism of P_{50} reduction is not clear at present, the changes are temperature dependent; the lower the temperature, the slower the P_{50} reduction. From 6 months to 1 year, there was a steady period with little change in HbV preserved at 4 °C and 23 °C. In the case of the storage of donated blood, the normal P_{50} value of about 28 Torr was significantly reduced to less than 20 Torr after 3 weeks of preservation due to the hydrolysis of 2,3-diphosphoglyceric acid and reduced glycolytic enzymatic activity at low temperature (Wells et al., 1981), thus the stored red cells soon after the transfusion do not effectively release oxygen until the enzymatic activity was restored. Therefore, the smaller changes in P_{50} observed in HbV preserved at 4 and 23 °C may be advantageous over blood transfusion. The significant increase in P_{50} after 1 year of preservation at 40 °C should be related to the drastic pH reduction inside the vesicles due to the hydrolysis of phospholipids which overwhelms the effects of PLP hydrolysis and leakage in this case.

In conclusion, we have confirmed that PEG modification and deoxygenation make it possible to store an Hb-vesicle suspension at ambient temperature for 1 year. PEG modification prevents intervesicular aggregation and preserves homogeneous dispersion, and deoxygenation prevents metHb formation. Utilization of saturated phospholipids as membrane components and homocysteine as a reductant also contribute to the stability. Generally, phospholipid vesicles are regarded as unstable capsules; however, the establishment of this pivotal technology will enhance the application of PEG-modified vesicles in other fields. The long-term preservation of oxygen carriers overcomes the limitation of the blood transfusion system and will contribute to benefiting clinical medicine.

ACKNOWLEDGMENT

The authors greatly acknowledge Mr. Shin-ichi Kawano (Shimadzu Co.) for measuring the LC-MS of lipid components. H. Sakai is a research fellow of the Japan Health Sciences Foundation. This work has been supported in part by the Health Science Research Grants

(Research on Advanced Medical Technology, Artificial Blood Project), the Ministry of Health and Welfare, Japan.

LITERATURE CITED

Balagopalakrishna, C., Manoharan, P. T., Abugo, O. O., and Rifkind, J. M. (1996) Production of superoxide from hemoglobin-bound oxygen under hypoxic conditions. *Biochemistry 35*, 6393−6398.

Brantley, R. E., Jr., Smerdon, S. J., Wilkinson, A. J., Singleton, E. W., and Olson, J. S. (1993) The mechanism of autoxidation of myoglobin. *J. Biol. Chem. 268*, 6995−7010.

Chung, J. E., Hamada, K., Sakai, H., Takeoka, S., and Tsuchida, E. (1995) Ligand exchange reaction of carbonylhemoglobin to oxyhemoglobin in a hemoglobin liquid membrane. *Nippon Kagaku Kaishi 2*, 123−127 (in Japanese).

Coukell, A. J., and Spencer, C. M. (1997) Poly(ethylene glycol)-liposomal doxorubicin. A review of its pharmacodynamic and pharmacokinetic properties, and therapeutic efficacy in the management of AIDS-related Kaposi's sarcoma. *Drugs, 53*, 520−538.

D'Agnillo, F., and Chang, T. M. S. (1998) Polyhemoglobin-superoxide dismutase-catalase as a blood substitute with antioxidant properties. *Nat. Biotechnol. 16*, 667−671.

Djordjevich, L., Mayoral, J., Miller, I. F., and Ivankovich, A. D. (1987) Cardiorespiratory effects of exchange transfusions with synthetic erythrocytes in rats. *Crit. Care Med. 15*, 318−323.

Gawryl, M. S., Houtchens, R. A., and Light, W. R. (1997) *Method for preserving a hemoglobin blood substitute*, U.S. Patent 5,-691,452.

Grit, M., and Crommelin, D. J. (1993) Chemical stability of liposomes: implications for their physical stability. *Chem. Phys. Lipids 64*, 3−18.

Hamada, K., Kose, T., Ohgushi, T., Sakai, H., Takeoka, S., Nishide, H., and Tsuchida, E. (1995) Assay sytems for the components of red cell substitutes. *Artif. Blood 3*, 96−101 (in Japanese).

Hosoi. F., Omichi, H., Akama, K., Awai, K., Endo, S., and Nakano, Y. (1997) Radiation-induced polymerization of phospholipid mixtures for the synthesis of artificial red blood cells. *Nucl. Instr. Methods Phys. Res. B 131*, 329−34.

Izumi, Y., Sakai, H., Hamada, K., Takeoka, S., Yamahata, T., Kato, R., Nishide, H., Tsuchida, E., and Kobayashi, K. (1996) Physiologic responses to exchange transfusion with hemoglobin vesicels as an artificial oxygen carrier in anesthetized rats: changes in mean arterial pressure and renal cortical tissue oxygen tension. *Crit. Care Med. 24*, 1869−73.

Kandler, R. L., and Spicuzza, J. C. (1994) Stable hemoglobin based composition and method to store same. United States Patent 5,353,773.

Kerwin, B. A., Akers, M. J., Apostol, I., Moore-Einsel, C., Etter, J. E., Hess, E., Lippincott, J., Levine, J., Mathews, A. J., Revilla-Sharp, P., Schubert, R., and Looker, D. L. (1999) Acute and long-term stability studies of deoxy hemoglobin and characterization of ascorbate-induced modifications. *J. Pharm. Sci. 88*, 79−88.

Kerwin, B. A., Heller, M. C., Levin, S. H., Randolph, H. W. (1998) Effects of Tween 80 and scrose on acute short-term stability and long-term storage at −20 °C of a recombinant hemoglobin. *J. Pharm. Sci. 87*, 1062−8.

Klibanov, A. L., Maruyama, K., Torchilin, V. P., and Huang, L. (1990) Amphipathic polyethylene glycols effectively prolongs the circulation time of liposomes. *FEBS Lett. 268*, 235−7.

Levy, A., Zhang, L., and Rifkind, J. M. (1988) Hemoglobin: a source of superoxide radical under hypoxic conditions. *Oxyradicals Mol. Pathol., Proc. Upjohn-UCLA Symp.* 11−25.

Matsumura, S., Yamaji, K., Ohki, H., Kosaka, K., and Iwashita, Y. (1992) Large scale production and characterization of lyophylized pyridoxalated hemoglobin polyoxyethylene (PHP). *Biomater. Artif. Cells Immobilization Biotechnol. 20*, 435−8.

Meyer, O., Kirpotin, D., Hong, K., Sternberg, B., Park, J. W., Woodle, M. C., and Papahadjopoulos, D. (1998) Cationic liposomes coated with polyethyle glycol as carriers for oligonucleotide. *J. Biol. Chem. 273*, 15621−7.

Middleton, H. M. (1986) Intestinal hydrolysis of pyridoxal 5′-phosphate in vitro and in vivo in the rat. Effect of protein binding and pH. *Gastroenterology 91*, 343−50.

Morell, S. A., Ayers, V. A., Grenwalt, T. J., and Hoffman, P. (1964) Thiols of the erythrocyte. *J. Biol. Chem. 239*, 2696−705.

Peterson, E. A., and Sober, H. A. (1954) Preparation of crystalline phosphorylated derivatives of Vitamin B_6. *J. Am. Chem. Soc. 76*, 169−175.

Phillips, W. T., Klipper, R. W., Awasthi, V. D., Rudolph, A. S., Cliff, R., Kwasiborski, V., and Goins, B. A. (1999) Poly-(ethylene glycol)-modified liposome-encapsulated hemoglobin: a long circulating red cell substitute. *J. Pharm. Exp. Ther. 288*, 665−70.

Rudolph, A. S., and Cliff, R. O. (1990) Dry storage of liposome-encapsulated hemoglobin: a blood substitute. *Cryobiology 27*, 585−590.

Rudolph, A. S., Sulpizio, A., Hieble, P., MacDonald, V., Chavez, M., and Feuerstein, G. (1997) Liposome encapsulation attenuates hemoglobin-induced vasoconstriction in rabbit arterial segments. *J. Appl. Physiol. 82*, 1826−35.

Sakai, H., Yuasa, M., Onuma, H., Takeoka, S., and Tsuchida, E. (2000a) Synthesis and physicochemical characterization of a series of hemoglobin-based oxygen carriers: objective comparison between cellular and acellular types. *Bioconjugate Chem. 11*, 56−64.

Sakai, H., Hara, H., Yuasa, M., Tsai, A. G., Takeoka, S., Tsuchida, E., and Intaglietta, M. (2000b) Molecular Dimensions of Hb-based O_2 Carriers Determine Constriction of Resistance Arteries and Hypertension in Conscious Hamster Model. *Am. J. Physiol. (Heart Circ. Physiol.)* (in press).

Sakai, H., Tsai, A. G., Kerger, H., Park, S.-I., Takeoka, S., Nishide, H., Tsuchida, E., and Intaglietta, M. (1998) Subcutaneous microvascular responses to hemodilution with red cell substitutes consisting of polyethylene glycol-modified vesicles encapsulating hemoglobin. *J. Biomed. Mater. Res. 40*, 66−78.

Sakai, H., Takeoka, S., Park, S.-I., Kose, T., Izumi, Y., Yoshizu, A., Nishide, H., Kobayashi, K., and Tsuchida, E. (1997) Surface-modification of hemoglobin vesicles with poly(ethylene glycol) and effects on aggregation, viscosity, and blood flow during 90%-exchange transfusion in anesthetized rats. *Bioconjugate Chem. 8*, 15−22.

Sakai, H., Hamada, K., Takeoka, S., Nishide, H., and Tsuchida, E. (1996) Physical properties of hemoglobin vesicles as red cell substitutes. *Biotechnol. Prog. 12*, 119−25.

Sakai, H., Takisada, M., Chung, J.-E., Takeoka, S., and Tsuchida, E. (1995) Modification of hemoglobin-vesicles with oligosaccharide chains. *Artif. Organs Today 4*, 309−16.

Sakai, H., Takeoka, S., Seino, Y., and Tsuchida, E. (1994) Suppression of methemoglobin formation by glutathione in a concentrated hemoglobin solution and in a hemoglobin-vesicles. *Bull. Chem. Soc. Jpn. 67*, 1120−5.

Sakai, H., Takeoka, S., Yokohama, H., Nishide, H., and Tsuchida, E. (1992) Encapsulation of Hb into unsaturated lipid vesicles and γ-ray polymerization. *Polymer Adv. Technol. 3*, 389−394.

Sampath, V., and Caughey, W. S. (1985) Prooxidant effects of glutathione in aerobic hemoglobin solutions. Superoxide generation from uncoordinated dioxygen. *J. Am. Chem. Soc. 107*, 4076−4078.

Satoh, T., Kobayashi, K., Sekiguchi, S., and Tsuchida, E. (1992) Characteristics of artificial red cells: hemoglobin encapsulated in poly-lipid vesicles. *ASAIO J. 38*, M580−M584.

Singh, M., Ferdous, A. J., and Jackson, T. L. (1999) Stealth monensis liposomes as a potentiator of adriamycin in cancer treatment. *J. Controlled Release 59*, 43−53.

Sou, K., Endo, T., Takeoka, S., and Tsuchida, E. (2000) Poly-(ethylene-glycol)-modification of the phospholipid vesicles by using the spontaneous incorporation of poly(ethylene glycol)-lipid into the vesicles. *Bioconjugate Chem. 11* (in press).

Szebeni, J., Di Iorio, E. E., Hauser, H., and Winterhalter, K. H. (1985) Encapsulation of hemoglobin in phospholipid lipisomes: characterization and stability. *Biochemistry 24*, 2827−932.

Szebeni, J., Hauser, H., Eskelson, C. D., Watson, R. R., Winterhalter, K. H. (1988) Interaction of hemoglobin derivatives with liposomes. Membrane cholesterol protects against the changes of hemoglobin. *Biochemistry 27*, 6425−34.

Takeoka, S., Ohgushi, T., Terase, K., Ohmori, T., and Tsuchida, E. (1996) Layer-controlled hemoglobin vesicles by interaction of hemoglobin with a phospholipid assembly. *Langmuir 12*, 1755−9.

Takeoka, S., Sakai, H., Kose, T., Mano, Y., Seino, Y., Nishide, H., and Tsuchida, E. (1997a) Methemoglobin formation in hemoglobin vesilces and reduction by encapsulated thiols. *Bioconjugate Chem. 8*, 539−44.

Takeoka, S., Ohgushi, T., Sakai, H., Kose, T., Nishide, H., and Tsuchida, E. (1997b) Construction of artificial methemoglobin reduction system in Hb vesicles. *Artif. Cells, Blood Substitutes, Immobilization Biotechnol. 25*, 31−41.

Tsuchida, E., Hasegawa, E., Kimura, N., Hatashita, M., and Makino, C. (1992) Polymerization of unsaturated phospholipids as large unilamellar liposomes at low temperature. *Macromolecules 25*, 207−212.

Tsuchida, E., Ed. (1998) Blood substitutes: present and future perspectives. Elsevier Science, Amsterdam.

Uziely, B., Jeffers, S., Isacson, R., Kutch, K., Wei-Tsao, D., Yehoshua, Z., Libson, E., Muggia, F. M., and Gabizon, A. (1995) Liposomal doxorubicin: antitumor activity and unique toxicities during two complementary phase I studies. *J. Clin. Oncol. 13*, 1777−1785.

Wang, L., Takeoka, S., Tsuchida, E., Tokuyama, S., Mashiko, T., Satoh, T. (1992a) Preparation of dehydrated powder of hemoglobin vesicles. *Polymer Adv. Technol. 3*, 17−21.

Wang, L., Morizawa, K., Tokuyama, S., Satoh, T., and Tsuchda, E. (1992b) Modulation of oxygen-carrying capacity of artificial red cells (ARC). *Polymer Adv. Technol. 4*, 8−11.

Wells, R. M., Hill, R. S., Woodfield, D. G. (1981) Changes of blood oxygen affinity in different CPD solutions during liquid storage. *Transfusion 21*, 709−714.

Woodle, M. C., and Lasic, D. D. (1992) Sterically stabilized liposomes. *Biochim. Biophys. Acta 1113*, 171−199.

Yamaoka, T., Tabata, Y., and Ikada, Y. (1994) Distribution and tissue uptake of poly(ethylene glycol) with different molecular weights after intravenous administration to mice. *J. Pharm. Sci. 83*, 601−606.

Yoshioka, H. (1991) Surface modification of haemoglobin-containing liposomes with poly(ethylene glycol) prevents liposome aggregation in blood plasma. *Biomaterials 12*, 861−864.

BC990173H

Fluorescent-Labeled Poly(ethylene glycol) Lipid Conjugates With Distal Cationic Headgroups

Tao Chen,[†,‡] Kim F. Wong,*[,†] David B. Fenske,[†] Lorne R. Palmer,[†] and Pieter R. Cullis[†,§]

Department of Biochemistry and Molecular Biology, University of British Columbia, 2146 Health Sciences Mall, Vancouver, BC, Canada V6T 1Z3, and Inex Pharmaceuticals Corporation, 100-8900 Glenlyon Parkway, Glenlyon Business Park, Burnaby, BC, Canada V5J 5J8. Received December 7, 1999;
Revised Manuscript Received February 11, 2000

The synthesis of a new class of fluorescent cationic poly(ethylene glycol) lipid conjugates (CPLs) is described. These lipids consist of a hydrophobic distearoyl-phosphatidylethanolamine (DSPE) anchor coupled to a highly fluorescent N_ϵ-dansyl lysine moiety, which is attached to a hydrophilic poly(ethylene glycol) (PEG) spacer that is linked to a cationic headgroup made of lysine residues. Introduction of the dansyl moiety allows rapid and accurate quantification of CPLs within lipid bilayers using fluorescence techniques. The synthetic scheme is straightforward, using repeated amino-carboxyl coupling reaction steps, with purification by precipitation. A series of dansylated CPLs was synthesized with zero, one, three, and seven lysine residues located at the distal end of the PEG chain, giving rise to CPLs with one, two, four, and eight distal positive charges, respectively. The structures of the CPLs were confirmed by ^{1}H NMR spectroscopy and chemical analysis. CPLs provide a means of introducing positive charge to a bilayer that is localized some distance from the membrane surface, and are of particular interest for nonviral gene delivery applications. The usefulness of CPLs is demonstrated by the enhanced in vitro cellular binding and uptake of liposomes containing CPL_4.

INTRODUCTION

To optimize the in vivo delivery of drugs using liposomal systems, general methods are required for increasing the interactions of liposomes with cells. To date, attempts to include specific targeting information on the liposome surface, such as antibody (*1*−*3*), vitamin (*4*−*8*), oligopeptide (*9*, *10*), or oligosaccharide (*10*) constructs specific for a particular membrane protein or receptor, have not been successful in achieving this goal, despite promising in vitro results. Many of these studies utilized poly(ethylene glycol) (PEG)[1] lipids with the ligands attached at the distal end of the PEG spacer, thereby physically removing the ligand from the vesicle surface and above any PEG coating present to impart long circulation lifetime characteristics.

This paper describes the synthesis of a new class of cationic lipids designed to enhance *nonspecific* targeting by increasing the electrostatic attraction between liposomes and cells. Such a role for cationic lipids such as DOTMA (*11*) or DODAC (*12*) has been demonstrated in DNA:liposome transfection complexes. Complexes are large aggregates formed as a result of electrostatic interactions between cationic liposomes and plasmid DNA. The presence of a slight excess of cationic lipid (relative to DNA) gives rise to a net positive charge that enhances interactions with cells. The key feature of the cationic poly(ethylene glycol) lipids (CPLs) described in the present paper is the presence of a multivalent cationic headgroup located at the distal end of a PEG spacer chain, which in turn is anchored in the membrane by attachment to a molecule of distearoyl-phosphatidylethanolamine (DSPE). By varying the length of this chain with respect to that of the surface PEG, it should be possible to achieve placement of the positive charge at some distance from the liposome surface, where interactions with cells would be maximized. The potential utility of CPL in the area of drug delivery may be strongly influenced by the type of lipid anchor, the variation in the chain length of the PEG spacer, and the number of positive charges on the headgroup. The former two parameters have been shown to influence the rate at which PEG-lipids will transfer between membranes (*13*), which could influence circulation longevity. To explore the role of the latter parameter, we have synthesized a series of dansylated CPL with zero, one, three, and seven lysine residues in the headgroup, giving rise to CPL with one, two, four, and eight positive charges, respectively. The presence of the highly fluorescent dansyl group

* To whom correspondence should be addressed. Phone: (604) 822-2649. Fax: (604) 822-4843. E-mail: kimwong@interchange.ubc.ca.

† University of British Columbia.

‡ Current address: Theralipids, Inc., 6100 Royalmount Ave., Montreal, PQ, Canada H4P 2R2.

§ Inex Pharmaceuticals Corporation.

[1]Abbreviations: BHK, baby hamster kidney; tBoc, *tert*-butyloxycarbonyl; tBoc-NH-PEG_{3400}-CO_2-NHS, tBoc protected and NHS activated PEG_{3400}; Chol, cholesterol; CPL, cationic poly(ethylene glycol) lipid conjugate; CPL_1, CPL with one positive charge; CPL_2, CPL with two positive charges; CPL_4, CPL with four positive charges; CPL_8, CPL with eight positive charges; DCC, *N*,*N*′-dicyclohexyl-carbodiimide; DCU, dicyclohexyl urea; DMEM, Dulbecco's Modified Eagle Medium; DODAC, *N*,*N*-dioleoyl-*N*,*N*-dimethylammonium chloride; DOTMA, *N*-[2,3-(dioleyloxy)propyl]-*N*,*N*,*N*-trimethylamine; FBS, fetal bovine serum; NHS, *N*-hydroxysuccinimide; di-tBoc-lysine-NHS, N_α,N_ϵ-di-tBoc-L-lysine-*N*-hydroxysuccinimide ester; DSPC, 1,2-distearoyl-*sn*-glycero-3-phosphocholine; DSPE, 1,2-distearoyl-*sn*-glycero-3-phospho-ethanolamine; LUV, large unilamellar vesicle; PBS, phosphate-buffered saline; PEG_{3400}, poly(ethylene glycol) with an average MW of 3400; Rh-PE, 1,2-dioleoyl-*sn*-glycero-3-phosphoethanolamine-*N*-(Lissamine Rhodamine B Sulfonyl); TFA, trifluoroacetic acid.

10.1021/bc990171x CCC: $19.00 © 2000 American Chemical Society
Published on Web 03/30/2000

Scheme 1. Structures of the Cationic-PEG-Lipids

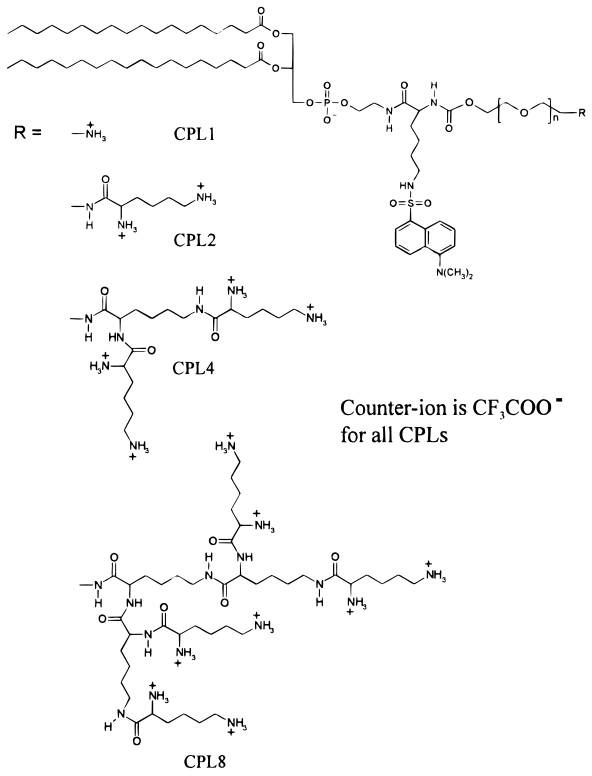

allows rapid and accurate quantification of the lipid using fluorescence techniques. All of the lipids contain a DSPE anchor coupled to N_ϵ-dansyl lysine, which is attached to a PEG spacer with a molecular weight of 3400. Aside from CPL_1, which possesses a headgroup made of a single primary amine, all others contain increasing numbers of lysine residues. The chemical structures of the CPLs are shown in Scheme 1. The potential usefulness of CPLs is demonstrated by enhanced in vitro cellular binding and uptake of CPL_4-LUVs.

EXPERIMENTAL PROCEDURES

Materials and Reagents. tBoc-NH-PEG_{3400}-CO_2-NHS was obtained from Shearwater Polymers (Huntsville, AL). N_α,N_ϵ-di-tBoc-L-lysine-*N*-hydroxysuccinimide ester, N_ϵ-dansyl-L-lysine, *N*-hydroxysuccinimide (NHS), and *N*,*N*′-dicyclohexyl-carbodiimide (DCC) were purchased from Sigma-Aldrich Canada (Oakville, ON). 1,2-Distearoyl-*sn*-glycero-3-phosphocholine (DSPC) and 1,2-distearoyl-*sn*-glycero-3-phosphoethanolamine (DSPE) were obtained from Northern Lipids (Vancouver, BC). Fluorescamine and rhodamine-DSPE (Rh-PE) were obtained from Molecular Probes (Eugene, OR). Cholesterol (Chol) was obtained from Sigma Aldrich Canada (Oakville, ON). Trifluoroacetic acid, diethyl ether, methanol, triethylamine, and chloroform were obtained from Fisher Scientific (Vancouver, BC). All reagents were used without further purification.

General Methods. All reactions were performed in 16 × 100 mm glass test tubes. ^{1}H NMR spectra were obtained employing a Bruker MSL 200 spectrometer operating at 200 MHz. Deuterated chloroform ($CDCl_3$) was used as the solvent in the NMR experiments. Proton chemical shifts (δ) were referenced to $CHCl_3$ set at 7.24 ppm. When signals were reasonably resolved, their intensities were integrated to allow an estimation of the number of protons. The chemical shifts of exchangeable amino group protons, observed between 7 and 8 ppm, are not given. These peaks were assigned on the basis of their removal by a D_2O exchange.

Phosphorus and fluorescamine assays were performed to confirm the ratio of primary amine per phosphate in each CPL as follows.

The phosphate concentration of the CPL was determined using the Fiske-Subarrow phosphorus assay (*14*). The primary amine concentration in the CPL was determined using the fluorophore fluorescamine. A fluorescamine solution (0.6 mg/mL) in acetone was prepared. An aliquot of CPL solution in HBS (2−4 μL) was made up to 250 μL with 200 mM sodium borate, pH 8.0. To this mixture, 50 μL of the fluorescamine solution was added dropwise with vortexing, followed by 1700 μL of water. The fluorescence of this solution was measured using a Perkin-Elmer LS50 Luminescence Spectrometer with λ_{ex} of 397 nm and λ_{em} of 475 nm and excitation and emission slit widths of 10 nm. The primary amine concentration of the CPL was determined from a lysine standard curve.

tBoc-NH-PEG_{3400}-CO_2-(N_ϵ-dansyl)lysine (1). tBoc-NH-PEG_{3400}-CO_2-NHS (500 mg, 147 μmol) in 3 mL of dry chloroform was added slowly to a solution of N_ϵ-dansyl-L-lysine (65 mg, 171 μmol) in 1 mL of methanol and 200 μL of triethylamine. After the reaction mixture was stirred at room temperature for 3 h, the solvent was removed under a N_2 stream and further dried under vacuum. The crude product was washed by first dissolving it in a minimum amount of chloroform with warming and then precipitating it out with the addition of 10 mL of diethyl ether. The ether was added while vortexing. Precipitation of **1** was accelerated by cooling. The precipitate was then pelleted by centrifugation, and the ether was discarded. This chloroform/ether wash and precipitation procedure was repeated. The dry solid was then dissolved in 4 mL of chloroform and cooled in an ice bath for 15 min. Methanol (2 mL) was added if this cooled solution was clear. If a precipitate (excess dansyl lysine) developed, it was filtered off prior to the addition of methanol. The chloroform/methanol solution was washed with 1.2 mL of 0.1 M HCl. The chloroform phase was extracted and dried, and the solid was redissolved in 6 mL of chloroform/methanol (2:1 v/v) and washed with 1.2 mL of distilled water. The chloroform phase was extracted and dried to a thick paste, and tBoc-NH-PEG-CO_2-(N_ϵ-dansyl)lysine (**1**) was precipitated with 10 mL of ether. After centrifugation and the removal of ether, the dried product was a light yellow solid.

Yield: 520 mg (93%). TLC (silica gel) chloroform/methanol (85:15 v/v): R_f 0.56. ^{1}H NMR ($CDCl_3$): δ 1.08 (t), 1.40 (s, 11H), 2.66 (s, 1H), 2.86 (s, 8H), 3.27 (q), 3.50 (t), 3.60 (s, 309H), 3.96 (t), 4.19 [m(broad)], 5.03 [s(broad), 1H], 5.22 (t, 1H), 5.43 (d, 1H), 7.16 (d, 1H), 7.51 (q, 2H), 8.19 (d, 1H), 8.27 (d), 8.50 (d, 1H) ppm.

Dansylated CPL_1-tBoc (3). First, tBoc-NH-PEG_{3400}-CO_2-(N_ϵ-dansyl)lysine-NHS (**2**) was prepared as follows. A solution of tBoc-NH-PEG_{3400}-CO_2-(N_ϵ-dansyl)lysine (**1**) (500 mg, 132 μmol) and NHS (31.5 mg, 274 μmol) in 2 mL of dry chloroform was added to DCC (42.8 mg, 207 μmol) dissolved in 1 mL of dry chloroform. The reaction mixture was stirred for 2 h at room temperature. The byproduct, dicyclohexyl urea (DCU), was filtered using a Pasteur pipet with a cotton plug. The filtrate, containing tBoc-NH-PEG_{3400}-CO_2-(N_ϵ-dansyl)lysine-NHS (**2**), was slowly added to a solution of DSPE (120.6 mg, 161 μmol) in 2 mL of dry chloroform and 200 μL of triethylamine. The dissolution of DSPE in dry chloroform and triethylamine required warming to 65 °C. After the reaction mixture was stirred at room temperature for 3 h, it was

dried, and chloroform/ether washed and precipitated as described earlier until the disappearance of DSPE on TLC as visualized with ninhydrin. This removal of excess DSPE required at least three washings. The product, dansylated CPL_1-tBoc (**3**), was dissolved in chloroform/methanol (2:1), washed with dilute HCl and water, and precipitated using ether as described for (**1**).

Yield: 575 mg (96%). TLC (silica gel) chloroform/methanol (85:15) R_f 0.58. ^{1}H NMR ($CDCl_3$): δ 0.85 (t, 4H), 1.22 (s, 48H), 1.41 (s, 10H), 1.55 (t), 2.27 [m(broad), 6H], 2.90 [m(broad), 6H], 3.04 (s, 8H), 3.27 (q), 3.61 (s, 275H), 4.14 [m(broad)], 4.32 (d), 4.38 (d), 5.05 [s(broad)], 5.23 [s(broad)], 5.58 [m(broad)], 7.37 (d, 1H), 7.49 [s(broad), 1H], 7.59 (t, 2H), 8.24 (d, 1H), 8.50 (d, 1H), 8.59 (d, 1H) ppm.

Dansylated CPL_1 (4). Trifluoroacetic acid (TFA) (2 mL) was added to a solution of dansylated CPL_1-tBoc (**3**) (550 mg, 121 μmol) in 2 mL of chloroform and stirred for 4 h at room temperature. The solution was concentrated to a thick paste and chloroform/ether washed three times. After the removal of ether, the solid was dissolved in 6 mL of chloroform/methanol (2:1) and washed with 1.2 mL of 5% sodium bicarbonate. The chloroform phase was extracted, dried, and redissolved in 6 mL of chloroform/methanol (2:1) and washed with 1.2 mL of distilled water. The chloroform phase was concentrated to a thick paste, and the purified CPL_1 (**4**) was obtained through a chloroform/ether wash and vacuum-dried.

Yield: 535 mg (97%). TLC (silica) chloroform/methanol/water (65:25:4) R_f 0.76. ^{1}H NMR ($CDCl_3$): δ 0.85 (t, 4H), 1.22 (s, 46H), 1.54 [m(broad), 8H], 2.23 (t, 6H), 2.84 (s, 9H), 3.16 [m(broad), 3H], 3.26 (t, 3H), 3.61 (s, 263H), 3.98 (q), 4.17 (t), 4.33 (d), 4.38 (d), 5.19 [s(broad)], 5.93 (d, 1H), 7.13 (d, 1H), 7.46 (t, 1H), 7.52 (t, 1H), 8.15 (d, 1H), 8.43 (t, 2H) ppm.

Dansylated CPL_2-tBoc (5). A solution of N_α,N_ϵ-di-tBoc-L-lysine-*N*-hydroxysuccinimide ester (105 mg, 236 μmol) in 2 mL of dry chloroform was gradually added to a solution of dansylated CPL_1 (**4**) (510 mg, 112 μmol) in 2 mL of chloroform containing 200 μL of triethylamine and stirred at room temperature for 3 h. The completion of the reaction was indicated by the disappearance of primary amine as visualized by ninhydrin assay on TLC. The reaction mixture was concentrated to a thick paste and chloroform/ether washed (~3 times) until the disappearance of excess N_α,N_ϵ-di-tBoc-L-lysine-*N*-hydroxysuccinimide ester as checked by TLC. The product was dissolved in 6 mL of chloroform/methanol (2:1) and washed with 1.2 mL of 0.1 M HCl. The chloroform phase was extracted, dried, redissolved in 6 mL of chloroform/methanol (2:1), and washed with 1.2 mL of distilled water. The chloroform phase was concentrated to a thick paste and the purified compound was obtained through a chloroform/ether wash and vacuum-dried.

Yield: 510 mg (96%). TLC (silica gel) chloroform/methanol (85:15) R_f 0.58. ^{1}H NMR ($CDCl_3$). δ 0.85 (t, 3H), 1.22 (s, 44H), 1.41 (s, 20H), 1.56 [m(broad)], 1.78 [m(broad)], 2.27 (m, 5H), 2.88 (s), 2.91 (s), 2.97 (s), 3.06 (s, 7H), 3.26 (t), 3.44 (t), 3.62 (s, 252H), 3.97 (t), 4.05 (d), 4.13 (m), 4.33 (d), 4.38 (d), 4.68 [s(broad)], 5.22 [s(broad)], 5.51 [s(broad)], 6.57 [t(broad), 1H], 7.39 (d, 1H), 7.51 [s(broad), 1H], 7.60 (t, 2H), 8.26 (d, 1H), 8.53 (d, 1H), 8.61 (d, 1H) ppm.

Dansylated CPL_2 (6). The synthesis of CPL_2 (**6**) was the same as that of CPL_1 (**4**) by deprotecting dansylated CPL_2-tBoc (**5**) (490 mg, 103 μmol).

Yield: 478 mg (97%). TLC (silica) chloroform/methanol/water (65:25:4) R_f 0.63. ^{1}H NMR ($CDCl_3$). δ 0.85 (t, 3H), 1.22 (s, 42H), 1.55 (m, 10H), 1.93 [s(broad), 4H], 2.24 (t, 5H), 2.85 (s, 8H), 3.26 (t, 3H), 3.61 (s, 271H), 3.95 (q), 4.17 (s), 4.34 (s), 5.18 [s(broad), 1H], 6.31 (d, 1H), 6.89 (s, 1H), 7.10 (d, 1H), 7.49 (m, 1H), 8.15 (d, 1H), 8.34 (d, 1H), 8.47 (d, 2H) ppm.

Dansylated CPL_4-tBoc (7). The synthesis of CPL_4-tBoc (**7**) was the same as that of CPL_2-tBoc (**5**) by reacting N_α,N_ϵ-di-tBoc-L-lysine-*N*-hydroxysuccinimide ester (170 mg, 383 μmol) with dansylated CPL_2 (**6**) (455 mg, 95 μmol).

Yield: 475 mg (96%). TLC (silica gel) chloroform/methanol (85:15) R_f 0.58. ^{1}H NMR ($CDCl_3$): δ 0.85 (t, 3H), 1.22 (s, 43H), 1.40 (s, 39H), 1.71 [m(broad), 6H], 2.27 (m, 5H), 2.88 (s), 2.90 (s), 2.95 (s), 3.05 (s, 10H), 3.25 (t, 3H), 3.43 (s), 3.61 (s, 262H), 3.97 (t), 4.05 (d), 4.15 (m), 4.32 (d), 4.37 (d), 4.51 [s(broad)], 4.75 [s(broad)], 4.90 [s(broad)], 5.23 [t(broad), 1H], 5.52 [s(broad)], 5.80 [s(broad), 1H], 7.15 [m(broad), 1H], 7.38 (d, 1H), 7.50 (s, 1H), 7.59 (t, 2H), 8.25 (d, 1H), 8.51 (d, 1H), 8.60 (d, 1H) ppm.

Dansylated CPL_4 (8). The synthesis of CPL_4 (**8**) was the same as that of CPL_1 (**4**) by deprotecting dansylated CPL_4-tBoc (**7**) (450 mg, 86 μmol).

Yield: 440 mg (97%). TLC (silica) chloroform/methanol/water (65:25:4) R_f 0.19. ^{1}H NMR ($CDCl_3$). δ 0.85 (t), 1.22 (s), 1.53 [m(broad)], 2.34 [m(broad)], 2.86 (s), 3.26 (t), 3.62 (s), 3.87 [s(broad)], 3.97 (t), 4.17 [s(broad)], 4.33 (d), 5.18 [s(broad)], 7.15 (d), 7.43 (s), 7.51 (t), 8.15 (d), 8.32 (d), 8.48 (d), 9.05 [s(broad)] ppm.

Dansylated CPL_8-tBoc (9). The synthesis of CPL_8-tBoc (**9**) was the same as that of CPL_2-tBoc (**5**) by reacting N_α,N_ϵ-di-tBoc-L-lysine-*N*-hydroxysuccinimide ester (70 mg, 158 μmol) with dansylated CPL_4 (**8**) (100 mg, 19 μmol).

Yield: 112 mg (96%). TLC (silica gel) chloroform/methanol (85:15) R_f 0.58. ^{1}H NMR ($CDCl_3$): δ 0.84 (t, 3H), 1.08 (s), 1.21 (s, 39H), 1.39 (s, 75H), 1.66 (m [broad]), 2.26 (m, 4H), 2.89 (s, 4H), 3.06 (s, 11H), 3.25 (t, 3H), 3.43 (s), 3.49 (s), 3.60 (s, 248H), 3.96 (t), 4.04 (d), 4.12 (t), 4.31 (d), 4.36 (m), 5.19 [m(broad)], 6.77 [m(broad), 1H], 6.91 [s(broad), 1H], 7.24 ($CHCl_3$), 7.41 (d), 7.50 [s(broad)], 7.60 (t), 8.25 (d, 1H), 8.53 (d, 1H), 8.63 (d, 1H) ppm.

Dansylated CPL_8 (10). The synthesis of CPL_8 (**8**) was the same as that of CPL_1 (**4**) by deprotecting dansylated CPL_8-tBoc (**9**) (50 mg, 8 μmol).

Yield: 48 mg (96%). TLC (silica) chloroform/methanol/water (65:25:4) R_f 0.13. ^{1}H NMR ($CDCl_3$): δ 0.85 (t, 3H), 1.22 (s, 34H), 1.52 [s(broad)], 2.23 [s(broad)], 2.86 (d), 3.27 (d), 3.61 (s, 274H), 3.96 (t), 4.18 [m(broad)], 7.14 [s(broad)], 7.24 ($CHCl_3$), 7.50 [m(broad)], 8.12−8.27 [s(broad)], 8.47 [m(broad)] ppm.

In Vitro Binding and Uptake. Large unilamellar vesicles (100 nm) composed of DSPC/Chol/rhodamine-PE/CPL_4 (49.5:45:0.5:5 mol %) and DSPC/Chol/rhodamine-PE (54.5:45:0.5 mol %) were prepared by extrusion as described by Hope et al. (*15*).

BHK cells, obtained from American Tissue Culture Collection (ATCC CCL-10, Rockville, MD), were plated in 12-well plates at 2.5×10^5 cells/well in DMEM (Gibco BRL, Burlington, ON) + 10% FBS (Gibco BRL, Burlington, ON) and allowed to grow overnight in an incubator at 37 °C with 5% CO_2. Samples (40 nmol) were incubated on the cells in DMEM + 10% FBS for 1, 2, 4, and 6 h. At each time point, the media was removed, the cells were washed twice with PBS, and lysed with 600 μL of lysis buffer (PBS containing 0.1% Triton X-100). Lipid uptake was quantified by measuring the rhodamine fluorescence in the lysate using $\lambda_{ex} = 560$ nm and $\lambda_{em} = 590$ nm with excitation and emission slit widths of 10 and 20 nm, respectively, using a Perkin-Elmer LS-50 Luminescence Spectrometer. Lipid uptake was normalized to the num-

Scheme 2. Sequential Synthesis of the CPLs[a]

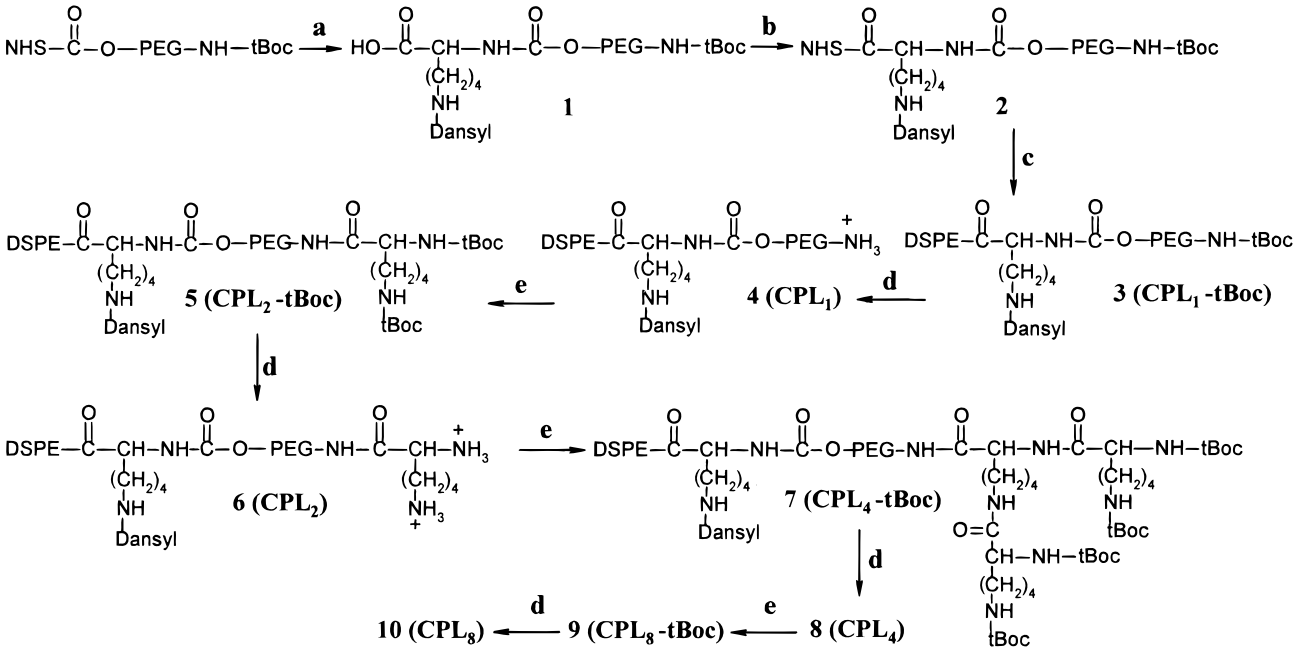

[a] Key: (a) N_ϵ-dansyl-L-lysine, triethylamine, methanol, chloroform, 3 h; (b) NHS, DCC, chloroform, 2 h; (c) DSPE, triethylamine, chloroform, 4 h; (d) TFA, chloroform, 4 h; (e) N_α,N_ϵ-di-tBoc-L-lysine-*N*-hydroxy-succinimide ester, triethylamine, chloroform, 3 h.

ber of cells using the BCA protein assay reagent kit (Pierce, Rockford, IL).

RESULTS AND DISCUSSION

The CPLs were synthesized by repeated coupling reaction steps involving amines and NHS-activated carbonate groups as outlined in Scheme 2. This consists of (a) incorporating the dansyl fluorescent label to the hydrophilic PEG spacer, (b) coupling of the DSPE anchor, and (c) attachment of the cationic headgroup to the lipid. The heterobifunctional PEG polymer tBoc-NH-PEG_{3400}-CO_2-NHS (MW 3400) was chosen for two reasons. First, it was commercially available. Second, it is insoluble in ether which provided a very convenient means of purifying its derivatives, **1**−**10**. Other reagents were used in excess to ensure the complete conversion of the PEG polymer to its derivatives. The excess reagents were soluble in ether and, therefore, could be removed by washing in ether during purification.

Incorporation of the fluorescent label, N_ϵ-dansyl lysine, to the PEG polymer by coupling the α-amino group of dansyl lysine with the NHS activated carbonate of PEG gave the lysine derivative **1**. The DSPE anchor was coupled via intermediate **2**, which was formed by the esterification of **1** using NHS and DCC. The resulting PEG lipid, **3**, was deprotected by removing the tBoc to form CPL_1, **4**, with one positive charge. The positive charges in the other CPLs are carried by the amino groups of lysine. Here, the NHS-activated and di-tBoc-protected lysine was attached to the free amino function of CPL_1 to form intermediate **5** which, upon deprotection, yielded CPL_2, **6**, with two positive charges. The attachment of two lysine residues to the amino groups of CPL_2 via intermediate **7** gave CPL_4, **8**, with four positive charges. Thus, CPL_8, **10**, with eight positive charges was synthesized with the attachment of four lysine residues as the headgroup. As can be seen, this provides a very convenient means of synthesizing multivalent CPLs that are of particular interest for nonviral drug delivery applications.

The structures of the purified intermediates and CPL in synthetic Scheme 2 were verified by ^{1}H NMR spectroscopy and chemical analysis. The ^{1}H NMR spectra showed well-resolved resonances for the PEG, tBoc, and acyl chains of DSPE at approximately 3.61, 1.41, and 1.21 ppm, respectively, and for the resonances of the dansyl moiety (aromatic protons at 7.1−8.5 ppm; methyl protons at 2.8−3.0 ppm). From the integrated signal intensities of the former three peaks, it was found that the ratio of tBoc/PEG or tBoc/DSPE was 1.0, 2.1, 4.0, and 8.1 for CPL_1-tBoc, CPL_2-tBoc, CPL_4-tBoc, and CPL_8-tBoc, respectively. As each tBoc is attached to an amino group, this gives the number of amino groups in the headgroup of each CPL relative to the CPL_1. That essentially identical results were obtained using the ratios of tBoc relative to both PEG and DSPE demonstrates the presence of lipid and polymer in correct proportion to the headgroup. The complete cleavage of the tBoc-protecting groups was verified by the loss of tBoc NMR peaks and chemical analysis, which determined the ratio of primary amine to phosphate in each of the CPL by using the fluorescamine and phosphorus assays. The amine/phosphate ratios for CPL_1, CPL_2, CPL_4, and CPL_8 were found to be 1.0, 2.2, 3.7, and 8.0, respectively. These corresponded well with the expected number of positive charge bearing amino groups of the respective CPLs.

A number of PEG-lipids similar to those described in the present paper have been designed to enhance liposomal targeting to cells. While some are intended for specific-targeting purposes, with folate (*4*), oligopeptide (*9*, *10*), or oligosaccharide (*10*) ligands present in the distal headgroups, cationic PEG-lipids have also been described. A nonfluorescent monovalent cationic amino-PEG-DSPE lipid similar to CPL_1 has been prepared previously and liposomes containing this lipid were found to possess prolonged circulation lifetimes (*16*). In addition, a separate study has reported the synthesis of a nonphospholipid anchored PEG with a distal divalent cationic headgroup (*17*). Finally, a dansyl-labeled PEG has previously been synthesized by Pendri et al. (*18*),

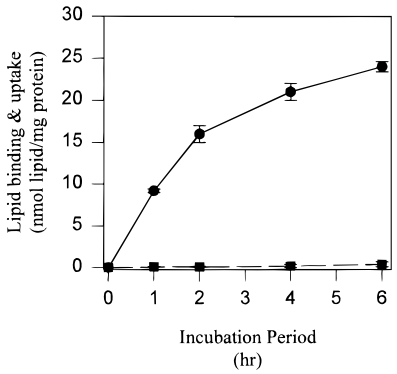

Figure 1. Time course for the binding and uptake of 20 mM DSPC/Chol/Rh-PE (54.5:45:0.5 mol %) LUV (■) and DSPC/Chol/Rh-PE/CPL_4 (49.5:45:0.5:5 mol %) LUV (●) by 1×10^5 BHK cells grown in DMEM + 10% FBS.

while Silvius and Zuckermann reported the synthesis of a fluorescent-labeled methoxyPEG-PE (*13*). The CPLs described here possess several attributes which may increase their usefulness relative to other cationic lipids. First, the phospholipid anchor will readily allow efficient incorporation of CPL into liposomal systems. Second, the dansyl label will permit accurate and convenient quantification of the CPL in the bilayer using fluorescence techniques. Finally, the valency of the cationic headgroup in the CPL can easily be modified using lysine residues.

To demonstrate that CPL enhance the interaction of liposomes with cells, we have incorporated CPL_4 into a common LUV system [DSPC/Chol/Rh-PE (54.5:45:0.5)], and have examined the time course of vesicle binding/uptake in BHK cells (Figure 1). In the presence of CPL_4 the cellular uptake of the liposomes is ~50 times greater than in its absence. These results demonstrate the potential utility of the CPL system. Further studies detailing the preparation of CPL-LUV systems and their application in the delivery of plasmid DNA to cells will be published elsewhere.

ACKNOWLEDGMENT

This work was supported by grants from the Medical Research Council of Canada (MRC).

LITERATURE CITED

(1) Meyer, O., Kirpotin, D., Hong, K., Sternberg, B., Park, J. W., Woodle, M. C., and Papahadjopoulos, D. (1998) Cationic liposomes coated with poly(ethylene glycol) as carriers for oligonucleotides. *J. Biol. Chem. 273*, 15621−15627.

(2) Kao, G. Y., Change, L. J., and Allen, T. M. (1996) Use of targeted cationic liposomes in enhanced DNA delivery to cancer cells. *Cancer Gene Ther. 3*, 250−256.

(3) Hansen, C. B., Kao, G. Y., Moase, E. H., Zalipsky, S., and Allen, T. M. (1995) Attachment of antibodies to sterically stabilized liposomes: evaluation, comparison and optimization of coupling procedures. *Biochim. Biophys. Acta 1239*, 133−144.

(4) Gabizon, A., Horowitz, A. T., Goren, D., Tzemach, D., Mandelbaum-Shavit, F., Qazen, M. M., and Zalipsky, S. (1999) Targeting Folate Receptor with Folate Linked to Extremities of Poly(ethylene glycol)-Grafted Liposomes: In Vitro Studies. *Bioconjugate Chem. 10*, 289−298.

(5) Lee, R. J., and Low, P. S. (1994) Delivery of liposomes into cultured KB cells via folate receptor-mediated endocytosis. *J. Biol. Chem. 269*, 3198−3204.

(6) Reddy, J. A., and Low, P. S. (1998) Folate-mediated targeting of therapeutic and imaging agents to cancers. *Crit. Rev. Ther. Drug Carrier Syst. 15*, 587−627.

(7) Holladay, S. R., Yang, Z., Kennedy, M. D., Leamon, C. P., Lee, R. J., Jayamani, M., Mason, T., and Low, P. S. (1999) Riboflavin-mediated delivery of a macromolecule into cultured human cells. *Biochim. Biophys. Acta 1426*, 195−204.

(8) Wang, S., and Low, P. S. (1998) Folate-mediated targeting of antineoplastic drugs, imaging agents, and nucleic acids to cancer cells. *J. Controlled Release 53*, 39−48.

(9) Zalipski, S., Puntambekar, B., Boulikas, P., Engbers, C. M., and Woodle, M. C. (1995) Peptide Attachment to Extremities of Liposomal Surface Grafted PEG Chains: Preparation of the Long-Circulating Form of Laminin Pentapeptide, YIGSR. *Bioconjugate Chem. 6*, 705−708.

(10) Zalipsky, S., Mullah N., Harding, J. A., Gittelman, J., Guo, L., and DeFrees, S. A. (1997) Poly(ethylene glycol)-Grafted Liposomes with Oligopeptide or Oligosaccharide Ligands Appended to the Termini of the Polymer Chains. *Bioconjugate Chem. 8*, 111−118.

(11) Felgner, P. L., Gadek, T. R., Holm, M., Roman, R., Chan, H. W., Wenz, M., Northrop, J. P., Ringold, G. M., and Danielson, M. (1987) Lipofection: a highly efficient, lipid-mediated DNA-transfection procedure. *Proc. Natl. Acad. Sci. U.S.A. 84*, 7413−7417.

(12) Zhang, Y. P., Sekirov, L., Saravolac, E. G., Tardi, P., Clow, K., Leng, E., Sun, R., Cullis, P. R., and Scherrer P. (1999) Stabilized plasmid-lipid particles for regional gene therapy: formulation and transfection properties. *Gene Ther. 6*, 1438−1447.

(13) Silvius, J. R., and Zuckermann, M. J. (1993) Interbilayer Transfer of Phospholipid-Anchored Macromolecules via Monomer Diffusion. *Biochemistry 32*, 3153−3161.

(14) Fiske, C. H., and Subbarow, Y. (1925) The colorimetric determination of phosphorous. *J. Biol. Chem. 66*, 375−400.

(15) Hope, M. J., Bally, M. B., Webb, G., and Cullis, P. R. (1985) Production of large unilamellar vesicles by a rapid extrusion procedure. Characterization of size distribution, trapped volume, and ability to maintain a membrane potential. *Biochim. Biophys. Acta 812*, 55−65.

(16) Zalipski, S., Brandeis, E., Newman, M. S., and Woodle, M. C. (1994) Long circulating, cationic liposomes containing amino-PEG-phosphatidylethanolamine. *FEBS Lett. 353*, 71−74.

(17) Schulze, U., Schmidt, H.-W., and Safinya, C. R. (1999) Synthesis of Novel Cationic Poly(ethylene glycol) Containing Lipids. *Bioconjugate Chem. 10*, 548−552.

(18) Pendri, A., Martinez, A., Xa, J., Shorr, R. G. L., and Greenwald, R. B. (1995) Poly(ethylene glycol) Fluorescent Linkers. *Bioconjugate Chem. 6*, 596−598.

BC990171X

Volume 10, Number 6, November/December

Bernhard Oswald, Leonid Patsenker, Josef Duschl, Henryk Szmacinski, Otto S. Wolfbeis, and Ewald Terpetsching*

SYNTHESIS, SPECTRAL PROPERTIES, AND DETECTION LIMITS OF REACTIVE SQUARAINE DYES, A NEW CLASS OF DIODE LASER COMPATIBLE FLUORESCENT PROTEIN LABELS

Page 925. In the address byline, FluorRx Inc., 979 Keystone Way, Carmel, Indiana 46032 should be University of Maryland School of Medicine, 725 West Lombard Street, Baltimore, Maryland 21201. In addition, in the footnotes at the lower left, ‡Fluorrx Inc. should be ‡Present address: FluorRx Inc., 979 Keystone Way, Carmel, IN 46032.

BC000019R

10.1021/bc000019r
Published on Web 05/15/2000

JULY/AUGUST 2000
Volume 11, Number 4

© *Copyright 2000 by the American Chemical Society*

Bioconjugate Chemistry

COMMUNICATIONS

Site Specific 1:1 Opioid:Albumin Conjugate with in Vitro Activity and Long in Vivo Duration

Darren L. Holmes,* Karen Thibaudeau, Benoît L'Archevêque, Peter G. Milner, Alan M. Ezrin, and Dominique P. Bridon*

ConjuChem, Inc., 225 President-Kennedy Avenue, Third Floor, Suite 3950, Montréal (Quebéc), Canada H2X 3Y8. Received February 29, 2000

A site-specific 1:1 dynorphin A-(1−13)-NH_2 derivative conjugated specifically to Cys 34 on human serum albumin (CCI-1035) was shown to be an opioid receptor agonist in vitro and to be a long lasting antinociceptive agent when administered intravenously to mice as assessed by an acetic acid writhing assay. When 10 μmol/kg of CCI-1035 was administered to mice, rapid antinociception was observed within 5 min following intravenous bolus injection and was sustained beyond 8 h. Antinociceptive activity was absent in a heat induced pain model using a mouse tail-flick assay. This finding represents the first report of a 1:1 albumin opioid conjugate retaining potent in vivo activity equal to or greater than dynorphin A, accompanied by a dramatic extension in duration of action. This novel site-specific bioconjugation technology produces an agent that may be useful for peripheral pain therapy.

Dynorphin A [Dyn A-(1−17)-OH], a heptadecapeptide of sequence H-Tyr-Gly-Gly-Phe-Leu^5-Arg-Arg-Ile-Arg-Pro^{10}-Lys-Leu-Lys-Trp-Asp^{15}-Asn-Gln-OH, was first isolated from porcine pituitary and recognized as a potent opioid agonist (*1*−*3*). Derivatives of Dyn A-(1−17)-OH, specifically Dyn A-(1−13)-NH_2, have also been shown to be very potent opioid receptor agonists (*4*−*8*). Of the three different types of opioid receptors, namely mu (μ), kappa (κ), and delta (δ), Dyn A derivatives have been shown to interact mainly at the μ and κ receptors (*9*). The pharmacology of dynorphin has been extensively studied, and antinociceptive activity has been convincingly demonstrated in several animal models; however, a clearly defined mechanism remains elusive and controversial (*4*, *10*). Although these peptides show remarkable antinociceptive activity in animals and humans, their rapid metabolism in vivo has precluded them from serious clinical development (*11*−*19*).

One of the major limitations of opioid therapy includes central mediated side effects. Evidence of central effects of dynorphin have appeared in current reports, although somewhat conflicting (*20*, *21*). Thus, the development of a peripherally acting opioid agonist would be extremely useful, although, challenging. This may be facilitated by the attachment of an opioid agonist to human serum albumin (HSA). It is known that HSA is present in the brain and CSF in very low concentrations (*22*, *23*) and that fluorescently labeled albumin can preferentially sequester into peripheral afferent nerve terminal dorsal cell bodies and the ascending tracts of the spinal cord (*24*). This forms the basis for the use of the Drug Affinity Complex (DAC) technology, which essentially involves

* To whom correspondence should be addressed.

10.1021/bc0000233 CCC: $19.00 © 2000 American Chemical Society
Published on Web 06/24/2000

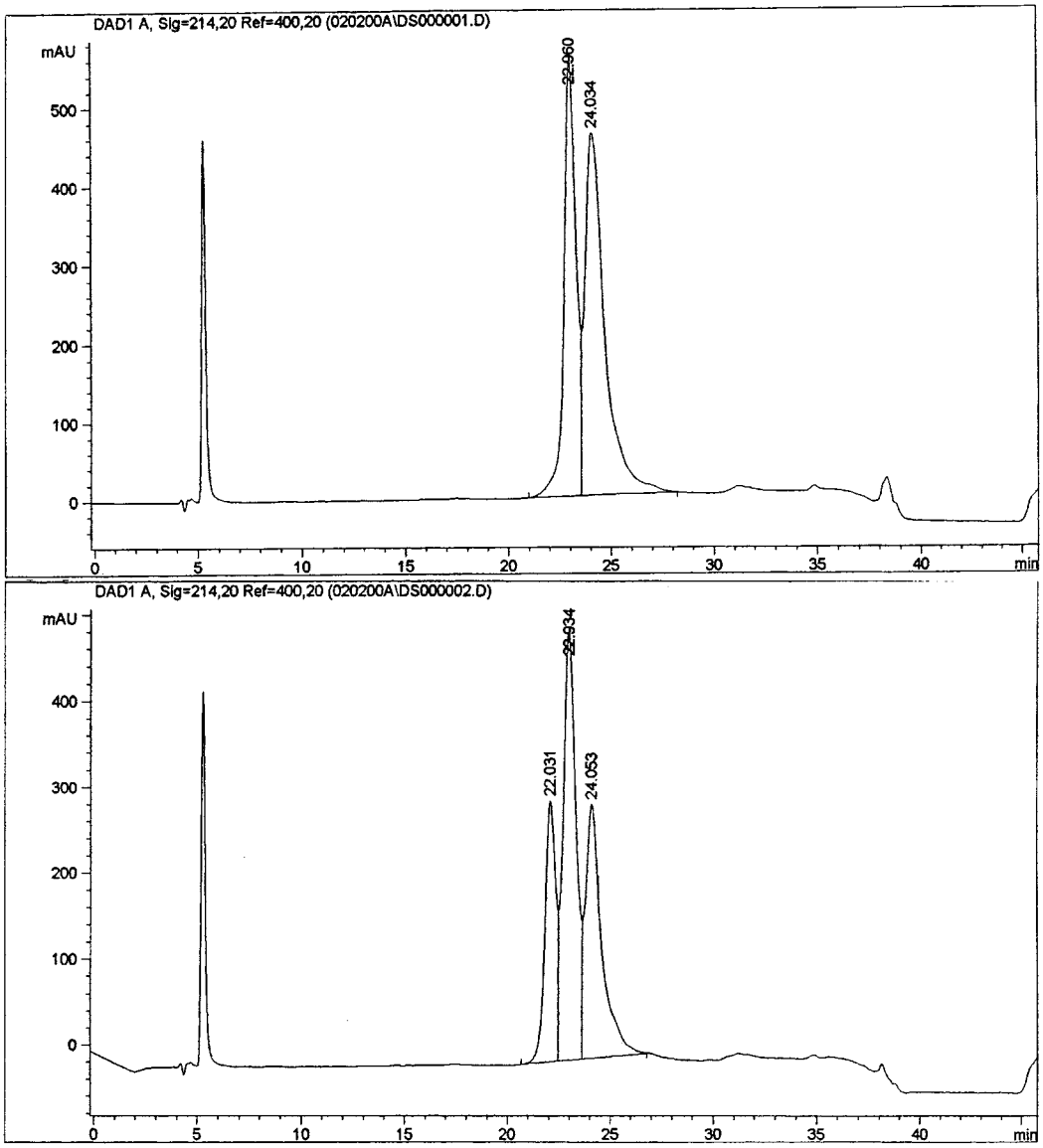

Figure 1. High-pressure liquid chromatogram of commercial 25% HSA[5] (top) and CCI-1035 (bottom). The peak at 22.0 corresponds to the conjugate; 22.9 corresponds to the half-cystine form; and the peak at 24.0 corresponds to the mercaptan form of albumin (see Figure 2).

the rapid and specific attachment of therapeutically useful agents to target carrier proteins using reactive chemistry (*25*). Application of this technology to opioid therapy requires that the DAC:opioid conjugates rapidly to plasma albumin and reaches the peripheral targets and facilitates antinociceptive activity. Albumin represents an ideal carrier as a drug conjugate because of its low CNS concentration and long bioavailability. The half-life of HSA is ~20 days and mouse serum albumin is ~1.2 days (*26*). As such, the bioconjugation of opioid peptides to albumin is designed to allow full retention of antinociceptive activity while adopting the circulating kinetics and distribution of the carrier protein. The focus of the initial experimentation was to define if a DAC:Dyn A-(1−13)-NH_2 construct could be prepared, if the resulting bioconjugate could retain the potent interaction with the opioid receptor in vitro and if the bioconjugate could provide antinociception of prolonged duration in vivo.

It is well-known that attachment of therapeutic or diagnostic agents to proteins give useful conjugates (*27*). However, most conjugates are polyvalent and nonspecific, where multiple random labeling of the protein is accomplished via cross-linking agents or by direct alkylation of free Lys residues of the protein (*28*). The DAC technology utilizes the abundance of circulating albumin in the plasma (ca. 45 g/L) (*23*) and site specifically attaching the DAC:opioid, via a maleimide, to form a stable thioether conjugate off the single free thiol residue at Cys 34[1] of HSA (*29*). It is anticipated that by selective mono-labeling the protein with an endogeneous peptide, as opposed to poly-labeling, the formed conjugate will behave similarly to the native albumin and not elicit an immunogenic response (*30*). The resulting conjugate's pharmacokinetic profile is then expected to resemble that of native albumin, therefore increasing the half-life of the antinociceptive agent comparable to that of native albumin. Thus, conjugation of a peptide to albumin is anticipated to provide stability to the peptide, prevent or dramatically reduce peptide metabolism, excretion, and enzymatic degradation, and greatly increase bio-

[1] The Cys residue at position 34 of HSA exists in several forms, about one-third of the albumin molecules carry half-cystine or half-glutathione in a ratio of about 4:1 and about 4 μM homocysteine is also found.

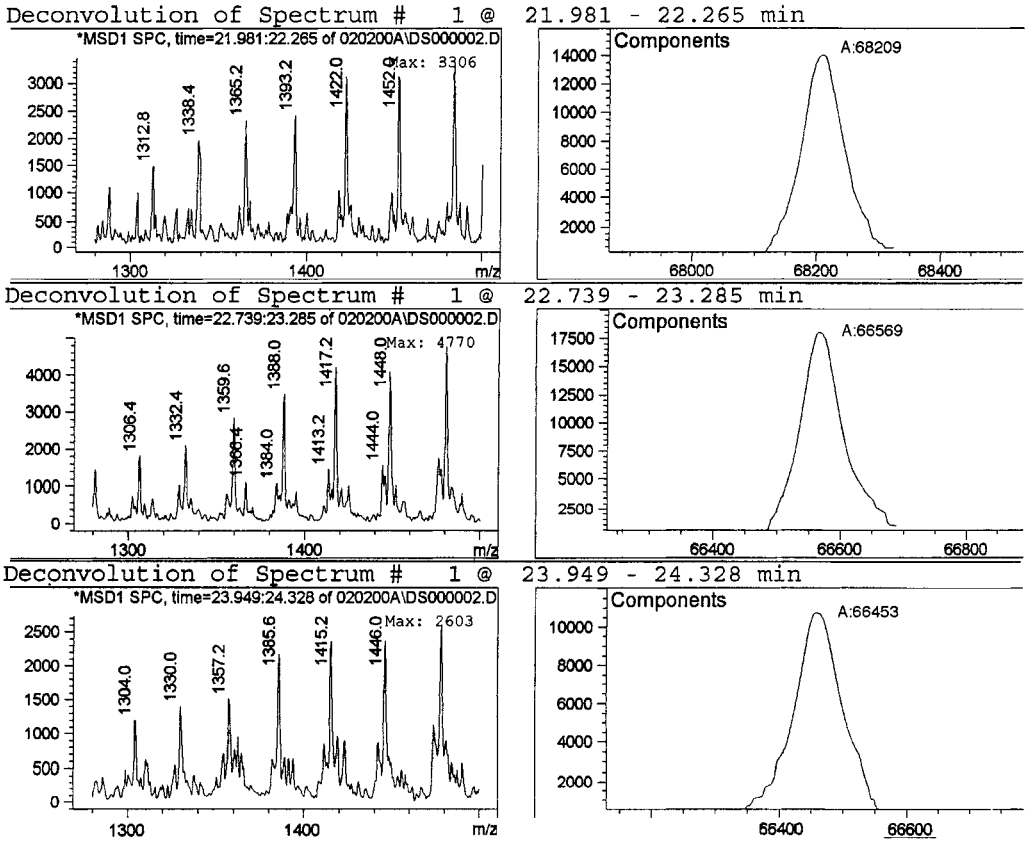

Figure 2. Mass spectra and deconvolution curve fitted protein mass spectra ± uncertainty interval of the DAC:opioid conjugate 68 209 ± 3 (top set); the half-cystine form of albumin 66 569 ± 7 (middle set); and the mercaptan form of albumin 66 453 ± 1 (bottom set).

availability and distribution while, retaining intrinsic activity at the opioid receptor level.

The Dyn A-(1−13)-NH_2 portion of the DAC:opioid was synthesized using solid-phase peptide synthesis (SPPS) (Scheme 1).[2] The incorporation of the maleimide entity, by attaching 3-maleimidopropionic acid to the ϵ-amino group of Lys at position 13 of the peptide chain, was accomplished using a methyltrityl (Mtt) protected amino acid derivative, Fmoc-Lys(Mtt)-OH,[3] for the terminal Lys residue in the solid-phase synthesis. The selective deprotection of the Mtt group with 1% trifluoroacetic acid (TFA) and 5% triisopropyl silane (TIS) in CH_2Cl_2 liberated the ϵ-amino group for coupling of 3-maleimidopro-

Scheme 1. Solid-Phase Synthesis of DAC:Opioid

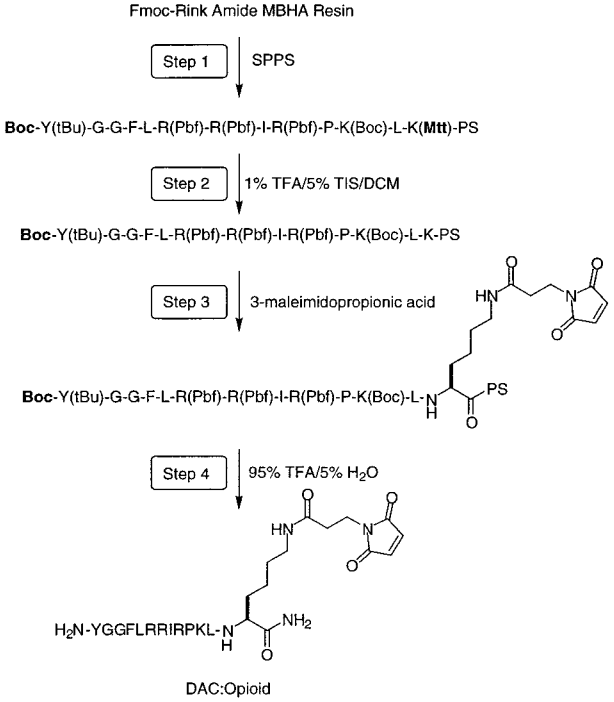

[2] Syntheses of all dynorphin A analogues were performed using manual solid-phase synthesis and an ABI 433A Peptide Synthesizer using Fmoc protected Rink Amide MBHA resin (NovaBiochem), 4 equiv of Fmoc protected amino acids, 4 equiv of a 0.45 M *O*-benzotriazol-1-yl-*N*, *N*, *N*′, *N*′-tetramethyluronium hexafluorophosphate (HBTU) and 1-hydroxybenzotriazole (HOBt) in *N*,*N*-dimethylformamide (DMF) solution and activation with 4 equiv of 2 M *N*,*N*,-diisopropylethylamine (DIEA) in 1-methyl-2-pyrrolidinone (NMP), and piperidine deprotection of Fmoc groups.

[3] Fmoc-Lys(Mtt)-OH was obtained from NovaBiochem.

[4] Resin cleavage and product isolation was performed using 95% TFA/2.5% TIS/2.5% H_2O, followed by precipitation by dry ice cold Et2O. The product was purified by preparative reversed phased HPLC using a Varian (Rainin) preparative binary HPLC system: gradient elution of 5−60% B [0.045% TFA in H2O (A) and 0.045% TFA in CH3CN (B)] over 60 min at 9.5 mL/min using a Dynamax C18, 60 Å, 8 μm, 21 mm × 25 cm column equipped with a Dynamax C18, 60 Å, 8 μm guard module and UV detector (Varian Dynamax UVD II) at λ 214 and 254 nm. The product had >95% purity with $t_R = 16.5$ min as determined by RP-HPLC mass spectrometry using a Hewlett-Packard LCMS-1100 series spectrometer equipped with a diode array detector and using electro-spray ionization, ESI-MS *m*/*z* for C82H133N26O17 (MH^+), calcd 1754.0, found 1754.9, $[M + H_2]^{2+}$ 877.8, $[M + H_3]^{3+}$ 585.5. Amino acid analysis: Gly 1.99 (2), Arg 2.95 (3), Pro 1.07 (1), Tyr 1.03 (1), Lys 2.01 (2), Ile 0.95 (1), Leu 2.01 (2), Phe 0.99 (1), MPA 1.07 (1); peptide content: 87%.

Scheme 2. Reaction of the DAC:Opioid with HSA to Form the Stable Thio Ether Conjugate CCI-1035

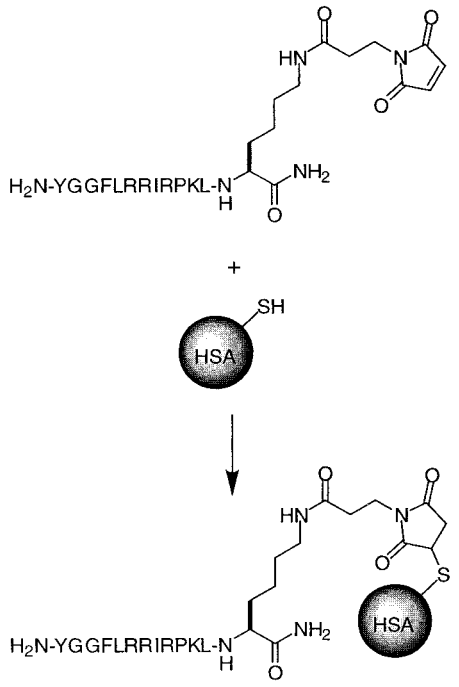

CCI-1035

pionic acid. The product was then cleaved from the resin by treatment with 95% TFA and purified to afford the DAC:opioid in >95% purity.[4] The conjugate, CCI-1035, was then prepared by dissolution of the DAC:opioid in water and adding to commercial 25% HSA[5] to a final concentration of ca. 1.0 mM conjugate (Scheme 2).[6] The proposed mono, site-specific labeling of the albumin was elucidated by mass spectrometry. Addition of the chemoselective maleimide to commercial 25% HSA[5], having molecular weights of 66 453 for the mercaptan form and 66 569 for the half-cystine form, produced a protein conjugate with a mass of 68 209, indicating the addition of one DAC:opioid (MW = 1754) to the mercaptan form of albumin (Figures 1 and 2). Since there is only one free thiol present at position 34 on albumin and that maleimides react exclusively with the thiol at this position, attachment at position 34 is presumed (*31*−*33*). Confirmation of single addition to the one free thiol on the mercaptan form of HSA is further demonstrated by the fact that there is no appearance of a conjugate in the LC chromatogram (Figure 1) or deconvolutions (Figure 2) with a molecular weight of 68 323 resulting from the half-cystine form reacting with the DAC:opioid. This finding eliminates any speculation that any disulfide bonds are broken or that an amino group is reacting with the maleimide, either of which could also give raise to the addition of multiple DAC:opioid molecules to albumin, which is not seen, and that the thiol group is essential for selective bioconjugation to occur.

In a nonspecific competition binding assay versus [^{3}H]-naloxone, both Dyn A-(1−13)-NH_2 and the conjugate gave identical inhibition of 10% at 0.01 μM and 90% inhibition at 1 μM, thus, proving opioid activity. The conjugate, CCI-1035, was then evaluated for its binding affinity to μ, κ, and δ opioid receptors using equilibrium competition binding assays.[7] The opioid binding affinities were determined using human recombinant CHO-K_1 cells for μ and κ receptors and CHO cells for the δ receptor (*34*−*36*). The affinities for μ, κ, and δ opioid receptors were determined by competitive inhibition of the radioligands [^{3}H]diprenorphin for μ and κ, and [^{3}H]natrindole for δ and results demonstrated opioid agonist activity. However, receptor selectivity could not be reproducibly determined.

Antinociceptive activity was evaluated in vivo using a standard acetic acid writhing assay.[7] Mice were systemically administered (bolus via tail vein) saline (10 mL/kg), 3 mg/kg (9.3 μmol/kg) morphine hydrochloride, 3 μmol/kg of Dyn A-(1−13)-NH_2, and 10 μmol/kg of CCI-1035. After time intervals of 5 min, 30 min, 1 h, 3 h, 8 h, and 24 h, 3% acetic acid was administered intraperitoneally and the number of acetic acid induced writhes were recorded over a 5-min interval for each mouse in groups of six Institute of Cancer Research (ICR) derived male or female mice. These data were then converted to percent inhibition and plotted against time (Figure 3).

Figure 3 reveals that the control groups of morphine and Dyn A-(1−13)-NH_2, as well as CCI-1035 all show activity at 5 min. Morphine and Dyn A-(1−13)-NH_2, however, are both inactive at times <3 h, whereas CCI-1035 is significantly active at 3 h and even after 8 h. These data show that the DAC:opioid conjugate, CCI-1035, exhibits an effect equal to that of morphine and Dyn A-(1−13)-NH_2, with the added advantage of improved duration of efficacy. The increased duration of action of CCI-1035 is hypothesized to be a result of the pharmacophore acquiring the metabolic rate and distribution of native albumin. The decrease in activity of CCI-1035 profiles that of albumin clearance in the mouse model, which is 1.2 days (*26*). In a separate study (data not shown) commercial 20% HSA did not show any appreciable antinociceptive activity, with % inhibition varying between 21% and 13% over the same time intervals used for CCI-1035.

Although 10 μmol/kg of CCI-1035 was administered intravenously, it is unclear how much of that amount elicited the antinociceptive response. From the efficacy data (Figure 3) a maximum response was achieved in 3 h, therefore a dose−response relationship (Figure 4) was determined using the writhing assay by challenging the mice with acetic acid 3 h post iv bolus injection of CCI-1035.[7] There is clear evidence of a dose−response with an activity observed as low as 0.1 to 10 μmol/kg, comparable to that of Dyn A-(1−13)-NH_2 (ED_{50} 1.1 μmol/kg) (*37*).

Thus, CCI-1035 produced a therapeutic agent that not only retained intrinsic potency but also seemed to

[5] Commercial 25% HSA, albumin (human) U. S. P., albutein 25% solution was obtained from Alpha Therapeutic Corporation. Product contains ca. 42% Cys 34 nonreduced (half-cystine) and ca. 58% Cys 34 free thiol (mercaptan form).

[6] In a 10-mL polypropylene centrifuge tube was added 55.0 μL of a 100 mM solution of the DAC:opioid in deionized water to 5.45 mL of commercial 25% (3.75 mM) human serum albumin. Vortexing for 10 s followed by incubation at RT for 3 h, then at 4 °C until further use, afforded a 1.0 mM solution of the conjugate as a mixture of conjugate, nonreduced albumin (half-cystine), albumin (mercaptan form) in a ratio of 22:44:33. Anal. RP-HPLC indicated no presence of the DAC:opioid and the product to be a mixture: t_R = 22.0 min, the conjugate (M^+ 68 209); t_R = 22.9 min, the half-cystine form (M^+ 66 569); and t_R = 24.0 min, the mercaptan form (M^+ 66 453) (Figures 1 and 2).

[7] Assays were performed at MDS Panlabs Taiwan, Ltd.

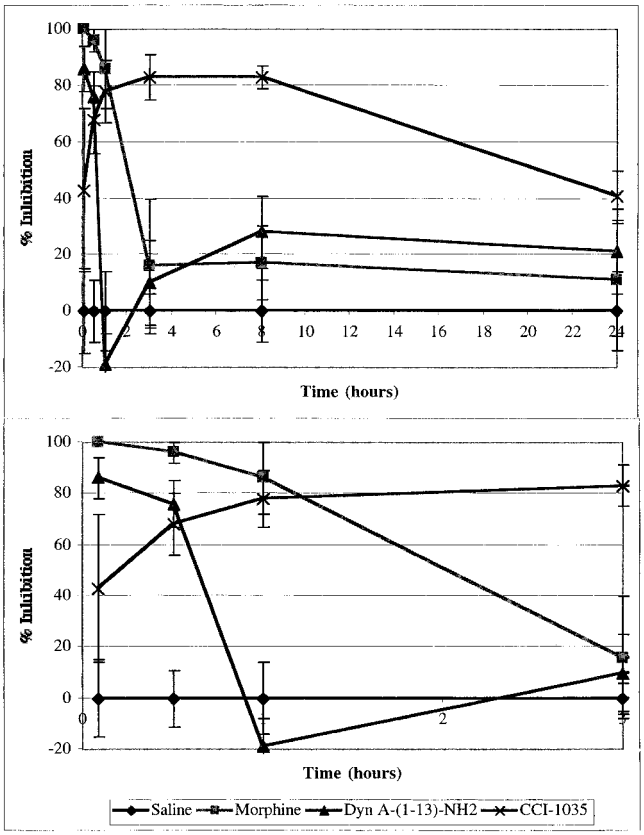

Figure 3. Antinociceptive effect using acetic acid induced writhing assay in mice from 5 min to 24 h (top) and expanded view of data from 0 to 3 h (bottom). Data represent mean ± SEM ($n = 6$); all values with % Inhibition >50% are significantly different from 0.09% NaCl group ($p < 0.01$, Student *t*-test); the value for CCI-1035 (10 μmol/kg) at 8 h is significantly different from morphine group (9.3 μmol/kg) ($p < 0.0005$, Student *t*-test). No appreciable activity was observed in this assay with 20% HSA.

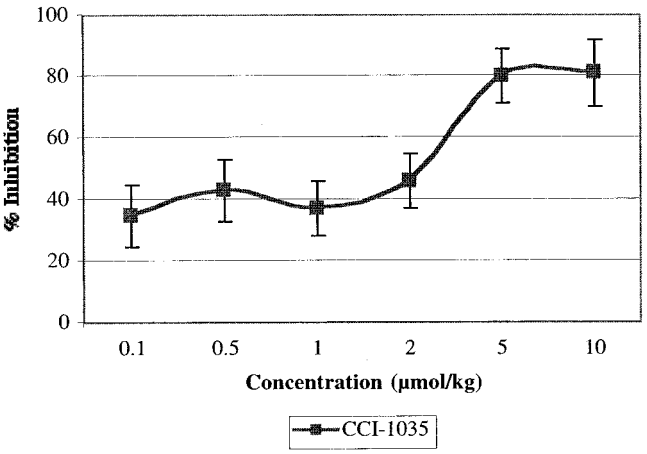

Figure 4. Dose−response relationship of CCI-1035 in mouse acetic acid writhing assay, 3 h post bolus intravenous injection. Data represent mean ± SEM ($n = 6$); all values for CCI-1035 with concentration < 5 μmol/kg are significantly different from 0.09% NaCl group ($p < 0.05$; Student *t*-test).

traverse the vascular interface, comparable to that of native albumin, and interact with the peripheral opioid receptors. These data indicate that in selected applications, conjugation with fractionated serum proteins may be utilized for ex vivo therapy for targets outside the vascular space.

Antinociceptive activity was also evaluated in vivo using a mouse tail-flick assay using the same compounds and concentrations similar to those in the acetic acid writhing assay.[7] Because it is known that dynorphin and its derivatives are inactive in this pain model (*20*) and that albumin has limited access across the blood brain barrier or traverse readily into the CSF, it was anticipated that CCI-1035 would show no antinociceptive activity in this model. In fact, neither Dyn A-(1−13)-NH_2 nor CCI-1035 showed any activity in this assay, and the only activity observed was with morphine.

This report is the first demonstration of a 1:1 dynorphin A derivative specifically conjugated to human serum albumin in an ex vivo fashion to produce an opioid receptor agonist. Additionally, bioconjugation to albumin prolonged the duration of antinociceptic activity in vivo beyond 8 h. Further work is ongoing to determine the actual pharmacokinetic profile, stability of the conjugate, naloxone reversibility, and activity in several other pain models. Application of the DAC technology to opioid therapy could generate a selective long acting opioid agonist, representing an improved therapeutic with controlled biodistribution.

ACKNOWLEDGMENT

We thank Dr. Angelica Fleser for performing the statistical analysis on the in vivo experimental data, Dalbir Sekhon for sample analyses, and Carolyn Finkle for her helpful suggestions.

Supporting Information Available: High-pressure liquid chromatography and mass spectral conditions, mass spec total ion chromatograms, and deconvolution data for 25% human serum albumin and CCI-1035. This material is available free of charge via the Internet at http://pubs.asc.org.

LITERATURE CITED

(1) Cox, B. M., Opheim, K. E., Teschenmacher, H., and Goldstein, A. (1975) A peptide-like substance from pituitary that acts like morphine. 2. Purification and properties. *Life Sci. 16*, 1777−1782.

(2) Goldstein, A., Tachibana, S., Lowney, L. I., Hunkapiller, M., and Hood, L. (1979) Dynorphin-(1−13), an extraordinarily potent opioid peptide. *Proc. Natl. Acad. Sci. U.S.A. 76*, 6666−6670.

(3) Goldstein, A., Fischli, W., Lowney, L. I., Hunkapiller, M., and Hood, L. (1981) Porcine pituitary dynorphin: Complete amino acid sequence of the biologically active heptadecapeptide. *Proc. Natl. Acad. Sci. U.S.A. 78*, 7219−7223.

(4) Naqvi, T., Haq, W., and Mathur, K. B. (1998) Structure−activity relationship studies of dynorphin A and related peptides. *Peptides 19*, 1277−1292.

(5) Arttamangkul, S., Ishmael, J. E., Murray, T. F., Grandy, D. K., DeLander, G. E., Kieffer, B. L., and Aldrich, J. V. (1997) Synthesis and Opioid Activity of Conformationally Constrained Dynorphin A Analogues. 2.[1] Conformational Constraint in the "Address" Sequence. *J. Med. Chem. 40*, 1211−1218.

(6) Chavkin, C., James, I. F., and Goldstein, A. (1982) Dynorphin Is a specific endogenous ligand of the κ opioid receptor. *Science 215*, 413−415.

(7) James, I. F., and Goldstein, A. (1984) Site-directed alkylation of multiple opioid receptors. I. Binding selectivity. *Mol. Pharmacol. 25*, 337−342.

(8) Garzon, J. G., Sanchez-Blazquez, P., Gerhart, J., Loh, H. H., and Lee, N. M. (1984) Dynorphin 1−13: interaction with other opioid ligand bindings in vitro. *Brain Res. 302*, 392−396.

(9) Snyder, K. R., Story, S. C., Heidt, M. E., Murray, T. F., DeLander, G. E., and Aldrich, J. V. (1992) Effect of Modification of the Basic Residues of Dynorphin A-(1−13) Amide on κ Opioid Receptor Selectivity and Opioid Activity. *J. Med. Chem. 35*, 4330−4333.

(10) Smith, A. P., and Lee, N. M. (1988) Pharmacology of Dynorphin. *Annu. Rev. Pharmacol. Toxicol. 28*, 123−140.

(11) Kreek, M. J., Schluger, J., Borg, L., Gunduz, M., and Ho, A. (1999) Dynorphin A1−13 causes elevation of serum levels of prolactin through an opioid receptor mechanism in humans: gender differences and implications for modulation of dopaminergic tone in the treatment of addictions. *J. Pharmacol. Exp. Ther. 288*, 260−269.

(12) Gambús, P. L., Schnider, T. W., Minto, C. F., Youngs, E. J., Billard, V., Brose, W. G., Hochhaus, G., and Shafer, S. L. (1998) Pharmacokinetics of intravenous dynorphin A(1−13) in opioid-naive and opioid-treated human volunteers. *Clin. Pharmacol. Ther. 64*, 27−38.

(13) Greenwald, M. K., Stitzer, M. L., and Haberny, K. A. (1997) Human pharmacology of the opioid neuropeptide dynorphin A(1−13). *J. Pharmacol. Exp. Ther. 281*, 1154−1163.

(14) Uneklabh, T., Sintavanarong, P., Wessagowit, V., and Lukanapichonchut, L. (1995) Clinical effect of dynorphin on heroin addicts. *J. Med. Assoc. Thai. 78*, 509−16.

(15) Giuffra, M., Mouradian, M. M., Davis, T. L., Ownby, J., and Chase, T. N. (1993) Dynorphin agonist therapy of Parkinson's disease. *Clin. Neuropharmacol. 16*, 444−447.

(16) Muller, S., and Hochhaus, G. (1995) Metabolism of Dynorphin A 1−13 in human blood and plasma. *Pharm. Res. 12*, 1165−1170.

(17) Muller, S., Dunker, R., and Hochhaus, G. (1996) Interspecies comparison of in vitro plasma degradation of dynorphin A 1−13. *Pharmazie 51*, 581−585.

(18) Muller, S., Grundy, B. L., and Hochhaus, G. (1996) Metabolism of Dynorphin A1−13 in Human CSF. *Neurochem. Res. 21*, 1213−1219.

(19) Muller, S., Ho, B., Gambus, P., Millard, W., and Hochhaus, G. (1997) An HPLC/RIA method for dynorphin A1−13 and its main metabolites in human blood. *J. Pharm. Biomed. Anal. 16*, 101−109.

(20) Pentel, P. R., Wananukul, W., Hooke, L. P., Jones, C. R. N., Hatsukami, D., Anderson, W. R., and Lee, N. M. (1995) Effects of high intravenous doses of dynorphin A(1−13) on tail flick latency and central nervous system histology in rats. *Pharmacol. Biochem. Behav. 51*, 387−390.

(21) Yaksh, T. L., and Noueihed, R. (1985) The physiology and pharmacology of spinal opiates. *Annu. Rev. Pharmacol. Toxicol. 25*, 433−462.

(22) Banks, W. A. and Broadwell, R. D. (1994) Blood to Brain and Brain to Blood Passage of Native Horseradish Peroxidase, Wheat Germ Agglutinin, and Albumin: Pharmacokinetic and Morphological Assessments. *J. Neurochem. 62*, 2404−2419.

(23) Peters, T. (1996) Metabolism: Albumin in the Body. In *All about albumin: biochemistry, genetics, and medical applications* (T. Peters, Ed.) pp 188−250, Academic Press, Inc., San Diego.

(24) Allen, D. T., and Kiernan, J. A. (1994) Permeation of Proteins from the Blood into Peripheral Nerves and Ganglia. *Neuroscience 59*, 755−764.

(25) Ezrin, A. M., Bridon, D. P., Holmes, D. L., and Milner, P. (1999) *Novel Conjugates of Opioids and Endogenous Carriers*, PCT, WO9924074.

(26) Dixon, F. J., Maurer, P. H., and Deichmiller, M. P. (1953) Half-Lives of Homologous Serum Albumins in Several Species. *Proc. Soc. Exp. Biol. Med. 83*, 287−288.

(27) Hermanson, G. T. *Bioconjugate Techniques*, Academic Press, San Diego, 1996.

(28) Kieffer, B. L., Black, D., and Hirth, C. G. (1993) ^{32}P-Labeled Opioid Peptides with High Affinity for the δ-Opioid Receptor. *Anal. Biochem. 215*, 1−8.

(29) Peters, T. (1996) Tertiary Structure and Physical Chemical Behavior. In *All about albumin: biochemistry, genetics, and medical applications* (T. Peters, Ed.) pp 24−54, Academic Press, Inc., San Diego.

(30) Park, K. B., Tingle, M. D., Grabowski, P. S., Coleman, J. W., and Kitteringham, N. R. (1987) Drug−protein conjugates--XI. Disposition and immunogenicity of dinitrofluorobenzene, a model compound for the investigations of drugs as haptens. *Biochem. Pharmacol. 36*, 591−599.

(31) Wu, C. W., and Yarbrough, L. R. (1976) N-(1-pyrene)-maleimide: a fluorescent cross-linking reagent. *Biochemistry 15*, 2863−2868.

(32) Hayashi, T., Shimoyama, Y., Kuwata, K., and Era, S. (1999) Investigation of slow dynamics of the sulfhydryl in the solution and gel states of bovine serum albumin: A vector electron paramagnetic resonance study. *Jpn. J. Physiol. 49*, 27−33.

(33) Yasuzawa, T., and Tomer, K. B. (1997) Structural determination of the conjugate of human serum albumin with a mitomycin C derivative, KW-2149, by matrix-assisted laser desorption/ionization mass spectrometry. *Bioconjugate Chem. 8*, 391−399.

(34) Maguire, P., Tsai, N., Kamal, J., Cometta-Morini, C., Upton, C., and Loew, G. (1992) Pharmacological profiles of fentanyl analogues at μ, δ and κ opiate receptors. *Eur. J. Pharmacol. 213*, 219−225.

(35) Simonin, F., Gavériaux-Ruff, C., Befort, K., Matthes, H., Lannes, B., Micheletti, G., Mattéi, M.-G., Charron, G., Bloch, B., and Kieffer, B. (1995) κ-Opioid receptor in humans: cDNA and genomic cloning, chromosomal assignment, functional expression, pharmacology, and expression pattern in the central nervous system. *Proc. Natl. Acad. Sci. U.S.A.* 92, 7006−7010.

(36) Wang, J.-B., Johnson, P. S., Persico, A. M., Hawkins, A. L., Griffin, C. A., and Uhl, G. R. (1994) Human μ opiate receptor−cDNA and genomic clones, pharmacologic characterization and chromosomal assignment. *FEBS Lett. 338*, 217−222.

(37) Hooke, L. P., He, L., and Lee, N. M. (1995) [Des-Tyr1]-dynorphin A-(2−17) has naloxone-insensitive antinociceptive effect in the writhing assay. *J. Pharmacol. Exp. Ther. 273*, 802−807.

BC0000233

© 2000 American Chemical Society, Bioconjugate Chem., Holmes bc0000233 Supporting Info Page 1

A Site Specific 1:1 Opioid:Albumin Conjugate with *In Vitro* Activity and Long *In Vivo* Duration

Darren L. Holmes*, Karen Thibaudeau, Benoît L'Archevêque,

Peter G. Milner, Alan M. Ezrin, and Dominique P. Bridon*

ConjuChem, Inc. 225 President-Kennedy Ave.,

Third Floor, Suite 3950,

Montréal (Quebéc), Canada H2X 3Y8

Supporting Information

* To whom correspondence should be addressed.

HPLC-MS Method Information

LC/MS METHOD FOR THE ANALYSIS OF HSA CONJUGATES.
Column Temperature: 50*C
Aquapore RP-300, 7u, 250x4.6mm

HP 1100 Quaternary Pump 1

Control
- Flow : 0.700 ml/min
- Stoptime : 46.00 min
- Posttime : Off

Solvents
- Solvent A : 0.0 % ( )
- Solvent B : Off
- Solvent C : 66.0 % (0.045% TFA in water)
- Solvent D : 34.0 % (0.045% TFA in ACN)

PressureLimits
- Minimum Pressure : 0 bar
- Maximum Pressure : 400 bar

Auxiliary
- Maximal Flow Ramp : 100.00 ml/min^2
- Primary Channel : Auto
- Compressibility : 100*10^-6/bar
- Minimal Stroke : Auto

Store Parameters
- Store Ratio A : Yes
- Store Ratio B : Yes
- Store Ratio C : Yes
- Store Ratio D : Yes
- Store Flow : Yes
- Store Pressure : Yes

HP 1100 Contacts Option

- Contact 1 : Open
- Contact 2 : Open
- Contact 3 : Open
- Contact 4 : Open

Timetable

Time	Solv.B	Solv.C	Solv.D	Flow	Pressure
0.00	0.0	66.0	34.0	0.700	
1.00	0.0	66.0	34.0	0.700	

25.00	0.0	58.8	41.2	0.700
30.00	0.0	50.0	50.0	0.700
35.00	0.0	5.0	95.0	1.000
41.00	0.0	5.0	95.0	1.000
45.00	0.0	66.0	34.0	1.000
46.00	0.0	66.0	34.0	0.700

HP 1100 Contacts Option Timetable
==========

Timetable is empty

==========
HP 1100 Quaternary Pump 1
==========

Control
- Flow : 0.700 ml/min
- Stoptime : 46.00 min
- Posttime : Off

Solvents
- Solvent A : 0.0 % ( )
- Solvent B : Off
- Solvent C : 66.0 % (0.045% TFA in water)
- Solvent D : 34.0 % (0.045% TFA in ACN)

PressureLimits
- Minimum Pressure : 0 bar
- Maximum Pressure : 400 bar

Auxiliary
- Maximal Flow Ramp : 100.00 ml/min^2
- Primary Channel : Auto
- Compressibility : 100*10^-6/bar
- Minimal Stroke : Auto

Store Parameters
- Store Ratio A : Yes
- Store Ratio B : Yes
- Store Ratio C : Yes
- Store Ratio D : Yes
- Store Flow : Yes
- Store Pressure : Yes

HP 1100 Contacts Option
==========

- Contact 1 : Open
- Contact 2 : Open
- Contact 3 : Open
- Contact 4 : Open

Timetable

Time	Solv.B	Solv.C	Solv.D	Flow	Pressure
0.00	0.0	66.0	34.0	0.700	
1.00	0.0	66.0	34.0	0.700	
25.00	0.0	58.8	41.2	0.700	
30.00	0.0	50.0	50.0	0.700	
35.00	0.0	5.0	95.0	1.000	
41.00	0.0	5.0	95.0	1.000	
45.00	0.0	66.0	34.0	1.000	
46.00	0.0	66.0	34.0	0.700	

HP 1100 Contacts Option Timetable

Timetable is empty

HP 1100 Diode Array Detector 1

Signals

Signal	Store	Signal,Bw	Reference,Bw [nm]
A:	Yes	214 20	400 20
B:	Yes	220 20	400 20
C:	Yes	254 20	400 20
D:	No	230 16	360 100
E:	No	280 16	360 100

Spectrum

Store Spectra	:	All
Range from	:	190 nm
Range to	:	400 nm
Range step	:	2.00 nm
Threshold	:	1.00 mAU

Time

Stoptime	:	As pump
Posttime	:	Off

Required Lamps

UV lamp required	:	Yes
Vis lamp required	:	No

Autobalance

Prerun balancing	:	Yes
Postrun balancing	:	No

Margin for negative Absorbance: 100 mAU

Peakwidth	:	> 0.4 min
Slit	:	4 nm

Analog Outputs

```
    Zero offset ana. out. 1:              5 %
    Zero offset ana. out. 2:              5 %
    Attenuation ana. out. 1:          1000 mAU
    Attenuation ana. out. 2:          1000 mAU


HP 1100 Contacts Option
=======================

    Contact 1              :      Open
    Contact 2              :      Open
    Contact 3              :      Open
    Contact 4              :      Open


================================================================================
                        Mass Spectrometer Detector
================================================================================


General Information
------- -----------

Use MSD                    : Enabled
Ionization Mode            : API-ES
Polarity                   : Positive
StopTime                   : asPump
Peakwidth                  : 1.00 min
Scan Speed Override        : Disabled
Fragmentor Ramp            : Disabled

[ Signal 1]

Tune File                  : atunes.tun
Time Filter                : Enabled
Data Storage               : Full

Scan Parameters

   Time |      Mass Range     | Gain|Frag- |Thres-| Step-
  (min) |    Low    |  High    | EMV |mentor| hold | size
 -------|-----------|----------|-----|------|------|-------
    0.00   1280.00   1500.00     1.0   125     100  0.40

[ MSZones]

Gas Temp                   : 350 C                 maximum 350 C
DryingGas                  : 13.0 l/min            maximum 13.0 l/min
Neb Pres                   : 20 psig               maximum 60 psig

VCap                       : 5000 V

================================================================================
                                FIA Series
================================================================================

FIA Series in this Method  :      Disabled
```

```
Time Setting
    Time between Injections :       0.80 min


================================================================================
                        HP 1100 Autosampler 1
================================================================================

Injection
    Injection Mode          :    Standard
    Injector volume         :          1.0 µl

Auxiliary
    Drawspeed               :          200 µl/min
    Ejectspeed              :          500 µl/min
    Draw position           :          0.0 mm

Time
    Stoptime                :      As Pump
    Posttime                :      Off


================================================================================
                      HP 1100 Column Thermostat 1
================================================================================

Temperature settings
    Left temperature        :      50.0*C
    Right temperature       :      Same as left
    Enable analysis         :      When Temp. is within setpoint +/-  0.8*C
    Store left temperature  :      Yes
    Store right temperature:       No

Time
    Stoptime                :      As pump
    Posttime                :      Off

Column Switching Valve      :      Column 1

Timetable is empty
```

High Pressure Liquid Chromatogram and integration of 25% HSA.

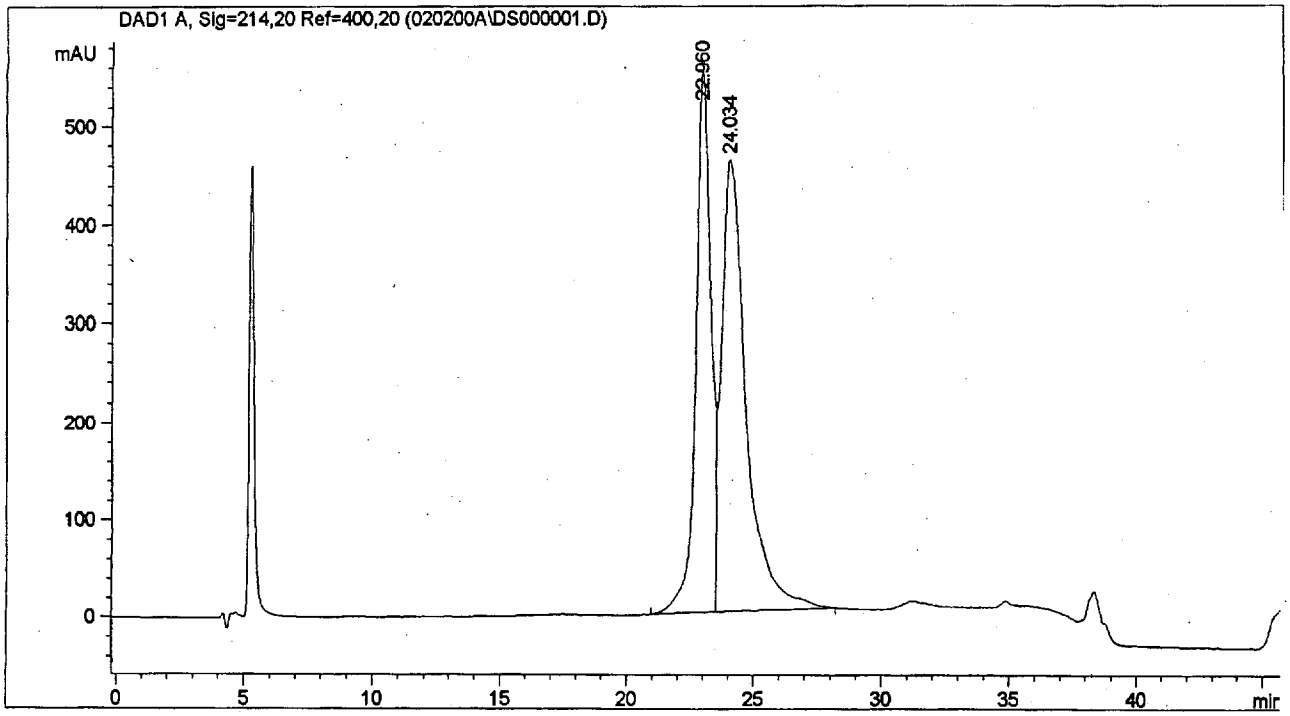


```
================================================================================
                              Area Percent Report
================================================================================

Sorted By             :      Signal
Multiplier            :      1.0000
Dilution              :      1.0000


Signal 1: DAD1 A, Sig=214,20 Ref=400,20

Peak RetTime Type  Width     Area      Height     Area
  #   [min]        [min]    [mAU*s]     [mAU]       %
----|-------|----|-------|----------|----------|--------|
   1  22.960 BV    0.6053 2.30079e4   553.15894  42.4032
   2  24.034 VB    1.0075 3.12520e4   460.65515  57.5968
Totals :                  5.42599e4  1013.81409

================================================================================
                              *** End of Report ***
```

High Pressure Liquid Chromatogram and integration of CCI-1035.

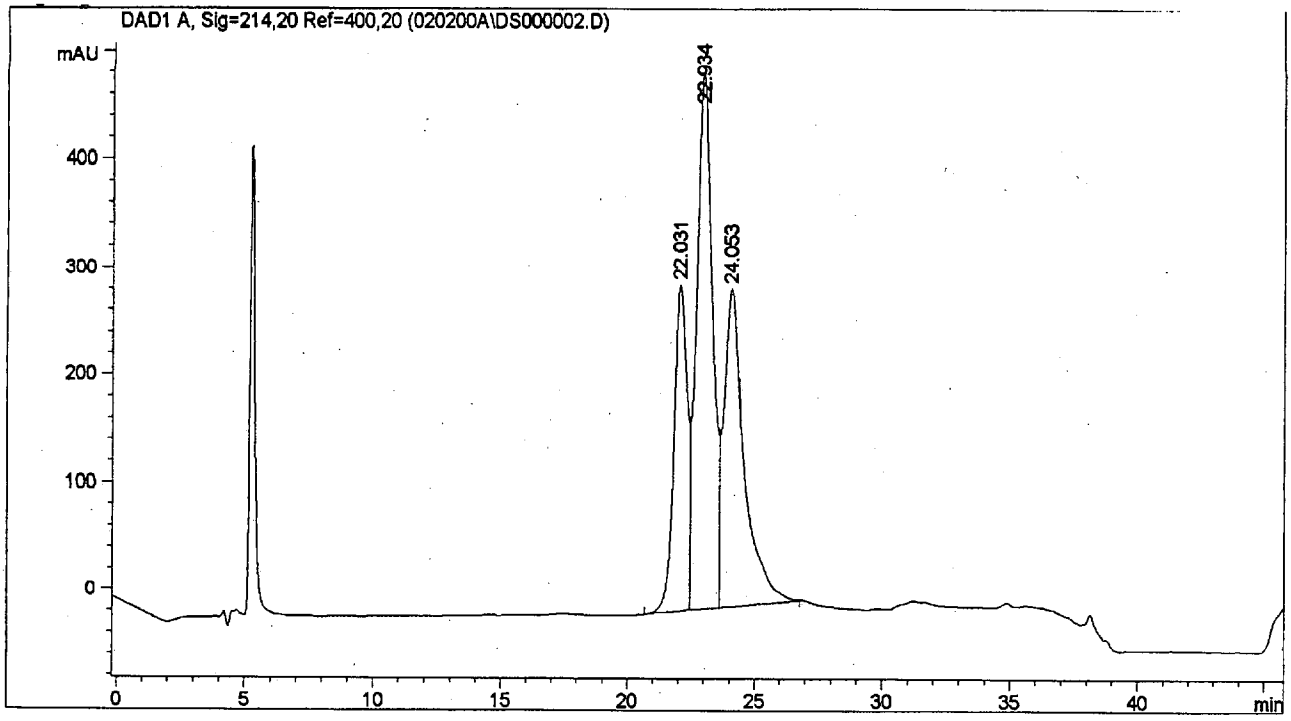


```
=====================================================================
                        Area Percent Report
=====================================================================

Sorted By             :      Signal
Multiplier            :      1.0000
Dilution              :      1.0000

Signal 1: DAD1 A, Sig=214,20 Ref=400,20

Peak RetTime Type  Width     Area      Height     Area
  #   [min]        [min]    [mAU*s]    [mAU]       %
----|-------|----|-------|----------|----------|--------|
   1  22.031 BV    0.5414 1.09857e4   304.13403  22.0831
   2  22.934 VV    0.6436 2.20186e4   498.25443  44.2612
   3  24.053 VB    0.7874 1.67427e4   296.23264  33.6558
Totals :                  4.97469e4  1098.62109

=====================================================================
                        *** End of Report ***
```

Deconvolution Parameters and Results for 25% HSA

Deconvolution Parameters

Adduct Ion:	+H (+), 1.0079 Da
Low MW:	50000
High MW:	70000
Maximum Charge:	50
Minimum Peaks in Set:	5
Retain Residual:	No
Ion PWHH:	0.6 Da
MW Agreement:	0.05 %
Noise Cutoff:	1000 counts
Abundance Cutoff:	10 %
MW Assign:	Curve fit
MW Assign Cutoff:	40 %
Envelope Cutoff:	50 %

Deconvolution of Spectrum # 1 @ 22.806 - 23.332 min

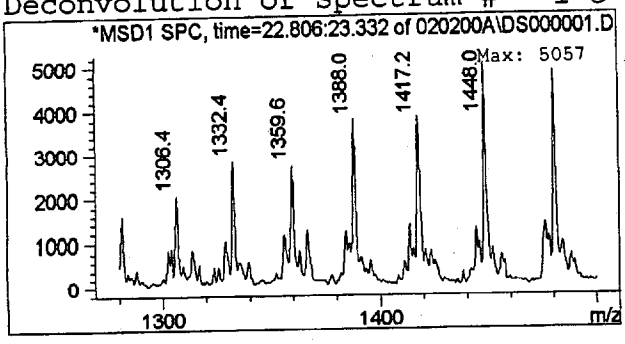

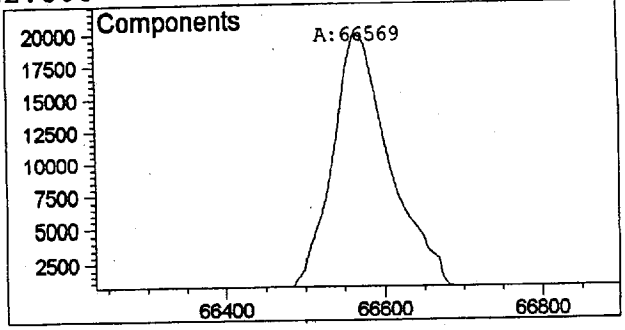

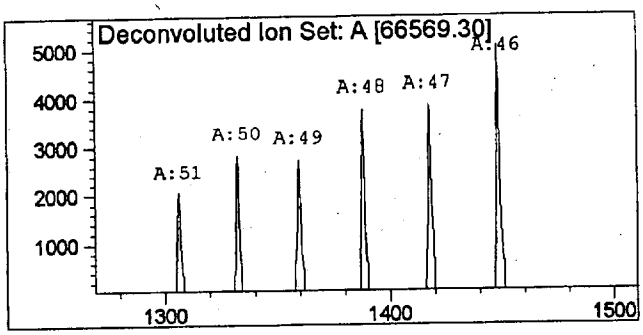

Component	Molecular Weight	Absolute Abundance	Relative Abundance
A	66569.30	19733	100.00

Component A Detail ---

Actual peak	Charge	Compound mass	Pred Peak (Avg)	Pred Peak (Fit)
1306.40	51	66575.00	1306.28	1306.29
1332.40	50	66569.61	1332.39	1332.39
1359.60	49	66571.01	1359.56	1359.57
1388.00	48	66575.62	1387.86	1387.87
1417.20	47	66561.03	1417.37	1417.38
1448.00	46	66561.64	1448.16	1448.17

Averaged Mass (Compound Mass): 66568.98 Std Deviation 6.36
Curve fitted mass: 66569.30 Uncertainty interval: 6.67

*** End of Report ***

Deconvolution of Spectrum # 1 @ 23.905 - 24.525 min

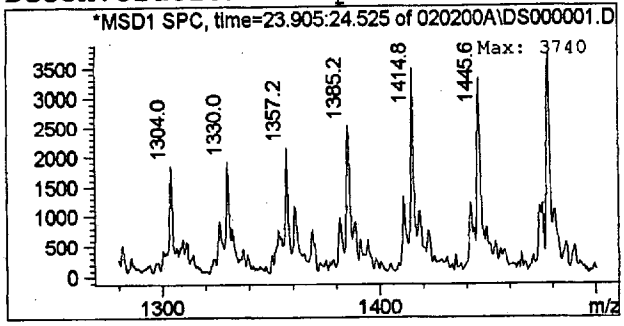

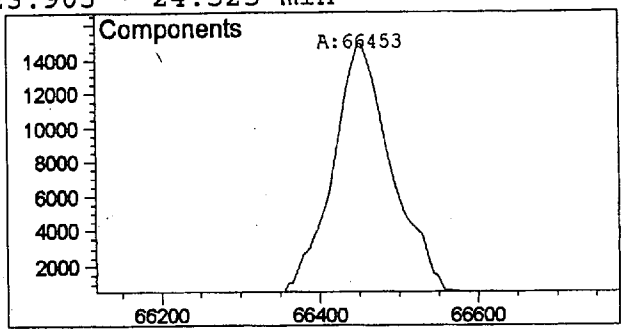

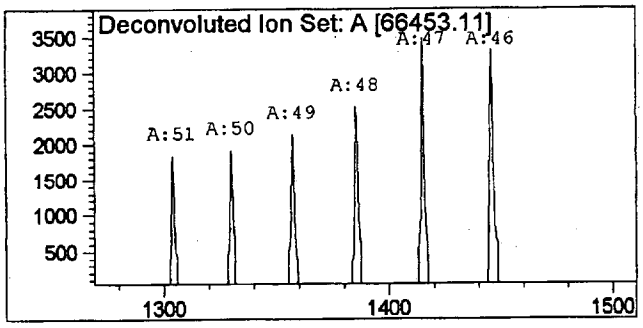

Component	Molecular Weight	Absolute Abundance	Relative Abundance
A	66453.11	14885	100.00

Component A Detail ---

Actual peak	Charge	Compound mass	Pred Peak (Avg)	Pred Peak (Fit)
1304.00	51	66452.60	1303.94	1304.01
1330.00	50	66449.60	1330.00	1330.07
1357.20	49	66453.41	1357.12	1357.19
1385.20	48	66441.22	1385.37	1385.45
1414.80	47	66448.23	1414.82	1414.90
1445.60	46	66451.24	1445.56	1445.64

Averaged Mass (Compound Mass): 66449.38 Std Deviation 4.43
Curve fitted mass: 66453.11 Uncertainty interval: 0.61

*** End of Report ***

Deconvolution Parameters and Results for CCI-1035

Deconvolution Parameters	
Adduct Ion:	+H (+), 1.0079 Da
Low MW:	50000
High MW:	70000
Maximum Charge:	50
Minimum Peaks in Set:	5
Retain Residual:	No
Ion PWHH:	0.6 Da
MW Agreement:	0.05 %
Noise Cutoff:	1000 counts
Abundance Cutoff:	10 %
MW Assign:	Curve fit
MW Assign Cutoff:	40 %
Envelope Cutoff:	50 %

Deconvolution of Spectrum # 1 @ 21.981 - 22.265 min

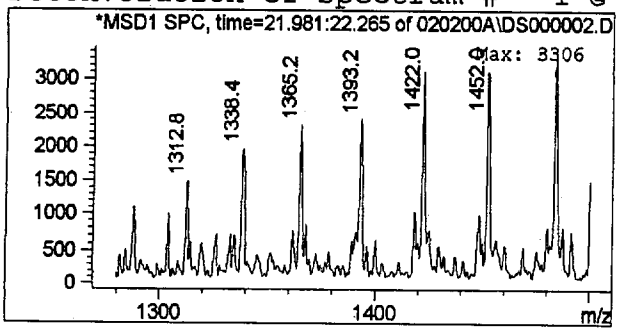

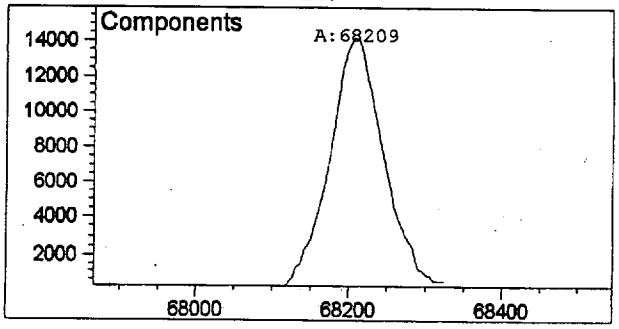

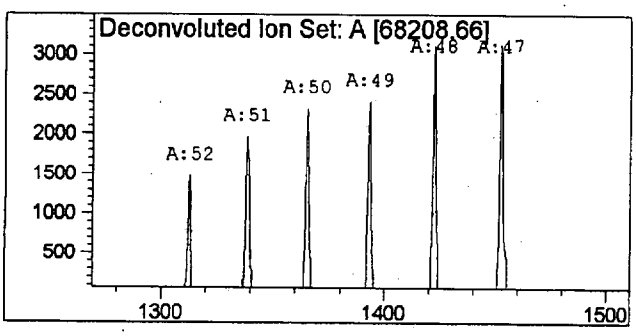

Component	Molecular Weight	Absolute Abundance	Relative Abundance
A	68208.66	14205	100.00

Component A Detail ---

Actual peak	Charge	Compound mass	Pred Peak (Avg)	Pred Peak (Fit)
1312.80	52	68213.19	1312.71	1312.71
1338.40	51	68207.00	1338.43	1338.43
1365.20	50	68209.60	1365.18	1365.18
1393.20	49	68217.41	1393.02	1393.02
1422.00	48	68207.62	1422.02	1422.02
1452.00	47	68196.63	1452.25	1452.26

Averaged Mass (Compound Mass): 68208.58 Std Deviation 7.02
Curve fitted mass: 68208.66 Uncertainty interval: 3.25

*** End of Report ***

Deconvolution of Spectrum # 1 @ 22.739 - 23.285 min

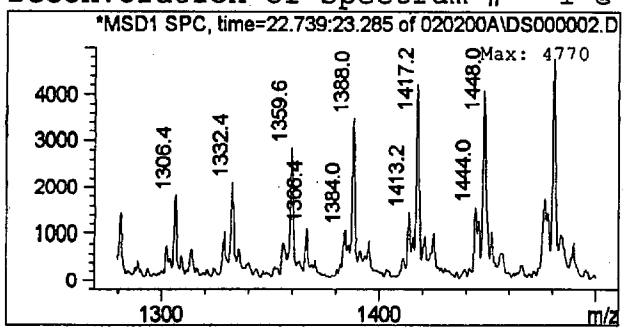

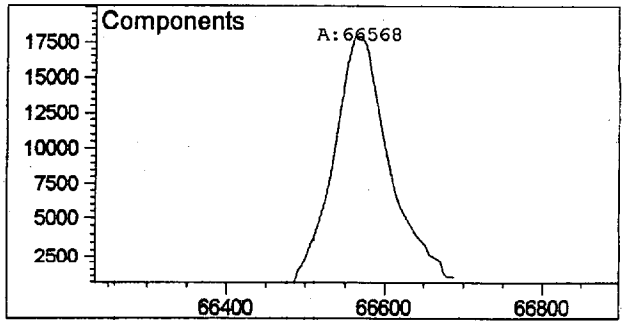

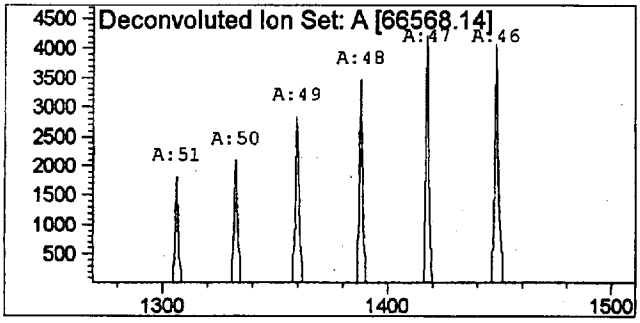

Component	Molecular Weight	Absolute Abundance	Relative Abundance
A	66568.14	17917	100.00

Component A Detail ---

Actual peak	Charge	Compound mass	Pred Peak (Avg)	Pred Peak (Fit)
1306.40	51	66575.00	1306.28	1306.27
1332.40	50	66569.61	1332.39	1332.37
1359.60	49	66571.01	1359.56	1359.54
1388.00	48	66575.62	1387.86	1387.84
1417.20	47	66561.03	1417.37	1417.35
1448.00	46	66561.64	1448.16	1448.14

Averaged Mass (Compound Mass): 66568.98 Std Deviation 6.36
Curve fitted mass: 66568.14 Uncertainty interval: 6.27

*** End of Report ***

Deconvolution of Spectrum # 1 @ 23.949 - 24.328 min

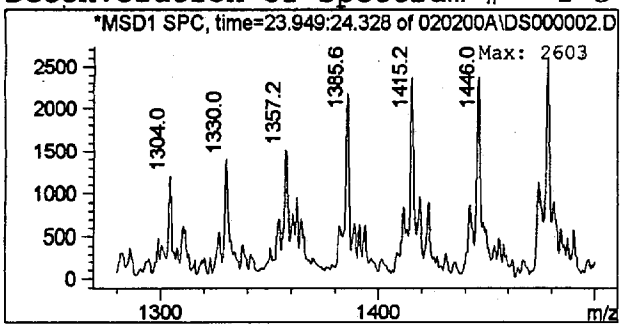

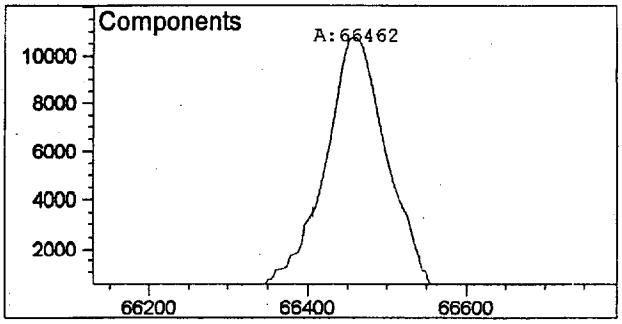

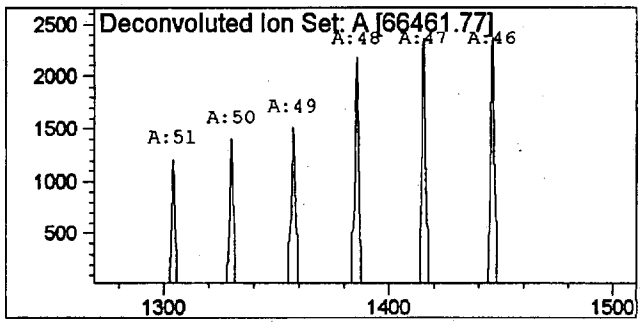

Component	Molecular Weight	Absolute Abundance	Relative Abundance
A	66461.77	10759	100.00

Component A Detail ---

Actual peak	Charge	Compound mass	Pred Peak (Avg)	Pred Peak (Fit)
1304.00	51	66452.60	1304.12	1304.18
1330.00	50	66449.60	1330.18	1330.24
1357.20	49	66453.41	1357.31	1357.37
1385.60	48	66460.42	1385.57	1385.63
1415.20	47	66467.03	1415.02	1415.09
1446.00	46	66469.64	1445.76	1445.83

Averaged Mass (Compound Mass): 66458.78 Std Deviation 8.24
Curve fitted mass: 66461.77 Uncertainty interval: 3.51

*** End of Report ***

Synthesis of Base-Substituted dUTP Analogues Carrying a Photoreactive Group and Their Application to Study Human Replication Protein A

Dmitri M. Kolpashchikov,[†] Tamara M. Ivanova,[†] Victor S. Boghachev,[†] Heinz-Peter Nasheuer,[‡] Klaus Weisshart,[‡] Alain Favre,[§] Pavel E. Pestryakov,[†] and Olga I. Lavrik*[,†]

Novosibirsk Institute of Bioorganic Chemistry, Siberian Division of the Russian Academy of Sciences, 630090 Novosibirsk, Russia, Institut Jacques Monod CNRS, 75251 Paris Cedex 05, France, and Institut für Molekulare Biotechnologie Jena, D-07708 Jena, Germany. Received July 12, 1999; Revised Manuscript Received March 22, 2000

Analogues of dUTP bearing a photoreactive 2-nitro-5-azidobenzoyl (NAB) group linked via spacers of varying length (n = 2, 4, 7−13 atoms) to the 5-position of the uridine ring (NAB-n-dUTP) were synthesized and characterized. DNA polymerase β efficiently incorporated these analogues into synthetic primer-template substrates in place of TTP, which allowed us to selectively introduce a photoreactive group at the 3′ primer terminus. After completing photoreactive primer synthesis, the reaction mixtures were irradiated with monochromatic UV light (315 nm) in the presence of human replication protein A (RPA), a heterotrimer consisting of three subunits with molecular mass 70 kDa (p70), 32 kDa (p32), and 14 kDa (p14), and were separated by SDS−PAGE. The photoreactive primers cross-linked directly with p70 and p32, but cross-linking of p14 was not achieved even by varying the length of the spacer group. The data speak in favor of the protection of p14 by other RPA subunits from the interaction with 3′-end of the primer. Cross-linking of substrates to pol β is inhibited when the analogue bears a short spacer (n = 2, 4, 7, and 8), but this is abrogated somewhat when longer spacers (n = 9−13) are examined. On the basis of these observations, we suggest that RPA and pol β form a complex on primer-template substrates.

INTRODUCTION

The utility of photoactivable reagents for mechanistic studies in molecular biology and biochemistry has been well documented (Meisenheimer and Koch, 1997). In particular, nucleotides carrying aryl azides have been widely used to investigate protein−nucleic acid and nucleic acid−nucleic acid interactions. Analogues of dUTP[1] (UTP) with a bulky group conjugated at the C5 on the pyrimidine ring are substrates for a number of DNA and RNA polymerases (Knorre et al., 1998), which makes them useful tools to study interactions between these substrates and components of the DNA replication machinery. Thus, the insight into the assembly of the replication (transcription) machinery might be deepened by the use of these photoreactive analogues.

The synthesis of 5-[*N*-(2-nitro-5-azidobenzoyl)-*trans*-3-aminopropenyl-1]-2′-deoxyuridine-5′-triphosphate (NAB-4-dUTP) has been described (Wlassoff et al., 1995) and was shown to effectively substitute for TTP in primer extension reactions catalyzed by a various DNA polymerases (Scherbik et al., 1996, Lavrik et al., 1998). Photoreactive primer-template synthesized in situ with this analogue was examined in photoaffinity-labeling experiments with human replication protein A (RPA) (Lavrik et al., 1998). RPA is a multisubunit protein involved in DNA replication, DNA repair, and recombination processes. It exists as a stable heterotrimer consisting of p70, p32, and p14 subunits (Wold, 1997). Incorporation of NAB-4-dUMP into DNA primer substrate demonstrated that the subunits could be cross-linked to the photoreactive nucleotide analogue, but cross-linking of p14 was not detected (Lavrik et al., 1998). Therefore, it was suggested that the p70 binds to the single-stranded region of the DNA duplex and that the p32 is situated near the 3′-end of the primer, while p14 located relatively far from the 3′ primer terminus.

To analyze the influence of spacer length between photoreactive group and 3′-end nucleotide on cross-linking to RPA, we synthesized dUTP analogues bearing photoreactive arylazido group attached by spacers of various length (NAB-n-dUTP, n = 2, 4, 7−13 atoms) between the uracil and the arylazido group and characterized their ability to cross-link to RPA. DNA polymerase β was used to incorporate these photoreactive dUTP analogues into primer-template substrate. Our conditions introduced a single photoreactive moiety at the 3′-end of the primer. Following UV irradiation, analysis of the cross-linking patterns allowed us to

* To whom correspondence should be addressed. Phone: (007-3832) 34-42-96. Fax: (007-3832) 33-36-77. E-mail: lavrik@niboch.nsc.ru.

[†] Novosibirsk Institute of Bioorganic Chemistry.

[‡] Institut für Molekulare Biotechnologie Jena.

[§] Institut Jacques Monod CNRS.

[1] Abbreviations: RPA, human replication protein A; pol β, mammalian DNA polymerase β; (d)NTP, 2′-deoxyribonucleoside-5′-triphosphates and nucleoside-5′-triphosphates; DMF, dimethylformamide; TEA, triethylamine; TEAB, triethylammonium bicarbonate; (d)UTP, 2′-deoxyuridine-5′-triphosphate and uridine-5′-triphosphate; DCC, *N*,*N*′-dicyclohexylcarbodiimide; NAB, 2-nitro-5-azidobenzoyl; SucOH, *N*-hydroxysuccinimide; SucONAB, *N*-hydroxysuccinimide ester of 2-nitro-5-azidobenzoic acid.

10.1021/bc990102i CCC: $19.00 © 2000 American Chemical Society
Published on Web 06/27/2000

identify interactions between RPA and the template-primer in the presence of pol β.

EXPERIMENTAL PROCEDURES

DMF, acetone, acetonitrile, pyridine, and triethylamine were purified and dried according to standard procedures. RPA was expressed in *Escherichia coli* and purified as described by Henricksen et al. (1994) and Nasheuer et al. (1992). Bovine serum albumin (BSA) was from Sigma. Rainbow-colored protein molecular mass markers were from Amersham. Prestained SDS−PAGE molecular mass markers were from Sigma. T_4 polynucleotide kinase was from New England Biolabs. [γ-^{32}P]ATP was from ICN. Synthetic oligonucleotides were obtained from GENSET or synthesized in the Institut Jacques Monod (Paris). Nensorb-20 columns were from Du Pont.

^{1}H NMR spectra were recorded with a Bruker WP-200 SY (200 MHz) and with a Bruker AC-200 (200.132 MHz) spectrometer. All ^{1}H chemical shifts are reported relative to TMS as an internal standard. ^{31}P NMR spectra were recorded on a Bruker AC-200 (81.015 MHz) spectrometer, and the ^{31}P chemical shifts are reported relative to 85% H_3PO_4 as an external standard. UV-absorption spectra were recorded on a Shimadzu UV-2100 (Japan). Analytical TLC was carried out on silica gel plates (Merck, DC-Alufolien Kieselgel 60 F_{254}) in $CHCl_3$/ethanol, 4:1 (v/v) (system A), dioxane/NH_4OH/water, 6:1:4 (v/v) (system B), and ethanol/NH_4OH, 4:1 (v/v) (system C). The compounds containing amino groups were visualized by ninhydrin reaction (1% ninhydrin, 2% acetic acid in methanol). Isolation and purification of the NAB-*n*-dUTP derivatives were performed by reversed-phase high-performance liquid chromatography using a LiChrosorb RP-18, 10 μm (Merck, Germany) 4.6 × 250 mm column, a Waters 600E, and a Waters 484 tunable absorbance detector. A linear gradient (2 mL/min) was from 0 to 30% acetonitrile in 0.05 M TEAB, pH 7.5. Computer molecular modeling simulations were carried out using MOPAC program.

5-(*trans*-3-Aminopropenyl-1)-2′-deoxyuridine-5′-triphosphate (**IV**) was prepared according to the procedure reported by Langer et al. (1981), *N*-hydroxysuccinimide esters of 2-nitro-5-azidobenzoic acid (SucONAB) was synthesized as described by Dobrikov et al. (1992a), 5-(aminomethyl)-2′-deoxyuridine (**I**) was obtained from thymidine in three steps using the method described earlier (Zarytova et al., 1991), and *N*-hydroxysuccinimide esters of *N*-trifluoroacetyl amino acids (**Va**−**g**, see Scheme 2) were obtained according to the method described for the synthesis of *N*-hydroxysuccinimide esters of amino acids (Anderson et al., 1964). *N*-(2-Nitro-5-azidobebzoyl)-4-aminobutyric acid (**VIa**), *N*-(2-nitro-5-azidobebzoyl)-5-aminopentanoic acid (**VIb**), *N*-(2-nitro-5-azidobebzoyl)-6-aminocaproic acid (**VIc**), *N*-(2-nitro-5-azidobebzoyl)-7-aminoheptanoic acid (**VId**), and *N*-(2-nitro-5-azidobebzoyl)-8-aminocaprylic acid (**VIe**) were obtained by benzoylation of amino group of corresponding amino acids by SucONAB in the presence of TEA according to the standart procedure (Anderson et al., 1964).

5-[*N*-(Trifluoroacetyl)-aminomethyl]-2′-deoxyuridine (II). The nucleoside **I** [72 mg (0.28 mmol)] was dissolved in 2 mL of methanol and was treated with 334 μL (2.80 mmol) of ethyltrifluoroacetate in the presence of 390 μL (2.80 mmol) TEA. The reaction mixture was left at room temperature for 24 h, pooled under reduced pressure, then dissolved in 5 mL of water. Product **II** was purified by passing through Dowex 50 WX 2. The fraction of nucleoside eluted by water was evaporated in a vacuum. The yield of compound **II** was 120 mg (87%). R_f 0.78 in system A; UV (H_2O) λ_{max} 268 nm (ϵ = 8800), λ_{min} 234 nm (ϵ = 3500); ^{1}H NMR (D_2O) δ 2.35 (m, H2′, 2H), 3.79 (m, H5′, 2H), 4.04 (m, H7, H4′, 3H), 4.45 (m, H3′, 1H), 6.26 (t, J = 6.0 Hz, H1′, 1H), 7.54 (s, H6, 1H).

Scheme 1

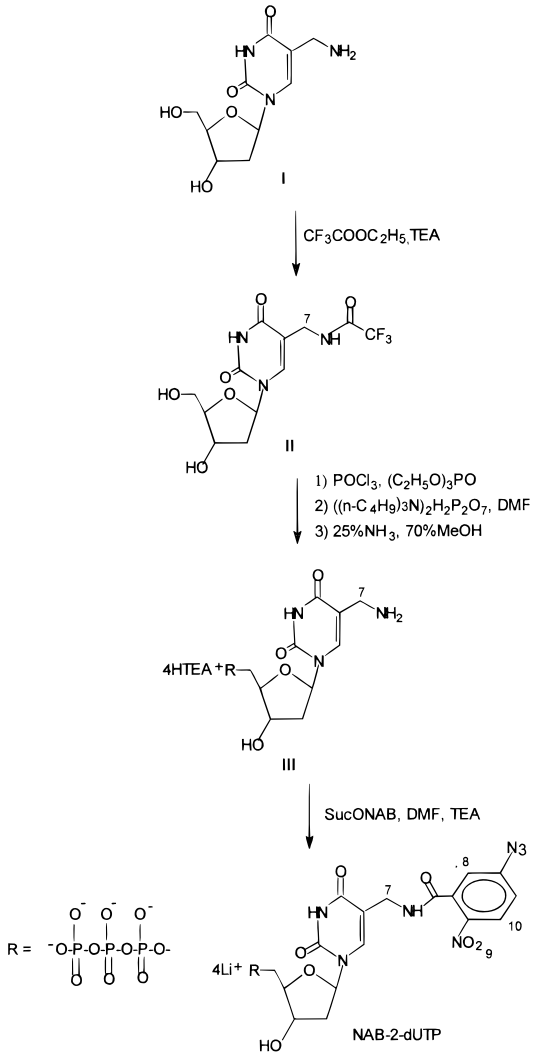

5-(Aminomethyl)-2′-deoxyuridine-5′-triphosphate (Triethylammonium salt) (III). Compound **III** was obtained from compound **II** using the method described earlier for the synthesis ATP (Ludwig et al., 1981). $POCl_3$ [21 μL (300 μmol)] was added to an ice-cooled suspension of **II** 35.3 mg (100 μmol) in 300 μL of triethyl phosphate. After 4 h at 4 °C, the reaction mixture was treated with a freshly prepared solution of 500 μL of 1 M bis(tri-*n*-butylammonium) pyrophosphate and 100 μL of tri-*n*-butylamine. When the phosphorylation was completed (about 1 min), 10 mL of 1 M triethylammonium bicarbonate was added. After 1 h at room temperature, the reaction mixture was pooled on a rotary evaporator and treated with 10 mL of concentrated aqueous ammonia for 3 h to remove the trifluoroacetic protecting group. The solution was evaporated and diluted with 15 mL of water, and the product was isolated by anion-exchange chromatography on DEAE-cellulose DE-32 (1 × 15 cm) using a gradient of triethylammonium bicarbonate (0.00−0.35 M, pH 7.5). The fraction containing compound **III** was evaporated and dried in a vacuum to give 30 μmol (30%) of **III**: R_f 0.15 in the system B; UV (H_2O) λ_{max} = 268 nm (ϵ = 8600), λ_{min} = 235 nm (ϵ = 3700); ^{31}P NMR (D_2O) δ −21.49 (t, J = 20 Hz, P_β, 1P), −11,16 (d, J = 20 Hz, P_α, 1P), −6.0 (d, J = 20 Hz, P_γ,

Scheme 2

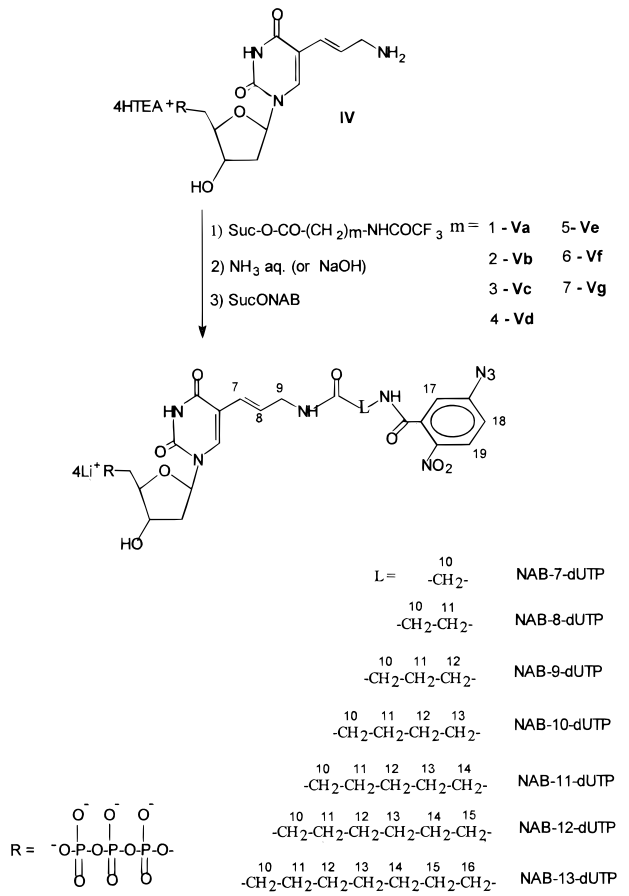

1P), ^{1}H NMR (D_2O) δ 1.24 [t, J = 7 Hz, CH_3 of $(C_2H_5)_3NH^+$, 36H], 2.40 (t, J = 5.5 Hz, H2′, 2H), 3.10 [q, CH_2 of $(C_2H_5)_3NH^+$, 24H], 3.96 (m, H7, H5′, 4H), 4.20 (m, H4′, H3′, 2H), 6.28 (t, J = 6 Hz, H1′, 1H), 8.29 (s, H6, 1H).

5-[*N*-(2-Nitro-5-azidobenzoyl)aminomethyl]-2′-deoxyuridine-5′-triphosphate (lithium salt) (NAB-2-dUTP). SucONAB [4.88 mg (16 mmol)] was added to the solution of compound **III** 34.4A_{268} (4 μmol) in a mixture of DMF (60 μL) and TEA (10 μL). The reaction mixture was left at room temperature for 4 h and then was loaded directly onto a column of DEAE-cellulose DE−32. The product NAB-2-dUTP was isolated by reversed-phase HPLC, precipitated with 2% $LiClO_4$ in acetone, and dried in a vacuum. The yield of NAB-*n*-dUTP was 89%. R_f 0.45 in system B; UV (H_2O) λ_{max} = 267 nm (ϵ = 10 000), 320 nm (ϵ = 8800), λ_{min} = 237 nm (ϵ = 8200), 293 nm (ϵ = 6300); ^{31}P NMR (D_2O) δ −19.97 (t, J = 20 Hz, P_β, 1P), −10.24 (d, J = 20 Hz, P_α, 1P), −4.3 (d, J = 20 Hz, P_γ, 1P); ^{1}H NMR δ (D_2O) 2.57 (d, J = 5.5 Hz, H2′, 2H), 4.27 (m, H7, H4′, H5′, 5H), 4.46 (m, H3′, 1H), 6.42 (t, J = 7 Hz, H1′, 1H), 7.32 (d, J = 2.3 Hz, H8, 1H), 7.48 (dd, J = 2.3 and 8.9 Hz, H9, 1H), 8.20 (s, H6, 1H), 8.49 (d, J = 8.9 Hz, H10, 1H).

5-[*N*-(*N*′-(2-Nitro-5-azidobenzoyl)-glycyl)-*trans*-3-aminopropenyl-1]-2′-deoxyuridine-5′-triphosphate (lithium salt) (NAB-7-dUTP). *N*-Hydroxysuccinimide ester of *N*-trifluoroacetyl glycine (**Va**) [5.4 mg (20 μmol)] was added to the solution of compound **IV** (10 μmol, 80A_{290}) in a mixture of 200 μL of DMF and 10 μL of TEA. After 1.5 h at room temperature, 2 mL of 2% $LiClO_4$ in acetone was added to the reaction mixture. The precipitate was isolated by centrifugation and washed by acetone two times. A total of 1 mL of 25% aqueous ammonia was added to the precipitate. After complete trifluoroacetyl protecting group removing (1 h 37 °C) by aqueous ammonia reaction mixture was evaporated under reduced pressure. The solid residue was dissolved in a 100 μL of mixture of DMF:H_2O:TEA (10:10:1) and treated with 13.1 mg (40 μmol) SucONAB. After 1.5 h at room temperature, the reaction mixture was treated by 2 mL of 2% $LiClO_4$ in acetone and washed by acetone, dried on air, dissolved in 1.5 mL of H_2O and applied on HPLC column. Fractions containing NAB-7-dUTP was evaporated, dissolved in 100 μL of H_2O, precipitated by 2% $LiClO_4$ in acetone, washed by acetone and ethyl ester, and dried on air. Yield 5.9 mg (75%); R_f 0.45 (system B); UV (H_2O) λ_{max} = 306 nm (ϵ = 14 100) λ_{min} = 264 nm (ϵ = 9900); ^{31}P NMR (D_2O) δ −19.65 (t, J = 20 Hz, P_β, 1P), −10.15 (d, J = 20 Hz, P_α, 1P), −4.18 (d, J = 20 Hz, P_γ, 1P), ^{1}H NMR (D_2O) δ 2.50 (t, J = 5.5 Hz, H2′, 2H), 3.78 [s, H $(CH_2)_{10}$, 2H], 4.05 (d, J = 5 Hz, H9, 2H) 4.25 (m, H3′, H4′, H5′, 4H), 6.2−6.4 (m, H1′, H7, H8, 3H), 7.40 (d, J = 2.3 Hz, H17, 1H), 7.49 (dd, J = 2.3 and 8.9 Hz, H18, 1H), 8.05 (s, H6, 1H), 8.35 (d, J = 8.9 Hz, H19, 1H).

5-[*N*-(*N*′-(2-Nitro-5-azidobenzoyl)-3-aminopropeonyl)-*trans*-3-aminopropenyl-1]deoxyuridine-5′-triphosphate (lithium salt) (NAB-8-dUTP) was synthesized from **IV** and *N*-hydroxysuccinimide ester of *N*-trifluoroacetyl β-alanine **(Vb)** according to the method described above for synthesis of compound NAB-7-dUTP. Yield 4.4 mg (53%); R_f 0.45 (system B); UV (H_2O) λ_{max} = 307 nm (ϵ = 14 300) λ_{min} = 265 nm (ϵ = 10 050); ^{31}P NMR (D_2O) δ −19.67 (t, J = 20 Hz, P_β, 1P), −10,16 (d, J = 20 Hz, P_α, 1P), −4.18 (d, J = 20 Hz, P_γ, 1P); ^{1}H NMR (D_2O) δ 2.34 (d, J = 5.5 Hz, H2′, 2H), 2.60 [t, J = 6.0 Hz, H of $(CH_2)_{10}$, 2H], 3.66 [s, H of $(CH_2)_{11}$, 2H], 4.15 (d, J = 5.0 Hz, H9, 2H) 4.20 (m, H3′, H4′, H5′, 4H), 6.22−6.34 (m, H1′, H7, H8, 3H), 7.05 (d, J = 2.3 Hz, H17, 1H), 7.36 (dd, J = 2.3 and 8.9 Hz, H18, 1H), 7.69 (s, H6, 1H), 8.18 (d, J = 8.9 Hz, H19, 1H).

5-[*N*-(*N*′-(2-Nitro-5-azidobenzoyl)-4-aminobutyryl)-*trans*-3-aminopropenyl-1]-2′-deoxyuridine-5′-triphosphate (lithium salt) (NAB-9-dUTP) was synthesized from **IV** and *N*-hydroxysuccinimide ester of *N*-trifluoroacetyl-4-aminobutyric acid **(Vc)** according to the method described above for synthesis of compound NAB-7-dUTP. Yield 3.0 mg (37%); R_f 0.45 (system B); UV (H_2O) λ_{max} = 305 nm (ϵ = 14 400) λ_{min} = 266 nm (ϵ = 10 100); ^{31}P NMR (D_2O) δ −19.73 (t, J = 20 Hz, P_β, 1P), −10.24 (d, J = 20 Hz, P_α, 1P), −4.27 (d, J = 20 Hz, P_γ, 1P), ^{1}H NMR (D_2O) δ 2.10 [m, H of $(CH_2)_{11}$, 2H], 2.35 [m, H2′, H $(CH_2)_{10}$, 2H], 3.39 [t, J = 6.0 Hz, H of $(CH_2)_{12}$, 2H], 3.99 (d, J = 7 Hz, H9, 2H) 4.20 (m, H3′, H4′, H5′, 4H), 6.16−6.35 (m, H1′, H7, H8, 3H), 7.15 (d, J = 2.3 Hz, H17, 1H), 7.29 (dd, J = 2.3 and 8.9 Hz, H18, 1H), 7.79 (s, H6, 1H), 8.18 (d, J = 8.9 Hz, H19, 1H).

5-[*N*-(*N*′-(2-Nitro-5-azidobenzoyl)-5-aminopentanoyl)-*trans*-3-aminopropenyl-1]-2′-deoxyuridine-5′-triphosphate (lithium salt) (NAB-10-dUTP) was synthesized from **IV** and *N*-hydroxysuccinimide ester of *N*-trifluoroacetyl-5-aminopentanoic acid **(Vd)** according to the method described above for synthesis of compound NAB-7-dUTP, but instead aqueous ammonia 2 M NaOH (1.5 h, 20 °C) was used for removing trifluoroacetyl protecting group. Yield 2.6 mg (29%); R_f 0.45 (system B); UV (H_2O) λ_{max} = 305 nm (ϵ = 14 450) λ_{min} = 266 nm (ϵ = 8200); ^{31}P NMR (D_2O) δ −19.80 (t, J = 20 Hz, P_β, 1P), −10.24 (d, J = 20 Hz, P_α, 1P), −4.25 (d, J = 20 Hz, P_γ, 1P), ^{1}H NMR (D_2O) δ 1.78 [m, H of $(CH_2)_{11,\ 12}$ 4H], 2.45 [m, H2′, H of $(CH_2)_{10}$, 2H], 3.48 [m, H of $(CH_2)_{13}$, 2H], 4.05 (d, J = 7 Hz, H9, 2H) 4.27 (m, H3′, H4′, H5′, 4H), 6.18−6.39 (m, H1′, H7, H8, 3H), 7.27 (d, J = 2.3 Hz, H17,

1H), 7.43 (dd, $J = 2.3$ Hz and 8.9 Hz, H18, 1H), 7.84 (s, H6, 1H), 8.30 (d, $J = 8.9$ Hz, H19, 1H).

5-[*N*-(*N′*-(2-Nitro-5-azidobenzoyl)-6-aminohexanoyl)-*trans*-3-aminopropenyl-1]-2′-deoxyuridine-5′-triphosphate (lithium salt) (NAB-11-dUTP) was synthesized from **IV** and *N*-hydroxysuccinimide ester of *N*-trifluoroacetyl-6-aminocaproic acid **(Ve)** according to the method described above for synthesis of compound NAB-7-dUTP, but instead aqueous ammonia 2 M NaOH (2 h, 20 °C) was used for removing trifluoroacetyl protecting group. Yield 1.7 mg (19%); R_f 0.45 (system B); UV (H_2O) $\lambda_{max} = 305$ nm ($\epsilon = 14\,400$) $\lambda_{min} = 266$ nm ($\epsilon = 10\,100$); ^{31}P NMR (D_2O) δ −19.84 (t, $J = 20$ Hz, P_β, 1P), −10.36 (d, $J = 20$ Hz, P_α, 1P), −4.35 (d, $J = 20$ Hz, P_γ, 1P), ^{1}H NMR (D_2O) δ 1.68 [m, H of $(CH_2)_{11,\ 12,\ 13}$ 6H], 2.40 [m, H2′, H $(CH_2)_{10}$, 4H], 3.45 [m, H of $(CH_2)_{14}$, 2H], 3.96 (m, H9, 2H) 4.25 (m, H3′, H4′, H5′, 4H), 6.15−6.36 (m, H1′, H7, H8, 3H), 7.09 (d, $J = 2.3$ Hz, H17, 1H), 7.24 (dd, $J = 2.3$ and 8.9 Hz, H18, 1H), 7.66 (s, H6, 1H), 8.18 (d, $J = 8.9$ Hz, H19, 1H).

5-[*N*-(*N′*-(2-Nitro-5-azidobenzoyl)-7-aminoheptanoyl)-*trans*-3-aminopropenyl-1]-2′-deoxyuridine-5′-triphosphate (lithium salt) (NAB-12-dUTP) was synthesized from **IV** and *N*-hydroxysuccinimide ester of *N*-trifluoroacetyl-7-aminoheptanoic acid **(Vf)** according to the method described above for synthesis of compound NAB-7-dUTP, but instead aqueous ammonia 2 M NaOH (2 h, 20 °C) was used for removing trifluoroacetyl protecting group. Yield 1.1 mg (12%); R_f 0.45 (system B); UV (H_2O) $\lambda_{max} = 304$ nm ($\epsilon = 14\,400$) $\lambda_{min} = 266$ nm ($\epsilon = 10\,100$); ^{31}P NMR (D_2O) δ −19.75 (t, $J = 20$ Hz, P_β, 1P), −10.30 (d, $J = 20$ Hz, P_α, 1P), −4.30 (d, $J = 20$ Hz, P_γ, 1P); ^{1}H NMR (D_2O) δ 1.46 [m, H of $(CH_2)_{12,13}$ 4H], 1.67 [m, H of $(CH_2)_{11,14}$ 4H], 2.37 [m, H2′, H $(CH_2)_{10}$, 4H], 3.42 [t, $J = 6$ Hz, H of $(CH_2)_{15}$, 2H], 3.97 (m, H9, 2H) 4.24 (m, H3′, H4′, H5′, 4H), 6.17−6.32 (m, H1′, H7, H8, 3H), 7.16 (d, $J = 2.3$ Hz, H17, 1H), 7.32 (dd, $J = 2.3$ and 8.9 Hz, H18, 1H), 7.73 (s, H6, 1H), 8.21 (d, $J = 8.9$ Hz, H19, 1H).

5-[*N*-(*N′*-(2-nitro-5-azidobenzoyl)-8-aminooctanoyl)-*trans*-3-aminopropenyl-1]-2′-deoxyuridine-5′-triphosphate (lithium salt) (NAB-13-dUTP) was synthesized from **IV** and *N*-hydroxysuccinimide ester of *N*-trifluoroacetyl-8-aminocaprylic acid **(Vg)** according to the method described above for synthesis of compound NAB-7-dUTP, but instead aqueous ammonia 2 M NaOH (2 h, 20 °C) was used for removing trifluoroacetyl protecting group. Yield 0.8 mg (9%); R_f 0.45 (system B); UV (H_2O) $\lambda_{max} = 307$ nm ($\epsilon = 14\,400$) $\lambda_{min} = 265$ nm ($\epsilon = 10\,100$). ^{31}P NMR (D_2O) δ −18.87 (t, $J = 20$ Hz, P_β, 1P), −10.32 (d, $J = 20$ Hz, P_α, 1P), −4.42 (d, $J = 20$ Hz, P_γ, 1P), ^{1}H NMR (D_2O) δ 1.42 (m, H of $(CH_2)_{12,\ 13,\ 14}$ 6H), 1.65 [m, H of $(CH_2)_{11,\ 15}$ 4H], 2.35 [m, H2′, H $(CH_2)_{10}$, 4H], 3.43 [m, H of $(CH_2)_{16}$, 2H], 3.98 (m, H9, 2H) 4.25 (m, H3′, H4′, H5′, 4H), 6.17−6.32 (m, H1′, H7, H8, 3H), 7.16 (d, $J = 2.3$ Hz, H17, 1H), 7.32 (dd, $J = 2.3$ and 8.9 Hz, H18, 1H), 7.73 (s, H6, 1H), 8.21 (d, $J = 8.9$ Hz, H19, 1H).

Radioactive Labeling of Oligonucleotide Primers. Dephosphorylated primers were 5′-phosphorylated with T_4 polynucleotide kinase as described (Sambrook et al., 1989). Unreacted [γ-^{32}P]ATP was separated by passing the mixture over a Nensorb-20 column using the manufacturer's suggested protocol.

Primer-Template Annealing. Lyophilized oligonucleotides were dissolved in 10 mM Tris-HCl, pH 7.4, and 1 mM EDTA and the concentrations were determined from their UV absorbance at 260 nm. Primer-templates were annealed at a molar ratio of 1:1 by heating at 90 °C for 3 min, and then the mixture was allowed to cool slowly to room temperature. The sequences of the primers and templates used were as follows:

5′-GGTTCGATATCGTAGTTCTAGTGTATAGCCCCTACC-3′

3′-CACATATCGGGGATGG-5′

Photochemical Cross-Linking. RPA was photoaffinity-labeled with photoreactive primer synthesized in situ using NAB-*n*-dUTP and pol β. Reaction mixtures (10 μL) contained 50 mM Tris-HCl, pH 7.8, 10 mM $MgCl_2$, 50 mM KCl, 1.4 μM pol β, 0.7 μM 5′-[^{32}P]primer-template, 10 μM NAB-*n*-dUTP, and RPA at a final concentration of 0.1−0.5 μM, as indicated. The reaction mixtures were incubated at 25 °C for 30−45 min to allow elongation of the primers. The mixtures were then spotted on Parafilm that was placed on ice and UV irradiated by a Bausch and Lomb monochromator equipped with an HBO W super pressure mercury lamp (315 nm) for 15 min. Then reactions were stopped by following addition of Laemmli buffer and heating. The photochemically cross-linked protein−DNA samples were separated by SDS−PAGE. Dried gels were subjected to autoradiography or quantified using a phosphorimager (Molecular Dynamics).

RESULTS

NAB-*n*-dUTP Synthesis and Characterization. The photochemical properties of the NAB group allow UV activation to be performed by near UV light, i.e., greater than 300 nm, which is beyond the absorbance of nucleic acids and proteins. Additionally, while this reactive group is very effective in the modification of proteins, it does not cross-link to DNA duplexes to any extent (Scherbik et al., 1997).

NAB-2-dUTP was obtained as shown in Scheme 1. Treatment of nucleoside **I** with ethyl trifluoroacetate results in formation of compound **II** with a protected amino group. The synthesis of compound **III** was carried out from nucleoside **II** according to the method described earlier (Ludwig, 1981) and summarized as follows. Reaction of the compound **II** with $POCl_3$ results in the formation of a nucleoside-5′-phosphorodichloridate that was treated with bis(tri-*n*-butylammonium) pyrophosphate to produce a nucleoside-5′-triphosphate. The treatment of the reaction mixture with concentrated aqueous ammonia permits the quantitative removal of the CF_3-CO residue from NH_2-group. The modified dUTP was purified and then converted to its triethylammonium salt (**III**). The photoreactive derivative (NAB-2-dUTP) was obtained by benzoylation of the aliphatic amino group of **III** with the *N*-hydroxysuccinimide ester of 2-nitro-5-azidobenzoic acid (SucONAB). The use of the triethylammonium salt of compound **III** permits us to carry out the reaction in DMF in the presence of triethylamine. This allowed us to achieve a high yield of the NAB-2-dUTP (near 90%) by using lower excess of SucONAB.

Compound **IV** (triethylammonium salt) (Scheme 2) was synthesized starting from dUTP, as previously described (Langer et al., 1981). The synthesis of compounds NAB-*n*-dUTP ($n = 7-13$) was initially carried out by the procedure as shown in Scheme 2. The only modification was that the trifluoroacetic group of NAB-*n*-dUTPs ($n = 7-9$) was removed by treatment with aqueous ammonia and that of NAB-*n*-dUTPs ($n = 10-13$) was removed by 2 M NaOH. The synthesis of NAB-*n*-dUTPs ($n < 10$) was quite efficient (30−75%), but the yield of the synthesis of nucleotide analogues with long spacers ($n = 11-13$) was reduced during the second stage of the synthesis (yield 10−20%). Two reasons might explain this result:

Scheme 3

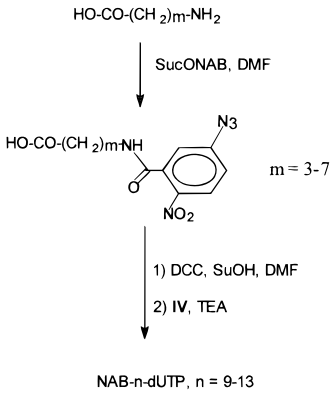

hydrolysis of the trifluoroacetic protecting group with NaOH did not completely remove the $COCF_3$ group, whereas the hydrolysis of the triphosphate group was already come out. Therefore, an alternative procedure to synthesize the analogues was created (Scheme 3). First, the amino groups of amino acids were acylated by SucONAB leading to the $HOOC(CH_2)_mNHNAB$ (m = 3, 4, 5, 6, 7). Next, the condensation of the latter compound with *N*-hydroxysuccinimide in the presence of DCC resulted in $SucOOC(CH_2)_mNHNAB$. Finally, the amino group of compound **IV** was acylated using $SucOOC(CH_2)_mNHNAB$ in the presence of TEA. This procedure increased the yield obtained for NAB-*n*-dUTPs with longer spacers (n = 9−13) to 80−90% (data not shown).

The NAB-*n*-dUTPs were characterized by UV and NMR (^1H, ^{31}P) spectra. Characteristic absorption spectra show superposition of the spectra of the corresponding modified nucleotides **III**, **VI**, and amides of 2-nitro-5-azidobenzoic acid (data not shown).

Photoreactive Primer-Template Duplex Synthesis. As described earlier, NAB-4-dUTP can be efficiently incorporated by HIV−RT (Scherbik et al., 1997), mammalian pol α, pol β, and Klenow fragment of *E. coli* DNA polymerase I (Lavrik et al., 1998). This property was utilized to synthesize a 5′-^{32}P-labeled primer by pol β, containing the photoreactive dNMP moiety, which was subsequently bound to RPA under UV-irradiation. The interactions between RPA and the primer-template in the presence of pol β represent a model for the interactions, which take place during DNA methabolism.

The primer elongation reactions were carried out under high-salt conditions to avoid the DNA unwinding by RPA which has been observed at low ionic strength (Georgaki et al., 1992). No differences in the efficiency of incorporation of the photoreactive analogue were observed either in the absence or in the presence of RPA (data not shown). Figure 1 shows that the initial primer (lane 1) is fully consumed in the reaction and that final product is obtained in the presence of both dTTP (lane 2) and NAB-*n*-dUTP (lanes 3−11). The decreased mobility of the primer in the denaturing gel electrophoresis correlated with the increased length of the spacer group.

Photo-Cross-Linking Experiments. The primers containing the respective photoreactive group at their 3′-ends were used for photoaffinity labeling of pol β and RPA. UV irradiation itself does not influence the specific activity of pol β (data not shown), and only labeling of pol β has been detected with each analogue in the absence of RPA (data not shown). Interestingly, two bands with different mobilities which corresponded to cross-linked pol β were detected when NAB-*n*-dUTPs with long spacers (n = 9−13) were used (Figure 2, lanes 7−10). The

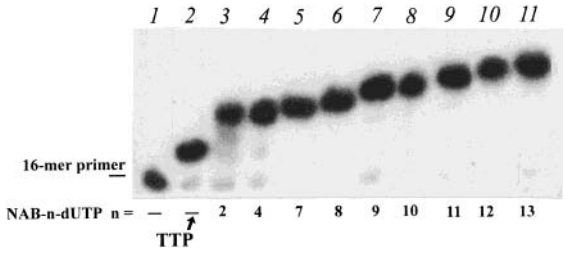

Figure 1. Substrate properties of NAB-*n*-dUTP. All reaction mixtures contained 50 mM Tris-HCl (pH 7.8), 10 mM $MgCl_2$, 50 mM KCl, 1.4 μM pol β, and 0.7 μM 5′-[^{32}P]primer-template (see Materials and Methods). Lane 1, without dNTP; lanes 2−11 contained 10 μM NAB-*n*-dUTP. Reaction mixtures were incubated for 30 min at 25° C. The reactions were terminated by adding 10 μL of 90% formamide, 50 mM EDTA, and 0.1% Bromophenol Blue. The mixtures were heated for 3 min at 80 °C, and products were separated by electrophoresis and visualized by autoradiography.

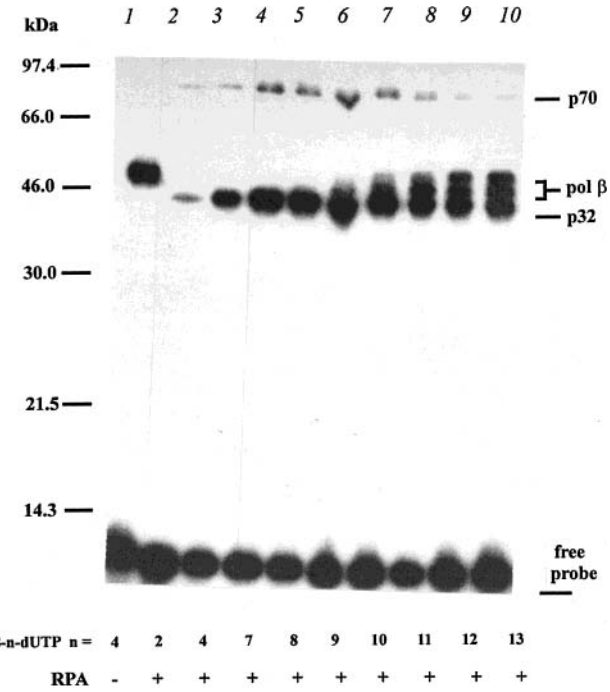

Figure 2. Photoaffinity labeling of RPA in the presence of pol β by photoreactive primers synthesized in situ. Reaction mixtures contained of 1.4 μM pol β, 50 mM Tris-HCl (pH 7.8), 10 mM $MgCl_2$, 50 mM KCl, and 0.7 μM 5′-[^{32}P]primer-template. In addition they contained 0.46 μM RPA and 10 μM NAB-*n*-dNTP when indicated. Reaction mixtures were incubated for 30 min at 25 °C and then UV-irradiated for 20 min (λ = 320 nm). The UV-cross-linked protein−DNA complexes were separated by SDS−PAGE and visualized by autoradiography. The positions of the free probe and protein markers are indicated.

same pattern was observed when DNA polymerase β was modified in the absence of RPA (data not shown). A possible explanation is that the photoreactive nucleotide might be forming cross-links to different amino acids of pol β. Chemical modification of individual protein at two different sites has been found to change the mobility of the modified proteins during SDS−gel electrophoresis (Yakubov et al., 1993).

Addition of RPA results in cross-linking of the primer to the p32 and p70 subunits with the p70 interaction being less intense (Figure 2). Furthermore, labeling of pol β was decreased for using the NAB-*n*-dUTPs with short spacers (n < 9), (Figure 2, lanes 2−5). In general, the cross-linking pattern of RPA subunits was not influenced by the spacer length. p14 subunit was not

labeled by any of the analogues under any condition used, whereas the subunits p32 and p70 were always cross-linked in these experiments (Figure 2). It is worth noting that each cross-linked protein is retarded by a value of 6−8 kDa in comparison to that of the unmodified protein. The labeling of pol β is inhibited in the presence of RPA, but in the case of NAB-*n*-dUTPs ($n = 9-13$), the decrease of pol β modification seems to be less emphasized in the presence of RPA (Figure 2, lanes 6−10), i.e., reagents with longer spacers introduced into the 3′-end of the primer are still able to modify pol β bound to DNA. These results could be explained by the assumption that the complexes pol β−RPA-primer-template exist in the reaction mixture. In this complex, pol β is situated at the large distance (approximately 16 Å) from 3′-end of primer and modified only by analogues with long spacer group.

DISCUSSION

Base-substituted analogues of dNTPs carrying arylazido groups provide new tools for photoaffinity labeling of the proteins interacting with nucleic acids. A number of aryl azides were used to obtain base-substituted photoreactive analogues of dUTP (Knorre et al., 1998). Synthesis of a photoreactive primer-template using NAB-4-dUTP as a substrate of various polymerases was reported earlier, and this primer−template was used to study RPA interaction with DNA duplex (Lavrik et al., 1998).

The main idea of the approach was to compare pattern of modification of RPA subunits using dUTP analogues with the spacers of various lengths. The results obtained in this work demonstrate that a single photoreactive moiety was incorporated at the 3′-end of the primer by pol β with equal efficiency for all the analogues used. We wanted to investigate whether p14 could be labeled by the analogues that had a different spacer length other than $n = 4$ that was used in the previous experiments (Lavrik et al., 1998). The length of the spacer carrying the photoreactive group was changed from 2 to 13 atoms that corresponds to a distance of 7.4 to 22.0 Å, respectively, from 5-position of the uridine to the azido group, according to molecular modeling simulations (data not shown). The absence of p14 cross-links using the analogues described here and by the analogues carrying other photoreactive groups attached to the 5-position of dUTP (manuscript in preparation) presumably speaks in favor of the protection of p14 by other RPA subunits from the interaction with the 3′-end of the primers.

In general, our data support the model of RPA interaction with DNA duplex template junction as suggested by an earlier report (Lavrik et al., 1998). For the interactions between the p70 and p32 subunits and the 3′-end of the primer, we propose the following model: the p70 subunit binds to the single-stranded template extension whereas the p32 subunit is located near 3′-end of the primer. The p14 subunit is situated relatively far from the primer, or alternatively, it is protected from modification by the p70 and p32 subunits. The functional significance of the location of p32 near the 3′-end of the nascent DNA is not understood. However, it has recently been shown that this subunit of RPA monitors the extension of RNA−DNA primers during the replication of SV-40 chromosomes (Mass et al., 1998).

RPA has been found to interact specifically with several DNA polymerases (Wold, 1997). RPA interacts with the primase subunits of the DNA polymerase α-DNA−primase complex (Dornreiter et al., 1992; Nasheuer et al., 1992). Until now, there was no direct evidence to suggest RPA−pol β interactions. On the basis of the results obtained here, we suggest that RPA binds to the pol β primer-template complex during DNA polymerization. In this complex pol β might bind to double-stranded part of partial DNA duplex or/and interact with RPA directly. This interaction might be important for function of base excision repair machinery.

This study highlights the functional capacities of photoreactive dUTP analogues carrying arylazido group, attached to the base by the linkers of various lengths, for examination of the interactions between duplex DNA, DNA polymerases, and other proteins involved in cellular DNA metabolism.

ACKNOWLEDGMENT

This work was supported in part by an INTAS grant (96-1778), by grants from RFBR-DFG, by a grant from Russian Foundation for Basic Research (98-04-49718, 98-04-49661, 99-04-040, 00-04-4930, and 99-04-49277), a grant from the scientific project of Young Scientists Program Siberian Division of Russian Academy of Scientists. We thank Svetlana N. Khodyreva, Richard D'Ari and Brian Van de Berg for the careful reading of the manuscript.

LITERATURE CITED

(1) Anderson, G. W., Zimmerman, J. E., and Callahan, F. M. (1964) The use of esters of N-hydroxysuccinimide in peptide synthesis. *J. Am. Chem. Soc. 86,* 1839−1842.

(2) Dobrikov, M. I., Gorn V. V., Zarytova, V. F., Levina, A. S., Prikhodjko, T. A., Shishkin, G. V., Tabatadze, D. R., and Zaalishvilli, M. M. (1992) Site-specific photomodification of nucleic acids by aryl azides and perfluoroaryl azide derivatives of oligonucleotides II. Study of nucleoside-specificity of modification. *Bioorgan. Khim. (Moscow) 18,* 1090−1098.

(3) Dobrikov, M. I., Prikhodjko, T. A., Safronov, I. V., and Shishkin, G. V. (1992a) Synthesis of photosensitive capron membranes. Photoimmobilization of DNA. *Sib. Chim. J. 2,* 18−23.

(4) Dobrikov, M. I., Zarytova, V. F., Komarova, N. I., Levina, A. S., Lokhov, S. A., Prikhodjko, T. A., Shishkin, G. V., Tabatadze, D. R., and Zaalishvilli, M. M. (1992b) Effective sequence-specific photomodification of nucleic acids by oligonucleotide derivatives bearing aromatic azido groups. *Bioorgan. Khim. (Moscow) 18,* 540−549.

(5) Dornreiter, I., Erdile, L. F., Gilbert, I. U., von Winkler, D., Kelly, T. J., and Fanning, E. (1992). Interaction of DNA polymerase α-primase with cellular replication protein A and SV40 T antigen. *EMBO J. 11,* 769−776.

(6) Doronin, S. V., Dobrikov, M. I., and Lavrik, O. I. (1992) Photolabeling of DNA polymerase α DNA primase complex based on catalytic competence of a dNTP reactive analogue. *FEBS Lett. 313,* 31−32.

(7) Doronin, S. V., Dobrikov, M. I., Buckle, M., Roux, P., Buc, H., and Lavrik, O. I. (1994) Affinity modification of human immunodeficiency virus reverse transcriptase and DNA template by photoreactive dCTP analogues. *FEBS Lett. 354,* 200−202.

(8) Georgaki, A., Strack, B., Podust, V., and Hübscher, U. (1992). DNA unwinding activity of replication protein A. *FEBS Lett. 308,* 240−244.

(9) Henricksen, L. A., Umbricht, C. B., and Wold, M. S. (1994) Recombinant replication protein A: expression, complex formation, and functional characterization. *J. Biol. Chem. 269,* 11121−11132.

(10) Langer, P. R., Waldrop, A. A., and Ward, D. C. (1981) Enzymatic synthesis of biotin-labeled polynucleotides: novel nucleic acid affinity probes. *Proc. Natl. Acad. Sci. U.S.A. 78,* 6633−6637.

(11) Lavrik, O. I., Prasad, R., Beard, W. A. Safronov, I. V., Dobrikov, M. I., Srivastava, D. K., Shishkin, G. V., Wood, T. G., and Wilson, S. H. (1996) dNTP binding to HIV-1 reverse transcriptase and mammalian DNA polymerase β as revealed by affinity labeling with a photoreactive dNTP analogue. *J. Biol. Chem. 271*, 21891−21897.

(12) Lavrik, O. I., Nasheuer, H. P., Weisshart, K. Wold, M. S., Prasad, R., Beard, W. A., Wilson, S. H., and Favre, A. (1998) Subunits of human replication protein A are cross-linked by photoreactive primers synthesized by DNA polymerases. *Nucleic Acids Res. 26*, 602−607.

(13) Knorre, D. G., Kudryashova, N. V., and Lavrik, O. I. (1998) Chemical approaches to investigation of template biosynthesis: study of replication and reversed transcription. *Russian Chem. Rev. (Moscow) 67*, 486-502.

(14) Laemmli, U. K. (1970) Cleavage of structural proteins during the assembly of the head of bacteriophage T4. *Nature 277*, 680−685.

(15) Ludwig, J. (1981) A new route to nucleoside-5′-triphosphates. *Acta Biochim. Biophys. Acad. Sci. Hung. 16*, 131−133.

(16) Mass, G., Nethanel, T., and Kaufmann, G. (1998) The middle subunit of replication protein A contacts growing RNA-DNA primers in replicating simian virus 40 chromosomes. *Mol. Cell Biol. 18*, 6399−6407.

(17) Meisenheimer, K. M., and Koch, T. H. (1997) Photo-cross-linking of nucleic acids to associated proteins. *Crit. Rev. Biochem. Mol. Biol. 32* (2), 101−140.

(18) Nasheuer, H. P., von Winkler, D., Schneider, C., Dornreiter, I., Gilbert, I., and Fanning, E. (1992) Purification and functional characterization of bovine RP-A in an in vitro SV40 replication system. *Chromosoma 102*, S52−S59.

(19) Sambrook, J., Fritsch, E. F., and Maniatis T. (1989) *Molecular Cloning: A Laboratory Manual*, 2nd ed., Cold Spring Harbor Laboratory Press, Plainview, NY.

(20) Scherbik, N. V., Khodyreva, S. N., Vlasov, V. A., Dobrikov, M. I., Dymshits, G. M., and Lavrik, O. I. (1997). Photoaffinity modification of HIV reverse transcriptase with deoxyuridine 5′-triphosphate analogue containing an arylazido group. *Mol. Biol. (Moscow) 31*, 344−352.

(21) Wlassoff, W. A., Dobrikov, M. I., Safronov, I. V., Dudko, R. Y., Bogachev, V. S., Kandaurova, V. V., Shishkin, G. V., Dymshits, G. M., and Lavrik, O. I. (1995) Synthesis and characterization of d(NTP) derivatives substituted with residues of different photoreagents. *Bioconjugate Chem. 6*, 352−360.

(22) Wold, M. S. (1997) Replication protein A: a heterotrimeric, single-stranded DNA-binding protein required for eukaryotic DNA metabolism. *Annu. Rev. Biochem. 66*, 61−92.

(23) Yakubov, L., Khald, Z., Zhang, L.-M., Truneh, A., Vlassov, V., and Stein, C. A. (1993) Oligodeoxynucleotides interact with recombinant CD4 at multiple sites. *J. Biol. Chem. 398*, 18818−18823.

(24) Zarytova, V. F., Komarova, N. I., Levina, A. S., Lokhov, S. G., Tabatadze, D. R., Khalimskaya, L. M., and Alexandrova, L. A. (1991) The synthesis of oligonucleotides carrying deoxyuridine C-5-modified with an aliphatic amino group. *Bioorgan. Khim. (Moscow) 17*, 1059−1065.

BC990102I

Enhanced Targeting Specificity to Tumor Cells by Simultaneous Recognition of Two Antigens

Marc Hillairet de Boisferon,[†] Olivier Raguin,[†] Monique Dussaillant,[†] William Rostène,[†] Jacques Barbet,[‡] and Anne Gruaz-Guyon*[,†]

INSERM U.339, Faculté de Médecine et Hôpital Saint-Antoine, Paris, France, and UPRES 2059, Faculté de Médecine, Université de la Méditerranée, Marseille, France. Received August 17, 1999; Revised Manuscript Received January 27, 2000

Radioimmunotherapy recently afforded convincing results for B-cell non-Hodgkin's lymphoma treatment with antibody specific for B-cell differentiation antigens. High doses of unlabeled or labeled antibodies are necessary to saturate specific sites on normal B-cells. We thus developed a new targeting strategy, taking advantage of dual binding cooperativity, to enhance the specificity of the radioactive uptake by tumor cells. This approach was evaluated using human Burkitt lymphoma cells (Ramos) which express both CD10 and CD20 antigens. Most normal cells express at most one of these two differentiation antigens but many hematological tumors, including most human B type acute lymphoblastic leukemia cells, express both. Cells pretargeted with two bispecific antibodies, one recognizing CD10 and a histamine derivative (HSG), the other recognizing CD20 and the DTPA-indium complex, bind cooperatively radiolabeled mixed-haptens (DTPA-HSG). Increased binding (about 5-fold compared to binding to only one of CD10 or CD20 antigens) is observed at 37 °C, demonstrating the feasibility of the technique. This binding enhancement is a slow process, not observed at 4 °C. Such a binding enhancement will increase specificity for targeting isotopes to double antigen positive tumor cells compared to nontumor tissue cells bearing only one of them. This approach might be used to increase tumor irradiation with minimal irradiation of normal cells.

INTRODUCTION

Radioimmunotherapy, a systemic radiotherapy using labeled monoclonal antibodies (mAb) to deliver radioisotopes to malignant cells, recently afforded convincing results for non-Hodgkin's lymphoma therapy (Corcoran et al., 1997; Wilder et al., 1996). These tumor cells, distributed in blood, bone marrow, lymph nodes and spleen, are readily accessible to labeled monoclonal antibodies. This and the relative radiosensitivity of lymphoma cells account for the efficacy of this blood borne therapy. The most encouraging results have been obtained using CD20 (Kaminski et al., 1993, 1996; Knox et al., 1996; Liu et al., 1998; Press et al., 1995), CD22 (Goldenberg et al., 1991; Juweid et al., 1995), CD37 (Kaminski et al., 1992; Press et al., 1993), and HLA-DR (DeNardo and DeNardo, 1995) as target antigens. Radioimmunotherapy has achieved complete response in almost half of the patients included in the numerous clinical studies concerning B-cell non-Hodgkin's lymphoma (Wilder et al., 1996). Results obtained in leukemia radioimmunotherapy, using antibodies directed to the interleukin-2 receptor (Waldman et al., 1994), HLA-DR (DeNardo et al., 1994), CD33 (Appelbaum et al., 1992; Jurcic et al., 1995; Scheinberg et al., 1991), and CD45 (Matthews et al., 1995), suggest that this technique may intensify anti-leukemia therapy before bone marrow transplant. The most impressive results were obtained when large amounts of labeled antibodies were used or when large amounts of unlabeled antibody were injected prior to a labeled antibody dose. The requirement for high doses or predosing with unlabeled antibody has been attributed to the necessary saturation of specific sites on normal cells. Indeed, in these approaches, target antigens are merely differentiation antigens, not specific for tumor cells.

Pretargeting has afforded very encouraging results in radioisotope targeting to solid tumors in animal models and in the clinic. The "Affinity Enhancement System" (AES), which uses unlabeled bispecific antibody, directed to a tumor antigen and to a hapten, and a labeled bivalent hapten (Le Doussal et al., 1990), is now recognized as a good candidate for the detection (Barbet et al., 1998; Chetanneau et al., 1994; De Labriolle-Vaylet et al., 2000; Le Doussal et al., 1993; Manetti et al., 1997; Vuillez et al., 1997) and treatment (Barbet et al., 1999; Gautherot et al., 1997; Hillairet de Boisferon et al., 1997) of neoplasms and particularly solid tumors. This technique is based on the enhanced affinity of the labeled hapten provided by the cooperativity of its simultaneous binding to two unlabeled bispecific antibodies at the surface of the target cell. Scintigraphy studies demonstrated improved tumor to normal tissue ratio compared to classical immunoscintigraphy using directly labeled antibodies (Le Doussal et al., 1990; Le Doussal et al., 1993). Encouraging radioimmunotherapy results have also been obtained in animal models of mouse lymphoma (Hillairet de Boisferon et al., 1997) and human colorectal carcinoma cell line grafted to nude mice (Gautherot et al., 1997) and in the clinic (Barbet et al., 1999). AES could be considered for the treatment of hematological diseases. However, the huge amounts of bispecific antibodies that would be necessary to saturate specific and nonspecific

* To whom correspondence should be addressed. Phone: (33) 1 40 01 14 66. Fax: (33) 1 43 43 89 46. E-mail: gruaz@adr.st-antoine.inserm.fr.

[†] INSERM U.339.

[‡] UPRES 2059.

10.1021/bc9901090 CCC: $19.00 © 2000 American Chemical Society
Published on Web 05/03/2000

binding sites on normal cells would make this approach too costly to be practical.

The scope of this work is to take advantage of the cooperativity of dual binding to enhance the specificity of the radioactivity uptake by the target tumor cell. The feasibility of enhanced binding to double antigen positive cells has been demonstrated in a model of mouse B-cells, using mixed 2,4-dinitrophenyl (DNP) × diethylenetriaminepentaacetic acid-indium [DTPA(In)] haptens. These hydrophobic haptens were efficiently targeted to normal mouse spleen cells using anti-Lyb-8.2 × anti-DTPA(In) and anti-IE^k × anti-DNP bispecific antibodies (Le Doussal et al., 1991). Subsequent studies proved that hydrophobic haptens were poorly delivered to target cells with more limited blood supply, such as tumor cells. Thus, we have designed and synthesized hydrophilic mixed-haptens, associating DTPA(In) and histamine-hemisuccinate coupled to glycine (HSG) (Janevik-Ivanovska et al., 1997). In this study, we first evaluated, in a macrophage model, the simultaneous binding to two distinct antibodies of a series of hydrophilic peptides, of various length and structure, bearing these two different haptens. Then, we investigated the ability of two of these mixed-haptens to simultaneously bind to two different bispecific antibodies [anti-CD10 × anti-HSG and anti-CD20 × anti-DTPA(In)] pretargeted to Ramos cells (human Burkitt lymphoma) which bear at their surface CD10 and CD20 antigens. The effect of cooperativity was studied by computer simulation of equilibrium binding isotherms.

MATERIAL AND METHODS

Cells. $P388D_1$ cells (ATCC, Rockville) are mouse macrophages which express receptors (Fc gamma RI and RII) for the IgG Fc fragment on the cell surface (Koren et al., 1975). These cells were grown in DMEM medium supplemented with 10% fetal calf serum (FCS), 1% glutamine, 1% nonessential amino acid, 1% sodium pyruvate, and 0.1% gentamycine at 37 °C in 5% CO_2. For binding experiments, the cells were harvested with trypsin-EDTA (0.05 and 0.02%, respectively) at 37 °C during 5 min. The cells were resuspended and washed once with culture medium and twice with binding medium [DMEM medium containing 0.2% of bovine serum albumin (BSA)]. The Ramos cell line (ATCC) is derived from a human Burkitt lymphoma known to express CD10 and CD20 at its surface. These cells were cultured in RPMI 1640 with 10% FCS, 1% glutamine, 1% nonessential amino acid, 1% sodium pyruvate, and 0.1% gentamycine at 37 °C in 5% CO_2. For binding experiments, the cells were washed twice with the binding medium (RPMI 1640 medium containing 0.2% of BSA). Before experiments, the viability of the cells was assessed by trypan blue exclusion. In all cases, viability was greater than 90%.

Mixed-Haptens. Peptides bearing one glycyl-succinyl-histamine hapten (HSG) and one diethylenetriaminepentaacetic acid (DTPA) were synthesized. The DTPA-HSG peptides (mixed-haptens) are listed in Table 1. As already described (Janevik-Ivanovska et al., 1997), mono-HSG peptides were synthesized by the step-wise solid-phase method using *tert*-butyloxycarbonyl, fluorenylmethyloxycarbonyl, and 2-chlorobenzyloxycarbonyl groups to protect α- or ϵ-amino groups depending on the position of the HSG hapten. The DTPA-HSG peptides were obtained by reacting DTPA dianhydride with the mono-HSG peptide. All peptides were purified by C18 reversed-phase chromatography.

Antibodies. All antibodies used in this work are mouse monoclonal immunoglobulins (IgG) kindly provided by Immunotech S. A. (France). The anti-HSG antibody (679.1MC7) is an $IgG_{1,\kappa}$ monoclonal antibody (Morel et al., 1990) and the antibody directed to the DTPA(In) complex (734) (Le Doussal et al., 1990) is an $IgG_{1,\lambda}$ monoclonal antibody. The anti-CD10 monoclonal antibody (ALB1 IOB5) is an $IgG_{2a,\kappa}$, and the monoclonal antibody (B9E9, HRC20), specific to the CD20 antigen, an $IgG_{2a,\kappa}$.

Table 1. Synthesized Mixed-Hapten[a]

Ac—Lys—Gaba—DTyr—Gaba—Lys—NH_2 (DTPA, HSG) AG 5.1	Ac—Lys—DTyr—Lys—NH_2 (DTPA, HSG) AG 5.0
HSG—Lys—DTyr—NH_2 (DTPA) AG 5.2	HSG—DTyr—Lys—NH_2 (DTPA) AG 5.3

[a] HSG, histamine-succinyl-glycyl; DTPA, diethylenetriaminepentaacetic acid; GABA, γ-amino-butyric acid.

Anti-CD20 × anti-DTPA(In) and anti-CD10 × anti-HSG bispecific antibodies were prepared by chemical coupling of the two reduced Fab′ fragments using *o*-phenylene-dimaleimide (Sigma) according to Glennie et al. (Glennie et al., 1987). Briefly, IgG was digested by pepsin (Sigma) (5% in 0.15 M acetate buffer, pH 4.0 for 2 h at 37 °C). The $F(ab')_2$ fragments were purified by preparative gel filtration on Superdex 200 (16 × 60 column, Pharmacia Biotech, France) in PBS pH 7.4. Fab′ fragments were obtained by reduction with 10 mM cysteamine (Sigma) in PBS (EDTA 10 mM, pH 7.4) during 1 h at 37 °C. Excess cysteamine was removed by gel filtration on a PD10 column (Pharmacia).

The Fab′ fragment directed to the hapten was incubated with excess *o*-phenylene-dimaleimide. Excess dimaleimide was removed by gel filtration on a PD10 column. The other Fab′ fragment directed to the cell antigen was incubated with the Fab-dimaleimide during 24 h at 4 °C. The conjugate (100 kDa) was separated from higher molecular weight material and nonreacted Fab′ fragments by preparative gel filtration on Superdex 200 (16 × 60 column) in PBS buffer.

Anti-DTPA(In) and anti-HSG Fab′ fragments were biotinylated and immobilized on avidin coated tubes (Immunotech S. A., France) to determine mixed-hapten immunoreactivity or equilibrium affinity constant.

Radiolabeling. The mixed-haptens (0.5 nmol) were labeled with indium-111 ($^{111}InCl_3$, 11.1 MBq, Cis Bio International, France) in 100 mM acetate−10 mM citrate buffer, pH 5.0, during 24 h (room temperature). Then, since the anti-DTPA(In) antibody is specific to the DTPA−indium complex, free DTPA groups were saturated with nonradioactive $InCl_3$ (5 nmol) in the same buffer. Excess free indium was removed on a Sep-Pak cartridge (Waters Milford) in acetate-citrate buffer, followed by elution of the labeled mixed-hapten in acetate-citrate buffer/methanol (50:50, v/v).

Radioiodination was performed by the chloramine T method. Before labeling, the free DTPA groups of each peptide were saturated with nonradioactive $InCl_3$ in 100 mM acetate−10 mM citrate buffer, pH 5.0. The solution of peptide (2 nmol, 100 μL) in 0.1 M phosphate buffer, pH 7.2, was incubated with $Na^{125}I$ (37 MBq, Amersham, France). The iodination was started by addition of 10 μL of chloramine T (1 mg/mL) in phosphate buffer. Reaction was stopped after 45 s by addition of 10 μL of sodium bisulfite (2 mg/mL) in water. Then the iodinated derivatives were separated by C18 reversed-phase HPLC with

H_2O/TFA 0.05% (A) and acetonitrile (B) with a linear gradient from 0 to 30% B during 40 min.

Antibodies (0.5 nmol) were labeled with iodine-125 (18.5 MBq) by the iodogen method (Salacinsky et al., 1981) and purified by gel filtration chromatography on a PD 10 column in PBS.

Quality Control. The fraction of each ^{125}I- or ^{111}In-labeled mixed-hapten able to bind to the anti-hapten antibodies (e.g., immunoreactivity) was determined by incubating trace amounts of the labeled peptide in anti-HSG or anti-DTPA(In) antibody-coated tubes (0.2 μg) for 1 h at 37 °C under shaking. Tubes were then washed twice with 0.9% NaCl, 0.02% Tween 20 and counted.

DTPA(In)- and HSG-coated tubes were prepared by incubating DTPA(In)-substituted biotinylated BSA or biotinylated mono-HSG peptide on avidin-coated tubes. Anti-hapten immunoreactivity was determined by incubating trace amounts of labeled bispecific antibody on HSG- or DTPA(In)-coated tubes.

Anti-CD10 or anti-CD20 immunoreactivity of each labeled antibody was determined from binding of trace amounts of the labeled antibody to increasing numbers of Ramos cells. ^{125}I-labeled antibodies (150 μL, 1×10^{-12} M) and 100 μL of cell suspension (1×10^5 to 1×10^7 cells) in a 350 μL final volume of RPMI/0.2% BSA were incubated during 1.5 h at 37 °C under shaking. Then, 100 μL of the suspension were centrifuged in triplicate for 2.5 min through a phthalate oil mixture (Dower et al., 1981). The radioactivity of the bottom of each tube containing the cell pellet and of 50 μL of the supernatant was then counted.

Determination of Antibody Binding Affinity. The equilibrium affinity constants (K_a) of the binding of antibodies to Ramos cells were determined by competition (three experiments in triplicate). The cell suspension (100 μL, 2×10^6 cells), ^{125}I-labeled antibodies (150 μL, 2.3×10^{-10} M), and 100 μL of increasing concentrations of unlabeled antibodies (3×10^{-6} to 3×10^{-10} M) were incubated together in RPMI/0.2% BSA. After 1.5 h at 37 °C under shaking, 100 μL of the suspension was centrifuged in triplicate for 2.5 min through a phthalate oil mixture as described above.

For the affinity constant determination of the binding of mixed-haptens to anti-hapten antibodies, trace amounts of ^{111}In-labeled mixed-haptens (1×10^{-10} M) were incubated in anti-DTPA(In)- or anti-HSG-coated tubes (0.01 μg) for 2 h at 37 °C with increasing concentrations of unlabeled mixed-haptens (1×10^{-6} to 1×10^{-10} M) in a final volume of 1 mL of PBS/0.2% BSA under shaking. Then, 100 μL of supernatant were taken off and counted. Tubes were washed twice with 0.9% NaCl and 0.02% Tween 20 and counted.

Demonstration of Antibody-Mediated Cooperative Binding of Mixed-Haptens. Binding experiments were performed on P388D$_1$ macrophage cells (1×10^5) in a final volume of 350 μL of binding medium. Radiolabeled mixed-haptens (2×10^{-10} M final concentration) were incubated with cells during 2.5 h at 37 °C under shaking in the presence of unlabeled anti-DTPA(In) IgG or anti-HSG IgG or an equimolar mixture of both IgGs (4×10^{-7} to 2.4×10^{-12} M final concentrations). Nonspecific binding was evaluated in the absence of antibodies. Then, 100 μL aliquots were centrifuged in triplicate through phthalate oil mixture as described above.

Binding experiments on Ramos cells were performed under the same conditions with a suspension of 2×10^6 cells in the presence of unlabeled anti-CD20 × anti-DTPA(In) or anti-CD10 × anti-HSG or an equimolar mixture of both bispecific antibodies (1×10^{-7} to 1×10^{-10} M final concentrations).

Binding and Internalization Kinetics. Ramos cells (2×10^6 cells) were incubated at 37 °C under shaking in 350 μL of culture medium containing 20 mM Hepes (pH 7.4) with iodinated mixed-hapten AG 5.0 and AG 5.2 (2×10^{-10} M) in the presence of a bispecific antibody concentration of 5.3×10^{-9} M and 1.6×10^{-8} M, respectively (final concentrations). At selected time intervals, 100 μL of cell suspension were applied to phthalate tubes and centrifuged to determine the total amount of radioactive peptide bound to the cells. Three different protocols were performed. Simultaneous incubation of antibodies and hapten was used in most experiments. When stated, antibodies were added to the cells first, incubated for 2 h, and the hapten was added without washing or after washing the cells free of unbound antibodies.

To determine the amount of tracer internalized in parallel, 350 μL of cell suspension was pelleted, resuspended in 350 μL binding buffer adjusted to pH 2.0 with 1 M HCl, incubated at 4 °C for 15 min under shaking and 100 μL of suspension were applied to phthalate tubes. This last procedure dissociated surface-bound ligands. Internalization was expressed as the percentage of the total incubated activity that remained bound to cells after acid wash.

Computer Simulations. The methodology introduced by Delaage and co-workers (Barbet et al., 1993; Bellon et al., 1973) is well suited to calculate binding equilibrium under complex situations. Basically, one adds up the concentrations of all interacting species, expressed as functions of free monomer concentrations, to form a partition function. For instance, if C_A, C_B, and C_C represent the free concentrations of species A, B, and C, respectively, and K_{AB} and K_{BC} are the affinity constants for the interactions of A with B and B with C, then one gets $C_A + C_B + C_C + K_{AB}C_AC_B + K_{BC}C_BC_C$. If C can bind to the AB complex, $K_{AB}K_{BC}C_AC_BC_C$ is added to the partition function. If binding involves cooperativity (or steric hindrance), a coefficient P_C is included and $P_CK_{AB}K_{BC}C_AC_BC_C$ is added instead. This is what was done for the complex involving the mixed-hapten, one molecule of each bispecific antibodies and one molecule of each membrane antigens and the term "cooperativity factor" refers to P_C. For simulation, the partition function [completed by subtracting the logarithmic terms, $A_o \ln(C_A)$, $B_o \ln(C_B)$, $C_o \ln(C_C)$, A_o, B_o, C_o being the total concentrations of each species] is minimized with respect to C_A, C_B, and C_C. The program can deal with any reasonable number of interacting species and possible complexes. Unknown parameters may be estimated by minimizing the sum of variance-weighted squared differences between calculated and experimental data. The program was used to estimate the affinity constants, number of binding sites per cell, and immunoreactivity from competition experiments. Then, the values determined for the affinity constants were used as fixed parameters, but binding site concentrations and the cooperativity factor were adjustable parameters in fitting the binding curves obtained in the experiments with mixed-hapten binding to Ramos cells in the presence of bispecific antibodies. All these calculations were performed by the program which uses Microsoft Excel 97 for input and output on a PC. This program is available on request to Jacques Barbet (UPRES 2059, Faculté de Médecine, Université de la Méditerranée, 27 Bd Jean Moulin, 13385, Marseille, France; e-mail: jacques.barbet@medecine.univ-mrs.fr).

Table 2. Equilibrium Affinity Constants and Immunoreactivity of Monoclonal IgGs and Bispecific Antibodies for Binding to CD10 or CD20 Antigens

antibody	affinity constant[b] K_a (M^{-1})	immunoreactivity to Ramos cells[a,b] (%)
IgG anti-CD10	$(3.6 \pm 0.4) \times 10^9$	25.9 ± 5.6
IgG anti-CD20	$(1.7 \pm 0.2) \times 10^9$	57.0 ± 8.2
anti-CD10 × anti-HSG	$(4.0 \pm 0.1) \times 10^8$	23.3 ± 2.3
anti-CD20 × anti-DTPA(In)	$(3.0 \pm 0.2) \times 10^8$	16.2 ± 0.6

[a] To determine immunoreactivity trace amounts of ^{125}I-labeled antibodies were incubated with increasing concentration of cells. [b] For each antibody, the immunoreactivity and the equilibrium binding constant were estimated simultaneously by nonlinear least-squares regression.

RESULTS

Determination of Antibody Equilibrium Affinity Constants. Equilibrium binding parameters of anti-CD10 and anti-CD20 IgGs and anti-CD20 × anti-DTPA-(In) and anti-CD10 × anti-HSG bispecific antibodies binding to Ramos cells were determined from three competition experiments run in triplicate. Nonspecific binding was evaluated with excess unlabeled anti-CD10 or anti-CD20 IgGs. For each antibody, the immunoreactivity was determined from binding experiments of the labeled antibody to increasing numbers of Ramos cells. Equilibrium binding constants and immunoreactivity were then determined from experimental results by fitting calculated to experimental bound-to-total ratios for all available data (Table 2). This was performed using an add-in to Microsoft Excel 97 developed by one of us (J.B.). Basically, this add-in uses variance-weighted nonlinear least-squares regression to estimate adjustable parameters and a description of multiple binding equilibria derived from Bellon et al. (1973) and Barbet et al. (1993).

The immunoreactivity of ^{125}I-labeled bispecific antibody against CD20 was found rather low (Table 2), whereas that of the corresponding ^{125}I-labeled IgG was significantly higher, the immunoreactivity of bispecific antibody against CD10 was similar to that of the corresponding IgG (Table 2). This was taken into account to determine the affinity constants. The affinity of intact IgGs was 5−9-fold higher than that of the respective monovalent bispecific antibodies (Table 2).

They were all in the nanomolar range, which is suitable for in vivo targeting applications. The immunoreactivity of ^{125}I-labeled bispecific antibodies against haptens was similar: 14% for anti-CD20 × anti-DTPA(In) and 13% for anti-CD10 × anti-HSG (data not shown).

Expression of the target antigens on Ramos cells varied from experiment to experiment in the 2.1×10^4 to 7.5×10^4 sites/cell range for CD10 and 1.6×10^4 to 1.5×10^5 for CD20.

Equilibrium Affinity Constant Determination of Mixed-Haptens Binding to Anti-Hapten Antibodies. Equilibrium affinity constants for the binding of mixed-haptens to anti-hapten antibodies were determined by competition (three experiments in triplicate). Binding of ^{111}In-labeled AG 5.1 mixed-hapten to anti-DTPA(In) or anti-HSG coated tubes was competed with increasing concentrations of unlabeled mixed-hapten. Binding constants were estimated by nonlinear least-squares regression as above. All measurements were performed at 37 °C with physiological salt concentrations to allow the use of these K_a values to analyze the binding of the mixed-haptens to Ramos cells in the presence of the bispecific antibodies (Table 3).

The highest K_a binding value to anti-HSG antibody was observed for HSG coupled to the epsilon-NH_2 of a lysine (1.9 ± 0.2 and $2.7 \pm 0.3 \times 10^9$ M^{-1} for AG 5.1 and AG 5.0, respectively). The anti-HSG K_a value decreased when HSG was coupled to the α-NH_2 of a lysine ($3.7 \pm 1.5 \times 10^8$ M^{-1} for AG 5.2) and was $2.2 \pm 0.1 \times 10^7$ M^{-1} for AG 5.3 when HSG was on the α-NH_2 of a tyrosine. The highest anti-DTPA(In) K_a value is observed for the mixed-haptens AG 5.3 and AG 5.1 ($1.9 \pm 0.2 \times 10^9$ M^{-1} and $1.9 \pm 0.3 \times 10^9$ M^{-1}, respectively). The affinity constants are $1.5 \pm 0.2 \times 10^9$ M^{-1} for AG 5.0 and $1.1 \pm 0.1 \times 10^9$ M^{-1} for AG 5.2. Immunoreactivity for binding to the anti-DTPA(In) or the anti-HSG antibodies were similar for ^{111}In- or ^{125}I-labeled mixed-haptens AG 5.0, AG 5.1, and AG 5.2 and ranged from 79 to 94% (Table 3). Due to its low affinity, the immunoreactivity of AG 5.3 for binding to the anti-HSG antibody could not be determined.

Binding to Macrophages of ^{111}In-Labeled Mixed-Haptens in the Presence of Anti-Hapten IgGs. The $P388D_1$ macrophage cells express receptors for the IgG Fc fragment at their surface (Koren et al., 1975). These receptors have a very low affinity for mouse IgG_1 (Haeffner-Cavaillon et al., 1979). The binding of ^{111}In-labeled mixed-haptens to $P388D_1$ cells incubated in the presence of increasing concentrations of each anti-DTPA(In) or anti-HSG or a mixture of both IgGs was studied. The experiment was repeated three times with similar results. Figure 1 shows typical curves. Mixed-hapten binding to $P388D_1$ cells pretargeted with only one anti-hapten IgG [anti-HSG or anti-DTPA(In)] was hardly detectable. In the presence of an equimolar mixture of the two anti-hapten antibodies, binding was dramatically increased for mixed-haptens AG 5.0, AG 5.1, and AG 5.2. Binding increased with increasing concentrations of the antibody mixture to reach a maximum. Then at higher antibody concentration, binding decreased as the labeled hapten was trapped by excess antibody in the supernatant. At the optimal IgG concentration (2.0×10^{-10} M), 13% of the mixed-hapten AG 5.0 and 11% of AG 5.1 were bound. The optimal IgG concentration for AG 5.2 binding was 1.8×10^{-9} M, with 12% of the mixed-hapten bound to the cells. In the presence of only one of each anti-

Table 3. Equilibrium Affinity Constants and Immunoreactivity of Mixed-Haptens for Anti-DTPA(In) and Anti-HSG Antibodies Coated Tubes

peptides	binding to anti-DTPA(In) mAb affinity constant (M^{-1})	binding to anti-HSG mAb affinity constant (M^{-1})	immunoreactivity to anti-DTPA(In) coated tubes (%)	immunoreactivity to anti-HSG coated tubes (%)
AG 5.1	$(1.9 \pm 0.3) \times 10^9$	$(1.9 \pm 0.2) \times 10^9$	89.4 ± 2.5	82.7 ± 0.5
AG 5.0	$(1.5 \pm 0.2) \times 10^9$	$(2.7 \pm 0.3) \times 10^9$	88.0 ± 6.1	93.9 ± 3.7
AG 5.2	$(1.1 \pm 0.1) \times 10^9$	$(3.7 \pm 1.5) \times 10^8$	84.8 ± 7.1	79.0 ± 1.2
AG 5.3	$(1.9 \pm 0.2) \times 10^9$	$(2.2 \pm 0.1) \times 10^7$	90.6 ± 2.7	*a*

[a] Due to its low affinity, the immunoreactivity of AG 5.3 for binding to the anti-HSG antibody could not be determined from maximal binding to tubes coated with excess anti-HSG.

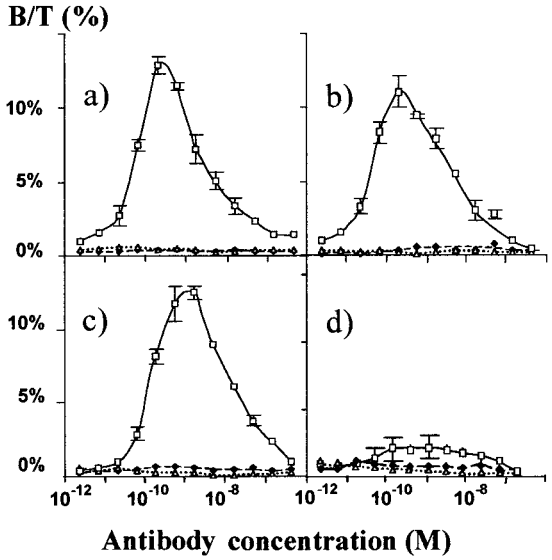

Figure 1. In vitro equilibrium binding of mixed-haptens to $P388D_1$ cells mediated by anti-hapten antibodies: $P388D_1$ cells were incubated for 2.5 h at 37 °C with ^{111}In-labeled mixed haptens AG 5.0 (a), AG 5.1 (b), AG 5.2 (c), or AG 5.3 (d) in the presence of increasing concentrations of anti-DTPA(In) IgG (dotted line), anti-HSG IgG (broken line) or an equimolar mixture of both IgGs (solid line). Cell suspension was centrifuged through phthalate oil, the supernatant and the cell pellet were counted. Mean bound/total labeled mixed-hapten (*B*/*T* %) ± sd unless smaller than point plotted (triplicate).

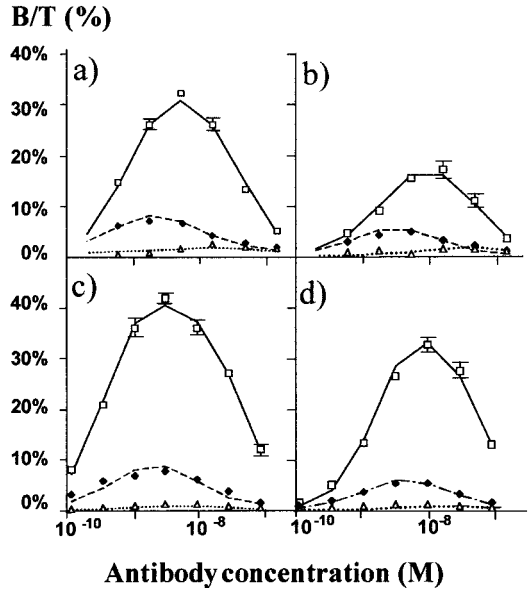

Figure 2. In vitro equilibrium binding of mixed-haptens to Ramos cells mediated by bispecific antibodies: Ramos cells were incubated for 2.5 h at 37 °C with ^{111}In-labeled mixed haptens AG 5.0 (a), AG 5.2 (b), or ^{125}I-labeled mixed-haptens AG 5.0 (c), AG 5.2 (d) in the presence of increasing concentrations of anti-CD20 × anti-DTPA(In) (dotted line), anti-CD10 × anti-HSG (broken line) or an equimolar mixture of both bispecific antibodies (solid line). Cell suspension was centrifuged through phthalate oil, the supernatant and the cell pellet were counted. Mean bound/total labeled mixed-hapten (*B*/*T* %) ± sd unless smaller than point plotted (triplicate).

hapten IgG at the same concentration less than 1% of the mixed-haptens was bound.

Interestingly, no binding increase was observed with AG 5.3. The observed binding of this peptide with the antibody mixture was roughly the sum of the binding in the presence of either the anti-DTPA(In) or the anti-HSG IgG. In contrast, with AG 5.0, AG 5.1, and AG 5.2, the simultaneous binding to both IgGs was roughly 14−17-fold the sum of the binding to one IgG, suggesting a cooperativity of the binding.

Binding to Ramos Cells of ^{111}In- and ^{125}I-Labeled Mixed-Haptens Mediated by Bispecific Antibodies. The ability of the anti-CD10 × anti-HSG and anti-CD20 × anti-DTPA(In) bispecific antibodies to target ^{111}In-labeled AG 5.0 and AG 5.2 to CD10 and CD20 expressing tumor cells was studied in binding experiments (at 37 °C, repeated twice) using human Burkitt lymphoma cells (Figure 2, panels a and b). Controls mimicking nontumor cells bearing only one antigen were performed by incubating Ramos cells with only one bispecific antibody. No more than 8% of AG 5.0 or AG 5.2 was bound in the presence of anti-CD10 × anti-HSG bispecific antibody only. Even less binding was observed with anti-CD20 × anti-DTPA(In) antibody alone. In the presence of an equimolar mixture of the two bispecific antibodies, increased binding was observed. At the optimal bispecific antibody concentrations (5.3×10^{-9} M for AG 5.0 and 1.6×10^{-8} M for AG 5.2), 32 and 18% of ^{111}In-labeled AG 5.0 and AG 5.2, respectively, were bound. The ^{125}I-labeled mixed-haptens AG 5.0 and AG 5.2 were targeted similarly to Ramos cells by bispecific antibody mixture under the same conditions with a maximal binding of 41 and 33%, respectively (Figure 2, panels c and d).

Binding of ^{125}I- and ^{111}In-labeled mixed-haptens at 37 °C in bivalent conditions (i.e., simultaneous binding to both antigens) was, respectively, about 5- and 4-fold higher than the sum of monovalent bindings (i.e., binding to only one antigen) in a wide range of bispecific antibody concentration, suggesting a cooperativity of the binding. This cooperativity was evaluated by computer simulation of the binding curves and nonlinear least-squares regression to estimate a cooperativity factor (see Materials and Methods). Affinity constants calculated in independent experiments were used to analyze experimental results. As the antigen expression on Ramos cells varied from experiment to experiment, the number of CD10 and CD20 sites per cell were fitted for each experiment. Typical curve fits are presented in Figure 2. Cooperativity factors were estimated to $(6.7 \pm 0.2) \times 10^3$ (mean ± sd) for ^{125}I-labeled 5.0, $(2.1 \pm 0.7) \times 10^3$ (mean ± sd) for ^{111}In-labeled 5.0, $(2.5 \pm 0.1) \times 10^3$ (mean ± sd) for ^{125}I-labeled AG 5.2, and $(1.6 \pm 1.3) \times 10^3$ (mean ± sd) for ^{111}In-labeled 5.2. As expected from the curves, the mixed-hapten ^{125}I-labeled AG 5.0 exhibited the highest cooperativity.

Influence of the Temperature on the Binding of ^{125}I-Labeled Mixed-Haptens to Ramos Cells. The binding of ^{125}I-labeled AG 5.0 to Ramos cells in the presence of optimal and suboptimal concentrations of bispecific antibodies was studied at 37 and 4 °C. In contrast to the increased targeting of ^{125}I-labeled AG 5.0 observed at 37 °C, in the presence of an equimolar mixture of bispecific antibodies at 4 °C, a simple additivity of the binding was observed at 3 different antibody concentrations (data not shown). Kinetic experiments performed at 4 °C with a 5.3×10^{-9} M concentration of one of each or a mixture of both bispecific antibodies showed that maximal binding of AG 5.0 (Figure 3a) reached a plateau after about 5 h of incubation in monovalent or bivalent conditions (half-life: about 53 min for binding to CD20, 18 min for binding to CD10, and 67 min for bivalent binding). No cooperativity was observed at 4 °C. Similar results were obtained with AG 5.2. These results suggest that low-temperature prevents a process involved in the observed binding enhancement at 37 °C.

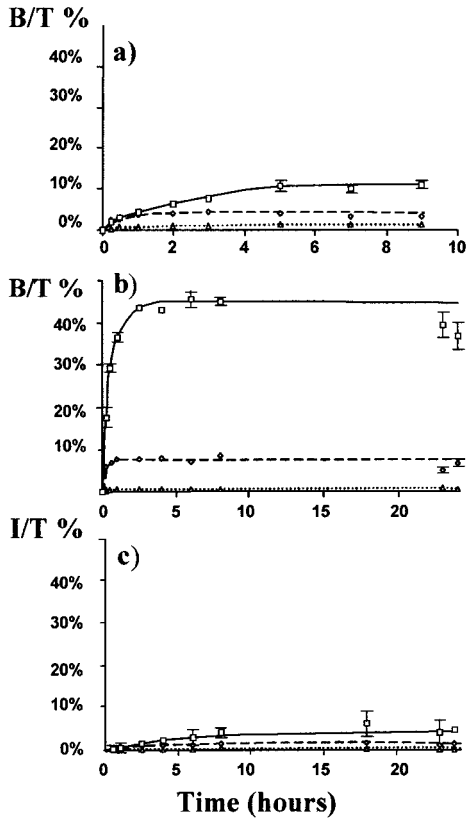

Figure 3. Kinetics of binding at 4 °C (a), 37 °C (b), and endocytosis at 37 °C (c) of ^{125}I-labeled mixed-hapten AG 5.0. Experiments were performed for various periods of time in the presence of the bispecific antibody concentration providing the maximal binding (5.3×10^{-9} M), anti-CD20 × anti-DTPA(In) (dotted line), anti-CD10 × anti-HSG (broken line) or an equimolar mixture of both bispecific antibodies (solid line). Fraction of radioactivity associated to the cells (*B*/*T* %) (a) and (b) or inside the cells (*I*/*T* %) (c) were counted (mean ± sd unless smaller than point plotted; triplicate).

Kinetics of ^{125}I-Labeled Mixed-Hapten Binding and Internalization to Ramos Cells at 37 °C. Binding and internalization experiments were performed on Ramos cells during 24 h with a 5.3×10^{-9} M concentration of one of each or a mixture of both bispecific antibodies and ^{125}I-labeled AG 5.0. Maximum binding of AG 5.0 was reached after 2.5 h incubation in the presence of an equimolar mixture of antibodies (half-life: about 25 min), whereas in monovalent binding conditions, binding was maximum after 15 min (half-life: about 4 min) (Figure 3b).

The amount of internalized ^{125}I-labeled AG 5.0 was measured in both monovalent and bivalent conditions (Figure 3c). Over 24 h, only a small fraction of tracer was internalized, but internalization was increased in the presence of the antibody mixture (5%) compared to monovalent conditions (less than 1.5%). Similar results were obtained with the AG 5.2 mixed-hapten.

Comparison between Mixing Reagents and Antibody Pretargeting. Almost identical ^{125}I-labeled AG 5.0 binding curves were obtained by mixing the labeled hapten and the antibodies (Figure 4a) or by preincubation of the antibodies for 2 h without washing before addition of the hapten (Figure 4b). Figure 4c shows the results obtained when cells were incubated first with the bispecific antibodies for 2 h and washed. Overall binding of the hapten was decreased under these conditions but cooperativity was maintained.

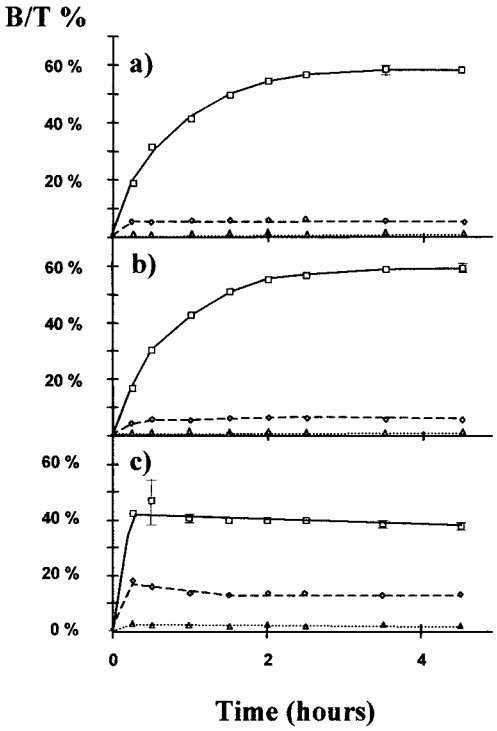

Figure 4. Binding of ^{125}I-labeled mixed-hapten AG 5.0 with pretargeting of antibodies. AG 5.0 (2×10^{-10} M) was incubated to Ramos cells together with a (5.3×10^{-9} M) bispecific antibody concentration (a) or after a preincubation of 2 h of the bispecific antibody without washing (b), or with a washing of the cells after the antibody preincubation (c). Binding was performed in the presence of anti-CD20 × anti-DTPA(In) (dotted line), anti-CD10 × anti-HSG (broken line), or an equimolar mixture of both bispecific antibodies (solid line). Mean bound/total labeled mixed-hapten (*B*/*T* %) ± sd unless smaller than point plotted (triplicate).

DISCUSSION

Numerous antibodies with high specificity to tumor antigens have been obtained since the introduction of monoclonal antibodies by Köhler and Milstein (1975). Nevertheless, despite the encouraging results of radioimmunotherapy in lymphomas, the treatment of solid tumors is limited by the irradiation of normal tissues. Unfavorable antibody pharmacokinetics, cross-reactions with normal tissues, and nonspecific binding sites account for the limited specificity of irradiation. The Affinity Enhancement System, which uses bispecific antibodies and mixed-haptens, has proven useful to enhance tumor to normal tissue uptake ratio (Chetanneau et al., 1994; Le Doussal et al., 1990), and preliminary results in radioimmunotherapy look promising (Barbet et al., 1999; Gautherot et al., 1997; Hillairet de Boisferon et al., 1997). The feasibility of targeting two antigens simultaneously expressed at the surface of the target cell has been demonstrated in a normal mouse B-cell model using 2,4-dinitrophenyl-derived haptens to target antigens (Le Doussal et al., 1991). In this system, antigen modulation precluded an accurate determination of the binding enhancement. In addition, the high hydrophobicity of the DNP hapten made it disappointing in tumor targeting experiments.

We demonstrated earlier that the histamine-hemisuccinate and the DTPA haptens are suitable to carry radioactive isotopes to tumor cells pretargeted with bispecific antibodies (Janevik-Ivanovska et al., 1997; Le Doussal et al., 1990). Both have low toxicity, high affinity to available antibodies and no cross-reactivity or non-

specific binding to body components, mostly because they are highly hydrophilic. For these reasons, HSG and DTPA were coupled to peptide connecting chains of various length and structure. A D-tyrosine residue was introduced in the backbone to allow iodine labeling, the C-terminal end of the peptide chain was amidated, the N-terminal was acetylated, and lysine side chains were substituted. This conferred the products extreme proteolysis resistance, as 6 h after injection to a mouse, 65% of AG 5.0 recovered in urine is immunoreactive (data not shown). The series of synthesized compounds is listed in Table 1. The binding affinity constants of mixed-hapten AG 5.1, AG 5.0 and AG 5.2 to anti-HSG [$(1.9 \pm 0.2) \times 10^9$ M^{-1}, $(2.7 \pm 0.3) \times 10^9$ M^{-1}, $(3.7 \pm 1.5) \times 10^8$ M^{-1}] and to anti-DTPA(In) antibodies [$(1.9 \pm 0.3) \times 10^9$ M^{-1}, $(1.5 \pm 0.2) \times 10^9$ M^{-1}, $(1.1 \pm 0.1) \times 10^9$ M^{-1}] are sufficiently high to perform two-step targeting with bispecific antibodies. The haptens may be labeled to a high specific activity with ^{111}In or ^{125}I without impairing their immunoreactivity (range 79−94). Recently, similar haptens have been labeled to a high specific activity (79 MBq/nmol) with iodine-131 (Barbet et al., 1999; Gautherot et al.,1997), a radioisotope suitable for therapeutic applications.

We used macrophages ($P388D_1$ cells) to investigate the ability of the mixed-haptens AG 5.0, AG 5.1, AG 5.2, and AG 5.3 to cross-link two different anti-hapten antibodies bound at the cell surface. $P388D_1$ macrophage cells express at their surface receptors for IgG_1 Fc fragment. These receptors have low affinity for monomeric mouse IgG_1 (Haeffner-Cavaillon et al., 1979). As a consequence, labeled mixed-haptens in the presence of increasing concentrations of anti-DTPA(In) or anti-HSG antibody show very limited binding. In the presence of IgG mixture, a dramatic increase of the binding of the mixed-haptens AG 5.0, AG 5.1, and AG 5.2 is observed, which is not simply additive, it is roughly 14−17-fold the sum of the monovalent binding. By contrast, AG 5.3 showed no significant binding cooperativity in the presence of the two IgGs. This results from the low affinity of this peptide for the anti-HSG antibody, attributed to an interaction between the histamine and the DTPA residues. As AG 5.1 structure was more complicated than that of the other mixed-haptens and the results obtained with this hapten were very similar to those obtained with AG 5.0, this peptide was not used for the following studies.

The Ramos cell line derived from a human Burkitt lymphoma, as do most human B type acute lymphoblastic leukemia cells, bears at its surface both CD10 and CD20 antigens. Most normal cells express at most one of these two differentiation antigens. Thus, an enhanced binding to cells bearing simultaneously both CD10 and CD20 would result in an enhanced specificity to these tumor cells. Binding experiments of labeled mixed-haptens to Ramos cells were performed in the presence of an equimolar mixture of both antibodies. Controls with only one antibody were run in parallel in order to mimic the binding to nontumor cells bearing only one antigen.

We demonstrated in previous studies that comparable tumor uptake was obtained with $F(ab')_2$−Fab′ and Fab′−Fab′ antibody conjugates (Le Doussal et al., 1990). In addition, Fab′−Fab′, which is cleared more rapidly from plasma than $F(ab')_2$−Fab′, allowed higher tumor to nontumor tissues ratios because of lower trapping of the bivalent hapten in plasma. For these reasons anti-CD20 × anti-DTPA(In) and anti-CD10 × anti-HSG Fab′−Fab′ were preferred to $F(ab')_2$−Fab′ antibody conjugates though these latter, as do IgGs, would have higher affinity for tumor cells.

The affinity of bispecific antibodies to the targeted antigens are higher than that of IgG_1 for Fc receptors. Consistently, the observed monovalent binding of AG 5.0 and AG 5.2 were higher on Ramos cells in the presence of bispecific antibodies than on macrophages pretargeted with a single IgG. Similar binding curves were observed at 37 °C for ^{111}In- and ^{125}I-labeled mixed-haptens in the presence of a mixture of anti-CD10 × anti-HSG and anti-CD20 × anti-DTPA(In) bispecific antibodies. Hapten binding to target cells was higher in the presence of both antibodies, and the binding curves obtained at 37 °C could not be explained by a simple additivity. Under bivalent binding conditions at 37 °C, binding was maximum after 2.5 h incubation, whereas monovalent binding reaches a maximum much quicker (about 15 min), suggesting that a slower process is involved in binding enhancement. Computer simulations showed that the simple hypothesis of cooperativity in the formation of complexes between the mixed-haptens and two bispecific antibody molecules bound to the target cell surface can account for the observed binding enhancement. By contrast, when the cooperativity factor is forced to 1.0 (no cooperativity) the calculated curves cannot fit satisfactorily the experimental data.

Interestingly, the binding of mixed-haptens in the presence of the two bispecific antibodies was strongly dependent on the incubation temperature. No significant difference was observed for maximal binding in monovalent conditions at 4 or 37 °C. In contrast to the enhanced binding observed at 37 °C under bivalent conditions, binding at 4 °C was simply additive. Internalization cannot account for the increased binding under bivalent conditions at 37 °C as only 5% of the incubated radioactivity was internalized after 24 h. The binding enhancement also appears to be a slow process, suggesting that it involves the diffusion of the target antigens in membranes. We can hypothesize that antigens diffuse freely driven by thermal diffusion and that bridging of two bispecific antibodies can occur statistically when they are closely located on the cell surface. Then, the enhanced stability of the complex would result from the restricted diffusion of the antigens, due to bivalent binding. More complex phenomenon could occur including capping in specialized areas on the cell surface.

These dual targeting reagents have been designed to enhance the specificity of pretargeting when tumor-specific antibodies are not available and antibodies to differentiation antigens are used instead. In pretargeting approaches, unlabeled bispecific antibodies are injected first, and the labeled hapten is injected a few days later when part of the circulating antibody has cleared. This situation is not easily reproduced in vitro. In all previous animal and clinical studies, the hapten was administered when significant concentrations of bispecific antibodies remained in the circulation. In some cases, both reagents have been administered simultaneously (Le Doussal et al., 1989, Manetti et al., 1997). This is the reason why in vitro binding experiments have been performed by simultaneous incubation of the antibodies and the hapten with the target cells. When the bispecific antibodies are preincubated with the cells before addition of the hapten, but not washed, hapten binding to target cells is essentially unchanged (Figure 4, panels a and b). When excess antibody is removed by washing the cells after preincubation, then hapten binding is reduced, because a fraction of the antibodies dissociates from the cells, but hapten binding cooperativity is clearly maintained (Figure 4c). In addition, the hydrophilicity of the labeled hapten should not be a drawback to the cooperative dual

binding, which is a slow process (maximum binding after 2.5 h), as excess antibody, in the plasma, will trap the hapten and reduce its clearance, as it was demonstrated earlier for haptens bearing two DTPA (Le Doussal et al., 1990). This shows that the mixed haptens should also be able to bind more tightly to cells expressing both target antigens in vivo in the context of pretargeting.

As a first step in the investigation of the potential of dual targeting for radioimmunotherapy, in vivo studies are now in progress in a model of SCID mice, i.v. grafted with Ramos cells which express CD10 and CD20 in this model as shown by autoradiographic studies. Such a binding enhancement will increase specificity for targeting isotopes to double antigen positive tumor cells and may be beneficial for targeting isotopes to B type acute lymphoblastic leukemia and Burkitt lymphoma, as well as other tumors coexpressing two markers of low specificity, and might increase tumor irradiation with minimal irradiation of normal cells.

ACKNOWLEDGMENT

We thank Pr. B. P. Roques for fruitful discussions and Immunotech for the generous supply of indispensable antibody reagent. We are grateful to Pr. S. Askienazy for research facilities. This work was supported in part by the Association pour la Recherche contre le Cancer through Grant 4042 allocated to A.G.G.

LITERATURE CITED

(1) Appelbaum, F. R., Matthews, D. C., Eary, J. F., Badger, C. C., Kellog, M., Press, O. W., Martin, P. J., Fisher, D. R., Nelp, W. B., Donnal Thomas, E., and Bernstein, I. D. (1992) The use of radiolabeled anti-CD33 antibody to augment marrow irradiation prior to marrow transplantation for acute myelogenous leukemia. *Transplantation 54* (5), 829−833.

(2) Barbet, J., Le Doussal, J. M., Gruaz-Guyon, A., Martin, M., Gautherot, E., and Delaage, M. (1993) Computer simulation of multiple binding equilibrium isotherms: application to the binding of bivalent ligands to antibodies interacting with cell surface Fc-receptors. *J. Theor. Biol. 165*, 321−340.

(3) Barbet, J., Peltier, P., Bardet, S., Vuillez, J. P., Bachelot, I., Denet, S., Olivier, P., Leccia, F., Corcuff, B., Huglo, D., Proye, C., Rouvier, E., Meyer, P., and Chatal, J. F. (1998) Radioimmunodetection of medullary thyroid carcinoma using indium-111 bivalent hapten and anti-CEA × anti-DTPA indium bispecific antibody. *J. Nucl. Med. 39*, 1172−1178.

(4) Barbet, J., Kraeber-Bodéré, F., Vuillez, J. P., Gautherot, E., Rouvier, E., and Chatal, J. F. (1999) Pretargeting with the Affinity Enhancement System for radioimmunotherapy. *Cancer. Biother. Radiopharm. 14*, 153−166.

(5) Bellon, B., Jelsch, J., and Delaage, M. (1973) Théorie des équilibres multiples pour les polymères. *Biochimie 55*, 1159−1162.

(6) Chetanneau, A., Barbet, J., Peltier, P., Le Doussal, J. M., Gruaz-Guyon, A., Bernard, A. M., Resche, I., Rouvier, E., Bourguet, P., Delaage, M., and Chatal, J. F. (1994) Pretargetted imaging of colorectal cancer recurrences using an ^{111}In-labeled bivalent hapten and a bispecific antibody conjugate. *Nucl. Med. Commun. 15*, 972−980.

(7) Corcoran, M. C., Eary, J., Bernstein, I., and Press, O. W. (1997) Radioimmunotherapy strategies for non-Hodgkin's lymphoma. *Ann. Oncol. 8* (Suppl. 1), 133−138.

(8) De Labriolle-Vaylet, C., Cattan, P., Sarfati, E., Wioland, M., Billotey, C., Brocheriou, C., Rouvier, E., De Rocquancourt, A., Rostène, W., Askienazy, S., Barbet, J., Milhaud, G., and Gruaz-Guyon, A. (2000) Successful surgical removal of occult metastases of medullary thyroïd carcinoma recurrences with the help of immunoscintigraphy and radioimmunoguided surgery. *Clin. Canc. Res. 6* (2), 363−371.

(9) DeNardo, G. L., Lewis, J. P., DeNardo, S. J., and O'Grady, L. F. (1994) Effect of Lym-1 radioimmunoconjugate on refractory chronic lymphocytic leukemia. *Cancer 73* (5), 1425−1432.

(10) DeNardo, G. L., and DeNardo, S. J. (1995) Treatment of B-lymphocyte malignancies with ^{131}I-Lym-1 and ^{67}Cu-2IT-BAT-Lym-1 and opportunities for improvement. In *Cancer Therapy with radiolabeled antibodies* (D. M. Goldenberg, Ed.) pp 217−227, CRC Press, Inc., Boca Raton, FL.

(11) Dower, S. K., DeLisi, C., Titus, J. A., and Segal, D. M. (1981) Mechanism of binding of multivalent immune complexes to Fc receptors. 1. Equilibrium binding. *Biochemistry 20*, 6326−6334.

(12) Gautherot, E., Bouhou, J., Le Doussal, J. M., Manetti, C., Martin, M., Rouvier, E., and Barbet, J. (1997) Therapy for colon carcinoma xenografts with bispecific antibody-targeted, iodine-131-labeled bivalent hapten. *Cancer 80*, 2618−2623.

(13) Glennie, M. J., McBride, H. M., Worth, A. T., and Stenvenson, G. T. (1987) Preparation and performance of bispecific F(ab′γ)$_2$ antibody containing thioether-linked Fab′γ fragments. *J. Immunol. 139*, 2367−2375.

(14) Goldenberg, D. M., Horowitz, J. A., Sharkey, R. M., Hall, T. C., Murthy, S., Goldenberg, H., Lee, R. E., Stein, R., Siegel, J. A., Izon, D. O., Burger, K., Swayne, L. C., Belisle, E., Hansen, H. J., and Pinsky, C. M. (1991) Targeting, dosimetry, and radioimmunotherapy of B-cell lymphomas with iodine-131-labeled LL2 monoclonal antibody. *J. Clin. Oncol. 9*, 548−564.

(15) Haeffner-Cavaillon, N., Dorrington, K. J., and Klein, M. (1979) Studies on the Fc gamma receptor of the murine macrophage-like cell line P388D$_1$. II. Binding of human IgG subclass proteins and their proteolytic fragments. *J. Immunol. 123* (5), 1914−1918.

(16) Hillairet de Boisferon, M., Manetti, C., Raguin, O., Gautherot, E., Rostène, W., Barbet, J., and Gruaz-Guyon, A. (1997) Pretargeted radioimmunotherapy using iodine-131-labeled bivalent hapten-bearing peptides. *LIPS 4*, 331−339.

(17) Janevik-Ivanovska, E., Gautherot, E., Hillairet de Boisferon, M., Cohen, M., Milhaud, G., Tartar, A., Rostène, W., Barbet, J., and Gruaz-Guyon, A. (1997) Bivalent hapten-bearing peptides designed for iodine-131 pretargeted radioimmunotherapy. *Bioconjugate Chem. 8* (4), 526−533.

(18) Jurcic, J. G., Caron, P. C., Nikula, T. K., Papadopoulos, E. B., Finn, R. D., Gansow, O. A., Miller, W. H., Jr., Geerlings, M. W., Warrell, R. P., Jr., Larson, S. M., and Scheinberg, D. A. (1995) Radiolabeled anti-CD33 monoclonal antibody M195 for myeloid leukemia. *Cancer Res. 55* (Suppl. 23), 5908−5910.

(19) Juweid, M., Sharkey, R. M., Markowitz, A., Behr, T., Swayne, L. C., Dunn, R., Hansen, H. J., Shevitz, J., Leung, S. O., and Rubin, A. D. (1995) Treatment of non-Hodgkin's lymphoma with radiolabeled murine, chimeric, or humanized LL2, an anti-CD22 monoclonal antibody. *Cancer Res. 55* (Suppl. 23), 5899s−5907s.

(20) Kaminski, M. S., Fig, L. M., Zasadny, K. R., Koral, K. F., DelRosario, R. B., Francis, I. R., Hanson, C. A., Normolle, D. P., Mudgett, E., Liu, C. P., Moon, S., Scott, P., Miller, R. A., and Wahl, R. L. (1992) Imaging, dosimetry, and radioimmunotherapy with iodine 131-labeled anti-CD37 antibody in B-cell lymphoma. *J. Clin. Oncol. 10*, 1696−1711.

(21) Kaminski, M. S., Zasadny, K. R., Francis, I. R., Milik, A. W., Ross, C. W., Moon, S. D., Crawford, S. M., Burgess, J. M., Petry, N. A., Butchko, G. M., Glenn, S. D., and Wahl, R. L. (1993) Radioimmunotherapy of B-cell lymphoma with [131I]anti-B1 (anti-CD20) antibody. *N. Engl. J. Med. 329*, 459−465.

(22) Kaminski, M. S., Zasadny, K. R., Francis, I. R., Fenner, M. C, Ross, C. W., Milik, A. W., Estes, J., Tuck, M., Regan, D., Fisher, S., Glenn, S. D. and Wahl, R. L. (1996) Iodine-131-anti-B1 radioimmunotherapy for B-cell lymphoma. *J. Clin. Oncol. 14* (7), 1974−1981.

(23) Knox, S. J., Goris, M. L., Trisler, K., Negrin, R., Davis, T., Liles, T. M., Grillo-López, A., Chinn, P., Varns, C., Ning, S. C., Fowler, S., Deb, N., Becker, M., Marquez, C., and Levy, R. (1996) Yttrium-90-labeled anti-CD20 monoclonal antibody therapy of recurrent B-cell lymphoma. *Clin. Cancer Res. 2*, 457−470.

(24) Köhler, G., and Milstein, C. (1975) Continuous cultures of fused secreting antibody of redefined specificity. *Nature 256*, 495−497.

(25) Koren, H. S., Handwerger, B. S., and Wunderlich, J. R. (1975) Identification of macrophage-like characteristics in a cultured murine tumor line. *J. Immunol. 114*, 894−897.

(26) Le Doussal, J. M., Gruaz-Guyon, A., Martin, M., Gautherot, E., Delaage, M., and Barbet, J. (1990) Targeting of indium 111-labeled bivalent hapten to human melanoma mediated by bispecific monoclonal antibody conjugates: imaging of tumors hosted in nude mice. *Cancer Res. 50*, 3445−3452.

(27) Le Doussal, J. M., Gautherot, E., Martin, M., Barbet, J., and Delaage, M. (1991) Enhanced in vivo targeting of an asymmetric bivalent hapten to double-antigen-positive mouse B-cells with monoclonal antibody conjugate cocktails. *J. Immunol. 146*, 169−175.

(28) Le Doussal, J. M., Chetanneau, A., Gruaz-Guyon, A., Martin, M., Gautherot, E., Lehur, P. A., Chatal, J. F., Delaage, M., and Barbet, J. (1993) Bispecific monoclonal antibody-mediated targeting of an indium-111-labeled DTPA dimer to primary colorectal tumors: pharmacokinetics, biodistribution, scintigraphy and immune response. *J. Nucl. Med. 34*, 1662−1671.

(29) Liu, S. Y., Eary, J. F., Petersdorf, S. H., Martin, P. J., Maloney, D. G., Appelbaum, F. R., Matthews, D. C., Bush, S. A., Durack, L. D., Fisher, D. R., Gooley, T. A., Bernstein, I. D., and Press, O. W. (1998) Follow-up of relapsed B-cell lymphoma patients treated with iodine-131-labeled anti-CD20 antibody and autologous stem-cell rescue. *J. Clin. Oncol. 16*, 3270−3278.

(30) Manetti, C., Rouvier, E., Gautherot, E., Loucif, E., Barbet, J., and Le Doussal, J. M. (1997) Targeting BCL_1 lymphoma with anti-idiotype antibodies: biodistribution kinetics of directly labeled antibodies and bispecific antibody-targeted bivalent haptens. *Int. J. Cancer 71*, 1000−1009.

(31) Matthews, D. C., Appelbaum, F. R., Eary, J. F., Fisher, D. R., Durack, L. D., Bush, S. A., Hui, T. E., Martin, P. J., Mitchell, D., Press, O. W., Badger, C. C., Storb, R., Nelp, W. B., and Bernstein, I. D. (1995) Development of a marrow transplant regimen for acute leukemia using targeted hematopoietic irradiation delivery by ^{131}I-labeled anti-CD45 antibody, combined with cyclophosphamide and total body irradiation. *Blood 85* (4), 1122−1131.

(32) Morel, A., Darmon, M., and Delaage, M. (1990) Recognition of imidazole and histamine derivatives by monoclonal antibodies. *Mol. Immunol. 27*, 995−1000.

(33) Press, O. W., Eary, J. F., Appelbaum, F. R., Martin, P. J., Badger, C. C., Nelp, W. B., Glenn, S., Butchko, G., Fisher, D. R., Porter, B., Matthews, D. C., Fisher, L. D., and Bernstein, I. D. (1993) Radiolabeled-antibody therapy of B-cell lymphoma with autologous bone marrow support. *N. Engl. J. Med. 329*, 1219−1224.

(34) Press, O. W., Eary, J. F., Appelbaum, F. R., Martin, P. J., Nelp, W. B., Glenn, S., Fisher, D. R., Porter, B., Matthews, D. C., Gooley, T. A., and Bernstein, I. D. (1995) Phase II trial of ^{131}I−B1 (anti-CD20) antibody therapy with autologous stem cell transplantation for relapsed B-cell lymphomas. *Lancet 346*, 336−340.

(35) Salacinsky, P. R., McLean, C., Sykes, J. E., Clement-Jones, V. V., and Lowry, P. J. (1981) Iodination of proteins and peptides using a solid-phase oxidizing agent 1,3,4,6-tetrachloro-3,6-diphenylglycoluryl (iodogen). *Anal. Biochem. 117*, 136−146.

(36) Scheinberg, D. A., Lovett, D., Divgi, C. R., Graham, M. C., Berman, E., Pentlow, K., Feirt, N., Finn, R. D., Clarkson, B. D., Gee, T. S., Larson, S. M., Oettgen, H. F., and Old, L. J. (1991) A phase I trial of monoclonal antibody M195 in acute myelogenous leukemia: specific bone marrow targeting and internalization of radionuclide. *J. Clin. Oncol. 9*, 478−490.

(37) Vuillez, J. P., Moro, D., Brichon, P. Y., Rouvier, E., Brambilla, E., Barbet, J., Peltier, P., Meyer, P., Sarrazin, R., and Brambilla, C. (1997) Two-step immunoscintigraphy for nonsmall-cell lung cancer staging using a bispecific anti-CEA/anti-indium-DTPA antibody and an indium-111-labeled DTPA dimer. *J. Nucl. Med. 38*, 507−511.

(38) Waldmann, T. A. (1994) Lymphokine receptors: a target for immunotherapy of lymphomas. *Ann. Oncol. 5* (Suppl. 1), 13−17.

(39) Wilder, R. B., DeNardo, G. L., and DeNardo, S. J. (1996) Radioimmunotherapy: recent results and future directions. *J. Clin. Oncol. 14*, 1383−1400.

BC9901090

Permeability of Yeast Cell Envelope to Fluorescent Galactosylated Telomers Derived from THAM

J. Coulon,[†] F. Thiebault,[†] C. Contino,[‡] A. Polidori,[‡] R. Bonaly,*[,†] and B. Pucci[‡]

Université Henri Poincaré, Nancy 1, UMR UHP-CNRS 7564, LCPE, Biochimie Microbienne, Faculté de Pharmacie, 5, rue A. Lebrun B.P. 403, 54001 Nancy Cedex, France, and Université d'Avignon, Laboratoire de Chimie Bioorganique et des Systèmes Moléculaires, Vectoriels, 33, rue Louis Pasteur, 84000 Avignon, France .
Received December 21, 1999; Revised Manuscript Received April 10, 2000

The work reported herein deals with the study of cellular recognition and permeability phenomena in yeasts. Various galactosylated organic telomers derived from trishydroxymethyl-aminomethane (THAM) and bearing fluorescent moieties were synthesized in order to measure their ability to cross the yeast cell envelope. Grafting fluorescent probes on the organic telomer backbone allowed us to study their specific behaviors toward the yeasts by fluorescence microscopy. Yeasts belonging to the genera *Kluyveromyces* and *Saccharomyces* were used for this study. With *Saccharomyces* yeast cells bearing mannose-specific lectins or lectin-like proteins, on their outer surface, all the galactosylated or nongalactosylated organic telomers passed through the cell envelope and invaded the cytoplasm. With *Kluyveromyces* yeast cells bearing galactose-specific lectins, the galactosylated organic telomers were blocked at the outer surface while the nongalactosylated derivatives crossed the cell envelope. Moreover, preincubation of *Kluyveromyces* yeasts with galactose or methylgalactose inhibited the cell surface anchorage of the organic telomers and allowed their penetration into the cytoplasm. When assays were performed on spheroplasts of both *Kluyveromyces* and *Saccharomyces* yeasts, no fixation on the surface could be observed, and all the derivatives went through the membrane and invaded the cytoplasm.

INTRODUCTION

The yeast envelope includes the cell wall and the membrane. The cell wall is a rigid structure made of heteropolyosides and proteins; it can be considered as an extra-cytoplasmic cell constituent permeability which has been investigated previously. De Nobel and Barnett (1991) showed that molecules with relative masses as great as 200 kDa or even 400 kDa often diffuse quite freely through intact yeast cell walls. Beside polyosides, yeast cell walls also contain several biologically active proteins such as hydrolases (invertase, acid phosphatase, and glucanases) that intervene in the nutrition processes of the cells and proteins (lectins, agglutinins, and flocculins) which are involved in cell−cell interaction and/or in molecular recognition phenomena. To date several heterologous proteins resulting from the construct of fusion have also been expressed on the surface of yeast cells. Enzymes such as α-galactosidase, lipase, and cutinase usually absent in *Saccharomyces cerevisiae* strains were incorporated into the cell wall using the α-agglutinin or flocculation C terminal fragment, which allowed their anchorage on the glucan. The peripheral cell location of these proteins has been demonstrated by immunofluorescence assays (Schreuder et al.,1996).

Lectins are carbohydrate-binding proteins. In many cases, these recognition proteins are shown to be located onto the surface of yeast cells and are involved in yeast flocculation (Basu et al., 1986; Critchley et al., 1987; Al-Mahmood et al., 1988; Al-Mahmood et al., 1991; Straver et al., 1994; El-Behhari et al., 1998). They specifically bind glycosidic polymers, which are anchored on the surface of adjacent yeast cells and so induce the flocculation phenomenon. Moreover, they can also recognize extracellular polysaccharides, oligosaccharides, and monosaccharides according to their respective specific structure.

In a recent work, we reported the synthesis of mono- or polygalactosylated organic telomers derived from trishydroxymethyl-aminomethane (THAM) (Polidori et al., 1994) and from galactosylated *N*-acryloyl ethanolamine (Coulon et al., 1998). We determined their recognition ability as ligand of the Kb CWL1 galactose specific lectin of the yeast *Kluyveromyces bulgaricus* (Coulon et al., 1998) and their surfactant properties in handling integral membrane proteins in solution (Chabaud et al., 1998).

Keeping in mind that *K. bulgaricus* cells bear galactose specific lectins on their outer surface (Al-Mahmood et al., 1991), we assumed that the galactosylated moieties grafted on the THAM organic telomers could act as ligands of this lectin and so interfere with its flocculating activity. One can also imagine that this complexation phenomenon at the outer surface of the yeast cell could inhibit or delay the intracellular penetration of such telomers.

In the present work, we used *K. bulgaricus*, *Kluyveromyces lactis*, and *S. cerevisiae* flocculent yeast strains in order to discriminate the fixation of neoglycoproteins and organic telomers on the yeast envelope. Neoglycoproteins are proteins [bovine serum albumin (BSA)] bearing fluorescent residues [in this case fluorescein isothiocyanate (FITC)] and specific covalently bonded sugar

* To whom correspondence should be adressed. Phone: 33-(0)3-83-17-88-42. Fax: 33-(0)3-83-17-88-79. E-mail: bonaly@pharma.u-nancy.fr.

[†] Université Henri Poincaré.

[‡] Université d'Avignon.

10.1021/bc990178e CCC: $19.00 © 2000 American Chemical Society
Published on Web 06/29/2000

Scheme 1

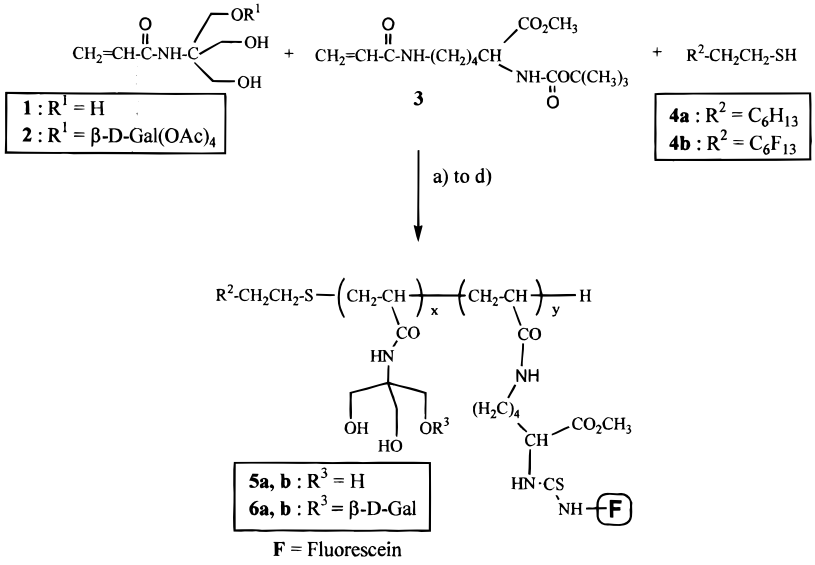

a) AIBN, MeOH, 65°C ; b) MeO⁻Na⁺, MeOH ; c) TFA, CH_2Cl_2, 0°C d) Fluorescein Isothiocyanate, DABCO, Pyridine, 50°C

residues (Monsigny et al., 1984). Organic telomers with MM between 1750 and 3400 Da are derived from THAM. All the synthetic compounds are labeled with fluorescent moieties. In these conditions, their recognition ability and therefore their cell envelope permeability in the various yeast strains can be visualized by fluorescence microscopy.

EXPERIMENTAL PROCEDURES

Synthesis of Monomers. Synthesis of THAM **1** and monogalactosylated THAM **2** was previously reported (Polidori et al., 1994).

Synthesis of *N*α-*tert*-(Butyloxycarbonyl) *N*ϵ-(Acryloyl)-L-lysine Methyl Ester 3. To a stirred solution of *N*α-*tert*-(butyloxycarbonyl)-L-lysine methyl ester acetate (4 g, 12,5 mmol) in freshly distilled dichloromethane at 0 °C was added diisobutylethylamine (DIEA) until a pH range between 8 and 9. Acryloyl chloride (1.87 mL, 23 mmol) was added dropwise at 0 °C, then the reaction mixture was stirred at room temperature for 24 h. The solution was successively washed with hydrochloric acid solution (1 mol/L) and water, dried over sodium sulfate, and concentrated to dryness in vacuo. The crude product was purified by column chromatography on silica gel (ethyl acetate/hexane 8/2 v/v). Compound **3** was isolated as a colorless oil with 76% yield. $[\alpha]_D = +7.5°$ (c, 1, $CHCl_3$). ^{1}H NMR ($CDCl_3$): δ 6.32 (^{1}H, dd, CH=); 6.15 (^{1}H, dd, CH_2=); 5.96 (^{1}H, t, CON*H*CH_2); 5.64 (^{1}H, dd, CH_2=); 5.17 (^{1}H, d, N*H*CH); 4.28 (^{1}H, m, CH); 3.34 (2H, q, CH_2-NH); 1.8−1.45 [6H, m, 3 (CH_2)]; 1.35 [9H, s, 3 (CH_3)]. ^{13}C NMR ($CDCl_3$): δ 173.23 (*C*O_2CH_3); 165.71 (CONH); 156.18 (CO urethane); 130.95 (CH_2=); 126.22 (CH=); 79.21 (C *tert*-butyl): 53.19 (CHα Lys); 52.29 (OCH_3); 39.14 (CH_2ϵLys); 35.47 ($CH_2$$\beta$Lys); 28.35 ($CH_3$*tert*-butyl); 22.81 ($CH_2$$\gamma$Lys).

Synthesis of Organic Telomers. A synthetic route of organic telomers derived from THAM labeled with fluorescein is presented in Scheme 1.

Telomerization reactions were achieved following the procedure previously described (Coulon et al., 1998). Monomers **3** and THAM **1** or monogalactosylated THAM **2** were reacted with different amounts of alkane or perfluoroalkanethiol telogen. The ratio (Ro) between the initial concentrations of the transfer reagent **4a** or **4b** and that of the monomers **1**−**3** are reported in Table 1. Telomerization reactions occurred in boiling methanol under a nitrogen atmosphere using AIBN as a radical initiator ([AIBN] = [Telogen]/2). They were pursued until each monomer disappeared (12−24 h). Organic telomers were purified by gel chromatography through a Sephadex LH60 column.

Table 1. Physicochemical Data of Fluorescent Telomer Synthesis

compd	R2	R3	Ro[a]	*x*/*y*	DPn = (*x* + *y*)	β-D-Gal. moieties	yield %[b]
5a	C_6H_{13}	H	1/6	2.66	5.5	0	48
5b	C_6F_{13}	H	1/6	1.75	5	0	61
6a	C_6H_{13}	β-D-Gal	1/6	3	8	≈6	30
6b	C_6F_{13}	β-D-Gal	1/6	2.35	7	≈5	37

[a] Ro = [Telogen **4a**,**b**]/[Monomers **1**−**3**]. [b] Over all yields of the telomers synthesis.

The relative proportions of each moiety called *x* and *y*, i.e., the average degree of polymerization (DPn = *x* + *y*) of macromolecules, were determined by ^{1}H NMR (solvent: DMSO-d_6) by comparing the area of typical signals ascribed to each monomer. Results were reported in Table 1.

Deacetylation of galactopyranosyl groups was performed at room temperature in methanol containing a catalytic amount of sodium methoxide. After treatment with a H^+-type resine (Amberlite IRC 50), filtration, and evaporation of the solvent, deacetylated telomer derivatives were isolated in quantitative yields.

After hydrolysis of *tert*-butyloxycarbonyl (BOC) groups with trifluoroacetic acid (TFA), fluorescein isothiocyanate was grafted via a thiourea bond to the lysine pendants. This last reaction was carried out at 50 °C in pyridine containing a catalytic amount of diazabicyclo[2,2,2]octane (DABCO). Fluorescent organic telomers were then purified by chromatography through a Sephadex G15 column and lyophilized.

Microorganisms and Culture Conditions. The flocculent yeast strains used were *K. lactis*, *S. cerevisiae* supplied from the Laboratoire de Microbiologie et Génétique, ENSAM (Montpellier, France), and *K. bulgaricus* (ATCC 96631). The *K. lactis* yeasts were grown aerobically (airflow, 40 L/h) at 25 °C for 24 h in a 2% glucose,

1% bactopeptone (Difco, Michigan) medium. *S. cerevisiae* and *K. bulgaricus* were grown under the same culture conditions in a 4% glucose, 0.4% bactopeptone (Difco, Michigan), 0.1% KH_2PO_4, 0.02% $MgSO_4,7H_2O$, and 0.02% $CaCl_2$ (Prolabo, Paris, France) medium.

Growth and Toxicity Assays. The effects of the organic telomers were tested on the growth of *K. bulgaricus*, *K. lactis*, and *S. cerevisiae*. The inoculum (10^7 cells/mL) was obtained from an overnight culture of the yeasts in liquid medium. The cultures were achieved aerobically at 25 °C in 100 mL Erlenmeyer flasks containing 20 mL of liquid culture medium supplemented with compounds to test. The Erlenmeyer flasks were stirred on a rotary shaker for 24 h. The growth of the yeasts was analyzed by measuring the absorbance at 620 nm with a Perkin-Elmer spectrophotometer.

All the THAM derivatives were solubilized in distilled water and sterilized using a 0.2 μm membrane. They were added to the culture medium at the concentrations of 1, 3, 4, 5, 6, and 8 mM at the same time as the inoculum.

Spheroplast Preparation. The yeasts were harvested at the end of the logarithmic growth phase by centrifugation at 1500*g* for 5 min at 4 °C. The cells were washed twice with distilled water, then twice with 1.2 M KCl. One gram of wet cells was suspended in 4 mL of 0.02 M phosphate buffer, pH 7.4, containing 0.01 M dithiothreitol and 2.0 mg/mL Pronase E (Merck). After incubation for 60 min at 30 °C under slight stirring (200 rpm) and centrifugation at 5000*g* for 1 min, the cells were washed three times and suspended in 4 mL of an isotonic buffer (0.15 M Na_2HPO_4, 0.08 M citric acid, 1.4 M KCl), pH 5.8, containing 20 mg of "Lysing-enzyme" (Sigma) and 5 mM dithiothreitol for 3 h at 30 °C under slight stirring. After centrifugation at 800*g*, the spheroplasts were washed twice with 1.2 M KCl and finally suspended in the isotonic buffer, pH 5.8.

The kinetics of spheroplast formation was followed by enumerating intact cells in a Malassez cell after contact for 10 min in distilled water, using an optic binocular microscope (SM-Lux-Leitz).

Extraction of a Galactose-Specific Lectin. The lectin was isolated from whole cells of *K. bulgaricus* ATCC 96631. After growth in a 2 L fermentor under aerobic conditions, cells were harvested by centrifugation at 3000*g* for 10 min at 4 °C, washed with Helm's buffer (150 mM CH_3COONa, 3.75 mM $CaCl_2$, and 3 mM NaN_3), pH 4.5, treated with 0.2 M D-galactose solution, and extensively washed with 0.01 M phosphate buffer, pH 7. Cells were then suspended at a concentration of 4% (w/v) in the same buffer supplemented with 5 mM EDTA and incubated at 37 °C for 90 min under slight stirring. The supernatant was collected by centrifugation at 3000*g* for 10 min and dialyzed at 4 °C for 48 h against distilled water and freeze-dried. The residual flocculating activity of the cells was assessed in a Helm's acetate buffer. If necessary, a second treatment was performed to obtain nonflocculating or deflocculated yeasts.

The titer of the so obtained lectin preparation was determined in glass tubes by mixing 150 μL of 2-fold serial dilution of lectin solution in Helm's acetate buffer pH 4.5 and 150 μL of a preliminary deflocculated yeast suspension (10^7 cells/mL) in the same buffer. After incubation for 30 min at room temperature, the lectinic titer corresponded to the reciprocal of the highest dilution of the lectin solution giving detectable aggregation or reflocculation of the preliminary deflocculated yeasts.

Reflocculation and Reflocculation Inhibition Assays. These assays were performed to specify the affinity of glucidic derivatives for the lectin.

Washing nonflocculating *K. bulgaricus* yeasts, obtained after lectin extraction, were suspended in Helm's acetate buffer to obtain 10^7 cells /mL. An aliquot of 150 μL of this cell suspension was added to 150 μL of lectinic solution titer 4. After 60 min of incubation at room temperature, yeast cell reflocculation was estimated by visual reading or optical microscope observation. The inhibition of this lectinic yeast reflocculation by glycosidic derivatives allowed to estimate the affinity of the latters for the lectin. For this purpose, a two-step assay was performed. First 150 μL of two-serial dilution of galactosylated organic telomers in Helm's acetate buffer was mixed with 150 μL of lectinic solution titer 4 and incubated for 60 min at room temperature. Then 150 μL of deflocculated yeast suspension was added and this mixture was incubated for 60 min at room temperature. The inhibitory concentration of the reflocculation (ICF) corresponded to the tube in which flocculation was visible. These tests allowed to specify the affinity of several glucidic derivatives for the lectin.

Fluorescence Measurement. The neoglycoprotein BSA-gal-FITC fluorescent probe used was provided by Sigma. This neoglycoprotein contains 15−20% mol of β-D-galactopyranose and 2−3 mol of fluorescein isothiocyanate/mol of protein.

Fluorescence microscopic observations were performed using a Zeiss Axioscope 50 microscope and a Zeiss MC80 camera. The photographs were achieved with Fugicolor 100 ASA color films. Measurements of probe and telomers concentration were followed with a SPEX Fluorolog II (λ_{exc} = 495 nm; λ_{em} = 520 nm) spectrofluorimeter.

The incorporation or the fixation of the fluorescent organic telomers in the yeast cells was observed by incubation of 100 μL of a cellular suspension (1×10^7 cells/mL, absorbance = 0.4) in the presence of 50 μL of 1 mM telomers for 15 min at 20 °C. After centrifugation at 4 °C, the pellet was suspended in 100 μL of distilled water, then the suspension was examined in order to determine the cell envelope crossing ability of the fluorescent derivatives.

To measure the inhibition by sugar on the fluorescent galactosylated organic telomer incorporation in flocculent yeast cells, three procedures were applied: (i) 500 μL of a cellular suspension (10^7 cells/mL), 100 μL of 1 mM fluorescent galactosylated telomer solution, and 100 μL of 1 mM sugar solution were mixed; after stirring for 2 min, the suspension was immediately examined by fluorescence microscopy; (ii) 500 μL of a cellular suspension (10^7 cells/mL) was incubated with 100 μL of 1 mM fluorescent galactosylated organic telomer solution for 15 min, then 100 μL of 1 mM sugar solution was added. After stirring for 2 min, the suspension was immediately examined by fluorescence microscopy; (iii) 500 μL of a cellular suspension (10^7 cells/mL) was incubated with 100 μL of 1 mM sugar solution for 15 min, then 100 μL of 1 mM fluorescent galactosylated organic telomer solution was added. After stirring for 2 min, the suspension was immediately examined by fluorescence microscopy, The tested sugars were galactose, methyl-β-D-galactose, glucose, and mannose (Sigma), and the assays were performed at 20 °C.

To observe the internalization speed of the fluorescent organic telomers into spheroplasts, preparations were performed as follows: *Kluyveromyces* and *Saccharomyces* spheroplast suspensions (10^7 cells/mL) in isotonic buffer, pH 5.8, were added to organic telomer solutions at

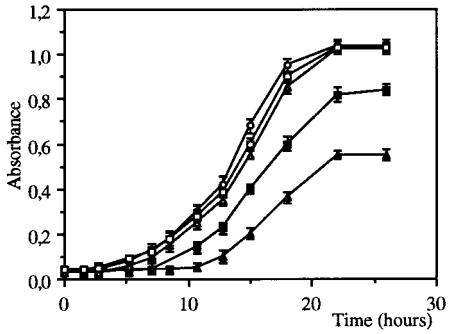

Figure 1. Growth of *K. bulgaricus* cells in the presence of the organic telomers at a concentration of 3 mM. (○) Control; (▲) compound **5a**; (△) compound **5b**; (■) compound **6a**; (□) compound **6b**.

concentrations from 0.1−1 mM. The mixtures were stirred for 1 min at 60 rpm, then incubated for several minutes at room temperature to achieve internalization kinetics of the fluorescent organic telomers.

The preparations were immediately examined by fluorescence microscopy after centrifugation for 4 min at 800*g*.

RESULTS AND DISCUSSION

Growth and Flocculation of the Yeasts in the Presence of Fluorescent Derivatives. The culture of the three yeast strains *K. bulgaricus*, *K. lactis*, and *S. cerevisiae* in the presence of telomers may be significantly altered at a concentration over 3 mM according to the derivatives nature.

Indeed, as shown in Figure 1, at a concentration of 3 mM in the medium, the organic telomers bearing an hydrocarbon tail (compounds **5a** and **6a**) hindered the growth of *K. bulgaricus*; the final biomass was diminished by about 70 and 30%, respectively. The galactosylated hydrocarbon compound (**6a**) appeared less toxic than the nongalactosylated one (**5a**). Similar results were obtained with *K. lactis* (figure not shown). These results can be explained if we take account for the detergency power of such surfactant.

The peripheral cell location of a galactose specific lectin at the surface of *K. bulgaricus* (Al-Mahmood et al., 1991) and *K. lactis* (El-Behhari et al., 1998) revealed a recognition of the saccharidic units of the galactosylated organic telomers **6a** and **6b**. This phenomenon could explain the decrease of toxicity of such compounds compared to the nongalactosylated one. Indeed, we can assume that this extracytoplasmic recognition of the galactosylated telomers (**6a**) checks the membrane insertion of the telomeric hydrocarbon tail and, thus, probably induces a loss of detergency. On the contrary, the nongalactosylated telomers **5a** and **5b** enter in the yeast cells. In the case of the telomer **5a**, the hydrocarbon tail can disturb their growth by altering the membrane structure, whereas the perfluoroalkyl one (**5b**), having no detergency character, can invade the cytoplasm with no effect on the cell growth.

It is noteworthy that in *S. cerevisiae*, bearing mannose-specific lectins at their surface, compound **(5a)** presented a detergency (or toxicity) comparable to that observed toward *Kluyveromyces* yeasts.

The organic telomers bearing a perfluoroalkyl tail (compounds **5b** and **6b**) showed no inhibitory effect on the growth of the three yeasts. This result can be related to previous observations with such perfluorosurfactants (Krafft and Riess, 1998). These compounds are neither hemolytic nor detergent (Zarif et al., 1993) and can keep membrane protein integrity.

Table 2. Inhibitory Concentration of the Flocculation (ICF) of Compounds 6a and 6b and Oligosaccharides

compds	ICF (mM)
5a	>500 mM
5b	>500 mM
6a	0.125 ± 0.025
6b	0.187 ± 0.031
methyl-β-D-galactoside	1.75 ± 0.25
galactose	3.12 ± 0.11
glucose	>300
mannose	>500 mM

[a] ICF, concentration of sugar derivatives or galactosylated polymers necessary to inhibit yeast flocculation. [b] Results are the mean of three independent experiments.

During all the growth assays, the yeasts were flocculent. However, we observed that galactosylated organic telomers **6a** or **6b** enhanced the flocculation of *K. bulgaricus*. The size of flocs in control flocculation disposed between slides was 0.85 ± 0.01 mm, and with galactosylated organic telomers, it was 12.45 ± 0.01 mm (Figure 2). This flocculation enhancement appeared to be due to the multiplicity of the galactose moieties on the organic telomers. These synthetic derivatives may play a role in intercellular ligand formation and favor cell−cell interactions. In the same way, Stratford (1992) observed that natural glycosylated compounds which are present in the culture medium may induce yeast flocculation.

Inhibition of Yeast Reflocculation by Galactosylated Telomers. Previous studies (Al-Mahmood et al., 1991) showed that *K. bulgaricus* yeasts bear on their outer surface a Kb CWL1 galactose-specific lectin involved in the flocculation phenomenon of these yeasts. To check the affinity of the telomers for this lectin, we used the reflocculation capacity of this lectin on nonflocculating *K. bulgaricus* cells obtained after lectin extraction. After preliminary incubation of lectin with various concentrations of galactose and galactosylated derivatives, flocculation of the lectin-treated yeasts was estimated, all the assays being performed in Helm's acetate buffer. Oligosaccharides are known to exhibit a higher affinity for lectins than free specific monosaccharides (Kawaguchi et al., 1980), and the presence of a hydrophobic aglycon on the sugar may also increase the affinity of the sugar for a lectin (Liener et al., 1986). As reported in Table 2, the galactosylated organic telomers **6a** and **6b**, respectively, bearing about 5 or 6 glycosidic units, had a 20−30-fold higher inhibitory efficiency on the lectin than galactose; so their lectinic affinity had to be higher than that of the free monosaccharide. This enhancement may be due either to a hydrophobic character afforded by grafting the galactose residues on the amphiphilic organic telomer (Coulon et al., 1998) or to the multiplication of saccharidic pendants on the macromolecular carrier and a possible cluster effect. However, it is noteworthy that the use of perfluoroalkyl galactosylated organic telomers, which exhibit higher hydrophobic and marked fluorophilic characters than the hydocarbon ones, did not reveal any modification of this affinity. Indeed, no differences could be observed between the two types of derivatives on the flocculation as well as on the reflocculation of *Kluyveromyces* cells. In these conditions, we can assume that the key parameter in this lectinic affinity is the multiplication of glycosidic units on the macromolecular carrier.

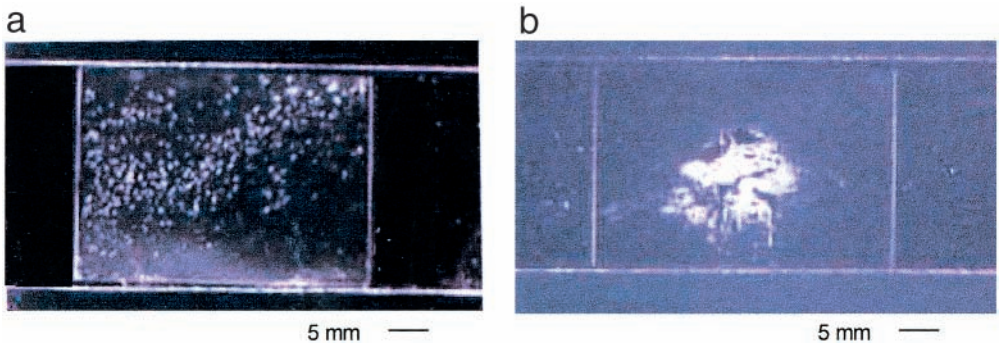

Figure 2. (a) Visualization of *K. bulgaricus* flocs without galactosylated organic telomer. (b) Visualization of *K. bulgaricus* flocs with galactosylated organic telomer.

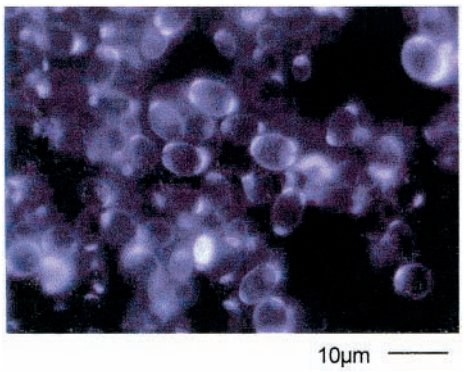

Figure 3. Visualization of *K. bulgaricus* cell wall by Calcofluor.

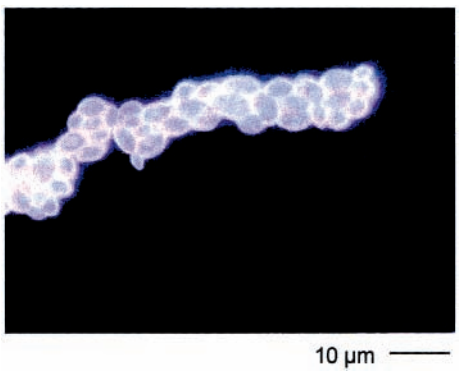

Figure 4. Anchorage of BSA-gal-FITC probe on the periphery of *K. bulgaricus* cells.

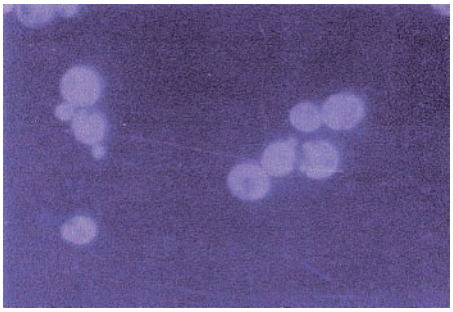

Figure 5. Homogeneous internalization of BSA-gal-FITC probe inside *S. cerevisiae* cells.

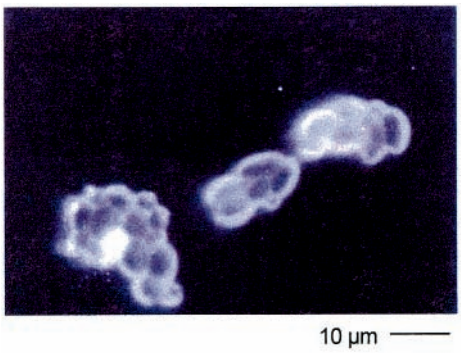

Figure 6. Anchorage of galactosylated organic telomers to the surface of *K. bulgaricus* cells.

As a matter of interest, if these assays were achieved on the *Saccharomyces* strain bearing a mannose-specific lectin, no effect on the flocculation of this yeast could be observed.

Fluorescence Microscopy Assays. Coloration of *K. bulgaricus* cells by calcofluor (Figure 3) was done in order to visualize the yeast cell wall. The lectin/glycosidic ligand complex implicated in the flocculation of *K. bulgaricus* could be visualized in vitro using fluorescent neoglycoprotein.

With flocculent *K. bulgaricus* and *K. lactis* strains, microscopic observations achieved in the presence of BSA-gal-FITC probe showed its homogeneous fixation on the periphery of the cells and no fluorescence could be observed inside the cells (Figure 4). Conversely, with *S. cerevisiae* no peripheral fixation was observed but an intracellular fluorescence was visualized (Figure 5).

Microscopic observations were also achieved using the galactosylated organic telomers at a concentration of 1 mM. As shown in Figure 6, it appeared that the galactosylated organic telomers **6a** and **6b** were bound and apparently blocked at the periphery of the yeast *K. bulgaricus*. The presence of a perfluoroalkyl chain (compound **6b**) instead of a hydrocarbon tail (compound **6a**) did not modify the binding properties of the derivatives onto the cell surface. When similar assays were achieved with nongalactosylated organic telomers, no binding on the periphery of the cells was observed, but all the yeast cells showed an intracellular fluorescence (Figure 7). Once more, no difference of internalization appeared between hydrocarbon organic telomer **5a** and perfluoroalkyl organic telomer **5b**. The same phenomena were observed with the flocculent *K. lactis* yeast strain tested under the same conditions (figures not shown).

Conversely, with *S. cerevisiae* bearing no galactose receptors but mannose specific lectins on their outer surface, all the galactosylated and nongalactosylated organic telomers were easily internalized (Figure 8).

These results confirm the presence of specific recognition components on the periphery of the yeast cells. These recognition components, lectins or lectin-like receptors, block the glycosidic derivatives at the cell wall level and do not allow their further internalization inside the cells. All these results validate our assumptions and clearly

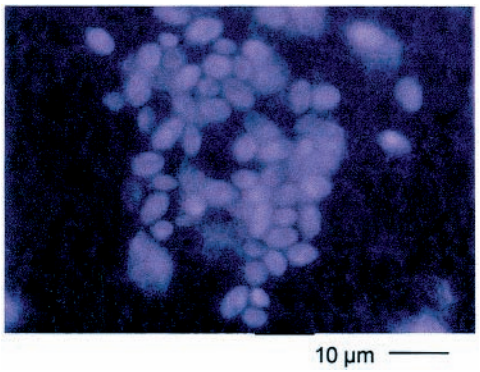

Figure 7. Homogeneous internalization of nongalactosylated organic telomers inside *K. bulgaricus* cells.

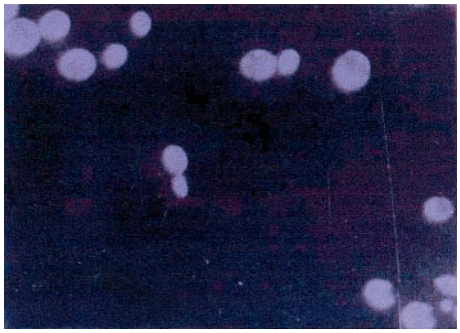

Figure 8. Homogeneous internalization of galactosylated or nongalactosylated organic telomers inside *S. cerevisiae* cells.

explain the respective inhibitory or toxic effect of nongalactosylated organic telomers on the growth of *Kluyveromyces* yeasts and of galactosylated ones on *Saccharomyces* strains. Moreover, they show the ability of specific lectin receptors located on the cell surface to bind galactosylated organic telomers and so eventually to ensure a cell recognition and vectorization process of glycosylated drugs on the yeast surface.

Permeability Measurement with Fluorescent Organic Telomers. These assays were performed on resting cells and on spheroplasts. Harvested at the end of their logarithmic growth phase, *K. bulgaricus* cells were incubated in the presence of a mixture of 1 mM methylgalactose, known to be a galactose-specific lectin inhibitor, and 1 mM fluorescent galactosylated organic telomers (compounds **6**) (first procedure described in Experimental Procedures). Organic telomers bound to the periphery of the cells, the concomitant presence of methylgalactose, and/or further addition of this latter derivative did not change peripheral binding of the organic telomers.

Moreover, when *K. bulgaricus* cells were incubated with 1 mM fluorescent galactosylated organic telomers alone (compounds **6**) (second procedure described in Experimental Procedures), the addition of 1 mM methylgalactose did not change peripheral binding of the galactosylated organic telomers.

This indicated a higher specific affinity of the galactosylated organic telomers for the *K. bulgaricus* peripheral lectin compared with that of methylgalactose. No fluorescence was observed inside the cells.

However, after preliminary incubation of *K. bulgaricus* cells with 1 mM methylgalactose alone (third procedure described in Experimental Procedures), then with fluorescent galactosylated organic telomers (compounds **6**), a very low peripheral fluorescence was observed and nearly 80% of the cells was intracellulary fluorescent. In

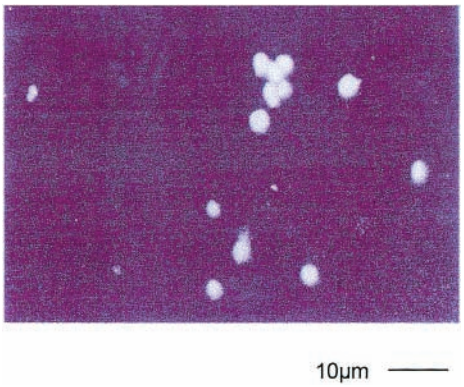

Figure 9. Internalization of galactosylated or nongalactosylated organic telomers inside *K. bulgaricus* spheroplasts.

this case, the accessibility of the peripheral receptors for the galactosylated organic telomers was diminished by methylgalactose preliminary fixed onto the cell outer surface, and the lack of free receptors on the yeast outer surface allowed internalization of galactosylated organic telomers into the cytoplasmic area, without any specific recognition process.

Spheroplasts, which are yeast cells without their cell wall, were also assayed in the presence of 1 mM galactosylated and nongalactosylated fluorescent organic telomers. Whether the spheroplasts were from *K. bulgaricus* or *S. cerevisiae*, for both galactosylated organic (compounds **6a** and **6b**) and nongalactosylated organic telomers (compounds **5a** and **5b**) no fluorescence could be observed on the periphery, all the organic telomers crossed the spheroplast envelope and invaded the intracellular area. In this case, however, as shown in Figure 9, organic telomer distribution was limited to the cytosol. This result may indicate that spheroplasts of *K. bulgaricus* and *S. cerevisiae* do not bear any specific lectinic receptors allowing organic telomer binding on their outer surface. However, it cannot be excluded that peripheral receptors exist, bind the organic telomers and swiftly if not instantaneously internalize them but at the concentration used, organic telomers are totaly internalized as showed in Figure 8.

To approach the internalization speed of the fluorescent organic telomers into the spheroplasts, kinetics were performed with concentrations from 0.1 to 1 mM. Internalization of all organic telomers occurred during the first 15 min of incubation with a homogeneous cytosol distribution. No difference could be observed between hydrocarbon and perfluoroalkyl organic telomers. After 50 min, the fluorescence decreased, due either to an efflux of these derivatives out of the spheroplasts or to their intracellular degradation (this is under investigation).

CONCLUSION

Yeast cell walls are mainly composed of peripheral phosphopeptidomannans (PPM), glucans, and to a lesser extent, chitin. These glycosidic polymers have been demonstrated to play several functions in recognition phenomena. Phosphopeptidomannans are considered as the predominant immunological determinants of yeast species (Fleet, 1991), they also are the ligands of receptors such as lectins, both being involved in yeast flocculation (Stratford, 1992). Peptidomannans may also form the α and a agglutinins responsible for mating agglutination (Lu et al., 1995). All the phenomena which involve these cell wall constituents are extracytoplasmic.

Glucans are responsible for cell wall rigidity and maintain the yeast cells morphological aspect, but some

glucans have been shown to serve as the target cell structures of natural killer (NK) cells. Indeed cells accumulating unprocessed N-linked glycan show an increased susceptibility to NK-mediated lysis (Dall'Olio et al., 1997).

The permeability of the yeast cell wall to neutral poly(ethylene glycol) polymers seems to depend markedly on the yeast strain as well as on its physiological conditions. During the exponential growth phase, the passage of very large molecules is quite evident, but electric charges, shape, and molecular mass of the macromolecules could affect their potential movement through the yeast wall (De Nobel and Barnett., 1991). However, these authors also hypothesized that glycosylation of macromolecules affects porosity and any specific yeast cell wall carrier systems. Such a hypothesis agrees with recognition mechanisms of glycosylated derivatives by cell wall carbohydrate-binding proteins, i.e., lectins, which have been shown to be present at the surface of several yeast strains; (i) cell wall lectin implicated in the flocculation of *K. bulgaricus* (Al-Mahmood et al., 1988, 1991); (ii) a mannose specific agglutin (certainly a lectin-like) involved in the flocculation of *S. cerevisiae* (Straver et al., 1994), (iii) a cell wall surface protein isolated and purified from the cells of flocculent *S. cerevisiae* (Shankar and Umesht-Kumar, 1994) and a galactose specific lectin involved in the flocculation of *K. lactis* (El-Behhari et al., 1998). Attioui (1994) used the flocculating yeast lectin recognition mechanism to target galactose-substituted cyclodextrins on flocculent *K. bulgaricus* cells bearing galactose specific lectins on their surface. Recently, Coulon et al. (1998) evidenced the efficient recognition of galactosylated organic telomers by the Kb CWL1 galactose-specific lectin isolated from *K. bulgaricus* and their possible use as tools for in vivo drug delivery.

Results reported in this work warrant several remarks and comments on the interaction between the yeast cells and extracellular compounds as well as on the yeast cell wall permeability or porosity for these compounds.

First, grafting fluorescent probes on a THAM-derived macromolecular backbone made it possible to observe the wall-crossing ability of the organic telomers and their cytosol biodistribution. This result confirms previous data obtained by ion microscopy (Chehade et al., 1998), i.e., the cell uptake and subcellular distribution of a perfluorinated organic telomer denoted FTAC, in two cell lines, rat fibroblasts and malignant murine B16 melanoma. This result also confirms that the fluorinated derivative is less toxic for yeast cells than the hydrocarboned derivatives.

Second, when glycosidic moieties are grafted on the organic telomers, their wall crossing ability depends on the presence of specific lectins on the outer yeast cell surface. In yeasts such as flocculent *K. bulgaricus* or *K. lactis* strains, the recognition of galactose substituted organic telomers by cell wall galactose-specific lectins induces their extra-cytoplasmic anchorage and affects their movement through the yeast wall. In this case, the polygalactosylated organic telomers show a lower toxic detergency effect on the membrane but may serve as extracellular specific ligands in cell−cell aggregation or flocculation phenomena mediated by a lectinic mechanism. Moreover, they may enhance cell−cell aggregation as, in their presence, larger flocs are obtained than in control flocculation.

The enzymatic elimination of the cell wall leads to spheroplasts and simultaneously discards the cell wall peripheral lectinic factors. The galactosylated organic telomers are internalized in the cytosol as easily as nonglycosylated ones.

The cell wall lectinic factors differ depending on yeast genera and/or yeast species and strains. They can be absent in mutant strains. This may explain the various porosity phenomena of yeasts for macromolecular compounds substituted with accessible glycosidic structures.

All the results in this present study clearly show the ability of glycosylated organic telomers to penetrate and to leave the intracellular compartment of the yeast cells as well as the role of the cell wall lectinic equipment in their specific recognition on the cell surface, and so in yeasts, cell wall lectinic receptors binding glycosylated polymers affect their intracellular penetration. This specific recognition mechanism may be applied to ensure specific cell targeting but also accounts for the various sensitivities of yeast strains toward glycosylated xenobiotics. However, such a discriminating targeting effect depends both on the nature of the xenobiotic saccharides and on the qualitative and quantitative peripheral lectinic equipment of the yeasts.

LITERATURE CITED

Al-Mahmood, S., Giummely, P., Bonaly, R., Delmotte, F., and Monsigny, M. (1988) *Kluyveromyces bulgaricus* yeast lectins. Isolation of *N*-acetylglucosamine and galactose-specific lectin, their relation with flocculation. *J. Biol. Chem. 263*, 3930−3934.

Al-Mahmood, S., Colin, S., and Bonaly, R. (1991) *Kluyveromyces bulgaricus* yeast lectins. Isolation of two galactose specific lectin forms from the yeast cell wall. *J. Biol. Chem. 266*, 20882−20887.

Attioui, F., Al-Omar, A., Leray, E., Parrot-Lopez, H., Finance, C., and Bonaly, R. (1994) Recognition ability and cytotoxicity of some oligosaccharidyl substituted β-cyclodextrin. *Biol. Cell 82*, 161−167.

Basu, J., Kundu, M., Mukherjee, K., and Chakrabarti, P. (1986) Release of a lectin from a fatty acid auxotroph of *Saccharomyces cerevisiae* grown in the presence of oleic acid. *Biochem. Biophys. Res. Commun. 136*, 596−602.

Chabaud, E., Barthélémy, P., Mora, N., Popot, J. L., and Pucci, B. (1998) Stabilization of integral-membrane proteins in aqueous solution using fluorinated surfactants. *Biochimie 80*, 515−530.

Chehade, F., Maurizis, J. C., Pucci, B., Pavia, A. A., Ollier, M., Veyre, A., Escaig, F., Jenguillaume, C., Dennebouy, R., Slodzian, G., and Hindie, E. (1996).Subcellular distribution of a new fluorinated biocompatible nonionic telomeric carrier. A study in cultured B16 melanoma and rat skin. *Cell Mol. Biol. 42*, 335−342.

Coulon, J., Bonaly, R., Pucci, B., Polidori, A., Barthelemy, P., and Contino, C. (1998) Cell targeting by glycosidic telomers. Specific recognition of the Kb CWL1 lectin by galactosylated telomers. *Bioconjugate Chem. 9*, 152−159.

Critchley, I. A., and Douglas, L. J. (1987) Isolation and partial characterization of an adhesin from *Candida albicans*. *J. Gen. Microbiol. 133*, 629−636.

Dall'Olio, F., Nariani, E., Tarozzi, A., Meneghetti, A., Chiricolo, T.Y., Lau, J., and Facchini, A. (1997) Expression of β-galactoside α 2−6 sialyl transferase does not alter the susceptibility of human colon cancer cells to NK-mediated cells lysis. *Glycobiology 7*, 507−513.

De Nobel, J. G., and Barnett, J. A. (1991) Passage of molecules through yeast cell walls: a brief essay-review. *Yeast 7*, 313−323.

El-Behhari, M., Ngonde-Ekome, J., Coulon, J., Pucci, B., and Bonaly, R. (1998) Comparative extraction procedures for a galactose-specific lectin involved in flocculation of *Kluyveromyces lactis* strains. *Appl. Microbiol. Biotechnol. 49*, 16−23.

Fleet, G. H. (1991) *The yeasts*, Vol. 4, pp 199−277, Academic Press, New York.

Kawaguchi, K., Kuhlenschmidt, M., Roseman, S., and Lee, Y.

(1980) Synthesis of some cluster galactosides and their effect on the hepatic galactose-binding system. *Arch. Biochem. Biophys. 205*, 388−395.

Krafft, M. P., and Riess, J. G. (1998) Highly fluorinated amphiphiles and colloidal systems, and their application in the biomedical field. A contribution. *Biochimie 80*, 489−514.

Liener, I. E., Sharon, N., and Goldstein, I. Y. (1986) The lectins: properties, functions and application in biology and medecine, Academic Press, Orlando, FL.

Lu, C. F., Montijn, R. C, Brown, J. L, Klis, F., Kurjan, J., Bussey, H., and Lipke, P. N. **(**1995) Glycosyl phosphatidylinositol-dependent cross-linking of α-agglutinin and β1,6-glucan in the *Saccharomyces cerevisiae* cell wall. *J. Cell Biol. 128*, 333−340.

Monsigny, M., Roche, A. C., and Midoux, P. (1984) Uptake of neoglycoproteins via membrane lectin(s) of L1210 cells evidenced by quantitative flow cytofluorometry and drug targeting. *Biol. Cell 51*, 187−196.

Polidori, A., Pucci, B., Maurizis, J. C., and Pavia, A. A. **(**1994) Synthesis of non ionic glycosidic surfactants derived from Tris(hydroxymethyl) amino methane. Preliminary assessment. *New J. Chem. 18*, 839−848.

Schreuder, M. P., Mooren, A. T. A., Toschka, N. Y., Verrips, C. T., and Klis, M. F. **(**1996) Immobilizing proteins on the surface of yeast cells. *Trends Biotech. 14*, 115−120.

Shankar, C. S., and Umesh-Kumar, S. (1994) A surface lectin associated with flocculation in brewing strain of *Saccharomyces cerevisiae*. *Microbiology 140*, 1097−1101.

Stratford, M. (1992) Yeast flocculation: a new perspective. *Adv. Microb. Physiol. 33*, 2−58.

Stratford, M. (1993) Yeast flocculation: flocculation onset and receptor availability. *Yeast 9*, 85−94.

Straver, M. H., Traas, V. M., Smit, G., and Kijne, J. W. (1994) Isolation and partial purification of mannose-specific agglutinin from Brewer's yeast involved in flocculation. *Yeast 10*, 1183−1193.

Zarif, L., Riess, J. G., Pucci, B., and Pavia, A. A. (1993) Biocompatibilty of alkyl and perfluoroalkyl telomeric surfactants derived from THAM. *Biomater. Artif. Cells Immobilization Biotechnol. 21*, 597−608.

BC990178E

Conjugation and Modeled Structure/Function Analysis of Lysozyme on Glycine Esterified Cotton Cellulose-Fibers

J. Vincent Edwards, Kandan Sethumadhavan, and Abul H. J. Ullah

FromUnited States Department of Agriculture, Agricultural Research Service, Southern Regional Research Center, Cotton Textile Chemistry Unit, New Orleans, Louisiana 70179-0687. Received October 18, 1999; Revised Manuscript Received March 20, 2000

The antimicrobial activity of lysozyme covalently bound to glycine-derivatized cotton cellulose was assessed in a 96-well format. Lysozyme was immobilized on glycine-bound cotton through a carbodiimide reaction. The attachment to cotton fibers was made through both a single glycine and a glycine dipeptide esterified to cotton cellulose. Higher levels of lysozyme incorporation were evident in the diglycine-linked cotton cellulose samples. The antibacterial activity of the lysozyme-conjugated cotton cellulose against *Bacillus subtilis* was assessed as a suspension of pulverized cotton fibers in microtiter wells. Inhibition of *B. subtilis* growth was observed to be optimal within a range of 0.14−0.3 mM (equivalent to 4−20 mg of lysozyme-bound cotton/mL) of lysozyme. Enhancement of activity over soluble lysozyme may result from the solid-phase protection afforded by the cellulose linkage of the glycoprotein against proteolytic lysis. Computational models of lysozyme based on its crystal structure attached through aspartate, glutamate, and COOH-terminal residues to cellopentaose-(3) Gly-*O*-6-glycyl-glycine ester were constructed. The models demonstrate no steric constraints to the active-site cleft from the glycine-conjugated cellulose chain when lysozyme is bound at the carboxylates of Asp-87, Glu-7, Asp-119, Asp-18, and COOH-terminal Leu-129. The more robust antibacterial activity of the enzyme when bonded to cotton fibers suggests good potential for biologically active enzymes on cotton-based fabrics.

INTRODUCTION

The immobilization of enzymes on textiles has received scarce attention. Immobilization of only α-amylase (*1*) and glucose oxidase (*2*) have been reported on a variety of fabrics. However, the potential utility of immobilizing numerous other enzymes on fabrics as a source of biologically active textile surfaces would offer highly selective functional properties while providing an environmentally acceptable textile finish. Here, we consider lysozyme as a model for enzyme activity on cotton cellulose.

C-type lysozyme is a 1,4-*β*-*N*-acetylmuramidase that derives its antibacterial activity from the selective lysis of the cell wall peptidoglycan at the glycosidic bond between the C-1 atom of *N*-acetylmuramic acid (NAM) and O-4 of *N*-acetylglucosamine (NAG) (*3*−*5*). The mechanism of action of lysozyme has been shown to occur through binding of tri-NAG in a cleft at the surface of the enzyme and subsequent carbonium ion-mediated hydrolysis of the glycosidic bond between the NAM and NAG residues (*6*−*8*). The mechanism of action of lysozyme is probably the best studied of any enzyme reported to date. Although lysozyme has been immobilized on numerous solid supports (*9*−*14*), its attachment to cotton cellulose and consideration of the relevant structure/function implications of surface protein and fiber contact points have not been reported. This paper reports the attachment of lysozyme to glycine-derivatized cotton cellulose and antimicrobial activity of the resulting conjugate. Structure/function molecular models are also examined to assess availability of the active-site conjugated lysozyme.

MATERIALS AND METHODS

Esterification of Cotton Cellulose with Fmoc-Glycine. Desized, scoured, bleached, and mercerized (an alkaline treatment of cellulose that results in the swelling of cellulose fibers) cotton twill was cut into circular disks (8.5 cm in) for the glycine esterification. Esterification was accomplished through base-catalyzed carbodiimide/HOBT[1] acylation. Cotton disks were pretreated with 20 mL of 25% TFA/DCM (10 min), washed with 5 × 20 mL of DCM, 2 × 20 mL, 10% DIPEA, 5 × 20 mL (5 min), and 2 × 20 mL of DCM. The cotton disks were vacuum-dried on a Buchner funnel and esterified in a beaker placed in an ultrasonic bath. Fmoc-glycine esterification was accomplished by reacting the cotton disks in a 20 mL DMF solution with 0.3 M Fmoc-glycine/DIC/HOBT and 0.03 M DMAP. One disk was removed, and a second glycine was reacted on the remaining cotton disk utilizing the following protocol. Acetylation of Fmoc-Gly-bound cellulose cotton was accomplished with acetic anhydride/NMI/DMF 1:2:3 (v/v/v) for 60 min. The cotton disks were washed with DMF (3 × 10 mL) and DCM (2 × 10 mL) and DCM (2 × 10 mL). Deprotection of Fmoc was accomplished in 20% piperidine/DMF, 15 min; wash (3 × DMF, 2 × DCM); coupling (0.3M Fmoc-glycine/HOBT/DIC in DMF, 90 min); wash (3 × DMF; 2 × DCM). To monitor completion of the glycine coupling step, 10 μL of a bromophenol blue/DMF solution was added during the coupling step.

[1] Abbreviations: HOBT, hydroxybenzotriazole; TFA, trifluoroacetic acid; DCM, methylene chloride; DIPEA, diisopropylethylamine; DMF, dimethylformamide; DIC, diisopropylcarbodiimide; DMAP, (dimethylamino)pyridine; NMI, *N*-methylimidazole; Fmoc, 9-fluorenylmethyloxycarbonyl.

10.1021/bc990141u Not subject to U.S. Copyright. Published 2000 by American Chemical Society
Published on Web 06/24/2000

Table 1. Levels of Lysozyme Conjugated To Fiber and Relative Antimicrobial Activity[a]

description of Gly-cellulose conjugate	analogue	percent protein on cotton fiber	activity of conjugate on fiber
lysozyme-Gly-cellulose	I	6.8% (4.7×10^{-7}mol)/mg of fiber	23.8 (OD $\times$ μmol^{-1})
lysozyme-Gly-Gly-cellulose	II	33.6% (2.3×10^{-6} mol)/mg of fiber	21.4 (OD $\times$ μmol^{-1})

[a] The levels of lysozyme conjugated to cotton cellulose and the relative activities as measured after 5 h of bacterial growth. Activity of the conjugate on fiber is reported at the 5-h time point as a ratio of optical density change (OD) over the total number of micromoles of lysozyme assayed per microtiter well. The freely dissolved lysozyme demonstrated a lower activity of 0.04 (OD $\times$ μmol^{-1}).

Immobilization of Lysozyme on Glycine-Cellulose Cotton. In 10 mL of dimethylformamide (DMF), 2.0 g of lysozyme was combined with HOBT (0.675 g) and *N*,*N*′diisopropylcarbodiimide (0.63 g), and the resulting solution was applied to two glycine-bound cotton disks. The reaction was allowed to proceed for 3 h, and the cotton disks were washed with DMF, ethanol, and methylene chloride. In a separate reaction, diisopropylethylamine (DIPEA) was added to neutralize the lysozyme solution to pH 7 prior to adding the coupling reagent. The protein levels on the cotton fiber samples were measured by the Kjeldahl method for elemental analysis of nitrogen.

Antibacterial Assay. *Bacillus subtilis* (NRRL NRS-744) was obtained from Agricultural Research Service, Peoria, IL 61604. The *B. subtilis* cultures were grown in the Luria broth medium containing 1% tryptone (DIFCO laboratories, Detroit), 0.5% NaCl, 0.5% yeast extract, and 15% Agar in sterile conditions. Seed cultures were grown in the same media (5 mL) without agar at 37 °C overnight. This was transferred to another flask containing 45 mL of fresh sterile medium and shaken at 37 °C for 5 h. The culture cells were obtained by centrifugation at 3000 rpm for 15 min. The pelleted cells were suspended in the same medium and recentrifuged once again. The bacteria were resuspended in 5 mL of the culture medium.

The antibacterial activity was measured based on the lysis of the *B. subtilis* cells, which leads to a drop in the optical density of the medium at 490 nm. The assays were done using 96-well culture plates and a Benchmark plate reader (Bio-Rad Laboratories) at 37 °C. The cotton twill samples were pulverized on a Wiley Mill of 80 mesh screen (150 μ size fibers) prior to assaying the fibers for antimicrobial activity. Five hundred milligrams of the lysozyme cross-linked fibers were suspended in 1 mL of medium for a 1−2 h period on a vortex mixer. The control wells contained 75 μL of *B. subtilis* bacteria and 125 μL of media with an optical density of approximately 1. Twenty-five microliters of the above fiber suspension and 75 μL of cells suspended in media were combined in 100 μL of culture media. Following these additions to the plate wells, the progress of the experiment was monitored at 490 nm every 15 min for 16 h. Values were normalized by subtracting the optical density contributed by addition of the fibers to the culture cells. This enabled comparison of wells with varying concentrations over the entire length of each test.

Models of Lysozyme-Bound Cellulose Pentasaccharide. Computational procedures were performed with DISCOVER and INSIGHT (Biosym Inc., San Diego) packages on a Silicon Graphics RS5000 Workstation. The initial configurations for the glycoprotein structures were prepared using INSIGHT with the crystal structure of lysozyme being selected from the Protein Data Bank. The starting structure of lysozyme was taken from the INSIGHT protein database file and was based on the crystal structure of lysozyme. Cellopentaose-(3) Gly-*O*-6-glycyl-glycine ester was also constructed in INSIGHT to mimic the extended conformation of a polysaccharide chain of cellulose esterified with a diglycine peptide as a linker. Cellopentaose-(3) Glc-*O*-6-glycyl-glycine ester was bonded to lysozyme at the side chain carboxylates of aspartate and glutamate residues. Charges were assigned to the polar residues based on the crystal structure of lysozyme. Energy minimization was accomplished by the method of steepest descent. Structures were minimized until the maximum derivative was less than 0.001 kcal/(mol Å). The consistent valence force field was used in all the potential energy calculations.

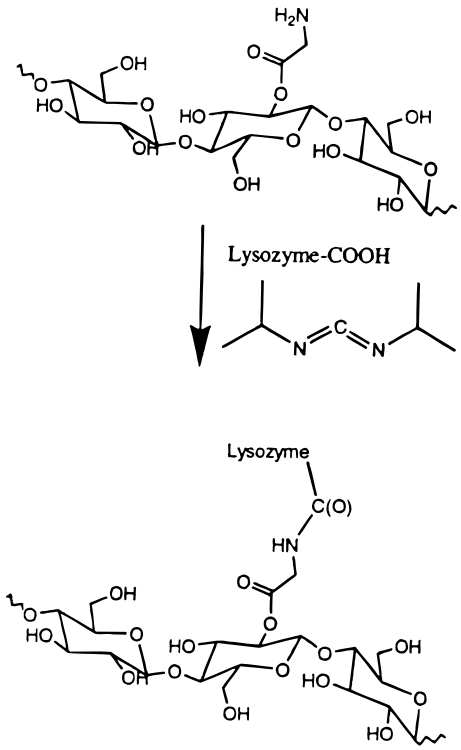

Figure 1. Carbodiimide-mediated reaction of lysozyme with cotton cellulose.

RESULTS

Analogues I and II are lysozyme linked to glycine and diglycine esterified cotton cellulose, respectively. The immobilization of lysozyme onto cotton cellulose was accomplished by reacting a 13 mM lysozyme solution in DMF to glycine esterified cotton cellulose. The reaction and representative structural linkages are illustrated in Figure 1. Lysozyme contains aspartate and glutamate residues on the protein surface (listed in Table 2). The carbodiimide activation of accessible side-chain carboxylates at those residues provides a variety of potential anchoring sites for amide bond formation between the aspartate/glutamate and glycine esterified cotton cellulose.

Protein levels of analogues I and II on the cotton cellulose were 6.8 and 33.6%, respectively, as shown in Table 1. Both the pH of the carbodiimide amide bond formation and the glycine linker influence the level of incorporation of lysozyme onto cellulose. A higher level

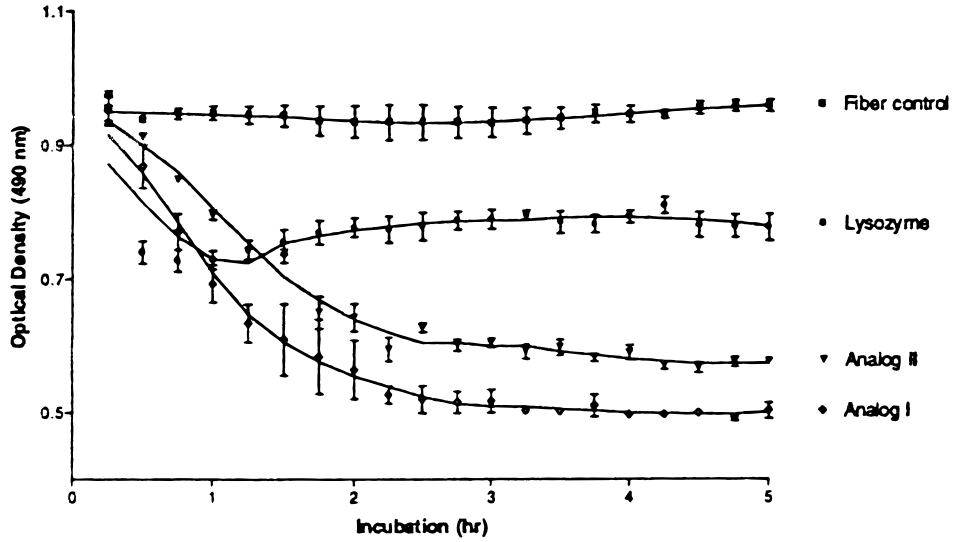

Figure 2. Time course of microbial growth for *B. subtilis* cells in the presence of two lysozyme-glycine cotton cellulose conjugates. Analogue I: lysozyme linked to cotton cellulose through a single glycine. Analogue II: lysozyme linked to cotton cellulose through diglycine. Lysozyme is freely dissolved (2.6×10^{-4} M). Control fiber is pulverized cotton twill. Samples of the lysozyme conjugates were prepared from a stock solution of 50 mg/800 μL. Aliquots having equivalent concentrations ranging from (0.6 to 2.6) $\times 10^{-4}$ M were suspended in media in a 96-well microtiter plate as described in Materials and Methods. Growth curves represent the average of three replicates. The experiment was carried out in triplicates and mean values were used to plot the graph.

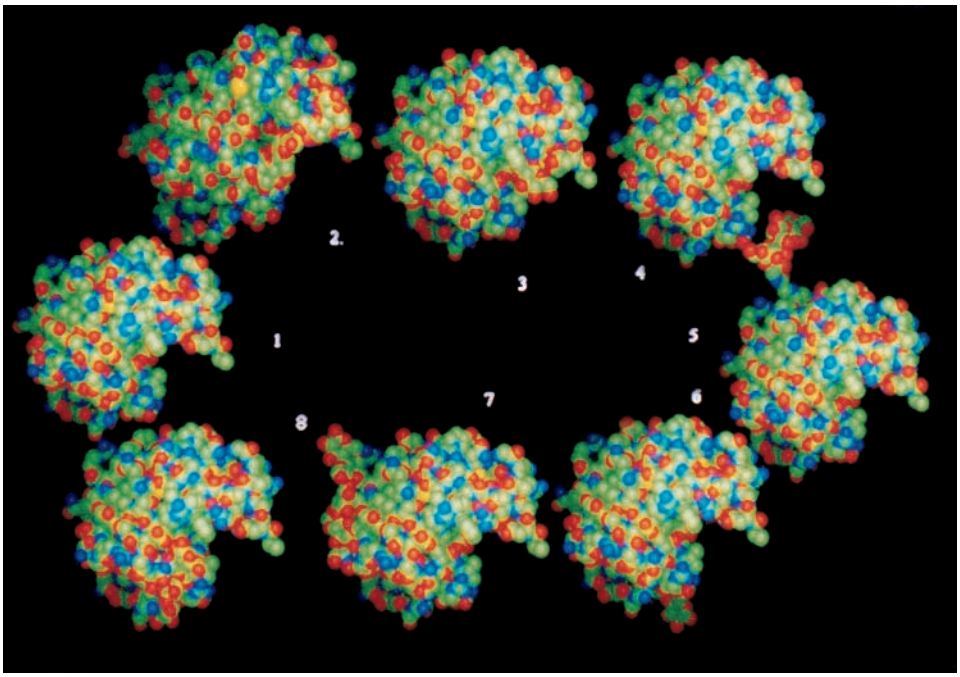

Figure 3. Molecular models of lysozyme-bound conjugates of cellopentaose-(3) Gly-*O*-6-glycyl-glycine ester. The eight structures shown are CPK models. Atom color types are as follows: oxygen (red); carbon (green); nitrogen (blue); sulfur (yellow): all models are oriented with the enzyme active site cleft in the right lower quadrant of the protein structure. The lysozyme (**1**) crystal structure may be compared with glycoprotein structures **2**−**8**. Amide linkages to the protein with the glycopeptide are the following: **1**, Lysozyme (unmodified); **2**, Asp-48; **3**, Asp-66; **4**, Glu-7; **5**, Asp-87; **6**, Asp-119; **7**, COOH-129; **8**, Glu-35.

of lysozyme on cotton cellulose was observed with analogue II containing the diglycine linker.

Inhibition of the growth of B. subtilis is shown in Figure 2, where cells were added to equivalent amounts of lysozyme-bound fibers. This was accomplished by adding lysozyme-bound fiber (analogue I and II) in quantities equivalent to the same molarity, lysozyme solutions. Analogues I and II gave similar profiles of inhibition over a 5-h period. The levels of inhibition observed for the cotton bound samples were longer lived than both comparable and higher lysozyme concentrations in solution.

The models constructed of lysozyme-bound cellulose were based on placing together the crystal structure-based model of lysozyme (*6*−*8*) with a minimized pentasaccharide analogue of glycyl-glycine ester. Formation of the amide bond between aspartate and glutamate residues of lysozyme and the cellulose fragment yielded a glycoprotein conjugate mimicking potential interactions of lysozyme with the polysaccharide chain of the bound cellulose. Models of lysozyme and seven of the glycoprotein adducts (structures **1**−**8**) are shown in Figure 3. Since Glu-35 (**8**) is involved in protonation of the D ring glycosidic oxygen of the polysaccharide backbone, attach-

Table 2. Aspartate and Glutamate Residues That May React with Glycine-Cellulose[a]

residue	surface/interior	±
Asp-18	surface	+
Asp-119	surface	+
Glu-7	surface	+
Glu-35*	interior	-
Asp-87	surface	+
Asp-101*	surface	-
Asp-52*	interior	-
Asp-48	surface	+
Asp-66	interior	±

[a] The aspartate and glutamate residues found in lysozyme are listed as being on the surface and interior of the protein. The ± indicates probability of either retaining (+) biological activity or interfering (−) at the active site with lysis. An asterisk indicates active-site residues involved in lysis of the cell wall polysaccharide (*).

ment at Glu-35 would completely block activity. The proximity of the Asp-48, conjugate cellulose chain (**2**), which lies parallel to the β-sheet structure of the protein, suggests steric hindrance to substrate binding. The Asp-66 conjugate structure (**3**) extends the cellulose chain across the opening of the active-site cleft, and would be expected to abrogate binding of the substrate. The Glu-7 (**4**) and Asp-129 (**7**) cellulose conjugates are in separate domains of the cellulose at linkages remote from the active-site cleft. The Asp-87 (**5**) conjugate places the cellopentaose backbone free from interaction with lysozyme.

DISCUSSION

This study outlines an approach to assessing an immobilized enzyme on cotton cellulose fibers. Lysozyme is perhaps one of the most well-characterized enzymes for it's mechanism of action and thus provides an opportunity to analyze the structure/function implications of cellulose linkers and subsequent enzyme activity. Lysozyme was attached through amide bond formation of aspartate and glutamate residues on the surface of the protein to accessible glycine esterified cellulose sites in the cotton cellulose fiber. The use of a carbodiimide coupling procedure wherein dimethylformamide was employed as a solvent resulted in significantly higher levels of protein cross-linking when diglycine was employed as a linker.

The immobilization of lysozyme has previously been studied with applications in the food preservative (*9*, *10*) and dairy industry (*11*, *12*). Immobilization of lysozyme on a variety of matrixes has been reported including chitosan and silica gel on a cross-linked polystyrene divinylbenzene matrix (*11*), silicate carriers (*13*), hydroxypropyl methyl cellulose acetate succinate (*14*) and dextran (*10*). Immobilization to these supports has included techniques such as the Maillard reaction (*10*), glutaraldehyde, Schiff base formation mediated with oxidized aldehydic dextran, or pyridino-4-aldehyde and BrCN (*13*), and carbodiimide coupling (*14*). To immobilize lysozyme on cotton cellulose we have employed a carbodiimide coupling onto glycine-derivatized cotton cellulose.

As shown in Figure 2 and Table 1, the antimicrobial activity observed on the lysozyme-bound cotton fibers was greater than that observed for lysozyme in solution. This may be due to the enhanced stability of the enzyme afforded by conjugation to cellulose. Improved stability against proteolytic digestion of proteases released during the course of the bacterial assay may account for this enhanced activity. This might be expected since anchoring of a protein to a solid-phase support can confer protection against proteolytic lysis of the protein (*15*).

The conformation of lysozyme (structure **1**) elucidated by X-ray crystal structure is depicted in Figure 3. A deep crevice or cleft containing the active site of the enzyme characterizes the lysozyme conformation. The cleft divides the molecule into two domains. One domain including residues 40− 85 contains primarily β-sheet structure. The other domain containing the amino- and COOH-terminal portions from residues 1 to 39 and 101 to 129 contains predominantly helical conformation. Three side-chain carboxylate residues, Glu-35, Asp-101, and Asp-52 are involved in the lytic activity of lysozyme. Examination of the crystal structure of lysozyme revealed that five of the residues (Table 2) not directly implicated in substrate lysis were distant from the catalytic-binding site of the enzyme. The fragment cellulose conjugates of the residues Asp-18, Asp-119, Glu-7, and Asp87 shown in the molecular models of the glycoprotein do not appear to present neighboring group interference at the active site. Two residues (Asp-48 and Asp-66) near the active site, however, demonstrate some potential for interference, as shown in Figure 3 (structure **2** and **3**). An examination of the conjugate structure of Asp-48 (**2**) revealed the cellopentaose backbone resides within 10 Å of the cleft where the B, C, and D rings of the cell wall peptidoglycan polysaccharide binds.

The attachment and subsequent biological activity of lysozyme to cotton cellulose suggests that enzymes may be conjugated to cotton through esterifiable residues on the surface while retaining activity. The efficacy of this approach to other enzymes on cotton cellulose will be the subject of future investigations.

LITERATURE CITED

(1) Shukala, S. R., and Athalye, A. R. Immobilizing Alpha-Amylase Onto Fibrous Supports. (1995) *Am. Dyest. Rep. 84* (7), 40−44.

(2) Kawakara, Y. Immobilizing Glucose Oxidase in Tussah Silk Fibers. (1999) *Text. Res. J. 69*, 2, 156.

(3) Salton, M. R. J., and Ghuysen, J. M. (1959) The structure of di- and tetra-saccharides released from cell walls by lysozyme and Streptomyces F_1 enzyme and the β (1−4) N-acetylhexosaminidase activity of these enzymes. *Biochim. Biophys. Acta 36*, 552−554.

(4) Salton, M. R. J., and Ghuysen, J. M. (1960) Acetylhexosamine Compounds Enzymically Released from *Micrococcus Lysodeikticus* Cell Walls. *Biochim. Biophys. Acta 45*, 355−363.

(5) Jeanloz, R. W., Sharon, N., and Flowers, H. M. (1963) The Chemical Structure Of A Disaccharide Isolated From *Micrococus lysodeikticus* Cell Wall. *Biochem. Biophys. Res. Commun. 13*, 20−25.

(6) Philips, D. C. (1966) The Three-Dimensional Structure of an Enzyme *Mol. Sci. Am. 215*, 78−90.

(7) Blake, C. C. F., Mair, G. A., North, A. C. T., Phillips, and Sarma, V. R. (1967) On the Conformation of Hen Egg-White Lysozyme Molecule. *Proc. R. Soc. Ser. B 167*, 365−377.

(8) Blake, C. C. F., Mair, G. A., North, A. C. T., Phillips, and Sarma, V. R. (1967) Crystallographic Studies of the Activity of Hen Egg-White Lysozyme. *Proc. R. Soc. Ser. B 167*, 378−388.

(9) Nakamura, S., Kato, A., and Kobayashi, K. New Antimicrobial Characteristics of Lysozyme-Dextran Conjugate. (1991) *J. Agric. Food Chem. 39*, 647−650.

(10) Hayashi, K., Kasumi, T., Kubo, N., Haraguchi, K., and Tsumura, N. (1989) Effects of N-Acetylmuramidase Streptomyces rutgersensis H-46 as a Food Preservative. *Agric. Biol. Chem. 53*, 3173−3177.

(11) Crapisi, A., Lante, A., Pasini, G., and Spettoli, P. (1993) Enhanced Microbial cell lysis by the use of lysozyme immobilized on different carriers. *Process Biochem. 28*, 17−21.
(12) Scott, D., Hammer, F. E., and Szalkucki, T. J. (1987) Bioconversions: enzyme technology. In *Food Biotechnology* (D. Knorr, Ed.) pp 413−419, Marcel Dekker, New York.
(13) Moser, I., Dworsky, P., Pittner, F. (1988) Degradation of Bacterial Cell Walls By Immobilized Lysozyme. *Appl. Biochem. Biotechnol. 19*, 243−249.
(14) Chen, J.-P., and Chen, Y.-C. (1997) Preparations of Immobilized Lysozyme With Reversibly Soluble Polymer For Hydrolysis of Microbial Cells. *Biores. Technol. 60*, 231−237.
(15) Kondo, A., Kishimura, M., Katoh, S., and Sado, E. (1997) Improvement of proteolytic resistance of immunoabsorbents by chemical modification with poly(ethylene glycol). *Biotechnol. Bioeng. 34* (4), 532−540.

BC990141U

Photochemical Immobilization of Anthraquinone Conjugated Oligonucleotides and PCR Amplicons on Solid Surfaces

Troels Koch,* Nana Jacobsen, Jef Fensholdt, Ulrich Boas, Mogens Fenger,† and Mogens H. Jakobsen

Exiqon A/S, Bygstubben 9, 2950 Vedbaek, Denmark, and Department of Clinical Biochemistry and Molecular Biology, University Hospital of Copenhagen, 2650 Hvidovre, Denmark. Received January 31, 2000; Revised Manuscript Received May 12, 2000

Ligand immobilization on solid surfaces is an essential step in fields such as diagnostics, bio sensor manufacturing, and new material sciences in general. In this paper a photochemical approach based on anthraquinone as the chromophore is presented. Photochemical procedures offer special advantages as they are able to generate highly reactive species in an orientation specific manner. As presented here, anthraquinone (AQ) mediated covalent DNA immobilization appears to be superior to currently known procedures. A synthetic procedure providing AQ-phosphoramidites is presented. These reagents facilitate AQ conjugation during routine DNA synthesis, thus enabling the AQ-oligonucleotides to be immobilized in a very convenient and efficient manner. AQ-conjugated PCR primers can be used directly in PCR. When the PCR is performed in solution, the amplicons can be immobilized after the PCR. Moreover, when the primers are immobilized prior to the PCR, a solid-phase PCR can be performed and the amplicons are thus produced directly on the solid support.

INTRODUCTION

Immobilization of DNA on solid supports has wide applications. Therefore, much attention has been devoted to this area, and consequently many different methods have been devised. The immobilization techniques range very broadly from passive immobilization (*1, 2*) to the more advanced covalent attachment procedures. Covalent immobilization is in many cases performed using chemically modified polymers, e.g., amino modification and subsequent coupling of the DNA in a separate reaction step (*3*−*9*). These techniques rely on consecutive manipulations and are often complex to handle.

Recently, Rehman et al. (*10*) published a copolymerization procedure where acrylamide monomers are linked to DNA and the conjugate is integrated via the polymerization on a suitable polymer. This procedure provides high loading of the ligand but is limited to a few solid supports on which the polymerization reaction can occur.

Covalent ligand immobilization via photoreactive species (photoprobes), i.e., the covalent link to the surface is mediated by the photoprobe during irradiation, offers the intriguing possibility of selective activation. In principle, this technique offers a generic and specific one-step procedure that is applicable for ligand immobilization on a wide range of surfaces. Traditionally psoralens, benzophenones, nitrene, and carbene precursors are used in photochemical immobilization reactions (*11*−*18*). However, all of these photoprobes suffer from several drawbacks. Carbenes and nitrenes are highly electrophilic species that react readily with water which severely reduces the immobilization yield in aqueous media. Psoralens react in 2 + 2 cycloadditions and can therefore only react with solid surfaces that contain exposed double bonds. Even though benzophenones react photochemically in radical-like reactions, and therefore do not react with water, they have nearly overlapping absorption spectra with the biological material and therefore an increased risk of photoinduced damage. Furthermore, the thermal reactivity of ketones, e.g., hydrate/imine formation, increases the risk of side reactions between the ketones and multifunctional bioligands dissolved in the aqueous medium.

Therefore, to reach the full potential of photochemical immobilization techniques, new classes of photoprobes have to be employed. Judged on the basic photochemical properties of tricyclic quinones, i.e., anthraquinones, this class of photoprobes provides interesting properties for ligand immobilization. (i) Excited anthraquinone is highly reactive and reacts with almost any C−H containing substrate (*19*). (ii) Anthraquinone reacts photochemically in radical reactions and therefore does not react with water (*20, 21*). (iii) Anthraquinone has much higher absorption coefficients above 300 nm, compared to most azides, diazirines, and benzophenones used in these procedures (*15, 22*−*23*); (iv) In contrast to ketones, the quinoid structure reduces significantly the reactivity of the carbonyl groups in the ground state.

In this paper, we describe a facile, orientation-specific, one-step technique for oligonucleotide photochemical immobilization using anthraquinone (Figure 1). This technique is useful for covalent attachment of DNA oligomers on a variety of solid surfaces. The photochemical properties of anthraquinone make bioligand immobilization possible on surfaces such as polystyrene, polycarbonate, polypropylene, Teflons, and silylated glass, which are frequently used in biotechnology.

MATERIAL AND METHODS

All chemical reagents and solvents were obtained from commercial suppliers and were used without further purification. NMR spectra were recorded at 400 MHz or at 250 MHz for ^{1}H NMR and at 62.9 MHz for ^{13}C NMR and at 202.33 MHz for ^{31}P NMR. δ-Values are in parts

* To whom correspondence should be addressed at Exiqon A/S. Phone: + 45-46-66-08-88. Fax: +45-46-66-18-88. E-mail: troels_koch@hotmail.com.

† University Hospital of Copenhagen.

10.1021/bc000011h CCC: $19.00 © 2000 American Chemical Society
Published on Web 06/24/2000

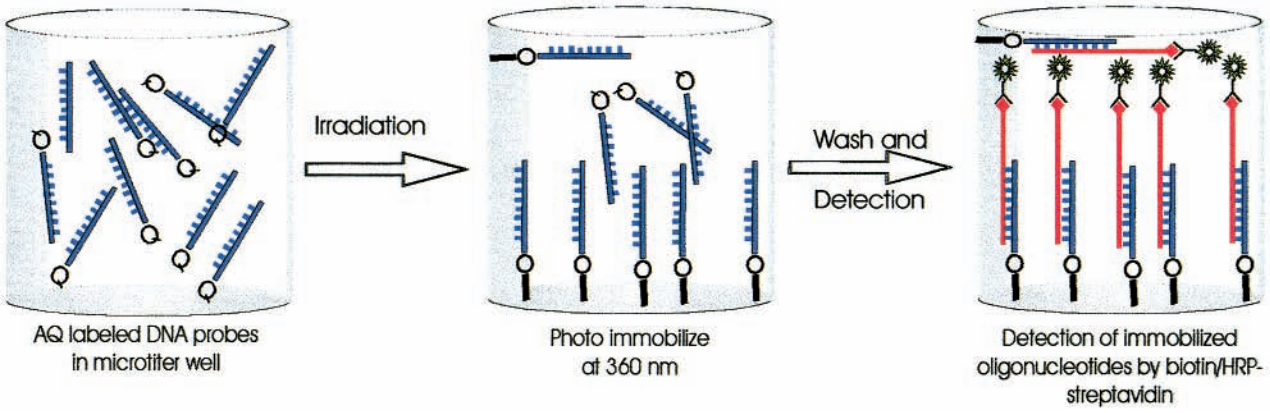

Figure 1. Photochemical immobilization of AQ-oligonucleotides.

per million relative to teramethylsilane as internal standard for ^{1}H NMR and ^{13}C NMR and relative to 85% H_3PO_4 as external standard for ^{31}P NMR.

MTP's[1] Polysorp (polystyrene) and TopYield (polycarbonate) were obtained from Nunc A/S, Denmark. Biotinylated primers were HPLC purified and obtained from DNA Technology, Denmark. The UV light source is the ULS-20-2 illuminator (UV Light Systems, Denmark) which is equipped with 28 Philips Cleo Compact 25W-S (14 bulbs located above and 14 bulbs below a glass plate sample holder).

Buffers. 6 × SSC: sodiumcitrate (90 mM), NaCl (900 mM), pH 7.0. SSCT: sodiumcitrate (15 mM), NaCl (150 mM), pH 7.0, Tween 20 (0.1% v/v). 2 × SSCT: sodiumcitrate (30 mM), NaCl (300 mM), pH 7.0, Tween 20 (0.1% v/v). TST: Tris (10 mM), NaCl (150 mM), pH 7.5, Tween 20 (0.1% v/v). PBST: standard phosphate saline buffer containing Tween 20 (0.05% v/v) was from Bie & Berntsen, Denmark. Agarose, analytical grade, was from Promega (WI).

Streptavidin-HRP was obtained from Pierce, IL. OPD was from KemEnTec A/S, Denmark. Taq-polymerase, 10 × PCR buffer and dNTPs, DIG-dUTP, anti-DIG-antibody, antifluorescein-antibody-HRP, and streptavidin-HRP were obtained from Boehringer Mannheim and Qiagen, Germany. Reagents for cloning PCR-fragments were obtained from Invitrogen, CA.

Oligonucleotides were synthesized on a DNA-synthesizer (Pharmacia Gene Assembler Special) using standard phosphoramidite coupling conditions according to the 0.2 μmol scale protocol. Standard 3′-deoxynucleoside CPG or polystyrene solid supports were used. This support and HEG linker was from KJ-Ross-Petersen A/S, Denmark.

Preparation of Anthraquinone Phosphoramidite Reagents. *N-(3-Hydroxypropyl)-2-anthraquinonecarboxamide (**2**).* To a stirred suspension of anthraquinone-2-carboxylic acid (**1**) (10.00 g, 39.64 mmol) in DMF (130 mL) was added BOP (17.54 g, 39.66 mmol) and triethylamine (11.05 mL, 79.28 mmol). The resulting mixture (initially a clear green solution) was stirred at room temperature for 10 min before drop wise addition of 3-amino-1-propanol (3.34 mL, 43.67 mmol). The reaction mixture (a clear brown solution) was stirred at room temperature in darkness for 17 h. The solution was slowly poured into ice containing water (300 mL). The precipitated material was isolated by filtration and recrystallized from boiling ethanol (96%) (ca. 200 mL) and resulted in the title compound **2** as a bright yellow solid (6.93 g, 57% yield).

^{1}H NMR (DMSO-d_6): δ 1.74 (2H, quintet, J = 6.52 Hz, CH_2), 3.25−3.44 (2H, m, CH_2), 3.50 (2H, broad t, J = 5.80 Hz, CH_2), 4.53 (1H, broad s, OH), 7.76−8.00 (2H, m, Ar), 8.04−8.36 (4H, m, Ar), 8.56 (1H, d, J = 1.55 Hz, Ar), 8.89 (1H, t, J = 5.42 Hz, NH).

^{13}C NMR (DMSO-d_6): δ 32.32, 36.96, 58.68, 125.50, 126.83, 126.85, 127.05, 132.79, 133.04, 133.08, 134.45, 134.66, 139.49, 164.62, 182.11.

*N-(3-(2-Cyanoethoxy(diisopropylamino)phosphinoxy)-propyl)-2-anthraquinone-carboxamide (**3**).* *N*-(3-Hydroxypropyl)-2-anthraquinone carboxamide (**2**) (1.00 g, 3.23 mmol) was suspended in anhydrous CH_2Cl_2 (30 mL) under N_2. *N*,*N*-Diisopropylethylamine (1.24 mL, 7.12 mmol) was added followed by dropwise addition of 2-cyanoethyl *N*,*N*-diisopropyl-phosphoramidochloridite (0.72 mL, 3.23 mmol). The resulting slightly turbid reaction mixture was stirred at room temperature for 25 min. The mixture was filtrated and diluted with ethyl acetate (100 mL) containing triethylamine (10 mL) and washed with saturated aqueous $NaHCO_3$ (2 × 20 mL). The organic solution was dried (Na_2SO_4) and evaporated under reduced pressure. The residue was dissolved in a minimum amount of CH_2Cl_2 and added dropwise to vigorously stirred ice cooled light petroleum ether (200 mL). The precipitated yellow powder was collected by filtration and dried overnight under high vacuum affording **3** (1.26 g, 77% yield). This compound could be stored under N_2 at −20 °C for several months without significant decomposition.

^{1}H NMR ($CDCl_3$): δ 1.17 (d, J = 6.86 Hz, CH_3), 1.87−2.15 (m, CH_2), 2.70 (t, J = 5.72 Hz, CH_2), 3.41−4.04 (m, CH_2, CH), 7.17 (broad t, J = 5.49 Hz, NH), 7.76−7.87 (m, Ar), 8.24−8.41 (m, Ar), 8.59 (d, J = 1.65 Hz, Ar).

^{13}C NMR ($CDCl_3$): δ 20.43, 20.54, 24.58, 24.69, 30.22, 30.33, 38.53, 43.03, 43.23, 58.19, 58.51, 62.45, 62.74, 117.90, 125.04, 127.39, 127.83, 133.15, 133.42, 134.39, 135.04, 139.80, 165.57, 182.50.

^{31}P NMR ($CDCl_3$): δ 148.49.

*2-(2-Cyanoethoxy(diisopropylamino)phosphinoxymethyl)-anthraquinone (**5**).* To a stirred suspension of 2-(hydroxymethyl)anthraquinone (**4**) (1.00 g, 4.20 mmol) in anhydrous CH_2Cl_2 (42 mL) under N_2 was added 2-cyanoethyl *N*,*N*,*N*′,*N*′-tetraisopropyl-phosphorodiamidite (1.33 mL, 4.20 mmol) followed by dropwise addition of tetrazole in CH_3CN (8.86 mL, 0.45 M). The reaction mixture was stirred at room temperature for 90 min, and the formed

[1] Abbreviations: AQ, anthraquinone; BOP, benzotriazol-1-yl-oxy-tris(dimethylamino)-phosphonium hexafluorophosphate; DIG, digoxigenin; DMT, dimethoxytrityl; HEG, hexaethyloxyglycol; HRP, horseradish peroxidase; MTP, microtiter plate; OPD, ortho-phenylenediamine.

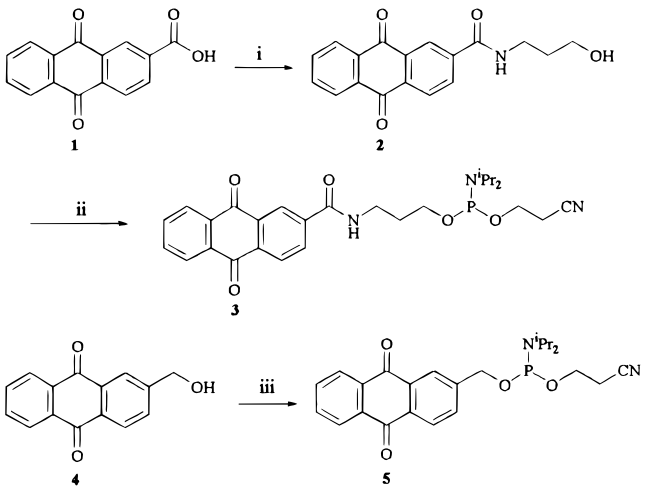

Figure 2. Synthesis of AQ-phosphoramidites. (i) 3-Amino-1-propanol, BOP, Et_3N, DMF. (ii) *N*,*N*-diisopropylphosphoramidochloridite, *N*,*N*-diisopropylethylamine, CH_2Cl_2. (iii) *N*,*N*,*N*′,*N*′-tetraisopropylphos-phorodiamidite, tetrazole, CH_2Cl_2, CH_3CN.

salts were removed by filtration. The filtrate was diluted with CH_2Cl_2 (50 mL) and washed with saturated aqueous $NaHCO_3$ (2 × 20 mL) and brine (20 mL). The organic solution was dried (Na_2SO_4) and evaporated under reduced pressure. The remaining yellow solid material was coevaporated with anhydrous CH_3CN and dried overnight under high vacuum yielding **5** as bright yellow solid (1.84 g, ∼100% yield).

^{1}H NMR ($CDCl_3$): δ 1.23 (d, J = 6.96 Hz, CH_3), 2.69 (t, J = 6.41 Hz, CH_2), 3.65−3.75 (m, CH), 3.84−3.97 (m, CH_2), 4.82−4.95 (m, CH_2), 7.77−7.82 (m, Ar), 8.27−8.32 (m, Ar).

^{13}C NMR ($CDCl_3$): δ 20.29, 20.35, 24.50, 24.57, 43.13, 43.26, 58.32, 58.51, 64.48, 64.66, 117.40, 125.03, 127.04, 127.10, 127.41, 132.01, 132.21, 132.48, 133.37, 133.39, 133.89, 133.96, 134.07, 145.95, 146.03, 182.68, 182.89.

^{31}P NMR ($CDCl_3$): δ 149.76.

In the following sections, $-(CH_2)_3-$ represents the linker used in amidite 3 and $-CH_2-$ represents the linker used in amidite 5.

Preparation of Anthraquinone Oligonucleotide Conjugates. The standard 2 min coupling time for unmodified deoxynucleoside phosphoramidites was increased to 5 min for DMT-HEG phosphoramidites. While still on the solid support, the 5′-OH termini of the oligonucleotides were coupled with the AQ-phosphoramidite reagents **3** or **5** (Figure 2) using the reagents as a solution in acetonitrile (0.1 M) and a 5 min coupling time. After completion of the synthesis, the oligonucleotides were cleaved from the solid support and the nucleobase protection groups removed by incubation with 32% NH_4-OH (when standard supports were used) or 32% NH_4-OH containing 1% LiCl (when Universal supports were used) at 55−60 °C for 10−15 h. The crude AQ-oligonucleotide conjugates were purified by reversed-phase HPLC (Waters, Delta Pack C-18, 100 Å, 15 μm, 300 × 3.9 mm ID) in a gradient from 100% triethylammonium acetate (0.05 M) at pH 7.4 to 100% H_2O/CH_3CN (1:1 v/v) from 0 to 15 min at a flow rate of 1.5 mL/min. Anthraquinone conjugation of DNA oligonucleotides delayed the elution for approximately 2 min compared to the unmodified oligonucleotide, and the specific retention times of the used oligonucleotides used in this paper are presented below (see Table 1).

Immobilization of Anthraquinone Conjugated Oligonucleotides in Microtiter Wells. AQ-oligonucleotides were dissolved in water, and the concentration was determined at 260 nm (AQ extinction coeficient, 50 000 OD at 260/M × cm^{-1}). It is important to note that anthraquinone-containing material must be kept in the dark during all nonphotochemical operations. Concentrations in the range of 0−24.3 μM (vide infra) were prepared in LiCl (0.2 M), and 100 μL was dispensed per well. Immobilization was performed by irradiation for 15 min 10 cm above the MTP. The MTPs were washed with 3 × 300 μL/well NaOH (0.4 M), Tween 20 (0.25% v/v), and with purified water. The MTPs were either used directly after this or stored at 4 °C. The plates were dried for 30 min at either room temperature or at 37 °C and stored. MTPs were equilibrated at room temperature for 30 min prior to use.

Detection Assay for Immobilized Oligonucleotides. Complementary biotinylated oligonucleotides were hybridized to the immobilized oligonucleotides during gentle agitation in the hybridization buffer (2 × SSCT) in 100 μL/well for 2 h at 37 °C. The MTPs were washed (1 x SSCT) in 3 × 300 μL/well at 37 °C, incubated in 100 μL/well with HRP-streptavidin (1 μg/mL), and diluted in PBST at room temperature for 15 min during gentle agitation. After washing with PBST (3 × 300 μL/well) colorimetric endpoint measurements were obtained after addition of 100 μL/well of the chromogenic mixture: OPD (0.66 mg/mL), citrate buffer (0.1 M) at pH 5.0, and H_2O_2 (0.012% v/v). The reaction was stopped with 100 μL/well H_2SO_4 (0.5 M,) and the absorbance at 492 nm was measured directly in the microtiter plate reader.

PCR-Amplification. The PCR reaction was performed in 100 μL 1 × PCR buffer containing 200 μM dNTPs (of each dATP, dCTP, dGTP, and dTTP), forward primer 5′-GTAAAACGACGGCCAGT-and reverse primer 5′-AACAGCTATGACCATG-3′ (0.2 μM of each), plasmid (50 ng/mL pUC19), Taq-polymerase (2.5 units), and MilliQ water. All PCR reactions were made on a Techne thermocycler using the following profile: (1) 3 min at 94 °C; (2) 30 cycles of 1 min at 45 °C, 1 min at 72 °C, 1 min at 94 °C; (3) 1 min at 45 °C and 10 min 72 °C; hold temperature: 4 °C. The PCR-amplifications were analyzed by agarose gel electrophoresis and detection was performed by ethidium bromide (10 μg/mL) in standard TAE buffer.

PCR Amplicon Capture. The following oligonucleotides were prepared: (1) 5′-AACAGCTATGACCATG-3′ (control), (2) AQ-$(CH_2)_3$-AACAGCTATGACCATG-3′; (3) AQ-$(CH_2)_3$-HEG-AACAGCTATGACCATG-3′; (4) AQ-$(CH_2)_3$-$(HEG)_2$-AACAGCTATGACCATG-3′.

Oligonucleotide 1−4 were prepared in the following dilution series: 25 μM, 8.3 μM, 2.7 μM, 0.9 μM, 0.3 μM, 0.1 μM, 34 nM, 11 nM, 3.0 nM, 1.0 nM, 0.4 nM, and 0.0 M. The oligonucleotides were immobilized by using the standard procedure described above.

Amplicons (approximately 7 ng ≈ 200 pmol) were diluted to 500 μL in MilliQ water, hot denatured (5 min, 95 °C), and then cooled on ice (10 min). Finally, biotinylated detection probe (1 nmol) and 2 × SSCT to a total volume of 10 mL was finally added. A total of 100 μL of this target solution was added per well and allowed to hybridize for 2 h at 37 °C during gentle agitation. Wells were washed 3 × 300 μL/well with 2 × SSCT. Detection was performed by incubating streptavidin-HRP (1 μg/mL) in PBST, 100 μL/well for 1 h. The wells were washed 3 × 300 μL in PBST, and developed with standard OPD assay for 30 min as described above.

Immobilization of AQ-Amplicons. Four different forward primers were synthesized: (1) 5′-GTAAAACGACGGCCAGT-3′ (control), (2) AQ-$(CH_2)_3$-GTAAAAC-

Table 1. Retention Times of Oligonucleotides Used in this Paper

		retention times (min)
1	5′-AACAGCTATGACCATG-3′ (control)	nd
2	AQ-$(CH_2)_3$-5′-AACAGCTATGACCATG-3′	9.831
3	AQ−$(CH_2)_3$-HEG−5′-AACAGCTATGACCATG-3′	10.710
4	AQ−$(CH_2)_3$-$(HEG)_2$−5′-AACAGCTATGACCATG-3′	10.710
1	5′-GTAAAACGACGGCCAGT-3′ (control)	nd
2	AQ−$(CH_2)_3$-5′-GTAAAACGACGGCCAGT-3′	9.331
3	AQ−$(CH_2)_3$-HEG−5′-GTAAAACGACGGCCAGT-3′	10.187
4	AQ−$(CH_2)_3$-$(HEG)_2$−5′-GTAAAACGACGGCCAGT-3′	10.704

GACGGCCAGT-3′, (3) AQ-$(CH_2)_3$-HEG-GTAAAACGACG-GCCAGT-3′, (4) AQ-$(CH_2)_3$-$(HEG)_2$-GTAAAACGACGGC-CAGT-3′.

PCR-amplification, as described above, was performed for each forward primer using the same reverse primer. As above, PCR amplifications were tested on standard agarose gel electrophoresis. Immobilization was performed by adding amplicon solution (ca. 36 ng of DNA) in 200 μL of LiCl (0.2 M) to a well. A total of 100 μL of this solution was taken out and 100 μL of LiCl (0.2 M) was added. This amplicon dilution method was repeated 10 times.

The amplicons were photochemically immobilized as described above and the amplicons were subsequently denatured in 200 μL/well NaOH (0.4 M) and Tween 20 (0.25% v/v). The wells were then washed 3 × 300 μL with 2 × SSCT. The denatured amplicons were hybridized to a sequence specific detection probe, 5′-biotin-ATGCCT-GCAGGTCGAC-3′. The detection assay described above was used to measure amplicon immobilization.

Solid-Phase PCR. A 810 bp fragment in exon 29 of apolipoprotein B was generated (forward primer ApoBE-S 5′-CTAACCTCTCTGAAAGACAACGTGC-3′; reverse primer ApoBE-3 5′-GATTGTGTTGATCTCATCTTGGATA-TA-3′). The forward primer was AQ modified (amidite **3**) in the 5′ end, [AQ-$(CH_2)_3$-HEG-forward primer], and immobilized in TopYiels plates. The PCR reaction was performed directly in the MTP's. The DNA fragment contains an EcoRI-polymorphism which has been related to atherosclerosis and coronary hearth disease (24). The fragment was cloned using the Topo TA Cloning kit.

The general procedure for solid-phase PCR is as follows. The ApoBE-S primer was modified and coupled to the microtiter wells in the amounts of 1.6−500 pmol in 100 μL/well. The PCR-mixture in 50 μL contained Taq-polymerase, buffer, and Q-solution from Qiagen, 200 μM dNTPs, 0.5 μM of primer ApoBE-3, and 0.05 μM of primer ApoBE-S. The cloned ApoB fragments or 100 ng of human genomic DNA was included as targets in the reaction. The reaction conditions were initialization by a 5 min denaturation step at 94 °C, followed by 35 cycles of 1 min denaturation at 94 °C, 1 min annealing at 62 °C, 1 min extension at 72 °C. A final extension step for 10 min at 72 °C was included. The wells were washed three times in TST buffer.

Five different detection modes of the PCR-product were tested. (**I**) Primer ApoBE-3 used in the PCR-reaction was 5′-end labeled with biotin and streptavidin-HRP-OPD was used as detection system. (**II**) The wells were treated with NaOH (0.2 M) and Tween 20 (0.1% v/v for 5 min), washed three times in NaOH (0.2 M) and Tween 20 (0.1% v/v), and washed three times with TST-buffer. A fluorescein-labeled detection probe (ApoBH2: fluorescein-5′-TCCTTAACTGAAAG, 0.5 μM) was added in 100 μL 6 × SSC. The wells were incubated at 50 °C for 60 min. Detection was performed with antifluorescein-antibody-HRP-OPD. (**III**) Performed as in **II**, but hybridization was performed in the thermocycler by heating to 94 °C for 2 min and cooling to 20 °C at a rate of 1 °C/min. (**IV**) DIG-dUTP (0.02 μM) was included in the PCR-reaction. After the PCR-reaction was completed, the wells were washed three times with TST buffer and the products were detected with anti-DIG-antibody-POD. (**V**) was performed as in **IV** but with prior NaOH-treatment as in **II**.

RESULTS

Preparation of 5′ Anthraquinone Conjugated Oligonucleotides. Initially we attempted to prepare a phosphoramidite derivative of *N*-(6-hydroxyhexyl)-2-anthraquinone carboxamide obtained from BOP-mediated coupling of anthraquinone-2-carboxylic acid 6-amino-1-hexanol. However, reaction of *N*-(6-hydroxyhexyl)-2-anthraquinone carboxamide with 2-cyanoethyl *N*,*N*,*N*′,*N*′-tetraisopropylphosphorodiamidite and tetrazole, gave a product which on attempted isolation led to decomposition. Filtration of the reaction mixture gave a crude product that could be used directly on the DNA synthesizer within a day.

Recently Gasper and Schuster (*25*) described the synthesis of *N*-(2-(methoxy-(di-isopropylamino)phosphinyl)ethyl)-2-anthraquinone, which they obtained as a viscous dark red oil after column chromatographic purification. Similarly, the corresponding *N*-pentyl-2-anthraquinone-carboxamide phosphoramidite was also prepared, but the product could not be purified completely by column chromatography.

We attempted to synthesize a cyanoethyl phosphoramidite analogue of the above-described methoxy protected *N*-ethyl-2-anthraquinone-carboxamide phosphoramidite. Reaction of *N*-(2-hydroxyethyl)-anthraquinone-carboxamide with 2-cyanoethyl *N*,*N*-diisopropyl phosphoramido chloridite in the presence of *N*,*N*-diisopropylethylamine or using the same procedure as was used for the hydroxyhexyl derivative above, gave initially a light yellow foam after flash chromatography. However, when this material was dried under high vacuum overnight a dark brown syrup was formed thus indicating decomposition.

Then *N*-(3-hydroxypropyl)-2-anthraquinonecarboxamide (**2**, Figure 2) was prepared by reaction of anthraquinone-2-carboxylic acid (**1**) activated with BOP and 3-amino-1-propanol. Phosphitylation of the alcohol **2** with 2-cyanoethyl *N*,*N*-diisopropyl phosphoramido chloridite in the presence of *N*,*N*-diisopropylethylamine gave after precipitation from petroleum ether the corresponding phosphoramidite reagent **3** as a yellow powder. In contrast to the unstable products obtained above, **3** remained stable at -20 °C for several months.

In addition, another stable AQ-phosphoramidite derivative **5** could be obtained in one step from commercially available 2-(hydroxymethyl)anthraquinone (**4**). Reaction of **4** with 2-cyanoethyl *N*,*N*,*N*′,*N*′-tetraisopropylphosphorodiamidite and tetrazole gave a bright yellow solid after aqueous workup and drying under high vacuum.

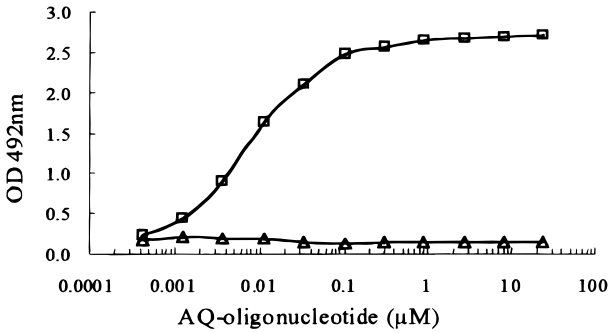

Figure 3. Immobilization efficiency as a function of AQ-oligonucleotide concentration: 0.0003, 0.0010, 0.004, 0.011, 0.033, 0.10, 0.30, 0.90, 2.70, 8.10, and 24.3 μM. The experiment is performed with a specific detection probe, i.e., complementary to the AQ-oligonucleotide (□), and an unspecific detection probe, i.e., not complementary to the AQ-oligonucleotide (△).

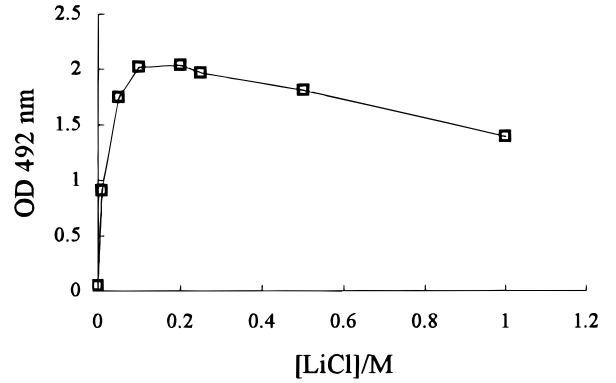

Figure 4. Immobilization of AQ-oligonucleotides (0.5 μM) as a function of LiCl concentration.

Oligomerization. Oligonucleotides containing anthraquinone covalently linked to 5′-terminus were synthesized on a DNA-synthesizer using standard phosphoramidite chemistry. While still on the solid support, the 5′-OH termini of the oligonucleotides were coupled with the HEG linker followed by coupling with either AQ-phosphoramidite reagent **3** or **5**. The AQ-oligonucleotide conjugates were cleaved from the solid support and the nucleobase protection groups removed by treatment with aqueous ammonium hydroxide. The crude anthraquinone modified oligonucleotides were purified by reversed-phase HPLC.

Immobilization of Oligonucleotides and PCR−Amplicons. Concentration dependent immobilization efficiency of AQ-oligonucleotides was tested in the range 0.0003−24.3 μM (Figure 3). Immobilization was performed in LiCl (0.20 M), and it appears that immobilization is very concentration dependent. It appears also from Figure 3 that hybridization is specific, i.e., the non-complementary detection probe did not recognize the immobilized AQ-oligomers. The salt concentration dependency was further examined (Figure 4). From this curve is seen that immobilization is very salt dependent and especially a minimum of salt is required, i.e., the curve has initially a very steep slope. The optimal salt concentration was assessed to ca. 0.2 M. The specificity of the salt dependency was analyzed, and immobilization studies were performed in LiCl, Li_2SO_4, $LiNO_3$, NaCl, NaH_2PO_4, KCl, KH_2PO_4, $MgCl_2$, $MgSO_4$, $(NH_4)_2CO_3$, and NH_4HCO_3. It was found that there was no significant difference among the salts, and therefore, the salt dependency of this immobilization method is of general nature (data not shown).

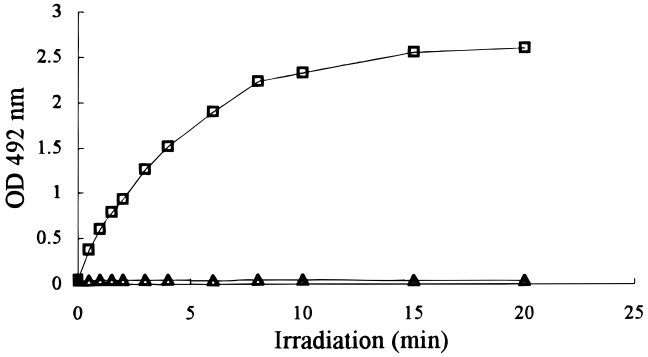

Figure 5. AQ-oligonucleotide (5 μM) immobilization as a function of irradiation time in LiCl [0.2 M (□)] and in MilliQ water (△).

Immobilization as a function of irradiation time was examined in LiCl (0.2 M) using 5 μM AQ-oligonucleotide (Figure 5). It was found that 15 min of irradiation was required to obtain maximal readout in the subsequent detection assay. In this experiment, the concentration was 5 μM, but additional experiments showed that the concentration could be significantly reduced. After these experiments, the optimal conditions for AQ-oligonucleotide immobilization were determined to be AQ-oligonucleotide (0.1 μM) in LiCl (0.2 M) and 15 min irradiation time. This immobilization procedure was successfully applied to other carbon containing polymers, e.g., polycarbonate, polypropylene, polyethylene, PVDF-Millipore membranes ("low background" membranes)(data not shown).

Recognition of immobilized probes is generally dependent on a certain spacing between the probe and the surface (*26*). Therefore, the hybridization properties of immobilized oligonucleotides were tested with different linker combinations. Two sets of linker variation experiments were performed: (I) detection of immobilized oligonucleotides with short detection probes and oligonucleotides (Figure 6); and (II) detection of immobilized oligonucleotides with long probes and PCR products (Figure 7).

Anthraquinone was conjugated to the 5′-position of the PCR primers and the conjugates were tested for their ability to be substrates in a PCR reaction. All AQ-constructs could act as primers in the standard PCR reaction, and the AQ-linked amplicons were subsequently photochemically immobilized to the solid surface. The immobilization efficiency of the AQ-amplicons was analyzed by amplicon specific detection probes (Figure 8). It appears that AQ-linked amplicon immobilization is not to any significant degree dependent on the linker between the AQ and the amplicon.

Solid-Phase PCR. The highest signal/noise ratio for covalently coupled oligonucleotides in microtiter wells was found when 0.1 μM of the oligomer was used during the immobilization step. Using higher as well as lower concentrations of the oligonucleotides decreased the sensitivity of the assay. In these immobilization experiments, detection mode **I** was used.

The five detection modes were tested in MTPs where the primers were immobilized at a concentration of 0.1 μM. Detection of the generated PCR amplicons was performed for each of the five modes for 60 min and the generated optical densities were measured (Figures 9 and 10). The prolonged detection step was needed because of the low signals obtained in procedure **I**−**III**. The largest signal was detected in mode **IV**, although the background

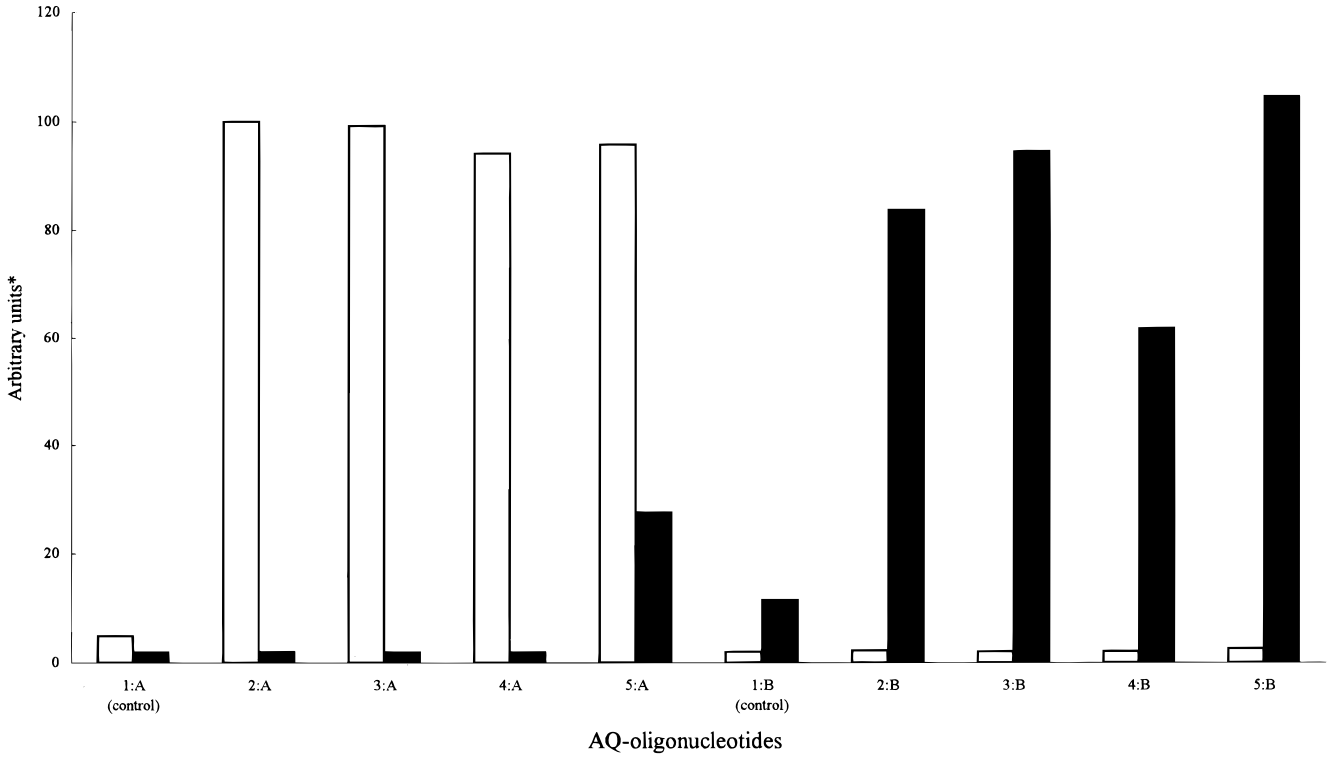

Figure 6. Linker dependency of AQ-oligonucleotide immobilization. (1) oligonucleotide without AQ, (2) AQ-$(CH_2)_3$-oligonucleotide (by amidite **3**), (3) AQ-$(CH_2)_3$-HEG-oligonucleotide (by amidite **3**), (4) AQ-$(CH_2)_3$-$(HEG)_2$-oligonucleotide (by amidite **3**), and (5) AQ-(CH_2)-oligonucleotide (by amidite **5**). The A-serie is with AQ−linkers conjugated to oligonucleotide: 5′-AACAGCTATGACCATG-3′; and the **B**-serie is with AQ−linkers conjugated to oligonucleotide: 5′-GTAAAACGACGGCCAGT-3′. Open bars represents detection with a biotinylated oligonucleotide complementary to the A serie. Filled bars represents detection with a biotinylated oligonucleotide complementary to the B serie. The arbitrary units collate to 100% specific detection by 2:A.

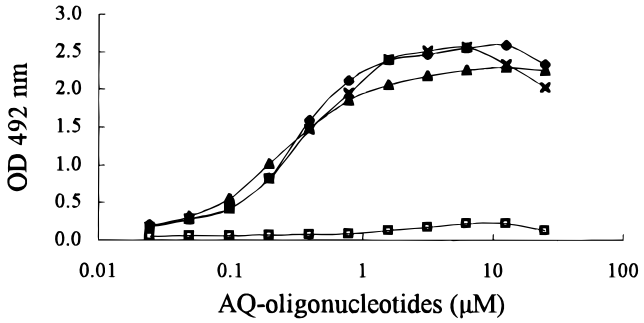

Figure 7. Linker dependency of amplicon capture (98 bp) as a function of AQ-oligonucleotide concentration during immobilization. (1) Oligonucleotide without AQ (□), (2) AQ-$(CH_2)_3$-oligonucleotide [by amidite 3 (△)], (3) AQ-$(CH_2)_3$-HEG-oligonucleotide [by amidite **3** (◆)], (4) AQ-$(CH_2)_3$-$(HEG)_2$-oligonucleotide [by amidite 3 (×)].

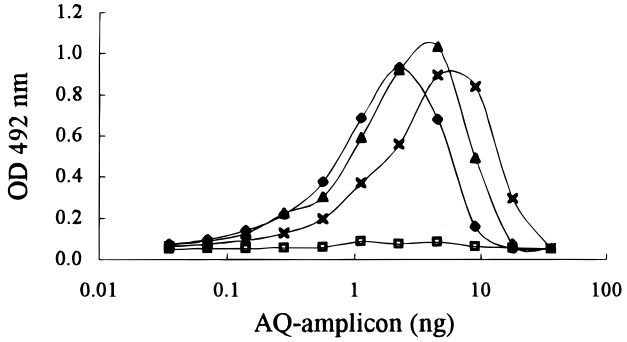

Figure 8. Immobilization of AQ-amplicons. (1) amplicon without AQ (□), (2) AQ-$(CH_2)_3$-amplicon [by amidite 3 (△)], (3) AQ-$(CH_2)_3$-HEG-amplicon [by amidite 3 (◆)], (4) AQ-$(CH_2)_3$-HEG_2-amplicon [by amidite 3 (×)].

was rather high. The signal/noise ratios were 2.6 (**I**), 18.6 (**II**), 21.2 (**III**), 3.0 (**IV**), and 3.9 (**V**).

DISCUSSION

Immobilization Mechanism. Excited quinones, such as anthraquinone, have the triplet n,π^*-state as the lowest excited state and are powerful electron acceptors (*19*, *20*, *27*). The presence of a hydrogen donor leads to rapid quinone reduction either by a one step hydrogen atom abstraction or by a two step electron/proton transfer (*28*). In both cases a radical pair is generated on the quinone and on the hydrogen donor (e.g., the polymer). Due to the aromatic nature of the di-one structure in quinones, the quinone-derived radical pairs combine by forming a carbon−oxygen bond with simultaneous aromatization of the quinone ring (*22*, *29*) (Figure 11), a reaction which is in contrast to the reaction of excited ketones.

The relative rate in hydrogen atom abstractions of excited anthraquinone is very high. The rate is of comparable magnitude as, e.g., chlorine and fluorine atoms (*19*, *30*). Therefore, the excited quinones will radicalize almost any polymer exposing C−H groups. After the hydrogen atom abstraction, the quinone will rapidly form a phenoxy radical which has a much-reduced reactivity. Excited anthraquinone will undergo this photochemistry if an appropriate hydrogen donor is present. If the hydrogen donor is not present, the excited quinone will convert to the groundstate through relaxation processes and retain the parent quinoid structure. This is in contrast to, e.g., azides where excitation, and subsequent nitrogen loss, leads to irreversible deactiva-

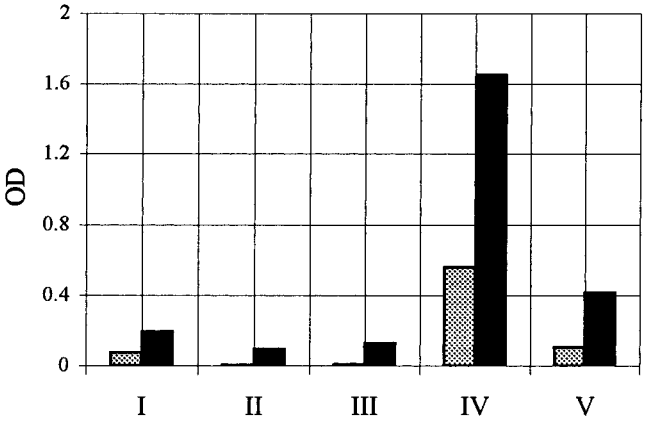

Figure 9. Solid-phase PCR. The PCR was performed as described in the text. The detection systems were (**I**) biotin-streptavidin-HRP-OPD; (**II**) NaOH (0.2 M) and Tween 20 (0.1% v/v) treatment before detection with a fluorescein labeled detection probe; (**III**) as in **II** but hybridization was performed in the thermocycler; (**IV**) DIG-dUTP included in the PCR and detected with anti-DIG-antibody; (**V**) as in **IV** but with prior NaOH-treatment as in **II**.

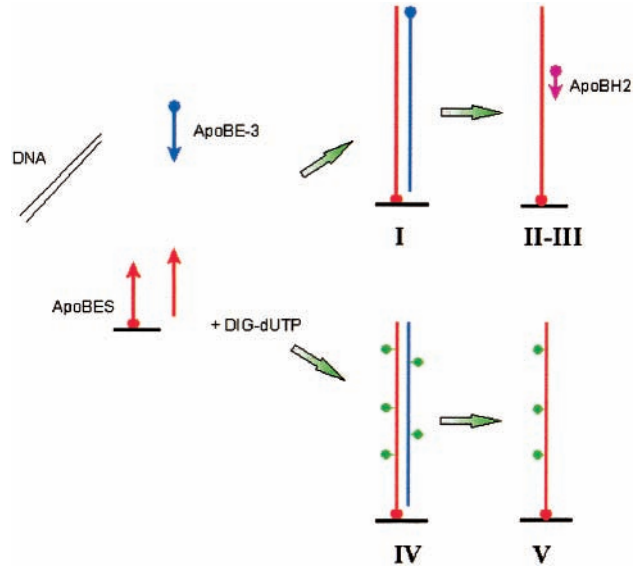

Figure 10. Solid-phase PCR setup. The left site of the figure shows the immobilized forward primer (ApoBES), the primers ApoBES and ApoBE-3 in a 1:10 ratio in solution, and the target DNA. In this basic setup a biotinylated (blue spot) immobilized PCR product will be generated (mode **I**), Denaturation of the this with NaOH removes the right-handed strand (blue strand). Detection of the generated PCR-product is done by hybridization with a specific fluorescein labeled primer (ApoBH2) (mode **II** or **III**) (grape arrow). In the lower panel DIG-dUTP is added in the PCR-reaction and both strands are labeled (mode **IV**). Denaturation of this product with NaOH produces a single stranded, DIG-labeled (green spots), immobilized PCR-product (mode **V**). Se text for further details.

tion of the starting material. Furthermore, if excitation leads to the formation of the overall reduced quinone, i.e., two consecutive hydrogen atom abstractions due to abundant activated hydrogens, the hydroanthraquinone will rapidly be oxidized by molecular oxygen and retain the parent quinoid structure. In this way anthraquinone can be "recycled" under certain circumstances, whereas other photoprobes, e.g., azides and benzophenone, will be irreversible deactivated after excitation under the same conditions.

We believe that the fast and efficient immobilization mediated by anthraquinone is due to these properties:

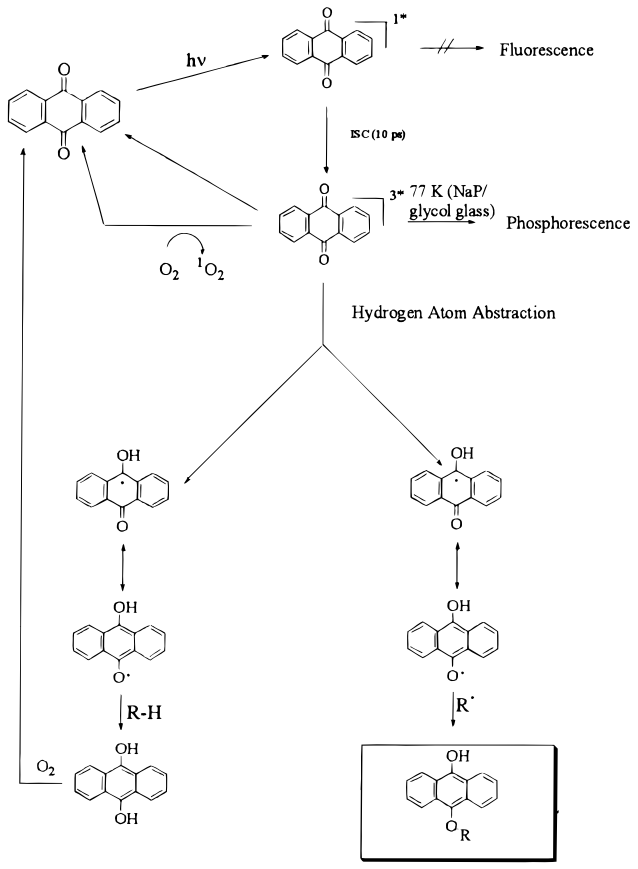

Figure 11. Photochemical pathways of anthraquinone.

(i) high absorption in the near UV region; (ii) creation of a highly reactive excited state; (iii) formation of a aroyl radical with much reduced reactivity; (iv) formation of a stable conjugated −OH/Ar−OR product; (v) "recyclable" chromophores (Figure 11).

Preparation of Anthraquinone Phosphoramidite Reagents. Many methods have been developed for attachment of reporter groups, including anthraquinone, to oligonucleotides (*31*). An efficient and convenient way of attaching anthraquinone to the 5′-terminus of an oligonucleotide is to convert the anthraquinone into a synthon that can be directly used in automated solid-phase DNA synthesis. There have only been reported a few examples of AQ-phosphoramidite reagents for 5′-terminus incorporation. AQ-ethyl piperazinyl phosphoramidite and AQ-hexamethylene-linked phosphoramidite reagents have been prepared and coupled to the 5′-OH terminus of oligonucleotides as the final step in a standard automated solid-phase synthesis (*32*, *33*). The resulting 5′-linked AQ-oligonucleotides were applied for attenuation or destruction of mammalian genetic expression or viral activity. Similarly 5′-end containing anthraquinone oligonucleotides have been prepared using phosphoramidite reagents derived from *N*-(2-hydroxyethyl)- and *N*-(5-hydroxypentyl)-2-anthraquinone carboxamide (*25*). The synthesized anthraquinone-modified oligonucleotides were used to establish that oxidative damage could migrate in double stranded DNA.

The synthesis of a large number of AQ-oligonucleotide conjugates using automated solid-phase chemistry requires easily accessible and relatively stable anthraquinone synthons. Our initial attempts to synthesize stable AQ-phosphoramidite reagents revealed that the above-mentioned reagents appeared to be very unstable. The synthesis of an AQ-phosphoramidite derivative by reac-

tion of *N*-(6-hydroxyhexyl)-2-anthraquinone carboxamide with 2-cyanoethyl *N*,*N*,*N*′,*N*′-tetraisopropylphosphorodiamidite and tetrazole gave a product that on attempted isolation led to decomposition. It is known that trivalent phosphorus compounds (electron donors) are reactive toward quinones (electron acceptors) resulting in charge-transfer complexes and ultimately in hydroquinone monoalkyl ethers (*34*, *35*). The hydroxyhexyl linker connecting the anthraquinone molecule and the phosphoramidite moiety could allow this intramolecular reaction to take place, and thus, somehow lead to decomposition. A shorter linker should therefore prevent this assumed interaction between the potentially reducing and oxidizing parts of the AQ-phosphoramidite reagent.

We attempted to prepare a cyanoethyl phosphoramidite analogue of *N*-(2-(methoxy-(diisopropylamino)-phosphinyl)ethyl)-2-anthraquinonecarboxamide previously reported (*25*). Reaction of *N*-(2-hydroxyethyl) anthraquinonecarboxamide with 2-cyanoethyl *N*,*N*-diisopropylphosphoramido-chloridite in the presence of *N*,*N*-diisopropylethylamine or using the same procedure as was used for the hydroxyhexyl derivative above, gave initially a bright yellow foam after flash chromatography. Drying this material under high vacuum overnight resulted in a highly viscous dark brown oil, indicating decomposition. Thus, the labile nature of this type of compound cannot be ascribed entirely to the length of the linker between the anthraquinone and the phosphoramidite functionality. However, it should be noted that even with the ethyl linker an intramolecular reaction is possible.

Despite being discouraged by these findings, *N*-(3-hydroxypropyl)-2-anthraquinonecarboxamide (Figure 2, **2**) was prepared by reaction of anthraquinone-2-carboxylic acid (**1**) activated with BOP and 3-amino-1-propanol. Phosphitylation of the alcohol **2** with 2-cyanoethyl *N*,*N*-diisopropylphosphoramidochloridite in the presence of *N*,*N*-diisopropylethylamine gave after precipitation from petroleum ether the corresponding phosphoramidite reagent **3** as a surprisingly stable yellow powder. This compound could be stored at −20 °C for several months without loss of reactivity.

In addition another stable AQ-phosphoramidite derivative **5** could be obtained in one step from commercially available 2-(hydroxymethyl)anthraquinone (**4**). Reaction of **4** with 2-cyanoethyl *N*,*N*,*N*′,*N*′-tetraisopropylphosphorodiamidite and tetrazole gave after aqueous workup a bright yellow solid. Judged on NMR analysis the purity of this material was found satisfying.

Immobilization of DNA on Polymer Surfaces. Biomolecules such as peptides and proteins conjugated with anthraquinone have successfully been photoimmobilized on solid surfaces in pure water (*36*, *38*). However, as demonstrated in this work, oligonucleotide immobilization is very salt dependent (Figure 4). One of the reasons for this solvent discrepancy between proteins/peptides and DNA relies on the charged nature of the nucleic acids. High ionic strength of the solvent will organize ions closely to the DNA which becomes strongly solvated, but the lipophilic AQ will be "salted out", i.e., the interaction with the DNA part will be reduced and the interaction with the lipophilic surface will thus be facilitated. The salt effect is of general nature, i.e., relating to a certain ion strength rather than to a specific ion effect.

The linker length between the anthraquinone and the oligonucleotides did not affect the hybridization efficiency to any considerable effect (Figure 6 and 7). This was surprising since it is often found that the probing efficiency of immobilized material is strongly dependent on a certain spacing (*26*). A reason for this could be that the oligonucleotides used here are adequately long to ensure that at least a minimal stable hybridization, e.g., at the distal parts of the immobilized oligomer, is sufficiently stable to be detected. In this way the parts of the oligonucleotide close to the surface will serve as linker.

The anthraquinone mediated immobilization appears to be rather insensitive to the size of the conjugate. This is illustrated in the example where anthraquinone is conjugated to PCR-primers (Figure 8). The PCR reactions could be performed with all conjugate constructs and the 98 bp amplicons could be directly immobilized. This was done using both the double stranded amplicons and the correponding denatured single stranded DNA equivalents. Recently, a procedure on how to produce arrays containing double stranded DNA has been published (*37*). In this report it was demonstrated that the most difficult issue was to ensure that each single spot contained the same length of double stranded DNA after the extension and hybridization procedure. By using our procedure the uniformity of the AQ-amplicons could be examined on gel electrophoresis and, e.g., purified before direct immobilizing to a solid surface.

The efficiency of the photochemical immobilization measured as mole per unit area has to be measured by using radioactive labels. It has not been determined in the present study, but the loading density in a very similar work using anthraquinone labeled PNA has been performed (*38*). By using ^{32}P-labeled PNA is was found that approximately 10 pmol of PNA could be immobilized in a microtiter well resulting in a binding density of 1 PNA/20 nm^2.

It is reasonable to assume that the binding density of oligonucleotide immobilization is similar to this. However, it is also important to note that the absolute density is only one measure of the efficiency because the *accessibility* of the immobilized material is often the critical measure in detecting the covalently linked ligands.

Solid-Phase PCR. In this experimental setup (Figures 9 and 10) the optimal PCR conditions were obtained when primers in the concentration of 0.1 μM were used during the immobilization. The signal/noise ratio was significantly reduced on either side of this optimum. The PCR included the immobilized primers in solution, but at 1/10th of the concentration of the reverse primer. This setup was necessary to obtain a detectable amount of PCR products, which is most probably due to steric restrictions in the annealing of DNA to the immobilized primers. The PCR products generated in solutions are exactly complementary to the immobilized oligomer in the 5′-end of the amplicon (ApoBE-S-primer end), with no 3′-end extensions. However, the reaction system is not simply a hybridization system of soluble amplicons because denaturation with NaOH (detection syst. **V**, Figure 9) removes the complementary strand from the immobilized extended PCR primer. Therefore, the immobilized primers are elongated by the polymerase.

The signal/noise ratio was highest for the two detection modes using fluorescein-labeled probes (**II**, **III**) (Figure 9). Mode **III** using gradual cooling of the annealing mixture was slightly better than the constant temperature annealing mode (**II**). The signal, however, was rather low (Figure 9). The signal increased considerably when DIG was incorporated at multiple sites in the PCR-product, but so did the background (**IV**); however, the signal/noise ratio could be improved by 33% if a denaturation step was performed to generate ssDNA prior to detection (**V**).

The PCR setup described above is essentially the same as for a standard PCR reaction, except that one of the primers was immobilized in MTPs. The relative amounts of primers included in the reaction are of utmost importance for the performance of a PCR reaction and it is therefore expected that optimization on these parameters will improve the amplification power significantly. If the signal could be improved a few fold, taken the present signal/noise ratios in consideration, the fluorescein-detection mode would be attractive for routine purposes. The detection systems using DIG derivatives have the highest signals. If restriction enzyme cuts are included in the procedure, the coupled/immobilized primer should be placed close to the restriction site to generate maximum difference in signal before and after the restriction cuts.

These experiments show that AQ immobilized primers can be used as substrates in a solid-phase PCR. Furthermore, the optimizing steps, which are necessary for all PCR-reactions, can be implemented in this format as well, whereby the procedure and detection methods are valid alternatives for classical solution based PCR reactions. This is an important feature for future automation purposes in, e.g., MTP or in micro array formats.

CONCLUSION

We have shown that anthraquinone conjugated to oligonucleotides can be used as a highly efficient photoprobe in immobilization procedures. The inherent photochemical properties of anthraquinone provide the opportunity for immobilization of polyfunctional biomolecules. Large molecules such as PCR amplicons are readily immobilized by the method. Immobilized PCR primers can be recognized by polymerases and can be used directly in solid-phase PCR reactions. The generality of the immobilization technique offers the opportunity to immobilize PCR primers on a large variety of polymers suitable for PCR platforms.

ACKNOWLEDGMENT

We are grateful for the scientific assistance provided by associate Professor Otto Dahl in the preparation of AQ-phosphoramidites.

LITERATURE CITED

(1) Nikiforov, T. T., and Rogers, Y.-H. (1995) The use of 96-well polystyrene plates for DNA hybridization-based assays: an evaluation of different approaches to oligonucleotide immobilization. *Anal. Biochem. 227*, 201−209.

(2) Hirayama, H., Tamaoka, J., and Horikoshi, K. (1996) Improved immobilization of DNA to microwell plates for DNA-DNA hybridization. *Nucleic Acids Res. 24*, 4098−4099.

(3) Zammatteo, N., Girardeaux, C., Delforge, D., Pireaux, J.-J., and Remacle, J. (1996) Amination of polystyrene microwells: application to the covalent grafting of DNA probes for hybridization assays. *Anal. Biochem. 236*, 85−94.

(4) Sheridan, P., Chang, C. A., and Running, J. (1993) *Process for immobilizing nucleic acid probes on polystyrene surfaces*, PCT Intl. Appl. WO 9313224, Chiron Corp., USA.

(5) Oroskar, A. A., Rasmussen, S., Rasmussen, H. N., Rasmussen, S., Sullivan, B. M., and Johansson, A. (1996) Detection of immobilized amplicons by ELISA-like techniques. *Clin. Chem. 42* (9), 1547−1555.

(6) Chrisey, L. A., Lee, G. U., and O'Ferrall, C. E. (1996) Covalent attachment of synthetic DNA to self-assembled monolayer films. *Nucleic Acid Res. 24*, 3031−3039.

(7) Joos, B., Kuster, H., and Cone, R. (1997) Covalent attachment of hybridizable oligonucleotides to glass supports. *Anal. Biochem. 247*, 96−101.

(8) Olejnik, J., Krzymanska-Olejnik, E., and Rothschild, K. J. (1998) Photocleavable aminotag phosphoramidites for 5′-termini DNA/RNA Labeling. *Nucleic Acid Res. 26*, 3572−3576.

(9) Proudnikov, D., Timofeev, E., and Mirzabekov, A. (1998) Immobilization of DNA in polyacrylamide gel for the manufacture of DNA and DNA-oligonucleotide microchips. *Anal. Biochem. 259*, 34−41.

(10) Rehman, F. N., Audeh, M., Abrams, E. S., Hammond, P. W., Kenney, M., and Boles, T. C. (1999) Immobilization of acrylamide-modified oligonucleotides by copolymerization. *Nucleic Acids Res. 27*, 649−655.

(11) Elsner, H. I., and Mouritsen, S. (1994) Use of Psoralens for Covalent Immobilisation of Biomolecules in Solid-Phase Assays. *Bioconjugate Chem. 5*, 463−467.

(12) Yan, M., Cai, S. X., Wybourne, M. N., and Keana, J. F. W. (1993) Photochemical Functionalization of Polymer Surfaces and the Production of Biomolecule-Carrying Micrometer-Scale Structures by Deep-UV Lithography Using 4-Substituted Perfluorophenyl azides. *J. Am. Chem. Soc. 115*, 814−816.

(13) Sigrist, H., Gao, H., and Wegmuller, B. (1992) Light-dependent covalent immobilization of biomolecules on "inert" surfaces. *BioTechnology 10*, 1026−1028.

(14) Gao, H., Kislig, E., Oranth, N., and Sigrist, H. (1994) Photolinker-polymer-mediated immobilization of monoclonal antibodies, F(ab′)2 and F(ab′) fragments. *Biotechnol. Appl. Biochem. 20*, 251−263.

(15) Clemence, J.-F., Ranieri, J. P., Aebischer, P., and Sigrist, H. (1995) Photoimmobilization of a Bioactive Laminin Fragment and Pattern-Guided Selective Neuronal Cell Attachment. *Bioconjugate Chem. 6*, 411−417.

(16) Sundarababu, G., Gao, H., and Sigrist, H. (1995) Photochemical Linkage of Antibodies to Silicon Chips. *Photochem. Photobiol. 61*, 540−544.

(17) Weiss, R. G., Ramamurthy, V., and Hammond, G. S. (1993) Photochemistry in Organized and Confined Media: A model. *Acc. Chem. Res. 26*, 530−536.

(18) Guire, P., and Dunkirk, S. G. (1993) *Method of biomolecule attachment to hydrophobic surfaces*, U.S. Patent 5,258,041, Bio-Metric Systems, Inc., United States.

(19) Maruyama, K., Ono, K., and Osugi, J. (1969) Relative Rate of Hydrogen Abstraction by the Triplet State. *Bull. Chem. Soc. Jpn. 42*, 3357−3369.

(20) El'tsov, A. V., Studzinskii, O. P., and Grebenkina, V. M. (1977) Photoinitiation of the Reactions of Quinones. *Russ. Chem. Rev. 46*, 185−227.

(21) Swayambunathan, V., and Periasamy, N. (1980) Photoreduction of Anthraquinone in Aqueous Micellar Solution. *J. Photochem. 13*, 325−334.

(22) Kudryasheva, N. S., Val'kova, G. A., Shigorin, D. N., and Gorelik, M. V. (1989) Photochemical Properties of Aromatic Carbonyl Compounds Belonging to Different Spectral Luminescence Groups of Molecular Systematics. *Russ. J. Phys. Chem. 63*, 91−94.

(23) Shcheglova, N. A., Shigorin, D. N., Krasnobaeva, P. I., Dokunikhin, N. S., and Galitsina, L. N. (1973) Relation between the structural Parameters of the Phosphor Molecules and of the Solvent Lattice and Luminescent Spectra of beta-Alkylanthraquinones. *Russ. J. Phys. Chem. 47*, 442−444.

(24) Myant, N. B., Gallagher, J., Barbir, M., Thomson, G. R. Wile, D., and Humphries, S. E. (1989) Restriction fragment length polymorphisms in the apo B gene in relation to coronary artery disease. *Atherosclerosis 77*, 193−210.

(25) Gasper, S. M., and Schuster, G. B. (1997) Intramolecular Photoinduced Electron Transfer to Anthraquinones Linked to Duplex DNA: The Effect of Gaps and Traps on Long-Range Radical Cation Migration. *J. Am. Chem. Soc. 119*, 12762−12771.

(26) Shchepinov, M. S., Case-Green, S. C., and Southern, E. M. (1997) Steric factors influencing hybridization of nucleic acids to oligonucleotide arrays. *Nucleic Acids Res. 25*, 1155−1161.

(27) Maruyama, K., Otsuki, T., and Naruta, Y. (1976) Photochemical Reaction of 9,10-Phenanthrenequinone with Hydro-

gen Donors. Behavior of Radicals in solution as Studied by CIDNP. *Bull. Chem. Soc. Jpn. 49*, 791−795.
(28) Formosinho, S. J. (1976) Photochemical Hydrogen Abstraction as Radiationless Transitions. *J. Chem. Soc., Faraday Trans. 2 72*, 1332−1339.
(29) Maruyama, K., Ono, K., and Osugi, J. (1972) The Photochemical Reaction of alpha-Diketones. *Bull. Chem. Soc. Jpn. 45*, 847−851.
(30) Brennan, J. F., and Beutel, J. (1969) Quinone Photochemistry. II. The Mechanism of photoreduction of 9,10-Phenanthrenequinone and 2-tert-Butyl-9,10-Anthraquinone in Ethanol. *J. Phys. Chem. 73*, 3245−3249.
(31) Beaucage, S. L. (1999) Attachment of Reporter Groups to DNA. In *Comprehensive Natural Products Chemistry* (E. T. Kool, Ed..) (Barton, D., and Nakanishi, K. Editors-in-Chief) Vol. 7, pp 153−250, Pergamon Press.
(32) Mori, K., Subasinghe, C., and Cohen, J. S. (1989) Oligodeoxynucleotide analogues with 5′-linked anthraquinone. *FEBS Lett. 249*, 213−218.
(33) Cohen, J. S., Mori, K., and Matsukura., M. (1990) *Novel Oligodeoxynucleotides with 5′-linked Chemical Groups, Method of Production Thereof and use Thereof*, WO 90/12802.
(34) Ramirez, F., and Dershowitz, S. (1959) Reaction of Trialkyl Phosphites and of Triaryl Phosphites with Chloranil. A New Synthesis of Hydroquinone Monoalkyl Ethers. *J. Am. Chem. Soc. 81*, 587−590.
(35) Ramirez, F., Chen, E. H., and Dershowitz, S. (1959) Reaction of Trialkyl Phosphites with *p*-Benzoquinone and with Other Symmetrically Substituted *p*-Quinones. A New Synthesis of Hydroquinone Monoalkyl Ethers. *J. Am. Chem. Soc. 81*, 4338−4342.
(36) Wiuff, C., Jauho, E. S., Stryhn, H., Andersen, L. O., Thaulov, K., Boas, U., and Jakobsen, M. H. (1999) Evaluation of a new ELISA for detection of antibodies against Salmonella, employing of lipopolysaccharide-derived antigens covalently attached to polystyrene. *Pept. Protein Res.* (in press).
(37) Bulyk, M. L., Gentalen, E., Lockhart, D. J., and Church, G. M. (1999) Quantifying DNA protein interactions by double-stranded DNA arrays. *Nat. Biotechnol. 17*, 573−577.
(38) Dyrbye, H., (1999) *PNA: Chemistry and Potential Diagnostic Application*, Masters Thesis, University of Copenhagen, Denmark.

BC000011H

Conjugation of Epitope Peptides with SH Group to Branched Chain Polymeric Polypeptides via Cys(Npys)

Gábor Mezö, Nikolett Mihala, David Andreu,† and Ferenc Hudecz*

Research Group of Peptide Chemistry, Hungarian Academy of Sciences, Eötvös L. University, H-1518, Budapest, Hungary, and Department of Organic Chemistry, University of Barcelona, Barcelona, Spain.
Received September 18, 1999; Revised Manuscript Received March 21, 2000

Since bioconjugates may play an important role as therapeutics in the future, the development of new and effective conjugation strategies is necessary. For the attachment of peptide-like molecules to carriers, there are two main coupling methods involving amide or disulfide bonds. Conjugation through an amide bond can be achieved in several well-defined ways known from peptide chemistry. However, the formation of disulfide bridges between cysteine-containing peptides and carrier molecules still has some problems. In this paper, we describe a novel approach in which the carrier polypeptide is modified by 3-nitro-2-pyridinesulfenyl (Npys)-protected cysteine and this derivative has been applied for conjugation of Cys-containing epitope peptides with poly(L-lysine)-based branched polypeptides. Considering the stability of Npys group in the presence of pentafluorophenol, Boc-Cys(Npys)-OPfp dervivative was selected for introduction to the N-terminal of branches of polypeptides backbone. The branches of the polymers were built up from oligo(DL-alanine) (poly[Lys(DL-Ala$_m$)], AK) and elongated by an optically active amino acid [poly[Lys(X$_i$-DL-Ala$_m$)], XAK]. We found that the nature of X (Glu, Ser, Thr) has great influence on the incorporation of the protected cysteine residue. Herpes simplex virus and adenovirus epitope peptides were conjugated to Boc-Cys(Npys)-modified polypeptides. Results indicate that the incorporation of epitope peptides depends on the number of Npys group on the polymers as well as on the presence/absence of Boc-protecting group on the Cys residue. This new class of Cys(Npys)-derivatized branched polypeptides is stable for a couple of months and suitable for effective preparation of epitope peptide conjugates possessing increased water solubility.

INTRODUCTION

The combination of macromolecules and small bioactive molecules has a wide range of applications, particularly in the development of polymeric therapeutics (*1*−*3*). In accordance with the strategy invented by Ringsdorf, both drug and targeting moieties are attached to the same carrier (*4*). In immunology, protein carriers are frequently applied to induce immune responses against covalently attached low molecular weight peptide epitopes, for monoclonal antibody production or for synthetic vaccine construction (*5*, *6)*. It has been also demonstrated that the effective synthetic vaccine must contain both B- and T-cell epitope sequences. These constructs usually consist of two different epitope peptides and a vehicle (e.g., macromolecule, liposome, and nanoparticle).

Ideally, the unambiguous conjugation of two different epitope peptides to a macromolecular carrier requires two unrelated coupling methods. The two most commonly used procedures for conjugation are based on amide and disulfide formation. There are many well-defined coupling methods for the attachment of biological active peptides to carriers through amide bonds (water-soluble carbodiimide (*7*), active ester (*8*), and BOP[1] (*9*). The conjugation via disulfide bridge is usually carried out by using heterobifunctional reagents such as SPDP (*10*) (Figure 1). However, the application of amino/thiol-type bifunctional compounds raises some problems. First of all, these molecules are usually connected to the carrier through amide bonds, which diminish the number of available amino functions on the macromolecule. In addition, this type of bifunctional reagent involves the introduction of a hydrophobic spacer moiety, which often decreases the water solubility of the parent macromolecule. Finally, the disulfide formation reaction between the activated thiol of the carrier and the cysteine-containing epitope peptide usually proceeds at neutral or slightly alkaline pH, which can give rise to side reactions such as oxidation (dimerization) of the HS-peptide.

An alternative strategy for disulfide-based conjugation is the application of Cys(Npys) as a coupling agent. The

* To whom correspondence should be addressed. Fax: 36-1-372 2620. Phone: 36-1-372 2828. E-mail: hudecz@szerves.chem.elte.hu.

† Department of Organic Chemistry.

[1] Abbreviations: Acp, E-aminocaproic acid; Boc, *tert*-butyloxycarbonyl; Bom, benzyoxymethyl; BOP, benzotriazol-1-yloxy-tris(dimethylamino)phosphonium hexafluorophosphate; BrZ, 2-bromobenzyl-oxycarbonyl; BSA, bovine serum albumin; Bzl, benzyl; cHex, cyclohexyl; ClZ, 2-chloro-benzyloxycarbonyl; DCC, *N*,*N*′-dicyclohexylcarbodiimide; DCM, dichloromethane; DCU, *N*, *N*′-dicyclohexylurea; DIEA, *N*,*N*′-diisopropylethylamine; DMF, *N*,*N*-dimethylformamide; $\overline{DP}_n$, *number average ratio of polymerization; DTT, dithiothreitol; FAB-MS, fast-atom bombardment mass spectrometry; HATU, 2-(7-aza-1H-benzotriazol-1-yl)-1,1,3,3-tetramethyluronium hexafluorophosphate; HOBt, 1-hydroxybenzotriazole; HPLC, high-performance liquid chromatography; HSV gD, Herpes simplex virus glycoprotein D; KLH, keyhole limpet hemocyanin; MBHA, 4-methylbenzhydrylamine; MBS*, *N*-(3-maleimido-benzoyloxy)-succinimide; Meb, 4-methylbenzyl; MeOH, methanol; Npys, 3-nitro-2-pyridinesulphenyl; SPDP, *N*-succinimidyl-3-(2-pyridyldithio)-propionate; TBTU, 2-(1H-benzotriazol-1-yl)-1,1,3,3-tetramethyluronium tetrafluoroborate; TFA, trifluor-acetic acid; TLC, thin-layer chromatography; Tos, tosyl; UV, ultraviolet.

10.1021/bc990116o CCC: $19.00 © 2000 American Chemical Society
Published on Web 06/10/2000

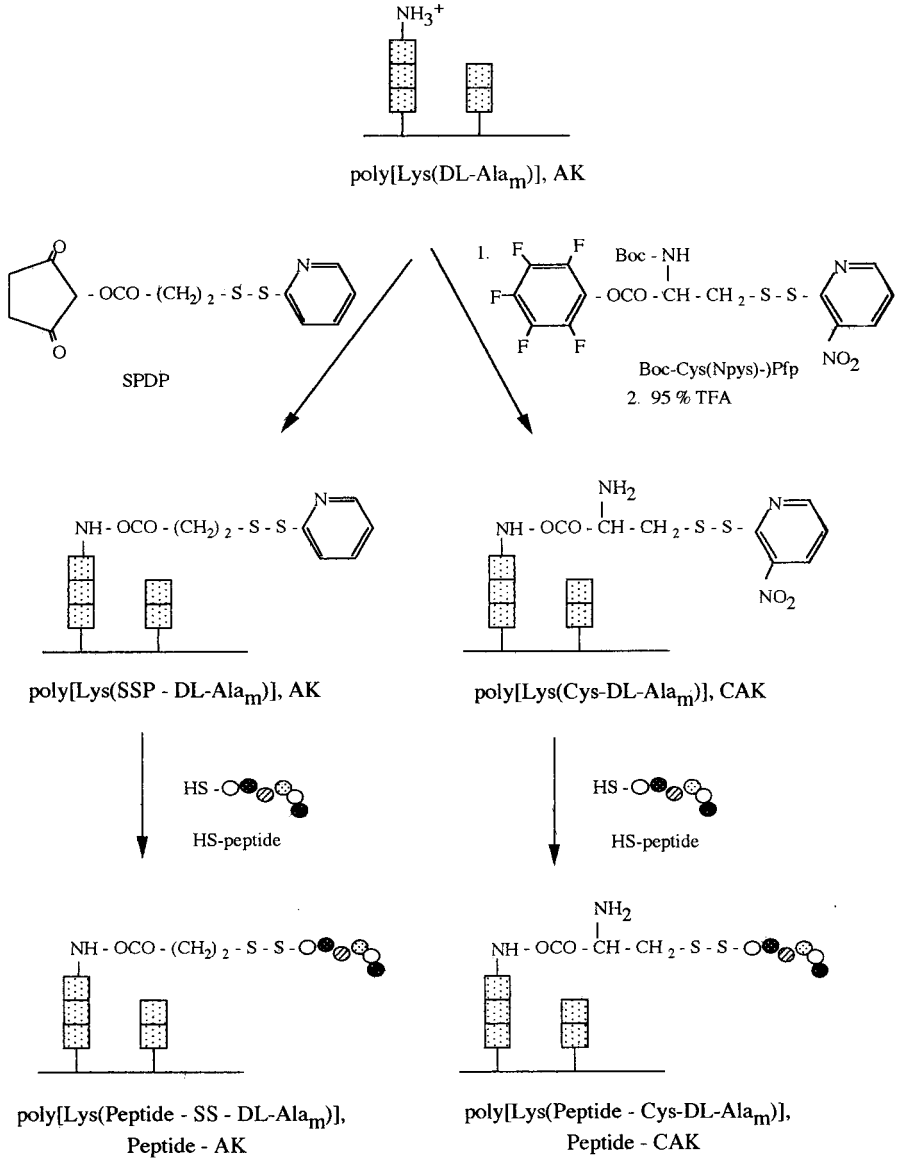

Figure 1. Outline of the synthesis of HS-oligopeptide conjugates with branched polypeptides by introduction disulpide bonds. Branched polypeptides were modified with heterobifunctional coupling reagent, SPDP or Cys(Npys).

Npys (3-nitro-2-pyridinesulfenyl) group was originally proposed as a protection for amino and/or hydroxyl functions during solid-phase peptide synthesis (*11*). The greatest potential of Npys, however, has gradually been realized to lie in the side-chain protection of Cys (*12*). Indeed, the most attractive feature of Npys is its dual character as an S-protecting and S-activating group.

Epitope peptides modified with Cys(Npys) residue at their C- or N-terminal were successfully conjugated to partially reduced BSA and KLH (*13*−*15*). The coupling procedure between the Cys(Npys) peptide and the free SH groups of the protein was carried out under acidic conditions (pH 4.5−7.0) to prevent the oxidation of the peptide and/or refolding of the reduced proteins. The aim of our studies reported here was the development of a new approach in which the macromolecular partner contains Cys(Npys) residues (Figure 2) and this derivative is conjugated with SH-oligopeptides. This strategy outlined in Figure 1 possesses several advantages: (i) the attachment of Cys(Npys) will not alter the number of amino groups on the macromolecule; (ii) it will allow direct peptide-carrier bonding without introduction of spacer entity and it will therefore preserve the solubility of the carrier; (iii) it will yield increased solubility since the optimal pH of this conjugation procedure is acidic (pH 4.5−7.0), and oxidation-related side reactions are suppressed.

In our laboratory, branched chain polymeric polypeptides with poly[L-Lys] backbone are used as macromolecular carriers (*16, 17*). The side chains of these polymers consist of a short oligo(DL-Ala) chain (3−6 amino acid residue) and an optically active amino acid residue at the N- or C-terminal part of the branches (poly[Lys(X_i-DL-Ala$_m$)] (XAK) and poly[Lys(DL-Ala$_m$-X_i] (AXK), where $i \approx 1$ and $m \approx 3$−6). These macromolecules were used earlier for the synthesis of epitope peptide conjugates to be used as antigens for the specific and sensitive detection of mucin1 glycoprotein-specific antibodies (*18*) and of *Mycobacterium tuberculosis* protein sensitized T cells (*19*). Branched polypeptide conjugates of epitope peptides derived from glycoprotein D of HSV have shown promising results as immunogens for vaccination of mice against lethal dose of HSV infection (*20*). For some of the artificial antigens described above we have utilized SPDP for the incorporation of Cys-peptide (*18*).

Here we present data on an alternative approach by utilizing Cys(Npys) residues on the side chains of four different XAK types branched chain polypeptides. Ap-

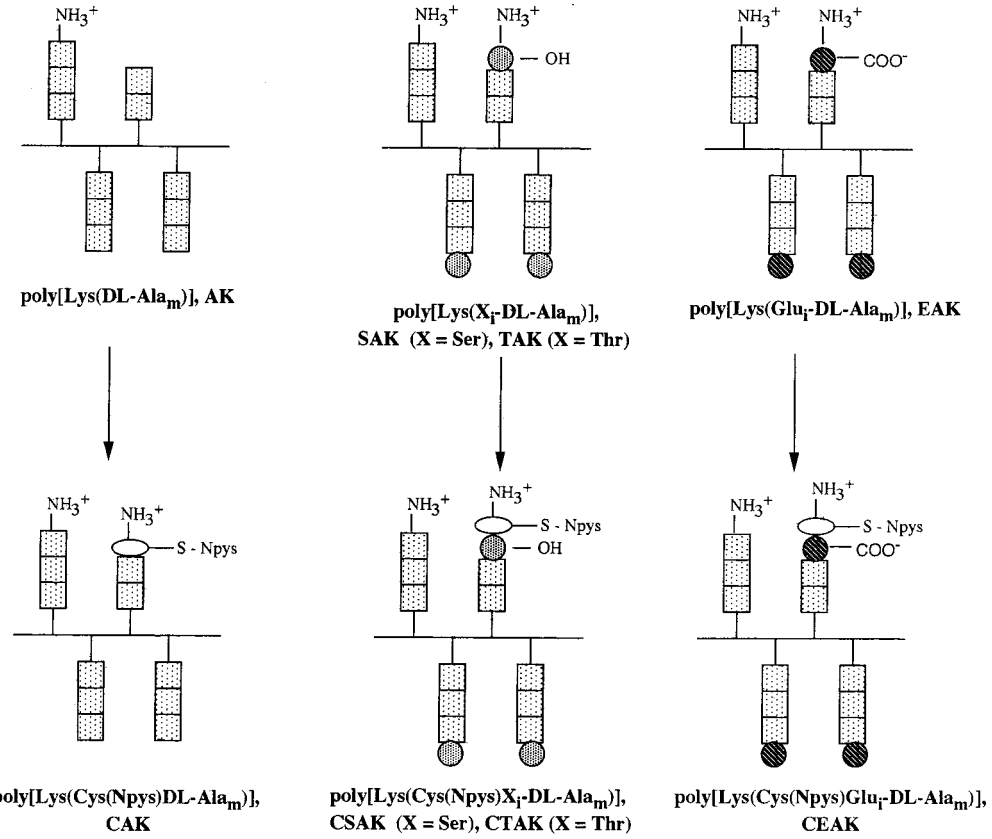

Figure 2. Schematic presentation of branched polypeptides used in this study.

propriate synthetic conditions developed for this methodology as well as the results of the synthesis of various conjugates applying Cys(Npys)-modified macromolecules and HS-peptide epitopes of viral origin are described. For this we have selected epitopes from glycoprotein D (gD) of Herpes simplex virus type 1 (^{9}LKNleADPNRFRGKDL^{22} and ^{276}SALLEDPVG^{284}) (*21*−*23*) and from adenovirus proteins AD2 (^{309}THLSYKPGKGDE^{320} and ^{399}NQAVDSYDPD^{408}) and AD41 (^{148}FIGTNINKDNGI^{159}) (*24*). In addition, we report for the first time on the preparation of a prototype conjugate in which two epitopes of gD type 1 joined by a dipeptide Acp-Cys spacer (where Acp is ϵ-amino caproic acid) are attached through the SH function of a single peptide to the Cys(Npys)-modified branched polypeptide (Figure 3).

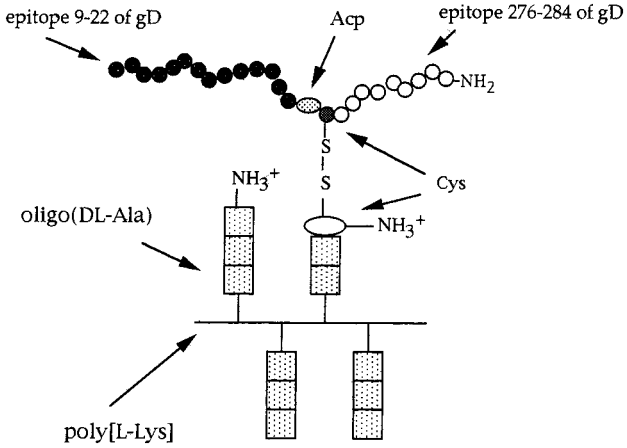

Figure 3. Schematic structure of a conjugate in which a single peptide containing epitopes corresponding to 9−22 and to 276−284 regions of glycoprotein D of HSV-1 is connected with carrier molecule. Two epitopes are joined by an Acp−Cys dipeptide spacer and the SH function of the peptide was used for conjugation with Cys(Npys) modified branched polypeptide.

EXPERIMENTAL PROCEDURES

Abbreviations used in this paper follow the rules of the IUPAC−IUB Commission of Biochemical Nomenclature (*25*) in accordance with the recommended nomenclature of graft polymers (*26*).[1]

Synthesis of Polymer Polypeptides. Branched polypeptides were synthesized as previously described (*16*, *17*, *27*). Briefly, poly[Lys] was prepared by the polymerization of N^{α}-carboxy-N^{ϵ}-benzyloxycarbonyl-lysine anhydride. After cleavage of the protecting groups poly[Lys(DL-Ala$_m$)] (AK) was prepared by grafting of short oligomeric DL-Ala side chains onto the ϵ-amino groups of poly[Lys]. Benzyloxycarbonyl-protected amino acids derivatives (*Z*-Ser-OPcp, *Z*-Thr-OPcp, and *Z*-Glu(OBzl)-OPcp) were coupled to the end of the side chains of AK by HOBt catalyzed active ester method (*28*). Blocking groups were removed completely with HBr in glacial acetic acid, as confirmed by UV spectroscopy at 254 nm resulted in poly[Lys(X$_i$-DL-Ala$_m$)] (XAK) polymers (where $i \leq 1$ and $m \approx 3-6$, X = Ser, Thr, or Glu). The composition of polypeptides was determined by amino acid analysis. The size and molecular weight of polymers were calculated from the amino acid composition and the sedimentation analysis of polylysine (*29*).

Synthesis of Epitope Peptides. Peptides (Table 1) were synthesized on MBHA resin (0.5 g, 1.1 mmol/g capacity) manually by Boc/Bzl strategy. The following protected amino acids were used: Asp(OcHex), Glu(OcHex), Thr(Bzl), Ser(Bzl), Tyr(BrZ), Lys(ClZ), Arg(Tos), His(Bom), and Cys(Meb). The protocol of the solid-phase synthesis was the following: (i) deprotection with 33% TFA/DCM (2 + 20 min); (ii) DCM washing (5 × 0.5 min); (iii) neutralization with 10% DIEA/DCM (3 × 1 min); (iv) DCM washing (4 × 0.5 min); (v) coupling 3 equiv of amino

Table 1. Characterization of Peptides Corresponding to Epitope(s) of HSV gD-1 or Adenovirus AD2, AD41 Proteins

amino acid sequence (code)	amino acid analysis found (calculated)	t_r (min)[a]	molar mass $[M + H]^+$
H-CSALLEDPVG-NH_2 HSV gD-1, Cys-276−284)	Asp, 0.95 (1); Ser, 0.90 (1); Glu, 1.12 (1); Pro, 0.99 (1); Gly, 1.12 (1); Ala, 1.00 (1); Val, 0.90 (1); Leu, 2.00 (2)	12.6[a]	1002.3 (1002.4)
H-LKNleADPNRFRGKDL-Acp-CSALLEDPVG-NH_2 (HSV gD-1, [Nle^{11}]-9−22-Acp-Cys-276−284)	Asx, 3.92 (4); Ser, 0.96 (1); Glu, 1.06 (1); Pro, 1.95 (2); Gly, 2.08 (2); Ala, 2.04 (2); Val, 1.00 (1); Nle, 1.00 (1); Leu, 4.04 (4); Phe, 1.00 (1); Lys, 2.08 (2); Arg, 1.96 (2)	16.4[a]	2740.0 (2740.2)
H-CTHLSZKPGKGDE-NH_2 (AD-2, Cys-309−320)	Asp, 0.98 (1); Thr, 0.97 (1); Ser, 0.96 (1); Glu, 1.05 (1); Pro, 1.01 (1); Gly, 2.04 (2); Leu, 1.00 (1); Tyr, 0.93 (1); His, 0.98 (1); Lys, 2.06 (2)	9.5[b]	1434.6 (1434.7)
H-CNQAVDSZDVD-NH_2 (AD-2, Cys-399−408)	Asx, 3.95 (4); Ser, 0.95 (1); Glu, 1.05 (1); Pro, 1.03 (1); Ala, 1.00 (1); Val, 0.97 (1); Tyr, 0.94 (1)	11.8[c]	1425.8 (1425.6)
H-CFIGTNINKDNGI-NH_2 (AD-41, Cys-148−159)	Asx, 3.94 (4); Thr, 0.96 (1); Gly, 2.02 (2); Ile, 3.03 (3); Phe, 1.01 (1); Lys, 1.02 (1)	17.9[c]	1407.7 (1407.5)

[a] Column: Phenomenex Jupiter C18 (250 × 4.6 mm, 10 μm, 300 Å). Eluent: (A) 0.1% TFA/water, (B) 0.1% TFA/AcN-water (80:20 v/v). Gradient: 0 min, 15% B; 5 min, 15% B; 35 min, 75%B. [b] Column: Vydac C4 (250 × 4.6 mm, 5 μm, 300 Å). Eluent: (A) 0.1% TFA/water, (B) 0.1% TFA/AcN-water (80:20 v/v). Gradient: 0 min, 10% B; 5 min, 10% B; 35 min, 50% B. [c] Column: Knaurt Eurosil Bioselect (250 × 4.0 mm, 5 μm, 300 Å). Eluent: (A) 0.1% TFA/water, (B) 0.1% TFA/AcN. Gradient: 0 min, 5% B; 25 min, 50%B. [d] Asx: Asn and Asp measured as aspartic acid.

acid−DCC−HOBt in DCM-DMF 4:1 or 1:4 mixture depends on the solubility of Boc-amino acid derivatives (60 min); (vi) DMF washing (1 × 0.5 min); (vii) DCM washing (2 × 0.5 min); (viii) ninhydrine assay. The peptides were cleaved from the resin by the aid of liquid HF in the presence of *p*-cresol and DTT (HF-*p*-cresol-DTT= 10 mL:1 g:0.1 g) for 1.5 h at 0 °C. The crude products were purified by HPLC using Delta Pak C_{18} semipreparative column (30 × 1.9 cm, 10 μm). The purified peptides were analyzed by HPLC, amino acid analysis and FAB-MS (Table 1).

Synthesis of Boc-Cys(Npys)-OPfp. A total of 500 mg (1.33 mmol) of Boc-Cys(Npys)-OH (Mw 375) and 245 mg (1.33 mmol) pentafluorophenol were dissolved in 5 mL of DCM, then 274 mg (1.33 mmol) of DCC dissolved in 2 mL of DCM was added to the solution. The reaction mixture was stirred in an ice bath for 15 min then for 2 h at RT. The reaction was followed by TLC. After cooling, the solution to 0 °C the precipitated DCU was filtered out, the solvent was evaporated, and the product was recrystallized from methanol. Yield 594 mg (83%) (Mw 541). Melting point: 96−99 °C. R_f = 0.65 (chloroform-methanol = 3:1); R_f = 0.92 (ethyl acetate). Optical rotation: $[\alpha]_D = -62.2$ (c = 1, DMF).

Synthesis of Branched Polypeptides with Cys-(Npys) Residues. The synthesis of poly[Lys(Cys-(Npys)$_i$-DL-Ala$_m$)] (CAK) is described in details. A total of 20 mg (57 μmol) of poly[Lys(DL-$Ala_{3.11}$)] (AK, $\overline{DP}_n$ = *66*, $\overline{Mw}_{monomer}$ 349) was dissolved in 0.5 mL d.i. water, and the solution was diluted with 3 mL of DMF. Equivalent amount (31 mg, 57 μmol) of Boc-Cys(Npys)-OPfp dissolved in 2 mL of DMF was added to the solution. The reaction mixture was stirred overnight at RT. The solvent was removed in vacuo (30 °C), and the remaining product was treated with ether (containing 10% DCM) several times for washing out the unreacted ester and the resulted pentafluorophenol. Yield: 35 mg. Boc-protection was removed in 5 mL of TFA-water (95:5, v/v) at 0 °C for 1h in the presence or absence of 5% *p*-cresol or thioanisole. The solution was concentrated in vacuo, then the remaining material was dissolved in water and dialyzed versus 0.1% acetic acid solution for 2 days followed by liophylization (yield 27 mg). The average degree of substitution was calculated from the UV absorption of Npys group at 350 nm (ϵ = 3930 M^{-1} cm^{-1} in DMF). The data were also corrected by peptide content of amino acid analysis measured from the same solution.

Other Cys(Npys) containing polymers were synthesized in the same way using poly[Lys(Ser$_{1.0}$-DL-$Ala_{3.1}$)] (SAK, $\overline{DP}_n$ = 66, $\overline{Mw}_{monomer}$ 428), poly[Lys(Glu$_{0.9}$-DL-$Ala_{3.1}$)] (EAK, $\overline{DP}_n$ = 66, $\overline{Mw}_{monomer}$ 465), or poly[Lys(Thr$_{1.0}$-DL-$Ala_{3.1}$)] (TAK, $\overline{DP}_n$ = 60, $\overline{Mw}_{monomer}$ 450). The starting molar ratio of Boc-Cys(Npys)-OPfp and the polymers as well as the average degree of incorporation to the branches are summarized in Table 2.

Conjugation of Epitope Peptides to Branched Polypeptides with Cys(Npys). Branched polypeptides containing Boc-Cys(Npys) (Boc-CAK or Boc-CSAK) were dissolved in DMF (A) or in DMF-0.06M phosphate buffer (pH 5.5) = 75:25 (v/v) mixture (B). Alternatively polymers without Boc protecting groups (CAK, CSAK) were dissolved in the 0.06 M phosphate buffer solution (C). A range of 1.2−1.4 equiv (calculated for the Npys content of the polymers) of Cys-epitope peptide dissolved in the same solvent was added to the polymer solution. The final concentration of the reaction mixture was 1 mg/mL for the polymer component. The mixtures were stirred for 4 h at RT. Then the solutions were filled in Visking tubes (cut off 8000−12000) and dialyzed for 2 days against 0.1% acetic acid. The conjugates containing Boc-protecting groups were deblocked with 95% TFA and then dialyzed and freeze-dried. In case of the presence of UV band at λ = 350 nm Npys groups were reacted with the 1.2 equiv excess of cysteine in 0.06 M phosphate buffer (pH 5.5) followed by dialysis and freeze-drying. The average degree of substitution of conjugates was calculated from amino acid composition and it is presented in Table 3.

The conjugate containing two epitopes joined by Acp-Cys spacer was prepared as follows. Boc-deprotected poly-[Lys(Cys$_{0.24}$-Ser$_{0.9}$-DL-$Ala_{3.1}$)] trifluoroacetate salt (10 mg, 16.5 μmol) was dissolved in 10 mL of 0.06 M phosphate buffer (pH 5.5). A total of 1.35 equiv amount of H-LKNleADPNRFRGKDL-Acp-CSALLEDPVG-NH_2 (14.8 mg, 5.4 μmol) calculated to the Npys content of polymer was added to the reaction mixture. The solution was stirred for 4 h at RT. The solution was filled in Visking tube (cut off 8000−12000) and dialyzed for 2 days against

Table 2. Incorporation of Boc-Cys(Npys) Residues into Branched Polypeptides

polymers	Boc-Cys(Npys)-Opfp/ polymer ratio (mol/mol)	amount of polymer (mg)	amount of Cys residue (mg)	average degree of substitiuon (%)[a]	
				I	II
poly[Lys(DL-$Ala_{3.1}$)] (AK)	0.25	20	7.8	26	27
	0.5	20	15.5	42	46
	0.75	20	23.3	65	73
	1.00	20	31.0	74	100
	1.50	20	46.5	75	nd
poly[Lys($Ser_{0.9}$-DL-$Ala_{3.1}$)] (SAK)	0.25	20	6.3	16	17
	0.50	20	12.7	24	24
	0.75	20	19.0	26	27
	1.00	20	25.3	28	27
	1.50	20	38.0	28	nd
poly[Lys($Glu_{0.9}$-DL-$Ala_{3.1}$)] (EAK)	0.50	20	11.7	37	40
	1.00	20	23.3	41	48
	1.50	20	35.0	42	54
poly[Lys($Thr_{1.0}$-DL-$Ala_{3.1}$)] (TAK)	1.00	10	12.0	11	nd

[a] Determined by UV analysis (I) and corrected with amino acid composition (II).

Table 3. Preparation and Characterization of Epitope Peptide-Branched Polypeptide Conjugates

polymer	Cys(Npys) substitution[a] (%)	amount of polymer (mg)	Cys(Npys) contant of polymer (mmol)	solvent	peptide	amount of peptide[b] (mg)	avarage substitution[c] (%)
Boc-CAK	100	5.0	7.1	A	H-CSALLEDPVG-NH_2	8.5	7
Boc-CAK	100	5.0	7.1	A	H-CFIGTNINKDNGI-NH_2	12.1	6
Boc-CAK	100	5.0	7.1	A	H-CTHLSYKPGKGDE-NH_2	15.1	6
CAK	27	5.0	2.2	C	H-CSALLEDPVG-NH_2	2.7	16
CAK	46	5.0	3.8	C	H-CSALLEDPVG-NH_2	4.6	42
CAK	100	5.0	8.3	C	H-CSALLEDPVG-NH_2	9.9	52
CAK	27	10.0	4.4	C	H-LKNleADPNRFRGKDL-Acp-CSALLEDPVG-NH2	14.8	26
Boc-CSAK	24	5.0	1.9	A	H-CSALLEDPVG-NH_2	2.3	18
Boc-CSAK	24	5.0	1.9	B	H-CSALLEDPVG-NH_2	2.3	25
CSAK	24	5.0	2.0	C	H-CNQAVDSYDPD- NH_2	2.8	20
CSAK	24	5.0	2.0	C	H-CSALLEDPVG-NH_2	2.4	21
CSAK	24	10.0	4.0	C	H-LKNleADPNRFRGKDL-Acp-CSALLEDPVG-NH_2	14.8	20

[a] Determined by UV analysis and corrected with amino acid composition. [b] Corresponding to 1.2 μmol of peptide. [c] Determined by amino acid analysis.

0.1% acetic acid. No Npys content was detected by UV spectroscopy in the conjugate after liophylization. The yield was 15 mg (86%). According to the amino acid analysis, 20% of side chains of branched polypeptide contained the bifunctional epitope peptide.

Analytical Methods. The amino acid composition of branched polypeptides, epitope peptides, and their conjugates was determined by amino acid analysis using a Beckman (Fullerton, CA) model 6300 amino acid analyzer. Prior to the analysis, samples were hydrolyzed in 6 M HCl in sealed and evacuated tubes at 110 °C for 24 h. Fast-atom bombardment mass spectrometry measurements were carried out on a Fisons (U.K.) VG-ZA-2SEQ tandem mass spectrometer equipped with a Cs^+ ion gun (30 keV). The peptide samples were dissolved in DMSO and mixed with glycerol matrix. Analytical HPLC was performed using reversed-phase columns on Knauer apparatus (H. Knauer, Bad Homburg, Germany). The instrument was assembled from two HPLC Pump 64, a Variable Wavelength Monitor, and functionalized by HPLC Software/Hardware Package Version 2.21 A. The types of columns, gradients, and solvents are shown in Table 1.

RESULTS AND DISCUSSION

The synthesis and simplified structure of branched chain polypeptides containing Cys(Npys) residue at the N-terminal of the side chains are outlined in Figures 1 and 2. These compounds were prepared for conjugation with HS-peptides comprising one or co-linearly two epitopes (Figure 3.). Prior to the incorporation of cysteine residue to the polymers, the stability of Npys group was studied in the presence of pentafluorophenol. Due to the contradictory results reported on the sensitivity of Npys group in the presence of HOBt during solid-phase peptide synthesis (*15*, *30*), we have attempted to avoid the in situ HOBt-catalyzed active ester method for the introduction of Boc-Cys(Npys) on the polypeptide branches. An alternative active ester approach was developed using Boc-Cys(Npys)-OPfp (*31*) prepared from Boc-Cys(Npys)-OH and pentafluorophenol by DCC condensation (*32*) and characterized. The reaction between Boc-Cys(Npys)-OPfp and the α-amino groups of the N-terminal amino acids of branched polypeptide yield pentafluorophenol as byproduct. Considering this, we have initiated a model experiment in which Boc-Cys(Npys)-OH was kept in DMF-water (9:1, v/v) mixture in the absence or presence of pentafluorophenol. This solvent is the preferred mixture for the coupling of protected amino acids to the branched polymers (*17*). On the basis of HPLC analysis of the solutions, we found no changes in the profile of Boc-Cys-(Npys)-OH for 1 day at RT (data not shown). These results indicate that the Npys group is stable under conditions applicable for Boc-Cys(Npys)-OPfp modification of polymeric polypeptides.

In the next set of experiments, the protected and activated cysteine residue was reacted with the branched polymers in the molar ratio of 0.25−1.5 mol/mol. The

average degree of substitution values is summarized in Table 2. These values were calculated from the UV absorption of the Npys chromophore containing polymers at $\lambda = 350$ nm using ϵ determined under conditions used for analysis. These values were corrected by the conjugate content of the same solution measured by amino acid analysis. The difference between these figures might be due to the water content of freeze-dried samples. The data of Table 2. indicate that the increase of input Boc-Cys(Npys)-OPfp/polymer ratio resulted in higher substitution in case of AK polymer. The application of 1:1 molar ratio was sufficient to achieve almost complete incorporation of Boc-Cys(Npys). Similar tendency was observed with EAK containing Glu at the end of the branches. But in this case, only 54% of the side chains could be modified even at 1.5 mol/mol input value. In contrast, the reaction between Boc-Cys(NPys)-OPfp and SAK resulted in only a small elevation of averge degree of substitution after increasing the input ratio from 0.25 to 0.75, and no further changes could be observed at 1.0 mol/mol ratio. Even more limited modification was detected with TAK polymer at the same input value. On the basis of the highest substitution figures achieved in these experiments, the following order could be established: AK (100%) > EAK (54%) > SAK (27%). The fairly low values for EAK and SAK could be indicative for the presence of noncovalent interactions (e.g., ionic- and H-bond) between side chains of the polymers. In case of EAK, the ionic forces between the α-amino group of the side-chain terminal Glu and the γ-COOH group of the neighboring, one could produce protonated amino groups and prevent the effective coupling of Boc-Cys(Npys)-OPfp to the side chains. The conformational properties, namely the tendency to form ordered structure of Ser-containing polymer indicated the presence of H-bond interaction between the side-chain terminals (*27*). In case of the other OH-amino acid containing polymer (TAK) where the incorporation of Boc-Cys(Npys) residues might be hindered not only by H-bonds but also by the bulky side chain of threonine.

Addition of MeOH to the reaction mixture or substitution of DMF by MeOH decreased the average degree of substitution of polymers studied. In case of SAK, these values were 25% in MeOH-DMF-water (45%−45%−10%) and 22% in MeOH-water (90%−10%) at 1:1 input molar ratio.

Epitope peptides elongated by Cys at their N-terminal were conjugated either to Boc-Cys(Npys)-polymers or to NH_2−Cys(Npys)-polymers. In the latter case, the N-protecting group was removed with 95% TFA/water in the presence or absence of scavangers. We found that the addition of 5% *p*-cresol or thioanisole to the cleavage mixture had no influence on the disulfide bond between SH of Cys and Npys moiety. Similarly no changes in the UV spectrum of the polymer could be observed after prolonged (2 days) dialysis of the N-deprotected polymer in 0.1% acetic acid solution. It should be noted that decrease of absorbance was detected when the dialysis was performed against distilled water.

For the conjugation of epitope peptides of HSV gD-1 (H-^{276}SALLEDPVG^{284}-NH_2) and two adenovirus proteins [H-^{148}FIGTNINKDNGI^{159}-NH_2 (AD41), H-^{309}THLSYK-PGKGDE^{320}-NH_2 (AD2) and H-^{399}NQAVDSYDPD^{408}-NH_2 (AD2)], two Cys(Npys)-polymers were selected. Both compounds (CAK and CSAK) were used in their Boc-protected forms as well as with free NH_2 groups at the end of the side chains, and the average degree of SH-peptide substitution was compared (Table 3). In the first set of experiments, polymer polypeptides with Boc-protecting groups were dissolved in DMF and reacted with SH-epitope peptides. In case of CAK, the average degree of substitution observed with three peptides of different composition and sequence was very low (6−7%). This indicates that the introduction of SH-peptides might not be favored in Boc-CAK containing Boc-Cys(Npys) residue at all of the side-chain terminal (100% substitution). In case of CSAK polymer, the SH-peptide incorporation was significantly higher in DMF (18%) or in DMF-0.06 M phosphate buffer (pH 5.5) mixture (25%). It should be noted that Boc-CSAK possesses Boc-Cys(Npys) moiety only on 24% of the branches. The comparison of data obtained with Boc-CAK and Boc-CSAK suggests that the steric hindrance caused by the presence of the large number of Boc-Cys(Npys) at the end of the side chains might prevent the incorporation of SH-peptides into polymers.

In case of CSAK containing no Boc-blocking groups, the average degree of SH-peptide incorporation was in the same range as compared to Boc-CSAK (Table 3). However, much higher average degree of substitution could be achieved with CAK polypeptide (16−52%) than with that of Boc-CAK (6−7%). These data underline that the removal of Boc-protecting group from a highly Boc-Cys(Npys) modified polypeptide (Boc-CAK vs CAK) could improve the disulfide exchange reaction between the polymer and SH-peptides. At the same time, there are no significant differences in reactivity of Cys(Npys)-polymers with or without Boc-group, when the average degree of Cys(Npys) content of the polymer is relatively modest (Boc-CSAK vs CSAK) (Figure 2).

We have also prepared a conjugate in which a 25-residue peptide is attached to Cys(Npys) polymers (Figure 2). The peptide was designed to combine two different epitopes of gD-1 HSV (^{9}LKNleADPNRFRGKDL^{22} and ^{276}SALLEDPVG^{284}) by a dipeptide spacer containing ϵ-aminocaproic acid residue (Acp) and Cys. In this dipeptide sequence, Acp connected the N^{α}-amino goup of C^{276}SALLEDPVG^{284} with the C^{α} -carboxy group of Leu residue in peptide ^{9}LKNleADPNRFRGKDL^{22}. Thiol group of Cys in the inner part of hybrid peptide containing two epitopes was used for conjugation to branched polypeptide. It has been demonstrated that the 9−21 sequence contains overlapping T- and B-cell epitopes (*21*, *22*), while 276−284 represents a B-cell epitope of the same protein (*21*). Immunization with protein (KLH or BSA) conjugates of peptide 8−23 (*33*) or Nle^{11}-substituted peptide 9−21 (*34*) produced high titer antibody response with virus neutralizing activity. We have also demonstrated that branched chain polypeptide conjugates either of peptide 276−284 or peptide 1−23 resulted in minimum 50% survival of mice infected by lethal dose of HSV virion (*23*, *35*). On the basis of these considerations, the 25-mer peptide was coupled in 0.06 M phosphate buffer to unprotected form of CAK and CSAK polymers containing 27 and 24% of Cys(Npys), respectively. In these cases, the average degree of substitution of branched polymers with the 25-mer peptide having Cys residue in central position was 26% in case of CAK and 20% in case of CSAK (Table 3). These data show that the use of AK- and SAK-based polymers with relatively low Cys(Npys) content (24−27%) results in epitope peptide conjugates in which almost all Npys group of the polymer could be replaced by the reaction of SH-peptides.

CONCLUSION

In this paper, a new method is described for the conjugation of branched polypeptides with cysteine con-

taining oligopeptides via Cys(Npys). We found that the efficacy of the incorporation of Cys(Npys) residue to the polymers using Boc-Cys(Npys)-OPfp depends mainly on the identity of the branch terminating amino acid, but the input molar ratio is also important. Bulky side chain of the N-terminal amino acid in the branches and/or its ability to participate in noncovalent interactions (ionic-, H-bond) decrease the incorporation of cysteine residue into the polymers. Cys(Npys)-modified polymers react effectively with cysteine-containing oligopeptides in a disulfide exchange reaction. However, the average degree of substitution was not increased significantly by elevation of the number of Cys(Npys) residue on the polymers. This suggests that determination of the optimal density of the reacting, namely Cys(Npys) group on the branched polypeptide is a crucial factor for the design and preparation of conjugates. Procedure described in this communication provides a new effective route for the conjugation through disulfide bond, which does not decrease the solubility of the carriers or the conjugates. In addition, our data suggest that this synthetic route is suitable for incorporation not only small oligopeptides with N-terminal SH groups but also relatively large peptide (25-mer) possessing Cys residue at the central region of the peptide.

ACKNOWLEDGMENT

These studies were supported by grants from the Hungarian Research Fund (OTKA T-14964 and T-03838), from the Hungarian Spanish Intergovernmental Program (5/1998) and from the Hungarian Ministry of Culture (MKM No. 0101/1997)

LITERATURE CITED

(1) Poznansky, M. J., and Cleland, L. G. (1980) Biological macromolecules as carriers of drugs and enzymes. In *Drug Delivery Systems* (R. L. Juliano, Ed.) pp 253−315, Oxford University Press, U.K..

(2) Seymour, L. W. (1992) Passive tumor targeting of soluble macromolecules and drug conjugates. *CRC Crit. Rev. Ther. Drug. Carrier Sys. 9,* 135−187.

(3) Maeda, H., and Matsumura, Y. (1989) Tumorotropic and lymphotropic principles of macromolecular drugs. *CRC Crit. Rev. Ther. Drug Carrier Sys. 6,* 193−210.

(4) Ringsdorf, H. (1975) Structure and properties of pharmacologically active polymers. *J. Polym. Sci. Polymer Symp. 51,* 135−153.

(5) Müller, G. M., Shapira, M., and Arnon, R. (1982) Anti-influenza response achived by immunization with a synthetic conjugates. *Proc. Natl. Acad. Sci. U.S.A. 79,* 5042−5046.

(6) Neurath, A. R., Kent, S. B. H., and Strick, N. (1982) Specificity of antibodies elicited by a synthetic peptide having a sequence in common fragment of virus protein the Hepatitis B surface antigen. *Proc. Natl. Acad. Sci. U.S.A. 79,* 7871−7875.

(7) Dean, C., Claassen, E., Gerritse, K., Zegers, N. D., and Boersma, W. J. A. (1990) A novel carbodiimide coupling method for synthetic peptides. *J. Immunol. Methods 129,* 119−125.

(8) Atassi, M. Z., Kazim, A. L., and Sakata, S. (1981) High yield coupling of peptides to protein carriers. *Biochim. Biophys. Acta 670,* 300−302.

(9) Mezö, G., Mezö, I., Pimm, M. V., Kajtár, J., Seprödi, A., Teplán, I., Kovács, M., Vincze, B., Pályi, I., Idei, M., Szekerke, M., and Hudecz, F. (1996) Synthesis, conformation, biodistribution and hormon related in vitro antitumor effect of GnRH antagonist branched polypeptide conjugate. *Bioconjugate Chem. 7,* 642−650.

(10) Carlsson, J., Drevin, H., and Axen, R. (1978) Protein thiolation and reversible protein−protein conjugation. N−Succinimidyl 3-(2-pyridyldithio) propionate, a new heterobifunctional reagent. *Biochem. J. 173,* 723−728.

(11) Matsueda, R., and Walter, R. (1980) 3-nitro-2-piridinesulfenyl (Npys) group. *Int. J. Pept. Protein Res. 16,* 392−401.

(12) Matsueda, R., Kimura, T., Kaiser, E. T., and Matsueda, G. R. (1981) 3-nitro-2-pyridinesulfenyl group for protection and activation of the thiol function of cystein. *Chem. Lett.* 737−740.

(13) Drijfhout, J. W., Perdijk, E. W., Weijer, W. J., and Bloemhoff, W. (1988) Controlled peptide−protein conjugation by means of 3-nitro-2-pyridinesulfenyl protection-activation. *Int. J. Pept. Protein Res. 32,* 161−166.

(14) Ponsati, B., Giralt, E., and Andreu, D. (1989) A synthetic strategy for simultaneous purification-conjugation of antigenic peptides. *Anal. Biochem. 11,* 389−395.

(15) Albericio, F., Andreu, D., Giralt, E., Navalpotro, C., Pedroso, E., Ponsati, B., and Ruiz-Gayo M. (1989) Use of the Npys thiol protection in solid-phase peptide synthesis. *Int. J. Pept. Protein Res. 34,* 124−128.

(16) Hudecz, F., and Szekerke, M. (1984) Synthesis of new branched polypeptides with poly(lysine) backbone. *Collect. Czech. Chem. Commun. 50,* 103−113.

(17) Mezö, G., Kajtár, J., Hudecz, F., and Szekerke, M. (1993) Carrier design: Conformational studies of amino acid (X) and oligopeptide (X-DL-Ala_m) substituted poly(L-lysine). *Biopolymers 33,* 873−885.

(18) Hudecz, F., and Price, M. R. (1992) Monoclonal antibody binding to peptide epitopes conjugated to synthetic branched polypeptide carriers. Influence of the carrier upon antibody recognition. *J. Immunol. Methods 147,* 201−210.

(19) Wilkinson, K. A., Vordermeier, M. H., Wilkinson, R., Iványi, J., and Hudecz, F. (1998) Synthesis and in vitro T cell immunogenicity of conjugates with dual specificities: attachment of epitope peptides of 16 kDa and 38 kDa proteins from M.tuberculosis to branched polypeptide. *Bioconjugate Chem. 9,* 539−547.

(20) Hudecz, F., Hilbert, Á., Mezö, G., Kajtár, J., and Rajnavölgyi, É. (1994) B-cell epitopes in Herpes simplex Virus-(HSV-1) glycoprotein D (gD). In *Synthetic peptides in the search for B-and T-cell epitopes* (Rajnavölgyi, É., Ed.) pp 157−169, R. G. Landes Company, Austin.

(21) Dietzschold, B., Eisenberg, R. J., Ponce deLeon, M., Golub, E., Hudecz, F., Varrichio, A., and Cohen, G. H. (1984) Fine structure analysis of type-specific and type common antigens sites of Herpes simplex virus glycoprotein D. *J. Virol. 52,* 431−435.

(22) Heber-Katz, E., Hollósi, M., Dietzschold, B., Hudecz, F., and Fasman, G. (1985) The T cell response to the glycoprotein D of the Herpes simplex virus: The significance of antigen conformation. *J. Immunol. 135,* 1385−1390.

(23) Hudecz, F., Hilbert, Á., Mezö, G., Mucsi, I., Kajtár, J., Bösze, Sz., Kurucz, I., and Rajnavölgyi, É. (1993) Epitope mapping of 273−284 region of HSV glycoprotein D by synthetic branched polypeptide carrier conjugates. *Pept. Res. 6,* 263−271.

(24) Ádám, É., Nász, I., Hudecz, F., Lengyel, A., Mezö, G., and Dobay, O. (1998) Characterisation of intertype specific epitopes on adenovirus hexone. *Arch. Virol. 142,* 1669−1682.

(25) IUPAC−IUB Commission on Biochemical Nomenclature. (1972) *Biochem. J. 127,* 753−756.

(26) IUPAC−IUB Commission on Biochemical Nomenclature. (1984) *Eur. J. Biochem. 138,* 9−37.

(27) Mezö, G., Kajtár, J., Nagy, I., Szekerke, M., and Hudecz, F. (1997) Carrier design: Synthesis and conformational studies of poly(L-lysine) based branched polypeptides with hydroxyl groups in the side chains. *Biopolymers 42,* 719−730.

(28) Mezö, G., Votavova, H., Hudecz, F., Kajtár, J., Sponar, J., and Szekerke, M. (1988) Conformation of branched polypeptides: The influence of DL-alanine oligomer spacers in the side chains. *Collect. Czech. Chem. Commun. 53,* 2843−2853.

(29) Hudecz, F., Kovács, P., Kutassi-Kovács, S., and Kajtár, J. (1984) GPC, CD and sedimentation analysis of poly-Lys and branched chain poly-Lys-poly-DL-Ala polypeptides. *Colloid Polym. Sci. 262,* 208−212.

(30) Matsueda, R., Higashida, S., Albericio, F., and Andreu, D. (1992) Compatibility of the S−(3-nitro-2-pyridinesulfenyl) protecting group with DCC/HOBt coupling chemistry. *Pept. Res. 5,* 262−264.

(31) Simmonds, R. G., Tupper, D. E., and Harris, J. R. (1994) Synthesis of disulfide-bridged fragments of omega-conotoxins GVIA and MVIIA. Use of Npys as a protecting/activating group for cysteine in Fmoc syntheses. *Int. J. Pept. Protein Res. 43*, 363−366.

(32) Kisfaludy, L., and Schön, I. (1983) Preparation of pentafluorophenyl esters of 9-fluoromethyloxycarbonyl amino acids for peptide synthesis. *Synthesis 1983*, 572−574.

(33) Dietzschold, B., Heber-Katz, E., Hudecz, F., Hollósi, M., Fasman, G., Eisenberg, R. J., and Cohen, G. H. (1985) In *Vaccines 85* (R. A. Lerner, R. M. Chanock, and F. Brown, Eds.) pp 227−234, Cold Spring Harbor Laboratory, Plainview, NY.

(34) Weijer, W. J., Drijfhout, J. W., Geerligs, H. J., Bloomhoff, W., Feijlbrief, M., Bos, C. A., Hoogerhout, P., Kerling, K. E. T., Popken-Boer, T., Slopsema, K., Wilterdrink, J. B., Welling, G. W., and Welling-Wester, S. (1988) Antibodies against synthetic peptides of Herpes simplex virus type-1 glycoprotein D and their capability to neutralize viral infectivity in vitro. *J. Virol. 62*, 501−510.

(35) Hilbert, Á., Hudecz, F., Mezö, G., Mucsi, I., Kajtár, J., Kurucz, I., Gergely, J., and Rajnavölgyi, É. (1994) The influence of branched polypeptide carriers on the immunogenicity of predicted epitopes of HSV-1 glycoprotein D. *Scand. J. Immunol. 40*, 609−617.

BC990116O

Steric Stabilization of poly-L-Lysine/DNA Complexes by the Covalent Attachment of Semitelechelic poly[*N*-(2-Hydroxypropyl)methacrylamide]

David Oupický,*,† Kenneth A. Howard,† Čestmír Koňák,‡ Philip R. Dash,† Karel Ulbrich,‡ and Leonard W. Seymour†

CRC Institute for Cancer Studies, University of Birmingham, Birmingham B15 2TA, U.K., and Institute of Macromolecular Chemistry, Academy of Sciences of the Czech Republic, Heyrovsky Sq. 2, 162 06 Prague 6, Czech Republic. Received October 21, 1999; Revised Manuscript Received February 25, 2000

The concept of steric stabilization was utilized for self-assembling polyelectrolyte poly-L-lysine/DNA (pLL/DNA) complexes using covalent attachment of semitelechelic poly[*N*-(2-hydroxypropyl)methacrylamide] (pHPMA). We have examined the effect of coating of the complexes with pHPMA on their physicochemical stability, phagocytic uptake in vitro, and biodistribution in vivo. The coated complexes showed stability against aggregation in 0.15 M NaCl and reduced binding of albumin, chosen as a model for the study of the interactions of the complexes with plasma proteins. The presence of coating pHPMA had no effect on the morphology of the complexes as shown by transmission electron microscopy. However, results of the study of polyelectrolyte exchange reactions with heparin and pLL suggested decreased stability of the coated complexes in these types of reactions compared to uncoated pLL/DNA complexes. Coated complexes showed decreased phagocytic capture by mouse peritoneal macrophages in vitro. Decreased phagocytosis in vitro, however, did not correlate with results of in vivo study in mice showing no reduction in the liver uptake and no increase in the circulation times in the blood. We propose that the rapid plasma elimination of coated pLL/DNA complexes is a result of binding serum proteins and also of their low stability toward polyelectrolyte exchange reactions as a consequence of their equilibrium nature.

INTRODUCTION

Polyelectrolyte polycation/DNA complexes are attracting considerable attention as a promising synthetic vector for gene delivery. However, despite substantial progress and considerable versatility and transfectional activity in vitro, simple polyelectrolyte gene delivery systems are quickly eliminated from the bloodstream following intravenous injection (plasma half-life typically less than 5 min) (Dash et al., 1999). The complexes are usually cleared quickly into the liver or spleen. Patterns of distribution in vivo indicate significant phagocytic capture by components of the reticuloendothelial system (RES), notably by tissue macrophages such as Kupffer cells (Dash et al., 1999). Rapid localization of DNA complexes in the RES (liver, spleen) prevents their targeting to non-RES tissues in a specific manner and results, therefore, in a severe limitation of their therapeutic potential. For targeted systemic delivery, a more prolonged plasma circulation of the vector is essential. It is, therefore, a central aim to decrease uptake by the RES in order to develop polymer-based DNA complexes with improved circulation times. In the design of long circulating DNA/polyelectrolyte complexes for gene delivery, we can be inspired by experiences obtained in the fields of similar particulate systems for drug delivery, notably liposomes and polymeric nanoparticles (Bazile et al., 1992; Illum et al., 1987; Lasic and Needham, 1995).

The interaction of similar particulate drug delivery systems with the cells of the RES is determined to a great extent by physicochemical properties of their surface and their size with larger particles being taken up faster (Moghimi, 1995; Monfardini and Veronese, 1998). The initial stages of phagocytosis involve the physical attachment of the particulate to the surface of the macrophage. An increase in particulate hydrophobicity is known to increase uptake by forming hydrophobic interactions between the particulate and the cell surface (Monfardini and Veronese, 1998), while particles with polar and charged surfaces have an increased circulation time and reduced uptake by RES organs (Gabizon and Papahadjopoulos, 1992). To avoid RES capture, it is, therefore, important to reduce the hydophobicity of the particles; however, it is known that materials with strong positive surface charge bind biological membranes nonspecifically, while those with strong negative charge can be substrates for phagocytosis via the macrophage polyanion receptor (Roser et al., 1998). Hence, it may also be important to avoid significant surface charge of the DNA complexes to prolong blood circulation.

Apart from nonspecific uptake of the particles by RES simply as a result of their physicochemical properties, adsorption of blood components onto particles also plays an important role. The blood contains a large number of proteins and glycoproteins that can function as opsonins (Moghimi, 1995). Rapid binding of one or more of these materials onto the complexes can occur and may have significant influence on the fate of the particulate. The first component adsorbed to the surface of positively charged complexes will probably be albumin, but other materials present in lower concentrations with higher

* To whom correspondence should be addressed. Phone: +44-121-414-3291. Fax: +44-121-414-3263. E-mail: davido@cancer.bham.ac.uk.

† CRC Institute for Cancer Studies.

‡ Institute of Macromolecular Chemistry.

10.1021/bc990143e CCC: $19.00 © 2000 American Chemical Society
Published on Web 06/16/2000

affinities for the surface will displace the first adsorbed layer as a function of time (Davis and Illum, 1988). One of the most successful strategies for obtaining long-circulating nanoparticles and liposomes has been polymer attachment [usually poly(ethylene glycol) (pEG)] at the particle surface, for creating a hydrophilic cloud reducing interactions with proteins and cells (steric stabilization). This so-called stealth technology has been successful in liposomes and nano- and microparticulate drug delivery systems (Lasic, 1997; Monfardini and Veronese, 1998).

The concept of using block or graft copolymers of cationic and hydrophilic nonionic monomers has been introduced by several groups as a new potential way in development of self-assembling polyelectrolyte gene delivery vectors (Katayose and Kataoka, 1997; Toncheva et al., 1998; Wolfert et al., 1996). The aim was to increase the hydrophilic character of the complexes and at the same time introduce a surface hydrophilic layer acting in a similar way as in stealth liposomes. However, in vivo biodistribution studies showed that these complexes are removed very quickly from the murine bloodstream similar to the complexes between DNA and simple polycations (Oupicky et al., 1999a). Unsuitable morphology of the complexes and protein binding at serum protein concentrations were proposed as the major reasons for their rapid removal (Oupicky et al., 1999a). A particular problem with this approach may reflect thermodynamic instability of the complexes resulting from necessary entrapment of hydrophilic chains of the block and graft copolymers within the polyelectrolyte core of the complex. To address this possibility and to examine its effect on the stability of the otherwise-hydrophobic core, in this study, we have allowed simple polyelectrolyte complexes to self-assemble before covalent linkage of the hydrophilic polymer, only to the surface of the polyelectrolyte particle.

Although significant attention is paid to the development of nonviral polyelectrolyte systems for gene delivery, most of the published works concentrate on in vitro study of the properties of the complexes. Relatively little information is available about suitability of these complexes for in vivo use (Chemin et al., 1998; Hashida et al., 1998; Laurent et al., 1999; Ogris et al., 1999). In this work, we therefore report the study of stability of the polyelectrolyte complexes of DNA with poly-L-lysine coated with hydrophilic pHPMA chains in aqueous NaCl solutions and their interaction with albumin. The results of the phagocytic uptake of pLL/DNA complexes by mouse peritoneal macrophages are discussed together with the biodistribution analysis in mice performed in order to obtain more information on the effect of the hydrophilic pHPMA coating on biological properties of complexes.

EXPERIMENTAL PROCEDURES

Materials. A circular 5.2 kb expression vector containing a SV40 promoter-driven luciferase reporter gene and ampicilin resistance was used in most experiments. This was prepared by growth in *Escherichia coli* DH5α and purified using Qiagen columns (Dorkin, U.K.). Following the final ethanol precipitation, the purity of the DNA was checked by agarose gel electrophoresis and 260/280 nm absorption. In the rest of the experiments, calf thymus DNA (ct-DNA) (sodium salt) was used. ct-DNA and poly-L-lysine hydrobromide (pLL) (molecular weight 19 600) were from Sigma Chemical Co. Semitelechelic poly[*N*-(2-hydroxypropyl)methacrylamide]s with carboxylic acid end group were prepared by radical polymerization as described in (Oupicky et al., 1999b).

Formation of pLL/DNA Complexes and Their Coating with poly(HPMA). All complexes in this study were prepared in water at DNA concentration 20 μg/mL (phosphate group concentration 61.5 nmol/mL). pLL was added to DNA solution in a single addition so the N:P ratio was 1.2 (pLL amino group concentration 73.8 nmol/mL). Freshly prepared solution of *N*-hydroxysuccinimidyl ester of carboxylic acid group terminated pHPMA (pHPMA-NHS) in water was then added to the complex solution followed by addition of Hepes buffer (pH 7.8) to reach final concentration 10 mM. The reaction was carried out at room temperature for at least 3 h before any other experiment. Two different molecular weights (number average) of pHPMA (8500 and 5000) and two different concentrations of them were used in the coating reaction (24.6 and 74 nmol/mL).

For the study of the dose effect on in vivo biodistribution, the coated complexes (pHPMA-pLL/DNA) were concentrated on Centricon-100 filters (Millipore). The increase of concentration to 120 μg/mL (determined by UV absorption) was achieved without any significant change in the size of the complexes.

Albumin-Induced Turbidity Assay. The ability of albumin (bovine serum albumin, Sigma) to cause the aggregation of the complexes was examined using a Perkin-Elmer (Buckinghamshire, U.K.) LS50B fluorimeter. The coated or uncoated complexes were both in 10 mM Hepes (pH 7.8). Albumin solution (30 mg/mL) was added stepwise to the complexes and changes in turbidity were monitored. Studies were performed at emission and excitation wavelengths set to the same value of 600 nm.

Polylysine-Induced Aggregation of Coated Complexes. The ability of pLL (19.6 kg/mol) to cause the aggregation of pHPMA-coated pLL/DNA complexes was monitored using commercial light-scattering equipment (Zetasizer, Malvern Instruments, U.K.). To the solution of coated complexes [prepared 24 h before the experiment using two different concentrations of pHPMA(8500)], two different amounts of pLL (final total concentration of pLL 30 and 75 μg/mL, i.e., 144.2 and 361 nmol/mL of pLL amino groups) were added to the solution immediately after an addition of NaCl (final concentration 0.15 M) and the changes in the size of the complexes were monitored.

Heparin Release of DNA. Heparin solution (12 μL, Heparin Sodium, Multiparin, 1000 units/mL; CP Pharmaceuticals Ltd. Wrexham, U.K.) was added to 15 μL of the solution of coated or uncoated complexes and left to incubate for 1 h. The complexes were then analyzed on 0.8% agarose gel (TBE buffer, 0.5 μg/mL ethidium bromide, 90 V, 45 min). To permit also quantitative analysis, DNA was spiked with ^{32}P-radiolabeled DNA as described below. The amount of DNA released was quantified using a Phosphoimager (Molecular Dynamics, Chesham, U.K.).

Transmission Electron Microscopy. The complexes were prepared in water at final DNA concentration of 20 μg/mL. A total of 10 μL of the solution was dispensed onto paraffin, and a piece of freshly cleaved mica (Agar Scientific, Stanstead, U.K.) was placed on top for 2 min. The mica was then removed and placed on a drop of 2% solution of uranyl acetate for a further 2 min. The mica was then washed twice in double-distilled water and allowed to dry before the sample was visualized by rotary shadowing with platinum (5° angle, 6 cm distance, rotation at 60 rpm) in a High Vacuum Coating Unit (Edwards, Crawley, U.K.) The sheet of mica was cut into sections and floated on water to release the sample that

was then picked up using sticky grids (carbon 200 mesh) and allowed to dry. The samples were then viewed using a JEOL 1200 EX Transmission Electron Microscope.

Static Light Scattering (SLS). Static light-scattering measurements were performed with a commercial Fica 40 apparatus in vertically polarized light at wavelength 632.8 nm and temperature 25 °C. The apparatus was calibrated with benzene at 90°. The intensities of scattered light at 45° (I_{45}), 90° (I_{90}), and 135° (I_{135}) have been measured for all the samples studied. Since the concentrations of particles and their refractive increments are not known, the intensity I_{90} normalized with intensity scattered by benzene at 90° is given for a qualitative discussion of results (I_{90} is roughly proportional to the weight-average molecular-weight of particles). Disymmetries I_{45}/I_{135} are used as a qualitative measure of particle sizes (radius of gyration).

Dynamic Light Scattering (DLS). Polarized DLS measurements were made in the angular range 30−135° using a light-scattering apparatus equipped with an He−Ne (632.8 nm) and Ar-ion laser (514.5 nm) and an ALV 5000, multibit, multi-tau autocorrelator covering approximately 10 decades in delay time. Most of the measurements were realized at the scattering angle 90°.

The inverse Laplace transform using the REPES (Jakes, 1995) method of constrained regularization is similar in many respects to the inversion routine CONTIN (Provencher, 1979). However, REPES directly minimizes the sum of the squared differences between the experimental and calculated intensity time correlation functions using nonlinear programming. This method uses an equidistant logarithmic grid with fixed components (here a grid 10 components/decade) and determines their amplitudes. As a result, a distribution function A(τ) of decay times is obtained. From the characteristic decay time, τ [the peak positions of A(τ)], the corresponding apparent average diffusion coefficient, D(90°), was calculated. The apparent average hydrodynamic radius, $R_H{}^a$, was calculated from D(90°) using the Stokes−Einstein equation (viscosity of water at 25 °C 0.894 cP), and the distribution of decay times A(τ) was recalculated on the distribution of hydrodynamic radii A($R_H{}^a$).

The experimental error of radius determination for the complexes was typically about 3%.

Alternatively, for the routine measurements, Malvern Instrument's Zetasizer 1000 system with a 70 mW external laser was used.

In Vitro Association of Complexes with Mouse Macrophages. Adult female BALB/c mice (25 g) were killed by cervical dislocation and injected intraperitoneally, under sterile conditions, with 5 mL of medium *199* containing 20% fetal calf serum (Gibco, Paisley, U.K.). The abdomen was then agitated gently, the peritoneum exposed and breached, and the medium removed using a syringe. The medium was then centrifuged (500*g*, 10 min) and the pellet resuspended in medium *199* containing 50% fetal calf serum. The cell suspension was then plated out into multiwell 6-well plates (480 000 cells/well). The macrophages were allowed to adhere for 2 h before medium (containing nonadherent cells) was removed. Fresh medium containing Amphotericin B (Sigma Chemical Co., Poole, U.K., 2.5 μg/mL), Penicillin, and Streptamycin (Sigma Chemical Co., Poole, U.K., 100 units/mL, 0.1 mg/mL, respectively) was then added to the cells. After 40 h, the cells were used in cellular association studies.

The complexes were formed with YOYO-1 labeled plasmid DNA (one YOYO-1 molecule/300 bp) using the same protocol as described above. Complexes were added at a DNA concentration of 20 μg/mL to plates containing adherent mouse macrophages in 50% *199* media, 50% FCS (75 μL of complexes/well). The complexes were added for various periods of time (0.5−1.5−3 h) after which the cells were removed by standard trypsin treatment, washed, and resuspended in PBS. Association of the complexes with cells was determined by the amount of YOYO-1/DNA detected with a Coulter EPICS XL flow cytometer using an argon ion laser set for excitation 488 nm and emission 520 nm. Cell groups were defined to exclude debris and duplets, and each cell type was gated individually against a negative control of cells without addition of complexes.

Table 1. Characteristics of Coated and Uncoated pLL/DNA Complexes

complex	$I_{90}{}^a$	$I_{45}/I_{135}{}^b$	$R_H{}^a$ (nm)^c
pLL/DNA	29	1.79	46
pHPMA(5500)-pLL/DNA	44	1.77	53
pHPMA(8500)-pLL/DNA	45	1.64	54

[a] Intensity of scattered light at 90° normalized with the intensity scattered by benzene. [b] Ratio of intensities of scattered light at 45 and 135°. [c] Hydrodynamic radius.

Radiolabeling of DNA Expression Vectors. Plasmid DNA was linearized with *Hin*dIII and then radiolabeled with [^{32}P]dCTP using the Ready-to-Go Oligolabeling kit (Pharmacia Biotech, St. Albans, U.K.). Unincorporated nucleotides were removed using MicroSpin columns (Pharmacia Biotech), and the purity of the labeled DNA was checked following agarose gel electrophoresis and quantitative analysis with a PhosphoImager (Molecular Dynamics, Chesham, U.K.).

In Vivo Biodistribution Study. pLL/DNA and pHPMA-pLL/DNA complexes were formed in water 12 h before the experiment using either ct-DNA or plasmid DNA containing a spike of ^{32}P-labeled DNA.

Before injection, glucose was added to a final concentration of 5% (w/v) to ensure iso-osmolarity. Complexes (0.2 mL) were administered via the tail vein to briefly anaesthetized 6-week-old female BALB/c mice. After 30 min, the animals were killed and dissected to permit determination of radioactivity distribution. The blood, lungs, liver, spleen, kidneys, intestines, and carcass (with tails being removed) were isolated, weighed, and dissolved in 10 M sodium hydroxide at 75 °C. Scintillation medium (20 mL) was added to each blood and tissue sample (1 mL) before geometry-corrected analysis of their contained radioactivity in a Packard scintillation counter. A bloodstream volume of 8.64 mL/100 g body weight was assumed (Seymour et al., 1991).

RESULTS

Coating of DNA Complexes and Their Morphology. The complexes were formed using only a slight excess of pLL (N:P ratio 1.2; ζ potential +20 mV) in order to limit the presence of free pLL, which would also react with pHPMA-NHS in the coating reaction. It has been shown that pLL/DNA complexes of this composition contain only a negligible amount of free pLL (Ward et al., 1999). On the other hand, using such a relatively low charge ratio results in complexes that are more susceptible to salt-induced aggregation. The coating reaction was therefore conducted in 10 mM Hepes buffer, pH 7.8. Under these conditions, only negligible aggregation of the complexes was observed during the coating reaction. The characteristics of the pLL/DNA complexes coated with pHPMA-NHS having number-average molecular weight 5500 and 8500, respectively, are given in Table 1. The

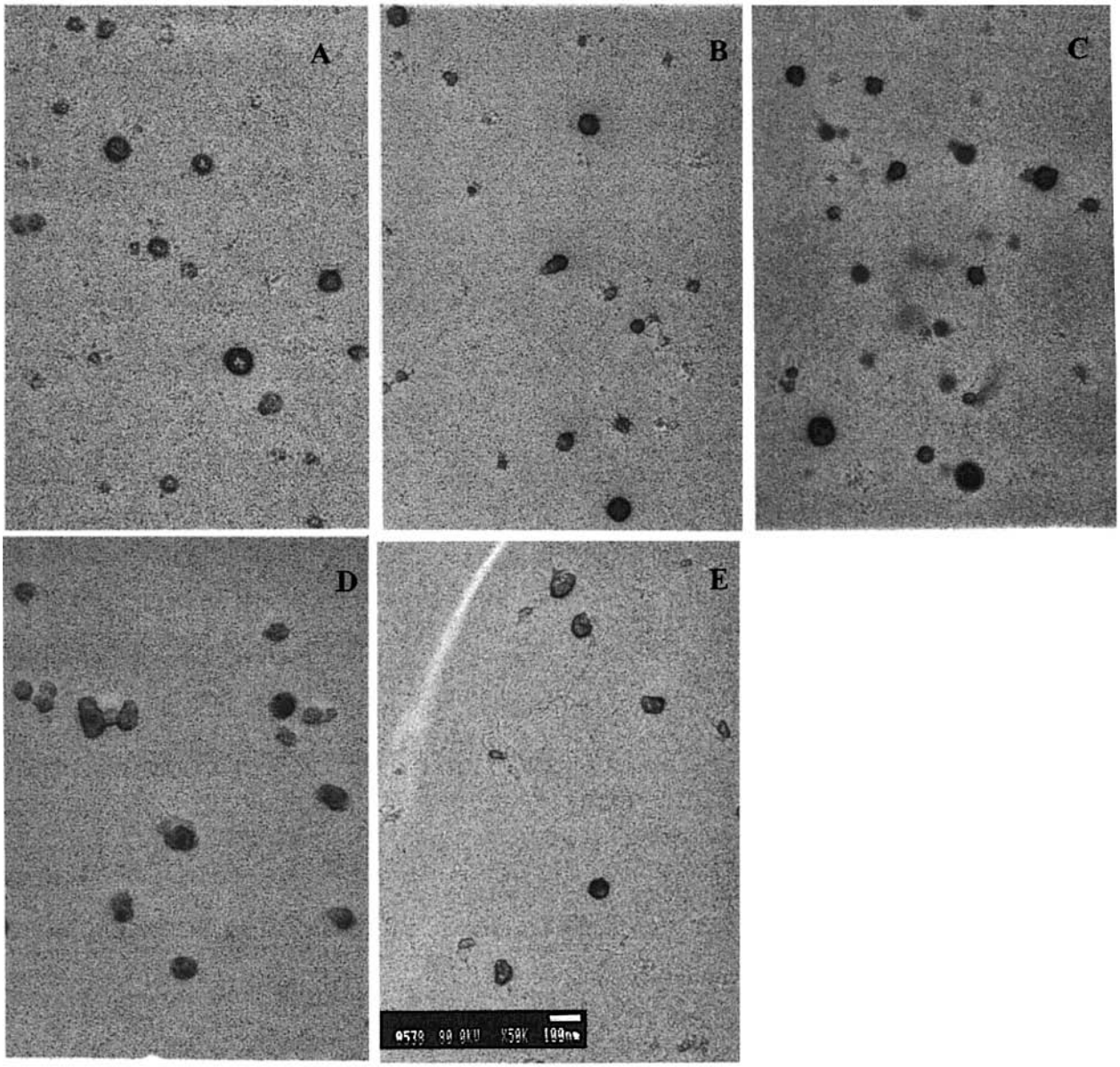

Figure 1. Transmission electron micrographs showing the morphology of plasmid and ct-DNA complexes coated with semitelechelic pHPMA(8500) at two different concentrations. (A) Uncoated pLL/ct-DNA; (B) pHPMA-pLL/ct-DNA (24.6 nmol/mL pHPMA-NHS); (C) pHPMA-pLL/ct-DNA (74 nmol/mL pHPMA-NHS); (D) pHPMA-pLL/plasmid DNA (24.6 nmol/mL pHPMA-NHS); (E) pHPMA-pLL/plasmid DNA (74 nmol/mL pHPMA-NHS); (50000× magnification).

coating slightly increased the hydrodynamic radius of complexes (1.17 times), and the scattered intensity (I_{90}) (proportional to molecular weight of particles) was also correspondingly increased (1.55 times). This increase shows that the molecular weight of pLL/DNA complexes is roughly proportional to $R_H^{2.7}$ of the complexes which is close to the model of solid spheres (exponent 3). Incubation of pLL/DNA complexes with pHPMA containing a nonreactive carboxylic acid end group did not cause any change in their size or molecular weight, confirming that the observed changes of particle parameters (Table 1) indicate covalent attachment of pHPMA-NHS to the pLL/DNA complexes. The covalent attachment of pHPMA-NHS was confirmed also by the decrease of amino group content [determined by TNBSA assay (Snyder and Sobocinski, 1975)] in pLL/DNA complexes after their coating with pHPMA-NHS. The data in Table 1 also demonstrate higher sensitivity of static light scattering methods compare to DLS and shows its importance in the study of these high-molecular-weight systems.

The idea of modifying pLL/DNA complexes with semitelechelic pHPMA-NHS assumes binding of the polymer to the surface of the complexes with little or no disturbance of the actual pLL/DNA complexes. However, the coating (especially when using high excess of coating polymer) may induce undesired changes in the morphology of the complexes. Figure 1 shows TEM pictures of pLL/DNA before and after coating with two different amounts of pHPMA(8500)-NHS. In no case was there a sign of any change in the morphology of the complexes. The complexes retained their spherical shape and also their diameter of about 100 nm.

Stability of Complexes in Salt. A combination of static and dynamic light scattering techniques was also used to examine the stability of complexes in 0.15 M NaCl. Table 2 shows the results of the stability measurements. The uncoated pLL/DNA complexes precipitated very fast, forming large aggregates almost immediately after the addition of NaCl, while the coated complexes were stable for at least 24 h. The scattered intensity I_{90}

Table 2. Effect of NaCl on Characteristics of Uncoated and Coated pLL/DNA Complexes[a]

complex	I_{90}[b]	I_{45}/I_{135}[c]	R_H[a] (nm)[d]
pLL/DNA	29	1.79	46
after 2 h			827
pHPMA(5500)-pLL/DNA	44	1.77	53
After 2 h	44	1.79	53
After 5.5 h	46	1.76	55
After 24 h	47	1.76	55
pHPMA(8500)-pLL/DNA	45	1.64	54
after 2 h	45	1.57	53
after 5.5 h	47	1.56	58
after 24 h	47	1.60	57

[a] Complexes were formed in water and coated in 10 mM Hepes (pH 7.8). NaCl was added after 12 h (final concentration 0.15 M). Changes of size and scattering intensities were measured 2, 5.5, and 24 h after NaCl addition. [b] Intensity of scattered light at 90 normalized with the intensity scattered by benzene. [c] Ratio of intensities of scattered light at 45 and 135°. [d] Hydrodynamic radius.

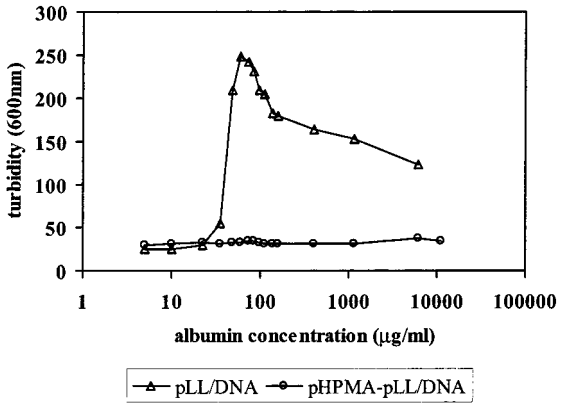

Figure 2. Albumin induced turbidity in the solution of pLL/ct-DNA complexes coated with pHPMA(8500) at the concentration 24.6 nmol/mL. Albumin solution (30 mg/mL) was added stepwise to the complexes and changes in turbidity were monitored at 600 nm.

of the coated complexes increased only by a few percent showing practically negligible aggregation. Neither types of parameters used for characterization of size of the complexes showed any significant change. This observation not only suggests the absence of aggregation but also indicates that no change in morphology of the complexes was induced at this stage (Provencher, 1979).

Interaction of Complexes with Albumin. The addition of albumin to pLL/DNA complexes in water results in significant turbidity that may be utilized as a convenient and simple measure of the stability of the complexes toward albumin interaction. Figure 2 compares pLL/DNA and pHPMA-pLL/DNA in this assay. While the addition of low concentration of albumin (<100 μg/mL) caused significant aggregation in uncoated complexes, in the case of coated complexes, no turbidity was observed up to 11 mg/mL of albumin. This shows that the presence of pHPMA stabilizes the complexes against albumin induced aggregation. However, the observed lack of increased turbidity of the coated complexes does not directly imply that albumin does not interact with the complexes. If albumin were simply to adsorb to the surfaces of the complexes, no aggregation would be observed, but it still could have an important effect on in vivo properties of the complexes.

Light-scattering techniques can contribute to better evaluating the effect of albumin on the DNA complexes. Table 3 demonstrates the effect of an addition of albumin (1 mg/mL) on characteristics of uncoated and coated

Table 3. Effect of Albumin and NaCl on Characteristics of Coated and Uncoated pLL/DNA Complexes[a]

complex	I_{90}[b]	I_{45}/I_{135}[c]	R_H[a] (nm)[d]
pLL/DNA	29	1.79	46
+albumin	86	1.69	53
+albumin + NaCl	327	5.1	199
pHPMA(5500)-pLL/DNA	44	1.77	53
+albumin	56	1.73	55
+albumin + NaCl	74	3.5	61
pHPMA(8500)-pLL/DNA	45	1.64	54
+albumin	58	1.54	53
+albumin + NaCl	60	1.65	57

[a] Complexes were formed in water and coated in 10 mM Hepes (pH 7.8). After 12 h, albumin was added (final concentration 1 mg/mL). Then NaCl (final concentration 0.15 M) was added to the solution of the complexes and albumin and changes of size and scattering intensities were measured. [b] Intensity of scattered light at 90° normalized with the intensity scattered by benzene. [c] Ratio of intensities of scattered light at 45 and 135°. [d] Hydrodynamic radius.

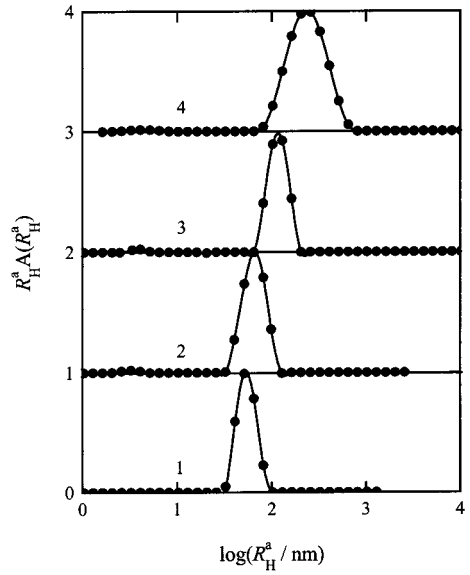

Figure 3. Effect of albumin and NaCl on distribution of hydrodynamic radii A(R_H^a) of uncoated pLL/DNA complexes: (1) complexes in water, (2) 0.3 h after addition of albumin (1 mg/mL), (3) 24 h after addition of albumin, (4) 5 h after addition of NaCl (0.15 M) to albumin containing solution of complexes.

complexes. The normalized intensity of scattered light I_{90} from the solution of complexes is again used instead of customary molecular weights because the concentration of albumin possibly incorporated into DNA complexes is unknown. Comparing the data in Tables 1 and 3, it can be seen that I_{90} increases several times and also the corresponding particle hydrodynamic radii increase accordingly in the case of uncoated pLL/DNA complexes. The average hydrodynamic radius of the uncoated complexes in the presence of 1 mg/mL of albumin increased by about 8 nm compared with the original complex (Table 3), but I_{90} increased almost 3 times, suggesting a large increase in molecular weight of the complexes due to their interaction with albumin. Dynamic light scattering offers also a possibility of determining directly the distribution of hydrodynamic radii of the complexes, which is more complex information than average values. The effect of albumin on the distribution of hydrodynamic radii of the uncoated complexes is given in Figure 3. An addition of albumin causes a shift of whole radii distribution to higher R_H^a values. We assume that the shift of the size distribution is caused predominantly by albumin binding on the surface of the complexes. NaCl addition results

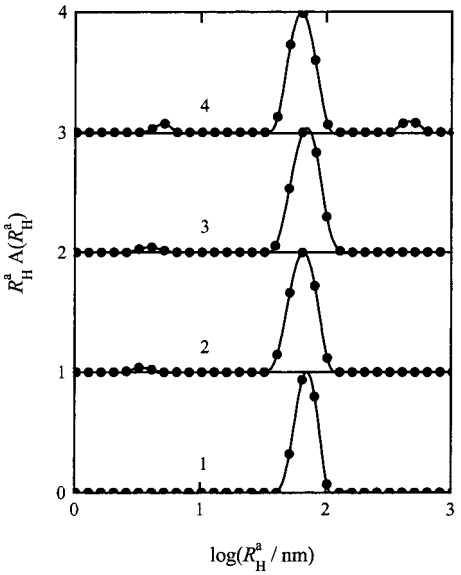

Figure 4. Effect of albumin and NaCl on distribution of hydrodynamic radii A(R_H^a) of coated pHPMA(8500)-pLL/DNA complexes (24.6 nmol/mL pHPMA(8500)-NHS): (1) complexes in distilled water; (2) 0.3 h after addition of albumin (1 mg/mL); (3) 24 h after addition of albumin, (4) 5 h after addition of NaCl (0.15 M) to albumin containing solution of complexes.

in aggregation of particles, which reflects in a shift of radii distribution to higher values and broadening of distribution. The presence of free albumin molecules can be identified with a small peak on A(R_H^a) at low R_H^a values.

Only a minor increase in the scattering intensity and size of the complexes was observed after albumin addition to the solution of coated complexes (Table 3 and Figure 4). The scattering intensity and sizes of the complexes were further increased when NaCl was added to the solution of complexes in the presence of albumin. However, whereas a marked increase was observed for the uncoated complexes, complexes coated with pHPMA(8500) show only minor changes.

A small aggregation effect was observed, particularly in the presence of both albumin and NaCl, in the solution of the complexes coated with pHPMA(5500) demonstrated by an increase of both the intensity and hydrodynamic radius in Table 3. The hydrodynamic radius of complexes coated with pHPMA(8500) exhibited a noticeably lower dependence on the albumin (1 mg/mL) and NaCl addition (Figure 4). Only small amount of aggregates could be detected after NaCl addition at high values of R_h^a (a small peak at high R_h^a values). Also the increase of I_{90} was significantly lower than in case of pHPMA(5500)-pLL/DNA. Thus, the pHPMA(8500)-pLL/DNA complexes were chosen for further study as they appear to be more stable than these coated with pHPMA(5500).

Exchange Reaction between the Complexes, Heparin, and pLL. The effect of polymer coating on the stability of the complexes against polyelectrolyte exchange reactions was studied in two systems. The ability of DNA to be released from complexes was studied by incubation of the complexes with heparin and the ability of pLL or pLL grafted with pHPMA to be replaced by competing polycation was studied by incubation with pLL of the same molecular weight.

The ability of the polyanion heparin sulfate to release plasmid DNA from its complexes with pLL was tested by monitoring appearance of free DNA by agarose gel

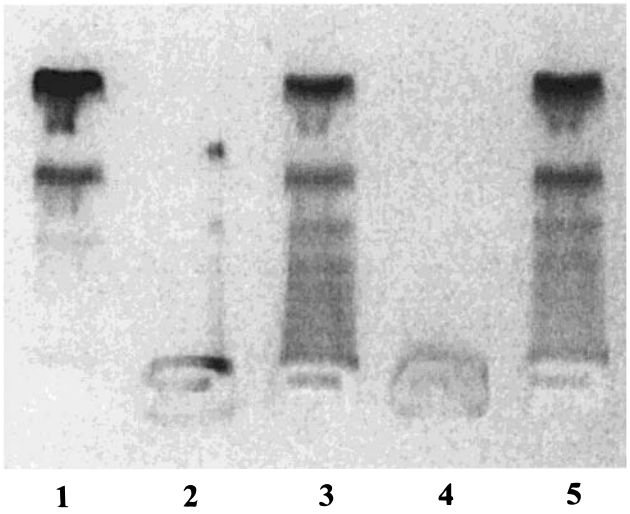

Figure 5. Agarose gel electrophoresis (0.8% gel; 0.5 μg/mL ethidium bromide) of pLL/plasmid DNA and pHPMA(8500)-pLL/plasmid DNA complexes incubated with heparin. Lane 1, free DNA; lane 2, pLL/DNA complexes; lane 3, pLL/DNA + heparin; lane 4, pHPMA-pLL/DNA; lane 5, pHPMA-pLL/DNA + heparin.

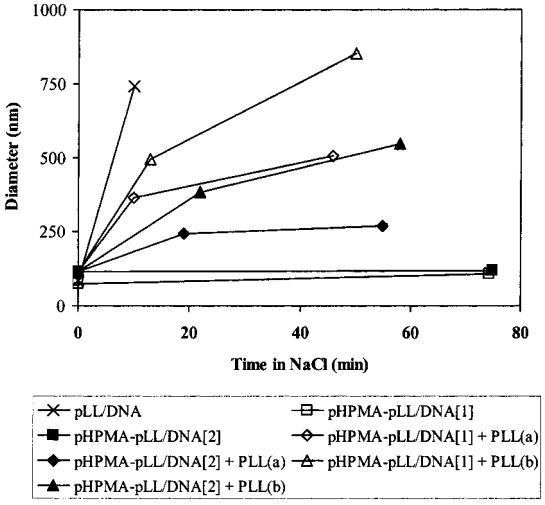

Figure 6. Aggregation of pLL/ct-DNA and pHPMA-pLL/ct-DNA complexes induced by an addition of pLL. pLL/DNA complexes were coated with pHPMA(8500) at two concentrations: 24.6 nmol/mL (pHPMA-pLL/DNA[1]) and 74 nmol/mL (pHPMA-pLL/DNA[2]). The coating reaction was left to proceed overnight. Then to the solution of the coated complexes NaCl was added (final concentration 0.15 M) followed by the addition of pLL—final concentration of pLL including pLL already present in the complexes—35 μg/mL pLL(a); 70 μg/mL pLL(b).

electrophoresis. Figure 5 shows that heparin was able to release free DNA in both cases studied, i.e., in case of both uncoated and pHPMA-coated pLL/DNA complexes. Ethidium bromide staining did not allow quantification of the amounts of DNA released in the two cases. To accomplish the quantitative analysis of DNA released, the DNA was spiked with ^{32}P-labeled plasmid DNA and the gel was analyzed with PhosphoImager. The analysis revealed that 83% of DNA was released from the uncoated complexes. Under the same experimental conditions, 97% of DNA was released from the coated complexes.

Addition of pLL to the coated complexes in the presence of 0.15 M NaCl resulted in immediate aggregation (Figure 6), although the coated complexes manifested very good stability against aggregation in salt (Table 2). The rate of the observed aggregation was found to be

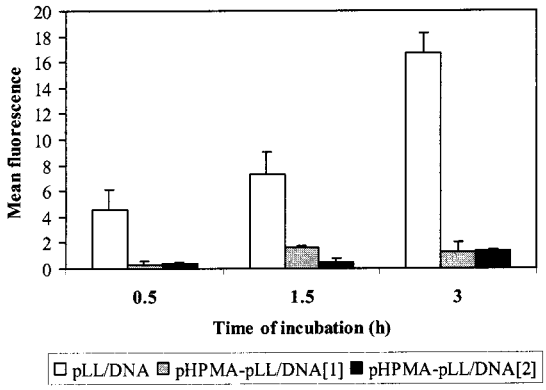

Figure 7. Cellular association of pLL/plasmid DNA complexes coated with pHPMA(8500) with murine peritoneal macrophages after incubation in 50% fetal calf serum. The increase in the mean fluorescence of the cells, assessed by flow cytometric analysis, was used as the measure of cellular association. The pLL/DNA complexes were coated at 24.6 and 74 nmol/mL of pHPMA(8500) (mean ± sd; $n = 3$).

dependent on the amount of pHPMA(8500) used for the coating and the concentration of free pLL added to the coated complexes (Figure 6). In this assay, the most stable complexes were those coated with higher concentration of pHPMA and the aggregation was also more rapid in the presence of higher concentrations of pLL.

In Vitro Association of the Complexes with Macrophages. Mouse peritoneal macrophages were used as an in vitro model for the study of the effect of pHPMA(8500) coating on the association with phagocytic cells.

Cell association of YOYO-1 labeled complexes was monitored using primary cultures of mouse peritoneal macrophages incubated in 50% fetal calf serum (Figure 7). Two concentrations of pHPMA(8500) were used for the coating; however, no obvious effect was observed. Analysis by FACS showed a significant decrease in complex association (~10 times) for both types of coated complexes in the whole time course of the study.

In Vivo Biodistribution of the Complexes. Reduced macrophage uptake in vitro encouraged further investigation of the coated complexes in vivo as it might be expected they show prolonged circulation times in the blood. The body distribution of the coated and uncoated pLL/DNA complexes containing ^{32}P-radiolabeled DNA was determined following intravenous injection into BALB/c mice using both plasmid and ct-DNA.

pLL/ct-DNA complexes were cleared rapidly from the bloodstream showing less than 10% of radioactivity in the blood after 30 min (Figure 8). Coating of these complexes with pHPMA(8500) resulted in even lower amount of radioactivity found in the blood (~3%). In both cases, there was some deposition in the carcass (~15%) and spleen (~10%), but the majority of radioactivity (over 60% of the recovered dose) was found in the liver. The coating of the complexes promoted even higher uptake by the liver, and consequently, reduced levels of radioactivity were found in all the organs isolated.

A similar experiment with plasmid DNA complexes (Figure 9) showed significantly higher levels of uncoated complexes remaining in the blood after 30 min (24.9 ± 4.1%). Coating of these complexes led again to a drop of the level of radioactivity in the blood to the levels similar to those found for coated ct-DNA complexes. The coating of the complexes led also to an increase in the liver uptake compared to uncoated complexes. Increasing the injected dose from 4 to 24 μg of DNA (using concentrated

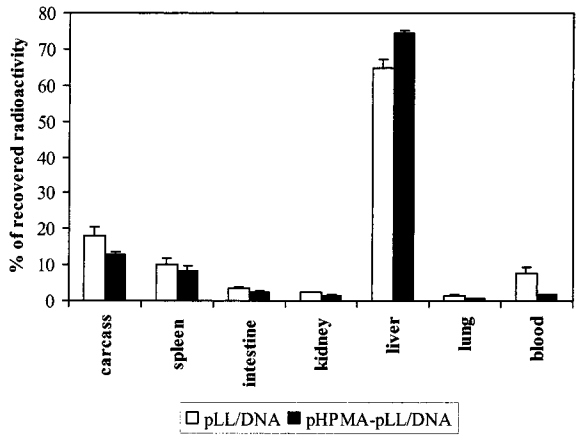

Figure 8. Body distribution of radioactivity determined in mice 30 min following intravenous injection of pLL/ct-DNA and pHPMA-pLL/ct-DNA [pHPMA(8500), 24.6 nmol/mL] coated complexes containing ^{32}P-labeled DNA. The complexes were administered at a dose of 4 μg of DNA/mouse in 5% glucose into the tail vein (mean ± sd; $n = 3$).

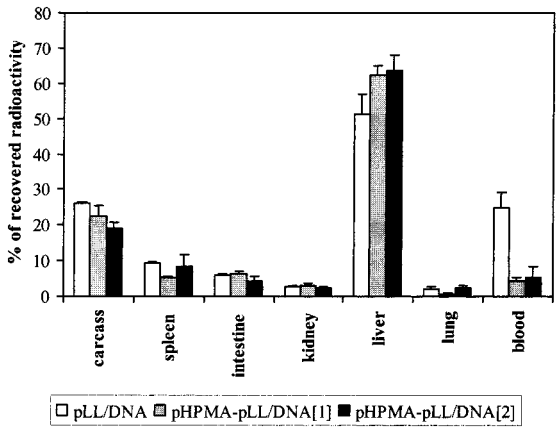

Figure 9. Body distribution of radioactivity determined in mice 30 min following intravenous injection of pLL/plasmid DNA or pHPMA-pLL/plasmid DNA [pHPMA(8500), 24.6 nmol/mL] coated complexes containing ^{32}P-labeled DNA. The complexes were administered at a dose of 4 μg of DNA (pLL/DNA and pHPMA-pLL/DNA[1]) or 24 μg of DNA (pHPMA-pLL/DNA[2])/mouse in 5% glucose into the tail vein (mean ± sd; $n = 3$).

coated complexes) had no significant effect on the levels of radioactivity found in the blood or the biodistribution pattern.

DISCUSSION

In this study, we have examined properties of pLL/DNA complexes coated with semitelechelic hydrophilic polymer pHPMA. pHPMA is known to be a nontoxic and nonimmunogenic polymer that was previously used in the field of drug delivery as a carrier of low-molecular-weight drugs (Duncan and Ulbrich, 1993), for surface modification of proteins (Oupicky et al., 1999c) and also in combination with cationic polymers for the formation of DNA complexes (Oupicky et al., 1999b). The properties of this polymer are in many ways similar to those of pEG. However, it has significant advantages in terms of its structural versatility enabling easy incorporation of various functionalities.

pLL/DNA complexes are usually prepared in water because of their tendency to aggregate in salt solutions. Several possible means of increasing stability of these complexes in salt solutions have been reported so far. Among them, using block and graft copolymers with

hydrophilic nonionic polymers found widespread use (Kabanov and Kabanov, 1995; Katayose and Kataoka, 1997; Seymour et al., 1998; Wolfert et al., 1996).

Another way of increasing their stability, known in colloid science as a steric stabilization, is to provide the complexes with a surface polymer layer. Such a layer can significantly affect interparticle forces; first, it can influence van der Waals attractive forces, and second, it can give rise to repulsion between the particles. The magnitude of repulsion arising from the presence of the adsorbed layer clearly depends on the density with which it covers the surface; the more thinly it is spread, the smaller its effectiveness in preventing the particles from approaching one another (Everett, 1988). The concept of steric stabilization has been exploited in the field of drug delivery as a way of preventing the particles from aggregation but also as a way of reducing their interactions with opsonins and components of RES which effectively increased circulation times of these particles (Davis and Illum, 1988). A similar approach has been reported only recently also for DNA complexes. It was reported that surface modification of DNA/polyethyleneimine complexes with pEG (5000 g/mol) results in an increased level of the complexes found in plasma 30 min after injection (~30% of the injected dose) (Ogris et al., 1999).

The coating reaction with succinimidyl reactive esters of pHPMA requires the presence of free amino groups accessible on the surface of the complexes. pLL/DNA complexes of the composition used in this study were already shown to bear surface positive charge (Wolfert et al., 1996). The presence of free amino groups suitable for reaction with acylating agents was also demonstrated by fluorescamine assay (Read et al., 1999).

The coating reaction proceeded under mild conditions leaving the complexes with slightly increased size and molecular weight due to the covalent binding of pHPMA. The morphology of the complexes was not changed as judged by TEM, and the complexes were still of roughly spherical shape.

Testing the stability of the coated complexes in salt showed steric stabilization using pHPMA of both molecular weights (5500 and 8500) and also using pHPMA(8500) at two different concentrations. The coating polymer reduced hydrophobic character of pLL/DNA complexes as demonstrated by their increased solubility in salts and also by successful preparation of concentrated solutions (containing 120 μg/mL DNA). DNA complexes designed for use as in vivo gene delivery systems should be stable in the body fluids, especially in the blood. We have studied the interaction of the complexes with serum albumin as a model serum protein. This can provide a useful indication of the changes in the properties of the complexes achieved by their modification with pHPMA. Studying the interaction with albumin can be important as it is likely that albumin is temporally the first component of blood binding similar particulate systems (Davis and Illum, 1988).

Albumin is able to bind to the pLL/DNA complexes forming ternary complexes (Dash et al., 1999). At a certain ratio, the ternary complexes are hydrophobic and excessive aggregation could be observed. The albumin-induced turbidity assay showed that coating the pLL/DNA complexes with pHPMA(8500) prevented albumin from causing such an aggregation of the complexes. More sensitive analysis of the interaction of the complexes with albumin (1 mg/mL) by static light scattering demonstrated similar results for uncoated pLL/DNA complexes, but also showed an increase in molecular weight of the coated complexes after incubation with albumin despite no simultaneous significant increase in their size. This result suggests that albumin can probably still bind to the coated complexes, although the binding is significantly reduced. Comparison of pHPMA with two different molecular weights showed that the higher molecular weight analogue is more effective in stabilization of the complexes against interaction with albumin especially in the presence of NaCl. Albumin was able to reduce the aggregation of pLL/DNA complexes, acting as a surface stabilizer (compare Tables 2 and 3). This suggests that although the uncoated pLL/DNA complexes showed only a low stability in salt solution or in low concentrations of albumin, their size could be well stabilized in the presence of much higher concentrations of proteins in the blood plasma.

Coating of the complexes with pHPMA may affect the release of free DNA in two ways. It might stabilize the complexes by preventing heparin from coming into a contact with pLL/DNA part of the coated complexes. However, study of the effects of the coating on polyelectrolyte exchange reactions showed that the surface polymer layer of pHPMA did not stabilize the complexes against replacing of DNA from the complexes. Moreover, quantitative analysis suggested that the coated complexes are even more susceptible to the exchange reaction with heparin than uncoated ones.

Studying similar type of exchange reaction using pLL added to the solution of the coated complexes, we have observed fast aggregation of the coated complexes in salt solution. The most likely explanation for the observed type of behavior is the exchange reaction of the added free pLL with surface pLL molecules of the complex grafted with pHPMA. As a result, complexes similar to uncoated pLL/DNA complexes are formed. The pHPMA grafted on pLL located on the surface of the complexes during coating reaction provided the complexes with increased stability against aggregation in salt but these grafted pLL molecules could be apparently replaced by competing pLL, demonstrating equilibrium nature of the polyelectrolyte complexes and also their tendency to precipitation, which is the preferred state of the complexes. These results show that while pHPMA is very effective in preventing the particles from aggregation, it cannot effectively block the access of single molecules (like heparin or pLL) to the core of the complexes as manifested by the ease of the exchange reactions.

To address the possibility that the coated complexes may be able to evade phagocytic capture, in vitro model representing phagocytic components of the RES was employed, in the form of mouse peritoneal macrophages. The substantial levels of cell-association shown by pLL/DNA complexes may reflect their net positive surface charge, promoting nonspecific association with cells and membranes as well as their hydrophobic nature and easy binding of various proteins that can promote the uptake. The particulate nature of pLL/DNA complexes may also promote physical attachment and subsequent phagocytosis. Coated complexes showed significantly decreased levels of capture possibly due to their higher hydrophilicity manifested by increased stability against salt induced precipitation. This may inhibit complex-cell attachment leading to a decrease in cell capture. Coating of the complexes by pHPMA may also create a physical barrier between the complex and cell surface resulting in steric hindrance analogous to stealth technology (Lasic et al., 1991) leading to reduced uptake.

In attempting to design systems capable of better pharmacokinetics, we have examined the biodistribution

of the pHPMA-coated and uncoated pLL/DNA complexes. There are several possible mechanisms that might contribute to the rapid blood clearance of pLL/DNA complexes, including rapid degradation by nucleases, activation of complement, opsonisation, and phagocytosis or filtering by capillary beds. However, it has been shown previously that DNA in the polyelectrolyte complexes is not degraded by nucleases and also no complement activation was observed for pLL/DNA complexes. Binding of plasma proteins was proposed as the most likely reason for the fast removal of pLL/DNA complexes from the blood (Dash et al., 1999). The injected complexes quickly bind albumin and other plasma proteins, forming an extended ternary complex with a net negative surface charge. This ternary complex still resists immediate degradation by serum nucleases but may promote phagocytic capture, particularly by Kupffer cells. We have shown in this study that complexes coated with semitelechelic pHPMA have demonstrated certain improved properties (increased stability in salt, against albumin induced aggregation, decreased albumin binding, and reduced phagocytic uptake) but these complexes have not, however, showed any prolongation in the circulatory times (Figures 6 and 7). On the contrary, in both cases studied (plasmid and ct-DNA), the polymer-coated complexes showed even lower levels in the blood after 30 min postinjection. The most remarkable difference was observed in case of plasmid pLL/DNA complexes—decrease from 25% (uncoated) to 3% (pHPMA-coated) of the complexes found in the blood after 30 min. The high level of plasmid pLL/DNA complexes found in the blood compare to ct-DNA complexes is a surprising finding and the reasons for such a difference are currently under investigation.

Despite all the improvements of properties of the complexes observed in in vitro experiments their in vivo behavior has not improved correspondingly. This suggests that the in vivo fate of the complexes may be significantly influenced by factors not reflected in the in vitro cell culture model. Among them high concentrations and wide variety of proteins and other molecules in plasma, together with contact with cell surfaces and enormous shear stress in the blood circulation may play an important role.

We propose that the equilibrium nature of the coated pLL/DNA complexes (manifested in the polyelectrolyte exchange reactions) might be one of the main reasons for their fast removal from the blood. The morphology of the coated complexes can be changed, as the pLL molecules grafted with pHPMA may be removed from the complexes quickly following entry serum leaving the complexes unprotected. An alternative explanation is conceivable, namely that higher doses [closer to the doses used in other particulate drug delivery systems (Oja et al., 1996)] are necessary in in vivo experiments to at least partly saturate RES.

There are several possible approaches to further stabilizing pLL/DNA complexes against polyelectrolyte exchange reactions. Several are being currently developed in our laboratories including enshrouding the complex with multifunctional hydrophilic polymer crosslinking the surface of the complexes (Dash et al., 2000).

ACKNOWLEDGMENT

The support of the EU by Grant ERBIC20CT97005 and of the Grant Agency of the Czech Republic by Grant 307/96/K226 is gratefully acknowledged.

LITERATURE CITED

(1) Bazile, D. V., Ropert, C., Huve, P., Verrecchia, T., Marland, M., Frydman, A., Veillard, M., and Spenlehauer, G. (1992) Body distribution of fully biodegradable [14C]-poly(lactic acid) nanoparticles coated with albumin after parenteral administration to rats. *Biomaterials 13*, 1093−1102.

(2) Chemin, I., Moradpour, D., Wieland, S., Offensperger, W.-B., Walter, E., Behr, J.-P., and Blum, H. E. (1998) Liver-directed gene transfer: a linear polyethylenimine derivative mediates highly efficient DNA delivery to primary hepatocytes in vitro and in vivo. *J. Viral Hepatitis 5*, 369−375.

(3) Dash, P. R., Read, M. L., Barrett, L. B., Wolfert, M. A., and Seymour, L. W. (1999) Factors affecting blood clearance and in vivo distribution of polyelectrolyte complexes for gene delivery. *Gene Ther. 6*, 643−650.

(4) Dash, P. R., Read, M. L., Fisher, K., Howard, K. A., Wolfert, M., Oupicky, D., Subr, V., Strohalm, J., Ulbrich, K., and Seymour, L. W. (2000) Decreased Binding to Proteins and Cells of Polymeric Gene Delivery Vectors Surface-Modified with a Multivalent Hydrophilic Polymer. *J. Biol. Chem. 275*, 3793−3802.

(5) Davis, S. S., and Illum, L. (1988) Polymeric microspheres as drug carriers. *Biomaterials 9*, 111−115.

(6) Duncan, R., and Ulbrich, K. (1993) Development of N−(2-hydroxypropyl)methacrylamide copolymer conjugates for delivery of cancer chemotherapy. *Macromol. Chem., Macromol. Symp. 70/71*, 157−162.

(7) Everett, D. H. (1988) *Basic Principles of Colloid Science*, The Royal Society of Chemistry, London.

(8) Gabizon, A., and Papahadjopoulos, D. (1992) The role of surface charge and hydrophilic groups on liposome clearance in vitro. *Biochim. Biophys. Acta 1103*, 94−100.

(9) Hashida, M., Takemura, S., Nishikawa, M., and Takakura, Y. (1998) Targeted delivery of plasmid DNA complexed with galactosylated poly(L-lysine). *J. Controlled Release 53*, 301−310.

(10) Illum, L., Jacobsen, L. O., Muller, R. H., Mak, E., and Davis, S. S. (1987) Surface characteristics and the interaction of colloidal particles with mouse peritoneal macrophages. *Biomaterials 8*, 113−117.

(11) Jakes, J. (1995) Regularized positive exponential sum (REPES) program—A way of inverting laplace transform data obtained by dynamic light scattering. *Collect. Czech. Chem. Commun. 60*, 1781−1797.

(12) Kabanov, A. V., and Kabanov, V. A. (1995) DNA Complexes with Polycations for the Delivery of Genetic Material into Cells. *Bioconjugate Chem. 6*, 7−20.

(13) Katayose, S., and Kataoka, K. (1997) Water-soluble polyion complex associates of DNA and poly(ethylene glycol)-poly(L-lysine) block copolymer. *Bioconjugate Chem. 8*, 702−707.

(14) Lasic, D. D. (1997) Recent developments in medical applications of liposomes: sterically stabilized liposomes in cancer therapy and gene delivery in vivo. *J. Controlled Release 48*, 203−222.

(15) Lasic, D. D., and Needham, D. (1995) The "stealth" liposome: A prototypical biomaterial. *Chem. Rev. 95*, 2601−2628.

(16) Lasic, D. D., Martin, F. J., Gabizon, A., Huang, S. K., and Papahadjopoulos, D. (1991) Sterically stabilized liposomes: a hypothesis on the molecular origin of the extended circulation times. *Biochim. Biophys. Acta 1070*, 187−192.

(17) Laurent, N., Wattiaux-De Coninck, S., Mihaylova, E., Leontieva, E., Warnier-Pirotte, M.-T., Wattiaux, R., and Jadot, M. (1999) Uptake by rat liver and intracellular fate of plasmid DNA complexed with poly-L-lysine or poly-D-lysine. *FEBS Lett. 443*, 61−65.

(18) Moghimi, S. M. (1995) Mechanisms regulating body distribution of nanospheres conditioned with pluronic and tetronic block copolymers. *Adv. Drug Delivery Rev. 16*, 183−193.

(19) Monfardini, C., and Veronese, F. M. (1998) Stabilization of substances in circulation. *Bioconjugate Chem. 9*, 418−450.

(20) Ogris, M., Brunner, S., Schuller, S., Kircheis, R., and Wagner, E. (1999) PEGylated DNA/transferrin-PEI complexes: reduced interaction with blood components, extended

circulation in blood and potential for systemic gene delivery. *Gene Ther. 6*, 595−605.
(21) Oja, C. D., Semple, S. C., Chonn, A., and Cullis, P. R. (1996) Influence of dose on liposome clearance: critical role of blood proteins. *Biochim. Biophys. Acta 1281*, 31−37.
(22) Oupicky, D., Konak, C., Dash, P. R., Seymour, L. W., and Ulbrich, K. (1999a) Effect of albumin and polyanion on the structure of DNA complexes with polycation containing hydrophilic nonionic block. *Bioconjugate Chem. 10*, 764−772.
(23) Oupicky, D., Konak, C., and Ulbrich, K. (1999b) DNA Complexes with Block and Graft Copolymers of N-(2-Hydroxypropyl)methacrylamide and 2-(Trimethylammonio)ethyl methacrylate. *J. Biomater. Sci., Polym. Ed. 10*, 573−590.
(24) Oupicky, D., Ulbrich, K., and Rihova, B. (1999c) Conjugates of Semitelechelic Poly[N−(2-hydroxypropyl)methacrylamide] with enzymes for Protein Delivery. *J. Bioact. Compat. Polym. 14*, 213−231.
(25) Provencher, S. W. (1979) *Makromol. Chem. 180*, 201.
(26) Read, M. L., Etrych, T., Ulbrich, K., and Seymour, L. W. (1999) Characterisation of the binding interaction between poly(L-lysine) and DNA using the fluorescamine assay in the formation of nonviral gene delivery vectors. *FEBS Lett. 461*, 96−100.
(27) Roser, M., Fischer, D., and Kissel, T. (1998) Surface-modified biodegradable albumin nano- and microspheres. II: effect of surface charge on in vivo phagocytosis and biodistribution in rats. *Eur. J. Pharm. Biopharm. 46*, 255−263.
(28) Seymour, L. W., Kataoka, K., and Kabanov, A. V. (1998) Cationic block copolymers as self-assembling vectors for gene delivery. In *Self-assembling Complexes for Gene Delivery: From Laboratory to Clinical Trials* (Kabanov, A. V., Felgner, P. L., and Seymour, L. W., Eds.) pp 219−239, John Wiley and Sons, New York.
(29) Seymour, L. W., Ulbrich, K., Wedge, S. R., Hume, I. C., Strohalm, J., and Duncan, R. (1991) N-(2-hydroxypropyl)-methacrylamide copolymers targeted to the hepatocyte galactose receptor: pharmacokinetics in DBA2 mice. *Brit. J. Cancer 63*, 859−866.
(30) Snyder, S. L., and Sobocinski, P. Z. (1975) An improved 2,4,6-trinitrobenzenesulfonic acid method for the determination of amines. *Anal. Biochem. 64*, 284−288.
(31) Toncheva, V., Wolfert, M. A., Dash, P. R., Oupicky, D., Ulbrich, K., Seymour, L. W., and Schacht, E. H. (1998) Novel vectors for gene delivery formed by self-assembly of DNA with poly(L-lysine) grafted with hydrophilic polymers. *Biochim. Biophys. Acta 1380*, 354−368.
(32) Ward, C. M., Fisher, K. D., and Seymour, L. W. (1999) A sensitive assay system for the determination of poly(L-lysine) concentration using turbidometry. *J. Bioact. Compat. Polym. 14*, 122−136.
(33) Wolfert, M. A., Schacht, E. H., Toncheva, V., Ulbrich, K., Nazarova, O., and Seymour, L. W. (1996) Characterization of vectors for gene therapy formed by self-assembly of DNA with synthetic block copolymers. *Hum. Gene Ther. 7*, 2123-2133.

BC990143E

Transglutaminase-Mediated Dual and Site-Specific Incorporation of Poly(ethylene glycol) Derivatives into a Chimeric Interleukin-2

Haruya Sato,* Keiji Yamamoto, Eiko Hayashi, and Yoshiyuki Takahara

Ajinomoto Company Inc., Central Research Laboratories, 1-1 Suzuki-cho, Kawasaki-ku, Kawasaki-shi, 210-8681, Japan. Received October 28, 1999; Revised Manuscript Received February 24, 2000

To expand the applications of poly(ethylene glycol) (PEG)−protein conjugates for clinical use, we have developed a novel method for dual and site-specific incorporations of PEG derivatives into proteins using a substrate peptide (AQQIVM, named TG2) and transglutaminase (TGase). In our previous studies, TG2 was shown to be a special peptide with two adjacent Gln substrates for guinea pig liver transglutaminase (G-TGase). We have now constructed a chimeric protein (named rTG2-IL-2) of human interleukin-2 (IL-2), in which TG2 was fused to the N-terminus of IL-2. For the G-TGase-catalyzed reaction, rTG2-IL-2 was dually and site-specifically modified with alkylamine derivatives of PEG (PEG10, average M_r 10 kDa) at both the Gln2 and Gln3 residues in the appended tag. To demonstrate the effectiveness of the G-TGase-catalyzed PEG-incorporation, we have compared the characteristics and the biological properties of PEG10−rTG2-IL-2 species with two PEG10 molecules attached to rTG2-IL-2 [$(PEG10)_2$−rTG2-IL-2] with that of $(PEG10)_2$−rhIL-2(R), in which PEG10 was randomly incorporated into rhIL-2 by a general procedure using a *N*-hydroxysuccinimidyl ester of PEG (PEG10-COOSu) (M_r 10 kDa). $(PEG10)_2$−rTG2-IL-2 was found to be superior in its in vitro bioactivities and equivalent in its pharmacokinetic profiles to $(PEG10)_2$−rhIL-2(R). Unlike most previous methods, this approach can place dual PEG chains at designed sites on chimeric proteins without decreasing their bioactivities. Thus, TGase-catalyzed PEG-incorporation would improve the therapeutic utility of PEG−protein conjugates.

INTRODUCTION

Covalent modification of proteins with poly(ethyleneglycol) [PEG,[1] also called polyoxyethylene (POE)] has emerged as the method of choice to overcome the major problems associated with protein therapeutics (*1*−*4*). Attachments of PEG to proteins can reduce their antigenicity and immunogenicity and improve their resistance to proteolysis, as well as prolong their circulating life (*5*−*7*). These properties are of great clinical interest, especially in the cases of relatively small proteins (*8*).

In most cases, monofunctional PEG derivatives, which contain a nonreactive methoxy terminus at one end and an amine-reactive group on the other end, are used for PEG attachment. Problems in controlling the conjugation chemistry frequently arise for the following reasons. (i) The number and the locations of the lysine residues vary greatly in native proteins. (ii) The reactive groups on the protein are randomly located.

Thus, the stoichiometry of the PEG−protein conjugates and the attachment sites of PEG to the proteins cannot be precisely controlled. These limitations can be circumvented by appropriately designing the protein and the functionalized PEG. Indeed, there are some examples of site-specific PEG-incorporation into proteins. The simplest method is N-terminal PEG-incorporation by lowering the pH, which takes advantage of the differences in the pK_a values of the α-amino group versus the ϵ-amino groups on the side chains of lysine residues (*9*). However, this method is not strictly site specific, because the incorporation cannot be restricted to only the N-terminus.

The most popular method is thiol-selective PEG modification. Genetic engineering allows the selective positioning of cysteine residues in polypeptide sequences, which when combined with their reactivity to maleimide-terminated PEG, offers an opportunity to assemble site-specifically modified PEG−protein conjugates (*10*−*14*). Similarly, an introduced N-terminal reactive carbonyl group at serine or threonine specifically reacts with an aminooxy-functionalized PEG to form a stable oxime bond (*15*). In addition to these methods, we have recently developed a novel enzymatic methodology using transglutaminase (TGase), in which a substrate Gln residue in an N or C-terminally appended tag in chimeric proteins is site-specifically modified with an alkylamine derivative of PEG, using guinea pig liver TGase (G-TGase) (*16*).

* To whom correspondence should be addressed. Phone: +81-44-244-5813. Fax: +81-44-244-9617. E-mail: haruya_satou@ajinomoto.com.

[1] Abbreviations: IL-2, interleukin 2; hIL-2, human IL-2; rhIL-2, recombinant human IL-2; TG2, AQQIVM (specific peptide for dual modification); TG2-IL-2, chimeric protein of IL-2 for dual and site-specific modification; rTG2-IL-2, recombinant TG2-IL-2; PEG, poly(ethyleneglycol); PEG10, poly(ethyleneglycol) donor substrate (MW 10 000); Boc, *tert*-butyloxycarbonyl; PEG10-Boc, PEG10 protected by Boc; PEG10-COOSu, *N*-hydroxysuccinimidyl ester of PEG10; PEG10−rhIL-2, conjugates between PEG10 and rhIL-2; PEG10−rTG2-IL-2, conjugates between PEG10 and rTG2-IL-2. $(PEG10)_n$−rhIL-2(R), PEG10-rhIL-2 species with *n* PEG10 molecules attached to rhIL-2. $(PEG10)_n$−rTG2-IL-2, PEG10-rTG2-IL-2 species with n PEG10 molecules attached to rTG-IL-2; TGase, transglutaminase; G-TGase, guinea pig liver TGase; SDS−PAGE, sodium dodecyl sulfate−polyacrylamide gel electrophoresis; Gln, glutamine: CTLL, cytotoxic T lymphocyte line; HOBt, 1-hydroxybenzotriazole; DCC, dicyclohexyl carbodiimide; HONSu, *N*-hydroxysuccineimide; TFA, trifluoroacetic acid; Gu-HCl, guanidine hydrochloride: MDC, monodansylcadaverine; Tris-HCl, tris(hydroxymethyl)aminomethane hydrochloride.

10.1021/bc990148b CCC: $19.00 © 2000 American Chemical Society
Published on Web 05/23/2000

Although these approaches are superior, due to the structural homogeneity of the constructed PEG−protein conjugates, there is one difficulty in chemically applying them to clinical uses. For small proteins, where the size is the rate-determining step in their in vivo clearance mechanism, only the size of the single PEG attached to these proteins will influence the pharmacokinetics of the conjugates (*15*, *17*, *18*). Thus, one can increase the circulatory half-life of these proteins by increasing the PEG mass or its molecular volume, either by enhancing its length or by adding multiple copies of PEG chains at one site in these site-specific methodologies. However, the above procedures present severe limitations, because of the broad molecular weight distribution of high molecular weight PEGs and the overall complexity of the synthesis of branched PEG derivatives (*19*). To overcome the limitations of current technologies, we have developed a methodology for dual and site-specific PEG incorporations into proteins on the basis of our enzymatic strategy.

For dual and site-specific modifications, the substrate sequence selected for the appended tag in the chimeric proteins was AQQIVM (named TG2). Our recent studies revealed that EAQQIVM (named FibN), which is derived from the N-terminus of fibronectin, is a special peptide with two adjacent Gln substrates for G-TGase (data not shown). Since the deletion of Glu1 in FibN does not affect the amine acceptor quality of the Gln residues in the G-TGase-catalyzed reaction, we have constructed a chimeric protein of interleukin 2 (rTG2-IL-2) by appending the TG2 sequence in place of the FibN at the N terminus.

In this paper, we report the stoichiometrically precise, dual, and site-specific incorporation of alkylamine derivatives of PEG (PEG10: average M_r, 10 kDa) into rTG2-IL-2 using G-TGase. We also compare the biological activities and the pharmacokinetics of purified PEG10−rTG2-IL-2 species with two PEG10 molecules site-specifically attached to rTG2-IL-2 [$(PEG10)_2$−rTG2-IL-2] with those of $(PEG10)_2$−rIL-2(R), in which two PEG10 molecules were randomly incorporated per mole of rhIL-2.

MATERIALS AND METHODS

G-TGase was purchased from Sigma Chemical Co., St. Louis, MO. The specific activity of G-TGase was 1.8 units/mg protein. α-Carboxymethyl-ω-methoxypolyoxyethylene, with an average molecular mass of 10 kDa, was purchased from Nippon Oils & Fats Co., Ltd., Japan. Preparation of the plasmid pTTG2IL2 encoding TG2-IL-2, transformation of *Escherichia coli* (*E. coli*) HB101 with the pTTG2IL2, and expression and purification of rTG2-IL-2 were done according to the same method used for rTG1-IL-2 (*16*). To prepare pTTG2IL2, two synthetic DNA fragments, 5′CGTTAAATGGCTCAGCAGATCGT3′ and 5′CATGACGATCTGCTGAGCCATTTAA3′, were obtained from Takara Shuzo Co., Ltd., Japan. Purified rTG2-IL-2 was analyzed by reversed-phase HPLC (RP-HPLC) and SDS−PAGE according to the same method used for rTG1-IL-2 (*16*). rhIL-2 was purified from inclusion bodies, as described by Tsuji et al. (*20*). Other chemicals were of reagent grade.

Synthesis of PEG10-Boc. The synthesis of PEG10 protected by Boc (PEG10-Boc) was done as described (*16*). α-Carboxymethyl-ω-methoxypolyoxyethylene (MW 10 000, 5.0 g, 0.5 mmol) was dissolved in 8 mL of dry *N*,*N*-dimethylformamide. After 1-hydroxybenzotriazole (HOBt; 0.135 g, 1.0 mmol) and dicyclohexylcarbodiimide (DCC; 0.206 g, 1.0 mmol) were sequentially added to the reaction solution, the mixture was stirred under an atmosphere of nitrogen at room temperature for 5 h. To the reaction mixture, N-Boc-1,5-diaminopentane (Fluka, Buchs, Switzerland; 0.202 g, 1.0 mmol) was added, and the resulting mixture was stirred under an atmosphere of nitrogen at room temperature for 36 h. After the solvent was removed at reduced pressure, the residue was purified by column chromatography on silica gel (step gradient 10/1 CH_2Cl_2/MeOH to 10/3/1 CH_2Cl_2/MeOH/H_2O) and yielded 3.7 g (73%) of PEG10-Boc as colorless crystals: R_f 0.61 (10/3/1 CH_2Cl_2/MeOH/H_2O); ^{1}H NMR ($CDCl_3$, 400 MHz) δ (ppm) 3.98 (2H, s), 3.74−3.58 (1054H, m), 3.38 (3H, s), 3.32−3.24 (2H, m), 3.16−3.06 (2H, m), 1.56−1.26 (6H, m), 1.44 (9H, s).

Synthesis of PEG10. After PEG10-Boc (0.69 g, 0.068 mmol) was dissolved in 6 mL of trifluoroacetic acid, the mixture was stirred at room temperature for 12 h. After the solvent was removed at reduced pressure, the colorless residue was dissolved in 10 mL of MeOH. The solution was then neutralized by the addition of sodium methoxide and was concentrated in vacuo. The residue was purified by column chromatography on silica gel (step gradient 10/1 CH_2Cl_2/MeOH to 10:3:1 CH_2Cl_2/MeOH/H_2O) and yielded 0.56 g (82%) of PEG10 as colorless crystals: R_f 0.58 (10/3/1 CH_2Cl_2/MeOH/H_2O); ^{1}H NMR (CDCl3, 400 MHz) δ (ppm) 4.03 (2H, s), 3.76−3.52 (1397H, m), 3.38 (3H, s), 3.33−3.27 (2H, m), 3.01−2.95 (2H, m), 1.56−1.30 (6H, m).

TGase-Catalyzed PEG10 Modification of rTG2-IL-2 and Purification of $(PEG10)_2$−rTG2-IL-2. The G-TGase-catalyzed PEG10 modification of rTG2-IL-2 was carried out with the following concentrations of reagents in 0.1 M Tris/HCl (pH 7.5) at 25 °C for 12 h: PEG10, 3.5 mM; $CaCl_2$, 10 mM; protein, 7 μM; and TGase, 0.3 units/mL. The amounts of the reaction buffer were 25 μL and 14 mL for the small- and large-scale reactions, respectively. In a control experiment, the modification of rhIL-2 was also carried out with the same reagent concentrations. Blanks were prepared in the absence of PEG10. At the end of the incubation for 12 h, the reaction mixtures were analyzed by SDS−PAGE under the same conditions used for rTG1-IL-2 (*16*). To remove the residual free PEG10, the reaction mixtures of rTG2-IL-2 and PEG10 were absorbed onto a Sep-Pak C8 cartridge (Millipore Co., Milford, MA) according to the same method used for rTG1-IL-2 (*16*). The eluted protein fractions were directly applied to a YMC-C8-AP column (4.6 × 150 mm; YMC Co., Ltd.), which was developed by a linear gradient of 54 to 60% acetonitrile containing 0.1% TFA for 30 min at a flow rate of 1 mL/min, followed by an isocratic wash at 80% acetonitrile containing 0.1% TFA for 10 min. Each fraction was collected, and the different protein peaks were separately pooled and analyzed by RP-HPLC, SDS−PAGE, and N-terminal sequencing. After the analysis, the fractions of the main peak were directly applied to a Molcut L LGC column (Millipore Co., Milford, MA) and the buffer was exchanged with Dulbecco's phosphate-buffered salaine (D-PBS) (pH 7.4). The samples were used for bioactivity and pharmacokinetic studies.

Reaction of the activated ester of PEG10 (PEG10-COOSu) and rhIL-2 and the purification of PEG10-COOSu modified rhIL-2. PEG10-COOSu was prepared according to the procedure of Gaertner et al. (*15*). Two grams of α-carboxymethyl-ω-methoxypolyoxyethylene (M_r 10 kDa, 0.2 mmol) were preactivated with 115 mg (1 mmol) of *N*-hydroxysuccinimide (HONSu) and 105 mg (0.5 mmol) of *N*,*N*′-dicyclohexylcarbodiimide (DCC) in 30 mL of ethyl acetate (EtOAc). After overnight incubation at 37 °C, the precipitated dicyclohexylurea was removed by centrifugation. The PEG derivative was precipitated

by cooling the solution to 4 °C. The precipitation was repeated three times to remove the excess HONSu and DCC, and finally the material was washed with cold EtOAc and ether and was dried in a vacuum desiccator. The yield of the PEG10-COOSu was 1.77 g (88%).

The PEG10-COOSu modification was carried out with the following concentrations of reagents in 1.25 mL of 0.2 M borate buffer (pH 8.5): PEG10-COOSu, 6.4 mM; protein, 64 μM. The PEG10-COOSu was gradually added to the rhIL-2 solution at a 100-fold M excess over 30 min, and the reaction was allowed to proceed for 12 h at 4 °C. The reaction mixtures were analyzed by SDS−PAGE. To remove the residual free PEG10, the reaction mixtures of rTG2-IL-2 and PEG10 were absorbed onto a Sep-Pak C8 cartridge (Millipore Co., Milford, MA) according to the same method used for rTG1-IL-2 (*16*). Then, separation and purification of the PEG-incorporated products were carried out according to the same procedure for the rTG2-IL-2 by RP-HPLC. A fraction of each peak was collected and directly applied to the Molcut II column to exchange the buffer with D-PBS for the following studies.

N-Terminal Sequence Analysis. The sequences of the N-terminal amino acids of rTG2-IL-2 and $(PEG10)_2$−rTG2-IL-2 were determined using a protein sequencer, (PSQ-1, Shimazu Co. Ltd., Japan). The phenylthiohydantoin (PTH) derivatives produced at each cycle were identified by HPLC reference to standard derivatives of the amino acids.

In Vitro Biological Assays. The bioactivities of rhIL-2, rTG2-IL-2, PEG10-modified rTG2-IL-2 [PEG10−rTG2-IL-2 and $(PEG10)_2$−rTG2-IL-2], and PEG10-COOSu-modified rhIL-2 [(PEG10)n−rhIL-2(R)] were determined by using the IL-2-dependent murine cell line CTLL-2 (*21*). The amount of IL-2 activity was determined in units per milligram by using the rhIL-2 standard (Collaborative Biomedical Products CO., Inc.) and was then expressed as the percent residual bioactivity as compared to the purified rhIL-2. All samples were tested in quadruplicate.

Pharmacokinetics of rhIL-2, rTG2-IL-2, $(PEG10)_2$−rTG2-IL-2, and $(PEG10)_2$−rhIL-2(R). Wistar rats (7W, male) were obtained from Charles River Breeding Labs (Japan). Each sample was intravenously injected as a bolus (10 μg as hIL-2/kg) in the jugular vein, and samples of blood were obtained at predetermined times, up to 24 h, with three groups. Each blood sample was transferred to a heparinized capillary tube at 4 °C and was centrifuged to obtain the plasma. An aliquot of the plasma was diluted with D-PBS, and the plasma concentrations of rTG2-IL-2 and rhIL-2 were determined by an ELISA procedure using the IL-2 Enzyme Immunoassay Kit (Cayman Chemical Co., Michigan, USA). The plasma half-life was estimated by using the nonlinear least-squares program Multi (Runge) (*22*).

Analytical Methods. SDS−PAGE was carried out with the PhastSystem (Amersham Pharmacia Biotech AB, Uppsala, Sweden) using a 20% (w/v) acrylamide gel under reducing conditions according to the same procedure used for rTG1-IL-2 (*16*). The concentrations of the unmodified and modified forms of rTG2-IL-2 and rhIL-2 were quantified by using an extinction coefficient ϵ_{280} of 1.2×10^4 M^{-1}.

RESULTS

Synthesis of PEG10. PEG10, in which one end of the linear polymer is modified with a straight chain alkylamine, was constructed. An analysis by ^{1}H NMR demonstrated that the product was the 1/1 binding product of α-(carboxymethyl)-ω-methoxypoly(oxyethylene) and 1,5-diaminopentane.

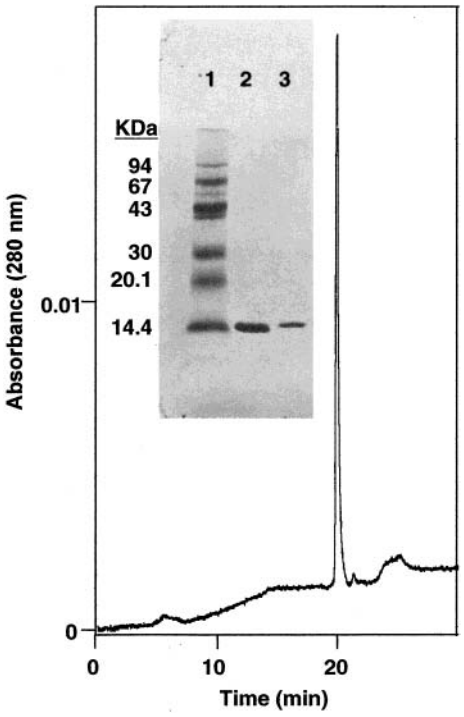

Figure 1. HPLC chromatogram of purified rTG2-IL-2 on a reversed-phase YMC-C8AP column. The analysis was achieved by a linear gradient of 48−80% acetonitrile containing 0.1% TFA over a 30 min. Inset shows the SDS−PAGE of the purified rTG2-IL-2. Lane 1: molecular weight markers. Lane 2: purified rhIL-2. Lane 3: purified rTG2-IL-2.

Expression and isolation of rTG2-IL-2. pTTG2IL-2, a direct expression plasmid of rTG2-IL-2, was constructed from pT13SNco by replacement of the *Cla*I/*Nco*I fragment with a synthetic DNA fragment. After transformation of *E. coli* strain HB101 with pTTG2IL-2, and growth in liquid culture, the chimeric protein (rTG2-IL-2) accumulated in the HB101/pTTG2IL-2 cells as inclusion bodies. Following the procedure for the preparation and purification of rTG2-IL-2, about 50 mg of rTG2-IL-2 was purified from the lysate of a 7.2 L *E. coli* culture. Purified rTG2-IL-2 gave only a single peak by analytical RP-HPLC and ran as a single band at 16 kDa, which was larger than rhIL-2 (15 kDa), in SDS−PAGE (Figure 1).

G-TGase-catalyzed PEG10 modification of rTG2-IL-2. At first, we compared the substrate reactivity between rTG2-IL-2 and rhIL-2 for G-TGase on a small reaction scale. Figure 2 shows the SDS−PAGE analysis of the PEG10-incorporated products for rTG2-IL-2 and rhIL-2. In the absence of PEG10, one new band was slightly visible at 30 kDa in addition to the unmodified rTG2-IL-2 (16 kDa), which presumably represents polymerization due to the intermolecular ϵ-(γ-glutamyl)-lysine cross-links for rTG2-IL-2 (lane 4). The high-molecular weight band that was observed at about 80 kDa could be due to G-TGase. The other minor bands in lanes 2 and 4 are derived from impurities in the G-TGase.

In the presence of PEG10, the rTG2-IL-2 band migrating at about 16 kDa was decreased, and two separate broad bands were observed (lane 5). Since RP-HPLC analysis of the reaction products showed that only two new peaks were observed (data not shown), these two bands, migrating at 32 and 60 kDa, presumably represent PEG10-incorporated rTG2-IL-2 molecules with molar ratios of 1:1 (PEG10−rTG2-IL-2) and 2:1 [$(PEG10)_2$−rTG2-IL-2], respectively. The attachment of one PEG10 molecule to rTG2-IL-2 causes a greater increase in size than that predicted from its molecular mass, presumably

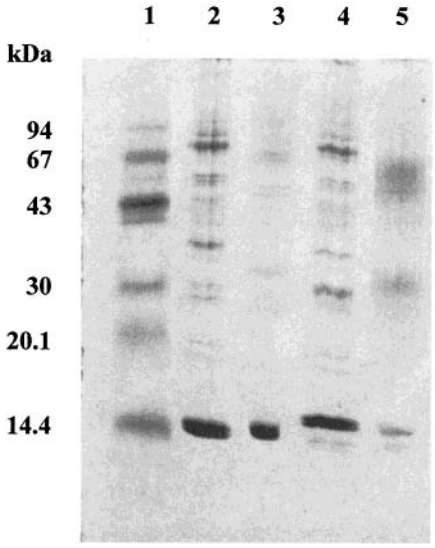

Figure 2. SDS−PAGE analysis of the G-TGase-catalyzed PEG10 modification of rhIL-2 and rTG2-IL-2. Lane 1, M_r marker. Lane 2, rhIL-2 + G-TGase. Lane 3, rhIL-2 + PEG10 + G-TGase. Lane 4, rTG2-IL-2 + G-TGase. Lane 5, rTG2-IL-2 + PEG10 + G-TGase.

due to the bulkiness of PEG10−rTG2-IL-2 conjugates. The increase with the second attachment of PEG10 is especially surprising (about 28 kDa). The reason for this finding might be a synergistic effect of the bulkiness of adjacent PEG10 molecules.

In contrast, no significant incorporation of PEG10 was seen for rhIL-2 (lane 3), suggesting that the PEG10 incorporation sites are located at the appended sequence in rTG2-IL-2. Although some minor protein bands are observed at about 28, 33, 50, and 65 kDa, these bands would not be derived from PEG10-incorporated rhIL-2, because there was no new peak for the reaction mixture of PEG10 and rhIL-2 in the RP-HPLC analysis (data not shown).

The G-TGase protein band was not visible in both lanes 3 and 5. One conceivable reason for the disappearance of the band would be due to PEG incorporation into G-TGase itself. A large amount of PEG molecules could react with G-TGase, and the PEG-incorporated G-TGase would migrate more slowly and broadly than the unmodified G-TGase. Although a faster component for rTG2-IL-2, which migrated at a position similar to that of rhIL-2, was observed, this minor band is derived from the G-TGase impurities.

To characterize the PEG10-incorporated products of rTG2-IL-2, we carried out a large-scale reaction between rTG2-IL-2 and PEG10. The separation of the modified and unmodified rTG2-IL-2 was carried out by RP-HPLC (Figure 3). Three separated peaks (X, Y, and Z) were observed. Since the large peak at about 5 min contained G-TGase, the G-TGase was easily removed from the reaction mixture.

SDS−PAGE analyses of each fraction of peaks X and Y actually showed a doublet (data not shown), probably due to the heterogeneity of the molecular distribution of PEG10 molecules. Thus, we collected the slower components of each peak to facilitate a uniform analysis of the molecular distribution of the conjugates. To demonstrate the heterogeneity of the PEG10 molecules, matrix-assisted laser desorption/ionization time-of-flight mass spectrometry (MALDI-TOFMS) would be useful.

After the collection, these protein peaks were examined again by SDS−PAGE (Figure 3). The protein band in

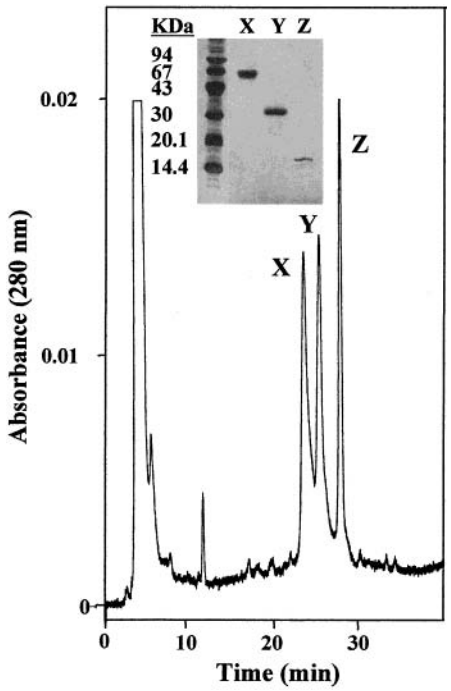

Figure 3. Separation of $(PEG10)_2$-rTG2-IL-2, PEG10-rTG2-IL-2, and unmodified rTG2-IL-2 using reversed-phase YMC−C8AP column. The separation was achieved by a linear gradient of 54−60% acetonitrile containing 0.1% TFA over a 30 min period, followed by an isocratic wash at 80% acetonitrile containing 0.1% TFA for 10 min. Peak X, $(PEG10)_2$-rTG2-IL-2. Peak Y, PEG10-rTG2-IL-2. Peak Z, unmodified rTG2-IL-2. Inset shows the SDS−PAGE of the collected fractions of peaks X−Z. Left lane, molecular mass markers. Lane X, collected fractions of peak X [$(PEG10)_2$-rTG2-IL-2]. Lane Y, collected fractions of peak Y (PEG10-rTG2-IL-2). Lane Z, collected fractions of peak Z (unmodified rTG2-IL-2).

peak Z, which migrates at 16 kDa, corresponds to the size of the unmodified rTG2-IL-2 (lane Z). The protein bands for peaks X and Y, which migrate at approximately 60 kDa (lane X) and 32 kDa (lane Y), respectively, correspond to the sizes of $(PEG10)_2$−rTG2-IL-2 and PEG10−rTG2-IL-2, respectively (yields 223 μg (15%) for $(PEG10)_2$−rTG2-IL-2 and 213 μg (14%) for PEG10−rTG2-IL-2). The ratios of $(PEG10)_2$−rTG2-IL-2/rTG2-IL-2 and PEG10−rTG2-IL-2/rTG2-IL-2 were lower in the RP-HPLC profile in Figure 3 than in the SDS−PAGE analysis of the small-scale reaction in Figure 2. One reason for this difference may be due to the insufficiency of the incubation in the large-scale reaction.

PEG10-COOSu Modification of rhIL-2. Figure 4 shows the RP-HPLC analysis of the reaction products between rhIL-2 and PEG10-COOSu. The protein peak for the unmodified rhIL-2 (peak d) was relatively small, and at least three new broad peaks (peaks a, b, and c) were observed. The electrophoretic pattern of the reaction mixture in SDS−PAGE demonstrated that the rhIL-2 band migrating at 15 kDa was relatively small, and at least four new bands were observed at about 100, 55−40, and 30 kDa, respectively (Figure 4, lane 3). A time course analysis by RP-HPLC for the PEG10-COOSu incorporation showed that peak c was the first new peak after few minutes, and peaks b and a were the second and third new peaks, respectively, which appeared after further incubation (data not shown), indicating that at least three kinds of PEG10−rhIL-2 conjugates were constructed over 12 h. Since the effect of attaching PEG10 molecules to rhIL-2 is to increase its hydrophilicity, the relative difference in the number of PEG incorporations

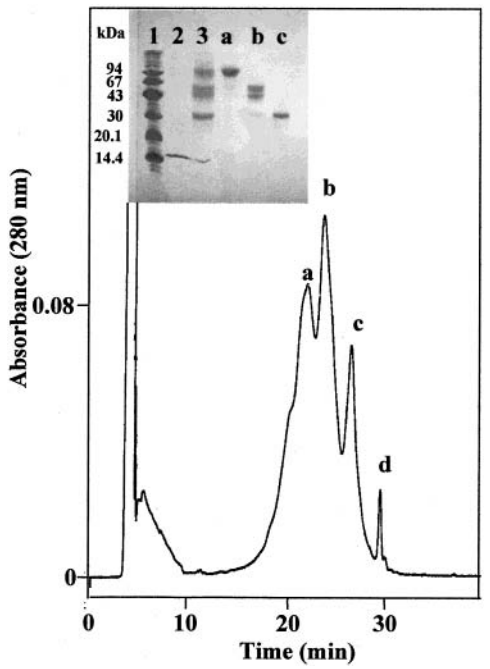

Figure 4. Separation of $(PEG10)_3$-rhIL-2(R), $(PEG10)_2$-rhIL-2(R), PEG10-rhIL-2(R), and unmodified rhIL-2 using reversed-phase YMC-C8AP column. The separation was achieved by a linear gradient of 54−60% acetonitrile containing 0.1% TFA over a 30 min period, followed by an isocratic wash at 80% acetonitrile containing 0.1% TFA for 10 min. Peak a, $(PEG10)_3$-rhIL-2(R). Peak b, $(PEG10)_2$-rhIL-2(R). Peak c, PEG10-rhIL-2(R). Peak d, unmodified rhIL-2. Inset shows the SDS−PAGE of the collected fractions of peaks a−d. Lane 1, molecular mass markers. Lane 2, purified rhIL-2. Lane 3, reaction mixture of rhIL-2 and PEG10-COOSu. Lane a, collected fractions of peak a [$(PEG10)_3$-rhIL-2(R)]. Lane b, collected fractions of peak b [$(PEG10)_2$-rhIL-2(R)]. Lane c, collected fractions of peak c [PEG10-rhIL-2(R)].

in the PEG−rhIL-2 conjugates would affect their retention times in RP-HPLC. Thus, we have assigned peaks a, b, and c as three, two, and one PEG incorporations within the rhIL-2 molecule [$(PEG10)_3$−rhIL-2(R), $(PEG10)_2$−rhIL-2(R), and PEG10−rhIL-2(R)], respectively. To confirm the assignment of each band on the SDS−PAGE completely, an independent method to measure the incorporation of PEG10, such as gel-filtration chromatography, should be employed.

SDS−PAGE analysis of each fraction of peaks a, b, and c actually showed a doublet (data not shown), a result similar to that found for the PEG−rTG2-IL-2 conjugates, as described before. Thus, we collected the slower components for each peak except for peak b, because the separation for peak b was impossible. After the collection, these protein peaks were examined again by SDS−PAGE (Figure 4, lanes a−c). The protein bands in peaks a and c, which migrate at 100 and 30 kDa, correspond to the sizes of $(PEG10)_3$−rhIL-2(R) and PEG10−rhIL-2(R), respectively. The doublet band in peak b, which migrates at 55 and 40 kDa, corresponds to the size of $(PEG10)_2$−rhIL-2(R) [yields 210 μg (17%) for $(PEG10)_3$−rhIL-2(R), 285 μg (23%) for $(PEG10)_2$−rhIL-2(R), and 154 μg (12%) for PEG10−rhIL-2(R)]. Although we can observe a faint protein band in the reaction mixture at around 25 kDa, this band would represent a minor product of PEG10−rhIL-2 (R), because this band was undetectable in peak c.

N-Terminal Sequence Analysis of $(PEG10)_2$−rTG2-IL-2. To determine the site of the modification in the G-TGase-catalyzed reaction, an N-terminal sequence analysis was carried out for purified $(PEG10)_2$−rTG2-IL-2 (Table 1). It revealed that the yields of PTH-Gln at cycles 2 and 3 for unmodified rTG2-IL-2 were 91 and 85%, respectively. In contrast, the yields of cycles 2 and 3 for $(PEG10)_2$−rTG2-IL-2 were 1.8 and 1.5%, respectively. Thus, we conclude that PEG10 couples site specifically at both Gln2 and Gln3 at the appended tag in rTG2-IL-2.

Table 1. N-Terminal Sequence Analysis of rTG2-IL-2 $(PEG10)_2$-rTG2-IL-2[a]

		recovery (%)[b]	
cycle	residue	rTG2-IL-2	$(PEG10)_2$-rTG2-IL-2
1	Ala	147	127
2	Gln	91	1.8
3	Gln	85	1.5
4	Ile	93	84
5	Val	98	92
6	Met	103	101
7	Ala	100	100

[a] A total of 100 pmol of rTG2-IL-2 and $(PEG10)_2$-rTG2-IL-2 wsa inserted into a PSQ-1 protein sequencer, and the recoveries of the first seven amino acid residues were determined for each. [b] The values shown are relative recoveries of PTH-amino acids. The values are normalized to Ala8 = 100%.

Table 2. IL-2 Bioactivity of PEG-Modified Proteins Bioactivity[a]

protein	units/mg	% activity[b]
rhIL-2	4.7×10^6	100
PEG10-rhIL-2(R)	3.5×10^6	74
$(PEG10)_2$-rhIL-2(R)	1.7×10^6	36
$(PEG10)_3$-rhIL-2(R)	0.3×10^6	6
rTG2-IL-2	3.4×10^6	72
PEG10-rTG2-IL-2	3.2×10^6	69
$(PEG10)_2$-rTG2-IL-2	3.4×10^6	72

[a] The amount of IL-2 activity was determined in units/mg by using the rhIL-2 standard on murine CTLL-2 cells. [b] The amount of % activity was expressed as the percent residual bioactivity as compared to the rhIL-2.

In Vitro Biological Assays. The bioactivities of the PEG10-modified proteins are shown in Table 2. The control, purified rhIL-2, has an activity of 4.7×10^6 units/mg as IL-2. The bioactivities of the PEG10-modified rhIL-2 molecules gradually decreased in proportion to the number of PEG10 incorporations relative to the unmodified rhIL-2 [PEG10−rhIL-2(R), 3.5×10^6 units/mg (74%); $(PEG10)_2$−rhIL-2(R), 1.7×10^6 units/mg (36%); and $(PEG10)_3$−rhIL-2(R), 0.3×10^6 units/mg (6%)]. In contrast, there was no decrease in the bioactivities of the PEG10-modified rTG2-IL-2 molecules as compared to the unmodified rTG2-IL-2 [rTG2-IL-2, 3.4×10^6 units/mg (72%); PEG10−rTG2-IL-2, 3.2×10^6 units/mg (69%); and $(PEG10)_2$−rTG2-IL-2, 3.4×10^6 units/mg (72%)], indicating that the dual and site-specific PEG10 modification did not significantly alter the overall structure of rTG2-IL-2. The small decrease in the bioactivity of the unmodified rTG2-IL-2, relative to the rhIL-2, may be due to some effects of the appended sequence at the terminus.

Pharmacokinetic Studies. Figure 5 shows the plasma levels of $(PEG10)_2$−rTG2-IL-2, $(PEG10)_2$−rhIL-2(R), rTG2-IL-2, and rhIL-2 injected i.v. into rats. The pharmacokinetic parameters of these proteins are shown in Table 3. Unmodified rTG2-IL-2 and rhIL-2 rapidly disappeared from the circulation, with half-lives ($T_{1/2,\alpha}$) of 2.9 and 5.5 min, respectively. In contrast, $(PEG10)_2$−rTG2-IL-2 and $(PEG10)_2$−rhIL-2(R) showed remarkably prolonged circulation, with half-lives ($T_{1/2,\beta}$) of 188 and 202 min, respectively. The total areas under the curves ($AUC_{0-\infty}$) for PEG10-modified rTG2-IL-2 and rhIL-2 were increased

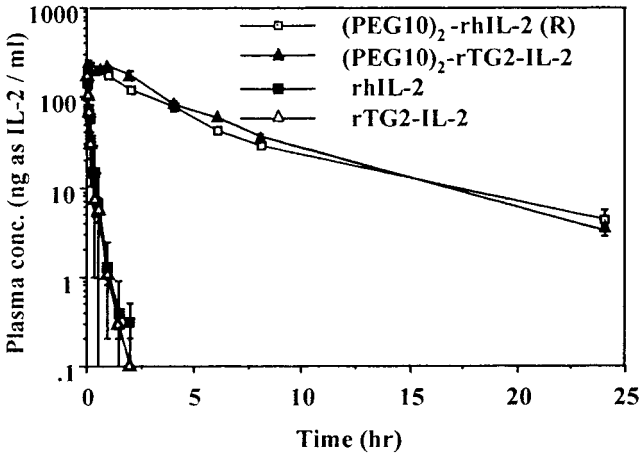

Figure 5. Plasma concentration time course of $(PEG10)_2$-rTG2-IL-2, $(PEG10)_2$-rhIL-2(R), rTG2-IL-2, and rhIL-2 in rats. The plasma concentrations were determined by ELISA after intravenous administration (10 μg as hIL-2/kg) into Wistar rats (7W, male). Data are presented as means ± standard deviations.

Table 3. Pharmacokinetics of Modified and Unmodified rhIL-2 or rTG2-IL-2

sample	$t_{1/2,\alpha}$[a]	$t_{1/2,\beta}$[a]	$AUC_{0-\infty}$
rhIL-2	5.5 ± 3.3	25.1 ± 15.2	19.4 ± 10.3
rTG2-IL-2	2.9 ± 0.9	16.3 ± 2.8	19.7 ± 2.7
$(PEG10)_2$-rhIL-2(R)		202.0 ± 8.5	919.8 ± 29.6
$(PEG10)_2$-rTG2-IL-2		187.9 ± 14.1	1030.6 ± 23.5

[a] The plasma half-life was estimated by using the nonlinear least squares program Multi (Runge).

about 50-fold over those of rTG2-IL-2 and rhIL-2. The results indicate that $(PEG10)_2$−rTG2-IL-2 possesses circulating properties that are identical to the randomly modified $(PEG10)_2$−rhIL-2(R).

DISCUSSION

An important goal for adding PEG molecules to therapeutic proteins is the extension of the protein's persistence in circulating blood. Since PEG modification is directly related to the in vivo circulating half-life of proteins, it is ideal to control the extent of the PEG modification of the target protein without decreasing its bioactivity. Our preliminary studies demonstrated that both of the adjacent Gln residues in the TG2 peptide were good substrates for G-TGase (*Analytical Biochemistry*, submitted for publication). Furthermore, only 2 mol of a fluorescent substrate, monodansylcadaverine (MDC) were incorporated per mole of rTG2-IL-2 in the enzymatic reaction (data not shown). On the basis of these observations, we have developed a methodology for dual and site-specific PEG modifications of proteins by using rTG2-IL-2 and G-TGase. Our results demonstrate the structural and biological efficiency of the G-TGase-catalyzed PEG modification over the random derivatization methods in the conjugation of proteins. Furthermore, the constructed $(PEG10)_2$−rTG2-IL-2 had a dramatically increased circulating half-life and preserved the rhIL-2 bioactivity.

We have designed a chimeric protein of hIL-2 (rTG2-IL-2) with a special substrate sequence at the terminus, using the following assumptions based on our previous studies of rTG1-IL-2 (16). (i) The addition of the TG2 sequence to the N-terminus does not affect the bioactivity or the original structure of hIL-2. (ii) The appended sequence maintains the unique properties of the adjacent glutaminyl substrates of TG2 in the G-TGase-catalyzed modification. Our IL-2 bioactivity studies showed that the overall structure of rTG2-IL-2 is quite similar to that of rhIL-2. Furthermore, the results of the 2/1 stoichiometric labeling of rTG2-IL-2 with PEG10 suggested that the appended tag maintains the flexibility of the peptide in the exposed segment of the polypeptide chain, without decreasing the substrate specificities. Thus, rhIL-2 is a suitable model for confirming our methodology of the dual and site-specific PEG modifications. To demonstrate the effectiveness of the G-TGase-catalyzed PEG incorporation, we have compared the characteristics and the biological properties of the $(PEG10)_2$−rTG2-IL-2 and $(PEG10)_2$−rhIL-2(R) conjugates.

Comparison of the SDS−PAGE profiles of the conjugates revealed different migration patterns. That is, $(PEG10)_2$−rhIL-2(R) showed a doublet band that mainly migrated at about 40 and 55 kDa, whereas $(PEG10)_2$−rTG2-IL-2 showed a band that migrated at 60 kDa. Although SDS−PAGE is not the most appropriate technique to characterize the effective size of each species, it clearly shows that constructs differing in topology, but not in average molecular weight, exhibit different apparent hydrodynamic radii (*15*). Thus, these differences are probably due to the structural heterogeneity and bulkiness of each conjugate.

Our pharmacokinetic studies showed that the extent of the prolonged circulating life of $(PEG10)_2$−rTG2-IL-2 is similar to that of $(PEG10)_2$−rhIL-2. Since the clearance rates of PEG−protein conjugates are mainly determined by their effective size, to escape glomerular filtration, this result is not consistent with the size difference between $(PEG10)_2$−rTG2-IL-2 and $(PEG10)_2$−rhIL-2 in SDS−PAGE. A reason for this inconsistency is proposed, as follows.

It is known that glomerular selectivity is based not only on the molecular size and shape but also on the charge of the molecule (*23*, *24*). In PEG−protein conjugates, large, negatively charged conjugates are retained longer in plasma than smaller, positively charged conjugates (*18*). On the basis of the assumption that the modifications with PEG10 and PEG10-COOSu do not alter the shapes of rTG2-IL-2 and rhIL-2 in this study, the charges of the proteins are affected only by the incorporation of PEG molecules. In rhIL-2, the PEG10-COOSu molecules are covalently attached to the lysine side chains of the protein, thereby progressively decreasing its isoelectric point (pI) upon modification. Hence, the net negative charge of the protein is increased in $(PEG10)_2$−rhIL-2(R). In contrast, in rTG2-IL-2, since the PEG10 molecules are covalently attached to the glutamine side chains of the protein in the G-TGase-catalyzed acyl transfer reaction, there is no change of its pI upon modification. Thus, regardless of the difference of the molecular sizes in SDS−PAGE, the negative charges within $(PEG10)_2$−rhIL-2(R) would prolong its circulating life, making it similar to the level of $(PEG10)_2$−rTG2-IL-2.

Since the properties of the PEG−protein product depend on its composition, in both the number and the positions of the attached PEG molecules, in most previous methods, the heterogeneity has been characterized in order to ensure product consistency (*25*). In particular, this product heterogeneity can play a crucial role in the licensing aspects of the PEG−protein conjugates as therapeutic agents. The N-terminal sequence analysis of $(PEG10)_2$−rTG2-IL-2 suggests that both of the adjacent Gln residues (Gln2 and Gln3) are site-specifically modified with PEG10. When using our methodology with a protein lacking reactive Gln residues for G-TGase, the PEG incorporation sites would be the substrate Gln

residues at the appended tag. Thus, our methodology would simplify the characterization studies of PEG−protein conjugates for verifying the lot-to-lot product consistency.

Furthermore, the site-specifically incorporated PEG−protein conjugates can be easily isolated from the reaction mixture. As shown in the RP-HPLC profiles of the reaction products for PEG10 and rTG2-IL-2, the constructed products presented two sharp, separate peaks, which were derived from the single and double PEG10-incorporated products of rTG2-IL-2. In contrast, the profiles for PEG10-COOSu and rhIL-2 were broad and complicated, due to the lack of control of the attachment sites and the incorporation numbers of PEG10-COOSu. This is another advantageous property of the PEG−protein conjugates as therapeutic conjugates.

The G-TGase-catalyzed incorporation of the PEG10 molecules to rTG2-IL-2 does not affect the bioactivity of rTG2-IL-2, whereas the random attachment of the PEG10 molecules gradually decreases the bioactivity of rhIL-2. In addition, rTG2-IL-2 was selectively modified with a PEG substrate with a higher molecular mass (average molecular mass, 20 kDa), without decreasing its bioactivity (data not shown). These observations indicate that the dual and site-specific PEG incorporation can provide a large panel of various sizes of PEG derivatives, for precise tuning of the biological activity and the plasma clearance of the target protein. Thus, our enzymatic PEG-incorporation would be generally applicable to the preparation of PEG−protein conjugates.

On the basis of these observations, the methodology described here is a new and attractive method to construct PEG−protein conjugates in cases where (a) the protein lacks reactive Gln residues, (b) the chimeric protein can be easily constructed, and (c) the chimeric protein can retain its bioactivity. This methodology is generally useful, as compared to the thiol-selective and the amino terminus-selective PEG-incorporations with large molecular weight PEG polymers (linear or branched), as detailed in the following points. (i) This method can increase the apparent molecular size of the PEG−protein conjugates more effectively, by using simple, linear PEG molecules with smaller molecular weights. (ii) The incorporation sites of this modification are limited to the substrate Gln residues.

Although we have selected the N terminus for appending the TG2 sequence, it would be possible to add the sequence to the C terminus of a protein. Furthermore, it would be possible to use other transglutaminases for the modification. For example, another TGase, microbial TGase, would display quite different structural requirements and reactivity than the liver enzyme for Gln substrates (*26*). Considering the therapeutic application of our PEG−protein conjugates, further studies will be necessary. With regard to this aspect, experiments to determine the immunogenicity and the antigenicity of the constructed chimeric protein and the modified derivatives would provide important points for their clinical uses (*27*).

Although the G-TGase-catalyzed PEG incorporation was studied for its utility in a therapeutic protein modification, there appear to be many practical applications for our methodology. For example, this approach can be extended to enzyme modification. Since it allows a doubling of the amount of PEG without a loss of the catalytic activity of the enzyme, the constructed PEG−enzyme conjugates present the potential of increased solubility in organic solvent and stability toward proteolysis and heating. In terms of these points, it would be possible to introduce other alkylamine derivatives of high molecular weight polymers, such as polysaccharides, which can be monofunctionalized at the reduced terminus with a reactive alkylamine (data not shown).

In conclusion, we have successfully developed a new methodology for dual and site-specific PEG incorporations into proteins. The high homogeneity of the PEG−protein conjugates and the ability to design conjugates with a predictable time course in plasma will improve the therapeutic indices of proteins.

LITERATURE CITED

(1) Abuchowski, A., van Es, T., Palczuk, N. C., and Davis, F. F. (1977) Alteration of immunological properties of bovine serum albumin by covalent attachment of poly(ethylene glycol). *J. Biol. Chem. 252* (11), 3578−3581.

(2) Abuchowski, A., McCoy, J. R., Palczuk, N. C., van Es, T., and Davis, F. F. (1977) Effect of covalent attachment of poly(ethylene glycol) on immunogenicity and circulating life of bovine liver catalase. *J. Biol. Chem. 252* (11), 3582−3586.

(3) Sato, H., Watanabe, M., and Iwashita, Y. (1995) Synthesis and characterization of superoxide dismutase−deferoxamine conjugate via polyoxyethylene. *Bioconjugate Chem. 6* (3), 249−254.

(4) Zalipsky, S. (1995) Functionalized poly(ethylene glycol) for preparation of biologically relevant conjugates. *Bioconjugate Chem. 6* (2), 150−165.

(5) Dreborg, S., and Akerblom, E. B. (1990) Immunotherapy with monomethoxypoly(ethylene glycol) modified allergens. *Crit. Rev. Ther. Drug. Carrier Syst. 6* (4), 315−365.

(6) Burnham, N. L. (1994) Polymers for delivering peptides and proteins. *Am. J. Hosp. Pharm. 51* (2), 210−218; quiz 228−229.

(7) Katre, N. V. (1990) Immunogenicity of recombinant IL-2 modified by covalent attachment of poly(ethylene glycol). *J. Immunol. 144* (1), 209−213.

(8) Hershfield, M. S. (1995) PEG-ADA replacement therapy for adenosine deaminase deficiency: an update after 8.5 years. *Clin. Immunol. Immunopathol. 76* (3, Part 2), S228−232.

(9) Kinstler, O. B., Brems, D. N., Lauren, S. L., Paige, A. G., Hamburger, J. B., and Treuheit, M. J. (1996) Characterization and stability of N-terminally PEGylated rhG-CSF. *Pharm. Res. 13* (7), 996−1002.

(10) Goodson, R. J., and Katre, N. V. (1990) Site-directed pegylation of recombinant interleukin-2 at its glycosylation site. *Biotechnology 8* (4), 343−346.

(11) Woghiren, C., Sharma, B., and Stein, S. (1993) Protected thiol-poly(ethylene glycol): a new activated polymer for reversible protein modification. *Bioconjugate Chem. 4* (5), 314−318.

(12) Kuan, C. T., Wang, Q. C., and Pastan, I. (1994) Pseudomonas exotoxin A mutants. Replacement of surface exposed residues in domain II with cysteine residues that can be modified with poly(ethylene glycol) in a site-specific manner. *J. Biol. Chem. 269* (10), 7610−7616.

(13) Benhar, I., Wang, Q. C., FitzGerald, D., and Pastan, I. (1994) Pseudomonas exotoxin A mutants. Replacement of surface-exposed residues in domain III with cysteine residues that can be modified with poly(ethylene glycol) in a site-specific manner. *J. Biol. Chem. 269* (18), 13398−13404.

(14) He, X. H., Shaw, P. C., Xu, L. H., and Tam, S. C. (1999) Site-directed poly(ethylene glycol) modification of trichosanthin: effects on its biological activities, pharmacokinetics, and antigenicity. *Life Sci. 64* (14), 1163−1175.

(15) Gaertner, H. F., and Offord, R. E. (1996) Site-specific attachment of functionalized poly(ethylene glycol) to the amino terminus of proteins. *Bioconjugate Chem. 7* (1), 38−44.

(16) Sato, H., Ikeda, M., Suzuki, K., and Hirayama, K. (1996) Site-specific modification of interleukin-2 by the combined use of genetic engineering techniques and transglutaminase. *Biochemistry 35* (40), 13072−13080.

(17) Beckman, J. S., Minor, R. L., Jr., White, C. W., Repine, J. E., Rosen, G. M., and Freeman, B. A. (1988) Superoxide dismutase and catalase conjugated to poly(ethylene glycol) increases endothelial enzyme activity and oxidant resistance. *J. Biol. Chem. 263* (14), 6884−6892.

(18) Knauf, M. J., Bell, D. P., Hirtzer, P., Luo, Z. P., Young, J. D., and Katre, N. V. (1988) Relationship of effective molecular size to systemic clearance in rats of recombinant interleukin-2 chemically modified with water-soluble polymers. *J. Biol. Chem. 263* (29), 15064−15070.

(19) Monfardini, C., Schiavon, O., Caliceti, P., Morpurgo, M., Harris, J. M., and Veronese, F. M. (1995) A branched monomethoxypoly(ethylene glycol) for protein modification. *Bioconjugate Chem. 6* (1), 62−69.

(20) Tsuji, T., Nakagawa, R., Sugimoto, N., and Fukuhara, K. (1987) Characterization of disulfide bonds in recombinant proteins: reduced human interleukin 2 in inclusion bodies and its oxidative refolding. *Biochemistry 26* (11), 3129−3134.

(21) Gillis, S., Ferm, M. M., Ou, W., and Smith, K. A. (1978) T cell growth factor: parameters of production and a quantitative microassay for activity. *J. Immunol. 120* (6), 2027−2032.

(22) Yamaoka, K., and Nakagawa, T. (1983) A nonlinear least squares program based on differential equations, MULTI (RUNGE), for microcomputers. *J. Pharmacobiodyn. 6* (8), 595−606.

(23) Kanwar, Y. S. (1984) Biophysiology of glomerular filtration and proteinuria. *Lab. Invest. 51* (1), 7−21.

(24) Deen, W. M., Satvat, B., and Jamieson, J. M. (1980) Theoretical model for glomerular filtration of charged solutes. *Am. J. Physiol. 238* (2), F126−F139.

(25) Snider, J., Neville, C., Yuan, L. C., and Bullock, J. (1992) Characterization of the heterogeneity of poly(ethylene glycol)-modified superoxide dismutase by chromatographic and electrophoretic techniques. *J. Chromatogr. 599* (1−2), 141−155.

(26) Kanaji, T., Ozaki, H., Takao, T., Kawajiri, H., Ide, H., Motoki, M., and Shimonishi, Y. (1993) Primary structure of microbial transglutaminase from Streptoverticillium sp. strain s-8112. *J. Biol. Chem. 268* (16), 11565−11572.

(27) Cheng, T. L., Wu, P. Y., Wu, M. F., Chern, J. W., and Steve, R. R. (1999) Accelerated clearance of poly(ethylene glycol)-modified proteins by anti-poly(ethylene glycol) IgM. *Bioconjugate Chem. 10*, 520−528.

BC990148B

Synthesis, Conjugation, and Radiolabeling of a Novel Bifunctional Chelating Agent for ^{225}Ac Radioimmunotherapy Applications

Lara L. Chappell,† Kim A. Deal,‡ Ekaterina Dadachova, and Martin W. Brechbiel*

Radioimmune & Inorganic Chemistry Section, DCS, NCI, NIH, Bethesda, MD, 20892. Received November 8, 1999; Revised Manuscript Received April 13, 2000

^{225}Ac ($t_{1/2}$ = 10 days) is an alternative α-emitter that has been proposed for radioimmunotherapy (RIT) due to its many favorable properties, such as half-life and mode of decay. The factor limiting use of ^{225}Ac in RIT is the lack of an acceptably stable chelate for in vivo applications. Herein is described the first reported bifunctional chelate for ^{225}Ac that has been evaluated for stability for in vivo applications. The detailed synthesis of a bifunctional chelating agent 2-(4-isothiocyanatobenzyl)-1,4,7,10,13,16-hexaazacyclohexadecane- 1,4,7,10,13,16-hexaacetic acid (HEHA-NCS) is reported. This ligand was conjugated to three monoclonal antibodies, CC49, T101, and BL-3 with chelate-to-protein ratios between 1.4 and 2. The three conjugates were radiolabeled with ^{225}Ac, and serum stability study of the [^{225}Ac]-BL-3-HEHA conjugate was performed.

INTRODUCTION

The treatment of cancer by the use of radiolabeled monoclonal antibodies continues to be attractive and supported by recent clinical reports (*1*). One variable that influences the effectiveness of radioimmunotherapy (RIT) in the treatment of cancer is the choice of the radionuclide and its associated emission characteristics (*2*). Solid tumors have been treated with β^-emitters such as ^{131}I ($t_{1/2}$ = 8.04 days) (*1a*) and ^{90}Y ($t_{1/2}$ = 64.1 h) (*1b*). The range of the β^- particle is several millimeters, and the majority of energy deposition does not occur immediately along the emission track (*3*). For example, the cytotoxicity attributed to the ^{90}Y radioimmunoconjugate of monoclonal antibody anti-Tac has been attributed to be a result of cross-fire and not a direct effect from the emission occurring at the cell surface (*4*, *5*). Therefore, these emissions have been proposed to be less useful for micrometastatic disease and lymphomas and also contribute to normal tissue toxicity (*6*).

In this case, an α-emitting radionuclide might be a better choice due to very high cytotoxcity, a short path-length emission, and immediate energy deposition that should minimize collateral cytotoxicity. Examples that have been studied are ^{213}Bi ($t_{1/2}$ = 46 min) (*7*, *8*) and ^{211}At ($t_{1/2}$ = 7.2 h) (*9*), and clinical trials employing these two radionuclides are ongoing (*10*, *11*). Challenges to the use of the former radionuclide is a short half-life potentially limiting tumor uptake and thus effectiveness, in addition to short supply and high cost. The general utility of the latter radionuclide, ^{211}At, in addition to possessing similar problems, albeit to a lesser degree, seems limited to being produced at facilities possessing an appropriate cyclotron. An alternative α-emitter that has been proposed for RIT is ^{225}Ac ($t_{1/2}$ = 10 days) which is a parent of ^{213}Bi (*12*). The decay process of ^{225}Ac includes four α-emissions and two β^--emissions to a stable ^{209}Bi daughter (Chart 1). As a very large amount of energy (∼28 MeV) is released during this process, much lower amounts of activity of the radionuclide are actually required to produce the desired effects and thus, this isotope demonstrates extreme cytotoxicity (*13*).

For RIT applications, ^{225}Ac must be linked as the metal complex to a monoclonal antibody (mAb) or immunoprotein via a suitable bifunctional chelating agent (*14*). The ^{225}Ac complex must be adequately thermodynamically and kinetically stable to minimize release of the isotope due to the extreme toxicity in vivo (*13*). Derivatives of acyclic polyaminocarboxylate ligands, such as ethylenediamine tetraacetic acid and diethylenetriamine pentaacetic acid (EDTA and DTPA), which form complexes with ^{225}Ac, have been demonstrated as far too labile in vivo (*15*). The use of calix[4]arene ligands has also been proposed for sequestration of ^{225}Ac in RIT applications (*16*). The first report demonstrated selectivity and extraction characteristics of the calix[4]arene derivative for ^{225}Ac, but presented no actual stability data (*16a*). The second report presented detailed results on the conjugation of a bifunctional calix[4]arene to a mAb and protein, immunoreactivity of the product, and studies on potential immunogenicity (*16b*). However, no data pertaining to actual stability, either in vitro or in vivo for the ^{225}Ac complex was presented, nor were any radiolabeling data included.

Previously, our laboratory has reported on the screening of chelating agents and potential development of more stable chelating agents for ^{225}Ac (*17*). A promising candidate that emerged from this study, 1,4,7,10,13,16-hexaazacyclohexadecane-1,4,7,10,13,16-hexaacetic acid (HEHA), was found to form an ^{225}Ac complex that was eliminated from the blood exceptionally rapidly, while also not permitting accumulation of ^{225}Ac in the target organs, i.e., liver and bone (*18*). Also, a substantial reduction in observable toxicity was noted during this comparison with other screened ^{225}Ac complexes (*19*). Upon the basis of this lead, an efficient synthesis and in vitro evaluation of a bifunctional version of this ligand was deemed to be the next logical step in the development

* To whom correspondence should be addressed. E-mail: martinwb@box-m.nih.gov.

† Current address: Department of Chemistry, SUNY at Oswego, Oswego, NY, 13126.

‡ Current address: The CNA Corporation, 4401 Ford Avenue, Alexandria, VA, 22302-8268.

10.1021/bc990153f CCC: $19.00 © 2000 American Chemical Society
Published on Web 06/28/2000

Chart 1. Decay Characteristics of ^{225}Ac

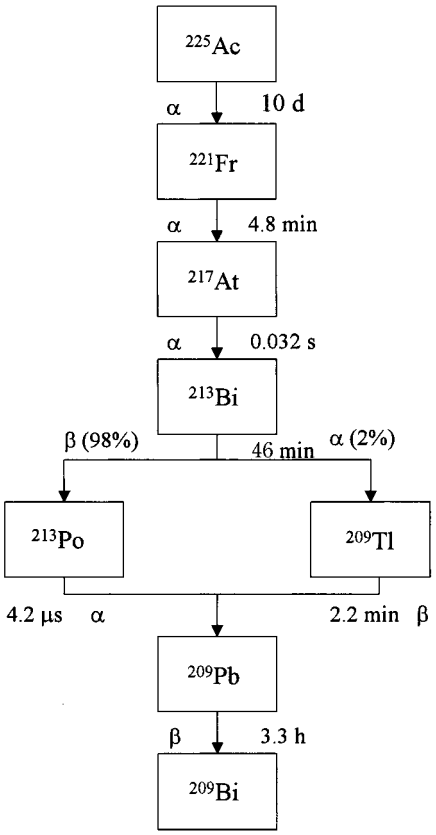

of a suitable chelating agent to test the hypothesis of using ^{225}Ac for RIT. Herein, we report the synthesis and characterization of the bifunctional C-functionalized HEHA ligand. This chelator has been conjugated to three mAbs, radiolabeled with ^{225}Ac, and the serum stability of one of the [^{225}Ac]HEHA-mAb conjugates evaluated.

EXPERIMENTAL SECTION

Materials and Methods. All materials were of reagent grade and used without further purification. Chromatography was performed on silica gel 60, 220−440 mesh ASTM (Fluka). Thin-layer chromatography (TLC) was performed on silica gel 60 F-254 plates (EM Reagents). All glassware used in the synthesis of the ligand after ester hydrolysis was acid-washed and rinsed with distilled deionized water.

^1H and ^{13}C NMR spectra were recorded on a Varian Gemini 300 instrument at ambient temperature. Chemical shifts are reported downfield relative to TMS ($CDCl_3$) or TSP (D_2O). Chemical ionization mass spectra (CI-MS) were measured using a Finnegan 3000 instrument. Fast atom bombardment mass spectra (FAB-MS) were measured using a Extrel 400 instrument. High-resolution FAB (HR-FAB) mass spectra were obtained on a JEOL SX102 mass spectrometer operated at an accelerating voltage of 10 kV. Samples were desorbed from a glycerol matrix using 6 keV xenon atoms. Mass measurements in HR-FAB are performed at 10 000 resolution. Analytical HPLC was performed on a Beckman gradient system equipped with model 114 M pumps controlled by System Gold software and a model 165 dual wavelength detector set at 254 and 280 nm. An Altex ODS C18 column (4.6 mm × 15 cm) with a 25 min gradient of 100% aqueous 0.05 M triethylammonium acetate to 100% methanol at a flow rate of 1 mL/min was used. Infrared spectra were obtained using a Bio-Rad FTS 45 spectrophotometer with the samples prepared as Nujol mulls.

HPLC purification of radiolabeled with ^{225}Ac conjugates, as well as HPLC analysis of samples from serum stability studies, were performed employing a Dionex system equipped with a model GPM-2 gradient pump, a Gilson model 112 UV monitor operating at 280 nm, an IN/US γ-RAM flow-through radioactivity detector, and a Gilson model 203 fraction collector. The size-exclusion HPLC column (TSK-Gel G3000SW, TosoHaas, Japan) eluted with PBS, pH 7.2, at 1 mL/min was used for these separations. Radioactive samples were counted in Minaxi γ-counter (Packard Instrument Company).

Synthesis. *4-Nitrophenylalaninylglycylglycine, methyl ester (**11**).* *N-tert*-Butoxycarbonyl-(D,L)-4-nitrophenylalanine (*20*) (20 g, 64.5 mmol), glycylglycine methyl ester hydrochloride (14.1 g, 77.2 mmol), Et_3N (11 mL, 77.2 mmol), and EDC (14.8 g, 77.2 mmol) were combined in anhydrous DMF (500 mL) and stirred at room-temperature overnight. The solvent was removed under vacuum, and EtOAc (500 mL) was added. The solution was extracted with H_2O (2 × 200 mL) and 5% $NaHCO_3$ (3 × 200 mL). The aqueous layers were back-extracted with EtOAc (2 × 150 mL), and this EtOAc portion was washed as above. The EtOAc layers were combined and washed with saturated NaCl solution (1 × 200 mL). The combined EtOAc solution was dried over anhydrous Na_2SO_4, filtered, and the filtrate reduced to dryness. The residue was taken up in boiling EtOAc (200 mL), and hexanes (300 mL) was added. The material initially separated as an oil which then turned to a white precipitate. This precipitate was chromatographed on silica gel with 10% MeOH in $CHCl_3$ elution. The first major band contained the product. Fractions containing product were combined and reduced to dryness to yield the product (13.16 g, 47%).

^1H NMR (DMSO-d_6) δ 1.27 (s, 9 H, *t*Bu), 2.88 (m, 1 H), 3.17 (m, 1 H), 3.64 (s, 3 H, $-OCH_3$), 3.79 (d, 2 H, J = 5.7), 3.88 (m, 2 H), 4.28 (m, 1 H), 7.09 (d, 1 H, J = 8.7, NH), 7.56 (d, 2 H, J = 9, Ar), 8.17 (d, 2 H, J = 8.7, Ar), 8.27 (t, 1 H, J = 5.9, NH), 8.33 (m, 2 H, J = 5.9, NH); ^{13}C NMR (DMSO-d_6) δ 28.04 (*t*Bu), 37.39, 40.54, 41.88, 51.77, 55.30, ($-OC(CH_3)_3$), 78.37 ($-OCH_3$), 123.30, 130.82, 146.43, 147.04 (Ar), 155.60, 169.62, 170.47, 171.81 (C(O)); MS (CI/NH_3) *m/e* 456 (M + NH_4^+). Anal. Calcd for $C_{19}H_{26}N_4O_8$: C, 52.05; H, 5.98; N, 12.78. Found: C, 51.79; H, 5.93; N, 12.60.

*N-tert-Butoxycarbonyl-4-nitro-phenylalaninylglycylglycine N-(2-Aminoethyl)-amide (**12**).* Methyl ester **11** (16.55 g, 37.8 mmol) in MeOH (100 mL) was added as a slurry by pipet to stirring ethylenediamine (250 mL, 3.7 mol), that had been freshly distilled from 3A sieves. The reaction mixture changed from colorless to pink, to deep red, and finally to brown and was left stirring for 3 days. The ethylenediamine was removed by vacuum rotary evaporation and the residue purified by column chromatography on silica gel with $CHCl_3$/MeOH/NH_4OH (12:4:1) elution.

^1H NMR (DMSO-d_6) δ 1.27 (s, 9 H, *t*Bu), 2.57 (t, 2 H, J = 6.3, $-CH_2NH_2$), 2.88 (m, 1 H), 3.06 (q, 2 H, J = 6.2), 3.17 (m, 1 H), 3.3 (br, 2 H), 3.69 (d, 2 H, J = 5.7), 3.76 (d, 2 H, J = 4.8), 4.24 (9 m, 1 H), 7.13 (d, 1 H, J = 8.7, NH), 7.56 (d, 2 H, J = 9.0, Ar), 7.74 (t, 1 H, J = 5.4, NH), 8.10 (t, 1 H, J = 5.9, NH), 8.16 (d, 2 H, J = 7.8, Ar), 8.35 (t, 1 H, J = 5.9, NH); ^{13}C NMR (DMSO-d_6) δ 27.97 (*t*Bu), 37.26, 41.21, 42.12, 42.24, 55.24 (-CH_2Ar), 78.37 ($-OC(CH_3)_3$)), 123.30, 130.82, 146.43, 146.97 (Ar), 155.60, 168.89, 169.32, 171.99 (C(O)); MS (CI/NH_3) *m/e* 467 (M^+ + 1). Anal. Calcd for $C_{20}H_{30}N_6O_7$: C, 51.49; H, 6.48; N, 18.01. Found: C, 50.88; H, 6.46; N, 17.83.

*N-(2-Aminoethyl)-4-nitro-phenylalaninylglycylglycine amide hydrochloride (**13**).* Dioxane (300 mL) was chilled in an ice bath and saturated with HCl (g) for 2 h. Carbamate **12** (8.95 g, 19.2 mmol) was added, and HCl (g) bubbled for an additional 30 min. The reaction mixture was stirred overnight, after which diethyl ether was added (200 mL) and the mixture chilled for 7 h. The solid was collected on a Büchner funnel, washed with ether, and dried under vacuum (10.6 g).

^{1}H NMR (DMSO-d_6) δ 2.87 (m, 2 H), 3.2−3.4 (m, 4 H), 3.5−3.9 (m, 4 H), 4.22 (m, 1 H), 7.62 (d, 2 H, J = 9, Ar), 8.13 (br, 2 H, NH), 8.20 (d, 2 H, J = 8.7, Ar), 8.40 (m, 1 H, NH), 8.48 (m, 1 H, NH), 9.11 (m, 1 H, NH); ^{13} C NMR (DMSO-d_6) δ 34.47, 36.60, 38078, 42.55, 53.60, 124.02, 131.67, 144.83, 147.34, 169.13, 169.98; MS (CI/NH_3) *m/e* 367 ($M + H^+$). Anal. Calcd for $C_{15}H_{22}N_5O_7$·2HCl·1.2dioxane·H_2O: C, 42.24; H, 6.37; N, 14.93. Found: C, 43.28; H, 6.50; N,14.99.

*1-(tert-Butoxycarbonyl)-5-(4-nitrobenzyl)-3,6,9,12,17-pentaoxo-1,4,7,10,13,16-hexaazacyclohexadecane (**14**).* Dioxane (3.7 L) was heated to 95 °C in a 5 L three-necked Morton flask. Hydrochloride **13** (4.39 g, 10 mmol) was dissolved in DMSO (35 mL), and Et_3N (4.6 mL, 33 mmol) was added. The mixture was stirred for 30 min and the Et_3N·HCl was removed by filtration. The filtrate was taken up into a gastight syringe and DMSO added to bring the final volume to 50 mL. *N-tert*-Butoxycarbonyl-iminodiacetic acid dihydroxysuccinnimyl ester (*20*) (4.27 g, 10 mmol) was dissolved in DMF, taken up into a gastight syringe and additional DMF was added to adjust the final volume to 50 mL. The syringes were loaded onto a syringe pump and added to the dioxane such that the addition was complete after 24 h. One more addition of 10 mmol in each reactant were added over a 24 h period. The reaction was heated for an additional 18 h and cooled to room temperature. The reaction was concentrated to thick oil under vacuum and the brown residue dissolved in $CHCl_3$ (500−600 mL). The $CHCl_3$ layer was washed with water (2 × 200 mL), saturated NaCl solution (1 × 100 mL), 5% HCO_3^- (5 × 150 mL), saturated NaCl solution (1 × 100 mL), 1 M HCl (2 × 100 mL), and saturated NaCl solution (1 × 100 mL). The $CHCl_3$ layer was dried over Na_2SO_4 and filtered, and the filtrate was reduced to dryness by rotary evaporation (crude yield 2.5 g). However, when purification by column chromatography on silica gel was performed, no product was isolated as determined by mass spectrometry and ^{1}H NMR spectroscopy.

*N-tert-Butyloxycarbonyliminodiacetyldiglycine Diethyl Ester (**1**).* *N-tert*-Butyloxycarbonyl-iminodiacetic acid (*21*)-(20 g, 85.8 mmol), glycine ethyl ester hydrochloride (24 g, 171.9 mmol), and triethylamine (24 mL, 172 mmol) were dissolved in anhydrous DMF (700 mL). EDC (34 g, 88.7 mmol) was added and the solution stirred 18 h at room temperature. The DMF was removed under vacuum, and the residue dissolved in ethyl acetate (600 mL). The ethyl acetate was extracted with water (1 × 200 mL), 5% $NaHCO_3$ (3 × 200 mL), brine (1 × 200 mL), 1 M HCl (1 × 200 mL), and brine (2 × 200 mL). The organic layer was dried over Na_2SO_4, filtered and concentrated to yield an oil (23 g, 66%).

^{1}H NMR (DMSO-d_6) δ 1.19 (t, 6 H, CH_3); 1,35 (s, 9 H, C(CH_3)$_3$); 3.30 (s, 2 H, CH_2); 3.32 (s, 2 H, CH_2); 3.88 (s, 2 H, CH_2); 3.91 (s, 2 H, CH_2); 4.08 (q, 4 H, CH_2CH$_3$); 8.80 (t, 2 H, N*H*); ^{13}C NMR (DMSO-d_6) δ 14.01, 27.73, 51.29, 21.77, 60.46, 79.76, 154.87, 169.86, 170.29, 170.41; MS (CI/NH_3) *m/e* 404 ($M^+ + 1$). Anal. Calcd for $C_{17}H_{29}N_3O_8$: C, 50.62; H, 7.24; N, 10.42. Found: C, 50.09; H, 7.10; N, 10.13.

*N-tert-Butyloxycarbonyliminodiacetyldiglycine (**2**).* To a stirred solution of NaOH (5.2 g, 131 mmol) in ethanol (200 mL) and H_2O (100 mL) was added dropwise diester **1** (23 g, 57 mmol) in ethanol (200 mL). The solution was stirred 60 h at room temperature followed by removal of ethanol under vacuum. The residual aqueous layer was extracted with ethyl acetate (1 × 200 mL). The aqueous layer was chilled to 0 °C and acidified to pH 2 with 3 M HCl (∼50 mL). To facilitate extraction, 20 g of NaCl was added and the aqueous layer was extracted with ethyl acetate repeatedly. The product began to precipitate in the organic layer and the organic layer was heated to maintain a clear solution before drying with sodium sulfate. After drying and filtration, concentration of the organic layer yielded the pure product as a white solid (14.59 g, 74%). The product was dried under vacuum at 70 °C for 24 h.

^{1}H NMR (DMSO-d_6) δ 1.34 (s, 9 H, C(CH_3)$_3$); 3.79 (s, 2 H, CH_2); 3.80 (s, 2 H, CH_2); 3.84 (s, 2 H, CH_2); 3.90 (s, 2 H, CH_2); 8.75 (m, 2 H, NH); ^{13}C NMR (DMSO-d_6) δ 27.79, 51.47, 51.96. 79.76, 154.99, 170.29, 171.26; MS (CI/NH_3) *m/e* 348 ($M^+ + 1$). Anal. Calcd for $C_{13}H_{21}N_3O_8$·HCl: C, 40.69; H, 5.77; N, 10.95. Found: C, 41.17; H, 5.61; N, 11.03.

*N-tert-Butyloxycarbonyliminodiacetyldiglycine Disuccinimidyl Ester (**3**).* Thoroughly dried diacid **2** (14 g, 40.3 mmol) and *N*-hydroxysuccinimide (10.2 g, 88.7 mmol) were stirred in DMF (250 mL) under argon. EDC (17 g, 88.7 mmol) was added and the solution stirred 18 h. The DMF was removed under vacuum, and the residue dissolved in ethyl acetate (600 mL). The organic layer was extracted with water (1 × 150 mL), 5% $NaHCO_3$ (3 × 200 mL), brine (1 × 200 mL), and brine (2 × 200 mL). The organic layer was dried with Na_2SO_4, filtered, and concentrated to yield a white solid (15.86 g, 73%). The product was thoroughly dried under vacuum at 70 °C prior to use in cyclization.

^{1}H NMR (DMSO-d_6) δ 1.34 (s, 9 H, C(CH_3)$_3$); 2.82 (s, 8 H, succinimide); 3.88 (s, 2 H, CH_2); 3.94 (s, 2 H, CH_2); 4.31 (s, 2 H, CH_2); 4.33 (s, 2 H, CH_2); 8.95 (t, 2 H, NH); ^{13}C NMR (DMSO-d_6) δ 25.19, 25.43, 27.74, 51.05, 79.89, 154.87. 166.53, 170.23, 170.54; MS (CI/NH_3) *m/e* 542 ($M^+ + 1$). Anal. Calcd for $C_{21}H_{27}N_5O_{12}$·1.5H_2O: C, 44.37; H, 5.31; N, 12.32. Found: C, 44.43; H, 5.54; N, 11.48.

*1-(tert-Butoxycarbonyl)-8-(4-nitrobenzyl)-3,6,9,14,17-pentaoxo-1,4,7,10,13,16-hexaazacyclohexadecane **(4).*** In a 5 L three-necked Morton flask, anhydrous dioxane (3.5 L) was heated to ∼90 °C. Disuccinimidyl ester **3** (5.42 g, 10 mmol) in DMF (50 mL) and *N*-(2-aminoethyl)-4-nitrophenylalaninamide (*19*) (2.52 g, 10 mmol) in DMF (50 mL) were each loaded in 50 mL gastight syringes and added to the dioxane so that the addition was complete after 24 h. Second and third additions were 10 and 5.5 mmol in each reactant, respectively. After the third addition, the reaction was heated for an additional 18 h and then cooled to room temperature. The reaction was concentrated to a thick brown oil under vacuum and the residue dissolved in chloroform (500 mL). The chloroform was washed with water (1 × 200 mL), 5% $NaHCO_3$, (2 × 200 mL), brine (1 × 200 mL), 1 M HCl (2 × 200 mL), brine (1 × 200 mL), and water (1 × 100 mL). The $CHCl_3$ layer was kept separate and reduced to dryness. A sticky, brown residue stuck to the inside of the separatory funnel was dissolved in MeOH and reduced to dryness. The residues isolated from the $CHCl_3$ and MeOH were each chromatographed on short silica gel columns with 10−20% MeOH in $CHCl_3$. Fractions that contained the product were combined (R_f = 0.55, silica gel, 20% MeOH in $CHCl_3$). This product was purified by column chroma-

tography on silica gel eluted with a 10%−20% MeOH in $CHCl_3$ gradient yielded the pure macrocycle as a tan solid (2.55 g, 19%).

^1H NMR (DMSO-d_6) δ 1.33 (s, 9 H, $C(CH_3)_3$), 2.8−4.0 (overlapping multiplets, 14 H); 4.5 (m, 1 H, CH); 7.47 (s, 2 H, Ar); 7.58 (t, 0.5 H, NH); 7.74 (d, 1.5 H, NH); 7.96 (d, 1 H, NH); 8.12 (d, 2 H, Ar); 9.14 (t, 0.5 H, NH); 9.21 (m, 1 H, NH); 9.36 (t, 0.5 H, NH)); ^{13}C NMR (DMSO-d_6) δ 27.74, 52.15, 53.36, 53.54, 79.22, 80.13, 123.36, 130.65, 146.37, 146.56, 154.69, 169.20, 170.66, 171.08, 171.27, 171.69; MS (CI/NH_3) *m/e* 564; ($M^+ + 1$) HPLC $t_R = 18.7$ min. Anal. Calcd for $C_{24}H_{33}N_7O_9 \cdot 2\ H_2O$: C, 48.08; H, 6.21; N, 16.35. Found: C, 48.28; H, 5.73; N, 15.87.

*2-(4-Nitrobenzyl)-3,8,11,15,18-pentaoxo-1,4,7,10,13,16-hexaazacyclohexadecane Hydrochloride (**5**).* Dioxane (50 mL) in a 250 mL three-necked round-bottom flask was chilled in an ice bath and saturated with HCl (g) for 2 h. Carbamate **4** (1.66 g, 2.9 mmol) was added and HCl (g) was bubbled through the reaction mixture for 1 h. The reaction stirred overnight (18 h) at room temperature. Diethyl ether (200 mL) was added and the reaction mixture chilled in the freezer for 6 h. The yellow precipitate was collected on a Büchner funnel, washed with diethyl ether, and vacuum-dried overnight. The product was isolated as a pale, yellow solid (1.9 g, >100%).

^1H NMR (DMSO-d_6) δ 3.0−3.3 (m, 7 H), 3.4 (m, 2 H), 3.70 (m, 3 H), 3.89 (m, 3 H), 4.44 (m, 1 H −CH−Ar), 7.54 (d, 2 H, Ar), 7.80 (t, 1 H, NH), 8.05 (t, 1 H, NH), 8.14 (d, 2 H, Ar) 8.20 (d, 1 H, NH), 8.96 (d of t, 2 H, NH); MS (CI/NH_3) *m/e* 464 ($M^+ + 1$); HPLC $t_R = 15.3$ min. Anal. Calcd for $C_{19}H_{25}N_7O_7 \cdot 1.5\ H_2O \cdot HCl \cdot$dioxane: C, 44.92; H, 6.06; N, 15.94. Found: C, 44.23; H, 5.90; N, 15.97.

*2-(4-Nitrobenzyl)-1,4,7,10,13,16-hexaazacyclohexadecane Hexahydrochloride **(6).*** The above product **5** (1.8 g, 3.0 mmol) and anhydrous THF (50 mL) was combined in a 100 mL two-necked round-bottom flask and chilled in an ice bath. To this suspension was added 1 M borane in THF (5−6 mL). The mixture was allowed to warm to room temperature and then heated at 50 °C. Over 3 days, additional 1 M borane in THF was added in 15, 5, and 10 mL portions, respectively, for a total of 36 mmol. The reaction mixture was evaporated to dryness and the yellow solid (1.55 g) dried under vacuum. This residue was transferred to a 250 mL three-necked flask and absolute EtOH (80 mL) was added. HCl(g) was bubbled through the reaction mixture for 2 h and then the reaction was heated at reflux for 17 h. After which, the reaction mixture was cooled to room temperature, Et_2O (150 mL) was added and the suspension was placed in the freezer overnight. The pale yellow precipitate was collected on a Büchner funnel, washed with diethyl ether and vacuum-dried (1.01 g, 54%).

^1H NMR (D_2O pH 1−2) δ 3.0−4.0 (m, 25 H, macrocycle, $-CH_2Ar$), 7.5 (m, 2 H, Ar), 8.25 (m, 2 H, Ar); MS (CI/NH_3) *m/e* 394 ($M^+ + 1$); HPLC $t_R = 17.8$ min. Anal. Calcd for $C_{19}H_{35}N_7O_2 \cdot 6HCl \cdot H_2O$: C, 36.21; H, 6.87; N, 15.56. Found: C, 36.06; H, 6.80; N, 14.59.

*Hexa-tert-butyl 2-(4-nitrobenzyl)-1,4,7,10,13,16-hexaazacyclohexadecane-1,4,7,10,13,16-hexaacetate (**7**).* Hexahydrochloride **6** (1.15 g, 1.83 mmol) was taken up in water (4 mL), and the pH raised to 13 by the addition of solid NaOH. The aqueous solution was extracted with $CHCl_3$ (4 × 100 mL). The combined $CHCl_3$ layers were dried over anhydrous Na_2SO_4 and the drying agent filtered. The free base was isolated as a yellow solid (593 mg, 80% recovery) after evaporation of the filtrate.

^1H NMR ($CDCl_3$) δ 1.6 (br, 6 H, NH); 2.2−3.4 (m, 25 H, macrocycle, CH_2Ar), 7.3 (m, 2 H, Ar), 8.05 (m, 2 H, Ar); ^{13}C NMR ($CDCl_3$) δ 38.39, 38.81, 46.34, 48.34, 48.53, 48.77, 49.07, 49.38, 52.41, 52.78, 58.67, 123.32, 123.57, 129.94, 146.34, 147.55.

The above free base (593 mg, 1.51 mmol) was dissolved in anhydrous DMF (10 mL), and *tert*-butyl bromoacetate (1.78 g, 9.1 mmol) was added. The reaction was allowed to stir in an ice bath and then warmed to room temperature over 1 h. An aqueous solution of Na_2CO_3 (965 mg in 20 mL of H_2O) was added, and the mixture was stirred for 2.5 h. Toluene (10 mL) was added, and the reaction mixture was stirred overnight (17 h). The reaction mixture was poured into a separatory funnel, and the aqueous layer drained. The toluene layer was saved. The aqueous layer was extracted with $CHCl_3$ (2 × 100 mL), and the combined $CHCl_3$ and toluene layers were reduced to dryness. The residue was determined to contain hexa-*tert*-butyl ester product by mass spectrometry. This residue was purified on two consecutive silica gel columns (2 × 10 cm) with a gradient from 5 to 10% MeOH in $CHCl_3$ and finally 10% NH_3(aq) in MeOH. Early fractions contained the hexa-*tert*-butyl ester product with some impurity. Later fractions contained only the hexa-*tert*-butyl ester product. These were combined, reduced to dryness, and vacuum-dried (462 mg, 29%).

^1H NMR ($CDCl_3$) δ 1.45 (overlapping s, 54 H, *t*Bu); 2.8−3.4 (m, 37 H, macrocycle, CH_2Ar), 7.46 (d, 2 H, Ar), 8.13 (d, 2 H, Ar); ^{13}C NMR ($CDCl_3$) δ 27.94, 52.05, 53.32, 55.33, 55.63, 55.99, 80.58, 123.20, 130.25, 146.21, 149.21, 149.37, 170.93, 171.65; MS (CI/NH_3) *m/e* 1078.6 ($M^+ + 1$), 1100.6 ($M^+ + Na$). Anal. Calcd for $C_{55}H_{94}N_7O_{14} \cdot 0.5\ H_2O$: C, 60.81; H, 8.81; N, 9.03. Found: C, 58.97; H, 8.44; N, 9.01.

*2-(4-Nitro-benzyl)-1,4,7,10,13,16-hexaazacyclohexadecane-1,4,7,10,13,16-hexaacetic Acid **(8).*** To a 10 mL round-bottom flask, hexa-*tert*-butyl 2-(4-nitrobenzyl)-1,4,7,10,13,16-hexaazacyclohexadecane-1,4,7,10,13,16-hexaacetate (166 mg, 0.15 mmol) was combined with concentrated HCl (5 mL) and heated at reflux for 6 h. The HCl(aq) was removed by rotary evaporation, and the residue taken up in water (1−2 mL) and was lyophilized to give the hexa-acid as a pale yellow solid (100 mg, 70%).

^1H NMR (D_2O, pH 1−2) δ 2.8−4.2 (m, 37 H), 7.48 (br, 2 H, Ar), 8.14 (br, 2 H, Ar); MS (CI/NH_3) *m/e* 742 ($M^+ + 1$); HPLC $t_R = 10.5$ min. Anal. Calcd for $C_{31}H_{47}N_7O_{14} \cdot 6$ HCl: C, 38.95; H, 5.59; N, 10.26. Found: C, 39.12; H, 5.66; N, 10.49.

*2-(4-Aminobenzyl)-1,4,7,10,13,16-hexaazacyclohexadecane-1,4,7,10,13, 16-hexaacetic acid (**9**).* A Schlenk flask was charged with 10% Pd/C (23.5 mg) and H_2O (3 mL) and fitted onto an atmospheric hydrogenator. The apparatus was flushed with H_2(g) two times to fully saturate the catalyst. A solution of hexaacetic acid **8** (76.6 mg, 0.080 mmol) in H_2O (3 mL) was injected via syringe into the flask. The hydrogenation was allowed to proceed until the uptake of H_2(g) ceased. The reaction mixture was filtered through a bed of Celite 577 packed in a medium glass fritted funnel. The filtrate was reduced to dryness by rotary evaporation and the residue taken up in water (1−2 mL). This was then lyophilized to give the aniline as a pale yellow solid (56 mg, 75%).

^1H NMR (D_2O, pH 1−2) δ 2.6−4.2 (m, 37 H), 7.46 (m, 4 H, Ar); ^1H NMR (D_2O, pH 13) δ 2.0−4.6 (m, 37 H), 6.83 (m, 2 H, Ar), 7.09 (m, 2 H, Ar); MS (CI/NH_3) *m/e* 712 ($M^+ + 1$); HPLC $t_R = 8.6$ min. $M - H^+$ calcd for $C_{31}H_{48}N_7O_{12}$: 710.3371. Found [HRFAB]: *m/e* = 710.3397, error = +5.0 ppm.

*2-(4-Isothiocyanatobenzyl)-1,4,7,10,13,16-hexaazacyclohexadecane-1,4,7,10,13, 16-hexaacetic acid (**10**).* A 1 M solution of $SCCl_2$ in $CHCl_3$ (50 mL) was added to aniline

9 (30.5 mg, 0.033 mmol) dissolved in H_2O (0.5 mL) in a vial. The mixture was stirred rapidly for 2 h at room temperature. The aqueous layer was decanted with a pipet into a round-bottom flask and the $CHCl_3$ layer washed with H_2O (3 × 0.5 mL). The combined aqueous portions were reduced to approximately 1 mL by rotary evaporation. The solution was then lyophilized to give the isothiocyanate as a pale yellow solid (30.9 mg, 96%).

^{1}H NMR (DMSO-d_6, pH 1−2) δ 3.0−4.0 (m, 37 H), 7.33 (br, 4 H, Ar); ^{1}H NMR (D_2O, pH 13) δ 2.2−3.4 (m, 37 H), 7.3 (m, 4 H, Ar); MS (FAB/glycerol) *m/e* 754 ($M^+ + 1$); IR (Nujol) 2034.1 cm^{-1}; HPLC t_R = 14.95 min. $M - H^+$ calcd for $C_{32}H_{46}N_7O_{12}S$. Found [HRFAB]: *m/e* = 752.2971, error = +6.1 ppm.

Antibody Conjugation. Purified monoclonal antibody CC49 (*22a*), which reacts with the human pancarcinoma antigen TAG-72 and its isotype-match BL-3 (*22b*), were supplied by Dr. J. Schlom, (Laboratory of Tumor Immunology and Biology, NCI, NIH); T101 antibody (*23*) was furnished by Dr. J. Carrasquillo (Nuclear Medicine Department, Clinical Center, NIH).

Antibody solutions were initially transferred to dialysis tubing (Spectra/Por CE DispoDialyers, MWCO 10 K, 5 mL) and were dialyzed against conjugation buffer, (1 L, 0.05 M CO_3^{-2}/HCO_3^{-1}, 0.15 M NaCl, 5 mM EDTA, pH 8.6) for 6 h at 4 °C. After dialysis, the protein concentration was determined spectrophotomerically. Extinction coefficients of 1.4, 0.65, and 1.3 mL/mg·cm were determined for mAbs BL-3, CC49, and T101, respectively, based on a mAb concentration from a protein determination using the Lowry method (*24*) with a bovine serum albumin standard. A solution of **10** in water was added to the antibody solution, such that initial molar ratio of ligand to antibody was 50-fold. The reaction mixture was allowed to stand at room-temperature overnight (18 h). The reaction mixture was transferred to Centricon (MWCO 30 K or 50 K) (Amicon) filtration units. Ammonium acetate buffer (0.15 M NH_4OAc, pH 7.0) was added to the filtration unit to a total volume of 2−2.5 mL, and the filtration units were centrifuged until the remaining volume was approximately 0.5 mL. Additional buffer was added, and this process was repeated for a total of six times. The final antibody concentration was measured spectrophotomerically and the ligand-to-protein ratio (*L*/*P*) was determined as previously described (*25*). In brief, the Pb(II) arsenazo III complex provided a colorometric assay that can be easily monitored. Pb(II) is efficiently and reproducibly transchelated from the dye to the mAb macrocycle conjugate thereby eliminating a radiolabeling assay.

Radiolabeling of HEHA-mAb Conjugates with ^{225}Ac. $^{225}Ac(NO_3)_3$ (2.2−4.0 mCi) was obtained from Oak Ridge National Laboratories (ORNL) as a solid. The solid was taken up in 0.1 M HCl (1 mL), such that the specific activity became 0.22−0.40 mCi/0.1 mL. For radiolabeling the conjugates, an aliquot of ^{225}Ac solution (0.05−0.2 mCi) was added to the vials containing 0.15 M NH_4OAc (0.3−0.4 mL) at pH 4.0, 5.0 or 7.0. The HEHA-mAb conjugate (0.3−0.4 mg) in 0.15 M NH_4OAc buffer, pH 7.0, was then added. The reaction mixture was incubated for 0.5 h at 37 °C.

Nonspecific protein binding was investigated by incubating 0.08 mCi of ^{225}Ac solution with 0.5 mg of bovine serum albumin (BSA) at pH 7.0 for 0.5 h at 37 °C and the assaying for labeling by HPLC.

Preliminary labeling yields were assessed using 10 cm ITLC-SG strips (Gelman Sciences) spotted with 1 μL of the reaction and developed in 0.15 M NH_4OAc buffer, pH 4.0. In this system, the labeled proteins are retained at the origin while ^{225}Ac acetate moves with the solvent front. The strips were dried, cut into 1-cm segments, and counted in the γ-counter. They were recounted 3 h later in order to obtain corrected labeling yields for ^{225}Ac after all of the ^{213}Bi that had been previously generated decayed.

The reaction was quenched with 0.1 M EDTA, pH 6.0 (4 μL), and [^{225}Ac]HEHA-mAb conjugate was purified on size exclusion HPLC column as described above. The protein fraction was collected and counted in a Capintec Radioisotope Calibrator and recounted 3 h later to calculate the specific activity of the product.

Serum Stability Studies. Purified [^{225}Ac]HEHA-mAb conjugate (200 μL) was incubated with fetal bovine serum (2 mL) for 3 days at 37 °C. Aliquots were withdrawn at times 0, 0.25, 1, 3, 5, 24, 48, and 72 h and analyzed by HPLC on size exclusion column as described above. The radioactive fractions containing high and low molecular weight components were collected and counted on a γ-counter immediately after elution and 3 h thereafter in order to determine if they were due to free ^{225}Ac or ^{213}Bi. If a particular fraction contained ^{225}Ac/^{213}Bi in equilibrium, the results obtained after 3 h counts were very close to the initial value. In the case of mostly ^{225}Ac being present, the counts increased 2-fold as the ^{213}Bi daughter grew in and ^{225}Ac/^{213}Bi reached equilibrium. Finally, the counts decreased 16-fold if mostly ^{213}Bi was present initially as 3 h are equal to ∼4 half-lives of ^{213}Bi. As a control, free ^{225}Ac was incubated in serum under the same conditions and aliquots checked by HPLC at the above time points.

RESULTS

Ligand Synthesis. An initial attempt at the synthesis of bifunctional HEHA was using the route outlined in Scheme 1, which has been denoted as the "5 + 1" cyclization. All attempts at cyclization using compound **13** and the BOC-iminodiacetate bis-active ester failed to yield any detectable, isolable amounts of desired macrocycle. Prompted by this result, a "3 + 3" cyclization was devised (Scheme 2). *tert*-Butyloxycarbonyl-iminodoacetic acid was extended in both directions through diimide coupling with ethyl glycine to produce diester **1**. Saponification and formation of the corresponding di-succinimidyl ester **3** prepared one-half of the targeted hexaaza-18-membered. The remaining component for the macrocyclization reaction, *N*-(2-aminoethyl)-4-nitrophenylalanine was readily available (*20*). Applying methods and conditions analogous to those previously reported (*21*) resulted in macrocycle **4** being isolated after chromatography in relatively good yield (20%).

The carbamate was then removed and the amides reduced with diborane, which after treatment with acid, yielded adequately pure cyclic polyamine as the presumed hexa-hydrochloride. Alkylation was found to be best accomplished by generation of the free base **6**, which was then reacted with *tert*-butyl bromoacetate adapting a procedure reported by Schumann, et al (*26*). The fully alkylated macrocycle was isolated by chromatography, the ester cleaved, and the nitro group then hydrogenated to produce aniline **9**. Treatment of the aniline with thiophosgene produced isothiocyanate **10**, which was isolated as a stable, yellow powder.

Conjugation. Monoclonal antibodies BL-3, T101, and CC49 were conjugated with **10** when using either a 10- or 50-fold molar ratio of ligand to mAb at pH 8.6. While an initial 10-fold molar ratio yielded conjugates with *L*/*P* final ratios ranging from 0.4 to 0.6, with 50-fold initial

Scheme 1. Attempted "5 + 1" Macrocyclization Route to Bifunctional HEHA[a]

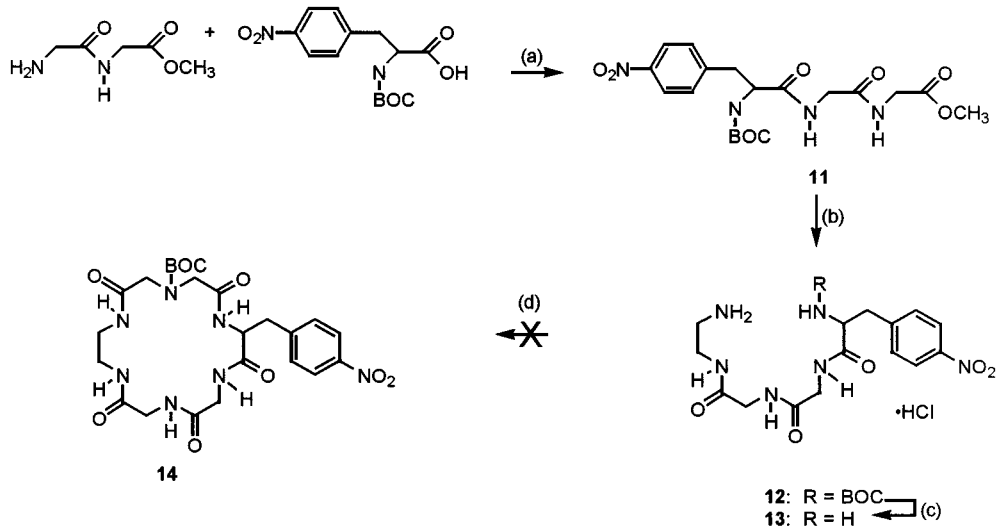

[a] (a) Et_3N, EDC, DMF, 47%. (b) Ethylenediamine, MeOH. (c) 1,4-Dioxane saturated with HCl(g). (d) 1,4-Dioxane, *N*-BOC-iminodiacetic acid di-OSu ester, 90 °C. BOC = *tert*-butyloxycarbonyl; EDC = 1-ethyl-3-(3-dimethylaminopropyl)carbodiimide; OSu = succinimidyl.

Scheme 2. Successful "3 + 3" Macrocyclization Route to Bifunctional HEHA[a]

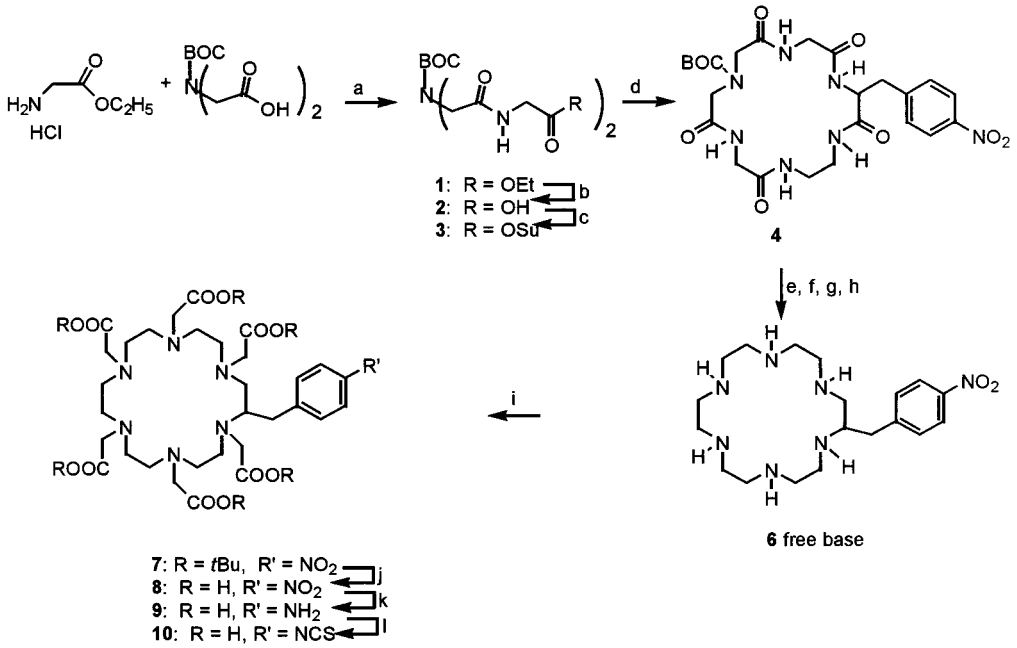

[a] Reagents and conditions: (a) NEt_3, EDC, DMF, 66%. (b) EtOH, H_2O, NaOH, 74%. (c) *N*-Hydroxysuccinimide, EDC, DMF, 73%. (d) *N*-(2-Aminoethyl)-4-nitrophenylalaninamide, 1,4-dioxane, 90 °C, 19%. (e) 1,4-Dioxane/HCl(g). (f) 1 M borane in THF, 50 °C. (g) EtOH/HCl(g). (h) NaOH(aq), extraction with $CHCl_3$. (i) $BrCH_2COOtBu$, DMF, Na_2CO_3, H_2O. (j) HCl(aq) reflux. (k) 10% Pd/C, H_2O. (l) $SCCl_2$, $CHCl_3$, H_2O. BOC = *tert*-butyloxycarbonyl; EDC = 1-ethyl-3-(3-dimethylaminopropyl)carbodiimide; OSu = succinimidyl.

excess of ligand to protein, final product *L*/*P* ratios of 2, 1.5, and 1.4 were obtained for the above mAbs, respectively.

Radiolabeling. The results of radiolabeling of HEHA-mAb conjugates are given in Table 1. During preliminary experiments, an incubation time of 30 min at 37 °C was found to produce the highest labeling yields while minimizing radiation damage to the antibody. No unspecific binding of ^{225}Ac to a free thiol group in BSA known to be responsible for unspecific binding of radiometals was detected. The labeling yields for ^{225}Ac were found to be dependent upon the pH of the reaction mixture with optimal results being obtained at pH 7.0. Labeling yields for ^{213}Bi, the ^{225}Ac daughter also present in the reaction mixture in equilibrium with ^{225}Ac, showed much less dependence on pH below 7.0. Preliminary experiments demonstrated that HEHA-mAb conjugates with a $L/P < 1.0$ resulted in decreased yields, generally lower than 30%. The data in Table 1 also shows that, by maintaining a $L/P \geq 1.0$, HEHA-mAb conjugates can be labeled with ^{225}Ac in 60−85% yield with specific activity of 200−400 μCi/mg protein, which should be easily sufficient to conduct therapy studies in animals.

Serum Stability. The results of serum stability studies of [^{225}Ac]HEHA-BL-3 conjugate in fetal bovine serum at 37 °C were performed in parallel with comparison to serum binding of free ^{225}Ac (Table 2 and Supporting Information). Free ^{225}Ac bound instantly, and essentially quantitatively, to serum proteins with a distinctive pattern of two peaks eluted at ~5.5 and 8.25 min. A

Table 1. Dependence of HEHA-MAb Labeling Yields with ^{225}Ac and ^{213}Bi on Conjugate Concentration, pH of Reaction Mixture, and Initial Activity of ^{225}Ac[a]

HEHA-MAb conjugate	amt of conjugate (μg)	pH	^{225}Ac activity (μCi)	^{213}Bi labeling (% yield)	^{225}Ac labeling (% yield)
HEHA-BL-3	300	7.0	50	80 ± 1	60 ± 3
$L/P = 2.0$	300	5.0	50	75 ± 3	43 ± 5
	300	4.0	50	67 ± 3	22 ± 2
	400	7.0	50	78 ± 2	75 ± 2
	400	7.0	100	82 ± 4	72 ± 5
	400	7.0	200	80 ± 4	85 ± 4
HEHA-T101	400	7.0	100	86 ± 5	90 ± 3
$L/P = 1.5$					

[a] Volume of reaction mixture was 0.4−0.6 mL; all yields are mean values of three experiments with SD; ^{213}Bi was present in reaction mixture in equilibrium with its parent ^{225}Ac.

Table 2. Results of Serum Stability Studies of [^{225}Ac]HEHA-BL-3 Conjugate in Fetal Bovine Serum at 37 °C[a]

time point (h)	^{225}Ac activity, associated with [^{225}Ac]HEHA-BL-3 conjugate (%)	^{213}Bi activity, associated with [^{225}Ac]HEHA-BL-3 conjugate (%)
0	100 ± 1	100 ± 1
0.4	99 ± 3	97 ± 2
1	77 ± 7	78 ± 4
3	73 ± 5	77 ± 3
5	69 ± 5	66 ± 3
24	<50	<50
48	<50	<50

[a] The values are the mean ($n = 3 \pm$ SD).

minor third component appeared at later time points eluting at ~6.8 min, with some trace amounts of radioactivity in the low molecular weight portion of the chromatogram attributable to the ^{213}Bi daughter. Select examples of the HPLC traces are shown in Figure 1. The radiolabeled HEHA-BL-3 construct, eluted at ~7.25 min, was the major component of what became a complex chromatogram after 5 h, with increased aggregate over time. Starting at the 1 h time point, a peak began to appear on the trailing slope of the [^{225}Ac]HEHA-BL-3 peak (~7.9 min) indicating the presence of species with molecular mass of ~75−100 kDa. After 5 h of incubation in serum, this peak increased to be approximately one-third of the [^{225}Ac]HEHA-BL-3 peak. By 24 h, less than 50% of ^{225}Ac was present in serum as the [^{225}Ac]HEHA-mAB conjugate.

DISCUSSION

Preliminary work in our laboratory involving screening chelating agents that formed complexes with ^{225}Ac for in vivo stability directed us to the HEHA ligand. This ligand was found to form an ^{225}Ac complex that was eliminated from the blood exceptionally rapidly, in addition to not accumulating significant amounts of the isotope in the liver and bone. Concomitantly, a substantial reduction in observable toxicity was detected during this comparison with other screened ^{225}Ac complexes (*17*, *19*).

The HEHA ligand had been conjugated to an immunoprotein through one of the acetate pendent group by formation of an isobutylcarboxycarbonic anhydride (*25*). However, this method did not provide a satisfactory conjugate and was not reproducible. Preparation of the HEHA ligand for conjugation by this method was inconvenient, and rigorous care was required in preparation of all the reagents used. Once prepared, the carboxycarbonic anhydride could not be stored and had to be used

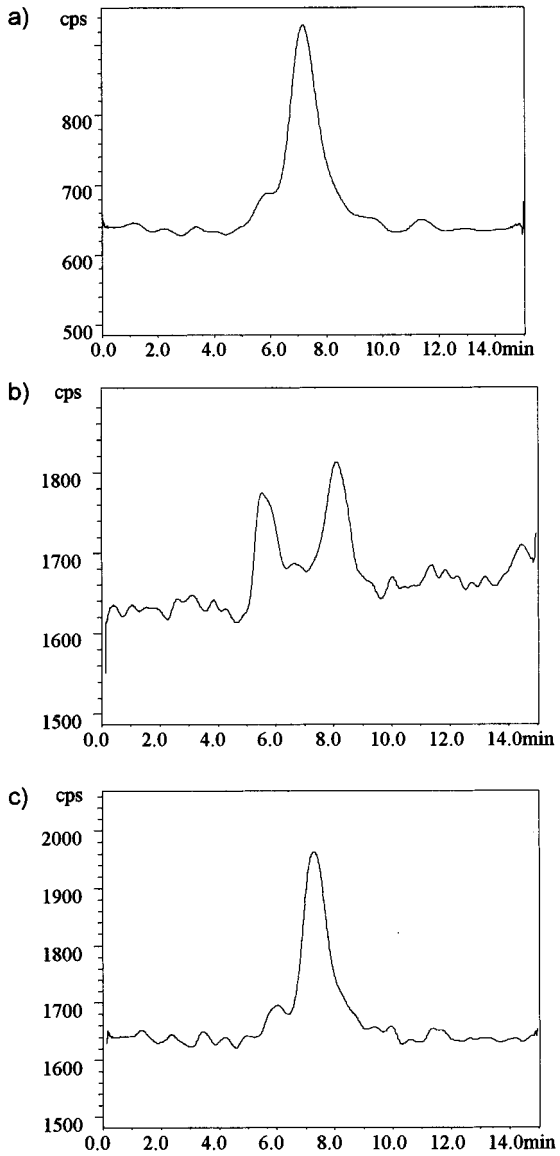

Figure 1. HPLC chromatograms of (a) [^{225}Ac]HEHA-BL-3 conjugate at $T = 0$ min, (b) free ^{225}Ac incubated in fetal bovine serum at $T = 15$ min, (c) [^{225}Ac]HEHA-BL-3 conjugate in fetal bovine serum at $T = 15$ min.

immediately. Finally, even when using a 100-fold excess of the ligand to immunoprotein, the product ligand/protein (L/P) ratios obtained were generally low with an $L/P = 0.7$ being the highest achieved (*25*). Concerns also existed about changing the coordination sphere and geometry of the HEHA ligand by using one of the carboxylates to form a protein conjugate. Conjugation of DOTA to immunoproteins employing one of the carboxylates has been reported in the literature (*27*). Changes in the ability of DOTA to coordinate Y(III) after such derivatization of the one of the acetate pendent groups of DOTA by linkage to *n*-butylamine, abbreviated as BD, had been reported (*28*). This yielded a chelate with an analogous coordination condition to a DOTA-protein conjugate where one of the carboxulates had been converted to an amide. This also produced a ligand that has different coordination properties than those of DOTA. This modification decreased the pK_a of one of the amine nitrogens of BD relative to DOTA, thereby the source of altered coordination chemistry and the rate of Y(III) loading of BD was approximately one-third to one-half that of the rate for DOTA at the same pH and temper-

ature (*28*). Recognizing the desirability of optimizing rapid formation kinetics when forming the radioimmunoconjugate, synthesis of a bifunctional C-functionalized analogue of HEHA was deemed desirable.

C-Functionalized tetraaza macrocycles have been synthesized by various routes (*29*−*31*). The synthesis of a C-functionalized DOTA [2-(4-nitrobenzyl-1,4,7,10-tetraazacyclododecane-1,4,7,10-tetraacetic acid] has also been reported previously by our group (*21*). Cyclization conditions that produced the best results for this ligand were the reaction of *N*-*tert*-butoxycarbonyl-iminodiacetic acid di-hydroxysuccinnimidyl ester (*21*) with *N*-(2-aminoethyl)-4-nitrophenylalaninamide (*20*) at modest dilution. An attractive aspect of this procedure was that this process permitted continuous addition of reactants to produce workable amounts of cyclization product. The polyaza macrocycle 18-[ane]-6 had been synthesized by Richman-Atkins chemistry (*32*). However, since our attempts to synthesize a C-functionalized 12-[ane]-4 by this methodology failed, we initially chose to employ a direct modification of our previously successful method (*21*) as outlined in Scheme 1. A five nitrogen component of the 18-[ane]-6 ring was to be reacted with a single nitrogen component to yield a product in which all of the nitrogens in the product would then be protected either as amides or carbamates. All attempts of the "5 + 1" cyclization (Scheme 1) failed to yield any detectable, isolable amounts of the desired hexaaza-18-membered macrocycle. One possible explanation for this failure might be having to overcome excessive entropy barriers to close the macrocycle using these reaction conditions. While thought entirely possible that a much slower addition rate with a higher dilution might promote formation of the desired 18-membered ring, the consensus was that this "5 + 1" route was not optimal and that a "3 + 3" cyclization would be more productive (Scheme 2). Returning to our original synthesis of the C-functionalized DOTA, one component employed for that macrocyclization chemistry, *N*-(2-aminoethyl)-4-nitrophenylalanine was immediately recognized as suitable for a "3 + 3" cyclization (*20*). The other cyclization component was reasonably accessible by extending an N-protected iminodiacetic acid with glycine to provide the two remaining nitrogens. Formation of the bis-active ester of this reagent and then applying essentially identical conditions and methods as previously employed produced the desired product in reasonably good yield. No attempts were made to optimize the reaction conditions beyond those reported herein and greater yields may well be possible.

After deprotection and careful reduction of the amides, adequately pure cyclic polyamine was obtained as the hydrochloride salt. After exploring several possible options, alkylation of the C-functionalized 18-[ane]-6 was best accomplished in a stepwise manner. The free base was first generated and briefly isolated, and then alkylated with *tert*-butyl bromoacetate through a modification of the procedure of Schumann et al. (*26*). After isolation of the fully alkylated macrocycle and deprotection of the carboxylic acids, hydrogenation, and treatment of the resultant aniline produced the final product.

The alkylation conditions reported by Schumann et al. (*26*) were found to have advantages over our earlier employed method for alkylation of a polyaza macrocycle with an alkyl bromoacetate. This had used a large excess of *tert*-butyl bromoactate in acetonitrile with solid anhydrous Na_2CO_3 and long reaction times, up to 1 week. Alternately, treatment with the same alkylating reagent in hot DMF (∼90 °C) with solid anhydrous Na_2CO_3 for 18−24 h was tested. While these methods in fact yielded the hexa-alkylated product, low yields (∼20%) complicated by the need for extensive chromatography to fully remove the partially alkylated products proved exceptionally challenging and tedious. Advantages of the Schumann method routinely included much shorter reaction times, 1 day vs 1 week, and simplified chromatography due to the greatly reduced production of partial alkylation products.

As reported here, mAbs BL-3, T101, and CC49 were conjugated with **10** to yield conjugates with ligand to protein product ratios as high as of 2, 1.5, and 1.4 were obtained for the above mAbs, respectively, when a 50-fold initial excess of ligand to protein was employed. There are numerous advantages to using **10** as compared to the HEHA-carboxycarbonic anhydride ligand for the conjugation to mAbs. Isothiocyanate **10** can be isolated, characterized, and stored as a powder in a desiccator for months at a time. The reagent needs only to be dissolved in water or conjugation buffer and added to the reaction mixture with no other required preparation. The conjugation of **10** with different mAbs worked very well and was reproducible. Three mAbs were chosen to demonstrate this: BL-3, T101, and CC49 and the HEHA-BL-3 conjugate was used for the ^{225}Ac serum stability studies. The other two mAbs (T101 and CC49) were conjugated to HEHA-NCS to demonstrate the generality of the conjugation method with other mAbs and that these conjugates can also be efficiently radiolabeled with ^{225}Ac.

The radiolabeling yields for ^{225}Ac were found to be dependent upon the pH of the reaction mixture with optimal results being obtained at pH 7.0, clearly showing the contribution of nonprotonated nitrogens of the HEHA macrocycle backbone into complexing ^{225}Ac. Interestingly, labeling yields for ^{213}Bi, the ^{225}Ac daughter also present in the reaction mixture in equilibrium with ^{225}Ac, showed much less dependence on pH below 7.0. This observation might be explained by the smaller size of Bi^{3+} cation in comparison with Ac^{3+} (103 and 112 pm, respectively) (*33*) making it easier for HEHA to encapsulate Bi^{3+} into the coordination sphere with even less contribution from the nitrogens of the macrocycle.

The ^{225}Ac radioimmunoconjugates thus formed with a $L/P \geq 1.0$ could be produced with specific activity of 200−400 μCi/mg of protein which should be easily sufficient to conduct therapy studies in animals. In accordance with the literature (*12*), 1 μCi of ^{225}Ac, together with its daughters, will supply a dose of 750 rad of energy to the tumor material, inducing a killing ratio of 99.99% of tumor cells. However, at this point, one must note that it remains completely undetermined as to whether the energy contributions from the daughter isotope decays can actually be included in such a calculation. The two daughters, ^{221}Fr ($t_{1/2}$ = 4.8 min) and ^{217}At ($t_{1/2}$ = 0.032 s), may be adequately short-lived to ensure that they do not significantly travel from the tumor site. However, ^{213}Bi, clearly has an adequate half-life to traffic and localize in the kidney (*18*). Proponents of the use of ^{225}Ac for RIT have put forth that the daughter may be formed as highly energetic, short-lived species that will bind to endogenous structures in vivo and thus minimize the departure of the ^{221}Fr and ^{217}At. It conceded that as highly improbable that the ligand forming the ^{225}Ac complex would survive the α-emission and associated recoil, and that any significant subsequent chelation of ^{221}Fr and ^{217}At daughters would occur. *However, the required experiments to determine the fate of the decay products of ^{225}Ac linked to an antibody in vivo simply have not been previously*

addressable due to the lack of a a suitable chelating agent for the parent radionuclide.

The results of serum stability studies of [^{225}Ac]HEHA-BL-3 conjugate in fetal bovine serum at 37 °C indicated that its integrity in plasma was adequate during very early time points. However, shortly thereafter, new radiolabeled protein species with both lower and higher molecular weight appeared and eventually developed into peaks with an area of approximately one-third of [^{225}Ac]-HEHA-BL-3. Similar results were obtained with the other conjugates and thus are not presented here. One possible explanation for these results may be the cutting of the mAb molecule into at least two pieces by the high LET radiation emitted in the process of cascade-like α-decay of ^{225}Ac to ^{213}Bi with concomitant increases in aggregated protein. A similar observation was reported by Mogul et al. (*34*) when the mAb CHA255 was labeled with high-specific activity ^{111}In, an Auger electron emitter, and observed protein backbone cleavage in the range from 5 to 30%. By 24 h, 42% of ^{225}Ac was still present in the serum as [^{225}Ac]HEHA complex. In support of this, we note that the protein peaks that were formed over time by the radioimmunoconjugate in serum do not correspond well with those peaks generated when ^{225}Ac was added to serum. Thus, simple broad transchelation to serum protein might not be the active mechanism by which loss of ^{225}Ac was observed. Examples of high LET radioimmunoconjugates evaluated by serum stability are few and the effects noted by Mogul et al. would predict that some apparent instability be observed for such materials.

Alternately, the [^{225}Ac]HEHA complex may very well not be stable in serum and thus HEHA may not be suitable for sequestering ^{225}Ac when conjugated to protein. Fortunately, ongoing experiments in murine models tend to indicate that the complex stability might be adequate to address the crucial question of the fate of the daughters in vivo. While use of a suitable isotope of Ac(III) would simplify this issue, detailed evaluation in murine models remains the only unambiguous method to resolve all aspects related to the ultimate use of ^{225}Ac as a therapeutic. Regardless of interpretation, therapeutic in vivo applications employing this specific derivative of HEHA would seem doubtful.

From analyzing the chromatograms of free ^{225}Ac incubated in plasma, it is clear that this isotope binds instantly to plasma proteins. This result has some significance as this binding to plasma and transport proteins could be a source of toxicity to normal tissue. Clearly the use of a stable complex is only one prerequisite to the use of ^{225}Ac and that potential adventitious binding to protein might require a very rigorous purification routine to minimize the extreme toxicity associated with this radioisotope.

CONCLUSIONS

We have synthesized the bifunctional chelating agent for ^{225}Ac, 2-(4-isothiocyanatobenzyl)-1,4,7,10,13,16-hexaazacyclohexadecane-1,4,7,10,13, 16-hexaacetic acid (HEHA-NCS) which was conjugated to three different mAbs. These conjugates were radiolabeled with ^{225}Ac with reasonably high yields and the serum stability in vitro was evaluated. Such results warrant further in vivo investigation of [^{225}Ac]HEHA-mAb conjugates as potential RIT agents and are currently ongoing to ascertain whether the RIT application is compromised by the formation of the daughters and their subsequent in vivo trafficking.

Supporting Information Available: The full series of HPLC chromatograms for the serum stability of the [^{225}Ac]HEHA antibody conjugate versus free ^{225}Ac. This material is available free of charge via the Internet at htttp://pubs.acs.org.

LITERATURE CITED

(1) (a) Zalutsky M. R., Moseley R. P., Coakham H. B., Coleman R. E., and Bigner D. D. (1989) Pharmacokinetics and tumour localisation of ^{131}I-labeled anti-tenascin monoclonal antibody 81C6 in patients with gliomas and other intracranial malignancies. *Cancer Res. 49*, 2807−2813. (b) Paganelli G., Grana C., Chino, M., Cremonesi, M., De Cicco, C., De Braud, F., Robertson, C., Zurrida, S., Casadio, C., Zoboli, S., Siccardi, A. G., and Veronesi, U. (1999) Antibody-guided three-step therapy for high grade glioma with yttrium-90 biotin. *Eur. J. Nucl. Med. 26*, 348−357. (c) Alvarez, R. D., Partridge, E. E., Khazaeli, M. B., Plott, G., Austin, M., Kilgore, L., Russell, C. D., Liu, T. H., Grizzle, W. E., Schlom, J., LoBuglio, A. F., and Meredith, R. F. (1997) Intraperitoneal Radioimmunotherapy of Ovarian Cancer with ^{177}Lu-CC49: A Phase I/II Study. *Gyn. Oncol. 65*, 94−101. (d) DeNardo, G. L., DeNardo, S. J., Kukis, D. L., O'Donnel, R. T., Shen, S., Goldstein, D. S., Kroger, L. A., Salako, Q., DeNardo, D. A., Mirick, G. R., Mausner, L. F., Srivastava, S. C., and Meares, C. F. (1998) Maximum Tolerated Dose of ^{67}Cu-2IT-BAT-LYM-1 for Fractionated Radioimmunotherapy of Non-Hodgkin's Lymphopma: A Pilot Study. *Anticancer Res. 18*, 2779−2788.

(2) Srivastava, S. C. (1996) Criteria for the selection of radionuclides for targeting nuclear antigens for cancer radioimmunotherapy. *Cancer Biother. Radiopharm. 11*, 43−50.

(3) McDevitt, M. R., Sgouros, G., Finn, R. D., Humm, J. L., Jurcic, J. G., Larson, S. M., and Scheinberg, D. A. (1998) Radioimmunotherapy with alpha-emitting nuclides. *Eur. J. Nucl. Med. 25*, 1341−1351.

(4) Waldmann, T. A., White, J. D., Carrasquillo, J. A., Reynolds, J. C., Paik, C. H., Gansow, O. A., Brechbiel, M. W., Jaffe, E. S., Fleisher, T. A., Goldman, C. K., Top, L. E., Bamford, R., Zaknoen, S., Roessler, S., Kasten-Sportes, C., Englang, R., Litou, H., Johnson, J. A., Jackson-White, T., Manns, A., Hanchard, B., Junghans, R. P., and Nelson, D. L. (1995) Radioimmunotherapy of IL-2Ra-Expressing Adult T-cell Leukemia with Yttrium-90 Labeled Anti-Tac. *Blood 86*, 4063−4075.

(5) O'Donoghue, J. A., Bardies, M., and Wheldon, T. E. (1995) Relationships between Tumor Size and Curability for Uniformly Targeted Therapy with Beta-Emitting Radionuclides. *J. Nucl. Med. 36*, 1902−1909.

(6) Jurcic, J. G., Caron, P. C., and Scheinberg, D. A. (1995) Monoclonal Antibody Therapy of Leukemia and Lymphoma. In *Advances in Pharmacology* (J. T. August, M. W. Anders, F. Murad, J. T. Coyle, Eds.) Vol. 33, pp 287−314, Academic Press, Inc., New York.

(7) Kennel, S. J., and Mirzadeh, S. (1998) Vascular targeted radioimmunotherapy with ^{213}Bi—an α-particle emitter. *Nucl. Med. Biol. 25*, 241−246.

(8) Nikula, T. K., McDevitt, M. R., Finn, R. D., Wu, C., Kozak, R. W., Garmestani, K., Brechbiel, M. W., Curcio, M. J., Pippin, C. G., Tiffany-Jones, L., Geerlings, M. W., Sr., Apostolidos, C., Molinet, R., Geerlings, M. W., Jr., Gansow, O. A., and Scheinberg, D. A. (1999) Alpha-Emitting Bismuth Cyclohexylbenzyl DTPA Constructs of Recombinant Humanized Anti-CD33 Antibodies: Pharmacokinetics, Bioactivity, Toxicity and Chemistry. *J. Nucl. Med. 40*, 166−176.

(9) (a) Zalutsky, M. R., McLendon, R. E., Garg, P. K., Archer, G. E., Schuster, J. M., and Bigner, D. D. (1994) Radioimmunotherapy of neoplastic meningitis in rats using an α-particle-emitting immunoconjugate. *Cancer Res. 54*, 4719−4725. (b) Zalutsky, M. R., Garg, P., Friedman, H. S., and Bigner, D. D. (1989) Labeling monoclonal antibodies and $F(ab')_2$ fragments with the α-particle emitting nuclide astatine-211: Preservation of the immunoreactivity and in vivo localization capacity. *Proc. Natl. Acad. Sci. 86*, 7149−7153.

(10) Scheinberg, D. A., Jurcic, J., Finn, R., Larson, S., McDevitt, M. R., Geerlings, M., Sgouros, G., Brechbiel, M., and Gansow,

O. A. (1998) *Clinical Applications of Targeted Alpha Particles for Cancer Therapy*, 215th National Meeting of the American Chemical Society, Dallas, TX.

(11) Zalutsky, M. R., Akabani, G., Cokgor, I., Friedman, H. S., Coleman, R. E., Friedman, A. H., McLendon, R. E., Reist, C. J., Pegram, C. N., Zhao, X.-G., and Bigner, D. D. (1998) Phase I trial of astatine-211 labeled human/mouse chimeric anti-tenascin antibody administered into malignant brain tumor resection cavities. Society of Neuro-Oncology Annual Meeting, San Francisco, CA. *Neuro-Oncology 1*, S65−S66.

(12) (a) Geerlings, M. W., Kaspersen, F. M., Apostolidis, C., and Van Der Hout, R. (1993) The feasibility of ^{225}Ac as a source of α-particles in radioimmunotherapy. *Nucl. Med. Commun. 14*, 121−125. (b) Geerlings, M. W., and Kaspersen F. M. Radioimmunotherapy using α-particles emission. U.S. Patent 5,246,691.

(13) Davis, I. A., Glowienka, K. A., Boll, R. A., Deal, K. A., Brechbiel, M. W., Stabin, M., Bochsler, P. N., Mirzadeh, S., and Kennel, S. J. (1999) Comparison of $^{225}Actinium$ Chelates: Tissue Distribution and Radiotoxicity. *Nucl. Med. Biol. 26*, 581−589.

(14) Gansow, O. A. (1991) Newer Approaches to the Radiolabeling of Monoclonal Antibodies by the Use of Metal Chelates. *Nucl. Med. Biol. 18*, 369−381.

(15) (a) Makarova, T. P., Sinitsyna, G. S., Stepanov, A. V., Shestakova, I. A., and Shestkov, B. I. (1972) Determination of the Complex Formation of Actinium 1. Determination of the Stability constants of Ethylenediaminetetraacetate Complexes of Actinium and its Separation from Lanthanum in Solutions of EDTA by the Method of Electromigration. *Radiochimiya 14*, 538−541. (b) Beyer, G. J., Offord, R. E., Kunzi, G., Jones, R. M. L., Ravin, U., Aleksandrova, Yu., Werlen, R. C., Macke, H., Lindroos, M., Jahn, S., and Tengblad, D. (1995) Biokinetics of Monoclonal Antibodies Labeled with Radio-Lanthanides and 225-Ac in Xenografted Nude Mice. *J. Labelled Cmpd. Radiopharm. 37*, 529−530.

(16) (a) Chen, X., Ji, M., Fisher, D. R., and Wai, C. M. (1998) Carboxylate-derived calixarenes with high selectivity for actinium-225. *Chem. Commun*. 377−378. (b) Gansey, M. H. B. G., de Haan, A. S., Bos, E. S., Verboom, W., and Reinhoudt, D. N. (1999) Conjugation, Immunoreactivity, and Immunogenicity of Calix[4]arenes; Model Study to Potential Calix[4]-arene-Based Ac3+ Chelators. *Bioconjugate Chem. 10*, 613−623.

(17) Deal, K. A., Davis, I. A., Mirzadeh, S., Kennel, S. J., and Brechbiel, M. W. (1999) Improved In Vivo Stability of Actinium-225 Macrocyclic Complexes. *J. Med. Chem. 42*, 2998−2992.

(18) Durbin, P. W. (1960) Metabolic characteristics within a chemical family. *Health Phys. 2*, 225−238.

(19) Kennel, S. J., personal communication.

(20) Brechbiel, M. W., Gansow, O. A., Atcher, R. W., Schlom, J., Esteban, J., Simpson, D. E., and Colcher, D. (1986) Synthesis of 1-(*p*-Isothiocyanatobenzyl) Derivatives of DTPA and EDTA. Antibody Labeling and Tumor-Imaging Studies. *Inorg. Chem. 25*, 2772.

(21) McMurry, T. J., Brechbiel, M. W., Kumar, K., and Gansow, O. A. (1992) Convenient Synthesis of Bifunctional Tetraaza Macrocycles. *Bioconjugate Chem. 3*, 108−117.

(22) (a) Muraro, R., Kuroki, M., Wunderlich, D., Poole, D. J., Colcher, D., Thor, A., Greiner, J. W., Simpson, J. F., Molinolo, A., Noguchi, P., and Schlom, J. (1988) Generation and characterization of B72.3 second generation monoclonal antobodies reactive with the tumor-associated glycoprotein 72 antigen. *Cancer Res. 48*, 4588−4596. (b) Colcher D., Esteban, J. E., Carrasquillo, J. A., Sugarbaker, P., Reynolds, J. C., Bryant, G., Larson, S. M., and Schlom, J. (1987) Complementation of intracavitary and intravenous administration of a monoclonal antibody (B72.3) in patients with carcinoma. *Cancer Res. 47*, 4218−4224.

(23) Carrasquillo, J. A., Raynolds, J. C., Bunn, P. A., Foon, K. A., Shuke, N., Schroff, R. W., Mulshine, J. L., Perentesis, P., Szymendera, J., Horowitz, M., and Larson, S. M. (1993) Pharmacokinetics of In-111 T101 (Anti-CD5) Monoclonal Antibody in Patients with Cutaneous T-Cell Lymphoma. *Antibody, Immunoconjugates, Radiopharm. 6*, 111−126.

(24) Lowry O. H., Rosebrough N. J., Farr A., and Randall A. J. (1951) Protein measurement with the folin phenol reagent. *J. Biol. Chem. 193*, 265−275.

(25) Dadachova, E., Chappell, L. L., and Brechbiel, M. W. (1999) Spectrophotometric Method for Determination of Bifunctional Macrocyclic Ligands in Macrocyclic Ligand−Protein Conjugates. *Nucl. Med. Biol. 26*, 977−982.

(26) Schumann, H., Bottger, U. A., Zietzke, K., Hemling, H., Kociok-Kohn, G., Pickardt, J., Hahn, F. E., Zschunke, A., Schiefner, B., Gries, H., Raduchel, B., and Platzek, J. (1997) 1,4,7,10,13,16,19,22-Octaazacyclotetracosane-1,4,7,10,13,16,19,22-octaacetic acid (H(8)OTEC) and 1,4,7,10,14,17,20,23-octaazacyclohexacosane-1,4,7,10,14,17,20,23-octaacetic acid (H(8)OHEC): Synthesis and characterization of two large macrocyclic polyamine polycarboxylic ligands and some of their copper(II) and lanthanide(III) complexes. *Chem. Ber.-Rec. 130*, 267−277.

(27) (a) Srivastava, S. C., Mausner, L. F., Mease, R. C., Meinken, G. E., Joshi, V., Kolsky, K., Sweet, M., and Steplewski, Z. (1995) Development and evaluation of copper-67 and samarium-153 labeled conjugates for tumor radioimmunotherapy. *Int. J. Pharmacog. 33*, 92−101. (b) Lewis, M. R., and Shively, J. E. (1998) Maleimidocysteineamido-DOTA Derivatives: New Reagents for Radiometal Chelate Conjugation to Antibody Sulfhydryl Groups Undergo pH-Dependent Cleavage Reactions. *Bioconjugate Chem. 9*, 72−86.

(28) Keire, D. A., and Kobayashi, M. (1999) NMR Studies of the Metal-Loading Kinetics and Acid−base Chemistry of DOTA and Butylamine-DOTA. *Bioconjugate Chem. 10*, 454−463.

(29) Takenouchi, K., Watanabe, K., Kato, Y., Koike, T., and Kimura, E. (1993) Novel Bifunctional Macrocyclic Chelating Agents Appended with Pendant-Type Carboxymethylamino Ligand and Nitrobenzyl Group and Stability of the $^{88}Y(III)$ Complexes. *J. Org. Chem. 58*, 1955−1958.

(30) Moi, M. K., Meares, C. F., and DeNardo, S. J. (1988) The peptide way to macrocyclic bifunctional chelating-agents − synthesis of 2-(*p*-nitrobenzyl)-1,4,7,10-tetraazacyclododecane-N,N′,N″,N‴-tetraacetic acid and study of its yttrium(III) complex. *J. Am. Chem. Soc. 110*, 6266−6267.

(31) Cox, J. P. L., Jankowski, K. J., Kataky, R., Parker, D., Beeley, N. R. A., Boyce, B. A., Eaton, M. A. W., Millar, K., Millican, At. T., Harrison, A., and Walker, C. (1989) Synthesis of a Kinetically Stable Y-90 Labeled Macrocycle antibody Conjugate. *J. Chem. Soc., Chem. Commun*. 797−789.

(32) Atkins, T. J., Richman, J. E., and Oettlye, W. F., (1988) Macrocyclic Polyamines: 1,4,7,10,13,16-Hexaazacyclooctadecane. In *Organic Synthesis Collective* (W. E. Noland, Ed.) Vol. 6, pp 652−662, John Wiley & Sons: New York, 1988.

(33) Shannon, R. D. (1976) Revised Effective Ionic Radii and Systematic Studies of Interatomic Distances in Halides and Chalcogenides. *Acta Crystallogr. 32*, 751−767.

(34) Mogul, R., and Meares, C. F. (1997) Mapping an Antibody Binding Site by Nuclear Decay *J. Am. Chem. Soc. 119*, 7169−7170.

BC990153F

© 2000 American Chemical Society, Bioconjugate Chem., Chappell bc990153f Supporting Info Page 1

Supporting Information for:

Synthesis, Conjugation and Radiolabeling of a Novel Bifunctional Chelating Agent for ^{225}Ac for Applications in Radioimmunotherapy.

Lara L. Chappell, Kim A. Deal, Ekaterina Dadachova, Martin W. Brechbiel

(Bioconjugate Chemistry)

Figure 1 Gel filtration HPLC chromatograms of ^{225}Ac-HEHA-BL-3 conjugate (left column) and free ^{225}Ac (right column) incubated in fetal bovine plasma at 37°C. a) UV trace of plasma proteins. Samples were analyzed at times b) 0; c) 15 min; d) 1 h; e) 3 h; f) 5 h; g) 24 h; and h) 48 h.

a)

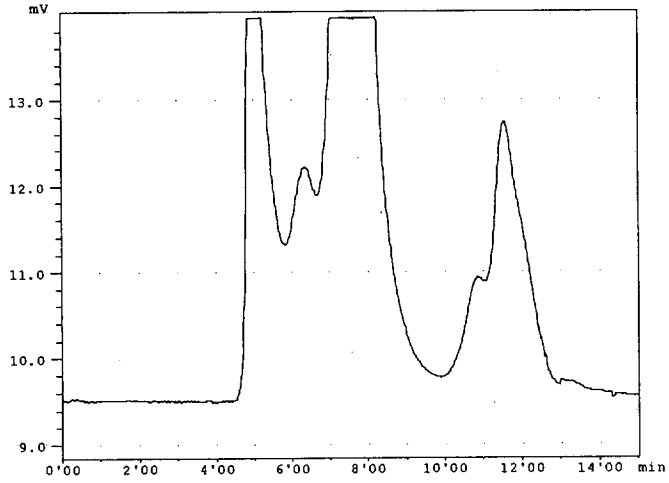

b)

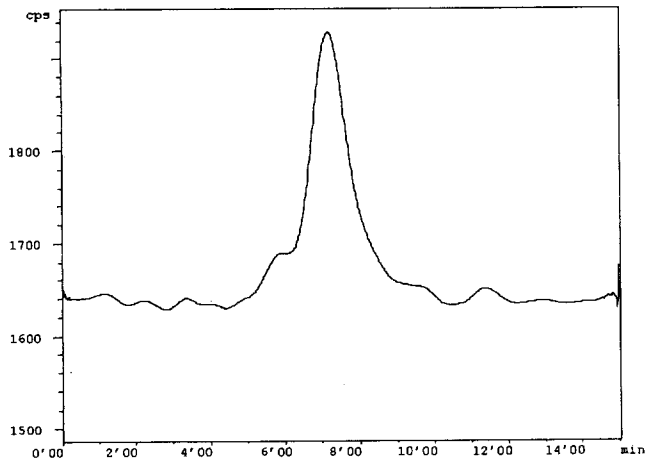

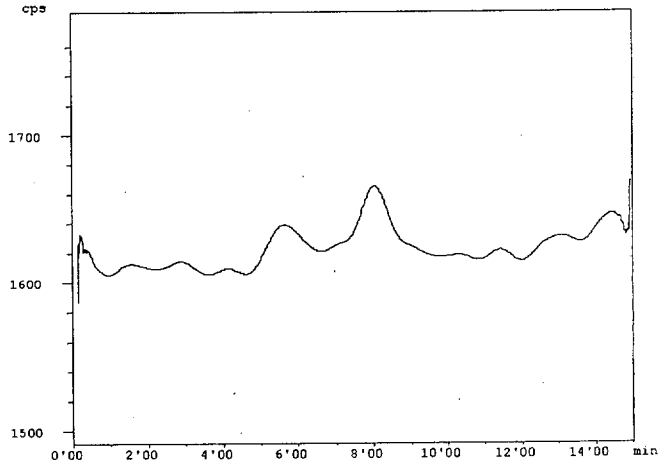

c)

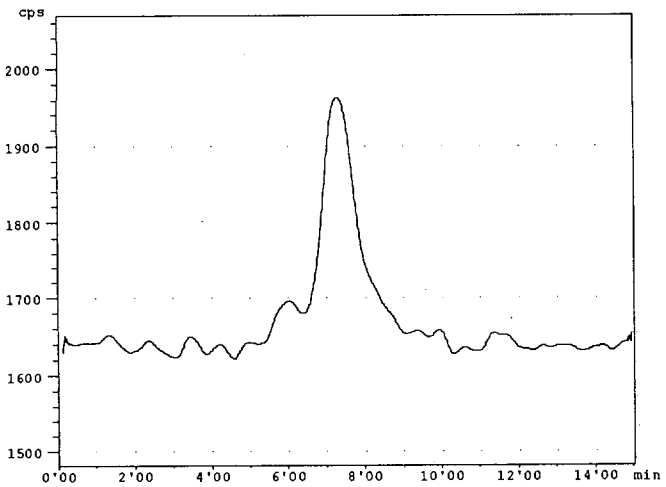
cps
2000
1900
1800
1700
1600
1500
0'00
2'00
4'00
6'00
8'00
10'00
12'00
14'00
min

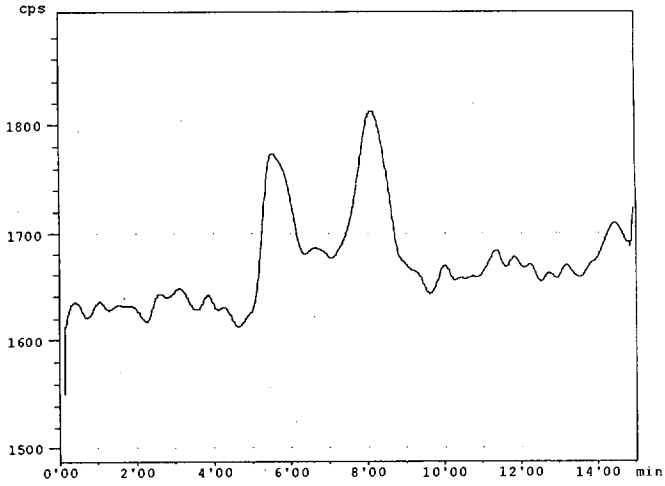
cps
1800
1700
1600
1500
0'00
2'00
4'00
6'00
8'00
10'00
12'00
14'00
min

d)

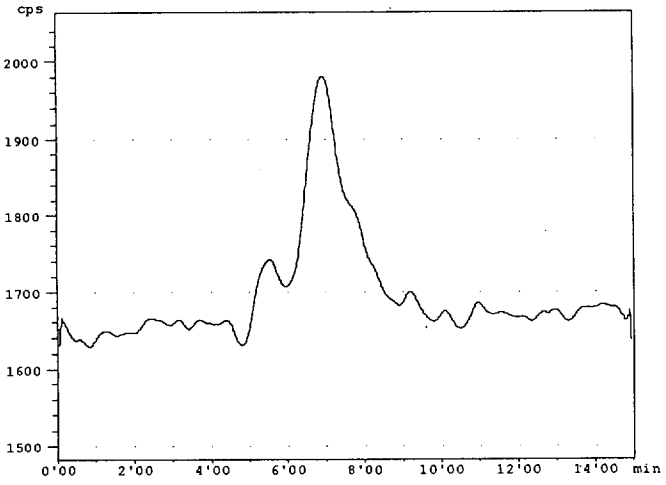
cps
2000
1900
1800
1700
1600
1500
0'00
2'00
4'00
6'00
8'00
10'00
12'00
14'00
min

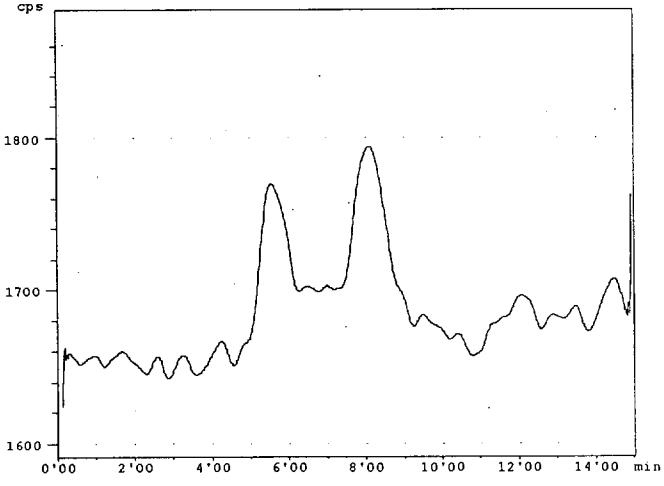
cps
1800
1700
1600
0'00
2'00
4'00
6'00
8'00
10'00
12'00
14'00
min

e)

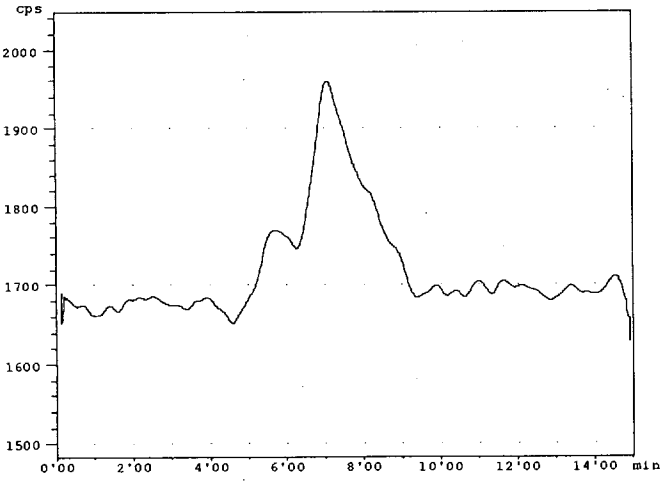
cps
2000
1900
1800
1700
1600
1500
0'00
2'00
4'00
6'00
8'00
10'00
12'00
14'00
min

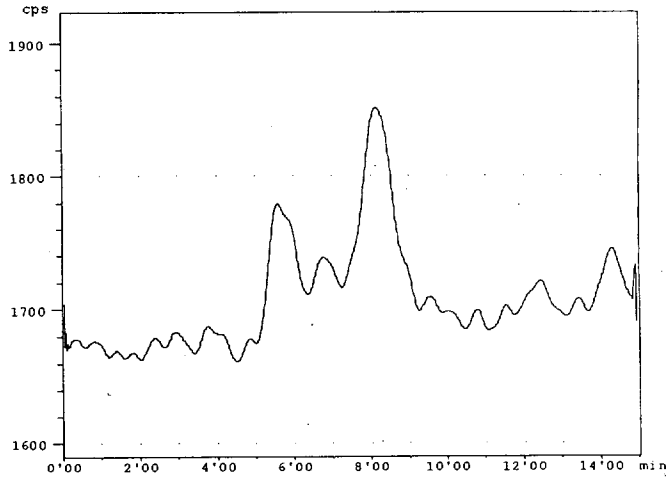
cps
1900
1800
1700
1600
0'00
2'00
4'00
6'00
8'00
10'00
12'00
14'00
min

f)

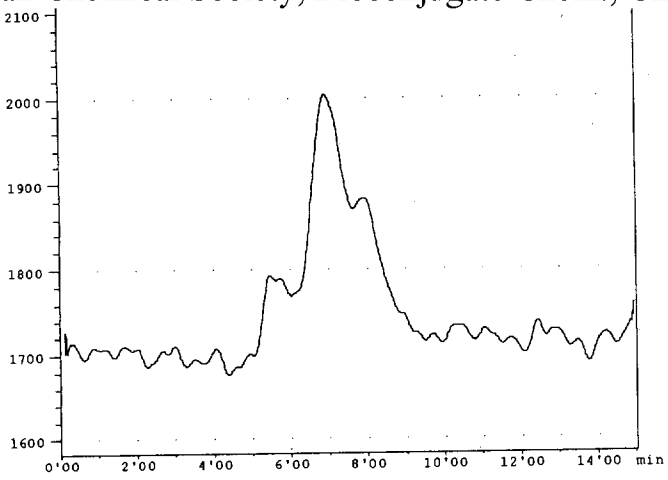
2100
2000
1900
1800
1700
1600
0'00
2'00
4'00
6'00
8'00
10'00
12'00
14'00
min

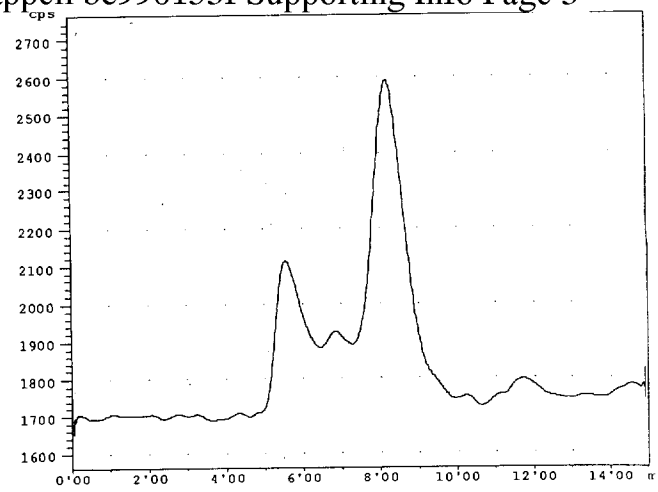
cps
2700
2600
2500
2400
2300
2200
2100
2000
1900
1800
1700
1600
0'00
2'00
4'00
6'00
8'00
10'00
12'00
14'00

g)

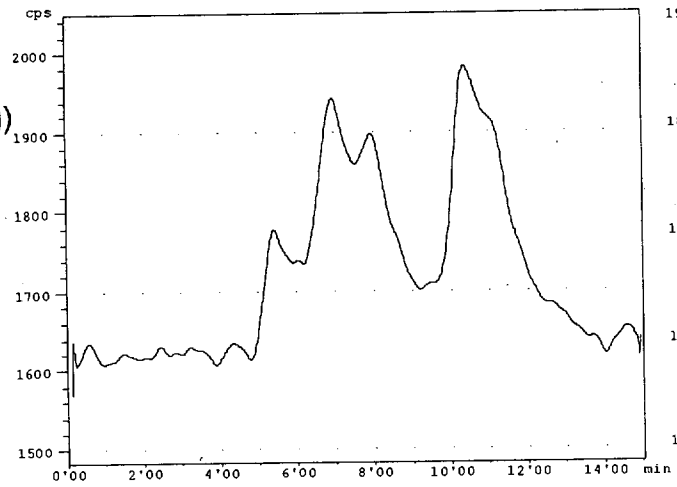
cps
2000
1900
1800
1700
1600
1500
0'00
2'00
4'00
6'00
8'00
10'00
12'00
14'00
min

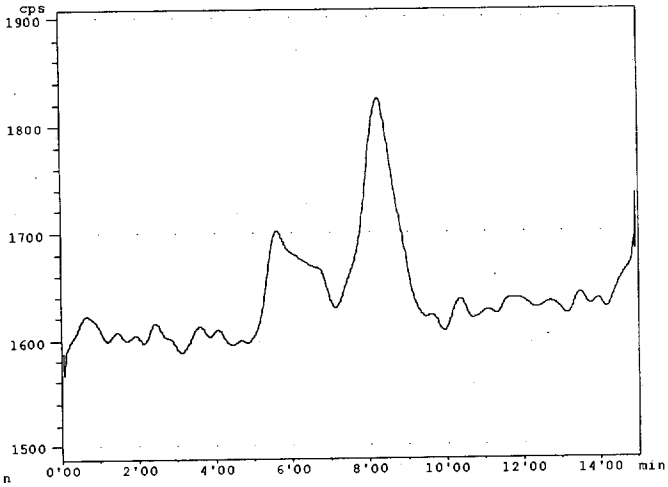
cps
1900
1800
1700
1600
1500
0'00
2'00
4'00
6'00
8'00
10'00
12'00
14'00
min

h)

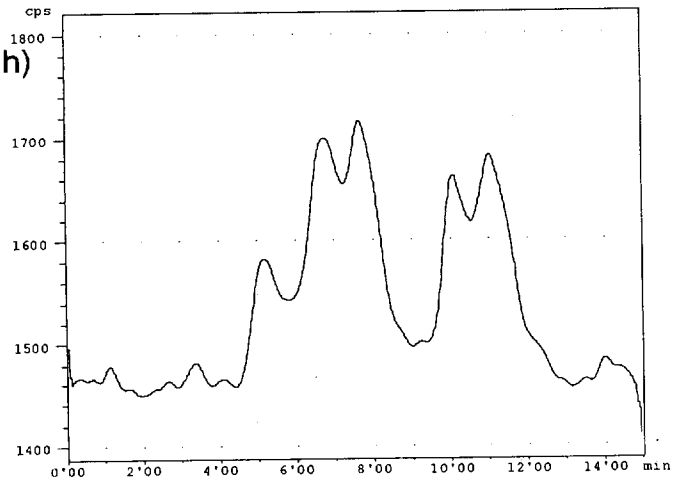
cps
1800
1700
1600
1500
1400
0'00
2'00
4'00
6'00
8'00
10'00
12'00
14'00
min

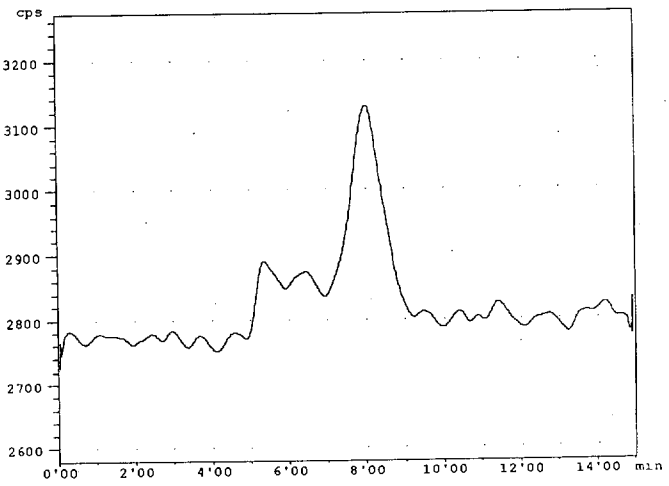
cps
3200
3100
3000
2900
2800
2700
2600
0'00
2'00
4'00
6'00
8'00
10'00
12'00
14'00
min

Mechanism of Intermolecular Purine-Purine-Pyrimidine Triple Helix Stabilization by Comb-Type Polylysine Graft Copolymer at Physiologic Potassium Concentration

Anwarul Ferdous,† Toshihiro Akaike, and Atsushi Maruyama*

Department of Biomolecular Engineering, Faculty of Bioscience and Biotechnology, Tokyo Institute of Technology, 4259 Nagatsuta, Midori-ku, Yokohama 226-8501, Japan. Received November 30, 1999; Revised Manuscript Received March 31, 2000

We previously reported a novel strategy to stabilize purine motif triplex DNA within a mammalian gene promoter at physiologically relevant pH, temperature, and potassium (K^+) concentrations by a comb-type poly(L-lysine)-*graft*-dextran copolymer [Ferdous et al., (1998) *Nucleic Acids Res. 26*, 3949−3954]. Here we describe the major contribution(s) of the copolymer to stabilize the purine motif triplex DNA at physiological K^+ concentrations. Self-aggregation through guanine-quartet formation of guanine-rich (G-rich) triplex-forming oligonucleotides (TFOs) has long been proposed for K^+-mediated inhibition of the purine motif triplex formation. However, this was not the case for the severe inhibitory effect of K^+ observed under our reaction conditions. Rather significant decrease in rate of triplex formation involving a G-rich TFO was a major factor to confer K^+ inhibition. Interestingly, in the presence of the copolymer the rate of triplex formation was tremendously increased and K^+-induced dissociation of preformed triplexes was not observed. Moreover, the triplex-promoting/stabilizing efficiency of the copolymer was amazingly higher than that of physiological concentrations of spermine. An absolute increase in binding constant of the TFO to the target duplex could therefore be the predominant mechanistic source for the copolymer-mediated triplex stabilization under physiological conditions in vitro.

INTRODUCTION

Over a decade, oligonucleotide-based strategy by triple helix (triplex) formation (i.e., the antigene strategy) through sequence-specific interaction of triplex-forming oligonucleotides (TFOs)[1] with the target duplex has attracted a great deal of attention for its possible role to alter gene functions (*1*−*8*). Unfortunately, extreme instability of both purine motif (*2*, *9*, *10*) and pyrimidine motif (*1*, *11*) triplexes under physiological conditions severely limited their therapeutic applications. In the pyrimidine-motif, pyrimidine-rich TFOs bind parallel to the homopurine strand of the duplex by Hoogsteen hydrogen bonding to form T·A:T and C^+·G:C triplets (*1*, *12*). Since the cytosine residues in the pyrimidine-rich TFOs are to be protonated to bind with the guanine of the G:C duplex, an acidic condition (pH < 6) is needed for the pyrimidine-motif triplex formation and thus impedes its utility in vivo (*1*, *11*, *12*). On the other hand, purine-rich TFOs run antiparallel to the homopurine strand and bind by reverse Hoogsteen hydrogen bonding to form A·A:T (or T·A:T) and G·G:C triplets (*2*, *9*, *10*). Despite the fact that physiological concentrations of various monovalent cations (M^+), particularly K^+ (*13*, *14*), severely inhibit the purine motif triplex formation, its stability at physiologic pH makes it more suitable to use in vivo.

For a long time, it has been proposed that an intra- and/or intermolecular self-association through guanine-quartet (G-quartet) and parallel or antiparallel homoduplex formation of G-rich TFOs confer K^+ inhibition of the purine motif triplex formation (*15*−*18*). But a decrease in rates of association and/or an increase in rates of dissociation of triplexes have also been suggested for K^+-mediated inhibition of triplex formation (*14*, *17*, *19*, *20*). We reported that a comb-type poly(L-lysine)-*graft*-dextran copolymer (Figure 1A), which hereafter will be referred to as the PLL−*g*-Dex copolymer, significantly stabilizes triplexes (*21*−*23*) and abrogates M^+ inhibition of the purine motif triplex formation involving a 30-mer target duplex from rat collagen α1 (I) gene promoter and its specific G-rich TFO, Pu (Figure 1B) (*22*, *23*). Although a chemical modification strategy of guanine in G-rich TFOs has been shown to increase triplex stability partially by reducing G-quartet formation (*20*, *24*−*28*), the putative mechanism(s) involved in the copolymer-mediated triplex stabilization with unmodified Pu is not yet clearly understood.

The main interest of our present study is, therefore, to define a mechanistic explanation for the copolymer-mediated triplex stabilization under physiologic [K^+]. Results from electrophoretic mobility shift assays (EMSAs) indicate that under our reaction conditions Pu is relatively insensitive to K^+ to form G-quartet structure. On the other hand, kinetic studies strongly suggest that tremendous decrease in the rate of triplex formation (i.e., the binding rate of Pu to duplex). However, addition of the copolymer in the reactions significantly increased the binding rate of Pu to duplex DNA (i.e., promotes triplex formation) and also decreased dissociation rate of Pu. Finally, the triplex-promoting/stabilizing efficiency of the

* To whom correspondence should be addressed. Phone and Fax: +81-45-924-5122. E-mail: amaruyam@bio.titech.ac.jp.

† Present address: University of Texas, Southwestern Medical Center at Dallas, Department of Internal Medicine, TX.

[1] Abbreviations: PLL-*g*-Dex, polylysine-*graft*-dextran copolymer; EMSA, electrophoretic mobility shift assay; G-rich, guanine-rich; M^+, monovalent cations; ODN, oligodeoxynucleotide; TFO, triplex-forming oligonucleotide; t-DNA, calf thymus DNA.

10.1021/bc990166t CCC: $19.00 © 2000 American Chemical Society
Published on Web 06/17/2000

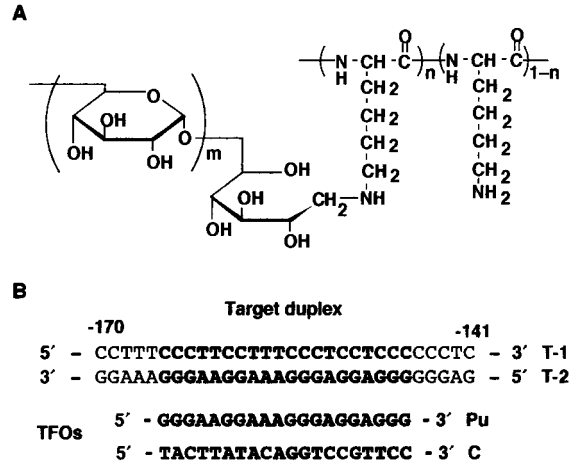

Figure 1. Schematic representations of the copolymer and ODNs used in this study. (A) Structural formula of the PLL-*g*-Dex copolymer. Preparation and characterization of the copolymer has been described previously in detail (*21*, *29*). Degree of substitution (*n*) is 0.2. Number-averaged polymerization degrees of PLL and dextran are 200 and 36.5 (*m*), respectively. (B) Sequences of the ODNs. ODN sequences of the target duplex (T-1 and T-2) and TFOs used in this study have been described before (*22*). In brief, T-2 was end-labeled and mixed with T-1 to prepare the labeled duplex for triplex analysis. Purine-rich (Pu) and control (C) TFOs are shown aligned with the triplex-forming target region in duplex (shown in bold).

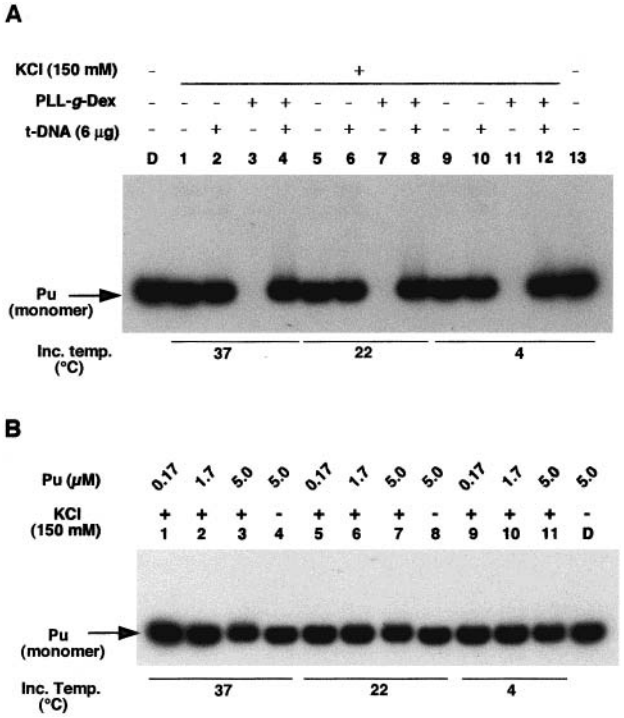

Figure 2. EMSA of Pu aggregation. (A) Pu does not form self-aggregates in the presence or absence of KCl and the copolymer. To effect self-aggregation, Pu (0.17 μM) containing trace amount of labeled Pu was mixed with control TFO for final 5 μM concentration of DNA in buffer containing 50 mM Tris-acetate (pH 7) and 10 mM $MgCl_2$ (buffer A). Reaction mixtures (9 μL) were incubated for 6 h at indicated temperatures (°C) either in the presence (+) or absence (−) of KCl and 2.5 μg of the copolymer (1 μM). Samples were resolved through 15% native polyacrylamide gel with (+) or without (−) adding thymus DNA (t-DNA). In lane D, formamide-denatured (10 min at 90 °C) sample was used without incubation. The gel was dried and exposed to Kodak Bio-max film at −80 °C. An arrow shows the position of monomeric form of Pu. (B) Effect of Pu concentration on K^+-induced self-aggregation. Reactions were carried out identically as described in panel A, except that Pu at the indicated final concentrations was incubated with (+) or without (−) KCl and then analyzed as above.

copolymer was remarkably higher than that of physiologic concentrations of spermine.

EXPERIMENTAL PROCEDURES

Oligonucleotides and t-DNA. Oligodeoxynucleotides (ODNs) for target duplex DNA (T-1 and T-2), purine-rich (Pu) and control (C) TFOs used in this study were obtained and processed as described previously (*22*). In brief, all ODNs were purified by gel electrophoresis on a 15% denaturing polyacrylamide gel, dissolved in 10 mM tris-acetate (pH 7.0), and quantitated by UV spectroscopy. Preparation of stock solution of calf thymus DNA (t-DNA) (Sigma-Aldrich, Japan) and its use to eliminate copolymer−DNA interaction before electrophoresis were described in detail (*22*, *23*).

Preparation of PLL-*g*-Dex Copolymer. Poly(L-lysine) HBr (PLL HBr, Mw = 4.5×10^4) and dextran T-10 (Dex) (Mn = 5.9×10^3) were obtained from Peptide Institute, Inc., Osaka, Japan and Pharmacia Biotech., Uppsala, Sweden, respectively. Preparation, isolation, and characterization of the PLL-*g*-Dex copolymer has been described in detail (*21*, *29*). Briefly, the copolymer (Dex content = 90 wt %, Mn = 2.5×10^5, as free salt) was prepared by a reductive amination reaction between PLL HBr and Dex in dimethyl sulfoxide using $NaBH_3$-CN as a catalyst.

Electrophoretic Mobility Shift Assays (EMSAs). *To analyze G-Quartet Formation of Pu.* Pu was end-labeled with [γ-^{32}P]ATP (Amersham) and T4 polynucleotide kinase and labeled Pu free from unincorporated [γ-^{32}P]ATP was purified on a Sephadex G-25 column (Pharmacia Biotech.) according to the manual. After freeze-drying, Pu was dissolved in 10 mM tris-acetate (pH 7.0) and was stored at −30 °C. All TFOs (Pu and C) were heated at 65 °C for 10 min to prevent self-aggregation and then quickly cooled on ice. To effect G-quartet formation, 10 nM labeled Pu was mixed with unlabeled Pu for the indicated final concentrations of Pu. Control TFO (C) was then added as carrier DNA to adjust the equimolar concentration (5 μM) of TFOs (Pu + C) as well as to avoid nonspecific adsorption of Pu to the tube walls and subsequent losses during processing. Required amount of control TFO was also added in all other experiments for final 5 μM concentration of TFOs as described (*22*). Reaction mixtures (9 μL) in 50 mM tris-acetate (pH 7.0) and 10 mM $MgCl_2$ (buffer A) were incubated for 6 h at different temperatures either in the presence or absence of KCl (150 mM) and the copolymer at a copolymer/DNA charge (P/D) ratio of 2 as described (*21*, *22*). After incubation, 2 μL of 50% glycerol solution containing bromophenol blue and 1 μL of reaction buffer with or without t-DNA (6 μg) were added. Samples were immediately resolved at room temperature by electrophoresis at 8 V/cm for 5 h through a 15% native polyacrylamide gel containing 2% glycerol, 45 mM tris-borate, 1 mM EDTA, and 10 mM KCl. This minimal K^+ concentration was also present in the electrophoresis buffer to maintain G-quartet integrity (*30*). Dried gels were then exposed to Kodak Biomax film at −80 °C.

For Triplex Assays in Which Pu Was Added with the Target Duplex with or without Preincubation in the Presence or Absence of K^+ and the Copolymer. Pu (0.34 μM) in 6 μL of buffer A was preincubated for 6 h at 37 °C in the presence or absence of 140 mM KCl and the copolymer as described above. Target duplex (3 ng) in buffer A (6 μL) with or without KCl (140 mM) was then

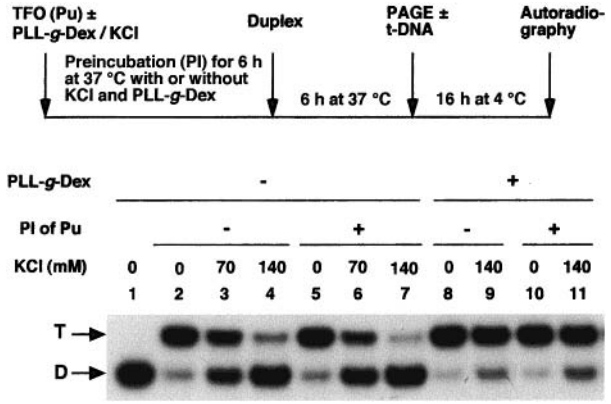

Figure 3. Coanalysis of self-aggregation and triplex formation by Pu. Reaction protocol that allowed coanalysis of KCl effects on Pu aggregation and triplex formation is shown diagrammatically above the gel. Reaction mixtures (6 μL) in buffer A containing Pu (0.34 μM) alone (lanes 5−7, 10, and 11), were preincubated (PI) for 6 h at 37 °C in the presence (+) or absence (−) of the copolymer and KCl (140 mM). Labeled duplex (3 ng) with (lanes 7 and 11) or without (lanes 1, 5, 6, and 10) 140 mM KCl in 6 μL of buffer A was then added and incubated for an additional 6 h to effect triplex formation at the indicated final concentrations of KCl. Triplex formation was also performed under the same conditions but without preincubating Pu (lanes 2−4, 8, and 9). t-DNA was added in reactions containing the copolymer and samples were electrophoresed to separate the duplex (D) and triplex (T) DNAs as described before (*22*).

added to the preincubated Pu to reach the final Pu concentration of 0.17 μM and further incubated for an additional 6 h for triplex formation at the indicated final concentrations of KCl. Triplex formation was also analyzed under identical conditions but by adding the target duplex and Pu with or without K^+ and the PLL−*g*-Dex copolymer simultaneously. Samples were resolved on a 15% native polyacrylamide gel prepared in buffer A containing 2% glycerol and triplex and duplex DNA bands were analyzed as described before (*22*).

To Monitor the Association Rates of Triplex Formation in the Presence or Absence of K^+ and Triplex Stabilizers. Triplex-forming reaction mixtures (9 μL) in buffer A containing 3 ng of target duplex, Pu (0.17 μM), and control TFO with or without KCl (140 mM), 1 mM spermine, and 1 μM of the copolymer (at *P*/*D* ratio of 2) were incubated at 37 °C for the indicated time period as shown in the figure. After each respective incubation time, triplex formation was analyzed as described above.

For Assays Monitoring K^+-Induced Dissociation of Preformed Triplexes. Triplex-forming reaction mixtures (6 μL) in buffer A containing target duplex, Pu, and control TFO with or without triplex stabilizers were incubated for 6 h at 37 °C to facilitate equivalent level of triplex formation (see, Figure 4). Then 3 μL of buffer A with or without KCl was added and dissociation of the preformed triplex DNA was monitored thereafter for the indicated time.

Calculation of Triplex Formation by EMSAs. The amount of radioactivity present in the duplex and triplex forms was determined with the Ambis System. The apparent fraction, θ, of the target duplex bound by Pu was calculated using the following equation:

$$\theta = S_{\text{triplex}}/(S_{\text{triplex}} + S_{\text{duplex}}) \qquad (1)$$

where S_{triplex} and S_{duplex} represent the radioactive signal for the triplex and duplex bands, respectively, as described previously (*26*).

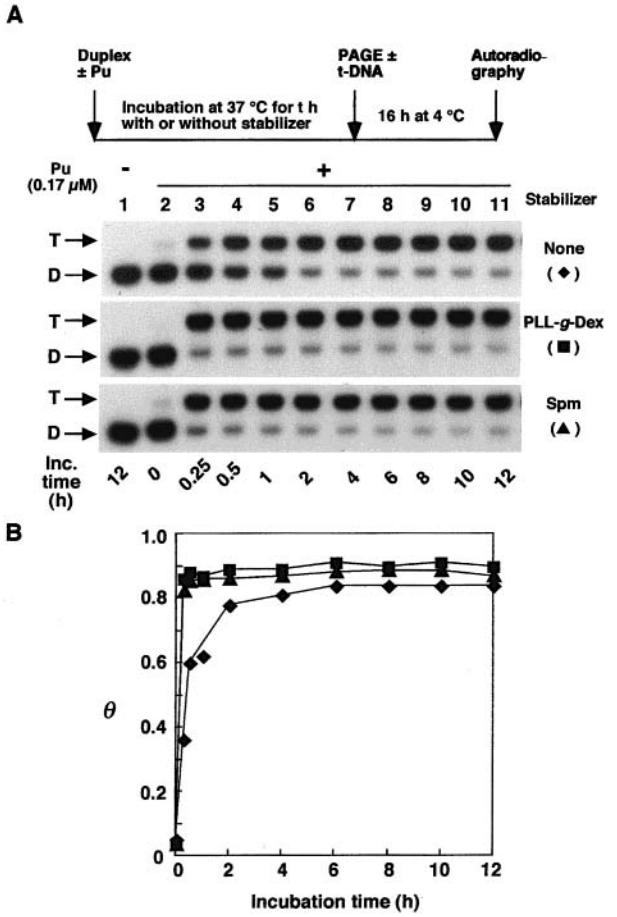

Figure 4. Kinetics of the purine motif triplex formation in the absence of KCl. (A) Analysis of triplex formation with or without triplex stabilizer. Kinetic analysis of triplex formation was performed according to the protocol shown above the gels. Labeled duplex (3 ng), Pu (0.17 μM), and control TFO were added together in 9 μL of buffer A and then incubated at 37 °C in the absence (None) or in the presence of either 2.5 μg of PLL-*g*-Dex copolymer (1 μM and *P*/*D* ratio is 2) or 1 mM spermine (Spm) as shown on the right side of each gel. Triplex formation after indicated time period (h) was analyzed as described in Figure 3. Arrows indicate the position of duplex (D) and triplex (T) DNAs. (B) Triplex formation curves in the presence or absence of stabilizers. The fraction of duplex in triplex form (θ) was calculated from eq 1 as described in Experimental Procedures and plotted against the incubation time. Each point represents an average of two independent experiments.

The apparent dissociation rate constant (k_{off}) for triplexes involving Pu was determined by taking the least-squares fitting of kinetic data to the eq 2 (*17*):

$$\theta_t/\theta_0 = e^{-k_{\text{off}}t} \qquad (2)$$

where t is the time after K^+ addition, θ_t is the apparent fraction of target duplex bound by Pu at time t, and θ_0 is the apparent fraction of target duplex bound by Pu at time zero. The relative k_{off} values were obtained from the following equation:

$$\text{rel } k_{\text{off}} = k_{\text{off}(K^+)}/k_{\text{off}(0)} \qquad (3)$$

where $k_{\text{off}(K^+)}$ is the value of k_{off} of the reaction mixture supplemented with KCl, and $k_{\text{off}(0)}$ is the value of k_{off} for the reaction mixture supplemented with buffer A.

RESULTS

Correlation between Self-Aggregation of Pu and Triplex Inhibition by K^+. Self-aggregation through

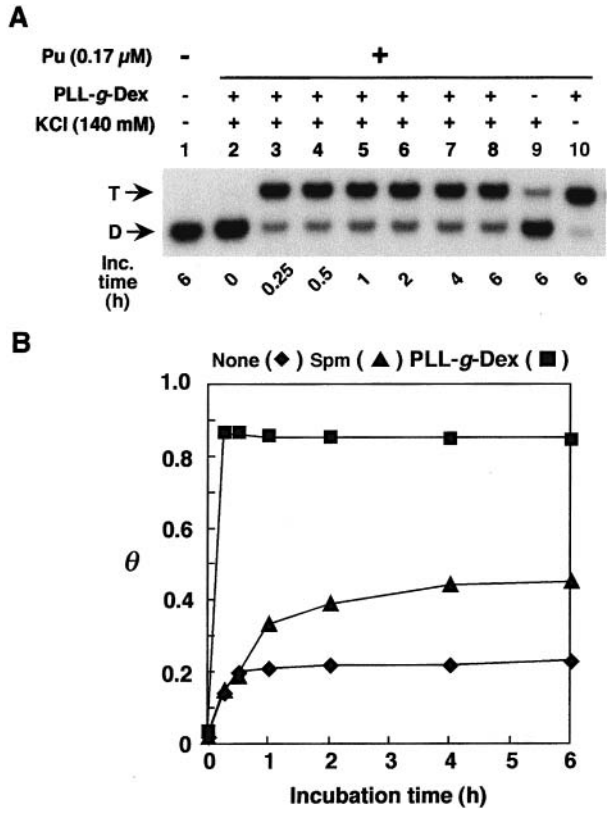

Figure 5. EMSA to analyze the effect of K^+ on association rates of triplex formation. (A) The copolymer accelerates the association rate of triplex formation in the presence of K^+. Kinetic analysis of triplex formation with or without triplex stabilizers was carried out identically as described in Figure 4 but in the presence of 140 mM KCl. Autoradiography of the gel for triplex formation in the presence (+) or absence (−) of PLL-*g*-Dex copolymer and K^+ after indicated time intervals (h) is shown. Identical experiments were performed with or without spermine (gels are not shown). (B) Triplex formation curves at 140 mM KCl in the presence or absence of triplex stabilizer. The fraction of duplex in triplex form (θ) was calculated and plotted against the time periods (h) as described in Figure 4B, except that θ in the absence of KCl under each condition (e.g., lane 10 for the copolymer) was considered to be 1 and calculated the values in the presence of KCl at each time point in the absence (None) or presence of 1 μM PLL-*g*-Dex copolymer and spermine (Spm). Each point represents an average of two independent experiments.

G-quartet, parallel and antiparallel homoduplex formation by G-rich ODNs has long been proposed to confer K^+ inhibition of the purine motif triplex formation (*15*−*18*). To explore this possibility, self-aggregation of Pu at physiologic [K^+] was tested. Figure 2A shows that Pu at 0.17 μM containing labeled Pu (∼10 nM) almost remains in monomeric form regardless of the presence or absence of KCl and the incubating temperature (cf. lane D with 1, 5, 9, and 13). Note that no retarded band was also observed in the presence of the copolymer and t-DNA (lanes 4, 8, and 12). Since higher concentrations of G-rich ODNs did favor G-quartet formation (*15*, *17*), self-aggregation of Pu at different concentrations was also analyzed but still failed to detect any retarded band (Figure 2B). These data suggest that K^+-mediated inhibition of triplex formation that we reported previously (*22*, *23*) and also observed in this study (see Figures 3 and 5) does not correlate with the self-aggregation hypothesis. However, the presence of the copolymer at higher concentrations (1.7−5 μM) of Pu with KCl slightly induced aggregation of Pu (data not shown).

Cheng and van Dyke (*31*) proposed that, in the presence of K^+, certain classes of self-associated species of G-rich ODNs had no apparent change in electrophoretic mobility to their monomeric form. Keeping this possibility in mind, an experiment for coanalysis of self-aggregation and triplex formation by Pu was designed in the presence or absence of K^+ and the copolymer. We found that triplex formation involving preincubated Pu in KCl, indeed, reduced slightly to that formed without preincubation (Figure 3, cf. lanes 3 and 4 with 6 and 7, respectively). Therefore, possibility of self-aggregation and/or unusual structure formation of Pu in the presence of K^+ cannot be totally overruled. However, this inhibitory effect was unaffected in the presence of the copolymer (cf. lanes 4, 7, 9, and 11) and spermine (data not shown). This suggests that the copolymer-mediated triplex stabilization at physiological [K^+] (cf. lanes 2, 4, and 9) may have nothing to do with self-aggregation and/or G-quartet formation of Pu.

Effect of the Copolymer on Kinetics of Triplex Formation. Since preincubation of Pu with K^+ neither formed aggregates nor significantly inhibited triplex formation (Figures 2 and 3), we, like others (*14*, *17*, *19*), presumed that K^+ affects either association or dissociation rates of triplex DNA to confer triplex inhibition. First, kinetics of triplex formation in the presence or absence of K^+ and triplex stabilizers were analyzed. As shown in Figure 4A, in the absence of K^+, the purine motif triplex DNA formed very rapidly (i.e., a matter of minutes) even at submicromolar concentration of Pu (0.17 μM). In addition, triplex formation reached to almost equilibrium with or without triplex stabilizers after 4−6 h incubation (Figure 4B). Note that the rate of triplex formation either in the presence of the copolymer or at the physiological concentration (1 mM) of spermine was indistinguishable.

Next we examined the kinetics of triplex formation at physiologic [K^+] either in the presence (see the gel) or absence (gels not shown) of the copolymer (Figure 5A). In all cases, the fraction of duplex in triplex form (θ) after 6 h incubation without KCl (e.g., lane 10) was considered to be 1 and compared to that formed in the presence of KCl after indicated incubation time. As shown graphically in Figure 5B, the rate of triplex formation was tremendously decreased and only 0.22 of θ was obtained after 6 h incubation of Pu with the target duplex (compare Figures 4 and 5). On the contrary, the rate of triplex formation in the presence of the copolymer was quite surprising under the same conditions. Triplex formation ($\theta \approx 0.9$) reached to plateau within 15 min of incubation (Figure 5A, lane 3) and remained fairly constant throughout the time course (lanes 3−8). Whereas, with 1 mM spermine only a modest increase in rate was observed after 1 h (Figure 5B), having consistency with a previous study (*32*). Therefore, even at 20-fold less in stabilizer/DNA charge ratio the triplex-promoting efficiency (i.e., increase the binding rate of Pu) of the copolymer at physiologic [K^+] is amazingly higher than that of spermine. These data are in good agreement with our previous observations (*22*, *23*).

Effect of the Copolymer on K^+-Induced Dissociation of Preformed Triplexes. It has been reported that triplex inhibition by K^+ occurs not only by slowing the rate of triplex formation but also by increasing the rate of triplex dissociation (i.e., destabilization of preformed triplexes) (*17*, *19*). Although the copolymer significantly abrogates the inhibitory effect of K^+ on rates of triplex formation (Figure 5), K^+-induced destabilization of preformed triplex DNA and the effect of the copolymer were

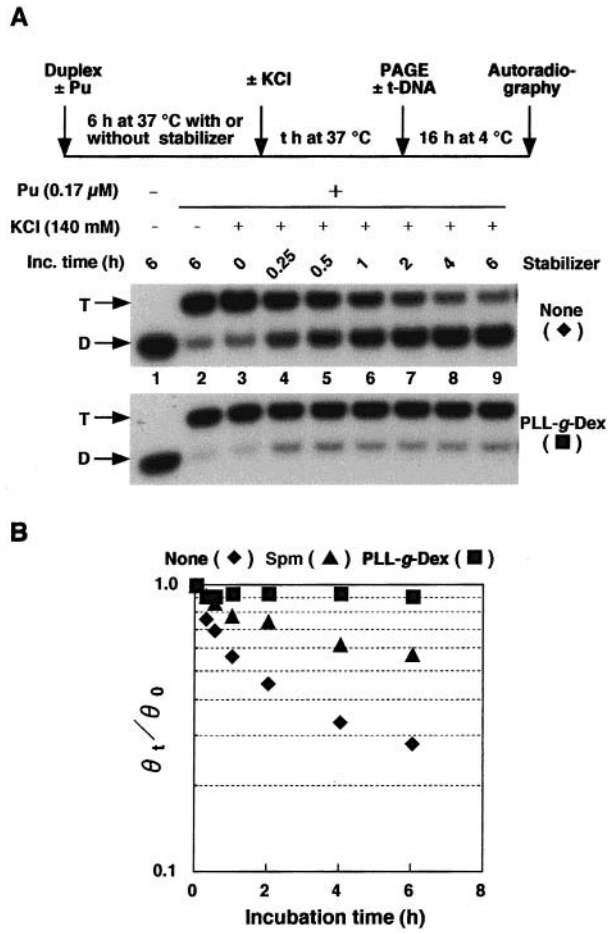

Figure 6. EMSA to analyze K^+-induced dissociation of preformed triplexes. (A) The copolymer decreases dissociation rate of preformed triplexes in the presence of K^+. Experiment for triplex formation and dissociation was carried out according to the scheme shown above the gels and also described in details under Experimental Procedures. Reaction mixtures (6 μL) containing labeled duplex and Pu in buffer A were incubated for 6 h at 37 °C either in the absence (None) or presence of PLL-*g*-Dex copolymer (gels are shown) and spermine (gel not shown). Triplex-forming reaction mixtures were then supplemented with 3 μL of buffer A (lane 2) or buffer containing KCl for 140 mM in final reaction volume and further incubated for indicated time periods (h) before electrophoretic analysis. (B) Triplex dissociation curves at 140 mM KCl in the presence or absence of triplex stabilizer. The fraction of duplex in triplex form (θ) in reactions without KCl was considered to be 1 and θ at time zero (θ_0) and at each time point (θ_t) after KCl addition was calculated, and θ_t/θ_0 values were fitted to eq 2 as described in Experimental Procedures. Each point represents an average of at least two independent experiments.

not clearly understood. To this end, target duplex and Pu in the presence or absence of triplex stabilizer but without KCl were first incubated for 6 h to reach the triplex formation to equilibrium under each reaction condition (see, Figure 4). Preformed triplexes were then supplemented with reaction buffer or buffer containing KCl. Samples were analyzed thereafter at different time points (Figure 6A). The value of θ without KCl was considered to be 1 and compared to quantify θ in each point after KCl addition. Results of experiments either in the presence or absence of the PLL−*g*-Dex copolymer and spermine are represented graphically in Figure 6B. To minimize the reassociation effect, initial time points were considered to calculate the apparent dissociation rate constants as described in Experimental Procedures and are listed in Table 1**.** While K^+-induced dissociation of preformed triplexes was slightly reduced (but not inhibited) in the presence of spermine, dissociation of preformed triplexes was not observed in the presence of the copolymer (see discussion). No detectable change in triplex formation is also observed when reactions were supplemented with buffer only (data not shown). Our results strongly suggest that the copolymer increased the association rate as well as decreased dissociation rate of the triplex to completely overcome the inhibitory effects of physiologic $[K^+]$.

Table 1. Comparison of Apparent k_{off} Values Obtained from Figure 6B[a]

stabilizer	k_{off} (s^{-1})	rel k_{off}
none	6.5×10^{-5}	1
spermine	2.8×10^{-5}	0.43
PLL-*g*-Dex	$<3.2 \times 10^{-6}$	<0.05

[a] Initial time points for triplex dissociation were considered to calculate the values of k_{off} from eq 2 as described in Experimental Procedures. Relative k_{off} (rel k_{off}) values were calculated from eq 3 as shown in Experimental Procedures.

DISCUSSION

In this study, we provide a mechanistic explanation for the purine motif triplex stabilization at physiologic $[K^+]$ by our previously reported PLL-*g*-Dex copolymer (Figure 1) (*22*, *23*). It is shown that inhibition of the purine motif triplex formation by K^+ involves decrease in binding rate of Pu to duplex (i.e., suppression of rates of triplex formation) (Figure 5). However, the rate of triplex formation in the presence of the copolymer was increased surprisingly, and K^+-induced dissociation of preformed triplexes was not observed. Moreover, despite more than 20-fold less in stabilizer/DNA charge ratio, triplex-promoting/stabilizing efficiency of the copolymer under physiologic $[K^+]$ was remarkably higher than that of physiological concentrations of spermine (Figures 5 and 6). This low triplex-stabilizing ability of oligocations (like spermine) was described as their competitive replacement by the coexiting M^+ (*22*, *33*). Finally, assay for coanalysis of self-aggregation and triplex formation (Figure 3) relay an important message that prior interaction of the copolymer with Pu does not affect its triplex-forming potentiality (Figures 2 and 3). It suggests that conjugation of Pu (i.e., TFOs) with the copolymer could be of future interest to investigate its effects on triplex stability in vitro and in vivo. The triplex-forming ability of the copolymer/ODN conjugates is being estimated in our laboratory.

Self-aggregation through G-quartet formation of G-rich TFOs was proposed as major phenomenon for K^+ inhibition of the purine motif triplex formation (*15*−*18*). Of late, several factors, like concentration (*15*, *17*), temperature (*34*), and especially the length and sequences of G-rich ODNs (*30*, *31*), have been proposed to have significant effect on self-association and G-quartet formation of G-rich ODNs. Unexpectedly, it was not the case for K^+ inhibition of triplex formation since the G-rich TFO (Pu) used in this study did not form G-quartet structure even at its varying concentrations and incubating at different temperatures (Figure 2). Triplex inhibition by K^+ without inducing G-quartet structure of G-rich ODN is not surprising since K^+ inhibition of the purine motif triplex formation by a mechanism that does not involve G-quartet formation is already reported (*14*). On the other hand, Cheng and van Dyke (*31*) proposed that on behalf of characteristic G-quartet structure, K^+ may induce G-TFOs to adopt an unusual structure. Coanalysis of self-aggregation and triplex formation (Figure 3) revealed that preincubation of Pu with K^+ slightly increased the

inhibitory effect of K^+ (Figure 3). It is possible that G-quartet/unusual structure formation by Pu is unstable and thus cannot be detected after gel electrophoresis. Note that this effect was unaffected in the presence of the copolymer (Figure 3). So further analysis (e.g., DMS assay) may help to understand aggregation but will not contribute very much toward our major interest mentioned before. Careful observation of previous studies (*15*, *17*, *31*) reveals that at higher concentrations of G-rich ODNs, despite more than 80% inhibition of triplex formation, only a minor fraction of the total ODNs was engaged in G-quartet structure while majority of them were in monomeric form at physiologic [K^+]. Taking together, coanalysis of self-aggregation and triplex inhibition at physiologic [K^+] may be necessary to evaluate the KCl effects. We, like others (*14*, *31*), presume that self-aggregation and/or G-quartet formation of G-rich ODNs in the presence of M^+ is sequence-specific and may not be the major effect for K^+ inhibition of the purine motif triplex formation.

Several groups have shown that K^+ inhibits the purine motif triplex formation either by reducing the rate of triplex formation (*14*, *19*, *20*) or by increasing the rate of dissociation of preformed triplexes (*17*, *19*). When analyzed under our reaction conditions, we, indeed, observed a drastic decrease in rates of triplex formation by K^+ (cf. Figures 4 and 5). However, the negative effect of K^+ on triplex formation was almost completely abrogated in the presence of the copolymer (Figures 5 and 6). Of interest, the copolymer reduced K^+-induced dissociation of the preformed triplex. Therefore, both absolute increase in association rate and decrease in K^+-induced dissociation rate are thought to be the primary contribution of the copolymer which compensates K^+-induced inhibition (Figures 5 and 6). Using a surface plasmon resonance sensor, we have recently shown that the copolymer stabilizes the pyrimidine motif triplex DNA at neutral pH absolutely by promoting the rate of triplex formation but having only a modest effect on dissociation rate (*35*). It suggests that the mechanism of the purine and the pyrimidine motif triplex stabilization by the copolymer is quite similar but may not be identical. The precise determination of association and dissociation rates of the purine motif triplex DNA with or without K^+ and the copolymer on a surface plasmon resonance sensor could help further understanding of the copolymer effect.

Although the precise mechanism(s) involved in triplex stabilization by the copolymer is not clearly understood, one plausible mechanism could be related with the counterion condensation effect (*36*). It has been suggested that triplex formation is accompanied by an increase in the counterion condensation, that is entropically unfavorable for triplex formation. On the other hand, the copolymer decreases the extent of counterion condensation since the association of polycationic materials with DNA is a counterion release process (*37*) which in turn increases the thermodynamic stability of triplexes. We recently demonstrated that the copolymer indeed reduces the counterion condensation effect to stabilize duplex and triplex DNA (*38*). Further, it may be plausible that the counterion releasing (ion exchange) behavior of the copolymer reduces nucleotide-K^+ interaction to relieve the inhitory effect of K^+. Of course, an unknown mechanism for the copolymer-mediated triplex stabilization cannot be overruled.

Promotion and stabilization of triplexes are considered, in general, as important issues for triplex-mediated modulation of gene functions (*8*). In addition to triplex stabilization, the graft copolymers with particular polysaccharide side chains exhibit as a potential candidate for cell-specific DNA carriers (*39*−*41*). Therefore, molecular designing of novel copolymer will certainly shed light on in vivo applicability of antigene strategy even though the triplex-promoting/stabilizing ability of the PLL-*g*-Dex copolymer in living cells is yet to be explored.

ACKNOWLEDGMENT

The authors gratefully acknowledge Drs H. Handa and K. Nagata of Tokyo Institute of Technology for their kind cooperation. Sincere thanks are due to N. Masato for technical assistance. This work was supported in part by a Grant-in-Aid (11167225) for Scientific Research on Priority Area (A) from the Ministry of Education, Science, Sports and Culture of Japan.

LITERATURE CITED

(1) Moser, H. E., and Dervan, P. B. (1987) Sequence-specific cleavage of double helical DNA by triple helix formation. *Science 238*, 645−650.

(2) Cooney, M. G., Czernuszewicz, Postel, E. H., Flint, S. J., and Hogan, M. E. (1988) Site-specific oligonucleotide binding represses transcription of the human c-myc gene in vitro. *Science 241*, 456−459.

(3) Maher, L. J. D., Wold, B., and Dervan, P. B. (1989) Inhibition of DNA binding proteins by oligonucleotide-directed triple helix formation. *Science 245*, 725−730.

(4) Helene, C. (1991) The anti-gene strategy: control of gene expression by triplex-forming-oligonucleotides. *Anticancer Drug. Des. 6*, 569−584.

(5) Postel, E. H., Flint, S. J., Kessler, D. J., and Hogan, M. E. (1991) Evidence that a triplex-forming oligodeoxyribonucleotide binds to the c-myc promoter in HeLa cells, thereby reducing c-myc mRNA levels. *Proc. Natl. Acad. Sci. U.S.A. 88*, 8227−8231.

(6) Volkmann, S., Jendis, J., Frauendrof, A., and Moelling, K. (1995) Inhibition of HIV-1 reverse transcription by triple-helix forming oligonucleotides with viral RNA. *Nucleic Acids Res. 23*, 1204−1212.

(7) Wang, G., Seidman, M. M., and Glazer, P. M. (1996) Mutagenesis in mammalian cells induced by triple helix formation and transcription-coupled repair. *Science 271*, 802−805.

(8) Beal, P. A., and Dervan, P. B. (1991) Second structural motif for recognition of DNA by oligonucleotide-directed triple-helix formation. *Science 251*, 1360−1363.

(9) For review, Vasquez K. M., and Wilson J. H. (2000) Triplex-directed site-specific genome modification. *Methods Mol. Biol. 133*, 183−200; Fox, K. R. (2000) Targeting DNA with triplexes. *Curr. Med. Chem. 7*, 17−37.

(10) Pilch, D. S., Levenson, C. and Shafer, R. H. (1991) Structure, stability, and thermodynamics of a short intermolecular purine-purine-pyrimidine triple helix. *Biochemistry 30*, 6081−6088.

(11) Rajagopal, P., and Feigon, J. (1989) Triple-strand formation in the homopurine:homopyrimidine DNA oligonucleotides d(G-A)4 and d(T-C)4. *Nature 339*, 637−640.

(12) Singleton, S. F., and Dervan, P. B. (1992) Influence of pH on the equilibrium association constants for oligodeoxyribonucleotide-directed triple helix formation at single DNA sites. *Biochemistry 31*, 10995−11003.

(13) Milligan, J. F., Krawczyk, S. H, Wadwani, S. and Matteucci, M. D. (1993) An antiparallel triple helix motif with oligodeoxynucleotides containing 2′-deoxyguanosine and 7-deaza-2′-deoxyxanthosine. *Nucleic Acids Res. 21*, 327−333.

(14) Cheng, A. J., and Van Dyke, M. W. (1993) Monovalent cation effects on intermolecular purine-purine-pyrimidine triple-helix formation. *Nucleic Acids Res. 21*, 5630−5635.

(15) Sen, D., and Gilbert, W. (1990) A sodium−potassium switch in the formation of four-stranded G4-DNA. *Nature 344*, 410−414.

(16) Jin, R. Z., Breslauer, K. J, Jones, R. A., and Gaffney, B. L. (1990) Tetraplex formation of a guanine-containing nonameric DNA fragment. *Science 250*, 543−546.
(17) Olivas, W. M., and Maher, L. J., III (1995) Competitive triplex/quadruplex equilibria involving guanine-rich oligonucleotides. *Biochemistry 34*, 278−284.
(18) Noonberg, S. B., Francois, J. C., Garestier, T., and Helene, C. (1995) Triplex formation with alpha anomers of purine-rich and pyrimidine-rich oligodeoxynucleotides. *Nucleic Acids Res. 23*, 1956−1963.
(19) Svinarchuk, F., Cherny, D., Debin, A., Delain. E., and Malvy, C. (1996) A new approach to overcome potassium-mediated inhibition of triplex formation. *Nucleic Acids Res. 24*, 3858−3865.
(20) Vasquez, K. M., Wensel, T. G., Hogan, M. E., and Wilson, J. H. (1995) High-affinity triple helix formation by synthetic oligonucleotides at a site within a selectable mammalian gene. *Biochemistry 34*, 7243−7251.
(21) Maruyama, A., Katoh, M., Ishihara, T., and Akaike, T. (1997) Comb-type polycations effectively stabilize DNA triplex. *Bioconjugate Chem. 8*, 3−6.
(22) Ferdous, A., Watanabe, H., Akaike, T., and Maruyama, A. (1998) Poly(L-lysine)-graft-dextran copolymer: amazing effects on triplex stabilization under physiological pH and ionic conditions (in vitro). *Nucleic Acids Res. 26*, 3949−3954.
(23) Ferdous, A., Watanabe, H., Akaike, T., and Maruyama, A. (1998) Comb-type copolymer: stabilization of triplex DNA and possible application in antigene strategy. *J. Pharm. Sci. 87*, 1400−1405.
(24) Olivas, W. M., and Maher, L. J., III (1995) Overcoming potassium-mediated triplex inhibition. *Nucleic Acids Res. 23*, 1936−1941.
(25) Gee, J. E., Revankar, G. R., Rao, T. S., and Hogan, M. E. (1995) Triplex formation at the rat neu gene utilizing imidazole and 2′-deoxy-6-thioguanosine base substitutions. *Biochemistry 34*, 2042−2048.
(26) Dagle, J. M., and Weeks, D. L. (1996) Positively charged oligonucleotides overcome potassium-mediated inhibition of triplex DNA formation. *Nucleic Acids Res. 24*, 2143-2149.
(27) Faruqi, A. F., Krawczyk, S. H., Matteucci, M. D., and Glazer, P. M. (1997) Potassium-resistant triple helix formation and improved intracellular gene targeting by oligodeoxyribonucleotides containing 7-deazaxanthine. *Nucleic Acids Res. 25*, 633−640.
(28) Joseph, J., Kandala, J. C., Veerapanane, D., Weber, K. T., and Guntaka, R. V. (1997) Antiparallel polypurine phosphorothioate oligonucleotides form stable triplexes with the rat alpha1(I) collagen gene promoter and inhibit transcription in cultured rat fibroblasts. *Nucleic Acids Res. 25*, 2182−2188.
(29) Maruyama, A., Watanabe, H., Ferdous, A., Katoh, M., Ishihara, T., and Akaike, T. (1998) Characterization of interpolyelectrolyte complexes between double-stranded DNA and polylysine comb-type copolymers having hydrophilic side chains. *Bioconjugate Chem. 9*, 292−299.
(30) Sen, D., and Gilbert, W. (1992) Guanine quartet structures. *Methods Enzymol. 211*, 191−199.
(31) Cheng, A. J., and Van Dyke, M. W. (1997) Oligodeoxyribonucleotide length and sequence effects on intramolecular and intermolecular G-quartet formation. *Gene 197*, 253−260.
(32) Musso, M., and van Dyke, M. W. (1995) Polyamine effects on purine-purine-pyrimidine triple helix formation by phosphodiester and phosphorothioate oligodeoxyribonucleotides. *Nucleic Acids Res. 23*, 2320−2327.
(33) Thomas, T., and Thomas, T. J. (1993) Selectivity of polyamines in triplex DNA stabilization. *Biochemistry 32*, 14068−14074.
(34) Basu, S., and Wickstrom, E. (1997) Temperature and salt dependence of higher order structure formation by antisense c-myc and c-myb phosphorothioate oligodeoxyribonucleotides containing tetraguanylate tracts. *Nucleic Acids Res. 25*, 1327−1332.
(35) Torigoe, H., Ferdous, A., Watanabe, H., Akaike, T., and Maruyama, A. (1999) Poly(L-lysine)-graft-dextran copolymer promotes pyrimidine motif triplex DNA formation at physiological pH. Thermodynamic and kinetic studies. *J. Biol. Chem. 274*, 6161−6167.
(36) Manning, G. S. (1978) The molecular theory of polyelectrolyte solutions with applications to the electrostatic properties of polynucleotides. *Q. Rev. Biophys. 11*, 179−246.
(37) Mascotti, D. P., and Lohman, T. M. (1990) Thermodynamic extent of counterion release upon binding oligolysines to single-stranded nucleic acids. *Proc. Natl Acad. Sci. U.S.A. 87*, 3142−3146.
(38) Maruyama, A., Ohnishi, Y., Watanabe, H., Torigoe, H., Ferdous, A., and Akaike, T. (1999) Polycation comb-type copolymer reduces counterion condensation effect to stabilize DNA duplex and triplex formation. *Colloids Surf., B 16*, 273−280.
(39) Asayama, S., Nogawa, M., Takei, Y., Akaike, T., and Maruyama, A. (1998) Synthesis of novel polyampholyte comb-type copolymers consisting of poly(L-lysine) backbone and hyaluronic acid side chains for a DNA carrier. *Bioconjugate Chem. 9*, 476−481.
(40) Takei, Y., Maruyama, A., Kuwano, S., Nishimura, Y., Asayama, S., Nogawa, M., Ikejima, K., Hori, M., Akaike, T., Lemasters, J. J., Watanabe, S., and Sato, N. (1999) Targeted gene transfer to sinusoidal endothelial cells and expression in vivo. *Transplant Proc.* 790−791.
(41) Park, J. U., Ishihara, T., Kano, A., Akaike, T., and Maruyama, A. (1999) Preparation of dendritic graft copolymer consisting of poly(L-lysine) and arabinogalactan as a hepatocyte specific DNA carrier. *Prep. Biochem. Biotechnol. 29*, 353−370.

BC990166T

In Vivo Transchelation of Copper-64 from TETA-Octreotide to Superoxide Dismutase in Rat Liver

Laura A. Bass, Mu Wang, Michael J. Welch, and Carolyn J. Anderson*

Mallinckrodt Institute of Radiology, Washington University School of Medicine, 510 South Kingshighway Boulevard, Campus Box 8225, Saint Louis, Missouri 63110. Received November 30, 1999; Revised Manuscript Received May 12, 2000

An understanding of the metabolic fate of radiometal-labeled peptides is important due to their application in the areas of diagnostic imaging and targeted radiotherapy. Radioisotopes of copper (^{64}Cu, $T_{1/2} = 12.7$ h; ^{67}Cu, $T_{1/2} = 62$ h) have been labeled to monoclonal antibodies (mAbs) and peptides and have applications in the areas of PET imaging and targeted radiotherapy of cancer. Copper-64-TETA-D-Phe^1-octreotide ([^{64}Cu]TETA-OC) has been shown to bind to the somatostatin receptor, both in vitro and in vivo, and this agent inhibited the growth of somatostatin-receptor positive tumors in rats. Copper-64-TETA-OC, however, showed a retention of activity in the blood, liver, and bone marrow, suggesting possible dissociation of ^{64}Cu from TETA-OC in vivo. The purpose of this study was to determine if ^{64}Cu dissociates from [^{64}Cu]TETA-OC and binds to the protein, superoxide dismutase (SOD) in rat liver. The liver metabolism of [^{64}Cu]TETA-OC was examined in normal rats using a gel-electrophoresis assay specific for SOD and size-exclusion chromatography. The major metabolite in rat liver at 20 h postinjection had a molecular weight of 32 kDa as shown by size-exclusion chromatography. A gel electrophoresis assay specific for the detection of SOD [nitro-blue tetrazolium (NBT)] showed that a ^{64}Cu-labeled protein isolated from rat liver homogenates comigrated with SOD. Evaluating the metabolic fate of copper radiopharmaceuticals demonstrated that Cu(II) dissociates from macrocyclic chelators such as TETA and binds to proteins in high concentrations, namely SOD in rat liver.

INTRODUCTION

An understanding of metabolism can aid in the design of radiopharmaceuticals for optimal retention in target tissues (such as tumors) and clearance through nontarget organs (such as the liver or kidneys). The information that can be obtained through in vivo metabolism studies includes the identification of the radiolabeled metabolites, which accumulate in both target and nontarget organs (*1*−*6*). An understanding of the metabolic fate of ^{64}Cu- and ^{67}Cu-labeled-monoclonal antibodies (mAbs) and peptides is of importance due to their applications in the areas of PET imaging (*7*−*10*) and targeted radiotherapy of cancer (*11*−*14*). The metabolites of radiometal-labeled radiopharmaceuticals determine the retention and clearance of the radionuclide in the target tissue(s) as well as the clearance organs.

The biodistribution and metabolism of several radiometal-peptide/mAb compounds have previously been investigated (*15*−*19*). These studies demonstrate that the in vivo metabolism of ^{111}In-labeled proteins and peptides is very different from that of analogous ^{64}Cu-labeled agents. Whereas ^{111}In-labeled peptides and mAbs are metabolized in the liver primarily to [^{111}In]chelate−amino acid moieties, the analogous ^{64}Cu-labeled chelator−biomolecule conjugates show significant dissociation of ^{64}Cu from the chelator followed by binding of the ^{64}Cu to 30−35 kDa proteins.

Superoxide disumutase (SOD) is a homodimeric enzyme of ∼ 32 kDa with each subunit containing one copper and one zinc atom believed to be bridged by an imidazole group (*20*). SOD is distributed widely in the cytosol of eukaryotic cells. This enzyme is especially abundant in the liver, kidney, adrenal, and red blood cells. SOD provides a defense mechanism against the potential toxicity of oxygen radicals by catalyzing the disproportionation of the superoxide ion to hydrogen peroxide and oxygen.

Rogers et al. analyzed the liver metabolism in rats of anti-colorectal carcinoma mAb 1A3 radiolabeled with ^{67}Cu through three different macrocyclic bifunctional chelators (BFCs) (*18*). Intact ^{67}Cu-labeled mAb BFC-1A3 conjugates and two other metabolites of the ^{67}Cu mAbs were observed. One of these metabolites was identified as [^{67}Cu]BFC-lysine by reversed-phase HPLC, while from size-exclusion chromatography, the higher molecular weight non-mAb species (∼35 kDa) was suggested to be the result of in vivo transchelation of ^{67}Cu from the BFC to superoxide dismutase (SOD). Since there are many biological proteins with a wide range of molecular weights to which copper can bind (*20*), this work was carried out to confirm transchelation of ^{67}Cu from [^{67}Cu]BFC conjugates of biological molecules to SOD in vivo in the rat liver.

The current focus of our research is the development of radiometal-labeled peptides for targeting tumor receptors for PET imaging and targeted radiotherapy (*8*, *14*). In the development of [^{64}Cu]TETA-D-Phe^1-octreotide ([^{64}Cu]TETA-OC, Figure 1) as an agent for targeted radiotherapy of somatostatin-receptor positive tumors, biodistribution studies in a tumor-bearing rat model demonstrated that there was a 10-fold greater concentration of [^{64}Cu]TETA-OC in the blood at longer time points (24 h) compared to [^{111}In]DTPA-OC (*8*). This observation,

* To whom correspondence should be addressed. Phone: (314) 362-8427. Fax: (314)362-9940. E-mail: AndersonCJ@mir.wustl.edu.

10.1021/bc990167l CCC: $19.00 © 2000 American Chemical Society
Published on Web 06/23/2000

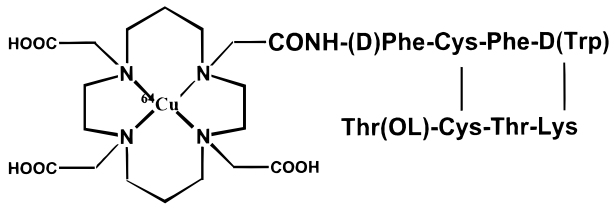

Figure 1. Structure of [^{64}Cu]TETA-OC.

along with the lack of liver clearance and increasing marrow uptake of [^{64}Cu]TETA-OC over time (out to 48 h) (*14*), suggests possible dissociation of ^{64}Cu from TETA-OC in vivo. To further examine the potential exchange of radioactive copper from BFC-biological molecule conjugates to SOD, we examined the liver metabolism of [^{64}Cu]TETA-OC in normal rats using gel-electrophoresis techniques, assays specific for SOD along with size-exclusion chromatography (*21*).

MATERIALS AND METHODS

Reagents and Instrumentation. Ultrapure ammonium dihydrogen phosphate was purchased from Johnson Matthey (Royston, England), and ultrapure ammonium acetate and amonium citrate was from Fluka (Ronkonkoma, NY). TETA-OC was synthesized as previously described (*14*). Sephadex G-25/50, riboflavin, SOD from bovine liver, and human erythrocytes and bovine serum albumin (BSA) were purchased from Sigma (St. Louis, MO). C-18 Sep-Pak cartridges were from Waters/Millipore (Burlington, MA). Mature female Sprague−Dawley rats were from Sasco (Omaha, NE). Copper-64 was produced at Washington University on a biomedical cyclotron (*22*). Bio-Spin-6 chromatography columns, Native Tris-Glycine Ready gels (10% resolving gel, 4% stacking gel), TWEEN-20, TEMED (*N*,*N*,*N*′,*N*′ tetramethylethylenediamine), Tris/glycine running buffer (10×), Tris/glycine/SDS running buffer (10×), native/denaturing sample buffer and nitrocellulose/PVDF membrane (0.2 μm) were purchased from Bio-Rad (Hercules, CA). Nitro-Blue tetrazolium (NBT) was purchased from Aldrich (Milwaukee, WI).

Organs were prepared using a Tekmar tissue homogenizer (Cincinnati, OH), a Branson Sonifier 185 cell disrupter, and a Sorvall RC2−B centrifuge. Pharmacia Superose 12 gel filtration columns were used in conjunction with a Pharmacia/LKB fast-protein liquid chromatography (FPLC) system (Piscataway, NJ) equipped with a UV−vis detector for analysis of liver homogenates. A set of eight calibration standards, with molecular masses ranging from 246 Da (cytidine) to 669 kDa (thyroglobulin), were used to calibrate the columns. A Beckman Gamma 8000 automated well-type γ counter was used to quantitate radioisotope in FPLC fractions. Radio-TLC was carried out using a Bioscan System 200 Imaging Scanner (Washington DC). Radioactive gels were analyzed via an InstantImager Electronic Autoradiography System from Packard Instrument Co. (Meriden, CT). BCA protein determination kit was obtained from Pierce (Rockford, IL).

Preparation of [^{64}Cu]TETA-OC, [^{64}Cu]SOD, and [^{64}Cu]BSA. Copper-64 chloride ($^{64}CuCl_2$) was diluted greater than 10-fold with 0.1 M NH_4OAc, pH 5.5. The [^{64}Cu]acetate was added to TETA-OC (1−10 μg) or SOD (1 mg), and the final volume adjusted to 1.0−1.5 mL with buffer. After incubation for 45 min at room temperature, [^{64}Cu]SOD (60 μCi) was purified using a G25/50 sephadex gel filtration column prepared in 0.1 M NH_4OAc. After a 60 min incubation at room temperature, [^{64}Cu]TETA-OC was purified using a Sep-Pak cartridge as previously described (*8*). Radiochemical purity was assayed by FPLC for [^{64}Cu]SOD and by HPLC and radio-TLC for [^{64}Cu]-TETA-OC.

For labeling to BSA (1 mg), $^{64}CuCl_2$ (60 μCi) was added to 0.1 M H_3PO_4, pH 8.3, and incubated for 15 min at room temperature. Purification was performed using a G25/50 sephadex gel filtration column prepared in 0.1 M H_3PO_4, pH 8.3. Radiochemical purity was assessed by FPLC.

In Vivo Metabolite Analysis in Sprague−Dawley Rats. Female Sprague−Dawley rats (n = 3−4) were injected via the tail vein with [^{64}Cu]TETA-OC (3−13 mCi; 5 μg) or [^{64}Cu]acetate (1−13 mCi), and livers were harvested 20 h postinjection. Prior to injection, the dose was diluted in 0.9% NaCl (saline). The liver was rinsed with precooled saline, blotted dry and treated with 5 mL of precooled 0.1 M NH_4OAc/EtOH mixture (35:65), homogenized (1 min), and sonicated (45 s). After centrifugation at 23500*g* for 30 min at 5 °C, the supernatants were removed. Organ blanks, where the [^{64}Cu]acetate or [^{64}Cu]TETA-OC was added directly to the liver prior to homogenization and centrifugation, were performed as controls. The total protein content of the liver supernatants was determined using the BCA method. All liver supernatants were analyzed by FPLC and gel electrophoresis (<200 μg of total protein loaded/lane). Some samples were also analyzed by radio-TLC on silica gel in 1:1 MeOH:10% NH_4OAc. For FPLC analysis, a 0.1−0.2 mL aliquot of the supernatant was injected on a Superose 12 gel filtration column. This column was eluted with 20 mM Hepes and 300 mM NaCl (pH 7.3) buffer at a flow rate of 0.4 mL/min, and the fractions were counted on a γ counter.

SOD Activity Gels. Fifty micrograms of total protein from the supernatant of liver homogenate samples or 1.5 μg of SOD standards (human and bovine) or BSA standard was applied to a 10% Tris/glycine Ready Gel and subjected to native polyacrilamide gel electrophoresis (PAGE). Radiolabeled agents and liver homogenates were analyzed by PAGE prior to analysis of radioactivity on the gel using the InstantImager. A separate native PAGE gel was run where the gel was submerged in 50 mL of 2.5 mM NBT at room temperature and shaken gently for 30 min. The gel was then transferred to a solution containing 28 mM TEMED, 2.8 mM riboflavin, and 36 mM potasssium phosphate (pH 7.8) and shaken gently at room temperature for 20 min. The gel was wrapped in plastic wrap and placed on a light source for 15−30 min. The gel stained blue at sites of $O_2^{\bullet}$, yet, staining was absent at sites of $O_2^{\bullet}$ scavenging, thus, white bands on a blue background indicated the presence of Cu/Zn−SOD (*21*).

RESULTS

Radiolabeling and Chromatography. TETA-OC was labeled with ^{64}Cu with a specific activity of ∼1500 mCi/μg. The radiochemical purity of ^{64}Cu-labeled TETA-OC was >95% as determined by HPLC and/or radio-TLC. The radiochemical purity of [^{64}Cu]SOD and [^{64}Cu]BSA was >95% as determined by FPLC. A radioactivity balance was performed for each sample run on the FPLC to determine if any activity remained trapped on the column. For all samples analyzed by FPLC, including standards and liver homogenates, there was little or no remaining activity left on the columns.

Analysis of Liver Extracts. *Standards.* A standard curve was constructed for each Superose column using

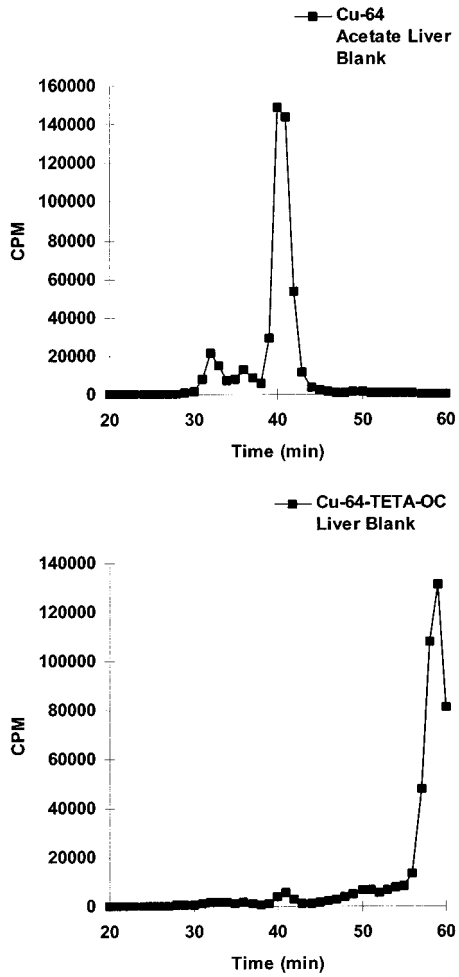

Figure 2. FPLC chromatograms of liver "blanks" of [^{64}Cu]-acetate and [^{64}Cu]TETA-OC added to liver homogenate ex vivo followed by homogenization and chromatographic analysis of the liver supernatant. (Top panel) [^{64}Cu]Acetate: peak 1, 32 min (10.7%), molecular mass ~150 kDa; peak 2, 36 min (7.5%), molecular mass ~45 kDa; peak 3, 40 min (81.8%), molecular mass ~11 kDa. (Bottom) [^{64}Cu]TETA-OC: peak 1, 41 min (3.4%), molecular mass ~8−10 kDa; peak 2, 50 min (10.6%), molecular mass <2 kDa; peak 3, 59 min (84%) molecular mass <2 kDa.

proteins of molecular masses ranging from 246 Da to 669 kDa. From this curve, the molecular masses of the [^{64}Cu]containing species formed in vivo were estimated. ^{64}Cu-labeled bovine SOD and ^{64}Cu-labeled human SOD standards eluted with the same retention time by FPLC (37 min). A [^{64}Cu]TETA-OC standard had a retention time of 58 min and was well-resolved from [^{64}Cu]SOD.

Ex Vivo Analyses. Organ blanks were carried out for [^{64}Cu]acetate and [^{64}Cu]TETA-OC to determine whether the species seen after i.v. injection were produced by the techniques used to extract the metabolites from the organs. In the case of "free" ^{64}Cu, we sought to determine whether ^{64}Cu would form [^{64}Cu]SOD in liver cell homogenates. FPLC (Figure 2, top) showed three species present in the liver blank: 11% eluted with a retention time of 32 min (molecular mass ~110 kDa), 8% eluted with a retention time of 36 min, which corresponded with [Cu]SOD, and 80% eluted at a longer retention time (40 min). Thus, the addition of free ^{64}Cu to liver tissue only forms a very small amount of [^{64}Cu]SOD. In the case of [^{64}Cu]TETA-OC (Figure 2, bottom), the organ blank eluted with the same retention time as the standard solution of [^{64}Cu]TETA-OC (58 min), demonstrating that the tissue homogenization process did not dissociate the ^{64}Cu from the TETA-OC.

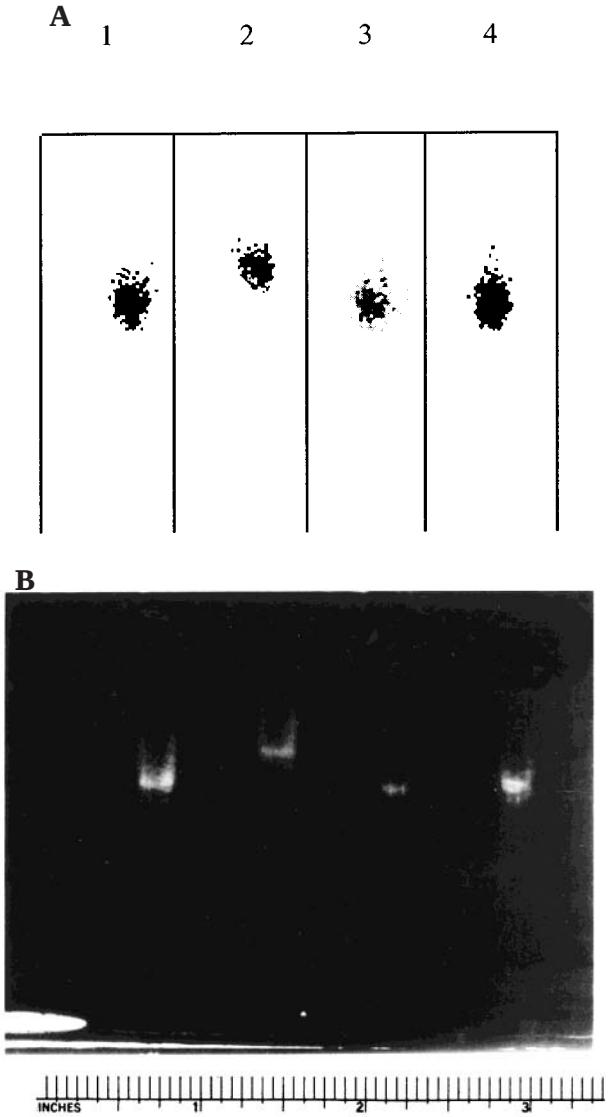

Figure 3. (A) Autoradiography showing ^{64}Cu-labeled bands of liver homogenate samples from rats injected with either [^{64}Cu]-TETA-OC or [^{64}Cu]acetate on native polyacrilamide gel electrophoresis. (B) Native polyacrilamide gel electrophoresis of the liver homogenate samples in A stained with NBT, riboflavin, and *N,N,N′,N′*-tetramethylethylenediamine for SOD activity. Lane 1, SOD from human erythrocytes (3.33 μg protein); lane 2, SOD from bovine liver (1.67 μg of protein); lane 3, liver homogenates from the rat injected with [^{64}Cu]TETA-OC (38.6 μg protein); lane 4: liver homogenates from the rat injected with [^{64}Cu]acetate (52 μg of protein).

[^{64}Cu]Acetate. To determine whether the i.v. administration of "free" ^{64}Cu (in the form of Cu-acetate) resulted in the formation of [^{64}Cu]SOD in the rat liver, [^{64}Cu]-acetate was injected in the rat, and the rat was sacrificed and the liver was removed 20 h postinjection. The liver was extracted using either phosphate-buffered saline (PBS), NH_4OAc (0.1 M, pH 5.5), or EtOH/PBS (75:25). Size-exclusion chromatography showed one ^{64}Cu-containing species eluting at approximately 35 kDa, independent of extraction media. These results agreed with those reported by Rogers et al. (*18*). The retention time of this species was equivalent to [^{64}Cu]SOD prepared in vitro using bovine or human SOD (Sigma). The gel electrophoresis of the liver homogenates indicated one radioactive band, which migrated slightly faster than the in vitro prepared ^{64}Cu-labeled bovine SOD, although it migrated identically to ^{64}Cu-labeled human SOD (Figure 3A). The

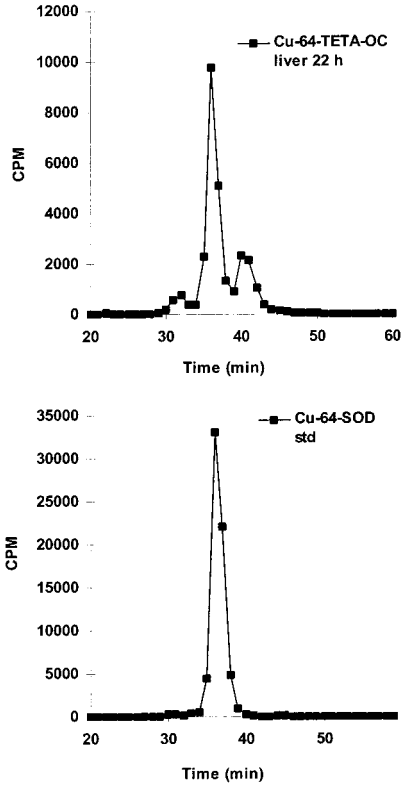

Figure 4. FPLC chromatograms of (top) liver homogenates from rats injected with (top) [^{64}Cu]TETA-OC compared to (bottom) [^{64}Cu]SOD standard. (Top panel) [^{64}Cu]TETA-OC: peak 1, 32 min (6.8%), molecular mass∼150 kDa; peak 2, 36 min (68.4%), molecular mass ∼32 kDa; peak 3, 40 min, molecular mass ∼11 kDa. (Bottom panel) [^{64}Cu]SOD standard: peak 1, 36 min (100%), molecular mass ∼32 kDa.

different migration patterns of human SOD1 mutants on native gels have been attributed to differences in charge (*23*). This is likely why we are seeing a difference between the migration of human vs bovine SOD. The NBT assay was performed on the gels and the migration distance of the radioactive bands corresponded to that for the white bands observed after NBT treatment (Figure 3B). A negative control was also run on a native gel with the NBT assay. Copper-64-labeled BSA was present on the autoradiograph of the native gel; however, a white band was not present after NBT treatment (data not shown).

[^{64}Cu]TETA-OC. In liver homogenates 20 h postinjection of [^{64}Cu]TETA-OC, approximately 69% of the ^{64}Cu eluted by FPLC as a ∼35 kDa species with 7% eluting as a higher molecular mass (∼100 kDa) species and 24% eluting as a lower molecular mass species (11−14 kDa). The majority of radiolabeled metabolites eluted identically to [^{64}Cu]SOD (Figure 4). Analysis of the gel after PAGE showed one ^{64}Cu-containing band, which migrated similarly to ^{64}Cu-labeled human SOD, but slightly faster than the bovine [^{64}Cu]SOD (Figure 3A). This band was also equivalent to the radioactive band observed in the liver homogenate after injection of [^{64}Cu]acetate. Assay of the gel with NBT exhibited white bands at migration distances equal to the radioactive bands, thus indicating the presence of Cu/Zn−SOD and its in vivo incorporation of ^{64}Cu (Figure 3B).

DISCUSSION

In the design of radiopharmaceuticals with optimal targeting for either specific organ systems or tumors, it is important to understand their metabolism in vivo. Duncan and Welch reported that [^{111}In]DTPA-conjugated glycoproteins were metabolized to [^{111}In]DTPA-lysine in the rat liver, confirming that transchelation of ^{111}In to proteins was not the major factor for the accumulation of ^{111}In in the liver (*15*). Studies carried out in our lab with ^{64}Cu-labeled chelator−protein and peptide conjugates showed a very different pattern of liver metabolism than what occurs with similar [^{111}In]labeled conjugates. Rogers et al. demonstrated that in rats [^{64}Cu]chelate−mAb conjugates were metabolized to [^{64}Cu]chelate−lysine conjugates in the kidney, but in the liver, transchelation of ^{64}Cu to a 32 kDa protein was the predominant metabolite (*18*). Due to our current interest in ^{64}Cu-labeled somatostatin analogues for diagnostic imaging (*8*, *10*) and targeted radiotherapy (*14*, *24*), we focused on the metabolism of [^{64}Cu]TETA-OC to determine if similar transchelation occurred in vivo in the rat liver.

Analyses were performed where the [^{64}Cu]acetate or [^{64}Cu]TETA-OC was added to whole livers ex vivo to differentiate between [^{64}Cu]SOD formed from in vivo processes vs that formed from extracellular incorporation of ^{64}Cu into SOD released upon lysing the cells. Addition of [^{64}Cu]acetate to rat liver ex vivo resulted in the formation of only a small amount of [^{64}Cu]SOD (Figure 2), whereas the [^{64}Cu]TETA-OC liver blank showed only intact agent. Seo and Ettinger reported that when ^{64}Cu-$(NO_3)_2$ was added to mouse hepatic cytosols, three major ^{64}Cu-binding fractions were detected (*25*). These fractions corresponded to molecular masses of 130 kDa and ∼50 kDa and metallothionein (MT) (∼17 kDa). Although we observed a similar chromatographic profile with rat whole liver homogenate, the amounts of each ^{64}Cu-labeled protein present were different than what Seo and Ettinger observed. The major peak at 40 min was possibly [^{64}Cu]MT. A potential reason for the lack of [^{64}Cu]SOD formation in rat liver ex vivo may be slow kinetics. Our in vivo data was obtained at 22 h postinjection, whereas the ex vivo homogenates were analyzed shortly after [^{64}Cu]acetate was added to the liver homogenates. Although these control experiments showed that [^{64}Cu]SOD does not form rapidly in rat liver homogenates ex vivo, they also demonstrated that the homogenization and sonication processes used to analyze the liver samples did not cause dissociation of ^{64}Cu from TETA-OC to form [^{64}Cu]SOD.

After the injection of either [^{64}Cu]acetate or [^{64}Cu]-TETA-OC, supernatants from rat liver homogenates were analyzed by FPLC and PAGE. The FPLC chromatograms of liver homogenates from rats injected with [^{64}Cu]acetate showed one ^{64}Cu-labeled protein present in the liver homogenate supernatant with a molecular mass of 32 kDa. These results are very similar to those of Terao and Owen (*26*), where they found that when ionic ^{67}Cu was injected into rats, 92.8% of the ^{67}Cu was bound to a protein with a molecular mass of 31 kDa (suggested to be either erythrocuprein, cytocuprin or SOD). Terao and Owen also found small amounts of ^{67}Cu labeled to proteins with molecular masses of 150 kDa [5.1%; probably ceruloplasmin (Cp)] and 11 kDa (2.2%; a sulfhydryl containing protein) (*26*), which we did not observe.

Rat liver homogenate supernatants from rats injected with [^{64}Cu]TETA-OC showed approximately three metabolites by FPLC, with the major metabolite having a molecular mass of 32 kDa (69%). The other two peaks corresponded to molecular masses of ∼150 kDa (7%) and ∼11 kDa (24%), which most likely correspond to ceruloplasmin and a sulfhydryl-containing protein such as metallothionein (*26*). Our results with [^{64}Cu]TETA-OC are very consistent with what has been reported with ionic ^{67}Cu by Terao and Owen and strongly suggest that

^{64}Cu dissociated from the TETA chelator and bound to proteins, primarily SOD.

The NBT assay was used to verify that the major radioactive band containing ^{64}Cu was associated with SOD. In the NBT method, riboflavin is used to generate $O_2^{\cdot}$, which is illuminated in the presence of TEMED and oxygen. NBT is photochemically reduced by $O_2^{\cdot}$ producing a blue color. SOD inhibits this reduction and thus is detected by a colorless band on a blue background. In rats injected with either [^{64}Cu]acetate or [^{64}Cu]TETA-OC, the radioactive bands comigrated with the colorless bands on the NBT assay, strongly suggesting that ^{64}Cu(II) bound to SOD in rat liver.

Further verification of the binding of ^{64}Cu to SOD in rat liver was attempted using Western blot analysis (data not shown). The use of SDS (non-native gel) causes proteins to unfold, and in our experiments, this appeared to cause the dissociation of ^{64}Cu from SOD. Therefore, we could not see a radioactive band for [^{64}Cu]SOD on a Western blot gel when SDS was present. Using native gel techniques (without SDS), we did not detect any binding of the SOD antibody to either human bovine SOD standards or to proteins in liver homogenates. With native gel techniques, the tertiary structure of proteins is intact. It is possible that in their intact state, there is no interaction between SOD and the anti-SOD antibody, and the antibody is only active against a denatured form of SOD.

DeNardo and colleagues have evaluated [^{67}Cu]BAT-2IT-Lym-1 in patients as an agent for RIT of lymphoma (*13*). They observed a flat, slow phase of blood clearance at about 3 days postinjection of [^{67}Cu]BAT-2IT-Lym-1, which was not observed with [^{131}I]Lym-1, suggesting that ^{67}Cu was incorporated into another protein. There was no evidence for binding of ^{67}Cu to albumin; however, ^{67}Cu was precipitated by anti-human Cp, with a maximum amount of [^{67}Cu]Cp observed on day 4 postinjection. It was hypothesized that ^{67}Cu was released from BAT-2IT-Lym-1 in the liver with subsequent formation of [^{67}Cu]Cp, and then [^{67}Cu]Cp was secreted back into the blood, which has also been suggested by Terao and Owen (*26*). These data agree with our results demonstrating that copper radionuclides dissociate from macrocyclic chelators in the liver and bind to proteins. The abundance of proteins such as SOD or Cp in the liver varies significantly between species, and rat liver has high concentrations of SOD (*27*). It has also been demonstrated that Cp can deliver copper to copper proteins such as SOD1 (*28*). We also observed a small amount of [^{64}Cu]Cp from the metabolism of [^{64}Cu]TETA-OC (~7%).

Possible explanations for the dissociation of copper radionuclides from bifunctional chelator-biomolecule conjugates are that the Cu(II) bifunctional chelator complexes may not be thermodynamically stable, or they may not be kinetically stable. Jones-Wilson and colleagues studied a series of six Cu(II) macrocyclic complexes and showed that some of the most thermodynamically stable complexes appeared to be the least stable in vivo (*29*), which argues for kinetic stability being more important.

In conclusion, using an assay specific for SOD, we have confirmed the formation of [^{64}Cu]SOD in the liver upon injection of [^{64}Cu]acetate and [^{64}Cu]TETA-OC into rats. Evaluating the metabolic fate of copper-radiopharmaceuticals has demonstrated that Cu(II) dissociates from macrocyclic chelates such as TETA and binds to proteins in high concentrations, namely SOD. Methods for circumventing the in vivo exchange of Cu(II) from such complexes is currently under investigation.

ACKNOWLEDGMENT

The authors would like to thank Todd Perkins and Dr. Deborah McCarthy for the production of ^{64}Cu, Lynne Jones and Elizabeth Sherman for technical assistance and W. Barry Edwards for helpful discussions. The authors would also like to thank Drs. Ruby Casareno and Jonathan Gitlin in the Department of Pediatrics at WUSM for their assistance with the SOD assays. This research was supported by the Department of Energy grant DE-FG02087ER60512 (M.J.W.) and the National Cancer Institute grant CA64475 (C.J.A.).

LITERATURE CITED

(1) Jones, P. L., Brown, B. A., and Sands, H. (1990) Uptake and Metabolism of ^{111}In-labeled Monoclonal Antibody B6.2 by the Rat Liver. *Cancer Res. 50*, 852s−856s.

(2) Geissler, F., Anderson, S. K., and Press, O. (1991) Intracellular Catabolism of Radiolabeled Anti-CD3 Antibodies by Leukemic T Cells. *Cell. Immunol. 137*, 96−110.

(3) Geissler, F., Anderson, S. K., Venkatesan, P., and Press, O. (1992) Intracellular Catabolism of Radiolabeled Anti-μ Antibodies by Malignant B-Cells. *Cancer Res. 52*, 2907−2915.

(4) Shih, L. B., Xuan, H., Aninipot, R., Stein, R., and Goldenberg, D. M. (1995) In Vitro and In Vivo Reactivity Of an Internalizing Antibody, Rs7, With Human Breast Cancer. *Cancer Res. 55*, S5857−S5863.

(5) Hofland, L. J., van Koetsveld, P. M., Waaijers, M., Zuyderwijk, J., Breeman, W. A. P., and Lamberts, S. W. J. (1995) Internalization of the Radioiodinated Somatostatin Analogue [125I-Tyr3]Octreotide by Mouse and Human Pituitary Cells: Increase by Unlabeled Octreotide. *Endocrinology 136*, 3698−3706.

(6) Novak-Hofer, H., Amstutz, H. P., Macke, H. R., Schwarzbach, R., Zimmermann, K., Morgenthaler, J. J., and Schubiger, P. A. (1995) Cellular Processing of Copper-67-labeled Monoclonal Antibody chCE7 by Human Neuroblastoma Cells. *Cancer Res. 55*, 46−50.

(7) Anderson, C. J., Connett, J. M., Schwarz, S. W., Rocque, P. A., Guo, L. W., Philpott, G. W., Zinn, K. R., Meares, C. F., and Welch, M. J. (1992) Copper-64-labeled antibodies for PET imaging. *J. Nucl. Med. 33*, 1685−1691.

(8) Anderson, C. J., Pajeau, T. S., Edwards, W. B., Sherman, E. L. C., Rogers, B. E., and Welch, M. J. (1995) In vitro and in vivo Evaluation of Copper-64-Labeled Octreotide Conjugates. *J. Nucl. Med. 36*, 2315−2325.

(9) Philpott, G. W., Schwarz, S. W., Anderson, C. J., Dehdashti, F., Connett, J. M., Zinn, K. R., Meares, C. F., Cutler, P. D., Welch, M. J., and Siegel, B. A. (1995) RadioimmunoPET: detection of colorectal carcinoma with positron-emitting copper-64-labeled monoclonal antibody. *J. Nucl. Med. 36*, 1818−1824.

(10) Dehdashti, F., Anderson, C. J., Trask, D. D., Bass, L. A., Schwarz, S. W., Cutler, P. D., McCarthy, D. W., and Lanahan, M. V. (1997) Initial Results with PET Imaging Using Cu-64-Labeled TETA-Octreotide in Patients with Carcinoid Tumor (abstract). *J. Nucl. Med. 38*, 103P.

(11) Connett, J. M., Anderson, C. J., Guo, L. W., Schwarz, S. W., Zinn, K. R., Rogers, B. E., Siegel, B. A., Philpott, G. W., and Welch, M. J. (1996) Radioimmunotherapy with a Cu-64-labeled monoclonal antibody: a comparison with Cu-67. *Proc. Natl. Acad. Sci. U.S.A. 93*, 6814−6818.

(12) DeNardo, G. L., Kukis, D. L., Shen, S., Mausner, L. F., Meares, C. F., Srivastava, S. C., Miers, L. A., and DeNardo, S. J. (1997) Efficacy and toxicity of 67Cu-2IT-BAT-Lym-1 radioimmunoconjugate in mice implanted with human burkitt's lymphoma (Raji). *Clin. Cancer Res. 3*, 71−79.

(13) DeNardo, G. L., DeNardo, S. J., Kukis, D. L., O'Donnell, R. T., Shen, S., Goldstein, D. S., Kroger, L. A., Salako, Q., DeNardo, D. A., Mirick, G. R., Mausner, L. F., Srivastava, S. C., and Meares, C. F. (1998) Maximum Tolerated Dose of 67Cu-2IT-BAT-LYM-1 for Fractionated Radioimmunotherapy of Non-Hodgkin's Lymphoma: A Pilot Study. *Anticancer Res. 18*, 2779−2788.

(14) Anderson, C. J., Jones, L. A., Bass, L. A., Sherman, E. L. C., McCarthy, D. W., Cutler, P. D., Lanahan, M. V., Cristel, M. E., Lewis, J. S., and Schwarz, S. W. (1998) Radiotherapy, Toxicity and Dosimetry of Copper-64-TETA-Octreotide in Tumor-Bearing Rats. *J. Nucl. Med. 39*, 1944−1951.

(15) Duncan, J. R., and Welch, M. J. (1993) Intracellular Metabolism of Indium-111-DTPA Labeled Receptor Targeted Proteins. *J. Nucl. Med. 34*, 1728−1738.

(16) Franano, F. N., Edwards, W. B., Welch, M. J., and Duncan, J. R. (1994) Metabolism of Receptor Targeted ^{111}In-DTPA-Glycoproteins: Identification of ^{111}In-DTPA-ϵ-lysine as the Primary Metabolic and Excretory Product. *Nucl. Med. Biol. 21*, 1023−1034.

(17) Rogers, B. E., Franano, F. N., Duncan, J. R., Edwards, W. B., Anderson, C. J., Connett, J. M., and Welch, M. J. (1995) Identification of Metabolites of In-111-DTPA-Monoclonal Antibodies and Antibody Fragments In Vivo. *Cancer Res. 55*, 5714s−5720s.

(18) Rogers, B. E., Anderson, C. J., Connett, J. M., Guo, L. W., Edwards, W. B., Sherman, E. L. C., Zinn, K. R., and Welch, M. J. (1996) Comparison of Bifunctional Chelates for Radiolabeling Monoclonal Antibodies with Copper Radioisotopes: Biodistribution and Metabolism. *Bioconjugate Chem. 7*, 511−522.

(19) Bass, L. A., Lanahan, M. V., Duncan, J. R., Erion, J. L., Srinivasan, A., Schmidt, M. A., and Anderson, C. J. (1998) Identification of the Soluble in vivo Metabolites of Indium-111-Diethylenetriaminepentaacetic Acid-D-Phe^1-Octreotide. *Bioconjugate Chem. 9*, 192−200.

(20) Linder, M. C. (1991) *Biochemistry of Copper*, Vol. 10, Plenum Press, New York.

(21) Beauchamp, C., and Fridovich, I. (1971) Superoxide dismutase: Improved Assays and an Assay Applicable to Acrylamide Gels. *Anal. Biochem. 44*, 276.

(22) McCarthy, D. W., Shefer, R. E., Klinkowstein, R. E., Bass, L. A., Margenau, W. H., Cutler, C. S., Anderson, C. J., and Welch, M. J. (1997) The Efficient Production of High Specific Activity Cu-64 Using a Biomedical Cyclotron. *Nucl. Med. Biol. 24*, 35−43.

(23) Borchelt, D. R., Lee, M. K., Slunt, H. S., Guarnieri, M., Xu, Z.-S., Wong, P. C., Brown, J. R. H., Price, D. L., Sisodia, S. S., and Cleveland, D. W. (1994) Superoxide Dismutase 1 with Mutations Linked to Familial Amyotrophic Lateral Sclerosis Possesses Significant Activity. *Proc. Natl. Acad. Sci. U.S.A. 91*, 8292−8296.

(24) Lewis, J. S., Lewis, M. R., Cutler, P. D., Srinivasan, A., Schmidt, M. A., Schwarz, S. W., Morris, M. M., Miller, J. P., and Anderson, C. J. (1999) Radiotherapy and Dosimetry of 64Cu-TETA-Tyr3-Octreotate in a Somatostatin Receptor-Positive Tumor-Bearing rat model. *Clin. Cancer Res. 5*, 3608−3616.

(25) Seo, H. C., and Ettinger, M. J. (1993) Identification and Purification of a Self-associating Copper-binding Protein from Mouse Hepatic Cytosols. *J. Biol. Chem. 268*, 1151−1159.

(26) Terao, T., and Owen, C. A. (1973) Nature of Copper Compounds in Liver Supernate and Biole of Rats: Studies with ^{67}Cu. *Am. J. Physiol. 224*, 682−686.

(27) Owen, C. A. (1982) *Biochemical Aspects of Copper: Copper Proteins, Ceruloplasmin, and Copper Protein Binding*, Noyes Publications, New Jersey.

(28) Goode, C. A., Dinh, C. T., and Linder, M. C. (1989) Mechanism of copper transport and delivery in mammals: review and recent findings. *Adv. Exp. Med. Biol. 258*, 131−144.

(29) Jones-Wilson, T. M., Deal, K. A., Anderson, C. J., McCarthy, D. W., Kovacs, Z., Motekaitis, R. J., Sherry, A. D., Martell, A. E., and Welch, M. J. (1998) The in vivo Behavior of Copper-64-Labeled Azamacrocyclic Compounds. *Nucl. Med. Biol. 25*, 523−530.

BC990167L

Synthesis and Characterization of a Sulfhydryl-Reactive Rhenium Metal−Ligand Complex

Jonathan D. Dattelbaum, Omoefe O. Abugo, and Joseph R. Lakowicz*

University of Maryland School of Medicine, Center for Fluorescence Spectroscopy, Department of Biochemistry and Molecular Biology, 725 West Lombard Street, Baltimore, Maryland 21201 . Received December 8, 1999; Revised Manuscript Received March 14, 2000

We describe the synthesis and spectral characterization of a rhenium metal−ligand complex. This complex reacts with sulfhydryl groups via an iodoacetamide side chain on the phenanthroline ligand and displays a high limiting anisotropy near 0.35 when excited at 442 nm. When covalently linked to human serum albumin, this complex displayed a mean decay time of about 1 μs. This decay time is appropriate for measuring rotational correlation times on the microsecond time scale as may occur for large macromolecular complexes.

INTRODUCTION

During the past 5 years there has been rapid development of transition metal−ligand complexes as biophysical probes and/or chemical sensors (*1*−*5*). The MLCs are typically composed of a central metal of Re, Ru, or Os and at least one diamine ligand. The photophysical properties of this class of molecules has been extensively studied (*6*−*9*). The MLCs display a number of favorable properties which facilitate their use as luminescence probes. The decay times are conveniently long, ranging from 10 ns to 10 μs. Most MLCs display polarized emission, allowing measurement of macromolecule hydrodynamics. The MLCs display large Stokes' shifts, which eliminates the problems of self-quenching often found with fluorescein and other fluorophores with small Stokes' shifts. And finally, most MLCs are highly stable, both photochemically and chemically.

While numerous MLCs have been synthesized and characterized, relatively few MLCs have been prepared in forms suitable for conjugation with proteins. In the present report, we extend the availability of conjugatable MLCs by the synthesis of a Re MLC which is reactive with sulfhydryl residues (Figure 1). As a chloride complex, this dye was found to have a reasonable quantum yield in dichloromethane and most especially displays a high fundamental anisotropy near 0.35 and is thus useful for anisotropy measurements of large proteins.

THEORY

Time-resolved intensity and anisotropy decays were recovered from the frequency-domain data, as described previously (*10*−*11*). Intensity decays were analyzed in terms of the multiexponential model

$$I(t) = \sum_i \alpha_i \exp(-t/\tau_i) \tag{1}$$

where α_i are the preexponential factors and τ_i the decay times. The fractional contributions of each decay component to the steady-state intensity are given by

$$f_i = \frac{\alpha_i \tau_i}{\sum_i \alpha_i \tau_i} \tag{2}$$

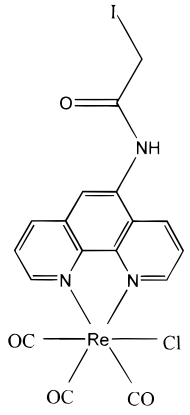

$Re(phen\text{-}IA)(CO)_3Cl$

Figure 1. Structure of the sulfhydryl reactive Re(phen-IA)-$(CO)_3Cl$ complex.

The mean lifetime is given by

$$\bar{\tau} = \sum_i f_i \tau_i = \frac{\sum_i \alpha_i \tau_i^2}{\sum \alpha_i \tau_i} \tag{3}$$

Anisotropy decays were analyzed in terms of the multicorrelation time (θ_k)

$$r(t) = \sum r_{0k} \exp(-t/\theta_k) \tag{4}$$

where r_{0k} is the amplitude of the kth correlation time. For a fully resolved anisotropy decay, one expects the recovered total anisotropy or the time zero anisotropy $r(0) = \sum r_{0k}$ to be equal to r_0, where r_0 is the fundamental anisotropy in the absence of rotational motions.

MATERIALS AND METHODS

Synthesis of Re(phen-IA)(CO)$_3$Cl. The synthesis of phen-IA is reported elsewhere (*12*). $Re(CO)_5Cl$ (76 mg, 210 mmol) (Aldrich Chemical Co., Milwaukee, WI) and phen-IA (78 mg, 215 mmol) were refluxed in toluene under argon in the dark for 6 h. The solution was cooled

10.1021/bc990174+ CCC: $19.00 © 2000 American Chemical Society
Published on Web 06/17/2000

to room temperature and kept overnight at 4 °C. The precipitated product was collected on a medium frit. Additional product was recovered by filtering the solution into ice cold hexane. Total yield was about 77%. The recovered product was further purified using preparative thin-layer chromatography. This was done on a silica plate using a mixture of 1.0:2.7:0.05 of methanol:chloroform:water as the mobile phase. The spot containing the pure Re−Cl was scraped off the plate at the end of the experiment and extracted from the silica matrix with a mixture of 7:3 of methanol: chloroform. FAB MS: m/z = 633.5 ([M − Cl]), 668.0 ([M]).

Modification of the cysteine residue of human serum albumin (Sigma) was accomplished by addition of 50 μL of a 20 mg/mL DMSO solution of Re(phen-IA)$(CO)_3Cl^+$ to 1 mL of the protein solution (5 mg/mL, 100 mM phosphate buffer, pH 7.3). The reaction proceeded overnight at 4 °C followed by gel filtration chromatography on a Sephadex G-25 column (Sigma, St Louis, MO) equilibrated in 10 mM Tris buffer, pH 8.0. The labeled protein was eluted with the 10 mM Tris buffer, pH 8.0, and dialyzed overnight with a 10 kDa Snakeskin cutoff tubing (Pierce, Rockfield, IL) against the same buffer at 4 °C. The dye-to-protein ratio was determined by the absorption of the photoluminescent complex and protein as previously described (*13*) and was found to be about 0.70. This will suggest minimal stearic problems during conjugation.

INSTRUMENTATION

Absorption spectra were measured on a Hewlett-Packard 8453 diode array spectrophotometer. All steady-state fluorescence measurements were performed using a SLM 8000 spectrofluorometer. Excitation anisotropy measurements for the MLCs were done in 9:1 glycerol: dichloromethane (DCM) at −70 °C using a Neslab Endocal methanol chiller attached to the SLM 8000 spectrofluorometer. Excitation for frequency-domain lifetime and anisotropy measurements was provided by the output from a Helium−cadmium laser (442 nm, Liconix 4280N), which was amplitude modulated at single frequencies between 10 kHz and 100 MHz with an electrooptical low-frequency modulator (K2.LF, ISS) and input into an ISS K2 frequency domain fluorometer (*13*). Emission was collected through a Corning 2-70 510 nm cutoff filter. Rhodamine B (Aldrich Chemical Co.) in water (τ = 1.68 ns) was used as a reference for the lifetime measurements.

RESULTS AND DISCUSSION

The absorption and emission spectra of Re(phen-IA)-$(CO)_3Cl$ (Re−Cl) are shown in Figure 2. Absorption maxima are seen near 410 and 280 nm, and the emission maximum near 600 nm. The large Stokes shift is typical of this class of luminophores. Its quantum yield in dichloromethane is 0.039 relative to $[Ru(bpy)_3]^{2+}$ in deoxygenated water (0.042). The extinction coefficients at 278, 325, and 380 nm are 23 100, 6450, and 3200, respectively.

Figure 2 also shows the excitation anisotropy spectra for Re−Cl. It was measured in 9:1 glycerol:DCM at −70 °C to prevent rotational diffusion during the excited-state lifetime. Re−Cl displays a high fundamental anisotropy of over 0.3 when excited at wavelengths above 400 nm. Fundamental anisotropy value of 0.338 was obtained at 442 nm for this complex. This large anisotropy, over 75% of the theoretical value of 0.4, makes this complex a useful polarization probe.

Figure 3 shows frequency-domain intensity decay of this complex when dissolved in DCM and when covalently linked to HSA. In DCM the intensity decays are single exponentials (Table 1). The decay times of the Re complex in DCM are sensitive to dissolved oxygen, which reduces the decay time from 436 ns in the absence of oxygen to 159 ns when in equilibrium with air. When bound to HSA, this complex displays a multiexponential

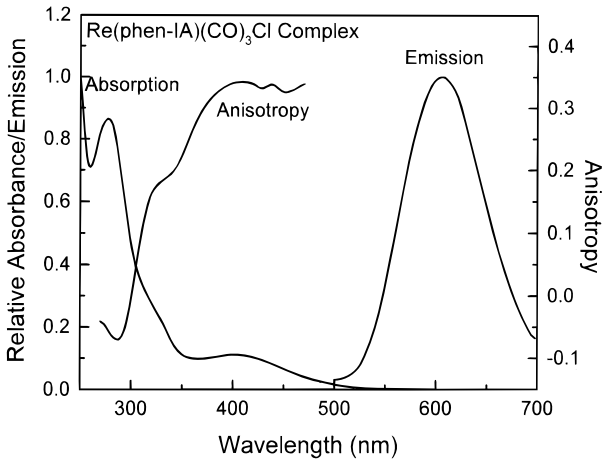

Figure 2. Absorption, emission and excitation anisotropy spectra of Re(phen-IA)$(CO)_3Cl$. Absorption and emission spectra were measured at room temperature in dichloromethane. Excitation anisotropy spectra were measured in 9:1 (v/v) glycerol/dichloromethane at −70 °C with emission at 500 nm.

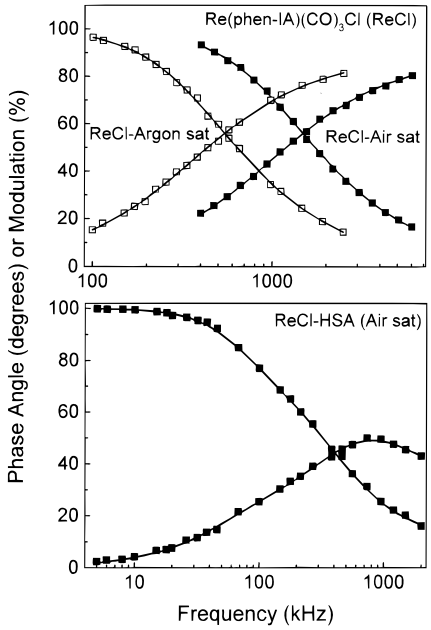

Figure 3. Representative frequency-domain intensity decays for the free Re−Cl complex and for HSA labeled with Re−Cl. Free Re−Cl measurements were made in dichloromethane while the labeled HSA was measured in aqueous solution. Excitation at 442 nm and observation above 500 nm.

Table 1. Intensity Decay Parameters of Free and HSA-Labeled Re(phen-IA)$(CO)_3Cl$

metal complex	τ_i (ns)	α_i	f_i	$\bar{\tau}$ (ns)	χ_R^2
Re−Cl in DCM[a](air)	159	1.000	1.00	159	2.64[b]
Re−Cl in DCM (argon)	436	1.000	1.00	436	4.74
Re−Cl−HSA (air)	2102	0.026	0.418		
	473	0.128	0.468		
	17.4	0.847	0.114	1101	4.73

[a] DCM, dichloromethane. [b] For calculation of χ_R^2 the uncertainties in the phase and modulation was assumed to be 0.2 and 0.005, respectively.

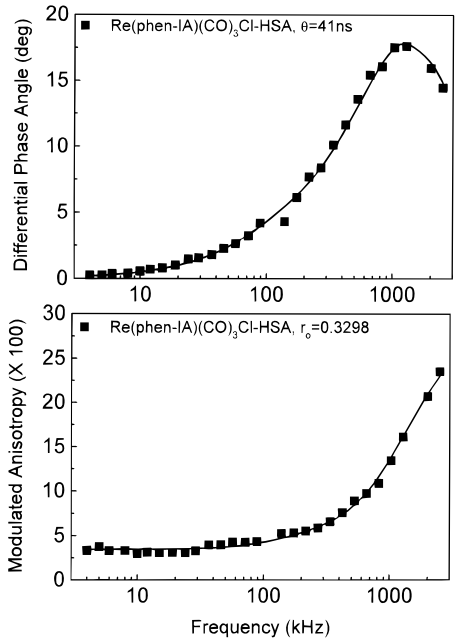

Figure 4. Frequency domain anisotropy decays of Re(phen-IA)$(CO)_3$Cl−HSA in aqueous solution. Excitation at 442 nm and observation above 500 nm.

decay (Figure 3), requiring three decay times for an acceptable fit. The mean decay time for the HSA-bound complex is 1101 ns. The much longer lifetime of the HSA-labeled complex when compared to the free probe indicates that the probe is well shielded within the protein and protected appreciably from oxygen quenching. This observed long lifetime also indicates that this probe could be used to measure long correlation times that would be expected for very large macromolecules.

To demonstrate the utility of this Re−Cl complex for measurement of microsecond of macromolecular hydrodynamics, its anisotropy decay was measured when bound to HSA. A rotational correlation time of 41 ns was recovered when bound to HSA. This result is in good agreement with that predicted by theory and previous experimental results (*13*−*15*). In addition, the initial anisotropy of 0.32 was close to that observed in vitrified glycerol solution at 442 nm (Table 1). This result suggests that this dye is covalently bound to HSA, and hence, its anisotropy decay reflects the overall rotation of the labeled HSA. (Figure 4).

Conclusion. We have synthesized and characterized a sulfhydryl reactive Re MLC, Re(phen-IA)$(CO)_3$Cl, that can be used to label cysteine residues in proteins. This complex is reactive with the sulfhydryl groups on proteins via an iodoacetamide side chain. This complex exhibited a long lifetime of 436 ns in an organic solvent and a high fundamental anisotropy of 0.34. The mean decay time was even longer when covalently bound to HSA, about 1101 ns. This long decay time makes this luminophore appropriate for measuring the correlation times of macromolecules of a similar time scale, as may be expected for moderate to large sized proteins. Its high anisotropy also makes it to be very useful in fluorescence polarization immunoassays of high molecular weight macromolecules (*17*−*19*).

It is also valuable to notice that this probe allows for time-resolved measurements with simple instrumentation. Wavelengths short enough to excite these complexes are available using light emitting diodes (*20*). Additionally, the light output of LEDs can be easily modulated to about 100 MHz (*20*−*23*), which is more than adequate for this long lifetime luminophore. Hence, the simple combination of this MLC luminophore and LED-based instrumentation can be used to study microsecond dynamics of macromolecules.

ACKNOWLEDGMENT

This work was supported by grants from the National Institutes of Health, RR-08119 and GM35154.

LITERATURE CITED

(1) Demas, J. N., and DeGraff, B. A. (1997). Applications of luminescent transition metal complexes to sensor technology and molecular probes. *J. Chem. Educ. 74* (6), 690−695.
(2) Demas, J. N., and DeGraff, B. A. (1991). Design and applications of highly luminescent transition metal complexes, *Anal. Chem. 63*, 829a−837a.
(3) Demas, J. N., and DeGraff, B. A. (1994). Design and applications of highly luminescent transition metal complexes. In *Topics in Fluorescence Spectroscopy: Probe Design and Chemical Sensing* (J. R. Lakowicz, Ed.) Vol. 4, pp 71−107 Plenum Press, New York.
(4) Lakowicz, J. R., Terpetschnig, E., Murtaza, Z., and Szmacinski, H. (1997) Development of long-lifetime metal−ligand probes for biophysics and cellular imaging, *J. Fluoresc. 7* (1), 17−25.
(5) Terpetschnig, E., Szmacinski, H., and Lakowicz, J. R. (1997) Long-lifetime metal−ligand complexes as probes in biophysics and clinical chemistry, *Methods in Enzymology 278*, 294−321.
(6) Kalayanasundaram, K. (1992) P*hotochemistry of Polypyridine and Porphyrin Complexes*, p 626, Academic Press, New York.
(7) Juris, A., Balzani, V., Barigelletti, F., Campagna, S., Belser, P., and Von Zelewsky, A. (1988) Ru(II) polypyridine complexes, photophysics, photochemistry, electrochemistry and chemiluminescence. *Coord.Chem. Rev. 84*, 85−277.
(8) Fredericks, S. M., Luong, J. C., and Wrighton, M. S. (1979) Multiple emissions from rhenium (I) complexes, Intraligand and charge-transfer emission from substituted metal carbonyl cations. *J. Am. Chem. Soc. 101* **(**24**)**, 7415−7417.
(9) Caspar, J. V., and Meyer, T. J. (1983) Applications of the energy gap law to nonradiative, excited-state decay. *J. Phys. Chem. 87*, 952−957.
(10) Lakowicz, J. R., and Gryczynski, I. (1991) Frequency-domain fluorescence spectroscopy. in *Topics in Fluorescence Spectroscopy, Vol 1, Techniques* (J. R. Lakowicz, Ed.) pp 293−355, Plenum Press, New York.
(11) Beechem, J. M., Gratton, E., Ameloot, M., Knutson, J. R., and Brand, L. (1991) The global analysis of fluorescence intensity and anisotropy decay data: Second-generation theory and programs. In *Topics in Fluorescence Spectroscopy, Vol 2, Principles* (J. R. Lakowicz, Ed.) Plenum Press, New York, pp 241−305.
(12) Sigman, D. S., Kuwabara, M. D., Chen, C. H. B., and T. W. Bruce (1991) Nuclease activity of 1,10-phenanthroline-copper in study of protein-DNA interactions. *Methods Enzymol.* 208, 414−433**.**
(13) Castellano, F. N., Dattelbaum, J. D., and Lakowicz, J. R. (1998) Long-lifetime Ru(II) complexes as labeling reagents for sulfhydryl groups. *Anal. Biochem. 255*, 165−170.
(14) Terpetschnig, E., Szmacinski, H., Malak, H., and Lakowicz, J. R. (1995) Metal−Ligand Complexes as a New Class of Long-Lived Fluorophores for Protein Hydrodynamics. *Biophys. J. 68*, 342−350.
(15) Terpetschnig, E., Dattelbaum, J. D., Szmacinski, H., and Lakowicz, J. R. (1997) Synthesis and spectral characterization of a thiol-reactive long- lifetime Ru(II) complex. *Anal. Biochem.* 251, 241−245**.**
(16) Lakowicz, J. R., Cherek, H., Gryczynski, I., Joshi, N., and Johnson, M. L. (1987) Enhanced resolution of fluorescence anisotropy decays by simultaneous analysis of progressively quenched samples. *Biophys. J.* 51, 755−768.
(17) Youn, H. J., Terpetschnig, E., Szmacinski, H., and Lakowicz, J. R. (1995) Fluorescence Energy Transfer Immunoassay

Based on a Long-Lifetime Luminescent Metal−Ligand Complex. *Anal. Biochem*. 232, 24−30.
(18) Terpetschnig, E., Szmacinski, H., and Lakowicz, J. R. (1995). Fluorescence Polarization Immunoassay of a High Molecular Weight Antigen Based on a Long-Lifetime Ru−Ligand Complex. *Anal. Biochem*. 227, 140−147.
(19) Terpetschnig, E., Szmacinski, H., and Lakowicz, J. R. (1996) Fluorescence polarization immunoassay of a high-molecular-weight antigen using a long wavelength-absorbing and laser diode-excitable metal-ligand complex. *Anal. Biochem*. 240, 54−59.
(20) Sipior, J., Carter, G. M., Lakowicz, J. R., and Rao, G. (1997) Blue light-emitting diode demonstrated as an ultraviolet excitation source for nanosecond phase-modulation fluorescence lifetime measurements *Rev. Sci. Instrum*. *68*(7), 2666−2670.
(21) Fantini, S., Franceschini, M. A., Fishkin, J. B., Barbieri, B., and Gratton, E. (1994) Quantitative determination of the absorption spectra of chromophores in strongly scattering media, A light-emitting diode based technique. *Appl. Opt*. *33* (22), 5204−5213.
(22) Lippitsch, M. E., and Wolfbeis, O. S. (1988) Fiber-optics oxygen sensor with the fluorescence decay time as the information carrier. *Anal. Chim. Acta 205*, 1-6.
(23) Sipior, J., Carter, G. M., Lakowicz, J. R., and Rao, G. (1996) Single quantum well light emitting diodes demonstrated as excitation sources for nanosecond phase-modulation fluorescence lifetime measurements. *Rev. Sci. Instrum*. *67* (11), 3795−3798.

BC990174+

Concepts for the Syntheses of Biotinylated Steroids. Part II: 17β-Estradiol Derivatives as Immunochemical Probes

Hagen Hauptmann,[†] Birgit Paulus,[†] Thomas Kaiser,[‡] and Peter B. Luppa*[,‡]

Institute for Organic Chemistry, Universität Regensburg, D-93053 Regensburg, Germany, and Institute for Clinical Chemistry and Pathobiochemistry, Klinikum rechts der Isar, Technische Uni-versität München, D-81675 München, Germany. Received December 14, 1999; Revised Manuscript Received February 28, 2000

Biotinylated 17β-estradiol (E2) derivatives are helpful probes for a better understanding of biospecific E2 interactions with steroid-binding proteins such as the estrogen receptor and anti-steroid antibodies. We describe synthetic strategies for the biotinylation of E2 toward the 3, 6α, and 7α positions using biotinyl-*N*-hydroxysuccinimide esters with different spacers, varying in structure and chain length. Key reaction for biotinylation at the 3 position is the regioselective ether formation of the phenolate E2 anion with a linker mesylate without protecting the 17β-hydroxyl group. The 6α position is accessible via a 3,17β protected 6α-hydroxy E2, prepared by stereospecific sodium borohydride reduction of 6-oxo E2. Direct cyanoethylation of the alcohol followed by reduction to the amine allows the biotinylation to 6α-*O*-coupled cyanoethyloxy linker E2 derivatives. Alternatively, 6α-*O*-coupled cyanoalkyloxy polyether linker E2 probes are obtained by a Williamson ether synthesis of the alcohol precursor with ω-*t*-butyl-dimethylsilyloxy-5-oxa-nonylmesylate. Cyanoethylation of the desilylated compound and further reduction of the nitrile led to the terminal amine. Reductive amination of the 3,17β acetylated 6-oxo E2 compound with 6-cyanoethyloxyhexyl ammonium acetate yields in a mixture of 6α/β-*N*-alkylated E2 nitriles. The epimers are separated by reversed-phase HPLC and the 6α-compound subsequently reduced to the terminal amine. The 7α-biotinylated E2 compound is derived from 7α-(11′-undecyl-*N*-methyl-*N*-butylamide) E2, which is already known from literature. Subsequently, the 3 and 17β positions are protected, and the amide is reduced to the 7α-(11′-undecanol) compound. Further cyanoethylation and reduction led to the 11′-amino-ethyloxyundecyl E2. Using ^{1}H NMR analysis, it could be shown that the biotin moiety of the biotinylated 6α- and 7α-E2 derivatives has an axial position which results in a vertical orientation of the substituent toward the α-face of the planar tetracyclic backbone. Thus, a negligible alteration of the original structure of the upper β-face offers the feasibility of applying the 6α- and 7α-derivatives as optimal tracers in competitive immunoassays.

INTRODUCTION

The design and synthesis of steroid derivatives is a field of major interest. The tools of organic chemistry enable the synthesis of 17β-estradiol (E2)[1] probes, which can help for a better understanding of the biospecific E2 interaction with steroid-binding proteins such as the estrogen receptor (ER) and anti-E2 antibodies as well as E2-binding serum globulin. An important application is the determination of E2 and related estrogens in human serum or urine by use of immunoassay methods for a series of endocrine disorders. Furthermore, the detection of the ER in tumor tissues is of outstanding interest as a prognostic factor in gynecological oncology. The study of ligand-binding properties of various E2 derivatives to the ER can provide insights in the molecular basis of the receptor physiology and yields hints for the pharmaceutical construction of novel antineoplastic agents.

Analytical and Biochemical Applications for Biotinylated E2 Derivatives. E2 probes labeled with prosthetic groups such as biotin can be used as immunochemical probes in a number of different applications, including immunoassays for the determination of E2 in serum. Whereas these compounds are already in use as tracers in steroid immunoassay techniques for endocrinological purposes (De Boever et al., 1986; Tiefenauer and Andres, 1990; Luppa et al., 1995; Adamczyk et al., 1998a; Meltola et al., 1999), the application of biotinylated E2 for the oncologically relevant determination of the ER in tumor tissues is still a future project.

Regarding the molecular interaction between the epitope represented by the steroidal E2 molecule and the paratope of a specific mono- or polyclonal anti-E2 antibody, a main aspect is the *specificity-to-structure* relationship. This term mirrors the *structure-to-activitity* relationship for the complexes of steroid hormones to the respective receptors. In both cases, crystallographic data are now available for the ligand-binding domain (LBD) of the ER (Brzozowski et al., 1997; Tanenbaum et al., 1998) and

* To whom correspondence should be addressed. Phone: +49 89 4140 4751. Fax: +49 89 4140 4875. E-mail: luppa@klinchem.med.tu-muenchen.de.

[†] Institute for Organic Chemistry.

[‡] Institute for Clinical Chemistry and Pathobiochemistry.

[1] Abbreviations: CDR, complementarity-determining regions; DDS-biotin, D-(+)-biotinyl-amino-3,6-dioxa-octanylaminocarbonylheptanoic acid-*N*-hydroxysuccinimide ester; DHP, dihydro-2H-pyrane; DMF, dimethylformamide; E2, 17β-estradiol; ER, estrogen receptor; HMPT, hexamethyl phosphoric acid triamide; LBD, ligand-binding domain; LC-biotin, D-(+)-biotinyl-ϵ-aminocaproic acid-*N*-hydroxysuccinimide ester; LSC, liquid solid chromatography; mp, melting point; MTBE, methyl-*t*-butyl ether; PE, petroleum ether; PPTS, pyridinum-*p*-toluenesulfonate; t_r, retention time; TBAF, tetrabutylammonium fluoride; TBDMS, *t*-butyl-dimethylsilyl; THF, tetrahydrofuran; THP, tetrahydropyrane.

10.1021/bc9901651 CCC: $19.00 © 2000 American Chemical Society
Published on Web 06/13/2000

for complementarity-determining regions (CDR) of F'_{ab}/steroid complexes (Arevalo et al., 1993a,b).

Considerations for the Derivatization of E2 at Different Ring Positions. The aim of this presentation is to summarize different organic chemical syntheses for the biotinylation of E2. This steroid is a lipophilic compound with a rigid and planar tetracyclic backbone. Detailed crystallographic data for E2 are given by Anstead et al. (1997). A crucial topic for the derivatization is the biochemical functionality of the derivatization position at the ring-core (Adamczyk et al., 1997). It depends on the special issue in which these steroidal derivatives are used. For immunoassay applications, E2 tracers can in principle be used with substituents at ring sites that are outside of the ligand-binding region of the respective anti-E2 antibody. Furthermore, the chemical structure of the spacer group linking the biotin residue to the steroid ring system is an important issue. The linker group has to minimize steric hindrances between the biotin moiety and the binding protein. Moreover, its chemical structure has a relevant influence on the process of antibody recognition: the structure must be similar to the linkage used in the immunization procedure.

E2 derivatives are best suited as biospecific adsorbents for the ER in an affinity chromatography system when substituted at the 7α-position (Bucourt et al., 1978). Analogues of E2 as ligands for the ER must bear hydrophobic substituents. Large substituents, however, are limited for binding to the LBD. It could be shown that substituents at positions 4, 7α, 11*β*, 12*β*, 14, 16α, and 17α lead to increased affinities, while, in contrast, substituents at positions 3, 6α, 6*β*, 9α, 16*β*, and 17*β* markedly diminish the affinity (Anstead et al., 1997; Hanson et al., 1998).

The challenge presented by the structural demands on the spacer group can be met through the synthesis of appropriate steroidal precursors and the careful selection of the biotinylation reagent. The 6 and 7 positions of the E2 ring are best suited when preparing immunochemical tracers for nonisotopic immunoassays. The principles for these chemical pathways will be described in detail.

EXPERIMENTAL PROCEDURES

General Methods. *Apparatus.* ^{1}H NMR spectra were recorded in $CDCl_3$ on a Bruker WM 250 (250 MHz) and on a Bruker ARX 400 (400 MHz), using Me_4Si for reference signal (δ 0.00 ppm); the data in Table 1 are reported in the following form: chemical shift (multiplicity, coupling constant in hertz if available, number of protons, position of proton). IR spectra were obtained from KBr or neat on a Mattson Genesis Series FT-IR spectrophotometer, and only characteristic IR bands are reported as wavenumbers (cm^{-1}). UV spectra were measured in MeOH on a Hitachi spectrophotometer U-2000. Optical rotation values were gained from a Perkin-Elmer 241 polarimeter, *c* is given in g/100 cm^{-3}. MS analyses were performed on a Finigan MAT 90 (FAB) and on a Varian MAT 112S and 311 A (EI). The preparative HPLC system consisted of an HPLC pump Knauer 64 (Knauer, Bad Homburg, Germany) and a UV detector ERC 7210 (ERC, Alteglofsheim, Germany). Preparative HPLC columns were from Bischoff Analysentechnik, Leonberg, Germany (Kromasil SC 100) and Knauer (Eurospher 100 C_{18}).

Chemicals. For column chromatography, silica gel (grain 0.063−0.200) from E. Merck (Darmstadt, Germany), neutral Al_2O_3 (aluminia N Super I, type W 200), and basic Al_2O_3 (aluminia B Super I, type W 200) from Woelm Pharma (Bad Honnef, Germany) were used. Thin-layer chromatography was performed using silica gel 60 F254 (0.2 mm) and neutral Al_2O_3 60 F254 type E (0.2 mm), both materials from Merck. E2 was from Sigma (Deisenhofen, Germany); 6-bromo-hexanol, tetrabutylammonium fluoride and *t*-butyl-dimethylchlorsilane were from Fluka (Buchs, Switzerland). D-(+)-Biotinyl-ε-aminocaproic acid-*N*-hydroxysuccinimide ester (LC-biotin) and D-(+)-biotinyl-amino-3,6-dioxaoctanyl-aminocarbonyl-heptanoic acid-*N*-hydroxysuccinimide ester (DDS-biotin) were purchased from Roche Molecular Biochemicals, Penzberg, Germany. All other laboratory chemicals were from Fluka.

Syntheses. Spectroscopic data of key intermediates and all end products of the described syntheses are presented in Table 1. All syntheses were carried out with 0.5−1.0 mmol of starting material.

1. Preparation of 17*β*-Hydroxy-3-(13′-biotinylaminocaproyl-5′,10′-dioxa-trideylamino-oxy)-estra-1,3,5(10)-triene (7). The synthesis of the 9-tetrahydropyranyloxy-5-oxa-nonylmesylate is described in Hauptmann et al. (2000).

17β-Hydroxy-3-(9′-tetrahydropyranyloxy-5′-oxa-nonyloxy)-estra-1,3,5-(10)-triene (**3**) (Miyashita et al., 1977; Gala et al., 1986). One equivalent of E2 (**1**) was dissolved in dry hexamethyl phosphoric acid triamide (HMPT) under N_2, 1 equiv of KH was added, and the mixture was stirred for 10 min at room temperature (rt). Then 1.1 equiv of 9-tetrahydropyranyloxy-5-oxa-nonylmesylate **2** was added to the solution dropwise until the reaction mixture turns into a brown gellike substance. After stirring for 18 h at room temperature, the mixture was quenched with H_2O and extracted twice with Et_2O. After removal of the solvent, the brownish oil was subjected to liquid solid chromatography (LSC) by use of alkaline Al_2O_3 as stationary phase and CH_2Cl_2:Et_2O (1:1, v/v) as the eluent. **3** was isolated as colorless oil, yield 75%.

17β-Hydroxy-3-(9′-hydroxy-5′-oxa-nonyloxy)-estra-1,3,5(10)-triene (**4**). One equivalent of **3** was dissolved in MeOH, and 0.1 equiv of pyridinum-*p*-toluenesulfonate (PPTS) was added. The solution was stirred for 65 h at room temperature. After removal of the solvent, the remaining oil was chromatographed at silica gel (SiO_2) (eluent CH_2Cl_2:ethyl acetate, 1:9, v/v). **4** was isolated as colorless oil, yield 95%.

17β-Hydroxy-3-(12′-cyano-5′,10′-dioxa-dodecyloxy)-estra-1,3,5(10)-triene (**5**) (Roy and Ray, 1995). One equivalent of **4** was dissolved under N_2 in acetonitrile. After addition of *t*-butanol, the clear solution was chilled on ice. Then 0.3 equiv of 1.0 mol/L of K-*t*-butanolate and 1.1 equiv of acrylonitrile ($d = 0.806$) were added, and the mixture was stirred for 15 min at 0 °C. The clear yellowish solution was quenched with H_2O and extracted twice with Et_2O. After LSC on SiO_2 (eluent ethyl actate:CH_2Cl_2, 1:4, v/v), **5** was isolated as main product, yield 70%. A dicyanoethylated compound as side product was discharged.

17β-Hydroxy-3-(13′-amino-5′,10′-dioxa-tridecyloxy)-estra-1,3,5(10)-triene (**6**) (Ray et al., 1991; Roy and Ray, 1995). Ten equivalents of $LiAlH_4$ was suspended at 0 °C under N_2 in dry Et_2O. One equivalent of **5**, dissolved in Et_2O, was added dropwise, and the gray suspension was stirred for further 90 min at room temperature. The suspension was again cooled to 0 °C, and a diluted $NaHCO_3$ solution added. The product was extracted with Et_2O and, after removal of the solvent, the residue was freeze-dried. **6** was isolated as colorless oil, yield 99%.

17β-Hydroxy-3-(13′-biotinylaminocaproyl-5′,10′-dioxa-trideylamino-oxy)-estra-1,3,5-(10)-triene (**7**) (Tiefenauer

Table 1. Spectroscopic Data of Key Intermediates and Final Products for the Syntheses of Biotinylated E2 Derivatives

compd	IR [$\bar{\nu}$ (cm^{-1})]	^{1}H NMR [δ (ppm)]	MS (FAB, 70 eV, *m*/*z*)	elementary analysis	UV [λ (nm), lgϵ]	$[\alpha]_D^{20}$, (c in MeOH)
4	3342 (OH), 3028 (CH_{arom}), 2926, 2868 ($CH_{aliphat}$), 1609, 1573 ($C{=}C_{conj}$), 1116 (C−O−C)	0.77 (s, 3 H, 18-CH_3), 2.83 (m, 2 H, 11-CH_2), 3.48 (m, 3 H, CH_2−O, OH), 3.64 (t, 2 H, CH_2−O), 3.70 (m, 2 H, CH_2−O), 3.96 (m, 2 H, CH_2−O), 6.62 (m, 1 H, 2-CH), 6.69 (dd, J = 8.5 Hz, J = 2.4 Hz, 1 H, 4-CH), 7.18 (d, J = 8.6 Hz, 1H, 1-CH)	417.4 (MH^+, 100%)	$C_{26}H_{40}O_4$ (416.60) calcd: C, 74.96; H, 9.86; found: C, 74.52; H, 9.71	281 nm, 3.15	
6	3600−3100 (OH), 3363, 3298 (NH_2), 3029 (CH_{arom}), 2926, 2867 ($CH_{aliphat}$), 1608, 1577 ($C{=}C_{conj}$), 1115 (C−O−C)	0.77 (s, 3 H, 18-CH_3), 2.63−2.87 (m, 4 H, 11-CH_2, CH_2−NH_2), 3.33−3.71 (m, 8 H, CH_2−O-), 3.97 (m, 2 H, CH_2−O-), 6.62 (d, J = 2.5 Hz, 1 H, 2-CH), 6.69 (dd, J = 8.5 Hz, J = 2.5 Hz, 1 H, 4-CH), 7.19 (d, J = 8.5 Hz, 1H, 1-CH)	474.4 (MH^+, 100%)	$C_{29}H_{47}O_4N$ (473.70) calcd: C, 73.53; H, 10.00; N, 2.96; found: C, 73.88; H, 9.87; N, 2.91	281 nm, 3.02	
7		0.77 (s, 3 H, 18-CH_3), 3.30−3.49 (m, 8 H, CH_2O), 3.95 (m, 2 H, CH_2O), 4.31 (m, 1 H, bio), 4.51 (m, 1 H, bio), 5.37 (m, 1 H, am-NH), 5.61 (s, 1 H, bio-NH), 6.46 (m, 1H, am-NH), 6.51 (d, J = 2.6 Hz, 1 H, 2-CH), 6.69 (dd, J = 8.5 Hz, J = 2.6 Hz, 1 H, 4-CH), 7.19 (d, J = 8.5 Hz, 1 H, 1-CH)	796 (MH^+, 100%)		281 nm, 3.09	+23°, 1.45
10	3429, 3298 (NH_2), 3028 (CH_{arom}), 2947, 2862 ($CH_{aliphat}$), 1609, 1576 ($C{=}C_{conj}$), 1115 (C−O−C), 1077, 1035, 1018, 975 (THP)	0.79 (d, 3 H, 18-CH_3), 2.85 (m, 2 H, −CH_2−NH_2), 3.70 (m, 2 H, CH_2−O), 3.91 (m, 2 H, CH_2−O), 4.56 (m, 1 H, O−CH−O), 4.66 (m, 1 H, O−CH−O), 5.32 (t, J = 3.1 Hz, 1 H, 6β-H), 5.36 (t, J = 3.1 Hz, 1 H, 6β-H), 6.91 (m, 1 H, 4-CH), 7.18 (m, 2 H, 1-CH, 2-CH)	514.5 (MH^+, 100%)	$C_{31}H_{47}O_5N$ (513.72) calcd: C, 72.45; H, 9.22; N, 2.73; found: C, 71.87; H, 9.30; N, 2.50	276 nm, 3.13	
11	3450−3250 (OH), 3403 (NH_2), 3032 (CH_{arom}), 2925, 2852 ($CH_{aliphat}$), 1696, 1647 (C=O), 1550 (am), 1116 (C−O−C)	0.79 (d, 3 H, 18-CH_3), 3.71 (m, 2 H, CH_2−O), 3.92 (m, 2 H, CH_2−O), 4.30 (m, 1 H, bio), 4.46 (m, 1 H, bio), 5.43 (t, J = 3.1 Hz, 1 H, 6β-H), 5.58 (s, 1 H, am-NH), 6.35 (m, 1 H, am-NH), 6.50 (m, 1 H, am-NH), 6.69 (s, 1 H, am-NH), 6.83 (m, 1 H, am-NH), 6.95 (m, 1 H, 4-CH), 7.13 (m, 1 H, 2-CH), 7.21 (m, 1 H, 1-CH)	859.3 (MH^+, 100%)		281 nm, 3.12	
14	3436 (OH), 3028 (CH_{arom}), 2963, 2859 ($CH_{aliphat}$), 1609, 1574 ($C{=}C_{conj}$), 1116 (C−O−C), 1178, 1032, 1011, 976 (THP)	0.79 (d, 3 H, 18-CH_3), 2.56 (s wide, 1 H, OH), 3.41−3.50 (m, 6 H, CH_2−O), 3.56−3.69 (m, 4 H, CH_2−O, CH_2−OH), 3.92 (m, 2 H, CH_2−O), 4.53 (m, 1 H, O−CH−O), 4.66 (m, 1 H, O−CH−O), 5.28 (t, J = 3.2 Hz, 1 H, 6β-H), 5.50 (t, J = 3.2 Hz, 1 H, 6β-H), 6.91 (m, 1 H, 4-CH), 7.17 (m, 2 H, 1-CH, 2-CH)	601.7 (MH^+, 100%)	$C_{36}H_{56}O_7$ (600.84) calcd: C, 71.97; H, 9.39; found: C, 71.02; H, 9.49	276 nm, 3.24.	
16	3371, 3306 (NH_2), 3030 (CH_{arom}), 2941, 2866 ($CH_{aliphat}$), 1609, 1575 ($C{=}C_{conj}$), 1114 (C−O−C), 1036, 1017, 977 (THP)	0.79 (d, 3 H, 18-CH_3), 2.78 (m, 2 H, −CH_2−NH_2), 3.32−3.48 (m, 8 H, CH_2−O), 3.51−3.74 (m, 4 H, CH_2−O), 3.91 (m, 2 H, CH_2−O), 4.54 (m, 1 H, O−CH−O), 4.65 (m, 1 H, O−CH−O), 5.30 (t, J = 3.2 Hz, 1 H, 6β-H), 5.49 (t, J = 3.2 Hz, 1 H, 6β-H), 6.91 (m, 1 H, 4-CH), 7.18 (m, 2 H, 1-CH, 2-CH)	658.7 (MH^+, 100%)	$C_{39}H_{63}O_7N$ (657.93) calcd: C, 71.20; H, 9.65; N, 2.13; found: C, 70.89; H, 9.41; N, 2.16	275 nm, 3.23	

Table 1 (Continued)

compd	IR [$\bar{\nu}$ (cm^{-1})]	^1H NMR [δ (ppm)]	MS (FAB, 70 eV, *m/z*)	elementary analysis	UV [λ (nm), lgϵ]	$[\alpha]_D^{20}$, (c in MeOH)
17	3312 (NH), 3029 (CH_{arom}), 2936, 2869 ($CH_{aliphat}$), 1702, 1645 (C═O), 1559 (am), 1116 (C−O−C)	0.76 (s, 3 H, 18-CH_3), 3.38−3.46 (m, 10 H, CH_2O), 4.30 (m, 1 H, bio), 4.50 (m, 1 H, bio), 4.55 (m, J = 10.0 Hz, J = 6.2 Hz, 6β-H), 6.70 (dd, J = 8.4 Hz, J = 2.6 Hz, 1 H, 4-CH), 6.97 (d, J = 2.2 Hz, 1 H, 2-CH), 7.11 (d, J = 8.5 Hz, 1 H, 1-CH)	1002.2 (MH^+, 100%)		281 nm, 3.02	
23	3450−3200 (OH), 3547, 3360 (NH_2), 2980, 2898 ($CH_{aliphat}$), 1618, 1579 (C═C_{conj}), 1116 (C−O−C)	0.76 (s, 2/3 (3H), 18-CH_3), 0.81 (s, 1/3 (3H), 18-CH_3), 3.43 (m, 2 H, CH_2−O), 3.61 (t, 2 H, CH_2−O), 3.71 (m, J = 2.3 Hz, 6α-H), 3.95 (m, J = 10.2 Hz, J = 7.1 Hz, 2/3 H, 6β-H), 6.70 (m, 1 H, 4-CH), 6.86 (m, 1 H, 2-CH), 7.15 (m, 1 H, 1-CH)	445.5 (MH^+, 100%)	$C_{27}H_{44}O_3N_2$ (444.66) calcd: C, 72.93; H, 9.97; N, 6.30; found: C, 72.77; H, 9.78; N, 5.22	281 nm, 3.17.	
24	3500−3200 (OH), 3294 (NH), 2932, 2853 ($CH_{aliphat}$), 1700, 1642 (C═O), 1552 (am)	0.75 (s, 3 H, 18-CH_3), 3.49 (m, 2 H, CH_2−O), 3.52 (m, 2 H, CH_2−O), 4.29 (m, 1 H, bio), 4.49 (m, 1 H, bio), 4.55 (dd, J = 10.1 Hz, J = 6.6 Hz, 1 H, 6β-H), 6.78 (dd, J = 8.4 Hz, J = 2.5 Hz, 1 H, 4-CH), 7.03 (d, J = 2.5 Hz, 1 H, 2-CH), 7.15 (d, J = 8.3 Hz, 1 H, 1-CH)	958.3 (MH^+, 100%)		281 nm, 3.08	+20°, 0.990
27	3450 (OH), 2963, 2851 ($CH_{aliphat}$), 610, 1575 (C═C_{conj}), 1126, 1076, 1035, 1021, 978 (THP)	2.73 (dd, J = 5.4 Hz, J = 17.5 Hz, 1 H, 6α-H), 2.87 (d, J = 17.5 Hz, 6β-H), 3.81 (t, 1 H, 17-CH), 4.66 (m, 1 H, −O−CH−O-), 5.38 (m, 1 H, −O−CH−O-), 6.76 (m, 1 H, 4-CH), 6.84 (m, 1 H, 2-CH), 7.19 (m, 1 H, 1-CH)	610.5 ($M^{\bullet+}$, 48%)	$C_{39}H_{62}O_5N$ (610.92) calcd: C, 76.67; H, 10.22; N, 2.29; found: C, 74.98; H, 10.19; N, 2.30		
29	3372, 3304 (NH), 2946, 2861 ($CH_{aliphat}$), 1609, 1576 (C═C), 1117 (C−O−C), 1035, 1028, 978 (THP)	2.75 (m, 3 H, −CH_2−NH_2, 6α-H), 2.87 (dd, J = 17.0 Hz, J = 4.8 Hz, 6β-H), 3.42 (t, 2 H, −CH_2−O), 3.50 (t, 2 H, CH_2−O-), 3.73 (m, 1 H, 17-CH), 4.65 (m, 1 H, −O−CH−O-), 5.35 (m, 1 H, −O−CH−O-), 6.71 (m, 1 H, 4-CH), 6.78 (m, 1 H, 2-CH), 7.17 (m, 1 H, 1-CH)	668.6 (MH^+, 21%)			
30	3295, 3094 (NH, OH), 2929, 2854 ($CH_{aliphat}$), 1700, 1644 (C═O), 1553 (am), 1115 (C−O−C)	0.78 (s, 3 H, 18-CH_3), 2.69 (d, J = 12.7 Hz, 1 H, 6α-H), 2.91 (dd, J = 12.7 Hz, J = 5.0 Hz, 6β-H), 3.67 (t, 1 H, 17-CH), 4.29 (m, 1 H, bio), 4.47 (m, 1 H, bio), 6.46 (m, J = 2.5 Hz, 1 H, 4-CH), 6.53 (dd, J = 2.7 Hz, 1 H, 2-CH), 7.07 (d, J = 8.4 Hz, 1 H, 1-CH)	839.5 (MH^+, 26%)		281 nm, 3.09	+14°, 1.77

[a] Abbreviations: bio, biotin; am, amide.

and Andres, 1990; Luppa et al. 1996). One equivalent of **6** was dissolved under N_2 in DMF. Three equivalents of NEt_3 and 1 equiv of LC-biotin were added and the solution was stirred for 18 h at room temperature. The solvent was removed and the residue chromatographed on SiO_2 (eluent MeOH:CH_2Cl_2, 1:4, v/v). The yield of **7** was 90%. A final purification was achieved by HPLC (column: Kromasil SC 100, 7 μm, 250 × 20 mm). Using MeOH:CH_2Cl_2 (1:6.14, v/v) as the eluent, the product has a retention time (t_r) of 10.7 min (flow, 7.8 mL/min).

2. Preparation of 3,17*β*-Dihydroxy-6α-(biotinyl-amino-3,6-dioxaoctanyl-aminocarbonyl-heptyl-3′-aminopropyloxy)-estra-1,3,5(10)-triene (11). *3,17β-(Bis-tetrahydropyranyloxy)-6α-(2′-cyanoethyloxy)-estra-1,3,5(10)-triene* (**9**). One equivalent of 3,17β-(bis-tetrahydropyranyloxy)-6α-hydroxy-estra-1,3,5(10)-triene (**8**) was dissolved under N_2 in dry acetonitrile and *t*-butanol (2:1, v/v) and cooled to 0 °C. After addition of 1.2 equiv of 1 mol/L of K-*t*-butanolate, 10 equiv of freshly distilled acrylonitrile (d = 0.806) was dropped slowly to the mixture. The solution was stirred for 20 min at 0 °C, neutralized with a diluted HCl solution, and extracted three times with Et_2O. After removal of the solvent, the product (**9**) was purified by LSC at SiO_2 using methyl-*t*-butyl ether:petroleum ether (MTBE:PE, 1:1, v/v) as the eluent, yielding 71% of a colorless oil.

3,17β-(Bis-tetrahydropyranyloxy)-6α-(3′-aminopropyloxy)-estra-1,3,5-(10)-triene (**10**) (Ray et al., 1991; Roy and Ray, 1995). Ten equivalents of $LiAlH_4$ was suspended under N_2 at 0 °C in dry Et_2O, and 1 equiv of nitrile (**9**) in Et_2O was slowly added. The reaction solution was stirred for 90 min at room temperature. After quenching the reaction by adding a diluted $NaHCO_3$ solution, the product was extracted three times with Et_2O and evaporated in the high vacuum. Yield, 98% of **10** as colorless solid, mp 62 − 64 °C.

3,17β-(Bis-tetrahydropyranyloxy)-6α-(biotinyl-amino-3,6-dioxa-octanylaminocarbonyl-heptyl-3′-aminopropyloxy)-estra-1,3,5(10)-triene (**11a**) (Tiefenauer and Andres, 1990; Luppa et al. 1996). The biotinylation was performed as already described in 1. One equivalent of amine **10** was allowed to react with 3 equiv of NEt_3 and 1 equiv of DDS-biotin. After chromatography at SiO_2 using CH_2Cl_2:MeOH (9:1, v/v) as the eluent, the product **11a** was isolated as a yellowish solid in a yield of 80%. Further purification by HPLC (eluent, 12% MeOH/CH_2Cl_2; flow, 9.8 mL/min; t_r, 10.6 min).

3,17β-Dihydroxy-6α-(biotinyl-amino-3,6-dioxaoctanyl-aminocarbonyl-heptyl-3′-aminopropyloxy)-estra-1,3,5(10)-triene (**11**) (Bernardy et al., 1979). The biotinylated compound **11a** was dissolved in acetic acid:MeOH:H_2O (4:2:1, v/v) and stirred for 15 h at room temperature. After removal of the solvent, the residue was freeze-dried by use of benzene, yield 99%. Further purification by HPLC (eluent, 12% MeOH/CH_2Cl_2; flow, 7.8 mL/min; t_r, 12.0 min).

3. Preparation of 3,17*β*-Dihydroxy-6α-(biotinyl-amino-3,6-dioxaoctanyl-aminocarbonyl-heptyl-5′,10′-dioxa-13′-aminotridecyloxy)-estra-1,3,5(10)-triene (17). *3,17β-(Bis-tetrahydropyranyloxy)-6α-(9′-dimethyl-t-butyl-silyloxy-5′-oxa-nonyloxy)-estra-1,3,5(10)-triene* (**13**). One equivalent of 3,17β-(bis-tetrahydropyranyloxy)-6α-hydroxy-estra-1,3,5(10)-triene (**8**) was dissolved under N_2 in dry HMPT:THF (1:1, v/v) and cooled to 0 °C. Then 1.1 equiv of KH and 1.5 equiv of 9-*t*-butyldimethylsilyloxy-5-oxa-nonyl-mesylate (**12**) were added dropwise and the solution was stirred for 90 min at room temperature. The reaction mixture turns to a gellike substance. After quenching with H_2O, the product was extracted three times with Et_2O. The solvent was removed and the residue was chromatographed at SiO_2 using Et_2O:PE (1:1, v/v) as the eluent. **13** was isolated as colorless oil, yield 60%.

3,17β-(Bis-tetrahydropyranyloxy)-6α-(9′-hydroxy-5′-oxa-nonyloxy)-estra-1,3,5(10)-triene (**14**) (Corey and Venkateswarlu, 1972a; Corey and Snider, 1972b). One equivalent of **13** was dissolved under N_2 in dry THF, 2 equiv of 1 mol/L tetrabutylammonium fluoride solution (TBAF) in THF was added, and the solution was stirred for 90 min at room temperature. After quenching with a saturated NaCl solution, the product was extracted three times with Et_2O. The solvent was removed, and the residue chromatographed at SiO_2 using Et_2O:PE (1:1, v/v) as the eluent. **14** was isolated as colorless oil, yield 95%.

3,17β-(Bis-tetrahydropyranyloxy)-6α-(12′-cyano-5′,10′-dioxa-dodecyloxy)-estra-1,3,5(10)-triene (**15**). The cyanoethylation was performed as already described in 2. One equivalent of **14** was allowed to react, after the LSC at SiO_2 (eluent Et_2O:PE, 1:1, v/v), the product **15** was isolated as colorless oil, yield 89%.

3,17β-(Bis-tetrahydropyranyloxy)-6α-(13′-amino-5′,10′-dioxa-tridecyloxy)-estra-1,3,5(10)-triene (**16**). The reduction of the nitrile was performed as already described in 2. One equivalent of **15** was allowed to react. The product **16** was isolated as colorless oil, yield 98%.

3,17β-(Bis-tetrahydropyranyloxy)-6α-(biotinyl-amino-3,6-dioxaoctanyl-aminocarbonylheptyl-5′-10′-dioxa-13′-aminotridecyloxy)-estra-1,3,5(10)-triene (**17a**). The biotinylation of the amine was performed as already described in 2. One equivalent of amine **16** was allowed to react with 3 equiv of NEt_3 and 1.1 equiv of DDS-biotin. After LSC at SiO_2 using CH_2Cl_2:MeOH (9:1, v/v) as the eluent, **17a** was isolated as yellowish solid, yield 79%. Further purification by HPLC (eluent, 12% MeOH/CH_2Cl_2; flow, 7.8 mL/min; t_r, 10.8 min).

3,17β-Dihydroxy-6α-(biotinyl-amino-3,6-dioxaoctanyl-aminocarbonyl-heptly-5′,10′-dioxa-13′-aminotridecyloxy)-estra-1,3,5(10)-triene (**17**). Cleavage of the THP protecting group was performed as described in 2. One equivalent of **17a** was allowed to react, yielding 98% **17**. The product was further purified by HPLC (eluent, 12% MeOH/CH_2Cl_2; flow, 7.8 mL/min; t_r, 12.0 min).

4. Preparation of 3,17*β*-Dihydroxy-6α-(biotinyl-amino-3,6-dioxaoctanyl-aminocarbonyl-7′-oxa-10′-aminodecylamine)-estra-1,3,5 (10)-triene (24). *3-(6-Bromohexyloxy)-propionitrile* (**18**). One equivalent of 6-bromo-l-hexanol (d = 1.38) was dissolved in dry THF, and 0.25 equiv of KH was added slowly, which causes a precipitate in a fine suspension. Subsequently, 1.5 equiv of freshly distilled acrylonitrile was added dropwise, and the solution was stirred for 1 h at room temperature. After acidification with diluted HCl, the solvent was removed, and the residue extracted three times with CH_2C1_2. The remaining yellowish oil was chromatographed at SiO_2 using CH_2C1_2 as the eluent. The product **18** was isolated as colorless oil, yield 90%.

3-(6-Azido-hexyloxy)-propionitrile (**19**). One equivalent of **18** was dissolved in EtOH 96%. After addition of 1.4 equiv of NaN_3, the clear solution was stirred for 15 h under reflux, and a colorless precipitate was being formed. After removal of the alcohol, the residue was extracted three times with MTBE. The yellowish oil was chromatographed at SiO_2 using Et_2O:PE (2:1, v/v) as the eluent. The product **19** was isolated as colorless oil, yield 94%.

3-(6-Aminohexyloxy)-propionitrile (**20**) (Mungall et al., 1975; Grunwell et al., 1976; Martin and Schmidt, 1993; Jadhav and Man, 1996). One equivalent of **19** was dissolved under N_2 in dry THF, and 1.1 equiv of Ph_3P and 1.5 equiv of H_2O were added. The solution was stirred for 2 h at room temperature. Then again 1.5 equiv of H_2O was added, the solution was stirred for further 2 h, and N_2 gas escaped. After removal of the solvent, the colorless oil was mixed with MTBE:PE (1:6, v/v). The precipitating substance was filtered and washed with PE. This procedure was repeated again. After final removal of the solvent, the residue was coated to basic Al_2O_3 and mounted on a chromatography column filled with basic Al_2O_3. Ph_3P remnants were eluted with Et_2O, and the product **20** as colorless oil was eluted with MeOH, yield 100% (still contaminated with 5−10% Ph_3P remnants).

3-Hydroxy-17β-acetoxy-6α/β-(9′-cyano-7′-oxa-nonyl-amine)-estra-1,3,5(10)-triene (**22**) (Bodmer et al., 1989). Ten equivalents of **20** was dissolved under N_2 in dry MeOH. Then 10 equiv of acetic acid (d = 1.05) abs. was added dropwise into the solution, and additionally molecular sieve was given to the solution. After stirring for 1 h at room temperature, the molecular sieve was filtered off and the clear solution transferred under N_2 in another flask. One equivalent of 3,17β-acetylated 6-oxo-E2 (**21**) was added, and the solution stirred for 10 min at room temperature. Then 6 equiv of $NaCNBH_3$ was added, and the reaction mixture was stirred under reflux for further 18 h. After removal of the MeOH, the residue was

Scheme 1. Synthetic Strategies for the 3-Biotinylation of E2

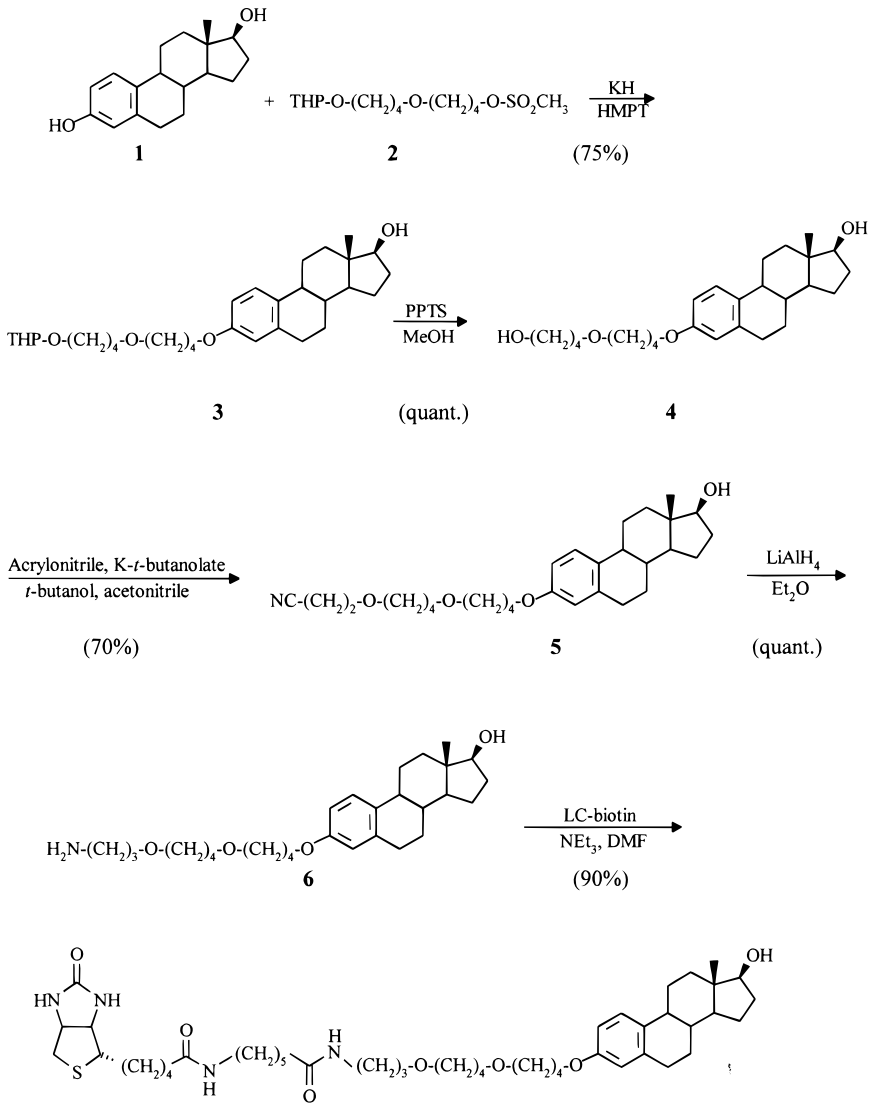

quenched with a saturated $NaHCO_3$ solution and extracted with Et_2O. After removal of the solvent, the product was chromatographed at SiO_2 using MTBE:MeOH:NEt_3 (94:5:1, v/v) as the eluent. The α/β-isomer mixture **22** was isolated as colorless oil, yield 68%.

3,17β-Dihydroxy-6α/β-(10′-amino-7′-oxa-pentadecyl-amine)-estra-1,3,5(10)-triene (**23**) (Ray et al., 1991; Roy and Ray, 1995). Ten equivalents of $LiAlH_4$ was suspended under N_2 in dry Et_2O and cooled to 0 °C. Then 1 equiv of nitrile **22**, dissolved in Et_2O, was added dropwise. The suspension was stirred for 90 min at room temperature and then quenched with a diluted $NaHCO_3$ solution. After extraction of the product with Et_2O and removal of the solvent, the residue was freeze-dried. The amine **23** was isolated as colorless solid, yield 98%, mp 35−38 °C.

3,17β-Dihydroxy-6α-(biotinyl-amino-3,6-dioxa-octanyl-aminocarbonyl-7′-oxa-10′-aminodecyl-amine)-estra-1,3,5(10)-triene (**24**). The biotinylation of the amine was performed as already described in 2. One equivalent of amine **23**, 3 equiv of NEt_3, and 1.1 equiv of DDS-biotin were allowed to react. After LSC at SiO_2 (eluent CH_2Cl_2:MeOH:NEt_3, 80:19:1, v/v), the product **24** was isolated as yellowish oil, yield 76%. Further purification of the α/β-epimers by HPLC (eluent, acetonitrile:H_2O, 7:3, v/v, with 0.075 mol/L ammonium acetate; flow, 9.9 mL/min; t_r, 27.8 min).

5. Preparation of 3,17β-Dihydroxy-7α-(14′-biotinyl-aminocaproyl-11′-oxa-tetradecyl-amine)-estra-1,3,5(10)-triene (30). *3,17β-Dihydroxy-7α-(11′-undecyl-N-methyl-N-butylamide)-estra-1,3,5(10)-triene* (**25**) was synthesized according to Tedesco et al. (1997).

3,17β-(Bis-tetrahydropyranyloxy)-7α-(11′-undecyl-N-methyl-N-butylamide)-estra-1,3,5(10)-triene (**26**). One equivalent of **25** in dry CH_2Cl_2 and 3 equiv of dihydro-2H-pyrane (DHP) were given to 0.186 equiv of PPTS, and the mixture was stirred for 16 h at room temperature. After addition of NEt_3, the solvent was removed. The residue was chromatographed at neutral Al_2O_3, using Et_2O:PE (2:1, v/v) as the eluent. **26** was isolated as colorless oil, yield 96%.

3,17β-(Bis-tetrahydropyranyloxy)-7α-(11′-undecanol)-estra-1,3,5(10)-triene (**27**). One equivalent of **26** in THF and a 1 mol/L solution of lithium triethyl-borohydride in THF were mixed together at 0 °C under N_2 and stirred for 20 h at 6 °C. After hydrolyzation with a saturated $NaHCO_3$ solution, the mixture was extracted three times with Et_2O. The solvent was removed and the remaining oil purified by LSC using SiO_2 as the stationary phase

and Et_2O as the solvent. **27** was isolated as colorless oil, yield 55%.

3,17β-(Bis-tetrahydropyranyloxy)-7α-(13′-cyano-11′-oxa-tridecyl)-estra-1,3,5(10)-triene (**28**). One equivalent of alcohol **27** was dissolved under N_2 in a mixture of dry acetonitrile, *t*-butanol, and CH_2Cl_2 (2.5:1:1.5, v/v). At 0 °C, first 10 equiv of acrylonitrile and then a 1 mol/L solution of K-*t*-butanolate in THF were added slowly and the reaction mixture was stirred for 15 min. Then the mixture was hydrolyzed with H_2O and extracted three times with Et_2O, and the solvent removed. The remaining oil was purified by LSC using SiO_2 as the stationary phase and Et_2O:PE (3:2, v/v) as the eluent, yielding **28** as a colorless oil (75%).

3,17β-(Bis-tetrahydropyranyloxy)-7α-(14′-amino-11′-oxa-tetradecyl)-estra-1,3,5(10)-triene (**29**). A suspension of 10 equiv of $LiAlH_4$ in Et_2O under N_2 at 0 °C was given to a solution of 1 equiv of the nitrile **28**, stirred for 4 h under reflux and then 16 h at room temperature. After quenching with a saturated $NaHCO_3$ solution, the product was continuously extracted overnight with Et_2O. The dried Et_2O solution was filtered on basic Al_2O_3 and again eluted with Et_2O. After removal of the solvent the product **29** was isolated as colorless resin, yield 96%.

3,17β-(Bis-tetrahydropyranyloxy)-7α-(14′-biotinyl-aminocaproyl-11′-oxa-tetradecylamine)-estra-1,3,5(10)-triene (**30a**). One equivalent of amine **29** and 1 equiv of LC-biotin were mixed under N_2 with 3 equiv of NEt_3 in DMF and stirred for 24 h at room temperature. The solvent was removed in the high vacuum, and the raw product purified by LSC on SiO_2 and 15% (v/v) MeOH/CH_2Cl_2 as the eluent. **30a** was isolated as colorless resin, yield 88%.

3,17β-Dihydroxy-7α-(14′-biotinyl-aminocaproyl-11′-oxa-tetradecylamine)-estra-1,3,5(10)-triene (**30**). One equivalent of **30a** was dissolved in a mixture of acetic acid, MeOH, and H_2O (4:2:1, v/v) and stirred for 22 h at room temperature. The solvent was removed in the high vacuum, and the raw product purified by LSC using SiO_2 as the stationary phase and MeOH:CH_2Cl_2 (4:1, v/v) as the eluent. The E2 derivative **30** was isolated as colorless resin, yield 92%. Further purification by HPLC (eluent, 14% MeOH/CH_2Cl_2, v/v; flow, 7.8 mL/min; t_r, 12.9 min).

RESULTS

The biotinylation reagents D-(+)-biotinyl-ε-aminocaproic acid-*N*-hydroxysuccinimide ester (LC-biotin) and D-(+)-biotinyl-amino-3,6-dioxa-octanyl-aminocarbonyl-heptanoic acid-*N*-hydroxysuccinimide ester (DDS-biotin) have been widely used for conjugating steroid analytes containing hydroxyl or amino groups to tracer molecules (Costello et al., 1979; Huber et al., 1994). We have recently reported on the synthesis of biotinylation 6-amino-E2 and 6-amino-estrone with the spacer −NHCO$(CH_2)_5$-NH− (Luppa et al., 1994). To obtain more variety in respect to length and chemical structure of the spacers, we decided to extend them by incorporation of ether chains. Methods were used to couple bifunctional spacer reagents to hydroxy, amino, and oxo functions. First, we studied the cyanoethylation of 3,17β-protected 6α-hydroxy-E2. Such reactions were already known from other hydroxy steroids (Ray et al., 1991; Roy and Ray, 1995). In this case, we obtained 6α-cyanoethyloxy-E2. To incorporate a more extended chain, we alkylated **8** in a Williamson reaction with 9-*t*-butyl-dimethyl-silyloxy-5-oxa-nonylmesylate. Cyanoethylation of the desilylated primary alcohol gave a cyanide. In a similar way, an ether unit was attached to the 3 position of E2. A straightforward synthesis of 7α-alkylated E2s by α-alkylation of 3,17-protected 6-oxo-E2 has been published recently (Tedesco et al., 1997). In our synthesis, we used 11-iodo-undecyl-*N*-butyl-*N*-methylamide as an electrophile for the 7-substitution. Deoxygenation and reduction of the amide to the alcohol were followed by cyanoethylation. 6-NH-R-linked spacer units were attached by reductive amination of 6-oxo-E2 with 6-aminocapronitrile and cyanoethyloxy-*n*-alkylamines. Mixtures of α/β-diastereomeres were obtained and separated by chromatography. All mentioned nitriles have been reduced to the amines and subsequently biotinylated. The procedures for the spacer reagents were described in detail.

Scheme 2. Synthetic Strategies for 6α-*O*-Biotinylated E2 Compounds, Derived from *O*-Coupled Cyanoethyloxy Linkers

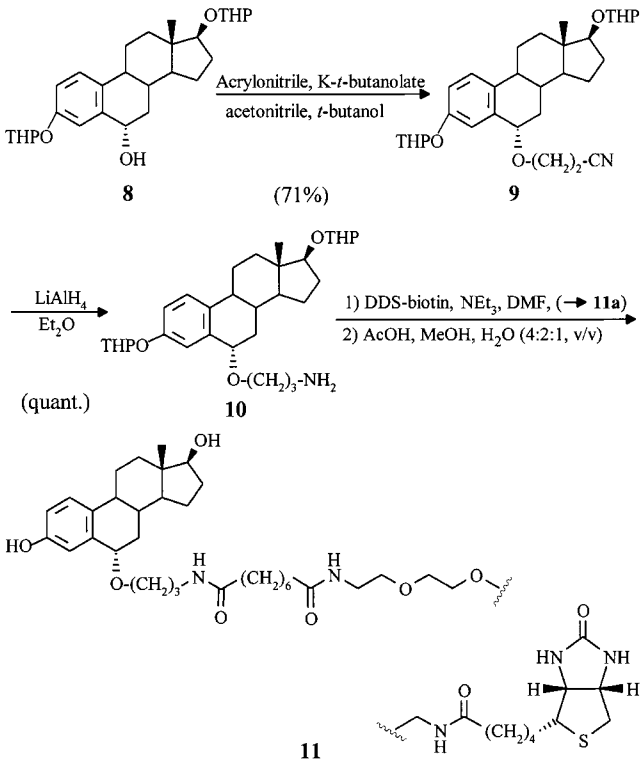

3-*O*-Biotinylated E2 (Scheme 1). The starting material E2 (**1**) was converted with potassium hydride to the potassium phenolate. Alkylation with **2**, cyanoethylation of the deprotected alcohol **4**, and reduction as described above gave the amine **6**. Biotinylation with LC-biotin completed the synthesis to give **7**.

6α-*O*-Biotinylated E2 Compounds, Derived from *O*-Coupled Cyanoethyloxy Linkers (Scheme 2). 6α-Hydroxylated E2 derivatives are easily prepared by stereospecific sodium borohydride reduction of the 6-oxo derivatives (Wintersteiner et al., 1963). 3,17-Di-tetrahydropyranyloxy-6α-hydroxy-E2 (**8**) was cyanoethylated with acrylonitrile in the presence of potassium-*t*-butoxide in a mixture of acetonitrile/*t*-butanol at 0 °C to give cyanide **9**. Reduction with lithium aluminumhydride to amine **10** and biotinylation with DDS-biotin yielded after hydroxylic deprotection the final product **11**.

6α-*O*-Biotinylated E2 Compounds, Derived from *O*-Coupled Cyanoalkyloxy Polyether Linkers (Scheme 3). The 6α-hydroxy-E2 derivative **8** was treated with 1 equiv of potassium hydride in HMPT and alkylated with 9-*t*-butyldimethylsilyloxy-5-oxa-nonylmesylate (**12**). Orthogonal protecting groups were necessary for the following steps. Desilylation with tetrabutylammonium-

Scheme 3. Synthetic Strategies for 6α-*O*-Biotinylated E2 Compounds, Derived from *O*-Coupled Cyanoalkyloxy Polyether Linkers

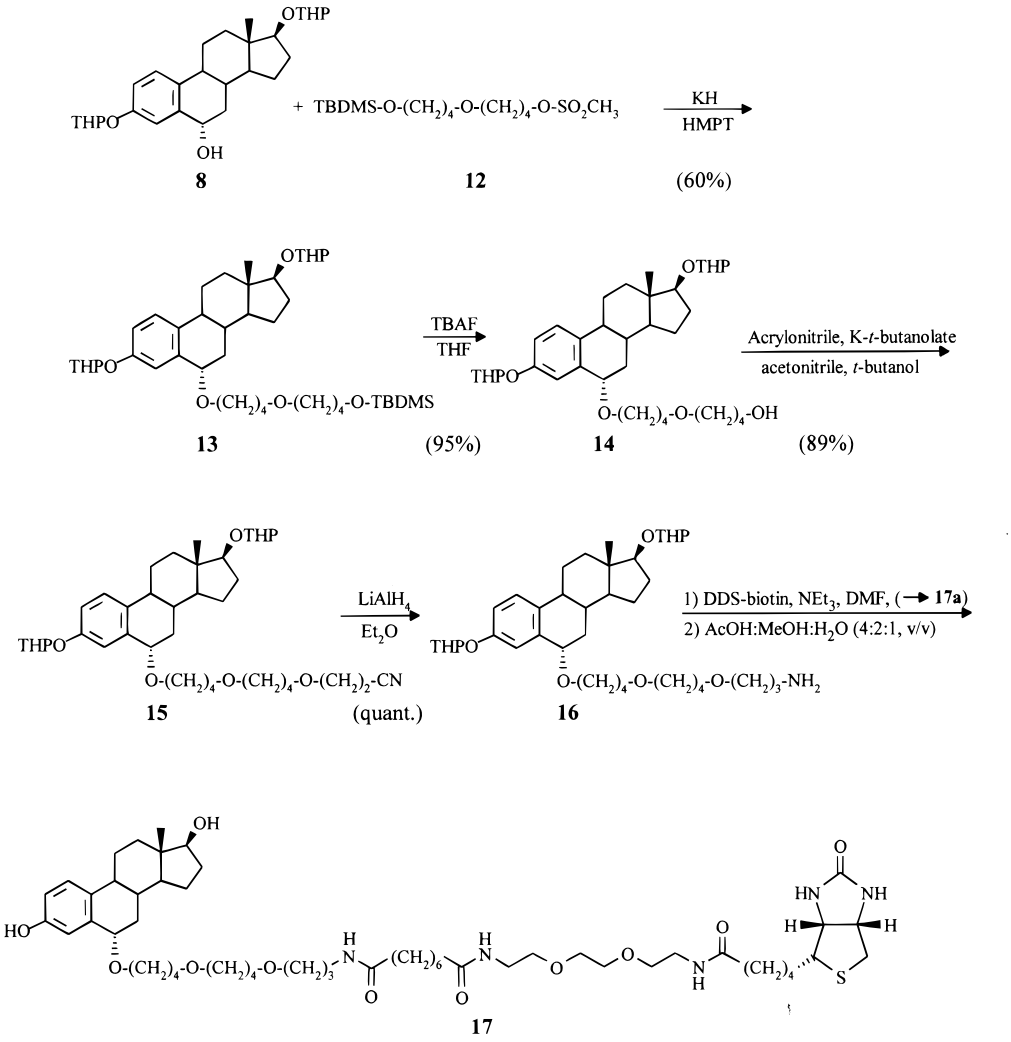

fluoride in THF and cyanoethylation, under the reaction conditions as described above, produces the cyanide **15**. Reduction to the amine **16** and biotinylation with DDS-biotin gave after hydroxylic deprotection the target molecule **17**.

6α-NH-Biotinylated E2 (Scheme 4). Reductive amination of 3,17*β*-diacetoxy-6-oxo-E2 (**21**) with the ammonium acetate derivative of **20** and sodium cyanoborohydride (Borch et al., 1971) in boiling methanol gave a mixture of the α/*β*-cyanides **22**. The α/*β*-ratio was about 5:1. The LSC inseparable mixture was used in the last two steps. **22** was reduced with lithium aluminumhydride to give the amines **23**, which were biotinylated with DDS-biotin to give the final product **24**, still being a diastereomeric mixture. The α-epimer was isolated by preparative RP-HPLC. The stereochemistry of the 6α-NH-linked epimer **24** was assigned on the basis of ^{1}H NMR spectroscopy. The results are in accordance to data of other reported 6α-substituted E2-derivatives (Luppa et al., 1994; Adamczyk et al., 1997). The characteristic proton coupling pattern for the 6*β*,7α,7*β*-ABX system exhibited the α-stereochemistry of the 6α-biotinylated E2 compound. The X-part of 6*β*-H for compound **24** was as follows: 4.55 ppm (dd, $^3J_{6\beta7\alpha} = 10.1$ Hz, $^3J_{6\beta7\beta} = 6.6$ Hz). This finding has to be compared to the ^{1}H NMR data concerning the 6*β*-H of the similar compound 6α-amino-E2, described by Adamczyk et al. (1997), showing coupling constants of 10.3 and 7.2 Hz at 4.54 ppm (1 H, d). In contrast, the 6α-H of 6*β*-amino-E2 shows a coupling constant of 1.8 Hz at 4.40 ppm (1 H, d) (Adamczyk et al., 1998a).

7α-CH$_2$-Biotinylated E2 (Scheme 5). 7α-(10′-*N*-butyl-*N*-methyl-carboxydecyl) E2 (**25**) was synthesized according to the protocol of Tedesco et al. (1997). The authors reported on the stereospecific formation of the α-compound by comparison of the spectroscopic data with those from the literature (Bowler et al., 1989). Lithium triethylborohydride reduced the amide **26** to the alcohol **27**, which was cyanoethylated to give the cyanide **28**. Reduction with lithium aluminumhydride produced the amine **29**, which was biotinylated with LC-biotin. Removing the hydroxylic tetrahydropyranyl protecting groups completed the synthesis.

DISCUSSION

Chemical modifications of E2 can easily be performed at the functional groups at position 3 and 17*β*. However, these two groups define in a high degree the identity of the estrogen. To preserve the epitope structure of the hapten, ring core-based modifications at the positions 6α and 7α are advisable for different investigations concerning the biospecific interaction of those immunochemical probes with steroid-binding proteins such as the ER and anti-E2 antibodies, as well as E2-binding serum globulin. We synthesized the 3-biotinylated E2 derivative **7** in

Scheme 4. Synthetic Strategies for 6α-NH-Biotinylated E2 Compounds

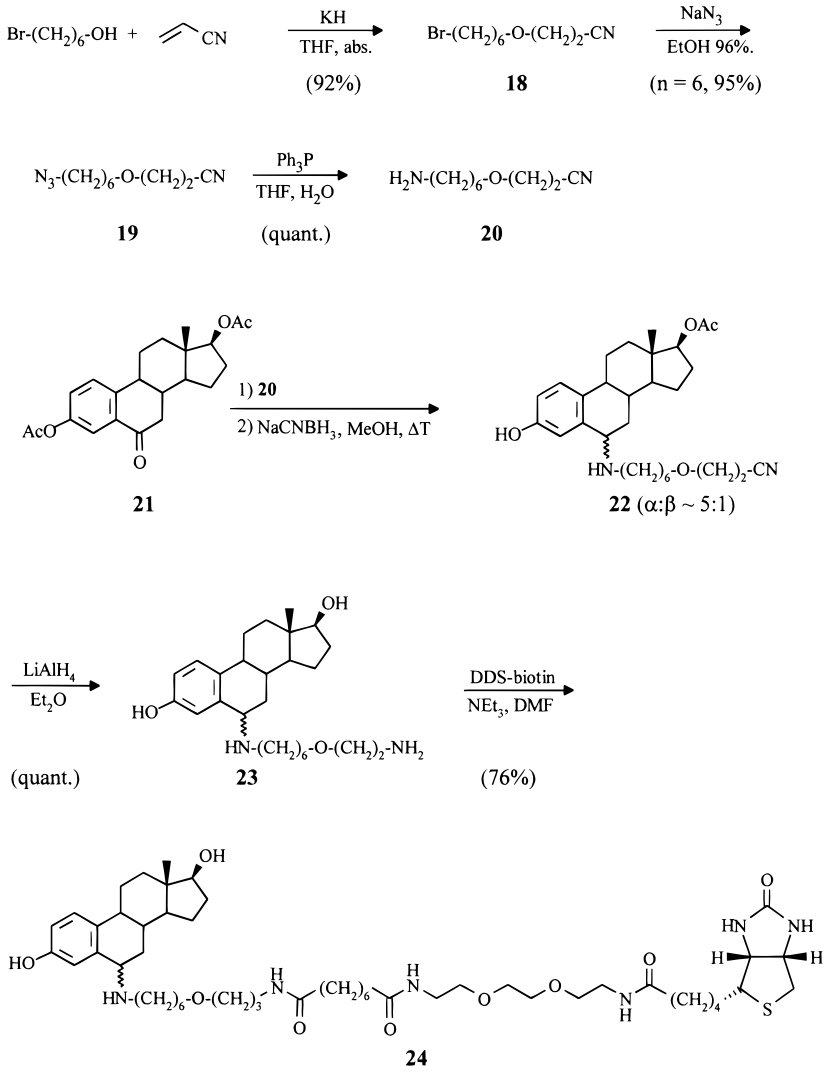

order to perform a detailed analysis of the position-specificity of different anti-E2 antibodies by use of a specific biosensor design (Kaiser et al., 2000).

Synthetic Strategies. The insertion of biotin in the E2 molecule was chosen due to the enormous advantages of the high binding affinity of the noncovalent interaction between biotin and (strept)avidin. This allows the application in many analytical assays that require the formation of a nearly irreversible and specific linkage between macromolecules (Wilchek and Bayer, 1990; Diamandis and Christopoulos, 1991). This paper presents synthetic approaches for the biotinylation of E2 at the positions 3, 6α, and 7α. Appropriate steroidal precursors varying in structure and chain length were prepared, convalently linked to the 3, 6α, and 7α position, and finally biotinylated.

The synthesis of the *3-O-biotinylated E2 derivative* started from the potassium E2 phenolate without protecting the 17*β*-hydroxyl function. A direct cyanoethylation of the phenolate could not be realized due to the fact that the phenolate itself is known as a good leaving group. Therefore, a Williamson ether synthesis with 9-THP-oxy-5-oxa-nonylmesylate was performed. Subsequently, a cyanoethylation of the THP-deprotected alcohol was applied. The reduction of the nitrile led to the amine compound (Scheme 1). For the synthesis of *6α-O-biotinylated E2 compounds*, we started from 6α-hydroxy-E2, which was easily prepared by stereospecific sodium borohydride reduction of 6-oxo E2. For all reactions at the 6α-hydroxyl group, the 3- and 17*β*-hydroxyl groups were THP protected. Cyanoethylation yielded short nitrile linkers which were further reduced to the respective amines (Scheme 2). For obtaining elongation of the spacer units, the 6α-hydroxyl group was alkylated with silyl-protected *ω*-hydroxy-alkyloxy-alkylmesylates (Williamson-type reaction). Further desilylation and cyanoethylation led to nitrile precursors of the amines, derived from *O*-coupled cyanoalkyloxy polyether linkers (Scheme 3). In a more convergent approach, we obtained *6α-NH-biotinylated E2 derivatives* by reductive amination of 3,17-acylated 6-oxo-E2 with cyanoethyloxyhexyl ammonium acetate. This reaction led to a 6α/*β* mixture of the amine products (Scheme 4).

A 3,17-protected 6-oxo-E2 was also used to induce an alkyl chain at the 7α-position of E2 to synthesize a *7α-CH_2-biotinylated E2 compound*. This synthetic pathway follows a procedure of Tedesco et al. (1997) who first described the selective 7α-alkyl substitution of 6-oxo E2 by an alkylation of the generated enolate followed by deoxygenation-deprotection with $BF_3 \cdot Et_2O/Et_3SiH$. The compound **25** was THP protected at the 3 and 17*β* positions and reduced to the 7α-undecanol derivative, and a chain elongation was performed using the above-described cyanoethylation, followed by a reduction to the respective amine (Scheme 5). Alternatively, Δ^6-estrogens can be used for 7α-alkylations in an efficient synthetic

Scheme 5. Synthetic Strategies for 7α-CH_2-Biotinylated E2 Compounds

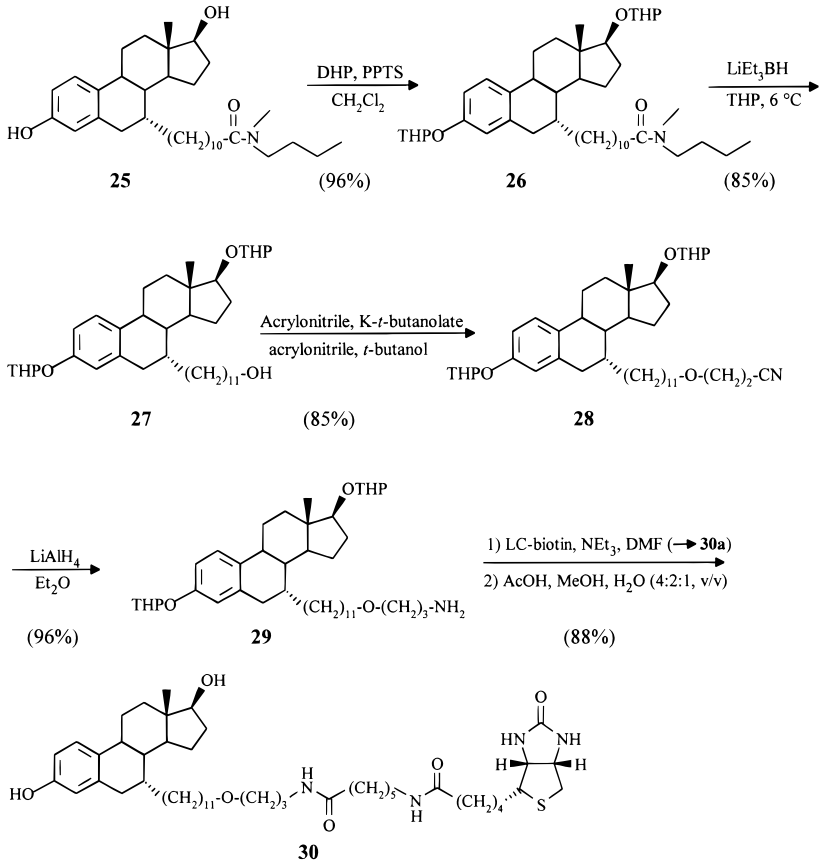

approach, as described by Rao and Wang (1997). Stereoselective approaches to C(7)-alkylated E2 derivatives were also described by Künzer et al. (1994). But these synthetic strategies were not followed by us as they are less stereoselective and versatile as the described route of Tedesco.

The stereochemistry of the 6- and 7-biotinylated E2 derivatives was already defined by using E2 educt compounds with fixed stereochemical configurations. Only the 6α-NH-E2 compound **22**, formed by the reductive amination of the 6-oxo E2 derivative **21**, resulted in a mixture of the α/β isomers (α/β ratio = 5:1). The 6α isomer was separated by RP-HPLC from the final product mixture **24**. In general, all described biotinylated E2 products were obtained in high overall yields apart from the respective intermediates of the reductive amination (Scheme 4).

Immunoassay Applications of Biotinylated E2 Derivatives. The analytical techniques for immunoassays now embrace a vast repertoire of different analytes (Gosling, 1990). For competitive steroid assays, there is demand for excellent sensitivity and specificity in a wide dynamic measuring range, especially in the reproductive endocrinology field (Price, 1998). These improvements can only be achieved through automation of the assays. An assumption for this is the availability of chemically stable and easy-to-handle steroid tracers. For steroid immunoassays, the major concern remains the degree of subtlety in the structural variability of the similar steroid families such as estrogens, androgens, gestagens, and corticoids. For an immunological reaction in a host animal, steroids have to be coupled to immunogenic proteins. The specificity of the resulting anti-steroid antibody reaction depends on the coupling position to the carrier protein; the ring position mainly determines the cross-reactivity of an antibody. When labeling steroids with isotopes or reporter enzymes at the ring positions 3 or 17 for the production of tracers in competitive immunoassays, analytical sensitivity and specificity is affected by a diminished ability for competition with the endogenous steroidal analyte (Kim et al., 1982; De Boever et al., 1986) due to altered epitope structures (Chames and Baty, 1998). Recently, we could depict that "nearly native" tracers lead to negligible alterations in comparison to the structure of the respective steroidal hapten (Luppa et al., 1995, 1997; Hauptmann et al., 2000). A 6α-biotinylated estrone derivative as tracer provides, e.g., high specificity for the determination of total estrone in serum through a better availability of the critical antigen sites. This was concluded from an intermethod comparison to an estrone RIA using a tritium-labeled tracer (Luppa et al., 1995) and is also in accordance to assumptions made by Fránek (1987).

For the often-used 6-carboxymethyloxime derivatives of E2, the altered hybridization (sp^2 vs sp^3) might be unfavorable, since the double bond in the chemical bridge denies free rotation. This may flatten the B-ring and gives rise to a mixture of syn- and anti-isomers (Rao et al., 1998). In case of amide bondages at the ring system, it should be noticed that the native electronic environment might be altered (Adamczyk et al., 1998b). By use of polyether or pure aliphatic spacer groups, also the hydrophilicity of these linkers must be considered. Care should be taken that the spacer is not too long, as this might result in a considerable loss of antibody binding through the diminished hydrophilicity of the tracer. This was concluded by Tiefenauer and Andres (1990), who discussed the structural requirements of biotinyl-E2 derivatives for optimal antibody binding.

The pivotal role of an optimized sterical tracer structure for the establishment of nonisotopic steroid immunoassays is appreciated by a new generation of E2 immunoassays such as the ACS:180 E2 (Aspeslet et al., 1998) in which 6-derivatized E2 tracers are applied. Also, other positions of the steroidal backbone can provide optimized structures for E2 tracers, like a 4-thioether derivative which was synthesized by Meltola et al. (1999). This tracer is highly useful in a time-resolved fluoroimmunoassay of E2.

According to monoclonal anti-steroid antibodies, the CDR interaction to steroidal ligands has been studied extensively (Rassaie et al., 1992; Yoon et al., 1993; Podestà and Montagnoli, 1994). Peptide residues within the combining site were found to play an important role for the antigen/antibody complementarity. These X-ray studies also gave additional insights into the structural adaptations in the CDR during the binding process (Arevalo et al., 1993a,b; Gani et al., 1994). Arevalo described a mechanism for the ligand-binding of progesterone with a specific anti-progesterone antibody. He could demonstrate that a tryptophan (Trp) residue of the CDR functions as surrogate ligand or shutter for the unoccupied hydrophobic-binding pocket. Induced by the binding process, the indole side chain of the Trp residue moves and enables an intimate binding with the β-face of the progesterone molecule, which takes place in the right anterior region of the binding pocket. Additionally, 3β-hemisuccinate and 3-carboxymethyloxime derivatives of progesterone were investigated, which showed also high affinites to the monoclonal anti-progesterone antibody. Thus, it can be stated that the steroidal ring regions B, C, and D enter in a semicircular shape into the CDR-binding pocket. The functional groups of the ligand are stabilized by conserved van der Waals and hydrogen-bond interactions to defined amino acid residues. Since the CDR shows also plasticity, changes in the rigid steroid backbone might be compensated. Nevertheless, changes in the chemical structure of the functional groups can lead to a loss of the antigen/antibody complementarity.

Ligand-Binding Studies of Biotinylated Steroid Derivatives to the ER. According to the unique characteristic of the ER within the steroid receptor superfamily, its pharmacophore accommodates various steroidal and nonsteroidal ligands (Anstead et al. 1997; Fuhrmann et al., 1998). The binding of ligands to the LBD of two subtypes ERα and ERβ is often studied by competition experiments using cytosolic preparations of tissue ERs using ^{3}H-E2 as a radioligand. Many potent estrogenic ligands have been found and studied extensively (Cummins, 1993). Radiolabeled receptor ligands such as 16α- or 16β-substituted ^{18}F derivatives of 17α-ethynyl-E2 show excellent receptor-mediated tumor imaging characteristics (Stalford et al., 1997). This scientific research encompasses both diagnosis and therapy of estrogen-dependent tumors. Thus, the application of biotinylated E2 compounds for the oncological relevant determination of the ERs in tumors would be worthwhile.

ACKNOWLEDGMENT

The authors thank the Fond der Deutschen Chemischen Industrie and the Bundesministerium für Bildung, Wissenschaft, Forschung und Technologie (Project 0311392) for financial grants.

LITERATURE CITED

Adamczyk, M., Mattingly, P. G., and Reddy, R. E. (1997) An efficient stereoselective synthesis of 6-α-aminoestradiol: preparation of estradiol fluorescent probes. *Steroids 62*, 462−467.

Adamczyk, M., Mattingly, P. G., and Reddy, R. E. (1998a) Synthesis of 6β-aminoestradiol and its biotin, acridinium, and fluorescein conjugates. *Steroids 63*, 130−134.

Adamczyk, M., Johnson, D. D., and Reddy, R. E. (1998b) Synthesis of 6β-[(2′-aminoethyl)carboxamidomethyl]estradiol and preparation of estradiol probes. *Bioconjugate Chem. 9*, 404−408.

Anstead, G. M., Carlson, K. E., and Katzenellenbogen, J. A. (1997) The estradiol pharmacophore: ligand structure-estrogen receptor binding affinity relationships and a model for the receptor binding site. *Steroids 62*, 268−303.

Arevalo, J. H., Stura, E. A., Taussig, M. J., and Wilson, I. A. (1993a) Three-dimensional structure of an anti-steroid Fab′ and progesterone-Fab′ complex. *J. Mol. Biol. 231*, 103−118.

Arevalo, J. H., Taussig, M. J., and Wilson, I. A. (1993b) Molecular basis of crossreactivity and the limits of antibody−antigen complementarity. *Nature 365*, 859−863.

Aspeslet, L. J., Chapelsky, L., Morrish, D., and Yatscoff, R. W. (1998) An evaluation of the new automated estradiol assay on the ACS:180. *J. Clin. Lig. Assay 21*, 340−344.

Bernardy, K. F., Floyd, M. B., Poletto, J. F., and Weiss, M. J. (1979) Synthesis of prostaglandins via conjugate addition of lithium *trans*-1-alkenyltrialkylalanate reagents. A novel reagent for conjugate 1,4-additions. *J. Org. Chem. 44*, 1438−1447.

Bodmer, D. M., Tiefenauer, L. X., and Andres, R. Y. (1989) Antigen- versus antibody-immobilized ELISA procedures based on a biotinyl-estradiol conjugate. *J. Steroid Biochem. 33*, 1161−1166.

Borch, R. F., Bernstein, M. D., and Durst, H. D. (1971) The cyanohydridoborate anion as a selective reducing agent. *J. Am. Chem. Soc. 93*, 2897−2904.

Bowler, J., Lilley, T. J., Pittam, J. D., and Wakeling, A. E. (1989) Novel steroidal pure anti-estrogens. *Steroids 54*, 71−99.

Brzozowski, A. M., Pike, A. C., Dauter, Z., Hubbard, R. E., Bonn, T., Engström, O., Öhman, L., Greene, G. L., Gustafsson, J. A., and Carlquist, M. (1997) Molecular basis of agonism and antagonism in the oestrogen receptor. *Nature 389*, 753−758.

Bucourt, R., Wignau, M., Torelli, V., Richard-Foyh, H., Geynet, C., Secco-Millet, C., Redeuilh, G., and Baulieu, E. (1978) New biospecific adsorbants for the purification of estradiol receptor. *J. Biol. Chem. 253*, 8221−8228.

Chames, P., and Baty, D. (1998) Engineering of an anti-steroid antibody: amino acid substitutions change antibody fine specificitiy from cortisol to estradiol. *Clin. Chem. Lab. Med. 36*, 355−359.

Corey, E. J., and Venkateswarlu, A. (1972a) Protection of hydroxyl groups as *tert*-butyl-dimethylsilyl derivates. *J. Am. Chem. Soc. 94*, 6190−6191.

Corey, E. J., and Snider, B. B. (1972b) A total synthesis of (±)-fumagillin. *J. Am. Chem. Soc. 94*, 2549−2550.

Costello, S. M., Felix, R. T., and Giese, R. W. (1979) Enhancement of immune cellular agglutination by use of an avidin−biotin system. *Clin. Chem. 25*, 1572−1580.

Cummins, C. H. (1993) Radiolabeled steroidal estrogens in cancer research. *Steroids 58*, 245−259.

De Boever, J., Kohen, F., Usanachitt, C., Vandekerckhove, D., Leyseele, D., and Vandewalle, L. (1986) Direct chemiluminescence immunoassay for estradiol in serum. *Clin. Chem. 32*, 1895−1900.

Diamandis, E. P., and Christopoulos, T. K. (1991) The biotin-(stept)avidin system: principles and applications in biotechnology. *Clin. Chem. 37*, 625−636.

Fránek, M. (1987) Structural aspects of steroid-antibody specificity. *J. Steroid Biochem.* 28, 95−108.

Fuhrmann, O., Parczyk, K., Klotzbücher, M., Klocker, H., and Cato, A. C. W. (1998) Recent developments in molecular action of anti-hormons. *J. Mol. Med. 76*, 512−524.

Gala, D., Steinman, M., and Jaret, R. S. (1986) Tetrahydropyrane as an efficient alcohol protecting group for the synthesis of penems: synthesis of Sch 34343. *J. Org. Chem. 51*, 4488−4490.

Gani, M., Coley, J., Piron, J., Humphreys, A. S., Arevalo, J., Wilson, I. A., and Taussig, M. J. (1994) Monoclonal antibodies against progesterone: effect of steroid-carrier coupling posi-

tion on antibody specificity. *J. Steroid Biochem. Mol. Biol. 48*, 277−282.

Gosling, J. P. (1990) A decade of development in immunoassay methodology [Review]. *Clin. Chem. 36*, 1408−1427.

Grunwell, J. F., Benson, H. D., Johnston, J. O., and Petrow, V. (1976) Antiprogestational agents. The synthesis of 7-alkyl steroidal ketones with anti-implantational and antidecidual activity. *Steroids 27*, 759−771.

Hanson, R. N., Napolitano, E., and Fiaschi, R. (1998) Novel high-affinity steroidal estrogenic ligands: synthesis and receptor binding of 11β-vinyl-17α-E/Z-phenylselenovinyl estradiols. *Steroids 63*, 479−483.

Hauptmann, H., Paulus, B., Kaiser, T., Herdtweck, E., Huber, E., and Luppa, P. B. (2000) Concepts for the syntheses of biotinylated steroids: part I. Testosterone derivatives as immunochemical probes. *Bioconjugate Chem. 11*, 239−252.

Huber, E., Zink, B., and Höss, E. (1994) Neues Biotinylierungsreagenz. Boehringer Mannheim GmbH, Patent DE 4302241 A1.

Jadhav, P. K., and Man, H. W. (1996) Synthesis of seven-membered cyclic oxamides: novel HIV-l protease inhibitors. *Tetrahedron Lett. 37*, 1153−1156.

Kaiser, T., Gudat, P., Stock, W., Pappert, G., and Luppa, P. (2000) Ligand-binding studies of monoclonal antibodies with immobilized biotinylated steroid derivatives on strepavidin matrixes using biosensor devices. *Biosens. Bioelectron.* (in press).

Kim, J. B., Barnard, G. J., Collins, W. P., Kohen, F., Lindner, H. R., and Eshhar, Z. (1982) Measurement of plasma estradiol-17β by solid-phase chemiluminescence immunoassay. *Clin. Chem. 28*, 1120−1124.

Künzer, H., Thiel, M., Sauer, G., and Wiechert, R. (1994) A new, stereoselective approach to C(7)-alkylated estra-1,3,5(10)-triene derivatives. *Tetrahedron Lett. 35*, 1691−1694.

Luppa, P., Birkmayer, C., and Hauptmann, H. (1994) Synthesis of 3-hydroxyestra-1,3,5(10)-trien-17-one and 3,17β-dihydroxyestra-1,3,5(10)triene 6α-*N*-(ϵ-biotinyl)caproamide, tracer substances for developing immunoassays for estrone and estradiol. *Bioconjugate Chem. 5*, 167−171.

Luppa, P., Hauck, S., Schwab, I., Birkmayer, C., and Hauptmann, H. (1995) 6α-Biotinylated estrone: novel tracer in competitive chemiluminescence immunoassay of estrone in serum. *Clin. Chem. 41*, 564−570.

Luppa, P., Hauck, S., Schwab, I., Birkmayer, C., and Hauptmann, H. (1996) Synthesis of 17β-hydroxy-androst-4-en-3-one-7α-(biotinyl-6-*N*-hexylamide), a conjugate useful for affinity chromatography and for testosterone immunoassays. *Bioconjugate Chem. 7*, 332−337.

Luppa, P., Hauck, S., Schmidmayr, S., Schwab, I., Birkmayer, C., Hauptmann, H., and Neumeier, D. (1997) Different 7α-biotinylated testosterone derivatives as tracers for competitive chemiluminescence immunoassays for testosterone in serum. *Clin. Chem. 43*, 2345−2352.

Martin, T. J., and Schmidt, R. R. (1993) Convenient chemical synthesis of CMP-*N*-acetyl-neuraminate (CMP-Neu-5-Ac)1, *Tetrahedron Lett. 34*, 1765−1768.

Meltola, N., Jauria, P., Saviranta, P., and Mikola, H. (1999) Synthesis of novel europium-labeled estradiol derivatives for time-resolved fluoroimmunoassays. *Bioconjugate Chem. 10*, 325−331.

Miyashita, M., Yoshikoshi, A., and Grieco, P. A. (1977) Pyridinium-*p*-toluenesulfonate. A mild and efficient catalyst for the tetrahydropyranylation of alcohols. *J. Org. Chem. 42*, 3772−3774.

Mungall, W. S., Greene, G. L., Heavner, G. A., and Letsinger, R. L. (1975) Use of azido group in the synthesis of 5′ terminal aminodeoxythymidine oligonucleotides. *J. Org. Chem. 40*, 1659−1662.

Podestà, A., and Montagnoli, G. (1994) Specificity in protein−ligand interactions: a model from estrone-antiserum binding. *Biochim. Biophys. Acta 1200*, 291−296.

Price, C. P. (1998) Progress in immunoassay technology. *Clin. Chem. Lab. Med. 36*, 341−347.

Rao, P. N., and Wang, Z. (1997) New synthesis of Δ^6-estrogens. *Steroids 62*, 487−490.

Rao, P. N., Wang, Z., Cessac, J. W., and Moore, O. H. (1998) Synthesis of new immunogens for estrone and estradiol-17β and antisera evaluation. *Steroids 63*, 141−145.

Rassaie, M. J., Kumari, G. L., Rao, P. N., Shrivastav, T. G., and Pandey, H. P. (1992) Influence of different combinations of antibodies and penicillinase-labeled testosterone derivatives on sensitivity and specificity of immunoassays. *Steroids 57*, 112−118.

Ray, R., Bouillon, R., Van Baelen, H., and Holick, M. F. (1991) Synthesis of 25-hydroxy-vitamin D_3 3β-3′-[*N*-azido-2-nitrophenyl)amino]propyl ether, a second-generation photoaffinity analogue of 25-hydroxyvitamin D_3: photoaffinity labeling of rat serum vitamin D binding protein. *Biochemistry 30*, 4809−4813.

Roy, A., and Ray, R. (1995) Aminopropylation of vitamin D hormone (1α,25-dihydroxy-vitamin D3), its biological precursors, and other steroidal alcohols: an anchoring moiety for affinity studies of sterols. *Steroids 60*, 530−533.

Stalford, A. C., Maggs, J. L., Gilchrist, T. L., and Park, B. K. (1997) The metabolism of 16-fluoroestradiols in vivo: chemical strategies for restricting the oxidative biotransformations of an estrogen-receptor imaging agent. *Steroids 62*, 750−761.

Tanenbaum, D. M, Wang, Y., Williams, S. P., and Sigler, P. B. (1998) Crystallographic comparison of the estrogen and progesterone receptor's ligand binding domains. *Proc. Natl. Acad. Sci. U.S.A. 95*, 5998−6003.

Tedesco, R., Katzenellenbogen, J. A., and Napolitano, E. (1997) An expeditious route to 7α-substituted estradiol derivatives. *Tetrahedron Lett. 38*, 7997−8000.

Tiefenauer, L. X., and Andres, R. Y. (1990) Biotinyl-estradiol derivatives in enzyme immunoassays: structural requirements for optimal antibody binding. *J. Steroid Biochem. 35*, 633−639.

Wilchek, M., and Bayer, E. A. (1990) Biotin-containing reagents. *Methods Enzymol. 184*, 123−138.

Wintersteiner, D., Moore, M., and Cohen, A. J. J. (1963) Stereochemical studies on 6−7-substituted derivatives of estra-3,17α diol. *J. Org. Chem. 29*, 1325.

Yoon, D. Y., Choi, M. J., Choe, I. S., Chung, T. W., and Byun, S. M. (1993) Influence of the conjugation site on the specificity of monoclonal antibodies to progesterone and on the performance of direct enzyme immunoassay. *Biochem. Mol. Biol. Int. 31*, 553−563.

BC9901651

Tris(3-mercaptopropyl)-*N*-glycylaminomethane as a New Linker to Bridge Antibody with Metal Particles for Biological Cell Separations

Olavi Siiman,*,† Alexander Burshteyn,‡ John A. Maples,‡ and James K. Whitesell§

Advanced Technology, Beckman Coulter, Inc., 11800 SW 147th Avenue, Miami, Florida 33196-2500, Reagents Applications & Development, Beckman Coulter, Inc., 11800 SW 147th Avenue, Miami, Florida 33196-2500, Department of Chemistry, North Carolina State University, Raleigh, North Carolina 27695-8204. Received December 14, 1999; Revised Manuscript Received April 14, 2000

Conjugates of nickel beads with CD8 and anti-red blood cell KC16 antibody were prepared by using the aminotrithiolate "spider" ligand, tris(3-mercaptopropyl)-*N*-glycylaminomethane, in its new function as a linker between the surface of nickel beads and antibody via activation of spider ligand attached to nickel beads with the common, heterobifunctional cross-linker, sulfosuccinimidyl 4-(*N*-maleimidomethyl)cyclohexane-1-carboxylate (sulfo-SMCC). Raw nickel beads were cleaned by either mild sonication in a bath or by stronger probe sonication to remove surface nickel oxide layers, before attachment of the spider ligand. Scanning electron micrographs of the nickel beads before and after probe sonication showed a marked change from a corrugated to a smooth bead surface. Analyses of the supernatants of conjugation mixtures for antibody gave surface densities of 2.5−5.2 mg/m^2 for CD8 and 0.6−12 mg/m^2 for KC16 antibody runs. The antibody-spider-nickel bead conjugates were used in magnetic bead depletions of targeted CD8+ lymphocytes or red blood cells (rbcs) in whole blood of normal donors. For CD8 cell depletions, the undepleted controls and supernatants of depleted samples were analyzed for CD8/CD4 cell populations by flow cytometry with appropriate fluorescent antibody markers. Enumeration of red blood cells, white blood cells (wbcs), and platelets (plts) in undepleted controls and supernatants of depleted samples were carried out on appropriate hematology counters. Whole blood titer results with various lots of either CD8-spider-nickel or KC16-spider-nickel bead conjugates showed varying degrees of depletion ability as indicated by bead-to-cell ratios of 2−32 for CD8 beads and by rbc-to-bead ratios of 1.2−10 for KC16 beads. Moreover, varying degrees of specificity of CD8 beads for CD8+ cells over CD4+ cells and of KC16 beads for rbcs over white blood cells and platelets were observed from the normalized nontargeted cell population figures in undepleted controls versus supernatants of depleted samples.

INTRODUCTION

Elemental nickel particles exhibit somewhat different ferromagnetic properties (*1*) depending upon their size, either above or below about 20 nm diameter. Typical Raney(porous) nickel particles produced on the industrial scale as a hydrogenation catalyst by thermal decomposition of nickel tetracarbonyl have an average diameter of 100−200 μm. Smaller particles in the 1−10 μm diameter range are also available. The disadvantage of using metallic particles in magnetic applications (*2*, *3*) is the tendency toward oxidation or other reactions caused by the elemental state of the metal combined with the high specific surface area common to all small particles. Nickel oxide layers on nickel particles could be removed by heat treatment; however, in order for decomposition of nickel oxide solid to its constituent elements in their standard states to be thermodynamically favorable, i.e., to have a negative standard free energy change, the temperature must be raised above 2540 K or 2270 °C, otherwise nickel oxide remains unchanged. This can be shown with standard entropy and enthalpy data (*4*) and use of the Gibbs−Helmholtz equation. Metallic particles can be stabilized by using alloying elements and additives, by protective organic coating, and by controlled oxidation of their surfaces, i.e., passivation. In previous work (*5*) on adsorption of antibody onto nickel beads and fixing the adsorbed antibody by cross-linking it with glutaraldehyde, attempts were made to enhance the nickel oxide layer with passivation by heat treatment at 250 °C to sterilize the beads and create more surface area for adsorption of antibody. An oxide coating on elemental solid nickel has long been used as a protective measure to prevent corrosion. Heating the nickel beads reduced the solubilization of nickel ions from the particles and did not alter the depletion performance of the antibody-coated beads. Nevertheless, a high level of leaching, about 100 μg of nickel/mL of 25% w/v solids nickel beads after 16 weeks of storage at 5 °C, of nickel ions from antibody-coated nickel beads suspended in BSA buffer still took place. Nickel oxide surfaces constantly exposed to buffered aqueous solution, unlike nickel surfaces exposed to air, are not immune to corrosion.

Therefore, we have explored ways of removing the nickel oxide coating from nickel beads, attaching a stabilizing linker to the nickel surface, and finally conjugating antibody covalently to the linker. Ultrasonication has recently been used to obtain clean, reactive metal surfaces (*6*). In this published description of the chemical effects of ultrasound on solids and surfaces, it was shown that one of the "world's worst" heterogeneous

* To whom correspondence should be addressed. E-mail: olavi.siiman@coulter.com.
† Advanced Technology, Beckman Coulter, Inc.
‡ Reagents Applications & Development, Beckman Coulter.
§ North Carolina State University.

10.1021/bc990176u CCC: $19.00 © 2000 American Chemical Society
Published on Web 06/08/2000

catalysts, Raney nickel right out of the bottle, could be irradiated with ultrasound to increase its reactivity by more than 100000-fold and regain Raney nickel-like activity. Auger depth profiling showed that the deep, passivating oxide coating on nickel particles before sonication was removed by irradiation with ultrasound. Thus, ultrasonication was adopted as the method of cleaning nickel bead surfaces to remove the nickel oxide coating.

To have a general method of preparing stable antibody-nickel bead conjugates useful in biological cell assays, monoclonal antibodies need to be covalently conjugated to chemically reactive groups on the surface of nickel beads. One way of accomplishing this conjugation to the nickel bead surface is to use a bifunctional linker molecule, part of which can be strongly attached to nickel on the particles while a different part of the linker can be chemically activated to allow conjugation of antibody. Preparation and characterization of the aminotrithiol, spider-like ligand, tris(3-mercaptopropyl)-*N*-glycylaminomethane, of composition, $C_{12}H_{26}N_2OS_3$, and structural formula, $H_2NCH_2CONHC(CH_2CH_2CH_2SH)_3$, was first reported in ref *7*. It was successfully used on a gold surface to bind strongly to its sulfhydryl groups and further provide NH_2 initiation sites for polymerization of alanine *N*-carboxyanhydride to form polyalanine helices that uniformly aligned themselves perpendicular to the surface. The spider ligand was further used (*8*) as a linker between polycrystalline gold surfaces and fluorescent (pyrenyl and fluorescamine) and redox-active (ferrocenyl) probes. This aminotrithiol ligand also has the potential to serve as a new heterobifunctional cross-linking agent by coordinating strongly to metal atoms on the surface of metal particles through its three sulfur atoms and allowing activation and conjugation of antibody through its amino group with a variety of established amino group activation reagents (*9*−*12*) such as sulfosuccinimidyl 4-(*N*-maleimidomethyl)cyclohexane-1-carboxylate, abbreviated as sulfo-SMCC.[1] The first use of the aminotrithiol ligand as such a linker was described (*13*) on gold nanoparticle-aminodextran-polystyrene latex beads. Various stages of addition of the aminotrithiol ligand and antibody to the latter beads were monitored with particle mobility versus pH measurements using the Coulter DELSA, Doppler electrophoretic light scattering analyzer. The soft base, highly polarizable sulfur atoms of low electronegativity, rather than the hard base, nonpolarizable nitrogen atom of high electronegativity, prefers to coordinate to the soft acid, metal atoms such as gold and silver. Nickel atoms on cleaned nickel bead surfaces also fall into the category of soft acid and thus should show similar, strong binding to the sulfur atoms in the aminotrithiol ligand. To be successful, the subsequent activation method for amino groups of the linker-coated nickel beads, and conjugation reaction to 2-iminothiolane-activated antibody, should not disturb the attachment of linker to the nickel beads or the single, dispersed particle status of the beads.

A review of the capabilities of various commercially available magnetic beads, most of which were previously classified in ref *14*, for depletion of targeted cells shows that Dynal, Inc. (Lake Success, NY) supplies magnetic beads with superior performance in immunomagnetic separations. DYNABEADS M-450, 4.5 μm diameter beads consisting of monosized polystyrene particles embedded with ferrofluid γ-Fe_2O_3 particles can be effectively used at a 3−10 bead-to-cell ratio in positive cell selection and at a 10−40 bead-to-cell ratio in negative cell selection. The nickel bead conjugates described herein and elsewhere (*15*) can be used either in magnetic separations or as heavy beads in separations by gravitational sedimentation as described in ref *5*. They compare favorably with the previous magnetic antibody-conjugated beads at bead-to-cell ratios ranging from 1/10 to 32.

MATERIALS AND METHODS

The monoclonal antibodies referred to herein are identifying designations used by Coulter Corporation, Miami, FL, for monoclonal antibodies made by Coulter Corporation. The term "CD" refers to "Cluster Designation" adopted by the International Workshops on Human Leukocyte Differentiation Antigens. A. T. C. C. is the American Type Culture Collection, Rockville, MD. CD8 (IgG1) antibody (clone SFCI21Thy2D3) was derived from hybridization of mouse NS/1-AG4 cells with spleen cells of BALB/cJ mice immunized with human thymocytes. KC16, a monoclonal antibody specific to red blood cells (*16*) (A. T. C. C. Deposit No. CRL 8994) is an IgG.

Calibrated pipets [e.g., Rainin pipetman (Gilson): P1000, P200, and P20], checked gravimetrically using distilled water and an analytical balance, were used. Typical accuracy with aqueous solutions for the midpoint of each range is <1.0, <0.3, and <0.1 μL.

Cleaning of Raw Nickel Beads by Ultrasonication. A total of 50 g of nickel powder, INCO (Suffern, NY 10901) type 123 (d_{50} = 7.4 μm, 2.42 g/cm^3 density, 0.50 m^2/g specific surface area) prepared by decomposition of nickel tetracarbonyl and obtained from Novamet Specialty Products Corp. (Wyckoff, NJ 07481) were suspended in 200 mL of 0.2 μm-filtered distilled water (DW) in a 250 mL tube. The mixture was roller mixed overnight and magnetically separated, and the supernatant containing fine particles was discarded. The residue was resuspended in 200 mL of DW in a 400 mL Pyrex, jacketed beaker, which was thermostated at a setting of 0 °C with a chilled, circulating 1:1 mixture of ethylene glycol−water from a Forma Scientific model 2006 circulator/cooler. The suspension of nickel beads in the jacketed beaker was then sonicated with a Braun Sonic 2000 ultrasonic probe set at maximum amplitude for efficient mixing of nickel beads for 8 h. During this period and at the end of the sonication period, the supernatant was separated from the nickel beads and discarded, and the residue resuspended in 200 mL of fresh DW 3−4 times.

Deprotection of *t*-BOC Spider Triacetate Linker Ligand. A full description of the preparation of the protected spider ligand, tris(3-acetylmercaptopropyl)-*N*-*t*-BOC-glycylaminomethane, is reported in ref *17*. A structural diagram of the protected ligand is shown in Figure 1.

Protocol 1. A total of 10 mg of protected ligand was dissolved in 5 mL of anhydrous methanol to give a colorless solution. A total of 2.5 mL of concentrated hydrochloric acid(36.5−38.0%) was then added to the solution of protected spider. The mixture was refluxed in a 50 mL round-bottom flask for 5 h to give a yellow solution having the odor of free sulfhydryl groups. The

[1] Abbreviations: *t*-BOC, *tert*-butoxycarbonyl; sulfo-SMCC, sulfosuccinimidyl 4-(*N*-maleimidomethyl)cyclohexane-1-carboxylate; IT, 2-iminothiolane; SEM, scanning electron microscope; Ab, antibody; IgG, immunoglobulin; CD, cluster designation; rbc, red blood cell; wbc, white blood cell; plt, platelet cell; DAP, 1,3-diaminopropane; ELISA, enzyme-linked immunosorbent assay; Ms, mouse; FITC, fluorescein isothiocyanate; RD1, R-phycoerythrin; Fl, fluorescence.

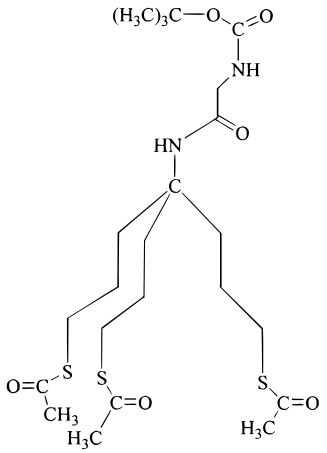

Figure 1. Structure of protected (*t*-BOC/triacetate) spider ligand.

acid-catalyzed hydrolysis mixture (final volume of 3.0 mL) of spider ligand was applied to the top of a Bio-Gel P-2 column, 1.1 cm × 30 cm, and eluted with DW. Fractions of the first band absorbing at 280 nm were collected and tested with Ellman's reagent, 5,5′-dithiobis-[2-nitrobenzoic acid], against a phosphate buffer blank. The reagent reacts with free sulfhydryl groups to form a highly colored chromophore with an absorbance at 412 nm (*18*). Fifteen minutes were allowed for development with Ellman's reagent. For a quantitative determination of sulfhydryl groups, a standard curve was run for L-cysteine to determine the linear response range for the complex. Twelve deprotected ligand fractions of 56 mL of total volume gave a corrected A_{412} reading of 0.549 for a mixture of 2500 μL of 0.1M sodium phosphate, pH 8.0 buffer, 250 μL of sample, and 200 μL of Ellman's reagent (Pierce Chemical Company, 4 mg in 1 mL of reaction buffer). Using a dilution factor of 11.8 and molar extinction coefficient of 14 150 L/mol cm at 412 nm, the sulfhydryl concentration is 0.458 mM, representing a yield of 44%.

Protocol 2. A total of 10 mg of *t*-BOC spider acetate was dissolved in 1 mL of absolute ethanol to give a colorless solution. A total of 100 μL of 1.0 M solution of sodium hydroxide in absolute ethanol was added and the resultant mixture was roller mixed overnight (18 h) at room temperature to produce a yellow solution. The latter product was purified on Bio-Gel P-2 to give three fractions of 14 mL of total volume with a corrected A_{412} reading of 0.354 or sulfhydryl concentration of 0.28 mM.

Scanning Electron Micrographs of Nickel Beads. Samples of raw nickel beads suspended at 25% w/v solids in distilled water and sonicated nickel bead suspension were prepared for scanning electron microscope (SEM) viewing by applying one drop of suspension to a metal stub coated with black conducting tape, spreading and removing most of the droplet with a pipet, and air-drying the remainder of the applied sample. SEM photos were taken using a Philips model XL40 FEG instrument. Figures 2 and 3 show SEM photos of raw nickel beads and sonicated nickel beads, respectively, taken with a 15 kV electron beam at 10000× magnification, and 50/50 mixed detection of backscatter/standard emission. The raw beads, $d_{50} = 7.4$ μm, showed a corrugated, crystallite surface of high surface area, which was smoothened on the macroscopic scale by sonication to yield nickel beads of about 1 μm smaller in diameter. This decrease in particle size can be related to previous Auger depth profiling (*5*), which showed a deep oxide coating before sonication and removal of the passivating nickel oxide layer after irradiation with ultrasound.

Coating of Cleaned Nickel Beads with Deprotected Spider Ligand. *Lot 49 Beads.* Three trials with 0.01, 0.003, and 0.001 mM sulfhydryl concentration of spider, protocol 1, and 5 mL of 25% w/v solids nickel beads, stored in DW purged with nitrogen gas in a refrigerator at 5 °C were prepared. Required volumes of 0.109, 0.033, and 0.011 mL of 0.458 mM spider sulfhydryl groups were added to nickel bead suspensions after removing equal volumes of supernatant, and the trial samples in 50 mL tubes were purged with nitrogen gas and roller mixed overnight for 16−24 h. Each sample was then washed five times with 1× PBS and resuspended to 5 mL with 1× PBS.

Lot 91 Beads. Three trials with 0.03, 0.01, and 0.003 mM sulfhydryl concentration of spider, protocol 2, and 10 mL of 25% w/v solids nickel beads were prepared. Required volumes of 1.07, 0.357, and 0.107 mL of 0.28 mM spider sulfhydryl groups were added to nickel bead suspensions after removing equal volumes of supernatant. The trial samples were then handled the same way as with lot 49 beads and finally resuspended to 10 mL with 1× PBS.

Conjugation of CD8 Antibody to Coated Nickel Beads. The general reaction scheme that was used to conjugate nickel beads coated with the spider ligand is shown in Figure 4.

Lot 49 Beads. A total of 1.5 μL of 10 mg/mL sulfo-SMCC solution was used per milliliter of 1% w/v solids of coated nickel beads to activate the aminotrithiolate-coated nickel beads. Thus, 0.188 mL of sulfo-SMCC solution was added to each trial sample, which were then roller mixed for 1 h with occasional brief sonication. All trials were washed five times with 1× PBS buffer solution and resuspended to 5 mL of total volume with 1× PBS.

A total of 15 mg of CD8 (0.400 mL) antibody concentrate in 0.503 mL of 1× PBS buffer solution was activated with 2-iminothiolane(IT) at a 15:1 = IT:Ab molar ratio, using 0.097 mL of 2 mg/mL IT solution. The reaction mixture in a 15 mL polystyrene centrifuge tube was roller mixed for 1 h and then applied to the top of a 30 mL G-50 Sephadex column, equilibrated with 1× PBS. The column was eluted with 1× PBS, and fractions of the first A_{280}-absorbing band containing IT-CD8 were pooled to yield 2.4 mL of 5.56 mg/mL IT-CD8 antibody solution.

Conjugations were run at 0.8 mg of IT-CD8/mL of 25% w/v solids beads, so that 0.719 mL of IT-CD8 solution was added to each of the three samples of 5 mL of sulfo-SMCC-activated nickel beads after removal of 0.719 mL of supernatant from each bead suspension. The mixtures were roller mixed for 2 h, and at the end of the conjugation period, 1 mL of each mixture was pipeted and filtered through a 0.2 μm low-protein binding filter disk. The A_{280} of each filtrate was measured to yield supernatant IT-CD8 concentrations of 0.444, 0.470, and 0.480 mg/mL, respectively. By difference, the surface concentrations of IT-CD8 were 0.356, 0.330, and 0.320 mg/mL or 2.85, 2.64, and 2.56 mg of CD8 antibody/m^2 of bead surface area, respectively, using the specific surface area of 0.50 m^2/g quoted by the manufacturer. These surface densities fall below the range 4.23−6.50 mg of CD8 antibody/m^2, that was previously (*19*) determined for IT-CD8 on diaminopropane (DAP)-coated polystyrene aldehyde/sulfate latex beads of about 2 μm diameter. The samples were blocked with 0.480 mL of 5 mg/mL L-cysteine solution in 1× PBS-(15 min), and then, 0.540 mL of 20 mg/mL iodoacetamide solution in 1× PBS and 0.100 mL of 1 M borate buffer

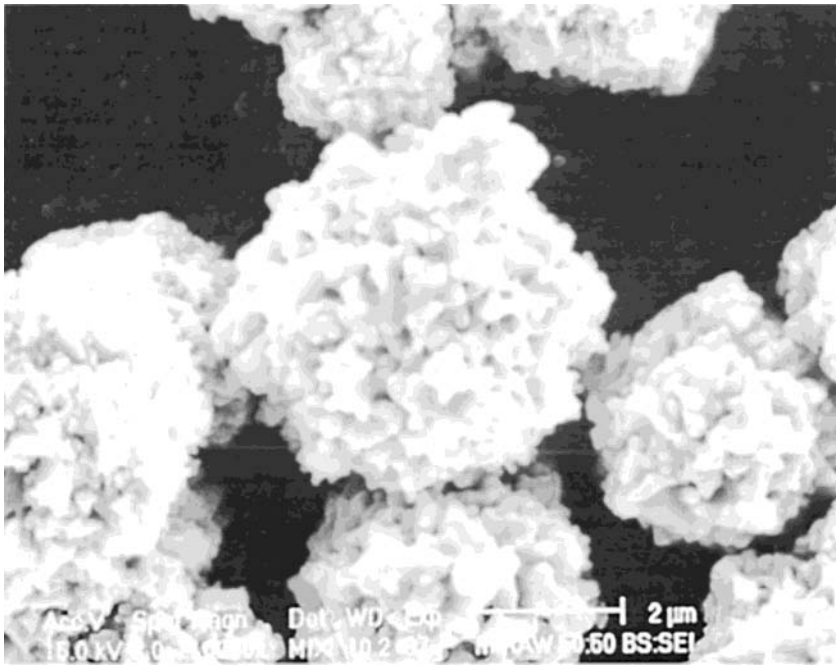

Figure 2. Scanning electron microscope photograph of raw nickel beads taken with 15.0 kV electron beam at 10000× magnification, and 50/50 mixed detection of backscatter/standard emission.

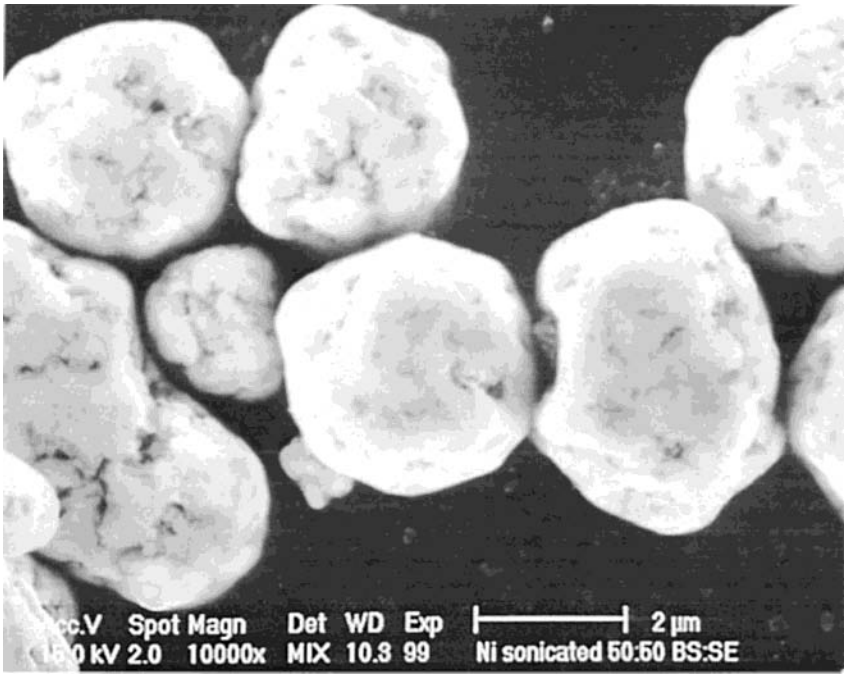

Figure 3. Scanning electron microscope photograph of sonicated nickel beads taken under the same conditions as in Figure 2.

solution, pH 9.8 (30 min). At the end of the blocking reactions, all three bead samples were separated by sedimentation, the supernatants were discarded, and the residues were washed three times with BSA buffer, 1%BSA/0.1% sodium azide in 1× PBS solution, resuspended in BSA buffer, roller mixed for 1 h, and stored in a refrigerator at about 5 °C for 16−24 h. The samples were then further washed three times with BSA buffer and the total volume of each sample was adjusted to 4 mL.

Lot 91 Beads. The activation-conjugation procedure for lot 91 beads was similar to the one used for lot 49 beads. A total of 0.357 mL of sulfo-SMCC solution was used per trial to activate the aminotrithiolate-coated nickel beads. After the 1 h activation period, all trials were washed five times with 1× PBS buffer solution and resuspended to 10 mL total volume with 1× PBS. A total of 30 mg of CD8 (0.799 mL) antibody concentrate in 1.007 mL of 1× PBS buffer solution was activated with IT, using 0.194 mL of 2 mg/mL IT solution. A total of 7 mL of 3.864 mg/mL purified IT-CD8 antibody solution was obtained.

For conjugations, 2.070 mL of IT-CD8 solution was added to each of the three samples of 10 mL of sulfo-SMCC-activated nickel beads after removal of 2.070 mL of supernatant from each bead suspension. After the conjugation period, filtrate IT-CD8 concentrations of 0.160, 0.182, and 0.364 mg/mL, respectively, were measured. By difference, the surface concentrations of IT-CD8 were 0.640, 0.618, and 0.436 mg/mL or 5.12, 4.94, and 3.49 mg CD8 antibody/m^2 of bead surface area,

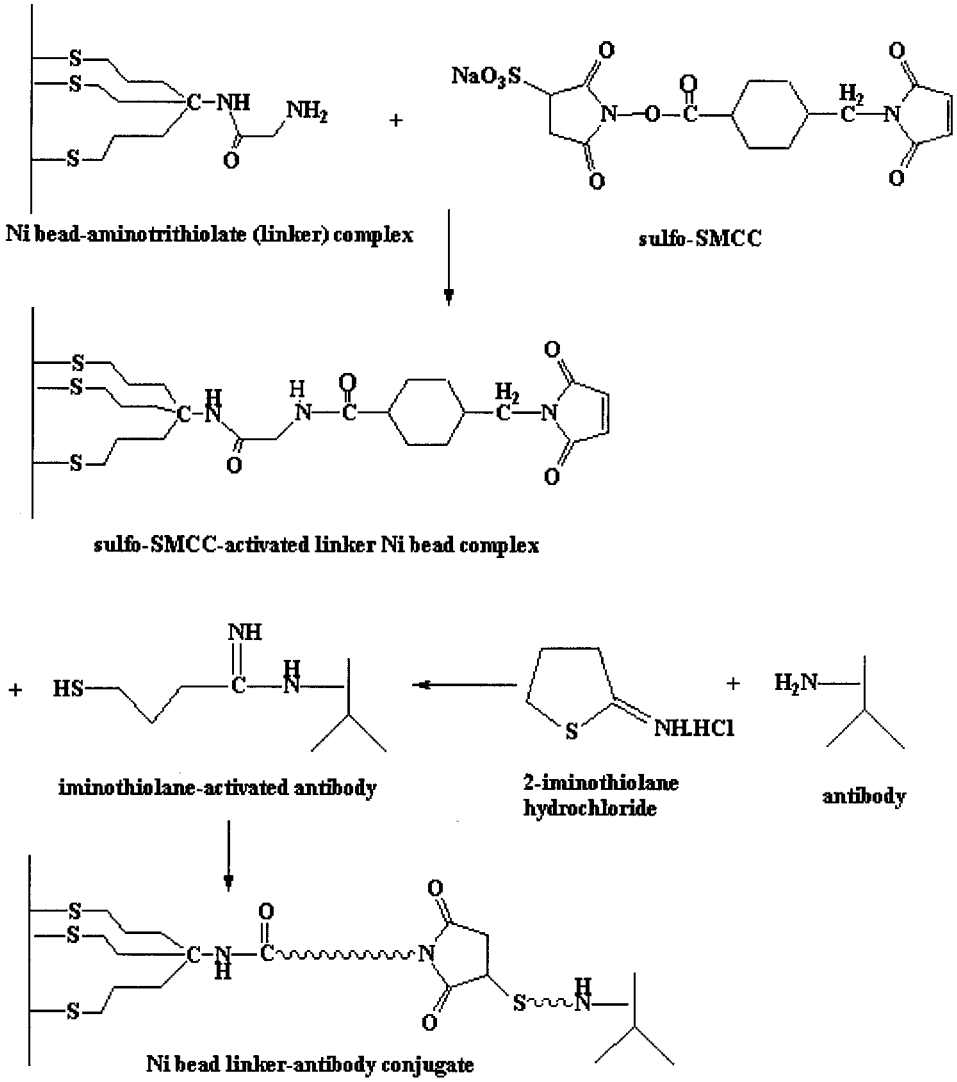

Figure 4. Reaction scheme for conjugation of antibody to spider ligand.

respectively. After the blocking reactions, the samples were washed as before for lot 49 beads, and the final total volume of each sample was adjusted to 10 mL.

Analyses of Supernatants of CD8-Nickel Bead Suspensions for Free Antibody and Nickel Ions. Average nickel content (*20*) of supernatants of CD8-nickel beads stored at 5 °C, room temperature (~22 °C), and 37 °C for 16 weeks was 29.7, 48.6, and 59.1 μg/mL, respectively. ELISA analyses (*21*) of supernatants for IgG1 antibody initially gave 0.719, 0.803, and 0.493 and then 5.10, 5.23, and 3.82 μg/mL after 16 weeks at 5 °C for three CD8-nickel bead samples. These supernatant concentrations compare with a range 0.1−3.6 μg/mL measured (*19*) for CD8-DAP-polystyrene latex bead conjugates in various media.

Control Runs for CD8 Adsorption on Ni Beads. To verify adsorption against specific reaction levels of CD8 antibody on sonicated and washed Ni beads, a series of runs with overnight roller mixing to adsorb IT at three different concentration levels on Ni beads followed by washing with 1× PBS five times and addition of either purified CD8 antibody or purified *S*-(β-aminoethyl)-IT-CD8 antibody derivative was carried out. The lowest concentration of IT (0.030 mM) on Ni beads (10 mL of 25% w/v solids) gave the largest amount (0.20 mg/mL or 1.6 mg/m^2) of CD8 antibody adsorbed on Ni beads. Two higher IT concentrations, 0.076 and 0.12 mM, gave much lower surface CD8 antibody concentrations of 0.073 and 0.068 mg/mL, respectively, or surface densities of 0.59 and 0.54 mg/m^2, for 0.90 mg/mL total CD8 antibody per trial. The concentration levels of CD8 antibody on Ni beads in this run are all substantially lower than levels in any of the conjugation runs for CD8 antibody with linker-coated Ni beads and are taken to reflect the intrinsic adsorption affinity of CD8 antibody for Ni beads. When the aminoethyl derivative of IT-CD8, obtained by reaction of IT-CD8 with *N*-(iodoethyl)-trifluoroacetamide (aminoethyl-8 reagent, Pierce Chemical Co.), was used at a total CD8 concentration of 0.80 mg/mL per trial with the same series of IT-coated Ni beads; then, surface CD8 concentrations were 0.79, 0.79, and 0.78 mg/mL, respectively, or about 3.1 mg/m^2 surface density per trial. Almost all of the aminoethyl derivative of IT-CD8 used in these latter trials was deposited on the surface of Ni beads.

Protocol for Nickel Bead Depletion of CD8-Cell Populations. Whole blood samples for CD8-cell depletion experiments were prepared as follows. CD8-linker-nickel bead suspensions were obtained from 25% w/v solids, with dilution with 1× PBS when needed, as 1, 2.5, 5, 10, 15, or 25% w/v solids suspensions. A total of 10−300 μL of suspension was used per 100 μL of whole blood from a normal donor. Undepleted controls and samples contained additional 1× PBS buffer, 300−10 μL, to

Table 1. Percentage CD8/CD4 Positive Cells in Undepleted Whole Blood and in Supernatants of Whole Blood Magnetically Depleted with Titers of Lot 49-1, -2, and -3 CD8-spider-nickel Bead Conjugates

	bead lot 49-1				bead lot 49-2				bead lot 49-3			
bead titer	% CD8+	% CD8 depleted	% CD4+	% CD4 norm.	% CD8+	% CD8 depleted	% CD4+	% CD4 norm.	% CD8+	% CD8 depleted	% CD4+	% CD4 norm.
0 μL	37.1	0	38.6	38.6	37.1	0	38.6	38.6	37.1	0	38.6	38.6
5	32.9	11.3	41.4	39.7	32.1	13.5	43.5	41.3				
10	30.9	16.7	43.7	41.0	28.9	22.1	44.3	40.7	30.7	17.3	42.8	40.1
20	27.7	25.3	45.1	40.9	23.9	35.6	48.0	41.7	27.6	25.6	43.5	39.4
30	25.7	30.7	45.4	40.2	23.8	35.8	48.5	42.0	21.0	43.4	50.0	41.9
40	25.8	30.5	46.6	41.3	21.1	43.1	48.7	40.9	18.7	49.6	51.2	41.8
50	21.2	42.9	49.4	41.5	20.6	44.5	49.2	41.1	15.4	58.5	51.3	40.2
75	22.0	40.7	48.8	41.4					15.1	59.3	54.2	42.3
100	23.6	36.4	47.9	41.4	18.1	51.2	51.6	41.8	14.5	60.9	50.3	38.9
200	0.5	98.7	59.4	37.7	0.5	98.7	60.6	38.4	0.3	99.2	60.6	38.3
300	0.1	99.7	59.6	37.5	0.2	99.5	60.9	38.4	0.0	100	61.3	38.6

maintain constant volume throughout the runs. The samples were then mixed on a Coulter model P1122 mixer for 2 min and magnetically separated with a multiposition Corning magnetic separator for 1 min. All supernatants of depleted samples were transferred to matching tubes, to which were added 10 μL of Coulter CYTO−STAT/COULTER CLONE CD4-RD1/CD8-FITC fluorescent marker, mixed for 10 min, and run on Coulter TQ-PREP, EPICS immunology workstation model U13337, in 35 s cycle to lyse rbcs and fix the cells. For each donor, three controls were prepared. The first, contained no antibody marker and was used to establish the position of wbc scatter. The second contained the dual fluorescent marker Coulter CYTO−STAT/COULTER CLONE Ms-IgG1-RD1/MsIgG1-FITC to determine background fluorescence, nonspecific cell fluorescence, and cell autofluorescence. PMT voltages were adjusted to give log-(fluorescence) values for the latter in the range of 0.1−1.0. The third contained the dual fluorescent label Coulter CYTO−STAT/COULTER CLONE CD4-RD1/CD8-FITC to establish overlap in emission spectra of the two labels and compensate for it. Each control consisted of 100 μL of whole undepleted blood from each donor and 10 μL of label or 1× PBS buffer, mixed gently for 10 min and run on Coulter TQ-Prep Workstation in 35 s cycle. All depleted samples and undepleted controls were analyzed on the Coulter EPICS XL-MCL or Profile II flow cytometer. Prior to runs, the flow cytometer was aligned with Coulter Flow-Check beads to give CV values less than 2.0%. Fluorescence intensity standardization was carried out with Coulter Flow-Set beads to obtain mean channel values of fluorescence intensity in the range of plus or minus one channel of FITC or RD1 intensity.

Preparation of KC16 Antibody-Spider-Nickel Bead Conjugates. *Run 1 (Lots 100-1, -2, and -3).* A total of 25 g of raw nickel beads was mixed with 10 mL of 0.2 μm filtered distilled water and sonicated in a bath for 7 h. The beads were then washed five times by magnetic separation with distilled water and resuspended to 10 mL total volume to give a 2.5% w/v solids bead suspension. The beads were then coated in three trials of 2 mL each in 15 mL tubes with 0.200, 0.600, and 1.200 mL of 0.33 mM spider (1.01 mM sulfhydryl groups as determined by Ellman's reagent) to give 0.092, 0.233, and 0.379 mM sulhydryl groups in the mixtures. The latter were roller mixed overnight and then washed five times with 1× PBS by magnetic separation. For activation of the spider-coated nickel beads, 7.5 μL of 10 mg/mL of sulfo-SMCC solution per trial was used. The mixtures were then roller mixed for 1 h, and washed five times with 1× PBS and resuspended in 1× PBS to a total volume of 2 mL. A total of 10 mg of KC16 antibody was activated in the same way as CD8 antibody to give 0.431 mL of 3.25 mg/mL IT-KC16 antibody. Conjugations were run at 0.700 mg/mL IT-KC16 antibody and 2.0 mL of total volume/trial. The fitrates at the end of the 2 h conjugation period gave 11.97, 10.34, and 11.30 mg of IT-KC16/m^2 surface density.

Run 2 (Lots 4-1, -2, and -3). A total of 30 mL of 10% w/v solids nickel bead suspension was probe sonicated for 8 h and washed five times with filtered distilled water. A total of 0.200, 0.600, and 1.200 mL of 0.33 mM spider solution/2.0 mL of nickel bead suspension was used to coat beads in each 10 mL of 10% w/v solids suspension. A total of 1.000 mL of 4.28 mg of IT-KC16/mL per 10.0 mL of total volume of 10% beads was used to give 2.22, 0.61, and 0.57 mg of IT-KC16/m^2 surface density in each trial, respectively.

RESULTS AND DISCUSSION

Depletion of CD8+ Lyphocytes from Whole Blood with CD8 Antibody-Spider-Nickel Bead Conjugates. Fluorescent counts from the CD8-FITC and CD4-RD1 markers were recorded for undepleted samples and for CD8-linker-nickel bead-depleted samples. The percentage depletion of CD8 cells was determined as (Fl counts,undepleted sample − Fl counts,depleted sample)/(Fl counts,undepleted sample) x 100. The percentage of CD8+ cells in lymphocytes, the percentage of CD8 depleted, the percentage of CD4+ cells in lymphocytes, and the normalized percentage of CD4 to account for removal of CD8 cells for 500 μL of whole blood and various titers from 5−300 μL of 2.5% w/v CD8-nickel bead suspension, lots 49-1, -2, and -3, are summarized in Table 1. Bead-to-cell ratios were calculated from the average volume/nickel particle of 2.12×10^{-10} cm^3 and, thus, average mass per particle of 5.13×10^{-10} g. Then, for 1 mL of 2.5% w/v solids nickel beads or 0.025 g of nickel beads, there will be 4.87×10^7 nickel particles/mL of 2.5% w/v solids beads. For a titer of 200 μL of 2.5% w/v solids beads, we have 9.74×10^6 beads. Lymphocytes per microliter of whole blood were enumerated on the Coulter STKS2B hematology analyzer as 1.64×10^3 for one donor. For 500 μL of whole blood per sample, this gave 8.2×10^5 lymphocytes. Flow cytometry analyses of the undepleted samples gave 37.1% CD8+ or 3.04×10^5 CD8+ lymphocytes for this donor. Therefore, the bead-to-cell ratio was calculated as 32. Results are graphically displayed in Figure 5 as the number of CD8 cells depleted versus bead-to-cell ratios for lot 49 beads. CD8 cells removed and bead-to-cell ratios showed a steady rise from $\sim 4 \times 10^4$ and $5-6 \times 10^4$ to $12-17 \times 10^4$ and $27-31 \times 10^4$, respectively, after which there was a sudden jump to 30×10^4 in the number of CD8 cells that were depleted.

Table 2. Percentage CD8/CD4 Positive Cells in Undepleted Whole Blood and in Supernatants of Whole Blood Magnetically Depleted with Titers of Lot 91-1, -2, and -3 CD8-spider-nickel Bead Conjugates

	bead lot 91-1				bead lot 91-2				bead lot 91-3			
bead titer	% CD8+	% CD8 depleted	% CD4+	% CD4 norm.	% CD8+	% CD8 depleted	% CD4+	% CD4 norm.	% CD8+	% CD8 depleted	% CD4+	% CD4 norm.
0 μL	48.8	0	22.3	22.3	48.8	0	22.3	22.3	48.8	0	22.3	22.3
10	26.8	45.1	29.0	22.6	35.6	27.0	25.4	22.0	40.7	17.8	25.1	22.9
20	27.9	42.8	28.0	22.1	22.2	54.5	29.2	21.4	34.4	29.5	26.5	22.7
30	15.8	67.6	31.8	21.3	6.6	86.5	32.1	18.6	16.9	65.4	32.2	21.9
40	3.0	93.8	34.3	18.6	6.1	87.5	34.1	19.5	17.2	64.8	32.0	21.9
50	6.5	86.7	33.8	19.5	2.8	94.3	36.1	19.5	11.4	76.6	35.2	22.0
75	0.9	98.2	36.1	18.8	0.7	98.6	35.9	18.6	9.2	81.1	35.0	21.1
100									3.3	93.2	36.2	19.7

Table 3. Percentage CD8/CD4 Positive Cells in Undepleted Whole Blood and in Supernatants of Whole Blood Magnetically Depleted with Titers of Lot 33-1, -2, and -3 CD8-spider-nickel Bead Conjugates

	bead lot 33-1				bead lot 33-2				bead lot 33-3			
bead titer	% CD8+	% CD8 depleted	% CD4+	% CD4 norm.	% CD8+	% CD8 depleted	% CD4+	% CD4 norm.	% CD8+	% CD8 depleted	% CD4+	% CD4 norm.
donor 52 598												
0 μL	31.3	0.0	45.9	45.9	31.3	0.0	45.9	45.9	31.3	0.0	45.9	45.9
10 μL, 1%	0.0	100	50.1	34.4	0.13	99.6	49.4	34.0	5.5	82.4	49.4	36.7
10 μL, 5%	0.0	100	47.3	32.5	0.0	100	46.7	32.0	0.0	100	49.9	34.3
10 μL, 10%	0.0	100	47.7	32.8	0.0	100	46.2	31.7	0.0	100	48.3	33.2
10 μL, 15%	0.0	100	46.9	32.2	0.0	100	47.2	32.4	0.0	100	47.0	32.3
10 μL, 25%	0.0	100	46.6	32.0	0.0	100	46.1	31.7	0.0	100	47.5	32.6
donor 52 936												
0 μL	26.5	0.0	48.8	48.8	26.5	0.0	48.8	48.8	26.5	0.0	48.8	48.8
10 μL, 1%	3.8	85.7	51.4	39.7	9.4	64.5	51.3	42.5	2.6	82.6	53.9	41.0
10 μL, 5%	2.3	91.3	51.6	39.1	0.0	100	50.8	37.3	0.0	100	52.1	38.3
10 μL, 10%	0.0	100	50.2	36.9	0.12	99.5	51.4	37.8	0.30	98.8	50.2	37.0
10 μL, 15%	0.0	100	49.8	36.6	0.12	99.5	48.6	35.8	0.068	99.7	50.0	36.8
10 μL, 25%	0.0	100	48.7	35.8	0.0	100	49.6	36.5	0.076	99.7	49.5	36.4

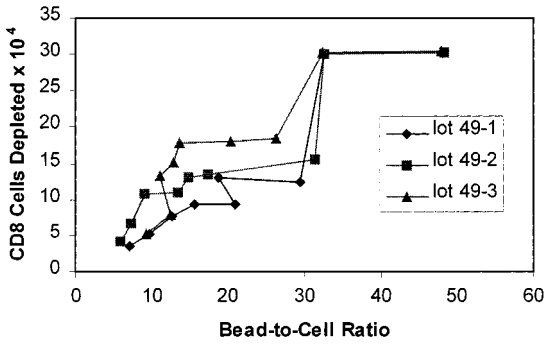

Figure 5. Progress of CD8+ lymphocyte cell depletion with single runs of lot 49-1, -2, and -3 CD8-spider-nickel bead conjugates plotted as CD8 cells depleted versus bead-to-cell ratio.

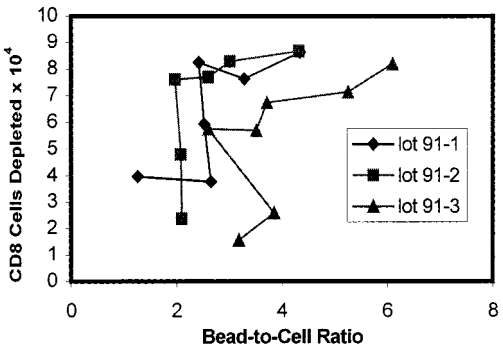

Figure 6. Progress of CD8+ lymphocyte cell depletion with single runs of lot 91-1, -2, and -3 CD8-spider-nickel bead conjugates plotted as CD8 cells depleted versus bead-to-cell ratio.

Similar results obtained for bead lots 91-1, -2, and -3 and 33-1, -2, and -3 are summarized in Tables 2 and 3, and for lot 91 beads, the number of CD8 cells depleted versus bead-to-cell ratios are graphically shown in Figure 6. Each lot of CD8 beads showed different targeted blood cell depletion characteristics. Note that the structure and size of aggregates of magnetic beads and cells that are typically formed on mixing beads with cells are not necessarily the same in each separate titer of beads added to whole blood in a particular run. The reversals apparent on two occasions in the graphs of Figure 6 are indicative of the degree of deviation per titer point in a run. Lot 49 beads showed the best specificity for CD8 cells over CD4 cells, as measured by the small deviations (0.0−9.6%) of the normalized percentage of CD4 in depleted samples compared to the percentage of CD4 in the undepleted control. However, the bead-to-cell ratio of about 30 at saturation (complete depletion of CD8 cells) was the highest of any lot. Lot 91 beads gave a better bead/cell ratio of 2−6 at saturation but the specificity (0.9−16.6% deviation in normalized percentage of CD4 values) for CD8 cells was worse. Lot 33 beads showed low bead-to-cell ratios based on 10 μL of 1% w/v solids beads, ranging from 3.5 to 4.2 for donor 52 598 (1.8×10^3 lymphocytes/μL) and 5.4 to 7.1 for donor 52 936 (1.6×10^3 lymphocytes/μL), but much worse specificity for CD8 cells.

Use of KC16 Antibody-Spider-Nickel Bead Conjugates in Depletion of Red Blood Cells from Whole Blood. One trial with KC16 antibody-conjugated to linker ligand coated nickel beads showed that 400 μL of whole blood was 95.68% depleted of red blood cells by 500 μL of 50% w/v solids beads. The rbcs were enumerated before (4.60×10^6 rbc/μL of whole blood) and after depletion with KC16 beads on the Coulter STKS2B hematology analyzer. There were 9.74×10^8 nickel particles/mL of 50% w/v solids beads, so that the titer of 500 μL of beads contained 4.87×10^8 nickel particles. Also, the number of rbcs depleted from 400 μL of whole

Table 4. Distribution of Cells in Undepleted Whole Blood and in Supernatants of Whole Blood Magnetically Depleted with Lot 4-1, -2, and -3 KC16-spider-nickel Bead Conjugates

	cell counts per microliter				
	Wbc × 10^3	Rbc × 10^6	Plt × 10^3	Rbc × 10^6, corr	% depletion, rbc
donor 41 518					
control	3.0	1.85	87	1.85	
lot 4−1	3.9	0.08	127	0.06	96.8
lot 4−2	4.0	0.46	128	0.33	82.2
lot 4−3	4.2	1.07	125	0.76	58.9
donor 53 418					
control	2.6	1.61	132	1.61	
lot 4−1	4.1	0.18	226	0.11	93.2
lot 4−2	3.4	1.31	176	1.00	37.9
lot 4−3	3.9	1.90	201	1.26	21.7

blood was $0.9568 \times 400\ \mu L \times 4.60 \times 10^6$ rbc/μL $= 1.76 \times 10^9$ rbc depleted. Therefore, the rbc-to-nickel bead ratio was 3.6.

In depletion of red blood cells from whole blood of another donor, 100 μL of 25% w/v solids beads (lot 100-1, -2, and -3) or 4.87×10^7 nickel beads, a 10 min mix with 400 μL of whole blood, and a 1 min magnetic separation showed 3.84×10^6 rbc/μL in the undepleted control for each trial, 2.60×10^6, 2.76×10^6, and 2.75×10^6 rbc/μL in the depleted trials to give 1.24×10^6, 1.08×10^6, and 1.09×10^6 rbc/μL depleted or 32.3, 28.1, and 28.4% rbc depleted. Thus, the rbc-to-bead ratios for depletion were 10, 8.9, and 9.0, respectively.

Results of a more detailed run with lot 4-1, -2, and -3 beads, showing cell counts per microliter for the undepleted control (400 μL of whole blood + 500 μL of 1× PBS) and the supernatants of depleted samples (control (400 μL of whole blood + 500 μL of 50% w/v KC16-spider-nickel bead suspension), are given in Table 4. Assuming that wbcs and plts are not depleted, a correction for the decrease in volume of supernatant after depletion was estimated from the percentage difference in cell counts for undepleted control and depleted sample for wbc and plt counts. This correction was averaged between wbc and plt counts, applied to calculate a corrected count for the samples depleted of rbcs, and allowed calculation of the percentage of rbc depletion as recorded in Table 4. For the two lot 4-1 depletions, the rbc-to-nickel bead ratios were calculated as 1.5 and 1.2, respectively.

Run 1 beads (lot 100) were not sonicated initially as severely as run 2 beads (lot 4), so that they remained as large as the original raw beads with more surface area due to the corrugated structure. This was reflected in the large surface densities of conjugated KC16 antibody and in the large rbc-to-bead ratios in depletions. Run 2 beads were smaller and had a smooth surface after probe sonication to give less surface area per bead. These properties served to yield surface densities of one-half or less for conjugated KC16 antibody and about 6−7-fold lower rbc-to-bead ratios in depletions. Nevertheless, the rbc-to-bead ratios for depletion are all the highest that have ever been observed. Other reported magnetic bead depletions of red blood cells from whole blood required many more beads than cells. For example, KC16-manganese ferrite beads (*14*) gave a bead-to-rbc ratio of 147.

LITERATURE CITED

(1) Kittel, C., and Galt, J. K. (1956) Ferromagnetic Domain Theory. *Solid State Phys. 3*, 437−564.

(2) Sharrock, M. P. (1990) Particulate Recording Media. *MRS Bulletin March*, 53−61.

(3) White, R. M. (1985) Opportunities in Magnetic Materials. *Science 229*, 11−15.

(4) *CRC Handbook of Chemistry and Physics* (1983−1984) pp D-50−D-93, 64th ed., CRC Press, Inc., Boca Raton, FL..

(5) Coulter, W. H., Zwerner, R. K., Schmittling, R. J., and Russell, T. R. *Method of Positive or Negative Selection of a Population or Subpopulation of a Sample Utilizing Particles and Gravity Sedimentation*, U.S. Patent No. 5,576,185, issued November 19, 1996.

(6) Suslick, K. S. (1995) Applications of Ultrasound to Materials Chemistry. *MRS Bulletin April*, 29−34.

(7) Whitesell, J. K., and Chang, H. K. (1993) Directionally Aligned Helical Peptides on Surfaces. *Science 261*, 73−76.

(8) Fox, M. A., Whitesell, J. K., and McKerrow, A. J. Fluorescence and Redox Activity of Probes Anchored through an Aminotrithiol to Polycrystalline Gold. *Langmuir 14*, 816−820.

(9) Wong, S. S. (1991) *Chemistry of Protein Conjugation and Cross-Linking*, p 279, CRC Press, Inc., Boca Raton, FL.

(10) Hermanson, G. T. (1996) *Bioconjugate Techniques*, pp 618−629, Academic Press, San Diego, CA.

(11) Aslam, M., and Dent, A. (1998) *Bioconjugation-Protein Coupling Techniques for the Biomedical Sciences*, Chapter 8, Grove's Dictionaries Inc., New York.

(12) *Pierce Catalog and Handbook* (1994, 1995) Life Science & Analytical Research Products, Pierce Chemical Company, Rockford, IL.

(13) Siiman, O., Gordon, K., Rodriguez, C. M., Burshteyn, A., Maples, J. A., and Whitesell, J. K. *Protein-Colloidal Metal-Aminodextran Coated Particle and Methods of Preparation and Use*, U.S. Patent 5,945,293, issued August 31, 1999.

(14) Siiman, O., Burshteyn, A., and Gupta, R. K. *Biodegradable Gelatin-Aminodextran Particle Coatings of and for Making Same*, U.S. Patent 5,466,609, issued November 14, 1995.

(15) Siiman, O., Burshteyn, A., Maples, J. A., and Whitesell, J. K. *Stable Protein-Nickel Particles and Methods of Production and Use Thereof*, International Patent application PCT/US98/20697 filed October 1, 1998, allowed September 24, 1999.

(16) Kortright, K. *Monoclonal antibody for recovery of leukocytes in human peripheral blood and method of recovery employing said monoclonal antibody*. U.S. Patent 4,752,563, issued June 1988.

(17) Whitesell, J. K, Chang, H. K., and Minton, M. A. Synthesis of *tris*-[3-Mercaptopropyl)methyl)]-N−(aminoacetyl) amide. *Tetrahedron* (submitted for publication).

(18) Ellman, J. C. (1959) Tissue sulfhydryl groups. *Arch. Biochem. Biophys. 82*, 70−77.

(19) Siiman, O., unpublished results.

(20) Nickel analyses were run by atomic absorption by G. G. Fletcher, Department of Biochemistry, McMaster University, Hamilton, Ontario, Canada.

(21) Maggio, E. T. (1985) *Enzyme-Immunoassay*, p 181, 4th ed., CRC Press, Boca Raton, FL.

BC990176U

Region-Selective Labeling of Antibodies as Determined by Electrospray Ionization-Mass Spectrometry (ESI-MS)

Maciej Adamczyk,* John Gebler, Kevin Shreder, and Jiang Wu

Department of Chemistry (9NM), Abbott Diagnostics Division, Abbott Laboratories, 100 Abbott Park Road, Abbott Park, Illinois 60064-6016. Received December 23, 1999; Revised Manuscript Received March 6, 2000

The electrospray ionization-mass spectrometry (ESI-MS) analysis of three sets of monoclonal antibody-acridinium-9-carboxamide conjugates is described. The conjugates (nine total) were enzymatically digested using papain and the resulting fragments [Fc heavy chain, Fab, or F(ab′)$_2$] were analyzed using liquid chromatography/ESI-MS. The average number of labels per fragment were calculated using Σ *nx*%, where *n* is the number of acridinium molecules covalently bound to the fragment and *x*% is the percent relative area of the corresponding peaks in the mass spectrum. When these values were normalized against the molecular weight of their respective region, antibody-dependent labeling patterns were observed. For antibodies **T** (anti-L−T$_4$) and **F** (anti-FITC), there was a preference for conjugation of the Fab region over the Fc region. For antibody **B** (anti-biotin), the trend was reversed.

INTRODUCTION

Antibody conjugates play a crucial role in diagnostics and medical applications (*1*). Typically, antibodies are covalently attached to a label which in turn endows the antibody with the ability to generate a signal or carry a biologically destructive payload (e.g., in "magic bullet" therapy). While it is clear that the incorporation ratio of label to protein plays an important role in the performance of a modified antibody (*2*−*4*), little more than the average incorporation of label is involved in the characterization of the typical conjugate. In the past, this minimal characterization has been due to the limited number of general techniques to measure other parameters, such as the distribution and location of labels on an antibody conjugate.

Traditionally, various spectroscopic techniques are used to determine label load of an antibody conjugate. However, each suffers from certain limitations that makes their use problematic. For example, while UV−vis spectroscopy is commonly employed, this technique cannot be readily used unless the label has a strong absorption distinct from that of the antibody. The use of dyes such as 2,4,6-trinitrobenzenesulfonate (TNBS) or Ellman's reagent [5,5′-dithio-bis(2-nitrobenzoic acid)] to titrate unmodified residues (e.g., amines or thiols, respectively) postconjugation can also be used (*5*, *6*). However, inaccuracies can arise from incomplete titrations and, at best, these colorimetric techniques offer only an indirect look at label load by showing how much of the antibody has *not* been modified.

By contrast, recent advancements in mass spectrometry (MS) have allowed a more informative and direct analysis of antibody conjugates. Once an antibody is labeled, a variety of species corresponding to a range of conjugates that vary by the covalent attachment of a single label can be observed. This *distribution* can then be used calculate a single average loading value (i.e., ratio of label to antibody). Using electrospray ionization-mass spectrometry (ESI-MS), Bennett et al. determined the label load and distribution of an isolated antibody Fab fragment labeled with biotin (*7*, *8*). Recently, Siegel et al. reported on the use of matrix-assisted laser desorption ionization (MALDI) to characterize the average loading number and distribution of antibody-calicheamicin conjugates (*9*). Interestingly, Seigel et al. also found that the analysis of intact antibody conjugates by ESI-MS was complicated by the difficult deconvolution of overlapping multiple charged peaks. This multiplicity was attributed to heterogeneity caused by glycosylation and labeling.

While issues such as label load and label distribution have been addressed, *where* labeling preferentially occurs is not part of the routine characterization of antibody conjugates. Because antibodies, like many proteins, can be divided into distinct regions responsible for structure, binding, and physiological effector functions (*10*), one could propose that different region-selective modifications of the same antibody would yield differences in conjugate performance. Such issues are critical in the immunodiagnostic and immunotheurapeutic fields. For example, modification of Fab residues near the antibody-binding site could adversely affect the affinity of an antibody. Indeed, variation in residues near the binding pocket but not directly contacting a hapten can still modulate the affinity of an antibody (*11*). Despite such concerns, general methods to characterize this "region-modification" are scarce. Because of the potential implications, we have developed and utilized an ESI-MS strategy to investigate whether an antibody-dependent preference exists for modification of the Fab region or Fc region during the labeling process.

RESULTS

Three different antibodies [anti-biotin (**B**, IgG2a); anti-FITC (**F**, IgG1); and anti-L−T$_4$ (**T**, IgG2a)] were conjugated with an acridinium label (**1**) at three different loading levels. The acridinium label was chosen because it provided a spectroscopic handle (visible $\lambda_{max} = 369$ nm) by which quantitative mass spectrometric data could be compared to quantitative UV−vis spectrophotometric data. Use of this label also results in a covalent amide

* To whom correspondence should be addressed. Phone: (847) 937-0225. Fax: (847) 938-8927. E-mail: maciej.adamczyk@abbott.com.

10.1021/bc990181y CCC: $19.00 © 2000 American Chemical Society
Published on Web 06/17/2000

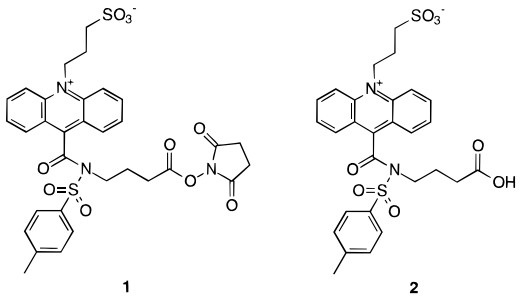

Figure 1.

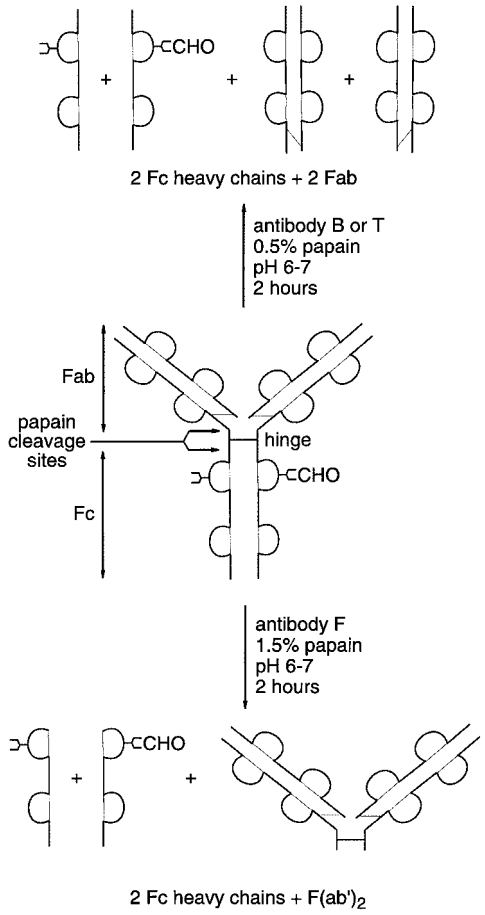

Figure 2. Summary of products obtained after papain digestion of antibodies **B**, **T**, and **F** (CHO = carbohydrate modification).

linkage to lysine residues which facilitates the long term stability of the conjugate. All antibodies were dialyzed exhaustively against PBS (100 mM sodium phosphate and 150 mM NaCl, pH 8.0) prior to conjugation. To each antibody (3.0 mg of mAb in 1.4 mL of PBS) was added 4, 8, or 16 equiv of the acridinium active ester **1** (reactions 1, 2, and 3, respectively) in 0.2 mL of DMF. Upon addition, the solutions were rapidly mixed and then allowed to stand overnight (18 h) in the dark. Each reaction was then purified using gel permeation chromatography, conditions in which the labeled antibody ($R_t \approx 8.3$ min) and unconjugated acridinium label ($R_t = 11.1$ min) were readily separated.

Postpurification, the antibody conjugates were enzymatically cleaved into Fc heavy chains and Fab [or $F(ab')_2$] using papain (*12*−*14*) (Figure 2). Digestion conditions were optimized to minimize nonselective cleavage (i.e., other than that near the hinge region) and disulfide exchange between antibody fragments. Cysteine, a necessary component for papain activation, was found to promote such exchanges. Consequently, the amount of cysteine present during the digestion was kept to a minimum. In the case of antibodies **B** and **T**, the use of a 0.5% solution (w/w) of papain at pH 6−7 for 2 h yielded Fc heavy chains and Fab. For these antibodies, the hinge region was not isolated under the experimental conditions, and its contribution was neglected. In the case of antibody **F** (IgG1), the use of a 1.5% solution (w/w) of papain under identical conditions of time, temperature, and pH yielded Fc heavy chains and $F(ab')_2$. Both mouse and rat IgGl antibodies have previously been observed to yield $F(ab')_2$ upon treatment with papain (*15*, *16*).

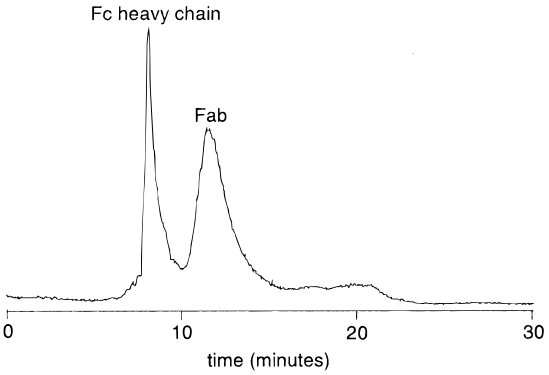

Figure 3. The total ion count chromatogram from LC/ESI-MS of the papain digested antibody conjugate **B1**.

A reversed-phase HPLC column, interfaced with the ion source of the mass spectrometer, was used for the separation of antibody fragments (*17*). Gradient elution using a water/acetonitrile mobile phase effectively removed salts and detergents from the whole antibody fragments while offering ready separation of Fc and Fab derived species (Figure 3). In general, baseline resolution was achieved between the Fc heavy chain and Fab for antibodies **B** and **F**. In the case of antibody **T**, there was some overlap between the peaks corresponding to the Fc heavy chain and $F(ab')_2$. Despite the presence of overlapping peaks, the unambiguous mass analysis of the digestion products was still possible (Table 1). By selection of the appropriate mass window (see Materials and Methods), the mass spectra profiles between the two species were readily distinguished. Importantly, postdigestion, no peak was observed for the native antibody. When injected alone, the whole antibodies eluted with a longer retention time than their postdigestion fragments and generated a readily detectable peak in the ion chromatogram. Therefore, the absence of a peak in the ion chromatogram corresponding to native antibody was taken as an indication that the enzymatic reactions had gone to completion.

The raw ESI-MS spectra for the Fc and Fab fragments of the antibody conjugate **B3** are shown in Figure 4. This particular conjugate exhibited the second highest level of acridinium incorporation among all the conjugates. Deconvolution of the spectra of multiply charged species to the mass domain for the Fc and Fab fragments of antibody **B** and its acridinium conjugates is shown in Figure 5. Prior to conjugation, only a single peak is observed for the Fab. Postconjugation with **1**, additional peaks corresponding to the acridinium conjugates are observed. The mass difference of each adjacent maxima in the peak modulation is ~568 Da corresponding to the addition of an acridinium to the anti-biotin antibody. At the acridinium active ester **1** to mAb ratio of 4:1, the native Fab is the most abundant species. As the ratio is increased to 16:1, the Fab covalently modified by two

Table 1. ESI-MS Characterization of the Papain Digested Native Antibodies T, B, and F

native antibody	molecular mass of Fab in daltons (% of total peak area)	molecular mass of $F(ab')_2$ in daltons (% of total peak area)	molecular mass of Fc heavy chain in daltons (% of total peak area)
anti-L−T4 (**T**)	47 620 (87%) 47 782 (13%)	n.o.[a]	25 710 (37%) 25 872 (54%) 26 035 (9%)
anti-biotin (**B**)	47 777 (100%)	n.o.	25 715 (44%) 25 878 (49%) 26 038 (7%)
anti-F1TC (**F**)	n.o.	95 664 (100%)	25 527 (5%) 25 715 (49%) 25 878 (29%) 26 038 (4%) 26 187 (8%) 26 350 (4%)

[a] n.o. = not observed.

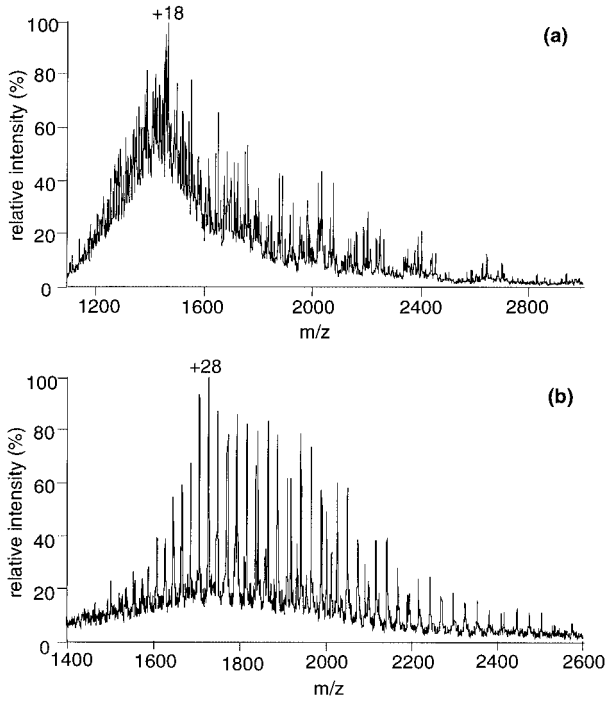

Figure 4. The raw ESI-MS spectra of the (a) Fc heavy chain and (b) Fab of antibody **B3** (ratio of acridinium label:antibody ~8.0).

acridinium labels becomes the most abundant species and the addition of as many as five acridinium labels is observed.

DISCUSSION

The average number of acridinium labels to each antibody fragment was computed using the equation $\sum nx\%$, where n is the number of acridinium molecules covalently bound to the fragment and $x\%$ is the percent relative area of the corresponding mass spectrum peaks. The calculation of the acridinium labels per region of glycosylated fragments took into account the contribution of all nonglycosylated and glycosylated peaks As expected, the Fc heavy chain was characterized by multiple components due to heterogeneous carbohydrate modification. The observed mass differences are consistent with modification of a heavy chain by a galactose or mannose residue (FW = 162). Because glycosylation of Fc heavy chains is asymmetric, the "single" heavy chain observed by ESI-MS is really a composite of both Fc heavy chains. For the Fab of antibody **T**, a major (87%) and minor (13%) peak which differed by a mass of 162 were observed (see Table 1). This Fab heterogeneity is consistent with either a ragged papain digest (*17*) or Fab glycosylation (*18*). Table 2 summarizes the distribution of each acridinium-conjugated fragment for the three antibodies, the average number of acridinium labels in the Fab and Fc regions, and the average number of acridinium labels per antibody.

Various factors need to be considered during the calculation of label load by ESI-MS. The determination of the distribution and average labeling value of conjugated species by ESI-MS is independent of drift in the instrument calibration because these values are calculated from the deconvoluted distribution of a single molecular ion envelope measurement. These values are also independent of the absolute concentration of conjugates. However, during the calculation of label-to-fragment ratio, the instrument response for each species in the distribution is presumed to be identical. In practice, the conjugation of an antibody fragment with the acridinium label **1** may alter its ionization efficiency and propensity to form sodium adducts.

To check how these factors effect the quantitative nature of the MS results, the total number of labels per antibody as determined by the MS method was compared to the value as determined with UV−vis spectroscopy, a common method to determine label load. When plotted against each other, these values were in good agreement and yielded a slope of 0.95 (Figure 6). Overall, the mass spectrometric data compare favorably with the coupling number obtained by UV−vis absorption spectrophotometry. On the basis of this correlation, we would assume that, on average, factors such as ionization efficiency and sodium adduct formation do not play a significant role in the determination of acridinium label load by ESI-MS.

To compare the extent of region-modification between the Fab and Fc region, the number of acridiniums per region were normalized against the MW of the nonglycosylated fragments (Figure 7). For the sake of comparison, the "Fab region" was defined as the $F(ab')_2$ for antibody **F** and the sum of two Fabs for antibodies **B** and **T**. Fc and Fc region are used synonymously. Normalization eliminates any error associated with the size of a fragment which may skew the apparent level of incorporation per region by virtue of a larger fragment simply having more nucleophilic lysine residues than a smaller fragment. For a hypothetical, completely randomized protein in which every amino acid residue capable of conjugation to the acridinium label **1** has identical reactivity, the ratio of labels per region would be expected to be similar for all reasonably large regions of that protein. For the conjugates studied here, there are clear antibody-dependent differences between the Fab and Fc

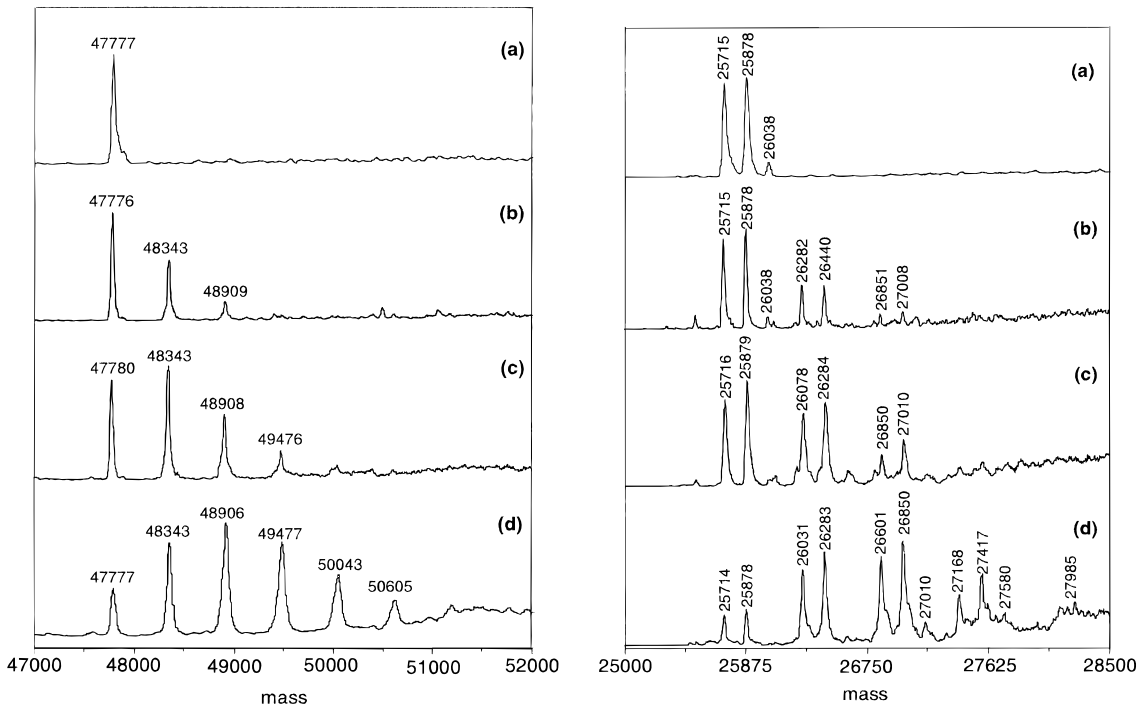

Figure 5. (Left panel) Deconvoluted spectra of Fab of antibody **B** before and after conjugation with 4, 8, and 16 equivalents of the acridinium active ester **1**. The calculated acridinium labels per Fab region are 0, 1.1, 2.1, and 4.4, respectively. (Right panel) Deconvoluted spectra of the Fc heavy chain of antibody **B** before and after conjugation with 4, 8, and 16 equivalents of the acridinium active ester **1**. The calculated number of acridinium labels per Fc are 0, 0.8, 1.8, and 3.6, respectively.

Table 2. Summary of Label Distribution and Load of the T, B, and F Antibody Conjugates as Determined by LC/ESI-MS

mAb conjugate[a]	label distribution of Fab or $F(ab')_2$[b]	label distribution of Fc heavy chain[b]	labels per Fab region[c]	labels per Fc region[c]	labels/antibody[d]
T1	0−3	0−2	1.69	1.08	2.8
T2	0−4	0−2	2.80	1.28	4.1
T3	1−7	0−3	6.30	2.19	8.5
B1	0−3	0−2	1.06	0.82	1.9
B2	0−3	0−3	2.10	1.75	3.9
B3	0−6	0−4	4.40	3.60	8.0
F1	0−4	0−1	1.25	0.46	1.7
F2	0−5	0−1	2.15	0.65	2.8
F3	2−9	0−3	5.80	1.74	7.5

[a] **T** = anti-L−T4 mAb; **B** = anti-biotin mAb; **F** = anti-FITC mAb. The numerals 1, 2, and 3 correspond to reactions in which 4, 8, or 16 equiv of the acridinium active ester **1**, respectively, were added. [b] The values shown indicate the range of conjugate species observed and used in the calculation of label load. For example, seven species were observed for the **B3** Fab, the lowest MW of which corresponded to unconjugated Fab and the highest MW of which corresponded to a species with six acridinium labels/Fab. For a detailed mass spectrum of the **B3** Fab, see Figure 5. [c] For the sake of comparison, the "Fab region" is defined as the $F(ab')_2$ for antibody **F** and the sum of two Fabs for antibodies **B** and **T** (Figure 2). "Fc region" and Fc are synonymous terms. By definition, an antibody Fc is composed of two Fc heavy chains. [d] Sum of the previous two columns.

regions. For antibodies **T** and **F**, there is a preference for conjugation of the Fab region over the Fc region. For antibody **B**, the trend is clearly reversed.

Several simple reasons could account for the observed region-selective labeling. First, and most likely, there could be more lysine residues present on one fragment versus the other. Since the variable region, by definition, does not have a defined sequence of residues, it may give the Fab region a disproportionate number of reactive residues relative to the Fc region. In this scheme, the reactivity of all lysines is assumed to be the same; what differs is the number of lysines. Alternatively, changes in conformation or microenvironment induced by the composition of the variable region could change the reactivity of specific lysine residues. In turn, this effect may create conjugatable sites on the Fab region that are more or less reactive than the "average" lysine residue present in Fc region. Finally, the answer may be a combination of these two proposals.

Mass spectrometry has opened new doors to the analysis of biological macromolecules. For example, antibody microheterogeneity caused by glycosylation and truncated amino acid residues has been observed by MS. In addition, both MALDI and ESI-MS have been applied to confirm the amino acid sequence of monoclonal antibodies (*19*−*26*). Such applications have demonstrated the ability of MS to structurally characterize proteins with a high degree of mass accuracy and precision.

As a tool for the analysis of protein conjugates, MS can now be routinely applied to a wide variety of systems. The label load and distribution of ligands covalently bound to proteins such as BSA, antibodies, and glucose 6-phosphate dehydrogenase have been readily characterized by MALDI and ESI-MS (*9*, *27*−*30*). One advantage of MS for the analysis of conjugates is that its use is independent of the spectroscopic nature of the label. While capillary gel electrophoresis has been applied to the analysis of doxorubicin modified antibody heavy and

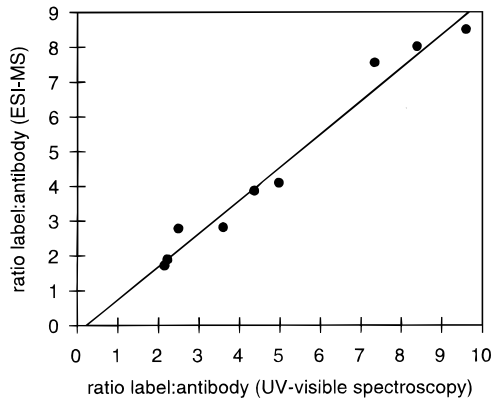

Figure 6. Plot of number of acridinium labels:antibody as estimated by ESI-MS versus the same values obtained by UV−vis spectroscopy. The slope of the best fit line is 0.95 and the correlation coefficient is 0.98.

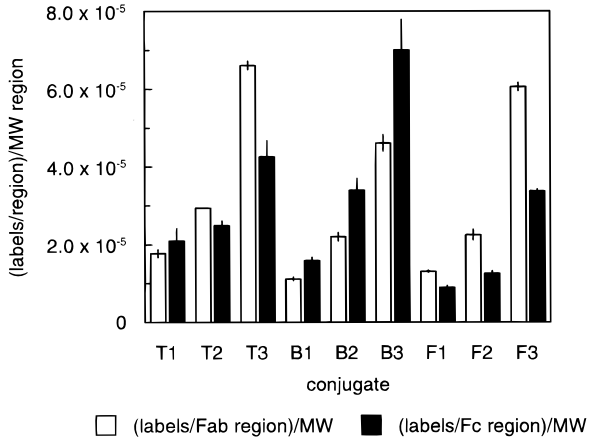

Figure 7. Region-modification for conjugates of antibodies **T**, **B**, and **F**. Bar graph of labels per region normalized by MW for each antibody conjugate. Each bar represents the average of two runs with the high and low value indicated by the error bar. Notice that the number of labels per Fab region or Fc region varies on a per MW basis. For antibodies **T** and **F** there is a preference for conjugation of the Fab region over the Fc region. For antibody **B**, the trend is clearly reversed.

light chains, the quantitative use of this technique requires a label that is both UV-active and fluorescent (*31*). No such requirement is needed for the ESI-MS approach shown here.

Characterization of antibody conjugates can play an important role in their development as immunoreagents. In the area of small organic molecules, issues of regioselectivity are well understood and manipulated to synthesize molecules with defined properties. In the case of biological macromolecules, this avenue has not been actively explored, perhaps because of the limited number of methods to investigate the phenomenon. The ESI-MS approach demonstrated here will allow for the ready analysis of the average labeling number, distribution, and the region-modification of various labels conjugated to monoclonal antibodies. Such analysis can be applied to study, prepare, and characterize antibody conjugates to ensure the production of high quality immunoreagents.

MATERIAL AND METHODS

Materials. The anti-L−T_4 (**T**, IgG2a), anti-biotin (**B**, IgG2a), and anti-fluorescein isothiocyanate (F1TC) (**F**, IgGI) monoclonal antibodies were obtained from the Abbott cell culture facility (Abbott Laboratories, Abbott Park, IL). Papain (10 mg/mL crystalline suspension from *Carica papaya*) was purchased from Boehringer-Mannheim (Indianapolis, IN). The syntheses of the acridinium active ester (**1**, Figure 1) and the acridinium free acid (2, Figure 1) are described elsewhere (*32*, *33*). Cysteine-HCl, EDTA, sodium hydroxide, formic acid, and guanidine-HCl were products of Sigma (St. Louis, MO). Sodium phosphate was purchased from Fisher Scientific (Fair Lawn, NJ). DMF was purchased from Aldrich Chemical Co. (Milwaukee, WI). DMF was purchased anhydrous and degassed prior to use with N2 gas to remove traces of dimethylamine. Microconcentrators (Microcon-10) were purchased from Millipore Corporation (Bedford, MA).

Preparation of Antibody-Acridinium-9-carboxamide Conjugates. General Procedure. To each antibody (3.0 mg of mAb in 1.4 mL of 100 mM sodium phosphate, 150 mM NaCl, pH 8.0) was added (a) 4, (b) 8, or (c) 16 equiv of the acridinium-9-carboxamide active ester **1** (Figure 1) in DMF (0.2 mL). Upon addition, the solutions were briefly vortexed then allowed to stand for 18 h in the dark. Each reaction was purified by HPLC using a SEC-250-5 gel permeation chromatography column (Bio-Rad, Hercules, CA) eluting with 100 mM sodium phosphate, 150 mM NaC1, 0.1% CHAPS, pH 6.3 (1.0 mL/min) and subsequently stored at 2−8 °C in the dark. Labeled antibody ($R_t \approx 8.3$ min) and unconjugated acridinium-9-carboxamide label ($R_t = 11.1$ min) were readily separated under these conditions.

The concentration of antibody conjugate was determined by UV−vis spectroscopy using the following formula:

$$[\text{conjugate}] = [A_{280} - (A_{369}/4.1)]/\epsilon_{280}$$

where A_{280} and A_{369} are the absorbance readings of the acridinium-9-carboxamide-antibody conjugates at the corresponding wavelengths; 4.1 is the A_{369}/A_{280} of the acid **2**, and ϵ_{280} (210 000 M^{-1} cm^{-1}) is the extinction coefficient of an IgG antibody at 280 nm (*34*). The ratio of acridinium label to antibody (**r**) conjugate was determined by UV−vis spectroscopy using the following formula:

$$r = \frac{A_{369}/\epsilon_{369}}{[A_{280} - (A_{369}/4.1)]/\epsilon_{280}}$$

where ϵ_{369} (14 700 M^{-1} cm^{-1}) is the extinction coefficient of the acridinium **2** at 369 nm.

Papain Digestion of Antibody Conjugates. Papain (10 μL of a 10 mg/mL suspension) was mixed with 90 μL of freshly prepared activation buffer (1 mM EDTA, 10 mM cysteine, and 50 mM sodium phosphate buffer, pH 7.0) and incubated at 37 °C for 10 min. The activated papain solution was added to 100 μL of anti-L−T_4 or anti-biotin conjugate solution (∼0.5 mg/mL) to give a papain/antibody ratio of 0.5% (w/w). The resulting solution was incubated at 37 °C for 2 h. The digestion mixture was desalted via ultrafiltration through a Microcon 10 (MWCO = 10K) and stored at −20 °C for LC/MS analysis. The digestions of the anti-FITC conjugates were performed following the same procedure, except the papain/antibody ratio was adjusted to 1.5% (w/w).

LC/ESI-MS Analysis of Fragments. The papain digests in 1N guanidine-HCl solution (2−5 μL) were injected onto a reversed-phase HPLC column (PLRP-S column, polystyrene/divinylbenzene, 1000 Å, 2.1 × 50 mm, Polymer Laboratories Ltd., Amherst, MA) at a flow rate of 0.1 mL/min. The mobile phases A and B contained 0.1% formic acid/H_2O and 0.1% formic acid/acetonitrile, respectively. A linear gradient elution was performed

from 90 to 10% A over 20 min. Typically, salts eluted at the void volume of the column (~4 min). The column was linked to a electrospray ion source which operated under the following conditions: ion spray voltage = 4800 V, orifice voltage = 50 V, nebulizing gas flow = 1.5 L/min, and TurboProbe jet (350 °C) air flow = 5 L/min. Mass analysis was carried out on a Sciex 100 mass spectrometer (Perkin-Elmer Sciex, Foster City, CA) equipped with a TurboIon spray source. The samples were scanned over m/z 1000−3000 with a total acquisition time of 5.0 s.

Molecular masses and their distributions of the fragments under both HPLC peaks were determined by converting the raw spectra of multiply charged species to the mass domain using the manufacture's deconvolution software (BioMultiview 1.3.1, Perkin-Elmer Sciex, Foster City, CA). The deconvolution mass window was chosen to be appropriate for the mass ranges of the expected antibody or antibody conjugate fragment. For example, for the digestion products of antibody **B** conjugates, mass windows of 25−28.5 kDa and 47−52 kDa were chosen to observe derivatives of the Fc heavy chain and Fab, respectively (see Figure 5). The mass domain was then saved as text files and imported into Grams software for further processing (Galactic Industries Co., Salem, NH). The peak intensity (area) corresponding to the respective acridinium conjugated antibody fragments were integrated and the contribution of each component in the distribution (relative intensity) was computed, assuming that the instrumental response is independent of the number of conjugates attached to the antibody. The average labeling number was then calculated from $\sum nx\%$, where n is the number of acridinium molecules covalently bound to the fragment and $x\%$ is the percent relative intensity of the corresponding mass spectrum peaks. For the calculation of total peak area, peak areas from both protonated molecules $[M + xH]^{x+}$ and sodium adducts $[M + xNa]^{x+}$ were included.

LITERATURE CITED

(1) Koppel, G. A. (1990) Recent advances with monoclonal antibody drug targeting for the treatment of human cancer. *Bioconjugate Chem. 1*, 13−23.

(2) Kanellos, J., Pietersz, G. A., and McKenzie, I. G. C. (1985) Studies of Methotrexate-Monoclonal Antibody Conjugates for Immunotherapy. *J. Natl. Cancer Inst. 75*, 319−329.

(3) Abraham, R., Moller, D., Senter, P., Hellström, I., and Hellström, K. E. (1991) The influence of periodate oxidation on monoclonal antibody avidity and immunoreactivity. *J. Immunol. Methods 144*, 77−86.

(4) Baldwin, R. W., Durrant, L., Embleton, M. J., Garnett, M., Pimm, M. V., Robins, R. A., Hardcastle, J. D., Armitage, N., and Ballantyne, K. (1985) Design and Therapeutic Evaluation of Monoclonal Antibody 791T/36-Methotrexate Conjugates. *Monoclonal Antibodies and Cancer Therapy*, pp 215−231, Alan R. Liss, Inc., New York.

(5) Sashidhar, R. B., Capoor, A. K., and Ramana, D. (1994) Quantitation of epsilon-amino group using amino acids as reference standards by trinitrobenzene sulfonic acid. A simple spectrophotometric method for the estimation of hapten to carrier protein ratio. *J. Immunol. Methods 167*, 121−127.

(6) Riddles, P. W., Blakeley, R. L., and Zerner, B. (1979) Ellman's reagent: 5,5′-dithiobis(2-nitrobenzoic acid)—a re-examination. *Anal. Biochem. 94*, 75−81.

(7) Bennett, K. L., Smith, S. V., Lambrecht, R. M., Truscott, R. J. W., and Sheil, M. M. (1996) Rapid characterization of chemically-modified proteins by electrospray mass spectrometry. *Bioconjugate Chem. 7*, 16−22.

(8) Bennett, K. L., Hick, L. A., Truscott, R. J. W., and Sheil, M. M. (1995) Optimum conditions for electrospray mass spectrometry of a monoclonal antibody. *J. Mass Spectrom. 30*, 769−771.

(9) Siegel, M. M., Tabei, K., Kunz, A., Hollander, I. J., Hamann, P. R., Bell, D. H., Berkenkamp, S., and Hillenkamp, F. (1997) Calicheamicin Derivatives conjugated to monoclonal antibodies: deterimination of loading values and distributions by infrared and UV matrix-assisted laseer desorption/ionization mass sectrometry and lectrospray ionization mass spectrometry. *Anal. Chem. 69*, 2716−2726.

(10) Clark, M. R. (1997) IgG Effector Mechanisms. *Chem. Immunol.*88−110.

(11) Wedemayer, G. J., Patten, P. A., Wang, L. H., Schultz, P. G., and Stevens, R. C. (1997) Structural Insights into the Evolution of an Antibody Combining Site. *Science 276*, 1665−1669.

(12) Milenic, D. E., Esteban, J. M., and Colcher, D. (1989) Comparison of methods for the generation of immunoreactive fragments of a monoclonal antibody (B72.3) reactive with human carinomas. *J. Immunol. Methods 120*, 71−83.

(13) Rousseaux, J., Biserte, G., and Bazin, H. (1980) The differential enzyme sensitivity of rat immunoglobulin G subclasses to papain and pepsin. *Mol. Immunol. 17*, 469−482.

(14) Boguslawski, S. J., Ledden, D. J., and Fredrickson, R. A. (1989) Improved procedure for preparation of $F(ab')_2$ fragments of mouse IgGs by papain digestion. *J. Immunol. Methods 120*, 51−56.

(15) Kurkela, R., Vuolas, L., and Vihko, P. (1988) Preparation of $F(ab')_2$ fragments from monoclonal mouse IgGI suitable for use in radioimaging. *J. Immunol. Methods 110*, 229−236.

(16) Rousseaux, J., Rousseaux-Prevost, R., and Bazin, H. (1983) Optimal Conditions for the Preparation of Fab and $F(ab')_2$ Fragments from Monoclonal IgG of Different Rat IgG Subclasses. *J. Immunol. Methods 64*, 141−146.

(17) Bennett, K. L., Smith, S. V., Truscott, R. J. W., and Sheil, M. M. (1997) Monitoring Papain Digestion of a Monoclonal Antibody by Electrospray Ionization Mass Spectrometry. *Anal. Biochem. 245*, 17−27.

(18) Grebenau, R. C., Goldenberg, D. M., Chang, C. H., Koch, G. A., Gold, D. V., Kunz, A., and Hansen, H. J. (1992) Microheterogeneity of a purified IgG1 Due to asymmetric FAB glycosylation. *Mol. Immunol. 29*, 751−758.

(19) Jiskoot, W., Werken, G. V. D., Martin, J. M. C., Green, B. N., Beuvery, E. C., and Crommelin, D. J. A. (1992) Application of electrospray mass spectrometry (ES-MS) for the analysis of monoclonal antibody Fc subunits. *Pharm. Res. 9*, 945−951.

(20) Ashton, D. S., Beddell, C. R., Cooper, D. J., Craig, S. J., Lines, A. C., Oliver, R. W. A., and Smith, M. A. (1995) Mass Spectrometry of the humanized monoclonal antibody CAMPATH 1H. *Anal. Chem. 67*, 835−842.

(21) Alexander, A. J., and Hughes, D. E. (1995) Monitoring of IgG antibody thermal stability by micellar electrokinetic capillary chromatography and matrix-assisted laser desorption/ionization mass spectrometry. *Anal. Chem. 67*, 3626−3232.

(22) Hirayama, K., Yuji, R., Yamada, N., Kato, K., Arata, Y., and Shimada, I. (1998) Complete and Rapid Peptide and Glycopeptide Mapping of mouse Monoclonal Antibody by LC/MS/MS Using Ion Trap Mass Spectrometry. *Anal. Chem. 70*, 2718−2725.

(23) Lewis, D. A., Guzzetta, A. W., Hancock, W. S., and Costello, M. (1994) Characterization of humanized Anti-TAC, an antibody directed against the interleukin 2 receptor, using electrospray ionization mass spectrometry by direct infusion, LC/MS, and MS/MS. *Anal. Chem. 66*, 585−595.

(24) Robert, G. D., Johnson, W. P., Burman, S., Anumula, K. R., and Carr, S. A. (1995) An Integrated Strategy for Structural Characterization of the Protein and Carbohydrate Components of Monoclonal Antibodies: Application to Anti-Respiratory Syncytial Virus MAb. *Anal. Chem. 67*, 3613−3625.

(25) Feng, R., and Konishi, Y. (1992) Analysis of Antibodies and Other Large Glycoproteins in the Mass Range of 150000−200000 Da by Electrospray Ionization Mass Spectrometry. *Anal. Chem. 64*, 2090−2095.

(26) Hagmann, M.-L., Kionka, C., Schreiner, M., and Schwer, C. (1998) Characterization of the $F(ab')_2$ fragment of a murine monoclonal antibody using capillary isoelectric focusing and

electrospray ionization mass spectrometry. *J. Chromatogr. A 816*, 49−58.
(27) Adamczyk, M., Buko, A., Chen, Y. Y., Fishpaugh, J. R., Gebler, J. C., and Johnson, D. D. (1994) Characterization of protein-hapten conjugates. 1. Matrix-assisted laser desorption ionization mass spectrometry of immuno BSA-hapten conjugates and comparison with other characterization methods. *Bioconjugate Chem. 5*, 631−635.
(28) Adamczyk, M., Gebler, J. C., and Mattingly, P. G. (1996) Characterization of protein-hapten conjugates. 2. Electrospray mass spectrometry of bovine serum albumin-hapten conjugates. *Bioconjugate Chem. 7*, 475−481.
(29) Siegel, M. M. (1996) *Determination of Loading Values and Distributions for Drugs Conjugated to Proteins and Antibodies by MALDI-MS and ESI-MS*. 211−226 ed., Vol. 61, Humana Press Inc., Totowa, NJ.
(30) Straub, K. M., and Levy, M. J. (1994) Characterization of hapten binding to immunoconjugates by electrospray ionization mass spectrometry. *Bioconjugate Chem. 5*, 194−198.
(31) Liu, J., Abid, S., and Lee, M. S. (1995) Analysis of monoclonal antibody chimeric BR96-doxorubicin immunoconjugate by sodium dodecyl sulfate-capillary gel electrophoresis with ultraviolet and laser-induced fluorescence detection. *Anal. Biochem. 229*, 221−228.
(32) Adamczyk, M., Fishpaugh, J., Mattingly, P. G., and Shreder, K. (1998) Tracermer (TM) signal generators: An arborescent approach to the incorporation of multiple chemiluminescent labels. *Bioorg. Med. Chem. Lett. 8*, 3595−3598.
(33) Adamczyk, M., Chen, Y.-Y., Mattingly, P. G., and Pan, Y. (1998) Neopentyl 3-triflyloxypropanesulfonate. A reactive sulfopropylation reagent for the preparation of chemiluminescent labels. *J. Org. Chem. 63*, 5636−5639.
(34) Mäkalä, O., and Seppälä, I. J. T. (1978) Immunochemistry. In *Handbook of Experimental Immunology* (D. M. Weir, Ed.) Blackwell Scientific Publications, Palo Alto, CA.

BC990181Y

In Vitro Interleukin-3 Binding to Leukemia Cells Predicts Cytotoxicity of a Diphtheria Toxin/IL-3 Fusion Protein

R. L. Alexander,[†] G. L. Kucera,[‡] B. Klein,[§] and A. E. Frankel*

Department of Physiology and Pharmacology, Department of Internal Medicine, Section on Hematology/Oncology, and Department of Cancer Biology, Wake Forest University School of Medicine, Wake Forest, North Carolina 27157, and Monsanto Company, St. Louis, Missouri. Received January 28, 2000; Revised Manuscript Received April 21, 2000

Patients with acute myeloid leukemia frequently develop chemotherapy resistant blasts. To overcome multidrug resistance, a diphtheria toxin fusion protein (DTIL3) was engineered by fusing the catalytic and translocation domains of diphtheria toxin (DT) to human interleukin-3 (IL-3). However, when blasts were isolated from patients and tested for colony growth inhibition by DTIL3, only a third of the samples showed sensitivity to the fusion protein. Prior to clinical development, we need to be able to identify which patients are likely to respond to therapy with DTIL3. In this report, we compared the inhibition of thymidine incorporation in human leukemia cell lines by DTIL3 to the IL-3 receptor number and affinity. We found DTIL3 was cytotoxic to four of the eight cell lines tested with half-maximal inhibition of thymidine incorporation (IC_{50}) from 1 to 50 pM. The IL-3 receptor density for these cell lines ranged from 0 to 2635 receptors per cell. The dissociation constant for an IL-3 high-affinity receptor agonist was 0.5 nM for cell lines with receptors. We found a correlation for the cell lines between the presence of high-affinity IL-3 receptors and sensitivity to DTIL3 ($p = 0.03$). These results suggest the variability in sensitivity of patient leukemic progenitors to DTIL3 may be due in part to the presence or absence of high-affinity IL-3 receptors.

INTRODUCTION

Acute myelogenous leukemia (AML), the most common acute leukemia in adults, is associated with a 70% complete remission (CR) rate after standard induction chemotherapy regimens (*1*). Intensive postremission therapy in combination with allogeneic bone marrow transplantation offers the possibility of cure to some of these individuals; however, fewer than 20% of all patients with the diagnosis of AML will have prolonged disease-free survival (*2*). Resistance to standard chemotherapeutic drugs is an important cause of the relapsed, refractory leukemia to which most patients succumb (*3*).

A number of identified drug resistance phenotypes are due to overexpression of specific proteins, and the concentration of these molecules in leukemic blasts has been correlated with response to cytotoxic chemotherapy (*4*−*8*). In several cases, the resistance protein transports out of the target cell or inactivates xenobiotics such as anthracyclines. Pharmacologic reversal of MDR-1-related anthracycline resistance has, to date, been associated with toxicities to marrow, gastrointestinal tract, and the central nervous system, as well as altered anthracycline pharmacodynamics and minimal improvements in response rate or disease-free survival (*9*). An antibody-targeted cytotoxic drug, anti-CD33-calicheamicin, was recently tested in a clinical trial and had reduced side effects (*10*). However, most patients rapidly developed resistance due to active drug efflux. Thus, novel agents that are cytotoxic to leukemic blasts and bypass multidrug resistance phenotypes are urgently needed.

One such class of therapeutics is protein toxins covalently linked to peptide ligands. The ligand directs the molecule to the surface of specific cell types. The toxin moiety then enters the cell and catalytically inactivates protein synthesis. Constructed protein toxins that target AML blasts include the following: anti-CD33-blocked ricin, anti-CD33-gelonin, diphtheria toxin-interleukin-3 (IL-3), anti-transferrin receptor-ricin A chain, granulocyte-macrophage colony-stimulating factor (GM-CSF)-ricin, GM-CSF−Pseudomonas exotoxin, and diphtheria toxin-GM-CSF (*11*−*21*). Each of these reagents inhibited protein synthesis by 50% (IC_{50}) in cell lines in a dose- and time-dependent manner. The least active drugs were anti-transferrin receptor-ricin A chain, GM-CSF-ricin, and GM-CSF−Pseudomonas exotoxin, with IC_{50}s of approximately 3×10^{-10} mol/L. Anti-CD33-blocked ricin and anti-CD33-gelonin had intermediate IC_{50}s of 1×10^{-10} mol/L, and diphtheria toxin-IL3 and diphtheria toxin-GM-CSF produced IC_{50}s of 3×10^{-11} mol/L. The variability in sensitivity that AML cell lines show to targeted toxins has been attributed to premature intracellular routing of ricin, ricin A chain, gelonin, and Pseudomonas exotoxin conjugates to lysosomes. In contrast, the diphtheria toxin fusion proteins are able to translocate to the cytosol from a prelysosomal intracellular compartment. Specificity of cell kill has been demonstrated for several of these conjugates, including anti-CD33-blocked ricin, anti-CD33-gelonin, diphtheria toxin-IL3, and diphtheria toxin-GM-CSF. Reductions in normal human or murine marrow progenitors were seen after toxin conjugate exposure, but, in each case, the effect was much smaller than that seen with AML progenitors (*17*, *19*, *20*).

A critical question is whether these chimeric proteins, which require functional cell surface receptors, intact intracellular routing pathways, and sensitive protein

* To whom correspondence should be addressed, Department of Cancer Biology.
[†] Department of Physiology and Pharmacology.
[‡] Department of Internal Medicine.
[§] Monsanto Company.

10.1021/bc000009q CCC: $19.00 © 2000 American Chemical Society
Published on Web 06/16/2000

synthesis machinery for intoxication, will kill malignant cells isolated directly from patients with leukemia. With several previously studied lymphoid malignancy-targeted toxins, including anti-CD5-ricin A chain and anti-CD25 (sFv)-Pseudomonas exotoxin, fresh leukemia cells were much less sensitive than cell lines (*22*, *23*). Cytotoxicity was enhanced for anti-CD5-ricin A chain by adding the monocarboxylic acid ionophore, monensin, and for anti-CD25-Pseudomonas exotoxin by prolonged incubation. Both of these interventions improve intracellular toxin transport to compartments optimal for translocation to the cytosol. Few similar experiments have been conducted with toxins targeted toward myeloid leukemia.

Interleukin-3 (IL-3) is a cytokine which supports the proliferation and terminal differentiation of multipotential and committed myeloid and lymphoid progenitors (*24*) but does not act on the most primitive hematopoietic stem cells (*25*). The IL3 receptor (IL3R) has been demonstrated by ^{125}I-labeled IL3 binding to human myeloid leukemic cells (*26*). Further, acute phase CML blasts proliferate in response to exogenous IL3 (*27*, *28*). In fact, CML progenitors have been reported to overexpress both IL3 and IL3R, yielding an autocrine loop that stimulates proliferation (*29*). This also occurs in certain autocrine transformed mouse leukemia cell lines (*30*). The IL3R is composed of α and β subunits (*31*). The binding of IL3 to its receptor causes rapid internalization of the ligand−receptor complex (*32*). Thus, based on the expression of IL3 receptors on blast cells isolated from patients with acute phase CML and AML and its rapid receptor-mediated endocytosis on receptor coupling, we chose to fuse IL3 to the catalytic and translocation domains of diphtheria toxin (DT).

To perform a comprehensive study of the sensitivity of diphtheria toxin-IL3, we investigated a series of cell lines that exhibited a range of responses to the toxin. We determined the IL3 receptor density and K_d for high-affinity IL-3 receptor agonist binding from each of the cell lines. Our data supports our hypothesis that cell lines that were responsive to the immunotoxin conjugate had far greater receptor density than cell lines that were less responsive to the treatment.

EXPERIMENTAL PROCEDURES

Cells. HL-60, CEM, and TK6 cell lines were suspended in RPMI 1640 media with L-glutamine and 10% fetal bovine serum (FBS). TF-1/GFP ΔRaf-1ER, TF-1, and AML193 cell lines were maintained in RPMI 1640 media with L-glutamine and 10% FBS, 1% nonessential amino acids (GIBCO-BRL, Grand Island, NY), 1% sodium pyruvate (GIBCO), 1% penicillin-streptomycin (GIBCO), and 50 ng/mL GM-CSF (Immunex, Seattle, WA). P815 cells were maintained in RPMI 1640 with L-glutamine and 10% FBS, 1% nonessential amino acids, 1% HEPES, 1% penicillin-streptomycin, 1% sodium pyruvate, and 0.1% mercaptoethanol. Cells were maintained in the log phase of cell growth in a humidified atmosphere of 5% CO_2-95% air at 37 °C. P815 Cells were kindly provided by Dr. Martha Alexander-Miller's Lab (WFUBMC, Department of Microbiology). TK6 cells were kindly provided by Dr. Steve Akman's Lab (WFUBMC, Section on Hematology/Oncology). TF-1 and TF-1/GFP ΔRaf-1ER cell lines were provided by Dr. James A. McCubrey (East Carolina University, Department of Microbiology).

Radioactively Labeled IL-3. A high-affinity IL-3 receptor ligand, SC-65461 (Searle Laboratories, Monsanto Company), with a 14 amino acid N-terminal extension containing two Tyr residues was used (*33*). The SC-65461 (5 μg) was iodinated using Iodogen (Pierce; Rockford, IL) and Na[^{125}I] (Amersham Pharmacia Biotech; Piscataway, NJ) as previously described (*34*) with a specific activity of 90.5 μCi/μg.

IL-3 Receptor Density. Aliquots of washed 1−6 × 10^6 cells in RPMI 1640 plus 2.5% bovine serum albumin, 20 mmol/L HEPES and 0.2% sodium azide were mixed with varying amounts of ^{125}I-labeled SC-65461 with or without excess (2 μg) unlabeled human IL-3 (SC-50341, Searle Laboratories, Monsanto Company) in a total volume of 170 μL. Cells were incubated at 37 °C for 40 min and then layered over a 200 μL of oil phthalate mixture (1 part dioctylphthalate and 1.5 parts dibutylphthalate, Aldrich, Milwaukee, WI). After centrifugation at 14 000 rpm for 2 min in a microfuge at room temperature, both pellets and supernatants were separated and radioactivity was counted in a *Packard Auto-Gamma 5650* gamma counter gated for ^{125}I with 50% counting efficiency. Background cpm was calculated by linear extrapolation from incubations with excess cold native IL-3 (SC-50341). Scatchard plots of specific bound/free versus specific bound cpm were made using *GraphPad Prism*, GraphPad Software, Inc., and *Microsoft Excel*, Microsoft Corporation. Linear regression and nonlinear regression analysis were calculated, and receptor densities of zero were recorded on the absence of specific ^{125}I binding or negative values of K_d. Radiolabeled saturation K_d (measured with the varying amounts of [^{125}I]SC-65461) was calculated on the concentration of SC-65461 giving half-maximal binding.

EC_{50} Analysis (Cold Saturation K_d). Aliquots of washed (1−6) × 10^6 cells in media were mixed with increasing amounts of unlabeled IL-3 (SC-50341), and a constant amount of ^{125}I-labeled SC-65461 in a total volume of 170 μL. Cells were incubated and counted (as above). Background cpm was calculated by linear extrapolation from incubations with excess unlabeled IL-3 (SC-50341). *GraphPad Prism*, GraphPad Software, Inc., was used for the nonlinear regression analysis. The concentration of unlabeled IL-3 reducing the [^{125}I]SC-50341 binding by 50% was the EC_{50} or unlabeled saturation K_d.

Cytotoxicity Assay. For thymidine incorporation inhibition assays, 5 × 10^4 cells were incubated in 100 μL of RPMI1640 with L-glutamine, 15% FBS, and 1% penicillin-streptomycin in Costar 96 well flat-bottomed plates. Twelve different concentrations of DTLIL3 were added to each column of the 96-well plate in 50 μL of media, and the cells were maintained at 37 °C/5% CO_2 for 48 h. Then 1 μCi [^{3}H]thymidine (NEN DuPont, Boston, MA) in 50 μL medium was added to each well, and incubation continued for an additional 18 h at 37 °C/5% CO_2. Cells were then harvested by a Skatron Cell Harvestor (Skatron Instruments, Lier, Norway) onto glass fiber mats and ^{3}H cpm were counted in an LKB liquid scintillation counter gated for ^{3}H. The calculated IC_{50}s were the concentrations of toxin which inhibited thymidine incorporation by 50% compared to control wells.

RESULTS

IL-3 Receptor Density. Because the IL-3 receptor population includes both high-affinity α and β chain complexes and low-affinity receptors consisting of the α subunit only, we analyzed the presence of both types of receptor complex on various cell lines. An example of one of the Scatchard plots is shown in Figure 1. Increasing amounts of radiolabeled high-affinity IL-3 receptor agonist (SC-65461) were added to saturate the binding sites on each cell line, and the Scatchard analysis of the first

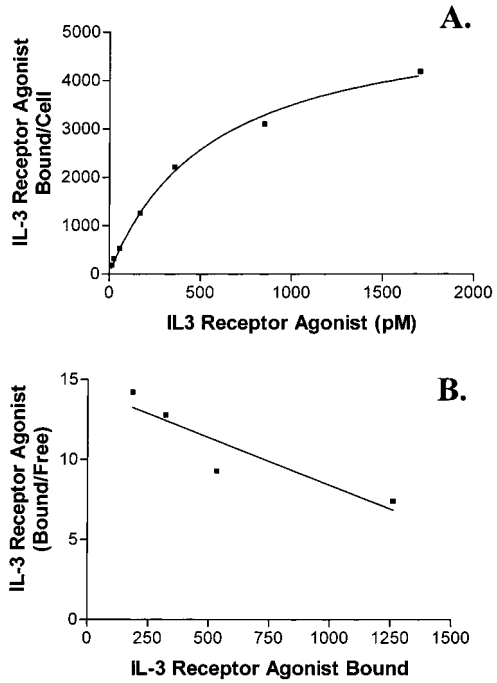

Figure 1. Saturation curve and scatchard analysis. Panel A shows a representative radiolabeled saturation curve of a receptor positive cell line (TF-1). The K_d value is in picomolar, and the plot represents the saturation of the binding sites on the TF-1 cell line. Panel B shows the Scatchard analysis of the first four data points from the saturation curve in panel A. The first four points were used because they represent the high-affinity receptor binding sites. The *x*-intercept is the receptor density per cell.

four data points produced an *x*-intercept value which was considered the receptor density of that particular cell line. The value of the *x*-intercept was considered to be zero if the slope of the Scatchard plot was positive, which indicated no detectable high-affinity receptors/cell. Certain cell lines such as TK6, P815, K562, and CEM cells showed little or no high-affinity receptors present. All other cell lines had detectable receptor densities with an average K_d of 563 ± 34.2 pM ($n = 14$). It should be noted that this K_d reflects the dissociation constant for the high-affinity IL-3 receptor agonist not the native IL-3 receptor. The receptor densities were TF-1/GFP ΔRaf-1ER, 2636 ± 774 receptors ($n = 4$); TF-1, 2384 ± 101 receptors ($n = 4$); AML193, 1863 ± 279 receptors ($n = 3$); HL-60, 703 ± 329 receptors ($n = 3$); TK6, 154 ± 52 receptors ($n = 4$); P815, 0.0 ± 0.0 receptors ($n = 3$); K562, 1 ± 1 receptor ($n = 3$); and CEM, 3 ± 3 receptors ($n = 3$). These data are represented in the bar graph in Figure 2.

IL-3 Binding Affinity. Two different nonequivalent measurements were made of IL-3 receptor binding affinity. In one case, we measured the binding affinity of the high-affinity receptor agonist SC-65461 using the radiolabeled saturation method. This was applied to all eight cell lines. The binding affinities were 563 ± 34.2 pM ($n = 14$) in the four cell lines tested. Four of the eight cell lines showed the presence of radiolabeled saturation K_ds of greater than 100 fold over TF-1 and were identified as receptor negative cell lines. Figure 3 illustrates the receptor density of each cell line. TF-1/GFP ΔRaf-1ER, TF-1, AML193, and HL-60 lines demonstrated greater receptor density than the other four cell lines TK6, P815, K562, and CEM.

To confirm these results, we performed a second binding assay using the unlabeled saturation method with human IL-3 (SC-50341) and [^{125}I]SC-65461 on a

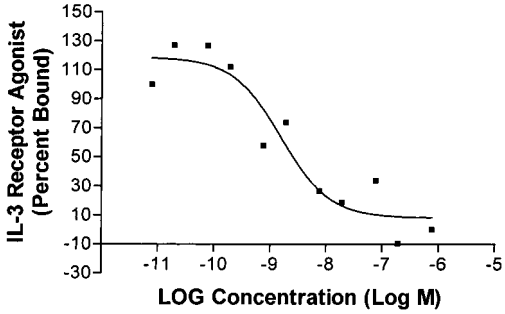

Figure 2. Unlabeled IL-3 (SC-65461) competition assay. This plot represents competition of unlabeled IL-3 and radioactively labeled [^{125}I]IL-3 receptor agonist (SC-65461) for IL-3 receptors on TF-1 cells. Increasing amounts of unlabeled SC-65461 were added to a constant amount of radiolabeled IL-3 in order to measure the K_d of IL-3. The percent bound of radiolabeled SC-65461 is plotted against the log of the concentration of unlabeled IL-3. $EC_{50} = 1.567 \times 10^{-9}$, $R^2 = 0.9038$.

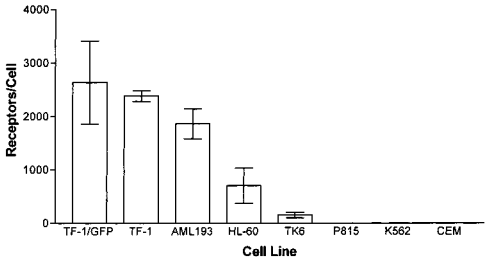

Figure 3. Receptor density of various cell lines. Receptor densities of the various cell lines tested are shown. The error bars represent the mean ± SEM, $n = 3$.

single cell line, TF-1. We found an EC_{50} or unlabeled saturation K_d equal to 1500 pM, which was 3-fold higher than the K_d seen with SC-65461.

The sensitivity of cell lines to DTIL3 was assayed by measuring the concentration of DTIL3 required to inhibit thymidine incorporation by 50% (IC_{50}). The IC_{50}s for thymidine incorporation inhibition with the eight cell lines were TF-1/GFP ΔRaf-1ER, 11 pM; TF-1, 17 pM; AML193, 28 pM; HL-60, 119 pM; TK6, >1400 pM; P815, >1400 pM; K562, >1400 pM; and CEM, >1400 pM (*35*). Receptor positive cell lines proved to have lower cytotoxicity IC_{50} values indicating greater sensitivity. Receptor negative cell lines had much higher cytotoxicity IC_{50} values and were less sensitive.

DISCUSSION

Our data previously showed that the DTIL-3 was toxic to several cell lines including TF-1, AML193, and HL-60 cells and nontoxic to TK6, K562, CEM, and P815 cell lines (IC_{50} > 1400 pM) (*35*). We were able to closely reproduce these sensitivities in this study. We wanted to determine if there was a correlation between cytotoxic IC_{50} values and high-affinity IL-3 receptor density on the previously tested cell lines. We hypothesized that the drug responsive cell lines would have a much greater receptor density than those cell lines that did not respond to the fusion toxin. To that end, we performed a series of saturation binding assays using ^{125}I-labeled IL-3 receptor agonist in order to measure the receptor density of the various cell lines.

The results of the binding assays supported our hypothesis. Cell lines that responded to the drug had far greater receptor density than those cell lines that did not respond to the fusion toxin. TF-1/GFP ΔRaf-1ER, TF-1, AML193, and HL-60 cell lines exhibited a large number of high-affinity receptors and were sensitive to DTIL3.

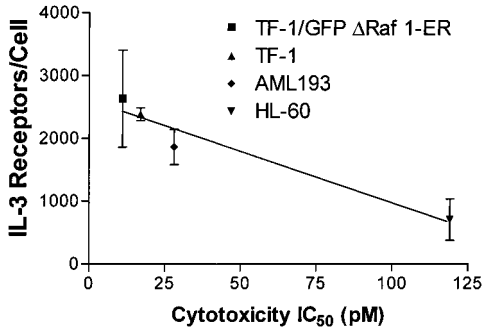

Figure 4. Cytotoxicity IC_{50} vs receptor density plot. the data shown represent a linear regression ($R^2 = 0.9411$) of the cytotoxicity IC_{50} values plotted against the receptor densities of the receptor positive cell lines (TF-1/GFP ΔRaf-1ER, TF-1, AML193, and HL-60). The points represent the mean ± SEM, $n = 3$. P value = 0.0299.

In contrast, CEM, K562, and P815 cell lines showed no binding of radiolabeled IL3 receptor agonist. TK6 cells exhibited a small number of receptors, but this number is in no way comparable to the receptor density of the receptor positive cell lines. These cell lines were insensitive to DTIL3. It is interesting to note that the higher the IC_{50} value, the lower the receptor density of the cell line, whereas a lower IC_{50} value gives a higher receptor density value. This information is of value because the correlation between IC_{50} value and receptor density can now be used to predict cytotoxicity in patients' leukemic blasts.

This novel activating agent would be of great benefit in patients who show multidrug resistance (MDR) to various types of leukemic chemotherapy. We can now measure IL-3 receptor density and use this as a predicting mechanism for which patients will or will not respond to the fusion toxin. Figure 4 shows a plot of receptor density and cytotoxicity IC_{50} values. The linear regression line shows a significant p value equal to 0.03, indicating a relationship between the cell line receptor density and cytotoxicity IC_{50}. Therefore, there is a direct correlation between the receptor density and IC_{50} value. Currently, we are investigating the relationship between IL-3 receptor density and clonogenicity on fresh leukemia patient blasts. There does seem to be a direct relationship between the patients' blasts colony inhibition to DTIL3 and the number of IL-3 receptors (data not shown). We plan to continue this line of testing to determine an accurate correlation between IL-3 receptor density and leukemic blast cell cytotoxicity to the DT-IL3 fusion protein.

ACKNOWLEDGMENT

This research was funded by support received from the American Cancer Society (IRG-93-035-6 to G.K.), the Leukemia Society of America (LSA6114 to A.F.), and the NIH (R01-CA-76178 to A.F.). The authors acknowledge the Monsanto Company (St. Louis, MO) and B.K. for their help in providing IL-3 and the Comprehensive Cancer Center-WFU Core Laboratories funded by NCI SCOR Grant CA12197: Tissue Culture Core Lab. Special thanks are extended to Scott Cramer, Ph.D., Jason Ramage, and Gilda Saluta.

LITERATURE CITED

(1) Schiffer, C. (1997) Acute myeloid leukemia in adults. In *Cancer Medicine* (J. Holland, E. Frie, R. Bast, D. Kufe, D. Marton, and R. Weichselbaum, Eds.) p 2617, Lea & Febiger, Philadelphia, PA.

(2) Rohatiner, A., and Lister, T. A. (1996) In *Acute myeloid leukemia in adults*. (E. S. Henderson, T. A. Lister, and M. F. Greaves, Eds.) p 479, Saunders, Philadelphia, PA.

(3) List, A. F. (1996) Role of multidrug resistance and its pharmacological modulation in acute myeloid leukemia. *Leukemia 10*, 937−942.

(4) Pirker, R., Wallner, J., Geissler, K., Linkesch, W., Haas, O. A., Bettelheim, P., Hopfner, M., Scherrer, R., Valent, P., and Havelec, L. (1991) MDR1 gene expression and treatment outcome in acute myeloid leukemia. *J. Natl. Cancer Inst. 83*, 708−712.

(5) Russo, D., Marie, J. P., Zhou, D. C., Faussat, A. M., Melli, C., Damiani, D., Michelutti, A., Michieli, M., Fanin, R., and Baccarani, M. (1994) Evaluation of the clinical relevance of the anionic glutathione-s-transferase (GST pi) and multidrug resistance (mdr-1) gene coexpression in leukemias and lymphomas. *Leuk. Lymphoma 15*, 453−468.

(6) Maung, Z. T., MacLean, F. R., Reid, M. M., Pearson, A. D., Proctor, S. J., Hamilton, P. J., and Hall, A. G. (1994) The relationship between bcl-2 expression and response to chemotherapy in acute leukaemia. *Br. J. Haematol. 88*, 105−109.

(7) List, A. F., Spier, C. S., Grogan, T. M., Johnson, C., Roe, D. J., Greer, J. P., Wolff, S. N., Broxterman, H. J., Scheffer, G. L., Scheper, R. J., and Dalton, W. S. (1996) Overexpression of the major vault transporter protein lung-resistance protein predicts treatment outcome in acute myeloid leukemia. *Blood 87*, 2464−2469.

(8) Leith, C. P., Kopecky, K. J., Godwin, J., McConnell, T., Slovak, M. L., Chen, I. M., Head, D. R., Appelbaum, F. R., and Willman, C. L. (1997) Acute myeloid leukemia in the elderly: assessment of multidrug resistance (MDR1) and cytogenetics distinguishes biologic subgroups with remarkably distinct responses to standard chemotherapy. A Southwest Oncology Group study. *Blood 89*, 3323−3329.

(9) Solary, E., Witz, B., Caillot, D., Moreau, P., Desablens, B., Cahn, J. Y., Sadoun, Pignon, B., Berthou, C., Maloisel, F., Guyotat, D., Casassus, P., Ifrah, N., Lamy, Y., Audhuy, B., Colombat, P., and Harousseau, J. L. (1996) Combination of quinine as a potential reversing agent with mitoxantrone and cytarabine for the treatment of acute leukemias: a randomized multicenter study. *Blood 88*, 1198−1205.

(10) Sievers, E. L., Appelbaum, F. R., Spielberger, R. T., Forman, S. J., Flowers, D., Smith, FO, Shannon-Dorcy, K., Berger, M. S., and Bernstein, I. D. (1999) Selective ablation of acute myeloid leukemia using antibody-targeted chemotherapy: a phase I study of an anti-CD33 calicheamicin immunoconjugate. *Blood 93*, 3678−3684.

(11) Roy, D. C., Griffin, J. D., Belvin, M., Blattler, W. A., Lambert, J. M., and Ritz, J. (1991) Anti-MY9-blocked-ricin: an immunotoxin for selective targeting of acute myeloid leukemia cells. *Blood 77*, 2404−2412.

(12) McGraw, K. J., Rosenblum, M. G., Cheung, L., and Scheinberg, D. A. (1994) Characterization of murine and humanized anti-CD33, gelonin immunotoxins reactive against myeloid leukemias. *Cancer Immunol. Immunother. 39*, 367−374.

(13) Xu, Y., Xu, Q., Rosenblum, M. G., and Scheinberg, D. A. (1996) Antileukemic activity of recombinant humanized M195-gelonin immunotoxin in nude mice. *Leukemia 10*, 321−326.

(14) Engert, A., Brown, A., and Thorpe, P. (1991) Resistance of myeloid leukaemia cell lines to ricin A-chain immunotoxins. *Leuk. Res. 15*, 1079−1086.

(15) Frankel, A. E., Hall, P. D., Burbage, C., Vesely, J., Willingham, M., Bhalla, K., and Kreitman, R. J. (1997) Modulation of the apoptotic response of human myeloid leukemia cells to a diphtheria toxin granulocyte-macrophage colony-stimulating factor fusion protein. *Blood 90*, 3654−3661.

(16) Perentesis, J. P., Waddick, K. G., Bendel, A. E., Shao, Y., Warman, B. E., Chandan-Langlie, M., and Uckun, F. M. (1997) Induction of apoptosis in multidrug-resistant and radiation-resistant acute myeloid leukemia cells by a recombinant fusion toxin directed against the human granulocyte macrophage colony-stimulating factor receptor. *Clin. Cancer Res. 3*, 347−355.

(17) Kreitman, R. J., and Pastan, I. (1997) Recombinant toxins containing human granulocyte-macrophage colony-stimulating factor and either pseudomonas exotoxin or diphtheria toxin kill gastrointestinal cancer and leukemia cells. *Blood 90*, 252−259.

(18) Chan, C. H., Blazar, B. R., Greenfield, L., Kreitman, R. J., and Vallera, D. A. (1996) Reactivity of murine cytokine fusion toxin, diphtheria toxin390-murine interleukin-3 (DT390-mIL-3), with bone marrow progenitor cells. *Blood 88*, 1445−1456.

(19) Chan, C. H., Blazar, B. R., Eide, C. R., Kreitman, R. J., and Vallera, D. A. (1995) A murine cytokine fusion toxin specifically targeting the murine granulocyte-macrophage colony-stimulating factor (GM-CSF) receptor on normal committed bone marrow progenitor cells and GM-CSF-dependent tumor cells. *Blood 86*, 2732−2740.

(20) Bendel, A. E., Shao, Y., Davies, S. M., Warman, B., Yang, C. H., Waddick, K. G., Uckun, F. M., and Perentesis, J. P. (1997) A recombinant fusion toxin targeted to the granulocyte-macrophage colony-stimulating factor receptor. *Leuk. Lymphoma 25*, 257−270.

(21) Perentesis, J. P., Bendel, A. E., Shao, Y., Warman, B., Davies, S. M., Yang, C. H., Chandan-Langlie, M., Waddick, K. G., and Uckun, F. M. (1997) Granulocyte-macrophage colony-stimulating factor receptor-targeted therapy of chemotherapy- and radiation-resistant human myeloid leukemias. *Leuk. Lymphoma 25*, 247−256.

(22) Hertler, A. A., Schlossman, D. M., Borowitz, M. J., Blythman, H. E., Casellas, P., and Frankel, A. E. (1989) An anti-CD5 immunotoxin for chronic lymphocytic leukemia: enhancement of cytotoxicity with human serum albumin-monensin. *Int. J. Cancer 43*, 215−219.

(23) Kreitman, R. J., Chaudhary, V. K., Waldmann, T., Willingham, M. C., FitzGerald, D. J., and Pastan, I. (1990) The recombinant immunotoxin anti-Tac(Fv)-Pseudomonas exotoxin 40 is cytotoxic toward peripheral blood malignant cells from patients with adult T-cell leukemia. *Proc. Natl. Acad. Sci. U.S.A. 87*, 8291−8295.

(24) Suda, T., Suda, J., Ogawa, M., and Ihle, J. N. (1985) Permissive role of interleukin 3 (IL-3) in proliferation and differentiation of multipotential hemopoietic progenitors in culture. *J. Cell. Physiol. 124*, 182−190.

(25) Ogata, H., Taniguchi, S., Inaba, M., Sugawara, M., Ohta, Y., Inaba, K., Mori, K. J., and Ikehara, S. (1992) Separation of hematopoietic stem cells into two populations and their characterization. *Blood 80*, 91−95.

(26) Park, L. S., Waldron, P. E., Friend, D., Sassenfeld, H. M., Price, V., Anderson, D., Cosman, D., Andrews, R. G., Bernstein, I. D., and Urdal, D. L. (1989) Interleukin-3, GM-CSF, and G-CSF receptor expression on cell lines and primary leukemia cells: receptor heterogeneity and relationship to growth factor responsiveness. *Blood 74*, 56−65.

(27) Miyauchi, J., Kelleher, C. A., Wong, G. G., Yang, Y. C., Clark, S. C., Minkin, S., Minden, M. D., and McCulloch, E. A. (1988) The effects of combinations of the recombinant growth factors GM-CSF, G-CSF, IL-3, and CSF-1 on leukemic blast cells in suspension culture. *Leukemia 2*, 382−387.

(28) Ailles, L. E., Gerhard, B., and Hogge, D. E. (1997) Detection and characterization of primitive malignant and normal progenitors in patients with acute myelogenous leukemia using long-term coculture with supportive feeder layers and cytokines. *Blood 90*, 2555−2564.

(29) Jian X, Lopez A, Holyoake T, Eaves A, and Eaves C. (1999) Autocrine production and action of IL-3 and GM-CSF in chronic myeloid leukemia. *Blood* (in press).

(30) Steelman, L. S., Algate, P. A., Blalock, W. L., Wang, X. Y., Prevost, K. D., Hoyle, P. E., and McCubrey, J. A. (1996) Oncogenic effects of overexpression of the interleukin-3 receptor on hematopoietic cells. *Leukemia 10*, 528−542.

(31) Hara, T., and Miyajima, A. (1992) Two distinct functional high affinity receptors for mouse interleukin-3 (IL-3). *EMBO J. 11*, 1875−1884.

(32) Nicola, N. A., Peterson, L., Hilton, D. J., and Metcalf, D. (1988) Cellular processing of murine colony-stimulating factor (Multi-CSF, GM-CSF, G-CSF) receptors by normal hemopoietic cells and cell lines. *Growth Factors 1*, 41−49.

(33) Thomas, J. W., Baum, C. M., Hood, W. F., Klein, B., Monahan, J. B., Paik, K., Staten, N., Abrams, M., and McKearn, J. P. (1995) Potent interleukin 3 receptor agonist with selectively enhanced hematopoietic activity relative to recombinant human interleukin 3. *Proc. Natl. Acad. Sci. U.S.A. 92*, 3779−3783.

(34) Cramer, S. D., Barnard, R., Engbers, C., Ogren, L., and Talamantes, F. (1992) Expression of the growth hormone receptor and growth hormone-binding protein during pregnancy in the mouse. *Endocrinology 131*, 876−882.

(35) Frankel, A., McCubrey, J. A., Miller, M., Delatte, S., Ramage, J., Kiser, M., Kucera, G. L., Alexander, R. L., Beran, M., Tagge, E. P., Kreitman, R. J., and Hogge, D. E. (2000) Diphtheria toxin fused to human interleukin-3 is toxic from patients with myeloid leukemias. *Leukemia 14*, 576−585.

BC000009Q

Biotin Reagents for Antibody Pretargeting. 4. Selection of Biotin Conjugates for in Vivo Application Based on Their Dissociation Rate from Avidin and Streptavidin

D. Scott Wilbur,* Ming-Kuan Chyan, Pradip M. Pathare, Donald K. Hamlin, Milah B. Frownfelter, and Brian B. Kegley

Department of Radiation Oncology, University of Washington, 2121 North 35th Street, Seattle, Washington 98195. Received March 6, 2000; Revised Manuscript Received May 10, 2000

An investigation was conducted to determine the affect of structural variation of biotin conjugates on their dissociation rates from Av and SAv. This information was sought to help identify optimal biotin derivatives for in vivo applications. Fifteen biotin derivatives were conjugated with a cyanocobalamin (CN−Cbl) derivative for evaluation of their "relative" dissociation rates by size exclusion HPLC analysis. Two biotin-CN−Cbl conjugates, one containing unaltered biotin and the other containing iminobiotin, were prepared as reference compounds for comparison purposes. The first structural variations studied involved modification of the biotinamide bond with a *N*-methyl moiety (i.e., sarcosine conjugate), lengthening the valeric acid side chain by a methylene unit (i.e., homobiotin), and replacing the biotinamide bond with thiourea bonds in two conjugates. The rate of dissociation of the biotin-CN−Cbl derivative from Av and SAv was significantly increased for biotin derivatives containing those structural features. Nine additional biotin conjugates were obtained by coupling amino acids or functional group protected amino acids to the biotin moiety. In the conjugates, the biotin moiety and biotinamide bond were not altered, but substituents of various sizes were introduced α to the biotinamide bond. The results obtained from HPLC analyses indicated that the rate of dissociation from Av or SAv was not affected by small substituents α to the biotinamide (e.g., methyl, hydroxymethyl, and carboxylate groups), but was significantly increased when larger functional groups were present. On the basis of the results obtained, it appears that biotin conjugates which retain an unmodified biotin moiety and have a linker molecule conjugated to it that has a small functional group (e.g., hydroxymethylene or carboxylate) α to the biotinamide bond are excellent candidates for in vivo applications. These structural features are obtained in the biotin amino acid conjugates: biotin-serine, biotin-aspartate, biotin-lysine, and biotin-cysteine. Importantly, these biotin derivatives can be readily conjugated with other molecules for specific in vivo applications. In our studies, these derivatives will be used in the design of new biotin conjugates to carry radionuclides for cancer therapy using the pretargeting approach.

INTRODUCTION

The very high binding affinities of biotin with the proteins avidin (*1*) and streptavidin (*2*) have made combinations of these reagents of particular interest to investigators developing chemical assays for a large variety of applications (*3*−*6*). Most of the assays that have been developed, or are under development, are conducted in vitro. However, some applications are being developed which utilize the high affinity of these chemicals for selective binding in vivo. One example of an in vivo application is an antibody-based multistep approach to delivering therapeutic radionuclides to cancer cells in patients, termed "pretargeting" (*7*−*17*). In the pretargeting studies, monoclonal antibody (mAb)[1] conjugates, streptavidin (SAv) and/or avidin (Av), and biotin conjugates are being evaluated in various combinations to maximize the amount of radionuclide delivered to cancer cells while minimizing the radiation dose to nontarget tissues in patients. Our group is developing new reagents that are optimized for use in the pretargeting approach to cancer therapy in patients. As part of that reagent development, we have focused an effort on determining which design factors make biotin conjugates optimal for in vivo use.

In our assessment, one of the most important design factors for biotin derivatives used in Targeted Radiotherapy is the requirement that the radionuclides bound to cancer cells be retained on those cells during the period of radioactive decay. In the pretargeting approach, retention of a radiolabeled biotin derivative on cancer cells is dependent on the dissociation rate of the mAb-SAv conjugate from its target antigen and on the dissociation rate of the biotin derivative from the mAb-SAv conjugate. The rate of dissociation of the biotin derivative containing the radionuclide is particularly important in vivo as endogenous biotin is always present (*18*−*20*). Administration of a large excess of avidin or streptavidin reagents can deplete endogenous biotin to allow binding of radiolabeled biotin with (strept)avidin on tumor cells. How-

* To whom correspondence should be addressed. Phone: (206) 685-3085. Fax: (206) 685-9630. E-mail: dswilbur@u.washington.edu.

[1] Abbreviations: Av, avidin; CN-Cbl, cyanocobalamin; EDC, 1-(3-dimethylaminopropyl)-3-ethylcarbodiimide hydrochloride; mAb, monoclonal antibody; r-SAv, recombinant streptavidin; rt, room temperature; (S)Av or (strept)avidin, denotes avidin or streptavidin; Sav, streptavidin; TCDI, 1,1-thiocarbonyldiimidazole; TFA, trifluoroacetic acid; TFP, tetrafluorophenyl; TFP-OH, tetrafluorophenol; TFP-OTFA, tetrafluorophenyl trifluoroacetate; TsCl, toluenesulfonyl chloride.

10.1021/bc000024v CCC: $19.00 © 2000 American Chemical Society
Published on Web 06/29/2000

ever, endogenous biotin is replenished and, therefore, will be available to bind in the place of any dissociated biotin derivative, effectively blocking its reassociation with the cancer cell. A decrease in quantity of radionuclides bound to cancer cells is problematic as it decreases the probability of killing those cells. Thus, in our studies to optimize biotin reagents for use in mAb-based pretargeting, it is important to have some idea of the dissociation rate of the biotin derivatives used relative to unmodified biotin. To assess the relative dissociation rates of biotin derivatives, we have recently investigated the use of biotin-dyes in an HPLC assay (*21*). From those studies, it was found that biotin derivatives which were conjugated with cyanocobalamin (CN−Cbl) could be used in a size exclusion HPLC analysis to determine their relative dissociation rates.

In this investigation, we have prepared twelve new biotin derivatives, conjugated them with CN−Cbl, and determined their relative dissociation rates from Av and SAv. The biotin derivatives chosen for evaluation were modified in locations that we believed would retain strong binding with Av and SAv. The structures of the biotin derivatives chosen for study were also based on our belief that they were likely to be stable to degradation by serum biotinidase (*22*, *23*). The biotin derivatives investigated contained modifications (1) in the length of side chain, (2) in the nature of bond between the linker and biotin moiety, and (3) in substituents on the methylene α to the biotinamide bond obtained by conjugation of biotin with a series of amino acids. As part of the investigation, three biotin-CN−Cbl derivatives previously tested (*21*) were included. The results obtained from the HPLC analyses conducted clearly indicate that certain structural modifications of biotin conjugates dramatically decrease their binding with (S)Av while other modifications have much less of an affect.

Reported herein is the rationale for the design of new biotin conjugates, their synthesis, results of relative dissociation rates as measured by HPLC analysis, and a discussion of the implications of those results with regards to the choice of biotin conjugates to be used for in vivo applications.

EXPERIMENTAL PROCEDURES

General. Solvents and chemicals obtained from commercial sources were analytical grade or better and were used without further purification. Solvents for HPLC analysis were obtained as HPLC grade and were filtered (0.2 μm) prior to use. Vitamin B_{12} (CN−Cbl); *d*-biotin, **4**; 4,7,10-trioxa-1,13-tridecanediamine; 2,3,5,6-tetrafluorophenol; toluenesulfonyl chloride; L-serine, **21**; and most other chemicals were purchased from Aldrich Chemical Co. (Milwaukee, WI). *O*-*tert*-Butyl-L-serine methyl ester hydrochloride, **19**; L-aspartic acid β-*tert*-butyl ester, **23**; and L-aspartic acid α-*tert*-butyl ester, **16**, were obtained from Calbiochem-Novabiochem Corp. (San Diego, CA). Iminobiotin NHS ester, **2b**, and recombinant streptavidin (r-SAv) were obtained from Sigma (St. Louis, MO). Avidin was purchased from Pierce (Rockford, IL). 2,3,5,6-Tetrafluorophenyl trifluoroacetate was prepared as previously described (*24*). Silica gel chromatography was conducted with 70−230 mesh 60 Å silica gel (Aldrich Chemical Co.). Melting points were obtained in open capillary tubes on a Mel-Temp II apparatus with a Fluke 51 K/J electronic thermometer and are uncorrected. ^{1}H NMR data, MS data, and HPLC chromatography were used to assess compound identity and purity (Data provided in the Supporting Information).

Spectral Analyses. ^{1}H NMR spectra were obtained on either a Bruker AC-200 (200 MHz), a Bruker AC-500 (500 MHz), or a Bruker AC-750 (750 MHz) instrument. Proton chemical shifts are expressed as parts per million using tetramethylsilane as internal standard ($\delta = 0.0$ ppm). IR data were obtained on a Perkin-Elmer 1420 infrared spectrophotometer. Some mass spectral data were obtained on a VG Analytical (Manchester, England) VG-70SEQ mass spectrometer with associated 11250J Data System using fast atom bombardment (FAB^+) at 8 keV in a matrix of MeOH/DMIX (thioglycerol/DMSO/TFAA 90/9/1) or 3NBA (3-nitrobenzyl alcohol). Other mass spectral data (ES^+) were obtained on a PE Biosystems Mariner Electrospray Time-of-Flight Mass Spectrometer.

Reversed-Phase Chromatography. HPLC separations of biotin derivatives and biotin-CN−Cbl conjugates were obtained on Hewlett-Packard quaternary 1050 gradient pumping system with a variable wavelength UV detector (254 and 360 nm) and a Varex ELSD MKIII evaporative light-scattering detector. Analysis of the HPLC data were conducted on Hewlett-Packard HPLC ChemStation software. All reactions were monitored by HPLC. Reversed-phase HPLC chromatography was carried out using an Alltech Altima C-18 column (5 μm, 250 mm × 4.6 mm) with a gradient solvent system at a flow rate of 1 mL/min. The gradient mixture was composed of MeOH (solvent A) and 0.1% aqueous HOAc (solvent B). Starting with 40% MeOH, the initial solvent mixture was held for 2 min, increased to 100% MeOH over the next 10 min, then held at 100% MeOH for 8 min. Retention times (t_R) are provided with the compound experimental.

Size Exclusion Chromatography. Size exclusion HPLC analyses were conducted on a system consisting of a Hewlett-Packard 1050 Multiple Wavelength Detector (280 nm), isocratic pump, and a Spherogel TSK 5000PW column (7.5 mm × 300 mm, 10 μm; stainless steel, Altex). The mobile phase was an aqueous solution containing 50 mM potassium phosphate (pH 6.8), 300 mM NaCl, 1 mM EDTA, and 1 mM NaN_3. A flow rate of 0.75 mL/min was used.

Preparation of 1. Preparation of **1** was accomplished by reaction of the *c*-lactone of CN−Cbl (*25*) with (neat) 4,7,10-trioxa-1,13-tridecanediamine at 50−55 °C for 1 h as previously described (*21*).

Preparation of 2a. Preparation of the TFP ester of biotin, **2a**, was accomplished as previously described (*26*).

Preparation of 2c. Preparation of the TFP ester of the biotin-sarcosine adduct, **2c**, was accomplished in situ as previously described (*23*).

Preparation of 2d. To a solution of 0.4 g (1.6 mmol) homobiotin, **9**, in 20 mL of DMF was added 0.23 mL (1.6 mmol) of Et_3N, followed by 484 mg (1.86 mmol) of TFP−OTFA. The reaction was stirred at room temperature for 30 min and the DMF was removed under vacuum. The residue was dissolved in $CHCl_3$, washed with H_2O and dried over anhydrous Na_2SO_4. The $CHCl_3$ was removed to yield a 550 mg (87%) of **2d** as a colorless solid. mp > 240 °C. ^{1}H NMR ($CDCl_3$, 500 MHz) δ 1.4 (m, 2H), 1.6−1.8 (m, 4H), 2.6 (t, $J = 3.6$ Hz, 2H), 2.7 (d, $J = 6.8$ Hz, 1H), 2.8 (dd, $J = 2.5$, 6.4 Hz, 1H), 3.1 (m, 1H), 4.3 (m, 1H), 4.5 (m, 1H), 5.73 (s, 1H), 6.02 (s, 1H), 6.9 (m, 1H). IR (KBr) 3240, 2920, 2840, 1780, 1700, 1520, 1480, 1080 cm^{-1}. HRMS mass calcd for $C_{17}H_{19}N_2O_3SF_4$ $(M + H)^+$: 407.1052. Found: 407.1038. HPLC: $t_R = 13.1$ min.

Preparation of 2e. To a 115 mg (0.535 mmol) quantity of norbiotinamine, **12**, dissolved in 5 mL of DMF was added 95 mg (0.535 mmol) of 1,1-thiocarbonyldiimi-

dazole. The reaction mixture was stirred at room temperature for 45 min, and the DMF was removed under vacuum. The resultant residue was dissolved in 0.5 mL of MeOH, and H_2O was added until a precipitate formed. The white precipitate was filtered, washed with H_2O, and dried under vacuum to give 76 mg (55%) of **2e**. mp 168−170 °C. ^{1}H NMR (DMSO-d_6, 200 MHz) δ 1.2−1.8 (m, 6H), 2.55 (d, J = 6.4 Hz, 1H), 2.9 (dd, J = 6.2, 2.5 Hz, 1H), 3.1 (m, 1H), 4.1 (m, 1H), 4.3 (m, 1H), 6.4 (d, J = 9 Hz, 2H). IR (KBr) 3240, 2920, 2840, 2200, 2120, 1700, 1470, 1340, 1270, 1160, 1100 cm^{-1}. HRMS mass calcd for $C_{10}H_{16}N_3OS_2$ $(M + H)^+$: 258.0735. Found: 258.0739. HPLC: t_R = 11.0 min.

Preparation of 2f. To a solution containing 100 mg of (0.437 mmol) biotinamine, **14**, in 15 mL of DMF was added 78 mg of (0.437 mmol) 1,1-thiocarbonyldiimidazole. The reaction mixture was stirred at room temperature for 2 h, and the DMF was removed under vacuum. The residue was dissolved in 5 mL of MeOH, and H_2O was added until a precipitate formed (3 vol). After storing the precipitate at 4 °C overnight, it was filtered, dried under vacuum, and triturated with MeOH to give 88 mg (74%) of biotin isothiocyanate, **2f**, as colorless solid. mp 122−124 °C. ^{1}H NMR (DMSO-d_6, 200 MHz) δ 1.2−1.8 (m, 8H), 2.55 (d, J = 6.2 Hz, 1H), 2.8 (dd, J = 6.2, 2.3 Hz, 1H), 3.1 (m, 1H), 3.64 (t, J = 3.2 Hz, 2H), 4.1 (m, 1H), 4.3 (m, 1H), 6.4 (d, J = 8.9 Hz, 2H). IR (KBr) 3220, 2910, 2840, 2160, 2080, 1690, 1460, 1210, 1060 cm^{-1}. HRMS mass calcd for $C_{11}H_{18}N_3OS_2$ $(M + H)^+$: 272.0891. Found: 272.0893. HPLC: t_R = 11.8 min.

Preparation of 2j. To a solution of *N*-biotinyl-*β*-*tert*-butyl ester-L-aspartic acid, **27** (2.20 g, 5.29 mmol), and tetrafluorophenol (0.88 g, 5.29 mmol) in 50 mL of anhydrous DMF was added EDC (1.52 g, 7.93 mmol) at room temperature. The reaction mixture was stirred at room temperature for 48 h, then the solution was triturated with water (200 mL), filtered, washed with water completely to give the crude *N*-biotinyl-*β*-*tert*-butyl ester-L-aspartic acid TFP ester, **2j**. The crude **2j** was purified by silica gel column chromatography (50 g) eluting with 30% EtOAc/Hex mixture to afford 1.74 g (58%) of a colorless solid. mp 85.2−86.4 °C dec ^{1}H NMR ($CDCl_3$, 200 MHz) δ 1.46 (s, 9 H), 1.43 (d, 2H), 1.72 (m, 4 H), 2.32 (t, 2 H), 2.72 (d, 2H), 2.87 (m, 1 H), 2.94 (m, 1H), 3.12 (m, 3H), 4.32 (m, 1H), 4.48 (m, 1H), 5.23 (m, 1H), 5.51 (s, 1H), 6.43 (d, 1H), 7.03 (m, 1H), 7.31 (d, 1H). HRMS calcd for $C_{24}H_{30}F_4N_3O_6S$ $(M + H)^+$: 564.1791. Found: 564.1793. HPLC: t_R = 13.1 min.

Preparation of 2n. To a solution of *N*-Biotinyl-*N*-*ϵ*-*tert*-Boc-L-Lysine, **28** (1.92 g, 4.06 mmol) and tetrafluorophenol (0.67 g, 4.06 mmol) in 50 mL of DMF was added EDC (0.86 g, 4.47 mmol). The reaction mixture was stirred at room temperature for 48 h, then the product was triturated with water (200 mL), filtered, washed with water thoroughly to give the crude product. The crude product was purified on a silica gel column (60 g) eluting with 30% EtOAc/hexane mixture to afford 1.14 g (45%) of the biotin-lysine-N-tBoc adduct, **2n**, as a colorless solid. mp 77.9−79.4 °C (dec). ^{1}H NMR ($CDCl_3$, 200 MHz) δ 1.44 (s, 9 H), 1.54 (d, 4H), 1.71 (m, 4H), 1.98 (m, 2H), 2.32 (t, J = 7.7 Hz, 2H), 2.71 (d, J = 12.8 Hz, 1H), 2.90 (m, 1H), 3.14 (d, 3H), 3.29−3.34 (m, 2 H), 4.33 (m, 1H), 4.50 (m, 1H), 4.86 (m, 1H), 5.71 (s, 1H), 6.52 (s, 1H), 6.72 (s, 1H), 7.02 (m, 1H), 7.44 (t, 1H). HRMS calcd for $C_{27}H_{37}F_4N_4O_6S$ $(M + H)^+$: 621.2370. Found: 621.2369. HPLC: t_R = 13.2 min.

Preparation of 3a. Preparation of the biotin-cyanocobalamin conjugate **3a** was accomplished by reaction of biotin TFP ester, **2a**, with **1** as previously described (*21*).

Preparation of 3b. Preparation of the iminobiotin-cyanocobalamin conjugate **3b** was accomplished by reaction of iminobiotin NHS ester, **2b**, with **1** as previously described (*21*).

Preparation of 3c. Preparation of the biotin-sarcosine-cyanocobalamin conjugate **3c** was accomplished by reaction of biotin-sarcosine TFP ester, **2c**, with **1** as previously described (*21*).

Preparation of 3d. To a solution of 100 mg of (0.063 mmol) CN−Cbl-*c*-lactone conjugate **1** dissolved in 10 mL of DMF was added 20 mg of (0.063 mmol) homobiotin TFP ester, **2d**, then 33 μL of (0.082 mmol) Et_3N. The reaction was stirred at room temperature for 4 h and the DMF was removed under vacuum. The residue was triturated in acetone and filtered to yield 108 mg (95%) of **3d** as a red solid, mp 198−200 °C (dec). ^{1}H NMR (CD_3OD, 750 MHz) δ 1.20 (s, 3H), 1.25 (d, J = 6.8 Hz, 3H), 1.37 (s, 3H), 1.39 (s, 3H), 1.43 (m, 6H), 1.46 (s, 3H), 1.62 (m, 6H), 1.75 (m, 6H), 1.88 (s, 3H), 1.94 (m, 2H), 2.05 (m, 4H), 2.18 (t, 4H), 2.25 (s, 3H), 2.26 (s, 3H), 2.36 (m, 1H), 2.47 (s, 3H), 2.48 (m, 2H), 2.55 (m, 2H), 2.60 (s, 3H), 2.67 (m, 4H), 2.88 (m, 4H), 3.11 (m, 1H), 3.25 (m, 4H), 3.30 (s, 3H), 3.33 (m, 2H), 3.40 (t, 2H), 3.52 (m, 4H), 3.59 (m, 8H), 3.76 (m, 1H), 3.90 (m, 1H), 4.08 (m, 1H), 4.17 (m, 1H), 4.30 (m, 1H), 4.48 (m, 1H), 4.66 (m, 1H), 6.04 (d, 1H), 6.28 (d, 1H), 6.50 (s, 1H), 7.14 (s, 1H), 7.25 (s, 1H). IR (KBr) 3340, 2920, 2860, 1660, 1570, 1500, 1360, 1210, 1140, 1080 cm^{-1}. MS (FAB^+) mass calcd for $C_{84}H_{126}N_{17}O_{20}CoPS$: 1814.82. Found: 1814.9 (M^+). HPLC: t_R = 8.6 min.

Preparation of 3e. To a solution of 150 mg of (0.095 mmol) CN−Cbl-*c*-lactone conjugate **1** dissolved in 10 mL of DMF was added 32 mg of (0.123 mmol) norbiotin isothiocyanate, **2e**, then 20 μL of (0.095 mmol) Et_3N. The reaction was stirred at room temperature for 48 h and the DMF was removed under vacuum. The residue was triturated in acetone and filtered to yield 163 mg (94%) of **3e** as a red solid. mp 205−207 °C (dec). ^{1}H NMR (CD_3OD, 750 MHz) δ 0.45 (s, 3H), 1.20 (s, 3H), 1.25 (d, J = 6.0 Hz, 3H), 1.37 (s, 3H), 1.39 (s, 3H), 1.44 (m, 2H), 1.46 (s, 3H), 1.62 (m, 6H), 1.75 (m, 3H), 1.81 (m, 3H), 1.88 (s, 3H), 1.95 (m, 2H), 2.05 (m, 3H), 2.15 (m, 4H), 2.25 (s, 3H), 2.26 (s, 3H), 2.37 (m, 1H), 2.47 (s, 3H), 2.45 (m, 2H), 2.54 (m, 2H), 2.60 (s, 3H), 2.66 (m, 4H), 2.85 (m, 2H), 2.92 (dd, 2H), 3.11 (m, 1H), 3.23 (m, 4H), 3.30 (s, 3H), 3.33 (m, 2H), 3.40 (t, 2H), 3.54 (m, 4H), 3.60 (m, 6H), 3.67 (m, 2H), 3.76 (m, 1H), 3.90 (m, 1H), 4.08 (m, 1H), 4.17 (m, 1H), 4.31 (m, 1H), 4.49 (m, 1H), 4.65 (m, 1H), 6.04 (d, 1H), 6.28 (d, 1H), 6.50 (s, 1H), 7.14 (s, 1H), 7.25 (s, 1H). IR (KBr) 3310, 2920, 2860, 2120, 1670, 1570, 1500, 1210, 1140, 1080 cm^{-1}. MS (FAB^+) mass calcd for $C_{83}H_{125}N_{18}O_{19}CoPS_2$: 1831.79. Found: 1831.67 (M^+). HPLC: t_R = 8.7 min.

Preparation of 3f. To a solution of 150 mg of (0.095 mmol) CN−Cbl-*c*-lactone conjugate **1** dissolved in 10 mL of DMF was added 34 mg of (0.123 mmol) biotin isothiocyanate, **2f**, then 20 μL of (0.095 mmol) Et_3N. The reaction was stirred at room temperature for 24 h, and the DMF was removed under vacuum. The residue was triturated in acetone and filtered to yield 140 mg (80%) of **3f** as a red solid. mp 200−202 °C (dec). ^{1}H NMR (CD_3OD, 750 MHz) δ 0.46 (s, 3H), 1.20 (s, 3H), 1.25 (d, J = 6.0 Hz, 3H), 1.37 (s, 3H), 1.39 (s, 3H), 1.43 (m, 3H), 1.46 (s, 3H), 1.59 (m, 4H), 1.64 (m, 2H), 1.74 (m, 2H), 1.81 (m, 4H), 1.88 (s, 3H), 1.91 (m, 1H), 1.96 (d, J = 13.7 Hz, 1H), 2.05 (m, 4H), 2.15 (m, 4H), 2.26 (s, 6H), 2.37 (d, J = 3.4 Hz, 1H), 2.45 (m, 2H), 2.47 (s, 3H), 2.55 (m, 2H), 2.60 (s, 3H), 2.64 (m, 2H), 2.70 (d, J = 12.8 Hz, 2H), 2.85 (m, 2H), 2.92 (dd, J = 5.1, 12.8 Hz, 2H), 3.10 (m, 1H),

3.23 (m, 4H), 3.30 (s, 3H), 3.34 (m, 2H), 3.40 (t, 2H), 3.54 (m, 4H), 3.60 (m, 6H), 3,67 (d, J = 14.7 Hz, 2H), 3.76 (m, 1H), 3.90 (m, 1H), 4.08 (m, 1H), 4.17 (m, 1H), 4.30 (m, 1H), 4.48 (dd, 1H), 4.65 (m, 1H), 6.04 (d, 1H), 6.28 (d, 1H), 6.50 (s, 1H), 7.14 (s, 1H), 7.25 (s, 1H). IR (KBr) 3340, 2920, 1660, 1570, 1490, 1210, 1110, 1060 cm^{-1}. MS (FAB^+) mass calcd for $C_{84}H_{127}N_{18}O_{19}CoPS_2$: 1845.80. Found: 1845.95 (M^+). HPLC: t_R = 9.2 min.

Preparation of 2g and 3g. To a solution containing 43 mg of (0.130 mmol) biotin-α-methylbutyrate, **17**, and 27 μL of (0.130 mmol) Et_3N in 10 mL of DMF was added 51 mg of (0.195 mmol) TFP−OTFA. The reaction was stirred at room temperature for 30 min to form the TFP ester of biotin-α-methylbutyrate, **2g**. To that solution was added a solution of 150 mg (0.095 mmol) of **1** and 10 μL of Et_3N in 10 mL of DMF. The reaction mixture was stirred at room-temperature overnight. The DMF was removed under vacuum, and the residue was triturated with acetone to give 140 mg (78%) of **3g** after removal of solvent. mp 194−196 °C (dec). ^1H NMR (CD_3OD, 750 MHz) δ 0.46 (s, 3H), 1.16, 1.25 (2xd, J = 6.8 Hz, 3H), 1.20 (s, 3H), 1.37 (s, 3H), 1.39 (s, 3H), 1.43 (m, 3H), 1.46 (s, 3H), 1.62 (m, 6H), 1.74 (m, 4H), 1.88 (s, 3H), 1.93 (m, 2H), 2.05 (m, 4H), 2.17 (t, 4H), 2.25 (s, 3H), 2.26 (s, 3H), 2.37 (m, 4H), 2.45 (m, 2H), 2.47 (s, 3H), 2.55 (m, 2H), 2.60 (s, 3H), 2.66 (m, 4H), 2.85 (m, 2H), 2.92 (dd, J = 4.3, 12.8 Hz, 2H), 3.10 (m, 1H), 3.22 (m, 4H), 3.30 (s, 3H), 3.33 (d, J = 11.1 Hz, 2H), 3.40 (t, J = 6.8 Hz, 2H), 3.51 (m, 4H), 3.59 (m, 6H), 3.64 (m, 2H), 3.76 (m, 1H), 3.90 (m, 1H), 4.08 (m, 1H), 4.17 (m, 1H), 4.23 (m, 1H), 4.30 (m, 2H), 4.48 (m, 1H), 4.65 (m, 2H), 6.04 (d, 1H), 6.28 (d, 1H), 6.50 (s, 1H), 7.14 (s, 1H), 7.25 (s, 1H). IR (KBr) 3340, 2920, 1660, 1570, 1500, 1400, 1210, 1110, 1080 cm^{-1}. MS (FAB^+) mass calcd for $C_{87}H_{130}N_{18}O_{21}CoPS$: 1885. Found: 1885 ($M^+$). HPLC: t_R = 8.2 min.

Preparation of 2h and 3h. TFP−OTFA (0.12 mL, 0.67 mmol) was added slowly to a mixture containing N-biotinyl-*O*-*tert*-butyl-serine, **25** (0.13 g, 0.34 mmol), Et_3N (0.14 mL, 1.01 mmol), and anhydrous CH_3CN (4.0 mL). The mixture was stirred at room temperature for 1 h, and then the volatile materials were evaporated under vacuum to give oily crude TFP ester, **2h**. The crude **2h** was redissolved in 3.0 mL of anhydrous DMF, then **1** (34.9 mg, 0.043 mmol) and Et_3N (0.10 mL, 0.72 mmol) were added at room temperature, respectively. The reaction mixture was stirred at room temperature for 16 h. The mixture was triturated with 20 mL of EtOAc and filtered to yield 77 mg (92%) of **3h** as a red solid. mp 187−190 °C (dec). ^1H NMR (CD_3OD, 200 MHz) δ 0.46 (s, 3H), 1.12 (s, 9H), 1.25 (m, 8H), 1.38 (d, 6H), 1.46 (s, 3H), 1.69 (m, 8H), 1.89 (s, 2H), 2.02 (m, 8H), 2.26 (s, 6H), 2.22−2.29 (m, 2 H), 2.38 (s, 1H), 2.47 (s, 3H), 2.52 (m, 2H), 2.60 (s, 3H), 2.66−3.27 (m, 11H), 3.30 (m, 16H), 3.41 (m, 4H), 3.52 (m, 4H), 3.59 (m, 4H), 3.63 (m, 2H), 3.70−3.99 (m, 2H), 4.09 (m, 1H), 4.18 (t, 1H), 4.32 (m, 1 H), 4.48 (m, 1H), 4.65 (m, 1H), 6.05 (s, 1H), 6.28 (d, 1H), 6.51 (s, 1H), 7.14 (s, 1H), 7.25 (s, 1H), 7.98 (s, 1H); MS (ES^+) mass calcd for $C_{90}H_{137}CoN_{18}O_{22}PS$ $(M + H)^+$: 1944. Found: 1944. HPLC: t_R = 9.8 min.

Preparation of 2i and 3i. TFP−OTFA (0.13 mL, 0.74 mmol) was dropped slowly to a solution of *N*-biotinyl-serine, **26** (0.37 mmol), and Et_3N (0.15 mL, 1.1 mmol) in anhydrous CH_3CN (2 mL) at room temperature. The solution was stirred at room temperature for 30 min, and then volatile materials were evaporated under vacuum to afford crude TFP ester, **2i**. The crude **2i** was redissolved in a solution of anhydrous DMF (2 mL) and Et_3N (0.15 mL, 1.1 mmol), then **1** (31.8 mg, 0.020 mmol) was added and stirred at room temperature for 16 h. The solution was triturated with 20 mL of ethyl acetate and filtered to give 36.2 mg (96%) of **3i** as a red solid. mp 196−199 °C dec ^1H NMR (CD_3OD, 200 MHz) δ 0.45 (s, 3H), 1.23 (m, 8H), 1.37 (d, 6H), 1.46 (s, 3H), 1.69 (m, 8H), 1.88 (s, 2H), 2.02 (m, 8H), 2.26 (s, 6H), 2.22−2.29 (m, 2 H), 2.37 (s, 1H), 2.47 (s, 3H), 2.53 (m, 2H), 2.60 (s, 3H), 2.66−3.27 (m, 11H), 3.30 (m, 16H), 3.41 (m, 4H), 3.52 (m, 4H), 3.59 (s, 4H), 3.63 (m, 2H), 3.71−3.95 (m, 2H), 4.09 (m, 1H), 4.18 (t, 1H), 4.30 (m, 1 H), 4.48 (m, 1H), 4.65 (m, 1H), 6.05 (s, 1H), 6.28 (d, 1H), 6.51 (s, 1H), 7.14 (s, 1H), 7.25 (s, 1H); MS (ES^+) mass calcd for $C_{86}H_{128}CoN_{18}O_{22}PSNa$ $(M + Na)^+$: 1911. Found: 1911. HPLC: t_R = 8.1 min.

Preparation of 3j. *N*-Biotinyl-*β*-*tert*-butyl-L-aspartate TFP ester, **2j** (8.0 mg, 14.15 μmol), was added to a solution of **1** (15.0 mg, 9.43 μmol) and Et_3N (2.6 μL, 18.86 μmol) in 1.5 mL of anhydrous DMF at room temperature. The reaction mixture was stirred at room temperature for 1 h, then 20 mL of ethyl acetate was added and stirred for an additional 10 min. The precipitate was filtered and washed with EtOAc to give 17.6 mg (95%) of **3j** as a red solid. mp 191−194 °C dec. ^1H NMR (CD_3OD, 200 MHz) δ 0.46 (s, 3H), 1.25 (m, 8H), 1.38 (d, 6H), 1.44 (s, 9 H), 1.46 (s, 3H), 1.69 (m, 8H), 1.89 (s, 2H), 2.02 (m, 8H), 2.26 (s, 6H), 2.22−2.29 (m, 2 H), 2.38 (s, 1H), 2.47 (s, 3H), 2.52 (m, 2H), 2.60 (s, 3H), 2.66−3.27 (m, 11H), 3.30 (m, 16H), 3.41 (m, 4H), 3.52 (m, 4H), 3.59 (m, 4H), 3.63 (m, 2H), 3.69−3.97 (m, 2H), 4.09 (m, 1H), 4.18 (t, 1H), 4.30 (dd, 1 H), 4.49 (dd, 1H), 4.65 (m, 1H), 6.05 (s, 1H), 6.28 (d, 1H), 6.51 (s, 1H), 7.14 (s, 1H), 7.25 (s, 1H); MS (ES^+) mass calcd for $C_{91}H_{137}CoN_{18}O_{23}PS$ $(M + H)^+$: 1973. Found: 1973. HPLC: t_R = 9.8 min.

Preparation of 2l and 3l. TFP−OTFA (0.085 mL, 0.49 mmol) was added dropwise to a solution of *N*-biotinyl-L-aspartic acid α-*tert*-butyl ester, **18** (0.17 g, 0.41 mmol) and Et_3N (0.17 mL, 1.23 mmol) in 4.0 mL of anhydrous CH_3CN at room temperature. The mixture was stirred at room temperature for 20 min, and then volatile materials were evaporated under vacuum to give the TFP ester **2l** as light-yellow oil. The crude **2l** was redissolved in 3.0 mL of anhydrous DMF, then **1** (0.0813 g, 0.0511 mmol) and Et_3N (0.17 mL, 1.23 mmol) were added. The reaction mixture was stirred at room temperature for 1 h, then 40 mL of ethyl acetate was added and stirred for an additional 10 min. The precipitate was filtered, washed with ethyl acetate, and evaporated to dryness to give 95 mg (94%) of **3l** as a red solid. mp 178−182 °C (dec). ^1H NMR (CD_3OD, 200 MHz) δ 0.46 (s, 3H), 1.24 (m, 8H), 1.38 (d, 6H), 1.45 (s, 9 H), 1.46 (s, 3H), 1.69 (m, 8H), 1.88 (s, 2H), 2.02 (m, 8H), 2.26 (s, 6H), 2.22−2.29 (m, 2 H), 2.37 (s, 1H), 2.47 (s, 3H), 2.52 (m, 2H), 2.60 (s, 3H), 2.66−3.27 (m, 11H), 3.30 (m, 16H), 3.41 (m, 4H), 3.52 (m, 4H), 3.58 (s, 4H), 3.63 (m, 2H), 3.68−3.96 (m, 2H), 4.09 (m, 1H), 4.18 (t, 1H), 4.31 (m, 1 H), 4.49 (m, 1H), 4.63 (m, 2H), 6.04 (s, 1H), 6.28 (d, 1H), 6.51 (s, 1H), 7.14 (s, 1H), 7.24 (s, 1H); MS (ES^+) mass calcd for $C_{91}H_{137}CoN_{18}O_{23}PS$ $(M + H)^+$: 1972. Found: 1972. HPLC: t_R = 9.6 min.

Preparation of 3n. *N*-Biotinyl-*N*-ε-*tert*-Boc-L-lysine tetrafluorophenyl ester, **2n** (8.8 mg, 14.15 μmol), was added to a solution of **1** (15.0 mg, 9.43 μmol) and Et_3N (18.86 μmol) in 1.5 mL of anhydrous DMF at room temperature. The reaction mixture was stirred at room temperature for 1 h, then 20 mL of EtOAc was added and stirred for 10 min. The precipitate was filtered and washed with EtOAc to afford 18.4 mg (96%) of pure **3n** as a red solid. mp 185−187 °C (dec). ^1H NMR (CD_3OD, 200 MHz) δ 0.46 (s, 3H), 1.26 (m, 8H), 1.38 (d, 6H), 1.43 (s, 9 H), 1.46 (s, 3H), 1.69 (m, 12H), 1.89 (s, 2H), 2.02 (m,

8H), 2.26 (s, 6H), 2.22−2.29 (m, 2 H), 2.38 (s, 1H), 2.47 (s, 3H), 2.52 (m, 2H), 2.60 (s, 3H), 2.66−3.27 (m, 13H), 3.30 (m, 16H), 3.41 (m, 4H), 3.52 (m, 4H), 3.59 (m, 4H), 3.63 (m, 2H), 3.69−3.97 (m, 2H), 4.09 (m, 1H), 4.18 (t, 1H), 4.30 (m, 1 H), 4.49 (m, 1H), 4.63 (m, 1H), 6.05 (s, 1H), 6.28 (d, 1H), 6.51 (s, 1H), 7.14 (s, 1H), 7.25 (s, 1H); MS (ES^+) mass calcd for $C_{94}H_{144}CoN_{19}O_{23}PS$ (M^+): 2029. Found: 2029. HPLC: $t_R = 10.1$ min.

Preparation of 3k, 3m, and 3o. Removal of t-Bu esters. The quantity of the t-Bu ester or N-tBoc protected biotin-CN−Cbl conjugate (**3j**, **3l**, or **3n**) was dissolved in neat trifluoroacetic acid and stirred at room temperature for 15 min. TFA was evaporated under vacuum. The crude product was redissolved in methanol (1 mL) and triturated with ethyl acetate (20−30 mL). The solid was filtered and dried under vacuum.

3k. A 20 mg quantity (10 μmol) dissolved in 1 mL of TFA gave 19 mg (98%) of a red solid after workup. mp 208−212 °C (dec). ^{1}H NMR (CD_3OD, 200 MHz) δ 0.45 (s, 3H), 1.24 (m, 8H), 1.38 (d, 6H), 1.46 (s, 3H), 1.69 (m, 8H), 1.89 (s, 2H), 2.02 (m, 8H), 2.26 (s, 6H), 2.22−2.29 (m, 2 H), 2.38 (s, 1H), 2.47 (s, 3H), 2.52 (m, 2H), 2.60 (s, 3H), 2.66−3.27 (m, 11H), 3.30 (m, 16H), 3.41 (m, 4H), 3.52 (m, 4H), 3.59 (m, 4H), 3.63 (m, 2H), 3.69−3.95 (m, 2H), 4.09 (m, 1H), 4.18 (t, 1H), 4.30 (dd, 1 H), 4.48 (dd, 1H), 4.64 (m, 1H), 6.04 (s, 1H), 6.28 (d, 1H), 6.51 (s, 1H), 7.14 (s, 1H), 7.25 (s, 1H); MS (ES^+) mass calcd for $C_{87}H_{129}CoN_{18}O_{23}PS$ $(M + H)^+$: 1916. Found: 1916. HPLC: t_R = 8.4 min.

3m. A 9 mg quantity (4.6 μmol) dissolved in 0.5 mL of TFA gave 7.9 mg (90%) of a red solid after workup. mp 204−207 °C (dec). ^{1}H NMR (CD_3OD) δ 0.46 (s, 3H), 1.25 (m, 8H), 1.38 (d, 6H), 1.46 (s, 3H), 1.69 (m, 8H), 1.89 (s, 2H), 2.02 (m, 8H), 2.26 (s, 6H), 2.22−2.29 (m, 2 H), 2.38 (s, 1H), 2.47 (s, 3H), 2.52 (m, 2H), 2.60 (s, 3H), 2.66−3.27 (m, 11H), 3.30 (m, 16H), 3.41 (m, 4H), 3.52 (m, 4H), 3.59 (m, 4H), 3.63 (m, 2H), 3.69−3.95 (m, 2H), 4.09 (m, 1H), 4.18 (t, 1H), 4.29 (dd, 1 H), 4.49 (dd, 1H), 4.64 (m, 1H), 6.04 (s, 1H), 6.28 (d, 1H), 6.51 (s, 1H), 7.14 (s, 1H), 7.25 (s, 1H); MS (ES^+) mass calcd for $C_{87}H_{126}CoN_{18}O_{22}PS$ $(M - H_2O)$: 1898. Found: 1898. HPLC: t_R = 7.7 min.

3o. A 9 mg quantity (4.5 μmol) dissolved in 0.5 mL of TFA gave 8 mg (93%) of a red solid after workup. mp 198−201 °C (dec). ^{1}H NMR (CD_3OD, 200 MHz) δ 0.45 (s, 3H), 1.24 (m, 8H), 1.38 (d, 6H), 1.46 (s, 3H), 1.69 (m, 12H), 1.89 (s, 2H), 2.04 (m, 8H), 2.26 (s, 6H), 2.25 (m, 2 H), 2.38 (s, 1H), 2.47 (s, 3H), 2.52 (m, 2H), 2.60 (s, 3H), 2.95 (m, 13H), 3.30 (m, 16H), 3.41 (m, 4H), 3.52 (m, 4H), 3.59 (m, 4H), 3.63 (m, 2H), 3.82 (m, 2H), 4.09 (m, 1H), 4.18 (t, 1H), 4.30 (m, 1 H), 4.48 (m, 1H), 4.64 (m, 1H), 6.05 (s, 1H), 6.28 (d, 1H), 6.51 (s, 1H), 7.14 (s, 1H), 7.25 (s, 1H); MS (ES^+) mass calcd for $C_{89}H_{136}CoN_{19}O_{21}PS$ $(M + H)^+$: 1930. Found: 1930. HPLC: t_R = 2.3 min.

Biotin Methyl Ester, 5. This compound was prepared by reaction of biotin, **4**, in methanolic HCl as previously described (*27*) to give a nearly quantitative yield of **5** as a colorless solid. mp 116−118 °C. HPLC: $t_R = 8.31$ min.

Biotinol, 6. This compound was prepared by reduction of a 1 g (3.88 mmol) of **5** with $LiAlH_4$ as previously described (*28*) to give 0.89 g (100%) of **6** as a colorless solid. mp 164−168 °C. HPLC: $t_R = 6.52$ min.

Biotinol-*p*-toluene Sulfonate, 7. A 0.7 g (3 mmol) quantity of biotinol, **6**, was dissolved in pyridine at 0 °C, and 1.14 g (6 mmol) toluenesulfonyl chloride was slowly added. The reaction mixture was stirred at 0 °C for 5 h and poured over crushed ice. The aqueous layer was extracted with CH_2Cl_2 (3 × 100 mL). The CH_2Cl_2 solution was washed with 2% aqueous HOAc then with aqueous saturated NaCl. The CH_2Cl_2 solution was then dried over anhydrous Na_2SO_4, filtered, and evaporated to yield 1.0 g (2.6 mmol, 87%) of **7** as a colorless solid. mp 145−147 °C. ^{1}H NMR ($CDCl_3$, 200 MHz) δ 1.3 (m, 2H), 1.6 (m, 2H), 2.4 (s, 3H), 2.65 (d, 1H), 2.85 (dd, 1H), 3.05 (m, 1H), 3.95 (m, 2H), 4.2 (m, 1H), 4.4 (m, 1H), 5.3 (s, 1H), 5.9 (s, 1H), 7.3 (d, 2H), 7.7 (d, 2H); IR (KBr) 3240, 2920, 1700, 1460, 1360, 1270, 1170, 1080 cm^{-1}. HRMS mass calcd for $C_{17}H_{25}N_2O_4S_2$ $(M + H)^+$: 385.1256. Found: 385.1232. HPLC: $t_R = 11.9$ min.

Biotin Nitrile, 8. This compound was prepared by reaction of 0.8 g (2.1 mmol) of **7** and NaCN in absolute alcohol as previously described (*29*) to give 0.30 g (60%) of **8** as a colorless solid. mp 153−154 °C. HPLC: $t_R = 5.7$ min.

Homobiotin, 9. A 230 mg (0.96 mmol) quantity of **8** in 15 mL of 1 N NaOH was heated to reflux for 3 h. The reaction mixture was acidified with concentrated HCl and a white precipitate formed. The precipitate was filtered, washed with water, and dried under vacuum to give a near quantitative yield of **9** as a colorless solid. mp > 240 °C. ^{1}H NMR (MeOH-d_4, 500 MHz) δ 1.4 (m, 2H), 1.55−1.8 (m, 4H), 2.2 (t, J = 3.3 Hz, 2H), 2.8 (d, J = 6.8 Hz, 1H), 3.0 (dd, J = 2.5, 6.6 Hz, 1H), 3.35 (m, 1H), 4.4 (m, 1H), 4.6 (m, 1H). IR (KBr) 3380, 3260, 2920, 1700, 1620, 1480, 1450, 1420, 1140, 1280, 1080 cm^{-1}. HRMS mass calcd for $C_{11}H_{19}N_2O_3S$ $(M + H)^+$: 259.1116; Found 259.1115. HPLC: $t_R = 7.4$ min.

Norbiotinamine N-tBoc, 11. This compound was prepared as previously described (*30*). Briefly, reaction of TFP ester, **2a**, with azide to form the acyl azide **10**, then rearrangement and trapping of the amine to give the N-tBoc protected norbiotinamine, **11**. HPLC: t_R = 10.7 min.

Norbiotinamine, 12. This compound was prepared by treatment of **11** with trifluoroacetic acid as previously described (*30*). ^{1}H NMR (MeOH-d_4, 200 MHz) δ 1.4−1.9 (m, 6H), 2.7 (d, J = 6.5 Hz, 1H), 2.8−3.0 (m, 3H), 3.1−3.3 (m, 1H), 4.3 (m, 1H), 4.5 (m, 1H). HRMS mass calcd for $C_9H_{18}N_3OS$ $(M + H)^+$: 216.1171; Found 216.1171. HPLC: $t_R = 2.8$ min.

Biotinamide, 13. To an ice-bath cooled solution containing 700 mg (1.8 mmol) of biotin TFP ester, **2a**, in 5 mL of DMF was added 30 mL of concentrated NH_4OH solution dropwise. After the addition, the reaction mixture was stirred in the ice bath for 5 min. Then the ice bath was removed and the reaction mixture was allowed to come to room temperature while stirring for 2 h. The white solid was filtered, washed with water and ether, and dried under vacuum to give a near quantitative yield of **13** as a white solid. mp 235−237 °C (dec). ^{1}H NMR (DMSO-d_6, 200 MHz) δ 1.1−1.8 (m, 6H), 2.0 (t, J = 3.6 Hz, 2H), 2.6 (m, 2H), 2.8 (dd, J = 6.2, 2.4 Hz, 1H), 3.1 (m, 1H), 4.1 (m, 1H), 4.3 (m, 1H), 6.4 (d, J = 5.7 Hz, 2H), 6.7 (s, 1H), 7.4 (s, 1H). IR (KBr) 3340, 3200, 2920, 1680, 1470, 1410, 1270, 1160, 1080 cm^{-1}. HRMS mass calcd for $C_{10}H_{18}N_3O_2S$ $(M + H)^+$: 244.1119. Found: 244.1111. HPLC: $t_R = 6.5$ min.

Biotinamine, 14. To a 300 mg (1.24 mmol) quantity of biotinamide, **13**, in 20 mL of THF was added 225 mg of (5.7 mmol) $LiAlH_4$. The suspension was refluxed for 24 h. Following this, the reaction mixture was cooled with an ice bath, and H_2O was added dropwise to destroy the excess $LiAlH_4$. The product was extracted with $CHCl_3$ (3 × 100 mL). The $CHCl_3$ solution was washed with H_2O then with aqueous saturated NaCl. The $CHCl_3$ solution was then dried over anhydrous Na_2SO_4, filtered, and evaporated to yield 280 mg (98%) of **14** as a colorless solid. mp 209−211 °C. ^{1}H NMR (MeOH-d_4, 500 MHz) δ 1.3−1.8 (m, 10H), 2.66 (t, J = 3.5 Hz, 2H), 2.74 (d, J =

Scheme 1. General Scheme for Preparation of Biotin-CN-Cbl Derivatives, 3a−o

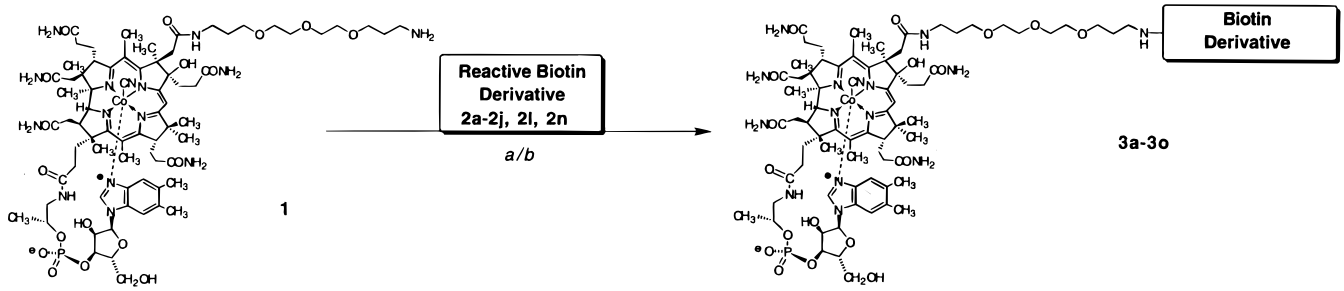

[a] DMF, Et_3N, rt, 1−16 h, 80−96%. [b] **3j**, **3l**, or **3n**,TFA, rt, 15 min, 90−98%.

6.3 Hz, 1H), 2.96 (dd, J = 6.5, 2.5 Hz, 1H), 3.3 (m, 1H), 4.3 (m, 1H), 4.5 (m, 1H). IR (KBr) 3220, 2920, 2840, 1690, 1570, 1470, 1320, 1250, 1160, 1090 cm^{-1}. HRMS mass calcd for $C_{10}H_{20}N_3OS$ $(M + H)^+$: 230.1327; Found 230.1318. HPLC: t_R = 2.8 min.

Preparation of 17. This compound was prepared by reaction of the biotin TFP ester **2a** with 3-aminobutyric acid, **15**, as previously described (*23*).

Preparation of 18. TFP−OTFA (0.14 mL, 0.82 mmol) was added slowly to a mixture containing *d*-biotin, **4**, (0.10 g, 0.41 mmol), Et_3N (0.17 mL, 1.23 mmol), and anhydrous DMF (12 mL) at room temperature. The mixture was stirred at room temperature for 10 min and then mixed with a solution of water (3 mL), acetone (5 mL), sodium hydrogen carbonate (0.172 g, 2.05 mmol), and α-*tert*-butyl-L-aspartic acid, **16**, (0.0924 g, 0.41 mmol). After the reaction mixture was stirred at room temperature for 6 h, volatile materials were evaporated under vacuum. The residue was washed with 20 mL of ethyl acetate and neutralized with 22 mL of 0.1 N HCl. After setting the precipitate at 5 °C for overnight, it was filtered, washed with water, and dried under high vacuum to yield 0.14 g (82%) of **18** as a colorless solid. mp 158−160 °C. ^1H NMR (CD_3OD, 200 MHz) δ 1.46 (s, 9 H), 1.49 (m, 2H), 1.66 (m, 4H), 2.27 (t, 2H), 2.78 (m, 2H), 2.97 (m, 1 H), 3.31 (m, 2H), 4.41 (dd, 1 H), 4.59 (dd, J = 5.0 Hz, 1 H), 4.75 (m, 1 H). HRMS calcd for $C_{18}H_{29}N_3NaO_6S$ $(M + Na)^+$: 438.1675. Found: 438.1675. HPLC: t_R = 9.2 min.

Preparation of 24. Biotin tetrafluorophenyl ester, **2a** (0.404 g, 1.03) was added slowly to a solution of *O*-*tert*-butyl-serine methyl ester **19** (0.218 g, 1.03 mmol) and Et_3N (0.43 mL, 3.09 mmol) in anhydrous DMF (5 mL) at room temperature. The reaction mixture was stirred at room temperature for 1 h and then was evaporated to dryness. The residue was purified by silica gel column chromatography (40 g) eluting with 5% MeOH/EtOAc to give 0.37 g (89%) of **24** as an oily solid. ^1H NMR ($CDCl_3$, 200 MHz) δ 1.14 (s, 9H), 1.48−1.84 (m, 6H), 2.31 (t, J = 7.0 Hz, 2H), 2.72−2.94 (m, 2H), 3.56 (dd, J = 3.3 Hz, 1H), 3.81 (m, 2H), (dd, J = 4.4 Hz, 1H), 4.53 (dd, J = 4.4 Hz, 1H), 4.72 (m, 1H), 5.19 (s, 1H), 5.84 (s, 1H). HRMS calcd for $C_{18}H_{32}N_3O_5S$ $(M + H)^+$: 402.2063. Found: 402.2061. HPLC: t_R = 10.5 min.

Preparation of 25. A solution containing potassium hydroxide (0.203 g, 3.62 mmol) *N*-biotinyl-*O*-*tert*-butyl-serine methyl ester, **24** (0.413 g, 1.03 mmol), methanol (5 mL), and water (5 mL) was stirred at 50−55 °C for 1 h. After the solution was cooled to room temperature, pH of the solution was adjusted to 4−5. Solvents were evaporated under vacuum, then the residue was taken up by methanol and evaporated to dryness. The crude product was purified by silica gel column chromatography (30 g) eluting with 20% MeOH/EtOAc to give 0.26 g (65%) of **25** as a colorless solid. mp 164−166 °C. ^1H NMR (DMSO-d_6, 200 MHz) δ 1.07 (s, 9H), 1.23−1.68 (m, 6H), 2.11 (t, J = 7.0 Hz, 2H), 2.43−2.60 (m, 2H), 2.82 (dd, J = 4.8 Hz, 1H), 3.08 (m, 1H), 3.41 (m, 1H), 3.99 (m, 1H), 4.12 (dd, J = 4.4 Hz, 1H), 4.30 (dd, J = 5.1 Hz, 1H), 6.40 (s, 1H), 6.55 (s, 1H), 7.35 (d, J = 7.3 Hz, 1H), 8.43 (s, 1H). HRMS calcd for $C_{17}H_{30}N_3O_5S$ $(M + H)^+$: 388.1906. Found: 388.1912. HPLC: t_R = 11.8 min.

Chart 1. Biotin Conjugates of CN-Cbl-*c*-lactone Used as Standards

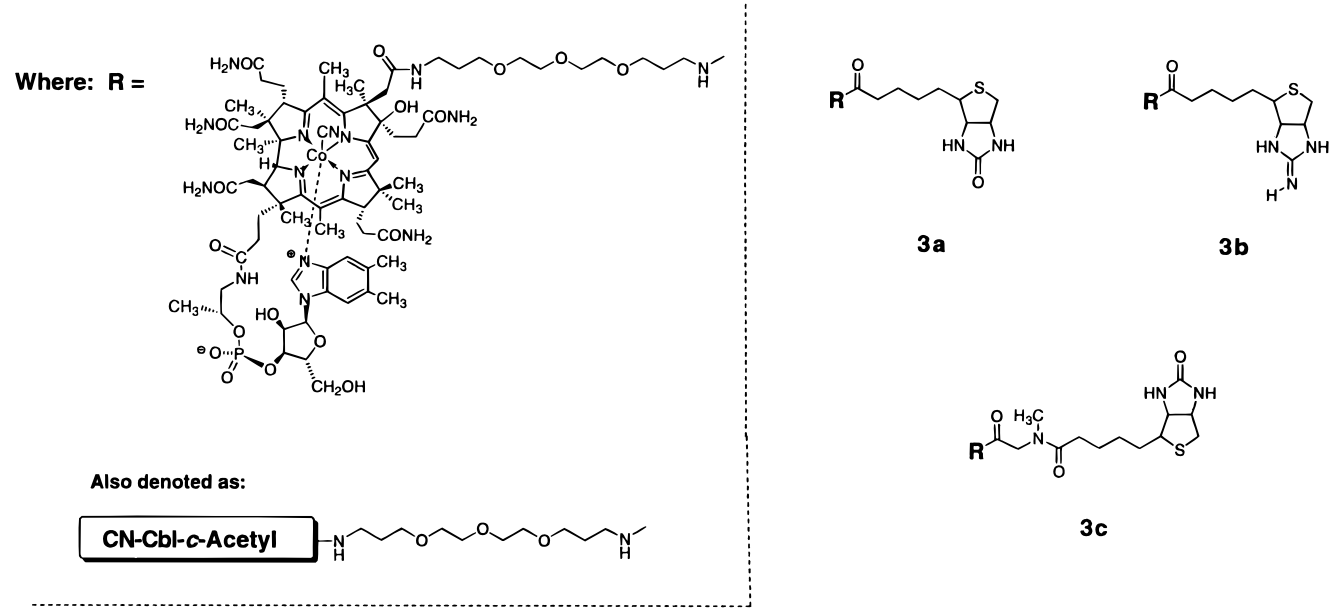

Chart 2. Biotin Conjugates of CN-Cbl-*c*-lactone Which Are Altered in Biotinamide Functionality

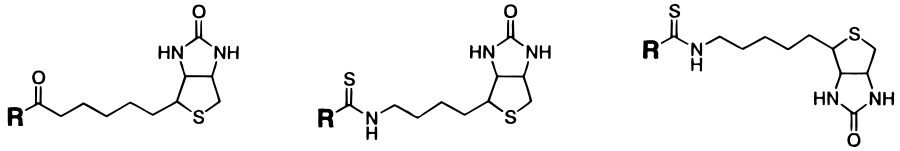

3d **3e** **3f**

Where R = CN-Cbl-*c*-Acetyl

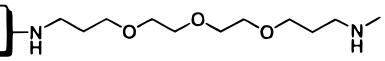

Preparation of 26. A mixture containing *N*-biotinyl-*O-tert*-butyl-serine methyl ester, **24** (0.15 g, 0.37 mmol), potassium hydroxide (0.062 g, 1.11 mmol), methanol (2 mL), and water (2 mL) was stirred at 55 °C for 30 min. The solution was taken to dryness under vacuum, then 1.5 mL of trifluoroacetic acid was added and stirred at room temperature for 16 h. Volatile materials were evaporated under vacuum, then the residue was purified by silica gel column chromatography (30 g) eluting with 50% MeOH/EtOAc to give 0.11 g (90%) of **26** as a colorless solid. mp 182−184 °C (dec). ^{1}H NMR (CD_3OD, 200 MHz) δ 1.49 (m, 2H), 1.68 (m, 4H), 2.31 (m, 2H), 2.70 (d, 1H), 2.94 (dd, 1H), 3.22 (m, 1H), 3.31 (m, 2H), 3.91 (d, 1H), 4.33 (m, 2H), 4.49 (dd, 1 H). HRMS calcd for $C_{13}H_{20}N_3Na_2O_5S$ $(M - H + 2Na)^+$: 376.0919. Found: 376.0924. HPLC: $t_R = 3.7$ min.

Preparation of 27. Biotin tetrafluorophenyl ester, **2a** (2.12 g, 5.39 mmol) was added to a solution containing L-aspartic acid β-*tert*-butyl ester, **22** (1.0 g, 5.29 mmol), sodium bicarbonate (1.47 g, 17.44 mmol), water (40 mL), and acetone (40 mL) at room temperature. The reaction mixture was stirred at room temperature for 16 h and then evaporated to dryness. The residue was washed with 60 mL of ethyl acetate and neutralized with 19.0 mL of 1.0 N HCl. After setting at 5 °C for overnight, the precipitate was filtered, washed with water and dried under high vacuum to yield 1.91 g (87%) of the biotin-aspartate-β-*O*-tBu ester adduct, **27** as a colorless solid. mp 167.6−168.5 °C. ^{1}H NMR (CD_3OD, 200 MHz) δ 1.45 (s, 9 H), 1.48−1.90 (m, 6 H), 2.22−2.30 (m, 2 H), 2.60−2.78 (m, 2 H), 2.83−2.97 (m, 1 H), 3.15−3.24 (m, 1 H), 3.29−3.32 (m, 1 H), 4.30 (dd, $J = 4.4$ Hz, 1 H), 4.48 (dd, $J = 5.0$ Hz, 1 H), 4.73 (dd, $J = 5.5$ Hz, 1 H). HRMS calcd for $C_{18}H_{29}N_3O_6S$ $(M + H)^+$: 416.1855. Found: 416.1868. HPLC: $t_R = 9.6$ min.

Preparation of 28. Biotin tetrafluorophenyl ester, **2a** (1.64 g, 4.18 mmol) was added to a solution of *N*-ϵ-*tert*-Boc-L-lysine, **23** (1.0 g, 4.06 mmol), sodium bicarbonate (1.13 g, 13.40 mmol), water (40 mL), and acetone (40 mL) at room temperature. The reaction mixture was stirred at room temperature for 16 h, then volatile materials were evaporated under vacuum. The residue was washed with 60 mL of ethyl acetate and neutralized with 14.0 mL of 1.0 N HCl. After the product set at 5 °C overnight, the product was filtered, washed with cold water, and dried under vacuum to yield 1.91 g (87%) of the biotin-

Chart 3. Biotin Conjugates of CN-Cbl-*c*-lactone Which Have Substituents Alpha to Biotinamide Functionality

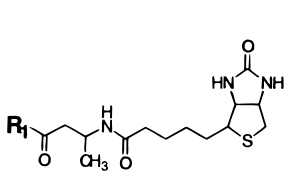

3g

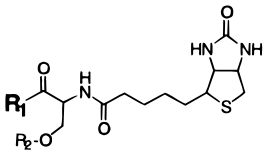

3h: R_2 = tBu
3i: R_2 = H

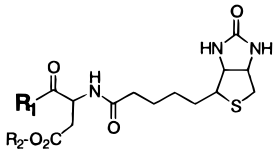

3j: R_2 = tBu
3k: R_2 = H

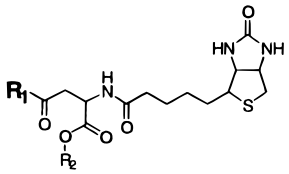

3l: R_2 = tBu
3m: R_2 = H

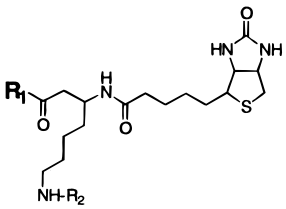

3n: R_2 = tBoc
3o: R_2 = H

Where R_1 = CN-Cbl-*c*-Acetyl

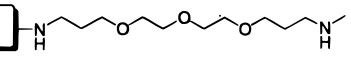

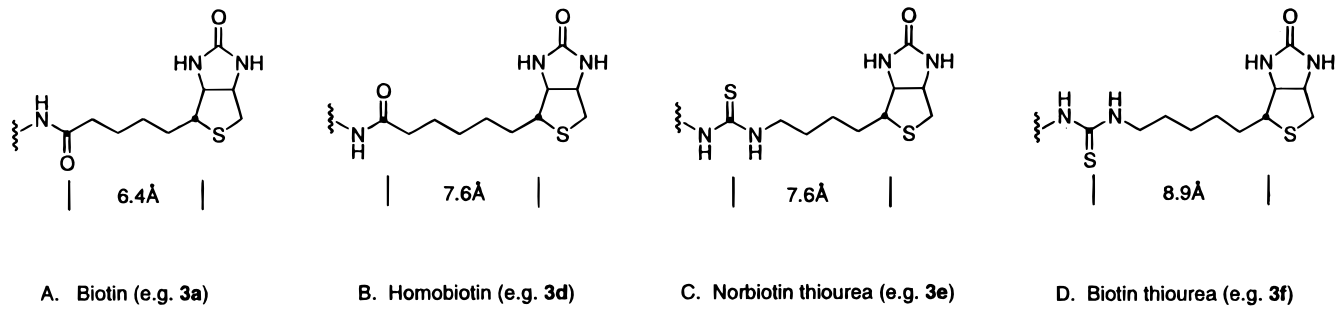

Figure 1. Distances from biotin ring structure to the carbonyl or thiocarbonyl functionality in biotin conjugates having altered biotinamide functionalities. Biotin is included for comparison. The distances shown were obtained from structural models in Chem3D (CambridgeSoft Corp., Cambridge, MA) after structural and energy minimization.

lysine-*N*-tBoc adduct, **28** as a colorless solid. mp 156.8−157.5 °C. ^{1}H NMR (CD_3OD, 200 MHz) δ 1.43 (s, 9 H), 1.48−1.90 (m, 10 H), 2.26 (t, J = 7.2 Hz, 2 H), 2.69 (d, J = 12.8 Hz, 1 H), 2.89−3.05 (m, 3 H), 3.16−3.26 (m, 1 H), 3.29−3.34 (m, 2 H), 4.26−4.34 (m, 2 H), 4.49 (dd, J = 4.8 Hz, 1 H). HRMS calcd for $C_{21}H_{36}N_4O_6S$ $(M + Na)^+$: 495.2253. Found: 495.2240. HPLC: t_R = 10.3 min.

Relative Dissociation Rate Analysis. To 300 μL of a 1 mg/mL solution of avidin (300 μg; 4.4 nmol) (or r-SAv) in a plastic microcentrifuge vial was added 4 equiv (18 nmol) of a biotin conjugate (**3a**−**o**) dissolved in 30 μL of a 10% aqueous DMSO solution. The avidin/biotin derivative mixture was incubated for 1 h at room temperature, and 100 μL of the solution was injected into the HPLC to assay binding. To the remaining avidin/biotin derivative solution was added 40 μL of a 1 mg/mL solution of biotin (40 μg; 164 nmol) in 10% aqueous DMSO. That solution was incubated for 1 h and 100 μL was removed for analysis by HPLC. The remaining solution was incubated for an additional 2 h, then another 100 μL was removed and analyzed by HPLC.

RESULTS

The primary goal of this research effort was to obtain information about how chemical modification of biotin conjugates affects their dissociation rate from Av and SAv. To attain that goal, several biotin derivatives were synthesized, conjugated with a cyanocobalamin (CN−Cbl) derivative (**1**), and their relative dissociation rates were measured by size exclusion HPLC analysis.

Compound Synthesis. A general synthetic route to preparing the biotin-CN−Cbl derivatives is shown in Scheme 1. The synthesis of the CN−Cbl derivative **1**, chosen for preparing the conjugates, is easily accomplished in high yield (>80%) by reacting the readily prepared *c*-lactone of CN−Cbl (*25*, *31*, *32*) with 4,7,10-trioxa-1,13-tridecanediamine at 55 °C for 1 h (*21*). This compound was conjugated with the modified biotin derivatives for evaluation in the HPLC analysis. Modifications of biotin included increasing the biotin side chain length (Chart 2), changing the type of bond used to conjugate the biotin moiety with a linker (Chart 2), and conjugation with amino acids to introduce substit-

Scheme 2. Synthesis of Homobiotin TFP Ester, 2d

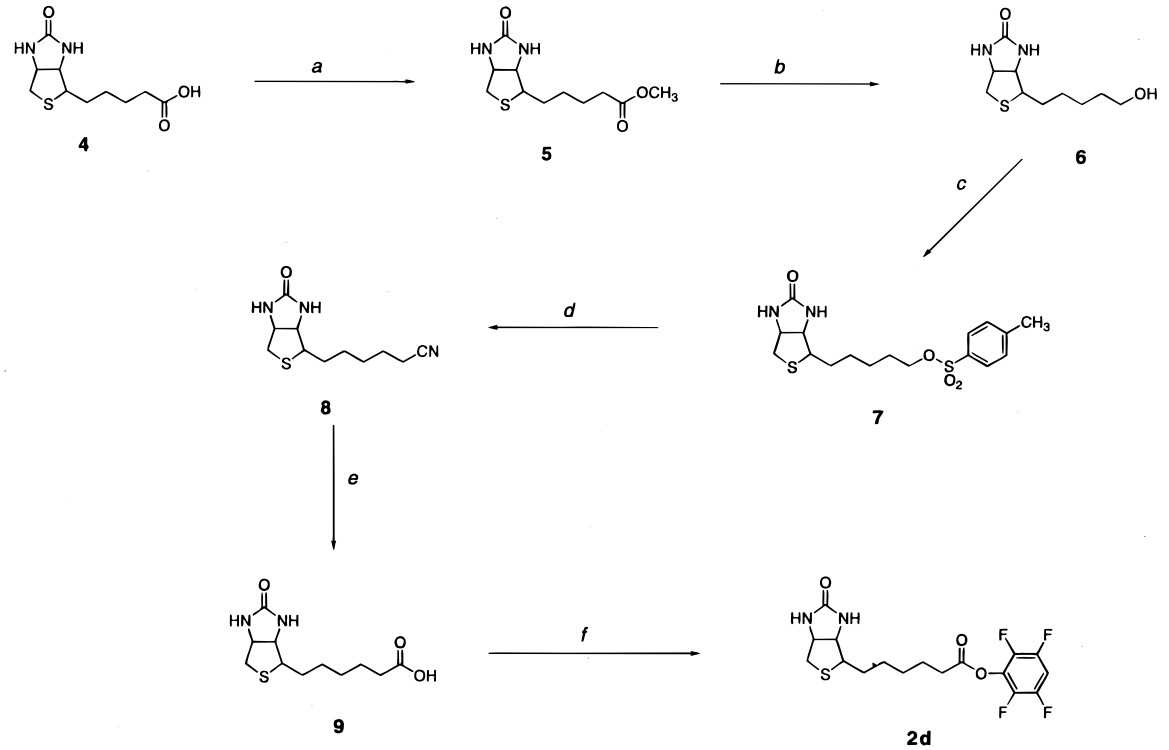

[a] MeOH, HCl, 99%. [b] $LiAlH_4$, 100%. [c] Pyridine, TsCl, 0 °C, 5 h, 87%. [d] NaCN, EtOH, 60%. [e] 1 N NaOH, Δ, 3 h, 99%. [f] DMF, Et_3N, TFP-OTFA, rt, 30 min, 87%.

Scheme 3. Synthesis of Norbiotin Isothiocyanate, 2e

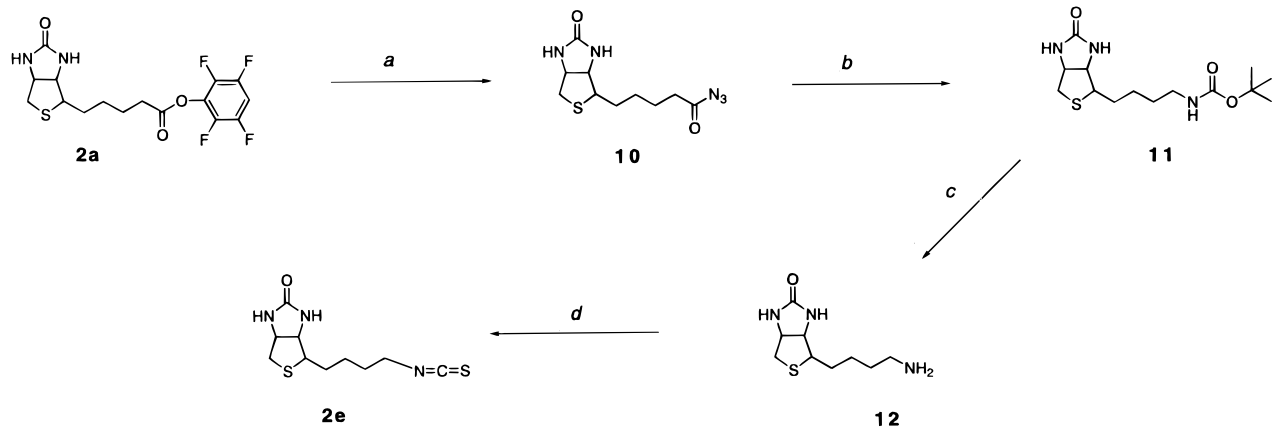

[a] NaN_3. [b]tBuOH, Δ. [c]TFA. [d]DMF, TCDI, rt, 45 min, 55%.

uents on the methylene group α to the biotinamide functionality (Chart 3).

Biotin-CN−Cbl Conjugates Used as Reference Compounds (3a, 3b, and 3c; Chart 1). Our previous studies demonstrated that the biotin-CN−Cbl conjugate, **3a**, which has no alteration in the biotin moiety or linker, has a very slow dissociation rate from Av and SAv, similar to that of biotin (*21*). Because of the very slow dissociation rate, **3a** was prepared for use as a reference compound. Similarly, our previous studies demonstrated that no binding was obtained with iminobiotin-CN−Cbl conjugate, **3b**, so it was prepared as a reference compound for biotin derivatives that have no retention. The previous studies also demonstrated that a biotin derivative which is modified with a methyl substituent on the biotinamide nitrogen, **3c**, had a measurable dissociation rate from Av and SAv over a 1−3 h period (*21*). Since we routinely incorporate the *N*-methylglycine moiety into our new biotin derivatives, **3c** was of particular interest as a reference compound for comparison purposes. Syntheses of **3a**, **3b**, and **3c** were accomplished in high yield by reaction of biotin TFP ester, **2a**, iminobiotin NHS ester, **2b**, or biotin-sarcosine TFP ester, **2c** with CN−Cbl derivative, **1** at room temperature for 4 h (*21*).

Biotin-CN−Cbl Conjugates That Have Altered Biotinamide Bonds (3d−f; Chart 2). Most biotin conjugates are prepared by reacting an activated ester of biotin with an amine containing moiety. If a primary aliphatic amine is conjugated, high binding affinity with Av and SAv is obtained, but in vivo applications are limited due to rapid cleavage of the biotinamide bond by biotinidase (*33*). Thus, our initial studies were focused on alteration of the biotinamide bond, either by moving it away from the biotin ring structure with insertion of a methylene group (Figure 1, panel B, increase of 1.2 Å) or by changing the nature of the biotinamide bond. Although it was uncertain whether addition of an extra methylene in the side chain of biotin, as is found in homobiotin (*34*), would be stabile to biotinidase cleavage, it was of interest to know if the rate of dissociation from Av and SAv would be affected by this change. Therefore, homobiotin tetrafluorophenyl ester, **2d**, was prepared as shown in Scheme 2. Reaction of **2d** with the CN−Cbl derivative, **1**, provided the homobiotin-CN−Cbl conjugate, **3d**, in 95% yield.

In a second approach, the biotinamide bond was replaced with a thiourea bond to assess how that modification affected the dissociation rate. We chose to prepare two biotin conjugates, **3e** and **3f**, containing thiourea bonds for the study. Not only was the nature of the biotinamide bond changed in biotin conjugates prepared, but the distance from the biotin ring structure to the hydrolyzable thiocarbonyl was increased 1.2−2.5 Å over that of the normal biotinamide bond (Figure 1, panels C and D). This fact, we believed, would help to stabilize the bonds toward biotinidase cleavage. One derivative, **3e**, was prepared from norbiotin isothiocyanate, **2e**, and the other derivative, **3f**, was prepared from biotin isothiocyanate, **2f**. The syntheses of **2e** and **2f** are shown in Schemes 3 and 4, respectively. Conjugations of **1** with norbiotin isothiocyanate,

Scheme 4. Synthesis of Biotin Isothiocyanate, 2f

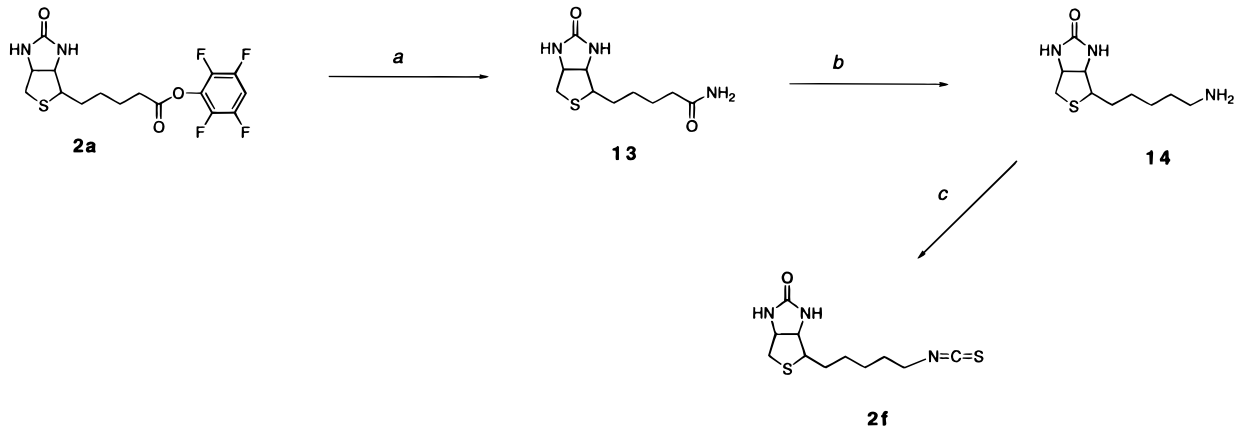

[a] DMF, concentrated NH_4OH, 0 °C to rt, 2 h, 99%. [b]THF, $LiAlH_4$, Δ, 24 h, 98%. [c]DMF, TCDI, rt, 2 h, 74%.

Scheme 5. Synthesis of Biotin-β-Amino Acid TFP Esters, 2g and 2l

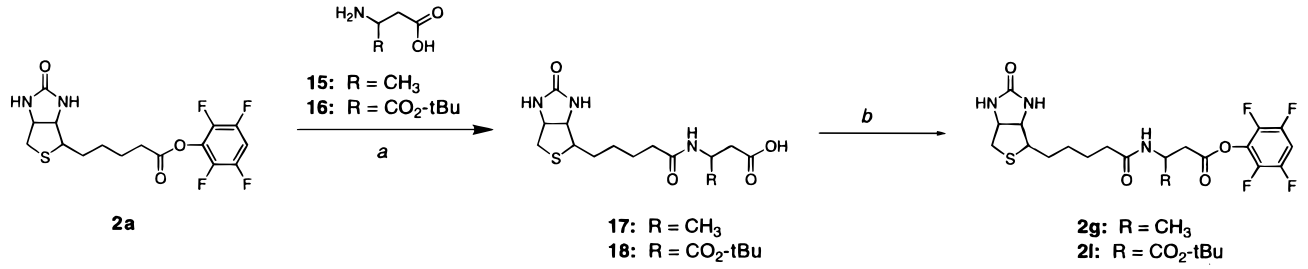

[a] **15**, DMF, Et_3N, rt, 24 h, 28%; **16**, H_2O, acetone, $NaHCO_3$, rt, 6 h, 82%. [b]TFP-OTFA, DMF, Et_3N, rt, 30 min.

2e, and biotin isothiocyanate **2f**, provided the CN−Cbl conjugates **3e** and **3f** in 94% and 80% yields, respectively.

Biotin-CN−Cbl Conjugates That Have Substituents Alpha to the Biotinamide Functionality (3g−o, Chart 3). Biotin conjugates which have functional groups of varying size α to the biotinamide bond were targeted for synthesis because previous studies had indicated that this modification might retain the high affinity binding and additionally result in stabilization toward biotinidase cleavage (*23*). The α substituents were obtained by incorporating amino acids or functional group protected amino acids between biotin and the hydrophilic linker. Three amino acid conjugates, **3g**, **3l**, and **3m** (Chart 3), were prepared from amino acids that had carboxylates beta to the amine (3-aminobutyric acid, **15**, and L-aspartic acid-α-tBu ester, **16**). The syntheses of these derivatives is shown in Scheme 5. Reaction of **15** or **16** with the TFP ester of biotin, **2a**, provided biotin adducts **17** and **18**. The TFP esters **2g** and **2l** were prepared in situ from **17** and **18**, then conjugated withCN−Cbl derivative **1** to provide **3g** and **3l** in 78 and 94% yields, respectively. Removal of the tBu ester from **2l** was accomplished in neat TFA to provide **3m** in 90% yield.

Three additional amino acid derivatives (a serine derivative, **19**; an aspartate derivative, **22**; and a lysine derivative, **23**) were conjugated with biotin TFP ester, **2a** as shown in Scheme 6. Some difficulties with the conjugations of biotin and serine, **21**, led to the use of the diprotected, methyl ester/tBu ether containing, derivative **19**. Reaction of biotin TFP ester, **2a**, with **19** provided the biotin serine methyl ester derivative **24** in 89% yield. Hydrolysis of the crude biotin conjugate, **24**, with KOH gave the free carboxylate **25** in 65% isolated yield. When the crude hydrolysis product was treated with TFA without isolation, a 90% yield of the fully deprotected biotin-serine conjugate, **26**, was obtained. To evaluate the difference in dissociation rates due to steric encumbrance, preparation of CN−Cbl conjugates of both **25** and **26** was desired. Conjugation of **25** with CN−Cbl derivative **1** was accomplished by in situ generation of the TFP ester, **2h**, followed by reaction with **1**. This reaction sequence provided the desired conjugate **3h** in 92% isolated yield. Conjugation of **26** was accomplished in the same manner, where in situ generated TFP ester **2i** was reacted with **1** to provide **3i** in 96% isolated yield.

Conjugation of L-aspartic acid, which has the beta-carboxylate protected as a t-Bu ester, **22**, results in a different biotin conjugate than conjugation of the α-carboxylate protected aspartate derivative, **18**. Reaction of biotin-TFP ester, **2a**, with **22** provided the conjugate **27** in 87% yield. Activation of **27** for conjugation was accomplished by preparing the TFP ester, **2j**, in 58% isolated yield. The biotin-aspartate TFP ester, **2j**, was subsequently conjugated with **1** to give **3j** in 95% isolated yield. The tBu ether moiety was removed from **3j** by reaction in TFA for 15 min to provide a 98% isolated yield of **3k**.

A conjugate containing biotin and lysine, **3o**, was prepared in which a free amine was present. Biotin conjugates containing lysine in that configuration were particularly attractive as they appeared to have the potential for conjugation of an additional moiety, provided the dissociation rate was not increased. Conjugation of the ϵ-*N*-tBoc protected L-lysine, **23**, with biotin TFP ester, **2a**, provided **28** in 87% yield. Conversion of **28** to its TFP ester was accomplished using EDC and

Scheme 6. Synthesis of Biotin-α-Amino Acid TFP Esters, 2h−j and 2n

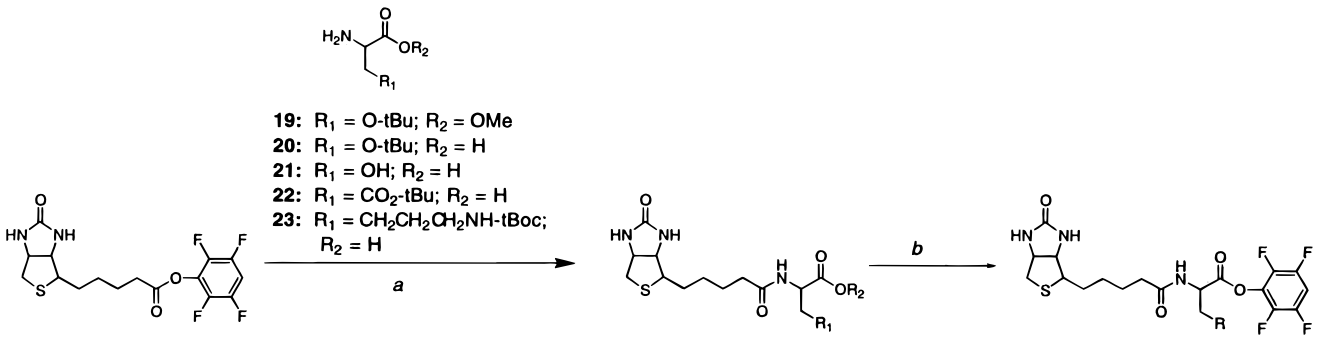

[a] **19**, DMF, Et_3N, rt, 1 h, 89%; **20**, KOH, MeOH, H_2O, 1 h, 55 °C, 65%; **21**, TFA, 16 h, 90%; **22** or **23**,H_2O, acetone, $NaHCO_3$, rt, 16 h, 87%. [b]**25** or **26**,TFP−OTFA, Et_3N, CH3CN, rt, 1 h; **27** or **28**, TFP−OH, DMF, EDC, rt, 48 h.

Table 1. Percentage of Biotin-CN−Cbl Dyes Bound[a] with Av or SAv at 1 and 3 h after Being Challenged by a Large Excess of Biotin[b]

biotin −CN−Cbl derivative	1 h	3 h
binding with Av		
3a	>98	>98
3b	0	0
3c	<5	0
3d	30	<10
3e	10	0
3f	<5	0
3g	>98	>98
3h	40	30
3i	>98	>98
3j	8	<5
3k	73	54
3l	49	27
3m	98	98
3n	29	17
3o	<5	0
binding with SAv		
3a	>98	>98
3c	30	<5
3e	50	15
3g	>98	>98
3k	70	36

[a] The quantity bound was measured by the peak areas of (S)Av-bound dye vs free dye at 360 nm. Retention times of bound and free dye were determined by standards. In some of the chromatograms, an additional small peak between the bound and free was noted. It is not clear what that peak is composed of. In those cases, the area of that peak was not included in the percentages shown. [b] A 53 M quantity of biotin was added to a solution containing 4 M equiv of biotin-CN−Cbl derivative bound with Av or SAv.

TFP−OH to provide **2n** in 45% isolated yield. Conjugation of **2n** with **1** provided **3n** in 96% yield. The tBoc protecting group was removed from **3n** with TFA to give **3o** in 93% yield.

HPLC Analyses for Relative Dissociation Rates. The relative rates of dissociation from Av were estimated by HPLC analysis for all biotin-CN−Cbl derivatives prepared [Chart 1 (**3a**−**c**), Chart 2 (**3d**−**f**), and Chart 3 (**3g**−**o**)]. Relative rates of dissociation from SAv were also evaluated for a few of the biotin-CN−Cbl derivatives (**3a**, **3c**, **3e**, **3g**, and **3k**). In the analyses, 4 M equiv of a biotin−dye conjugate were added to 1 M equiv of Av or SAv, and the solution was incubated at room temperature for 1 h. At that time, an aliquot was removed for size exclusion HPLC analysis ($t = 0$). Following that analysis, 53 M equiv of biotin was added to the Av/dye mixture, and aliquots were taken at 1 and 3 h post-biotin addition for HPLC analyses. HPLC peak areas for bound and free biotin-CN−Cbl dye were used to obtain percentages. The percent bound was calculated by dividing peak area for the protein-bound dye by the total peak area (bound and free) for dye (362 nm). Percentages of biotin-CN−Cbl conjugates bound with Av or SAv are tabulated in Table 1.

A large variation in the percent of biotin-CN−Cbl dye bound with Av or SAv was noted within the 3 h assay period. With the exception of the iminobiotin derivative, **3b**, all of the biotin-CN−Cbl derivatives were fully bound with Av and SAv when no biotin was present. As in our previous studies, unmodified biotin-CN−Cbl derivative **3a** did not dissociate from either Av or SAv at a detectable rate in the assay period when a large excess of biotin was introduced. The homobiotin derivative, **3d**, and the derivatives that contained thiourea bonds, **3e** and **3f**, dissociated rapidly when biotin was added. Biotin derivatives that have substituents α to the biotinamide bond, e.g., the α-methyl derivative **3g**, the α-hydroxymethylene derivative **3i**, and α-carboxylate derivative **3m**, all had no detectable dissociation in the presence of biotin within the 3 h test period. In contrast to this, biotin-CN−Cbl derivatives which contained the larger substituents, α-acetate, **3k**, and α-butylamine, **3o**, dissociated relatively rapidly. Interestingly, the biotin-CN−Cbl derivatives which had substituents α to the biotinamide containing the very bulky tBu ether, **3h**, tBu esters **3j**, **3l** and tBoc group, **3n**, appeared to be more tolerated than the derivatives that had changes in the biotinamide bond (**3c**−**f**). Another interesting observation is that removal of the bulky N-tBoc group in the protected lysine adduct, **3n,** to give the free amine, **3o**, resulted in a very rapid dissociation rate. This increase in the dissociation rate must reflect a difficulty in binding with the positive amine derivative. Since Av has a high pI [e.g., 10 (*1*)], the observed dissociation rate may be due to repulsion of charges. Although there were some differences in the dissociation rates of biotin-CN−Cbl derivatives when bound with SAv versus Av (Table 1), the trend for a biotin derivative to have either a slow dissociation or a more rapid dissociation was retained.

DISCUSSION

The high affinity binding of biotin with Av ($K = 10^{15}$ M^{-1}) (*2*, *35*, *36*) and SAv ($K = 10^{13}$−10^{14} M^{-1}) (*2*, *37*) makes these compounds particularly attractive for conjugates used in the cancer pretargeting approach. While the binding affinities might be expected to decrease when biotin is conjugated with another molecule, it seems reasonable that with the appropriately designed biotin conjugates, high affinity binding can be retained. This statement is based on the observation that many biotin conjugates have been prepared which have an apparent high affinity for Av and/or SAv and on the fact that in biotin derivatives, which have an unmodified bicyclic biotin ring structure, most of the "hydrogen-bonding network" is retained (*38*). The design of biotin conjugates for this application appeared to be quite simple in the initial examination, however, as studies have progressed it has become apparent that there are specific requirements that must be met in the design of new biotin conjugates for in vivo application. Those requirements include (1) high water solubility, (2) incorporation of a spacer between biotin and the molecule to which it is attached, and (3) incorporation of a functional group that blocks the biotinamide cleavage by biotinidase without significantly decreasing binding affinity with Av or SAv.

Water solubility has not been a concern in biotin derivatives prepared to carry radiometals (*39*−*44*). However, our initial investigations to design biotin conjugates for pretargeting halogen radionuclides were hampered by the very low water solubility of biotin derivatives. This difficulty was overcome by introducing a hydrophilic molecule between the biotin moiety and the molecule that was being conjugated (*23*, *26*, *45*, *46*). In addition to increasing water solubility, the hydrophilic linking molecule acts as a spacer between the biotin moiety and its conjugated molecule. A number of research efforts have demonstrated that introduction of a spacer moiety between biotin and certain molecules can improve binding with Av and/or SAv (*47*−*53*). Therefore, in our optimization of biotin derivatives, we generally include a hydrophilic linker molecule between biotin and the molecule with which it is to be conjugated.

Our initial in vitro studies were also hampered by an instability of biotin conjugates. This instability appeared

to be brought about by cleavage of biotin by the enzyme biotinidase (*22*, *33*, *54*−*56*). Other investigators had indicated that modification of the biotinamide bond with a methyl group blocked this cleavage (*57*), and our own studies confirmed that finding (*23*). Since obtaining that result, we have made a number of biotin derivatives that contain the hydrophilic linker and also contain the *N*-methyl biotinamide functionality to provide in vivo stability. More recently, we examined the relative association and dissociation rates of some biotin derivatives, including the *N*-methyl derivative by HPLC analyses (*21*). While only small differences were observed in the association rates, significant increases in the rate of dissociation of biotin conjugates from Av and SAv were observed.

Rapid dissociation rates of biotin derivatives from Av or SAv can be problematic for in vivo application, particularly in pretargeting of radionuclides for therapy. Although the rate at which radiolabeled biotin molecules are released from a tumor site is dependent on a number of factors, the rate of dissociation from Av or SAv is perhaps the most important factor. It is our belief that in an optimal therapy situation, the pretargeted mAb-SAv conjugate is homogeneously distributed in the tumor and all of the available biotin binding sites are filled with radiolabeled biotin derivatives. When all of the available biotin binding sites are filled, a homogeneous distribution of the radionuclide is obtained in the tumor. If only a portion of the biotin binding sites on the tumor-bound mAb-SAv conjugate are filled, it unlikely that a homogeneous distribution will be obtained. The biotin binding sites on cells nearest to the blood vessels will be filled to a higher extent than those further from the blood vessels. This situation has previously been described for high affinity mAbs as having a "binding site barrier" (*58*). When some of the biotin binding sites are unfilled, the dissociation rate is not as important since avidity will play a role in keeping the radiolabeled biotin derivative in the tumor. However, when the biotin binding sites are filled, either by the initial radiolabeled biotin derivative or by endogenous biotin, then the dissociation rate of the biotin derivative is of paramount importance in tumor retention.

Dissociation rates of biotin derivatives from Av and SAv have previously been accurately measured using [^{14}C]biotin[2] or [^{3}H]biotin (*37*, *59*). In our studies, an accurate value for the dissociation rates was not required, so we chose to use a rapid nonradioactive HPLC assay to measure relative dissociation rates of biotin derivatives over a 3−4 h period (*21*). In previous studies, it was demonstrated that relative dissociation rates could be obtained by challenging biotin-cyanocobalamin (biotin-CN−Cbl) conjugates that were bound to Av or SAv with a large excess (e.g., >50 M equiv) of biotin. On the basis of those studies, we chose to prepare biotin derivatives conjugated with a CN−Cbl derivative, **1**, as shown in Scheme 1.

In our initial approach to biotin modification, we hypothesized that structural modification of the biotinamide bond might provide stability toward biotinidase cleavage while retaining the high binding affinity. The very simple modification of extending the side chain of biotin by one methylene unit to form the homobiotin derivative, **3d**, was examined first. Surprisingly, the homobiotin derivative was found to have a rapid dissociation rate relative to an unmodified biotin derivative, **3a** (Table 1). Our next approach to biotin modification was to change the type of bond connecting biotin and the linker from the biotinamide bond to a thiourea bond. Two thiourea bonded biotin derivatives, **3e** and **3f**, were prepared and evaluated. These derivatives demonstrated even faster dissociation rates than the homobiotin derivative. The results obtained in the initial studies indicate that the biotin moiety and the biotinamide bond should not be altered if retention of the very high affinity binding is desired.

Biotin derivatives which have amino acids conjugated to biotin were also of interest in our binding study. The interest in biotin-amino acid derivatives was brought about by a previous literature report (*59*) and our own experiences, which indicated that biotinidase cleavage may be blocked if the conjugates has substituents α to the biotinamide bond. Rosebrough reported that after reaction of the sulfhydryl group, the biotin derivative formed from conjugation of cysteine and biotin was stable to biotinidase cleavage (*60*). The biotin derivative formed in that study has a carboxylate α to the biotinamide. In our own studies, it was noted that conjugation of biotin with 3-aminobutyric acid provided a substantial decrease in the rate of biotin cleavage by biotinidase (*23*). We were particularly interested in determining how the size and nature of functional group α to the biotinamide functionality affected the dissociation rate. Thus, a series of derivatives which contained substituents α to the biotinamide bond were prepared (Chart 3). The series included a methyl (**3g**), a hydroxymethylene (**3i**), an acetate (**3k**), a carboxylate (**3m**), and a butylamine (**3o**). The synthetic routes to the targeted biotin derivatives required that tBu ether, tBu ester, and N-tBoc protecting groups be used. The biotin derivatives which contained the protecting groups were also conjugated with the CN−Cbl moiety. While not of primary interest, evaluating those biotin derivatives (**3h**, **3j**, **3l**, and **3n)** permitted an analysis of the effect of bulky protecting group on the dissociation rate. The results obtained from the HPLC analyses indicate that the smaller substituents, the methyl, hydroxymethylene and carboxylate groups do not increase the dissociation rate, whereas larger substituents such as an acetate or a butylamine group increase the dissociation rate significantly. As expected, a significant steric effect was also noted for biotin derivatives containing the tBu and tBoc protecting groups.

The goal of this investigation was to obtain information on how modifications of biotin conjugates affected their dissociation rates from Av and SAv such that biotin derivatives which retained very slow dissociation rates could be identified. It seems likely that there are other modifications than those studied that could retain slow dissociation rates from Av and SAv and also possess biotinidase stability. However, once it was determined in these studies that the biotin moiety must remain unaltered to retain a slow dissociation rate, our efforts were directed solely at evaluating the effect of substituents α to the biotinamide bond. In contrast to biotin derivatives used for in vitro assays, such as previously reported radioiodinated biotin derivatives (*61*−*65*), we believe that structural modifications will be required in designing optimal biotin derivatives. Although some of the previously reported radiohalogenated (*66*−*72*) and metal binding biotin derivatives (*13*, *39*, *40*, *42*, *43*, *73*−*77*) have been successfully applied to pretargeting without incorporating all of the structural parameters of biotin conjugates listed above, full optimization of the biotin conjugate structure for in vivo use should provide a more efficacious reagent when applied to Targeted Radiotherapy.

On the basis of previous studies, we have developed a number of radiolabeled biotin derivatives that contain a

Chart 4. Preferred Biotin Derivatives for in Vivo Applications

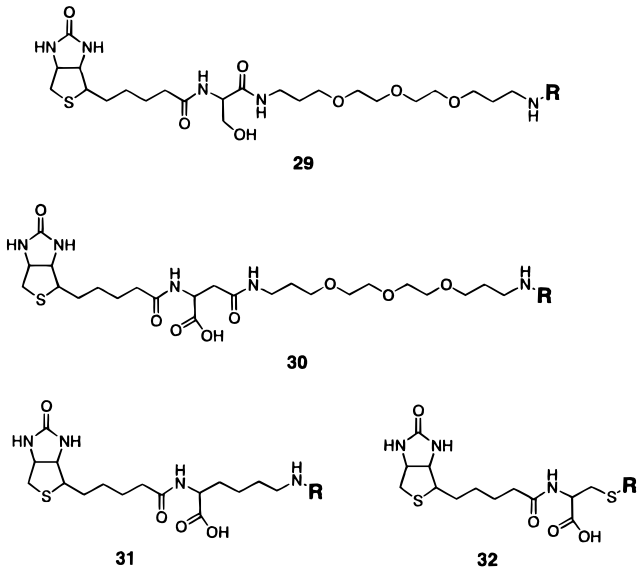

N-methyl biotin moiety (*78*). The data obtained in this study indicates that the dissociation rates from Av and SAv are significantly increased when biotin conjugates contain a biotinamide bond that has been modified as a *N*-methyl derivative. However, it must be emphasized that these data alone do not indicate that *N*-methyl biotinamide derivatives will not be useful for in vivo application. Indeed, Axworthy et al. (*77*) have demonstrated that a Y-90 labeled *N*-methyl biotin derivative can be successfully used in a pretargeting approach for cancer therapy in the mouse model. The dissociation rates are not the only factors in determining if a biotin derivative will be useful in vivo, and dissociation rates are not fully predictive of tumor retention in vivo as other factors, such as avidity, affect the retention of biotin derivatives in a tumor. Relative dissociation rates do, however, provide a parameter that can be optimized for in vivo use as most applications that utilize the biotin/SAv binding pair do so because of the high affinity of these compounds.

On the basis of the studies herein, biotin derivatives in which the structure of biotin is not modified but contains a linker molecule that has a small substituent, such as a hydroxymethylene or carboxylate group, α to the biotinamide bond should provide excellent candidates for in vivo applications. Incorporation of structural features that result in slow dissociation from Av or SAv alone does not result in compounds that are optimized. For example, although high binding affinity was obtained with the derivative containing an α methyl group (**3g**), our previous studies indicated that it was not completely stable to biotinidase degradation (*23*) making that configuration nonoptimal for in vivo use. Other biological factors, such as half-life in blood, metabolic pathway, and routes of excretion also play a role in obtaining the optimal biotin derivative for in vivo applications. Ultimately, optimization of biotin derivatives for in vivo applications must have these parameters included.

Our present choice of biotin derivatives is shown in Chart 4. Coupling serine with biotin provides an α-hydroxymethylene containing derivative, **29**. Coupling biotin with either an aspartate, lysine, or cysteine can provide an α-carboxylate as these adducts, **30**, **31**, and **32**, can be conjugated to other molecules (**R**) through their carboxylate, amine, or sulfhydryl groups (respectively). The biotin-serine conjugate **29** and biotin-aspartate **30** are shown with our preferred hydrophilic linker as part of the biotin derivative. The biotin-lysine conjugate, **31**, and biotin-cysteine conjugate, **32**, might be more effectively used for conjugation with molecules that are ionized or have an inherent high water solubility. Importantly, we have conducted studies with radioiodinated derivatives that have shown the α-hydroxymethylene and α-carboxylate functionalities effectively block cleavage by biotinidase (*79*).

In Summary. Fifteen biotin derivatives were prepared and conjugated with a CN−Cbl derivative, **1**. The relative dissociation rates of those compounds were measured by size exclusion HPLC. The HPLC analyses provided definitive data on how the various modifications in the biotin structure affected the dissociation rates from Av. Only the unmodified biotin conjugate, **3a**, and the modified conjugates that contained a methyl (**3g**), hydroxymethylene (**3i**), or carboxylate (**3m**) retained the slow dissociation rate found with biotin. Slightly different values were obtained when SAv was used rather than Av, but the trends for slow dissociation were the same as found with Av. From these data, we propose that the best biotin conjugates for in vivo applications are those that have a hydroxymethylene or a carboxylate α to the biotinamide bond. Biotin derivatives with these structural features retain high binding affinities. In other studies, we have demonstrated that biotin derivatives with these structural features are also stable to biotinidase cleavage.

ACKNOWLEDGMENT

We thank Dr. Ross Lawrence (Department of Medicinal Chemistry, University of Washington) for efforts in obtaining mass spectral data. We are grateful for the financial support provided by the Department of Energy, Medical Applications and Biophysical Research Division, Office of Health and Environmental Research under Grant DE-FG03-98ER62572.

Supporting Information Available: HPLC chromatograms, NMR spectra, and mass spectra of all new or not fully characterized compounds (**3d**−**o**, **2e**, **2f**, **2j**, **2n**, **7**, **9**, **13**, **18**, **24**−**26**, **28**). This material is available free of charge via the Internet at http://pubs.acs.org.

LITERATURE CITED

(1) Green, N. M. (1975) Avidin. *Adv. Protein Chem. 29*, 85−133.
(2) Green, N. M. (1990) Avidin and Streptavidin. *Methods Enzymol. 184*, 51−67.
(3) Bayer, E. A., and Wilchek, M. (1980) The Use of the Avidin−Biotin Complex as a Tool in Molecular Biology. *Methods Biochem. Anal. 26*, 1−45.
(4) Bayer, E. A., and Wilchek, M. (1996) The Avidin−Biotin System. In *Immunoassay* (E. P. Diamandis, and T. K. Christopoulos, Eds.) pp 237−267, Academic Press, San Diego.
(5) Diamandis, E. P., and Christopoulos, T. K. (1991) The Biotin-(Strept)Avidin System: Principles and Applications in Biotechnology. *Clin. Chem. 37*, 625−636.
(6) Wilchek, M., and Bayer, E. A. (1990) Introduction to Avidin−Biotin Technology. *Methods Enzymol. 184*, 5−45.
(7) Hnatowich, D. J., Virzi, F., and Rusckowski, M. (1987) Investigations of Avidin and Biotin for Imaging Applications. *J. Nucl. Med. 28*, 1294−1302.
(8) Paganelli, G., Riva, P., Deleide, G., Clivio, A., Chiolerio, F., Scassellati, G. A., Malcovati, M., and Siccardi, A. G. (1988) In Vivo Labeling of Biotinylated Monoclonal Antibodies by Radioactive Avidin: A Strategy to Increase Tumor Radiolocalization. *Int. J. Cancer 2*, 121−125.

(9) Paganelli, G., Pervez, S., Siccardi, A. G., Rowlinson, G., Deleide, G., Chiolerio, F., Malcovati, M., Scassellati, G. A., and Epenetos, A. A. (1990) Intraperitoneal Radio-Localization of Tumors Pre-Targeted by Biotinylated Monoclonal Antibodies. *Int. J. Cancer 45*, 1184−1189.

(10) Paganelli, G., Magnani, P., Zito, F., Villa, E., Sudati, F., Lopalco, L., Rossetti, C., Malcovati, M., Chiolerio, F., Seccamani, E., Siccardi, A. G., and Fazio, F. (1991) Three-step monoclonal antibody tumor targeting in carcinoembryonic antigen-positive patients. *Cancer Res. 51*, 5960−5966.

(11) Paganelli, G., Malcovati, M., and Fazio, F. (1991) Monoclonal Antibody pretargetting techniques for tumour localization: the avidin−biotin system. *Nucl. Med. Commun. 12*, 211−234.

(12) Fritzberg, A. R., Kasina, S., Rao, T. N., Vanderheyden, J.-L., and Srinivasan, A. (1997) *Metal-Radionuclide-Labeled Proteins and Glycoproteins for Diagnosis and Therapy*, U.S. Patent 5,616,692.

(13) Goodwin, D. A., and Meares, C. F. (1997) Pretargeting: General Principles. *Cancer (Suppl.) 80*, 2675−2680.

(14) Goodwin, D. A., Meares, C. F., and Osen, M. (1998) Biological properties of biotin-chelate conjugates for pretargeted diagnosis and therapy with the avidin/biotin system. *J. Nucl. Med. 39*, 1813−1818.

(15) Sakahara, H., and Saga, T. (1999) Avidin−biotin system for delivery of diagnostic agents. *Adv. Drug Del. 37*, 89−101.

(16) Stoldt, H. S., Aftab, F., Chinol, M., Paganelli, G., Luca, F., Testori, A., and Geraghty, J. G. (1997) Pretargeting Strategies for Radio-immunoguided Tumour Localisation and Therapy. *Eur. J. Cancer 33*, 186−192.

(17) Zhu, H., Jain, R. K., and Baxter, L. T. (1998) Tumor Pretargeting for Radioimmunodetection and Radioimmunotherapy. *J. Nucl. Med. 39*, 65−76.

(18) Mock, D. M. (1999) Biotin status: which are valid indicators and how do we know? *J. Nutr. 129*, 498S−503S.

(19) Zempleni, J., and Mock, D. M. (1999) Biotin biochemistry and human requirements. *J. Nutr. Biochem. 10*, 128−138.

(20) Wang, H., and Pevsner, J. (1999) Detection of endogenous biotin in various tissues: novel functions in the hippocampus and implications for its use in avidin−biotin technology. *Cell Tissue Res. 296*, 511−516.

(21) Wilbur, D. S., Pathare, P. M., Hamlin, D. K., Frownfelter, M. B., Kegley, B. B., Leung, W.-Y., and Gee, K. R. (2000) Evaluation of Biotin-Dye Conjugates for Use in an HPLC Assay to Assess Relative Binding of Biotin Derivatives with Avidin and Streptavidin. *Bioconjugate Chem. 11*, 584−598.

(22) Hymes, J., Fleischhauer, K., and Wolf, B. (1997) Biotinidase in Serum and Tissues. *Methods Enzymol. 279*, 422−434.

(23) Wilbur, D. S., Hamlin, D. K., Pathare, P. M., and Weerawarna, S. A. (1997) Biotin reagents for antibody pretargeting. Synthesis, radioiodination, and in vitro evaluation of water soluble, biotinidase resistant biotin derivatives. *Bioconjugate Chem. 8*, 572−584.

(24) Gamper, H. B., Reed, M. W., Cox, T., Virosco, J. S., Adams, A. D., Gall, A. A., Scholler, J. K., and Meyer, R. B. (1993) Facile Preparation of Nuclease Resistant 3′ Modified Oligodeoxynucleotides. *Nucleic Acids Res. 21*, 145−150.

(25) Pathare, P. M., Wilbur, D. S., Heusser, S., Quadros, E. V., McLoughlin, P., and Morgan, A. C. (1996) Synthesis of cobalamin-biotin conjugates that vary in the position of cobalamin coupling. Evaluation of cobalamin derivative binding to transcobalamin II. *Bioconjugate Chem. 7*, 217−232.

(26) Wilbur, D. S., Hamlin, D. K., Vessella, R. L., Stray, J. E., Buhler, K. R., Stayton, P. S., Klumb, L. A., Pathare, P. M., and Weerawarna, S. A. (1996) Antibody fragments in tumor pretargeting. Evaluation of biotinylated Fab′ colocalization with recombinant streptavidin and avidin. *Bioconjugate Chem. 7*, 689−702.

(27) Sundberg, S. A., Barrett, R. W., Pirrung, M., Lu, A. L., Kiangsoontra, B., and Holmes, C. P. (1995) Spatially-Addressable Immobilization of Macromolecules on Solid Supports. *J. Am. Chem. Soc. 117*, 12050−12057.

(28) Alves, A. M., Holland, D., and Edge, M. D. (1989) A Chemical Method of Labeling Oligodeoxyribonucleotides with Biotin: A Single Step Procedure Using a Solid-Phase Methodology. *Tetrahedron Lett. 30*, 3089−3092.

(29) Hofmann, K., Chen, C., Bridgwater, A., and Axelrod, A. E. (1947) Furan and Tetrahydrofuran Derivatives. VII. The Synthesis and Biological Activity of a Number of Oxybiotin Homologues. *J. Am. Chem. Soc. 69*, 191−195.

(30) Szalecki, W. (1996) Synthesis of Norbiotinamine and Its Derivatives. *Bioconjugate Chem. 7*, 271−273.

(31) Wagner, F. (1965) Reactions of the cyano and alkyl cobalamins. *Proc. R. Soc. London, Ser. A 288*, 344−347.

(32) Lien, E. L., Ellenbogen, L., Law, P. Y., and Wood, J. M. (1974) Studies on the Mechanism of Cobalamin Binding to Hog Intrinsic Factor. *J. Biol. Chem. 249*, 890−894.

(33) Pispa, J. (1965) Animal Biotinidase. *Ann. Med. Exp. Biol. Fenniae 43*, 3−40.

(34) Ruis, H., Brady, R. N., McCormick, D. B., and Wright, L. D. (1968) Bacterial Degradation of Biotin. II. Catabolism of ^{14}C-Homobiotin and ^{14}C-Norbiotin. *J. Biol. Chem. 243*, 547−551.

(35) Green, N. M. (1963) Avidin. 3. The Nature of the Biotin-Binding Site. *Biochem. J. 89*, 599−609.

(36) Green, N. M. (1966) Thermodynamics of the Binding of Biotin and some Analogues of Avidin. *Biochem. J. 101*, 774−780.

(37) Chilkoti, A., and Stayton, P. S. (1995) Molecular Origins of the Slow Streptavidin−Biotin Dissociation Kinetics. *J. Am. Chem. Soc. 117*, 10622−10628.

(38) Klumb, L. A., Chu, V., and Stayton, P. S. (1998) Energetic roles of hydrogen bonds at the ureido oxygen binding pocket in the streptavidin−biotin complex. *Biochemistry 37*, 7657−7663.

(39) Virzi, F., Fritz, B., Rusckowski, M., Gionet, M., Misra, H., and Hnatowich, D. J. (1991) New indium-111 labeled biotin derivatives for improved immunotargeting. *Int. J. Rad. Appl. Instrum. B 18*, 719−726.

(40) Jeong, J. M., Kinuya, S., Paik, C. H., Saga, T., Sood, V. K., Carrasquillo, J. A., Neumann, R. D., and Reynolds, J. C. (1994) Application of High Affinity Binding Concept to Radiolabel Avidin with Tc-99m Labeled Biotin and the Effect of pI on Biodistribution. *Nucl. Med. Biol. 21*, 935−940.

(41) Hashmi, M., and Rosebrough, S. F. (1995) Synthesis, Pharmacokinetics, and Biodistribution of ^{67}GA Deferoxamineacetyl-Cysteinylbiotin. *Drug Metab. Dispos. 23*, 1362−1367.

(42) Chang, F., Rusckowski, M., Qu, T., and Hnatowich, D. J. (1997) Early Results in the Irrational Design of New Bifunctional Chelators. *Cancer (Suppl.) 80*, 2347−2353.

(43) Renn, O., Goodwin, D. A., Studer, M., Moran, J. K., Jacques, V., and Meares, C. F. (1996) New Approaches to Delivering Metal-Labeled Antibodies to Tumors: Synthesis and Characterization of New Biotinyl Chelate Conjugates for Pre-Targeted Diagnosis and Therapy. *J. Controlled Release 39*, 239−249.

(44) Karacay, H., Sharkey, R. M., Govindan, S. V., McBride, W. J., Goldenberg, D. M., Hansen, H. J., and Griffiths, G. L. (1997) Development of a Streptavidin-Anti-Carcinoembryonic Antigen Antibody, Radiolabeled Biotin Pretargeting Method for Radioimmunotherapy of Colorectal Cancer. Reagent Development. *Bioconjugate Chem. 8*, 585−594.

(45) Wilbur, D. S., Pathare, P. M., Hamlin, D. K., and Weerawarna, S. A. (1997) Biotin Reagents for Antibody Pretargeting. 2. Synthesis and in Vitro Evaluation of Biotin Dimers and Trimers for Cross-linking of Streptavidin. *Bioconjugate Chem. 8*, 819−832.

(46) Wilbur, D. S., Pathare, P. M., Hamlin, D. K., Stayton, P. S., To, R., Klumb, L. A., Buhler, K. R., and Vessella, R. L. (1999) Development of new biotin/streptavidin reagents for pretargeting. *Biomol. Eng. 16*, 113−118.

(47) Costello, S. H., Felix, R. T., and Giese, R. W. (1979) Enhancement of Immune Cellular Agglutination by Use of An Avidin−Biotin System. *Clin. Chem. 25*, 1572−1580.

(48) Hofmann, K., Titus, G., Montibeller, J. A., and Finn, F. M. (1982) Avidin Binding of Carboxyl-Substituted Biotin and Analogues. *Biochemistry 21*, 978−984.

(49) Shao, M. C., Chin, C. C., Caprioli, R. M., and Wold, F. (1987) The regulation of glycan processing in glycoproteins. The effect of avidin on individual steps in the processing of biotinylated glycan derivatives. *J. Biol. Chem. 262*, 2973−2979.

(50) Bernstein, K. E., Welsh, S. L., and Inman, J. K. (1990) A Deeply Recessed Active Site in Angiotensin-Converting Enzyme is Indicated From The Binding Characteristics of Biotin-Spacer-Inhibitor Reagents. *Biochem. Biophys. Res. Commun. 167*, 310−316.
(51) Smith, J. S., Miller, B. T., Knock, S. L., and Kurosky, A. (1991) Biotinylated Peptides/Proteins. 1. Determination of Stoichiometry of Derivatization. *Anal. Biochem. 197*, 247−253.
(52) Polli, J. W., and Billingsley, M. L. (1991) Preparation, characterization and biological properties of biotinylated derivatives of calmodulin. *Biochem. J. 275*, 733−743.
(53) Basak, A., Jean, F., Dugas, H., and Lazure, C. (1994) Biotinylation of an Enkephalin-Containing Heptapeptide via Various Spacer Arms. Synthesis, Comparative Binding Studies toward Avidin, and Application as Substrates in Enzymatic Reactions. *Bioconjugate Chem. 5*, 301−305.
(54) Chauhan, J., Ebrahim, H., Bhullar, R. P., and Dakshinamurti, K. (1985) Human Serum Biotinidase. *Ann. N. Y. Acad. Sci. 447*, 386-388.
(55) Wolf, B., Hymes, J., and Heard, G. S. (1990) Biotinidase. *Methods Enzymol. 184*, 103−111.
(56) Hymes, J., and Wolf, B. (1996) Biotinidase and Its Roles in Biotin Metabolism. *Clin. Chim. Acta 255*, 1−11.
(57) Axworthy, D. B., Theodore, L. J., Gustavson, L. M., and Reno, J. M. (1997) Biotinidase-Resistant Biotin-DOTA Conjugates. U.S. Patent 5,608,060.
(58) Fujimori, K., Covell, D. G., Fletcher, J. E., and Weinstein, J. N. (1990) A Modeling Analysis of Monoclonal Antibody Percolation Through Tumors: A Binding-Site Barrier. *J. Nucl. Med. 31*, 1191−1198.
(59) Piran, U., and Riordan, W. J. (1990) Dissociation Rate Constant of the Biotin-Streptavidin Complex. *J. Immunol. Methods 133*, 141−143.
(60) Rosebrough, S. F. (1993) Plasma Stability and Pharmacokinetics of Radiolabeled Deferoxamine-Biotin Derivatives. *J. Pharmacol. Exp. Ther. 265*, 408−415.
(61) Groman, E. V., Rothenberg, J. M., Bayer, E. A., and Wilchek, M. (1990) Enzymatic and Radioactive Assays for Biotin, Avidin, and Streptavidin. *Methods Enzymol. 184*, 208−217.
(62) Livaniou, E., Evangelatos, G. P., and Ithakissios, D. S. (1987) Radioiodinated Biotin Derivatives for In Vitro Radioassays. *J. Nucl. Med. 28*, 1430−1434.
(63) Livaniou, E., Evangelatos, G. P., and Ithakissios, D. S. (1987) Biotin radioligand assay with an 125I-labeled biotin derivative, avidin, and avidin double-antibody reagents. *Clin. Chem. 33*, 1983−1988.
(64) Evangelatos, S. A., Kakabakos, S. E., Evangelatos, G. P., and Ithakissios, D. S. (1993) Determination of serum biotinidase activity with biotinyl derivatives of Iodotyramines as substrates. *J. Pharm. Sci. 82*, 1228−1231.
(65) Garlick, R. K., and Giese, R. W. (1988) Avidin binding of radiolabeled biotin derivatives. *J. Biol. Chem. 263*, 210−215.
(66) Khawli, L. A., and Kassis, A. I. (1992) *m*-[^{125}I]Iodoaniline: a Useful Reagent for Radiolabeling Biotin. *Nucl. Med. Biol. 19*, 297−301.
(67) Najafi, A., and Peterson, A. (1993) Preparation and in vitro evaluation of "no-carrier-added" ^{18}F-labeled biotin. *Nucl. Med. Biol. 20*, 401−405.
(68) Shoup, T. M., Fischman, A. J., Jaywook, S., Babich, J. W., Strauss, H. W., and Elmaleh, D. R. (1994) Synthesis of Fluorine-18-Labeled Biotin Derivatives: Biodistribution and Infection Localization. *J. Nucl. Med. 35*, 1685−1690.
(69) Kortylewicz, Z. P., Baranowska-Kortylewicz, J., Adelstein, S. J., Carmel, A. D., and Kassis, A. I. (1994) Radiolabeled Biotin Amides from Triazenyl Precursors: Synthesis, Binding, and In-Vivo Properties. *J. Labelled Compd. Radiopharm. 34*, 1129−1146.
(70) Foulon, C. F., Adelstein, S. J., and Kassis, A. I. (1996) One-step synthesis of radioiodinated biotin derivatives. *Bioorg. Med. Chem. Lett. 6*, 779−784.
(71) Foulon, C. F., Schoultz, B. W., and Zalutsky, M. R. (1997) Preparation and Biological Evaluation of an Astatine-211 Labeled Biotin Conjugate: Biotinyl-3-[^{211}At]astatoanilide. *Nucl. Med. Biol. 24*, 135−143.
(72) Foulon, C. F., Alston, K. L., and Zalutsky, M. R. (1997) Synthesis and Preliminary Biological Evaluation of (3-Iodobenzoyl)norbiotinamide and ((5-Iodo-3-pyridinyl)carbonyl)-norbiotinamide: Two Radioiodinated Biotin Conjugates with Improved Stability. *Bioconjugate Chem. 8*, 179−186.
(73) Rowlinson-Busza, G., Hnatowich, D. J., Rusckowski, M., Snook, D., and Epenetos, A. A. (1993) Xenograft Localization Using Pretargeted Streptavidin-conjugated Monoclonal Antibody and ^{111}In-Labeled Biotin. *Antibody, Immunoconjugates, Radiopharm. 6*, 97−109.
(74) Modorati, G., Brancato, R., Paganelli, G., Magnani, P., Pavoni, R., and Fazio, F. (1994) Immunoscintigraphy with three step monoclonal pretargeting technique in diagnosis of uveal melanoma: preliminary results. *Br. J. Ophthalmol. 78*, 19−23.
(75) Alvarez-Diez, T. M., Polihronis, J., and Reilly, R. M. (1996) Pretargeted Tumour Imaging with Streptavidin Immunoconjugates of Monoclonal Antibody CC49 and ^{111}In-DTPA-Biocytin. *Nucl. Med. Biol. 23*, 459−466.
(76) Breitz, H. B., Weiden, P. L., Beaumier, P. A., Axworthy, D. B., Seiler, C., Su, F.-M., Graves, S., Bryan, K., and Reno, J. M. (2000) Clinical Optimization of Pretargeted Radioimmunotherapy with Antibody-Streptavidin Conjugate and ^{90}Y-DOTA-Biotin. *J. Nucl. Med. 41*, 131−140.
(77) Axworthy, D. B., Reno, J. M., Hylarides, M. D., Mallett, R. W., Theodore, L. J., Gustavson, L. M., Su, F., Hobson, L. J., Beaumier, P. L., and Fritzberg, A. R. (2000) Cure of human carcinoma xenografts by a single dose of pretargeted yttrium-90 with negligible toxicity. *Proc. Natl. Acad. Sci. U.S.A. 97*, 1802−1807.
(78) Wilbur, D. S., Hamlin, D. K., Pathare, P. M., and Weerawarna, S. A. (1997) Biotin reagents for antibody pretargeting. Synthesis, radioiodination and in vitro evaluation of water soluble, biotinidase resistant biotin derivatives. *Bioconjugate Chem. 8*, 572−584.
(79) Wilbur, D. S., Hamlin, D. K., Chyan, M.-K., Pathare, P. M., and Kegley, B. B. (2000) Biotin Reagents in Antibody Pretargeting. 5. Additional Studies of Biotin Conjugate Design to Provide Biotinidase Stability. *Bioconjugate Chem.* (manuscript in preparation).

BC000024V

© 2000 American Chemical Society, Bioconjugate Chem., Wilbur bc000024v Supporting Info Page 1

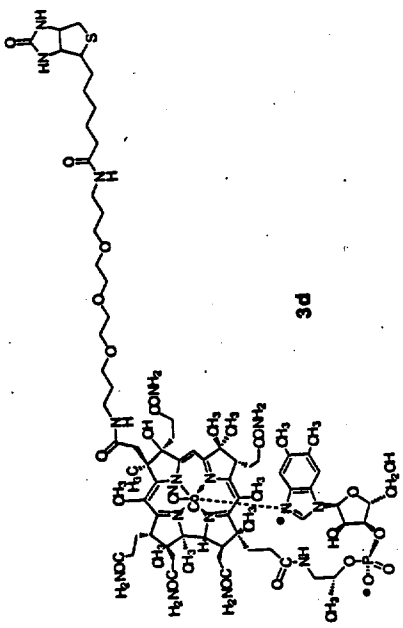

3d

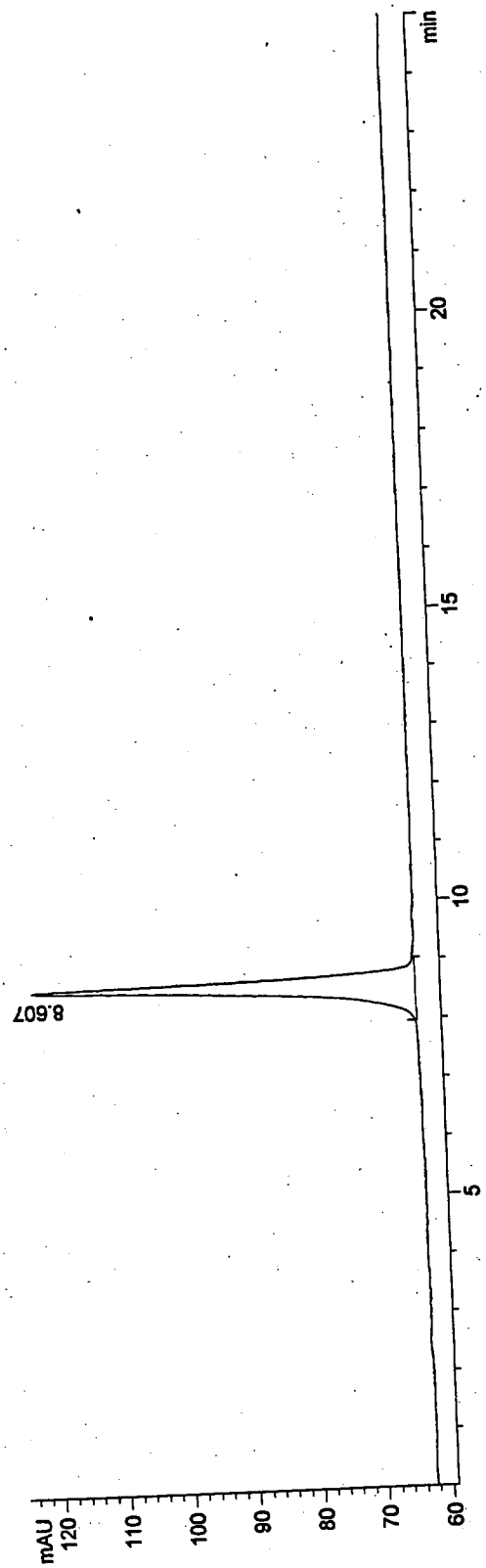

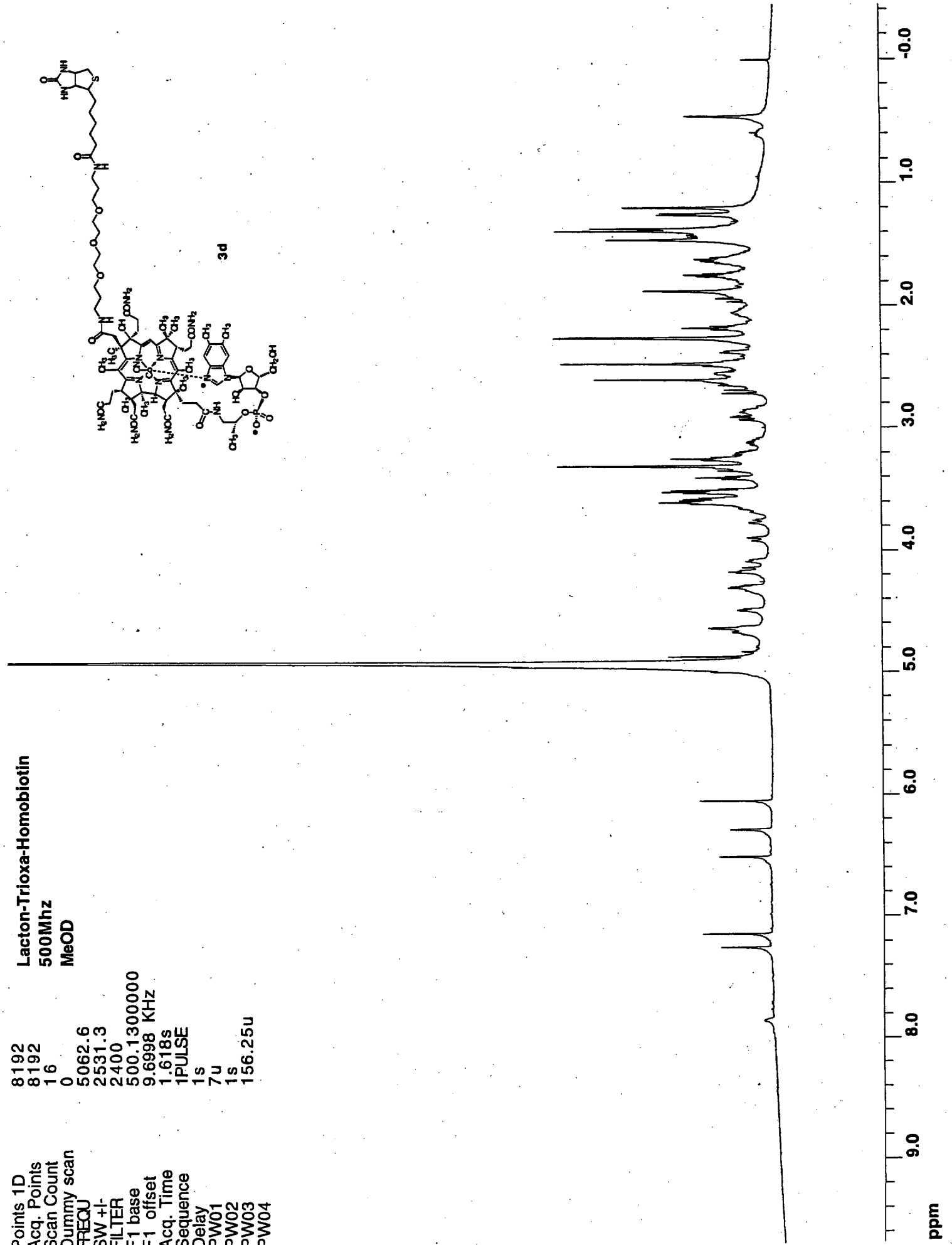
Lacton-Trioxa-Homobiotin
500Mhz
MeOD
Points 1D 8192
Acq. Points 8192
Scan Count 16
Dummy scan 0
FREQU 5062.6
SW +/- 2531.3
FILTER 2400
F1 base 500.1300000
F1 offset 9.6998 KHz
Acq. Time 1.618s
Sequence 1PULSE
Delay 1s
PW01 7u
PW02 1s
PW03 156.25u
PW04
3d
9.0
8.0
7.0
6.0
5.0
4.0
3.0
2.0
1.0
-0.0
ppm

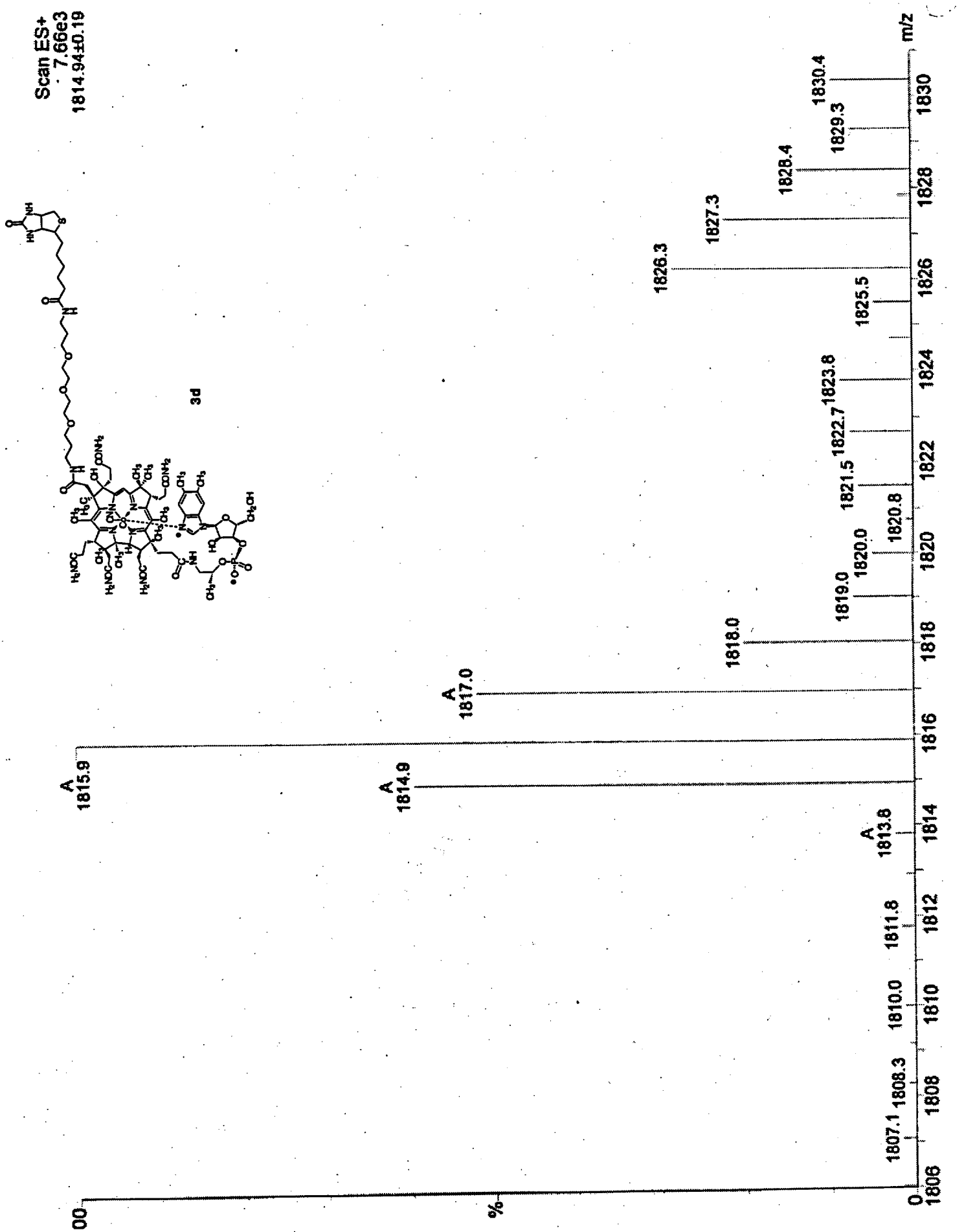
Scan ES+
7.66e3
1814.94±0.19
3d
100
%
0
m/z
1806
1807.1
1808
1808.3
1810
1810.0
1811.8
1812
1813.8
1814
1814.9
1815.9
1816
1817.0
1818
1818.0
1819.0
1820
1820.0
1820.8
1821.5
1822
1822.7
1823.8
1824
1825.5
1826
1826.3
1827.3
1828
1828.4
1829.3
1830
1830.4

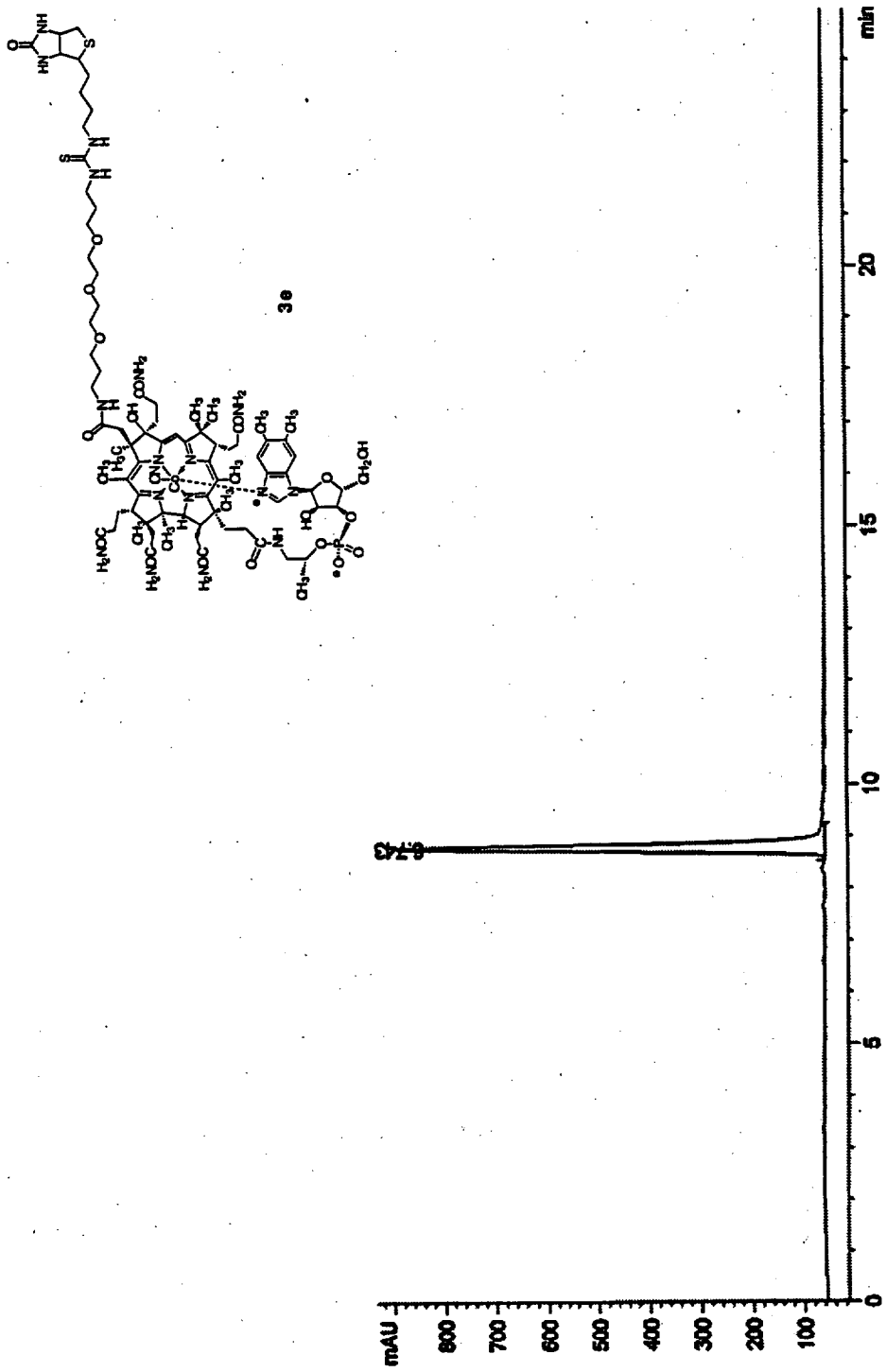
3e
mAU
800
700
600
500
400
300
200
100
0
5
10
15
20
min

© 2000 American Chemical Society, Bioconjugate Chem., Wilbur bc000024v Supporting Info Page 5

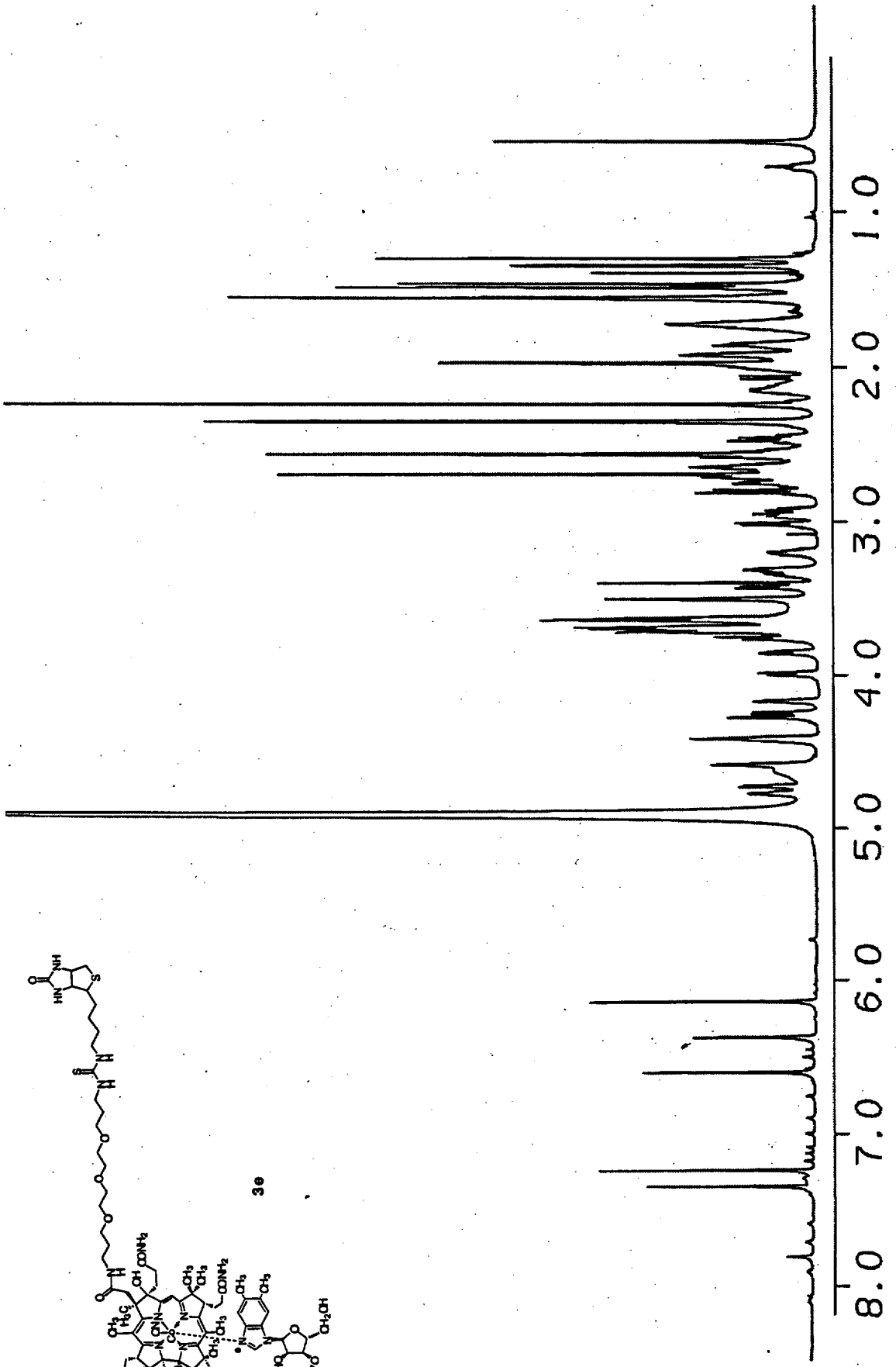

3e

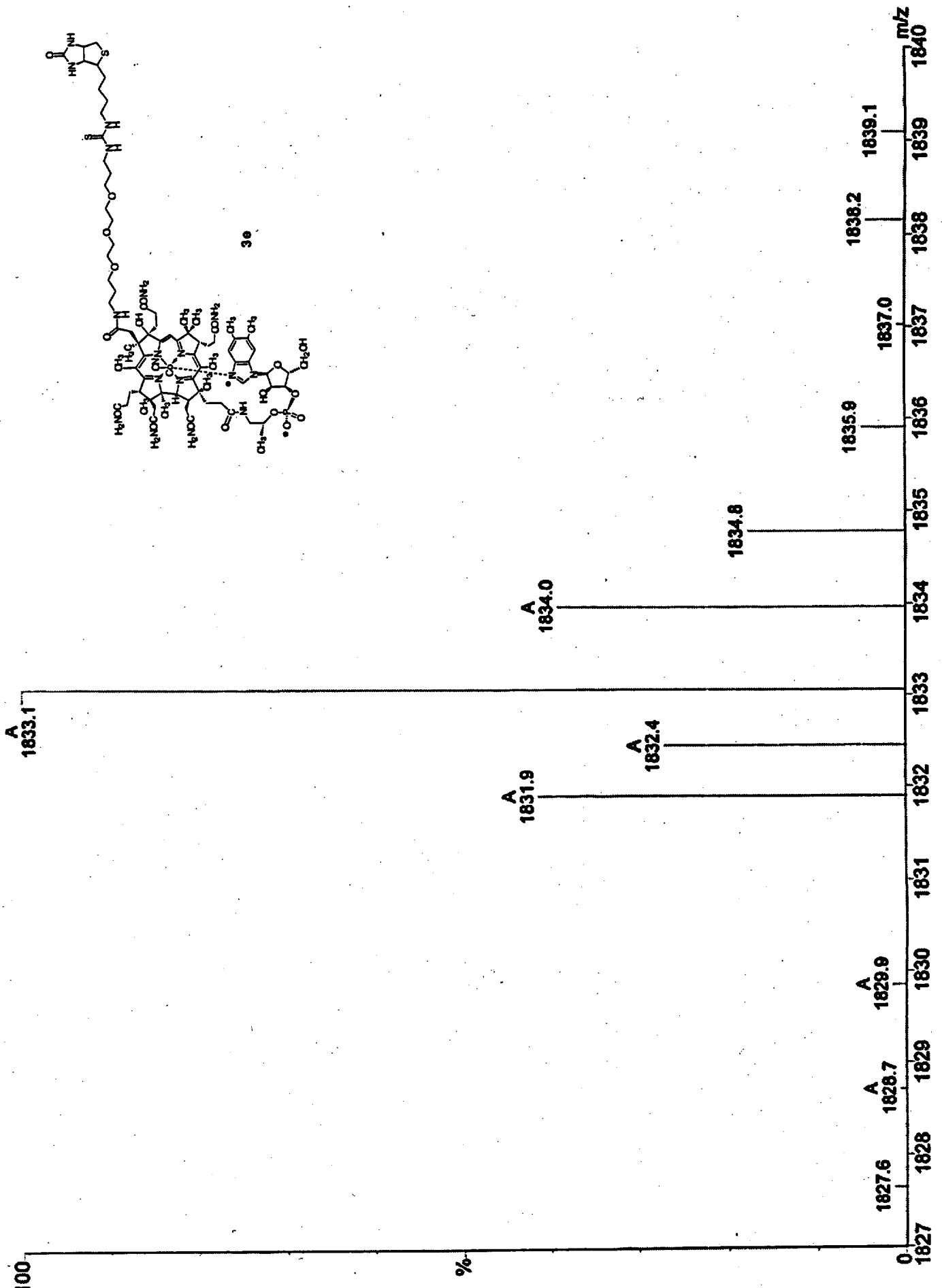
3e
100
%
0
1827
1828
1829
1830
1831
1832
1833
1834
1835
1836
1837
1838
1839
1840
m/z
1827.6
A 1828.7
A 1828.9
A 1831.9
A 1832.4
A 1833.1
A 1834.0
1834.8
1835.9
1837.0
1838.2
1839.1

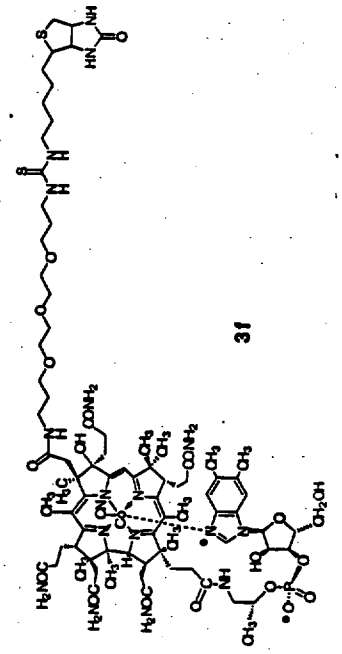

31

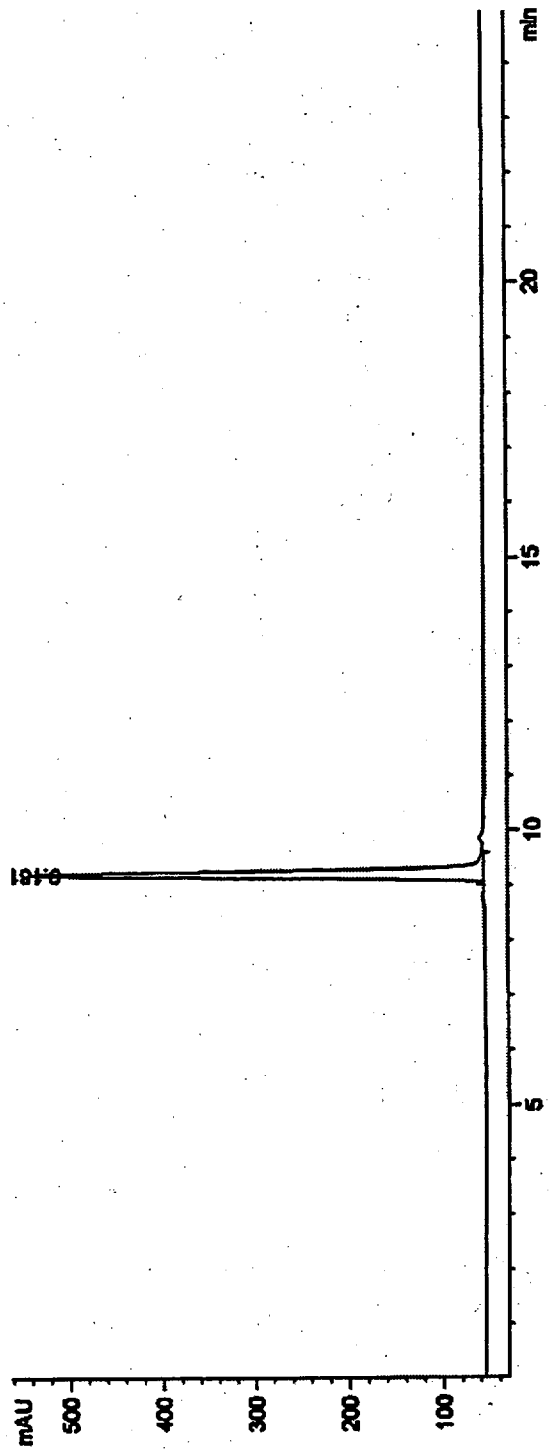

© 2000 American Chemical Society, Bioconjugate Chem., Wilbur bc000024v Supporting Info Page 8

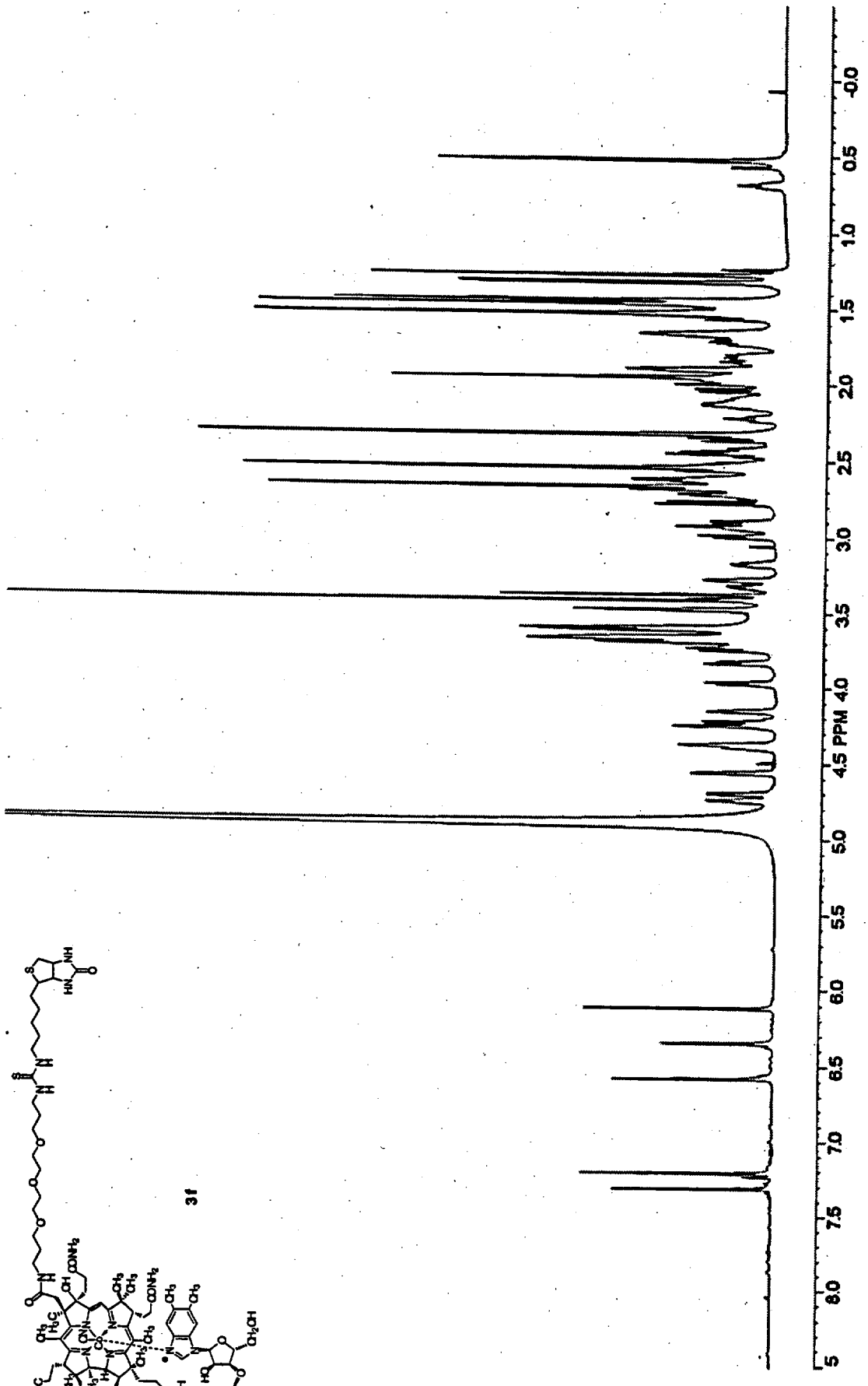

© 2000 American Chemical Society, Bioconjugate Chem., Wilbur bc000024v Supporting Info Page 9

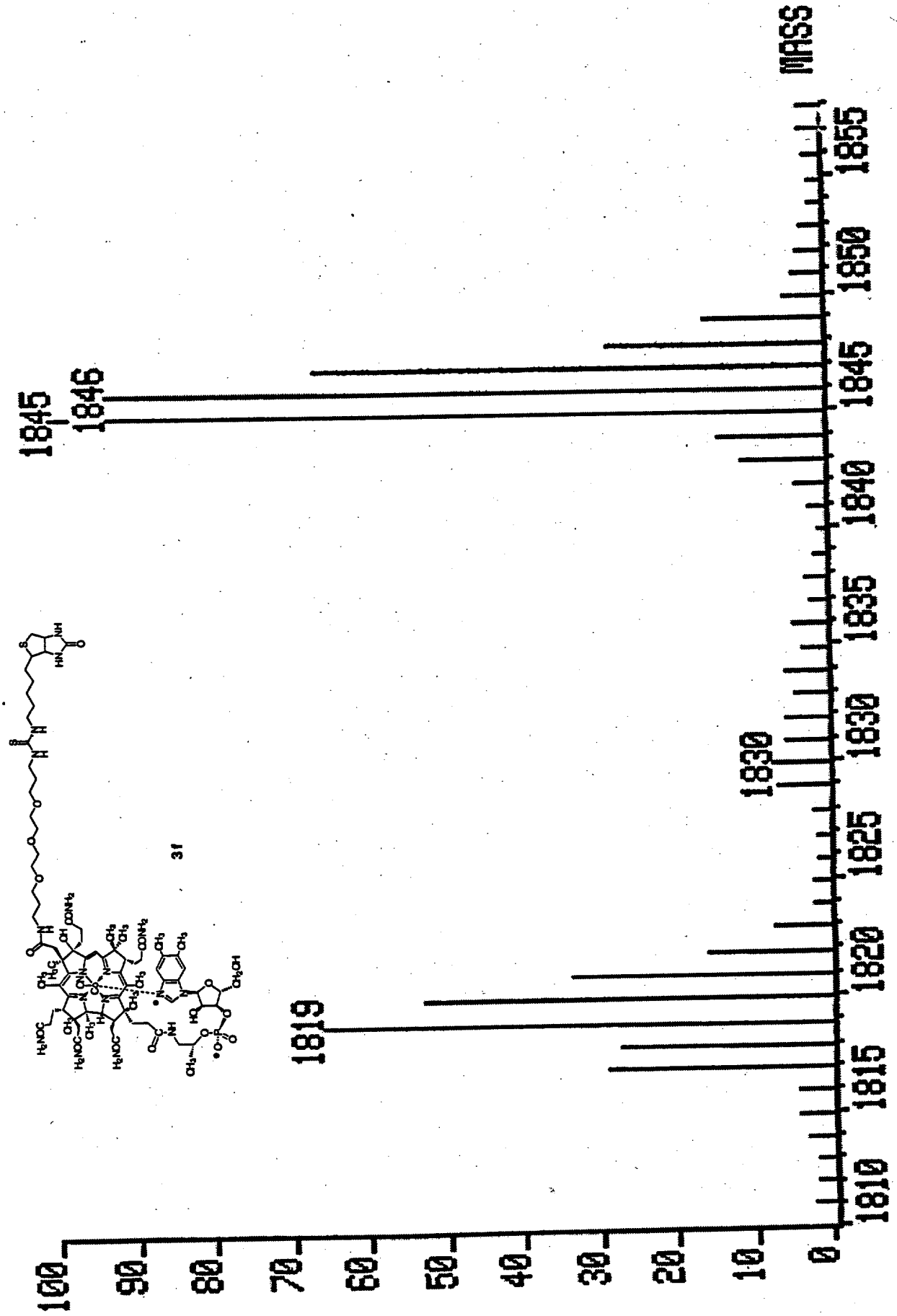

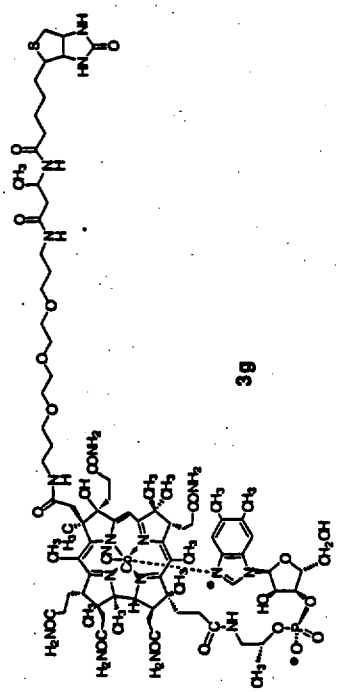

3g

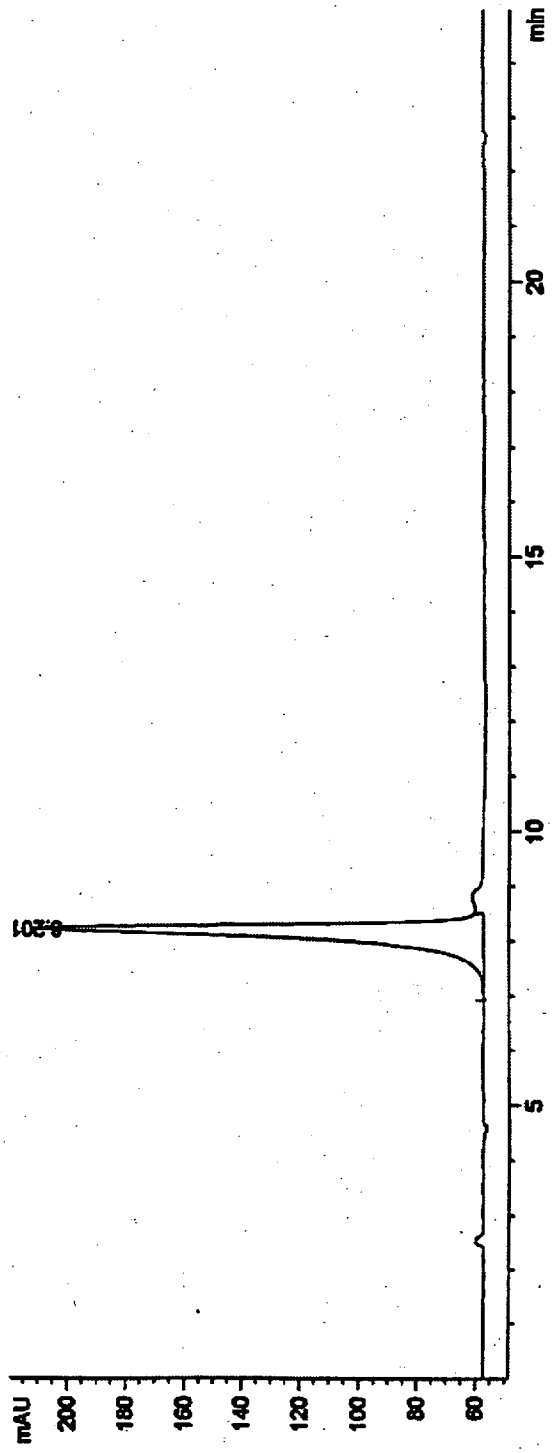

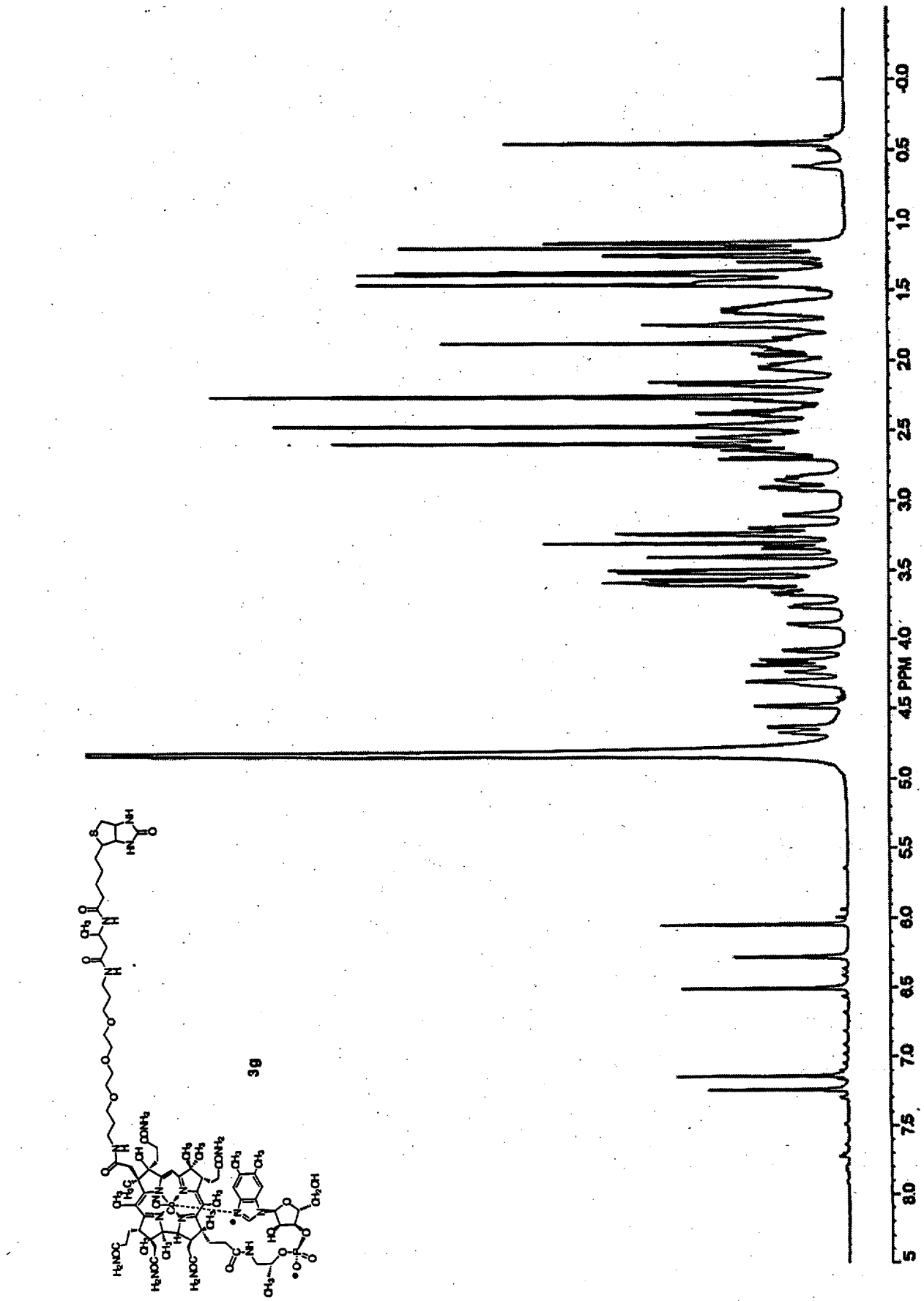
3g
8.0
7.5
7.0
6.5
6.0
5.5
5.0
4.5 PPM 4.0
3.5
3.0
2.5
2.0
1.5
1.0
0.5
0.0

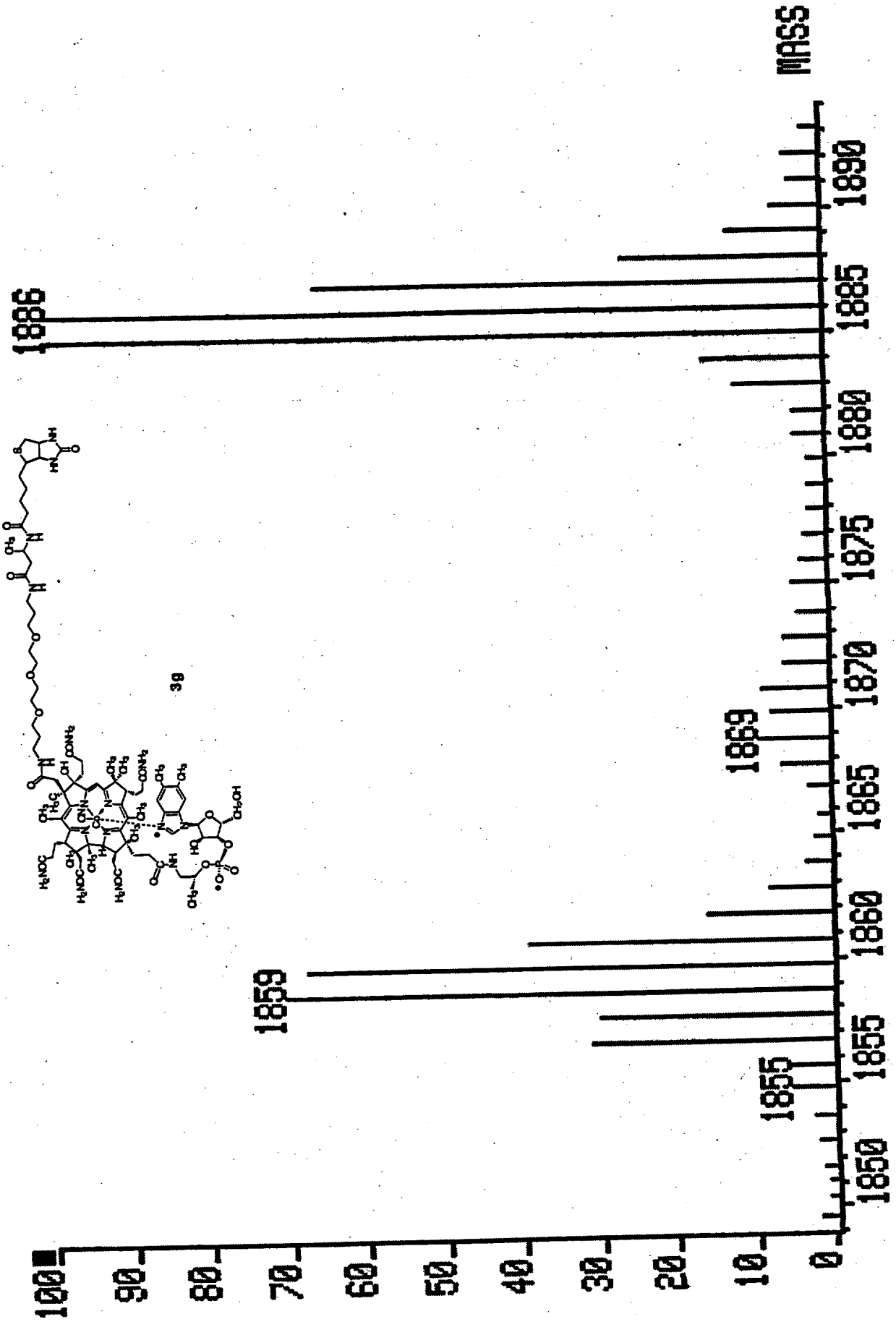
MASS
1886
1859
1859
1855
1850
1855
1860
1865
1870
1875
1880
1885
1890
100
90
80
70
60
50
40
30
20
10
0
3g

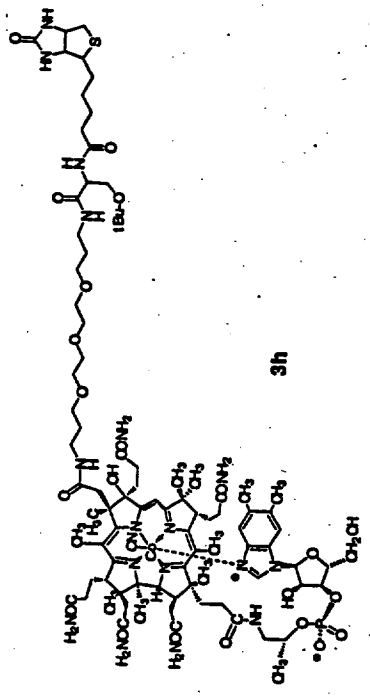

3h

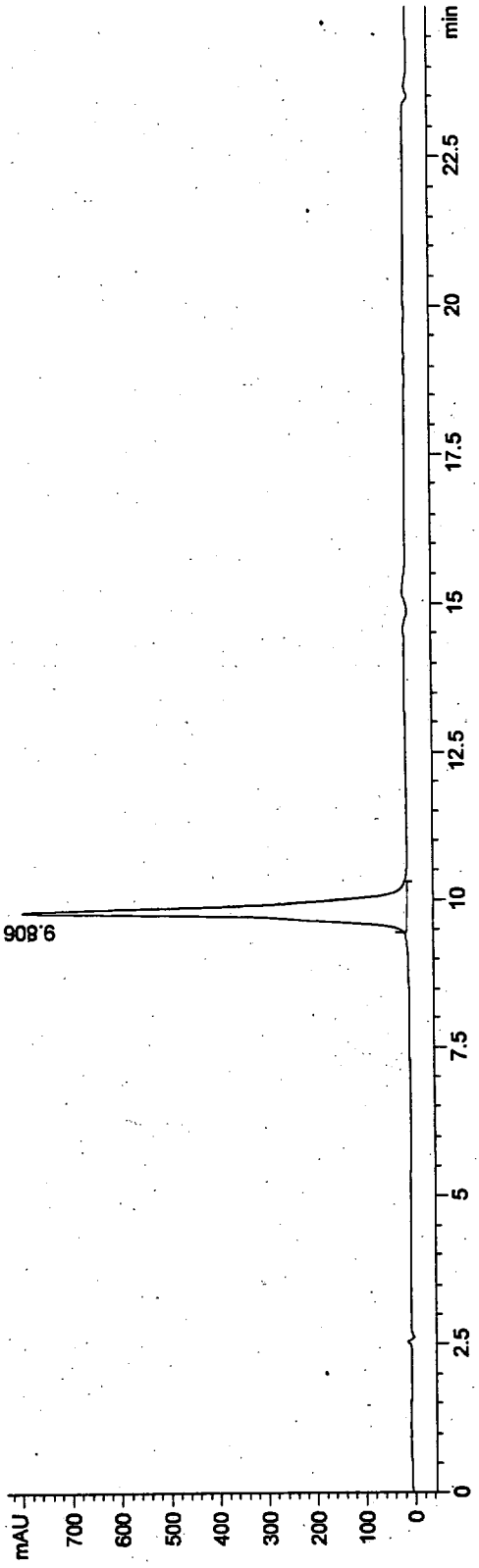
9.806
mAU
700
600
500
400
300
200
100
0
0
2.5
5
7.5
10
12.5
15
17.5
20
22.5
min

© 2000 American Chemical Society, Bioconjugate Chem., Wilbur bc000024v Supporting Info Page 14

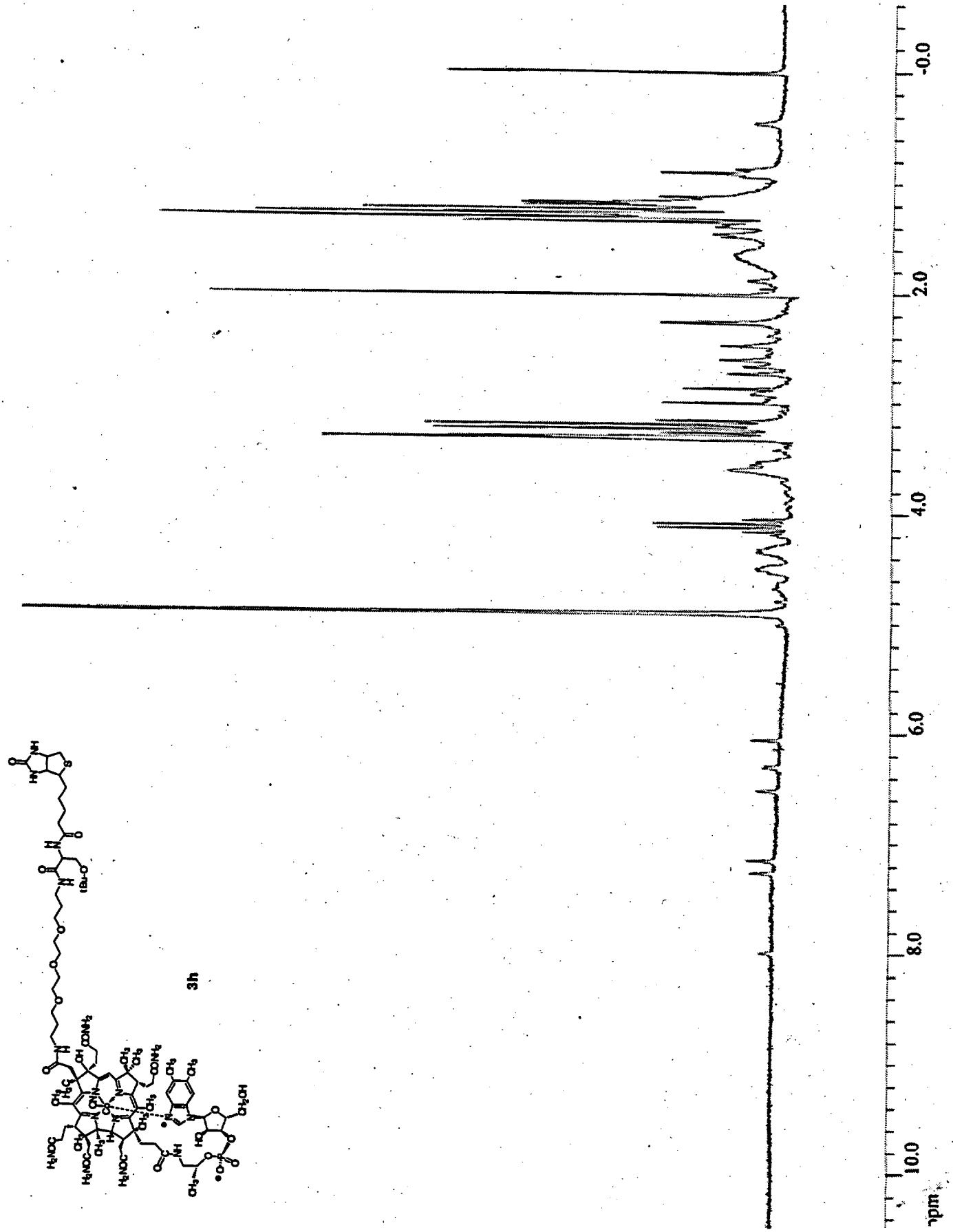

© 2000 American Chemical Society, Bioconjugate Chem., Wilbur bc000024v Supporting Info Page 15

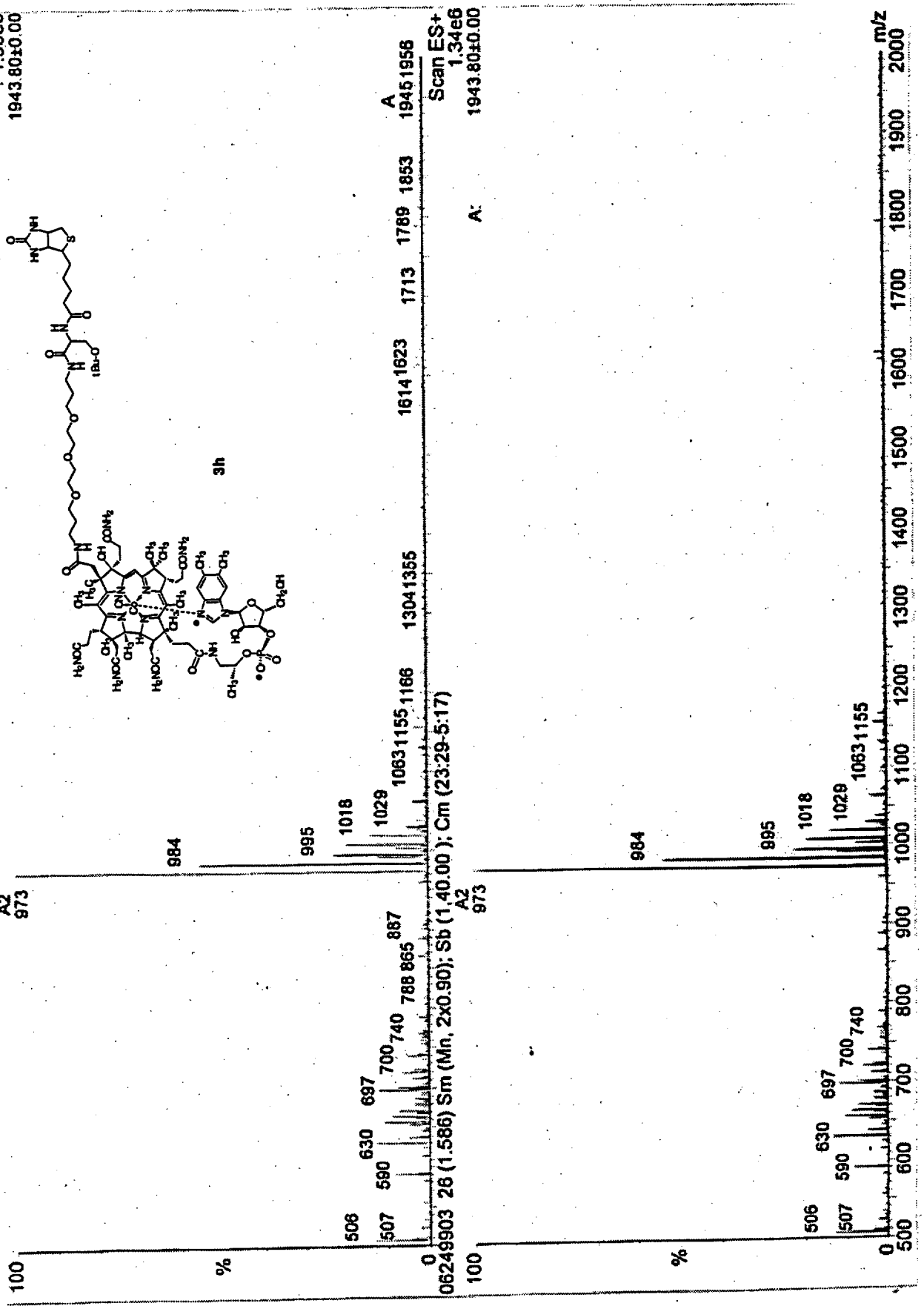

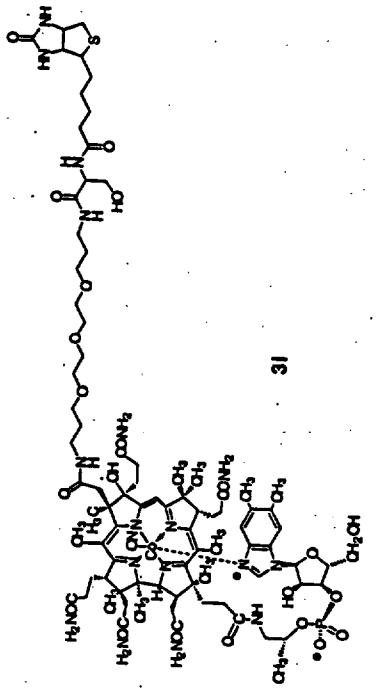

3l

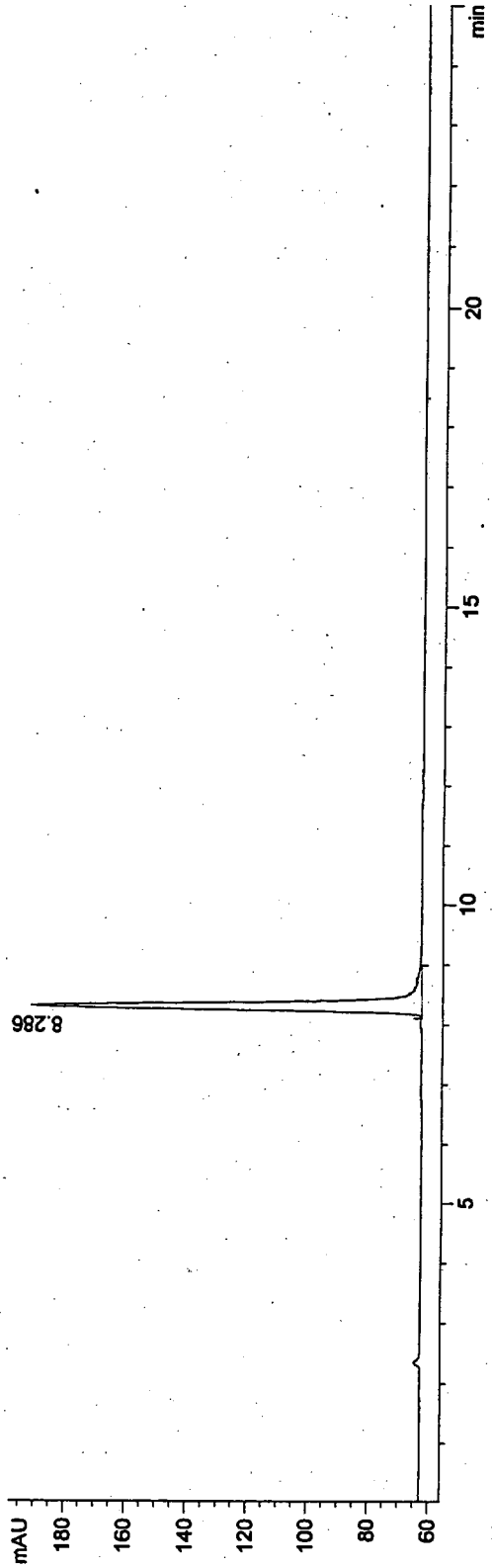

© 2000 American Chemical Society, Bioconjugate Chem., Wilbur bc000024v Supporting Info Page 17

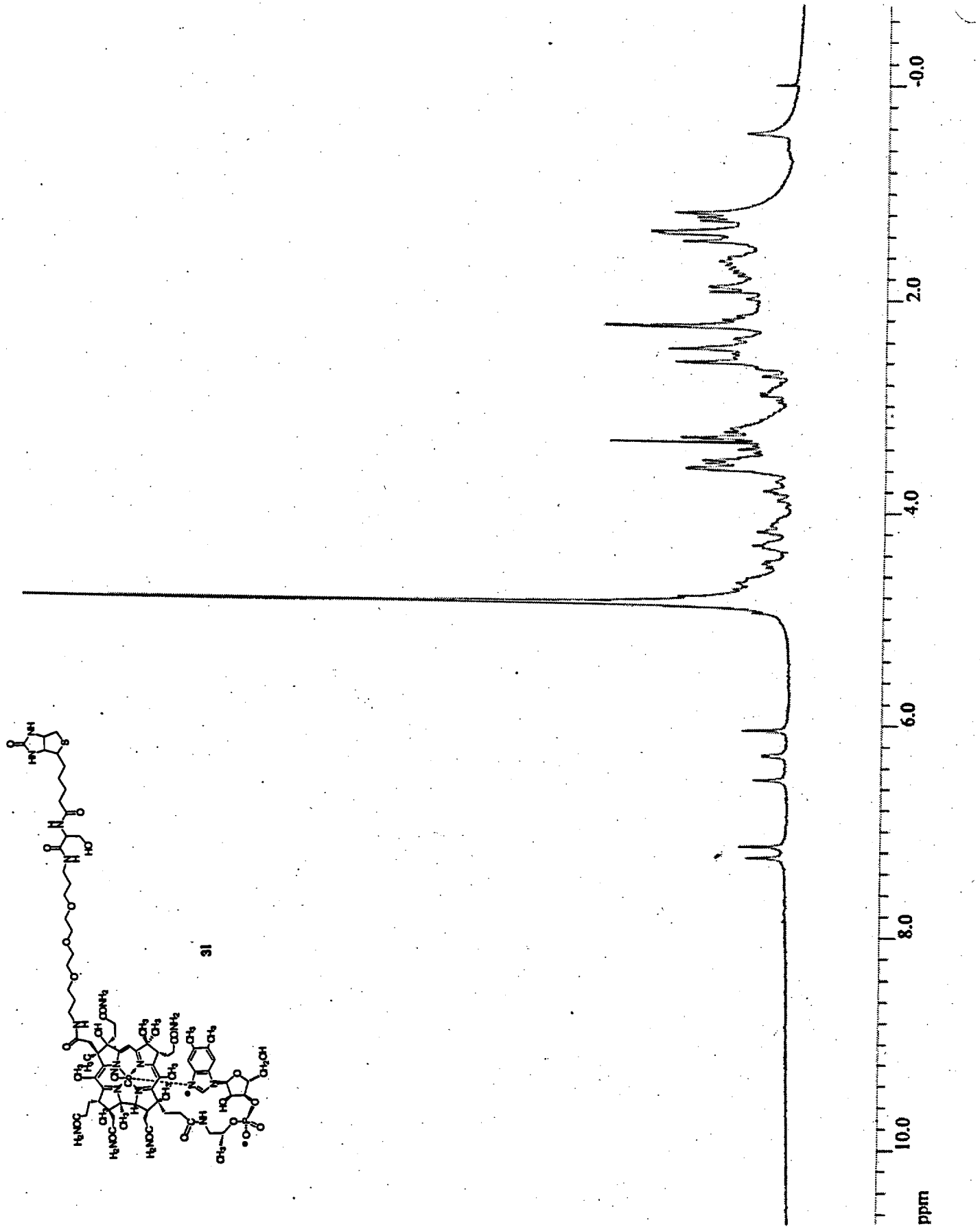

© 2000 American Chemical Society, Bioconjugate Chem., Wilbur bc000024v Supporting Info Page 18

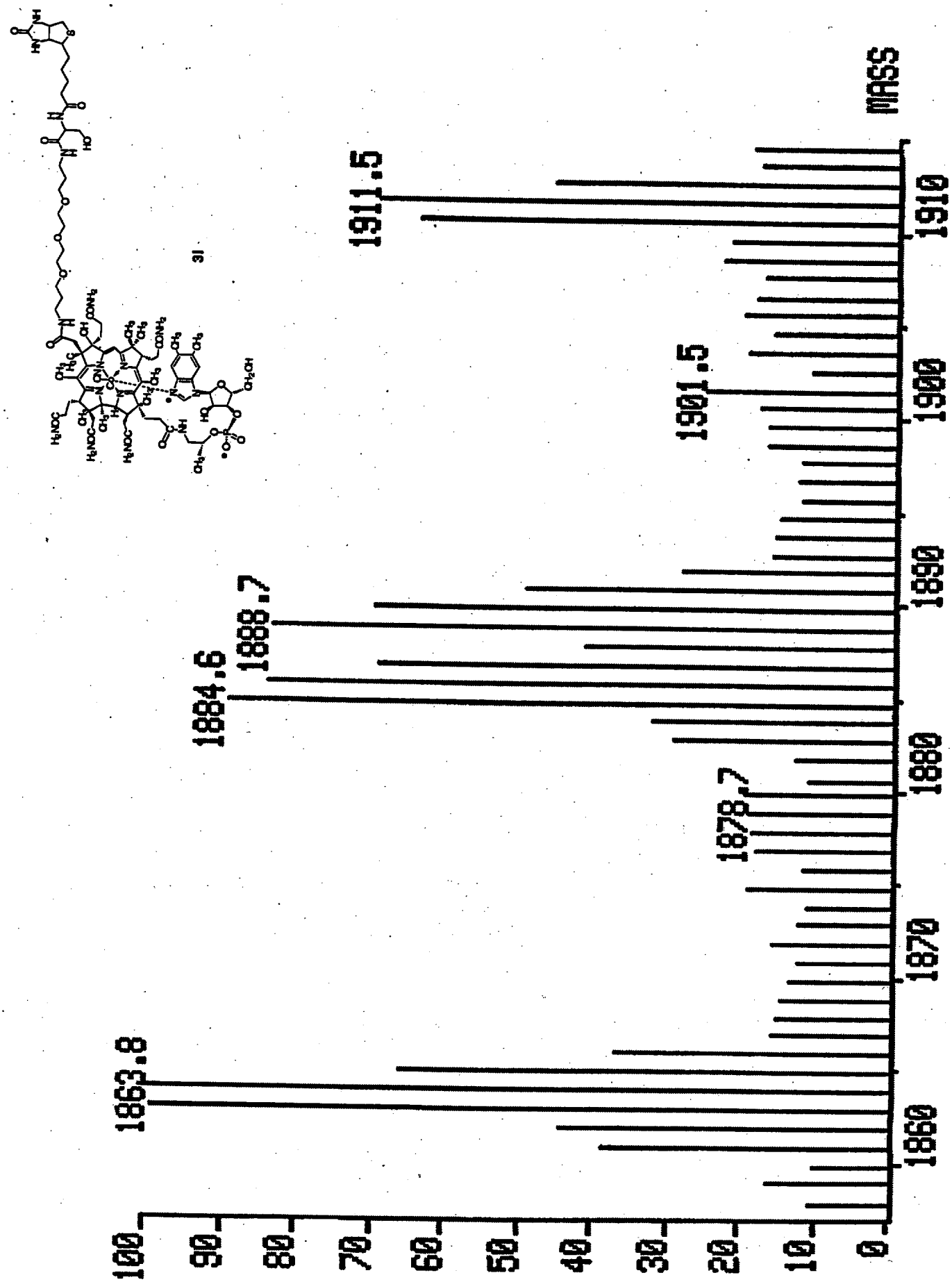

© 2000 American Chemical Society, Bioconjugate Chem., Wilbur bc000024v Supporting Info Page 19

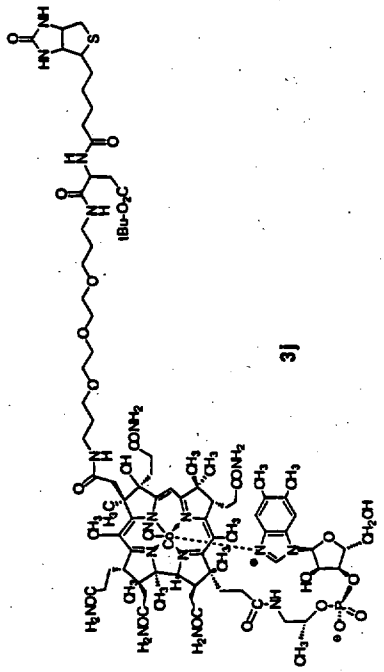

3j

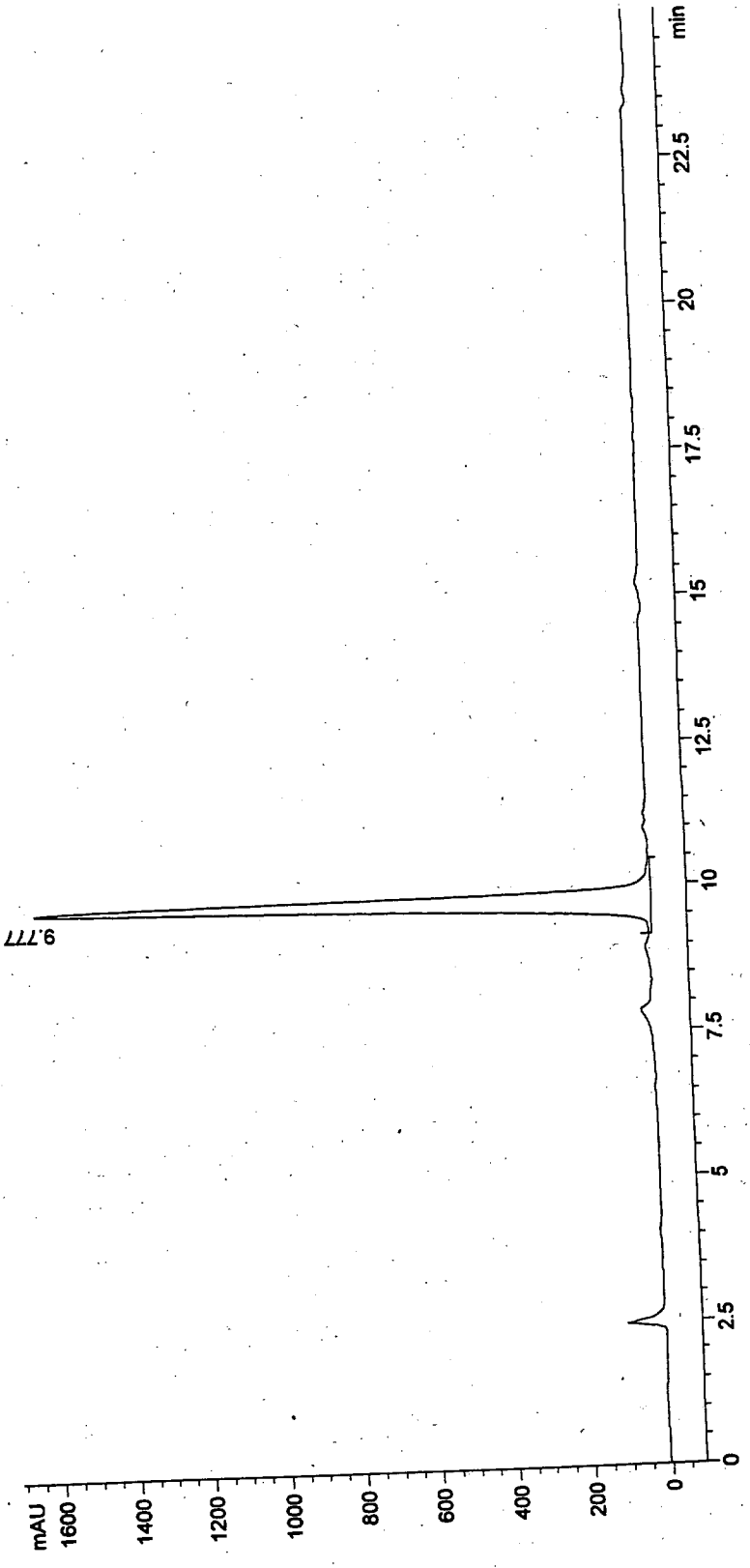

© 2000 American Chemical Society, Bioconjugate Chem., Wilbur bc000024v Supporting Info Page 20

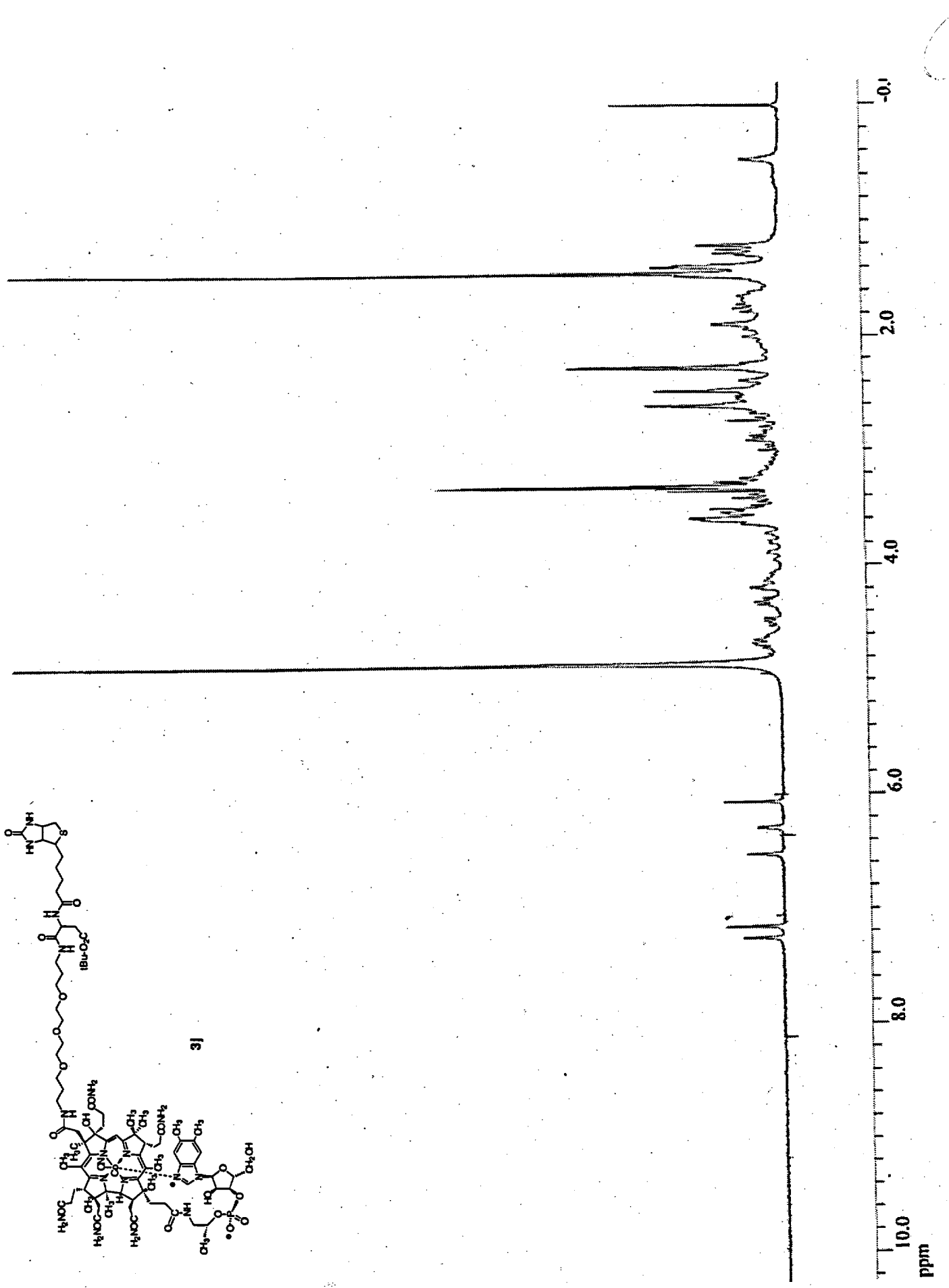

© 2000 American Chemical Society, Bioconjugate Chem., Wilbur bc000024v Supporting Info Page 21

© 2000 American Chemical Society, Bioconjugate Chem., Wilbur bc000024v Supporting Info Page 22

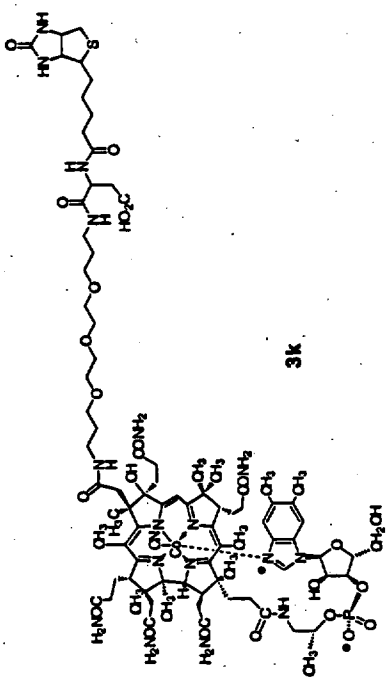

3k

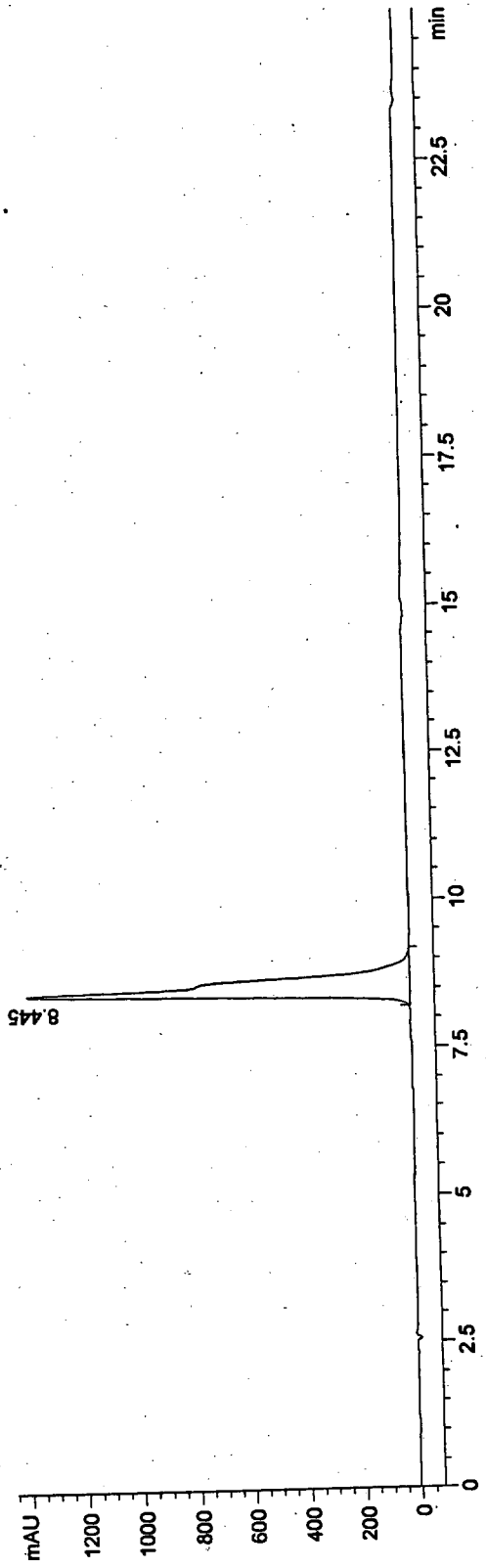

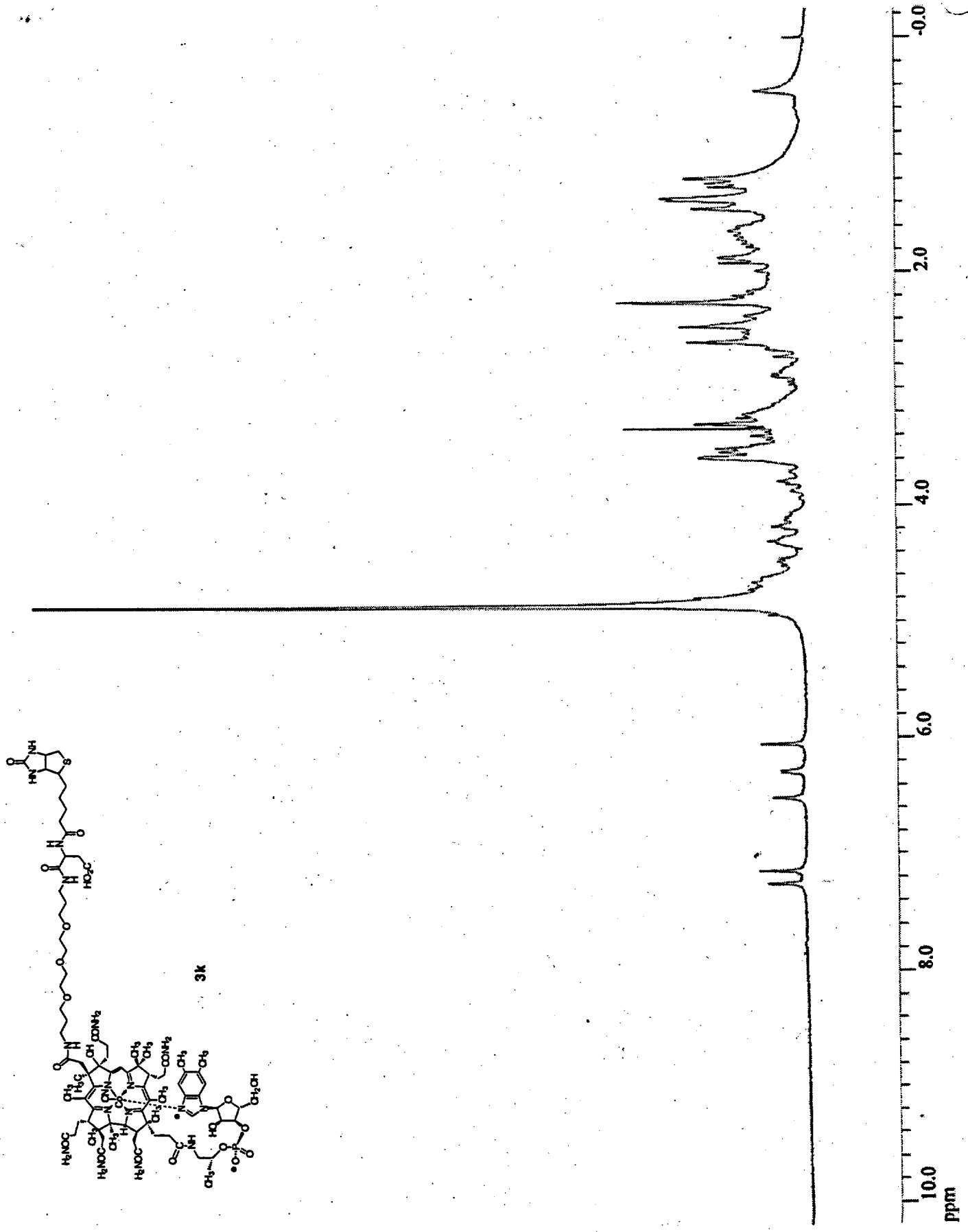
3k
-0.0
2.0
4.0
6.0
8.0
10.0
ppm

© 2000 American Chemical Society, Bioconjugate Chem., Wilbur bc000024v Supporting Info Page 24

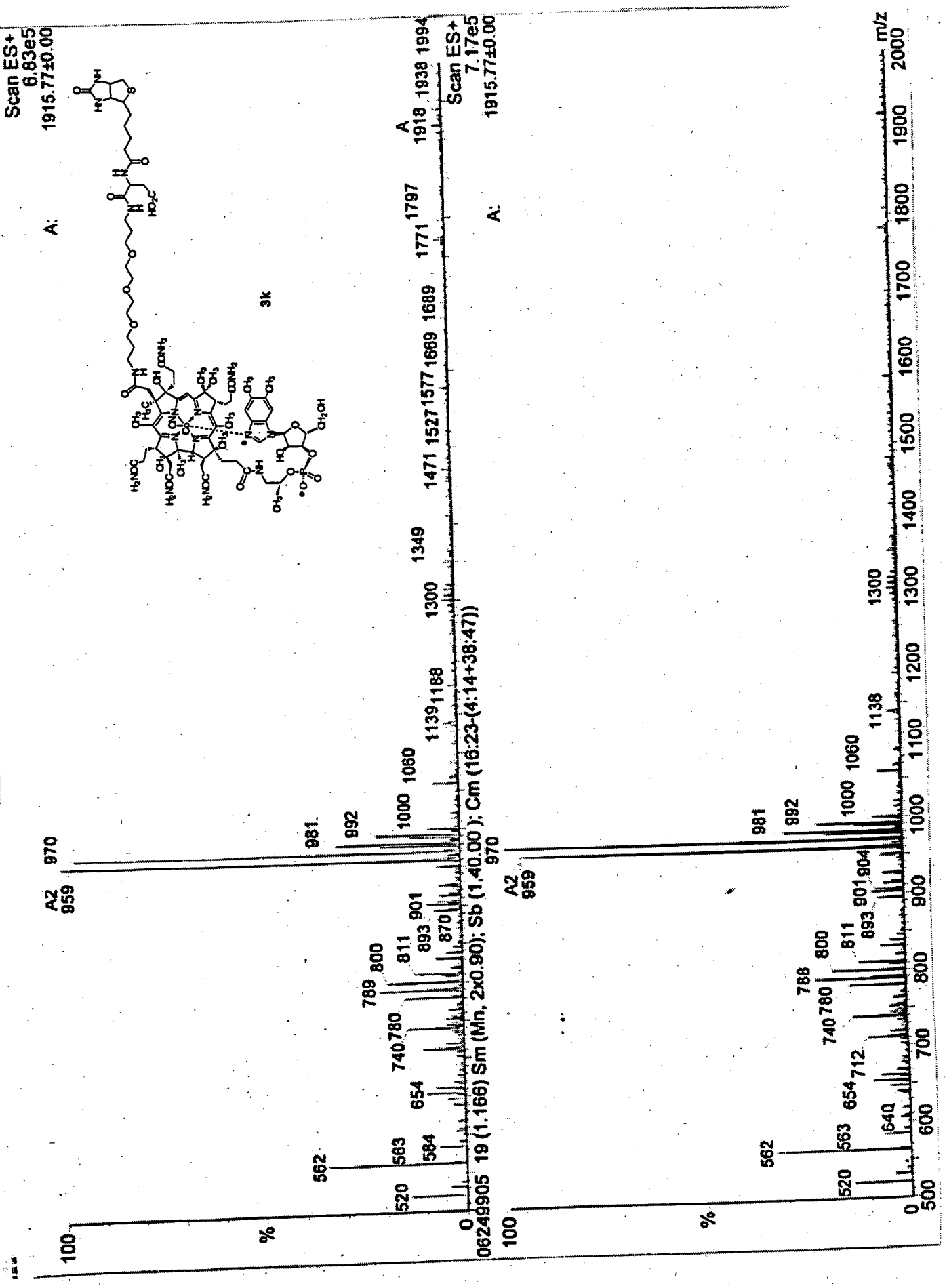

© 2000 American Chemical Society, Bioconjugate Chem., Wilbur bc000024v Supporting Info Page 25

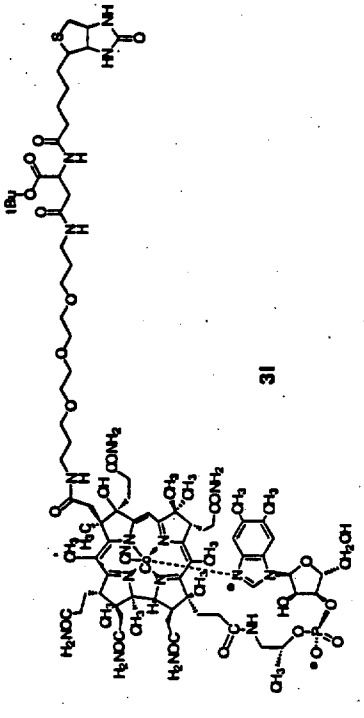

31

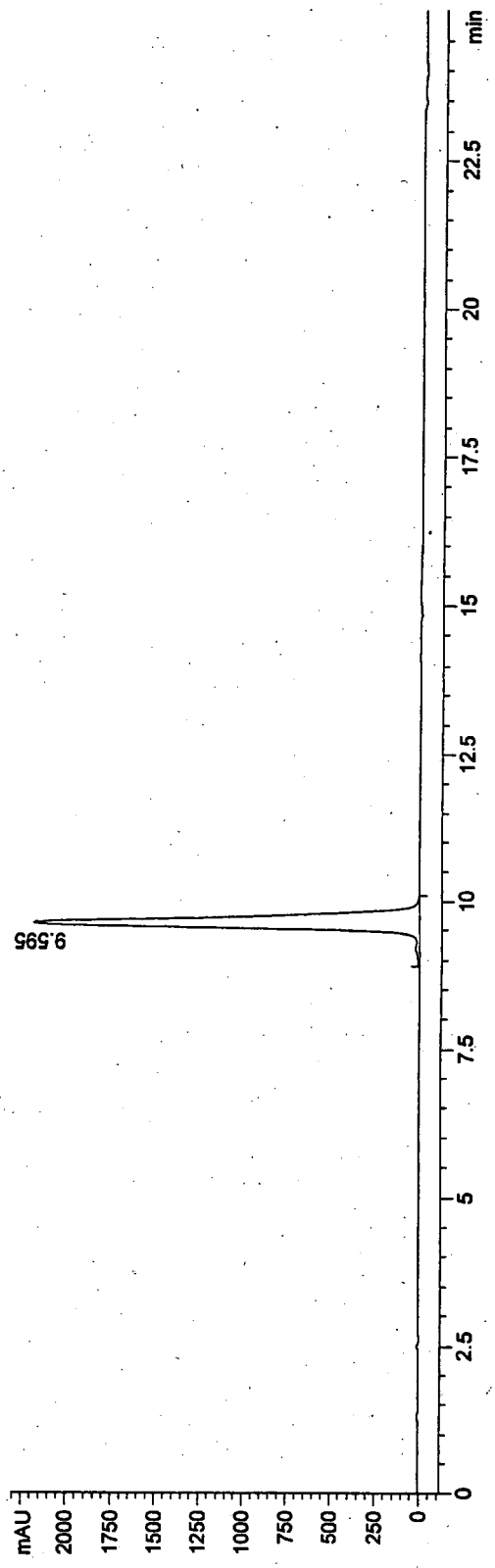

© 2000 American Chemical Society, Bioconjugate Chem., Wilbur bc000024v Supporting Info Page 26

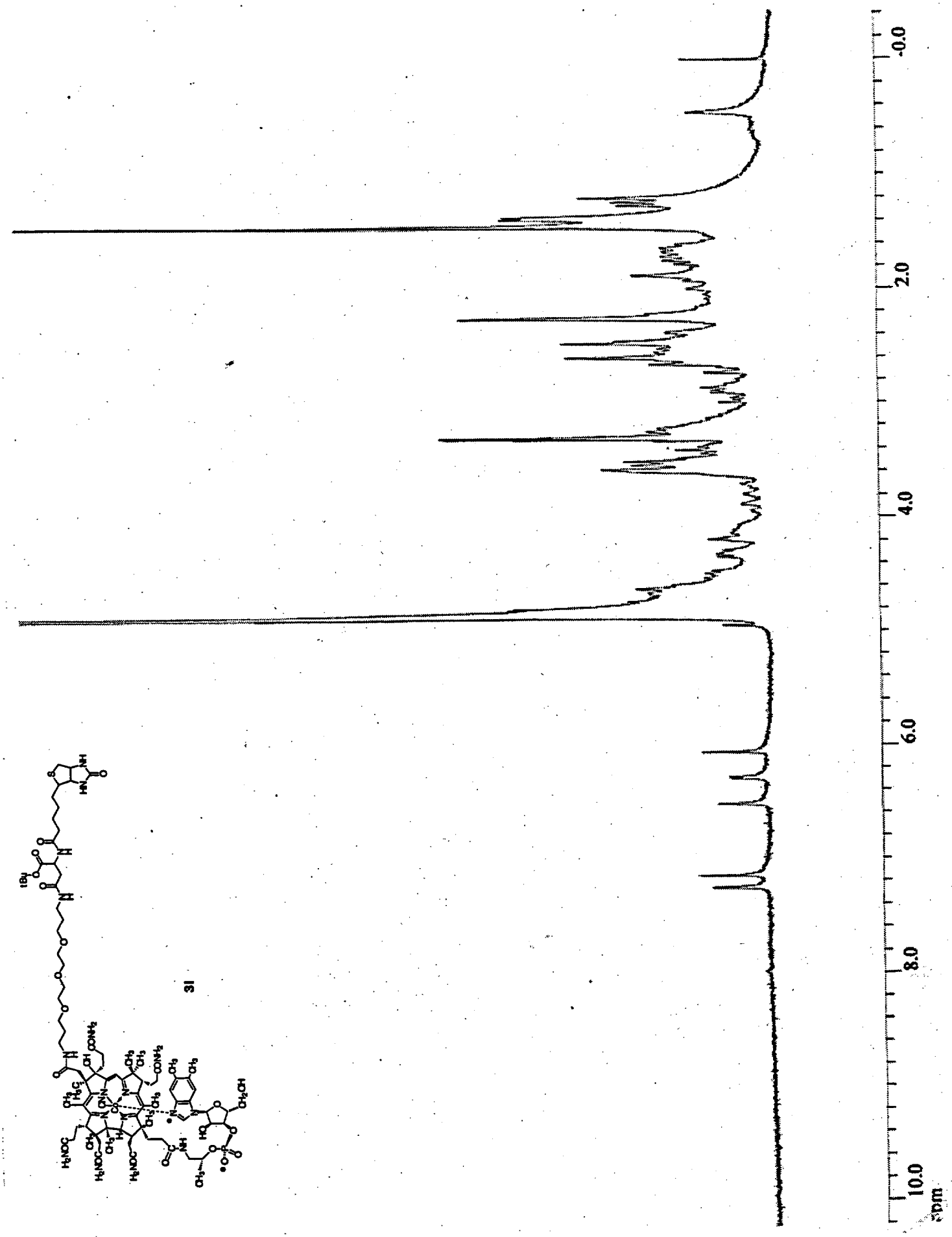

© 2000 American Chemical Society, Bioconjugate Chem., Wilbur bc000024v Supporting Info Page 27

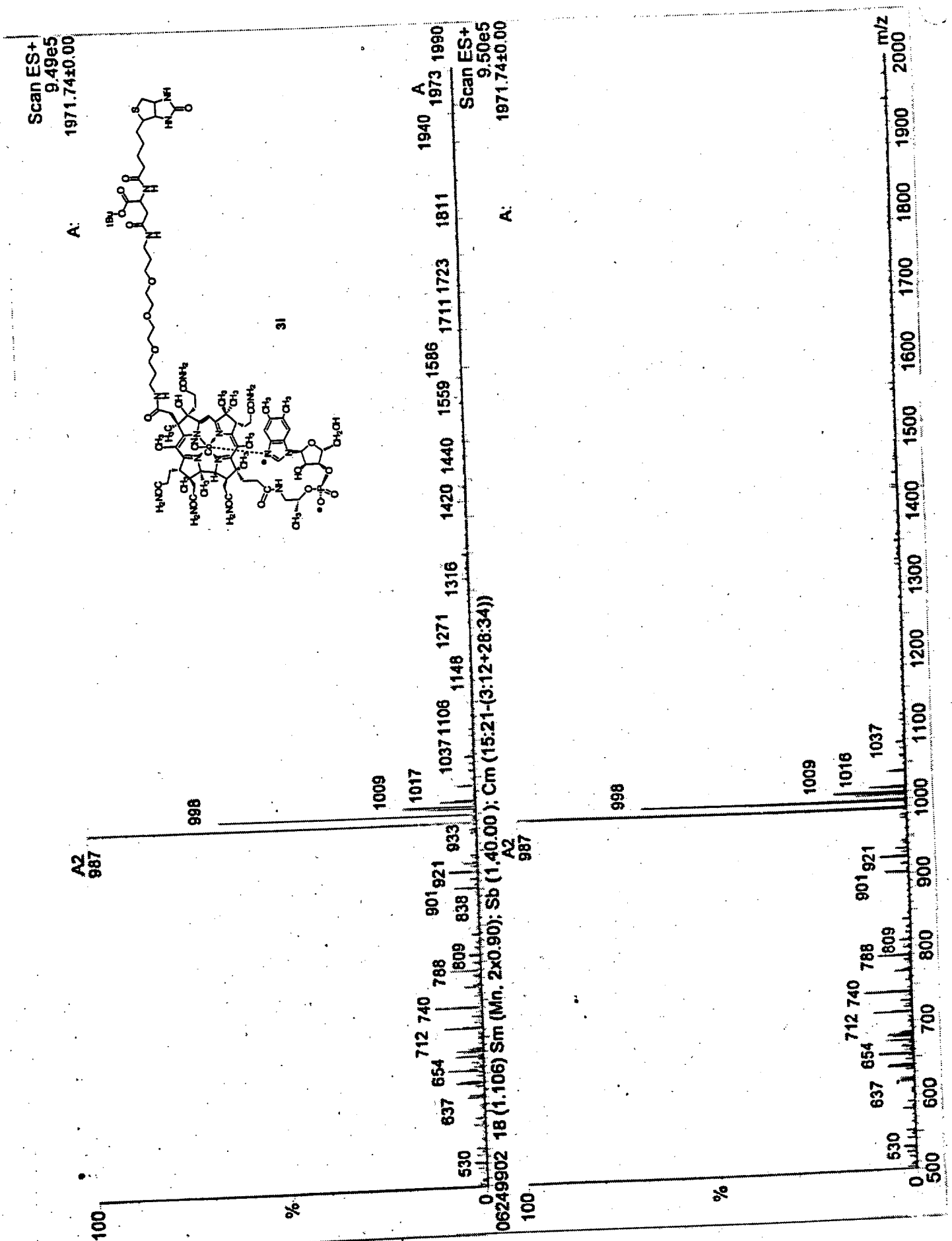

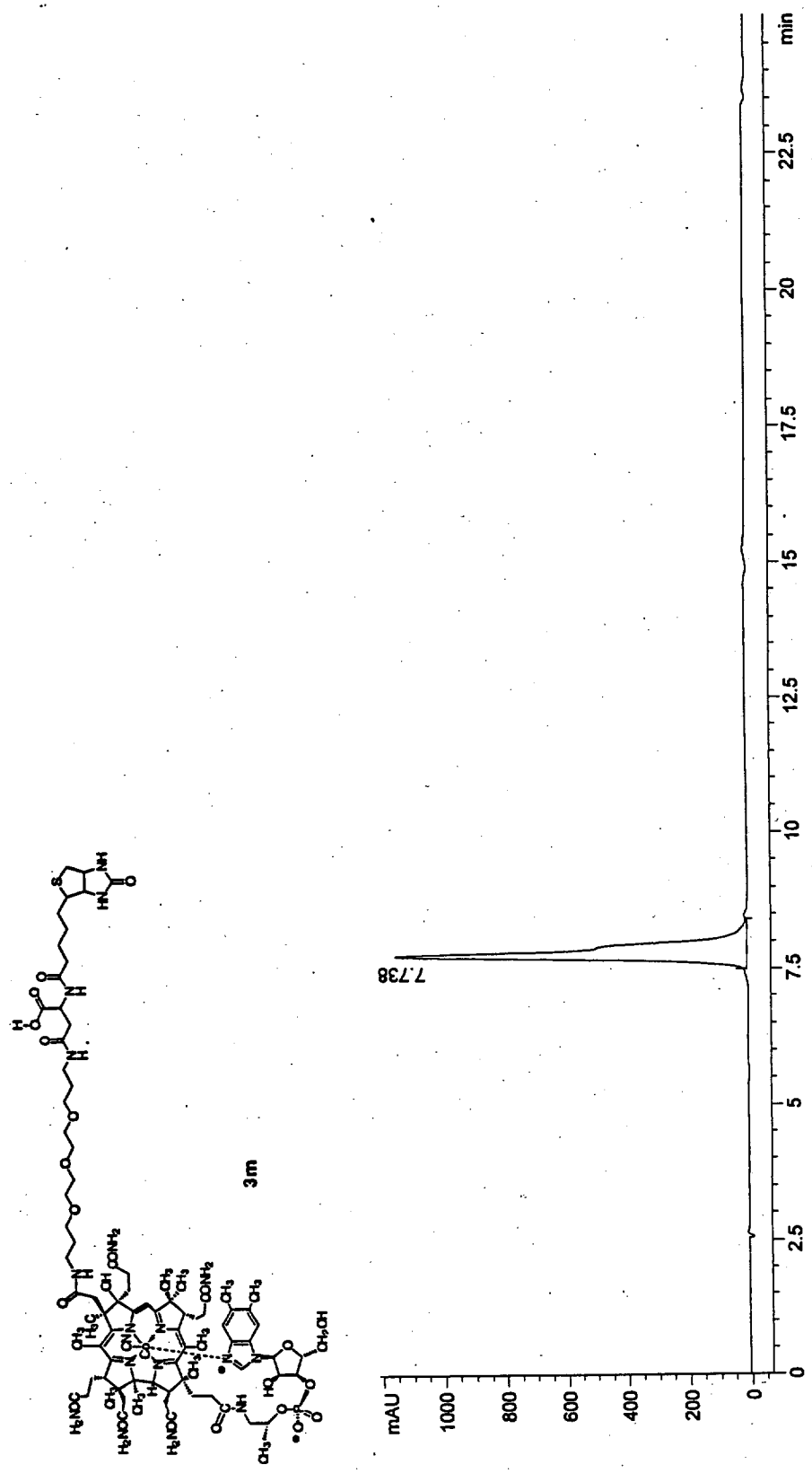
3m
7.738
mAU
1000
800
600
400
200
0
0
2.5
5
7.5
10
12.5
15
17.5
20
22.5
min

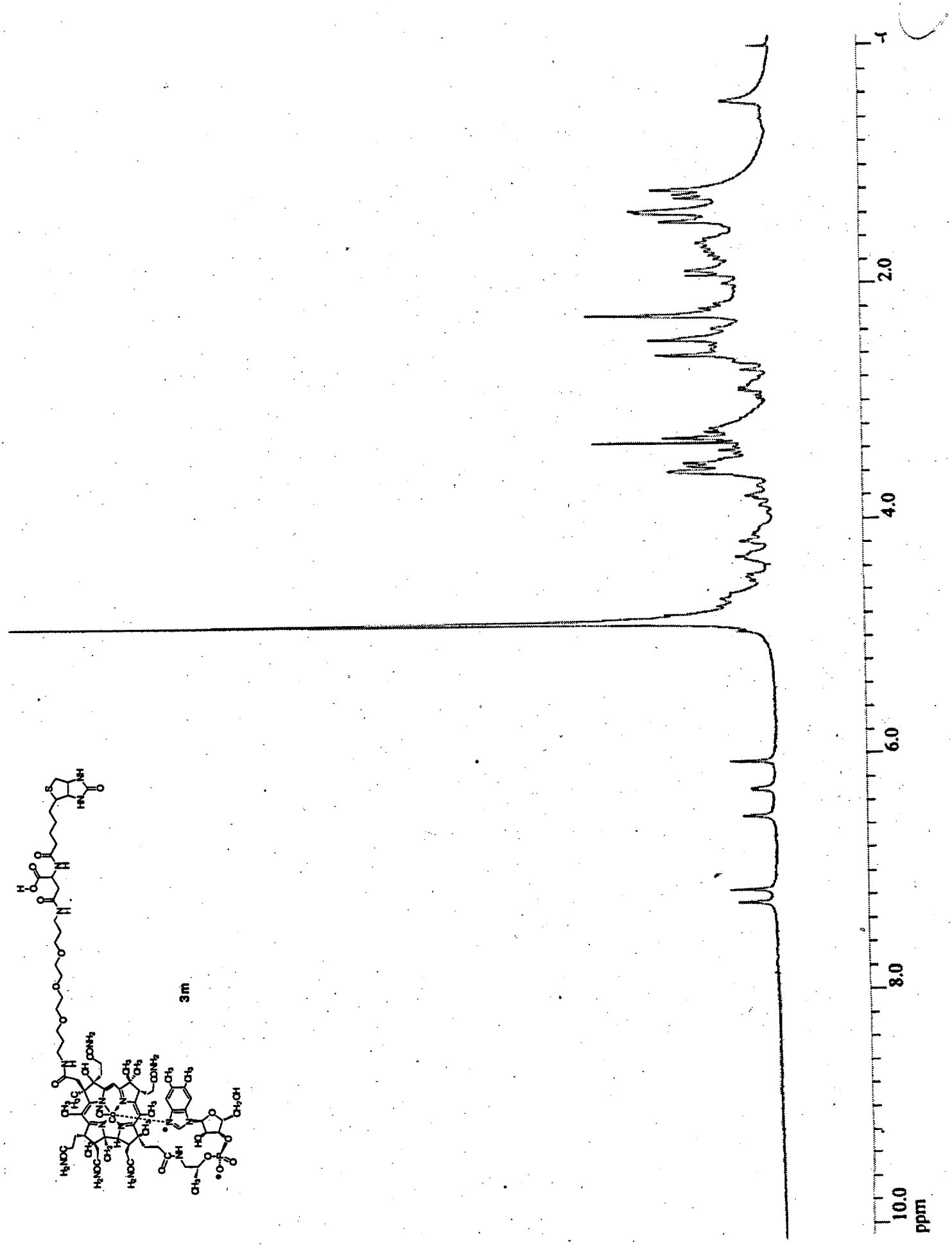
3m
2.0
4.0
6.0
8.0
10.0
ppm

© 2000 American Chemical Society, Bioconjugate Chem., Wilbur bc000024v Supporting Info Page 30

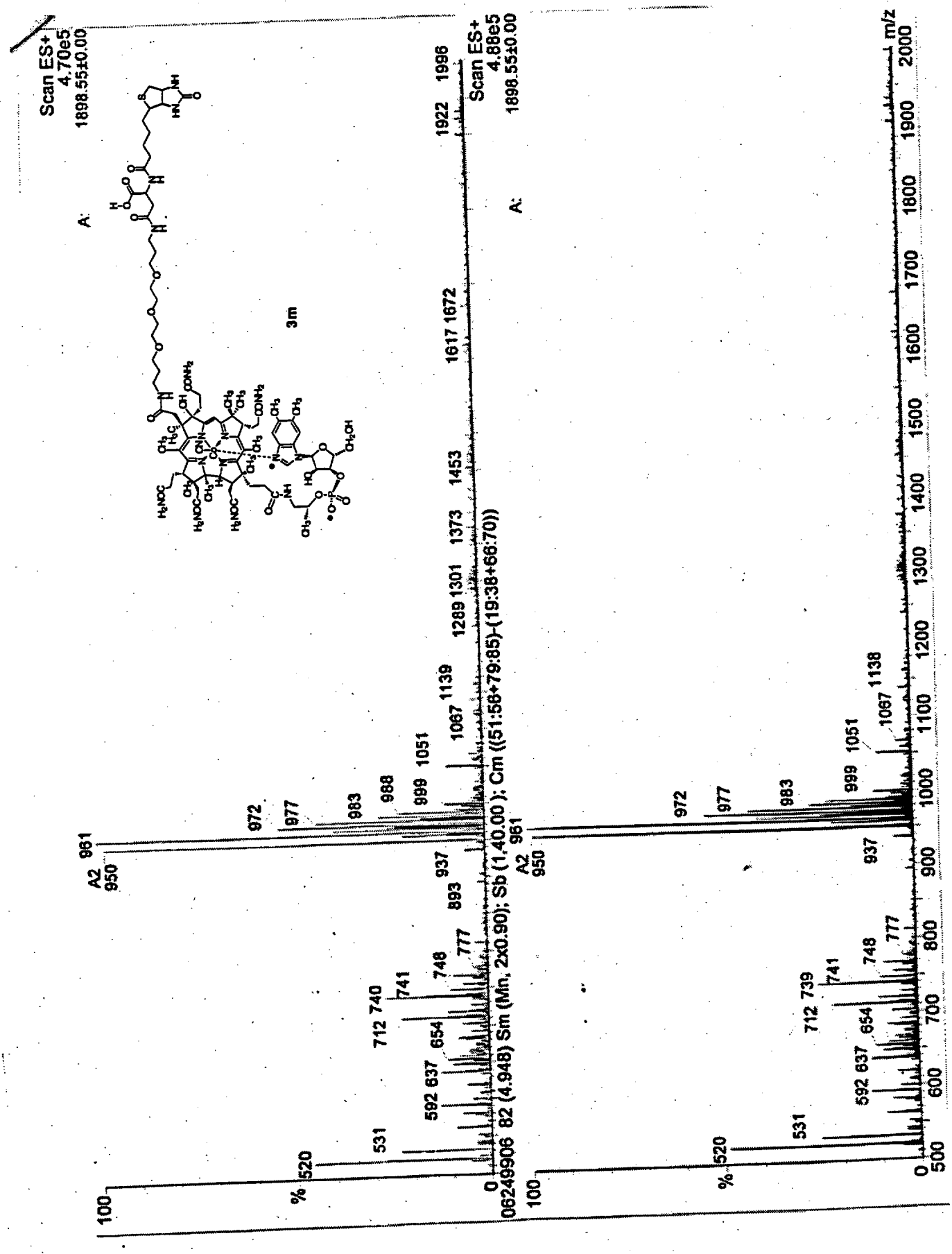

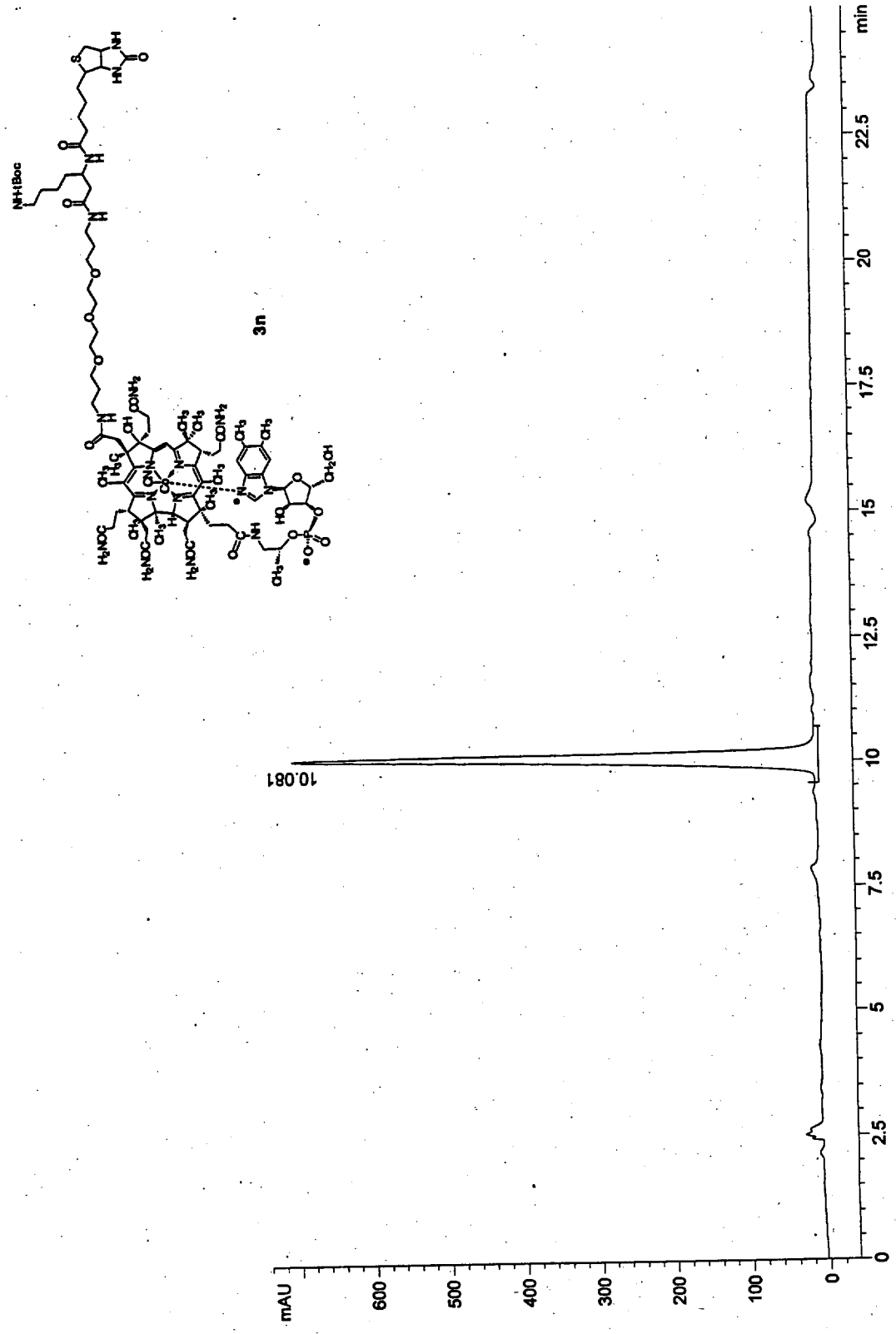
3n
10.081
mAU
600
500
400
300
200
100
0
min
0
2.5
5
7.5
10
12.5
15
17.5
20
22.5

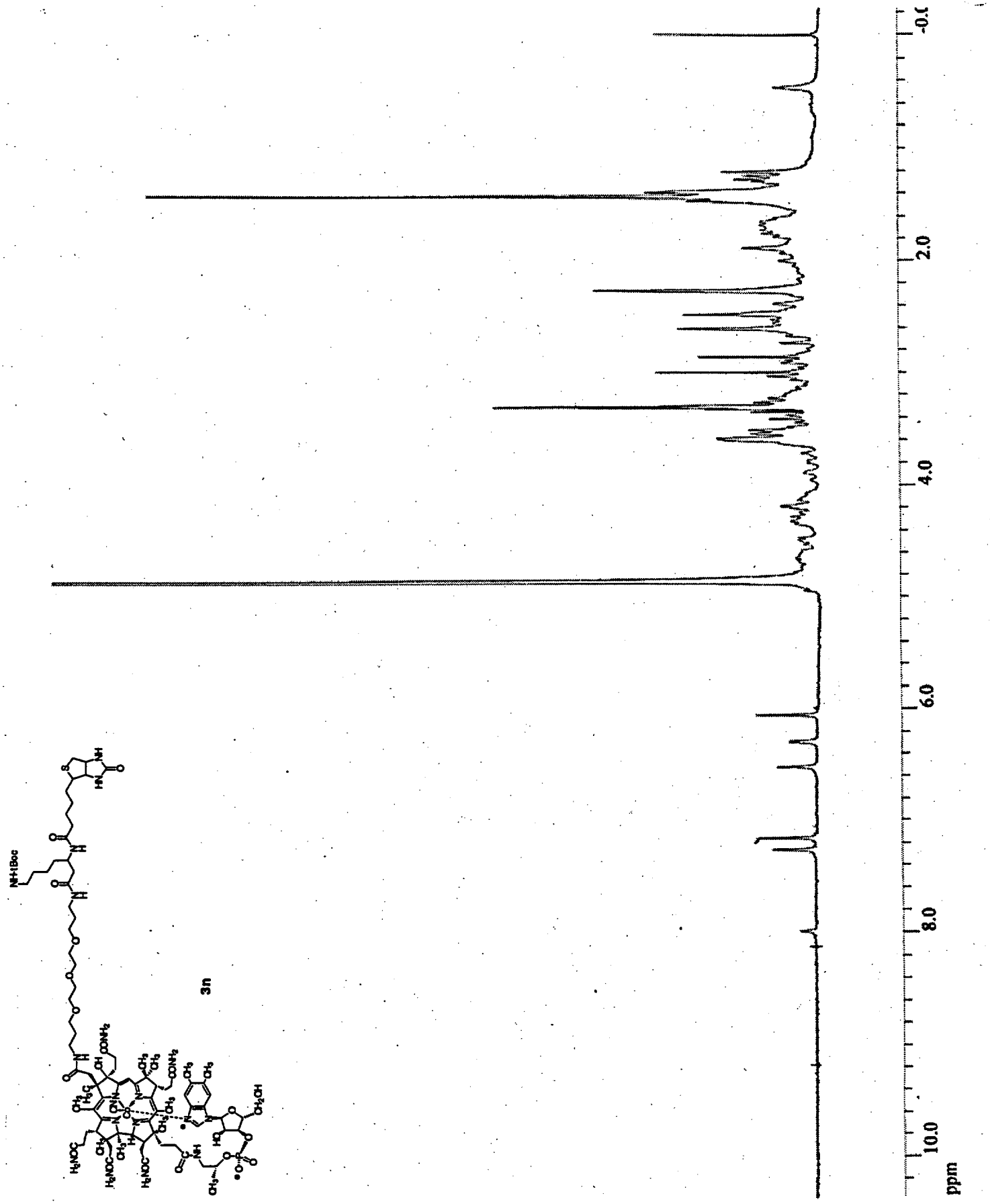
NH-tBoc
3n
10.0
8.0
6.0
4.0
2.0
ppm

© 2000 American Chemical Society, Bioconjugate Chem., Wilbur bc000024v Supporting Info Page 33

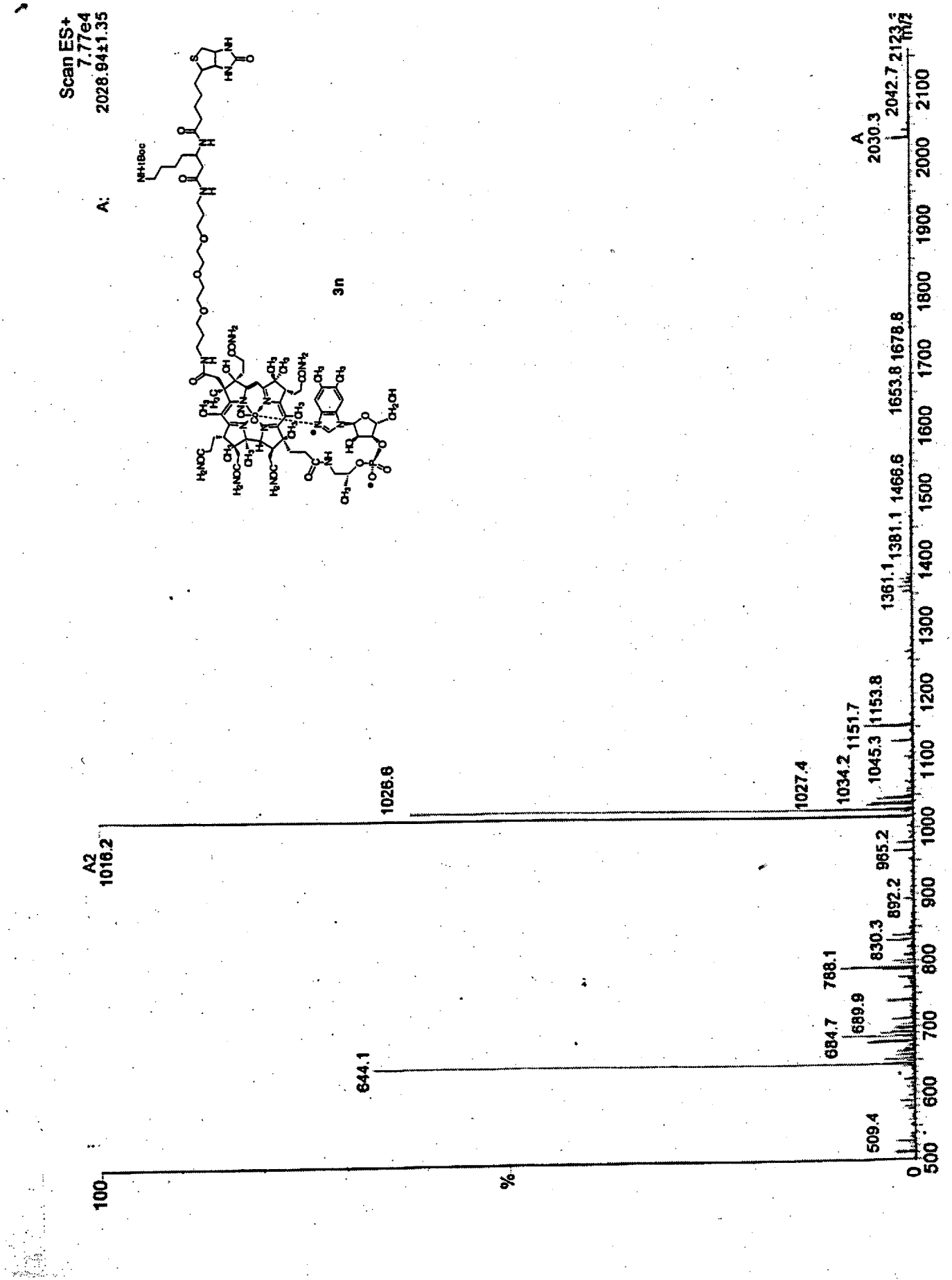

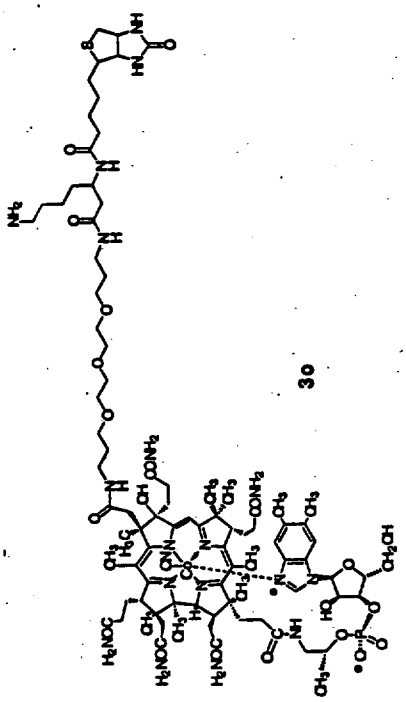

30

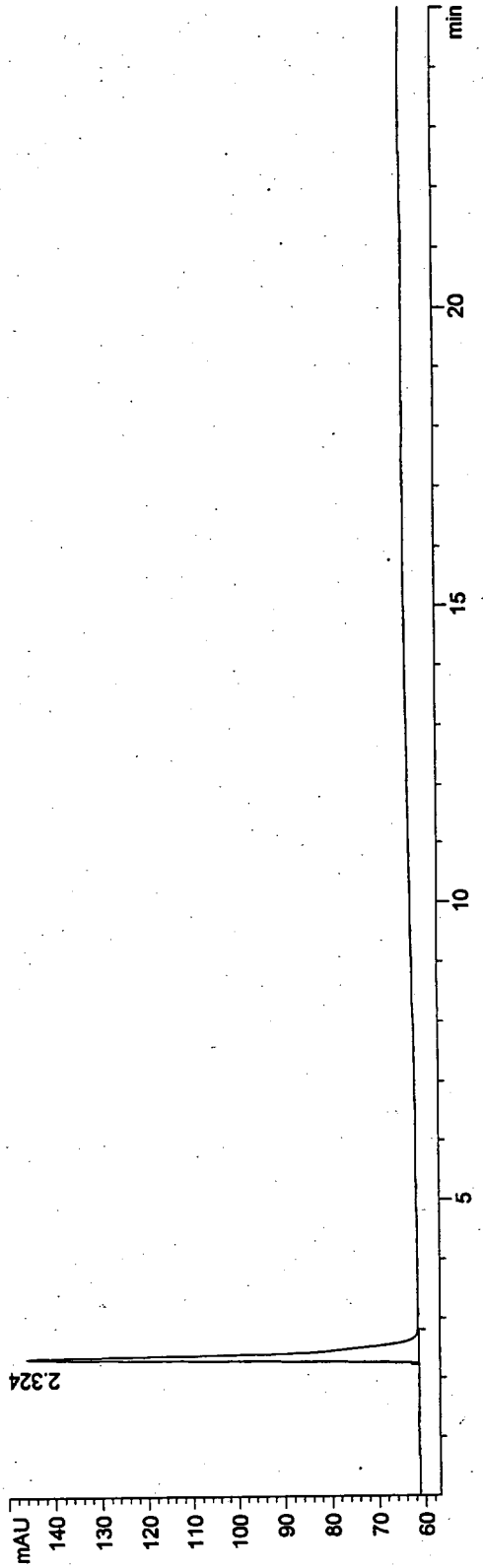

© 2000 American Chemical Society, Bioconjugate Chem., Wilbur bc000024v Supporting Info Page 35

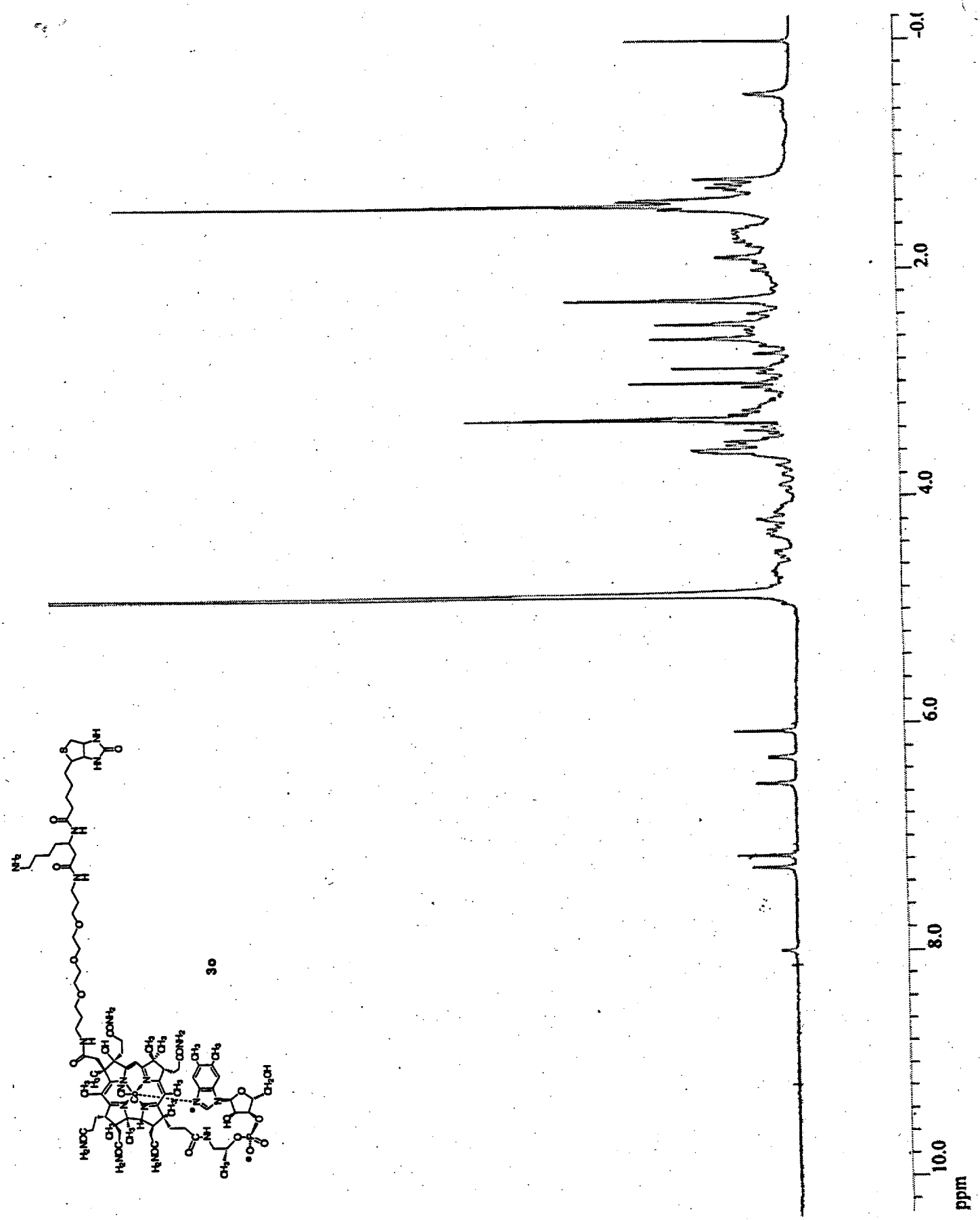

© 2000 American Chemical Society, Bioconjugate Chem., Wilbur bc000024v Supporting Info Page 36

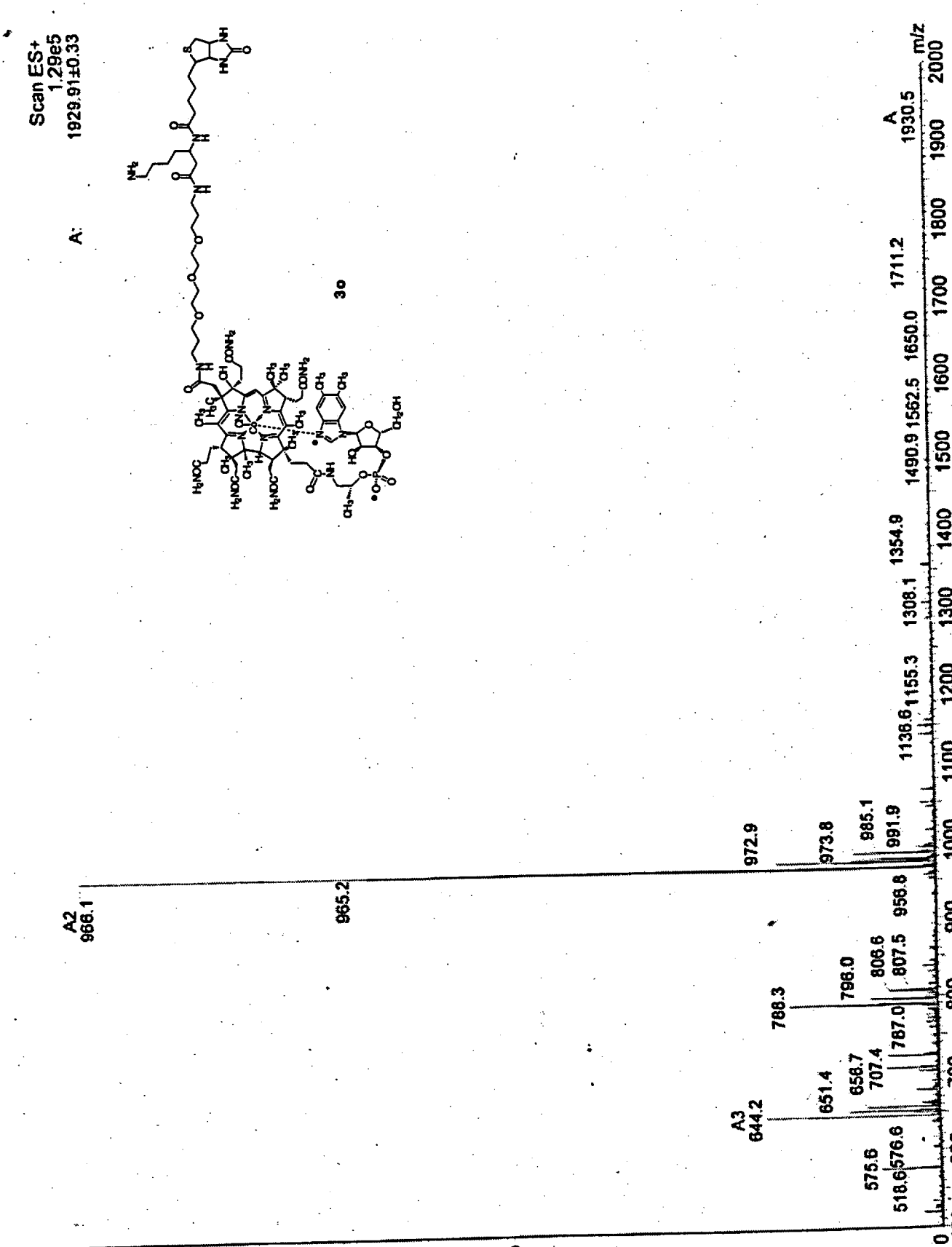

© 2000 American Chemical Society, Bioconjugate Chem., Wilbur bc000024v Supporting Info Page 37

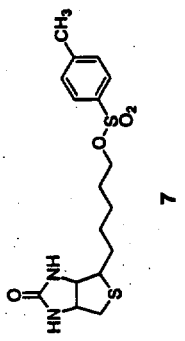

7

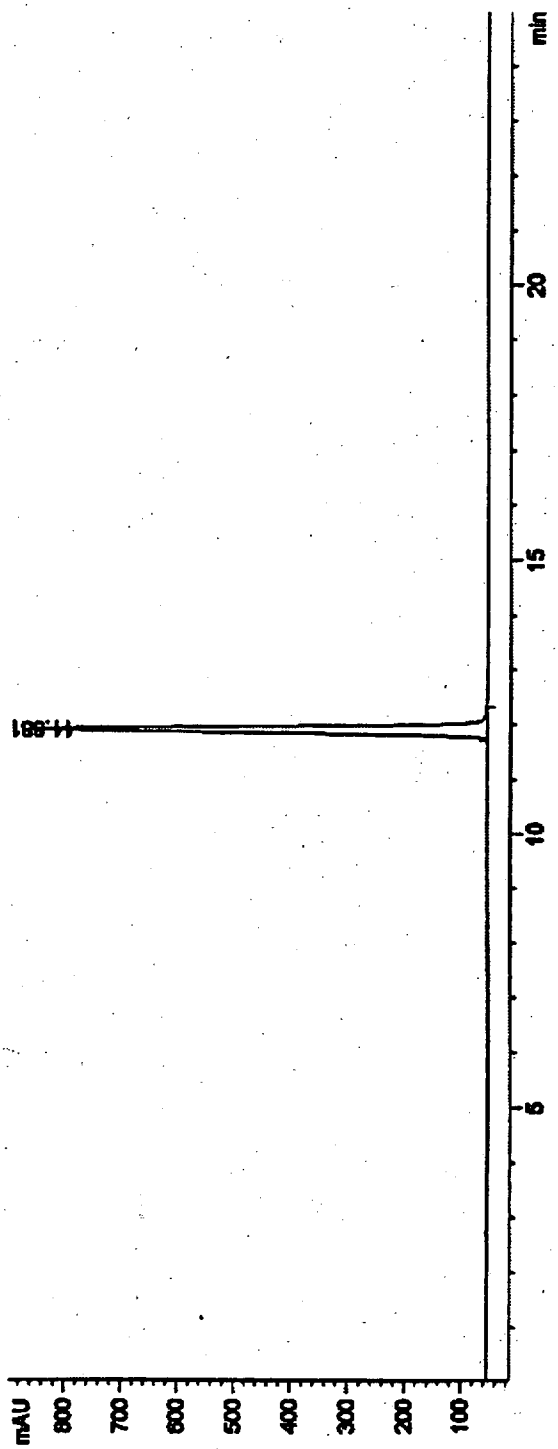

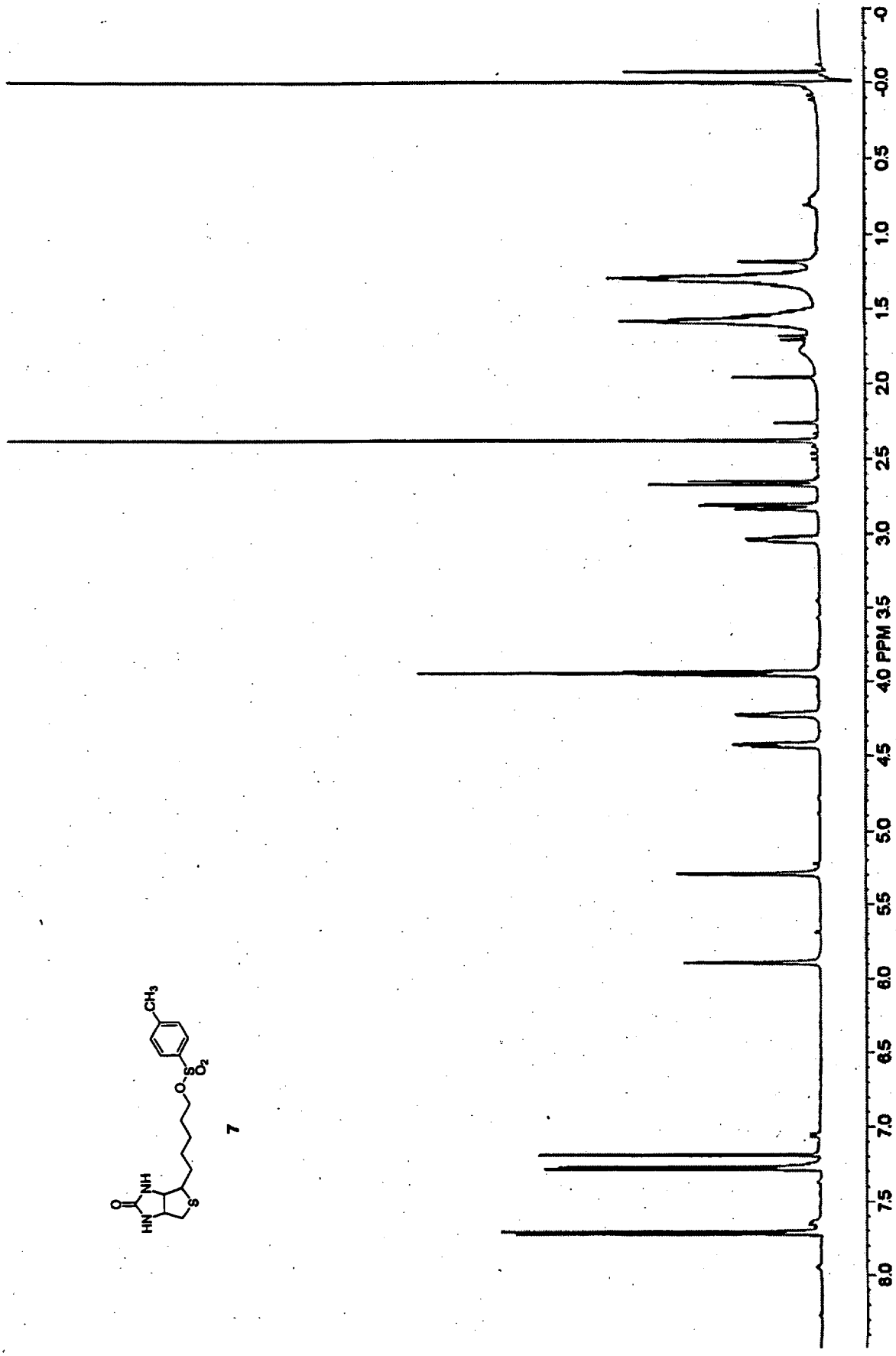
-0
-0.0
0.5
1.0
1.5
2.0
2.5
3.0
3.5
4.0 PPM
4.5
5.0
5.5
6.0
6.5
7.0
7.5
8.0
8.0
CH3
SO2
O
NH
HN
O
S

7

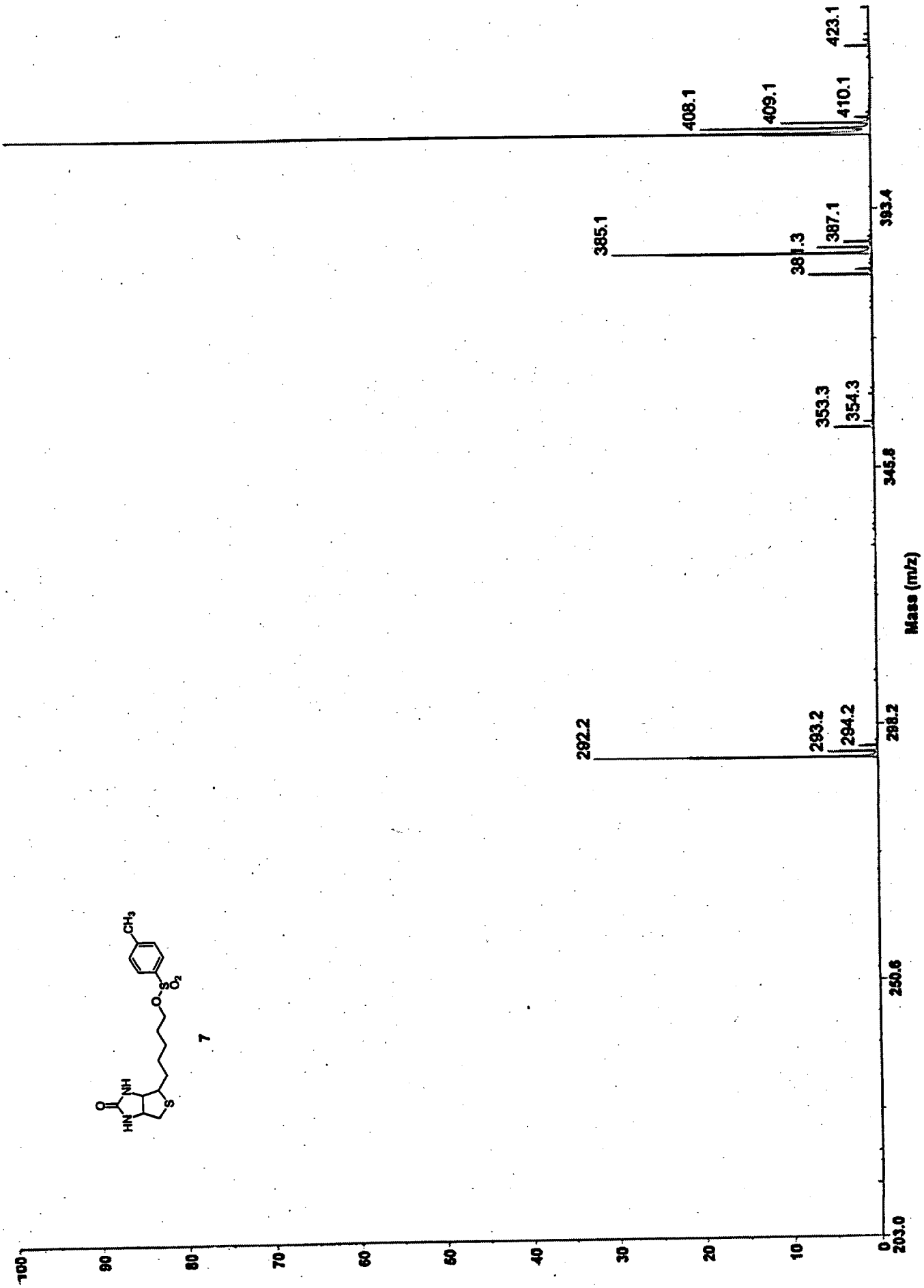
407.1
+ Na
408.1
409.1
410.1
423.1
385.1
387.1
393.4
353.3
354.3
346.8
292.2
293.2
294.2
298.2
Mass (m/z)
250.6
203.0
100
90
80
70
60
50
40
30
20
10
0
7

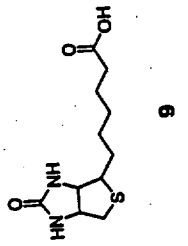

9

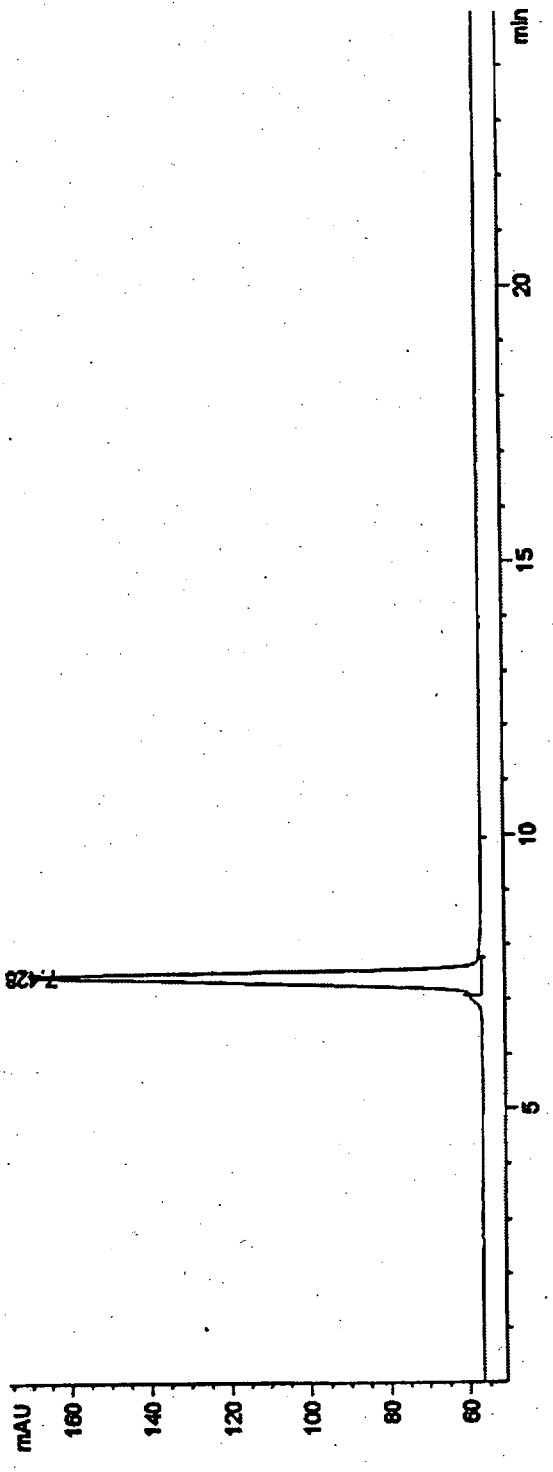

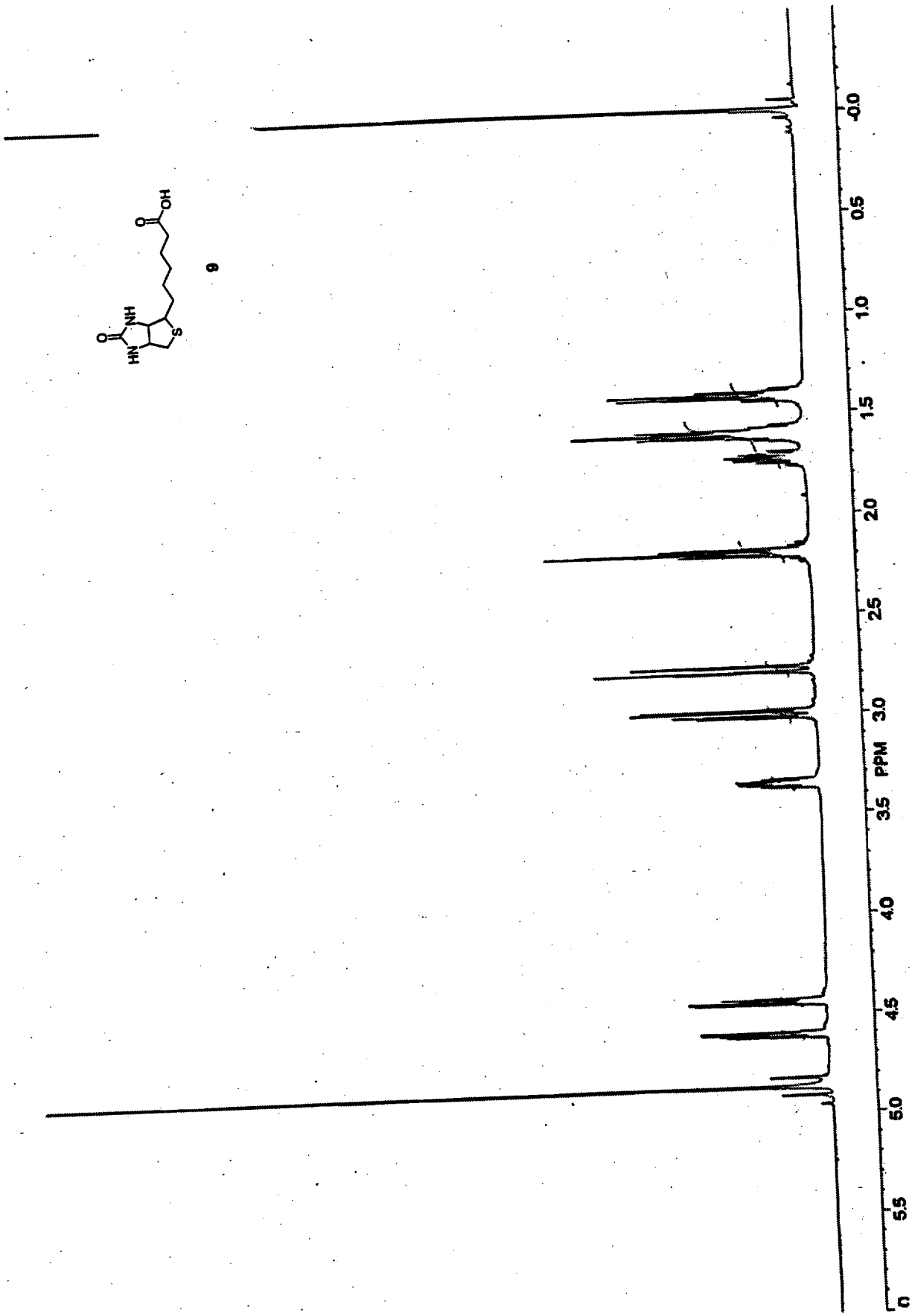
9
-0.0
0.5
1.0
1.5
2.0
2.5
3.0
3.5
PPM
4.0
4.5
5.0
5.5
0

© 2000 American Chemical Society, Bioconjugate Chem., Wilbur bc000024v Supporting Info Page 42

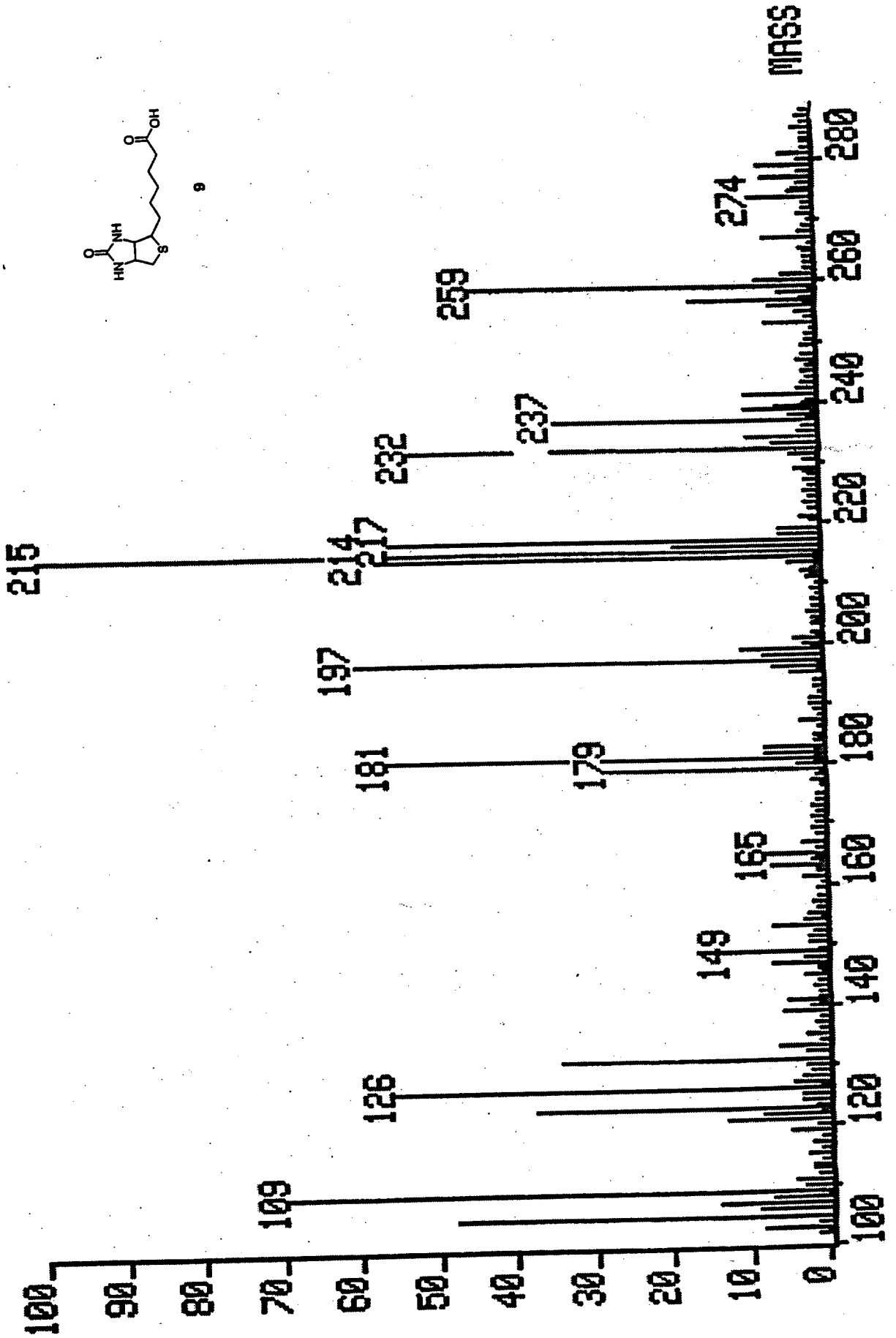

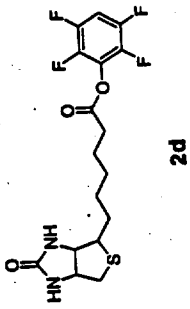

2d

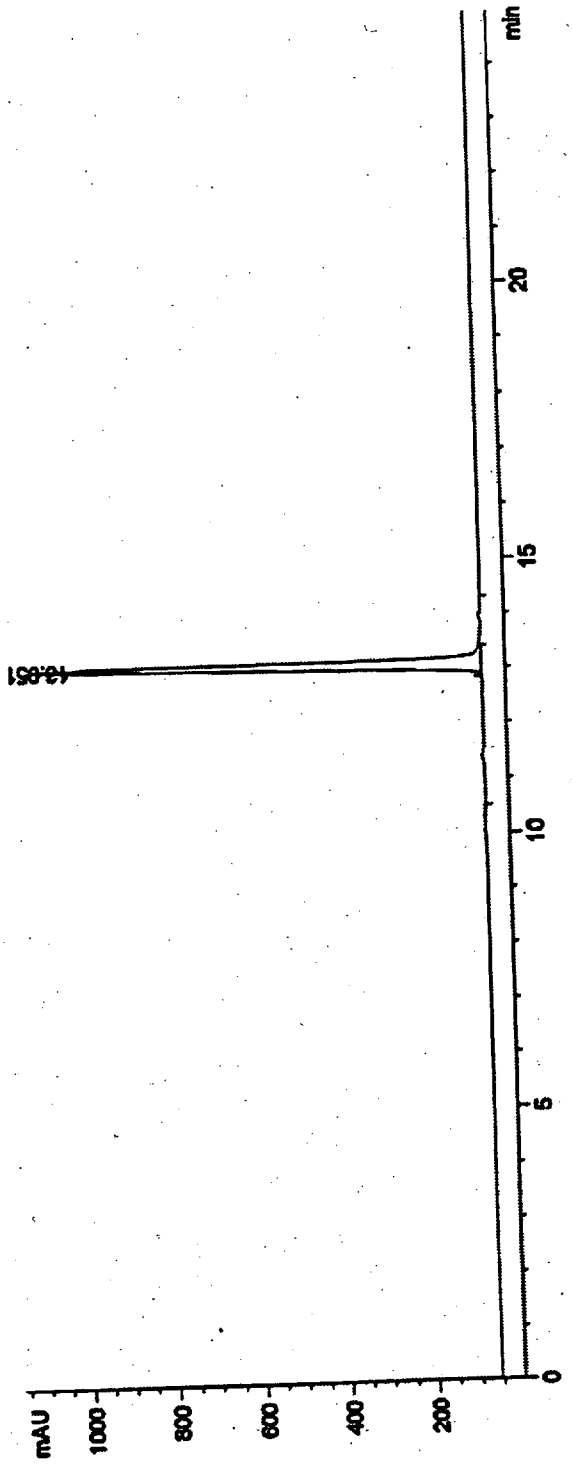

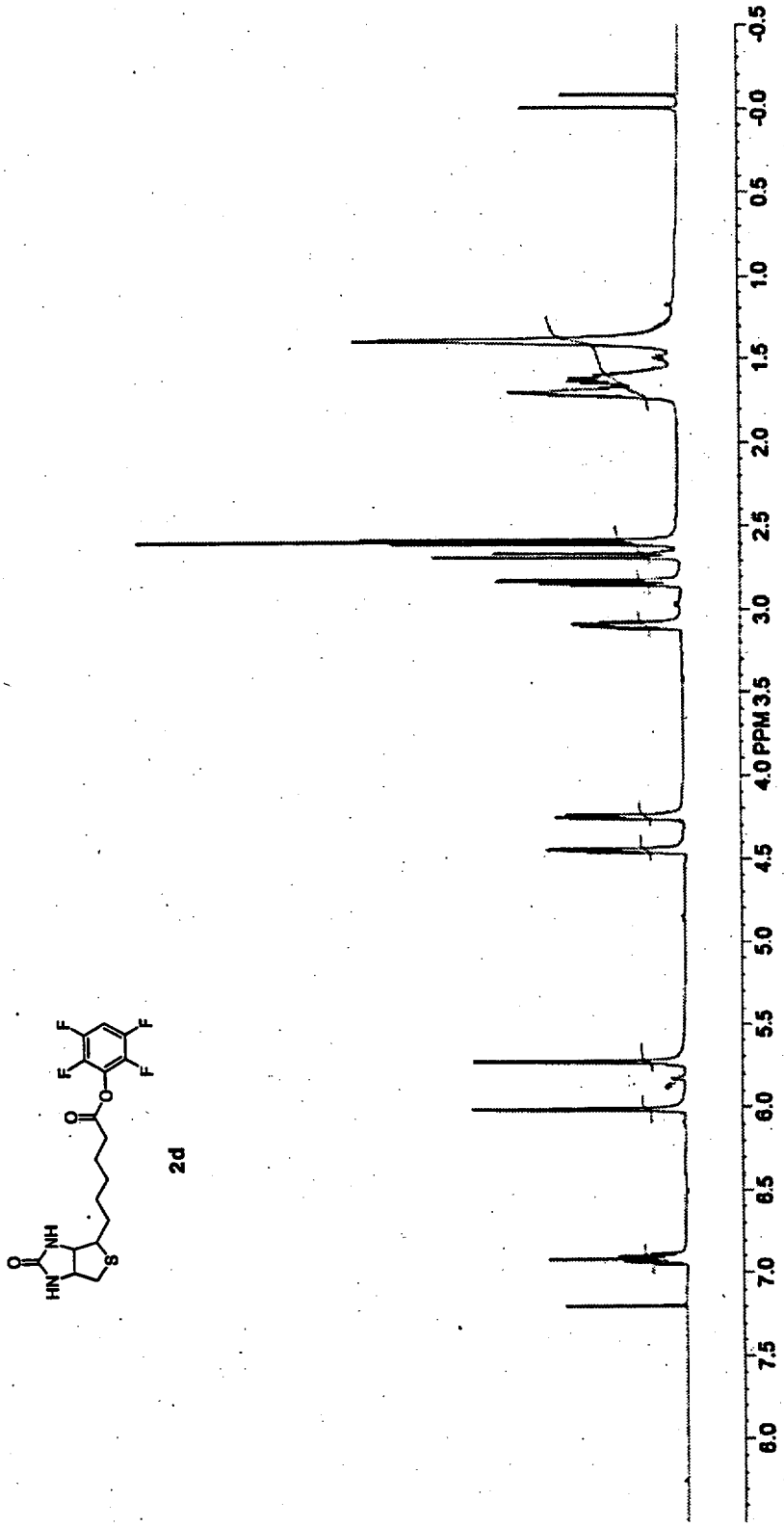
F
F
F
F
O
O
NH
HN
O
S
2d
-0.5
-0.0
0.5
1.0
1.5
2.0
2.5
3.0
3.5
4.0 PPM
4.5
5.0
5.5
6.0
6.5
7.0
7.5
8.0

© 2000 American Chemical Society, Bioconjugate Chem., Wilbur bc000024v Supporting Info Page 45

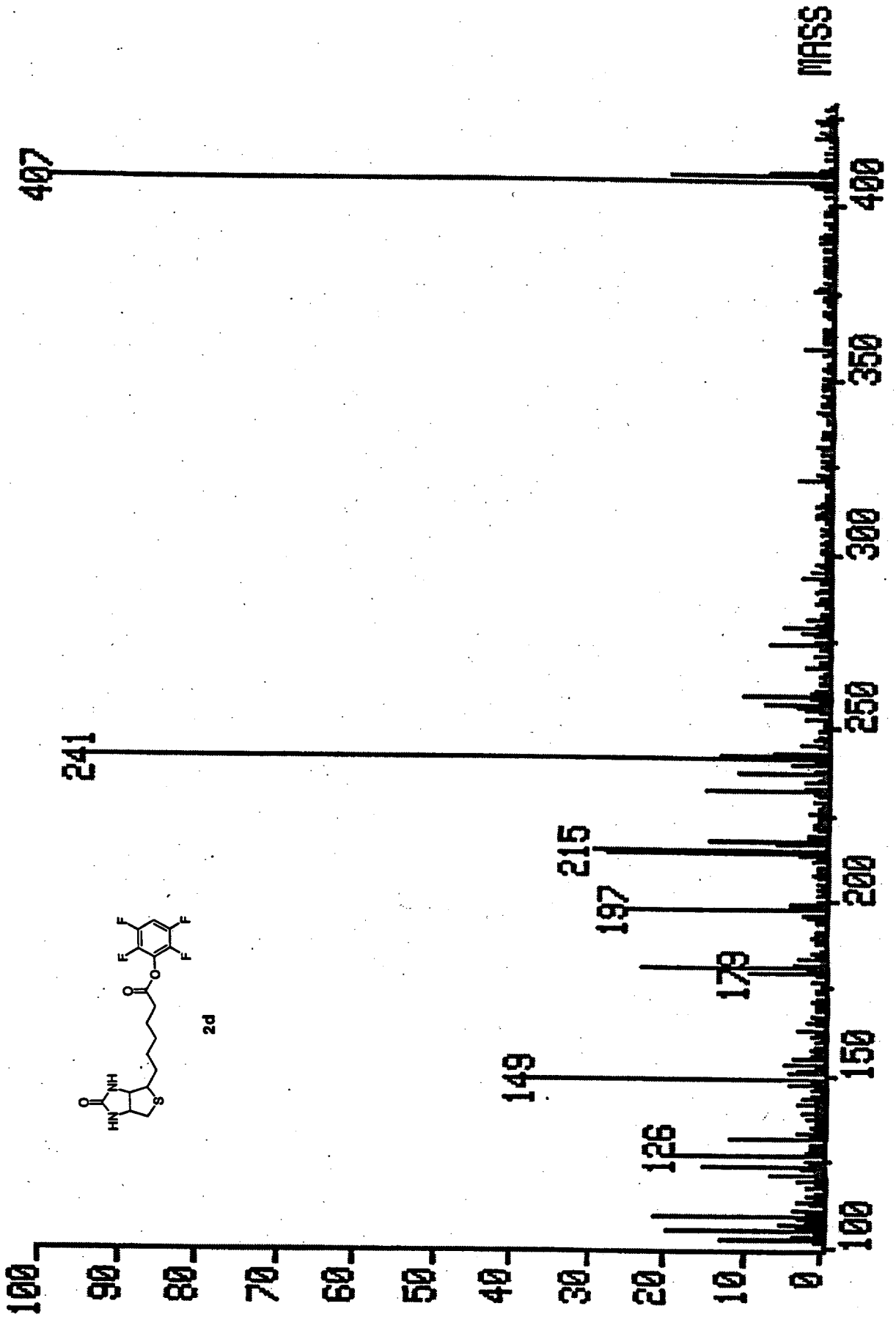

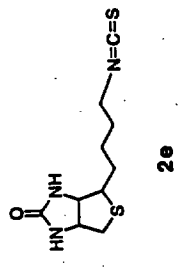

2e

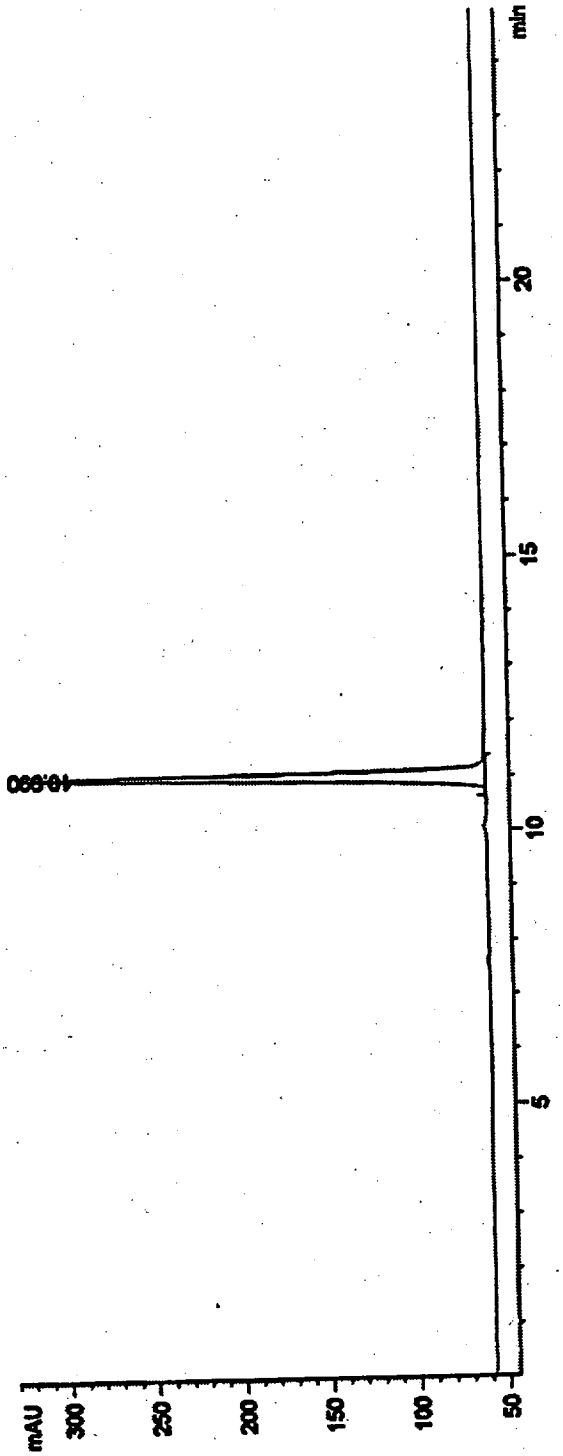

© 2000 American Chemical Society, Bioconjugate Chem., Wilbur bc000024v Supporting Info Page 47

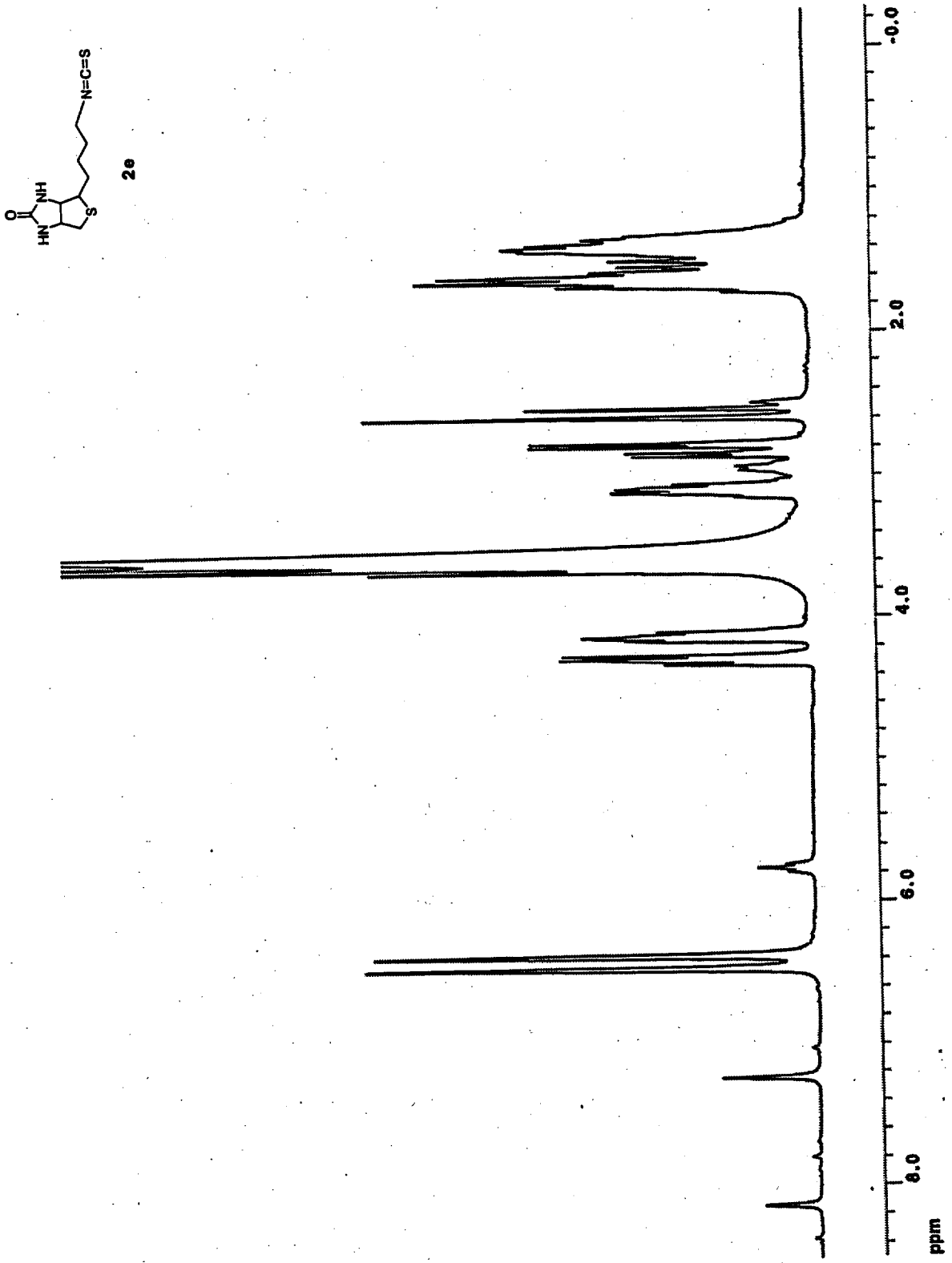

© 2000 American Chemical Society, Bioconjugate Chem., Wilbur bc000024v Supporting Info Page 48

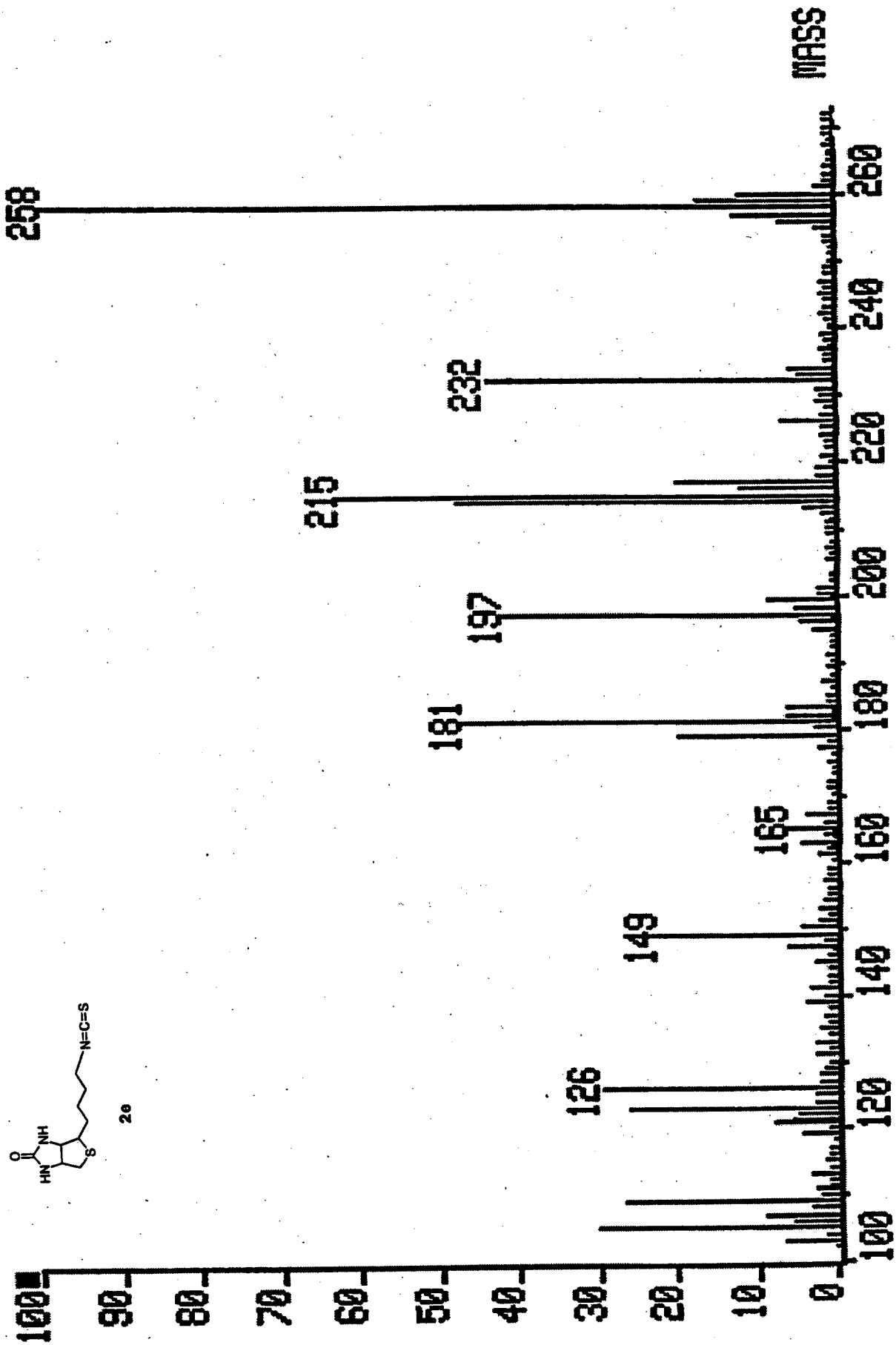

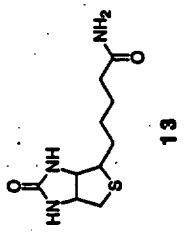

13

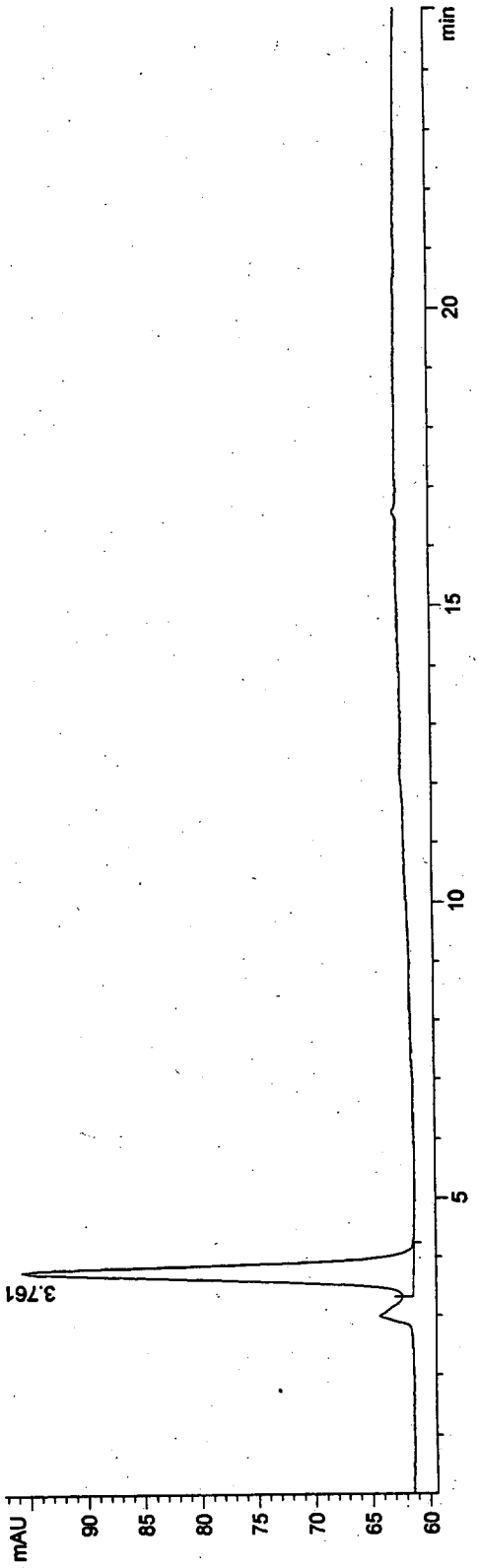

© 2000 American Chemical Society, Bioconjugate Chem., Wilbur bc000024v Supporting Info Page 50

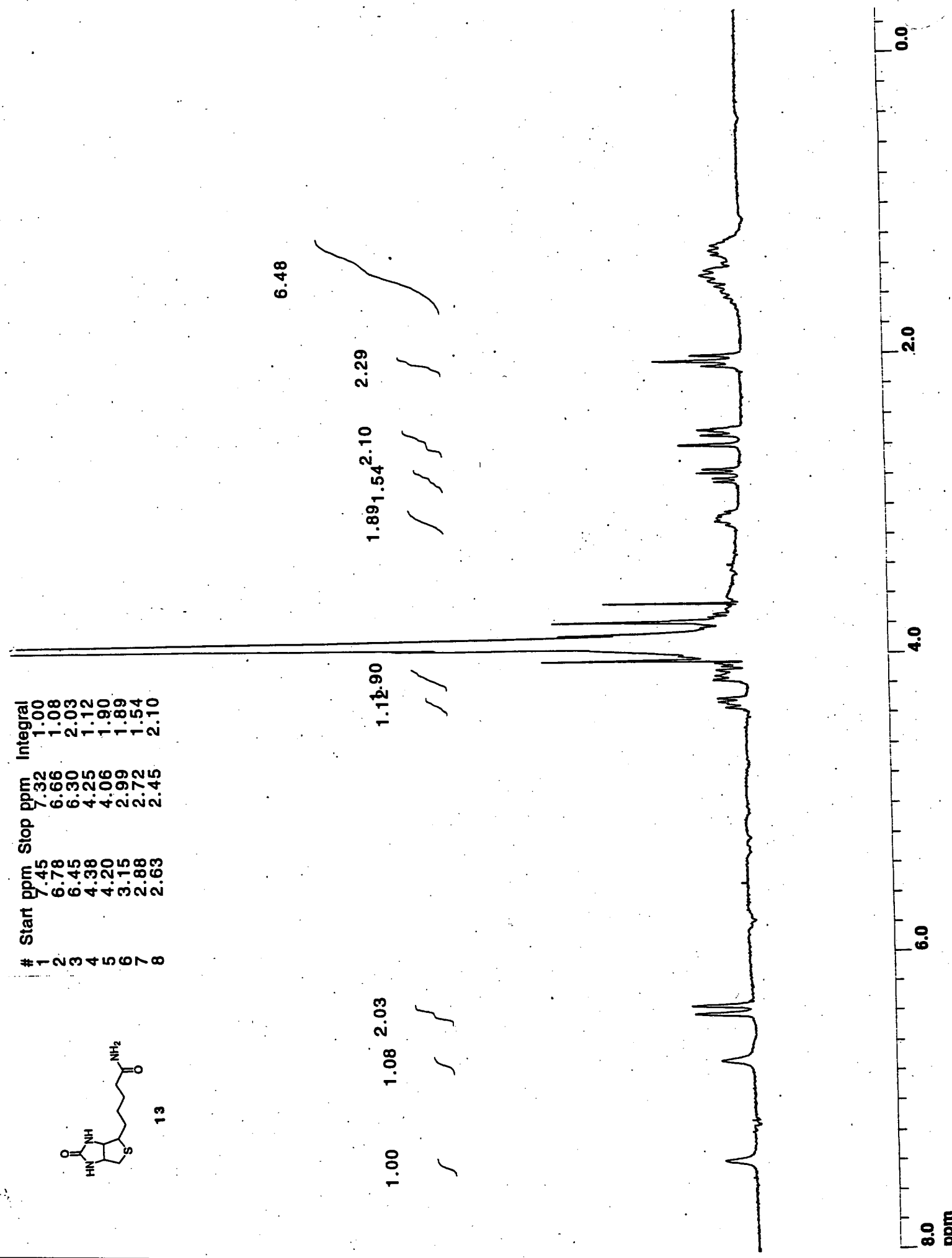

© 2000 American Chemical Society, Bioconjugate Chem., Wilbur bc000024v Supporting Info Page 51

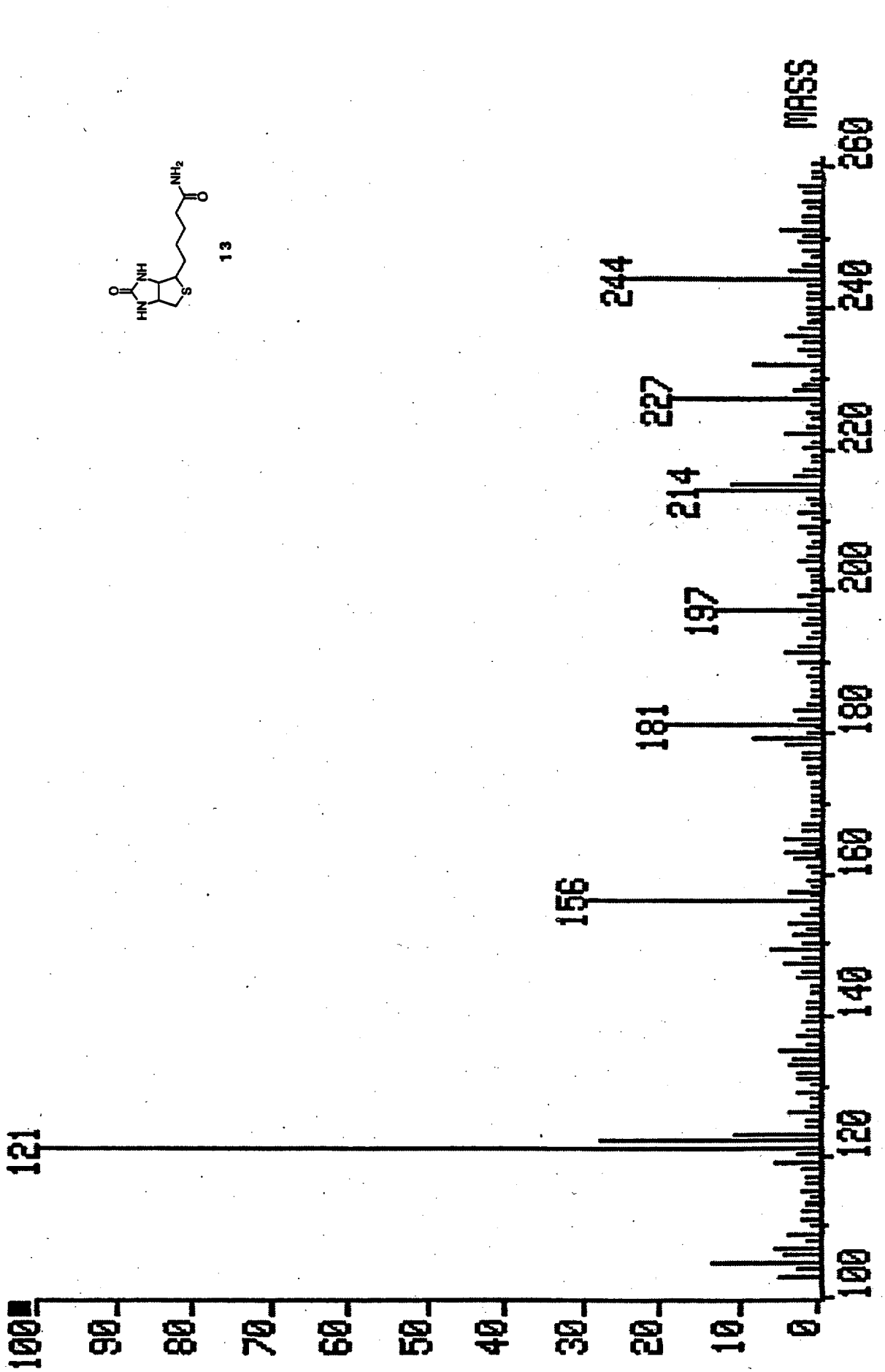

13

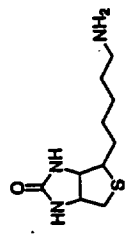

14

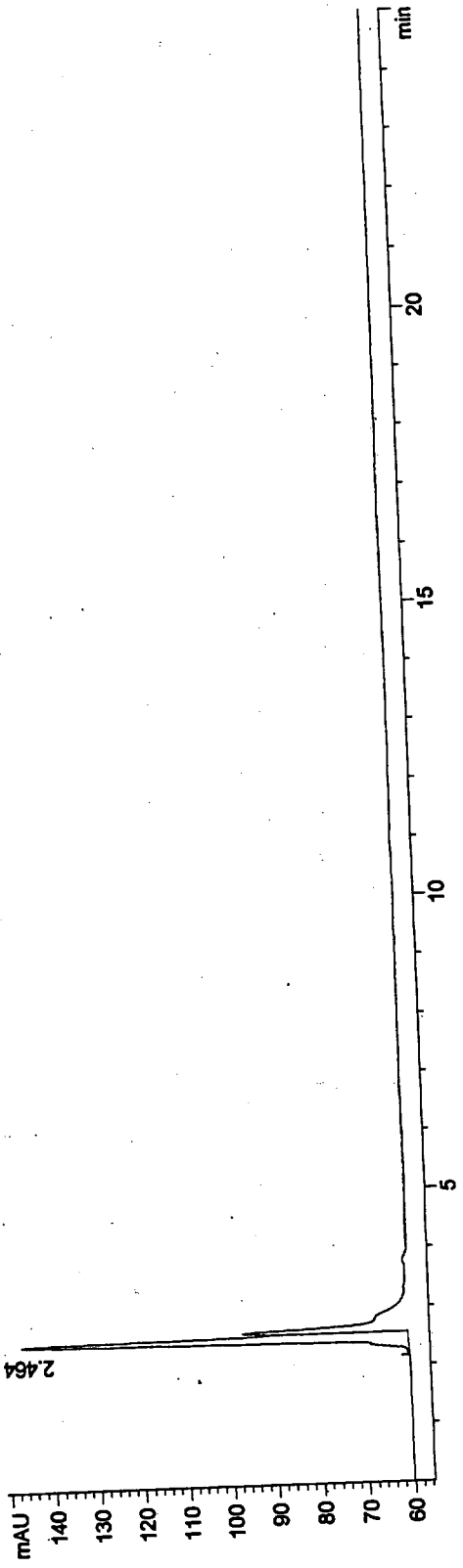

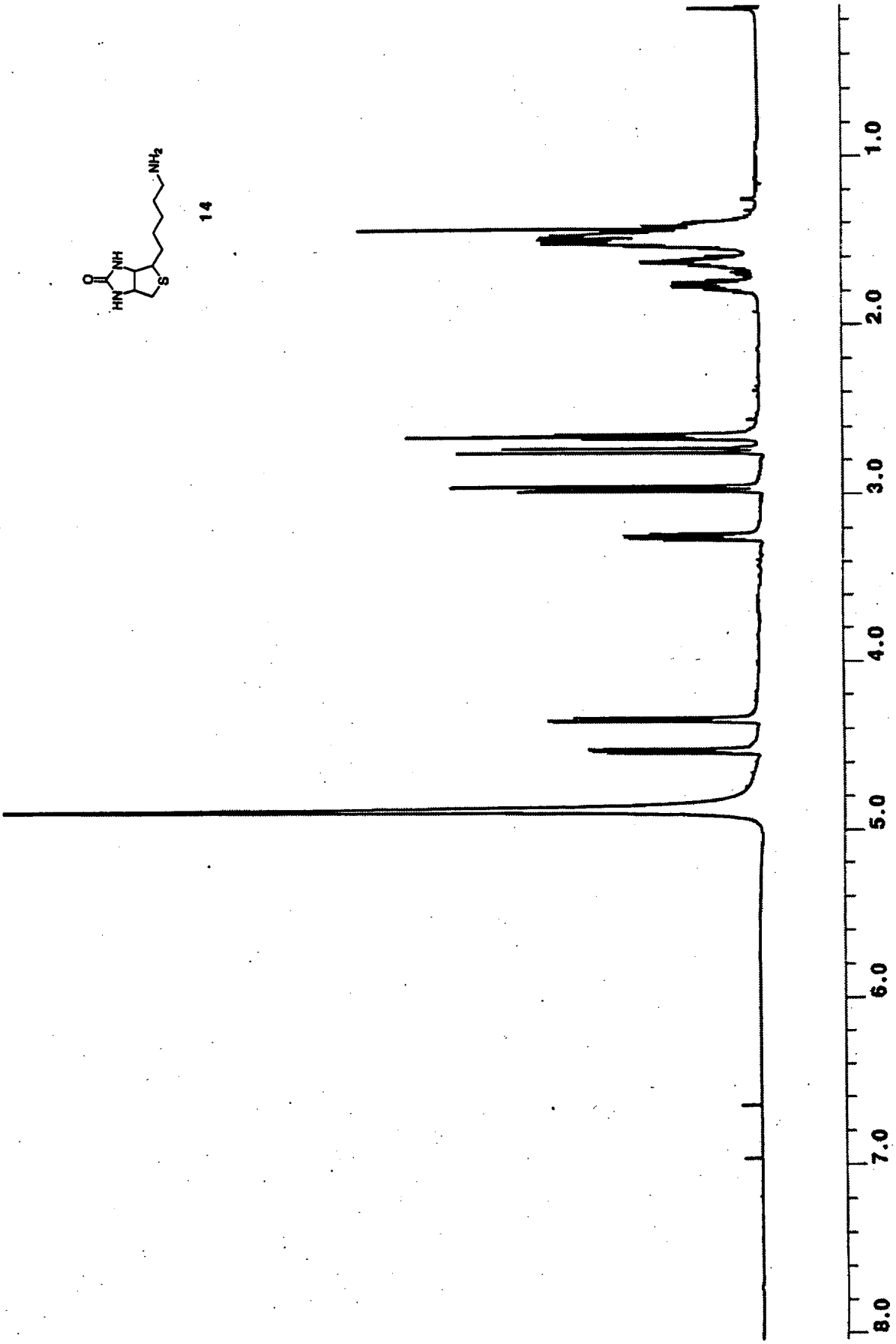
NH2
NH
HN
O
S
14
1.0
2.0
3.0
4.0
5.0
6.0
7.0
8.0

© 2000 American Chemical Society, Bioconjugate Chem., Wilbur bc000024v Supporting Info Page 54

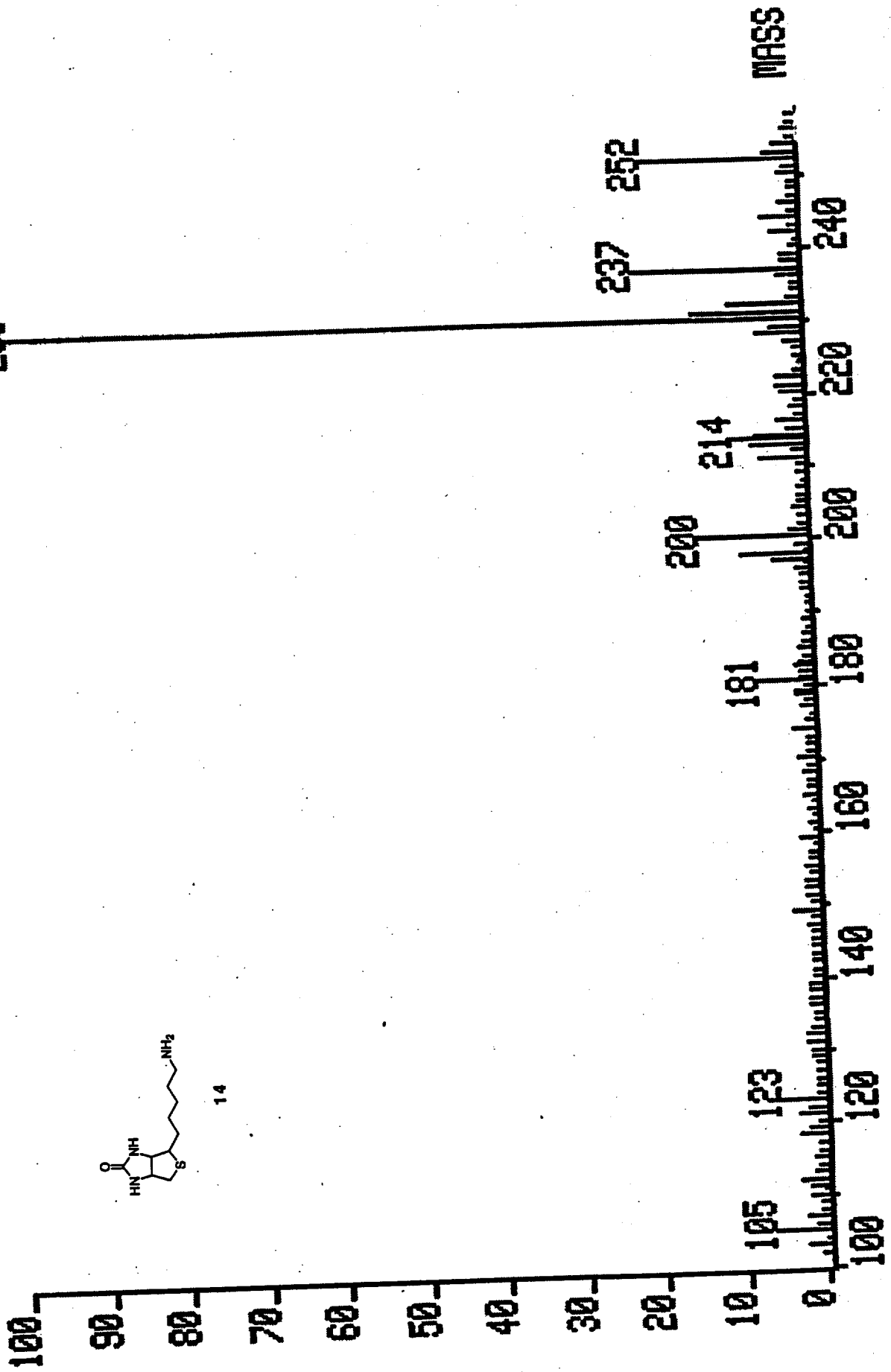

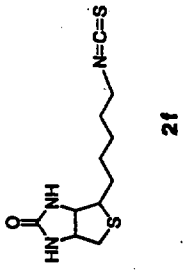

21

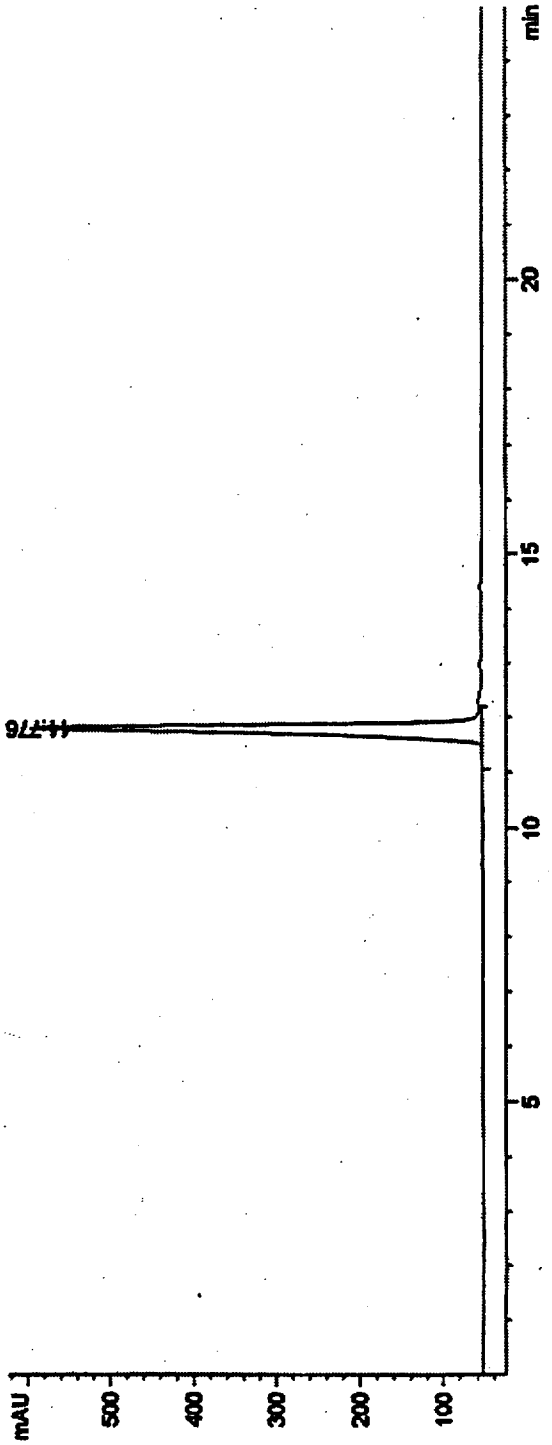

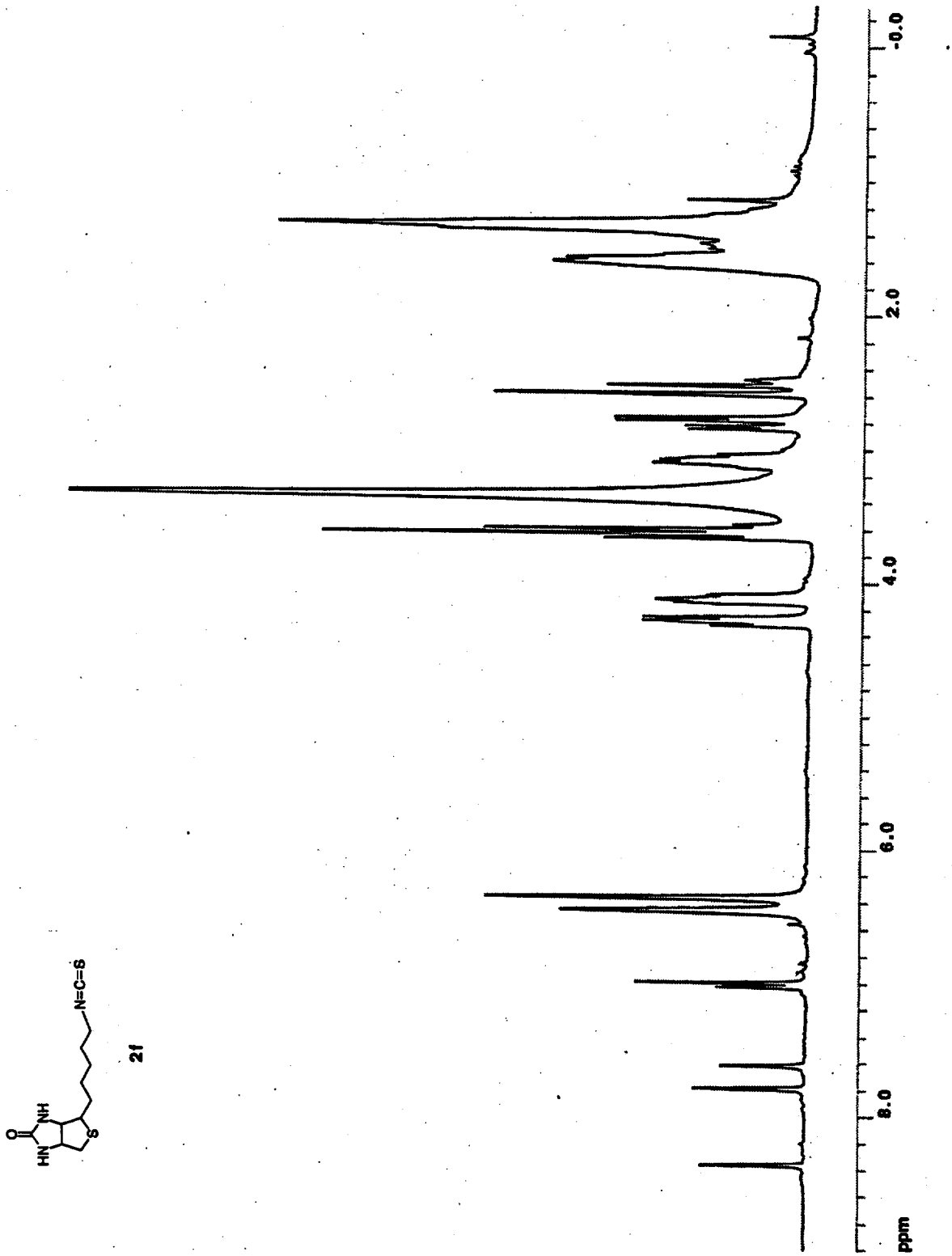
21
N=C=S
NH
HN
O
S
-0.0
2.0
4.0
6.0
8.0
ppm

© 2000 American Chemical Society, Bioconjugate Chem., Wilbur bc000024v Supporting Info Page 57

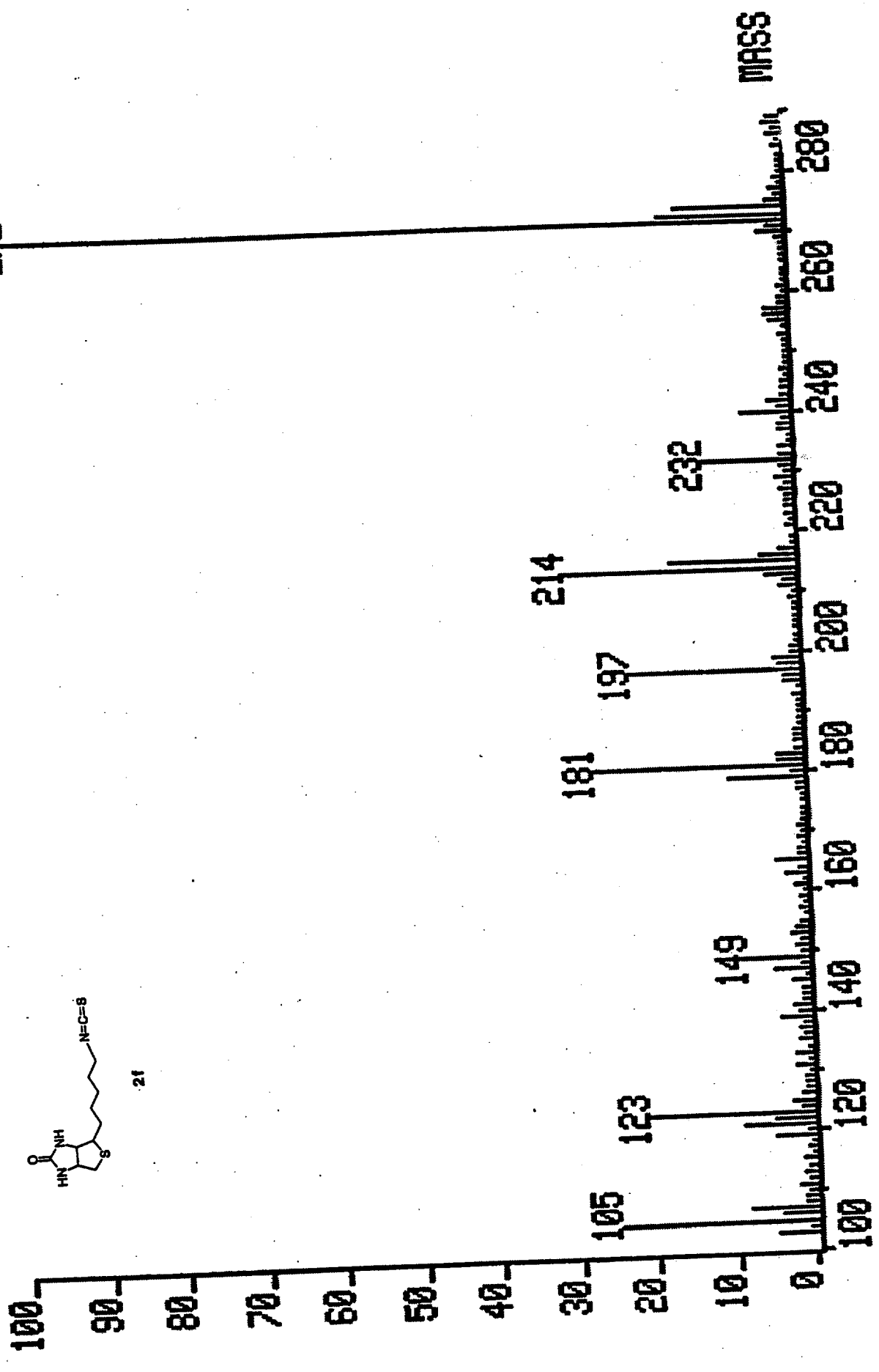

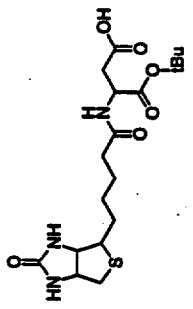

18

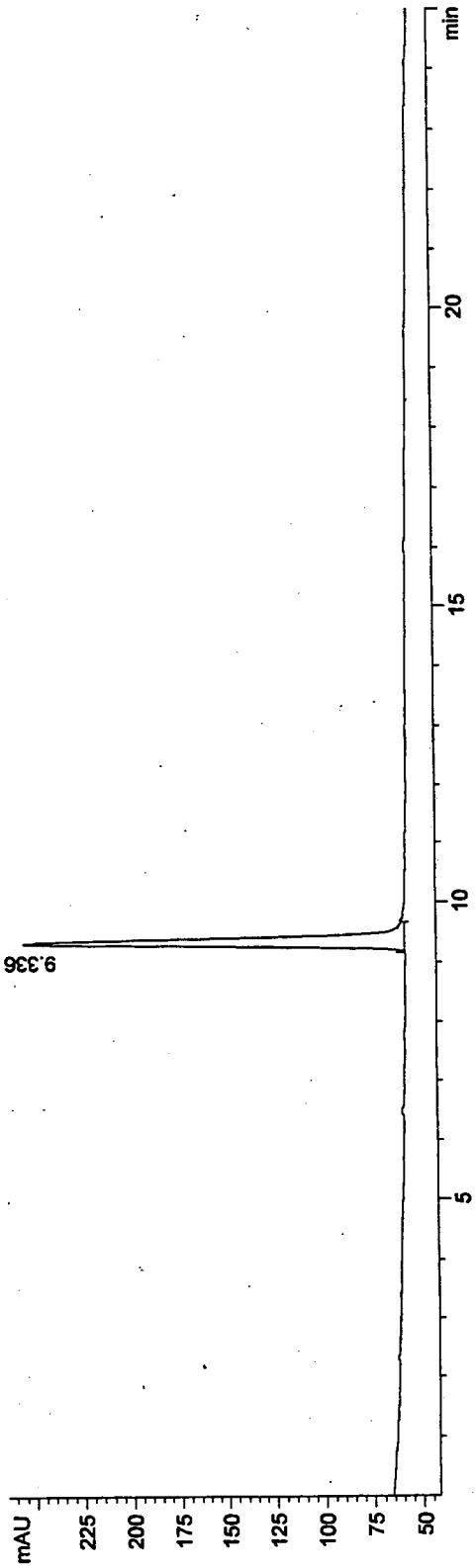

© 2000 American Chemical Society, Bioconjugate Chem., Wilbur bc000024v Supporting Info Page 59

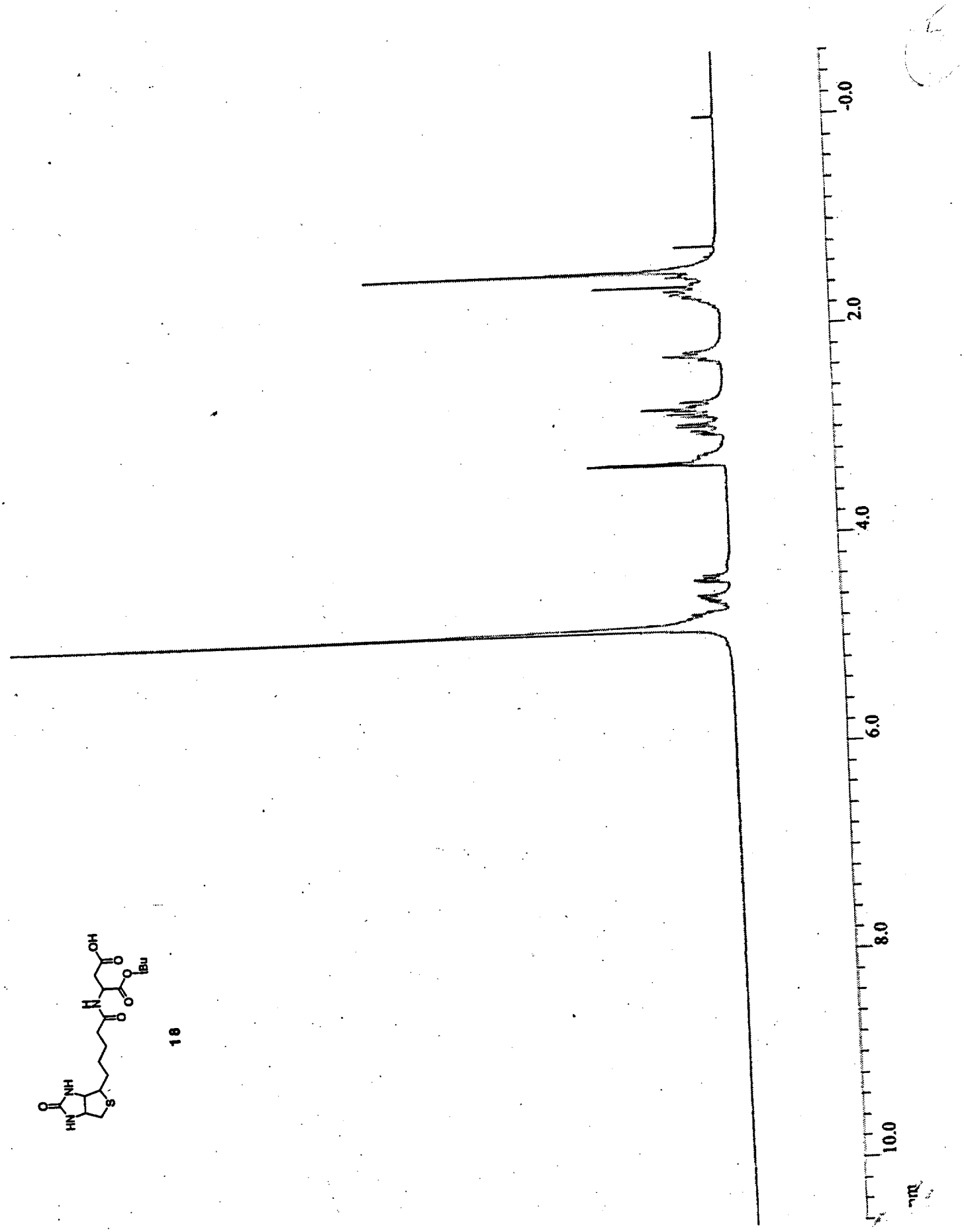

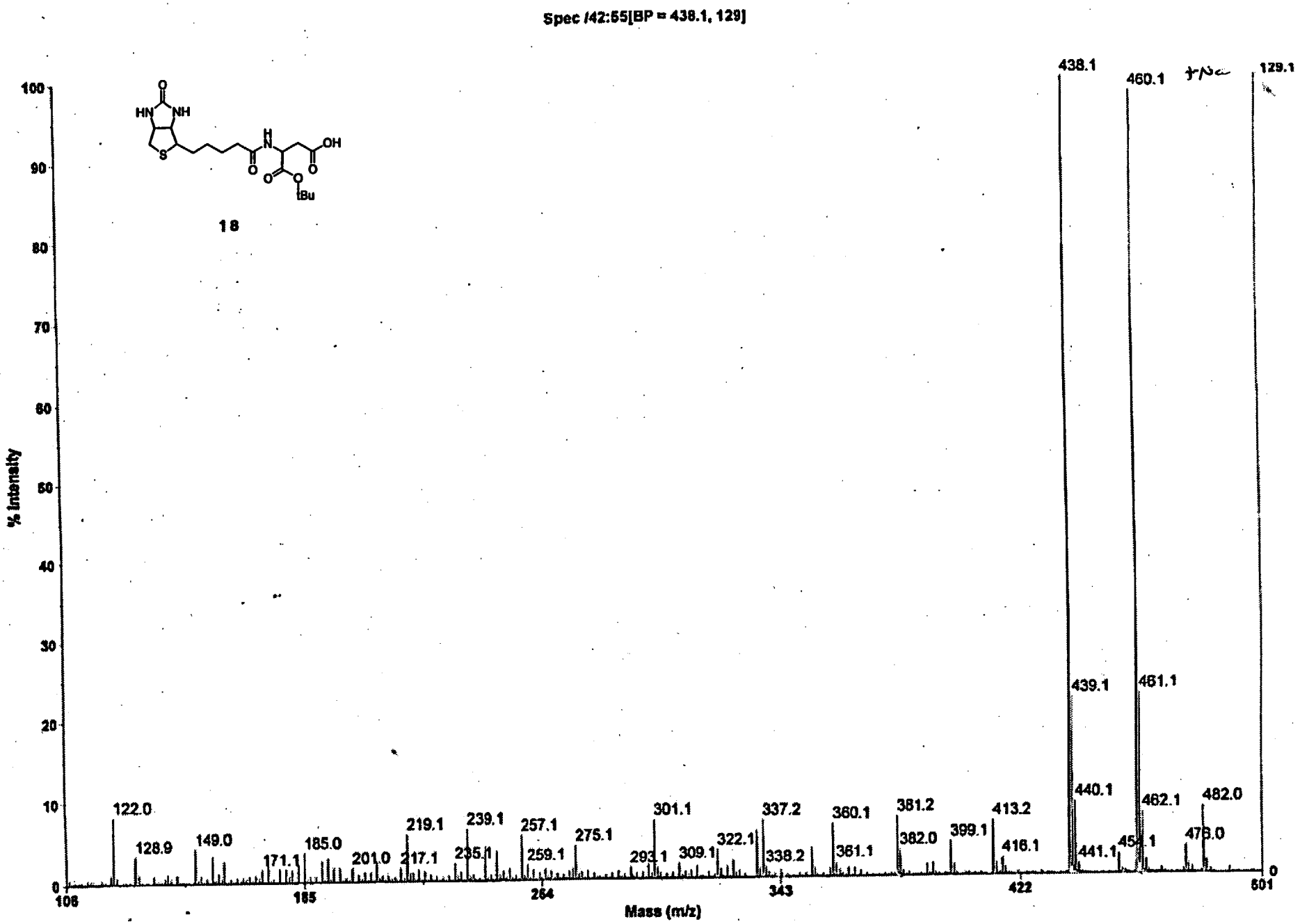

© 2000 American Chemical Society, Bioconjugate Chem., Wilbur bc000024v Supporting Info Page 60

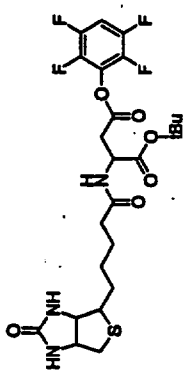

21

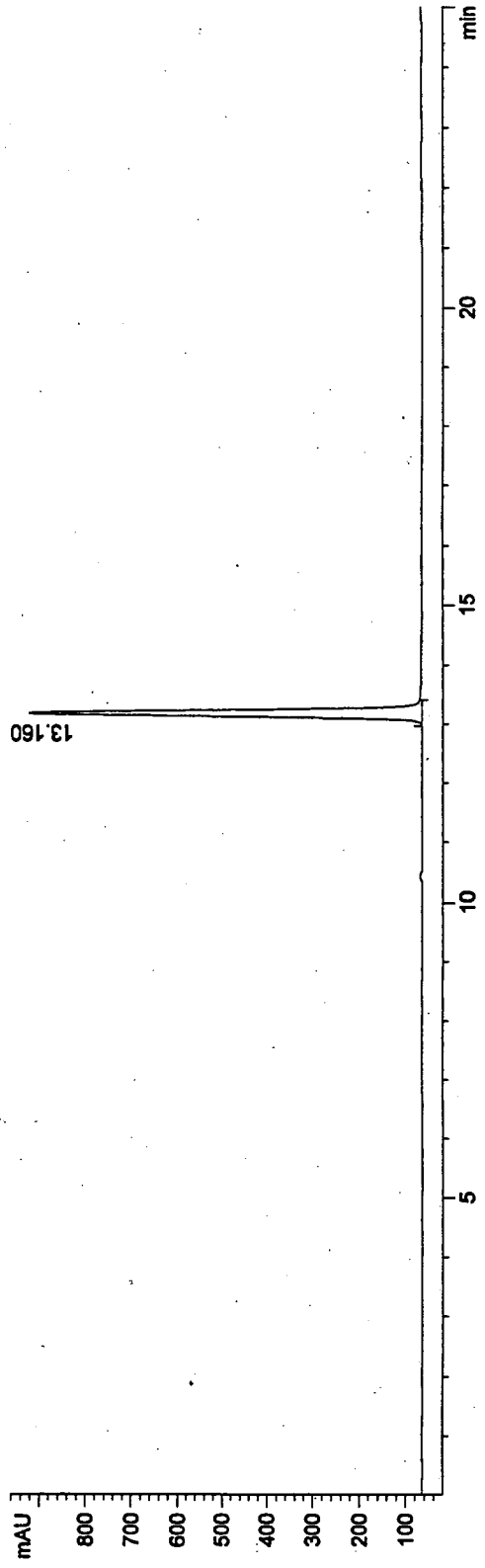

© 2000 American Chemical Society, Bioconjugate Chem., Wilbur bc000024v Supporting Info Page 62

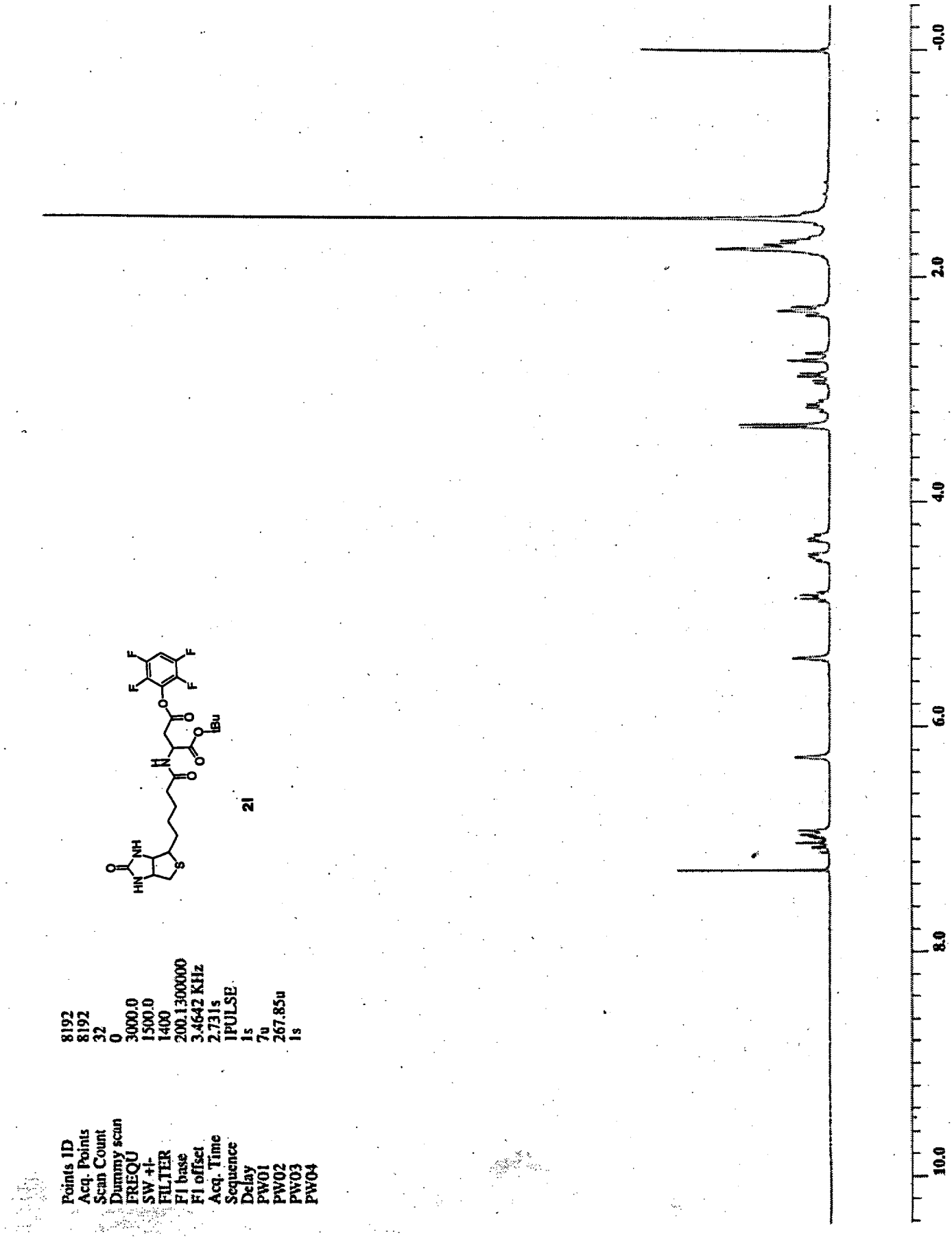

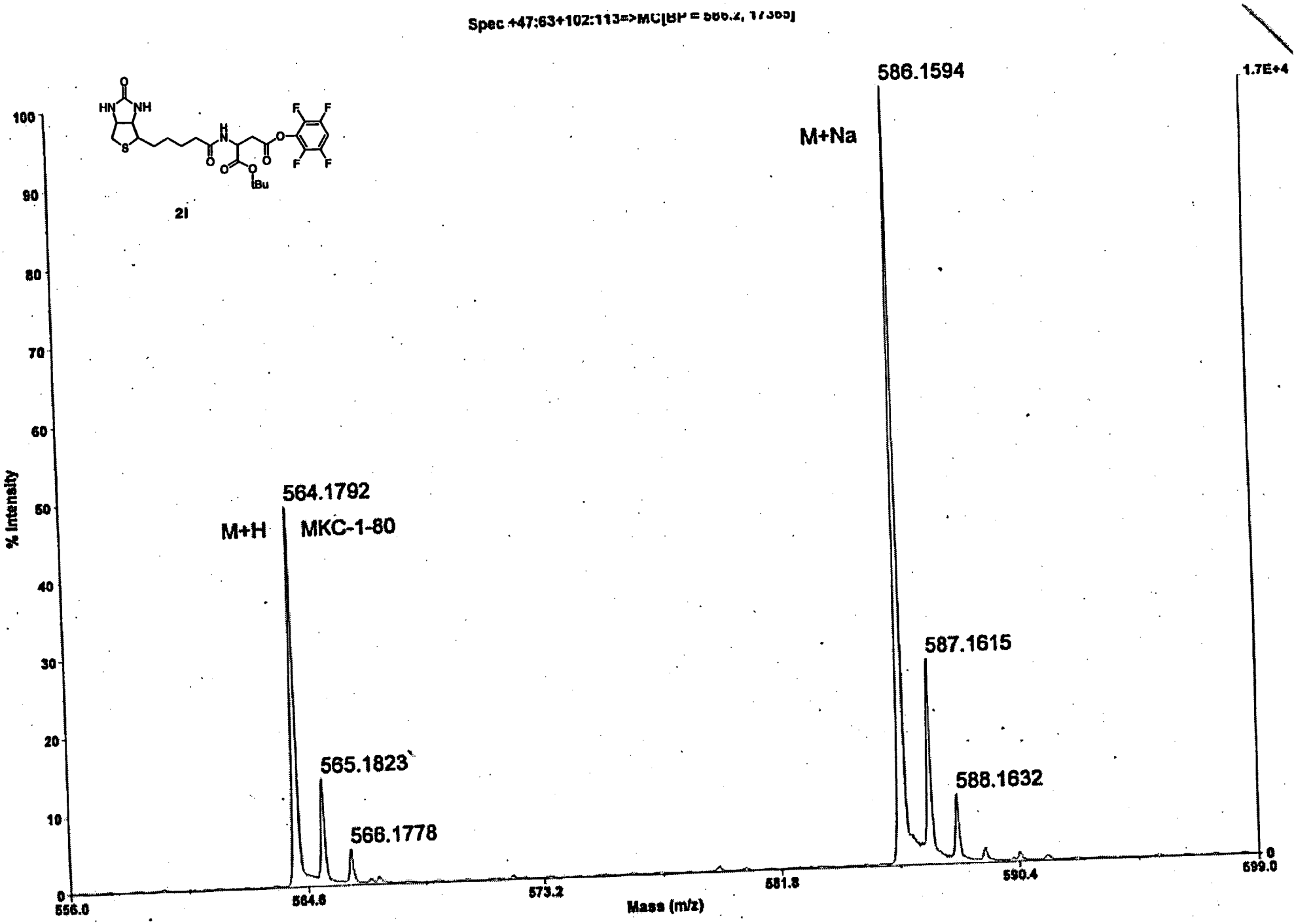

© 2000 American Chemical Society, Bioconjugate Chem., Wilbur bc000024v Supporting Info Page 63

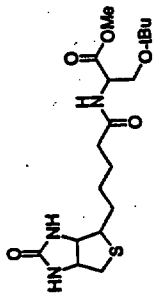
O-tBu
OMe
NH
HN
S

24

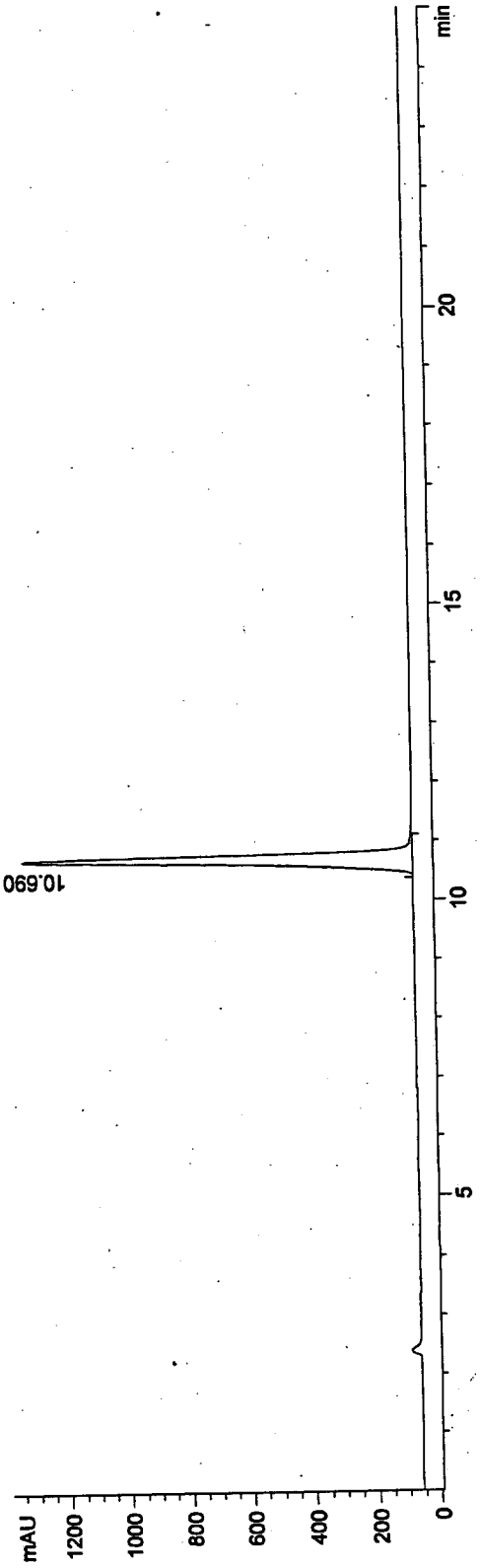
min
10.690
mAU
0
200
400
600
800
1000
1200
5
10
15
20

© 2000 American Chemical Society, Bioconjugate Chem., Wilbur bc000024v Supporting Info Page 65

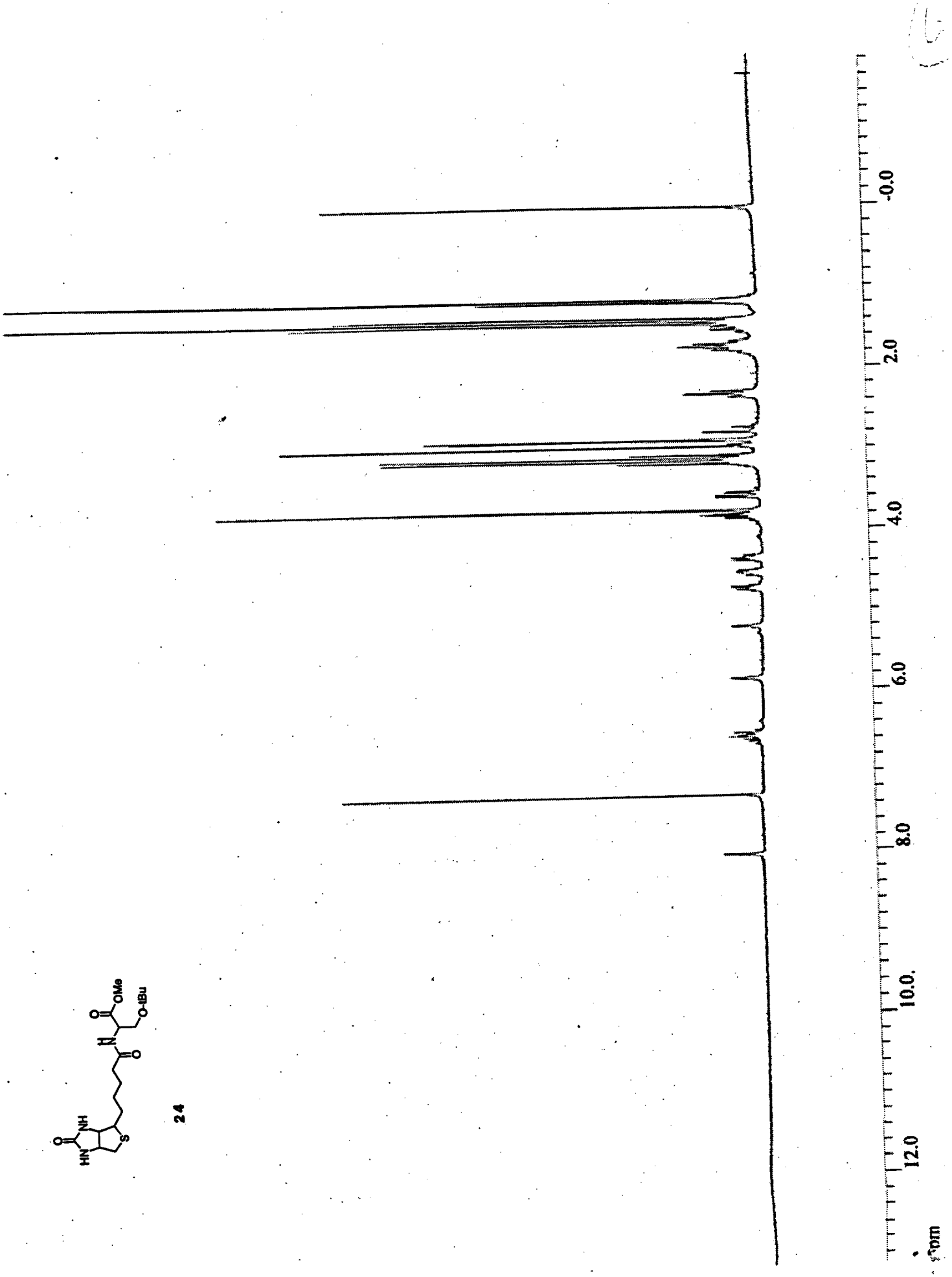

24

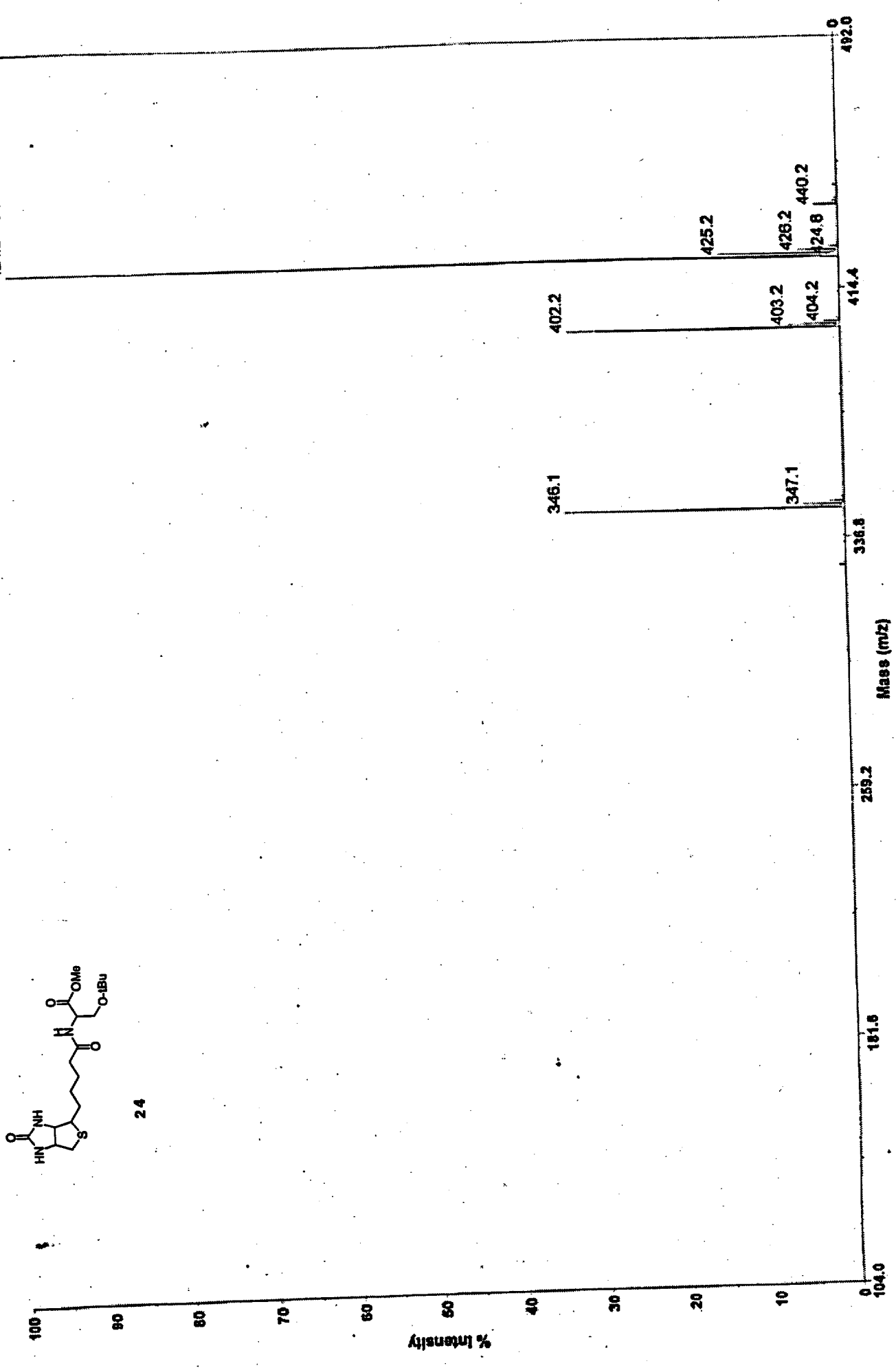
3907.8
424.2
+Na
425.2
426.2
424.8
440.2
402.2
403.2
404.2
414.4
346.1
347.1
336.8
259.2
181.8
104.0
492.0
Mass (m/z)
% Intensity
100
90
80
70
60
50
40
30
20
10
0
OMe
O-tBu
NH
HN
S
24

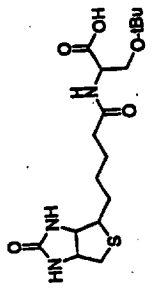

25

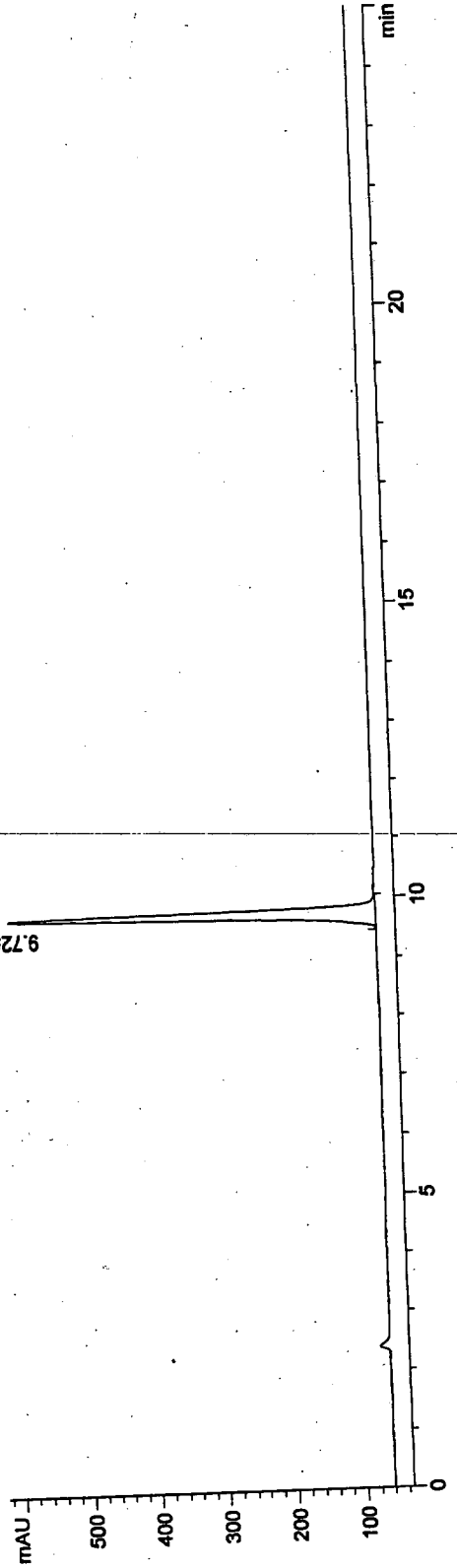

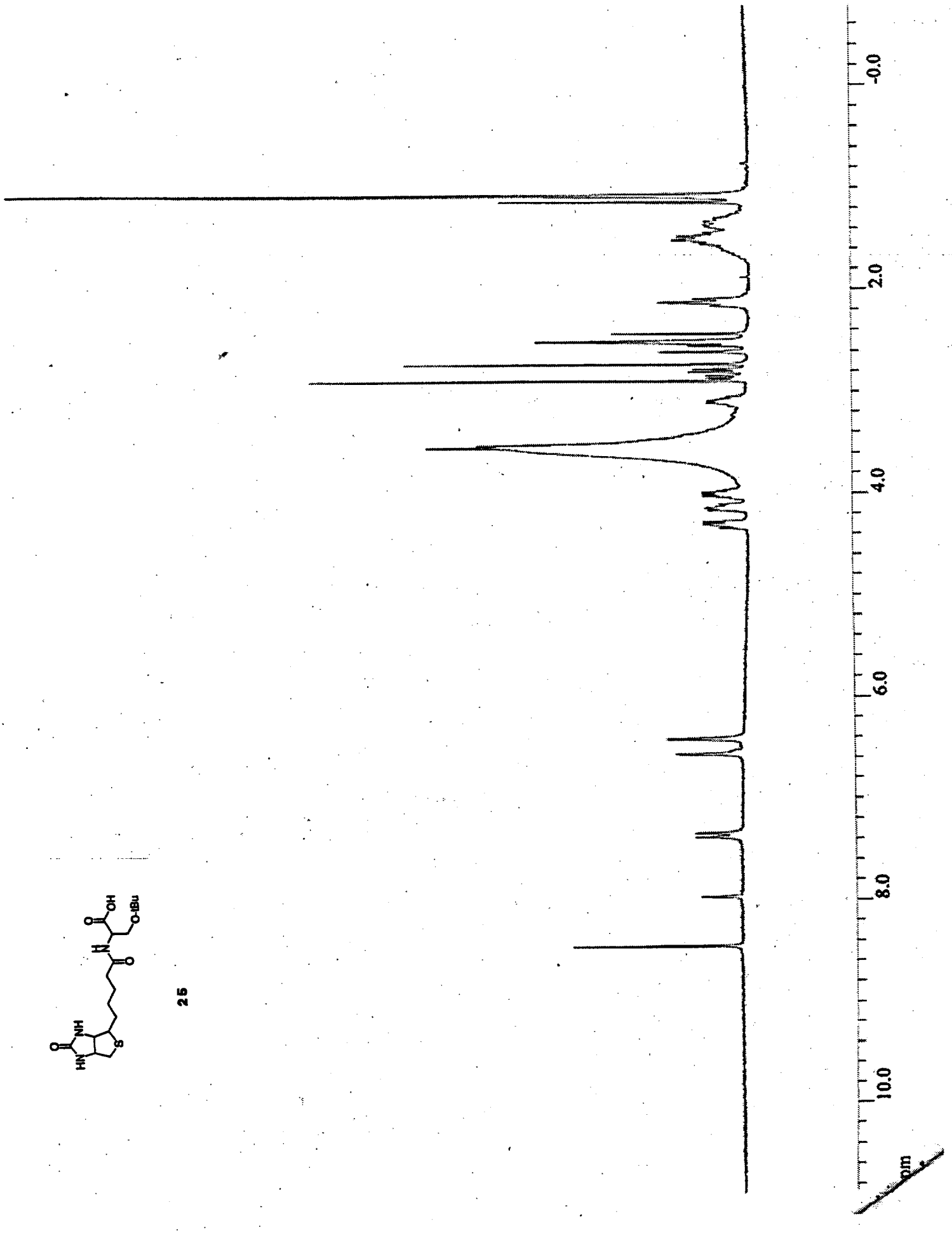

25

© 2000 American Chemical Society, Bioconjugate Chem., Wilbur bc000024v Supporting Info Page 69

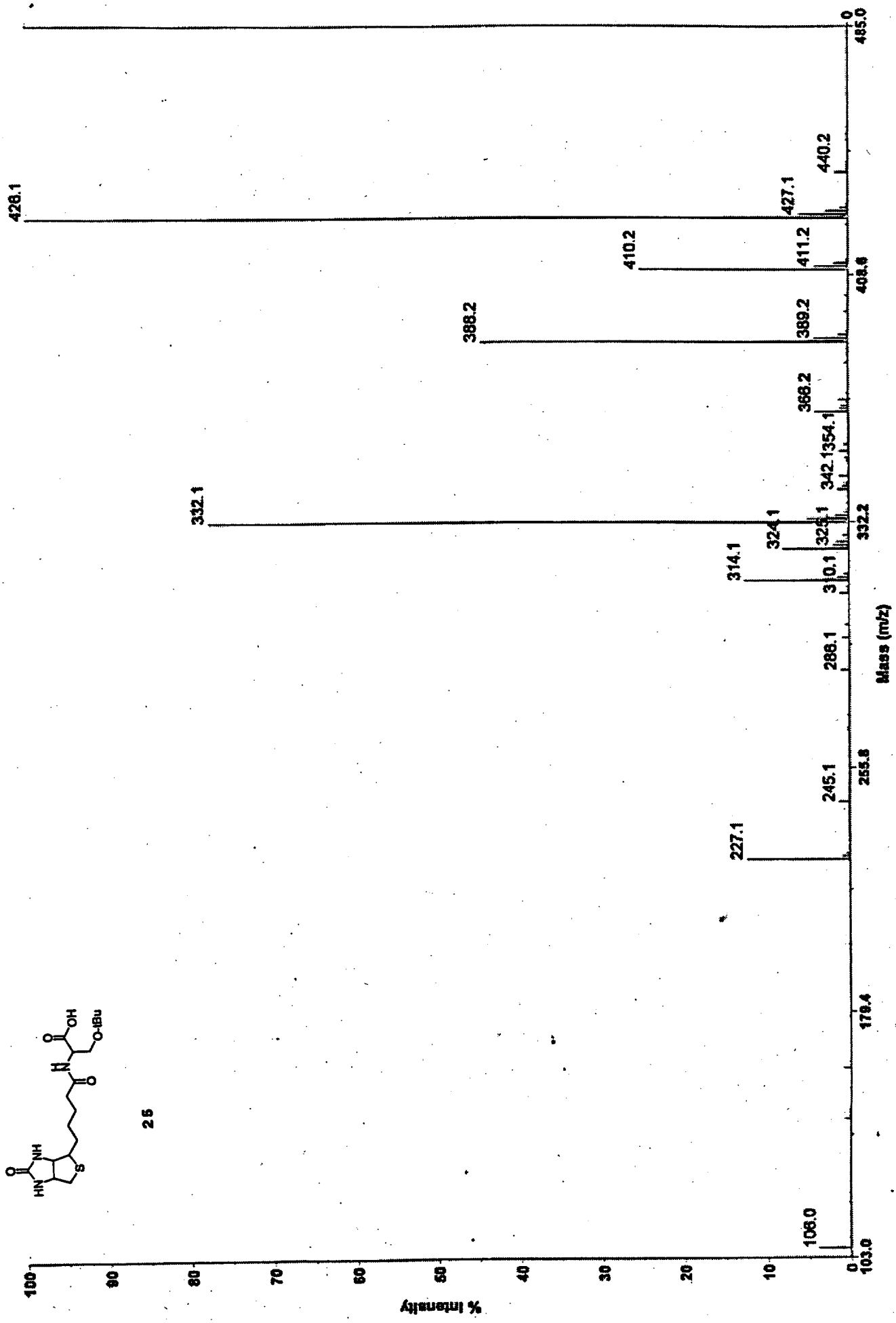

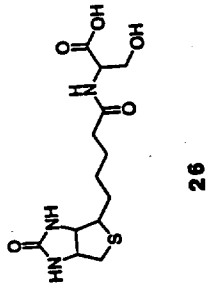

26

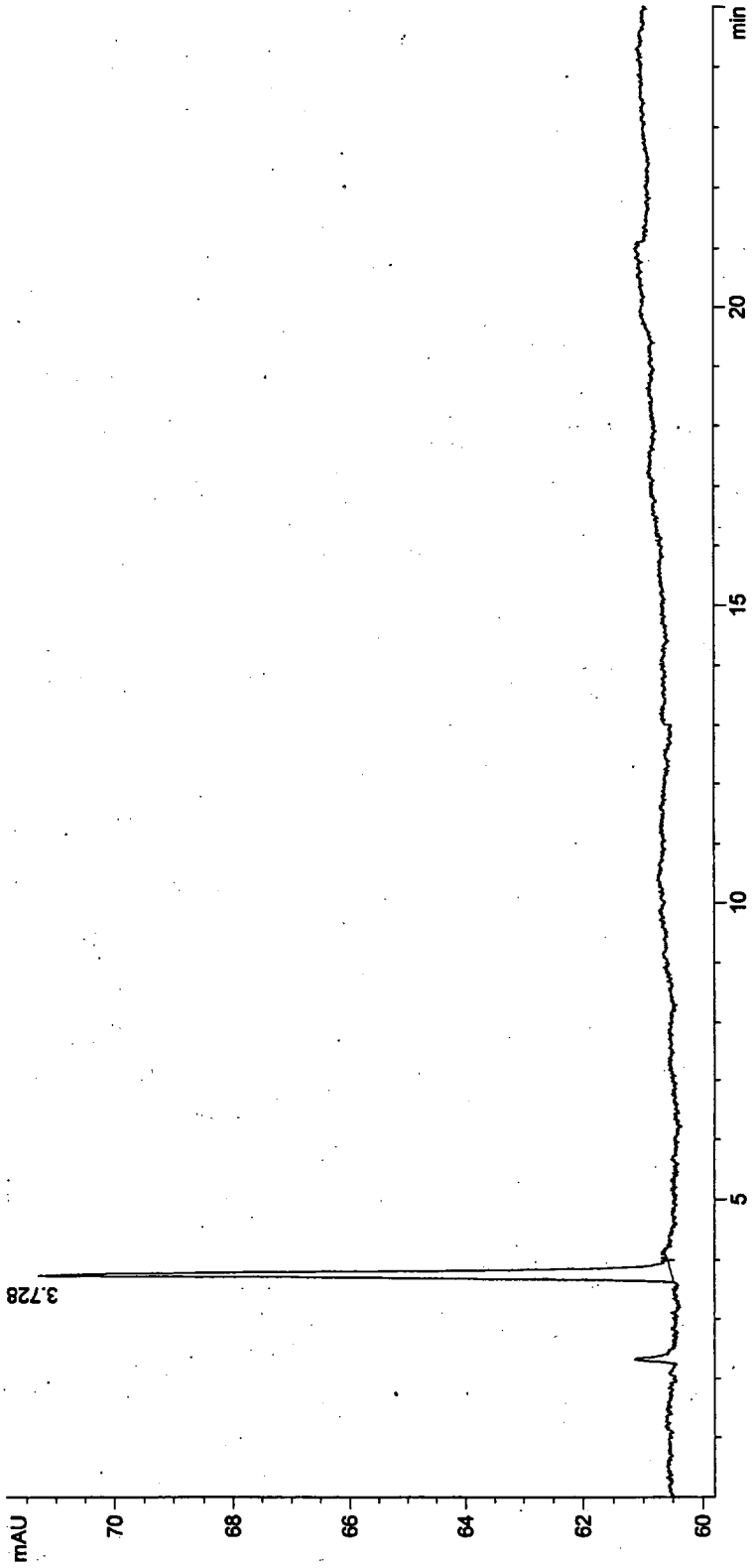

© 2000 American Chemical Society, Bioconjugate Chem., Wilbur bc000024v Supporting Info Page 71

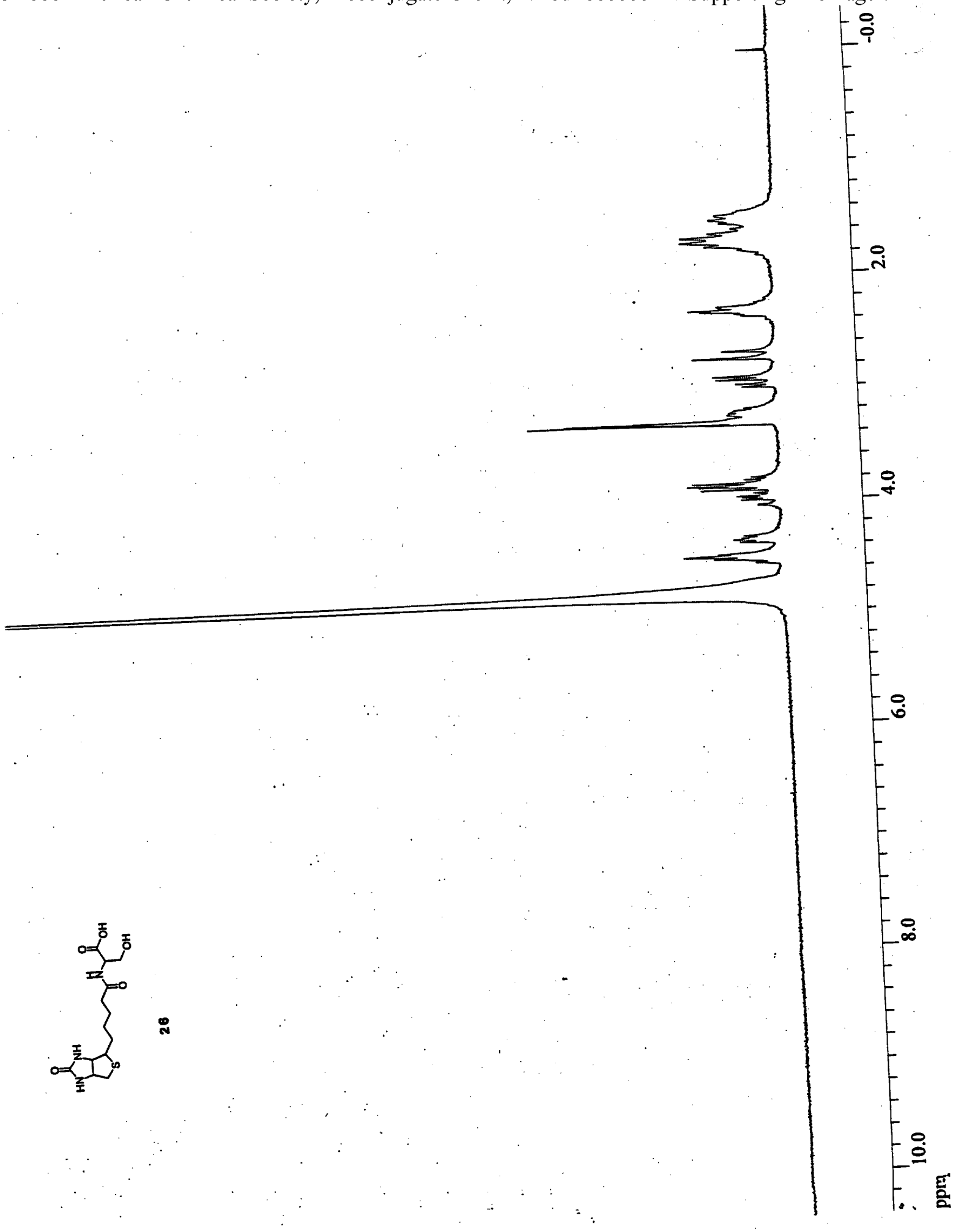

26

© 2000 American Chemical Society, Bioconjugate Chem., Wilbur bc000024v Supporting Info Page 72

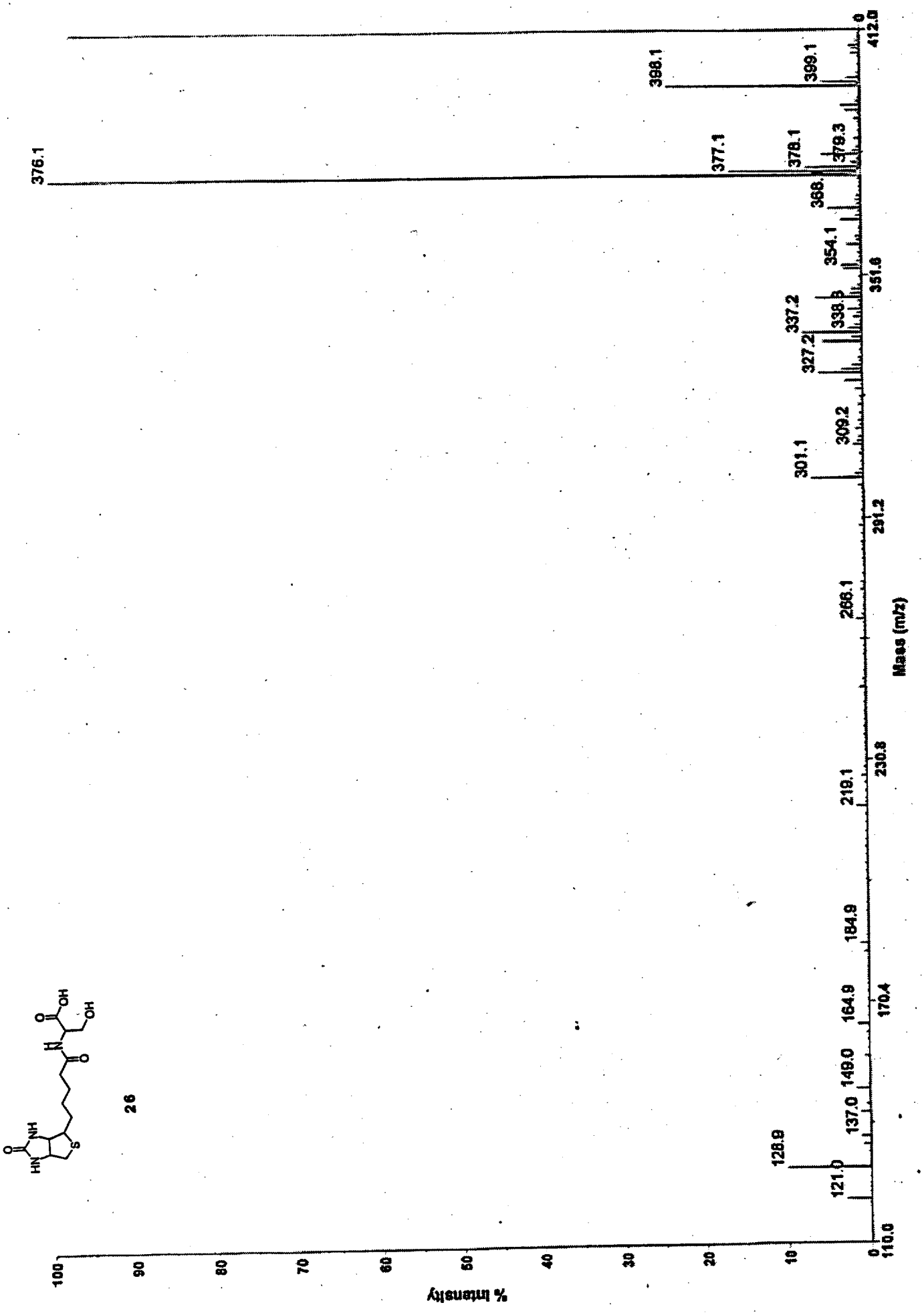

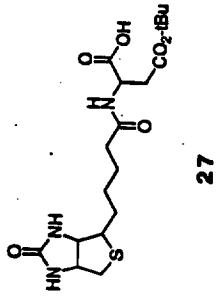
OH
O
CO2-tBu
H
N
O
NH
HN
O
S

27

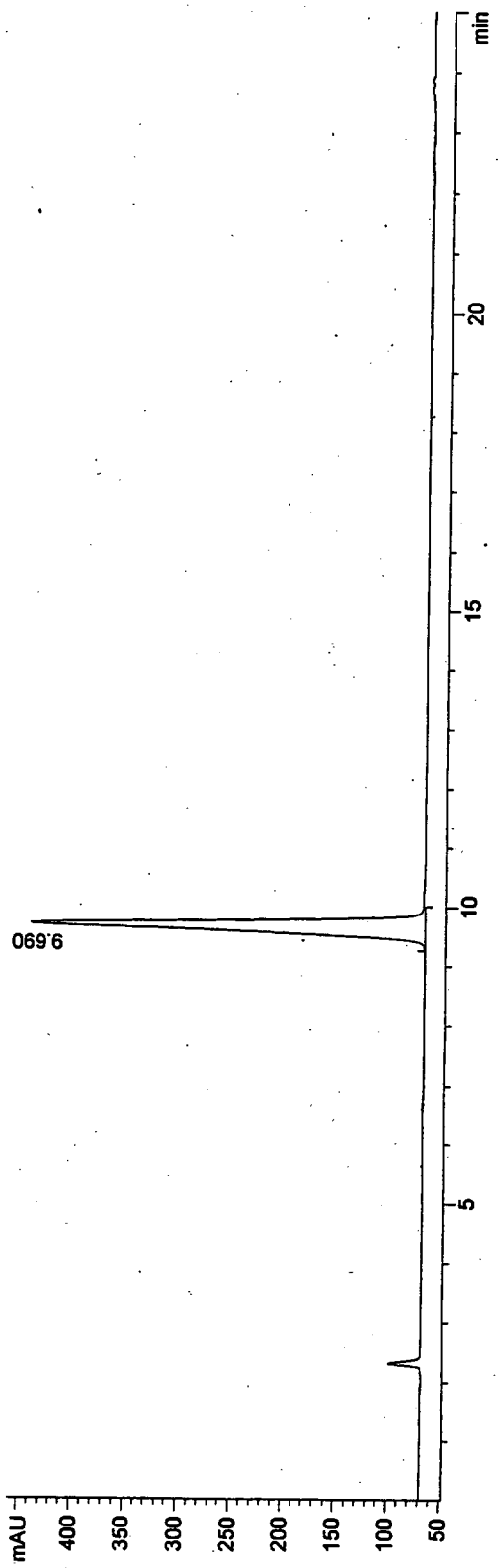
9.690
min
5
10
15
20
mAU
400
350
300
250
200
150
100
50

© 2000 American Chemical Society, Bioconjugate Chem., Wilbur bc000024v Supporting Info Page 74

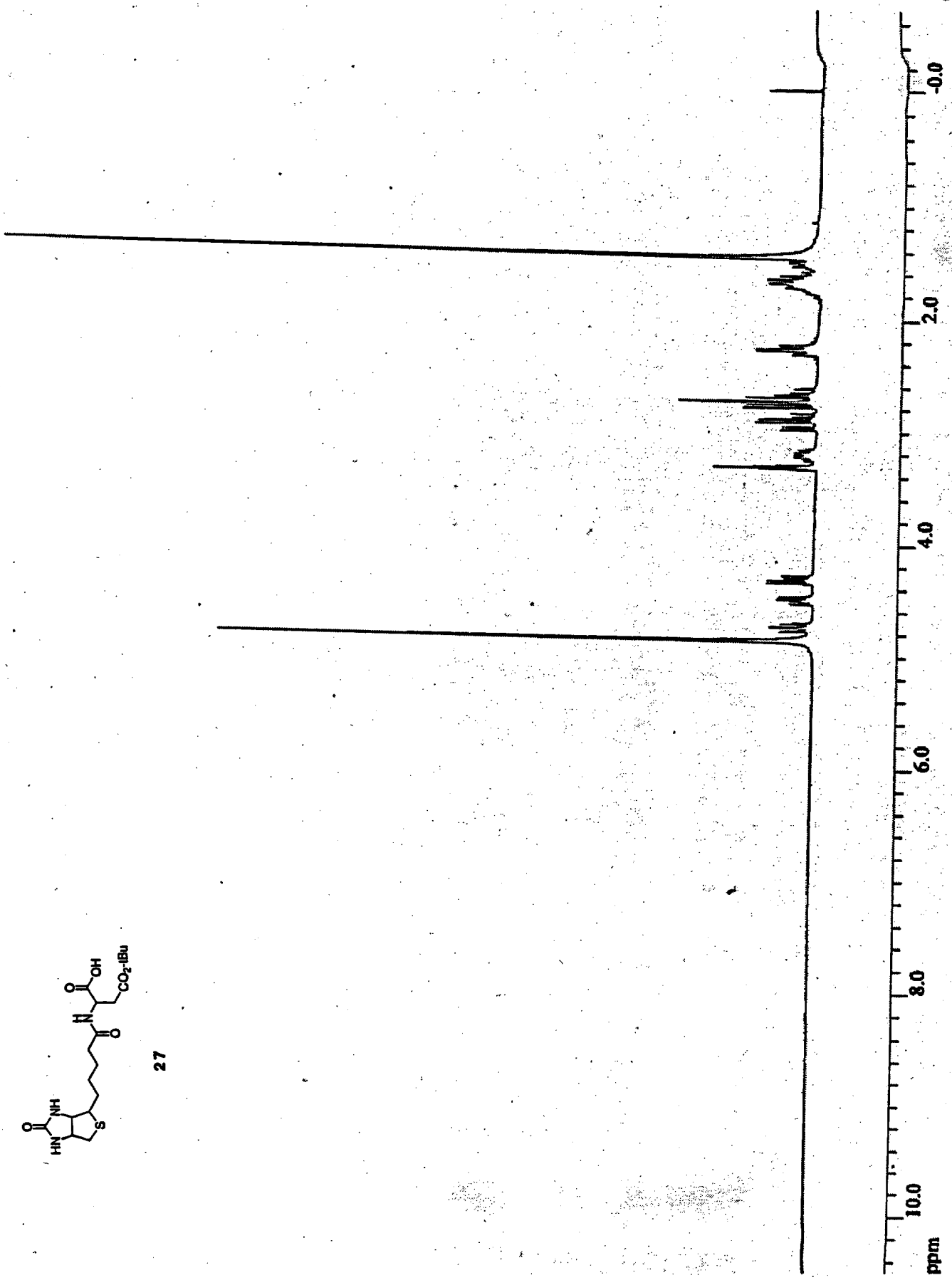

27

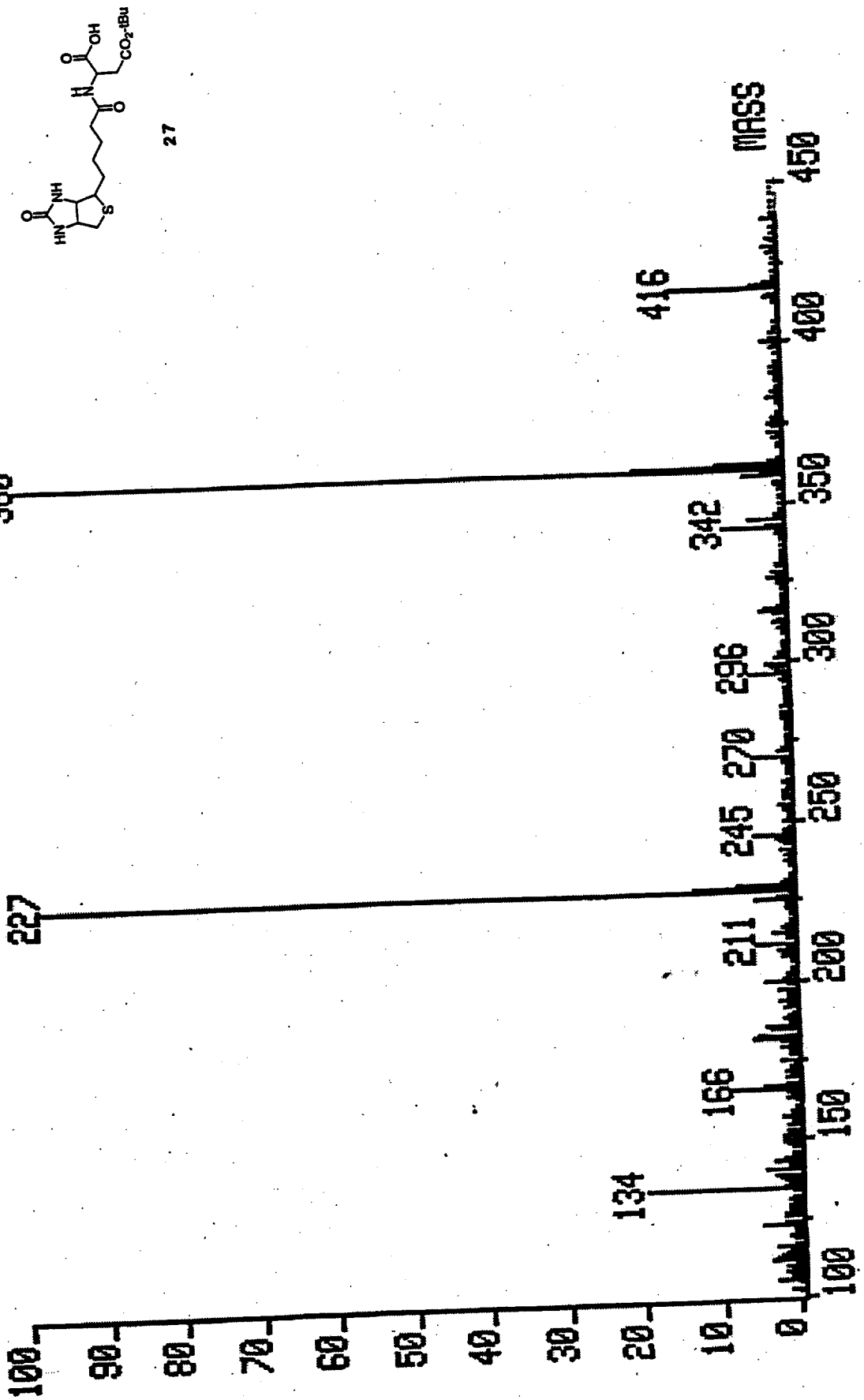
27
MASS
100
90
80
70
60
50
40
30
20
10
0
100
134
150
166
200
211
227
245
250
270
296
300
342
350
360
400
416
450

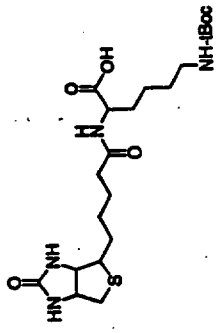

28

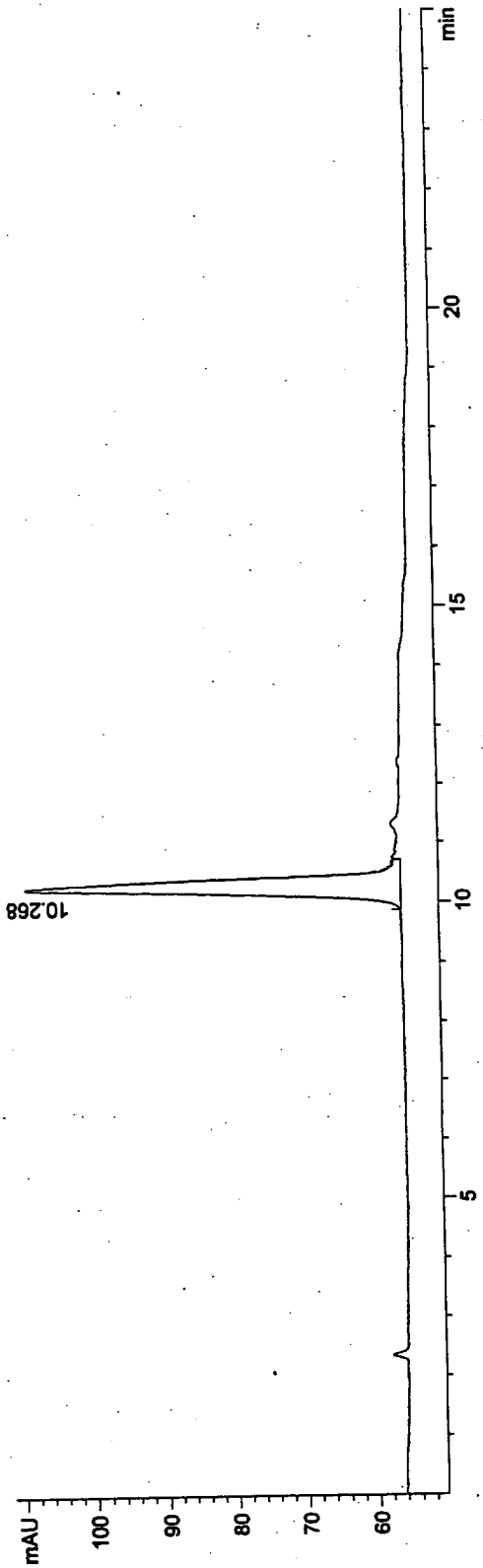

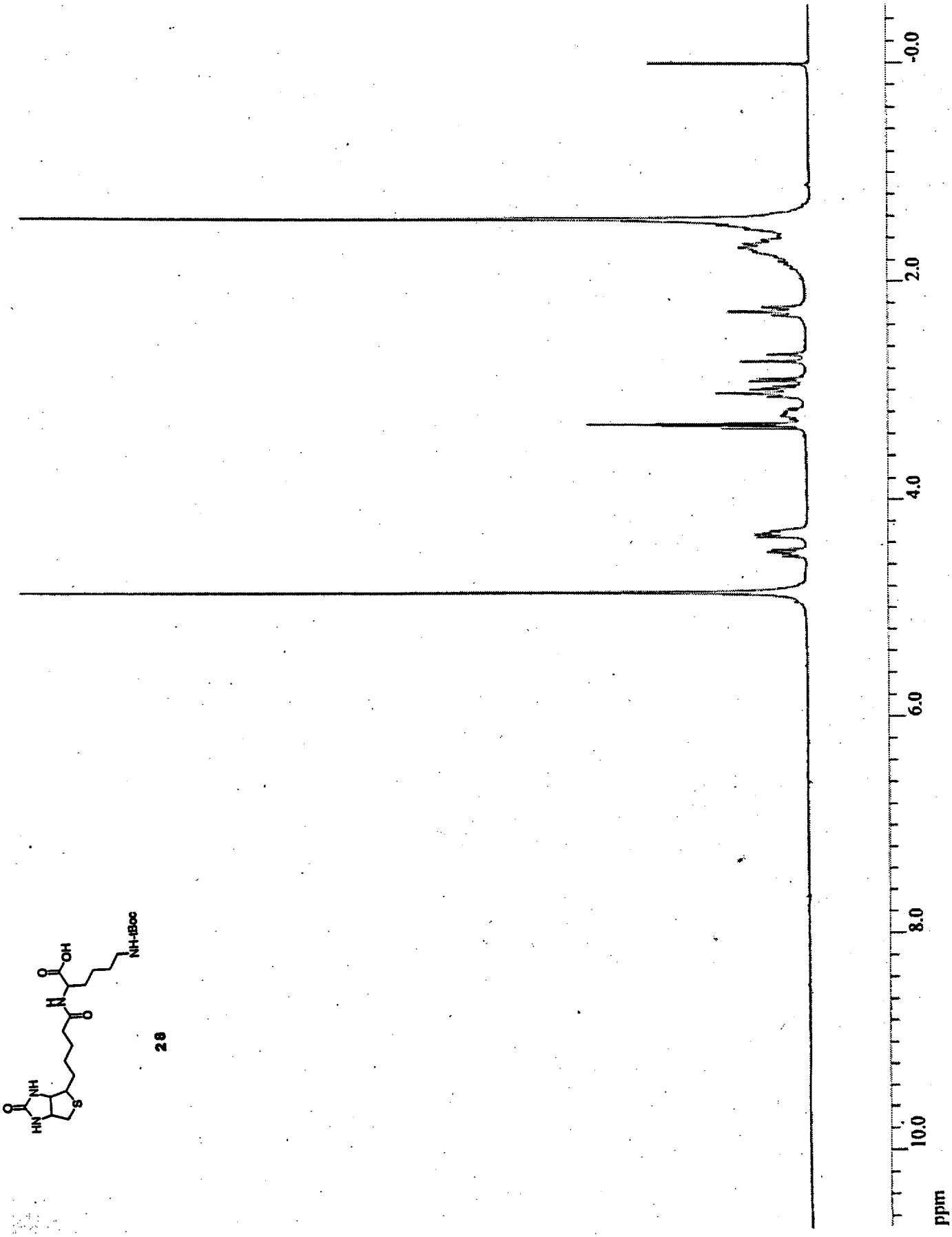
NH-tBoc
OH
28
-0.0
2.0
4.0
6.0
8.0
10.0
ppm

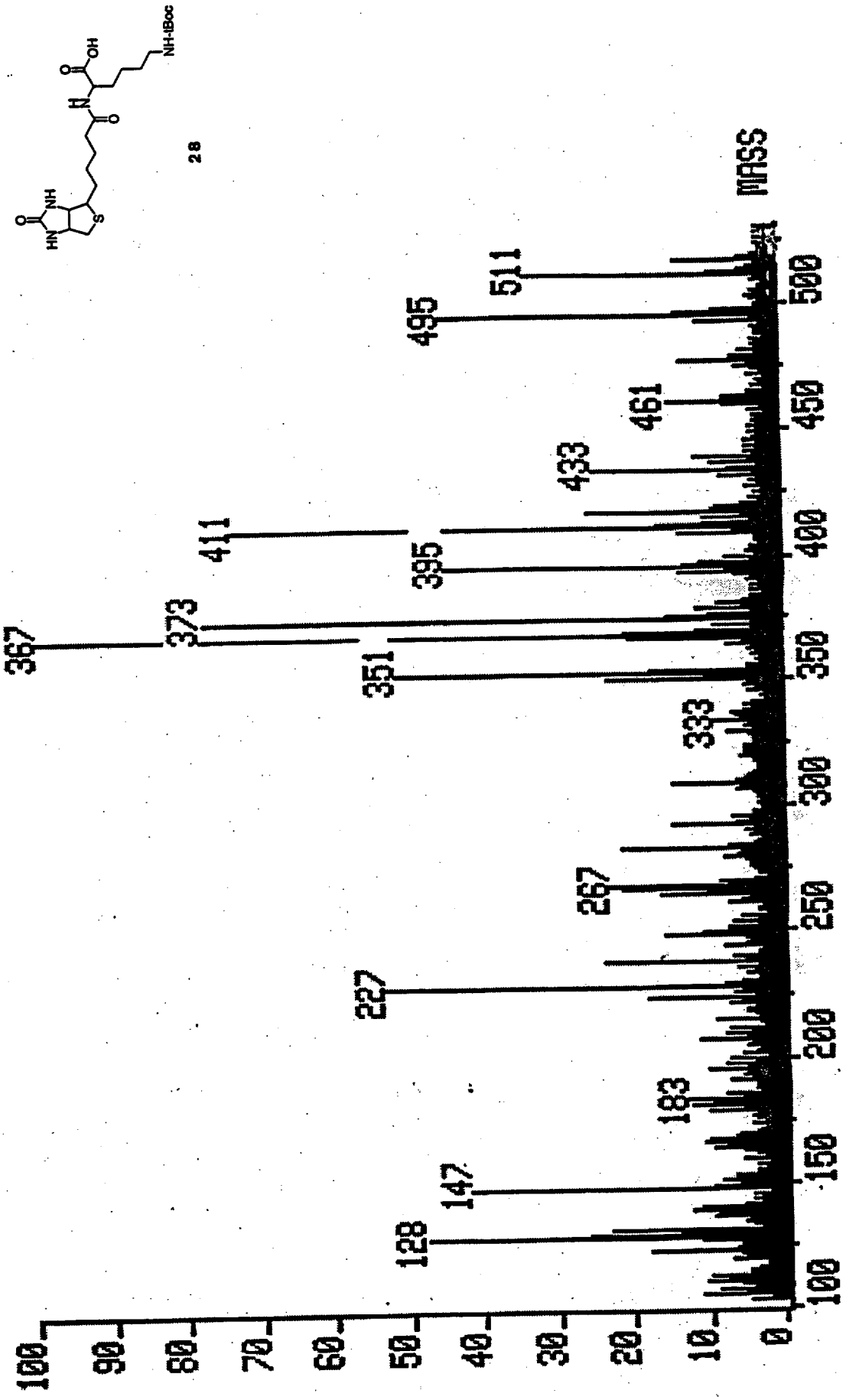
NH-tBoc
OH
NH
HN
S
28
MASS
100
90
80
70
60
50
40
30
20
10
0
100
128
147
150
183
200
227
250
267
300
333
350
351
367
373
400
395
411
433
450
461
495
500
511

© 2000 American Chemical Society, Bioconjugate Chem., Wilbur bc000024v Supporting Info Page 79

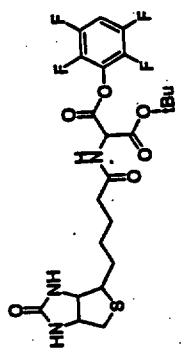

21

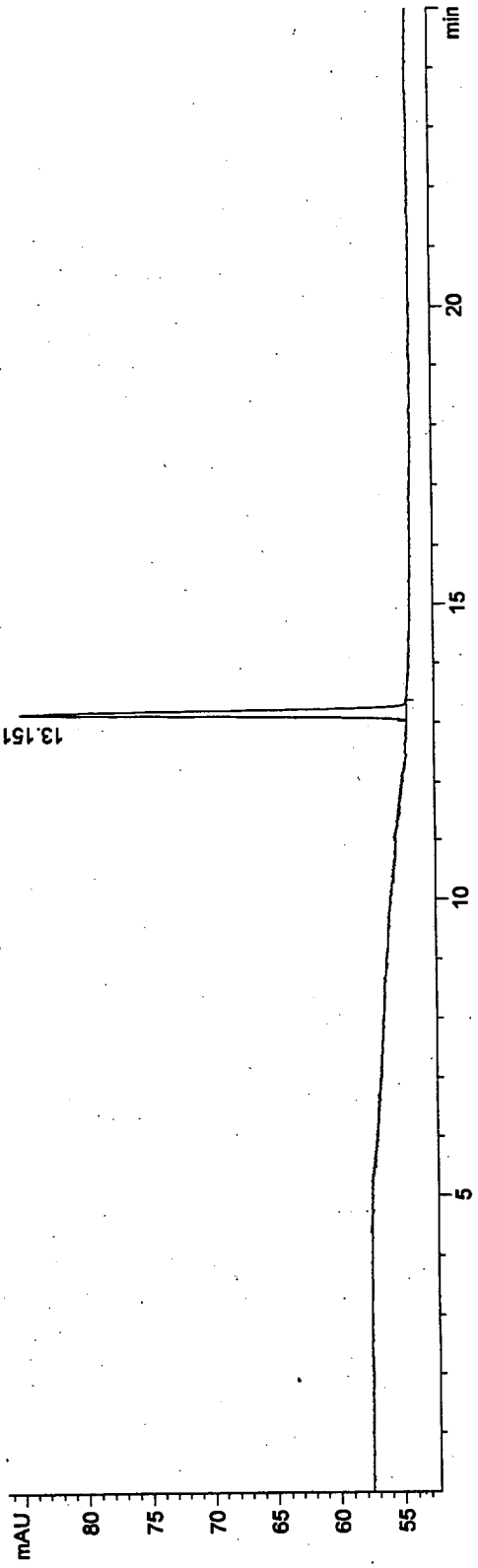

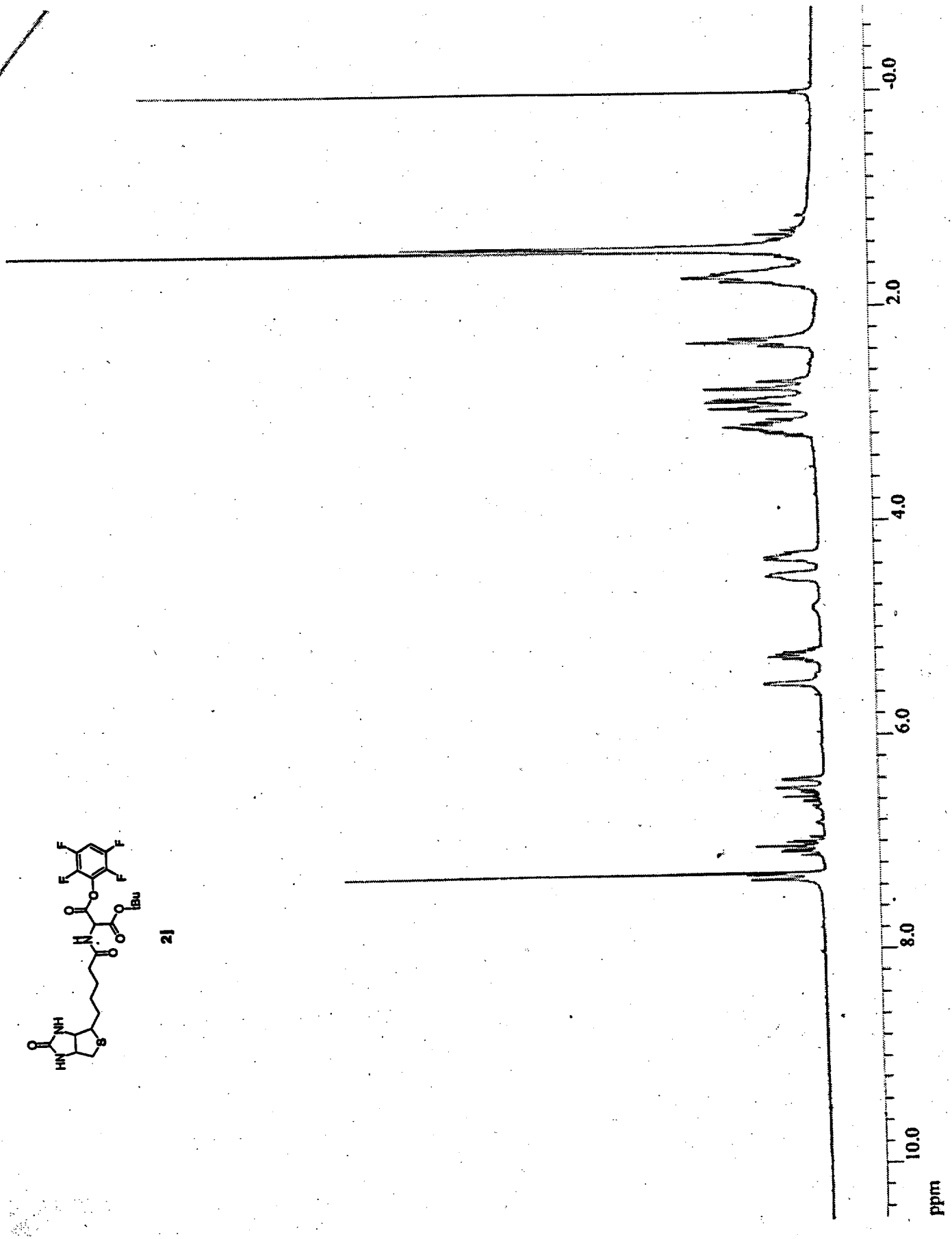

21

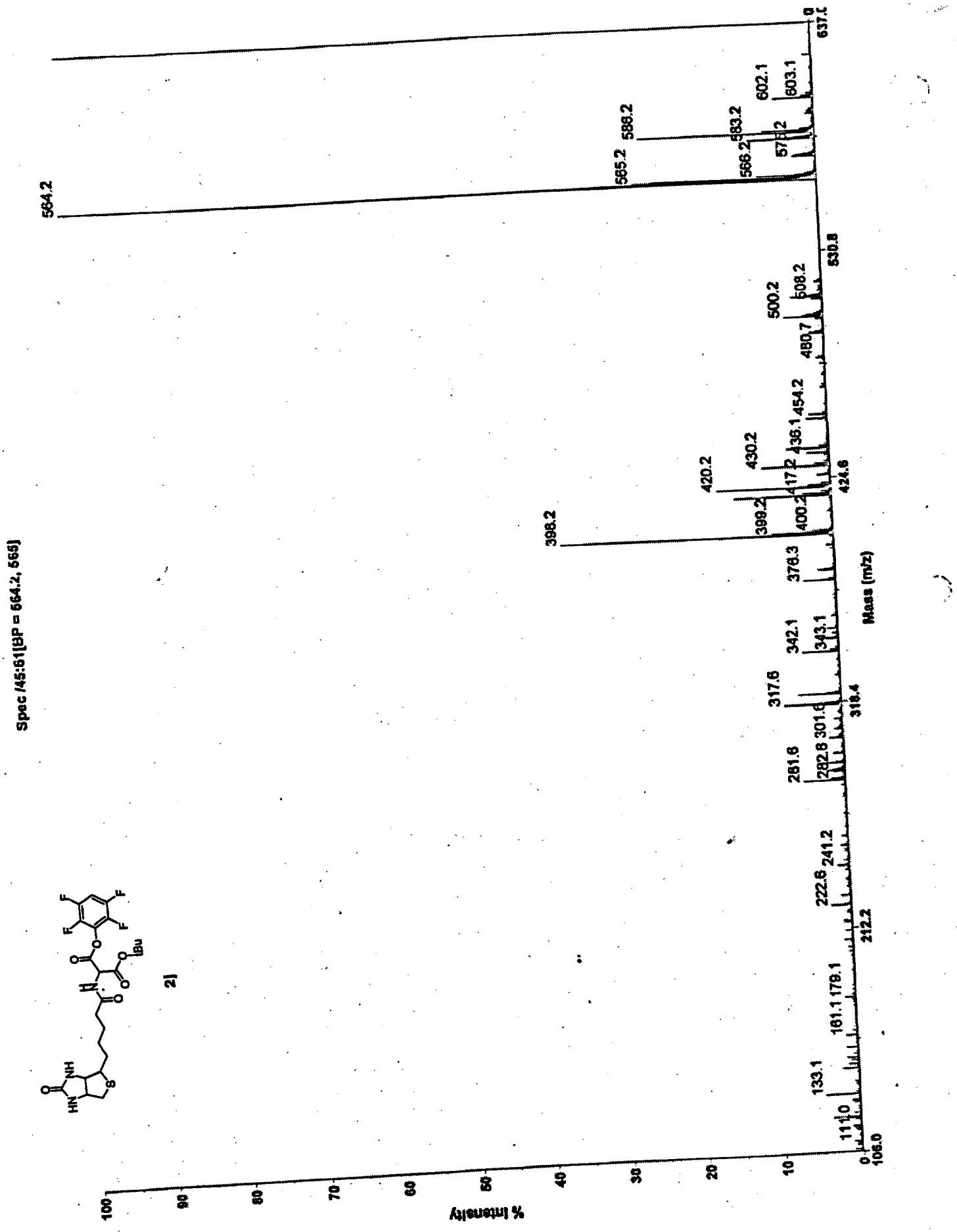
Spec #45:61[BP = 564.2, 565]
564.2
565.2
586.2
583.2
602.1
603.1
637.0
530.8
500.2
508.2
480.7
454.2
436.1
430.2
420.2
424.6
398.2
399.2
400.2
376.3
342.1
343.1
317.6
318.4
281.6
282.8
301.6
241.2
222.6
212.2
178.1
181.1
133.1
111.0
106.0
% Intensity
Mass (m/z)
2]

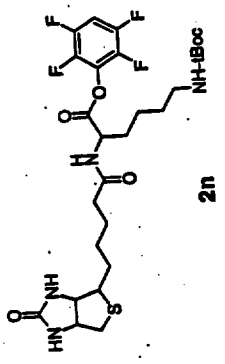
F
F
F
F
O
NH-tBoc
N
H
O
NH
HN
O
S

2n

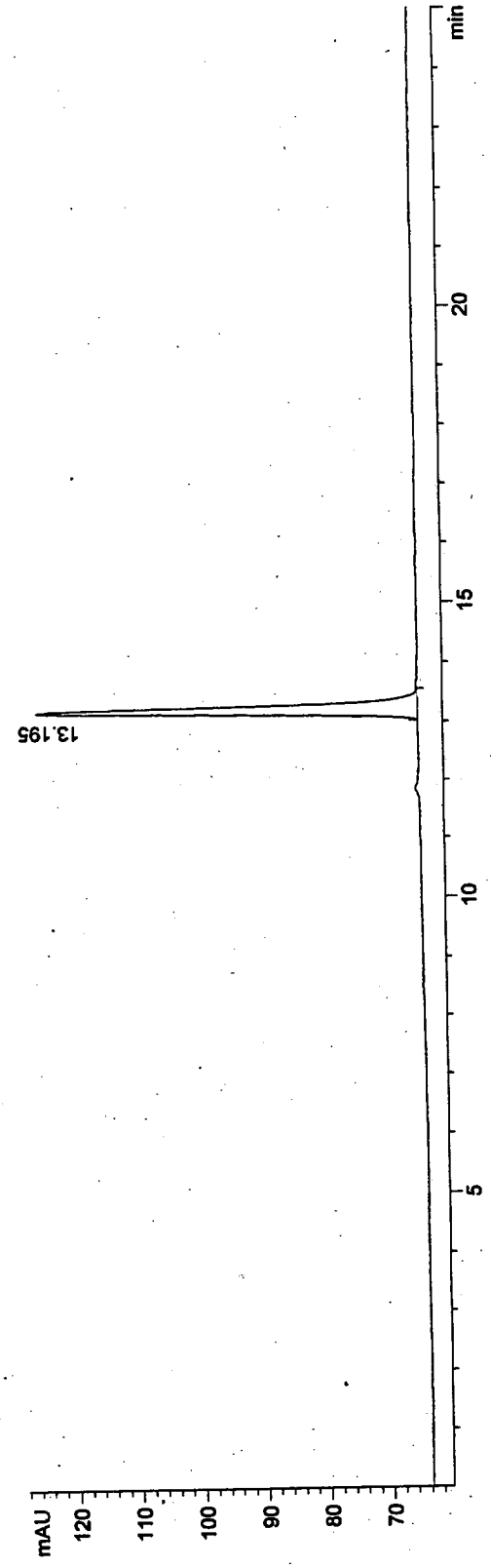
min
20
15
10
5
13.195
mAU
120
110
100
90
80
70

© 2000 American Chemical Society, Bioconjugate Chem., Wilbur bc000024v Supporting Info Page 83

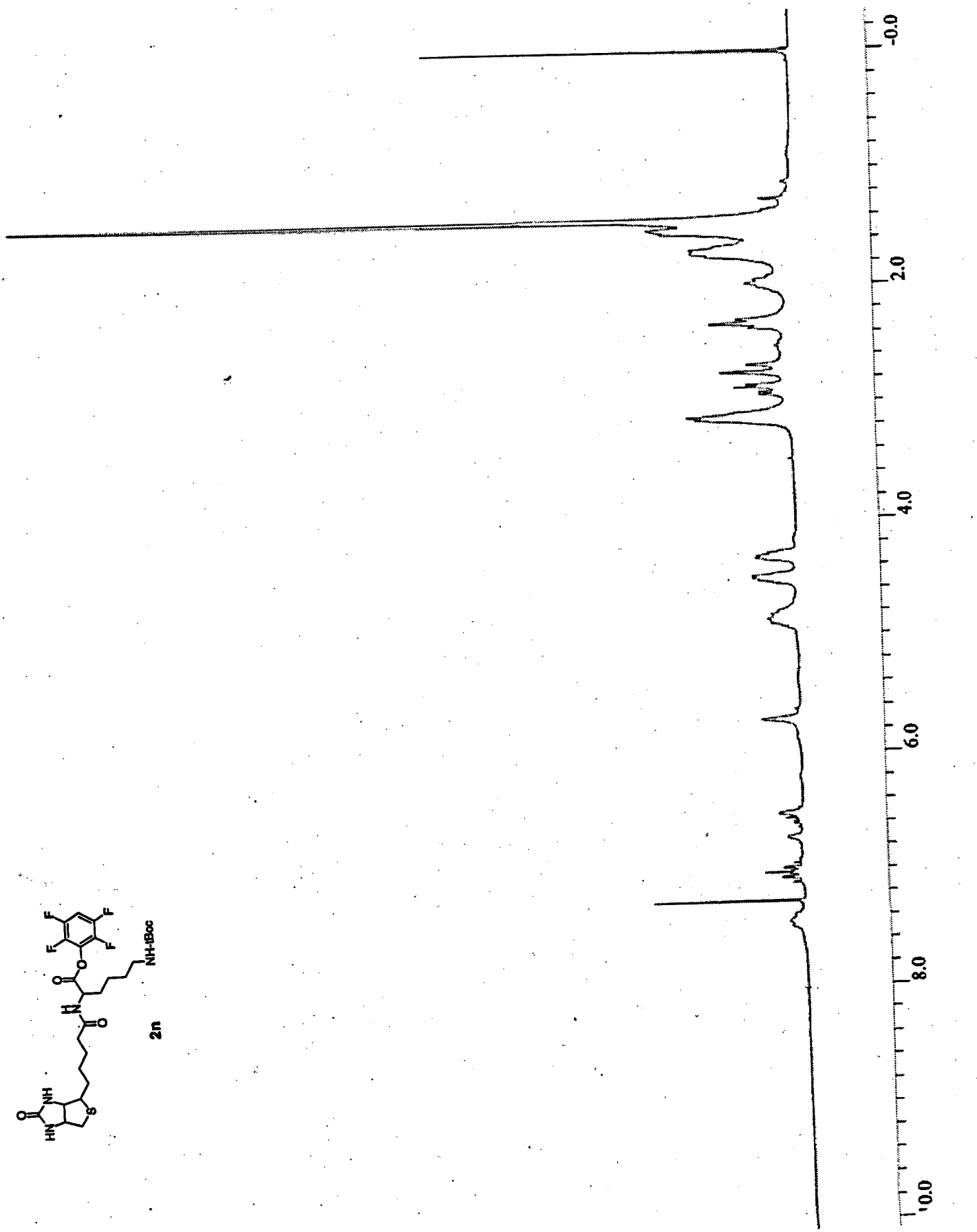

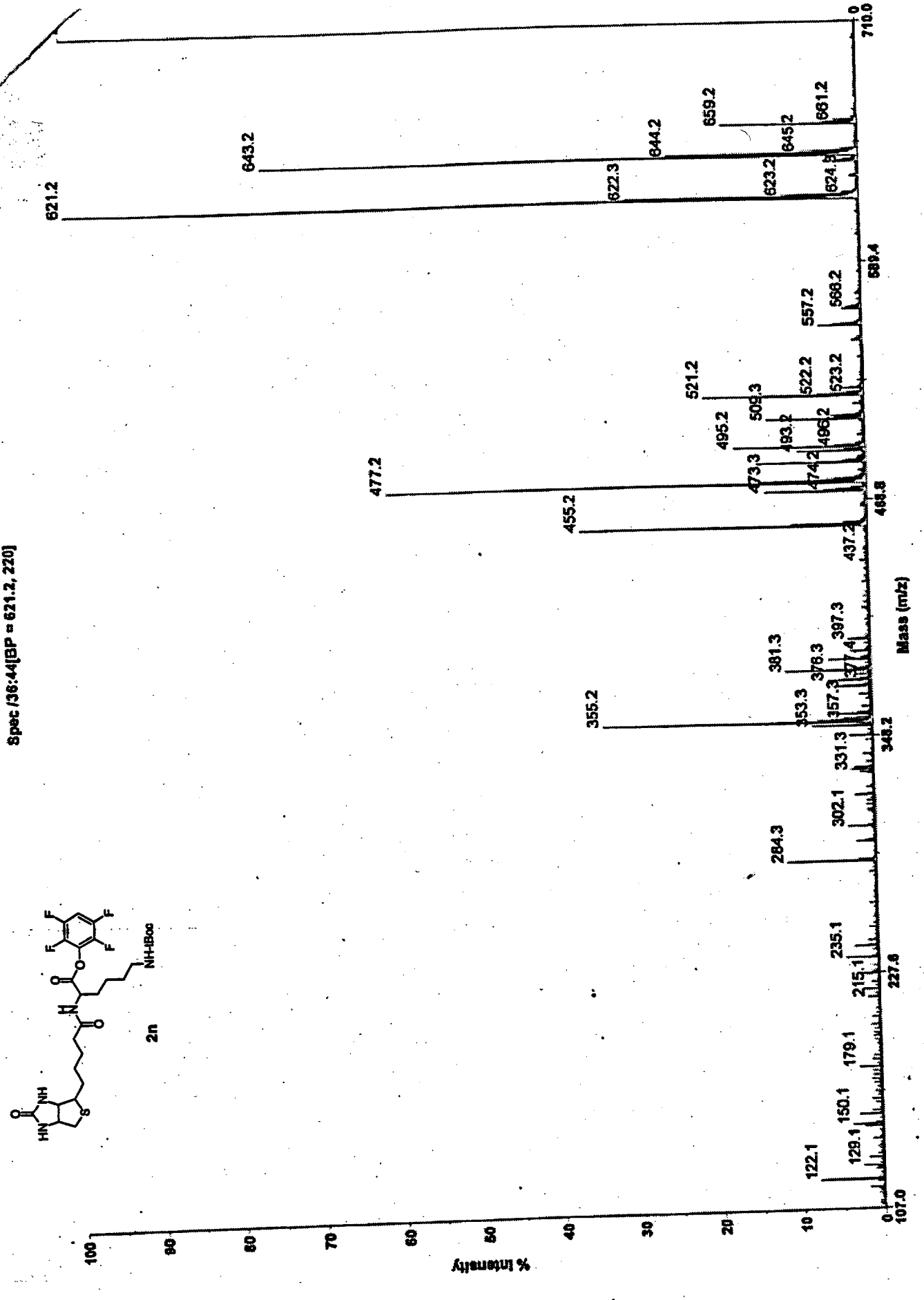
Spec #36:44[BP = 621.2, 220]
% Intensity
Mass (m/z)
2n
NH-Boc
621.2
643.2
622.3
644.2
623.2
645.2
659.2
661.2
624.2
710.0
557.2
566.2
521.2
522.2
523.2
495.2
509.3
496.2
477.2
473.3
474.2
455.2
437.2
397.3
381.3
378.3
355.2
353.3
357.3
348.2
331.3
302.1
284.3
235.1
215.1
227.8
179.1
150.1
129.1
122.1
107.0

Evaluation of Biotin−Dye Conjugates for Use in an HPLC Assay To Assess Relative Binding of Biotin Derivatives with Avidin and Streptavidin

D. Scott Wilbur,*,† Pradip M. Pathare,† Donald K. Hamlin,† Milah B. Frownfelter,† Brian B. Kegley,† Wai-Yee Leung,‡ and Kyle R. Gee‡

Department of Radiation Oncology, University of Washington, Seattle, Washington 98195, and Molecular Probes, Inc., Eugene, Oregon 97402 . Received January 23, 2000; Revised Manuscript Received May 10, 2000

In this investigation, studies were conducted to determine if size exclusion HPLC could be used to assess relative association rates (on-rates) and dissociation rates (off-rates) of biotin derivatives from avidin (Av) and streptavidin (SAv). For easy detection and quantification of biotin derivatives, molecules that can be detected by UV absorbance were conjugated to biotin. Concern that conjugation of the chromophoric moieties (dyes) might affect biotin binding with Av and SAv or might interact with the HPLC column led to evaluation of 10 biotin−dye conjugates. The dyes conjugated with biotin included dansyl, cyanocobalamin (CN−Cbl), coumarin 343, Lissamine-rhodamine, fluorescein, Cascade Blue, Lucifer Yellow, Oregon Green, tetramethylrhodamine, and Alexa Fluor 594. The biotin−dye conjugates were initially evaluated to determine their peak characteristics on two different size exclusion HPLC columns. Measurement of the percent of biotin−dye conjugate bound with Av in the presence of an equal quantity of biotin provided an association rate relative to biotin. All of the biotin−dyes tested had association rates within a factor of 3× (slower) that of biotin. The relative dissociation rate of biotin−dye conjugates was assessed by challenging the biotin conjugate bound to Av or SAv with a large excess of biotin. All of the initial biotin−dye conjugates tested bound Av and SAv tightly resulting in very slow dissociation rates. From the biotin−dye conjugates studied, biotin−CN−Cbl, **6b**, was selected as the best conjugate for the HPLC assay. To test the HPLC assay, an iminobiotin−CN−Cbl conjugate, **13a**, and a biotin−sarcosine−CN−Cbl conjugate, **13b**, were synthesized. The fact that the iminobiotin does not bind with Av at physiological pH was easily detected in the size exclusion HPLC assay. The biotin−sarcosine−CN−Cbl conjugate was expected to have a more rapid dissociation rate than the other biotin−dye conjugates. This was confirmed in that HPLC assay. Although **13b** bound tightly with Av in the absence of added biotin, it was completely released within 1 h when challenged by an excess of biotin. A slower dissociation of **13b** was noted with SAv. The results obtained indicate that CN−Cbl conjugates of biotin derivatives can be used to determine relative on-rates and off-rates of biotin derivatives with Av and SAv. The studies also demonstrated that the biotin−CN−Cbl conjugate, **6b**, can be used as a reference compound to compare on-rates and off-rates of nonchromophoric biotin derivatives.

INTRODUCTION

The number of applications that use biotin and one of its high affinity binding proteins, avidin (Av)[1] and streptavidin (SAv), have increased tremendously over the past two decades (*1*−*4*). Most applications of this technology require that biotin be derivatized by conjugation with another molecule. Consequently, a large number of biotin derivatives have been prepared for in vitro and in vivo applications. In our studies, biotin conjugates are being prepared which serve as carriers of radionuclides in monoclonal antibody (mAb)[1]-based tumor pretargeting for cancer diagnosis and therapy (*5*−*8*). The biotin/streptavidin (SAv) binding pair was chosen for this application as they bind with such high affinity (e.g., 10^{13} M^{-1}) (*9*) that the radionuclide containing biotin moiety should remain bound with mAb−SAv conjugate on tumor cells over the decay period of most radionuclides of interest.

In vivo applications of biotin derivatives are constrained by the cleavage of biotinamide bonds by the enzyme biotinidase (*10*−*12*), but modifications of the biotin conjugate can be made to block that cleavage (*13*−*15*). In the course of our studies, a radioiodinated, biotinidase stabilized, biotin conjugate which contained a *N*-methylbiotinamide functionality was bound in streptavidin-coated wells and then challenged by adding a large excess of biotin. That experiment was conducted to confirm that the dissociation rate (or "off-rate") of the radiolabeled biotin conjugate was very slow, as required for in vivo cancer targeting. However, when examined at 1 h post-biotin addition, less than 20% of the radioactivity remained bound (unreported results). Since endogenous biotin will be present in patients being treated with radionuclides delivered to cancer cells via

* To whom correspondence should be addressed. Phone: (206) 685-3085. Fax: (206) 685-9630. E-mail: dswilbur@u.washington.edu.

† Department of Radiation Oncology.

‡ Molecular Probes, Inc.

[1] Abbreviations: Av, avidin; CN−Cbl, cyanocobalamin; DCC, dicyclohexylcarbodiimide; DIPCDI, diisopropylcarbodiimide; HOAc, acetic acid; *i*-PrOH, 2-propanol; mAb, monoclonal antibody; NCS, *N*-chlorosuccinimide; NHS, *N*-hydroxysuccinimide; NMM, *N*-methylmorpholine; PBS, phosphate-buffered saline; rt, room temperature; (strept)avidin and (S)Av, denotes avidin or streptavidin; SAv, streptavidin; TFP, tetrafluorophenyl; TFP−OTFA, tetrafluorophenyl trifluoroacetate.

10.1021/bc0000031 CCC: $19.00 © 2000 American Chemical Society
Published on Web 06/29/2000

Chart 1. Biotin−Dye Conjugates Prepared

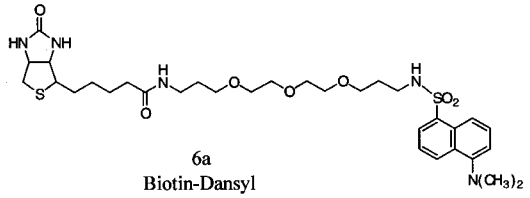

6a
Biotin-Dansyl
λ_{max} = 328 nm

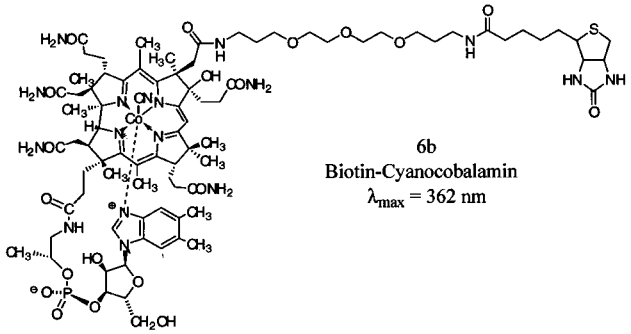

6b
Biotin-Cyanocobalamin
λ_{max} = 362 nm

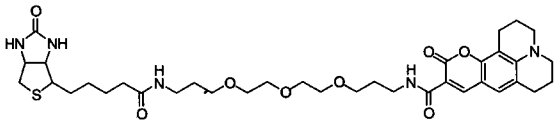

6c
Biotin-Coumarin
λ_{max} = 448 nm

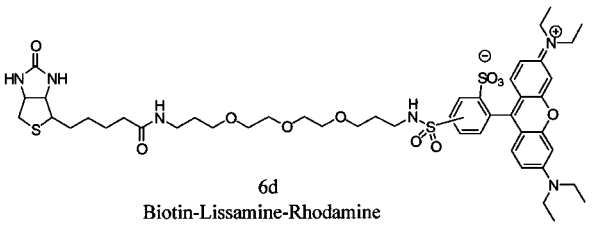

6d
Biotin-Lissamine-Rhodamine
λ_{max} = 564 nm

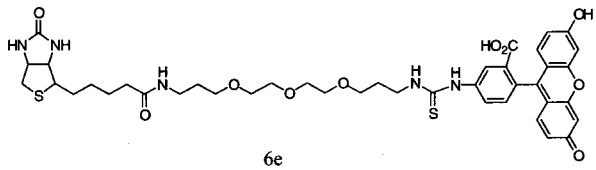

6e
Biotin-Fluorescein
λ_{max} = 499 nm

the pretargeting approach, this finding was troubling. From the results of this simple experiment, it became apparent that an important question to ask when designing new biotin derivatives is how changes in biotin structure and its conjugates affect binding with Av or SAv.

The results obtained in our radiolabeled *N*-methylbiotinamide binding studies prompted us to develop a method for assessing binding of a biotin conjugate with Av and SAv relative to unaltered biotin or another biotin derivative. Size exclusion HPLC was chosen for the analysis as it is relatively rapid, allows evaluation under nonequilibrium conditions, and is readily available to most research groups. Although radiolabeled biotin derivatives could be used in such an assay, we were most interested in developing a method that did not rely on radioactivity for detection. An alternative is to conjugate a UV absorbing molecule (i.e., dye) to biotin for detection. Thus, it was thought that an HPLC assay to evaluate relative binding characteristics of new biotin derivatives might be obtained when an appropriate biotin−dye was used. Consideration of the requirements for a biotin−dye conjugate in this application led to setting criteria that the biotin−dye should (1) have a similar association rate with streptavidin as that of unaltered biotin; (2) have high aqueous solubility; (3) not interact with HPLC column material such that the peak shapes of the free biotin−dye and the Av-biotin−dye are symmetrical and the peak areas are easily quantified; (4) have an elution time that is reasonably short (near where Av or SAv elute); (5) have little absorbance in the wavelength measuring protein quantity (280 nm); (6) have a large extinction coefficient that permits detection of small quantities; and (7) be relatively easy to prepare or obtain.

It was not obvious a priori which biotin−dye conjugates would be best for use in the HPLC assay, so a series of biotin−dye conjugates was prepared for evaluation. Five biotin−dye conjugates (Chart 1) and five biocytin conjugates (Chart 2) were prepared. Of those compounds, it was found that the biotin−cyanocobalamin (CN−Cbl) conjugate **6b** had the most desirable properties for the HPLC analysis. Once that had been determined, two additional biotin−CN−Cbl derivatives, iminobiotin−CN−Cbl, **13a**, and biotin−sarcosine−CN−Cbl, **13b**, were prepared for comparison in the assays. HPLC assays were conducted with biotin−dye conjugates to evaluate their rate of association relative to biotin, and their rate of dissociation in the presence of excess biotin.

Reported herein are the syntheses of the biotin−dye conjugates and their evaluation in competitive binding studies. From the studies, two HPLC-based assays have been developed that can be used routinely to assess biotin derivative binding relative to unaltered biotin or another biotin derivative.

EXPERIMENTAL PROCEDURES

General. Solvents and chemicals obtained from commercial sources were analytical grade or better and were used without further purification. Solvents for HPLC analysis were obtained as HPLC grade and were filtered (0.2 μm) prior to use. Dansyl chloride, **4a**; Vitamin B_{12}, (CN−Cbl); coumarin 343, **4c**; fluorescein isothiocyanate isomer 1, **4e**; 4,7,10-trioxa-1,13-tridecanediamine, **2**; 2,3,5,6-tetrafluorophenol; and most other chemicals were purchased from Aldrich Chemical Co. (Milwaukee, WI). Lissamine rhodamine B sulfonyl chloride and mixed isomers, **4d**, were obtained from Molecular Probes, Inc.

Chart 2. Biocytin−Dye Conjugates Prepared

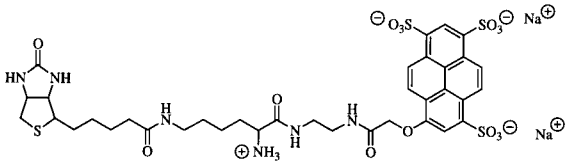

11a
Biocytin Cascade Blue ®
λ_{max} = 400 nm

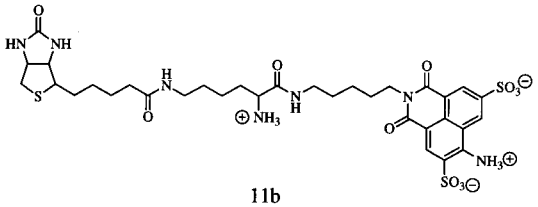

11b
Biocytin Lucifer Yellow
λ_{max} = 428 nm

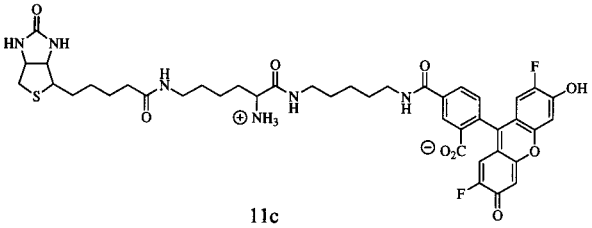

11c
Biocytin Oregon Green®
λ_{max} = 495 nm

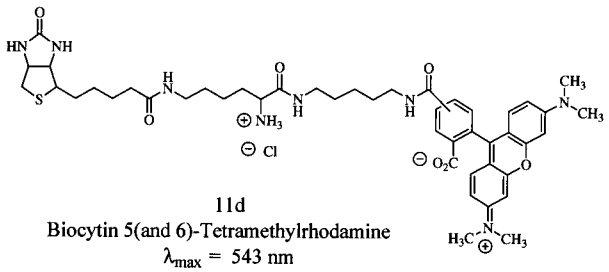

11d
Biocytin 5(and 6)-Tetramethylrhodamine
λ_{max} = 543 nm

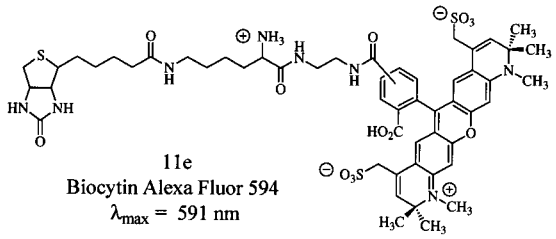

11e
Biocytin Alexa Fluor 594
λ_{max} = 591 nm

(Eugene, OR).[2] Iminobiotin NHS ester, **12a**, and recombinant streptavidin were obtained from Sigma (St. Louis, MO). Avidin was obtained from Pierce (Rockford, IL). 2,3,5,6-Tetrafluorophenyl trifluoroacetate (TFP−OTFA) was prepared as previously described (*16*). Biocytinamine adducts, Cascade Blue ethylenediamine, **9a**; Lucifer Yellow cadaverine, **9b**; Oregon Green 488 cadaverine, **9c**; tetramethylrhodamine cadaverine, **9d**; and Alexa Fluor 594 NHS ester were obtained from Molecular Probes, Inc. (Eugene, OR) (*2*). Silica gel chromatography was conducted with 70−230 mesh 60 Å silica gel (Aldrich Chemical Co.). Melting points were obtained in open capillary tubes on a Mel-Temp II apparatus with a Fluke 51 K/J electronic thermometer and are uncorrected. ^{1}H NMR data, MS data, and HPLC chromatography were used to assess compound identity and purity (data provided in the Supporting Information).

Spectral Analyses. ^{1}H NMR were obtained on a Bruker instrument: AC-200 (200 MHz), AC-400 (400 MHz), AC-500 (500 MHz), or AC-750 (750 MHz). Proton chemical shifts are expressed as parts per million using tetramethylsilane as internal standard (δ = 0.0 ppm). Due to the complex spectra of cyanocobalamin derivatives, NMR data for those compounds (**5b**, **6b**, **13a**, and **13b**) are provided as complete spectra in the supporting data. IR data were obtained on a Perkin-Elmer 1420 infrared spectrophotometer. Mass spectral data of the biotin−dye conjugates were obtained on a VG Analytical (Manchester, England) VG-70SEQ mass spectrometer with associated 11250J Data System using fast atom bombardment (FAB$^+$) at 8 keV in a matrix of MeOH/DMIX (Thioglycerol/DMSO/TFAA: 90/9/1) or 3NBA (3-nitrobenzyl alcohol). Mass spectral data for the biocytin−dye conjugates were obtained using FAB$^+$ on a Micromass ZMD electrospray instrument connected to a Waters2690 Alliance HPLC.

Chromatography. HPLC separations of dyes (**4**), dye conjugates (**5**), and biotin−dye conjugates (**6**) were obtained on Hewlett-Packard quaternary 1050 gradient pumping system with a variable wavelength UV detector (254 nm) and a Varex ELSD MKIII evaporative light-scattering detector. Analysis of the HPLC data were conducted on Hewlett-Packard HPLC ChemStation software. Reversed-phase HPLC chromatography was carried out using an Alltech Altima C-18 column (5 μm, 250 mm × 4.6 mm) with a gradient solvent system at a flow rate of 1 mL/min. The gradient mixture was composed of MeOH (solvent A) and 1% aqueous HOAc (solvent B). Starting with 40% MeOH, the initial solvent mixture was held for 2 min, increased to 100% MeOH over the next 10 min and then held at 100% MeOH for 5 min. Retention times (t_R) under these conditions for biotin conjugates are provided with the individual compounds. All biotin conjugation reactions were monitored by HPLC.

HPLC separations of biocytin−dye conjugates **11a−e** were obtained using a Waters 2690 Alliance instrument with UV detection at 254 nm. Analytical separations were conducted on a C18 Microsorb MV 4.6 × 250 mm column using a linear 5 to 95% gradient of acetonitrile/0.1 M ammonium acetate unless noted otherwise. The pH of the separations varied, so that value is included with the

[2] Biocytin−dye conjugates were prepared at Molecular Probes, Inc., Eugene, OR.

Table 1. Retention Times and Peak Widths for Biotin−Dye Conjugates and Avidin on Size-Exclusion HPLC Chromatograms

biotin derivative	Protein Pak 300SW retention time[a] (peak width[b])	Spherogel TSK 5000PW retention time[a] (peak width[b])
6a, dansyl	ND[c]	ND
6b, cyanocobalamin	32 min (5 min)	18 min (2 min)
6c, coumarin	ND	ND
6d, lissamine-rhodamine[d]	ND	ND
6e, fluorescein	49 min[e] (4 min)	ND (60 min[e], 5+ min)
11a, Cascade Blue	25 and 26 min (2 min)	17 and 19 min (3.5 min)
11b, Lucifer Yellow	29 min (3 min)	27 min (5 min)
11c, Oregon Green	34 min (4 min)	29 min (5+ min)
11d, tetramethylrhodamine	ND	ND
11e, Alexa Fluor 594	ND	18 and 20 min (7 min)
Avidin[f]	18 min (2 min)	14 min (2 min)

[a] The retention time values are rounded to the next whole number. [b] Peak width is taken at baseline and is rounded to the next whole number. In chromatograms containing two peaks, the width of both peaks is taken. [c] ND indicates that no peak was detected in the 45 min (Protein Pak column) or 30 min (TSK 5000PW column) run time. [d] The biotin−lissamine−rhodamine conjugate caused a degradation of the column which took several injections of avidin to restore. [e] The retention times of the biotin-fluorescein conjugate were obtained past the end of the run times as this conjugate is routinely used by investigators. [f] The retention time for avidin is provided for comparison.

experimental for each compound. The compound retention times (t_R) and purity are provided with the experimental for each compound. Separations for preparative purification was conducted on a Waters Prep 2000 instrument.

Size exclusion HPLC analyses used in the (strept)-avidin binding experiments were conducted on a system consisting of a Hewlett-Packard 1050 Multiple Wavelength Detector (280 nm), isocratic pump, and one of three different size exclusion columns. Those columns included (1) a TSK-GEL G3000SW size exclusion column (7.5 mm × 600 mm, 10 μm; stainless steel, TosoHaas, Montgomeryville, PA); (2) a Protein Pak 300SW column (8.0 × 300 cm; 10 μm; glass; Waters Associates, Milford, MA); or (3) a Spherogel TSK 5000PW column (7.5 mm × 300 mm, 10 μm; stainless steel, Altex)[3]. The majority of the studies was carried out on the Spherogel TSK 5000PW column. The mobile phase was an aqueous solution containing 50 mM potassium phosphate (pH 6.8), 300 mM NaCl, 1 mM EDTA, and 1 mM NaN_3. A flow rate of 0.75 mL/min was used. The retention times for Av or SAv and the biotin−dye conjugates varied depending on the column used. Retention times for biotin−dye conjugates are provided in Table 1.

Biotin Tetrafluorophenyl Ester, 1. This compound was prepared from biotin and tetrafluorophenyl trifluoroacetate (TFP−OTFA) as previously described (*17*).

***N*-(13-Amino-4,7,10-trioxatridecanyl)biotinamide, 3.** This compound was prepared from reaction of biotin TFP ester, **1**, and 4,7,10-trioxatridecane-1,13-diamine, **2**, as previously described (*17*).

Biotin-Dansyl Conjugate, 6a. To a solution containing 4 g (18.5 mmol) of trioxatridecanediamine, **2**, and 0.5 mL of Et_3N in 5 mL of EtOAc was added 500 mg (1.85 mmol) of dansyl chloride in 50 mL of EtOAc dropwise over a 1 h period. After the addition, the EtOAc was removed under vacuum. The residue was washed with 150 mL of ether to remove excess **2** and was placed on a silica column (2.5 cm × 35 cm). The column was eluted with 50 mL of EtOAc and then 50 mL fractions of EtOAc:MeOH at mixtures of 90:10, 80:20, and 70:30. The fractions containing product were taken to dryness and then suspended in CH_3CN and filtered. The filtrate was dried under vacuum to yield 200 mg (24%) of the dansyl-trioxatridecanediamine adduct, **5a**. This material was 95% pure by HPLC and was used in the next step without further purification.

To a solution of **5a** (200 mg, 0.442 mmol) and 125 μL of Et_3N (0.9 mmol) in 25 mL of DMF was added 173 mg of (0.442 mmol) biotin TFP ester, **1**, in 25 mL of DMF dropwise over a 10 min period. The reaction mixture was stirred at room temperature for 2 h (followed by HPLC), and then the DMF was removed under vacuum. The residue was dissolved in 150 mL of $CHCl_3$ and washed with saturated $NaHCO_3$ solution (2 × 20 mL) and H_2O (20 mL). The $CHCl_3$ solution was dried over anhydrous Na_2SO_4, filtered, and the $CHCl_3$ was removed under vacuum to give a quantitative yield (300 mg) of **6a**, mp 61−63 °C. ^{1}H NMR (MeOH-d_4, 300 MHz) δ 1.4 (m, 2H), 1.6−1.9 (m, 8H), 2.2 (t, J = 3.5 Hz, 2H), 2.7 (d, J = 6.6 Hz, 1H), 2.9−3.1 (m, 12H), 3.15−3.4 (m, 8H), 3.50−3.65 (m, 8H), 4.3 (m, 1H), 4.5 (m, 1H), 7.3 (d, J = 3.6 Hz, 1H), 7.6 (m, 2H), 8.2 (d, J = 3.6 Hz, 1H), 8.4 (d, J = 4.2 Hz, 1H), 8.57 (d, J = 4.05 Hz, 1H). UV: λ_{max} 328 nm. IR (KBr) 3280, 2920, 1690, 1450, 1320, 1260, 1140, 1080 cm^{-1}. HPLC: t_R = 12.0 min. HRMS mass calcd for $C_{32}H_{50}N_5O_7S_2$ (M + H): 680.3152. Found: 680.3126.

Cyanocobalamin-*c*-lactone, 4b. This compound was prepared from cyanocobalamin by reaction with NaI and NCS in HOAc as previously described (*18*).

Cyanocobalamin-*c*-lactone Adduct with Trioxatridecanediamine, 5b. A 1.0 g (0.739 mmol) quantity of CN−Cbl-*c*-lactone, **4b**, was dissolved in 50 mL of trioxatridecanediamine, **2**, and heated to 50−55 °C for 1 h. After cooling to room temperature, acetone was added (200 mL) and the solid was collected to yield 0.95 g (82%) of **5b**, mp 251−254 °C (dec). ^{1}H NMR (MeOH-d_4, 750 MHz) (NMR spectrum provided in Supporting Information). HPLC: t_R = 2.4 min. MS (FAB$^+$) mass calcd for $C_{73}H_{109}N_{15}O_{18}CoP$: 1573.7. Found: 1574 (M$^+$).

Biotin−Cyanocobalamin Conjugate, 6b. To a solution of 500 mg (0.318 mmol) of **5b** and 44 μL of Et_3N (0.318 mmol) in 10 mL of DMF was added 130 mg (0.382 mmol) of biotin TFP ester, **1**. The reaction was stirred at room temperature for 4 h (followed by HPLC), and the DMF was removed under vacuum. The residue was washed with acetone to yield 460 mg (80%) of **6b**, mp 207−211 °C (dec). ^{1}H NMR (MeOH-d_4, 750 MHz) (NMR spectrum provided in Supporting Information). HPLC: t_R = 5.2 min. MS (FAB$^+$) mass calcd for $C_{83}H_{123}N_{17}O_{20}$-CoPS is 1799. Found: 1800 (M + H).

[3] The Spherogel TSK 5000PW column was obtained from Altex. An equivalent column (TSKgel 5000PW) can be obtained from TOSOHAAS (Montgomeryville, PA).

Biotin−Coumarin Conjugate, 6c. A 100 mg (0.35 mmol) quantity of coumarin 343 was dissolved in 40 mL of DMF and 50 μL of Et_3N was added. To that solution was added 110 mg of TFP−OTFA, and the resultant solution was stirred at room temperature for 4 h. A 156 mg (0.350 mmol) quantity of biotin-trioxatridecanediamine, **3**, was added to the reaction solution, and it was stirred at room temperature for 1 h. The DMF was removed under vacuum, and the residue was loaded onto a silica column (2.5 cm × 35 cm). The column was eluted with EtOAc and then EtOAc:MeOH. Fractions containing the product (by HPLC analysis) were combined and evaporated to give 100 mg (40%) of **6c** as a redish brown solid, mp > 220 °C. ^{1}H NMR ($CDCl_3$, 500 MHz) δ 1.4 (m, 2H), 1.6−2.1 (m, 12H), 2.2 (s, 2H), 2.7−2.95 (m, 6H), 3.15 (s, 1H), 3.35 (s, 6H), 3.5−3.8 (m, 14H), 4.3 (m, 1H), 4.5 (m, 1H), 5.9 (m, 1H), 6.55 (m, 1H), 6.8 (s, 1H), 7.0 (s, 1H), 8.6 (d, 1H), 8.9 (s, 1H). UV−vis: λ_{max} 448 nm. IR (KBr) 3300, 2920, 1690, 1510, 1440, 1360, 1300, 1210, 1170, 1100 cm^{-1}. HPLC: t_R = 13.5 min. HRMS mass calcd for $C_{36}H_{52}N_5O_8S$ (M + H): 714.3537. Found: 714.3505.

Biotin−Lissamine-rhodamine Conjugate, 6d. A 133 mg (0.34 mmol) quantity of Lissamine rhodamine B sulfonyl chloride, **4d**, was added to 1.5 g (5.4 mmol) trioxatridecanediamine, **2**, and the reaction mixture was stirred at room temperature for 1 h. EtOAc was added (100 mL) to the reaction mixture, and the organic layer was discarded. The residue was loaded on a column (2.5 cm × 25 cm) and eluted with EtOAc with increasing percentage of MeOH. The fractions containing product were combined and evaporated to dryness to yield 50 mg (19%) of the Lissamine-rhodamine-trioxatridecanediamine adduct, **5d**. (Note: an additional 170 mg was obtained from the column when it was eluted with MeOH containing 1% HOAc. However, this material was a mixture by HPLC analysis).

A 50 mg quantity (0.066 mmol) of **5d** was dissolved in 10 mL of DMF, and 10 μL (0.066 mmol) of Et_3N was added. To that solution was added 26 mg (0.066 mmol) of biotin TFP ester, **1**. The reaction mixture was stirred at room temperature overnight, and the DMF was removed under vacuum. The residue was triturated with EtOAc and the resultant solid was dissolved in H_2O and filtered. Lyophilization of the filtrate yielded 60 mg (92%) of **6d** as a violet colored solid, mp 154−158 °C (dec). ^{1}H NMR (MeOH-d_4, 300 MHz) δ 1.0−2.0 (m, 22H), 2.2 (t, J = 8.75 Hz, 2H), 2.6−4.0 (m, 27H), 4.3 (m, 1H), 2.4 (m, 1H), 6.4 (m, 2H), 6.7 (d, J = 10.5 Hz, 1H), 6.9−7.2 (m, 3H), 7.9 (m, 1H), 8.2 (s, 1H), 8.5 (s, 1H). UV−vis: λ_{max} 564 nm. IR (KBr) 3300, 2920, 1690, 1590, 1510, 1460, 1410, 1330, 1180, 1030 cm^{-1}. HPLC: t_R = 11.1 min. HRMS mass calcd for $C_{47}H_{67}N_6O_{11}S_3$ (M + H): 987.4030. Found: 987.4021.

Biotin−Fluorescein Conjugate, 6e. To 300 mg (0.77 mmol) of fluorescein isothiocyanate, **4e**, dissolved in 20 mL of DMF was added 110 μL (0.77 mmol) of Et_3N. To this mixture was added 357 mg of (0.8 mmol) trioxatridecanylbiotinamide, **3**, and the reaction mixture was stirred at room temperature overnight. The DMF was removed under vacuum, and the solid residue was washed with $CHCl_3$ and then ether. The solid was placed on a silica column (2.5 cm × 25 cm) and was eluted with EtOAc and then EtOAc:MeOH mixtures. The desired product eluted with mixtures containing 8:2/7:3 EtOAc:MeOH. The fractions containing product by HPLC analysis were combined and after removal of solvent gave 0.5 g (78%) of **6e** as an orange colored solid (or yellow powder), mp 182−185 °C (dec). ^{1}H NMR (MeOH-d_4, 500 MHz) δ 1.2 (m, 2H), 1.5 (m, 2H), 1.55−1.8 (m, 6H), 2.0 (m, 2H), 2.2 (t, J = 3.5 Hz, 2H), 2.7 (d, J = 6.5 Hz, 1H), 2.9 (dd, J = 6.25, 2.5 Hz, 1H), 3.2 (m, 1H), 3.3 (t, J = 3.5 Hz, 2H), 3.5−3.8 (m, 15H), 4.3 (m, 1H), 4.5 (m, 1H), 6.6 (dd, J = 8.5, 2.5 Hz, 2H), 6.7 (m, 4H), 7.2 (d, J = 4.5 Hz, 1H), 7.8 (brd, 1H), 8.16 (s, 1H). UV−vis: λ_{max} 499 nm. IR (KBr) 3300, 2920, 1740, 1680, 1600, 1450, 1250, 1180, 1110 cm^{-1}. HPLC: t_R = 10.8 min. HRMS mass calcd for $C_{41}H_{50}N_5O_{10}S_2$ (M + H): 836.2999. Found: 836.2982.

***N-t*-BOC-biocytin succinimidyl ester, 8.** To a cloudy mixture of *N*-t-BOC-biocytin (**7**, 1.50 g, 3.26 mmol) (*19*) in isopropyl alcohol/DMF (1:1, 100 mL) was added *N*-hydroxysuccinimide (0.44 g, 3.82 mmol) and diisopropylcarbodiimide (0.52 mL, 3.5 mmol). After 8 h, TLC showed about 70% reaction. More *N*-hydroxysuccinimide (0.87 mmol) and carbodiimide (0.65 mmol) were added; 2 h later, TLC showed complete reaction. The volatile materials were removed under vacuum, and the residue dissolved in chloroform (25 mL). The resulting solution was added dropwise to ethyl ether/hexanes (1:1, 100 mL). The resulting white precipitate was collected and dried under vacuum to give 1.7 g (93%) of **8** as a semistable colorless powder that was used without further purification: R_f 0.75 ($CHCl_3$/MeOH/AcOH; 15:3:1). ^{1}H NMR (DMSO-d_6) δ 4.30 (t, 1H), 4.12 (t, 1H), 3.79 (m, 1H), 3.08 (m, 1H), 2.99 (m, 2H), 2.80 (s, 4H), 2.50 (br s, 2H), 2.03 (t, 2H), 1.8−1.2 (m, 21H); LRMS (FAB$^+$) 569 (M$^+$, 15), 472 (biocytin, 35), 350 (100).

Biocytin-Cascade Blue Conjugate, 11a. To a solution of Cascade Blue ethylenediamine (**9a**, 1.20 g, 1.92 mmol) in 35 mL of water was added *N*-methylmorpholine (0.22 mL, 2.0 mmol). A solution of **8** (1.11 g, 2.00 mmol) in 10 mL of DMF was added dropwise over 5 min. The resulting pale brown solution was stirred overnight and then charged with a fresh portion of **8** (0.67 g, 1.2 mmol). After another hour, TLC indicated that the reaction was complete. The reaction solution was extracted with 10% methanol/chloroform (10 × 20 mL) to remove the free *N*-hydroxysuccinimide and then concentrated under vacuum to a yellow foam. The crude product was purified by chromatography on Sephadex LH-20 using water as eluant to afford 2.0 g of **10a** as a yellow foam.

The carbamate **10a** (2.0 g, 1.9 mmol) was suspended in 4 M HCl-dioxane (Aldrich, 20 mL). The resulting mixture was stirred overnight. The volatile material was removed under vacuum, and the residue was purified by chromatography on Sephadex LH-20 using water as eluant to give 1.24 g (69%) of **11a** as a pale yellow powder: R_f 0.26 (dioxane/2-propanol/water/NH_4OH; 15:53:13:14). ^{1}H NMR (D_2O) δ 9.22 (s, 1H), 9.1 (m, 3H), 8.7 (d, 1H), 8.16 (s, 1H), 4.15 (s, 1H), 3.90, (s, 1H), 3.70 (s, 1H), 3.0 (m, 6H), 2.45 (s, 1H), 2.25 (s, 1H), 1.7 (m, 6H), 1.15 (m, 8H), 0.60 (m, 2H). UV−vis: λ_{max} 400 nm (ϵ 31 000, 50 mM potassium phosphate, pH 8). HPLC: pH 4.7, t_R = 12.1 min. MS (FAB$^+$) 913 (M$^+$, 95), 415 (100).

Biocytin−Lucifer Yellow Conjugate, 11b. To a solution of Lucifer Yellow cadaverine (**9b**, 0.45 g, 0.84 mmol) in 20 mL of water was added a solution of **8** (0.47 g, 0.84 mmol) in 2 mL of DMSO and 2 drops of *N*-methylmorpholine. The resulting cloudy yellow mixture was stirred overnight, whereupon TLC showed some product formation (**10b**) but considerable hydrolysis of **8** to **7** was noted. A fresh portion of **8** (0.47 g) in 2 mL of DMSO was added, and the reaction mixture stirred overnight. This cycle was repeated four times, until TLC showed consumption of the starting **9b**. The reaction mixture was concentrated under vacuum. The residue was dissolved in 35% methanol/water, followed by extraction with chloroform (8 × 25 mL). The aqueous phase was concentrated under vacuum to give a yellow residue,

which was purified by chromatography on Sephadex LH-20 using water as eluant to give 0.91 g of **10b** as a yellow powder, contaminated with *N*-hydroxysuccinimide. The carbamate **10b** (0.70 g, 0.72 mmol) was stirred in 4 M HCl/dioxane (10 mL) for 2 h and then concentrated under vacuum. The residue was chromatographed repeatedly on Sephadex LH-20, using water as eluant, to give 0.28 g (45%) of pure **11b** as a yellow powder: R_f 0.52 (dioxane/i-PrOH/water/ammonium hydroxide; 15:58:13:14). ^{1}H NMR (D_2O) δ 9.02 (s, 1H), 8.79 (s, 1H), 8.71 (s, 1H), 4.45 (m, 1H), 4.15 (m, 1H), 4.03 (t, 2H), 3.96 (t, 1H), 3.45 (m, 1H), 3.13 (m, 3H), 2.7 (m, 2H), 2.61 (m, 1H), 2.12 (t, 2H), 1.79 (m, 2H), 1.71 (m, 2H), 1.65 (m, 2H), 1.5−1.2 (m, 10H), 1.03 (m, 2H). UV−vis: λ_{max} 428 nm (ϵ 10 800, pH 7 buffer). HPLC: pH 4.7, t_R = 14.0 min. MS (FAB$^+$) 850 (M^+, 75), 811 ($M^+ - K^+$, 100).

Biocytin−Oregon Green Conjugate, 11c. To a solution of Oregon Green 488 cadaverine (**9c**, 5-isomer, 0.52 g, 1.05 mmol) and sodium carbonate (0.25 g, 2.4 mmol) in 1:1 water/dioxane (80 mL) was added a solution of **8** (0.85 g, 1.4 mmol) in dioxane/DMF (20 mL/2 mL) dropwise over 30 min. The reaction solution was stirred an additional hour, whereupon TLC indicated that the reaction was complete. Concentration under vacuum gave a residue that was dissolved in water (100 mL) and then washed with EtOAc (100 mL) and chloroform (100 mL). The aqueous portion was treated with aqueous citric acid until a precipitate formed, followed by extraction with EtOAc. The extract was dried under vacuum to give a yellow gum, which was purified by flash chromatography on silica gel using chloroform/methanol (9:1 to 85:15, containing 0.02% TFA) to give 0.75 g (75%) of **10c** as an orange foam.

To a solution of **10c** (0.74 g, 0.78 mmol) in EtOAc (20 mL) was added concentrated HCl (3 mL). The resulting mixture was stirred overnight, and the volatile materials were removed under vacuum. The residue was purified by flash chromatography on silica gel using 20% methanol/chloroform (containing 0.02% TFA) to give **11c** as a yellow gum in quantitative yield. Analytically pure material was obtained by preparative HPLC using a Phenomenex Prodigy Prep ODS (10 μm, 50 × 250 mm) column, eluting with a linear gradient of 20 to 30% acetonitrile in 25 mM ammonium acetate (pH 7.0) over 40 min. Pure fractions were pooled and evaporated repeatedly from methanol to give **11c** as an orange powder: R_f 0.08 (MeCN/H_2O/HOAc; 8:1:1). ^{1}H NMR (D_2O) δ 8.45 (d, 1H), 8.00 (d, 1H), 7.32 (d, 1H), 6.7 (m, 4H), 4.45 (m, 1H), 4.30 (m, 1H), 3.68 (t, 2H), 3.53 (t, 2H), 3.2 (m, 3H), 2.91 (dd, 1H), 2.65 (dd, 1H), 2.18 (t, 2H), 1.9−1.3 (m, 18H). ^{19}F NMR (D_2O) δ 131.0 (m). UV−vis: λ_{max} 495 nm (ϵ 68 800, pH 9 buffer). HPLC: pH 4.7, t_R = 14.9 min. MS (FAB$^+$) 851 (M^+ − Cl, 100), 426 (40).

Biocytin−Tetramethylrhodamine Conjugate, 11d. To a solution of tetramethylrhodamine cadaverine (**9d**, 5 and 6 isomers, 0.51 g, 0.99 mmol) in DMF (14 mL, anhydrous) under nitrogen were added **8** (0.55 g, 0.99 mmol) and *N*-methylmorpholine (0.10 g, 0.99 mmol). The resulting solution was stirred at room temperature overnight and then concentrated under vacuum. The resulting red gum was dissolved in chloroform and precipitated by addition of toluene. The carbamate **10d** was then isolated by filtration as 0.85 g (89%) of a red powder, as a mixture of regioisomers.

A 0.41 g (0.43 mmol) portion of **10d** was suspended in 9 mL of dioxane; 2.0 mL of 4 M HCl/dioxane was added. The resulting mixture was stirred overnight, and then the supernatant decanted. The residual solids were dried under vacuum and then partially purified by chromatography on Sephadex LH-20 using water as eluant. Further purification was afforded by preparative HPLC using a Hamilton PRP-1 column (10 μm particle size) with elution by acetonitrile in 1% ammonium hydroxide in water (20 to 40% linear gradient over 45 min). Pure fractions were pooled and concentrated under vacuum to give **11d** as 0.21 g (54%) of a red powder: R_f 0.25 (dioxane/i-PrOH/water/ammonium hydroxide; 15:58:13:14). ^{1}H NMR (D_2O) δ 8.29 (s, 1H), 8.01 (m, 1H), 7.78, 7.40 (s, d, 1H) 7.15 (d, 2H), 6.79 (m, 2H), 6.49 (br s, 2H), 4.55 (m, 1H), 4.29 (m, 1H), 3.53 (t, 1H), 3.35 (m, 4H), 3.1 (m, 14H), 2.89 (m, 1H), 2.67 (m, 1H), 2.10 (m, 2H), 1.8−1.1 (m, 18H). UV−vis: λ_{max} 543 nm (ϵ 92,500, MeOH). HPLC: C18 Luna 4.6 × 250 mm column, pH 7, t_R = 17.7 min. MS (FAB$^+$) 869 (M^+, 100), 515 (100).

Biocytin−Alexa Fluor 594 Conjugate, 11e. To a solution of Alexa Fluor 594 succinimidyl ester (*20*) (0.5 g, 0.52 mmol) in DMF (10 mL) at 0 °C was added a solution of *N*-t-Boc ethylenediamine (0.33 g, 2.1 mmol) in 2 mL of DMF. The resulting mixture was stirred for 30 min and then concentrated under vacuum. Purification of the resulting purple residue by flash chromatography using 15% H_2O/CH_3CN gave the Alexa Fluor 594 *N*-t-Boc-ethylenediamine adduct.

Trifluoroacetic acid (8 mL) was added to the Alexa Fluor 594 *N*-t-Boc-ethylenediamine adduct (0.25 g, 0.29 mmol) at 0 °C. The resulting mixture was stirred for 30 min and then concentrated to dryness under vacuum. The residue (**9e**) was dissolved in DMF (10 mL), followed by addition of **8** (0.32 g, 0.58 mmol) and triethylamine (0.30 mL, 4.0 mmol). The resulting mixture was stirred at room temperature for 2 h and then concentrated under vacuum. The residue was purified by flash chromatography on silica gel using water/acetonitrile (0 to 15%) as eluant, giving 0.30 g (84%) of carbamate **10e** as a red solid. Trifluoroacetic acid (8 mL) was added to **10e** (0.30 g, 0.24 mmol) at 0 °C. The resulting mixture was stirred for 30 min, whereupon TLC indicated that the reaction was complete. The volatile material was removed under vacuum, and the residue dissolved in dilute sodium bicarbonate solution. The solution was evaporated to dryness, and the residue purified by chromatography on coarse silica gel using water in acetonitrile (0 to 20%) as eluant, giving 172 mg (63%) of **11e** as a hygroscopic purple powder, made up of a mixture of 5- and 6-regioisomers: R_f 0.18 (H_2O/CH_3CN; 3:7). ^{1}H NMR (DMSO-d_6) δ 8.40 (s, 1H), 8.17 (d, 1H), 7.96 (two d, 2H), 7.78 (two t, 2H), 7.43 (s, 1H), 7.21 (d, 1H), 6.59 (s, 2H), 6.53 (d, 2H), 6.43 (s, 2H), 6.39 (br s, 4H), 6.30 (s, 2H), 5.53 (s, 2H), 5.49 (s, 2H), 4.29 (m, 2H), 4.11 (m, 2H), 3.3 (m, 10H), 3.2−2.7 (m, 22H), 2.55 (two 2, 2H), 2.02 (q, 4H), 1.6−1.15 (m, 44H). UV−vis: λ_{max} 591 nm (ϵ 79,700, pH 7 buffer). HPLC: 0 to 60% gradient, pH 7, t_R = 20.9, 22.0 min (92% pure).

Iminobiotin−Cyanocobalamin Conjugate, 13a. To a solution containing 200 mg (0.127 mmol) of CN−Cbl-*c*-lactone conjugate **5b** and 20 μL (0.127 mmol) of Et_3N was added 53 mg (0.130 mmol) of the NHS ester of iminobiotin, **12a**. The reaction mixture was stirred at room temperature for 4 h, and the DMF was removed under vacuum. The residue was loaded onto a preparative C18 column, and the product was eluted with a 3:4 mixture of MeOH:H_2O. Removal of solvent from the fractions containing product gave 130 mg (57%) of **13a**, mp 165−168 °C (dec). ^{1}H NMR (MeOH-d_4, 750 MHz) (NMR spectrum provided in Supporting Information). IR (KBr) 3360, 2920, 1660, 1570, 1500, 1400, 1360, 1210, 1140, 1080 cm^{-1}. t_R = 8.0 min. MS (FAB$^+$) mass calcd for $C_{83}H_{124}N_{18}O_{19}CoPS$: 1799. Found: 1799 (M +).

Biotin−Sarcosine-Cyanocobalamin Conjugate, 13b. To a solution of 120 mg (0.382 mmol) of biotin−sarcosine adduct (*15*) and 60 μL (0.458 mmol) of Et_3N in 10 mL of DMF was added 120 mg (0.458 mmol) of TFP−OTFA. The reaction was stirred at room temperature for 20 min to form the TFP ester of biotin−sarcosine, **12b**. In another flask, 500 mg of (0.318 mmol) CN−Cbl-*c*-lactone conjugate **5b** was dissolved in 10 mL of DMF and 44 μL of (0.318 mmol) Et_3N was added. The biotin−sarcosine TFP ester solution was added to the solution containing **5b**, and the resultant solution was stirred at room temperature for 4 h (followed by HPLC). The solvent was removed under vacuum, and the residue was washed with acetone. The resultant solid was dissolved in MeOH:H_2O (60:40) and was placed on a C-18 column. The column was eluted with 80:20 MeOH:H_2O to give 387 mg of (65%) **13b** after removal of solvent, mp 172−174 °C (dec). ^{1}H NMR (MeOH-d_4, 750 MHz) (NMR spectrum provided in Supporting Information). IR (KBr) 3320, 2920, 1660, 1570, 1400, 1360, 1210, 1110, 1080 cm^{-1}. HPLC: t_R = 8.1 min. MS (FAB$^+$) mass calcd for $C_{73}H_{109}N_{15}O_{18}CoP$: 1871. Found: 1871 (M+).

HPLC Analysis of Binding of Conjugates 6a−f, 11a-e, 13a, and 13b with Avidin and Streptavidin. The biotin−dye conjugates were covered from light with aluminum foil during the analyses. UV absorption was used for detection with dual wavelength monitoring. Absorption of the proteins Av and SAv was monitored at 280 nm and absorption of the biotin−dye conjugates was monitored at their λ_{max} (indicated in Charts 1 and 2). Percentages of bound and free biotin−dye conjugates were obtained directly from peak areas of the bound or free biotin−dye conjugate divided by the sum of their areas times 100.

Biotin−Dye Binding: Initial binding studies were conducted by addition of four molar equiv of the biotin−dye conjugate to solutions containing 1 equiv of avidin or streptavidin. That mixture was allowed to incubate for 1 h at room temperature. Aliquots (100 μL) of the protein/biotin−dye mixture were injected onto the size exclusion column and chromatograms were obtained.

Competitive "On-Rate" Analyses. *Method A: Biotin−Dye Competing with Biotin*. A 20 μL aliquot of a mixture containing 5.9 nmol of biotin and 5.9 nmol of a biotin conjugate (**6a**−**f**, **11a**−**e**) in 10% aqueous DMSO solution[4] was added to 100 μL of a 1 mg/mL solution of avidin (100 μg; 1.5 nmol) in PBS. The solution was mixed and then incubated for 1 h at room temperature. After that time, a 100 μL aliquot was removed by syringe and analyzed by HPLC. The percent of dye coeluting with the avidin peak represents the amount of biotin−dye bound in the competitive binding study.

Method B: Biotin Derivative Competing with Biotin−CN−Cbl, ***6b***. A 20 μL aliquot of a mixture containing 5.9 nmol of a biotin derivative (e.g., biotin sarcosine adduct) and 5.9 nmol of **6b** in 10% aqueous DMSO solution[4] was added to 100 μL of a 1 mg/mL solution of avidin (100 μg; 1.5 nmol) in PBS. The solution was mixed and then incubated for 1 h at room temperature. After that time, a 100 μL aliquot was removed by syringe and analyzed by HPLC. The percent of dye coeluting with the avidin peak subtracted from 100% provides the amount of biotin derivative bound in the competitive binding study.

Competitive "Off-Rate" Analyses. *Method A: Biotin−Dye Displacement by Biotin*. To 300 μL of a 1 mg/mL solution of avidin (300 μg; 4.4 nmol) in a microcentrifuge vial was added 4 equiv (18 nmol) of a biotin conjugate (**6a**−**f**, **11a**−**e**) dissolved in 30 μL of a 10% aqueous DMSO solution. The avidin/biotin derivative mixture was incubated for 1 h at room temperature and 100 μL of the solution was injected into the HPLC to assay binding. To the remaining avidin/biotin derivative solution was added 40 μL of a 1 mg/mL solution of biotin (40 μg; 164 nmol) in 10% aqueous DMSO. That solution was incubated for 1 h, and 100 μL was removed for analysis by HPLC. The remaining solution was incubated for an additional 2−3 h, and then another 100 μL was removed and analyzed by HPLC. (In some studies, HPLC chromatograms were also obtained at 24 h postmixing to ascertain the change in percent biotin bound at that timepoint).

Method B: Biotin Derivative Displacement by Biotin−CN−Cbl, ***6b***. To 400 μL of a 1 mg/mL solution of avidin (400 μg; 5.9 nmol) in a microcentrifuge vial was added 2−3 equiv (12−18 nmol) of biotin or a biotin derivative (e.g., biotin−sarcosine adduct) dissolved in 40 μL of a 10% aqueous DMSO solution. The avidin/biotin derivative mixture was incubated for 1 h at room temperature, and then biotin−CN−Cbl derivative, **6b** (27 nmol) in 40 μL of water was added. That solution was incubated for 10 min, and 100 μL was removed for analysis by HPLC. Additional 100 μL aliquots were removed and analyzed by HPLC at 1, 3, and 24 h postaddition of **6b**.

RESULTS

Preparation of the Biotin−Dye Conjugates. Initially, five biotin−dye conjugates (**6a**−**e**) and five biocytin dye conjugates (**11a**−**e**) were prepared for evaluation of the chromophore to be used in the size exclusion HPLC analyses. The biotin−dye conjugates contained an unaltered biotin moiety and biotinamide bond to ensure that they would bind tightly with avidin. Biotin−dye conjugates **6a**−**e** (Chart 1) contained the 4,7,10-trioxatridecane-1,13-diamine moiety, **2**, as a linker and biotin−dye conjugates **11a**−**e** (Chart 2) contained a lysine (biocytin) and either an ethylenediamine or a pentanediamine (i.e., cadaverine) moiety as linkers.

Biotin−dye conjugates **6a**−**e** were prepared by one of two general reaction routes as depicted in Scheme 1. Low yields of biotin−dyes were obtained in many of the reactions; however, for these studies, there was no need to optimize the reaction yields. Biotin−dyes **6c** and **6e** were prepared via Route A (Scheme 1). Biotin−dye **6c** was prepared from reaction of *N*-(13-amino-4,7,10-trioxatridecanyl)biotinamide, **3**, with an in situ formed tetrafluorophenyl (TFP) ester of commercially available coumarin 343 in 40% yield. Similarly, reaction of **3** with commercially available fluorescein isothiocyanate, **4e**, gave **6e** in 78% yield. Biotin−dyes **6a**, **6b**, and **6d** were prepared via Route B (Scheme 1). To prepare **6a**, dansyl chloride was reacted in neat trioxadiamine, **2**, to give **5a** in 24% yield. This was followed by reaction of the purified **5a** with the TFP ester of biotin, **1**. Similarly, **6d** was prepared by reacting Lissamine-rhodamine sulfonyl chloride in **2** to give **5d** in 19% purified yield, which was subsequently reacted with **1**. Preparation of the cyanocobalamin **6b** is shown in Scheme 3. Formation of the cyanocobalamin-*c*-lactone, **4b**, was accomplished by reac-

[4] Solutions of 10% DMSO were used for consistency even though most of the biotin−dye and biocytin−dye conjugates were water soluble. Also, for consistency, 10% aqueous DMSO solutions were used for biotin and its derivatives that do not have dyes conjugated (e.g., biotin, iminobiotin, biotin−sarcosine). After mixing with Av or SAv solution, the final assay solution contained 1.7% DMSO in the competitive "on-rate" analyses and 2.3% DMSO in the competitive "off-rate" analyses.

Scheme 1. Synthetic Routes for Preparing Hydrophilic Biotin−Dye Conjugates

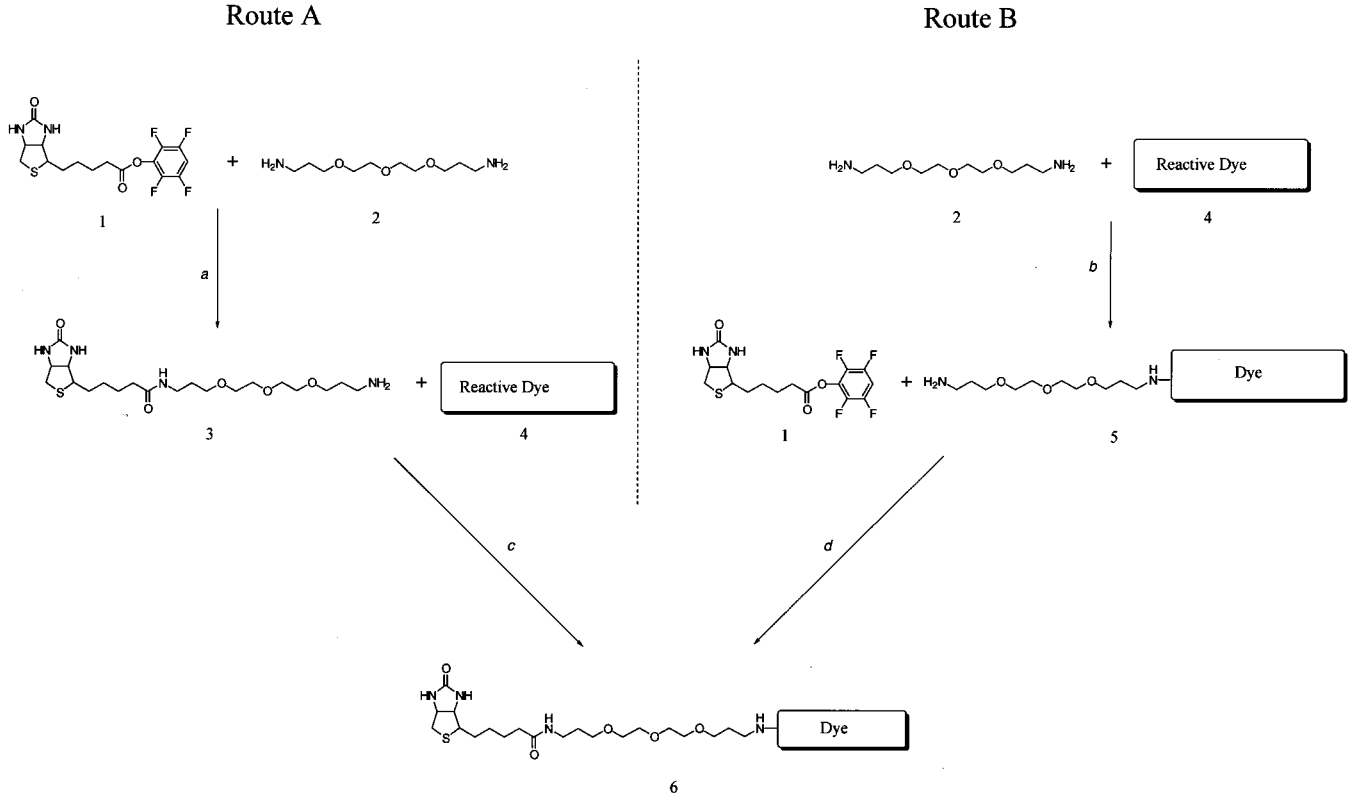

[a] DMF, Et_3N. [b]Et_3N, rt, 1 h. [c]DMF, Et_3N, rt; reaction times vary. [d]DMF, Et3N, rt; reaction times vary.

Scheme 2. Synthetic Route for Preparing Biocytin−Dye Conjugates

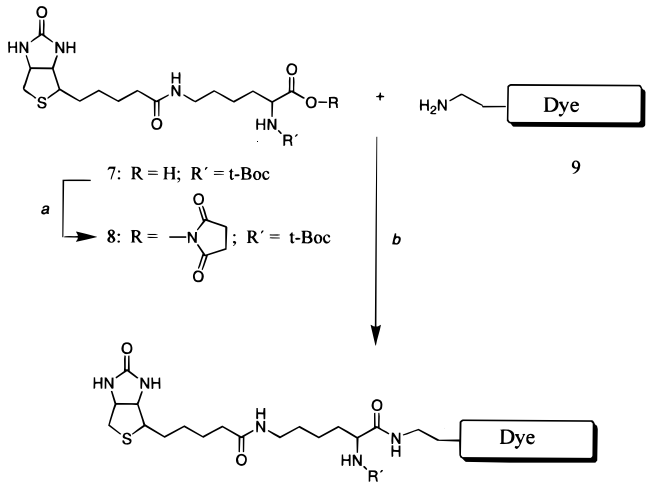

[a] DMF, *i*-PrOH, NHS, DIPCDI, rt, 10 h. [b][1] H_2O, DMF, NMM, rt or Na_2CO_3, H_2O, dioxane, rt; [2] 4 M HCl, dioxane, rt or EtOAc, concentrated HCl

tion of cyanocobalamin with iodine monochloride and acetic acid as previously reported (*18*) Reaction of the lactone with trioxadiamine, **2**, provided the adduct, **5b**, which was readily conjugated with biotin TFP ester, **1**, to give the desired biotin−CN−Cbl, **6b**, in 66% overall yield. Preparation of the iminobiotin conjugate, **13a**, and biotin−sarcosine conjugate, **13b**, also followed the sequence shown in Scheme 3. The NHS ester of iminobiotin, **12a**, can be readily prepared (*21*) (Scheme 4) or obtained from commercial sources, but the TFP ester of biotin−sarcosine is best prepared in situ just prior to reaction (*15*). Reaction of **5b** and iminobiotin NHS ester, **12a**, provided **13a** in 57% purified yield. Similarly, the biotin−sarcosine TFP ester, **12b**, reacted with **5b** to provide **13b** in 65% purified yield.

The biocytin−dye adducts **11a**−**e** were prepared by reaction of the NHS ester of *N*-t-Boc protected biocytin, **8**, with alkylamine derivatives of the fluorescent dyes, **9**, as depicted in Scheme 2. The final step in each reaction sequence was removal of the t-Boc protecting group. The overall yields ranged from 45 to 75%.

Choice of Biotin−Dye Conjugate for the HPLC Analysis. The first studies were focused on obtaining information on the size exclusion HPLC properties of the biotin−dye conjugates (**6a**−**e**, **11a**−**e**). Initial HPLC analyses were conducted on a TSK-GEL G3000SW column, which was 60 cm in length. This column proved to be too long as it took up to 1 h to complete an analysis. To decrease the analysis time, shorter (i.e., 30 cm) columns were used in most of the studies. Since it was anticipated that the biotin−dye conjugates might interact differently with different column matrixes, evaluations of the biotin−dye conjugates were conducted on two different size exclusion columns. One column (Protein Pak 300SW) had a silica based support and the other column (TSK 5000PW) had a hydrophilic polymer support. The retention times and peak width (at baseline) of the biotin−dye conjugates measured at their λ_{max} are provided in Table 1. The retention time and peak width of avidin measured at 280 nm is also provided for comparison. Retention times were longer on the Protein Pak column so run times of 45 min were used. Run times of 30 min were adequate for studies on the TSK 5000PW column.

An evaluation of the association and dissociation rates of biotin−dye conjugates with Av relative to that of unaltered biotin was conducted on each of the biotin−

Scheme 3. General Scheme for Preparation of Biotin Conjugates Containing CN−Cbl-*c*-lactone-trioxatridecanediamine

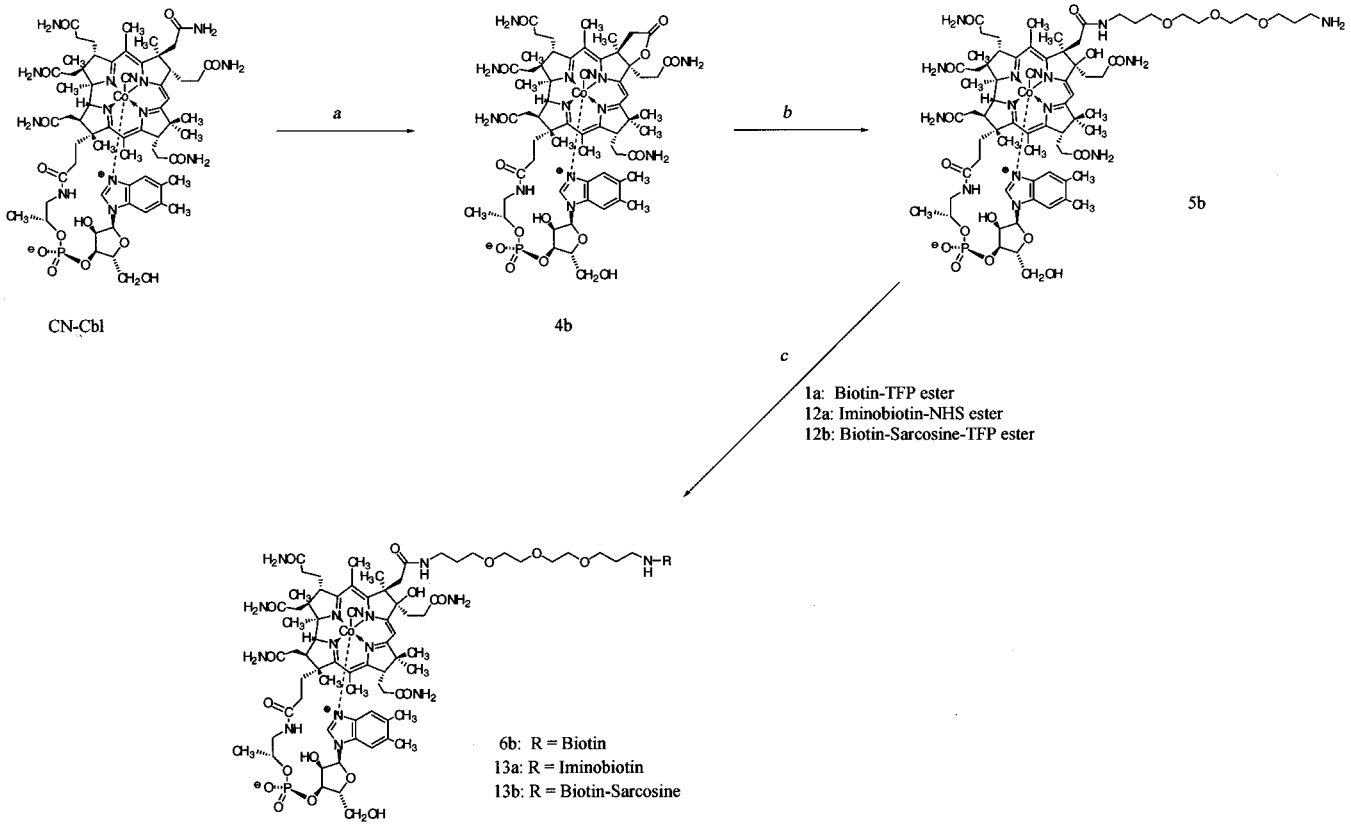

[a] NCS, NaI, HOAc, rt. [b]2, 50−55 °C, 1 h. [c]DMF, Et_3N, rt, 4 h.

Scheme 4. Preparation of Iminobiotin NHS Ester, 12a, and Biotin−Sarcosine TFP Ester, 12b.

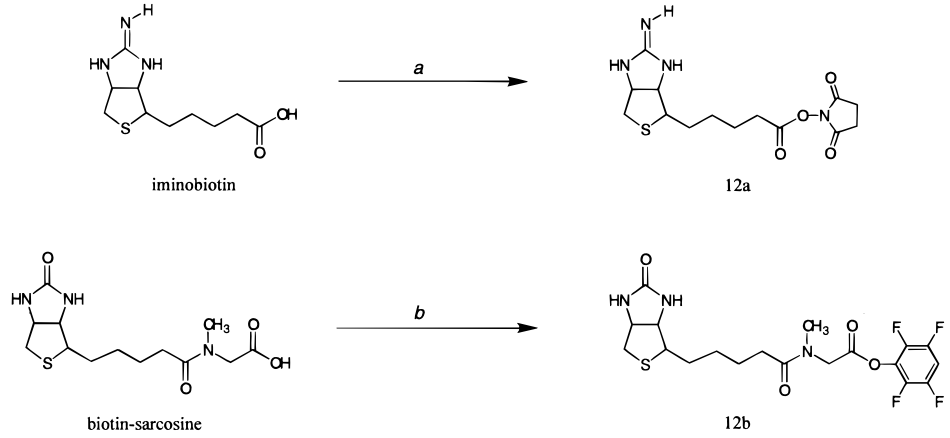

[a] NHS, DCC, 4 °C, 1 h. [b]TFP−OAc, DMF, Et_3N, rt, 20 min.

dye conjugates that were detectable in a 30 min run time (i.e., **6b**, **6e**, **11a**, **11b**, **11c**, and **11e**). Initially, the binding of 4 equiv of each biotin−dye conjugate with Av was assessed to demonstrate that complete binding could be achieved. In some binding assays, small quantities of free biotin−dye conjugate were noted, but decreasing the quantity of biotin−dye to 3 equiv demonstrated that >95% was bound for each compound. The slight excess observed in some runs was attributed to experimental errors in aliquoting.

After evaluating binding of the biotin−dye conjugates with Av, an analysis was conducted to determine competitive binding of the biotin−dye conjugates in the presence of unaltered biotin. In that analysis, equal quantities (4 M equiv each) of biotin−dye conjugate and biotin were mixed and then added to Av. This mixture was incubated for 1 h at room temperature and then an aliquot of the reaction mixture was injected onto the HPLC column and eluted. The percentages of biotin−dye conjugate bound with Av are provided in Table 2. Equivalent association rates would result in 50% of the biotin−dye being bound with Av. The results indicate that all of the biotin−dye conjugates have association rates that are similar to that of unaltered biotin. The biotin−CN−Cbl conjugate, **6b**, has the slowest association rate relative to biotin resulting in 18% bound. However, the percentage bound can be increased to approximately 42% by simply increasing the ratio of **6b**: biotin to 2:1. This is shown in the chromatograms C and D in Figure 1.

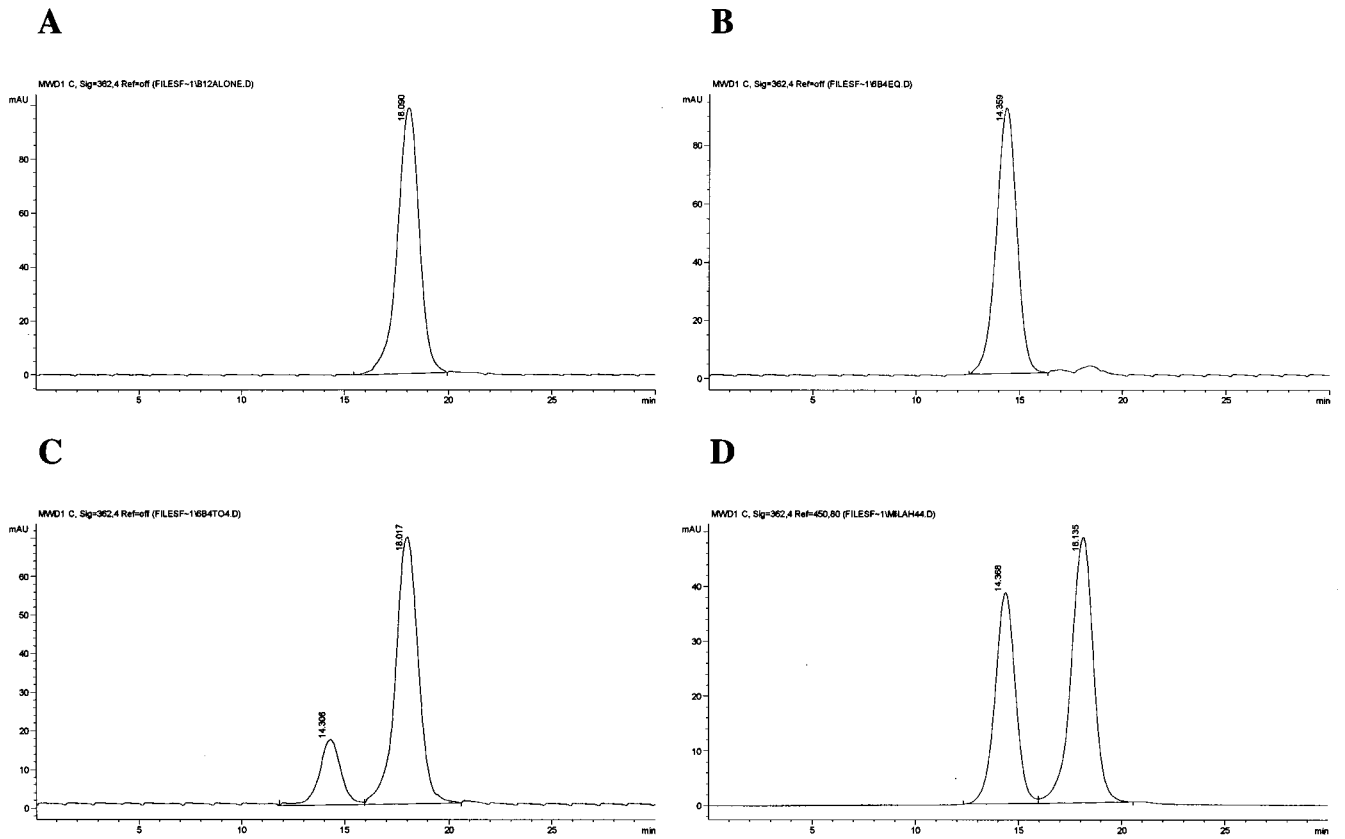

Figure 1. Chromatograms showing the association rates of **6b** and **13a** relative to biotin: (A) the elution of biotin−CN−Cbl conjugate, **6b**, by itself (t_R = 18.1 min); (B) 4 equiv of **6b** bound with Av (t_R = 14.4 min); (C) the results of a competitive binding of 4 equiv of **6b** and 4 equiv of biotin [t_R = 14.3 min (18%) and 18.0 min (82%)]; and (D) the results of a competitive binding of 4 equiv of **6b** and 2 equiv of biotin [t_R = 14.4 min (42%) and 18.1 min (58%)].

Table 2. Percentage of Biotin−Dye Conjugates Bound with Avidin as Measured by Size-Exclusion HPLC

biotin derivative	association assay[a] % Av bound at 1 h	dissociation assay[b] change in % bound at 3 h (%)
6b, cyanocobalamin	20	<5
11a, Cascade Blue	30	<5
11b, Lucifer Yellow	44	<5
11c, Oregon Green	48	<5
11e, Alexa Fluor 594	30	<5

[a] To a mixture of 4 equiv of the biotin−dye conjugate and 4 equiv of biotin was added 1 equiv (4 equiv binding capacity) of Av. This mixture was incubated for 1 h at room temperature. A value of 50% is obtained if the association rate is equivalent to that of biotin. [b] Four equivalents of biotin−dye conjugate are bound with Av, after 1 h, 53 equiv of biotin are added and the mixture is incubated at room temperature for 3 h. No change (or <5% change) indicates that the biotin−dye conjugate has a very high affinity for Av.

The competitive association assay can also be conducted with a biotin−dye conjugate as the reference compound (rather than biotin). As an example, competitive binding of **6b** with the unconjugated biotin derivative, biotin−sarcosine (Scheme 4), resulted in 33% of **6b** bound to Av after 1 h incubation. This result is very similar to the competitive binding of **6b** with biotin (Table 2).

On the basis of a number of factors, including our desire to minimize the HPLC run time, it was determined that the biotin−cyanocobalamin derivative (CN−Cbl) **6b** had the most favorable characteristics for the size exclusion analysis. With **6b**, the percent bound and free can be quantified very rapidly, and the results were found to be reproducible over several runs. However, it was not certain that the extinction coefficients for protein bound **6b** were the same as that for **6b** in solution. Therefore, it was important to assess the linearity of the UV response for bound and free. To determine this, varying quantities (1−8 equiv) of biotin−CN−Cbl, **6b**, were added to a set quantity of Av and the HPLC peak areas at 280 nm (protein) and 362 nm (CN−Cbl) were assessed. A least-squares fit plot of peak area (362 nm) vs equiv of **6b** added is shown in Figure 2. It can be noted that a nearly linear relationship is obtained, indicating that the extinction coefficient is the same for bound and free **6b**.

Assessment of Relative Dissociation Rates of Biotin−Dye Conjugates. Relative dissociation rates were determined by binding 4 equiv of the biotin−dye conjugate with Av and then challenging that conjugate with a large excess (i.e., 53 equiv)[5] of biotin. Only minor changes in the percent bound were observed over a 24 h period in the initial biotin−dye conjugates studied (i.e., **6b**, **6e**, **11a**−**c**, and **11e**).

Measurement of biotin derivatives that had diminished binding with Av was conducted to demonstrate that the HPLC assay worked as expected. Two additional biotin−CN−Cbl conjugates were prepared. An iminobiotin conjugate, **13a**, was chosen as it was not expected to bind with Av under physiological conditions (i.e., pH 7) (*22*). This was confirmed in our assay as no protein bound iminobiotin−CN−Cbl conjugate was detected by HPLC

[5] Calculation of the number of equivalents of biotin added in the competitive assay was done as follows. The original 330 μL solution contained 4.4 nmol of Av. A 100 μL aliquot of this solution was removed for binding analysis, resulting in 3.1 nmol (1 equiv) of Av remaining. To this solution was added 164 nmol of biotin (53 equiv).

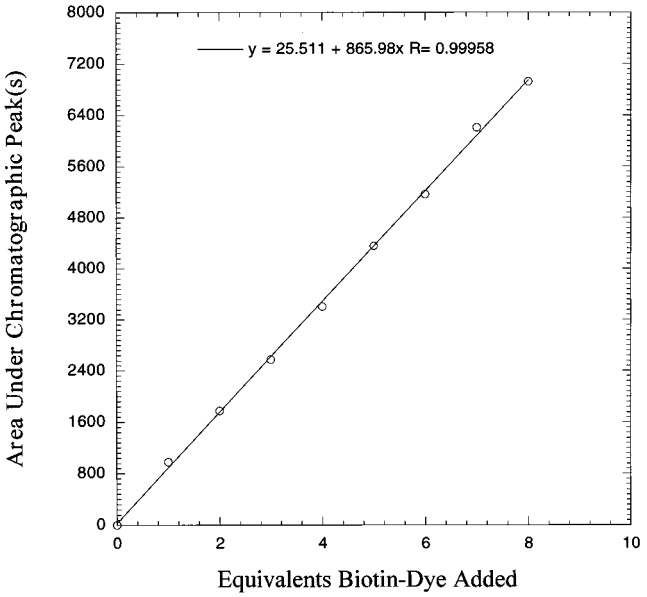

Figure 2. Graph plotting the least-squares fit of total area under the HPLC peak(s) measured at 362 nm for bound and free **6b** after 1−8 equiv are incubated for 1 h at room temperature with 1 equivalent of Av. The linearity of chromatographic response (R = 0.99958) indicates that there is no (or minor) differences in extinction coefficients for bound and free **6b**.

even in the absence of biotin. A biotin−sarcosine conjugate, **13b**, was chosen as the second conjugate as it was expected to have a measurable dissociation rate relative to that of biotin−CN−Cbl conjugate **6b**. Although **13b** bound Av completely and remained bound over time in the absence of biotin, less than 10% remained bound after 1 h, and none remained bound at 3 h when challenged with 53 equiv of biotin (Figure 3, chromatograms C and D). This rapid off-rate correlated well with the observation previously obtained with streptavidin bound radiolabeled biotin−sarcosine adduct (*15*; unreported results). This result can be contrasted with the results obtained for **6b**, where very little (<3%) change was noted after 3 h in the presence of excess biotin (Figure 3, chromatograms A and B).

An alternate method for assaying dissociation rates relative to another biotin−dye (e.g., **6b**) can be obtained by prebinding 3−4 equiv of the biotin derivative and then adding 4 equiv of a reference biotin−dye (e.g., **6b**) and monitoring the percent bound to Av with time. If the dissociation rate of the biotin derivative is slow, then little change would be expected in the percent biotin−dye bound within a 24 h period. In contrast to that, if the biotin derivative dissociation rate is faster than the dissociation rate of the reference biotin−dye, there will be a measurable change in the quantity bound to Av after a 24 h incubation time. An example of this assay is shown in Figure 4, where there was no change (i.e., <1%) over a 24 h period in the amount of **6b** bound to Av when biotin was prebound, but a large change (20−53%) in the amount of **6b** bound to Av was observed when biotin−sarcosine was prebound.

While most of the HPLC analyses were conducted with Av, in some experiments, SAv was used. Of particular interest was whether there was a measurable difference in association rates or dissociation rates of biotin derivatives between binding with Av or binding with SAv. In examination of association rates of some biotin−dye conjugates, there appeared to be only small differences, with those possibly being caused by run to run variances due to experimental error. However, it was possible to detect a fairly substantial difference in the dissociation rate of **13b** when bound with SAv compared with that observed with Av. Interestingly, the dissociation rate from SAv was slower than observed for Av, with 44% remaining bound at 1 h and 14% remaining bound at 3 h addition of excess biotin (Figure 3, chromatograms E and F). We are attempting to find a basis for this slower dissociation rate through computer modeling of Av and SAv with **13b**.

DISCUSSION

Measurement of the changes in rates of association and dissociation of a biotin conjugate with Av or SAv can provide important information about how a particular biotin conjugate may work for an application in comparison with another biotin conjugate. In our in vivo application of biotin derivatives for targeted radiotherapy of cancer, it is essential that radioactivity delivered to cancer cells be bound with SAv in a manner that it does not come free during the period of the radionuclide decay. Thus, optimization of a biotin derivative to carry a radionuclide in our studies includes determining the rate of dissociation of that biotin derivative relative to biotin and other biotin derivatives. However, for our purposes, it is not necessary to obtain an accurate value for the dissociation rate, rather to assess whether the rate is similar to, or different from, that of biotin or another biotin derivative under study.

In this study, we sought to develop an assay that was simple to conduct and would allow direct determination of relative association and dissociation of biotin derivatives at neutral pH and under nonequilibrium conditions, mimicking in vivo binding. Although thermodynamic parameters can be calculated for binding of biotin and biotin derivatives with Av (*22*−*24*) and SAv (*25*), a more direct and easily performed assay for determination of relative binding was desired. Methods of measuring bound vs free biotin using fluorescent polarization (*26*) and Raman spectroscopy (*27*) were not attractive due to the equipment required. Although we routinely prepare radiolabeled biotin derivatives, methods using radiolabeled biotin, such as competitive binding assays (*28*) and isotope dilution (*29*) were not attractive due to the handling difficulties associated with radionuclides. Postcapillary affinity detection of biotin derivatives was attractive (*30*), but we did not have the equipment for that analytical method. Similarly, HPLC systems which used postcolumn affinity detection (*31*) were of interest, but were more complex than we required. Since our primary interest in the assay was to determine the percentage of biotin derivative Av or SAv bound with time, it was thought that such a system could be measured directly by the use of size exclusion HPLC. To make the assay easy to use in the normal laboratory setting, we chose to conjugate the biotin derivatives with a chromophore for detection by UV. Although this seemed to be a reasonable approach to obtaining relative binding, there was some concern about the effects of the chromophoric moiety on the measurement of relative binding.

Due to the concern that the nature of the chromophoric moiety would alter the binding assay, we chose to prepare and evaluate a number of different biotin−dye conjugates. We also chose to evaluate the biotin−dye conjugates on two different size exclusion columns, one being silica based and the other being organic polymer based. As in our previous studies of biotin derivatives (*15*, *17*, *3*,*2*) five biotin−dye conjugates incorporated the ether containing linker, 4,7,10-trioxatridecane-1,13-diamine, **2**,

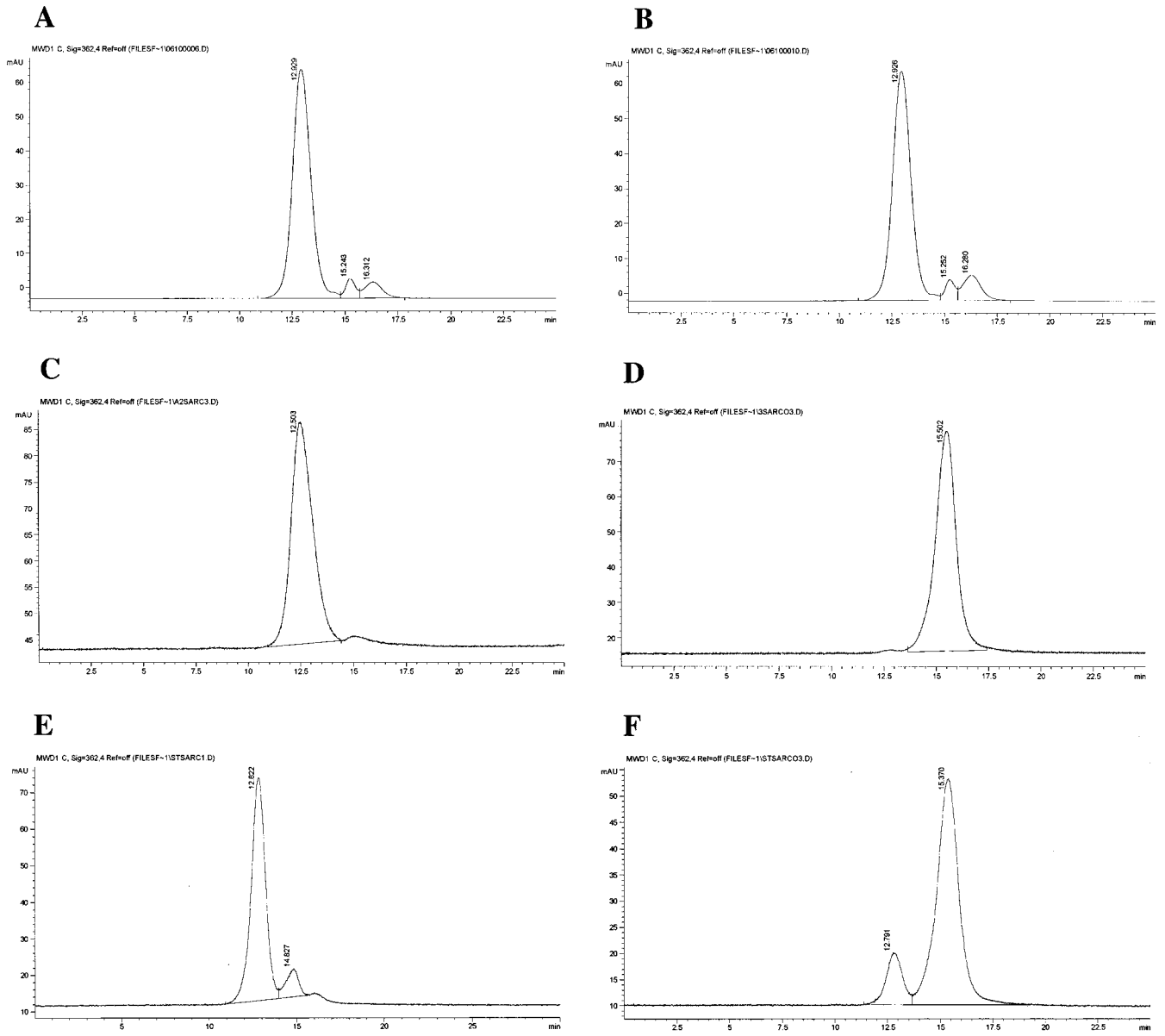

Figure 3. Chromatograms showing dissociation rates of biotin−CN−Cbl conjugates **6b** with Av and **13b** with Av and SAv: (A) the biotin−CN−Cbl conjugate, **6b**, bound to Av prior to addition of biotin [t_R = 12.9 min (90%), t_R = 15.2 min (4%), t_R = 16.3 min (6%)]. It should be noted that the peak at 15.2 min may contain a nonbinding CN−Cbl containing impurity and the peak at 16.3 min is **6b** in excess of 4 equiv; (B) the biotin−CN−Cbl conjugate, **6b**, bound to Av 3 h after incubation with 53 equiv of biotin [t_R = 12.9 min (87%), t_R = 15.2 min (4%), t_R = 16.3 min (9%)]; (C) the biotin−sarcosine−CN−Cbl conjugate, **13b**, bound to Av prior to addition of biotin (t_R = 12.5 min); (D) the biotin−sarcosine−CN−Cbl conjugate, **13b**, bound to Av 3 h after incubation with 53 equiv of biotin (t_R = 15.5 min); (E) the biotin−sarcosine−CN−Cbl conjugate, **13b**, bound to SAv prior to addition of biotin (t_R = 12.8 min); and (F) the biotin−sarcosine−CN−Cbl conjugate, **13b**, bound to SAv 3 h after incubation with 53 equiv of biotin [t_R = 12.8 min (14%) and 15.4 min (86%)].

as a 17 Å spacer[6] between biotin and the chromophore (Chart 1). In addition to being a spacer moiety, **2** also decreases the hydrophobicity of the biotin moiety. In contrast, biocytin−dye derivatives (Chart 2) can incorporate simple aliphatic linkers without concern about decreasing water solubility because they contain ionized functional moieties. The linker between biotin and the conjugated molecule in the biocytin compounds studied include a lysine-ethylenediamine linker (12 Å spacer)[6] and a lysine-cadaverine linker (16 Å spacer).[6] Even with the hydrophilic linker, biotin−dyes **6a**, **6c**, and **6e** had low aqueous solubility making it necessary to dissolve them in DMSO prior to using them in the assay. For consistency, all of the biotin−dye conjugates tested were dissolved in 10% aqueous DMSO. The biotin solution was also made in 10% DMSO as a 1 mg/mL solution was desired, and its solubility in water is only 0.22 mg/mL (*33*). After dilution into the Av or SAv solutions, the final concentration of DMSO was 1.7% in the competitive on-rate analyses and 2.3% in the competitive off-rate analyses. Binding analyses were also conducted with **6b** and **13b** which contained no DMSO. Those analyses gave the same results as analyses containing the small amount of DMSO.

Initial HPLC studies were focused on elution characteristics of the biotin−dye conjugates. Our goal was to find a biotin−dye conjugate that had a peak shape and

[6] The length of the linker between the biotin carbonyl and the conjugated moiety is estimated in the fully linearized form. The values were obtained after energy minimization of the chemical models in ChemDraw 5.0 (CambridgeSoft Corporation, Cambridge, MA).

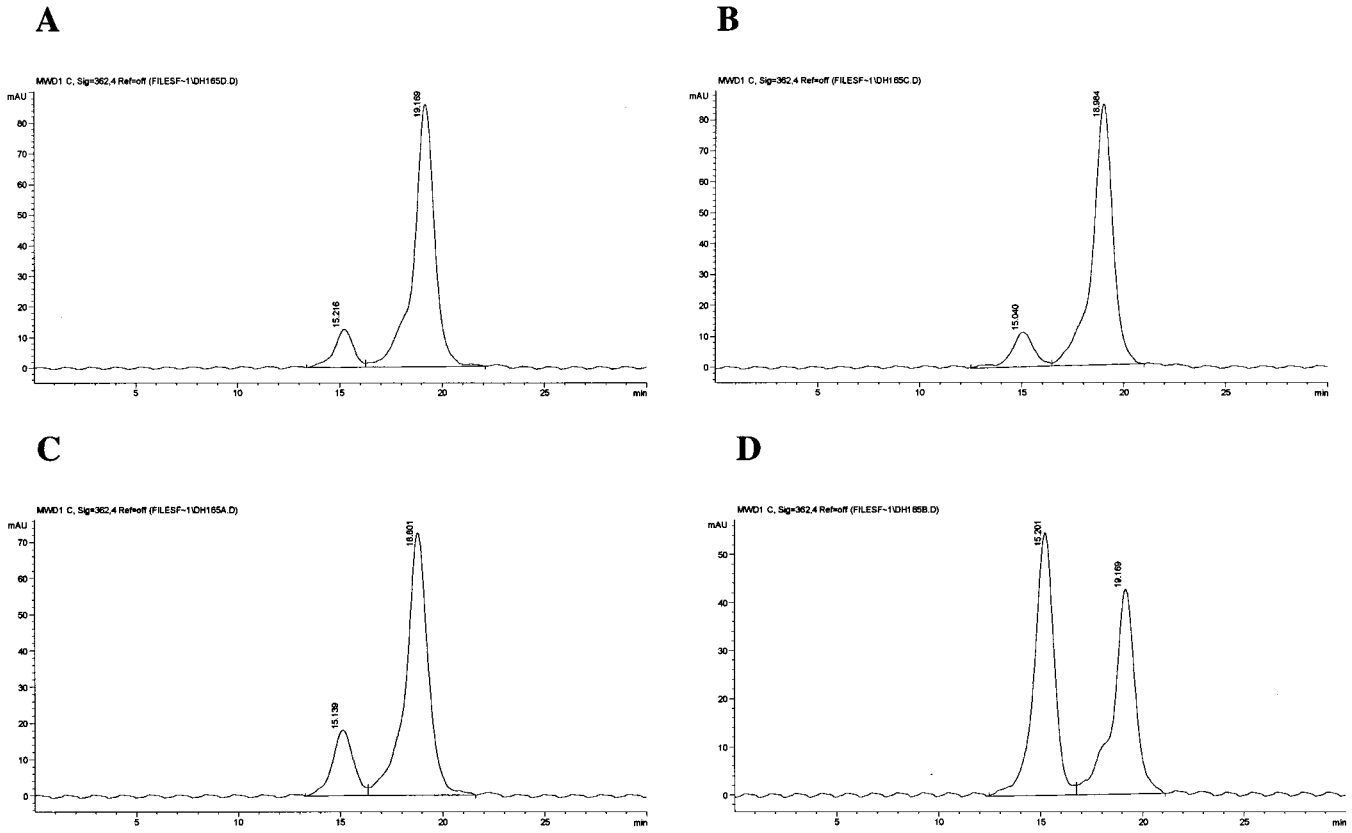

Figure 4. Chromatograms showing dissociation of biotin or biotin−sarcosine in the presence of 4 equiv of **6a**: (A) the biotin−CN−Cbl conjugate, **6b**, bound to Av and free 10 min after its addition to Av prebound with 3−4 equiv of *biotin* [t_R = 15.2 min (13%) and 19.2 min (87%)]; (B) the biotin−CN−Cbl conjugate, **6b**, bound to Av and free 24 h after its addition to Av prebound with 3−4 equiv of *biotin* [t_R = 15.0 min (13%) and 19.0 min (87%)]. (C) the biotin−CN−Cbl conjugate, **6b**, bound to Av and free 10 min after its addition to Av prebound with 3−4 equiv of *biotin-sarcosine* [t_R = 15.1 min (20%) and 18.8 min (80%)]; (D) the biotin−CN−Cbl conjugate, **6b**, bound to Av and free 24 h after its addition to Av prebound with 3−4 equiv of *biotin-sarcosine* [t_R = 15.2 min (53%) and 19.2 min (47%)].

an elution time similar to that of Av such that the analysis would take less than 30 min to run and could be easily quantified by peak integration. To minimize the cost, most binding studies were conducted with avidin. The analysis was conducted by simply eluting the biotin−dye conjugates without Av or SAv present. Analyses on the silica-based size exclusion column (Protein Pak 300SW) demonstrated that biocytin-Cascade Blue, **11a**, and biocytin-Lucifer Yellow, **11b**, have elution characteristics suitable for application in the analyses (Table 1). Their retention times were within the desired 30 min run time and peak widths were small enough to provide good quantification. Analysis of the biotin−dyes on a hydrophilic polymer based column (TSK 5000PW) provided very different results. While **11a** and **11b** also eluted within the 30 min time frame, the cyanocobalamin derivative, **6b**, was the best candidate for this application as it had a relatively short retention time (18 min) and narrow peak width (2 min).

The biotin derivatives **6a**, **6c**, **6d**, and **11d** did not elute from either column during the run times (30 or 45 min). This fact made them undesirable for the assay. Although these derivatives were eliminated from the assay, Av binding studies were conducted with them. Interestingly, their binding with Av altered its retention on the size exclusion column, either through a process of interaction with the matrix or through dissociation of its tetrameric structure.[7] The biotin−fluorescein conjugate, **6e**, had a retention time that exceeded the desired 30 min run time. However, since biotin derivatives containing fluorescein are commercially available and are used for other applications, an effort was made to determine if this compound could be used even if it did not have optimal properties. Retention times of 49 and 60 min were observed on the two columns (Table 1). The long retention times and broad peak widths appear to make **6e** a poor candidate for the analysis.

Association rates of biotin−dye conjugates with Av relative to biotin were obtained in a competitive binding assay. In that analyses, equal quantities (4 M equiv each) of biotin−dye conjugates and unaltered biotin were mixed, and then Av was added. After incubation for 1 h at room temperature, an aliquot of the reaction mixture was injected onto the HPLC column and eluted. The 1 h time point was chosen as it was thought that time would ensure complete binding of biotin or biotin−dye conjugate. The ability to determine relative association rates was predicated on having a very slow dissociation rate relative to the association rate. The dissociation rates of biotin or the biotin−dye conjugates studied was expected to be very slow relative to the 1 h timepoint. This expectation was based on the fact that the half-time for dissociation of biotin from Av is around 200 days at 25 °C (*22*). Although half-time for dissociation of biotin from streptavidin is much faster [i.e., 2.9 days (*23*)], it is also long with respect to the 1 h time point. The biocytin−dye conjugates had 30−48% bound to Av (Table 2), which

[7] The conclusion that Av may have dissociated into monomeric form came from the fact that the chromatographic peak (measured at 280 nm) eluted much later (e.g., >18 min) than usual (e.g., 15 min). Smaller proteins have similar elution times.

indicated that they had association rates very near to that of biotin. The biotin−CN−Cbl conjugate, **6b**, had the least bound (18%) of the biotin derivatives tested in the presence of an equal quantity of biotin. However, when a 2:1 ratio of **6b**:biotin was competed in the association assay, approximately 42% of **6b** bound. Thus, it appears that the rate of association of **6b** is approximately half that of biotin. The small differences in association rates seen between the biotin−dyes tested did not provide a basis for selecting one over another.

Another HPLC analysis provided data on the dissociation rate of biotin−dye conjugates. A fairly short (i.e., 1−4 h) time period was used in the assay as it was thought that measurable differences in dissociation within that period would likely result in observable differences in the in vivo tumor retention of radiolabeled biotin derivatives. Although this analysis did not provide valid kinetic data, it did provide data that indicated the off-rate was fast or slow relative to another biotin derivative. All of the initial biotin−dye conjugates studied (**6a**−**e**, **11a**−**e**) contained biotin conjugated to a linker moiety through an aliphatic primary amine. Biotin−dye conjugates which are linked to other molecules through an aliphatic primary amine would be expected to have dissociation kinetics similar to that of unmodified biotin (*22*). Indeed, all of the initial biotin dyes conjugates studied have slow off-rates, similar to unconjugated biotin.

A choice of biotin−dye conjugate had to be made to develop assays for determining relative association and dissociation rates. Solely on the basis of HPLC characteristics, the biotin−dye conjugates were limited to **6b**, **11a**, and **11b**. While it appears that **11a** and **11b** might be used with the Protein Pak 300SW column for HPLC assays to relative association and dissociation rates of biotin derivatives, the fact that the assays could be conducted within 20−25 min if **6b** were used on the TSK 5000PW column, and that the peak widths allowed good quantification, made that combination more attractive for our studies. The criteria set for selection of an ideal biotin−dye was met with **6b**. It is highly soluble in aqueous solution (i.e., >10 mg/mL). The peak shape of free **6b** is similar to that of the proteins Av or SAv on the size exclusion column used, and the elution time is only slightly longer than that of Av and SAv. This indicates that there is little interaction of the CN−Cbl moiety with the organic polymer-based column. The rates of association and dissociation of **6b** with Av and SAv are similar to unconjugated biotin. Although the CN−Cbl moiety is a large molecule, it appears to have only a minor effect on the very rapid association rate of **6b**, and 4 equiv readily binds with Av or SAv. Importantly, the biotin−CN−Cbl derivative **6b**, and the other CN−Cbl conjugates, **13a** and **13b**, were easily prepared in good overall chemical yields.

There are two different approaches to obtaining relative association and dissociation rates with biotin−CN−Cbl derivatives. The first approach (method A) is to prepare CN−Cbl conjugates of the biotin derivatives that are to be evaluated and assess their association and dissociation rates relative to biotin. This approach was taken with the biotin−CN−Cbl derivatives, **6b**, **13a**, and **13b**. Additional biotin derivatives have been evaluated using this assay. Those results are described in another paper (*34*). The second approach (method B) is to measure the association and dissociation rates of biotin derivatives relative to a biotin−CN−Cbl derivative that has binding characteristics similar to unconjugated biotin, e.g., **6b**. It appears that either approach will provide data that will help determine if the binding characteristics of biotin derivatives have been altered by conjugation or other modification of biotin. Because large differences in dissociation rates can be seen in shorter periods of time when CN−Cbl derivatives are prepared and evaluated, it seems that this approach may be beneficial when a series of derivatives are being tested. However, if **6b** can be synthesized or is made available through commercial sources,[8] it might be easier to compare biotin derivatives to it rather than synthesize CN−Cbl conjugates of biotin derivatives. The biocytin-dye conjugates **11a** and **11b** are commercially available and may also work well when used as reference biotin compounds.

In Summary. We have demonstrated that relative association and dissociation rates of biotin−dyes with Av or SAv can be assessed by HPLC. Of the 10 biotin−dye conjugates prepared and evaluated for use in a size exclusion HPLC assay, two biocytin dye conjugates and one biotin−dye conjugate had elution properties that made them attractive for use in the assays. We chose the biotin−CN−Cbl conjugate **6b** for use in our continuing studies as its use permits short analyses times. Two additional biotin−CN−Cbl derivatives, an iminobiotin−CN−Cbl conjugate, **13a**, and a biotin−sarcosine−CN−Cbl conjugate, **13b**, were also prepared and evaluated in the HPLC binding assays. These derivatives also functioned well, demonstrating that biotin derivatives can be conjugated with CN−Cbl and effectively used to determine association and dissociation rates relative to biotin or another biotin derivative. We also demonstrated that an alternative approach, wherein nonchromophoric biotin derivatives were assessed relative to **6b** (rather than biotin). This approach required more time to observe the differences in dissociation rates than did the assay where CN−Cbl conjugates of the biotin derivatives were prepared. Applications of the assays described herein will permit rapid evaluation of the relative association and dissociation rates of new biotin derivatives. This information should help delineate whether conjugation or modification of biotin compounds has compromised their binding affinity.

ACKNOWLEDGMENT

We thank Dr. Ross Lawrence (Department of Medicinal Chemistry, University of Washington) for efforts in obtaining mass spectral data. We are grateful for the financial support provided by the Department of Energy, Medical Applications and Biophysical Research Division, Office of Health and Environmental Research under Grant DE-FG03-98ER62572.

Supporting Information Available: HPLC chromatograms, NMR spectra, and mass spectra of biotin−dye conjugates **5b** and **6a**−**e** and NMR spectra of biocytin-dye conjugates **11a**−**e** are provided. This material is available free of charge via the Internet at http://pubs.acs.org.

LITERATURE CITED

(1) Wilchek, M., and Bayer, E. A. (1989) Avidin−Biotin Technology Ten Years On: Has It Lived up to Its Expectations? *Trends Biochem. Sci. 14*, 408−412.

(2) Wilchek, M., and Bayer, E. A. (1990) Introduction to Avidin−Biotin Technology. *Methods Enzymol. 184*, 5−45.

[8] A commercial source, Quanta BioDesigns (Dublin, OH), is planning to make **6b** available for sale. The biocytin-dye conjugates **11a**−**e** are available from Molecular Probes, Inc. (Eugene, Oregon).

(3) Savage, M. D., Mattson, G., Desai, S., Nielander, G. W., Morgensen, S., and Conklin, E. J. (1992) *Avidin−Biotin Chemistry: A Handbook*, Pierce Chemical Company, Rockford, IL.
(4) Hermanson, G. T. (1996) Avidin−Biotin Systems. *Bioconjugate Techniques*, pp 570−592, Academic Press, San Diego.
(5) Hnatowich, D. J., Virzi, F., and Rusckowski, M. (1987) Investigations of Avidin and Biotin for Imaging Applications. *J. Nucl. Med. 28*, 1294−1302.
(6) Paganelli, G., Malcovati, M., and Fazio, F. (1991) Monoclonal Antibody pretargetting techniques for tumour localization: the avidin−biotin system. *Nucl. Med. Commun. 12*, 211−234.
(7) Fritzberg, A. R. (1998) Antibody Pretargeted Radiotherapy: A New Approach and a Second Chance. *J. Nucl. Med. 39*, 20N, 21N, 22N, 36N.
(8) Goodwin, D. A., and Meares, C. F. (1997) Pretargeting: General Principles. *Cancer (Suppl.) 80*, 2675−2680.
(9) Perez-Luna, V. H., O'Brien, M. J., Opperman, K. A., Hampton, P. D., Lopez, G. P., Klumb, L. A., and Stayton, P. S. (1999) Molecular recognition between genetically engineered streptavidin and surface-bound biotin. *J. Am. Chem. Soc. 121*, 6469−6478.
(10) Pispa, J. (1965) Animal Biotinidase. *Ann. Med. Exptl. Biol. Fenniae 43*, 3−40.
(11) Chauhan, J., Ebrahim, H., Bhullar, R. P., and Dakshinamurti, K. (1985) Human Serum Biotinidase. *Ann. N. Y. Acad. Sci. 447*, 386-388.
(12) Hymes, J., Fleischhauer, K., and Wolf, B. (1997) Biotinidase in Serum and Tissues. *Methods Enzymol. 279*, 422−434.
(13) Axworthy, D. B., Theodore, L. J., Gustavson, L. M., and Reno, J. M. (1997) Biotinidase-Resistant Biotin-DOTA Conjugates. United States Patent 5,608,060.
(14) Rosebrough, S. F. (1993) Plasma Stability and Pharmacokinetics of Radiolabeled Deferoxamine-Biotin Derivatives. *J. Pharmacol. Exp. Ther. 265*, 408−415.
(15) Wilbur, D. S., Hamlin, D. K., Pathare, P. M., and Weerawarna, S. A. (1997) Biotin reagents for antibody pretargeting. Synthesis, radioiodination, and in vitro evaluation of water soluble, biotinidase resistant biotin derivatives. *Bioconjugate Chem. 8*, 572−584.
(16) Gamper, H. B., Reed, M. W., Cox, T., Virosco, J. S., Adams, A. D., Gall, A. A., Scholler, J. K., and Meyer, R. B. (1993) Facile Preparation of Nuclease Resistant 3′ Modified Oligodeoxynucleotides. *Nucleic Acids Res. 21*, 145−150.
(17) Wilbur, D. S., Hamlin, D. K., Vessella, R. L., Stray, J. E., Buhler, K. R., Stayton, P. S., Klumb, L. A., Pathare, P. M., and Weerawarna, S. A. (1996) Antibody fragments in tumor pretargeting. Evaluation of biotinylated Fab′ colocalization with recombinant streptavidin and avidin. *Bioconjugate Chem. 7*, 689−702.
(18) Pathare, P. M., Wilbur, D. S., Heusser, S., Quadros, E. V., McLoughlin, P., and Morgan, A. C. (1996) Synthesis of Cobalamin-Biotin Conjugates That Vary in the Position of Cobalamin Coupling. Evaluation of Cobalamin Derivative Binding to Transcobalamin II. *Bioconjugate Chem. 7*, 217−232.
(19) Bodanszky, M., and Fagan, D. T. (1977) Synthesis of Biocytin-Containing Peptides. *J. Am. Chem. Soc. 99*, 235−239.
(20) Panchuk-Voloshina, N., Haugland, R. P., Bishop-Stewart, J., Bhalgat, M. K., Millard, P. J., Mao, F., and Leung, W. Y. (1999) Alexa dyes, a series of new fluorescent dyes that yield exceptionally bright, photostable conjugates. *J. Histochem. Cytochem. 47*, 1179−1188.
(21) Fudem-Goldin, B., and Orr, G. A. (1990) 2-Iminobiotin-Containing Reagent and Affinity Columns. *Methods Enzymol. 184*, 167−173.
(22) Green, N. M. (1975) Avidin. *Adv. Protein Chem. 29*, 85−133.
(23) Green, N. M. (1990) Avidin and Streptavidin. *Methods Enzymol. 184*, 51−67.
(24) Swamy, M. J. (1995) Thermodynamic Analysis of Biotin Binding to Avidin. A High Sensitivity Titration Calorimetric Study. *Biochem. Mol. Biol. Int. 36*, 219−225.
(25) Klumb, L. A., Chu, V., and Stayton, P. S. (1998) Energetic roles of hydrogen bonds at the ureido oxygen binding pocket in the streptavidin−biotin complex. *Biochemistry 37*, 7657−7663.
(26) Schray, K. J., Artz, P. G., and Hevey, R. C. (1988) Determination of avidin and biotin by fluorescence polarization. *Anal. Chem. 60*, 853−855.
(27) Torreggiani, A., and Fini, G. (1998) The binding of biotin analogues by streptavidin: a Raman spectroscopic study. *Biospectroscopy 4*, 197−208.
(28) White, H. B., 3rd (1997) Competitive binding assays for biotin-binding proteins. *Methods Enzymol. 279*, 464−466.
(29) Bhullar, R. P., Lie, S. H., and Dakshinamurti, K. (1985) Isotope Dilution Assay for Biotin. *Ann. N. Y. Acad. Sci. 447*, 122−128.
(30) Kelly, J. A., Reddy, K. R., and Lee, C. S. (1997) Mechanistic studies of postcapillary affinity detection for capillary zone electrophoresis based on the biotin-streptavidin system. *Anal. Chem. 69*, 5152−5158.
(31) Oosterkamp, A. J., Irth, H., Thaden, U. R., and van der Greef, J. (1997) Theoretical concepts of on-line liquid chromatographic-biochemical detection systems. *J. Chromatogr. 787*, 37−46.
(32) Wilbur, D. S., Pathare, P. M., Hamlin, D. K., and Weerawarna, S. A. (1997) Biotin reagents for antibody pretargeting. 2. Synthesis and in vitro evaluation of biotin dimers and trimers for cross-linking of streptavidin. *Bioconjugate Chem. 8*, 819−832.
(33) Budavari, S., O'Neil, M. J., Smith, A., and Heckelman, P. E., Eds. (1989) *The Merck Index*, 11th ed., p 192, Merck & Co., Inc., Rahway, NJ.
(34) Wilbur, D. S., Pathare, P. M., Hamlin, D. K., Chyan, M.-K., and Brian B. Kegley (2000) Biotin Reagents for Antibody Pretargeting. 4. Selection of Biotin Conjugates for In Vivo Application Based on Their Dissociation Rate with Avidin and Streptavidin. *Bioconjugate Chem. 11*, 539−583.

BC0000031

© 2000 American Chemical Society, Bioconjugate Chem., Wilbur bc0000031 Supporting Info Page 1

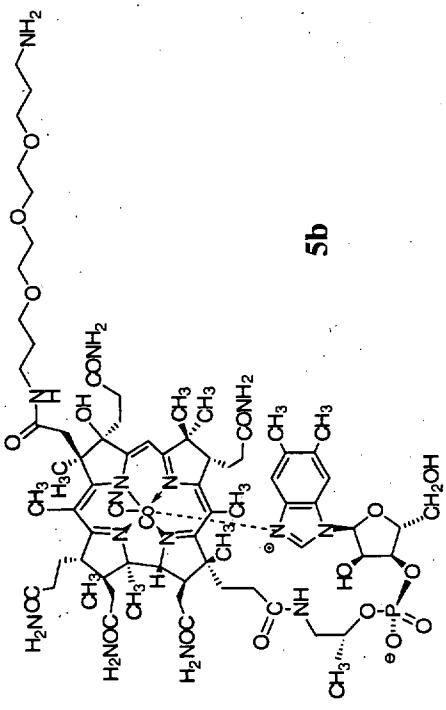

5b

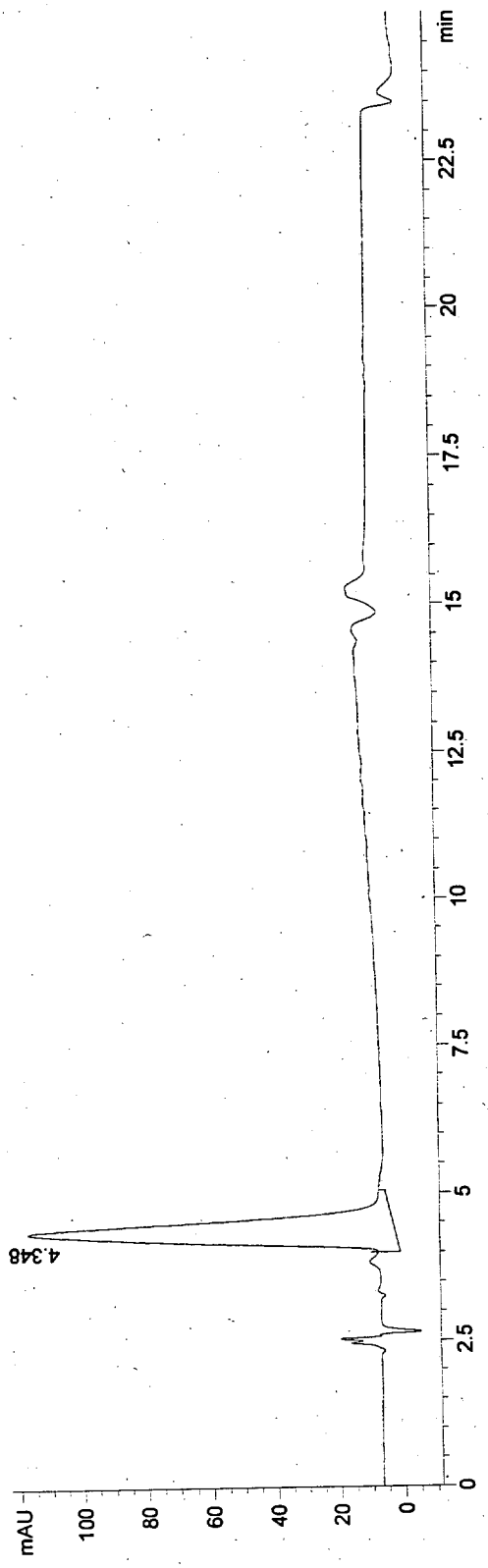

© 2000 American Chemical Society, Bioconjugate Chem., Wilbur bc0000031 Supporting Info Page 2

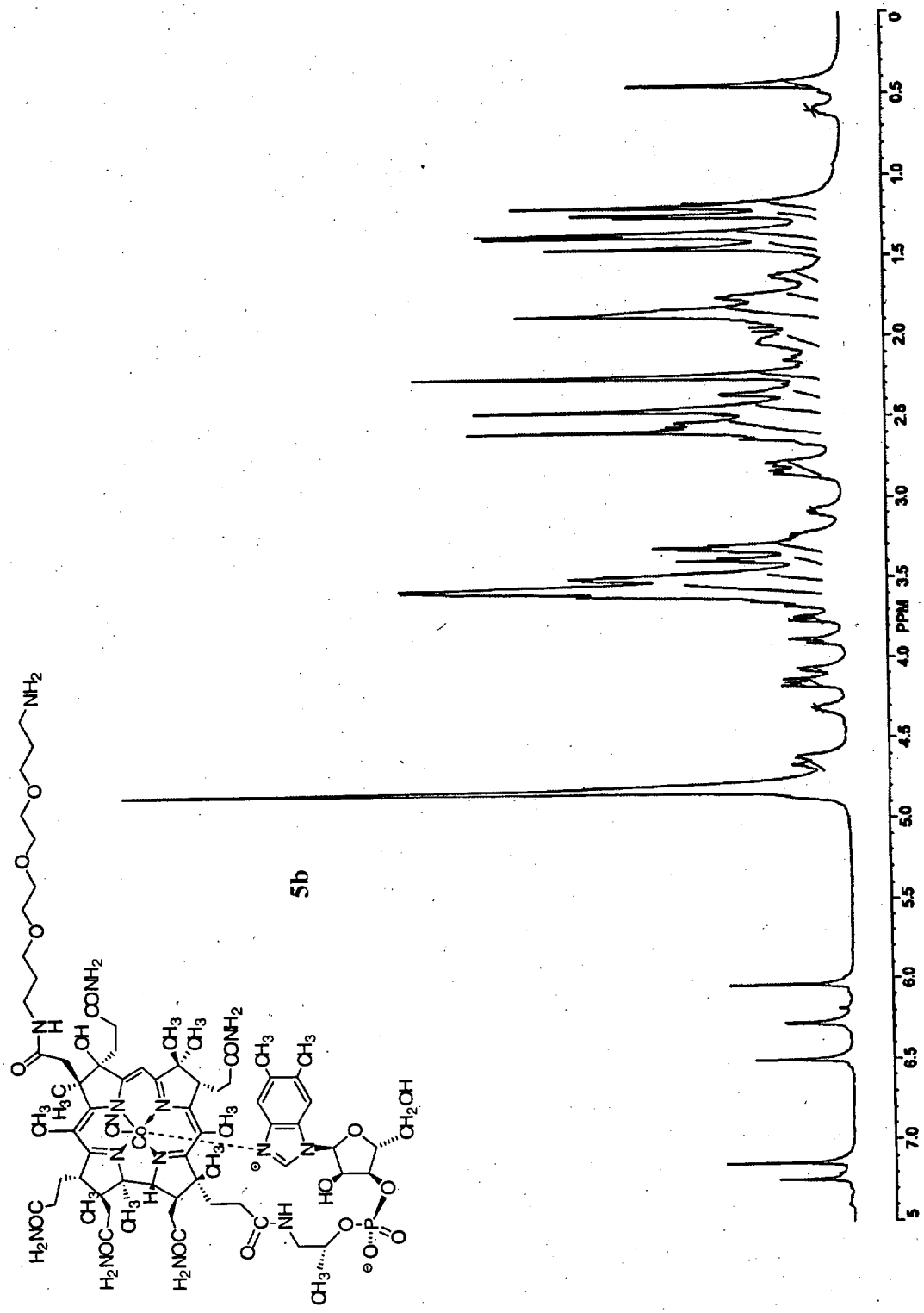

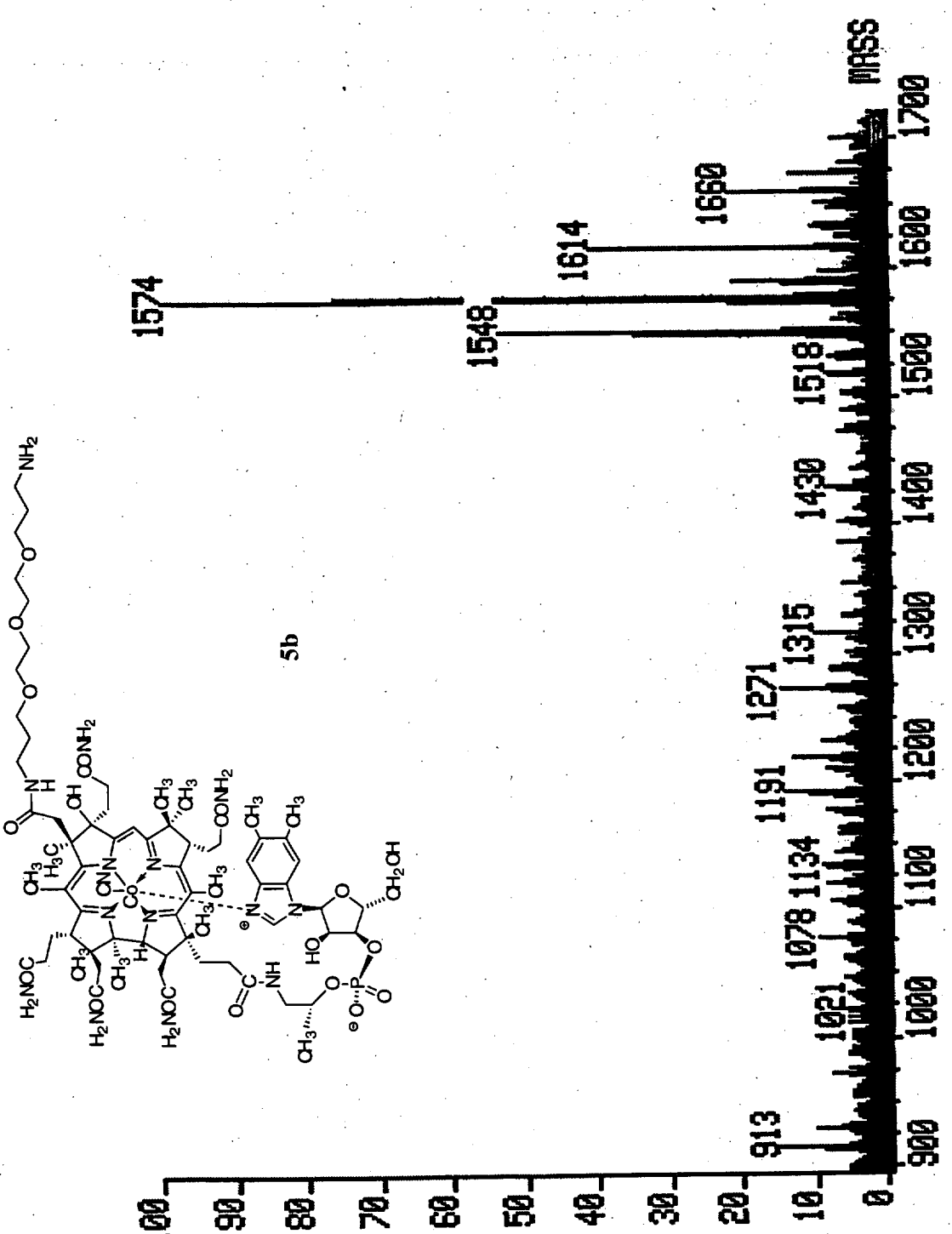
5b
MASS
913
1021
1078
1134
1191
1271
1315
1430
1518
1548
1574
1614
1650
900
1000
1100
1200
1300
1400
1500
1600
1700
0
10
20
30
40
50
60
70
80
90
100

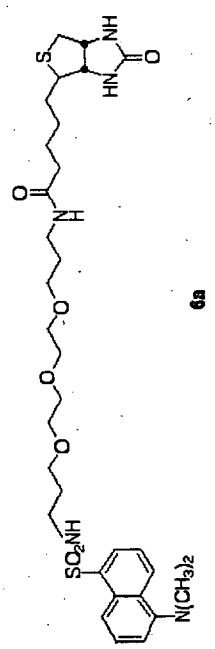
NH
S
HN
O
O
N
H
O
O
O
O
O
SO2NH
N(CH3)2

6a

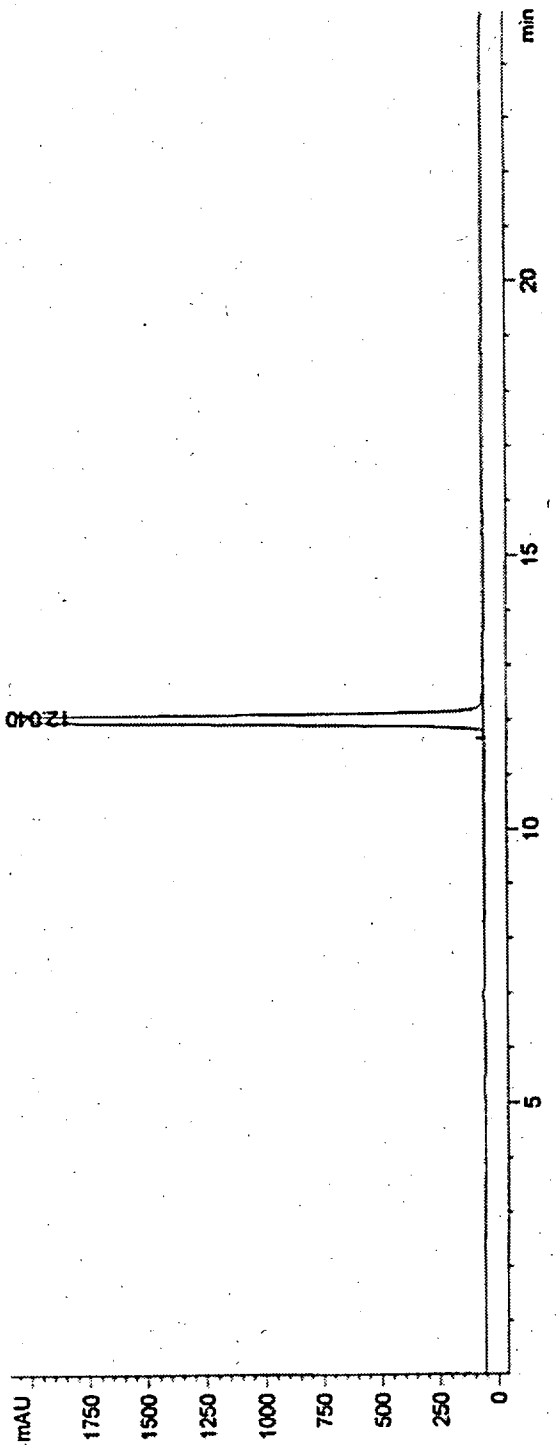
12.040
min
20
15
10
5
0
mAU
1750
1500
1250
1000
750
500
250
0

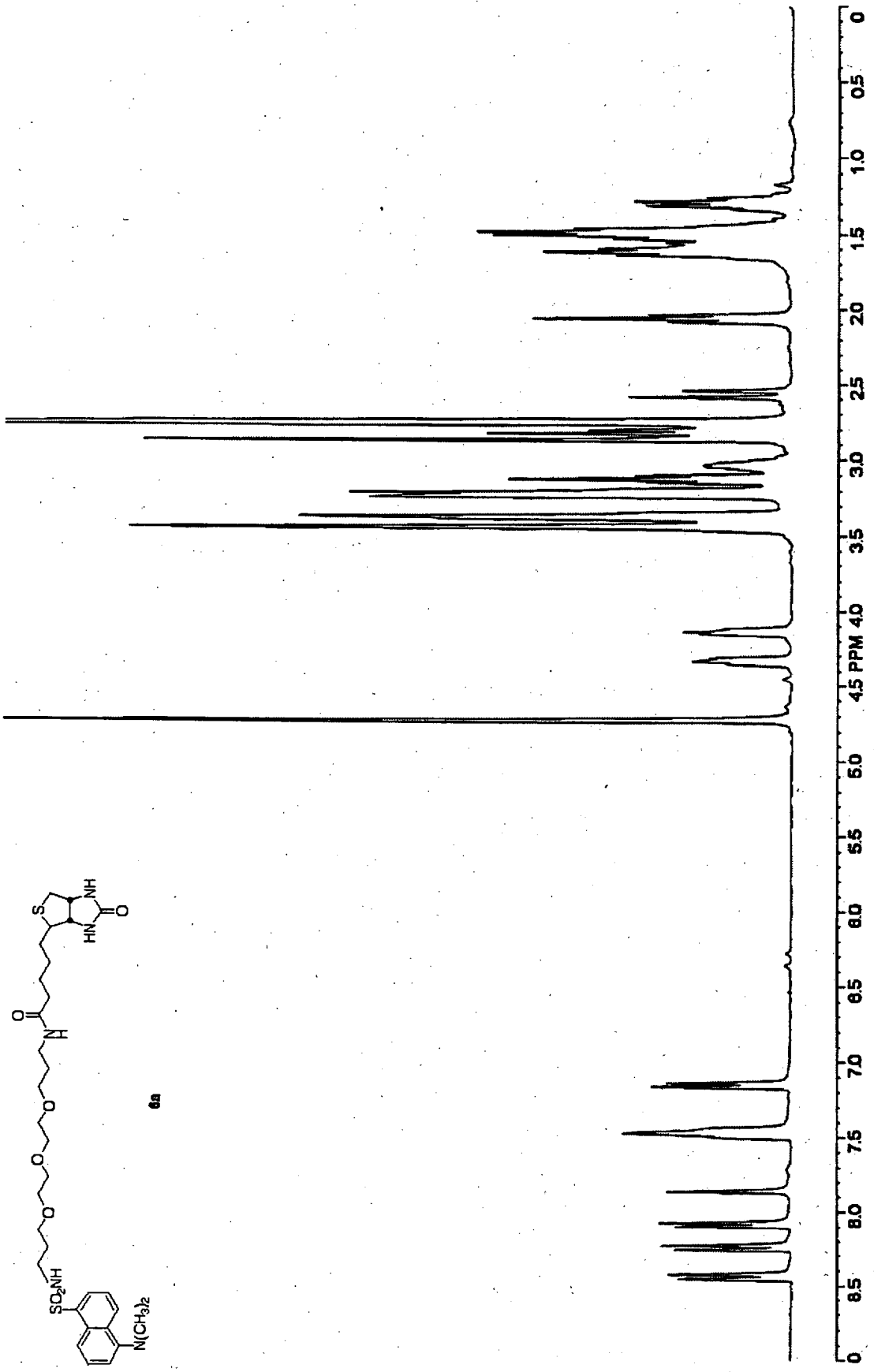
S
NH
HN
O
O
N
H
O
O
O
O
SO2NH
N(CH3)2
6a
0
0.5
1.0
1.5
2.0
2.5
3.0
3.5
4.0
4.5 PPM
5.0
5.5
6.0
6.5
7.0
7.5
8.0
8.5
0

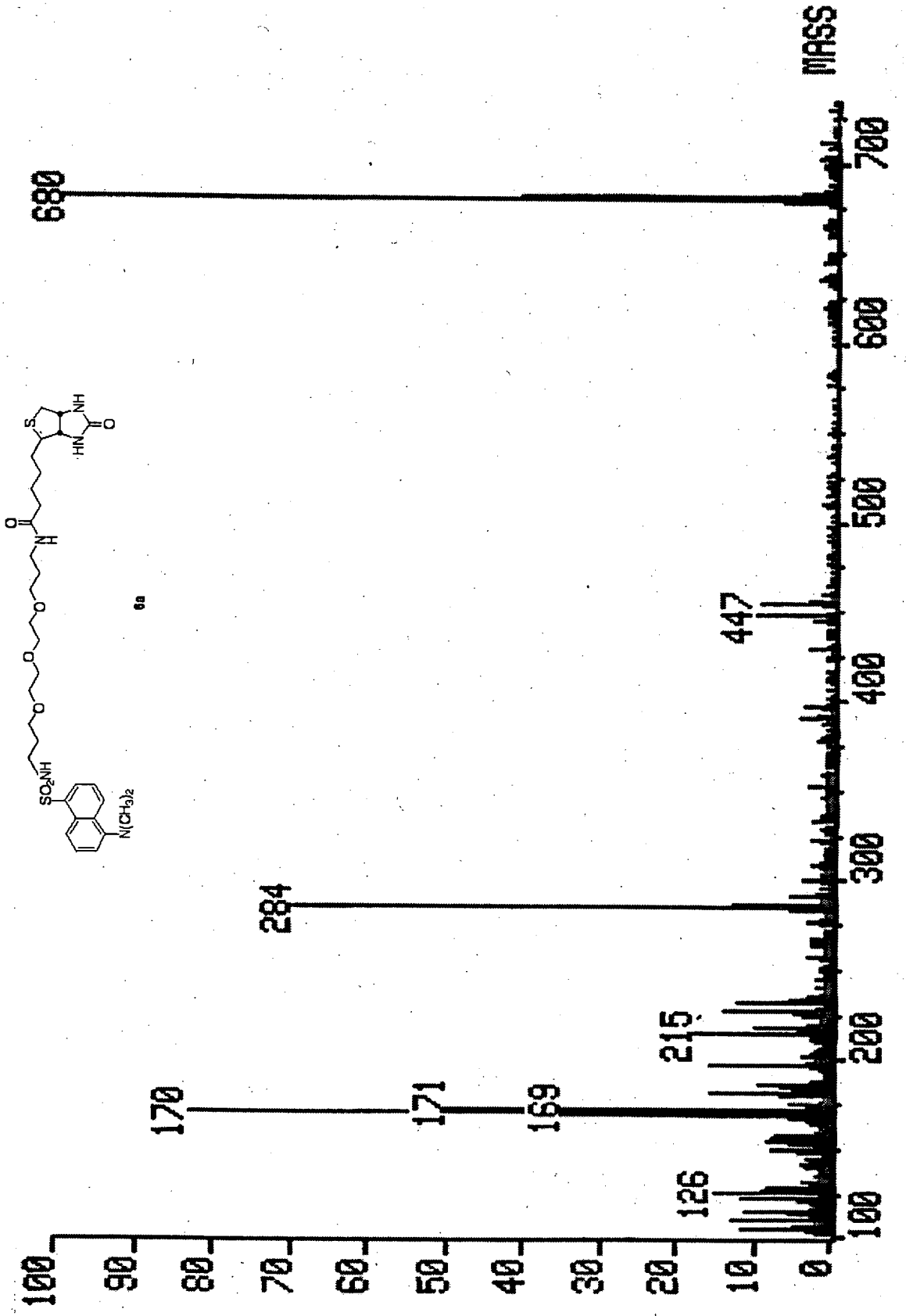
MASS
100
90
80
70
60
50
40
30
20
10
0
100
126
169
170
171
200
215
284
300
400
447
500
600
680
700
6a

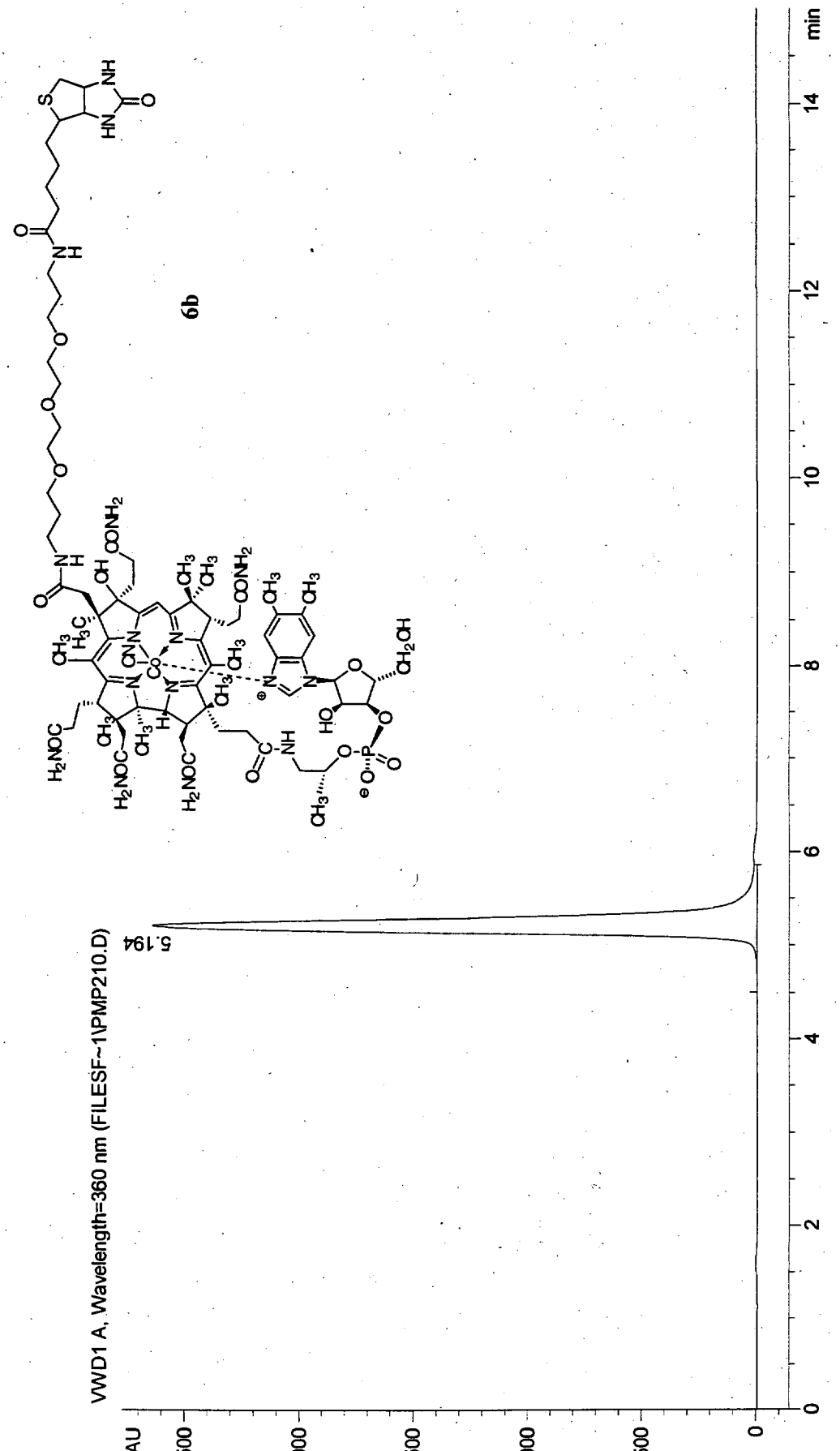
6b
VWD1 A, Wavelength=360 nm (FILESF~1\PMP210.D)
5.194
mAU
2500
2000
1500
1000
500
0
0
2
4
6
8
10
12
14
min

© 2000 American Chemical Society, Bioconjugate Chem., Wilbur bc0000031 Supporting Info Page 8

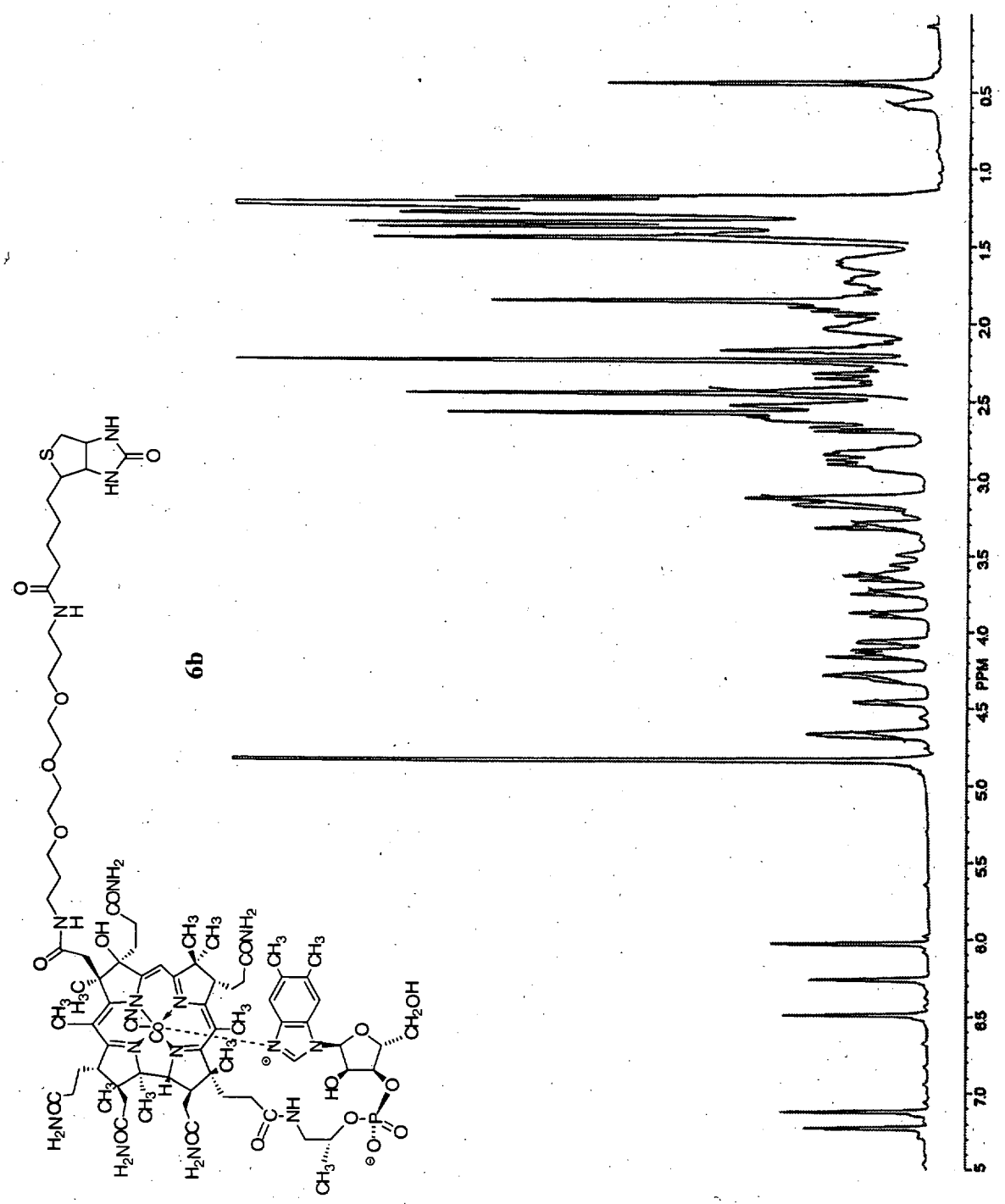

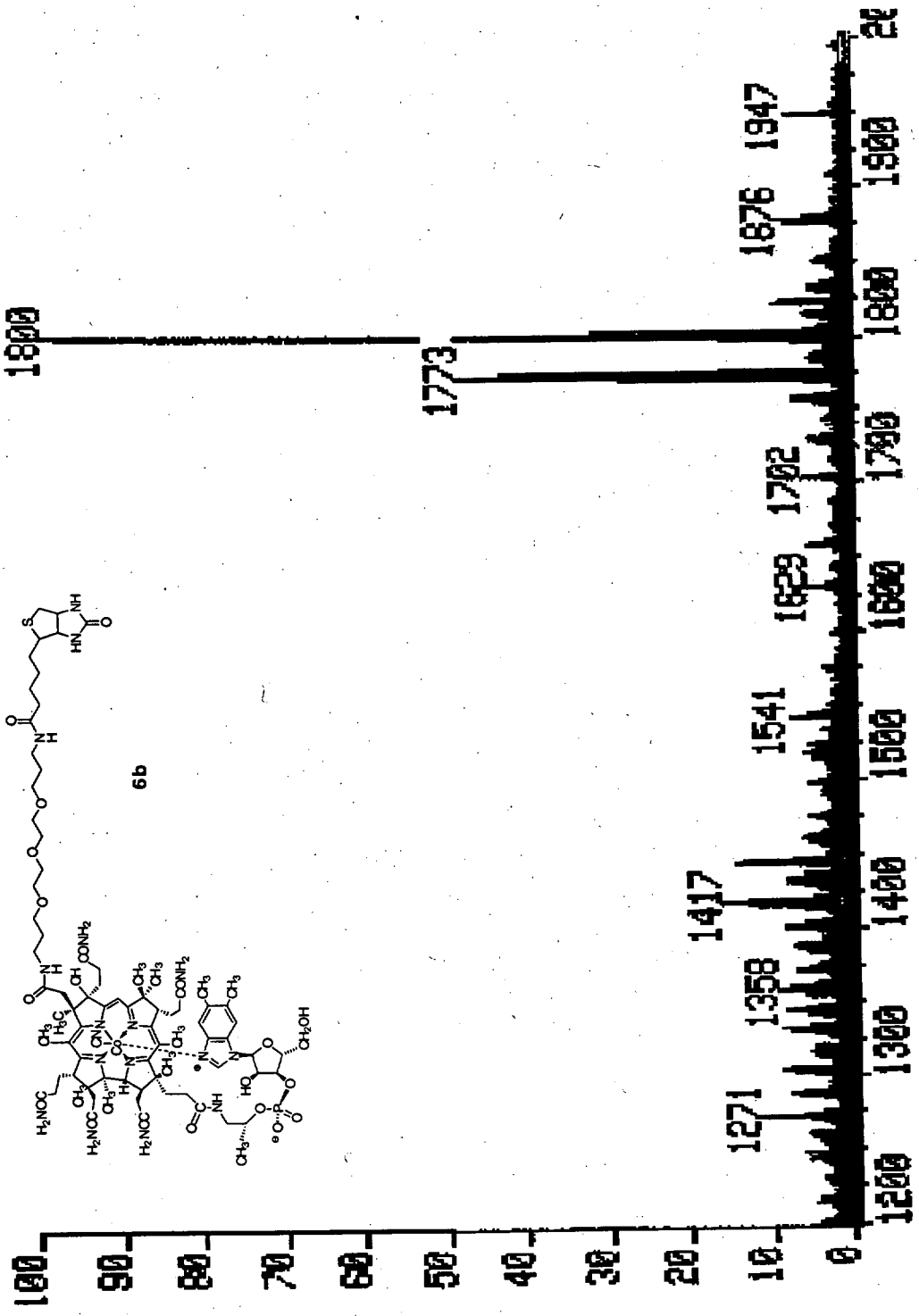
6b
1800
1773
1876
1947
1702
1623
1541
1417
1358
1271
100
90
80
70
60
50
40
30
20
10
0
1200
1300
1400
1500
1600
1700
1800
1900

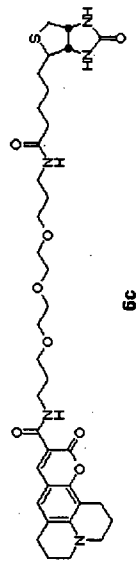

6c

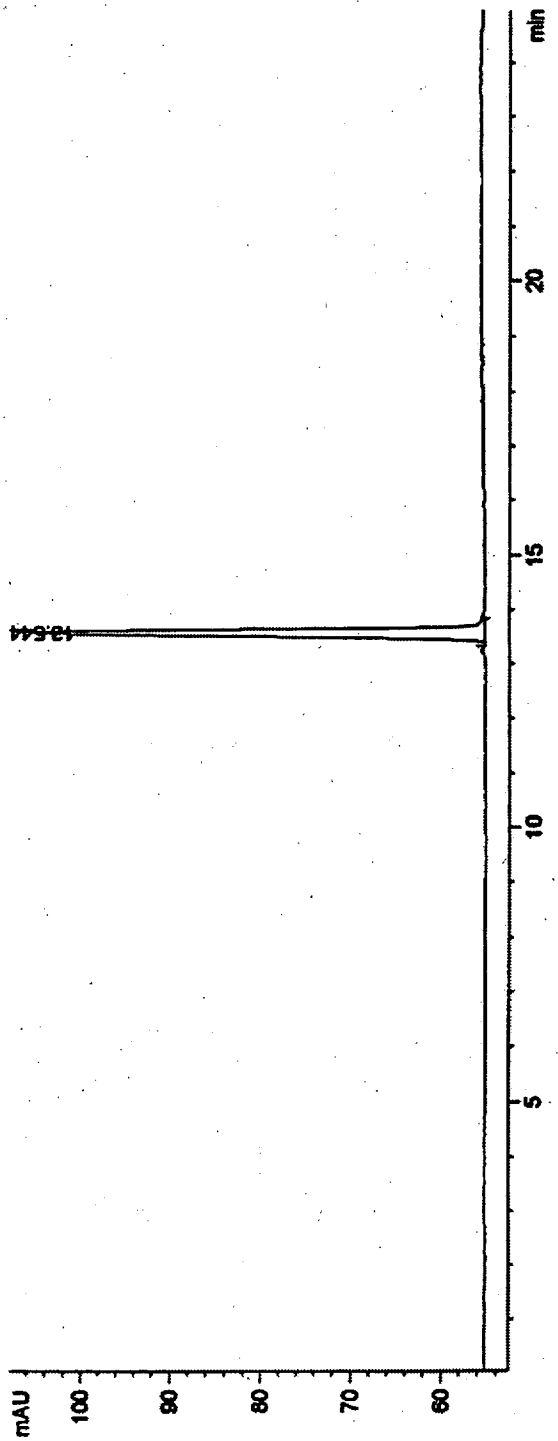

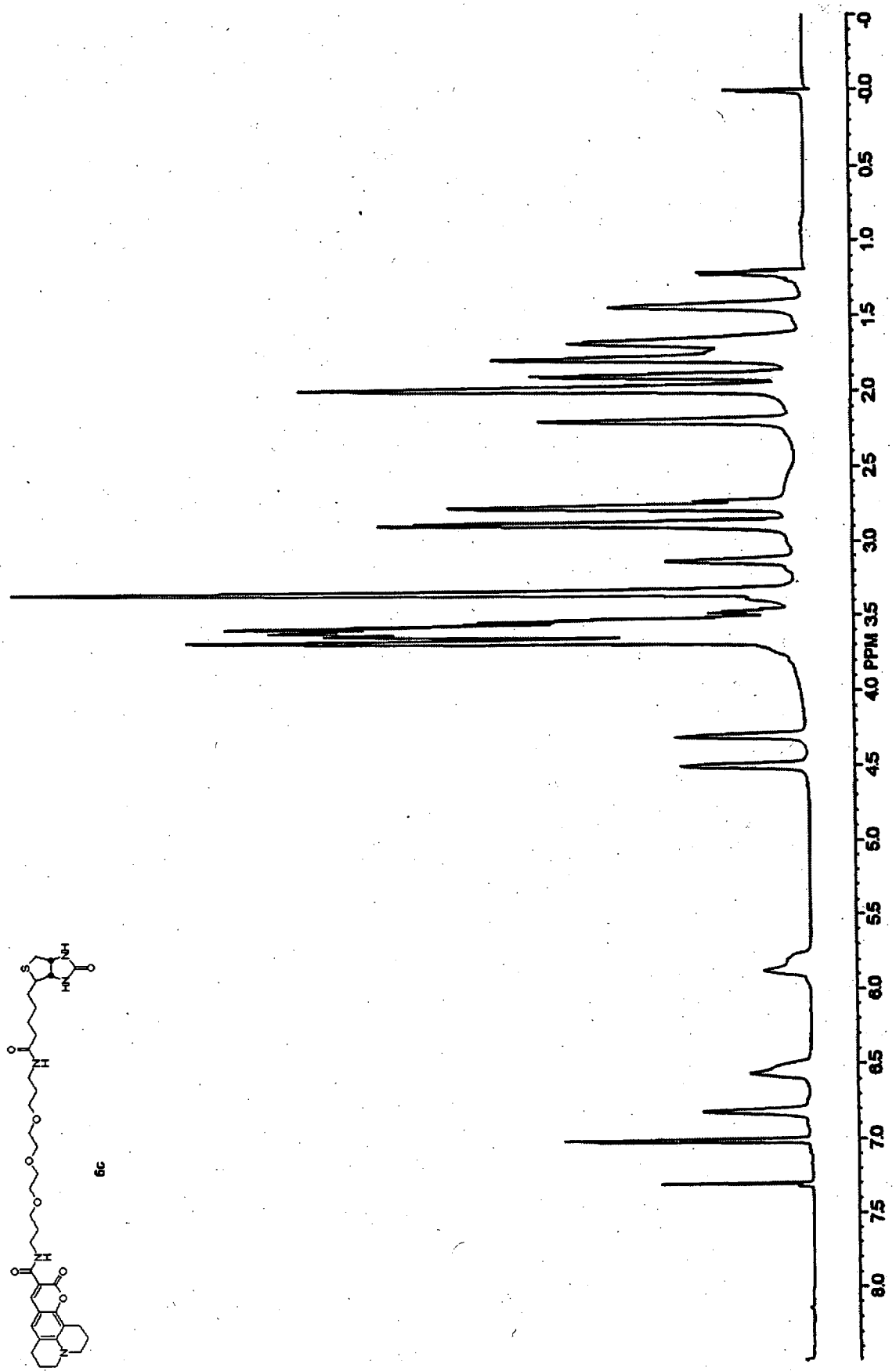
6c
-0
-0.0
0.5
1.0
1.5
2.0
2.5
3.0
3.5
4.0 PPM
4.5
5.0
5.5
6.0
6.5
7.0
7.5
8.0

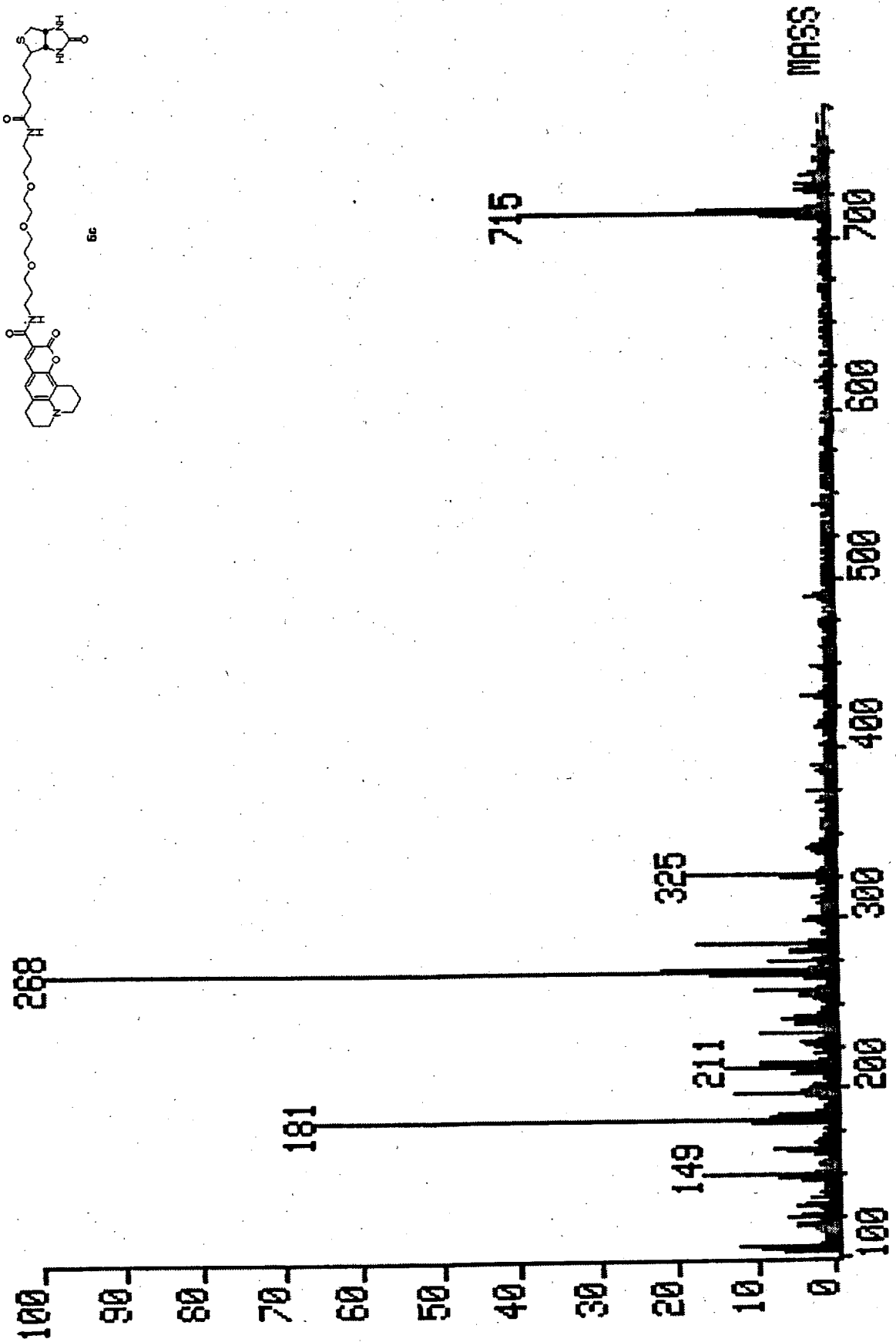
6c
MASS
715
325
268
211
181
149
100
700
600
500
400
300
200
100
90
80
70
60
50
40
30
20
10
0

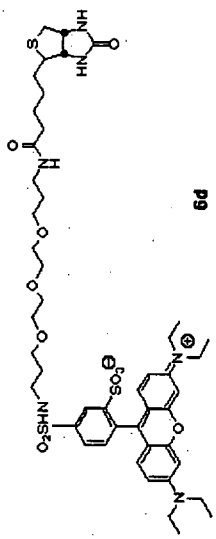

6d

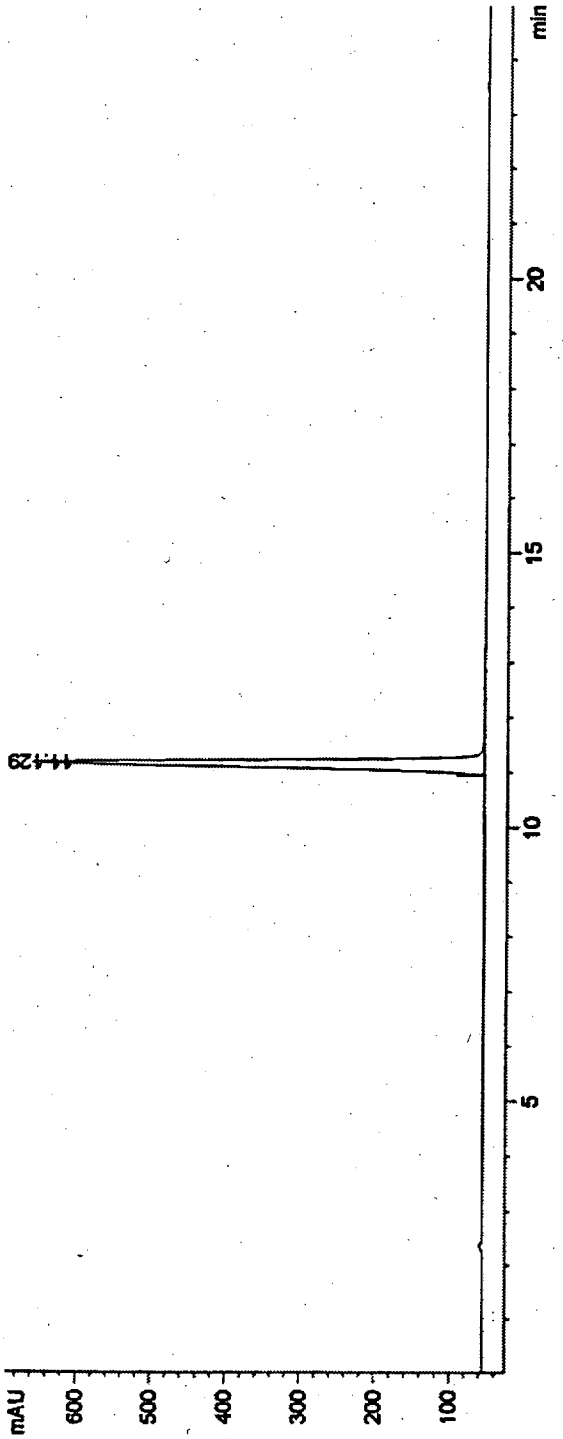

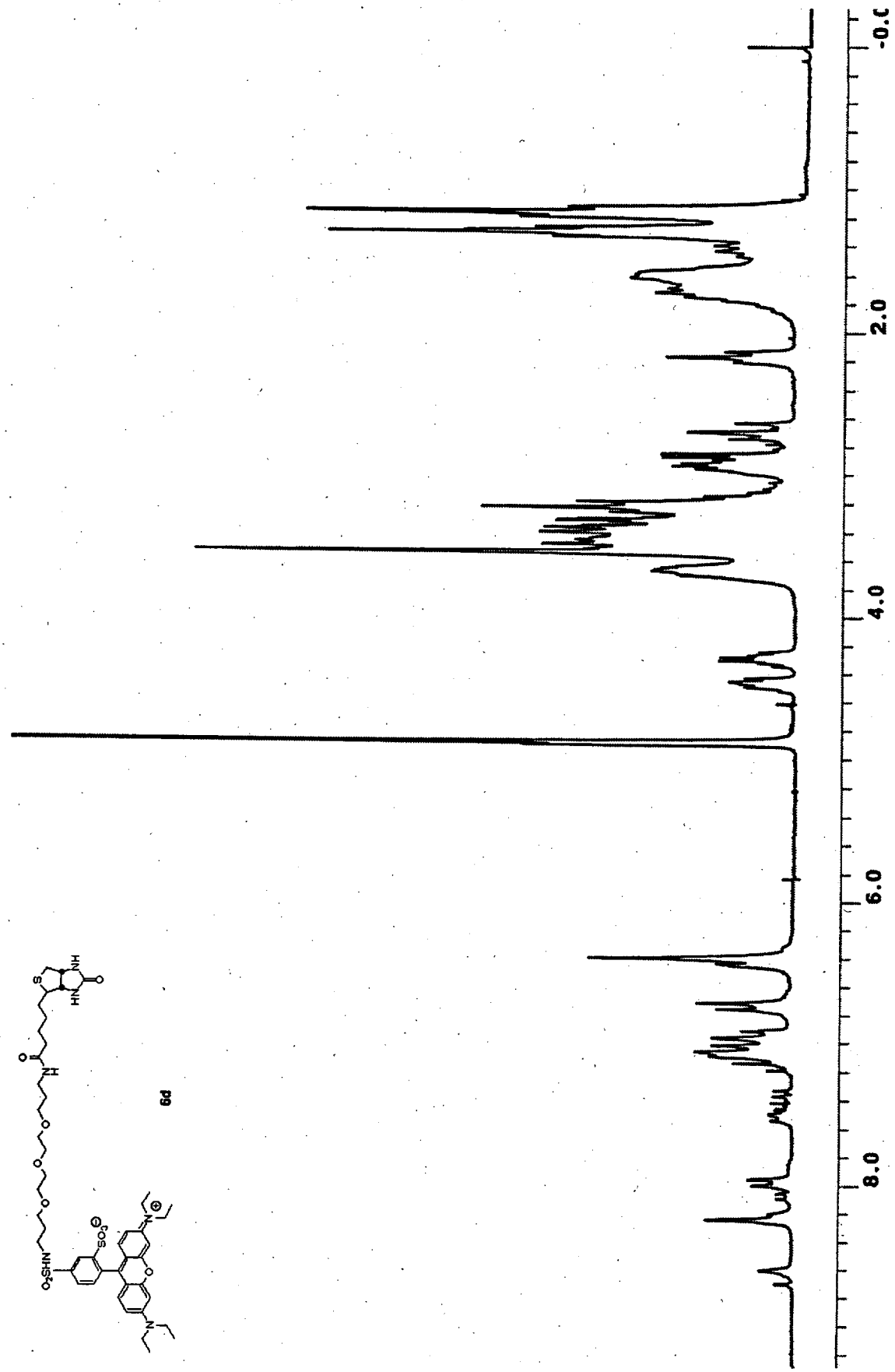
6d
8.0
6.0
4.0
2.0

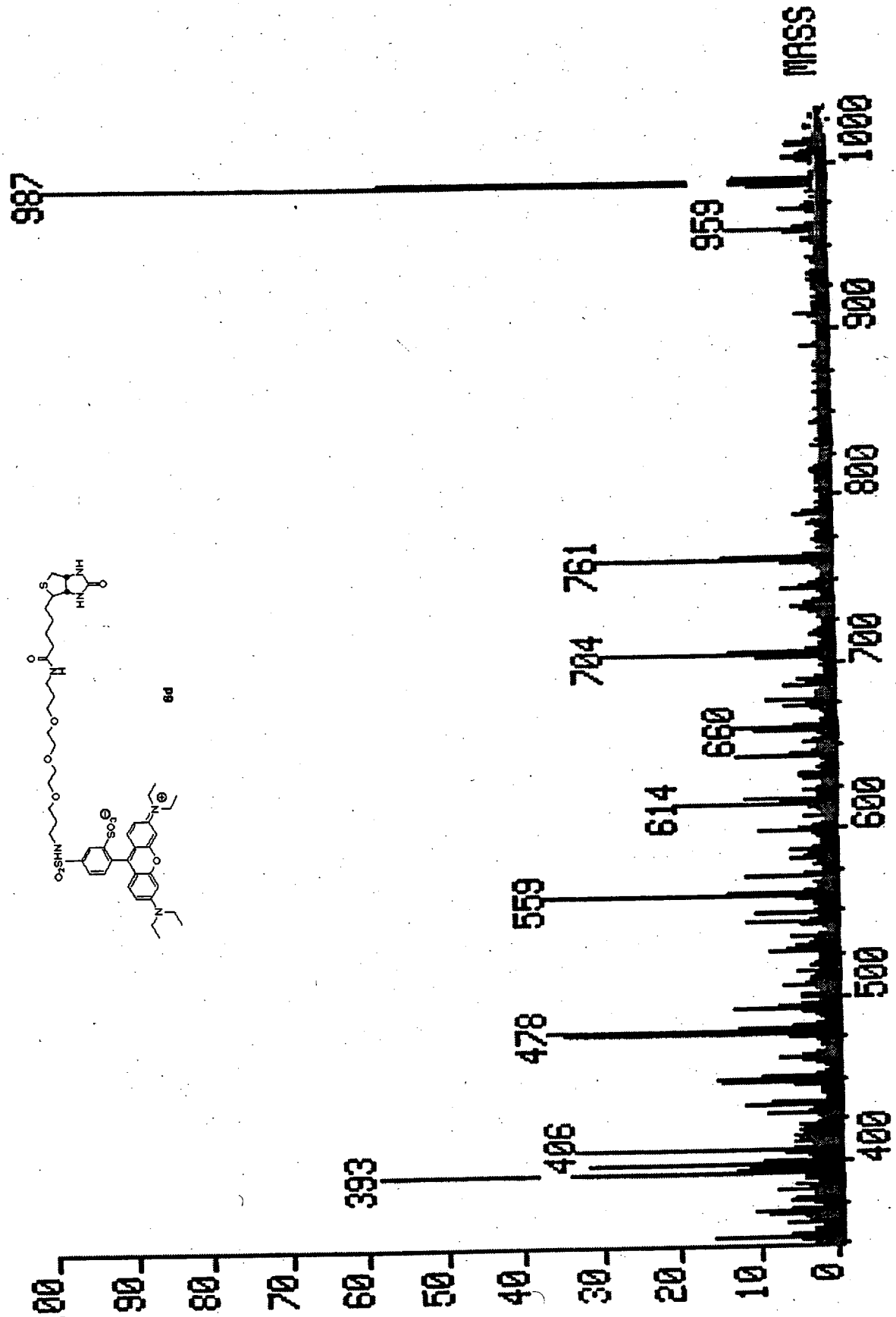
MASS
100
90
80
70
60
50
40
30
20
10
0
400
500
600
700
800
900
1000
393
406
478
559
614
660
704
761
959
987

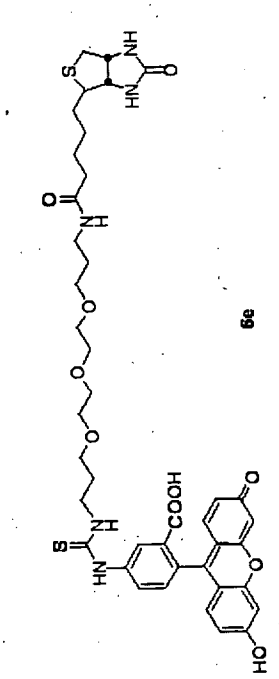
6e

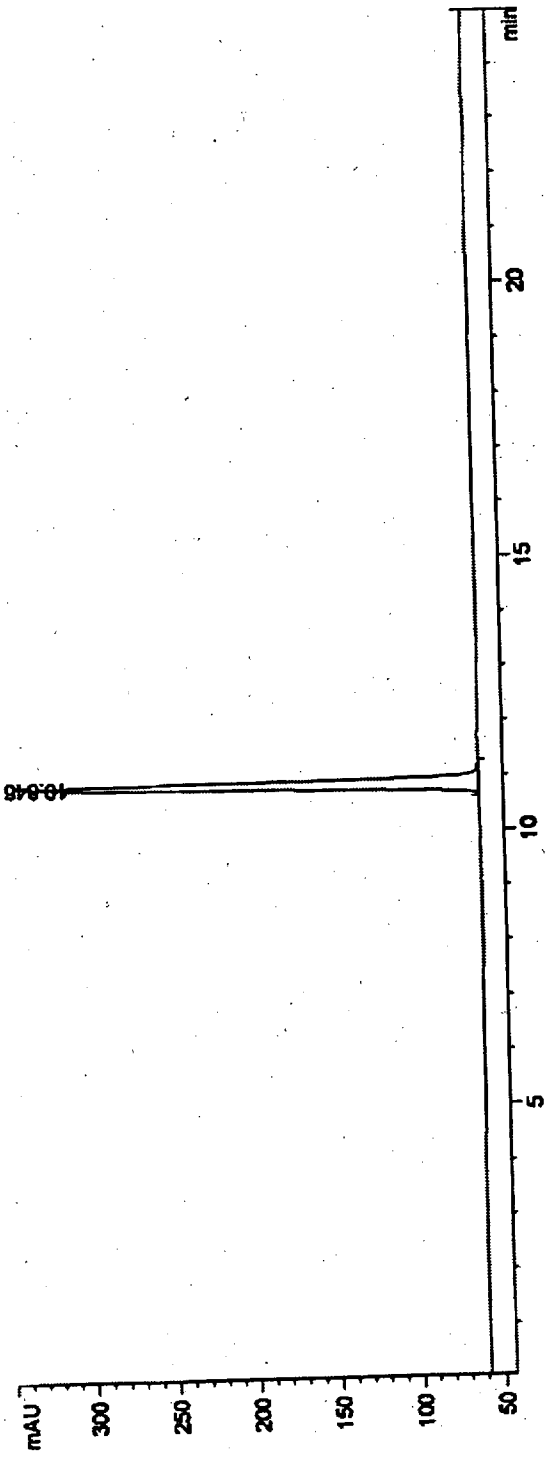
10.646
min
5
10
15
20
mAU
50
100
150
200
250
300

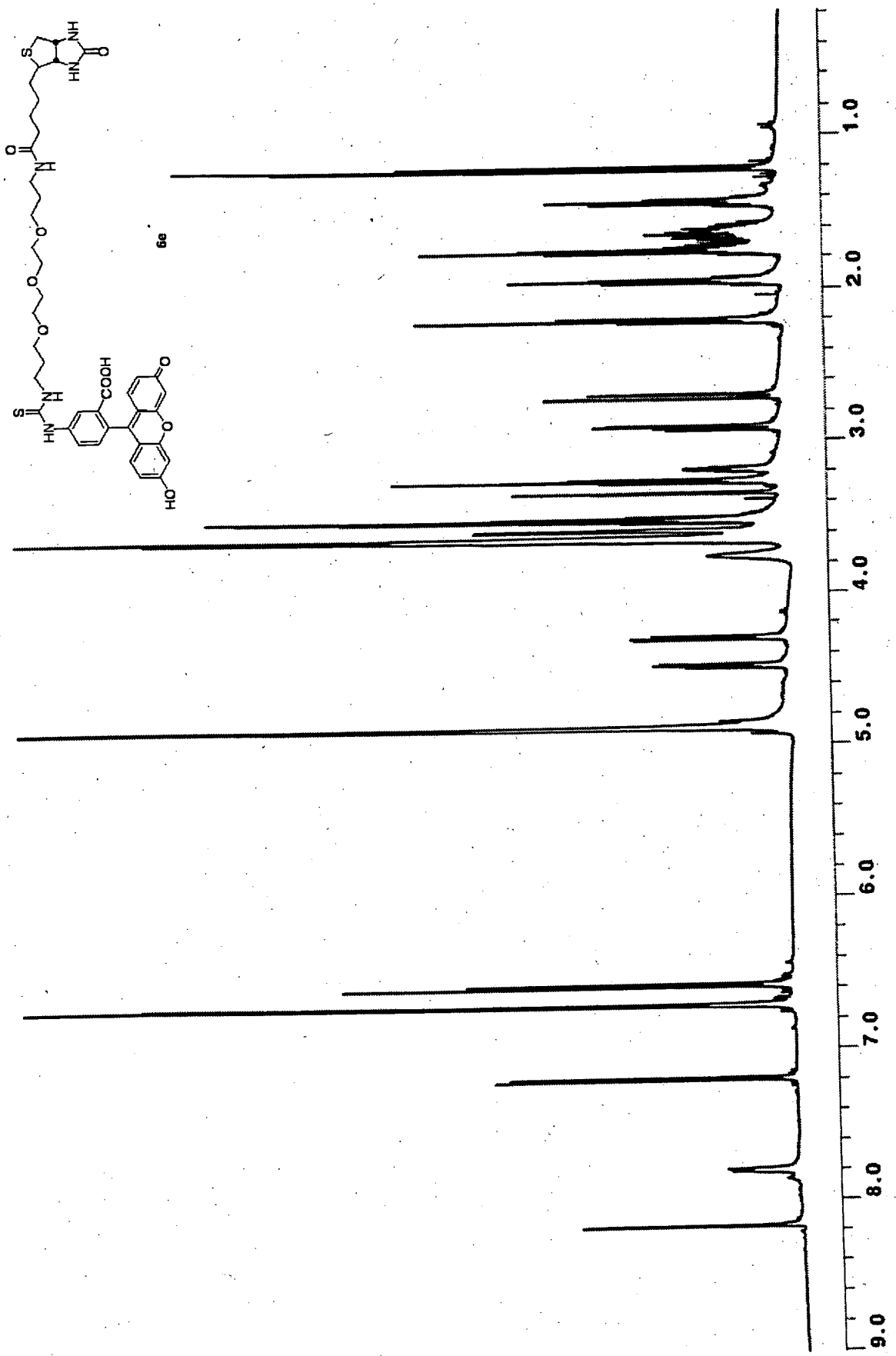
6e
1.0
2.0
3.0
4.0
5.0
6.0
7.0
8.0
9.0

© 2000 American Chemical Society, Bioconjugate Chem., Wilbur bc0000031 Supporting Info Page 18

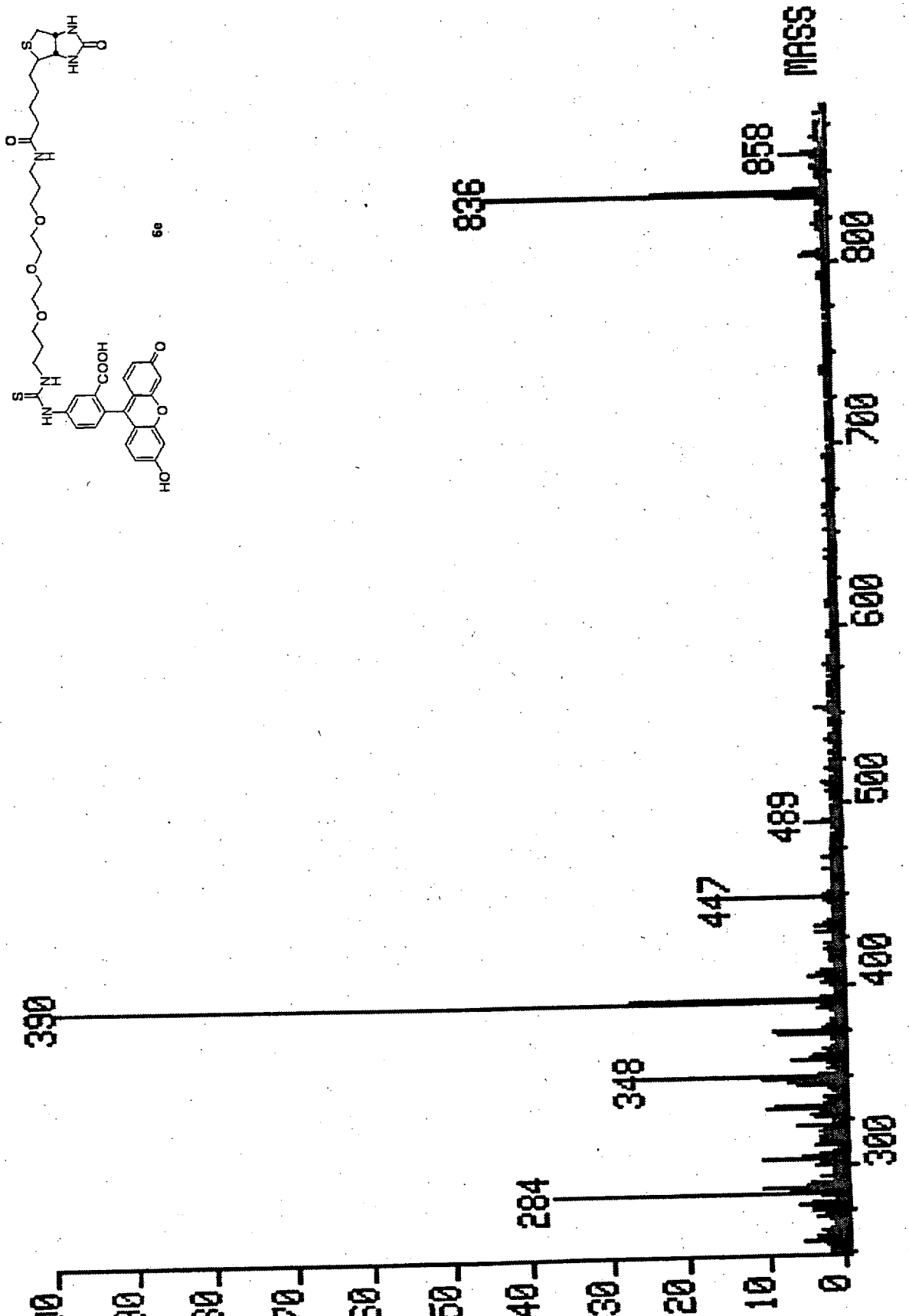

© 2000 American Chemical Society, Bioconjugate Chem., Wilbur bc0000031 Supporting Info Page 19

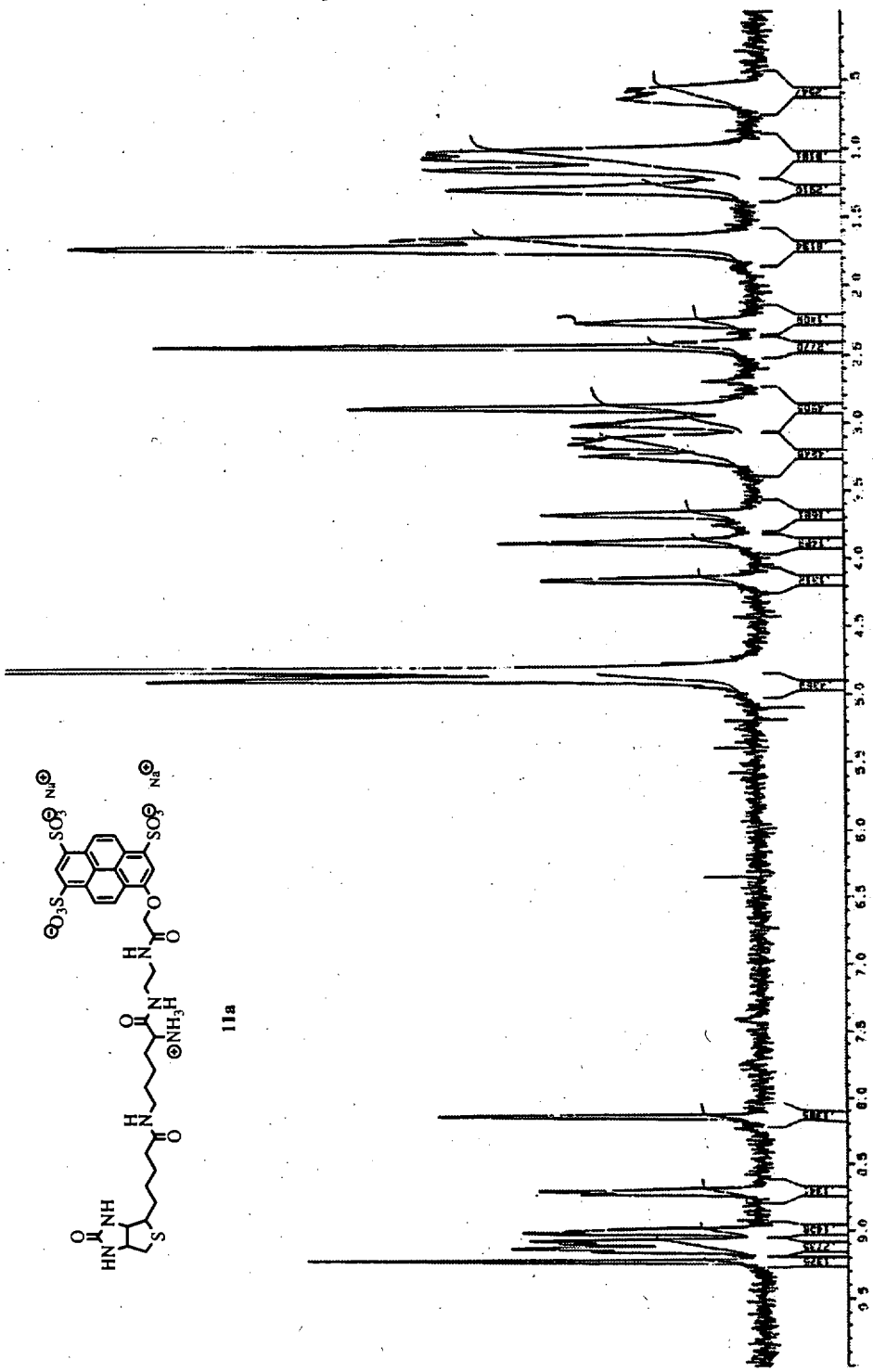

11a

© 2000 American Chemical Society, Bioconjugate Chem., Wilbur bc0000031 Supporting Info Page 20

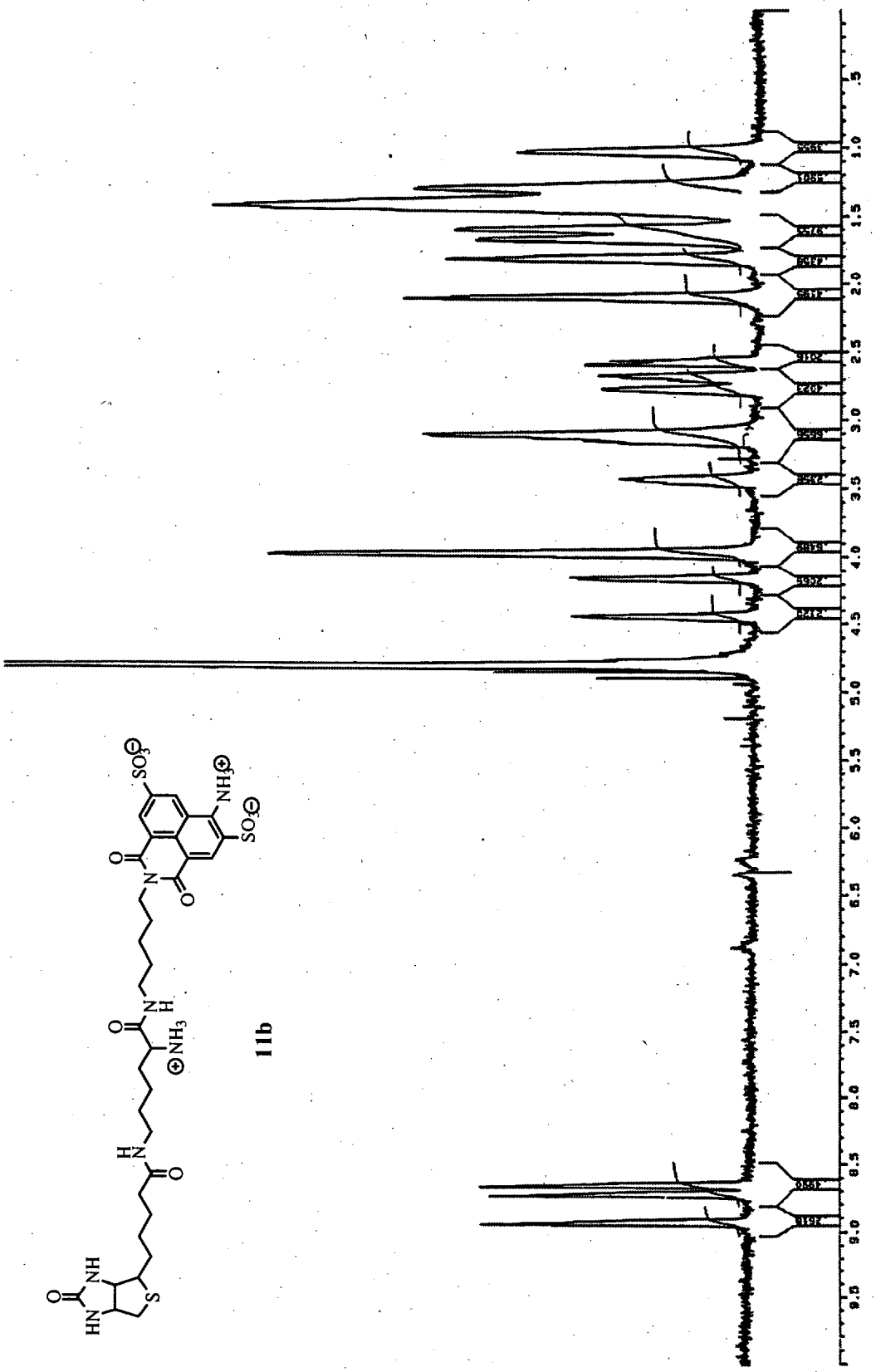

11b

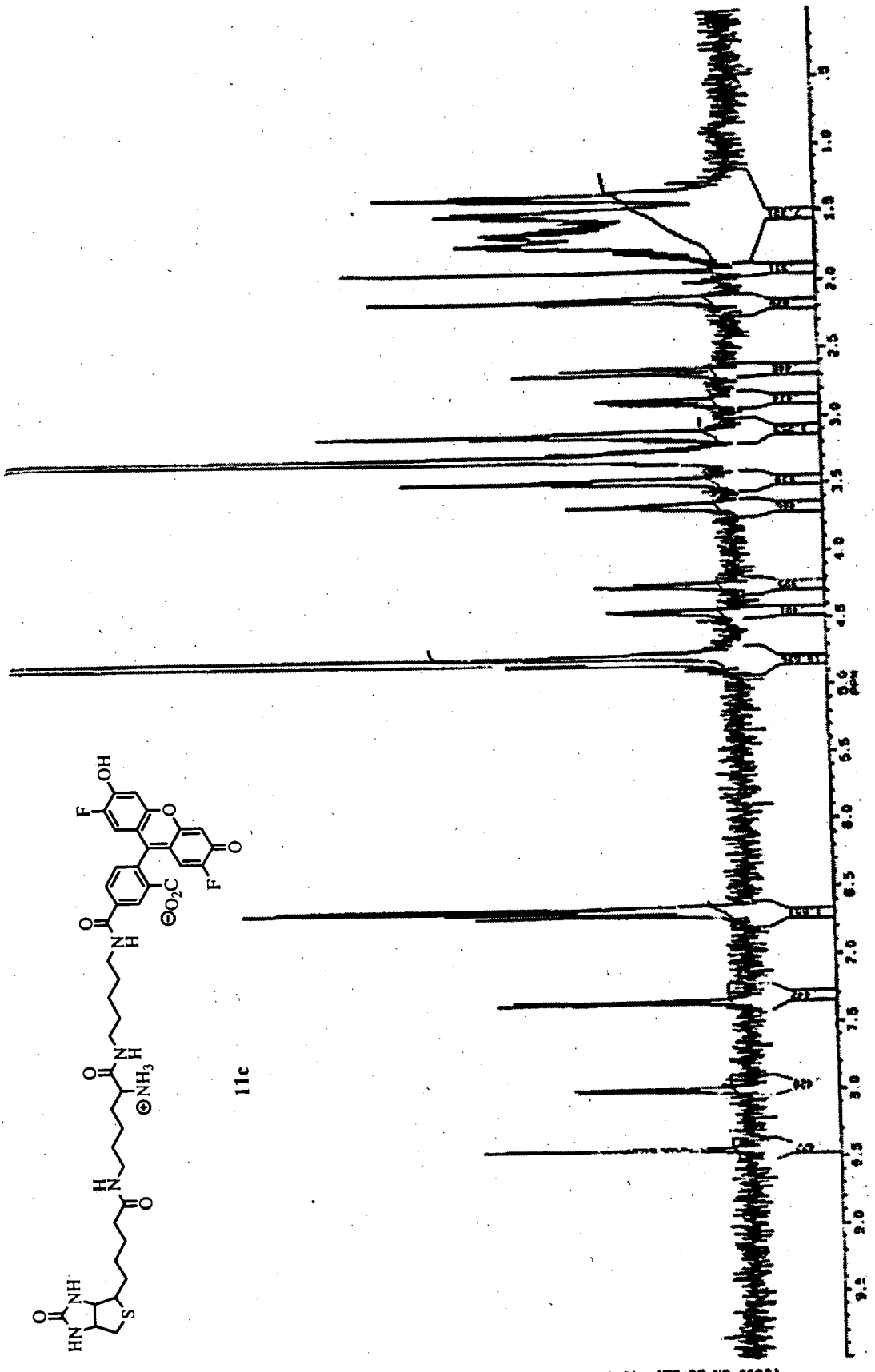
11c
07/23/98 TUE 08:51 [TX/RX NO 6892]

© 2000 American Chemical Society, Bioconjugate Chem., Wilbur bc0000031 Supporting Info Page 22

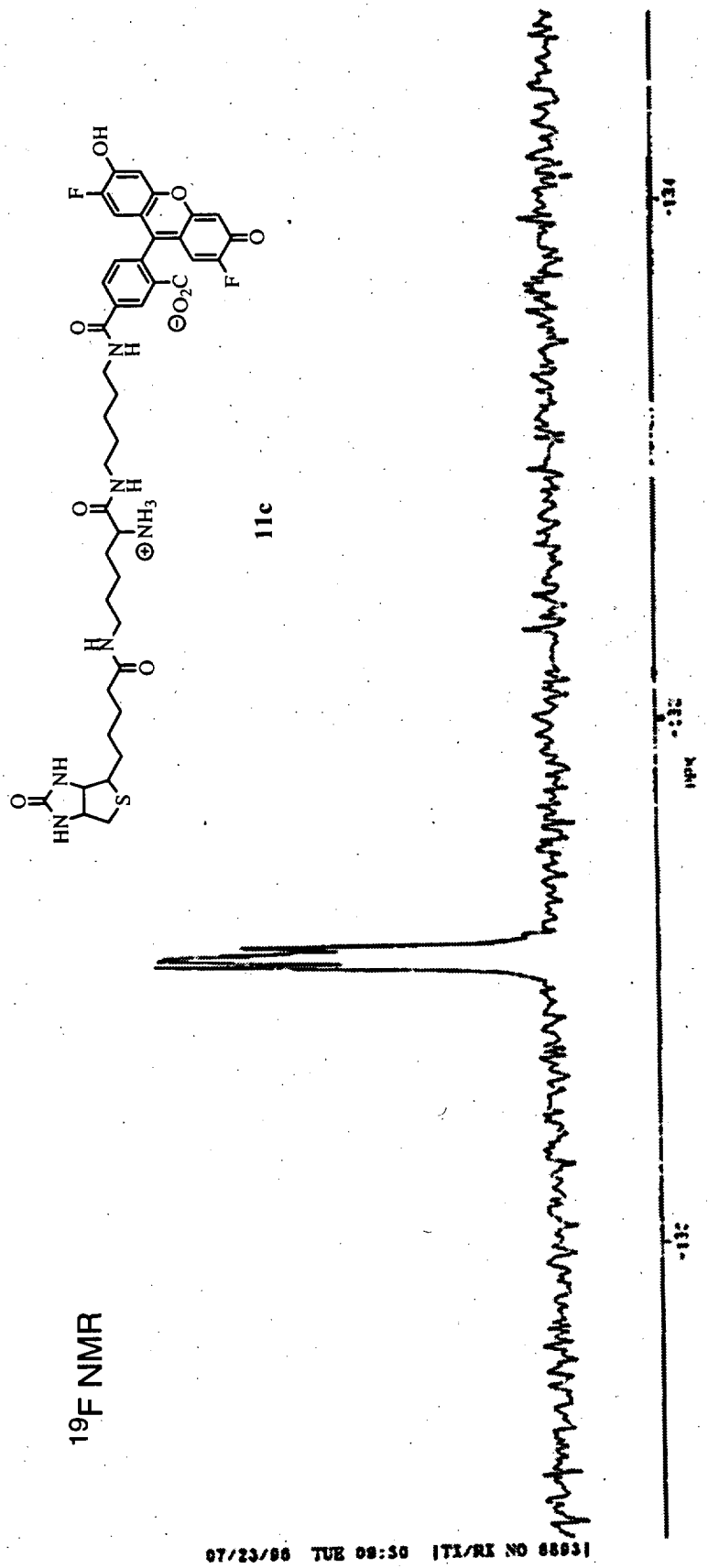

© 2000 American Chemical Society, Bioconjugate Chem., Wilbur bc0000031 Supporting Info Page 23

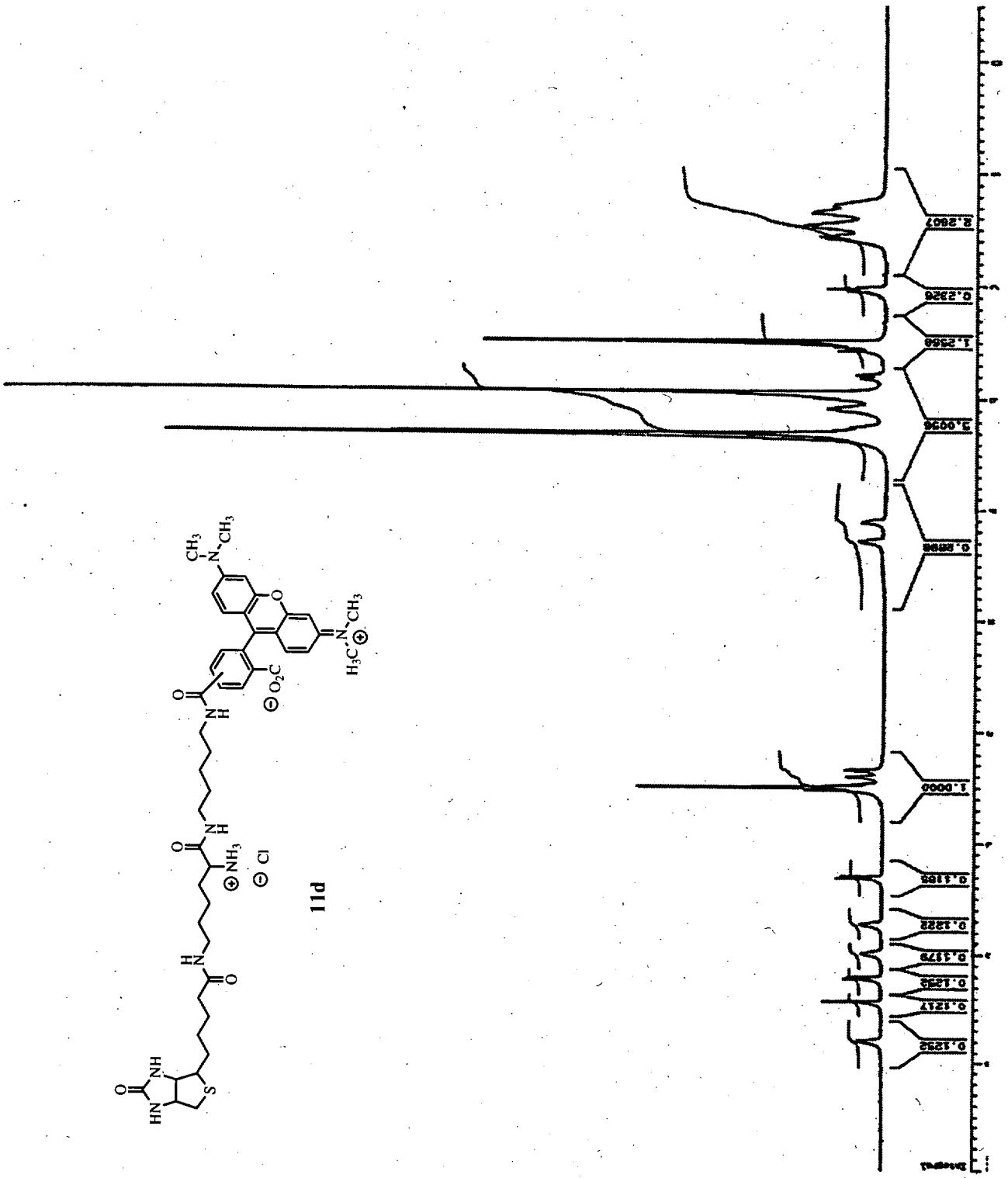

11d

© 2000 American Chemical Society, Bioconjugate Chem., Wilbur bc0000031 Supporting Info Page 24

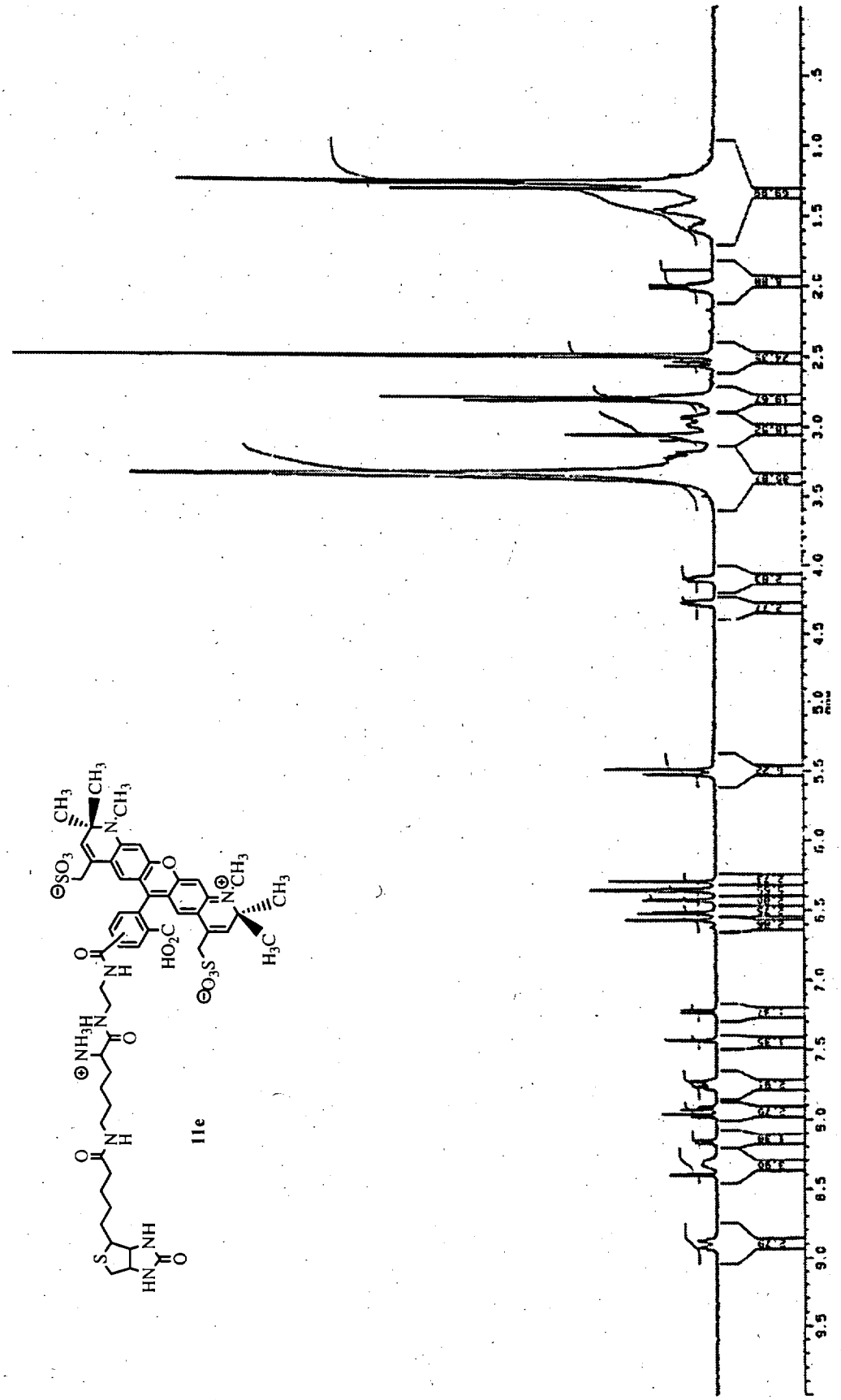

11e

© 2000 American Chemical Society, Bioconjugate Chem., Wilbur bc0000031 Supporting Info Page 25

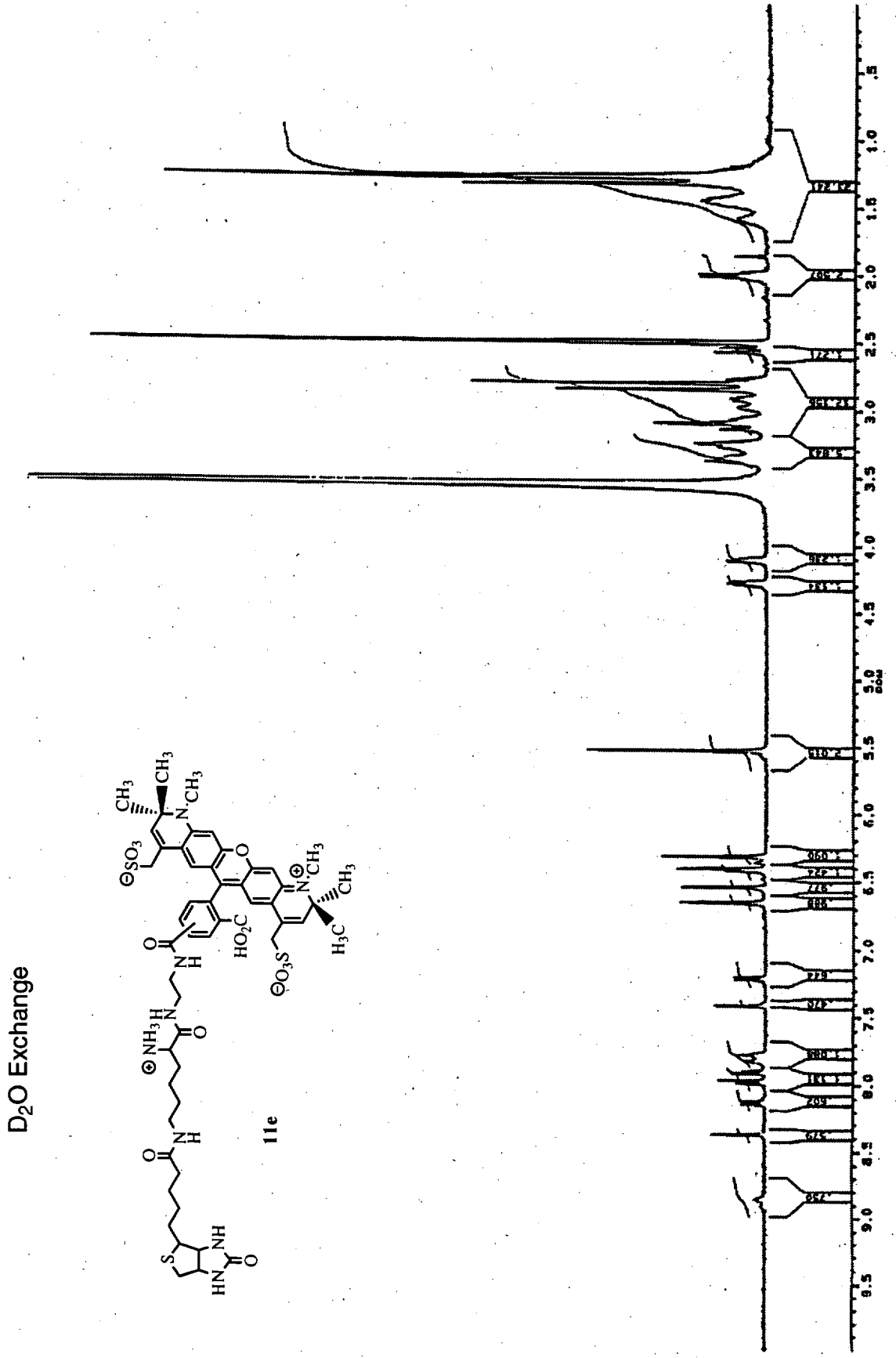

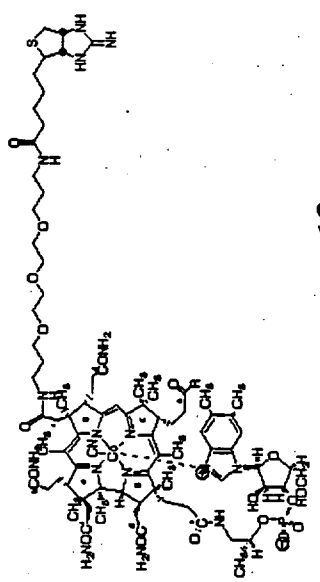

13a

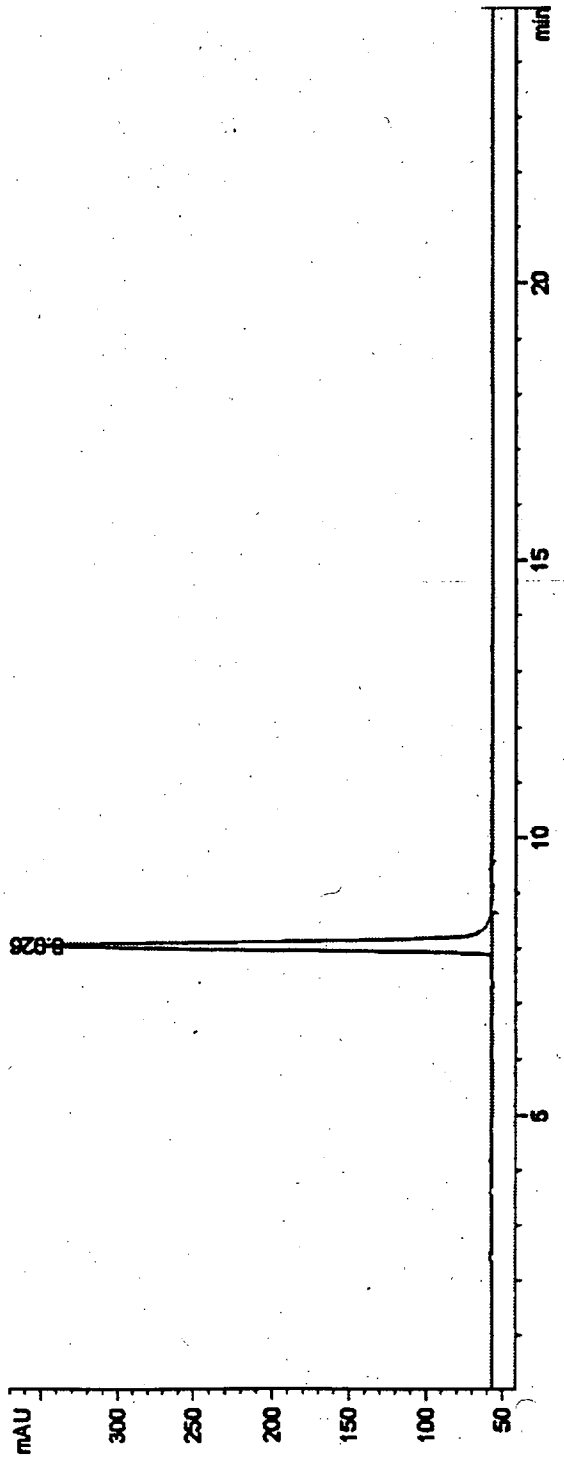

© 2000 American Chemical Society, Bioconjugate Chem., Wilbur bc0000031 Supporting Info Page 27

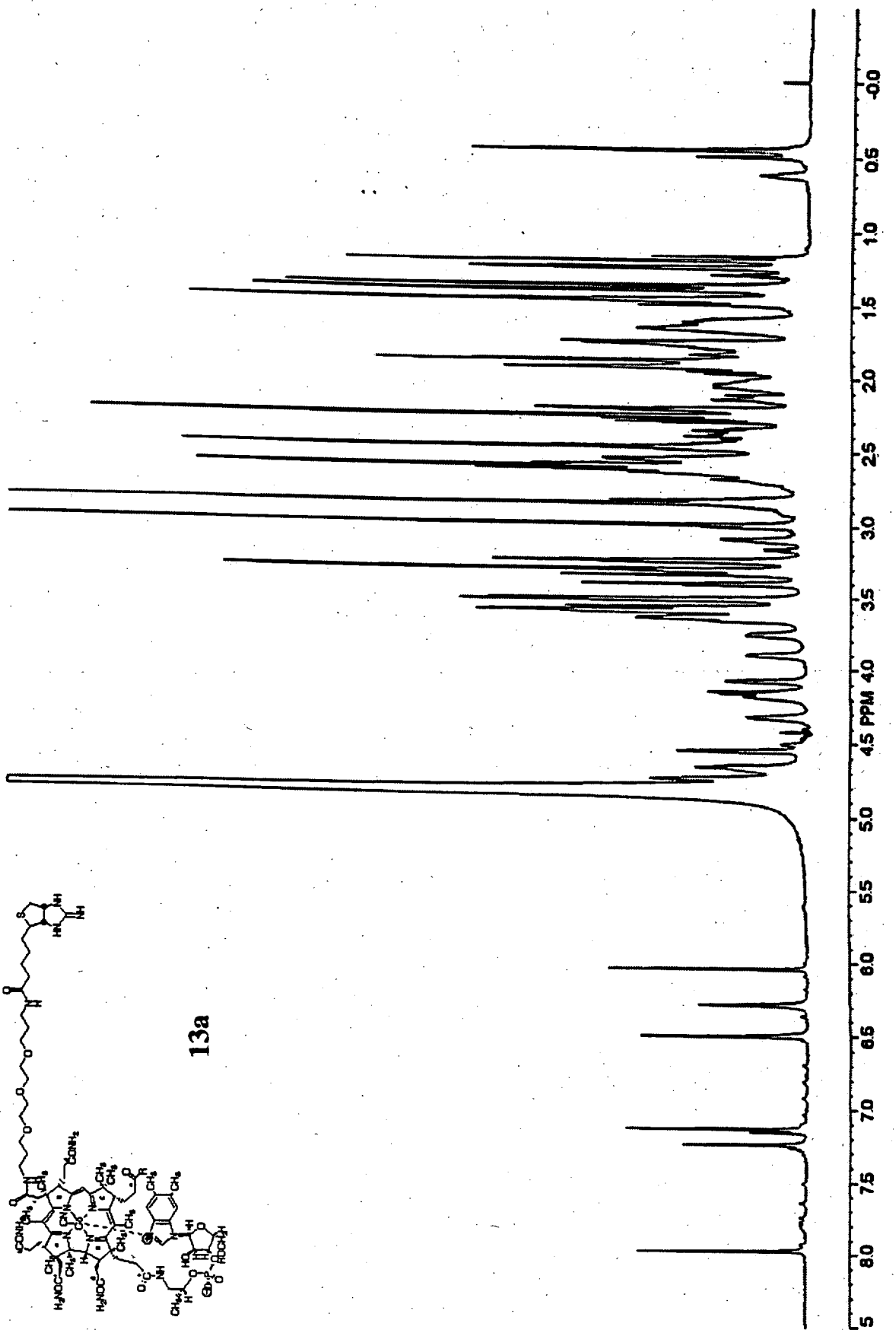

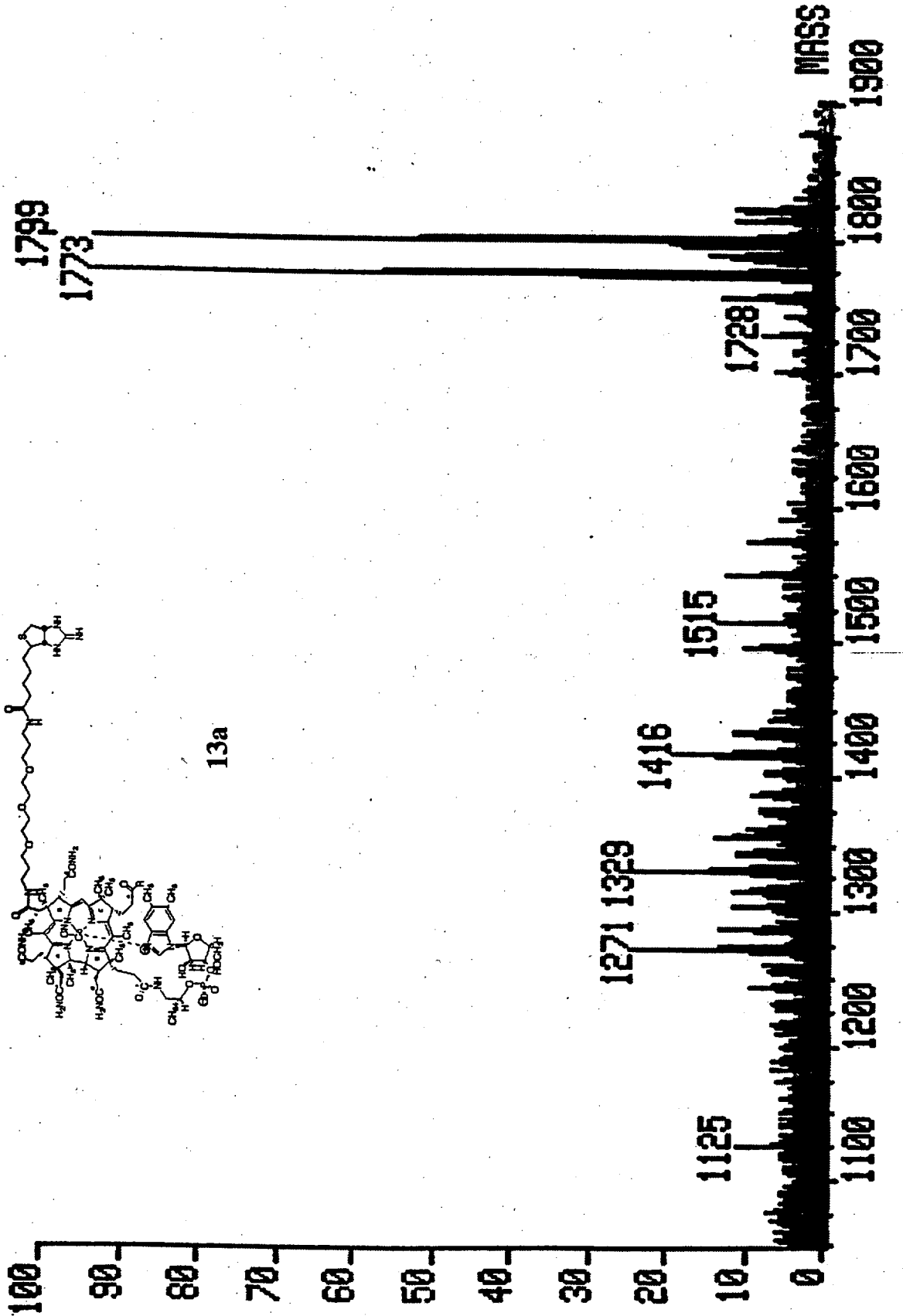
13a
MASS
1799
1773
1728
1515
1416
1329
1271
1125
100
90
80
70
60
50
40
30
20
10
0
1100
1200
1300
1400
1500
1600
1700
1800
1900

© 2000 American Chemical Society, Bioconjugate Chem., Wilbur bc0000031 Supporting Info Page 29

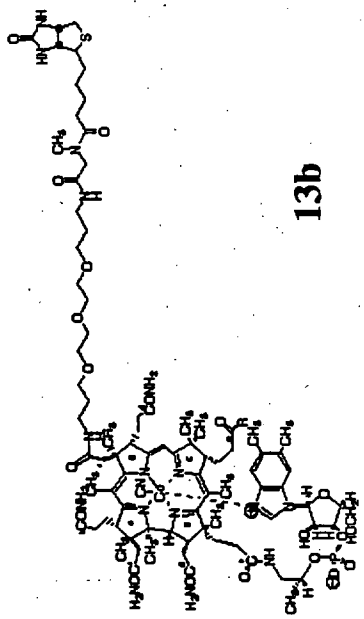

13b

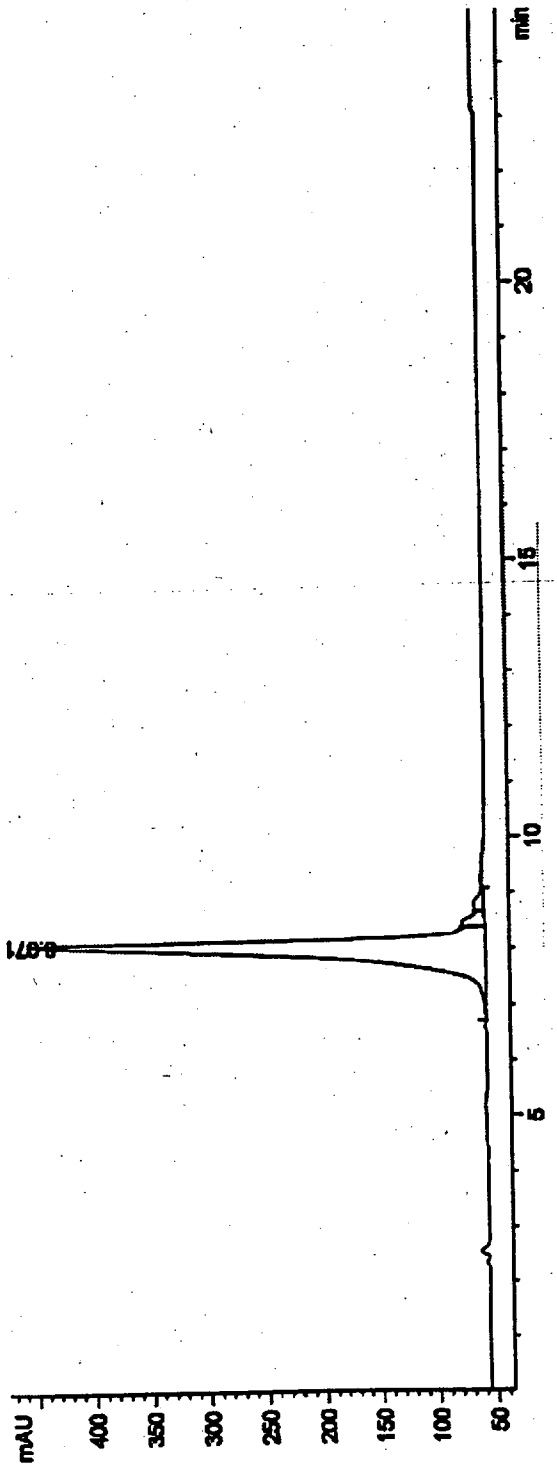

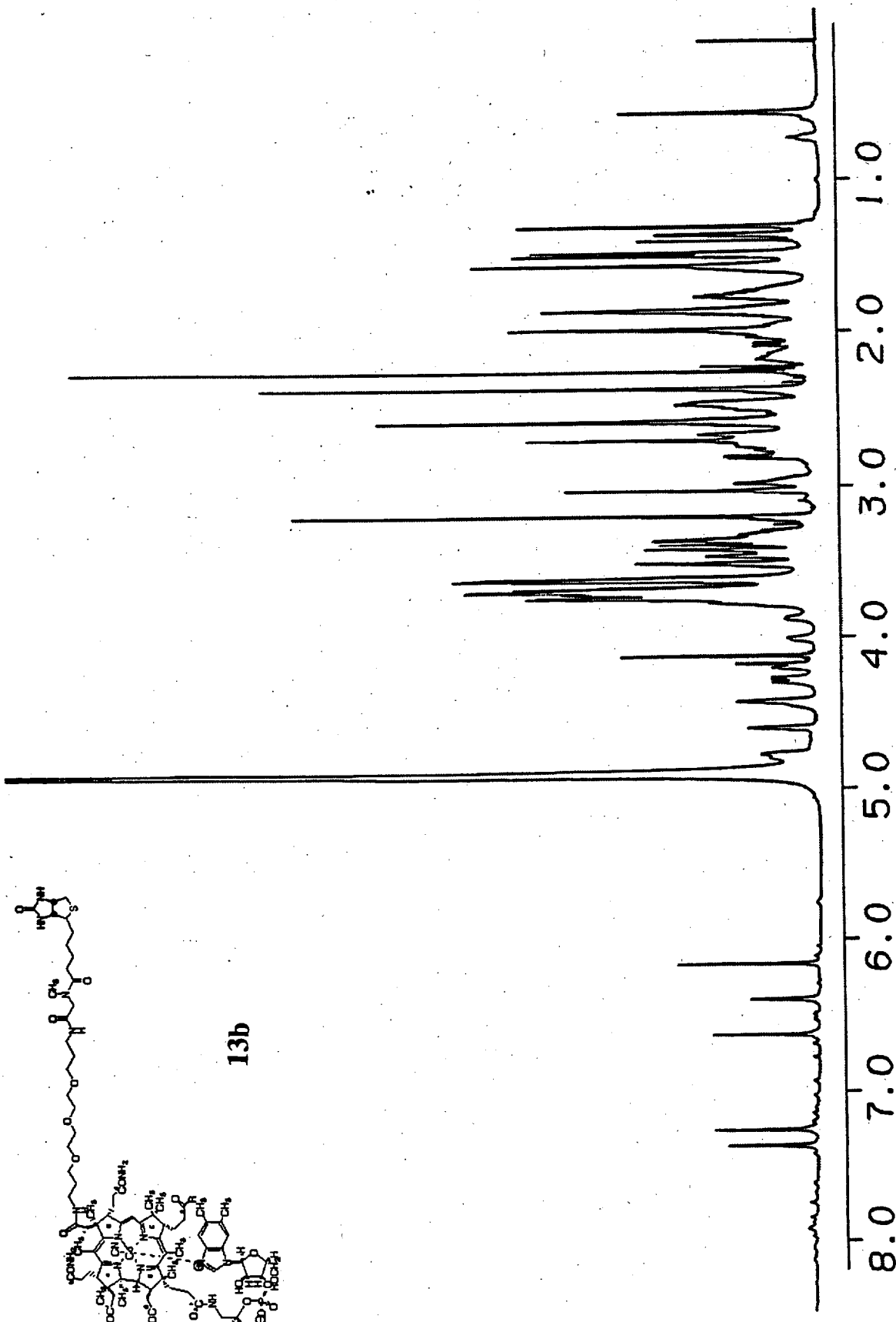
13b
8.0
7.0
6.0
5.0
4.0
3.0
2.0
1.0

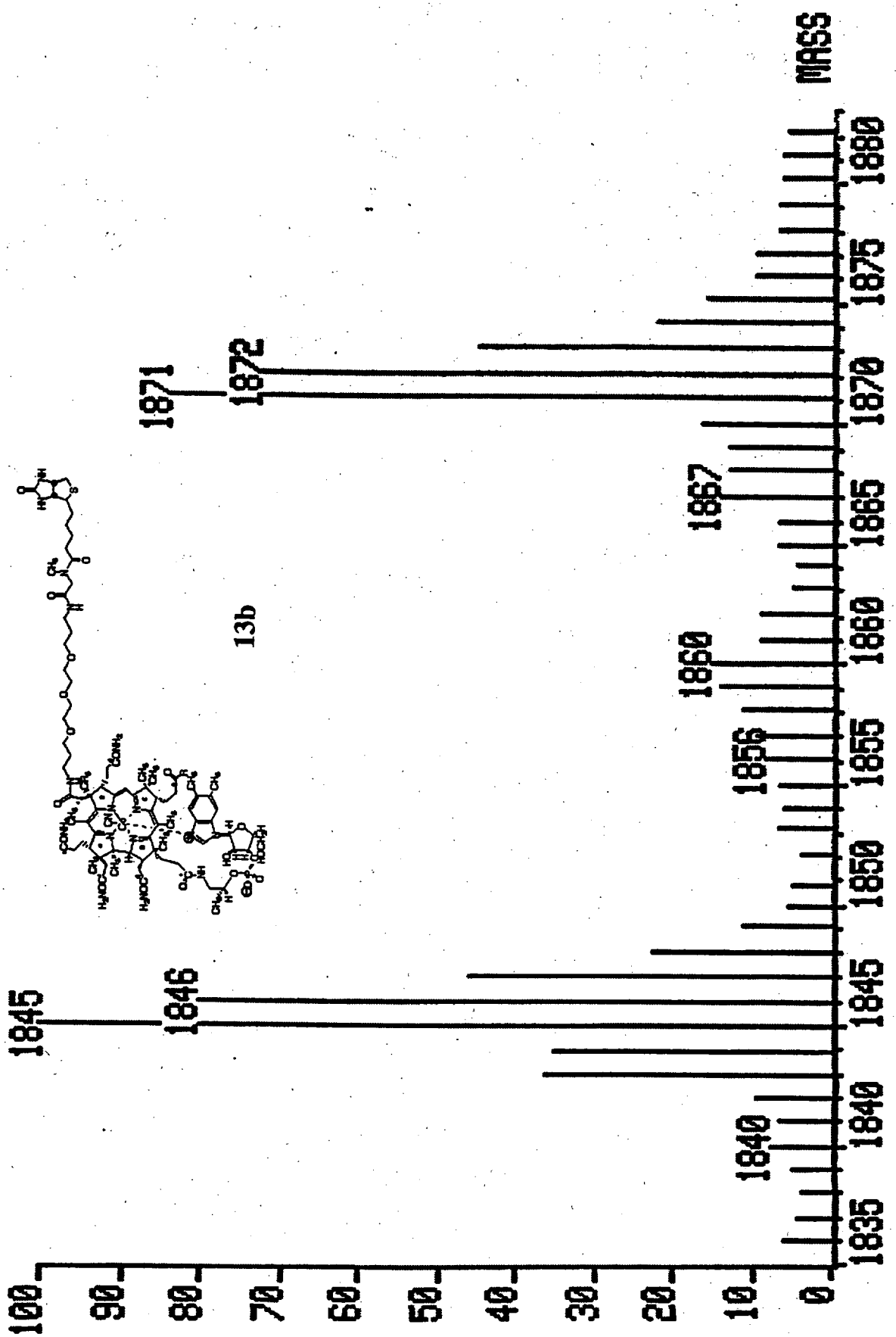
MASS
1880
1875
1870
1865
1860
1855
1850
1845
1840
1835
1871
1872
1867
1860
1856
1845
1846
1840
100
90
80
70
60
50
40
30
20
10
0
13b

Preparation of an Imidazole-Conjugated Oligonucleotide

Marc Beban and Paul S. Miller*

Department of Biochemistry and Molecular Biology, School of Public Health Johns Hopkins University, 615 North Wolfe Street, Baltimore, Maryland 21205. Received January 22, 2000; Revised Manuscript Received March 31, 2000

Postsynthetic modification of an oligonucleotide with an imidazole functional group was achieved by formation of an amide bond between the functional group and a single 2′-amino-2′-deoxyuridine, d-aU, of the oligonucleotide. The succinimidyl ester of *N*-glutaryl-histamine was synthesized under anhydrous conditions and added to the oligonucleotide in an acetonitrile-containing buffer at pH 8.0. Formation of the conjugate was assayed by digestion with snake venom phosphodiesterase and bacterial alkaline phosphatase, followed by reversed-phase HPLC to resolve constituent nucleosides. The disappearance of a peak corresponding to d-aU and the appearance of a peak that coelutes with authentic 2′-(*N*-glutaryl-*N*′-histaminyl)-2′-deoxyuridine confirmed the formation of the conjugate. Imidazole-conjugated oligonucleotides may have utility as antisense agents capable of hydrolyzing RNA.

INTRODUCTION

Oligonucleotides and their analogues can provide a scaffold of chemically reactive sites to which may be tethered a variety of functional groups. Conjugates between oligonucleotides and functional groups result in hybrid molecules that retain properties of each moiety (Goodchild, 1990). As a result, oligonucleotide-conjugates can be created that have altered biophysical properties (e.g., binding affinity, hydrophobicity, and fluorescence), chemical reactivity (e.g., radical generating or hydrolytic activity), or both (e.g., cross-linking). Some conjugates improve upon the intrinsic qualities of oligonucleotides, such as affinity for their complementary target (Asseline, et al., 1984) whereas others impart new properties such as chemical reactivity (Lee, et al., 1988; Chu and Orgel, 1985; Francois, et al., 1988).

Site-specific modifications may be introduced into oligonucleotides either through modified nucleosides during automated synthesis, or through postsynthetic modification of the oligonucleotide (Goodchild, 1990; Agrawal, 1994; Chu and Orgel, 1994). Automated synthesis is advantageous because it allows a controlled, site-specific introduction of the modification without formation of side products. However, the synthesis of protected nucleoside analogues for automated synthesis may be complicated, and the protection and/or deprotection schemes for the functional group may be incompatible with the chemistry of automated synthesis.

Postsynthetic modification is useful in initial attempts at derivatizing oligonucleotides or oligonucleotide analogues. Selective postsynthetic modification of terminal phosphates can be achieved using carbodiimide chemistry to generate activated phosphates such as phosphorimidazolides (Chu, et al., 1983). Subsequent nucleophilic attack by bifunctional primary amines provides a terminal nucleophilic site through which conjugates can be generated by amide or disulfide bond chemistry (Chu and Orgel, 1994). Terminal hydroxyls can be derivatized using *N*,*N*′-carbonyldiimidazole. This generates a reactive imidazole carbamate intermediate of the oligonucleotide (Bonfils, et al., 1992; Komiyama and Inokawa, 1994; Ushuijima, et al., 1998). Subsequent displacement of the imidazole by an amine generates a stable carbamate derivative of the oligonucleotide.

It is also possible to derivatize oligonucleotides postsynthetically at internal sites. To do this, it is necessary to have a unique, chemically reactive site in order to avoid formation of undesired adducts. Commercially available modified bases may be incorporated into oligonucleotides at specific sites during automated synthesis. Masked primary amines can be deprotected and derivatized postsynthetically (Haralambidis, et al., 1987). Alternatively, selective derivatization of unmodified bases can be achieved in the presence of base analogues. For instance, the selective, bisulfite-catalyzed transamination of cytosine in an oligonucleotide-containing bisulfite insensitive 5-methylcytosine has been reported (Miller and Cushman, 1992). Additionally, oligonucleotide analogues containing aminoalkyl linkers at an internal site in place of a nucleotide have been derivatized to give conjugates active in cleaving RNA (Reynolds, et al., 1996).

In this paper, we describe a simple procedure for preparing an oligodeoxyribonucleotide that is conjugated with an imidazole functional group. The procedure allows placement of the imidazole function at any position within the oligonucleotide.

EXPERIMENTAL PROCEDURES

Protected deoxyribonucleoside phosphoramidites and reagents for oligonucleotide synthesis were purchased from Glenn Research. All chemicals and solvents were of reagent grade or better. Reversed-phase high-performance liquid chromatography was carried out on an analytical scale using a Microsorb C_{18}, 5 μm particle size, 100 Å pore size, 4.6 × 150 mm column and on a preparative scale using a Microsorb C_{18}, 5 μm particle size, 100 Å pore size, 10.0 × 250 mm column, both purchased from Rainin Instruments Inc. ^{1}H NMR spectra were acquired on a Bruker AMX 300 spectrometer. Chemical shifts are reported in parts per million (d) and referenced to the proton chemical shifts of deuterated solvent.

* To whom correspondence should be addressed. Phone: (410) 955-3489. Fax: (410) 955-2926. E-mail: pmiller@jhsph.edu.

10.1021/bc000004t CCC: $19.00 © 2000 American Chemical Society
Published on Web 06/13/2000

Preparation of Histamine. Histamine was prepared from its dihydrochloride salt (Lancaster Chemical Co.) using strong anion-exchange chromatography. A column containing Amberlite IRA-400 quaternary amine resin (Fisher Chemical Co.) was washed with at least 3 column volumes of 0.1 N sodium hydroxide in 20% aqueous dioxane. The resin was washed with at least 3 column volumes of 0.5 N sodium hydroxide and 0.1 N sodium hydroxide. The resin was then washed with ddH_2O until the pH of the eluent was equal to that of the ddH_2O. A solution of histamine dihydrochloride in ddH_2O was loaded onto the column and eluted with ddH_2O. Fractions were pooled and dried under vacuum. Histamine was recovered in 82% yield. The identity of the compound was confirmed by ^1H NMR in D_2O (H2, 7.35 δ, singlet; H4. 6.70 δ, singlet; H7, 2.77 δ, triplet; H6, 2.52 δ, triplet). A 1 M stock solution in ddH_2O was prepared, and the molar extinction coefficient was determined ($\Sigma_{208nm} = 4540\ M^{-1}\ cm^{-1}$). This stock solution was stored at 4 °C.

Preparation of 2′-(*N*-Glutaryl-*N*′-histaminyl)-2′-deoxyuridine (4). The reaction was carried out in two steps. In the first step, equal volumes of a 100 mM solution of 2′-amino-2′-deoxyuridine and a 500 mM solution of disuccinimidyl glutarate (Pierce Chemical Co.) each in DMSO[1] were combined and reacted for 5 min at room temperature. Aliquots were quenched with EDA and saved for RP-HPLC analysis. In the second step, an equal volume of 1 M histamine in DMSO was added to the d-aU/DSG reaction solution and aliquots were quenched with EDA 30, 35, and 60 min later. The bulk of the reaction was quenched with an equal volume of 0.5 N sodium hydroxide. Samples from the EDA-quenched reactions were assayed at 260 nm by RP-HPLC using a 10 mL linear gradient of 2 to 6.5% acetonitrile in 50 mM sodium phosphate, pH 5.8, at a flow rate of 1 mL/min.

The bulk of the reaction was purified by preparative RP-HPLC using a 40 mL linear gradient of 2 to 6.5% acetonitrile in 50 mM sodium phosphate, pH 5.8, at a flow rate of 2 mL/min. The column was monitored at 280 nm. HPLC purified **4** was desalted on a Microsorb C_{18} preparative guard column (10 × 65 mm, 5 μm particle size, 100 Å pore size, Rainin Instrument Co.). The conjugate was evaporated to dryness; the residue was dissolved in a solution containing 2% acetonitrile in 50 mM sodium phosphate, pH 5.8; and the solution was loaded onto the column equilibrated with 2% acetonitrile in 50 mM sodium phosphate, pH 5.8. The column was washed with 10 mL of water, and the conjugate was eluted with 50% aqueous acetonitrile.

The structure of **4** was confirmed by ^1H NMR in D_2O: H6 (7.65 δ), H5 (5.81 δ), H1′ (5.69 δ), H3′ (4.15 δ), H4′ (4.00 δ), H5′ (3.65 δ), H2′ (4.40 δ), H2″ (8.25 δ), H4″ (7.00 δ), H7″ (3.25 δ), H6″ (2.72 δ), H10″, H12″ (2.05 δ and 1.95 δ), and H11″ (1.60 d). The double primes denote the *N*-glutaryl-histamine portion of the molecule.

Preparation of a 2′-Amino-Derivatized Oligonucleotide (10). A 2′-amino-derivatized oligodeoxyribonucleotide, d-AAAGAAAAGAAGAAAU*CG (**10**), where U* is 2′-amino-2′-deoxyuridine, was synthesized on an ABI 392 automated DNA/RNA synthesizer using standard phosphoramidite chemistry. The d-aU residue was introduced using the commercially available protected 2′-trifluoroacetamido-2′-deoxyuridine phosphoramidite. The oligonucleotide was deprotected by treatment with concentrated ammonium hydroxide at 65 °C for 5 h and purified by preparative RP-HPLC.

Synthesis of the Succinimidyl Ester of N-Glutarylhistamine. An aliquot of the 1 M histamine stock solution in water was evaporated under vacuum, and the residue was evaporated three times with anhydrous methanol. The residue was dissolved in DMSO to give a 1.5 M solution. This solution was combined with 2 M DSG dissolved in DMSO to give a final solution of 0.5 M DSG and 0.2 M histamine. After incubating for 13 h at room temperature, samples were diluted as necessary using 0.08% aqueous trifluoroacetic acid. The reaction was assayed by RP-HPLC at 215 nm using a gradient that consisted of 2 mL of 0.08% TFA followed by 15 mL of a linear gradient of 0 to 30% acetonitrile in 0.08% TFA at a flow rate of 1 mL/min. Aliquots of the reaction mixture were also treated with 5 N sodium hydroxide for 24 h at 37 °C and assayed by RP-HPLC as described above.

Preparation of Imidazole Conjugated Oligonucleotide. Ten A_{260} units (~50 nmol) of oligonucleotide **10** was dissolved in 5 μL of 50% acetonitrile in 50 mM sodium phosphate, pH 8.0. The oligonucleotide was heated at 37 °C for 15 min, and then combined with 15 μL the succinimidyl ester of *N*-glutarylhistamine prepared as described above. The solution was incubated overnight at 37 °C. The reaction mixture was then treated with 50 μL of 0.5 N sodium hydroxide for 30 min at 37 °C and then diluted into 50 mM sodium phosphate, pH 5.8. The solution was analyzed by RP-HPLC at 260 nm using 27 mL of a linear gradient of 5 to 15% acetonitrile in 50 mM sodium phosphate, pH 5.8 at a flow rate of 1 mL/min.

The imidazole-conjugated oligonucleotide was purified by preparative scale RP-HPLC using 74 mL of a linear gradient of 5 to 15% acetonitrile in 50 mM sodium phosphate, pH 5.8. The column was monitored at 280 nm. The solution containing the purified oligonucleotide was evaporated to dryness; the residue was dissolved in 50 mM sodium phosphate, pH 5.8; and the solution was loaded onto a Microsorb C_{18} preparative guard column that had been equilibrated with 50 mM sodium phosphate, pH 5.8. The column was washed with 10 mL of water and the oligonucleotide eluted with 50% aqueous acetonitrile.

An aliquot containing 0.1 A_{260} unit of the purified oligonucleotide was evaporated to dryness and the residue was dissolved in 48 μL of a solution containing 10 mM Tris/2 mM magnesium chloride, pH 8.0. The solution was treated with 0.1 unit of snake venom phosphodiesterase and 15 units of bacterial alkaline phosphatase for 18 h at 37 °C. The reaction mixture was diluted into 50 mM sodium phosphate, pH 5.8, and analyzed by RP-HPLC using 3 mL of a linear gradient from 0 to 5% acetonitrile in 50 mM sodium phosphate pH 5.8; followed by 5 mL of 5% acetonitrile in 50 mM sodium phosphate, pH 5.8; and followed by 10 mL of a linear gradient of 5 to 50% acetonitrile in 50 mM sodium phosphate, pH 5.8, at 1 mL/min.

RESULTS AND DISCUSSION

An oligodeoxyribonucleotide, **10,** was prepared that contains a d-aU residue near the 3′-end of the oligonucle-

[1]Abbreviations: BAP, bacterial alkaline phosphatase; d-aU, 2′-amino-2′-deoxyuridine; ddH_2O, distilled, deionized water; DMSO, dimethyl sulfoxide; DSG, disuccinimidyl glutarate; EDA, ethylenediamine; NHS, *N*-hydroxysuccinimide; RP-HPLC, reversed-phase high-performance liquid chromatography; SVPD, snake venom phosphodiesterase; TFA, trifluoroacetic acid.

Scheme 1[a]

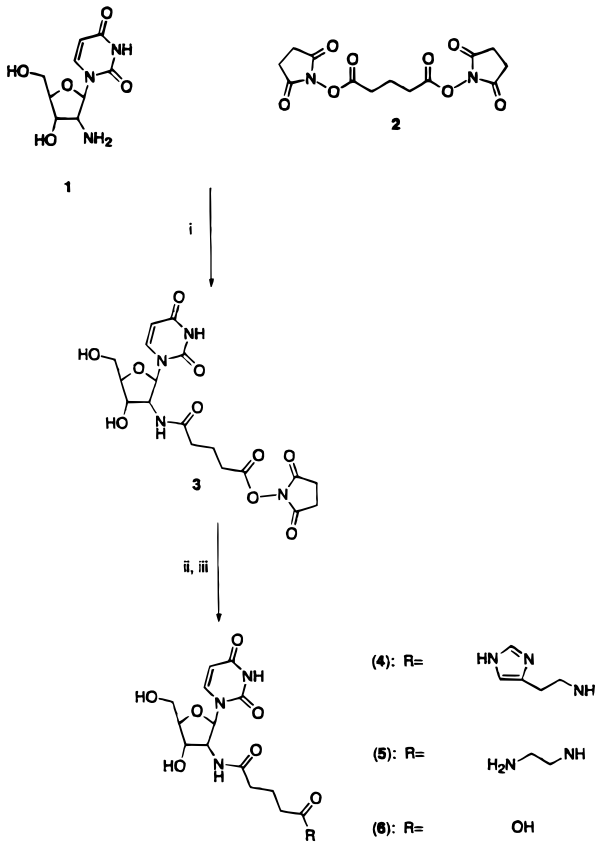

[a] (i) DMSO. (ii) 500 mM histamine in DMSO, **4**, or EDA, **5**, or 250 mM sodium hydroxide, **6**. (iii) RP-HPLC.

otide. The d-aU provides a primary amine to which may be tethered functional groups using conjugation chemistry. The general strategy was to generate the activated ester of the functional group to be derivatized, and then introduce that to the d-aU under conditions amenable to amide bond formation. The carboxylate of the *N*-glutrylhistamine provides a site for generating activated electrophilic centers that can subsequently react with the nucleophilic d-aU to give an amide linkage.

Test conjugation reactions were first carried out at the nucleoside level on d-aU itself. The nucleoside served as both a model reaction for coupling to the d-aU containing oligonucleotide and as a way to generate standards for a RP-HPLC assay used to follow the oligonucleotide conjugation reaction. Commercially available disuccinimidyl glutarate, DSG, was used to form the succinimidyl ester of 2′-(*N*-glutaryl)-2′-deoxyuridine as shown in Scheme 1. This was accomplished by reacting d-aU (**1**) with a 10-fold excess of DSG (**2**) in dry DMSO. Formation of the NHS ester of 2′-(*N*-glutaryl)-2′-deoxyuridine (**3**) was monitored by first quenching aliquots of the reaction with ethylenediamine and analyzing the products by C-18 RP-HPLC. This procedure converts the NHS-activated ester of **3** to aminoethyl derivative **5**. As shown in Figure 1 (panels A and B), d-aU is resolved from **5** whereas 2′-*N*-glutaryl-2′-deoxyuridine (**6**), which would result upon hydrolysis of the succinimidyl ester, coelutes with d-aU under these conditions.

In the second step of the reaction, histamine in DMSO was added to a final concentration of 500 mM. This yielded 87% of 2′-(*N*-glutaryl-*N*′-histaminyl)-2′-deoxyuridine (**4**) after 30 min of incubation. As shown in Figure 1 (panels C, D, and E), the product was well resolved from

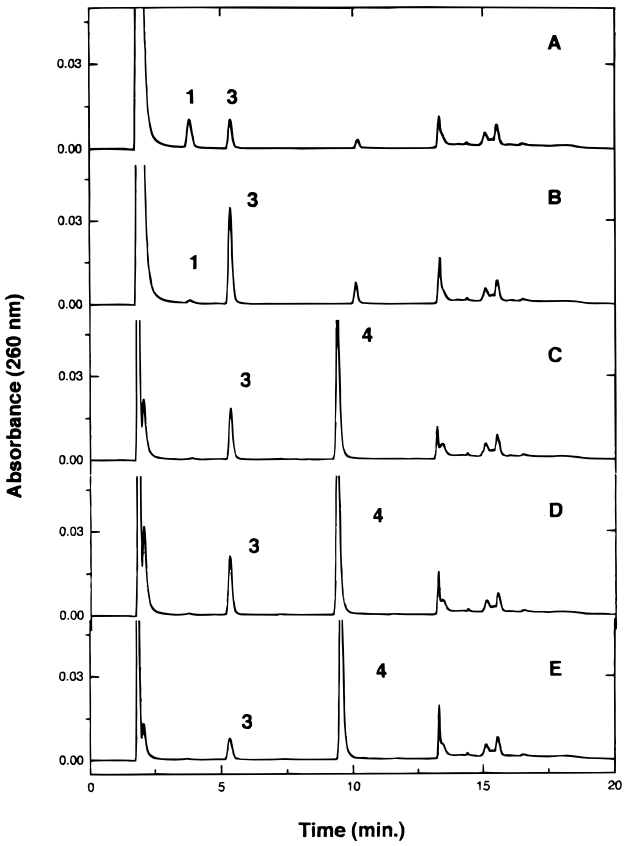

Figure 1. Reversed-phase chromatograms of the glutaryl derivatives of 2′-amino-2′-deoxyuridine. Solutions of DSG and d-aU in DMSO were combined and aliquots were quenched with EDA 0 min (panel A) or 5 min (panel B) after mixing. The remaining reaction was treated with histamine in DMSO and aliquots were quenched with EDA 0 min (panel C), 5 min (panel D), or 30 min (panel E) after addition of histamine. The reactions were analyzed by RP-HPLC as described in the Experimental Procedures. The peaks are **1**, 2′-amino-2′-deoxyuridine (**1**); **3**, the aminoethyl derivative of 2′-(*N*-glutaryl-*N*′-histaminyl)-2′-deoxyuridine (**5**); and **4**, 2′-(*N*-glutaryl-*N*′-histaminyl)-2′-deoxyuridine (**4**).

side products and from the incompletely reacted succinimidyl ester **3.** The product was readily purified by preparative-scale RP-HPLC, and was characterized by ^{1}H NMR in D_2O.

Although the reaction shown in Scheme 1 worked well when applied to the nucleoside, d-aU, it could not be applied successfully to the derivatization of d-aU contained oligonucleotide **10**. To generate the oligonucleotide conjugate, it was necessary to first generate the succinimidyl ester of *N*-glutarylhistamine (**8**) as shown in Scheme 2. Histamine (**7**) was combined with DSG (**2**) to give the activated ester of **8**, and bis-histaminylglutarate (**9**). The progress of the reaction was assayed by RP-HPLC using an acetonitrile gradient in 0.08% trifluoroacetic acid. As shown by the chromatograms in Figure 2, this gradient is capable of separating the activated ester of **8** from bis-histaminylglutarate (**9**), and from histamine (**7**) and DSG (**2**) as well. Treatment of the crude reaction with sodium hydroxide confirmed the identity of the peaks in the chromatogram. Thus as expected, **9** is stable to sodium hydroxide whereas **8** disappears and an earlier eluting peak is evident.

Oligonucleotide **10** was coupled with **8**, generated in situ as described above, in a 50% acetonitrile/sodium phosphate buffer at pH 8.0 as shown in Scheme 3. The crude reaction mixture was then analyzed by RP-HPLC

Scheme 2

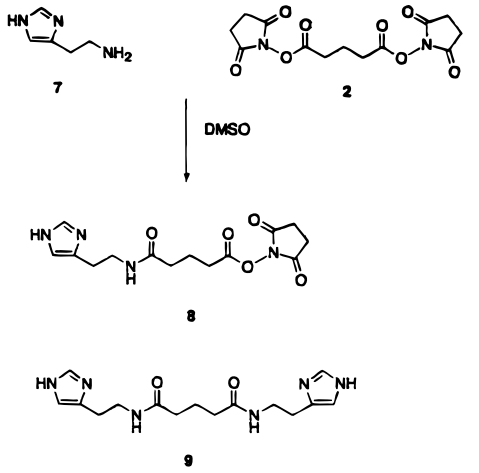

after quenching with sodium hydroxide. The chromatogram of the crude reaction mixture (Figure 3, panel A) showed the formation of a new peak eluting with a retention time of 15 min. This peak was purified by preparative RP-HPLC; rechromatographed to confirm its purity (Figure 3, panel B), and coinjected with underivatized oligonucleotide to confirm that it was a distinct species (Figure 3, panel C).

The purified conjugated oligonucleotide was hydrolyzed to its component nucleosides by digestion with a combination of snake venom phosphodiesterase and bacterial alkaline phosphatase. The digest was analyzed by RP-HPLC using conditions that are capable of resolving the

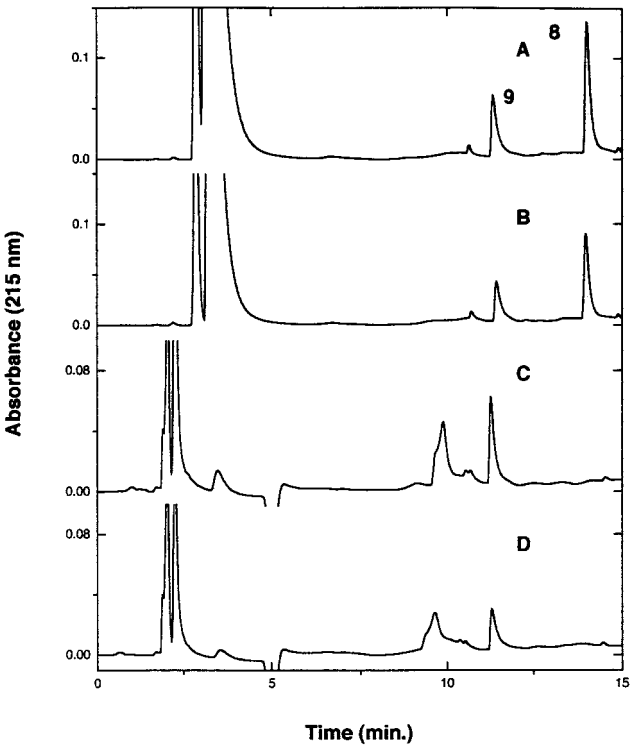

Figure 2. Formation of the succinimidyl ester of *N*-glutarylhistamine. Solutions of DSG and histamine in DMSO were mixed and aliquots were assayed directly 1 h (panel A) or 13 h (panel B) after mixing. Alternatively the reactions were quenched with sodium hydroxide 1 h (panel C) or 13 h (panel D) after mixing. The reactions were analyzed by RP-HPLC as described in the Experimental Procedures. The peak labeled **8** is the succinimidyl ester of *N*-glutarylhistamine and the peak labeled **9** is bis-histaminylglutarate.

Scheme 3[a]

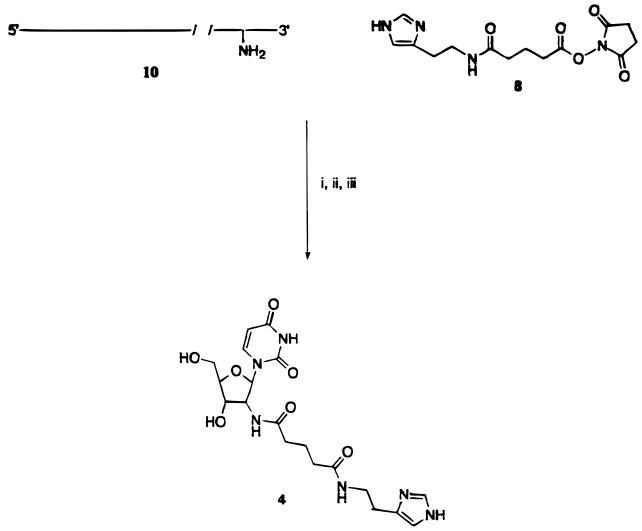

[a] (i) **10** in 50% acetonitrile/sodium phosphate buffer, pH 8.0 combined with **8** in DMSO. (ii) SVPD/BAP. (ii) RP-HPLC.

expected nucleosides as shown in Figure 4, panel A. As expected, digestion of underivatized oligonucleotide **10** produced d-C, d-G, d-A, and d-aU (see panel B) whereas the digest of the derivatized oligonucleotide lacked the peak corresponding to d-aU and showed the appearance of a new peak that eluted between d-G and d-A (see panel C). Coinjection of the oligonucleotide conjugate digest with authentic d-aU and 2′-(*N*-glutaryl-*N*′-histaminyl)-2′-deoxyuridine (**4**) standards confirmed that this new peak is 2′-(*N*-glutaryl-*N*′-histaminyl)-2′-deoxyuridine.

Site specific hydrolysis of RNA has been mediated by oligonucleotides covalently modified with functional groups designed to mimic the active site of RNAse A. Chemical

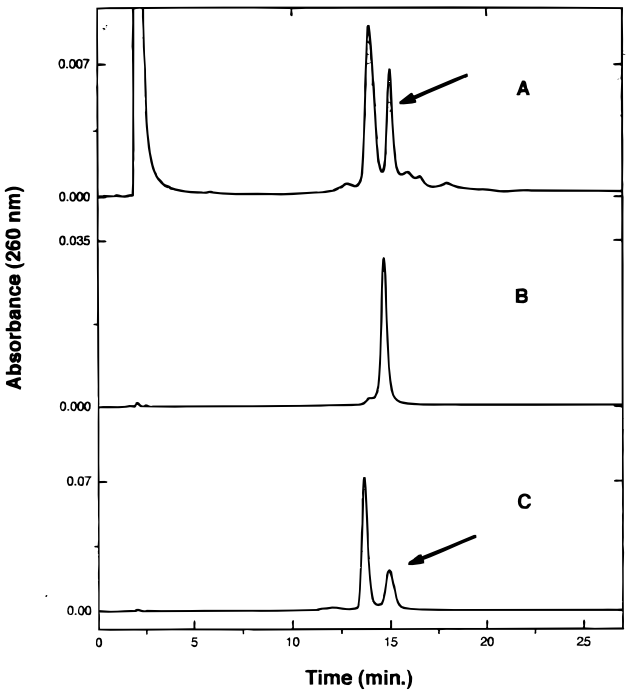

Figure 3. Reaction of oligonucleotide **10** with the succinimidyl ester of *N*-glutarylhistamine. Panel A shows the crude reaction mixture; panel B shows the purified conjugated oligonucleotide and panel C a coinjection of **10** and the conjugated oligonucleotide. The reactions were analyzed by RP-HPLC as described in the Experimental Procedures.

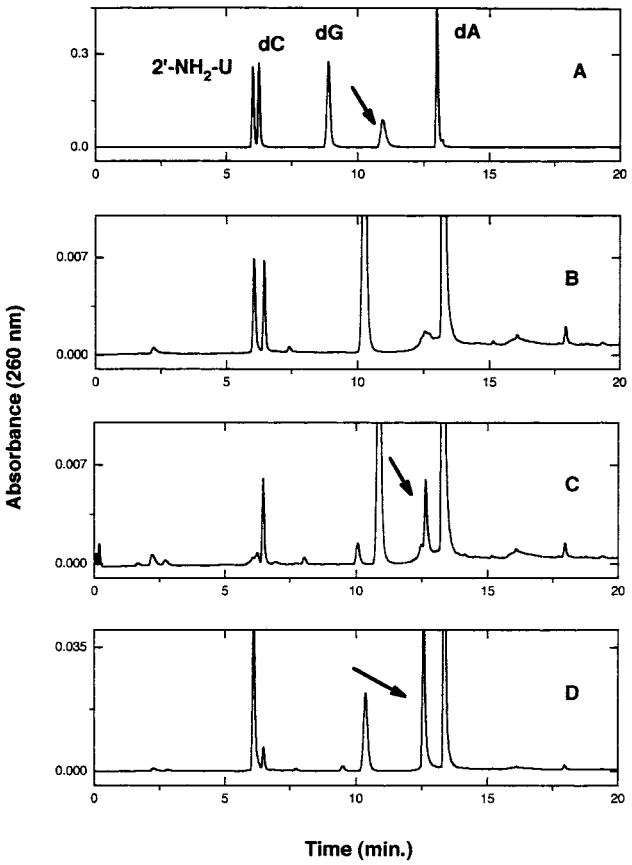

Figure 4. Enzymatic digestion of the imidazole-conjugated oligonucleotide. Panel A shows a chromatogram of a mixture of d-aU, d-C, d-G, 2′-(*N*-glutaryl-*N*′-histaminyl)-2′-deoxyuridine, **4**, (indicated by the arrow), and dA standards; panel B shows a chromatogram of the digest of oligonucleotide **10**; panel C shows a chromatogram of the digest of the imidazole-conjugated oligonucleotide and panel D shows a coinjection of conjugated oligonucleotide digest and d-aU and (**4**). The reactions were analyzed by RP-HPLC as described in the Experimental Procedures.

moieties containing two imidazoles, or two amines, or an imidazole and an amine, tethered to an oligonucleotide, have been used to specifically target RNA, and result in site-specific hydrolysis (Reynolds, et al., 1996; Ushijima, et al., 1998). Modeling studies indicate that an imidazole, tethered to the d-aU residue of oligonucleotide **10** by the eight atom glutaryl linker can be positioned in the minor groove of a duplex formed by **10** and a complementary RNA oligonucleotide. In this conformation, the imidazole is in close enough proximity to a 2′-hydroxyl of the RNA backbone to abstract a proton of the hydroxyl. Such proton abstraction in conjunction with other functional groups could promote site-specific cleavage of the RNA target. Experiments to test this possibility are currently in progress.

ACKNOWLEDGMENT

The research described in this report was supported by a grant from the National Institutes of Health, GM57140.

LITERATURE CITED

Agrawal, S. (1994) Functionalization Of Oligonucleotides With Amino Groups And Attachment OF Amino Specific Reporter Groups. In *Methods in Molecular Biology, Vol. 26: Protocols for Oligonucleotide Conjugates* (S. Agrawal, Ed.) Humana Press, Inc., Totowa.

Asseline, U., Delarue, M., Lancelot, G., Toulme, F., Thuong, N. T., Montenay-Garestier, T., and Helene, C. (1984) Nucleic Acid-Binding Molecules With High Affinity And Base Sequence Specificity: Intercalating Agents Covalently Linked To Oligodeoxynucleotides. *Proc. Natl. Acad. Sci. U.S.A. 81*, 3297−3301.

Bonfils, E., Depierreux, C., Midoux, P., Thuong, N. T., Monsigny, M., and Roche, A. C. (1992) Drug Targeting: Synthesis And Endocytosis Of Oligonucleotide-Neoglycoprotein Conjugates. *Nucleic Acids Res. 20*, 4621−4629.

Chu, B. C. F., and Orgel, L. E. (1985) Nonenzymatic Sequence-Specific Cleavage Of Single-Stranded DNA. *Proc. Natl. Acad. Sci. U.S.A. 82*, 963−967.

Chu, B. C. F., and Orgel, L. E. (1994) Postsynthesis Functionalization Of Oligonucleotides. in *Methods in Molecular Biology, Vol. 26: Protocols for Oligonucleotide Conjugates* (S. Agrawal, Ed.) Humana Press, Inc., Totowa.

Chu, B. C. F., Wahl, G. M., and Orgel, L. E. (1983) Derivatization Of Unprotected Polynucleotides. *Nucleic Acids Res. 11*, 6513−6522.

Francois, J.-C, Saison-Behmoaras, T., Chassignol, M., Thuong, N. T., Sun, J., and Helene, C. (1988) Periodic Cleavage Of Poly(dA) By Oligothymidylates Covalently Linked To The 1,10-Phenanthroline-Copper Complex. *Biochemistry 27*, 2272−2276.

Goodchild, J. (1990) Conjugates Of Oligonucleotides And Modified Oligonucleotides: A Review Of Their Synthesis And Properties. *Bioconjugate Chem. 1* (3), 165−191.

Haralambidis, J., Chai, M., and Tregear, G. W. (1987) Preparation Of Base-Modified Nucleosides Suitable For Non-Radioactive Label Attachment And Their Incorporation Into Synthetic Oligodeoxyribonucleotides. *Nucleic Acids Res. 15*, 4857−4876.

Komiyama, M., and Inokawa, T. (1994) Selective Hydrolysis Of tRNA By Ethylenediamine Bound To A DNA Oligomer. *J. Biochem. 116*, 719−720.

Miller, P. S., and Cushman, C. D. (1992) Selective Modification Of Cytosines In Oligodeoxyribonucleotides. *Bioconjugate Chem. 3*, 74−79.

Reynolds, M. A., Beck, T. A., Say, P. B., Schwartz, D. A., Dwyer, B. P., Daily, W. J., Vaghefi, M. M., Metzler, M. D., Klem, R. E., and Arnold, L. J. (1996) Antisense Oligonucleotides Containing An Internal Non-Nucleotide-Based Linker Promote Site-Specific Cleavage of RNA. *Nucleic Acids Res. 24*, 760−765.

Ushijima, K., Hidetaka, G., Kazumi, H., Shirakawa, M., Kagosima, K., Takai, K., and Takaku, H. (1998) Site-Specific Cleavage Of tRNA By Imidazole And/Or Primary Amine Groups Bound At The 5′-End Of Oligodeoxyribonucleotides. *Biochim. Biophys. Acta 1379*, 217−233.

BC000004T

Bioconjugate Chemistry

SEPTEMBER/OCTOBER 2000
Volume 11, Number 5

© Copyright 2000 by the American Chemical Society

REVIEWS

Preparation and Applications of Peptide−Oligonucleotide Conjugates

Ching-Hsuan Tung*

Center for Molecular Imaging Research, Massachusetts General Hospital, Harvard Medical School, 149 13th Street, room 5406, Charlestown, Massachusetts 02129

Stanley Stein

Center for Advanced Biotechnology and Medicine, 679 Hoes Lane, Piscataway, New Jersey 08854. Received March 23, 2000

I. INTRODUCTION

Oligonucleotides constitute a class of potential therapeutic agents that can be used to target mRNA (antisense strategy), double-stranded DNA (triple-helix strategy), and even proteins [aptamer strategy (*1*)] (Figure 1). Further improvements in certain properties, however, may be required before the therapeutic value of oligonucleotides can be realized. Properties to be considered include cell-specific delivery, cellular uptake efficiency, intracellular distribution, stability against degradation, binding strength, target specificity, and mechanism of target inactivation. Achievement of these desired improvements is being addressed in many different ways. Most notable is the use of replacements for the phosphodiester linkage, such as in the phosphorothioate analogue of DNA, to gain more nuclease resistant analogues.

Proteins are versatile enough to impart virtually any desired biological property, and have been used as enhancers of certain properties in oligonucleotides. For example, polylysine conjugates of ligands for cell surface receptors, such as transferrin (*2*−*4*) and/or adenovirus particles (*5*) have been used to prepare DNA complexes, which have been shown to possess greater cellular uptake efficiency. Unfortunately, the large size and complex structure of proteins can add considerable uncertainty to this approach. However, peptides can often substitute for whole proteins to mimic certain biological functions, in this case to improve the potency of oligonucleotides. Rather than forming ionic complexes between the oligonucleotide and the peptide, the peptide is preferably covalently linked to the oligonucleotide. This gives a more consistent product in which the desired properties can be carefully controlled by structural variations. This report will review the different methods of preparation of such peptide−oligonucleotide conjugates and some initial studies on the use of these compounds.

II. PREPARATION OF PEPTIDE−OLIGONUCLEOTIDE CONJUGATE (POC)

Both peptide and oligonucleotide synthesis are well-developed methods. Using a DNA synthesizer, oligonucleotides can be prepared conveniently on a research or production scale. Automated peptide synthesis, also available on a research or production level, is somewhat more complicated than oligonucleotide synthesis because of the diverse physical and chemical properties of different amino acids. Preparing peptide−oligonucleotide conjugate (POC) is even less straightforward. The chemistries used on peptide and DNA synthesizers are not fully compatible with each other. The challenge is how to synthesize a desired POC using a convenient method that can be easily scaled up, if necessary. There are two different approaches, which have been studied exten-

* To whom correspondence should be addressed. Phone: (617) 726-5788. Fax: (617) 726-5708. E-mail: tung@helix.mgh.harvard.edu.

10.1021/bc0000334 CCC: $19.00 © 2000 American Chemical Society
Published on Web 09/18/2000

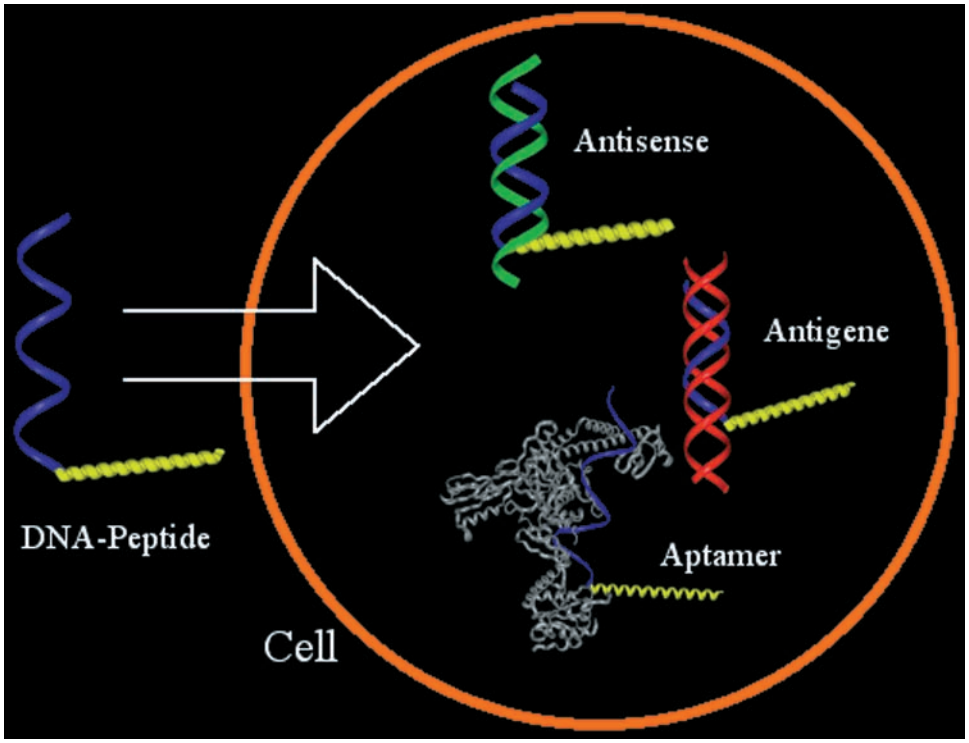

Figure 1. Appending a biologically active peptide (yellow) may improve efficacy of an oligonucleotide (blue). A peptide−oligonucleotide conjugate can bind to an mRNA (green), a gene (red) or a protein (gray) in an antisense, an antigene or an aptamer application, respectively.

sively, for preparing POCs. One is total in-line synthesis and the other is fragment conjugation.

A. In-Line Synthesis. The most direct way of preparing POCs would be in-line synthesis. In this approach, the peptide and oligonucleotide are synthesized sequentially on automatic synthesizers. For peptide synthesis, Fmoc (9-fluorenylmethyloxycarbonyl) chemistry has been used most frequently for in-line synthesis, since its reaction condition is much milder than Boc (*tert*-butyloxycarbonyl) chemistry. In typical Fmoc chemistry, the N-terminus and side chains of the amino acids are protected by Fmoc and *tert*-butyl groups, respectively. On each cycle, the Fmoc group is removed with 20% piperidine. After synthesis, the peptide is cleaved from the support and side chain deprotected with 90% trifluoroacetic acid (TFA).

In various studies, the peptide was usually assembled first on the solid support, followed by oligonucleotide synthesis. In 1987, Haralambidis et al. first reported a solid phase synthesis of POCs for the purpose of preparing nonradioactive DNA probes (*6*). Fmoc and phosphoramidite chemistry was used sequentially on a controlled pore glass (CPG) support. A ω-hydroxycarboxylic acid was used to convert the amino group at the N-terminus of the peptide into a hydroxyl group, which then served as a linker between the peptide and oligonucleotide components. After completion of the POC synthesis, TFA/ethanedithiol was applied to deprotect the peptide, and aqueous ammonia treatment was then used to simultaneously deprotect the oligonucleotide portion and cleave the conjugate from the CPG. Thereafter, the lysine sidechain amino groups became ready for further reaction with the fluorescent reporter groups (*7*−*9*). These POCs were used as nonradioactive PCR primers (*10*). Applying the same approach, with only a minor change in DNA synthesis, they prepared POCs containing viral fusion peptide sequences at the 3′ end of an oligonucleotide (*11*).

To skip harsh TFA treatment, various peptide sidechain protecting groups were suggested. Base-labile protection groups were applied in POC synthesis (*12*−*16*). For example, the hydrazine removable 1-(4,4-dimethyl-2,6-dioxocyclohex-1-ylidene) ethyl (Dde) group was used with Fmoc chemistry on both CPG and Fractosil supports (*12*). The Dde group is stable to 20% piperidine treatment, which is used for removal of the Fmoc group at each coupling cycle, but can be removed later using ethanolamine or hydrazine solution. In another example, a modified t-Boc chemistry was used to prepare the peptide portion. Base labile Fmoc and 9-fluorenylmethyl (Fm) groups were utilized as the amino acid side chain protecting groups. Thus, with this combination, the DNA was not exposed to strong acid (*14*−*16*).

Bifunctional branch linkers having one amino group for peptide synthesis and one hydroxyl group for oligonucleotide synthesis have also been used (Figure 2) (*17*, *18*). Fmoc chemistry was used to synthesize peptides either on Teflon or high load PEG-PS beads, while the standard phosphoramidite chemistry was used for oligonucleotide synthesis. To prevent harsh ammonia treatment, different conjugate cleavage and oligonucleotide deprotection approaches were developed. A method previously used to prepare methylphosphonate DNA was adopted, based on ethylenediamine in absolute ethanol (1:1) for 1 h at 55 °C (*17*). The other approach used more base labile protecting groups on the exocyclic amines, namely 2-(acetoxymethyl)benzoyl for dA and dG, and acetyl for dC. These protecting groups can be removed with 50 mM K_2CO_3 in methanol (*18*).

The preparation by in-line solid-phase synthesis of a POC consisting of two oligonucleotides connected by a peptide linker (i.e., DNA-peptide-DNA) was reported (*19*). The chemistry was more challenging, since one oligonucleotide, the peptide, and then the other oligonucleotide had to be assembled sequentially. The allyl phosphoramidite was used as a substitute for the usual cyanoethyl phosphoramidite during the first oligonucleotide synthesis on a sarcosine modified CPG. At the end of the oligonucleotide, 5′-amino-5′-deoxythymidine was

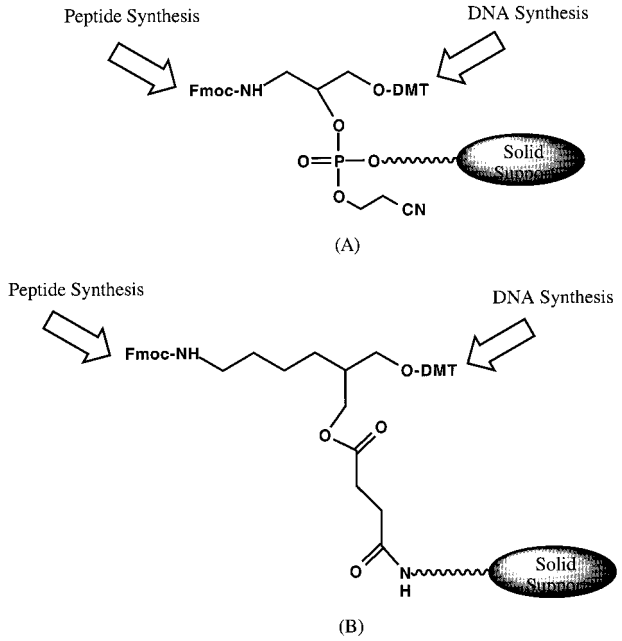

Figure 2. Branched supports for in-line synthesis of POCs (*17*, *18*). For peptide synthesis, the Fmoc protecting group would be removed under basic conditions initially and then after each amino acid coupling cycle. Subsequently, for oligonucleotide synthesis, the DMT protecting group would be removed under acidic conditions initially and then after each nucleotide coupling cycle.

incorporated to have an amino group for subsequent peptide synthesis, which was done by Fmoc chemistry. The usual β-cyanoethyl phosphoramidite chemistry was used for the second oligonucleotide synthesis. Since only dT and Ala were used in this conjugate, no base and side-chain deprotection step was needed. Cleavage from the solid support and removal of the allyl and cyanoethyl phosphate protecting groups were simultaneously achieved using aqueous ammonia.

In-line synthesis could be most direct for preparing POCs, but finding the right combination of protecting groups is the key problem. So far, in our opinion, there is no published method suitable for all POC syntheses. The incompatibilities between peptidic and oligonucleotidic protecting groups during the sequential assemblies lead to a restricted choice of sequences that can be prepared. In most reported methods, the POC still has to be exposed to aqueous ammonia and 90% trifluoroacetic acid to remove the protecting groups on the nucleotides and amino acids. Potential damage to the peptide or oligonucleotide component of the POC is possible, although, recently, it has been reported that the aqueous ammonia treatment does not cause racemization or peptide bond cleavage (*11*, *15*).

B. Fragment Conjugation. In each example of in-line synthesis cited above, there are always certain limitations due to the incompatibilities of the peptide and oligonucleotide chemistries. The conjugation approach could help prevent exposure of the oligonucleotide to strong acidic condition (e.g., 90% trifluoroacetic acid) or the peptide to strong basic condition (e.g., ammonia solution). By this method, the peptide and the oligonucleotides are synthesized, cleaved from their solid supports, deprotected and purified, separately. Therefore, the most appropriate synthetic chemistry can be used for each component without concern for incompatibility. The purified oligonucleotide and peptide can then be joined together, such as by one of the linkages shown in Figure 3. Ready-to-use amino linkers and thiol linkers for oligonucleotide 3′ and/or 5′-terminal modification are commercially available. Peptides can be functionalized by adding a cysteine residue at the N-terminus, C-terminus, or even at an internal position. Since both functionalized oligomers can be prepared conveniently from commercially available reagents, the conjugation approach could be applicable for most laboratories.

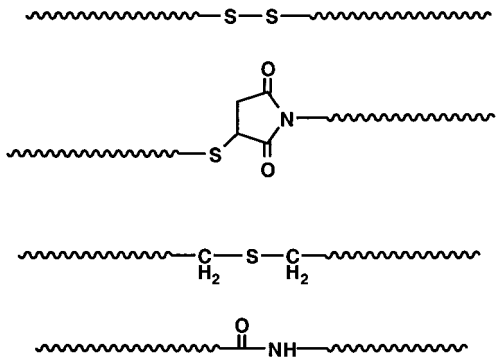

Figure 3. Commonly used linkages in fragment conjugation: disulfide, maleimide, thioether, and amide bonds (from top to bottom).

The disulfide bond between a pair of cysteine residues is a potentially reversible linkage commonly found in proteins, and by analogy, this bond has been used to prepare POCs (*20*−*25*). Instead of using a reversible linker, peptides, and oligonucleotides have been covalently attached using many nonreversible linkages, such as thioether and maleimide. Bifunctional cross-linkers typically have an active ester to react with an amino group, and a maleimide or an iodoacetyl group to react with a thiol group. The first step of the conjugation begins by reacting the activated ester with the amino group at basic pH, which could be either on the oligonucleotide (*21*, *26*−*28*) or on the peptide (*11*, *29*−*31*). Then the second component is attached to the activated first component through a thiol-specific reaction.

Several purification steps are required for the preparation of a POC by the conjugation approach. The peptide and oligonucleotide are separately synthesized and purified. Excess cross-linking reagent must be removed after the first reaction between the activated ester and the amino group. Gel filtration chromatography (*21*), ion-exchange chromatography (*26*, *27*), membrane filtration (*28*), and reversed-phase chromatography (*29*) have all been reported. An additional step is then needed to purify the final product after the thiol-specific step of the conjugation reaction.

Recently, two solid-phase activation methods have been developed to simplify preparation of POCs. The activate esters, bromoacetic anhydride (*30*) or succinimido 3-maleimido propanoate (*31*), were attached to the N-terminus of the peptide while on the solid support. After cleavage and one step of purification, the activated peptide was ready for reaction with a thiol-containing oligonucleotide. Similarly, a cysteine analogue was attached to an oligonucleotide for simplied POC preparation (*25*).

Although the coupling reactions look straightforward, there are also some limitations to the conjugation approach. The solubility of oligonucleotides is quite consistent regardless of sequence, but different peptides may have totally different properties which will reflect on the coupling reaction. Most of the conjugation reactions were done in a mixture of aqueous and organic solutions. Unfortunately, not all peptides are readily soluble in such

solutions (*11*). For example, hydrophobic peptides require organic solvent, but oligonucleotides are water soluble. In addition nonspecific interactions between the peptide and oligonucleotide reactants can also be problematic. Our studies indicated that highly cationic (i.e., positively charged) peptides interacted with negatively charged DNA, causing precipitation. This problem could be partially resolved by having a high concentration of salt in the reaction mixture (*32*, *33*).

Since the acidic condition might be harmful to the oligonucleotide, plus considering the complexity of the peptide protecting groups, fragment conjugation on the DNA solid support has also been proposed (*34*−*36*). The peptide was prepared and purified, then coupled to an oligonucleotide on the solid support (*36*, *37*). The purified peptide can be attached to an amino functionalized oligonucleotide through a stable amide linkage (*34*, *35*) or used as a nucleophile to react with an oligonucleotide and cleave it off an oxime resin (*37*). The fragment coupling method may provided a mild approach for POC synthesis, however, the selection of peptide sequences is still restricted.

A unique method for preparing POCs, template-directed ligation, was reported by Bruick et al. (*38*). Prepurified, unprotected peptide with an activated thioester at its C-terminus was temporarily tethered to a 5′-thiol terminated oligonucleotide through a thioester linkage. When this thioester-linked intermediate and a second oligonucleotide, which had a 3′-amino group, were simultaneously hybridized to adjacent sequences on a complementary template, the peptide migrated from the first to the second oligonucleotide, thereby forming a stable amide linkage with the second oligonucleotide.

In general, the reaction conditions of fragment conjugation are milder than those of direct synthesis. However, fragment conjugation requires multiple steps of preparation and purification, causing significant loss. Therefore, the overall yield is usually lower.

C. Purification and Analysis. HPLC is used most frequently for purifying POCs. In reversed-phase HPLC, if the peptide is highly hydrophobic, the complex tends to elute later than the oligonucleotide (*11*, *28*). On the other hand, if the peptide is quite hydrophilic, the oligonucleotide will dominate the elution, and both the oligonucleotide and conjugate will elute at similar positions (*27*, *30*, *31*). To aid in reversed-phase HPLC purification, the hydrophobic Fmoc group of the synthetic peptide (*26*) was utilized in a manner similar to that used in the trityl-on/trityl-off two-step oligonucleotide purification (Figure 4). The Fmoc group from the peptide synthesis was retained on the N-terminus by skipping the final piperidine deprotection step. Because of the hydrophobicity of the Fmoc group, the Fmoc-on peptide and Fmoc-on peptide−oligonucleotide conjugate eluted similarly at a higher percentage of organic solution than did the unreacted oligonucleotide. Thereafter, the Fmoc-group was conveniently removed with piperidine, and the POC eluted with a retention time similar to that previously observed for the unreacted oligonucleotide, which had been removed in the previous chromatography step. Alternatively, a trityl-on/trityl-off two-step purification method has been applied to the purification of a POC synthesized by the in-line strategy (*11*).

Anion-exchange chromatography provides an alternate method for POC preparation, especially for multiply cationic peptides (*33*). After conjugation, the POCs with various net charges can be separated from the parent oligonucleotides in a salt gradient. Since the separation principle of anion-exchange chromatography differs from

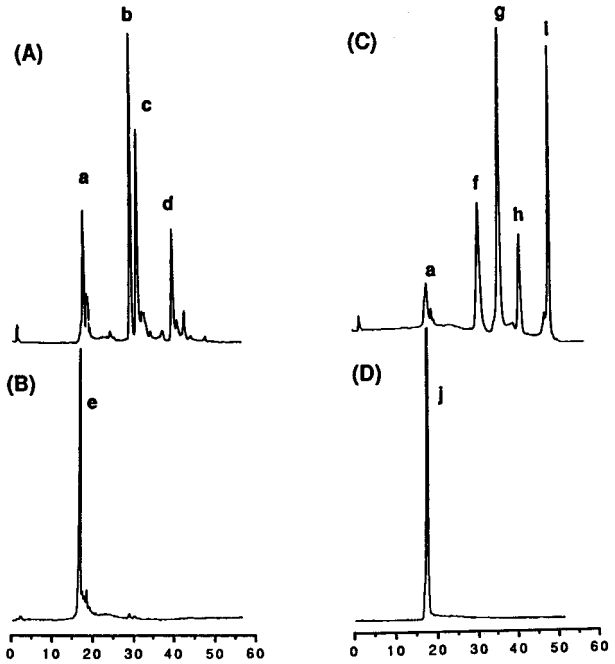

Figure 4. Reversed-phase HPLC purification of POCs. Chromatography was on a 25 × 0.46 cm PRP-1 (polymer-based reversed-phase) column (Hamilton) at a flow rate of 1 mL/min using a gradient of increasing acetonitrile (1%/min) in 0.1 M triethylammonium acetate, pH 9.7. (Panel A) Separation of the reaction mixture of the 3′-iodo-activated 12-mer DNA and Fmoc-$(\delta Orn)_{12}$-Cys-NH_2. The product at 29 min (peak b) was collected and the Fmoc group was cleaved. Rechromatography gave the purified product (panel B). (Panel C) Separation of the reaction mixture of the 3′,5′-diiodo-activated 12-mer DNA with Fmoc-$(\delta Orn)_3$-Cys-NH_2. The product at 39 min (peak h) was collected and the Fmoc groups were cleaved. Rechromatography gave the purified final product (panel D). The abscissa and ordinate represent time in minutes and absorbance at 258 nm, respectively. The peaks are labeled as follows: a, unreacted DNA; b, Fmoc-$(\delta Orn)_{12}$-Cys(NH_2)-DNA; c, Fmoc-$(\delta Orn)_{12}$-Cys(NH_2); d, $[(\delta Orn)_{12}$-Cys$(NH_2)]_2$ (i.e., disulfide dimer of peptide); e, $(\delta Orn)_{12}$-Cys-NH_2-DNA; f, Fmoc-$(\delta Orn)_3$-Cys(NH_2)-DNA; g, Fmoc-$(\delta Orn)_3$-Cys(NH_2); h, [Fmoc-$(\delta Orn)_3$-Cys$(NH_2)]_2$-DNA; i, [Fmoc-$(\delta Orn)_3$-Cys$(NH_2)]_2$; j, $(\delta Orn)_3$-Cys$(NH_2)]_2$-DNA. Adapted from Zhu et al. (*27*).

that of reversed phase, complementary information about the POC can be obtained conveniently.

Polyacrylamide gel electrophoresis (PAGE) is also commonly used for purifying and analyzing POCs. Depending on the amino acid composition of the appended peptide, the charge/mass ratio of the POC will be different from that of the original oligonucleotide. For example, POCs containing positively charged peptides migrate considerably slower than the corresponding unconjugated oligonucleotide, as shown in a series of arginine peptides conjugated to a 9-mer oligonucleotide or linked between a pair of 9-mer oligonucleotides (Figure 5) (*33*). As expected, the mobility decreased in proportion to the number of positive charges. When the overall charge of the POC is close to neutral, there is essentially no mobility in the gel. The more recently introduced capillary electrophoresis (CE) is also available for analyzing POCs. Like the traditional PAGE, the capillary is filled with polyacrylamide gel, often in urea, then the separation is done in a high voltage field. Interestingly, the migration pattern in CE may differ markedly from that found in PAGE (*11*). Thus, HPLC, PAGE, and CE provide independent, alternative methods for monitoring the conjugation reaction and for analyzing the products.

Enzymatic assays have been used to characterize POCs. For example, a POC was resistant to snake venom

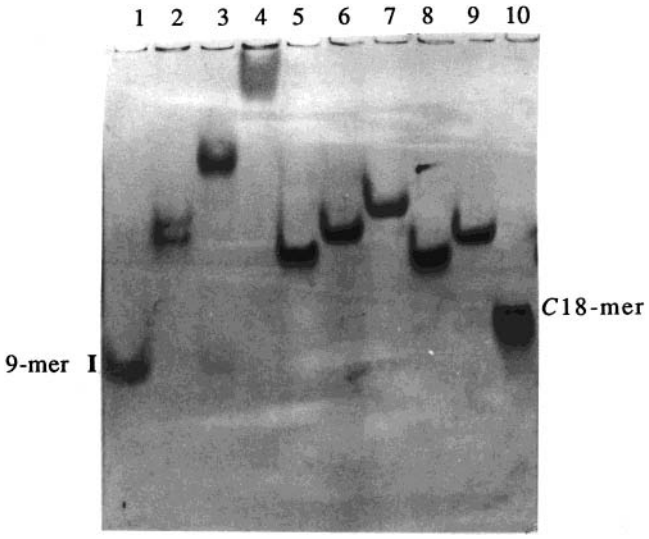

Figure 5. Electrophoretic mobility of oligoarginine−oligonucleotide conjugates. Two different 9-mer oligonucleotides, one linked through its 5′-terminus (I) and the other through its 3′-terminus (II) were covalently coupled to oligoarginine peptides of 3, 5, and 7 residues, each peptide having an additional residue of cysteine at the C-terminus or at both termini. D-Arg was used in combination with L-Arg (alternating residues) in certain instances. A nondenaturing (no urea) 20% polyacrylamide gel was run in Tris-borate buffer, pH 8 and then stained with silver. (Lane 1) 9-mer **I**, (lane 2) R_3−I, (lane 3) R_5−I, (lane 4) R_7−I, (lane 5) II−R_3−I, (lane 6) II−R_5−I, (lane 7) II−R_7−I, (lane 8) II−(D/L)R_3−I, (lane 9) II-(D/L)-R_5-I, (lane 10) complementary 18-mer. Adapted from Wei et al. (*33*).

phosphodiesterase when the 3′-terminus was blocked by linker and peptides, but was subject to partial hydrolysis by spleen phosphodiesterase and P1 nuclease (*6*). Complete hydrolysis by snake venom phosphodiesterase and alkaline phosphatase was also reported (*14*, *39*, *40*). Furthermore, trypsin has been applied to digest the cationic peptide and confirm the structure of a POC (*28*).

As commonly done for peptide characterization, amino acid analysis (AAA) can be used to analyze POCs. The correct amino acid composition was typically found for POCs, except for glycine (*11*, *17*, *25*, *29*, *30*). It had been suspected that glycine might be produced during hydrolysis of the oligonucleotide (*11*, *17*, *29*, *30*). To study this unknown glycine (*41*), four nucleosides were hydrolyzed separately by gas-phase hydrolysis for 48 h and analyzed by ion-pair reversed-phase HPLC with postcolumn fluorometric detection using *o*-phthaldialdehyde/2-mercaptoethanol (*42*). A peak at the glycine position was found only in the deoxyadenosine hydrolysate, but not in the deoxyguanosine, deoxycytidine, or thymidine hydrolysates. This peak was consistently observed in hydrolysates of several different oligonucleotides and POCs in a yield of about 0.5 mol of glycine/mol of deoxyadenosine in the oligonucleotide. In addition, it was also observed that the commercially available 3′ and 5′ amino linkers produce their own specific peaks on AAA of a POC hydrolysate (Figure 6). These specific peaks from deoxyadenosine and the linkers may serve as markers to characterize and quantitate POCs.

Two techniques, electrospray ionization (ESI) (*9*, *11*, *30*, *43*) and matrix-assisted laser desorption−ionization/time-of-flight (MALDI-TOF) (*12*, *18*, *19*, *38*) mass spectrometry, have been used to characterize POCs (*44*). Usually, the negative ion mode was used to detect the molecular ion of the POC. The carboxylic acid matrixes, sinapinic acid (*18*), 4-hydroxy-α-cyano-cinnamic (*15*, *44*), and 3-hydroxypicolinic acid (*38*), as well as the non-carboxylic acid matrix, 2,4,6-trihydroxyacetophenone/diammonium salt (*13*) were used for MALDI-TOF analysis. It was suggested that matrix selection for MALDI may be according to the mass ratio between peptide and oligonucleotide (*44*). Both methods gave quite accurate mass determinations, being within a few daltons of the calculated mass for POCs in the range of 9000 Da. However, MALDI-TOF is about an order more sensitive than ESI (*44*). Clearly, mass spectral analysis should become a standard method for characterizing peptides, oligonucleotides, and POCs.

III. APPLICATIONS OF PEPTIDE−OLIGONUCLEOTIDE CONJUGATES

POCs have drawn increasing attention during the past few years. A prominent potential application is antisense therapy, but POCs can be utilized in many different fields (Table 1). A brief summary of some novel designs and applications of POCs is given below.

A. Cellular Delivery. Delivery of an oligonucleotide to its target may be critical to its therapeutic efficacy. An important goal, therefore, is enhancement of transmembrane penetration and localization to the subcellular compartment containing the nucleic acid targets. Oligonucleotide uptake efficiency has been improved by covalent attachment to polylysine or by simply making an ionic, noncovalent complex with polylysine and its derivatives (*45*, *46*). Positively charged surfaces of such complexes or conjugates may adhere to the negatively charged cell surface, resulting in improved transport efficiency. Furthermore, the polycationic component might induce leakage from endosomes, thereby preventing lysosomal entrapment (*47*).

Recently, several well-defined POCs were proposed to improve cellular delivery efficiency. Varying from cell surface receptor binding peptides to nuclear localization peptides all have been investigated for POCs. Receptors on the cell surface were the first type of target used to enhance oligonucleotide delivery. Examples include the Fc receptor binding peptide, TQPREEQYNSTFRV, derived from the putative receptor binding site of rat IgG γ2b (*31*), the tripeptide, Z-D-Phe-L-Phe-Gly (Z = benzyloxycarbonyl), which is a specific inhibitor of cell fusion and hemolysis (*17*), and GCSKAPKLPAALC, a peptide antagonist to the insulin-like growth factor 1 receptor (IGF1−R) (*18*).

The use of appended water-soluble vitamins, such as vitamin B_6 (*48*), has been proposed to improve cellular uptake and bypass lysosomal entrapment. A method for preparing POCs with tethered vitamin B_6 was developed (*49*). In this procedure, pyridoxal was coupled to the N-terminus of an ornithine isopeptide. The pyridoxyl-peptide was then linked via its cysteine thiol group to an iodoacetylated oligonucleotide.

Cell specific intracellular delivery of antisense agents was proposed by attaching the neoglycopeptide, YEE(ahGalNAc)$_3$, to the terminus of methylphosphonate DNAs by a thioether linkage (*50*, *51*). Specificity of delivery, which is to asialoglycoprotein receptors on the cell surface of the human hepatocellular carcinoma, was demonstrated by using cell lines differing in this receptor. The receptor-mediated uptake mechanism of the POC was demonstrated by a competition assay in which adding a 100-fold excess of free ligand inhibited uptake (*50*). The compound was further tested in mice. After tail vain injection of a low picomole amount of the conjugate, 70% of the injected dose accumulated in the liver within 15 min. Conversely, little of the unglycosylated control POC was found in the liver (*51*).

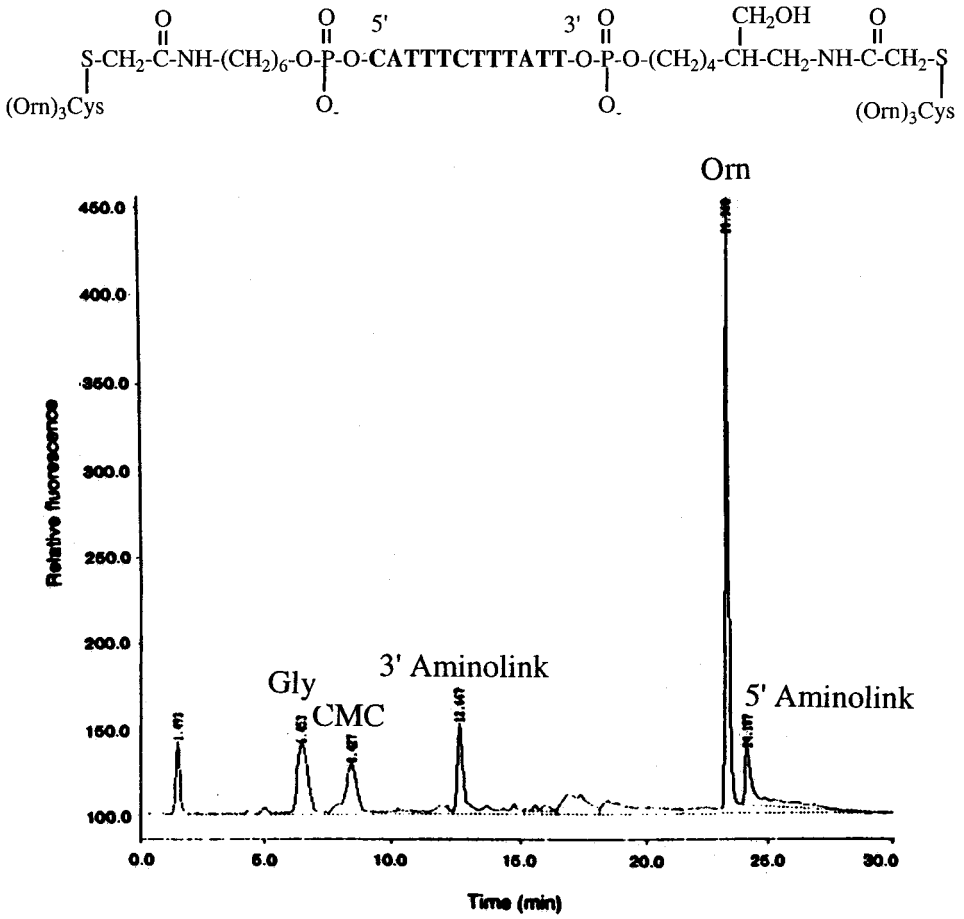

Figure 6. Amino acid analysis of a POC. The structure of the POC is shown. After hydrolyzing in an atmosphere of constant boiling HCl, the hydrolysate was resolved by ion-pair reversed-phase HPLC and detected by postcolumn fluorometric reaction of amino groups on the analytes. Adapted from Zhu et al. (*41*).

The N-terminal region of the transmembrane glycoprotein, gp41, of HIV-1 has been found to be critical to the viral replication cycle. Mutations in this region, which is known to participate in virus/cell membrane fusion, inhibit infection, syncytium formation and cytopathy. The putative fusion peptide derived from this region of gp41, AVGAIGALFLGFLGAAG, and its shorter version, ALFLGFLGAAG, were separately attached to the 3′ terminus of anti-HIV-1 oligonucleotides for the purposes of facilitating trans-membrane delivery and protecting against 3′-exonuclease degradation (*11*). Interestingly, the C-terminus of the same protein has a second membrane fusion and lysis peptide, DRVIEVVQGAYRAIRNIPRRIRQG. It was proposed for oligonucleotide delivery, too (*25*). In this same paper, another fragment, PTSQSRGDPTGPKE, derived from the C-terminus of the HIV tat protein, which has a similar membrane fusion property, was also described (*25*).

It is generally believed that oligonucleotides are transported into cells by an endocytic uptake mechanism. In this pathway, oligonucleotides could be trapped in endosomes, then lysosomes, resulting in degradation by nucleases and, hence, poor therapeutic activity. Influenza viruses have a natural mechanism to overcome lysosomal entrapment. A viral protein fusion domain will cause formation of aggregates as the pH in the endosome decreases. Fusion of the endosomal and viral membranes then occurs, resulting in leakage and entry of the nucleocapsid into the cytosol. Accordingly, the fusion peptide of the influenza hemagglutinin envelope protein, GLFEAIAGFIENGWEGMIDGGGY, has been used for antisense oligonucleotide delivery (*21*) and gene delivery (*52*). The peptide was linked to an anti-TAT (and a nonsense control) phosphodiester oligonucleotide or to the phosphorothioate oligonucleotide, S-dC_{28}, through either a reducible disulfide bond or a nonreducible thioether bond. A 5−10-fold increase in anti-HIV-1 activity was obtained for the conjugates of both the antisense and nonsense phosphodiester oligonucleotides when they were tested in HIV infected CEM-SS lymphocytes.

Endoplasmic reticulum (ER) retaining signal peptides, KDEL and YGEEDTSEKDEL, were proposed for use in improving the trafficking efficiency of oligonucleotides (*29*, *30*). It was suggested that an appended ER recognition signal peptide would allow the endocytosed oligonucleotide to escape from endosomes into ER or Golgi compartments and eventually into the cytosol or nucleus. An oligonucleotide complementary to the translation initiation region of the gag mRNA of HIV-1 was conjugated to ER signal peptides in a two-step conjugation method using either a thioether or a disulfide linkage. Antisense activity was tested in HIV-1 infected human peripheral blood mononuclear cells by measuring reverse transcriptase activity. It was found that the thioether-linked conjugate is three times more potent than the oligonucleotide, whereas the disulfide linked POC is three times less potent than the oligonucleotide itself (*29*).

Nuclear localization is essential for achieving inhibition of transcription via triple helix formation (antigene function). Furthermore, nuclear localization may be preferable for antisense function, since the target pre-mRNA or mRNA in transit to the cytoplasm may be subject to RNase H degradation. A variety of nuclear localization sequences (NLS) may be found in proteins.

Table 1. Peptides Used in POCs

peptide function	peptide sequence	ref
delivery		
cell surface binding		
Fc receptor binding peptide	TQPREEQYNSTFRV	*31*
antagonist to IGF-1 receptor	D-GCSKAPKLPAALC	*18*
β-endophin receptor ligand	YGGFLRRG	*38*
hepatocyte specific delivery	YEE(ah-GalNAc)3	*50*, *51*
cell fusion and hemolysis inhibitor	Z−D-Phe-L-Phe-Gly	*17*
ER retaining	YKDEL	*29*
	YGEEDTSEKDEL	*30*
nuclear localization signal (NLS)	AAKRVKLG	*38*
	QAKKKKLDK	*14*
	-PKKKRKV-	*15*, *20*, *28*, *56*
	CNSAAFEDLRVLS	*28*
	MNKIPIKDLLNPQC	*28*
cell membrane fusion		
viral fusion peptide	AVGAIGALFLGFLGAAG	*11*
Cα-gp41 fusion peptide	DRVIEVVQGAYRAIRNIPRRIRQG	*25*
HIV TAT C-terminus peptide	PTSQSRGDPTGPKE	*25*
lysosomal fusion		
hemagglutinin envelope fusion peptide	GLFEAIAGFIENGWEGMIDGGGYC	*21*
membrane translocation plus nuclease localization signal		
antennapedia peptide	RQIKIWFQNRRMKWKKEN	*24*, *69*
engineered	AAVALLPAVLLALLAPVQRKRQKLMP	*72*
engineered	MGLGLHLLVLAAALQGAKKKRKV	*71*
DNA binding		
cationic peptide	CGGSPKKSPKK	*22*
	CAGAAKKAGAAKK	*22*
	CAAKKAAKKAAKK	*22*
	CTPKRPRGRPKK	*23*
	CAAGAKKAAGAKK	*23*
	KKAAKKACAKKAAKK	*23*
	CAAKKAAKKAAKKAAKK	*23*
	CAARRAARRAARR	*23*
	CAARRAARRAARRAARR	*23*
	(δ-Orn)$_n$-Cys, $n = 3, 8, 12$	*27*
	Cys-(Arg)$_n$-Cys, $n = 3, 5, 7$	*78*
cationic peptide library		*43*, *85*
DNA minor groove (A/T rich) binder	*N*-methylpyrrole carboxamide peptides	*96*
	Dihydropyrroloindole peptides	*97*
bridge peptide	AAAAAA	*19*
	Cys-(Arg)$_n$-Cys, $n = 3, 5, 7$	*78*
RNA binding		
TAR binding	RKKRRQRRRC	*84*
cationic peptide	KKKKKKKK	*93*
artificial nuclease		
	K and H	*108*
	GGH	*26*, *106*
	(LKKL)3	*12*
	HGH	*13*
	KGH	*13*
	HKG	*107*
other		
α-helix peptide	LARLLARLLARL	*31*
probe handle	AKAKAKAKAKA	*6*
	KKKFKn, $n = 0-2$	*9*
c-myc tag peptide	AEQKLISEEDLN	*40*
mass tag		*112*
human neutrophil elastase inhibitor	*N*-methoxysuccinyl-Ala-Ala-Pro-Val	*94*

Nuclear transport sequences derived from SV-40, PKKKRKV (*15*, *20*, *28*, *53*) from nucleoplasmin, QAKKKKLDK (*14*), from influenza virus nucleoprotein, NSAAFEDLRVLS, from yeast α2 protein, MNKIPIKDLLNPQ (*28*), and AAKRVKLG (*38*) have all been covalently tethered to oligonucleotides. For example, a 3′-hexanol-modified 24-mer antisense oligonucleotide, complementary to the mRNA for calmodulin, was reported to alter regulation of membrane ion channels and swimming behavior of single-celled freshwater *ciliate paramecium* (*28*). The oligonucleotide, or its derivatives, was delivered by electroporation, and the effect on swimming behavior was measured. Interestingly, none of the nuclear signal peptide conjugates tested influenced swimming, but the antisense oligonucleotide itself, the antisense oligonucleotide with an amino linker, the antisense oligonucleotide with a single cysteine and the antisense oligonucleotide with a nontargeting peptide, LALAK, did influence swimming behavior. It was suggested that binding to the nuclear transport receptor might sequester the POC (*28*). Recently, Zanta et al. demonstrated that a single copy but not multiple copies of SV40 NLS is able to direct plasmid DNA into the nucleus (*54*, *55*).

Neves et al. prepared a POC with a triple helix forming oligonucleotide and a NLS as an aid for plasmid DNA delivery (*56*). In their design, the NLS, GAGPKKKRKV, was anchored to the 3′ end of the psoralen-labeled oligonucleotide. A homopurine region for triplex formation was cloned into the plasmid at a designated position.

When the oligonucleotide recognizes its target and forms triple helix, the psoralen will become cross linked with the plasmid DNA and bring in an NLS to direct plasmid transportation.

For antisense or antigene applications, the final destination of oligonucleotides could be the nucleus. However, the above-mentioned methods overcome only part of the delivery barrier. Learning from nature, there are some membrane translocational peptides that can cross not only cellular membrane but also nuclear membrane, such as Antennapedia peptide (*57*), HIV tat peptide (*58*), VP22 herpesvirus protein (*59*) and several de novo designed sequences (*60*, *61*). These peptides have been applied to delivery of various payloads in vitro and in vivo (*62*−*68*). In cell culture, a conjugate of an oligonucleotide and the Antennapedia peptide, RQIKIWFQNRRMKWKKEN, which was derived from the third helix of the Antennapedia homeodomain, was able to demonstrate an antisense effect by inhibiting amyloid precursor protein expression at the 40 nM level (*24*). In a separate study, the Antennapedia peptide conjugated oligonucleotide against Cu/Zn superoxide dismutase showed a 100-fold better effect in culture than did the oligonucleotide by itself (*69*). Using the same targeting peptide, peptide nucleic acid (PNA) was efficiently taken up into Bowes cells and its in vivo effect of suppressing expression of functional galanin was also observed after intrathecal administration in rats (*70*).

Currently, Antennapedia and tat peptides are the two most studied membrane translocational signals. They have shown some success in various applications, but there has been little progress on oligonucleotide delivery. One possible reason, in our opinion, is the positive charges on the peptides. Both Antennapedia and tat peptides are highly positively charge peptides, while the oligonucleotides are fully negatively charged compounds. Severe charge interaction may cause aggregation or even precipitation. Thus, a better synthetic approach is needed before further studies can be performed.

Other de novo designed carrier peptides include a hydrophobic fragment of *caiman crocodylus* Ig(v) light chain with an appended NLS from SV40, MGLGLHLLVLAAALQGAKKKRKV (*71*). A membrane permeable signal of the Kaposi fibroblast growth factor with a transcription nuclear factor κB, AAVALLPAVLLALLAPVQRKRQKLMP (*72*), also showed better cellular delivery of oligonucleotides by fluorescence microscopy.

B. Hybrid Stabilization. The strength of hybridization between 2 or more polyanionic oligonucleotide strands is diminished by charge repulsion. One approach to eliminating this charge repulsion effect is to replace the phosphodiester bond with a nonionic linkage, such as in the methylphosphonate or PNA analogues of DNA. Indeed, it has been shown that PNA:DNA or PNA:RNA hybrids are more stable than the corresponding DNA:DNA or DNA:RNA hybrids (*73*). Even further, DNA analogues containing positively charged internucleoside bonds have been prepared (*74*−*76*). The concept is to realize stronger hybridization between the complementary strands due to a charge attraction effect. Instead of modifying the nucleic acid backbone, another approach is to append polycationic moieties to the antisense strand.

A 15-mer oligonucleotide, having a sequence complementary to the initiation region of vesicular stomatitis virus, was covalently linked to poly-L-lysine through an *N*-morpholine ring by sequential periodic acid oxidation of a 3′-terminal ribose, reaction with poly-L-lysine and sodium cyanoborohydride reduction (*77*). The antisense activity of this POC was achieved at a dose as low as

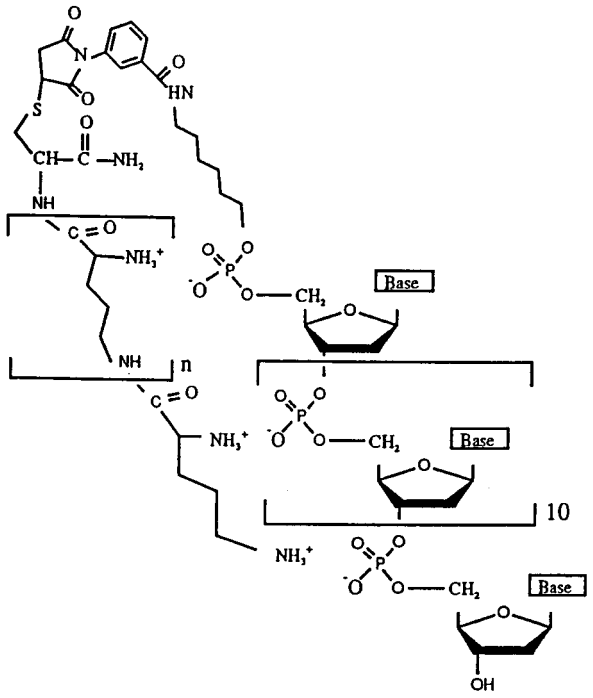

Figure 7. Structure of an oligo(δ)ornithine−oligonucleotide POC. The alignment is depicted to demonstrate the possibility of intramolecular ion pairing. Adapted from Zhu et al. (*32*).

100 nM. Whether the increase in potency was due to stronger target mRNA binding or enhanced cellular uptake, or both, is unknown. In this approach, multiple copies of the oligonucleotide become attached to the amino groups on polylysine in a random and positionally variable manner. As an alternative, we investigated the use of short and well-defined oligocationic peptides (*27*, *32*). An ornithine isopeptide, which was linked from the side-chain amino group to the carboxyl group, was selected first for studying the charge neutralization effect (Figure 7). Since the linear distance between the negatively charged phosphate groups on DNA and that between the α-amino groups on the oligo(δ)ornithine isopeptide are similar, ion-pairing should be possible. A series of ornithine isopeptides of different lengths was linked to a 12-mer antisense oligonucleotide. Thermostability of the POC with its complementary target was found to increase with peptide length with an average increase of about 0.5 °C/ornithine residue. This local charge interaction was observed even in 3 M sodium chloride at neutral pH. A circular dichroism experiment showed that the DNA:POC duplex retained the B-form structure. Site-specific cleavage with RNase H demonstrated that the POC hybridized specifically with its complementary RNA sequence and that the appended peptide did not interfere with RNase H activity, which may be crucial to an effective antisense drug.

A comparable series of oligoarginine peptides of 3, 5, and 7 residues was appended to a 9-mer oligonucleotide (*33*). An average increase in T_m of 2 °C/arginine residue was observed for duplexes with complementary single-stranded DNA (*78*). The charge and hydrogen bonding interactions provided by the guanidine side chain groups in arginine peptides appear to be stronger than those provided by the α-amino groups in oligo(δ)ornithine isopeptides. This difference in thermal stability between appended oligo(δ)ornithine isopeptides and oligoarginine peptides remains to be confirmed using the same oligonucleotide sequences. In a similar study, a small cationic pentapeptide library was prepared using Arg, Lys, Orn,

and His (*43*). It was found that Arg binds tighter than other cationic peptide and histidine peptide is sensitive to pH changes around neutrality.

In other studies, cationic peptides derived from sequences in DNA-binding proteins were disulfide-linked to oligonucleotides and were evaluated by their ability to compete with digestion of the target double-stranded DNA by an oligonucleotide-staphylococcal nuclease conjugate (*22*). The peptides, AGAAKKAGAAKK and AAKKAAKKAAKK, were designed based on staphylococcal nuclease which has 22 lysine residues, including several dilysine repeats on its surface. A tandem repeat of SPKK, GGGSPKKSPKK, which is an A/T rich binding peptide, was also prepared for the same purpose. However, none of these cationic peptide conjugates was able to competitively block the oligonucleotide-staphylococcal nuclease activity. The authors suggested that the binding might depend on structure, not simply on charge. Although these cationic peptides did not block the oligonucleotide-staphylococcal nuclease, they did accelerate hybridization of the appended oligonucleotide to the target strand (23). Compared to the unmodified oligonucleotide, the best peptide, AAKKAAKKAAKKAAKK, was observed to increase the association constant by 48000-fold, as measured by annealing rate of primer on a polymerase chain reaction (PCR). This was even 4-fold faster than for the oligonucleotide-staphylococcal nuclease conjugate. A shorter version, AAKKAAKKAAKK, and an arginine-substituted version, AARRAARRAARRAARR, both had a substantial drop in association constant of more than several 100-fold.

Two oligonucleotides with an appropriate spacer can bind cooperatively and monomerically to two noncontiguous regions of RNA (*79*) or duplex DNA (*80*−*83*). We prepared conjugates in which two oligonucleotides were bridged by cationic oligoarginine peptides (*78*). The oligoarginine peptide could not only act as a spacer, but could also contribute to the affinity. In comparison to the use of a neutral linker, a POC having two 9-mer oligonucleotides linked by an oligoarginine peptide was found to bind tighter to a noncontiguous target single-stranded DNA. The strength of binding, as evaluated by thermostability, was dependent on both the length of the peptide and the spacing between the complementary sites within the target strand. Sequence specificity for target RNA was demonstrated by RNase H footprinting of the RNA/DNA duplex regions.

The repulsive effect of three anionic strands may be of greater significance than for two strands. In triple strand formation, most frequently, the target is a homopurine−homopyrimidine duplex DNA tract and the third strand is either a homopyrimidine or homopurine oligonucleotide that binds according to Hoogsteen or reverse Hoogsteen hydrogen bonding. In vitro, triple strand formation requires the presence of a relatively high concentration of cations, such as at least 1 mM spermine or 10 mM magnesium. We have shown by melting curves that appended polyamines can substantially increase triplex formation capability of an oligonucleotide and can eliminate the requirement for cations in solution (*84*). This work has been extended to peptides (*85*). A series of tetracationic peptides were appended to the triplex-forming strand. As with the polyamines, these POCs showed an enhancement in triplex-formation. In this study, we found that an oligonucleotide as short as a 15-mer, with an attached cationic tetrapeptide, can form a stable triplex without the assistance of other cations, such as magnesium, in phosphate-buffered saline. To date, all of these hybridization stabilizing compounds, except PNA, have been tested only in cell-free assays using physical measurements. The next rational experiments would be to investigate their binding efficiency in cell culture.

C. Structure Recognition. Sequence specificity is important, especially for a clinical product, to avoid unintentional interaction with a nontarget RNA. Statistically, at least a 17-mer is required for a sequence to be unique within the human genome (*86*). An antisense oligonucleotide of shorter length would be expected to have numerous possible hybridization sites in the RNA population of a cell, and most of them would be in nontarget RNAs. In the case of a longer antisense oligonucleotide, the T_m for a duplex with an RNA having one or more mismatches might be sufficiently high to get hybridization to numerous nontarget RNAs. Furthermore, short DNA/RNA hybrids are capable of stimulating RNase H (*84*, *87*), so hybridization of even a portion of the antisense DNA to an RNA target could lead to inappropriate degradation. The tendency of antisense oligonucleotides to cause misdirected cleavage of nontarget RNAs by RNase H has been demonstrated in Xenopus oocytes (*88*). Besides, unexpected nonantisense mechanisms of inhibition have also been reported (*86*, *89*).

Accordingly, other approaches for improving target specificity may be necessary. An impressive example is a bicyclic oligonucleotide that can form a triplex with a single-stranded target by coincident Watson−Crick and Hoogsteen base pairing, providing exceptional specificity and affinity (*90*). Alternatively, there are many proteins that can recognize specific sequences and structures of nucleic acids. Attaching peptide fragments corresponding to these recognition sequences might be an ideal way of increasing the specificity of an oligonucleotide. For example, binding and, hence, antigene activity might be improved by adding a peptide that can recognize a short region of double-stranded DNA in proximity of a homopurine/homopyrimidine stretch. Similarly, antisense activity and specificity might be improved by appending an RNA recognition peptide to a short oligonucleotide.

We have demonstrated by RNase H footprinting this dual specificity concept using the HIV-1 Tat peptide/TAR RNA interaction domains (*84*), which represent a well-studied system (*91*). The TAR RNA has a long duplex stem that is interrupted by a 3-base bulge and a 6-base loop. The new design of the antisense agent is based on both sequence and secondary structure of TAR RNA. An oligonucleotide which base pairs with the single-stranded loop by Watson−Crick hydrogen bonding and an arginine rich peptide, RKKRRQRRR, which recognizes the stem-bulge structure were covalently attached through a flexible tether (Figure 8). It was found that all three parts of this POC (oligonucleotide, linker, and peptide) contribute to the potential antisense activity. Length and direction of the linker could change the RNase H cleavage pattern and efficiency. The 5′-C_{12} amino linker was the best among the three linkers tested. A 6-mer oligonucleotide (no appended peptide), complementary to the 6-base loop of TAR, was capable of stimulating cleavage of RNase H (50% of the TAR was hydrolyzed under the experimental conditions). About 10% RNA cleavage was observed for a complementary 5-mer, but RNase H activity was not observed with a 4-mer oligonucleotide (Figure 9). However, a conjugate of this 4-mer with the Tat peptide was able to stimulate RNase H cleavage of the TAR RNA, with about 3% of the TAR being hydrolyzed under the experimental conditions. Base substitution in the TAR RNA at the peptide recognition site or at the loop site eliminated the RNase H degradation

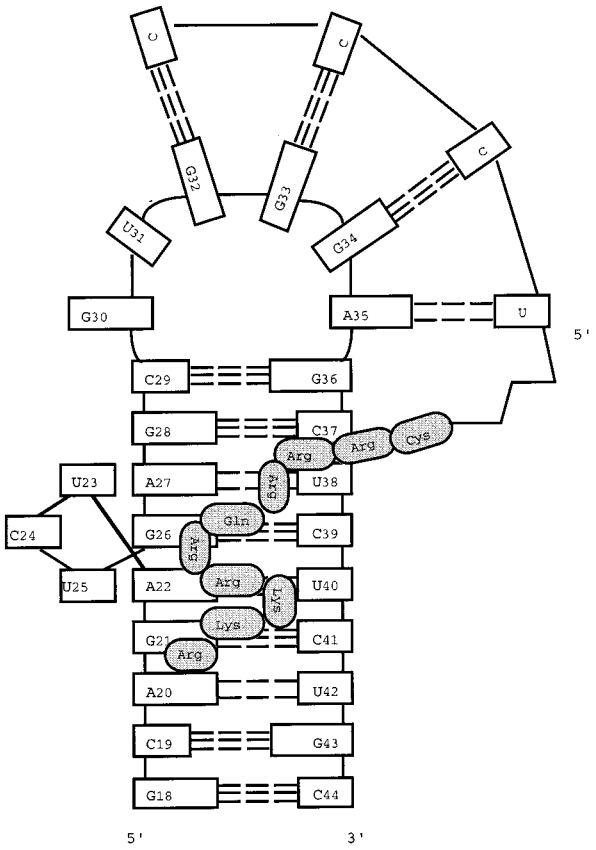

Figure 8. Representation of a dual-specificity antisense agent binding to target RNA. The Tat protein binding domain peptide is known to interact with the UCU unpaired bulge and the neighboring double-stranded stem region. An appended oligonucleotide may base pair with the single-stranded 6-base loop region, thereby stimulating cleavage by RNase H.

(Figure 9). These results demonstrate that the desired antisense target specificity may be achieved with such dual-site recognition strategy. It should be possible to extend this technique to other RNA targets, since highly specific, folded binding sites for small ligands can be present or induced to be present in RNA (*92*).

The concept of dual recognition of an RNA hairpin loop by a POC was investigated using computer modeling (*93*). An octalysine peptide was attached to the center of an oligonucleotide, having 4 nucleotides at each end, through either a D- or L-aspartic alcohol spacer. This pair of 4-nucleotide arms was designed to base pair with the overhanging sequences of an RNA having a hairpin loop, with the intent of achieving electrostatic contacts between the octalysine peptide and the hairpin region. On the basis of computer calculations, the L-aspartic alcohol linker distorted some electrostatic interactions between the positively charged lysine peptide and the phosphate groups on the stem of the RNA hairpin; therefore, the D isomer would be preferred (*93*).

In a variation of the dual specificity approach, library synthesis methodology was used to screen for an oligonucleotide that would bind to the enzyme, neutrophil elastase (*94*). Although oligonucleotides with strong affinity for the enzyme were identified, they did not inhibit its activity. A preselected weak tetrapeptide inhibitor, which was screened from a phage library approach, was applied in this study (*95*). One of these high-affinity, noninhibitory DNA ligands was covalently linked to the tetrapeptide inhibitor of elastase, *N*-methoxysuccinyl-Ala-Ala-Pro-Val. The inhibition efficiency of this POC aptamer was nearly 5 orders of magnitude higher than for the peptide itself. The length of the spacer was found to be critical to the design of the POC inhibitor. When the peptide was linked directly to the DNA ligand without any spacer, no significant improvement in inhibitory activity was observed.

In an antigene approach, *N*-methylpyrrole carboxamide polyamides, which bind to the minor groove of an A/T rich region of double-stranded DNA, were covalently attached to oligothymidine or oligodeoxyadenosine (*96*). The stability of the conjugate was increased with the number of the *N*-methylpyrrole carboxamide residues. Better thermostability was found when the *N*-methylpyrrole carboxamide was linked to the thymidine strand. Since the peptide recognizes only the A−T base pair, the T_m of G−C paired double-stranded DNA was not increased by an appended *N*-methylpyrrole carboxamide. Similar minor groove binding peptides, dihydropyrroloindole peptides, and oligonucleotide conjugates were also prepared and tested on DNA and RNA targets (*97*). The T_m of DNA−RNA complexes was raised significantly by the dihydropyrroloindole peptide conjugates, but was much lower than for the DNA−DNA duplexes. Constrained polyamides have been shown to have even greater affinity for double-stranded DNA, and rules for designing these polyamides have been established to provide the sequence specificity (*98*, *99*).

D. Artificial Nuclease. Instead of depending on recruitment of cellular RNase H, an oligonucleotide with hydrolytic activity against the complementary RNA strand would be ideal for antisense applications (*100*). These nuclease properties would be especially important to backbone-modified oligonucleotide analogues, such as PNA, methylphosphonate or 2′ alkylated RNA, none of which stimulate RNase H activity. Several nucleases have been covalently attached to oligonucleotides for this purpose (*101*). For therapeutic applications, however, a small nuclease mimic would be more realistic than a large enzyme, and specificity for RNA cleavage must be maintained to avoid possible mutagenic effects on chromosomal DNA or toxic consequences from interaction with other cellular components. Studies on the catalytic mechanism of ribonuclease A (*102*) revealed that two imidazole groups on histidine residues and one amino group on lysine are essential for the hydrolytic activity. The imidazole groups act as general acids and bases, whereas the amino group stabilizes the transition state of the RNA hydrolysis reaction. A series of small nuclease mimics which contain intercalator, imidazole, and amino groups with different spacing were reported by us (*103*) and others (*104*, *105*). The intercalators were designed to bring the catalytic groups into the desired geometry and were found to be critical for achieving ribonuclease activity. Limited cleavage was observed, especially when only two groups, either two imidazoles or one imidazole and one amino group, were used. It was also found that cleavage is sensitive to RNA secondary structure. Unfortunately, obtaining appreciable sequence-specific cleaving activity with peptide−intercalator conjugates of oligonucleotides was not achieved.

Short peptides containing imidazole and amino groups but no intercalators, GGH (*26*, *106*), HGH and KGH (*13*), and HKG (*107*), were appended to the oligonucleotides. Site-specific ribonuclease activity was found using an HKG peptide placed in the middle of an oligonucleotide, and similar catalytic activity was observed for an analogue having two imidazole groups (*107*). Although the hydrolytic activity was weak, with less than 10% of the target RNA being cleaved after 5 days of incubation, this was the first report of significant sequence-specific

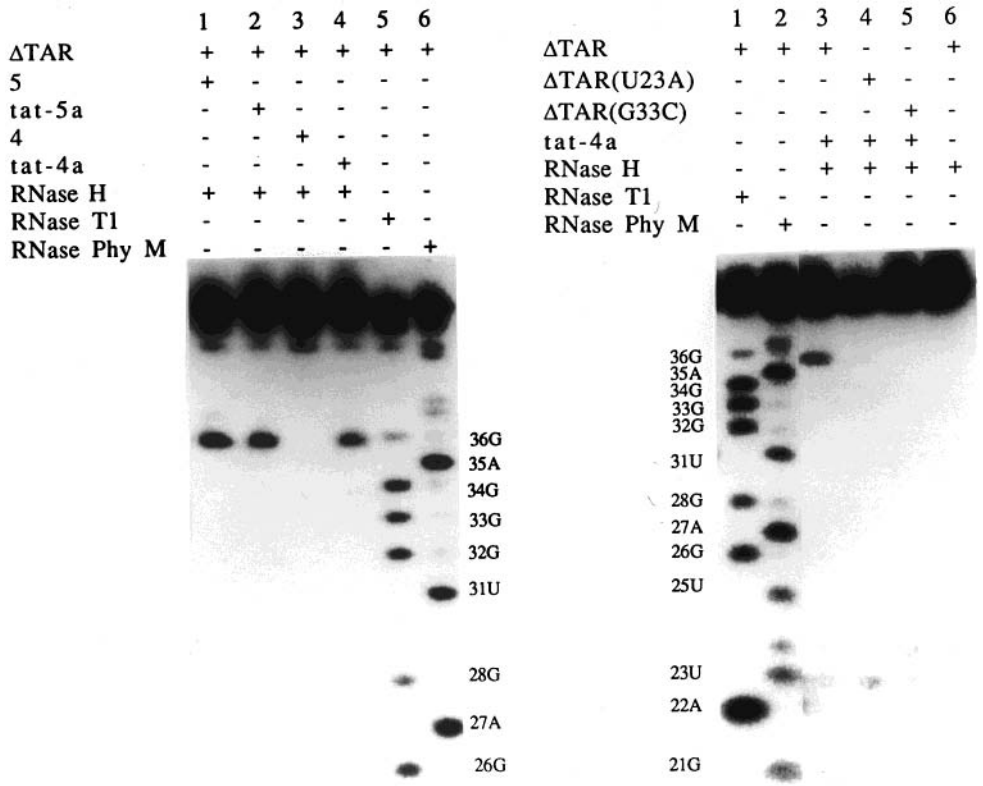

Figure 9. RNase H cleavage assay. The 5′-[^{32}P]phosphorylated 27-mer RNA target (ΔTAR) is shown in Figure 8. The designations "4" and "5" refer to oligonucleotide length, whereas "tat-4a" and "tat-5a" refer to the corresponding POCs. Identification of the bands in this autoradiogram is made by comparison to the cleavage ladder controls (T1 and Phy M ribonucleases). Intact ΔTAR is the top band. The left panel shows that the 5-mer antisense oligonucleotide stimulates site-specific RNase H digestion whether free or appended to the tat peptide. However, the 4-mer antisense oligonucleotide stimulates RNase H cleavage only when appended to the tat peptide. The right panel demonstrates specificity of each component in the POC. A mutant ΔTAR having a base change resulting in mismatch with the antisense oligonucleotide (G33C) is not cleaved, whereas a mutant ΔTAR having a base change resulting in loss of tat peptide binding (U23A) is also not cleaved. Adapted from Tung et al. (*84*).

artificial ribonuclease activity. Achievement of nuclease activity was also attempted by putting imidazole and amino groups at separate positions on oligonucleotides (*108*−*110*). Site-specific cleavage on tRNA up to 50% within 18 h was obtained (*110*). Unfortunately, the kinetics of these synthetic mimics is still far below the natural nucleases. Theoretically, kinetics can be improved by arranging imidazole and other reacting groups into more conformationally constrained positions which are geometrically close to the active site of the enzyme. Of course, it is possible to append to oligonucleotides more reactive reagents, such as a copper (II) chelate, which was shown to hydrolyze RNA in a sequence specific manner (*111*). It is not clear whether this chelate could be maintained in vivo, or whether more reactive chemical groups would have nonspecific toxic effects.

IV. CONCLUSION

Rational drug design is a promising new approach for therapeutics. Sequence specificity, according to Watson−Crick and/or Hoogsteen base pairing rules, constitutes a rational means for inhibiting a particular target nucleic acid associated with a particular disease. POCs can also utilize the nucleic acid recognition properties inherent to peptides. Furthermore, other attributes, such as cell targeting and enhanced cellular uptake and nuclear localization may be contributed by the appended peptide in a POC. The many examples cited in this review illustrate these potential advantages. Perhaps, the utilization of some of these concepts will eventually contribute to the successful application of oligonucleotides to human therapeutics.

Besides their potential use for therapeutic applications, POCs can serve as research tools. Several novel applications have been demonstrated, for example, as fluorescent probes (*7*−*9*), PCR primers (*10*, *21*), and molecular tags for various applications (*40*, *112*). With increased specificity and strength of target binding, POCs may be useful in diagnostic applications or as affinity purification reagents.

During the past several years, many investigators have focused on methods for preparing POCs. However, in our opinion, current synthetic methods, both in-line synthesis and fragment conjugation, are far from being mature. More robust approaches for POC synthesis need to be established. The introduction of automatic DNA and peptide synthesis has contributed to the biotechnology revolution. Automatic in-line synthesis of POCs may have similar impact. Currently, the biggest challenge is to develop new protecting groups which will be compatible with peptide and oligonucleotide synthesis. On the other hand, extensive testing and evaluation of POCs in biological systems is equally demanded. During the preparation of this review, we found that most of the studies on POCs included only synthesis, whereas only a limited number of POCs have been thoroughly studied for their biological effects. Therefore, a concerted effort

by both synthetic chemists and biologists is needed to advance the field of POCs.

ACKNOWLEDGMENT

The authors would like to thank Dr. Chia-Lin Chyan for assisting in Figure 1. This work was supported in part by NIH Grant R21DK55713 (CT).

LITERATURE CITED

(1) Hermann, T., and Patel, D. J. (2000) Adaptive recognition by nucleic acid aptamers. *Science 287*, 820−5.

(2) Wagner, E., Zenke, M., Cotten, M., Beug, H., and Birnstiel, M. L. (1990) Transferrin-polycation conjugates as carriers for DNA uptake into cells. *Proc. Natl. Acad. Sci. U.S.A. 87*, 3410−4.

(3) Wagner, E., Cotten, M., Foisner, R., and Birnstiel, M. L. (1991) Transferrin-polycation−DNA complexes: the effect of polycations on the structure of the complex and DNA delivery to cells. *Proc. Natl. Acad. Sci. U.S.A. 88*, 4255−9.

(4) Citro, G., Perrotti, D., Cucco, C., D'Agnano, I., Sacchi, A., Zupi, G., and Calabretta, B. (1992) Inhibition of leukemia cell proliferation by receptor-mediated uptake of c-myb antisense oligodeoxynucleotides. *Proc. Natl. Acad. Sci. U.S.A. 89*, 7031−5.

(5) Wagner, E., Zatloukal, K., Cotten, M., Kirlappos, H., Mechtler, K., Curiel, D. T., and Birnstiel, M. L. (1992) Coupling of adenovirus to transferrin-polylysine/DNA complexes greatly enhances receptor-mediated gene delivery and expression of transfected genes. *Proc. Natl. Acad. Sci. U.S.A. 89*, 6099−103.

(6) Haralambidis, J., Duncan, L., and Tregear, G. W. (1987) The solid-phase synthesis of oligonucleotides containing a 3′-peptide moiety. *Tetrahedron Lett. 28*, 5199−5202.

(7) Haralambidis, J., Duncan, L., Angus, K., and Tregear, G. W. (1990) The synthesis of polyamide-oligonucleotide conjugate molecules. *Nucleic Acids Res. 18*, 493−9.

(8) Haralambidis, J., Angus, K., Pownall, S., Duncan, L., Chai, M., and Tregear, G. W. (1990) The preparation of polyamide-oligonucleotide probes containing multiple nonradioactive labels. *Nucleic Acids Res. 18*, 501−5.

(9) Tong, G., Lawlor, J. M., Tregear, G. W., and Haralamibids, J. (1995) Oligonucleotide−polyamide hybrid molecules containing multiple pyrene residues exhibit significant excimer fluorescence. *J. Am. Chem. Soc. 117*, 12151−8.

(10) Tong, G., Lawlor, J. M., Tregear, G. W., and Haralamibids, J. (1993) The synthesis of oligonucleotide−polyamide conjugate molecules suitable as PCR primers. *J. Org. Chem. 58*, 2223−31.

(11) Soukchareun, S., Tregear, G. W., and Haralambidis, J. (1995) Preparation and characterization of antisense oligonucleotide−peptide hybrids containing viral fusion peptides. *Bioconjugate Chem. 6*, 43−53.

(12) Truffert, J. C., Lorthioir, O., Asseline, U., Thuong, N. T., and Brack, A. (1994) On-line solid-phase synthesis of oligonucleotide−peptide hybrids using silica supports. *Tetrahedron Lett. 35*, 2353−6.

(13) Truffert, J. C., Asseline, U., Brack, A., and Thuong, N. T. (1996) Synhtesis, purification and characterization of two peptide−oligonucleotide conjugates as potential artificial nucleases. *Tetrahedron 52*, 3005−16.

(14) de la Torre, B. G., Avino, A. M., Tarrason, G., Royo, M., Albericio, F., and Eritja, R. (1994) Stepwise solid-phase synthesis of oligonucleotide−peptide hybrids. *Tetrahedron Lett. 35*, 2733−6.

(15) de La Torre, B. G., Albericio, F., Saison-Behmoaras, E., Bachi, A., and Eritja, R. (1999) Synthesis and binding properties of oligonucleotides carrying nuclear localization sequences. *Bioconjugate Chem. 10*, 1005−12.

(16) Robles, J., Beltran, M., Marchan, V., Perez, Y., Travesset, I., Pedroso, E., and Grandas, A. (1999) Towards nucleopeptides containing any trifunctional amino acid. *Tetrahedron 55*, 13251−64.

(17) Juby, C. D., Richardson, C. D., and Broussear, R. (1991) Facile preparation of 3′ oligonucleotide−peptide conjugates. *Tetrahedron Lett. 32*, 879−882.

(18) Basu, S., and Wickstrom, E. (1995) Solid-phase synthesis of a D-peptide-phosphorothioate oligodeoxynucleotide conjugate from two arms of a poly(ethylene glycol)-polystyrene support. *Tetrahedron Lett. 36*, 4943−6.

(19) Bergmann, F., and Bannwarth, W. (1995) Solid phase synthesis of directly linked peptide-oligodeoxynucleotide hybrids using standard synthesis protocols. *Tetrahedron Lett. 36*, 1839−42.

(20) Eritja, R., Pons, A., Escarceller, M., Giralt, E., and Albericio, F. (1991) Synthesis of defined peptide−oligonucleotide hybrids containing a nuclear transport signal sequence. *Tetrahedron 47*, 4113−20.

(21) Bongartz, J. P., Aubertin, A. M., Milhaud, P. G., and Lebleu, B. (1994) Improved biological activity of antisense oligonucleotides conjugated to a fusogenic peptide. *Nucleic Acids Res. 22*, 4681−8.

(22) Corey, D. R., Munoz-Medellin, D., and Huang, A. (1995) Strand invasion by oligonucleotide-nuclease conjugates. *Bioconjugate Chem. 6*, 93−100.

(23) Corey, D. R. (1995) 48000-fold acceleration of hybridization by chemically modified oligonucleotides. *J. Am. Chem. Soc. 117*, 9373−4.

(24) Allinquant, B., Hantraye, P., Mailleux, P., Moya, K., Bouillot, C., and Prochiantz, A. (1995) Downregulation of amyloid precursor protein inhibits neurite outgrowth in vitro. *J. Cell Biol. 128*, 919−27.

(25) Soukchareun, S., Haralambidis, J., and Tregear, G. (1998) Use of Nalpha-Fmoc-cysteine(S-thiobutyl) derivatized oligodeoxynucleotides for the preparation of oligodeoxynucleotide-peptide hybrid molecules. *Bioconjugate Chem. 9*, 466−75.

(26) Tung, C. H., Rudolph, M. J., and Stein, S. (1991) Preparation of oligonucleotide−peptide conjugates. *Bioconjugate Chem. 2*, 464−5.

(27) Zhu, T., Tung, C. H., Breslauer, K. J., Dickerhof, W. A., and Stein, S. (1993) Preparation and physical properties of conjugates of oligodeoxynucleotides with poly(delta)ornithine peptides. *Antisense Res. Dev. 3*, 349−56.

(28) Reed, M. W., Fraga, D., Schwartz, D. E., Scholler, J., and Hinrichsen, R. D. (1995) Synthesis and evaluation of nuclear targeting peptide-antisense oligodeoxynucleotide conjugates. *Bioconjugate Chem. 6*, 101−8.

(29) Arar, K., Monsigny, M., and Mayer, R. (1993) Synthesis of oligonucleotide−peptide conjugates containing a KDEL signal sequence. *Tetrahedron Lett. 34*, 3087−90.

(30) Arar, K., Aubertin, A. M., Roche, A. C., Monsigny, M., and Mayer, R. (1995) Synthesis and antiviral activity of peptide−oligonucleotide conjugates prepared by using N alpha-(bromoacetyl)peptides. *Bioconjugate Chem. 6*, 573−7.

(31) Ede, N. J., Tregear, G. W., and Haralambidis, J. (1994) Routine preparation of thiol oligonucleotides: application to the synthesis of oligonucleotide−peptide hybrids. *Bioconjugate Chem. 5*, 373−8.

(32) Zhu, T., Wei, Z., Tung, C. H., Dickerhof, W. A., Breslauer, K. J., Georgopoulos, D. E., and Leibowitz, M. J., et al. (1993) Oligonucleotide-poly-L-ornithine conjugates: binding to complementary DNA and RNA. *Antisense Res. Dev. 3*, 265−75.

(33) Wei, Z., Tung, C. H., Zhu, T., and Stein, S. (1994) Synthesis of oligoarginine-oligonucleotide conjugates and oligoarginine-bridged oligonucleotide pairs. *Bioconjugate Chem. 5*, 468−74.

(34) Zubin, E. M., Romanova, E. A., Volkov, E. M., Tashlitsky, V. N., Korshunova, G. A., Shabarova, Z. A., and Oretskaya, T. S. (1999) Oligonucleotide−peptide conjugates as potential antisense agents. *FEBS Lett. 456*, 59−62.

(35) Peyrottes, S., Mestre, B., Burlina, F., and Gait, M. J. (1998) The synthesis of peptide−oligonucleotide conjugates by a fragment coupling approach. *Tetrahedron 54*, 12513−22.

(36) Grandas, A., Robles, J., and Pedroso, E. (1995) Phosphitylation of primary carboxamides − synthesis of peptide−oligonucleotide conjugates with acylphosphoramidate linkers. *Nucleosides Nucleotides 14*, 825−8.

(37) Fujii, M., Hasegawa, T., and Koujima, I. (1997) Preparation of DNA-peptide conjugate using oxime resin. *Nucleic Acids Symp. Ser. 37*, 71−2.

(38) Bruick, R. K., Dawson, P. E., Kent, S. B., Usman, N., and Joyce, G. F. (1996) Template-directed ligation of peptides to oligonucleotides. *Chem. Biol. 3*, 49−56.
(39) de la Torre, B. G., Avino, A. M., Escarceller, M., Royo, M., Albericio, F., and Eritja, R. (1993) Use of base-labile protected derivative of 6-mercaptohexanol for the preparation of oligonucleotides containing a thiol group at the 5′-end. *Nucleosides Nucleotides 12*, 993−1005.
(40) Gottschling, D., Seliger, H., Tarrason, G., Piulats, J., and Eritja, R. (1998) Synthesis of oligodeoxynucleotides containing N4-mercaptoethylcytosine and their use in the preparation of oligonucleotide−peptide conjugates carrying c-myc tag-sequence. *Bioconjugate Chem. 9*, 831−7.
(41) Zhu, T., Peng, Y., Lackland, H., and Stein, S. (1993) Confirmation of oligonucleotide−peptide structure by amino acid analysis. *Anal. Biochem. 214*, 585−7.
(42) Meltzer, N. M., Tous, G. I., Gruber, S., and Stein, S. (1987) Gas-phase hydrolysis of proteins and peptides. *Anal. Biochem. 160*, 356−61.
(43) Harrison, J. G., and Balasubramanian, S. (1998) Synthesis and hybridization analysis of a small library of peptide-oligonucleotide conjugates. *Nucleic Acids Res. 26*, 3136−45.
(44) Jensen, O. N., Kulkarni, S., Aldrich, J. V., and Barofsky, D. F. (1996) Characterization of peptide−oligonucleotide heteroconjugates by mass spectrometry. *Nucleic Acids Res. 24*, 3866−72.
(45) Clarenc, J. P., Degols, G., Leonetti, J. P., Milhaud, P., and Lebleu, B. (1993) Delivery of antisense oligonucleotides by poly(L-lysine) conjugation and liposome encapsulation. *Anticancer Drug Des. 8*, 81−94.
(46) Bordier, B., Perala-Heape, M., Degols, G., Lebleu, B., Litvak, S., Sarih-Cottin, L., and Helene, C. (1995) Sequence-specific inhibition of human immunodeficiency virus (HIV) reverse transcription by antisense oligonucleotides: comparative study in cell-free assays and in HIV-infected cells. *Proc. Natl. Acad. Sci. U.S.A.. 92*, 9383−7.
(47) Boussif, O., Lezoualc'h, F., Zanta, M. A., Mergny, M. D., Scherman, D., Demeneix, B., and Behr, J. P. (1995) A versatile vector for gene and oligonucleotide transfer into cells in culture and in vivo: polyethylenimine. *Proc. Natl. Acad. Sci. U.S.A. 92*, 7297−301.
(48) Zhang, Z. M., and McCormick, D. B. (1991) Uptake of N-(4′-pyridoxyl)amines and release of amines by renal cells: a model for transporter-enhanced delivery of bioactive compounds. *Proc. Natl. Acad. Sci. U.S.A. 88*, 10407−10.
(49) Zhu, T., and Stein, S. (1994) Preparation of vitamin B6-conjugated peptides at the amino terminus and of vitamin B6-peptide−oligonucleotide conjugates. *Bioconjugate Chem. 5*, 312−5.
(50) Hangeland, J. J., Levis, J. T., Lee, Y. C., and Ts'o, P. O. (1995) Cell-type specific and ligand specific enhancement of cellular uptake of oligodeoxynucleoside methylphosphonates covalently linked with a neoglycopeptide, YEE(ah-GalNAc)3. *Bioconjugate Chem. 6*, 695−701.
(51) Hangeland, J. J., Flesher, J. E., Deamond, S. F., Lee, Y. C., Ts, O. P., and Frost, J. J. (1997) Tissue distribution and metabolism of the [32P]-labeled oligodeoxynucleoside methylphosphonate-neoglycopeptide conjugate, [YEE(ah-GalNAc)3]-SMCC-AET-pUmpT7, in the mouse. *Antisense Nucleic Acid Drug Dev. 7*, 141−9.
(52) Plank, C., Oberhauser, B., Mechtler, K., Koch, C., and Wagner, E. (1994) The influence of endosome-disruptive peptides on gene transfer using synthetic virus-like gene transfer systems. *J. Biol. Chem. 269*, 12918−24.
(53) Branden, L. J., Mohamed, A. J., and Smith, C. I. (1999) A peptide nucleic acid-nuclear localization signal fusion that mediates nuclear transport of DNA. *Nat. Biotechnol. 17*, 784−7.
(54) Zanta, M. A., Belguise-Valladier, P., and Behr, J. P. (1999) Gene delivery: a single nuclear localization signal peptide is sufficient to carry DNA to the cell nucleus. *Proc. Natl. Acad. Sci. U.S.A. 96*, 91−6.
(55) Sebestyen, M. G., Ludtke, J. J., Bassik, M. C., Zhang, G., Budker, V., Lukhtanov, E. A., and Hagstrom, J. E., et al. (1998) DNA vector chemistry: the covalent attachment of signal peptides to plasmid DNA. *Nat. Biotechnol. 16*, 80−5.
(56) Neves, C., Byk, G., Scherman, D., and Wils, P. (1999) Coupling of a targeting peptide to plasmid DNA by covalent triple helix formation. *FEBS Lett. 453*, 41−5.
(57) Derossi, D., Joliot, A. H., Chassaing, G., and Prochiantz, A. (1994) The third helix of the Antennapedia homeodomain translocates through biological membranes. *J. Biol. Chem. 269*, 10444−50.
(58) Frankel, A. D., and Pabo, C. O. (1988) Cellular uptake of the tat protein from human immunodeficiency virus. *Cell 55*, 1189−93.
(59) Elliott, G., and O'Hare, P. (1997) Intercellular trafficking and protein delivery by a herpesvirus structural protein. *Cell 88*, 223−33.
(60) Avrameas, A., Ternynck, T., Nato, F., Buttin, G., and Avrameas, S. (1998) Polyreactive anti-DNA monoclonal antibodies and a derived peptide as vectors for the intracytoplasmic and intranuclear translocation of macromolecules. *Proc. Natl. Acad. Sci. U.S.A. 95*, 5601−6.
(61) Lin, Y. Z., Yao, S. Y., Veach, R. A., Torgerson, T. R., and Hawiger, J. (1995) Inhibition of nuclear translocation of transcription factor NF-kappa B by a synthetic peptide containing a cell membrane-permeable motif and nuclear localization sequence. *J. Biol. Chem. 270*, 14255−8.
(62) Phelan, A., Elliott, G., and O'Hare, P. (1998) Intercellular delivery of functional p53 by the herpesvirus protein VP22. *Nat. Biotechnol. 16*, 440−3.
(63) Morris, M. C., Vidal, P., Chaloin, L., Heitz, F., and Divita, G. (1997) A new peptide vector for efficient delivery of oligonucleotides into mammalian cells. *Nucleic Acids Res. 25*, 2730−6.
(64) Aldrian-Herrada, G., Desarmenien, M. G., Orcel, H., Boissin-Agasse, L., Mery, J., Brugidou, J., and Rabie, A. (1998) A peptide nucleic acid (PNA) is more rapidly internalized in cultured neurons when coupled to a retro-inverso delivery peptide. The antisense activity depresses the target mRNA and protein in magnocellular oxytocin neurons. *Nucleic Acids Res. 26*, 4910−6.
(65) Singh, D., Bisland, S. K., Kawamura, K., and Gariepy, J. (1999) Peptide-based intracellular shuttle able to facilitate gene transfer in mammalian cells. *Bioconjugate Chem. 10*, 745−54.
(66) Bhorade, R., Weissleder, R., Nakakoshi, T., Moore, A., and Tung, C. H. (2000) Macrocyclic Chelators with Paramagnetic Cations Are Internalized into Mammalian Cells via a HIV−Tat Derived Membrane Translocation Peptide. *Bioconjugate Chem. 11*, 301−305.
(67) Schwarze, S. R., Ho, A., Vocero-Akbani, A., and Dowdy, S. F. (1999) In vivo protein transduction: delivery of a biologically active protein into the mouse. *Science 285*, 1569−72.
(68) Lewin, M., Carlesso, N., Tung, C. H., Tang, X. W., Cory, D., Scadden, D. T., and Weissleder, R. (2000) Tat peptide-derivatized magnetic nanoparticles allow in vivo tracking and recovery of progenitor cells. *Nat. Biotechnol. 18*, 410−4.
(69) Troy, C. M., Derossi, D., Prochiantz, A., Greene, L. A., and Shelanski, M. L. (1996) Downregulation of Cu/Zn superoxide dismutase leads to cell death via the nitric oxide-peroxynitrite pathway. *J. Neurosci. 16*, 253−61.
(70) Pooga, M., Soomets, U., Hallbrink, M., Valkna, A., Saar, K., Rezaei, K., and Kahl, U., et al. (1998) Cell penetrating PNA constructs regulate galanin receptor levels and modify pain transmission in vivo. *Nat. Biotechnol. 16*, 857−61.
(71) Chaloin, L., Vidal, P., Lory, P., Mery, J., Lautredou, N., Divita, G., and Heitz, F. (1998) Design of carrier peptide−oligonucleotide conjugates with rapid membrane translocation and nuclear localization properties. *Biochem. Biophys. Res. Commun. 243*, 601−8.
(72) Antopolsky, M., Azhayeva, E., Tengvall, U., Auriola, S., Jaaskelainen, I., Ronkko, S., and Honkakoski, P., et al. (1999) Peptide−oligonucleotide phosphorothioate conjugates with membrane translocation and nuclear localization properties. *Bioconjugate Chem. 10*, 598−606.
(73) Egholm, M., Buchardt, O., Christensen, L., Behrens, C., Freier, S. M., Driver, D. A., and Berg, R. H., et al. (1993) PNA hybridizes to complementary oligonucleotides obeying the Watson-Crick hydrogen-bonding rules. *Nature 365*, 566−8.

(74) Browne, K. A., Dempcy, R. O., and Bruice, T. C. (1995) Binding studies of cationic thymidyl deoxyribonucleic guanidine to RNA homopolynucleotides. *Proc. Natl. Acad. Sci. U.S.A. 92*, 7051−5.

(75) Jung, P. M., Histand, G., and Letsinger, R. L. (1994) Hybridization of alternating cationic/anionic oligonucleotides to RNA segments. *Nucleosides Nucleotides 13*, 1597−605.

(76) Fathi, R., Huang, Q., Coppola, G., Delaney, W., Teasdale, R., Krieg, A. M., and Cook, A. F. (1994) Oligonucleotides with novel, cationic backbone substituents: aminoethylphosphonates. *Nucleic Acids Res. 22*, 5416−24.

(77) Lemaitre, M., Bayard, B., and Lebleu, B. (1987) Specific antiviral activity of a poly(L-lysine)-conjugated oligodeoxyribonucleotide sequence complementary to vesicular stomatitis virus N protein mRNA initiation site. *Proc. Natl. Acad. Sci. U.S.A. 84*, 648−52.

(78) Wei, Z., Tung, C. H., Zhu, T., Dickerhof, W. A., Breslauer, K. J., Georgopoulos, D. E., and Leibowitz, M. J., et al. (1996) Hybridization properties of oligodeoxynucleotide pairs bridged by polyarginine peptides. *Nucleic Acids Res. 24*, 655−61.

(79) Cload, S. T., Richardson, P. L., Huang, Y.-H., and Scherpatz, A. (1993) Kinetic and thermodynamic analysis of RNA binding by tethered oligonucleotide probes: alternative structure and conformational changes. *J. Am. Chem. Soc. 115*, 5005−14.

(80) Ono, A., Chen, C. N., and Kan, L. S. (1991) DNA triplex formation of oligonucleotide analogues consisting of linker groups and octamer segments that have opposite sugar−phosphate backbone polarities. *Biochemistry. 30*, 9914−2.

(81) Durand, M., Peloille, S., Thuong, N. T., and Maurizot, J. C. (1992) Triple-helix formation by an oligonucleotide containing one (dA)12 and two (dT)12 sequences bridged by two hexaethylene glycol chains. *Biochemistry 31*, 9197−204.

(82) Beal, P. A., and Dervan, P. B. (1992) Recognition of double helical DNA by alternate strand triple helix formation. *J. Am. Chem. Soc. 114*, 4976−82.

(83) Kessler, D. J., Pettitt, B. M., Cheng, Y. K., Smith, S. R., Jayaraman, K., Vu, H. M., and Hogan, M. E. (1993) Triple helix formation at distant sites: hybrid oligonucleotides containing a polymeric linker. *Nucleic Acids Res. 21*, 4810−5.

(84) Tung, C. H., Wang, J., Leibowitz, M. J., and Stein, S. (1995) Dual-specificity interaction of HIV-1 TAR RNA with Tat peptide-oligonucleotide conjugates. *Bioconjugate Chem. 6*, 292−5.

(85) Tung, C. H., Breslauer, K. J., and Stein, S. (1996) Stabilization of DNA triple-helix formation by appended cationic peptides. *Bioconjugate Chem. 7*, 529−31.

(86) Branch, A. D. (1998) A good antisense molecule is hard to find. *Trends. Biochem. Sci. 23*, 45−50.

(87) Fakler, B., Herlitze, S., Amthor, B., Zenner, H. P., and Ruppersberg, J. P. (1994) Short antisense oligonucleotide-mediated inhibition is strongly dependent on oligo length and concentration but almost independent of location of the target sequence. *J. Biol. Chem. 269*, 16187−94.

(88) Woolf, T. M., Melton, D. A., and Jennings, C. G. (1992) Specificity of antisense oligonucleotides in vivo. *Proc. Natl. Acad. Sci. U.S.A. 89*, 7305−9.

(89) Stein, C. A. (1995) Does antisense exist? *Nat. Med. 1*, 1119−21.

(90) Chaudhurt, N. C., and Kool, E. T. (1995) Very high affinity DNA recognition by bicyclic and cross-linked oligonucleotides. *J. Am. Chem. Soc. 117*, 10434−42.

(91) Frankel, A. D. (1992) Peptide models of the Tat-TAR protein-RNA interaction. *Protein Sci. 1*, 1539−42.

(92) Yang, Y., Kochoyan, M., Burgstaller, P., Westhof, E., and Famulok, M. (1996) Structural basis of ligand discrimination by two related RNA aptamers resolved by NMR spectroscopy. *Science 272*, 1343−7.

(93) Sahasrabudhe, P. V., and Gmeiner, W. H. (1996) The affinity of an oligodeoxynucleotide−peptide conjugate for an RNA hairpin loop depends on stereochemistry at the DNA-peptide junction. *J. Biomol. Struct. Dyn. 13*, 585−91.

(94) Lin, Y., Padmapriya, A., Morden, K. M., and Jayasena, S. D. (1995) Peptide conjugation to an in vitro-selected DNA ligand improves enzyme inhibition. *Proc. Natl. Acad. Sci. U.S.A. 92*, 11044−8.

(95) Roberts, B. L., Markland, W., Ley, A. C., Kent, R. B., White, D. W., Guterman, S. K., and Ladner, R. C. (1992) Directed evolution of a protein: selection of potent neutrophil elastase inhibitors displayed on M13 fusion phage. *Proc. Natl. Acad. Sci. U.S.A. 89*, 2429−33.

(96) Sinyakov, A. N., Lokhov, S. G., Kutyavin, I. V., Gamper, H. B., and Meyer, R. B. (1995) Exceptional and selective stabilization of A−T rich DNA-DNA duplexes by N-methylpyrrole carboxamide peptides conjugated to oligodeoxynucleotides. *J. Am. Chem. Soc. 117*, 4995−6.

(97) Lukhtanov, E. A., Kutyavin, I. V., Gamper, H. B., and Meyer, R. B., Jr. (1995) Oligodeoxyribonucleotides with conjugated dihydropyrroloindole oligopeptides: preparation and hybridization properties. *Bioconjugate Chem. 6*, 418−26.

(98) Cho, J., Parks, M. E., and Dervan, P. B. (1995) Cyclic polyamides for recognition in the minor groove of DNA. *Proc. Natl. Acad. Sci. U.S.A. 92*, 10389−92.

(99) Dervan, P. B., and Burli, R. W. (1999) Sequence-specific DNA recognition by polyamides. *Curr. Opin. Chem. Biol. 3*, 688−93.

(100) Haner, R., and Hall, J. (1997) The sequence-specific cleavage of RNA by artificial chemical ribonucleases. *Antisense Nucleic Acid Drug Dev. 7*, 423−30.

(101) Uchiyama, Y., Inoue, H., Ohtsuka, E., Nakai, C., Kanaya, S., Ueno, Y., and Ikehara, M. (1994) DNA-linked RNase H for site-selective cleavage of RNA. *Bioconjugate Chem. 5*, 327−32.

(102) Breslow, R., and Xu, R. (1993) Recognition and catalysis in nucleic acid chemistry. *Proc. Natl. Acad. Sci. U.S.A. 90*, 1201−7.

(103) Tung, C. H., Wei, Z., Leibowitz, M. J., and Stein, S. (1992) Design of peptide-acridine mimics of ribonuclease activity. *Proc. Natl. Acad. Sci. U.S.A. 89*, 7114−8.

(104) Podyminogin, M. A., Vlassov, V. V., and Giege, R. (1993) Synthetic RNA-cleaving molecules mimicking ribonuclease A active center. Design and cleavage of tRNA transcripts. *Nucleic Acids Res. 21*, 5950−6.

(105) Shinozuka, K., Shimizu, K., Nakashima, Y., and Sawai, H. (1994) Synthesis and RNA cleaving activities of polyamine derived novel artificial ribonuclease. *Bio. Med. Chem. Lett. 4*, 1979−82.

(106) De Napoli, L., Messere, A., Montesarchio, D., Piccialli, G., Benedetti, E., Bucci, E., and Rossi, F. (1999) A new solid-phase synthesis of oligonucleotides 3′-conjugated with peptides. *Bioorg. Med. Chem. 7*, 395−400.

(107) Reynolds, M. A., Beck, T. A., Say, P. B., Schwartz, D. A., Dwyer, B. P., Daily, W. J., and Vaghefi, M. M., et al. (1996) Antisense oligonucleotide containing an internal, nonnucleotide-based linker promote site-specific cleavage of RNA. *Nucleic Acids Res. 24*, 760−65.

(108) Bashkin, J. K., McBeath, R. J., Modak, A. S., Sample, K. R., and Wise, W. B. (1991) Synhtesis and characterization of oligonucleotide peptide. *J. Org. Chem. 56*, 3168−76.

(109) Prakash, T. P., Krishnakumar, R., and Ganesh, K. N. (1993) Approaches to nuclease models: synthesis and conformational studies of dTprA conjugated with histamine at C8(A) and ethylenediamine at C5′(T). *Nucleosides Nucleotides 12*, 713−28.

(110) Ushijima, K., Gouzu, H., Hosono, K., Shirakawa, M., Kagosima, K., Takai, K., and Takaku, H. (1998) Site-specific cleavage of tRNA by imidazole and/or primary amine groups bound at the 5′-end of oligodeoxyribonucleotides. *Biochim. Biophys. Acta 1379*, 217−23.

(111) Bashkin, J. K., Frolova, E. I., and Sampath, U. (1994) Sequence-specific cleavage of HIV mRNA by a ribozyme mimic. *J. Am. Chem. Soc. 116*, 5981−2.

(112) Olejnik, J., Ludemann, H. C., Krzymanska-Olejnik, E., Berkenkamp, S., Hillenkamp, F., and Rothschild, K. J. (1999) Photocleavable peptide-DNA conjugates: synthesis and applications to DNA analysis using MALDI-MS. *Nucleic Acids Res. 27*, 4626−4631.

BC0000334

Translocation Properties of Novel Cell Penetrating Transportan and Penetratin Analogues

Maria Lindgren,[†] Xavier Gallet,[‡] Ursel Soomets,[†,§] Mattias Hällbrink,[†] Ebba Bråkenhielm,[†] Margus Pooga,[†,||] Robert Brasseur,[‡] and Ülo Langel*[,†]

Department of Neurochemistry and Neurotoxicology, Arrhenius Laboratories, Stockholm University, S-106 91 Stockholm, Sweden, Centre de Biophysique Moléculaire Numérique, Faculté Universitaire des Agronomiques, Passage des déportés 2, 5030 Gembloux, Belgium, Department of Biochemistry, Tartu University, Ravila 19, 50411, Tartu, Estonia, and Estonian Biocenter, Riia 23, 51010, Tartu, Estonia. Received November 12, 1999; Revised Manuscript Received May 1, 2000

Novel analogues of the cell-penetrating peptides penetratin and transportan were synthesized. The distribution of the biotin-labeled peptides in Bowes melanoma cell line has been investigated by indirect fluorescence with fluorescein-streptavidin detection. The time course of uptake of ^{125}I-labeled transportan analogues has been characterized in the same cell line. Molecular modeling was used to analyze the penetration and the orientation of molecules in a simulated biological membrane. The results, both from molecular modeling and fluorescence studies, imply that penetratin and transportan do not enter the cells by related mechanisms and that they do not belong to the same family of translocating peptides.

INTRODUCTION

A number of techniques has been developed to deliver different cellular effectors into cells. The majority of techniques of delivery are invasive, like electroporation and microinjection. Liposome encapsulation and receptor-mediated endocytosis are milder methods, but also suffer from serious drawbacks, in particular, low delivery yield. As a new candidate with fewer drawbacks stands the class of transporting peptides with an ability to enter the cells in an energy-independent manner and also to bring certain macromolecules into the cells (for review see ref *1*).

Recently, a rapidly expanding family of peptide-based cellular transporters has been developed by several research groups. The initial work was carried out on a 16 amino acid long peptide derived from the third helix of the Antennapedia homeodomain protein crossing plasma membranes with high efficacy in an energy independent manner (*2*, *3*). This opened up new possibilities for the development of useful and efficient carrier vectors. Indeed, this peptide, the first member of the family of peptide transport vectors today known as penetratins, has now been shown to deliver small proteins, DNA (*4*), and PNA[1] oligomers into cells (*5*). Structure/function studies have been carried out on penetratin in order to define the structural requirements and the mechanism of the cell penetration and to improve the carrier efficacy of the peptides (*6*, *7*).

Transportan (*8*), a 27 amino acid long chimeric peptide, introduced by our group, is a combination of the N-terminal fragment of the neuropeptide galanin and the membrane interacting wasp venom peptide mastoparan. A Lys[13] residue connects these two bioactive peptides, and its ε-amino group is used for coupling of cargoes. Transportan, like penetratin, efficiently crosses plasma membranes in an energy independent manner (*8*).

In this paper, the two translocating peptides, penetratin and transportan, and their novel analogues, have been tested for their ability to enter Bowes melanoma cells by using indirect fluorescence and ^{125}I-labeled or fluorophor-labeled peptides. Additionally, molecular modeling was used to analyze the interaction of peptides with membranes. This theoretical approach reveals that penetratin and transportan may not insert into the phospholipid bilayer in the same manner and may have different orientation in the membrane.

EXPERIMENTAL PROCEDURES

Peptide Synthesis. The peptides were synthesized in a stepwise manner in a 0.1 mmol scale on a model 431A peptide synthesizer (Applied Biosystems) using *t*-Boc strategy of solid-phase peptide synthesis. *tert*-Butyloxycarbonyl amino acids were coupled as hydroxybenzotriazole esters to a *p*-methylbenzylhydrylamine (MBHA) resin (Bachem, Switzerland) to obtain C-terminally amidated peptides. Biotin was coupled manually to ε-amino group of Lys after orthogonal deprotection from Fmoc-group, using 3-fold excess of HOBt and TBTU activated biotin (Chemicon, Sweden) in DMF to the peptide on resin. Deprotection of the side chains from formyl and benzyl groups was carried out using the low TFMSA method. The peptides were cleaved with liquid HF at 0 °C for 30 min in the presence of *p*-cresol or thiocresol/*p*-cresol as scavengers when Met was present. The purity

* To whom correspondence should be addressed. Phone: 46-8-161793. Fax: 46-8-161371. E-mail: ulo@neurochem.su.se.
[†] Department of Neurochemistry and Neurotoxicology.
[‡] Centre de Biophysique Moléculaire Numérique.
[§] Department of Biochemistry.
[||] Estonian Biocenter.

[1] Abbreviations: PNA, peptide nucleic acid; HOBt, hydroxybenzotriazole, TBTU, 2-(1H-benzotriazole-1-yl)- 1,1,3,3- tetramethyluronium tetrafluoroborate, FITC; fluorescein-5-isothiocyanate, GRAVY; grand average of hydrophathicity, RAMSES; rapid analysis master/salves extensible system, MHP; molecular hydrophobic potentials, TFMSA; trifluoromethane sulfonic acid, HF; hydrofluoric acid, ER; endoplasmatic reticulum, ABZ; anthranilic acid, HKR; Hepes Krebs Ringer buffer.

10.1021/bc990156s CCC: $19.00 © 2000 American Chemical Society
Published on Web 09/18/2000

Table 1. Comparison of Cell Penetrating Properties of Penetratin and Its Novel Analogues in Bowes Cells[a]

peptide	uptake indirect fluorescence
biotinyl-penetratin(1−16)-[$N^{1\alpha}$-biotinyl]-pAntp(43−58) (*6*), biotinyl-RQIKIWFQNRRMKWKK amide	+
[$N^{1\alpha}$-biotinyl]-[D-Pro^8]-ent-Penetratin−amide, biotinyl-all-D-RQIKIWFPNRRMKWKK amide	++
[$N^{1\alpha}$-biotinyl]-Arg-Phe-Trp-Ile-Asn-Lys−penetratin(8−16) amide, biotinyl-RFWINKQNRRMKWKK amide	+
[$N^{1\alpha}$-biotinyl, Leu^6]−penetratin, biotinyl-RQIKILFQNRRMKWKK amide	−
[bis-$N^{1\alpha}$−biotinyl,$N^{16\epsilon}$-penetratin (1-15)]−biotinyl-penetratin(1−16), biotinyl-RQIKIWFQNRRMKWK-[biotinyl-RQIKIWFQNRRMKWKK] amide	++

[a] Cells were incubated with 10 μM peptides at 37 °C for 60 min. The uptake efficiency is estimated fluorescence intensity and relative to the transportan original sequence [(++) comparable uptake to that of transportan, (+) a peptide with half the intensity compared to transportan, (−) no noticeable difference from control cells, that is without addition of peptide].

of the peptides was > 98% as demonstrated by HPLC on an analytical Nucleosil 120-3 C_{18} RP-HPLC column (0.4 × 10 cm). The molecular masses of the peptides were determined with a Plasma Desorption Mass Spectrometer (Bioion 20, Applied Biosystem) and the calculated values were obtained in each case.

Iodination. Peptide iodination was carried out by the chloramine T method (*9*). $Na^{125}I$ (specific activity 16.1 mCi/mg, concentration 0.1 mCi/mL) was mixed with 5 equiv of the peptides, and phosphate buffer was added in 10-fold excess. The chloramine T solution was prepared at a concentration of 2 mg/mL in phosphate buffer, pH 7.4. After 2 min of incubation, the reaction was stopped by adding sodium metabisulfit (2.4 mg/mL in phosphate buffer, pH 7.4). The peptides were purified on a reversed-phase, RP, column SEP-PAK 51910 (Millipore) using stepwise gradient of acetonitrile in water. The iodination was performed using 1 mCi $Na^{125}I$ and 4.9 nmol of biotinylated peptide for transportan and transportan 2, while transportan 3 was iodinated using 5 mCi of $Na^{125}I$ and 12.6 mmol, respectively. The fractions with the highest specific activity of radiolabeled peptides were used in the experiments.

Cells. The human Bowes melanoma cell line was cultivated in minimal essential medium with Earl-salts (MEM) supplemented with 10% foetal calf serum, 2 mM L-glutamine, 100 IU/mL penicillin and 100 μg/mL streptomycin in air with CO_2 enriched to 5% at 37 °C. Bowes cells were grown on round glass coverslips in a 24 well plate to approximately 50% confluence.

Cellular Penetration of Biotinyl-Labeled Peptides. The medium containing serum was exchanged for a serum-free medium, and a water solution of the biotinyl-peptides was added directly into the medium. The cells were then incubated for different time periods in 5% CO_2 enriched air at 37 °C. The cells were washed twice with PBS, fixed, and permeabilized with methanol for 10 min at −20 °C, washed again with PBS, and incubated for 1 h in a 5%(w/v) solution of bovine serum albumin in PBS in order to decrease unspecific binding. The peptides were visualized by staining with streptavidin-FITC (Amersham, U.K.) in the same solution for 1 h at room temperature. The cell nuclei were stained with Hoechst 33 258 (0.5 μg/mL) for 5 min, after which the coverslips were washed five times with PBS and mounted in 20% glycerol in PBS. As an control the same procedure was performed with an alternative fixation method: 3% *p*-formaldehyde in PBS 15 min and then pearmabilised for 3 min on ice with 30 mM Hepes buffer with 0.5% Triton X-100 (Sigma). This was done to distinguish membrane associated peptides from internalized peptides. The images were obtained by Zeiss Axioplan 2 microscope (Carl Zeiss Inc., Germany) equipped with a cooled digital CCD camera C4880 (Hamamatsu Photonics, Japan) or by a laser scanning confocal microscope (model LSM 510; Carl Zeiss Inc., Sweden) equipped with an Ar laser (488 nm), a He/Ne laser (543 nm), a 63 × 1.4 oil immersion objective. The Ar and He/Ne lasers were operated at 8 and 60% power, respectively. Images were processed using Adobe Photoshop 3.0 software (Adobe systems Inc., CA).

Cellular Penetration of ^{125}I-Labeled Peptides. Bowes cells were grown to 70−80% confluence in 75 cm^2 flask. The cells were scraped off and centrifuged at 1500 rpm for 10 min. The supernatant was discarded and the pellet resuspended in 2 mL of Hepes-buffered Krebs Ringer solution (HKR), pH 7.4 (5 mM Hepes, 137 mM NaCl, 2.68 mM KCl, 2.05 mM $MgCl_2 \cdot 6H_2O$, 1.8 mM $CaCl_2 \cdot 2H_2O$) with the addition of 1 mg/mL BSA. The cell suspension was aliquoted and the iodinated peptides were added to reach an activity of 1 million cpm/tube. The samples were incubated in a water bath at 37 °C up to 240 min. The samples were centrifuged through a mixture of 40% dioctylphthalate and 60% dibutylphthalate. The fractions were counted in γ-counter (Packard). Penetration of $Na^{125}I$ into Bowes cells was measured to estimate the intactness of cells and nonspecific binding.

Comparison of Transportan and Penetratin Uptake. Approximately 70.000 detached Bowes cells were incubated in HKR containing 10 μM ABZ-labeled peptides for 30 min in 37 °C and subsequently treated with 0.25% trypsin for 4 min to remove surface-bound peptide. The cells were harvested by centrifugation and washed twice. The fluorescence intensity was measured in a Hitachi F-2000 fluorescence spectrophotometer. As a control, peptides treated with trypsin prior to incubation with the cells, were used.

Prediction Programs. The characteristics presented in Table 3 are calculated using Prot Param prediction program (*10*). Statistical analysis of 44 proteins has revealed that there are certain dipeptides that occur in proteins in correlation with the stability of the protein (*11*). A weight value of instability to each of the 400 different dipeptides has been assigned. Using these weight values it is possible to compute an instability index (*11*). A protein whose instability index is smaller than 40 is predicted as stable, a value above 40 predicts that the protein may be unstable.

The estimated half-life is based on the findings that the N-terminal amino acid residue of a peptide plays an important role in determining its ubiquitin-mediated proteolytic stability in vivo (*12*−*14*). The set of individual amino acids can thus be ordered with respect to the half-lives that they confer when present at the amino terminus of a protein.

Table 2. Comparison of Cellular Uptake and Localization of Novel Transportan Analogues in Bowes Cells[a]

name	uptake indirect fluorescence
[$N^{13\varepsilon}$-biotinyl]transportan (*8*), GWTLNSAGYLLGK[biotinyl]INLKALAALAKKIL amide	++
[$N^{13\varepsilon}$-biotinyl]transportan 2, [GWTLNSAGYLLGK[biotinyl]INLKAKAALAKKLL amide[b]	++
[$N^{9\varepsilon}$-biotinyl]transportan 3, $C_6H_5CH_2CO$-Y(Me)FQNRPRYK[biotinyl]-(Ahx)[c]-INLKALAALAKKIL-amide	+
[$N^{13\varepsilon}$-biotinyl]transportan 4, GWTLNSAGYLLGK[biotinyl]FLPLILRKIVTAL amide[d]	−
[$N^{13\varepsilon}$-biotinyl,Pro^6]transportan or transportan 5, GWTLNPAGYLLGK[biotinyl]INLKALAALAKKIL amide	+
[$N^{13\varepsilon}$-biotinyl,Pro^6,Pro^7]−transportan or transportan 6, GWTLNPPGYLLGK[biotinyl]INLKALAALAKKIL amide	+

[a] Cells were incubated with 10 μM peptides at 37 °C for 60 min. The uptake efficiency is estimated and relative to the transportans original sequence [(++) comparable uptake to that of transportan, (+) a peptide with half the intensity compared to transportan, (−) no noticeable difference from control cells, that is without addition of peptide]. [b] Mas17, inactive mastoparan analogue, INLKAKAALAKKLL amide. [c] Synthetic vasopressin antagonist, $C_6H_5CH_2CO$−Y(Me)FQNRPRY, Ahx 6-aminohexanoic acid. [d] Membrane associating hornet venom crabrolin, FLPLILRKIVTAL amide.

Table 3. Physicochemical Properties of Penetratin and Transportan and the Improved Analogue Transportan 2[a]

characteristics	penetratin	transportan	transportan 2
1. no. of amino acids	16	27	27
2. pI	12.31	10.18	10.30
3. no. of charged amino acids	7+/0-	3+/0-	5+/0-
4. maximal reported cargo	55-mer DNA oligo (*4*)	21-mer PNA (*5*)	biotin
5. estimated half-life (in mammalian reticulocytes, in vitro) (h)	1	30	30
6. aliphatic index	48.75	148.52	134.07
7. GRAVY	−1.731	0.633	0.322
8. instability index	46.6	0.04	−7.09

[a] Prediction program ProtParam (http://expasy.hcuge.ch/cgi-bin/protparam) has been applied in calculations (*10*).

By statistical analysis (*15*), it has been shown that the aliphatic index, which is defined as the relative volume of a protein occupied by an aliphatic side chain, is significantly higher for proteins of thermophilic bacteria as to proteins found in other species. The aliphatic index may be regarded as a positive factor for the increase of thermostability of globular proteins.

GRAVY (*16*) or grand average of hydropathy values for a protein is achieved by sum the hydropathy values of all the amino acids and dividing by the number of residues in the sequence. The GRAVY score differs significantly for membrane embedded (high values), membrane bound and soluble proteins (usually negative values).

Membrane Interaction Modeling. The structure of each peptide (Tables 1 and 2) was predicted using the Stereo alphabet procedure. To each of the *n* amino acids of the sequence, six pairs of (ϕ,ψ) angles were attributed: −60°,−40° (right α-helix); −160°,160° (β-sheet); −140°,-80° (intermediary structure between β-sheet and 3^{10} helix); −80°,160° (helix of the polyproline); −80°,80° (3^{10} helix), and 60°,60° (left. α-helix). These structures correspond to the minimal energy states of an alanine residue on the van der Waals and electrostatic energy maps (*17*). The energy of each of the 6^n combinations was calculated and the conformations of minimal energy were recorded. They were submitted to a Simplex minimization procedure. This calculation was carried out in a medium of intermediate dielectric constant of a hydrophobic/hydrophilic interface (*18*). Nonpeptidic parts of molecules (biotin, amide group) were added using the Hyperchem 5.0 software (Autodesk, Sausalito, Ca).

In the Impala procedure (*19*), an empirical function *C* is used to describe the water−lipid interface. Considering that the properties of the membrane are constant in the plane of the bilayer, *C* varies along the *z* axis, normal to the lipid bilayer and has its origin ($z = 0$) at the center of the membrane.

$$C(z) = 1/[1 + \exp[\alpha(|z| - z_o)]]$$

With α and z_o defined so that $C \approx 1$ for $z < 18.5$ and $z > 18.5$ and $C \approx 0$ for $-13.5 < z < 13.5$. The interaction between the peptides and the lipids are described by the sum of two restraint functions:

$$E_{int} = -\sum_{(i=1,n)} S_i E_{tr_i} C(z_i)$$

E_{int} simulates the hydrophobic effect depending on the accessible surface of the peptides, and S_i is the atomic free energy of transfer from a hydrophobic to a hydrophilic phase E_{tr_i} and the position z_i of each atom *i*.

The second term mimics the solvophobic effect in the lipid phase:

$$E_{lip} = a_{lip} \sum_{(i=1,n)} S_i C(z_i)$$

where a_{lip} is an empirical constant.

The term E_{lip} tends to minimize the interactions between the peptide and the lipid if they are not as favorable as lipid/lipid interactions are. The conformation of peptides was fixed and their position and orientation were tested by running a Monte Carlo procedure of 10^5 steps at 310 K. Maximal rotations of 5 °C and translations of 1 Å were allowed. The Tammo procedure (*19*) was used to calculate the starting position of peptides at a single water/lipid interface taking into account the hydrophobic and the hydrophilic center of molecules. The peptide orientation of minimal energy was retained.

Calculations were performed on RAMSES (Rapid Analysis Master/Salves Extensible System), parallel hardware of 21 Tracor Europa Pentium Pro PC connected by a 100 megabyte network and controlled by a HP Vectra VA Pentium Pro. The calculation software have been developed in our laboratory (*19*). Molecular visualizations were

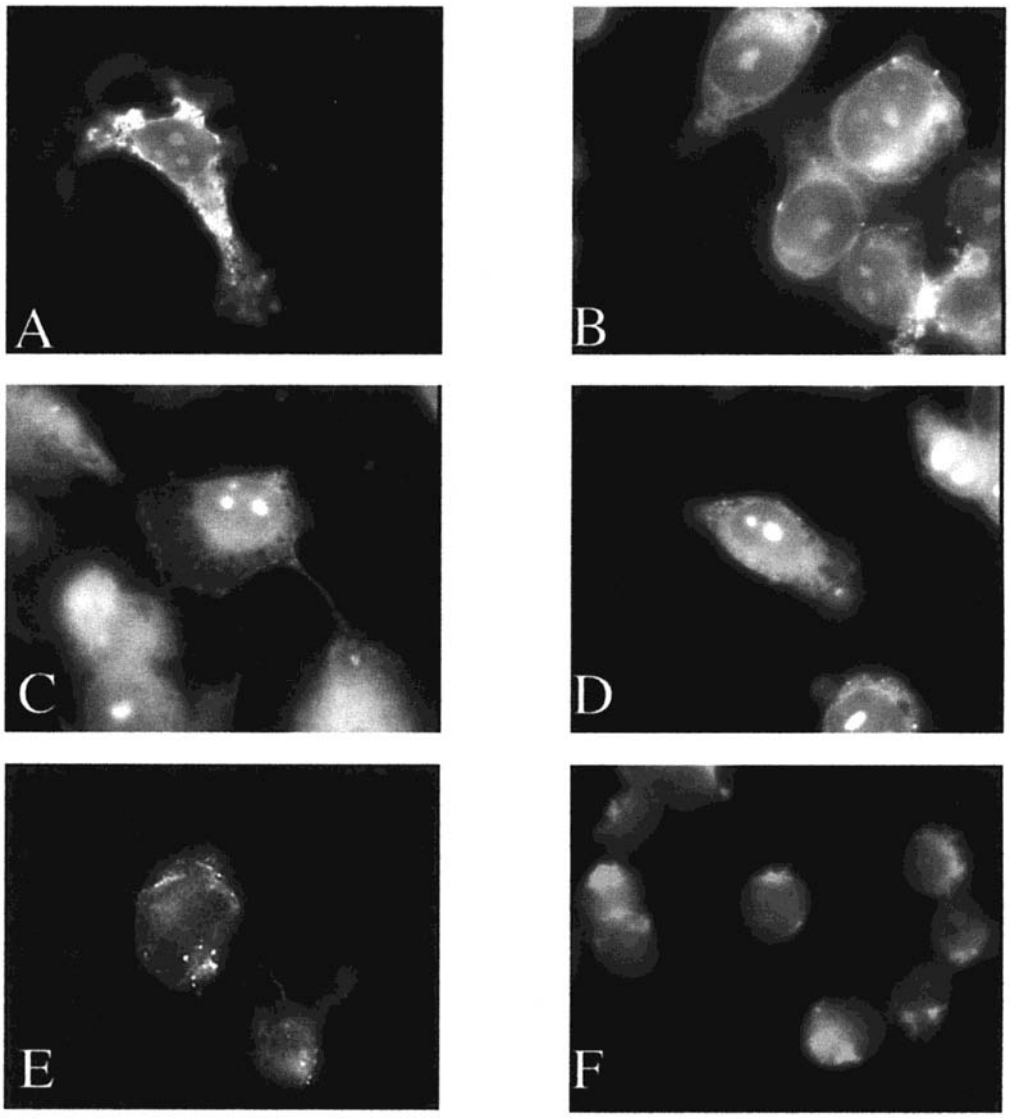

Figure 1. Internalization of biotinyl-peptides, by Bowes melanoma cells visualized by staining with streptavidin-FITC. Cells were incubated with 10 μM peptides for 30 min. (A and B) Transportan at 37 and 4 °C, respectively. (C and D) Penetratin at 37 and 4 °C, respectively. (E) transportan 3 at 37 °C and (F) control cells without any peptide added.

performed using WinMGM 2.0 software (*20*) from Ab Initio Technology (Obernai, France).

RESULTS

The new biotinyl-penetratin analogues [$N^{1\alpha}$-biotinyl]-[D-Pro^8]-*ent*-penetratin and [$N^{1\alpha}$-biotinyl-$N^{16\epsilon}$-penetratin-(1−15)]-penetratin(1−16) showed somewhat higher intracellular concentrations as judged by fluorescence microscopy of bound streptavidin-FITC than the biotinyl-penetratin(1−16) (Table 1).The peptides [$N^{1\alpha}$-biotinyl]-Arg-Phe-Trp-Ile-Asn-Lys-penetratin(8−16) and [$N^{1\alpha}$-biotinyl,Leu^6]-penetratin showed detectable but lower intracellular concentrations (Table 1).

All the new transportan analogues, except transportan 4 (Table 2), were also found to translocate into Bowes cells, both at 4 and at 37 °C. The peptides seem to associate with intracellular membranous structures, such as the ER and Golgi, but were also detectable in the cytosol. Transportan 3 treated cells had somewhat lower fluorescent signal as compared to transportan, while transportan 2 showed a comparable signal (Table 2). These data are in accordance with data obtained with iodinated peptides (Figure 2). Transportan 4 had the lowest penetration capability of all the peptides in this study.

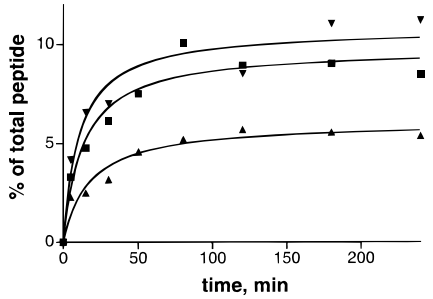

Figure 2. Cellular uptake of [^{125}I]transportan and its [^{125}I]-analogues into Bowes melanoma cells. Cells were incubated at 37 °C with 10 nM [^{125}I]transportan (■), 10 nM [^{125}I]transportan 2 (▼), 10 nM [^{125}I]transportan 3 (▲). Points are experimental; curves were fitted with the aid of the nonlinear regression program (GraphPad Software, Inc.).

The two transportan analogues with proline substitutions did give weaker staining than the original peptide but comparable signal to transportan 3. The order of cellular uptake by immuno fluorescence was transportan

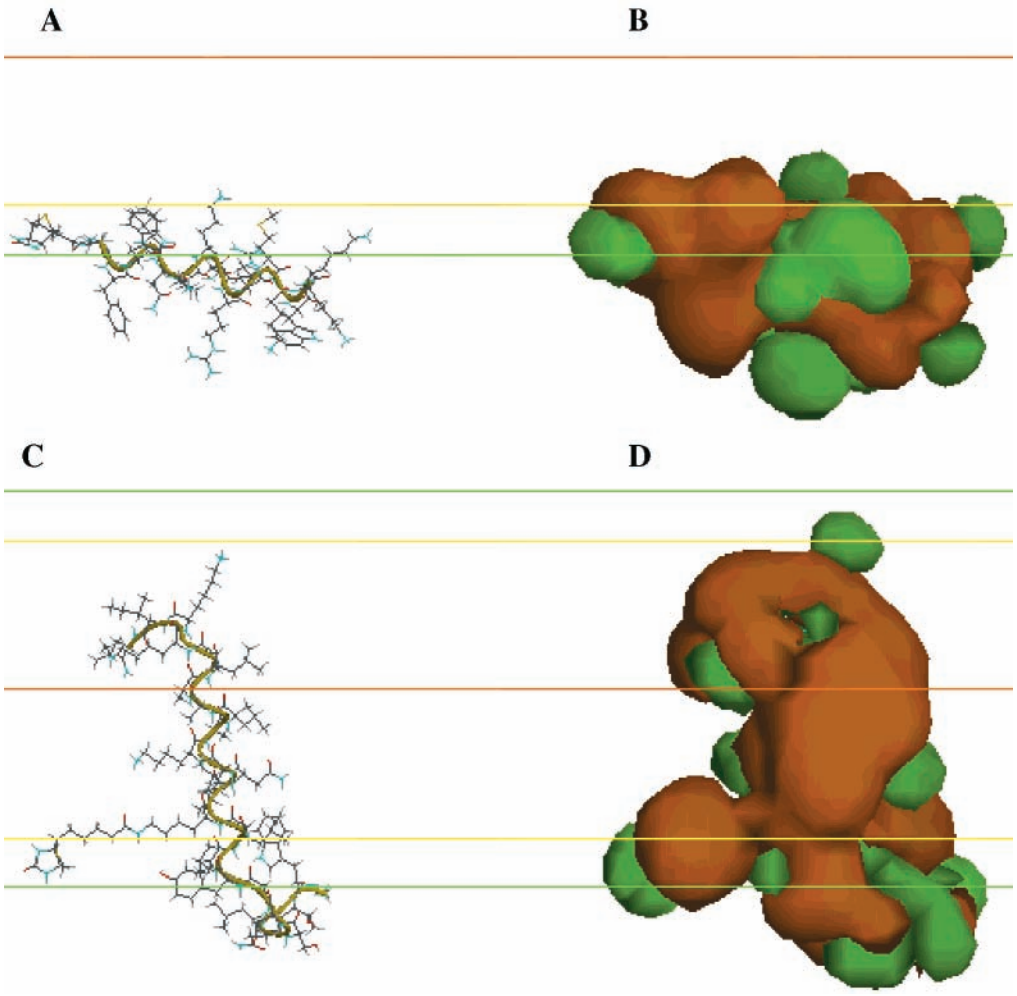

Figure 3. Interaction of calculated peptides with a membrane model. The orange line denotes the center of the bilayer ($z = 0$). Yellow line ($z = 13.5$ Å), green line ($z = 18$ Å). The environment is completely hydrophilic bellow the green line and completely hydrophobic above the yellow line. (A) Orientation of [$N^{1\alpha}$-biotinyl]Arg-Phe-Trp-Ile-Asn-Lys-penetratin(8−16) parallel to the membrane surface. The yellow ribbon shows the secondary structure of the peptide. (B) Calculation of the molecular hydrophobic potentials, MHP, around this peptide in the same orientation as in panel A. Orange surfaces are associated with hydrophobic isopotentials and green patches with hydrophilic isopotentials domains. (C) Orientation of [$N^{13\epsilon}$-biotinyl]transportan normal to the membrane surface. (D) Calculation of MHP around the peptide in the same orientation as in panel C.

and transportan 2 > transportan 3, transportan 5, and transportan 6 > transportan 4.

Peptide iodination on tyrosine was successfully carried out with transportan, transportan 2 and transportan 3, the peptides with demonstrated cellular localization (cf. above). The time courses of the uptake of [^{125}I]transportan, −2, −3 by Bowes melanoma cells are shown in Figure 2. All [^{125}I]transportans are internalized even at 10 nM concentration and time courses of cell penetration of the peptides are comparable. The maximum uptake for labeled transportan and transportan 2 are nearly identical, 9.8 ± 0.6 and 10.7 ± 0.8% of total peptide, respectively, while the same value for transportan 3 is significantly lower, 6.0 ± 0.4% of total peptide added. The efficiency and time course of uptake are in accordance with earlier result shown for transportan (*8*).

The ABZ-labeled transportan and penetratin were used to compare the amount of internalized peptide at equilibrium. The amount of internalized peptide corresponded to 6.7 ± 0.3% for transportan and 3.3 ± 0.4 for penetratin of the total added peptide thus the cellular concentration of transportan should be about two times higher than for penetratin, this is in accordance with the immunofluorecsence data (Figure 4).

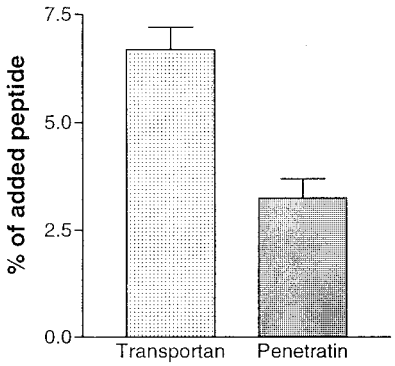

Figure 4. Percent of added transportan and penetratin.

In fluorescence studies, it was earlier shown (*21*) that using a strong fixative such as methanol could cause diffusion of internalized small molecules such as peptides. Therefore, the alternative formaldehyde fixative should be used to better preserve the cells internal structure and peptide localization as compared to nonfixed cells. Therefore both protocols for fixation of cells were used in this study, and they did give the same result.

Comparison of Penetratin and Transportan. Both penetratin and transportan enter the cells with high

efficiency but the staining pattern with FITC-streptavidin (Figure 1) is somewhat different. The plasma membrane is visualized by both peptides while the nuclear membrane staining is visible with transportan only. Penetratin does show nuclear localization, as do all the penetratin analogues, but has an more diffuse staining of the cell interior. It is possible that transportans higher affinity for cellular membrane structures could allow the membranes to act as a sink for the peptide which would explain its higher intracellular concentration.

Both penetratin and transportan internalize in an energy independent manner (Figure 1.). They have more common properties than that of cellular uptake but they also differ in several. Penetratin is a part of a protein while transportan is a synthetically combined sequence of two biologically active naturally occurring peptides, which may explain their differences in stability (see Table 3). Penetratin is 16 amino acids long while transportan is 27, although shorter penetratin contains almost the double amount of basic/positively charged residues, which are known to be cleavage sites for proteases.

Results from the ProtParam prediction programs (*10*) give the half-life of degradation for transportan to 30 h in eucaryotic cells, while the corresponding value for the penetratin sequence is only 1 h. The great difference in estimated stability should be taken into consideration when choosing a transporting peptide for a certain application.

The GRAVY values (Table 3) (*16*) suggest that the penetratin sequence would not be found in a membrane-spanning part of the protein while transportan is in the GRAVY range of integral membrane proteins such as the rhodopsins (0.70 for bacteriorhodopsin and 0.28 for bovine rhodopsin). This, and the fact that transportan is a hydrophobic peptide, would explain transportans localization into membranous structures such as ER and the Golgi.

In the membrane interaction model, penetratin was rejected out of the bilayer while transportan spanned the membrane with an angle of 65° to the surface plane (Figure 3). In contrast, both peptides do enter the cells, as shown by fluorescence, iodination, and various biological effects. The great difference in physicochemical properties of transportan and penetratin, and the fact that they both do penetrate into cells, support the idea of these two peptides translocating the plasma membrane in different manner.

Penetratin has been shown to deliver a 55 nucleotide long DNA oligomer (*22*) into cells while transportan has internalized with a 21mer of PNA, as cargo (*5*). The cargo size limit of both the peptides remains to be determined.

Membrane Interaction. Molecular modeling studies were performed on five sequences of penetratin (Table 1) and four sequences of transportan (Table 2). Modeling of secondary structure of peptides reveal that, peptides adopt an α-helical conformation although their end parts have a coiled structure, particularly for the N-terminus of [$N^{13\epsilon}$-biotinyl]transportan, transportan 2 and 4. This conformation is probably determined by the orientation of the bulky tryptophan side chain.

Among the five analogues of penetratin tested with the Impala procedure, two peptides, biotinyl-penetratin(1−16) and [bis-$N^{1\alpha}$-biotinyl,$N^{16\epsilon}$-penetratin(1−15)]-penetratin(1−16), were rejected out of the lipid bilayer. The most stable position of the [$N^{1\alpha}$-biotinyl]-[D-Pro^8]-ent-penetratin peptide is an oblique orientation according to the membrane plane. Its N-terminal end including the biotinyl group is buried into the apolar phase when the main part of the peptide is located out of the bilayer. The peptide [$N^{1\alpha}$-biotinyl]Arg-Phe-Trp-Ile-Asn-Lys-penetratin(8−16) lies flat at the membrane interface pointing some polar and charged side chains (Arg1, Gln7, Asn8, and Lys14) toward the area corresponding to the phospholipid polar heads (Figure 3A). The [$N^{1\alpha}$-biotinyl, Leu^6]-penetratin peptide remains out of the membrane. It adopts an oblique orientation and only its N-terminal part (Arg1, Gln2, Ile3, and Arg10) interacts with the bilayer.

The most surprising result was obtained for the [$N^{13\epsilon}$-biotinyl]transportan which span the membrane with an angle of 65° with regard to the surface plane (Figure 3C). Only a part of the N-terminal end (Thr3 to Gly8) remains out of the bilayer, when the aromatic side chain (Trp2 and Tyr9) are located at the membrane interface. Calculation of molecular hydrophobic potentials [(MHP (*23*)] displays a rather hydrophilic N-terminal side (Figure 3D). The transportan 2 peptide lies flat at the interface between the phospholipid polar heads and the hydrophobic core, with most of the polar residues pointing toward the membrane outside. Due to its unusual structure (two peptides separated by an alkyl chain), the transportan 3 peptide displays a specific orientation. The N-terminal part with its four aromatic groups remains out of the membrane when the C-terminal peptide lies in the hydrophobic core, pointing its three lysine residues into the phospholipid polar heads area. The transportan 4 peptide is slightly tilted with regard to the membrane interface. It lies in the area corresponding to the phospholipid heads with an angle of 22°.

The presence of proline residues gave a kinked helical structures to [$N^{1\alpha}$-biotinyl]-[D-Pro^8]-ent-penetratin and [$N^{13\varepsilon}$-biotinyl]transportan 4. The proline analogues have coiled structure in the N-terminal domain due to the helix-breaker ability of the proline residues. Nevertheless, this conformation is stabilized in the transportan 5 by π-stacking interactions between the aromatic side chains of tyrosine and tryptophane residues. At the C-terminal ends of transportan 5 and transportan 6, the carbonyl group interacts with the amino group of the last but one lysine residue according to the running sequence. Due to the sequence similarity the proline analogues, transportan 5 and transportan 6, exhibit almost identical orientations in the membrane interaction model. They span the phospholipid leaflets with angles of 54 and 76°, respectively. For both molecules, the biotinyl group, the polar (Thr3, Asn5) and aromatic (Trp2, Tyr9) residues in the N-terminal end lay in the phospholipid polar heads area when the Lys25 residues is anchored in the opposite equivalent area. The α-helical content of the proline analogues were estimated to be much lower than compared to the other peptides in this study, thus the helix breaker, proline, had a great influence on internalization of the transportan peptide. This is in agreement with Scheller et al. (*24*) who showed that the amphilicity of the α-helix is of great importance for cellular penetration.

DISCUSSION

In view of the fact that the intracellular concentrations of [$N^{1\alpha}$-biotinyl,Pro^8]-penetratin, where glutamine has been substituted with a proline residue, and of the D-amino acid analogue were somewhat higher as compared to the original peptide, a new analogue was designed containing both of these modifications. The resulting peptide, the [$N^{1\alpha}$-biotinyl]-[D-Pro^8]-*ent*-penetratin-amide, indeed showed the highest intracellular staining, followed by indirect immunofluorescence, of all of the penetratin analogues tested (Table 1) although this

cannot be interpreted unambiguously. The higher intracellular concentration could be a result of lower degradation because of the lack of lysozymes that can digest the peptide bonds between D-amino acids, and not of more effective internalization.

An all-D-amino acid peptide with the sequence RFWINK-amide was found by screening a peptide library for μ-opioid receptor agonists and found to exhibit long lasting opoid effects in vivo (*25*). This implicates that the peptide crosses the blood−brain barrier. Because of the similarities in amino acid contents between the first part of penetratin and the opioid agonist, the N-terminal was substituted in its L-amino acid form resulting in the [$N^{1\alpha}$-biotinyl]Arg-Phe-Trp-Ile-Asn-Lys-penetratin(8−16) amide. The uptake was rather low, but still it would be interesting to study by which degree this peptide, in its enantio form, can pass the blood-brain-barrier.

[$N^{1\alpha}$-biotinyl,Leu^6]penetratin was designed to test the significance of the aromatic residue tryptophan, which seems to be of great importance as the uptake was lowered, probably due to loss of the stabilizing Trp−membrane interaction (Figure 3).

Penetratin has been proposed to internalize as a dimer (*6*); therefore, the branched peptide, [bis-$N^{1\alpha}$-biotinyl,$N^{16\varepsilon}$-penetratin (1−15)]-biotinyl-penetratin(1−16), was synthesized. Indeed, this peptide does show a higher intracellular concentration than the original sequence. Whether this is caused by the dimeric nature of the peptide or the two binding sites for streptavidin, which could lead to slower degradation and thereby would leave one binding site intact, is not clear.

Currently, a model has been proposed for the cell penetration of penetratin which also is thought to apply for a fragment of the Tat protein (*6*), another cell penetrating peptide. This model suggests that the basic residues in the peptide can engage in ionic interactions with the negatively charged phospholipids in the cell membrane, causing a local invagination in the plasma membrane leading to local reorganization of the lipid bilayer, resulting in the formation of inverted micelles. These would enclose the peptide and its cargo in a hydrophilic environment to finally release them on the cytosolic face of the membrane.

Polycationic sequences are considered to exert their membrane destabilizing activity by interacting with negatively charged phospholipids in the plasma membrane. This is considered to result in internalization of the cationic peptides, possibly by the mechanism of non specific absorptive mediated endocytosis. The approach of polycationization could thus be used for targeting peptides to the cytoplasm of cells with a high rate of absorptive endocytosis. The peptides' ability to disorganize biological membranes also explains why many polycationic peptides are cytotoxic at high concentrations. This is the main drawback of this family of cell penetrating peptides, consequently amphipathic peptide toxins may not be able to function as carriers by themselves, due to high cytotoxicity, but rather be part of larger chimeras, such as transportan.

Transportan (*8*) has been shown to cross the plasma membrane of all animal cell lines tested so far at both 37 and 4 °C, thus implicating that the transport of the peptide is neither energy dependent nor receptor mediated. The internalization of transportan is not blocked by endocytosis inhibitors such as phenylarsine oxide or hyperosmolar sucrose solution, and the maximal intracellular concentration is reached after about 20 min. Transportan has, moreover, been coupled to a 21-mer PNA and this construct has been shown to penetrate cells (*5*).

In the penetration studies performed, transportan and transportan 2 give comparable signals by indirect fluorescence (Table 2) and iodination (Figure 2). The difference between these peptides are the C terminal part where transportan 2 contains the inactive mastoparan analogue, Mas 17 (*26*).

In transportan 3, the galanin part of the peptide is exchanged by the synthetic vasopressin antagonist to elucidate the receptor dependency of the internalization. The peptide was primarily found in the plasma membrane but not in the nucleus nor in internal membrane structures (Figure 1). The transportan 4 did not enter the cells in any detectable amount, hence the mastoparan part with its ampiphatic properties seems to be of great importance for the ability of this type of peptides to translocate the cellular membranes. In conclusion, the novel cell-penetrating transportan analogues should contain the mastoparan part while the galanin part could be modified whitout complete loss of internalization activity.

The molecular-modeling analysis shows that the peptides may use different ways to penetrate into the membrane. In our calculations, biotinyl-penetratin(1−16) and [bis-$N^{1\alpha}$-biotinyl,$N^{16\epsilon}$-penetratin(1−15)]-penetratin(1−16) were unable to insert into the bilayer demonstrate due to that those peptides contain a large number of basic residues which make them extremely hydrophilic. As proposed above, an unusual interaction mechanism may exist between those residues and the negative charges of the phospholipid heads that allows penetratin to destabilize the membrane and to penetrate into its hydrophobic core. The information concerning their translocation is not included in their amino acid sequences and the issue should be addressed in further studies.

Due to their amphiphilic character, most of the α-helical peptides adopt a flat or a slightly oblique orientation with regard to the membrane interface. Indeed, for biotinyl-penetratin(1−16), [$N^{1\alpha}$-biotinyl]-[D-Pro^8]-ent-penetratin, [$N^{1\alpha}$-biotinyl]Arg-Phe-Trp-Ile-Asn-Lys-penetratin(8−16), [$N^{1\alpha}$-biotinyl,Leu^6]-penetratin and, especially, transportan 4, the polar and charged amino acids are located on one side of the helix. The difference of orientation for the first two penetratin analogues indicate that an inverted chirality and the introduction of a proline residue may drastically change their mode of penetration. Amphiphilic peptides are adsorbed on the membrane surface and could cross progressively the lipid bilayer. This character of some peptides is displayed by the calculation of MHP (Figure 3B).

The [$N^{13\varepsilon}$-biotinyl]transportan spans the lipid bilayer entirely with regard to an angle of 65°. This peptide has the most hydrophobic sequence and encloses only four polar amino acids while penetratin contains seven arginine or lysine residues. Furthermore, aromatic residues (Trp2 and Tyr9) lie at the membrane interface and stabilize the peptide insertion.

To conclude, the different modifications of the chimeric transportan, such as Mas 17 in transportan 2 and the vasopressin antagonist part in transportan 3, do not alter the peptides ability to translocate, while modifications of the amphipathic α-helical C-terminal, as mastoparan substituted to crabrolin in transportan 4 do. Crabrolin is, like mastoparan, a hemolytic peptide toxin and it has been shown to form α-helical structure (*27*), but the differences in sequence are sufficient to eliminate the

cellular uptake. The low internalization of the two proline substituted analogues further suggest the importance of the C-terminal α- helical structure of transportan. The penetratin analogues, on the other hand, were modified in a different manner. The single amino acid modifications did not alter the penetration ability, except for the Trp replaced with Leu in [$N^{1\alpha}$-biotinyl,Leu^6]penetratin, which made the N-terminus interact with the bilayer. The all-D analogue would be a useful transporter peptide if a longer effect would be desired. Even though the bispenetratin, like all the penetratins, is relatively hydrophilic it does enter the cells. The membrane interaction model implies that transportan's arrangement and features of its amino acids will explain the translocating property, while the penetratin sequence does not reveal its mode of penetration. Thus, it seems that penetratin and transportan are not belonging to the same family of translocating peptides and that they do not enter the cells by identical mechanisms.

ACKNOWLEDGMENT

We would like to thank Cecilia Kut (Södertörn University) for her help in preparing the fluorescence microphotographs. This work was supported by the European Community Biotechnology, BI104-98-0227, by EU MAST III CT97-0156, Swedish Research Council for Engineering Sciences (TFR), the Swedish Research Council for Natural Sciences (NFR), and also by the Swedish Institute (Visby program). M.P. is also supported by the Estonian Science Foundation (ETF 4007). R.B. is Directeur de Recherche FNRS (Fonds National de la Recherche Scientifique). X.G. is supported by the Interuniversity Poles of Attraction Program—Belgian State, Prime minister's Office—Federal Office for Scientific, Technical and Cultural Affairs', contract no. P.4/03.

LITERATURE CITED

(1) Lindgren, M., Hällbrink, M., Prochiantz, A., and Langel, Ü. (2000) Cell penetrating peptides. *Trends Pharm. Sci.* 21, 99−103.

(2) Bloch-Gallego, E., Le Roux, I., Joliot, A. H., Volovitch, M., Henderson, C. E., and Prochiantz, A. (1993) Antennapedia homeobox peptide enhances growth and branching of embryonic chicken motoneurons in vitro. *J. Cell. Biol. 120,* 485−492.

(3) Perez, F., Joliot, A., Bloch-Gallego, E., Zahraoui, A., Triller, A., and Prociantz, A. (1992) Antennapedia homeobox as a signal for the cellular internalization and nuclear addressing of a small exogenous peptide. *J. Cell. Sci. 102*, 392−396.

(4) Prochiantz, A. (1996) Getting hydrophilic compounds into cells: lessons from homeopeptides. *Curr. Opin. Neurobiol. 6*, 629−634.

(5) Pooga, M., Soomets, U., Hällbrink, M., Valkna, A., Saar, K., Rezaei, K., Kahl, U., Hao, J.-X., Xu, X.-J., Wiesenfeld-Hallin, Z., Hökfelt, T., Bartfai, T., and Langel, Ü. (1998) Cell penetrating PNA constructs regulate galanin receptor levels and modify pain transmission in vivo. *Nat. Biotech. 16*, 857−861.

(6) Derossi, D., Joliot, A., Chassaing, G., and Prochiantz, A. (1994) The third helix of the Antennapedia homeodomain translocates through biological membranes. *J. Biol. Chem. 269,* 10444−10450.

(7) Derossi, D., Calvet, S., Trembleau, A., Brunissen, A., Chassaing, G., and Prochiantz, A. (1996) Cell Internalization of the Third Helix of the Antennapedia Homeodomain Is Receptor-independent. *J. Biol. Chem. 271,* 18188−18193.

(8) Pooga, M., Hällbrink, M., Zorko, M., and Langel, Ü. (1998) Cell penetration by transportan. *FASEB J. 12*, 67−77.

(9) Gavin, J. R., Roth, J., Jen, P., and Freychet, P. (1972) Insulin receptors in human circulating cells and fibroblasts. *Proc. Natl. Acad. Sci. U.S.A. 69*, 747−751.

(10) Appel, R. D., Bairoch, A., and Hochstrasser, D. F. (1994) A new generation of information retrieval tools for biologists: the example of the ExPASy WWW server. *Trends Biochem. Sci. 19*, 258−260.

(11) Guruprasad, K., Reddy, B. V. B., and Pandit, M. W. (1990) Correlation between stability of a protein and its dipeptide composition: a novel approach for predicting in vivo stability of a protein from its primary sequence. *Protein Eng. 4*, 155−161.

(12) Bachmair, A., Finley, D., and Varshavsky, A. (1986) In vivo half-life of a protein is a function of its amino-terminal residue. *Science 234*, 179−186.

(13) Ciechanover, A., and Schwartz, A. L. (1989) How are substrates recognized by the ubiquitin-mediated proteolytic system? *Trends Biochem. Sci. 14*, 483−488.

(14) Tobias, J. W., Shrader, T. E., Rocap, G., and Varshavsky, A. (1991) The N-end rule in bacteria. *Science 254*, 1374−1377.

(15) Ikai, A. (1980) Thermostability and aliphatic index of globular proteins. *J. Biochem. 88*, 1895−1898.

(16) Kyte, J., and Doolittle, R. F. (1982) A simple method for displaying the hydropathic character of a protein. *J. Mol. Biol. 157*, 105−132.

(17) Lins, L., Brasseur, R., De Pauw, M., J. P., V. B., Ruysschaert, J. M., Rosseneu, M., and Vanloo, B. (1995) Helix-helix interaction in reconstituted high-density lipoproteins. *Biochim. Biophys. Acta 1258*, 10−18.

(18) Brasseur, R., and Ruysschaert, J. M. (1986) Conformation and mode of organization of amphiphilic membrane components: a conformational analysis. *Biochem. J. 238*, 1−11.

(19) Ducarme, P., Rahman, M., and Brasseur, R. (1998) IMPALA: a simple restraint field to simulate the biological membrane in molecular structure studies. *Proteins 30*, 357−371.

(20) Rahman, M., and Brasseur, R. (1994) WinMGM: a fast CPK molecular graphics program for analyzing molecular structure. *J. Mol. Graphics 12*, 212−218.

(21) Pichon, C., Monsigny, M., and Roche, A.-C. (1999) Intracellular localisation of oligonucleotides: influence of fixative protocols. *Antisense Nucleic Acid Drug Dev. 9*, 89−93.

(22) Ojcius, D., and Young, J. D. (1991) Cytolytic pore-forming proteins and peptides: is there a common structural motif? *Trends Biochem. Sci. 16*, 225−229.

(23) Brasseur, R. (1991) Differentiation of lipid-associating helices by use of three-dimensional molecular hydrophobicity potential calculations. *J. Biol. Chem. 266*, 16120−16127.

(24) Scheller, A., Oehlke, J., Wiesner, B., Dathe, M., Krause, E., Beyermann, M., Melzig, M., and Bienert, M. (1999) Structural requirements for cellular uptake of α-helical amphipathic peptides. *J. Pept. Sci. 5*, 185−194.

(25) Dooly, C. T., Chung, N. N., Wilkes, B. C., Schiller, P. W., Bidlack, J. M., Pasternak, G. W., and Houghten, R. A. (1994) An all D-amino acid opioid peptide with central analgestic activity from a combinatorial library. *Science 266*, 2019−2022.

(26) Soomets, U., Hällbrink, M., Zorko, M., and Langel, Ü. (1997) From galanin and mastoparan to galparan and transportan. *Curr. Top. Pept. Protein Res. 2*, 83−113.

(27) Krishnakumari, V., and Nagaraj, R. (1997) Antimicrobial and hemolytic activities of crabrolin, a 13-residue peptide from the venom of the European hornet, *Vespa crabro*, and its analogues. *J. Pept. Res. 50*, 88−93.

BC990156S

General Method to Label Antisense Oligonucleotides with Radioactive Halogens for Pharmacological and Imaging Studies

Bertrand Kühnast,[†,‡] Frédéric Dollé,[‡] Salvatore Terrazzino,[†,‡] Bernard Rousseau,[§] Christian Loc'h,[‡] Françoise Vaufrey,[‡] Françoise Hinnen,[‡] Isabelle Doignon,[†,‡] Florence Pillon,[§] Christelle David,[‡] Christian Crouzel,[‡] and Bertrand Tavitian*[,†,‡]

INSERM U334, Service Hospitalier Frédéric Joliot, Service des Molécules Marquées, CEA/DSV, France.
Received December 28, 1999; Revised Manuscript Received April 3, 2000

Evaluation of oligonucleotides for biomedical applications requires different in vivo and in vitro approaches (pharmacokinetics, biodistribution, macro- and microimaging, metabolism, ...), that are performed with different radioisotopes according to the temporal and spatial resolution needed. A method to introduce radioactive isotopes of halogens (fluorine, bromine, and iodine) in a small and stable molecule has been developed. Radiosynthons can then be conjugated with any given oligonucleotide in one step to create the appropriate radiotracer. This general radiolabeling procedure for oligonucleotides is efficient to synthesize ^{18}F-, ^{76}Br-, and ^{125}I-oligonucleotides for biological needs. Applications of the method to biodistribution, metabolism, in vivo and ex vivo imaging of ^{125}I- and ^{18}F-labeled oligonucleotides are reported.

INTRODUCTION

Due to their excellent targeting capacities and easiness of synthesis in high diversity, oligonucleotides are extensively used in vitro as ligands for nucleic acids [antisense oligonucleotides (Crooke and Lebleu, 1993)], proteins and small molecules [aptamer oligonucleotides (Gold et al., 1997)]. Although the seductive idea to use oligonucleotides in vivo for therapy, diagnostic, imaging, etc (Agrawal, 1996) appeared more than 30 years ago (Belikova et al., 1967), these applications are still in their infancy and it appears that tremendous efforts are still necessary to develop these compounds as pharmaceuticals (Stein and Cheng, 1993). Natural oligonucleotides show poor stability, affinity and membrane passage, and it is now clear that oligonucleotides are spatially structured in vivo and that some sequences confer noncanonical biological properties to oligonucleotides. Numerous chemical modifications of the natural oligonucleotides aimed at improving their biological stability and bioavailability have been proposed and thousands of sequences tested (Agrawal et al., 1990; Chen et al., 1990; Miller, 1991; Giles and Tidd, 1992; Larrouy et al., 1992; Kawasaki et al., 1993; Monia et al., 1993; Sanghvi et al., 1993; Zhao et al., 1993; Iribarren et al., 1994; Jorgensen et al., 1994; Nielsen et al., 1994; Agrawal et al., 1995; Moulds et al., 1995; Stein et al., 1997). Eventually, the biological activity and the putative benefit of any modification of oligonucleotides expected to exert a specific action in a living organism can only be fully appreciated through in vivo or ex vivo studies.

As a means to explore the targeting ability and pharmacokinetics of oligonucleotides directly in vivo, noninvasive imaging is a method of choice and several groups have reported labeling methods with γ emitters (Dewanjee et al., 1994; Hnatowich et al., 1995; Cammilleri et al., 1996; Charlton et al., 1997; Reed et al., 1997; Hjelstuen et al., 1998; Fujibayashi et al., 1999) and with positron emitters for positron emission tomography (PET) (Dollé et al., 1997; Hedberg et al., 1997; Tavitian et al., 1998; Hedberg et al., 1998; Yngve et al., 1999).

We previously described a general method for labeling oligonucleotides based on the efficient coupling of fluorobenzylbromoacetamide with oligonucleotides bearing a phosphorothioate monoester group at the 3'end. Radiolabeling is performed in two steps: (1) radiosynthesis of a synthon designed for high reactivity and stable incorporation of radiohalogens (Wilbur et al., 1989); and (2) regioselective conjugation of the synthon to the oligonucleotide in reaction times compatible with the half-life of isotopes. Using the positron emitter fluorine-18 (half-life 109.8 min), we imaged the biodistribution of oligonucleotides during several hours in vivo with PET. Quantitative imaging of oligonucleotides bearing different chemical modifications was performed using the same ^{18}F-synthon, demonstrating that this approach is relevant for in vivo oligonucleotide evaluation (Tavitian et al., 1998).

With the aim to encompass the whole pannel of in vivo and ex vivo imaging techniques and to improve temporal and spatial resolution, we describe here a method to introduce radioactive isotopes of other halogens (bromine and iodine) in the same synthon that was used for fluorine. The radiosynthon can then be conjugated with a given oligonucleotide in one step to create the appropriate radiotracer labeled with any radioactive isotope of iodine and bromine: iodine-123, iodine-125, iodine-131, and bromine-76, in addition to fluorine-18. Applications are illustrated by results of (1) a biodistribution and metabolic study in which the same oligonucleotide was labeled with fluorine-18 and iodine-125 and co-injected to mice for comparative analyses; and (2) an imaging study in which the radioactivity localization observed in

* To whom correspondence should be addressed: INSERM U334, CEA−SHFJ, 4 place du général Leclerc, F-91401 Orsay cedex, France. Phone: +33 1 69867779. Fax: +33 1 69867739. E-mail:tavitian@shfj.cea.fr.

[†] INSERM U334.

[‡] Service Hospitalier Frédéric Joliot.

[§] Service des Molécules Marquées.

10.1021/bc990183i CCC: $19.00 © 2000 American Chemical Society
Published on Web 08/31/2000

vivo with a ^{18}F-oligonucleotide and PET was refined with the corresponding ^{125}I-oligonucleotide and ex vivo microautoradiography.

EXPERIMENTAL SECTION

1. General. *1.1. Chemicals.* Chemicals were purchased from Aldrich, Sigma, and ICN Biomedicals and were used without further purification.

A 9mer phosphodiester oligonucleotide (ACCGATCCG$^{3'}$-p_s) purchased from Genset (Paris, France) was chosen as a model for the coupling reaction with the isotope-carrying molecule. An 18mer phosphodiester oligonucleotide (AGAATACAGGGTCCAAAT$^{3'}$-p_s) from Eurogentec (Seraing, Belgium) was used for further confirmation of the validity of radiolabeling and for biological studies. This sequence is complementary to nucleotides 1209−1227 of the env sequence of the Lilly and Steeves strain of murine SFFV Freind erythroleukemia virus (Moreau-Gachelin et al., 1986), but has no known complementary sequence in mammalian cDNA databases (Tavitian et al., 1998).

1.2. Analytical Methods. Thin layer chromatography (TLC) was run on precoated plates of silica gel $60F_{254}$ (Merk). The compounds were localized at 254 nm using a UV lamp. Flash chromatography was conducted on silica gel 63-200 μm (Merck) at 0.3 bar (compressed air).

HPLC analyses and purifications (HPLC A to G) were performed on the following HPLC systems. Pumps: Pu1, 600 controller gradient system (Waters); Pu2, 501 (Waters); Pu3, gradient pump (Merck). UV detectors: Uv1, multiwavelength 490E (Waters); Uv2, 1100 Series (Hewlett-Packard); Uv3, 486 (Waters); Uv4, UV Detector (Merck). Radioactivity detectors: Ra1, Geiger Muller detector; Ra2, Flow One Scintillation Analyzer (Packard) equipped with a liquid scintillation or PET cell for radioactivity monitoring; Ra3, LB 2040 (Berthold). The columns used were the following: Co1, semipreparative C18 μBondapak Waters (300 × 7.8 mm, porosity 10 μm); Co2, analytical C18 μBondapak Waters (300 × 3.9 mm, porosity 10 μm); Co3, semipreparative HR Silica Prep Nova-Pak Waters (300 × 7.8 mm, porosity 6 μm). Solvents were determined as follows: A, triethylammonium acetate (TEAA) 100 mM (pH 7); B, acetonitrile; C, CH_2Cl_2; D, EtOAc; E, aqueous NaH_2PO_4 (0.01 M). **HPLC A**: HPLC system, Pu1/Uv1/Ra1; HPLC column, Co1. HPLC solvents and conditions: A/B gradient, linear in 5 min from 95/5 (A/B) to 90/10 (A/B), then linear in 10 min from 90/10 (A/B) to 85/15 (A/B), then wash-out for 10 min at 50/50 (A/B); flow rate, 6 mL/min; detection at 254 nm. **HPLC B**: HPLC system, Pu1/Uv1/Ra1; HPLC column: Co1; HPLC solvents and conditions: A/B gradient, linear in 5 min from 95/5 (A/B) to 90/10 (A/B), then linear in 15 min from 90/10 (A/B) to 80/20 (A/B), then wash-out for 10 min at 50/50 (A/B); flow rate, 6 mL/min; detection at 254 nm. **HPLC C**: HPLC system, Pu2/Uv3/Ra1; HPLC column, Co3. HPLC solvents and conditions: isocratic C/D (95/5); flow rate, 5.0 mL/min; detection at 254 nm. **HPLC D**: HPLC system, Pu2/Uv3/Ra1; HPLC column, Co2. HPLC solvents and conditions: isocratic E/B (60/40); flow rate, 1.0 mL/min; detection at 254 nm. **HPLC E**: HPLC system, Pu3/Uv4/Ra3; HPLC column, Co1. HPLC solvents and conditions: isocratic E/B (60/40); flow rate, 6.0 mL/min; detection at 254 nm. **HPLC F**: HPLC system, Pu3/Uv4/Ra3; HPLC column, Co1. HPLC solvents and conditions: A/B gradient, linear in 5 min from 95/5 (A/B) to 90/10 (A/B), then linear in 15 min from 90/10 (A/B) to 80/20 (A/B), then wash-out for 10 min at 50/50 (A/B); flow rate, 6 mL/min; detection at 254 nm. **HPLC G**: HPLC system, Pu1/Uv2/Ra2; HPLC column, Co2. HPLC solvents and conditions: A/B gradient, linear in 3 min from 95/5 (A/B) to 90/10 (A/B), then linear in 27 min from 90/10 (A/B) to 70/30 (A/B), then wash-out for 10 min at 50/50 (A/B); flow rate, 1.5 mL/min; detection at 254 nm.

NMR spectra were recorded on a Bruker AMX (300 MHz) apparatus using the hydrogenated residue of the deuterated solvents (DMSO-d_6, δ 2.50 ppm; CD_2Cl_2, δ 5.32 ppm) and/or TMS as internal standards for ^{1}H NMR as well as the deuterated solvents (DMSO-d_6, δ 39.5 ppm; CD_2Cl_2, δ 53.8 ppm) and/or TMS as internal standards for ^{13}C NMR and TMP as internal standard for ^{31}P NMR. The chemical shifts are reported in ppm, downfield from TMS.

The mass spectra (MS) DCI/NH_4^+ were measured on a Finigan-Map 4600 apparatus, a Nermag R10-10 apparatus. Electrospray ionization (negative mode) were measured on a Quattro VG (Fison, Manchester, U.K.) and mass were calculated from a distribution of differently charged oligonucleotides.

1.3. Isotopes Availability. Fluorine-18. No-carrier-added aqueous [^{18}F]fluoride ion was produced on a CGR-MeV 520 cyclotron by irradiation of a 2 mL water target using a 20 MeV proton beam on 95% enriched [^{18}O]water [^{18}O-(p,n)^{18}F] and was transferred to the appropriate hot cell. Typical production: 700−800 mCi (25.9−29.6 GBq) of [^{18}F]F^- at the end of bombardment for a 20 μA, 30 min (36 000 μC) irradiation. A complete description of the target hardware and operation can be found in reference (Dollé et al., 1999).

Bromine-76. No-carrier-added bromine-76 was produced on a CGR-MeV 520 cyclotron by irradiation of a 1.8 g natural arsenic using a 30 MeV ^{3}He beam [^{75}As-(^{3}He,2n)^{76}Br] and was transferred to the appropriate hot cell. The target was kept for 15 h before work up to allow for the decay of ^{75}Br ($t_{1/2}$, 1.6 h) formed during the irradiation [^{75}As(^{3}He,3n)^{75}Br]. Typical production: 9−10 mCi (333−370 MBq) of NH_4[^{76}Br]Br for a 15 μA, 120 min (108 000 μC) irradiation.

Iodine-125. Na[^{125}I]I (1 mCi, 37 MBq) was purchased from Amersham Pharmacia Biotech (France).

1.4. Others. Radiosyntheses using fluorine-18 were performed in a 5 cm-lead-shielded cell using a computer assisted Zymate robot system (Zymark corporation). For bromine-76, radiosyntheses were performed in a 5 cm-lead-shielded cell. Iodine-125 radiosyntheses were performed in gloveboxes. Microwave activations were performed with a MicroWell 10 oven (2.45 GHz), Labwell AB, Sweden.

2. Chemistry. *2.1. Preparation of Unlabeled N-(4-Halogenobenzyl)-2-bromoacetamide (**2a**−**c**). General Procedure To Synthesize Unlabeled N-(4-Halogenobenzyl)-2-bromoacetamide (**2a**−**c**).* To a solution containing 4-halogenobenzylamine (**1a**−**c**) and of *N*-methylmorpholine (1 equiv; MW, 101.15) in 100 mL of CH_2Cl_2 was added dropwise bromoacetyl bromide (1 equiv, MW, 201.86) while maintaining the temperature under 30 °C. After addition, the reaction mixture was stirred at room-temperature overnight. The mixture was then filtered and concentrated to dryness, and the residue was chromatographed on silica gel. Elution with heptane/EtOAc (90/10 to 60/40) gave pure *N*-(4-halogenobenzyl)-2-bromoacetamide (**2a**−**c**) as solids.

*N-(4-Fluorobenzyl)-2-bromoacetamide (**2a**).* The procedure described above was used with 4-fluorobenzylamine (**1a**) to provide pure *N*-(4-fluorobenzyl)-2-bromoacetamide (**2a**) [see Dollé et al. (1997) for details and analytical characterization].

Table 1.[a]

ONs	sequence	X	anal. yield	R_t (min)	MS calc.	MS found
5a	ACCGATCCG	F	85-90%	12.0-12.5	2994.0	2994.2
b	ACCGATCCG	Br	85-90%	15.0-15.5	3005.0	3005.3
c	ACCGATCCG	I	58-90%	16.0-16.5	3052.0	3051.4
6a	AGAATACAGGGTCCAAAT	F	70-75%	14.0-14.5	5801.0	5799.4
b	AGAATACAGGGTCCAAAT	Br	70-75%	16.0-16.5	5862.0	5879.0
c	AGAATACAGGGTCCAAAT	I	70-75%	17.0-17.5	5909.0	5914.5

[a] **5a**: *N*-(4-flurobenzyl)-2-(ACCGATCCG3′-p_s)-acetamide. **5b**: *N*-(4-bromobenzyl)-2-(ACCGATCCG3′-p_s)-acetamide. **5c**: *N*-(4-iodobenzyl)-2-(ACCGATCCG3′-p_s)-acetamide. **6a**: *N*-(4-flurobenzyl)-2-(AGAATACAGGGTCAAAT3′-p_s)-acetamide. **6b**: *N*-(4-bromobenzyl)-2-(AGAATACAGGGTCCAAAT3′-p_s)-acetamide. **6c**: *N*-(4-iodobenzyl)-2-(ACAATACAGGGTCCAAAT3′-p_s)-acetamide.

*N-(4-Bromobenzyl)-2-bromoacetamide (**2b**).* The procedure described above was used with 1.5 g of 4-bromobenzylamine (**1b**) hydrochloride (6.7 mmol), 600 μL of *N*-methylmorpholine and 580 μL of bromoacetyl bromide to provide 560 mg of pure *N*-(4-bromobenzyl)-2-bromoacetamide (**2b**) as a white solid (yield 65%). R_f (heptane/EtOAc 50/50): 0.26. ^{1}H NMR (DMSO-d_6, 298K): δ 8.76 (s, H); 7.52 (d, J = 8.4 Hz, 2H); 7.22 (d, J = 8.4 Hz, 2H); 4.27 (d, J = 6 Hz, 2H); 3.33 (s, 2H). ^{13}C NMR (DMSO-d_6, 298 K): δ 165.9 [C]; 137.5 [C]; 132.1 [CH]; 129.8 [CH]; 121.8 [C]; 43.8 [CH_2]; 29.5 [CH_2]. MS (DCI/NH_4^+) $C_9H_9NOBr_2$: 323 [M + NH_4^+], 325 [M + NH_4^+], 327 [M + NH_4^+].

*N-(4-Iodobenzyl)-2-bromoacetamide (**2c**).* The procedure described above was used with 500 mg of 4-iodobenzylamine (**1c**) (2.2 mmol), 170 μL of *N*-methylmorpholine, and 200 μL of bromoacetyl bromide to provide 230 mg of pure *N*-(4-iodobenzyl)-2-bromoacetamide as a yellow solid (yield 63%). R_f (heptane/EtOAc 50/50): 0.27. ^{1}H NMR (CD_2Cl_2, 298K): δ 7.67 (d, J = 8.1 Hz, 2H); 7.04 (d, J = 8.1 Hz, 2H); 6.80 (bs, $w_{1/2}$ = 23.5 Hz, 1H); 4.38 (d, J = 6 Hz, 2H); 3.89 (s, 2H). ^{13}C NMR (CD_2Cl_2, 298K): δ 165.8 [C]; 165.0 [C]; 138.1 [CH]; 129.9 [CH]; 93.1 [C]; 43.8 [CH_2]; 29.57 [CH_2]. MS (DCI/NH_4^+) C_9H_9NOBrI: 373 [M + NH_4^+]; 371 [M + NH_4^+].

*2.2. Conjugation of Oligonucleotides with N-(4-Halogenobenzyl)-2-bromoacetamide. General Procedure for Conjugating N-(4-Halogenobenzyl)-2-bromoacetamide to a 3′Phosphorothioate Monoester Oligonucleotide (**5a**−**c**, **6a**−**c**).* An OD of 100 (1 OD is the UV absorbance of 33 μg of an oligonucleotide regardless of the sequence of bases) of 9mer or 18mer phosphodiester 3′ phosphorohtioate monoester (**3**, **4**) oligonucleotide in water was reacted with an excess (3 equiv) of *N*-(4-halogenobenzyl)-2-bromoacetamide (**2a**−**c**) in 1.0 mL of a 1/1 (v/v) mixture of methanol and PBS (0.1 M, pH 8) for 30 min at 120 °C. The solvents were evaporated, and the compound was purified by RP-HPLC for **5a**, **5b**, **6a**, and **6b**, HPLC A, and for **5c** and **6c**, HPLC B. For all synthesized oligonucleotides [**5a**−**c**, **6a**−**c** (Table 1)], the ^{31}P NMR spectra (recorded in D_2O, at 298.0 K) can be resumed as follows: δ +15.2 [−OP(O)(OH)(S-acetamide)]; −4.0 [−OP(O)-(OH)O−]. This general procedure was used with ACCGATCCG$^{3'}$-p_S (**3**) or AGAATACAGGGTCCAAAT$^{3'}$-p_s (**4**) and the corresponding *N*-(4-halogenobenzyl)-2-bromoacetamide (**2a**−**c**) to provide *N*-(4-halogenobenzyl)-2-(ACCGATCCG$^{3'}$-p_S)-acetamide (**5a**−**c**) and *N*-(4-halogenobenzyl)-2-(AGAATACAGGGTCCAAAT$^{3'}$-p_s)-acetamide (**6a**−**c**), respectively.

*2.3. Synthesis of Precursors for Radiolabeling. 2.3.1 Precursor for Fluorination. 4-Cyano-N,N,N-trimethylanilinium Trifluoromethanesulfonate (**8**).* A solution of 21.1 g of 4-dimethylaminobenzonitrile (**7**) (144 mmol) and 22.6 mL of methyl trifluoromethanesulfonate (1.4 equiv, 200 mmol) in 300 mL of dry benzene was refluxed for 5 h under an argon atmosphere. The solid residue was filtered off and dissolved in 300 mL of water. This aqueous solution was washed once with 200 mL of CH_2Cl_2, once with 200 mL of $CHCl_3$ and concentrated to dryness. The residue was recrystallized twice from CH_2Cl_2 containing a few drops of MeOH to give 36.6 g of pure 4-cyano-*N*,*N*,*N*-trimethylanilinium trifluoromethanesulfonate (**8**) as pale yellow needles (82% yield). R_f (MeOH/AcOH, 50/50): 0.4. ^{1}H NMR (DMSO-d_6, 338.0 K): δ 8.30−8.00 (2b, 4H); 3.70 (s, 9H). ^{13}C NMR (DMSO-d_6, 338.0K): δ 150.0 [C]; 133.9 [CH]; 121.8 [CH]; 120.6 [q, J = 325 Hz, CF_3]; 116.9 [C]; 113.2 [C]; 56.4 [CH_3].

*2.3.2. Precursor for Bromination and Iodination. 4-Trimethysilylbenzylamine Hydrochloride (**9**).* A total of 1.5 g of 4-bromobenzylamine (**1b**) (6.74 mmol) was dissolved in 20 mL of dry THF, and the solution was cooled in a dry ice/ethanol bath to −78 °C. A total of 3 mL of butyllithium in hexanes (10.0 M) was then added dropwise (4.5 equiv, 30.3 mmol) under argon. After 1 h of reaction, 3.2 mL of trimethylsilyl chloride (3.3 equiv, 22.24 mmol) was added and the solution was stirred overnight at room temperature. The yellow solution with a white solid was then hydrolyzed with 10 mL of water to obtain a limpid yellow solution. The 4-trimethylsilylbenzylamine was extracted from the basic aqueous layer with 2 × 50 mL of diethyl ether. The organic layer was washed with 2 × 100 mL of brine, dried over Na_2SO_4, and concentrated under vacuum without heating. The resultant yellow oil was purified on silica gel column. Elution with AcOEt/MeOH (90/10) gave 423 mg of pure 4-trimethysilylbenzylamine. The 4-trimethysilylbenzylamine thus obtained was diluted with diethyl ether and cooled with an ice bath. Hydrogen chloride in diethyl ether was added to precipitate quantitatively 509 mg of 4-trimethysilylbenzylamine hydrochloride (**9**) (35% yield). R_f ($CHCl_3$/MeOH 80/20): 0.30.^{1}H NMR (CD_3OD, 298K): δ 7.62 (d, J = 6.0 Hz, 2H); 7.50 (d, J = 6.0 Hz, 2H); 4.16 (s, 2H); 0.30 (s, 9H). ^{13}C NMR (CD_3OD, 298 K): δ 142.8 [C], 135.1 [CH], 134.9 [C], 129.3 [CH], 44.3 [CH_2], −1.1 [CH]. MS (DCI/NH_4^+) $C_{10}H_{18}NSiCl$: 197 [M + NH_4^+]; 180 [M + H^+].

*N-(4-Trimethylsilylbenzyl)-2-bromoacetamide (**10**).* To a solution of 400 mg of 4-trimethysilylbenzylamine hydrochloride (**9**) (1.85 mmol) and 170 μL of *N*-methylmorpholine (1 equiv) in 15 mL of CH_2Cl_2 in ice under argon was added dropwise 160 μL of bromoacetylbromide (1 equiv). The solution was stirred overnight at room temperature. The solution was then filtered and washed with 2 × 20 mL of brine before concentrating solvants under vacuum. The obtained brown solid was purified on silica gel column, eluted with dichloromethane/AcOEt (95/5) to provide 377 mg of a white solid of *N*-(4-trimethylsilylbenzyl)-2-bromoacetamide (**10**) (65% yield). R_f (heptane/EtOAc 50/50): 0.40 ^{1}H NMR (CD_2Cl_2, 298 K): δ 7.50 (d, J = 6 Hz, 2H); 7.26 (d, J = 6 Hz, 2H); 6.92 (bs,

$w_{1/2}$ = 22.5 Hz, 1H); 4.40 (d, J = 6 Hz, 2H); 3.85 (s, 2H); 0.25 (s, 9H). ^{13}C NMR (CD_2Cl_2, 298 K): δ 165.9 [C]; 140.2 [C]; 138.7 [C]; 134.1 [CH]; 127.3 [CH]; 44.3 [CH_2]; 29.5 [CH_2], −1.1 [CH]. MS (DCI/NH_4^+): $C_{12}H_{18}NOSiBr$: 319 [M + NH_4^+]; 317 [M + NH_4^+]; 302 [M + H^+]; 300 [M + H^+].

3. Radiochemistry. *3.1. Procedures for Labeling of the Precursors. 3.1.1. Fluorination. N-(4-[^{18}F]Fluorobenzyl)-2-bromoacetamide ([^{18}F]**2a**). Preparation of the K[^{18}F]-F−K_{222}−Complex.* To recover and recycle the [^{18}O]water target, the 2 mL of aqueous [^{18}F]fluoride from the target were passed through an anion-exchange resin (AG1 × 8, Bio-Rad, 100−200 mesh). See Dollé et al. (1999) for more practical details. The [^{18}F]fluoride ion was then eluted from the resin using 1.0 mL of a 4.5 mg/mL aqueous K_2CO_3 solution. After addition of 11.0−15.0 mg of Kryptofix K_{222} (4,7,13,16,21,24-hexaoxa-1,10-diazabicyclo[8.8.8]-hexacosane), the resulting solution was then gently concentrated to dryness at 145−150 °C under a nitrogen stream for 10 min to give no-carrier-added K[^{18}F]F−K_{222} complex as a white semisolid residue.

Procedure A: Conventional Heating. The residue was then dissolved in 200 μL of freshly distilled DMSO and transferred to a 2 mL reaction vial containing 8 mg of the triflate salt of 4-trimethylammoniumbenzonitrile (**8**). The evaporation tube was rinsed twice with 200 μL of DMSO which was then added to the previous reaction mixture. Resolubilization yields were about 60−80% of the original [^{18}F]fluoride ion. The reaction vial was then tightly sealed with a Teflon cap and heated in a heating block without stirring at 180−200 °C for 20 min.

The experimental conditions used for the reduction of the cyano function ($LiAlH_4$ in refluxing THF) and condensation of the formed amine with bromoacetyl bromide were identical to those described in reference Dollé et al., 1997 and Kühnast et al., 2000. The *N*-(4-[^{18}F]fluorobenzyl)-2-bromoacetamide ([^{18}F]-**2a**) thus synthesized was purified by HPLC: HPLC C: t_R: 5.0−5.5 min. Typically, 66−95 mCi (2.4−3.5 GBq) of pure [^{18}F]-**2a** (and up to 114 mCi (4.2 GBq)) could be obtained in 85−95 min starting from a 600−650 mCi (22.2−24.0 GBq) aliquot of a cyclotron [^{18}F]F^- production batch.

Procedure B: Microwave Activation. Freshly distilled DMSO (600 μL) containing 8 mg of the labeling precursor (**8**) was directly added into the tube containing the dried K[^{18}F]F−K_{222}-complex. The tube (not sealed) was placed in a microwave oven. Microwaves, 100 W, were applied to the system for 1 min. The remainder of the synthesis used the same procedure as described above.

3.1.2. Bromination and Iodination. Preparation of NH_4[^{76}Br]Br. After 15 h of decay, the target was dissolved in 40 mL of concentrated H_2SO_4 at 180 °C. The solution was cooled (50 °C) and treated with an aqueous solution of chromic acid (4.2 g in 12 mL of water). The radioactive [^{76}Br]Br was swept out with a nitrogen stream and trapped at room temperature in 2 mL of 1.0 M aqueous NH_4OH. This solution was evaporated to dryness at 15−20 °C for 15−20 min to give no-carrier-added NH_4[^{76}Br]-Br, which was used without further purification.

*N-(4-[^{76}Br]Bromobenzyl)-2-bromoacetamide ([^{76}Br]**2b**).* A total of 500 μg of *N*-(4-trimethylsilylbenzyl)-2-bromoacetamide (**10**) (1.6 μmol) in 125 μL of MeOH was reacted with 340 μCi (12 MBq) of NH_4[^{76}Br]Br in MeOH and 360 μg of Chloramine T (1.6 μmol) and 100 μL of HCl 0.1 N. After 5 min of reaction at room temperature, the reaction was quenched by addition of an excess of sodium metabisulfite. The *N*-(4-[^{76}Br]bromobenzyl)-2-bromoacetamide ([^{76}Br]**2b**) thus synthesized was purified by RP-HPLC: HPLC D, t_R = 12.0−12.5 min. This purification provided 255 μCi (0.9 MBq) of pure *N*-(4-[^{76}Br]bromobenzyl)-2-bromoacetamide ([^{76}Br]**2b**). The solvents were then evaporated under a stream of nitrogen.

*N-(4-[^{125}I]Iodobenzyl)-2-bromoacetamide ([^{125}I]**2c**).* A total of 500 μg of *N*-(4-trimethylsilylbenzyl)-2 bromoacetamide (**10**) (1.6 μmol) in 125 μL of MeOH was reacted with 1 mCi (37 MBq) of Na[^{125}I]I, 360 μg of Chloramine T (1.6 μmoles), and 100 μL of HCl 0.1 N. After 30 min reaction at room temperature, the reaction was quenched by addition of an excess of sodium metabisulfite. The *N*-(4-[^{125}I]iodobenzyl)-2-bromoacetamide ([^{125}I]**2c**) thus synthesized was purified by semipreparative RP-HPLC: HPLC E, t_R = 8.5−9.0 min. This purification provided 630 μCi (24 MBq) of pure *N*-(−4-[^{125}I]iodobenzyl)-2-bromoacetamide ([^{125}I]**2c**). The solvents were then evaporated under a stream of nitrogen.

*3.2. General Procedure for Labeling Oligonucleotides (**3**, **4**).* 9mer and 18mer (**3**, **4**) oligonucleotide at 30 OD (ca. 1 mg) in water were added to a vessel containing the dried purified *N*-(4-[*labeled*]halogenobenzyl)-2-bromoacetamide ([*labeled*]**2a**−**c**) and diluted in 1 mL of a 1/1 (v/v) mixture of methanol/PBS (0.1 M, pH 8). After 10 min of reaction at 120 °C, the solvents were evaporated under a stream of nitrogen and labeled oligonucleotides-([*labeled*]**5a**−**c** and [*labeled*]**6a**−**c**) were purified from unlabeled oligonucleotides (**3**, **4**) and unreacted *N*-(4-[*labeled*]halogenobenzyl)-2-bromoacetamide ([*labeled*]-**2a**−**c**) by RP-HPLC using the same conditions as for 9mer and 18mer oligonucleotides cold references (HPLC A for the [^{18}F]fluorooligonucleotide and [^{76}Br]bromooligonucleotide **5a**, **6a**, **5b**, and **6b**; HPLC F for the [^{125}I]-iodooligonucleotide **5c** and **6c**). Pure labeled 9mer or 18mer oligonucleotides were collected and desalted on a G25 Sephadex Column (Amersham Pharmacia Biotech) after evaporation of the solvents, yielding a radiochemically pure solution for the animal studies.

4. Biological Applications. *4.1. In Vitro Studies.* Freshly collected mouse plasma (200 μL) was incubated at 37 °C with 50 μL of ^{125}I-labeled oligonucleotide (6.4 kBq) in saline buffer. Aliquots of 50 μL were sampled at 15 min, 60 min, 120, 180, and 300 min and radioactivity was extracted and processed on RP-HPLC as described below.

4.2 Animals. Male Swiss mice (20−30 g), male Sprague−Dawley rats (200 g), and a male adult baboon (7.5 kg) were housed separately at constant temperature (21 °C) and relative humidity (60%) under a regular light/dark schedule. Food and water were freely available. Procedures involving animals were in conformity with institutional guidelines that are in compliance with current French and European laws and policies.

*4.3 Biodistribution. [^{125}I]9mer Oligonucleotide [^{125}I]**5c**.* Male Swiss mice (20−30 g) were injected with 11 μCi (0.41 MBq) of [^{125}I]9mer oligonucleotide in the tail vein. Animals were sacrificed at 5 min, 1 h, and 4 h, and the kidneys, liver, spleen, heart, lung, brain, muscle, blood, and adrenals immediately collected. Aliquots of these organs were weighed and radioactivity was counted on a γ counter (Cobra, Packard). Radioactivity was expressed as percentage of injected dose per gram of organ (% ID/g) and reported as the mean ± standard deviation. Alternate samples of the kidneys, liver and lungs were frozen for analysis of their metabolites as described below.

*[^{18}F]-18mer Oligonucleotide and [^{125}I]18mer Oligonucleotide [^{125}I]**6c** and [^{18}F]**6a**.* Mice were injected in the tail vein simultaneously with 160 μCi (6 MBq) of [^{18}F]-18mer oligonucleotide and 2.5 μCi (0.09 MBq) of [^{125}I]-18mer oligonucleotide in the same syringe. Animals were

sacrified 5 min, 1 h, 4, h, and 15 h after injection, and the kidneys, liver, heart, lung, brain, spleen, adrenals, muscles, thyroid, and blood were immediately collected. Samples of each organ were weighed and radioactivity was counted on a γ counter Cobra (Packard). Fluorine-18 radioactivity was immediately counted on a 450−650 keV energy window, while iodine-125 radioactivity was counted after fluorine-18 decay on a 15−35 keV energy window. Linearity of the counter on the two energy windows was checked. Radioactivity was expressed as percentage of injected dose per gram of organ (% ID/g) and reported as the mean ± standard deviation.

5. Metabolism. *5.1. Plasma Extraction and RP-HPLC Analysis.* One volume of phenol/$CHCl_3$ (v/v) and four volumes of Tris-EDTA (pH 8) were added to 200 μL of rat plasma and the mixture centrifuged at 13 000 rpm (12 500 g) for 10 min. Pellet was extracted again with an additionnal 200 μL of Tris-EDTA, and supernatants were collected, vacuum-dried, and dissolved in a known volume of TEAA before injection on analytical RP-HPLC: HPLC G.

5.2. Tissue Extraction and RP-HPLC Analysis. Upon removal, kidneys and liver were frozen in dry ice and kept at −80 °C. Tissues were homogenized in buffer (Tris-HCl 0.02 M; EDTA 0.02 M; NaCl 0.1 M; NP40 0.5%) and centrifuged 2 min at 13 000 rpm. Supernatants were digested overnight with proteinase K (2 mg/mL; 10 units/mg solid) at 37 °C and extracted with phenol/chloroforme as described above. Extracted supernatants were concentrated by lyophilization and dissolved in a known volume of TEAA for RP-HPLC analysis (HPLC G).

6. Imaging. *6.1. Ex Vivo Autoradiography.* Male Sprague−Dawley rats (200 g) were injected with 40 μCi (1.5 MBq) of [^{125}I]18mer oligonucleotide in the tail vein and sacrificed at 5 min after injection. Kidneys were removed and frozen in isopentane at −50 °C. Tissue sections were cut at 20 μm on a cryostat (Leitz, France), melted on glass slides (Superfrost/Plus, O.Kinder GmbH, Germany), immersed with Carnoy fixative [EtOH 60%, $CHCl_3$ 30%, acetic acid 10% (v/v/v)] during 10 min at room temperature, and allowed to dry overnight at room temperature. The slides were dipped into a NTB2 autoradiography emulsion (Kodak, France) and exposed for 30 days before revelation and counterstaining with Cresyl violet. They were observed at 125-fold magnification with a Olympus U-MCB microscope and digitally photographed using Analysis-Pro (Olympus).

6.2 In Vivo PET Imaging. Positron emission tomography was performed as previously described (Tavitian et al., 1998). Briefly, 1.2 mCi of [^{18}F]18mer oligonucleotide (mean specific radioactivity 426 mCi/μmol) were injected IV to a male adult baboon placed under isoflurane anesthesia in a Siemens ECAT EXACT HR+ camera and whole body images acquired in 3D mode.

RESULTS AND DISCUSSION

1. Chemistry. The method to label short length oligonucleotides with fluorine-18 described in Dollé et al. (1997) is based on the coupling of a 3′ end phosphorothioate monoester oligonucleotide with a fluorobenzylacetamide compound. This coupling method has been here applied with success to oligonucleotides of various lengths and with other halogens than fluorine.

1.1. Preparation of N-(4-halogenobenzyl)-2-bromoacetamide. 4-halogenobenzylamine (**1a**−**c**) were reacted with bromoacetyl bromide in the presence of *N*-methylmorpholine to give unlabeled *N*-(4-halogenobenzyl)-2-bromoacetamide (**2a**−**c**) in yields of 60 to 65% (Scheme 1).

Scheme 1

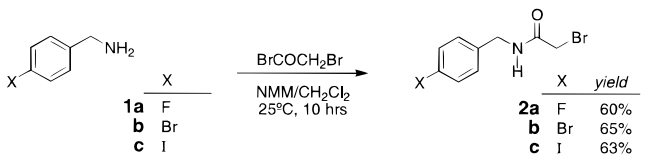

1.2. Conjugation of oligonucleotides with N-(4-halogenobenzyl)-2-bromoacetamide. The reference unlabeled 3′substituted oligonucelotides were prepared as described in Scheme 2, starting with two oligonucleotidic sequences: (i) a 9mer oligonucleotide (ACCGATCCG$^{3'}$-ps) (**3**) a model small oligonucleotide with manageable size, well-balanced A/C/G/T ratio, and absence of palindromic sequences; (ii) a 18mer oligonucleotide (AGAATACA-GGGTCCAAAT$^{3'}$-ps) (**4**) for in vivo biodistribution studies in rat. Both 9mer and 18mer were " orphan " oligonucleotides with no known complementary sequences in mammals. Known quantities of oligonucleotides **3** and **4** were reacted with *N*-(4-halogenobenzyl)-2-bromoacetamide **2a**−**c** for 30 min at 120 °C. RP-HPLC purification gave **5a**−**c** and **6a**−**c** as the highly predominant products. Apparently, the length of the oligonucleotide influenced slightly the yield of the conjugation reaction (85−90% and 70−75% yield for **5a**−**c** and **6a**−**c**, respectively), although comparing the obtained yields can hardly be done: the double molar amount of the short oligonucleotide has been used to the long one. The unlabeled compounds were analyzed by RP-HPLC: as expected, **5a**−**c** and **6a**−**c**, had longer retention times than the starting oligonucleotides (**3** and **4**) due to their increased lipophilicity following the addition of the halogenobenzyl substituent. The regioselectivity of coupling was checked by ^{31}P NMR: as expected, the chemical shift of the 3′ end phosphorus atom was shifted from +42.0 ppm in the phosphorothioate monoester group to +15.2 ppm in the 3′ end phosphorothioate diester group. Other internucleosidic phosphodiester groups were between −3.5 and −4.0 ppm. These values are in agreement with published ^{31}P NMR literature (Gorenstein, 1984; Gorenstein, 1992).

1.3. Preparation of Precursors for Halogenation. 1.3.1. Precursor for Fluorine-18 Labeling. The first radiochemical step in the fluorine-18 radiosynthesis (Scheme 5) corresponded to the introduction of the fluorine using a nucleophilic aromatic substitution. A cyano function was chosen as para-activator of the aromatic ring and *N*,*N*,*N*-trimethylammonium was chosen as leaving group for this substitution, not only for its high potential as leaving group in comparison with a corresponding halo or better nitro substituent, but also for the expected superior precursor separation from the reaction product [4-[^{18}F]-fluorobenzonitrile (**11**)] in HPLC due to the differences in the physicochemical properties. Thus, 4-cyano-*N*,*N*,*N*-trimethylanilinium trifluoromethanesulfonate (**8**) was prepared from commercial 4-dimethylaminobenzonitrile in 82% yield (Scheme 3).

1.3.2. Precursor for Bromine-76 and Iodine-125 Labeling. Direct isotope exchange was possible but presented the drawback to yield radioactive molecules with low specific activities and to contaminate the final product with high amounts of carriers. Trimethylsilylbenzyl or trimethylstannylbenzyl compounds are good candidates for electrophilic bromination and iodination due to the strong reactivity if the C-silicon or C-tin bound with an oxidant agent. Halodesilylation produced a non carrier added *N*-(4-halogenobenzyl)-2-bromoacetamide in good radiochemical yields and easy to purify from the precursor (Vaidyanathan et al., 1993; Loc'h et al., 1994).The

Scheme 2

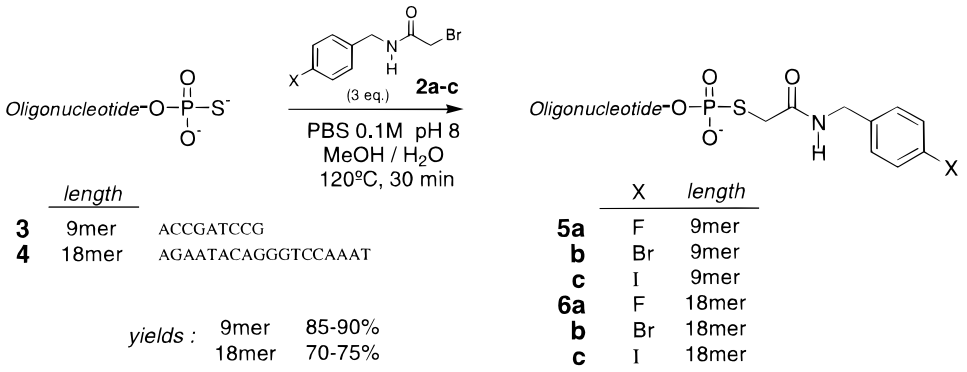

Scheme 3

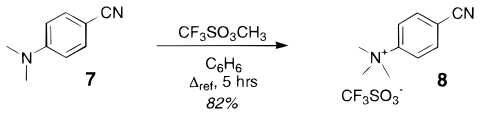

synthesis of the *N*-(4-trimethylsilylbenzyl)-2-bromoacetamide precursor (**10**) for bromination and iodination was done in two steps: (i) introduction of the trimethylsilyl group on the parabromo-activated aromatic benzylamine (**1b**). Displacement of the bromine atom by lithium was induced by the strong base *n*-butyllithium, added in excess to allow deprotonation of the amine that occurred first. Trimethylsilyl chloride was then added to substitute lithium by trimethylsilyl group and to provide the stable 4-trimethylsilylbenzylamine, which was precipitated as stable 4-trimethylsilylbenzylamine hydrochloride (**9**) by addition of hydrogen chloride in diethyl ether (yield 40%). (ii) 4-Trimethylsilylbenzylamine hydrochloride (**9**) was reacted in dichloromethane with *N*-methylmorpholine and bromoacetyl bromide to provide the precursor *N*-(4-trimethylsilylbenzyl)-2-bromoacetamide (**10**) for radiohalogenation in a yield of 65% (Scheme 4).

2. Radiochemistry. *2.1 Labeling of the Precursors (Scheme 5). Fluorination.* The first radiochemical step, the introduction of fluorine-18, was performed in hot DMSO (at 180 °C, using conventional heating) for 20 min using the activated [^{18}F]KF−K_{222} complex (incorporation yields of 80−85%). It has also been performed using microwave activations (100 W) for 1 min, giving the desired [^{18}F]fluorobenzonitrile (**11**) in up to 95% yield. The use of microwave activations allowed the reduction of synthesis time and critical point with short half-life isotopes and the improvement of the yield of incorporation of fluorine-18. The second and third steps (reduction of the cyano function using $LiAlH_4$ in refluxing THF and condensation of the amine obtained with bromoacetyl bromide) were identical to those described in Dollé et al. (1997). Semipreparative HPLC gave pure [^{18}F]*N*-(4-fluorobenzyl)-2-bromoacetamide [^{18}F]**2a** (coelution with authentic synthesized unlabeled reference compound). [^{18}F]**2a** was produced in 20−30% decay-corrected yield based on the starting [^{18}F]fluoride (Scheme 5).

Bromination and Iodination. Trimethylsilylbenzoacetamide (**10**) on treatment with NH_4[^{76}Br]Br or Na[^{125}I]I and chloramine T produced the corresponding radiobrominated and radioiodinated products in 5 and 30 min, respectively. The crude was directly injected onto RP-HPLC to collect pure *N*-(4-[^{76}Br]bromobenzyl)-2-bromoacetamide ([^{76}Br]**2b**) or *N*-(4-[^{125}I]iodobenzyl)-2-bromoacetamide ([^{125}I]**2c**) in yields of 75 and 65% respectively (Scheme 5).

2.2 Halogeno-Labeled Oligonucleotides. Halogenobenzylbromoacetamides (**2a**−**c**) were radiolabeled prior to any linkage with the oligonucleotides. This route allows the use of commercial available 3′-end phosphorothioate monoester oligonucleotide, sparing an impairment of the oligonucleotide by oxidizing or temperature conditions of labeling, and a more efficient purification of the labeled probe, in contrast to the alternative route of synthesizing oligonucleotides bearing the labeling precursor at the 3'end prior to label. Non reacted *N*-(4-[*labeled*]halogenobenzyl)-2-bromoacetamide is easily separated from labeled and nonlabeled oligonucleotide by RP-HPLC because of the difference of size and lipophilicity of the molecules, whereas separation of the labeled oligonucleotide from bearing-precursor-oligonucleotide is more difficult.

Conjugation of oligonucleotides (**3** and **4**) with the desired RP-HPLC purified [*labeled*]-halogenobenzylbromoacetamide ([^{18}F]**2a**, [^{76}Br]**2b**, or [^{125}I]**2c**) (Scheme 6) occurred in a mixture of MeOH/PBS 0.1M pH 8 for 30 min at 120 °C (yields 45−55%). The labeled probes were then purified by RP-HPLC (followed by NAP-10 desalting procedure) to provide pure [*labeled*]-oligonucleotides 9mer (**5a**−**c**) and 18mer (**6a**−**c**).

The rapid and mild conditions of conjugation of oligonucleotides to the labeled halogenobenzylbromoacetamide respected the chemical structure of oligonucleotides and was compatible with the half-life of fluorine-18. The whole synthetic procedure for fluorine-18 allowed to obtain 15−25 mCi (555−925 MBq) of pure labeled oligonucleotide ([^{18}F]**5a** and [^{18}F]**6a**) in 180 min (7−13% decay-corrected yield) with a specific radioactivity of 3−5 Ci/μmol (111−195 GBq/μmol) (decay-corrected from end of bombardment). The procedure for labeling oligonucleotides with fluorine-18 is largelly automated and the production of ^{18}F-labeled oligonucleotides is nearly performed in routine. For iodine-125, 350−400 μCi (12.9−14.8 MBq) of labeled oligonucleotide **5c** and **6c** were obtained starting from 1 mCi (37 MBq) of Na[^{125}I]I. The radioactive yield for the whole procedure was 35%, providing for both 9mer and 18mer oligonucleotides, pure radioactive probes [^{125}I]**5c**, [^{125}I]**6c** with a specific radioactivity of 1 Ci/μmol (37 GBq/μmol).

As a control, an aliquot of the radioactive probes was coinjected with unlabeled reference onto analytical RP-HPLC. Radioactive and UV detection demonstrated that [*labeled*]oligonucleotides eluted at the same retention time as authentic synthesized unlabeled reference compounds.

3. Biodistribution. For all three labeled oligonucleotides ([^{125}I]**5c**, [^{125}I]**6c**, and [^{18}F]**6a**), the biodistribution in mice was typical of phosphodiester oligonucleotides (Table 1). Apart from the thyroïd, radioactivity concentrations were highest in the blood, plasma and in the two major excretion organs, the kidneys and liver. They were

Scheme 4

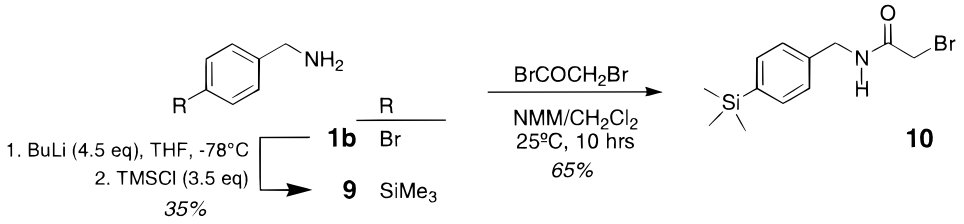

Scheme 5

fluorine-18 labeling

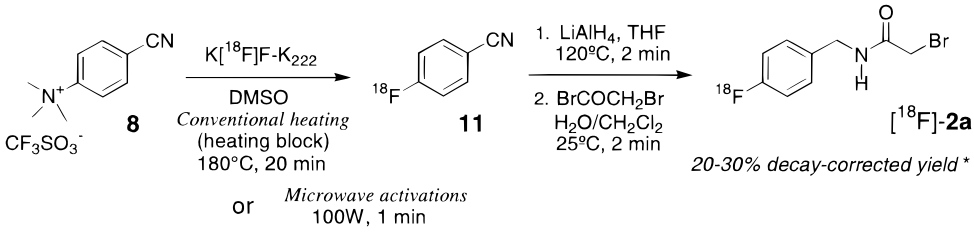

bromine-76 and iodine-125 labeling

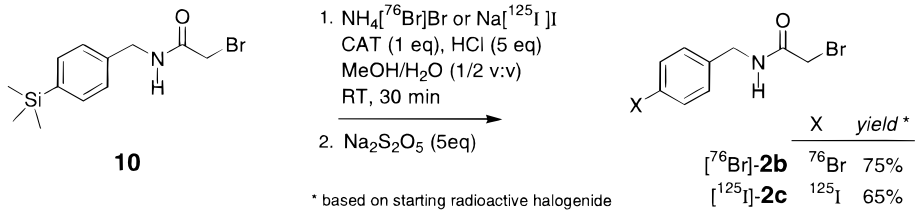

Scheme 6

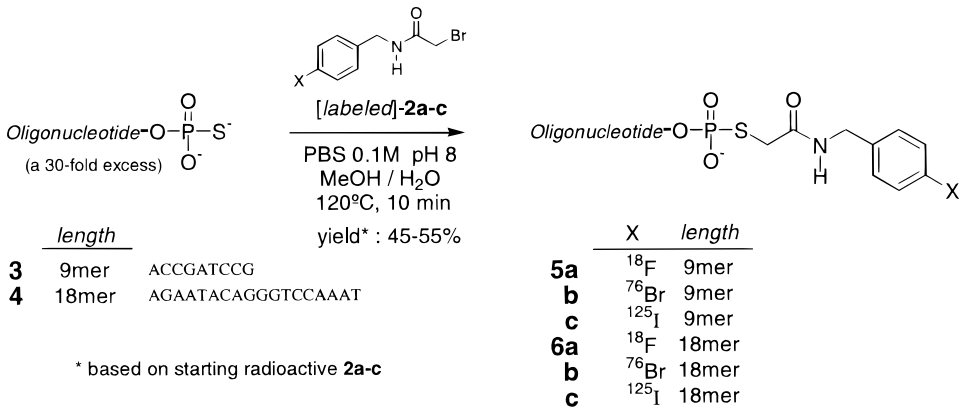

low in all other organs, with the lowest amount found in the brain, reflecting the low blood-brain barrier passage of oligonucleotides. In all these organs, the radioactivity concentrations declined rapidly over time, with no significant uptake in any organ, leading to only minute amounts detectable at 4 h after administration. As previously reported (Tavitian et al., 1998), in vivo degradation of phosphodiester oligonucleotides leads to radioactivity being recovered predominantly in labeled metabolites rapidly after i.v. injection to animals (see below), and accordingly there were no significant differences between the different compounds. In particular, the time course of radioactivity concentrations were similar for the ^{125}I-labeled 9mer and 18mer ([^{125}I]**5c** and [^{125}I]-**6c**) oligonucleotides. In contrast, comparison between the [^{125}I]- and [^{18}F]18mer ([^{125}I]**6c** and [^{18}F]**6a**) showed that the iodinated form led, as expected, to much higher concentrations in the thyroid gland than the fluorinated oligonucleotide. Uptake in this organ increased at late times, probably reflecting the affinity for iodine transporters of a degradation product of the [^{125}I]oligonucleotides. Another difference was that the two [^{125}I]oligonucleotides ([^{125}I]**5c** and [^{125}I]**6c**) led to higher radioactivity concentrations at later times in all organs, while at the early time point (5 min), higher radioactivity concentrations were found in the liver and kidneys after [^{18}F]-oligonucleotide injection. This suggests that the metabolites formed from the [^{125}I]18mer and [^{18}F]18mer have different biodistributions in vivo.

4. **Metabolism.** *4.1. In Vitro and in Vivo Metabolism of [^{125}I]9mer Oligonucleotide ([^{125}I]**5c**).* The yield of extraction of radioactivity from plasma with phenol/chloroforme was about 80%. RP-HPLC analysis of the incubated oligonucleotides in plasma displayed that the radioactive probe was progressively degraded. A total of 78% of intact probe was recovered after 15 min incubation, whereas only 35% radioactivity corresponded to starting oligonucleotide after 300 min incubation. In vivo, the metabolism was quite different since in plasma collected from injected animals, intact oligonucleotide did

Table 2. Biodistribution of Radioactivity in Mice after i.v. Injection of Labeled Oligonucleotides[a]

A. ^{125}I-Labeled 9mer Oligonucleotide [^{125}I]**5c**

	5 min	1 h	4 h
kidneys	11.3 ± 2.4	3.7 ± 0.1	1.1 ± 0.2
liver	8.2 ± 0.5	4.8 ± 0.1	1.1 ± 0.3
spleen	2.5 ± 0.1	1.5 ± 0.07	0.5 ± 0.06
heart	5.3 ± 2	2.1 ± 0.1	0.5 ± 0.2
lung	5.8 ± 0.1	3.4 ± 0.4	0.8 ± 0.3
brain	1.1 ± 0.1	1.5 ± 0.01	0.3 ± 0.1
muscle	3 ± 1.9	1.3 ± 0.06	0.52 ± 0.01
blood	11.1 ± 1.3	3.2 ± 0.3	0.8 ± 0.1
plasma	20.4 ± 5.1	4.3 ± 0.1	1.1 ± 0.1

B. ^{125}I-Labeled 18mer Oligonucleotide [^{125}I]**6c**

	5 min	1 h	4 h	15 h
kidneys	11.5 ± 0.8	4.7 ± 0.7	1.5 ± 0.3	0.1 ± 0.02
liver	8.7 ± 0.6	3.6 ± 0.3	1.5 ± 0.4	0.3 ± 0.1
spleen	1.8 ± 0.2	1.2 ± 0.1	0.4 ± 0.1	0.01 ± 0.00
heart	2.9 ± 0.5	1.5 ± 0.4	0.9 ± 0.1	0.02 ± 0.01
lung	7.3 ± 0.5	3.8 ± 1.6	1.3 ± 0.2	0.5 ± 0.07
brain	0.3 ± 0.03	1 ± 0.3	0.7 ± 0.1	0.01 ± 0.00
muscle	1.5 ± 0.3	1.3 ± 0.03	0.49 ± 0.05	0.06 ± 0.01
blood	8.4 ± 0.9	2.2 ± 0.3	0.9 ± 0.2	0.04 ± 0.00
plasma	16.5 ± 2.5	3.4 ± 0.1	1.1 ± 0.2	0.04 ± 0.01
thyroid	15.7 ± 2	14.2 ± 2.2	61 ± 5.5	49.7 ± 1.5
adrenals	3 ± 0.5	1.4 ± 0.2	0.8 ± 0.3	0.17 ± 0.02

C. ^{18}F-Labeled 18mer Oligonucleotide [^{18}F]**6a**

	5 min	1 h	4 h
kidneys	20.7 ± 1.7	2 ± 0.1	0.6 ± 0.02
liver	10.5 ± 0.4	1.66 ± 0.09	0.5 ± 0.01
spleen	0.89 ± 0.03	0.86 ± 0.04	0.14 ± 0.03
heart	1.3 ± 0.2	0.9 ± 0.3	0.18 ± 0.06
lung	3.4 ± 0.3	1.4 ± 0.3	0.27 ± 0.05
brain	0.18 ± 0.01	0.7 ± 0.3	0.2 ± 0.05
muscle	1.3 ± 0.2	0.84 ± 0.09	0.2 ± 0.07
blood	2.8 ± 0.05	0.5 ± 0.1	0.19 ± 0.01
plasma	4.9 ± 0.06	0.8 ± 0.2	0.22 ± 0.04
thyroid	1.8 ± 0.2	0.8 ± 0.2	0.23 ± 0.01
adrenals	1.5 ± 0.3	0.9 ± 0.1	0.3 ± 0.1

[a] All values are expressed in percent of injected dose per gram tissue and are the mean of three to four animals ± standard deviation.

not represent more than a few percent of the extracted radioactivity 5 min after injection and no intact probe was detected at 1 and 4 h.

In vivo, the oligonucleotide was essentially degraded in a "in front" eluting peak and slower eluting species than the starting probe. In organs (kidneys, liver, and lungs), the yields of radioactivity extraction were low and did not exceed 45%. Analysis by HPLC showed that no intact probe was recovered at any times and that the patterns of metabolites at 4 h were similar to those observed in plasma at 4 h. The different patterns of degradation of oligonucleotides in vitro and in vivo demonstrate that the metabolism is not only due to the plasmatic nucleases but also to tissular enzymes.

*4.2. [^{18}F]- and [^{125}I]18mer Oligonucleotide ([^{125}I]**6c** and [^{18}F]**6a**).* Metabolism was studied in plasma with both the fluorinated and iodinated probes whereas it was studied in organs (kidneys and liver) only for the iodinated probe because of the too short half-life of fluorine-18. Chromatograms showed a rapid degradation of the probes in plasma. Five minutes after injection, none of the starting oligonucleotide was recovered in plasma. In kidneys, less than 5% of the radioactivity was associated with the starting oligonucleotide at 5 min after injection and the probe was totally degraded at 1 h. In liver, no intact oligonucleotide was detected at any time. The rapid and total degradation of phosphodiester oligonucleotide has already been established (Sands et al., 1994; Sands et al., 1995; Tavitian et al., 1998). Since the [^{18}F]18mer and [^{125}I]18mer ([^{125}I]**6c** and [^{18}F]**6a**) oligonucleotides were administered simultaneously, differences in the biodistributions can be attributed to differences in the phamacokinetics of the fluorinated and iodinated metabolites.

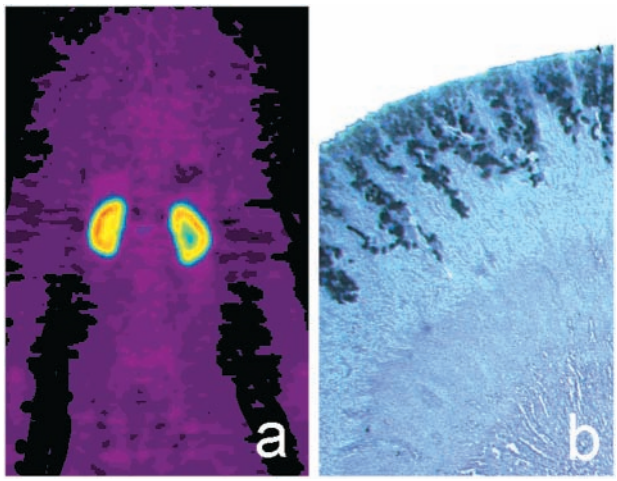

Figure 1. Distribution of radioactivity in the kidneys shown by in vivo PET imaging with the ^{18}F-oligonucleotide [^{18}F]**6a** injected in a monkey (a) is corroborated by ex vivo autoradiography of the kidney after ^{125}I-oligonucleotide [^{125}I]**6c** injection in a rat (b). Both images represent distribution of the radioactivity 5 min after tracer administration.

5. Comparative Imaging. A major reason for replacing fluorine-18 with another isotope is the necessity to correlate the images obtained in vivo with PET with the cellular distribution of the radiotracer. Even with the "high resolution" (HR) camera used in this study, that has a spatial resolution of ca. 100 mm^3 (Bendriem et al., 1992), it is difficult to determine the precise localization of radioactivity after [^{18}F]oligonucleotide injection in the primate. For instance, the resolution of PET images is too low to state positively the exact localization of the radioactivity in an organ such as the kidneys (Figure 1A). Autoradiography with a low-energy isotope is needed to increase spatial resolution to the cellular level, but since the technique requires the sacrifice of the animal it was performed in rodents rather than in a monkey. Indeed, micro-autoradiography of rat kidney sections obtained 5 min after [^{125}I]18mer injection (Figure 1B) showed that the radioactivity was present in the cortex of the organ, demonstrating that at early times the compound is subject to glomerular filtration. At this resolution level, it is possible to visualize distribution in the periglomerular space, suggesting an uptake of the radiotracer and/or of its metabolites by the previously described "oligonucleotide channel" of the brush border (Hanss et al., 1998).

CONCLUSION

The objective of this work was to develop a general, noncarrier added method for labeling oligonucleotides with radioactive halogens for use in radiopharmacology. We aimed at designing a method as universal as possible to be applied to any sequence and oligonucleotide chemistry, that could be performed with the different isotopes relevant to the variety of in vivo and ex vivo imaging and analytical techniques required for the development of oligonucleotides as pharmaceuticals.

Radiolabeling is performed in two steps, (1) radiolabeling of a synthon designed for high reactivity and stable

incorporation of halogens; and (2) regioselective conjugation of the synthon to the oligonucleotide. Performing the radiosynthesis of the synthon separately from the synthesis of the oligonucleotide allows (1) high yield incorporation in an activated C6 aromatic ring of the halogen through the use of harsh conditions that would not be compatible with the stability of the oligonucleotides; (2) purification of the synthon from other radioactive byproducts by HPLC; and (3) the possibility to work with any oligonucleotide obtained in-house or commercially, without tedious unblocking steps to protect the oligonucleotides from unwanted reactions. The coupling reaction itself is designed to be rapid and efficient in conditions compatible with the chemical stability of the oligonucleotides and the half-life of isotopes. In this respect, it is noteworthy that we obtained excellent coupling yields in times as short as 10−30 min. Since the synthon addition does not hamper biological properties of the oligonucleotides in vitro, including hybridization to the complementary target (Deverre et al., 1997; Tavitian et al., 1998), these novel radioprobes can be considered as valuable indicators of oligonucleotides fate in living organisms.

The family of radioprobes that can now be produced with this methodology encompasses the whole pannel of in vivo and ex vivo imaging techniques, complementing and refining studies on oligonucleotides' pharmacology: fluorine-18, a positron emitter used in PET ($t_{1/2}$ = 110 min); iodine-125, a low energy Auger electron emitter used for high-resolution autoradiography ($t_{1/2}$ = 59.9 days); iodine-123, a γ emitter used in SPECT ($t_{1/2}$ = 13.2 h); iodine-131, a γ emitter for imaging and therapy ($t_{1/2}$ = 8 days) and bromine-76, a positron emitter with a relatively long half-life ($t_{1/2}$ = 16.1 h). Access to isotopes with longer half-lifes allows to extend the times during which biodistribution and metabolism can be studied, in vivo with PET or SPECT or ex vivo in small animals, while low-energy isotopes allow to perform high-resolution imaging with autoradiography. In addition, iodine-123 and iodine-131 labeling allow for extension of oligonucleotide imaging to γ cameras.

The present work was conducted with the natural phosphodiester backbone as template compounds. Phosphodiester oligonucleotides are instable in vivo and cannot be used as such without incorporation into vectors with protective effects. However, the labeling method can now be applied to oligonucleotides bearing modifications on their ribose phosphate backbones or nucleobases, to yield radioactive probes in sufficient quantity with high specific radioactivity (Kühnast et al., 2000), opening the possibility to image the pharmacodistribution and analyze the metabolites of virtually any present or future modification aimed at improving the biodisponibility of oligonucleotides. This will certainly prove useful for drug and radiotracer design and development of oligonucleotides.

ACKNOWLEDGMENT

The authors wish to thank cyclotron operators Mr. Daniel Gouel and Mr. Christophe Peronne for performing the irradiations, as well as Drs Didier Gasparutto, Alain Valleix, Sven Klussmann, and Henri Virelizier for MS recording. This study was supported by a grant from the *Ministère de l'Enseignement Supérieur et de la Recherche* (ACC SV12 no. 2654) and a BIOMED-2 contract (BMH4-CT96-1067).

LITERATURE CITED

Agrawal, S. (1996) *Antisense therapeutics*, Humana Press, Totawa.

Agrawal, S., Tang, J. Y., and Brown, D. M. (1990) Analytical study of phosphorothioate analogues of oligodeoxynucleotides using high-performance liquid chromatography. *J. Chromatogr. 509*, 396−399.

Agrawal, S., Zhang, X., Lu, Z., Zhao, H., Tamburin, J. M., Yan, J., Cai, H., Diasio, R. B., Habus, I., and Jiang, Z. (1995) Absorption, tissue distribution and in vivo stability in rats of a hybrid antisense oligonucleotide following oral administration. *Biochem. Pharmacol. 50*, 571−576.

Belikova, A., Zarytova, V., and Grineva, N. (1967) Synthesis of ribonucleosides and diribonucleoside phosphates containing 2-chloro-ethylamine and nitrogen mustard residues. *Tetrahedron Lett. 8*, 3557−3562.

Bendriem, B., Trebossen, R., Frouin, V., Lamer, O., Brulon, V., and Syrota, A. (1992) Evaluation of a PET scanner in 2D and 3D acquisition mode. *IEEE Proc. 14*, 1837−1840.

Cammilleri, S., Sangrajrang, S., Perdereau, B., Brixy, F., Calvo, F., Bazin, H., and Magdelenat, H. (1996) Biodistribution of iodine-125 tyramine transforming growth factor α antisense oligonucleotide in athymic mice with a human mammary tumour xenograft following intratumoral injection. *Eur. J. Nucl. Med. 23*, 448−452.

Charlton, J., Sennello, J., and Smith D. (1997) In vivo imaging of inflammation using an aptamer inhibitor of human neutrophil elastase. *Chem. Biol. 4*, 809−816.

Chen, T.-L., Miller, P. S., Ts'o, P. O., and Colvin, O. M. (1990) Disposition and metabolism of oligodeoxynucleoside methylphosphonate following a single iv injection in mice. *Drug Metab. Dispos. 18*, 815−818.

Crooke, S. T., and Lebleu, B. (1993) *Antisense research and applications*, CRC Press, Boca Raton.

Deverre, J. R., Boutet, V., Boquet, D., Ezan, E., Grassi, J., and Grognet, J. M. (1997) A competitive enzyme hybridization assay for plasma determination of phosphodiester and phosphorothioate antisense oligonucleotide. *Nucleic Acids Res. 25*, 3584−3589.

Dewanjee, M. K., Ghafouripour, A. K., Kapadvanjwala, M., Dewanjee, S., Serafini, A. N., Lopez, D. M., and Sfakianakis, G. N. (1994) Noninvasive imaging of c-myc oncogene messenger RNA with indium-111-antisense probes in a mammary tumor-bearing mouse model. *J. Nucl. Med. 35*, 1054−1063.

Dollé, F., Hinen, F., Vaufrey, F., Tavitian, B., and Crouzel, C. (1997) A general method for labeling oligodeoxynucleotides with 18F for in vivo PET imaging. *J. Labelled Compd. Radiopharm. 39*, 319−330.

Dollé, F., Dolci, L., Valette, H., Hinnen, F., Vaufrey, F., Guenther, I., Fuseau, C., Coulon, C., Bottlaender, M., and Crouzel, C. (1999) Synthesis and nicotinic acetylcholine receptor in vivo binding properties of 2-fluoro-3-[2(s)-2-azetidinylmethoxy]pyridine: a new positron emission tomography ligand for nicotinic receptors. *J. Med. Chem. 42*, 2251−2259.

Fujibayashi Y., Yoshimi, E., Sakahara, H., Saga, T., Konishi, J., Yonekura, Y., and Yokoyama, A. (1999) A novel 111-In-labeled antisense DNA probe with multi-chelating sites (mcs-probe) showing high specific radioactivity and labeling efficiency. *Nucl. Med. Biol. 26*, 17−21.

Giles, R. V., and Tidd, D. M. (1992) Increased specificity for antisense oligodeoxynucleotide targeting of RNA cleavage by RNase H using chimeric methylphosphonodiester/phosphodiester structures. *Nucleic Acids Res. 20*, 763−770.

Gold, L., Brown, D., He, Y., Shtatland, T., Singer, B. S., and Wu, Y. (1997) From oligonucleotide shapes to genomic SELEX: novel biological regulatory loops. *Proc. Natl. Acad. Sci. U.S.A. 94*, 59−64.

Gorenstein, D. (1984) *Phosphorous-31 NMR: principles and applications*, Academic Press, New York.

Gorenstein, D. (1992) *Handbook of organophosphorous chemistry: advances in phosphorous-31 NMR*, Marcel Dekker, Inc, New York.

Hanss, B., Leal-Pinto, E., Bruggeman, L., Copeland, T., and Klotman, P. (1998) Identification and characterization of a

cell membrane nucleic acid channel. *Proc. Natl. Acad. Sci. U.S.A. 95*, 1921−1926.

Hedberg, E., and Langstrom, B. (1997) Synthesis of 4-([18F]-fluoromethyl)phenyl isothiocyanate and its use in labeling oligonucleotides. *Acta Chem. Scand. 51*, 1236−1240.

Hedberg, E., and Langstrom, B. (1998) 18F-Labeling of oligonucleotides using succinimido 4-[18F]fluoro-benzoate. *Acta Chem. Scand. 52*, 1034−1039.

Hjelstuen, O. K., Tonnesen, H., Bremer, P. O., and Verbruggen, A. M. (1998) 3′-Tc-Labeling and biodistribution af a CAPL antisense oligodeoxynucleotide. *Nucl. Med. Biol. 25*, 651−657.

Hnatowich, D. J., Winnard, P., Virzi, T., Fogarasi, M., Sano, T., Smith, C. L., Cantor, C. R., and Rusckowski, M. (1995) Technetium-99m labeling of DNA oligonucleotides. *J. Nucl. Med. 36*, 2306−2314.

Iribarren, A. M., Cicero, D. O., and Neuner, P. J. (1994) Resistance to degradation by nucleases of (2′S)-2′-deoxy-2′−C-methyloligonucleotides, novel potential antisense probes. *Antisense Res. Dev. 4*, 95−98.

Jorgensen, P. N., Stein, P. C., and Wengel, J. (1994) Synthesis of 3′−C−(hydroxymethyl)thymidine − Introduction of a novel class of deoxynucleosides and oligodeoxynucleotides. *J. Am. Chem. Soc. 116*, 2231−2232.

Kawasaki, A. M., Casper, M. D., Freier, S. M., Lesnik, E. A., Zounes, M. C., Cummins, L. L., Gonzalez, C., and Cook, P. D. (1993) Uniformly modified 2′-deoxy-2′-fluoro phosphorothioate oligonucleotides as nuclease-resistant antisense compounds with high affinity and specificity for RNA targets. *J. Med. Chem. 36*, 831−841.

Kühnast, B., Dollé, F., Vaufrey, F., Hinnen, F., Crouzel, C., and Tavitian, B. (2000) Fluorine-18 labeling of oligonucleotides bearing chemically modified ribose-phosphate backbones. *J. Labelled Compd. Radiopharm.* (in press).

Larrouy, B., Blonski, C., Boiziau, C., Stuer, M., Moreau, S., Shire, D., and Toulme, J. J. (1992) RNase H-mediated inhibition of translation by antisense oligodeoxyribonucleotides: use of backbone modification to improve specificity. *Gene 121*, 189−194.

Loc'h, C., Mardon, K., Valette, H., Brutesco, C., Merlet, P., Syrota, A., and Mazière, B. (1994) Preparation and pharmacological characterization of [76Br]-meta-bromobenzylguanidine. *Nucl. Med. Biol. 21*, 49−55.

Miller, P. S. (1991) Oligonucleoside methylphosphonates as antisense reagents. *Biol. Technol. 9*, 358−362.

Monia, B. P., Lesnik, E. A., Gonzalez, C., Lima, W. F., McGee, D., Guinosso, C. J., Kawasaki, A. M., Cook, P. D., and Freier, S. M. (1993) Evaluation of 2′-modified oligonucleotides containing 2′-deoxy gaps as antisense inhibitors of gene expression. *J. Biol. Chem. 268*, 14514−14522.

Moreau-Gachelin, F., D'Auriol, L., Robert-Lezenes, J., Galibert, F., Tambourin, P., and Tavitian, A. (1986) Analysis of integrated proviral DNA sequences with an octadecanucleotide probe designed for specific identification of spleen focus-forming virus in the mouse genome. *J. Virol. 57*, 349−352.

Moulds, C., Lewis, J. G., Froehler, B. C., Grant, D., Huang, T., Milligan, J. F., Matteucci, M. D., and Wagner, R. W. (1995) Site and mechanism of antisense inhibition by C-5 propyne oligonucleotides. *Biochemistry 34*, 5044−5053.

Nielsen, P. E., Egholm, M., and Buchardt, O. (1994) Peptide nucleic acid (PNA)−A DNA mimic with a peptide backbone. *Bioconjugate Chem. 5*, 3−7.

Reed, M. W., Panyutin, I. G., Hamlin, D., Lucas, D. D., and Wilbur, D. S. (1997) Synthesis of ^{125}I-labeled oligonucleotides from tributylstannylbenzamide conjugates. *Bioconjugate Chem. 8*, 238−243.

Sands, H., Gorey-Feret, J., Ho, S. P., Bao, Y., Cocuzza, A. J., Chidester, D., and Hobbs, F. W. (1995) Biodistribution and metabolism of internally 3H-labeled oligonucleotides. II. 3′, 5′-blocked oligonucleotides. *Mol. Pharmacol. 47*, 636−646.

Sands, H., Gorey-Feret, L. J., Cocuzza, A. J., Hobbs, F. W., Chidester, D., and Trainor, G. L. (1994) Biodistribution and metabolism of internally 3H-labeled oligonucleotides. I. Comparison of a phosphodiester and a phosphorothioate. *Mol. Pharmacol. 45*, 932−943.

Sanghvi, Y. S., Hoke, G. D., Freier, S. M., Zounes, M. C., Gonzalez, C., Cummins, L., Sasmor, H., and Cook, P. D. (1993) Antisense oligodeoxynucleotides: synthesis, biophysical and biological evaluation of oligodeoxynucleotides containing modified pyrimidines. *Nucleic Acids Res. 21*, 3197−3203.

Stein, C. A., and Cheng, Y. C. (1993) Antisense oligonucleotides as therapeutic agents − is the bullet really magical? *Science 261*, 1004−1012.

Stein, D., Foster, E., Huang, S. B., Weller, D., and Summerton, J. (1997) A specificity comparison of four antisense types: morpholino, 2′-O-methyl RNA, DNA, and phosphorothioate DNA. *Antisense Nucleic Acid Drug Dev. 7*, 151−157.

Tavitian, B., Terrazzino, S., Kühnast, B., Marzabal, S., Stettler, O., Dollé, F., Deverre, J., Jobert, A., Hinnen, F., Bendriem, B., Crouzel, C., and Di Giamberardino, L. (1998) In vivo imaging of oligonucleotides with positron emission tomography. *Nat. Med. 4*, 467−471.

Vaidyanathan, G., and Zalutsky, M. (1993) No carrier added synthesis of meta-[131I]iodobenzylguanidine. *Appl. Radiat. Isot. 44*, 621−628.

Wilbur, D. S., Hadley, S. W., Hylarides, M. D., Abrams, P. G., Beaumier, P. A., Morgan, A. C., Reno, J. M., and Fritzberg, A. T. (1989) Development of a stable radioiodinating reagant to label monoclonal antibodies for radiotherapy of cancer. *J. Nucl. Med. 30*, 216−226.

Yngve, U., Hedberg, E., Lovqvist, A., Tolmachev, V., and Langstrom, B. (1999) Synthesis of N-succinimidyl 4-[76Br]-bromobenzoate and its use in conjugation labeling of macromolecules. *Acta Chem. Scand. 53*, 508−512.

Zhao, Q., Matson, S., Herrera, C. J., Fisher, E., Yu, H., and Krieg, A. M. (1993) Comparison of cellular binding and uptake of antisense phosphodiester, phosphorothioate, and mixed phosphorothioate and methylphosphonate oligonucleotides. *Antisense Res. Dev. 3*, 53−66.

BC990183I

pH-Sensitive Cationic Polymer Gene Delivery Vehicle: *N*-Ac-poly(L-histidine)-graft-poly(L-lysine) Comb Shaped Polymer

Jonathan M. Benns,[†] Joon-Sig Choi,[‡] Ram I. Mahato,[†] Jong-Sang Park,[‡] and Sung Wan Kim*[,†]

Center for Controlled Chemical Delivery, Department of Pharmaceutics and Pharmaceutical Chemistry, University of Utah, Biomedical Polymers Research Building, 30 South 2000 East Street, Room 201, Salt Lake City, Utah 84112, Department of Chemistry, Seoul National University, Seoul, 151-742, Korea.
Received February 17, 2000; Revised Manuscript Received May 1, 2000

Advancing biotechnology spurs the development of new pharmaceutically engineered gene delivery vehicles. Poly(L-histidine) {PLH} has been shown to induce membrane fusion at endosomal pH values, whereas PLL has a well documented efficacy in polyplex formation. Therefore, *N*-Ac-poly(L-histidine)-graft-poly(L-lysine) {PLH-*g*-PLL} was synthesized by grafting poly(L-histidine) to poly(L-lysine) {PLL}. PLH-*g*-PLL formed polyplex particles by electrostatic interactions with plasmid DNA {pDNA}. The mean particle size of the polyplexes was in the range of 117 ± 6 nm to 306 ± 77 nm. PLH-*g*-PLL gene carrier demonstrated higher transfection efficacy in 293T cells than PLL at all equivalent weight ratios with pDNA. The inclusion of chloroquine as an endosomolytic agent enhanced transfection for both PLL and PLH-*g*-PLL gene carriers. PLH-*g*-PLL enhanced β-galactosidase expression compared to PLL, but still increased in efficacy when chloroquine was included.

INTRODUCTION

In the past decade, drug therapies have moved into a realm which includes the use of genes to combat illness. The theory behind the use of genetic material encoding vital proteins is simple; let the patient make their own therapeutic proteins. The efficacy of nonviral gene therapy relies upon the ability to deliver plasmid DNA into a cell nucleus to function as a gene. However, there are many obstacles in utilizing gene delivery for therapeutic treatments, consequently the introduction of new delivery vehicles for transfection continues. Many of the new delivery vehicles have been built on previous designs in an attempt to improve efficacy. One of the problems is the necessity for the ability to introduce plasmid DNA into the specific cell types (*1*−*5*). The other major issue in efficient gene expression is the release of the DNA from the endosomal compartment into the cytoplasm after transfection of the cell has taken place (*1*, *6*). Gene transfer depends on the ability to preferentially target specific cell types and allow release of the DNA into the cytoplasm with limited toxic side effects (*7*). Pharmaceutically engineered gene delivery vehicles cannot provide effective expression if the entire entity is transferred into the lysosomal compartment, which breaks down the plasmid. Although chloroquine has proven to aid in the release of the plasmid DNA into the cytoplasm, it has been found to be toxic and thus cannot be used in vivo. Therefore, there is a growing need for endosomal disrupting agents for enhanced release of the plasmid into the cytoplasm.

Viruses are known for their ability to be extremely efficient in delivering genes to the particular cells that are needed for the survival and progression of the viral species (*8*). Progressing knowledge of the virus and its ability to replicate, and the further understanding of the molecular mechanisms in which its genetic code is integrated into the cell has paved the path for viral based gene delivery (*7*, *9*−*11*). A perfect synthetic virus with no serious health-related side effect concerns led researchers in the direction pointing to the development of cationic polymer-based gene delivery vectors, which mimic the functions of a virus. Cationic polymers have been shown to form complexes (polyplex) with plasmids via ionic interaction (*12*−*16*). Although cationic polymers such as poly(L-lysine) {PLL} have been shown to efficiently condense DNA and protect DNA from nuclease attack, there are some disadvantages (*17*). PLL does not induce or facilitate the endosomal release of DNA. PLL possesses ϵ-amine groups, which can be linked to targeting ligands or pH-sensitive entities giving multifunctional capabilities.

Aggregation and lack of a targeting moiety has been somewhat circumvented by the attachment of other polymers and compounds to PLL forming co-block or comb-shaped polymers. Receptor-mediated endocytosis was found to increase transfection with PLL when the polymer was tethered to galactose, where the endocytosis occurred via the asialoglycoprotein receptor (*13*, *14*, *16*). Also, the transferrin receptor has been shown to be effective in increasing transfection ability (*18*−*20*). Recently, the folate binding protein has been exploited for receptor mediated endocytosis when folic acid has been tethered to cationic polymers (*21*−*24*).

Membrane fusion has been studied for the purpose of creating the opportunity for escape of material from a cellular compartment membrane (*20*, *25*). Viral envelopes have been noted to fuse with the endosomal and/or lysosomal compartment membranes. This fusion of the membrane occurs after the virus protein envelope had been internalized by receptor-mediated endocytosis, and by subsequent exposure to the acidic washes inside the respective compartments. This leads to the release of the

* To whom correspondence should be addressed. Phone: (801) 581-6801. Fax: (801) 581-7848. E-mail: Rburns@deans.pharm.utah.edu.
[†] Center for Controlled Chemical Delivery.
[‡] Department of Chemistry.

10.1021/bc0000177 CCC: $19.00 © 2000 American Chemical Society
Published on Web 09/18/2000

viral genome into the cytoplasm was as a result of the membrane fusion event (*26*−*29*). While multivalent inorganic cations have been employed for membrane fusion phenomena, cationic polymers have been found to perform the same function with higher efficiencies (*30*, *31*). The cationic polymers of poly(L-lysine) (PLL) and poly(L-histidine) (PLH) were both determined to have membrane fusion capability (*32*). PLL induced fusion occurs only in pH regions outside normal physiological conditions, whereas membrane fusion takes place at physiological pH values when PLH is used. The extent of PLH fusion increases as pH of the environment decreased, coinciding with the biological activity of the endosome (*33*). Histidine residues have been substituted into PLL chains giving pH-sensitive characteristics to the polymer and subsequently increasing transfection (*34*, *35*). In the pursuit of an ideal pharmaceutically engineered polymeric gene delivery system, a *N*-Ac-poly(L-histidine)-graft-poly(L-lysine) comb shaped polymer (PLH-*g*-PLL) was synthesized with the hypothesis of improved endosomal escape via membrane fusion, and subsequently increasing gene expression in cultured cells.

MATERIALS AND METHODS

Materials. Fmoc-im-benzyl-L-histidine, p-alkoxybenzyl alcohol resin, poly(L-lysine) PLL, ~8000 Da, ethidium bromide, *N*-(2-hydroxyethyl)piperazine-*N*′-{2-ethanesulfonic acid} (HEPES), 3-{4,5-dimethylthiazol-2-yl}-2,5- diphenyltetrazoliumbromide (MTT), chloroquine, O-nitrophenyl-*β*-D-galactopyranoside (ONPG), and *N*-hydroxysuccinimide were all purchased from Sigma Chemical Co. (St. Louis, MO). Piperidine, dimethyl sulfoxide (DMSO), trifluoroacetic acid (TFA), and dicyclohexacarbodiimide (DCC) were purchased from Aldrich (Milwaukee, WI). Plasmid pSV-*β*-gal (EMBL accession no. X65335), DNA size marker, and bacterial JM 109 strain were purchased from Promega (Madison, WI). Fetal bovine serum (FBS), Dulbecco's Modified Eagle's Medium (DMEM), trypsin-EDTA 0.25%, and Dulbecco's phosphate-buffered saline (DPBS) were purchased from Hyclone (Logan, UT). QIAfilter Plasmid Kit was purchased from Qiagen (Boulder, CO). *N*-Hydroxybenzotriazole (HOBT), *N*-*N*-diisopropylethylamine (DIPEA), and 2-(1H−benzotriazole-1-yl)-1,1,3,3-tetramethyluroniumhexafluorophosphate (HBTU) were from AnaSpec, Inc. (San Jose, CA). Dialysis tubing (MWCO 6000−8000) was from Spectrum Medical Industries, Inc. (Los Angeles, CA).

Synthesis of *N*-Acetyl-poly(im-benzyl-L-histidine). Poly(im-benzyl-L-histidine) was prepared by solid-phase peptide synthesis using Fmoc-chemistry. A *p*-alkoxybenzyl alcohol resin was used as a solid support. Briefly, the coupling reaction was conducted with HOBT/HBTU/DIPEA using Fmoc-im-benzyl-L-histidine as a monomer. Piperidine (30%) was used for Fmoc-deprotection. Each coupling and deprotection reaction was repeated 18 times and monitored by ninhydrin tests. The terminal amino group was acylated with acetic anhydride and the polypeptide was detached from the resin with 90% TFA. Cold ether was added to this solution, and the precipitate was washed with ether and dried. The product of this synthesis was a poly-histidine with approximately 18 linked histidines.

Synthesis of *N*-Acetyl-poly(im-benzyl-L-histidine)-NHS ester. *N*-hydroxysuccinimide (0.069 g) and DCC (0.049 g) were added to solution of *N*-acetyl-poly(im-benzyl-L-histidine) (25 mg) dissolved in DMF. The mixture was constantly stirred for 80 min at 30 °C. Dicyclohexylurea (DCU) formed as a solid was removed by filtering-off. Cold ether was added to the solution and the precipitate was obtained. The precipitate was washed further with cold ether.

Synthesis of *N*-Ac-poly(L-histidine)-graft-poly(L-lysine). First *N*-acetyl-poly(im-benzyl-L-histidine)-NHS ester (2.4 mmol) was dissolved in 0.6 mL of DMF, then 5 mg of poly(L-lysine) was added to this solution. After shaking the mixture for 4 h at room temperature, the product was precipitated in cold ether. The im-benzyl group of the imidazole was deprotected by Na/NH_3 method. The polymer was dialyzed overnight using the MWCO 6000−8000 dialysis tubing, followed by freeze-drying. *N*-Ac-poly(L-histidine)-graft-poly(L-lysine) was obtained and ^1H NMR was used to determine conjugation. PLL was determined to have 25% of its ϵ-amine groups tethered to the histidine polymer.

Amplification and Purification of Plasmid DNA (pSV-*β*-gal). Plasmid DNA encoding *β*-galactosidase (pSV-*β*-gal) was used as the reporter gene in this study. The plasmid pSV-*β*-gal was electrophorated into *E. coli* JM 109 bacterial strain using an electrophorator (ECM 600, BTX). The transformed cells were grown in larger quantities (0.5−1 L) of LB broth supplemented with 100 μg/mL ampicillin. The plasmid DNA was purified using the QLAfilter plasmid purification kit from QIAgen and the purified plasmid was diluted in sterilized water. The purity was confirmed by 1% agarose gel electrophoresis followed by ethidium bromide staining and DNA concentration was measured by UV absorption at 260 nm.

Band Retardation. PLH-*g*-PLL/plasmid polyplexes were prepared using 1−100 μg for each molecular weight *N*-Ac-poly(L-histidine)-graft-poly(L-lysine) comb shaped polymer and 1 μg of pSV-*β*-gal. The samples were incubated at room temperature for 30 min to ensure formation of the polyplex. The Easy-Cast Electrophoresis System (Owl Scientific Inc., Woburn, Ma) was setup with a sample buffer TBE (45 mM Tris-borate, 1 mM EDTA, pH 8.0) on a 1% (w/v) agarose gel. The run was taken at 100 V for 90 min, using an Electrophoresis Constant Power Supply (Pharmacia Fine Chemical Model ECPS 3000/150), until the marker and polyplex solutions had run enough length to identify band weights. Following electrophoresis, the gel was stained with ethidium bromide (0.5 μg/mL) for 30 min. Ethidium bromide allows the use of an ultra-violet illuminator to show the location of the DNA and various levels of polyplex formation (*36*).

Ethidium Bromide Displacement. The ability of *N*-Ac-poly(L-histidine)-graft-poly(L-lysine) to effectively condense DNA was monitored by observing the fluorescence quenching of the DNA-ethidium bromide interaction. Solutions were made with 1 mg/mL of DNA and 1 mg/mL of ethidium bromide. The solutions were incubated on the counter for 15 min to ensure interactions between DNA and the ethidium bromide. The range of polymer concentrations tested in ability to quench fluorescence was 0.1−20 mg. The solutions were made to the volume of 1 mL by dilution with a buffer (20 mM Hepes, 0.015 M NaCI, pH 7.4). The complete solutions incubated for 30 min prior to fluorescence testing to allow the Coulombic interactions of the polymer to displace ethidium bromide from the plasmid DNA. The relative fluorescence intensity was measured on an ISS Photon Counting Spectrofluorometer (ISS Inc., Champaign, IL). The spectrofluorometer was operated with an excitation wavelength (λ_{ex}) of 488 nm and emission wavelength (λ_{em}) of 590 nmn (*2*).

Dynamic Laser Light Scattering. The sizes of the polyplexes formed by increasing weight ratios of PLL and PLH-*g*-PLL were determined using dynamic laser light scattering. Each polyplex was formed by adding a poly-

mer solution and DNA solution (each filtered through 0.2 μm filters) into sterile ddH_20 then vortexing the solution and letting the complex formation take place for 20 min. The polyplexes were formed with PLL in dilute (0.02 mg/mL) and concentrated (0.05 mg/mL) solutions to determine if there was concentration dependence in complexation. The PLH-*g*-PLL polyplex formation was done under a corresponding median concentration. Polyplex diameters were measured using a Lexel Corp model 95 ion-argon laser (Palo Alto, CA) filtered for 514.5 nm, a Brookhaven Instrument Inc. BI-100 M Goniometer, and a BI-2030 Autocorrelator (Holtsville, NY). A Brookhaven correlator program written in QuickBASIC performed all calculations.

Acid−Base Titration. The ability of the gene carriers (PLH-*g*-PLL and PLL) to protonate and obtain a positive charge over a 10 to 2 pH range was determined by acid−base titration. Each polymer was made into a 30 mL solution with a 0.2 mg/mL concentration. The solution was then titrated to a pH of 10 with 1 M NaOH where the pH was measured using a Coming pH meter 340. The solution was then titrated with 1 N HCI given in various volume increments. The pH profile was obtained for each polymer and graphs of the data were generated.

In Vitro Transfection. The 293T transformed immortalized cell line was used for transfection and cell viability tests. The cell line was grown in polystyrene tissue culture flasks containing DMEM supplemented with 10% FBS, penicillin (100 units/mL), streptomycin (100 units/mL), gentamycin (50 μg/mL) in a 37 °C and 5% CO_2 environment. When transfection and/or cell viability experiments were conducted, the cells were plated in 3.5 cm diameter dishes. This was done after the cells had become about 80% confluent in the culture flasks. The cells were decanted of media and washed twice with DPBS and then trypsinized with 0.25% trypsin-EDTA for 8 min or until the cells were observed to detach from the culture flask under a microscope. The cells were then collected, diluted, and counted using a hemocytometer. The appropriate cell concentration (8×10^5 cells/dish) was then placed in the wells in the plating process. For transfection studies, PLL and PLH-*g*-PLL solutions were prepared and filtered through 0.2 μm polycarbonate membrane filters. The polymer solutions were then mixed with pSV-β-gal in ddH_20 and incubated for 20 min at room temperature. The polyplexes were added to media supplemented with 10% FBS. Chloroquine at a 100 pM final concentration was then added to appropriate solutions. The media in each dish was replaced with the transfection solution. The plated cells were then incubated with the polymer/DNA solution for 4 h. After the incubation period was completed, the polyplex solutions were removed and replaced with media. The plated cell culture was then incubated for an additional 36 h.

ONPG Assay for Expressed β-Galactosidase. β-Galactosidase expression from the cells transfected with PLL and PLH-*g*-PLL polyplexes was determined spectrophotometrically at 420 nm using a modified ONPG method (*2*, *36*). Briefly, 300 μL of a 1.33 mg/mL ONPG in a 2× buffer was added to cells, which had been broken down by 300 μL of lysis buffer, and incubated for 4 h. β-Galactosidase hydrolyzes the colorless substrate into yellowish o-nitrophenyl. The absorbance was measured in a 150 μL cuvette at 420 on a Perkin-Elmer UV/VIS/NIR lambda 19 spectrophotometer.

X-gal Assay for Expressed β-Galactosidase. β-Galactosidase expression was also determined by X-gal staining and counting of stained cells. After the 36 h incubation period, the cells were washed twice with ddH_2O and fixed with 1.25% glutaraldahyde for 20 min. The fixed cells were then washed four times with DPBS. The X-gal stain solution was prepared and 1.75 mL was added to the fixed cells. The cells were stained for 4 h until the transfected cells had turned blue. Following staining, the stain solution was removed and the cells were washed twice with DPBS and preserved with a glycerol water solution. The blue cells were then counted under the microscope.

Cell Viability. The cytotoxicity of the polyplexes was determined on 293T cell line using a MTT assay (*2*, *3*). The cells were plated in 3.5 cm diameter dishes at 8×10^6 cells/well. A MTT solution in DPBS was made at 2 mg/mL and filtered. The MTT solution (180 μL) was added to the cell culture 36 h after removal of transfection solution. The MTT solution was removed and 3.5 mL of DMSO was added so that any crystals formed by the living cells due to the presence of MTT would dissolve. The solvating of the crystals by DMSO allows for absorbance to be taken at 570 nm. The absorbance was measured in a 150 μL cuvette on a Perkin-Elmer UV/VIS/NIR lambda 19 spectrometer.

RESULTS

Synthesis of *N*-Ac-poly(L-histidine)-graft-poly(L-lysine). Poly (im-benzyl-L-histidine), an 18-mer linear polymer, was synthesized. There was not any free amine groups open for each step of polymerization, as determined by ninhydrin tests. After the final grafting of linear PLH to PLL was completed, the protecting groups were removed. A schematic of PLH-*g*-PLL synthesis is shown in Figure 1. ^{1}H NMR was used to determine the percent of PLL ϵ-amine groups conjugated to PLH molecules. ^{1}H NMR (D_2O, 300.1 MHz, 300 K): δ 7.45, 6.67 (m, imidazole-H of histidine), 4.36 (m, α-CH of histidine), 4.14 (m, α-CH of lysine), 2.78 (m, β-CH_2 of histidine), 2.52 (m, ϵ-CH_2 of lysine), 1.77 (s, CH_3 of acetyl), 1.64, 1.35, 1.19 (m, $(CH_2)_3$ of lysine. Analysis of proportionality of hydrogen atoms on respective sites indicated that 25% of the PLL ϵ-amine groups were conjugated to linear PLH molecules forming a comb shaped polymer.

Band Retardation Assay. The resulting gel electrophoresis when PLH-*g*-PLL complexed with pSV-β-gal was prepared and viewed with the aid of ethidium bromide association fluorescence (not shown). With an exclusion of the two terminal lanes, PLH-*g*-PLL concentration was increased compared to a constant amount of DNA. The increasing concentrations of this polymer decreased the electrophoretic mobility of plasmid DNA. No mobility of the DNA was observed at the polymer/DNA weight ratios above 20 (w/w). This decrease in electrophoretic mobility of the pDNA is due to the increasing DNA condensation and compaction.

Ethidium Bromide Displacement Assay. The ability of *N*-Ac-poly(L-histidine)-graft-poly(L-lysine) to condense DNA was tested with the ethidium bromide displacement assay. The more effective the polymer was in condensing plasmid DNA, the lower the relative fluorescence would be. The quenching of ethidium bromide/DNA interaction fluorescence by PLH-*g*-PLL was monitored by a spectrofluorometer. From Figure 2 it can be seen that the increasing concentrations of PLH-*g*-PLL increased the quenching of ethidium bromide fluorescence. At a low polymer/DNA ratio, there is little exclusion of ethidium bromide demonstrating minimal complexation and condensation. The data shows that increasing polymer concentration increases the ability to condense

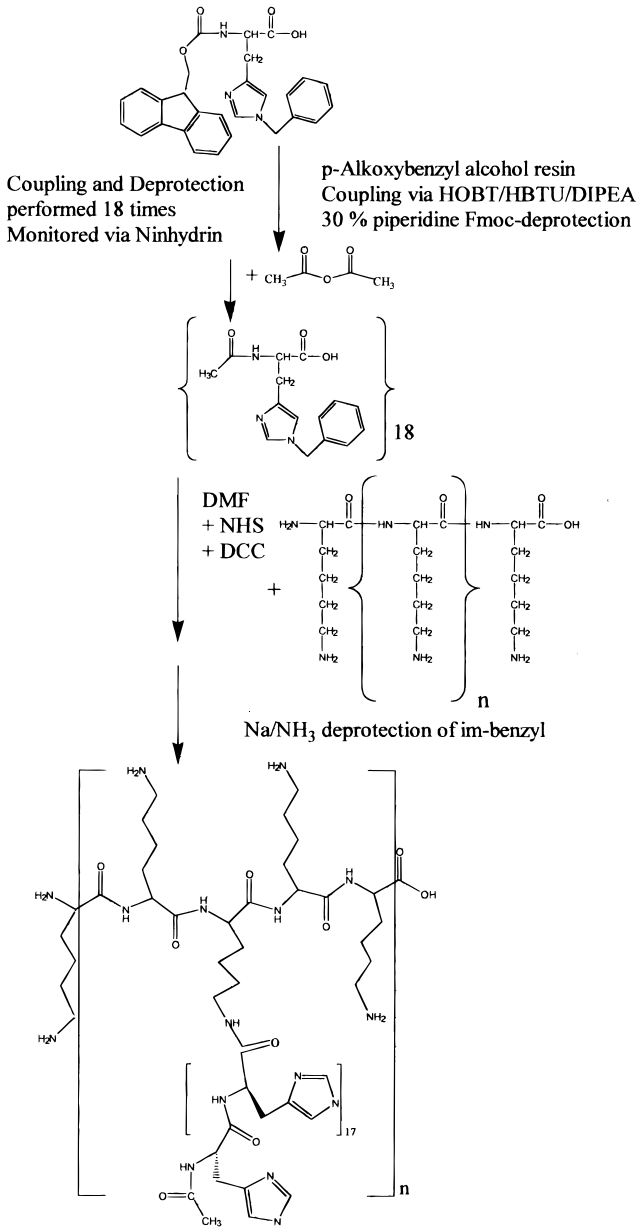

Figure 1. Schematic for synthesis of *N*-Ac-poly(L-histidine)-graft-poly(L-lysine) {PLH-*g*-PLL}.

DNA and subsequently hinders interactions with ethidium bromide. This is in good agreement with band retardation data.

Dynamic Laser Light Scattering. The particle size of polyplexes was determined by dynamic laser light scattering. The PLL polyplex particles were formed by increasing polymer/DNA weight ratios and in concentrated and dilute solutions. The size change with increasing polymer amount (PLL and PLH-*g*-PLL) at constant DNA can be seen in Figure 3. When PLH-*g*-PLL was used to compact pDNA, the polyplex size decreased as polymer concentration increased (Figure 3). PLH-*g*-PLL did not compact pDNA as effectively as PLL, however at higher weight ratios, PLH-*g*-PLL was just as effective as PLL. The polyplex size did not drastically decrease further at higher weight ratios.

Acid−Base Titration. The acid−base titration profile was obtained for PLL, PLH, and PLH−PLL, and shown in Figure 4. The initial high pH protonation of the ϵ-amine groups of PLL can be seen as a horizontal trend above pH 8. However, the titration curve trend turns

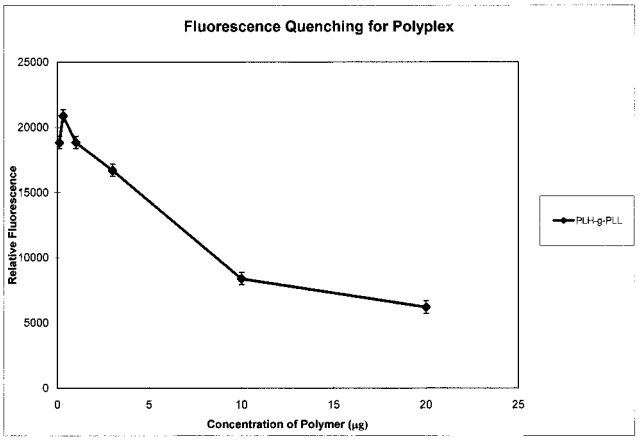

Figure 2. Effect of polymer concentration on DNA condensation. The solutions were incubated for 30 min to ensure polyplex formation. Error bars are the standard deviation of data points for the same polyplex solution.

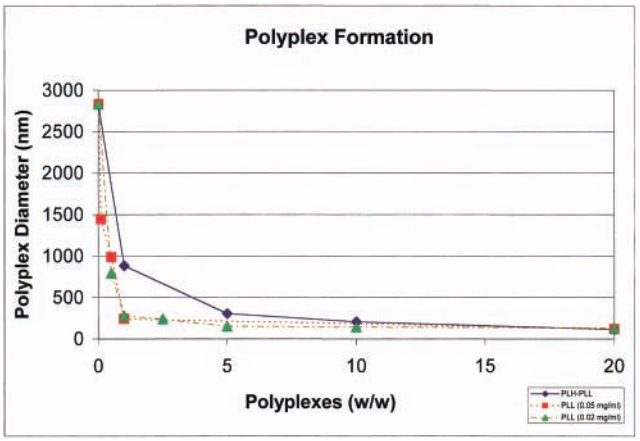

Figure 3. Effect of polymer concentration on particle size of pSV-*β*-gal polyplexes prepared using PLL and *N*-Ac-poly(L-histidine)-graft-poly(L-lysine). The solutions were incubated for 30 min to ensure polyplex formation. Error bars are the standard deviation of data points for the same polyplex solution taken at different times.

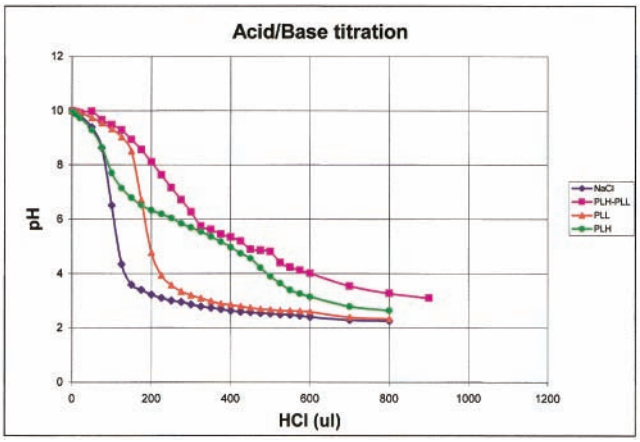

Figure 4. Acid−Base titration profile of 0.1 M NaCI, PLL, PLH, and PLH−PLL.

nearly vertical suggesting little buffering capacity of PLL. Unlike PLL, PLH showed considerable buffer capacity over almost the entire pH. The imidazole of histidine has a pK_a around 6.0 and this pK_a indicates that PLH protonates and becomes a strong polycation in the endosomal pH range. When PLH and PLL are combined, the titration curve gives the basic buffering capacity of

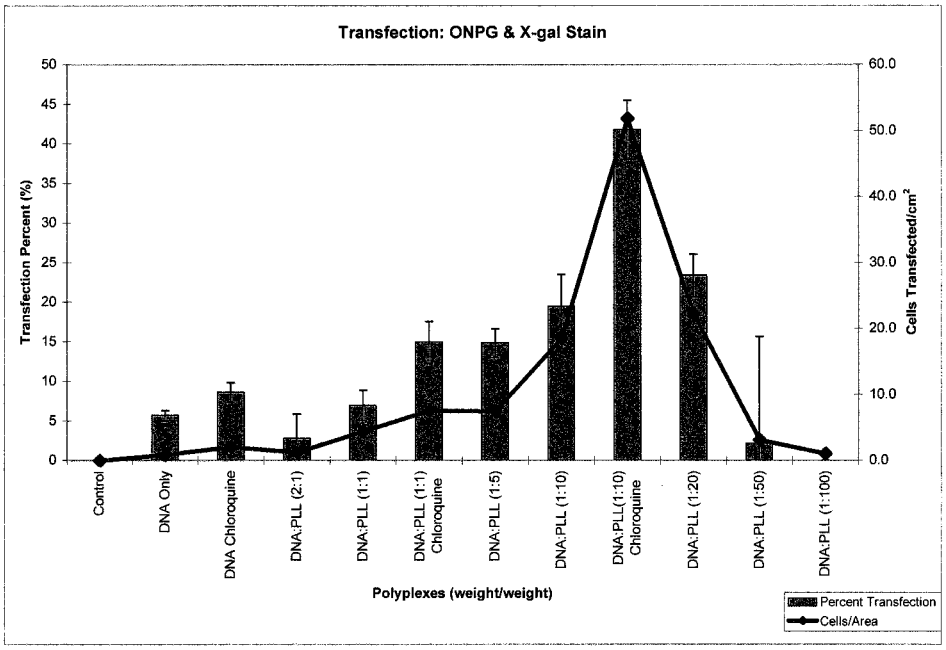

Figure 5. Effect of polymer concentration efficiency of polyplexes prepared with PLL and pSV-β-gal. Transfections were carried out using 293T cultured cells. The *x*-axis defines the polymer/DNA weight/weight ratio, with poly(L-lysine) (PLL) and with or without the aide of chloroquine. The left *y*-axis is obtained from absorbance from ONPG assay given in transfection percent, which is the absorbance percentage of that obtained by a calcium phosphate precipitation positive control. The right *y*-axis is defined as cells transfected/cm^2 counted after X-gal staining. Results are presented as mean ± standard deviation of three assays.

PLL and the endosomal pH buffering capacity of PLH. This result is in good agreement with previous reports where partially substituted PLL with histidine polymers had both DNA condensing and endosomolytic properties (*37*). Figure 4 supports the previous data that PLH-*g*-PLL retains the complexation and compaction ability associated with PLL, but also induces endosomal pHL protonation.

Transfection. Transfection was performed on 293T cells with the polyplexes prepared at different polymer/DNA ratios using poly(L-lysine) and *N*-Ac-poly(L-histidine)-graft-poly(L-lysine). Transfection efficiency was determined using ONPG and X-gal methods. Furthermore, each series of experiments included a calcium precipitation transfection solution as a positive control where its transfection ability was considered to be 100%. The absorbances taken from the polymer solutions were compared to those obtained from the calcium precipitation method, and reported as a percent of calcium precipitation. Figure 5 shows the effect of PLL/DNA weight ratio on transfection in vitro. For a given amount of DNA (9 μg/well), an increase in PLL concentration increased the transfection to a maximum with 20 weight ratio. Subsequent increase in polymer concentration decreased activity of β-galactosidase due to cell death. This trend was obtained by both assay schemes employed. The change in the absorbance is directly proportional to the β-galactosidase enzyme productivity of the transfected cells.

The absorbance increased for each polymer concentration when chloroquine was included in the transfection solution. β-Galactosidase concentration was a maximum when chloroquine was included and polyplexes were prepared at a polymer/DNA ratio of 10 (w/w) (Figure 5).

The effect of PLH-*g*-PLL/DNA weight ratio on transfection was studied using pSV-β-gal complexed with PLH-*g*-PLL. Transfection solutions had increasing amounts of polymer at a constant amount of DNA up to a maximum PLH-*g*-PLL/DNA ratio of 20. An increase in PLH-*g*-PLL polymer concentration increased the transfection (Figure 6). Transfection solutions containing PLH-*g*-PLL were compared to those that included only PLL. PLH-*g*-PLL showed better transfection efficiency for equivalent weight ratios of PLL. For equivalent weight ratios, PLH-*g*-PLL has less cationic polymer molecules. A less amount of polymer molecules was taken to prove that poly(histidine) grafted to PLL increased the transfection efficiency of the gene delivery vehicle.

The corresponding PLH-*g*-PLL transfection solutions were also given the endosomal disrupting agent chloroquine to determine if there would be any further endosomal escape of the polyplexes. Enhanced transfection efficiency, above that provided by the histidine residues, was observed for each of the PLH-*g*-PLL polyplex systems in the presence of chloroquine. The increase in transfection when chloroquine was included demonstrates that the grafted histidine polymers are not improving the endosomal escape potential to a maximum. However, PLH grafts improved the efficacy of the PLL cationic polymer molecules. The use of the ONPG and X-gal stain methods gave supporting data for comparison. Multiple assays indicating similar transfection profiles supports the hypothesis that grafting PLH to PLL enhances endosomal escape by the gene delivery vehicle and therefore increased the ability of the transfected cell to express the encoded protein.

Cell Viability. The efficacy of a gene carrier is partly dependent on the corresponding toxicity of the polymer and polyplex solutions. The wells containing cells in only media with no treatment of polymer or polyplexes were used as a positive control with a cell viability of 100%. The cell viability was determined for the cells treated with PLL/DNA polyplexes prepared at different weight ratios of PLL ranging from 1 to 100 (Figure 7). The solutions with increased amount of PLL over 20 times the amount of DNA were toxic to 293T cells. Although the increase in PLL concentration enhanced transfection, it was also toxic to the cells. The relative cell viability of

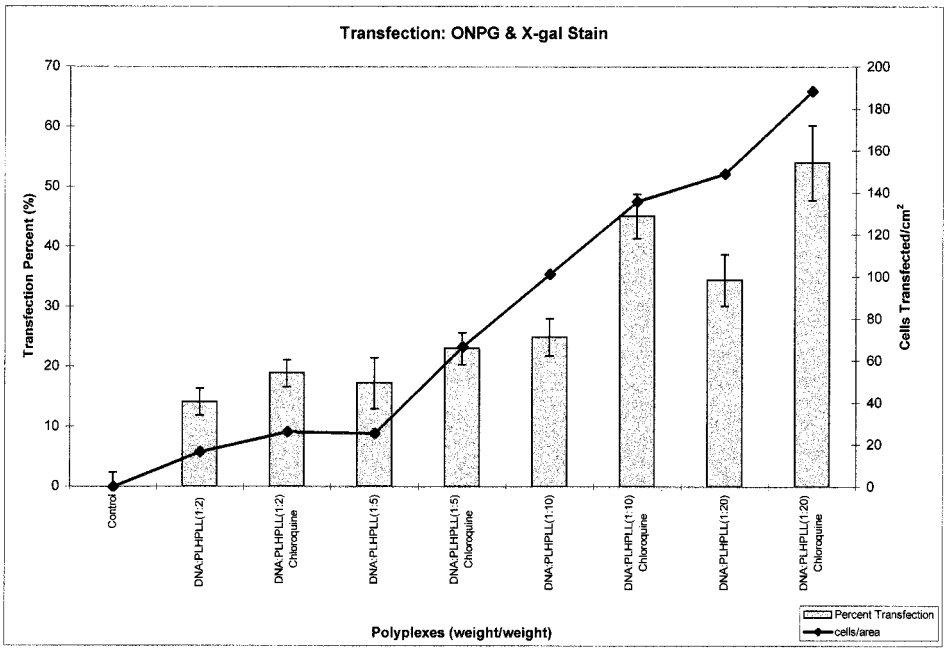

Figure 6. Effect of polymer concentration on transfection efficiency on 293T cells with polyplexes prepared using *N*-Ac-poly(L-histidine)-graft-poly(L-lysine) {PLH-*g*-PLL} and pSV-*β*-gal. The *x*-axis defines the polymer/DNA weight/weight ratio, *N*-Ac-poly(L-histidine)-graft-poly(L-lysine) {PLH-*g*-PLL} and with or without the aide of chloroquine. The left *y*-axis is obtained from absorbance from ONPG assay given in Transfection Percent, which is the absorbance percentage of that obtained by a calcium phosphate precipitation positive control. The right *y*-axis is defined as cells transfected/cm^2 counted after X-gal staining. Data are represented as the mean ± SD of three assays.

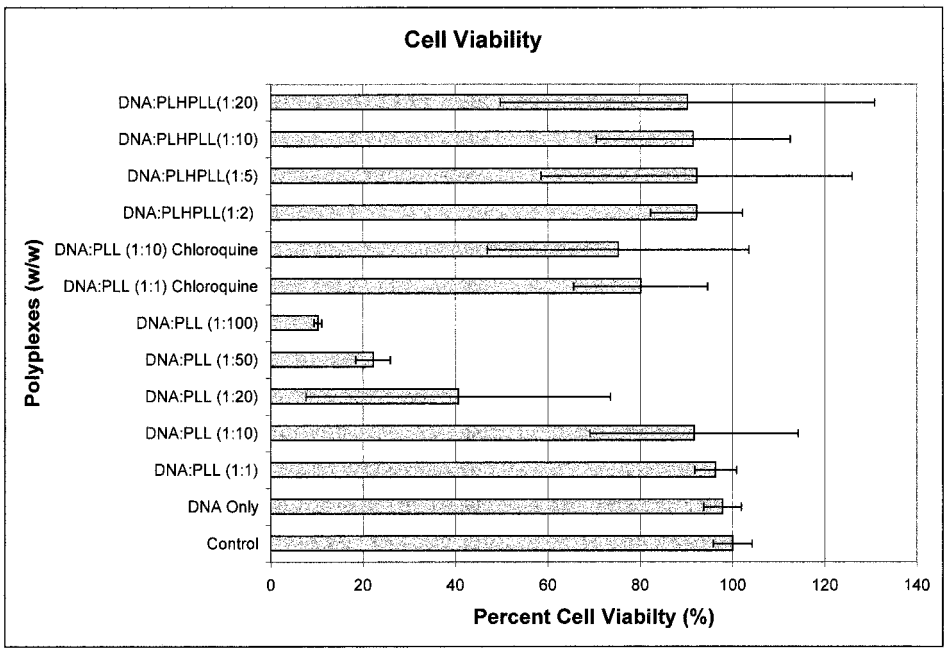

Figure 7. Cell viability percent of 293T cultured cells transfected with polyplexes prepared with pSV-*β*-gal and either PLL or PLH-*g*-PLL. PLL represents poly(L-lysine), PLHPLL represents *N*-Ac-poly(L-histidine)-graft-poly(L-lysine). The *x*-axis also indicates if transfection solution contained chloroquine. The error bars are the standard deviation of three assays.

the polyplexes prepared at a PLL/DNA weight ratio of 10 was ~80%. Generally, there was increase in toxicity with increase in polymer concentration. However, at the optimal PLL/DNA ratio of 10, the cell viability stayed in a range acceptable and greater than 70%.

PLL/DNA polyplexes prepared at w/w ratios of 1 and 10 were studied for toxicity in the presence of chloroquine. The inclusion of chloroquine in the solution increased the toxicity, while only ~40% cell viability for the cells treated with polyplexes with PLL/DNA of 20 w/w.

The toxicity of PLH-*g*-PLL polyplexes was also determined using 293T cells (Figure 7). The toxicity of the solutions was increased as the polymer concentration in the polyplex vector was increased. However, the relative cell viability was still greater than 80%.

DISCUSSION

Nonviral vectors require the entry of plasmid DNA into the cells and then further entry into the nucleus to function as a gene. These nonviral vectors must overcome at least four limiting barriers. The first barrier is

targeting the gene delivery vehicle to the desired area in vivo, while avoiding degradation by the physiological defense system. Also, by limiting which cells will endocytose the vector, the specific cells needed to produce the encoded protein will have a higher probability of successful transfection. The second barrier is the need to introduce DNA into the specific desired cell type efficiently and safely. Efficiency is in the level of transfection and transgene expression, which includes the ability to preferentially target specific cell types and allow pDNA release into the cytoplasm with limited toxic side effects (*1*). Without an in vivo targeting capability, the future of gene delivery would be limited to ex vivo methods of transfection. The introduction of in vivo procedures lacking an effective targeting moiety could lead to widespread random insertion of the genetic material into cells all over the human body. The third barrier is the release of DNA from the endosomal compartment. The plasmid DNA in the pharmaceutically engineered gene delivery vehicle cannot provide effective expression if the entire entity is transferred into the lysosomal compartment and subsequently degraded (*38*). Fusogenic peptides derived from different viruses have been used to enhance the escape of gene delivery vehicles from the endosome (*20*). These peptides are amino acid sequences found on virus particles that have pH dependent conformations allowing for cytoplasm targeting. Along these lines, other pH sensitive components such as chloroquine and poly(histidine) have been utilized with increased transfection efficiency (*34*, *35*, *39*). The fourth barrier is the translocation of the DNA into the nucleus. The transfer of the genetic material into the nucleus can be accomplished with a nuclear localization signal peptide. However, this nuclear localization step in gene delivery is not fully understood and steps are continuing to progress to advance this area (*40*).

In this study, *N*-Ac-poly(L-histidine)-graft-poly(L-lysine) {PLH-*g*-PLL} cationic polymer was synthesized (Figure 1) and characterized in terms of DNA condensing, particle size of polyplex, toxicity, and transfection in vitro (*4*, *5*, *36*). PLH-*g*-PLL is a PLL backbone with 25% of its ϵ-amine group's graft with PLH by analysis with ^{1}H NMR. The reactions were monitored via ninhydrin assay to indicate if there were primary amines present. The use of mass spectral analysis would have been a better way to do a more thorough characterization of intermediates in the polymer synthesis. However, the reaction scheme does not allow other side reactions, although it may change the polydispersity of the final product. The linking of PLH to PLL was a limiting step in this synthesis; therefore, proton-NMR was used to determine the conjugation percentage by comparing histidine and lysine residues. The polydispersity of PLH may not be exact to yield an 18 mer polymer, but with accurate weighing of reagents and careful synthesis the ninhyrdrin assay should indicate complete reactions.

Higher weight ratios of PLH-*g*-PLL/plasmid DNA effectively retarded the electrophoretic mobility (data not shown). This suggests that PLH-*g*-PLL did not relinquish the ability of PLL to condense DNA. These data was consistent with other conjugated PLL carriers (*2*, *34*).

Both polymers efficiently condensed DNA into small polyplexes. PLL and PLH-*g*-PLL exhibited fluorescence quenching with increasing polymer concentration as determined from the ethidium bromide displacement assay (Figure 3). This fluorescence quenching shows increasing DNA compaction with an increase in polymer concentration. This supports the evidence provided by the retarded gel electrophoreses.

The PLH-*g*-PLL showed a similar compaction profile with less magnitude in comparison to PLL. The optimal condensation of PLH-*g*-PLL was higher with a polymer/DNA ratio of 20. PLH-*g*-PLL polymer had less ability to condense DNA, as poly(L-histidine) is not charged at pH 7.4 and does not complex with plasmid at neutral pH (*35*). However, polyplexes of diameter 117 nm were formed when 20 times excess polymer was used (Figure 4). This happens because at lower ratios of PLH-*g*-PLL/pDNA, PLH-*g*-PLL has 25% of the ϵ-amine groups unavailable for protonation. Also histidine residues are attached to PLL affects a low weight ratio compaction of DNA by decreasing the amount of amines for a given weight.

PLL as shown in Figure 4 had the ability to protonate at pH values above physiological conditions and also showed a steep decrease through neutral to acidic pH. The PLH profile was indicative of a neutral polymer at high pH and began to protonate at pH 6.5−5.0 and buffered the system through this range. The pH, where buffering capability occurred, was that of physiological endosomal pH values. The resulting profile obtained from PLH with PLL was observed to be a summation of the two titrations, and indicates the addition of both properties with negligible loss of either compaction or endosomnal protonation. Protonation of histidine polymers within the physiological pH range is significant for endosomal disruption, where the pK_a of polyhistidine and the titration profile are consistent with desired properties given by previous reports (*28*, *33*−*35*). Poly(L-histidine) has been shown to induce fusion of lipid bi-layers in a slightly acidic medium upon protonation of the imidazole groups by increasing 16 interactions between the polymeric cation and the negatively charged membrane phospholipid (*32*, *33*). In addition, PLH was found to be more fusogenic in acidic medium than PLL.

The inclusion of chloroquine increased the transfection efficiency, which is consistent with previously reported results (*2*, *5*, *39*). The transfection ability of the polyplex reached a maximum value for the vector complexed with PLH-*g*-PLL, and when chloroquine was also added to the system (Figure 6). Both PLL and PLH-*g*-PLL demonstrated increasing transfection efficiency as the amount of polymer increased, β-galactosidase concentration in 293T cells increased. All polymer solutions increased transfection efficacy when chloroquine was added to aid in endosomal escape (*39*). PLH-*g*-PLL/DNA complexes prepared at weight ratio of 20 was most effective, especially when chloroquine was included. Our findings on enhanced transfection with PLH-*g*-PLL is in good agreement with Midoux and Monsigny (1999) (*35*) who demonstrated that the partial substitution of poly(L-lysine) ϵ-amine groups with histidine residues significantly enhanced transfection. In their studies, optimal conditions for transfection was found when PLL substitution level was 38 ± 5% (*34*). The additional increase in transfection with inclusion of chloroquine demonstrates that there is still room for improvement in the polymeric gene carrier. The endosomal disruption of PLH-*g*-PLL is a step in the right direction for enhanced gene transfer. Scientists have also reported that the amphipathic peptide HSWYG {Gly-Leu-Phe-His-Ala-Ile-Ala-His-Phe-Ile-His-Gly-Gly-Trp-His-Gly-Leu-Ile-His-Gly-Trp-Tyr-Gly} containing five histidine residues, also permeabilizes cell membranes at endosomal pH values (*38*). The generation of cationic charges via protonation of several imidazole groups inside the endosome is a suitable approach to allow DNA to be released into the cytosol (*34*). Therefore, the transfection efficiency will be increased from the enhanced ability of DNA to escape the endosomal com-

partment and be translocated into the nucleus for transcription.

CONCLUSION

The pharmaceutically engineered pH-sensitive *N*-Ac-poly(L-histidine)-graft-poly(L-lysine) comb shaped polymer {PLH-*g*-PLL} showed improved transfection in 293T cells in comparison to a poly(L-lysine) {PLL} control, possibly due to enhanced endosomal release of DNA. The endosomal escape usually occurs via a membrane fusion, buffering, or a nonspecific endosomotropic function. There was successful transfection and transgene expression for higher weight ratios of *N*-Ac-poly(L-histidine)-graft-poly-(L-lysine) comb shaped polymer. The pursuit of viable gene delivery vehicles should continue in biocompatible polymer designs until a nonviral gene delivery vector is produced with high efficiency in cell targeting and transport into the cellular cytoplasm leading to efficient expression of transfected pDNA.

ACKNOWLEDGMENT

The authors would like to thank Expression Genetic, Inc. for supporting this work in furthering the designs of cationic polymer gene carriers.

LITERATURE CITED

(1) Benns, J. M., and Kim, S. W. (2000) Tailoring New Gene Delivery Designs for Specific Targets. *J. Drug Targeting 8*, 1−12.

(2) Choi, Y. H., Liu, F., Park, J. S., and Kim, S. W. (1998) Lactose-poly(ethylene glycol)-grafted poly-L-lysine as hepatoma cell- tapgeted gene carrier. *Bioconjugate Chem. 9*, 708−718.

(3) Kim, J. S., Kim, B. I., Maruyama, A., Akaike, T., and Kim, S. W. (1998) A new nonviral DNA delivery vector: the terplex system. *J. Controlled Release 53*, 175−182.

(4) Kim, J. S., Maruyama, A., Akaike, T., and Kim, S. W. (1998) Terplex DNA delivery system as a gene carrier. *Pharm. Res. 15*, 116−121.

(5) Lentz, M. J., and Kim, S. W. (1998) Terplex system for delivery of DNA and oligonucleotides. In *Self Assembling Complexes for Gene Delivery* (A. V. Kabanov, P. L. Felgner, and L. W. Seymour, Eds.) John Wiley & Sons Ltd., New York.

(6) Mulligan, R. C. (1993) The basic science of gene therapy. *Science 260*, 926−932.

(7) Ledley, F. D. (1996) Pharmaceutical approach to somatic gene therapy. *Pharm. Res. 13*, 1595−1614.

(8) Smith, A. E. (1995) Viral vectors in gene therapy. *Annu. Rev. Microbiol. 49*, 807−838.

(9) Shimotohno, K., and Temin, H. M. (1981) Formation of infectious progeny virus after insertion of herpes simplex thymidine kinase gene into DNA of an avian retrovirus. *Cell 26*, 67−77.

(10) Wei, C. M., Gibson, M., Spear, P. G., and Scolnick, E. M. (1981) Construction and isolation of a transmissible retrovirus containing the src gene of Harvey murine sarcoma virus and the thymidine kinase gene of herpes simplex virus type 1. *J. Virol. 39*, 935−944.

(11) Tabin, C. J., Hoffmann, J. W., Goff, S. P., and Weinberg, R A. (1982) Adaptation of a retrovirus as a eucaryotic vector transmitting the herpes simplex virus thymidine kinase gene. *Mol. Cell. Biol. 2*, 426−436.

(12) Dorudi, S., Northover, J. M., and Vile, R. G. (1993) Gene transfer therapy in cancer. *Br. J. Surg. 80*, 566−572.

(13) Plank, C., Zatloukal, K., Cotten, M., Mechtler, K., and Wagner, E. (1992) Gene transfer into hepatocytes using asialoglycoprotein receptor mediated endocytosis of DNA complexed with an artificial tetra-antennary galactose ligand. *Bioconjugate Chem. 3*, 533−539.

(14) Chiou, H. C., Tangco, M. V., Levine, S. M., Robertson, D., Kormis, K., Wu, C. H., and Wu, G. Y. (1994) Enhanced resistance to nuclease degradation of nucleic acids complexed to asialoglycoprotein-polylysine carriers. *Nucleic Acids Res. 22*, 5439−5446.

(15) Wadhwa, M. S., Knoell, D. L., Young, A. P., and Rice, K. G. (1995) Targeted gene delivery with a low molecular weight glycopeptide carrier. *Bioconjugate Chem. 6*, 283−291.

(16) Wilson, J. M., Grossman, M., Wu, C. H., Chowdhury, N. R, Wu, G. Y., and Chowdhury, J. R. (1992) Hepatocyte-directed gene transfer in vivo leads to transient improvement of hypercholesterolemia in low-density lipoprotein receptor-deficient rabbits. *J. Biol. Chem. 267*, 963−967.

(17) Laemmli, U. K. (1975) Characterization of DNA condensates induced by poly(ethylene oxide) and polylysine. *Proc. Natl. Acad. Sci. U.S.A. 72*, 4288−4292.

(18) Wagner, E., Zenke, M., Cotten, M., Beug, H., and Birnstiel, M. L. (1990) Transferrin-polycation conjugates as carriers for DNA uptake into cells. *Proc. Natl. Acad. Sci. U.S.A. 87*, 3410−3414.

(19) Wagner, E., Cotten, M., Foisner, R., and Birnstiel, M. L. (1991) Transferrin-polycation-DNA complexes: the effect of polycations on the structure of the complex and DNA delivery to cells. *Proc. Natl. Acad. Sci. U.S.A. 88, 4255−4259.*

(20) Wagner, E., Plank, C., Zatloukal, K., Cotten, M., and Birnstiel, M. L. (1992) Influenza virus hemagglutinin HA-2 N-terminal fusogenic peptides augment gene transfer by transferrin-polylysine-DNA complexes: toward a synthetic virus-like gene-transfer vehicle. *Proc. Natl. Acad. Sci. U.S.A. 89*, 7934−7938.

(21) Mislick, K. A., Baldeschwieler, J. D., Kayyem, J. F., and Meade, T. J. (1995) Transfection of folate-polylysine DNA complexes: evidence for lysosomal delivery. *Bioconjugate Chem. 6*, 512−515.

(22) Leamon, C. P., Weigl, D., and Hendren, R. W. (1999) Folate copolymer-mediated transfection of cultured cells. *Bioconjugate Chem. 10*, 947−957.

(23) Reddy, J. A., Dean, D., Kennedy, M. D., and Low, P. S. (1999) Optimization of folate-conjugated liposomal vectors for folate receptor-mediated gene therapy. *J. Pharm. Sci. 88*, 1112−1118.

(24) Reddy, J. A., and Low, P. S. (1998) Folate-mediated targeting of therapeutic and imaging agents to cancers. *Crit. Rev. Ther. Drug Carrier Syst. 15*, 587−627.

(25) Plank, C., Oberhauser, B., Mechtler, K., Koch, C., and Wagner, E. (1994) The influence of endosome-disruptive peptides on gene transfer using synthetic virus-like gene transfer systems. *J. Biol. Chem. 269*, 12918−12924.

(26) Maeda, T., Kawasaki, K., and Ohnishi, S. (1981) Interaction of influenza virus hemagglutinin with target membrane lipids is a key step in virus-induced hemolysis and fusion at pH 5.2. *Proc. Natl. Acad. Sci. U.S.A. 78*, 4133−4137.

(27) White, J., Kartenbeck, J., and Helenius, A. (1980) Fusion of Semliki forest virus with the plasma membrane can be induced by low pH. *J. Cell Biol. 87*, 264−272.

(28) White, J., and Helenius, A. (1980) pH-dependent fusion between the Semliki Forest virus membrane and liposomes. *Proc. Natl. Acad. Sci. U.S.A. 77*, 3273−3277.

(29) Tycko, B., and Maxfield, F. R (1982) Rapid acidification of endocytic vesicles containing alpha 2- macroglobulin. *Cell 28*, 643−651.

(30) Gad, A. E., Silver, B. L., and Eytan, G. D. (1982) Polycation-induced fusion of negatively charged vesicles. *Biochim. Biophys. Acta 690*, 124−132.

(31) Lampe, P. D., and Nelsestuen, G. L. (1982) Myelin basic protein-enhanced fusion of membranes. *Biochim. Biophys. Acta 693*, 320−325.

(32) Uster, P. S., and Deamer, D. W. (1985) pH-dependent fusion of liposomes using titratable polycations. *Biochemistry 24*, 1−8.

(33) Wang, C. Y., and Huang, L. (1984) Polyhistidine mediates an acid-dependent fusion of negatively charged liposomes. *Biochemistry 23*, 4409−4416.

(34) Midoux, P., and Monsigny, M. (1999) Efficient gene transfer by histidylated polylysine/pDNA complexes. *Bioconjugate Chem. 10*, 406−411.

(35) Pichon, C., Roufa, M. B., Monsigny, M., and Midoux, P. (2000) Histidylated oligolysines increase the transmembrane passage and the biological activity of antisense oligonucleotides. *Nucleic Acids Res. 28*, 504−512.

(36) Choi, Y. H., Liu, F., Kim, J. S., Choi, Y. K., Park, J. S., and Kim, S. W. (1998) Poly(ethylene glycol)-grafted poly-L-lysine as polymeric gene carrier. *J. Controlled Release 54*, 39−48.

(37) Tang, M. X., and Szoka, F. C. (1997) The influence of polymer structure on the interactions of cationic polymers with DNA and morphology of the resulting complexes. *Gene. Ther. 4*, 823−32.

(38) Midoux, P., Kichler, A., Boutin, V., Maurizot, J. C., and Monsigny, M. (1998) Membrane permeabilization and efficient gene transfer by a peptide containing several histidines. *Bioconjugate Chem. 9*, 260−267.

(39) Wolfert, M. A., and Seymour, L. W. (1998) Chloroquine and amphipathic peptide helices show synergistic transfection in vitro. *Gene Ther. 5*, 409−414.

(40) Zanta, M. A., Belguise-Valladier, P., and Behr, J. P. (1999) Gene delivery: a single nuclear localization signal peptide is sufficient to carry DNA to the cell nucleus. *Proc. Natl. Acad. Sci. U.S.A. 96*, 91−96.

BC0000177

Dimerization of Human Growth Hormone in the Presence of Metal Ions

Gervydas Dienys,[†] Jolanta Sereikaitė,*[,‡] Virgis Lukša,[‡] Ona Jarutienė,[†] Edita Mištinienė,[‡] and Vladas-Algirdas Bumelis[‡]

Faculty of Chemistry, Vilnius University, Lithuania, and Institute of Biotechnology, Graičiūno 8, Vilnius 2028, Lithuania. Received August 25, 1999; Revised Manuscript Received February 10, 2000

Zn^{2+} and Co^{2+} ions are known to promote human growth hormone reversible dimerization. In these studies, dimerization was also shown to be initiated by nine other metal ions: Cd^{2+}, Hg^{2+}, Cu^{2+}, Ag+, Au^{3+}, Au+, Pd^{2+}, Ni^{2+}, and Pt^{4+}. In some cases (Hg^{2+}, Ag^{+}, Au^{3+}, and Ni^{2+}) formation of higher oligomers also took place. In addition further detailed investigation of dimerization in the presence of Zn^{2+} ions was carried out.

Human growth hormone (hGH)[1] is a polymorphic hormone. Several forms are found in the pituitary gland (*1*−*3*). The 22 kDa form is the most prevalent. The 20 kDa form, though, which lacks residues 32−46, amounts to approximately 15% of that present. There are several dimeric forms, all of which have a molecular mass of 45 kDa (10−20% of the total hGH). Some are dimers, formed by intermolecular disulfide bonding. Upon reduction with 2-mercaptoethanol, or oxidation with performic acid, they are converted into 22 kDa monomers. Another dimeric form of hGH was also detected which was resistant to reduction by 2-mercaptoethanol (*1*). Reversible dimerization of hGH takes place in the presence of Zn^{2+} ions, as thoroughly investigated by B. C. Cunningham and T. W. Patapoff, et al., using size-exclusion chromatography and sedimentation equilibrium methods (*4*, *5*). Zn^{2+} forms a 1:1 complex with hGH. Two globules of such a complex then associate to form a dimer with a dissociation constant, $K_d = 2.6$ mM. Mutational analysis was then used to identify the coordination site of Zn^{2+} and to determine the binding surface between two monomeric globules (*4*). Indeed, B. C. Cunningham, et al., proposed that the Zn^{2+}-hGH dimer may be the major storage form of hGH in vivo. hGH is synthesized and secreted into storage granules before its release from the anterior pituitary. The concentration of hGH and Zn^{2+} in these granules is greater than 1 mM. Practically all the hGH would be expected to be in dimeric form under such conditions, the dimer being more resistant to denaturation during storage than the monomeric form (*4*). Co^{2+} has previously been reported to effectively substitute for Zn^{2+} in the hGH dimer (*4*). We therefore screened a range of metal ions in order to find, whether others could also induce dimerization of hGH. We report the results in this paper. Cross-linking of the subunits by the trifunctional agent 1,3,5-triacryloyl-hexahydro-s-triazine (TAT) was used to identify the formation of dimers (*6*).

MATERIALS AND METHODS

Chemicals. Recombinant human growth hormone expressed in *Escherichia coli* with the N-terminal Phe residue deleted was obtained from Biofa AB (Lithuania). Protein markers for sodium dodecyl sulfate−polyacrylamide gel electrophoresis (SDS−PAGE) were obtained from Pharmacia. TAT was prepared as described by T. L. Gresham and T. R. Steadman (*7*) and recrystallized from water. Acetic acid, trifluoroacetic acid, $ZnCl_2$, $NiCl_2 \times 6H_20$, $CuCl_2$, $AlCl_3 \times 6H_20$, $HgCl_2$, and $PdCl_2$ were obtained from Fluka, while acetonitrile for reversed phase high-performance liquid chromatography (RP-HPLC), $FeCl_3 \times 6H_20$ were obtained from Sigma. Trypsin (sequencing grade) was obtained from Boehringer Mannheim. Other metal salts were obtained from Reachim (Russia).

Dimerization of hGH by Metal Ions and Cross-Linking by TAT. A total of 0.4 mL of the reaction mixture, containing 0.014 mM of hGH and from 0.014 to 1.4 mM of metal ions in 0.05 M borate buffer, pH 9.2, was incubated for 5 min at 30 °C and then 0.1 mL of 9 mM TAT solution was added. After incubation for 3 h at 30 °C the reaction mixture was cooled to 5 °C and extensively dialyzed. Subsequently, the reaction mixture was analyzed by SDS−PAGE to identify cross-linked protein forms.

SDS−PAGE. SDS−PAGE was carried out on the Mighty Small electrophoresis unit (Hoefer Scientific Instruments) according to the method of Laemmli (*8*). The acrylamide concentration used in the gel was 9.5%. Dithiothreitol (50 mM in the sample) was added to reduce −S−S− bonds. Proteins were stained with Coomassie Brilliant Blue R-250 and the gels were scanned at 633 nm using the Dual-Wavelength TLC scanner (CS 930, Shimadzu).

Modification of hGH by TAT. The reaction mixture containing 0.035 mM of hGH and 3.7 mM of TAT in 0.05 M borate buffer, pH 9.2, was incubated at 30 °C. Samples were withdrawn after incubation for 5, 15, 30, 60, 150, and 300 min and the reaction was stopped by acidification to pH 5.0. Samples were analyzed by electrospray ionization mass spectrometry (ESI-MS) or used for trypsin digestion and peptide mapping.

* To whom correspondence should be addressed. Phone: (370 2) 602112. Fax: (370 2) 602116. E-mail: Sereik@ibt.lt.

[†] Vilnius University.

[‡] Institute of Biotechnology.

[1] Abbreviations: hGH, human growth hormone; TAT, 1,3,5-triacryloyl-hexahydro-s-triazine; SDS−PAGE, sodium dodecyl sulfate−polyacrylamide gel electrophoresis; RP-HPLC, reversed-phase high-performance liquid chromatography; ESI-MS, electrospray ionization mass spectrometry.

10.1021/bc990112j CCC: $19.00 © 2000 American Chemical Society
Published on Web 08/17/2000

Table 1. Cation Effects on the Cross-Linking of hGH: $(hGH)_2$ as a Percentage of Total[a]

	molar ratio hGH/cation	
cation	1/1	1/10
Zn^{2+}	69.4 ± 1.8[b]	67.7 ± 2.7[b]
Cd^{2+}	61.2 ± 5.9	76.2 ± 7.6
Co^{2+}	8.5 ± 1.9	18.3 ± 1.1
Hg^{2+}	38.3 ± 4.5	
Cu^{2+}	1.6 ± 1.4	30.9 ± 5.9
Au^{3+}	10.1 ± 1.7	33.0 ± 1.2
Au^{+}	3.4 ± 2.7	4.9 ± 6.4
Pd^{2+c}	29.6 ± 3.9	1.6 ± 1.5
Ni^{2+}	2.6 ± 1.9	10.8 ± 4.5
Pt^{4+}	1.4 ± 0.8	1.1 ± 0.6

[a] pH 9.2, 3 h at 30 °C. [b] Standard deviations for three to five identical parallel experiments are given. [c] 12.7 ± 2.8, when hGH/cation = 1/5.

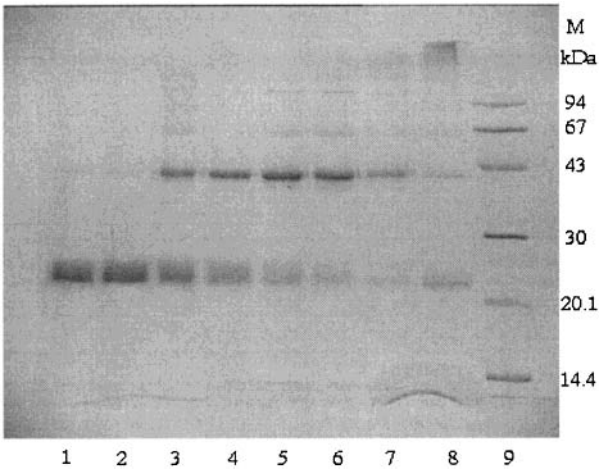

Figure 1. SDS−PAGE (9.5%) of hGH cross-linked by TAT in the presence of metal ions (0.05 M borate buffer, pH 9.2, 3 h at 30 °C; initial concentrations: hGH, 0.014 mM; TAT, 1.8 mM). Lanes 1−3, molar ratio hGH/Ag^{+}, 1/1, 1/3, and 1/10, respectively; lanes 4−8, molar ratio hGH/Hg^{2+}, 1/1, 1/2, 1/3, 1/5, and 1/10, respectively; lane 9, protein markers.

The kinetics of modification of hGH amino groups were followed by measuring the reaction mixture concentration of free amino groups every 30 min over a period of 5 h, using the 2,4,6-trinitrobenzene sulfonic acid method (*9*) described by Jonušienė et al. (*10*). Three kinetic runs were carried out for each reaction. When the kinetics of modification of dimeric hGH were investigated, the reaction mixture contained 0.07 mM Zn^{2+}.

Trypsin Digestion and Peptide Mapping. Before trypsin digestion all samples of hGH were purified by RP-HPLC as described below under sample preparation for mass spectrometry. Lyophilized hGH was dissolved in 1% ammonium bicarbonate, pH 7.9−8.0, to a final concentration of 1 mg/mL. A total of 100 μL of the trypsin solution (0.5 mg/mL) was added to 500 μL of the hGH solution and the sample was incubated for 4 h at 37 °C. Digestion was stopped by freezing (−20 °C).

RP-HPLC tryptic mapping was performed using the reversed phase column Hi-Pore RP-318 (250 × 4.6 mm, Bio-Rad). A linear gradient of 0% B to 20% B for 20 min, 20% B to 25% B for 20 min, 25% B to 50% B for 25 min, 50% B to 80% B for 15 min at flow rate of 1 mL/min was applied, where eluent A was 0.1% trifluoroacetic acid in water, and eluent B was 0.1% trifluoroacetic acid in acetonitrile/water (90/10, v/v). UV absorption was monitored at 215 nm.

Sample Preparation for Mass Spectrometry. All samples prior to mass spectrometry were purified by RP-HPLC using reversed-phase column Hi-Pore RP-304 (250 × 4.6 mm, Bio-Rad); solvent A, 0.1% trifluoracetic acid in water; solvent B, 0.1% trifluoroacetic acid in acetonitrile/water (90/10, v/v). The column was initially equilibrated with solvent A at a flow rate of 1 mL/min. After injection the column was eluted with a 5 min linear gradient to 50% B followed by a 60 min linear gradient to 80% B. The chromatographic analysis was performed on a HP 1100 Series HPLC system. Collected peaks were lyophilized and dissolved in acetonitrile/water/acetic acid (49.5/49.5/1, v/v/v).

Table 2. Cross-Linked hGH Forms in the Presence of Ag^{+}(percentage of the total hGH)[a]

	molar ratio hGH/Ag^{+}	
form of hGH	1/1	1/10
$(hGH\text{-}Ag^{+})_2$	8.5 ± 1.1[b]	30.7 ± 3.8[b]
$(hGH\text{-}Ag^{+})_3$	2.0 ± 0.8	7.8 ± 2.3
higher oligomers	0	9.4 ± 7.2

[a] pH 9.2, 3 h at 30 °C. [b] Standard deviations for three parallel experiments are given.

Table 3. Modification of hGH by TAT[a]

reaction time (min)	no. of modified lysine amino groups		no. of TAT molecules coupled with hGH molecule[c]
	hGH	$(hGH)_2$	
5	0.17[b] ± 0.02	0.22[b] ± 0.02	0.35
15	0.50[b] ± 0.06	0.62[b] ± 0.01	0.78
30	0.89 ± 0.35	1.23 ± 0.20	1.26
60	1.79 ± 0.54	2.28 ± 0.05	2.14
90	2.62 ± 0.42	3.40 ± 0.25	
150	3.99 ± 0.49	4.79 ± 0.17	
210	5.02 ± 0.44	5.71 ± 0.06	
300	6.06 ± 0.06	6.58 ± 0.14	

[a] pH 9.2, 30 °C, 3.7 mM TAT. [b] Calculated from the pseudofirst-order rate constants $(6.40 \pm 0.81) \times 10^{-5}$ s^{-1} and $(8.06 \pm 0.05) \times 10^{-5}$ s^{-1}. [c] Calculated from ESI-MS data.

Electrospray Ionization Mass Spectrometry. The HP 1100 Series mass selective detector was used for the acquisition of the electrospray ionization mass spectra. All spectra were in the positive ion mode, over mass range 300−3000 *m*/*z*.The samples were delivered to the analyzer using a 400 μL/min flow of acetonitrile/water/acetic acid (49.5/49.5/1, v/v/v). The working conditions were the following: capillary voltage, 4500 V; fragmentor voltage, 170 V; drying gas flow, 13 L/min; and temperature, 350 °C. The nebulizer pressure used was 25 psi. Nitrogen was used for drying and nebulizing.

RESULTS AND DISCUSSION

It is well-known, that formation of protein oligomers in solution can be investigated by the cross-linking of the subunits and subsequent SDS−electrophoresis (*11*−*13*). We used TAT a convenient cross-linking agent (*6*) to screen of the ability of a range of metal ions to induce dimerization of hGH. All experiments were performed under standard conditions (pH 9.2, 30 °C, concentration of hGH, 0.014 mM). The molar ratio hGH/cation used was from 1/1 to 1/100. 30 metal ions were tested, 11 of them induced dimerization of hGH at least to some extent (Table 1). Each of the 11 formed a compact group downward and to the left of zinc in the periodic table of chemical elements. Cross-linking did not take place in the presence of Mg^{2+}, Al^{3+}, Ca^{2+}, Ba^{2+}, Pb^{2+}, Fe^{2+}, Fe^{3+}, Mn^{2+}, Cr^{3+}, Sr^{2+}, Ga^{3+}, Zr^{4+}, Tl^{+}, In^{3+}, Rh^{3+}, Ru^{3+}, Nd^{3+}, La^{3+}, and Eu^{3+}. Thus there was no significant dimerization of hGH in solutions containing these cations.

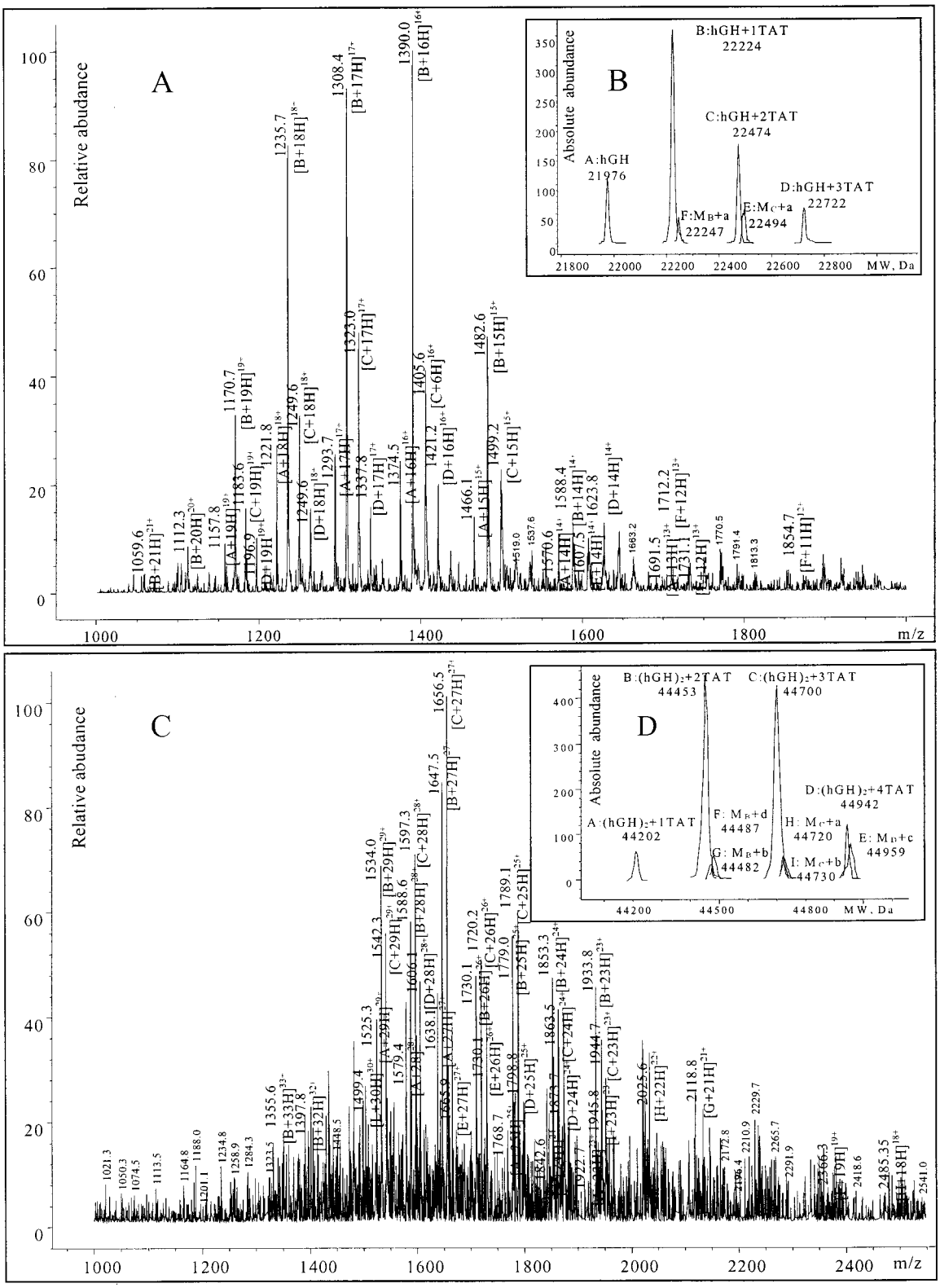

Figure 2. Mass spectrum (A) and components of hGH (B), modified by TAT (pH 9.2, 30 min at 30 °C). Mass spectrum (C) and components (D) of cross-linked dimers $(hGH{-}Zn^{2+})_2$ (pH 9.2, 30 min at 30 °C). In panels B and D, a = hydrogen atom replaced by Na^+; b = $(hGH)_2$ associated with Zn^{2+}; c = with H_2O; and d = with $2H_2O$.

According to their respective modes of action the ions given in the Table 1 may be divided into four groups. Dimer formation was most effectively initiated by Zn^{2+} and Cd^{2+}. An equimolar amount of each of these ions was sufficient to generate nearly complete cross-linking of hGH to form dimers. Excess $Zn^{2+}$and Cd^{2+} did not enhance the rate of cross-linking.

Less than 10% of the cross-linked hGH dimer was formed, however, in the presence of equimolar amounts of Co^{2+}, Cu^{2+}, Pt^{4+}, and Au^{+}. The yield of cross-linked dimer increased though, if excess metal ions were used and/or the duration of the reaction time was extended. For example, using a 1/10 molar ratio of hGH/Cu^{2+} the yield of cross-linked dimers was 31% after 3 h, 46% after

Table 4. Components of the TAT−hGH Modification Reaction Mixture[a,b]

components of the reaction mixture[c]	reaction time (min)			
	5	15	30	60
hGH	65	32	16	2
hGH + 1TAT	35	57	51	33
hGH + 2TAT		11	24	30
hGH + 3TAT			9	21
hGH + 4TAT				10
hGH + 5TAT				4

[a] pH 9.2, 30 °C. [b] Initial concentrations of hGH, 0.035 mM; TAT, 3.7 mM. [c] Percentage from the amount of total hGH + *n*TAT.

Table 5. Composition of Cross-Linked Dimers $(hGH{-}Zn^{2+})_2$[a,b]

components of the dimer mixture[c]	reaction time (min)	
	30	60
$(hGH{-}Zn^{2+})_2$ + 1TAT	3	5
$(hGH{-}Zn^{2+})_2$ + 2TAT	44	25
$(hGH{-}Zn^{2+})_2$ + 3TAT	36	32
$(hGH{-}Zn^{2+})_2$ +4TAT	17	23
$(hGH{-}Zn^{2+})_2$ + 5TAT		14
$(hGH{-}Zn^{2+})_2$ + 6TAT		1

[a] pH 9.2, 30 °C. [b] Concentrations of hGH − 0.014 mM, Zn^{2+}, 0.028 mM; TAT, 1.8 mM. [c] Percentage from the amount of total $(hGH{-}Zn^{2+})_2$ + *n*TAT.

6 h, and 68% after 20 h. The dimeric form was the only product of cross-linking, no higher oligomers were formed.

Together with $(hGH)_2$, cross-linked trimers and higher oligomers of hGH were formed in the presence of Ni^{2+}, Ag^+, Hg^{2+}, and Au^{3+}. Hg^{2+} ions were particularly effective in promoting the formation of higher oligomers (Figure 1). When equivalent concentrations of $Hg^{2+}$and hGH were used, only dimeric (approximately 40%) and monomeric hGH were found in the reaction mixture. When the ratio of hGH/Hg^{2+} was changed from 1/2 to 1/5, monomeric hGH nearly disappeared and bands of $(hGH)_3$ and higher oligomers became visible. Further increases in Hg^{2+} concentration resulted in higher oligomers as the main products, while the concentration of monomeric hGH increased again. Apparently, excessive complexation of Hg^{2+} distorted the contact surface for dimer formation (Figure 1, lane 8). Ag^+ ions induced formation of $(hGH)_3$ even more effectively than Hg^{2+} ions (Figure 1, lanes 1−3; Table 2). Higher oligomers were formed only at hGH/Ag^+ ≤ 1/10.

Pd^{2+} ions were noted for their peculiarity. Pd^{2+} could not be included in any of the three groups of ions discussed above. Approximately 30% of $(hGH)_2$ was formed at hGH/Pd^{2+} = 1/1. Even a small excess of Pd^{2+} though diminished the formation of $(hGH)_2$. Higher oligomers were not formed.

Indeed at very high concentrations of nearly all cations (hGH/cation = 1/100) the efficacy of $(hGH)_2$ cross-linking was diminished, even if higher oligomers were not formed. For example, the yields of $(hGH)_2$ at metal ion ratios of 1/1, 1/10, and 1/100 were for Co^{2+}, 8.5 ± 1.9, 18.3 ± 1.1, and 14.9 ± 1.7; for Cu^{2+}, 1.6 ± 1.4, 30.9 ± 5.9, and 26.6 ± 4.3, respectively.

To characterize this cross-linking of hGH on a molecular level we carried out a detailed investigation of the cross-linking process in the presence of Zn^{2+} ions. The kinetics of modification of amino groups by TAT were measured both for monomeric and dimeric hGH, using 2,4,6-trinitrobenzene sulfonic acid as an analytical reagent (*9*, *10*). It was found that the pseudofirst-order rate constants at the beginning of the reaction were (6.40 ± 0.81) × 10^{-5} s^{-1} for hGH and (8.06 ± 0.05) × 10^{-5} s^{-1} for $(hGH{-}Zn^{2+})_2$ (pH 9.2, 30 °C, 3.7 mM of TAT). The number of modified amino groups was also nearly the same during the course of the reaction (Table 3), to indicate that the reactivity of amino groups was not seriously disturbed by dimerization. Apparently there is no lysine residues on the contact surface of hGH globules in $(hGH)_2$.

There are nine lysine residues in the hGH molecule. Together with the N-terminal proline residue, there are therefore 10 potential points with which TAT might react. ESI-MS was therefore used to identify and quantitatively estimate modified monomeric hGH species, containing 1, 2, 3, and so on molecules of coupled TAT (Figure 2, panels A and B; Table 4). The average number of TAT molecules, coupled with hGH, over increasing reaction times, is given in Table 3. During the first half hour of the reaction the average number exceeded the number of modified lysine amino groups (Table 3), an observation explained by the fact that modification of the N-terminal proline is not exposed using the 2,4,6-trinitrobenzene sulfonic acid method (*10*). Proline is modified much faster than the primary amino groups of lysine residues because of a lower pK_a and a higher activity of secondary as compared to primary amines (*14*).

Cross-linked dimers $(hGH{-}Zn^{2+})_2$ formed by the action of TAT on hGH in the presence of Zn^{2+} ions were separated on RP-HPLC and were analyzed by ESI-MS (Figure 2, panels C and D; Table 5). The data clearly indicate that major modifications of hGH are not needed

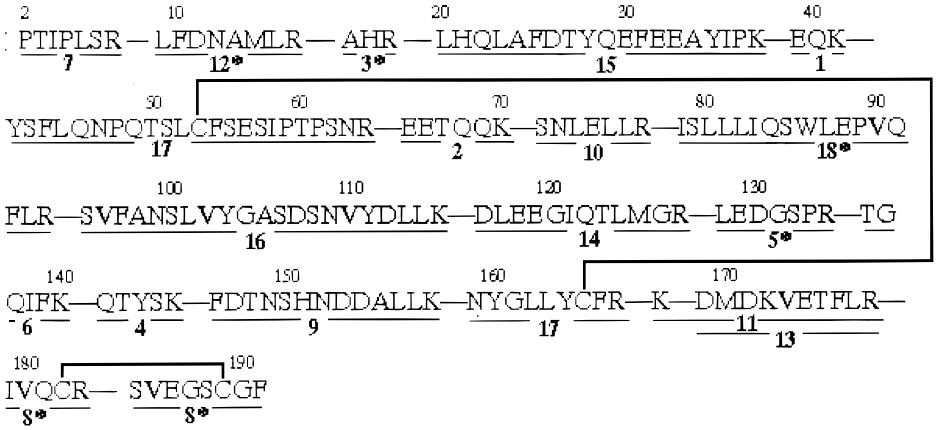

Figure 3. Peptides formed by tryptic hydrolysis of unmodified hGH. Bold ciphers correspond to the numbers of peptides in Figure 4. The asterisk marks peptides without Lys residues.

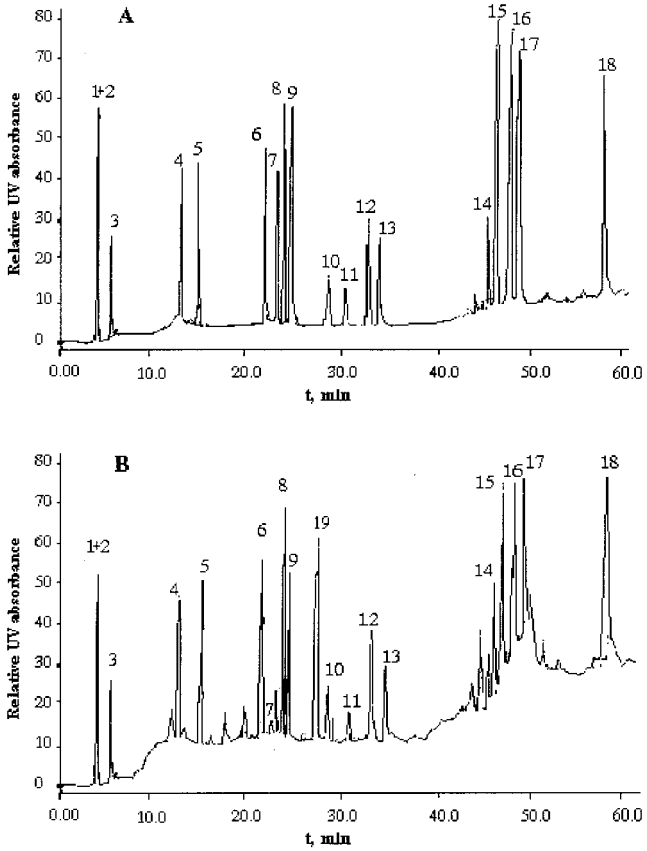

Figure 4. RP-HPLC separation of peptides obtained by tryptic hydrolysis of unmodified (A) and modified hGH (B, pH 9.2, 60 min at 30 °C, 3.7 mM TAT).

Table 6. Mass List for the Unmodified Peptides

peptide no.	amino acid sequences of peptides	mass from amino acid sequence (Da)	mass from ESI-MS (Da)
1	EQK	403.4	403.7
2	EETQQK	761.8	761.5
3	AHR	382.4	382.3
4	QTYSK	625.7	625.4
5	LEDGSPR	772.8	772.5
6	TGQIFK	692.8	692.7
7	PTIPLSR	782.9	782.6
8	IVQCR + SVEGSCGF	1400.6	1399.8
9	FDTNSHNDDALLK	1489.6	1489.1
10	SNLELLR	843.9	843.7
11	KDMDKVETFLR	1381.6	1381.1
12	LFDNAMLR	979.1	978.5
13	DMDKVETFLR	1253.4	1252.8
14	DLEEGIQTLMGR	1361.5	1361.1
15	LHQLAFDTYQEFEEAYIPK	2340.6	2342.6
16	SVFANSLVYGASDSNVYDLLK	2263.5	2262.2
17	YSFLQNPQTSLCFSESIPTPSNR + NYGLLYCFR	3763.2	3762.5
18	ISLLLIQSWLEPVQFLR	2055.5	2055.2

for dimer cross-linking, two to three molecules of TAT are enough.

Finally, the relative activities of hGH amino groups and the N-terminal proline were estimated by the method of tryptic digestion. Unmodified hGH was cleaved into 18 peptides after complete tryptic hydrolysis (Figure 3). All except two small and very hydrophilic peptides 1 and 2, which were eluted as one peak with void volume were separated by RP-HPLC (Figure 4A). Peptides were identified by ESI-MS (Table 6) (*15*). When ϵ-amino groups of lysine residues were modified by the addition of TAT peptidic bonds Lys−X were protected from cleavage by trypsin. Some chromatogram peaks became smaller and some new peaks appeared (Figure 4B). The new peak 19 (Figure 4B) was identified as N-terminal peptide 7 plus 1 molecule of TAT (calculated mass, 1032.5 Da; mass from ESI-MS, 1031.7 Da). Five peptides (*3*, *5*, *8*, *12*, *18*) marked by an asterisk in Figure 3 and in Table 7 did not, however, contain lysine at either of the hydrolyzed peptidic bonds. The relative peak areas of these five peptides remained constant during modification of hGH, while relative yields of other peptides were reduced (Table 7). The N-terminal peptide 7 disappeared most rapidly, to prove once more that the N-terminal proline residue is the most reactive nucleophilic group of the hGH molecule. The next most rapidly modified were the Lys-145 and Lys-158 amino groups (Table 8). All three most active groups are situated near the contact surface, between hGH globules in the dimeric structure (*4*), and therefore, they are mainly responsible for cross-linking.

Table 7. Relative Yields of Peptides Obtained by Tryptic Hydrolysis of TAT Modified hGH (mol of peptide/mol of hydrolyzed protein)

	time of modification by TAT (min)			
peptide	0	60	150	300
3*[a]	0.96	0.93	0.94	0.90
4	0.90	0.71	0.11	0.12
5*	0.68	0.68	0.68	0.68
6	0.96	0.88	0.38	0.15
7	0.77	0.04	0.0015	0.001
8*	0.66	0.69	0.66	0.66
9	0.75	0.34	0.07	0.02
10	0.37	0.30	0.20	0.14
11	0.17	0.11	0.006	0.02
12*	0.80	0.80	0.80	0.80
13	0.51	0.36	0.23	0.13
14	0.36	0.42	0.46	0.51
15	1.00	0.86	0.65	0.43
16	1.00	0.90	0.49	0.38
17	0.77	0.42	0.27	0.006
18*	0.83	0.84	0.81	0.80

[a] Peptides without Lys residues.

Table 8. TAT Reactivity of hGH Amino Groups

amino acid residue	share of the reacted amino groups (%)	
	after 60 min	after 150 min
N-terminal (Pro)	95	99
Lys 158	55	91
Lys 145	45	91
Lys 168	34	65
Lys 70	19	46
Lys 140	17	64
Lys 38	14	35
Lys 115	10	51

Structural studies are needed in order to explain hGH dimer formation. The most likely scenario is that coordination with metal ions induces conformational changes of hGH globules (*16*) and makes them subject to dimerization.

LITERATURE CITED

(1) Lewis, U. J., Peterson, S. M., Bonewald, L. F., Seavey, B. K., and Vanderlaan, W. P. (1977) An Interchain disulfide dimer of human growth hormone. *J. Biol. Chem. 252*, 3697−3702.

(2) Lewis, U. J., Bonewald L. F., and Lewis L. J. (1980) The 20,000-Dalton variant of human growth hormone: location of the amino acid deletions. *Biochem. Biophys. Res. Commun. 92, 511−516.*

(3) Mokridge, J. W., Aston, R., Morell, D. J., and Holder A. T. (1998) Cross-linked growth hormone dimers have enhanced biological activity. *Eur. J. Endocrinol. 138*, 449−459.

(4) Cunningham, B. C., Mulkerrin, M. G., and Wells, J. A. (1991) Dimerization of human growth hormone by zinc. *Science 253*, 545−548.
(5) Patapoff, T. W., Mrsny, R. J., and Lee, W. A. (1993) The application of size exclusion chromatography and computer simulation to study the thermodynamic and kinetic parameters for short-lived dissociable protein aggregates. *Anal. Biochem. 212*, 71−78.
(6) Dienys, G., Sereikaite, J., Gavenas, G., Kvederas, R., and Bumelis, V. A. (1998) Cross-linking of protein subunits by 1,3,5-triacryloyl-hexahydro-s-triazine. *Bioconjugate Chem. 9*, 744−748.
(7) Gresham, T. L., and Steadman, T. R. (1949) Triazines from formaldehyde and nitriles. *J. Am. Chem. Soc. 71*, 1872−1873.
(8) Laemmli, U. K. (1970) Laemmli cleavage of structural proteins during the assembly of the head of bacteriophage T4. *Nature 227*, 680−685.
(9) Satake, K., Okuyma, T., Ohashi, M., and Shinoda, T. (1960) The spectrophotometric determination of amine, amino acid and peptide with 2,4,6-trinitrobenzene-1-sulfonic acid. *J. Biochem. 47*, 654−657.
(10) Jonušienė, Z., Dienys, G., and Steponavicius, J. (1988) Determination of amino groups in proteins and peptides with 2,4,6-trinitrobenzene sulfonic acid. *Zh. Anal. Khim. 43*, 536−540.
(11) Geiselmann, J., Seifried, S. E., Yager, T. D., Liang, C., and Hippel, P. H. (1992) Physical properties of the *Escherichia coli* transcription termination factor rho. 2. Quaternary structure of the rho hexamer. *Biochemistry 31*, 121−132.
(12) Horiguchi, T., Miwa, Y., and Shigesada, K. (1997) The quaternary geometry of transcription thermination factor rho: assignment by chemical cross-linking. *J. Mol. Biol. 269*, 514−528.
(13) Loster, K., and Josic, D. (1997) Analysis of protein aggregates by combination of cross-linking reactions and chromatographic separations. *J. Chromatogr. B 699*, 439−461.
(14) Gavenas, G., Dienys, G., and Adomėnienė, O. (1984) Kinetics of nucleophilic addition of piperidine and glycine to N-substituted and N,N-disubstituted acrylamides. *Org. React. 21*, 295−303.
(15) Glocker, M. O., Borchers, C., Fiedler, W., Suckau, D., and Przybylski, M. (1994) Molecular characterization of surface topology in protein tertiary structures by amino-acylation and mass spectrometric peptide mapping. *Bioconjugate Chem. 5*, 583−590.
(16) Eichhorn, G. L. (1993) Conformational change induced by metal ions through coordination. *Coord. Chem. Rev. 128*, 167−173.

BC990112J

A Novel Amine−Dioxime Chelator for Technetium-99m: Synthesis and Evaluation of 2-Nitroimidazole-Containing Analogues as Markers for Hypoxic Cells

Zi-Fen Su,[†,‡] James R. Ballinger,[‡,§,||] A. M. Rauth,*[,†,‡] Douglas N. Abrams,[⊥] and Mervyn W. Billinghurst[⊥]

Departments of Medical Biophysics and Pharmaceutical Sciences, University of Toronto, 610 University Avenue, Toronto, Ontario M5G 2M9, Canada, Division of Experimental Therapeutics, Ontario Cancer Institute, 610 University Avenue, Toronto, Ontario M5G 2M9, Canada, and Department of Radiopharmacy, Health Sciences Centre, 820 Sherbrooke Street, Winnipeg, Manitoba R3A 1R9, Canada. Received December 7, 1999; Revised Manuscript Received May 10, 2000

A novel amine−dioxime chelator for ^{99m}Tc has been developed. It offers the advantages of ease of synthesis and flexibility in alteration of lipophilicity. Labeling by stannous reduction of pertechnetate takes place rapidly and efficiently at room temperature and is stable for 24 h. The ^{99m}Tc:ligand ratio is believed to be 1:2. Seven different alkyl moieties were used to achieve a range of lipophilicities. Three series of compounds were prepared: 2-nitroimidazoles as potential hypoxia-targeting agents, 4-nitroimidazoles as a less easily reduced isomer, and untargeted anilines. In an in vitro model of cellular hypoxia, the 2-nitroimidazole compounds all showed selective accumulation whereas 4-nitroimidazoles showed variable selectivity and aniline showed no selectivity. These experiments demonstrate the potential utility of the 2-nitroimidazole derivatives of the amine−dioxime class of chelator as hypoxia-targeting agents.

INTRODUCTION

Technetium-99m (^{99m}Tc) is the most widely used radionuclide in nuclear medicine because of its ready availability on-site from a ^{99}Mo/^{99m}Tc generator, short half-life of 6 h, reasonable cost, suitable γ energy of 140 keV, and flexibility of application (*1*). Being a metal, ^{99m}Tc does not form covalent bonds with targeting molecules, but rather must be attached via a chelating group. In the last 15 years, several new classes of metal chelators have been developed and exploited in the design of radiopharmaceuticals; these vary in their ease of synthesis, ease of incorporation of ^{99m}Tc, strength of chelation, and flexibility of application. These include diamino-dithiol (*2*−*4*), bis amine−oxime (*5*−*7*), and boronic acid adducts of technetium oxime (BATO) complexes (*8*), all of which form neutral, lipophilic complexes with ^{99m}Tc, "hiding" the metal within the structure and allowing the physicochemical properties of the complex to be determined by pendant groups rather than the metal.

Although these chelators are used in a variety of radiopharmaceuticals, they can suffer from certain limitations: Because of the structural requirements for chelation, they may be limited in flexibility in terms of what parts of the chemical structure can be altered to achieve targeting. The lipophilicity of derivatives may not vary over a wide range and may be difficult to adjust; for example, the bis amine−oxime and BATO chelators tend to be extremely lipophilic, and this has led to unsatisfactory results with targeting groups such as somatostatin on PnAO (*9*) and 2-nitroimidazole on BATO (*10*). Many are asymmetrical and form two or more isomers with Tc═O; these isomers can be difficult to separate and may have different properties (*11*). Finally, some of these chelates, especially the bis amine−oximes, have limited stability in vitro and in vivo (*12*, *13*).

Two classes of oxime-containing chelators have been used as radiopharmaceuticals. The bis amine−oxime or PnAO class is used in the brain perfusion agent exametazime or HMPAO (*5*) and the hypoxia agents BMS181321 and BRU59-21 (*6*, *7*). These are neutral, lipophilic complexes, which form at room temperature under stannous reduction, although the first two compounds have only limited stability postlabeling. In contrast, the BATO chelates formed by template synthesis from vicinal dioximes (e.g., dimethylglyoxime, cyclohexanedione dioxime) and a boronic acid (e.g., methyl boronic acid, boric acid) (*8*) to form neutral, lipophilic complexes are extremely stable. These are also prepared by stannous reduction but require heating for the desired complex to form. Two ^{99m}Tc BATO complexes formed from vicinal dioximes have been reported by Su et al. (*14*). These formed lipophilic, cationic complexes with ^{99m}Tc upon reduction with sodium borohydride but did not show sufficient myocardial localization to be useful for imaging (*14*). In the present series of compounds, stannous reduction of pertechnetate to TcO^{3+} was used to prepare neutral complexes with amine−dioximes.

One area in which lipophilicity is believed to play an important role is hypoxia imaging (*15*). Cellular hypoxia is believed to be an important factor in resistance of tumors to radiation and other forms of therapy. It is also

* To whom correspondence should be addressed. Phone: (416) 946-2977. Fax: (416) 946-2984. E-mail: rauth@oci.utoronto.ca.
[†] Departments of Medical Biophysics.
[‡] Ontario Cancer Institute.
[§] Pharmaceutical Sciences.
[||] Present address: Department of Nuclear Medicine, Addenbrooke's Hospital, Hills Road, Cambridge CB2 2QQ, United Kingdom.
[⊥] Department of Radiopharmacy.

10.1021/bc9901705 CCC: $19.00 © 2000 American Chemical Society
Published on Web 08/22/2000

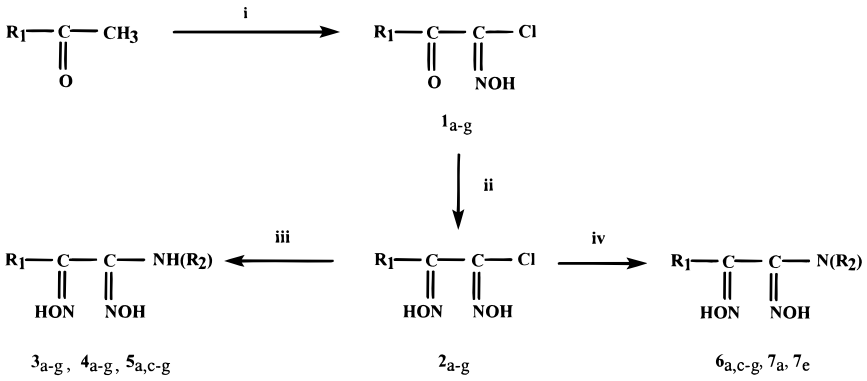

Compounds	R_1	R_2				
		$\mathbf{3}_{a-g}$	$\mathbf{4}_{a-g}$	$\mathbf{5}_{a,c-g}$	$\mathbf{6}_{a,c-g}$	$\mathbf{7}_a$, $\mathbf{7}_e$
$\mathbf{3}_a$, $\mathbf{4}_a$, $\mathbf{5}_a$, $\mathbf{6}_a$, $\mathbf{7}_a$	CH_3-	-C_2H_4-2NI	-C_2H_4-4NI	-C_6H_5	imidazole	$(C_2H_5)_2$
$\mathbf{3}_b$, $\mathbf{4}_b$,	C_2H_4-	-C_2H_4-2NI	-C_2H_4-4NI	---	---	---
$\mathbf{3}_c$, $\mathbf{4}_c$, $\mathbf{5}_c$, $\mathbf{6}_c$	C_3H_7-	-C_2H_4-2NI	-C_2H_4-4NI	-C_6H_5	imidazole	---
$\mathbf{3}_d$, $\mathbf{4}_d$, $\mathbf{5}_d$, $\mathbf{6}_d$	*iso*C_4H_9-	-C_2H_4-2NI	-C_2H_4-4NI	-C_6H_5	imidazole	---
$\mathbf{3}_e$, $\mathbf{4}_e$, $\mathbf{5}_e$, $\mathbf{6}_e$, $\mathbf{7}_e$	$(CH_3)_3C$-	-C_2H_4-2NI	-C_2H_4-4NI	-C_6H_5	imidazole	$(C_2H_5)_2$
$\mathbf{3}_f$, $\mathbf{4}_f$, $\mathbf{5}_f$, $\mathbf{6}_f$	C_6H_5-	-C_2H_4-2NI	-C_2H_4-4NI	-C_6H_5	imidazole	---
$\mathbf{3}_g$, $\mathbf{4}_g$, $\mathbf{5}_g$, $\mathbf{6}_g$	$C_6H_5C_2H_4$-	-C_2H_4-2NI	-C_2H_4-4NI	-C_6H_5	imidazole	---

Figure 1. Synthetic scheme of three classes of chelating agents, $\mathbf{3}_{a-g}$, $\mathbf{4}_{a-g}$, and $\mathbf{5}_{a,c-g}$, $\mathbf{6}_{a,c-g}$, $\mathbf{7}_a$, and $\mathbf{7}_e$.

important to detect hypoxic but viable tissue following myocardial or cerebral infarction. 2-Nitroimidazoles are a class of compounds, which are reduced enzymatically and selectively retained in hypoxic tissue. For both therapeutic and diagnostic applications of 2-nitroimidazoles, optimization of lipophilicity has been important (*15*, *16*). It has recently been suggested that the optimum octanol/water partition coefficient (PC) for a hypoxia imaging agent is ~1, although the compounds which have been evaluated clinically have PC values which range from 0.4 for [^{18}F]fluoromisonidazole to 40 for BMS181321 (*15*). In the present report, the flexibility of the amine–dioxime has been used to design ^{99m}Tc complexes with a wide range of PC values. The lead series contained 2-nitroimidazole as a hypoxia-targeting group. Two series of control compounds, which contained 4-nitroimidazole and aniline groups, were compared with the 2-nitroimidazoles. 4-Nitroimidazoles, which have lower electron affinity than 2-nitroimidazoles, would not be as efficiently reduced and bound. Aniline analogues were also prepared and have no hypoxia-targeting group. These three series of compounds have been synthesized, ^{99m}Tc complexes prepared and analyzed, and the behavior of the complexes in an in vitro model of cellular hypoxia was evaluated.

EXPERIMENTAL PROCEDURES

Materials and Instruments. Acetone, 2-butanone, 2-pentanone, 2-methyl-3-pentanone, *tert*-butyl methyl ketone, acetophenone, benzylacetone, 2-nitroimidazole, 4-nitroimidazole, 2-bromoethylphthalimide, hydrazine hydrate, phthalic acid dinonyl ester, and dibutyl phthalate were purchased from Aldrich Chemical Co. Hydroxylamine hydrochloride, aniline, *N*,*N*-dimethylformamide (DMF), and silica gel (120–200 mesh) were bought from VWR Canlab. Imidazole, diethylamine, triethylamine, diethylenetriaminepentaacetic acid (DTPA), and bovine serum albumin (BSA) were purchased from Sigma-Aldrich Canada Ltd. Stannous chloride dihydrate was obtained from BDH Chemicals. Na^{99m}TcO$_4$ was obtained from a ^{99}Mo/^{99m}Tc generator (DuPont Pharma).

Analysis and purification of ^{99m}Tc-labeled compounds was carried out on a Beckman model 125 System Gold (Fullerton, CA) reversed-phase high-pressure liquid chromatography (HPLC) system with Zorbax SB or Beckman ODS 4.6 × 250 mm 5 μm C_{18} columns. UV and radiometric detectors were connected in series. H_2O/MeOH and 0.02 M, pH 4.6, NH_4OAc/MeOH were used as mobile phases (flow rate, 1.0 mL/min). Tests of the binding of the ^{99m}Tc tracers to BSA were performed using a size exclusion column, TSK–Gel 7.8 × 300 mm from Toso-Haas (Japan), with 0.05 M, pH 6.7, phosphate buffer (either 0.7 or 1.0 mL/min) as mobile phase. ^{1}H NMR spectra were recorded on a 300 MHz Bruker or a 500 MHz Varian UNITYPlus-500 spectrometer with tetramethylsilane as reference. High-resolution mass spectra were recorded on a Micromass 70–250S (double focusing) spectrometer.

General Procedure for Preparing 1-Chloro-1,2-dione-1-oxime ($\mathbf{1}_{a-g}$, Figure 1). A flask containing 2.5 equiv of NOCl (*17*) in 200–300 mL of carbon tetrachloride or diethyl ether was set in a −10 °C ice–salt bath. To the solution was added dropwise 1 equiv of the α-methyl ketone. The ice–salt bath was removed after the completion of the addition, and the mixture was stirred at room temperature. The reaction took place slowly with release of gas during the first few hours and then become more vigorous. The temperature of the reaction mixture was maintained at 20–27 °C by means of the ice bath. The mixture was stirred at room temperature for 2 h further after the completion of the reaction. The crystalline precipitate was collected by filtration, washed with a minimum amount of carbon tetrachloride, and dried in a desiccator under vacuum. Yields: 1-chloro-1-oxime-acetone-2 ($\mathbf{1}_a$), 83%; 1-chloro-1-oxime-butanone-2 ($\mathbf{1}_b$), 72%; 1-chloro-1-oxime-pentanone-2 ($\mathbf{1}_c$), 84%; 1-chloro-

1-oxime-4-methylpentanone-2 (**1$_d$**), 79%; 1-chloro-1-oxime-pinaclone-2 (**1$_e$**), 84%; 1-chloro-1-oxime-acetophenone-2 (**1$_f$**), 94%; 1-chloro-1-oxime-phenylacetone-2 (**1$_g$**), 79%.

General Procedure for Preparing 1-Chloro-1,2-dione Dioxime (2$_{a-g}$, Figure 1). 1-chloro-1,2-dione-1-oxime (**1$_{a-g}$**) was dissolved in 2−3-fold by weight of water and chilled in an ice bath. To the solution was added 4 equiv of hydroxylamine hydrochloride dissolved in a minimum amount of water (*18*, *19*). The ice bath was removed after the completion of addition. The reaction was stirred at room temperature for 3 h, at 50−60 °C for 30 min, and then stored in a fume hood at room temperature. The crystalline product was collected by filtration, washed with water, dried in a desiccator, and purified by recrystallization from ethanol/water.

*1-Chloro-1,2-propanedione Dioxime (**2$_a$**).* Yield 53%. ^{1}H NMR (DMSO-d_6): δ 12.53 (s, 1H, =NO**H**), 11.98 (s, 1H, =NO**H**), 2.03 (s, 3H, −C**H**$_3$).

*1-Chloro-1,2-butanedione Dioxime (**2$_b$**).* Yield 39%. ^{1}H NMR (DMSO-d_6): δ 12.51 (s, 1H, =NO**H**), 11.95 (s, 1H, =NO**H**), 2.57 (q, 2H, CH_3C**H**$_2$C=NOH), 1.0 (t, 3H, C**H**$_3CH_2$−).

*1-Chloro-1,2-pentanedione Dioxime (**2$_c$**).* Yield 44%. NMR (DMSO-d_6): δ 12.51 (s, 1H, =NO**H**), 11.94 (s, 1H, =NO**H**), 2.57 (q, 2H, C_2H_5C**H**$_2$−), 1.48 (m, 2H, CH_3C**H**$_2CH_2$−), 0.874 (t, 3H, C**H**$_3C_2H_4$−).

*1-Chloro-4-methyl-pentanedione(1,2) Dioxime (**2$_d$**).* Yield 27%. ^{1}H NMR (DMSO-d_6): δ 12.50 (s, 1H, =NO**H**), 11.94 (s, 1H, =NO**H**), 2.0 [m, 1H, $(CH_3)_2C$**H**CH_2−], 0.857 [d, 6H, (C**H**$_3)_2$−].

*1-Chloro-3,3-dimethyl-butanedione(1,2) Dioxime (**2$_e$**).* Yield 68%. ^{1}H NMR (DMSO-d_6): δ 12.23 (s, 1H, =NO**H**), 11.32 (s, 1H, =NO**H**), 1.14 [s, 9H, (C**H**$_3)_3$C−].

*1-Chloro-2-phenyl-ethanedione(1,2) Dioxime (**2$_f$**).* Yield 81%. ^{1}H NMR (DMSO-d_6): δ 12.55 (s, 1H, =NO**H**), 12.09 (s, 1H, =NO**H**), 7.29−7.39 (m, 5H, C$_6$**H**$_5$−).

*1-Chloro-4-phenyl-butanedione(1,2) Dioxime (**2$_g$**).* Yield 38%. ^{1}H NMR (DMSO-d_6): δ 12.57 (s, 1H, =NO**H**), 12.08 (s, 1H, =NO**H**), 7.19−7.27 (m, 5H, C$_6$**H**$_5$−), 2.76−2.84 (m, 4H, phenyl-C**H**$_2$C**H**$_2$−).

2-(2-Nitro-1*H*-imidazolyl)ethylamine. The title compounds were prepared as reported by Hay et al. (*20*) with some modifications. 2-Nitroimidazole (2.0 g, 17.7 mmol) and 2-bromoethylphthalimide (4.72 g, 18.6 mmol) were added to a suspension of K_2CO_3 (2.44 g, 18.6 mmol) in 60 mL of DMF. The mixture was stirred at 110 °C for 2 h and then cooled to room temperature. After removing the solvents by rotary evaporation under vacuum, 150 mL of water was added to the residue. The precipitate was collected, washed by water, and dried in a desiccator under vacuum to give 3.19 g (63%) of 2-(2-nitro-1*H*-imidazolyl)ethylphthalimide. ^{1}H NMR (300 MHz, DMSO-d_6): δ 7.83 (s, 4H, Ar**H**), 7.59 (d, J = 1.0 Hz, 1H, imidazole), 7.06 (d, J = 1.1 Hz, 1H, imidazole), 4.61 (broad, 2H, $-CH_2C$**H**$_2$−imidazole), 4.06 (broad, 2H, −C**H**$_2CH_2$−imidazole).

The phthalimide (3.19 g) was dissolved in 60 mL of ethanol and heated to reflux. To the solution was added 1.12 g (22 mmol) of hydrazine hydrate in 10 mL of ethanol. The mixture was stirred under reflux for 2 h. After cooling to room temperature, the reaction mixture was set in an ice bath. The precipitate was removed by filtration, and the filtrate was brought to dryness by rotary evaporation. The compound was purified by flash chromatography on a silica gel column (4 cm × 80 cm) with petroleum ether and diethyl ether as eluents to yield 1.18 g (72%) of the title compound. ^{1}H NMR (DMSO-d_6): δ 7.61 (s, 1H, imidazole), 7.15 (s, 1H, imidazole), 4.35 (t, J = 6.1 Hz, 2H, $-CH_2C$**H**$_2$−imidazole), 2.90 (t, 2H, J = 6.1 Hz, −C**H**$_2CH_2$−imidazole).

2-(4-nitro-1*H*-imidazolyl)ethylamine. This compound was prepared in a similar manner. Yield of 2-(4-nitro-*1*H-imidazolyl)ethylphthalimide, 3.0 g (39%), mp 237−8 °C. Yield of 2-(4-nitro-1*H*-imidazolyl)ethylamine, 1.4 g (90%). ^{1}H NMR (300 MHz, DMSO-d_6): δ 8.38 (s, 1H, imidazole), 7.82 (s, 1H, imidazole), 4.02 (t, J = 6.0, 2H, $-CH_2C$**H**$_2$−imidazole), 2.89 (t, J = 6.0, 2H, −C**H**$_2CH_2$−imidazole).

General Procedures for Preparing 1-*N*-[2-(2-nitro-1*H*-imidazolyl)ethylamine]-1,2-alkanedione Dioxime (3$_{a-g}$, Figure 1). On a 0.2−1.0-g scale, a mixture of 2-(2-nitro-1*H*-imidazolyl)ethylamine with 2 equiv of triethylamine in 10 mL of anhydrous methanol was set in an ice bath. To the solution was added 1 equiv of 1-chloro-1,2-alkanedione dioxime (**2$_{a-g}$**). After the completion of addition, the mixture was stirred at room temperature for 3 h and then at 50−60 °C for another 3 h. The solvent was removed by rotary evaporation under vacuum. The residue was placed on a silica gel column and eluted first with 200 mL of dichloromethane and then with 500 mL of diethyl ether which removed most of the product. The ether was removed by rotary evaporation under vacuum. The residue was collected, washed with hot isopropyl ether, and dried in a desiccator under vacuum. **3$_b$** was further purified by HPLC on a Beckman ODS C_{18} 4.6 × 250 mm column with H_2O/MeOH as eluent. **3$_f$** was washed with a minimum amount of 50/50 MeOH/H_2O to remove the dark brown impurities.

*1-N-[2-(2-Nitro-1H-imidazolyl)ethylamine]-1,2-propanedione Dioxime (**3$_a$**).* Yield 92.6%, mp 168−9 °C (dec). ^{1}H NMR (300 MHz, DMSO-d_6): δ 11.22 (s, 1H, =NO**H**), 9.98 (s, 1H, =NO**H**), 7.41 (d, J = 0.86 Hz, 1H, imidazole ring), 7.14 (d, J = 0.93 Hz, 1H, imidazole ring), 5.68 (t, 1H, −N**H**C$_2$H$_4$−), 4.46 (t, J = 5.62 Hz, 2H, −C**H**$_2$−imidazole), 3.72 (m, 2H, −NHC**H**$_2CH_2$−), 1.80 (s, 3H, C**H**$_3$C=NOH). High-resolution MS (electron impact, EI) found for $C_8H_{12}N_6O_4$ (M^+): 256.0919. Calcd: 256.0920.

*1-N-[2-(2-Nitro-1H-imidazolyl)ethylamine]-1,2-butanedione Dioxime (**3$_b$**).* Yield 47%, mp 169−170 °C (dec). ^{1}H NMR (DMSO-d_6): δ 11.17 (s, 1H, =NO**H**), 9.98 (s, 1H, =NO**H**), 7.42 (d, J = 0.98 Hz, 1H, imidazole ring), 7.14 (d, J = 0.97 Hz, 1H, imidazole ring), 5.68 (t, J = 6.84 Hz, 1H, −N**H**C$_2$H$_4$−), 4.46 (t, J = 5.62 Hz, 2H, −C**H**$_2$−imidazole), 3.68 (m, 2H, −NHC**H**$_2CH_2$−), 2.36 (q, J = 7.49 Hz, CH_3C**H**$_2$C=NOH, 0.92 (t, J = 7.46 Hz, C**H**$_3CH_2$−). High-resolution MS (EI) found for $C_9H_{14}N_6O_4$ (M^+): 270.1064. Calcd: 270.1077.

*1-N-[2-(2-Nitro-1H-imidazolyl)ethylamine]-1,2-pentanedione Dioxime (**3$_c$**).* Yield 49%, mp 128−9 °C (dec). ^{1}H NMR (300 MHz, DMSO-d_6): δ 11.15 (s, 1H, =NO**H**), 9.96 (s, 1H, =NO**H**), 7.42 (s, 1H, imidazole ring), 7.14 (s, 1H, imidazole ring), 5.67 (t, J = 6.70 Hz, 1H, −N**H**C$_2$H$_4$−), 4.46 (t, J = 5.55 Hz, 2H, −C**H**$_2$−imidazole), 3.68 (m, 2H, −NHC**H**$_2CH_2$−), 2.34 (t, 2H, CH_3C**H**$_2$C=NOH), 1.36 (m 2H, CH_3C**H**$_2CH_2$−), 0.824 (t, 3H, C**H**$_3C_2H_4$−). High-resolution MS (EI) found for $C_{10}H_{16}N_6O_4$ (M^+): 284.1228. Calcd: 284.1233.

*1-N-[2-(2-Nitro-1H-imidazolyl)ethylamine]-4-methyl-pentanedione(1,2) Dioxime (**3$_d$**).* Yield 43%, mp 156−7 °C (dec). ^{1}H NMR (300 MHz, DMSO-d_6): δ 11.13 (s, 1H, =NO**H**), 9.94 (s, 1H, =NO**H**), 7.43 (d, J = 0.92 Hz, 1H, imidazole ring), 7.13 (d, J = 1.0 Hz, 1H, imidazole ring), 5.66 (t, J = 6.69 Hz, 1H, −N**H**C$_2$H$_4$−), 4.17 (t, J = 5.35 Hz, 2H, −C**H**$_2$−imidazole), 3.66 (m, 2H, −NHC**H**$_2CH_2$−), 2.30 [d, 2H, $(CH_3)_2CHC$**H**$_2$−], 1.82 [m, 1H, $(CH_3)_2C$**H**$_2$-CH_2−], 0.80 [d, 6H, (C**H**$_3)_2$CH−]. High-resolution MS (EI) found for $C_{11}H_{18}N_6O_4$ (M^+): 298.1394. Calcd: 298.1390.

*1-N-[2-(2-Nitro-1H-imidazolyl)ethylamine]-3,3-dimethyl-butanedione(1,2) Dioxime (**3$_e$**).* Yield 41%, mp 164−5 °C (dec). ^{1}H NMR (300 MHz, DMSO-d_6): δ 10.90 (s, 1H, =NO**H**), 9.40 (s, 1H, =NO**H**), 7.53 (d, J = 0.93 Hz, 1H, imidazole ring), 7.13 (d, J = 0.93 Hz, 1H, imidazole ring), 5.98 (t, J = 6.43 Hz, 1H, −N**H**C$_2$H$_4$−), 4.49 [t, J = 5.71 Hz, 2H, −C**H**$_2$(imidazole)], 3.23 (m, 2H, −NHC**H**$_2$CH$_2$−), 0.96 [s, 9H, (C**H**$_3$)$_3$C−]. High-resolution MS (EI) found for $C_{11}H_{18}N_6O_4$ (M^+): 298.1386. Calcd: 298.1390.

*1-N-[2-(2-Nitro-1H-imidazolyl)ethylamine]-2-phenyl-ethanedione(1,2) Dioxime (**3$_f$**).* Yield 83%, mp 132−133 °C (dec). ^{1}H NMR (300 MHz, DMSO-d_6): δ 11.05 (s, 1H, =NO**H**), 9.86 (s, 1H, =NO**H**), 7.42−7.31 (m, 5H, phenyl ring), 7.38 (d, J = 0.97 Hz, imidazole ring), 7.14 (d, J = 1.22 Hz, 1H, imidazole ring), 6.02 (t, J = 6.60 Hz, 1H, −N**H**C$_2$H$_4$−), 4.39 (t, J = 5.74 Hz, 2H, −C**H**$_2$−imidazole), 3.50 (m, 2H, −NHC**H**$_2$CH$_2$−). High-resolution MS (EI) found for $C_{13}H_{14}N_6O_4$ (M^+): 318.1081. Calcd: 318.1077.

*1-N-[2-(2-Nitro-1H-imidazolyl)ethylamine]-4-phenyl-butanedione(1,2) Dioxime (**3$_g$**).* Yield 80%, mp 173−4 °C (dec). ^{1}H NMR (DMSO-d_6): δ 11.30 (s, 1H, =NO**H**), 10.05 (s, 1H, =NO**H**), 7.39 (d, J = 0.78 Hz, 1H, imidazole ring), 7.26−7.13 (m, 6H, imidazole and phenyl rings), 5.68 (t, J = 6.82 Hz, 1H, −N**H**C$_2$H$_4$−), 4.45 (t, J = 5.71 Hz, 2H, −CH$_2$C**H**$_2$−imidazole), 3.68 (m, 2H, −C**H**$_2$CH$_2$−imidazole). 2.65 (broad, 4H, phenyl−C**H**$_2$C**H**$_2$−). High-resolution MS (EI) found for $C_{15}H_{18}N_6O_4$ (M^+): 346.1392. Calcd: 346.1390.

General Procedures for Preparing 1-*N*-[2-(4-Nitro-1*H*-imidazolyl)ethylamine]-1,2-alkanedione Dioxime (4$_{a-g}$, Figure 1). The preparation of these compounds was similar to that of compounds **3$_{a-g}$**.

*1-N-[2-(4-Nitro-1H-imidazolyl)ethylamine]-1,2-propane-dione Dioxime (**4$_a$**).* Yield 32%, mp 192−3 °C (dec). ^{1}H NMR (DMSO-d_6): δ 11.29 (s, 1H, =NO**H**), 10.09 (s, 1H, =NO**H**), 8.26 (d, J = 1.41 Hz, 1H, imidazole ring,), 7.72 (d, J = 1.35 Hz, 1H, imidazole ring), 5.68 (t, J = 6.77 Hz, 1H, −N**H**C$_2$H$_4$−), 4.14 (t, J = 5.81 Hz, 2H, −C**H**$_2$−imidazole), 3.64 (m, 2H, −NHC**H**$_2$CH$_2$−), 1.82 (s, 3H, C**H**$_3$C=NOH). High-resolution MS (EI) found for $C_8H_{12}N_6O_4$ (M^+): 256.0914. Calcd: 256.0920.

*1-N-[2-(4-Nitro-1H-imidazolyl)ethylamine]-1,2-butane-dione Dioxime (**4$_b$**).* Yield 21%, mp 180−1 °C (dec). ^{1}H NMR (DMSO-d_6): δ 11.21 (s, 1H, =NO**H**), 10.07 (s, 1H, =NO**H**), 8.26 (d, J = 1.33 Hz, 1H, imidazole ring), 7.72 (d, J = 1.33 Hz, 1H, imidazole ring), 5.68 (t, J = 6.71 Hz, 1H, −N**H**C$_2$H$_4$−), 4.15 (t, J = 5.78 Hz, 2H, −C**H**$_2$−imidazole), 3.61 (m, 2H, −NHC**H**$_2$CH$_2$−), 2.38 (q, 2H, CH$_3$C**H**$_2$C=NOH), 0.91 (t, 3H, C**H**$_3$CH$_2$−). High-resolution MS (EI) found for $C_9H_{14}N_6O_4$ (M^+): 270.1084. Calcd: 270.1078.

*1-N-[2-(4-Nitro-1H-imidazolyl)ethylamine]-1,2-pentane-dione Dioxime (**4$_c$**).* Yield 34%, mp 131−2 °C (dec). ^{1}H NMR (DMSO-d_6): δ 11.21 (s, 1H, =NO**H**), 10.07 (s, 1H, =NO**H**), 8.27 (d, J = 1.44 Hz, 1H, imidazole ring), 7.72 (d, J = 1.35, 1H, imidazole ring), 5.60 (t, J = 6.65 Hz, 1H, −N**H**C$_2$H$_4$−), 4.15 (t, J = 5.76 Hz, 2H, −C**H**$_2$−imidazole), 3.61 (m, 2H, −NHC**H**$_2$CH$_2$−), 2.33 (t, 2H, CH$_3$CH$_2$C**H**$_2$−), 1.35 (q, 2H, CH$_3$C**H**$_2$CH$_2$−), 0.81 (t, 3H, C**H**$_3$C$_2$H$_4$−). High-resolution MS (EI) found for $C_{10}H_{16}N_6O_4$ (M^+): 284.1230. Calcd: 284.1233.

*1-N-[2-(4-Nitro-1H-imidazolyl)ethylamine]-4-methyl-pentanedione(1,2) Dioxime (**4$_d$**).* Yield 81%, mp 173−4 °C (dec). ^{1}H NMR (DMSO-d_6): δ 11.19 (s, 1H, =NO**H**), 10.06 (s, 1H, =NO**H**), 8.28 (d, J = 1.35 Hz, 1H, imidazole ring), 7.73 (d, J = 1.36 Hz, 1H, imidazole ring), 5.67 (t, J = 6.61 Hz, 1H, −N**H**C$_2$H$_4$−), 4.17 (t, J = 5.75 Hz, 2H, −C**H**$_2$−imidazole), 3.60 (m, 2H, −NHC**H**$_2$CH$_2$−), 2.30 [d, 2H, (CH$_3$)$_2$CHC**H**$_2$−], 1.72 [m 1H, (CH$_3$)$_2$C**H**$_2$CH$_2$−], 0.78 [d, 6H, (C**H**$_3$)$_2$CH−]. High-resolution MS (EI) found for $C_{11}H_{18}N_6O_4$ (M^+): 298.1381. Calcd: 298.1390.

*1-N-[2-(5-Nitro-1H-imidazolyl)ethylamine]-3,3-dimethyl-butanedione(1,2) Dioxime (**4$_e$**).* Yield 19%, mp 163−4 °C. ^{1}H NMR (DMSO-d_6): δ 10.91 (s, 1H, =NO**H**), 9.46 (s, 1H, =NO**H**), 8.33 (d, J = 1.32 Hz, 1H, imidazole ring), 7.78 (d, J = 1.38 Hz, 1H, imidazole ring), 6.03 (t, J = 6.26 Hz, 1H, −N**H**C$_2$H$_4$−), 4.21 (t, J = 5.63 Hz, 2H, −C**H**$_2$−imidazole), 3.15 (m, 2H, −NHC**H**$_2$CH$_2$−), 0.98 [s, 9H, (C**H**$_3$)$_3$C−]. High-resolution MS (EI) found for $C_{11}H_{18}N_6O_4$ (M^+): 298.1396. Calcd: 298.1390.

*1-N-[2-(4-Nitro-1H-imidazolyl)ethylamine]-2-phenyl-ethanedione(1,2) Dioxime (**4$_f$**).* Yield 86%, mp 203−4 °C (dec). ^{1}H NMR (DMSO-d_6): δ 11.61 (s, 1H, =NO**H**), 9.96 (s, 1H, =NO**H**), 8.17 (d, J = 1.35, 1H, imidazole ring), 7.67 (d, J = 1.32 Hz, imidazole ring), 7.39−7.30 (m, 5H, phenyl ring), 6.03 (t, J = 6.57 Hz, 1H, −N**H**C$_2$H$_4$−), 4.10 (t, J = 5.64 Hz, 2H, −C**H**$_2$−imidazole), 3.45 (m, 2H, −NHC**H**$_2$CH$_2$−). High-resolution MS (EI) found for $C_{13}H_{14}N_6O_4$ (M^+): 318.1092. Calcd: 318.1077.

*1-N-[2-(2-Nitro-1H-imidazolyl)ethylamine]-4-phenyl-butanedione(1,2) Dioxime (**4$_g$**).* Yield 20%, mp 185−6 °C (dec). ^{1}H NMR (DMSO-d_6): δ 11.35 (s, 1H, =NO**H**), 10.16 (s, 1H, =NO**H**), 8.25 (d, J = 1.28 Hz, 1H, imidazole ring), 7.75 (d, J = 1.28 Hz, 1H, imidazole ring), 7.28−7.12 (m, 5H, phenyl rings), 5.70 (t, J = 6.82 Hz, 1H, −N**H**C$_2$H$_4$−), 4.12 (t, J = 5.72 Hz, 2H, −C**H**$_2$−imidazole), 3.62 (m, 2H, −NHC**H**$_2$CH$_2$−). 2.66 (broad, 4H, −C**H**$_2$C**H**$_2$−). High-resolution MS (EI) found for $C_{15}H_{18}N_6O_4$ (M^+): 346.1393. Calcd: 346.1390.

General Procedures for Preparing 1-*N*-Aniline-1,2-alkanedione Dioxime (5$_{a,c-g}$, Figure 1). Three equivalents of aniline was diluted in 7−15 mL of isopropyl ether and placed in an ice bath. To the solution was added 1 equiv of **2$_{a-g}$** (0.5−8 g scale) dissolved in a minimum amount of methanol. The mixture was stirred at 0 °C for 1 h, at room temperature for 1 h, and then at 50−60 °C for 1 h. After cooling to room temperature, the crystalline precipitate ($C_6H_5NH_2$·HCl) was removed by filtration. The filtrate was brought to dryness. The residue was dissolved in a minimum amount of methanol and placed on a silica gel column. The column was eluted first with 200 mL of dichloromethane and then with 200 mL of diethyl ether. The ether was removed and the residue was collected and dried in desiccator under vacuum.

*1-N-Aniline-1,2-propanedione Dioxime (**5$_a$**).* Yield 29%. ^{1}H NMR (DMSO-d_6): δ 11.31 (s, 1H, =NO**H**); 10.65 (s, 1H, =NO**H**); 7.86 (s, 1H, −N**H**C$_6$H$_5$); 7.17−6.77 (m, 5H, −C$_6$**H**$_5$); 1.90 (s, 3H, −C**H**$_3$). High-resolution MS (EI) found for $C_9H_{11}N_3O_2$ (M^+): 193.0854. Calcd: 193.0851.

*1-N-Aniline-1,2-pentanedione Dioxime (**5$_c$**).* Yield 49%, mp 60−62 °C (dec). ^{1}H NMR (DMSO-d_6): δ 11.25 (s, 1H, =NO**H**); 10.61 (s, 1H, =NO**H**); 7.80 (s, 1H, −N**H**C$_6$H$_5$); 7.16−6.78 (m, 5H, −C$_6$**H**$_5$); 2.50 (t, 2H, −C**H**$_2$CH$_2$CH$_3$); 1.48 (m, 2H, −CH$_2$C**H**$_2$CH$_3$); 0.88 (t, 3H, −CH$_2$CH$_2$C**H**$_3$). High-resolution MS (EI) found for $C_{11}H_{15}N_3O_2$ (M^+): 221.1163. Calcd: 221.1164.

*1-N-Aniline-4-methyl-pentanedione(1,2) Dioxime (**5$_d$**).* Yield 33%. ^{1}H NMR (DMSO-d_6): δ 11.27 (s, 1H, =NO**H**); 10.61 (s, 1H, =NO**H**); 7.80 (s, 1H, −N**H**C$_6$H$_5$); 7.18−6.79 (m, 5H, −C$_6$**H**$_5$); 2.29 [d, 2H, −C**H**$_2$CH(CH$_3$)$_2$]; 1.95 [m, 1H, −CH$_2$C**H**(CH$_3$)$_2$]; 0.87 [d, 6H, −CH$_2$CH(C**H**$_3$)$_2$]. High-resolution MS (EI) found for $C_{12}H_{17}N_3O_2$ (M^+): 235.1317. Calcd: 235.1321.

*1-N-Aniline-3,3-dimethyl-butanedione(1,2) Dioxime (**5$_e$**).* Yield 37%, mp 161−2 °C (dec). ^{1}H NMR (DMSO-d_6): δ 11.15 (s, 1H, =NO**H**); 10.04 (s, 1H, =NO**H**); 8.15 (s, 1H, −N**H**C$_6$H$_5$); 7.15 (t, 2H, phenyl); 7.05 (d, 2H, phenyl); 6.88

(t, 1H, phenyl); 0.97 [s, 9H, $(CH_3)_3C-$]. High-resolution MS (EI) found for $C_{12}H_{17}N_3O_2$ (M^+): 235.1314. Calcd: 235.1321.

*1-N-Aniline-2-phenyl-ethanedione(1,2) Dioxime (**5$_f$**).* Yield 41%, mp 57−8 °C (dec). ^{1}H NMR (DMSO-d_6): δ 11.63 (s, 1H, =NO**H**); 10.55 (s, 1H, =NO**H**); 8.16 (s, 1H, −N**H**C_6H_5); 7.45−6.88 (m, 10H, −C_6**H**$_5$, −NHC_6**H**$_5$). High-resolution MS (EI) found for $C_{14}H_{13}N_3O_2$ (M^+): 255.1009. Calcd: 255.1008.

*1-N-Aniline-4-phenyl-butanedione(1,2) Dioxime (**5$_g$**).* Yield 20%, mp 126−7 °C (dec). ^{1}H NMR (DMSO-d_6): δ 11.41 (s, 1H, =NO**H**); 10.71 (s, 1H, =NO**H**); 7.85 (s, 1H, −N**H**C_6H_5); 7.28−6.75 (m, 10H, −C_6**H**$_5$, −NHC_6**H**$_5$). High-resolution MS (EI) found for $C_{16}H_{17}N_3O_2$ (M^+): 283.1323. Calcd: 283.1321.

General Procedures for Preparing 1-*N*-Imidazole-1,2-alkanedione Dioxime (6$_{a,c-g}$, Figure 1). To a 2:1 methanol/diethyl ether solution of compounds **1$_{a-g}$**, which was set in a water bath, were added dropwise 1 equiv of imidazole and triethylamine dissolved in 2:1 methanol/diethyl ether. The temperature was maintained at room temperature during the addition. After stirring at room temperature for 2 h, the mixture was heated to 60 °C for 10 min. The crystalline precipitate was filtered, washed with water, and used for the next reaction. The raw 1-*N*-imidazole-1,2-alkanedione monoxime was dissolved in a minimum amount of methanol and placed in a water bath. To the solution was added 1.2 equiv of NH_2OH, which was prepared by neutralizing $NH_2OH\cdot$HCl with NaOH. The reaction mixture became cloudy after the addition of NH_2OH. A minimum amount of methanol was added to make the cloudy mixture clear. The mixture was stirred at 60 °C for 15 min, then placed in a fume hood overnight. The precipitate was removed by filtration. The filtrate was brought to dryness and the residue was dissolved in hot methanol/water. Precipitation occurred on cooling. The precipitate was collected, washed with water, and dried in a desiccator under vacuum.

*1-N-Imidazole-1,2-propanedione Dioxime (**6$_a$**).* Yield 11%, mp 214−5 °C (dec). ^{1}H NMR (DMSO-d_6): δ 13.05 (s, 1H, =NO**H**); 12.13 (s, 1H, =NO**H**); 9.24 (s, 1H, imidazole); 7.80 (s, 1H, imidazole); 7.46 (1H, imidazole); 2.12 (s, 3H, −C**H**$_3$).

*1-N-Imidazole-1,2-pentanedione Dioxime (**6$_c$**).* Yield 6.3%, mp 174−5 °C (dec). ^{1}H NMR (DMSO-d_6): δ 12.20 (s, 1H, =NO**H**); 11.82 (s, 1H, =NO**H**); 7.70 (s, 1H, imidazole); 7.20 (s, 1H, imidazole); 6.96 (s, 1H, imidazole); 2.62 (t, 2H, CH_3C**H**$_2CH_2-$).

*1-N-Imidazole-4-methyl-pentanedione(1,2) Dioxime (**6$_d$**).* Yield 10%, mp 149−150 °C (dec). ^{1}H NMR (DMSO-d_6): δ 12.22 (s, 1H, =NO**H**); 11.83 (s, 1H, =NO**H**); 7.70 (s, 1H, imidazole); 7.20 (s, 1H, imidazole); 6.96 (s, 1H, imidazole); 2.56 [s, 1H, $(CH_3)_2CHC$**H**$_2-$]; 2.10 [m, 1H, $(CH_3)_2C$**H**CH2−]; 0.95 [d, 6H, $(C$**H**$_3)_2CHCH_2-$].

*1-N-Imidazole-3,3-dimethyl-butanedione(1,2) Dioxime (**6$_e$**).* Yield 13%, mp 181−2 °C (dec). ^{1}H NMR (DMSO-d_6): δ 11.91 (s, 1H, =NO**H**); 11.41 (s, 1H, =NO**H**); 8.14 (s, 1H, imidazole); 7.37 (s, 1H, imidazole); 6.99 (s, 1H, imidazole); 1.12 [s, 9H, $(C$**H**$_3)_3C-$].

*1-N-Imidazole-2-phenyl-ethanedione(1,2) Dioxime (**6$_f$**).* Yield 11%, mp 153−4 °C (dec). ^{1}H NMR (DMSO-d_6): δ 12.21 (s, 1H, =NO**H**); 11.98 (s, 1H, =NO**H**); 7.91 (s, 1H, imidazole); 7.38−7.43 (m, 6H, C_6H_5-, imidazole); 6.99 (s, 1H, imidazole).

*1-N-Imidazole-4-phenyl-butanedione(1,2) Dioxime (**6$_g$**).* Yield 13.6%, mp 166−7 °C (dec). ^{1}H NMR (DMSO-d_6): δ 12.23 (s, 1H, =NO**H**); 11.94 (s, 1H, =NO**H**); 7.61 (s, 1H, imidazole); 7.13−7.30 (m, 6H, C_6**H**$_5-$, imidazole); 6.93 (d, 1H, J = 0.93, imidazole), 2.80−2.96 (m, 4H, phenyl−C_2**H**$_4-$).

1-*N*-Diethyl-1,2-propanedione Dioxime (7$_a$). To a solution of diethylamine (1.27 g, 17.4 mmol) in 7 mL of aectonitrile, which was set in an ice bath, was added dropwise 1.0 g (5.8 mmol) of **2$_a$** dissolved in 10 mL of methanol. The temperature of the reaction mixture was kept below 15 °C during the addition. The reaction mixture was stirred at room temperature for 4 h after the completion of addition. The crystalline precipitate (diethylamine HCl) was removed by filtration. The filtrate was brought to dryness, the residue was dissolved in a minimum amount of methanol and loaded on a silica gel column. The column was eluted first with 100 mL of dichloromethane and then with 250 mL of diethyl ether. The ether eluate was brought to dryness and the waxlike residue was dried in a desiccator under vacuum to give 1.0 g (99%) product. ^{1}H NMR (DMSO-d_6): δ 11.04 (s, 1H, =NO**H**); 8.82 (s, 1H, =NO**H**); 3.06 [q, 4H, $-N(C$**H**$_2CH_3)_2$]; 1.87 [s, 3H, C**H**$_3C(=NOH)-$]; 1.01 [t, 6H, $-N(CH_2C$**H**$_3)_2$].

1-*N*-Diethyl-1,2-propanedione Dioxime (7$_e$). This compound was prepared in a way similar to that of **7$_a$**. Yield 1.0 g (66%). ^{1}H NMR (DMSO-d_6): δ 10.54 (s, 1H, =NO**H**); 8.68 (s, 1H, =NO**H**); 2.96 [m, 4H, $-N(C$**H**$_2CH_3)_2$]; 1.13 [s, 9H, $(C$**H**$_3)_3C-$]; 1.04 [t, 6H, $-N(CH_2C$**H**$_3)_2$].

^{99m}Tc Labeling of Compounds 3$_{a-g}$, 4$_{a-g}$, and 5$_{a,c-g}$. The ^{99m}Tc labeling of these three classes of chelating agents was performed by two methods.

Method I. To a 3 mL tube were added 40−100 μg of chelating agent (in 10−25 μL of methanol), 100 μL of 0.1 M, pH 4.6, NH_4OAc buffer, 100 μL of saline, 92 μL of 0.1 N NaOH, 2−1000 MBq of $Na^{99m}TcO_4$ (in 20−200 μL saline), and 10 μg of $SnCl_2$ (in 10 μL of 1 N HCl). The chelation took a few minutes to complete. The radiochemical yield and purity of the ^{99m}Tc-labeled compounds was tested by HPLC on a C_{18} reversed-phase column, with either 0.02 M, pH 4.6, NH_4OAc/MeOH, or H_2O/MeOH as mobile phase, gradient 50% H_2O to 10% H_2O over 20 min, flow rate 1.0 mL/min.

Method II. To a 3-mL tube were added 40−100 μg of chelating agent (in 10−25 μL of methanol), 200 μL of 10 mg/mL of pentasodium DTPA, 2−1000 MBq of $Na^{99m}TcO_4$ (in 20−200 μL of saline), and 50 μL of Sn-DTPA, which was prepared by mixing 10 μL of 20 mg/mL $SnCl_2$ in 1 N HCl with 500 μL of 10 mg/mL pentasodium DTPA. The chelation took a few minutes to complete. The radiochemical yield and purity of the ^{99m}Tc-labeled compounds were analyzed by HPLC under the conditions stated above.

^{99m}Tc Labeling of Compounds 6$_{a,c-g}$, 7$_a$, and 7$_e$. Attempts were made to label compounds **6$_{a,c-g}$**, **7$_a$**, and **7$_e$** with ^{99m}Tc under the conditions described in Methods I and II. The labeling efficiency was tested by HPLC as above.

^{99m}Tc Labeling of Mixed Ligands. Two chelating agents (either **3$_{a-g}$** plus **4$_{a-g}$** or **3$_{a-g}$** plus **5$_{a,c-g}$**) were mixed together and labeled with ^{99m}Tc by either Method I or Method II. The labeling efficiency was determined by HPLC under the conditions stated above.

Stability Test of the ^{99m}Tc Tracers in Phosphate Buffer and in BSA. The ^{99m}Tc tracers were mixed with an equal volume of either PBS or 0.5 M, pH 7.4, phosphate buffer at room temperature for a period up to 24 h and were analyzed by reversed-phase HPLC. The stability of one volume of ^{99m}Tc complexes in 5 vol of 50 mg/mL BSA in PBS were incubated at 37 °C for a period up to 24 h and tested by size-exclusion HPLC.

Partition Coefficient (PC) Measurement. ^{99m}Tc-labeled compounds were isolated by HPLC with H_2O/MeOH as eluent. After removing the solvent by rotary evaporation under vacuum, the residue was dissolved in 1.0 mL of saline plus 0.5 mL of ethanol. Aliquots of 10 μL were placed in a tube containing 1.0 mL of *n*-octanol and 1.0 mL of PBS, and vortexed for 1 min. Aliquots of 0.6 mL of each phase were transferred to 1.5-mL microcentrifuge tubes and centrifuged at 12000*g* for 2 min. The radioactivity in triplicate 100 μL samples from each phase was counted in a Picker Pace-1 γ well counter. The PC values were calculated by dividing the mean counts in the *n*-octanol phase by the counts in the PBS phase.

Studies of Cellular Accumulation of ^{99m}Tc Complexes. The in vitro model for the evaluation of hypoxia markers has been described elsewhere (*21*). This model was used to test the cellular accumulation of the 20 ^{99m}Tc complexes of $\mathbf{3}_{a-g}$, $\mathbf{4}_{a-g}$, and $\mathbf{5}_{a,c-g}$ under aerobic and hypoxic conditions. Chinese hamster ovary (CHO) cells grown in suspension culture in α minimal essential medium (α-MEM) containing 10% (v/v) of fetal bovine serum were resuspended in fresh α-MEM at a concentration of (1−2) × 10^6 cells/mL and incubated at 37 °C. The aerobic and hypoxic conditions were generated by stirring the cell suspension under an atmosphere of air or nitrogen, respectively (both containing 5% CO_2). The ^{99m}Tc tracer (2−10 MBq) was added to the suspension and aliquots were removed at different time intervals over the course of 6 h. Triplicate aliquots of 100 μL were transferred to 1.5 mL microcentrifuge tubes containing 1 mL of an oil mixture (phthalic acid dinonyl ester:dibutyl phthalate, 2:3) and centrifuged at 12000*g* for 2 min. Aliquots of 30 μL of the supernatant were removed for radioactivity counting. The remaining supernatant and most of the oil were removed by aspiration. The tip of the tube containing the cell pellet was clipped into a counting tube and the radioactivity in the cell pellet and supernatant sample was measured in a γ well counter. Curves of C_{in}/C_{out} under aerobic and hypoxic conditions, where C_{in} and C_{out} represented the radioactivities in the cell pellet and in the equivalent volume of supernatant, respectively, as a function of time were plotted as described previously (*21*).

RESULTS

Synthesis of the Chelating Agents. The intermediate 1,2-alkanedione monoximes ($\mathbf{1}_{a-g}$) were prepared by bubbling NOCl through a solution of the corresponding α-methyl ketone with dry diethyl ether or carbon tetrachloride (Figure 1). NOCl reacted with acetone, 2-butanone, 2-pentanone, 2-methyl-3-pentanone, and *tert*-butyl-methyl ketone vigorously at room temperature. However, the reaction of NOCl with acetophenone and benzylacetone proceeded rather slowly and took several days to complete. The yields of the seven dione monoxime compounds ranged from 72 to 94%. Care has to be taken in the preparation of $\mathbf{1}_b$ because significant amounts of byproduct, which was shown to be 2,3-butanedione monoxime, could be produced during the reaction of NOCl with 2-butanone. This byproduct could be diminished by carefully maintaining the temperature of reaction mixture at 20−25 °C. The compounds $\mathbf{1}_{a-g}$ were hygroscopic and it is advisable to convert $\mathbf{1}_{a-g}$ into the more stable $\mathbf{2}_{a-g}$ as soon as possible.

The oxo group of $\mathbf{1}_{a-g}$ could be converted into an oxime by hydroxylamine hydrochloride (Figure 1). Compounds $\mathbf{2}_{a-g}$ separated as crystals from the reaction mixture on standing in a fume hood at room temperature. They were soluble in common organic solvents, such as alcohol, acetone and acetonitrile, and were more stable than $\mathbf{1}_{a-g}$ on storage. The byproduct, 2,3-butandione dioxime, was less soluble in ethanol, acetonitrile, and cold methanol than the desired product $\mathbf{2}_b$; thus, 2,3-butandione dioxime could be separated from $\mathbf{2}_b$ by extracting the latter into acetonitrile.

The chlorine of $\mathbf{2}_{a-g}$ was active and could be substituted by either primary or secondary amines (Figure 1). This nucleophilic substitution was performed with 2-(2-nitro-1*H*-imidazolyl)ethylamine ($\mathbf{3}_{a-g}$), 2-(4-nitro-1*H*-imidazolyl)-ethylamine ($\mathbf{4}_{a-g}$), aniline ($\mathbf{5}_{a,c-g}$), imidazole ($\mathbf{6}_{a,c-g}$), and diethylamine ($\mathbf{7}_a$, $\mathbf{7}_e$). The rate of substitution depended on the activity of the proton of the amine or imine, or the substituents on the imidazole ring. For example, imidazole was able to replace the chlorine of either $\mathbf{1}_{a-g}$ or $\mathbf{2}_{a-g}$, while 2-(2-nitro-1*H*-imidazolyl)ethylamine and 2-(4-nitro-1*H*-imidazolyl)ethylamine were not. No product could be isolated from the reaction of 2-nitroimidazole or 4-nitroimidazole with $\mathbf{1}_{a-g}$ or $\mathbf{2}_{a-g}$. The solubility of the three classes of compounds in ethanol increased in the order: $\mathbf{4}_{a-g} < \mathbf{3}_{a-g} < \mathbf{5}_{a,c-g}$.

The NMR data demonstrated that the chemical shifts of the two protons on the oxime groups were dependent on the R_2 groups (Figure 1). In comparison with those of $\mathbf{2}_{a-g}$ (12.0 ppm and 12.2−13.0 ppm for the two protons of the =NOH groups), the oxime protons of $\mathbf{3}_{a-g}$, $\mathbf{4}_{a-g}$, and $\mathbf{5}_{a,c-g}$ were shifted to higher field (10.0−10.7 ppm and 11.0−11.7 ppm), while those of $\mathbf{6}_{a,c-g}$ (11.4−12.1 ppm and 11.9−13.1 ppm) were little affected. The imidazole group of $\mathbf{6}_{a,c-g}$ might play a role as an electron-withdrawing group that is similar to the chlorine atom of $\mathbf{1}_{a-g}$. However, the two oxime protons of $\mathbf{7}_a$ and $\mathbf{7}_e$ were significantly shifted to higher field (8.7−8.8 ppm and 10.5−11.0 ppm). It is interesting to note that two of the three protons of a free imidazole ring are chemically equivalent as two single lines were seen on ^{1}H NMR: 7.0 ppm (s, 2H) and 7.6 ppm (s, 1H). They became chemically nonequivalent when they combined with $\mathbf{2}_{a-g}$ to form compounds $\mathbf{6}_{a,c-g}$. Three single lines (7.0, 7.2, and 7.7 ppm) on the ^{1}H NMR of $\mathbf{6}_{c-g}$ were observed and assigned to the three protons on the imidazole ring. It should be mentioned that the three imidazole protons of $\mathbf{6}_a$ appeared at 7.6, 7.8, and 9.2 ppm, which oriented at lower field than those of $\mathbf{6}_{c-g}$. The configuration of $\mathbf{6}_a$ might be different from its analogues in the series. Unlike $\mathbf{6}_{a,c-g}$, the protons of the imidazole ring of $\mathbf{3}_{a-g}$ and $\mathbf{4}_{a-g}$ exhibited weak coupling (0.8−0.9 Hz and 1.3−1.4 Hz). The proton attached to the 1-N position (1-N proton) could be detected by ^{1}H NMR. The 1-N protons of $\mathbf{3}_{a-g}$ and $\mathbf{4}_{a-g}$ appeared at 6.0 ppm, while that of $\mathbf{5}_{a,c-g}$ was at 7.8 ppm and fell in a region for protons of aromatic compounds.

All 20 chelating agents, $\mathbf{3}_{a-g}$, $\mathbf{4}_{a-g}$, and $\mathbf{5}_{a,c-g}$, have been analyzed by high-resolution mass spectrometry. The detected molecular ions have displayed good agreement (error limits within 5 ppm) with the calculated molecular weights of the compounds.

^{99m}Tc Labeling of Compounds $\mathbf{3}_{a-g}$, $\mathbf{4}_{a-g}$, $\mathbf{5}_{a,c-g}$, $\mathbf{6}_{a,c-g}$, $\mathbf{7}_a$, and $\mathbf{7}_e$. The ^{99m}Tc labeling of these chelating agents was carried out using either $SnCl_2$ or Sn-DTPA as reducing agent for $Na^{99m}TcO_4$. The chelation of $\mathbf{3}_{a-g}$, $\mathbf{4}_{a-g}$, and $\mathbf{5}_{a,c-g}$ to ^{99m}Tc was complete within a few minutes at room temperature, as shown by HPLC analysis with two solvent systems. ^{99m}Tc chelates of $\mathbf{3}_{a-g}$ and $\mathbf{4}_{a-g}$ exhibited a single radioactive peak on the chromatogram, while $\mathbf{5}_{a,c-g}$ showed a minor peak (5−10%) on the tail of the main peak. The retention time (t_R) of a ^{99m}Tc chelate depended on the nature of the mobile

Table 1. Retention Time, Radiochemical Purity, and Yield of 20 ^{99m}Tc Complexes Containing 2-Nitroimidazole (3_{a-g}), 4-Nitroimidazole (4_{a-g}), or Aniline (5_{a-g}) with R_1 Defined in Figure 1[a]

	3_{a-g}			4_{a-g}			$5_{a,c-g}$		
R_1	t_R (min)	purity (%)	yield (%)	t_R (min)	purity (%)	yield (%)	t_R (min)	purity (%)	yield (%)
CH_3-	11.03	100	94	11.22	99	97	13.19	92	80
C_2H_5-	11.74	100	84	11.28	98	97			
C_3H_7-	11.93	100	92	11.56	99	98	15.54	87	80
isoC_4H_9-	12.45	100	89	12.04	99	95	17.67	86	77
$(CH_3)_3C$-	12.97	98	90	11.73	99	96	19.47	95	91
C_6H_5-	11.81	100	88	11.36	99	95	15.52	93	82
$C_6H_5C_2H_4$-	13.40	97	90	12.83	96	91	19.17	98	88

[a] The complexes were prepared by Method II, and radiochemical purity was analyzed by HPLC on a C_{18} column with H_2O/MeOH as mobile phase; gradient, 50 to 10% H_2O over 20 min; flow rate, 1.0 mL/min. Yield was calculated as percent recovery of injected activity in the collected HPLC peak.

phases used for HPLC, but the radiochemical yield and purity remained similar. Compounds $\mathbf{3}_{a-g}$ and $\mathbf{4}_{a-g}$ are similar in structure, as are the ^{99m}Tc complexes of each pair of isomers. For example, $\mathbf{3}_a$ and $\mathbf{4}_a$ are one pair of isomers, and their ^{99m}Tc complexes are another pair of isomers. Each pair of isomers showed similar retention time on HPLC. The t_R of the ^{99m}Tc complexes of $\mathbf{3}_{a-g}$ increased in the order of $\mathbf{3}_a < \mathbf{3}_b < \mathbf{3}_f < \mathbf{3}_c < \mathbf{3}_e < \mathbf{3}_d < \mathbf{3}_g$, which is in accordance with the t_R of the chelating agents themselves. The ^{99m}Tc complexes of $\mathbf{4}_{a-g}$ presented the same order of t_R as well. Figure 2 presents the HPLC analysis of ^{99m}Tc complexes of $\mathbf{3}_f$ and $\mathbf{4}_f$, representative of the remaining 12 complexes containing 2- or 4-nitroimidazole groups. The 20 ^{99m}Tc complexes of $\mathbf{3}_{a-g}$, $\mathbf{4}_{a-g}$, and $\mathbf{5}_{a,c-g}$ were prepared using either $SnCl_2$ or Sn-DTPA as reducing agent, and analyzed by HPLC. The retention times, purities, and radiochemical yields are summarized in Table 1. The purity of a ^{99m}Tc complex was measured by HPLC, while its radiochemical yield was calculated by comparing the radioactivity injected with that collected in the major peak. It is noted that $\mathbf{5}_{a,c-g}$ exhibited longer retention times than $\mathbf{3}_{a-g}$ and $\mathbf{4}_{a-g}$, which suggests that $\mathbf{5}_{a,c-g}$ are more lipophilic than $\mathbf{3}_{a-g}$ and $\mathbf{4}_{a-g}$, though the latter have higher molecular weights. Similarly, the ^{99m}Tc complexes of $\mathbf{5}_{a,c-g}$ showed longer t_R than $\mathbf{3}_{a-g}$ and $\mathbf{4}_{a-g}$.

The attempted labeling of $\mathbf{6}_{a,c-g}$, $\mathbf{7}_a$, and $\mathbf{7}_e$ with ^{99m}Tc by using either $SnCl_2$ or Sn-DTPA as reducing agent was unsuccessful. No labeled compound was detected by HPLC and only ^{99m}Tc colloids resulted from these labelings.

Stability of the ^{99m}Tc Complexes of 3_{a-g}, 4_{a-g}, and $5_{a,c-g}$ in PBS/PB and BSA. All the ^{99m}Tc complexes were stable in PBS and 0.5 M PB at room temperature for a period up to 24 h (data not shown). When incubated in BSA PBS solution at 37 °C for a period up to 24 h (data not shown), most of the ^{99m}Tc complexes of 2- and 4-nitroimidazole showed less than 20% binding to BSA. The exceptions were $\mathbf{3}_e$, and $\mathbf{4}_d$, which showed significant BSA binding, 43 and 34% respectively. In addition, $\mathbf{3}_g$ and $\mathbf{4}_g$ exhibited approximately 65% breakdown in BSA. In contrast, the ^{99m}Tc complexes of $\mathbf{5}_{a,c-g}$ showed 95−100% binding to BSA but no evidence of breakdown. The degree of BSA binding of these ^{99m}Tc tracers appeared to be independent of the incubation time.

Structural identification of ^{99m}Tc Chelates of 3_{a-g}, 4_{a-g}, and $5_{a,c-g}$. The chemical structure of a ^{99m}Tc chelate could theoretically be determined by elemental analysis, NMR, and MS, but it is not feasible to prepare weighable amounts of a ^{99m}Tc chelate for this purpose because even as little as 1 mg of ^{99m}Tc can emit 1×10^5 GBq γ radiation (*22*). Alternatively, the chemical structure could be determined by using ^{99}Tc, but its long half-life ($t_{1/2} = 2.1 \times 10^5$ years) and emissions (294 keV β^-) restrict its use in chemical and radiopharmacy laboratories. Nevertheless, the structural identification of ^{99m}Tc chelates of $\mathbf{3}_{a-g}$, $\mathbf{4}_{a-g}$, and $\mathbf{5}_{a,c-g}$ has been attempted as described below, with the particular goal of determining the ^{99m}Tc:ligand ratio.

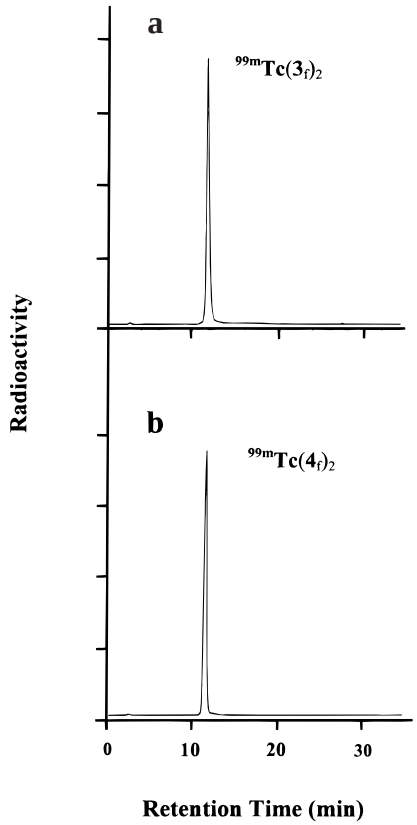

Figure 2. HPLC of ^{99m}TcO($\mathbf{3}_f$)$_2$ and ^{99m}TcO($\mathbf{4}_f$)$_2$. The complexes were prepared by Method II. The analysis was carried out on Beckman ODS C_{18} 4.6 × 250 mm column, with H_2O/MeOH as mobile phase. Flow rate 1.0 mL/min, gradient 50 to 10% H_2O over 20 min.

The labeling of any one of $\mathbf{3}_{a-g}$ and $\mathbf{4}_{a-g}$ with ^{99m}Tc in the presence of either $SnCl_2$ or Sn-DTPA was complete and efficient, with only one single peak detected by HPLC (Table 1 and Figure 2). Interestingly, three peaks were observed on HPLC after labeling a mixture of two chelating agents, one from the $\mathbf{3}_{a-g}$ series and another from either $\mathbf{4}_{a-g}$ or $\mathbf{5}_{a,c-g}$ series, for example, with ^{99m}Tc in the presence of the same reducing agent. Two examples of the HPLC analysis of the mixed-ligand ($\mathbf{3}_b + \mathbf{4}_g$ and $\mathbf{3}_g + \mathbf{4}_b$) labeling with ^{99m}Tc are shown in Figure 3. Three peaks were detected by HPLC upon labeling a mixture of either $\mathbf{3}_b$ (60 μg, 0.22 μmol) and $\mathbf{4}_g$ (80 μg, 0.23 μmol) or $\mathbf{3}_g$ (80 μg, 0.23 μmol) and $\mathbf{4}_b$ (60 μg,

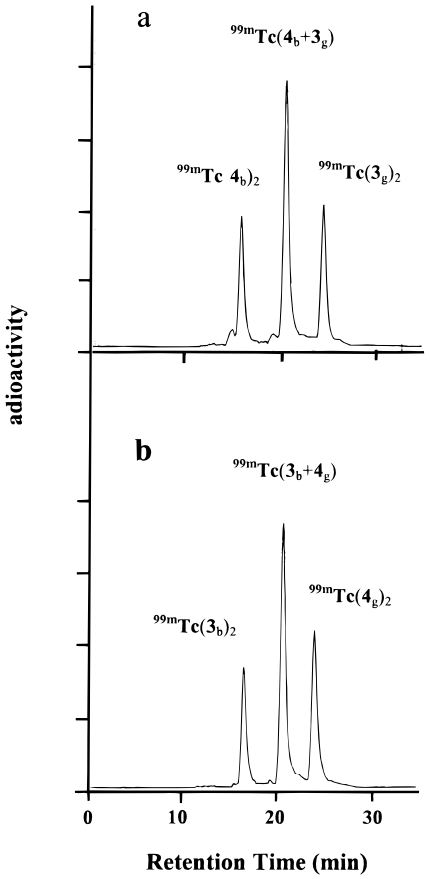

Figure 3. HPLC of the mixed-ligands labeling with ^{99m}Tc. Upper panel: 0.22 μmol of $\mathbf{4_b}$ mixed with 0.23 μmol $\mathbf{3_g}$. Lower panel: 0.22 μmol of $\mathbf{3_b}$ mixed with 0.23 μmol of $\mathbf{4_g}$. The labelings were performed by Method I. The analysis was carried out on Beckman ODS C_{18} 4.6 × 250 mm column, with 0.02 M, pH 4.6, NH_4OAc/MeOH as mobile phase. Flow rate 1.0 mL/min, gradient 50 to 10% NH_4OAc buffer over 20 min.

0.22 μmol) with ^{99m}Tc in the presence of $SnCl_2$. Following isolation of the three peaks by HPLC, removal of the solvents by rotary evaporation under vacuum, redissolution of the residue in a mixture of saline and ethanol, and reinjection into HPLC, three peaks in the same pattern and with the same retention times were exhibited in Figure 3. The peaks of ^{99m}Tc($\mathbf{3_b}$)$_2$, ^{99m}Tc($\mathbf{4_g}$)$_2$, ^{99m}Tc($\mathbf{4_b}$)$_2$, and ^{99m}Tc($\mathbf{3_g}$)$_2$ in Figure 3 were identified because their retention times were similar to the four corresponding ^{99m}Tc complexes analyzed under the same conditions. The middle peaks on the upper and lower chromatograms of Figure 3 were assigned as the mixed-ligand ^{99m}Tc chelates ^{99m}Tc($\mathbf{3_b}$ + $\mathbf{4_g}$) and ^{99m}Tc($\mathbf{3_g}$ + $\mathbf{4_b}$), respectively. This assignment was further confirmed by coinjecting the ^{99m}Tc-labeled mixed-ligands with the four single-ligand complexes separately. That is, upon mixing ^{99m}Tc($\mathbf{3_b}$)$_2$ with ^{99m}Tc-labeled mixed-ligand ($\mathbf{3_b}$ + $\mathbf{4_g}$) products and injecting into HPLC, the peak height of ^{99m}Tc($\mathbf{3_b}$)$_2$ and ^{99m}Tc($\mathbf{3_b}$ + $\mathbf{4_g}$) in Figure 3 increased accordingly. The same result was observed upon the co-injection of the other three single ^{99m}Tc tracers mixed with the corresponding ^{99m}Tc-labeled mixed-ligand products. In addition, the peak height of ^{99m}Tc($\mathbf{3_b}$)$_2$ in Figure 3 varied in accordance with the change of the molar ratio of $\mathbf{3_b}$ in the mixture. A similar result was also observed with the other three chelating agents, $\mathbf{3_g}$, $\mathbf{4_b}$, and $\mathbf{4_g}$. Therefore, the middle of the three peaks in the upper and lower chromatograms of Figure 3 must be the ^{99m}Tc mixed-ligand complexes ^{99m}Tc($\mathbf{4_b}$ + $\mathbf{3_g}$) and ^{99m}Tc($\mathbf{3_b}$ + $\mathbf{4_g}$),

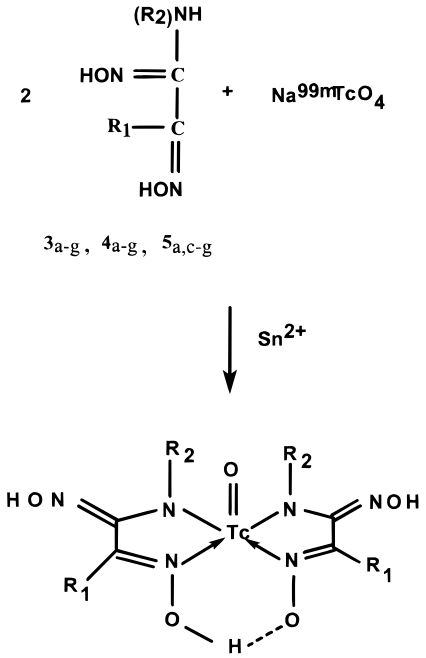

Figure 4. Proposed structures of ^{99m}Tc complexes of $\mathbf{3_{a-g}}$, $\mathbf{4_{a-g}}$, and $\mathbf{5_{a,c-g}}$.

respectively. All this evidence supported the assumption that the ratio of ^{99m}Tc:ligand is 1:2.

However, it was not certain whether it was the four oxime groups of the two chelating agents that chelate ^{99m}Tc. As stated earlier, the ^{99m}Tc labeling of $\mathbf{6_{a,c-g}}$ under similar conditions was not successful. The imidazole group of $\mathbf{6_{a,c-g}}$, directly linked to the α-carbon without any spacer, might hinder the α-oxime group to chelate ^{99m}Tc. However, steric hindrance by the imidazole group of $\mathbf{6_{a,c-g}}$ is not likely the explanation because ^{99m}Tc labeling of $\mathbf{7_a}$ and $\mathbf{7_e}$ was unsuccessful as well, yielding mostly ^{99m}Tc colloids that could not be detected by HPLC. Compounds $\mathbf{7_a}$ and $\mathbf{7_e}$ contain a diethylamine group attached to the α-carbon, which is not considered a more significant hindrant for the α-oxime group than the aniline group of $\mathbf{5_{a,c-g}}$, which chelated ^{99m}Tc well. Therefore, it appears that the proton on the nitrogen linked to the α-carbon is important for chelation of ^{99m}Tc and the α-oxime group of $\mathbf{3_{a-g}}$, $\mathbf{4_{a-g}}$, and $\mathbf{5_{a,c-g}}$ might not play a role in chelating ^{99m}Tc under these labeling conditions. The chelation of ^{99m}Tc might be through the β-oxime group and the nitrogen atom linked to the α-carbon of the chelating agents. $\mathbf{6_{a,c-g}}$ and $\mathbf{7_a}$ and $\mathbf{7_g}$ could not chelate ^{99m}Tc because there is no proton on the nitrogen attached to the α-carbon of these molecules. The structure of ^{99m}Tc($\mathbf{3_{a-g}}$)$_2$, ^{99m}Tc($\mathbf{4_{a-g}}$)$_2$, or ^{99m}Tc($\mathbf{5_{a,c-g}}$)$_2$ is consequently proposed in Figure 4.

Partition Coefficient (PC) Determination of ^{99m}Tc($\mathbf{3_{a-g}}$)$_2$. The PC values of the seven ^{99m}Tc($\mathbf{3_{a-g}}$)$_2$ complexes, before and after HPLC purification, were determined (Table 2). The HPLC-purified ^{99m}Tc complexes, after removing the solvents and redissolving in a mixture of saline and ethanol, and reinjecting into HPLC under the same condition, revealed the same retention times as those without HPLC purification. This suggests that purification did not change the composition of the ^{99m}Tc($\mathbf{3_{a-g}}$)$_2$ complexes. The PC values of the seven ^{99m}Tc complexes purified by HPLC increased in the order as: ^{99m}Tc($\mathbf{3_a}$)$_2$ < ^{99m}Tc($\mathbf{3_b}$)$_2$ < ^{99m}Tc($\mathbf{3_f}$)$_2$ < ^{99m}Tc($\mathbf{3_c}$)$_2$ < ^{99m}Tc($\mathbf{3_e}$)$_2$ < ^{99m}Tc($\mathbf{3_d}$)$_2$ < ^{99m}Tc($\mathbf{3_g}$)$_2$, which is similar to that of their retention times on HPLC (Table 1). The data in Table 1 demonstrated that a chelating agent which

Table 2. Octanol/PBS Partition Coefficients of Seven ^{99m}Tc Complexes Containing the 2-Nitroimidazole Group (3_{a-g}) with R_1 Defined in Figure 1[a]

	partition coefficient	
R_1	unpurified	purified
CH_3-	0.11 ± 0.01	0.11 ± 0.01
C_2H_5-	0.49 ± 0.05	0.51 ± 0.02
C_3H_7-	4.76 ± 0.35	5.70 ± 0.58
isoC_4H_9-	23.7 ± 1.70	26.2 ± 1.91
$(CH_3)_3C$-	2.63 ± 0.16	2.82 ± 0.18
C_6H_5-	5.70 ± 0.52	4.92 ± 0.14
$C_6H_5C_2H_4$-	107 ± 8	108 ± 17

[a] The complexes were prepared by Method II and purified by HPLC on a C_{18} column with H_2O/MeOH as mobile phase. Ten microliters of each purified ^{99m}Tc complex or labeling mixture (unpurified) were partitioned between 1.0 mL of *n*-octanol and PBS. Each value is mean of three determinations ± SEM.

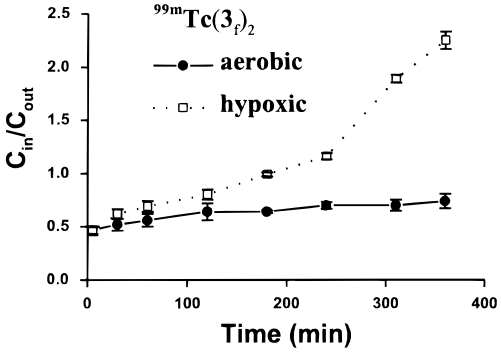

Figure 5. Accumulation of ^{99m}TcO($\mathbf{3_f}$)$_2$ in Chinese hamster ovary cells under aerobic and hypoxic conditions as a function of time. C_{in} stands for the radioactivity concentration inside cells, while C_{out} stands for radioactivity in supernatant. Each point is mean of three measurements and the error bars are SEM.

exhibited a longer retention time on reversed-phase HPLC usually formed a ^{99m}Tc complex with a longer retention time. However, ^{99m}Tc($\mathbf{3_e}$)$_2$ seemed to be an exception in the series as it showed an unexpectedly lower PC than its analogues. This result with ^{99m}Tc($\mathbf{3_e}$)$_2$ was also noted in the PC determination of the samples without HPLC purification (Table 2). In fact, the data in Table 2 suggest that it is the alkyl chain length of a chelating agent, rather than molecular weight, which plays an important role in determining the lipophilicity of the corresponding ^{99m}Tc complex. For example, the PC of ^{99m}Tc($\mathbf{3_f}$)$_2$ is almost equal to ^{99m}Tc($\mathbf{3_c}$)$_2$ even though the former has a higher molecular weight.

Cellular Accumulation of the ^{99m}Tc Complexes of 3_{a-g}, 4_{a-g}, and $5_{a,c-g}$ under Hypoxic and Aerobic Conditions. Samples of each ^{99m}Tc complex of $\mathbf{3_{a-g}}$, $\mathbf{4_{a-g}}$, or $\mathbf{5_{a,c-g}}$ were added to CHO cells incubated under hypoxic or aerobic conditions. Aliquots were removed from the cell suspension as a function of time, spun through oil to separate the cells from the supernatant medium, and the radioactivity in the cell pellet (C_{in}) and supernatant (C_{out}) were measured in a well counter. The C_{in}/C_{out} ratio under hypoxic and aerobic conditions was plotted as a function of time. Figure 5 is a plot of the data obtained with ^{99m}Tc($\mathbf{3_f}$)$_2$ and is representative of the remaining six ^{99m}Tc complexes which contain the 2-nitroimidazole group. The accumulation of ^{99m}Tc($\mathbf{3_f}$)$_2$ increased with time in both aerobic and hypoxic cells, but the increase in hypoxic cells was greater than in aerobic cells. For example, the C_{in}/C_{out} values at 5 min for aerobic and hypoxic cells were 0.47 and 0.46, respectively, while at 6 h the C_{in}/C_{out} for aerobic cells was 0.74 and for hypoxic cells was 2.25, representing a 3-fold hypoxic/aerobic differential. The remaining six ^{99m}Tc tracers of this series also demonstrated higher accumulation in hypoxic cells than in aerobic cells at 6 h. The hypoxic/aerobic differentials at 6 h were 2.6, 3.1, 2.2, 1.7, 1.4, and 2.4 for ^{99m}Tc($\mathbf{3_a}$)$_2$, ^{99m}Tc($\mathbf{3_b}$)$_2$, ^{99m}Tc($\mathbf{3_c}$)$_2$, ^{99m}Tc($\mathbf{3_d}$)$_2$, ^{99m}Tc($\mathbf{3_e}$)$_2$, and ^{99m}Tc($\mathbf{3_g}$)$_2$, respectively. These data are illustrated in the upper panel of Figure 6, where the C_{in}/C_{out} values in hypoxic and aerobic cells at 6 h are plotted against the HPLC retention time of the complex.

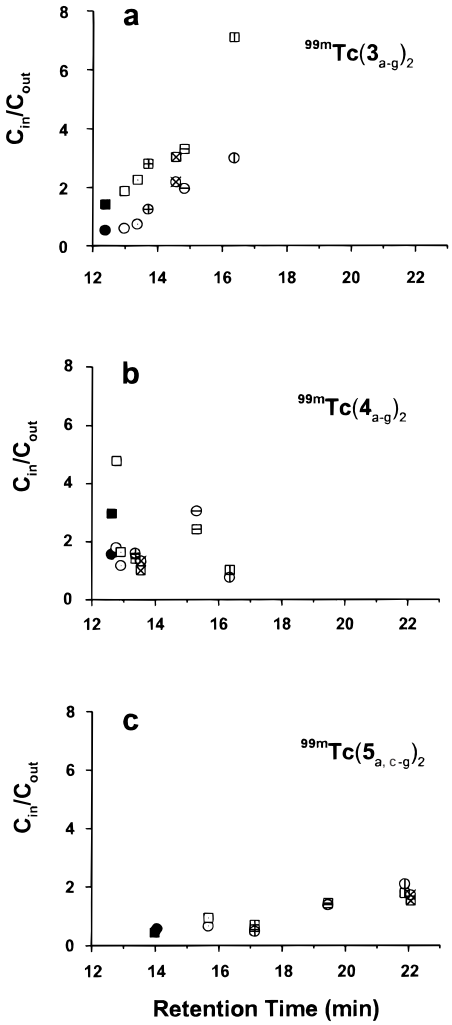

Figure 6. The accumulation of ^{99m}TcO($\mathbf{3_{a-g}}$)$_2$ (panel a), ^{99m}TcO($\mathbf{4_{a-g}}$)$_2$ (panel b), and ^{99m}Tc($\mathbf{5_{a,c-g}}$)$_2$ (panel c) in Chinese hamster ovary cells under aerobic and hypoxic conditions at 6 h time point. The complexes were prepared by Method I, analyzed by HPLC on Beckman ODS C_{18} 4.6 × 250 mm column, with 0.02 M, pH 4.6, NH_4OAc/MeOH as mobile phase. Flow rate 1.0 mL, gradient 30 to 10% NH_4OAc buffer over 20 min. (Circle) Under aerobic condition. (Square) Under hypoxic condition. Solid symbols stand for ^{99m}Tc complexes of $\mathbf{3_a}$, $\mathbf{4_a}$, and $\mathbf{5_a}$; open symbols stand for ^{99m}Tc complexes of $\mathbf{3_b}$ and $\mathbf{4_b}$; dot-centered symbols stand for ^{99m}Tc complexes of $\mathbf{3_f}$, $\mathbf{4_f}$, and $\mathbf{5_f}$; plus-centered (+) symbols stand for ^{99m}Tc complexes of $\mathbf{3_c}$, $\mathbf{4_c}$, and $\mathbf{5_c}$; cross-centered (×) symbols stand for ^{99m}Tc complexes of $\mathbf{3_e}$, $\mathbf{4_e}$, and $\mathbf{5_e}$; horizontal-line-centered (−) symbols stand for ^{99m}Tc complexes of $\mathbf{3_d}$, $\mathbf{4_d}$, and $\mathbf{5_d}$; vertical-line-centered (|) symbols stand for $\mathbf{3_g}$, $\mathbf{4_g}$, and $\mathbf{5_g}$.

The 4-nitroimidazole group of ^{99m}Tc($\mathbf{4_{a-g}}$)$_2$ is more difficult to reduce than 2-nitroimidazole (*10*). This is reflected in the lower hypoxic/aerobic differentials at 6 h for ^{99m}Tc($\mathbf{4_{a-g}}$)$_2$ than for their ^{99m}Tc($\mathbf{3_{a-g}}$)$_2$ counterparts. The results are plotted in the middle panel of Figure 6. Among the seven compounds, only ^{99m}Tc($\mathbf{4_a}$)$_2$

and ^{99m}Tc($\mathbf{4_b}$)$_2$ showed significant hypoxic/aerobic differentials of 1.9 and 2.6, while ^{99m}Tc($\mathbf{4_f}$)$_2$ and ^{99m}Tc($\mathbf{4_d}$)$_2$ showed differentials of only 1.4 and 1.3, respectively. The remaining three ^{99m}Tc complexes, ^{99m}Tc($\mathbf{4_c}$)$_2$, ^{99m}Tc($\mathbf{4_e}$)$_2$, and ^{99m}Tc($\mathbf{4_g}$)$_2$ exhibited no differential in cellular accumulation under hypoxic and aerobic conditions.

It was anticipated that ^{99m}Tc($\mathbf{5_{a,c-g}}$)$_2$ would show equal accumulation in hypoxic and aerobic cells because they do not contain a hypoxia-targeting group, such as the 2-nitroimidazole or 4-nitroimidazole groups of ^{99m}Tc($\mathbf{3_{a-g}}$)$_2$ and ^{99m}Tc($\mathbf{4_{a-g}}$)$_2$. The lower panel of Figure 6 confirms this assumption; the C_{in}/C_{out} values of aerobic and hypoxic cells for the six complexes of ^{99m}Tc($\mathbf{5_{a,c-g}}$) were almost equal at 6 h.

DISCUSSION

Propyleneamine oxime (PnAO) is a well-known chelating agent for ^{99m}Tc, forming a stable and lipophilic complex (*23*−*25*). PnAO chelates ^{99m}Tc via two amine nitrogen atoms and two oxime nitrogen atoms. The three positive charges of the ^{99m}TcO^{3+} core are neutralized during complexation with the release of three protons: two amine protons and one hydroxyl proton. The hydroxyl proton is released by the formation of an intramolecular hydrogen bond between the two hydroxyl groups of PnAO. The hydrogen bond significantly increases the stability of ^{99m}Tc−PnAO class of complexes. One example of this class of complexes is ^{99m}Tc−(hexamethyl propyleneamine oxime) or HMPAO, which is used as a brain imaging agent (*5*). ^{99m}Tc−[PnAO-1-(2-nitroimidazole)] or BMS181321 is another PnAO-based ^{99m}Tc complex, which contains a 2-nitroimidazole group and has shown selective accumulation in hypoxic cells (*6*). However, in vivo studies indicated that the clearance of BMS181321 from the blood and background tissues is slow, due to its high lipophilicity (PC = 40), which limited its usage as a hypoxia imaging agent (*21*). Analogues with lower lipophilicity are under investigation (*7*).

Lipophilicity is an important factor in the biological behavior of a ^{99m}Tc complex. Complexes of inadequate lipophilicity have difficulty crossing biological membranes by passive diffusion, have a low volume of distribution, and tend to be cleared rapidly from the body by renal excretion. To develop a ^{99m}Tc based complex for imaging tumor hypoxia, ^{99m}Tc complexes which possess specific functional groups for targeting, such as 2-nitroimidazole, and appropriate lipophilicity are required. However, it is difficult to modify the lipophilicity of ^{99m}Tc−PnAO type complexes or to prepare a ^{99m}Tc−PnAO complex that bears two homo- or hetero-functional groups, such as two 2-nitroimidazole groups or one 2-nitroimidazole and one 4-nitroimidazole group. However, this can be readily achieved using the dioxime class of ligand reported in this paper.

All 20 ligands, $\mathbf{3_{a-g}}$, $\mathbf{4_{a-g}}$, and $\mathbf{5_{a,c-g}}$, can efficiently chelate ^{99m}Tc in the presence of either $SnCl_2$ or Sn-DTPA in a pH range 4.6−9 at room temperature. The chemical yields and purities of the chelation were shown to be high by HPLC analysis (Table 1). The true radiochemical yields of the ^{99m}Tc complexes could be even higher than those presented in Table 1 because some highly lipophilic ^{99m}Tc complexes ($\mathbf{3_g}$, $\mathbf{4_g}$, and $\mathbf{5_{a,c-g}}$, for example) were retained to some extent on the column which decreased their recovery from the HPLC system. The ^{99m}Tc complexes were stable for 24 h in saline at room temperature without the need for an antioxidant. The ability of the dioxime to chelate ^{99m}Tc in the presence of an excess of the strong chelating agent DTPA (Method II) further attests to the strength of the ^{99m}Tc−dioxime complex. ^{99m}Tc labeling of $\mathbf{3_{a-g}}$ and $\mathbf{4_{a-g}}$ showed a single peak on HPLC and no isomers were evident. The ^{99m}Tc complexes of $\mathbf{5_{a,c-g}}$ could be different from those of $\mathbf{3_{a-g}}$ and $\mathbf{4_{a-g}}$ in structure. On HPLC a minor peak (about 5−10% in radiochemical yield) appeared on the tail of the main peak of ^{99m}Tc complexes of $\mathbf{5_{a,c-g}}$. Whether or not the minor peak is an isomer of ^{99m}Tc($\mathbf{5_{a,c-g}}$)$_2$ remains to be confirmed. Aside from the ^{99m}Tc complexes of $\mathbf{3_e}$, $\mathbf{4_e}$, and $\mathbf{5_e}$, which exhibited comparatively broad peaks, the ^{99m}Tc complexes of the remaining 17 ligands produced symmetrical peaks on HPLC. Judging from the results in Table 1, the tertiary butyl group of $\mathbf{3_e}$, $\mathbf{4_e}$, and $\mathbf{5_e}$ did not act as a significant steric hindrant in chelation of ^{99m}Tc.

The ratio of ^{99m}Tc to chelating agent in these 20 complexes is believed to be 1:2 based on analysis of the ^{99m}Tc complexes of mixed ligands, and there is no evidence to indicate the formation of 1:3 complexes (Figure 3). It is also believed that the ^{99m}Tc is chelated by the nitrogen atom of the oxime group on the β-carbon and the nitrogen atom linked to the α-carbon, not by the two nitrogen atoms of the two oxime groups, to form a complex with a square pyramidal configuration with the oxo group at the apex. If this is the case, there are two dπ−pπ bonds formed between ^{99m}Tc and the nitrogen of the β-dioximes, and two σ bonds formed between ^{99m}Tc and nitrogen at the α-carbon. In addition to the σ bonds, there could be dπ−pπ conjugations between ^{99m}Tc, the α-carbon, the nitrogen of the α-oxime, and the nitrogen at the α-carbon. If this is the case, the two ^{99m}Tc−N bonds would be shorter than usual ones and stronger. The proton on the nitrogen that is attached to the α-carbon of $\mathbf{3_{a-g}}$, $\mathbf{4_{a-g}}$, and $\mathbf{5_{a,c-g}}$ is vitally important for the chelation of ^{99m}Tc. Without it, no chelation of ^{99m}Tc took place, as was seen with $\mathbf{6_{a,c-g}}$, $\mathbf{7_a}$, and $\mathbf{7_e}$, despite their two oxime groups and one nitrogen atom attached to the α-carbon. This evidence further supports the proposed structure of the ^{99m}Tc complexes in Figure 4. This proposed structure suggests there might exist an intermolecular hydrogen bond between the two hydroxyl groups on the same side, which could enhance the stability of the ^{99m}Tc chelate. The three positive charges of the TcO^{3+} core are therefore neutralized upon chelation. This proposed structure is different from the vicinal dioxime complexes of transition metal ions, such as Ni^{2+}, Co^{2+}, Pd^{2+}, and Cu^{2+}, where the metal ions are chelated at pH 1−7 by the two nitrogen atoms of the oxime groups or by the two oxygen atoms of the oxime groups to form complexes in square planar geometry (*26*). Dioximes are also able to chelate ^{99m}Tc in the presence of $NaBH_4$ to form a boronic acid adduct of ^{99m}TcCl(dioxime)$_3$ or BATO complex (*8*, *10*, *14*).

The dioxime ligands presented in this report offer two potential advantages over PnAO. First, a ^{99m}Tc complex containing two different functional groups, by means of mixed-ligand labeling techniques, can be conveniently prepared. Two examples, ^{99m}Tc($\mathbf{3_b}$ + $\mathbf{4_g}$) and ^{99m}Tc($\mathbf{3_g}$ + $\mathbf{4_b}$), are illustrated in Figure 3. The second advantage is that it is possible to prepare a series of ^{99m}Tc complexes, by means of combinations of ligands, with various lipophilicities. The lipophilicity of a ^{99m}Tc complex is described by its octanol/water partition coefficient (PC). The PC values of the seven complexes of ^{99m}Tc($\mathbf{3_{a-g}}$)$_2$, shown in Table 2, range from 0.11 for ^{99m}Tc($\mathbf{3_a}$)$_2$ to 107 for ^{99m}Tc($\mathbf{3_g}$)$_2$, a 3 orders of magnitude difference over the series of complexes. The PC values of the ^{99m}Tc complexes appeared to be proportional to the length of the carbon chain rather than the molecular

weight. In a plot of log(PC) values (Table 2) as a function of length of carbon chain (number of the carbons of a *n*-alkyl chain, *n*), a straight line is evident (figure not shown) described by the equation log PC = 0.86*n* − 1.88. Consequently, a ^{99m}Tc complex with a longer carbon chain, *n*-butyl for example, would have an even higher PC value (36.3) than that of ^{99m}Tc($\mathbf{3_d}$)$_2$ (PC = 26.2). A similar result has been observed in the study of ^{99m}Tc−PnAO complexes (*27*), where a relationship of the lipophilicity and length of carbon chain on the backbone of the chelating agents was described as log PC = 0.88*n* + 0.322. Accordingly, the PC of a ^{99m}Tc−PnAO complex with two *n*-propyl groups on the backbone would be 916, which is 160-fold greater than that of ^{99m}Tc($\mathbf{3_c}$)$_2$. This implies that altering the alkyl groups on the backbone cannot finely modify the PC of a ^{99m}Tc−PnAO.

Ten of the 14 2- and 4-nitroimidazole ^{99m}Tc complexes showed low binding (0−17%) to high concentration of BSA. Two complexes, ^{99m}Tc($\mathbf{3_e}$)$_2$ (43%) and ^{99m}Tc($\mathbf{4_d}$)$_2$ (34%), showed intermediate levels of BSA binding. Two complexes, ^{99m}Tc($\mathbf{3_g}$)$_2$ and ^{99m}Tc($\mathbf{4_g}$)$_2$, exhibited 65% breakdown in BSA and of the remaining activity 57−88% bound to BSA. In contrast, the ^{99m}Tc complexes of $\mathbf{5_{a,c-g}}$ showed no breakdown but high levels of binding to BSA (95−100%). This high level of binding might be the main cause of the low C_{in}/C_{out} values observed for this series (Figure 6c).

The cellular uptake of the 20 ^{99m}Tc complexes under aerobic and hypoxic conditions was investigated in an in vitro model as described above. The radioactivity associated with the CHO cells was measured as a function of incubation time. The cellular uptake of the ^{99m}Tc complexes under aerobic and hypoxic conditions at the 5 min and 6 h time points, and the hypoxic/aerobic differential at 6 h, in relation to the functional groups and the PC values will be the focus of this discussion.

At 5 min, there is equal uptake of a ^{99m}Tc complex by aerobic and hypoxic CHO cells. This is the case for all the 20 ^{99m}Tc complexes. However, the initial uptake value of each series of ^{99m}Tc complexes, such as ^{99m}Tc($\mathbf{3_{a-g}}$)$_2$, ^{99m}Tc($\mathbf{4_{a-g}}$)$_2$ and ^{99m}Tc($\mathbf{5_{a,c-g}}$)$_2$, differed from each other and mainly depended on the functional groups and the lipophilicity. The accumulation of ^{99m}Tc($\mathbf{3_f}$)$_2$, representative of the series, in aerobic and hypoxic CHO cells as a function of time is plotted in Figure 5. The uptake of the complex in aerobic and hypoxic cells was equal at 5 min. At 6 h, the ratio of radioactivity in the aerobic cells to that in the medium (C_{in}/C_{out}) was 1.6-fold greater than that at 5 min, while the C_{in}/C_{out} under hypoxic conditions revealed a much greater increase of 4.9-fold, resulting in a hypoxic/aerobic differential of 3-fold. In general, the initial cellular uptakes under both aerobic and hypoxic conditions of the ^{99m}Tc complexes of $\mathbf{3_{a-g}}$ increased in sequence with their retention times on HPLC. The upper panel of Figure 6 shows the accumulation of radioactivity in CHO cells after 6 h incubation with the complexes of ^{99m}Tc($\mathbf{3_{a-g}}$)$_2$ under either aerobic or hypoxic conditions. The C_{in}/C_{out} ratio of the seven ^{99m}Tc tracers exhibited a trend which followed the order of their retention times on HPLC, or the PC values. All showed hypoxic/aerobic differentials significantly greater than 1.

The in vitro results obtained with the 4-nitroimidazole series $\mathbf{4_{a-g}}$ are presented in the middle panel of Figure 6. Contrary to what was seen in the $\mathbf{3_{a-g}}$ series, there is not as good a relationship between C_{in}/C_{out} at 6 h and HPLC retention time or PC value. In addition, only two of the $\mathbf{4_{a-g}}$ complexes show hypoxic/aerobic differentials significantly greater than 1. This was attributed to the inefficient enzymatic reduction of the 4-nitroimidazole moiety in $\mathbf{4_{a-g}}$.

Finally, in the untargeted aniline series $\mathbf{5_{a,c-g}}$ presented in the lower panel of Figure 6, there is a relationship between C_{in}/C_{out} at 6 h and HPLC retention time, but no hypoxic/aerobic differentials were observed due to the lack of a hypoxia-specific targeting mechanism. Thus, only the $\mathbf{3_{a-g}}$ series of complexes containing 2-nitroimidazole all showed selective accumulation in hypoxic cells and are potentially useful for imaging hypoxic cells in vivo. However, it must be noted that the hypoxic/aerobic differentials observed in this series of compounds are modest in comparison with other reports of hypoxia imaging agents (*6*, *7*, *21*). The present series of compounds represent a proof of principle and a first step toward a hypoxia imaging agent.

CONCLUSIONS

A novel amine−dioxime chelator for ^{99m}Tc has been reported which forms stable 1:2 ^{99m}Tc:ligand complexes in high yield on stannous reduction at room temperature. Lengthening the alkyl chain allowed tailoring of the lipophilicity of the ^{99m}Tc complex. Complexes containing a 2-nitroimidazole moiety showed selective accumulation in hypoxic cells in vitro whereas those with 4-nitroimidazole or aniline did not. This work has shown the preparation and utility of the novel amine−dioxime chelator.

ACKNOWLEDGMENT

The ligands were synthesized under grants from the Heart and Stroke Foundation, Squibb Radiology Research Fund, and Winnipeg Health Sciences Centre Research Foundation. Radiolabeling and evaluation of the complexes was performed under operating grants from the Medical Research Council of Canada and the National Cancer Institute of Canada.

LITERATURE CITED

(1) Dewanjee, M. K. (1990) The chemistry of ^{99m}Tc-labeled radiopharmaceuticals. *Semin. Nucl. Med. 20*, 5−27.

(2) Vallabhajosula, S., Zimmerman, R. E., Picard, M., Stritzke, P., Mena, I., Hellman, R. S., Tikofsky, R. S., Stabin, M. G., Morgan, R. A., and Goldsmith, S. J. (1989) Technetium-99m ECD: A new brain imaging agent: In vivo kinetics and biodistribution studies in normal human subjects. *J. Nucl. Med. 30*, 599−604.

(3) Meegalla, S. K., Plossl, K., Kung, M. P., Chumpradit, S., Stevenson, D. A., Kushner, S. A., McElgin, W. T., Mozley, P. D., and Kung, H. F. (1997) Synthesis and characterization of technetium-99m-labeled tropanes as dopamine transporter-imaging agents. *J. Med. Chem. 40*, 9−17.

(4) Meltzer, P. C., Blundell, P., Jones, A. G., Mahmood, A., Garada, B., Zimmerman, R. E., Davison, A., Holman, B. L., and Madras, B. K. (1997) A technetium-99m SPECT imaging agent which targets the dopamine transporter in primate brain. *J. Med. Chem. 40*, 1835−1844.

(5) Nowotnik, D. P., Canning, L. R., Cumming, S. A., Harrison, R. C., Higley, B., Nechvatal, G., Pickett, R. D., Piper, I. M., Bayne, V. J., and Forster, A. M. (1985) Development of a ^{99}Tc^{m}-labeled radiopharmaceutical for cerebral blood flow imaging. *Nucl. Med. Commun. 6*, 499−506.

(6) Linder, K. E., Chan, Y. W., Cyr, J. E., Malley, M. F., Nowotnik, D. P., and Nunn, A. D. (1994) TcO(PnAO-1-(2-nitroimidazole)) [BMS-181321], a new technetium-containing nitroimidazole complex for imaging hypoxia: synthesis, characterization, and xanthine oxidase-catalyzed reduction. *J. Med. Chem. 37*, 9−17.

(7) Johnson, L. L., Schofield, L., Mastrofrancesco, P., Donahay, T., and Nott, L. (1998) Technetium-99m-nitroimidazole uptake in a swine model of demand ischemia. *J. Nucl. Med. 39*, 1468−1475.

(8) Treher, E. N., Francesconi, L. C., Gougoutas, J. Z., Malley, M. F., and Nunn, A. D. (1989) Mono-capped tris dioxime complexes of technetium(III): Synthesis and structural characterization of $TcX(dioxime)_3B-R$(X = Cl, Br; dioxime = dimethylglyoxime, cyclohexanedionedioxime; R = CH_3, C_4H_9). *Inorg. Chem. 28*, 3411−3416.
(9) Maina, T., Stolz, B., Albert, R., Bruns, C., Koch, P., and Macke, H. (1994) Synthesis, radiochemistry and biological evaluation of a new somatostatin analogue (SDZ 219-387) labelled with technetium-99m. *Eur. J. Nucl. Med. 21*, 437−444.
(10) Linder, K. E., Chan, Y. W., Cyr, J. E., Nowotnik, D. P., Eckelman, W. C., and Nunn, A. D. (1993) Synthesis, characterization, and in vitro evaluation of nitroimidazole-BATO complexes: new technetium compounds designed for imaging hypoxic tissue. *Bioconjugate Chem. 4*, 326−333.
(11) Meegalla, S. K., Plossl, K., Kung, M. P., Stevenson, D. A., Mu, M., Kushner, S., Liable-Sands, L. M., Rheingold, A. L., and Kung, H. F. (1998) Specificity of diastereomers of [^{99m}Tc]TRODAT-1 as dopamine transporter imaging agents. *J. Med. Chem. 41*, 428−436.
(12) Billinghurst, M. W., Abrams, D. N., and Lawson, M. S. (1991) Stabilization of [^{99m}Tc]HMPAO - 1. Ethanolic preparation. *Appl. Radiat. Isot. 42*, 607−612.
(13) Ballinger, J. R., and Gulenchyn, K. Y. (1991) Alternative formulations of technetium-99m HMPAO. *Appl. Radiat. Isot. 42*, 315−316.
(14) Su, Z. F., Linse, K. H., Steinmetz, H. J., and Schwochau, K. (1992) Preparation and evaluation of cationic ^{99}Tc/^{99m}Tc dimethoxy- and diethoxy-hexanedione dioxime complexes. *J. Labelled Compd. Radiopharm. 31*, 61−70.
(15) Chapman, J. D., Engelhardt, E. L., Stobbe, C. C., Schneider, R. F., and Hanks, G. E. (1998) Measuring hypoxia and predicting tumor radioresistance with nuclear medicine assays. *Radiother. Oncol. 46*, 229−237.
(16) Brown, J. M., and Workman, P. (1980) Partition coefficient as a guide to the development of radiosensitizers which are less toxic than misonidazole. *Radiat. Res. 82*, 171−190.
(17) Morton, J. R., and Wilcox, H. W. (1953) *Inorganic Syntheses*, vol. IV, p 48, McGraw-Hill Book Co., New York.
(18) Rheinboldt, H., and Schmitz-Dumont, O. (1925) *Justus Liebigs Ann. Chem. 444*, 113−135.
(19) Behrend, R., and Schmitz, J. (1893) *Justus Liebigs Ann. Chem. 277*, 320.
(20) Hay, M. P., Wilson, W. R., Moselen, J. W., Palmer, B. D., and Denny, W. A. (1994) Hypoxia-selective antitumor agents. 8. Bis(nitroimidazolyl)alkanecarboxamides: a new class of hypoxia-selective cytotoxins and hypoxic cell radiosensitizers. *J. Med. Chem. 37*, 381−391.
(21) Ballinger, J. R., Wan Min Kee, J., and Rauth, A. M. (1996) In vitro and in vivo evaluation of a technetium-99m-labeled 2-nitroimidazole (BMS181321) as a marker of tumor hypoxia. *J. Nucl. Med. 37*, 1023−1031.
(22) Schwochau, K. (1994) Technetium radiopharmaceuticals - fundamentals, synthesis, structure, and development. *Angew. Chem., Int. Ed. Engl. 33*, 2258−2267.
(23) Troutner, D. E., Volkert, W. A., Hoffman, T. J., and Holmes, R. A. (1983) A tetradentate amine oxime complex of Tc-99m. *J. Nucl. Med. 24*, P10.
(24) Troutner, D. E., Volkert, W. A., Hoffman, T. J., and Holmes, R. A. (1984) A neutral lipophilic complex of ^{99m}Tc with a multidentate amine oxime. *Int. J. Appl. Radiat. Isot. 35*, 467−470.
(25) Jurisson, S., Schlemper, E. O., Troutner, D. E., Canning, L. R., Nowotnik, D. P., and Neirinckx, R. D. (1986) Synthesis, characterization, and X-ray structural determinations of technetium(V)-oxo-tetradentate amine oxime complexes. *Inorg. Chem. 25*, 543−549.
(26) Singh, R. B., Garg, B. S., and Singh, R. P. (1979) Oximes as spectrophotometric reagents - a review. *Talanta 26*, 425−444.
(27) Neirinckx, R. D., Nowotnik, D. P., Pickett, R. D., Harrison R. C., Ell, P. J. (1986) Development of a lipophilic Tc-99m complex useful for brain perfusion evaluation with conventional imaging equipment. In *Amphetamines and pH Shift Agents: Basic Research and Clinical Results* (H. Biersack and C. Winkler, Eds.) pp 59−70, Walter de Gruyter.

BC9901705

Antiproliferative Effect of a Lectin- and Anti-Thy-1.2 Antibody-Targeted HPMA Copolymer-Bound Doxorubicin on Primary and Metastatic Human Colorectal Carcinoma and on Human Colorectal Carcinoma Transfected with the Mouse *Thy-1.2* Gene

B. Říhová,*,† M. Jelínková,† J. Strohalm,‡ M. Šťastný,† O. Hovorka,† D. Plocová,‡ M. Kovář,† L. Dráberová,§ and K. Ulbrich‡

Institute of Microbiology, Academy of Sciences of the Czech Republic, 142 20 Prague 4-Krč, Czech Republic, Institute of Macromolecular Chemistry, Academy of Sciences of the Czech Republic, 162 06 Prague 6-Dejvice, Czech Republic, and Institute of Molecular Genetics, Academy of Sciences of the Czech Republic, 142 20 Prague 4-Krč, Czech Republic . Received December 7, 1999; Revised Manuscript Received June 3, 2000

The aim of this study was to compare the potential of two plant lectins [peanut agglutinin (PNA) and wheat germ agglutinin (WGA)], monoclonal antibody (anti-Thy-1.2), its $F(ab')_2$ fragments, and galactosamine as targeting moieties bound to the polymer drug carrier to deliver a xenobiotic, doxorubicin, to selected cancer cell lines. We have used primary (SW 480, HT 29) and metastatic (SW 620) human colorectal cancer cell lines and a transfectant, genetically engineered SW 620 cell line with mouse gene *Thy-1.2* (SW 620/T) to test the possibility of marking human cancer with xenogeneic mouse gene and use it for effective site-specific targeting. The targeting moieties and doxorubicin were conjugated to a water-soluble copolymer based on *N*-(2-hydroxypropyl)methacrylamide (HPMA) acting as a carrier responsible for controlled intracellular release of the targeted drug. FACS analysis showed a strong binding of WGA−FITC to all tested cell lines. Binding of PNA−FITC was considerably weaker. The in vitro antiproliferative effect of lectin-targeted HPMA carrier-bound doxorubicin evaluated as [^{3}H]TdR incorporation reflected both the intensity of the binding and the different sensitivity of the tested cancer cells lines to doxorubicin. The antiproliferative effect of conjugates targeted with WGA was comparable to that with the conjugates targeted with the anti-Thy-1.2 monoclonal antibody or their $F(ab')_2$ fragments. The magnitude of the cytotoxic effect of HPMA−doxorubicin targeted with PNA was lower in all tested cell lines. While the conjugates with WGA were more cytotoxic, the conjugates with PNA were more specific as their binding is limited to cancer cells and to the sites of inflammation. Noncytotoxic conjugates with a very low concentration of doxorubicin and targeted with PNA, anti-Thy-1.2, or their $F(ab')_2$ fragments exerted in some lines (SW 480, SW 620) low mitogenic activity. The *Thy-1.2* gene-transfected SW 620 metastatic colorectal cancer cell line was sensitive to the antiproliferative effect of Thy-1.2-targeted doxorubicin as was shown for the Thy-1.2$^+$ EL4 cell line and for Thy-1.2$^+$ concanavalin A-stimulated mouse T lymphocytes. These results represent the first indication of the suitability of transfection of human cancer cells with selected targeting genes for site-specific therapy of malignancies.

INTRODUCTION

Mouse monoclonal antibodies directed against tumor cell surface antigens have the potential to localize selectively within the tumor after systemic administration (Goldenberg et al., 1980). However, a number of clinical trials that were conducted to evaluate the therapeutic efficacy of such mAbs per se have shown relatively limited antitumor effects (Houghton et al., 1985). Recent therapeutic approaches to the treatment of cancer have focused on developing novel delivery systems to increase the therapeutic indices of anticancer agents by targeting them to malignant cells. The lack of specificity of conventional chemotherapy for malignant cells with severe dose-limiting side effects has led to the development of a new class of compounds called immunotoxins (Neville and Youle, 1982; Raso, 1982; Vitetta et al., 1982; Hertler and Frankel, 1989) and other drug delivery

* To whom correspondence should be addressed: Institute of Microbiology AS CR, Vídeňská 1083, 142 20 Prague 4-Krč, Czech Republic. Telephone: +420 2 475 2267. Fax: +420 2 472 11 43. E-mail: Rihova@biomed.cas.cz.

† Institute of Microbiology, Academy of Sciences of the Czech Republic.

‡ Institute of Macromolecular Chemistry, Academy of Sciences of the Czech Republic.

§ Institute of Molecular Genetics, Academy of Sciences of the Czech Republic.

[1] Abbreviations: AIBN, 2,2′-azobisisobutyronitrile; Con A, concanavalin A; DCCI, *N*,*N*′-dicyclohexylcarbodiimide; DMF, *N*,*N*-dimethylformamide; DMSO, dimethyl sulfoxide; DOX-HCL, doxorubicin hydrochloride; FITC, fluorescein isothiocyanate; FPLC, fast protein liquid chromatography; FCS, fetal calf serum; GPC, gel permeation chromatography; [^{3}H]TdR, [^{3}H]-thymidine; HPMA, *N*-(2-hydroxypropyl)methacrylamide; HPLC, high-performance liquid chromatography; Ma, methacryloyl; mAbs, monoclonal antibodies; NK cells, natural killer cells; ONp, *p*-nitrophenoxy; OPA, *o*-phthaldialdehyde; PBS, phosphate-buffered saline; RI, refractive index; PNA, peanut agglutinin; TEA, triethylamine; WGA, wheat germ agglutinin.

10.1021/bc9901696 CCC: $19.00 © 2000 American Chemical Society
Published on Web 09/18/2000

systems for antitumor therapy (Duncan, 1992). These drug delivery systems are directed against epitopes present on tumor cells and carry drugs interfering with tumor cell growth. Such tumor-selective cytotoxic conjugates are also produced by a conjugation of the anthracycline antibiotic doxorubicin to the water-soluble polymeric carrier based on *N*-(2-hydroxypropyl)methacrylamide (Kopeček et al., 1991) and targeted with carbohydrates (Duncan et al., 1987, 1988), antibody (Říhová and Kopeček, 1985; Říhová et al., 1988, 1992, 1996; Šťastný et al., 1997; Jelínková et al., 1998; Omelyanenko et al., 1998a,b), or growth hormones (O'Hare et al., 1993) to avoid nonspecific damage of nonmalignant cells and toxicity to healthy tissues.

Lectins are plant proteins or glycoproteins that bind to specific sugars in the surface glycoproteins and glycolipids of eukaryotic cells. Weaver and Bailey (1987) demonstrated a rapid receptor-mediated endocytosis of concanavalin A, and Hussain et al. (1997) suggested that lectins can be utilized for intestinal drug targeting in vivo. Altered lectin binding is common in malignant and premalignant epithelia (Ryder et al., 1994). Cancer cells often express different carbohydrates on their surfaces, which are involved in NK cell cosignaling and consequently in cancer cell eradication. It was reported that the normal adult colonic epithelium expresses receptors for wheat germ agglutinin (WGA), while neoplastic or inflammatory colonic epithelium binds peanut agglutinin (PNA) (Boland and Roberts, 1988). Wirth et al. (1998) described the usefulness of WGA as a targeting carrier protein of doxorubicin for the treatment of colon carcinoma, and Wroblewski et al. (1999) reported that conjugation of WGA and PNA to the polymeric carrier poly(HPMA) does not destroy their binding affinity to target carbohydrates.

However, spontaneous human cancers often do not express surface antigens suitable for targeting. Thus, we also address the question of whether transfection of human colorectal carcinoma with the mouse *Thy-1.2* gene would result in a xenogeneic-gene-marked cancer target suitable for site-specific drug delivery. The Thy-1.2 (CDw90) alloantigen is a GPI-anchored surface protein with an M_w of about 25−35 kDa, which is expressed on thymocytes and mouse peripheral T cells and on neurons. It is involved in T activation process. Thy-1.2 glycoprotein was used for efficient targeting in mouse T lymphocytes and mouse EL4 T cell lymphoma (Říhová et al., 1996, 2000; Jelínková et al., 1998).

Thus, the purpose of this study was (a) to investigate the targeting capacities of two lectins, WGA and PNA, in several tumor cell lines and in normal concanavalin A-stimulated T lymphocytes, (b) to compare the targeting capacity of lectins with galactosamine, the monoclonal anti-Thy-1.2 antibody and its F(ab′)$_2$ fragment, and (c) to determine if the metastatic human colorectal cancer cell line SW 620 transfected with the mouse *Thy-1.2* gene is sensitive to the antiproliferative effect of anti-Thy-1.2 monoclonal antibodies-targeted HPMA carrier-bound doxorubicin. The sensitivity of transfected cell line SW 620/T was compared with the sensitivity of Thy-1.2$^+$ EL4 mouse T cell lymphoma and with normal Thy-1.2$^+$ splenocytes activated with concanavalin A.

MATERIALS AND METHODS

Chemicals. 1-Aminopropan-2-ol, methacryloyl chloride, glycyl-L-phenylalanine, L-leucylglycine, 4-nitrophenol, triethylamine, *N*,*N*-dimethylformamide, *N*,*N*′-dicyclohexylcarbodiimide, 2,2′-azobisisobutyronitrile, phthalaldehyde, 5-thio-D-glucose, galactosamine, and dimethyl sulfoxide were from Fluka AG (Buchs, Switzerland). Doxorubicin hydrochloride was obtained as a kind gift from Pharmacia-Farmitalia Carlo Erba, and peanut agglutinin and wheat germ agglutinin were from Sigma-Aldrich. All other chemicals and solvents were analytical grade. The organic solvents were dried and purified by conventional procedures and distilled before use. Stock solutions of samples and/or drug were made in PBS and diluted further in the medium.

Table 1. Characteristics of Polymer Precursors and Antibody (Lectin)-Targeted Poly(HPMA) Conjugates of Doxorubicin

sample	structure	M_w[a] (kDa)	ONp[a] (mol %)	DOX (wt %)	TM[b] (wt %) ± SD
1	P(GFLG-DOX)(GFLG-a-Thy1.2 (mAb))	16.4	9.0	4.5	25 ± 2
2	P(GFLG-DOX)(GFLG-a-Thy1.2-F(ab′)$_2$)	16.4	9.0	4.5	25 ± 2
3	P(GFLG-DOX)(GFLG-gal)	25.1	8.8	6.4	6.2 ± 0.9
4	P(GFLG-DOX)(GFLG-WGA)	18.8	8.7	4.2	25 ± 2
5	P(GFLG-DOX)(GFLG-PNA)	18.8	8.7	4.2	25 ± 2
6	P-GFLG-WGA	17.8	6.2	0	25 ± 2
7	P-GFLG-PNA	17.8	6.2	0	25 ± 2

[a] Polymer precursor. [b] Targeting moieties: monoclonal antibody anti-Thy-1.2, its F(ab′)$_2$ fragment, PNA, WGA, or galactosamine.

Synthesis of Monomers. *N*-(2-Hydroxypropyl)methacrylamide was prepared by the reaction of methacryloyl chloride with 1-aminopropan-2-ol in freshly distilled methylene chloride containing suspended anhydrous sodium hydrogencarbonate as described by Ulbrich et al. (2000). Mp: 70 °C. Anal. Calcd: C, 58.72; H, 9.15; N, 9.78. Found: C, 58.79; H, 9.02; N, 9.75.

Methacryloylglycyl-DL-phenylalanyl-L-leucylglycine 4-nitrophenyl ester (Ma-GlyPheLeuGly-ONp) was prepared as previously described (Rejmanová et al., 1983). Mp: 134−136 °C. Amino acid analysis: 2.06:0.53:0.48:1.00: 0.02 Gly:L-Phe:D-Phe:L-Leu:D-Leu.

Synthesis of Polymer Conjugates. Polymer conjugates with antibody, its F(ab′)$_2$ fragment, galactosamine, or lectins (samples 1−7, Table 1) were prepared by two- or three-step synthesis. In the first step, polymer precursors differing in the content of reactive ester groups were prepared. Polymer precursors were prepared by radical precipitation copolymerization of HPMA with Ma-GlyPheLeuGly-ONp (initiator AIBN, 0.6 wt %; concentration of monomers, 12.5 wt %; content of Ma-GlyPheLeuGly-ONp in the reaction mixture, 9 or 6 mol %; temperature, 60 °C; polymerization time, 24 h) as described previously (Rejmanová et al., 1983). The content of oligopeptide side chains terminated in 4-nitrophenoxy groups was determined in the copolymer by UV spectrophotometry (DMSO, ϵ = 9500 L mol^{-1} cm^{-1}, λ = 274 nm), and weight- and number-average molecular masses, M_w and M_a, respectively, were determined by liquid chromatography after aminolysis of reactive groups with 1-aminopropan-2-ol

[FPLC Pharmacia, Superose 6, phosphate buffer containing 0.5 M NaCl, calibration using poly(HPMA) fractions].

In the second step, HPMA conjugates with WGA or PNA (samples 6 and 7) were obtained by aminolytic reaction of the polymer precursor in aqueous solution. The polymer precursor was dissolved in distilled water (10−15 wt %) under stirring after cooling to 10 °C and adding a solution of the respective lectin in phosphate buffer (15−25 mg/mL). The pH of the reaction mixture was adjusted to 8.2 under stirring at 10 °C by adding a saturated solution of $Na_2B_4O_7$ (end-point titration; pH-stat radiometer). The course of the reaction was controlled by the consumption of the borate solution. After the reaction had been completed, the polymer−lectin conjugate was purified by gel filtration (Sephadex G-25) and transferred into phosphate buffer. The conjugate was characterized by GPC and electrophoresis, and the content of the protein in the conjugate was estimated using amino acid analysis.

In the second step of the synthesis of the drug-containing conjugates (samples 1−5), DOX was bound to the polymer via aminolysis of a part of reactive ester groups. The respective polymer precursor was dissolved in DMSO (15 wt %), and 50 mol % DOX-HCl (relative to the ONp content in the precursor) was added. Under stirring, 1 equiv of TEA (related to DOX-HCl) was added in four small portions. The reaction mixture was stirred in the dark at room temperature for 2 h; the solution was filtered, and the polymer was obtained by precipitation into an acetone/diethyl ether mixture. Free, unreacted DOX was removed by gel filtration of the polymer solution in methanol using a Sephadex LH-20 column.

In the third step, the polymer containing DOX and remaining ONp groups, dried in a vacuum, was dissolved in distilled water (10−15 wt %) and conjugated with the respective protein using the procedure described above. The content of DOX in the conjugate was estimated spectrophotometrically; the conjugate was characterized by GPC and electrophoresis, and the content of the protein in the conjugate was estimated using amino acid analysis.

Conjugate 3 containing galactosamine as a targeting moiety was prepared by an aminolytic reaction of the rest of ONp groups of the DOX-bearing polymer (as described above) with galactosamine in DMSO as described previously (Duncan et al., 1987).

Methods of Purification and Characterization of Conjugates. Polymer−drug intermediates were freed of low-molecular mass impurities (such as free DOX or 4-nitrophenol) by gel filtration using a Sephadex LH-20 column (100 cm × 3.4 cm) with methanol elution. The conjugates with antibody or lectin were purified using a Sephadex G-25 column eluted with phosphate buffer (pH 7.4). Samples were kept in the frozen state (−30 °C) until biological evaluation could be carried out.

Conjugates containing both the targeting moiety and the drug were characterized and tested for the content of free polymer, drug, or protein by GPC using a Sepharose 4B/6B 100 cm × 1.6 cm column (UV and RI detection) or FPLC with a system equipped with a Superose 6 column, and by electrophoresis (Pharmacia-LKB Phast System, SDS−PAGE, gradient gels 4−15) (Říhová and Kopeček, 1985). The protein content in the conjugates was estimated by amino acid analysis (LDC Analytical, precolumn OPA derivatization, calibration with the respective protein) and the DOX content by UV spectrophotometry in water (ϵ = 11 500 mol L^{-1} cm^{-1}, λ = 485 nm). Neither GPC nor electrophoresis showed significant amounts of free antibody, free lectin, or free drug in the conjugates.

GPC was carried out on a Sepharose 4B/6B column (1.6 cm × 100 cm) using phosphate buffer (pH 7.2) at a flow rate of 2 mL/min, via RI and UV detection.

The composition of amino acids in Ma-GlyPheLeuGly-ONp and the content of proteins in the conjugates were determined by amino acid analysis with precolumn OPA derivatization on an LDC Analytical analyzer using the reverse-phase column (Tessek SGX C18, 250 mm × 4 mm), via elution with a solvent gradient of sodium acetate buffer and methanol, and fluorescence detection with a model 4100 fluoromonitor (LDC Analytical). Before analysis, the samples were hydrolyzed with 6 M HCl at 115 °C for 16 h. The hydrolysate was dried over NaOH and, prior to the analysis, dissolved in distilled water. The concentration and the ratio of amino acids were determined using OPA−3-mercaptopropionic acid derivatization, with detection at an emission wavelength of 229 nm and an excitation wavelength of 450 nm. The optical purity of amino acids was determined using OPA−5-thio-D-glucose derivatization, with detection at an emission wavelength of 450 nm and an excitation wavelength of 229 nm.

Targeting Moieties. Two lectins were used in this study: PNA from *Arachis hypogea*, which binds to galactose β-1,3-*N*-acetylgalactosamine, and WGA from *Triticum vulgare*, which binds to *N*-acetyl-D-glucosamine. Both lectins as well as their fluorescein isothiocyanate (FITC) analogues were obtained from Sigma-Aldrich. Monoclonal antibody directed against Thy-1.2 mouse alloantigen, clone 1aG4/C5, is of the IgG_3 isotype (Dráber et al., 1980). Antibodies were produced in BALB/c mice by injection of hybridoma clone 1aG4/C5 and purified from mouse ascites fluid by a combination of 2-fold 45% SAS precipitation and protein A affinity chromatography (Říhová et al., 1996). The concentration was determined by spectrophotometry (λ = 280 nm), and their purity was assessed by SDS−PAGE. mAb reactivities were checked before use by indirect immunofluorescence using FITC-labeled anti-mouse IgG_3 and FACSorter (Becton Dickinson, Mountain View, CA) against appropriate cell lines. The $F(ab')_2$ fragment of anti-Thy-1.2 antibodies was produced by digestion with pepsin as described previously (Říhová et al., 2000).

Cell Lines. The following cell lines were used: human colorectal cancer cell line SW 480 (primary), human colorectal cancer cell line SW 620 (metastatic), human colorectal cancer cell line HT 29 (primary), and mouse EL4 T cell lymphoma ($H\text{-}2^b$ origin), all of them purchased from the American Type Culture Collection (ATCC, Rockville, MD).

(Thy-1.2$^+$) SW 620 Transfectant Cells. *Cells*. SW 620 cells were originally cultured in L-15 medium supplemented with 10% fetal calf serum (FCS). The cells were gradually adapted to grow in RPMI-1640 medium supplemented with 10% FCS and antibiotics and cloned in this medium. Clones with improved cloning efficiency were recloned, and cell lines with a relatively high cloning efficiency (about 30%) were used in these experiments.

Plasmids. Two plasmid vectors were used. Plasmid pThy-1.2, a pUC13-derived vector containing the 8.1 kb *Eco*RI fragment derived from the genomic bacteriophage library of MOPC41 plasmacytoma (Evans et al., 1984), was kindly obtained from G. A. Evans of The Salk Institute of Biological Studies (La Jolla, CA). For selection of transfected cells, we used plasmid pSTneoB in which the bacterial aminoglycosyl 3′-phosphotransferase type II (AGPT) gene is under the control of tandem promoters

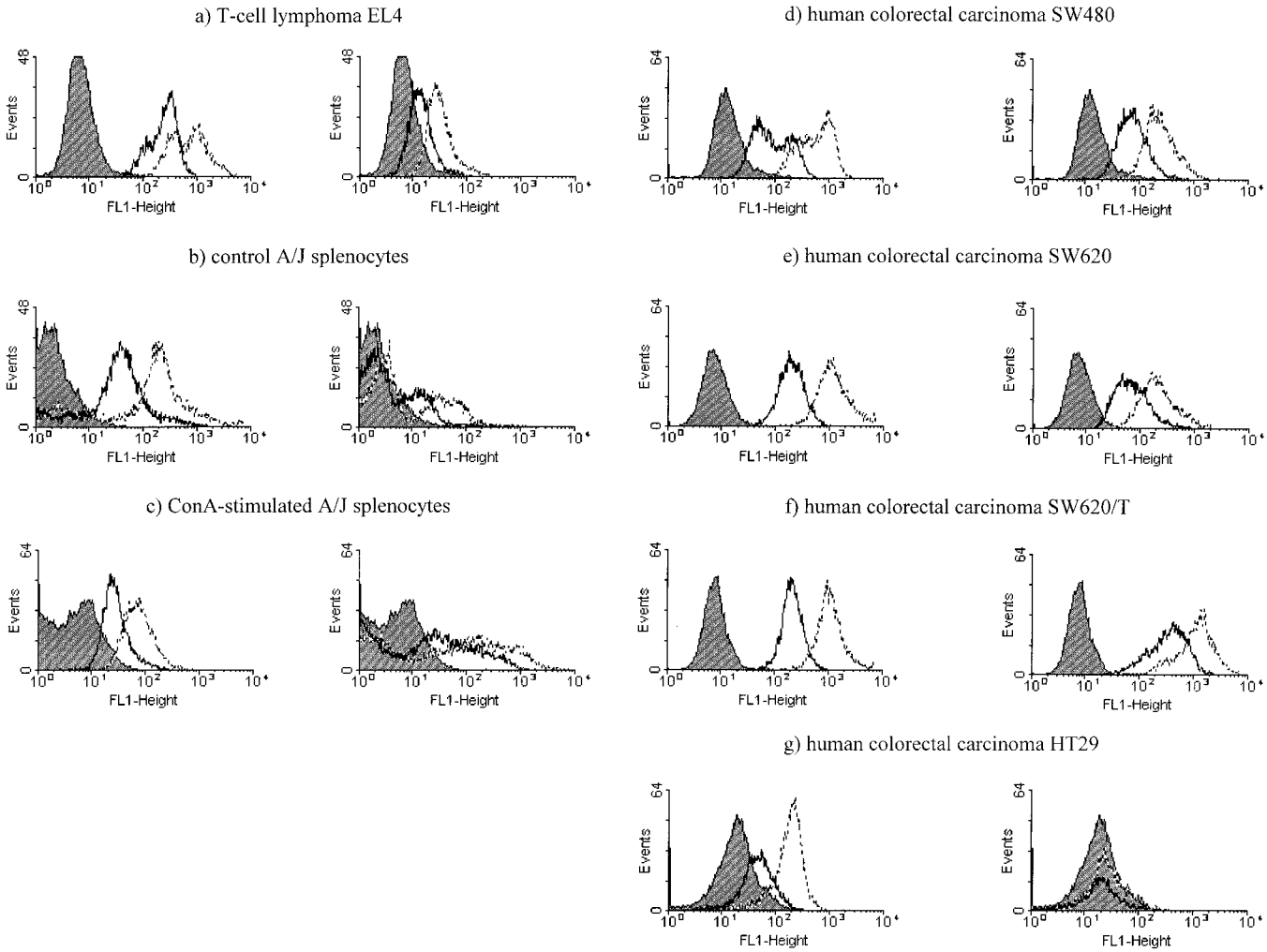

Figure 1. (a−g) Flow cytometry analysis of WGA and PNA expression in EL4, SW 480, SW 620, SW 620/T, and HT 29 human colorectal cancer cell lines and in control and concanavalin A-stimulated A/J splenocytes. Cells were treated with WGA−FITC and PNA−FITC: left, WGA−FITC; right, PNA−FITC; gray, control cells; dotted line (left), 400 ng/mL WGA−FITC; dotted line (right), 10 μg/mL PNA−FITC; solid line (left), 80 ng/mL WGA−FITC; solid line (right), 2 μg/mL PNA−FITC.

of SV40 and HSVtk (Katoh et al., 1987). This vector, which confers resistance to the neomycin analogue G418 on mammalian cells, was kindly provided by K. Katoh of Kyoto University (Kyoto, Japan). Both plasmids were isolated by the alkaline lysis method and by two equilibrium centrifugations in CsCl (Sambrook et al., 1989).

DNA Transfection and G418 Selection. DNA transfection was performed by a modification of the method of Chen and Okayama (1987). SW 620 cells (6×10^5) were aliquoted into 60 mm tissue culture dishes and incubated in culture medium. After 24 h, the medium was replaced with fresh culture medium and 0.5 mL of plasmid mix was added. Plasmid mix was prepared by mixing 9 μg of pThy-1.2 and 1 μg of pSTneoB in 0.5 mL of BES buffer containing 25 mM BES (pH 7.0), 140 mM NaCl, 0.75 mM Na_2HPO_4, and 125 mM $CaCl_2$. After incubation for 6 h at 37 °C and in 5% CO_2 in air, the medium was removed and 2 mL of 25% DMSO in BES buffer was added. After 4 min, the DMSO was removed, the cells were washed twice with PBS, and culture medium was added. The next day, the cells were trypsinized and transferred into three 60 mm tissue culture dishes with culture medium containing 1 mg/mL G418 (Geneticin, Sigma Chemical Corp., St. Louis, MO). Detached cells were removed by washing on the third, sixth, ninth, and fifteenth day after DNA transfection, and G418-resistant colonies were isolated 21 days after transfection.

The colonies were expanded and tested for the presence of surface Thy-1.2 by indirect immunofluorescence using 1aG4/C5 mAb (Dráber et al., 1980) and FACSorter analysis. Initial screening showed that only a small fraction of transfected cells exhibited surface fluorescence, and therefore, Thy-1.2$^+$ cells were enriched by a two-step immunomagnetic separation procedure using 1aG4/C5 mAb in the first step and Dynabeads M-450 coated with goat anti-mouse IgG (Dynal A. S., Oslo, Norway) in the second step. After purification, the cells were cloned and recloned in the absence of G418, and only subclones in which more than 95% of the cells expressed surface Thy-1.2, as determined by FACSorter analysis (see above), were used in further experiments (Figure 1).

Tissue Culture Condition. Routine culture and all experiments with cancer cell lines were conducted at 37 °C in a humidified atmosphere of 5% CO_2/95% air in RPMI 1640 medium (Gibco Laboratories) supplemented with 10% v/v heat-inactivated fetal calf serum (FCS) selected for low mitogenicity, 2 mM L-glutamine (Gibco Laboratories), 50 mM 2-mercaptoethanol (Fluka), 100 units/mL penicillin, and 100 μg/mL streptomycin.

Mice. Mice of inbred strain A/J were obtained from the breeding colony of the Institute of Physiology (Academy of Sciences of the Czech Republic) and kept in standard housing. The mice were used when they were

12 weeks old. All experiments were approved by the Animal Welfare Committee of the Institute of Microbiology of the Academy of Sciences of the Czech Republic.

Fluorescence-Activated Cell Sorter Analysis (FACS). Flow cytometric measurements were carried out on a FACSorter as described previously (Říhová et al., 1996, 2000). Labeled cells were analyzed using a forward versus side scatter gate for the inclusion of single-cell populations and exclusion of debris and cell aggregates. At least 5000 cells were tested for each measurement.

Cytotoxicity Assay. Inhibition of [^{3}H]thymidine incorporation was used to evaluate the cytostatic action of targeted HPMA conjugates of doxorubicin in vitro as described previously (Říhová et al., 1992). Tumor cells were harvested from the exponential phase of growing cultures, centrifuged for 10 min at 800*g*, resuspended in fresh medium (RPMI 1640), and counted by hemocytometer. NUNCLON 96-well FB tissue culture plates (NUNC) were seeded with 0.1 mL of cell suspension (EL4 at a density of 5×10^5 cells/mL for 24 h; SW 620, SW 480, SW 620/T, and HT 29 at a density of 1×10^5 cells/mL for 72 h; splenocytes at a density of 5×10^6 cells/mL for 72 h), and various concentrations of free doxorubicin, doxorubicin bound to HPMA targeted with lectins, mAbs, their F(ab′)$_2$ fragment or galactosamine, and nontargeted HPMA-bound lectins were added to the wells to achieve the desired concentrations and a final well volume of 0.25 mL. Triplicate wells were used for each test condition. At the end of the incubation period, 1 μCi/50 μL of [^{3}H]-thymidine (Amersham Corp.) was added per well, followed by incubation for 6 h. Cells were then collected using a cell harvester (Tomtec) onto glass fiber filters (filtermat, Wallac). When the mixture was dried, a sheet of solid scintillator-Meltilex (Wallac) was placed together with a filtermat containing 96 samples in a sample bag and run together through a heat sealer (Microsealer, Wallac) in MicroBeta TriLux (Wallac).

Statistical Analysis. The Wilcoxon's statistics (multiple-comparison method) and a Student's *t* test were used to evaluate the differences between experimental groups. *P* values of <0.05 were taken to be statistically significant.

RESULTS

Characterization of Targeted Poly(HPMA) Copolymer Carrier-Bound Doxorubicin. Characteristics of all synthesized conjugates are given in Table 1. All DOX-bearing conjugates contained <0.1 wt % free DOX (related to the total DOX content). Neither electrophoresis nor GPC revealed the presence of a detectable amount of free protein in the conjugates. The molecular mass of anti-Thy-1.2-targeted conjugates (M_w) was approximately 600 kDa, and the distribution of molecular masses was very broad (close to 5) as a result of branching reactions, which cannot be eliminated during the aminolytic reaction of the polyfunctional polymer with polyfunctional glycoprotein. The use of the anti-Thy-1.2 F(ab′)$_2$ fragment resulted in the lower molecular mass of the conjugate ($M_w \approx 400$ kDa) and also a more narrow distribution of molecular masses. Conjugates targeted with lectins exhibited lower molecular masses than antibodies ($M_w \approx 300$ kDa) with a polydispersity of ~3. The molecular mass ($M_w = 28\,000$ Da) and polydispersity (1.5) of sample 3 were very close to the data obtained for the polymer precursor.

Binding of WGA−FITC and PNA−FITC to SW 620, SW 620/T, SW 480, HT 29, and EL4 Cancer Cell Lines and to Con A-Activated and Nonactivated (Control) Mouse T Lymphocytes. Before the use of a targeted drug for cytotoxic assays could be extended, it was necessary to estimate the capacity of binding of targeting moieties to different cancer cell lines and to normal and Con A-stimulated T lymphocytes selected as a target. Primary, metastatic, and Thy-1.2-transfected human colorectal cell lines SW 480, SW 620, and SW 620/T exhibited similar binding of WGA−FITC and PNA−FITC. The level of PNA binding was considerably lower. A very low level of binding of WGA−FITC and no binding of PNA−FITC were observed with the HT 29 human colorectal cell line. Binding of WGA−FITC to EL4 mouse T cell lymphoma was comparable with that to SW 480 and SW 620 cell lines, and the level of binding to both forms of splenocytes (control and Con A-stimulated) was lower. A low level of binding of PNA−FITC to control splenocytes significantly increased after stimulation with Con A (Figure 1b,c). The results of FACS analysis further show that the SW 620/T line binds to a great extent anti-Thy-1.2 monoclonal antibody. Similar binding was observed with Thy-1.2$^+$ mouse T lymphocytes and with Thy-1.2$^+$ mouse T cell lymphoma EL4. No such binding was detected with the parent SW 620 cancer cell line (Figure 2).

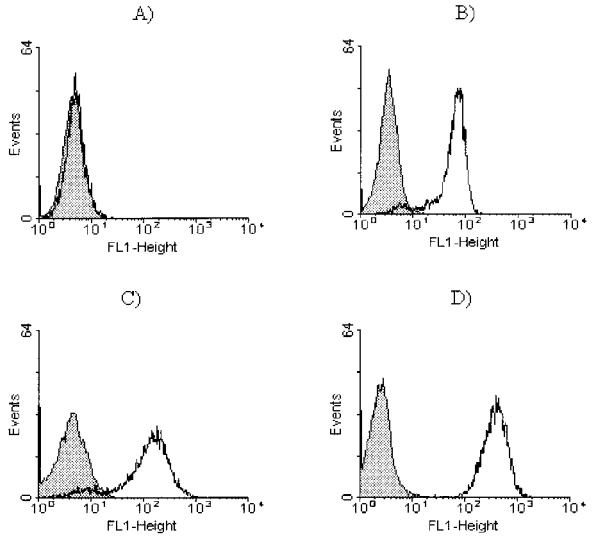

Figure 2. Flow cytometry analysis of Thy-1.2 expression in the SW 620 human colorectal cancer cell line, the SW 620 cell line transfected with the *Thy-1.2* gene (SW 620/T), mouse T lymphocytes, and mouse T cell lymphoma EL4. The cells were reacted with 1aG4/C5 anti-Thy-1.2 mAb (10 μg/mL) followed by FITC-labeled rabbit anti-mouse IgG3. In controls, the first antibody was TEC-11 IgG3 (Dráberová and Dráber, 1991) which does not bind to RBL cells: (A) human colorectal carcinoma SW 620, (B) human colorectal carcinoma SW 620 transfected with the *Thy-1.2* gene (SW 620/T), (C) mouse T lymphocytes, and (D) mouse T cell lymphoma EL4.

Influence of Targeting Moieties on the Cytostatic Activity of Targeted Poly(HPMA)-Bound Doxorubicin in SW 620, SW 620/T, SW 480, HT 29, and EL4 Cancer Cell Lines and in Mouse T Lymphocytes in Vitro. The effect of targeted doxorubicin on tumor cell growth was investigated by [^{3}H]TdR incorporation. In vitro inhibition of cell proliferation of SW 620, SW 620/T, and SW 480 cancer cell lines by HPMA copolymer-carrier-bound doxorubicin targeted with lectins (WGA and PNA), galactosamine, or anti-Thy-1.2 monoclonal antibody or with its F(ab′)$_2$ fragments is shown in Figures 3−5. The corresponding concentrations of doxorubicin required for 50% inhibition of cell proliferation (IC_{50}) for SW 620, SW 620/T, SW 480, HT29, and EL4 cancer cell lines and for concanavalin A-activated mouse T lympho-

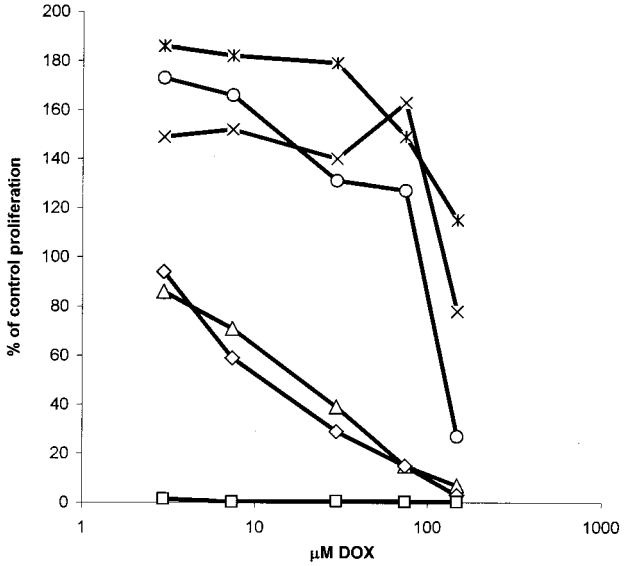

Figure 3. Cytostatic effect of targeted HPMA-bound doxorubicin in the human colorectal cancer SW 620 cell line: (×) DOX-HPMA-anti-Thy-1.2 (sample 1), (∗) DOX-HPMA-anti-Thy-1.2−F(ab')$_2$ (sample 2), (○) DOX-HPMA-gal (sample 3), (◇) DOX-HPMA-WGA (sample 4), (△) DOX-HPMA-PNA (sample 5), and (□) doxorubicin (DOX). $p < 0.001$ for sample 1. $p < 0.01$ for sample 2. $p < 0.05$ for sample 3. $p < 0.01$ for sample 4. $p < 0.05$ for sample 5 (all via a Student's *t* test).

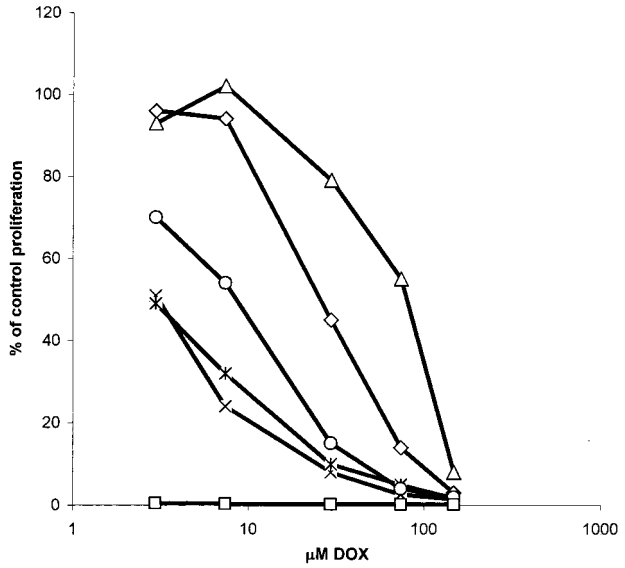

Figure 4. Cytostatic effect of targeted HPMA-bound doxorubicin in the human colorectal cancer SW 620/T cell line: (×) DOX-HPMA-anti-Thy-1.2 (sample 1), (∗) DOX-HPMA-anti-Thy-1.2−F(ab')$_2$ (sample 2), (○) DOX-HPMA-gal (sample 3), (◇) DOX-HPMA-WGA (sample 4), (△) DOX-HPMA-PNA (sample 5), and (□) doxorubicin (DOX). $p < 0.05$ for sample 1. $p < 0.001$ for sample 2. $p < 0.005$ for sample 3. $p < 0.01$ for sample 4. $p < 0.05$ for sample 5 (all via a Student's *t* test).

cytes are summarized in Table 2. A very high concentration of doxorubicin (>100 μM) was cytostatic in all tested conjugates, and it inhibited cancer cell proliferation in all studied tumor cell lines (Figures 3−5). The exceptions were anti-Thy-1.2-targeted conjugates in cancer cell line SW 620. Conjugates of HPMA copolymer carrier-bound doxorubicin, targeted with monoclonal antibodies against Thy-1.2 alloantigen or targeted with their F(ab')$_2$ fragments, specifically inhibited cancer cell proliferation in vitro only in a metastatic human colorectal cancer cell line transfected with Thy-1.2 alloantigen (Figure 4), in

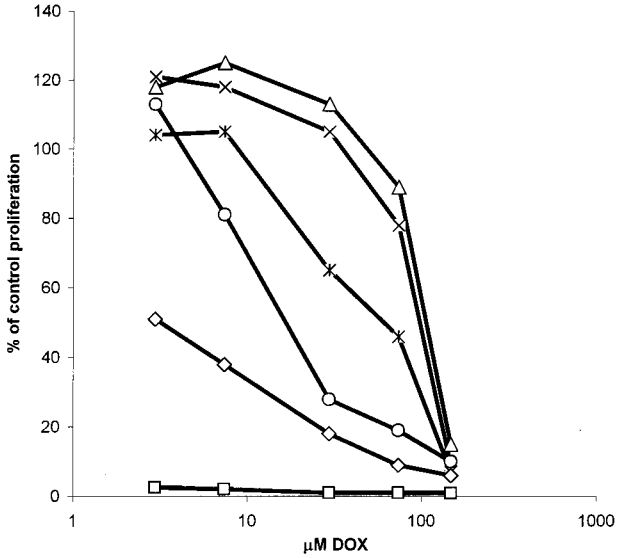

Figure 5. Cytostatic effect of targeted HPMA-bound doxorubicin in the human colorectal cancer SW 480 cell line: (×) DOX-HPMA-anti-Thy-1.2 (sample 1), (∗) DOX-HPMA-anti-Thy-1.2−F(ab')$_2$ (sample 2), (○) DOX-HPMA-gal (sample 3), (◇) DOX-HPMA-WGA (sample 4), (△) DOX-HPMA-PNA (sample 5), and (□) doxorubicin (DOX). $p < 0.05$ for sample 1. $p < 0.002$ for sample 2. $p < 0.05$ for sample 3. $p < 0.01$ for sample 4. $p < 0.05$ for sample 5 (all via a Student's *t* test).

Table 2. IC_{50} Values Determined in Cancer Cell Lines SW 620, SW 620/T, SW 480, HT 29, and EL4 and in Con A-Stimulated T Cells

sample	cancer cell line	IC_{50} concentration (μM DOX) ± SD
P–GFLG-DOX	SW 620	150 ± 30.9
	SW 620/T	2.96 ± 0.63
P–GFLG-a-Thy 1.2	SW 480	111.1 ± 34.4
	HT 29	150 ± 42
	EL4	5.18 ± 1.29
	T cells (Con A)	2.96 ± 0.71
P–GFLG-DOX	SW 620	150 ± 34.7
	SW 620/T	2.96 ± 1.01
P–GFLG-F(ab′)$_2$	SW 480	74.1 ± 22.2
	HT 29	150 ± 24.8
	EL4	5.18 ± 1.50
	T cells (Con A)	2.96 ± 1.02
P–GFLG-DOX	SW 620	87 ± 20.01
	SW 620/T	7.4 ± 2.07
P–GFLG-gal	SW 480	14.8 ± 4.29
	HT 29	95 ± 32.3
	EL4	29 ± 6.96
P–GFLG-DOX	SW 620	14.8 ± 4.58
	SW 620/T	14.8 ± 3.92
P–GFLG-WGA	SW 480	2.96 ± 0.98
	HT 29	9.2 ± 2.94
	EL4	74 ± 23.68
	T cells (Con A)	11.1 ± 2.77
P–GFLG-DOX	SW 620	22.2 ± 5.10
	SW 620/T	74.1 ± 20.74
P–GFLG-PNA	SW 480	111.1 ± 29.99
	HT 29	112 ± 33.6
	EL4	148.1 ± 42.94
	T cells (Con A)	29.6 ± 7.40
DOX	SW 620	0.0518 ± 0.022
	SW 620/T	0.109 ± 0.034
	SW 480	0.09 ± 0.042
	HT 29	0.0518 ± 0.024
	EL4	0.22 ± 0.082
	T cells (Con A)	0.22 ± 0.099

Thy-1.2$^+$ EL4 mouse T cell lymphoma, and in Thy-1.2$^+$ Con A-stimulated mouse T lymphocytes (Table 2). Conjugates of HPMA copolymer-bound doxorubicin targeted with PNA and WGA lectins inhibited proliferation of

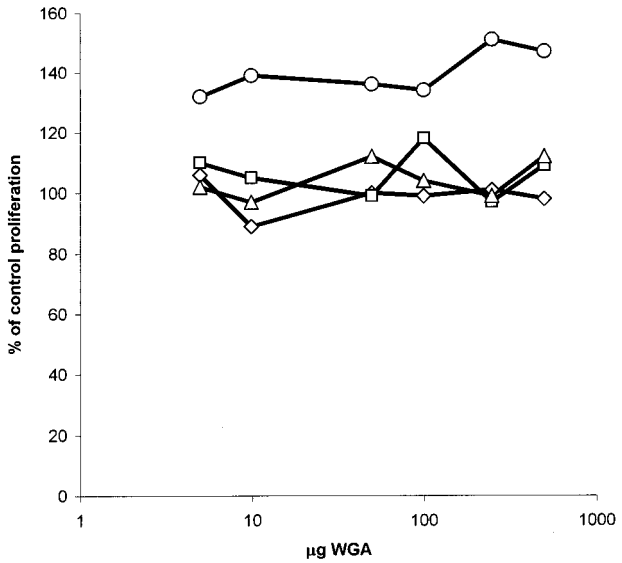

Figure 6. Effect of HPMA-bound WGA (sample 6) on proliferation of different cancer cell lines: (◇) SW 620, (□) SW 620/T, (△) SW 480, and (○) EL4.

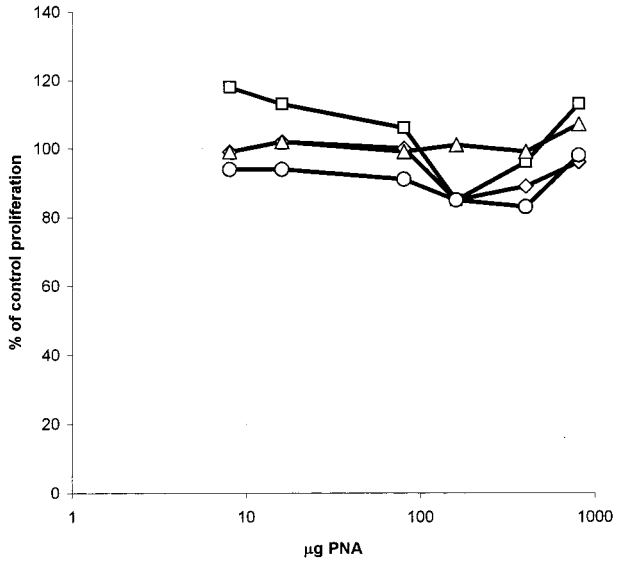

Figure 7. Effect of HPMA-bound PNA (sample 7) on proliferation of different cancer cell lines: (◇) SW 620, (□) SW 620/T, (△) SW 480, and (○) EL4.

target cells in a dose-dependent manner and had similar cytotoxicities in the metastatic SW 620 cell line (Figure 3 and Table 2), while the 2−40-fold lower cytotoxicity of the PNA-targeted drug was observed in EL4, Con A-stimulated A/J splenocytes, SW 620/T, HT 29, and SW 480 cancer cell lines (Figures 3−5 and Table 2). For instance, the IC_{50} for PNA-targeted HPMA-bound doxorubicin in the SW 480 cell line was 111.1 μM, while the IC_{50} for WGA-targeted HPMA-bound doxorubicin was only 2.96 μM. Similarly, the IC_{50} for the HT 29 cell line was 112 μM for PNA-targeted HPMA-bound doxorubicin, while a value of only 9.2 μM was estimated for WGA-targeted doxorubicin. The extent of cytotoxicity does not always reflect the extent of binding of PNA-targeted conjugates. We have observed slight but definite decreases in cytotoxicity of the SW 620/T cell line to PNA-targeted doxorubicin if compared with parent cell line SW 620. The IC_{50} for PNA-targeted doxorubicin was 22.2 μM in the SW 620 cell line; in transfectant SW 620/T cells, it was 74.1 μM (Table 2 and Figures 3 and 4), while the binding of PNA−FITC to SW 620/T cells was more intense (Figure 1e,f). On the other hand, SW 620/T was more sensitive to the galactosamine-targeted doxorubicin. The IC_{50} for SW 620 cells was 87 μM, while in SW 620/T transfectant cells, it was only 7.4 μM (Table 2 and Figures 3 and 4). No cytotoxicity or mitogenic activity against SW 620, SW 620/T, and SW 480 cancer cell lines was observed with WGA- and PNA-bound HPMA copolymer carrier without doxorubicin (Figures 6 and 7). By contrast, detectable stimulation of cell proliferation was observed with HPMA−WGA conjugates in the EL4 cell line (Figure 6) and surprisingly and repeatedly in metastatic cancer cell line SW 620 with a low concentration of doxorubicin conjugates of HPMA targeted with monoclonal antibodies, their F $(ab')_2$ fragments, or galactosamine (Figure 3).

DISCUSSION

Lectins are capable of interacting specifically with certain oligosaccharides (Sharon and Lis, 1972) which makes them prospective targeting moieties in site-specific drug delivery, since the glycosylation pattern of cells is often altered upon malignant transformation. The normal colon shows little binding of PNA, whereas inflammatory colon and colonic carcinomas show binding of PNA (Yuan et al., 1986; Caldero et al., 1989; Ryder et al., 1994). Specific PNA binding was also observed in nasopharyngeal carcinomas regardless of their histopathologic type (Huang et al., 1996) and in malignant melanomas, where the extent of PNA binding, but not WGA binding, correlates somehow with the metastatic potential (Zebda et al., 1994; Dore et al., 1997).

In previous in vitro studies, the binding capacity of anti-Thy-1.2 monoclonal antibodies and binding of WGA and PNA were assessed by flow cytometric determination of the cell-bound fluorescence intensity. Lectin and anti-Thy-1.2 monoclonal antibody exhibited dose-dependent binding to target cells with the only exception. In the SW 620/T cell line, the levels of binding were almost equal. The level of binding of anti-Thy-1.2 antibody and WGA exceeded that of PNA−lectin. In most reported cases, a direct correlation was reported between the intensity of binding of the targeted cytostatic drugs or immunotoxins to target cells and their respective cytotoxicites were observed, although anomalies were also seen (Bjorn et al., 1985; LeMaistre et al., 1987). We have observed comparable binding of PNA−FITC to human colorectal cancer cell lines SW 620 and SW 480, while the pronounced cytotoxicity of PNA-targeted HPMA-bound doxorubicin was observed only in the SW 620 cell line and in Con A-stimulated mouse T lymphocytes. Similarly, a very low level of binding of WGA−FITC was observed with the HT29 cell line, while the cytotoxicity of WGA-targeted doxorubicin was high (Table 2). These discrepancies between the intensity of binding and cytotoxicities may reflect different processing and intracellular release of the targeted drug in different cancer cell lines (Marks et al., 1990). It was described in immunotoxins that the cellular internalization rate and intracellular destination are more critical factors in targeted drug efficacy than the number and binding of cell surface receptors (Goldmacher et al., 1989; Recht et al., 1996).

A very high concentration of targeted doxorubicin (over 100 μM) inhibited in vitro cancer cell proliferation in most studied tumor cell lines. It is obvious that at this concentration the inhibition of cell proliferation reflects not only specific binding and internalization of the targeted drug but also nonspecific accumulation (fluid-phase pinocytosis) of tested compounds as certain inhibi-

tion with anti-Thy-1.2-targeted conjugate was also observed in the SW 480 cancer cell line, which does not express Thy-1.2 xenoantigen (Figure 5). Specific inhibition of proliferation reflects metabolic consequences of receptor-mediated internalization of targeted drug−copolymer carrier conjugates and depends on the number of cell surface receptors and the affinity constant of the receptor−ligand complex as well as on the rate of complex internalization (Říhová, 1998). Nonspecific inhibition mainly reflects the fluid-phase uptake of the conjugate into the cancer cells which is proportional to the concentration of the extracellular material. However, the concentration of extracellular material is not the only factor influencing the nonspecific inhibitory effect. The same high concentration of antibody-targeted doxorubicin which causes in the SW 480 cell line significant inhibition is considerably less toxic in cell line SW 620. The other factors which could be responsible for different nonspecific effects of very high concentrations of polymer-bound drug in the SW 620 line and the SW 480 line are the different compositions of the cell surface (SW 620 is a cell line of metastatic human colorectal cancer, while SW 480 is a cell line of a primary human colorectal cancer) and different intracellular fates.

Our results further demonstrate that both lectin-targeted conjugates containing doxorubicin are cytotoxic in vitro. WGA- and antibody-targeted prodrugs of doxorubicin have been shown to be more cytotoxic for cancer cell lines and Con A-activated A/J T cells than the corresponding PNA-targeted prodrugs. Control experiments were performed to rule out the possibility that the cytotoxic effect may arise from WGA or PNA bound to the HPMA copolymer carrier. We have not observed the contribution of WGA or PNA to the antiproliferative effect of the whole conjugate as WGA or PNA bound to the HPMA copolymer without doxorubicin did not affect cancer cell proliferation (Figures 6 and 7). Throughout the whole range of tested doses (4.96−495.9 μM doxorubicin), no decrease and only a small increase in thymidine incorporation were seen only in mouse EL4 T cell lymphoma. Thus, the cytostatic activity of lectin-targeted doxorubicin derives from the conjugated drug.

We have compared the cytostatic effect of PNA- and WGA-targeted doxorubicin in different cancer cell lines and in concanavalin A-stimulated A/J T lymphocytes. The $\leq$40-fold difference which was observed in the IC_{50} values in tested lines is probably due to (a) different internalization rates of the ligand−receptor complexes, (b) differences in the expression and availability of PNA- and WGA-binding glycoproteins, and/or (c) differences in their intracellular fates (Ryder et al., 1994). The different accessibility of different surface receptors due to the expression of a new protein marker is probably also the explanation for the different sensitivity of the parent cell line SW 620 and its *Thy-1.2* transfectant (SW 620/T) to the antiproliferative effect of PNA- and galactosamine-targeted doxorubicin. Experiments are in progress to explain these different sensitivities of SW 620 and SW 620/T cell lines.

The targeting efficacy of WGA conjugates is comparable to that of conjugates targeted by monoclonal antibodies or their $F(ab')_2$ fragments. However, while the conjugates with WGA are more cytotoxic, the conjugates with PNA are more specific as their strong binding is limited to cancer cells and to the sites of inflammation (Yuan et al., 1986; Boland and Roberts, 1988; Caldero et al., 1989; Ryder et al., 1994; Zebda et al., 1994; Huang et al., 1996; Dore et al., 1997; Wirth et al., 1998). The slight expression of PNA on healthy cells was reported for memory B cells (Lahvis and Cerny, 1997), spermatids and spermatozoa (Lee and Damjanov, 1985), urothelium (Ward et al., 1987), Schwann cell membrane (Corbo et al., 1993), and some embryonic cells (Stringa et al., 1997; Buse and Seifert, 1998). Thus, lectin-prodrug targeting is a promising approach for the delivery of drugs or vaccines to the gastrointestinal tract. The gastrointestinal stability of lectins makes lectin-targeted HPMA conjugates useful for peroral administration which offers local and more convenient therapy not only for colorectal carcinoma but also for other colon-associated diseases.

We further demonstrated that transfection of human cancer cells with a mouse gene, controlling the synthesis of the unique cell surface marker Thy-1.2, provides a good target for site-specific therapy. The cytostatic action of anti-Thy-1.2- or $F(ab')_2$-targeted doxorubicin bound to poly(HPMA) is specific. Such evidence is derived from the experiments with Thy-1.2^+ cells, such as mouse T lymphocytes, EL4 mouse T cell lymphoma, or the *Thy-1.2*-transfected SW 620 metastatic human colorectal cancer cell line. The IC_{50} for the transfected SW 620 cell line is comparable with that observed with naturally Thy-1.2-expressing EL4 mouse T cell lymphoma and with that for concanavalin A-stimulated A/J mouse T lymphocytes. The same is true for conjugates targeted with $F(ab')_2$ fragments of anti-Thy-1.2 monoclonal antibody. On the other hand, conjugates of doxorubicin bound to the HPMA copolymer carrier and targeted with antibodies or their $F(ab')_2$ fragments which are not detectable on the surface of SW 620, SW 480, or HT 29 cell lines do not interfere in therapeutic doses of doxorubicin with cell proliferation.

Our data indicate that targeting of HPMA copolymer-bound doxorubicin is a promising approach for tumor cell eradication. The major problem of targeted drug therapy is the specificity of targeting molecules. Improved expression of certain oligosacharides on the surface of tumor cells such as Gal(β1−3)GalNAc can be used to identify tumor cells by lectins (PNA). And such lectins can therefore act as targeting moieties. Surface antigens specific for tumor cells can be detected with even higher specificity with monoclonal antibodies. Recent progress in gene therapy-based approaches offers another possibility of overcoming the problem with the absence of specific tumor markers in certain tumors. This approach is based on transfer of selected genes, such as CD 66a (Luo et al., 1999), into tumor cells and then utilization of these gene products as a target of mAb in a similar way as Thy-1.2 in this paper. It is very likely that in future combined strategies will be available in which gene therapy will be used to suppress tumor and to mark it with markers which can be used for tumor cell targeting.

The results have shown (a) the potential role for lectins as targeting moieties in cytostatic therapy of human colorectal carcinoma and (b) that the xenogeneic gene transfected into human colorectal carcinoma can serve as a target in site-specific anticancer therapy.

ACKNOWLEDGMENT

This research was supported by the Ministry of Industry and Trade (Grant PZ-Z2/24/99) and by the Grant Agency of the Czech Republic (Grant 307/96/K226). We thank Dr. Petr Dráber for valuable discussion and Ms. Hana Semorádová and Ms. Helena Mišurcová for their excellent technical assistance.

LITERATURE CITED

Bjorn, M. J., Ring, D., and Frankel, A. (1985) Evaluation of monoclonal antibodies for the development of breast cancer immunotoxins. *Cancer Res. 45*, 1214−1221.

Boland, C. R., and Roberts, J. A. (1988) Quantitation of lectin binding sites in human colon mucins by use of peanut and wheat germ agglutinins. *J. Histochem. Cytochem. 36*, 1305−1307.

Buse, E., and Seifert, H. (1998) Glycoconjugate expression during early mouse oculogenesis. *Histochem. J. 30*, 819−827.

Caldero, J., Campo, E., Ascaso, C., Ramos, J., Panades, M. J., and Rene, J. M. (1989) Regional distribution of glycoconjugates in normal, transitional and neoplastic human colonic mucosa. A histochemical study using lectins. *Virchows Arch. A: Pathol. Anat. Histopathol. 415*, 347−356.

Chen, C., and Okayama, H. (1987) High-efficiency transformation of mammalian cells by plasmid DNA. *Mol. Cell. Biol. 7*, 2745−2752.

Corbo, M., Quattrini, A., Latov, N., and Hays, A. P. (1993) Localization of GM1 and Gal(β1−3)GalNAc antigenic determinants in peripheral nerve. *Neurology 43*, 809−814.

Dore, J. F., Maisonneuve, P., Cattaruzza, M. S., Autier, P., Cochran, A. J., and Boyle, P. (1997) A molecular epidemiological approach to the study of expression of a metastasis marker in primary melanomas and its correlation with individual patient's risk of recurrence or metastasis. *Melanoma Res. 7* (Suppl. 2), S121−S125.

Dráber, P., Zikán, J., and Vojtíšková, M. (1980) Establishment and characterization of permanent murine hybridomas secreting monoclonal anti-Thy-1 antibodies. *J. Immunogenet. 7*, 455−474.

Dráberová, L., and Dráber, P. (1991) Functional expression of the endogeneous Thy-1 gene and the transfected murine Thy-1.2 gene in rat basophilic leukemia cells. *Eur. J. Immunol. 21*, 1583−1590.

Duncan, R. (1992) Drug-polymer conjugates: potential for improved chemotherapy. *Anticancer Drugs 3*, 175−210.

Duncan, R., Kopečková-Rejmanová, P., Strohalm, J., Hume, I., Cable, H. C., Pohl, J., Lloyd, J. B., and Kopeček, J. (1987) Anticancer agents coupled to *N*-(2-hydroxypropyl)methacrylamide copolymers. I. Evaluation of daunomycin and puromycin conjugates in vitro. *Br. J. Cancer 55*, 165−174.

Duncan, R., Kopečková, P., Strohalm, J., Hume, I. C., Lloyd, J. B., and Kopeček, J. (1988) Anticancer agents coupled to *N*-(2-hydroxypropyl)methacrylamide copolymers. II. Evaluation of daunomycin conjugates in vivo against L1210 leukaemia. *Br. J. Cancer 57*, 147−156.

Evans, G. A., Ingraham, H. A., Lewis, K., Cunningham, K., Seki, T., Moriuchi, T., Chang, H. C., Silver, J., and Hyman, R. (1984) Expression of the Thy-1 glycoprotein gene by DNA-mediated gene transfer. *Proc. Natl. Acad. Sci. U.S.A. 81*, 5532−5536.

Goldenberg, D. M., Kim, E. E., DeLand, F. H., van Nagell, J. R., Jr., and Javadpour, N. (1980) Clinical radioimmunodetection of cancer with radioactive antibodies to human chorionic gonadotropin. *Science 208*, 1284−1286.

Goldmacher, V. S., Scott, C. F., Lambert, J. M., McIntyre, G. D., Blattler, W. A., Collnhson, A. R., Stewart, J. K., Chong, L. D., Cook, S., Slayter, H. S., et al. (1989) Cytotoxicity of gelonin and its conjugates with antibodies is determined by the extent of their endocytosis. *J. Cell Physiol. 141*, 222−234.

Hertler, A. A., and Frankel, A. E. (1989) Immunotoxins: a clinical review of their use in the treatment of malignancies. *J. Clin. Oncol. 7*, 1932−1942.

Houghton, A. N., Mintzer, D., Cordon-Cardo, C., Welt, S., Fliegel, B., Vadhan, S., Carswell, E., Melamed, M. R., Oettgen, H. F., and Old, L. J. (1985) Mouse monoclonal IgG3 antibody detecting GD3 ganglioside: a phase I trial in patients with malignant melanoma. *Proc. Natl. Acad. Sci. U.S.A. 82*, 1242−1246.

Huang, H., Jiang, D., and Li, Z. (1996) Metastatic potential correlates with cell surface carbohydrate profiles of nasopharyngeal carcinoma. *Chung Hua Erh Pi Yen Hou Ko Tsa Chih 31*, 165−167.

Hussain, N., Jani, P. U., and Florence, A. T. (1997) Enhanced oral uptake of tomato lectin-conjugated nanoparticles in the rat. *Pharm. Res. 14*, 613−618.

Jelínková, M., Strohalm, J., Plocová, D., Šubr, V., Šťastný, M., Ulbrich, K., and Říhová, B. (1998) Targeting of human and mouse T-lymphocytes by monoclonal antibody-HPMA copolymer-doxorubicin conjugates directed against different T-cell surface antigens. *J. Controlled Release 52*, 253−270.

Katoh, K., Takahashi, Y., Hayashi, S., and Kondoh, H. (1987) Improved mammalian vectors for high expression of G418 resistance. *Cell Struct. Funct. 12*, 575−580.

Kopeček, J., Rejmanová, P., Strohalm, J., Ulbrich, K., Říhová, B., Chytrý, V., Lloyd, J. B., and Duncan, R. (1991) Synthetic polymeric drugs. U.S. Patent 5,037,883.

Lahvis, G. P., and Cerny, J. (1997) Induction of germinal center B cell markers in vitro by activated CD4+ T lymphocytes: the role of CD40 ligand, soluble factors, and B cell antigen receptor cross-linking. *J. Immunol. 159*, 1783−1793.

Lee, M. C., and Damjanov, I. (1985) Lectin binding sites on human sperm and spermatogenic cells. *Anat. Rec. 212*, 282−287.

LeMaistre, C. F., Edwards, D. P., Krolick, K. A., and McGuire, W. L. (1987) An immunotoxin cytotoxic for breast cancer cells in vitro. *Cancer Res. 47*, 730−734.

Luo, W., Tapolsky, M., Earley, K., Wood, C. G., Wilson, D. R., Logothetis, C. J., and Lin, S. H. (1999) Tumor-suppressive activity of CD66a in prostate cancer. *Cancer Gene Ther. 6*, 313−321.

Marks, A., Ettenson, D., Bjorn, M. J., Lei, M., and Baumal, R. (1990) Inhibition of human tumor growth by intraperitoneal immunotoxins in nude mice. *Cancer Res. 50*, 288−292.

Neville, D. M., Jr., and Youle, R. J. (1982) Monoclonal antibody-ricin or ricin A chain hybrids: kinetic analysis of cell killing for tumor therapy. *Immunol. Rev. 62*, 75−91.

O'Hare, K. B., Duncan, R., Strohalm, J., Ulbrich, K., and Kopečková, P. (1993) Polymeric drug-carriers containing doxorubicin and melanocyte-stimulating hormone: in vitro and in vivo evaluation against murine melanoma. *J. Drug Targeting 1*, 217−229.

Omelyanenko, V., Kopečková, P., Gentry, C., and Kopeček, J. (1998a) Targetable HPMA copolymer-adriamycin conjugates. Recognition, internalization, and subcellular fate. *J. Controlled Release 53*, 25−37.

Omelyanenko, V., Gentry, C., Kopečková, P., and Kopeček, J. (1998b) HPMA copolymer-anticancer drug-OV-TL16 antibody conjugates. II. Processing in epithelial ovarian carcinoma cells in vitro. *Int. J. Cancer 75*, 600−608.

Raso, V. (1982) Antibody mediated delivery of toxic molecules to antigen bearing target cells. *Immunol. Rev. 62*, 93−117.

Recht, L. D., Raso, V., Davis, R., and Salmonsen, R. (1996) Immunotoxin sensitivity of Chinese hamster ovary cells expressing human transferrin receptors with differing internalization rates. *Cancer Immunol. Immunother. 42*, 357−361.

Rejmanová, P., Pohl, J., Baudyš, M., Kostka, V., and Kopeček, J. (1983) Polymers containing enzymatically degradable bonds, VIII. Degradation of oligopeptide sequeces in poly[*N*-(2-hydroxypropyl)methacrylamide] copolymers by bovine cathepsin B. *Makromol. Chem. 184*, 2009−2020.

Říhová, B., and Kopeček, J. (1985) Biological properties of targetable poly[*N*-(2-hydroxypropyl)methacrylamide]-antibody conjugates. *J. Controlled Release 2*, 289−310.

Říhová, B., Kopečková, P., Strohalm, J., Rossmann, P., Větvička, V., and Kopeček, J. (1988) Antibody-directed affinity therapy applied to the immune system: in vivo effectiveness and limited toxicity of daunomycin conjugated to HPMA copolymers and targeting antibody. *Clin. Immunol. Immunopathol. 46*, 100−114.

Říhová, B., Jegorov, A., Strohalm, J., Mat'ha, V., Rossmann, P., Fornůsek, L., and Ulbrich, K. (1992) Antibody-targeted cyclosporin A. *J. Controlled Release 19*, 25−40.

Říhová, B., Strohalm, J., Plocová, D., Šubr, V., Šrogl, J., Jelínková, M., Šírová, M., and Ulbrich, K. (1996) Cytotoxic and cytostatic effects of anti-Thy1.2 targeted doxorubicin and cyclosporin A. *J. Controlled Release 40*, 303−319.

Říhová, B. (1998) Receptor-mediated targeted drug or toxin delivery. *Adv. Drug Delivery Rev. 29*, 273−289.

Říhová, B., Jelínková, M., Strohalm, J., Šubr, V., Plocová, D., Hovorka, O., Novák, K., Plundrová, D., Germano, Y., and Ulbrich, K. (2000) Polymeric drugs based on conjugates of synthetic and natural macromolecules, II. Anti-cancer activity of antibody or $(Fab')_2$-targeted conjugates and combined therapy with immunomodulators. *J. Controlled Release 64*, 241−261.

Ryder, S. D., Smith, J. A., Rhodes, E. G., Parker, N., and Rhodes, J. M. (1994) Proliferative responses of HT29 and Caco2 human colorectal cancer cells to a panel of lectins. *Gastroenterology 106*, 85−93.

Sambrook, J., Fritsch, E. F., and Maniatis, T. (1989) *Molecular cloning. A laboratory manual*, Cold Spring Harbor Laboratory Press, Cold Spring Harbor, NY.

Sharon, N., and Lis, H. (1972) Lectins: cell-agglutinating and sugar-specific proteins. *Science 177*, 949−959.

Šťastný, M., Ulbrich, K., Strohalm, J., Rossmann, P., and Říhová, B. (1997) Abnormal differentiation of thymocytes induced by free cyclosporine is avoided when cyclosporine bound to *N*-(2-hydroxypropyl)methacrylamide copolymer carrier is used. *Transplantation 63*, 1818−1827.

Stringa, E., Love, J. M., McBride, S. C., Suyama, E., and Tuan, R. S. (1997) In vitro characterization of chondrogenic cells isolated from chick embryonic muscle using peanut agglutinin affinity chromatography. *Exp. Cell Res. 232*, 287−294.

Ulbrich, K., Šubr, V., Strohalm, J., Plocová, D., Jelínková, M., and Říhová, B. (2000) Polymeric drugs based on conjugates of synthetic and natural macromolecules, I. Synthesis and physico-chemical characterisation. *J. Controlled Release 64*, 63−79.

Vitetta, E. S., Krolick, K. A., and Uhr, J. W. (1982) Neoplastic B cells as targets for antibody-ricin A chain immunotoxins. *Immunol. Rev. 62*, 159−183.

Ward, G. K., Stewart, S. S., Price, G. B., and Mackillop, W. J. (1987) Cellular heterogeneity in normal human urothelium: quantitative studies of lectin binding. *Histochem. J.*, 337−344.

Weaver, L. T., and Bailey, D. S. (1987) Effect of the lectin concanavalin A on the neonatal guinea pig gastrointestinal mucosa in vivo. *J. Pediatr. Gastroenterol. Nutr. 6*, 445−453.

Wirth, M., Fuchs, A., Wolf, M., Ertl, B., and Gabor, F. (1998) Lectin-mediated drug targeting: preparation, binding characteristics, and antiproliferative activity of wheat germ agglutinin conjugated doxorubicin on Caco-2 cells. *Pharm. Res. 15*, 1031−1037.

Wroblewski, S., Kopečková, P., Říhová, B., and Kopeček, J. (1999) Lectin-HPMA copolymer conjugates: potential oral drug carriers for targeting diseased tissues. *Macromol. Chem. Phys. 199*, 2601−2608.

Yuan, M., Itzkowitz, S. H., Boland, C. R., Kim, Y. D., Tomita, J. T., Palekar, A., Bennington, J. L., Trump, B. F., and Kim, Y. S. (1986) Comparison of T-antigen expression in normal, premalignant, and malignant human colonic tissue using lectin and antibody immunohistochemistry. *Cancer Res. 46*, 4841−4847.

Zebda, N., Bailly, M., Brown, S., Dore, J. F., and Berthier-Vergnes, O. (1994) Expression of PNA-binding sites on specific glycoproteins by human melanoma cells is associated with a high metastatic potential. *J. Cell Biochem. 54*, 161−173.

BC9901696

Immobilization of Lipid Vesicles on Polymer Support via an Amphiphilic Peptidic Anchor: Application to a Membrane Enzyme

Aline Percot, X. X. Zhu, and Michel Lafleur*

Département de chimie, Université de Montréal, C.P. 6128, succursale Centre-ville, Montréal, Québec H3C 3J7, Canada. Received December 23, 1999; Revised Manuscript Received April 27, 2000

To immobilize lipid vesicles on a polymer support, we have used a peptidic anchor with the following sequence: Ala-Ala-Leu-Leu-Leu-Ala-Ala-Ala-Ala-Ala-Ala-Ala-Ala-Ala-Ala-Ala-Ala-Ala-Ala-Ala-Ala-Ala-Ala-Ala-Ala-Ala-Trp-Lys-Lys-Lys-Lys-Lys-Lys. This amphiphilic peptide was previously designed in our group to interact spontaneously and strongly with vesicles without perturbing their permeability. At the end of the solid-phase peptide synthesis, the peptide was left on the polymer beads and this novel polymer−peptide system was used for vesicle immobilization. It was shown that this polymer−peptide system could immobilize as much as 200 μmol of lipids per gram of dry resin. The amount of immobilized vesicles was decreased by a reduction of the proportion of the negatively charged lipids in the vesicles, indicating the importance of electrostatic interactions in the immobilization of the vesicles. The integrity of the vesicles was mostly preserved after the immobilization. This new polymer−peptide system was used easily and successfully to immobilize a membrane-bound enzyme, γ-glutamyl transpeptidase. The activity of the membrane-bound enzyme was studied by monitoring the release of *p*-nitroaniline. The activity of the enzyme was still retained, even after being re-used eight times, indicating the strong immobilization of the enzyme in its active form. The polymer−peptide support could be regenerated by washing with ethanol and reused.

INTRODUCTION

The immobilization of lipid vesicles on a solid support can lead to a wide range of applications including chromatographic techniques (*1*−*4*), controlled drug release systems (*5*−*7*), immobilizing devices for cells (*8*), and enzymatic reactions (*9*−*11*). Several approaches have been developed for the immobilization of lipid membranes, including covalent binding (*1*) and entrapment (*11*−*13*). However, most of the existing techniques imply chemical modifications (*1*) or detergent dialysis (long and perturbing for biomolecule as enzyme) (*11*−*13*).

In the present study, we present an alternative device providing a strong, spontaneous, and simple way to immobilize vesicles. A peptidic anchor covalently attached to a polymer resin is used to bind lipid vesicles through electrostatic and hydrophobic interactions. We have previously designed an amphiphilic peptide with the sequence Ala-Ala-Leu-Leu-Leu-Ala-Ala-Ala-Ala-Ala-Ala-Ala-Ala-Ala-Ala-Ala-Ala-Ala-Ala-Ala-Ala-Ala-Ala-Ala-Ala-Ala-Trp-Lys-Lys-Lys-Lys-Lys-Lys ($A_2L_3A_{19}WK_6$) (*14*). This peptide has a hydrophobic segment of 24 amino acids and a short hydrophilic part made of six lysine residues. A tryptophan was inserted between the hydrophilic and the hydrophobic segment to help the positioning of the peptide in the membrane (*15*) and to serve as a convenient fluorescent probe (*16*). This amphiphilic peptide was found to interact spontaneously and strongly with various types of membranes (zwitterionic and negatively charged) without perturbing their permeability. Therefore, it is a suitable anchoring peptide in our newly designed polymer−peptide supports. Even though the hydrophobic segment plays a role in the membrane affinity, the binding of vesicles by this peptide has been shown to be strongly dependent on the electrostatic interactions and can be enhanced by the presence of anionic lipids in the bilayer (*14*). The sense of the peptide was also an important parameter when the peptide was grafted on a solid surface. In our system, the *C*-terminal bearing lysine is attached on the polymer resin and acts as a biocompatible spacer between the polymer surface and the hydrophobic segment.

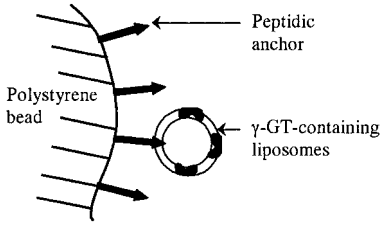

Figure 1. Schematic representation of the peptide-polymer system which is used to immobilize the enzyme-containing liposomes.

The 31 amino acid peptide $A_2L_3A_{19}WK_6$ can be attached onto a functional polymeric resin by solid-phase peptide synthesis (SPPS) without the final cleavage, leaving resin beads coated with the peptides (Figure 1). The polymer support in this application should have good thermal and mechanical stability and good resistance to solvent or microbial attack. The polystyrene (PS) beads used for SPPS are stable and insoluble in aqueous buffer. The strong amide bond formed between the polymer and the peptide is also stable and is resistant to mild treatments such as ethanol washing. To evaluate the potential use of this polymer−peptide system as an efficient vesicle-supporting system, we have studied its affinity for bilayers of various lipid compositions. In addition, to examine the effect of the charges of the peptidic anchor, two polymer−peptide systems were synthesized. In one case, the ϵ-amino side group of lysine and the side chain

* To whom correspondence should be addressed. Fax: (514) 343-7586. E-mail: michel.lafleur@UMontreal.CA.

10.1021/bc9901806 CCC: $19.00 © 2000 American Chemical Society
Published on Web 08/12/2000

of tryptophan were deprotected at the end of the peptide synthesis so that the lysine residues carried positive charges (deprotected $A_2L_3A_{19}WK_6$). In the other case, the protecting groups were left on at the end of the synthesis leading to neutral residues (protected $A_2L_3A_{19}WK_6$). The membrane-immobilization ability and the permeability of the immobilized vesicles were studied for both grafted peptides.

Immobilization of enzymes on insoluble supports offers the great advantages of continuous operation, improved enzyme stability and reusability, and easy recovery of the product. Most of the devices developed for enzyme immobilization involve direct attachment of the enzyme on a polymeric support (*17*, *18*). This is appropriate for water-soluble enzymes, but many enzymes exist in cell membranes and a bilayer environment is needed for them to remain active (*19*, *20*). Generally, liposomes can be formed and trapped in a polymer matrix by the detergent removal method, by freeze−thawing, or by cross-linking (*21*, *22*). These techniques are complicated to perform and may perturb the activity of the enzymes. The polymer−peptide system developed here can be easily used to immobilize membrane-bound enzymes. γ-Glutamyl transpeptidase (γ-GT) was used as a model membrane enzyme. It was incorporated in vesicles that were subsequently immobilized on the polymer support. The activity of the immobilized enzyme was tested for repeated operations in a batch reactor. We report here the results of a novel biocatalytic system consisting of a membrane enzyme reconstituted in lipid vesicles immobilized on polymer beads via a peptidic anchor.

MATERIALS AND METHODS

Material. 1-Palmitoyl-2-oleoyl-*sn*-glycero-3-phosphatidylcholine (POPC) and 1-palmitoyl-2-oleoyl-*sn*-glycero-3-phosphatidylglycerol (POPG) were purchased from Avanti Polar Lipids (Birmingham, AL), sulforhodamine B (SRB) from Molecular Probes Inc. (Eugene, OR), and ethylenediaminetetraacetic acid (EDTA) from Aldrich (Milwaukee, WI). The 4-(2′,4′-dimethoxyphenyl-Fmoc-aminomethyl)phenoxyacetamido-ethyl (Fmoc Amide) resin and the methylbenzhydrylamine (MBHA) resin were purchased from Perkin-Elmer Applied Biosystems (Foster City, CA). 4-(2-Hydroxyethyl)-1-piperazineethanesulfonic acid (HEPES) and Triton X-100, L-γ-glutamyl-*p*-nitroanilide, glycylglycine, bovine kidney γ-glutamyl transpeptidase (EC 2.3.2.2), and a protein assay kit were purchased from Sigma (St. Louis, MO).

Peptide Synthesis. The peptides were synthesized using the standard procedures for solid-phase chemistry (*23*). Automated synthesis was carried out on an Advanced ChemTech synthesizer 396 MPS. Both peptides were synthesized with the 9-fluorenylmethoxycarbonyl (Fmoc) strategy. The protected peptide was synthesized on the Fmoc Amide resin whereas the deprotected peptide was synthesized on the MBHA resin. The deprotection step was achieved by classical treatment of the beads with trifluoroacetic acid (92.5 %) and triisopropylsilane (2.5%). In the case of the protected polymer−peptide system, the *tert*-butyloxycarbonyl (Boc) protective groups were not eliminated from the side amino groups for the lysines and the tryptophan. At the end of the synthesis, both the protected and unprotected peptides were left covalently attached on the resin.

Binding Studies. Lipid stock solutions were prepared by dissolving each lipid in a 95/5 (v/v) benzene/methanol solvent and the lipid mixtures were obtained by mixing appropriate volumes of the stock solutions. The lipids were then lyophilized from the benzene/methanol solutions and hydrated with the binding buffer (20 mM HEPES, 100 mM NaCl, 2 mM EDTA, pH 7.4). Large unilamellar vesicles (LUVs) were prepared as previously described by extrusion through polycarbonate filters of 100 nm pore size (*24*).

The amount of vesicles bound to the polymer beads was determined by a centrifugation assay. The dry polymer beads (around 5 mg) were hydrated with the binding buffer for 15 min. The LUVs were added to the polymer beads to obtain a final lipid concentration of ca. 10 mM, and a final volume of ca. 3 mL. They were incubated in the presence of the beads at room temperature for 3 h with constant agitation. The samples were then centrifuged (10 min, 2200*g*) to settle the polymer beads. The quantity of immobilized lipids was determined by measuring the phospholipid concentration in the supernatant using the Fiske-SubbaRow phosphorus assay (*25*). A control experiment showed that, in the absence of the polymer, all the lipids remained in the supernatant after incubation and centrifugation.

Leakage Experiments. Two methods were used to estimate the integrity of the immobilized vesicles. In both approaches, the release of a dye (SRB) entrapped in the vesicles was measured. SRB-containing vesicles were prepared by hydrating the lipids (POPC:POPG 50:50, molar ratio) with a dye-containing buffer (20 mM HEPES, 60 mM NaCl, 2 mM EDTA, pH 7.4, 30 mM SRB). They were immobilized on the polymer beads according to the protocol described above. The immobilized and unbound vesicles were separated by a centrifugation step.

First, the polymer−peptide beads with the immobilized vesicles were washed with ethanol to solubilize and recover all the immobilized lipids and the entrapped SRB. The SRB fluorescence intensity of the ethanol washing, as well as the quantity of lipids, was measured. The fluorescence intensity relative to the amount of lipid (arbitrary unit per mole of lipid, au/mol) representative of the concentration of SRB trapped in the vesicles was calculated for free and immobilized vesicles. Second, in another set of experiments, Triton-X (0.1 vol %), a membrane-perturbing agent, was added to stirred beads on which vesicles were immobilized. Before the addition of the surfactant, the fluorescence of the SRB inside the vesicles was quenched because of its high concentration (*26*), and the perturbation of the permeability was monitored by the increased SRB fluorescence intensity in the cell.

The fluorescence measurements were performed at 25 °C on a SPEX Fluorolog-2 spectrometer equipped for sample stirring. The fluorescence intensity of SRB was monitored with an excitation wavelength of 565 nm, an emission wavelength of 586 nm and a response time of 0.3 s. The excitation and emission band-path widths were set at 1.5 and 0.5 nm, respectively.

Preparation and Immobilization of γ-GT-Bound Liposomes. γ-GT was dissolved in the binding buffer (0.4 mg/mL). The protein concentration was determined by a modified Lowry protein assay with deoxycholate and trichloroacetic acid (*27*). To obtain γ-GT reconstituted in lipid bilayers, solid lipids (POPC:POPG 50:50, molar ratio) were hydrated with the enzyme-containing buffer. The lipid suspension (ca. 30 mM) was then freeze−thawed and extruded to obtain vesicles with a diameter of 100 nm. In parallel, about 10 mg of the dry peptide-coated beads were incubated in 1 mL of binding buffer. Afterward, an aliquot of the γ-GT-lipid suspension was added to the polymer beads. The samples were incubated at room temperature for 3 h with constant agitation. To

eliminate unbound enzymes and lipid vesicles, the polymer beads were washed three times with the binding buffer. After these washings, no lipid was found in the supernatant and only a residual enzyme activity could be detected. A cyclic activity assay was performed with these polymer beads bearing the γ-GT-containing vesicles. A solution (2.8 mL) containing 20 mM HEPES (pH 7.4), 100 mM NaCl, 2 mM EDTA, 14.3 mM glycylglycine, and 0.5 mM L-γ-glutamyl-*p*-nitroanilide was added to the polymer beads directly in a UV cell. This enzymatic reaction transforms the substrate L-γ-glutamyl-*p*-nitroanilide into *p*-nitroaniline as product, which should be released to the media. The amount of *p*-nitroaniline produced from the reaction was measured on a Varian Cary (1 Bio) UV−vis Spectrophotometer at 410 nm for 10 min. An extinction coefficient of 8.80×10^3 M^{-1} cm^{-1} for *p*-nitroaniline was used (*11*). The temperature was controlled with a water-jacketed cell holder connected to a circulating bath thermostated at 25 °C. The mixture was periodically stirred vigorously, and the polymer beads settled after each stirring step. The absorbance was measured as an indication of the amount of *p*-nitroaniline released in the supernatant. An absolute activity could be calculated for the immobilized membrane-bound γ-GT and was expressed as micromoles of *p*-nitroaniline liberated per minute per milliliter of hydrated resin. At the end of each enzymatic reaction, the supernatant containing the remaining substrate and the product was removed. The resin was washed by 1 mL of binding buffer, and fresh substrate was added to perform another cycle of the enzymatic reaction.

A control experiment was done with the same enzyme-containing buffer but without lipids to quantify the residual activity due to the enzyme directly adsorbed on the polymer−peptide system. The measured activities of the membrane-bound γ-GT and the adsorbed γ-GT were normalized to the activity of the membrane-bound enzyme during the first cycle.

Control experiments were also done to verify that the detected activity was due to the immobilized enzymes and not to the enzymes released during the activity assay. At steps $N = 0$, 5, and 10, the resin was treated exactly the same way as in an activity assay (10 min incubation at 25 °C with stirring), but with no substrate added to the mixture. After this treatment, an activity assay was done on the recovered supernatant.

As a reference, the activity of the free enzyme in buffer was measured and its specific activity was expressed as micromoles of *p*-nitroaniline liberated per minute per milligram of protein.

RESULTS AND DISCUSSION

Immobilization of Liposomes. The performance of the polymer−peptide system was evaluated for the immobilization of fluid membranes with various lipid compositions. The liposomes were made of POPC, a zwitterionic lipid, and POPG, a negatively charged lipid, allowing a modulation of the interfacial charge of the vesicles. To examine the contribution of electrostatic interactions, we compared the immobilization capacities of the polymer beads grafted with the peptide in its deprotected and protected forms. A control experiment was also carried out with the bare resin without attached peptides.

Figure 2 shows the amount of immobilized lipids for membranes with varying proportions of the negatively charged lipids. The amount of immobilized lipids increases with increasing POPG content in the lipid

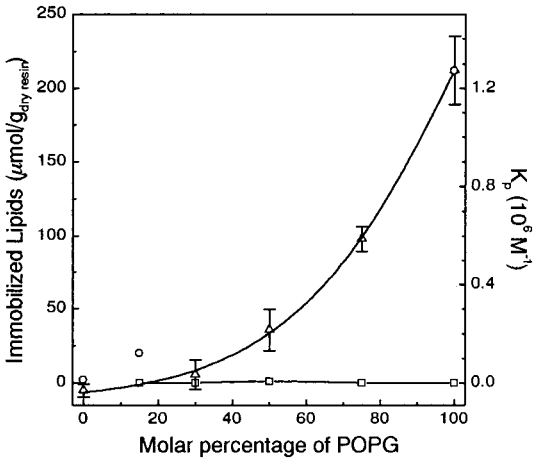

Figure 2. Quantity of immobilized lipids on the polymer support grafted with the deprotected $A_2L_3A_{19}WK_6$ peptidic anchor (△) and on the support grafted with protected $A_2L_3A_{19}WK_6$ (□) as a function of the POPG content in the vesicles made of POPC:POPG mixtures. The error bars represent the standard deviation on at least 3 measurements. The binding constant (K_p) of the free peptide (○) are shown for three POPC:POPG systems (*14*). The left and right vertical axes were normalized relative to the highest value (i.e., that obtained for pure POPG).

mixture for the polymer with the deprotected peptide $A_2L_3A_{19}WK_6$. In the case of pure POPG vesicles, this support system can immobilize as much as 200 μmol of lipids/g of dry resin. For the bare resin, no lipids were retained in the pellet (data not shown), indicating that the peptidic anchors grafted on the polymer beads are essential in the immobilization of the vesicles. For the polymer beads coated with the protected $A_2L_3A_{19}WK_6$, almost no lipids were immobilized on the resin (less than 1 μmol/g of dry resin), indicating the importance of the electrostatic interactions between the solid support and the vesicles during the immobilization. The charges on both the peptide and the vesicle surface are very important to an efficient immobilization. The crucial role of electrostatics was already observed in the interactions between membranes and this peptide in its free form (*14*). The binding constant (K_p) of the free peptide to various POPC:POPG vesicles was estimated from the initial slope of the binding isotherms of the free peptide (*14*). As shown in Figure 2, this binding constant increases with the POPG content in the bilayer. For the free peptide, the affinity is 120 times higher for the POPG vesicles than for the POPC vesicles. This is consistent with the data obtained for the grafted peptide, where the quantity of immobilized lipid varies from insignificant quantity for POPC up to 200 μmol/$g_{dry\ resin}$ for POPG vesicles. The low affinity of the free peptide for the zwitterionic vesicles ($K_p \approx 1.1 \times 10^4$ M^{-1}) helps to explain the fact that the polymer−peptide system did not bind zwitterionic vesicles.

The integrity of the immobilized vesicles was verified by encapsulating a fluorescent probe in POPC:POPG (50:50) vesicles. First, SRB and the lipids immobilized on the polymer beads were solubilized by vigorous washing with ethanol. The intensity of the SRB fluorescence divided by the quantity of lipids in the ethanol washing is representative of the concentration of encapsulated SRB. This parameter has been determined for the free vesicles (by diluting an aliquot in ethanol) and for the immobilized ones. For free vesicles containing 30 mM SRB, a fluorescence intensity per lipid of $(1.07 \pm 0.04) \times 10^{13}$ au/mol was obtained. For the immobilized vesicles, it was $(0.6 \pm 0.1) \times 10^{13}$, representing on average 57% of the SRB remained in the bound vesicles. To verify that the

SRB was indeed entrapped in the vesicles, in a second set of experiments, we added a surfactant to the pellet and measured the SRB fluorescence intensity. A rapid increase of the fluorescence intensity was observed after the addition of Triton. This showed that a significant quantity of SRB was still encapsulated at a high concentration in the vesicles after the immobilization step and that the SRB could be released by a membrane-disrupting detergent. However, this increase is hard to quantify because of the diffusion of the polymer beads. In addition, the integrity of the vesicles cannot be determined precisely because the SRB probe interacts with our solid support as inferred from a residual pink color of the beads, even after the ethanol washing. Therefore, the value obtained for the remaining entrapped SRB upon immobilization is underestimated. We can conclude from both results that the majority of the encapsulated SRB remains in the vesicles and that the vesicles immobilized on our polymer−peptide system can be used as small containers for further applications.

Enzymatic Reaction of Reconstituted γ-GT in Liposomes Immobilized on the Polymer−Peptide System. Vesicles containing POPC:POPG (50:50) were used as a matrix for the enzyme reconstitution. The enzyme-containing vesicles were then immobilized onto the resin bearing the deprotected $A_2L_3A_{19}WK_6$. After being washed to eliminate the unbound vesicles and enzymes, the beads were ready to be used as a biocatalytic system. This method is much simpler and less time-consuming than most of the classical immobilization methods as they need dialysis steps or chemical attachment of the enzyme (*9*−*11*).

The activity of the immobilized membrane-bound γ-GT was estimated to be 0.3 μmol min^{-1} mL^{-1} of hydrated resin for the initial cycle. This activity is in the same range as the activity detected by Gotoh et al. (*9*) for the membrane-bound γ-GT immobilized by dialysis on Sepharose. The activity of the free enzyme under the same conditions (buffer, pH, and temperature) was around 13 μmol mg^{-1} min^{-1}. If we assume that the activity is not affected by the reconstitution in the bilayer or by the immobilization step, we could estimate that the quantity of active enzyme immobilized on the resin was about 0.02 mg/mL of hydrated resin. It should be noted that this amount corresponds to the "efficient" enzyme, which is likely limited to the enzyme present in the external layer of the membrane (*11*).

In Figure 3, the enzyme activity relative to that of the initial cycle (0.3 μmol min^{-1} mL^{-1} of hydrated resin) is plotted versus the number of cycles in a batch reactor approach as described in Materials and Methods. Significant activity was retained even after 12 cycles (more than 20% of the initial activity). We can observe a linear loss of activity with the increasing number of cycles. This decrease of activity could result from a physical loss of enzyme from the system or from a deactivation of the enzyme retained in the system. To identify the origin of this decrease, the release of the enzyme during the activity assay was examined (see Materials and Methods). The activity measured on the supernatant actually corresponds to the loss of activity observed between two successive cycles. Therefore, the decrease of activity is most likely due to the physical loss of the enzyme. We could not detect any lipid in the supernatants, but because of the small amount of lipids involved, we could not distinguish whether the enzyme was released in its free form or along with lipid vesicles. The measured activities of the supernatant were much smaller than those observed with the polymer beads, clearly indicating

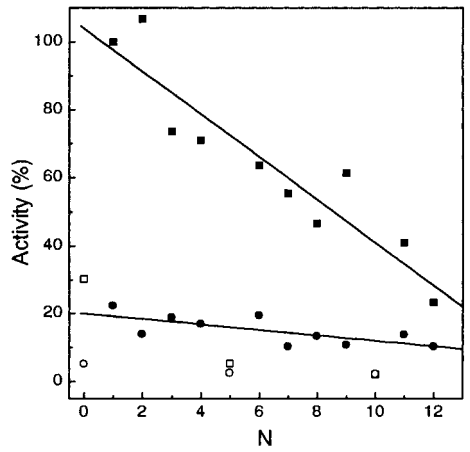

Figure 3. Relative activity for the immobilized membrane-active enzyme γ-GT (■) and for the adsorbed enzyme (●) on the polymer-deprotected $A_2L_3A_{19}WK_6$ system plotted as a function of the number of utilization cycles (*N*). As a control experiment, the loss of the enzyme was periodically probed ($N = 0$, 5, and 10) by measuring the enzymatic activity in the supernatant for the experiments involving the immobilized enzyme (□) and the adsorbed enzyme (○). The activity assay was made at 25 °C and the absorbance was measured at 410 nm.

that most of the enzymatic reaction was performed by the enzyme reconstituted in the vesicles immobilized on the resin.

To confirm that the enzymatic activity was due to the membrane-bound γ-GT and not to the γ-GT directly adsorbed on the resin, a control experiment was made without any lipids. The resin support was incubated with the enzyme under the same conditions, and the activity of the adsorbed enzyme was measured for repeated cycles in the same way. Even for $N = 1$, the activity detected was only 20% of the activity detected for membrane-bound enzyme. As shown in Figure 3, the activity decreased linearly with the number of cycles, as in the case of the membrane-bound enzyme.

The polymer−peptide system allows easy recovery of the products and the reutilization of the enzyme. The durability of the immobilized enzyme is very important for the applications. More than 50% of its initial activity was still retained after eight cycles. It is important to note that this polymer−peptide system can be reused. After 12 cycles of use, the resin can be regenerated by washing with ethanol and lyophilization and reused with similar performances.

CONCLUSIONS

We have developed and characterized a polymer−peptide system able to immobilize lipid vesicles. The amphiphilic peptidic anchor grafted on the resin was responsible for the immobilization of the liposomes and the interactions involved were mostly electrostatic. The quantity of immobilized vesicles increased with the content of negatively charged lipids in the bilayer and reached 200 μmol/g of dry resin for POPG vesicles. Upon immobilization, the permeability of the vesicles was mostly maintained, and the vesicles could be used as small containers. This carrier can be easily regenerated by washing with ethanol and reused.

This polymer−peptide support is versatile since the peptide can interact strongly and spontaneously with many types of lipids. A membrane-active enzyme was shown to have retained its activity after being immobilized through vesicles bound to the polymer support via an amphiphilic peptide. This system offers an alter-

native method for enzyme immobilization and has several advantages compared with immobilization strategies by covalent binding or physical adsorption, including the preservation of the conformation and activity of membrane-active enzymes, the possibility to immobilize water-insoluble enzymes and minimal diffusion effects for the enzymes attached to the surface of the polymer beads. We have tested one model membrane-active enzyme with the new support system in this study. It is obvious that this type of polymer−peptide support may be potentially used for the immobilization of biological membranes and even cells, as drug carriers and column packing materials for the separation of biomolecules.

ACKNOWLEDGMENT

Financial support from the Natural Sciences and Engineering Research Council (NSERC) of Canada and Fonds FCAR from the Province of Quebec is gratefully acknowledged.

LITERATURE CITED

(1) Pidgeon, C., and Venkataram, U. V. (1989) Immobilized artificial membrane chromatography: supports composed of membrane lipids. *Anal. Biochem. 176*, 36−47.
(2) Ong, S., Qiu, X., and Pidgeon, C. (1994) Solute interactions with immobilized artificial membranes. *J. Phys. Chem. 98*, 10189−10199.
(3) Yang, Q., and Lundahl, P. (1994) Steric immobilization of liposomes in chromatographic gel beads and incorporation of integral membrane proteins into their lipid bilayers. *Anal. Biochem. 218*, 210−221.
(4) Zhang, Y., Xiao, Y., Kellar, K. J., and Wainer, I. W. (1998) Immobilized nicotinic receptor stationary phase for on-line liquid chromatographic determination of drug-receptor affinities. *Anal. Biochem. 264*, 22−25.
(5) Stevenson, W. T. K., and Sefton, M. V. (1994) Recent developments in polymer-based controlled release technology for therapeutic purposes. *Trends Polym. Sci. 2*, 98−104.
(6) Wu, X. S., Hoffman, A. S., and Yager, P. (1992) Conjugation of phosphatidylethanolamine to poly(*N*-isopropylacrylamide) for potential use in liposomal drug delivery systems. *Polymer 33*, 4659−4662.
(7) Bochot, A., Fattal, E., Gulik, A., Couarraze, G., and Couvreur, P. (1998) Liposomes dispersed within a thermosensitive gel: a new dosage form for ocular delivery of oligonucleotides. *Pharm. Res. 15*, 1364−1369.
(8) Kino, Y., Sawa, M., Kasai, S., and Mito, M. (1998) Multiporous cellulose microcarrier for the development of a hybrid artificial liver using isolated hepatocytes. *J. Surg. Res. 79*, 71−76.
(9) Gotoh, T., and Kikuchi, K. (1998) Immobilization of biological membranes by sonication and freeze−thawing. *J. Chem. Eng. Jpn. 31*, 860−863.
(10) Monsan, P., and Combes, D. (1988) Enzyme stabilization by immobilization. *Methods Enzymol. 137*, 584−612.
(11) Gotoh, T., Shidara, M., Iwanaga, T., Kikuchi, K., and Hozawa, M. (1994) Immobilization of γ-glutamyl transpeptidase, a membrane enzyme, in gel beads via liposome entrapment. *J. Ferment. Bioeng. 77*, 268−273.
(12) Wallstén, M., Yang, Q., and Lundahl, P. (1989) Entrapment of lipid vesicles and membrane protein−lipid vesicles in gel bead pores. *Biochim. Biophys. Acta 982*, 47−52.
(13) Yang, Q., Wallstén, M., and Lundahl, P. (1990) Lipid-vesicle-surface chromatography. *J. Chromatogr. 506*, 379−389.
(14) Percot, A., Zhu, X. X., and Lafleur, M. (1999) Design and characterization of anchoring amphiphilic peptides and their interactions with lipid vesicles. *Biopolymers 50*, 647−655.
(15) Landolt-Marticorena, C., Williams, K. A., Deber, C. M., and Reithmeier, R. A. F. (1993) Nonrandom distribution of amino acids in the transmembrane segments of human type I single span membrane proteins. *J. Mol. Biol. 229*, 602−608.
(16) Georghiou, S., Thompson, M., and Mukhopadhyay, A. K. (1982) Melittin-phospholipid interaction studied by employing the single tryptophan residue as an intrinsic fluorescent probe. *Biochim. Biophys. Acta 688*, 441−452.
(17) Ding, Z., Chen, G., and Hoffman, A. S. (1998) Unusual properties of thermally sensitive oligomer-enzyme conjugates of poly(*N*-isopropylacrylamide)-trypsin. *J. Biomed. Mater. Res. 39*, 498−505.
(18) Chen, G., and Hoffman, A. S. (1993) Preparation and properties of thermoreversible, phase-separating enzyme-oligo(*N*-isopropylacrylamide) conjugates. *Bioconjugate Chem. 4*, 509−514.
(19) Gennis, R. B., and Jonas, A. (1977) Protein−lipid interactions. *Annu. Rev. Biophys. Bioeng. 6*, 195−238.
(20) Coleman, R. (1973) Membrane-bound enzymes and membrane ultrastructure. *Biochim. Biophys. Acta 300*, 1−30.
(21) Messing, R. A. (1975) *Immobilized Enzymes for Industrial Reactors*, Academic Press, New York.
(22) Weetall, H. H. (1975) *Immobilized Enzymes, Antigens, Antibodies, and Peptides*, Marcel Dekker, Inc., New York.
(23) Grant, G. A. (1992) *Synthetic Peptides: a user's guide*, W. H. Freeman and Company, New York.
(24) Benachir, T., Monette, M., Grenier, J., and Lafleur, M. (1997) Melittin-induced leakage from phosphatidylcholine vesicles is modulated by cholesterol: a property used for membrane targeting. *Eur. Biophys. J. 25*, 201−210.
(25) Fiske, C. H., and SubbaRow, Y. (1925) The colorimetric determination of phosphorus. *J. Biol. Chem. 66*, 375−400.
(26) El Jastimi, R., and Lafleur, M. (1999) A dual-probe fluorescence method to examine selective perturbations of membrane permeability by melittin. *Biospectroscopy 5*, 133−140.
(27) Peterson, G. L. (1977) A simplification of the protein assay method of Lowry et al. which is more generally applicable. *Anal. Biochem. 83*, 346−356.

BC9901806

Caged Chemotactic Peptides

Michael C. Pirrung* and Sandra J. Drabik

Department of Chemistry, Levine Science Research Center, Box 90317, Duke University, Durham, North Carolina 27708-0317

Jasimuddin Ahamed and Hydar Ali

Department of Pathology, School of Dental Medicine, University of Pennsylvania, Philadelphia, Pennsylvania 19104. Received January 11, 2000; Revised Manuscript Received May 31, 2000

This work has as its ultimate goal the creation of a concentration spike of a chemoattractant peptide in a time-resolved and spatially defined way using a light pulse. This strategy requires "caging" the peptide with a photochemically removable group. Model studies used alanine ethyl ester in reductive amination with nitrobenzaldehydes to form two different *N*-nitrobenzyl derivatives. An fMLF peptide bearing these two N-terminal nitrobenzyl groups was also prepared. The yield and kinetics of their deprotection to return the fMLF peptide were determined. It was established that the caged peptides have vastly reduced biological activity as chemoattractants, as designed.

INTRODUCTION

Chemotaxis is the directed movement of cells along a chemical gradient. It is displayed by a variety of prokaryotic and eukaryotic cells including bacteria, cellular slime molds, and leukocytes (neutrophils) (*1*), which respond to factors derived from complement, bacterially derived lipids, or *N*-formylated peptides. The cellular mechanism by which neutrophils rapidly move to sites of infection signaled by chemoattractants remains enigmatic. Even though the receptors involved have been sequenced and many of the molecules involved in neutrophil adherence and traction identified, the essential mechanisms that control and regulate the neutrophil motor remain obscure.

The ability of short *N*-formylated peptides to induce chemotaxis in mammalian leukocytes was originally discovered by Schiffmann et al. (*2*). Extensive follow-on biological studies have ensued (*3*). Chemotactic peptides act at a highly specific receptor, the formyl peptide receptor (FPR), located in the plasma membrane of neutrophils (*4*). Interaction of the peptide with the G-protein-linked receptor can initiate a number of intracellular events including lysosomal enzyme release, superoxide formation, and redistribution of cations, especially Ca^{2+}. Much of the early research focused on the rabbit neutrophil, while more recently the human receptor has been under investigation (*5*). It has been cloned and expressed (*6*), and receptor subtypes of the hFPR are known (*7*).

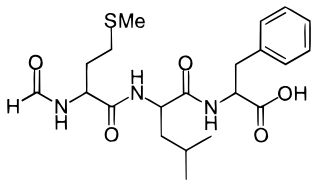

f-Met-Leu-Phe,
a chemotactic peptide

Numerous reports have discussed structure/activity relationships and conformational studies of *N*-formyl peptide analogues, including backbone-modified peptides (*8*). A variety of synthetic peptides have been prepared and tested for chemotactic activity, and novel agonists have been discovered using autocrine peptide library methods (*9*). The most active chemotactic peptide is *N*-formyl-L-methionine-L-leucine-L-phenylalanine (fMLF) which has an ED_{50} for chemotaxis of 8×10^{-11} M. Freer and co-workers provided detailed studies of peptides with substitutions at positions one (Met) and three (Phe) (*10*), as well as at position two (Leu) and C-terminal modifications (*11*). Biological activity appears to reside, in order of importance, in (a) the formyl group, (b) methionine at position one, and (c) phenylalanine at position three. The leucine residue can be replaced by other aliphatic residues. Strategies for conjugation of chemotactic peptides to reactive or fluorescent groups based on these structure/activity relationships have been developed (*12*).

Because of the role of the chemotaxis receptor in time/space functions of the cell, techniques that address time/space relationships are needed to study the FPR. As an example, the intracellular movement of the FPR during chemotaxis has been monitored through fluorescence microscopy (*13*). Once occupied by ligand, the receptor rapidly signals and is then desensitized and internalized, making it difficult to study. Novel chemotactic peptide analogues would allow a closer focus on the cellular functions of neutrophil leukocytes. For example, a caged (inactive) peptide that could be activated rapidly in situ would allow the regulation of these cellular events to be studied with greater precision. This concept draws on earlier studies of bacterial chemotaxis using caged amino acids (*14*).

The caging of peptides and proteins has been a subject of significant recent interest (*15*). The peptides that have been caged include those that inhibit cAMP-dependent protein kinase, calmodulin, myosin light chain kinase, and neuropeptide Y. The proteins that have been caged include G-actin, myosin, thrombin, and ion channels. As

10.1021/bc000001g CCC: $19.00 © 2000 American Chemical Society
Published on Web 08/25/2000

powerful as these methods have been in time-resolved studies of cell motility, inter alia, in most cases the caged derivative can only be prepared by direct reaction of the native biomolecule with a chemical derivatizing reagent. As this process is generally conducted in aqueous solution, the diversity of chemical reactions that can be used for derivatization is limited, limiting the types of linking chemistry and photoremovable groups that may be used. In the work described here, chemical synthesis enables the preparation of an optimal compound that would be unavailable from the native peptide.

On the basis of earlier work showing that substitutions of photoremovable groups at the C-terminus of the chemotactic peptide do not affect its activity (W. A. Sherwin, unpublished material), direct functionalization of the *N*-formyl residue was instead performed. Early efforts to exploit the dimethoxybenzoin carbamate photoremovable group previously developed in our laboratory (*16*) failed at the final formylation stage, requiring an alternative protecting group. Some of the most effective photoremovable groups are nitrobenzyl derivatives, which upon irradiation undergo an internal redox process to produce a hemiaminal (*17*). This decomposes to provide the free amide and a nitrosoaldehyde. To maximize the long-wavelength absorption of the arene, electron-donating groups are used.

RESULTS

To assess the utility of nitrobenzyl chemistry for protection of the formyl peptide N-terminus, alanine ethyl ester was used as a model. The most reliable method for preparation of its *N*-nitrobenzyl derivatives proved to be reductive amination with nitroveratraldehyde (reaction 1) or nitropiperonaldehyde (reaction 2).

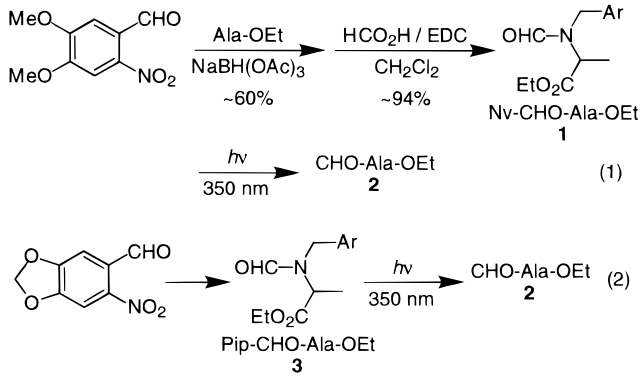

The resulting secondary amines can be formylated with in situ-generated formic anhydride. Because of the superior photochemical deprotection properties of nitrobenzyl derivatives with benzylic methyl substitution (*18*) or electron-withdrawing groups (*19*), a number of efforts were made to prepare such derivatives of Ala-OEt. However, it was not possible to reductively aminate Ala-OEt with nitroacetophenones to incorporate a benzylic methyl group, and while nucleophiles such as cyanide could be added to the nitrobenzaldehyde imines, the resulting secondary amines could not be formylated. Photochemical deprotection of the two *N*-nitrobenzyl formylalanines in acetonitrile in a Rayonet photochemical reactor with 350 nm lamps proceeded cleanly and at similar rates (0.42 s^{-1}), as analyzed by HPLC.

The preparation of the caged peptides was accomplished by applying a similar reductive amination protocol to synthetic MLF−OMe (reactions 3 and 4) to produce the *N*-nitroveratryl or *N*-nitropiperonyl peptides.

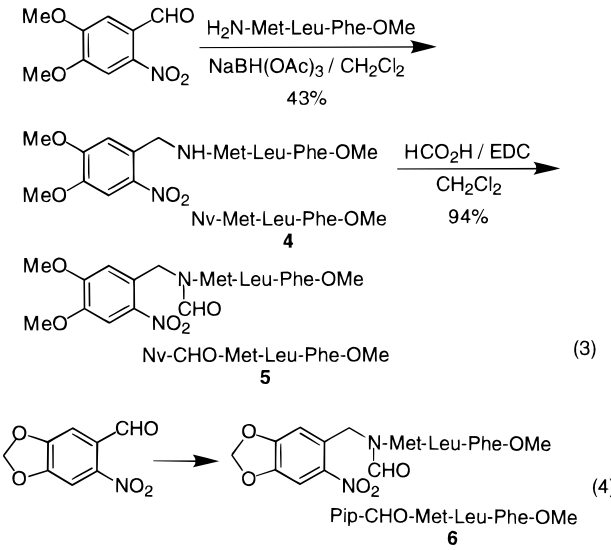

Formylation by the formic anhydride procedure produces Nv-CHO-MLF and Pip-CHO-MLF as the methyl esters, which are readily hydrolyzed to the acids (~70%).

The photochemical deprotection reaction was shown to return the fMLF peptide ester by its isolation in good yield (reaction 5). Negligible amounts of methionine

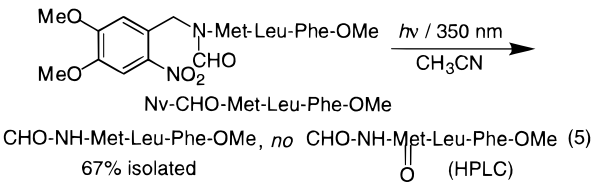

oxidation, a side reaction sometimes of concern in photochemical deprotection processes, were observed, as determined by HPLC and MS analysis in comparison to the known compound (*20*) (authentic sample synthesized from methionine sulfoxide).

The rates of the deprotection of Nv-CHO-MLF-OH and Pip-CHO-MLF-OH were determined using HPLC analysis. A modest but interesting 4−5-fold acceleration of deprotection is observed (to 1.9−2.4 s^{-1}) as compared to the simple alanine ester model. The quantum yields of deprotection of the two chemotactic peptides were determined using HPLC analysis of two-component photochemical reactions containing a nitrobenzyl amide whose deprotection has a known quantum yield. While Φ for the caged chemotactic peptides is relatively low (2 and 4%), these quantum yields are comparable to those of other nitrobenzyl-caged biological effectors and should not limit the utility of these caged peptides in studying leukocyte chemotaxis.

The ability of the peptide methyl esters to trigger β-hexosaminidase secretion in rat basophilic leukemia (RBL-2H3) cells stably expressing fMLF receptors was evaluated using an assay previously reported (*21*). Figure 1 shows the data for NV-fMLF−OMe and fMLF−OMe. All data are summarized below. The N-substitution leads to a 3−4 orders of magnitude drop in activity, meaning that photochemical deprotection of these caged chemo-

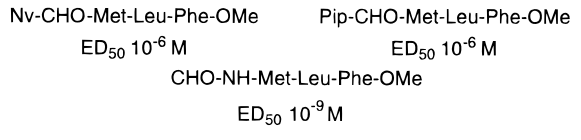

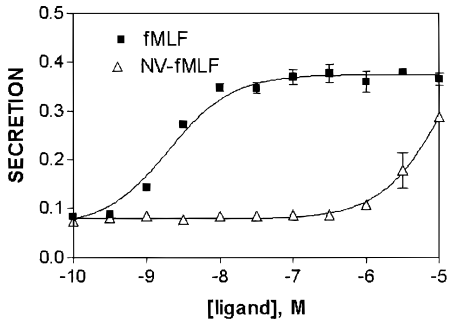

Figure 1. Secretion of β-hexosaminidase by N-formyl peptides in RBL-2H3 cells expressing fMLF receptors. RBL-2H3 cells were stimulated with fMLF−OMe and NV-fMLF−OMe compounds at different concentrations for 10 min. The OD was taken at 400 nm wavelengths in a ELISA reader. Values are the mean of single triplicate determinations and representative of three separate experiments.

tactic peptides should permit activation of leukocytes to chemotaxis on microsecond time scales, the rate of photochemical removal of nitrobenzyl groups after a light pulse.

ACKNOWLEDGMENT

Financial support provided by NIH AI-42151. The assistance of L. LaBean in administrative support of this work is greatly appreciated.

Supporting Information Available: Experimental descriptions. This material is available free of charge via the Internet at http://www.pubs.acs.org.

LITERATURE CITED

(1) Harvath, L. (1989) *Annu. Rep. Med. Chem. 24*, 233−241. Didsbury, J. R., Uhing, R. J., and Snyderman, R. (1992) In *Mononuclear Phagocytes* (R. van Furth, Ed.) pp 413−424, Kluwer, Amsterdam, .

(2) Schiffmann, E., Corcoran, B. A., and Wahl, S. M. (1975) *Proc. Natl. Acad. Sci. U.S.A. 72*, 1059−1062.

(3) Prossnitz, E. R., and Ye, R. D. (1997) *Pharmacol. Ther.* 73−102. Hallett, M. B. (1997) *Bioessays 19*, 615−621. Snyderman, R., Smith, C. D., and Verghese, M. W. (1986) *J. Leukoc. Biol. 40*, 785−800. Ali, H., Richardson, R. M., Haribabu, B., and Snyderman, R. (1999) *J. Biol. Chem. 274*, 6027−6030.

(4) Becker, E. L., Bleich, H. E., Day, A. R., Freer, R. J., Glasel, J. A., Latina, M., and Visintainer, J. (1979) *Biochemistry 18*, 4656−4668.

(5) Bommakanti, R. K., Klotz, K.-N., Dratz, E. A., and Jesaitis, A. J. (1993) *J. Leukoc. Biol. 54*, 572−577. Lala, A., Gwinn, M., and De Nardin, E. (1999) *Eur. J. Biochem. 264*, 495−499.

(6) Boulay, F., Tardif, M., Brouchon, L., and Vignais, P. (1990) *Biochemistry 29*, 11123−11133.

(7) Murphy, P. M., and McDermott, D. (1991) *J. Biol. Chem. 266*, 13560−13567. Schulz, P., Stannel, P., Voight, M., Jakobs, K. H., and Gierschick., P. (1992) *Biochem. J. 384*, 207−212. Prossnitz, E. R., Zuehenberger, O., Cochrane, C. G., and Ye, R. D. (1992) *Biochem. Biophys. Res. Commun. 179*, 471−476. Murphy, P. M., Ocelik, T., Kenney, R. R., McDermott, D., and Francke, R. (1992) *J. Biol. Chem. 267*, 7637−7643. Ye, R. D., Cavanaugh, S. L., Zuehenberger, O., Prossnitz, E. R., and Cochrane, C. G. (1992) *Biochem. Biophys. Res. Commun. 184*, 582−589. Bao, L., Gerard, N. P., Eddy, R. L., Jr., Shows, T. B., and Gerard, C. (1992) *Genomics 13*, 437−440. Hartt, J, K., Barish, G., Murphy, P. M. and Gao, J. L. (1999) *J. Exp. Med. 190*, 741−747.

(8) Michel, A. G., Lajoie, G., and Hassani, C. A. (1990) *Int. J. Pept. Protein Res. 36*, 489. Sauvé, G., Rao, V. S., Lajoie, G., and Belleau, B. (1985) *Can. J. Chem. 63*, 3089. Cavisshioni, G., Vertuani, G., Scatturin, A., and Spisani, S. (1994) *Bioorg. Med. Chem. Lett. 4*, 1551−1554.

(9) Klein, C., Paul, J. I., Sauve, K., Schmidt, M. M., Arcangeli, L., Ransom, J., Trueheart, J., Manfredi, J. P., Broach, J. R., and Murphy, A. J. (1998) *Nat. Biotechnol. 16*, 1334−1337.

(10) Freer, R. J., Day, A. R., Radding, J. A., Schiffmann, E., Aswanikumar, S., Showell, H. J., and Becker, E. L. (1980) *Biochemistry 19*, 2404−2410.

(11) Freer, R. J., Day, A. R., Muthukumaraswamy, N., Pinon, D., Wu, A., Showell, H. J., and Becker, E. L. (1982) *Biochemistry 21*, 257−263.

(12) Vilven, J. C., Domalewski, M., Prossnitz, E. R., Ye, R. D., Muthukumaraswamy, N., Harris, R. B., Freer, R. J., and Sklar, L. A. (1998) *J. Recept. Signal Transduct. Res. 18*, 187−221.

(13) Servant, G., Weiner, O. D., Neptune, E. R., Sedat, J. W., and Bourne, H. R. (1999) *Mol. Biol. Cell 10*, 1163−1178.

(14) Khan, S., Spudich, J. L., McCray, J. A., and Trentham, D. R. (1995) *Proc. Natl. Acad. Sci. U.S.A. 92*, 9757−9761. Jasuja, R., Keyoung, J., Reid, G. P., Trentham, D. R., and Khan, S. (1999) *Biophys. J. 76*, 1706−1719.

(15) Marriot, G., and Walker, J. W. (1999) *Trends Plant. Sci. 4*, 330−334.

(16) Pirrung, M. C., and Huang, C.-Y. (1995) *Tetrahedron Lett. 36*, 5883.

(17) Pillai, V. N. R. (1997) *Organic Photochemistry 8*, 225−323. Pillai, V. N. R. (1980) *Synthesis* 1−26.

(18) Holmes, C. P. (1997) *J. Org. Chem. 62*, 2370−2380. Barth, A., Corrie, J. E. T., Gradwell, M. J., Maeda, Y., Mantele, W., Meier, T., (1997) Trentham, D. *J. Am. Chem. Soc. 119*, 4149−4159.

(19) Hess, G. P., and Grewer, C. (1998) *Methods Enzymol. 291*, 443−473.

(20) Toniolo, C., Bonora, G. M., Freer, R. J., Kennedy, S. P., Pittenger, K. L., and Becker, E. L. (1989) *Peptides 9*, 1195−1205.

(21) Ali, H., Richardson, R. M., Tomhave, E. D., Didsbury, J. R., and Snyderman, R. (1993) *J. Biol. Chem. 268*, 24247−24254.

BC000001G

Experimental.

Synthesis of *tert*-butyloxycarbonyl-L-methionine-L-leucine-L-phenylalanine methyl ester (Boc-Met-Leu-Phe-OMe or Boc-MLF-OMe). Peptides were assembled via standard EDC [1-(3-dimethylaminopropyl)-3-ethylcarbodiimide hydrochloride] mediated couplings [with HOBT (1-hydroxybenzotriazole) to suppress racemization]. *tert*-Butyloxycarbonyl (t-Boc) was used as an amino protecting group, and was removed with TFA prior to coupling. Boc-Leu-OH (2.0g) was dissolved in 70 mL of dichloromethane and 2 mL of DMF. The resulting solution was cooled to 0 °C on an ice bath. EDC (1.69 g, 1.1 eq) and HOBt (1.19 g, 1.1 eq) were added and the reaction mixture was kept at 0 °C for 15 min. Phenylalanine methyl ester hydrochloride (HCl-NH_3-Phe-OMe, 1.73 g) was dissolved in 40 mL dichloromethane and treated with triethylamine (1.12 mL, 1 eq) to liberate the free amine. This solution was added dropwise to the leucine solution. The mixture was allowed to stir overnight. The reaction was quenched with the addition of an equal volume of 1 N sodium bicarbonate. The organic layer was separated and washed with brine. The solution was dried with sodium sulfate and the solvent removed *in vacuo*. The dimer recrystallized from dichloromethane and hexane to give 2.81 g (89 %) as a white solid. Boc-Met-OH (0.90 g) was dissolved in 25 mL of dichloromethane. The resulting solution was cooled to 0 °C on an ice bath. EDC (0.69 g, 1.0 eq) and HOBt (0.49 g, 1.0 eq) were added and the reaction mixture was kept at 0 °C for 15 min. Boc-Leu-Phe-OMe (1.4 g) was dissolved in a solution of 25 mL of trifluoroacetic acid and 12.5 mL dichloromethane. After stirring for 45 min, the solvent was removed *in vacuo*. The yellow oil that remained was dissolved in 40 mL dichloromethane and the solvent was evaporated *in vacuo* to remove excess TFA. The process was repeated twice yielding the trifluoroacetate salt, which was used without further purification. The above trifluoroacetate salt was dissolved in 20 mL dichloromethane. One equivalent of triethylamine (0.5 mL) was added to liberate the free amine. The amine was added dropwise to a stirring solution of the Boc protected methionine. The mixture was allowed to stir overnight. The reaction mixture was transferred to separatory funnel and washed with an equal volume of 1M bicarbonate, 1 M citric acid, brine, and water. The organic layer was dried

with sodium sulfate and the solvent was removed *in vacuo*. The tripeptide was isolated as a white solid (1.7 g, 90 %) was used without further purification.

Reductive Amination of Met-Leu-Phe Ester. Boc-MLF-OMe (1.0 g) was dissolved in a solution of 10 mL of trifluoroacetic acid and 20 mL dichloromethane. After stirring for 45 min, the solvent was removed *in vacuo*. The yellow oil that remained was dissolved in 40 mL dichloromethane and the solvent was removed *in vacuo* to remove excess TFA. This process was repeated twice yielding the trifluoroacetate salt, which was used without further purification. The TFA salt was dissolved in 10 mL dichloromethane. One equivalent of triethylamine (0.89 mL) was added to liberate the free amine. The amine was added dropwise to a stirring solution of the aromatic aldehyde (1.2 eq) in dichloromethane. After 5 min, sodium triacetoxyborohydride (neat, 3 eq) was added. The flask was covered with foil and allowed to stir for 3-5 d, until TLC indicated the absence of starting material. The reaction was quenched by addition (with vigorous stirring) of saturated sodium bicarbonate solution. The organic layer was separated and washed with bicarbonate, then brine. The organic layer was dried with sodium sulfate and the solvent was removed *in vacuo*. The material was purified via flash chromatography using dichloromethane/ethyl acetate as eluant.

N-(6-Nitro-3,4-dimethoxy)benzyl L-methionine-L-leucine-L-phenylalanine methyl ester (Nv-MLF-OMe, 4). The above procedure was followed, giving 0.50 g (43 %) of the title compound as a yellow syrup, R_f 0.34, 90:10 dichloromethane:ethyl acetate. ^{1}H-NMR ($CDCl_3$): δ 7.65 (d, J = 8.8, 1H), 7.20 (m, 6H), 7.01 (d, J = 7.6, 1H), 4.69 (dd, J = 7.2, 6.0, 1H), 4.55 (m, 1H), 3.91 (s, 3H), 3.85 (s, 3H), 3.81 (d, J = 12.4, 1H), 3.62 (s, 3H), 3.54 (d, J = 12.4, 1H), 3.19 (dd, J = 2.8, 5.0, 1H), 3.06 (dd, J = 5.6, 10.5, 1H), 2.95 (dd, J = 7.0, 10.5, 1H), 2.50 (m, 2H), 1.99 (s, 3H), 1.97 (m, 2H), 1.48 (m, 2H), 1.73 (m, 1H), 0.85 (d, J = 6.4, 3 H), 0.83 (d, J = 6.4, 3 H). ^{13}C NMR ($CDCl_3$): δ 173.4, 171.8, 171.6, 153.42, 147.85, 140.90, 135.79, 129.22, 128.96, 128.31, 126.82, 114.23, 107.76, 61.56, 56.61, 56.10, 53.38, 52.05, 50.76, 50.40, 41.33, 37.71, 32.88, 60.46, 24.63, 22.69, 21.77, 15.17. HRMS: MH^+ $C_{30}H_{43}O_8N_4S$ calc 619.2802; found

619.2800. IR 3291.7 (br), 1745.2(s), 1650.0 (s), 1643.4 (s), 1518.7 (s), 1329.4 (w), 1273.9 (m), 1217.3(w) cm^{-1}.

N-(6-Nitro-3,4-methylenedioxy)benzyl L-methionine-L-leucine-L-phenylalanine methyl ester (Pip-MLF-OMe). The above procedure was followed, giving 0.35 g (61 %) of the title compound as a yellow syrup, R_f 0.21, 90:10 dichloromethane:ethyl acetate. ^{1}H-NMR ($CDCl_3$): δ 7.51 (s, 1H), 7.49 (d, J = 7.5 hz, 1H), 7.2 (m, 6H), 6.97 (s, 1H), 6.68 (d J = 8.1, 1H), 6.10 (s, 2H), 4.85 (dd J = 10.1 and 6.15, 1H), 4.46 (m, 1H), 3.76 (s, 2H), 3.71 (s, 3H), 3.21 (dd, J = 6.4 and 4.9), 3.15 (dd, J = 5.6 and 13.8, 1H), 3.06 (dd, J = 6.6 and 13.8, 1H), 2.53 (dd, J = 8.0 and 8.0), 2.07 (s, 3H), 2.03 (m, 2H), 1.82 (m, 1H), 1.61 (m, 2H), 0.93 (d, J = 6.8, 3H), 0.90 (d, J = 6.8, 3H). ^{13}C NMR ($CDCl_3$): δ 173.40, 171.51, 151.85, 147.14, 142.68, 135.66, 131.47, 129.09, 128.36, 126.88, 111.14, 105.64, 12.90, 61.26, 53.28, 52.29, 51.29, 50.41, 41.02, 37.95, 32.83, 30.65, 24.86, 21.91, 15.41. HRMS: MH^+ $C_{29}H_{38}O_8N_4S$ calc 603.2489; found 603.2471. IR 3278.5 (br), 2954.2 (br), 2913.55 (w), 1744.3 (s, br), 1638.4 (s), 1504.0 (s), 1482.3 (m), 1256 (s), 1035.0 (w), 700.5 (w) cm^{-1}.

Peptide N-formylation. Formic acid (2.2 eq, 96 % ACS reagent grade) was added to dichloromethane (approximately 30 mL per mmol) at 0 °C. EDC (1.1 eq) was added and the reaction mixture was allowed to stir for 10 min. The amine was dissolved in dichloromethane and added dropwise to the solution. The mixture was stirred overnight, allowing the ice to melt. The mixture was quenched with the addition of a solution of saturated sodium bicarbonate. The organic layer was washed with brine, separated, dried ($NaSO_4$), and the solvent removed *in vacuo*. The product was observed as a mixture of conformers (TLC indicated a single spot). The material was used without further purification.

N-Formyl-N-(6-nitro-3,4-dimethoxy)benzyl L-methionine-L-leucine-L-phenylalanine methyl ester (Nv-CHO-MLF-OMe, 5). The above procedure was followed, giving 0.37 g (94 %) of the title compound as a yellow syrup, R_f 0.65, 90:10 dichloromethane:ethyl acetate. ^{1}H-NMR ($CDCl_3$): δ 8.55 and 8.25 (s, 1H), 7.69 and 7.571 (s, 1H), 7.27 (m, 3H), 7.08 (m, 2H), 7.02 and 6.98 (s, 1H), 6.77 and 6.53 (d, J = 8.1 and 7.8, 1H),

6.46 and 6.29 (d, J = 8.1 and 7.8, 1H), 5.10 (d, J = 16.1, 1H), 4.83 (m, 1H), 4.81 (m, 1H), 4.76 and 4.46 (m and dd, J = 7.4, 7.4, 1H), 4.26 (m, 1H), 3.97 and 3.94 (s, 3H), 3.92 (s, 3H), 3.71 and 3.69 (s, 3H), 3.07 (m, 2H), 2.48 (m, 2H), 2.18 (m, 3H), 2.05 and 2.04 (s, 3H), 1.41 (m, 3H), 0.89 and 0.85 (d, J = 6.1, 3H), 0.82 and 0.80 (d, J = 6.1, 3H). ^{13}C NMR ($CDCl_3$): δ (171.51 and 171.30), (170.87 and 170.75), (169.43 and 169.13), (164.71 and 163.82), 153.34, (148.63 and 147.87), 140.71, (135.67 and 135.35), 129.08, (128.50 and 128.38), (127.09 and 126.93), 125.51, (113.19 and 111.66), (108.74 and 107.78), 60.94, (57.00 and 56.70), (56.42 and 56.30), (53.24 and 53.14), (52.28 and 52.18), 49.20, 44.70, (41.26 and 40.68), 37.77, (30.62 and 30.30), 27.60, (24.78 and 24.68), (22.86 and 22.59), 22.03 and 21.81), 15.35. HRMS: MH^+ $C_{31}H_{43}O_9N_4S$ calc. 647.2750; found 647.2753. IR 3298.5 (br), 1744.5 (s), 1649.99 (s), 1519.889 (s), 1331.0 (w), 1274.5 (s), 1218.2 (w), 1061.89 (w) cm^{-1}.

N-Formyl-N-(6-nitro-3,4-methylenedioxy)benzyl L-methionine-L-leucine-L-phenylalanine methyl ester (Pip-CHO-MLF-OMe, 6). The above procedure was followed, giving 0.12 g (90 %) of the title compound as a yellow syrup, R_f 0.41, 90:10 dichloromethane:ethyl acetate. ^{1}H-NMR ($CDCl_3$): δ (8.49 and 8.15, s 1H), (7.57 and 7.51, s 1H), 7.24 (m, 4H), 7.08 (m, 3H), (6.91 and 6.84, s, 1H), 6.63 (d J = 8.1), 6.08 (m, 2H), 4.93 (d, J = 16.9), 4.86 (d, J = 16.9), 4.80 (m, 1H), (4.66 and 4.34, m 1H), 4.28 (m, 1H), (3.70 and 3.68, s, 3H), 3.07 (m, 2H), 2.44 (m, 2H), 2.19 (m, 3H), 2.04 (s, 3H), 1.52 (m, 3H), (0.88 and 0.85 d, J = 6.6, 6.0), (0.85 and 0.83 d, J = 6.0, 6.3). ^{13}C NMR ($CDCl_3$): δ (171.41 and 171.27), 171.01 and 170.90), 168.93, (164.67 and 163.95), (152.14 and 152.04), (147.67 and 146.83), (142.23 and 141.98), (135.61 and 135.38), 128.79, (128.37 and 128.29), (126.95 and 126.84), (109.23 and 108.02), (106.17 and 105.50), (103.21 and 102.88), 59.72, 56.12, (53.24 and 53.14), (52.31 and 52.21), (52.14 and 51.84), 48.15, 44.31, (41.06 and 40.61), 37.68, (30.36 and 30.12), (30.12 and 29.88), 27.73, 24.66, (22.72 and 22.56), (22.07 and 21.88), 15.25. HRMS: MH^+ $C_{30}H_{39}O_9N_4S$ calc 631.2438; found 631.2442. IR: 3289.6 (br), 2916.7 (w), 2869.8 (w), 1714.9 (s), 1780.3 (s, br), 1522.4 (m), 1484.1 (w), 1436.4 (w), 1331.2 (w), 1259.0 (m), 1034.7 (w) cm^{-1}.

Ester Hydrolysis. The methyl ester (0.57 mmol) was dissolved in a mixture of tetrahydrofuran (9 mL), methanol (2.9 mL), and water (0.9 mL). The resulting solution was cooled to 0 °C with an ice bath and lithium hydroxide (119 mg, 5 eq) was added (as a solid). The reaction was kept at 0 °C and was monitored via TLC. After 3-4 h, TLC indicated that no methyl ester remained. The reaction was quenched with an equal volume of 1N $KHSO_4$ and 25 mL of dichloromethane was added. The organic layer was separated, washed with saturated brine, and dried with sodium sulfate. The solvent was removed *in vacuo.*

N-Formyl-N-(6-nitro-3,4-dimethoxy)benzyl L-methionine-L-leucine-L-phenylalanine (Nv-CHO-MLF-OH). The above procedure was followed, giving 0.26 g (73 %) of the title compound as a white solid, which was used without further purification. ^{1}H-NMR ($CDCl_3$): δ (8.21 and 8.17, s 1H), (7.68 and 7.56 s, 1H), 7.48 (d, J = 8.4), 7.20 (m, 6H), (7.02 and 6.91, s, 1H), 5.02 (d J = 16.2), 4.79 (m, 2H), 4.52 (d, J = 7.5), (4.35 and 4.15, m, 1H), (3.95 and 3.93, s, 3H), (3.90 and 3.89, s, 3H), 3.16 (m, 1H), (3.02 and 2.97 dd, J = 14.4, 6.6 and 14.4, 6.6), 2.40 (m, 2H), 2.17 (m, 1H), 2.02 (s, 3H), 1.92 (m, 1H), 1.42 (m, 3H), 0.84 and 0.79 (d J = 5.7, 6.0), (0.79 and 0.77, d, J = 6.0, 6.0). ^{13}C NMR ($CDCl_3$): δ 173.16, 171.93, 169.50, 164.71, 153.48, (148.80 and 147.99), 140.74, (135.92 and 135.61), (129.32 and 129.22), 128.42, 126.94, 125.07, (113.42 and 111.69), (108.79 and 107.83), 60.30, 56.78, (56.52 and 56.35), 53.64, (52.60 and 52.0), 49.76, 44.18, (41.06 and 40.51), 36.96, 30.63, (30.30 and 30.11), 24.82, (22.83 and 22.58), (22.04 and 21.77), 15.40. HRMS: MH^+ $C_{30}H_{41}O_9N_4S$ calc 633.2594; found 633.2599. IR 3303.2 (br) 2958.0 (br), 1729.9 (s), 1713.3(s), 1680.8(s), 1659.34(s), 1650.16(s), 1643.63(s),

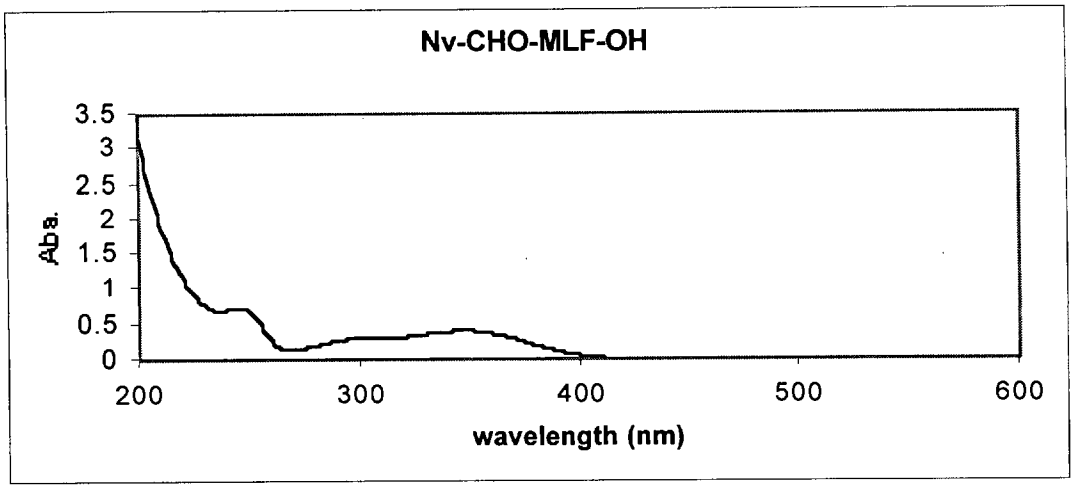

1555.6 (m), 1536.7, 1519.0, 1503.9, 1453.8 (m), 1332.8 (m), 1219.1, (m) 1062.29 (w), 986.32(w), 872.95(w), 797.1(w), 735.68v, 701.32(w) cm^{-1}. The UV spectrum is shown.

N-Formyl-N-(6-nitro-3,4-methylenedioxy)benzyl L-methionine-L-leucine-L-phenylalanine (Pip-CHO-MLF-OH). The above procedure was followed, giving 0.06 g (71 %) of the title compound as a white solid. The product was purified using preparative TLC (Analtech 20 X 20 cm 1000 microns silicagel GF uniplate) eluted with ethyl acetate containing 1 % acetic acid. The material of interest was scraped off and removed from the silica with ethyl acetate (R_f = 0.4). ^{1}H-NMR ($CDCl_3$): δ 8.17 and 8.10 (s, 1H), 7.57 and 7.49 (s, 1H), 7.23 (m, 5H), 6.93 (s, br), 6.81 (s, 1H), 6.09 and 6.06 (s, 2H), 4.79 (m, 3H), 4.50 (m, 1H), 4.30 and 4.18 (m, 1H), 3.21 (m, 1H), 3.05 (dd, J = 9.0 and 6.0, 1H), 2.35 (m, 2H), 2.10 (m, 2H), 1.97 (s, 3H), 1.40 (m, 3H), 0.86 and 0.83 (d, J = 7.2 and 5.4, 6H). ^{13}C NMR ($CDCl_3$) δ (152.26 and 152.10), 147.94, 147.02, (142.45 and 142.07), 135.86, 129.38, 128.34, 126.93, 109.66, 108.25, (106.32 and 105.57), (103.36 and 103.00), 60.04, 53.72, 52.03, 43.92, (41.05 and 40.63), 37.37, (30.49 and 30.27), 29.42, 27.62, 24.74, (22.81 and 22.64), (22.05 and 21.86), 15.36. HRMS: MH^+ $C_{29}H_{37}O_9N_4S$ calc 617.2281; found 617.2275. IR 3220.94 (br), 2945.6 (w), 2932.7 (w), 1680.95 (s, br), 1666.8 (s), 1660.0 (s), 1593.2 (w), 1530.9 (s), 1509.3 (s), 1486.2 (w), 1333.3 (m), 1263.6 (s), 1200.9 (m), 1135.0 (w) 1036.2 (w) cm^{-1}. The UV spectrum is shown.

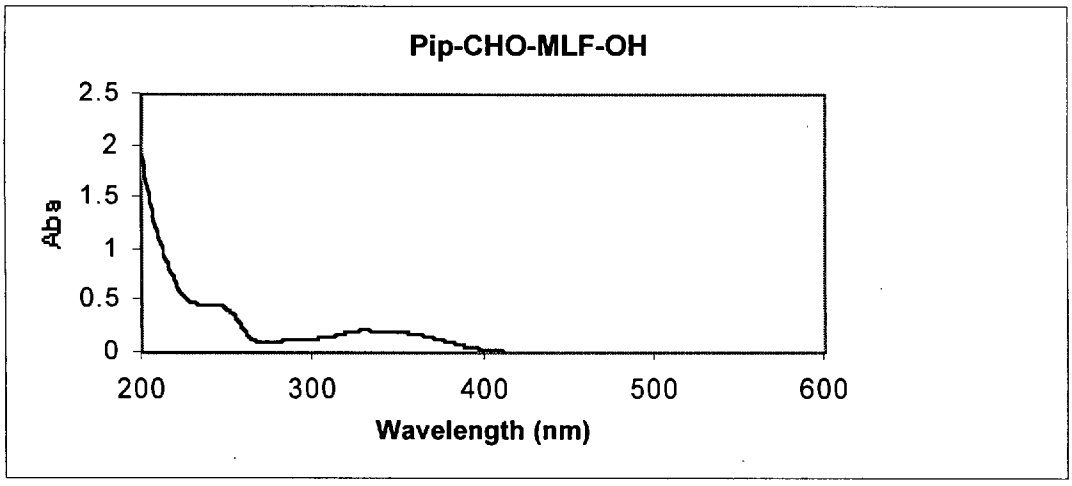

Preparative HPLC. An Alltech Econosil 10 μ C18 10 X 250 mm column was used. Conditions unless otherwise specified: flow rate of 3.5 mL/min, UV detection at 220 nm,

solvents (water and acetonitrile) were filtered prior to use and degassed *via* a helium sparge. Approximately 20mg of crude material was injected for each run. The following gradient was used to separate Pip-CHO-MLF-OH: Solvent A: H_2O with 0.1 % trifluoroacetic acid; Solvent B: CH_3CN with 0.1 % trifluoroacetic acid; 0 min, 40% B; 20 min, 95% B. The material of interest had a retention time of 9.8 min.

Analytical HPLC. An Alltech Econosil 5 μ C18 4.6 X 250 mm column was used. Conditions unless otherwise specified: flow rate of 1 mL/min, UV detection at 220 nm, solvents (water and acetonitrile) were filtered prior to use and degassed via a helium sparge.

Irradiation of Nitrobenzylformylalanines. A 0.01 M solution of each alanine derivative (Pip-CHO-Ala-OEt and Nv-CHO-Ala-OEt) was prepared in acetonitrile. The solution was irradiated (with rapid magnetic stirring) in a Pyrex round bottom flask in a Rayonet reactor fitted with 350 nm UV lamps. Reaction progress was followed by diluting a 25 μL aliquot of the solution with an additional 75 μL of solvent, loading 10 μL of this diluted solution into a 20 μL loop, and injecting it into the HPLC operating at a flow rate of 1.2 mL/min. An isocratic elution system was used for Nv-CHO-Ala-OEt: 85 % A/15 %B. The retention times are 3.7 min (Nv-CHO-Ala-OEt) and 3.0 min (CHO-Ala-OEt). The following elution gradient was utilized for Pip-CHO-Ala-OEt: 0 min, 0% B; 10 min, 10% B. The retention times are 10.7 min (Pip-CHO-Ala-OEt) and 5.3 min (CHO-Ala-OEt). The area of the resulting peaks was used to determine amount of starting material remaining and was used in graphical data. Plots of time vs. moles for each photolysis show first order decay. Plots of time vs. ln moles are linear with a 0.42 s^{-1} rate at the same flux.

Irradiation of Caged Chemotactic Peptides. The derivatized peptides (Nv-CHO-MLF-OH and Pip-CHO-MLF-OH) were irradiated in a manner similar to that described above. A 5 mM solution in acetonitrile was irradiated (with rapid magnetic stirring) in a Pyrex round bottom flask in a Rayonet reactor fitted with 350 nm UV lamps. The progress of the reaction was followed by taking 15 μL aliquots of the reaction mixture at the following time points: 0, 3, 8, 15, 30, 90, 120, 150 min, which were injected via a 20 μL loop. The following gradient was

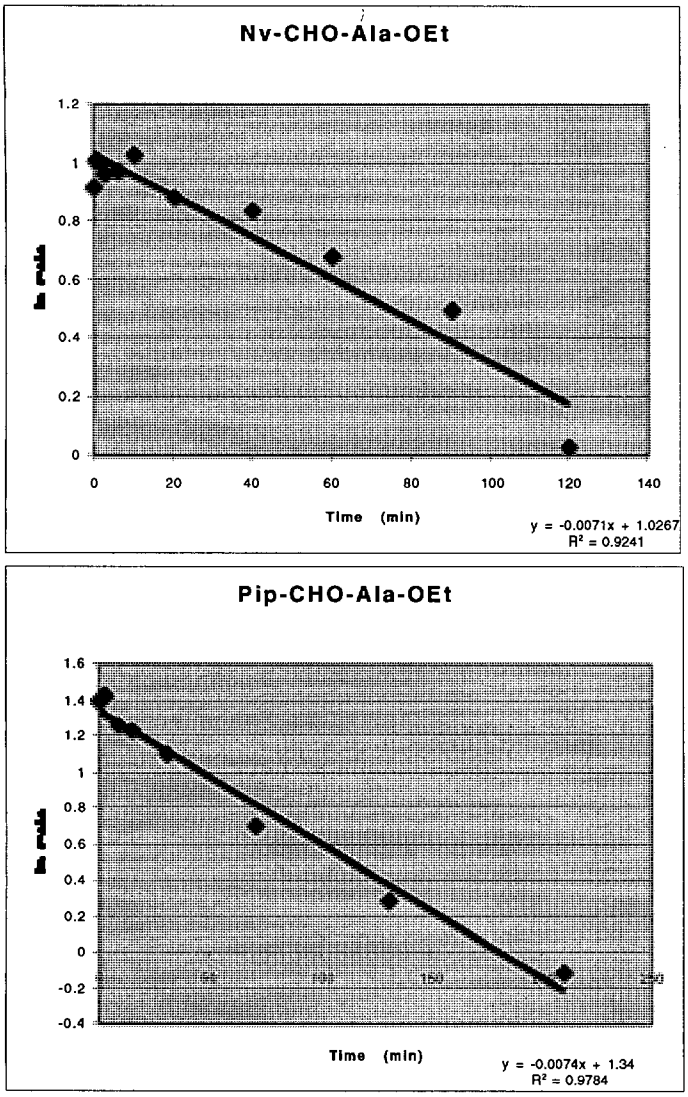

utilized: 0 min, 20% B; 20min, 90% B; 30min, 95% B. Compounds were identified according to their characteristic retention times as compared with known standards as follows: CHO-M(O)LF-OH, 6.3 min; CHO-MLF-OH 7.9 min; NV-NH-Ac10.8 min; Nv-CHO-MLF-OH, 11.1 min; Pip-CHO-MLF-OH 11.6 min. A plot of time vs. moles for each photolysis shows a first order decay. A plot of time vs. ln moles is linear. The rate for Nv-CHO-MLF-OH is 1.89 s^{-1}, while that for Pip-CHO-MLF-OH is 2.41 s^{-1}.

Quantum yield determination. Both derivatives were irradiated alone (data shown above) and with an equimolar concentration of Nv-NH-Ac (in the same flask) to determine quantum yield. Two separate experiments were conducted with Nv-CHO-MLF-OH. They are shown below: A

quantum yield of 0.024 is obtained. The photolysis of Pip-CHO-MLF-OH was carried out in the same manner as that of Nv-CHO-MLF-OH. Analysis of the data give a quantum yield of 0.041.

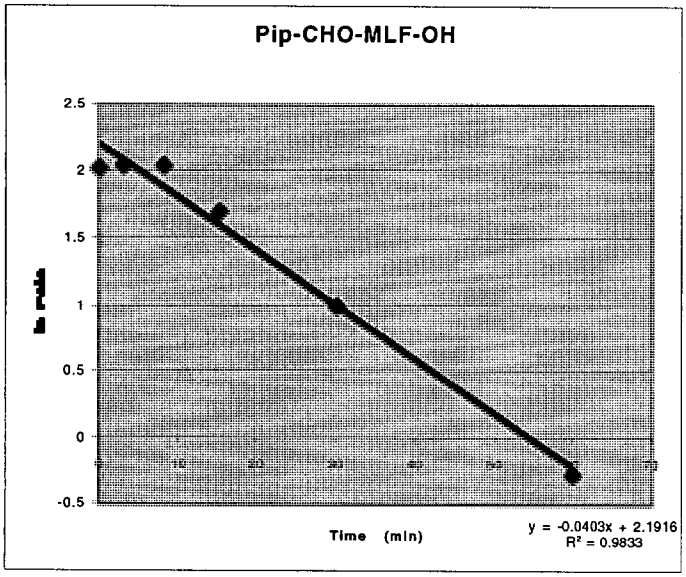

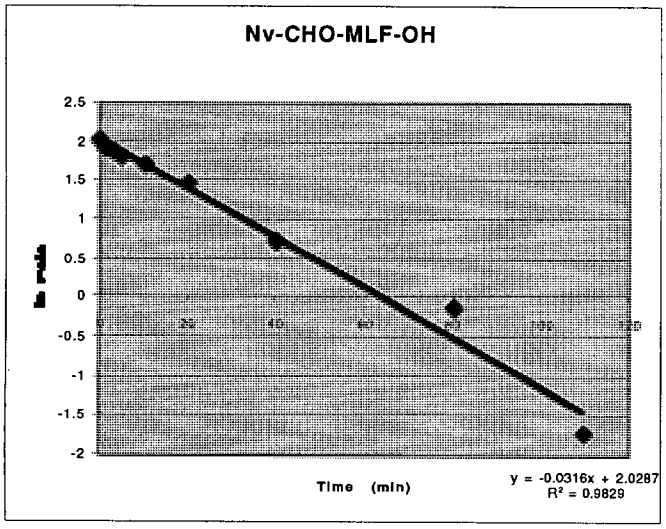

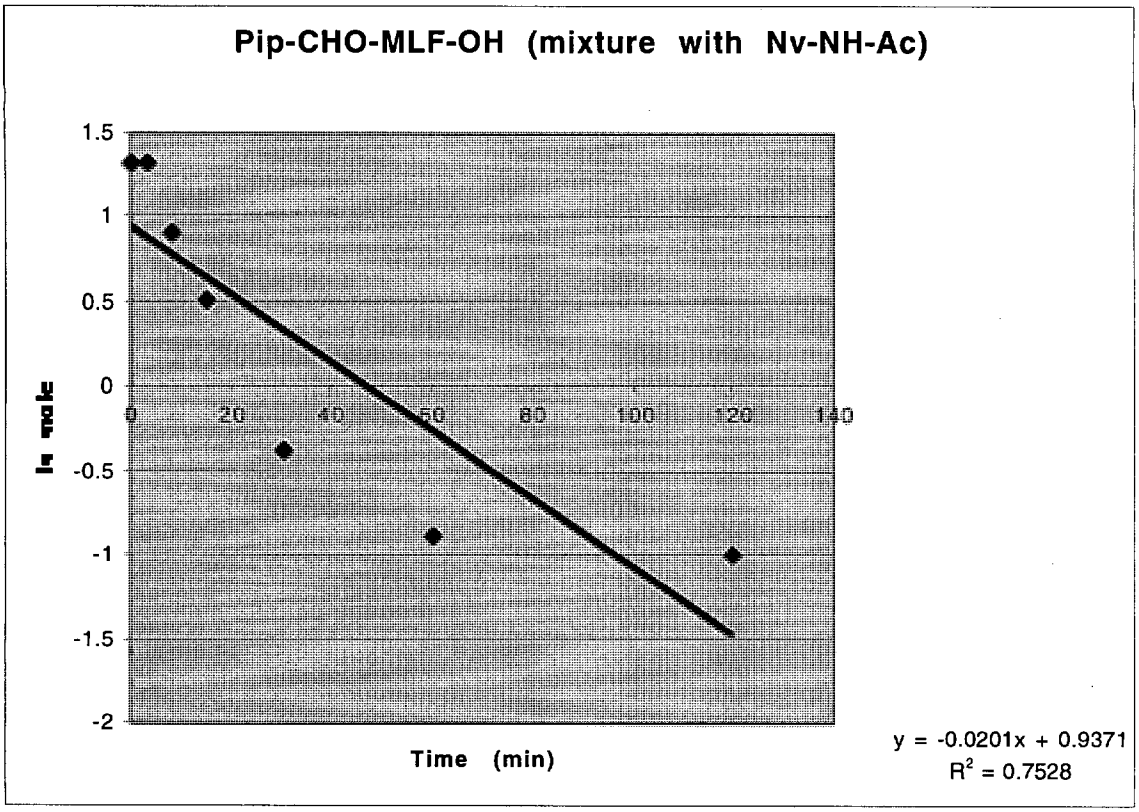
Pip-CHO-MLF-OH (mixture with Nv-NH-Ac)
1.5
1
0.5
0
-0.5
-1
-1.5
-2
0
20
40
60
80
100
120
140
ln mole
Time (min)
y = -0.0201x + 0.9371
R2 = 0.7528

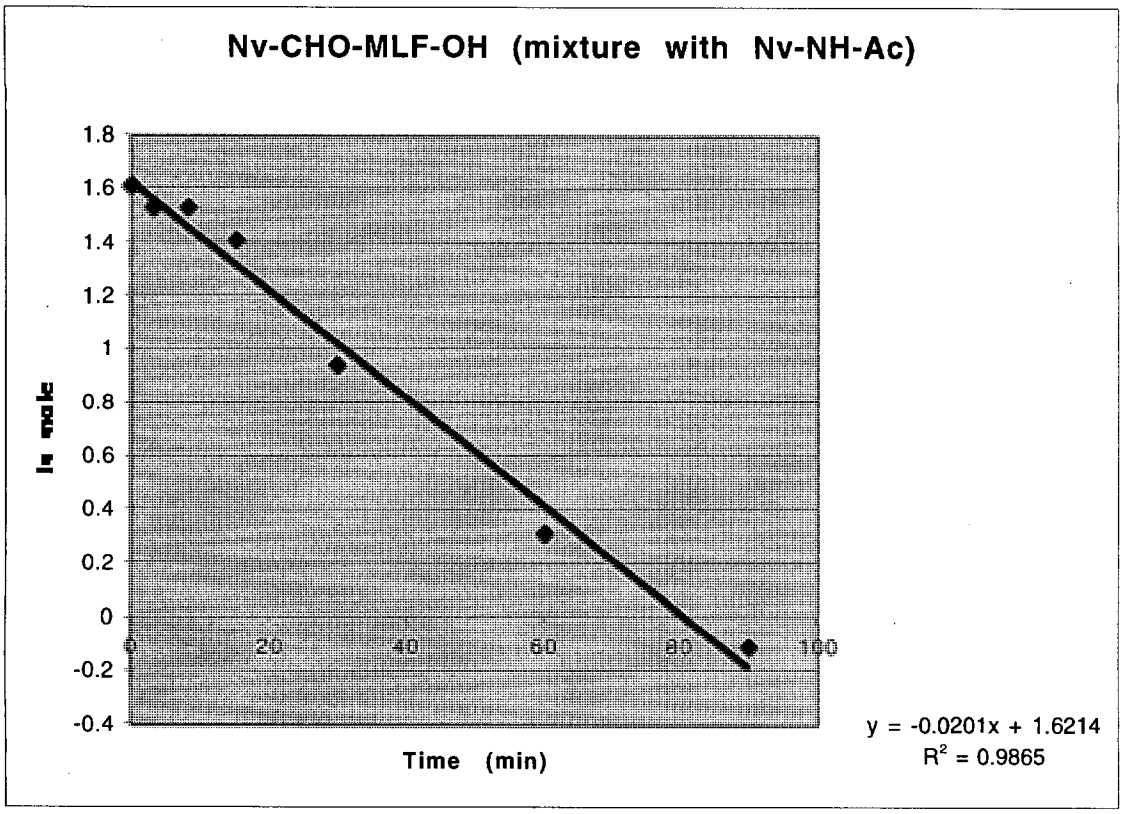
Nv-CHO-MLF-OH (mixture with Nv-NH-Ac)
1.8
1.6
1.4
1.2
1
0.8
0.6
0.4
0.2
0
-0.2
-0.4
0
20
40
60
80
100
Time (min)
y = -0.0201x + 1.6214
R2 = 0.9865

Cell culture and secretion assay. A rat basophilic leukemia RBL-2H3) cell line stably expressing fMLF receptors was used for this study. Cells were cultured in 96-well tissue culture plates overnight. Cells were then washed with HEPES-buffered saline containing 0.1%BSA and treated with and without fMLF or NV-fMLF. β-Hexosaminidase release was assessed as previously reported.[21]

© 2000 American Chemical Society, Bioconjugate Chem., Pirrung bc000001g Supporting Info Page 13

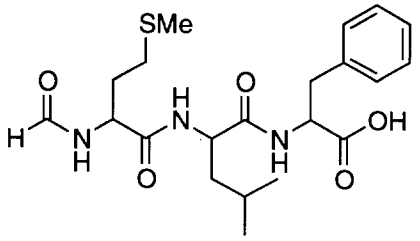

f-Met-Leu-Phe,
a chemotactic peptide

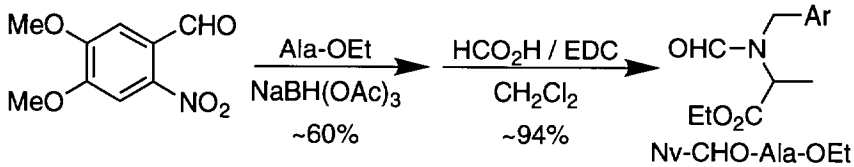

Nv-CHO-Ala-OEt
1

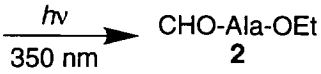

(1)

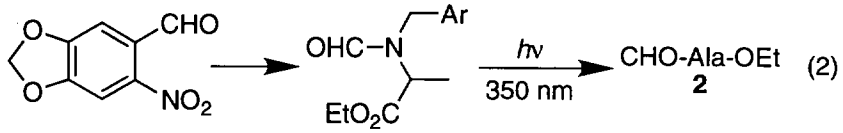

(2)

Pip-CHO-Ala-OEt
3

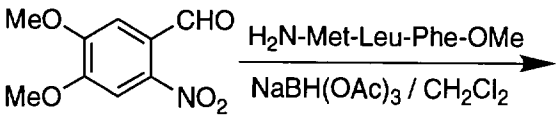

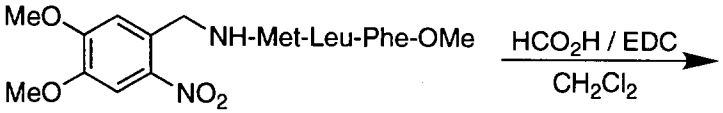

Nv-Met-Leu-Phe-OMe
4

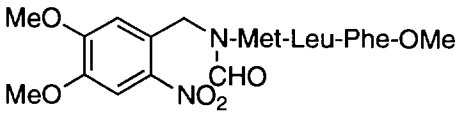

Nv-CHO-Met-Leu-Phe-OMe
5

(3)

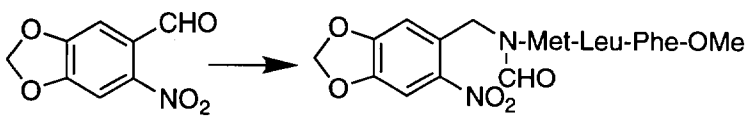

(4)

Pip-CHO-Met-Leu-Phe-OMe
6

© 2000 American Chemical Society, Bioconjugate Chem., Pirrung bc000001g Supporting Info Page 14

Nv-CHO-Met-Leu-Phe-OMe
ED_{50} 10^{-6} M

Pip-CHO-Met-Leu-Phe-OMe
ED_{50} 10^{-6} M

CHO-NH-Met-Leu-Phe-OMe
ED_{50} 10^{-9} M

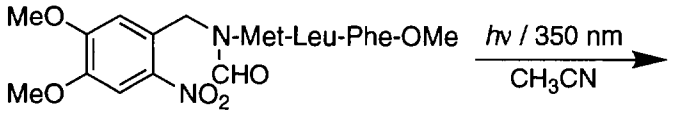

Nv-CHO-Met-Leu-Phe-OMe

CHO-NH-Met-Leu-Phe-OMe, *no* 67% isolated

CHO-NH-Met-Leu-Phe-OMe (5) (HPLC)

For graphical abstract:

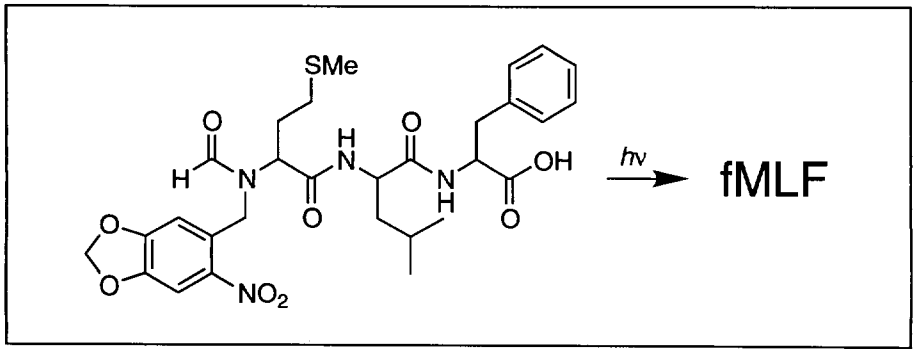

A Novel Selenocystine-*β*-Cyclodextrin Conjugate That Acts as a Glutathione Peroxidase Mimic

Xiaojun Ren,[†,‡] Junqiu Liu,[†] Guimin Luo,*[,†] Yan Zhang,[†] Yuanming Luo,[†] Ganglin Yan,[†] and Jiacong Shen[‡]

Key Laboratory of Molecular Enzymology and Engineering, Jilin University, Changchun 130023, China, and Key Laboratory of Supramolecular Structure & Spectroscopy, Jilin University, Changchun 130023, P. R. China . Received January 28, 2000; Revised Manuscript Received May 1, 2000

A novel artificial glutathione peroxidase mimic consisting of a selenocystine-di-*β*-cyclodextrin conjugate (selenium-bridged-6,6′-amino-selenocystine-6,6′-deoxy-di-*β*-cyclodextrin), in which selenocystine is bound to the primary side of *β*-cyclodextrin through the two amino nitrogen groups of selenocystine, was synthesized. The glutathione peroxidase activities of the mimic-catalyzed reduction of H_2O_2, *tert*-butylhydroperoxide, and cumene hydroperoxide by glutathione are 4.1, 2.11, and 5.82 units/*μ*mol, respectively. The first activity was 82 and 4.2 times as much as that of selenocysteine and ebselen, respectively. Studies on the effect of substrate binding on the glutathione peroxidase activity suggest that it is important to consider substrate binding in designing glutathione peroxidase mimics. The detailed steady-state kinetic studies showed that the mimic-catalyzed reduction of H_2O_2 by glutathione followed a ping−pong mechanism, which was similar to that of the native glutathione peroxidase.

INTRODUCTION

Glutathione peroxidase (GPX)[1] (EC 1.11.1.9) comprises four identical subunits. Each subunit approximates 21 000 Da and contains a selenocysteine (SeCys) residue, which is the catalytically active group (*1*). The crystal structure of the enzyme has been determined by X-ray diffraction method (*2*). The enzyme catalyzes the reduction of a variety of hydroperoxides. It is believed that many diseases are accompanied or even caused by "oxidative stress", a situation characterized by excessive formation of reactive reduced oxygen metabolites (superoxide anionic radical, hydrogen peroxide, and hydroxyl radical) (*3*, *4*). To scavenge reactive reduced oxygen, antioxidant pharmacotherapy has emerged as remedy for pathological states characterized by an overwhelmed antioxidant defense system. GPX plays a vital important role in scavenging active oxygen. However, the native GPX has some shortcomings such as instability, poor availability, and high molecular weight, which have limited its application. Therefore, many GPX mimics have been synthesized. They include catalytic antibodies (*5*, *6*), semisynthetic enzyme (*7*, *8*), ebselen (*9*), diaryl diselenides (*10*), α-(phenylselenenyl) ketones (*11*), diaryl ditellurides (*12*), diaryl tellurides (*13*), cyclic selenamides (*14*, *15*), and transition metal complex (*4*). Among them, ebselen is the best-known GPX mimic. This interesting molecule has been researched extendedly from pulse-radiolytic studies on radical reactivity through its biological properties in organs to clinical settings (*16*, *17*).

Enzymes promote very fast reactions by bringing the reacting groups together under the special conditions of the enzyme−substrate complex, but it is clear that a major part of rate enhancement observed is simply due to the way that the functional groups involved are brought together (*18*). General conclusions from work on models are that efficient catalysis involves an initial binding interaction between the substrate and the enzyme (*19*). Cyclodextrins are cyclic oligosaccharides consisting of a hydrophobic cavity with which many complexes can be formed via host−guest chemistry. This property has been extensively exploited in the past as enzyme mimics, catalyzing various reactions (*20*, *21*). The effect of an amino group on the antioxidant activity has been extensively investigated with enzyme model (*22*), but the effect of the substrate binding on the antioxidant activity has not been studied using enzyme model. In this report, *β*-cyclodextrin (*β*-CD) modified by selenocystine (SeCyss) was prepared and used as native GPX model to investigate the function of hydrophobic substrate binding. The GPX activities and kinetic studies of the mimic were described. These results reveal that the mimic is a much more efficient catalyst than ebselen, SeCys, and some of the compounds based on diary diselenides.

EXPERIMENTAL PROCEDURES

Instrumental. The characterization was performed with a Varian Unity-400 NMR Spectrometer, a Bruker IFS-FT66V Infrared Spectrometer and a Perkin-Elmer 240 DS Elemental Analyzer. The content and valence of selenium were determined by means of an ESCALAB MKII X-ray Photoelectron Spectrometer. The enzyme activities were measured using a Shimadzu UV-3100 Spectrophotometer.

Materials. *β*-CD, *p*-toluene sulfochloride (TsCl) and *tert*-butylhydroperoxide (*t*-BuOOH) were purchased from

* To whom correspondence should be addressed. E-mail: gmluo@mail.jlu.edu.cn. Fax: 86-431-8923907. Phone: 86-431-8922331-3698.

† Key Laboratory of Molecular Enzymology and Engineering.

‡ Key Laboratory of Supramolecular Structure & Spectroscopy.

[1] Abbreviations: *t*-BuOOH, *tert*-butylhydroperoxide; CuOOH, cumene hydroperoxide; *β*-CD, *β*-cyclodextrin; disecysCD, selenium-bridged-6,6′-amino-selenocystine-6,6′-deoxy-*β*-cyclodextrin; DMF, *N*,*N*-dimethylformamide; EDTA, etheylenediaminetetraacetic acid; NADPH, *β*-nicotinamide adenine dinucleotide phosphate, reduced form; GPX, glutathione peroxidase; GSH, glutathione; PhSeSePh, diphenyl diselenide; SeCys, selenocysteine; SeCyss, selenocystine; TsCl, *p*-toluene sulfochloride.

10.1021/bc0000076 CCC: $19.00 © 2000 American Chemical Society
Published on Web 08/31/2000

Scheme 1

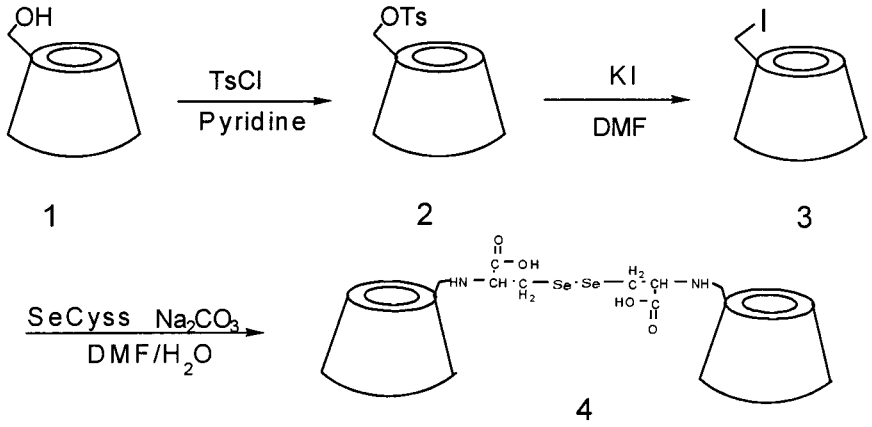

Tianjin Chemical Plant. Sodium borohydride, glutathione (GSH), β-nicotinamide adenine dinucleotide phosphate (NADPH), SeCyss, cumene hydroperoxide (CuOOH), and GSH reductase (type III) were obtained from sigma. Sephadex G-25 was purchased from Pharmacia. Potassium iodide was obtained from Northeast Pharmaceutical Headquarter Factory. β-CD was recrystallized twice from water and dried for 12 h at 120 °C in a vacuum. Analytical grade pyridine was predried by refluxing over KOH for 12 h, then over extremely anhydrous BaO for 12 h, and distilled just before use. *N*,*N*-Dimethylformamide (DMF) was dried over P_2O_5 for several days at room temperature. Then DMF was decanted, shaken with KOH pellets, and then distilled under reduced pressure. All the other materials were used without further purification. Buffers were prepared with distilled, deionized water.

Synthesis of Selenium-Bridged-6,6′-Amino-selenocystine-6,6′-deoxy-β-cyclodextrin (disecysCD). The synthesis route of disecysCD is shown in Scheme 1. The regiospecific monotosylation of 6-position hydroxyl of β-CD was carried out according to the ref *23* to synthesize 6-OTs-6-deoxy-β-CD **2**. 6-Iodo-6-deoxy-β-CD **3** was synthesized by using the reaction of 6-OTs-6-deoxy-β-CD and potassium iodide in dried DMF at 80 °C (*24*). The synthesis of disecysCD **4** was accomplished as follows. SeCyss (10 mg, 0.03 mmol) in water solution (4 mL) containing Na_2CO_3 (13 mg, 0.12 mmol) was added to 6-iodo-6-deoxy-β-CD (400 mg, 0.32 mmol) in DMF (4 mL). The mixture was bubbled using pure nitrogen for 30 min. Under the protection of pure nitrogen, the mixture was kept for 20 h at 65 °C, and then was oxidized in air, finally purified by centrifugation and Sephadex G-25 column ($\Phi 5 \times$ A50 cm) chromatography ($\lambda = 254$) using distilled, deionized water as eluent. The product solution was freeze-dried and the lyophilized powder was fresh yellow product with 27% yield.

Characterization of DisecysCD. The structure of disecysCD was analyzed by means of elemental analysis, IR, ^{1}H NMR. The data were shown as follows. Anal. calcd for $C_{90}H_{148}O_{72}N_2Se_2 \cdot 6H_2O$: C, 40.39; H, 6.03; N, 1.05. Found: C, 40.50; H, 5.89; N, 1.06. IR (KBr): 3364 (−OH), 2929, 2854 (CH, CH_2), 1671 (C═O), 1615, 1155, 1085, 1029 (−O−). ^{1}H NMR (400 MHz, D_2O) d: 5.07−4.82 (m, 14H, 1-H), 3.90−3.59 (m, 54H, 3-, 5-, 6-H, and CH of SeCyss), 3.57−3.33 (m, 28H, 2-, 4-H), 3.30−2.60 (m, 8H, 6-H and CH_2 of SeCyss).

Determination of the Se Content and the Valence of DisecysCD. The Se content and valence of the mimic were determined by X-ray photoelectron spectroscopy (*25*). The energy of the exciting X-ray was 1253.6 eV (Mg, Kα). $C_{1s} = 285.0$ eV was served as standard. The scans were performed five times. The Se3d electron binding energy of disecysCD was 54.8 eV, which approaches the binding energy 55.1 eV of SeCyss. This result is consistent with our previous observations in 6-SeCD, a GPX mimic containing diselenium bridge (*26*), indicating that the selenium in disecysCD presents in the form of diselenium bridge (−Se−Se−). The ratio of C/Se and C/N was also given by the experiment as follows: C/Se, 45.9:1 (calcd 45:1), and C/N, 45.5:1 (calculated 45:1), indicating that 1 mol of the mimic contains 2 mol of selenium and nitrogen.

Measurement of the binding constant for complexation of GSH by 6-OTs-6-deoxy-β-CD. The binding constant between 6-OTs-6-deoxy-β-CD and GSH in a pH 7.0, 50 mM potassium phosphate buffer was determined by following the absorption at 274 nm of 6-OTs-6-deoxy-β-CD (6.0×10^{-5} M) as a function of the concentration of GSH (1.2×10^{-3} M, 1.8×10^{-3} M, 2.4×10^{-3} M, 6×10^{-3} M) (*27*). The binding constant was found to be 1.01×10^2 M.

Determination of the GPX Activity of DisecysCD. The GPX activity of disecysCD was measured using coupled test procedure assay (*10*). The reaction was carried out at 37 °C in 500 μL of the solution containing 50 mM potassium phosphate buffer, pH 7.0, 1 mM ethylenediaminetetraacetic acid (EDTA), 1 mM sodium azide, 1 mM GSH, 1 unit of GSH reductase, and 10−50 μM disecysCD. The mixture was preincubated for 10 min, and then 0.25 mM NADPH solution was added and incubated for 3 min at 37 °C. Thereafter, the reaction was initiated by addition of 0.5 mM hydroperoxides. Organic hydroperoxides were dissolved in methanol, which did not affect the activity assay. The activity was determined by the decrease of NADPH absorption at 340 nm. Appropriate controls were run without enzyme mimic and were subtracted. The activity unit of the mimic is defined as the amount of the mimic that utilizes 1 μmol of NADPH/min. The activity is expressed in units per micromole of enzyme mimic.

Assay of Kinetics of DisecysCD. The assay of kinetics of disecysCD was similar to that of native GPX (*28*). The initial rates were determined by observing the change of NADPH absorption at 340 nm at several concentrations of one substrate while the concentration of the other substrate was kept constant. All kinetic experiments were performed in 0.5 mL of the reaction solution containing 50 mM potassium phosphate buffer, pH 7.0, 1 mM EDTA, 1 unit of GSH reductase, 0.25 mM NADPH, and appropriate concentration of GSH, H_2O_2, and disecysCD. The reaction conditions and operation

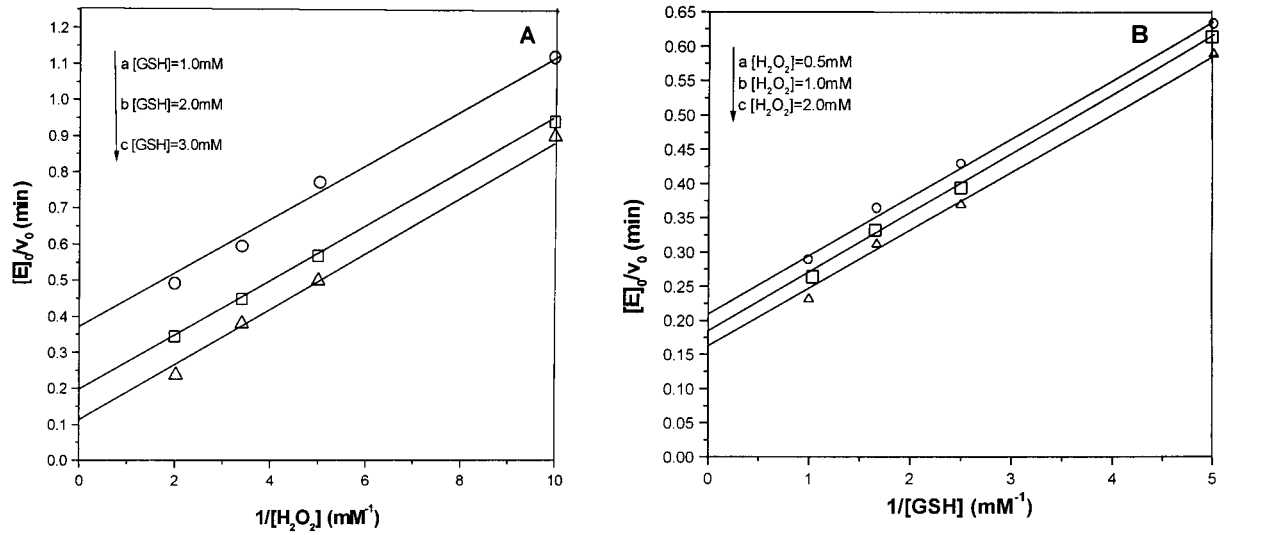

Figure 1. Double-reciprocal plots of the initial velocity vs the concentration of the substrates. (A) $[E]_0/V_0$ (min) vs $1/[H_2O_2]$ (mM^{-1}) for 2 μM disecysCD, at [GSH] = 1.0 mM (○), 2.0 mM (□), and 3.0 mM (△). (B) $[E]_0/V_0$ (min) vs 1/[GSH] (mM^{-1}) for 10 μM disecysCD, at $[H_2O_2]$ = 0.5 mM (○), 1.0 mM (□), and 2.0 mM (△).

Table 1. GPX Activities of DisecysCD and Other Species

species	hydroperoxide	activity (units/μmol)
SeCys	H_2O_2	0.05
Ebselen	H_2O_2	0.99
PhSeSePh	H_2O_2	1.95
DisecysCD[a,b]	H_2O_2	4.13 (0.2)
	t-BuOOH	2.11 (0.25)
	CuOOH	5.82 (0.25)
β-CD[a,b]	H_2O_2	0.03 (0.01)
β-CD + SeCys[a,b]	H_2O_2	0.11 (0.05)

[a] Reactions were carried out in 50 mM potassium phosphate buffer, pH 7.0, at 37 °C, 1 mM GSH, 0.5 mM H_2O_2. [b] Standard deviations are shown in parentheses.

Table 2. Kinetic Parameters for the GPX Activity of DisecysCD[a,b]

$[H_2O_2]$ (mM)	k_{cat}(app) (min^{-1})	K_{GSH}(app) (M)	k_{cat}(app)/K_{GSH}(app) (M^{-1} min^{-1})
0.5	4.8 ± 0.5	$(0.42 \pm 0.02) \times 10^{-3}$	$(1.14 \pm 0.04) \times 10^4$
1.0	5.3 ± 0.2	$(0.47 \pm 0.03) \times 10^{-3}$	$(1.13 \pm 0.08) \times 10^4$
2.0	6.3 ± 0.4	$(0.55 \pm 0.02) \times 10^{-3}$	$(1.15 \pm 0.03) \times 10^4$
[GSH] (mM)	k_{cat}(app) (min^{-1})	$K_{H_2O_2}$(app) (M)	k_{cat}(app)/$K_{H_2O_2}$(app) (M^{-1} min^{-1})
1.0	2.8 ± 0.2	$(0.22 \pm 0.01) \times 10^{-3}$	$(1.27 \pm 0.04) \times 10^4$
2.0	5.1 ± 0.5	$(0.38 \pm 0.06) \times 10^{-3}$	$(1.34 \pm 0.01) \times 10^4$
3.0	9.1 ± 02	$(0.72 \pm 0.03) \times 10^{-3}$	$(1.26 \pm 0.03) \times 10^4$

[a] Reactions were carried out in 50 mM potassium phosphate buffer, pH 7.0, at 37 °C. [b] The data in the table were obtained from the plots in Figure 1.

procedure were basically same as that described in Determination of the GPX Activity of DisecysCD. The reaction was initiated by addition appropriate concentration of H_2O_2. The nonenzymatic reaction affecting the measurement of the initial rate was taken into account and subtracted to obtain exact kinetic values.

RESULTS

GPX Activities of DisecysCD. The GPX activity was monitored using the modified Wilson's method. The noenzymatic reaction was taken into account and then subtracted to obtain the exact activity. The GPX activities of the disecysCD-catalyzed reduction of a variety of hydroperoxides by GSH were listed in Table 1 and the GPX activity of other species were included for comparison.

From the Table 1, the GPX activity of disecysCD for the reduction of H_2O_2 by GSH was found to be 4.13 units/μmol, indicating that disecysCD displays a higher GPX activity than SeCys (*5*), ebselen (*10*), and diphenyl diselenide (PhSeSePh) (*10*). At 1 mM GSH and 0.5 mM H_2O_2, the initial rates of the reduction of H_2O_2 by GSH were 9.0×10^{-6} M min^{-1} for disecysCD (2 μM), 2.1×10^{-6} M min^{-1} for ebselen (2 μM), 4.7×10^{-7} M min^{-1} for SeCys (2 μM), 4.2×10^{-7} M min^{-1} for β-CD (2 μM), and 5.8×10^{-7} M min^{-1} for β-CD + SeCys (2 μM). The spontaneous reaction rate was determined to be 3.6×10^{-7} M min^{-1}. These data show that disecysCD, ebselen, SeCys, β-CD, and β-CD + SeCys accelerate the reaction by 25-, 6-, 1.3-, 1.2-, and 1.6-fold, respectively. The disecysCD also catalyzes the reduction of organic hydroperoxides such as *t*-BuOOH and CuOOH. The spontaneous reaction rates of the reduction of these hydroperoxides were found to be lower than that of H_2O_2. The GPX activities of disecysCD for reduction of *t*-BuOOH and CuOOH by GSH were determined to be 2.11 and 5.82 units/μmol, respectively.

Kinetics of the DisecysCD-Catalyzed Reduction of H_2O_2 by GSH. To probe the mechanism of the disecysCD-catalyzed reduction of H_2O_2 by GSH, comprehensive kinetic studies were carried out. The initial rates for the reduction of H_2O_2 by GSH were determined as a function of substrate concentration, varying one substrate concentration while the other fixed. Michaelis−Menten kinetics were observed for both substrates under all the conditions investigated. The apparent kinetic parameters obtained at several GSH and H_2O_2 concentrations are summarized in Table 2. Double-reciprocal plots of the initial velocity vs the concentration of the substrates yielded families of parallel lines for both substrates (Figure 1), consistent with a ping-pong mechanism involving at least one covalent enzyme intermediate. The relevant steady-state equation for this system is

$$\frac{v_0}{[E]_0} = \frac{k_{max}[GSH][H_2O_2]}{K_{GSH}[H_2O_2] + K_{H_2O_2}[GSH] + [H_2O_2][GSH]} \quad (1)$$

where k_{max} is a pesudo-first-order rate constant and $K_{H_2O_2}$ and K_{GSH} are the Michaelis constants for H_2O_2 and GSH,

respectively. From the data in Table 2, $k_{max} = 14.3 \pm 0.8$ min^{-1}, $K_{H_2O_2} = 2.06 \pm 0.15$ mM, and $K_{GSH} = 0.59 \pm 0.10$ mM. Thus, $k_{max}/K_{H_2O_2} = 6.9 \times 10^3$ min^{-1} M^{-1} and $k_{max}/K_{GSH} = 2.4 \times 10^4$ min^{-1} M^{-1}.

DISCUSSION

A coupled test procedure was performed to assay the GPX activities of disecysCD. The oxidized GSH formed in catalytic reaction was reduced to reduced GSH by adding NADPH in the presence of GSH reductase (eqs 2 and 3)

$$2GSH + ROOH \xrightarrow{\text{enzyme}} GSSG + ROH + H_2O \quad (2)$$

where R = H,*t*-butyl,cumenyl

$$GSSG + NADPH + H^+ \xrightarrow{\text{Reductase}} 2GSH + NADP^+ \quad (3)$$

The amount of oxidized GSH was measured in terms of the decrease of NADPH absorbance at 340 nm. At the NADPH concentration used, the coupled reaction was a zero-order reaction with respect to NADPH and the oxidation of GSH was the rate-limiting step. After adding a variety of hydroperoxides to the reaction solution, a linear-dependent decrease of NADPH was found during the initial 10 min of the reaction. The reaction mixture was preincubated with GSH to obtain the maximum activities. In our experiment, the GPX activities of disecysCD for reduction of H_2O_2, *t*-BuOOH, and CuOOH were enhanced 1.5, 1.2, and 1.8-fold by preincubation with GSH, respectively.

The only marginal GPX activity was observed in reduction of H_2O_2 by GSH in the presence of SeCys that is the catalytically active group of the native GPX, and addition of β-CD appreciably enhanced the GPX activity. It should be noted that β-CD itself was as the catalyst, suggesting that the hydrophobic cavity of β-CD play an important in the catalytic cycle. When SeCyss was bound to the primary face of β-CD, the disecysCD-catalyzed reduction of H_2O_2 by GSH was considerably accelerated and the GPX activity of disecysCD was 82-fold more actives than that of SeCys. Enhancement of rate by disecysCD was explained by correlating the crystal structure of the native enzyme with the properties of β-CD. Clearly, the ability to bind this thiol substrate is essential for the enzyme activity. In the vicinity of the reactive group of the native GPX, some aromatic amino acid residues that can form hydrophobic environment facilitate substrate GSH binding (*2*). Analysis of the incubation solution containing GSH and cyclodextrin using electrospray mass spectrometry and tandem mass spectrometry reveals that cyclodextrin itself could bind GSH to form intramolecular complex (*29*). Binding of GSH by 6-OTs-6-deoxy-β-CD was investigated by spectrophotometric titration and binding constant was found to be 1.01×10^2 M. These observations suggest that cyclodextrin and cyclodextrin's derivative bind GSH to form the intramolecular complex. Cyclodextrins provide hydrophobic cavity to bind the substrate GSH and bring the catalytic group and GSH together, then the initial binding interaction between disecysCD and GSH accelerates the reaction of GSH and H_2O_2 (*19*). The hydrophobic action of cavity of β-CD plays a vital role in rate enhancement. So it is not surprising to discover that the GPX activity of conjugate disecysCD was more active than that of SeCys, ebselen, and PhSeSePh. The GPX activity of disecysCD could be enhanced by improving the ability to bind another substrate hydroperoxide. Cyclodextrins have stronger ability to bind shape/size-fit organic molecule (the aromatic group in CuOOH) than that for shape/size-unfit organic molecule (the *tert*-butyl group in *t*-BuOOH) in the cavity (*30*). The substrate CuOOH could take advantage of the cavity of disecysCD more effectively, thus the GPX activity for CuOOH is 2.8-fold than that for *t*-BuOOH. These results show that to bind substrate is a major problem that should be considered in the development of artificial imitation of GPX.

Scheme 2

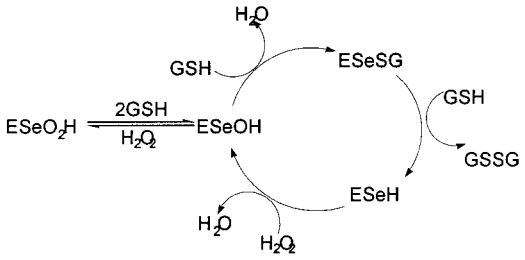

The kinetic data for disecysCD can be a triple-transfer mechanism and may be described by Dalziel's parameter (*31*).

$$\frac{[E]_0}{v_0} = \Phi_0 + \frac{\Phi_{GSH}}{[GSH]} + \frac{\Phi_{H_2O_2}}{[H_2O_2]} \quad (4)$$

The form of the rate equation obtained is identical with that of native GPX in vivo except for the presence of the Φ_0 term, which is negligible in the native GPX cycle. According to the native GPX cycle shown in Scheme 2, one can easily obtain the rate equation described as eq 5 (*32*).

$$\frac{[E]_0}{v_0} = \frac{\Phi_{GSH}}{[GSH]} + \frac{\Phi_{H_2O_2}}{[H_2O_2]} \quad (5)$$

Similarity of the rate equation between disecysCD and the native GPX clearly suggest that disecysCD may exactly follow the native GPX cycle.

An initially slow rate of H_2O_2 consumption was observed in disecysCD-catalyzed the reduction of H_2O_2 by GSH without preincubation with GSH. We interpret this rate lag as initially slow reaction of disecysCD and GSH (eq 6).

$$CDCysSeSeCysCD + GSH \leftrightarrow CDCysSeH + CDCysSeSG \quad (6)$$

Indeed, the lag time was reduced as GSH concentration was increased. In the studies of PhSeSePh mechanism, the interconversion of *S*-(phenylselenyl) glutathione, benzenselenolate, and benzeneselenenic acid has been proposed in the catalytic cycle (*33*). According to these observations, our disecysCD should adapt the similar mechanism proposed for PhSeSePh. In this mechanism (Scheme 3), the CDCysSeSeCysCD (disecysCD) lies off the main catalytic cycle, and the main catalytic cycle is consistent with the native GPX.

The kinetic parameters for the native GPX, acting on H_2O_2 and GSH, at pH 7.0 and 37 °C, are $\Phi_{H_2O_2} = 0.93 \times 10^{-10}$ M min and $\Phi_{GSH} = 2.13 \times 10^{-8}$ M min (*28*). The equivalent kinetic parameters for disecysCD, acting on H_2O_2 and GSH, at pH 7.0 and 37 °C, are $\Phi_{H_2O_2} = 1.5 \times 10^{-4}$ M min, and $\Phi_{GSH} = 4.2 \times 10^{-5}$ M min, by inspection of eq 1. These parameters can be directly compared, since they were measured at the same pH and temperature for the same substrate. Native GPX is believed to have

Scheme 3

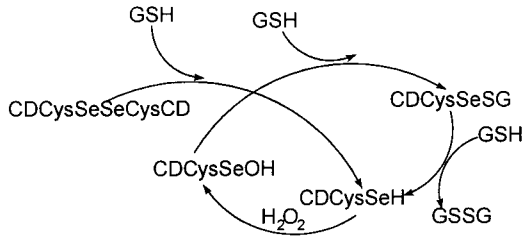

evolved to optimal efficiency for the decomposition of H_2O_2, having an apparent second-order rate constant for the reaction between H_2O_2 and enzyme of the order of 10^{10} M^{-1} min^{-1}. DisecysCD falls far short of this ideal, giving an equivalent rate constant for hydroperoxide consumption of approximately 7×10^3 M^{-1} min^{-1}. The rate of reaction between the two enzymes and their respective substrate GSH were also different, as evidenced by the values of Φ_{GSH} above. This shows that disecysCD is far less efficient than the native GPX.

In the eq 4, Φ_0 has a finite value for disecysCD but is equal to zero for GPX. This indicates that there is no accumulation of catalytic intermediates for the native GPX, but such intermediates do build up in case of disecysCD (*34*). Our kinetic data suggest that the attack of GSH on CDCysSeSG may be rate determining to some degree and hence that CDCysSeSG would be accumulated, which is agreement with the reactivity of the intermediates. Among the intermediates, selenenyl sulfide (CDCysSeSG) could be synthesized and separated (*33*, *35*). Because the concentration of CDCysSeH would be low under steady-state conditions, the low concentration of the selenolate may be responsible for the slow rate of decomposition of H_2O_2, which reacts with this disecysCD intermediate. On the basis of the discussion above, it may be possible to design an artificial enzyme model, which could make use of the enzyme's binding energy to conquer the rate-determining step and hence resolve this question.

On the basis of above discussions, it is important to consider binding substrate in designing GPX mimics. Our enzyme model, which only has hydrophobic environment, is simpler than native enzyme, which not only has hydrophobic environment (Phe and Trp) but also has two Arg residues and one Gln residue, which form salt-bridge and hydrogen bond with GSH to help binding GSH. On the basis of molecular design, it is possible to obtain strong substrate binding by modification of cyclodextrin overcoming the rate-determining step. The information obtained in this study should be useful for understanding the native enzyme and the design and synthesis of highly active enzyme models with GPX activity.

ACKNOWLEDGMENT

This study was supported by the High Technology Research Development Plan (no. 863-103-13-01-05).

LITERATURE CITED

(1) Mills, G. C. (1957) Hemoglobin catabolism. I. Glutathione peroxidase, an erythrocyte enzyme which protects hemoglobin from oxidase breakdown. *J. Biol. Chem. 229*, 189−197.

(2) Epp, O., Ladenstein, R., and Wendel, A. (1983) The refined structure of the selenoenzyme glutathione peroxidase at 0.2-nm resolution. *Eur. J. Biochem. 133*, 51−69.

(3) Doroshow, J. H. (1995) Glutathione peroxidase and oxidative stress. *Toxicology Lett. 82/83*, 395−398.

(4) Spector, A., Wang, G. M., and Wang, R. R. (1993) Photochemically induced cataracts in rat lenses can be prevented by AL-3823A, a glutathione peroxidase mimic. *Proc. Natl. Acad. Sci. U.S.A. 90*, 7485−7489.

(5) Luo, G. M., Zhu, Z. Q., Ding, L., Gao, G., Sun, Q. A., Liu, Z., Yang, T. S., and Shen, J. C. (1994) Generation of selenium-containing abzyme by using chemical mutation. *Biochem. Biophys. Res. Common. 198*, 1240−1247.

(6) Ding, L., Liu, Z., Zhu, Z. Q., Luo, G. M., Zhao, D. Q., and Ni, J. Z. (1998) Biochemical characterization of selenium-containing catalytic antibody as a cytosolic glutathione peroxidase mimic. *Biochem. J. 332*, 251−255.

(7) Wu, Z. P., and Hilvert, D. (1990) Selenosubtilisin as a glutathione peroxidase mimic. *J. Am. Chem. Soc. 112*, 5647−5648.

(8) Muller, S. B., Muller, S., Dorsselaer, A. V., Böck, A., and Branlant, G. (1998) Substituting selenocysteine for active site cysteine 149 of phosphorylating glyceraldehyde 3-phosphate dehydrogenase reveals a peroxidase activity. *FEBS. Lett. 439*, 241−245.

(9) Müller, A., Cadenas, E., Graf, P., and Sies, H. (1984) A novel biologically active seleno-organic compound. I. Glutathione peroxidase-like activity in vitro and antioxidant capacity of PZ51 (ebselen). *Biochem. Pharmacol. 33*, 3235−3239.

(10) Wilson, S. R., Zucker, P. A., Huang, R. R. C., and Spector, A. (1989) Development of synthetic compounds with glutathione peroxidase activity. *J. Am. Chem. Soc. 111*, 5936−5939.

(11) Cotgreave, I. A., Moldeus, P., Brattsand, R., Hallberg, A., Andersson, C. M., and Engman, L. (1992) α-(phenylselenenyl) acetophenone derivatives with glutathione peroxidase-like activity, a comparison with ebselen. *Biochem. Pharmacol. 43*, 793−802.

(12) Engman, L., Stern, D., Cotgreave, I. A., and Andersson, C. M. (1992) Thiol peroxidase activity of diaryl ditellurides as determined by a ^1H NMR method. *J. Am. Chem. Soc. 114*, 9737−9743.

(13) Engman, L., Stern, D., and Deleman, M. (1994) Thiol peroxidase activity of diorganyl tellurides. *J. Org. Chem. 59*, 1973−1979.

(14) Reich, H. J., and Jasperse, C. P. (1987) Organoselenium chemistry. redox chemistry of selenocysteine model systems. *J. Am. Chem. Soc. 109*, 5549−5551.

(15) Back, T. G., and Dyck, B. P. (1997) A novel camphor-derived selenamide that acts as a glutathione peroxidase mimetic. *J. Am. Chem. Soc. 119*, 2079−2083.

(16) Sies, H. (1993) Ebselen, a selenoorganic compound as glutathione peroxidase mimic. *Free Radical Biol. Med. 14*, 313−323.

(17) Parnham, M. J., Leyck, S., Graf, E., Dowling, E. J., and Blake, D. R. (1991) The pharmacology of ebselen. *Agents Actions 32*, 4−9.

(18) D'Souza, V. T., and Bender, M. L. (1987) Miniature organic models of enzyme. *Acc. Chem. Res. 20*, 146−152.

(19) Kirby, A. J. (1996) Enzyme mechanisms, Models, and Mimics. *Angew. Chem., Int. Ed. Engl. 35*, 707−724.

(20) Murakami, Y., Kikuchi, J. I., Hisaeda, Y., and Hayashida, O. (1996) Artificial enzyme. *Chem. Rev. 96*, 721−758.

(21) Breslow, R., and Dong, S. D. (1998) Biomimetic reactions catalyzed by cyclodextrins and their derivatives. *Chem. Rev. 98*, 1997−2011.

(22) Iwaoka, M., and Tomoda, S. (1994) A model study on the effect of an amino group on the antioxidant activity of glutathione peroxidase. *J. Am. Chem. Soc. 116*, 2557−2561.

(23) Matsui, Y., and Okimoto, A. (1978) The binding and catalytic properties of a positively charged cyclodextrin. *Bull. Chem. Soc. Jpn. 51*, 3030−3034.

(24) Tabushi, I., Kuroda, Y., and Mochizuki, A. (1980) The first successful carbonic anhydrase model prepared through a new route to regiospecifically bifunctionalized cyclodextrin. *J. Am. Chem. Soc. 102*, 1152−1153.

(25) Chiu, D., Tappel, A. L., and Millard, M. M. (1977) Improved procedure for X-ray photoelectron spectroscopy of selenium-glutathione peroxidase and application to rat liver enzyme. *Arch. Biochem. Biophys. 184*, 209−214.

(26) Liu, J. Q., Gao, S. J., Luo, G. M., Yan, G. L., and Shen, J. C. (1998) Artificial imitation of glutathione peroxidase with

6-selenium-bridged β-cyclodextrin. *Biochem. Biophys. Res. Commun. 247*, 397−400.

(27) Benesi, H. A., and Hildebrand, J. H. (1949) A spectrophotometric investigation of the interaction of iodine with aromatic hydrocarbons. *J. Am. Chem. Soc. 71*, 2703−2707.

(28) Flohé, L., Loschen, G., Günzler, W. A., and Eichele, E. (1972) Glutathione peroxidase, V the kinetic mechanism. *Hoppe-Seyler's Z. Physiol. Chem. 353*, 987−999.

(29) Sun, W. X., Liu, J. Q., Cui, M., Song, F. R., and Liu, S. Y. (1999) Cyclodextrin-catalyzed oxidation of glutathione in solution and in an ion trap. *Rapid Commun. Mass Spectrom. 13*, 950−953.

(30) Wenz, G. (1994) Cyclodextrins as building blocks for supramolecular structure and functional units. *Angew. Chem., Int. Ed. Engl. 33*, 803−822.

(31) Engel, P. C. (1981) Enzyme kinetics, the steady-state approach. In *Enzyme substitution or ping-pong mechanism* (W. J. Brammar and M. Edidin, Eds.) pp 62−66, Chapman and Hall, London and New York.

(32) Flohé, L. (1989) The selenoprotein glutathione peroxidase. *Glutathione: chemical, biochemical, medical aspects* (D. Dolphin, R. Poulsin, and O. Avramovic, Eds.) pp 643−731, John Wiley & Sons, New York.

(33) Engman, L., Andersson, C., Morgenstern, R., Andersson, C. M., and Hallberg, A. (1994) Evidence for a common selenolate intermediate in the glutathione peroxidase-like catalysis of α-(phenylselenenyl) ketones and diphenyl diselenide *Tetrahedron 50*, 2929−2938.

(34) Ganther, H. E., and Kraus, R. J. (1984) Oxidation states of glutathione peroxidase. *Methods Enzymol. 107*, 593−602.

(35) Bell, I. M., Fisher, M. L., Wu, Z. P., and Hilvert, D. (1993) Kinetic studies on the peroxidase activity of selenosubtilisin. *Biochemistry 32*, 3754−3762.

BC0000076

Poly(DMAEMA-NVP)-*b*-PEG-galactose as Gene Delivery Vector for Hepatocytes

Dong Woo Lim,[†] Young Il Yeom,[‡] and Tae Gwan Park*,[†]

Department of Biological Sciences, Korea Advanced Institute of Science and Technology, Taejon 305-701, South Korea and Gene Therapy Research unit, Korea Research Institute of Bioscience and Biotechnology, Taejon 305-600, South Korea. Received February 8, 2000; Revised Manuscript Received June 18, 2000

A block copolymer composed of cationic polymer and poly(ethylene glycol) (PEG) was used as a DNA carrier. Poly(2-(dimethylamino)ethyl methacrylate (DMAEMA)-*co*-*N*-vinyl-2-pyrrolidone (NVP)) having a terminal carboxylic group was synthesized by free radical polymerization using an initiator, 4,4′-azobis(4-cyanovaleric acid). The terminal carboxylic acid was activated by *N*-hydroxysuccinimide (NHS) with dicyclohexylcarbodiimide (DCC) and then conjugated with PEG-bis(amine). For specific gene targeting to asialoglycoprotein receptor of hepatocytes, a galactose moiety was incorporated into the PEG terminal end of poly(DMAEMA-NVP)-*b*-PEG by reductive coupling using lactose and sodium cyanoborohydride. RSV luciferase plasmid was used as a reporter gene, and in vitro gene transfection efficiency was measured in HepG2 human hepatocarcinoma cells. Poly(DMAEMA-NVP)-*b*-PEG-galactose/DNA complexes formed at 0.5−2 polymer/plasmid weight ratio had compacted structures around 200 nm particle size and exhibited slightly negative surface charge. These complexes were coated with a cationic, pH sensitive, endosomolytic peptide, KALA, to generate positively charged poly(DMAEMA-NVP)-*b*-PEG-galactose/DNA/KALA complex particles. In the presence of serum proteins, both the PEG block and the galactose moiety of poly(DMAEMA-NVP)-*b*-PEG-galactose greatly enhanced the gene transfection efficiency, which was very close to that of Lipofectamine plus. Irrespective of the presence of serum proteins, as the KALA/DNA weight ratio increased, the transfection efficiency of poly(DMAEMA-NVP)-*b*-PEG-galactose was enhanced due to the pH dependent endosomal disruptive property of KALA. This study demonstrates that sufficient transfection efficiency as high as that of commercial agent could be attained by judicious formulation of molecular engineered poly(DMAEMA-NVP)-*b*-PEG-galactose in combination with an endosomolytic peptide, KALA.

INTRODUCTION

A wide range of nonviral gene delivery vectors has been used to deliver plasmid DNA or anti-sense oligonucleotides into mammalian cells. Cationic lipids, cationic polymers, and peptides were molecularly engineered to form self-assembled intermolecular complexes with DNA. It is important to efficiently condense negatively charged macromolecular DNA to nanoparticulates with oppositely charged molecules. For an efficient cell transfection, they should be nanosized particulates less than 200 nm in diameter having a positive surface charge to permit a facile adsorptive endocytosis of the complexes through cell membrane. Nonspecific binding of cationic complexes to anionic cell surface proteoglycans present in cell membrane plays a pivotal role in transporting the DNA complex particulates into cell cytoplasm.

Synthetic polymers such as polyethyleneimine (PEI), polyamidoamine, poly-L-lysine (PLL), and poly(2-(dimethylamino)ethyl methacrylate) (DMAEMA) have been extensively used to deliver plasmid DNA into mammalian cells (*1*−*5*). Most of them are cationic polyelectrolytes for the compaction of DNA. In particular, DMAEMA, has been recently studied in detail as a potential DNA carrier. PolyDMAEMA condenses plasmid DNA mainly through an ionic interaction, resulting in various transfection efficiencies depending on polymer/DNA weight ratio (*4*−*6*). It was also suggested that hydrogen bonding between carbonyl groups of DMAEMA unit and amine groups of base pairs of DNA additionally contributes to the condensation of plasmid DNA (*7*). Nonionic water-soluble polymer, poly(*N*-vinyl-2-pyrrolidone) (NVP) was also used as a DNA transfection carrier (*8*, *9*). It was reported that the C═O group of NVP unit and the NH group of DNA base pairs formed hydrogen bonding for DNA compaction (*10*). While these synthetic polymers show relatively high gene transfection efficiency in the absence of serum proteins, they exhibit greatly reduced transfection efficiency in the presence of serum proteins. This is because nonspecific protein adsorption occurs onto the positively charged surface of polymer/DNA complex particles, which hampers their adsorptive endocytic transport into cells (*11*, *12*). To overcome this problem, poly(ethylene glycol) (PEG) conjugated cationic polymers were used to suppress the nonspecific protein adsorption. Different types of PEG-grafted and PEG-blocked polymers were examined to enhance an in vitro gene transfection efficiency. PEG-grafted PLL, PEG-blocked PLL, and PEG-grafted PEI effectively reduced the interaction with serum proteins and resulted in higher transfection efficiency in the presence of serum proteins (*13*−*17*). Recently, it was reported that pegylation of PEI/DNA complexes reduced plasma protein binding to a great extent and showed prolonged circulation in blood when injected intravenously (*18*). To further enhance the transfection efficiency

* To whom correspondence should be addressed. Phone: +82 42 869 2621. Fax: +82 42 869 2610. E-mail: tgpark@sorak.kaist.ac.kr.

[†] Department of Biological Sciences.

[‡] Gene Therapy Research unit.

10.1021/bc000014u CCC: $19.00 © 2000 American Chemical Society
Published on Web 08/31/2000

to a specific cell, a targeting moiety against a specific receptor present in cell membrane has been conjugated to various polymeric gene carriers to deliver DNA by a receptor-mediated endocytosis. For instance, galactosylated PLL and PEI have been used to selectively deliver plasmid DNA to hepatocytes having specific galactose-binding receptors in their cell membrane, asialoglycoprotein receptor (*19*−*22*). Another important consideration for increasing the transfection efficiency is the rapid escape of the polymer/DNA complex particulates from endosomal compartment to the cytoplasmic region before ultimate degradation in lysosome. For this purpose, endosomolytic and fusogenic peptides such as GALA and KALA were included in the formulation of polymer/DNA complexes (*23*−*25*). A cationic oligopeptide KALA (WEAK-LAKA-LAKA-LAKH-LAKA-LAKA-LKAC-EA), undergoing a pH dependent conformational change from random coil to amphiphatic α-helical structure, showed a great fusogenic activity against endosomal membrane and used by itself as a plasmid DNA carrier (*26*, *27*).

In this study, the above-mentioned diverse approaches for enhancing the transfection efficiency were combined to produce an optimized gene carrier directed for hepatocytes. Two structural units of polymeric gene carriers, DMAEMA and NVP, were free radically copolymerized by using a carboxyl group containing azo-initiator, 4,4′-azobis(4-cyanovaleric acid). The terminal carboxylic group was conjugated with PEG bis(amine) to yield poly-(DMAEMA-NVP)-*b*-PEG. For a specific gene targeting to asialoglycoprotein receptor of hepatocytes, a galactose moiety was incorporated into the amino terminal end of PEG by reductive coupling using lactose and sodium cyanoborohydride. RSV luciferase plasmid DNA used as a reporter gene, was first compacted by poly(DMAEMA-NVP)-*b*-PEG-galactose to yield nanosized complexes having slightly negative surface charge and then the resulting complexes were coated with the cationic, endosomal disruptive peptide, KALA, for efficient receptor mediated endoytosis as well as for enhanced endosomal membrane disruptive activity. Cell transfection efficiencies were evaluated in HepG2 cells in terms of the different types of poly(DMAEMA-NVP) derivatives, the weight ratio of polymer/plasmid, and the coating amount of fusogenic peptide. Cytotoxicities of various poly(DMAEMA-NVP) derivatives and KALA were also examined.

MATERIALS AND METHODS

Materials. 2-(Dimethylamino)ethyl methacrylate and *N*-vinyl-2-pyrrolidone were purchased from Polysciences (Warrington, PA) and distilled under reduced pressure before use. 4,4′-Azobis(4-cyanovaleric acid), 1,3-dicyclohexylcarbodiimide (DCC), *N*-hydroxysuccinimide (NHS), PEG-bis(amine) (MW 3350), lactose, and sodium cyanoborohydride were obtained from Sigma (St. Louis, MO). Dialysis membrane (MW cutoff, 10000) was purchased from Spectrum (Houston, Texas). Phosphate-buffered saline (PBS), Dulbecco's Modified Eagle's Medium (DMEM), fetal bovine serum (FBS), L-glutamine, penicillin-streptomycin, trypsin-EDTA, and Lipofectamine plus were the products of Gibco-BRL (Grand Island, NY). HepG2 human hepatocarcinoma cells were provided by the Korean Cell Line Bank (Seoul, Korea). Micro BCA protein assay reagent kit was obtained from Pierce (Rockford, IL) and luciferase assay system was the products of Promega (Madison, WI). Plasmid RSV luciferase was extracted from transformed *Escherichia coli* by a standard alkaline lysis technique (*28*), and purified by an ultracentrifugation in an equilibrium cesium chloride gradient. The purity of plasmid DNA preparations was determined by running an aliquot on 0.8% agarose gel electrophoresis and the concentration was determined by measuring the absorbance ratio at 260/280 nm using a spectrophotometer (Beckman, DU650).

Synthesis and Conjugation of Poly(DMAEMA-NVP)-*b*-PEG-galactose. Five grams of 2-(dimethylamino)ethyl methacrylate and *N*-vinyl-2-pyrrolidone at a molar feed composition of 1:1.42 (weight ratio 1:1) was dissolved in 40 mL of distilled, deionized water and charged into a round-bottomed flask. After nitrogen gas purging, 50 mg of an initiator, 4,4′-azobis(4-cyanovaleric acid) (monomer/initiator weight ratio of 100/1) dissolved in ethanol, was added. Free radical copolymerization was carried out at 60 °C for 3 h under nitrogen atmosphere. A carboxylic acid terminal end group of poly(DMAEMA-NVP) was activated by NHS with DCC in DMF at room temperature for 3 days at a molar ratio of 1:2:2, respectively and then conjugated to primary amine groups of PEG-bis(amine) in 0.1 M sodium tetraborate buffer at pH 9.0 for 24 h. PEG-bis(amine) was used at 4-fold molar amount of NHS-activated poly(DMAEMA-NVP) to generate a free amine group in the PEG end. Poly(DMAEMA-NVP)-*b*-PEG-NH_2 (100 mg; 2.5 μmol) and lactose (36 mg; 100 μmol) were dissolved in 20 mL of 0.1 M sodium tetraborate buffer at pH 9.0. After the addition of sodium cyanoborohydride (31 mg; 500 μmol), the mixture was reacted for 2 days at 40 °C with stirring. The product was purified by dialyzing against distilled, deionized water (MW cutoff, 10000) and then freeze-dried.

Characterization of Poly(DMAEMA-NVP) Derivatives. ^{1}H NMR spectra were taken with a Brucker DRX 300 NMR operating at 300.13 MHz by using a solvent, D_2O, and chemical shifts were measured in parts per million by using 3-(trimethyl-silyl) propionic-2,2,3,3-d_4 acid (TSP) sodium salt as an internal reference. Gel permeation chromatography (GPC) was carried out with a Waters 510 HPLC pump system connected with 410 differential refractometer using Bio-Silect 250-5 column (300 × 7.6 mm, Bio-Rad) as a size-exclusion column. Distilled and deionized water was used as a mobile phase at a flow rate of 1.0 mL/min. Molecular weight was determined by using vitamin B-12 (MW 1350), equine myoglobin (MW 17 000), chicken ovalbumin (MW 44 000), bovine γglobulin (MW 158 000), and thyroglobulin (MW 670 000) as a series of molecular weight markers. A potentiometric titration for the cationic copolymers was measured with 0.1 M HCl by using a pH meter (710A, Orion)

Synthesis and Purification of Fusogenic Peptide, KALA. KALA (WEAK-LAKA-LAKA-LAKH-LAKA-LAKA-LKAC-EA) was synthesized by using a peptide synthesizer (Applied Biosystems, 430A). The peptide was cleaved from the resin with trifluoroacetic acid (TFA) in the presence of phenol, ethanedithiol (EDT), and thioanisole and separated from the resin by filtration followed by precipitation with diethyl ether. The resulting white solid was dissolved at 20 mg/mL in distilled, deionized water and purified by reversed-phase HPLC on the C_{18} column using the following conditions: solvent A, 0.05% TFA in water; solvent B, 0.05% TFA in acetonitrile:water (80:20); gradient 0 to 20% B for 4 min, 20 to 60% B for 20 min, gradient 60 to 100% B for 22 min, and 100 to 0% B for 30 min at a flow rate 1.5 mL/min; the eluate was monitored at 220 nm. The concentration of peptide stock solution was determined by a micro-BCA method.

Gel Retardation Assay of Poly(DMAEMA-NVP) Derivatives/DNA Complexes. Complexes between poly-(DMAEMA-NVP) derivatives and DNA were formed by adding 10 μL of various polymer solutions, ranging from

0.005 to 0.1 μg/μL in deionized water into 2 μL of plasmid solution (0.5 μg/μL in water). The reason for using deionized water for the formation of complexes was to maximize the polyelectrolyte complexation between the two species in the absence of any buffer salts and was to prevent the formation of aggregates. The poly(DMAEMA-NVP) derivatives/DNA complexes were incubated for 30 min at 37 °C and subsequently run on a 0.8% agarose gel. The retardation of their complexes was visualized by ethidium bromide staining.

Size and Surface Charge of Poly(DMAEMA-NVP)-*b*-PEG-galactose/DNA Complexes. Various amounts of poly(DMAEMA-NVP)-*b*-PEG-galactose dissolved in deionized water were added drop by drop into deionized water containing a fixed amount of plasmid DNA, and incubated for 30 min at 37 °C, which corresponds to the polymer/plasmid weight ratio ranging from 0.25 to 8. The size and ζ-potential of self-assembled complex particulates formed between poly(DMAEMA-NVP)-*b*-PEG-galactose and plasmid DNA in aqueous solution at various polymer/plasmid ratios were measured by a dynamic light scattering instrument (Zetaplus, Brookhaven, NY) equipped with a He−Ne laser at a wavelength of 632.2 nm. To analyze the size and surface ζ-potential changes in case of adding KALA to the poly(DMAEMA-NVP)-*b*-PEG-galactose/plasmid complex, various amounts of KALA were slowly dropped into the polymer/plasmid complex with the variation of KALA/DNA weight ratio from 0 to 4.

Gene Transfection Efficiency of Self-Assembled Complex of Plasmid and Poly(DMAEMA-NVP) Derivatives with Fusogenic Peptide, KALA. HepG2 human hepatocarcinoma cells were grown in Dulbecco's Modified Eagles Medium, supplemented with 10% fetal bovine serum, 100 units/mL penicillin-streptomycin, and 2 mM L-glutamine at 37 °C in a humidified atmosphere under 5% CO_2. To express asialoglycoprotein receptors in HepG2 cells as much as possible, HepG2 cell line with low passage was used. The cultured HepG2 cells were plated in a 24-well plate at an initial density of 50 000 cells/well 24 h prior to transfection. Two micrograms of plasmid were first complexed with various amounts of poly(DMAEMA-NVP) derivatives for 15 min at 37 °C with gentle vortexing and subsequently coated with KALA by adding various amounts of KALA in a dropwise manner at the above condition. The complexes were also incubated for 15 min at 37 °C to allow the formation of stabilized polymer/DNA/KALA nanoparticulates. Cells were transfected in 200−300 μL of serum-free DMEM by addition of 40−80 μL of water containing polymer/DNA/KALA complexes. Lipofectamine plus consisting of two reagents was used with a slight modification, as a control gene carrier (*29*). Two micrograms of plasmid, precomplexed with 6 μL of the plus reagent in 100−150 μL of serum-free DMEM for 15 min at 37 °C, was combined with 4 μL of Lipofectamine reagent in 100−150 μL of serum-free DMEM. DNA/plus/lipofectamine reagent complexes were incubated for 15 min at 37 °C and then added to each well. For the gene transfection under serum-free condition, the cells were incubated for 6 h in the serum-free transfection medium, and then the medium was removed and replaced by fresh medium containing 10% FBS. For the gene transfection in the presence of serum proteins, as soon as various gene delivery complexes in the serum free medium were added into each well, 10% FBS was added to each well with gentle stirring. All other procedures were the same as the previous methods. The cells were incubated for additional 42 h, when they reached 70−80% of confluency. Luciferase gene expression was determined by using a luciferase assay system. Luminescence activity was recorded for 15 s in a Lumat LB 9501 luminometer (Berthold, Wildbach, Germany) and expressed as the number of relative light units (RLU) per milligram of cell protein. Protein concentration per well was measured by a Micro-BCA protein assay.

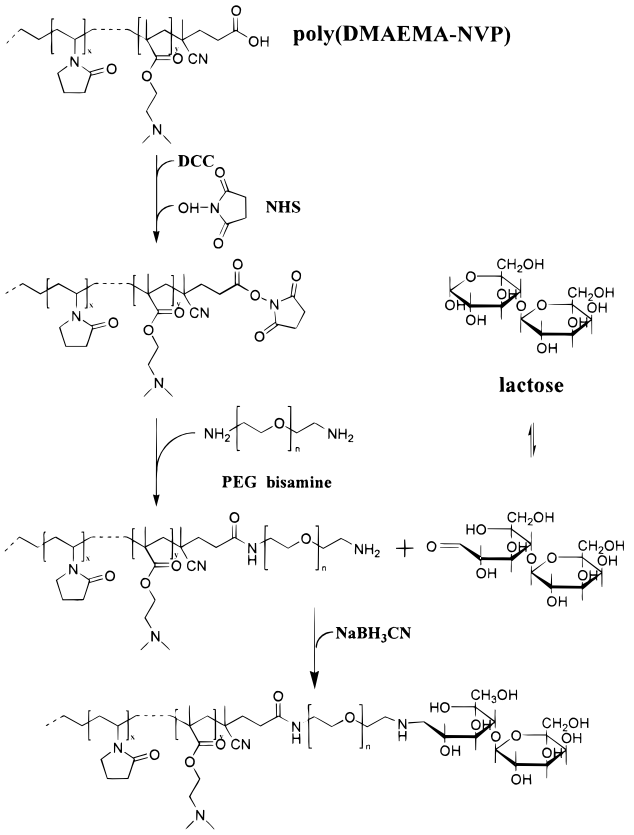

Figure 1. Schematic representation of poly(DMAEMA-NVP)-*b*-PEG-galactose synthesis.

Cytotoxicity of Gene Delivery Vectors against HepG2 Cells. HepG2 cells were grown in 96 well plates at an initial density of 20 000 cells/well in 0.2 mL of growth medium. The cells were grown for 48 h, after which the growth medium was removed and replaced by the growth medium containing various amounts of polymeric gene delivery vectors. After 48 h of incubation, the metabolic activity of HepG2 cells in each well was measured by using thiazolyl blue (3-[4,5-dimethylthiazol-2-yl]-2,5-diphenyltetrazolium bromide, MTT) assay (*30*). One hundred microliters of fresh growth medium and 10 μL of 5 mg/mL MTT stock solution, dissolved in PBS and filtered through a sterilized 0.22 μm filter, were added to each well. After 4 h of incubation at 37 °C, the cells were broken up by adding 100 μL of cell lysis buffer [10% (w/v) SDS (sodium dodecyl sulfate), 45% DMF (*N*,*N*-dimethyl formamide), 45% water, pH 4.7] to each well and scraped well, and then that plate was incubated at 37 °C for 1 day. The optical densities were measured at 590 nm in a microplate reader (Bio-Rad, model 550).

RESULTS AND DISCUSSION

Figure 1 shows a schematic illustration of synthetic route for poly(DMAEMA-NVP)-*b*-PEG-galactose. The copolymer composed of DMAEMA and NVP unit having a terminal carboxylic acid was synthesized by using an

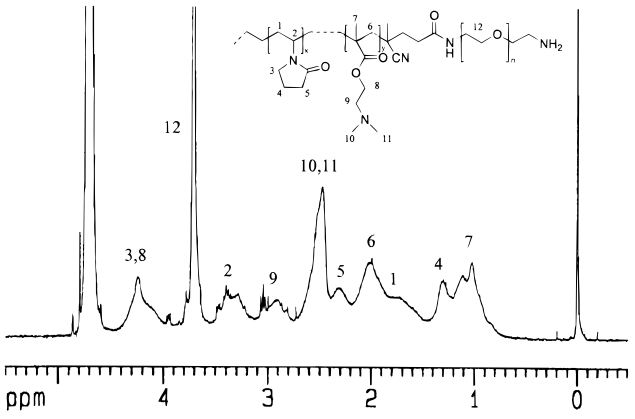

Figure 2. 300 MHz ^{1}H NMR spectra of poly(DMAEMA-NVP)-*b*-PEG in D_2O. Chemical shifts were measured in ppm by using 3-(trimethyl-silyl) propionic-2,2,3,3-d_4 acid (TSP) sodium salt as an internal reference.

azo-initiator, 4,4′-azobis(4-cyanovaleric acid). The conjugation of PEG-bis(amine) was performed by activating the terminal carboxylic acid of poly(DMAEMA-NVP) by NHS and DCC. The NHS-activated poly(DMAEMA-NVP) dissolved in DMF, was slowly added into 0.1 M sodium tetraborate buffer containing an excessive molar amount of primary amine groups of PEG-bis(amine) to generate poly(DMAEMA-NVP)-*b*-PEG with a terminal free primary amine group in the PEG end. Last, the terminal galactose moiety at the PEG end was introduced by a reductive amination coupling of lactose using sodium cyanoborohydride. Unconjugated PEG-bis(amine) (MW 3350) and other chemicals for conjugation were thoroughly removed by dialysis against water (MW cutoff 10000). An ^{1}H NMR spectrum of poly(DMAEMA-NVP)-*b*-PEG is shown in Figure 2, where protons of DMAEMA and NVP unit in the random copolymer structure are assigned, in good agreement with the spectra previously reported (*31*). A single PEG proton peak ($-CH_2-CH_2-O-$) appeared at 3.7 ppm, demonstrating the generation of a di-block copolymer, poly(DMAEMA-NVP)-*b*-PEG. While the molar feed ratio of DMAEMA in the polymerization recipe was 0.41, the molar fraction of DMAEMA in the copolymer structure of poly(DMAEMA-NVP) was 0.47, as determined by calculating the relative areas of characteristic proton peaks in *N*,*N*′-dimethyl group of DMAEMA unit (10, 11 peaks in Figure 2) and $-CH_2$ group of pyrrolidone ring of NVP structural unit (4 or 5 peak in Figure 2), respectively. Weight and number average molecular weight of the di-block copolymer, as determined by aqueous GPC, were 44 000 and 41 000, respectively. Since the molecular weight value was determined by aqueous GPC using various proteins as standards, an unexpectedly narrow value of molecular weight distribution might be obtained. The aqueous GPC profile of the di-block copolymer exhibited a single peak, suggesting that unreacted PEG was removed during the dialysis step. Average pK_a value of poly(DMAEMA-NVP)-*b*-PEG, defined as the pH value at which 50% of tertiary amine groups of DMAEMA structural unit in the random copolymer was protonated, was around 6.5, indicating that the copolymer might show a slight "proton sponge" effect when located within acidic endosomal membrane after endocytosis as previously hypothesized (*32*). The titration curve of the block copolymer, poly(DMAEMA-NVP)-*b*-PEG, which was performed in deionized water, is shown in Figure 3.

It should be noted that the copolymer of DMAEMA-NVP was likely to have a nonrandom sequence of

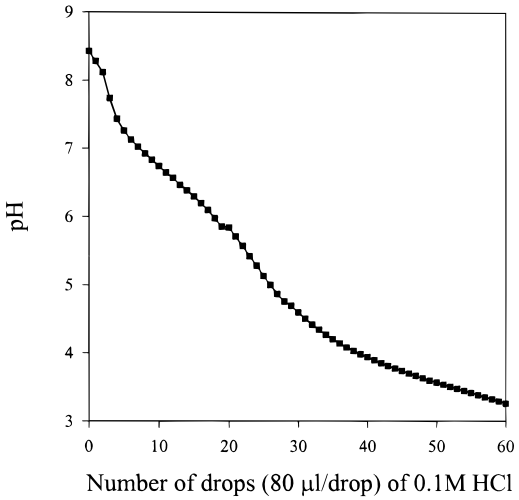

Figure 3. Potentiometric titration curve for poly(DMAEMA-NVP)-*b*-PEG titrated by 0.1 M HCl.

DMAEMA and NVP along the polymer backbone because reactivity ratios of the two monomers during the copolymerization are quite different. It was reported that the reactivity ratio of DMAEMA was much higher than NVP, resulting in the preferential polymerization of DMAEMA over NVP with the generation of a blocky structure (*33*). Additionally, it was probable that an ester linkage of DMAEMA, which was exposed in deionized water for polymerization, was hydrolyzed by a base catalysis mechanism. In this case, a hydrolyzed product, methacrylic acid, was likely to incorporate in the copolymer backbone. It was reported that the monomer, DMAEMA was very hydrolytically unstable in an aqueous medium, while polyDMAEMA was not (*34*). Thus, it cannot be ruled out the possibility that PEG chain was grafted to the incorporated methacrylic acid moiety of poly(DMAEMA-NVP) backbone instead of producing the proposed block copolymer structure. Since the hydrolytic rate of DMAEMA might compete with the polymerization kinetic rate, it is not clear how much methacrylic acid was incorporated in the copolymer structure. While a block copolymer, poly(DMAEMA-NVP)-*b*-PEG, was intended to synthesize in this study, poly(DMAEMA-NVP)-*g*-PEG could be formed competitively. A more rigorous study for elucidating the copolymer structure will be necessary.

To demonstrate the interaction between positively charged poly(DMAEMA-NVP) and negatively charged plasmid DNA, a gel retardation assay was performed by electrophoresis on 0.8% agarose gel. As shown in Figure 4, three topologically different plasmid DNA species, i.e., supercoiled, linear, and open circular form, could be observed from bottom to top of lanes 2 and 3. Complete retardation of complexes was observed when the polymer and plasmid DNA were compacted at a very low polymer/plasmid weight ratio, above 0.5. In addition, poly(DMAEMA-NVP)-*b*-PEG/plasmid complexes also showed a complete retardation at a range of 0.5−1 polymer/plasmid weight ratio, which was very similar to poly(DMAEMA-NVP)/plasmid complexes (data not shown). This demonstrates that the PEG block had no profound effect on the complex formation between cationic polymers and anionic plasmid DNA by ionic interaction. The condensing capacity of these polymers toward plasmid DNA was also evaluated by a dynamic light scattering (DLS) method. According to the DLS analysis, poly(DMAEMA-NVP)-*b*-PEG-galactose started to compact plasmid DNA at the copolymer/plasmid weight ratio of

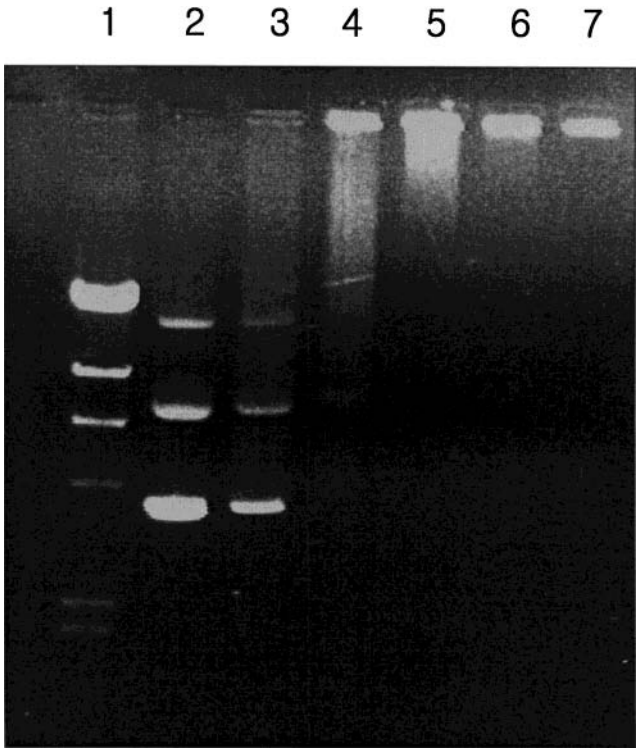

Figure 4. Compaction of DNA with poly(DMAEMA-NVP) demonstrated in a gel retardation assay (0.8% agarose gel electrophoresis); lane 1, DNA size marker (*λ-Hin*dIII); lane 2, DNA only; and lanes 3−7, poly(DMAEMA-NVP)/DNA complexes at different weight ratios. Lane 3, 0.05; lane 4, 0.1; lane 5, 0.25; lane 6, 0.5; lane 7, 1.

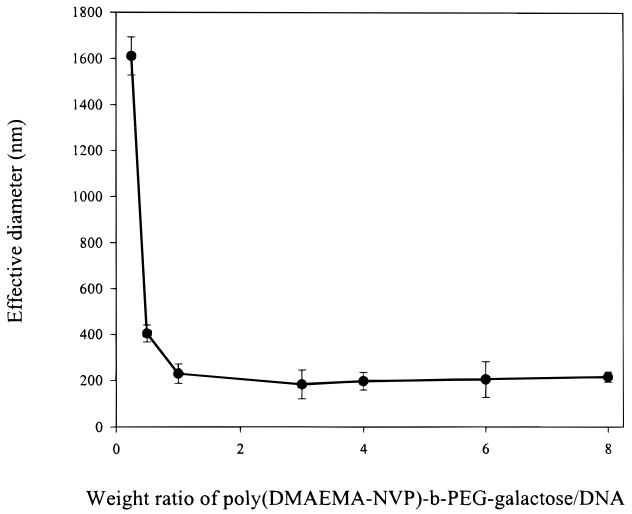

Figure 5. Effective particle diameter (nm) of complexes formed between DNA and poly(DMAEMA-NVP)-*b*-PEG-galactose as a function of poly(DMAEMA-NVP)-*b*-PEG-galactose/DNA weight ratio at a fixed plasmid DNA amount. Each point was expressed as a mean value ± SD in duplicate experiments.

0.5 and produced around 200 nm size nanoparticles at the weight ratio of 1.0, as shown in Figure 5. Therefore, the poly(DMAEMA-NVP) derivatives could effectively compact plasmid DNA at a very low range between 0.5 and 1 polymer/DNA weight ratio, which was in good agreement with the fact that poly(DMAEMA-NVP) random copolymer had the ability of compacting DNA at very low polymer/DNA ratios, as previously reported (*35*). Figure 6 shows the surface ζ-potential of poly(DMAEMA-NVP)-*b*-PEG-galactose/plasmid complex particles with and without coating of the cationic, pH-dependent,

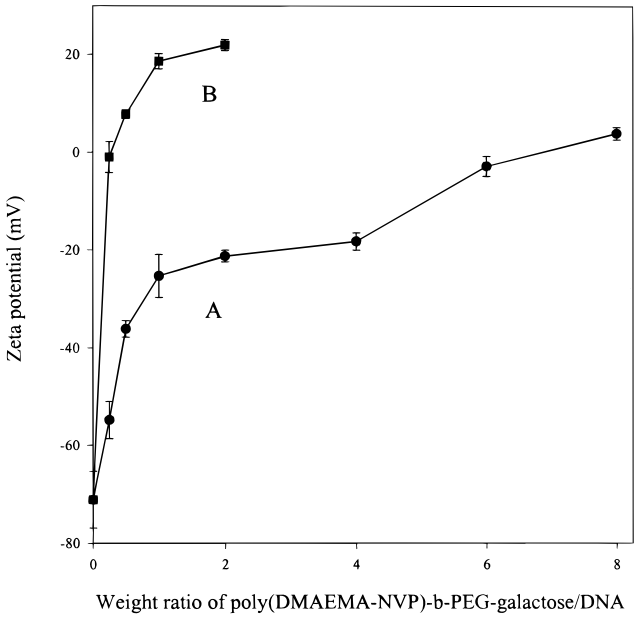

Figure 6. ζ-Potential of (A) self-assembled complex of DNA and poly(DMAEMA-NVP)-*b*-PEG-galactose and (B) the poly(DMAEMA-NVP)-*b*-PEG-galactose/DNA complex coated with KALA (KALA/DNA weight ratio = 4) as a function of poly(DMAEMA-NVP)-*b*-PEG-galactose/DNA weight ratio at a fixed plasmid DNA amount. Each point was expressed as a mean value ± SD in duplicate experiments.

α-helical peptide, KALA. It shows that the complex particles formed up to polymer/plasmid weight ratio of 6 exhibited negative surface charge while maintaining their compacted structures around 200 nm in size, suggesting that the amount of cationic polymer to neutralize anionic plasmid DNA was insufficient under the conditions of complex formation adopted in this study. When KALA (KALA/DNA weight ratio = 4) was coated onto these polymer/DNA complex particles, the ζ-potential values turned abruptly into positive charge, ranging from around 0 mV to about 20 mV. Furthermore, as the polymer/DNA weight ratio increased, the surface ζ-potential of poly(DMAEMA-NVP)-*b*-PEG-gal/DNA/KALA complexes tended to show a saturation value of 26.6 ± 3.8 mV. These optimized poly(DMAEMA-NVP)-*b*-PEG-galactose/DNA/KALA complex nanoparticles, as schematically shown in Figure 7, were used for further cell transfection experiments. The proposed DNA delivery system can be summarized as follows. First, the poly(DMAEMA-NVP)-*b*-PEG-galactose/DNA complex particles having a diameter of around 200 nm with negative surface charge were generated and then coated with positively charged fusogenic KALA peptide onto the surface of the polymer/DNA complexes to produce the polymer/DNA/KALA complex nanoparticles with net positively charged surface. This molecular architecture might permit not only a facile nonspecific adsorptive endocytosis but also allow a superior endosomal membrane escaping activity because of KALA surface coating. Additionally, these polymer/DNA/KALA composite nanoparticles are expected to have both enriched PEG chains located on the surface for the minimization of serum protein adsorption and galactose targeting moiety at the end of PEG chain for enhancing the receptor-mediated endocytosis against asialoglycoprotein receptors existing in the cell membrane of hepatocytes.

In vitro transfection efficiencies of luciferase plasmid DNA, which was first compacted with poly(DMAEMA-NVP), poly(DMAEMA-NVP)-*b*-PEG, and poly(DMAEMA-

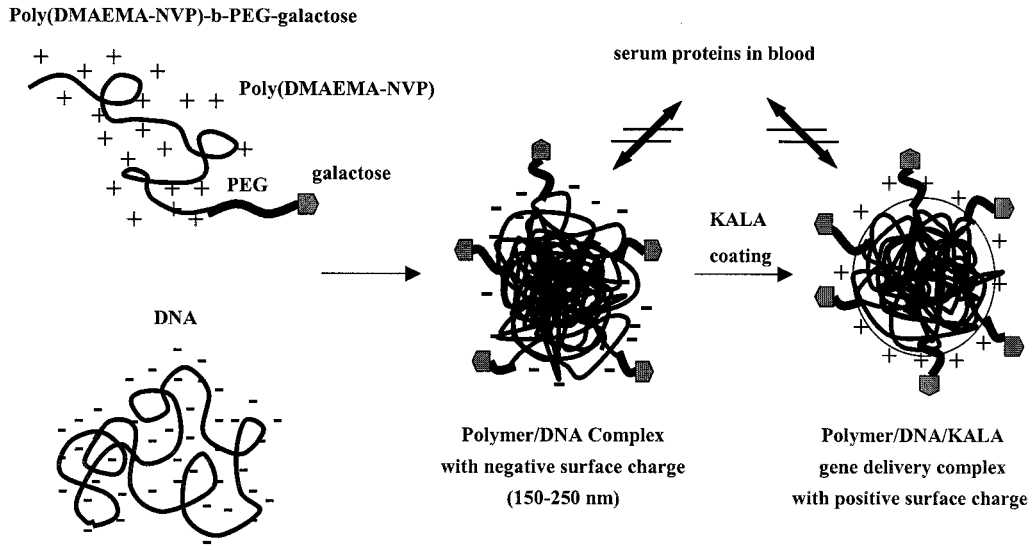

Figure 7. Schematic representation of poly(DMAEMA-NVP)-*b*-PEG-galactose/DNA/KALA complex formulated for an efficient gene transfection. Plasmid DNA highly compacted with poly(DMAEMA-NVP)-*b*-PEG-galactose exhibits slightly negative surface charge, which could be coated with α-helical, amphiphatic KALA at pH 7.5 by ionic interaction, resulting in net positively charged surface.

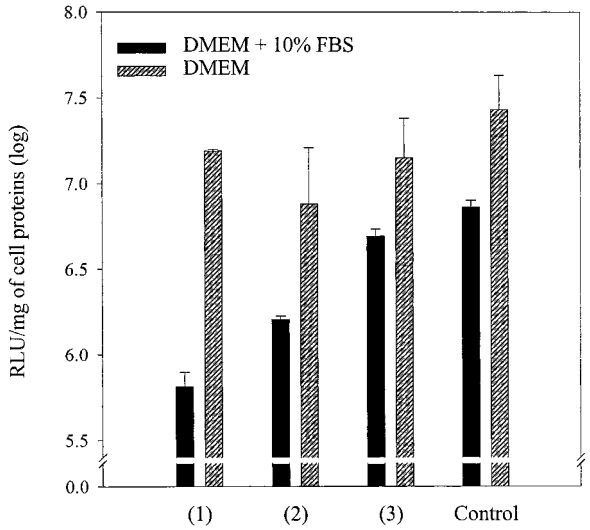

Figure 8. Transfection efficiencies against HepG2 cells of (1) poly(DMAEMA-NVP), (2) poly(DMAEMA-NVP)-*b*-PEG, and (3) poly(DMAEMA-NVP)-*b*-PEG-galactose. To prepare poly(DMAEMA-NVP) derivatives/DNA/KALA complexes, 2 μg of DNA was mixed with 1 μg of poly(DMAEMA-NVP) derivatives and then 8 μg of KALA was added to the complex. Lipofectamine plus was used as a control gene carrier. Each point was expressed as a mean value ± SD in duplicate experiments.

NVP)-*b*-PEG-galactose and then surface-coated with KALA, were evaluated against a HepG2 cell line in order to see the effects of the PEG block and the galactose targeting moiety in the presence and absence of serum proteins. It is shown in Figure 8 that in the presence of serum proteins (10% FBS), both the PEG block and the galactose moiety synergistically enhanced the gene transfection efficiency of poly(DMAEMA-NVP)-*b*-PEG-galactose, which is closely approaching that of Lipofectamine plus. It can be expected that in the presence of serum proteins, the PEG block spacer and the terminal galactose moiety exposed onto the surface of polymer/DNA/KALA complex prevented the nonspecific serum protein adsorption and increased the receptor mediated endocytosis, respectively. Poly(DMAEMA-NVP)/DNA/KALA complex demonstrates the lowest transfection efficiency possibly due to more pronounced protein adsorption onto the surface of the complex particles, leading to net negatively charged surface and consequently resulting in the reduction of adsorptive endocytosis through cell membrane. In the absence of serum proteins, however, the PEG block as well as the galactose moiety in the polymer structure have no significant effects on the transfection efficiency, while demonstrating much higher tranfection efficiencies than in the presence of serum proteins. This is likely to occur because the gene transfection efficiencies of poly(DMAEMA-NVP) and its derivatives are sufficiently high by themselves without serum proteins, masking the PEG effect on the transfection. It appears that the suppression of surface protein adsorption by the PEG chains in the presence of serum proteins increases the gene transfection efficiency mainly due to maintaining the positive surface charge, which facilitated the adsorptive endocytosis process. Concomitantly, the surface exposed terminal galactose moieties of the polymer/DNA/KALA complex were likely to additionally contribute to the receptor-mediated process. To confirm whether the receptor mediated endocytosis process indeed took place, transfecting the proposed DNA carrier to different cell lines lacking asialoglycoprotein receptors or transfecting it to HepG2 cells in the presence of free galactose in the medium would be necessary. Figure 9 shows the gene transfection efficiency of poly(DMAEMA-NVP)-*b*-PEG-galactose as a function of polymer/plasmid weight ratio. It is noteworthy that KALA by itself can condense plasmid DNA and exhibits some transfection activity, which is consistent with the previous finding of using KALA as a DNA transfection agent (*26*). It can be seen that up to the poly(DMAEMA-NVP)-*b*-PEG-galactose/DNA weight ratio of 0.5, the transfection efficiency increases, but decreases thereafter. The slightly decreased transfection efficiency at the weight ratio of 0.75 might be due to a dose-dependent cytotoxic effect of the polymer, although the cytotoxicity of polymer is minimal as will be discussed later. Thus, these data suggest that relatively small amount of the synthesized polymer can be used to efficiently compact plasmid DNA to the size of nanoparticulates with a negative surface charge and then a minimal amount of KALA could be ionically coated on the surface of the polymer/DNA complexes, resulting in positively surface-charged polymer/DNA/KALA complexes with an endosomal disruptive activity. This additionally reveals that the proposed

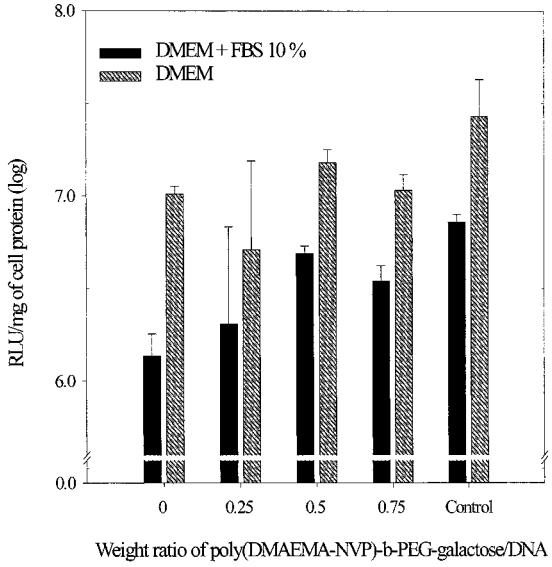

Figure 9. Transfection efficiency of poly(DMAEMA-NVP)-*b*-PEG-galactose against HepG2 cells as a function of poly-(DMAEMA-NVP)-*b*-PEG-galactose/DNA weight ratio. A total of 2 μg of DNA was mixed with various amounts of poly(DMAEMA-NVP)-*b*-PEG-galactose, and then 8 μg of KALA was added to the complex. Lipofectamine plus was used as a control gene carrier. Each point was expressed as a mean value ± SD in duplicate experiments.

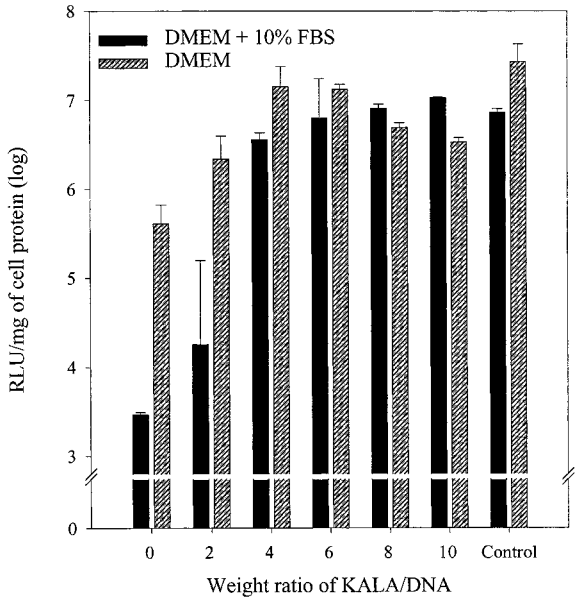

Figure 10. Transfection efficiency of poly(DMAEMA-NVP)-*b*-PEG-galactose against HepG2 cells as a function of KALA/DNA weight ratio. A total of 2 μg of DNA was mixed with 1 μg of poly(DMAEMA-NVP)-*b*-PEG-galactose and various amounts of KALA were added to the complex. Lipofectamine plus was used as a control gene carrier. Each point was expressed as a mean value ± SD in duplicate experiments.

approach of DNA compaction with the polymer and subsequent KALA coating is an efficient way to reduce the cytotoxic effect of cationic polymers to cells.

Poly(DMAEMA-NVP)-*b*-PEG-galactose/DNA complexes formulated with increasing weight ratios of fusogenic peptide KALA/plasmid, exhibited greatly enhanced transfection efficiencies regardless of KALA amounts to be coated as shown in Figure 10. The polymer/DNA complexes without coating of fusogenic peptide, KALA, showed higher transfection efficiency in the absence of serum proteins than in the presence of serum proteins.

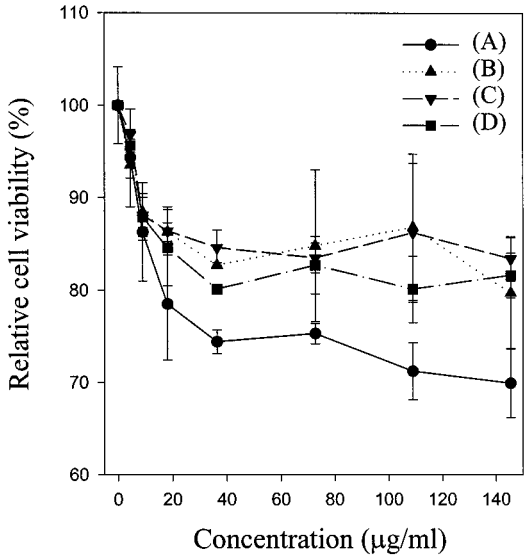

Figure 11. Effects of various polymeric gene carriers on relative HepG2 cell viability. (A) Poly(DMAEMA-NVP), (B) Poly-(DMAEMA-NVP)-*b*-PEG, (C) Poly(DMAEMA-NVP)-*b*-PEG-galactose, and (D) fusogenic peptide, KALA were used. HepG2 cells were incubated with culture medium containing polymers for 2 days. Each point was expressed as a mean value ± SD in triplicate experiments.

However, in the presence of serum proteins, the polymer/DNA complexes exhibited more enhanced transfection efficiency with increasing KALA coating amount. Irrespective of the presence of serum proteins, as the KALA/DNA weight ratio increased, poly(DMAEMA-NVP)-*b*-PEG-galactose/DNA/KALA complexes enhanced transfection extents in a similar pattern, due to the pH dependent endosomal disruptive property of KALA. It is conceivable that an endosomal disruptive activity of KALA is a dominant factor in the gene expression rather than the endocytosis of the complexes into cells, since there is no difference in transfection efficiencies with and without serum proteins. In particular, with the increasing amount of KALA, luciferase expression in the presence of serum proteins is almost similar or superior to Lipofectamine plus. Last, it should be mentioned that poly(DMAEMA-NVP)-*b*-PEG-galactose exhibited much reduced cytotoxicity than other polymeric gene carriers as measured by MTT assay, which is shown in Figure 11. Both poly(DMAEMA-NVP)-*b*-PEG and poly(DMAEMA-NVP)-*b*-PEG-galactose demonstrate reduced cytotoxicity compared to poly(DMAEMA-NVP). This can be attributed to the masking effect of cationic charges in the polymer by PEG chains against cells. The fusogenic peptide, KALA showed comparable cytotoxicity to PEG blocked polymeric gene carriers, such as poly(DMAEMA-NVP)-*b*-PEG and poly(DMAEMA-NVP)-*b*-PEG-galactose. The introduction of NVP structural units in the poly-DMAEMA additionally lowered the overall cytotoxic effect of cationic polymers used for gene carriers as similarly reported previously (*35*).

CONCLUSION

This study demonstrates that sufficient transfection efficiency as high as a commercially available agent could be attained by carefully designing the molecular structure of cationic poly(DMAEMA-NVP)-*b*-PEG with a targeting moiety, galactose at the end of PEG block and coating the polymer/DNA complex with a pH dependent, endosomal disruptive peptide, KALA.

ACKNOWLEDGMENT

This work was supported in part by the grants (HMP-99-B-02-0002 and 98-G-08-02-A-16) from the Ministry of Health and Welfare and the Ministry of Science and Technology, Republic of Korea.

LITERATURE CITED

(1) Remy, J.-S., Abdallah, B., Zanta, M. A., Boussif, O., Behr, J. P., and Demeneix, B. (1998) Gene transfer with lipospermines and polyethyleneimines. *Adv. Drug Delivery Rev. 30*, 85−95.

(2) Haensler, J., and Szoka, F. C. (1993) Polyamidoamine cascade polymers mediate efficient transfection of cells in culture. *Bioconjugate Chem. 4*, 372−379.

(3) Zauner, W., Ogris, M., and Wagner, E. (1998) Polylysine-based transfection systems utilizing receptor-mediated delivery. *Adv. Drug Delivery Rev. 30*, 97−113.

(4) Cherng, J.-Y., Wetering, P. V. D., Talsma, H., Crommelin, D. J. A., and Hennink, W. E. (1996) Effect of size and serum proteins on transfection efficiency of poly((2- dimethylamino)-ethyl methacrylate)-plasmid nanoparticles. *Pharm. Res. 13*, 1038 1042.

(5) Cherng, J.-Y., Wetering, P. V. D., Talsma, H., Crommelin, D. J. A., and Hennink, W. E. (1997) Freeze-drying of poly-((2-dimethylamino)ethyl methacrylate)-based gene delivery systems. *Pharm. Res. 14*, 1838−1841.

(6) Wetering, P. V. D., Cherng, J.-Y., Talsma, H., and Hennink, W. E. (1997) Relation between transfection efficiency and cytotoxicity of poly((2-dimethylamino)ethyl methacrylate)-plasmid complexes. *J. Controlled Release 49*, 59−69.

(7) Wetering, P. V. D., Moret E. E., Schuurmans-Nieuwenbroek, N. M. E., Steenbergen, M. J. V., and Hennink, W. E. (1999) Structure−activity relationships of water-soluble cationic methacrylate/methacrylamide polymers for nonviral gene delivery. *Bioconjugate Chem. 10*, 589−597.

(8) Kollidon, V. B. (1993) *Poly(vinylpyrrolidone) for the pharmaceutical industry*, BASF Aktiengesellschaft Feinchemie, Ludwigshafen.

(9) Gombotz, W. R., Pankey S. C., Phan, D., Drager, R., Donaldson, K., Antonsen, K. P., Hoffman, A. S., and Raff H. V. (1994) The stabilization of human IgM monoclonal antibody with poly(vinylpyrrolidone). *Pharm. Res. 11*, 624−632.

(10) Mumper, R. J., Duguid, J. G., Anwer, K., Barron, M. K., Nitta, H., and Rolland, A. P. (1996) polyvinyl derivatives as a novel interactive polymers for controlled gene delivery to muscle. *Pharm. Res. 13*, 701−709.

(11) Godbey, W. T., Wu, K. K., and Mikos, A. G. (1999) Poly-(ethylenimine) and its role in gene delivery. *J. Controlled Release 60*, 149−160.

(12) Erbacher, P., Remy, J.-S., and Behr, J.-P. (1999) Gene transfer with synthetic virus-like particles via the integrin-mediated endocytosis pathway. *Gene Ther. 6*, 138−145.

(13) Choi, Y. H., Liu, F., Kim J. S., Choi, Y. K., Park, J. S., and Kim, S. W. (1998) Polyethylene glycol-grafted poly-L-lysine as polymeric gene carrier. *J. Controlled Release 54*, 39−48.

(14) Kwon, G. S., and Okano, T. (1999) Soluble self-assembled block copolymers for drug delivery. *Pharm. Res. 16*, 597−600.

(15) Katayose, S., and Kataoka, K. (1997) Water soluble polyion complex associates of DNA and poly(ethylene glycol)-poly(L-lysine) block copolymers. *Bioconjugate Chem. 8*, 702−707.

(16) Katayose, S., and Kataoka, K. (1998) Remarkable increase in nuclease resistance of plasmid DNA through supramolecular assembly with poly(ethylene glycol)-poly(L-lysine) block copolymer. *J. Pharm. Sci. 87*, 160−163.

(17) Vinogradov, S., Bronich, T. K., and Kavanov, A. V. (1998) Self-assembly of polyamine-poly(ethylene glycol) copolymers with phosphorothioate oligonucleotides. *Bioconjugate Chem. 9*, 805−812.

(18) Ogris, M., Brunner, S., Schüller, S., Kircheis, R., and Wagner, E. (1999) Pegylated DNA/transferring-PEI complexes: reduced interaction with blood components, extended circulation in blood and potential for systemic gene delivery. *Gene Ther. 6*, 595−605.

(19) Wu, C. H., and Wu, G. Y. (1998) Receptor-mediated delivery of foreign genes to hepatocytes. *Adv. Drug Delivery Rev. 29*, 243−248.

(20) Hashida, M., Takemura, S., Nishikawa, M., and Takakura, Y. (1998) Targeted delivery of plasmid DNA complexed with galactosylated poly (L-lysine). *J. Controlled Release 53*, 301−310.

(21) Choi, Y. H., Liu, F., Park, J. S., and Kim, S. W. (1998) Lactose-poly(ethylene glycol)-grafted poly L-lysine as hepatoma cell targeted gene carrier. *Bioconjugate Chem. 9*, 708−718.

(22) Zanta, M. A., Boussif, O., Adib, A., and Behr, J. P. (1997) *In vitro* gene delivery to hepatocytes with galactosylated polyethyleneimine. *Bioconjugate Chem. 8*, 839−844.

(23) Plank, C., Oberhauser, B., Mechtler. K., Koch, C., and Wagner, E. (1994) The influence of endosome-disruptive peptides on gene transfer using synthetic virus-like gene transfer systems. *J. Biol. Chem. 269*, 12918−12924.

(24) Wolfert, M. A., and Seymour, L. W. (1998) Chloroquine and amphiphatic peptide helices show synergistic transfection *in vitro. Gene Ther. 5*, 409−414.

(25) Wagner, E. (1998) Effects of membrane-active agents in gene delivery. *J. Controlled Release 53*, 155−158.

(26) Wyman, T. B., Nicol F., Zephalti, O., Scaria P. V., Plank C., and Szoka, F. C. (1997) Design, Synthesis, and Characterization of a cationic peptide that binds to nucleic acids and permeabilizes bilayers. *Biochemistry 36*, 3008−3017.

(27) Duguid, J. G., Li, C., Shi, M., Logan, M. J., Alila, H., Rolland, A., Tomlinson, E., Sparrow, J. T., and Smith, L. C. (1998) A physicochemical approach for predicting the effectiveness of peptide-based gene delivery systems for use in plasmid-based gene therapy. *Biophys. J. 74*, 2802−2814.

(28) Sambrook, J., Fritsch, E. F., and Maniatis, T. (1989) *Molecular cloning 1*, pp 1.33-1.52, Cold Spring Harbor Laboratory Press, Plainview, NY.

(29) Life Technologies Co. (1999) Lipofectamine Plus Reagent, Technical Bulletin.

(30) Putnam, D., and Langer, R. (1999) Poly(4-hydroxy-L-proline ester); low-temperature polycondensation and plasmid DNA complexation. *Macromolecules 32*, 3658−3662.

(31) Deboudt, K., Delporte, M., and Loucheux, C. (1995) Copolymers of N-vinyl-2-pyrrolidone and 2-(dimethylamino)-ethyl methacrylate, 1. *Macromol. Chem. Phys. 196*, 279−290.

(32) Pouton, C. W., and Seymour, L. W. (1998) Key issues in nonviral gene delivery. *Adv. Drug Delivery Rev. 34*, 3−19.

(33) van de Wetering, P., Schuurmans-Nieuwenbroek, N. M. E., van Steenbergen, M. J., Crommelin D. J. A., and Hennink, W. E. (2000) Copolymers of 2-(dimethylamino)ethyl methacrylate with ethoxytriethylene glycol methacrylate or N-vinyl-pyrrolidone as gene transfer agents. *J. Controlled Release 64*, 193−203.

(34) van de Wetering, P., Zuidam, N. J., van Steenbergen M. J., van der Houwen, O. A. G. J., Underberg, W. J. M., and Hennink, W. E. (1998) A Mechanistic study of the hydrolytic stability of poly(2-(dimethylamino)ethyl methacrylate). *Macromolecules 31*, 8063−8068.

(35) van de Wetering, P., Cherng, J.-Y., Talsma, H., Crommelin D. J. A., and Hennink, W. E. (1998) 2-(dimethylamino)ethyl methacrylate based (co)polymers as gene transfer agents. *J. Controlled Release 53*, 145−153.

BC000014U

Anomalous Fluorescence Enhancement of Cy3 and Cy3.5 versus Anomalous Fluorescence Loss of Cy5 and Cy7 upon Covalent Linking to IgG and Noncovalent Binding to Avidin

Hermann J. Gruber,* Christoph D. Hahn, Gerald Kada, Christian K. Riener, Gregory S. Harms, Werner Ahrer,† Thomas G. Dax,† and Hans-Günther Knaus‡

Institute of Biophysics and Institute of Chemistry, J. Kepler University, Altenberger Strasse 69, A-4040 Linz, Austria, and Institute of Biochemical Pharmacology, Peter Mayr Strasse 1, A-6020 Innsbruck, Austria. Received February 11, 2000; Revised Manuscript Received June 8, 2000

This study provides a critical examination of protein labeling with Cy3, Cy5, and other Cy dyes. Two alternate situations were tested. (i) Antibodies were covalently labeled with Cy dye succinimidyl ester at various fluorophore/protein ratios and the fluorescence of the labeled antibodies was compared to that of free Cy dye. (ii) Fluorescent biotin derivatives were synthesized by derivatizing ethylenediamine with one biotin and one Cy3 (or Cy5) residue. The fluorescence properties of these biotin−Cy dye conjugates were examined at all ligand/(strept)avidin ratios ($0 \leq n \leq 4$). The results showed an astounding discrepancy between Cy3 and Cy5: Cy3-labeled antibodies fluoresced very well, even at high Cy3/protein ratios, and the same applied to (strept)avidin with up to four bound biotin−Cy3 conjugates. In contrast, antibodies with six covalently bound Cy5 labels (obtained with the recommended procedure) were almost nonfluorescent, only at 2−3 Cy5 labels/IgG some moderate fluorescence was obtained. By analogy, the biotin−Cy3 conjugate fluoresced intensely, even at high ligand/avidin ratio, in contrast to the weakly fluorescing biotin−Cy5 conjugate. Three mechanisms are responsible for the discrepancy between Cy3 and Cy5. (i) Attachment of Cy3 to a protein's surface causes an anomalous enhancement in fluorescence (by 2−3-fold) while no enhancement occurs with Cy5. (ii) Mutual quenching of IgG-bound Cy dyes by resonance energy transfer is much more pronounced for Cy5 labels than for Cy3. (iii) In IgG with six bound Cy5 labels, about one-third of the labels adopt a nonfluorescent state which is characterized by a large UV−vis absorption maximum at 600 nm instead of at 650 nm. Cy3.5 was found to mimick the properties of Cy3, while Cy7, and to some extent also Cy5.5, were similar to Cy5. In conclusion the Cy dye series is divided into two groups: Antibodies with multiple Cy3 or Cy3.5 labels yield bright fluorescence while extensive quenching occurs in antibodies labeled with Cy5 and Cy7.

INTRODUCTION

Immunofluorescence microscopy has been, and still is, an indispensable tool of cell biology and histology. It provides for specific visualization of one or two particular target proteins in live or fixed cells while all other biomolecules remain invisible, except for unavoidable autofluorescence of biomatter (Aubin, 1979; Benson et al., 1979; Marelius, 1995; Wolfbeis and Leiner, 1985). Usually the fluorescent labels are coupled to the lysine residues of the target-specific antibodies in a statistical way, and high fluorophore/antibody ratios are generally preferred for two purposes.: (i) to maximize the fluorescence signal from each antibody molecule and (ii) to minimize the fraction of unlabeled or too weakly labeled antibodies in the total pool. Beyond some optimal fluorophore/antibody ratio, however, the fluorescence signal per antibody will decrease, rather than increase, due to resonance energy transfer between fluorophores on one protein molecule (Steinberg, 1971).

The parameters of optimal labeling are well documented for fluorescein, TMR, Texas Red, as well as the Bodipy and Alexa dye series (Goding, 1976; Haugland, 1995; Haugland, 1996). In contrast, no explicit information of that kind is available on the Cy dye series. This is unfortunate because Cy3 and Cy5 are most promising labels for single molecule fluorescence microscopy (SMFM),[1] Cy3 because of exceptional brilliance (Mujumdar et al., 1993; Wessendorf and Brelje, 1992) and outstanding photostability (G. S. Harms, unpublished results) and Cy5 (or Cy7) because of excitation at wavelengths above

* To whom correspondence should be addressed at the Institute of Biophysics at J. Kepler University. Phone: +43 (732) 2468-9271. Fax: +43 (732) 2468-822. E-mail: hermann.gruber@jk.uni-linz.ac.at.

† Institute of Chemistry.

‡ Institute of Biochemical Pharmacology.

[1] Abbreviations: Biotin-4-Cy, biotin-4-Cy3 and/or biotin-4-Cy5; biotin-4-Cy3 and *biotin-4-Cy5* denote the structures shown in Scheme 1; biotin-4-fluorescein, 5-(and 6)-[2-(biotinoyl)-aminoethylaminocarbonyl]-fluorescein; BSA, bovine serum albumin; Cy3-PE, Cy3-labeled phosphatidylethanolamine; DIEA, *N*,*N*-diisopropyl-*N*-ethylamine; DMF, dimethylformamide; EGF, epidermal growth factor; HgTx, hongotoxin; HgTx-A19C, mutant of HgTx in which alanine-19 is replaced by cysteine; Ig, bovine gamma globulins; IgG, goat immunoglobulin G; Ig(G), bovine Ig or goat IgG; MS, mass spectrometry; NHS, *N*-hydroxysuccinimide; PEG, poly(ethylene glycol); RT, room temperature (22−25 °C); SbTMU, *O*-(*N*-succinimidyl)-*N*,*N*,*N*′,*N*′-bis-(tetramethylene)-uronium hexafluorophosphate; SDS, sodium dodecyl sulfate; (strept)avidin, avidin and/or streptavidin; SMFM, single molecule fluorescence microscopy; TMR, tetramethylrhodamine. See Supporting Information for abbreviations of Cy dyes.

10.1021/bc000015m CCC: $19.00 © 2000 American Chemical Society
Published on Web 08/31/2000

600 nm where autofluorescence of biomatter is much reduced (Aubin, 1979; Benson et al., 1979; Marelius, 1995; Wolfbeis and Leiner, 1985).

In the present study, the parameters of antibody labeling with Cy dyes were critically examined. To our great surprise the Cy dye series was found to be divided into two groups with widely different fluorescence properties, imposing limitations on the use of Cy5 and Cy7 for immunfluorescence microscopy, especially in SMFM.

EXPERIMENTAL PROCEDURES

Materials. Analytical-grade materials were used as long as they were commercially available. Cy3-, Cy3.5-, Cy5-, and Cy5.5-monofunctional dye, as well as Cy7-bifunctional dye, QAE Sephadex A-25, and PD-10 columns were obtained from Amersham Pharmacia Biotech. Bovine Ig (γ globulins), goat IgG, BSA, *d*-biotin, avidin, and streptavidin were purchased from Sigma. LiChroprep gel was obtained from Merck.

Buffers. Buffer A contained 100 mM NaCl, 50 mM NaH_2PO_4, and 1 mM EDTA (pH 7.5 adjusted with NaOH). Buffer B was a 3/1 mixture of buffer A and 2 M NaCl. Buffer C contained 150 mM Na_2CO_3 (pH 9.3 adjusted with H_3PO_4). Buffer D contained 150 mM NaCl and 5 mM NaH_2PO_4 (pH 7.4 adjusted with NaOH).

Measurement of Cy Dye Concentrations. The molar extinction coefficients of the Cy dyes in methanolic solution are known ($\epsilon_{550} = 150\,000\ M^{-1}\ cm^{-1}$ for Cy3, $\epsilon_{581} = 150\,000\ M^{-1}\ cm^{-1}$ for Cy3.5, $\epsilon_{650} = 250\,000\ M^{-1}\ cm^{-1}$ for Cy5, $\epsilon_{678} = 250\,000\ M^{-1}\ cm^{-1}$ for Cy5.5, and $\epsilon_{750} = 250\,000\ M^{-1}\ cm^{-1}$, for Cy7, according to the manufacturer's data sheets). Here it was found that the absorption changed very little when the Cy dyes were dissolved in aqueous buffer. Covalent attachment of the Cy dyes to protein was also seen to have little effect, except for a small bathochromic shift (see Figure 7 and Figures 8A and 9A in the Supporting Information). Unless stated otherwise, all Cy dye concentrations (including those of biotin-4-Cy3 and *biotin-4-Cy5*) were calculated from the absorbance values at λ_{max}, assuming the above cited molar extinction coefficients.

Covalent Labeling of Proteins with Cy Dyes. Goat IgG, bovine Ig, or BSA were reacted with Cy3-, Cy3.5-, Cy5-, or Cy5.5-monofunctional dye, as well as with Cy7-bifunctional dye, either according to the manufacturer's recommendations (solid symbols in Figures 1−3) or at lower dye/protein ratios (open symbols in Figures 1−3). One portion of Cy dye ("to label 1 mg of protein") was dissolved in 50 μL of DMSO, and from this stock solution a series of dye/DMSO solutions was prepared which corresponded to a consecutive dilution by a factor of 2 in each dilution step (as an exception, the first two dilution steps were by a factor of 4 in the Cy5 series in Figure 2). Labeling was started by mixing 0.2 mL of protein (1 mg/mL in buffer C) with 10 μL of dye/DMSO solution and vortexing was repeated after 10 and 20 min. After 30 min reaction time at RT (with mixing after 10 and 20 min) the protein with bound Cy dye was separated from unreacted Cy dye by gel filtration in buffer A [same protocol as used for avidin (see Supporting Information)]. The protein concentrations in the void peak were calculated from A_{280} ($\epsilon_{280} = 210\,000\ M^{-1}\ cm^{-1}$ for goat IgG according to the manufacturer's data sheet; $\epsilon_{280} = 174\,000\ M^{-1}\ cm^{-1}$ for bovine Ig, determined experimentally; $\epsilon_{280} = 44\,300\ M^{-1}\ cm^{-1}$ for BSA, Elgersma et al., 1990), taking into account the absorbance contribution from covalently bound Cy dye at 280 nm ($0.08 \times A_{550}$ for Cy3, $0.24 \times A_{580}$ for Cy3.5, $0.05 \times A_{650}$ for Cy5, and $0.18 \times A_{680}$ for Cy5.5, according to the manufacturer's instructions; $0.11 \times A_{750}$ for Cy7, determined from the absorption spectrum of Cy7-bifunctional dye in buffer A). The Cy dye concentrations in the protein peaks were measured by absorbance as described above.

Synthesis of Biotin-4-Cy3 and *Biotin-4-Cy5* (see Scheme 1 and Supporting Information). All operations were carried out under dim light, and light was further excluded by wrapping flasks and glass columns with aluminum foil. Cy3-monofunctional dye (1.4 μmol) or Cy5-monofunctional dye (1.0 μmol) was dissolved in 1 mL of DMF containing 8.4 mg SbTMU (20.4 μmol, Bannwarth and Knorr, 1991), and 5 μL neat DIEA (57 μmol) was added. After 40 min of stirring at RT this mixture was added to dry biotin-NH-CH_2-CH_2-NH_3^+ Cl^- [prepared according to Garlick and Giese (1988)]. Another 20 μL of neat DIEA (230 μmol) was added and stirring was continued under argon for 1 h at RT. The solvent was removed and the dry residue sequentially chromatographed on QAE Sephadex A-25 (Gruber et al., 1997), on LiChroprep gel (Gruber et al., 2000), and on an HPLC C-18 column (Vydac no. 218TP510) as described in the Supporting Information. The compounds were found to be pure by HPLC and by electrospray MS, and the correct molecular structures were proven by NMR spectroscopy (see Supporting Information).

Fluorescence Measurements of Cy-Dye-Labeled Immunoglobulins and of Biotin-4-Cy3 and *Biotin-4-Cy5* in Absence and Presence of (Strept)avidin. All measurements were done in buffer A at 25 °C. Cy dye-labeled goat IgG or bovine Ig were consistently diluted to 50 nM Cy label concentration (according to absorbance at λ_{max}, see above). In the control experiments, the fluorescence of commercial Cy3- and Cy5-monofunctional dye or Cy7-bifunctional dye was also measured at 50 nM chromophore concentration.

For characterization of biotin-4-Cy3 and *biotin-4-Cy5*, 2 mL of 40 nM avidin [freshly prepared from the standardized 1.75 μM avidin stock solution (see Supporting Information)] or 2 mL 40 nM streptavidin [freshly prepared from the standardized 3.03 μM stock solution (see Supporting Information)] were stirred in the cuvette and 2 μL volumes of biotin-4-Cy3 [12.3 μM stock solution (see Supporting Information)] or *biotin-4-Cy5* [16.7 μM stock solution (see Supporting Information)] were successively added from a Hamilton syringe at 3 min intervals and Cy dye fluorescence at the end of each 3 min interval was recorded (see Figure 4).

RESULTS

Fluorescence Properties of Cy3-, Cy3.5-, Cy5-, Cy5.5-, and Cy7-Labeled Proteins. All samples of labeled protein were diluted to the same Cy label concentration (50 nM according to Cy dye absorption) and the fluorescence signals were compared to the fluorescence intensities of 50 nM free Cy dye in buffer (see Figures 1A, 2A, and 3A). At the lowest numbers of covalently bound Cy labels per Ig(G), many protein molecules were actually unlabeled and most of the labeled protein molecules carried a single Cy dye only. Extrapolation to 0 labels/Ig(G), therefore, gave the fluorescence of exactly mono-labeled Ig(G) in comparison to free fluorophore in buffer. As can be seen in Figures 1A, 2A, and 3A, Ig(G) molecules with a single Cy5 or Cy5.5 label (extrapolation of the dashed lines to $x = 0$) or with a single Cy7 label (extrapolation of the dotted line in Figure 2A to $x = 0$) had almost the same fluorescence

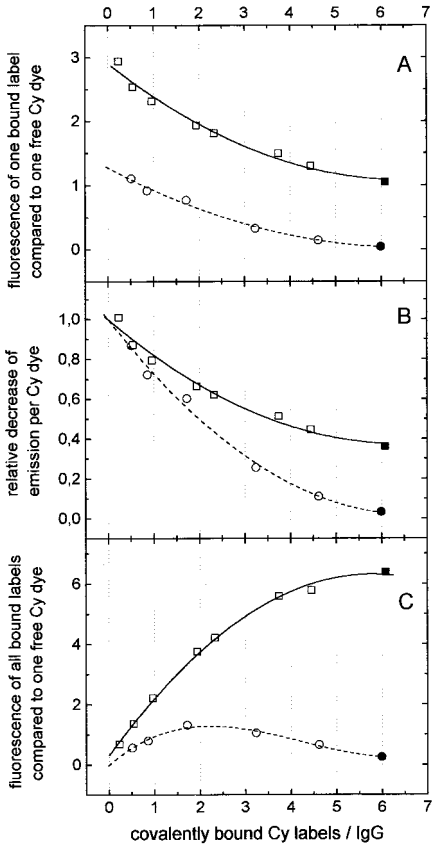

Figure 1. Covalent labeling of goat IgG with Cy3 (squares)- or Cy5-monofunctional dye (circles). IgG (1 mg/mL in buffer C) was reacted for 30 min at RT with amine-reactive Cy dye, either according to the manufacturer's instructions (solid symbols) or at lower dye/protein ratio (open symbols) and IgG with covalently bound Cy dye was separated from unreacted Cy dye by gel filtration. (A) IgG with covalently bound Cy dye was diluted to 50 nM Cy3 or Cy5 concentration (according to absorbance at 550 or 650 nm), and the fluorescence yield of IgG-bound label was compared to that of 50 nM free Cy3- or Cy5-monofunctional dye, respectively. Cy3 or Cy5 were excited at 530 or 630 nm, and the emission was measured at 565 or 665 nm, respectively. (B) Progressive fluorescence decrease of IgG-bound Cy3 (squares) or Cy5 labels (circles). The ordinate values from panel A were divided by the extrapolated intensities at 0 labels/protein in panel A. (C) The cumulative fluorescence yield of one labeled IgG molecule was calculated by multiplying the average fluorescence yield of one IgG-bound fluorophore (ordinate values in panel A) by the average number of fluorophores per IgG (see Experimental Procedures). The solid symbols in (A−C) indicate results obtained by the standard procedure.

yield as free Cy5, Cy5.5, or Cy7, respectively. Higher numbers of Cy5 or Cy7 labels, however, led to such a rapid drop in fluorescence (dashed and dotted lines in Figures 1A and 2A) that even the cumulative fluorescence of all Ig(G)-bound labels together started to drop beyond 3 fluorophores/protein (dashed and dotted lines in Figures 1C and 2B). It is concluded that, in practice, antibody molecules should carry no more than 2−4 Cy5 or Cy7 labels which is far less than obtained with the recommended procedure (solid circles and triangles in Figures 1 and 2). A more favorable result was obtained with Cy5.5. While, in general, Cy5.5 (circles in Figure 3) followed a similar pattern as Cy5 (circles in Figures 1 and 2), much less quenching occurred in antibodies labeled with ∼5 Cy5.5 labels/protein molecule (solid circle in Figure 3B), thus the stoichiometry of Cy5.5 over IgG is less critical, and higher levels of fluorescence per antibody can be achieved with Cy5.5 than with Cy5.

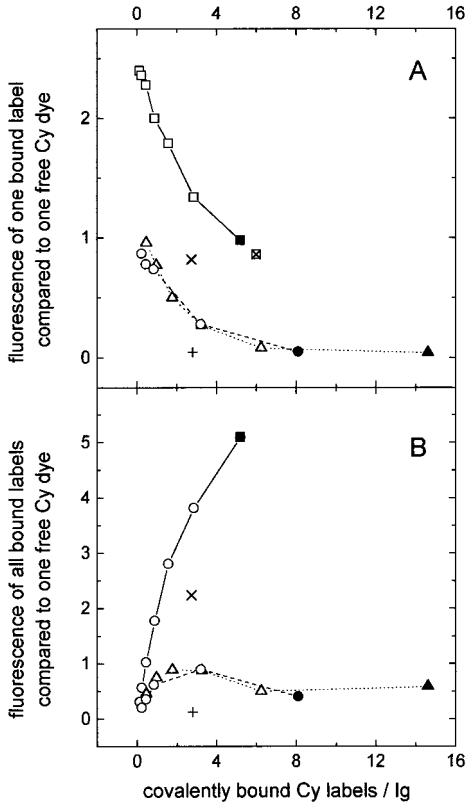

Figure 2. Covalent labeling of bovine Ig with Cy3 (squares), Cy5 (circles), and Cy7 (triangles). Ig (1 mg/mL in buffer C) was reacted for 30 min at RT with amine-reactive Cy dye, either according to the manufacturer's instructions (solid symbols) or at lower dye/protein ratio (open symbols) and Ig with covalently bound Cy dye was separated from unreacted Cy dye by gel filtration. (A) Gel-filtered Ig with covalently bound Cy dye was diluted to 50 nM Cy3, Cy5, or Cy7 concentration, and the fluorescence yield of Ig-bound label was compared to that of 50 nM free Cy3, Cy5, and Cy7, respectively. Excitation was at 530, 630, or 730 nm and the emission was measured at 570, 670, or 770 nm, respectively. (B) The cumulative fluorescence yield of one labeled Ig molecule was calculated by multiplying the average fluorescence yield of one Ig-bound fluorophore (ordinate values in panel A) by the average number of fluorophores per Ig (see Experimental Procedures). The solid symbols in (A and B) indicate results obtained with bovine Ig by the standard procedure. Labeling of BSA (at 1 mg/mL) with Cy3 (×) or Cy5 (+) by the standard procedure is also shown in (A and B).

To our great surprise, extremely bright fluorescence was seen in Cy3- and Cy3.5-labeled antibodies. At high fluorophore/antibody ratio (see solid squares in Figures 1C, 2B, and 3B) each individual Cy3 or Cy3.5 label fluoresced with the same average intensity as one free Cy3 or Cy3.3 dye in buffer (see solid squares in Figures 1A, 2A, and 3A). At lower numbers of Cy dye per Ig(G) the fluorescence per Cy3 or Cy3.5 was even higher (solid lines in Figures 1A, 2A, and 3A). Extrapolation to 0 labels/protein indicated that goat IgG with a single Cy3 label was three times more fluorescent (solid line in Figure 1A), bovine Ig with a single Cy3 label was 2.5 times more fluorescent (solid line in Figure 2A) than free Cy3 in buffer, and a similar enhancement in fluorescence was seen at low Cy3.5 numbers per IgG (solid line in Figure 3A).

The fluorescence of Cy dye-labeled BSA followed the same general pattern as observed with Ig(G). BSA with 2.7 bound Cy3 labels fluoresced quite well (× in Figure 2) while BSA with 2.8 Cy5 labels was almost nonfluorescent (+ in Figure 2). The lower fluorescence of Cy3-BSA (× in Figure 2A) in comparison to Cy3-Ig (squares

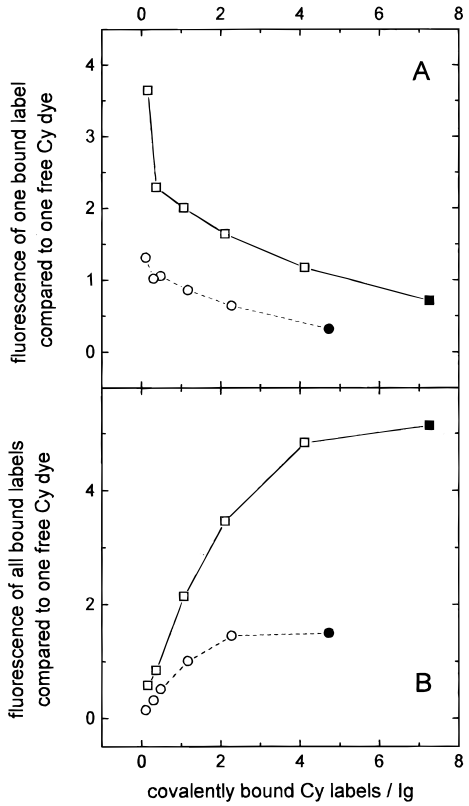

Figure 3. Covalent labeling of goat IgG with Cy3.5- (squares) or Cy5.5-monofunctional dye (circles). IgG (1 mg/mL in buffer C) was reacted for 30 min at RT with amine-reactive Cy dye, either according to the manufacturer's instructions (solid symbols) or at lower dye/protein ratio (open symbols) and IgG with covalently bound Cy dye was separated from unreacted Cy dye by gel filtration. (A) IgG with covalently bound Cy dye was diluted to 50 nM Cy3.5 or Cy5.5 label concentration (according to absorbance at 580 or 680 nm), and the fluorescence yield of IgG-bound label was compared to that of 50 nM free Cy3.5- or Cy5.5-monofunctional dye, respectively. Cy3.5 or Cy5.5 were excited at 560 or 655 nm, and the emission was measured at 600 or 700 nm, respectively. (B) The cumulative fluorescence yield of one labeled IgG molecule was calculated by multiplying the average fluorescence yield of one IgG-bound fluorophore (ordinate values in panel A) by the average number of fluorophores per IgG (see Experimental Procedures). The solid symbols in (A and B) indicate results obtained by the standard procedure.

in Figure 2A) was largely explained by the different size of the two proteins. BSA with 2.7 Cy3 labels was to be compared to Ig having the same average mutual distance of Cy3 labels on the protein. Taking into account the elongated structures of both BSA (Andrade et al., 1992) and IgG, the average Cy3−Cy3 distance should roughly correlate with the mass ratios of Cy3 over protein. In other words, BSA with 2.7 bound Cy3 was expected to have similar fluorescence as Ig with 6 bound Cy3 labels. The corresponding data point was generated by extrapolation (crossed square in Figure 2A) and indeed the calculated fluorescence yield almost coincided with the observed fluorescence of BSA with the same Cy3/protein mass ratio (× in Figure 2A). These data indicate that the dramatic difference between Cy3 on one hand and Cy5 (or Cy7) on the other was not a peculiarity of antibody labeling but a general consequence of statistical protein labeling with amine-reactive Cy dyes.

In the following, it was tested whether the anomalous enhancement of Cy3 fluorescence would also occur when Cy3 was noncovalently linked to the surface of (strept)-avidin via biotin anchors. As described below, the answer to this question was indeed positive, giving rise to discovery of the first small biotin derivative with strong fluorescence in the (strept)avidin-bound state (Gruber et al., 1997, 1998; Kada et al., 1999).

Synthesis and Characterization of Biotin-4-Cy3 and *Biotin-4-Cy5*. Biotin-4-Cy3 and *biotin-4-Cy5* were prepared by the same route as previously described for biotin-4-fluorescein (Kada et al., 1999), except that an excess of biotin-NH-CH_2-CH_2-NH_2 had to be reacted with a small amount of Cy dye, due to the high cost of the latter. The large excess of biotin-NH-CH_2-CH_2-NH_2 and of the other reagents was efficiently removed by a combination of anion exchange (Gruber et al., 1997) and reversed phase chromatography (Gruber et al., 2000). Complete activation of commercial Cy dye with SbTMU (step 1 in Scheme 1) and the essentially complete Cy dye

Scheme 1. Syntheses of Biotin-4-Cy3 and *Biotin-4-Cy5* from Commercial Cy3- and Cy5-Monofunctional Dye

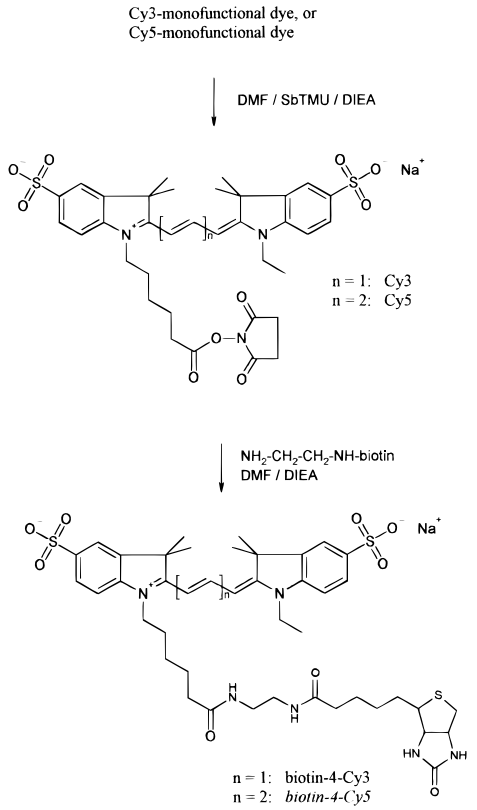

coupling to biotin-NH-CH_2-CH_2-NH_2 (step 2 in Scheme 1) guaranteed that every Cy dye was linked to a biotin moiety. Residual traces of free Cy dye were easily removed because binding to QAE-Sepharose was tighter (Gruber et al., 1997) and binding to LiChroprep gel was less tight (Gruber et al., 2000) than observed with the products.

The correct structures of biotin-4-Cy3 and *biotin-4-Cy5* were proven by NMR and electrospray MS (see Supporting Information). In both cases, binding studies with avidin showed that 100% of the colored material was specifically bound by avidin (see Supporting Information), i.e., every Cy dye was chemically linked to a biotin group via an ethylenediamine spacer (see Scheme 1). The molar concentrations of biotin-4-Cy3 and *biotin-4-Cy5* were also accurately measured by quantitative assessment of binding site occupation in standardized avidin and streptavidin samples, using endogeneous tryptophane fluorescence in (strept)avidin to monitor ligand binding (see Supporting Information).

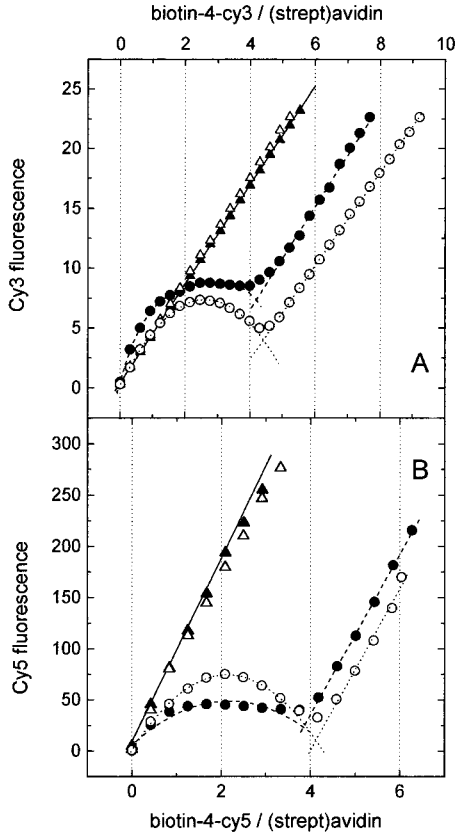

Figure 4. Fluorescence of biotin-4-Cy3 and *biotin-4-Cy5* in the presence (circles) or absence (solid lines) of avidin or streptavidin. Avidin (40 nM, solid circles) or streptavidin (40 nM, open circles) was titrated with increasing amounts of biotin-4-Cy3 (panel A) or *biotin-4-Cy5* (panel B) while monitoring Cy3 fluorescence (excitation at 530 nm, emission at 570 nm) or Cy5 fluorescence (excitation at 630 nm, emission at 665 nm), respectively. In the presence of 8 μM *d*-biotin neither avidin (solid triangles) nor streptavidin (open triangles) had an effect on the fluorescence of biotin-4-Cy3 or *biotin-4-Cy5*. For the sake of clarity, only the linear fits (solid lines) through the control data points (absence of avidin and streptavidin) are shown.

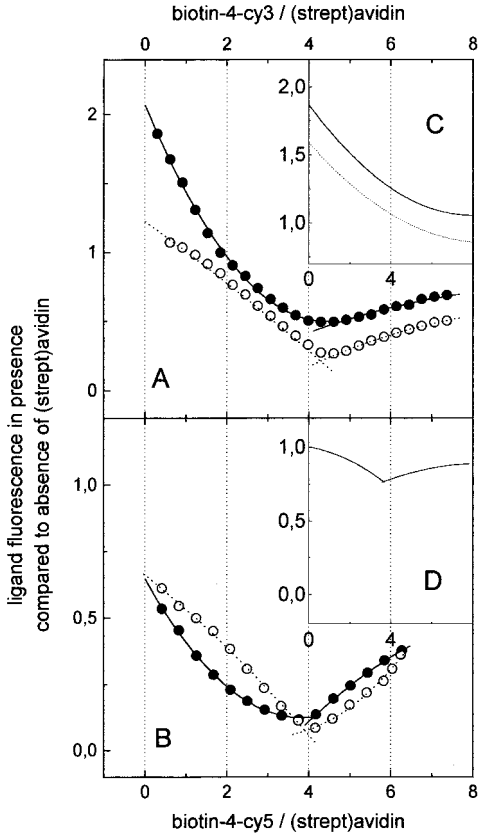

Figure 5. Persistence of biotin-4-Cy3 fluorescence (A) and *biotin-4-Cy5* fluorescence (B) after binding to avidin (solid circles) or streptavidin (open circles). The data were calculated by dividing fluorescence in the presence of (strept)avidin (circles in Figure 4) by fluorescence in absence of protein (solid lines in Figure 4). For comparison, the effect of avidin (solid lines) and streptavidin (dotted line) upon the fluorescence of a biotin-PEG_{800}−Cy3 conjugate (C) and a biotin-PEG_{1900}−Cy5 conjugate (D) is shown in the insets; the data are taken from Gruber et al. (1996).

Fluorescence of Biotin-4-Cy3 and *Biotin-4-Cy5* before/after Binding to Avidin and Streptavidin. (Strept)avidin samples with known *functional* concentrations (see Supporting Information) (=biotin-binding sites/4) were titrated with biotin-4-Cy3 or *biotin-4-Cy5* working solutions. The *functional* concentrations (=biotin group concentration) of the latter were also known from prior standardization (see Supporting Information). Cy dye fluorescence was measured during cumulative titrations and plotted versus known ligand/protein ratios (see Figure 4). In the absence of (strept)avidin (solid lines) or when (strept)avidin had been pre-blocked with *d*-biotin (triangles) the addition of biotin-4-Cy3 or of *biotin-4-Cy5* gave rise to a steep linear increase in Cy dye fluorescence, as expected for absence of interaction with (strept)avidin.

When functional avidin or streptavidin was titrated with *biotin-4-Cy5* (solid or open circles in Figure 4B, respectively) a similar profile was obtained as with all previously tested short biotin-fluorophore conjugates (Gruber et al., 1997; Gruber et al., 1998; Kada et al., 1999): Between 0 and 2 ligands/(strept)avidin the fluorescence signal showed a weak rise, whereas further addition of *biotin-4-Cy5* caused a *decrease* in fluorescence, minimal fluorescence occurring at 4 ligands/(strept)avidin tetramer. The steep linear rise at >4 ligands/protein was parallel to the control series (solid line and triangles in Figure 4B) and evidently derived from the intense fluorescence of unbound ligands which were in excess. The relative extent of (strept)avidin-induced fluorescence quenching is shown in Figure 5B. At the smallest ligand/protein ratio a large fraction of (strept)avidin molecules carried no ligand at all and most of the remaining (strept)avidins were occupied by a single *biotin-4-Cy5* molecule. Extrapolation to 0 ligands/(strept)avidin in Figure 4B obviously gave an estimate for the fluorescence of (strept)avidin tetramers with a single bound *biotin-4-Cy5* molecule (~65% in comparison to the fluorescence of unbound *biotin-4-Cy5*, see Figure 5B). In 4:1 complexes with (strept)avidin, however, *biotin-4-Cy5* fluorescence was quenched by ~90% (see Figure 5B). The loss in *biotin-4-Cy5* fluorescence at high ligand/protein ratio resembled the loss in Cy5 fluorescence observed at high Cy5/IgG ratios (circles in Figures 1A and 2A); the similarity was even more pronounced when the cumulative fluorescence yields were plotted for different ratios of *biotin-4-Cy5* over (strept)avidin (compare Figure 6B with the circle series in Figure 1C). In both cases the optimal fluorescence yield was seen at ~2 bound Cy5 labels/protein.

In contrast to the biotin−Cy5 conjugate, biotin-4-Cy3 excelled with bright fluorescence even after binding to avidin and streptavidin (see Figures 4A, 5A, and 6A). In the case of avidin the anomalous fluorescence increase reached a factor of ~2 when a single biotin-4-Cy3 molecule was bound per tetramer (extrapolation of the solid line in Figure 5A to 0 ligands/avidin) while this

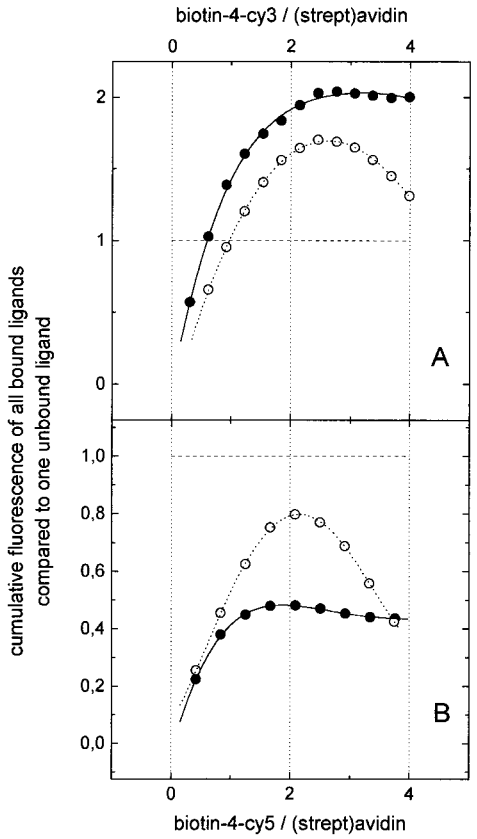

Figure 6. Total Cy3 or Cy5 fluorescence from one avidin (solid circles) or streptavidin molecule (open circles) with $0 \leq n \leq 4$ bound biotin-4-Cy3 (A) or *biotin-4-Cy5* (B), normalized to the fluorescence of one free biotin-4-Cy3 or *biotin-4-Cy5* molecule, respectively. These cumulative fluorescence yields were calculated by multiplying the average fluorescence yield of one (strept)avidin-bound ligand (ordinate values in Figure 5A and Figure 5B) by the average number of bound ligands (abscissa values in Figure 5A and Figure 5B), respectively.

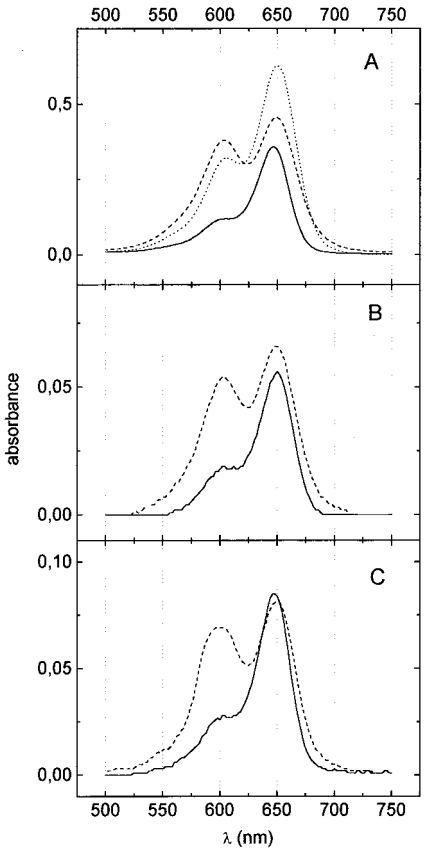

Figure 7. Absorption spectra of free and protein-bound Cy5-labels. (A) Goat IgG with 6.0 bound Cy5 labels/protein in absence (dashed line) and in the presence of 1% SDS (dotted line). The spectrum of free Cy5-monofunctional dye is shown for comparison (solid line). (B) Goat IgG with 6.0 bound Cy5 labels (same sample as in panel A) has been diluted with 9 volumes of buffer A (dashed line). For comparison, goat IgG with 0.5 bound Cy5 labels/protein is shown (solid line). (C) Free *biotin-4-Cy5* (0.29 μM, solid line) is compared with an equimolar mixture of *biotin-4-Cy5* and avidin (both 0.5 μM, dashed line).

effect was small in case of streptavidin (extrapolation of the dotted line in Figure 5A to 0 ligands/streptavidin). Admittedly some Cy3 quenching did occur at >2 ligands/(strept)avidin (Figure 5A) but the cumulative fluorescence at $2 \leq n \leq 4$ ligands/protein was always larger than that of one free biotin-4-Cy3 (Figure 6A), with a plateau at 2-fold fluorescence in the case of avidin (solid circles). Comparison with the square series in the Figures 1C and 2B reveals that Cy3 fluorescence saturated much faster at high ligand/avidin ratios than at comparable Cy3/Ig(G) ratios. Nevertheless the remarkable superiority of Cy3 over Cy5 (compare squares with circles in Figures 1C and 2B) was retained when switching from covalent Cy dye labeling to noncovalent binding of short biotin−Cy dye conjugates to (strept)avidin (compare Figure 6A with Figure 6B).

Absorption and Fluorescence Spectra of Cy5 Labels at High Ratios of Label/Protein. One reason for the brilliant fluorescence of Cy3-labeled antibodies (and of avidin-bound biotin-4-Cy3) has already been identified: Binding of one Cy3 label to a protein's surface generally caused an anomalous fluorescence increase by a factor of 3 (Figure 1A), 2.5 (Figure 2A), or 2 (solid line in Figure 5A). However, this was not the only reason proteins with a large number of Cy3 labels were much more fluorescent than proteins with the same number of Cy5 labels (see Figures 1C, 2B, and 6). Figure 1B demonstrates that Cy5 fluorescence suffers from much stronger "quenching" at high fluorophore/protein ratio than does Cy3. This effect was most pronounced in the case of covalently labeled IgG (see Figure 1B). Attachment of 6 Cy5/IgG caused a 97% (!) drop in fluorescence yield per Cy5 label (open circles) while 36% of initial fluorescence per Cy3 label was retained in IgG with 6 Cy3 labels (solid squares). A similar pattern was observed with avidin and streptavidin, i.e., quenching of biotin-4-Cy3 was consistently weaker than of *biotin-4-Cy5* (not shown).

The moderate quenching of Cy3 at higher degrees of protein labeling (squares in Figure 1B) was comparable to quenching in fluorescein- or TMR-labeled proteins (Goding, 1976; Haugland, 1995). Resonance energy transfer between the fluorophores on the identical protein molecule is known to be the main mechanism of quenching in this case (Steinberg, 1971). The anomalous extent of Cy5 quenching (circles in Figure 1B), however, was caused by an additional mechanism besides resonance energy transfer: At high degrees of Cy5 labeling the regular absorption maximum at ~650 nm was reduced, an additional absorption maximum at ~600 nm was observed (see dashed spectra in Figure 7), and the latter derived from a nonfluorescent state of Cy5 (see Figures 8 and 9 in the Supporting Information).

The normal absorption spectrum of free Cy5 dye is shown in Figure 7A (solid trace). Almost the same spectrum was obtained for IgG with 0.5 bound Cy5 labels (solid trace in Figure 7B) and for free *biotin-4-Cy5* (solid trace in Figure 7C). IgG with 6 bound Cy5 labels,

however, gave an absorption spectrum with two similar absorption maxima at ~600 nm and at ~650 nm (dashed trace in Figure 7A), and the same profile was obtained after 10-fold dilution with buffer (dashed trace in Figure 7B). The anomalous effect was largely reversed when SDS was added at a final concentration of 1% (dotted trace in Figure 7A), i.e., when the protein was partially unfolded. This process took several minutes at RT and it did not occur in 0.1% SDS.

Further characterization of Cy5-labeled IgG and of avidin-bound *biotin-4-Cy5* gave the following results (see Supporting Information). (i) The spectra in Figure 7 were linear composites of a single absorption peak at 600 nm plus the normal spectrum of Cy5 (λ_{max} = 650 nm). (ii) The 600 nm absorption peak corresponded to a completely nonfluorescent state of protein-bound Cy5 residues. (iii) The nonfluorescent state was caused by intramolecular Cy5−Cy5 label interactions only and not by Cy5−protein interaction.

Upon the basis of these findings, it was possible to assess the relative contribution of the nonfluorescent state to fluorescence reduction at high Cy5/protein ratios. Figure 7A shows that the normal absorption peak at 650 nm was increased by a factor of 1.4 when IgG with 6 Cy5 labels (dashed trace) was treated with 1% SDS (dotted trace). This means that ~30% of all Cy5 labels had been in the nonfluorescent state before the addition of SDS, while 70% of all IgG-bound Cy5 labels had been in their normal condition, i.e., in a potentially fluorescent state. Nevertheless the actual extent of Cy5 quenching was as high as 97% (open circle at 6 Cy5/IgG in Figure 1B). From this follows that quenching of Cy5 fluorescence in highly Cy5-labeled proteins is mostly due to resonance energy transfer, while only a minor fraction of bound Cy5 labels adopts a nonfluorescent state, causing some additional reduction in fluorescence yield.

DISCUSSION

The present study provides a critical examination of protein labeling with Cy dyes. The results showed an astounding discrepancy between Cy3 and Cy3.5 on one hand and Cy5 and Cy7 on the other: Cy3- and Cy3.5-labeled antibodies fluoresced very well, even at high fluorophore/protein ratios (see Figures 1C, 2B, and 3B), whereas Cy5- and Cy7-labeled antibodies showed weak fluorescence, with a critical "optimum" at 2−3 labels/protein (see Figures 1C and 2B).

The exceptional fluorescence of Cy3- and Cy3.5-labeled antibodies and the noncritical role of fluorophore/protein ratio derived from fortunate coincidence of two effects: (i) covalent attachment of Cy3 or Cy3.5 labels to antibodies generally resulted in nearly 3-fold fluorescence enhancement (extrapolation of the solid lines in Figures 1A, 2A, and 3A to low fluorophore/protein ratio) which did not occur with the other Cy dyes, and (ii) mutual intramolecular quenching between Cy3 (or Cy3.5) labels by resonance energy transfer was much weaker than between the other Cy dyes (see Figure 1B, 2B, and 3B).

Fortunately the anomalous increase in Cy3 fluorescence was also observed when a very short biotin−Cy3 conjugate was noncovalently bound to (strept)avidin (see Figure 5A) and high fluorescence was still observed when up to four biotin-4-Cy3 were bound per (strept)avidin tetramer (see Figure 6A). Thus, biotin-4-Cy3 was discovered to be the first *small* fluorescent biotin derivative with strong fluorescence in the (strept)avidin-bound state. All other previously tested fluorescent biotin derivatives had suffered from strong quenching in the bound state unless the fluorophores were linked to biotin via long PEG spacers (Gruber et al., 1997, 1998; Marek et al., 1997; Kada et al., 1999). In conclusion, biotin-4-Cy3 appears well suited for specific and intense postlabeling of immobile (strept)avidin molecules and subsequent fluorescence detection.

The findings of the present study are particularly relevant to SMFM where detection of single probe molecules depends on fluorophores with high fluorescence yield, high photostability, and long excitation wavelength. Cy5, Cy5.5, and Cy7 can be excited at >600 nm where the autofluorescence background of live cells is lower by orders of magnitude as compared to the excitation range of TMR, Cy3, and Cy3.5 (Aubin, 1979; Benson et al., 1979; Marelius, 1995; Wolfbeis and Leiner, 1985). In fact, a Cy5-labeled phospholipid (Cy5-PE; Schütz et al., 1999; Schütz et al., 2000a) and a 1:1 conjugate of Cy5 and hongotoxin (Gruber et al., 2000; Schütz et al., 2000b) were the first single molecules visualized by far-field microscopy in live cells. Nevertheless Cy3-labeled antibodies are also expected to be useful for SMFM on live cells because (i) the cumulative signal from 5 to 6 Cy3 labels/protein is very high (see Figures 1C and 2B), (ii) the fluorescence signal (counts/ms) of a single Cy3 (Cy3-PE in a lipid membrane; G. Harms, unpublished results) is about 5-fold stronger than that of TMR−PE or Cy5-PE, and (iii) Cy3-PE proved to be 2−3-fold more stable to photobleaching than TMR−PE or Cy5-PE (G. Harms, unpublished results). Meanwhile single copies of a 1:1 EGF−Cy3 conjugate have also been observed on living cells (Sako et al., 2000), thus antibodies labeled with 6 Cy3 residues should be even easier to resolve despite the autofluorescence background.

The anomalous fluorescence enhancement of protein-bound Cy3 labels can tentatively be explained by simple assumptions. The fluorescence quantum yield of Cy3 is known to depend on solvent polarity and especially on viscosity; in ethanol Cy3 is ~2 and in glycerol ~10 times more fluorescent than it is in water (Mujumdar et al., 1993). If we assume that proteins contain surface patches with moderate Cy3-affinity then we expect two consequences: (i) intact Cy3 succinimidyl ester should preadsorb toward these sites and subsequently the activated hexanoic acid side chain of Cy3 should couple to some lysine residue that is within reach, and (ii) the so-coupled Cy3 residue will further stay adsorbed to the same patch most of the time, and the fluorescence of Cy3 will be enhanced by the low polarity of the site (as seen in ethanol), as well as by the reduction in conformational mobility of Cy3 (as observed in glycerol). The same concept also accounts for the enhancement of biotin-4-Cy3 fluorescence upon binding to avidin (see Figure 5A, solid circles). Obviously, the $-NH-CH_2-CH_2-NH-CO-(CH_2)_5-$ spacer (see Scheme 1) between the avidin-bound biotin residue and the chromophore of Cy3 allows the latter to reach a "Cy3-philic" patch on avidin. Streptavidin does not have such a site within reach of a bound biotin-4-Cy3 (see Figure 5A, open circles). Yet streptavidin can also enhance Cy3 fluorescence when a biotin-PEG_{800}−Cy3 conjugate is bound (Figure 5C, dotted line), i.e., the "Cy3-philic" patches on streptavidin are far away from the biotin-binding sites and only the PEG_{800} spacer gives the Cy3 label sufficient tether to reach it.

When a large protein is labeled with Cy3 succinimidyl ester the abundance of lysine residues provides for a high probability that Cy3 gets coupled to a surface patch which enhances Cy3 fluorescence. In contrast, there should be little chance for favorable Cy3-protein interaction if a small protein/peptide with a single free cysteine residue

is labeled with a thiol-reactive Cy3 derivative. To check this point we actually labeled a cysteine mutant of hongotoxin (HgTx-A19C; Schütz et al., 2000a) with a maleimide derivative of Cy3 (prepared as described for Cy5, Gruber et al., 2000). At 50 nM concentration this Cy3-HgTx conjugate showed only 55% of the fluorescence of 50 nM Cy3 succinimidyl ester or of 50 nM Cy3-maleimide derivative (data not shown). This finding, and the results for streptavidin-bound biotin-4-Cy3 (Figure 5A, open circles) proved that the anomalous enhancement of Cy3 fluorescence indeed depends on protein surface patches with *particular* properties and is not a general consequence whenever Cy3 is linked to the surface of a protein.

In contrast to Cy3, the fluorescence of Cy5 labels was neither enhanced nor much reduced when linked to a protein with a 1:1 stoichiometry. This was deduced from the relative fluorescence yield at low Cy5/antibody ratios (circles in Figures 1A and 2A) and from the observation that the 1:1 conjugate of HgTx-A19C with Cy5 showed the same fluorescence yield as free Cy5 succinimidyl ester (Gruber et al., 2000). On the other hand, the linking of ≥2 Cy5 labels to a single protein molecule was found to cause severe "quenching" (see circles in Figures 1A, 2A, and 5B).

The minor reason for low fluorescence at high Cy5/antibody ratio was appearance of a nonfluorescent state of Cy5 which showed a unique absorption spectrum, with a single absorption peak at 600 nm (see dashed lines in Figure 7). Interestingly, the fraction of Cy5 labels in the nonfluorescent state was linearly dependent on Cy5/antibody ratio, ranging from exactly 0% at the extrapolated number of 0.0 Cy5/antibody to 30% at 6 Cy5 labels/antibody molecule (see Figure 10A in the Supporting Information). From this dependence on Cy5/protein ratio, we conclude that (i) the nonfluorescent state can only be caused by a second Cy5 label which is located on the same protein molecule and (ii) the spatial distribution of Cy5 labels over the antibody surface must be far from random. In case of random distribution there would be no chance for Cy5−Cy5 interaction at very low Cy5/antibody ratios (e.g., at 0.1 or 0.2 Cy5/protein): even in the rare case of an antibody molecule with two Cy5 labels the average Cy5−Cy5 distance would be too large for direct Cy5−Cy5 contact and too large also for dipole−dipole interaction through space (dependent on r^{-6}). We therefore propose that the nonfluorescent state of protein-bound Cy5 derives from a Cy5 dimer, the two hexanoic acid side chains being covalently linked to properly spaced lysine residues on the protein. In aqueous solution Cy5 analogues lacking the sulfonate residues are well-known for dimer formation (Mujumdar et al., 1993), thus if positively charged side chains on the protein happen to compensate for the negative charges of the sulfonate groups (see Scheme 1), such a Cy5 dimer may well be stabilized to the extent that even in 1% SDS it takes minutes to break the Cy5−Cy5 and the Cy5−protein interactions (see Figure 7A). We suspect that the first Cy5 preadsorbs to such a positively charged site on the protein, covalently binds to a lysine, subsequently attracts a second Cy5 succinimidyl ester, and the latter also gets anchored to another lysine the position of which permits to retain the tight dimer geometry. If such an optimally positioned second lysine residue is not within reach, then the adsorbed second Cy5 succinimidyl ester molecule would still have a high chance for covalent reaction with some nearby lysine residue; the strict dimer could no longer persist but, due to the short Cy5−Cy5 distance, there should be strong resonance energy transfer between the two neighboring Cy5 residues, resulting in strong fluorescence quenching. In other words, the anomalously strong fluorescence quenching at high Cy5/antibody ratios (see circles in Figures 1A and 2A) seems to derive from "catalysis" of Cy5 attachment by already protein-bound Cy5 labels, leading to clusters of Cy5 even at rather low Cy5/protein ratios. As expected, this problem was much reduced in case of Cy5.5 the chromophore of which carries four, rather than two sulfonate groups; in comparison to Cy5, less quenching (solid circle in Figure 3A) and higher cumulative fluorescence (solid circle in Figure 3B) was seen at five Cy5.5 labels/antibody.

We are aware that the above presented hypotheses for anomalous enhancement of Cy3 fluorescence and anomalous quenching of Cy5 fluorescence are not yet proven by the available data but the concepts provide a first basis for discussion and for further strategies to get more fluorescence yield from Cy dye-labeled probes, needed to simplify single molecule studies in living cells and other systems.

ACKNOWLEDGMENT

We are indebted to Prof. Wolfgang Buchberger, Prof. Heinz Falk, and Prof. Norbert Müller for use of HPLC and spectrometer facilities. Helpful suggestions by one of the reviewers and advice by Prof. Karl Grubmayr is gratefully acknowledged. This work was supported by the Austrian Research Funds (Project P-12663 MED) and EU Biomed 2 Project BMH4-CT97-2118.

Supporting Information Available: Experimental details and supporting results (Table 1, Figures 8−14). This material is available free of charge via the Internet at http://pubs.acs.org.

LITERATURE CITED

Andrade, J. D., Hlady, V., Wei, A.-P., Ho, C.-H., Lea, A. S., Jean, S. I., Lin, Y. S., and Stroup, E. (1992) Proteins at interfaces: principles, multivariate aspects, protein resistant surfaces, and direct imaging and manipulation of adsorbed proteins. *Clin. Mater. 11*, 67−84.

Aubin, J. E. (1979) Autofluorescence of viable cultured mammalian cells. *J. Histoch. Cytoch. 27*, 36−43.

Bannwarth, W., and Knorr, R. (1991) Formation of carboxamides with *N*,*N*,*N*′,*N*′-tetramethyl (succinimido) uronium tetrafluoroborate. *Tetrahedron Lett. 9*, 1157−1160.

Benson, R. C., Mayer, R. A., Zaruba, M. E., and McKhann, G. M. (1979) Cellular autofluorescence - is it due to flavins? *J. Histoch. Cytoch. 27*, 44−48.

Elgersma, A. V., Zsom, R. L., Norde, W., and Lyklema, J. (1990) The adsorption of bovine serum albumin on positively and negatively charged polystyrene latices. *J. Colloid Interface Sci. 138*, 145−156.

Garlick, R. K., and Giese, R. W. (1988) Avidin binding of radiolabeled biotin derivatives. *J. Biol. Chem. 263*, 210−215.

Goding, J. W. (1976) Conjugation of antibodies with fluorochromes: modification to the standard methods. *J. Immunol. Methods 13*, 215−226.

Gruber, H. J., Marek, M., Schindler, H., and Kaiser, K. (1997) Biotin-fluorophore conjugates with poly(ethylene glycol) spacers retain intense fluorescence after binding to avidin and streptavidin. *Bioconjugate Chem. 8*, 552−559.

Gruber, H. J., Kada, G., Marek, M., and Kaiser, K. (1998) Accurate titration of biotin-binding sites in avidin and streptavidin with biotin-fluorophore conjugates. *Biochim. Biophys. Acta 1381*, 203-212.

Gruber, H. J., Kada, G., Pragl, B., Riener, C., Hahn, C. D., Harms, G. S., Ahrer, W., Dax, T. G., Hohenthanner, K., and Knaus, H. G. (2000) Preparation of thiol-reactive Cy5 deriva-

tives from commercial Cy5 succinimidylester. *Bioconjugate Chem. 11*, 161−166.
Haugland, R. P. (1995) Coupling of monoclonal antibodies with fluorophores. *Methods Mol. Biol. 45*, 205−221.
Haugland, R. P. (1996) *Handbook of fluorescent probes and research chmichals*, Molecular Probes, Inc.
Kada, G., Falk, H., and Gruber, H. J. (1999) Accurate measurement of avidin and streptavidin in crude biofluids with a new, optimized biotin-fluorescein conjugate. *Biochim. Biophys. Acta 1427*, 33−43.
Marek, M., Kaiser, K., and Gruber, H. J. (1997) Biotin-pyrene conjugates with poly(ethylene glycol) spacers are convenient fluorescent probes for avidin and streptavidin. *Bioconjugate Chem. 8*, 560−566.
Marelius, J. (1995) Autofluorescence imaging of living cells. MSc Thesis at Uppsala University, School of Engineering.
Mujumdar, R. B., Ernst, L. A., Mujumdar, S. R., Lewis, C. J., and Waggoner, S. S. (1993) Cyanine dye labeling reagents: sulfoindocyanine succinimidyl esters. *Bioconjugate Chem. 4*, 105−111.
Sako, Y., Minoguchi, S., and Yanagida, T. (2000) Single molecule imaging of EGFR signaling on the surface of living cells. *Nat. Cell Biol. 2*, 168−172.
Schütz, G. J., Schindler, H., and Schmidt, T. (1999) Diffusion of single lipid molecules in cell membranes. *Biophys. J. 76*, A57.
Schütz, G. J., Kada, G., Pastushenko, V. P., and Schindler, H. (2000a) Properties of lipid microdomains in a muscle cell membrane visualized by single molecule microscopy. *EMBO J. 19*, 892−901.
Schütz, G. J., Pastushenko, V. P., Gruber, H. J., Knaus, H.-G., Pragl, B., and Schindler, H. (2000b) 3D Imaging of individual ion channels in live cells at 40 nm resolution. *Single Mol. 1*, 25−31.
Steinberg, I. Z. (1971) Long-range nonradiative transfer of electronic excitation energy in proteins and polypeptides. *Annu. Rev. Biochem. 40*, 83−114.
Wessendorf, M. W, and Brelje, T. C. (1992) Which fluorophore is brightest? A comparison of the staining obtained using fluorescein, tetramethylrhodamine, lissamine rhodamine, texas red, and cyanine 3.18. *Histochemistry 98*, 81−85.
Wolfbeis, O. S., and Leiner, M. (1985) Mapping of the total fluorescence of human blood serum as a new method for its characterization. *Anal. Chim. Acta 167*, 203-215.

BC000015M

Abbreviations of Cy dyes. Cy3-monofunctional dye (= Cy3-mono-O-Su), sodium 1-[5-(*N*-succinimidyloxycarbonyl)-pent-1-yl]-2-[3-(3,3-dimethyl-1-ethyl-5-sulfonato-indolin-2-ylidene)-1-propen-1-yl]-3,3-dimethyl-3*H*-indolium-5-sulfonate; Cy3.5-monofunctional dye (= Cy3.5-mono-O-Su), trisodium 1-[5-(*N*-succinimidyloxycarbonyl)-pent-1-yl]-2-[3-(3,3-dimethyl-1-ethyl-5,7-disulfonato-benzo[e]indolin-2-ylidene)-1-propen-1-yl]-3,3-dimethyl-5-sulfonato-3*H*-benzo[e]indolium-7-sulfonate; Cy5-monofunctional dye (= Cy5-mono-O-Su), sodium 1-[5-(*N*-succinimidyloxycarbonyl)-pent-1-yl]-2-[5-(3,3-dimethyl-1-ethyl-5-sulfonato-indolin-2-ylidene)-1,3-pentadien-1-yl]-3,3-dimethyl-3*H*-indolium-5-sulfonate; Cy5.5-monofunctional dye (= Cy5.5-mono-O-Su), sodium 1-[5-(*N*-succinimidyloxycarbonyl)-pent-1-yl]-2-[5-(3,3-dimethyl-1-ethyl-5,7-disulfonato-benzo[e]indolin-2-ylidene)-1,3-pentadien-1-yl]-3,3-dimethyl-5-sulfonato-3*H*-benzo[e]indolium-7-sulfonate; Cy7-bifunctional dye, sodium 1-[5-(*N*-succinimidyloxycarbonyl)-pent-1-yl]-2-[7-(3,3-dimethyl-1-ethyl-5-sulfonato-indolin-2-ylidene)-1,3,5-heptatrien-1-yl]-3,3-dimethyl-3*H*-indolium-5-sulfonate;

Characterization of Protein-Bound Cy5 Labels by UV-vis Absorption and Fluorescence Spectroscopy. As shown in Figure 7 (see main article), simultaneous attachment of 6 Cy5 labels per IgG molecule led to appearance of a new absorption peak (λ_{max} ~ 600 nm) in addition to the normal absorption maximum of Cy5 (λ_{max} ~ 650 nm). For quantitative analysis, the normalized absorption spectra of IgG with different ratios of Cy5 label/protein were summarized in Figure 8A, and the dose-response function (peak ratio *versus* degree of Cy5 labeling) is shown in Figure 10A. Comparison of the absorption spectra (Figure 8A) with fluorescence excitation spectra (Figure 8B) revealed that the new absorption peak at ~600 nm did not contribute to Cy5 fluorescence as detected at 665 nm. The same observations were made with avidin and *biotin-4-Cy5* at various molar ratios (compare Figures 9A and 9B). To further exclude the possibility that the 600 nm peak gave any fluorescence at all, the excitation wavelength was also fixed to 600 nm and the emission was examined between 600 nm and 800

nm. However, both IgG with 6 Cy5 labels and avidin with 4 *biotin-4-Cy5* ligands gave only the normal emission spectrum of Cy5 (data not shown), with the low intensity as expected from excitation of Cy5 at 600 nm instead of at 630 nm (see Figures 8B and 9B). From the above data it was unequivocally concluded that the new absorption peak at ~600 nm seen in highly Cy5-labeled proteins derived from some "new state" of Cy5 which did not fluoresce at all.

Figures 10A and 10B finally demonstrate that the anomalous appearance of the 600 nm absorption peak solely derived from mutual interaction of Cy5 labels bound to the identical protein molecule. As argued in context with Figures 1B, 2B, 3B, and 5AB (see main article), extrapolation of the plotted function to 0 fluorophores per protein molecule gave the peak ratio (A_{600}/A_{650}) that would be observed from a homogeneous population of protein molecules carrying no more than one Cy5 label. Surprisingly, this extrapolated value for exactly mono-labeled IgG (solid line in Figure 10A) was identical with the peak ratio observed from free Cy5 dye (solid circle in Figure 10A). By analogy, the extrapolated peak ratio for a single *biotin-4-Cy5* ligand on an avidin molecule (solid line in Figure 10B) was identical to the peak ratio of free *biotin-4-Cy5* (solid circle in Figure 10B). In other words: the anomalous appearance of additional absorption at ~600 nm had nothing to do with the fact that some Cy5 dye was linked to the surface of a protein and was solely due to Cy5-Cy5 interaction because it only occurred when more than one Cy5 label was bound per protein.

It should be mentioned that some indication of the analogous phenomenon (additional absorption at ~500 nm at expense of the regular ~550 nm absorption maximum) was also seen with protein-bound Cy3 (and Cy5.5) labels and with avidin-bound biotin-4-Cy3 ligands at high Cy3/protein ratios - but the extent was by no means comparable to the effects on Cy5 labels.

A Comment on the Measurement of Protein-Bound Cy5 Labels. Admittedly the anomalous decrease of 650 nm absorption was ignored when quantifying the number of Cy5 labels per Ig(G). In this way only those Cy5 labels were counted which had retained their

fluorescence (see above). In 1 % SDS the *total* number of Cy5 labels per Ig(G) would have been measured. From a comparison of the dashed with the dotted trace in Figure 7A we can estimate that the total number of Cy5 labels per IgG would have been 8.3 when measured in 1 % SDS, rather than 6.0. Consequently we would have diluted with more buffer to arrive at a nominal concentration of 50 nM Cy5 label before measuring fluorescence yield in Figure 1A. The net effect would have been a 40 % higher abscissa value and a 40 % lower ordinate value of the solid circle in Figure 1A, and similar but smaller shifts would have occured with all open circles in Figure 1A. From the linear dependence of A_{600}/A_{650} on the number of Cy5/IgG (Figure 10A) we predicted the positions of the circles in Figure 1A as they would have been obtained by the "SDS method" (data not shown). The result: in spite of different locations these corrected data were positioned on the same fit line (dashed curve in Figure 1A) as the presently shown open and closed circles. In other words: the same dependence of fluorescence yield per Cy5 label (dashed line in Figure 1A) and of cumulative fluorescence yield (dashed line in Figure 1C) on the number of Cy5/IgG was obtained whether the fraction of non-fluorescent Cy5 labels was ignored (measurement of A_{600}/A_{650} in absence of SDS) or included (measurement of A_{600}/A_{650} in presence of 1 % SDS).

Synthesis of Biotin-NH-CH_2-CH_2-NH_3^+ Cl^-. Biotin-NH-CH_2-CH_2-NH_3^+ Cl^- was synthesized as described (Garlick and Giese, 1988). The product was pure by TLC. ^{1}H-NMR (D_2O, 500 MHz) δ: 4.64 (1H, m, position 6a in biotin) 4.46 (1H, m, position 3a in biotin) 3.53 (2H, t, J = 5.9 Hz, CH_2-NH_3^+) 3.38 (1H, m, position 4 in biotin) 3.17 (2H, t, J = 5.9 Hz, CO-NH-CH_2-CH_2-NH_3^+) 3.03 (1H, dd, J_{vic} = 5.0 Hz, J_{gem} = 13.1 Hz, position 6_I in biotin) 2.82 (1H, d, J = 13.1 Hz, position 6_{II} in biotin) 2.33 (2H, t, J = 7.3 Hz, CH_2-CH_2-CH_2-CH_2-CO-NH in biotin side chain) 1.53-1.83 (4H, m, CH_2-CH_2-CH_2-CH_2-CO-NH in biotin side chain) 1.32-1.53 (2H, m, CH_2-CH_2-CH_2-CH_2-CO-NH in biotin side chain).

TLC. Merck plastic sheets (silica gel 60) without fluorescent indicator were used. Eluents I, II, and III contained 70 parts of chloroform, 30 parts of methanol, and 4 parts of conc. ammonia, or water, or acetic acid, respectively. Cy dyes were visible without staining, other components were stained with iodine vapor.

Tentative Assignment of the proton NMR Signals in Position 6 of Biotin. The molecular structure of biotin is shown in Figure 14A. We believe that the NMR signals of proton $H6_I$ and $H6_{II}$ (at 3.03 and 2.82 ppm in the above spectrum) can be assigned to the absolute positions as indicated in Figure 14A. This conclusion is drawn from AM1 calculations using the MOPAC package (MOPAC 6.0 DEC-3100 Edition 1990, FJ Seiler Res. Lab., US Air Force Academy CO80840; Dewar et al., 1985), where coordinates derived from a force field calculation served as an input. The ring fragment of the so-obtained geometry is shown in Figure 14B. The most important feature is the close similarity between the dihedral angle of H3a and H4 (19°) and between the dihedral angle of H6a and the *cis*-H6 (20°). Consequently we would expect similar vicinal coupling constants in the NMR spectrum. The multiplet of H4 at 3.38 ppm contains a vicinal coupling constant of 4.6 Hz; the doublet of a doublet of the *cis*-H6 at 3.03 ppm ($H6_I$ in Figure 14A) shows very similar vicinal coupling (5.0 Hz) besides strong geminal coupling (13.1 Hz). The doublet at 2.82 ppm, on the other hand, must be attributed to the *trans*-H6 ($H6_{II}$ in Figure 14A) which only couples to its geminal, but not to its vicinal neighbour. This behaviour can be explained by the dihedral angle between H6a and the *trans*-H6 (141°). As the Karplus relation is known to be different for five- as compared to six-membered rings, it is likely that the minimum occurs at 141° and therefore the coupling between these two protons would become too small for being observed.

Synthesis of Biotin-4-Cy3 (see Scheme 1). Cy3-monofunctional dye (1.4 µmol) was dissolved in 1 mL of DMF containing 8.4 mg SbTMU (20.4 µmol, Bannwarth and Knorr, 1991), and 5 µL neat DIEA (57 µmol) was added. After 40 min of stirring at RT this mixture

was added to dry biotin-NH-CH_2-CH_2-NH_3^+ Cl^- (see above), another 20 µL neat DIEA (228 µmol) was added and stirring was continued under argon for 1 h at RT. The solvent was removed and the dry residue was dissolved in 5 mL 2 mM Na_2HPO_4 (pH 6.5 adjusted with NaOH). This solution was loaded on a QAE Sephadex A-25 column (1.5 x 8.5 cm, Cl^- form, prewashed in distilled water, see Gruber et al., 1997) at a flow rate of 1 mL/min. After washing with 10 mL portions of water, 40, 80, 160, 320, and 640 mM NaCl (without phosphate) the colored product was eluted with 1280 mM NaCl. The product fraction was adjusted to 2.5 % solvent B (100 % solvent B was a 5/2 mixture of ethanol and n-propanol [Feldhoff, 1991]; 100 % solvent A was 0.1 % acetic acid in water) and loaded on a LiChroprep column (1.5 x 3.5 cm, prewashed in 5 % solvent B, see Gruber et al., 2000) at a flow rate of 2 mL/min. After washing with 12 mL portions of 5, 10, 15, 20, and 25 % of solvent B the product was eluted with 30 % solvent B. After removal of solvent the dry residue was redissolved in methanol and dried down in a smaller flask.

Biotin-4-Cy3 (1.0 µmol out of the 1.2 µmol obtained from the LiChroprep column) was further purified by preparative HPLC on a Vydac C-18 column (# 218TP510, 250 x 10 mm, 2 mL/min, 0.1 % acetic acid instead of trifluoroacetic acid in all eluents). When applying a 30 min gradient from 5 to 50 % acetonitrile pure biotin-4-Cy3 (0.7 µmol according to Cy3 absorbance) was eluted at 16.5-17 min after the start of the gradient. The solvent was removed and the structure of biotin-4-Cy3 was confirmed by ^{1}H-NMR (see below). In parallel, a small aliquot was purified on an analytical Vydac C-18 column (# 218TP54, 250 x 4 mm, 1 mL/min), using the same elution protocol as above. Pure biotin-4-Cy3 was eluted 13 min after the start of the gradient, as detected by UV-vis absorption and by direct analysis of the eluent with electrospray MS. Only two m/e peaks were detected which exactly met expectation for the monoanion (897) and dianion (448) of biotin-4-Cy3.

^{1}H-NMR (D_2O, 500 MHz) δ: 8.59 (1H, t, J = 13.5 Hz, β proton of the methin bridge) 7.83-7.97 (4H, m, positions 4 and 6 of the indolin residues) 7.44 (2H, t, $J_{ortho} = J_{para}$ = 7.6 Hz, position 7 of the indolin residue) 6.43 (2H, m, α and α' protons of the methin bridge) 4.53 (1H, m, position 6a in biotin) 4.34 (1H, m, position 3a in biotin) 4.1-4.23 (4H, m, CH_2 of the *N*-ethyl group and N-CH_2-CH_2-CH_2-CH_2-CH_2-CO in Cy3 side chain) 3.21 (5H, s, CO-NH-CH_2-CH_2-NH-CO and position 4 in biotin) 2.86 (1H, m, position 6_I in biotin) 2.61 (1H, d, J = 12.8 Hz, position 6_{II} in biotin) 2.24 (2H, m, CH_2-CH_2-CH_2-CH_2-CO-NH in biotin side chain) 2.15 (2H, m, N-CH_2-CH_2-CH_2-CH_2-CH_2-CO in Cy3 side chain) 2.07 (~4H, s, acetic acid from reversed phase chromatography) 1.89 (2H, m, N-CH_2-CH_2-CH_2-CH_2-CH_2-CO in Cy3 side chain) 1.79 (12 H, s, four methyl groups of Cy3 residue) 1.44-1.70 (6H, m, CH_2-CH_2-CH_2-CH_2-CO-NH in biotin side chain, N-CH_2-CH_2-CH_2-CH_2-CH_2-CO in Cy3 side chain) 1.22-1.44 (7H, m, CH_2-CH_2-CH_2-CH_2-CO-NH in biotin side chain, N-CH_2-CH_2-CH_2-CH_2-CH_2-CO in Cy3 side chain, and CH_3 of the N-ethyl group).

Synthesis of *Biotin-4-Cy5*. The procedure was the same as described for biotin-4-Cy3, except that 1.0 µmol Cy5-monofunctional dye were used in place of Cy3-monofunctional dye (see above). LiChroprep chromatography gave 0.84 µmol of partially pure product according to Cy5 absorbance. 0.65 µmol were subjected to preparative HPLC, yielding 0.33 µmol of pure product. Only two m/e peaks were detected in electrospray MS which exactly met expectation for the monoanion (924) and dianion (461) of *biotin-4-Cy5*.

^{1}H-NMR (D_2O, 500 MHz) δ: 8.05-8.18 (2H, m, β and β' protons of the methin bridge) 7.80-7.94 (4H, m, positions 4 and 6 of the indolin residues) 7.39 (2H, t, $J_{ortho} = J_{para}$ = 9.7 Hz, position 7 of the indolin residue) 6.66 (2H, m, γ and γ' protons of the methin bridge) 6.37 (2H, m, α and α' protons of the methin bridge) 4.53 (1H, m, position 6a in biotin) 4.32 (1H, m, position 3a in biotin) 4.09-4.20 (4H, m, CH_2 of the *N*-ethyl group and N-CH_2-CH_2-CH_2-CH_2-CH_2-CO in Cy5 side chain) 3.21 (4H, s, CO-NH-CH_2-CH_2-NH-CO) 3.18 (1H, m,

position 4 in biotin) 2.86 (1H, m, position 6_I in biotin) 2.62 (1H, d, J = 12.7 Hz, position 6_{II} in biotin) 2.24 (2H, t, J = 6.5 Hz, CH_2-CH_2-CH_2-CH_2-CO-NH in biotin side chain) 2.15 (2H, t, J = 7.0 Hz, N-CH_2-CH_2-CH_2-CH_2-CH_2-CO in Cy3 side chain) 2.06 (~2H, s, acetic acid from reversed phase chromatography) 1.87 (2H, m, N-CH_2-CH_2-CH_2-CH_2-CH_2-CO in Cy3 side chain) 1.74 (12 H, s, four methyl groups of Cy3 residue) 1.44-1.70 (6H, m, CH_2-CH_2-CH_2-CH_2-CO-NH in biotin side chain, N-CH_2-CH_2-CH_2-CH_2-CH_2-CO in Cy3 side chain) 1.22-1.44 (7H, m, CH_2-CH_2-CH_2-CH_2-CO-NH in biotin side chain, N-CH_2-CH_2-CH_2-CH_2-CH_2-CO in Cy3 side chain, and CH_3 of the N-ethyl group).

Test for Specific Binding of Biotin-4-Cy3 and *Biotin-4-Cy5* towards Avidin. Specific binding towards avidin was demonstrated by incubation of biotin-4-Cy3 or *biotin-4-Cy5* with excess of avidin and subsequent gel filtration. In particular, avidin (~6 nmol according to ε_{282} = 96500 M^{-1} cm^{-1}; Green, 1990) and fluorescent biotin derivative (2.4 nmol biotin-4-Cy3 or 1.7 nmol *biotin-4-Cy5*, estimated from absorbance at 550 nm or 647 nm) were incubated in 0.2 mL buffer A for 30 min at RT, diluted with 0.3 mL of buffer A and loaded on a PD-10 column (~10 mL bed of Sephadex G-25M) which had been pre-equilibrated in buffer B (the high salt concentration in buffer B minimized binding of the positively charged avidin molecules to Sephadex G-25 which contains some residual COOH groups). The column was washed with buffer B (2 x 1 mL), and the eluent was discarded. Avidin was completely eluted by adding 2 mL of water on top of the column. Free ligand was eluted with another 10 mL of water. In the control run avidin (~6 nmol) was pre-blocked with *d*-biotin (270 nmol, 5 min incubation) before the fluorescent biotin derivative (~2 nmol) was added. Measured absorbance values at 282 nm were corrected for the small absorbances of Cy3 or Cy5 (as described for IgG in the main article) before calculating the avidin concentrations in the column fractions.

The results are shown in Table 1. In the absence of *d*-biotin all fluorescent ligands were bound to avidin (void peaks in Table 1). The incomplete recovery of biotin-4-Cy3 and *biotin-4-Cy5* from the PD-10 column (75-90 %) did not derive from incomplete binding to avidin but from adsorption to the Sephadex gel since neither biotin-4-Cy3 nor *biotin-4-Cy5* was observed in the "salt peak" when avidin was not blocked by *d*-biotin (see Table 1). The data were, therefore, consistent with 100 % bindability of biotin-4-Cy3 and *biotin-4-Cy5* towards avidin. Absence of non-specific binding was demonstrated by complete block of ligand binding in the presence of a large excess of *d*-biotin. In this case no fluorescent ligand co-migrated with avidin, and all nonadsorbed ligands were recovered in the "salt peak" (see Table 1).

Measurement of Biotin-Binding Sites in Stock Solutions of Avidin and Streptavidin. The primary standard was a 16 mM *d*-biotin stock solution prepared by dissolving 99 % pure *d*-biotin in DMSO. Aliquots were stored at -25 °C. The 16 µM *d*-biotin working solution was prepared by accurate dilution with buffer A.

Avidin and streptavidin were dissolved in buffer A (at ~2 to 3 µM *nominal* concentration by weight) and stored at 4 °C for up to one week, or at -25 °C for up to one month without refreezing. The concentration of *functional* avidin or streptavidin (= biotin binding sites/4) was determined by titration with *d*-biotin while monitoring the tryptophane fluorescence of (strept)avidin (Lin and Kirsch, 1979; Gruber et al., 1998). Buffer A (1920 µL) was mixed with 80 µL ~2 µM avidin stock solution and 5 µL aliquots of 16 µM *d*-biotin standard were successively added from a Hamilton syringe (see Figure 11A). The nearly linear decrease in tryptophane fluorescence mirrored progressive binding of *d*-biotin to avidin and the break-point at 34.9 µL *d*-biotin (558 pmol) indicated stoichiometric binding of 4 biotin molecules per avidin tetramers. Consequently the amount of avidin in the cuvette was calculated to be 140 pmol and the *functional* concentration of avidin in the *nominally* ~2 µM stock solution was determined as 140 pmol / 80 µL = 1.75 µM. Triplicate experiments gave a *functional*

concentration of 1.75 ± 0.03 μM in the avidin stock solution and 3.01 ± 0.03 μM in the streptavidin stock solution (not shown).

Measurement of Biotin Groups in the Stock Solutions of Biotin-4-Cy3 and *Biotin-4-Cy5*. Fortunately tryptophane quenching in avidin could also be used to monitor stoichiometric binding of the new fluorescent ligands biotin-4-Cy3 and *biotin-4-Cy5* towards avidin (in contrast to biotin-PEG-Cy dye conjugates; Gruber et al., 1997; Kaiser et al., 1997), as is demonstrated in Figure 11B. Buffer A (1954 μL) and 46 μL of 1.75 μM avidin stock solution (80 pmol avidin = 320 pmol of biotin-binding sites) were mixed and stirred in the cuvette, and 2 μL aliquots of a *nominally* 16 μM stock solution (according to UV-vis absorbance) of biotin-4-Cy3 (circles in Figure 11B) or *biotin-4-Cy5* (triangles in Figure 11B) were successively added from a Hamilton syringe at 3 min intervals (necessary for completion of ligand binding after each addition) while monitoring tryptophane quenching in avidin. Saturation of the 320 pmol of biotin-binding sites was achieved with 19.1 μL of *nominally* 16 μM *biotin-4-Cy5* (see triangles in Figure 11B), thus the *functional* concentration of *biotin-4-Cy5* in the stock solution was 320 pmol / 19.1 μL = 16.7 μM. This result agreed well with the *nominal* concentration of 16 μM that had been estimated from absorbance at 647 nm, assuming the same molar extinction coefficient as published for free Cy5-monofunctional dye.

A much larger discrepancy between *nominal* and *functional* concentration was observed with biotin-4-Cy3. 26.0 μL of *nominally* 16 μM biotin-4-Cy3 was necessary to saturate 320 pmol of biotin-binding sites (see circles in Figure 11B), corresponding to a *functional* concentration of 320 pmol / 26.0 μL = 12.3 μM in the stock solution of biotin-4-Cy3. In principle, the 12.3 μM biotin group content in the *nominally* 16 μM stock solution of biotin-4-Cy3 could have resulted from one or both of the following reasons: (i) The molar extinction coefficient (ε_{550}) of biotin-4-Cy3 may be much higher than 150000 M^{-1} cm^{-1} which is the known value for underivatized Cy3-monofunctional dye; or (ii) the stock solution of biotin-4-

Cy3 could have contained additional Cy3 chromophores that were not linked to biotin residues. The latter possibility, however, was excluded by TLC, HPLC, electrospray MS, and by the observed 100 % bindability of all Cy3 chromophores in biotin-4-Cy3 towards avidin (see Table 1 and corresponding text in these Supplements). It is, therefore, concluded that the molar extinction coefficients of biotin-4-Cy3 is ~195000 M^{-1} cm^{-1} and that both the biotin group content and the Cy3 chromophore content in the stock solution of biotin-4-Cy3 was 12.3 µM. Similar unpredictable shifts in the molar extinction coefficient of fluorophores have been observed with many other biotin-fluorophore conjugates (Gruber et al., 1997; Gruber et al., 1998; Kada et al., 1999).

Dissociation Kinetics of *Biotin-4-Cy5* from Avidin. As shown in Figure 7C (see original article) and Figure 9A, progressive binding of *biotin-4-Cy5* to avidin tetramers was accompanied by a steady increase in the 600 nm absorption peak, at the expense of the normal absorption maximum at 650 nm. Figure 10B depicts the nonlinear relationship between the ratio of the two absorption maxima ($r = A_{600}/A_{650}$) and the average number of ligands (n) that are bound per avidin tetramer. The data were fitted by the expression

$$r = 0.33 + 0.985 / (1 + 0.79 / n) \qquad (1)$$

(see solid line in Figure 10B). Inversion gave an expression which allowed to calculate the average number of bound ligands (n) in other experiments where only the ratio r of the absorption maxima is known:

$$n = 0.79 / [0.985 / (r - 0.33) - 1] \qquad (2)$$

This empirical expression provided for explicit monitoring of the dissociation kinetics of *biotin-4-Cy5* from an initial complex of avidin with 4 bound *biotin-4-Cy5* molecules (Figure 12). Irreversible dissociation of *biotin-4-Cy5* was caused by addition of a 100-fold excess of *d*-biotin which irreversibly occupied each biotin-binding site on avidin when a fluorescent *biotin-*

4-Cy5 molecule had dissociated spontaneously. As expected, the dissociation of *biotin-4-Cy5* molecules was accompanied by a decrease in the anomalous 600 nm absorption maximum (squares in Figure 12A) and concomitant revovery of the normal 650 nm absorption maximum of Cy5 chromophores (circles in Figure 12A). The ratio $r = A_{600}/A_{650}$ (Figure 12B) was then converted into the average number (n) of *biotin-4-Cy5* molecules that were still bound per avidin tetramer (Figure 12C) by means of equation (2). The time course of *biotin-4-Cy5* dissociation could be fitted to a bi-exponential decay: 2.8 ligands per avidin tetramer appeared to dissociate with a faster time constant (0.31 h) and the remaining 1.2 ligands per avidin tetramer appeared to dissociate with a roughly 10-fold longer time constant (4.7 h).

When viewed in a semiquantitative way the observed bi-exponential dissociation kinetics was quite informative. For proper interpretation it was necessary to explain why equation (2) yielded a rather imperfect conversion of the A_{600}/A_{650} values in Figure 12B into ligand numbers per avidin tetramer (Figure 12C). Equation (2) is the inversion of equation (1) which has been derived from stepwise titration of avidin tetramers with increasing amounts of *biotin-4-Cy5* (Figures 9A and 10B). The manual mixing process after each addition of *biotin-4-Cy5* (see Figures 9A and 10B) was certainly slower than the association kinetics of the ligands. Thus after each addition of *biotin-4-Cy5* some local excess of ligands over binding sites must have occured for a certain time in the vicinity of the pipette tip, giving rise to formation of higher fractions of avidin tetramers with 2, 3, and 4 bound ligands than would have occurred in the case of very fast mixing. During the 10 min intervals only a fraction of the non-equilibrium distribution could relax, as is obvious from Figure 12C; full relaxation would have required titration intervals of several days! Consequently the forward titration shown in Figure 10B gave an imperfect relationship between A_{600}/A_{650} and the average number of *biotin-4-Cy5* molecules bound per avidin tetramer.

For the above reasons it is justified to understand Figure 12C in the sense that two out of four bound *biotin-4-Cy5* molecules dissociated with a faster time constant (~0.5 h) while the remaining two ligands on the avidin tetramer dissociated with ~10-fold slower kinetics. Such biphasic dissociation has been observed with most biotin derivatives (Finn et al., 1980; Finn et al., 1984; Finn and Hofmann, 1985; Gruber et al., 1997; Gruber et al., 1998; Hofmann et al., 1983; Lavielle et al., 1983; Romovacek et al., 1983) and it is known to derive from the pairwise arrangements of biotin-binding sites in avidin (and streptavidin) tetramers (Green et al., 1971; Green, 1990; Hendrickson et al., 1989; Livnah et al., 1993; Pugliese et al., 1993). The linear distance between the carboxyls of two adjacently bound biotin residues is 20 Å (see Figure 13). Figure 13 also shows the dimensions of two adjacently bound *biotin-4-Cy5* molecules drawn on proper scale. From this sketch it is obvious that there is much steric interaction between neighbouring Cy5 residues. Binding of one *biotin-4-Cy5* molecule will, therefore, hamper the association of another *biotin-4-Cy5* to the neighbouring binding site. For the same reason, one out of two adjacently bound ligands will dissociate much faster than the single remaining ligand in the same pair of binding sites.

The whole avidin tetramer contains *two pairs* of biotin-binding sites (not shown in Figure 13). The distance between non-neighbouring sites is known to be 30 Å and the shortest connection of two non-neighbouring sites over the protein's surface would be even much larger (Hendrickson et al., 1989; Livnah et al., 1993, Pugliese et al., 1993). Under such geometric conditions absolutely no steric interaction between *biotin-4-Cy5* molecules is possible which are bound to non-neighbouring sites on avidin. Based on these geometric considerations, two out of four bound *biotin-4-Cy5* molecules are expected to dissociate more rapidly while the remaining two ligands stay bound on a longer time scale. As argued above, the time course shown in Fig. 13C is fully compatible with such biphasic dissociation kinetics within the inherent uncertainties of the experiment.

LITERATURE CITED IN THE SUPPLEMENTS ONLY

Dewar, M. J. S., Zoebisch, E. G., Healy, E. F., and Stewart, J. J. P. (1985) AM1: A new General Purpose Quantum Mechanical Molecular Model. *J. Am Chem. Soc. 107*, 3902-3909

Feldhoff, R. (1991) Why not ethanol-based solvents for RP-HPLC of peptides and proteins? *Techniques in Protein Chemistry 17*, 55-63.

Finn, F. M., Titus, G., Montibeller, J. A., and Hofmann, K. (1980) Hormone-receptor studies with avidin and biotinylinsulin-avidin complexes. *J. Biol. Chem. 255,* 5742-5746.

Finn, F. M., Titus, G., and Hofmann, K. (1984) Ligands for insulin receptor isolation. *Biochemistry 23,* 2554-2558.

Finn, F. M., and Hofmann, K. H. (1985) Synthesis of biotinyl derivatives of peptide hormones and other biological materials. *Methods Enzymol. 109,* 418-445.

Green, N. M., Konieczny, L., Toms, E. J., and Valentine, R. C. (1971) The use of bifunctional biotinyl compounds to determine the arrangement of subunits in avidin. *Biochem J. 125,* 781-791.

Green, N. M. (1990) Avidin and streptavidin. *Methods Enzymol. 184*, 51-67.

Hendrickson, W. A., Pähler, A., Smith, J. L., Satow, Y., Merrit, E. A., and Phizackerley, R. P. (1989) Crystal structure of core streptavidin determined from multiwavelength anomalous diffraction synchroton radiation. *Proc. Natl. Acad. Sci. U.S.A. 86*, 2190-2194.

Hofmann, K., Titus, G., Montibeller, J. A., and Finn, F. M. (1982) Avidin binding of carboxyl-substituted biotin and analogues. *Biochemistry 21,* 978-984.

Kaiser, K., Marek, M., Haselgrübler, T., Schindler, H., and Gruber, H. J. (1997) Basic Studies on Heterobifunctional Biotin-PEG Conjugates with a 3-(4-Pyridyldithio)propionyl Group on the Second Terminus. *Bioconjugate Chem. 8,* 545-551

Lavielle, S., Chassaing, G., and Marquet, A. (1983) Avidin binding of biotinylated analogues of substance P. *Biochim. Biophys. Acta 759,* 270-277.

Lin, H. J., and Kirsch, J. F. (1979) A rapid, sensitive fluorometric assay for avidin and biotin. *Methods Enzymol. 62,* 287-289.

Livnah, O., Bayer, E. A., Wilchek, M., and Sussman, J. L. (1993) Three-dimensional structures of avidin and the avidin-biotin complex. *Proc. Natl. Acad. Sci. U.S.A. 90,* 5076-5080.

Pugliese, L., Coda, A., Malcovati, M., and Bolognesi, M. (1993) Three-dimensional structure of the tetragonal crystal form of egg-white avidin in the functional complex. *J. Mol. Biol. 231,* 698-710.

Romovacek, H., Finn, F. M., and Hofmann, K. (1983) Avidin binding of biotinylated corticotropins. *Biochemistry 22,* 904-909.

Table 1: Specificity of ligand binding towards avidin. Avidin (~6 nmol according to A_{282}) was incubated with fluorescent ligand (~2 nmol according to absorption at λ_{max}) and gel filtered on a PD-10 column. In the control runs, avidin had been pre-blocked with 270 nmol of *d*-biotin before fluorescent ligand was added.

PD-10 column:	**void peak**	**"salt peak"**
biotin-4-Cy3	5.9 nmol avidin	0.0 nmol avidin
	1.8 nmol biotin-4-Cy3 *a)*	0.0 nmol biotin-4-Cy3
d-biotin + biotin-4-Cy3	6.0 nmol avidin	0.0 nmol avidin
	0.0 nmol biotin-4-Cy3	1.9 nmol biotin-4-Cy3 *a)*
biotin-4-Cy5	5.8 nmol avidin	0.0 nmol avidin
	1.5 nmol *biotin-4-Cy5* *a)*	0.0 nmol *biotin-4-Cy5*
d-biotin + biotin-4-Cy5	6.2 nmol avidin	0.0 nmol avidin
	0.0 nmol *biotin-4-Cy5*	1.5 nmol *biotin-4-Cy5* *a)*

a) Free biotin-4-Cy3 and free *biotin-4-Cy5* showed the expected absorption maxima at 550 nm and at 647 nm, while the λ_{max} values in the avidin-bound state were 552 nm and 652 nm, respectively.

Figure 8: Comparison between absorption and excitation spectra of Cy5-labeled IgG. (A) Normalized absorption spectra of free Cy5-monofunctional dye (solid line) and of goat IgG with 0.5 (dashed line), 4.6 (dotted line) and 6.0 (dash-dot line) bound Cy5 labels per protein. (B) Fluorescence excitation spectra of free Cy5-monofunctional dye (solid line) and of goat IgG with 0.5 (dashed line), 0.9 (dotted line), 1.7 (dash-dot line), 3.2 (dash-dot-dot line), 4.6 (short dash line), and 6.0 (short dot line) bound Cy5 labels per protein. Emission was detected at 665 nm and the narrow scattering peaks around 665 nm were removed from all spectra for the sake of clarity.

Figure 9: Comparison between absorption and excitation spectra of avidin-bound *biotin-4-Cy5* at various protein/ligand ratios. (A) Normalized absorption spectra of free *biotin-4-Cy5* (thick solid line) and of avidin tetramers with 0.1 (thin solid line), 1 (dashed line), 2 (dotted line), 3 (dash-dot line), and 4 (dash-dot-dot line) bound *biotin-4-Cy5* molecules. 1.2 mL of buffer A containing 600 pmol *functional* avidin was mixed with increasing amounts of 14.5 µM *biotin-4-Cy5* (10 min intervals) to give the desired ligand/protein ratios and each spectrum was recorded at the end of a 10 min interval. (B) Fluorescence excitation spectra of free *biotin-4-Cy5* (solid line, 40 nM free ligand) and of avidin tetramers (40 nM) with an average of 1 (dashed line), 2 (dotted line), 3 (dash-dot line), and 4 (dash-dot-dot line) bound *biotin-4-Cy5* molecules. Emission was detected at 665 nm and the narrow scattering peaks around 665 nm were removed from all spectra for the sake of clarity.

Figure 10: Dependence of anomalous Cy5 absorption at 600 nm on the number of Cy5 labels per protein. (A) Peak ratios A_{600}/A_{650} of goat IgG with various numbers of bound Cy5 labels per protein (open circles, same samples as in Figures 1 and 8). Free Cy5-monofunctional

dye is shown for comparison (solid circle). (B) Peak ratios A_{600}/A_{650} of avidin tetramers with various numbers of bound *biotin-4-Cy5* molecules (open circles, same samples as in Figure 9). Free *biotin-4-Cy5* is shown for comparison (solid circle).

Figure 11: Titration of the biotin-binding sites in avidin with *d*-biotin or biotin-4-Cy3 or *biotin-4-Cy5*. (A) Avidin (2 mL, ~80 nM *nominal* concentration by weight) was titrated with a 16 µM *d*-biotin standard by cumulative additions at 40 sec intervals. The tryptophans in avidin were excited at 290 nm and fluorescence was monitored at 340 nm. From the breakpoint at 34.9 µL a *functional* avidin concentration of 70 nM was calculated. (B) Avidin (2 mL, 40 nM *functional* concentration) was titrated with a 16 µM stock solution (*nominal* concentration by absorbance) of biotin-4-Cy3 (circles, excitation at 530 nm, emission at 570 nm) or *biotin-4-Cy5* (triangles, excitation at 630 nm, emission at 665 nm). From the breakpoints at 26.1 µL and 19.1 µL the *functional* concentrations of the biotin-4-Cy3 and *biotin-4-Cy5* stock solutions were calculated to be 12.3 µM and 16.7 µM, respectively.

Figure 12: Displacement of *biotin-4-Cy5* from avidin tetramers. (A) 1.2 mL 0.5 µM avidin (0.6 nmol tetramers) was mixed with 166 µL 14.5 µM *biotin-4-Cy5* (2.4 nmol ligands) and equilibrated for 10 min at 25 °C. At t = 0 h 15 µL 16 mM *d*-biotin was added and absorbance at 600 nm (squares) and 650 nm (circles) was monitored for 22 h. (B) The ratio A_{600}/A_{650} was calculated from panel (A). (C) The number of bound *biotin-4-Cy5* molecules per avidin tetramer was calculated from A_{600}/A_{650} as described in the text.

Figure 13: Schematic representation of one pair of biotin-binding sites in an avidin tetramer. In reality the relative orientation of two neighbouring binding pockets is not parallel but this aspect is irrelevant for the purpose of this drawing. What counts for the interaction of two adjacently bound *biotin-4-Cy5* molecules (shown in proper scaling) is the linear distance between the two biotin carboxyls (20 Å, see dashed line) and the fact that the carboxylic groups of two adjacently bound biotins can be physically connected by a 22-atom spacer (Green, 1990).

Figure 14: Molecular structure of *d*-biotin. (A) Stereochemical structure and atomic numbering of biotin. (B) Prediction of ring fragment conformation from semi-empirical calculations (see text).

© 2000 American Chemical Society, Bioconjugate Chem., Gruber bc000015m Supporting Info Page 19

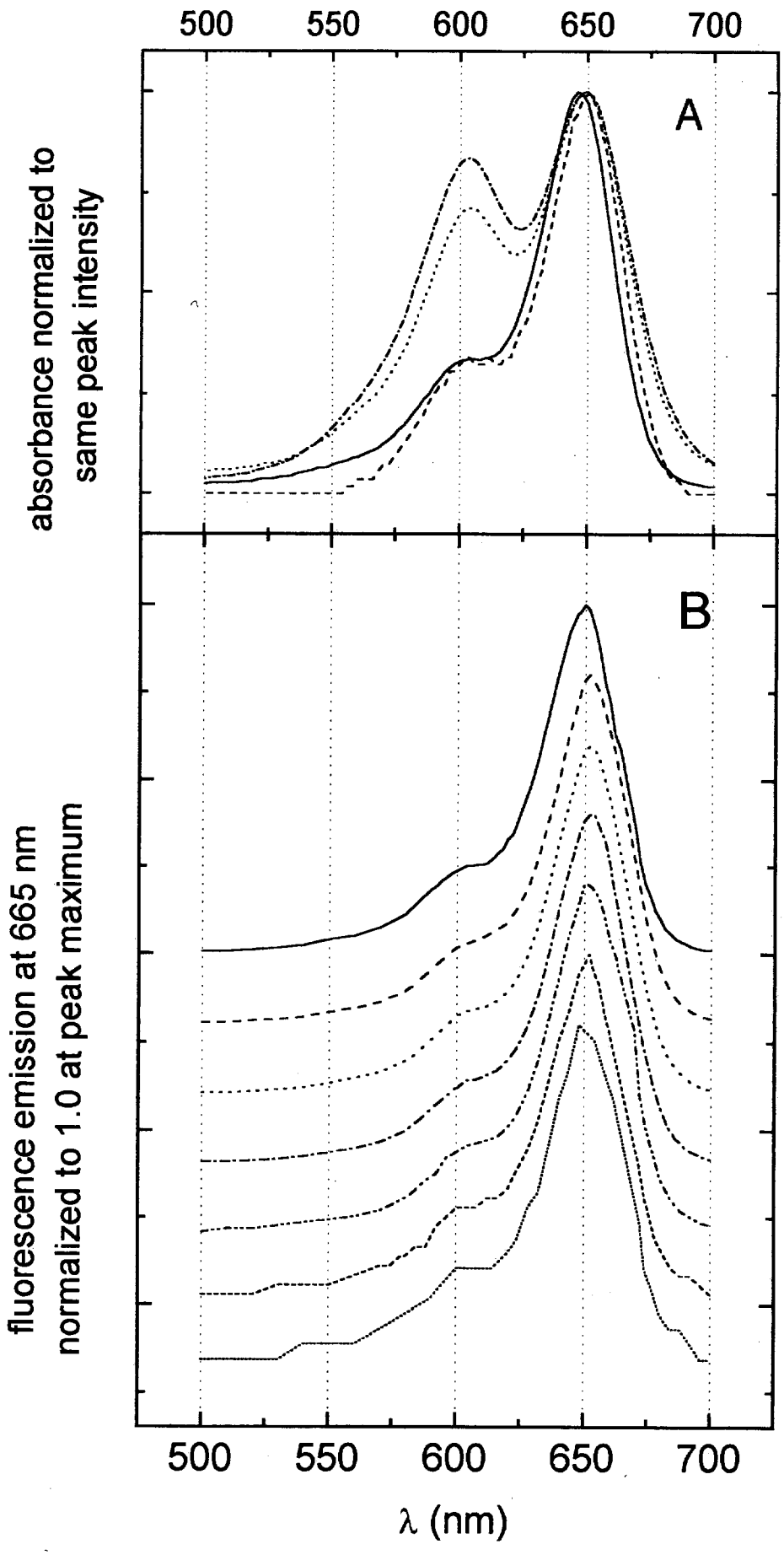

© 2000 American Chemical Society, Bioconjugate Chem., Gruber bc000015m Supporting Info Page 20

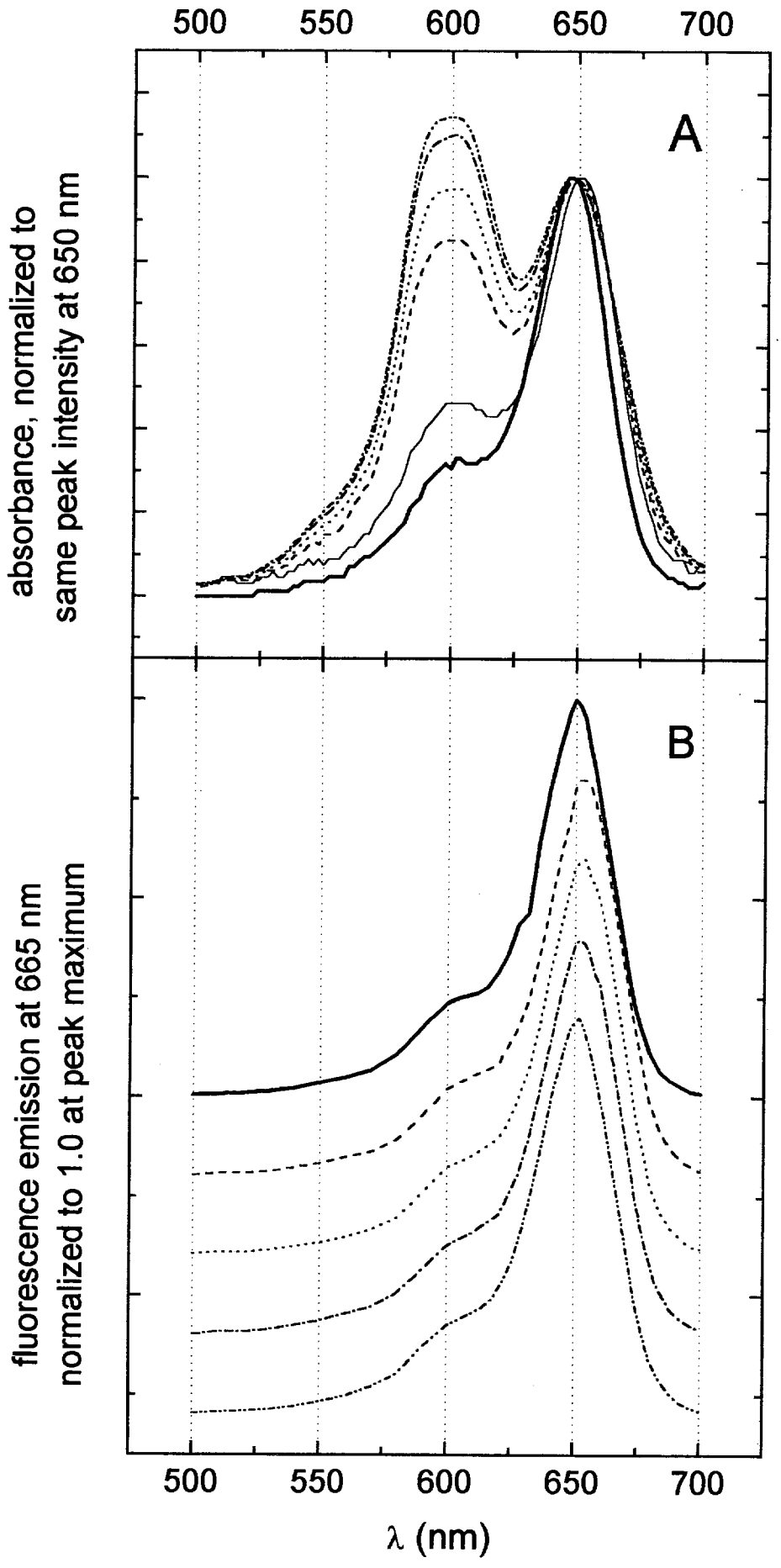

© 2000 American Chemical Society, Bioconjugate Chem., Gruber bc000015m Supporting Info Page 21

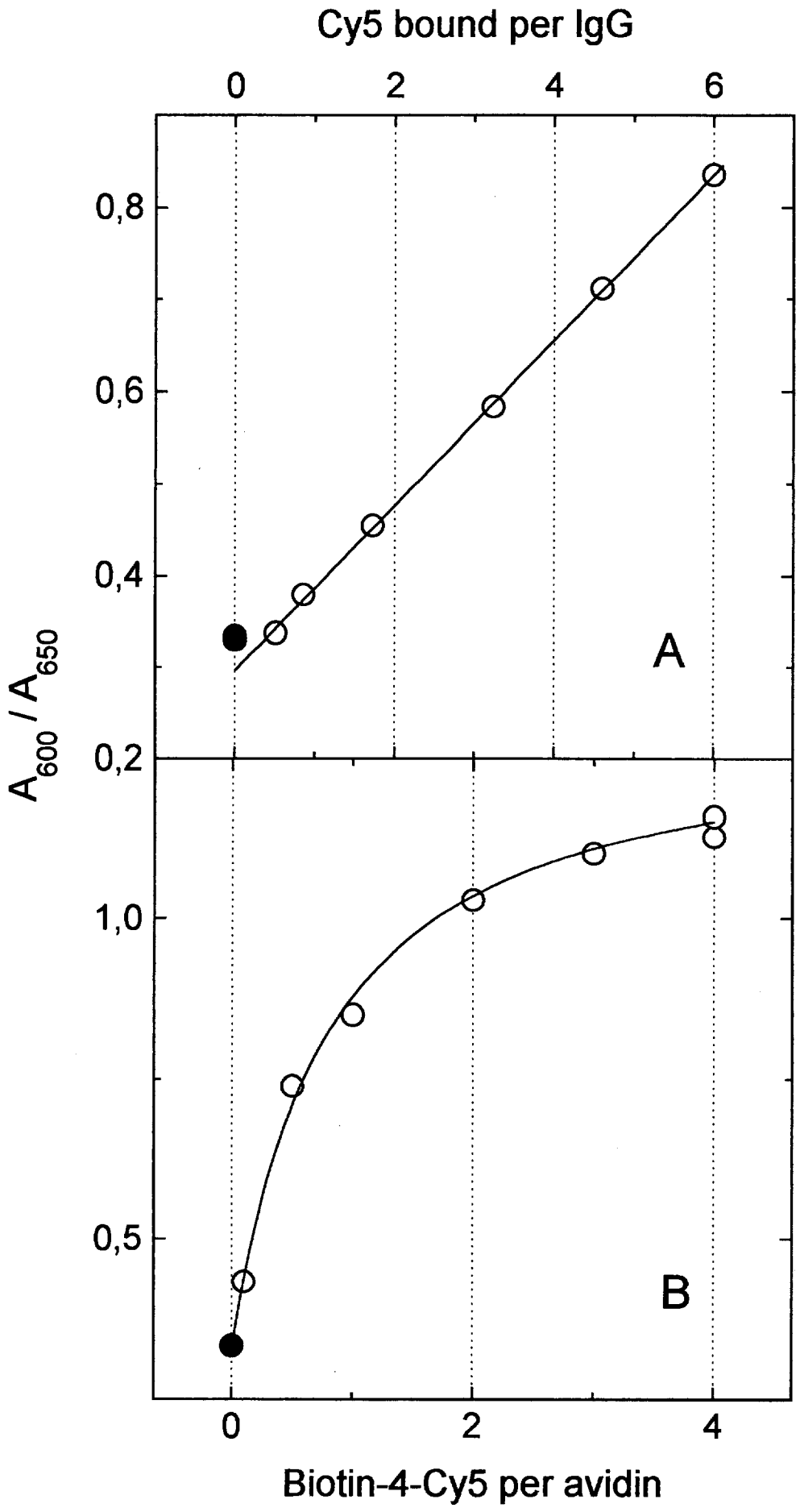

© 2000 American Chemical Society, Bioconjugate Chem., Gruber bc000015m Supporting Info Page 22

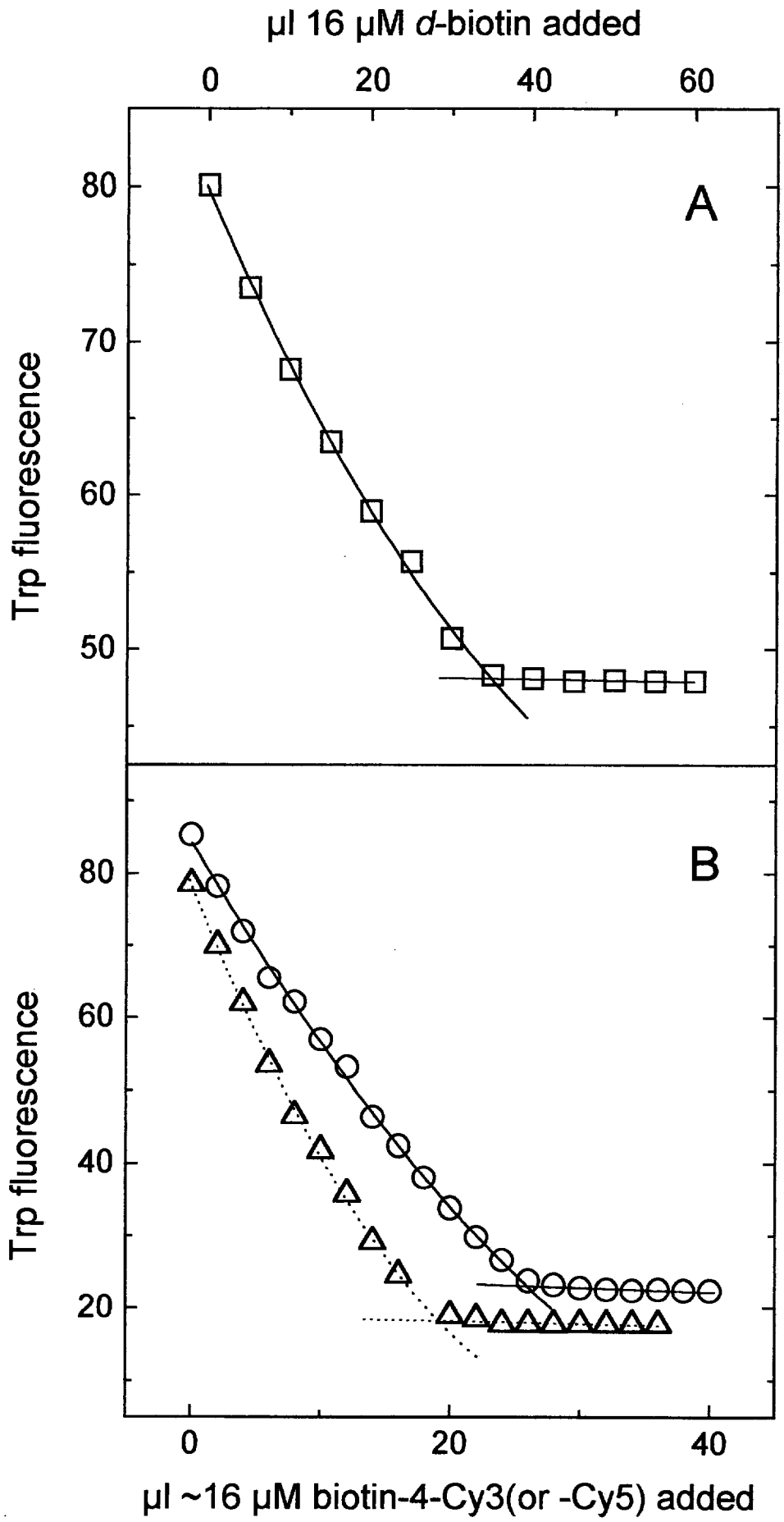

© 2000 American Chemical Society, Bioconjugate Chem., Gruber bc000015m Supporting Info Page 23

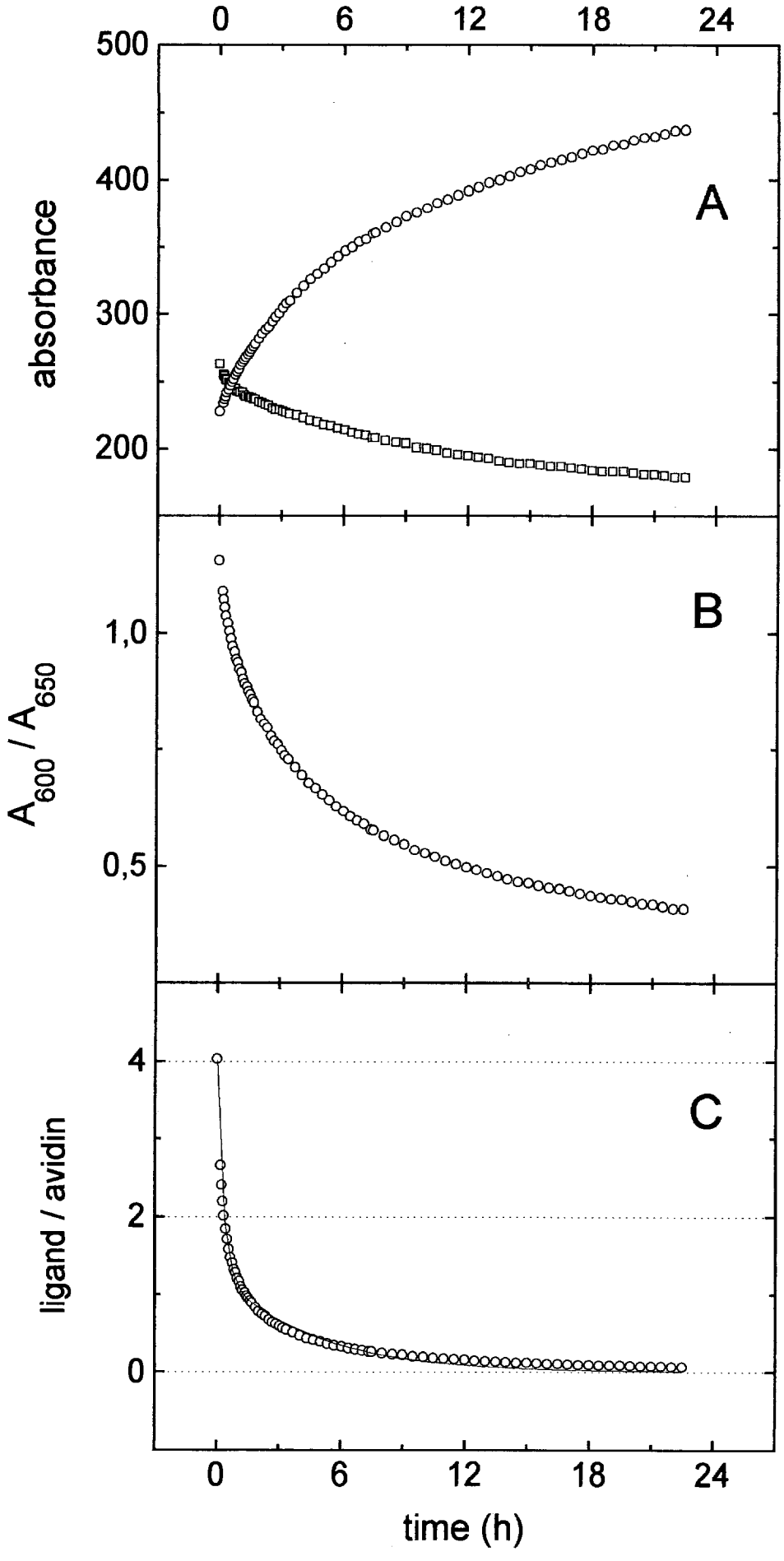

© 2000 American Chemical Society, Bioconjugate Chem., Gruber bc000015m Supporting Info Page 24

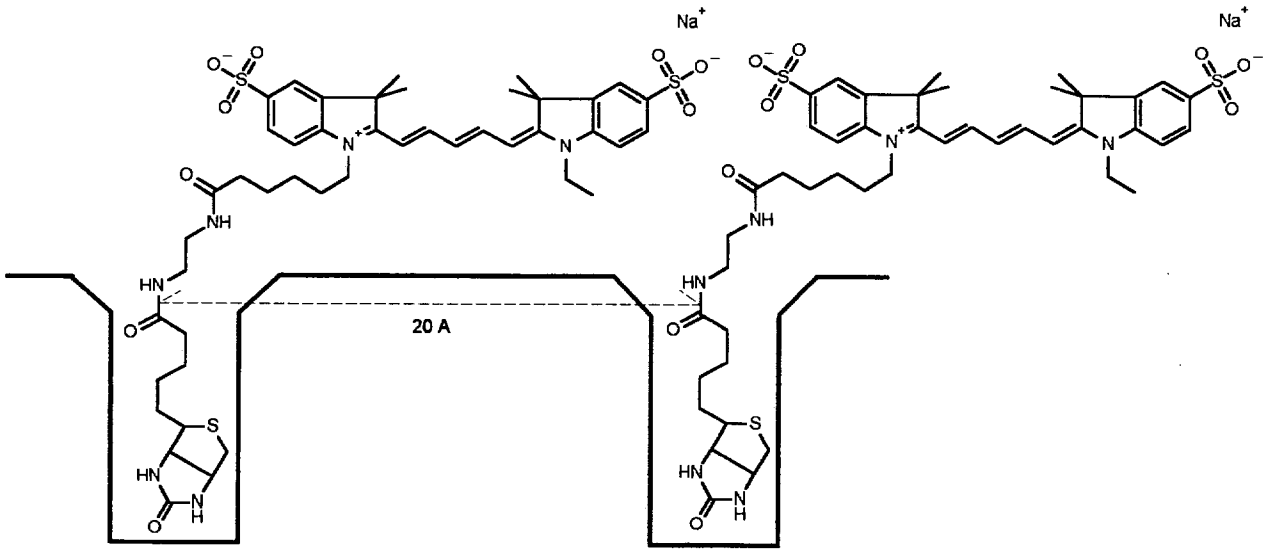

A:

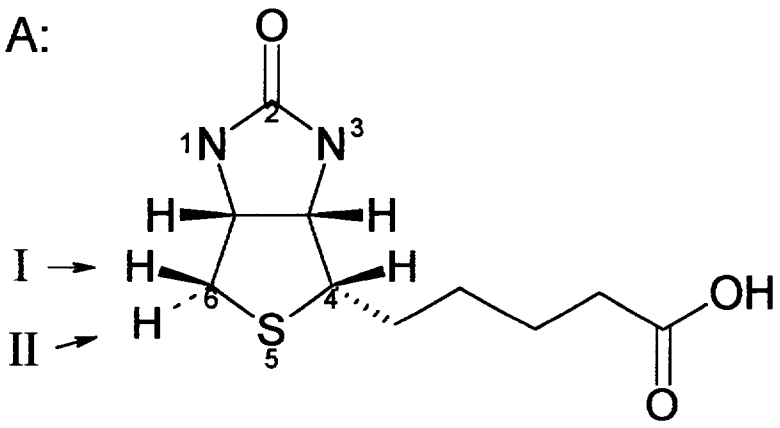

B:

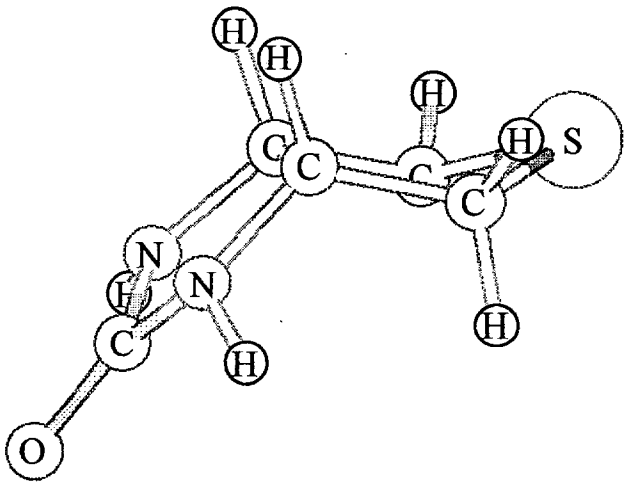

Surface Modification of Diaspirin Cross-linked Hemoglobin (DCLHb) with Chondroitin-4-sulfate Derivatives. Part 1

Ton T. Hai,* David E. Pereira,† Deanna J. Nelson,† Jim Catarello, and Ana Srnak

Corporate Research and Technical Services, Baxter Healthcare Corporation, 25212 West State Route 120, Round Lake, Illinois 60073-9799. Received February 21, 2000; Revised Manuscript Received June 25, 2000

Synthetic methodology was developed for the preparation of chondrotin-4-sulfate reagents that could be specifically attached to the surface of diaspirin cross-linked hemoglobin (DCLHb), a chemically stabilized human hemoglobin. The surface-modified hemoglobin solutions had a significantly higher colloidal osmotic pressures (COP) than DCLHb. The P_{50} of the modified DCLHb was dependent upon the reactive end group of the chondrotin-4-sulfate reagents that was used for the protein modification. Modification of DCLHb with the chondroitin-4-sulfate derivatives containing the maleimide end group **23** provided a hemoglobin with a P_{50} value of 23 mmHg, while the P_{50} of hemoglobins prepared from chondroitin-4-sulfate derivatives containing the aldehyde end group **13** and **18** remained unchanged from that of DCLHb.

INTRODUCTION

Extracellular human hemoglobin is a protein composed of four polypeptide subunits, two α chains and two β chains, each with one heme associated with it. In the hemoglobin tetramer, each α chain is associated with a β chain to form two stable α-β dimers, which in turn associate to form the tetramer with a molecular weight of about 64 500. The subunits are noncovalently associated through van der Waals forces, hydrogen bonds and salt bridges.

Human hemoglobin is not suitable for use as an oxygen delivering therapeutic agent for several reasons. First, the oxygen affinity of extracellular human hemoglobin is too high and, therefore, does not effectively deliver oxygen to tissues. Second, in the circulation, extracellular hemoglobin dissociates into α-β dimers. High concentrations of these dimers overwhelm the haptoglobin scavenging system and accumulate in the tubules of the kidney, where they are nephrotoxic. These shortcomings may be overcome by the stabilization of the tetrameric hemoglobin through intramolecular cross-linking between the dimeric subunits of the native hemoglobin. One such chemically modified hemoglobin is diaspirin cross-linked hemoglobin (DCLHb), which is intramolecularly cross-linked between the α chains (lysine $99_{\alpha1}$−lysine $99_{\alpha2}$) by a fumarate bridge (*1*, *2*). Although stabilization of the tetrameric hemoglobin molecule by chemical modification was successful in addressing the above shortcomings, the full potential of extracellular hemoglobin solutions as an oxygen delivering therapeutic agent could not be met by tetrameric hemoglobin solutions.

A primary drawback of chemically modified tetrameric hemoglobins, such as DCLHb, was the limited duration of the hemoglobin in the circulatory system. A hemoglobin of this size, approximately 64 500, is able to traverse cellular pores in the membrane of the circulatory system and enter interstitial spaces between endothelial cells lining the lumen of the circulatory system. As a result, tetrameric hemoglobin can leave the intravascular space at a rate that is greater than that which is desired for optimal therapeutic utility. DCLHb has an elimination half-life of 2.5 h for a 25- and 50 mg/kg dose and an elimination half-life of 3.3 h for a 100-mg/kg dose in man (*3*).

Therefore, further modifications to the hemoglobin that have the effect of increasing the molecular size of the resulting hemoglobin composition have been developed to extend the circulatory duration of the hemoglobin molecules. These additional modifications can be divided into two groups: polymerization and surface modification. DCLHb has been polymerized with PEG and polyamide cross-linking agents in this laboratory (*4*, *5*) and human hemoglobin has been polymerized with other reagents, such as, glutaraldehyde and an *o*-raffinose derived dialdehyde (*6*).

Less investigated is the surface modification of hemoglobin. Surface modification of hemoglobin is accomplished with monofunctional derivatization reagents that react with either the 44 available lysine ϵ-amino groups and terminal amino groups or the two thiol groups of the cysteines at position 93 of the β-chains (β-93-Cys). Both human and bovine hemoglobin have been surface modified with monofunctional poly(ethylene glycol) derivatives (*7*). This modification is reported to extend the circulating half-life of the modified hemoglobin molecules. An area of hemoglobin surface modification that has not been extensively explored is the use of hydrophilic, anionic reagents. Hemoglobin molecules surface modified with a reagent that could impart a global negative surface charge to the molecule would be expected to be repulsed from the surface of the endothelial cells lining the lumen of the circulatory system. It has been reported in the literature that macromolecules with an anionic molecular charge have a decrease rate of vascular endothelial and glomerular permeability (*8*−*11*). Thus, a surface-modified hemoglobin with a global negative charge may be less likely to cross through capillary junctions or glomerular pores, thereby, extending the circulatory half-life of the hemoglobin composition (*12*).

* To whom correspondence should be addressed. Phone: (847) 270-5837. Fax: (847) 270-5897. E-mail: ton_hai@baxter.com.

† Current address: Magellan Laboratories Inc., P.O. Box 13341, Research Triangle Park, NC 27709.

10.1021/bc000021i CCC: $19.00 © 2000 American Chemical Society
Published on Web 08/25/2000

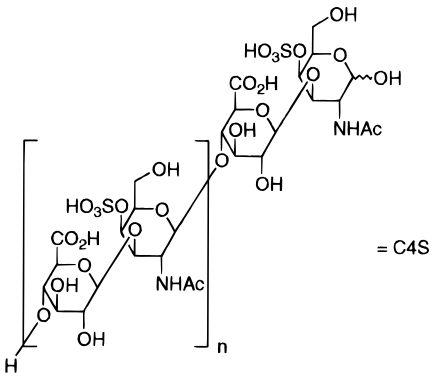

1

Figure 1.

For these reasons, we chose to modify the surface of DCLHb with an anionic polysaccharide that would not only increase the size of the hemoglobin but also impart a global negative charge to the protein. In addition to imparting a negative charge, the polysaccharide needs to be nonimmunogenic and biocompatible. A polysaccharide that met these criteria was chondroitin-4-sulfate, one of the most abundant mucopolysacharides in the human body (*13*). Chondroitin-4-sulfate (C4S) is a long, unbranched polysaccharide chain composed of a repeating disaccharide structure containing uronic acid and hexosamine moieties. Chondroitin-4-sulfate molecules are strongly polyanionic due to the carboxylic acid and sulfate groups that are regularly spaced along the polymer backbone. The structure of chondroitin-4-sulfate (**1**) is shown in Figure 1.

EXPERIMENTAL PROCEDURES

General. Diaspirin cross-linked hemoglobin (DCLHb), Plasma Lyte A, and Lactated Ringer's irrigation solution were obtained from Baxter Healthcare Corporation, Deerfield, IL. Chondroitin-4-sulfate (injection grade, average MW of 50 000) was purchased from Maruha Corporation, Japan. All other commercial reagents were of the highest purity available. All solvents used were of HPLC grade. NMR spectrometry was performed on either a Bruker 270 MHz or a 300 MHz spectrometer.

Analytical Methods. Thin-layer chromatography (TLC) was performed with Whatman MK6F silica gel 60 Å TLC plates. The products were eluted with 2-propanol: ammonium hydroxide: water (6:1:3, v/v/v). The plates were analyzed with UV light or stained with either ninhydrin or 2,3,5-triphenylphenyltetrazolium chloride (TTC) (*25*). The TTC spray solution was freshly prepared before use by combining one part 4% methanolic TTC solution with 1 part 1 N NaOH solution. The sprayed plate was heated for 5−10 min at 100 °C. Reducing sugars produce a red color upon development.

Analytical RP-HPLC was performed on a Vydac Protein C_4 column (5 μm, 4.6 × 250 mm). The mobile phase was delivered at 1 mL/min. as a linear gradient of B (CH_3CN:H_2O:TFA, 60:40:0.1, by volume) in A (CH_3CN:H_2O:TFA, 20:80:0.1, by volume) as follows: (1) 50% B to 55% B over 20 min, (2) 55% B to 75% B over 10 min; and (3) 75% B to 85% B over 10 min. Analytes were detected by measuring the absorbance at 220 nm.

Size exclusion chromatography (SEC) was performed with a Superdex 200 (Pharmacia Biotech) SEC Column. A mobile phase of 50 mM phosphate buffer pH 7.0 containing 0.15 M NaCl at delivered a flow rate of 0.7 mL/min was used. SEC was also performed with a TSK G4000SW and G3000 SW columns (7.5 × 300 mm, Toso Haas) connected in series. Analytes were eluted with a binary mobile phase (50 mM phosphate, pH 6.5/2-propanol, 9:1 by volume) delivered at a flow rate of 1 mL/min. In both cases, analytes were detected by measuring the absorbance at 220 nm for chodroitin-4-sulfate and at 280 nm for hemoglobin products.

Sample preparation for chondroitin sulfate analysis: a 5 mg of the C4S sample was dissolved in 0.5 mL of Nanopure water, and the solution was filtered through a 0.2 μm filter. A 20 μL aliquot of the solution was loaded on the column. Sample preparation for hemoglobin analysis: a 7 μL aliquot of the hemoglobin solution was added to 0.5 mL of Nanopure water and the solution was filtered through a 0.2 μm filter. A 20 μL aliquot of the solution was loaded on the column.

Oxygen equilibrium curves were recorded by reoxygenation of nitrogen equilibrated deoxyhemoglobin in 0.1 M Bis-Tris buffer (pH 7.4 at 37 °C) in the spectral cuvette of a Hemox Analyzer (TCS Medical Products Co., Huntington Valley, PA). The oxygen pressure at which hemoglobin is half saturated (P_{50}) and the subunit cooperativity (n_{40-60}) were calculated from the oxygen equilibrium curves. The concentrations of oxy-, deoxy-, and methemoglobin were calculated from their absorbance at three wavelengths (630, 576, and 560 nm) using the reported molar extinction coefficients (*14*). Total hemoglobin concentration was calculated by summation of the concentrations of these components, and percent methemoglobin (MetHb) was calculated as its portion of the total hemoglobin concentration. The number of reactive thiols on the polyDCLHb molecules was determined by the method of Neis et al. (*15*).

Red Cell Aggregation Testing. A simple in vivo test in which red cell aggregation was monitored was used for assessing the biocompatibilty with blood of the chemically modified DCLHb. In this test, human blood was diluted with physiological electrolyte solution (negative control) or chemically modified DCLHb solution (test solution) and then incubated. Solutions containing 10, 30, and 50% (by volume) of the chemically modified DCLHb solution were prepared and tested in this way. If there was no interaction between the test solution and the red cells or platelets, the red cells were dispersed randomly through the sample and a score of "none" was recorded. However, if there were interactions between the test sample and red cells platelets, aggregates and/or platelet "clumps" were observed. A score of "very few", "few", "1", and "2" served to define increasing degrees of red cell aggregation of the chemically modified DCLHb solution.

Chondroitin-4-sulfate-4K (2). Chondroitin-4-sulfate (400.8 g) was dissolved in 5 L of 0.5 N HCl. The solution was heated at 65 °C for about 24 h. The solution was cooled in an ice bath to RT. The pH was adjusted to 7.6 with 5 N NaOH. To the solution was added 12 L of ethanol. The mixture was stirred for 3 h under ice bath cooling. The solvent was decanted and 4 L of ethanol was added. The mixture was stirred to obtain a solid. The solid was collected and washed with ethanol (2 × 500 mL) followed by ethyl ether (1 × 500 mL). The solid was vacuum-dried to give 343.5 g of product having MW of 4000 (*16*). The compound had a SEC a retention time of 26.3 min obtained on a Superdex 200 (Pharmacia Biotech) SEC column.

Diethylene Glycol Bis(3-aminopropyl)ether Mono-*tert*-butyl Carbonate (4). Diethylene glycol bis(3-aminopropyl)ether (**3**) (528.0 g, 2.4 mol) was dissolved in 2 L of dichloromethane. A solution of di-*tert*-butyl dicar-

bonate (261.4 g, 1.2 mol) in 1 L of dichloromethane was added dropwise over 4.5 h. The solution was stirred for 1 h and then extracted with 1 L of water. The organic phase was evaporated to an oil. The oil was dissolved in 2 L of water and the pH was adjusted to 5 with 5 and 1 N HCl. The solution was extracted with 1 L of dichloromethane. The pH of the aqueous phase was adjusted to 13 with 1 N NaOH. The solution was extracted with dichloromethane (4 × 750 mL). The extracts were combined and dried with $MgSO_4$. The solution was evaporated to give 241.3 g (31%) of viscous oil product.

^{1}H NMR ($CDCl_3$): δ 1.39 (s, 9-H); 1.67 (m, 4-H); 2.75 (t, 2-H, J = 6.75 Hz); 3.17 (q, 2-H, J = 6.2 Hz); 3.51 (m, 14-H) 5.19 (s, 1-H). ^{13}C NMR ($CDCl_3$): δ 28.3; 33.2; 39.5; 69.3; 69.5; 70.1; 70.4; 70.5; 78.7; 156.0; impurity resonances at 29.5; 38.4; 70.0. Anal. calcd for $C_{15}H_{32}N_2O_5$: C, 56.23; H, 10.07; N, 8.74. Found: C, 56.87; H, 9.86; N, 8.36.

Chondroitin-4-sulfate Derivative 5. Compound **2** (222.0 g, 55.0 mmol) and **4** (150.1 g, 470.5 mmol) were dissolved in 1.2 L of sterile water for irrigation, USP, and the solution pH was adjusted to 8.3 with 1 N HCl. Ethanol (600 mL) was added to the solution followed by borane−pyridine complex (57 mL). The solution was heated at 40 °C for 4 days. The solution was cooled to RT and the pH was adjusted to 10 using 5 N NaOH followed by 1 N NaOH. Ethanol (12 L) was added to solution with stirring. After stirring 3 h, the mixture was allowed to stand for 1 h. The solvent was decanted and the solid was collected and washed with ethanol (2 × 500 mL) followed by ethyl ether (1 × 500 mL). The solid was vacuum-dried to give 210.7 g (89%) of product.

^{1}H NMR (D_2O): δ 1.38 (s); 1.70 (t, J = 6.48 Hz); 1.98 (s); 3.09 (t, J = 6.48 Hz); 3.29−3.75 (m); 3.95 (m); 4.04 (m); 4.12 (m); 4.17 (m); 4.45 (m). ^{13}C NMR (D_2O): δ 25.4; 30.6; 31.6; 39.9; 53.6; 53.8; 54.4; 63.8; 70.3; 70.5; 71.2; 71.1; 72.4; 74.6; 75.3; 75.4; 75.5; 76.5; 77.4; 77.8; 77.9; 78.1; 78.4; 79.0; 79.2; 82.5; 82.8; 83.1; 83.7; 103.6; 104.2; 106.3; 106.6; 106.9; 107.1; 161.1; 177.2; 177.4; 177.5; 177.8; 178.8; 178.9.

Chondroitin-4-sulfate Derivative 6. Compound **5** (184.2 g) was dissolved in 750 mL of water and 750 mL of 1 N HCl. The pH of the solution was adjusted to 0.85 with 1 N HCl. The solution was stirred at RT for 24 h. The solution was evaporated from about 1.8 L to a volume of about 1 L. The solution was diluted with ethanol (8 L) and the mixture was stirred for 2 h. The precipitate was collected and washed with ethanol (250 mL) and then with ethyl ether (250 mL). The solid was vacuum-dried to give 143.9 g (79%) of **6**.

^{1}H NMR (D_2O): δ 1.89 (m); 3.09 (t, J = 6.48 Hz); 3.29−3.75 (m); 3.93 (m); 4.06 (m); 4.14 (m); 4.51 (m); 4.69 (m). ^{13}C NMR (D_2O): δ 23.1; 23.5; 26.4; 27.6; 38.7; 47.4; 48.4; 52.0; 52.2; 52.7; 62.0; 63.7; 68.5; 68.7; 69.4; 70.5; 70.6; 72.3; 72.4; 73.1; 73.3; 73.5; 73.7; 74.5; 74.8; 75.5; 75.6; 76.0; 76.1; 81.0; 99.2; 102.4; 104.8; 105.0; 105.3; 105.4; 172.4; 172.6; 173.6; 173.8; 173.7; 176.0; 176.2.

Methyl 4-Thia-7-diethoxy-heptanoate (10). Methyl 3-mercaptopropionate (**8**) (120.0 g, 1.0 mol) was added to a mixture of potassium carbonate (250.0 g, 1.8 mol) in 1 L of DMF. 3-Chloropropionaldehyde diethyl acetal (**9**) (194.6 g, 1.17 mol) was added to the mixture. The mixture was heated to 85 °C for 5 h. An additional 10.0 g portion of the acetal and 10.1 g of potassium carbonate was added. The mixture was heated for an additional 1.5 h at 85 °C. The mixture was cooled to about 20 °C and ethyl ether (1 L) was added to the mixture. Water (1 L) was added to the mixture while the mixture was well stirred. The phases were separated and the aqueous phase was extracted with ethyl ether (1 × 1 L; 1 × 500 mL). The combined extracts were extracted with a 5% potassium carbonate solution (800 mL). The organic phase was dried with $MgSO_4$ and filtered, and the filtrate was evaporated to an liquid. The product was collected by distillation from 115 to 120 °C at 0.2 mm Hg to give 186.1 g (74%) of product.

^{1}H NMR ($CHCl_3$): δ 1.19 (t, J = 7.1 Hz, 6-H); 1.86 (q, J = 7.7 Hz, 2-H); 2.59 (m, 4-H), 2.76 (m, 2-H); 3.45 (m, 2-H); 3.64 (m, 5-H); 4.57 (t, J = 5.6 Hz, 1-H). ^{13}C NMR ($CHCl_3$): δ 14.7; 26.3; 26.5; 33.0; 33.9; 51.0; 60.8; 100.9; 171.5. Anal. calcd for $C_{11}H_{22}O_4S$: C, 52.77; H, 8.86; S, 12.81. Found: C, 52.37; H, 8.66; S,12.71.

4-Thia-7-diethoxy-heptanoic Acid (11). Methyl 4-thia-7-diethoxy-heptanoate (**10**) (250.3 g, 1.0 mol) was dissolved in ethanol (600 mL). Potassium hydroxide (61.8 g, 1.1 mol) in water (200 mL) was added in one portion. After stirring for 45 min, the solvent was evaporated to two-thirds of the starting volume. To the remaining solution was added 500 mL of water. The solution was extracted with ethyl ether (2 × 300 mL). The aqueous phase was collected, and ethyl ether (500 mL) was added. The mixture was stirred vigorously as 5 N HCl (182 mL) was slowly added. The phases were separated and the aqueous phase was extracted with ethyl ether (2 × 300 mL). The extracts were combined and extracted with 1.00 N NaOH (1 × 72 mL) to remove impurities. The organic phase was dried with $MgSO_4$ and evaporated to provide 183.6 g (78%) of **11** as viscous oil.

^{1}H NMR ($CDCl_3$): δ 1.15 (t, J = 7.0 Hz, 6-H); 1.86 (q, J = 6.8 Hz, 2-H); 2.54 (t, J = 7.5 Hz, 2-H); 2.60 (t, J = 6.8 Hz, 2-H); 2.73 (q, J = 7.0 Hz, 2-H); 3.48 (m, 2-H); 3.61 (m, 2-H); 4.57 (t, J = 5.6 Hz, 1-H). ^{13}C NMR ($CDCl_3$): δ 15.3; 25.5; 26.3; 27.3; 31.8; 33.5; 61.6; 101.4; 167.1; 168.9. Anal. calcd for $C_{10}H_{20}O_4S$: C, 50.77; H, 8.30; S, 13.57; Found: C, 50.89; H, 8.30; S, 13.41.

N−Succinimidyl 4-Thia-7-diethoxy-heptanoate (12). 4-Thia-7-diethoxy-heptanoic acid (**11**) (153.9 g, 0.65 mol) and triethylamine (72.9 g, 0.72 mol) were combined in 1 L of acetonitrile. *N*,*N*′-Disuccinimidyl carbonate (184.6 g, 0.72 mol) was added as a solid in portions. The resulting solution was stirred at RT overnight. The solution was evaporated to an oil, and the oil was dissolved in 1 L of chloroform. The solution was extracted with 5% $NaHCO_3$ (2 × 500 mL). The organic phase was treated with activated carbon, and the mixture was dried with $MgSO_4$. The mixture was filtered through a pad of $MgSO_4$, and the filtrate was evaporated to give 186.5 g (95%) of **12** as an oil. The oil was used without further purification.

^{1}H NMR ($CDCl_3$): δ 1.19 (t, J = 7.0 Hz, 6-H); 1.89 (q, J = 6.7 Hz, 2-H); 2.60 (t, J = 7.5 Hz, 2-H); 2.85 (m, 12-H); 3.49 (m, 2-H); 3.62 (m, 2-H); 4.58 (t, J = 5.6 Hz, 1-H). ^{13}C NMR ($CDCl_3$): δ 15.2; 25.5; 26.2; 27.3; 31.8; 33.5; 61.5; 101.4; 167.1; 168.9. Anal. calcd for $C_{14}H_{23}NO_6S$: C, 50.43; H, 6.95; N, 4.20. Found: C,49.89; H, 6.61; N, 3.77.

Chondroitin-4-sulfate Derivative 7. Compound **6** (140.0 g, 35.0 mmol) was dissolved in 1.2 L of water. The pH of the solution was adjusted to 9 with 5 N NaOH. *N*-Succimidyl 4-thia-7-diethoxy-heptanoate **12** (58.8 g, 170.0 mmol) in 500 mL of DMF was added dropwise. After the addition was complete, the solution was stirred 4 h at RT. The solution was concentrated to 500 mL. Ethanol (4 L) was added to the solution. The solvent was decanted from the resulting oil. Ethanol (4 L) was added to the oil and the mixture was kept at 5 °C. The solvent was decanted. The remaining mixture was centrifuged to give a gellike pellet. The pellet was diluted with acetone and evaporated to a semisolid. Ethyl ether was

added, and the mixture was allowed to stand for 1 h. The mixture was filtered, and the gellike solid was dried under vacuum at room temperature. The solid was collected to give 104.7 g (71%) of **7**.

^{1}H NMR (D_2O): δ 1.18 (m); 1.76 (m); 1.91 (m); 2.05 (s); 2.57 (m); 2.61 (m); 2.79 (m); 2.99 (s); 3.29−3.75 (m); 3.95 (m); 4.09(m); 4.15 (m); 4.21 (m); 4.49 (m); 7.91 (s). ^{13}C NMR (D_2O): δ 15.5; 17.9; 22.9; 23.1; 23.6; 26.2; 26.4; 27.3; 27.8; 29.3; 32.5; 34.2; 36.7; 37.4; 38.0; 51.9; 52.1; 52.6; 53.1; 58.5; 62.1; 63.9; 64.0; 68.6; 68.7; 69.4; 69.5; 70.4; 70.6; 72.9; 73.5; 73.6; 73.8; 74.6; 74.7; 75.7; 76.0; 76.3; 76.4; 77.2; 77.4; 77.7; 80.6; 81.1; 81.3; 82.2; 101.9; 102.4; 103.0; 104.3; 104.5; 104.8; 105.2; 105.3; 166.0; 175.4; 175.6; 175.7; 176.1; 176.3; 176.5; 176.9; 177.0; 178.0.

Chondroitin-4-sulfate Aldehyde 13. Compound **7** (104.3 g) was dissolved in a solution of 750 mL of sterile water and 750 mL of 1 N HCl. The pH of the solution was adjusted to 2 with 1 N HCl. The solution was stirred for 3.5 h. The reaction solution was concentrated to about 100 mL. Acetone (250 mL) was added to precipitate the product as an oil. The solvent was decanted and an additional 250 mL of acetone was added. The mixture was agitated, and the solvent was decanted. To the resulting semisolid was added an additional 250 mL of acetone. The mixture was allowed to stand for 1 h. The resulting solid was collected, washed with 100 mL of acetone, and dried under vacuum to give 113.6 g of **13**.

^{1}H NMR (D_2O): δ 1.75 (m); 2.02 (s); 2.51 (m); 2.58 (m); 2.79 (m); 3.29−3.75 (m); 3.95 (m); 4.04 (m); 4.12 (m); 4.17 (m); 4.54 (m); 5.08 (s); 9.64(s). ^{13}C NMR (D_2O): δ 22.9; 23.1; 23.5; 36.7; 37.4; 51.9; 52.1; 52.7; 62.0; 68.4; 68.68.7; 69.4; 70.4; 70.6; 72.3; 73.1; 73.3; 73.5; 74.7; 75.5; 75.7; 76.0; 76.8; 77.0; 77.2; 80.9; 81.1; 90.7; 102.3; 102.5; 104.4; 104.7; 104.9; 105.3; 172.6; 172.9; 173.8; 173.9; 174.0; 175.5; 175.7; 176.0; 176.2; 207.4. Compound exists in the aldehyde and hydrated form (90.8 and 207.4 resonances).

***N*-(4-Diethoxybutyryl)succinamic Acid (15).** 4-Aminobutyraldehyde diethylacetal (**14**) (5.3 g, 32.9 mmol) was dissolved in 10 mL of chloroform. A solution of succinic anhydride (3.3 g, 33.0 mmol) in 20 mL of chloroform was added dropwise. The oil was used without further purification. ^{1}H NMR ($CDCl_3$): δ 1.15 (m, 12-H); 2.00 (m, 8-H); 2.63 (m, 8-H); 3.45 (m, 2-H); 3.56 (m, 2-H); 3.69 (m, 4-H); 5.07 (d, J = 4.05 Hz, 1-H); 5.45 (d, J = 5.19 Hz, 1-H); 7.25 (s, 2-H). ^{13}C NMR ($CDCl_3$): δ 15.1; 15.2; 21.0; 22.8; 28.7; 28.8; 29.1; 29.3; 31.4; 31.6; 45.7; 46.0; 62.2; 64.3; 85.8; 87.6; 171.9; 172.0; 176.5. Impurity resonances: 176.4; 58.1; 28.6; 18.0.

***N*-Succinimidyl *N*-(4-Diethoxybutyryl)succinamate (16).** Disuccinimidyl carbonate (6.5 g, 25.3 mmol) was added as a solid to a solution of *N*-(4-diethoxy)butyrylsuccinamic acid (**15**) (6.0 g, 23.0 mmol) and triethylamine (2.6 g, 25.3 mmol) in acetonitrile. The solution was stirred overnight at room temperature. The solution was evaporated to an oil. The oil was dissolved in chloroform (75 mL) and extracted with water (2 × 25 mL). The organic phase was extracted with 5% $NaHCO_3$ (2 × 25 mL) and then dried over anhydrous $MgSO_4$. The mixture was filtered, and the filtrate was concentrated under vacuum to give **16** as an oil. The oil was used without further purification.

^{1}H NMR ($CDCl_3$): δ 1.11 (m, 6-H); 1.53 (m, 4-H); 2.62 (s, 4-H); 3.42 (m, 6-H); 3.56 (m, 2-H); 4.35 (dd, 1-H); 4.40 (t, 1-H). ^{13}C NMR ($CDCl_3$): δ 15.1; 22.9; 25.4; 27.9; 30.7; 61.4; 102.1; 168.7; 168.9; 177.1. Anal. calcd for $C_{16}H_{26}N_2O_7$: C, 53.62; H, 7.31; N, 7.82. Found: C, 53.07; H, 7.01; N, 8.00.

Chondroitin-4-sulfate Derivative 17. Compound **6** (10.0 g, 2.5 mmol) was dissolved in 100 mL of water, and the solution pH was adjusted to 9.3 with 1 N NaOH. A solution of *N*-oxysuccinimidyl *N*-(4-diethoxy)butyrylsuccinamate (**16**) (4.5 g, 12.5 mmol) in 10 mL of DMF was added to the reaction solution. The solution was stirred for 3 h at room temperature. The solution was concentrated under vacuum to a volume of about 25 mL. To the solution was added 1 L of ethanol. The mixture was cooled to 5 °C and allowed to stand overnight. The solvent was decanted, and the solid was collected by filtration. The solid was washed with ethanol (25 mL) and then with ethyl ether (2 × 25 mL). The solid was dried under vacuum to give 6.8 g (64%) of **17**.

^{1}H NMR (D_2O): δ 1.24 (m); 1.76 (m); 2.06 (br. s); 2.49 (m); 2.72 (s); 3.2−4.20 (br. s); 4.49. ^{13}C NMR (D_2O): 14.3; 14.9; 15.4; 23.6; 26.2; 29.3; 31.0; 31.4; 32.5; 33.0; 37.4; 39.0; 52.0; 52.6; 62.1; 63.6; 64.1; 68.5; 68.8; 69.2; 69.4; 70.4; 70.6; 72.6; 72.9; 73.8; 74.7; 75.7; 76.0; 76.4; 76.6; 77.2; 77.4; 80.7; 81.0; 81.3; 101.9; 104.5; 104.8; 105.1; 105.3; 108.7; 175.3; 175.6; 175.7; 176.0; 177.0; 177.1; 178.7.

Chondroitin-4-sulfate Aldehyde 18. Compound **17** (5.5 g, 1.4 mmol) was dissolved in 25 mL of water, and the solution pH was adjusted to 1.5 with 1 N HCl. The solution was stirred at RT for 4 h. The solution was concentrated under vacuum to a volume of about 10 mL, and then acetone (50 mL) was added. The solvent was decanted, and an additional 50 mL of acetone was added. The solvent was again decanted, and 50 mL of acetone was added. The mixture was stirred and the solid was collected. The solid was dried under vacuum to give 5.0 g (83%) of **18**.

^{1}H NMR (D_2O): δ 1.14 (m); 1.74; (br. s); 1.80 (br. s); 2.47 (br. s); 2.61 (br. s); 2.75 (br. s); 3.20−4.16 (m); 4.56 (br. s); 5.63 (s). ^{13}C NMR (D_2O): δ 14.5; 15.0; 22.9; 23.1; 23.5; 26.3; 28.4; 31.4; 37.5; 46.8; 47.7; 52.2; 52.8; 62.0; 68.5; 68.7; 69.5; 69.9; 70.4; 70.7; 72.3; 73.5; 74.5; 74.6; 74.8; 75.4; 75.6; 75.7; 76.0; 76.1; 76.4; 77.0; 77.3; 80.4; 81.1; 8`.9; 82.7; 102.5; 104.5; 104.8; 105.0; 172.3; 172.5; 173.4; 173.6; 175.8; 176.0; 176.2; 183.0.

***N*-Succinimidyl 2-Formylphenoxyacetate (20).** 2-Formylphenoxyacetic acid (**19**) (18.0 g, 0.1 mol) and *N*-hydroxysuccinimide (13.0 g, 0.11 mol) were combined in 300 mL of acetonitrile. 1,3-Dicyclohexylcarbodiimide (24.1 g, 0.12 mol) in 100 mL of acetonitrile was added. The resulting mixture was stirred for 3 h and then filtered. The filtrate was concentrated to dryness under vacuum, and tetrahydrofuran (THF; 50 mL) was added. The solid was collected by filtration, and the filtrate was reduced in volume to about 15 mL. The precipitated solid was collected, combined with the first crop, and dried to give 22.8 g (82%) of **20**.

^{1}H NMR (DMSO-d_6): δ 2.82 (s, 4-h); 5.54 (s, 2-H); 7.16 (t, J = 7.43 Hz, 1-H); 7.25 (d, J = 8.42 Hz, 1-H); 7.71 (m, 2-H); 10.41 (s, 1-H). ^{13}C NMR (D_2O): δ 25.2, 63.7, 122.2, 124.8, 136.2, 159.3, 165.3, 169.9, 188.8. Anal. calcd for $C_{11}H_{22}O_4$: C, 56.32; H, 4.00; N, 5.05. Found: C, 56.44; H, 4.00; N, 4.92.

Chondroitin-4-sulfate Aldehyde 21. Compound **6** (8.0 g, 2.0 mmol) in water (60 mL) was added dropwise to a solution of *N*-oxysuccimidyl 2-formylphenoxyacetate (**20**) (3.3 g, 12 mmol) in DMF (100 mL) over 1.5 h. The solution was stirred at RT for 1 h, and then the solution was concentrated to dryness under vacuum. The residue was dissolved in 60 mL of water, and the solution was filtered. Ethanol (500 mL) was added to the filtrate to precipitate the product. The product was washed with ethanol (25 mL) and dried to give 3.6 g (43%) of product.

^{1}H NMR (D_2O): δ 1.78; 1.99; 3.32; 3.47; 3.59; 3.66; 3.75; 3.97; 4.06; 4.18; 4.45; 7.046 (d); 7.19 (t); 7.69 (t); 7.84 (d).

Table 1. Surface Modification of DCLHb with 23

molar ratio of **23**/DCLHb	peak maxima[a] (retention time, min)	P_{50} (mm Hg)	n (40−60)	C4S/Hb[b]
DCLHb	19.6	31	2.7	NA
5/1	17.6	21	2.1	NA
10/1	16.9	21	1.9	NA
15/1	16.3	23	1.9	NA
20/1	15.8	22	1.8	7.0/1
25/1	15.4	22	1.9	7.8/1
30/1	15.1	22	1.8	9.8/1
35/1	14.9	23	1.8	10.7/1
40/1	14.7	23	1.9	NA

[a] SEC column: TSKG3000 and TSKG4000 in series. [b] Determined by NMR.

^{13}C NMR (D_2O): δ 23.6; 27.6; 29.3; 37.5; 38.7; 52.1; 52.7; 62.2; 68.6; 69.4; 70.5; 70.6; 72.9; 73.5; 73.8; 74.8; 75.7; 76.1; 76.4; 76.4; 77.3; 77.5; 81.1; 81.4; 101.9; 105.2; 105.4; 114.4; 123.3; 125.4; 132.0; 138.5; 160.5; 171.7; 175.4; 175.7; 176.1; 177.1; 194.7.

Chondroitin-4-sulfate Maleimide 23. A solution of **6** (7.0 g, 1.75 mmol) in a solution of 46 mL of water and the solution pH were adjusted to 9 with 5 N NaOH. DMF (23 mL) was added to the solution of **6**, and the solution was added to a stirred solution of *N*-succinimidyl maleimidopropionate (**22**) (2.78 g, 10.5 mmol) in solution of 140 mL of DMF and 10 mL of water at a rate of 4−5 mL/min. After the addition, the solution was stirred for an additional 1 h. The reaction mixture was concentrated to dryness. The residue was dissolved in water and filtered to remove an insoluble solid. The filtrate was diluted with ethanol to precipitate the product. The solid was dried to give 5.83 g (80%) of **23**.

^{1}H NMR (D_2O): δ 1.78 (br. s); 1.80 (br. s); 2.14; 2.56 (br. s) 3.24−4.17 (m); 4.07; 4.28; 4.55; 4.57; 6.95 (s). ^{13}C NMR (D_2O): δ 23.1; 23.7; 26.3; 26.5; 29.3; 35.7; 36.0; 37.5; 47.1; 47.4; 50.6; 52.1; 62.2; 64.0; 68.7; 69.5; 70.5; 70.7; 72.0; 72.9; 73.6; 73.8; 74.8; 75.6; 76.1; 76.5; 76.8; 77.5; 80.1; 81.1; 81.4; 82.3; 102.0; 102.5; 103.9; 104.6; 104.9; 105.2; 105.4; 135.7; 173.7; 173.7; 173.8; 174.5; 175.9; 175.8; 176.1; 176.4; 17.1; 178.6.

Surface Modification of DCLHb with Chondroitin-4-sulfate Containing Aldehyde End Groups. A solution of DCLHb in 0.1 M borate, pH 9.0, was deoxygenated by vacuum/nitrogen cycles for 1.5 h at room temperature. A solution of **13**, **18**, or **21** in water and borane−pyridine complex (borane-pyridine/**2** in a molar ratio of 5/1) were added so that the final concentration of DCLHb was 6 g/dL in borate buffer, pH 9.0. The reaction mixture was stirred at room temperature under nitrogen for 24 h and dialyzed against Plasma-Lyte A to give the final product. The results are summarized in Tables 2 and 3 and Figure 2.

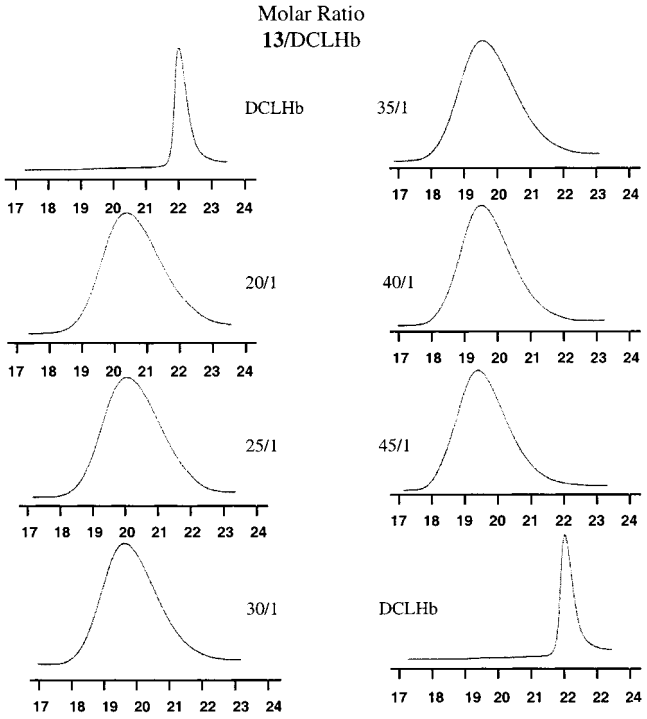

Figure 2.

Surface Modification of DCLHb with Chondroitin-4-sulfate Containing Maleimide End Groups. A solution of DCLHb in 0.1 M HEPES, pH 8.0, was deoxygenated by vacuum/nitrogen cycles for 1.5 h at room

Table 2. Effect on P_{50} and Coopertivity by the Surface Modification of DCLHb by 13 and 18

	DCLHb-**13** conjugate			DCLHb-**18** conjugate
molar ratio of **13** or **18**/DCLHb	peak maxima[a] (retention time, min)	P_{50} (mmHg)	n (40−60)	peak maxima[a] (retention time, min)
DCLHb	22.0	30	2.7	22.0
20/1	20.3	31	2.3	20.7
25/1	20.0	32	2.4	20.5
30/1	19.5	33	2.3	20.3
35/1	19.4	33	2.4	20.1
40/1	19.2	32	2.2	19.7
45/1	19.5	31	2.2	19.7

[a] SEC column: Superdex 200.

Table 3. Physical Characteristics of Surface Modified DCLHb with 13

		DCLHb-**13** conjugate molar ratio of **13**/DCLHb		
	DCLHb	25/1	35/1	40/1
total Hb (g/dL)	10.3	7.1	6.9	7.1
% MetHb	2.0	8.0	11.7	17.2
pH at 37 °C	7.38	7.44	7.37	7.48
COP (mmHg)	43	92	124	123
viscosity (cp)	1.2	1.5	2.0	1.6
osmolality (mOsm/Kg)	286	290	338	296
cell aggregation[a]	none seen	none seen	none seen	none seen

[a] Results of 50% CS-DCLHb concentration.

temperature. A solution of **23** in water and borane−pyridine complex (borane−pyridine/**2** in a molar ratio of 5/1) were added so that the final concentration of DCLHb was 6 g/dL in 0.1 M HEPES, pH 8.0. The hemoglobin solution was stirred at room temperature under nitrogen, and the reaction was monitored by SEC (column: TSK G3000SW and TSK G4000SW in series). SEC indicated that the surface modification of DCLHb was completed within 6 h. The reaction mixture was dialyzed against Plasma Lyte A to give the final product. The results are summarized in Table 1.

RESULTS AND DISCUSSION

Synthesis of Monofunctional Chondroitin-4-sulfate Derivatives. Chondroitin-4-sulfate has a MW of 50 000. A solution of hemoglobin surface modified with chondroitin-4-sulfate molecules with this high of MW would result in a solution too viscous to be used as a therapeutic solution. Therefore, the MW of chondroitin-4-sulfate was reduced to 4000 via acid-catalyzed hydrolytic cleavage at 65 °C. The hydrolysis was stopped at the time the size exclusion chromatography (SEC) profile of the reaction product was comparable with the SEC profile of a chondroitin-4-sulfate standard with a MW of 4000 provided by Biorelease, Inc. (*16*). The hydrolysis method provided Chondroitin-4-sulfate (C4S) (**2**) with reproducible product distributions as determined by SEC and yields.

It has been reported in the literature that the reducing terminus of a disaccharide or polysaccharide can be directly derviatized with a primary amine by reductive amination under mild conditions (*17*−*19*). We took advantage of this chemistry to introduce a primary amine to the reducing terminus of chondroitin-4-sulfate. The reductive amination was achieved by treatment of chondroitin-4-sulfate (**2**) with the monoprotected diamine diethylene glycol bis(3-aminopropyl)ether mono-*tert*-butyl carbonate (**4**) in the present of a reducing agent depicted in Scheme 1. The choice of the reducing agent for this transformation was critical. Sodium cyanoborohydride has been successfully used for the reductive amination of carbohydrates (*17*−*21*). However, for large-scale syntheses the use of poisonous sodium cyanoborohydride is unattractive as is the workup, because care must be exercised with respect to the sodium cyanide and hydrogen cyanide byproducts. The use of sodium cyanoborohydride could be avoided by the use of borane-pyridine complex. Cabacungan et al. (*22*) found that borane−pyridine complex has a higher reducing capacity than sodium cyanoborohydride for the reductive methylation of N-α-acetyl-lysine with formaldehyde. In addition, borane−pyridine complex does not readily reduce aldehydes (*23*, *24*). Therefore, the reduction of the reducing terminus of chondroitin-4-sulfate during the reductive amination reaction could also be avoided by the use of borane-pyridine complex. The aminated product **5** was prepared by the treatment chondroitin-4-sulfate (**2**) with **4** in the present of borane-pyridine complex under alkaline conditions at 40 °C over four days. The reaction was terminated when the detection with 2,3,5-triphenyltetrazolium chloride (TTC) of the reducing terminus was negative (*25*). The diethylene glycol bis(3-aminopropyl)-ether (**3**) was monoprotected with a *tert*-butyl carbonate group using di-*tert*-butyl dicarbonate (Scheme 1). The BOC protecting group was removed by acid hydrolysis from **5** to give the deprotected product **6**.

The primary amine of **6** was coupled to both alkyl and aromatic aldehyde moieties via an amide linkage. 4-Thia-7-diethoxy-heptanoyl was covalently linked to **6** as outlined in Scheme 2. Treatment of **6** with *N*-succinimidyl 4-thia-7-diethoxy-heptanoate (**12**) gave **7** in moderate yields. *N*-Succinimidyl 4-thia-7-diethoxy-heptanoate (**12**) was synthesized by a three step method (Scheme 3). Methyl 3-mercaptopropionate (**8**) was allowed to react

Scheme 1[a]

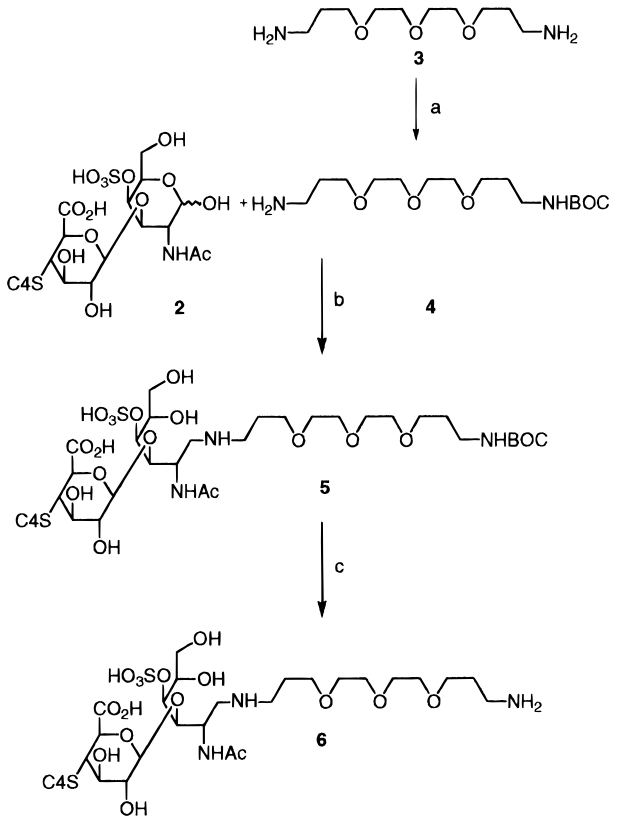

[a] (a) Di-*tert*-butyl carbonate, CH_2Cl_2; (b) borane-pyridine, EtOH, 40 °C, 4 days; (c) HCl, 24 h.

Scheme 2[a]

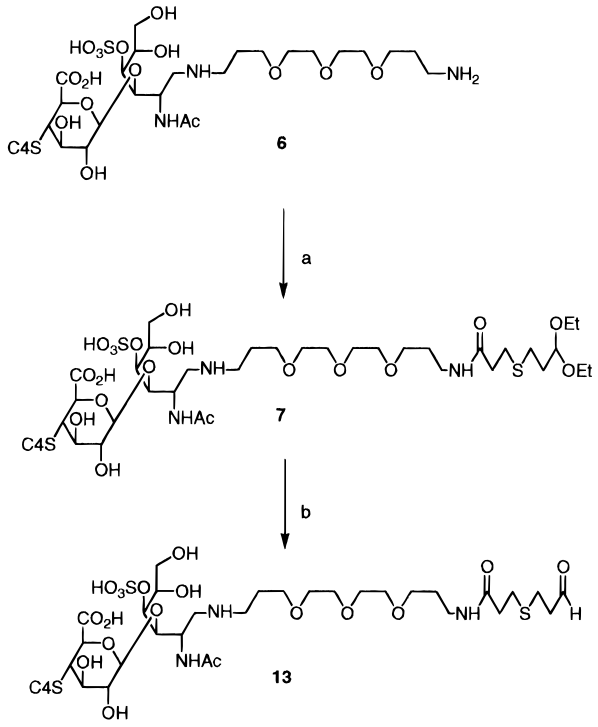

[a] **12**, pH 9, DMF-water; (b) HCl, water.

Scheme 3[a]

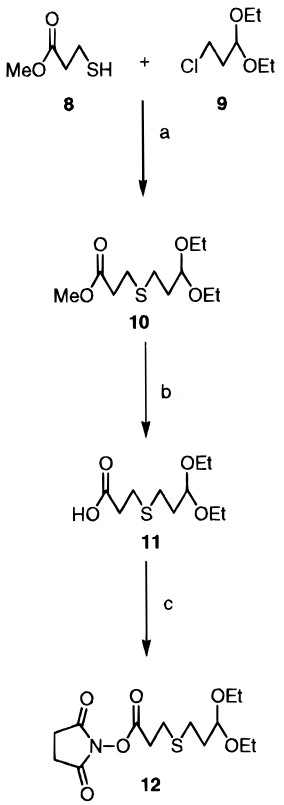

[a] (a) K_2CO_3, DMF, 85 °C; (b) KOH, ethanol water; (c) disuccinimidyl carbonate, triethylamine, acetolnirile.

with 3-chloropropionaldehyde diethyl acetal (**9**) in the presence of potassium carbonate to give methyl 4-thia-7-diethoxy-heptanoate (**10**). Methyl 4-thia-7-diethoxy-heptanoate (**10**) was hydrolyzed to the free acid (**11**) with potassium hydroxide in aqueous ethanol. Treatment of the free carboxylic acid with disuccinimidyl carbonate provided *N*-succinimidyl 4-thia-7-diethoxy-heptanoate (**12**) in good yields. The target compound **13** was prepared by the deprotection of the aldehyde group of **7** by acid hydrolysis.

The coupling of the aldehyde groups with amino groups on the surface of proteins is dependent upon the distance of the aldehyde to a heteroatom on the reagent chain as demonstrated by Harris and Sedaghat-Herati (*26*). They showed that PEG propionaldehyde (PEG-OCH_2CH_2CHO) was more reactive toward the protein amino groups than was PEG acetaldehyde (PEG-OCH_2CHO). To test the reactivity of a reagent with a greater distance between the aldehyde group and a heteroatom, a chondroitin-4-sulfate derivative containing a butyraldehyde end group (**18**) was prepared. The carboxylic acid of *N*-(4-ethoxybutyryl)-succinamic acid (**15**) was activated with *N*-hydroxysuccinimide to provide **16** that was readily coupled to the primary amino group of **6** to afford the target compound **17**. The ethoxy groups of **17** were removed under acidic conditions to provide **18** (Schemes 4 and 5).

In addition to alkyl aldehydes, we also wanted to investigate the utility of employing aromatic aldehydes and maleimide groups for the attachment of chondroitin-4-sulfate to DCLHb. The chondroitin-4-sulfate derivative **21**, terminating with an aromatic aldehyde, was prepared from *N*-sucinimidyl 2-formylphenaoxyacetic acid and **6** shown in Scheme 6. A maleimide moiety was conveniently coupled to **6** using *N*-succinimidyl maleimidopropionate (**22**) to provide **23** (Scheme 7).

Scheme 4[a]

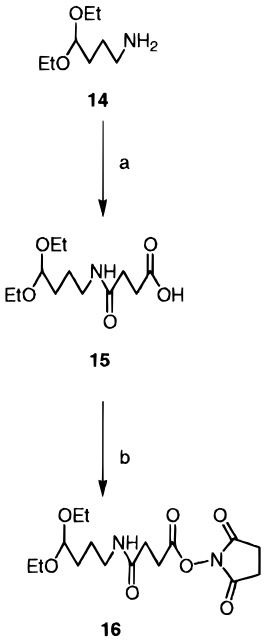

[a] (a) Succinic anhydride, $CHCl_4$; (b) DSC, Et_3N, CH_3CN.

Scheme 5[a]

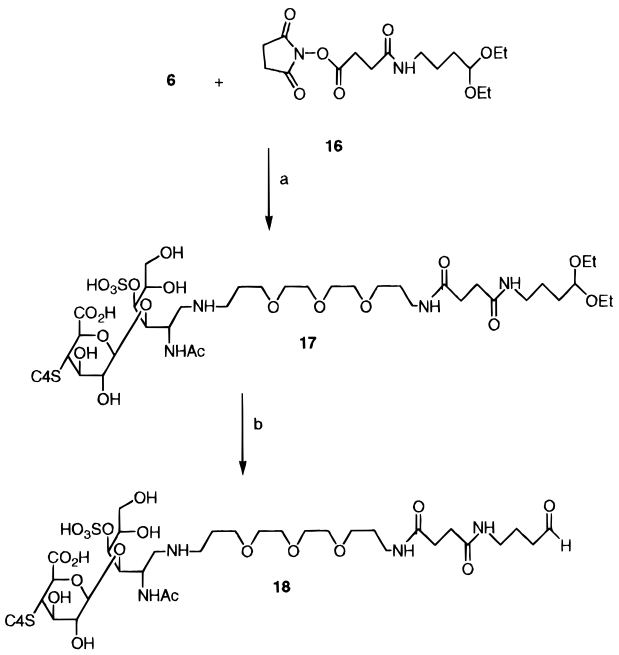

[a] (a) DMF-water; (b) HCl.

Modification of DCLHb with Chondroitin-4-sulfate Derivatives. The typical surface modification of DCLHb with the maleimide derivative **23** was accomplished by the reaction of deoxyDCLHb in HEPES buffer, pH 8, with the chondrotin-4-sulfate derivative under a nitrogen atmosphere at room temperature over the course of 6 h. The results are summarized in Table 1. The data indicates that **23** surface-modified DCLHb provides a product that exhibited a single peak by SEC with a shorter retention time than that of DCLHb. The greater the **23**/DCLHb molar ratio, the more extensively surface modified the products are as detected by the decrease in the product SEC retention times. The P_{50} and n (cooperativity) values are in the range 21−23 mm Hg

Scheme 6[a]

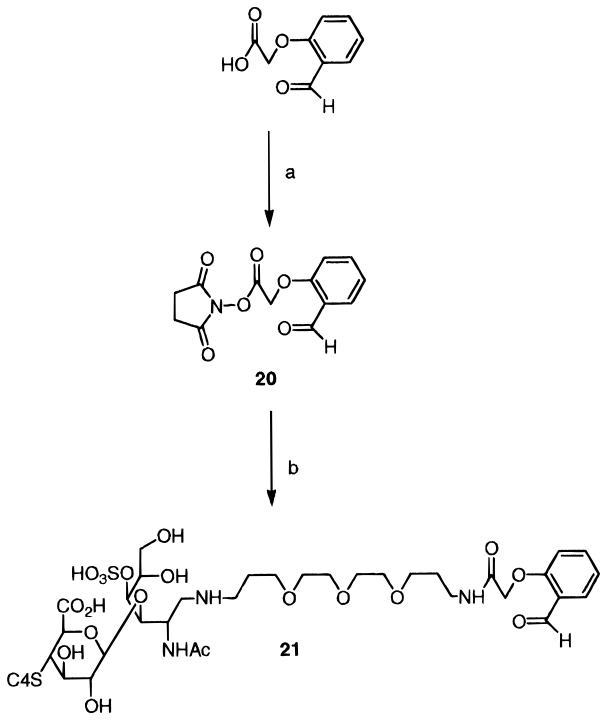

[a] (a) DCC, *N*-hydroxysuccinimide; CH_3CN; (b) **6**, DMF-water.

Scheme 7[a]

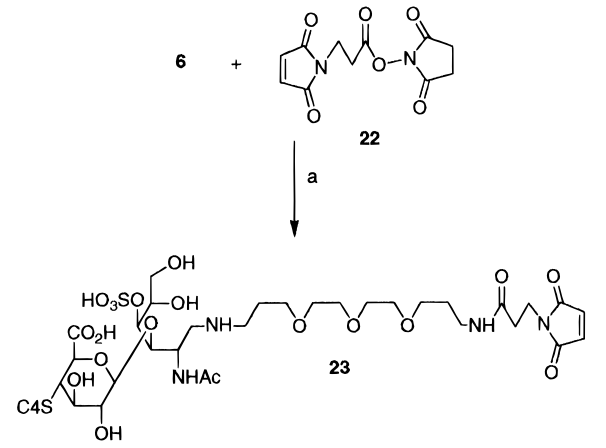

[a] (a) DMF-water.

and 1.9−2.1, respectively. The decrease in the P_{50} of the surface-modified DCLHb product solutions was expected and is due to the alkylation of β-cys93 residues by **23** (*27*, *28*). The maleimide group is known to alkylate both thiol and amino groups although the reagent will preferentially react with a thiol group and, indeed, this was the case. It was found that 30−35% of the added **23** would react with the surface of DCLHb as determined by NMR spectrometry (*29*). Since the *N*-acetyl groups of chondroitin-4-sulfate give an isolated and distinct resonance at 2 ppm in a ^{1}H NMR spectrum, this resonance was used to quantitate the number of chondroitin-4-sulfate moieties attached to the protein. The method involved generating a standard curve of integrals of the *N*-acetyl groups of **6** in a DCLHb solution. The degree of alkylation of DCLHb by **23** was determined by the measurement of the resonance at 2 ppm and relating that value to the standard curve.

It has been demonstrated that the reductive amination of a protein or peptide is most effective using cyanoborohydride or borane−pyridine under slightly alkaline conditions (pH 7−9) (*18*, *21*, *30*). Thus, the surface modification of DCLHb with aldehydes **13**, **18**, and **21** was performed under deoxy conditions in borate buffer, pH of 9, in the presence of borane−pyridine. The latter was selected to avoid the toxicity associated with sodium cyanoborohydride. Since borane−pyridine complex does not readily reduce aldehyde groups at neutral or alkaline pH (*24*), the reagent can be added along with the aldehyde allowing the Schiff bases that are formed to be reduced during the course of the reaction.

The data indicate that **13** and **18** effectively surface-modified DCLHb. The surface-modified DCLHb showed a single, broad peak by SEC with the retention time in the range 19−20 min as shown in Figure 2. The P_{50} and *n* values of the products are the range of 31−33 mm Hg and 2.2−2.6, respectively. These values indicate that the surface modification of DCLHb with **13** or **18** do not greatly perturb the conformation of the protein. The chondroitin-4-sulfate derivative that contains a butyraldehyde end group, **18**, is as active as the chondroitin-4-sulfate derivative with the propionaldehyde end group (**13**) toward the surface modification of DCLHb. The aromatic aldehyde containing derivative **21** also modified DCLHb; however, the modified product was rapidly oxidized to metHb during the reaction workup. The mechanism of this rapid oxidation is unknown.

The physical properties of DCLHb modified with **13** are presented in Table 3. The two most distinguishing features of the modified DCLHb are the colloidal osmotic pressure (COP) and red blood cell aggregation data. The COP of the **13**-DCLHb conjugates were 2−3-fold greater than that of DCLHb. The high COP can be attributed to the highly hydrated chondroitin-4-sulfate moieties attached to the protein surface.

Red blood cell aggregation was determined by mixing known concentrations of the modified hemoglobin products with red blood cells. Red cell aggregation (*31*) has been observed with some polyDCLHb solutions prepared by polymerization with bifunctional polyamide reagents (*5*). *In* vitro, RBCs are also known to form red cell aggregates when they are suspended in saline solution in the presence of a wide variety of macromolecules such as serum proteins (*32*), dextran (*33*−*38*), polylysine (*34*−*38*), poly(ethylene glycol) (*34*, *35*), poly(vinylpyrrolidone) (*37*), polysaccharides (*36*), and polyglutamic acid (*36*). Several mechanisms of red cell aggregate formation have been proposed (*33*, *35*−*44*), including size-dependent interaction of the macromolecule with the red cell membrane, changes in the surface charge or charge density of the red cell membrane induced by the adherent macromolecule, and the volume excluded effect of the polymer. Since DCLHb-chodroitin-4-sulfate conjugates do not cause red cell agregation even though the products' COP are high, the volume-excluded mechanism of cell aggregation cannot be invoked. The negatively charged surface of DCLHb-chodronitin-4-sulfate conjugates may prevent red cell aggregation.

In conclusion, chondrotin-4-sulfate reagents that could be readily attached to the surface of diaspirin cross-linked hemoglobin (DCLHb) were prepared. Synthetic methodology has been developed that allows for the modification of proteins, such as DCLHb, through alkylation of protein thiols or amino groups by the chondroitin-4-sulfate derivatives. The modification of proteins with chondroitin-4-sulfate would add an global negative charge that has the potential to alter the in vivo properties of the proteins and, possibly, increase their therapeutic utility.

LITERATURE CITED

(1) Hai, T. T., Nelson, D. J., and Srnak, A. (1992) Process for the production of cross-linked hemoglobin in the presence of sodium tripolyphosphate. U.S. Patent 5,128,452.

(2) Chatterjee, R., Welty, E. V., Walder, R. Y., Pruitt, S. L., Roger, P. H., Arnone, A., and Walder, J. A. (1986) Isolation and characterization of a new hemoglobin derivative cross-linked between the α chains (Lysine $99_{\alpha 1}$-Lysine $99_{\alpha 2}$). *J. Biol. Chem. 261*, 9929−9937.

(3) Przybelski, R. J., Daily, E. K., Kisichi, J. C., Mattia-Goldberg, C., Bounds, M. J., and Colburn, W. A. (1996) Phase I study of the safety and pharamcologic effects of diaspirin cross-linked hemoglobin solution. *Crit. Care Med. 24*, 1993−2000.

(4) Hai, T. T., Pereira, D. E., Nelson, D. J., and Srnak, A. (1998) Polymerization of Diaspirin Cross-linked Hemoglobin (DCLHb) with PEG activated with Benzenesulfonate bearing electron-withdrawing groups. *Tetrahedron 55*, 2147−2156.

(5) Hai, T. T., Pereira, D. E., and Nelson, D. J. (1999) Polymerization of Diaspirin Cross-linked Hemoglobin (DCLHb) with water soluble, nonimmunogenic polyamide cross-linking agents. *Bioconjugate Chem. 10*, 1013−1020.

(6) Chang, M. S. T. (1999) Future prospects for artificial blood. *Trends Biotechnol. 17*, 61−67, and references therein.

(7) Nho, K., Zalipsky, S., and Davis, F. (1993) Chemically modified hemoglobin as an effective, stable nonimmunogenic red cell substitute. U.S. Patent 5,234,903.

(8) Rennke, H. G., Cotran, R. S., and Venkatachalam, M. A. (1975) Role of molecular charge in glomerular permeability. *67*, 638−646, and other references.

(9) Sibley, C. P., Bauman, K. F., and Firth, J. A. (1983) Molecular charge as a determinant of macromolecule permeability across the capillary endothelium of the guinea-pig placenta. *Cell Tissue Res. 229*, 365−377.

(10) Schneeberger, E. E. (1988) Interaction of plasma proteins with negatively charged sites on the pulmonary capillary endothelium of the rat. *Cell Tissue Res. 251*, 417−423.

(11) Pietra, G. G., Fishman, A. P., Lanken, P. N., Sampson, P., and Hansen-Flaschen, P. (1982) Permeability of endothelium to neutral and charged macromolecules. *Ann. N. Y. Acad. Sci. 401*, 241−247.

(12) Bunn, H. F. (1993) The use of hemoglobin as a blood substitute. *42*, 112−117.

(13) Fransson, L. (1982) In *Mammalian Glycosaminoglycans in The Polysaccharides* (G. O. Aspinal, Ed.) Vol. 3, pp 351−358.

(14) Van Assendelft, O. W., and Zijlstra, W. G. (1975) Extinction coefficients for use in equations for the spectrophotometric analysis of hemoglobin mixtures. *Anal. Biochem. 69*, 43−48.

(15) Neis, J. M., Van Gemert, P. J. L., Roelofs, H. M. J., and Henderson, P. T. H. (1984) Disappearance of free SH-groups in hemoglobin of man, rat and rabbit after exposure to alkylating agents in vitro. *Toxicology 31*, 319−327.

(16) Unpublished results. MW was determined by sedimentation velocity. Biorelease, Inc. 8A Industrial Way, Salem, NH 03079.

(17) Kamicker, B. J., Schwartz, B. A., Olson, R. M., Drinkwitz, D. C., and Gray, G. R. (1977) Proteins containing reductively aminated disaccharides: Immunchemical characterization. *Arch. Biochem. Biophys. 183*, 393−398.

(18) Schwartz, B. A., and Gray, G. R. (1977) Proteins containing reductively aminated disaccharides, Synthesis and chemical characterization. *Arch. Biochem. Biophys. 181*, 542−549.

(19) Mann, J. S., Huang, J. C., and Keana, J. F. W. (1992) Molecular amplifiers: Synthesis and Functionalization of a Poly(aminopropyl)dextran bearing a uniquely reactive terminus for univalent attachment to biomolecules. *Bioconjugate Chem. 3*, 154−159.

(20) Gray, G. R. (1974) The direct coupling of oligosaccharides to proteins and derivatized gels. *Arch. Biochem. Biophys. 163*, 426−428.

(21) Raja, R. H., LeBouf, R. D., Stone, G. W., and Weigel, P. H. (1984) Preparation of alkylamine and ^{125}I-Radiolabeled derivatives of hyaluronic acid uniquely modified at the reducing end. *Anal. Biochem. 139*, 168−177.

(22) Cabacungan, J. C., Ahmed, A. I., and Feeney, R. E. (1982) Amine boranes as alternative reducing agents for the reductive alkylation of proteins. *Anal. Biochem. 124*, 272−278.

(23) Moormann, A. E. (1993) Reductive amination of piperidines with aldehydes using borane pyridine. *Synth. Commun. 23*, 789−795.

(24) Pelter, A., and Mosser, R. M. (1984) Reductive aminations of ketones and aldehydes using borane-pyridine. *J. Chem. Soc., Perkin Trans. 1* 717−720.

(25) Fisher, F. G., and Dorfel, H. (1954) Die quantitative Bestimmung reduzierender Zuker auf Papierchromatogrammen. *Hoppe-Seylers Z. Physiol. Chem. 297*, 164−178.

(26) Harris, J. M., and Sedaghat-Herati, M. R. (1993) Preparation and the use of poly(ethylene glycol) propionaldehyde. U.S. Patent 5,252,714.

(27) Riggs, A. (1961) The binding of N-ethylmaleimide by human hemoglobin and its effect upon the oxygen equilibrium. *J. Biol. Chem. 236*, 1948−1954.

(28) Garel, M. G., Beuzard, Y., Domenget, C., Martin, J., Galacteros, F., and Rosa, J. (1982) Binding of 21 thiol reagents to human hemoglogin in solution and intact cells. *Eur. J. Biochem. 123*, 513−519.

(29) Jackson, C. J., Charlton, J. L., Kuzmnski, K., Lang, G. M., and Sehon, A. H. (1987) Synthesis, isolation and characterization of conjugates of ovalbumin with PEG using cyanuric chloride as the coupling agent. *Anal. Biochem. 165*, 114−127.

(30) Geoghegan, K. F., Cabacungan, J. C., Dixon, H. B. F., and Feeney, R. E. (1981) Alternative reducing agents for reductive methylation of amino groups in proteins. *Int. J. Pept. Res. 17*, 345−352.

(31) Unpublished results.

(32) Fordyke, D. R., Palfree, R. G. E., and Takeda, A. (1982) Formation of erythrocyte rouleaux in preheated normal serum: roles of albumin polymers and lysophophadidylcholine. *Can. J. Chem. 60*, 705−711.

(33) Chien, S., and Kung-Ming, J. (1973) Ultra structural basis of the mechanism of rouleaux formation. *Microvasc. Res. 5*, 155−166.

(34) Tilley, D., Coakley, W. T., Gould, R. K., Payne, S. E., and Hewison, L. A. (1987) Real time observations of polylysine, dextran and poly(ethylene glycol) induced mutual adhesion of erythrocytes held in suspension in an ultrasonic standing wave field. *Eur. Biophys. J. 14*, 499−507.

(35) Van Oss, C. J., and Coakley, W. T. (1988) Mechanism of successive modes of erythrocyte stability and instability in the presence of various polymers. *Cell Biophys. 13*, 141−150.

(36) Meda, N., and Shiga, T. (1985) Inhibition and acceleration of erythrocyte aggregation induced by small macromolecules. *Biochim. Biophys. Acta 843*, 128−136.

(37) Sewchand, L. S., and Bruckschwaiger, D. (1980) Observed differences in dextran and poly(vinylpyrrolidone) as rouleaux-inducing agents. *Can. J. Physiol. Pharmacol. 58*, 271−274.

(38) Buxbaum, K., Evans, E., and Brooks, D. E. (1982) Quantitation of surface affinities of red blood cells in dextran solution and plasma. *Biochemistry 21*, 3235−3239.

(39) Meda, N., Kon, K., Imaizumi, K., Sekiya, M., and Shiga, T. (1983) Alteration of rheological properties of human erythrocytes by cross-linking of membrane proteins. *Biochim. Biophys. Acta 735*, 104−122.

(40) Skalak, R. (1984) Aggregation and disaggregation of red blood cells. *Biorheology 21*, 463−476.

(41) Fabry, T. L. (1987) Mechanism of erythrocyte aggregation an sedimentation. *Blood 70*, 1572−1576.

(42) Kobuchi, Y., Ito, T., and Ogiwara, A. (1988) A model for rouleaux pattern formation of red blood cells. *J. Theor. Biol. 130*, 129−145.

(43) Tuszinski, J. A. (1988) On possible mechanisms of rouleaux formation in human erythrocytes. *J. Theor. Biol. 132*, 369−373.

(44) Chien, S., Feng, S., Vayo, M., Sung, L. A., Usami, S., and Skalak, R. (1990) The dynamics of shear disaggregation of red blood cells in a flow channel. *Biorheology 27*, 135−147.

(45) Rowlands, S., Sewchand, L. S., and Enns, G. (1983) A quantum mechanical interaction of human erythrocytes. *Can. J. Physiol. Pharmacol. 60*, 52−59.

BC000021I

Linker-Mediated Modulation of the Chemiluminescent Signal from N^{10}-(3-Sulfopropyl)-*N*-sulfonylacridinium-9-carboxamide Tracers

Maciej Adamczyk,* Yon-Yih Chen, Jeffrey R. Fishpaugh, Phillip G. Mattingly, You Pan, Kevin Shreder, and Zhiguang Yu

Abbott Laboratories, Diagnostics Division, Department of Chemistry D9NM, Building AP 20, 100 Abbott Park Road, Abbott Park, Illinois 60064-6016. Received March 20, 2000; Revised Manuscript Received May 1, 2000

Four chemiluminescent *N*-sulfonylacridinium-9-carboxamide active esters (**17**−2**0**) were prepared from the corresponding acids and coupled to both of the aminated phenobarbital (**13**) and *N*-(6-aminohexyl)-phenytoin (**16**) haptens. The level of signal produced by chemiluminescent *N*-sulfonylacridinium-9-carboxamide phenobarbital and phenytoin tracers in a solid-phase immunoassay format was found to be modulated by at least 20-fold by the judicious choice of the reactive acridinium-hapten linking group.

INTRODUCTION

The linker group used to connect a label to a small molecule hapten or a macromolecule can have a profound influence on the performance of the bioconjugate. Linkers can contribute to "bridge-binding" interactions (*1*−*11*) between tracers and antibodies when the same linker is used both in the immunogen and tracer. In this phenomenon, the antibody recognizes the commonly used linker in addition to or to the exclusion of the hapten. Frequently the length of the linker must be optimized to ensure accessibility of the bioconjugate for a binding interaction or to otherwise maximize the signal from the label (*8*, *9*, *12*−*20*). At others times, the linker must be modified to increase the solubility of the bioconjugate. In these cases, the linker group remains intact once the bioconjugate is formed, i.e., no covalent bonds are intentionally formed or broken. It is advantageous at other times to incorporate a linker that can be selectively cleaved, thus separating the label from the hapten or macromolecule (*21*−*24*).

We have recently reported on the synthesis and characterization of a new class of highly hydrophilic N^{10}-(3-sulfopropyl)-*N*-sulfonyl-acridinium-9-carboxamide chemiluminescent labels (*25*, *26*) (**1**, Figure 1). The linker groups used in bioconjugates with these labels are *not* chemically inert; in fact, they might be expected to exert a profound influence on the chemiluminescent reaction. As shown in the figure, on treatment with basic hydrogen peroxide, N^{10}-(3-sulfopropyl)-*N*-sulfonyl-acridinium-9-carboxamide labeled tracers or conjugates give rise to the light emitting N^{10}-(3-sulfopropyl)-9-acridone (**6**) with loss of the linking group (**5**) (*27*). Examination of unconjugated N^{10}-(3-sulfopropyl)-*N*-sulfonyl-acridinium-9-carboxamides showed that changing the R and R′ groups in the linker could result in a greater than 20-fold change in the chemiluminescence lifetime of the label, while the total light output remained essentially constant (*26*). If the linker-dependent variability displayed in solution by the unconjugated label were to be duplicated once the label was incorporated into an assay, two effects would be expected. Conjugates using the slower emitting labels would require longer read times to harvest the maximum amount of signal and therefore exhibit a negative impact on the throughput of the assay. Alternatively, signal could be sacrificed for shorter read times and higher throughput, but with the result of poorer sensitivity. For assays designed for analytes present in the microgram per millilter concentration range, however, less signal may be a beneficial characteristic. Many automated chemiluminescent detectors are tuned for maximum sensitivity and are likely to be overwhelmed by the signal generated in assays for high-concentration analytes.

To assess the magnitude of these effects, haptens for the high-concentration analytes phenobarbital (*28*) and phenytoin (*29*−*32*) were conjugated to N^{10}-(3-sulfopropyl)-*N*-sulfonyl-acridinium-9-carboxamides via representative linking groups from the previous model study (*26*). The effect of the linker on the observed signal using a short read time was evaluated in a microtiter plate chemiluminescent immunoassay format using the complementary sheep polyclonal antibodies specific for the respective tracers.

MATERIALS AND METHODS

Sheep polyclonal *anti*-phenobarbital and *anti*-phenytoin were obtained from the Abbott Laboratories antibody production facility (Abbott Laboratories, Abbott Park, IL). Phenobarbital and phenytoin calibrators were taken from the Abbott AxSYM assay kits for those analytes. Reagent-grade sheep polyclonal IgG[1] was purchased from Sigma Chemical Co. (St. Louis, MO.) The HiTrap protein G affinity column (5 mL) was purchased from Amersham Pharmacia (Piscataway, NJ). The FPLC system used consisted of a liquid chromatography controller (LCC-500, Pharmacia LKB) control unit (UV-1) and optical unit (LKB, UV-1). The MicroLumat Plus microplate lumi-

* To whom correspondence should be addressed. Phone: (847) 937-0225. Fax: (847) 938-8927. E-mail: maciej.adamczyk@abbott.com.

[1] Abbreviations: IgG, immunoglobulin G; HPLC, high-performance liquid chromatography; TMS, tetramethylsilane; ESI-MS, electrospray ionization mass spectrometry; RP, reversed phase; THF, tetrahydrofuran; DMF, dimethylformamide; TFA, trifluoroacetic acid; PBS, phosphate-buffered saline; DTPA, diethylenetriaminepentaacetic acid.

10.1021/bc0000280 CCC: $19.00 © 2000 American Chemical Society
Published on Web 07/19/2000

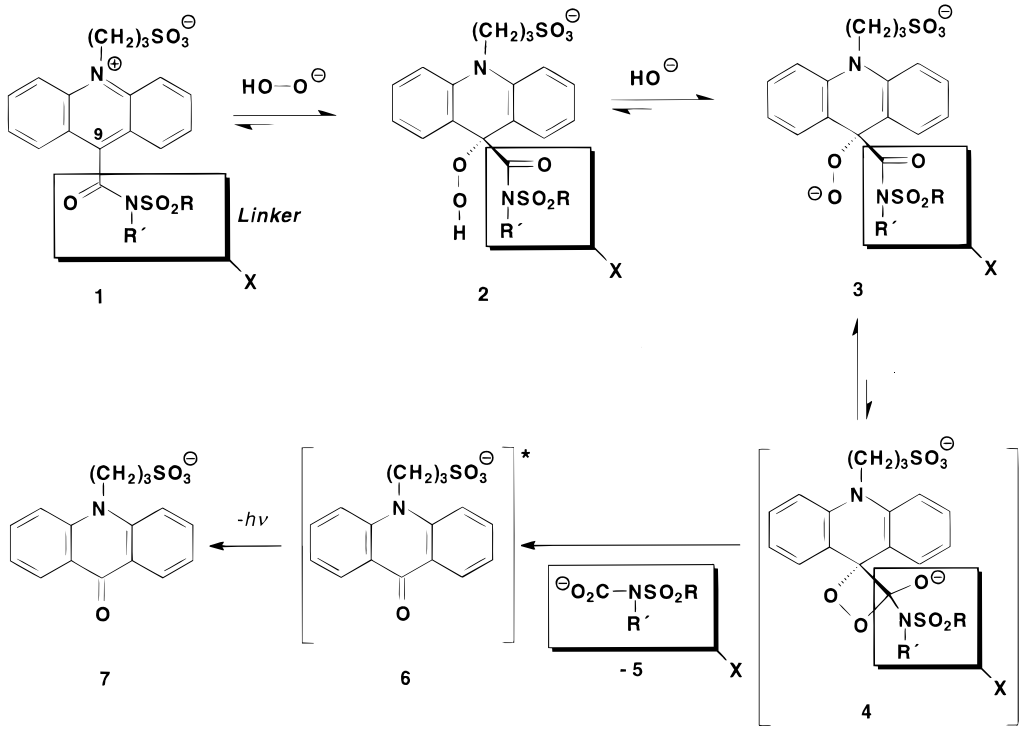

Figure 1. Reaction of N^{10}-(3-sulfopropyl)-*N*-sulfonyl-acridinium-9-carboxamides with basic hydrogen peroxide.

nometer LB 96V equipped with WinGlow software and the microtiter plates were obtained from EG&G Berthold (Gaithersburg, MD).

All reagents for synthesis were purchased from Aldrich Chemical Co. (Milwaukee, WI) or Sigma Chemical Co. and used without further purification, except where noted. All the solvents employed were of HPLC grade purchased from EM Science (Gibbstown, NJ) and used as received. ^{1}H NMR (300 MHz) and ^{13}C NMR (75 MHz) spectra were recorded on a Varian Gemini spectrometer in the solvent noted; chemical shifts (δ) are reported in parts per million relative to TMS; coupling constants (J) are reported in hertz. Mass spectra were obtained on a Perkin-Elmer Sciex API 100 electrospray mass spectrometer in the positive ion mode unless noted otherwise. Reversed-phase (RP) analytical HPLC was performed using a Waters μBondapak C_{18} 10 μm (8 mm × 100 mm) column eluting at 2 mL/min (elution solvent ratio v/v reported) with UV detection at 254 nm, unless otherwise stated. Preparative RP-HPLC was performed using a Waters μBondapak C_{18} 10 μm (40 mm × 100 mm) column eluting at 45 mL/min (elution solvent ratio v/v reported) with UV detection at 254 nm, unless otherwise stated. IUPAC names of new compounds were obtained using the ACD/ILab Web service version 3.5 at http://www.acdlabs.com/ilab.

Diethyl 2-Phenyl-2-[6-(tetrahydro-2H-pyran-2-yloxy)hexyl]malonate (9). To a suspension of KH (3.19 g, 35% w/w, 27.9 mmol) in THF (20 mL) was added diethyl phenylmalonate **8** (4.39 g, 18.60 mmol) in DMF (20 mL). After stirring for 1 h, 1-bromo-6-tetrahydropyranyloxyhexane (4.93 g, 18.6 mmol) in THF (8 mL) and DMF (8 mL) was added and the resulting mixture was heated to reflux for 14 h. The reaction solution was cooled, then poured into water (50 mL), and extracted with dichloromethane (3 × 50 mL). The extract was dried over anhydrous sodium sulfate, filtered, and evaporated in vacuo to give a brown oil which was purified by column chromatography (silica gel, 10−20% ethyl acetate in hexane). Fractions were pooled then evaporated in vacuo to afford **9** (3.78 g, 48%). ^{1}H NMR ($CDCl_3$): 7.43−7.28 (5 H, m), 4.55 (1 H, t, J = 3), 4.22 (4 H, m), 3.84 (1 H, m), 3.71 (1 H, m), 3.68 (1 H, m), 3.36 (1 H, m), 2.27 (1 H, m), 1.68 (1 H, m), 1.52 (7 H, m), 1.28 (7 H, m), 1.20 (6 H, m). ESI-MS: m/z 437 $(M + NH_4)^+$. Analytical HPLC (8 mm × 100 mm Nova-Pak HR C_{18}, 0.05% trifluoroacetic acid in acetonitrile/0.05% aqueous trifluoroacetic acid, 80:20): 3.91 min, >90%.

5-Phenyl-5-[6-(tetrahydro-2H-pyran-2-yloxy)hexyl]-2,4,6(1H,3H,5H)-pyrimidinetrione (10). Sodium (0.7 g, 30.5 mmol) was dissolved in ethanol (8 mL). Urea (0.602 g, 10.03 mmol) and **9** (3.66 g, 8.72 mmol) were then added. The resulting solution was heated to reflux for 14 h. Ice was added, and the solution was acidified with concentrated HCl to pH 1. The solution was extracted with dichloromethane (4 × 50 mL). The extract was dried over anhydrous sodium sulfate, filtered, and evaporated in vacuo to give a yellow oil which was purified by column chromatography (silica gel, 25−75% ethyl acetate in hexane). Fractions were pooled then evaporated in vacuo to afford **10** (1.21 g, 36%). ^{1}H NMR ($CDCl_3$): 7.35 (5 H, m), 4.56 (1 H, q, J = 3.5), 3.87 (1 H, m), 3.71 (1 H, m), 3.51 (1 H, m), 3.36 (1 H, m), 2.40 (1 H, m), 1.69 (2 H, m), 1.52 (8 H, m), 1.25 (9 H, m). ESI-MS: (negative ion) m/z 387 $(M - H)^-$. Analytical HPLC (8 mm × 100 mm Nova-Pak HR C_{18}, 0.05% trifluoroacetic acid in acetonitrile/0.05% aqueous trifluoroacetic acid, 45:55): 5.33 min, >90%.

5-(6-Hydroxyhexyl)-5-phenyl-2,4,6(1H,3H,5H)-pyrimidinetrione (11). A solution of **10** (1.21 g, 3.12 mmol) in THF (6 mL) and HCl (2 N, 6 mL) was stirred for 4 h. The reaction mixture was extracted with dichloromethane (40 mL × 5). The combined extracts were dried over anhydrous sodium sulfate, filtered, and evaporated in vacuo to give a light yellow oil which was purified by column chromatography (silica gel, 30−75% ethyl acetate in hexane). Fractions were pooled and then evaporated in vacuo to afford **11** (0.276 g, 30%). ^{1}H NMR (CD_3OD): 7.36 (5 H, m), 3.31 (2 H, m), 2.32 (2 H, m), 1.51 (2 H, m), 1.37 (6 H, m). ESI-MS: (negative ion) m/z 303 $(M - H)^-$.

Analytical HPLC (8 × 100 mm, Nova-Pak HR C_{18}, 0.05% trifluoroacetic acid in acetonitrile/0.05% aqueous trifluoroacetic acid, 30:70): 3.45 min, >99%.

6-(2,4,6-Trioxo-5-phenylhexahydro-5-pyrimidinyl)hexyl 2-[(*tert*-Butoxycarbonyl)amino]ethylcarbamate (12). To a solution of **11** (274 mg, 0.901 mmol) in THF (5 mL) was added phosgene in toluene (1.93 N, 10 mL, 19.3 mmol). After stirring for 3 h, the reaction mixture was evaporated in vacuo. The residue was redissolved in THF (10 mL) and cooled to 0 °C. *tert*-Butyl *N*-(2-aminoethyl)carbamate (624 mg, 3.9 mmol) was added and the solution was stirred for 2 h. After removing the solvent in vacuo, the residue was purified by column chromatography (silica gel, 60−75% ethyl acetate in hexane). Fractions were pooled then evaporated in vacuo to afford **12** (426 mg, 96%). ^{1}H NMR ($CDCl_3$): 9.49 (1 H, br), 7.36 (5 H, m), 5.39 (1 H, br), 5.02 (1 H, br), 4.02 (2 H, m), 3.25 (4 H, m), 2.40 (2 H, m), 1.53 (2 H, m), 1.42 (9 H, s), 1.25 (6 H, m). ESI-MS (negative ion): *m*/*z* 489 $(M - H)^-$. Analytical HPLC (8 × 100 mm Nova-Pak HR C_{18}, 0.05% trifluoroacetic acid in acetonitrile/0.05% aqueous trifluoroacetic acid, 40:60): 5.83 min, >99%.

6-(2,4,6-Trioxo-5-phenylhexahydro-5-pyrimidinyl)hexyl 2-Aminoethylcarbamate (13). To a solution of **12** (152 mg, 0.310 mmol) in dichloromethane (2 mL) was added trifluoroacetic acid (2 mL). After stirring for 15 min, the reaction mixture was evaporated in vacuo to afford **13**. ^{1}H NMR (CD_3OD): 7.38 (5H, s), 4.04 (2 H, t, J = 6), 3.36 (2 H, t, J = 6), 3.02 (2 H, t, J = 6), 2.34 (2 H, m), 1.61 (2 H, m), 1.39 (8 H, m). ESI-MS: *m*/*z* 391 $(M + H)^+$. Analytical HPLC (8 × 100 mm prep Nova-Pak HR C_{18}, 0.05% trifluoroacetic acid in acetonitrile/0.05% aqueous trifluoroacetic acid, 25:75): 3.52 min, >99%. The residue was dissolved in DMF (4 mL), and the solution (0.08 mmol/mL) was retained for use in later reactions.

3-(6-Bromohexyl)-5,5-diphenyl-2,4-imidazolidinedione (15) (*33*). Potassium hydroxide (628 mg, 10.0 mmol) was added to a suspension of 5,5-diphenylhydantoin (**14**, 2.52 g, 10.0 mmol) in absolute ethanol (50 mL). The reaction mixture was stirred for 2 h under a nitrogen atmosphere at ambient temperature. Removal of solvents in vacuo afforded the desired phenytoin potassium salt. The salt was added to a solution of 1,6-dibromohexane (24.4 g, 100 mmol) in acetonitrile (70 mL). The mixture was refluxed under a nitrogen atmosphere for 22 h, cooled, and poured into 1:1 ethyl acetate/water (150 mL). The two layers were separated. The aqueous layer was extracted with ethyl acetate (2 × 50 mL). The combined organic extracts were washed with brine (25 mL), dried over anhydrous sodium sulfate, and evaporated in vacuo to give an oily residue. The residue was purified by flash chromatography (silica gel, 20−50% ethyl acetate in hexanes) to afford the bromide **15** (2.03 g, 45%). ^{1}H NMR ($CDCl_3$): 7.41−7.34 (10 H, m), 6.55 (1 H, s), 3.58 (2 H, t, J = 7.3), 3.34 (2 H, t, J = 6.8), 1.77 (2 H, p, J = 7.1), 1.66 (2 H, p, J = 7.4), 1.44 (2 H, p, J = 7.4), 1.30 (2 H, p, J = 7.3). ESI-MS: *m*/*z* $(M + NH_4)^+$ 432, 434.

3-(6-Aminohexyl)-5,5-diphenyl-2,4-imidazolidinedione Trifluoroacetate Salt (16). Ammonium hydroxide (13 mL, 65 mmol) was added to a solution of 3-(6-bromohexyl)-5,5-diphenyl-2,4-imidazolidinedione (**15**) (415 mg, 1.00 mmol) in water (15 mL) and dioxane (30 mL). After stirring for 2 days at reflux, the solvents were removed in vacuo to give an oil. Purification by preparative reversed-phase HPLC (acetonitrile/0.03% aqueous trifluoroacetic acid, 30:70) afforded the desired amine TFA salt **16** (122 mg, 35%). ^{1}H NMR ($CDCl_3$): 7.94 (2 H, br s), 7.61 (1 H, s), 7.31 (10 H, s), 3.49 (2 H, t, J = 6.9), 2.84 (2 H, br s), 1.64−1.53 (4 H, m), 1.38−1.16 (4 H, m). ESI-MS: $(M + H)^+$ 352. Analytical HPLC (acetonitrile/0.03% aqueous trifluoroacetic acid, 30:70): 10.65 min, 99.8%.

Preparation of N^{10}-(3-Sulfopropyl)-*N*-sulfonylacridinium-9-carboxamide Active Esters. *3-[9-({{4-[(2,5-Dioxo-1-pyrrolidinyl)oxy]-4-oxobutyl}[(4-methylphenyl)-sulfonyl]amino}-carbonyl)-10-acridiniumyl]-1-propanesulfonate (**17**).* 9-[[(3-Carboxypropyl)[(4-methylphenyl)-sulfonyl]amino]-carbonyl]-10-(3-sulfopropyl)-acridinium inner salt (*25*) (8.00 g, 13.68 mmol) was suspended in DMF (80 mL) and pyridine (11 mL). A solution of *N*-trifluoroacetoxysuccinimide (*34*) (29 g, 137 mmol) in DMF (80 mL) was added. All the solids gradually dissolved after which a yellow precipitate formed. After stirring for 24 h in the dark, the precipitate was collected by filtration and washed sequentially with ethyl acetate (200 mL), cold ethanol (60 mL), and again with ethyl acetate (2 × 200 mL). Further drying in vacuo afforded the desired active ester **17** (9.5 g, 99%). ^{1}H NMR ($CDCl_3$): 9.00 (2 H, m), 8.44 (2 H, m), 8.19 (1 H, d, J = 8.4), 8.50−7.80 (4 H, m), 7.67 (1 H, d, J = 8.5), 7.17 (2 H, m), 5.63 (2 H, m), 4.30 (2 H, m), 3.01 (2 H, t, J = 7.0), 2.87 (4 H, s), 2.32 (3 H, s), 1.74 (2 H, m). Analytical RP-HPLC (4.6 × 300 mm μBondapak C_{18}, acetonitrile/0.1% aqueous formic acid, 30:70, 1 mL/min, 254 nm): 4.34 min, 97%. ESI-MS: *m*/*z* 683 $(M + H)^+$. Anal. calcd for $C_{32}H_{31}N_3O_{10}S_2$: C, 56.38; H, 4.58; N, 6.16; S, 9.41. Found: C, 56.15; H, 4.70; N, 6.24; S, 9.31.

*3-(9-{[Isopropyl({4-[4-oxo-4-(2,3,4,5,6-pentafluorophenoxy)butyl]phenyl}sulfonyl)amino] carbonyl}-10-acridiniumyl)-1-propanesulfonate (**18**).* 3-(9-{[{[4-(3-Carboxypropyl)phenyl]sulfonyl} (isopropyl)-amino]carbonyl}-10-acridiniumyl)-1-propanesulfonate inner salt (*26*) (100 mg, 0.16 mmol) and pentafluorophenyl trifluoroacetate (550 μL, 3.2 mmol) were dissolved in dimethylformamide (2 mL). Pyridine (260 μL, 3.2 mmol) was added, and the solution was stirred for 16 h. Afterward, the reaction mixture was evaporated in vacuo and the residue was triturated with diethyl ether (4 × 5 mL). The remaining solid was purified by preparative RP-HPLC (μ-Bondapak C_{18}, acetonitrile/0.05% aqueous TFA 45:55, λ = 254 nm, 70 mL/min) to afford the desired active ester **18** (52%). ^{1}H NMR ($CDCl_3$): 9.10−8.90 (2 H, m), 8.50−8.30 (2 H, m), 8.30−7.25 (8 H, m), 5.82 (2 H, m), 4.44 and 3.70 (1 H, m), 4.37 and 3.64 (2 H, m), 1.62 and 1.43 (6 H, d, J = 6.7), 3.0−1.20 (10 H, m). ^{13}C NMR ($CDCl_3$): δ 173.2, 168.9, 165.5, 164.1, 160.2, 159.7, 153.1, 150.7, 150.3, 149.6, 148.6, 142.8, 141.4, 141.2, 141.0, 140.3, 140.0, 139.5, 139.3, 137.8, 137.7, 136.7, 136.1, 133.9, 131.3, 129.8, 129.7, 129.4, 129.1, 129.0, 128.3, 127.4, 126.7, 124.9, 122.3, 122.1, 119.9, 119.6, 119.3, 117.7, 113.9, 57.0, 55.1, 50.8, 50.5, 47.8, 34.7, 34.5, 32.4, 32.3, 25.7, 25.6, 24.8, 21.7, 19.9, 19.4, 17.3. ESI-MS: *m*/*z* 779.4 $(M + H)^+$. Analytical HPLC (4.6 × 300 mm μBondapak C_{18}, acetonitrile/0.05% aqueous trifluoroacetic acid, 50:50, 1 mL/min): 14.58 min, >95%.

*3-[9-({(Isopropylsulfonyl)[4-oxo-4-(2,3,4,5,6-pentafluorophenoxy)butyl]amino}carbonyl)-10-acridiniumyl]-1-propanesulfonate (**19**).* 3-(9-{[(3-Carboxypropyl)(isopropylsulfonyl)amino]carbonyl}-10-acridiniumyl)-1-propanesulfonate inner salt (*26*) was treated as in the preparation of **18**, to afford the desired active ester **19** (82%). ^{1}H NMR ($CDCl_3$): 9.10−8.90 (2 H, m), 8.50−8.35 (2 H, m), 8.20−7.85 (4 H, m), 5.83 (2 H, s), 4.80−1.50 (11 H, m), 1.68 and 1.21 (6 H, d, J = 6.8). ^{13}C NMR ($CDCl_3$): 168.6, 168.2, 167.0, 165.2, 152.5, 149.2, 141.7, 141.0, 140.2, 136.1, 129.9, 129.2, 127.3, 126.7, 122.6, 120.1, 119.7, 57.1, 55.7, 50.9, 50.6, 47.7, 46.9, 30.5, 29.1, 25.4, 24.6, 23.5, 16.2, 16.1. ESI-MS: *m*/*z* 703.8 $(M + H)^+$. Analytical HPLC (4.6

× 300 mm μBondapak C_{18}, acetonitrile/0.05% aqueous trifluoroacetic acid, 50:50, 1 mL/min): 5.08 min, >95%.

*3-[9-({(Mesitylsulfonyl)[4-oxo-4-(2,3,4,5,6-pentafluorophenoxy)butyl]amino}carbonyl)-10-acridiniumyl]-1-propanesulfonate (**20**).* 3-(9-{[(3-Carboxypropyl)(mesitylsulfonyl)amino]carbonyl}-10-acridiniumyl)-1-propanesulfonate inner salt (*26*) was treated as in the preparation of **18**, to afford the desired active ester **20** (88%). ^{1}H NMR ($CDCl_3$): 9.10−8.90 (2 H, m), 8.50−8.30 (2 H, m), 8.00−7.70 (4 H, m), 7.16 and 6.48 (2 H, s), 5.85 (2 H, m), 4.37 and 3.64 (2 H, m), four singlets: 2.81, 2.41, 2.10 and 1.89 (9 H), 3.50−1.80 (8 H, m). ^{13}C NMR ($CDCl_3$): 168.3, 168.2, 165.7, 165.0, 150.5, 149.5, 146.1, 145.0, 141.7, 141.2, 140.8, 140.2, 140.1, 140.0, 139.5, 132.8, 132.6, 132.5, 130.0, 128.6, 128.1, 126.8, 122.6, 122.5, 120.1, 119.4, 50.8, 47.8, 47.3, 46.1, 30.7, 29.5, 25.7, 25.1, 23.9, 22.9, 22.0, 21.2, 20.9. ESI-MS: *m/z*: 779.4 $(M + H)^+$. Analytical HPLC (4.6 × 300 mm μBondapak C_{18}, acetonitrile/0.05% aqueous trifluoroacetic acid, 50:50, 1 mL/min): 9.5 min, >95%.

Preparation of N^{10}-(3-sulfopropyl)-*N*-sulfonylacridinium-9-carboxamide tracers 21−28. *General Method.* N^{10}-(3-Sulfopropyl)-*N*-sulfonylacridinium-9-carboxamide active ester (**17**−**20**) (0.050 mmol) was added to a solution of the phenobarbital (**13**) or phenytoin (**16**) hapten (0.05 mmol) in 1:1 dimethylformamide/100 mM phosphate buffer (3 mL, pH 8) and mixed for 17 h under a nitrogen atmosphere in the dark. The solvents were removed in vacuo, and the residue was purified by preparative reversed-phase HPLC (acetonitrile/0.03% aqueous trifluoroacetic acid). Fractions were pooled and lyophilized to afford the tracers as yellow powders.

*3-{9-[2-[(4-Methylphenyl)sulfonyl]-6,11-dioxo-18-(2,4,6-trioxo-5-phenylhexahydro-5-pyrimidinyl)-12-oxa-2,7,10-triazaoctadec-1-anoyl]-10-acridiniumyl}-1-propanesulfonate (**21**)* was prepared from phenobarbital hapten **13** and acridinium active ester **17** (36%). ^{1}H NMR (CD_3-OD): 8.94 (2 H, d, J = 13), 8.42 (2 H, t, J = 7), 8.19 (0.5 H, d, J = 9), 8.00 (1.5 H, d, J = 8), 7.91 (0.5 H, t, J = 9), 7.85 (1.5 H, t, J = 7), 7.78 (0.5 H, d, J = 8), 7.63 (0.5 H, d, J = 8), 7.35 (1 H, s), 7.31 (4 H, s), 7.14 (3 H, s), 6.87 (2 H, br), 4.24 (2 H, t, J = 7), 3.98 (2 H, m), 3.24 (4 H, m), 2.76−2.63 (4 H, m), 2.44 (2 H, t, J = 7), 2.35 (3 H, s), 2.26 (4 H, m), 1.64 (4 H, m), 1.28 (8 H, m). ESI-MS: *m/z* 957 $(M)^+$. Analytical HPLC (0.05% trifluoroacetic acid in acetonitrile/0.05% aqueous trifluoroacetic acid, 40:60): 5.18 min, >98%.

*3-(9-{[Isopropyl({4-[4-oxo-4-({2-[({[6-(2,4,6-trioxo-5-phenylhexahydro-5-pyrimidinyl)hexyl]oxy}-carbonyl)amino]-ethyl}amino)-butyl]phenyl}sulfonyl)amino]carbonyl}-10-acridiniumyl)-1-propanesulfonate (**22**))* was prepared from phenobarbital hapten **13** and acridinium active ester **18** (47%). ^{1}H NMR (CD_3OD): 8.93 (2 H, d, J = 9), 8.46 (2 H, t, J = 7), 8.23 (0.25 H, d, J = 9), 8.12 (1.75 H, d, J = 9), 8.00 (2 H, m), 7.81 (0.25 H, d, J = 8), 7.61 (0.25 H, d, J = 8), 7.32 (8.5 H, br), 5.71 (2 H, br), 3.94 (2 H, t, J = 6), 3.26 (7 H, m), 2.71−2.58 (4 H, m), 2.26 (4 H, m) 1.89 (2 H, t, J = 8), 1.72 (6 H, d, J = 6), 1.46 (2 H, m), 1.28 (8 H, m). ESI-MS: *m/z* 985 $(M)^+$. Analytical HPLC (0.05% trifluoroacetic acid in acetonitrile/0.05% aqueous trifluoroacetic acid, 40:60): 6.85 min, >98%.

*3-{9-[2-(Isopropylsulfonyl)-6,11-dioxo-18-(2,4,6-trioxo-5-phenylhexahydro-5-pyrimidinyl)-12-oxa-2,7,10-triazaoctadec-1-anoyl]-10-acridiniumyl}-1-propanesulfonate (**23**)* was prepared from phenobarbital hapten **13** and acridinium active ester **19** (59%). ^{1}H NMR (CD_3OD): 9.01 (1.5 H, d, J = 10), 8.89 (0.5 H, d, J = 10), 8.49 (2 H, m), 8.29 (2 H, m), 8.06 (2 H, m), 7.36 (3 H, s), 7.32 (2 H, s), 5.77 (1 H, br), 5.71 (1 H, br), 4.51 (1 H, m), 4.18 (1 H, m), 3.99 (1 H, t, J = 7), 3.92 (1 H, t, J = 7), 3.56 (1 H, m), 3.26 (4 H, m), 2.71 (4 H, m), 2.61 (1 H, m), 2.44 (2 H, m), 2.33 (2 H, m), 2.24 (1 H, m), 1.64 (3 H, d, J = 7), 1.60 (2 H, m), 1.35 (8 H, m), 1.20 (3 H, d, J = 7). ESI-MS: *m/z* 909 $(M)^+$. Analytical HPLC (0.05% trifluoroacetic acid in acetonitrile/0.05% aqueous trifluoroacetic acid, 40:60): 4.00 min, >98%.

*3-{9-[2-(Mesitylsulfonyl)-6,11-dioxo-18-(2,4,6-trioxo-5-phenylhexahydro-5-pyrimidinyl)-12-oxa-2,7,10-triazaoctadec-1-anoyl]-10-acridiniumyl}-1-propanesulfonate (**24**)* was prepared from phenobarbital hapten **13** and acridinium active ester **20** (30%). ^{1}H NMR (CD_3OD): 8.96 (0.5 H, d, J = 10), 8.17 (1.5 H, d, J = 9), 8.42 (2 H, m), 8.10 (1.5 H, d, J = 8), 8.01 (0.5 H, t, J = 7), 8.88 (2 H, m), 7.33 (2 H, s), 7.32 (3 H, s), 7.25 (1 H, s), 6.46 (1 H, s), 5.72 (0.5 H, br), 5.62 (1.5 H, br), 4.40 (1.5 H, br), 4.01 (1.5 H, t, J = 7), 3.86 (0.5 H, t, J = 7), 3.49 (0.5 H, br), 3.25 (4 H, m), 2.68 (2 H, m), 2.49 (0.5 H, d, J = 7), 2.40 (3 H, s), 2.36 (2 H, m), 2.24 (2 H, m), 2.07 (3 H, s), 1.82 (3 H, s), 1.78 (2 H, m), 1.64 (1.5 H, d, J = 7), 1.54 (4 H, m), 1.29 (8 H, m). ESI-MS: *m/z* 985 $(M)^+$. Analytical HPLC (0.05% trifluoroacetic acid in acetonitrile/0.05% aqueous trifluoroacetic acid, 40:60): 6.73 min, >97%.

*3-[9-({(4-{[6-(2,5-Dioxo-4,4-diphenyl-1-imidazolidinyl)-hexyl]amino}-4-oxobutyl)[(4-methylphenyl)sulfonyl]amino}-carbonyl)-1,2,3,4-tetrahydro-10-acridiniumyl]-1-propanesulfonate (**25**)* was prepared from phenytoin hapten **16** and acridinium active ester **17** (78%). ^{1}H NMR (CD_3-OD): 8.91 (2 H, d, J = 9.20), 8.20−7.78 (6 H, m), 7.39−7.28 (10 H, m), 7.24−7.15 (4 H, m), 5.77−5.68 (2H, m), 4.26−4.17 (2 H, m), 3.55−3.44 (2 H, m), 3.28−3.15 (2 H, m), 2.71−2.54 (2 H, m), 2.50−2.22 (2 H, m), 2.39 (3 H, s), 1.79−0.70 (1 H, m), 1.66−1.23 (9 H, m), 1.16−1.02 (2 H, m). ESI-MS: *m/z* 918 $(M + H)^+$. Analytical HPLC (acetonitrile/0.03% aqueous trifluoroacetic acid, 45:55): 7.38 min, >99%.

*3-(9-{[{[4-(4-{[6-(2,5-Dioxo-4,4-diphenyl-1-imidazolidinyl)hexyl]amino}-4-oxobutyl)phenyl]-sulfonyl}(isopropyl)-amino]carbonyl}-10-acridiniumyl)-1-propanesulfonate (**26**)* was prepared from phenytoin hapten **16** and acridinium active ester **18** (71%). ^{1}H NMR (acetonitrile-d_3): 8.79−8.76 (2 H, m), 8.26−7.40 (7 H, m), 7.39−7.24 (10 H, m), 6.94−6.59 (1 H, br m), 5.77−5.68 (2 H, m), 4.79−4.74 (1 H, m), 3.50−3.38 (2 H, m), 3.26−3.15 (2 H, m), 3.04−3.02 (2 H, m), 2.79−2.49 (4 H, m), 2.16−2.03 (2 H, m), 1.83−1.77 (2 H, m), 1.68 (6 H, d, J = 6.7), 1.58−1.49 (2 H, m), 1.38−1.10 (10 H, m). ESI-MS: *m/z* 947 $(M + H)^+$. Analytical HPLC (acetonitrile/0.1% aqueous trifluoroacetic acid/water 50:5:45): 5.4 min, >99%.

*3-(9-{[(4-{[6-(2,5-Dioxo-4,4-diphenyl-1-imidazolidinyl)-hexyl]amino}-4-oxobutyl)(isopropylsulfonyl)-amino]carbonyl}-10-acridiniumyl)-1-propanesulfonate (**27**)* was prepared from phenytoin hapten **16** and acridinium active ester **19** (46%). ^{1}H NMR (D_2O/acetonitrile-d_3, 1:1): 8.89−8.78 (2 H, m), 8.45−8.40 (2 H, m), 8.23−8.15 (2 H, m), 8.04−7.94 (2 H, m), 7.40−7.29 (10 H, m), 5.66−5.60 (2 H, m), 4.46−4.11 (1 H, m), 3.48−3.07 (6 H, m), 2.90−2.31 (4 H, m), 1.52 and 1.30 (6 H, d, J = 7, ratio 2.4/1), 1.51−0.90 (12 m). ESI-MS: *m/z* 871 $(M + H)^+$. Analytical HPLC (acetonitrile/0.1% aqueous trifluoroacetic acid/water 40:5:55): 9.1 min, >99%.

*3-(9-{[(4-{[6-(2,5-Dioxo-4,4-diphenyl-1-imidazolidinyl)-hexyl]amino}-4-oxobutyl)(mesitylsulfonyl)-amino]carbonyl}-10-acridiniumyl)-1-propanesulfonate (**28**)* was prepared from phenytoin hapten **16** and acridinium active ester **20** (26%). ^{1}H NMR (D_2O:acetonitrile-d_3, 1:1): 8.82 (1 H, d, J = 9.2), 8.69 (1 H, d, J = 9.3), 8.44−8.32 (2 H, m), 8.03−7.91 (2 H, m), 7.84 (2 H, d, J = 8.9), 7.37−7.28 (12 H, m), 7.23 (1 H, s), 6.40 (1 H, s), 5.63−5.43 (2 H, m),

Scheme 1. Preparation of Phenobarbital Hapten 13

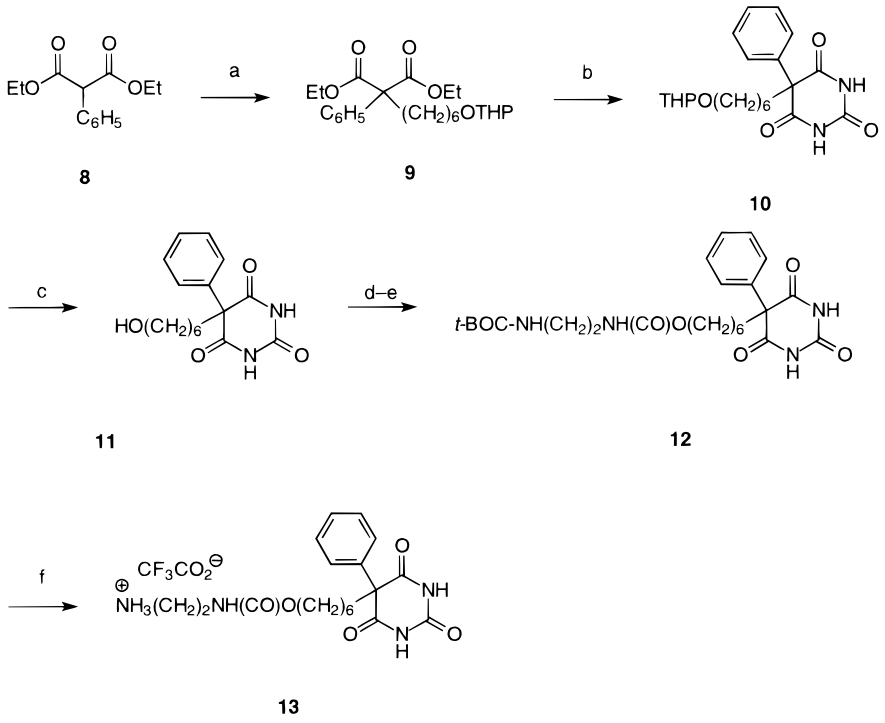

[a] 1-Bromo-6-tetrahydropyranyloxyhexane, KH, THF/DMF, reflux, 14 h. [b]Urea, NaOEt. [c]2 N aqueous HCl, THF. [d]Phosgene. [e]*tert*-Butyl *N*-(2-aminoethyl)carbamate. [f]TFA.

Scheme 2. Preparation of Phenytoin Hapten 16

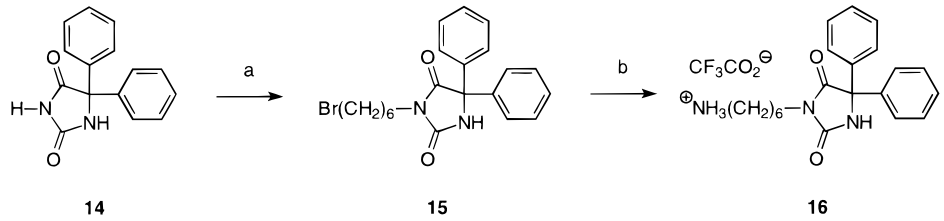

[a] (i) Potassium hydroxide, ethanol; (ii) 1,6-dibromohexane, acetonitrile, reflux. [b](i) Ammonium hydroxide, dioxane, reflux; (ii) preparative HPLC.

4.38−4.30 (1 H, m), 3.44 (2 H, t, J = 7.1), 3.19−3.05 (4 H, m), 2.65−2.25 (4 H, m), 2.00 (3 H, s), 1.75 (6 H, s), 1.73−1.68 (1 H, m), 1.64−1.18 (8 H, m), 1.13−1.01 (2 H, m). ESI-MS: m/z 352 $(M + H)^+$. Analytical HPLC (acetonitrile/0.03% aqueous trifluoroacetic acid, 45:55): 10.65 min, >99%.

Antibody purification. Sheep serum proteins were precipitated by the slow, dropwise addition of saturated NH_4SO_4 until a final concentration of 50% saturated NH_4SO_4 was reached. The sample was then allowed to stand for 12 h at 4−8 °C. The precipitate was then pelleted using ultracentrifugation, the supernatant discarded, and the pellet taken up in PBS (10 mL, 100 mM sodium phosphate, 150 mM NaCl, pH 7.0). The mostly dissolved serum proteins were clarified by filtration (0.2 μm polyethersulfone syringe filter, Nalge Nunc International, Rochester, NY) and then dialyzed exhaustively against PBS. The resulting solution was loaded onto a HiTrap protein G column (0.5 mL/min) that had been equilibrated with sodium phosphate buffer (20 mM, pH 7.0). When the A_{280} of the eluant returned to background, the bound antibodies were eluted with aqueous glycine-HCl (100 mM, pH 2.7, 3 mL/min). Fractions with an A_{280} > 0.1 AU were pooled, immediately neutralized with Tris buffer (1 M, pH 9.0), and then dialyzed exhaustively against PBS. The antibody solutions were concentrated to 5−10 mg/mL using ultracentrifugation (Centriprep 30, Millipore, Bedford, MA) and stored at −78 °C prior to use. Concentration of the antibody stock solutions was determined using an extinction coefficient of 1.4 $(mg/mL)^{-1}\ cm^{-1}$ (*35*).

Chemiluminescence Evaluation of Phenobarbital (21−24) and Phenytoin (25−28) Tracers on Binding with Antibodies. *Immobilization of the Antibodies.* Each antibody (*anti*-phenobarbital, *anti*-phenytoin, and control sheep polyclonal serum) was diluted with sodium bicarbonate buffer (100 mM, pH 9.6) to afford the desired concentration stock solution (2.5 μg/mL). Each antibody solution was dispensed into the microtiter plate (200 μL/well) and incubated at ambient temperature (2 h) to allow for passive immobilization. After the antibody solution was aspirated, the each well was then treated with 2% nonfat dry milk dissolved in PBS buffer (pH 7.2, 200 μL/well) for 1 h.

Determining Microtiter Plate-Bound Antibody Binding Capacity. All tracers were first dissolved in absolute ethanol to afford the desired concentration stock solutions (0.5 mM). Each stock solution was serially diluted with 2% nonfat dry milk dissolved in PBS buffer to make tracer solutions ranging from 5.0 μM to 10 pM. Tracer solutions (150 μL/well) were added to each well of the corresponding immobilized antibody and incubated at

Table 1. Acridinium-Labeled Tracers

Hapten	N^{10}-(3-Sulfopropyl)-*N*-sulfonylacridinium-9-carboxamide active ester	Tracer Structure
Phenobarbital (**13**)	**17**	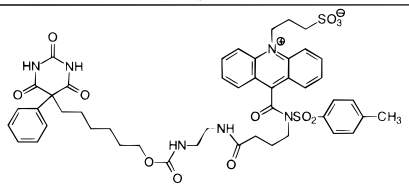 **21**
	18	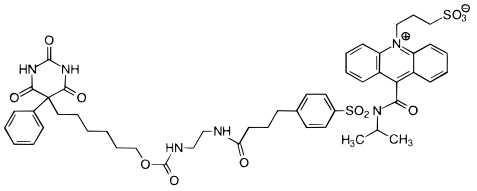 **22**
	19	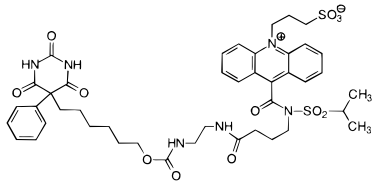 **23**
	20	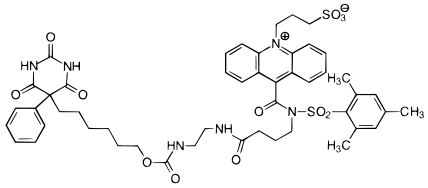 **24**
Phenytoin (**16**)	**17**	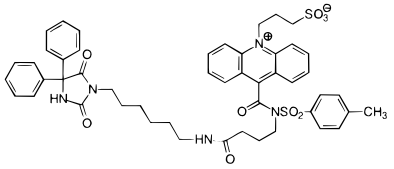 **25**
	18	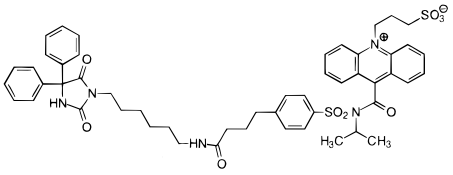 **26**
	19	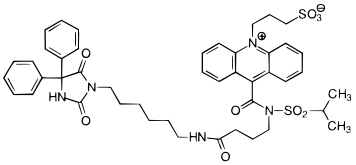 **27**
	20	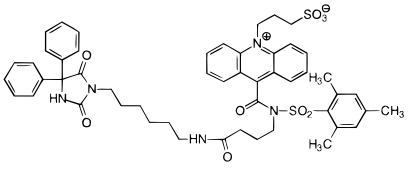 **28**

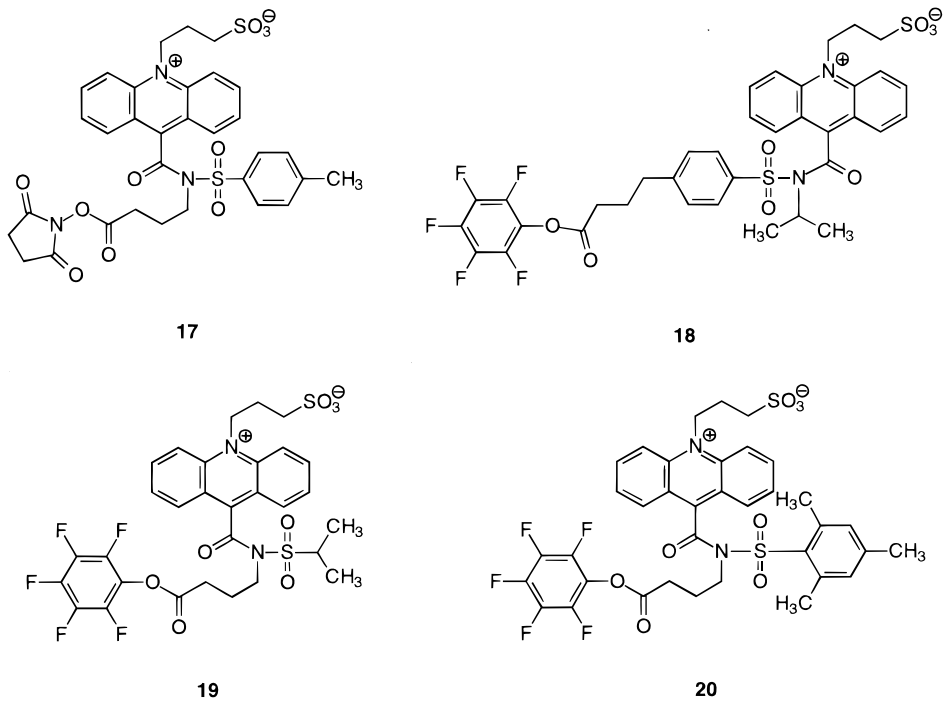

Figure 2. N^{10}-(3-Sulfopropyl)-*N*-sulfonylacridinium-9-carboxamide active esters.

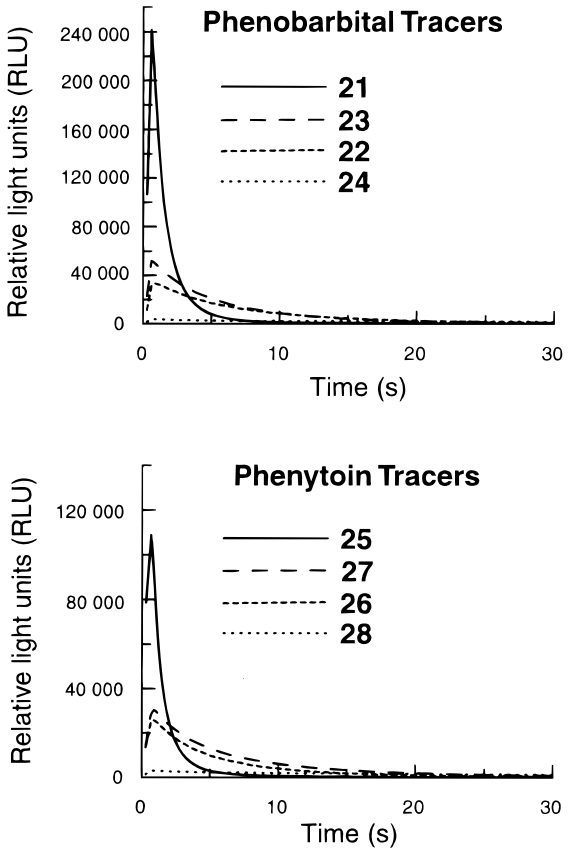

Figure 3. Typical chemiluminescent emission vs time profile for each linker modified tracer. Each microtiter well was coated with polyclonal *anti*-phenobarbital or *anti*-phenytoin antibody solution (2.5 μg/mL, 200 μL/well). Phenobarbital tracers (**21**−**24**, 250 nM, 150 μL/well) and phenytoin tracers (**25**−**28**, 100 nM, 150 μL/well) were incubated with the immobilized antibodies for 1 h. Chemiluminescence was recorded for 30 s.

ambient temperature for another 1 h. Afterward, the plate was thoroughly washed (PBS, 0.1% Tween-20, 6 × 1 min). The plate was transferred to the luminometer, and each well was sequentially triggered [200 μL, 1:1 solution A (0.35 M sodium hydroxide, 2% Triton X-100)/ solution B (0.008 N HNO_3, 1.32% H_2O_2, 0.09% DTPA)]. Chemiluminescence emission from each well was recorded for 30 s. A typical chemiluminescent emission vs time profile for each tracer (**21**−**24**, 250 nM; **25**−**28**, 100 nM) is shown in Figure 3. Plots of the total chemiluminescent emission (initial 3 s) first vs tracer concentration are shown in Figure 4. Nonspecific chemiluminescence background from control sheep polyclonal serum was subtracted to get the specific chemiluminescence signal for the *anti*-hapten antibody/tracer complex. Relative chemiluminescence output was calculated by comparing the saturated responses of each phenobarbital or phenytoin tracer to that of tracers **21** and **25**, respectively, and is reported in Table 2.

Assessing the Effect of Linker Chemistry on Antibody Affinity (IC_{50}). Solutions (150 μL), each containing a phenobarbital tracer (**21**−**24**) (1.0 μM) and phenobarbital (100 μM-10 nM), were dispensed into separate microtiter wells and incubated at ambient temperature for 1 h with the immobilized *anti*-phenobarbital antibody. The plate was thoroughly washed (PBS, 0.1% Tween-20, 6 × 1 min). Bound tracer was triggered, and chemiluminescence was measured for 30 s. The signal at each analyte concentration was normalized using the noninhibited chemiluminescence signal as the reference. The IC_{50} value for each tracer was determined from a plot (Figure 5) of normalized signal vs analyte concentration using this four parameter logistic (GraFit 3.0) (*36*):

$$Y = \frac{a}{1 + (x/\mathrm{IC}_{50})^{s}} + \text{background}$$

where *a* is the maximum *y* range, *s* is a slope factor, and *x* represents the concentration of analyte.

The experiment was repeated with phenytoin tracers **25**−**28**.

Effect of Signal Modulation on the Chemiluminescence Dose/Response Curve. Each phenobarbital acridinium tracer (**21**−**24**) was diluted into 2% nonfat dry milk in

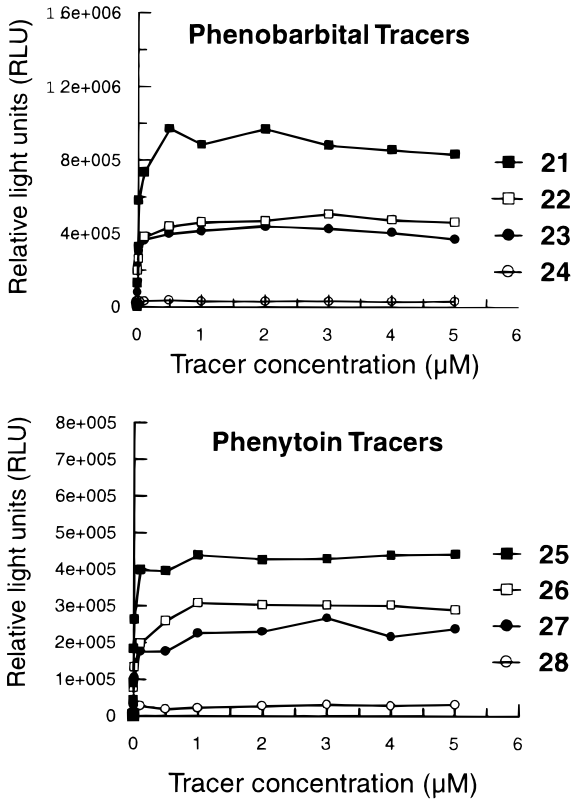

Figure 4. Total chemiluminescent emission vs tracer concentration. After polyclonal *anti*-phenobarbital or *anti*-phenytoin antibody was immobilized (2.5 μg/mL, 200 μL/well), each tracer solution with concentration ranging from 0.001, 0.01, 0.1, 1.0, 10, 100 nM, 1.0, 2.0, 3.0, 4.0, to 5.0 μM was incubated (150 μL/well). The saturated chemiluminescence response of each tracer was averaged and normalized to obtain the relative chemiluminescence output.

Table 2. Linker Affect on Chemiluminescent Signal and Antibody Affinity

compd	relative signal (3 s)	IC_{50} (μM)
phenobarbital tracers		
21	1.00	5.5
22	0.57 ± 0.14	1.8
23	0.49 ± 0.11	2.1
24	0.04 ± 0.01	2.3
phenytoin tracers		
25	1.00	14.0
26	0.65 ± 0.07	7.7
27	0.54 ± 0.07	9.2
28	0.06 ± 0.03	14.6

PBS buffer, pH 7.2, to obtain a stock solution (250 nM). To each well of the *anti*-phenobarbital coated plate were added a tracer (145 μL) and one of six phenobarbital calibrators (0, 5, 10, 20, 40, and 80 μg/mL, 5 μL). The plate was incubated for 1 h and washed, and the chemiluminescence was recorded for 3 s (Figure 6).

Evaluation of the phenytoin tracers **25**−**28** was conducted similarly. The concentration of each phenytoin tracer solution was 100 nM, and the concentration of the phenytoin calibrators were 0, 2.5, 5, 10, 20, and 40 μg/mL.

RESULTS

Preparation of Haptens and Chemiluminescent Tracers. Each hapten was prepared by standard protocols. Thus, phenobarbital hapten **13** was prepared in six steps from diethyl phenylmalonate **8** (Scheme 1), while

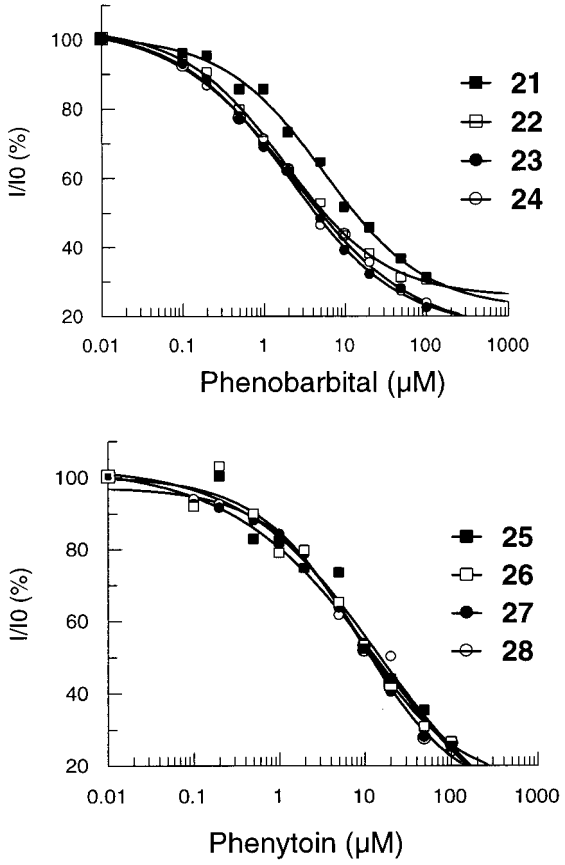

Figure 5. The effect of linker chemistry on antibody avidity (IC_{50}). The total concentration of each tracer was fixed at 1.0 μM. Phenobarbital or phenytoin was diluted into each tracer stock (1.0 μM) to get final phenobarbital or phenytoin concentration of 0.01, 0.1, 0.2, 0.5, 1.0, 2.0, 5.0, 10, 20, 50, and 100 μM. The normalized chemiluminescence count (I/I_0) was plotted against each inhibitor concentration.

diphenylhydantoin **14** afforded the desired phenytoin hapten **16** in two steps (Scheme 2).

The requisite active esters of the chemiluminescent acridinium salts **17**−**20** (Figure 2) were prepared from the corresponding free acids (*25*, *26*). *N*-Hydroxysuccinimide active ester **17** precipitated from the reaction of the free acid with *N*-trifluoroacetoxysuccinimide in nearly quantitative yield. Pentafluorophenyl active esters **18**-**20** were isolated in 52−88% yield as lyophilized powders after purification by preparative reversed-phase HPLC.

Reaction of the phenobarbital and phenytoin aminated haptens **13** and **16** with each of the chemiluminescent acridinium salt active esters **17**−**20** in buffered aqueous DMF afforded the chemiluminescent tracers **21**-**28** listed in Table 1 in 26−78% yield after preparative RP-HPLC.

Evaluation of Chemiluminescent Phenobarbital and Phenytoin Tracers with Polyclonal Antibodies. Purified sheep *anti*-phenobarbital, *anti*-phenytoin IgGs, and a control sheep antisera were dispensed into the wells of a white polystyrene microtiter plate (500 pg/well) and incubated for 2 h. Afterward, the plate was overcoated with a 2% solution of nonfat dry milk in PBS buffer to minimize nonspecific binding of the acridinium tracers. Solutions of the complementary chemiluminescent tracers were added to each well (150 μL, 10 pM to 5 μM, corresponding to 1.5 fmol to 750 pmol/well). After incubation and washing, the chemiluminescence was triggered and recorded for 30 s. From this experiment both the chemiluminescence profile of the tracers in the

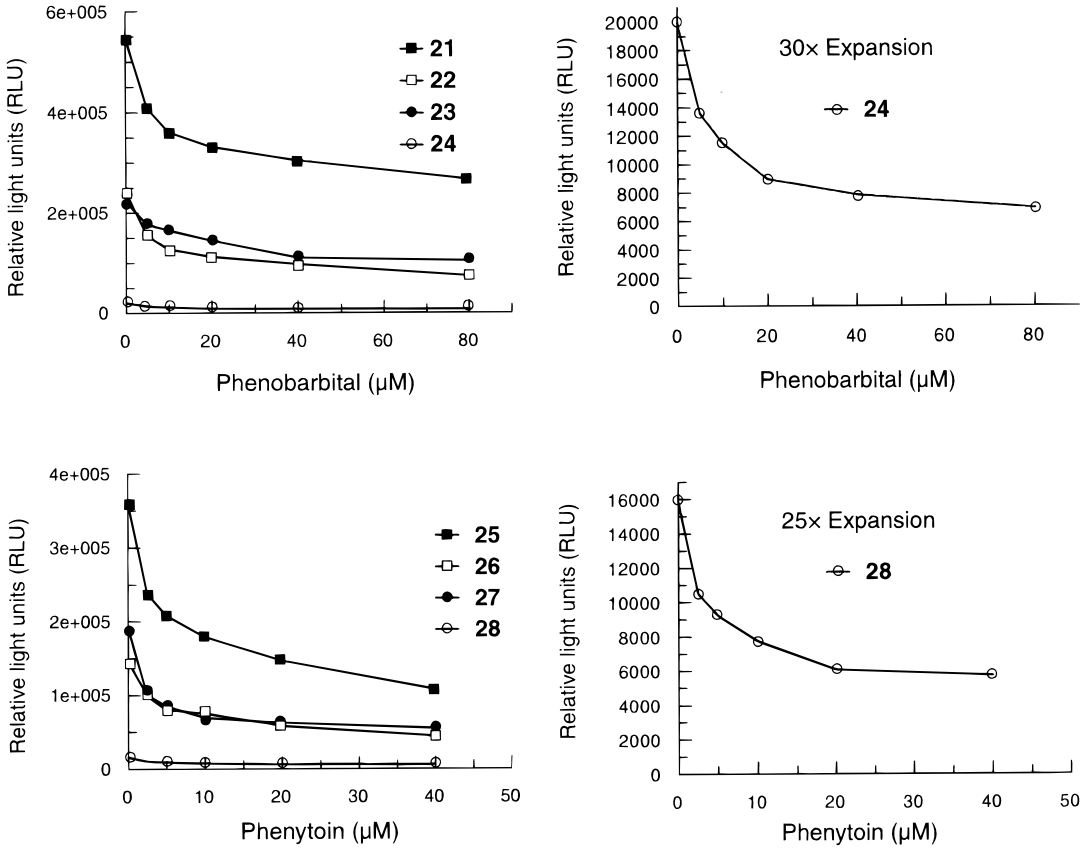

Figure 6. Linker-mediated signal modulation in a solid-phase chemiluminescence assay. Each tracer series, **21**−**24** (145 μL, 250 nM) and **25**−**28** (145 μL, 100 nM) was incubated with the complementary immobilized antibody and calibrators (5 μL of 0, 5, 10, 20, 40, and 80 μg/mL for phenobarbital; 0, 2.5, 5, 10, 20, and 40 μg/mL for phenytoin) for 1 h. Chemiluminescence was then triggered and recorded for 3 s.

presence of the corresponding antibodies and the binding capacity of the immobilized antibodies could be determined.

Thus, the change in the chemiluminescence signal from each tracer (**21**−**28**) over the observation period paralleled that which was recorded for the unconjugated *N*-sulfonylacridinium-9-carboxamide acids (*26*) in the absence of antibody. Figure 3 illustrates this point for a single concentration of the phenobarbital (**21**−**24**, 37.5 pmol) and phenytoin (**25**−**28**, 15 pmol) tracers, respectively. The chemiluminescence signal from phenobarbital tracer **21** and phenytoin tracer **25**, both derived from acridinium label **17**, peaked within 2 s and was essentially exhausted within 6 s. At the other extreme, tracers **24** and **28**, derived from active ester **20** had a nearly constant lower-level glow over the entire observation period. Even so, regardless of the linker used to attach the acridinium nucleus, the total harvested signal remained essentially constant (data not shown). Therefore, as a practical demonstration of the signal modulating effect of the linkers, subsequent experiments used only the signal recorded in the first three seconds of the chemiluminescent reaction.

Figure 4 shows that the immobilized antibodies were saturated once the concentration of chemiluminescent tracer reached about 1 μM. A comparison of the chemiluminescence signal at saturation also demonstrated the effect of the linker chemistry. The signals for the tracers in each series were normalized to the phenobarbital tracer **21** or phenytoin tracer **25**, respectively. As shown in Table 2, the signal of phenobarbital tracers **22** and **23**, which possessed the more sterically demanding isopropyl-substituted linkers, were reduced nearly 50%, while the light emission from **24** that carried the even more sterically hindered mesityl group, was decreased to only 4% of **21**. Phenytoin tracers demonstrated the same trend.

The linker chemistry had little effect on the binding interaction of the tracers with the antibodies, as evidenced by the slight differences in the observed inhibition constant (IC_{50}) in the presence of free phenobarbital or phenytoin. Solutions containing each tracer (1.0 μM) and fixed concentrations of the free analytes (0, 0.01, 0.1, 0.2, 0.5, 1.0, 2.0, 5.0, 10, 20, 50, and 100 μM) were allowed to compete for the available antibody binding sites on the microtiter plate, causing a decrease in the observed chemiluminescence signal. For each tracer, the chemiluminescence signal at each inhibitor concentration was normalized to the uninhibited chemiluminescence signal (Figure 5). IC_{50} values (Table 2) of three phenobarbital tracers **22**−**24** were very similar (1.8, 2.1, and 2.3 μM, respectively). Phenobarbital tracer **21** has an IC_{50} of 5.5 μM. The inhibition constants of phenytoin tracers **25**−**28** were also close to each other, ranging from 7.7 to 14.6 μM.

Modulating Effect of Acridinium Linker Chemistry in an Immunoassay Format. The polyclonal *anti*-phenobarbital and *anti*-phenytoin antibodies were immobilized on the microtiter plate as described above (500 pg/well). To generate calibration curves, each tracer series **21**−**24** (145 μL, 250 nM) and **25**−**28** (145 μL, 100 nM) was incubated with the complementary immobilized antibody and calibrators (5 μL of 0, 5, 10, 20, 40, and 80 μg/mL for phenobarbital; 0, 2.5, 5, 10, 20, and 40 μg/mL for phenytoin) for 1 h. Chemiluminescence was then triggered and recorded for 3 s. The integrated chemilumi-

nescence signals were plotted vs calibrator concentrations (Figure 6). Calibration curves from the four tracers in each series have similar shapes and are roughly parallel to each other. In both series, the *N*-sulfonylacridinium-9-carboxamide tracers bearing the mesityl-substituted linker showed the most pronounced attenuation of signal, while the isopropyl derivatives produced an intermediate signal.

DISCUSSION

It was previously demonstrated that chemiluminescent *N*-sulfonylacridinium-9-carboxamide labels all produce the same excited-state acridone (**6**, Figure 1**)** but have different light-generating profiles in solution that are governed by the steric and electronic properties of the linking group (*26*). In an immunoassay for low-molecular weight analytes, these labels must be conjugated to hapten molecules to form tracers that interact further with antibodies and the sample containing the analyte of interest. Commonly, these chemiluminescent immunoassays (CLIA) are heterogeneous, i.e., the antibody component is immobilized on a solid support such as a microtiter plate or microparticles. The noncovalent tracer/antibody complex may dissociate under the stringent conditions of the chemiluminescent reaction. If so, the chemiluminescence profile of the tracer in a heterogeneous immunoassay should parallel profile of the unconjugated label in solution; the signal generated would be affected by the linker substituents. In the absence of dissociation, the linking group may be sufficiently long to allow the triggering reagents access to the acridinium nucleus unhindered by the antibody. On the other hand, the tracer molecule may be deeply docked into the antigen-binding region of the antibody, making the tracer less accessible to the triggering reaction. The chemiluminescence profile of the tracer might then be different from that of the corresponding unconjugated acridinium label. Additionally, the interaction with the antibody could have a leveling effect, masking differences due to the chemical reactivity of the linking group.

In this study, the data support the first or second scenario. Four *N*-sulfonylacridinium-9-carboxamide labels, each having linking groups with distinctive steric and electronic properties, were chosen and conjugated to phenobarbital and phenytoin haptens. A chemiluminescence immunoassay was developed for characterizing their light-generating and binding properties. Both phenobarbital and phenytoin tracers showed the same trend seen in the unconjugated labels: the tracers with the least sterically hindered linker, phenobarbital **21** and phenytoin **25**, had the fastest light-emission therefore the most signal within the first three seconds. The tracers with the most sterically hindered linkers, phenobarbital **24** and phenytoin **28**, had dramatically attenuated chemiluminescence within the first three seconds. Their light outputs dropped to about 5% compared to the tracers **21** and **25**. There were no obvious changes in binding interaction between the tracers and antibodies that could be attributed changes in the linker chemistry, as indicated by the inhibition constants (IC_{50}). Even though the IC_{50} value of phenobarbital tracer **21** was about three times higher than the other three phenobarbital tracers, the thermodynamic difference is negligible.

CONCLUSION

Chemiluminescent labels were developed because they offered lower detection limits than fluorescent or enzymatic labels and were more convenient to use than radiolabels. While assays and instrumentation have been fine-tuned to maximize sensitivity, clinically relevant analytes such as phenobarbital and phenytoin are often present in high concentration. So high, that assays that employ high yield chemiluminescent labels often can produce too much signal, overwhelming the instrument detector. The present study indicates that the level of signal produced by *N*-sulfonylacridinium-9-carboxamide tracers in a solid-phase immunoassay format can be modulated by at least 20-fold by the judicious choice of the acridinium-hapten linking group.

LITERATURE CITED

(1) Gallacher, G., Hansell, M., and Landon, J. (1989) An improved label for amphetamine fluoroimmunoassay. *Ther. Drug Monit. 11*, 607−11.

(2) Nordblom, G. D., Webb, R., Counsell, R. E., and England, B. G. (1981) A chemical approach to solving bridging phenomena in steroid radioimmunoassays. *Steroids 38*, 161−73.

(3) Nordblom, G. D., Counsell, R. E., and England, B. G. (1984) A specific radioimmunoassay for androstenedione with reduced bridge-binding. *Steroids 44*, 275−82.

(4) Tiefenauer, L. X., Bodmer, D. M., Frei, W., and Andres, R. Y. (1989) Prevention of bridge binding in immunoassays: a general estradiol tracer structure. *J. Steroid Biochem. 32*, 251−7.

(5) Allen, R. M., and Redshaw, M. R. (1978) The use of homologous and heterologous ^{125}I-radioligands in the radioimmunoassay of progesterone. *Steroids 32*, 467−86.

(6) De Boever, J., Kohen, F., and Bosmans, E. (1993) Antibody binding efficiency of differently labeled steroid hormones. *Anal. Chim. Acta 275*, 81−7.

(7) Ersoy, O., Fleck, R., Sinskey, A., and Masamune, S. (1998) Antibody-catalyzed cleavage of an amide bond using an external nucleophilic cofactor. *J. Am. Chem. Soc. 120*, 817−8.

(8) Kaiser, K., Marek, M., Haselgrubler, T., Schindler, H., and Gruber, H. J. (1997) Basic studies on heterobifunctional biotin-PEG conjugates with a 3-(4-pyridyldithio)propionyl marker on the 2nd terminus. *Bioconjugate Chem. 8*, 545−51.

(9) Luppa, P., Bruckner, C., Schwab, I., Hauck, S., Schmidmayr, S., Birkmayer, C., Paulus, B., and Hauptmann, H. (1997) 7-α-Biotinylated testosterone derivatives as tracers for a competitive chemiluminescence immunoassay of testosterone in serum. *Clin. Chem. 43*, 2345−52.

(10) Mitsuma, M., Kambegawa, A., Okinaga, S., and Arai, K. (1987) A sensitive bridge heterologous enzyme immunoassay of progesterone using geometrical isomers. *J. Steroid Biochem. 28*, 83−8.

(11) Tiefenauer, L. X., and Andres, R. Y. (1984) Prevention of bridge binding effects in haptenic immunoassay systems exemplified by an iodinated radioimmunoassay for melatonin. *J. Immunol. Methods 74*, 293−8.

(12) Benson, S. C., Zeng, Z., and Glazer, A. N. (1995) Fluorescence energy-transfer cyanine heterodimers with high affinity for double-stranded DNA. I. Synthesis and spectroscopic properties. *Anal. Biochem. 231*, 247−55.

(13) Gruber, H. J., Marek, M., Schindler, H., and Kaiser, K. (1997) Biotin-fluorophore conjugates with poly(ethylene glycol) spacers retain intense fluorescence after binding to avidin and streptavidin. *Bioconjugate Chem. 8*, 552−9.

(14) Johnson, G. M., Albarella, J. P., and Petry, C. (1997) Heterobifunctional cross-linkers containing 4,9-dioxa-1, 12-dodecanediamine spacers. *Bioconjugate Chem. 8*, 447−52.

(15) Lown, J. W., Gunn, B. C., Chang, R.-Y., Majumdar, K. C., and Lee, J. S. (1978) Bis-intercalative binding to DNA of novel bis (10-methyl) acridinium chlorides and its dependence on chain length of linker. *Can. J. Biochem. 56*, 1006−15.

(16) Marek, M., Kaiser, K., and Gruber, H. J. (1997) Biotin-pyrene conjugates with poly(ethylene glycol) spacers are convenient fluorescent-probes for avidin and streptavidin. *Bioconjugate Chem. 8*, 560−6.

(17) Randolph, J. B., and Waggoner, A. S. (1997) Stability, specificity and fluorescence brightness of multiply labeled fluorescent DNA probes. *Nucleic Acids Res. 25*, 2923−9.

(18) Russell-Jones, G. J., Westwood, S. W., and Habberfield, A. D. (1995) Vitamin B12 mediated oral delivery systems for GCSF and EPO. *Bioconjugate Chem. 6*, 459−65.

(19) Russell-Jones, G. J., and Westwood, S. W. (1996) Vitamin B12 conjugates with EPO, analogues thereof and pharmaceutical compositions. *Patent U.S.* 5,548,064.

(20) Albarella, J. P., Minegar, R. L., Patterson, W. L., Dattagupta, N., and Carlson, E. (1989) Monoadduct forming photochemical reagents for labeling nucleic acids for hybridization. *Nucleic Acids Res. 17*, 4293−308.

(21) Gildea, B. D., Coull, J. M., and Koster, H. (1990) A versatile acid-labile linker for modification of synthetic biomolecules. *Tetrahedron Lett. 31*, 7095−8.

(22) Leikauf, E., Barnekow, F., and Koester, H. (1995) Heterobifunctional trityl derivatives as linking reagents for the recovery of nucleic acids after labeling and immobilization. *Tetrahedron 51*, 3793−802.

(23) Soukup, G. A., Cerny, R. L., and Maher, L. J. (1995) Preparation of oligonucleotide-biotin conjugates with cleavable linkers. *Bioconjugate Chem. 6*, 135−8.

(24) Olejnik, J., Krzymanskaolejnik, E., and Rothschild, K. J. (1998) Photocleavable aminotag phosphoramidites for 5′-termini dna/rna. *Nucleic Acids Res. 26*, 3572−6.

(25) Adamczyk, M., Chen, Y.-Y., Mattingly, P. G., and Pan, Y. (1998) Neopentyl 3-triflyloxypropanesulfonate. A reactive sulfopropylation reagent for the preparation of chemiluminescent labels. *J. Org. Chem. 63*, 5636−9.

(26) Adamczyk, M., Chen, Y.-Y., Mattingly, P. G., Moore, J. A., and Shreder, K. (1999) Modulation of the chemiluminescent signal from N^{10}-(3-sulfopropyl)-*N*-sulfonylacridinium-9-carboxamides. *Tetrahedron 55*, 10899−914.

(27) Adamczyk, M., Fishpaugh, J. R., Gebler, J. C., Mattingly, P. G., and Shreder, K. (1998) Detection of reaction intermediates by flow injection electrospray ionization mass spectrometry: reaction of chemiluminescent *N*-sulfonylacridinium-9-carboxamides with hydrogen peroxide. *Eur. Mass Spec. 4*, 121−5.

(28) Oeltgen, P. R., Shank, W. A. J., Blouin, R. A., and Clark, T. (1984) Clinical evaluation of the Abbott TDx fluorescence polarization immunoassay analyzer. *Ther. Drug Monit. 6*, 360−7.

(29) Takayasu, S., Maeda, M., and Tsuji, A. (1985) Chemiluminescent enzyme immunoassay using beta-D-galactosidase as the label and the bis(2,4,6-trichlorophenyl)oxalate-fluorescent dye system. *J. Immunol. Methods 83*, 317−25.

(30) Dasgupta, A., Warner, B. F., and Datta, P. (1999) Use of alkaline phosphatase to correct the underestimation of fosphenytoin concentration in serum measured by phenytoin immunoassays. *Am. J. Clin. Pathol. 111*, 557−62.

(31) Dasgupta, A., Datta, P., Redlich, G., and Limmany, A. (1997) Analytical performance of a new chemiluminescent phenytoin (ACS:180) assay. *Ther. Drug Monit. 19*, 191−4.

(32) Jarzabek, J. I., and Kampa, I. S. (1999) Adaptation of total phenytoin reagent pack for measuring free phenytoin levels with the Abbott AxSYM immunoassay analyzer. *Ther. Drug Monit. 21*, 134−6.

(33) Hudkins, R. L., and DeHaven-Hudkins, D. L. (1994) Phenytoin derivatives as potent σ ligands. *Bioorg. Med. Chem. Lett. 4*, 2185−8.

(34) Sakaibara, S., and Inukai, N. (1965) The trifluoroacetate method of peptide synthesis. I. The synthesis and use of trifluoroacetate reagents. *Bull. Chem. Soc. Jpn. 38*, 1979−84.

(35) Ey, P. L., Prowse, S. J., and Jenkin, C. R. (1978) Isolation of pure IgG1, IgG2a and IgG2b immunoglobulins from mouse serum using protein A-Sepharose. *Immunochemistry 15*, 429−36.

(36) Halfman, C. J. (1981) Concentrations of binding protein and labeled analyte that are appropriate for measuring at any analyte concentration range in radioimmunoassays. *Methods Enzymol. 74*, 481−97.

BC0000280

Synthesis and Characterization of Novel Spin-Labeled Photoaffinity Nonnucleoside Analogues of ATP as Structural and EPR Probes for Myosin

Xiaoru Chen,[†] Jean Grammer,[†] Roger Cooke,[‡] Edward Pate,[§] and Ralph G. Yount*,[†]

School of Molecular Biosciences, Department of Pure and Applied Mathematics, Department of Chemistry,-Washington State University, Pullman, Washington 99164, and Department of Biochemistry and Biophysics & CVRI, University of California, San Francisco, California 94143. Received March 21, 2000

Two new spin-labeled photoreactive nonnucleoside ATP analogues, 1-(4-azido-2-nitrophenyl)amino-3-(1-oxyl-2,2,5,5-tetramethylpyrrolidinyl-3-carbamido)-2-propyl triphosphate (SL-NANTP) and 2-(4-azido-2-nitrophenyl)amino-2,2-(1-oxyl-2,2,6,6-tetramethyl-4-piperidylidene)di(oxymethylene) ethyl triphosphate (SSL-NANTP), were synthesized and characterized. This study aims to develop a second generation of NANTP-based analogues containing immobile spin labels that can be used to monitor conformational changes in myosin during the contractile cycle of muscle. Previous studies have shown that both a photoaffinity nonnucleoside ATP analogue, 2-[(4-azido-2-nitrophenyl)amino] ethyl triphosphate (NANTP) [Nakamaye et al. (1985) *Biochemistry 24*, 5226−5235], and a photoaffinity ATP analogue, 3′(2′)-*O*-4-[4-oxo-(4-amino-2,2,6,6-tetramethyl-piperidino-1-oxyl)-4-benzoyl] benzoyl adenosine 5′-triphosphate (SL-Bz_2ATP) [Wang et al. (1999) *J. Muscle Res. Cell Motil. 20*, 743−753], behave like ATP in their interactions with myosin. Remarkably, photolabeled myosin recovers all of its normal enzymatic properties after treatment with actin in the presence of MgATP [Luo et al. (1995) *Biochemistry 34*, 1978−1987]. For SL-NANTP, the spin label moiety is attached to NANTP via an aminomethyl side chain. In SSL-NANTP, attachment is via a restricted spiro ring. The two new probes interact with myosin subfragment-1 (S1) in a manner analogous to ATP, and after photoincorporation, labeled S1 recovers full activity after treatment with actin and MgATP. The electron paramagnetic resonance (EPR) spectrum resulting from S1 photolabeled with SL-NANTP shows a very high degree of probe mobility. However, the EPR spectrum of S1 photolabeled with SSL-NANTP shows that the probe is highly immobilized with respect to S1, constrained to move within a cone of angle 52° (full-width, half-max). Unlike the parent, NANTP, which photolabels on the 23 kDa tryptic fragment of S1, SSL-NANTP photolabels on the 20 kDa fragment. Its highly immobile nature means that it is potentially a useful reporter group to monitor cross-bridge motion in muscle fibers.

INTRODUCTION

Electron paramagnetic resonance (EPR)[1] has been a frequently employed method to monitor possible conformational changes of myosin and actin that may occur during active contraction of muscle (reviewed in refs *1* and *2*). The most commonly used target for EPR spin probes is the reactive thiol on the heavy chain of myosin termed SH1 (Cys-707 in rabbit skeletal myosin) (*3*−*7*). SH1 on skeletal myosin can be modified with *N*-(1-oxyl-2,2,6,6-tetramethyl-4-piperidinyl)iodoacetamide (IASL) to provide an immobile probe that can monitor changes in the orientation of myosin heads (*8*). A significant disadvantage to this approach is that chemical modification of SH1 changes the properties of myosin (*8*, *9*) and potentially affects the active tension of muscle fibers (*5*, *10*). Moreover, SH1 is known from the crystal structure of myosin subfragment 1 (S1) to lie in a region between the globular motor domain and the light chain binding domain (*11*). Recently, it was reported that a large and distinct rotation of the myosin light chain domain occurs upon muscle contraction when Cys-108 of the regulatory light chain (RLC) was labeled with a cysteine-specific spin probe, 3-(5-fluoro-2,4-dinitroanilino)-2,2,5,5-tetramethyl-1-pyrrolidinyloxy (*12*). This indicates that movement of the tail portion of myosin heads is important in force generation. Similar probes to monitor possible

* To whom correspondence should be addressed at the Department of Chemistry. E-mail: yount@wsu.edu. Phone: (509) 335-3442. Fax: (509) 335-9688.

[†] School of Molecular Biosciences.

[‡] Department of Biochemistry and Biophysics & CVRI.

[§] Department of Pure and Applied Mathematics.

[1] Abbreviations: EPR, electron paramagnetic resonance; IASL, *N*-(1-oxyl-2,2,6,6-tetramethyl-4-piperidinyl)iodoacetamide; RLC, regulatory light chain; FDNASL, 3-(5-fluoro-2,4-dinitroanilino)-2,2,5,5-tetramethyl-1-pyrrolidinyloxy; S1, myosin subfragment 1; ATP, adenosine triphosphate; Bz_2ATP, 3′-*O*-(4-benzoyl)benzoyl-ATP; SL-Bz_2ATP, 3′(2′)-0-4-[4-oxo-(4-amino-2,2,6,6-tetramethyl-piperidino-1-oxyl)-4-benzoyl] benzoyl adenosine 5′-triphosphate; 4-amino-TEMPO, 4-amino-2,2,6,6-tetramethyl-l-piperidinyloxy; NANTP, 2-[(4-azido-2-nitrophenyl)amino]ethyl triphosphate; SL-NANTP, 1-(4-azido-2-nitrophenyl)-amino-3-(1-oxyl-2,2,5,5-tetramethylpyrrolidinyl-3-carbamido)-2-propyl triphosphate; SSL-NANTP, 2-(4-azido-2-nitrophenyl)-amino-2,2-(1-oxyl-2,2,6,6-tetramethyl-4-piperidylidene)di(oxymethylene) ethyl triphosphate; SPC, salicylphosphorochloridite; Tris base, 2-amino-2-(hydroxymethyl)-1,3-propanediol; MALDI-MS, matrix-assisted laser desorption/ionization mass spectroscopy; SL-ester, 1-oxyl-2,2,5,5-tetramethylpyrrolidinyl-3-carboxylic acid *N*-hydroxysuccinimide ester; TEAB, triethylammonium bicarbonate; AcSSL-NANTP, 2-(4-azido-2-nitrophenyl)amino-2,2-(acetoxy-2,2,6,6-tetramethyl-4-piperidylidene)di(oxymethylene) ethyl triphosphate; SL-ATP, 2′, 3′-*O*-(1-oxyl-2, 2,6,6-tetramethyl-4-piperidylidene)adenosine 5′-triphosphate.

10.1021/bc000032b CCC: $19.00 © 2000 American Chemical Society
Published on Web 08/31/2000

movement of the motor domain have depended on spin-labeled ATP analogues (*13*−*15*). The disadvantage to this approach is that a large and sharp spectral signal arises from unbound ATP analogue and overlaps with the desired spectral components from the probe bound at the active site of myosin. This problem potentially can be overcome by use of spin-labeled ATP photoaffinity analogues. As reported previously, it is possible to specifically photolabel rabbit skeletal myosin at Ser-324 with a photoreactive ATP analogue, Bz_2ATP (*16*) and then reactivate the enzyme by treatment with actin and MgATP (*17*). This approach then when combined with a spin label attached to the photoreactive ATP analogue means it should be possible to introduce a site specific label at the active site. As a first step, we have synthesized and studied the spin-labeled photoaffinity ATP analogue, SL-Bz_2ATP (*18*). A photoreactive p,p′-dicarboxybenzophenone moiety is attached to the 2′(3′) hydroxyls of ATP via an ester linkage, and the spin label 4-amino-TEMPO is amidated to the second carboxyl group. SL-Bz_2ATP is a substrate for S1 and myosin in muscle fibers. It can be covalently incorporated at the active site with high specificity and yield, and the photolabeled myosin retains characteristic enzymatic properties. However, the EPR spectrum of SL-Bz_2ATP photolabeled muscle fibers showed that this probe is too mobile to provide orientational information about myosin heads during contraction (*18*).

A second synthetic approach utilizing the smaller nonnucleoside ATP analogue based on NANTP (*19*) was initiated. NANTP is a photoreactive ATP analogue, 2-[(4-azido-2-nitrophenyl)amino]ethyl triphosphate that is a substrate for myosin, Fl ATPase and kinesin (Pate et al., unpublished data). It behaves like ATP when it reacts with myosin (*19*) and supports active tension and shortening of muscle fibers (*20*). Interestingly, it specifically photolabels Trp-130 in the 23 kDa of rabbit skeletal S1 (*21*). After treatment, with actin to weaken analogue binding, NANDP-labeled S1 has normal ATPase activity in the presence of MgATP (*17*).

With these considerations in mind, we set out to design and synthesize new analogues of NANTP containing a nitroxide spin probe in addition to its nitrophenyl azide photoaffinity group. The synthesis and characterization of 1-(4-azido-2-nitrophenyl)amino-3-(1-oxyl-2, 2,5,5-tetramethylpyrrolidinyl-3-carbamido)-2-propyl triphosphate (SL-NANTP) and 2-(4-azido-2-nitrophenyl)amino-2,2-(1-oxyl-2,2,6,6-tetramethyl-4-piperidylidene)di(oxymethylene) ethyl triphosphate (SSL-NANTP) are described here. These two new nonnucleoside ATP analogues are substrates for myosin, and the respective NANDP products are stably trapped at the active site by the phosphate analogues AlF_4^- or vanadate. While the EPR spectrum of photoincorporated SL-NANDP showed the probe to be too mobile to act as a reporter group, comparable labeling of S1 with SSL-NANDP gives a highly immobile spectrum, suitable to monitor conformational changes in myosin heads. In addition, SSL-NANDP was found to photolabel the carboxyl terminal 20 kDa tryptic fragment of S1 rather than the 23 kDa amino terminal fragment labeled by NANDP (*21*), showing that both of these major tryptic fragments, 23 and 20 kDa, function to make up part of the nucleotide binding site of myosin. This use of photoreactive spin-labeled substrates then represents a second method to do site-specific spin labeling that potentially can be used to report myosin head movement even in complex systems such as glycerinated muscle fibers.

MATERIALS AND METHODS

Microanalyses were carried out by Desert Analytics (Tucson, AZ) with a Perkin-Elmer 240C Elemental Analyzer. UV spectra were recorded on a Varian 2200 spectrometer. ^1H NMR spectra were recorded on a Bruker AMX 300 and referenced to HOD (4.70 ppm) or TMS (0.0 ppm). ^{31}P NMR spectra were obtained on a Varian VXR-500 spectrometer by using 85% phosphoric acid as an external standard. EPR spectra of synthesized compounds were obtained on a Varian E-3 spectrometer using an ER 3200 cavity. Low-resolution mass spectra of the compounds without phosphate were recorded on a 7070 EHF VG analytical mass spectrometer. Low-resolution mass spectra of the compounds with phosphate were recorded on a matrix-assisted laser desorption/ionization mass spectrometer (MALDI) from PerSeptive Biosystems. High-resolution mass spectra of the final probes with phosphate were obtained at the Mass Spectrometry Center (University of Washington, Seattle, WA) on a PE Biosystems (Foster City, CA) Mariner electrospray-TOF run in negative ion mode with a mobile phase of 1:1 CH_3CN/H_2O. Thin-layer chromatographic analyses (TLC) were done on aluminum backed silica gel 60 F_{254} thin-layer chromatography plates (EM Industries, Inc.) using solvent A [isobutyric acid/H_2O/concentrated NH_4OH (66:33:1)] or as described. Analyses of total phosphate and acid-labile phosphate were done as described previously (*22*). Flash chromatography used TLC silica gel (Aldrich, average particle size = 2−25 gm) in a 4.2 (w) × 5.2 (h) cm sintered glass funnel.

HPLC analysis was performed on a Spherisorb C18 column (100 × 4.6 mm). Eluant A, 100 mM triethylammonium acetate, pH 6.2; eluant B, 100 mM triethylammonium acetate, pH 6.2, in 90% acetonitrile; gradient 0 to 50% over 50 min at a flow rate of 1 mL/min. Capillary electrophoresis (CE) was performed on a Pace 5500 (Beckman) using a 50 cm × 75 μm uncoated capillary. Buffer: 20 mM sodium phosphate, pH 7.5; 20 kV, normal polarity; 20 °C; 215 nm.

4-Oxo-TEMPO, chymotrypsin, and Li_3ADP were from Sigma Chemical Co.; 4-fluoro-3-nitrophenyl azide was synthesized from 4-fluoro-3-nitroaniline (Aldrich) as described by Guillory and Jeng (*23*). Other reagents not from Aldrich were BCA protein assay reagents (Pierce); sodium orthovanadate and Tris base (Fischer); Ultima-gold scintillation Fluid (Packard); [^{32}P]phosphoric acid (NEN). The boiling point of the petroleum ether used was 35−60 °C.

Bis(tri-*n*-butylammonium) pyrophosphate was prepared as described by Moffatt (*24*) as follows: the solution of tetrasodium pyrophosphate decahydrate (4.46 g, 10 mmol) in cold water (100 mL) was applied to Dowex 50WX8 in the H^+-form. This column was eluted with water at 4 °C. The fractions with pH below 5 (pH paper) were pooled (approximately 200 mL) and added into a vigorously stirred solution of tributylamine (3.70 g, 20 mmol) in ethanol (40 mL) in an ice bath. The solvents were removed by rotary evaporation and then coevaporated twice with ethanol (20−30 mL each time) at 30 °C. The last traces of water/ethanol were removed by coevaporating twice with anhydrous dimethylformamide (DMF) dried over molecular sieves. The residue was dissolved in DMF (20 mL) to form a light yellowish solution which was stored in a brown bottle under argon at −20 °C until used.

Myosin subfragment 1 (S1) (115 000 g/mol) was prepared by a modification of the method of Okamoto and Sekine (*25*) as previously described (*26*) and stored in 50

mM Tris, 100 mM KCI, pH 8.0, at 4 °C (S1 buffer). F-actin was purified from rabbit skeletal muscle as described (*27*).

Analytical Procedures. Protein concentrations were determined by the BCA protein assay or Coomassie Blue (Pierce) using unmodified S1 as the standard as previously described (*28*); $\epsilon_{280}^{1\%} = 7.5\ cm^{-1}$ (*29*). ATPase assays were performed as described previously (*30*), except that release of inorganic phosphate was measured at 2 and 8 min after the addition of S1 to the assay mixture.

1-Oxyl-2,2,5,5-tetramethylpyrrolidinyl-3-carboxylic acid N-hydroxysuccinimide ester (SL-ester). SL-ester was synthesized by the general procedures of Hoffman et al. (*31*). 1-Oxyl-2, 2,5,5-tetramethylpyrrolidinyl-3-carboxylic acid (3-carboxy-proxyl) (0.53 g, 2.85 mmol) and *N*-hydroxysuccinimide (0.331 g, 2.88 mmol) were dissolved in the mixed solvent of ethyl acetate (10 mL) and DMF (3 mL) and cooled in an ice bath. A solution of *N*,*N*′-dicyclohexylcarbodiimide (0.595 g, 2.89 mmol) in ethyl acetate (4 mL) was added dropwise with stirring. After 2 h, the reaction mixture was taken out of the ice bath and stirred overnight at room temperature. Solvents were removed by rotary evaporation at 30 °C and the residue was fractionated by reduced pressure flash column chromatography using the solvents ethyl acetate/petroleum ether (1:3, 1:2, and then 1:1, v/v) as eluents. A light yellowish solid (0.63 g) was obtained from the eluent of ethyl acetate/petroleum ether (1:1, v/v). TLC: one spot, $R_f = 0.42$ (ethyl acetate/petroleum ether, 1:1, v/v). Yield: 78%. Melting point (mp): 185−186 °C. Electron ionization mass spectroscopic (EI-MS) analysis *m/e* (M^+) found 283 (calcd, $C_{13}H_{19}O_5N_2$, 283). The EPR spectrum of the pure solid sample was recorded at 9.46 GHz and showed a typical nitroxyl radical spectrum with a singlet centered at 3381.0 G.

1-Amino-3-(4-azido-2-nitrophenyl)amino-2-propanol (1). 1,3-diamino-2-propanol (3.0 g, 33.34 mmol) was dissolved in 100 mL of 80% DMF/20% H_2O and cooled in an ice bath. A solution of 4-fluoro-3-nitrophenyl azide (1.82 g, 10 mmol) in DMF (25 mL) was added dropwise with stirring in a period of 20−30 min. A deep-red solid was precipitated from the solution. After 0.5 h, the reaction mixture was taken out of the ice bath and stirred overnight at room temperature. The deep-red solid was harvested by filtration and washed several times with methanol (10 mL each time). TLC of the solid product in solvent A showed one spot ($R_f = 0.58$). The filtrate was concentrated to dryness by rotary evaporation at 30 °C, and the residue recrystalized from methanol to produce the second portion of pure product **1**. Product: 2.02 g, mp 81−82 °C. Yield 80%. EI-MS *m/e* (M^+) found 252 (calcd, $C_9H_{12}O_3N_6$, 252). ^{1}H NMR (CD_3COCD_3): δ 1.17−1.27 (br, 2 H, NH_2), 2.74 (br s, 1 H, OH), 2.90−3.25 (m, 2 H, CH_2), 3.34−3.52 (m, 2 H, CH_2), 4.10−4.13 (m, 1 H, CH), 7.13−7.25 (m, 2 H, phenyl H), 7.70 (d, 1 H, phenyl H), 8.10 (br s, 1 H, NH). Anal. ($C_9H_{12}N_6O_3$) C, H, N.

1-(4-Azido-2-nitrophenyl)amino-3-(1-oxyl-2,2,5,5-tetramethylpyrrolidinyl-3-carbamido)-2-propanol (2). To a solution of 1-amino-3-(4-azido-2-nitrophenyl)-amino-2-propanol (0.504 g, 2 mmol) in DMF (20 mL) was added dropwise SL-ester (0.566 g, 2 mmol) dissolved in 10 mL of ethyl acetate through a dropping funnel with a pressure-equalization arm at room temperature. After stirring overnight, the solvents were removed by rotary evaporation at 30 °C, and the residue isolated by reduced pressure flash column chromatography using acetone/petroleum ether (1:3 and then 1:2, v/v) as eluents. Product: deep-red amorphous solid, 0.70 g, mp 137−138 °C. Yield: 83%. TLC: one spot, $R_f = 0.46$ (acetone/petroleum ether, 1:2, v/v). Chemical ionization mass spectroscopic analysis (CI-MS) *m/e* (M^+) found 420 (calcd, $C_{18}H_{26}O_5N_7$, 420). The EPR analysis of the pure solid sample was performed at a frequency of 9.46 GHz and showed a typical nitroxide spectrum with a singlet centered at 3381.0 G. The compound was further characterized by reduction to the hydroxylamine as described below. Anal. ($C_{18}H_{26}N_7O_5$) C, H, N.

To obtain ^{1}H NMR spectrum, the nitroxy group of compound 2 was reduced to the *N*-hydroxyl derivative as described (*32*). To a solution of compound **2** (0.1 g, 0.24 mmol) in chloroform (1 mL) 2 mL of 0.2 M phenylhydrazine in chloroform was added. This mixture was stirred for 1 h and then the solvent was removed. The residue was purified by flash chromatography using acetone/petroleum ether (1:3 and then 1:2, v/v) as eluents. Product: deep-red solid, 50 mg. TLC: one spot, $R_f = 0.46$. ^{1}H NMR ($CDCl_3$): δ 1.12 (s, 3 H, CH_3), 1.18 (s, 3 H, CH_3), 1.22 (s, 6 H, CH_3), 1.74−1.78 (d, 2H, CCH_2C), 2.01−2.08 (t, 1 H, CHCO), 2.70 (br s, 1 H, OH), 2.90−3.10 (m, 2 H, CH_2), 3.36−3.50 (m, 2 H, CH_2), 4.10−4.13 (m, 1 H, CH−O), 7.10−7.21 (m, 2 H, phenyl H), 7.65 (d, 1 H, phenyl H), 8.10 (br s, 1 H, NH). CI-MS *m/e* (M^+) found 421 (calcd, $C_{18}H_{27}O_5N_7$, 421).

1-(4-Azido-2-nitrophenyl)amino-3-(1-oxyl-2, 2, 5, 5-tetramethylpyrrolidinyl-3-carbamido)-2-propyl triphosphate (SL-NANTP). SL-NANTP was synthesized according to the procedures of Ludwig and Eckstein (*33*−*35*) by which nucleoside triphosphates were synthesized. Compound **2** (0.39 g, 0.93 mmol) was dissolved in anhydrous dioxane/pyridine (8 mL, 3/1, v/v) in a rubber septum capped vessel under argon and cooled in an ice bath. A freshly prepared solution of SPC (0.207 g, 1 mmol) in anhydrous dioxane (2 mL) was injected through the septum and the resulting solution vigorously stirred for 10 min in an ice bath and another 10 min at room temperature. A solution of 0.5 M tetra(tri-*n*-butylammonium) pyrophosphate in anhydrous DMF (4 mL, 2 mmol) was injected into the reaction system cooled in an ice bath. After stirring for 10 min, a solution of 1% iodine in pyridine/water (98/2, v/v) (20 mL, 1.6 mmol) was added to oxidize phosphite to phosphate. After stirring for an additional 10 min in an ice bath and then for 30 min at room temperature, the excess iodine was destroyed by addition of 6 mL of 5% aqueous solution of sodium bisulfite. The reaction mixture was concentrated to dryness by rotary evaporation at 30 °C. The residue was dissolved in H_2O (20 mL), and the solution cooled in an ice bath, and a concentrated ammonium hydroxide solution (40 mL) was added to hydrolyze the cyclic triphosphate. After 2 h, the reaction mixture was taken out of the ice bath and stored overnight at 4 °C. Argon was bubbled for 0.5 h to remove ammonia. The solution was evaporated to dryness by rotary evaporation at 30 °C, and the residue was dissolved in H_2O (30 mL) (pH 6.95). One-half of this solution was applied to DEAE Sephadex A-25 (Aldrich, 40−120 gm) in a column (3.2 × 50 cm) and eluted with a linear gradient of 0.3 to 0.6 M triethylammonium bicarbonate (TEAB) at 4 °C (flow rate = 3.5 mL/min, 4.8 min/fraction, total elution time = 24 h). Pyrophosphate was eluted in fractions 95−141, and the deep-red product in fractions 149−173. A total of two runs of the DEAE Sephadex A-25 column were performed, and the fractions containing product SL-NANTP as determined by TLC (solvent A) were pooled. Water and triethylammonium bicarbonate were removed by rotary evaporation at 30 °C. The product showed a single spot on TLC with solvent A ($R_f = 0.48$). HPLC analysis

(>97% pure): t_R = 27.8 min. CE analysis (>97% pure): t_R = 9.9 min. Yield: 0.20 mmol, 21.6% (based on its molar extinction coefficient of 4680 M^{-1} cm^{-1} at 473 nm).

Phosphate assays showed that the ratio of total phosphate to acid labile phosphate was 1.49; theory, 1.50. UV spectrum (water, pH 7.20): λ_{max} at 261 and 473 nm. Molar extinction coefficients calculated from total phosphate assays were 24 360 ± 440 M^{-1} cm^{-1} at 261 nm and 4680 ± 80 M^{-1} cm^{-1} at 473 nm. High-resolution negative electrospray MS *m/e* $(M - H)^-$ found 659.0911 (calcd, M − H, $C_{18}H_{28}O_{14}N_7P_3$, 659.0907). The EPR spectrum of the solution of SL-NANTP dissolved in methanol recorded at 9.46 GHz showed a typical nitroxide spectrum with a triplet centered at 3378.3 G and a hyperfine splitting of 17.5 G.

To obtain NMR spectra free of triethylamine, SL-NANTP was precipitated as the sodium salt by addition of NaI acetone solution (1 M) and washed several times with cold acetone as described previously (*21*). A portion of SL-NANTP (0.2 mL, 23 mM, and pH 7.0) was reduced to the hydroxyamine derivative by addition of 50 μL of 100 mM ascorbic acid (pH 7.0) (*13*). Negative MALDI-MS using α-cyano-4-hydroxy-cinnamic acid as matrix found *m/e* $(M - H)^-$ 660.09 (calcd, $C_{18}H_{29}O_{14}N_7P_3$, 660.10) (*36*). ^1H NMR (D_2O): δ 1.26 (s, 3 H, CH_3), 1.39 (s, 3 H, CH_3), 1.42 (s, 3 H, CH_3), 1.43 (s, 3 H, CH_3), 1.82−1.86 (d, 2 H, CCH_2C), 2.10−2.21 (m, 1 H, CHCO), 2.96−3.18 (m, 2 H, CH_2), 3.59−3.72 (m, 2 H, CH_2), 4.53−4.57 (m, 1 H, CH−O), 7.20−7.30 (m, 2 H, phenyl H), 7.82 (d, 1 H, phenyl H). ^{31}P NMR (D_2O): −9.70 (d, γ−P), −11.25 (d, α−P) and − 22.34 (t, β−P).

2-(Hydroxymethyl)-2-(4-azido-2-nitrophenyl)amino-1,3-propanediol (3). To a solution of 4-fluoro-3-nitrophenyl azide (7.50 g, 41.0 mmol) dissolved in 26 mL of 80% DMF/20% H_2O, 2-amino-2-(hydroxymethyl)-1,3-propanediol (Tris base) (4.84 g, 20.0 mmol) was added. After stirring for 8 days, the solvents were removed with rotary evaporation at room temperature. The residue was isolated by flash chromatography using acetone/petroleum ether (1:2 and then 1:1). Product: 0.75 g, orange solid, mp 153−154 °C. Yield 26.5%. TLC showed one spot, R_f = 0.32 (acetone/petroleum ether, 1:1). ^1H NMR ($CDCl_3$): δ 1.48 (br s, 3 H, OH), 3.86 (s, 6 H, CH_2), 6.90−7.28 (m, 2 H, phenyl), 7.70 (d, 1 H, phenyl H), 8.30(s, 1 H, NH). EI-MS *m/e* (M^+) found 283 (calcd, $C_{10}H_{13}O_5N_5$, 283). Anal. ($C_{10}H_{13}N_5O_5$) C, H, N.

2-(4-Azido-2-nitrophenyl)amino-2,2-(1-acetoxy-2,2,6,6-tetramethyl-4-piperidylidene)di(oxymethylene) ethanol (5). 1-Acetoxy-4-methoxy-2,2,6,6-tetramethyl-1,2,5,6-tetrahydropyridine **(4)** was prepared according to the method of Alessi et al. (*32*). A total of 2.6 g (11.45 mmol) of compound **4** was added into a solution of compound **3** (0.3 g, 1.06 mmol) in tetrahydrofuran (THF) (5 mL), followed by a catalytic amount of *p*-toluenesulfonic acid monohydrate. After the reaction solution was stirred for 6 days, THF was removed by rotary evaporation at room temperature. The residue was isolated by flash chromatography using ethyl acetate/petroleum ether (1:3, 1:2, and then 1:1) as eluents. Product: 0.16 g, orange solid, mp 135−136 °C. Yield 31.6%. TLC: one spot at R_f = 0.37 (ethyl acetate/petroleum ether, 1:1). ^1H NMR ($CDC1_3$): δ 1.01 (s, 6 H, CH_3), 1.19 (s, 3 H, CH_3), 1.21 (s, 3 H, CH_3), 1.50 (br s, 1 H, OH), 1.77−1.86 (t, 2 H, CH_2), 1.98−2.06 (m, 5 H, CH_2 and CH_3CO), 3.76 (m, 6 H, CH_2), 7.0−7.39 (m, 2 H, phenyl H), 7.79 (d, 1 H, phenyl H), 8.34 (s, 1 H, NH). CI-MS *m/e* $(M + 1)^+$ found 479 (calcd, $C_{21}H_{30}O_7N_6$, 478). Anal. ($C_{21}H_{30}N_7O_6$) C, H, N.

2-(4-Azido-2-nitrophenyl)amino-2,2-(1-acetoxy-2,2,6,6-tetramethyl-4-piperidylidene)di(oxymethylene) Ethyl Triphosphate (AcSSL-NANTP). The phosphorylation of the spiroketal intermediate **5** and the subsequent displacement reaction were done as described previously (*19*, *20*). Phosphorus oxychloride (0.15 mL, 1.6 mmol) was pipetted into a solution of N-acetoxy spiro ketal **5** (0.19 g, 0.4 mmol) in trimethyl phosphate (3 mL) in a glovebag under argon at room temperature. The reaction flask was sealed with a septum, an argon balloon was connected to the reaction flask to exclude moisture, and the reaction flask was immersed in an ice-bath immediately. After 8 h with stirring, the reaction solution was injected into a solution of bis(tri-*n*-butylammonium) pyrophosphate in DMF (6.4 mL, 3.2 mmol) and tri-*n*-butylamine (1.52 mL, 6.4 mmol) under argon and precooled in an ice bath. After 10 min, 1 M TEAB (25 mL) was added, and this mixture was left overnight at 4 °C. The solvents were removed with rotary evaporation at 30 °C. TEAB was removed by coevaporating with methanol. The residue was dissolved in water (30 mL), and this solution applied to DEAE Sephadex A-25 (Aldrich, 40−120 gm) column (3.2 cm × 50 cm). The product was eluted with a linear gradient of 0.3 to 0.6 M TEAB (5 L total volume, pH 7.60) at 4 °C with a flow rate of 3.5 mL/min, and 16.8 mL fractions were collected. The major peak, AcSSL-NANTP, was eluted at 0.46 M TEAB buffer. The product fractions were pooled and taken to dryness by rotary evaporation at 30 °C. The residue was coevaporated three times with methanol to remove TEAB. Product: deep red solid, 0.2 mmol (based on the molar extinction coefficient ϵ_M of 4100 M^{-1} cm^{-1} at 464 nm). Yield: 50.0%. TLC: one spot at R_f = 0.32 (solvent A). HPLC analysis (>97% pure): t_R = 31.6 min. CE analysis (>97% pure): t_R = 8.4 min. Mass spectroscopic analysis (negative MALDI) found *m/e* $(M - H)^-$ 717.42 (calcd, $C_{2l}H_{32}O_{16}N_6P_3$, 717.43) (*36*). ^1H NMR(D_2O): δ 1.21 (s, 6 H, CH_3), 1.26 (s, 3 H, CH_3), 1.39 (s, 3 H, CH_3), 1.66−1.72 (t, 2 H, CH_2), 2.01−2.12 (m, 5 H, CH_2 and CH_3CO), 3.64 (m, 6 H, CH_2), 7.02−7.30 (m, 2 H, phenyl H), 7.80 (d, 1 H, phenyl H). ^{31}P NMR (D_2O): −10.20 (d, γ−p), −11.10 (d, α-p), −22.81 (t, β-p).

2-(4-Azido-2-nitrophenyl)amino-2,2-(1-oxyl-2,2,6,6-tetramethyl-4-piperidylidene)di(oxymethylene) ethyl triphosphate (SSL-NANTP). SSL-NANTP was prepared from AcSSL-NANTP by a method modified from Alessi et al. (*14*). A solution of potassium hydroxide (0.55 g) in methanol (10 mL) was added into a reaction flask containing AcSSL-NANTP (164 μmol), methanol (15 mL), and water (15 mL). After the reaction mixture was saturated with oxygen, it was connected to an oxygen balloon and vigorously stirred for 8 days. A few drops of glacial acetic acid were added to bring the pH to 7.0. This solution was applied to a DEAE Sephadex, A-25 (Aldrich, 40−120 μM) column (3.2 cm × 50 cm) and eluted with a linear gradient of 0.3 to 0.6 M TEAB (5 L total volume, pH 7.60) at 4 °C and a flow rate of 3.5 mL/min. The red fractions containing the product were pooled and concentrated to dryness with rotary evaporation at 30 °C. The last traces of TEAB were removed by coevaporating three times with methanol (50 mL each). The yield was 156 μmol (95%) (based on ϵ_M 4100 M^{-1} cm^{-1} at 464 nm). TLC showed one spot at R_f = 0.32 (solvent A). HPLC analysis (>97% pure): t_R = 32.3 min. CE analysis (>97% pure): t_R = 10.6 min.

High-resolution mass spectroscopy (negative electrospray) *m/e* $(M - H)^-$ found 674.0911 (calcd, $C_{19}H_{29}O_{15}N_6P_3$, 674.0904). Phosphate assays showed that the ratio of total phosphate to acid labile phosphate was 1.47; theory, 1.50. UV (water, pH 7.0): λ_{max} at 464 and 262 nm. Molar

extinction coefficients calculated from the total phosphate assay were 4100 ± 30 M^{-1} cm^{-1} at 464 nm and 25 480 ± 360 M^{-1} cm^{-1} at 262 nm. The EPR analysis of the solution of the product in methanol recorded at 9.45 GHz showed a typical nitroxide spectrum with a triplet centered at 3375 G and a hyperfine splitting of 16.0 G.

To obtain NMR spectra free of triethylamine, SSL-NANTP was converted to the sodium salt as described (*22*). A small portion of the solution of the product in water (2.3 μmol, pH 7.0) was reduced with a solution of sodium ascorbate in water (2.3 μmol, pH 7.30) and then dried with a speed vacuum. The residue was dissolved in D_2O for running ^{31}P NMR which showed three sets of peaks: −8.70 (d, γ−p), −10.80 (d, α−p), −22.24 (t, β−p). ^1H NMR (D_2O): δ 1.20 (s, 6 H, CH_3), 1.24 (s, 3 H, CH_3), 1.38 (s, 3 H, CH_3), 1.70−1.78 (t, 2 H, CH_2), 2.03−2.15 (m, 2 H, CH_2), 3.68 (m, 6 H, CH_2), 7.01−7.22 (m, 2 H, phenyl H), 7.82 (d, 1 H, phenyl H). Negative MALDI mass spectroscopic analysis found $(M - H)^-$ 675.12 (calcd, $C_{19}H_{30}O_{15}N_6P_3$, 675.10) (*36*).

Synthesis of 2-(4-Azido-2-nitrophenyl)amino-2,2-(1-oxyl-2,2,6,6-tetramethyl-4-piperidylidene)di(oxymethylene) ethyl [β-^{32}P]diphosphate ([^{32}P]SSL-NANDP). [^{32}P]SSL-NANDP was prepared by coupling of [^{32}P]phosphate to 2-(4-azido-2-nitrophenyl)amino-2,2-(1-oxyl-2,2,6,6-tetramethyl-4-piperidylidene)di(oxymethylene) ethyl monophosphate (SSL-NANMP) as described (*19*, *21*). Yield 76% (based on the molar extinction coefficient of 4100 M^{-1} cm^{-1} at 464 nm). Specific activity 63 000 cpm/nmol. After 5 months, a small amount of [^{32}P]-SSL-NANDP was reduced by sodium ascorbate to obtain NMR spectra. ^1H NMR (D_2O) δ 1.10 (s, 6 H, CH_3), 1.24 (s, 3 H, CH_3), 1.37(s, 3 H, CH_3), 1.69−1.75 (t, 2 H, CH_2), 2.04−2.12 (m, 2 H, CH_2), 3.68 (m, 6 H, CH_2), 7.02−7.20 (m, 2 H, phenyl H), 7.81 (d, 1 H, phenyl H). ^{31}P NMR (D_2O): −9.62 (d, β−P), −12.20 (d, α−P). Negative MALDI mass spectroscopic analysis found $(M - H)^-$ 594.10 (calcd, $C_{19}H_{28}O_{12}N_6P_2$, 594.12). SSL-NANMP was prepared by a similar method as for synthesis of SSL-NANTP, except that 1 N NaOH was added to pH 7.30 to hydrolyze the dichlorophospate to the monophosphate instead of addition of pyrophosphate. NMR analysis of SSL-NANMP reduced by sodium ascorbate: ^1H NMR (D_2O) δ 1.11 (s, 6 H, CH_3), 1.21 (s, 3 H, CH_3), 1.36(s, 3 H, CH_3), 1.68−1.76 (t, 2 H, CH_2), 2.01−2.12 (m, 2 H, CH_2), 3.67 (m, 6 H, CH_2), 7.03−7.23 (m, 2 H, phenyl H), 7.80 (d, 1 H, phenyl H). ^{31}P NMR (D_2O): 0.387 (s). Negative MALDI mass spectroscopic analysis found $(M - H)^-$ 514.12 (calcd, $C_{19}H_{27}O_9N_6P$, 514.16).

Vanadate Trapping and Photoincorporation of SSL-NANDP and SL-NANDP onto Rabbit Skeletal Myosin S1. For SSL-NANTP trapping, S1 (26.1 μM) was incubated with 2 mM $NiC1_2$, 0.1 mM [^{32}P]SSL-NANDP, and 1 mM sodium orthovanadate or an equivalent volume of S1 buffer (control) at 25 °C. After 40 min, EDTA (pH 8.0) and ATP were added to 20 and 5 mM, respectively, and the samples purified by Sephadex G-50 spin columns in S1 buffer (50 mM Tris, 100 mM KCI, pH 8.0 at 4 °C). The purified S1·Ni·[^{32}P]SSL-NANDP·Vi complex was irradiated at 0 °C for 16 min using a Hanovia 450 W medium-pressure Hg lamp. To avoid photodamage and nonspecific labeling, a Pyrex filter and a Schott 408 filter were used to remove most of the radiation below 400 nm. To determine the amount of trapping, samples of the complex and the control before irradiation were counted by liquid scintillation and the protein concentrations were measured by use of Coomassie blue. To determine the amount of covalent incorporation, known samples of the complex after irradiation were precipitated by addition of perchloric acid to 5%, centrifuged and the pellets were analyzed for radioactivity.

For SL-NANTP trapping, S1 (34 μM) was incubated with 2 mM $MgCl_2$ and 0.2 mM SL-NANTP in S1 buffer for 10 min at 25 °C followed by addition of 5 mM NaF and 1 mM $AlCl_3$ or an equivalent volume of S1 buffer (control). After 40 min at 25 °C, EDTA and pyrophosphate were added to 20 and 1.8 mM, respectively, and the samples purified by Sephadex G-50 spin columns in S1 buffer (for ATPase assays) or S1 buffer with NaCl replacing the KCl. The purified S1·MgSL·NANDP·AlF_4 complex in NaCl−S1 buffer was irradiated at 0 °C for 4 min using a Hanovia 450 W medium-pressure Hg lamp. To determine the amount of trapping and covalent incorporation, samples of the complex before and after irradiation were precipitated by addition of cold perchloric acid to 5% and microcentrifuged, and the OD_{261} of the neutralized supernatent was measured. The extinction coefficient at 261 nm for the photolyzed SL-NANDP was determined by measuring the OD_{261} of a sample of SL-NANDP followed by irradiation of the sample and remeasuring the OD_{261} and was determined to be 11 880 M^{-1} cm^{-1}.

SDS−PAGE Analysis. Myosin S1 samples were analyzed by SDS−PAGE on 18 × 20 cm 12% gels according to the procedure of Laemmli (*37*). Protein bands were visualized by staining with a solution of Coomassie blue (1.61 g of Coomassie blue in 1 L of methanol, 1 L of water, and 200 mL of glacial acetic acid). Gel strips containing the bands of interest were excised and placed in 20 mL glass vials. Ultimagold (Packard) (10 mL) was added, and the radioactivity was determined.

EPR Spectroscopy. After irradiation in the presence of SL-NANTP or SSL-NANTP and Pi analogue, the S1 solution is a mixture of covalently photolabeled S1, unmodified S1, and trapped but unmodified S1. The spectrum of covalently bound diphosphate analogue is desired. Irradiated samples were treated with actin at low ionic strength to release trapped Pi analogue and noncovalently bound SSL-NANDP or SL-NANDP before adding excess ATP to dissociate S1 and photolabeled S1 from the actin as previously described by Luo et al. (*17*). The samples were then centrifuged, and the supernatant was purified by gel filtration (*17*). The protein solution was dialyzed into a buffer containing 0.12 M KOAc, 5 mM $Mg(OAc)_2$, 40 mM MOPS, 1 mM EGTA, pH 7.0, and then concentrated to 65 μM S1-SL-NANDP or S1-SSL-NANDP by centrifugation through a semipermeable membrane (Centricon, 30 kDa cutoff). A sample in a 50 μL glass capillary was placed in the center of a TE_{011} cavity.

Experiments were done at room temperature, 21−23 °C. EPR measurements were performed with an ER/200D EPR spectrometer from IBM Instruments, Inc. (Danbury, CT). First derivative, X-band spectra were recorded using 50 s, 125 G wide sweeps with the following instrument settings: microwave power, 25 mW; gain, 1.0×10^5−1.0×10^6; center field, 3478−3480 G; time constant, 200 ms; frequency, 9.3 GHz; modulation, 1 gauss at a frequency of 100 kHz. Each spectrum is the average of 25 distinct sweeps from an individual experimental preparation.

RESULTS AND DISCUSSION

Synthesis of SL-NANTP. The purpose of this study is to develop a series of second generation spin-labeled photoaffinity nonnucleoside ATP analogues based on NANTP. The plan is to photolabel the residues of myosin

Scheme 1: Synthesis of SL-NANTP

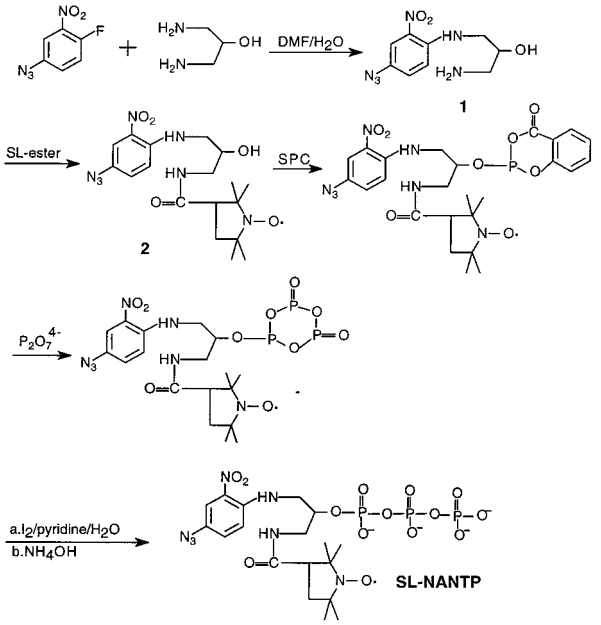

Scheme 2: Synthesis of SSL-NANTP

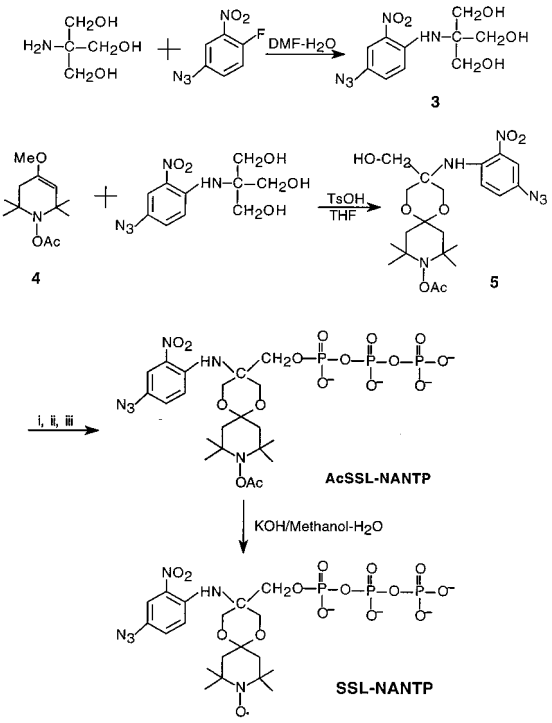

specifically near the active site so that motion of the head (or part of the head) can be monitored spectroscopically during the contraction process. The key step in the synthesis of SL-NANTP was phosphorylation of intermediate **2**. Phosphorus oxychloride has been used in the past as a phosphorylating reagent for primary alcohols to synthesize ATP analogues (*19*, *20*). Initially, we tried to use phosphorus oxychloride to phosphorylate the secondary alcohol of intermediate **2** without success, possibly because of steric hindrance. Salicylphosphorochloridite (SPC) has been previously employed as a phosphorylating reagent for the preparation of ATP analogues (*33*−*35*). This reagent is capable of undergoing three nucleophilic displacement reactions. We have exploited this multifunctionality in the synthesis of SL-NANTP. The sequence of the synthetic reactions is shown in Scheme 1. The synthesis proceeds via the phosphorylation of intermediate **2** by SPC. This is followed by displacement of the leaving group with pyrophosphate, oxidation of phosphite by iodine, and hydrolysis of the cyclic meta-triphosphate by concentrated ammonium hydroxide. The total yield from phosphorylation of intermediate **2** to the final product SL-NANTP was around 22%, which compares favorably with other syntheses that used phosphorus oxychloride.

The ^{31}P NMR and ^{1}H NMR spectra of SL-NANTP are very broad because of the presence of the nitroxide spin label. Reduction of the nitroxide of SL-NANTP with ascorbic acid yields the hydroxyamine derivative whose ^{31}P NMR and ^{1}H NMR spectra confirmed the predicted structure.

Synthesis of SSL-NANTP. The route used to synthesize SSL-NANTP, in which the free radical is attached to NANTP via a spiro ketal group, is shown in Scheme 2. The most important steps in the synthesis of SSL-NANTP were the syntheses of the triol intermediate **3** and *N*-acetoxy spiroketal intermediate **5**. Because Tris base is only soluble in water whereas 4-fluoro-3-nitrophenyl azide is not, a mixture of 80% DMF and 20% water was chosen as the reaction solvent. Tris base was still not completely soluble, which resulted in long reaction times (8 days) and relatively low yields (26%). Nevertheless, Tris base was chosen for several reasons. First, Tris base contains three hydroxyl groups and an amino group which are necessary to attach the spin label to NANTP via a spiroketal ring. Second, Tris base is the simplest compound suitable for our design, which makes the synthesized probe SSL-NANTP more likely to be a substrate for myosin. And third, Tris base is a convenient and cheap reagent. The *N*-acetoxy spiroketal intermediate **5** was synthesized by the reaction of the triol intermediate **3** and the enol ether spin label precursor **4** in the presence of the catalyst, *p*-toluenesulfonic acid monohydrate, by a procedure similar to that of Alessi et al. (*14*, *32*). Because the steric hindrance to the reaction of the two hydroxyl groups of the intermediate **3** with enol ether **4** is large, the reaction proceeded slowly. However, using the chemistry we have described, intermediate **5** could be prepared smoothly. The *N*-acetoxy triphosphate derivative, AcSSL-NANTP, was prepared by phosphorylation of the intermediate **5** with $POCl_3$ followed by the addition of tributylammonium pyrophosphate (*19*) or tributylammonium phosphate (*38*) to form the tri- and diphosphate products, respectively. In our experiments, the yield from the tributylammonium pyrophosphate reaction was much higher (50%) than that from tributylammonium phosphate (10%). To oxidize AcSSL-NANTP to the free radical probe SSL-NANTP, it was helpful to saturate the reaction solution with oxygen and to keep it in an oxygen atmosphere to accelerate the reaction. Alternatively, the final product SSL-NANTP was also prepared by oxidation of the intermediate **5** to the free radical nitroxide followed by phosphorylation with $POCl_3$ and reaction with tributylammonium pyrophosphate, but the yield was lower (36%).

SSL-NANTP and SL-NANTP Are Substrates for Myosin. It was first important to verify that SSL-NANTP and SL-NANTP bound to myosin in a manner similar to ATP. The hydrolysis studies of SSL-NANTP, SL-NANTP, and ATP by S1 are summarized in Table 1. S1 cleaved SSL-NANTP in the presence of Ca^{2+} and K^{+}/EDTA at the rate of 208% and 16% of that with ATP, respectively. The hydrolysis rates for SL-NANTP in the presence of Ca^{2+} and K^{+}/EDTA were 76% and 1.5% of that with ATP, respectively. In the presence of actin, V_{max}

Table 1. Reaction Rates for SSL-NANTP and SL-NANTP as substrates for S1[a]

assay conditions	ATP (μmol of Pi/ mg/min)	SSL-NANTP (μmol of Pi/ mg/min)	SL-NANTP (μmol of Pi/ mg/min)
K^+	5.39 ± 0.20	0.89 ± 0.13	0.08 ± 0.01
Ca^{2+}	1.18 ± 0.04	2.45 ± 0.07	0.90 ± 0.10
Mg^{2+}/actin	5.68 ± 0.14	2.83 ± 0.02	not determined

[a] S1 and actin-activated ATPase activities were determined from liberated Pi assayed using the methods of Wells and Yount (*42*) and White (*43*). Assays were measured at 25 °C with the following conditions. Ca^{2+}ATPase: 152 mM KC1, 15.2 mM $CaCl_2$, 152 mM Tris, 7.6 mM SSL-NANTP or SL-NANTP or ATP, 0.35 μM S1, pH 7.70. K^+/EDTA ATPase: 50 mM Tris, 5 mM EDTA, 0.6 M KC1, 5 mM SSL-NANTP or ATP, 0.35 μM S1, pH 7.50. Actin-activated Mg^{2+}ATPase: 10 mM Tris, 3 mM $MgCl_2$, 3 mM SSL-NANTP or SL-NANTP or ATP, 5.6 μM S1, pH 7.90, with 4.0−119 μM actin.

Table 2. Trapping and Incorporation of SSL-NANDP in S1

sample[a]	% ATPase[b]	% trapped SSL-NANDP/S1	% covalent SSL-NANDP/S1
control	98.0	2.5	
Vi/Ni^{2+} trapped	31.0	66.0	13.5

[a] The S1·Ni^{2+}·SSL-NANDP·Vi complex was prepared and irradiated as described as under Materials and Methods. [b] The NH_4^+-EDTA ATPase activity of the purified S1·Ni.SSL-NANDP·Vi complex and control sample were determined as previously described (*42*), except that the release of inorganic phosphate was measured after 2 and 8 min. These were then compared to standard S1.

Table 3. Trapping and Incorporation of SL-NANDP in S1

sample[a]	% ATPase[b]	% trapped SL-NANDP/S1	% covalent SL-NANDP/S1
control	101.0	4.4	
AlF_4 trapped	22.4	89.7	38.5

[a] The S1·Mg^{2+}·SL-NANDP·AlF_4 complex was prepared and irradiated as described as under Materials and Methods. [b] The NH_4^+-EDTA ATPase activity of the purified S1·Mg^{2+}·SL-NANDP·A1F_4 complex and control sample were determined as described in Table 2 and were then compared to standard S1.

for the MgSSL-NANTPase was 50% of MgATPase. These results show that both SSL-NANTP and SL-NANTP are substrates for S1 with properties similar to ATP.

Trapping and Covalent Photoincorporation of SSL-NANDP and SL-NANDP into S1. The specificity of labeling is an important consideration in the photoincorporation of ATP analogues in myosin. It has been shown that trapping of nucleotide analogues prior to irradiation is essential to obtain specific photolabeling of the active site of myosin (*25*, *26*, *19*). S1 was incubated with [^{32}P]SSL-NANDP and Vi as described in Methods and Materials, and untrapped SSL-NANDP and Vi were then removed by gel centrifugation columns. It was found that 66% of the sites were occupied. After photoirradiation and removal of unbound SSL-NANDP by actin treatment, S1 was covalently labeled at 13.5% of the sites (see Table 2). Here the Ni^{2+} acts to prevent vanadate-promoted photooxidation of myosin that occurs in the presence of Mg^{2+} (*26*). If S1 was treated with SL-NANTP, $MgCl_2$ and AlF_4^-, almost 90% of the active sites were trapped, and 38% of the active sites were subsequently photolabeled (See Table 3).

EPR Spectroscopy of Photoincorporated SL-NANTP and SSL-NANTP. Figure 1 shows EPR spectra obtained from S1 photolabeled with SL-NANDP (dashed line) and SSL-NANDP (solid line). The three sharp peaks (P2, P3, and the central large peak) in the SL-NANDP spectrum are indicative of a probe that is covalently attached to the protein. However, the probe is highly mobile with respect to the protein, undergoing rapid, nanosecond rotation. The low-field shoulder at P1 in the SL-NANDP spectrum does indicate a very small, more highly immobilized population of probes. This component is too small to be of use in orientational studies, however.

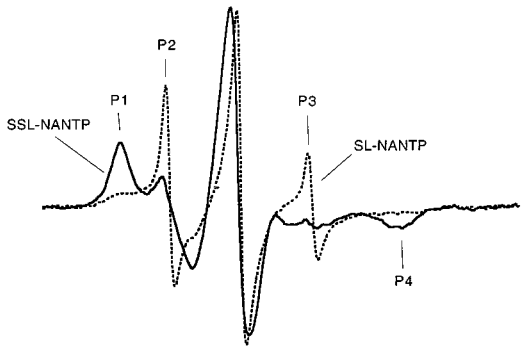

Figure 1. EPR spectra of SL-NANDP (dashed line) and SSL-NANDP (solid line) covalently attached to S1 in solution. The spectra are the average of 25 distinct, 125 mT wide sweeps.

The solid line in Figure 1 is the EPR spectrum obtained from S1-SSL-NANDP. The splitting between the low field peak, P1, and the high field dip, P4, is 65.5 ± 0.5 G (mean ± SEM, 4 obs) indicating a covalently attached probe that is highly immobilized with respect to S1. The analysis of Griffith and Jost (*39*) indicates the probe constrained to move within a cone of angle approximately 52° (full-width, half-max). The small superimposed peaks at P2 and P3 show an additional, small (<5%) highly mobile component. This probably is the result of a small degree of nonspecific labeling.

Our goal is to develop EPR photoaffinity probes for use in orientational studies of myosin. The high degree of mobility seen in the spectrum of S1-SL-NANDP makes this probe unusable for this purpose, and further characterization was not done. However, due to the high degree of immobilization of the S1-SSL-NANDP spectrum, it was of interest to localize SSL-NANDP on S1.

Localization of [^{32}P]SSL-NANDP on Myosin S1. The heavy chain of S1 can be partially digested with trypsin into three characteristic fragments, the NH_2-terminal 23-kDa fragment, the central 50-kDa fragment and the COOH-terminal 20-KDa fragment (*40*). Previously, Trp-130 on 23-kDa fragment of rabbit skeletal muscle myosin (*26*) and its equivalent amino acid, Arg-128 of scallop myosin, have been shown to be specifically photolabeled by NANDP (*41*). Our initial hypothesis was that SSL-NANDP would also specifically label Trp-130. As seen in Figure 2, all of the label, prior to trypsinization, was in the parent heavy-chain fragment 95-kDa and none in the light chains (Figure 2A). Surprisingly, after trypsinization for 15 min, the label was found to be essentially all in the COOH-terminal 20-kDa fragment. The 23- and 50-kDa fragments were not labeled (Figure 2B). These results demonstrated that a residue(s) in the 20-kDa fragment were the major site of photolabeling, and that elements of this fragment, like those of the 23 kDa and 50 kDa fragments, are close to the active site.

CONCLUSION

Two new spin-labeled photoaffinity, nonnucleoside ATP analogues have been synthesized and characterized. Both are based upon a previously characterized, photoaffinity probe, NANTP. For SL-NANTP, the spin label moiety is

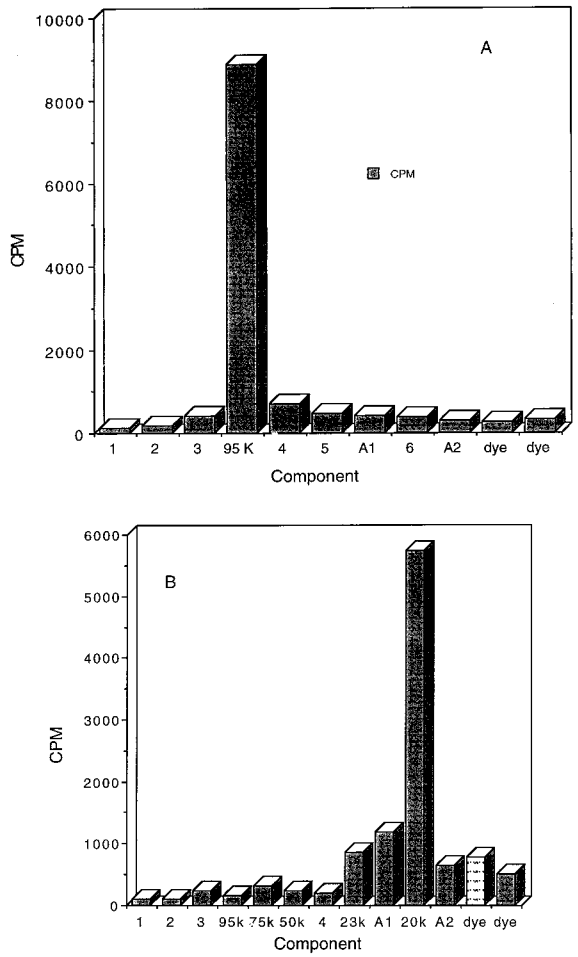

Figure 2. SSL-NANDP specifically labeled 20 kDa of myosin. S1 was trapped and photolabeled with [^{32}P]SSL-NANDP as described under Materials and Methods. The photolabeled S1 was analyzed by gel electrophoresis using a 12% SDS polyacrylamide gel before (panel A) and after (panel B) partially digestion with trypsin (1:100 w:w of trypsin to S1). The gels were stained with Coomassie Blue and sliced into fragments. The fragments were analyzed for radioactivity by scintillation counting.

attached to NANTP via an aminomethyl side chain. In SSL-NANTP, the attachment is via a restricted spiro ring. These two new probes are substrates for S1 and can be trapped at the active site of S1 with phosphate analogues. Both photolabeled S1 with good yields. Attachment of the spin probe moiety using an aminomethyl side chain resulted in a probe that was too mobile after photoincorporation to be of significant use in orientational studies. The more restrictive spiro ring in SSL-NANTP resulted in a highly immobilized probe once attached covalently to S1. Its degree of immobilization is comparable to that observed for EPR probes covalently attached at SH1 (Cys-707) that have been used to monitor myosin head motion (*2*−*10*). Surprisingly, SSL-NANTP specifically labeled the 20 kDa fragment of rabbit skeletal myosin S1, instead of 23 kDa, where NANTP photolabels. However, unlike the SH1-modified myosin, photolabeled S1 appears to retain its normal enzymatic properties. SSL-NANTP offers the possibility of a benign, site-specific probe that can report changes in motor domain orientation within an intact muscle fiber.

ACKNOWLEDGMENT

This project was supported by NIH Grants DK 05195 (R.G.Y.), AR39643 (E.P.), and AR42895 (R.C.). We are grateful to G. Reid Asbury, Drs. William Siems and Qing Wu (Washington State University) for their help in low-resolution mass spectroscopic analyses, and Dr. Ross Lawrence (University of Washington) for high-resolution mass spectroscopic determinations.

Supporting Information Available: Tables of Elemental Analytical Data and Chromatograms. This material is available free of charge via the Internet at http://pubs.acs.org.

LITERATURE CITED

(1) Cooke, R. (1986) The mechanism of muscle contraction. *CRC Crit. Rev. Biochem. 21*, 53−118.
(2) Thomas, D. D. (1987) Spectroscopic probes of muscle cross-bridge rotation. *Annu. Rev. Physiol. 49*, 691−709.
(3) Mendelson, R. A., Morales, M. F., and Botts, J. (1973) Segmental flexibility of the S-1 moiety of myosin. *Biochemistry 12*, 2250−2255.
(4) Thomas, D. D., and Cooke, R. (1980) Orientation of spin-labeled myosin heads in glycerinated muscle fibers. *Biophys. J. 32*, 891−906.
(5) Fajer, P. G., Fajer, E. A., Brunsvold, N. J., and Thomas, D. D. (1988) Effects of AMPPNP on the orientation and rotational dynamics of spin-labeled muscle cross-bridges. *Biophys. J. 53*, 513−524.
(6) Berger, C. L., and Thomas, D. D. (1993) Rotational dynamics of actin-bound myosin heads in active myofibrils. *Biochemistry 32*, 3812−3821.
(7) Roopnarine, O., and Thomas, D. D. (1995) Orientational dynamics of Indane dione spin-labeled myosin heads in relaxed and contracting skeletal muscle fibers. *Biophys. J. 68*, 1461−1471.
(8) Seidel, J. C., Chopek, M., and Gergely, J. (1970) Effect of nucleotides and pyrophosphate on spin labels bound to S1 thiol groups of myosin. *Biochemistry 9*, 3265−3272.
(9) Reisler, E. (1982) Sulfhydryl modification and labeling of myosin. *Methods Enzymol. 85*, *84*−*93*.
(10) Crowder, M., and Cooke, R. (1982) The effect of myosin sulphydryl modification on the mechanics of fibre contraction. *J. Muscle Res. Cell Motil. 5*, 131−146.
(11) Rayment, I., Rypniewski, W. R., Schmidt-Base, K., Smith, R., Tomchick, D. R., Benning, M. M., Winkelmann, D. A., Wesenberg, G., and Holden, H. M. (1993) Three-dimensional structure of myosin subfragment-1: A molecular motor. *Science 261*, 50−57.
(12) Baker, J. E., Brust-Mascher, I., Ramachandran, S., LaConte, L. E. W., and Thomas, D. D. (1998) A large and distinct rotation of the myosin light domain occurs upon muscle contraction. *Proc. Natl. Acad. Sci. U.S.A. 95*, 2944−2949.
(13) Crowder, M. S., and Cooke, R. (1987) Orientation of spin-labeled nucleotides bound to myosin in glycerinated muscle fibers. *Biophys. J. 51*, 323−333.
(14) Alessi, D. R., Corrie, J. E. T., Fajer, P. G., Ferenczi, M. A., Thomas, D. D., Trayer, I. P., and Trentham, D. R. (1992) Synthesis and properties of a conformationally restricted spin-labeled analog of ATP and its interaction with myosin and skeletal muscle. *Biochemistry 31*, 8043−8054.
(15) Wilson, G. J., Shull, S. E., Naber, N., and Cooke, R. (1997) Myosin head interactions in Ca^{2+}-activated skinned rabbit skeletal muscle. *J. Biochem. (Tokyo) 122*, 563−571.
(16) Mahmood, R., Elzinga, M., and Yount, R. G. (1989) Serine-324 of myosin's heavy chain is photoaffinity-labeled by 3′-(2′)-O-(4-benzoylbenzoyl)adenosine triphosphate. *Biochemistry 28*, 3989−3995.
(17) Luo, Y., Wang, D., Cremo, C. R., Pate, E., Cooke, R., and Yount, R. G. (1995) Photoaffinity ADP analogs as covalently attached reporter groups of the active site of myosin subfragment 1. *Biochemistry 34*, 1978−1987.
(18) Wang, D., Luo, Y., Grammer, J., Pate, E., Cooke, R., and Yount, R. G. (1999) Synthesis of a spin-labeled photoaffinity ATP analogue and its use to specifically photolabel myosin cross-bridges in skeletal muscle fibers. *J. Muscle Res. Cell Motil. 20*, 743−753.
(19) Nakamaye, K. L., Wells, J. A., Bridenbaugh, R. L., Okamoto, Y., and Yount, R. G. (1985) 2-[(4-Azido-2-nitrophenyl)-

amino]ethyl triphosphate, a novel chromophoric and photoaffinity analogue of ATP. Synthesis, characterization and interaction with myosin subfragment 1. *Biochemistry 24*, 5226−5235.
(20) Wang, D., Pate, E., Cooke, R., and Yount, R. (1993) Synthesis of nonnucleotide ATP analogues and characterization of their chemomechanical interaction with muscle fibers. *J. Muscle Res. Cell Motil. 14*, 484−497.
(21) Okamoto, Y., and Yount, R. G. (1985) Identification of an active site peptide of skeletal myosin after photoaffinity labeling with N-(4-azido-2-nitrophenyl)-2-aminoethyl diphosphate. *Proc. Natl. Acad. Sci. U.S.A. 82*, 1575−1579.
(22) Yount, R. G., Babcock, D., Ballantyne, W., and Ojala, D. (1971) Adenylyl imidodiphosphate, an adenosine triphosphate analogue containing a P- -N- -P linkage. *Biochemistry 10*, 2484−2489.
(23) Guillory, R. J., and Jeng, S. J. (1977) Arylazido nucleotide analogues in a photoaffinity approach to receptor site labeling. *Methods Enzymol. 46*, 259−288.
(24) Moffatt, J. G. (1964) A general synthesis of nucleoside-5′ triphosphates. *Can. J. Chem. 42*, 599−604.
(25) Okamoto, Y., and Sekine, T. (1985) A streamlined method of subfragment one preparation from myosin. *J. Biochem. (Tokyo) 98*, 1143−1145.
(26) Grammer, J. C., Cremo, C. R., and Yount, R. G. (1988) UV-induced vanadate-dependent modification and cleavage of skeletal myosin subfragment 1 heavy chain. 1: Evidence for active site modification. *Biochemistry 27*, 8408−8415.
(27) Pardee, J. D., and Spudich, J. A. (1982) Purification of muscle actin. *Methods Enzymol. 85*, 164−181.
(28) Wells, J. A., Werber, M. M., Legg, J. I., and Yount, R. G. (1979) Inactivation of myosin subfragment one by cobalt(II)/cobalt(III) phenanthroline complexes. I. Incorporation of Co(III) by in situ oxidation of Co(II). *Biochemistry 18*, 4793−4799.
(29) Wagner, P. D., and Weeds, A. G. (1977) Studies on the role of myosin alkali light chains. Recombination and hybridization of light chains and heavy chains in subfragment-1 preparations. *J. Mol. Biol. 109*, 455−473.
(30) Wells, J. A., Werber, M. M., and Yount, R. G. (1979) Inactivation of myosin subfragment one by cobalt(II)/cobalt(III) phenanthroline complexes. 2. Cobalt chelation of two critical SH groups. *Biochemistry 18*, 4800−4805.
(31) Hoffman, B. M., Schofield, P., and Rich, A. (1969) Spin-labeled transfer RNA. *Proc. Natl. Acad. Sci. U.S.A. 62*, 1195−1202.
(32) Alessi, D. R., Corrie, J. E. T., Feeney, J., Trayer, I. P., and Trentham, D. R. (1991) Conformationally restricted spin labeled nucleotides: a model study of the synthesis and properties of the 2′,3′-O-spiro ketal of uridine and 4-oxo-2,2,6,6-tetramethyl-1-piperidyloxy. *J. Chem. Soc., Perkin Trans. 1*, 2243−2247.
(33) Ludwig, J., and Eckstein, F. (1989) Rapid and efficient synthesis of nucleoside 5′-O-(1-thiotriphosphates), 5′-triphosphates and 2′,3′-cyclophosphorothioates using 2-chloro-4H-1,3,2-benzodioxaphosphorin-4-one. *J. Org. Chem. 54*, 631−635.
(34) Ludwig, J., and Eckstein, F. (1991) Synthesis of nucleoside 5′-O-(1,3-dithiotriphosphates) and 5′-O-(1,1-dithiotriphosphates). *J. Org. Chem. 56*, 1777−1783.
(35) Ludwig, J., and Eckstein, F. (1991) Stereospecific synthesis of guanosine 5′-O-(1,2-dithiotriphosphates). *J. Org. Chem. 56*, 5860−5865.
(36) Chen, X., Siems, W. F., Asbury, G. R., and Yount, R. G. (1999) Fingerprint patterns from laser-induced azido photochemistry of spin-labeled photoaffinity ATP analogues in matrix-assisted laser desorption/ionization mass spectrometry. *J. Am. Soc. Mass Spectrom. 10*, 1337−1340.
(37) Laemmli, U. K. (1970) Cleavage of structural proteins during the assembly of the head of bacteriophage T4. *Nature 227*, 680−685.
(38) Mishra, N. C., and Broom, A. D. (1991) A novel synthesis of nucleoside 5′-triphosphates. *J. Chem. Soc., Chem. Commun.* 1276−1277.
(39) Griffith, O. H., and Jost, P. C. (1976) Lipid spin labels in biological membranes. In *Spin Labeling Theory and Applications* (L. J. Berliner, Ed.) pp 454−523, Academic Press, NY.
(40) Balint, M., Wolf, I., Tarcsafalvi, A., Gergely, J., and Sreter, F. A. (1978) *Arch. Biochem. Biophys. 190*, 793−799.
(41) Kerwin, B. A., and.Yount, R. G. (1992) Photoaffinity labeling of scallop myosin with 2-[(4-azido-2-nitrophenyl)-amino]ethyl diphosphate: identification of an active site arginine analogous to tryptophan-130 in skeletal muscle myosin. *Bioconjugate Chem. 3*, 328−336.
(42) Wells, J. A., and Yount, R. G. (1979). Active site trapping of nucleotides by cross-linking two sulfhydryls in myosin subfragment 1. *Proc. Natl. Acad. Sci. U.S.A. 76*, 4966−4970.
(43) White, H. D. (1982) Special instrumentation and techniques for kinetic studies of contractile systems. *Methods Enzymol. 85*, 698−708.

BC000032B

Responsive Hybrid Hydrogels with Volume Transitions Modulated by a Titin Immunoglobulin Module

Li Chen,[†] Jindřich Kopeček,[‡] and Russell J. Stewart*,[†]

Department of Bioengineering and Department of Pharmaceutics and Pharmaceutical Chemistry, 20 South 2030 East, Room 506, University of Utah, Salt Lake City, Utah 84112. Received May 3, 2000; Revised Manuscript Received July 11, 2000

The I28 immunoglobulin (Ig)-like module of human cardiac titin, an elastic muscle protein, was used to cross-link acrylamide (AAm) copolymers into hybrid hydrogels. Cross-linking was accomplished through metal coordination bonding between terminal histidine tags (His tags) of the I28 module and metal-chelating nitrilotriacetic acid (NTA)-containing side chains on the copolymer. In solution, the β-sheet structure of the I28 module unfolded with a transition midpoint of about 58 °C as the temperature was elevated. Hydrogels cross-linked with the I28 module demonstrated positive temperature responsiveness; they swelled to 3 times their initial volume at temperatures above the melting temperature of the cross-links. Positive temperature responsiveness is unusual for synthetic hydrogels. The I28 hybrid hydrogels demonstrate that cross-linking synthetic polymers with natural, well-characterized protein modules is a practical strategy for creating new materials with unique environmental responsiveness predictably determined by the mechanical properties of the protein cross-links. These new materials may be useful for controlled chemical delivery.

INTRODUCTION

Stimuli-responsive hydrogels undergo volume transitions in response to physical or chemical changes in their environment. A remarkable number of hydrogels have been developed that are responsive to changes in pH, ionic strength, biochemicals, solvent, temperature, electric and magnetic fields, and light (*1*). The extensive interest in responsive hydrogels stems in large part from the broad range of their potential applications. Responsive hydrogels have been used as selective absorbents (*2*), as matrixes for immobilization of enzymes (*3*), as reservoirs for controlled release of chemicals and drugs (*4*), and as microactuators (*5*). The majority of responsive hydrogels have been created using conventional methods of chemical and physical cross-linking of a relatively small number of synthetic polymers, especially (methyl)-acrylates and their copolymers.

As an alternative approach to synthesizing stimuli-responsive hydrogels, we are interested in cross-linking synthetic water-soluble polymers with recombinant protein modules to create hybrid hydrogels with environmental responsiveness that has not been observed in purely synthetic hydrogels. The rationale behind this approach is that the unique properties of the protein module cross-links, like well-defined structures, consistent mechanical properties, and cooperative folding and unfolding, may allow hydrogels to be designed with new, more pronounced, or uniquely controlled responses to environmental stimuli. The defined structures and properties of the cross-links will allow the hydrogel response to be directly related to the structure of the cross-links. Via adjustment of the amino acid sequence of the cross-links, it should be possible to fine-tune the responsiveness of the hybrid hydrogel for a specific application, perhaps much more precisely than previously possible through conventional polymer synthesis. As an example of a hybrid hydrogel, we recently reported a thermally responsive hybrid hydrogel that was assembled by cross-linking a copolymer of *N*-(2-hydroxypropyl)methacrylamide (HPMA) with synthetic and natural coiled-coil domains (*6*). These hydrogels collapsed sharply to about 10% of their equilibrium volume at a temperature that corresponded to a temperature-induced conformational transition in the coiled-coil cross-links. Responsive hydrogels have also been cross-linked with intact antibody molecules (*7*).

In this paper, we describe a new hybrid hydrogel assembled by cross-linking an acrylamide copolymer with a single immunoglobulin (Ig)-like domain from the elastic muscle protein, titin. Titin is a gigantic, modular protein consisting of more than 200 Ig and fibronectin type III domains. Structurally, the repeating titin Ig domain is a sandwich of two antiparallel β-sheets held together by hydrophobic interactions between the β-sheets in the core of the domain and by hydrogen bonds between the β-strands forming the β-sheets (*8*). Lately, a number of research groups have used optical tweezers (*9*, *10*) or AFMs (*11*−*13*) to stretch individual molecules of native titin, or recombinant segments of titin containing defined numbers of titin Ig domains, to investigate the molecular basis of titin's elasticity. The most prominent feature of the force-extension profiles generated in these experiments was a sawtooth pattern of exponential increases in force, followed by stress relaxation at a force threshold of about 200 pN. The number of events in the pattern corresponded to the number of Ig domains and the approximately 30 nm periodicity corresponded to the length of a stretched-out Ig domain, providing evidence that the events were due to the sequential stress denaturation of individual Ig domains. Steered molecular

* Corresponding author. Phone: (801) 581-8581. Fax: (801) 581-8966. E-mail: rstewart@ee.utah.edu.

[†] Department of Bioengineering.

[‡] Department of Pharmaceutics and Pharmaceutical Chemistry.

10.1021/bc000046h CCC: $19.00 © 2000 American Chemical Society
Published on Web 08/15/2000

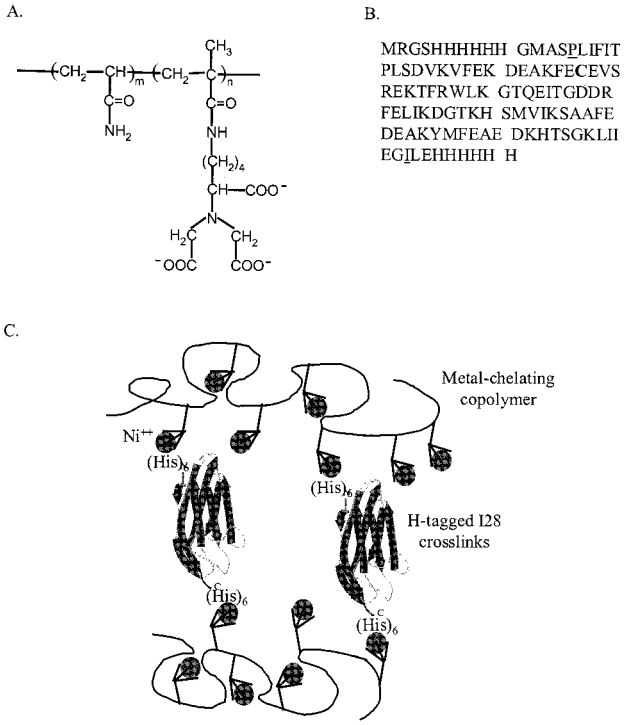

Figure 1. Assembly of the I28 cross-linked hydrogel. (A) Chemical structure of metal-chelating copolymer poly(AAm-*co*-MABNTA). The polymer was prepared by copolymerizing AAm with the metal-chelating comonomer MABNTA in Tris buffer (pH 8.9) under nitrogen, using ammonium persulfate and *N*,*N*,*N*′,*N*′-tetramethylenediamine as the redox initiator. (B) Protein sequence of the recombinant titin I28 cross-linker H-I28-H. The protein contains His tags at both ends. Single-letter abbreviations for amino acids are used: M, methionine; R, arginine; G, glysine; S, serine; H, histidine; A, alanine; P, proline; L, leucine; I, isoleucine; F, phenylalanine; T, threonine; D, aspartic acid; V, valine; K, lysine; E, glutamic acid; C, cysteine; W, tryptophan; Q, glutamine; Y, tyrosine. The underlined amino acid residues mark the start or end of the human cardiac titin I28 segment. The recombinant protein module contains 111 amino acids with a predicted molecular mass of 12.2 kDa. (C) Structure of the hybrid hydrogel. The hydrogel was formed through metal complex formation by the pendant metal-chelating ligand, NTA-Ni^{2+}, on the polymer and the terminal His tags of the protein.

dynamic simulations suggested that a folded Ig domain when pulled from its ends resists stretching until hydrogen bonds between β-strands begin rupturing near a threshold force, which is followed by a sudden drop in force and complete unraveling of the domain structure (*14*).

Our objective was to create a hydrogel in which the chemical potential of the hydrogel polymer matrix generates the driving force stretching titin Ig modules from their ends. The titin Ig module, in turn, would control the swelling of the polymer matrix. The cooperative unfolding of the Ig module cross-links would lead to a unique hydrogel swelling profile in response to environmental conditions. Our strategy for assembling an Ig module cross-linked hydrogel is diagrammed in Figure 1. Cross-linking is through noncovalent, metal coordination bonds between pendant metal-chelating nitrilotriacetic acid (NTA) groups on the polymer side chain and terminal histidine residues (His tag) of the titin Ig module. This convenient protein binding scheme has been applied extensively in recombinant protein purification (*15*), in protein immobilization at interfaces (*16*, *17*), and recently in hybrid hydrogel assembly (*6*).

EXPERIMENTAL PROCEDURES

Construction of the pET24a-I28 Expression Plasmid. A segment of DNA encoding the I28 Ig domain of human cardiac titin was PCR amplified from a plasmid kindly provided by A. Pastore. The I28 PCR product was digested with *Nhe*I and *Xho*I (Promega) and ligated into a pET21a *Escherichia coli* expression vector (Novagen) that had been previously modified to add histidine tags at both the amino and carboxyl ends of the expressed protein. The construct was verified by restriction enzyme digestion analysis and DNA sequencing (Figure 1B). The double-His-tagged I28 insert was transferred to the kanamycin resistant pET24a plasmid.

Expression and Purification of I28. For expression, the pET24a-I28 plasmid was transformed into *E. coli* strain BL21(DE3) (Novagen, Inc.). Single colonies were selected and grown overnight at 37 °C in LB medium (5 mL) containing 50 μg/mL kanamycin. LB cultures (500 mL) with 50 μg/mL kanamycin were then inoculated with the overnight cultures and grown at 37 °C until the A_{600} reached approximately 0.8 (about 2 h). Expression was induced with 0.1 mM isopropyl β-D-thiogalactopyranoside (IPTG) for 4 h at 37 °C or for 6 h at 30 °C. The induced cells were pelleted (Beckman JA 10 rotor, 4500 rpm, 30 min) and stored at −70 °C.

To purify the double-His-tagged I28 (H-I28-H), the cell pellets were resuspended in binding buffer [10 mM Tris and 200 mM sodium chloride (pH 7.4)] containing 20 μg/mL lysozyme, 1 mM phenylmethanesulfonyl fluoride (PMSF), and 0.1% Triton X-100. The cell suspension was sonicated on ice four times for 10 s using an ultrasonic demembranator (Fisher Scientific) to lyse the cells. After centrifugation at 4 °C, the clarified lysate was loaded onto a Ni-NTA (Qiagen, Inc.) column pre-equilibrated with binding buffer. The column was washed with binding buffer with 60 mM imidazole. H-I28-H was eluted with binding buffer with 300 mM imidazole. The H-I28-H fractions were combined and exchanged into 20 mM HEPES buffer with 150 mM NaCl (pH 7.4). The protein was concentrated, frozen in liquid nitrogen, and stored at −70 °C.

Sedimentation Equilibrium. H-I28-H samples were dialyzed into PBS buffer (pH 7.4) with 5 mM dithiothreitol (DTT). Three H-I28-H solutions with A_{280} values of 0.70, 0.35, and 0.18 were analyzed simultaneously in a Beckman Optima XL-A analytical ultracentrifuge with an An-60 Ti rotor. Centrifugation was carried out at 20 °C at three speeds, 25K, 32K, and 38K rpm. Protein sedimentation was assessed at 280 nm. Data analysis was performed using the nonlinear regression program NONLIN (*23*).

Circular Dichroism Spectroscopy. H-I28-H CD spectra were generated using a quartz rectangular cuvette with a path length of 0.1 cm and a volume of 300 μL in an Aviv 62DS CD spectrometer equipped with a thermoelectric temperature control system. Data were collected using the program Star3.0. Wavelength scans were performed at 25 °C, in 0.5 nm steps, and 5 s data averaging at each step. Scans for each sample were repeated at least five times and averaged. In the thermal stability experiments, the CD signal at 215 nm was monitored as the temperature was ramped from 30 to 90 °C in 1 °C increments. The sample was equilibrated for 2 min at each temperature, and the signal was averaged for 1.5 min.

Fluorescence Spectrometry. The fluorescence of the single tryptophan residue in H-I28-H was investigated using an ISS Grey multifrequency fluorometer with an

excitation wavelength of 293 nm. The fluorescence spectra of H-I28-H were determined under native conditions in PBS buffer [20 mM $NaPO_4$, 150 mM NaCl, and 5 mM DTT (pH 7.4)] and under denaturing conditions in PBS buffer with 5 M urea. For the denaturation experiment, spectra were recorded after 20 h at room temperature. The fluorescence spectra of H-I28-H cross-links in a hydrogel were collected at room temperature in PBS buffer and after heating the cuvette at 85 °C overnight.

Synthesis of a Metal-Chelating Acrylamide Copolymer [Poly(AAm-*co*-MABNTA)]. The metal-chelating monomer 2-methacrylamidobutyl nitrilotriacetic acid (MABNTA) was synthesized as described previously (*24*). The final product had a melting point of 104−107 °C, and a molecular mass of 329.7 Da determined by electrospray ionization mass spectrometry. ^{1}H NMR analysis (DMSO-d_6, 200 MHz): δ 1.33−1.59 [m, 6.9H, $CH_2(C\underline{H}_2)_3$], 1.82 (s, 3H, $C\underline{H}_3$), 3.05 (t, 1.7H, CO-NH-$C\underline{H}_2$), 3.40 [t, 1H, CH_2-$C\underline{H}$(COOH)-N], 3.53 [3.3H, N-($C\underline{H}_2$-$C\underline{O}O)_2$], 5.28, 5.60 (s, s, 2H, $C\underline{H}_2$=), 7.87 (1H, CO-N$\underline{H}$), 12.40 [s, 3H, (COO$\underline{H}$)$_3$].

Copolymerization (total monomer, 2.6 wt %) of acrylamide (AAm, Polysciences, Inc., chemzymes ultrapure, 86.5 mol %) and MABNTA (13.5 mol %) was carried out in Tris buffer (pH 8.9) at room temperature, under nitrogen for 24 h, using ammonium persulfate (Fisher Scientific, electrophoresis grade, 7 wt %) and *N*,*N*,*N*′,*N*′-tetramethylenediamine (Bio-Rad, electrophoresis grade) as the redox initiator. The copolymer was dialyzed against water and lyophilized. Weight and number-average molecular masses were measured by size exclusion chromatography on a fast protein liquid chromatography system equipped with a Superose 6 (10/30) column (Pharmacia, Piscataway, NJ) and a light-scattering detector (MiniDawn, Wyatt). The column was calibrated using poly(HPMA) standards with narrow polydispersity. The percentage of NTA side chains in the copolymer was determined by proton NMR (500 MHz) and by acid−base titration using a 10 mL ABU80 autoburet and a PHM84 research pH meter.

Assembly of I28 Cross-Linked Hydrogels. The metal-chelating acrylamide copolymer was charged with nickel by mixing the copolymer and nickel sulfate in 20 mM HEPES buffer (pH 7.4) and 150 mM NaCl at a 1:1 molar ratio of Ni^{2+} to NTA side chains. A gel formed initially before the mixture was thoroughly mixed, likely because of cross-linking between NTA side chains. With continued mixing, the gel completely dissolved. The pH of the solution was adjusted to 7.8 with NaOH. To assemble the hybrid hydrogels, the H-I28-H protein from a 110 mg/mL stock solution was mixed with the Ni-charged copolymer solution to give approximately 2 mol % protein cross-linking. As a control, the same amount of H-I28-H was mixed with the chelating copolymer in the absence of Ni^{2+}. A chemically cross-linked control was prepared by copolymerizing the same ratio of acrylamide and MABNTA comonomers with 2.5 mol % *N*,*N*′-methylenebisacrylamide (Polysciences, Inc., chemzymes ultrapure) under the same conditions used for preparing the titin cross-linked copolymer.

Temperature Responsiveness of I28 Cross-Linked Hydrogels. Small pieces of the hydrogels were immersed in PBS buffer [20 mM $NaPO_4$ and 150 mM NaCl (pH 7.4)] in a quartz cuvette with a jacket connected to a water bath to control the temperature. The gels were observed by brightfield microscopy (Nikon Eclipse E800) and recorded on videotape. The dimensions of the gel were measured from digitized images using Scion Image (Scion Corp.) software. The average rate of temperature increase was 2 °C/min, with the equilibration time being about 1 h at each recorded temperature. The temperature of the water bath was calibrated by measuring the temperature inside the cuvette with a thermocouple. The volume swelling ratio is the ratio of the hydrogel volume at an elevated temperature to the volume at 29 °C. Three samples were measured at each time.

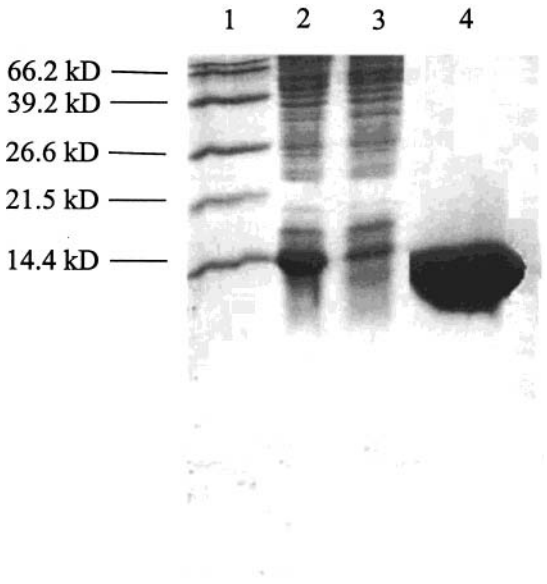

Figure 2. H-I28-H purification: lane 1, molecular mass markers; lane 2, soluble proteins from the cell lysate; lane 3, flow-through of the Ni-NTA agarose column; lane 4, purified H-I28-H.

RESULTS

Characterization of the H-I28-H Protein Module. The I28 Ig module from human cardiac titin was chosen because it was previously cloned, biochemically characterized, and had a reasonable melting temperature, 58 °C (*18*). During the subcloning process, His tags were added to both the carboxyl and amino termini of the I28 Ig module, which we term H-I28-H. The His-tagged Ig module was expressed efficiently in *E. coli* and was purified by metal affinity chromatography from *E. coli* lysates. By SDS−PAGE (Figure 2), the molecular mass of the Ig module was estimated to be about 12 kDa, in good agreement with the calculated molecular mass of 12.2 kDa based on the sequence. The native mass of H-I28-H was analyzed by sedimentation equilibrium in PBS buffer [20 mM phosphate, 150 mM NaCl, and 5 mM DTT (pH 7.4)]. The sedimentation data (not shown) were well-fit by an equation for a single ideal species with a molecular mass of 11.4 kDa. Comparison of the native molecular mass to the calculated molecular mass of 12.2 kDa suggested that H-I28-H was a stable, nonaggregating monomer in physiological conditions we used in our experiments.

The secondary structure and thermal stability of H-I28-H were investigated by CD spectroscopy. The CD spectrum of H-I28-H had a negative peak at about 213 nm (Figure 3A) characteristic of β-sheet structure (*19*), suggesting that the recombinant His-tagged I28 module was in its native conformation, which is comprised primarily of β-sheet. Thermal stability was investigated by monitoring the CD signal at 215 nm as the temperature was raised from 30 to 90 °C. In agreement with previously published stability studies of the I28 module (*18*), the H-I28-H module underwent thermal denaturation with a transition midpoint of about 58 °C (Figure 3B).

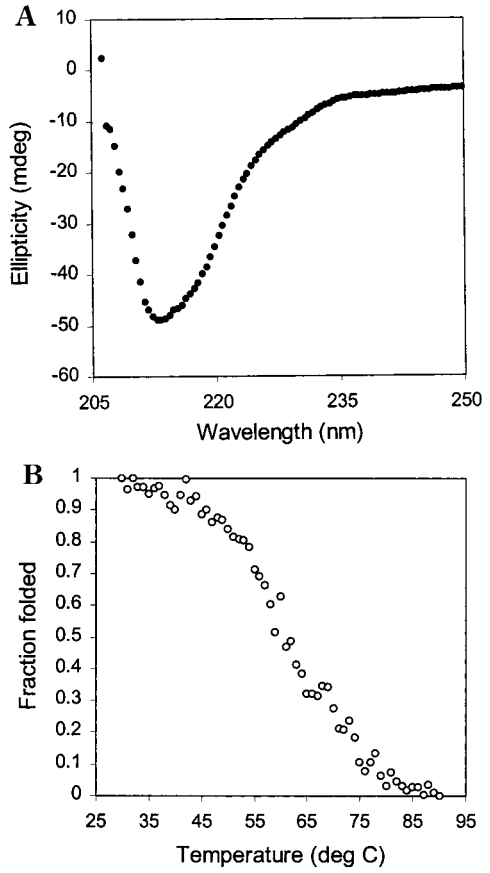

Figure 3. (A) CD spectra of H-I28-H at 25 °C in phosphate-buffered saline (pH 7.2). (B) Thermal denaturation of H-I28-H monitored by ellipticity at 215 nm.

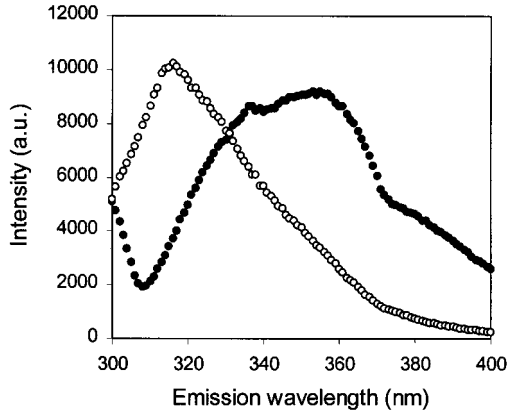

Figure 4. Intrinsic fluorescence of the single tryptophan residue of H-I28-H determined in the native state in phosphate-buffered saline (○) and after denaturation in phosphate-buffered saline and 5 M urea (●). The excitation wavelength was 293 nm.

The I28 module contains a single tryptophan (W) residue that is highly conserved in titin's Ig domains. From the structure of the titin Ig domains (*8*), the single W residue is known to be buried in the hydrophobic core between the two β-sheets of the Ig fold. Tryptophan residues that are fully exposed to water fluoresce maximally at about 350 nm, whereas Ws buried in a hydrophobic environment fluoresce at about 330 nm (*20*). Fluorescence spectrometry in the presence and absence of denaturant (Figure 4) confirmed that the W residue of H-I28-H was buried; in 5 M urea, the peak emission was at 350 nm, compared to peak emission at 317 nm in PBS.

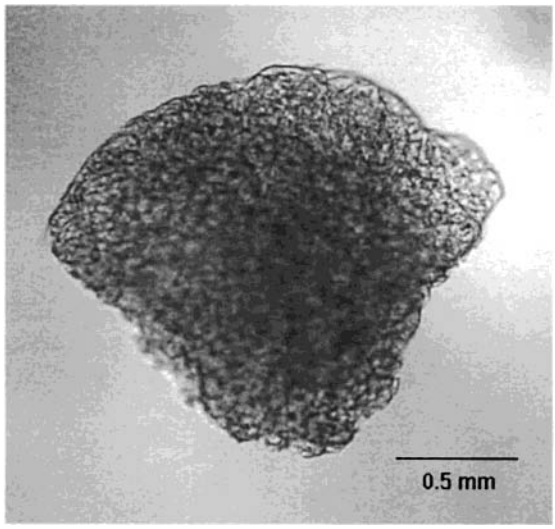

Figure 5. Photograph of a titin I28 cross-linked hydrogel. The thickness of the gel was less than 1 mm.

Characterization of the Metal-Chelating Acrylamide Copolymer [Poly(AAm-*co*-MABNTA)]. The chemical structure of the chelating MABNTA monomer was confirmed by ^{1}H NMR spectroscopy. After copolymerization with acrylamide, the copolymer number and weight-average molecular mass were 11 and 14 kDa, respectively. The percent of chelating monomers in the copolymer was determined by ^{1}H NMR and acid−base titration of the three COOH groups of the MABNTA units. During titration, a single neutral point was observed (not shown). If it is assumed that all three COOH groups in the MABNTA side chains were neutralized, the copolymer contained 10.0 mol % MABNTA. The same mol % of MABNTA was obtained by ^{1}H NMR.

Assembly of I28 Hybrid Hydrogels. When poly(AAm-*co*-MABNTA) chelated with a stoichiometric amount of Ni^{2+} was mixed with an H-I28-H solution at a cross-linking ratio of about 2 mol %, gels formed immediately. The I28 cross-linked hydrogels were translucent, macroscopically homogeneous, and relatively rigid (Figure 5). The gels remained intact for more than 30 days submerged in PBS buffer. In control experiments in which poly(AAm-*co*-MABNTA) was mixed with I28 in the absence of Ni^{2+}, no gels formed, confirming that gel formation occurred through metal coordination bonds. Additional control experiments were carried out in the absence of I28 and with substoichiometric amounts of Ni^{2+} to investigate gel formation by cross-linking between NTA side chains. When poly(AAm-*co*-MABNTA) chelated with a stoichiometric amount of Ni^{2+} was mixed with unchelated poly(AAm-*co*-MABNTA) at final NTA to Ni^{2+} ratios of 1.7:1 and 2.5:1, soft gels formed. However, these soft gels dissolved in excess PBS buffer, or when Ni^{2+} was added to raise the NTA to Ni^{2+} ratio toward 1:1. The control experiments suggest that the stable gel formation that we observed with Ni^{2+}-chelated poly(AAm-*co*-MABNTA) and H-I28-H was predominantly due to specific cross-linking between the His tags of H-I28-H and the NTA side chains of the copolymer.

Temperature Response of the Hybrid Hydrogels. The dimensions of the I28 cross-linked hydrogels were recorded as the hydrogels were heated under a video microscope. Via measurement of the distance between three triangular points on the gel, it appeared that the gel swelled isotropically (not shown). Therefore, the

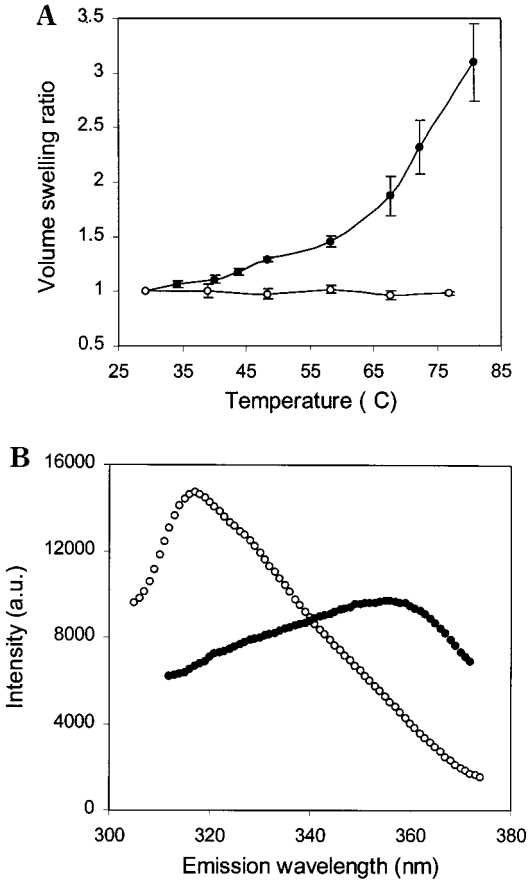

Figure 6. (A) Temperature responses of hydrogels in phosphate-buffered saline (pH 7.2). The volume swelling ratio is the ratio of hydrogel volume at an elevated temperature to the volume at 29 °C: (●) titin I28 cross-linked hydrogel (10 mol % NTA comonomer and 2 mol % protein cross-link) and (○) chemically cross-linked hydrogel (10 mol % NTA comonomer and 2.5 mol % BisAAm). The gels were heated in a jacketed quartz cuvette connected to a water bath. The average rate of temperature increase was 2 °C/min, with an equilibration time of about 1 h. The temperature of the water bath was calibrated by measuring the temperature inside the cuvette with a thermocouple. The dimensions of the gel were measured from digitized video images using Scion Image (Scion Corp.) software. (B) Intrinsic fluorescence of the H-I28-H cross-linked hydrogel at room temperature (○) and after heating the gel at 85 °C (●). The excitation wavelength was 293 nm.

volume swelling ratio,

$$Q = (L/L_0)^3 \quad (1)$$

, was calculated as where L/L_0 is the ratio of the length to the initial length. As the temperature was increased from 30 to 80 °C, the hybrid hydrogel swelled to about 3 times its initial equilibrium volume (Figure 6A). In contrast, a chemically cross-linked control gel, prepared with the same level of MABNTA (10 mol %) and a similar amount of cross-linking agent (2.5 mol %) as the hybrid gels, did not change in volume over the same temperature range. The temperature transition was not reversible since 12 h after returning the gel to room temperature the volume of the temperature-swelled hydrid hydrogel did not change.

The structure of the H-I28-H cross-links inside the hydrogel was investigated using the fluorescence of the I28 W residue as a reporter. At room temperature, the fluorescence maximum of the I28 cross-linked hydrogel was 317 nm (Figure 6B), corresponding to the fluorescence maximum of the protein in PBS buffer without denaturant (Figure 4), which suggested that the I28 cross-links were in their native structure. After the gel was heated at 85 °C, the fluorescence maximum shifted to 360 nm, corresponding to the denatured state of I28, providing evidence that gel swelling occurred due to the denaturation of the I28 cross-links.

DISCUSSION

The titin protein has unique viscoelastic properties that arise from the highly ordered molecular structure of the modules of which it is comprised. Our goal was to take advantage of the consistent structure and predictable mechanical properties of one of titin's well-characterized structural modules, an Ig module, to create a hydrogel with unique environmental responsiveness. We constructed a double-His-tagged single I28 Ig domain, which we produced in *E. coli*. The recombinant I28 domain was correctly folded into its native structure as judged by its molecular mass in solution, its secondary structure, its thermal stability, and intrinsic fluorescence spectra.

Hydrogels readily formed when the H-I28-H protein was mixed with the Ni^{2+}-chelated acrylamide copolymer. The metal coordination cross-linking strategy provides a convenient and effective method for assembling hybrid hydrogels. One of the major advantages of this strategy is that hydrogels are formed in aqueous buffer, at neutral pH, at ambient temperature, and in the absence of redox initiators (radicals) that can damage proteins. The metal coordination linkage between His tags and NTA is quite robust; the H-I28-H cross-linked gels were stable submerged in buffer for more than 30 days. One concern about the strategy could be the potential for Ni^{2+} cross-linking between NTA side chains. In control experiments, in which Ni^{2+} was added to the chelating copolymer with a substoichiometric ratio of Ni^{2+} to NTA side chains, soft gels formed at high polymer concentrations. These gels dissolved in excess buffer or as nickel sulfate was added. After the chelating polymer had been preloaded with a stoichiometric amount of Ni^{2+}, the NTA−NTA cross-links were minimized during hydrogel assembly and cross-linking most likely occurred predominantly through metal coordination between His tags and NTA.

The H-I28-H cross-linked gel responded to rising temperature by swelling isotropically more than 3-fold over the temperature range of 30−80 °C (Figure 6). The equilibrium volume increased significantly above 58 °C, the melting temperature of the H-I28-H protein determined by CD spectroscopy (Figure 3B), suggesting that the swelling was due to the thermally induced unfolding of the H-I28-H cross-links. The fluorescence maximum at 350 nm from the heated gel confirmed that the H-I28-H domain was unfolded in the temperature-swollen gels (Figure 6B). A chemically cross-linked gel of the chelating acrylamide copolymer did not change in volume over the same temperature range (Figure 6A). Swelling due to disruption of the metal coordination bonds at elevated temperatures can be ruled out by previously reported hybrid hydrogels that were cross-linked by metal coordination with a His-tagged coiled coil that had a melting temperature of >100 °C. These gels did not change in volume over the temperature range of 25−90 °C (*6*).

The positive temperature response of the I28 hybrid hydrogel is unusual. Most temperature-responsive hydrogels demonstrate negative thermal responses; they shrink at elevated temperatures. A common example is chemically cross-linked poly(*N*-isopropylacrylamide)

[p(NIPAAm)] which shrinks near the LCST of pNIPAAm due to hydrophobic interactions among its side chains that become stronger as the temperature increases. Hydrogels of chemically cross-linked polymers and copolymers of other *N*,*N*′-alkyl-substituted acrylamides, such as *N*-ethylacrylamide or *N*,*N*′-dimethylacrylamide, also have similar but less sharp negative thermosensitivity (*21*). An exception is poly(acrylic acid)-containing hydrogels, which swell with elevated temperature at low pH due to disruption of hydrogen bonding between acrylic acid and acrylamide side chains (*22*). The poly(acrylic acid) hydrogels are not temperature-responsive at pHs significantly greater than the pK_a of the carboxylic acid side chains, i.e., neutral pH. Therefore, the I28 cross-linked hydrogels may be unique in demonstrating a substantial positive temperature response at neutral pH.

In the single titin molecule stretching experiments, some Ig modules were observed to consistently unfold at lower forces than others (*11*). Likewise, biochemical stability studies with isolated titin Ig modules demonstrated that there can be dramatic variations in stability between modules (*18*). For example, the melting temperature of the I27 module was 72.6 °C, compared to 35.3 °C for the I11 module. The variable stability of homologous titin Ig modules suggests that small changes in amino acid sequence can have pronounced effects on module stability. It may be possible, therefore, to select natural Ig modules as cross-links to create hydrogels for a particular application that respond at a specified temperature. The temperature response could be adjusted over a wide range of temperatures. Furthermore, since the Ig module structure is known (*8*), it is likely that the thermal stability of the Ig modules can be adjusted in a predictable manner by altering a few key amino acids within the domain. By using multiple-Ig module cross-links, it may be possible to assemble hydrogels that undergo volume transitions at multiple temperatures.

In addition to its temperature response, we expect that the I28 cross-linked hybrid hydrogel may respond to other stimuli as well, like ionic strength. As the ionic strength is lowered, the osmotic pressure inside the polyanionic acrylamide copolymer gel will exert increasing force on the I28 cross-links. At a critical ionic strength, the swelling force exerted by the polymer matrix may exceed the threshold force needed to rupture the I28 structure, leading to the cooperative unraveling of the I28 modules. The sudden expansion of the hydrogel cross-links from 4 to ∼30 nm, as seen in the titin stretching experiments (*11*), could result in a pronounced step in the volume transition. The novel swelling profile in response to changes in temperature, and potentially other environmental conditions, along with the potential for adjusting the response over a wide range of environmental conditions, suggests that the I28 cross-linked hybrid hydrogels may have applications in controlled chemical delivery. The gels may be particularly useful for controlled delivery of biologically active proteins because of the mild hydrogel assembly conditions.

The Ig cross-linked hybrid hydrogels demonstrate that well-defined protein modules can be used to mechanically modulate the intrinsic response of a synthetic copolymer matrix in a predictable manner. Biology is a vast resource of predesigned, prefolded protein modules, with well-characterized structures and properties, which can be recombined and modified using the tools of molecular biology. Cross-linking synthetic water-soluble copolymers with recombinant protein modules offers a new approach and a new inventory of molecular materials with which to design responsive hydrogels for a wide variety of applications.

ACKNOWLEDGMENT

We thank Dr. Annelisa Pastore for the human I28 plasmid. This work was supported by grants from the National Science Foundation (BES 9807287).

LITERATURE CITED

(1) Tanaka, T. (1992) Phase transitions of gels. *Polyelectrolyte Gels: Properties, Preparation, and Applications* (R. S. Harland and R. K. Prud'homme, Eds.) ACS Symposium Series 480, p 1, American Chemical Society, Washington, DC.

(2) Tanaka, T., Wang, C., Pande, V., Grosberg, A. Y., English, A., Masamune, S., Gold, H., Levy, R., and King, K. (1996) Polymer gels that can recognize and recover molecules. *Faraday Discuss. 102*, 201−206.

(3) Albin, G., Horbett, T. A., and Ratner, B. D. (1985) Glucose sensitive membranes for controlled delivery of insulin: Insulin transport studies. *J. Controlled Release 2*, 153−164.

(4) Langer, R. (1998) Drug delivery and targeting. *Nature 392* (Suppl.), 5−10.

(5) Osada, Y., Okuzaki, H., and Hori, H. (1992) A polymer gel with electrically driven motility. *Nature 355*, 242−244.

(6) Wang, C., Stewart, R. J., and Kopeček, J. (1999) Hybrid hydrogels assembled from synthetic polymers and coiled-coil protein domains. *Nature 397*, 417−420.

(7) Miyata, T., Asami, N., and Uragami, T. (1999) A reversibly antigen-responsive hydrogel. *Nature 399*, 766−769.

(8) Pfuhl, M., and Pastore, A. (1995) Tertiary structure of an immunoglobulin-like domain from the giant muscle protein titin: a new member of the I set. *Structure 3*, 391−401.

(9) Tskhovrebova, L., Trinick, J., Sleep, J. A., and Simmons, R. M. (1997) Elasticity and unfolding of single molecules of the giant muscle protein titin. *Nature 387*, 308−312.

(10) Kellermayer, M. S. Z., Smith, S. B., Granzier, H. L., and Bustamante, C. (1997) Folding-unfolding transitions in single titin molecules characterized with laser tweezers. *Science 276*, 1112−1116.

(11) Rief, M., Gautel, M., Oesterhelt, F., Fernandez, J. M., and Gaub, H. E. (1997) Reversible unfolding of individual titin immunoglobulin domains by AFM. *Science 276*, 1109−1112.

(12) Marszalek, P. E., Lu, H., Li, H., Carrion-Vazquez, M., Oberhauser, A. F., Schulten, K., and Fernandez, J. M. (1999) Mechanical unfolding intermediates in titin modules. *Nature 402*, 100−103.

(13) Carrion-Vazquez, M., Oberhauser, A. F., Fowler, S. B., Marszalek, P. E., Broedel, S. E., Clarke, J., and Fernandez, J. M. (1999) Mechanical and chemical unfolding of a single protein: a comparison. *Proc. Natl. Acad. Sci. U.S.A. 96*, 3694−3699.

(14) Lu, H., Isralewitz, B., Krammer, A., Vogel, V., and Schulten, K. (1998) Unfolding of titin immunoglobulin domains by steered molecular dynamics simulation. *Biophys. J. 75*, 662−671.

(15) Hochuli, E., Döbeli, H., and Schacher, A. (1987) New metal chelate adsorbent selective for proteins and peptides containing neighbouring histidine residues. *J. Chromatogr. 411*, 177−184.

(16) Sigal, G. B., Bamdad, C., Barberis, A., Strominger, J., and Whitesides, G. M. (1996) A Self-Assembled Monolayer for the Binding and Study of Histidine-Tagged Proteins by Surface Plasmon Resonance. *Anal. Chem. 68*, 490−497.

(17) Ho, C., Limberis, L., Caldwell, K. D., and Stewart, R. J. (1998) A metal-chelating pluronic for immobilization of histidine-tagged proteins at interfaces: immobilization of firefly luciferase on polystyrene beads. *Langmuir 14*, 3889−3894.

(18) Politou, A. S., Gautel, M., Improta, S., Vangelista, L., and Pastore, A. (1996) The elastic I-band region of titin is assembled in a 'modular' fashion by weakly interacting Ig-like domains. *J. Mol. Biol. 255*, 604−616.

(19) Towell, J. F., III, and Manning, M. C. (1994) Analysis of protein structure by circular dichroism spectroscopy. In *Analytical Applications of Circular Dichroism* (N. Purdie and H. G. Brittain, Eds.) p 175, Elsevier Science, Amsterdam.
(20) Jiskoot, W., Hlady, V., Naleway, J. J., and Herron, J. N. (1995) Application of fluorescence spectroscopy for determining the structure and function of proteins. In *Physical Methods to Characterize Pharmaceutical Proteins* (J. N. Herron, W. Jiskoot, and D. J. A. Crommelin, Eds.) p 1, Plenum Press, New York.
(21) Okano, T., Bae, Y. H., Jacobs, H., and Kim, S. W. (1990) Thermally on−off switching polymers for drug permeation and release. *J. Controlled Release 11*, 255−265.
(22) Katono, H., Maruyama, A., Sanui, K., Ogata, N., Okano, T., and Sakurai, Y. (1991) Thermo-responsive swelling and drug release switching of interpenetrating polymer networks composed of poly(acrylamide-*co*-butyl methacrylate) and poly(acrylic acid). *J. Controlled Release 16*, 215−228.
(23) Johnson, M. L., Correia, J. J., Yphantis, D. A., and Halvorson, H. R. (1981) Analysis of data from the analytical ultracentrifuge by nonlinear least-squares techniques. *Biophys. J. 36*, 575−588.
(24) Tang, A., Wang, C., Stewart, R., and Kopeček, J. (2000) Self-assembled peptides exposing epitopes recognizable by human lymphoma cells. *Bioconjugate Chem. 11*, 363−371.
BC000046H

Bioconjugate Chemistry

NOVEMBER/DECEMBER 2000
Volume 11, Number 6

© Copyright 2000 by the American Chemical Society

COMMUNICATIONS

Transition Metal Derivatives of Peptide Nucleic Acid (PNA) Oligomers—Synthesis, Characterization, and DNA Binding

Jeroen C. Verheijen,[‡] Gijs A. van der Marel,[‡] Jacques H. van Boom,*[,‡] and Nils Metzler-Nolte*[,§]

Leiden Institute of Chemistry, P.O. Box 9502, 2300 RA Leiden, The Netherlands, and Max-Planck-Institut für Strahlenchemie, Stiftstrasse 34-36, Mülheim/Ruhr, Germany. Received June 28, 2000

This work describes the first automated solid-phase synthesis of metal derivatives of peptide nucleic acid (PNA) oligomers and their interaction with DNA and PNA. PNA constitutes a relatively young and very promising class of DNA analogues with excellent DNA and RNA binding properties. However, PNA lacks a suitable handle that would permit its sensitive detection on its own as well as when hybridized with complementary oligonucleotides. Metal complexes, on the other hand, offer high potential as markers for biomolecules. In this paper, we describe the synthesis of PNA heptamers (tggatcg-gly, where gly is a C-terminal glycine carboxylic acid amide) with two covalently attached metal complexes at the PNA N-terminus, namely a ferrocene carboxylic acid derivative and a tris-(bipyridine)ruthenium(II) derivative. We show how all synthesis steps may be carried out with high yield on a DNA synthesizer, including attachment of the metal complexes. The conjugates were characterized by HPLC (>90% purity) and ESI-MS. Binding studies of the purified Ru-PNA heptamer to complementary DNA and PNA and comparison to the isosequential metal-free acetyl PNA heptamer proves that the attached metal complex has an influence on the stability (UV-T_m) and structure (CD spectroscopy) of the conjugates, possibly by disruption of the nearby A:T base pair.

Many human diseases can nowadays be traced to genetic dispositions such as mutations of a single base in the DNA, deletions or translations of a whole sequence, or even multiple genetic disorders. Consequently, genetic diagnostics are becoming increasingly important and common (*1*). Technically, the presence of a certain DNA sequence is detected by hybridization with a complementary DNA sequence which carries a radioactive or fluorescence marker that will permit the detection of the hybridization event. Though commonly employed, this scheme is far from ideal in a number of aspects. Stability and sequence specificity, as well as binding affinity of natural DNA, are often worse than desired. The use of radioactive markers is undesirable for obvious reasons. In addition, the signal from fluorescence markers is sometimes difficult to quantify, and indeed fluorescence may be quenched all together under unfavorable circumstances.

Much effort has been directed to the development of DNA analogues with improved properties. A promising DNA analogue, dubbed PNA (peptide nucleic acid), was published by Nielsen et al. in 1991 (*2*). PNA strands bind complementary RNA and ss-DNA stronger than homologous DNA with likewise increased mismatch discrimina-

* To whom correspondence should be addressed. (J.H.v.B.) Fax: +31 71 527 4307. E-mail: j.boom@chem.leidenuniv.nl. (N.M.-N.) New address: Institut für Pharmazeutische Chemie, Universität Heidelberg, Im Neuerheimer Feld 364, D-69120 Heidelberg. Fax: +49 6227 546430. E-mail: Nils.Metzler-nolte@urz.uni-heidelberg.de.

[‡] Leiden Institute of Chemistry.

[§] Max-Planck-Institut für Strahlenchemie.

10.1021/bc0000740 CCC: $19.00 © 2000 American Chemical Society
Published on Web 11/20/2000

Table 1. Binding Properties of Ru-PNA 6b with Complementary PNA or DNA[a]

entry	duplex	type	T_m (°C) (melting)	T_m (°C) (annealing)
1	Ac-tggatcg-gly (**9**) gly-acctagc-Ac (**8**)	PNA·PNA	61.4	61.4
2	Ru-tggatcg-gly (**6b**) gly-acctagc-Ac (**8**)	Ru-PNA·PNA	59.7 ($\Delta T_m = -1.7$ °C)	59.4 ($\Delta T_m = -2.0$ °C)
3	Ac-tggatcg-gly (**9**) 3′-ACCTAGC-5′ (**7**)	PNA·DNA	41.3	40.3
4	Ru-tggatcg-gly (**6b**) 3′-ACCTAGC-5′ (**7**)	Ru-PNA·DNA	39.0 ($\Delta T_m = -2.3$ °C)	36.0 ($\Delta T_m = -4.3$ °C)

[a] All temperatures were determined by UV spectroscopy (UV-T_m). Hybridization studies were performed in a phosphate buffered solution at pH 7, with a NaCl concentration of 100 mM. Heating and cooling rate was 0.5 °C/min after equilibration at the starting temperature (20 and 90 °C). Gly denotes a C-terminal glycine carboxamide, capital and small letters stand for DNA and PNA, respectively.

Scheme 1. Synthesis of Metal-PNA Oligomers[a]

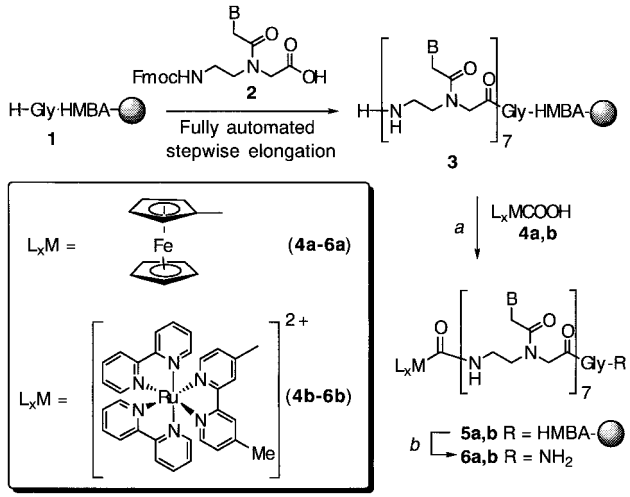

[a] (a) 2-(7-Azabenzotriazol-1-yl)-1,1,3,3-tetramethyluronium Hexa-fluorophosphate (HATU), *N*,*N*-di-*iso*-Propylethylamine (DiPEA), 30 min. (b) NH_3/MeOH, 50 °C, 16 h.

tion (*3*−*5*). Transition-metal complexes, on the other hand, hold great promise for sensitive detection by improved fluorescent properties or in electrochemical assays (*6*−*12*). We have recently published the first transition-metal derivatives of PNA monomers (*13*). In the following, we describe the automated solid-phase synthesis of transition-metal derivatives of PNA oligomers as well as their characterization and interaction with complementary DNA and PNA. To the best of our knowledge, apart from a single cationic manganese porphyrin PNA conjugate that was shown to effect sequence-specific oxidative DNA cleavage upon addition of $KHSO_5$ by Nielsen and Meunier (*14*), no systematic studies on PNA oligomers with covalently bound transition-metal complexes have been reported up to the present date.

Two metal complexes were selected for attachment to immobilized PNA oligomers, namely ferrocene derivative **4a** and tris(bipyridine)ruthenium(II) complex **4b**. Both complexes are very stable, undergo reversible one-electron oxidation, and exhibit characteristic UV−vis absorptions that will facilitate their detection for instance during HPLC purification. In addition, Ru complexes have become important tools for the study of electron transport in DNA (*15*, *16*). It should be noted that the octahedral ruthenium complex **4b** exists as a racemic mixture of topological stereoisomers (Λ and Δ). The synthesis of the metal−PNA conjugates (M-PNAs) **6a**,**b** is depicted in Scheme 1 and starts with the assembly of a PNA heptamer according to a well-established solid-phase synthesis protocol (*17*) using Fmoc/*N*-acyl protected PNA monomers **2** [*B* = A(Bz), C(Bz), G(^{i}Bu), T] (*18*). The metal complex **4** was coupled to the terminal amino group of PNA heptamer **3**. To this end, a standard PNA coupling cycle was slightly adapted by increasing the coupling time to 30 min and omitting the capping step. Subjection of the resulting immobilized M-PNA **5** to methanolic ammonia resulted in cleavage from the resin with simultaneous deprotection of the exocyclic amines. The crude mixtures were filtered, concentrated and analyzed by HPLC-MS. In both cases, the HPLC diagram of the crude mixture showed one major product **6** with the correct mass (>90% by HPLC, see Supporting Information). In case of the Ru-PNA complex **6b**, HPLC detection was performed using dual wavelength monitoring (254 and 370 nm). Only the Ru complex has an appreciable absorption at the latter wavelength and it is of interest to note that only one HPLC peak was observed at both wavelengths simultaneously which corresponded to the desired product.

Purification by RP-HPLC furnished the homogeneous complexes. Unfortunately, the solubility of the uncharged, lipophilic ferrocene conjugate **6a** in neutral aqueous buffer was rather low, precluding further studies. Since we have a special interest in conjugates of PNA with bulky chiral metal complexes, Ru-PNA **6b** was selected for further characterization. The UV−vis spectrum of **6b** was essentially the sum of the UV−vis spectrum of metal complex **4b** (with characteristic MLCT bands around 454 nm) and the known spectrum of mixed-sequence PNA oligomers. The duplex stability with complementary DNA (**7**) and PNA (**8**) was determined by monitoring the UV absorption upon heating or cooling of equimolar mixtures in phosphate buffered solutions at pH 7 (UV-T_m). Comparison to isosequential native PNA (**9**) reveals that the presence of the bulky ruthenium complex is fully compatible with duplex formation (Table 1). Thus, the melting temperature (T_m) of the Ru−PNA·PNA duplex (entry 2) was only 1.7 °C lower than that of the corresponding PNA·PNA duplex (entry 1), whereas the drop in T_m was 2.3 °C with complementary DNA (compare entries 3 and 4). This drop in T_m is about the value generally accepted for one A:T base pair. Furthermore, in the latter case a small but significant T_m-hysteresis is observed (3 °C, entry 4). A similar phenomenon was described earlier for the melting behavior of various PNA analogues (*19*, *20*). Clearly, the forward kinetics of duplex formation and the duplex stability are diminished by the bulky Ru complex, possibly by disrupting the hydrogen bonding of the N-terminal A:T base pair.

An appreciable effect of the bulky Ru complex on the secondary structure of the duplex was observed by CD spectroscopy. A positive Cotton effect with maximum at 266 nm is observed for the PNA·DNA system (Figure 1), corresponding to the expected B-DNA like helix (*21*). When the acetyl group is replaced by a Ru-complex (as

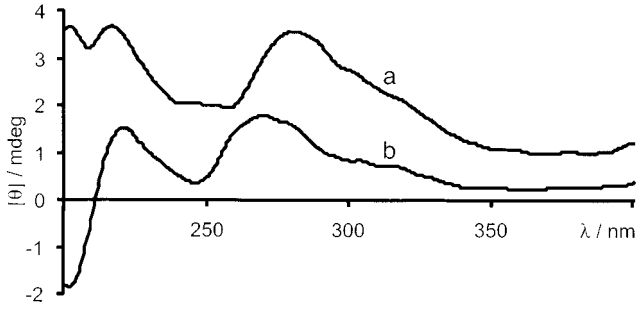

Figure 1. CD spectra of **6b**·DNA (a) and Ac-PNA·DNA (b).

in **6b**), the maximum at 266 nm shifts to 280 nm. In addition, the observed Cotton effect is rather weak, which may be ascribed to the following two reasons. A full helical turn in a PNA·DNA duplex takes 13 base pairs (*22*). Since in this study only heptamers are used, the secondary structure may not be fully developed. More interestingly, it should be remembered that a racemic mixture of both topological isomers of Ru−PNA **6b** is used. Therefore, duplexation with DNA gives an equimolar mixture of diastereoisomers, each giving rise to their own CD signals. Giese and co-workers have recently described the synthesis of diastereomerically pure DNA conjugates of tris(phenanthroline)ruthenium complexes (*23*). There is an ongoing debate as to which way optically pure Ru complexes of this type interact with DNA (*15*, *24*). Investigations into the preparation and hybridization properties of chirally pure Ru-PNA complexes are currently in progress.

In conclusion, we have demonstrated that the synthesis of metal PNA conjugates with high yield and purity is feasible by standard solid support peptide synthesis methods. The stability of a ruthenium-PNA conjugate binding to complementary DNA is only slightly less than for a nonmetalated PNA strand, allowing the metal complex to act as a marker for PNA·DNA binding. Studies on the synthesis and behavior of enantiomerically pure metal−PNA conjugates are underway and will be reported in due course.

ACKNOWLEDGMENT

This work was supported by the Council for Chemical Sciences of The Netherlands Organization for Scientific Research (CW-NWO) and the Fond der Chemischen Industrie. We thank Hans van den Elst for recording the HPLC-MS spectra. N.M.N. is grateful to Prof. K. Wieghardt for generous support of this work.

Supporting Information Available: Experimental details and HPLC chromatograms of **6a** and **6b**. This material is available free of charge via the Internet at http://pubs.acs.org.

LITERATURE CITED

(1) Stryer, L. (1995) *Biochemistry*, W. H. Freeman and Company, New York.
(2) Nielsen, P. E., Egholm, M., Berg, R. H., and Buchardt, O. (1991) Sequence selective recognition of DNA by strand displacement with a thymine-substituted polyamide. *Science 254*, 1497−1500.
(3) Eriksson, M., and Nielsen, P. E. (1996) PNA-nucleic acid complexes. Structure, stability and dynamics. *Q. Rev. Biophys. 29*, 369−394.
(4) Nielsen, P. E. (1998) Structural and biological properties of peptide nucleic acids (PNA). *Pure Appl. Chem. 70*, 105−110.
(5) Nielsen, P. E. (1999) Peptide Nucleic Acid. A Molecule with Two Identities. *Acc. Chem. Res. 32*, 624−630.
(6) Cass, A. E. G., Davis, G., Francis, G. D., Hill, H. A. O., Aston, W. J., Higgins, I. J., Plotkin, E. V., Scott, L. D. L., and Turner, A. P. F. (1984) Ferrocinium-coupled Glucose Oxidase Electrode. *Anal. Chem. 56*, 667−671.
(7) Schuhmann, W., Ohara, T. J., Schmidt, H.-L., and Heller, A. (1991) Electron Transfer between Glucose Oxidase and Electrodes via Redox Mediators Bound with Flexible Chains to the Enzyme Surface. *J. Am. Chem. Soc. 113*, 1394−1397.
(8) Tao, G., Katz, E., and Willner, I. (1997) Enantioselective bioelectrocatalyzed oxidation of glucose by glucose oxidase at chiral-monolayer-electrodes. *J. Chem. Soc., Chem. Commun.* 2073−2074.
(9) Ryabov, A. D., Goral, V. N., Gorton, L., and Csöregi, E. (1999) Electrochemically and Catalytically Active Reconstituted Horseradish Peroxidase with Ferrocene-Modified Hemin and an Artificial Binding Site. *Chem. Eur. J. 5*, 961−967.
(10) Ihara, T., Nakayama, M., Murata, M., Nakano, K., and Maeda, M. (1997) Gene Sensor using Ferrocenyl Oligonucleotide. *J. Chem. Soc., Chem. Commun.* 1609−1610.
(11) Wang, J., Palecek, E., Nielsen, P. E., Rivas, G., Cai, X. H., Shiraishi, H., Dontha, N., Luo, D. B., and Farias, P. A. M. (1996) Peptide nucleic acid probes for sequence-specific DNA biosensors. *J. Am. Chem. Soc. 118*, 7667−7670.
(12) Wang, J. (1998) DNA biosensors based on peptide nucleic acid (PNA) recognition layers. A review. *Biosens. Bioelectron. 13*, 757−762.
(13) Hess, A., and Metzler-Nolte, N. (1999) Transition metal labels on peptide nucleic acid (PNA) monomers. *J. Chem. Soc., Chem. Commun.* 885−886.
(14) Bigey, P., Sönnichsen, S. H., Meunier, B., and Nielsen, P. E. (1997) DNA Binding and Cleavage by a Cationic Manganese Porphyrin-Peptide Nucleic Acid Conjugate. *Bioconjugate Chem. 8*, 267−270.
(15) Holmlin, R. E., Dandliker, P. J., and Barton, J. K. (1997) Ladungsübertragung durch den DNA-Basenstapel. *Angew. Chem. 109*, 2830−2848; *Angew. Chem., Int. Ed. Engl. 36*, 2714−2730.
(16) Diederichsen, U. (1997) Ladungstransport in DNA: eine Kontroverse. *Angew. Chem. 109*, 2411−2413; *Angew. Chem., Int. Ed. Engl. 36*, 2317−2319.
(17) Verheijen, J. C., Deiman, B. A. L. M., Yeheskiely, E., van der Marel, G. A., and van Boom, J. H. (2000) Efficient Hydrolysis of RNA by a PNA-Diethylenetriamine Adduct. *Angew. Chem. 112*, 377−380; *Angew. Chem., Int. Ed. 39*, 369−372.
(18) Bergmann, F., Bannwarth, W., and Tam, S. (1995) Solid Phase Synthesis of Directly Linked PNA-DNA-Hybrids. *Tetrahedron Lett. 36*, 6823−6826.
(19) Kuwahara, M., Arimitsu, M., and Sisido, M. (1999) Sequence-Specific Hybridization between Two Different Types of Peptide Nucleic Acids. *Bull. Chem. Soc. Jpn. 72*, 1547−1552.
(20) Ceulemans, G., Van Aerschot, A., Rozenski, J., and Herdewijn, P. (1997) Oligonucleotides with 3-hydroxy-*N*-acetylprolinol as Sugar Substitute. *Tetrahedron 53*, 14957−14974.
(21) Leijon, M., Gräslund, A., Nielsen, P. E., Buchardt, O., Nordén, B., Kristensen, S. M., and Eriksson, M. (1994) Structural Characterization of PNA-DNA Duplexes by NMR. Evidence for DNA in a B-like Confomation. *Biochemistry 33*, 9820−9825.
(22) Eriksson, M., and Nielsen, P. E. (1996) Solution structure of a peptide nucleic acid-DNA duplex. *Nat. Struct. Biol. 3*, 410−413.
(23) Meggers, E., Kusch, D., and Giese, B. (1997) An efficient synthesis of enantiomerically pure Delta- and Lambda-ruthenium(II)-labeled oligonucleotides. *Helv. Chim. Acta 80*, 640−652.
(24) Kim, H.-H., Lincoln, P., Nordén, B., and Tuite, E. (1997) Absence of chiral discrimination in the interaction of tris-(diphenylphenanthroline)ruthenium(II) with DNA. *J. Chem. Soc., Chem. Commun.* 2375−2376.

BC0000740

© 2000 American Chemical Society, Bioconjugate Chem., Verheijen bc0000740 Supporting Info Page 1

SUPPLEMENTARY MATERIAL

Bioconjugate Chemistry

Transition Metal Derivatives of Peptide Nucleic Acid (PNA) Oligomers - Synthesis, Characterization and DNA Binding

Jeroen C. Verheijen, Gijs A. van der Marel, and Jacques H. van Boom, and Nils Metzler-Nolte*

Experimental section

*Solid-phase synthesis of M-PNA adducts **6a,b**:* All solvents (Biosolve, DNA synthesis grade) were used as received. Ferrocene carboxylic acid was purchased from Aldrich, the Ru complex **4b** was prepared following published procedures (Peek et al., *Int. J. Pept. Prot. Res.*, 38, **1991**, 114 - 123). Solid phase synthesis was performed on a Pharmacia Gene Assembler using highly cross-linked polystyrene beads as the solid support (loading: 26-28 μmol/g) on a 1 μmol scale. The support was functionalized with a glycine moiety via a *p*-hydroxymethylbenzoic acid linker. Assembly of the PNA part was established using solutions of 0.3 M of monomers **2** or **4a,b** in dimethylformamide, 0.3 M D*i*PEA in acetonitrile/dimethylformamide (1/1, v/v) and 0.3 M HATU in acetonitrile/dimethylformamide (1/1, v/v). Prior to coupling, the monomers were pre-activated for 1 min by mixing equal amounts of the PNA monomer (15 equiv per μmol support), HATU and D*i*PEA solutions. The protocol for one PNA chain extension cycle consisted of (1) wash: acetonitrile/dimethylformamide (1/1, v/v), 2.5 mL; (2) coupling: PNA + HATU + DiPEA in acetonitrile/dimethylformamide (1/1, v/v), 15 min; (3) wash: acetonitrile/dimethylformamide (1/1, v/v), 2.5 mL (4) capping: Ac_2O/lutidine/*N*-methylimidazole/tetrahydrofuran (1/1/1/7, v/v/v/v), 2.0 mL; (5) wash: acetonitrile/dimethylformamide (1/1, v/v), 2.5 mL; (6) Fmoc deprotection: 20% piperidine in

acetonitrile/dimethylformamide (1/1, v/v), 3 min; (7) wash: acetonitrile/dimethylformamide (1/1, v/v), 2.5 mL. For metal complexes **4a,b** the coupling time in step 2 was increased to 30 min and step 4 (capping) was omitted. After the last elongation step, the oligomers were cleaved from the support with concomitant deprotection of the exocyclic amino groups by treatment with methanolic ammonia (1.5 mL) at 50 °C for 16 h. HPLC-MS analysis was carried out on a Jasco LCMS system equipped with an Altima C-18 column (4.6 x 150 mm) with mass detection on a Perkin Elmer Sciex API 165 equipped with an Electrospray Interface (ESI). RP-HPLC purification of **6a,b** was performed on a Jasco HPLC system equipped with a LiChrospher 100 RP-18 endcapped column (4.0 x 250 mm). In all cases, gradient elution was performed by building up a gradient starting with buffer A (0.1% TFA in water) and applying buffer B (0.1% TFA in acetonitrile/water, 9/1, v/v) with a flow rate of 1.0 mL/min.

Thermal melting studies: Melting temperatures (T_m) were determined with equimolar mixtures of PNA **9** or Ru-PNA **6b** and complementary DNA **7** or PNA **8** at a concentration of 3 μM, in a 10 mM phosphate buffer, pH=7.0, containing NaCl (100 mM) and EDTA (0.1 mM). Prior to recording the melting profile, the solutions were heated at 90 °C for several minutes and then cooled to 20 °C over 2.0 h. The mixtures were kept at 20 °C for 1 h and heated to 80 °C at a rate of 0.5 °C per minute while the A_{260} was recorded against temperature. Prior to recording the annealing profile, the mixtures were heated at 90 °C for several minutes. The mixtures were cooled to 20 °C at a rate of 0.5 °C per minute while the A_{260} was recorded againts temperature. The T_m values were determined as the maxima of the first-derivative plots of absorbance versus temperature.

CD measurements: CD spectra were recorded on a JASCO J715 instrument at room temperature and calibrated against a standard camphor sulphate solution, using equimolar mixtures of PNA **9** or Ru-PNA **6b** and complementary DNA **7** or PNA **8** at a concentration of 3 μM, in a 10 mM phosphate buffer, pH=7.0, containing NaCl (100 mM) and EDTA (0.1 mM).

HPLC Chromatograms of **6a** (top) and **6b** (bottom) with observed mass of the main peak (ESI-MS data directly from HPLC-MS)

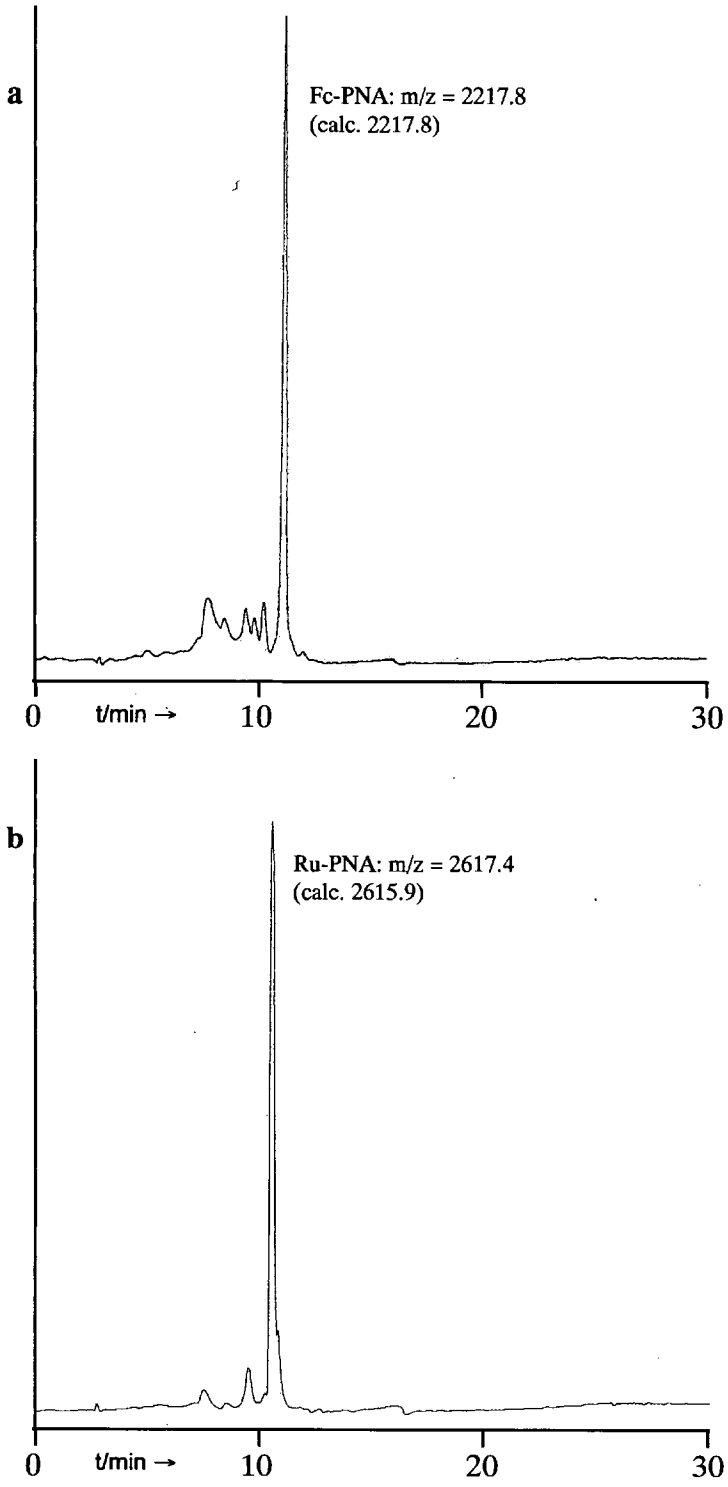

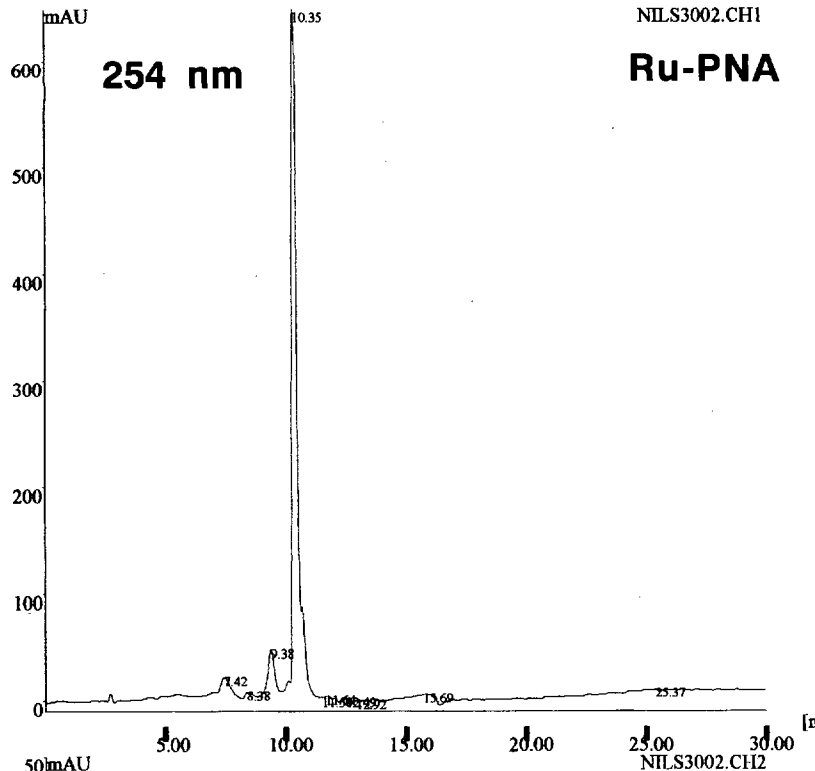

File name : NILS3002.CH1
Info :

Vial # = 1 Rack # = 1
Acqu. Date :19-May-99 9:05:2
Curr. Date :19-May-99 11:00:2
User : HANS
Control Method : 0590%370

#	Rt	Area
1	7.42	434.00
2	8.38	108.00
3	9.38	751.00
4	10.35	7053.41
5	11.50	2778.41
6	11.64	-697.65
7	12.49	-495.80
8	12.92	-114.61
9	15.69	144.00
10	25.37	195.00

Total Area of Peak = 10156

Injection Volume = 25.00 µl

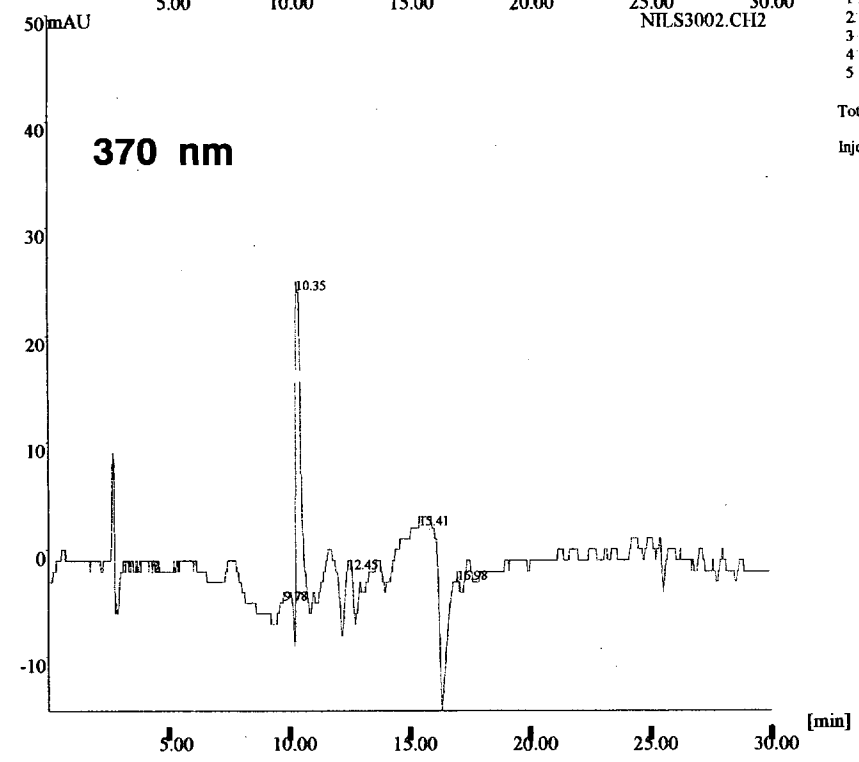

File name : NILS3002.CH2
Info :

Vial # = 1 Rack # = 1
Acqu. Date :19-May-99 9:05:2
Curr. Date :19-May-99 11:00:2
User : HANS
Control Method : 0590%370

#	Rt	Area
1	9.78	137.00
2	10.35	479.50
3	12.45	130.00
4	15.41	219.50
5	16.98	144.75

Total Area of Peak = 1111

Injection Volume = 25.00 µl

Melting Curves

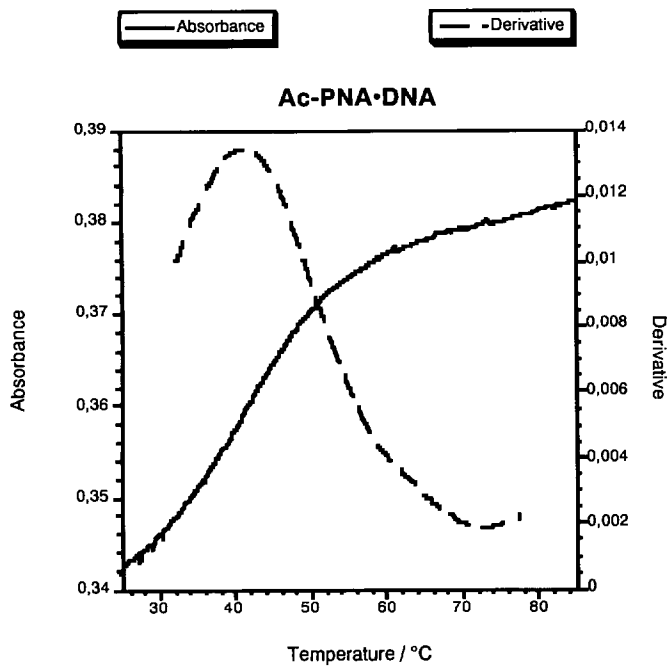

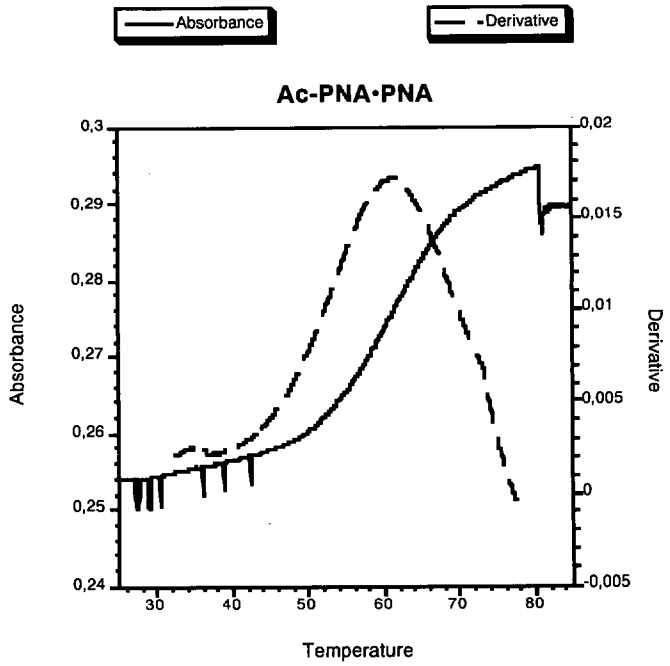

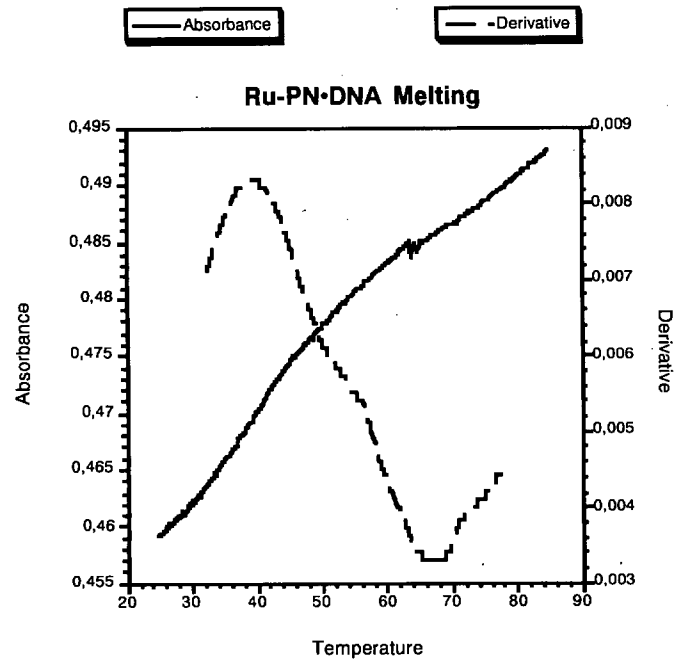

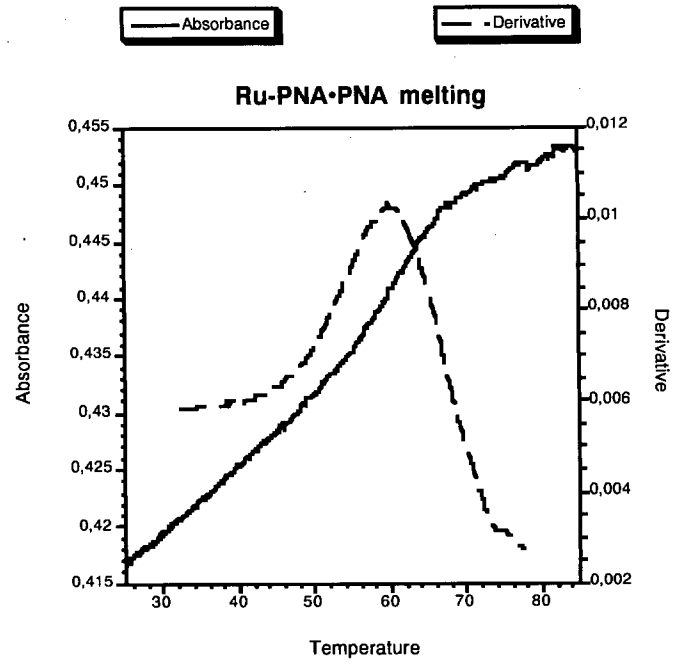

Example melting curves are shown for each type of conjugate together with the first derivative. For determination of Tm, an average of at least two measurements was taken. No annealing data are shown in this material but the overall appearance of the annealing curves is very similar to the melting curves. See experimental section and table 1 for details.

Bioconjugate Chemistry

NOVEMBER/DECEMBER 2000
Volume 11, Number 6

© Copyright 2000 by the American Chemical Society

COMMUNICATIONS

Transition Metal Derivatives of Peptide Nucleic Acid (PNA) Oligomers—Synthesis, Characterization, and DNA Binding

Jeroen C. Verheijen,[‡] Gijs A. van der Marel,[‡] Jacques H. van Boom,*[,‡] and Nils Metzler-Nolte*[,§]

Leiden Institute of Chemistry, P.O. Box 9502, 2300 RA Leiden, The Netherlands, and Max-Planck-Institut für Strahlenchemie, Stiftstrasse 34-36, Mülheim/Ruhr, Germany. Received June 28, 2000

This work describes the first automated solid-phase synthesis of metal derivatives of peptide nucleic acid (PNA) oligomers and their interaction with DNA and PNA. PNA constitutes a relatively young and very promising class of DNA analogues with excellent DNA and RNA binding properties. However, PNA lacks a suitable handle that would permit its sensitive detection on its own as well as when hybridized with complementary oligonucleotides. Metal complexes, on the other hand, offer high potential as markers for biomolecules. In this paper, we describe the synthesis of PNA heptamers (tggatcg-gly, where gly is a C-terminal glycine carboxylic acid amide) with two covalently attached metal complexes at the PNA N-terminus, namely a ferrocene carboxylic acid derivative and a tris-(bipyridine)ruthenium(II) derivative. We show how all synthesis steps may be carried out with high yield on a DNA synthesizer, including attachment of the metal complexes. The conjugates were characterized by HPLC (>90% purity) and ESI-MS. Binding studies of the purified Ru-PNA heptamer to complementary DNA and PNA and comparison to the isosequential metal-free acetyl PNA heptamer proves that the attached metal complex has an influence on the stability (UV-T_m) and structure (CD spectroscopy) of the conjugates, possibly by disruption of the nearby A:T base pair.

Many human diseases can nowadays be traced to genetic dispositions such as mutations of a single base in the DNA, deletions or translations of a whole sequence, or even multiple genetic disorders. Consequently, genetic diagnostics are becoming increasingly important and common (*1*). Technically, the presence of a certain DNA sequence is detected by hybridization with a complementary DNA sequence which carries a radioactive or fluorescence marker that will permit the detection of the hybridization event. Though commonly employed, this scheme is far from ideal in a number of aspects. Stability and sequence specificity, as well as binding affinity of natural DNA, are often worse than desired. The use of radioactive markers is undesirable for obvious reasons. In addition, the signal from fluorescence markers is sometimes difficult to quantify, and indeed fluorescence may be quenched all together under unfavorable circumstances.

Much effort has been directed to the development of DNA analogues with improved properties. A promising DNA analogue, dubbed PNA (peptide nucleic acid), was published by Nielsen et al. in 1991 (*2*). PNA strands bind complementary RNA and ss-DNA stronger than homologous DNA with likewise increased mismatch discrimina-

* To whom correspondence should be addressed. (J.H.v.B.) Fax: +31 71 527 4307. E-mail: j.boom@chem.leidenuniv.nl. (N.M.-N.) New address: Institut für Pharmazeutische Chemie, Universität Heidelberg, Im Neuerheimer Feld 364, D-69120 Heidelberg. Fax: +49 6227 546430. E-mail: Nils.Metzler-nolte@urz.uni-heidelberg.de.

[‡] Leiden Institute of Chemistry.

[§] Max-Planck-Institut für Strahlenchemie.

10.1021/bc0000740 CCC: $19.00 © 2000 American Chemical Society
Published on Web 11/20/2000

Table 1. Binding Properties of Ru-PNA 6b with Complementary PNA or DNA[a]

entry	duplex	type	T_m (°C) (melting)	T_m (°C) (annealing)
1	Ac-tggatcg-gly (**9**) gly-acctagc-Ac (**8**)	PNA·PNA	61.4	61.4
2	Ru-tggatcg-gly (**6b**) gly-acctagc-Ac (**8**)	Ru-PNA·PNA	59.7 ($\Delta T_m = -1.7$ °C)	59.4 ($\Delta T_m = -2.0$ °C)
3	Ac-tggatcg-gly (**9**) 3′-ACCTAGC-5′ (**7**)	PNA·DNA	41.3	40.3
4	Ru-tggatcg-gly (**6b**) 3′-ACCTAGC-5′ (**7**)	Ru-PNA·DNA	39.0 ($\Delta T_m = -2.3$ °C)	36.0 ($\Delta T_m = -4.3$ °C)

[a] All temperatures were determined by UV spectroscopy (UV-T_m). Hybridization studies were performed in a phosphate buffered solution at pH 7, with a NaCl concentration of 100 mM. Heating and cooling rate was 0.5 °C/min after equilibration at the starting temperature (20 and 90 °C). Gly denotes a C-terminal glycine carboxamide, capital and small letters stand for DNA and PNA, respectively.

Scheme 1. Synthesis of Metal-PNA Oligomers[a]

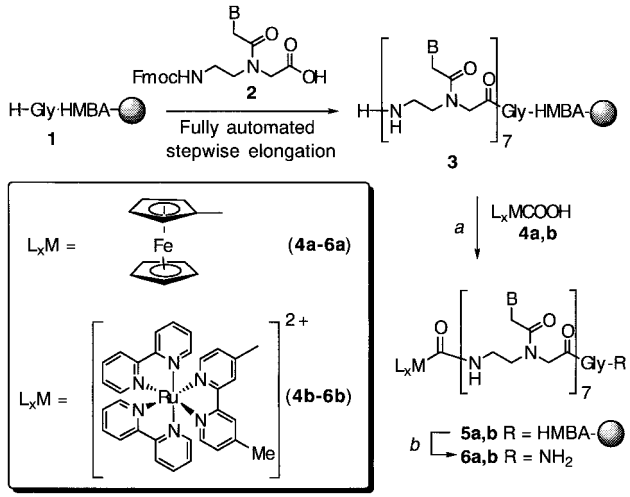

[a] (a) 2-(7-Azabenzotriazol-1-yl)-1,1,3,3-tetramethyluronium Hexa-fluorophosphate (HATU), *N*,*N*-di-*iso*-Propylethylamine (DiPEA), 30 min. (b) NH_3/MeOH, 50 °C, 16 h.

tion (*3*−*5*). Transition-metal complexes, on the other hand, hold great promise for sensitive detection by improved fluorescent properties or in electrochemical assays (*6*−*12*). We have recently published the first transition-metal derivatives of PNA monomers (*13*). In the following, we describe the automated solid-phase synthesis of transition-metal derivatives of PNA oligomers as well as their characterization and interaction with complementary DNA and PNA. To the best of our knowledge, apart from a single cationic manganese porphyrin PNA conjugate that was shown to effect sequence-specific oxidative DNA cleavage upon addition of $KHSO_5$ by Nielsen and Meunier (*14*), no systematic studies on PNA oligomers with covalently bound transition-metal complexes have been reported up to the present date.

Two metal complexes were selected for attachment to immobilized PNA oligomers, namely ferrocene derivative **4a** and tris(bipyridine)ruthenium(II) complex **4b**. Both complexes are very stable, undergo reversible one-electron oxidation, and exhibit characteristic UV−vis absorptions that will facilitate their detection for instance during HPLC purification. In addition, Ru complexes have become important tools for the study of electron transport in DNA (*15*, *16*). It should be noted that the octahedral ruthenium complex **4b** exists as a racemic mixture of topological stereoisomers (Λ and Δ). The synthesis of the metal−PNA conjugates (M-PNAs) **6a**,**b** is depicted in Scheme 1 and starts with the assembly of a PNA heptamer according to a well-established solid-phase synthesis protocol (*17*) using Fmoc/*N*-acyl protected PNA monomers **2** [*B* = A(Bz), C(Bz), G(^{i}Bu), T] (*18*). The metal complex **4** was coupled to the terminal amino group of PNA heptamer **3**. To this end, a standard PNA coupling cycle was slightly adapted by increasing the coupling time to 30 min and omitting the capping step. Subjection of the resulting immobilized M-PNA **5** to methanolic ammonia resulted in cleavage from the resin with simultaneous deprotection of the exocyclic amines. The crude mixtures were filtered, concentrated and analyzed by HPLC-MS. In both cases, the HPLC diagram of the crude mixture showed one major product **6** with the correct mass (>90% by HPLC, see Supporting Information). In case of the Ru-PNA complex **6b**, HPLC detection was performed using dual wavelength monitoring (254 and 370 nm). Only the Ru complex has an appreciable absorption at the latter wavelength and it is of interest to note that only one HPLC peak was observed at both wavelengths simultaneously which corresponded to the desired product.

Purification by RP-HPLC furnished the homogeneous complexes. Unfortunately, the solubility of the uncharged, lipophilic ferrocene conjugate **6a** in neutral aqueous buffer was rather low, precluding further studies. Since we have a special interest in conjugates of PNA with bulky chiral metal complexes, Ru-PNA **6b** was selected for further characterization. The UV−vis spectrum of **6b** was essentially the sum of the UV−vis spectrum of metal complex **4b** (with characteristic MLCT bands around 454 nm) and the known spectrum of mixed-sequence PNA oligomers. The duplex stability with complementary DNA (**7**) and PNA (**8**) was determined by monitoring the UV absorption upon heating or cooling of equimolar mixtures in phosphate buffered solutions at pH 7 (UV-T_m). Comparison to isosequential native PNA (**9**) reveals that the presence of the bulky ruthenium complex is fully compatible with duplex formation (Table 1). Thus, the melting temperature (T_m) of the Ru−PNA·PNA duplex (entry 2) was only 1.7 °C lower than that of the corresponding PNA·PNA duplex (entry 1), whereas the drop in T_m was 2.3 °C with complementary DNA (compare entries 3 and 4). This drop in T_m is about the value generally accepted for one A:T base pair. Furthermore, in the latter case a small but significant T_m-hysteresis is observed (3 °C, entry 4). A similar phenomenon was described earlier for the melting behavior of various PNA analogues (*19*, *20*). Clearly, the forward kinetics of duplex formation and the duplex stability are diminished by the bulky Ru complex, possibly by disrupting the hydrogen bonding of the N-terminal A:T base pair.

An appreciable effect of the bulky Ru complex on the secondary structure of the duplex was observed by CD spectroscopy. A positive Cotton effect with maximum at 266 nm is observed for the PNA·DNA system (Figure 1), corresponding to the expected B-DNA like helix (*21*). When the acetyl group is replaced by a Ru-complex (as

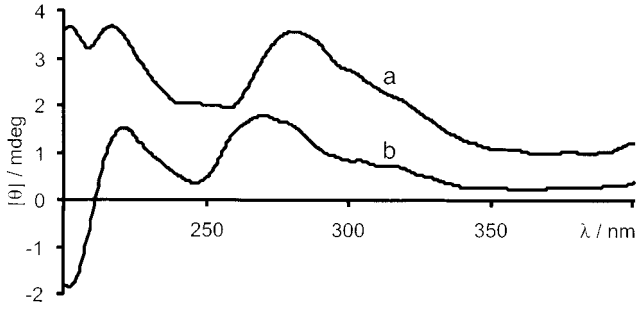

Figure 1. CD spectra of **6b**·DNA (a) and Ac-PNA·DNA (b).

in **6b**), the maximum at 266 nm shifts to 280 nm. In addition, the observed Cotton effect is rather weak, which may be ascribed to the following two reasons. A full helical turn in a PNA·DNA duplex takes 13 base pairs (*22*). Since in this study only heptamers are used, the secondary structure may not be fully developed. More interestingly, it should be remembered that a racemic mixture of both topological isomers of Ru−PNA **6b** is used. Therefore, duplexation with DNA gives an equimolar mixture of diastereoisomers, each giving rise to their own CD signals. Giese and co-workers have recently described the synthesis of diastereomerically pure DNA conjugates of tris(phenanthroline)ruthenium complexes (*23*). There is an ongoing debate as to which way optically pure Ru complexes of this type interact with DNA (*15*, *24*). Investigations into the preparation and hybridization properties of chirally pure Ru-PNA complexes are currently in progress.

In conclusion, we have demonstrated that the synthesis of metal PNA conjugates with high yield and purity is feasible by standard solid support peptide synthesis methods. The stability of a ruthenium-PNA conjugate binding to complementary DNA is only slightly less than for a nonmetalated PNA strand, allowing the metal complex to act as a marker for PNA·DNA binding. Studies on the synthesis and behavior of enantiomerically pure metal−PNA conjugates are underway and will be reported in due course.

ACKNOWLEDGMENT

This work was supported by the Council for Chemical Sciences of The Netherlands Organization for Scientific Research (CW-NWO) and the Fond der Chemischen Industrie. We thank Hans van den Elst for recording the HPLC-MS spectra. N.M.N. is grateful to Prof. K. Wieghardt for generous support of this work.

Supporting Information Available: Experimental details and HPLC chromatograms of **6a** and **6b**. This material is available free of charge via the Internet at http://pubs.acs.org.

LITERATURE CITED

(1) Stryer, L. (1995) *Biochemistry*, W. H. Freeman and Company, New York.
(2) Nielsen, P. E., Egholm, M., Berg, R. H., and Buchardt, O. (1991) Sequence selective recognition of DNA by strand displacement with a thymine-substituted polyamide. *Science 254*, 1497−1500.
(3) Eriksson, M., and Nielsen, P. E. (1996) PNA-nucleic acid complexes. Structure, stability and dynamics. *Q. Rev. Biophys. 29*, 369−394.
(4) Nielsen, P. E. (1998) Structural and biological properties of peptide nucleic acids (PNA). *Pure Appl. Chem. 70*, 105−110.
(5) Nielsen, P. E. (1999) Peptide Nucleic Acid. A Molecule with Two Identities. *Acc. Chem. Res. 32*, 624−630.
(6) Cass, A. E. G., Davis, G., Francis, G. D., Hill, H. A. O., Aston, W. J., Higgins, I. J., Plotkin, E. V., Scott, L. D. L., and Turner, A. P. F. (1984) Ferrocinium-coupled Glucose Oxidase Electrode. *Anal. Chem. 56*, 667−671.
(7) Schuhmann, W., Ohara, T. J., Schmidt, H.-L., and Heller, A. (1991) Electron Transfer between Glucose Oxidase and Electrodes via Redox Mediators Bound with Flexible Chains to the Enzyme Surface. *J. Am. Chem. Soc. 113*, 1394−1397.
(8) Tao, G., Katz, E., and Willner, I. (1997) Enantioselective bioelectrocatalyzed oxidation of glucose by glucose oxidase at chiral-monolayer-electrodes. *J. Chem. Soc., Chem. Commun.* 2073−2074.
(9) Ryabov, A. D., Goral, V. N., Gorton, L., and Csöregi, E. (1999) Electrochemically and Catalytically Active Reconstituted Horseradish Peroxidase with Ferrocene-Modified Hemin and an Artificial Binding Site. *Chem. Eur. J. 5*, 961−967.
(10) Ihara, T., Nakayama, M., Murata, M., Nakano, K., and Maeda, M. (1997) Gene Sensor using Ferrocenyl Oligonucleotide. *J. Chem. Soc., Chem. Commun.* 1609−1610.
(11) Wang, J., Palecek, E., Nielsen, P. E., Rivas, G., Cai, X. H., Shiraishi, H., Dontha, N., Luo, D. B., and Farias, P. A. M. (1996) Peptide nucleic acid probes for sequence-specific DNA biosensors. *J. Am. Chem. Soc. 118*, 7667−7670.
(12) Wang, J. (1998) DNA biosensors based on peptide nucleic acid (PNA) recognition layers. A review. *Biosens. Bioelectron. 13*, 757−762.
(13) Hess, A., and Metzler-Nolte, N. (1999) Transition metal labels on peptide nucleic acid (PNA) monomers. *J. Chem. Soc., Chem. Commun.* 885−886.
(14) Bigey, P., Sönnichsen, S. H., Meunier, B., and Nielsen, P. E. (1997) DNA Binding and Cleavage by a Cationic Manganese Porphyrin-Peptide Nucleic Acid Conjugate. *Bioconjugate Chem. 8*, 267−270.
(15) Holmlin, R. E., Dandliker, P. J., and Barton, J. K. (1997) Ladungsübertragung durch den DNA-Basenstapel. *Angew. Chem. 109*, 2830−2848; *Angew. Chem., Int. Ed. Engl. 36*, 2714−2730.
(16) Diederichsen, U. (1997) Ladungstransport in DNA: eine Kontroverse. *Angew. Chem. 109*, 2411−2413; *Angew. Chem., Int. Ed. Engl. 36*, 2317−2319.
(17) Verheijen, J. C., Deiman, B. A. L. M., Yeheskiely, E., van der Marel, G. A., and van Boom, J. H. (2000) Efficient Hydrolysis of RNA by a PNA-Diethylenetriamine Adduct. *Angew. Chem. 112*, 377−380; *Angew. Chem., Int. Ed. 39*, 369−372.
(18) Bergmann, F., Bannwarth, W., and Tam, S. (1995) Solid Phase Synthesis of Directly Linked PNA-DNA-Hybrids. *Tetrahedron Lett. 36*, 6823−6826.
(19) Kuwahara, M., Arimitsu, M., and Sisido, M. (1999) Sequence-Specific Hybridization between Two Different Types of Peptide Nucleic Acids. *Bull. Chem. Soc. Jpn. 72*, 1547−1552.
(20) Ceulemans, G., Van Aerschot, A., Rozenski, J., and Herdewijn, P. (1997) Oligonucleotides with 3-hydroxy-*N*-acetylprolinol as Sugar Substitute. *Tetrahedron 53*, 14957−14974.
(21) Leijon, M., Gräslund, A., Nielsen, P. E., Buchardt, O., Nordén, B., Kristensen, S. M., and Eriksson, M. (1994) Structural Characterization of PNA-DNA Duplexes by NMR. Evidence for DNA in a B-like Confomation. *Biochemistry 33*, 9820−9825.
(22) Eriksson, M., and Nielsen, P. E. (1996) Solution structure of a peptide nucleic acid-DNA duplex. *Nat. Struct. Biol. 3*, 410−413.
(23) Meggers, E., Kusch, D., and Giese, B. (1997) An efficient synthesis of enantiomerically pure Delta- and Lambda-ruthenium(II)-labeled oligonucleotides. *Helv. Chim. Acta 80*, 640−652.
(24) Kim, H.-H., Lincoln, P., Nordén, B., and Tuite, E. (1997) Absence of chiral discrimination in the interaction of tris-(diphenylphenanthroline)ruthenium(II) with DNA. *J. Chem. Soc., Chem. Commun.* 2375−2376.

BC0000740

Synthesis of a Stable and Specific Surface Plasmon Resonance Biosensor Surface Employing Covalently Immobilized Peptide Nucleic Acids

Martin Burgener,* Michael Sänger, and Urs Candrian

R+D Unit and Section for Vaccines, Division of Biologicals, Swiss Federal Office of Public Health, P.O. Box, CH-3003 Berne, Switzerland . Received January 18, 2000; Revised Manuscript Received July 5, 2000

Biosensors allow the real-time and label-free observation of biochemical reactions between various ligands including antigen−antibody reactions and nucleic acids hybridizations. In our studies, we used a surface plasmon resonance biosensor to elucidate the hybridization characteristics of a peptide nucleic acid (PNA) ligand immobilized on sensor surfaces either through covalent or streptavidin−biotin coupling. A biotin-labeled PNA was employed in the latter approach whereas the covalent immobilization included the following steps: A maleimide group was attached to the N-terminal of the PNA using *N*-succinimidyl 4-(*N*-maleimidomethyl)-cyclohexane-1-carboxylate (SMCC). To generate free thiol groups for coupling, a carboxylated dextran matrix of the sensor surface was activated with *N*-hydroxysuccinimide (NHS) and *N*-ethyl-*N*′-(dimethylaminopropyl)-carbodiimide (EDC) and thiolated by addition of cystamine dihydrochloride followed by reduction with 1,4-dithioerythrite (DTE). Finally, the modified PNA was coupled to the sulfhydryl groups of the activated dextran matrix. Repetitive hybridizations of a single-stranded synthetic DNA oligomer to the PNAs demonstrated the superior stability of covalent immobilization compared to noncovalent immobilization. Differentiation of point mutations in the analyte molecule was accomplished at 40 °C using guanidine thiocyanate concentrations of 1.5−1.7 M. In further experiments, we showed that a perfectly matched PNA allows the detection of a single-stranded DNA at a sensitivity of less than 1% in a background of single-stranded DNA having a single C to T point mutation in the region complementary to the PNA. Consequently, covalently bound PNAs provide a stable and reproducible environment for the development of mutation-specific DNA analysis assays.

INTRODUCTION

Detection and characterization of nucleic acids allow the identification of biological samples and are of central interest in many fields of molecular biology. The analysis relies on the sensitive and specific hybridization of oligonucleotide probes to nucleic acid target molecules. The hybridization of a primer to a template molecule is the central step in all amplification reactions such as polymerase chain reaction (PCR), reactions based on reverse transcription as well as DNA sequencing reactions. Southern blotting and DNA-based ELISAs rely also on the hybridization of a probe to a target sequence. In all those techniques, the final nucleic acid duplex is detected but the actual hybridization process is not monitored. The end-point determination requires direct labeling of the probe with radioactive isotopes, chemiluminescent, or fluorescent molecules. Alternatively, indirect detection is achieved by introducing marker molecules like biotin or antigenic sites that can be recognized with streptavidin and antibodies which are modified to allow color reactions (*1*). Only recently, instruments such as Taq-Man from Perkin-Elmer and the Lightcycler from Roche that allow real time monitoring of PCR have been introduced (*2*, *3*). But in most formats performed with these instruments, labeling of hybridization oligonucleotides is still required.

One area, in which nucleic acid analysis will become important in the future is the quality assurance of vaccines, e.g., live attenuated poliovirus vaccines. These vaccines were developed decades ago by Sabin and are known to be capable of reversion to neurovirulence (*4*). Therefore, each vaccine production lot is tested for neurovirulence by direct inoculation of poliovirus into the central nervous system of susceptible primates (*4*). The molecular basis for neurovirulence of poliovirus vaccine strains is the reversion of attenuating point mutations such as the backmutation from T to C at nucleotide position 472 of the Sabin poliovirus serotype 3. Assays based on PCR and restriction enzyme digestion of amplification products have been developed to detect this backmutation. One such test to assess the consistency of production at a molecular level is the so-called MAPREC (mutant analysis by polymerase chain reaction and restriction enzyme cleavage) in vitro assay. A disadvantage of the MAPREC assay, which is time and labor consuming and uses radiolabeled oligonucleotides, is the fact that it depends on the nucleotide sequence around the mutation (*4*). An adaptation of the assay to other mutations may therefore be difficult or even impossible.

In the past years, biosensor technology has been developed rapidly and it is now possible to elucidate nucleic acids interactions (*5*). Kinetic properties of hybridizations can be determined due to the ability to observe the interaction of ligand and analyte in real time, providing important knowledge for all hybridization based investigations (*6*). Applications of biosensor technology in the field of nucleic acids analysis include the detection of point mutations (*7*), the simultaneous screening of nucleic acid samples on high-density DNA arrays

* To whom correspondence should be adressed.

10.1021/bc0000029 CCC: $19.00 © 2000 American Chemical Society
Published on Web 10/21/2000

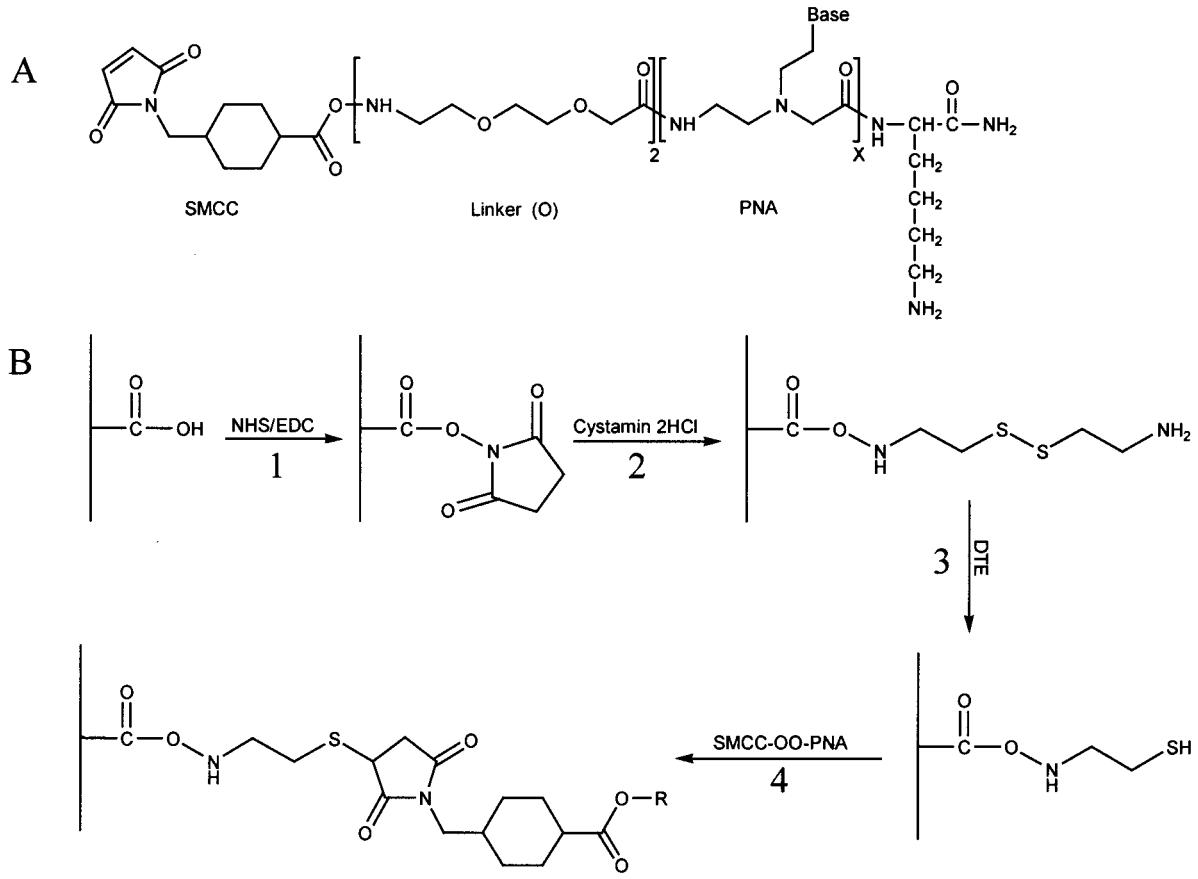

Figure 1. (A) Chemical structure of the SMCC-OO-PNA-Lys molecule. The X corresponds to the number of bases. (B) Scheme of surface modification of the carboxymethylated dextran layer. Activation of surface (1), derivatization of surface with cystaminium dihydrochloride (2), reduction of cystamine disulfides to thiols (3), coupling of PNA (4). (R is equal to OO-PNA).

(*8*), and the detection of products of the PCR employing DNA−DNA hybridization (*9*, *10*).

In our studies, we used a Biacore biosensor, based on surface plasmon resonance (SPR), to investigate as a model the mutation specific hybridization of poliovirus nucleic acids. SPR measurements are rapid and can be performed within minutes without the need for specific labels. The detection system relies on the measurement of changes in the refractive index, which is proportional to the mass of the bound analyte. With the Biacore instrument, premanufactured streptavidin-coated matrix surfaces are often used (*11*, *12*). Such surfaces allow the coupling of biotinylated DNA ligands. However, it was found that this approach does not produce stable ligand−surfaces complexes (*12*), a result that has been reproduced in our laboratory (not published). Since a high reproducibility of results is of central interest in kinetic evaluation as well as in concentration measurements, manufacture of stable sensor surfaces containing nucleic acid probes is indispensable.

We therefore replaced the insufficiently stable streptavidin−biotin-mediated attachment of nucleic acid ligands to the biosensor surface by direct covalent coupling of the ligand to the dextran surface. In addition, instead of the conventional oligonucleotide ligand, a peptide nucleic acid (PNA) was used (*13*, *14*). Due to it's unique chemical properties, application of PNAs in molecular biology has proven to be a very attractive approach for different assays (*15*−*17*): PNAs are not cleaved by common nucleases and restriction enzymes and are therefore more stable than oligonucleotides, have a higher affinity for nucleic acids than DNA, can invade DNA duplexes under low salt concentrations and build very stable triplexes with DNA (*14*, *18*). As a consequence of these properties, PNAs are more specific in the detection of point mutations, which has been shown by Wang et al. employing an electrochemical biosensor (*19*). Our work demonstrates that it is feasible to synthesize a stable, covalently linked PNA sensor surface complex able to detect point mutations in analyte oligonucleotides thus combining the advantages of real time label-free analysis with superior specificity and reproducibility.

EXPERIMENTAL PROCEDURES

Materials. All ligand and analyte oligonucleotides, except Oligo neg, were designed to cover position 472 in the domain V of the 5′ untranslated region (UTR) of Poliovirus Serotype 3, Sabin Strain. This position (boldface in the sequences below), is responsible for the attenuated phenotype, as well as reversion to neurovirulence. Oligo T and Oligo C correspond to the cDNA sequence of vaccine and revertant strain, respectively. Oligo neg was designed not to match any other sequence neither ligand, nor analyte. Oligo T, 5′-GGG TTG CAG CTG CCT GCT CCA TGG TTA G**A**A TTA GCC GCA TTC AGG-3′; Oligo C, 5′-GGG TTG CAG CTG CCT GCT CCA TGG TTA G**G**A TTA GCC GCA TTC AGG-3′; Oligo neg, 5′-ATG GCA CGC ACG ATA AAC TAG ACG CAC GAG TGA AAG ATA AAT GGC-3′.

All DNA-oligonucleotides were used as analytes and were synthesized by Microsynth, Balgach, Switzerland. Polio-PNA-SMCC, SMCC-OO-GGC TAA T**C**C TAA CCA-O-Lys-NH_2 (Figure 1), and Polio-PNA-Biotin, Bio-OO-GGC TAA T**C**C TAA CCA-Lys-NH_2, were used as Ligands (O = linker unit) and were synthesized by PE Biosystems (Framingham, MA).

All experiments were performed on a Biacore X biosensor, from Biacore, Uppsula, Sweden. Carboxymethylated-sensor chips (CM chips), streptavidin-sensor chips (SA chips), *N*-hydroxysuccinimide (NHS), *N*-ethyl-*N*′-(dimethylaminopropyl)-carbodiimide (EDC), ethanolamine and HBS buffer (10 mM HEPES, pH 7.4, 150 mM NaCl, 3.4 mM EDTA, 0.005% (v/v) surfactant P20) were purchased from Biacore.

Cystamine dihydrochloride, *N*-ethylmaleimide (NEM), guanidine thiocyanate (GuSCN), and 1,4-dithioerythritol (DTE) were from Merck, Darmstadt, Germany.

Experimental data were evaluated with Biaevolution 3.0.2, Biacore, and Gauss 3.2.38, Aptech Systems, Maple Valley, WA.

Immobilization of Biotinylated PNAs (SA-PNA Chip). All solutions are in water, expect otherwise stated. All immobilizations were carried out in HBS buffer, 25 °C, and at a flow rate of 5 μL/min. The SA chip was twice exposed to 20 μL of 50 mM sodium hydroxide to precondition the surface. Polio-PNA-Biotin (0.1 μM in 20 mM sodium phosphate buffer, pH 7.0) was immobilized to a level of about 600 RU. Not bound ligand was removed by washing with 20 μL of 50 mM NaOH.

Standard Procedure for Covalent Immobilization of PNAs (CM-PNA Chip). A total of 15μL of 50 mM NHS and 200 mM EDC was injected to yield a NHS-activated CM-Matrix. By injecting 15 μL of a 40 mM cystamine dihydrochloride, cystamine dihydrochloride was covalently bound via amine coupling (Figure 1). Surplus-active groups were deactivated using 20 μL of 1 M ethanolamine. Bound cystamine was reduced by injecting 15 μL of 100 mM DTE. Polio-PNA-SMCC (5 μM in 20 mM sodium phosphate buffer, pH 7.0) was immobilized to a level of about 600 RU. Free sulhydryl groups were deactivated by injecting 20 μL of 20 mM NEM, 1 M NaCl, 20 mM sodium phosphate buffer, pH 7.0. Not bound ligand was removed by washing with 20 μL of 50 mM NaOH.

Stability of Specific Sensor Surfaces. All hybridization experiments were carried out in 1.6 M GuSCN, 0.1 M sodium phosphate buffer, pH 7.0, 0.15 M NaCl (GuSCN buffer) as running buffer, at 40 °C and a flow rate of 10 μL/min. The regeneration solution was 50 mM of NaOH. Oligo C was dissolved in running buffer to obtain serial dilutions ranging from 39 nM to 20 μM. A total of 30 μL of each dilution was injected. Each dilution series was repeated four times on each sensor surface (SA-PNA and CM-PNA chip).

A calibration curve employing Oligo C (40 nM to 40 μM) in GuSCN buffer was established for both sensor surfaces (SA-PNA and CM-PNA chip). The curves were fitted to the equation $f(R) = R_{Hi} - [(R_{Hi} - R_{Lo})/(1 - (x/A_2)^{A_1})]$ as used in the Biaevaluation 3.0.2 software. Eighteen consecutive injections of 30 μL of 5 μM Oligo C in GuSCN buffer were performed on the SA-PNA chip. Using the first derivation of $f(R)$, $f'(R) = R_{Hi} - R_{Lo})A_2x^{(A_2-1)}/(1 + (\frac{x}{A_1})^{A_2})^2 \cdot A_1{}^{A_2}$, the concentration with the same slope as the 5 μM oligo C based on the SA calibration curve was determined for the CM-PNA calibration curve (3.8 μM). Eighteen consecutive injections of 30 μL of 3.8 μM oligo C in GuSCN buffer were performed on the CM-PNA chip.

Specificity of PNA−DNA Hybridization. A total of 30 μL of 2 μM Oligo C, Oligo T, and Oligo neg was separately injected in 0.1 M sodium phosphate buffer, pH 7.0, 0.15 M NaCl with increasing GuSCN concentrations (from 0 to 2.4 M in 0.3 M steps). Running buffer was HBS. The regeneration solution was 50 mM NaOH.

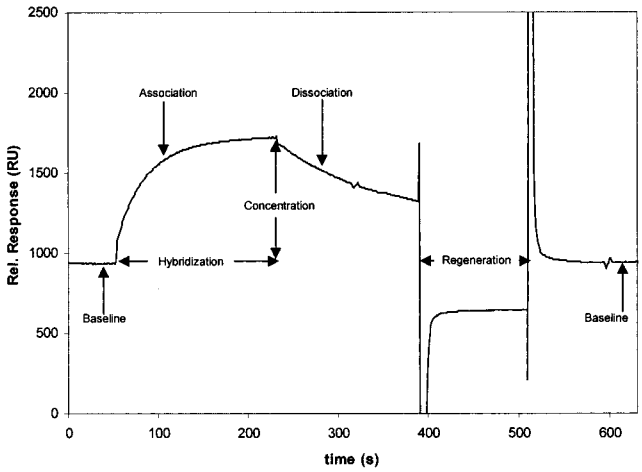

Figure 2. SPR response from a single measurement-cycle. The plot represents the difference between the analytical cell compared to the reference cell. The concentration corresponds to the maximal response signal. For experimental details see the Experimental Procedures.

Mixtures of Oligo C, Oligo T, and Oligo neg were produced to measure the specific detection of Oligo C. The amount of Oligo C compared to Oligo T was 100, 50, 10, 5, 2.5, 1, and 0.75%. The concentration of Oligo C was kept at 0.2 μM and Oligo neg was used to adjust the total amount of DNA to 26.6 μM. As controls served 100% Oligo T (40 μM) and 100% Oligo neg (40 μM). All oligos were dissolved in GuSCN buffer. A total of 30 μL of each DNA mixture was injected and the measurement cycle including hybridization, and regeneration (Figure 2) was repeated several times.

RESULTS

Synthesis of PNA Chips. As described in the Experimental Procedures, a PNA−oligonucleotide specific for the 5′ UTR of the poliovirus serotype 3 revertant, which contains a T to C mutation at nucleotide position 472, was used as a probe. The PNA was coupled to the sensor surface as follows. In one method, the PNA labeled with biotin was immobilized on a sensor chip precoated with streptavidin as previously published by Sawata et al. (*9*) (SA-PNA chip). In an alternative approach, we developed a standard procedure for the covalent binding of the PNA, modified at its N-terminal with a maleimide group, to a carboxylated dextran matrix of a sensor surface (CM-PNA chip) (Figure 1). As shown in Figure 3, this synthesis, encompassing several steps, was performed and monitored directly on the Biacore X biosensor. Six immobilizations followed by hybridization with Oligo C at an analyte concentration of 20 μM demonstrated the reproducibility of the standard immobilization procedure (2072 RU, se=23.2; excluding an extreme value of 1606 RU). Increase of NHS/EDC concentration or injection volume yielded higher PNA binding capacity, whereas increasing concentration or injection volume of cystamine dihydrocloride did not influence the binding capacity (data not shown).

Stability of PNA Sensor Chips. The stability of both types of PNA sensor chips was evaluated by hybridizing the complementary Oligo C to the immobilized PNA. For each type of PNA sensor chip, the hybridization of increasing concentrations of target DNA was measured and the dilution series was repeated four times. The resulting hybridization curves are shown in Figure 4. Clearly, each series of measurements with the SA-PNA chip yielded curves with decreased signal intensities

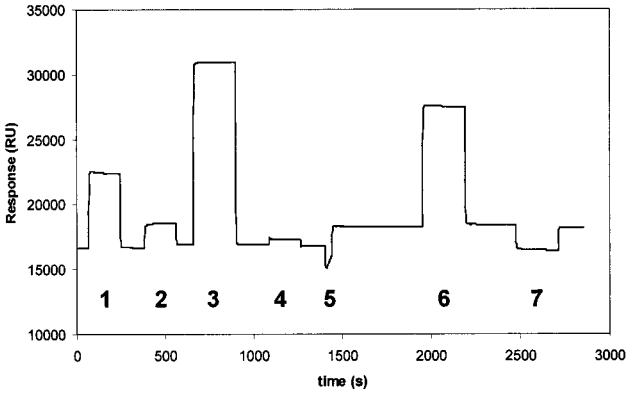

Figure 3. SPR sensogram of covalent immobilization of PNA to a CM surface. NHS activated CM Matrix (1), amine coupling of cystamine (2), deactivation of surplus NHS groups (3), reduction of cystamine to yield free sulfhydryl groups (4), covalent immobilization of Polio-PNA-SMCC (5), deactivation of free sulfhydryl groups using NEM (6), removal not bound PNA with NaOH Injection (7).

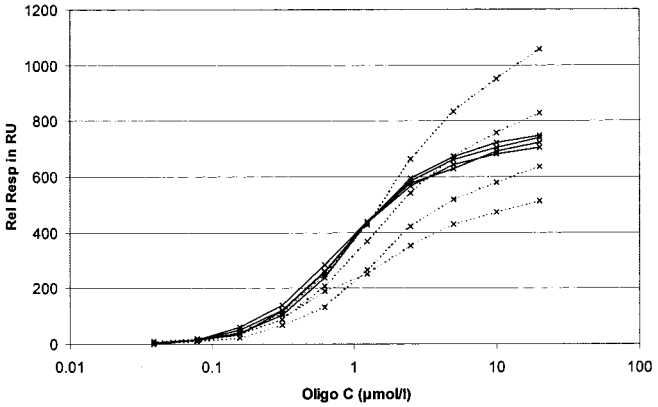

Figure 4. Overlay of concentration curves (SPR response) from four consecutive experiments with hybridization of increasing amounts of Oligo C to both, the CM-PNA chip (dashed line) and the SA-PNA chip (solid line) in GuSCN buffer. The Oligo C concentration was ranging from 39nM to 20μM.

indicating a progressive loss of hybridization capacity. At the highest target DNA concentration, the signal intensity obtained during the fourth measurement was only 48% of the one observed during the first measurement. In contrast, the chip with the covalently bound PNA gave quite consistent results through all four measurement series (94%). This result was confirmed by hybridizing constant concentrations to both types of PNA chips (Figure 5). The concentration of Oligo C was adjusted to 5 μM and 3.8 μM for the SA-PNA chip and the CM-PNA chip, respectively, to correspond to the same calibration curve slope. The chosen concentrations deliver Response signals at about 75% of the maximal saturation. The mean signal loss from one hybridization experiment to another was 2.2% for the SA-CM chip, whereas for the CM-PNA chip only 0.2%. For the 18 experiments, the last measurement reached 96 and 68% of the first for the CM-PNA chip and the SA-PNA chip, respectively.

Specificity of PNA−DNA Hybridization.. In these experiments, the CM-PNA chip was exclusively used because of its superior stability. When perfectly matched target molecules (Oligo C) as well as species with a single mismatch (Oligo T) at the 472 position were hybridized in standard salt buffer (0.1 M sodium phosphate, 0.15 M sodium chloride) to the PNA, the ligand was not specific for the analyte. Addition of the chaotropic salt guanidin thiocyanate improved the specificity of the hybridization

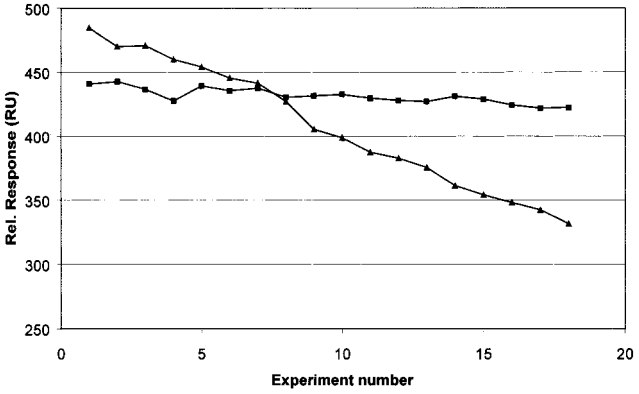

Figure 5. SPR response from 18 hybridization experiments with Oligo C for both, the CM-PNA chip (■) and the SA-PNA chip (▲). The concentration of Oligo C was 5 μM for the SA-PNA chip hybridization and 3.8 μM for the CM-PNA chip, respectively.

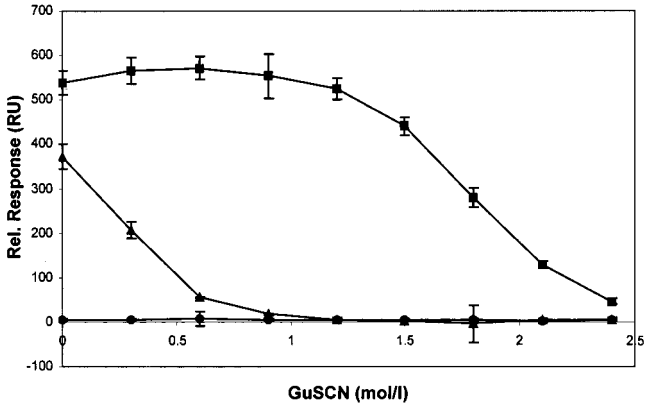

Figure 6. Determination of GuSCN concentration for specific detection of perfect match hybridization (SPR response on the CM-PNA chip). Concentration for all oligos was adjusted to 2 μM. GuSCN concentration was ranging from 0 to 2.4 M. Oligo C (■), Oligo T (▲), and Oligo neg (●). Bars indicate the confidence interval (significance level $\alpha = 0.05$).

substantially (Figure 6). At a concentration of 1.6 M GuSCN, the signal obtained with the mismatched oligonucleotide did not exceed the background signal (Oligo neg) whereas the hybridization of the perfectly matched oligonucleotide was only slightly weaker than in the buffer without GuSCN.

Sensitivity of PNA−DNA Hybridization. Again, the CM-PNA chip was used for these experiments. All hybridizations were performed in buffer containing the 1.6 M GuSCN buffer to ensure high specificity. Under these conditions, the detection of complementary Oligo C at a concentration of 0.2 μM was demonstrated with increasing amounts of the mismatched Oligo T. During the hybridization, the DNA concentration was kept constant at 26.6 μM using Oligo neg of completely unrelated sequence. As shown in Table 1, the increasing amounts of Oligo T (one mismatch) did not increase the background, and Oligo C could still be detected in the 0.75% assay, indicating that the hybridization of Oligo C was not disturbed by high background. Paradoxically, a slight increase in signal intensity was noticed with increasing amounts of mismatched oligonucleotide in mixture, although both controls, 100% oligo T and 100% Oligo neg, respectively, produced no detectable signals.

DISCUSSION

In our work we evaluated the potential of a SPR biosensor for the mutation specific characterization of

Table 1. Hybridization of Analyte Mixtures to the CM-PNA Chip

		0.2 μM Oligo C mixed with Oligo T (% Oligo C)[a]								
	0.2 μM Oligo C	100%	50%	10%	5%	2.5%	1%	0.75%	100% Oligo T[b]	100% Oligo neg[b]
RU[c]	188 ± 23	162 ± 50	155 ± 50	172 ± 37	194 ± 14	208 ± 4	227 ± 15	232 ± 25	−5.6 ± 3.8	−7.6 ± 5.6

[a] In all mixtures, total DNA concentration was adjusted to 26.6 μM with Oligo neg. [b] Concentration was kept at 40 μM. [c] Data represent mean and confidence interval (significance level $\alpha = 0.05$).

poliovirus nucleic acids. The suitability of SPR for the analysis and characterization of nucleic acids has been shown before (*8*, *9*). However, these authors failed to demonstrate the stability and the specificity at the level of point mutations of their approach based on ligand bound by the biotin−streptavidin interaction to the sensor surface. In our work, we could prove that such a surface does not give reproducible results due to loss of binding capacity of the sensor surface. There are three possible explanations for this effect: (a) loss of ligand, (b) inactivation of ligand, or (c) incomplete regeneration of the surface. In additional experiments (data not published), we could demonstrate that the reduced capacity could almost completely be replenished by immobilizing new ligand, favoring the loss of ligand explanation (while the other effects may play a minor role). Since the biotin−streptavidin binding is not a covalent one, its kinetics will depend on the conditions of the reaction; harsh conditions (e.g., regeneration of sensor surface with NaOH) may lead to a decreased association constant, therefore, destabilizing the streptavidin−biotin complex and leading to loss of ligand. This will finally lead to an decreased capacity of the sensor surface for the ligand and a lower resonance signal. We could solve this problem by attaching the PNA ligand covalently to the sensor surface. For this purpose, we developed a chemical synthesis consisting of several standardized reaction steps that could be performed within minutes and monitored online on the SPR apparatus. Increased PNA immobilization could be achieved altering NHS/EDC concentrations or injection volume, but this did not result in increased sensitivity.

In our experiments, we showed that the use of a PNA as ligand and a hybridization buffer containing a high concentration of the chaotropic salt guanidine thiocyanate results in a highly sequence specific system. We envision that adoption of our approach to other sequences requires the optimization of the GuSCN concentration only. To achieve this, experiments as shown in Figure 6, which can be completed within hours, have to be done. However, this remains to be proven even if the poliovirus sequence used in this study as a model contains internal complementary structures that make hybridization assays more difficult to perform. Furthermore, our approach is not sufficiently sensitive at this time. Target nucleic acid concentrations in the sensitivity experiment (Table 1) were 0.2 μM with a total DNA concentration of 40 μM. Compared to this, a typical PCR may contain amplified DNA at a concentration of 0.1 μM. Would one attempt to detect a mutated fragment at a level of less than 1%, the biosensor approach described in this paper would have to be 400 times more sensitive. The data presented in Table 1 may point to a solution of this problem, showing that 0.2 μM complementary Oligo C alone gave a lower signal compared to the measurement when the same concentration was mixed with 26.6 μM Oligo T with a single mismatch. Binding of this oligonucleotide to the PNA ligand can be excluded since we showed that high concentration does not yield signals even slightly above background. Thus, this observation is not due to unspecific target DNA adsorption to the sensor surface because the total DNA concentration was kept constant during the experiment and control probes produced no signal. Since our oligonucleotides, the perfectly matched as the one with a point mutation contain internal complementary sequences, we propose at this time the following hypothesis: we have proven that perfectly matched target molecules only bind to the PNA ligand. Since these molecules are substantially longer than the ligand, parts of their sequences, with internal complementarily, remain exposed and available for hybridization with free analyte in the solution. The molecules with a single mismatch in the part of the sequence complementary to the PNA ligand are able to hybridize to exposed sequences to which they are perfectly complementary. This increases the mass of the molecule bound to the PNA ligand and results according to the principals of SPR in a stronger signal. We currently investigate this phenomena and evaluate its potential to be used to obtain improved sensitivity.

ACKNOWLEDGMENT

We thank Prof. Dr. Th. Seebeck for his interest in this work and helpful discussions. This work was supported by a grant from the Swiss Defence Procurement Agency (Grant 321.001.96.53.06.03).

LITERATURE CITED

(1) Wagener, C. (1997) Molecular diagnostics. *J. Mol. Med. 10*, 728−744.

(2) Livak, K. J., Flood, S. J., Marmaro, J., Giusti, W., and Deetz, K. (1995) Oligonucleotides with fluorescent dyes at opposite ends provide a quenched probe system useful for detecting PCR product and nucleic acid hybridization. *PCR Methods Appl. 4*, 357−362.

(3) Wittwer, C. T., Ririe, K. M., Andrew, R. V., Davis, D. A., Gundry, R. A., and Balis, U. J. (1997) The LightCycler: a microvolume multisample fluorimeter with rapid temperature control. *Biotechniques 22*, 176−181.

(4) Wood, D. J., and Macadam, A. J. (1997) Laboratory tests for live attenuated poliovirus vaccines. *Biologicals 25*, 3−15.

(5) Ziegler, C., and Gopel, W. (1998) Biosensor development. *Curr. Opin. Chem. Biol. 2*, 585−591.

(6) Gotoh, M., Hasegawa, Y., Shinohara, Y., Shimizu, M., and Tosu, M. (1995) A new approach to determine the effect of mismatches on kinetic parameters in DNA hybridization using an optical biosensor. *DNA Res. 2*, 285−293.

(7) Nilsson, P., Persson, B., Larsson, A., Uhlan, M., and Nygren, P. A. (1997) Detection of mutations in PCR products from clinical samples by surface plasmon resonance. *J. Mol. Recognit. 10*, 7−17.

(8) Sapolsky, R. J., Hsie, L., Berno, A., Ghandour, G., Mittmann, M., and Fan, J. B. (1999) High-throughput polymorphism screening and genotyping with high-density oligonucleotide arrays. *Genet. Anal. 14*, 187−192.

(9) Kai, E., Sawata, S., Ikebukuro, K., Iida, T., Honda, T., and Karube, I. (1997). Novel DNA detection system of flow injection analysis (*2*). The distinctive properties of a novel system employing PNA (peptide nucleic acid) as a probe for specific DNA detection. *Nucleic Acids Symp. Ser. 37*, 321−322.

(10) Sawata, S., Kai, E., Ikebukuro, K., Iida, T., Honda, T., and Karube, I. (1999). Application of peptide nucleic acid to the direct detection of deoxyribonucleic acid amplified by polymerase chain reaction. *Biosens. Bioelecton. 14*, 397−404.
(11) Wood, S. J. (1993) DNA-DNA hybridization in real time using BIAcore. *Microchem. J. 47*, 330−337.
(12) Persson, B., Stenhag, K., Nilsson, P., Larsson, A., Uhlen, M., and Nygren, P. A. (1997) Analysis of oligonucleotide probe affinities using surface plasmon resonance: a means for mutational screening. *Anal. Biochem. 246*, 34−44.
(13) Nielsen, P. E., Egholm, M., and Buchardt, O. (1994) Peptide nucleic acid (PNA). A DNA mimic with a peptide backbone. *Bioconjugate Chem. 5*, 3−7.
(14) Corey, D. R. (1997) Peptide nucleic acids: expanding the scope of nucleic acid recognition. *Trends Biotechnol. 15*, 224−229.
(15) Orum, H., Nielsen, P. E., Egholm, M., Berg, R. H., Buchardt, O., and Stanley, C. (1993) Single base pair mutation analysis by PNA directed PCR clamping. *Nucleic Acids Res. 21*, 5332−5336.
(16) Weiler, J., Gausepohl, H., Hauser, N., Jensen, O. L., and Hoheisel, J. D. (1997) Hybridisation based DNA screnning on peptide nucleic acid (PNA) oligomer arrays. *Nucleic Acids Res. 25*, 2792−2799.
(17) Demers, D. B., Curry, E. T., Egholm, M., and Sozer, A. C. (1995) Enhanced PCR amplification of VNTR locus D1S80 using peptide nucleic acid (PNA). *Nucleic Acids Res. 23*, 3050−3055.
(18) Peffer, N. J., Hanvey, J. C., Bisi, J. E., Thomson, S. A., Hassman, C. F., Noble, S. A., and Babiss, L. E. (1993) Strand-invasion of duplex DNA by peptide nucleic acid oliomers. *Proc. Natl. Acad. Sci. U.S.A. 90*, 10648−10652.
(19) Wang, J., Rivas, G., Cai, X., Chicharro, M., Parrado, C., Dontha, N., Begleiter, A., Mowat, M., Palecek, E., and Nielsen, P. E. (1997) Detection of point mutation in the p 53 gene using a peptide nucleic acid biosensor. *Anal. Chim. Acta 344*, 111−118.

BC0000029

Photopatterning of Antibodies on Biosensors

Xiao-hui Liu, Hsu-kun Wang,† James N. Herron,† and Glenn D. Prestwich*

Department of Medicinal Chemistry and Department of Pharmaceutics and Pharmaceutical Chemistry, 30 South 2000 East, Room 201, The University of Utah, Salt Lake City, Utah 84112-5820. Received January 27, 2000; Revised Manuscript Received May 5, 2000

The immobilization of biomolecules on surfaces in defined micropatterns has become increasingly important for the development of new diagnostic devices and high-throughput genetic and drug screening protocols. We describe the synthesis and testing of thiol-reactive, photoactivatable linkers that will permit laser micropatterning or photolithographic patterning of surfaces. In these linkers, a benzophenone photophore is tethered through a variable-length poly(ethylene glycol) hydrophilic spacer to a maleimide group. Spacers containing one to five ethylene glycol units were examined. Antibodies were photoimmobilized on polystyrene waveguides and the resulting biosensors were used for fluorescence immunoassays. The spacer with five ethylene glycol units optimally decreased the steric interactions among large molecules (antibodies and antigens) and increased binding capacity and response rate of the biosensor. Two different sandwich assay protocols were examined. In the first, the antigen and fluorescently labeled second antibody were added sequentially to the biosensor ("stepwise"). In the second, the antigen and antibody were premixed before injection into the biosensor ("premixed"). The stepwise protocol gave a significantly higher response than that of the premixed protocol. Although the premixed protocol is more convenient, the stepwise protocol provides enhanced sensitivity.

INTRODUCTION

Micropatterning of surfaces with biomolecules has become important in applications that include medical diagnostic assays, high-throughput screens for drug discovery, drug toxicity screening, and genetic screening. In each application, a surface is patterned with a two-dimensional array of chemically distinct molecules. Two general approaches have emerged for patterning surfaces: (i) direct dispensing (or "spotting") of the different biomolecules on their appropriate positions in the array using a microfluidic system, and (ii) photopatterning of biomolecules on the surface using either photoactivatable cross-linkers or photodeprotection of masked or "caged" reactive functional groups (*1*). In many respects, the spotting approach is easier and faster than photopatterning. However, it is susceptible to both reduced biological activity (of the immobilized ligands) and nonspecific binding resulting from unoriented immobilization of the biomolecules by physical adsorption. Also, spotting limits the diversity of molecules that can be immobilized by photopatterning. In contrast, the heterobifunctional reagents employed in photopatterning permit site-directed coupling of biomolecules to the surfaces to provide optimal orientation for maximal bioactivity (*2*, *3*). In addition, cross-linkers can be used to covalently attach biomolecules to surfaces that are coated with thin films of hydrophilic polymers, e.g., poly(ethylene glycol) (PEG)[1] or triblock copolymers such as the Pluronic family (*4*, *5*). These site-specific cross-linking strategies can reduce nonspecific binding to proteins and other blood components.

Numerous heterobifunctional, photoactivatable cross-linking agents for protein conjugation have been reported (*6*, *7*) and many are commercially available. Most of these compounds contain aryl azides as the photophore. Benzophenone (BP)-containing reagents, however, have also been developed and used for photoimmobilization (*8*−*10*). BPs can be manipulated in ambient light and can be activated at wavelengths that cause little damage to proteins. Importantly, BPs also cross-link with higher efficiency than other photoreactive functionalities (*11*, *12*). 4-Maleimidobenzophenone (BPMI) is a commercially available thio-reactive, photoactivatable linker that is potentially useful for photoimmobilization of biopolymers on surfaces (*13*, *14*). However, this reagent is not optimal for tethering macromolecules to surfaces because the two functional groups are rigidly held within less than 8 Å of each other. We reasoned that introduction of a hydrophilic spacer would allow generation of fluorescence biosensors in which increased accessibility of the immobilized antibody to soluble antigens improved sensitivity. PEG was selected for the spacer because of its high water solubility, conformational flexibility, and biocompatibility. We report herein the preparation of a series of four BP-oligo(ethylene glycol)-maleimides (BP-EG*n*-MI, $n = 1, 2, 3, 5$) and their use to photopattern surfaces with antibodies in a site-specific manner. Sensors that were the most responsive were obtained when the BP-EG*n*-MI was first coupled to the biomolecule and the bioconjugate was subsequently photoimmobilized on the waveguide surface.

* To whom correspondence should be addressed. Phone: (801) 585-9051. Fax: (801) 585-9053. E-mail: gprestwich@deans.pharm.utah.edu.

† Department of Pharmaceuticals and Pharmaceutical Chemistry.

[1] Abbreviations: anti-BSA, anti-bovine serum albumin; anti-FL, anti-fluorescein; anti-hCG, anti-human chorionic gonadotrophin; BP, benzophenone; BPMI, 4-maleimidobenzophenone; DEAD, diethyl azodicarboxylate; DIAD, diisopropyl azodicarboxylate; DTT, dithiothreitol; FITC, fluorescein isothiocyanate; hCG, human chorionic gonadotrophin; PBS, phosphate-buffered saline; PEG, poly(ethylene glycol); PS, polystyrene.

10.1021/bc000006d CCC: $19.00 © 2000 American Chemical Society
Published on Web 09/21/2000

EXPERIMENTAL PROCEDURES

General. Tetrahydrofuran (THF) was distilled from sodium/benzophenone immediately prior to use. All reactions were conducted in oven-dried glassware. Column chromatography was performed using silica gel (60 Å, 240−400 mesh ASTM) from Whatman Co. (Hillsboro, OR). BPMI (Molecular Probes, Inc., Eugene, OR) and FluoroLink Cy5 (Amersham Life Science, Inc., Arlington Heights, IL) were used as supplied. All other organic reagents were obtained from Aldrich Chemical Co. (Milwaukee, WI).

Antibodies. Antibodies of several different specificities were employed in these studies: anti-bovine serum albumin (anti-BSA), anti-human chorionic gonadotrophin (anti-hCG), and anti-fluorescein (anti-FL). Anti-BSA was a murine monoclonal antibody (mAb) obtained from Sigma Chemical Co. (Milwaukee, WI). It was labeled with FluoroLink Cy5 (*13*). Two different anti-hCG antibodies (anti-hCGA and anti-hCGB) were used; each reacts with a different epitope on hCG, and thus the two antibodies can be employed in a sandwich immunoassay. Both anti-hCG antibodies were a generous gift of Akzo-Nobel Chemicals, Inc. (Dobbs Ferry, NY). Anti-hCGA was cleaved into monovalent half molecules using 2-mercaptoethylamine (*15*). This procedure produces several reactive thiol groups in the hinge region that were used for site-specific immobilization. Anti-hCGB was labeled with FluoroLink Cy5 to give the second antibody for the sandwich immunoassays.

The anti-fluorescein antibody (anti-FL 9-40) belongs to the $IgG_1(\kappa)$ subclass and exhibits an affinity of about 1×10^7 M^{-1} at 25 °C (*16*). The hybridoma cell-line that secretes this antibody was obtained from Professor Edward W. Voss, Jr. (University of Illinois at Urbana−Champaign). Anti-FL 9-40 was produced in murine ascites fluid and purified (*13*). Purified anti-FL 9-40 was then digested with pepsin to produce $(Fab')_2$ fragments, which were then reduced to Fab′ fragments using dithiothreitol (DTT) (*13*). The Fab′ fragments contain thiol groups at the C-terminal end that were used for site-specific immobilization.

Antigens. BSA was labeled with both fluorescein isothiocyanate (FITC) and FluoroLink Cy5. The labeling was carried out as follows: BSA (2 mg) was reacted with FITC (20-fold molar excess) in sodium carbonate buffer, pH 8.0, at room temperature for 2 h and the BSA-FL was separated by a PD-10 column with phosphate-buffered saline (PBS) as eluent. Then the BSA-FL was allowed to react with Cy5 dye in sodium carbonate buffer, pH 9.3, at room temperature for 30 min; the product, Cy5-BSA-FL, was purified again by a PD-10 column using PBS buffer as eluent. UV−vis: $\lambda_{max} = 278$, 496, and 652 nm; calculation based on extinction coefficients indicated a BSA:FL:Cy5 ratio of 1:0.7:0.7. BSA and hCG were obtained from Sigma.

Synthetic Methods. 2-(2-Fluorenylmethoxycarbonyl-aminoethoxy)-ethanol (1) (*17*). A solution of 9-fluorenylmethyl chloroformate (1.00 g, 3.86 mmol) in 30 mL of dry THF was cooled in an ice bath. 2-(2-Aminoethoxy)-ethanol (810 mg, 7.70 mmol, dissolved in 20 mL of dry THF) was added slowly. The mixture was stirred in the ice bath for 20 min and at room temperature for 20 min. After filtration to remove the amine salt, the solution was condensed to give 1.26 g (100%) of the carbamate **1** as white semisolid. ^{1}H NMR ($CDCl_3$, 200 MHz) δ 3.40 (m, 2H, CH_2N), 3.56 (m, 4H, 2-CH_2O−), 3.70 (m, 2H, −OCH_2−), 4.22 (t, $J = 7$ Hz, 1H, −CH−), 4.40 (d, $J = 7$ Hz, 2H, −CH_2OCO), 7.29 (m, 4H, 4H−Ar), 7.57 (d, $J = 7.6$ Hz, 2H, 2H−Ar), 7.75 (d, $J = 7.6$ Hz, 2H, 2H−Ar). ^{13}C NMR ($CDCl_3$, 200 MHz) δ 195.9, 156.5, 143.9, 141.3, 127.6, 127.0, 124.9, 120, 72.2, 70.0, 66.5, 61.6, 47.2, 40.8. EI-MS *m/z* 327(M^+, 0.19), 196 (0.2), 180 (2.0), 179 (21.9), 178 (100), 165 (7.2). HRMS (EI) (*m/z*) calcd for $C_{19}H_{21}NO_4$ (M^+) 327.1470; found 327.1456.

4-(2-(2-Fluorenylmethoxycarbonyl-aminoethoxy)-ethoxy)-benzophenone (2). 4-Hydroxybenzophenone (624 mg, 3.15 mmol), 2-(2-fluorenylmethoxycarbonyl-aminoethoxy)-ethanol (**1**, 1.00 g, 3.05 mmol), and Ph_3P (948 mg, 3.6 mmol) were dissolved in 24 mL of dry THF and cooled to 0 °C under N_2. Diethyl azodicarboxylate (DEAD) (0.6 mL, 3.79 mmol) was added slowly. The mixture was stirred for 3 h then stored at room temperature overnight. After concentration in vacuo, the residue was purified on SiO_2 (ethyl acetate−hexanes 1:3 to 1:1) to give 1.21 g (78%) of compound **2** as a pale yellow oil. ^{1}H NMR ($CDCl_3$, 200 MHz) δ 3.46 (m, 2H, CH_2N), 3.64 (m, 2H, −OCH_2−), 3.85 (m, 2H, −CH_2O−), 4.20 (m, 3H, −OCH_2-, −CH−), 4.36 (d, $J = 6.6$ Hz, −CH_2CO−), 6.98 (m, 2H, Ar), 7.2−7.8 (15H, Ar). ^{13}C NMR ($CDCl_3$, 200 MHz) δ 195.5, 162, 156.2, 143.9, 141.0, 138.0, 132.5, 131.9, 129.7, 128.2, 127.6, 127.0, 125.0, 120.0, 114.0, 70, 69.3, 67.5, 68.9, 62.5, 47.2, 41.0. EI-MS *m/z* 508 ($M^+ + 1$, 0.02) 463 (0.05), 311 (7.5) 256 (14.8) 198 (28.8), 178 (100). CI-MS: *m/z* 508 ($M^+ + 1$, 1.04), 314 (15.9), 286 (95), 199 (44.5) 179 (100), 105 (20). HRMS (EI) (*m/z*) calcd for $C_{32}H_{30}NO_5$ ($M^+ + 1$) 508.2124; found 508.2136.

4-(2-(2-Aminoethoxy)ethoxy)-benzophenone (3) (*17*). Compound **2** (872 mg, 1.72-mmol) was dissolved in 5 mL of piperidine and stirred for 40 min at room temperature. Then the solution was concentrated in vacuo, and the residue was dissolved in dichloromethane and washed with water (20 mL × 2). The organic layer was dried over $MgSO_4$, concentrated, and purified on SiO_2 (ethyl acetate:methanol:ammonium hydroxide 100:2:1) to give 400 mg (81.6%) of **3** as a pale yellow oil. ^{1}H NMR ($CDCl_3$, 200 MHz) δ 2.99 (t, $J = 5.3$ Hz, 2H, CH_2N), 3.58 (t, $J = 5.3$ Hz, 2H, −OCH_2−), 3.85 (t, $J = 5.0$ Hz, 2H, −CH_2O−), 4.20 (t, $J = 5.0$ Hz, 2H, −OCH_2−), 6.99 (m, 2H, Ar), 7.50 (m, 3H, Ar), 7.75 (m, 4H, Ar). ^{13}C NMR ($CDCl_3$, 200 MHz) δ 195.5, 162.4, 138.0, 132.5, 131.6, 130.2, 129.7, 128.1, 114.0, 73.6, 69.2, 67.5, 41.7. EI−MS: *m/z* 285 (M^+, 2.29), 256 (50.7), 198 (100), 121 (19.2), 105 (24.4), 98 (15.4). HRMS (EI) (*m/z*) calcd for $C_{17}H_{19}NO_3$ (M^+) 285.1365; found 285.1358.

N-Substituted Maleamic Acid (4) (*18*). A reaction mixture containing compound **3** (100 mg, 0.35 mmol), and maleic anhydride (35 mg, 0.35 mmol) in 0.7 mL of glacial acetic acid was stirred for 20 h. The mixture was purified on SiO_2 (ethyl acetate:acetic acid, 100:3) to afford 110 mg (82%) of **4** as a colorless oil. ^{1}H NMR ($CDCl_3$, 200 MHz) δ 3.65 (t, $J = 5.4$ Hz, 2H, −CH_2N), 3.72 (t, $J = 5.4$ Hz, 2H, −OCH_2−), 3.92 (t, $J = 4.4$ Hz, 2H, −CH_2O−), 4.20 (t, $J = 4.4$ Hz, 2H, −OCH_2−), 6.10 (d, $J = 14.8$ Hz, 1H, CH =), 6.35 (d, $J = 14.8$ Hz, 1H, =CH), 6.98 (m, 2H, Ar), 7.50(m, 3H, Ar), 7.80 (m, 4H, Ar). EI-MS *m/z* 383-(M^+, 4.32), 365 (19.5), 312 (9.3), 256 (29.2), 242 (48.5), 198 (93), 165 (23), 121 (100), 105 (56.8). HRMS (EI) (*m/z*) calcd for $C_{21}H_{21}NO_6$ (M^+) 383.1369; found 383.1374.

BP-EG2-MI (5). A reaction mixture containing maleamic acid **4** (85 mg, 0.22 mmol) in 0.3 mL of acetic anhydride and sodium acetate (25 mg, 3 mmol) was heated at 90 °C for 2 h. It was cooled to room temperature and quenched with 10 mL of water. The aqueous solution was extracted with ethyl acetate (10 mL × 2). The combined organic extracts were dried (Na_2SO_4) and concentrated in vacuo. The residue was purified on SiO_2 (ethyl acetate:hexane 3:1) to give 67 mg (83%) of the pure product **5** as

a colorless oil. ^{1}H NMR ($CDCl_3$, 200 MHz) δ 3.72 (m, 4H, $-OCH_2CH_2N=$), 3.82 (m, 2H, $-CH_2O-$), 4.13 (t, J = 4.4 Hz, 2H, $-OCH_2-$), 6.64 (s, 2H, CH=CH), 6.93 (m, 2H, Ar), 7.50 (m, 3H, Ar), 7.75 (m, 4H, Ar). ^{13}C NMR ($CDCl_3$, 200 MHz) δ 195.4, 170.5, 162.3, 139.1, 134.0, 132.4, 131.6, 130.2, 129.6, 129.1, 114.0, 68.8, 68.0, 67.5, 67.3, 67.0, 38.0, 36.9, 20.4. EI-MS *m/z* 365 (M^+, 68.4), 288 (4.26), 224 (21.7), 198 (32.5), 124 (100), 105 (32). HRMS (EI) (*m/z*) calcd for $C_{21}H_{19}NO_5$ (M^+) 365.1263; found 365.1247.

4-Hydroxyethoxybenzophenone (6). 4-Hydroxybenzophenone (300 mg, 1.513 mmol), ethylene glycol (281 mg, 4.54 mmol), and Ph_3P (595 mg, 2.27 mmol) were dissolved in 20 mL of dry THF and cooled to 0 °C under N_2. Diisopropyl azodicarboxylate (DIAD) (0.34 mL, 2.27 mmol) was added slowly. The mixture was stirred at 0 °C for 3 h then stored at room temperature for 24 h. After concentration in vacuo, the residue was purified on SiO_2 (ethyl acetate:hexane 1:1) to afford 201 mg (55%) of compound **6** as a colorless oil. ^{1}H NMR ($CDCl_3$, 200 MHz) δ 4.0 (t, J = 4.6 Hz, 2H, $-CH_2O-$), 4.16 (t, J = 4.6 Hz, 2H, $-OCH_2-$), 6.96 (d, J = 8.8 Hz, 2H, Ar), 7.24−7.56 (m, 3H, Ar), 7.71−7.84 (m, 4H, Ar). ^{13}C NMR ($CDCl_3$, 200 MHz) δ 195.6, 162.3, 138.0, 132.5, 131.9, 130.3, 129.7, 128.2, 114.0, 69.4, 61.1. EI-MS *m/z* 242.1 (M^+, 63.9), 165.1 (35.4), 121.0 (100), 105.0 (34.4), 77 (22.9). HRMS (EI) (*m/z*) calcd for $C_{15}H_{14}O_3$ (M^+) 242.0943, found 242.0930.

BP-EG1-MI (7) (*19*, *20*). DIAD (0.056 mL, 0.371 mmol) was added to a solution containing 4-hydroxyethoxybenzophenone (**3**, 60 mg, 0.248 mmol), maleimide (96 mg, 0.99 mmol), and Ph_3P (97 mg, 0.371 mmol) in 3 mL of dry THF precooled to 0 °C. The mixture was stirred at 0 °C for 3 h, then allowed to stand at room temperature for 24 h. After concentration in vacuo, the residue was purified on SiO_2 (ethyl acetate:hexane 1:2) to afford 51 mg (32%) of BP-EG1-MI **7** as pale yellow oil. ^{1}H NMR ($CDCl_3$, 200 MHz) δ 3.96 (t, J = 5.5 Hz, 2H, CH_2), 4.20 (t, J = 5.5 Hz, 2H, CH_2), 6.73 (s, 2H, CH=CH), 6.90 (d, J = 8.8 Hz, 2H, Ar), 7.24−7.55 (m, 3H, Ar), 7.69−7.80 (m, 4H, Ar). ^{13}C NMR ($CDCl_3$, 200 MHz) 195.6, 170.4, 161.7, 138.1, 135.0, 134.2, 132.5, 131.9, 130.5, 129.7, 128.2, 114.1, 70.0, 64.7, 37.0, 21.9. EI-MS *m/z* 321.3 (14.4), 211.2 (5.82), 124.1 (100), 105.1 (8.4). HRMS (EI) (*m/z*) calcd for $C_{19}H_{15}NO_4$ (M^+) 321.1001, found 321.1007.

4-Tri(ethylene glycol) Benzophenone (8). 4-Hydroxybenzophenone (500 mg, 2.52 mmol), tri(ethylene glycol) (378 mg, 2.52 mmol), and Ph_3P (758 mg, 2.88 mmol) were dissolved in 24 mL of dry THF and cooled to 0 °C under N_2. DEAD (0.48 mL, 3.03 mmol) was added slowly. The mixture was stirred at 0 °C for 3 h, then allowed to stand at room temperature overnight. After condensation, the residue was purified on SiO_2 (ethyl acetate-petroleum ether) to afford 327 mg (58%) of compound **8** as a colorless oil. ^{1}H NMR ($CDCl_3$, 200 MHz) δ 3.61 (t, J = 3.35 Hz, 2H, CH_2OH), 3.72 (m, 6H, 3-CH_2-), 3.89 (t, J = 4.9 Hz, 2H, $-CH_2O-$), 4.20 (t, J = 4.9 Hz, 2H, $-OCH_2-$), 6.96 (d, J = 8.9 Hz, 2H, Ar), 7.44−7.55 (m, 3H, Ar), 7.70−7.62 (m, 4H, Ar). ^{13}C NMR ($CDCl_3$, 200 MHz) δ 195.5, 162.2, 138.1, 132.5, 132.1, 131.7, 130.2, 129.7, 128.6, 128.3, 128.1, 114.0, 72.4, 70.8, 70.2, 69.4, 67.5, 61.6. EI-MS *m/z* 331.1 (0.14), 277 (74.0), 198 (26.7), 183 (9.16), 121 (16.3), 105 (50.4), 77 (24.7), 45 (100). HRMS (EI) (*m/z*) calcd for $C_{19}H_{22}O_5$ (M^+) 330.1467; found 330.1473.

BP-EG3-MI (9). DEAD (0.05 mL, 0.309 mmol) was added to a solution containing 4-tri(ethylene glycol) BP (**8**, 100 mg, 0.303 mmol), maleimide (30 mg, 0.309 mmol), and Ph_3P (81 mg, 0.309 mmol) in 2 mL of dry THF that was precooled to 0 °C. The reaction was performed and worked up as described for compound **7** to afford 32 mg (27%) of BP-EG3-MI **9** as a colorless oil. ^{1}H NMR ($CDCl_3$, 200 MHz) δ 3.62−3.72 (m, 8H), 3.64 (t, J = 4.5 Hz, 2H, CH_2), 4.18 (t, J = 5 Hz, 2H, CH_2), 6.66 (s, 2H, CH=CH), 6.95 (d, J = 8.88 Hz, 2H, Ar), 7.45−7.49 (m, 3H, Ar), 7.71−7.82 (m, 4H, Ar). ^{13}C NMR ($CDCl_3$, 200 MHz) δ 195.0, 171.5, 162.4, 134.1, 132.5, 131.9, 129.7, 128.1, 114.1, 106.5, 103.5, 102.5, 70.8, 70.0, 69.5, 67.9, 67.6, 37.1, 13.0. EI-MS *m/z* 409.4 (10.3), 224.2 (11.6), 168.2 (4.5), 124.1 (100), 105.1 (31.06). HRMS (EI) (*m/z*) calcd for $C_{10}H_{23}NO_6$ (M^+) 409.1525; found 409.1523.

4-Penta(ethylene glycol) Benzophenone (10). 4-Hydroxybenzophenone (250 mg, 1.26 mmol), penta(ethylene glycol) (734 mg, 3.78 mmol), and Ph_3P (331 mg, 1.26 mmol) were dissolved in 8 mL of dry THF and cooled to 0 °C under N_2. DEAD (0.2 mL, 1.26 mmol) was added slowly and stirred at 0 °C for 3 h, then continuous stirring at room temperature for 2 days. After concentration in vacuo, the residue was purified on SiO_2 (ethyl acetate: hexane 1:1 to ethyl acetate:methanol 20:1) to afford 163 mg (34%) of compound **10** as a colorless oil. ^{1}H NMR ($CDCl_3$, 200 MHz) δ 3.57−3.76 (m, 16H, 8CH_2), 3.85 (t, J = 5 Hz, 2H, $-CH_2-$), 4.20 (t, J = 4.6 Hz, 2H, $-CH_2-$), 6.96 (d, J = 8.8 Hz, 2H, Ar), 7.45−7.52 (m, 3H, Ar), 7.71−7.82(m, 4H, Ar). ^{13}C NMR ($CDCl_3$, 200 MHz) δ 195.5, 162.4, 138.2, 132.4, 131.6, 130.2, 129.6, 128.1, 114.1, 72.5, 70.8, 70.5, 70.2, 69.4, 67.5, 61.6. EI-MS *m/z* 388.2 (1.85), 300.2 (7.93), 286.1 (10.4), 224.0 (22.6), 198.1 (21.9), 147.0 (6.9), 121.0 (15.8), 105.0 (60.6), 45.0 (100).

BP-EG5-MI (11). DIAD (0.043 mL, 0.286 mmol) was added into a solution containing 4-penta(ethylene glycol) BP (**1**, 80 mg, 0.191 mmol), maleimide (74 mg, 0.764 mmol), and Ph_3P (75 mg, 0.286 mmol) in 3 mL of dry THF that was precooled to 0 °C. The reaction was performed and worked up as described above to afford 36 mg (38%) of BP-EG5-MI **11** as a pale yellow oil. ^{1}H NMR ($CDCl_3$, 200 MHz) δ 3.58−3.74 (m, 16H), 3.87 (t, J = 5.2 Hz, 2H, CH_2), 4.20 (t, J = 4.4 Hz, 2H, CH_2), 6.67 (s, 2H, CH=CH), 6.95 (d, J = 8.8 Hz, 2H, Ar), 7.24−7.55 (m, 3H, Ar), 7.71−7.62 (m, 4H, Ar). ^{13}C NMR ($CDCl_3$, 200 MHz) 195.5, 170.6, 162.4, 138.2, 134.1, 132.5, 131.9, 130.2, 129.7, 128.1, 114.1, 70.8, 70.6, 70.5, 70.0, 69.5, 67.7, 67.6, 37.1. EI-MS *m/z* 472.2 (0.64), 30.1 (6.56), 286.1 (10.6), 268.1 (4.98), 224.0 (19.6), 198.1 (7.58), 124.0 (100), 105.0 (41.2). HRMS (EI) (*m/z*) calcd for $C_{27}H_{31}NO_8$ (M^+) 497.2050; found 497.2027.

Photoimmobilization of Antibodies on Biosensor Waveguides. Photoimmobilization of BP-EG*n*-MI (*n* = 0, 1, 2, 3, 5) and Antibody Immobilization. The biosensor waveguide is a 2.54 × 2.54 cm clear polystyrene (PS) slide with a molded lens for the coupling of excitation light (*13*, *14*, *21*). The surfaces were tested either on clean PS or PS-coated (adsorbed) with Pluronic P105. The waveguides were mounted on metallic coating trays. Stock solutions of linkers (10 μM) were prepared in DMF and diluted into buffer. An aliquot (1 mL) of a given BP-EG*n*-MI cross-linker (150 nM in 0.1 M $NaPO_4$, pH 6.0) was applied to cover the surface of each tray. The trays were then irradiated (360 nm, 1.9 mW/cm^2) at 4 °C for 45 min. After the photochemical reaction, the surfaces were washed three times with 0.1 M NaH_2PO_4 buffer, pH 6.0 containing 5 mM EDTA.

Freshly prepared anti-FL Fab′ (1 mL, 3 mM in 0.1 M $NaPO_4$ buffer, pH 6.0, with 5 mM EDTA) was applied onto each of the freshly washed surfaces, and the reaction between the free thiol group and the maleimide double bond was allowed to proceed at 4 °C overnight. After the reaction the surfaces were postcoated with a solution of 0.5 BSA and 0.1% trehalose in PBS buffer at room temperature for 30 min and dried in vacuo.

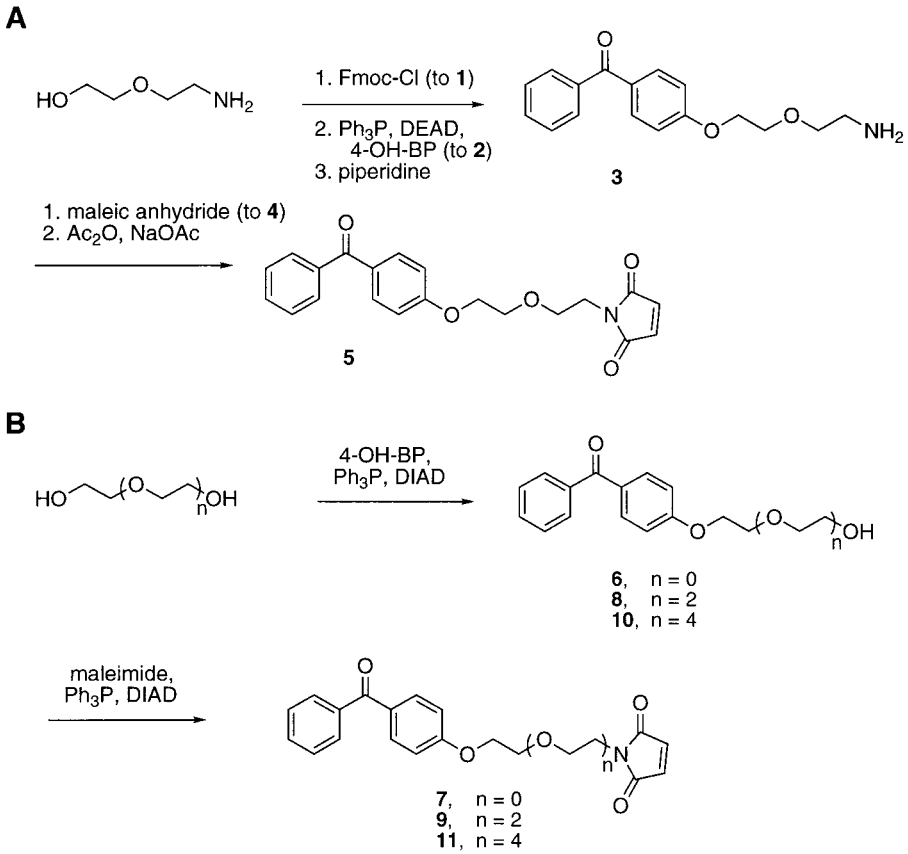

Figure 1. Synthesis of BP-EG*n*-MI (n = 0, 1, 2, 3, 5).

In other experiments (routes 3 and 4), the order of addition was reversed. Thus, PB-EG*n*-MI reagents were first coupled to a half-molecule of anti-hCG-A and the BP-containing bioconjugates were subsequently photoimmobilized on the PS surfaces.

Biosensor Assays. Both direct antigen binding assays (for FL-BSA-Cy5) and sandwich assays (for both FL-BSA and hCG) were employed. For the direct antigen binding assay, FL-BSA-Cy5 acted as both antigen and tracer. A waveguide surface coated with anti-FL Fab′ was assembled into the flow cell, and the flow cell was mounted into the instrument. A solution of FL-BSA-Cy5 at a given concentration was pumped into the flow cell and the binding of FL-BSA-Cy5 was recorded over time with a CCD camera. Cy5 fluorescence was excited at 635 nm using a red semiconductor laser. Fluorescence emission was detected at 670 nm using an interference filter (Omega). For sandwich assays having FL-BSA as the antigen, FL-BSA was allowed to react with the sensor surface for 5 min, and then the surface was flushed with PBS buffer to remove the unbound antigen. Tracer solution (anti-BSA-Cy5) was then injected, and the sandwich formation was monitored using the CCD camera. Alternatively, the antigen and the tracer solutions could be premixed and injected. For the hCG assays, waveguides coated with the half-molecule of anti-hCG-A antibody were allowed to react with hCG for 5 min, tracer-antibody (anti-hCG-B−Cy5) was injected into the flow cell, and sandwich formation was monitored with a CCD camera. In some cases, hCG and tracer antibody (anti-hCG-B−Cy5) were premixed before injection into the flow cell. Details of the assay technique have been previously described (*13, 14, 21*).

Photopatterning of a Waveguide Surface. A clean waveguide surface was covered by a gasket in the shape of the letter "U", and the photolinker-antibody solution-BP-EG5-MI-1/2 anti-hCG-A (150 nM in PBS) was added to the "U". The entire unit was irradiated (360 nm, 1.9 mW/cm^2) at 4 °C for 45 min. The surface was then washed with 10 mM phosphate buffer, pH 7.4, and the entire surface was postcoated with 10% StabilCoat (BSI Corporation, Eden Prairie, MN). The surface was incubated with hCG (3.5 nM) for 30 min at room temperature and binding of anti-hCG-B-Cy5 (1 nM) for another 30 min at room temperature. The surface was washed with deionized water and air-dried. A fluorescence image of the "U" was obtained using CCDOPS 1.061(SBIG, Santa Barbara, CA).

RESULTS AND DISCUSSION

Four new BP-EG*n*-MI (n = 1, 2, 3, 5) cross-linkers were synthesized using two different routes (*17*−*20*). BP-EG2-MI (Figure 1A) was prepared in five steps from 2-(2-aminoethoxy)ethanol. After protection as the Fmoc derivative **1**, the BP ether **2** was formed by Mitsunobu coupling with 4-hydroxybenzophenone. Deprotection with piperidine gave free amine **3**, and the maleimide moiety was introduced by acylation with maleic anhydride followed by cyclization of maleamic acid **4** to the final product **5**. A more efficient route was subsequently developed for the remaining heterobifunctional reagents, BP-EG*n*-MI (n = 1, 3, 5). Using sequential Mitsunobu reactions (Figure 1B), first the 4-hydroxybenzophenone and then maleimide moieties were sequentially coupled to the ends of any given PEG. Although the yield of the first coupling is complicated by the production of a bis-BP ether byproduct, this was removed by chromatography and gave a net overall increase in synthetic yield in fewer steps. Each compound was characterized by ^{1}H and ^{13}C NMR. The final compounds, BP-EG*n*-MI, were not soluble in water but were prepared as 10 μM DMF

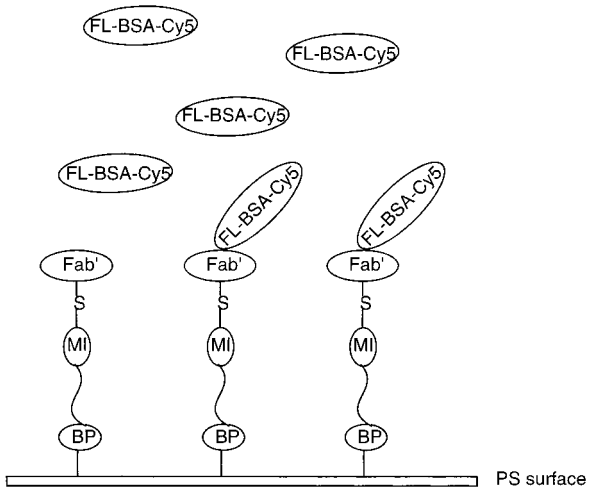

Figure 2. Schematic diagram of photoimmobilization and biosensor assays. BP-EG*n*-MI reagents were first coupled to anti-FL Fab′, then the BP-containing bioconjugates were photoimmobilized on PS or Pluronic P105-coated PS surfaces. In the direct antigen binding assay, FL-BSA-Cy5 acted as both antigen and tracer. In the sandwich assay (not shown), FL-BSA (used as antigen) was injected into the flow cell and allowed to react with the immobilized antibodies for 5 min. A solution containing anti-BSA-Cy5 was then injected into the flow cell, and binding to the immobilized antigen−antibody complex was monitored with a CCD camera.

solutions, then diluted to 150 nM in 0.1 M NaH_2PO_4 (pH 6.0) buffer for subsequent photoimmobilization experiments.

Uncoated (clean) and P105-coated PS surfaces reacted differently with BP-EG*n*-MIs. The cross-linker-antibody conjugates covalently coupled to the uncoated PS surface to give an essentially homogeneous monolayer. In contrast, the P105-coated PS had many PEG chains that could either react with or prevent hydrophobic adsorption of the bioconjugates. As a result, attachment of the antibody was reduced, and antigen-containing sites appeared unavailable for binding. The poor reproducibility of biosensor response for antibodies photoimmobilized onto P105-coated PS (data not shown) led us to abandon this approach. Several different approaches were thus compared to obtain the analytical system illustrated diagrammatically in Figure 2.

In Figure 3, route 1 involves initially photoimmobilizing the BP-EG*n*-MI (n = 0, 1, 2, 3, 5) onto PS surfaces and subsequent incubation with anti-FL Fab′ fragment at 4 °C overnight to produce a monolayer of BP-EG*n*-MI−Fab′ conjugates (see Figure 2). After postcoating with BSA to block regions of unmodified PS, a FL-BSA-Cy5 solution was passed over the surface in the flow cell, and fluorescence emission was recorded. The results are shown in Figure 4. Among the five BP-EG*n*-MIs, BP-EG5-MI and BPMI gave the best binding rates and highest capacities, while BP-EG1-MI, BP-EG2-MI, and BP-EG3-MI gave essentially identical specific binding properties. Specific binding is a function of antibody orientation and density. At present, the particular steric and orientational factors that cause high specific binding by the EG0 and EG5 ligands and the reduced binding of the EG1, EG2, and EG3 ligands remain unclear.

The effectiveness of the different BP-EG*n*-MIs at reducing nonspecific binding was evaluated (route 2, Figure 3). Figure 5 shows that with no coating on the PS surface, FL-BSA-Cy5 absorbed rapidly and gave a strong increase in fluorescence. In contrast, after the photoimmobilization of BP-EG*n*-MI onto the PS, the

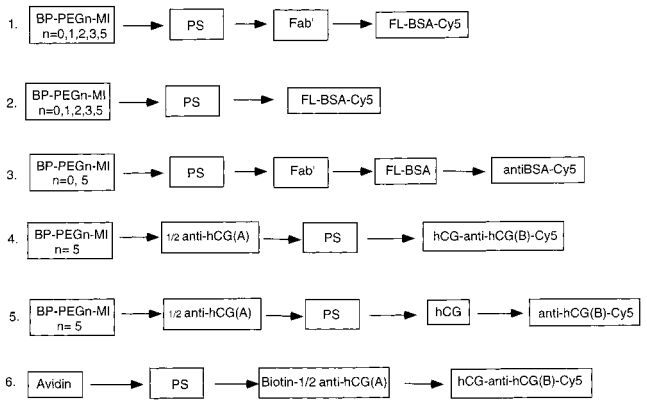

Figure 3. Protocols used for photoimmobilization and biosensor assays on PS surfaces. In route 1, each of the BP-EG*n*-MI cross-linkers was photoimmobilized on a waveguide surface, followed by reaction with anti-FL Fab′. The ability of the immobilized Fab′ fragment to bind antigen (FL-BSA-Cy5) was then tested. Routes 1 and 2 are direct antigen binding assays; routes 3−6 are sandwich assays.

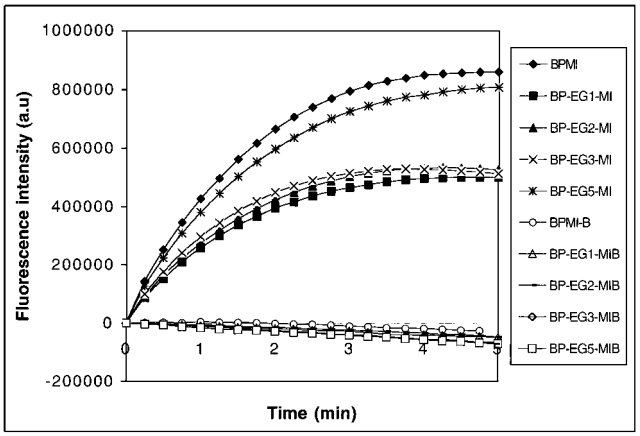

Figure 4. Effect of ethylene glycol spacer length on the antigen-binding activity of Fab′ fragment immobilized with the BP-EG*n*-MI cross-linkers. The immunoassay was performed as in route 1 (Figure 3). In the control experiments (labeled BP-EG*n*-MIB), the different BP-EG*n*-MI cross-linkers were photoimmobilized, followed directly by postcoating BSA; however, no Fab′ fragment was immobilized. Nonspecific binding was examined by injecting various concentrations of FL-BSA-Cy5 into the flow cell. Each data point is the mean of six independent determinations. Error bars are displayed but not readily visible since their size is comparable to the plot symbols. The time courses for the controls ("MIB") are overlapped at the baseline.

nonspecific binding of FL-BSA-Cy5 decreased significantly with an increasing number of ethylene glycol units. However, if the surface was further treated with BSA (without Fab′), the binding of FL-BSA-Cy5 was negligible (BP-EG*n*-MIB). Therefore, the nonspecific binding of FL-BSA-Cy5 on BP-EG5-MI-coated surfaces was higher than desired and postcoating the surface with BSA was still necessary prior to performing the biosensor assay.

Since comparable results were observed for BP-EG5-MI and BPMI in Figure 4, we examined a third protocol (route 3, Figure 3) using a sandwich immunoassay. Following photoimmobilization and chemical linking of the anti-FL Fab′, FL-BSA and anti-BSA-Cy5 solutions were allowed to react with the PS waveguide sequentially at 5 min intervals. Two different concentrations (1 and 10 nM) of anti-BSA were examined. In the case of stepwise immunoassay, the rate of binding to the BP-EG5-MI surface was four times faster than for the BPMI surface (Figure 6). This demonstrates that the penta-(ethylene glycol) unit spacer can decrease the steric

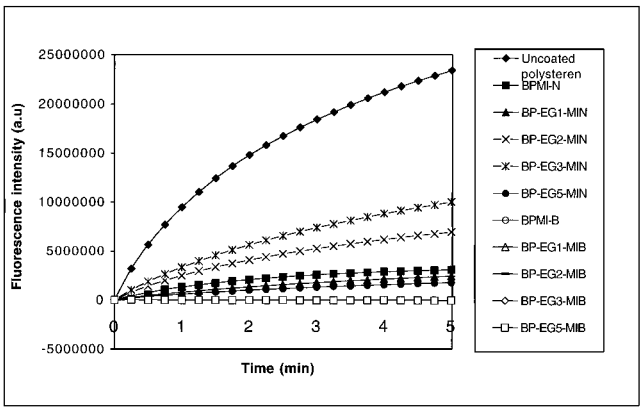

Figure 5. Effects of ethylene glycol spacer and post-coating on the nonspecific adsorption of BSA to PS surfaces. The binding sequence on the waveguide is shown in route 2 (Figure 3). The time courses for the controls are overlapped at the baseline. See text for experimental details and Figure 4 legend for details of data presentation.

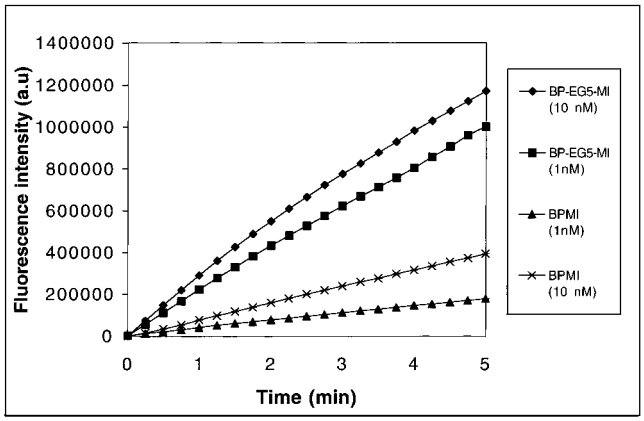

Figure 6. Effect of ethylene glycol spacer length on the antigen-binding capacity of anti-FL antibodies immobilized with BP-EG5-MI and BPMI. The binding sequence used in this experiment is shown in route 3 (Figure 3). Two different concentrations of anti-BSA (1 and 10 nM) were employed. See text and Figure 4 legend for details.

hindrance for the antigen to approach the antibody epitopes, and thereby enhance the antigen-binding capacity and resultant sensitivity of a biosensor.

To evaluate the feasibility and generality of BP-EG5-MI use in fluorescence biosensors, we examined routes 4, 5, and 6 (Figure 3) using a fluorescence immunoassay for hCG. In routes 4 and 5, BP-EG5-MI was allowed to react with the monovalent half-molecule of anti-hCG-A. Then, these half-antibody conjugates were photoimmobilized on a PS waveguide for subsequent immunoassays. The photoimmobilization strategy was compared to the classic avidin−biotin coupling chemistry in route 6.

In addition, two different assay protocols were compared. In the first protocol (stepwise), hCG was allowed to react with immobilized antibodies for 5 min, and then a Cy5-labeled second antibody (also reactive with hCG) was added. Its binding to the immobilized antigen−antibody complex was monitored using the biosensor. In the second protocol (premixed), hCG and the Cy5-labeled second antibody were premixed and then the binding rate of the complex was monitored with the biosensor. Figure 7 shows that the stepwise assay gave a 2-fold increase in binding rate relative to the premixed assay. This phenomenon may be due to the ease of binding of smaller molecules (antigen) to give high density on the surface. For the binding of hCG/anti-hCG-B-Cy5 onto BP-EG5-

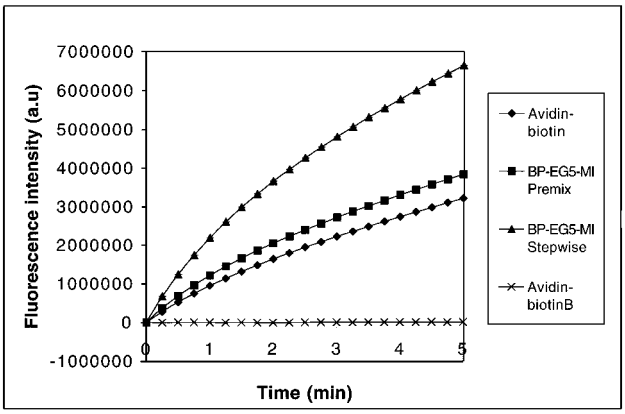

Figure 7. Comparison of photoimmobilization and avidin/biotin immobilization. The binding sequences on the waveguide are shown in routes 4, 5, and 6 (Figure 3). See text and Figure 4 legend for details.

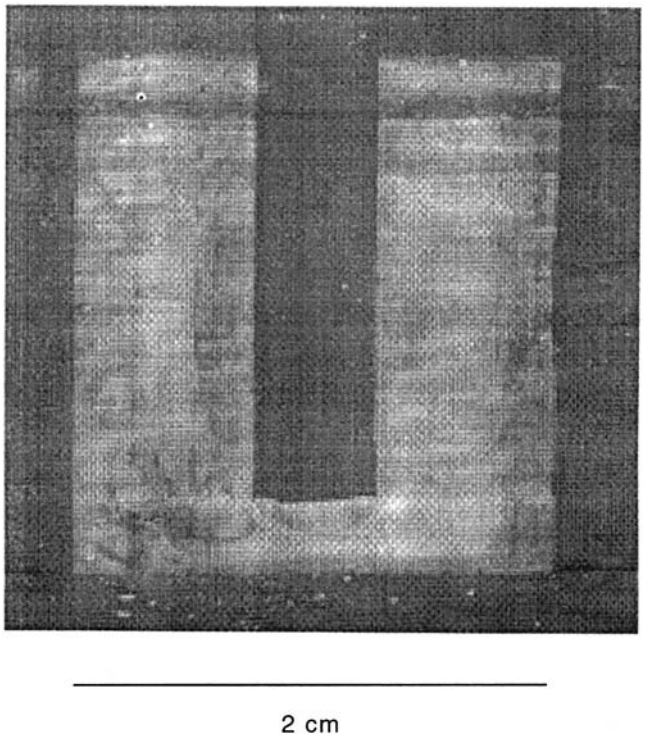

Figure 8. Photopatterning of a planar waveguide biosensor. See text for details.

MI-1/2 anti-hCG-A coated PS surfaces, the rate was slightly higher than that of a parallel reaction using avidin−biotin-1/2 anti-hCG-A-coated surfaces. This demonstrated that BP-EG5-MI was the photo-cross-linker with strongest potential for practical applications.

Immunosensors used in clinical diagnostic assays generally require no surface regeneration as they are being developed as "single-use" devices for point-of-care applications. However, regeneration of the immunologically active surface may be desirable for biosensors used in remote and/or continuous sensing applications (e.g., food process monitoring, environmental testing, biological warfare detection). Previously, we studied the reversibility of antigen binding to antibodies and Fab′ fragments immobilized to silica surfaces coated with PEG (*22*). These studies showed that there was an inverse correlation between reversibility and the surface density of immobilized antibody and/or Fab′ fragment. Thus, for

reusable sensors, it may be advantageous to control the surface density by using the BP-EG5-MI photo-cross-linker.

Finally, we demonstrated that it was possible to use BP-EG*n*-MI for photopatterning. Figure 8 shows the image of a "U" created on a PS surface by irradiation of a template-confined solution of BP-EG5-MI coupled to a half-antibody of hCG-A.

In summary, the biosensor assays described above demonstrated that BP-EG5-MI was an excellent heterobifunctional cross-linker for the photopatterning of biomolecules onto PS surfaces. The optimal conditions for the photoimmobilization and the biosensor assays included the following steps. First, the half-molecule of anti-hCG-A antibody was coupled to the maleimide moiety of BP-EG5-MI. Second, the conjugated antibody is photoimmobilized onto PS via the BP moiety, and the surface was postcoated with BSA. Third, antigen was incubated on the surface for 5−10 min. Fourth, the tracer solution was allowed to flow over the surface in a flow cell, and laser excitation resulted in emission of a detectable signal. Biosensors, with photopatterned antibodies prepared in this way, have important applications for continuous sensing of analytes and in clinical diagnostic assays.

ACKNOWLEDGMENT

This work was supported by an award from the Center for Biopolymers at Interfaces (to G.D.P. and J.N.H.), by start-up funds from The University of Utah (to G.D.P.), and by Public Health Service award HL 32123 (to J.N.H.).

LITERATURE CITED

(1) Sigrist, H., Collioud, A., Clémence, J.-F., Gao, H., Luginbühl, R., Sänger, M., and Sundarababu, G. (1995) Surface immobilization of biomolecules by light. *Opt. Eng. 34*, 2329−2348.

(2) Herbert, C. B., McLernon, T. L., Hypolite, C. L., Adams, D. N., Pikus, L., Huang, C. C., Fields, G. B., Letourneau, P. C., DiStefano, M. D., and Hu, W. S. (1997) Micropatterning gradients and controlling surface densities of photoactivatable biomolecules on self-assembled monolayers of oligo(ethyleneglycol) alkanethiolates. *Chem. Biol. 4*, 731−737.

(3) Hypolite, C., McLernon, T., Adams, C., Chapman, K., Herbert, C., Huang, C., DiStefano, M., and Hu, W. (1997) Formation of microscale gradients of protein using heterobifunctional photolinkers. *Bioconjugate Chem. 8*, 658−663.

(4) Roberts, C., Chen, C., Mrksich, M., Martichonok, V., Ingber, D., and Whitesides, G. (1998) Using mixed self-assembled monolayers presenting RGD and $(EG)_3OH$ groups to characterize long-term attachment of bovine capillary endothelial cells to surfaces. *J. Am. Chem. Soc. 120*, 6548−6555.

(5) Nakamura, T., Nagasaki, Y., and Kataoka, K. (1998) Synthesis of heterobifunctional poly(ethylene glycol) with a reducing monosaccharide residue at one end. *Bioconjugate Chem. 9*, 300−303.

(6) Brunner, J. (1993) New photolabeling and cross-linking methods. *Annu. Rev. Biochem. 62*, 483−514.

(7) Ji, T. (1979) The application of chemical cross-linking for studies on cell membranes and the identification of surface reporters. *Biochim. Biophys. Acta 559*, 39−69.

(8) Dormán, G., and Prestwich, G. D. (2000) Using photolabile ligands in drug discovery and development. *Trends Biotech. 18*, 64−77.

(9) Olszewski, J. D., Dormán, G., Elliott, J. T., Hong, Y., Ahern, D. G., and Prestwich, G. D. (1995) Tethered benzophenone reagents for the synthesis of photoactivatable ligands. *Bioconjugate Chem. 6*, 395−400.

(10) Rozsnyai, L., Benson, D., Fodor, S., and Schultz, P. (1992) Photolithographic immobilization of biopolymers on solid supports. *Angew. Chem., Int. Ed. Engl. 31*, 759−761.

(11) Prestwich, G. D., Dormán, G., Elliott, J. T., Marecak, D. M., and Chaudhary, A. (1997) Benzophenone photoprobes for phosphoinositides, peptides, and drugs. *Photochem. Photobiol. 65*, 222−234.

(12) Dormán, G., and Prestwich, G. D. (1994) Benzophenone photophores in biochemistry. *Biochemistry 33*, 5661−5673.

(13) Herron, J., Wang, H., Durtschi, J., Caldwell, K., Christensen, D., Chang, I., and Huang, S. (1998) Orientation and activity of immobilized antibodies. In *Biopolymers at interfaces* (M. Malmsten, Ed.) pp 221-280, Marcel Dekker, New York.

(14) Herron, J., Christensen, D., Wang, H., Caldwell, K., Janatova, J., and Huang, S. (1997) *Apparatus and methods for multi-analyte homogeneous fluoroimmunoassays*. U.S. Patent 5,677,196.

(15) Hermanson, G. T. (1996) Antibody modification and conjugation. In *Bioconjugate Techniques*, pp 460−492, New York.

(16) Bates, B. M., Ballard, D. W., and Voss, E. W., Jr. (1985) Comparative properties of monoclonal antibodies comprising a high-affinity anti-fluorescyl idiotype family. *Mol. Immunol. 22*, 871−877.

(17) Carpino, L., and Han, G. (1972) The 9-fluorenylmethoxycarbonyl amino-protecting group. *J. Org. Chem. 37*, 3404−3409.

(18) Kalgutkar, A., Crews, B., and Marnett, L. (1996) Design, synthesis, and biochemical evaluation of N-substituted maleimides as inhibitors of prostaglandin endoperoxide synthases. *J. Med. Chem 39*, 1692−1703.

(19) Boeckler, C., Frisch, B., and Schuber, F. (1998) Design and synthesis of thiol-reactive lipopeptides. *Bioorg. Med. Chem. Lett. 8*, 2055−2058.

(20) Walker, M. (1994) The Mitsunobu reaction: a novel method for the synthesis of bifunctional maleimide linkers. *Tetrahedron Lett. 35*, 665−668.

(21) Herron, J. N., Wang, H.-K., Terry, J. D., Durtschi, L., Tan, M. E., Astill, R., Smith, S., and Christensen, D. A. (1998) Rapid clinical diagnostics assays using injection molded planar waveguides. *Proc. SPIE−Int. Soc. Opt. Eng. 3259*, 54−64.

(22) Huang, S.-C., Caldwell, K. D., Lin, J.-N., Wang, H.-k., and Herron, J. N. (1996) Site-specific immobilization of monoclonal antibodies using spacer-mediated attachment. *Langmuir 12*, 4202−4298.

BC000006D

Novel Tat-Peptide Chelates for Direct Transduction of Technetium-99m and Rhenium into Human Cells for Imaging and Radiotherapy

Valery Polyakov, Vijay Sharma, Julie L. Dahlheimer, Christina M. Pica, Gary D. Luker, and David Piwnica-Worms*

Laboratory of Molecular Radiopharmacology, Department of Radiology and Department of Molecular Biology and Pharmacology, Washington University Medical School, St. Louis, Missouri 63110. Received January 28, 2000; Revised Manuscript Received July 10, 2000

Rapid and efficient delivery of radioactive metal complexes to the cell interior would enable novel applications in medical imaging and radiotherapy. Membrane permeant peptide conjugates incorporating HIV-1 Tat transactivation protein sequences (GRKKRRQRRR) and an appropriate peptide-based motif (ϵ-KGC) that provides an N_3S donor core for chelating technetium and rhenium were synthesized. Oxotechnetium(V) and oxorhenium(V) Tat−peptide complexes were prepared by facile transchelation reactions with permetalates, tin(II) chloride and sodium glucoheptonate. RP-HPLC showed two major [^{99m}Tc]Tat−peptide species (**4**) that differed in retention time by ∼2 min corresponding to two [Re]-Tat−peptide species (**7**) shown to have identical mass, consistent with formation of two isomers, likely the oxo-metal diastereomers. [^{99m}Tc]Tat−peptides were stable to transchelation in vitro. In human Jurkat cells, [^{99m}Tc]Tat−peptide **4** showed concentrative cell accumulation (30-fold greater than extracellular concentration) and rapid uptake kinetics ($t_{1/2}$ < 2 min) in a diastereomeric-comparable manner. Paradoxically, uptake was enhanced in 4 °C buffer compared to 37 °C, while depolarization of membrane potential as well as inhibition of microtubule function and vesicular trafficking showed no inhibitory effect. Cells preloaded with **4** showed rapid washout kinetics into peptide-free solution. Modification of [^{99m}Tc]Tat−peptide by deletion of the N-terminus Gly with or without biotinylation minimally impacted net cell uptake. In addition, the C-terminus thiol of the prototypic Tat−peptide was labeled with fluorescein-5-maleimide to yield conjugate **8**. Fluorescence microscopy directly localized conjugate **8** to the cytosol and nuclei (possibly nucleolus) of human Jurkat, KB 3-1 and KB 8-5 tumor cells. Preliminary imaging studies in mice following intravenous administration of prototypic [^{99m}Tc]Tat−peptide **4** showed an initial whole body distribution and rapid clearance by both renal and hepatobiliary excretion. Analysis of murine blood in vivo and human serum ex vivo revealed >95% intact complex, while murine urine in vivo showed 65% parent complex. Thus, these novel Tat−peptide chelate conjugates, capable of forming stable [Tc/Re(V)]complexes, rapidly translocate across cell membranes into intracellular compartments and can be readily derivatized for further targeted applications in molecular imaging and radiotherapy.

INTRODUCTION

Peptide-based imaging and radiotherapeutic agents offer high molecular target specificity and a great degree of flexibility in their design (*1*−*4*). Peptide-based imaging agents, exemplified by the commercially available agents Octreoscan and Acutech (*5*−*7*), often are composed of a domain for targeting cell-surface receptors and a moiety for stable chelation of desired radiometals (*1*, *2*). Among these, technetium-99m (^{99m}Tc) is the most commonly used isotope in medical imaging (*3*). Readily available through ^{99}Mo/^{99m}Tc generator systems, ^{99m}Tc has an ideal photon energy for imaging applications and possesses a short half-life (6 h) compatible with the pharmacokinetics in vivo of many biological and clinical applications (*1*, *3*, *8*, *9*). In addition, chelation chemistry for ^{99m}Tc has received much attention because these donor cores also enable radiotherapy using the chemically analogous ^{186}Re/^{188}Re species (*10*). Targeting of peptide-based imaging agents largely has been limited to extracellular or externally oriented membrane receptors because charge, size, and pharmacokinetic considerations of conventional peptide constructs do not enable translocation across cellular membranes (*2*). The dielectric constant of the lipid bilayer of the plasma membrane poses a formidable barrier to the entry of charged compounds into cells (*11*). Because targeted delivery of peptide agents to intracellular compartments would enable a broad range of novel applications in medical imaging and radiotherapy, a peptide conjugate capable of incorporating medically relevant metals while permeating the plasma membrane is highly desired.

Several transduction sequences capable of permeating the plasma membrane of cells and thereby enabling delivery of biomolecules and various “cargos” have been reported recently. These include the third helix of the homeodomain of Antennapedia (*12*), a peptide derived from the heavy chain variable region of an anti-DNA monoclonal antibody (*13*), and several viral proteins including Herpes simplex virus VP22 (*14*), HIV-1 Rev protein and HTLV-1 Rex protein basic domains (*15*), and HIV-1 Tat protein basic domain (*16*, *17*). Although the exact mechanisms of membrane transduction are not well

* To whom correspondence should be addressed. Phone: (314) 362-9356. Fax: (314) 362-0152. E-mail: piwnica-wormsd@mir.wustl.edu.

10.1021/bc000008y CCC: $19.00 © 2000 American Chemical Society
Published on Web 09/21/2000

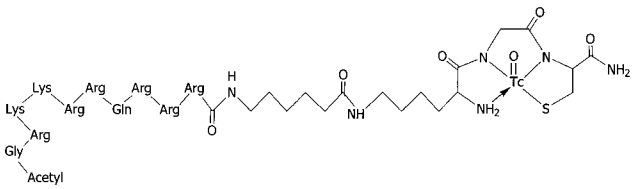

Figure 1. Structure of a [^{99m}Tc]Tat−peptide complex.

characterized, they generally have been described as achiral and independent of a receptor (*12*, *18*). Membrane transduction peptides have been shown to deliver into cells a variety of polypeptides (*14*, *17*, *19*), immunoreactive epitopes (*20*), fluorescent probes (*21*), and derivatized superparamagnetic iron oxide nanoparticles (*22*).

Herein we report a Tat−peptide basic motif for transduction of peptide chelates across plasma membranes as a delivery vehicle for imaging and radiotherapeutic isotopes. We designed prototypic peptides that constituted in their simplest form two functional domains, a membrane permeant peptide sequence derived from HIV-1 Tat protein residues 48−57 (GRKKRRQRRR) and a peptide-based chelator able to coordinate isotopes of metals useful in medical imaging and therapy (Figure 1). Novel radiolabeled Tat−peptide chelates are shown to rapidly and quantitatively concentrate by over 30-fold within the cytoplasm and nucleus of living human cells.

EXPERIMENTAL PROCEDURES

Peptide Synthesis. Peptide conjugate **1** (Gly-Arg-Lys-Lys-Arg-Arg-Gln-Arg-Arg-Arg-AHA-ϵ-Lys-Gly-Cys) was prepared by solid-phase peptide synthesis using all L *N*-α-FMOC-protected amino acids and standard BOP/HOBt coupling chemistry, except for the ϵ-Lys residue which used an *N*-α-tBOC, *N*-ϵ-FMOC-Lys to direct peptide coupling to the ϵ-amine. AHA represents 6-aminohexanoic acid as an aliphatic linker between the Tat 48−57 residues and the peptide chelating moiety. For peptides **2** and **3**, the N-terminus Gly was omitted. Peptides were either N-terminus acetylated (**1** and **2**) or biotinylated (**3**), C-terminus amidated (**1**, **2**, and **3**), and deprotected by standard methods. Peptides were purified (>94%) by preparative C_{18} reversed-phase HPLC using as eluent 0.1% trifluoroacetic acid in water (0.1% TFA/H_2O) modified with 0.1% trifluoroacetic acid in 90% acetonitrile/10% water [0.1% TFA/(90% CH_3CN/H_2O)] by a linear gradient (5−40% over 40 min) flowing at 1.0 mL/min. A single HPLC peak was observed for each peptide conjugate. The identity of peptide conjugates **1**−**3** was confirmed by amino acid analysis [**1**, 14 amino acids (Gln 1; Gly 2; Cys 1; Lys 3, Arg 6, AHA 1); **2** and **3**, 13 amino acids (Gln 1; Gly 1; Cys 1; Lys 3; Arg 6, AHA 1] and electrospray mass spectrometry (**1**, *m*/*z* 1839.0, calcd $C_{74}H_{143}N_{37}O_{16}S_1$, 1839.3; **2**, *m*/*z* 1782.8, calcd $C_{72}H_{140}N_{36}O_{15}S_1$, 1782.2; **3**, *m*/*z* 1965.6, calcd $C_{80}H_{151}N_{38}O_{16}S_2$, 1965.5).

Preparation of Radiolabeled [^{99m}Tc^{V}O]Tat−Peptide. Tat−peptide conjugates were labeled with ^{99m}Tc by ligand exchange using [^{99m}Tc]glucoheptonate as the ligand exchange reagent (Scheme 1) (*7*). A commercially available stannous glucoheptonate radiopharmaceutical kit [Sn(II)Cl_2·2H_2O, 0.14 mg; sodium glucoheptonate, 200 mg; Glucoscan, DuPont Pharma, Billerica, MA] was reconstituted with 1.0 mL of [^{99m}Tc]Na(TcO_4) (50 mCi) in isotonic saline obtained by eluting a commercial radionuclide ^{99}Mo/^{99m}Tc generator and allowed to stand for 15 min at room temperature. In a small glass vial, to a 10 μL aliquot of Tat−peptide conjugate stock solution

Scheme 1

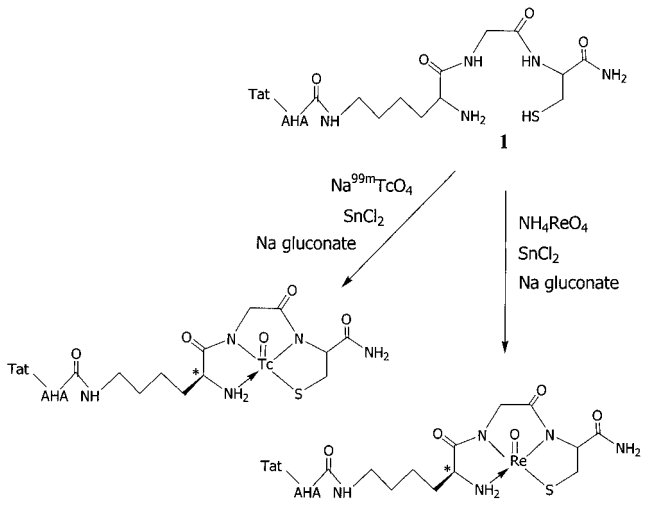

(10 mg dissolved in 1 mL of 0.9% saline or water), [^{99m}Tc]-glucoheptonate solution (15−50 μL), and sufficient water to generate a final volume of 100 μL were added, and the reaction was allowed to proceed at room temperature for 15 min. Radiochemical yields (>95%) of oxotechnetium [^{99m}Tc]Tat−peptide complexes were determined by TLC using silica gel developed with either 15% TFA or H_2O as indicated and scanning radiometric detection (Bioscan, Inc., Washington DC). By TLC with TFA, [^{99m}Tc]Tat complexes **4**, **5**, and **6** from peptides **1**, **2**, and **3**, respectively, each showed an $R_f \approx 0.45$, readily distinguished from [^{99m}Tc]glucoheptonate ($R_f = 0.95$) and [^{99m}Tc]TcO_4^- ($R_f = 0.95$). By TLC with H_2O, [^{99m}Tc]Tat complexes remained at the origin while [^{99m}Tc]glucoheptonate and [^{99m}Tc]TcO_4^- moved with the solvent front. Radiochemical purity (>90%) was determined by radiometric RP-HPLC using the solvent gradient system described above as well as a linear gradient (0−60% over 60 min) also flowing at 1.0 mL/min. Specific activity was estimated to be 2×10^8 mCi/mol.

Preparation of [Re^{V}O]Tat−Peptide. [Re]Tat−peptide conjugates also were obtained through ligand exchange using [Re]glucoheptonate as the ligand exchange reagent (7). To 0.1 mL of a freshly prepared stock solution [sodium α-D-glucoheptonate, 200 mg, 0.81 mmol and tin(II)chloride dihydrate, 18.4 mg, 0.082 mmol in 1 mL of distilled water] was added 0.1 mL of a stock solution (ammonium perrhenate, 14.9 mg, 0.055 mmol in 1 mL of water), and the mixture allowed to stand for 15 min at room temp. To the mixture was added the appropriate Tat−peptide conjugate (1 mg, ~0.4 μmol) in water, and the reaction allowed to proceed at room temperature for 30 min. RP-HPLC analysis was performed using the solvent gradient system described above and the desired fractions collected. Identity of isolated [Re]Tat−peptide complexes was confirmed by electrospray mass spectrometry (acetyl-Gly-Arg-Lys-Lys-Arg-Arg-Gln-Arg-Arg-Arg-AHA-ϵ-Lys-Gly-Cys[Re] (**7**), *m*/*z* 2039.0, calcd $C_{74}H_{140}N_{37}O_{17}Re_1S_1$, 2038.4).

Preparation of Tat−Peptide-Fluorescein. Tat−peptide conjugates were labeled on the C-terminal thiol with fluorescein maleimide (FM) as described previously (*21*). Briefly, in a small glass vial, Tat−peptide conjugate (1 mg) was dissolved in phosphate buffered saline (PBS, pH 7.4) and reacted with 1.2 eq of fluorescein maleimide dissolved in dimethylformamide for 2 h in the dark at room temperature. Fluorescent peptide was purified by RP-HPLC (single peak; purity >97%) using the above

gradient conditions and lyophilized in the dark. Identity of the desired fluorescein tagged Tat−peptide was confirmed by electrospray mass spectrometry (acetyl-Gly-Arg-Lys-Lys-Arg-Arg-Gln-Arg-Arg-Arg-AHA-ϵ-Lys-Gly-Cys-FM (**8**), *m/z* 2266.0, calcd $C_{98}H_{156}N_{38}O_{23}S_1$, 2266.6; acetyl-Arg-Lys-Lys-Arg-Arg-Gln-Arg-Arg-Arg-AHA-ϵ-Lys-Gly-Cys-FM (**9**), *m/z* 2210.0, calcd $C_{96}H_{153}N_{37}O_{22}S_1$, 2209.6).

Cell Culture. Monolayers of human epidermoid carcinoma KB 3-1 cells and the colchicine-selected KB 8-5 derivative cell lines were grown at 37 °C in an atmosphere of 5% CO_2 as previously described (*23*, *24*). For experiments, cells were plated in 100-mm Petri dishes containing seven 25-mm glass coverslips on the bottom and grown to subconfluence in DMEM (GIBCO, Grand Island, NY) supplemented with L-glutamine (1%), penicillin/streptomycin (0.1%), and heat-inactivated fetal calf serum (10%) in the absence or presence of 10 ng/mL colchicine, respectively.

Human Jurkat leukemia cells were maintained in RPMI also supplemented with L-glutamine, penicillin/streptomycin, and 10% fetal calf serum at 37 °C in an atmosphere of 5% CO_2 (*25*).

Cellular Uptake and Washout Studies of [^{99m}Tc]-Tat−Peptide Conjugates. Control solution for tracer uptake experiments was a modified Earle's balanced salt solution (MEBSS) containing (mM): 145 Na^+, 5.4 K^+, 1.2 Ca^{2+}, 0.8 Mg^{2+}, 152 Cl^-, 0.8 $H_2PO_4^-$, 0.8 SO_4^{2-}, 5.6 dextrose, 4.0 HEPES, and 1% bovine calf serum (vol/vol), pH 7.4 ± 0.05. A 130 mM K^+/20 mM Cl^- solution was made by equimolar substitution of potassium methanesulfonate for NaCl as described (*26*).

Kinetic experiments of [^{99m}Tc]Tat−peptide complexes were performed in Jurkat leukemia cells suspended in MEBSS with minor modifications of methods described in the literature (*27*). Transport experiments were performed in siliconized microfuge tubes and initiated by addition of 732.5 μL cells at 5×10^6 cells/ml to 10 μL of MEBSS containing [^{99m}Tc]Tat−peptide complex and 7.5 μL of vehicle alone or of any added drug in vehicle at 100-fold the desired concentration. Unless stated otherwise, [^{99m}Tc]Tat−peptide complex was added to MEBSS accompanied by molar excess unlabeled Tat−peptide as obtained directly from the labeling procedure; final total peptide concentration was typically 0.5−1 μM (50 nmol/mCi; 10 μCi/mL). Tubes were incubated in a 37 °C water bath with occasional mixing. The reaction was terminated by spinning 250 μL aliquots from the reaction for 10 s through 800 μL of a 75:25 mixture of silicon oil (density = 1.050; Aldrich) and mineral oil (density = 0.875; Acros). An aliquot of the aqueous phase was obtained to normalize extracellular concentration of the Tc-peptide to cell-associated activity, then the oil and aqueous phases were aspirated and the cell pellet extracted in 0.5 mL of 1% SDS, 10 mM sodium borate. For peptide washout experiments, cells were first incubated to plateau uptake (10 min) in MEBSS loading buffer (37 °C), collected by rapid centrifugation and the pellet resuspended in 750 μL peptide-free MEBSS (4 °C) to clear extracellular tracer. Following another rapid spin, the cell pellet was resuspended in peptide-free MEBSS (37, 25, or 4 °C) for various times and the experiment terminated as above. All cell extracts were assayed for protein by BCA analysis (Pierce Chemical Co.) using bovine serum albumin as the protein standard. Cell extracts, stock solutions, and extracellular buffer samples were assayed for gamma activity in a well-type sodium iodide gamma counter (Cobra II, Beckman; 130−165 keV window). Absolute concentration of total [Tc]Tat−peptide complex in solution was determined from the specific activity of Tc, based on equations of Mo/Tc generator equilibrium (28). Transport data are reported as pmol of peptide_i (mg protein)$^{-1}$ (μM_o)$^{-1}$, wherein peptide_i represents total peptide within the cells and (μM_o)$^{-1}$ represents concentration of total peptide in the extracellular buffer (*29*). Data are generally reported as mean ± SEM.

Fluorescence Microscopy. Exponentially growing Jurkat cells were incubated in fresh media or MEBSS containing the fluorescein labeled Tat−peptide conjugate (0.5−1 μM) at 37 or 4 °C for 10−20 min. Cells were then cytospun onto glass slides, fixed at room temperature or on ice by direct addition of 4% (v/v) paraformaldehyde in PBS to the adherent cells for 10 min and then rinsed three times with PBS (1 min each). Similarly, human KB 3-1 and KB 8-5 epidermoid carcinoma cells growing on coverslips or chamber slides were incubated in MEBSS containing the fluorescein labeled Tat−peptide conjugate at 37 °C for 10 min, then fixed in 4% paraformaldehyde at room temperature and rinsed three times with PBS. Cells were then mounted with anti-fading mounting medium following the recommended procedures of the manufacturer (Vector). Distribution of fluorescein conjugates was analyzed on a Zeiss epifluorescence microscope or laser-scanning confocal fluorescence imaging system coupled to a Nikon microscope equipped with a CCD interfaced to a PC (*30*).

Stability of Radiolabeled Peptide in Vitro and in Vivo. The stability in vitro of [^{99m}Tc]Tat−peptide **4** in aqueous buffers between pH 4 and 9 was evaluated by incubation of radiolabeled peptide (10 mg/mL) for 1 h at RT in HEPES (10 mM) or Tris base (50 mM) buffer pH adjusted with HCl or NaOH, followed by TLC and scanning radiometric analysis. Additional effects of reduced glutathione (2.5 mM), cysteine (10 μM and 2.5 mM) or EDTA (2.5 mM) on radiolabeled Tat−peptide stability was performed by addition of competing chelator to buffers at each pH. Stability in vitro was further assessed by radio-TLC after incubation of [^{99m}Tc]Tat−peptide for 1 h at 37 °C in human serum, bovine calf serum, murine urine, culture media containing 10% fetal calf serum as well as MEBSS transport buffer.

In addition, human Jurkat cells were incubated with [^{99m}Tc]Tat−peptide **4** in MEBSS transport buffer for 1 h at 37 °C, centrifuged, and the cell pellet lysed in modified mammalian lysis buffer {100 mM NaCl; 50 mM Tris base (pH 8); 2 mM dithiothreitol; 0.5% NP-40; 1 mM phenylmethylsulfonylfluoride; 10 μg/mL leupeptin; 10 μg/mL aprotinin}. Radio-TLC analysis of both extracellular buffer and cell lysate was performed. Furthermore, stability in vivo of radiolabeled Tat−peptide was characterized by radio-TLC analysis of serum and urine samples 30 min after intravenous administration of 270 μCi of [^{99m}Tc]Tat−peptide **4** to FVB mice.

Biodistribution and Imaging Studies. Vertebral animal procedures were approved by the appropriate institutional review committee. Distribution of [^{99m}Tc]-Tat−peptide complex **4** in tissues of Balb/c mice was determined as previously described (*31*, *32*). Mice were anesthetized by metofane inhalation and injected with **4** (2 μCi in 50 μL saline) via bolus injection through a tail vein. Animals were sacrificed by cervical dislocation at 5, 30, 60, and 120 min postinjection ($n = 3$ each). Blood samples were obtained by cardiac puncture and tissues harvested rapidly. Gamma activity in organ samples was counted for 1 min, or until two standard deviations of sampling were below 0.5%. Data are expressed as percent of injected dose (% id) per organ [(organ μCi) (injected μCi)$^{-1}$ × 100] or % id per gram of tissue [(tissue μCi) (injected μCi)$^{-1}$ (g tissue)$^{-1}$ × 100].

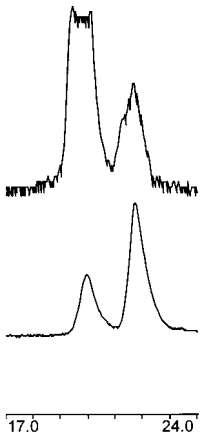

Figure 2. Radiometric (top) and UV (bottom) RP-HPLC chromatograms of [^{99m}Tc]Tat−peptide complex **4** and [Re]Tat−peptide complex **7**, respectively. Isolation and mass spectrometry of each Re species revealed identical masses (*m*/*z* 2039.0) consistent with formation of syn and anti isomers upon chelation of the metal.

For imaging studies, Balb/c mice also were lightly anesthetized with metofane inhalation. [^{99m}Tc]Tat−peptide complex **4** (200 μCi in 50 μL saline) was injected via a tail vein into mice positioned under a gamma scintillation camera (Siemens Basicam, Siemens Medical Systems, Iselin, NJ; 5 mm pinhole collimator; 20% energy window centered over 140 keV photopeak of Tc-99m). Sequential posterior images of mice were collected for 3 min each at 1, 30, and 60 min postinjection of the radiotracer with the mouse recovering and being reanesthetized just prior to each timepoint. A 256 × 256 image matrix with correction for radioactive decay was used on a PC platform and standard image analysis software. No corrections were made for scatter or attenuation. Whole body distribution of the complexes are presented with gray scale images.

RESULTS

Chemistry. Tat−peptide conjugates were synthesized by standard solid-phase methods and their corresponding ^{99m}Tc- and Re-complexes were obtained by ligand exchange using [^{99m}Tc]glucoheptonate or [Re]glucoheptonate, respectively (Scheme 1). Incorporation of a metal into the N_3S donor core has been shown to result in the formation of three five-membered rings and create a chiral center (*33*). Such structures typically resemble a square pyramid with the nitrogens at the base and the oxygen in the apical position (*33*) and are known to be stable (*34*). Radiochemical yield (>95%) and purity (>90%) of the oxotechnetium complexes were determined by TLC using silica gel with scanning radiometric detection and by radiometric RP-HPLC, respectively. By TLC, [^{99m}Tc]Tat peptide complexes were readily distinguished from [^{99m}Tc]glucoheptonate and [^{99m}Tc]TcO_4^- which moved at or near the solvent front. RP-HPLC analysis and radiometric detection of [^{99m}Tc]Tat−peptide **4** revealed two closely eluting peaks (Figure 2). Similarly, RP-HPLC analysis and UV detection of [Re]Tat−peptide **7** also revealed two eluting peaks with retention times differing by ∼2 min (Figure 2), close to the radiometric peaks observed with the ^{99m}Tc-labeled species. Furthermore, a second gradient system revealed similar results. Each Re peak was isolated and the identity of the oxorhenium Tat−peptide complex confirmed by mass spectrometry. Because both peaks had identical mass (*m*/*z* 2039.0 each; calcd 2038.4), we concluded that each represented an

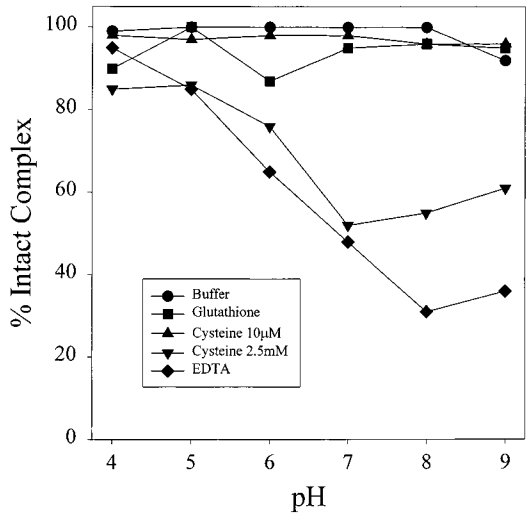

Figure 3. Effect of pH and competing chelation compounds on stability of radiolabeled Tat−peptide. Following incubation of [^{99m}Tc]Tat−peptide complex **4** for 1 h at RT in HEPES or Tris buffer adjusted to the indicated pH in the absence (●) or presence of reduced glutathione [2.5 mM (■)], cysteine [10 μM (▲)], cysteine [2.5 mM (▼)], or EDTA [2.5 mM (♦)], percent intact complex was determined by radio-TLC.

isomer of the N_3S chelation moiety in relation to the metal−oxygen bond due to participation of the chiral α-C atom of lysine in the chelation ring (*2*, *33*, *35*). The data were consistent with formation of the two anticipated diastereoisomers, the apical oxygen being syn and anti relative to the side chain of the Lys residue (see the asterisk in Scheme 1), as validated with analogous N_3S structures.

Separation of the isomers of Re−Tat−peptide complex **7** was accomplished by RP-HPLC and the kinetics of interconversion studied in aqueous solution at RT. For analysis, an HPLC fraction (assigned to isomer a) was collected, lyophilized, resuspended in water or PBS and monitored over 48 h. Interconversion of isomer a was not observed in deionized water. However, in PBS (pH 7.4), the emergence of isomer b was evident after 1 h at RT and a peak ratio of ∼2:1 (isomer a:isomer b) was observed at 2 h. After 48 h, the ratio remained ∼2:1, the inverse of the original mixture of **7** (see Figure 2). Thus, while PBS facilitated interconversion of the chelate, equilibrium was not observed with the peptide conjugate over this time interval. A proposed mechanism for interconversion of an analogous isolated N_3S chelate involves the coordination of a water molecule in the sixth position on the metal, trans to the metal−oxo bond (*33*).

To study the stability of the Tat−peptide chelate conjugates in vitro, radio-TLC analysis of [^{99m}Tc]Tat−peptide **4** was examined after incubation of peptide in buffered solution ranging in pH from 4 to 9 (Figure 3). As shown, [^{99m}Tc]Tat−peptide **4** was very stable to transchelation between pH 4−9, a physiologically relevant range of pH values likely to be encountered in vivo. Percent intact complex remained >97% over 1 h. The presence of reduced glutathione (2.5 mM; ∼100000-fold molar excess over labeled peptide complex), a competing physiologic chelator with modest binding affinity, showed no effect. Furthermore, [^{99m}Tc]Tat−peptide **4** remained >96% intact in the presence of physiological concentrations of the strong chelator cysteine (10 μM; ∼1000-fold molar excess), even under alkaline conditions. However, under extreme conditions of highly concentrated cysteine (2.5 mM) or EDTA (2.5 mM), evidence of over 50% transchelation was observed at pH ≥7. Additionally,

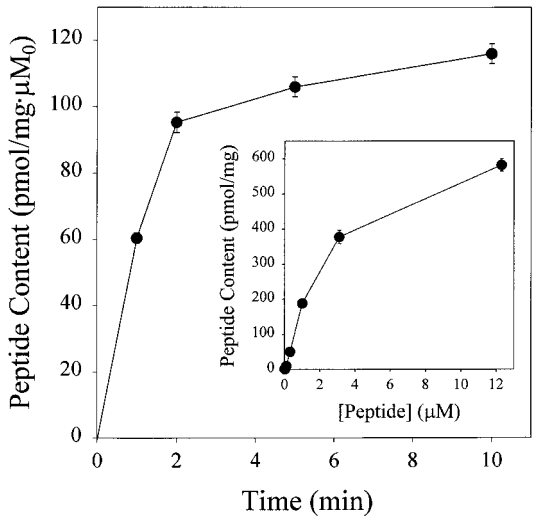

Figure 4. Kinetics of [^{99m}Tc]Tat−peptide complex **4** accumulation into human Jurkat cells. Cells were incubated in MEBSS loading buffer for the indicated times, washed, and cell-associated activity determined. Each point represents the mean of three to four determinations; bars represent ± SEM when larger than the symbol. Plot is representative of four independent experiments. (Inset) Concentration dependence of plateau accumulation of **4**. Twenty minute net uptake values at the indicated extracellular concentrations of **4** are plotted.

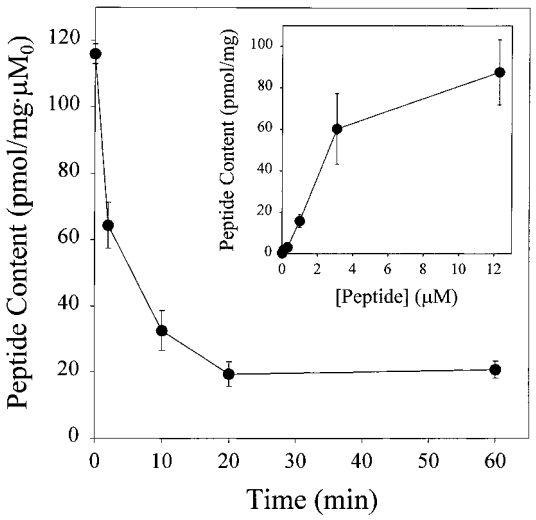

Figure 5. Washout kinetics of [^{99m}Tc]Tat−peptide complex **4** from human Jurkat cells at 37 °C. Cells were incubated (10 min) in MEBSS loading buffer (37 °C), washed, and then incubated in peptide-free MEBSS (37 °C). Cell-associated activity as a function of time in washout buffer is shown. Each point represents the mean of three to four determinations; bars represent ± SEM when larger than the symbol. Plot is representative of three independent experiments. (Inset) Concentration dependence of cellular residual activity of **4**. Sixty minute washout residual values after cell loading at the indicated extracellular concentrations of **4** are plotted.

incubation of [^{99m}Tc]Tat−peptide in human serum, bovine serum, cell culture media or MEBSS transport buffer for 1 h at 37 °C showed no evidence of metabolites or transchelation reactions by TLC (H_2O) (data not shown), further suggesting that the [^{99m}Tc]Tat−peptide was resistant to the action of serum proteases and natural chelators.

Cellular Transport Kinetics of [^{99m}Tc]Tat−Peptides. We first examined the overall uptake kinetics of [^{99m}Tc]Tat−peptide **4** in human Jurkat leukemia cells. Jurkat cells rapidly accumulated **4**, approaching a plateau in less than 5 min (Figure 4). This exceeded by an order of magnitude the uptake kinetics previously reported for an organometallic hydrophobic cation, [^{99m}Tc]-Sestamibi, which also is known to localize intracellularly (*29*, *36*). Steady-state values for the [^{99m}Tc]Tat−peptide complex were 116 ± 3 pmol (mg protein)$^{-1}$ (μM_o)$^{-1}$ (n = 4). Given a typical cell water space of 4 μL (mg protein)$^{-1}$ (*23*), this would indicate an intracellular/extracellular ratio for complex **4** of ∼30, consistent with the complex being rapidly concentrated within cells. Furthermore, TLC analysis of cell lysates showed >95% intact complex (data not shown).

To further characterize transport of the complex, plateau accumulation of [^{99m}Tc]Tat−peptide **4** in Jurkat cells (10 min incubation) was determined as a function of extracellular concentration of the agent by addition of increasing amounts of radiolabeled peptide to the buffer (at a fixed specific activity). While readily detectable at concentrations as low as 7 nM, cell content of **4** rose in proportion to the extracellular concentration of the complex. There was evidence of concentration saturation as extracellular concentrations rose into the 8 μM range (Figure 4, inset). The shape of the concentration-dependence curve implied the existence of a diffusive component and a saturable binding component to the overall uptake mechanism (*31*). Curve fitting of the data (*37*) suggested a half-maximal value of 2 μM for the saturable component.

Washout of [^{99m}Tc]Tat−peptide complex **4** also showed very rapid kinetics. Washout was ∼90% complete within 20 min (Figure 5). This may have favorable impact on signal-to-noise for nontarget tissues regarding use of this general class of agents in vivo. However, a residual compartment of slowly exchanging or retained activity was observable for longer time points. This residual was a function of extracellular peptide concentration (Figure 5, inset). Because the Arg-rich Tat protein basic domain is known to bind to viral RNA, this residual compartment may represent binding to analogous nuclear components in human cells, but this remains to be ascertained.

The radiosynthetic reaction for the Tat−peptide complexes inherently yields a mixture of isomeric [^{99m}Tc]Tat−peptide complexes (as described above) as well as ∼10000-fold molar excess unlabeled Tat−peptide conjugate. The latter arises as a consequence of the extremely high specific activity of the radiolabeling isotope ^{99m}Tc (*3*). To determine whether human cells could distinguish between putative syn and anti isomers of purified Tat−peptide complexes, fractions containing pure isomers of [^{99m}Tc]Tat−peptide complex **4** were isolated by RP-HPLC, lyophilized and each added to MEBSS buffer for accumulation experiments into Jurkat cells (10 min incubation, a short time compared to the solution interconversion times shown above). In Jurkat cells, the 10-min uptake of purified [^{99m}Tc]Tat−peptide isomer b was ∼60% of the uptake of isomer a (Table 1). However, in the same cells, when 20000-fold molar excess unlabeled Tat−peptide conjugate was added to purified [^{99m}Tc]Tat−peptide isomers in buffer, thereby simulating standard peptide mixtures, 10-min uptake of isomer b was now ∼80% of the uptake of isomer a. In addition, no consistent stereospecific trend was observed for the washout residual (Table 1). Thus, while net accumulation of putative syn and anti isomers of [^{99m}Tc]Tat−peptide complex **4** were not exactly equal, conformation per se produced only modest effects on the net cell uptake and washout of these [^{99m}Tc]Tat−peptide complexes. Furthermore, the 3−4-fold enhancement of cellular accumulation of purified isomers of [^{99m}Tc]Tat−peptide in the presence of

Table 1. Uptake and Washout of Isomers of [^{99m}Tc]Tat−peptide 4 in Human Jurkat Cells[a]

peptide	isomer a	isomer b
10-min net uptake [pmol (mg protein)$^{-1}$ (μM$_o$)$^{-1}$]		
purified [^{99m}Tc]Tat-peptide	62.8 ± 4.1	36.6 ± 5.2
added unlabeled peptide	185.9 ± 10.9	149.2 ± 4.5
30-min washout residual [pmol (mg protein)$^{-1}$ (μM$_o$)$^{-1}$]		
purified [^{99m}Tc]Tat-peptide	10.8 ± 1.1	7.9 ± 1.4
added unlabeled peptide	11.2 ± 0.8	23.8 ± 4.8

[a] Cells were incubated in MEBSS loading buffer (10 min; 37 °C) containing HPLC-purified isomers of **4** in the absence or presence of ~20000-fold molar excess unlabeled peptide, and then analyzed, or washed and then incubated in peptide-free MEBSS (30 min; 37 °C) prior to analysis. Cellular content of **4** is expressed as [pmol (mg protein)$^{-1}$ (μM$_o$)$^{-1}$]. Values represent the mean ± SEM of three to four determinations each.

Table 2. Effect of Various Drugs on Net Uptake of [^{99m}Tc]Tat−peptide 4 in Human Jurkat Cells

drug	10-min net uptake [pmol (mg protein)$^{-1}$ (μM$_o$)$^{-1}$]
control MEBSS	79.1 ± 2.0
0.1% DMSO vehicle	94.4 ± 20.2
Colchicine (100 ng/mL)	96.5 ± 11.8
Taxol (1 μM)	72.0 ± 4.3
Nocodozole (5 μg/mL)	66.8 ± 1.7
Cytochalasin D (1 μM)	76.2 ± 1.9
Brefeldin A (2.5 μg/mL)	79.4 ± 9.8
Wortmannin (100 nM)	82.9 ± 10.0

[a] Cells were incubated in MEBSS loading buffer (10 min; 37 °C) containing **4** and the indicated drugs prior to analysis. See the legend of Table 1 for details.

20000-fold molar excess unlabeled peptide (Table 1) obviates a simple receptor−ligand interaction for the net cell uptake process on one hand and simple diffusion on the other hand. These data provide evidence for a translocation mechanism with overall high capacity and a modest degree of positive cooperativity.

Because several membrane permeant peptides have been reported to accumulate within cells by mechanisms related to cytoskeletal function (*14*), several inhibitors known to impact microtubules, actin filaments, and various cytoskeletal-mediated vesicular transport pathways were tested. In Jurkat cells, neither the microtubule-disrupting agents colchicine (100 ng/mL), taxol (1 μM), nocodozole (5 μg/mL), the filament-disrupting agent cytochalasin D (1 μM), the trans-Golgi transport inhibitor brefeldin A (2.5 μg/mL), nor the phosphatidylinositol-3 kinase inhibitor wortmannin (100 nM) had any significant effect on net cell uptake of [^{99m}Tc]Tat−peptide **4** (Table 2). Thus, the pathway for accumulation of [^{99m}Tc]-Tat−peptide was unlikely to be mediated by a microtubulin or cytoskeletal-mediated transport mechanism. Furthermore, ice-cold buffer (4 °C) not only failed to inhibit uptake, but modestly enhanced net accumulation of the complex over time (Figure 6). In addition, after loading in 37 °C buffer, washout into ice-cold buffer was only modestly inhibitory (Figure 7). These data point to an unique cell membrane translocation pathway not highly dependent on endocytosis, vesicular trafficking or cellular metabolism.

To further examine potential mechanisms of localization, Jurkat cells were incubated with standard [^{99m}Tc]-Tat−peptide **4** in control MEBSS or buffer comprised of 130 mM K^+/20 mM Cl^- plus valinomycin (1 μg/mL), a potassium ionophore (*29*). When cells are incubated in this high K^+ buffer, electrical potentials of the mitochondrial membrane ($\Delta\Psi$), and plasma membrane (E_m) are depolarized toward zero, eliminating the inward driving force for uptake of cationic molecules (*38*). While Tat−peptide has amphiphilic cationic properties (*21*), net uptake of [^{99m}Tc]Tat−peptide complex **4** under isoelectric conditions was actually 42 ± 3% greater than control (data not shown), rather than decreased, indicating that the mechanism of Tat−peptide accumulation was independent of membrane potential.

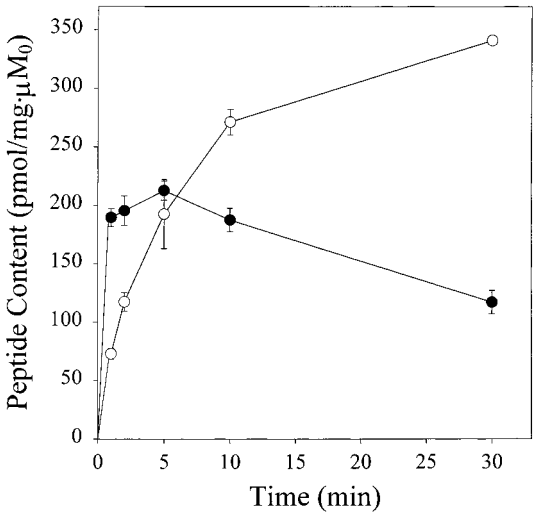

Figure 6. Effect of temperature on accumulation of [^{99m}Tc]-Tat−peptide complex **4** into human Jurkat cells. Cells were incubated in MEBSS loading buffer at 37 °C (●) or 4 °C (○) for the indicated times, washed, and cell-associated activity determined. Each point represents the mean of four determinations, except the 30 min point at 4 °C (n = 1); bars represent ± SEM when larger than the symbol. Plot is representative of two independent experiments.

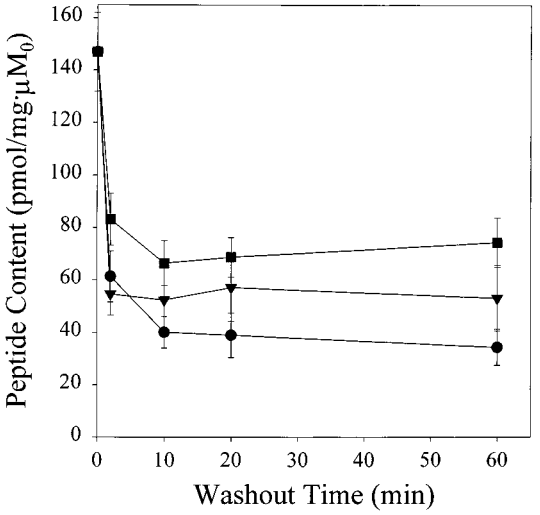

Figure 7. Effect of temperature on washout of [^{99m}Tc]Tat−peptide complex **4** from Jurkat cells. Cells were incubated (10 min) in MEBSS loading buffer (37 °C), washed, and then incubated in peptide-free MEBSS at 37 °C (●), 25 °C (▼), or 4 °C (■). Cell-associated activity as a function of time in washout buffer is shown. Each point represents the mean of three to four determinations; bars represent ± SEM when larger than the symbol.

The effect of N-terminus modifications on cellular uptake of the [^{99m}Tc]Tat−peptide conjugates was also explored. Deletion of the N-terminus Gly as in [^{99m}Tc]-Tat−peptide **5** modestly reduced both Tat−peptide net uptake and the washout residual in Jurkat cells (Table 3), but resulted in an increased net uptake/washout ratio.

Table 3. Effect of N-Terminus Modification on Net Uptake and Washout of [^{99m}Tc]Tat−peptides in Human Jurkat Cells

	[pmol (mg protein)$^{-1}$ (μM$_0$)$^{-1}$]	
peptide	20-min net uptake	30-min washout residual
[^{99m}Tc]Tat-peptide **4**	77.9 ± 3.5	24.3 ± 7.6
[^{99m}Tc]Tat-peptide **5**	61.7 ± 6.1	11.0 ± 1.8
[^{99m}Tc]Tat-peptide **6**	42.7 ± 3.2	24.3 ± 6.3

[a] Cells were incubated in MEBSS loading buffer (20 min; 37 °C) containing **4**, **5,** or **6**, and then analyzed, or washed and then incubated in peptide-free MEBSS (30 min; 37 °C). Cell content of peptide was determined as indicated. See the legend of Table 1 for details.

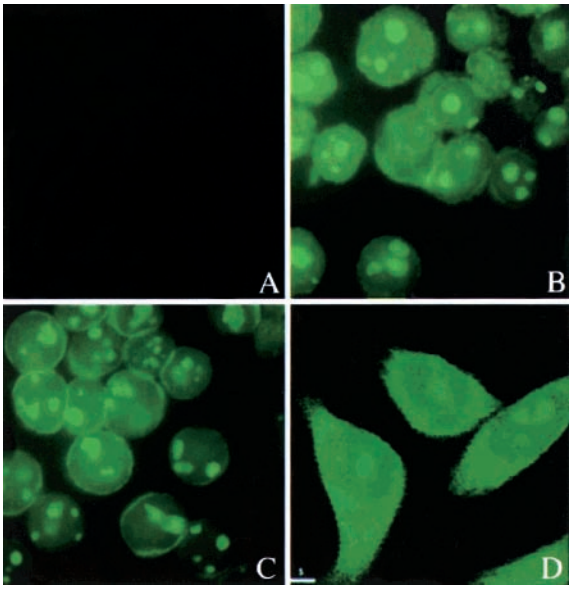

Figure 8. Cellular accumulation of fluorescein labeled Tat−peptide conjugate (**8**) in human Jurkat and KB-3-1 tumor cells. Cells were incubated with substrate for 10−20 min at 37 or 4 °C as indicated followed by fixation. Panels show fluorescence micrographs of Jurkat cells incubated at 37 °C in buffer containing fluorescein maleimide (1 μM) alone (A), at 37 °C in buffer containing **8** (B), and at 4 °C in buffer containing **8** (C) as well as a confocal micrograph of KB-3-1 cells incubated at 37 °C in buffer containing **8** (D). Note green fluorescence from labeled peptide residing in both cytosolic and nuclear (putative nucleolar) components. The cytosolic compartment containing fluorescent peptide, while more obvious in KB-3-1 tumors cells, appears as a rim surrounding the Jurkat cell nuclei, typical of lymphocytic cell types. Panel D, bar = 5 μm; panels A−C, magnified ~2× panel D.

However, N-terminus biotinylation of the shortened peptide (**6**) decreased net uptake while increasing the washout residual resulting in a lower uptake/washout ratio (Table 3).

Fluorescence Microscopy. While the tracer experiments advantageously determined cell-associated radioactivity in a quantitative manner, the exact subcellular location of [^{99m}Tc]Tat−peptides cannot be evaluated by population-based γ-counting techniques. To directly localize and thereby prove intracellular distribution of the Tat−peptide chelate construct, uptake experiments were performed with a fluorescein derivatized Tat−peptide conjugate (**8**) using suspension cultures of human Jurkat cells. As expected, cells did not show internalization of fluorescein maleimide when the nonconjugated fluorophore was added to the media or MEBSS alone (Figure 8A). However, fluorescence microscopy revealed diffuse cytoplasmic and focal nuclear accumulation of the fluorescein derivatized Tat−peptide in all Jurkat cells (Figure 8B). Overall, the multifocal nuclear staining pattern was suggestive of nucleolar localization of the conjugate. Interestingly, the same uptake and localization pattern was observed at 4 °C (Figure 8C). In both KB 3-1 epidermoid carcinoma cells (Figure 8D) and *MDR1* P-glycoprotein-expressing multidrug resistant KB 8-5 cells (data not shown), a cytoplasmic and focal nuclear accumulation pattern also was observed, providing evidence for the ubiquitous nature of tumor cell uptake for this Tat−peptide conjugate. The results in KB 8-5 cells also suggested that P-glycoprotein, an efflux pump of many hydrophobic cationic compounds (*39*), was not involved in the cell permeation pathway of Tat−peptides. Peptide **9** also showed a similar subcellular localization pattern (data not shown). Overall, the fluorescence staining pattern provided direct evidence for the intracellular localization of these novel Tat−peptide chelate based imaging and radiotherapeutic agents.

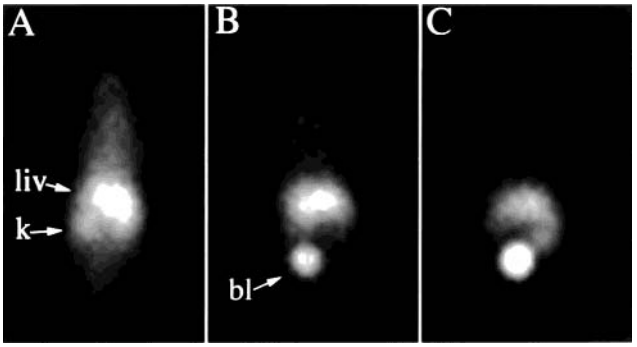

Figure 9. Scintigraphic gray scale images of [^{99m}Tc]Tat−peptide complex **4** in a Balb/c mouse. Following bolus intravenous injection of **4**, posterior images of the mouse were obtained with a gamma scintillation camera. Representative planar images obtained 3 min (A), 30 min (B), and 60 min (C) postinjection are shown. Rapid whole body distribution is followed by predominantly renal clearance of the [^{99m}Tc]Tat−peptide complex and appearance in the urinary bladder. Arrows demarcate liver (liv), kidneys (k), and bladder (bl).

Whole Body Imaging and Biodistribution Analysis. Exploiting the 140 keV emission photon of ^{99m}Tc, preliminary imaging of Balb/c mice was performed by gamma scintigraphy following tail vein bolus injection of [^{99m}Tc]Tat−peptide complex **4** (200 μCi). The complex was observed to rapidly distribute throughout the body, in a pattern initially consistent with organ perfusion (Figure 9). Of note, dynamic analysis of serial images as well as biodistribution data (Table 4) revealed that the complex reached peak organ levels within the first few minutes after injection and displayed modestly rapid blood clearance, favorable pharmacokinetic properties for potential uses of these complexes as imaging agents. Over the subsequent 2 h, [^{99m}Tc]Tat−peptide complex **4** was cleared by both renal and hepatobiliary excretion with activity appearing in the urinary bladder and bowel (Figure 9 and Table 4).

Analysis of [^{99m}Tc]Tat−peptide stability in vivo also was performed. In FVB mice, radio-TLC analysis of serum and urine samples 30 min after intravenous injection of [^{99m}Tc]Tat−peptide **4** revealed >95% intact complex in serum, but only 65% intact complex in the urine. However, direct addition of [^{99m}Tc]Tat−peptide **4** to murine urine samples ex vivo for 1 h at 37 °C showed no evidence of transchelation, thus localizing the observed transmetalation/metabolic reactions to the renal parenchyma in situ.

Table 4. Biodistribution of [^{99m}Tc]Tat−peptide 4 in Balb/c Mice

	5 min	30 min	60 min	120 min
		% id/organ		
blood	12.22 ± 0.78	4.67 ± 0.13	2.82 ± 0.17	1.58 ± 0.05
lung	1.95 ± 0.03	0.89 ± 0.03	0.43 ± 0.06	0.29 ± 0.03
liver	23.73 ± 1.47	30.15 ± 0.96	26.05 ± 0.67	18.36 ± 0.33
spleen	1.21 ± 0.01	0.45 ± 0.02	0.36 ± 0.01	0.33 ± 0.00
kidney	13.55 ± 0.68	10.57 ± 1.00	6.67 ± 0.38	4.61 ± 0.01
muscle	17.08 ± 0.88	9.97 ± 1.09	9.00 ± 3.44	2.42 ± 0.41
fat	2.89 ± 0.40	1.20 ± 0.18	0.67 ± 0.14	0.37 ± 0.03
heart	0.82 ± 0.05	0.20 ± 0.01	0.10 ± 0.01	0.05 ± 0.00
brain	0.13 ± 0.01	0.06 ± 0.00	0.04 ± 0.01	0.03 ± 0.00
bone	14.19 ± 0.54	10.69 ± 0.51	7.24 ± 0.24	4.98 ± 0.08
small intestine	8.16 ± 0.36	5.01 ± 0.41	10.74 ± 0.70	17.12 ± 0.87
large intestine	3.42 ± 0.28	0.89 ± 0.08	0.55 ± 0.01	1.84 ± 0.19
skin	8.48 ± 0.59	9.41 ± 0.18	5.10 ± 0.29	1.88 ± 0.09
		% id/gram		
blood	10.81 ± 0.92	4.07 ± 0.01	2.62 ± 0.24	1.38 ± 0.07
lung	17.13 ± 0.79	7.66 ± 0.37	4.09 ± 0.77	2.60 ± 0.23
liver	22.65 ± 1.47	27.64 ± 0.57	26.60 ± 1.70	17.25 ± 0.48
spleen	18.81 ± 1.22	7.20 ± 0.43	5.48 ± 0.52	4.88 ± 0.19
kidney	49.53 ± 4.06	36.94 ± 4.08	25.08 ± 1.60	16.99 ± 0.53
muscle	3.02 ± 0.19	1.75 ± 0.23	1.62 ± 0.56	0.42 ± 0.08
fat	3.06 ± 0.48	1.25 ± 0.17	0.73 ± 0.13	0.38 ± 0.03
heart	9.42 ± 0.78	2.17 ± 0.12	1.09 ± 0.11	0.59 ± 0.03
brain	0.39 ± 0.05	0.18 ± 0.01	0.11 ± 0.02	0.08 ± 0.01
bone	5.03 ± 0.40	3.73 ± 0.23	2.69 ± 0.18	1.73 ± 0.04
small intestine	6.77 ± 0.38	4.73 ± 0.27	10.13 ± 0.94	15.50 ± 0.67
large intestine	4.49 ± 0.42	1.26 ± 0.15	0.85 ± 0.06	2.82 ± 0.30
skin	4.47 ± 0.11	4.92 ± 0.08	2.83 ± 0.17	0.98 ± 0.05

[a] Mean ± SEM of three determinations at each time point. Error values of 0.00 indicate <0.005.

DISCUSSION

Design of Membrane Permeant Imaging and Radiotherapeutic Peptides. HIV-1 Tat transactivation protein is a potent viral transcriptional regulator capable of rapid translocation through the cell membrane (*21*, *40*). Tat is efficiently taken up by cells and interacts with trans-activation responsive region (TAR) RNA, a stem-loop structure located at the 5′-end of nascent HIV-1 transcripts (*41*). A small region of the HIV-1 Tat protein centered on a cluster of basic amino acids (residues 47−58) suffices to confer this permeation property (*21*). Given the many constraints that large molecular weight compounds may impose on pharmacokinetics and tissue penetration in vivo (*42*), we were attracted to this domain as a small candidate permeation motif likely to confer favorable translocation properties to imaging and radiotherapeutic peptide chelates.

Prototypic all L-peptides were synthesized containing two functional domains, a membrane permeant peptide sequence derived from Tat protein and a peptide-based chelator able to coordinate the desired imaging and therapeutic radionuclides. Among several choices available for the chelator moiety (*2*), a convenient starting point for these prototypic peptides was the ϵ-Lys-Gly-Cys sequence which generates an amino diamido thiol (N_3S) chelating core for an incoming TcO^{3+} or ReO^{3+} metallic species (*6*, *33*). Advantages of this sequence include (a) an appropriate ϵ-Lys residue which is readily available as a protected precursor for solid-phase peptide synthesis, (b) amino acid chain extension off the ϵ-amine of Lys confers rotational freedom between the membrane permeation and chelating domains of the peptide conjugate, (c) the chelation moiety is readily radiolabeled at room temperature using a facile transchelation reaction, and significantly, (d) this chelation moiety has proven favorable pharmacokinetic and metabolic properties in the clinical development of other targeted peptide agents (*6*, *43*). In this regard, cysteine, a naturally occurring and strong chelating compound for technetium, is a commonly used competitive compound for in vitro stability studies of ^{99m}Tc labeled compounds (*44*). In the present study, while 100000-fold molar excess cysteine produced 50% transchelation, the more physiologic challenge of 1000-fold molar excess cysteine (10 μM) showed little evidence of transchelation. These results are comparable to a recent stability report of an analogous N_3S chelating moiety (*34*), wherein 1000-fold molar excess cysteine for 24 h at room temperature (phosphate buffer, pH 7.4) resulted in no detectable transchelation of the ^{99m}Tc labeled conjugate. Other natural chelators also were without effect and, thus, we conclude that the ϵKGC chelation moiety, in accordance with published data in vitro and in vivo (*7*), is sufficiently stable to warrant further exploration for labeling [^{99m}Tc]Tat−peptides. Future studies will explore additional combinations of Tat peptide with interesting chelation moieties (*2*), including histidine (*45*), which readily coordinates Tc/Re(I)-carbonyl compounds.

Tissue penetration is a significant factor limiting efficacy of large macromolecules in vivo (*46*). Significantly, the data in this report now reduce by one amino acid the minimum Tat peptide basic motif sufficient for membrane transduction of a conjugated cargo. For example, previous studies have utilized HIV-1 Tat protein amino acid residues 48−60 (*21*), 48−59 (*47*), residues 47−57 (*19*), and residues 48−57 (*22*). Deletion of the N-terminus Gly as in [^{99m}Tc]Tat−peptide complex **5** (representing Tat protein amino acid residue 48) only minimally impacted net cell uptake compared to **4**. Thus, Tat protein amino acid residues 49−57 appear sufficient to impart the desired membrane translocation properties. However, further analysis of the minimally required motif would be of great interest as the smallest possible permeation sequence likely would show favorable pharmacokinetics in vivo.

In Vivo Imaging with Peptide Complexes. Low molecular weight peptides and antibody fragments provide rapid tumor targeting and uniform distribution in

tumor tissues (*48*). While such characteristics render low molecular weight peptides attractive vehicles for the delivery of radioactivity to tumor tissues and organs for both targeted imaging and radiotherapy, problems have been encountered. High and persistent localization of radioactivity is often observed in the kidneys, which compromises tumor visualization in the kidney region and limits therapeutic potential (*49*, *50*). As discussed by Arano et al. (*51*), radiolabeled low molecular weight peptides and antibody fragments would become much more useful for targeted imaging and therapy if the renal radioactivity levels could be reduced without impairing those in the target tissue. Previous studies have indicated that after glomerular filtration radiolabeled low molecular weight peptides and antibody fragments are likely resorbed by proximal tubules via luminal endocytosis (*52*, *53*). The long residence times of nontransported radiometabolites generated after lysosomal proteolysis of the radiolabeled fragments in renal cells also were reported to be responsible for the persistent renal radioactivity levels (*49*, *53*). The rapid renal clearance observed for the [^{99m}Tc]Tat−peptide complexes suggests that lysosomal proteolysis is not relevant to the overall excretion pathway of [^{99m}Tc]Tat−peptides in vivo and may favorably impact whole body imaging and therapeutic applications with these complexes.

Given the nuclear localization and RNA binding properties of Tat (*41*, *54*), an appealing potential use of our novel [^{99m}Tc]Tat−peptide complexes would entail chelation of ^{186}Re or^{188}Re for delivery of therapeutic radiopharmaceuticals directly to the cell nucleus. Combined with appropriate targeting constructs, this might enable efficient delivery of gamma irradiation doses directly to RNA/DNA pools within tumors. It should also be possible to synthesize alternative Tat−peptide conjugates using DTPA or DOTA, chelates suitable for other incoming radiotherapeutic and relaxivity metals, for applications in radiotherapy and magnetic resonance imaging.

CONCLUSION

In summary, a new class of peptide-based membrane permeant radiopharmaceuticals incorporating Tat−peptide basic sequences and a convenient peptide motif for chelation of metal isotopes was designed and synthesized. These potential imaging and radiotherapeutic agents are capable of rapid transduction through the plasma membrane of a variety of human cells and are shown to accumulate in a highly concentrative manner. Fluorescence microscopy of fluorescein-tagged Tat−peptide conjugates directly verified the cytosolic and focal nuclear localization of these agents. These prototypic [^{99m}Tc]Tat−peptide complexes can be easily derivatized for further targeted applications.

ACKNOWLEDGMENT

We thank Delynn Silvestros for support with gamma scintigraphy, Carolyn Crankshaw for technical assistance, and Mike Berne of Tufts University for peptide synthesis. Mass spectra were obtained from the Washington University Resource for Biomedical and Bioorganic Mass Spectrometry. This work was supported by U.S. National Institutes of Health Grants RO1 CA82841 and P20 CA86251.

LITERATURE CITED

(1) Hom, R., and Katzenellenbogen, J. (1997) Technetium-99m-labeled receptor-specific small-molecule radiopharmaceuticals: recent developments and encouraging results. *Nucl. Med. Biol. 24*, 485−498.

(2) Liu, S., and Edwards, D. (1999) ^{99m}Tc-labeled small peptides as diagnostic radiopharmaceuticals. *Chem. Rev. 99*, 2235−2268.

(3) Jurisson, S., and Lydon, J. (1999) Potential technetium small molecule radipharmaceuticals. *Chem. Rev. 99*, 2205−2218.

(4) Anderson, C., and Welch, M. (1999) Radiometal-labeled agents (non-technetium) for diagnostic imaging. *Chem. Rev. 99*, 2219−2234.

(5) Krenning, E., Kwekkeboom, D., Bakker, W., Breeman, W., Kooij, P., Oei, H., van Hangen, M., Postema, P., de Jong, M., and Reubi, J. (1993) Somatostatin receptor scintigraphy with [In-111-DTPA-D-Phe] and [I123-Tyr]octreotide: the Rotterdam experience with more than 1000 patients. *Eur. J. Nucl. Med. 20*, 716−731.

(6) Pearson, D., Lister-James, J., McBride, W., Wilson, D., Martel, L., Civitello, E., and Dean, R. (1996) Thrombus imaging using technetium-99m-labeled high-potency GPIIb/IIIa receptor antagonists. Chemistry and initial biological studies. *J. Med. Chem. 39*, 1372−1382.

(7) Lister-James, J., Vallabhajosula, S., Moyer, B., Pearson, D., McBride, B., De Rosch, M., Bush, L., Machac, J., and Dean, R. (1997) Pre-clinical evaluation of technetium-99m platelet receptor-binding peptide. *J. Nucl. Med. 38*, 105−111.

(8) Abrams, M., and Murrer, B. (1993) Metal compounds in therapy and diagnosis. *Science 261*, 725−730.

(9) Schwochau, K. (1994) Technetium radiopharmaceuticals − fundamentals, synthesis, structure and development. *Angew. Chem., Int. Ed. Engl. 33*, 2258−2267.

(10) Volkert, W., and Hoffman, T. (1999) Therapeutic radiopharmaceuticals. *Chem. Rev. 99*, 2269−2292.

(11) Flewelling, R., and Hubbell, W. (1986) The membrane dipole potential in a total membrane potential model: applications to hydrophobic ion interactions with membranes. *Biophys J. 49*, 541−552.

(12) Derossi, D., Calvet, S., Trembleau, A., Brunissen, A., Chassaing, G., and Prochiantz, A. (1996) Cell internalization of the third helix of the Antennapedia homeodomain is receptor-independent. *J. Biol. Chem. 271*, 18188−18193.

(13) Avrameas, A., Ternynck, T., Nato, F., Buttin, G., and Avrameas, S. (1998) Polyreactive anti-DNA monoclonal antibodies and a derived peptide as vectors for the intracytoplasmic and intranuclear translocation of macromolecules. *Proc Natl Acad Sci U.S.A. 95*, 5601−5606.

(14) Elliot, G., and O'Hare, P. (1997) Intercellular trafficking and protein delivery by a Herpesvirus structural protein. *Cell 88*, 223−233.

(15) Kubota, S., Siomi, H., Satoh, T., Endo, S., Maki, M., and Hatanaka, M. (1989) Functional similarity of HIV-1 rev and HTLV-1 rex proteins: identification of a new nucleolar-targeting signal in rev protein. *Biochem. Biophys. Res. Commun. 162*, 963−970.

(16) Frankel, A., and Pabo, C. (1988) Cellular uptake of the tat protein from human immunodeficiency virus. *Cell 55*, 1189−1193.

(17) Fawell, S., Seery, J., Daikh, Y., Moore, C., Chen, L., Pepinsky, B., and Barsoum, J. (1994) Tat-mediated delivery of heterologous proteins into cells. *Proc Natl Acad Sci U.S.A. 91*, 664−668.

(18) Derossi, D., Chassaing, G., and Prochiantz, A. (1998) Trojan peptides: the penetratin system for intracellular delivery. *Trends Cell Biol. 8*, 84−87.

(19) Nagahara, H., Vocero-Akbani, A., Synder, E., Ho, A. L., DG, Lissy, N., Becker-Hapak, M., Ezhevsky, S., and Dowdy, S. (1998) Transduction of full-length TAT fusion proteins directly into mammalian cells: TAT-p27^{Kip1} induces cell migration. *Nat. Med. 4*, 1449−1452.

(20) Schluesener, H. (1996) Protection against experimental nervous system autoimmune diseases by a human immunodeficeincy virus-1 Tat peptide-based polyvalent vaccine. *J. Neurosci. Res. 46*, 258−262.

(21) Vives, E., Brodin, P., and Lebleu, B. (1997) A truncated HIV-1 Tat protein basic domain rapidly translocates through the plasma membrane and accumulates in the cell nucleus. *J. Biol. Chem. 272*, 16010−16017.

(22) Josephson, L., Tung, C.-H., Moore, A., and Weissleder, R. (1999) High-efficiency intracellular magnetic labeling with novel superparamagnetic-Tat peptide conjugates. *Bioconjugate Chem. 10*, 186−191.
(23) Piwnica-Worms, D., Chiu, M., Budding, M., Kronauge, J., Kramer, R., and Croop, J. (1993) Functional imaging of multidrug-resistant P-glycoprotein with an organotechnetium complex. *Cancer Res. 53*, 977−984.
(24) Akiyama, S. I., Fojo, A., Hanover, J. A., Pastan, I., and Gottesman, M. M. (1985) Isolation and genetic characterization of human KB cell lines resistant to multiple drugs. *Somatic Cell. Mol. Genet. 11*, 117−126.
(25) Peng, C.-Y., Graves, P., Thoma, R., Wu, Z., Shaw, A., and Piwnica-Worms, H. (1997) Mitotic and G2 checkpoint control: regulation of 14-3-3 protein binding by phosphorylation of Cdc25C on serine-216. *Science 277*, 1501−1505.
(26) Piwnica-Worms, D., Jacob, R., Horres, C. R., and Lieberman, M. (1983) Transmembrane chloride flux in tissue-cultured chick heart cells. *J. Gen. Physiol. 81*, 731−748.
(27) Bosch, I., Crankshaw, C., Piwnica-Worms, D., and Croop, J. (1997) Characterization of functional assays of P-glycoprotein transport activity. *Leukemia 11*, 1131−1137.
(28) Lamson, M., Kirscher, A., Hotte, C., Lipsitz, E., and Ice, R. (1975) Generator-produced $^{99m}Tc-TcO_4^-$: carrier free? *J. Nucl. Med. 16*, 639−641.
(29) Piwnica-Worms, D., Kronauge, J., and Chiu, M. (1990) Uptake and retention of hexakis (2-methoxy isobutyl isonitrile) technetium(I) in cultured chick myocardial cells: mitochondrial and plasma membrane potential dependence. *Circulation 82*, 1826−1838.
(30) Rao, V., Dahlheimer, J., Bardgett, M., Snyder, A., Finch, R., Sartorelli, A., and Piwnica-Worms, D. (1999) Choroid plexus epithelial expression of MDR1 P-glycoprotein and multidrug resistance-associated protein contribute to the blood-cerebrospinal fluid drug-permeability barrier. *Proc. Natl. Acad. Sci. U.S.A. 96*, 3900−3905.
(31) Herman, L. W., Sharma, V., Kronauge, J. F., Barbarics, E., Herman, L. A., and Piwnica-Worms, D. (1995) Novel hexakis(areneisonitrile)technetium(I) complexes as radioligands targeted to the multidrug resistance P-glycoprotein. *J. Med. Chem. 38*, 2955−2963.
(32) Sharma, V., Beatty, A., Wey, S.-P., Dahlheimer, J., Pica, C., Crankshaw, C., Bass, L., Green, M., Welch, M., and Piwnica-Worms, D. (2000) Novel gallium(III) complexes transported by *MDR1* P-glycoprotein: potential PET imaging agents for probing P-glycoprotein-mediated transport activity in vivo. *Chem. Biol. 7*, 335−343.
(33) Wong, E., Fauconnier, T., Bennett, S., Valliant, J., Nguyen, T., Lau, F., Lu, L., Pollak, A., Bell, R., and Thornback, J. (1997) Rhenium(V) and technetium(V) oxo complexes of an $N_2N'S$ peptidic chelator: evidence of interconversion between the syn and anti conformations. *Inorg. Chem. 36*, 5799−5808.
(34) Decristoforo, C., and Mather, S. (1999) Preparation, Tc-99m-labeling, and in vitro characterization of HYNIC and N_3S modified RC-160 and [Tyr^3]octreotide. *Bioconjugate Chem. 10*, 431−438.
(35) Meegalla, S., Plossl, K., Kung, M.-P., Chumpradit, S., Stevenson, D., Kushner, S., McElgin, W., Mozley, P., and Kung, H. (1997) Synthesis and characterization of technetium-99m-labeled tropanes as dopamine transporter-imaging agents. *J. Med. Chem. 40*, 9−17.
(36) Piwnica-Worms, D., Rao, V., Kronauge, J., and Croop, J. (1995) Characterization of multidrug-resistance P-glycoprotein transport function with an organotechnetium cation. *Biochemistry 34*, 12210−12220.
(37) Sharma, V., Crankshaw, C., and Piwnica-Worms, D. (1996) Effects of multidrug resistance (*MDR1*) P-glycoprotein expression levels and coordination metal on the cytotoxic potency of multidentate (N_4O_2) ethylenediamine-bis[propyl-(R-benzylimino)]metal(III) cations. *J. Med. Chem. 39*, 3483−3490.
(38) Sharma, V., and Piwnica-Worms, D. (1999) Metal complexes for therapy and diagnosis of drug resistance. *Chem. Rev. 99*, 2545−2560.
(39) Ambudkar, S., Dey, S., Hrycyna, C., Ramachandra, M., Pastan, I., and Gottesman, M. (1999) Biochemical, cellular, and pharmacological aspects of the multidrug transporter. *Annu. Rev. Pharmacol. Toxicol. 31*, 361−398.
(40) Mann, D., and Frankel, A. (1991) Endocytosis and targeting of exogenous HIV-1 Tat protein. *EMBO 10*, 1733-1739.
(41) Jones, K., and Peterlin, B. (1994) Control of RNA initiation and elongation at the HIV-1 promoter. *Annu. Rev. Biochem. 63*, 717−743.
(42) Hobbs, S., Monsky, W., Yuan, F., Roberts, W., Griffith, L., Torchilin, V., and Jain, R. (1998) Regulation of transport pathways in tumor vessels: role of tumor type and microenvironment. *Proc. Natl. Acad. Sci. U.S.A. 95*, 4607−4612.
(43) Lister-James, J., Moyer, B., and Dean, R. (1997) Pharmacokinetic considerations in the development of peptide-based imaging agents. *Q. J. Nucl. Med. 41*, 111−118.
(44) Hnatowich, D., Virzi, F., Fogorasi, M., Rusckowski, M., and Winnard, P. (1994) Can a cysteine challenge assay predict the in vivo behavior of Tc-99m-labeled antibodies? *Nucl. Med. Biol. 21*, 1035−1044.
(45) Waibel, R., Alberto, R., Willuda, J., Finnern, R., Schibli, R., Stichelberger, A., Egli, A., Abram, U., Mach, J.-P., and Pluckthun, A., et al. (1999) Stable one-step technetium-99m labeling of His-tagged recombinant proteins with a novel Tc-(I)-carbonyl complex. *Nat. Biotechnol. 17*, 897−901.
(46) Wolf, G., Fischman, A., Boucher, Y., and Jain, R. (1999) Enhancement of fluid filtration across tumor vessels: implications for delivery of macromolecules. *Proc. Natl. Acad. Sci. U.S.A. 96*, 3137−3142.
(47) Efthymiadis, A., Briggs, L., and Jans, D. (1998) The HIV-1 Tat nuclear localization sequence confers novel nuclear import properties. *J. Biol. Chem. 273*, 1623−1628.
(48) Yokota, T., Milenic, D., Whitlow, M., Wood, J., Hubert, S., and Schlom, J. (1993) Microautoradiographic analysis of the normal organ distribution of radioiodinated single-chain Fv and other immunoglobulin forms. *Cancer Res. 53*, 3776−3783.
(49) Choi, C., Lang, L., Lee, J., Webber, K., Yoo, T., Chang, H., Le, N., Jagoda, E., Paik, C., and Pastan, I., et al. (1995) Biodistribution of 18F- and 125I-labeled anti-Tac disulfide-stabilized Fv fragments in nude mice with interleukin 2 alpha receptor-positive tumor xenografts. *Cancer Res. 55*, 5323−5329.
(50) Behr, T., Becker, W., Bair, H., Klein, M., Stuhler, C., Cidlinsky, K., Wittekind, C., Scheele, J., and Wolf, F. (1995) Comparison of complete versus fragmented technetium-99m-labeled anti-CEA monoclonal antibodies for immunoscintigraphy in colorectal cancer. *J. Nucl. Med. 36*, 430−441.
(51) Arano, Y., Fujioka, Y., Akizawa, H., Ono, M., Uehara, T., Wakisaka, K., Nakayama, M., Sakahara, H., Konishi, J., and Saji, H. (1999) Chemical design of radiolabeled antibody fragments for low renal radioactivity levels. *Cancer Res. 59*, 128−134.
(52) Silbernagl, S. (1988) The renal handling of amino acids and oligopeptides. *Physiol. Rev. 68*, 911−1007.
(53) Duncan, J., and Welch, M. (1993) Intracellular metabolism of ^{111}In-DTPA labeled receptor targeted proteins. *J. Nucl. Med. 34*, 1728−1738.
(54) Harada, K., Martin, S., Tan, R., and Frankel, A. (1997) Molding a peptide into an RNA site by in vivo peptide evolution. *Proc. Natl. Acad. Sci. U.S.A. 94*, 11887−11892.

BC000008Y

Kinetics of CO and O_2 Binding to Human Serum Albumin-Heme Hybrid

Teruyuki Komatsu, Yasuko Matsukawa, and Eishun Tsuchida*

Department of Polymer Chemistry, Advanced Research Institute for Science & Engineering, Waseda University, Tokyo 169-8555, Japan. Received February 14, 2000; Revised Manuscript Received April 21, 2000

The kinetics of the CO and O_2 binding to the synthetic hemoprotein, recombinant human serum albumin (rHSA) incorporating *eight* 2-[8-{*N*-(2-methylimidazolyl)}octanoyloxymethyl]-5,10,15,20-tetrakis(*o*-pivalamido)phenylporphinatoiron(II)s (FePs) [rHSA-FeP(8)] have been investigated by laser flash photolysis. Time dependence of the absorption change accompanied the CO rebinding to rHSA-FeP(8) was composed of three phases. The fastest component was the axial base elimination, and the long-lived biphasic decay corresponds to the direct recombination of CO to the five-N-coordinated FePs in rHSA. The rate constants of the fast and slow phases of the CO association [k_{on}^{CO}(fast), k_{on}^{CO}(slow)] were determined to be 4.9×10^6 M^{-1} s^{-1} and 6.7×10^5 M^{-1} s^{-1}, respectively. The initial amplitude after the laser pulse gave the concentration ratio of the fast and slow phases ($n = 3$); (i) two of the eight FePs exhibited the slow rate constants and (ii) they are presumably accommodated in the second and fifth binding sites of FeP in the albumin structure. The absorption decay following the O_2 photodissociation of rHSA-FeP(8) also showed the same behavior. Thermodynamically, the large $\Delta G^{\ddagger}$ of the slow phase of the CO rebinding, which mainly comes from the enthalpic factor, suggests the appearance of additional steric hindrance on the central metal iron of FeP. Furthermore, orientation of the porphyrin plane in rHSA was predicted by molecular simulation, which supports the experimental data from the kinetic observations.

INTRODUCTION

The binding kinetics of small gaseous ligands (CO, O_2, or NO) to hemoproteins, e.g., myoglobin (Mb) and hemoglobin (Hb), have been widely studied for many years and it is still of current interest for the development of their mutant derivatives (Gibson 1970; Olson et al., 1971, 1988; Sawicki et al., 1977; Sharma et al., 1976; Steinmeier et al., 1975). For instance, the main features of the binding processes of Mb can be described as a scheme including two intermediate states in which the ligand molecule is inside the protein, but has not yet bound to the iron center of the heme. Much research has been carried out to interpret these transient states in terms of the stereochemistry of the Mb molecule (Ansari et al., 1985; Austin et al., 1975; Jongeward et al., 1988; Sato et al., 1990). A variety of theoretical simulations have also been undertaken to study the response of the ligand and protein structure to the photodissoiation (Case et al., 1979; Kottalam et al., 1988).

We have recently found that the recombinant human serum albumin (rHSA) incorporating the tetraphenylporphinatoiron(II) derivative linked a covalently bound axial base, 2-[8-{*N*-(2-methylimidazolyl)}octanoyloxymethyl]-5,10,15,20-tetrakis(α,α,α,α-*o*-pivalamido)phenylporphinatoiron(II) (FeP) (rHSA-FeP) can reversibly bind and release O_2 under physiological conditions (in aqueous media, pH 7.3, 37 °C) like Hb and Mb (Komatsu et al., 1999; Tsuchida et al., 1997, 1999). It is noteworthy that the obtained rHSA-FeP hybrid shows a good compatibility with the human whole blood and can quantitatively transport O_2 in vivo (Tsuchida et al., 2000). That is, rHSA-FeP is now one of the most promising materials as a totally synthetic red cell substitute. Interestingly, laser flash photolysis to the dioxygenated rHSA-FeP leads to nonexponential relaxation of the O_2-photodissociated products on a microsecond time scale (Tsuchida et al., 1999). This paper describes the rebinding kinetics of CO and O_2 to this synthetic hemoprotein and its thermodynamic properties. Furthermore, molecular simulation allows us to predict the orientation of the porphyrin plane in the albumin structure, which supports the kinetic observations.

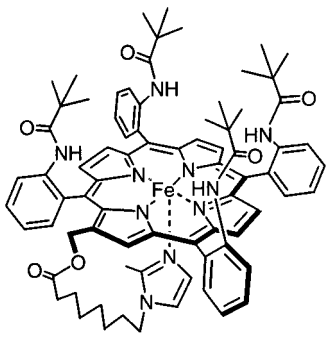

FeP

EXPERIMENTAL PROCEDURES

Materials and Prepration. The synthetic heme, 2-[8-{*N*-(2-methylimidazolyl)}octanoyloxymethyl]-5,10,15,20-tetrakis(*o*-pivalamido)phenylporphinatoiron(II) (FeP) was prepared according to our previously reported procedures (Tsuchida et al., 1995). A recombinant human serum albumin (rHSA; 25 wt %) was obtained from WelFide Corporation (Sumi et al., 1993). The rHSA-FeP solution

* To whom the correspondence should be addressed. CREST investigator, JST. Phone: +81 3-5286-3120. Fax: +81 3-3205-4740. E-mail: eishun@mn.waseda.ac.jp.

10.1021/bc000016e CCC: $19.00 © 2000 American Chemical Society
Published on Web 09/30/2000

was prepared by the following procedure. Aqueous ascorbic acid (120 mM, 10 μL) was added to an ethanol solution of Fe(III)P (60 μM, 20 mL) under a CO atmosphere to reduce the central ferric ion of FeP. The obtained six-coordinate carbonyl Fe(II)P in ethanol was slowly added to the phosphate buffer solution (30 mM, pH 7.3) of rHSA (3.75 μM, pH 7.3, 40 mL) through the wall of the round flask. The mixture was then dialyzed with a cellulose membrane against phosphate buffer (pH 7.3) for 2 h and another 16 h at 4 °C. The ethanol content was finally reduced to less than 95 ppm, affording an aqueous solution of rHSA-FeP(8) [[FeP]: 20 μM, FeP/rHSA = 8 (mol/mol)].

Laser Flash Photolysis. CO and O_2 bindings to FeP were expressed by

$$\mathrm{FeP} + \mathrm{L} \underset{k^{\mathrm{L}}_{\mathrm{off}}}{\overset{k^{\mathrm{L}}_{\mathrm{on}}}{\rightleftharpoons}} \mathrm{FeP\text{-}L} \qquad (1)$$

$$[K^{\mathrm{L}} = k^{\mathrm{L}}_{\mathrm{on}}/k^{\mathrm{L}}_{\mathrm{off}}]$$

where L is CO or O_2. The association rate constants of these gaseous ligands ($k^{\mathrm{L}}_{\mathrm{on}}$) were obtained from the rebinding kinetics following photodissociation of CO or O_2 by laser flash photolysis [Continium Surelight I-10 (Nd:YAG laser SHG: 532 nm, 6 ns pulse width)]. In particular, a CO/O_2 competitive binding technique was employed for the determination of $k^{\mathrm{O_2}}_{\mathrm{on}}$ (Tsuchida et al., 1993; Collman et al., 1983; Traylor et al., 1985). The Xenon lamp (150 W) was used as the monitor light source. The time dependence of the absorption changes that accompanied the CO or O_2 recombination were detected by a Hamamatsu Photonics R636 photomultiplier, and the relaxation curves were fitted to triple-exponentials. A KOFLOC Gas Blender GB-3C prepared the mixture gas with the desired partial pressure. For the solubility of CO and O_2 in water at 25 °C, we used the values of 0.94 and 1.25 mM, respectively. Gas concentrations were always at least 10 times that of the FeP concentration, therefore, the pseudo-first-order approximation could be applied throughout. The cuvette of the sample ([FeP]: 20 μM) was fixed into a thermostated holder and the temperature was mainteined from 10 to 35 °C for the Arrhenius equation in order to obtain the activation energy parameters.

Binding Equilibria. The gaseous-binding affinity (partial pressure at half binding for FeP, $P^{\mathrm{L}}_{1/2} = 1/[K^{\mathrm{L}}]$) was determined by spectral changes at various partial pressures of CO or O_2 as in previous reports (Tsuchida et al., 1993; Collman et al., 1983). The FeP concentrations of 20 μM were normally used for the UV−vis absorption spectroscopy. The UV−vis absorption measurements were performed using a Shimadzu V-570 spectrometer within the range of 350−700 nm.

Molecular Simulations. The orientation of FeP in the hydrophobic cavity of rHSA was predicted by the ESFF force field simulation using an Insight II system (Molecular Simulations Inc.) on a Silicon Graphics O_2 computer. First, the domain for FeP was preliminarily predicted using the domain analysis program. The initial structure in which FeP was placed in the crevice between IB and IIA, namely the hemin site, was proposed. The potential energy was obtained after the energy minimization with 100 steps of the conjugate gradient method assuming a dielectric constant of 1.0. Random numbers automatically produced the degrees of freedom of FeP and the residues within the length of 12 Å from the porphyrin center were permitted to move.

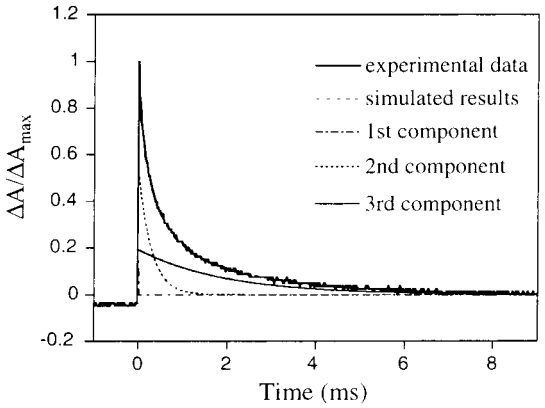

Figure 1. Absorption decay of CO rebinding to rHSA-FeP(8) after the laser flash photolysis at 25 °C. The kinetics was composed of three phases and the relaxation curve was fitted by triple-exponentials.

RESULTS AND DISCUSSION

CO-Binding Kinetics. We have shown earlier that a maximum of *eight* FeP molecules are incorporated into certain domains of human serum albumin with binding constants from a K_1 of 1.2×10^6 to a K_8 of 1.3×10^4 M^{-1} (Tsuchida et al., 1997, 1999). Three of the eight sites were estimated to be subdomains IB−IIA (hemin site), IIA (bilirbin site), and IIIA (typical palmitic acid site), respectively. For convenience, the eight binding sites of FeP are now named the *first site* to the *eighth site* in order of their magnitudes of the binding constants (K_1−K_8). As a matter of course, the microenvironment around the each FeP in albumin should not be identical. Therefore, one can expect the multiple binding processes of CO and O_2 with this synthetic hemoprotein. Flash photolysis experiments were then carried out to characterize the CO- and O_2-binidng behavior of rHSA-FeP in detail. First, an aqueous solution of rHSA incorporating eight carbonyl-FePs [rHSA-FeP(8)], which displayed absorption maxima at 427 and 539 nm, was irradiated. The time dependence of the absorption change [ΔA(t)] at 443 nm after the laser flash photolysis showed nonexponential kinetics (Figure 1), which was independent of the monitoring wavelength and the laser pulse intensity. On the basis of the careful inspection of the relaxation curve, it could be fitted to triple-exponentials using eq 2,

$$\Delta A(t) = C_1 \exp(-k_1 t) + C_2 \exp(-k_2 t) + C_3 \exp(-k_3 t) \quad (2)$$

where k_1, k_2, and k_3 are apparent rate constants for the each reaction. The fastest component with a k_1 of 2.4×10^5 s^{-1} was relatively minor (C_1: 0.16) and found to be independent of the CO concentration. This kinetics should be related to an axial base elimination (Geibel et al., 1978), so that the latter biphasic decay corresponds to the direct rebinding process of CO to the five-N-coordinated FeP in rHSA (deoxy form). The k_2 and k_3 values yield the association rate constants for the fast and slow phases [$k^{\mathrm{CO}}_{\mathrm{on}}$(fast), $k^{\mathrm{CO}}_{\mathrm{on}}$(slow)] (Table 1); the $k^{\mathrm{CO}}_{\mathrm{on}}$(slow) ($6.7 \times 10^5$ M^{-1} s^{-1}) became one-seventh of $k^{\mathrm{CO}}_{\mathrm{on}}$(fast) ($4.9 \times 10^6$ M^{-1} s^{-1}). Interestingly, the absorption decay during the CO recombination of rHSA-FeP(1) was almost monophasic ($k_{\mathrm{on}} = 4.7 \times 10^6$ M^{-1} s^{-1}). Therefore, it can be supposed that the CO-association rate of FeP is largely affected by the protein environments surrounding the metal center of FeP, e.g., steric hindrance of the amino acid residues and difference in polarity.

Table 1. Association and Dissociation Rate Constants of CO and O_2 to rHSA-FeP in Phosphate Buffer (pH 7.3) at 25 °C

	CO		O_2			
	10^{-6} k_{on}(fast) (M^{-1} s^{-1})	10^{-6} k_{on}(slow) (M^{-1} s^{-1})	10^{-7} k_{on}(fast) (M^{-1} s^{-1})	10^{-7} k_{on}(slow) (M^{-1} s^{-1})	10^{-2} k_{off}(fast) (s^{-1})	10^{-2} k_{off}(slow) (s^{-1})
rHSA-FeP(2)	4.5 [69]	0.65 [31]	3.4 [67]	0.94 [33]	7.4	2.0
rHSA-FeP(4)	4.7 [65]	0.66 [35]	3.2 [63]	1.0 [37]	7.2	2.2
rHSA-FeP(8)	4.9 [73]	0.67 [27]	3.4 [73]	0.95 [27]	7.5	2.0
Hb(T-state)α[a]	0.22		0.29		1.8	

[a] In brackets (%); the percentage of the fast and slow components in CO- or O_2-rebinding to the five-N-coordinated FeP in rHSA, which is estimated from the amplitude of $\Delta A(t=0)$. [b] pH 7, 20 °C (Sawicki et al., 1977; Steinmeier et al., 1975).

Table 2. Free-Energy Changes and Activation Parameters of the CO Association to rHSA-FeP(8) in Phosphate Buffer (pH 7.3) at 25 °C

	phase	10^{-6} k_{on}^{CO} (M^{-1} s^{-1})	$\Delta G^{\ddagger}$ (kJ mol^{-1})	$\Delta H^{\ddagger}$ (kJ mol^{-1})	$\Delta S^{\ddagger}$ (J mol^{-1} K^{-1})
rHSA-FeP(8)	fast	4.9	43	19	−80
	slow	0.67	49	23	−83
FeP (in toluene)		6.9	44 (:$\Delta G_I^{\ddagger}$)	13	−104

We then calculated the concentration ratio of the fast and slow phases (n) from the initial amplitude after the laser pulse [$\Delta A(t=0)$]. For the rHSA-FeP(8), the n value was approximately three, indicating two of the eight FePs exhibited the slow rate constants [k_{on}^{CO}(slow)]. The absorption decays of rHSA-FeP(2) and rHSA-FeP(4) also obeyed the triple-exponentials in which the second and third components again showed the clear CO-concentration dependence. The determined k_{on}^{CO}(fast) and k_{on}^{CO}(slow) were all the same as those of rHSA-FeP(8). On the basis of the n values of rHSA-FeP with different numbers of FeP/rHSA [1, 2, 4, 8 (mol/mol)], it takes into account that two of the eight FePs with the slow rate constant reside in the second and fifth binding sites of the FePs in the albumin structure, i.e., "slow site". Of course, since the numbers of FePs bound represent average numbers, we made two assumptions; (1) the binding numbers of FeP in an rHSA are identical to the mixture ratio, and (2) in the case of rHSA-FeP(4), for example, the two states (I, II) exist in the solution; I state in which FePs occupy the first to the fourth binding sites (66%), and II state in which FePs occupy the first to the third binding sites and the fifth site (34%).

To interpret the reaction profile, the activation parameters and free energy changes ($\Delta G^{\ddagger}$) of the CO rebinding to rHSA-FeP(8) were measured (Table 2). The Arrhenius plots of each relaxation component showed a straight line in the temperature range of 15−35 °C. $\Delta G^{\ddagger}$ of the slow phase (49 kJ mol^{-1}) was significantly higher than that of the fast phase (43 kJ mol^{-1}), and its enthalpy term mainly contributes to the destabilization of the transition state. This result suggests that an additional steric hindrance opposes the binding of CO. In a protein, the multiple free energy barriers generally regulate the entering or leaving of the gaseous ligand. We then proposed a double-barrier model in which CO encounters two barriers on its way from water to the binding site of FeP (Figure 2). **A** is the FeP−CO bound state, **S** is the dissociated state and **B**, is an intermediate state that is only transiently populated. The external barrier II is attributed to the matrix disturbance of the free diffusion of CO from the outer aqueous phase. Once within the pocket of the serum albumin, CO has to overcome energy barrier I for the bond formation. In general, the association rate constants of CO with synthetic hemes and hemoproteins are low compared with those of O_2 or NO and far below the diffusion limit at room temperature (Austin et al., 1975; Sharma et al., 1976; Tetreau et al., 1990). Therefore, the overall reaction rates of CO with rHSA-FeP should be governed by the height of barrier I. The $\Delta G^{\ddagger}$ of the CO binding to FeP in homogeneous toluene solution was determined to be 44 kJ mol^{-1}, which is identical to that of the fast component of rHSA-FeP(8) [$\Delta G^{\ddagger}$(fast): 43 kJ mol^{-1}]. At the "fast sites", the rHSA structure does not interfere with the CO recombination. In contrast, the height of the barrier increased at the slow site and the CO rebinding could be opposed by the steric hindrance of the bulky amino acid residues located over the porphyrin plane.

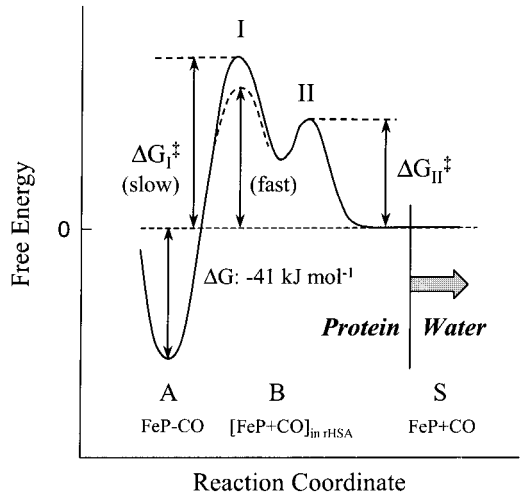

Figure 2. Double-barrier model for CO rebinding to rHSA-FeP. $\Delta G_I^{\ddagger}$ and $\Delta G_{II}^{\ddagger}$ refer to the top of barriers I and II relative to the reactants. The overall reaction rate is determined by $\Delta G_I^{\ddagger}$.

O_2-Binding Kinetics. The O_2-binding kinetics of rHSA-FeP showed exactly the same trend observed in the CO recombination. The absorption decay [$\Delta A(t)$] of rHSA-FeP(8) following the O_2 photodissociation was again fitted by triple-exponentials. The fastest relaxation with the apparent rate constant of k_1 (less than 10%) was independent of the O_2 concentration. This reaction is considered to be the unfavorable base elimination (Geibel et al., 1978). The slopes of the linear plots of k_2 and k_3 versus [O_2] yield two association rate constants for the fast and slow phases [$k_{on}^{O_2}$(fast), $k_{on}^{O_2}$(slow)] (Table 1). The differences in the $k_{on}^{O_2}$(fast) and $k_{on}^{O_2}$(slow) values are significantly smaller than that observed in CO. As predicted, the O_2-binding kinetics of rHSA-FeP(1) obeyed a single-exponential (k_{on} = 3.2 × 10^7 $M^{-1}s^{-1}$). The n values for rHSA-FeP [FeP/rHSA = 2, 4, 8 (mol/mol)] were the same as those of the CO recombination. Conse-

Table 3. CO- and O_2-Binding Affinities of rHSA-FeP in Phosphate Buffer (pH 7.3) at 25 °C

	CO		O_2	
	10^{-1} $P_{1/2}$(fast) (Torr)	10^{-1} $P_{1/2}$(slow) (Torr)	$P_{1/2}$(fast) (Torr)	$P_{1/2}$(slow) (Torr)
rHSA-FeP(4)	1.1	1.1	13	13
rHSA-FeP(8)	1.2	1.2	14	13

quently, the second and the fifth binding sites of FeP are again assigned to the *slow sites* for O_2 binding.

CO- and O_2−Binding Affinities. The CO- and O_2-binding affinities ($P_{1/2}$ is the gaseous pressure at half ligand-binding for FeP) of rHSA-FeP were determined based on the UV−vis absorption spectral changes by the CO and O_2 titrations. According to the results of the kinetics experiments, the $P_{1/2}$ values were divided by two components using eq 3,

$$Y = A(K(\text{fast})[\text{L}]/(1 + K(\text{fast})[\text{L}])) + B(K(\text{slow})[\text{L}]/(1 + K(\text{slow})[\text{L}])) \quad (3)$$

where Y is total CO and O_2 saturation of FeP in rHSA, $K(\text{fast}) = [P_{1/2}(\text{fast})]^{-1}$, $K(\text{slow}) = [P_{1/2}(\text{slow})]^{-1}$, and $A/B = n$. The obtained $P_{1/2}$(fast) and $P_{1/2}$(slow) of the CO and O_2 bindings to rHSA-FeP(4) and rHSA-FeP(8) did not show any significant difference (Table 3). Furthermore, the O_2 dissociation rate constants in the slow sites [k_{off}(slow)] became smaller than those of the fast sites (Table 1). Since the O_2-binding affinities were constant, the dissociation of O_2 from the dioxygenated FeP is also retarded in the slow sites.

Molecular Simulations. The three-dimensional structure of these synthetic hemoproteins has not yet been solved, although we have attempted to prepare its single crystal. Molecular simulation, however, allows us to predict the orientation of the guest molecule in rHSA. If the CO- and O_2-binding plane of FeP, i.e., the four-pivalamido substituted face of the porphyrin, looks toward the albumin surface and there is no steric hindrance of the protein matrix above, the association rates should not be disturbed. This is actually observed in the *fast site*. The most stable structure of rHSA-FeP, in which FeP was placed in the subdomains IB−IIA (hemin site), has been simulated by the ESFF force field. The first position of FeP was preliminary predicted using the domain analysis program (see experimental). In the converged state with the lowest potential energy, the four-pivalamido face turns to the outside (Figure 3). In addition, there seems to be a pathway for the small gaseous ligands from the bulk water to the porphyrin plane. This site could be the *fast site* for the CO and O_2 bindings to FeP. These simulation results preliminary support the experimental data based on the kinetic observations.

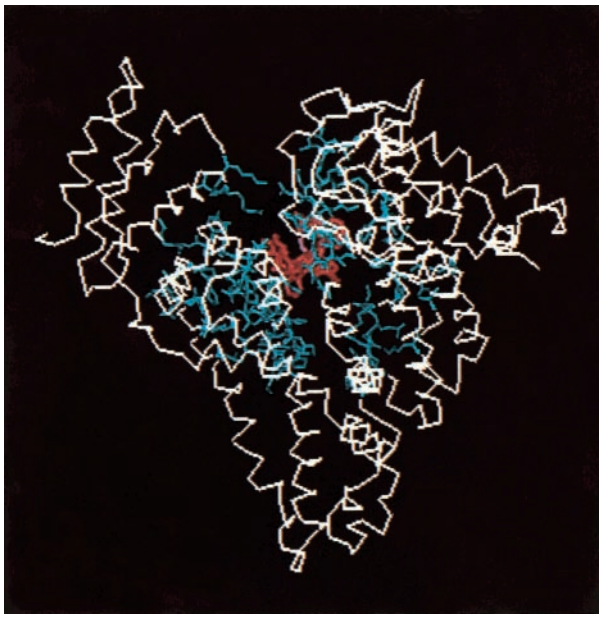

Figure 3. Molecular simulation image of the most stable conformation of dioxygenated rHSA-FeP(1) in which FeP is placed into the well-known hemin site. The backbones and amino acid residues within the length of 12 Å from the porphyrin center are permitted to move and colored blue. The four-pivalamido groups on the porphyrin ring plane obviously face the outside bulk water.

In conclusion, the CO- and O_2-binding kinetics of the recombinant human serum albumin incorporating *eight* tetraphenylporphinatoiron(II) derivatives are composed of three phases, in which the long-lived biphasic decay corresponds to the direct recombination of CO and O_2 to the five-N-coordinated FePs in rHSA. Two of the eight sites of FeP (the second and fifth binding sites) are estimated to be the *slow sites* for the CO and O_2 associations. A thermodynamic study revealed that the large $\Delta G^{\ddagger}$ of the slow phase in the CO recombination is brought about by the enthalpic factor. The association of the gaseous ligands to the porphyrin in the slow site is probably interfered by the steric hindrance of the amino acid residues of the protein interior. Furthermore, the predicted structure of the rHSA-FeP hybrid by molecular simulation supports the experimental results from the kinetic observations. This procedure can presumably be useful for understanding the CO- and O_2-binding behaviors on a shorter time scale.

ACKNOWLEDGMENT

This work was partially supported by the Core Research for Evolutional Science and Technology, JST, Health Science Research Grants (Artificial Blood Project) of the Ministry of Health and Welfare, Japan, and a Grant-in-Aid for Scientific Research (11650935) form the Ministry of Education, Science, Culture and Sports, Japan.

LITERATURE CITED

(1) Ansari, A., Berendzen, J., Bowne, S. F., Frauenfelder, H., Iben, J. E. T., Sauke T. B., Shyamsunder, E., and Young, R. D. (1985) Protein States and Protein Quakes. *Proc. Natl. Acad. Sci. U.S.A. 82*, 5000−5004.

(2) Austin, R. H., Beeson, K. W., Eisenstein, L., Faruenfelder, H., and Gunsalus, I. C. (1975) Dynamics of Ligand Binding to Myoglobin. *Biochemistry 14*, 5355−5373.

(3) Case, D. A., and Karplus, M. (1979) Dynamics of Ligand Binding to Heme Proteins. *J. Mol. Biol. 132*, 343−368.

(4) Collman, J. P., Brauman, J. I., Iverson, B. L., Sessler, J. L., Morris, R. M., and Gibson, Q. H. (1983) O_2 and CO Binding to Iron(II) Porphyrins: A Comparison of the "Picket Fence" and "Pocket" Porphyrins. *J. Am. Chem. Soc. 105*, 3052−3064.

(5) Jongeward, K. A., Magde, D., Taube, D. J., Marsters, J. C., Traylor, T. G., and Sharma, V. S. (1988) Picosecond and Nanosecond Geminate Recombination of Myoglobin with CO, O_2, NO, and Isocyanate. *J. Am. Chem. Soc. 110*, 380−387.

(6) Geibel, J., Cannon, J., Campbell, D., and Traylor, T. G. (1978) Model Compounds for R-State and T-State Hemoglobins. *J. Am. Chem. Soc. 100*, 3575−3585.

(7) Gibson, Q. H. (1970) The Reaction of Oxygen with Hemoglobin and the Kinetic Basis of the Effect of Salt on Binding of Oxygen. *J. Biol. Chem. 245*, 3285−3288.

(8) Komatsu, T., Hamamatsu, K., Wu, J., and Tsuchida, E. (1999) Physicochemical Properties and O_2-Coordination Structure of Human Serum Albumin Incorporating Tetrakis(*o*-pivalamido)phenylporphyrinatoiron(II) Derivatives. *Bioconjugate Chem. 10*, 82−86.

(9) Kottalam, J., and Case D. A. (1988) Dynamics of Ligand Escape from the Heme Pockets of Myoglobin. *J. Am. Chem. Soc. 110*, 7690−7697.

(10) Olson, J. S., Sadersen, M. E., and Gibson, Q. H. (1971) The Dissociation of the First Oxygen Molecule from Some Mammalian Oxyhemoglobin. *J. Biol. Chem. 246*, 5919−5923.

(11) Sato, F., Shiro, Y., Sakaguchi, Y., Suzuki, T., Iizuka, T., and Hayashi, H. (1990) New Transient Species of Sperm Whale Myoglobin in Photodissociation of Dioxygen from Oxymyoglobin. *J. Biol. Chem. 265*, 2004−2010.

(12) Sawicki, C. A., and Gibson G. H. (1977) Properties of the T State of Human Oxyhemoglobin Studied by Laser Photolysis. *J. Biol. Chem. 252*, 7538−7547.

(13) Sharma, V. S., Schmidt, M. R., and Ranney, H. M. (1976) Dissociation of CO from Carboxyhemoglobin. *J. Biol. Chem. 251*, 4267−4272.

(14) Steinmeier, R. C., Parkhurst, L. J. (1975) Kinetic Studies on the Five Principle Components of Normal Adult Human Hemoglobin. *Biochemistry 14*, 1564−1573.

(15) Sumi, A., Ohtani, W., Kobayashi, K., Ohmura, T., Yokoyama, K., Nishida, M., and Suyama, T. (1993) Purification and Physicochemical Properties of Recombinant Human Serum Albumin. *Biotechnology of Blood Proteins* (C. Rivat and J.-F. Stoltz, Ed.) Vol. 227, pp 293−298, John Libbey Eurotext (Montrouge).

(16) Tetreau, C., Momentau, M., and Lavalette, D. (1990) Influence of Distal Steric Hindrance on Multiple Energy Barriers in Ligand Binding to Heme Model Compounds. *Inorg. Chem. 29*, 1727−1731.

(17) Traylor, T. G., Tsuchiya, S., Campbell, D., Mitchell, M., Stynes, D., and Koga, N. (1985) Anthracene Heme Cyclophanes. Steric Effects in CO, O_2, and RNC Binding. *J. Am. Chem. Soc. 107*, 604−614.

(18) Tsuchida, E., Komatsu, T., Arai, K., and Nishide, H. (1993) Synthesis and Dioxygen-Binding Properties of Doble-sided Porphyrinatoiron(II) Complexes Bearing Covalently Bound Axial Imidazole. *J. Chem. Soc., Dalton Trans. 1993*, 2465−2469.

(19) Tsuchida, E., Komatsu, T., Kumamoto, S., Ando, K., and Nishide, H. (1995) Synthesis and O_2-Binding Properties of Tetraphenylporphyrinatoiron(II) Derivatives Bearing a Proximal Imidazole Covalently Bound at the β-pyrrolic Position. *J. Chem. Soc., Perkin Trans. 2 1995*, 747−753.

(20) Tsuchida, E., Ando, K., Maejima, H., Kawai, N., Komatsu, T., Tekeoka, S., and Nishide, H. (1997) Properties of and Oxygen Binding by Albumin-Tetraphenyl-porphinatoiron(II) Derivative Complexes. *Bioconjugate Chem. 8*, 534−538.

(21) Tsuchida, E., Komatsu, T., Matsukawa, Y., Hamamatsu, K., and Wu, J. (1999) Human Serum Albumin Incorporating Tetrakis(*o*-pivalamido)phenylporphinatoiron(II) Derivative as a Totally Synthetic O_2-Carrying Hemoprotein. *Bioconjugate Chem. 10*, 797−802.

(22) Tsuchida, E., Komatsu, T., Hamamatsu, K., Matsukawa, Y., Tajima, A., Yoshizu, A., Izumi, Y., and Kobayashi, K. (2000) Exchange Transfusion with Albumin-Heme as an Artificial O_2-Infusion into Anesthetized Rats: Physiological Responses, O_2-Derivery, and Reduction of the Oxidized Hemin Sites by Red Blood Cells. *Bioconjugate Chem. 11*, 46−50.

BC000016E

Design and Synthesis of Novel Glycopolythiophene Assemblies for Colorimetric Detection of Influenza Virus and *E. coli*

Myung-Gi Baek,* Raymond C. Stevens, and Deborah H. Charych†

Lawrence Berkeley National Laboratory, Materials Sciences Division, Berkeley, California 94720

A novel family of glycopolythiophenes containing sialic acid or mannose ligands were prepared and evaluated for their ability to bind lectins, virus, and bacteria. For the set of glycopolythiophenes studied, the spacer-length between the polymer backbone and the ligand was varied to optimize binding interactions. The glycopolymers were blue-shifted (absorbance of ca. 400 nm) relative to the corresponding homo-polythiophenes (absorbance ca. 440 nm), suggesting a twisted conformation for the glycopolymers. The altered conformation is likely due to electrostatic or H-bonding interactions between the polymer chains, arising from the carbohydrate ligand. Further conformational changes in the polythiophene backbone were detected by the binding of specific receptors; lectins (wheat germ agglutinin, concanavalin A), Influenza virus, and *Escherichia coli*. The binding interactions result in an unusual red-shift in the visible absorption of the polymer backbone, suggesting a lengthening of the effective conjugated length upon interaction of the ligand with its congnate receptor. These conjugated glycopolymeric systems offer a potentially new platform for the detection of molecular binding interactions.

INTRODUCTION

In the past few decades, new types of organic polymers such as polyacetylene, polydiacetylene, polypyrrole, polyaniline, and polyphenylene have received increased attention due to the high demand for materials capable of performing various optical and electronic functions. Important properties of these materials include electroconductivity, liquid crystallinity, nonlinear optical effects, and novel chromatic properties (*1*−*4*). These conjugated polymers exhibit high electrical conductivity with good thermal stability. For their preparation, synthetic efforts were geared toward minimizing structural defects (e.g., broad molecular weight distribution, branching, crosslinking, etc.). Polythiophene is an important member of this class of π-conjugated polymers. Due to a planar−nonplanar conformational transition of the π-conjugated system, these materials exhibit a variety of optical transitions upon external stimuli such as heat (*5*−*8*), light (*9*), metals (*10*, *11*), chemicals (*12*), and proteins (*13*, *14*). These effects have been termed thermochromism, photochromism, ionochromism, or biochromism, respectively. Another important polymer of this class is polydiacetylene. Ligand-derivatized versions of self-assembling polydiacetylenes have been studied extensively for their biochromic properties (*15*, *37*, *38*−*43*). For example, sialic-acid-derivatized polydiacetylenes detect influenza virus hemagglutinin by a color change from blue to red (*15*, *42*). Other derivatives have been shown to detect toxin (*37*, *43*). The chromic transitions of both polydiacetylene and polythiophene can be strongly correlated with the electronic structure and the conformation of the polymer backbone. Indeed, theoretical studies have shown that a high degree of planarity along the polymer chains leads to better electrical properties (*16*). However, the rearrangement of the polymer backbone also strongly depends on the conformational state of the side chains (*17*, *18*). In addition, aggregation of polythiophene chains induces the formation of π-stacks in the macromolecular assembly and generates enhanced electronic and photonic properties (*9*, *18*, *19*). Therefore, the degree of π-conjugation of the polymer chains and their susceptibility to external stimuli are critical if the material is to be used as a sensory device (*20*).

Applications of polythiophene-based biosensors require that the material must be tailored to biological environments. This requires the incorporation of biologically active species, such as proteins, peptides, lipids, or carbohydrates in the polymeric system. In particular, carbohydrates are attractive because they are relatively small when compared to proteins and are expressed externally from the cell surface as a component of glycoproteins, glycolipids, and capsular polysaccharides (*21*). Carbohydrates are involved in key recognition events (*22*−*24*) with a variety of receptor proteins such as hormones, enzymes, toxins, lectins, antibodies, viruses, and bacteria. Carbohydrates are also involved in numerous biological processes (*25*) such as cell growth, recognition and differentiation, cancer metastasis, inflammation, and pathogen-entry. Finally, the hydrophilicity of the carbohydrate moieties facilitates water solubility of the polymeric material. Thus, the carbohydrate moieties are excellent candidates for creating new types of biochromic polythiophene materials. For example, an analogue of sialic acid is the receptor-specific carbohydrate for the influenza virus hamagglutinin (*22*, *26*−*29*). In addition, certain mannose residues recognize some bacterial species, such as *Escherichia coli* and *Salmonella* (*30*−*35*). In particular, Type I piliated *E. coli* is a pathogen responsible for many urinary tract infections and is a mannose-specific bacteria (*31*−*33*, *35*). Considering the interactions of sialic acid and mannose toward these specific pathogen proteins, we designed and synthesized

* To whom correspondence should be addressed. Present address: Chemical Biology Program, Steacie Institute for Molecular Science, National Research Council of Canada, Ottawa, Ontario, K1A 0R6, Canada.

† Present address: Chiron Technologies, Life Science Center, MS 4.5, 4560 Horton Ave., Emeryville, CA, 94706.

10.1021/bc000026f CCC: $19.00 © 2000 American Chemical Society
Published on Web 11/03/2000

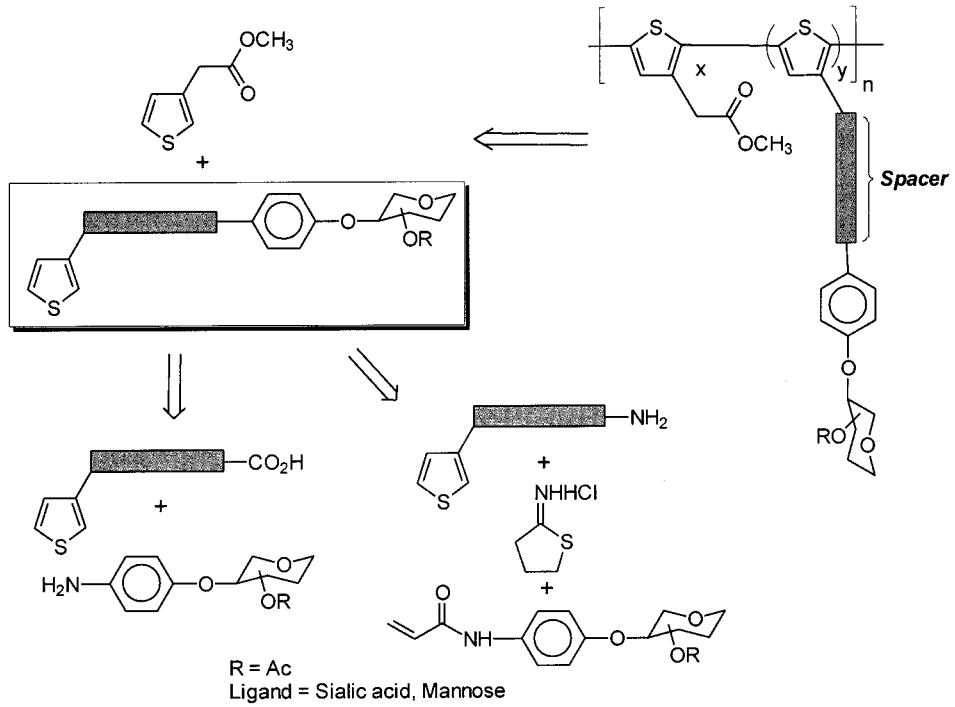

Figure 1. Retrosynthetic analysis of glycopolythiophenes.

a series of new thiophene-carbohydrate monomers with well-defined spacer-lengths (side chains) to optimize protein binding. Subsequent copolymerization of the thiophene-carbohydrate monomer with methyl (3-thienyl) acetate (**7**) as a comonomer gave a series of novel glycopolythiophenes (glyco-PTs) (Figure 1). In addition, the multivalent display of carbohydrates on the glyco-PTs overcomes the characteristic low binding affinity of the individual carbohydrates to their receptor proteins. The glyco-PTs were tested for their ability to undergo absorption shifts after the addition of proteins. The mannose-glyco-PTs were studied with *Concanavalin A* (Con A), biotin-labeled Con A, and *E. coli* (HB101 strain), whereas the sialic acid-glyco-PTs were investigated with *Triticum Vulgaris* (Wheat germ) and Influenza virus (A/B).

EXPERIMENTAL PROCEDURES

General Procedures. Air- and moisture-sensitive reactions were carried out in dried glasswares under nitrogen atmosphere. Chloroform was distilled from phosphorus pentoxide. Methanol was degassed under high vacuum until no gas bubbles were observed and handled under nitrogen prior to use. Sialic acid and *p*-nitrophenyl mannopyranoside were obtained from Rose Scientific Ltd. 3-Thiopheneacetic acid was obtained from Acros. *Triticum Vulgaris* (Wheat germ), *Concanavalin* A (Con A), biotin-labeled Con A (Sigma), and streptavidin (Pierce) were used as received. Influenza virus was obtained from Department of Health Service, Public Health Laboratory, San Diego. *E. coli* (HB101) was obtained from department of Plant and Microbial Biology, UC−Berkeley. All other reagents were used as received from Aldrich. NMR spectra were recorded with a Bruker AMX-300 (300 MHz), VBAM-400 (400 MHz), or AMX-500 (500 MHz) spectrometer. Optical rotations were recorded with Perkin-Elmer Polarimeter (model 241). UV−vis absorption spectroscopy was performed on Shimadzu Spectrophotometer (model UV-1601).

Succinimidyl (3-Thienyl)acetate (9). To a solution of 3-thiopheneacetic acid (1 g, 7.8 mmol) in $CHCl_3$ (25 mL) was slowly added thionyl chloride (0.6 mL, 1 equiv) at room temperature. The resulting solution was refluxed for 1 h. After cooled to 0 °C, the mixture of *N*-hydroxysuccinimide (0.9 g, 1 equiv) and DIPEA (2.8 mL, 1 equiv) in $CHCl_3$ (20 mL) was slowly added and the reaction was continued another 2 h. The solution was diluted with $CHCl_3$ (20 mL), washed with water, then, dried over Na_2SO_4. After solvent was removed by rotary evaporator, the residue was purified by silica gel column chromatography ($CHCl_3$/MeOH, 40/1) or recrystallized ($CHCl_3$/hexane, 1/1) to afford yellowish powder in 71% yield (1.32 g, 5.5 mmol). MS (EI) 240.0 (MH^+); ^{1}H NMR ($CDCl_3$) δ 7.30 (dd, 1H, ^4J = 3.0 Hz, ^4J = 4.90 Hz, thiophene), 7.26 (m, 1H, thiophene), 7.06 (dd, 1H, J = 1.3 Hz, ^4J = 4.9 Hz, thiophene), 3.94 (s, 2H, CH_2), 2.76 (s, 4H, $2CH_2$); ^{13}C NMR ($CDCl_3$) δ 169.5, 166.7, 131.1, 128.5, 126.6, 124.2, 32.7, 25.9.

4-[(3-Thienyl)acetamido]butanoic acid (12). To a solution of thiophene active ester (**9**) (1.1 g, 4.6 mmol) and 4-aminobutanoic acid (**10**) (0.48 g, 4.6 mmol) in $CHCl_3$ (50 mL) was added couple of drops of DIPEA, and the resulting solution was stirred overnight at room temperature. A white precipitate was filtered off, and the filtrate was condensed under reduced pressure. Without further workup, the residue was purified by silica gel column chromatography ($CHCl_3$/MeOH, 10/1) to give a white solid in 67% yield (0.7 g, 3.1 mmol). MS (EI) 228.0 (MH^+); mp 77.3−77.6 °C; ^{1}H NMR (CD_3OD) δ 7.27 (dd, 1H, J = 3.0 Hz, ^4J = 4.7 Hz, thiophene), 7.11 (m, 1H, thiophene), 6.95 (dd, 1H, J = 1.1 Hz, ^4J = 4.8 Hz, thiophene), 3.44 (s, 2H, thiophene-CH_2), 3.14 (t, 2H, J = 6.9 Hz, amide-CH_2), 2.22 (t, 2H, J = 7.4 Hz, CH_2-acid), 1.70 (m, 2H, CH_2); ^{13}C NMR (CD_3OD) δ 178.2, 174.0, 136.8, 129.4, 126.9, 123.6, 40.1, 38.6, 32.3, 25.9.

6-[(3-Thienyl)acetamido]caproic acid (13). Thiophene active ester (**9**) (1 g, 4.2 mmol) and 6-aminocaproic acid (**11**) (0.55 g, 4.2 mmol) were coupled as described above to give white solid in 90% yield (0.97 g, 3.8 mmol). MS (EI) 255.0 (M^+); mp 78.6−79.5 °C; ^{1}H NMR (CD_3OD) δ 7.33 (1H, dd, thiophene), 7.17 (1H, m, thiophene), 7.01 (1H, dd, thiophene), 3.49 (s, 2H, thiophene-CH_2), 3.16 (t,

2H, $J = 6.9$ Hz, amide-CH_2), 2.25 (t, 2H, $J = 7.4$ Hz, CH_2-acid) 1.63−1.42 (m, 4H, $2CH_2$), 1.36−1.28 (m, 2H, CH_2); ^{13}C NMR (CD_3OD) δ 177.6, 173.8, 136.9, 129.5, 126.9, 123.6, 40.5, 38.7, 35.0, 30.2, 27.6, 25.9.

2-[(3-Thienyl)acetamido]-1-aminoethane (16). To a solution of ethylenediamine (356 μL, 5.3 mmol) in $CHCl_3$ (200 mL) was added thiophene active ester (**9**) (1.0 g, 4.4 mmol) in $CHCl_3$ (30 mL) by dropwise fashion for 2 h period at room temperature. The mixture was stirred overnight at the same condition. A precipitate was filtered off and the filtrate was extracted with 1 M HCl-(aq) (30 mL × 5). The aqueous layer was combined and evaporated under reduced pressure. The residue was purified by silica gel column chromatography ($CHCl_3$/MeOH/2-propanol, 5/3/2) to give white hygroscopic solid in 83% yield (3.7 g, 20 mmol). MS (EI) 184 (M^+); mp 89.7−92.1 °C; ^{1}H NMR (CD_3OD) δ 7.34 (dd, 1H, thiophene), 7.20 (m, 1H, thiophene), 7.04 (dd, 1H, thiophene), 3.54 (s, 2H, CH_2), 3.25 (t, 2H, $J = 6.3$ Hz, CH_2), 2.73 (t, 2H, $J = 6.3$ Hz, CH_2); ^{13}C NMR (CD_3OD) δ 174.3, 136.8, 129.5, 126.9, 123.7, 42.9, 42.0, 38.6.

8-[(3-Thienyl)acetamido]-1-octylamine (17). 1,8-Octanediamine (0.78 g, 5.4 mnol) and **9** (1.2 g, 1 equiv) were coupled as described above to give yellowish resin in 96% yield (1.4 g, 5.2 mmol). MS (EI) 268 (M^+); ^{1}H NMR (CD_3OD) δ 7.31 (dd, 1H, thiophene), 7.13 (broad s, 1H, thiophene), 6.98 (dd, 1H, thiophene), 3.45 (s, 2H, thiophene-CH_2), 3.11 (m, 2H, amide-CH_2), 2.82 (m, 2H, CH_2-amine), 1.43 (m, 8H, $4CH_2$); ^{13}C NMR (CD_3OD) δ 173, 137.0, 129.4, 126.8, 123.6, 40.9, 40.6, 38.7, 30.4, 30.2, 30.1, 28.6, 27.8, 27.5.

8-[(3-Thienyl)acrylamido]-1-octylamine (20). To a solution of **18** (1.1 g, 4.4 mmol) and **19** (0.7 g, 1 equiv) in $CHCl_3$ (30 mL) was added HOBt (0.7 g, 1.2 equiv) at ice water temperature. The solution was stirred for 15 min, then DIPEA (pH 9) and EDC (1 g, 1.2 equiv) were added. The reaction was continued for 6 h at room temperature. The reaction mixture was diluted with $CHCl_3$ (30 mL), washed successively with saturated $NaHCO_3$(aq) and water, then dried over Na_2SO_4. The solution was briefly condensed and the residue was purified by silica gel column chromatography (EtOAc/hexane, 4/1) to give yellowish solid. Subsequently, the solid was treated with TFA (30% in CH_2Cl_2) for 3 h at room temperature to give light yellow solid in overall 87% yield (1.07 g, 3.8 mmol). mp 147.2−147.9 °C; ^{1}H NMR ($CDCl_3$) δ 7.58 (broad s, thiophene), 7.50 [d, 1H, $J_{trans} = 15.5$ Hz, =CH−C(O)NH], 7.42 (m, 1H, $J = 2.9$ Hz, $^4J = 5.0$ Hz, thiophene), 7.33 (broad d, 1H, thiophene), 6.42 (d, 1H, thiophene-CH=), 3.26 (t, 2H, $J = 7.2$ Hz, CH_2), 2.88 (t, 2H, $J = 7.7$ Hz, CH_2), 1.62 (m, 2H, CH_2), 1.53 (m, 2H, CH_2), 1.35 (m, 6H, 3 CH_2); ^{13}C NMR ($CDCl_3$) δ 183.3, 167.5, 137.9, 126.9, 126.6, 124.7, 133.9, 120.1, 39.3, 39.1, 29.0, 28.7, 27.1, 26.5, 25.9.

***p*-[(3-Thienyl)acetamido]phenyl Methyl (5-Acetamido-4,7,8,9-tetra-*O*-acetyl-3,5-dideoxy-D-glycero-α-D-galacto-2-nonulopyranosid)onate (21).** To a solution of **1** (0.4 g, 0.7 mmol) and thiopheneacetic acid (90 mg, 1 equiv) in CH_2Cl_2 (5 mL) was added DIPEA (pH 9) and TBTU (0.27 g, 1.2 equiv). The resulting solution was stirred for 5 h at an ambient temperature. The solution was diluted with CH_2Cl_2 (10 mL) and washed successively with saturated $NaHCO_3$, water, and dried over Na_2SO_4. Solvent was eliminated by rotary evaporator, and the residue was purified by silica gel column chromatography ($CHCl_3$/MeOH, 10/1) to give ivory foam solid in 90% yield (0.43 g, 0.62 mmol). MS (positive FAB) 707.3 (MH^+); mp 58.5−60.7 °C; ^{1}H NMR ($CDCl_3$) δ 8.33 (s, 1H, NH), 7.33 (d, 2H, $J_{om} = 8.6$ Hz, Ar-ortho), 7.23 (dd, 1H, $J = 2.8$ Hz, $^4J = 4.9$ Hz, thiophene), 7.12 (broad s, 1H, thiophene), 6.98 (dd, 1H, $J = 1.2$ Hz, $^4J = 4.9$ Hz, thiophene), 6.91 (d, 2H, Ar-meta), 6.41 (d, 1H, $J_{N5} = 9.8$ Hz, NH), 5.31 (m, 2H, H-7, H-8), 4.85 (ddd, 1H, $J_{45} = 10.2$ Hz, $J_{43e} = 4.7$ Hz, $J_{43a} = 11.7$ Hz, H-4), 4.31 (dd, 1H, $J_{56} = 10.7$ Hz, H-6), 4.21 (dd, 1H, $J_{9a9b} = 10.3$ Hz, H-9a), 4.06 (m, 2H, H-5, H-9b), 3.63 [s, 3H, C(O)O−CH_3], 3.51 (s, 2H, CH_2-thiophene), 2.64 (dd, $J_{3e4} = 4.4$ Hz, $J_{3e3a} = 12.9$ Hz, H-3e), 2.10 (dd, 1H, $J_{3a4} = 11.2$ Hz, H-3a), 2.02, 2.01, 1.93, 1.92, 1.79 (5 s, 15H, 5 AcO); ^{13}C NMR ($CDCl_3$) δ 171.0, 170.9, 170.4, 170.3, 169.3, 168.2, 150.2, 135.0, 134.7, 128.8, 126.7, 123.5, 121.2, 120.9, 100.5, 73.5, 69.4, 69.3, 67.6, 62.3, 53.1, 49.2, 39.1, 38.8, 23.3, 21.2, 21.0.

Compound 22. 22 was prepared from **1** and **12** using the peptide coupling protocol. Yield 75%; FAB (+)−MS 791.3 (MH^+); ^{1}H NMR ($CDCl_3$) 6.28 (t, 1H, $J_{NCH2} = 5.6$ Hz, NH), 5.85 (d, 1H, $J_{N5} = 9.9$ Hz, NH), 3.28 [m, 2H, CH_2−HNC(O)], 2.29 [t, 2H, $J = 6.0$ Hz, HNC(O)-CH_2], 1.78 (m, 2H, CH_2); ^{13}C NMR ($CDCl_3$) 39.3, 38.3, 34.9, 28.9. Other chemical shifts are same as **21**.

Compound 23. 23 was prepared from **1** and **13** using the peptide coupling protocol. Yield 86%; MS (positive FAB) 820.3 (MH^+); mp 71−73 °C; ^{1}H NMR ($CDCl_3$) δ 6.18 (t, 1H, $J_{NCH2} = 5.7$ Hz, NH), 6.12 (d, 1H, $J_{N5} = 9.9$ Hz, NH), 3.11 [m, 2H, CH_2−HNC(O)], 2.22 [m, 2H, HNC(O)-CH_2], 1.58 (m, 2H, CH_2), 1.39 (m, 2H, CH_2), 1.24 (m, 2H, CH_2); ^{13}C NMR ($CDCl_3$) δ 39.3, 36.9, 28.9, 27.8, 26.1. Other chemical shifts are same as **21**.

Compound 24. 24 was prepared from **3** and **13** using the peptide coupling protocol. Yield 60%; MS (positive FAB) 951.5 (MH^+); mp 76−77 °C; ^{1}H NMR ($CDCl_3$) δ 8.61 (s, 1H, NH), 7.99 (s, 1H, NH), 7.47 (d, 2H, $J_{om} = 8.9$ Hz, Ar-ortho), 7.31 (dd, 1H, $^4J = 4.9$ Hz, $^4J = 2.9$ Hz, thiophene), 7.12 (m, 1H, thiophene), 6.98 (m, 3H, Ar-meta, thiophene), 6.29 (m, 1H, NH), 5.81 (m, 1H, NH), 5.34 (broad s, 1H, H-7, H-8), 4.92 (ddd, 1H, $J_{45} = 10.2$ Hz, $J_{43e} = 4.7$ Hz, $J_{43a} = 11.7$ Hz, H-4), 4.33 (m, 2H, H-6, H-9), 4.11 (m, 2H, H-5, H-9b), 3.63 [s, 3H, C(O)O−CH_3], 3.57 (s, 2H, CH_2-thiophene), 3.42 (m, 2H, CH_2), 3.19 (m, 2H, CH_2), 2.89 (t, 2H, hidden, CH_2), 2.65 (m, 7H, H-3e, $3CH_2$), 2.15 (dd, 1H, $J_{3a4} = 11.2$ Hz, $J_{3e4} = 4.6$ Hz, H-3a), 2.10, 2.09, 2.02, 2.01, 1.88 (5 s, 15H, 5AcO), 1.58 (m, 2H, CH_2), 1.41 (m, 2H, CH_2), 1.25 (m, 2H, CH_2); ^{13}C NMR ($CDCl_3$) δ 176.9, 173.3, 170.9, 170.3, 170.0, 167.9, 162.6, 149.8, 134.9, 134.8, 128.5, 126.7, 120.8,, 123.4, 120.7, 100.3, 73.3, 69.3, 68.9, 67.4, 62.0, 52.9, 49.4, 37.9, 39.4, 38.5, 38.1, 37.4, 36.5, 36.3, 31.9, 31.4, 29.1, 27.3, 26.1, 25.1, 23.2, 21.0, 20.8.

Compound 25. 25 was prepared from **1** and **19** using the peptide coupling protocol. Yield 82%; MS (positive FAB) 719.2 (MH^+); mp 79.3−81.1 °C; ^{1}H NMR ($CDCl_3$) δ 7.62 [d, 1H, $J_{trans} = 15.5$ Hz, HNC(O)CH=], 6.51 (m, 2H, =CH-thiophene, NH), 5.34 (m, 2H, H-7, H-8), 4.88 (ddd, 1H, $J_{45} = 10.2$ Hz, $J_{3e4} = 4.7$ Hz, $J_{3a4} = 11.7$ Hz, H-4), 4.34 (dd, 1H, $J_{6ab} = 10.5$ Hz, H-6), 4.24 (dd, 1H, $J_{9ab} = 12.4$ Hz, H-9a), 4.06 (m, 2H, H-9b, H-5), 3.51 (s, 3H, CO_2-CH_3), 2.50 (hidden, 1H, H-3e), 2.13 (hidden, 1H, H-3a), (5 s, 15H, AcO); ^{13}C NMR ($CDCl_3$) δ 171.1, 170.9, 170.4, 170.3, 168.2, 166.0, 151.2, 138.2, 135.5, 127.7, 127.1, 125.5, 121.0, 100.6, 73.5, 69.4, 67.7, 62.3, 53.1, 49.2, 38.3, 23.2, 21.2, 21.1. Other chemical shifts are same as **24**.

***p*-[(3-Thienyl)acetamido]phenyl-α-D-2,3,4,6-tetra-*O*-acetyl mannopyranoside (26).** To a solution of 4-aminophenyl-α-D-mannopyranoside (**4**) (2.0 g, 4.6 mmol) and thiopheneacetic acid (**6**) (0.6 g, 4.6 mmol) in CH_2Cl_2 (50 mL) were added DIPEA (0.8 mL) and TBTU (1.8 g, 5.5 mmol). The resulting solution was stirred for 4 h at room temperature. The solution was diluted with CH_2-

Cl_2 (20 mL) and washed successively with saturated $NaHCO_3$(aq) and water and then dried over Na_2SO_4. The solution was condensed under reduced pressure, and the residue was purified by silica gel column chromatography (EtOAc/hexane, 2/1) to give light yellowish amorphous solid in 83% yield (2.1 g, 3.8 mmol). MS (positive FAB) 564 (MH^+), 586.3 (MNa^+); mp 62.5−64.0 °C; ^{1}H NMR ($CDCl_3$) δ 7.35 (m, 3H, Ar-ortho, thiophene), 7.19 (m, 1H, thiophene), 7.03 (d, 1H, J = 4.9 Hz, thiophene), 6.98 (d, 2H, J_{om} = 9.0 Hz, Ar-meta), 5.50 (dd, 1H, J_{23} = 3.4 Hz, J_{34} = 10.0 Hz, H-3), 5.41 (d, 1H, J_{12} = 1.9 Hz, H-1), 5.39 (dd, 1H, J_{23} = 3.3 Hz, H-2), 5.34 (dd, 1H, J_{34} = 10.0 Hz, $J_{45} \leq$ 1 Hz, H-4), 4.24 (dd, 1H, J_{56a} = 5.4 Hz, J_{6ab} = 12.4 Hz, H-6a), 4.04 (m, 2H, H-5, H-6b), 3.71 (s, 2H, CH_2), 2.16, 2.02, 2.01, 2.00 (4 s, 4 AcO); ^{13}C NMR ($CDCl_3$) δ 176.0, 170.6, 170.0, 169.7, 168.7, 156.0, 134.4, 133.0, 128.4, 127.0, 123.7, 121.5, 117.0, 96.1, 69.3, 69.1, 68.9, 65.9, 62.1, 38.9, 20.9, 20.8, 20.7.

Compound 27. 27 was prepared from **4** and **12** using the peptide coupling protocol. Yield (quantitative); MS (positive FAB) 649 (NH^+); ^{1}H NMR ($CDCl_3$) δ 9.04 (broad s, 1H, NH), 7.50 (d, 2H, J_{om} = 9.1 Hz, Ar-ortho), 7.28 (dd, 1H, J = 3.0 Hz, ^4J = 4.9 Hz, thiophene), 7.09 (broad s, 1H, thiophene), 6.96 (m, 3H, Ar-meta, thiophene), 6.25 (broad t, 1H, NH), 5.51 (dd, 1H, J_{23} = 8.4 Hz, J_{34} = 10.0 Hz, H-3), 5.43 (d, 1H, J_{12} = 1.9 Hz, H-1), 5.40 (dd, 1H, J_{23} = 3.5 Hz, H-2), 5.32 (dd, 1H, J_{34} = 10.0 Hz, $J_{45} \leq$ 1 Hz, H-4), 4.24 (dd, 1H, J_{56a} = 5.0 Hz, J_{6ab} = 12.1 Hz, H-6a), 4.08−4.00 (m, 2H, H-5, H-6b), 3.56 (s, 2H, thiophene-CH_2), 3.28 (m, 2H, CH_2-amide), 2.28 (m, 2H, carbonyl-CH_2), 2.16, 2.01, 2.00, 1.99 (4 AcO), 1.79 (m, 2H, CH_2); ^{13}C NMR ($CDCl_3$) δ 171.9, 171.1, 170.6, 170.0, 169.9, 169.7, 156.0, 134.6, 133.9, 128.4, 126.7, 123.5, 121.2, 116.9, 96.1, 69.4, 69.1, 68.9, 65.9, 62.1, 38.9, 38.6, 38.1 34.5, 26.2, 20.9, 20.7.

Compound 28. 28 was prepared from **4** and **13** using the peptide coupling protocol. Yield quantitative; MS (positive FAB) 677 (MH^+); ^{1}H NMR ($CDCl_3$) δ 7.95 (broad s, 1H, NH), 5.78 (broad t, 1H, NH), 5.51 (dd, 1H, J_{23} = 3.4 Hz, J_{34} = 10.0 Hz, H-3), 5.40 (m, 2H, H-1, H-2), 5.33 (dd, 1H, J_{34} = 10.0 Hz, $J_{45} \leq$ 1, H-4), 4.24 (dd, 1H, J_{56a} = 4.8 Hz, J_{6ab} = 11.9 Hz, H-6a), 4.05 (m, 2H, H-5, H-6b), 3.54 (s, 2H, thiophene-CH_2), 3.18 (m, 2H, CH_2-amide), 2.26 [m, 2H, C(O)-CH_2], 2.16, 2.02, 2.01, 2.00 (4 AcO), 1.66 (m, 2H, CH_2), 1.45 (m, 2H, CH_2), 1.28 (m, 2H, CH_2); ^{13}C NMR ($CDCl_3$) δ 171.7, 171.3, 170.8, 170.6, 170.0, 169.7, 156.0, 134.9, 133.6, 128.4, 126.7, 123.4, 121.3, 116.9, 96.1, 69.4, 69.1, 68.9, 65.9, 62.1, 38.9, 38.6, 38.1, 26.2, 20.9, 20.7. Other chemical shifts are same as **26**.

Compound 29. 29 was prepared from **4** and **19** using the peptide coupling protocol. Yield 70%; MS (positive FAB) 576 (MH^+); mp 63.1−63.8 °C; ^{1}H NMR ($CDCl_3$) δ 7.89 (broad s, 1H, NH), 7.68 [d, 1H, J_{trans} = 15.4 Hz, C(O)-NH−CH=], 7.55 (d, 2H, J_{om} = 8.3 Hz, Ar-ortho), 7.40 (dd, 1H, J = 3.0 Hz, ^4J = 4.9 Hz, thiophene), 7.28 (broad s, 1H, thiophene), 7.20 (broad d, 1H, thoiophene), 7.00 (d, 2H, Ar-meta), 6.40 (1H, d, =CH-thiophene), 5.53 (dd, 1H, J_{23} = 3.5 Hz, J_{34} = 10.0 Hz, H-3), 5.41 (m, 2H, H-1, H-2), 5.34 (dd, 1H, J_{34} = 9.9 Hz, $J_{45} \leq$ 1, H-4), 4.25 (dd, 1H, J_{56a} = 5.1 Hz, J_{6ab} = 12.0 Hz, H-6a), 4.09−4.02 (m, 2H, H-5, H-6b), 2.17, 2.03, 2.02, 2.01 (4 AcO); ^{13}C NMR ($CDCl_3$) δ 175.1, 173.0, 170.6, 170.0, 169.8, 156.0, 137.7, 133.6, 135.7, 127.6, 126.9, 125.0, 121.4, 120.5, 117.1, 96.1, 69.4, 69.1, 68.9, 66.0, 62.1, 26.2, 20.9, 20.7. Other chemical shifts are same as **26**.

Compound 32. To a solution of 3-thiophenehydrazide (**30**) (0.2 g, 1.42 mmol) and 2-iminothiolane hydrochloride (**31**) (0.2 g, 1 equiv) in degassed MeOH (5 mL) was saturated with N_2 gas and added couple of drops of DIPEA. The resulting solution was stirred for 3 h at room temperature. *p*-Acrylamidophenyl methyl (5-acetamido-4,7,8,9-tetra-*O*-acetyl-3,5-dideoxy-D-glycero-α-D-galacto-2-nonulopyranoside) onate (**2**) (0.45 g, 0.7 mmol) in degassed $CHCl_3$ (5 mL) was injected slowly and continued the reaction overnight at the same condition. Solvent was briefly evaporated and the residue was dissolved in $CHCl_3$ (20 mL), washed with saturated $NaHCO_3$ and water and then dried over Na_2SO_4. The solution was condensed and the residue was purified by silica gel column chromatography ($CHCl_3$/MeOH, 10/1) to give a dark violet solid in 51% yield (0.33 g, 0.36 mmol). MS (positive FAB) 880.2 $(M\text{-}Cl)^+$; mp 103.5−104.7 °C; ^{1}H NMR ($CDCl_3$) δ 2.82 [broad t, 2H, HNC(O)-CH_2], 2.67 (broad t, 2H, CH_2−S), 2.53 [m, 4H, S−CH_2, CH_2−C(NH)], 1.85 (m, 2H, CH_2); ^{13}C NMR ($CDCl_3$) δ 49.2, 36.5, 35.3, 30.5, 27.6. Other chemical shifts are same as **21**.

Compound 33. 33 was prepared from **2** and **16** with 2-iminothiolane hydrochloride (**31**) using successive the ring opening and the peptide coupling protocol. Yield 44%; MS (positive FAB) 922.3 $(M - Cl)^+$; mp 115.2−116.7 °C; ^{1}H NMR ($CDCl_3$) δ 3.57 (s, 2H, CH_2-thiophene), 3.35 [broad s, 4H, HN−CH_2CH_2−HNC(O)], 2.74 [NHC(O)-CH_2], 2.67 (broad s, 2H, CH_2−S), 2.52 (broad s, 2H, S−CH_2), 2.48 [broad s, 2H, CH_2−C(NH)], 1.84 (m, 2H, CH_2); ^{13}C NMR ($CDCl_3$) δ 42.7, 37.4, 37.1, 32.0, 31.4, 27.8, 27.1, 26.5. Other chemical shifts are same as **21**.

Compound 34. 34 was prepared from **2** and **17** with iminothiolane hydrochloride (**31**) using successive the ring opening and the peptide coupling protocol. Yield 78%; MS (positive FAB) 1006.5 $(M - Cl)^+$; mp 69.3−71.2 °C; ^{1}H NMR ($CDCl_3$) δ 3.39−3.35 [m, 7H, CH_2-thiophene, CH_2−HNC(O), C(O)O−CH_3], 3.09 [m, 2H, C(NH)NH−CH_2], 2.86 [m, 6H, HNC(O)-$CH_2CH_2SCH_2$], 2.49 [m, 3H, H-3e, CH_2−C(NH)NH], 1.99 (m, 1H, H-3a), 1.86 (m, 2H, CH_2), 1.50 (m, 2H, CH_2), 1.34 (m, 2H, CH_2), 1.10 (m, 8H, $4CH_2$); ^{13}C NMR ($CDCl_3$) δ 50.6, 42.5, 39.6, 37.9, 37.3, 30.7, 29.2, 28.8, 27.7, 27.5, 26.4. Other chemical shifts are same as **21**.

Compound 35. 35 was prepared from **5** and 3-thiophenehydrazide (**30**) with iminothiolane hydrochloride (**31**) using successive the ring opening and the peptide coupling protocol. Yield 41%; MS (positive FAB) 737.0 $(M - Cl)^+$; mp 69.7−70.4 °C; ^{1}H NMR ($CDCl_3$) δ 2.72 [broad t, 2H, HNC(O)-CH_2], 2.57 (broad t, 2H, CH_2−S), 2.43 [m, 4H, S−CH_2, CH_2−C(NH)], 1.80 (m, 2H, CH_2); ^{13}C NMR ($CDCl_3$) δ 44.3, 37.1, 30.5, 27.4, 26.5. Other chemical shifts are same as **36**.

Compound 36. 36 was prepared from **5** and **16** with iminothiolane hydrochloride (**31**) using successive the ring opening and the peptide coupling protocol. Yield 53%; MS (positive FAB) 779.4 $(M - Cl)^+$; mp 86.3−87.8 °C; ^{1}H NMR ($CDCl_3$) δ 9.50 (s, 1H, NH), 8.99 (s, 1H, NH), 8.75 (s, 1H, NH), 7.95 (s, 1H, NH), 7.53 (d, 2H, J = 8.9 Hz, Ar-ortho), 7.20 (broad d, 1H, thiophene), 7.07 (broad d, 1H, thiophene), 6.95 6.92 (m, 3H, thiophene, Ar-meta), 5.48 (dd, 1H, J_{23} = 3.3 Hz, J_{34} = 10.1 Hz, H-3), 5.42 (d, 1H, J_{12} = 1.8 Hz, H-1), 5.39 (dd, 1H, H-2), 5.33 (dd, J_{34} = 10.1 Hz, $J_{45} \leq$ 1, H-4), 4.22 (dd, 1H, J_{56a} = 4.7 Hz, J_{6ab} = 12.3 Hz, H-6a), 4.02 (m, 2H, H-5, H-6b), 3.51 (s, 2H, CH_2-thiophene), 3.38 [broad s, 4H, HN−CH_2CH_2−HNC-(O)], 2.76 [NHC(O)-CH_2], 2.64 (broad s, 2H, CH_2−S), 2.53 (broad s, 2H, S−CH_2), 2.44 [broad s, 2H, CH_2−C(NH)], 2.16, 2.02, 2.00, 1.99 (4 s, 12H, 4 AcO), 1.86 (m, 2H, CH_2); ^{13}C NMR ($CDCl_3$) δ 175.6, 171.8, 170.7, 170.5, 170.1, 169.7, 168.0, 152.0, 134.5, 133.7, 128.5, 126.2, 123.3, 121.6, 116.9, 96.1, 69.3, 69.1, 68.9, 65.9, 62.1, 42.8, 37.5, 37.3, 32.1, 31.4, 27.6, 27.1, 26.2, 20.9, 20.7.

Compound 37. 37 was prepared from **5** and **17** with iminothiolane hydrochloride (**31**) using successive the ring opening and the peptide coupling protocol. Yield 43%; MS (positive FAB) 863.5 $(M - Cl)^+$; mp 69.3−71.2 °C; ^{1}H NMR ($CDCl_3$) δ 3.19 [m, 2H, CH_2−HNC(O)], 3.07 [m, 2H, C(NH)NH−CH_2], 2.12, 1.98, 1.96 (3 s, 12H, AcO), 1.84 (m, 2H, CH_2), 1.50 (m, 2H, CH_2), 1.34 (m, 2H, CH_2), 1.15 (m, 8H, 4 CH_2); ^{13}C NMR ($CDCl_3$) δ 50.6, 42.9, 39.6, 37.8, 37.3, 30.7, 29.2, 28.7, 27.6, 27.5, 26.4. Other chemical shifts are same as **36**.

Compound 38. 38 was prepared from **5** and **20** with iminothiolane hydrochloride (**31**) using successive the ring opening and the peptide coupling protocol. Yield 35%; MS (positive FAB) 875.5 $(M - Cl)^+$; mp 88.7−90.0 °C; ^{1}H NMR ($CDCl_3$) δ 7.45 [d, 1H, J_{trans} = 15.4 Hz, HNC-(O)-CH=], 6.48 (d, 1H, =CH-thiophene), 3.25 [m, 4H, CH_2−HNC(O)], 3.07 [m, 2H, C(NH)NH−CH_2], 2.15, 2.01, 2.00, 1.99 (4 s, 12H, AcO), 1.85 (m, 2H, CH_2), 1.54 (m, 2H, CH_2), 1.42 (m, 2H, CH_2), 1.23−1.14 (m, 8H, 4 CH_2); ^{13}C NMR ($CDCl_3$) δ 137.8, 121.6, 50.6 42.9, 39.8, 37.3, 37.3, 30.7, 29.2, 28.8, 27.6, 27.5, 26.4. Other chemical shifts are same as **36**.

Polymerization. *Oxidative Polymerization by $FeCl_3$.* To a suspension of $FeCl_3$ (4 equiv) in dry $CHCl_3$ was saturated with N_2 and slowly added a solution of carbohydrate-thiophene monomer and methyl (3-thienyl)-acetate (**7**) (mole ratio, 1/5) in dry $CHCl_3$ over 2−3 h period. The resulting emulsion was stirred for 3 days at room temperature under N_2. The solution was then poured into MeOH (20 mL), and the brownish solid was filtered, then briefly washed with MeOH. Polymer obtained was washed thoroughly by Soxhlet extraction using MeOH. The residue was dried under reduced pressure to give red-brownish solid. [for sialic acid glycopolymers; 31−50% (w/w), for mannose glycopolymers; 28−46% (w/w)].

Poly[methyl (3-thienyl)acetate] (39). To a solution of $FeCl_3$ (22.4 g, 0.1 mol) in dry $CHCl_3$ (50 mL) was saturated with N_2 and slowly added **7** (4.9 g, 34.4 mmol) in dry $CHCl_3$ (20 mL) over 5 h period. The resulting emulsion was stirred for 3 days at room temperature under N_2. MeOH (50 mL) was directly added, and the solution was stirred another couple of hours. A dark brown solid was filtered and briefly washed with MeOH. Polymer was then thoroughly washed by Soxhlet extraction using MeOH. The residue was dried under reduced pressure to give dark brownish solid (3.3 g) in 67% (w/w) yield. ^{1}H NMR ($CDCl_3$) δ 7.20 (broad t, 1H, thiophene), 3.75−3.61 (m, 5H, CH_2, CH_3).

Poly(thiopheneacetic acid) (40). To a solution of **39** (0.3 g) in MeOH (20 mL) was added NaOH (85 mg, 1.2 equiv), and the mixture was refluxed overnight. The dark red homogeneous solution was cooled to ice water temperature and acidified by concentrated HCl. The precipitate was filtered, thoroughly washed with water, and then dried under high vacuum to give light brown solid (0.27 g) in 90% (w/w) yield.

Deprotection of Glycopolymers. The glycopolythiophene-*co*-methyl ester (0.2 g) was suspended in $CHCl_3$ (10 mL), and $CH_3O^-Na^+$/MeOH (25 wt %) was added to adjust pH ∼9. The solution was stirred for 7 h at room temperature. The solution was briefly dried under reduced pressure, then treated with 0.3 M aqueous NaOH solution (7 mL) for another 5−10 h at room temperature. The insoluble portion was filtered off through Celite pad and the filtrate was dialyzed (12 000 MW cutoff) against distilled water (2 L) for 3 days. This solution was employed for the assays without further purification.

Bioassays of Glyco-PTs with Proteins. Biochromic capability of glyco-PTs were evaluated with various proteins such as lectins, virus, and bacteria depending on carbohydrate ligands. It was found that 15−20 μL of protein stock solution was optimal, producing a detectable color change within 4−5 h. To maximize color change, incubation time was given up to 12 h. However, longer incubation times resulted in precipitation of the glyco-PT-protein complexes.

Precipitation Assays with Lectins (ConA and WGA). A glycopolymer stock solution was diluted 1:4−5 in 0.01 M phosphate buffer (pH 7.3), and 300 μL of the solution was transferred to a 500 μL eppendorf tube. A total of 20 μL of stock solution prepared from lectin (1 mg/mL, 0.01 M PBS) was mixed and incubated at room temperature for 12 h. Visible absorption spectra were recorded and compared with the same concentration of the mother solution as a negative control. Each test was performed in duplicate.

Precipitation Assays with *Concanavalin* A-Biotin-Streptavidin. A glycopolymer stock solution was diluted 1:4−5 in 0.01 M phosphate buffer (pH 7.3), and 300 μL of the solution was transferred to two of the 500 μL eppendorf tubes. A total of 20 μL of stock solution prepared from biotin-labeled Con A (1 mg/mL, 0.01 M PBS) was mixed and preincubated at room temperature for 1 h. Subsequently, 20 μL of Streptavidin (1 mg/mL, 0.01 M PBS) was added, and the resulting solution was incubated at room temperature for 10−12 h. Visible absorption spectra were recorded and compared with the same concentration of the mother solution as a negative control. A slight precipitate was detected visually within 24 h after addition of streptavidin. Each test was performed in duplicate.

Colorimetric Assay with *Esherichia coli*, strain HB101. *E. coli* HB101 (pSH2) were grown for 24 h in static LB broth, and the solution was gently centrifuged and collected a clear supernatant before use. A glycopolymer stock solution was diluted 1:4−5 in 0.01 M phosphate buffer (pH 7.3), and 300 μL of the solution was transferred to a 500 μL eppendorf tube. After centrifugation of the stock solution, 20 μL of supernatant *E. coli* HB101 was mixed and incubated at room temperature for 12 h. The visible absorption spectra were recorded and compared with the same concentration of the mother solution as a negative control. The darker red color of *E. coli*-treated mannose-PTs was verified visually with the brownish colored mother solution. Each test was performed in duplicate.

Colorimetric Assays with Influenza Virus A/B. A glycopolymer stock solution was diluted 1:4−5 in 0.01 M phosphate buffer (pH 7.3), and 300 μL of the solution was transferred to a 500 μL eppendorf tube. A total of 20 μL of the stock solution of Influenza Virus A or B was mixed and incubated at 4 °C for 2−6 h. The visible absorption spectrum was recorded and compared with the same concentration of the mother solution as a negative control. The darker red color of Influenza-virus-treated sialic acid-PTs was verified visually with the brownish colored mother solution. Each test was performed in duplicate.

RESULTS AND DISCUSSION

General Procedures for Synthesis of Carbohydrate Monomers. Suitably functionalized sialic acid and mannose moieties at the O-linked aromatic aglycon (**1**, **2**, **3**, **4**, and **5**) were prepared according to literature procedures (*26*, *36*) (Figure 2). Aromatic aglycon was used

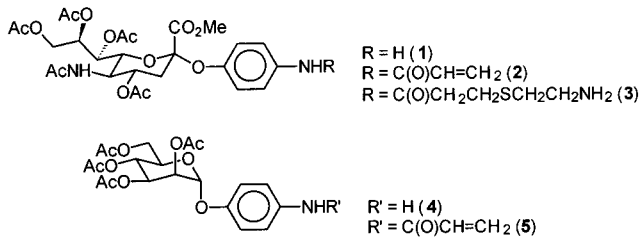

Figure 2. Structure of carbohydrate ligands bearing aromatic aglycon.

Scheme 1. Synthesis of Thiophene Esters

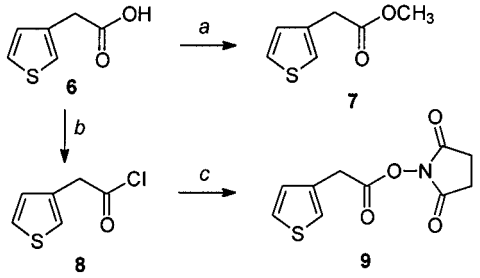

[a] $SOCl_2$/MeOH, 0 °C → r.t., 3 h, 88%. [b] $SOCl_2$/dioxane, r.t. [c] NHS, DIPEA/$CHCl_3$, 0 °C, 75%.

as the mannose ligand since a hydrophobic pocket mainly composed of tyrosine (Tyr) residues in the mannose specific protein stabilizes the carbohydrate by $\pi-\pi$ interactions with the hydrophobic substituent of the aglycon (*60*). For sialic acid, the aromatic aglycon enhances the binding of sialoside ligand to hemagglutinin and prevents the neuraminidase of the influenza virus, from cleaving the O-linked glycosidic bond (*26*, *27*, *29*). On the basis of the fixed carbohydrate structures, two series of thiophene-carbohydrate monomers were synthesized, derived from the thiophene esters shown in Scheme 1.

In the first set of experiments, amine and carboxylic acid terminated thiophene intermediates were prepared (Scheme 2) and subsequently coupled with carbohydrate moieties. In the second set, the distance between thiophene and carbohydrate was extended by iminothiolane hydrochloride (**30**) and a thiol was generated after extension. These thiols were prepared in situ and coupled with **2** or **5** by Michael-type addition to give another set of thiophene−carbohydrate monomers. The two types of carbohydrate moieties are summarized in Tables 1 and 2. Commercially available 3-thiopheneacetic acid (**6**, Acros, Organics, Fisher Scientific) was converted into the corresponding methyl ester (**7**) in 88% yield by thionyl chloride in methanol. Thiopheneacetyl chloride (**8**) was prepared in situ, by thionyl chloride in dioxane. Direct addition of *N*-hydroxysuccinimide (NHS) in the presence of diisopropylethylamine (DIPEA) at 0 °C afforded thiophene active ester (**9**) in 75% overall yield. Product **9** was stable under the dry condition and could be prepared in bulk quantities.

Carboxylic acid functionalized thiophenes, **12** and **13** with the hydrocarbon spacers, were prepared by nucleophilic addition of bifunctionalized **10** and **11** to **9** in 95% yields (Scheme 2). In a similar manner, **9** was reacted with diamines **14** and **15**, under highly dilute conditions. Dimerized byproduct was removed by silica gel chromatography to give the amines **16** and **17** in 83 and 96% yields, respectively. Product **17** was also obtained from **6** and mono-Boc protected **18** by peptide coupling and subsequent deprotection by 30% trifluoroacetic acid (TFA) in CH_2Cl_2. To extend the π-conjugation in the polymer

Scheme 2. Synthesis of Acid-Base Functionalized Thiophenes

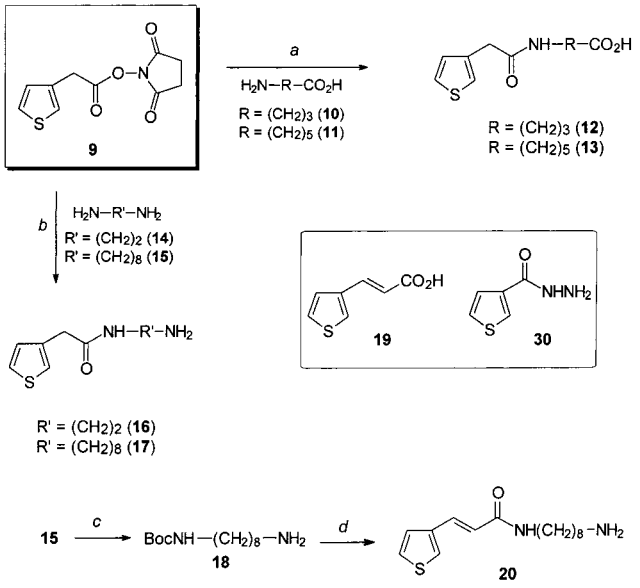

[a] cat. DIPEA/$CHCl_3$, r.t., 95%. [b] $CHCl_3$ (highly diluted), r.t., overnight, 83−96%. [c] BOC-ON, Et_3N/$CHCl_3$, r.t., 52%. [d] (i) 3-(3-Thienyl)acrylic acid (**19**), HOBt/EDC, DIPEA, $CHCl_3$, r.t., 6 h, 93%, (ii) 30% TFA/CH_2Cl_2, r.t., 3 h, 93%, (iii) 1 M NaOH, quantitative.

Table 1. Short Spacer of Thiophene-carbohydrate Monomers Prepared by Peptide Coupling

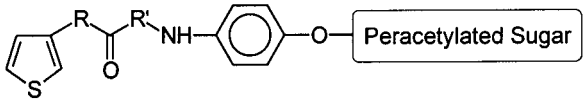

R	R′	sialic acid (%)	mannose (%)
CH_2		**21** (90)	**26** (83)
CH_2	$(CH_2)_3C(O)$	**22** (75)	**27** (quantitative)
CH_2	$(CH_2)_5C(O)$	**23** (86)	**28** (quantitative)
CH_2	$(CH_2)_5C(O)NH(CH_2)_2S$-$(CH_2)_2C(O)$	**24** (60)	N/A[a]
CH=CH		**25** (82)	**29** (70)

[a] Not available.

Table 2. Long Spacer of Thiophene-Carbohydrate Monomers Prepared Using Imminothiolane Hydrochloride

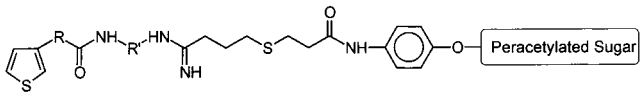

R	R′	sialic acid (%)	mannose (%)
		32 (51)	**35** (41)
CH_2	$(CH_2)_2$	**33** (44)	**36** (53)
CH_2	$(CH_2)_8$	**34** (78)	**37** (43)
CH=CH	$(CH_2)_8NHC(NH)(CH_2)_3S$-$(CH_2)_2C(O)NH$	N/A[a]	**38** (35)

[a] Not available.

to the spacer, 3-(3-thienyl)acrylic acid (**19**) was used, followed by treatment with TFA to afford the thiophene free amine (**20**), in 93% yield. No polymerization of the acrylic functional group was detected during synthesis and the results were confirmed by NMR. Carboxylic acid functionalized thiophenes, **6**, **12**, **13**, and **19**, were coupled with carbohydrate moieties, **1**, **3** or **4** by *O*-benzotriazol-

Scheme 3. Oxidative Polymerization with $FeCl_3$

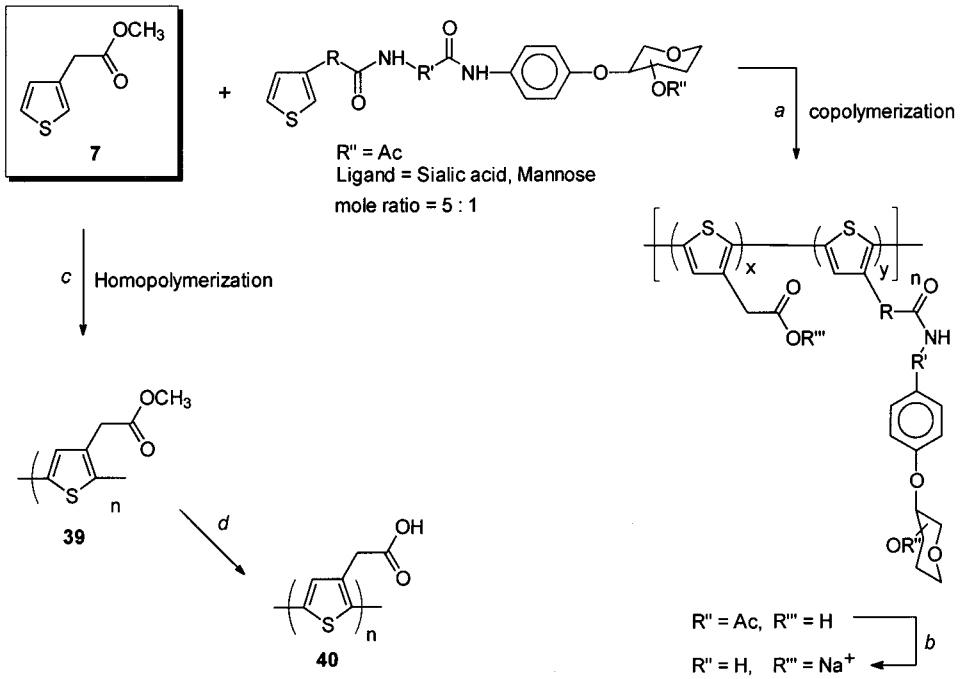

[a] (i) $FeCl_3$, dry $CHCl_3$, N_2, r.t., 2−3 days, (ii) Shoxlet extraction/MeOH. [b] MeO^-Na^+/MeOH/$CHCl_3$ (pH 9), 7 h, (ii) 0.3 M NaOH(aq), r.t., 5−10 h, (iii) dialysis/water (MW 12 000 cutoff). [c] (i) $FeCl_3$ (4 equiv), dry $CHCl_3$, N_2, r.t., 3 days, (ii) Shoxlet extraction/MeOH, 67% (w/w). [d] (i) NaOH (1.2 equiv)/MeOH, reflux, 5 h, (ii) HCl, 0 °C, 90% (w/w).

1-yl-*N*,*N*,*N*′,*N*′-tetramethyluronium tetrafluoroborate (TBTU) strategy to afford the series of thiophene-spacer (side chain)-carbohydrates, **21**, **22**, **23**, **24**, **25** for sialic acid and **26**, **27**, **28**, and **29** for mannose. The yields were 60−90% for the sialic acid residue and 70% quantitative for the mannose residue, respectively (Table 1).

For a mimic of the lipid−carbohydrate monomer used in previous studies of biochromism (*15*, *37*, *41*, *42*), more elongated spacers were designed and synthesized using the iminothiolane hydrochloride (**31**) strategy (Table 2). Ring opening nucleophilic addition of **31** was initiated by the free amine bearing thiopene derivatives, **16**, **17**, **20**, and **30** in the presence of diisopropylethylamine (DIPEA) and degassed methanol to generate a series of mercapto-thiophene intermediates. Subsequent addition of **2** or **5** derived Michael-type addition of a thiol to the acrylamido functional group to afford the second set of thiophene-spacer-carbohydrate species, **32**, **33**, **34** for sialic acid and **35**, **36**, **37**, and **38** for mannose in 51−78% and 35−53% yields, respectively. All structures were confirmed by NMR (^1H, ^{13}C) and mass spectra.

General Procedures for Polymer Formation. The formation of carbohydrate-modified polythiophene was carried out primarily by (co-) polymerization of the thiophene−carbohydrate monomers, and the thiophene methyl ester (**7**), using $FeCl_3$ as a promoter (Scheme 3).

The homopolymer, poly(methyl 3-thiopheneacetate), **39** (Scheme, 3), was prepared from chemical oxidative polymerization of **7** in $CHCl_3$ (*13*, *49*). **39** was purified by Soxhlet extraction with methanol for 3 days to eliminate the low molecular weight portion and any residual promoter to afford 67% (w/w) yield. Subsequently, **39** was further refluxed in the presence of NaOH in methanol for 5 h and acidified with concentrated HCl at 0 °C to give **40** in 90% (w/w) yield.

A series of thiophene−carbohydrate monomers was copolymerized with **7** by $FeCl_3$ in dry $CHCl_3$ followed by Soxhlet extraction with methanol to afford the corresponding glycopolythiophene derivatives in 50−76% (w/w) yields. The ratio of **7** to thiophene−carbohydrate applied was 5/1. The structural regularity of some glycopolythiophenes having reasonable solubility in organic solvent were determined by ^1H NMR spectral data. Mostly, they possessed a randomly distributed chain structure and presented a broad distribution of signals over the whole range of the spectra (*44*−*46*).

Conversion of these glycopolythiophenes into the corresponding deprotected analogues was accomplished as follows. Fully protected glycopolythiophenes were treated with MeO^-Na^+ in MeOH/$CHCl_3$ mixture for 7−9 h, and subsequently, an excess of aqueous NaOH was reacted for 5−10 h at room temperature depending on the polymers. The heterogeneous solution turned into a homogeneous red-brown solution when deesterification was complete. The solution was dialyzed (molecular weight 12 000 cutoff) against water to eliminate excess NaOH and low molecular weight portion and lyophilized to afford brownish solid, **41**, **42**, **43**, **44**, **45**, **46**, **47**, and **48** for sialic acid-PTs in 31−50% (w/w) yields and **49**, **50**, **51**, **52**, **53**, **54**, **55**, and **56** for mannose-PTs in 28−48% (w/w) yields, respectively (Table 3). However, these dried polymers were poorly soluble in aqueous solution again and NaOH was required to induce solubility.

Biochromic Effects. As recently reported (*13*), polythiophene derivatives that display biotin were synthesized and shown to undergo colorimetric transitions in response to binding of streptavidin. The degree of conjugation in the polythiophene backbone is influenced by external stimuli (*5*−*14*, *47*−*51*) and usually involves planar−nonplanar transitions. Another important driving force for the conformational change of the polymer backbone is electrostatic interactions, leading to aggregation, gelation, or even crystallization (*12*, *52*, *53*). As reported by McCullough et al. (*12*), regioregular polythiophenes having carboxylic acid side chains on an ethylene spacer showed significant H-bonding that contributes to extended π-orbital overlap along the main

Table 3. Structure of Polythiophene-*co*-carbohydrate Polymers Prepared with $FeCl_3$

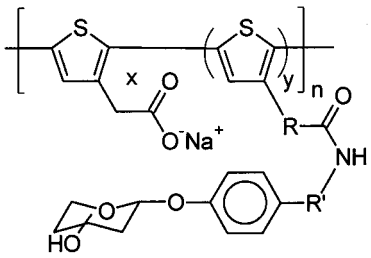

R	R′	sialic acid (%, w/w)[b]	mannose (%, w/w)[b]
CH_2		**41** (48)	**49** (30)
CH_2	$(CH_2)_3C(O)NH$	**42** (31)	**50** (48)
CH_2	$(CH_2)_5C(O)NH$	**43** (50)	**51** (43)
CH_2	$(CH_2)_2NHC(NH)(CH_2)_3S(CH_2)_2C(O)NH$	N/A[a]	**52** (28)
CH_2	$(CH_2)_8NHC(NH)(CH_2)_3S(CH_2)_2C(O)NH$	**44** (37)	**53** (31)
CH_2	$(CH_2)_2NHC(O)(CH_2)_2S(CH_2)_2NHC(NH)(CH_2)_3S(CH_2)_2C(O)NH$	**45** (41)	N/A[a]
CH_2	$(CH_2)_5C(O)NH(CH_2)_2S(CH_2)_2C(O)NH$	**46** (36)	N/A[a]
CH═CH	$(CH_2)_8NHC(NH)(CH_2)_3S(CH_2)_2C(O)NH$	N/A[a]	**54** (40)
CH═CH		**47** (49)	**55** (32)
	$NHC(NH)(CH_2)_3S(CH_2)_2C(O)NH$	**48** (30)	**56** (46)

[a] Not available. [b] Weight percent yields of polymers.

chain. In that particular work, the absorption maximum of the polymer was 560 nm.

In the polymers described herein, the nonregioregular polythiophene homopolymer derivative (**40**), containing a methylene spacer between the backbone and the acid group, showed a maximum absorption at 440 nm. This comparison suggests that regioregularity and the nature of the functionalized side chain are important factors in determining the conformation of the polymer backbone (*10*, *11*, *17*, *18*, *47*−*49*).

Concanavalin A (Con A) is a lectin that binds terminal α-D-mannosyl residues (*54*, *60*) and has been previously used as a model for the study of mannose-lectin interactions. Similarly, *Triticum Vulgaris* (wheat germ agglutinin) is a sialic-acid (NeuAc)-binding lectin (*55*). On the basis of these binding specificities, the series of glycopolythiophenes were examined for their ability to bind and detect these lectins. All of the glycopolythiophene derivatives produced a main absorption peak around 400−430 nm indicating that the degree of conjugation of the polymer backbone is reduced relative to the parent homopolymer (**40**). The blue-shift of the glycopolymer absorption suggests a more nonplanar conformation of the backbone. These relative absorption shifts compared to **40** strongly depend on the nature of the substituent in the polymer side chain. This agrees well with previous results that demonstrate the effect of side-chain bulk on polymer backbone planarity (*11*, *17*, *18*).

To demonstrate the biochromic capability of these glycopolythiophenes, several bioassays were performed. We hypothesized, based on previous studies (*7*, *10*−*15*, *17*, *53*), that the degree of planarity in the polymer backbone could depend on electrostatic, H-bonding, steric, or van der Waals interactions within or between polymer. These interactions are expected to be disrupted or altered upon receptor binding.

The steric effects produced by bulky carbohydrates in the glyco-PTs should also be considered (*18*, *56*, *57*). These possible interactions can amplify or reduce the sensing capability of the polymers by planar-nonplanar transitions. Therefore, we tested sialic acid-PTs (series I) and mannose-PTs (series II) to determine the ability of these materials to interact with WGA and Con A,

Table 4. Series I, UV−Vis Spectroscopic Data of Sialic Acid-PTs with the Receptor Proteins

polymer (sialic acid)	λ_{max} (nm) (in aqueous)	$\Delta\lambda_{max}$ (nm) WGA	Influenza A[a]	Influenza B[a]
40	440	0	+4	+3
41	408	+1	+6	+15
42	429	−4	+5	+6
43	429	−2	+10	+10
44	401	0	+15	+15
45	415	0	+27	+32
46	416	0	0	+3
47	411	0	+4	0
48	422	−6	+14	+17

[a] Assays were performed at 4 °C.

Table 5. Series II, UV−Vis Spectroscopic Data of Mannose-PTs with the Receptor Proteins

polymer (mannose)	λ_{max} (nm) (in aqueous)	$\Delta\lambda_{max}$ (nm) Con A[a]	C-B-S[b]	*E. coli* (HB 101)
40	440		+2	+5
49	411		+5	+16
50	405		+1	+8
51	401		0	+18
52	410		+6	+27
53	405		+4	+21
54	405		+7	+23
55	408		+8	+25
56	415		+1	+32

[a] Precipitates were obtained after addition of Con A. [b] C-B-S stands for Con A-biotin-streptavidin.

respectively (Tables 4 and 5). In the case of series I (Table 4), compounds **42**, **43**, and **48** exhibit a distinct blue-shift of the maximum absorption wavelength upon addition of WGA. The other polymers in this series remain unchanged. This indicates that the carbohydrate−protein interaction occurs, but there is a relatively small change in the conformation of the polymers upon protein addition. Increasing the lectin concentration does not affect the absorption shift. Eventually, the solution precipitates after a few hours. We expected polymer **47** would be more sensitive than the others due to the extension of the polymer π-conjugation system to the side chain. However, it showed no absorption shift upon addition of WGA.

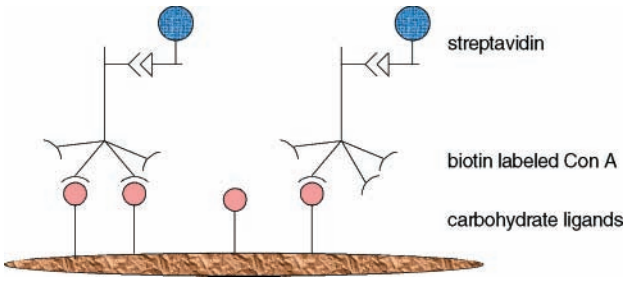

Figure 3. Schematic representation of the double sandwiched biochromic sensory device based on mannose-PT.

Similarly, the glyco-PTs of series II were also examined with Con A (Table 5). All polymers formed a red-brown precipitate regardless of the concentration of the polymer solution. Indeed, these precipitates were the complexes of mannose-polythiophene and Con A (*58*), and precipitation seems to have occurred before the absorption change. This may be due to the higher density of the binding site in Con A (4 subunits/molecule) and also higher its molecular weight (102 000 kDa) than that of WGA (2 subunits/molecule, 36 000 kDa). The Con A effectively cross-links the mannose-PTs before the observation of an absorption shift.

To minimize the problem of precipitation, we used a biotinylated Con A, complexed to streptavidin. This complex, when bound to the mannose-PT helps stabilize the polymer−protein complex, presumably by inhibiting cross-linking.

Using this motif, a small but significant biochromic response was observed upon the addition of streptavidin (Figure 3). A red-shift of up to 8 nm was observed upon the addition of the protein complex (Table 5). The result suggests that the binding of biotin-labeled Con A/streptavidin increases the π-conjugated system of polymer backbone. This result agrees qualitatively with a similar report by Leclerc et al. (*13*) where biotin-containing polythiophene was incubated directly with avidin to generate a biochromic response. However, in that report, the protein binding produced a blue-shift of the polymer backbone absorption.

We were interested in determining whether the size and valency of the binding receptor has any influence on the optical shifts observed with these glyco-PTs. To that end, we investigated the interactions of influenza virus A and B and *E. coli* (HB101 strain) with the sialic acid-PTs and mannose-PTs, respectively. The interaction of these agents with these sugars are well-documented in the literature (*22*, *26*, *27*, *29*, *31*, *33*−*35*). Interestingly, all assays indicated an absorption maximum wavelength shift that was substantially higher than that of the lectins. This wavelength shift was to the red, and in the range of 0 to +27 nm for Influenza virus A, 0 to +32 nm for Influenza virus B, and +8 to +32 nm for *E. coli*. For the sialic acid-PTs, polymer **45** showed the largest wavelength shift upon addition of both influenza A and B (+27 and +32 nm, respectively) (Figure 4). For the mannose-PTs, polymer **56** showed the largest wavelength shift (+32 nm) after *E. coli* binding (Figure 5). The wavelength shift was observed with the naked eye, as a color change to dark red. The direction of the wavelength shift is contradictory to those previously reported (*12*, *13*, *15*, *37*). In the case of the sialic acid-PT series, **41**, **42**, and **47**, having a relatively short side chain showed the weakest wavelength shifts. Morever, **47** exhibited the weakest degree of transition (+4 nm for influenza A, 0 nm for influenza B), most likely because of the inability of the virus to access the carbohydrate on the short

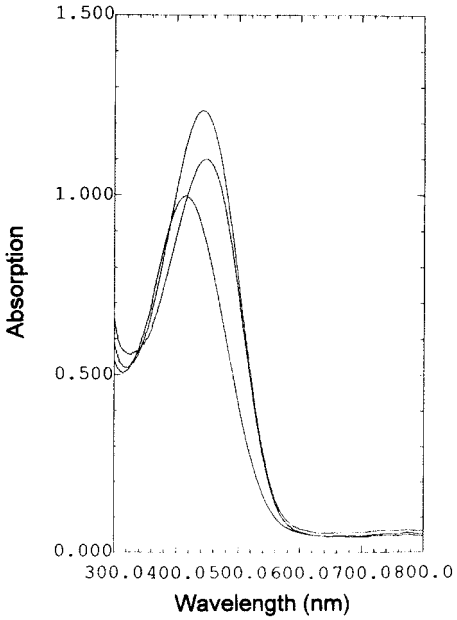

Figure 4. UV−vis spectra of sialic acid-PT (**45**) before and after addition of Influenza virus. Influenza virus A (top), Influenza virus B (middle), and no virus (bottom).

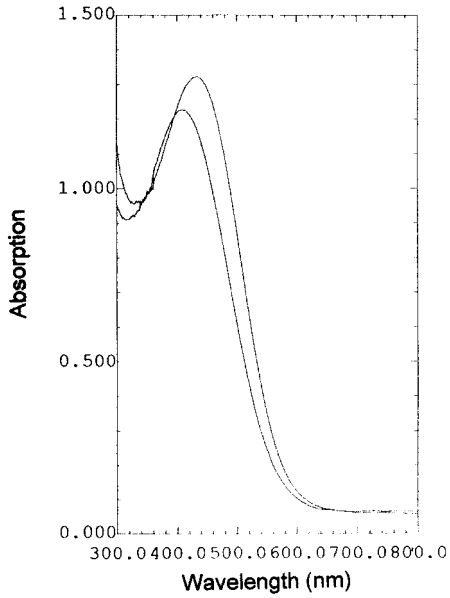

Figure 5. UV−vis spectra of mannose-PT (**56**) before and after addition of *E. coli*. with *E. coli* (top) and without *E. coli* (bottom).

linker. The other polymers, **44**, **45**, and **48** having longer side chains, exhibited $\Delta\lambda_{max}$ values up to 27 nm for influenza A and 32 nm for influenza B, with an observed color change to dark red (Figure 6). Polymer **43**, which has an intermediate side chain length indicated a wavelength shift of 10 nm.

A similar trend was observed for the mannose-PTs where the absorption maximum shifts were, in general, more significant than the sialic acid-PTs. Interestingly, **55** showed a strong absorption maximum shift to the red by 25 nm. Similar side-chain lengths of **49** and **50** showed somewhat smaller $\Delta\lambda_{max}$ values, +16 and +8 nm, respectively. These results suggest that, upon highly cooperative interactions between the carbohydrate and receptor protein, the degree of conjugation of the glycopolythiophene backbone is increased and the chain is rearranged to a more extended π-conjugated system. In general, the polymers with the longer side chains exhibit greater shift,

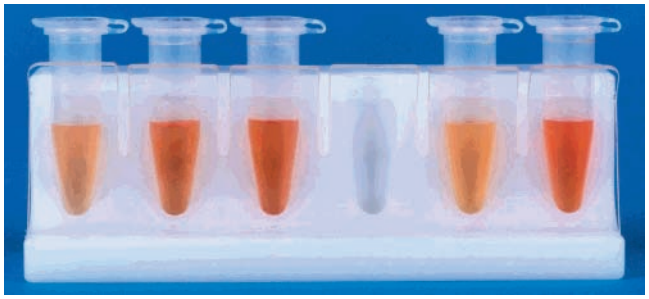

Figure 6. Color Change of Polythiophenes by addition of the receptor protein. From the left side, Sialic aicd-PT (**45**), **45** with Influenza virus A, **45** with Influenza virus B, blank, Mannose-PT (**56**), and **56** with *E. coli*.

again suggesting a higher degree of transition to the more planar conformer (see for example, **52**−**56**).

The unusual red-shift of these polymers upon interaction with protein, virus, or bacteria may be explained in a simple sense, by a nonplanar to planar transition of the polymer backbone. Because these polymers are soluble polymers in free solution [unlike previous biochromic studies with polydiacetyle ne where ordered assemblies such as vesicles or LB films were used (*15*, *38*−*41*)], it is likely that numerous intermolecular interactions can occur. The acidic groups in the polymer backbone and carbohydrate side chains can easily engage in electrostatic or H-bonding interactions. The favorable energetics of these interactions could exceed that of efficient π-orbital overlap of the backbone. Therefore, twisting of the polymer backbone is favored under these conditions. Indeed, these types of interactions are supported by the fact that the homopolymer **40**, already has an absorption maximum that is significantly more in the red compared all of the carbohydrate-modified polymers (**41**−**56**). This is not completely unexpected given the high propensity of carbohydrates to engage in H-bonding interactions. However, upon binding of the cognate receptor, such as lectin, virus, or *E. coli*, the intermolecular interactions between the carbohydrate side chains are disrupted. This would be reasonable since the binding interaction has a higher affinity than the simple intermolecular forces occurring between carbohydrates. Once the intermolecular interactions are disrupted, the polymer assumes a more extended conformation, with decreased twisting of the polymer backbone. The increased π-orbital overlap of this extended conformation results in the observed red-shift. In addition, the multivalent nature of the influenza virus and *E. coli* receptors can bind multiple sites on the polymer, further amplifying the changed conformation. This agrees with the greater shifts observed for these particles, in comparison to that of the simple lectins.

CONCLUSIONS

Water-soluble glycopolythiophenes containing sialic acid or mannose ligands have been synthesized by oxidative copolymerization of methyl (3-thienyl)acetate (**7**) and thiophene-carbohydrate monomers. The ability of these materials to detect lectins, influenza virus, and *E. coli* was evaluated by visible absorption spectrometry. The biochromic properties were dependent on the structure of polymers and the nature of the binding receptors (e.g., divalent versus multivalent). Due to the presence of the carbohydrate ligands on the polymer backbone, each chain has lower degree of π-conjugation than the corresponding homopolythiophene. These intermolecular interactions play a critical role in the unusual red shifts observed upon interaction with the cognate receptors. Once the virus or bacterium binds, the intermolecular interactions that produce a twisted polymer backbone are disrupted, and a more planar polymer backbone results. In general, the longer the side chain between the carbohydrate and the polymer backbone, the greater the absorption maximum shift. This may be related to optimized fit of the ligand to the receptor pocket. It is possible that these effects could be amplified by the preparation of more regioregular species, or thiophenes oligomers (*59*). Further optimization of these systems may result in enhanced detection of biological macromolecules.

ACKNOWLEDGMENT

This research was supported by the Director, Office of Energy Research, Office of Basic Energy Sciences and Division of Materials Sciences. We thank Dr. Y. H. Choi and K. H. Kim for their generous gift of *E. coli* HB101 (pSH2). We also would like to thank Dr. M. Alper, Director of the Biomolecular Materials Program for his support.

LITERATURE CITED

(1) Skotheim, T. A., Ed. (1986) *Handbook of Conducting Polymers*, Marcel Dekker, New York.
(2) Piao, X. L., Kim, J.-S., Yun, Y.-K., Hong, S.-K., and Jin, J.-I. (1997) Combined type liquid crystalline polymers composed of poly(ρ-phenylene terephthalate) main chain and azobenzene mesogenic side groups attached through polymethylene spacers. *Macromolecules 30*, 2294−2299.
(3) Roncali, J. (1997) Synthetic principles for band gap control in linear π-conjugated systems. *Chem. Rev. 97*, 173−205.
(4) Ueberhofen, K., Deutesfeld, A., Koynov, K., and Bubeck, C. (1999) Nonlinear optical waveguide spectroscopy of a conjugated polymer: poly(ρ-phenylenevinylene) *J. Opt. Soc. Am. B Opt. Phys. 16*, 1921−1935.
(5) Leclerc, M., Fréchette, M., Bergeron, J.-Y., Ranger, M., Lévesque, I., and Faïd, K. (1996) Chromic phenomena in neutral polythiophene derivatives. *Macromol. Chem. Phys. 197*, 2077−2087.
(6) Roux, C., Faïd, K., and Leclerc, M. (1994) Polythiophene derivatives: smart materials. *Polymer News 19*, 6−10.
(7) Lévesque, I., and Leclerc, M. (1995) Ionochromic effects in regioregular ether-substituted polythiophenes. *J. Chem. Soc., Chem. Commun. 7*, 2293−2294.
(8) Graf, D. D., Duan, R. G., Campbell, J. P., Miller, L. L., and Mann, K. R. (1997) From monomers to π-stacks. A comprehensive study of the structure and properties of monomeric, π-dimerized, and π-stacked forms of the cation radical of 3′,4′-dibutyl-2′,5′-diphenyl-2,2′:5′,2′-terthiophene. *J. Am. Chem. Soc. 119*, 5888−5899.
(9) Hosaka, N., Tachibana, H., Shiga, N., Matsumoto, M., and Tokura, Y. (1999) Photoinduced phase transformation in polythiophene. *Phys. Rev. Lett. 82*, 1672−1675.
(10) Masella, M. J., and Swager, T. M. (1993) Designing conducting polymer-based sensors: selective ionochromic response in crown ether containing polythiophenes. *J. Am. Chem. Soc. 115*, 12214−12215.
(11) Crawford, K. B., Goldfinger, M. B., and Swager, T. M. (1998) Na^+ specific emission changes in an ionophoric conjugated polymer. *J. Am. Chem. Soc. 120*, 5187−5192.
(12) McCullough, R. D., Ewbank, P. C., and Loewe, R. S. (1997) Self-assembly and disassembly of regioregular, water soluble polythiophenes: chemoselective ionochromatic sensing in water. *J. Am. Chem. Soc. 119*, 633−634.
(13) Faïd, K., and Leclerc, M. (1996) Functionalized regioregular polythiophenes: towards the development of biochromic sensors. *J. Chem. Soc., Chem. Commun*. 2761−2762.
(14) Pande, R., Kamtekar, S., Ayyagari, M. S., Kamath, M., Marx, K. A., Kuma, J., Tripcthy, S. K., and Kaplan, D. L. (1996) A biotinylated undecylthiophene copolymer bioconjugate for surface immobilization: creating an alkaline phos-

phatase chemoluminescence-based biosensor. *Bioconjugate Chem. 7*, 159−164.

(15) Charych, D. H., Nagy, J. O., Spevak, W., and Bednarski, M. D. (1993) Direct colorimetric detection of a receptor−ligand interaction by a polymerized bilayer assembly. *Science 261*, 585−588.

(16) Bredas, J. L. (1985) Relationship between band gap and bond length alternation in organic conjugated polymers. *J. Chem. Phys. 82*, 3809−3811.

(17) Roncali J. (1992) Conjugated poly(thiophene): synthesis, functionalization, and applications. *Chem. Rev. 92*, 711−738.

(18) McCullough, R. D. (1998) The chemistry of conducting polythiophenes. *Adv. Mater. 10*, 93−116.

(19) Zerbi, G., Chierichetti, B., and Ingänas, O. (1991) Thermochromism in polyalkylthiophenes: molecular aspects from vibrational spectroscopy. *J. Chem. Phys. 94*, 4646−4658.

(20) Marsella, M. J., Carroll, P. J., and Swager, T. M. (1995) Design of chemoresistive sensory materials: polythiophene-based pseudopolyrotaxanes. *J. Am. Chem. Soc. 117*, 9832−9841.

(21) Sharon, N. (1975) Complex Carbohydrates: *Their Chemistry, Biosynthesis and Functions*, Addison−Wesley, Reading MA.

(22) Reutter, W., Köttgen, E., Bauer, C., and Gerok, W. (1982) In *Sialic acids, Chemistry, Metabolism and Function* (R. Schauer, Ed.) Cell biology monograph series, Vol. 10, Springer-Verlag, Vienna.

(23) Goldstein, I. J., and Poretz, R. D. (1986) In *The lectins. Properties, Functions and Applications in Biology and Medicine* (I. E. Liener, N. Sharon, and I. J. Goldstein, Eds.) Academic press, Orlando, Florida.

(24) Sharon, N., and Lis, H. (1993) Carbohydrates in cell recognition. *Sci. Am.* January, 82−89.

(25) Lee, Y. C., and Lee, Reiko T. (1994) *Neoglycoconjugates: preparation and applications*, Academic press.

(26) Roy, R., Andersson, F. O., Harms, G., Kelm, S., and Schauer, R. (1992) Synthesis of esterase-resistant 9-O-acetylated polysialoside as inhibitor of influenza C virus hemagglutinin. *Angew. Chem., Int. Ed. Engl. 31*, 1478−1481.

(27) Toogood, P. L., Galliker, P. K., Glick, G. D., and Knowles, J. R. (1991) Monovalent sialosides that bind tightly to influenza A virus. *J. Med. Chem. 34*, 3138−3140.

(28) Roy, R., Zannini, D., Meunier, S. J., and Romanowska, A. (1993) Synthetic oligosaccharides: indispensable probes for the life sciences. *ACS Symp. Ser. 560*, 104−119.

(29) Spaltenstein, A., and Whitesides, G. (1991) Polyacrylamides bearing pendant α-sialoside groups strongly inhibit agglutination of erythrocytes by influenza virus. *J. Am. Chem. Soc. 113*, 686−687.

(30) Firon, N., Ofek, I., and Sharon, N. (1983) Carbohydrate specificity of the surface lectin of *Escherichia coli, Klebsiella pneumoniae*, and *Salmonella typhimurium*. *Carbohydr. Res. 120*, 235−249.

(31) Bertozzi, C. R., and Bednarski, M. D. (1992) A receptor-mediated immune response using synthetic glycoconjugates. *J. Am. Chem. Soc. 114*, 5543−5546.

(32) Old, D. C. (1972) Inhibition of the interaction between fimbrial hamagglutinins and erythrocytes by D-mannose and other carbohydrates. *J. Gen. Microb. 71*, 149−157.

(33) Firon, N., Ofek, I., and Sharon, N. (1984) Carbohydrate-binding sites of the mannose-specific fimbrial lectins of enterobacteria. *Infect. Immun. 43*, 1088−1090.

(34) Venegas, M. F., Navas, E. L., Gaffney, R. A., Duncan, J. L., Anderson, B. E., and Schaetter, A. J. (1995) Binding of type 1-piliated *Escherichia coli* to Vaginal mucus. *Infect. Immun. 63*, 416−422.

(35) Madison, B., Ofek, I, Clegg, S., and Abraham, S. N. (1994) Type 1 fimbrial shafts of *Escherichia coli* and *klebsiella pneumoniae* influence sugar-binding specificities of their fimH adhesions. *Infect. Immun. 62*, 843−848.

(36) Page, D., Aravind, S., and Roy, R. (1996) Synthesis and lectin binding properties of dendritic mannopyranoside. *Chem. Commun.* 1913−1914.

(37) Pan, J., and Charych, D. H. (1997) Molecular recognition and colorimetric detection of cholera toxin by poly(diacetylene) liposome incorporating Gm1 ganglioside. *Langmuir 13*, 1365−1367.

(38) Jonas, U., Shah, K., Norvez, S., and Charych, D. (1999) Reversible color switching and unusual solution polymerization of hydrazide-modified diacetylene lipids. *J. Am. Chem. Soc. 121*, 4580−4588.

(39) Okada, S., Jelinek, R., and Charych, D. (1999) Induced color change of conjugated polymeric vesicles by interfacial catalysis of phospholipase A_2. *Angew. Chem., Int. Ed. 38*, 655−659.

(40) Jelinek, R., Okada, S., Norvez, S., and Charych, D. (1998) Interfacial catalysis by phospholipases at conjugated lipid vesicles: colorimetric detection and NMR spectroscopy. *Chem. Biol. 5*, 619−629.

(41) Okada, S., Peng, S., Spevak, W., and Charych, D. (1998) Color and chromism of polydiacetylene vesicles. *Acc. Chem. Res. 31*, 229−239.

(42) Reichert, A., Nagy, J., Spevak, W., Charych, D. (1995) Polydiacetylene liposomes functionalized with sialic acid bind and colorimetrically detect influenza virus. *J. Am. Chem. Soc. 117*, 829−830.

(43) Charych, D., Cheng, Q., Reichert, A., Kuziemko, G., Stroh, M., Nagy, J., Spevak, J., and Stevens, R. (1996) A litmus test for molecular recognition using artificial membranes. *Chem. Biol. 3*, 113−120.

(44) McCullough, R. D., and Loewe, R. D. (1992) Enhanced electrical conductivity in regioselectively synthesized poly(3-alkylthiophenes). *J. Chem. Soc., Chem. Commun.* 70−72.

(45) Chen, T. A., and Rieke, R. D. (1992) The first regioregular head-to-tail poly(3-hexylthiophene-2,5-diyl) and a regiorandom isopolymer: Ni vs Pd catalyst of 2(5)-bromozinco)-3-hexylthiophene polymerization. *J. Am. Chem. Soc. 114*, 10087−10088.

(46) McCullough, R. D., Tristram-Nagle, S., Williams, S. P., Loewe, R. D., and Jayaraman, M. (1993) Self-orienting head-to tail poly(3-alkylthiophenes): new insights on structure−property relationships in conducting polymers. *J. Am. Chem. Soc. 115*, 4910−4911.

(47) Leclerc, M., Lévesque, I., Goldenberg, L., and Petty, M. C. (1997) Processing-induced chromism in thin films of polythiophene derivatives. *Macromol. Rapid Commun. 18*, 733−737.

(48) Faïd, K., Fréchette, M., Ranger, M., Mazerolle, L., Lévesque, I., and Leclerc, M. (1994) Chromic phenomena in regioregular and nonregioregular polythiophene derivatives. *Chem. Mater. 7*, 1390−1396.

(49) Chayer, M., Faïd, K., and Leclerc, M. (1997) Highly conducting water-soluble polythiophene derivatives. *Chem. Mater. 9*, 2902−2905.

(50) Li, X.-C., Sirringhaus, H., Garnier, F., Holmes, A. B., Moratti, S. C., Feeder, N., Clegg, W., Teat, S. J., and Friend, R. H. (1998) A highly π-stacked organic semiconductor for thin film transistors based on fused thiophenes. *J. Am. Chem. Soc. 120*, 2206−2207.

(51) Roux, C., and Leclerc, M. (1992) Rod-totail transition in alkoxy-substituted polythiophenes. *Macromolecules 25*, 2141−2144.

(52) Pincus, P., and De Gennes, P. G. (1978) Nematic polymers. *J. Polym. Sci., Polym. Symp. 65*, 85−90.

(53) Rughooputh, S. D. D., Hotta, S., Heeger, A. J., and Wudl, F. (1987) Chromism of soluble polythiophenes. *J. Polym. Sci., Part B: Polym. Phys. 25*, 1071−1078.

(54) Gunther, G. R. (1973) Concanavalin A derivatives with altered biological activities. *Proc. Nat. Acad. Sci. U.S.A. 70*, 1012−1016.

(55) Nagata, Y., and Burger, M. M. (1974) Weat germ agglutinin: molecular characteristics and specificity for sugar binding. *J. Biol. Chem. 249*, 3116−3122.

(56) Yamamoto, T., Komarudin, D., Arai, M., Lee, B.-L., Suganuma, H., Asakawa, N., Inoue, Y., Kubota, K., Sasaki, S., Fukuda, T., and Matsuda, H. (1998) Extensive studies on π-stacking of poly(3-alkylthiophene-2,5-diyl)s and poly(4-alkylthiazole-2,5-diyl)s by optical spectroscopy, NMR analysis,

light scattering analysis, and X-ray crystallography. *J. Am. Chem. Soc. 120*, 2047−2058.
(57) Lee, C., Kim, K. J., and Rhee, S. B. (1995) The effects of ester substitution and alkyl chain length on the properties of polythiophenes. *Synth. Met. 69*, 295−296.
(58) Pagé, D., and Roy, R. (1996) Synthesis of divalent α-D-mannopyranosylated clusters having enriched binding affinities towards concanavalin A and pea lectins. *Bioorg. Med. Chem. Lett. 6*, 7165−1770.
(59) Elandaloussi, E., Frère, P., Richomme, P., Orduna, J., Garin, J., and Roncali, J. (1997) Effect of chain extension on the electrochemical and electronic properties of π-conjugated soluble thienylenevinylene oligomers. *J. Am. Chem. Soc. 119*, 10774−10784.
(60) Hardman, K. D. (1979) The carbohydrate binding site of concanavalin A. *ACS Symp. Ser. 88*, 12−26.

BC000026F

Genetically Synthesized Antibody-Binding Protein Self-Assembled on Hydrophobic Matrix

Tsutomu Sugihara, Gi Hun Seong, Eiry Kobatake, and Masuo Aizawa*

Department of Biological Information, Graduate School of Bioscience and Biotechnology, Tokyo Institute of Technology, Nagatsuta, Midori-ku, Yokohama 226-8501, Japan. Received March 23, 2000; Revised Manuscript Received July 16, 2000

A unique antibody-binding protein, (E12B2)n, was genetically synthesized, which was characterized by a hydrophobic peptide, E12, at one terminus and an antibody-binding peptide, B2, at the other. It was clarified by atomic force microscopy (AFM) imaging that this protein was efficiently self-assembled on a hydrophobic solid surface. (E12B2)n self-assembled on a microplate exhibited an excellent performance of antibody-binding affinity. The proposed design of antibody-binding protein seems promising in immobilizing antibody molecules on hydrophobic solid surfaces.

INTRODUCTION

Immobilization of antibody molecules on a solid surface is a widely used technique in various fields such as immunoassays, immunosensors, and affinity chromatography (*1*−*3*). In these systems, it is essential to assemble antibody molecules stably on a solid surface in a highly oriented manner with retaining their antigen-binding affinity.

Antibody molecules may be stably immobilized by covalent bonding to the solid surface. However, it often results in a loss of their antigen-binding affinity. Although simple adsorption offers an easy method for immobilization, it results in partial or complete denaturation of adsorbed molecules (*4*−*10*).

One of the methods is to immobilize antibody molecules indirectly on the solid surface via antibody-binding proteins, including staphylococcal protein A (SpA) and protein G (*11*−*18*), which specifically recognize and bind the Fc region of numerous mammalian immunoglobulin G (IgG) with leaving the Fab regions available for antigen binding. In this method, direct damage of antibody molecules due to immobilization may be avoided, and the orientation of Fab regions can be controlled. However, immobilization of such antibody-binding proteins on the solid surface should suffer from the inactivation of their antibody-binding abilities.

To overcome these disadvantages, a novel antibody-binding protein has been designed in such a manner as a hydrophobic peptide unit in sequence may surround the surface loop of the antibody-binding domain to be self-assembled on the hydrophobic solid surface. The B domain of SpA (*19*−*21*) and elastin-based polyhexapeptide repeat (Ala-Pro-Gly-Val-Gly-Val), E (*22*−*24*), were sequenced to construct the designed protein. The structural gene for 2-repeat of the B domain (B2) was ligated to the gene for 12-repeat of elastin-based poly-hexapeptide (E12) in frame. The 2-repeat of the B domain has been confirmed to exhibit enough binding affinity to stably immobilize the Fc region of IgG, while the 12-repeat of E is expected to provide the protein with hydrophobicity strong enough to be self-assembled on a hydrophobic solid surface. The synthesized gene was expressed in *Escherichia coli* and purified with affinity chromatography. The structure of resulting protein was designated E12B2. Two-repeat and four-repeat of E12B2, designated $(E12B2)_2$ and $(E12B2)_4$, respectively, were also constructed. The self-assembled protein molecules on a hydrophobic solid surface were individually visualized and evaluated by atomic force microscopy (AFM) imaging, which could reveal the rationality of our designing the antibody-binding protein. Furthermore, antibody-binding ability of (E12B2)n assembled on a hydrophobic plastic surface was investigated.

EXPERIMENTAL PROCEDURES

Materials. Plasmid pET-32 (c), *E. coli* BL21 (DE3) competent cells, enterokinase, and EKapture Agarose were purchased from Novagen (Madison, W1). Ni-NTA agar was purchased from Qiagen (Hilden, Germany). Nontreatment-type 96-wells microtiter plate (FALCON 1172) was obtained from Becton Dickinson Labware (Franklin Lakes, NJ). Block Ace was purchased from Snow brand milk products Co., Ltd. (Sapporo, Japan). Bovine serum albumin (BSA) was obtained from Sigma Chemical Co. (St. Louis, MO). Rabbit anti-BSA antibody was purchased from Intercell Technologies Inc. (Hopewell, NJ). Peroxidase conjugated protein A (SpA-POD) was obtained from Wako Pure Chemicals Industries, Ltd. (Osaka, Japan), peroxidase was purchased from Toyobo (Osaka, Japan), and rabbit anti-peroxidase (horseradish) antibody was purchased from Rockland (Gilbertsville, PA).

Plasmid Construction. In the previous study, we constructed the plasmid designated pKK−B2 (*25*), which was inserted a 2-repeat of the gene encoding the B domain of SpA. This inserted fragment (B2) was amplified with polymerase chain reaction (PCR) by using the synthesized DNA primer containing *Bam*HI site and the reverse primer containing *Bgl*II and *Eco*RI sites. This amplified fragment (B2) was digested with *Bam*HI and *Eco*RI and inserted into the *Bgl*II−*Eco*RI site of pGEX-E12 (*26*), which was encoding GST and the 12-repeat of the APGVGV sequence. The resulting plasmid was designated pGEX-E12B2. A *Bam*HI−*Eco*RI fragment of

* To whom correspondence should be addressed. E-mail: maizawa@bio.titech.ac.jp. Phone: +81-45-924-5759. Fax: +81-45-924-5779.

10.1021/bc000031j CCC: $19.00 © 2000 American Chemical Society
Published on Web 11/02/2000

the pGEX-E12B2 was inserted at *Bgl*II−*Eco*RI site of the same plasmid, and pGEX-$(E12B2)_2$ was constructed. This procedure was repeated for pGEX-$(E12B2)_2$, and pGEX-$(E12B2)_4$ encoding a 4-repeat of $(APGVGV)_{12}$-$(B\ domain)_2$ sequence was constructed. Finally, each fragment of *Bam*HI−*Eco*RI from pGEX-E12B2, pGEX-$(E12B2)_2$, and pGEX-$(E12B2)_4$ was inserted into the pET-32 (c) at the same site as a fusion with the gene of thioredoxin in frame. The resulting plasmids were designated pET-E12B2, pET-$(E12B2)_2$, and pET-$(E12B2)_4$, respectively.

Expression and Purification of Proteins. *E. coli* BL21 (DE3) cells were transformed with the plasmids pET-E12B2, pET-$(E12B2)_2$, and pET-$(E12B2)_4$ and they were grown in LB medium supplemented with 50 μg/mL ampicillin to $OD_{660} = 0.5$ at 37 °C. After induction with 1 mM isoproplylthio-β-galactoside (IPTG), cells were cultured for another 4 h at 20 °C. They were harvested by centrifugation, washed with lysis buffer (10 mM imidazole, 300 mM NaCl, and 50 mM phosphate, pH 8.0) and disrupted by sonication. After centrifugation, the supernatant was applied to the Ni-NTA Agar to purify the fusion protein with thioredoxin by using the affinity of histidine-tag at N-terminus. The purified fusion protein was cleaved site-specifically with enterokinase to cut off the thioredoxin moiety for 16 h at 21 °C. After cleavage reaction, thioredoxin and enterokinase were removed by applying Ni-NTA Agar and EKapture Agarose. The resulting proteins possessing reciprocally 1, 2, and 4-repeated sequences were designated E12B2, $(E12B2)_2$, and $(E12B2)_4$, respectively. These proteins were dialyzed with phosphate-buffered saline (PBS). Purified samples of E12B2, $(E12B2)_2$, and $(E12B2)_4$ were analyzed by SDS−PAGE and Western blotting.

AFM Imaging of Self-Assembled (E12B2)n on HOPG or Mica Surface. Purified (E12B2)n protein was dissolved in PBS to a final concentration of 100 nM in PBS. Twenty microliters of the solution containing (E12B2)n protein was incubated on a freshly cleaved highly oriented pyrolytic graphite (HOPG) or mica for 1 h at 37 °C, which was washed with 1 mL of distilled water and dried shortly in a stream of compressed and filtered air. All samples were further dried in a 2 L glass desiccator in the presence of P_2O_5 for 10 min.

The samples were imaged with an AFM of NanoScope III MultiMode system (Digital Instruments, Santa Barbara, CA) in the tapping mode in air. The tip of the cantilever is modulated sinusoidally to touch briefly the surface as it scans the surface of the sample. Standard silicon cantilevers of 125 μm in length were used. Cantilever oscillation frequency was tuned to the resonance frequency of the cantilever (280−350 kHz). The 512 × 512 pixel images were captured with a scan size between 1.0 and 2.0 μm at a scan rate of 1−2 scan lines/s. The area of (E12B2)n self-assembled on substrates was determined with the NanoScope image analysis package.

Competitive ELISA. One hundred microliters of rabbit anti BSA antibody (10 μg/mL) was added to the wells of microplate coated with BSA and incubated for 1 h at 37 °C. After these wells were washed several times with phosphate-buffered saline including 0.1% Tween 20 (PBS-T), 100 μL of 0.25% Block Ace in PBS-T was added to the wells and they were incubated for 1 h at 37 °C. These wells were washed several times with PBS-T. Thus, antibody molecules were coated on the surface with orientation as displaying their Fc region to liquid phase.

The various concentrations of (E12B2)n solution including 0.25 μg/mL SpA-POD were reacted on the microplate coated with rabbit IgG for 1 h at 37 °C. After these wells were washed several times with PBS-T, 50 μL of 0.5 mg/mL *o*-phenylene diamine in 50 mM acetate buffer (pH 5.0) and 50 μL of 0.06% hydrogen peroxide were added to the wells. This enzyme reaction was stopped with 50 μL of 4 M H_2SO_4. The absorbance of the reaction mixture at 490 nm was measured with a microplate-reader (Bio-Rad, Hercules, CA).

Antibody Binding Assay on Each Protein-Coated Microplate. One hundred microliters of solution of each SpA, E12B2, $(E12B2)_2$, and $(E12B2)_4$ was added to the individual well of a 96-well nontreatment-type microtiter plate (Falcon 1172) in various concentrations, and they were incubated for 1 h at 37 °C. After these wells were washed several times with PBS-T, 100 μL of 0.25% Block Ace in PBS-T was added to the wells, and they were incubated for 1 h at 37 °C. These wells were washed several times with PBS-T. Thus, these protein-coated microplates were designated SpA-plate, E12B2-plate, $(E12B2)_2$-plate, and $(E12B2)_4$-plate.

One hundred microliters of 10 μg/mL rabbit anti-peroxidase antibody solution was reacted to SpA-plate, E12B2-plate, $(E12B2)_2$-plate, and $(E12B2)_4$-plate, and they were incubated for 1 h at 37 °C. All wells were washed several times with PBS-T, then 100 μL of 10 μg/mL peroxidase was added to the wells and incubated for 1 h at 37 °C. After these wells were washed several times with PBS-T, peroxidase enzyme reaction was done according to the previous procedure.

Antibody Assembling Ability on $(E12B2)_4$-Coated and Noncoated Plate. One hundred microliters of rabbit anti-peroxidase antibody solution was added to the $(E12B2)_4$-coated microplate and noncoated microplate in various concentrations, and they were incubated for 1 h at 37 °C. All wells were washed several times with PBS-T and then blocked with 0.25% Block Ace. One hundred microliters of 10 μg/mL peroxidase was added to the wells, and they were incubated for 1 h at 37 °C. After these wells were washed several times with PBS-T, peroxidase enzyme reaction was done according to the previous procedure.

RESULTS

Plasmid Construction and Protein Purification. Designed antibody-binding proteins, E12B2, $(E12B2)_2$, and $(E12B2)_4$, were produced in *E. coli* by using the GST-fusion system. However, no desired proteins were produced in both soluble and insoluble fractions of *E. coli* (data not shown). Then the fusion partner was changed from GST to thioredoxin. Through the use of this system, E12B2, $(E12B2)_2$, and $(E12B2)_4$ were produced in larger amounts in the soluble fraction than the insoluble fraction. SDS−PAGE analysis of these purified samples revealed the single band in the predicted molecular mass, approximately 21, 42, and 84 kDa, respectively (Figure 1A). Western blotting analysis revealed the same pattern of protein band as SDS−PAGE analysis (Figure 1B).

AFM Imaging of Self-Assembled (E12B2)n on HOPG or Mica Surface. Each solution of (E12B2)n was assembled on HOPG and mica plates as hydrophobic and hydrophilic surfaces, respectively, and they were observed by AFM (Figure 2). From these images, the ratio of covered area with (E12B2)n was calculated (Table 1). Assembling amounts of proteins on the HOPG surface increased with an increase of E12B2 unit (Figure 2, panels A−C). In the case of $(E12B2)_4$, almost the whole surface (87.88%) of the HOPG was covered with the proteins (Figure 2C). In contrast, the protein was scarcely assembled on the mica surface (Figure 2, panels D−F). The $(E12B2)_4$ was assembled on hydrophobic HOPG

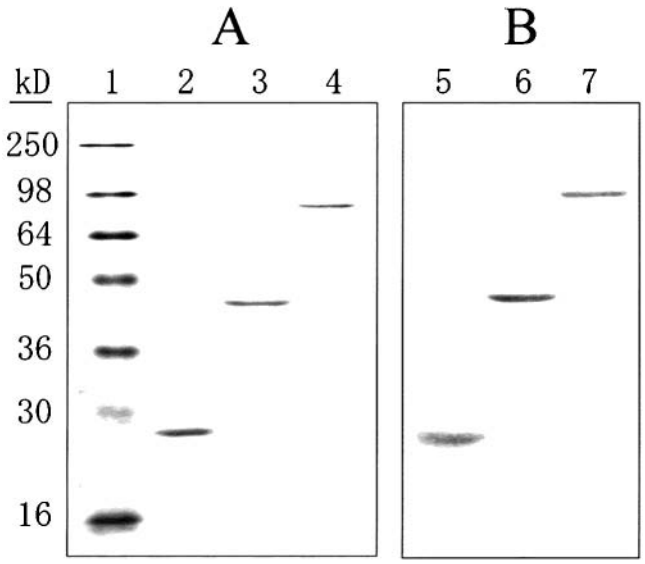

Figure 1. (A) SDS−PAGE analysis of purified E12B2, $(E12B2)_2$, and $(E12B2)_4$. Purified proteins were separated by electrophoresis in 12% SDS−polyacrylamide gel. The gel was stained with coomassie brilliant blue. (1) molecular weight marker, (2) E12B2, (3) $(E12B2)_2$, (4) $(E12B2)_4$, (B) Western blotting of E12B2, $(E12B2)_2$, and $(E12B2)_4$. These proteins were transferred to PVDF membrane and probed alkaline phosphatase-conjugated rabbit IgG. (5) E12B2, (6) $(E12B2)_2$, (7) $(E12B2)_4$.

surface about 200 times more than hydrophilic mica surface (Figure 2, panels C and F).

Competitive ELISA. The antibody-binding ability of (E12B2)n in liquid phase was investigated by comparing with SpA. The various concentrations of (E12B2)n or SpA solution including SpA-POD (0.25 μg/mL) were reacted to rabbit IgG immobilized microplate. The amount of reacted SpA-POD to immobilized IgG was estimated by peroxidase activity. They are plotted against protein concentrations as shown in Figure 3. The antibody-binding ability of E12B2 was lower than that of SpA. However, that of $(E12B2)_2$ was slightly higher than that of SpA. Furthermore, $(E12B2)_4$ gave an excellent antibody-binding ability, which was about 10 times higher than that of SpA.

Antibody Binding Assay on Each Protein-Coated Microplate. The antibody-binding ability of (E12B2)n on a solid phase was investigated by enzyme immunoassay. At first, (E12B2)n were coated on the microplate surface in various concentrations. A constant amount of rabbit anti-peroxidase antibody was reacted to each protein-coated microplate and then peroxidase was added. Amount of immobilized peroxidase was estimated by peroxidase activity, which reflected the amount of assembled (E12B2)n retained antibody binding ability on the microplate surface. They are plotted against protein concentrations as shown in Figure 4. A large amount of E12B2 over 100 nM was required for saturated assembling on the microplate surface. However, the required amount of (E12B2)n for assembling was dramatically reduced by repeating E12B2 sequence. In the case of $(E12B2)_4$, less than 10 nM of protein concentration was sufficient for saturated assembling. To compare with the other IgG-binding protein, the same experimental procedure was done in the case of SpA. The antibody binding ability of SpA in solid phase was slightly lower than that of $(E12B2)_2$. In the following study, the sufficient amount of $(E12B2)_4$ was coated on a microplate for immobilizing antibody.

Antibody Assembling Ability on $(E12B2)_4$-Coated and Noncoated Plate. The antibody assembling ability of the $(E12B2)_4$-coated plate was investigated by comparing with that of the noncoated plate. Rabbit anti-peroxidase antibody was reacted to $(E12B2)_4$-coated and noncoated microplate in various concentrations, then peroxidase was added. Amount of immobilized peroxidase was estimated by peroxidase activity, which reflected the amount of immobilized antibody molecule on the microplate. The results for $(E12B2)_4$ are shown in Figure 5. Antibody could be assembled on microplate surface by physical adsorption. However, the antibody-assembling ability on $(E12B2)_4$-coated microplate was more efficiently by than noncoated one.

DISCUSSION

In this study, we have designed and constructed a unique antibody-binding protein, (E12B2)n, which was characterized by a hydrophobic peptide unit.These proteins tried to be produced in *E. coli* by using the GST-fusion system. However, no desired proteins were produced in both soluble and insoluble fractions of *E. coli* (data not shown). Then the fusion partner was changed from GST to thioredoxin which could increase drastically the solubility of heterologous proteins synthesized in the *E. coli* cytoplasm and result in an increased accumulation of the fusion protein to higher levels. Furthermore, since the host *E. coli* BL21 (DE3) has a gene for T7 RNA polymerase under the control of tac promoter in their chromosomal DNA, production of T7 RNA polymerase is induced with IPTG. As the result, an enhanced expression of the gene under T7 promoter is induced by adding IPTG (*27*). Through the use of this system, E12B2, $(E12B2)_2$, and $(E12B2)_4$ were produced in larger amounts in the soluble fraction than in the insoluble fraction. These proteins were purified by Ni-NTA affinity chromatography from the soluble fraction, and thioredoxin was removed by cleavage reaction with enterokinase. Purified samples were dialyzed with PBS.

Simple adsorption of protein molecules on solid surface is mostly dependent on the hydrophobic interaction between protein molecule and solid surface. Since (E12B2)n has the hydrophobic peptide, E12, in their structure, they should be efficiently self-assembled on the hydrophobic solid surface by hydrophobic interaction. To investigate the assembling efficiency of (E12B2)n onto the hydrophobic and hydrophilic surfaces, each protein was assembled on HOPG and mica plates as the hydrophobic and hydrophilic surfaces, respectively, and was visualized by AFM (Figure 2). (E12B2)n was assembled preferably on the HOPG hydrophobic surface. And more, assembling amounts of proteins on the HOPG surface increased with an increase of E12B2 unit (Table 1). In contrast, the protein was scarcely assembled on the mica surface. These results suggest that (E12B2)n are self-assembled on the HOPG surface through strong hydrophobic interaction between the E12 sequence and the hydrophobic solid surface. Generally, the interaction between molecule and surface of HOPG are very weak (*28*). Therefore, Droz et al. modified the surface of HOPG by glow discharge to assemble IgG (*29*). However, E12B2 was assembled homogeneously without any modification of HOPG surface. It is a distinctive feature of this protein.

The antibody-binding ability of (E12B2)n was compared with that of SpA. Competitive ELISA and antibody binding assay revealed that the 4-repeat of E12B2 sequence, $(E12B2)_4$, was superior in antibody binding to SpA in both liquid and solid phases, although $(E12B2)_2$ was comparable with SpA. In the following study, $(E12B2)_4$ was coated as an antibody-binding matrix on a hydrophobic solid surface.

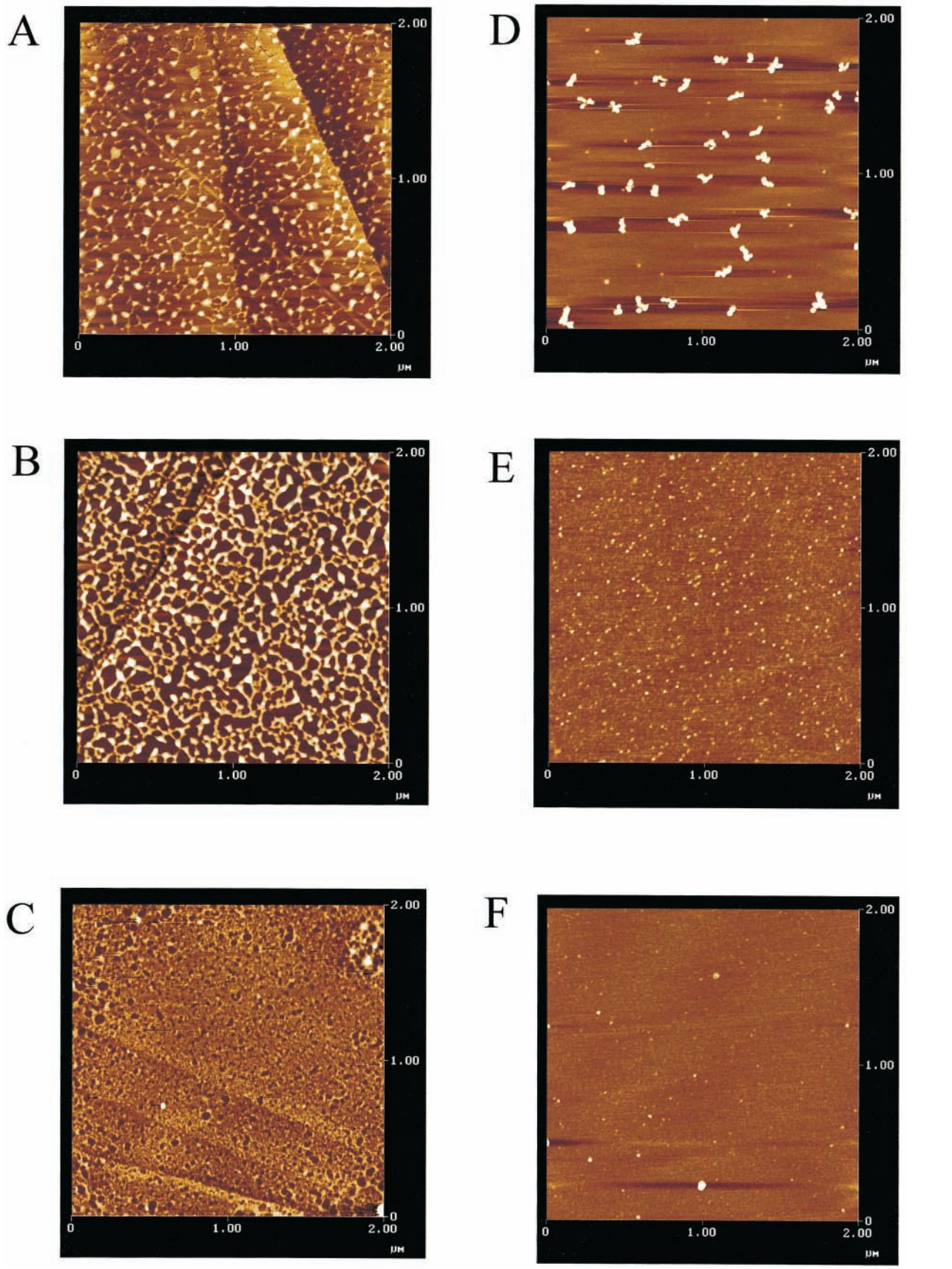

Figure 2. AFM imaging of assembling (E12B2)n on HOPG or mica surface. When adding 100 nM of (E12B2)n solution, assembled (E12B2)n was imaging by atomic force microscopy. (A) E12B2 on HOPG, (B) $(E12B2)_2$ on HOPG, (C) $(E12B2)_4$ on HOPG, (D) E12B2 on Mica, (E) $(E12B2)_2$ on Mica, (F) $(E12B2)_4$ on Mica.

In general immunoassy methods, antibody was assembled on a microplate surface by simple adsorption. Therefore, the antibody-assembling ability of the $(E12B2)_4$-coated plates was investigated by comparing with that of the noncoated plate. As shown in Figure 5, antibody molecule was more effectively immobilized on the

Table 1. Ratio of Covered Areas by (E12B2)n on HOPG or Mica Surface[a]

	HOPG (%)	mica (%)
E12B2	26.18	4.36
$(E12B2)_2$	50.18	3.60
$(E12B2)_4$	87.88	0.45

[a] The area of (E12B2)n self-assembled on structure was determined with bearing of the NanoScope image analysis package.

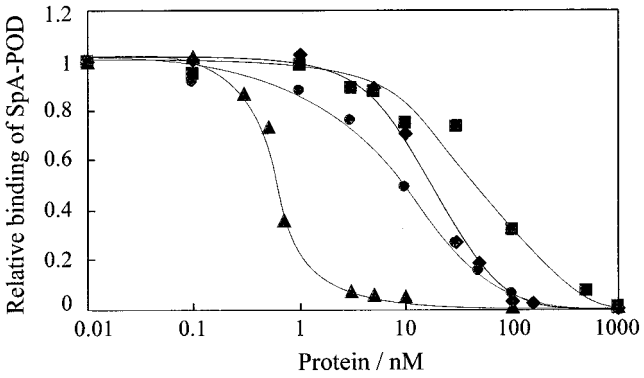

Figure 3. Antibody-binding activity of E12B2, $(E12B2)_2$, $(E12B2)_4$, and SpA. The binding of SpA-POD with each protein to rabbit IgG adsorbed on microplate surface was measured in the presence of competing protein. The absorbance at 490 nm at each concentration of competing protein was divided by the absorbance without the protein, and the value was plotted against the logarithmic of molar concentration of each protein. Values are the mean ± SD from four independent assays. E12B2 (■), $(E12B2)_2$ (●), $(E12B2)_4$ (▲), and SpA (◆).

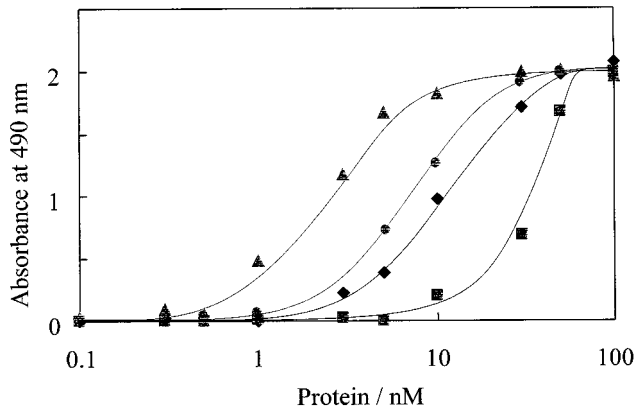

Figure 4. The absorbances by peroxidase reaction were plotted against the adding protein concentrations. These curves reflected the amount of assembled protein molecules on microplate surface. E12B2 (■), $(E12B2)_2$ (●), $(E12B2)_4$ (▲), and SpA (◆).

$(E12B2)_4$-coated microplate than noncoated microplate. In the model case of immunoassay, we tried the sandwich ELISA for targeting mouse IgM on $(E12B2)_4$-coated or noncoated microplate. The required amount of primary antibody for assembling on microplate surface is reduced with $(E12B2)_4$ coating (data not shown). These results suggest that (E12B2)n, especially $(E12B2)_4$, is a good material for assembling antibody on a hydrophobic matrix.

CONCLUSION

Genetically synthesized protein, (E12B2)n, showed an excellent performance of antibody binding on the hydrophobic solid surface. The antibody immobilization is simply carried out by coating the hydrophobic solid surface with (E12B2)n, which is followed by affinity binding of antibodies. (E12B2)n will find a wide application in immunoassays, immunosensors, and affinity chromatography.

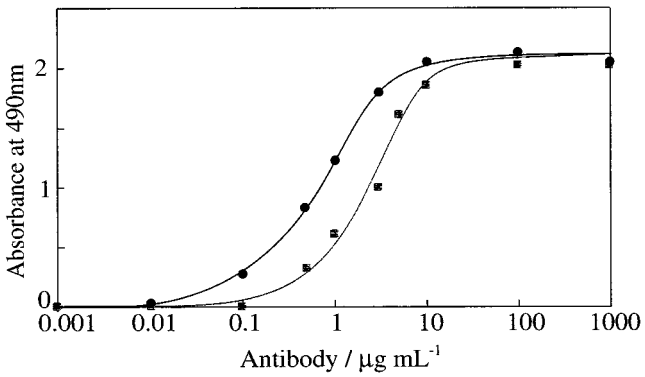

Figure 5. The absorbances by peroxidase reaction were plotted against the adding antibody concentration. These curves were reflected the amount of assembled antibody molecules on $(E12B2)_4$-coated (●) or noncoated microplate (■).

LITERATURE CITED

(1) Lu, B., Smyth, M. R., and O'Kennedy, R. (1996) Oriented immobilization of antibodies and its applications in immunoassays and immunosensors. *Analyst 121* (3), 29R−32R.

(2) Rabbany, S. Y., Donner, B. L., and Ligler, F. S. (1994) Optical immunosensors. *Crit. Rev. Biomed. Eng. 22* (5−6), 307−346.

(3) Jack, G. W. (1994) Immunoaffinity chromatography. *Mol. Biotechnol. 1* (1), 59−86.

(4) (4) Matson, R. S., and Little, M. C. (1988) Strategy for the immobilization of monoclonal antibodies on solid-phase supports. *J. Chromatogr. 458*, 67−77.

(5) Butler, J. E., Ni, L., Nessler, R., Joshi, K. S., Suter, M., Rosenberg, B., Chang, J., Brown, W. R., and Cantarero, L. A. (1992) The physical and functional behavior of capture antibodies adsorbed on polystyrene. *J. Immunol. Methods 150* (1−2), 77−90.

(6) Cantarero, L. A., Butler, J. E., and Osborne, J. W. (1980) The adsorptive characteristics of proteins for polystyrene and their significance in solid-phase imunoassays. *Anal. Biochem. 105* (2), 375−382.

(7) Schwab, C., and Bosshard, H. R. (1992) Caveats for the use of surface-adsorbed protein antigen to test the specificity of antibodies. *J. Immunol. Methods 147* (1), 125−134.

(8) Suter, M., and Butler, J. E. (1986) The immunochemistry of sandwich ELISAs. II. A novel system prevents the denaturation of capture antibodies. *Immunol. Lett. 13* (6), 313−316.

(9) Hollander, Z., and Katchalski-Katzir, E. (1986) Use of monoclonal antibodies to detect conformational alterations in lactate dehydrogenase isoenzyme 5 on heat denaturation and on adsorption to polystyrene plates. *Mol. Immunol. 23* (9), 927−933.

(10) Dierks, S. E., Butler, J. E., and Richerson, H. B. (1986) Altered recognition of surface-adsorbed compared to antigen-bound antibodies in the ELISA. *Mol Immunol. 23* (4), 403−411.

(11) Turkova, J. (1999) Oriented immobilization of biologically active proteins as a tool for revealing protein interactions and function. *J. Chromatogr. B 722* (1−2), 11−31.

(12) Kikuchi, J., Mitsui, Y., Asakura, T., Hasuda, K., Araki, H., and Owaku, K. (1999) Spectroscopic investigation of tertiary fold of staphylococcal protein A to explore its engineering application. *Biomaterials 20* (7), 647−654.

(13) Penzol, G., Armisen, P., Fernandez-Lafuente, R., Rodes, L., and Guisan, J. M. (1998) Use of dextrans as long and hydrophilic spacer arms to improve the performance of immobilized proteins acting on macromolecules. *Biotechnol. Bioeng. 60* (4), 518−523.

(14) Denizli, A., Rad, A. Y., and Piskin, E., (1995) Protein A immobilized polyhydroxyethyl methacrylate beads for affinity sorption of human immunoglobulin G. *J. Chromatogr. B 668* (1), 13−19.

(15) Piskin, E., Ayhan, H., Bulmus, E. V., Rad, A. Y., Falkenhagen, D., and Weber, C. (1996) Protein A carrying monosize PMMA microbeads for the removal of HIgG from human plasma. *Int. J. Artif. Organs 19* (5), 311−317.

(16) Kobatake, E., Ikariyama, Y., and Aizawa, M. (1995) Production of the chimeric-binding protein, maltose-binding protein−protein A, by gene fusion. *J. Biotechnol. 38* (3), 263−268.

(17) Anderson, G. P., Jacoby, M. A., Ligler, F. S., and King, K. D. (1997) Effectiveness of protein A for antibody immobilization for a fiber optic biosensor. *Biosens. Bioelectron. 12* (4), 329−336.

(18) Ljungquist, C., Jansson, B., Moks, T., and Uhlen, M. (1989) Thiol-directed immobilization of recombinant IgG-binding receptors. *Eur. J. Biochem. 186* (3), 557−561.

(19) Uhlen, M., Guss, B., Nilsson, B., Gatenbeck, S., Philipson, L., and Lindberg, M. (1984) Complete sequence of the staphylococcal gene encoding protein A. A gene evolved through multiple duplications. *J. Biol. Chem. 259* (3), 1695−1702.

(20) Gouda, H., Torigoe, H., Saito, A., Sato, M., Arata, Y., and Shimada, I. (1992) Three-dimensional solution structure of the B domain of staphylococcal protein A: comparisons of the solution and crystal structures. *Biochemistry 31* (40), 9665−9672.

(21) Deisenhofer, J. (1981) Crystallographic refinement and atomic models of a human Fc fragment and its complex with fragment B of protein A from Staphylococcus aureus at 2.9- and 2.8-A resolution. *Biochemistry 20* (9), 2361−2370.

(22) Urry, D. W., Cunningham, W. D., and Ohnishi, T. (1974) Studies on the conformation and interactions of elastin. Proton magnetic resonance of the repeating pentapeptide. *Biochemistry 13* (3), 609−616.

(23) Renugopalakrishnan, V., Khaled, M. A., Rapaka, R. S., and Urry, D. W. (1978) Proton magnetic resonance and conformational energy calculations of repeat peptides of tropoelastin. A permutation of the hexapeptide. *Biochim. Biophys. Acta 536* (2), 421−428.

(24) Urry, D. W., Onishi, T., Long, M. M., and Mitchell, L. W. (1975) Studies on the conformation and interactions of elastin: nuclear magnetic resonance of the polyhexapeptide. *Int. J. Pept. Protein Res. 7* (5), 367−378.

(25) Kanno, S., Kobatake, E., Yanagida, Y., Haruyama, T., and Aizawa, M. (2000) Assembling of engineering IgG-binding protein on gold surface for highly oriented antibody immobilization. *J. Biotechnol. 76* (2−3), 207−214.

(26) Kobatake, E., Onoda, K., Yanagida, Y., Haruyama, T., and Aizawa, M. (1999) Design of the thermostable cell adhesion protein. *Bio/Techniques 13*, 23−27.

(27) LaVallie, E. R., DiBlasio, E. A., Kovacics, S., Grant, K. L., Schendel, P. F., and MaCoy, J. M. (1993) A thioredoxin gene fusion expression system that circumvents inclusion body formation in the *E. coli.* cytoplasm. *Bio/Technology 11*, 187−193.

(28) Salmeron M., Beebe T., Odriozola J., Wilson T., Ogletree D. F., and Siekhaus W. (1990) Imaging of biomolecules with the scanning tunneling microscopy: problems and prospects. *J. Vac. Sci. Technol. A 8*, 635−641.

(29) Droz E., Taborelli M., Descouts P., and Wells T. N. C. (1994) Influence of aurface and protein modification on immunoglobulin G adsorption observed by scanning force microscopy. *Biophys. J. 67*, 1316−1323.

BC000031J

Oligonucleotide–Polymer Conjugates: Effect of the Method of Synthesis on Their Structure and Performance in Diagnostic Assays

Claire Minard-Basquin, Carole Chaix,* Christian Pichot, and Bernard Mandrand

UMR 2142 CNRS/bioMérieux, ENS Lyon, 46 allée d'Italie, 69364 Lyon Cedex 7, France.
Received January 31, 2000; Revised Manuscript Received June 25, 2000

Oligonucleotide–polymer conjugates have been described to improve the sensitivity of an enzyme-linked oligosorbent assay diagnostic test. To understand the influence of their structure and conformation in solution on the efficiency of the test during the capture step, two different ways of synthesizing these conjugates were compared. The first consisted of coupling 5′ amino modified oligonucleotides to poly(maleic anhydride-*alt*-methylvinyl ether) and poly(maleic anhydride-*alt*-ethylene). The second resulted from direct synthesis of oligonucleotides from poly(maleic anhydride-*alt*-ethylene) previously grafted onto a controlled pore glass support. The different conjugates were analyzed by size-exclusion chromatography and viscometry. The former method for conjugate synthesis produced aggregates, which was not the case for the latter. These conjugates were then used in the capture phase of a hybridization assay using a HBV DNA target, on a bioMérieux VIDAS instrument. Different parameters were studied, such as the purity of the conjugate solution and the number of oligonucleotides per polymer chain. The amount of conjugate coated on the solid-phase receptacle surface at the time of the capture phase was evaluated by radioactive labeling. Finally, it was demonstrated that conjugates produced an amplification factor of 50 versus the capture oligonucleotide probe used as the reference. The detection limit reached 10^8 copies/mL.

INTRODUCTION

Hepatitis B virus (HBV) disease is a major worldwide health problem, affecting millions of people. The diagnosis of the infection traditionally depends on various serologic HBV markers. However, the quantitation of HBV DNA in serum by molecular hybridization represents the most informative method for determining viral replication and serum infectivity (*1*). In the past, different hybridization assays for HBV DNA measurement have been developed. Dot blot (*2*) and liquid hybridization (*3*) were first employed, but were found to lack sensitivity. Later on, the polymerase chain reaction (PCR) efficiently improved the limits of HBV DNA detection. However, this very sensitive method often lacked reproducibility and stringent conditions were also required to avoid contamination (*4*). In this context, new signal amplification strategies were investigated as an alternative to target enzymatic amplification. These methods enabled direct measurement of HBV DNA in serum, allowing its quantitation. First of all, it was envisioned to develop modified oligonucleotides used as probes carrying multiple nonradioactive labels, e.g., fluorophore (*5*) or biotin (*6*), with the purpose of increasing sensitivity. Furthermore, to reduce nonspecific binding, another hybridization assay was developed that used branched DNA (bDNA) (*7*–*9*). More recently, oligonucleotide dendrimers were described to amplify radioactive or fluorescent signals in hybridization tests (*10*).

In this context, our laboratory focused early on the detection of viral nucleic acid material using the ELOSA technique (enzyme-linked oligosorbent assay) (Figure 1) (*11*). The principle of this test is (i) to isolate the DNA target using a capture oligonucleotide (ON) probe immobilized on a solid support and (ii) to detect and quantify the DNA target using a detection probe labeled by an enzyme. With this strategy, oligonucleotide-polymer conjugates used as probes for both capture and detection of the nucleic acid target (*12*, *13*) have been described to improve the sensitivity of the test on a bioMérieux VIDAS immunoanalysis instrument (Figure 2). In the capture step, oligonucleotide–polymer conjugates were used to increase the coating of the probe on the solid support. Likewise, in the detection step, oligonucleotide–polymer conjugates have been described to improve detection signal due to an increase in the enzyme concentration. These conjugates were previously obtained by the coupling of 5′ amino modified oligonucleotides onto polymer reactive functions. Several polymers have been investigated such as poly(*N*-vinylpyrrolidone-*N*-acryloxysuccinimide) (P[NVPNAS]) (*14*), maleic anhydride copolymers (*15*), *N*-(2,2-dimethoxyethyl)-*N*-methacrylamide (*16*) and 6-deoxy-6-methacryloylamido-D-glucopyranose (*17*). It has been demonstrated that conjugates obtained

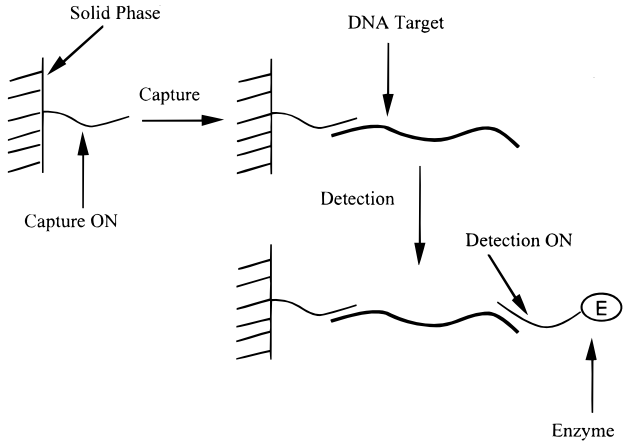

Figure 1. ELOSA sandwich test.

* To whom correspondence should be addressed.

10.1021/bc000010p CCC: $19.00 © 2000 American Chemical Society
Published on Web 09/28/2000

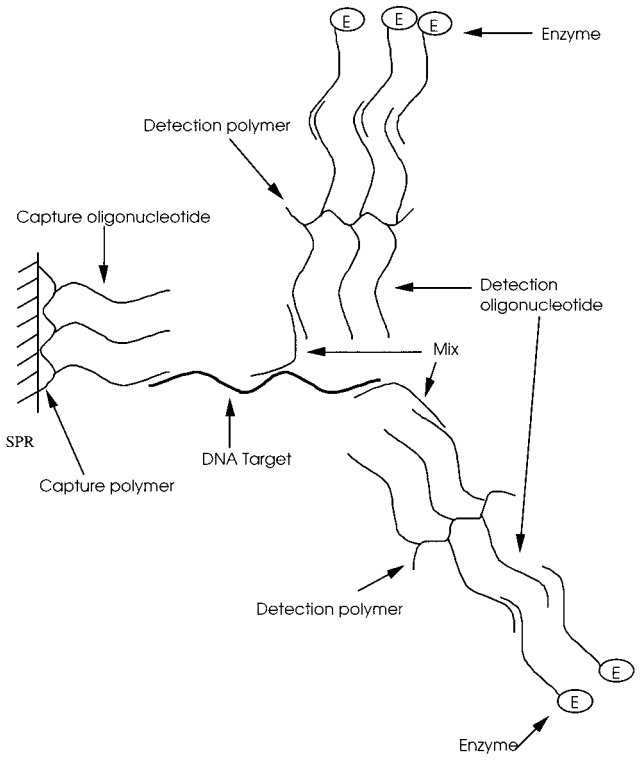

Figure 2. Sandwich hybridization assay with capture and detection amplification.

with the poly(maleic anhydride-*alt*-methylvinyl ether) (P[MAMVE]) copolymer increased the sensitivity of an ELOSA diagnostic test in the capture phase (*18*) and that the P[NVPNAS] conjugate copolymer used in the detection step also enhanced detection signal (*18*). However, the coupling method has shown some drawbacks. Indeed, the coupling reaction led to the formation of aggregates that entrapped ONs and hindered their accessibility. Several hypotheses were put forward to explain such aggregate formation: (i) cross-linking of several polymer chains (*19*) and/or (ii) coupling side reactions induced by exocyclic amine functions of the nucleic bases (*18*, *20*). To avoid the aggregation process observed during the coupling reaction and to control biomolecule orientation onto the polymer chain, a new method of conjugate synthesis has been recently described (*21*). Direct synthesis of oligonucleotides has been performed on the poly(maleic anhydride-*alt*-ethylene)(P[MAE]) and the P[MAMVE] (Figure 3) previously grafted on a solid support (controlled pore glass). P[MAE] was preferred to P[MAMVE] because of its good stability under ammonia treatment used for nucleic base deprotection. To compare the two families of conjugates, both synthesis methods were carried out (Figure 4). Conjugates were analyzed by SEC and SEC-MALLS−viscometry with the aim of evaluating their structure in solution. They were then tested in the capture phase of the HBV DNA sandwich hybridization diagnostic assay. The correlation between their structure and their ability to amplify the DNA detection signal is discussed in this work. Different parameters were examined, such as the influence of the free ON part and the number of ONs per copolymer chain. Finally, conjugates were compared by running an ELOSA sandwich test with a range of concentrations of the HBV DNA target. This experiment allowed us to estimate the real influence of conjugates on the sensitivity limits of the test. Moreover, the amount of conjugate coated on the SPR surface during the capture phase was evaluated by radioactive labeling.

P[MAMVE]
$\overline{Mn}$ = 67000 g/mol

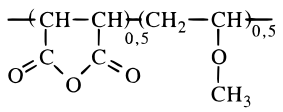

P[MAE]
$\overline{Mn}$ = 27000 g/mol

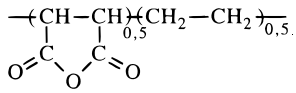

P[NVPNAS]
$\overline{Mn}_{app}$ = 35000 g/mol

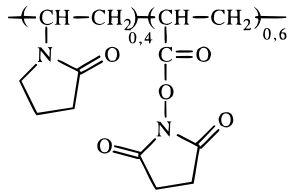

Figure 3. Linear structure of copolymer ($\overline{Mn}_{app}$ = apparent number average molecular weight).

EXPERIMENTAL SECTIONPROCEDURES

Materials. P[MAE] was obtained from Aldrich. P[MAMVE] was obtained from PolyScience Inc. Their number average molecular weight ($\overline{M}$n) of 27 000 and 67 000 g/mol, respectively, was determined by size-exclusion chromatography (SEC) in organic solvent (DMSO) using poly(ethylene oxide) standards. P[NVPNAS] (*22*) was obtained by free radical polymerization in *N*,*N*-dimethylformamide (DMF). The copolymer was characterized by UV spectroscopy and by ^{13}C nuclear resonance spectroscopy to determine respectively its composition and the monomer sequence distribution. The apparent number average molecular weight ($\overline{M}$n$_{,app}$) of 35 000 g/mol was determined by SEC coupled to a multiangle laser light scattering detector (conditions described below) with a d*n*/d*c* of 0.2 mL/g.

Anhydrous dimethyl sulfoxide (DMSO) and DMF were purchased from Aldrich. Oligonucleotide syntheses were carried out on an Expedite System Instrument (Millipore). SEC analyses were performed using a Waters UltraHydrogel 500 column or a Waters UltraHydrogel 500 column and a Waters UltraHydrogel 2000 column on line, a Kontron HPLC 420 pump running in a 0.1 M phosphate buffer, pH 6.8, and a Kontron 430 UV detector. Detection was achieved by absorbance at 260 nm which corresponded to the λ_{max} adsorption of the oligonucleotide. Viscometry analyses were performed using SEC coupled to a multiangle laser light scattering detector and coupled to an on line viscometer in a triple detector configuration (SEC-MALLS−viscometry). Two associated columns (Waters UltraHydrogel 500 and 2000) were connected to a Spectra-physics isochrome pump running in a 0.1M phosphate buffer/20 mM NaCl, pH 6.6. For the detection part, a seventeen angle DAWN DSP (WYATT Technology) operating at 690 nm, a viscometer H502 (Viscotek) and a Waters 510 differential refractometer were used on line.

(α-^{32}P)ddATP was obtained from Amersham and (γ-^{32}P)ATP from NEN. Terminal transferase was purchased from Boehringer Mannheim and T4 polynucleotide kinase from Ozyme. Radioactivity was counted with a Liquid Scintillation Analyzer 1900 TR (Packard).

Conjugates Obtained by ON Coupling. Conjugates were obtained according to the protocol described by Ladavière et al. (*15*). Oligonucleotides (ONs) used in this part (ON1, Table 1), were synthesized by standard DNA cyanoethyl *N*,*N*-diisopropylamino phosphoramidite chemistry. ONs were modified at their 5′ position by an

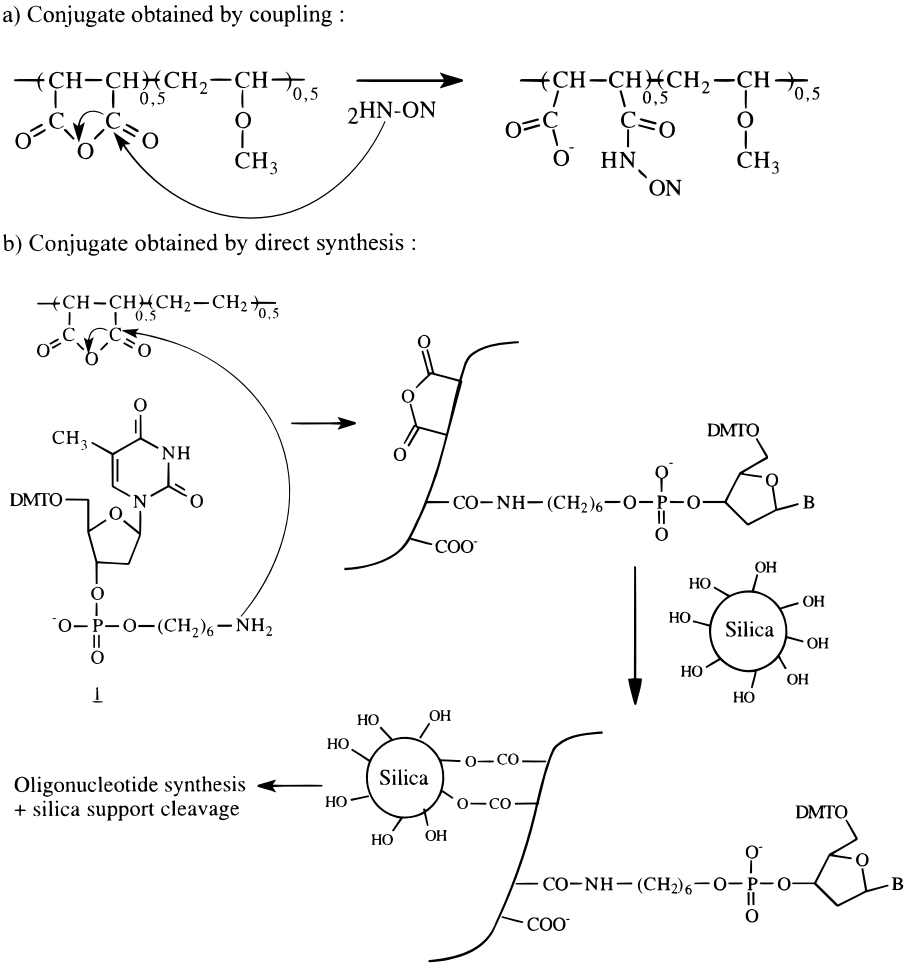

Figure 4. Conjugate synthesis methods.

Table 1. ON Sequences

ON number	sequence (5′−3′)	name
ON1	TCAATCTCGGGAATCTCAATGTTAG	capture ON
ON1b	TCAATCTCGGGAATCTCAATGTTAGTTTTT	capture ON
ON2	AACGCTACTACTATTAGTAG	detection ON
ON3	CTACTAATAGTAGTAGCGTT	complementary of ON2

Table 2. Reaction Conditions for Conjugates Obtained by Coupling

conjugate	polymer used	amount of polymer introduced[a] (mg)	amount of ON introduced[b] (nmol)	coupling yield (%)	ONs/copolymer chain[c]
[1]	P[MAMVE]	0.15	10.5	64	3
[2]	P[MAMVE]	0.15	15	84	6
[3]	P[MAMVE]	0.101	15	94	9
[4]	P[MAMVE]	0.071	15	87	12
[5]	P[MAMVE]	0.07	15	88	13
[6]	P[MAMVE]	0.07	15	93	13
[7]	P[MAMVE]	0.011	30	10	18
[8]	P[MAE]	0.058	15	85	6
[9]	P[NVPNAS]	0.021	15	75	19

[a] Amount of polymer introduced in the mixture. [b] Amount of ON introduced in the mixture (ON1 for P[MAMVE] and ON3 for P[NVPNAS]). [c] see Characterization of Conjugates part.

aminohexyl arm for coupling to the copolymer. The appropriate amount of polymer (P[MAMVE]) or (P[MAE]) was first dissolved in 1 mL of DMSO at 37 °C. Dried ON1 was dissolved in 7 μL of 0.1M sodium borate/0.5 M sodium chloride buffer pH 9.3. Then, 10 μL of the polymer solution and 143 μL of DMSO were added. The reaction was carried out for 3 h at 37 °C. Before use, the solvents were removed under vacuum, and the conjugates resuspended in water. Coupling conditions were described in Table 2.

For P[NVPNAS], the coupling protocol differed (*23*). Dried 5′ amino modified ON2 (15 nmol) was dissolved in 10 μL of 0.1M sodium borate buffer, pH 9.3. Then 21 μL of polymer solution at 1 mg/mL in DMF and 70 μL of DMF were added. The reaction was carried out for 2 h at 50 °C. After drying, conjugates were resuspended in water and purified by SEC.

Conjugates Obtained by Direct ON Synthesis on CPG Support. Conjugates were synthesized according to the protocol described by Chaix et al. (*21*). The P[MAE] used in this strategy was first functionalized with different amounts of the nucleotide initiator of ON synthesis (Figure 4). In a second step, the resulting polymer was grafted onto a hydroxylated CPG support. The amount

Table 3. Conjugates Obtained by Direct Synthesis

conjugate	conjugate purity (%)[a]	minimal ONs/ copolymer chain[b]
[10]	100	11
[11]	88	19
[12]	70−88	36
[13]	95	62
[14]	93	65
[15]	23	81
[16]	16	87
[17]	79	87
[18]	80	92
[19]	68	109

[a] Conjugate purity was determined by SEC compared to free ON population. [b] Estimated minimal number (see Characterization of Conjugates part).

of starter nucleotide bound to CPG via the polymer was established by trityl cation measurement (*21*). It was estimated to be from 1.49 to 4.25 μmol/gram of support, according to the quantities of nucleotide introduced in the mixture. ON1b (Table 1) was synthesized from this functionalized CPG by standard DNA cyanoethyl *N*,*N*-diisopropylamino phosphoramidite chemistry on an Expedite Nucleic Acid Synthesis Instrument (Millipore). Conjugates were recovered in solution after ammonia treatment (NH_4OH 30%, 16 h at 60 °C). Before use, conjugates were dried under vacuum, resuspended in water and purified by filtration on Centricon (cutoff 100 000 g/mol). The structure and purity of the conjugates used are summarized in Table 3.

Detection of HBV DNA by ELOSA Test. *Molecular Tools To Run Sandwich Test.* The capture probe consisted of an ON−polymer conjugate carrying an oligonucleotide sequence complementary to HBV DNA from position 2430 to 2454 (ON1, Table 1). The conjugate was diluted at 150 nM in 4× phosphate buffer saline (PBS) (10× PBS is 1.37 M NaCl, 27 mM KCl, 43 mM Na_2HPO_4, and 14 mM KH_2PO_4).

The target used was a PCR product of HBV DNA (double-stranded 2339 bp) cloned in pBR 322 and purified by agarose gel electrophoresis as previously described by Erout et al. (*23*). The PCR target was diluted in PEG buffer (0.1 M sodium phosphate pH 7, 0.5 M NaCl, 0.65% Tween, 0.14 mg/mL DNA salmon sperm, 2% PEG 4000). Before use, the target was denatured in 1.4 N NaOH (5 min at room temperature) and neutralized by 1.4 N acetic acid.

The intermediate ONs (mix) contained 17 ONs complementary to 17 highly conserved regions of HBV sequence. These 17 ONs have an identical non-HBV sequence of 20 nucleotides in length in their 3′ position (ON3, Table 1). The mix was diluted at 26.85 nM, for each ON, in PEG buffer.

The detection phase used a conjugate ON2−P[NVPNAS], complementary to the non-HBV common sequence of the mix (ON3), and complementary to a probe covalently linked to an enzyme (alkaline phosphatase) (ON3-AP). The conjugate ON2−P[NVPNAS] and the ON3-AP were diluted at 15 nM in PEG buffer.

The enzyme detection substrate used was 4-methylumbelliferyl phosphate (4-MUP). The washing buffer used was PBS-Tween (1X PBS with 0.5% Tween).

HBV DNA Test on VIDAS. Detection was performed using a bioMérieux VIDAS immunoanalysis instrument. The test was based on sandwich hybridization (*24*, *25*) using specific probes complementary to highly conserved regions of the HBV DNA sequence. For the capture phase, the conjugate ON1(1b)−copolymer was coated on the inside of a disposable conical VIDAS solid-phase receptacle (SPR) by passive adsorption (*23*). After 1 h of coating at 37 °C, the SPRs were washed with PBS-Tween to remove the uncoated conjugates. The hybridization test was performed for 3h at 37 °C during which the following steps occurred: capture of the target by ON1(1b)−copolymer conjugate, washing, incubation with the mix, washing, incubation with ON2−P[NVPNAS] conjugate, washing, incubation with ON3-AP and AP substrate. The enzymatic reaction converted the substrate into a detectable fluorescent signal expressed in Relative Fluorescent Units (RFU) by the VIDAS detector.

Quantitation of the ON Number Adsorbed onto the VIDAS Solid-Phase Receptacle (SPR). *^{32}P Labeling.* The conjugates obtained by the coupling reaction and the 5′ amino modified oligonucleotide (ON1, Table 1) were labeled in their 3′ position as follows: 30 pmol of conjugate (concentration of nucleic acid part measured at 260 nm) or ON were mixed with 4 μL of 5× reaction buffer (5× reaction buffer is comprised of 1 M potassium cacodylate, 1.25 mM Tris-HCl, bovine serum albumin, 1.25 mg/mL, pH 6.6 at 25 °C), 2 μL of 25 mM cobalt chloride solution, 1 μL of terminal transferase (25 units), and 3 μL of (α-^{32}P)ddATP (30 μCi). The final volume was adjusted to 20 μL with water. The reaction was left for 1 h at 37 °C. The enzyme was then inactivated at 70 °C for 10 min. The conjugate was purified by two filtrations with 500 μL of water on Centricon (cutoff, 100 000 g/mol). The 5′ amino modified ON1 was purified using a G25 column.

The conjugates obtained by ON direct synthesis were labeled in their 5′ position. 30 pmol of the conjugate nucleic acid material were mixed with 2 μL of 10× T4 polynucleotide kinase buffer (1× final concentration is 70 mM Tris-HCl, 10 mM $MgCl_2$, 5 mM DTT, pH 7.6 at 25 °C), 1 μL of T4 polynucleotide kinase (10 units), 3 μL (γ-^{32}P)ATP (15μCi). The final volume was adjusted to 20 μL with water. The reaction was left for 1 h at 37 °C. The enzyme was inactivated at 70 °C for 10 min. The conjugates were purified by two filtrations with 500 μL of water on Centricon (cutoff, 100 000 g/mol).

After purification, the specific activity of each product was measured.

Coating. To a conjugate or ON solution at 150 nM (concentration of nucleic acid part measured at 260 nm) in PBS 4×, 300 000 counts/minute (cpm) of labeled conjugates or ON were introduced, respectively (total volume of the reaction = 600 μL). A total of 300 μL of solution was introduced into the VIDAS conical SPRs sealed at the narrow extremity. SPRs were made of Polystyrene−polybutadiene plastic. The coating was realized by aspirating and dispensing the liquid in the SPR (35 times) for 50 min with a pipetman. SPRs were then washed twice with 300 μL of PBS-Tween, and counted in a liquid scintillation analyzer. Data are summarized in Figure 12.

RESULTS AND DISCUSSION

Conjugates Obtained by the ON Coupling Reaction. Conjugates were produced by coupling ON1 on P[MAMVE] or P[MAE]. Different amounts of ON or polymer were introduced to obtain conjugates with various ON/polymer ratios and purity levels. The reaction was controlled by SEC analysis. Experimental conditions and the corresponding coupling yields are summarized in Table 2.

Figure 5 shows an example of SEC analysis for the coupling of ON1 to P[MAMVE] copolymer, in which three different populations were separated by chromatography. The first population (peak 1) was eluted as an excluded

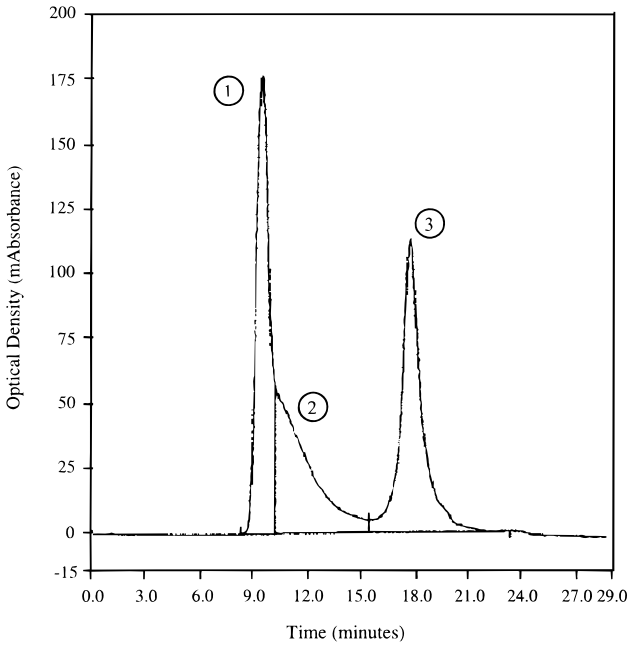

Figure 5. SEC analysis of ON1−PMAMVE conjugate (conjugate [1]) using Waters UltraHydrogel 500 column in 0.1M phosphate buffer pH 6.8. (Flow = 0.5 mL/min) Three populations appeared: (1) excluded peak, (2) lower molecular weight conjugate, (3) free oligonucleotide.

peak corresponding to high molecular weight conjugates. As demonstrated by Ladavière et al. (*15*), this population showed a very high molecular weight (more than 2 000 000 g/mol) when analyzed by SEC coupled to a multiangle laser light scattering detector (SEC-MALLS). The second population eluted (peak 2) corresponded to conjugate with lower molecular weight and the last population (16 min. to 22 min) to residual ONs (peak 3). From that analysis, the coupling yield (*R*) has been defined as the ratio of ON−copolymer versus the total amount of ON introduced in the reaction mixture:

$$R = \frac{\text{area(ON/polymer)}}{\text{area(ON/polymer)} + \text{area(freeON)}} = \frac{\text{area(peak1} + \text{peak2)}}{\text{area (peak1} + \text{peak2)} + \text{area(peak3)}} \quad (1)$$

This calculation takes into account that at 260 nm, the molar extinction coefficient of the ON bound to conjugate is the same as for free ON (*15*). The ratio *R* enables determination of the average number *N* of ONs per copolymer chain according to:

$$N = \frac{n\text{ON}}{n\text{copolymer}} \times R \quad (2)$$

where n_{ON} and $n_{copolymer}$ are the amount in moles of the ON and copolymer introduced in solution, respectively.

Conjugates Obtained by ON Direct Synthesis. Before running ON synthesis on an Expedite DNA synthesis instrument, polymer functionalized CPG was performed as follows: First, the nucleotide **1** coupling yield on polymer was optimized at 90% in a 4 h reaction in DMSO (*21*). Second, hydroxyl-CPG was added to the solution and grafting of the nucleotide activated polymer was performed for 24 h (Figure 4).

According to the amount of nucleotide initially introduced into the reaction mixture, different functionalized CPGs were obtained, from 1.49 to 4.25 μmol of 1 per gram of support. ON1b were then synthesized from these functionalized supports with a sequence differing from ON1 by a supplement of five thymidine in the 3′ position. Indeed, in direct synthesis, ONs were developed from 3′ to 5′. So, this short oligothymidine spacer was necessary to distance the ON1 sequence from the polymer chain, thereby avoiding steric hindrance phenomena. Conjugates were recovered in solution by ammonia treatment, and analyzed by SEC. Results are summarized in Table 3.

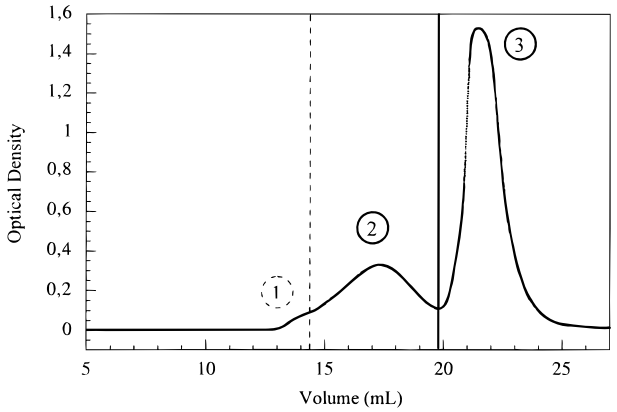

Figure 6. SEC analysis of ON1b-PMAE conjugate (conjugate [15]) using Waters UltraHydrogel 500 and 2000 columns on line in 0.1M phosphate buffer pH 6.8. (Flow = 0.5 mL/min) Two main populations were observed: (2) conjugate, (3) parasite population.

Figure 6 shows an example of SEC analysis of a ON1b−P[MAE] conjugate. As we can see, three kinds of peaks are also observed. The first population of conjugates formed a weak shoulder at the excluded volume (14 min in the chromatographic conditions). But the main population of conjugates was under peak 2 and corresponded to lower masses. Finally, a third population (peak 3) was identified as free ON by ^{32}P labeling (*26*). This latter result was unexpected and was attributed to the following phenomena. (i) An adsorption of both nucleotide **1** and phosphoramidite monomers on the support initiated uncontrolled DNA synthesis. Nucleotide **1** was adsorbed on the CPG surface during the preparation of functionalized support and phosphoramidite monomers during the first cycle of ON synthesis (*26*). (ii) Some starter nucleotide (**1**) was coupled to the polymer by its nucleic base exocyclic amine function. Indeed, by capillary electrophoresis, it appeared that almost 10% of the nucleotide **1** was bound via this more labile link and was cleaved under ammonia treatment (unpublished results). (iii) It was also demonstrated that about 20% of the amide bond between polymer and starter was broken during ammonia treatment (*27*). Consequently, to approximate the real number *N* of ONs per copolymer chain, the initial equivalent number of nucleotides incorporated on P[MAE] (considering the coupling reaction yield) was reduced to 30% (step one, Figure 4). The estimations of the number of ONs per polymer chain are summarized in Table 3.

Conjugate Structure. From SEC analyses in 0.1 M phosphate buffer, pH 6.8, it can be observed that conjugates obtained using the two different methods of synthesis exhibit different structures. Indeed, it was shown that conjugates obtained by the coupling reaction mainly produced aggregates of high molecular weight. For instance, the percentage of aggregates was close to 100% in the case of the P[NVPNAS] coupling reaction with ONs (results not shown). In contrast, no excluded peak was observed for conjugates obtained by direct synthesis, which tends to prove that no aggregated structure was formed.

Table 4. Conjugate Structure

conjugate	*a* parameter	$R_{g,app}$ (nm)	% of conjugate population[a]
[2] (peak 1)	0.36	78	55
[2] (peak 2)	0.81	38	45
[5] (peak 1)	0.34	81	73
[5] (peak 2)	0.73	38	27
[15] (peak 1)	0.38	106	27
[15] (peak 2)	0.73	47	73

[a] UV detection.

Conjugates were also analyzed by SEC coupled to a multiangle laser light scattering detector and a viscometer on line. This analytical system enabled the estimation of the *a* parameter from the Mark−Houwink−Sakurada relationship: $[\eta] = KM^a$ (*28*) and measurement of the radius of gyration, for populations of conjugates separated by chromatography (two columns, UltraHydrogel 500 and 2000). These data provide information concerning the structure of conjugates in 0.1 M phosphate buffer/20 mM NaCl, pH 6.6. For those obtained by the ON coupling reaction strategy, two populations were previously identified (Figure 5). SEC-MALLS−viscometry analyses revealed some differences in their conformation, as reported in Table 4. Whereas the aggregates (peak 1) had an apparent radius of approximately 78 nm for conjugate [2] and 81 nm for conjugate [5] with a compact random coil form ($a \approx 0.3$), the lower molecular weight conjugate population eluted from 10 to 16 min (peak 2) had a smaller apparent radius of gyration of approximately 38 nm with a more expanded random coil form ($a \approx 0.8$). As the proportion of aggregates was predominant (>50%), the conjugates were considered to be essentially in a random coil form in solution with a relatively compact structure. On the other hand, SEC analyses of conjugates obtained by ON direct synthesis (Figure 6) and data obtained by SEC-MALLS−viscometry system (Table 4) showed the presence of a small amount of aggregates which eluted close to the excluded volume of 14 min in the experiment (peak 1, Figure 6). This population had an apparent radius of gyration of 106 nm with a compact random coil form ($a \approx 0.38$). However, the main population of conjugates had an apparent radius of gyration of approximately 47 nm with a more expanded random coil form ($a \approx 0.8$). This latter population corresponded to the nonaggregated ON−polymer conjugates, as confirmed by the apparent number average molecular weight ($\overline{M}n_{,app}$) of 345 000 g/mol measured by SEC-MALLS in 0.1 M phosphate buffer, pH 6.8.

In Figure 7, we have attempted to depict conjugate conformation in aqueous media. Regarding the form parameter and the apparent radius of gyration calculated from viscometry and light-scattering experiments, different structures can be proposed. For conjugates obtained by the coupling reaction, the conformation was essentially in a compact random coil form. With an apparent radius of gyration of 80 nm, it could be suggested that in this case, ON−polymer conjugate chains were essentially entangled, forming huge and compact aggregates (Figure 7). On the other hand, the strategy of direct ON synthesis produced conjugates in a more expanded form with an apparent radius of gyration around 40 nm. This time we supposed that the molecule could simply be folded up on itself maintaining a nonassociated expanded structure in solution.

It was also demonstrated that the number of ONs per copolymer chain varied from one method to another. For conjugates obtained by the coupling reaction, this number rose from 3 to 18. It was not possible to graft a larger amount of ONs per polymer chain because of the decrease in the coupling yield. Indeed, referring to the last experiment that led to 18 ONs/P[MAMVE] chain, the observed coupling yield was already down to 10%. In contrast, conjugates obtained by direct synthesis contained a larger number of ON, from 11 to 109. However, conjugates were not pure, with either method, since a percentage of free ONs was evidenced. So, to examine the influence of free ONs on the VIDAS signal, conjugates were purified at different stages. After characterization, all these conjugates have been used in hybridization assays in order to evaluate their performances in the capture phase.

Use of the ON−Copolymer Conjugates in the Detection of HBV DNA. An efficient sandwich hybridization assay on the automated VIDAS immunoanalysis instrument has been previously developed by bioMérieux and our laboratory (*29*), using specific probes to detect highly conserved regions of HBV DNA. Optimized probe sequences used for the capture and detection phases of the test are described in Table 1. In the capture phase, ON1 and ON1b were used, according to the conjugate synthesis method. The ON−copolymer conjugates described previously were tested for their ability to improve the detection limits of HBV DNA target (Figure 2). ON1−P[MAMVE], ON1−P[MAE], and ON1b−P[MAE] resulting from the two different methods of synthesis were evaluated at the capture phase. ON1−P[MAMVE] conjugate obtained by the coupling method was used as the reference for the diagnostic test described here, as it was considered to be the best candidate to improve capture phase efficiency (*18*). In both cases, the same ON3−P[NVPNAS] conjugate was used in the detection step.

Effect of Free ON on VIDAS Signal. As discussed above, conjugates were contaminated by free ONs. Consequently, it was necessary to study the effect of the conjugate purity on the VIDAS signal. To do so, the two conjugates ([7] and [16]) were progressively purified by successive filtrations, using Centricon with a 100 000 g/mol cutoff, and the purity checked by SEC analysis. For both conjugates, ELOSA experiments were run at all stages of the purification. The test was performed using 10^{10} copies/mL of HBV target (*30*). As we can see on Figure 8, the effect of the free ON part on the signal differed from one conjugate to another. For conjugates obtained by the coupling reaction, the effect was minor (Figure 8a). An increase of 1.1 of the RFU was observed with an increase from 10 to 87% of the conjugate purity. In contrast, for conjugates obtained by direct synthesis, the effect was not negligible (Figure 8b). the RFU signal increased with conjugate purity up to 60%, and then remained stable. To clearly understand the real action of the free ON part in mixtures of conjugates at the capture step, various ELOSA experiments were run, by addition of a percentage of 5′ aminolinked free ON increasing progressively (from 10 to 100%) to an initial solution of conjugates purified at about 93%. Conjugate [6] (Table 2) for conjugate obtained by the coupling reaction and conjugate [14] (Table 3) for the conjugate obtained by direct synthesis were used. RFU signals were recorded and summarized in Figure 9. It appeared that from 7 to 60% of ON in the capture solution, no effect on the RFU signal was observed for conjugate obtained by the coupling reaction, whereas for conjugate obtained by direct synthesis, the free ON population immediately reduced the signal intensity. Thus, in this latter case, a competition was evidenced between ONs and conjugates

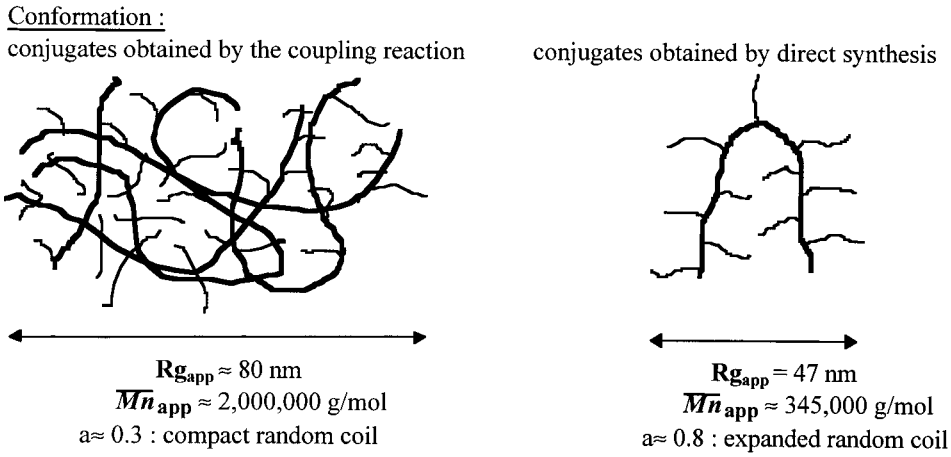

Figure 7. Modeling of conjugate conformation in 0.1 M phosphate buffer/20 mM NaCl pH 6.6. $R_{g,app}$ = apparent radius of gyration and a = form parameter calculated from the Mark−Houwink-Sakurada relationship: $[\eta] = KM^a$.

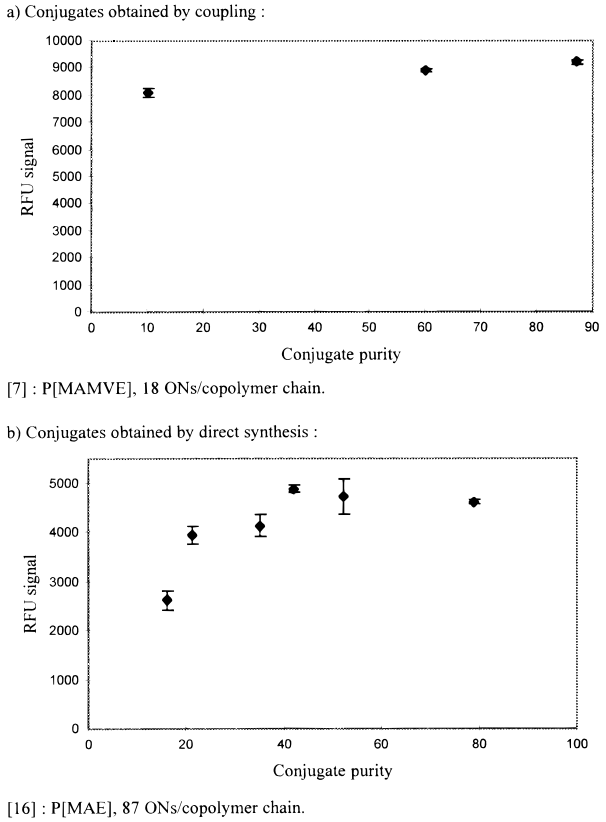

Figure 8. Effect of the conjugate purity on the VIDAS signal. Mean values of duplicate measurements.

for adsorption onto the SPR surface during the capture step. Above 60% of ON in solution, both signals rapidly decreased.

From these studies, it can be concluded that conjugates obtained by the coupling reaction could be used without any purification up to a level of 60% of ONs in the crude product. In contrast, conjugates obtained by direct synthesis required a purification step, because of competition between free ONs and conjugates for coating onto the SPR surface.

Effect of the ON Number per Polymer Chain on the VIDAS Signal. As emphasized in the conjugate structure part, the number of ONs per copolymer chain changed from one conjugate to another, according to the method of synthesis. The effect of this difference on the VIDAS signal was therefore assessed. For all conjugates used

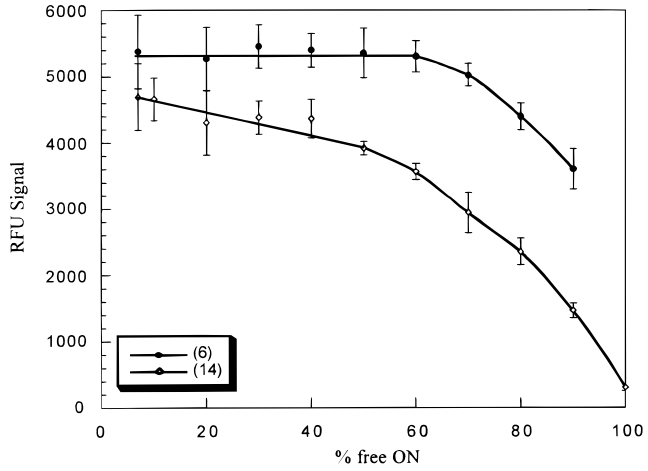

Figure 9. Effect of the percentage of free ON in the capture solution on the VIDAS signal. Mean values of duplicate measurements for a set of three experiments. [6]: P[MAMVE] (obtained by coupling, 93% conjugate purity, 13 ON/copolymer chain). [14]: P[MAE] (obtained by direct synthesis, 93% conjugate purity, 65 ON/copolymer chain).

in the experiment, purity was raised to 60% (from 68 to 88%) to directly correlate the result with the influence of the ONs tethered to the copolymer chain. The hybridization test was performed using 10^{10} copies/mL of HBV target. As shown in Figure 10, conjugates exhibited different behaviors. For conjugates obtained by the coupling reaction (Figure 10a), the RFU signal was increased until 12 ONs/copolymer chain and then remained stable. The rise in the signal could be explained by both the increase in the number of ONs and the aggregated form. Indeed, the higher the number of ONs per polymer chain, the more numerous the aggregates observed on chromatography. For conjugate [1], the percentage of aggregated form was close to 55% whereas for conjugate [4], it was close to 80%. Consequently, it seemed that aggregates might play an important role in the capture phase of the ELOSA test. For conjugates obtained by direct synthesis (Figure 10b), the signal intensity remained stable for experiments run with conjugates [11], [12], and [18] (from 19 to 92 ONs/chain). Concerning the most functionalized conjugate (109 ONs bound to a polymer chain that bears around 210 maleic anhydride-ethylene units), the decrease was certainly due to steric hindrance phenomena. Finally, two conjugates obtained by the coupling reaction ([4] and [8]) and two conjugates obtained by direct synthesis ([10] and [18])

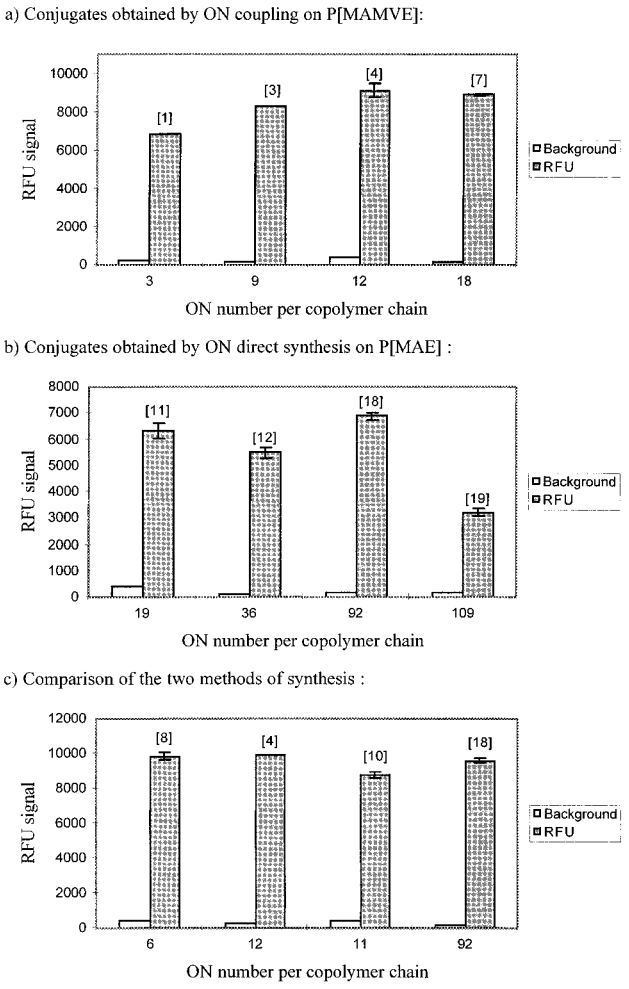

Conjugates [8], [10], [18] : P[MAE] ; conjugate [4] : P[MAMVE]

Figure 10. Effect of the number of ONs per polymer chain on the VIDAS signal. Mean values of duplicate measurements. The purity of all conjugates was raised to 60%.

were compared (Figure 10c). For conjugate [8] synthesized with P[MAE], no more than 6 ONs by chain can be obtained. Indeed, as in the case of P[MAMVE], it was not possible to couple a larger amount of ON because of the coupling yield decrease. To control the effect of the copolymer on the VIDAS signal, the two conjugates obtained by the coupling reaction ([4] and [8]) were compared. As can be seen, the RFU signal was identical with both P[MAE] conjugate [8] and P[MAMVE] conjugate [4]. In both cases, the maximum of ONs per polymer chain was reached, leading to the formation of aggregates. As previously discussed, these two parameters (high ON number and aggregate form) were essential for the improvement of test sensitivity. But no other effect was observed on the signal in relation to the length or the comonomer nature of the polymer used. Conjugate [10] was obtained by direct synthesis. In this case, the ON number on P[MAE] was low (11 ONs/chain) and the resulting VIDAS signal was compared to experiments run with conjugates [4] and [8]. It was observed that the signal for conjugate [10] was slightly inferior to those with conjugates [4] and [8]. But, when the number of ONs per chain was increased (conjugate [18]), the RFU signal was partly recovered.

In conclusion, a higher number of ONs for conjugates obtained by direct synthesis could balanced the "aggregate" parameter that improves VIDAS sensitivity.

Comparison of the Two Conjugates. Conjugates [4] and

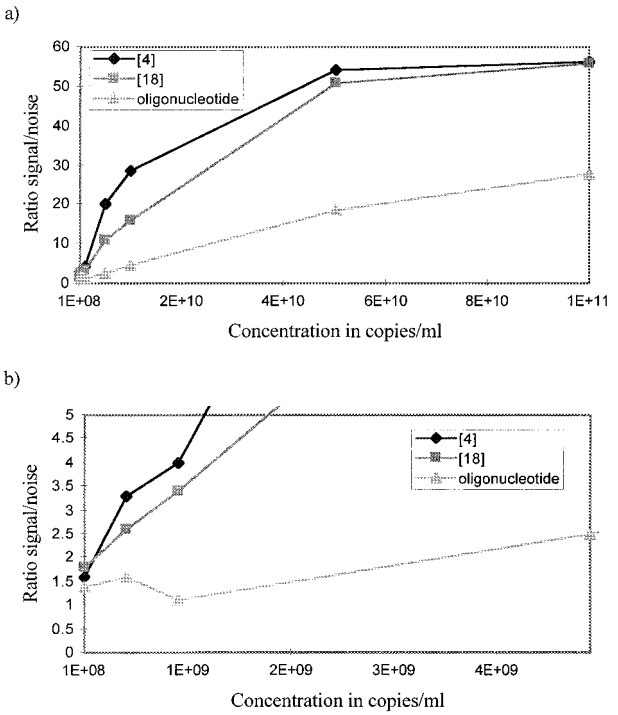

Figure 11. Comparison of conjugates in VIDAS. [4]: P[MAMVE] (obtained by coupling, 87% conjugate purity, 12 ON/copolymer chain). [18]: P[MAE] (obtained by direct synthesis, 80% conjugate purity, 92 ON/copolymer chain).

[18] were compared in a hybridization test using a set of diluted HBV targets from 10^8 to 10^{11} copies/mL. The capture oligonucleotide (ON1, Table 1) was used as a control.

In Figure 11, the signal/noise ratio versus the concentration of HBV target is represented. As can be seen, the ratio increased with the concentration of targets to reach a plateau at 5×10^{10} copies/mL. To determine the sensitivity limit of the conjugates, a cutoff of 2 for the signal/noise ratio, was applied. As shown in Figure 11b, sensitivity was the same for both conjugates, i.e., about 10^8 copies/mL, whereas the capture oligonucleotide used as reference had a sensitivity limit near to 5×10^9 copies/mL. Hence, an amplification factor of 50 was reached by using the conjugates in the capture step.

In conclusion, conjugates obtained by direct synthesis were as efficient as those obtained by the coupling reaction. In both cases, the detection limit was close to 10^8 copies/mL, using P[NVPNAS] conjugate in the detection step.

Quantitation of the ON Number Adsorbed onto the VIDAS SPRs. To clearly understand what occurred during the coating step, an attempt was made to quantify the number of ONs adsorbed on the SPR surface. To do so, radioactive labeling of nucleic acid material was envisioned. The conjugate obtained by the coupling reaction ([5]) and ON1 used as the control were labeled at their 3′ position, whereas conjugates obtained by ON direct synthesis ([10] and [13]) were labeled at their 5′ position. After purification, these "hot" molecules were mixed with a solution of "cold" compounds, at 150 nM. In this case, the concentration of radiolabeled molecules added was negligible. After coating and washing, SPRs radioactivity was measured and the number of picomoles (N) adsorbed were determined according to the following equation:

$$N = \frac{\omega}{A_s} \times \frac{1}{R} \quad (3)$$

where ω is the number of counts per minute (cpm) of the SPR, A_s, the specific activity (cpm/pmol) of compounds, and R, the ratio of the amount of labeled product versus the total amount introduced.

Moreover, it was controlled that neither the SPR screen radioactive signal nor the presence or absence of liquid in the SPR disturb the measure.

As can be seen in Figure 12, a major difference is observed between conjugates and ON1. Indeed, about 1 pmol was adsorbed on the SPR for ON1, whereas from 3 to 7 pmol of nucleic acid material were adsorbed using conjugates. This result was in agreement with VIDAS experiments, which have demonstrated that the use of conjugates versus ON enhanced the signal. Between the conjugates [5] and [13], no difference was clearly evidenced. The conjugate obtained by the coupling reaction gave an average value of 6.4 pmol and about 5.3 pmol of oligonucleotides were coated with the conjugate obtained by the second method. It was also remarked that the standard deviation of ±3.1 pmol observed for conjugate [5] after six experiments seemed to emphasize a lower reproducibility of the coating in this case. Results were correlated with VIDAS experiments where the detection limit was the same with both conjugates, but the signal at 10^{10} copies/mL was slightly higher with conjugate [5] (results not shown). The number of ONs per chain for conjugate [5] was much lower than that of conjugate [13], signifying that the layer of conjugates coated onto the surface was more important in the first case. On the contrary, conjugate [13] obtained by ON direct synthesis was less efficiently adsorbed on the SPR surface, but the resulting amount of ONs coated was almost the same as for conjugate [5]. Between conjugates [5] and [10], a significant difference was observed. Indeed, an average of 2.8 pmol of ONs were coated with conjugate [10] obtained by direct synthesis. In this case, the number of ONs per chain was the same for both conjugates. So the difference in coating could be explained by their difference of structure. Unlike conjugate [10], conjugate [5] was essentially in an aggregated form. It appeared that this latter conformation favored conjugate coating on the SPR surface. Between conjugates [10] and [13], a real difference in coating was also observed. Indeed, for conjugate [13] twice as many picomoles of ONs were adsorbed. As their structure was the same, this difference could be explained by their number of ONs bound to the copolymer chain. These results were in agreement with VIDAS experiments where the signal was higher for conjugate [13] (VIDAS signal was identical for conjugates [13] and [18]).

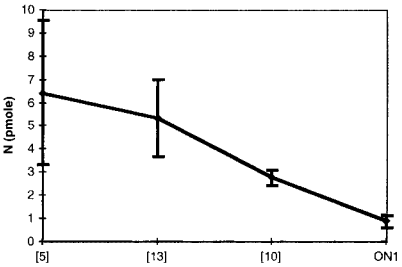

	$N_{[5]}$[a]	$N_{[13]}$[b]	$N_{[10]}$[c]	N_{ON1}[d]
Mean Value	6.4 ± 3.1	5.3 ± 1.7	2.8 ± 0.3	0.9 ± 0.3

Figure 12. Evaluation of the number (N) of picomoles adsorbed on the SPR surface by ^{32}P labeling. Number of picomoles adsorbedon the SPR for conjugates (a) [5], (b) [13], (c) [10], and (d) ON1, respectively. Mean values of six experiments.

CONCLUSION

The goal of this study was to assess the effect of conjugate (ONs−polymer) structure on their capacity to increase the detection signal of an ELOSA type diagnostic test.

For this purpose, two different methods of synthesis were studied. One method consisted of coupling 5′ amino modified ONs to P[MAMVE] or P[MAE] reactive polymer and the second methods relied on direct synthesis of ONs from the P[MAE] polymer previously grafted onto CPG support.

It was evidenced by SEC and SEC-MALLS−viscometry that the first method led to a main population of aggregated conjugates, in a compact coil conformation in solution, whereas the second strategy produced nonaggregated conjugates, in an expanded random coil form. Another difference was in the number of ONs linked to the polymer chain. The coupling method allowed a limited number of ONs per chain to be tethered (18 ONs/P[MAMVE], 6 ONs/P[MAE]) in order to keep a correct coupling yield. In contrast, the latter strategy was more efficient, permitting a range from 11 to 109 ONs per P[MAE] chain.

Both conjugates were evaluated for amplification of the detection signal of an HBV DNA hybridization sandwich test developed on a bioMérieux VIDAS instrument. Only the capture step of the test was investigated in this work and the improvement of detection sensitivity was demonstrated with both conjugates. Then, the effect of the free ON population present in the crude products of synthesis was evaluated. A low influence was observed for conjugates from the first method meaning that aggregated conjugates were adsorbed preferentially onto the surface of the VIDAS SPR, during the coating step. In contrast, conjugates obtained by ON direct synthesis appeared to be in competition with free ON population. Their nonaggregated structure was closer to that of a nucleic acid fragment and the higher the percentage of free ON population, the poorer the signal. Finally, it was demonstrated that the use of P[MAE] instead of P[MAMVE] for conjugates obtained by the coupling reaction did not affect the capture efficiency of the test.

After selection of the best conjugates from the two different methods and optimization of their purity, the detection limits of the ELOSA test were improved by both conjugates by a factor 50 compared to the capture oligonucleotide probe used as the reference. At this stage of the work, the question was to know whether one type of conjugate was adsorbed more efficiently on the SPR surface, offering more ONs to capture DNA target, thereby improving test sensitivity, or, on the contrary, one of them simply offered after coating a majority of more accessible ONs for the capture step. An experiment of ^{32}P labeling of the ONs linked to the polymer chain demonstrated that in fact the amount of oligonucleotides coated on the surface was almost the same for both conjugates. As the number of ONs per chain was much lower for the macromolecules obtained by the coupling reaction, this signified that the thickness of the conjugate layer on the SPR surface was much more important in this case. This can be explained by the aggregated compact structure which may favor the adsorption of a bulky layer of conjugates. Regarding capture phase effectiveness, a higher number of ONs tethered to the polymer chain can balanced the lack of aggregates for

conjugates obtained by ON direct synthesis. On the contrary, the second kind of conjugates obtained by direct synthesis may flatten onto the SPR surface because of its more expanded conformation, thereby limiting the amount of molecule coated and possibly, to some extent, the accessibility of few ONs.

In conclusion, it should be interesting to investigate the synthesis of artificial aggregates which could be grafted onto the surface of a CPG support to develop direct ON synthesis. This kind of macrostructure, with a high number of tethered ONs, should be a suitable candidate as a probe for the capture phase of an ELOSA diagnostic test.

ACKNOWLEDGMENT

We wish to thank J. M. Lucas and A. Domard for viscometry analyses and helpful discussions. We also thank M. H. Charles for her precious help in VIDAS experiments, G. Oriol and V. Cheney for ^{32}P labeling, training and advice, and the Fondation Merieux for financial support.

LITERATURE CITED

(1) Bonino, F., Hoyer, B., Nelson, J., Engle, R., Verme, G., and Gerin, J. (1981) Hepatitis B virus DNA in the sera of HBsAg carriers: a marker of active hepatitis B virus replication in the liver. *Hepatology 1* (5), 386-391.

(2) Nair, P. M., Tong, M. J., Stevenson, D., Roskamp, D., and Boone, C. (1986) A pilot study on the effects of prednisone withdrawal on serum hepatitis B virus DNA and HBeAg in chronic active hepatitis B. *Hepatology 6* (6), 1319−1324.

(3) Hwang, S. J., Lee, S. D., Lu, R. H., Chan, C. Y., Lai, L., Co, R. L., and Tong, M. J. (1996) Comparison of three different hybridization assays in the quantitative measurement of serum hepatitis B virus DNA. *J. Virol. Methods 62*, 123−129.

(4) Kessler, H. H., Pierer, K., Santner, B. I., Vellimedu, S. K., Stelzl, E., Lackner, H., Moser, A., and Marth, E. (1998) Quantitative detection of hepatitis B virus DNA with a new PCR assay. *Clin. Chem. Lab. Med. 36* (8), 601−604.

(5) Haralambidis, J., Angus, K., Pownall, S., Duncan, L., Chai, M., and Tregear, G. W. (1990) The preparation of polyamide-oligonucleotide probes containing multiple nonradioactive labels. *Nucleic Acids Res. 18* (3), 501−505.

(6) Pieles, U., Sproat, B. S., and Lamm, G. M. (1990) A protected biotin containing deoxycytidine building block for solid-phase synthesis of biotinylated oligonucleotides. *Nucleic Acids Res. 18* (15), 4355−4360.

(7) Urdea, M. S., Running, J. A., Horn, T., Clyne, J., Ku, L. and Warner, B. D. (1987) A novel method for the rapid detection of specific nucleotide sequences in crude biological samples without blotting or radioactivity; application to the analysis of hepatitis B virus in human serum. *Genes 61*, 253−264.

(8) Horn, T., and Urdea, M. S. (1989) Forks and combs and DNA: the synthesis of branched oligodeoxyribonucleotides. *Nucleic Acids Res. 17* (17), 6959−6967.

(9) Urdea, M. S. (1994) Branched DNA signal amplification. Does bDNA represent post-PCR amplification technology? *BioTechnology 12*, 926−928.

(10) Shchepinov, M. S., Udalova, I. A., Bridgman, A. J., and Southern, E. M. (1997) Oligonucleotide dendrimers: synthesis and use as polylabeled DNA probes. *Nucleic Acids Res. 25* (22), 4447−4454.

(11) Mallet, F., Hebrard, C., Brand, D., Chapuis, E., Cros, P., Allibert, P., Besnier, J. M., Barin, F., and Mandrand, B. (1993) Enzyme-linked oligosorbent assay for detection of polymerase chain reaction-amplified human immunodeficiency virus type 1. *J. Clin. Microbiol. 31* (6), 1444−1449.

(12) Mabilat, C., Cros, P., Erout, M. N., Thiercy, J. M., Pichot, C., and Mandrand, B. (June 1993) French Pat. 9,307,797.

(13) Mandrand, B., Cros, P., Delair, T., Charles, M. H., Erout, M. N., and Pichot, C. (September 1993), French Pat. 9,311,-006.

(14) Erout, M. N., Elaissari, A., Pichot, C., Cros, P., and Kurfurst, R. (1996) Characterization of the grafting reaction between oligodeoxyribonucleotides and N-vinylpyrrolidone/N-acryloxysuccinimide copolymers by size exclusion chromatography and free solution capillary electrophoresis. *Int. J. Polym. Anal. Charact. 2*, 253−269.

(15) Ladavière, C., Véron, L., Delair, T., Domard, A., Pichot, C., and Mandrand, B. (1997) Reactive polymers in diagnostics: syntheses and characterizations of nucleic acid probes and (maleic anhydride-co-methyl vinyl ether) polymers. *J. Appl. Polym. Sci. 65*, 2567−2577.

(16) Véron, L., De Bignicourt, M. C., Delair, T., Pichot, C., and Mandrand, B. (1996) Syntheses of poly(N-(2,2-dimethoxyethyl)-N-methyl acrylamide) for the immobilization of oligonucleotides. *J. Appl. Polym. Sci. 60*, 235−244.

(17) Delair, T., Badey, B., Domard, A., Pichot, C., and Mandrand, B. (1997) Syntheses and characterization of conjugates of nucleic acid probes and 6-aminoglucose-based polymers. *Polym. Adv. Technol. 8*, 297−304.

(18) Delair, T., Charles, M. H., Cros, P., Laayoun, A., Mandrand, B., and Pichot, C. (1998) Synthesis and characterization of nucleic acid-(co)polymer conjugates: application to diagnostics. *Polym. Adv. Technol. 9*, 349−361.

(19) Ladavière, C. (1998) Doctorat thesis, Université Claude Bernard, Lyon.

(20) Ferraton, N., Delair, T., Laayoun, A., Cros, P., and Mandrand, B. (1997) Covalent immobilization of nucleic acid probes onto reactive synthetic polymers. *J. Appl. Polym. Sci. 66*, 233−242.

(21) Chaix, C., Minard-Basquin, C., Delair, T., Pichot, C., and Mandrand, B. (1998) Oligonucleotide synthesis on maleic anhydride copolymers covalently bound to silica spherical support and characterization of the obtained conjugates. *J. Appl. Polym. Sci. 70* (12), 2487−2497.

(22) Erout, M. N., Elaissari, A., Pichot, C., and Llauro, M. F. (1996) Radical initiated copolymers of N-vinylpyrrolidone and n-acryloxysuccinimide: kinetic and microstructure studies. *Polymer 37* (7), 1157−1165.

(23) Erout, M. N., Troesch, A., Pichot, C., and Cros, P. (1996) Preparation of conjugates between oligonucleotides and N-vinylpyrrolidone/N-acryloxysuccinimide copolymers and applications in nucleic acid assays to improve sensitivity. *Bioconjugate Chem. 7* (5), 568−575.

(24) Allibert, P., Cros, P., and Mandrand, B. (1992) Automated detection of nucleic acid sequences of HPV 16, 18 and 6/11. *Eur. J. Biomed. Technol. 14*, 152−155.

(25) Mabilat, C., Desvarenne, S., Panteix, G., Machabert, N., Bernillon, M. H., Guardiola, G., and Cros, P. (1994) Routine identification of *Mycobacterium tuberculosis* complex isolates by automated hybridization. *J. Clin. Microbiol. 32* (11), 2702−2705.

(26) Minard-Basquin, C., Chaix, C., Pichot, C., and Mandrand, B. (1999) Oligonucleotide synthesis on linear reactive polymer grafted onto solid support, medical diagnostics applications. *Nucleosides Nucleotides 18* (6, 7), 1285−1287.

(27) Unpublished results.

(28) Houwink, R. (1940) *J. Prakt. Chem. 157*, 15.

(29) Troesch, A., unpublished results.

(30) It is important to notice that, in the range of target concentrations from 10^{10} to 10^{12} copies/mL, the relative fluorescent unit (RFU) signal drastically increases to saturate at about 10 000. Consequently, RFU signal fluctuated a lot in this very sensitive area, from 1 day to another. Therefore, results recorded from one series of experiments run at the same time could easily be compared, whereas those corresponding to tests run on different days could not be correlated. In this context, only data obtained from the same set of assays have been compared and discussed in this work.

BC000010P

High-Generation Polycationic Dendrimers Are Unusually Effective at Disrupting Anionic Vesicles: Membrane Bending Model

Zhi-Yi Zhang and Bradley D. Smith*

Department of Chemistry and Biochemistry, University of Notre Dame, Notre Dame, Indiana 46556. Received February 17, 2000; Revised Manuscript Received June 15, 2000

The membrane disruption properties of high generation (G4 to G7) poly(amidoamine) (PAMAM) dendrimers are evaluated and compared to linear poly(lysine). The G6 and G7 dendrimers are unusually effective at inducing leaky fusion of anionic, large unilamellar vesicles, as determined by standard fluorescence assays for lipid mixing, leakage, and contents mixing. Both G7 dendrimer and poly(lysine) are able to disrupt sterically stabilized vesicles that are coated with poly(ethylene glycol). A G7 dendrimer/DNA complex with a 1:1 concentration ratio of dendrimer surface amines to DNA phosphate groups is unable to induce leakage of 3:7 POPA-PE vesicles; however, extensive leakage is observed when the surface amine to phosphate stoichiometry is ≥3:1. Thus, the DNA/dendrimer complexes that typically induce high levels of cell transfection are also able to induce high levels of vesicle leakage. The G7 dendrimer does not induce membrane phase separation in 3:7 POPA-PE vesicles, but an inverse hexagonal phase is observed by ^{31}P NMR. The enhanced membrane disruption is interpreted in terms of a membrane bending model. A rigid, polycationic dendrimer sphere uses electrostatic forces to bend a malleable, anionic membrane and induce bilayer packing stresses. This bending model is biomimetic in the sense that protein-induced membrane bending is currently thought to be an important factor in the fusion mechanism of influenza virus.

INTRODUCTION

Dendritic polymers have a promising future as drug delivery vehicles (*1*, *2*) and as cell transfection agents (*3*−*14*). The hope is that dendrimers will enhance efficacy by improving delivery issues such as targeting, stability, and bioavailability. At present, the field is in its infancy, and the literature contains little discussion of how delivery is likely to occur at the molecular level. In particular, the current understanding of how dendrimers interact with bilayer membranes is quite weak. A major problem is the complexity and heterogeneity of the biomembrane matrix which makes it difficult to interpret results. Similarly, enhanced cell transfection has been reported using polydisperse mixtures of fractured dendrimers as DNA carriers (*3*); however, it is difficult to rationalize these results without knowing more about these complex delivery systems. In an effort to better understand the underlying supramolecular chemistry, we have chosen to study the interaction of monodisperse dendrimers with vesicle membranes.

This paper describes the effects that commercially available polycationic polyamidoamine (PAMAM)[1] dendrimers have on anionic unilamellar vesicles. The PAMAM dendrimers have an ethylenediamine core (Scheme 1) and are prepared by an iterative sequence of reactions (*2*). The number of surface amine groups doubles with each generation and the dendrimer diameter increases incrementally (Table 1). Generations 4 (G4) and below have open structures and ellipsoidal shapes, whereas G5 and above have closed-shell structures and are spherical (*2*, *15*). The goal of the study was to ascertain if PAMAM dendrimers interact with vesicle membranes in a size- or shape-dependent manner. We have evaluated the membrane disruption ability for dendrimer generations G4 to G7, and we find that, compared to linear poly(lysine), the higher generations are unusually effective at disrupting anionic vesicle membranes. A biomimetic membrane bending model is proposed to explain this observation.

EXPERIMENTAL PROCEDURES

All phospholipids including NBD-PE and Rh-PE were purchased from Avanti Polar Lipids. Py-PE, Py-C10-HPM, R18, ANTS, and DPX (Molecular Probes), poly(lysine) HBr salts (Sigma, polydispersity of 1.2), and 49KD-poly(glutamic) acid sodium salt (Sigma, polydispersity of 1.2) were purchased and used without further purification. The 4.7 kb pEGFP-N1 vector (Clontech) was propagated in *Escherichia coli* and purified using a QIAGEN tip and the associated QIAGEN protocol. Fluo-

* To whom correspondence should be addressed. Phone: (219) 631 8632. Fax: (219) 631 6652. E-mail: smith.115@nd.edu.

[1] Abbreviations: ANTS, 1-aminonaphthalene-3,6,8-trisulfonate; DMPC, 1,2-dimyristoyl-sn-glycero-3-phosphocholine; DPX, *N*,*N*′-*p*-xylenebis(pyridinium bromide); HPTS, 8-hydroxypyrene-1,3,6-trisulfonic acid; NBD-Taurine, *N*-(7-nitrobenz-2-oxa-1,3-diazol-4-yl)aminoethanesulfonic acid; LUVs, large unilamellar vesicles; NBD-PE, 1,2-dipalmitoyl-sn-glycero-3-phosphoethanolamine- *N*-(7-nitrobenz-2-oxa-1,3-diazol-4-yl); PAMAM, polyamidoamine; PE, phosphatidylethanolamine (egg); PEG, poly(ethylene glycol); PEG-2000-DOPE, 1,2-dioleoyl-sn-phosphatidylethanolamine-*N*-(poly(ethylene glycol)2000); POPA, 1-palmitoyl-2-oleoyl-sn-glycero-3-phosphatidic acid; POPC, 1-palmitoyl-2-oleoyl-sn-glycero-3-phosphocholine; POPS, 1-palmitoyl-2-oleoyl-sn-glycero-3-phosphoserine; PS, phosphatidylserine (bovine brain); Py-C10-HPM, 1-hexadecanoyl-2-(1-pyrenedecanoyl)-sn-glycero-3-phosphomethanol; Py-PE, 1-hexadecanoyl-2-(1-pyrenedecanoyl)-sn-glycero-3-phosphoethanolamine; R18, octadecyl rhodamine B chloride; Rh-PE, 1,2-dipalmitoyl-sn-glycero-3-phosphoethanolamine-*N*-(lissamine rhodamine B sulfonyl); SUVs, small unilamellar vesicles; TES, *N*-tris(hydroxymethyl)methyl-2-aminoethanesulfonic acid.

10.1021/bc000018z CCC: $19.00 © 2000 American Chemical Society
Published on Web 09/19/2000

Scheme 1

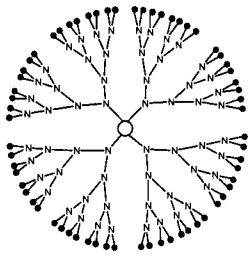

G4-PAMAM Dendrimer

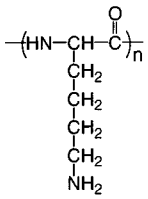

Poly(lysine)

○ = N-$(CH_2)_2$-N

N–N = N-$(CH_2)_2$-CO-NH-$(CH_2)_2$-N

N–● = N-$(CH_2)_2$-CO-NH-$(CH_2)_2$-NH_2

Table 1. Polymer Sizes

polymer	molecular weight	no. of surface amines	mean diameter (nm)
G4-PAMAM	14 215[a]	64[a]	
G5-PAMAM	28 826[a]	128[a]	4.3[c]
G6-PAMAM	58 048[a]	256[a]	6.9[c]
G7-PAMAM	116 493[a]	512[a]	8.0[c]
7.5K-poly(lysine)	7500[b]	36[b]	
34K-poly(lysine)	34 300[b]	164[b]	
100K-poly(lysine)	99 500[b]	476[b]	

[a] Theoretical value. [b] Average value, polydispersity around 1.2. [c] Experimental values reported in ref *15*.

rescence measurements were recorded on a Perkin-Elmer LS 50B instrument and all experiments were conducted at 25 °C.

PAMAM Dendrimers. The dendrimers were purchased from Dendritech. An ongoing concern in dendrimer science is sample purity. It is not straightforward to unambiguously establish the structural purity of high-generation dendrimers. The two most likely impurites are larger dendrimer−oligomers and smaller low-generation structures. A chromatographic analysis of the G7 dendrimers used in this study, conducted by the vendor, indicated that the sample was approximately 90% monodendrimer, 7% oligodendrimer, and 3% low-generation material. Thus, we cannot rule out the possibility that a fraction of the membrane disruption activity induced by the G7 dendrimer sample may be due to a small amount of highly active oligodendrimer impurity. However, even if this is true, the proposed model for dendrimer-induced membrane disruption would be essentially unchanged.

Vesicle Preparation. A solution of lipids in chloroform was evaporated using a rotary evaporator (<30 °C), and the resulting film was dried under vacuum for at least 1 h. The vesicles were dispersed in (1) 25 mM ANTS in 40 mM NaCl/5 mM TES (pH 7.4), (2) 90 mM DPX in 5 mM TES (pH 7.4), or (3) 12.5 mM ANTS/45 mM DPX/20 mM NaCl/5 mM TES (pH 7.4) with the aid of a Vortex mixer. Pyrex glass beads were added before vortexing to facilitate removal of the lipid film from the sides of the flask. The resulting opaque dispersion was frozen in an ethanol/dry ice bath and then allowed to thaw in a water bath at 35−40 °C. This freeze−thaw cycle was repeated 10 times. The resulting mixture was extruded, at room temperature, 29 times through a 19 mm polycarbonate filter (Nucleopore) typically with 100 nm diameter pores using a hand-held Basic LiposoFast device purchased from Avestin. The size of vesicles was routinely checked by dynamic light scattering using a Coulter N4 plus instrument. Separation of untrapped marker compound was achieved by dialysis (15 000 MW cutoff) against 150 mM NaCl.

Lipid Mixing Assays. Extents of lipid mixing were determined using three types of fluorescence probe dilution assays (*16*, *17*). The first two assays use anionic probes whereas the third uses a zwitterionic probe.

NBD-PE/Rh-PE Assay. One population of vesicles contained the probes NBD-PE and Rh-PE (0.6% each), whereas another population was unlabeled. Excitation was set at 470 nm and fluorescence emission was measured at 530 nm using a 515 nm filter. Labeled vesicles were mixed with an equal population of unlabeled vesicles (final lipid concentration was 50 μM) in 3 mL, pH 7.4, of buffer (100 mM NaCl/5 mM TES). Lipid mixing results in an increase in NBD-PE fluorescence intensity due to diminished quenching as the two probes are diluted. The residual fluorescence was taken as 0% lipid mixing, and 100% mixing was set using vesicles containing 0.3% of the probes. Control experiments showed that NBD-PE fluorescence is not affected by interactions with the polycations. For example, addition of polycations to solutions of probe-containing vesicles that had been disrupted with Triton X-100 produced no change in fluorescence.

R18 Assay. Excitation was set at 560 nm and fluorescence emission was measured at 590 nm. The 2% R18 labeled vesicles (5 μM) were mixed with unlabeled vesicles (45 μM) in 3 mL of 100 mM NaCl/5 mM TES (pH 7.4) buffer. The initial fluorescence was taken as 0% lipid mixing and 100% mixing was determined by addition of Triton X-100 to give 0.5%(w/v).

Py-PE assay. Excitation was set at 320 nm and fluorescence emission was measured at 395 and 470 nm. The ratio of I_{470nm}(ex) to I_{395nm}(mon) was determined as a function of time. The 5% labeled vesicles (5 μM) were mixed with unlabeled vesicles (45 μM) in 3 mL of 100 mM NaCl/5 mM TES (pH 7.4) buffer. Vesicles (50 μM) containing 0.5% of Py-PE were used to calibrate the ratio of I_{470nm}(ex)/I_{395nm}(mon) corresponding to 100% lipid mixing.

Leakage Assay. The fluorophore ANTS and its collisional quencher DPX were co-encapsulated in a single population of vesicles. Leakage results in an increase in ANTS fluorescence intensity due to dimished quenching as the two probes are diluted (*17*). Control experiments established that both dendrimer and poly(lysine) slightly enhance the fluorescence of ANTS but the presence of excess poly(glutamate) restores the original fluorescence intensity. Excitation was set at 355 nm and fluorescence emission was measured at 530 nm using a 515 nm filter. At $t = 0$ s, vesicles (50 μM lipid) containing ANTS/DPX were dispersed in 3 mL of 100 mM NaCl/5 mM TES (pH 7.4) buffer, and the residual fluorescence was taken as 0% leakage. At $t = 100$ s, the system was treated with polycation, and at $t = 300$ s, poly(glutamate) was added to eliminate extraneous signal due to polycation/ANTS interaction. The fluorescence intensity corresponding to 100% leakage was determined by addition of 0.3% (w/v) Triton X-100.

Contents Mixing Assay. Attempts to measure aqueous contents mixing using the Tb^{3+}/DPA asssay (*17*) were unsuccessful due to light scattering problems. The use of sodium inositol hexaphosphate as a vesicle deaggregation agent was not helpful in our hands (*18*). The calcein/Co^{2+} assay (*19*) could not be employed due to precipitation of a dendrimer/Co^{2+} complex. A problem with the ANTS/DPX assay (*17*) was enhancement of leaked ANTS fluorescence upon interaction with the

dendrimer; however, the presence of excess poly(glutamate) reverses the polycation/ANTS interaction and restores the original ANTS emission spectrum. At $t = 0$ s, vesicles containing ANTS were mixed in 3 mL of 100 mM NaCl/5 mM TES (pH 7.4) buffer with an equal concentration of vesicles containing DPX (final lipid concentration was 50 μM). At $t = 100$ s, the system was treated with polycation, and at $t = 300$ s, poly(glutamate) was added. The initial fluorescence was taken as 0% contents mixing, and a solution of ANTS/DPX-containing vesicles (50 μM) in 3 mL of 100 mM NaCl/5 mM TES (pH 7.4) buffer was used for the calibration of 100% contents mixing.

^{31}P NMR. Aqueous lipid dispersions were prepared by vortexing 50 mM POPA/PE (3:7) in 1.0 mL of an aqueous buffer (100 mM NaCl, 5 mM TES, pH 7.4) and then adding of G7-PAMAM dendrimer or 100K-poly(lysine) (10 mM of surface amines). Prior to the NMR measurements, 0.1 mL of D_2O was introduced into the samples. The ^{31}P NMR spectra (121 MHz) were acquired at 25 °C using a phase-cycled Hahn spin−echo sequence (*20*). In each case, about 1000 scans were collected with a recycling delay of 3 s and line broadening of 100 Hz. The chemical shifts are relative to small phosphatidylcholine vesicles at 0 ppm.

Dendrimer Internalization Assays. Three different methods were used to detect dendrimer entry into 3:7 POPA/PE vesicles.

HPTS/DPX Assay (21). A dispersion (311 μL) of G7-PAMAM, the water-soluble anionic dye HPTS, and 3:7 POPA/PE vesicles (200 nm) was incubated for 200 s at 25 °C and then added to a gently stirred solution of 40 mM DPX (2689 μL) (final concentrations: G7-PAMAM surface amine 10 μM, HPTS 1.0 μM, and phospholipids 1.0 mM). The intensity of the HPTS emission at 510 nm was measured using the pH-independent excitation wavelength of 413 nm (I). In a separate experiment, the HPTS intensity was measured for a sample that contained water instead of 40 mM DPX (I_{100}). Finally, aqueous Triton X-100 was added (0.5% w/v) to the DPX containing sample and the intensity of the HPTS emission at 413 nm was remeasured (I_0). The percentage of internalized HPTS was calculated as $(I - I_0)/(I_{100} - I_0) \times 100\%$.

NBD-Taurine Assay. To a mixture of G7-PAMAM (5 μM of surface amine) and NBD-taurine (0.5 μM) in 3 mL of buffer (100 mM NaCl, 5 mM TES, pH 7.4) were added 3:7 POPA/PE vesicles (50 μM; 100, 200, or 400 nm). After incubation at 25 °C for 200 s, the dispersion was treated with poly(glutamate) (250 μM of surface carboxylate), and then 200 s later, the intensity of the NBD-taurine emission at 530 nm using excitation wavelength of 470 nm was measured (I_{100}). Sodium dithionite (30 mM) was added and the NBD-taurine emission was measured after 10 min (I). Finally, aqueous Triton X-100 was added (0.5% w/v) and the NBD-taurine emission was measured (I_0). The percentage of internalized NBD-taurine was calculated as $(I - I_0)/(I_{100} - I_0) \times 100\%$.

NBD-G7 Assay. An NBD−dendrimer conjugate (10% NBD−G7) with 10% of the surface dendrimer amines labeled with NBD was prepared by stirring a mixture of G7-PAMAM (9.1 mg, 40 μmol surface amine) and 7-nitrobenz-2-oxa-1,3-diazol-4-chloride (NBD-Cl, 0.8 mg, 4.0 μmol) in methanol (500 μL) in the dark at room temperature for 18 h. TLC (silica gel/chloroform) indicated that the NBD-Cl was consumed. The solvent was evaporated to give a yellow solid which was used without purification. To a solution of 10% NBD−G7 (10 μM of surface amine) in 3 mL of buffer (100 mM NaCl, 5 mM TES, pH 7.4) was added 3:7 POPA/PE vesicles (200 nm, 1.0 mM). After incubation at 25 °C for 200 s, the intensity of the 10% NBD−G7 emission at 530 nm was measured using excitation wavelength of 470 nm (I_{100}). Sodium dithionite (30 mM) was added and the emission was measured after 10 min (I). Finally, aqueous Triton X-100 was added (0.5% w/v) and the 10% NBD−G7 emission was measured (I_0). The percentage of internalized 10% NBD−G7 was calculated as $(I - I_0)/(I_{100} - I_0) \times 100\%$.

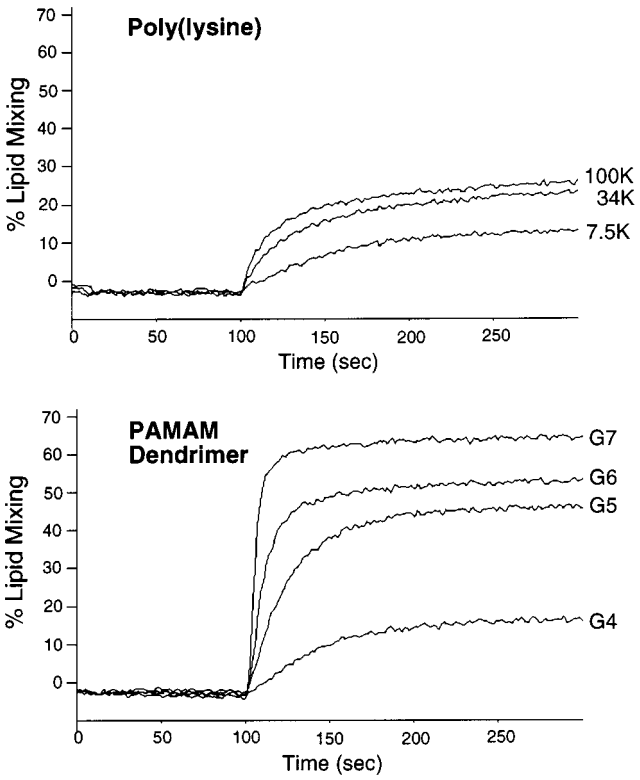

Figure 1. Lipid mixing of 3:7 POPA/PE vesicles at pH 7.4 and 25 °C. A population of vesicles containing NBD-PE/Rh-PE was mixed with an equal amount of unlabeled vesicles (final [phospholipid] = 50 μM), and treated with polycation at $t = 100$ s. In each case, the concentration of polymer surface amines was 10 μM.

RESULTS

Lipid Mixing. The polycation-induced intermixing of lipid bilayers was monitored using three different fluorescence probe dilution assays (*16, 17*) Generally, the resonance energy transfer pair of NBD-PE and Rh-PE was employed. Since these probes are anionic and the fusogens are polycationic, it was important to eliminate the possibility of artifacts due to probe transfer, phase separation, and probe/polycation interaction. Therefore, a number of the lipid-mixing experiments were repeated using the R18 probe or the zwitterionic Py-PE. In essentially all cases, the lipid mixing results were found to be probe independent.

The first vesicles examined were anionic, large unilamellar vesicles (LUVs, 100 nm diameter) composed of 3:7 POPA/PE. Two equal populations of 3:7 POPA/PE vesicles were mixed at $t = 0$ s (final concentration of phospholipid was 50 μM). One population contained the NBD-PE and Rh-PE, whereas the other was unlabeled. An aliquot of polymer was added at $t = 100$ s, to give a final concentration of polymer surface amines of 10 μM. As shown in Figure 1 and Table 2 (entry 1), the extent of lipid mixing increased only slightly with the molecular weight of poly(lysine), but increased markedly with dendrimer molec-

Table 2. Extents (%) of Lipid Mixing, Leakage, and Contents Mixing[a]

entry	assay	vesicle composition	G4 PAMAM	G5 PAMAM	G6 PAMAM	G7 PAMAM	7.5K poly(lysine)	34K poly(lysine)	100K poly(lysine)
1	lipid mixing	POPA-PE 3:7	16[b]	46[b]	53	64	13[b]	24	26
2	lipid mixing	POPS-PE 3:7				45			10
3	lipid mixing	POPA-POPC 3:7	c	c	c	2	0	c	c
4	lipid mixing	PS-POPC 3:7	c	c	c	0	c	c	c
5	lipid mixing	POPA-POPC 4:1	b	0	7	25	3	11	14
6	lipid mixing	PS-POPC 4:1	0	4	7	20	0		0
7	lipid mixing	PS	c	c	c	18	c	c	0
8	leakage	POPA-PE 3:7	5[b]	6	37	58	4	4	4
9	contents mixing	POPA-PE 3:7	11[b]	6	6	4	19	12	12

[a] 100 nm unilamellar vesicles, total lipid concentration = 50 μM, concentration of polymer surface amines = 10 μM. [b] Precipitation occurred after measurement. [c] Rapid precipitation obscured measurement.

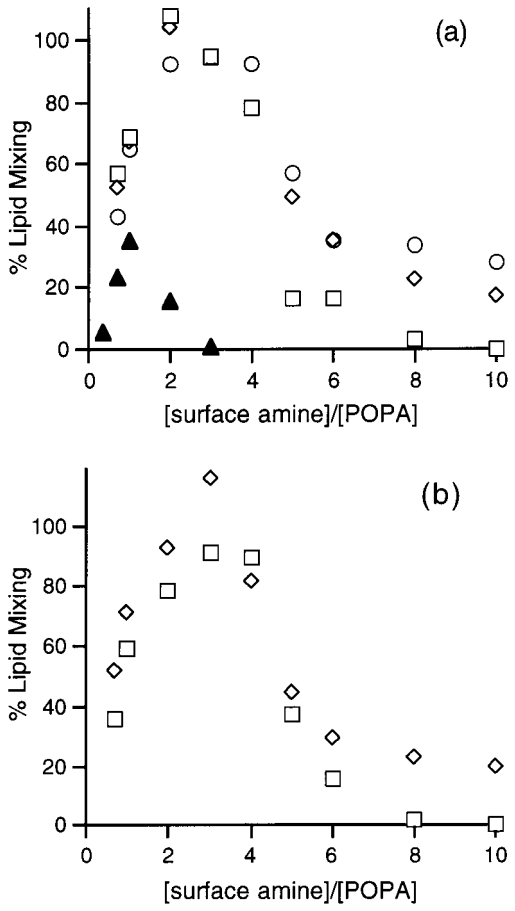

Figure 2. Lipid mixing as a function of the concentration ratio of polymer surface amines to POPA (100 nm, [phospholipid] = 50 μM, pH 7.4, 25 °C) (a) 3:7 POPA/PE vesicles: (▲) 100K-poly(lysine), NBD-Rh assay; (◇) G7-PAMAM, NBD-Rh assay; (○) G7-PAMAM, Py-PE assay; (□) G7-PAMAM, R18 assay. (b) 3:7 POPA/PE vesicles containing 2% PEG-2000-DOPE: (◇) G7-PAMAM, NBD-Rh assay; (□) G7-PAMAM, R18 assay. Uncertainty ± 5% units.

ular weight. Furthermore, a high-generation dendrimer was more effective than a poly(lysine) with a similar number of surface amines. When excess poly(glutamate), a strong binder of polycations (*22*), was added to the vesicles before the polymer, no lipid mixing occurred, indicating that electrostatic interactions are driving vesicle aggregation and the subsequent lipid mixing.

The effect of polycation concentration on lipid mixing was examined using G7 dendrimer and 100K-poly(lysine). As shown in Figure 2a, the general trend is the same for both polycations; that is, the extent of lipid mixing of 3:7 POPA/PE vesicles initially increases with concentration, reaches a maximum, and then decreases (*18*, *23*, *24*) At low concentrations, the polycations cross-link and aggregate the anionic vesicles, but at higher concentrations the polycations coat the vesicles and hinder close approach. In the case of poly(lysine), lipid mixing was a maximum when the concentration ratio of surface amine to POPA was 1, an observation that has been noted before (*23*). In the case of G7 dendrimer, lipid mixing was maximal when the ratio of surface amine to POPA was about 3. The higher charge ratio is likely due to the rigid and spherical structure of the dendrimer which can only contact a vesicle with a fraction of its available surface amines. Thus, a higher concentration of surface amines is needed to reach the optimal level of cross-linking and charge neutralization.

The results of vesicle composition studies are summarized in Table 2 (entries 1−7). When the fusion inhibitor POPC (*18*, *25*) was used instead of PE, almost no lipid mixing was observed with G7 dendrimer (compare entries 1 and 3). However, significant lipid mixing occurred when the fraction of POPA was increased (compare entries 3 and 5). Interestingly, there was little or no lipid mixing induced by 100K-poly(lysine) when PS was used instead of POPA (compare entries 1 and 2 and 5 and 6) or even when the LUVs were composed of 100% PS (entry 7). This observation is in agreement with a previous study using LUVs (*18*), but contrasts with a report that poly(lysine) is able to fuse SUVs containing PS (*23*).

As summarized in Table 3, the presence of 2% PEG-2000-DOPE in 3:7 POPA/PE vesicles greatly decreases the extent of lipid mixing induced by $CaCl_2$ (entry 10). In this case, aggregation of the sterically hindered vesicles, a requisite step for fusion, is greatly inhibited (*26*). In contrast, both G7-PAMAM dendrimer (entries 12 and 13) and 100K-poly(lysine) (entries 14 and 15) are still able to induce the sterically stabilized vesicles to undergo significant amounts of lipid mixing. A study of lipid mixing as a function of G7 dendrimer concentration resulted in a bell-shaped profile that closely matches that seen with conventional 3:7 POPA/PE vesicles (Figure 2).

The effect of added NaCl on polycation-induced lipid mixing of 3:7 POPA/PE vesicles is summarized in Table 4. Surprisingly, the extent of lipid mixing increases with increasing NaCl concentration. This relationship is the reverse to that observed with Ca^{2+}-mediated fusion (*27*).

Leakage. Leakage was measured using the ANTS/DPX fluorescence assay (*17*) As shown in Figure 3 and Table 2 (entry 8), low and high molecular weight poly(lysine) induced very little leakage. The same result was obtained with the low-generation dendrimers but the G6 and G7 dendrimers induced rapid and drastic leakage. When excess poly(glutamate) was added before the polycations no leakage occurred. Leakage from conventional and sterically stabilized 3:7 POPA/PE vesicles was

Table 3. Extents (%) of Cation-Induced Lipid Mixing of Conventional and Sterically Hindered Vesicles[a]

entry	assay	cation	charge ratio (±)[b]	conventional (3:7, POPA/PE)[a]	sterically hindered[a]
10	R18	$CaCl_2$ (1 mM)		86	7
11	NBD-PE Rh-PE	$CaCl_2$ (20 mM)			6
12	R18	G7 PAMAM	1:1	69	59
13	NBD-PE Rh-PE	G7 PAMAM	1:1	83	71
14	R18	100K poly(lysine)	1:1	39	15
15	NBD-PE Rh-PE	100K poly(lysine)	1:1	41	35

[a] Conventional vesicles were 3:7 POPA/PE (100 nm, 50 μM phospholipid, pH 7.4, 25 °C). Sterically hindered vesicles contained an additional 2% PEG-2000-DOPE, lipid mixing uncertainty ± 5%. [b] Concentration ratio of polycation surface amines to POPA.

Table 4. Effect of NaCl Concentration on Extent (%) of Polycation-Induced Lipid Mixing of 3:7, POPA/PE Vesicles[a]

[NaCl] (mM)	G7 PAMAM[b]	100K poly(lysine)[b]
100	56	34
200	78	35
300	74	33
400	78	42
500	67	41

[a] [phospholipid] = 50 μM, 5 mM TES buffer, pH 7.4, 25 °C, lipid mixing uncertainty ± 5%. [b] Concentration ratio of polycation surface amines to POPA was 2:3.

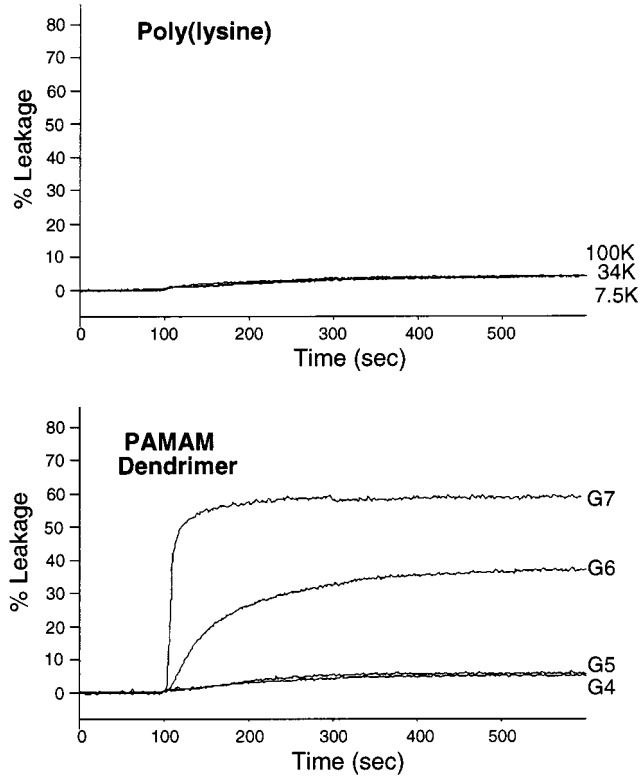

Figure 3. Leakage from 3:7 POPA/PE vesicles (100 nm, [phospholipid] = 50 μM, pH 7.4, 25 °C) containing ANTS/DPX. The vesicles were treated with polymer at t = 100 s (in each case, the concentration of polymer surface amines was adjusted to 10 μM), and with poly(glutamate) (500 μM carboxylates) at t = 300 s.

monitored as a function of G7-PAMAM concentration. As shown in Figure 4, both systems exhibit bell-shaped dependencies that are very similar to the lipid mixing profiles in Figure 2.

The leakage of ANTS/DPX from 3:7 POPA/PE vesicles at pH 7.4 (100 mM NaCl/5 mM TES) and 25 °C induced by complexes of DNA and G7 dendrimer is shown in Figure 5. DNA (pEGFP-N1 vector, 4.7 kb, the plasmid codes for enhanced green fluorescent protein and is commonly used to measure cell transfection efficiency)

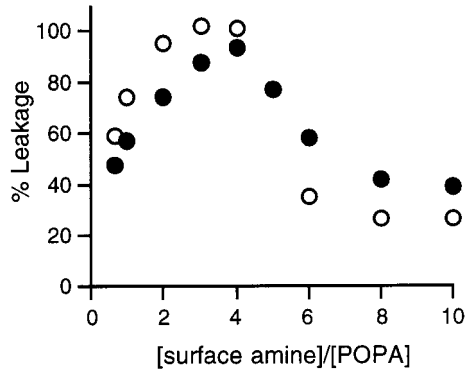

Figure 4. Leakage as a function of the concentration ratio of G7-PAMAM surface amines to POPA (pH 7.4, 25 °C); (○) 3:7 POPA/PE vesicles (100 nm, [phospholipid] = 50 μM); (●) sterically hindered 3:7 POPA/PE vesicles containing 2% PEG-2000-DOPE. Uncertainty ± 5%age units.

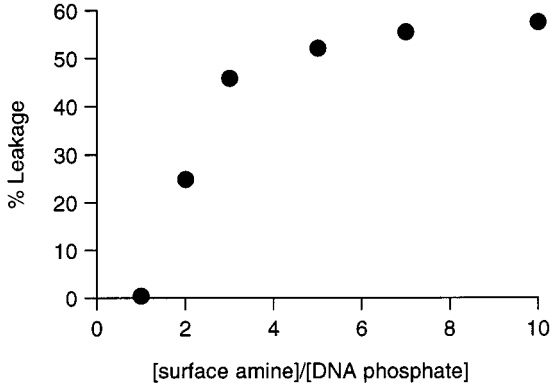

Figure 5. Leakage from 3:7 POPA/PE vesicles (100 nm, 50 μM lipid, pH 7.4, 25 °C) containing ANTS/DPX, induced by G7 dendrimer/DNA complexes at different concentration ratios of dendrimer surface amine to DNA phosphate groups. In each case, the concentration of G7 dendrimer surface amines was 10 μM.

and G7 dendrimer were mixed at different concentration ratios of dendrimer surface amine to DNA phosphate group. After 5 min, the dendrimer/DNA complexes were added to the vesicles (50 μM phospholipid) at pH 7.4 (100 mM NaCl/5 mM TES). In each case, the final concentration of G7 dendrimer surface amines was 10 μM. No leakage was observed when the surface amine/DNA phosphate ratio was unity, whereas the leakage induced by a surface amine/DNA phosphate ratio of 3:1 was 80% of the extensive leakage induced by G7 dendrimer alone. Previous work has shown that monodisperse particles are formed when the surface amine/DNA phosphate ratio is 3:1, with diameters around 100 nm and ζ-potentials of +50 mV (*28*−*30*).

Contents Mixing. The amount of contents mixing of 3:7 POPA/PE vesicles, determined using the ANTS/DPX assay (*17*), is summarized in Table 2 (entry 9). Poly(lysine) induced a modest amount of contents mixing at

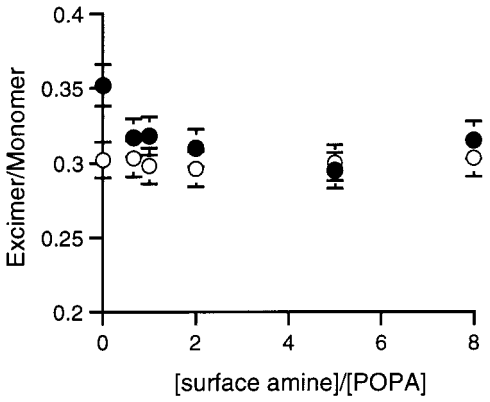

Figure 6. Excimer/monomer ratio as a function of the concentration ratio of G7-PAMAM surface amines to POPA (3:7 POPA/PE vesicles, 100 nm, 50 μM phospholipid, pH 7.4, 25 °C); (○) Py-PE; (●) Py-C10-HPM.

about the same rate as lipid mixing (see Figure 1). Very little contents mixing was observed with G6 and G7 dendrimers because leakage was so rapid and extensive.

Membrane Fluidity. Pyrene-containing lipids are used as probes to detect lateral phase separation and changes in membrane fluidity (*31*, *32*). Polycations have been shown to induce phase separation in certain anionic membranes, which is reflected by an increase in the pyrene excimer/monomer ratio (*31*), whereas in other cases, an observed decrease in excimer/monomer ratio has been interpreted as a decrease in the rate of lateral diffusion (*31*, *32*). Two pyrene-containing probes were used in this study, zwitterionic Py-PE and anionic Py-C10-HPM. Addition of increasing amounts of G7 dendrimer to 3:7 POPA/PE vesicles containing 5% Py-PE (50 μM lipid, pH 7.4) resulted in no detectable change in the excimer/monomer ratio (Figure 6). Addition of increasing amounts of G7 dendrimer to 3:7 POPA/PE vesicles (50 μM lipid, pH 7.4) containing 5% Py-C10-HPM produced a U-shaped dependence, with an initial decrease in the excimer/monomer ratio followed by a subsequent increase (Figure 6). The data indicates that G7 dendrimer does not induce phase separation in 3:7 POPA/PE vesicles, does not effect the lateral diffusion of the zwitterionic PE, but does slow the diffusion of the anionic POPA. The U-shaped dependence on excimer/monomer ratio has been noted before (*31*−*33*) and is attributed to the gradual delocalization of positive sites as the membrane surface becomes saturated with polycation.

^{31}P NMR spectroscopy. ^{31}P NMR line shapes are often used to identify changes in membrane morphologies (*34*). For example, ^{31}P NMR was employed in conjuction with freeze−fracture techniques to show that the near-spherical polycationic protein, cytochrome *c*, induces anionic cardiolipin-containing membranes to undergo a phase change from bilayer to inverse hexagonal, H_{II} (*35*). In contrast, linear poly(lysine) does not induce such a morphology change to inverse membrane curvature (*36*). A similar result is seen in Figure 7, which shows the change in ^{31}P NMR line shapes upon treatment of 3:7 POPA/PE vesicles (50 mM lipid, pH 7.4, 5 mM TES, 100 NaCl) with polycation. In the absence of polycation the typical bilayer pattern is observed (Figure 7A). Addition of poly(lysine) (10 mM of surface amines) results in precipitation with no major change in line shape (Figure 7B). Addition of G7-PAMAM dendrimer (10 mM of surface amines) also produces a precipitate, but there is concomitant formation of hexagonal II phase as reflected by the reduced line width and the characteristic reverse peak asymmetry (Figure 7C) (*34*, *35*)

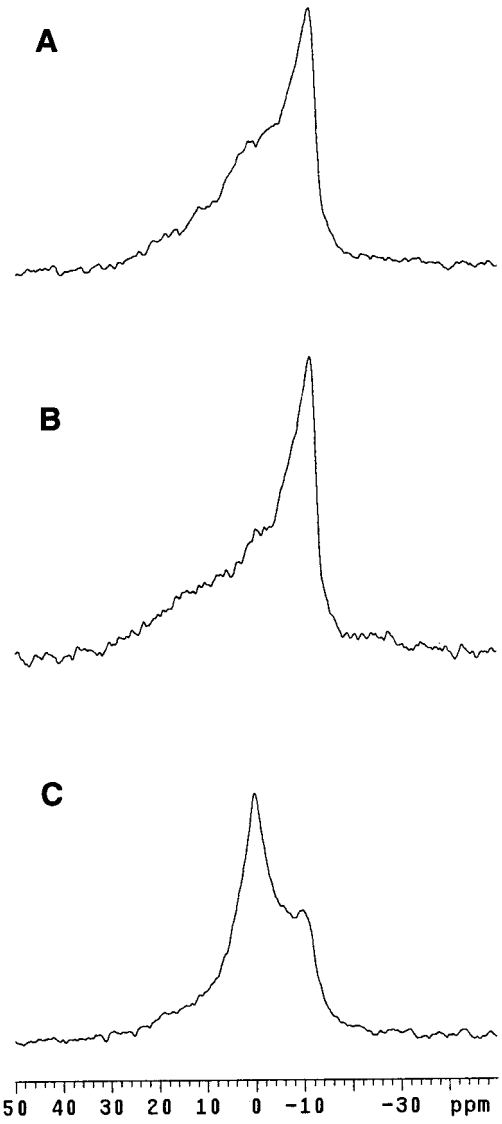

Figure 7. ^{31}P NMR spectra of 3:7, POPA/PE vesicles (50 mM phospholipid) in 5 mM TES, 100 mM NaCl, pH 7.4, 25 °C. (A) no addition, (B) addition of 100K-poly(lysine) (10 mM surface amines), (C) addition of G7-PAMAM dendrimer (10 mM surface amines).

No Dendrimer Internalization. Three related assays were used to determine if the G7-PAMAM dendrimers were internalized by 3:7 POPA/PE vesicles at pH 7.4. The first method was recently described by Tedesco and Matile (*21*). Vesicles (3:7 POPA/PE, 200 nm) were treated with dendrimer (at low surface amine to POPA) and the anionic fluorescent dye HPTS. If the dendrimers entered the vesicle by an endovesiculation mechanism, then presumably some HPTS should also be internalized at the same time. The internalized HPTS can be detected because it is protected from the externally added quencher DPX (*21*). The second method employed the anionic water soluble dye NBd-taurine as a replacement for HPTS and used externally added sodium dithionite as a chemical quencher of the NBD-taurine (*37*) Both methods were unable to produce evidence for internalization of the anionic dyes. A third method resorted to covalent attachment of the NBD dye to the PAMAM dendrimer. A dendrimer−NBD conjugate (10% NBD−G7) was prepared with 10% of the surface dendrimer amines labeled with NBD. Incubation of the 10% NBD−G7 conjugate with excess 3:7 POPA/PE vesicles, and subsequent chemical quenching by dithionite again showed no evi-

dence for internalization of the NBD−G7 conjugate. We conclude that the dendrimers are not internalized into a protective environment within the vesicles, although the results do not rule out the possibility that dendrimers enter the vesicles but remain accessible to the quenching probes.

DISCUSSION

Membrane Disruption Using Poly(Lysine). Peptidyl polycations such as poly(lysine) are well-known to bind tightly to anionic vesicles [each basic residue contributes about 1 kcal/mol to the membrane binding energy (*38*, *39*)] and promote vesicle−vesicle interaction. The specific outcome (aggregation, leakage, lipid mixing, contents mixing) depends on the composition and size of the vesicles. For example, poly(lysine) promotes the aggregation and complete fusion of anionic SUVs (*23*, *40*), whereas treatment of LUVs with poly(lysine) usually results in hemifusion, i.e., lipid mixing only and no mixing of aqueous contents (*18*, *41*). The increased fusogenicity of SUVs is attributed to the greater membrane curvature strain (*42*).

During the course of this study we confirmed a previous report (*18*) that poly(lysine) is able to promote the lipid mixing of PA-containing LUVs more effectively than PS-containing LUVs (entries 1, 2, 5−7, Table 2). This may be due to the different structures that poly(lysine) forms on the membrane surfaces. It is well-established that poly(lysine) is a random coil in neutral solution, but adopts a β-sheet on a PA membrane surface (*43*−*45*), and forms α-helices on a PS membrane surface (*46*). The same conformations but with reduced content are also observed in mixed PA−PC (*47*) and PS−PC (*46*) vesicles. In addition, there is evidence that poly(lysine) induces significant lateral phase separation in PA−PC vesicles (*44*, *45*, *48*) but not so in PS−PC (*46*) or PS−PE vesicles (*32*). Thus, poly(lysine) β-sheets on a PA surface appear to induce more lipid mixing than α-helices on a PS surface. The β-sheet structures may force a closer approach of apposed dehydrated surfaces, and/or increase the number of surface defects due to lateral phase separation (*49*).

Membrane Disruption Using PAMAM Dendrimers. High-generation PAMAM dendrimers are unusually effective at disrupting anionic vesicles. Specifically, G6 and G7 dendrimers rapidly induce large amounts of lipid mixing and leakage of aqueous contents (Figures 1 and 3). They are much more effective than low-generation PAMAM dendrimers or poly(lysine) of any molecular weight, even when the polymer concentrations are adjusted so that the number of exposed surface amines is constant. For example, G7 dendrimer (20 nM of polymer) induces four times more lipid mixing and twelve times more leakage in 3:7 POPA-PE vesicles (50 μM total lipid) than an 8-fold higher concentration of G4 dendrimer (160 nM of polymer).

Both G7-PAMAM and 100K-poly(lysine) are able to disrupt sterically hindered, PEG-containing vesicles that are otherwise resistant to Ca^{2+}-induced fusion (Table 3, Figure 2, and Figure 4). Apparently, the polycations are able to overcome the surface hydration barrier provided by the external PEG chains and force the apposed membranes to undergo lipid mixing. Similarly, Ca^{2+}-mediated fusion is strongly inhibited by increasing NaCl concentrations (*27*), but the lipid mixing induced by PAMAM dendrimers and poly(lysine) actually increases with NaCl concentration (Table 4). Na^+ ions are thought to affect fusion in opposing ways (*50*). They can associate with the anionic bilayer surface and promote lipid mixing because of charge neutralization. Conversely, they can inhibit vesicle aggregation by increasing the thickness of the repulsive hydration layer at the membrane surface (*50*). It appears that even in the presence of high NaCl concentrations, 100K-poly(lysine) and especially G7-PAMAM dendrimer are still able to cross-link the vesicles (*38*, *39*) and, because of increased charge neutralization, induce enhanced lipid mixing.

In general, the best cell transfection results with PAMAM dendrimers are observed with high-generation homologues and when the ratio of dendrimer surface amines to DNA phosphate groups is greater than unity (*3*−*14*, *29*). The dendrimer/DNA complexes formed under these conditions are irregular polycationic aggregates (*29*, *51*). We find that a G7 dendrimer/DNA complex with a 1:1 concentration ratio of dendrimer surface amines to DNA phosphate groups is unable to induce leakage of 3:7 POPA-PE vesicles; however, extensive leakage is observed when the surface amine to phosphate stoichiometry is $\geq$3:1 (Figure 5). Thus, the polycationic DNA/dendrimer complexes that typically induce high levels of cell transfection also induce the highest levels of vesicle leakage. The dendrimer/vesicle interaction is strongly dependent on the vesicle membrane composition. The polycationic dendrimers disrupt different types of anionic vesicles, especially PE-containing vesicles (Table 2). They do not disrupt zwitterionic PC vesicles (*52*, *53*) or anionic vesicles containing a high fraction of PC (Table 2). This membrane selectivity may explain some of the differences in transfection efficiencies and cell toxicities observed with different cell lines (*3*−*14*).[2]

Membrane Bending Model. Why are the higher generation dendrimers better at disrupting anionic membranes? Although a definitive answer cannot be provided at this time, it is worth emphasizing that high-generation PAMAM dendrimers are monomolecular weight polycations with spherical shapes of known diameters (Table 1) and that these structural attributes greatly simplify any analysis of their supramolecular properties. What can be stated with some certainty is that the observed membrane disruption is not due to a simple detergent effect. PAMAM dendrimers are highly water-soluble polycations [essentially all of the surface amine groups are protonated at neutral pH (*54*)]. The outer surface of a high-generation PAMAM dendrimer is highly congested and unlikely to be deeply penetrated by a phospholipid (*2*, *15*, *55*, *56*). Recent EPR studies show that there is very little interaction between G2-PAMAM dendrimers and zwitterionic DMPC vesicles (*52*). A modest interaction is observed with G7 dendrimers which leads to a partially perturbed bilayer structure, but the integrity of the membrane is preserved (*52*).

With anionic vesicles, the interaction is an electrostatic attraction between a malleable, anionic bilayer membrane (radius of curvature $\sim$50 nm), and a rigid, cationic dendrimer sphere (radius of curvature $\sim$4 nm). This leads to dendrimer-induced membrane bending as shown in Figure 8. When a polycationic dendrimer binds to the

[2] The vesicle disruption events reported in this paper are much faster than the process of cell transfection which occurs over a period of hours. However, it should be noted that the vesicles were typically composed of POPA/PE, an unnatural vesicle composition that was used specifically because of its relative instability and the expectation that the vesicles would magnify any disruption effect. At present it is not known if high generation PAMAM dendrimers have a special ability to disrupt biological membranes.

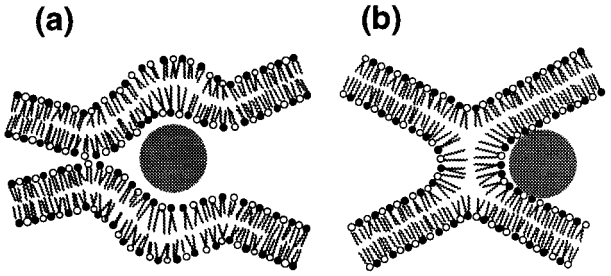

Figure 8. Schematic representation of dendrimer-induced bending of bilayer membranes. Lipids with black headgroups represent anionic phospholipids, the others may be zwitterionic phospholipids. (a) Cross section of a polycationic dendrimer that cross-links the exterior surfaces of two anionic vesicles. Electrostatic forces bend the bilayer surfaces and induce local regions of inverse curvature. (b) Cross-section of a polycationic dendrimer bound to two hemifused vesicles at the periphery of the vesicle-vesicle contact point.

exterior of an anionic vesicle, electrostatic forces bend the bilayer surface (*57*), and induce a local region of inverse curvature (*58*), which in turn induces packing stresses (*59*). If a dendrimer is situated at the connection point of two or more vesicles (Figure 8a) then the packing stresses lead to enhanced lipid mixing. Lipid mixing at a contact point on one side of the dendrimer produces the hemifused intermediate shown in Figure 8b. The structure has inversely curved surfaces at the periphery of the vesicle−vesicle contact point (*57*−*60*). We propose that high-generation polycationic dendrimers facilitate lipid mixing by electrostatically stabilizing these inversely curved, anionic surfaces (Figure 8b).[3] The crucial structural factors are the dendrimer's polycationic charge, rigid spherical shape, and highly congested exterior surface. The following observations support this hypothesis. (i) The vesicle disruption effect is specific for high-generation PAMAM dendrimers and is diminished with low-generation dendrimers or linear poly(lysine) of any molecular weight. (ii) Vesicle disruption is greatly diminished when POPC is used instead of PE (Table 2, compare entries 1−4). The PC headgroup is larger and more heavily hydrated than the PE headgroup (*58*) and it is energetically more costly for bilayers containing PC to adopt inverse curvature (*18*, *57*−*60*). (iii) ^{31}P NMR (Figure 7) shows that G7 dendrimer acts like the near-spherical polycationic protein, cytochrome *c* (*35*), and induces bilayer membranes to adopt an inverse hexagonal II phase. Linear poly(lysine) does not induce such a change to inverse curvature. (iv) The area per surface amine for PAMAM dendrimers decreases with each generation, and by G7 is about 70 Å^2/surface amine (see Figure 37 in ref *2*) which is close to the headgroup area for a typical fluid-phase bilayer membrane. Thus, the matched spacing between surface groups may lead to optimal charge neutralization and optimal membrane bending strain. (v) The dendrimer-induced membrane bending model is biomimetic in the sense that protein-induced membrane bending is thought to be an important factor in the fusion mechanism of Influenza virus (*62*, *63*).

[3] The hemifused intermediate shown in Figure 8b is often referred to as a stalk, and is an intermediate in the stalk fusion mechanism. However, the stalk hypothesis describes the fusion of uncharged membranes where electrostatic effects are minimal. Thus, this study of anionic membranes is not a test of the stalk hypothesis, but it does raise the possibility that some biological fusion systems may operate by a mechanism that is similar to that described in Figure 8b (*61*).

In addition to membrane bending, other factors may be contributing to the dendrimer's enhanced vesicle disruption ability. One possibility is lateral phase separation, which is thought to be an important factor in Ca^{2+}-mediated fusion (*50*). Polycations have been shown to induce phase separation in a number of anionic membrane compositions (*33*, *44*, *45*, *48*, *64*) but not so in others (*32*, *46*). We are unable to detect dendrimer-induced phase separation in 3:7 POPA/PE vesicles (Figure 6), but we cannot rule out transient microdomains. Another factor that cannot be discounted at present is an interaction between the dendrimer and the membrane surface. Poly(lysine) is thought to be situated above the polar headgroup region of the membrane, with perhaps a water monolayer between (*38*, *39*, *65*). An unusual structural feature with high generation PAMAM dendrimers is the densely packed spherical surface, which may not be properly hydrated for steric reasons. Thus, the dendrimers may possess an unusual ability to interact with, or dehydrate, the polar headgroups at the bilayer surface which may lead to enhanced fusion.

Drug Delivery and Cell Transfection. The membrane bending model suggests that dendrimers may be useful as fusion catalysts. Indeed, a polycationic G9 dendrimer was recently shown to dramatically enhance the fusion of reteroviral-infected murine cells (*66*). Thus, it may be possible to use dendrimers to improve vesicle-mediated drug delivery. The dendrimers could promote vesicle−cell fusion which would allow vesicle-encapsulated drugs to enter the cell.

As drug delivery vehicles, dendrimers can be viewed as either endo receptors with the drugs encapsulated in the dendrimer internal cavities (*1*, *2*, *56*) or they can be used as exo receptors with drugs bound to the dendrimer surfaces. An example of the latter approach is cell transfection. The recent commercial availability of PAMAM dendrimers has led to their increased use as cell transfection agents (*3*−*13*). Cell transfection is a complicated multistep process, but in many cases, it appears that transfection is mediated by endocytosis, and there is evidence that exit from the endosome is the step that controls transfection efficiency (*28*). Our results show that high generation PAMAM dendrimers have an unusual ability to disrupt bilayer membranes, which suggests that they may be able to permeate from endosomes. We tested this idea by trying to detect dendrimer entry into vesicles. Our lack of success does not necessarily mean that PAMAM dendrimers cannot pass through endosomal membranes.[2] It may be that the outward curvature of the vesicles prevents dendrimer influx. In the case of endosomal exit, the transport process is efflux which should be more favorable because the membrane curvature is reversed. Nonetheless, our inability to detect dendrimer internalization emphasizes the point that other cell transfection mechanisms have been proposed. For example, the enhanced transfection has been attributed to the dendrimer acting as a proton sponge in the acidic endosomes which leads to osmotic swelling and endosome lysis (*3*). Another possibility is increased resistance to DNA degradation (*29*, *30*). Finally, fractured dendrimers have been reported with enhanced transfection activities, an observation attributed to their more flexible structures (*3*, *8*). It is apparent that further studies are needed to clearly delineate the factors controlling gene delivery using PAMAM dendrimers (*29*, *30*, *51*).

CONCLUSION

We find that high-generation, polycationic PAMAM dendrimers are able to disrupt anionic vesicles much better than low-generation dendrimers or linear poly(lysine). The high-generation dendrimers also have a special ability to induce anionic membranes to adopt inverse curvature. The results are rationalized in terms of a dendrimer-induced membrane bending model. Although the model is somewhat speculative, it does provide a simple physical picture that suggests how polycationic dendrimers may act in various drug delivery and cell transfection applications.

ACKNOWLEDGMENT

We thank Y. Vandenburg for preparing the DNA plasmid samples and Dr. J. Zajicek for assistance with the ^{31}P NMR. This work was supported by the National Institutes of Health (GM 59078).

LITERATURE CITED

(1) Kim, Y., and Zimmerman, S. C. (1998) *Curr. Opin. Chem. Biol. 2*, 733−742.
(2) Tomalia, D. A., and Durst, H. D. (1993) in *Topics in Curr. Chem.* (E. Weber, Ed.) pp 193−313, Springer-Verlag, Berlin.
(3) Tang, M. X., Redemann, C. T., and Szoka, F. C. (1996) *Bioconjugate Chem. 7*, 703−714.
(4) Kukowska-Latallo, J. F., Bielinska, A. U., Johnson, J., Spindler, R., Tomalia, D. A., and Baker, J. R. (1996) *Proc. Natl. Acad. Sci. U.S.A. 93*, 4897−4902.
(5) Goncz, K. K., Kunzelmann, K., Xu, Z. D., and Gruenert, D. C. (1998) *Hum. Mol. Gen. 7*, 1913−1919.
(6) Qin, L. H., Pahud, D. R., Ding, Y. Z., Bielinska, A. U., Kukowska-Latallo, J. F., Baker, J. R., and Bromberg, J. S. (1998) *Hum. Gene Ther. 9*, 553−560.
(7) Alahari, S. K., DeLong, R., Fisher, M. H., Dean, N. M., and Juliano, R. L. (1998) *J. Pharm. Exp. Ther. 286*, 419−428.
(8) Ruponen, M., Yla-Herttuala, S., and Urtti, A. (1999) *Biochim. Biophys. Acta 1415*, 331−341.
(9) Turnen, M. P., Hiltunen, M. O., Ruponen, M., Virkamaki, L., Szoka, F. C., Urtti, A., and Yla-Hertuala, S. (1999) *Gene Ther. 6*, 6−11.
(10) Hudde, T., Rayner, S. A., Comer, R. M., Weber, M., Issacs, J. D., Waldmann, H., Larkin, D. P. F., and George, A. J. T. (1999) *Gene Ther. 6*, 939−943.
(11) Dunphy, E. J., Redman, R. A., Herweijer, H., and Cripe, T. P. (1999) *Hum. Gene Ther. 10*, 2407−2417.
(12) Toth, I., Sakthivel, T., Widerspin, A. F., Bayele, H., O'Donnell, M., Perry, D. J., Pasi, K. J., Lee, C. A., and Florence, A. T. (1999) *S.T.P. Pharma Sci. 9*, 93−99.
(13) Kukowska-Latallo, J. F., Chen, C. L., Eichman, J., Bielinska, A. U., and Baker, J. R. (1999) *Biochem. Biophys. Res. Commun. 264*, 253−261.
(14) Loup, C., Zanta, M., Caminade, A., Majoral, J., and Meunier, B. (1999) *Chem. Eur. J. 5*, 3644−3650.
(15) Jackson, C. J., Chanzy, H. D., Booy, F. P., Drake, B. J., Tomalia, D. A., Bauer, B. J., and Amis, E. J. (1998) *Macromolecules 31*, 6259−6265.
(16) Düzgünes, N, Allen, T. M., Fedor. J., and Paphadjopoulos, D. (1987) *Biochemistry 26*, 8435−8442.
(17) Düzgünes, N., and Wilschut, J. (1993) *Methods Enzymol. 220*, 3−14.
(18) Bondeson, J., and Sundler, R. (1990) *Biochim. Biophys. Acta 1026*, 186−194.
(19) Kendall, D. A., and MacDonald, R. C. (1982) *J. Biol. Chem. 257*, 13892−13898.
(20) Rance, M., and Byrd, A. (1983) *J. Magn. Reson. 52*, 221−240.
(21) Tedesco, M., and Matile, S. (1999) *Bioorg. Med. Chem. 7*, 1373−1379.
(22) Gad, A, Bental, M., Elyahiv, G., and Weinberg, H. (1985) *Biochemistry 24*, 6277−6282.
(23) Walter, A., Steer, C. J., and Blumenthal, R. (1986) *Biochim. Biophys. Acta 861*, 319−330.
(24) Oku, N., Yamaguchi, N., Yamaguchi, N., Shibamoto, S., Ito, F., and Nango, M. (1986) *Biochem. J. 100*, 935−944.
(25) McIntosh, T. J., Kulkarni, K. G., and Simon, S. A. (1999) *Biophys. J. 76*, 2090−2098.
(26) Holland, J. W., Hui, C., Cullis, P. R., and Madden, T. D. (1996) *Biochemistry 35*, 2618−2624.
(27) Düzgünes, N., Nir, S., Wiscut, J., Bentz, J., Newton, C., Portis, A., and Papahadjoloulos, D. (1981) *J. Membr. Biol. 59*, 115−125.
(28) Rolland, A. P. (1998) *Crit. Rev. Ther. Drug Carrier Sys. 15*, 143−198.
(29) Bielinska, A. U., Kukowska-Latallo, J. F., and Baker, J. R. (1997) *Biochim. Biophys. Acta 1353*, 180−190.
(30) Bielinska, A. U., Chen, C. L., Johnson, J., and Baker, J. R. (1999) *Bioconjugate Chem. 10*, 843−850.
(31) Junker, M., and Creutz, C. E. (1993) *Biochemistry 32*, 9968−9974.
(32) Epand, R. M., and Lim, W. (1995) *Biosci. Rep. 15*, 151−160.
(33) Bradley, A. J., Maurer-Spurej, E., Brooks, D. E., and Devine, D. V. (1999) *Biochemistry 38*, 8112−8123.
(34) Yeagle, P. L. (1996) in *Handbook of Nonmedical Applications of Liposomes, Vol. II., Models for Biological Phenomena* (D. D. Lasic and Y. Barenholz, Eds.) Chapter 5, CRC, Boca Raton.
(35) DeKrujiff, B., and Cullis, P. R. (1980) *Biochim. Biophys. Acta 602*, 477−490.
(36) DeKrujiff, B., and Cullis, P. R. (1980) *Biochim. Biophys. Acta 601*, 235−240.
(37) Balch, C., Morris, R., Brooks, E., and Sleight, R. G. (1994) *Chem. Phys. Lipids 70*, 205−212.
(38) Ben-Tal, N., Honig, B., Peitzsch, R. M., Denisov, G., and McLaughlin, S. (1996) *Biophys. J. 71*, 561−575.
(39) Kim, J., Mosior, M., Chung, L. A., Wu, H., and McLaughlin, S. (1991) *Biophys. J. 60*, 135−148.
(40) Gad, A. E., Silver, B., and Eytan, G. D. (1982) *Biochim. Biophys. Acta 690*, 124−132.
(41) Gad, A. E., Bental, M., Elyashiv, M., and Weinberg, H. (1985) *Biochemistry 24*, 6277−6282.
(42) Talbot, W. A., Zheng, L. X., and Lentz, B. R. (1997) *Biochemistry 36*, 5827−5836.
(43) Takahashi, H., Yasue, T., Ohki, K., and Hatta, I. (1996) *Mol. Membr. Biol. 13*, 233−240.
(44) Fukushima, K., Sakamoto, T., Tsuji, J., Kondo, K., and Shimozawa, R. (1994) *Biochim. Biophys. Acta 1191*, 133−140.
(45) Laroche, G., Carrier, D., and Pézolet, M. (1988) *Biochemistry 27*, 6220−6228.
(46) Fukushima, K., Muraoka, Y., Inoue, T., and Shimozawa, R. (1989) *Biophys. Chem. 34*, 83−90.
(47) Fukushima, K., Muraoka, Y., Inoue, T., and Shimozawa, R. (1988) *Biophys. Chem. 30*, 237−244.
(48) Hartmann, W., Galla, H.-J., and Sackmann, E. (1977) *FEBS Lett. 78*, 169−172.
(49) Lentz, B. (1994) *Chem. Phys. Lipids 73*, 91−106.
(50) Leckband, D. E., Helm, C. A., and Israelachvili, J. (1993) *Biochemistry 32*, 1127−1140.
(51) Ottaviani, M. F., Sacchi, B., Turro, N. J., Chen, W., Jockusch, S., and Tomalia, D. A. (1999) *Macromolecules 32*, 2275−2282.
(52) Ottaviani, M. F., Matteini, P., Brustolon, M., Turro, N. J., Jockusch, S., and Tomalia, D. A. (1998) *J. Phys. Chem. B 102*, 6029−6039.
(53) Ottaviani, M. F., Daddi, R., Brustolon, M., Turro, N. J., and Tomalia, D. A. (1999) *Langmuir 15*, 1973−1980.
(54) Ottaviani, M. F., Montalti, F., Romanelli, M., Turro, N. J., and Tomalia, D. A. (1996) *J. Phys. Chem. 100*, 11033−11042.
(55) Watkins, D. M., Sayed-Sweet, Y., Klimash, J. W., Turro, N. J., and Tomalia, D. A. (1997) *Langmuir 13*, 3136−3141.
(56) Jansen, J. F. G. A., Meijer, W. W., and De Babandander-van den Berg, E. M. M. (1995) *J. Am. Chem. Soc. 117*, 4417−4418.
(57) Chernomordik, L. V., and Zimmerberg, J. (1995) *Curr. Opin. Struct. Biol. 5*, 541−547.

(58) Epand, R. M., and Polozov, I. (1996) in *Handbook of Nonmedical Applications of Liposomes, Vol. II., Models for Biological Phenomena* (D. D. Lasic and Y. Barenholz, Eds.) Chapter 7, CRC, Boca Raton.
(59) McIntosh, T. J., Kulkarni, K. G., and Simon, S. A. (1999) *Biophys. J. 76*, 2090−2098.
(60) Siegel, D. P. (1999) *Biophys. J. 76*, 291−313.
(61) Weber, T., Zemelman, B. V., McNew, J. A., Westerman, B., Gmachi, M., Parlati, F., Söllner, T. H., and Rothman, J. E. (1998) *Cell 92*, 759−772.
(62) Koslov, M. M., and Chernomordik, L. V. (1998) *Biophys. J. 75*, 1384−1396.
(63) Markosyan, R., Melikyan, G. B., and Cohen, F. S. (1999) *Biophys. J. 77*, 943−952.
(64) Densiov, G., Wanaski, S., Luan, P., Glaser, M., and McLaughlin, S. (1998) *Biophys. J. 74*, 731−744.
(65) Kleinschmidt, J. H., and Marsh, D. (1997) *Biophys. J. 73*, 2546−2555.
(66) Xu, G. P., Solaiman, F., Zink, M. A., and Hodgson, C. P. (2000) *Cancer Gene Ther.* 7, 53−58.

BC000018Z

Synthesis of Multiacyl Poly(ethylene glycol) for the Conjugation of Cytochrome *c* to Phospholipid Vesicle

Haruki Ohkawa, Yuji Teramura, Shinji Takeoka, and Eishun Tsuchida*

Department of Polymer Chemistry, Advanced Research Institute for Science and Engineering, Waseda University, Tokyo 169-8555, Japan. Received March 6, 2000; Revised Manuscript Received August 14, 2000

To conjugate water-soluble macromolecules on the surface of phospholipid vesicles, we synthesized a poly(ethylene glycol) (PEG)-lipid having four acyl chains using a lysine (Lys)-type monodendron structure. One end of the diamino-PEG was amidified with Lys, and then two amino groups of the Lys moiety were amidified with two Lys derivatives which had been acylated with two stearoyl groups. The other end of the PEG was activated with a triazine group or a pyridyldithio group. The hydrate of the lipid mixture of dipalmitoylphosphatidylcholine, cholesterol, dipalmitoylphosphatidylglycerol, and the PEG-lipid at a molar ratio of 5/5/1/0.3 was extruded in order to prepare the phospholipid vesicles with the average diameter of 270 ± 20 nm. The coupling ratio of cytochrome *c* with the PEG-lipid was monitored by HPLC, detecting the pyridyl 2-thione liberated from the pyridyldithio group and determining it to be 26% on the basis of the incorporated PEG-lipid.

INTRODUCTION

Phospholipid vesicles or liposomes acting as vehicles for water-soluble, insoluble, or amphiphilic substances are one of the potent candidates for drug delivery systems (DDS). There are many reports on vesicles bearing immunoglobulins (immunoliposomes) or receptor proteins (proteoliposomes) that produce such site-directories (*1*−*4*). In general, these proteins are covalently coupled to the surface of the vesicles using hydrophobic anchors such as fatty acids, diacylphosphatidylethanolamine, or diacylphosphatidylinositol via various conjugation techniques. For the incorporation of transferrin (80 kDa) (*5*) or immunoglobulin G (150 kDa) (*6*), four or five acyl chains are considered to be desirable as anchors rather than two acyl chains or one diacylphospholipid.

On the other hand, the incorporation of poly(ethylene glycol) (PEG) on the surface of the vesicle, so-called PEGylation, is a useful method for the stabilization of vesicles (*7*−*9*). This modification is effective for the long-term preservation of the vesicle dispersion or the prolongation of the lifetime of the intravenously injected vesicles. However, PEGylation should mask the recognition abilities of the site-directing vesicles because it prevents the interaction of foreign molecules with the vesicular surface. Therefore, the functional water-soluble molecules should be coupled with the terminal of the PEG extending from the surface of the vesicle. There are various coupling methods, i.e., *N*-hydroxysuccinimide (NHS)-activated (*10*), triazine-activated (*11*), or isocyanate-activated PEG (*12*) to target the amino group, and pyridyldithiopropionate (PDP)-activated PEG (*13*−*15*) to target the mercapto groups via a thiol-disulfide exchange reaction (*16*).

Though the coupling with PEG-diacylphosphatidylethanolamine is useful for the incorporation of small molecules such as amino acids (*17*, *18*) or folic acid (*19*), it would sometimes be difficult for the incorporation of functional water-soluble macromolecules. This is because the hydrophobic anchor is too small to tether the large molecules onto the surface of the bilayer membrane. In fact, a considerable amount of the PEG-lipid should dissociate from the surface if the molecular weight of the PEG is greater than 5000 (*20*), and when the molecular weight was 12 500, at least four stearoyl chains should be necessary for stable conjugation. Silvius and Zuckermann reported the influence of the PEG molecular weight and the acyl chain length of the PEG-lipids on the interbilayer transfer rate (*21*). They insisted on the importance of the hydrophobicity of the anchor part for effectively decreasing the transfer rate.

We have synthesized new PEG derivatives with a reactive group at one terminal of the PEG and a large multiacyl hydrophobic group at the other terminal of the PEG using a lysine-dendron structure. Its hydrophobicity could be adjusted by changing the generation number of the dendron which would be sufficient to allow the receptor proteins to be immobilized on the surface of the vesicles (*20*).

In this study, we synthesized a tetraacyl PEG-lipid, where the PEG terminal was activated with PDP or triazine, and cytochrome *c* as a typical water-soluble protein marker was conjugated with the surface of the vesicle via the PEG-lipid by modification of a method reported by Haselgrübler *et al* (*22*).

EXPERIMENTAL SECTION

Materials. NH_2-PEG-NH_2 (MW 1900) was purchased from Fluka Chemical Co. (Switzerland) and reprecipitated twice from ether. L-Lysine, dicyclohexylcarbodiimide (DCC), triazinetrichloride, and *N*-hydroxysuccinimide (NHS) were purchased from Kanto Chemical Co. (Tokyo, Japan). The triazine was purified by recrystallization twice from methanol. The others were used without purification. 9-Fluorenylmethyl chloroformate (Fmoc-Cl), di-*tert*-butyl dicarbonate [$(Boc)_2O$], dithiothreitol (DTT), succinimidylpyridyldithiopropionate (SPDP), and cytochrome *c* were purchased from Wako Pure Chemicals Industries, Ltd. (Osaka, Japan). These reagents were used without further purification. Presome (DPPC/cholesterol/DPPG: 5/5/1, by mol) was purchased from Nippon Fine Chemical Co. (Takasago, Japan).

* To whom all correspondence should be addressed.

10.1021/bc000025n CCC: $19.00 © 2000 American Chemical Society
Published on Web 10/21/2000

Methods. (i) Thin Layer Chromatography. Plastic sheets coated with 0.2 mm silica gel 60 without a fluorescent indicator (Merck, Germany) were used for thin-layer chromatography. Eluent I was a mixture of chloroform, methanol, and water at a ratio of 8/3/1 by vol. Eluents II and III were the mixtures of chloroform and methanol at ratios of 4/1 and 9/2, respectively. Spots were detected with I_2. The existence of amino groups was detected by spraying a 10 wt % aqueous ninhydrine solution and heating to around 100 °C.

(ii) Synthesis of HO-Lys-(Boc)$_2$. According to the conventional method, L-Lys was dissolved in dioxane, $(Boc)_2O$ was added and stirred for 6 h. After the confirmation of the disappearance of the TLC spot stained by ninhydrine, the mixture was reprecipitated from hexane and recrystallized twice from hexane/ethyl acetate. Yield: 75%. R_f value, IR, ^{1}H NMR data were consistent with the literature (*20*).

(iii) Synthesis of NH$_2$-PEG-Lys-(Boc)$_2$. NH_2-PEG-NH_2 (5.49 g, 2.89 mmol) was dried in vacuo for 3 h at 70 °C. HO-Lys-$(Boc)_2$ (1.00 g, 2.89 mmol), DCC (656 mg, 3.18 mmol), NHS (366 mg, 3.18 mmol), and (dimethylamino)-pyridine (DMAP, 353 mg 2.89 mmol) were then dissolved in dry chloroform (20 mL) and stirred for 1 h at 5 °C. After filtration to eliminate dicyclohexylurea (DCU), the solution was added dropwise to the solution of NH_2-PEG-NH_2 dissolved in 15 mL of dry chloroform. The reaction mixture was stirred for 6 h at room temperature (RT), followed by evaporation and reprecipitation from cold ether (−20 °C). The precipitate was dissolved in chloroform and subjected on silica gel with flash chromatography (eluent I). After eluting with 100 mL of solvent, the silica gel including NH_2-PEG-Lys-$(Boc)_2$ was picked up and eluted again with 200 mL of solvent. The solution was evaporated, dried in vacuo, and NH_2-PEG-Lys-$(Boc)_2$ (3.22 g) was obtained as a pale yellow highly viscous liquid. Yield: 50%. R_f (eluent I) 0.35−0.50; IR (cm^{-1}, film on NaCl) 3510, 2868, 1648, 1100; ^{1}H NMR ($CDCl_3$, 500 MHz) δ 1.09−1.28 (m, 8H, $-CH_3$, 2-aminopropyl/$-CH_2$, γ-lysine), 1.42−1.48 (m, 20H, $-CH_3$, Boc/ $-CH_2$, δ-lysine), 2.62 (broad, amine), 3.60 (broad, PEG).

(iv) Synthesis of Fmoc-PEG-Lys-(Boc)$_2$. NH_2-PEG-Lys-$(Boc)_2$ (1.00 g, 0.45 mmol) was dissolved in dry chloroform (10 mL) and stirred for 30 min under an argon atmosphere. Fmoc-Cl (190 mg, 0.76 mmol) and DMAP (31 mg, 0.25 mmol) were then added and stirred for 13 h at RT. After the confirmation of the disappearance of the TLC spot stained by ninhydrine, the precipitate was filtered, evaporated and dissolved in 40 °C of benzene. The precipitate was filtered and reprecipitated twice from cold ether (−20 °C). The filtrate was dried in vacuo and purified by flash chromatography (eluent II), and 890 mg of Fmoc-PEG-Lys-$(Boc)_2$ was then obtained as a pale yellow highly viscous liquid. Yield: 81%, R_f (eluent II) 0.35−0.50; IR (cm^{-1} film on NaCl) 3332, 2868, 1714, 1648, 1108; ^{1}H NMR ($CDCl_3$, 500 MHz) δ 1.09−1.28 (m, 8H, $-CH_3$, 2-aminopropyl/$-CH_2$, γ-lysine), 1.42−1.48 (m, 20H, $-CH_3$, Boc/ $-CH_2$, δ-lysine), 2.62 (broad, amine), 3.60 (broad, PEG), 7.22−7.69 (m, 8H, Fmoc)

(v) Deprotection of the Boc Groups. Fmoc-PEG-Lys-$(Boc)_2$ (800 mg, 0.326 mol) was dissolved in a mixture of chloroform (10 mL) and trifluoroacetic acid (TFA, 15 mL) and stirred for 4 h at −20 °C under nitrogen atmosphere. The white precipitate was filtered off and precipitated twice from cold ether (−20 °C). The precipitate was dissolved in 100 mL of benzene and freeze-dried. Fmoc-PEG-Lys (688 mg) was obtained as a pale yellow gellike solid. Yield: 94%. Deprotection was confirmed from a ninhydrine test and the disappearance of Boc signal on ^{1}H NMR.

(vi) Synthesis of Lys-(stearoyl)$_2$. Lys-$(stearoyl)_2$ was synthesized according to our previous method (*20*). Lys (5.00 g, 34.2 mmol) was dispersed in dry benzene including benzyl alcohol (14.6 g, 135 mmol) and *p*-toluenesulfonic acid (14.7 g, 85.4 mmol) and refluxed for 7 h, removing the produced water until the turbid Lys dispersion became transparent. The reaction mixture was reprecipitated three times from ether. At this stage, the carboxyl group of Lys was protected with benzyl ester (yield: 91%). R_f (eluent II) 0.80; IR (cm^{-1}, film on NaCl) 3331, 2915, 1748, 1641; ^{1}H NMR ($CDCl_3$, 500 MHz) δ 0.85 (t, 6H, $-CH_3$, stearoyl), 1.27(m, 58H, $-CH_2$/$-CH_2$, γ-lysine), 1.46 (m, 2H, $-CH_2$, δ-lysine), 1.58 (m, 4H, N$-$CO$-$C$-CH_2$), 1.66−1.81 (m, 2H, $-CH_2$, β-lysine), 2.20 (dt, 4H, $-$N$-$CO$-CH_2$), 3.16(m, 2H, $-CH_2$, ϵ-lysine), 5.18 (s, 2H, $-CH_2-C_6H_5$), 7.35 (m, 5H, $-C_6H_5$).

To this ester (1.28 g, 2.20 mmol) dissolved in chloroform, the equivalent amount of triethylamine, 2.2 equiv amounts of stearic acid and DCC were added and stirred for 8 h at RT. Bzl-O-Lys-$(stearoyl)_2$ was then obtained with a high yield (1.29 g, 71%). This compound was deprotected under a NaOH condition. After recrystallization from chloroform three times, 934 mg of Lys-$(stearoyl)_2$ was obtained. Yield: 88%. Deprotection was confirmed from the disappearance of signals assigned to a benzyl group with ^{1}H NMR.

(vii) Synthesis of NH$_2$-PEG-Lys-(Lys)$_2$-(stearoyl)$_4$. Lys-$(stearoyl)_2$ (571 mg, 0.841 mmol), DCC (178 mg, 0.861 mmol), and NHS (99 mg, 0.861 mmol) were dissolved in a mixture of chloroform (15 mL) and TEA (1 mL) and stirred for 2 h at 5 °C. DCU was eliminated by filtration, then Fmoc-PEG-Lys (688 mg, 0.306 mmol) was added and stirred for 36 h at RT. The solvent was evaporated, and the reaction mixture was dissolved in chloroform and precipitated twice from ether. The filtrate was then extracted with methylene chloride (300 mL) and dried in vacuo. Thus, Fmoc-PEG-Lys-$(Lys)_2$-$(stearoyl)_4$ was obtained. R_f (eluent III) 0.68 (not stained by ninhydrine); IR (cm^{-1}, film on NaCl) 3318, 2917, 2850, 1714, 1625, 1108; ^{1}H NMR ($CDCl_3$, 500 MHz) δ 0.84 (t, 6H, $-CH_3$, stearoyl), 1.09−1.28 (m, $-CH_3$, 2-aminopropyl/$-CH_2$, γ-lysine/$-CH_2$, stearoyl), 1.42−1.48 (m, 6H, $-CH_2$, δ-lysine), 1.58 (m, 4H, N$-$CO$-$C$-CH_2$), 1.66−1.81 (m, 6H, $-CH_2$, β-lysine), 2.20 (dt, 8H, $-$N$-$CO$-CH_2$), 3.16(m, 6H, $-CH_2$, ϵ-lysine), 3.60 (broad, PEG), 7.22−7.69 (m, 8H, Fmoc).

Fmoc-PEG-Lys-$(Lys)_2$-$(stearoyl)_4$ was dissolved in the mixture of 0.1 N NaOHaq, methanol, and chloroform (10/5/0.5, by vol) and stirred for 3 h at 5 °C. The precipitate (Fmoc salt) was removed by filtration, dried in vacuo, and 378 mg of NH_2-PEG-Lys-$(Lys)_2$-$(stearoyl)_4$ was obtained as a pale yellow solid. Total yield: 37%. Deprotection was confirmed from a ninhydrine test and disappearance of Fmoc signal in ^{1}H NMR.

(viii) Synthesis of Triazine-PEG-Lys-(Lys)$_2$-(stearoyl)$_4$ (A). Triazinetrichloride (10.5 mg, 5.69×10^{-2} mmol) was dissolved in 3 mL of dry acetonitrile and substituted with nitrogen gas. The solution was cooled to −20 °C with an ice-NaCl bath. To the solution a dry acetonitrile solution containing NH_2-PEG-Lys-$(Lys)_2$-$(stearoyl)_4$ (A) (50 mg, 1.43×10^{-2} mmol) and diisopropylethylamine (2.22 mg, 1.72×10^{-2} mmol) was added dropwisely and stirred for 8 h. The mixture was washed with 700 mL of cold ether until unreacted triazinetrichloride was completely eliminated. The filtrate was extracted with benzene and freeze-dried. Triazine-PEG-Lys-$(Lys)_2$-$(stearoyl)_4$ (48.0

mg) was obtained as a pale yellow powder. Yield: 95%. R_f (eluent II) 0.33−0.51 (not stained by ninhydrine); IR (cm^{-1}, film on NaCl) 3318, 2917, 2850, 1624, 1109; ^1H NMR ($CDCl_3$, 500 MHz) δ 0.84 (t, 6H, $-CH_3$, stearoyl), 1.09−1.28 (m, $-CH_3$, 2-aminopropyl/$-CH_2$, γ-lysine/$-CH_2$, stearoyl), 1.42−1.48 (m, 6H, $-CH_2$, δ-lysine), 1.58 (m, 4H, N−CO−C−CH_2), 1.66−1.81 (m, 6H, $-CH_2$, β-lysine), 2.20 (dt, 8H, −N−CO−CH_2), 3.16(m, 6H, $-CH_2$, ϵ-lysine), 3.60 (broad, PEG).

(ix) Synthesis of PDP−PEG-Lys-(Lys)$_2$-(stearoyl)$_4$ (B). NH_2-PEG-Lys-$(Lys)_2$-$(stearoyl)_4$ (127 mg, 3.79×10^{-2} mmol) was dissolved in 2 mL of a mixed solvent containing chloroform, methanol, and 0.1 N−NaOH in a volume ratio of 10/5/0.4 and stirred under a nitrogen atmosphere for 1h. SPDP (14.8 mg, 4.75×10^{-2} mmol) was then added and stirred for 13 h at 5 °C. Benzene was added to the mixture, freeze-dried, and reprecipitated twice from ether. PDP−PEG-Lys-$(Lys)_2$-$(stearoyl)_4$ (B) (101 mg) was thus obtained as a white powder without any byproducts. Yield: 75%. R_f (eluent II) 0.44−0.59 (not stained by ninhydrine); IR (cm^{-1}, film on NaCl) 3318, 2917, 2850, 1714, 1624, 1109; ^1H NMR ($CDCl_3$, 500 MHz) δ 0.84 (t, 6H, $-CH_3$, stearoyl), 1.09−1.28 (m, $-CH_3$, 2-aminopropyl/$-CH_2$, γ-lysine/$-CH_2$, stearoyl), 1.42−1.48 (m, 6H, $-CH_2$, δ-lysine), 1.58 (m, 4H, N−CO−C−CH_2), 1.66−1.81 (m, 6H, $-CH_2$, β-lysine), 2.20 (dt, 8H, −N−CO−CH_2), 3.16(m, 6H, $-CH_2$, ϵ-lysine), 3.60 (broad, PEG), 7.05−8.43 (m, 4H, $-C_5NH_4$).

(x) Preparation of Vesicles Modified with A and B. Presome (53.9 mg, 97.5 mol %) and A (8.5 mg, 2.5 mol %) or B (8.5 mg, 2.5 mol %) were dissolved in 200 mL of benzene and freeze-dried. The mixed lipid powder was then dispersed into 100 mL of phosphate-buffered saline (PBS) and stirred for 5 h. After concentration to 15 mL by ultrafiltration (cutoff: 120 000, 45 mmϕ, Advantec Co.), the vesicles were prepared by an extrusion method. The final pore size of the membrane filters (FM series Fuji Film Co. Tokyo) were 220 nm to prepare the vesicles of about 250 nm in average diameter, which was measured by a dynamic light-scattering method (COULTER submicron particle analyzer, model; N4−SD). The incorporation ratio of the PEG-lipids (A and B) was measured by the ^1H NMR spectrum, where the choline methyl protons of DPPC were detected at 3.33 ppm (in $CDCl_3$), and the methylene protons of the PEG chain at 3.65 ppm (*23*).

(xi) Conjugation with Cytochrome c: A-Vesicle. A solution (2 mL) containing 1 mg of cytochrome *c* was added to the A-vesicle dispersion (3 mL) and stirred at 5 °C. After 0.5, 1, and 2 h, 20 μL of dispersion was sampled for an HPLC [LC-8A, Shimadzu Co., Japan, column: TSK-GEL $G3000SW_{XL}$ 7.8 mmϕ × 300 mmh, flow-rate: 1 mL/min, solvent: PBS (pH 7.4)] measurement detected at 210 and 330 nm. Cytochrome *c* was detected at 330 nm.

B-Vesicle. First, a mercapto group was introduced to cytochrome *c* by SPDP as described previously (*16*). An ethanol solution (50 μL) containing SPDP (1.6×10^{-4} mmol) was added to cytochrome *c* (2 mg, 1.6×10^{-4} mmol) dissolved in 1 mL of PBS, and stirred for 1 h at RT. Excess DTT was added and stirred for 0.5 h at 5 °C. The cytochrome *c* was purified by gel permeation chromatography (Sepharose G-25: Pharmacia). Conjugation of the cytochrome *c* to the B-vesicle was carried out in the same way as A-vesicle. The amount of cytochrome *c* conjugated to the B-vesicle was estimated by quantitation of the 2PT formed by thiol-disulfide exchange, which had a specific absorbance at 343 nm. The reaction was monitored with HPLC detected at 210 and 343 nm. After 3 h, 1 mL of the reaction mixture was sampled, and DTT (0.3 mg) was added and stirred for 0.5 h to detect the amount of the unreacted PDP group from 2TP. The HPLC measurement was then carried out to study the reaction ratio of the PDP group, namely, the amount of cytochrome *c* conjugated with the surface of the vesicle via disulfide linkage.

RESULTS AND DISCUSSION

Synthesis of PEG Derivatives. To immobilize proteins on the surface of the vesicle, we designed PEG-lipids having a triazine or a PDP, which can react with the amino group or the mercapto group of the proteins, respectively. An orthogonal synthetic procedure was applied for the syntheses of the PEG-lipids using the diamino-PEG, Fmoc, and Boc as protecting groups (Scheme 1).

Lysine, of which two amino groups were protected with Boc, was bound to one terminal amino group of the PEG. This reaction was performed using a DCC-additive method. The low yield was caused by the difficult purification though flash chromatography was utilized for the purification. During elution, the bands of the PEG derivatives were broadened and overlapped each other. Next, the reaction of the other terminal amino group of the PEG with Fmoc-Cl stoichiometrically proceeded. The deprotection of the Boc groups was carried out with TFA, and the resulting amino groups were reacted with two equivalent amounts of distearoyl lysine using a DCC-additive method. Thus, a PEG derivative with four acyl chains at one end and a Fmoc group at the other end was obtained. Four acyl chains were confirmed based on the ^1H NMR spectra, where the integral ratio of the Fmoc group to the terminal methyl groups of the acyl chains was 8/12 (Figure 1A).

The PEG derivative with four acyl chains was treated with NaOH for the deprotection of the Fmoc group to obtain NH_2-PEG-Lys-$(Lys)_2$-$(stearoyl)_4$. The deprotection was confirmed with TLC using a ninhydrine-staining method. The intermolecular hydrogen bonding at the lysine dendron group might reduce the solubility in chloroform, which was indicated by the IR spectra where the C=O stretching band appeared in 1624 cm^{-1}. The low solubility or gelation of the compound made the treatment difficult. Since purification was not performed by chromatography, it was reprecipitated from cold methylene chloride. Very interestingly, the solubility of the compound became high if the terminal amino group was changed to the triazine or PDP group. This suggests the involvement of the terminal amino group in the intermolecular hydrogen bonding.

The activation of the PEG derivatives was accomplished according to Scheme 2. An excess amount of triazine was added to the solution of NH_2-PEG-Lys-$(Lys)_2$-$(stearoyl)_4$ for the synthesis of only the monosubstituted derivative. After a reaction in dried acetonitrile, the unreacted triazine was removed by precipitation with ether until the TLC spot attributed to triazine disappeared. A single spot on the TLC indicated no impurities.

The activation with SPDP was performed under basic conditions and a nitrogen atmosphere so as not to produce byproducts such as disulfide derivatives or the protonated pyridyl group. We did not use pyridine as a base because it is difficult to remove the pyridine without heating. The PDP group is weak against heat treatment. When we used aqueous NaOH as the base, the solvent and impurities could be easily removed by filtration after freeze-drying the solution and dissolving it in benzene. On the basis of the ^1H NMR spectrum (Figure 1B), the

Scheme 1. Synthesis of NH_2-PEG-Lys-$(Lys)_2$-$(stearoyl)_4$

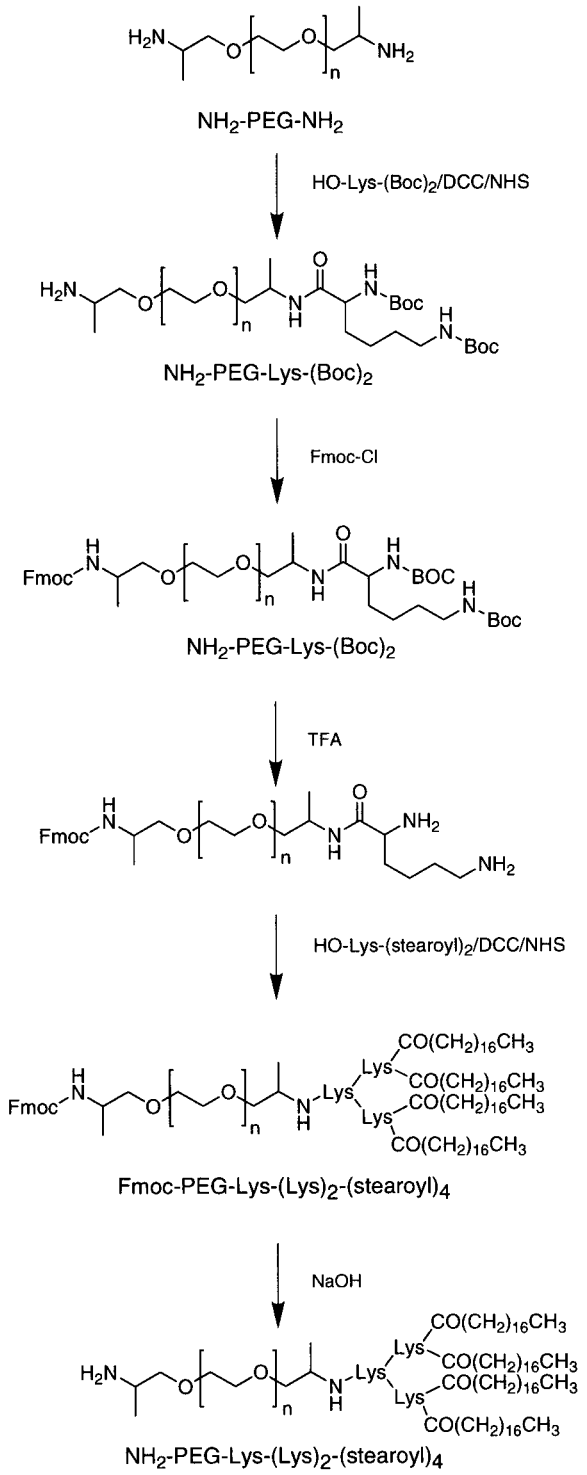

integral ratio of the peaks at 7.05−8.43 (PDP) and 0.84 ppm (CH_3 protons of stearoyl chains) shows that the PDP group was almost quantitatively attached to the other terminal of the PEG.

Preparation of vesicles modified with A and B. We found that the mixed lipids containing the tetraacyl PEG-lipids was hard to hydrate, therefore, we hydrated the lipids with a large volume of PBS and concentrated it by ultrafiltration before extrusion. Vesicles with diameters of 258 nm (**A**-vesicles), and 290 nm (**B**-vesicles) were prepared by the extrusion method. Extrusion through membrane filters with a 3μm pore size was difficult when

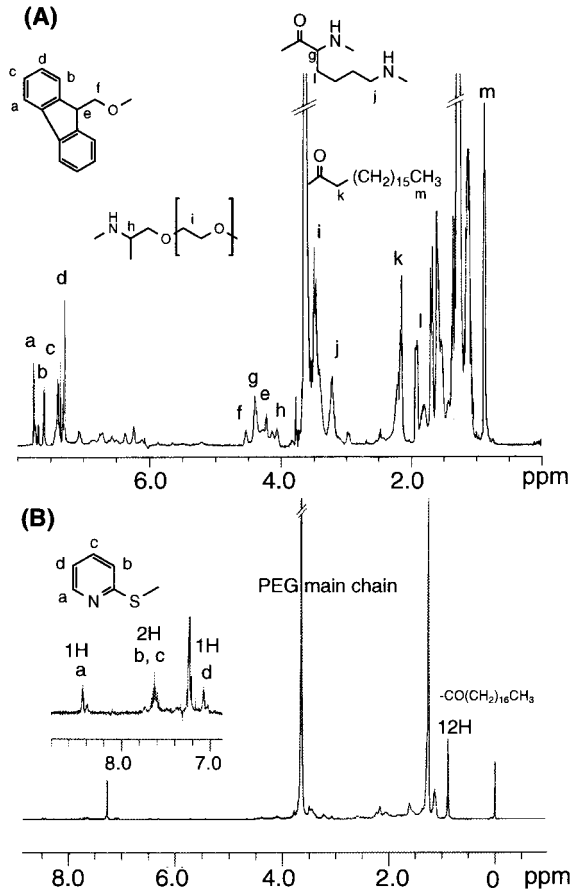

Figure 1. ^{1}H NMR spectrum (500 MHz) of PEG derivatives. (A) Fmoc-PEG-Lys-$(Lys)_2$-$(stearoyl)_4$ in $CDCl_3$ (enlarged). The Fmoc group has specific signals around 7.2−7.7 ppm. The integral ratio of Fmoc protons to methyl protons belonging to the stearoyl chain was 8/12, indicating that four acyl chains were attached at the other termini of PEG. (B) PDP-PEG-Lys-$(Lys)_2$-$(stearoyl)_4$ in $CDCl_3$. Inset is an enlargement of the signals around 7.0−8.4 ppm, which were assigned to a PDP group. This indicates that the Fmoc group was substituted with a PDP group.

compared with the extrusion of vesicles without the PEG-lipid. It is suggested that a part of the PEG-lipids would not completely dissolve due to the strong intermolecular hydrophobic interaction and hydrogen bonding (*20*).

As shown in Figure 2, the PEG-lipid (B) was incorporated into the vesicle; a signal from the PDP group could be detected at around 7.3 ppm together with the methylene peak of the PEG (3.64 ppm) and the choline methyl peak of the phospholipids (3.32 ppm). This indicates the existence of PDP groups on the surface of the vesicles. In the same way, it is considered that triazine groups exist on the A-vesicles, though the ^{1}H NMR signals assigned to the triazine could not be detected (triazine does not have any protons). Instead, the amount of PEG existing on the surface of the A-vesicle can be estimated from the ^{1}H NMR spectra (*23*). The incorporation ratios of the PEG-lipids, A and B, into the vesicle were 54 and 61%, respectively, indicating some were filtered out. We are now trying the incorporation of the PEG-lipid to the vesicles after preparation of the vesicles or the detergent dialysis method in order to improve the incorporation ratio. It is noted that the diameter of the vesicles did not change for at least 2 months as shown in Table 1, suggesting that PEG chains extending from the surface of the vesicle should contribute to the high dispersing ability.

Scheme 2. Activation of NH_2-PEG-Lys-$(Lys)_2$-$(stearoyl)_4$ with Triazine or SPDP for Synthesis of Amino or Mercapto-Attacking Reagents

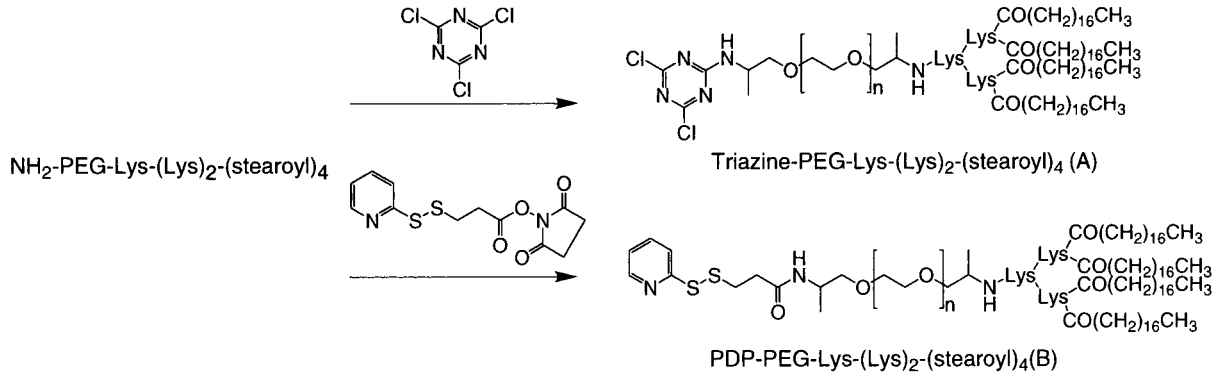

Table 1: Characterization of Vesicles Containing A and B

	A	B
diameter[a] (nm)	258 ± 42	290 ± 45
diameter[b] (nm)	263 ± 69	302 ± 51
diameter after conjugation (nm)	361 ± 140[c]	304 ± 66[d]
incorporation ratio[e] (%)	54	61
molar ratio of PEG (mol%)	1.4	1.5
exposed PEG[f] (mol%)	0.35	0.38

[a] Measured after extrusion. [b] Measured 2 months after. [c] Measured after 3 h mixing. Increase of diameter was observed. [d] Measured after 3 h mixing. [e] Quantitated by ^{1}H-NMR spectra (500 MHz, in $CDCl_3$). [f] Calculated as the vesicle with two bilayer membranes.

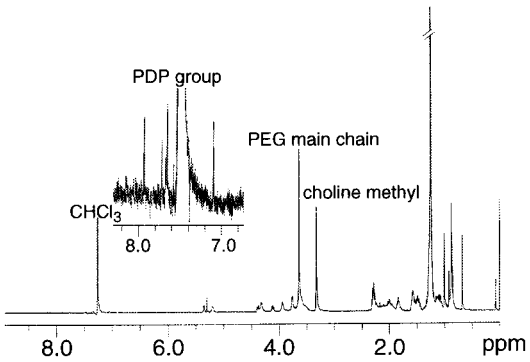

Figure 2. ^{1}H NMR spectrum (500 MHz) of the vesicle containing PDP activated PEG-lipid B in $CDCl_3$. The signals assigned to the methyl protons of the phosphatidylcholine and methylene protons of PEG were detected together with that of the PDP group, indicating the incorporation of the PEG-lipid into the phospholipid vesicle.

Conjugation with Cytochrome c to the Vesicle. The conjugation of cytochrome *c* to the surface of the vesicles via the triazine-activated PEG-lipid (A) was monitored by HPLC. As shown in Figure 3, the elution times of the vesicle and cytochrome *c* were 5 and 10 min, respectively. The coupling between the PEG-lipid and cytochrome *c* was completed within 30 min because the peak of cytochrome *c* did not change after 30 min. After 3 h, the integral value of the vesicle peak increased due to the increase in the diameter of the vesicles to 361 ± 140 nm (Table 1). This would not be caused by the aggregation of vesicles but by the cross-linking of vesicles through cytochrome *c* and the triazine group of PEG on the surface of the vesicles. Therefore, we added amino acids such as glycine in order to deactivate the remaining activated group.

In the case of the triazine-activated vesicles, though cytochrome *c* was surely detected in the vesicle fraction

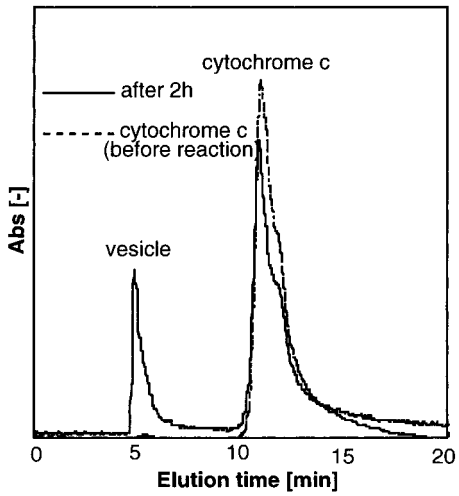

Figure 3. Conjugation of cytochrome *c* to the A-vesicle. The elution speed was 1 mL/min. For the detection of cytochrome *c*, 330 nm was used. The solid line is the elution curve of the mixture after 2 h reaction. The dotted line is the elution curve of the cytochrome *c* solution, containing the same amount of cytochrome *c* as the reaction mixture.

Table 2: Quantitation of Consumed PDP Groups by HPLC Analysis

A: consumed PDP after 3 h mixing	2.54×10^{-8} mol
B: consumed PDP by DTT	7.19×10^{-8} mol
yield: $[A/(A + B)] \times 100$	26.3%

by HPLC, it is difficult to distinguish the cationic cytochrome *c* merely adsorbed on the negatively charged surface of the vesicles from that covalently bound to the surface. We used the PDP-activated vesicle (B-vesicle) because the 2PT release was accompanied by the reaction of the PDP-activated PEG with cytochrome *c*. 2PT shows a specific absorption band at 343 nm as evidence of coupling. By combination with HPLC, 2PT is isolated and quantified in order to determine the amount of the coupled proteins (*24*). We adopted the constant elution curve obtained after 3 h mixing for analysis. The elution times of the vesicles, cytochrome *c*, and 2PT were 5, 10, and 15 min, respectively, as shown in Figure 4. The concentration of the unreacted PDP groups exposed on the surface of the vesicle was measured by adding excess DTT. Although DTT also shows a small absorption at 343 nm (*24*), the elution time (13 min) of DTT was different from that of 2PT (15 min in HPLC). The yield was then calculated from the ratio of the integral values of the peak assigned to 2PT (Table 2).

As a result, 26% of the PDP groups reacted with the cytochrome *c*, because the number of bilayer membranes

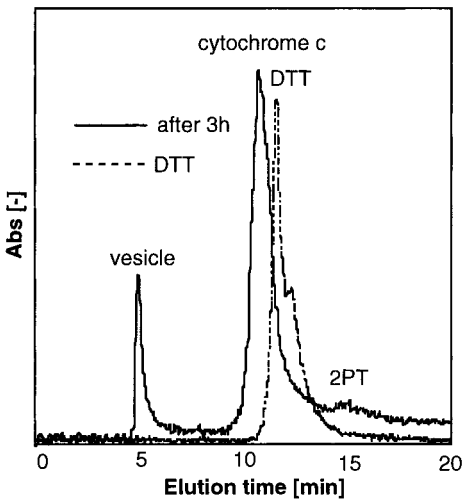

Figure 4. Conjugation of cytochrome *c* to the B-vesicle. The elution speed was 1 mL/min. The detection wavelength was 343 nm which was the λ_{max} of 2PT. The solid line is the elution curve of the mixture after 3h reaction. Peaks assigned to the vesicle, cytochrome *c*, and 2PT were detected after 5, 10, and 15 min, respectively. The dotted line is the elution curve of DTT. The difference in the elution times of DTT (13 min) and 2PT (15 min) allows to determine the amount of 2PT namely cytochrome *c* conjugated to the B-vesicle.

of the vesicles (250 nm) prepared by an extrusion method is approximately two as described in the literature (*25*). A 1.53 mol % amount of the PEG-lipid (B) would be incorporated into the vesicles, and 0.38 mol % was calculated to be exposed outside the vesicles. The consumed PEG-lipid was then at most 0.10 mol % (0.38 mol % × 0.26); namely, the concentration of cytochrome *c* on the surface of the vesicle was 0.10 mol % on the basis of the lipids existing on the surface of the vesicle. This means that about 400 cytochrome *c* molecules were conjugated on one vesicle. Such a low yield was also reported in a similar experiment for the conjugation of IgG to a vesicle (*22*).

The relatively low reaction ratio (26%) of cytochrome *c* conjugation might be explained in terms of the location of the PDP groups. Namely, one possibility is that the hydrophobic PDP group would exist in the core region of the entangled PEG and be shielded by the steric hindrance of the PEG chain. The other is that the hydrophobic PDP group would be inserted into the hydrophobic part of the bilayer membrane. If the coupling of cytochrome *c* with the PEG-lipid (B) would be carried out by using mixed micelles comprising surfactants such as sodium cholate, which are not bilayer forming surfactants, the reaction ratio should be improved in the case of the latter hypothesis.

We isolated the cytochrome *c*-conjugated vesicles by ultracentrifugation (33 000 rpm, 1 h) and applied them to the HPLC (210, 330 nm for detection) after redispersion. Only one peak was detected in the void volume, which was attributed to the vesicles. The same experiment was performed for the vesicles comprising DPPC/choresterol/DPPG/DPPE (5/5/1/0.29) where cytochrome *c* was conjugated with the DPPE by SPDP in the same way. We confirmed a new peak besides the peak in the void volume in the HPLC elution curve after every ultracentrifugation (data not shown). It was considered to be the assemblies of the cytochrome *c*-conjugated DPPE, indicating that some portion of the cytochrome *c*-conjugated DPPE would be dissociated from the vesicles. The above data support the stable conjugation of cytochrome *c* on the surface of the vesicle by the tetraacyl PEG-lipid rather than by the diacyl PEG-lipid. This trend agrees with the data that the PEG, with a molecular weight of 12 500 (approximately as large as that of cytochrome *c*), would be stably conjugated on the surface of the vesicles if coupled with the tetraacyl anchor (*20*).

CONCLUSIONS

An effective incorporation of the large hydrophobic part into PEG-lipids was designed in order to realize the conjugation of large water-soluble macromolecules or receptor proteins on the surface of the vesicle. We synthesized heterobifunctional PEG derivatives with four stearoyl chains attached to the terminal of a lysine dendron with PDP or triazine as the reactive groups at the other terminal of the PEG, and confirmed the coupling of cytochrome *c* to the activated PEG-lipids in the bilayer membrane. The stable conjugation of larger macromolecules would be possible if the generation number of lysine dendrons would be increased for the further introduction of acyl chains.

ACKNOWLEDGMENT

This work was supported by Health Science Research Grants (Artificial Platelets), Research on Advanced Medical Technology, Ministry of Health and Welfare, Japan and grants-in-aid from the Ministry of Education, Science, Sports, and Culture, Japan (No. 11877172, 12558112).

LITERATURE CITED

(1) Heath, T. D., and Martin, F. J. (1986) The development and application of protein-liposome conjugation techniques. *Chem. Phys. Lipids 40*, 347−358.

(2) Chua, M. M., Fan, S. T., and Karush, F. (1984) Attachment of immunoglobulin to liposomal membrane via protein carbohydrate. *Biochim. Biophys. Acta 800*, 291−300.

(3) Ansell, S. M., Tardi, P. G., and Buchkowsky S. S. (1996) 3-(2-pyridyldithio)propionic acid hydrazide as a cross-linker in the formation of liposome-antibody conjugates. *Bioconjugate Chem. 7*, 490−496.

(4) Martin, F. J., and Papahadjopoulos, D. (1982) Irreversible coupling of immunoglobulin fragments to preformed vesicles.-An improved method for liposome targeting. *J. Biol. Chem. 257*, 286−288.

(5) Afzelius, P., Demant, E. J. F., Hansen, G. H., and Jensen, P. B. (1989) Covalent modification of serum transferrin with phospholipid and incorporation into liposomal membranes. *Biochim. Biophys. Acta 979*, 231−238.

(6) Huang, A., Tsao, Y. S., Kennel, S. J., and Huang, L. (1982) Characterization of antibody covalently coupled liposomes. *Biochim. Biophys. Acta 716*, 140−150.

(7) Klibanov, A. L., Maruyama, K., Torchilin, V. P., and Huang, L. (1990) Amphipatic poly(ethylene glycol)s effectively prolong the circulation time of liposome, *FEBS Lett. 268*, 235−237.

(8) Sakai, H., Takeoka, S., Park, S. I., Kose, T., Nishide, H., Izumi, Y., Yoshizu, A., Kobayashi, K., and Tsuchida, E. (1997) Surface modification of hemoglobin vesicles with poly(ethylene glycol) and effects on aggregation, viscosity, and blood flow during 90% exchange transfusion in anesthetized rats. *Bioconjugate Chem. 8*, 23−30.

(9) Zalipsky, S. (1995) Functionalized poly(ethylene glycol) for preparation of biologically relevant conjugates. *Bioconjugate Chem. 6*, 150−165.

(10) Harris, J. M., (1990) Introduction to biotechnical and biomedical applications of poly(ethylene glycols). In *poly(ethylene glycol), Chemistry: Biotech. Biomed. Appl.* (J. M. Harris, Ed.) pp 1−14, Plenum Press, New York.

(11) Takahashi, K., Ajima, A., Yoshimoto, T., Okada, M., Matsushima, A., and Inada, Y. (1985) Chemical reactions by poly(ethylene glycol) modified enzymes in chlorinated hydrocarbons. *J. Org. Chem. 50*, 3414−3415.

(12) Greenwald, R. B., Pendri, A., and Bolikal, D. (1995) Highly water soluble taxol derivatives: 7-poly(ethylene glycol) carbamates and carbonates. *J. Org. Chem. 60*, 331−336.
(13) Bettinger, T., Remy, J. S., Erbacher, P., and Behr, J. P. (1998) Convenient polymer-supported synthetic route to heterobifunctional polyethylene glycols. *Bioconjugate Chem. 9*, 842−846.
(14) Kaiser, K., Marek, A., Haselgrübler, T., Schindler, H., and Gruber, H. J. (1997) Basic studies of heterobifunctional biotin-PEG conjugates with a 3-(4-pyridyldithio)propionyl marker on second terminus. *Bioconjugate Chem. 8*, 545−551.
(15) Herman, S., Loccufier, J., and Schacht, E. (1994) End-group modification of α-hydro-ω-methoxy-poly(oxyethylene), 3-facile methods for introduction of a thiol-selective reactive end-group. *Macromol. Chem. Phys. 195*, 203−209.
(16) Carlsson, J., Drevin, H., and Axen, R. (1978) Protein thiolation and reversible protein−protein conjugation- Succinimidyl 3-(2-pyridyldithio)propionate, a new heterobifunctional reagent. *Biochem. J. 173*, 723−737.
(17) Schulze, U., Schmidt, H. W., and Safinya, C. R. (1999) Synthesis of novel cationic poly(ethylene glycol) containing lipids. *Bioconjugate Chem. 10*, 548−552.
(18) Zalipsky, S., Mullah, N., Harding, J. A., Gittelman, J., Guo, L., and Defrees, S. A. (1997) Poly(ethylene glycol)-grafted liposomes with oligopeptide or oligosaccharide ligands appended to the termini of the polymer chains. *Bioconjugate Chem. 8*, 111−118.
(19) Gabizon, A., Horowitz, A. T., Goren, D., Tzemach, D., Mandelbaum-Shavit, F., Qazen, M. M., and Zalipsky, S. (1999) Targetting folate receptor with folate linked to extremities of poly(ethylene glycol)-grafted liposomes: in vitro studies. *Bioconjugate Chem. 10*, 289−298.
(20) Takeoka, S., Mori, K., Ohkawa, H., Sou, K., and Tsuchida, E. (2000) Synthesis and assemblies of poly(ethylene glycol)-lipids with mono-, di-, and tetraacyl chains and a poly(ethylene glycol) chain of various molecular weights. *J. Am. Chem. Soc. 122*, 7927−7935.
(21) Silvius, J. R., and Zuckermann, M. J. (1993) Interbilayer transfer of phospholipid-anchored macromolecules via monomer diffusion. *Biochemistry 32*, 3153−3161.
(22) Haselgrübler, T., Amerstorfer, A., Schindler, H., and Gruber, H. J. (1995) Synthesis and applications of a new poly(ethylene glycol) derivatives for the cross-linking of amine with thiols. *Bioconjugate Chem. 6*, 242−248.
(23) Yoshioka, H. (1991) Surface modification of haemoglobin-containing liposomes with poly(ethylene glycol) prevents liposome aggregation in blood plasma. *Biomaterials 12*, 861−864.
(24) Na, D. H., Woo, B. H., and Lee, K. C. (1999) Quantitative analysis of derivatized proteins prepared with pyridyl disulfide-containing cross-linkers by high-performance liquid chromatography. *Bioconjugate Chem. 10*, 306−310.
(25) Takeoka, S., Ohgushi, T., Terase, K., Ohmori, T., and Tsuchida, E. (1996) Layer-controlled hemoglobin vesicles by interaction of hemoglobin with a phospholipid assembly. *Langmuir 12*, 1755−1759.
(26) Roberts, W. L., Kim, B. H., and Resenberry, T. L. (1987) Differences in the glycolipid membrane anchors of bovine and human erythrocyte acetylcholinesterases. *Proc. Natl. Acad. Sci. U.S.A. 22*, 7817−7821.
(27) Rifkin, M. R., and Landsberger, F. R. (1990) Trypanosome variant surface glycoprotein transfer to target Membranes: a model for the pathogenesis of trypanosomiasis. *Proc. Natl. Acad. Sci. U.S.A. 87*, 801−805.

BC000025N

Anchor-Chain Molecular System for Orientation Control in Enzyme Immobilization

Wen-Hai Shao,† Xian-En Zhang,* Hong Liu, and Zhi-Ping Zhang

Wuhan Institute of Virology, Chinese Academy of Sciences, Wuhan, 430071, P. R. China

Anthony E. G. Cass

Department of Biochemistry, Imperial College of Science, Technology & Medicine, South Kensington, London SW7 2AY, U.K. Received March 20, 2000; Revised Manuscript Received July 13, 2000

An anchor-chain molecular system was constructed for controlled orientation and high activity in enzyme immobilization. A streptavidin recognition peptide (streptag) coding sequence was fused to the 3′ end of the phoA gene, which codes for *E. coli* alkaline phosphatase (EAP). Both the wild-type (WT) and the Asp-101 → Ser (D1O1S) mutant were modified with the streptag sequence with or without the insertion of a flexible linker peptide [-(Gly-Ser)$_5$-] coding sequence. The fused genes were cloned into the vector pASK75 and expressed in the periplasm of the host cell *Escherichia coli* SM547. The proteins were released by osmotic shock and purified by ion-exchange chromatography. Enzyme activities of all proteins were measured spectrophotometrically with *ρ*-nitrophenyl phosphate as the substrate. Specific activities of D101S-streptag and D101S-linker-streptag enzymes were increased 25- or 34-fold over the WT, respectively. These fusion proteins were then immobilized on microtiter plates through streptag−streptavidin binding reaction. After immobilization, the D101S-linker-streptag enzyme displayed the highest residual activity and the ratio of enzyme activities of the linker to nonlinker enzymes was 8.4. These results show that the addition of a linker peptide provides a spacer so as to minimize steric hindrance between the enzyme and streptavidin. The method provides a solution for controlled enzyme immobilization with high recover activity, which is especially important in construction of biosensors, biochips, or other biodevices.

INTRODUCTION

Understanding the properties of immobilized proteins is critical to the optimal design of biosensors, bioseparations, bioreactors, and the production of bioelectronic devices will undoubtedly demand much better control of the positioning and assembly of biomolecular materials as well as high retention of biological activity. Protein patterning, the defined spatial localization of molecules on a surface, is a powerful approach to generate molecular arrays for analytical or bioelectronic applications and similarly demands a high degree of molecular control over the orientation of the molecules on the surface.

In most circumstances, however, immobilization chemistries require a significant amount of enzyme. Likewise, immobilized enzymes very often show reduced reaction rates and product yields (*1*). This is mainly due to the multisite attachment, multiple orientations, and steric hindrance that result from nonspecific chemical cross-linking of protein to surface. Attempts have been made to solve the problems by more precisely defined protein−surface interations. Examples include site-specific attachment to gold surfaces by introducing a single cysteine residue into the cysteine-free enzyme (*2*), orientational control of enzymes by the use of nonporous hydroxyalkyl methacrylate solid support (*3*), and oriented immobilization of antibodies by the use of immobilized protein A or G (*4*).

One of the most promising methods is to use fusion protein technology. Fusion proteins, comprising separate protein sequences have been widely used as aids to expression and purification of recombinant proteins. The gene for the protein of interest is fused to a sequence that codes for a protein or peptide, which in turn binds to a specific molecular structure on the surface. Many of these expression/purification systems are commercially available, and their basic characteristics have been reviewed (*5*). These fusion sequences can also be used to immobilize proteins on surfaces for sensing or molecular electronic applications. The efficiency of immobilization depends on the carrier, immobilization method, and initial enzyme concentration. Gritsch et al. (*6*) described the binding of a poly (His) fusion protein to surfaces coated with metal-chelating self-assembled lipid monolayers. Recently, a method was described for photopatterning surfaces with biotin (*7*) and biotinylated EAP bound via a streptavidin bridge. An alternative to biotinylation is to use a streptavidin binding peptide sequence (streptag). The streptag sequence was created by selection from a genetic fusion peptide library by its ability to bind to streptavidin in a specific and reversible manner (*8*). Streptavidin is usually preferred to avidin, due to its lower nonspecific binding characteristics and high resistance to denaturation (*9*).

An EAP-streptag fusion protein system has been characterized (*10*) and, although the activity of the fusion protein was lower than WT, the work demonstrated the potential use of the avidin−biotin system for protein immobilization under mild conditions.

Escherichia coli alkaline phosphatase (EC 3.1.3.1, EAP) is a homodimeric zinc metalloprotein that has been

* To whom correspondence should be addressed. Phone/Fax: +86 (0)27 87641492. E-mail: x.zhang@pentium.whiov.ac.cn.

† Current address: Department of Biology, Xuzhou Normal University, Jiangsu province, 221009, P. R. China.

10.1021/bc000029s CCC: $19.00 © 2000 American Chemical Society
Published on Web 11/01/2000

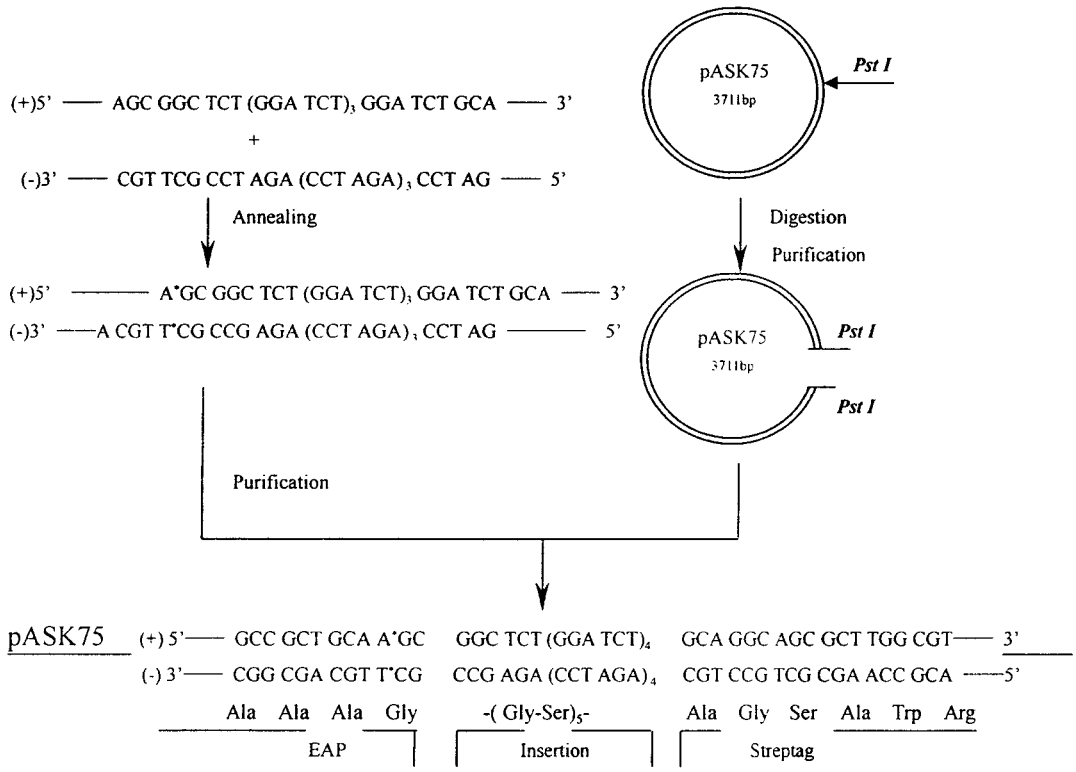

Figure 1. Strategy of linker insertion. An asterisk (*) indicates modified amino acid residues, which leads to elimination of the restriction enzyme site at the 5′ termination of linker. The insertion fragment must be designed to be subject to the enzyme *Pst*I. The synthesized oligos contain an overlap at both ends to adapt to the catalytic reaction of *Pst*I.

extensively characterized (*11*−*13*). Its broad substrate specificity means that the enzyme activity can be readily measured when immobilized using either colorimetric or fluorescent end-point detection. The major drawback of the enzyme in analytical applications is its relatively low activity. Several point mutations in the vicinity of the active site have been shown to alter the enzymatic activity. In particular, data from the introduction of a serine hydroxyl group at position 101 suggests that the mutant enzyme achieves a quicker catalytic turnover by allowing faster product release (*14*, *15*).

Since direct fusion of streptag to EAP led to a 50% loss of enzyme activity (*7*), we sought to improve on this by inserting a linker peptide between the C-terminus of EAP and the streptag sequence. This was thought to provide a sufficiently flexible spacer for both proteins to remain in native conformation. This may improve the control of the orientation of enzyme during immobilization, so resulting in a high recovery activity.

EXPERIMENTAL PROCEDURE

Materials. Agar, agarose, ampicillin (Amp), *ρ*-nitrophenyl phosphate (pNPP), and streptavidin were purchased from Sigma Chemical Co. Tryptone and yeast extract were obtained from England OXOID. Restriction endonucleases were products of either GIBCO BRL or Promega Co. Kits used for the extraction of plasmid and the isolation of DNA fragments from agarose gels were purchased from QIAGEN. T4 DNA ligase was obtained from GIBCO BRL.

A stirred cell system used for protein concentration was purchased from FILTRON. A Titertek Uniscan microplate reader was used to measure the activity of the immobilized enzymes. Purification was accomplished using a Q Sepharose (Sigma) ion-exchange chromatography column. The single strand oligonucleotide coding for the linker peptide was commercially obtained from Sangon (Shanghai, China). The *E. coli* strain SM547 and the plasmid pEK48 kindly donated by professor Kantrowitz and pASK75 was purchased from Biometra.

Construction of Fusion Proteins. The EAP-streptag fusion proteins were generated by cloning phoA into the plasmid pASK75 (*10*). The linker peptide oligonucleotide was annealed into double-strand DNA prior to mixing with pASK75, which had been previously cut with *Pst*I (Figure 1). The mixture was treated with T4 DNA ligase overnight at 14 °C, followed by transforming into competent *E. coli* SM547 cells and plating on LB medium plates containing 100 *μ*g/mL Amp and 40 *μ*g/mL 5-bromo-4-chloro-3-indolyl phosphate (BCIP) (w/v). Twelve of the blue colonies (displaying EAP activity) were selected, and plasmid DNA was isolated. Each of the plasmid candidates was first checked for the correct size by agarose gel electrophoresis and then analyzed by PCR. A plasmid, which contained the correct inserted linker peptide sequence, was isolated. The construction of plasmids containing the mutation was accomplished by cutting both plasmid pASK75 and the D1O1S mutant plasmid pEK48 (X.-E. Zhang et al., unpublished results) with the restriction enzymes *Tth*111 I and *Bstx*I. Digestion with these enzymes produced a fragment of the *pho*A gene containing the mutational site. The strategy was to replace the fragment from the mutant plasmid pEK48. To ensure that the fragment from the WT gene was not able to religate, the pASK75 backbone was removed from an agarose gel after electrophoresis using QIAquick Gel Extraction Kit. Transformation into competent *E. coli* SM547 cells was performed. The mixture was plated on LB medium plate. The isolation of the target plasmid was accomplished as before. DNA sequencing results also confirmed that the linker peptide and the new mutational sites were introduced.

Protein Purification. Cells were grown at 37 °C in LB medium containing 100 *μ*g/mL Amp with shaking

until the absorbance at 600 nm reached 0.5. Expression was then induced by the addition of isoprophylthio-β-D-galactoside (IPTG) (for cells containing pEK48) or Tetracycline (for cells containing pASK75) to a final concentration of 1 mM or 0.2 μg/mL (w/v), respectively. After the bacterial cells were grown for 20 h, they were harvested by centrifugation. The fusion protein was released by osmotic shock according to the method of Brockman and Heppel (*16*). The supernatant containing the fusion proteins were combined and purified using Q Sepharose ion-exchange chromatography.

Initially, the column was washed with 20% ethanol (v/v) and then equilibrated with 10 mM Tris (TMZP buffer, 100 mM Tris containing 1×10^{-3} M $MgCl_2$, 1×10^{-4} M NaH_2PO_4, 3.1×10^{-3} M NaN_3, and 1×10^{-5} M $ZnSO_4$, pH 7.4). The protein was applied to the column in the same buffer and unbound protein was eluted with equilibration buffer. The protein was eluted using a salt gradient in the TMZP buffer, and 8 mL fractions were collected and tested for EAP activity. Proteins were concentrated using the FILTRON stirred cell system. Final protein preparations were stored at −20 °C in TMZP buffer. Protein concentration and purity were determined by using Bio-Rad Assay Kit with bovine serum albumin as the standard and SDS−PAGE, respectively.

Kinetic Assays. EAP is catalytically active at relatively high pH values. The enzyme is most active at pH 10.0, and accordingly, all reactions were carried out at that pH in 1 M Tris buffer. ρNPP was used as an EAP substrate to measure the enzymatic activities spectrophotometrically and, hence, determine the kinetic parameters. The release of ρ-nitrophenolate (ρNP) was monitored at 405 nm. A total of 3 μL of enzyme solution was added to the microtiter wells containing 33 μL of 3 M Tris-HCl (pH 10.0) and 64 μL of ρNPP (50 mM Tris-HCI buffer; 1 mM $MgCl_2$; pH 10.0). The reaction mixture was incubated for 1 min at 25 °C. The absorbance at 405 nm in each well of the plate was then read after subtraction of the blank value for each dilution.

The activity assays after immobilization were performed as described below. A total of 100 μL of 100 μg/mL streptavidin was applied to each well of the microtiter plate and incubated for 1 h at 4 °C. The plate was washed three times with distilled water and subsequently blocked for 4 h in 3% BSA solution (w/v). After washing, 100 μL of 10 μg/mL EAP fusion protein was added and incubated for 30 min. Unbound enzyme was removed by washing three times. Finally, 100 μL of ρNPP solution (20 mM ρNPP and 1 M Tris-HCl, pH 10.0) was added. The color signal was developed for 2 min. The absorption values were determined using a microplate reader and data were reported as A_{405} values for the sample wells after subtraction of the blank value. The measurements were repeated three times.

Protein Immobilization. One microliter of 100 μg/mL streptavidin was applied to each well of the glass slide and incubated for 4 h at 4 °C. After removal of the solution, the plate was blocked with 3% BSA solution (w/v), and incubated for 4 h. After washing, 1 μL of 10 μg/mL EAP fusion protein was applied and incubated for 2 h. Unbound enzymes were removed by washing three times with distilled water. Finally, 1 μL of NBT/BCIP (another EAP substrate, diluted 4:4:25 in buffer supplied by the HuaMei manufacturer) was added. Color change was seen within 10 min. Unless stated otherwise, the experiments were performed at room temperature (25 °C).

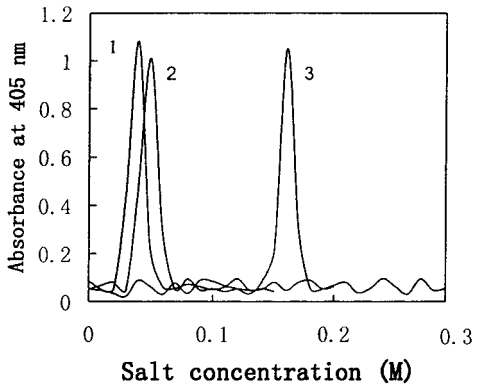

Figure 2. Elution pattern of the proteins. Peak 1, EAP-streptag; peak 2, EAP; peak 3, EAP-linker- streptag.

RESULTS

Alteration of Elution Peak. All proteins had the same elution peak profile, but required different ionic strengths of the eluting buffer. The WT and fusion protein containing streptag can be eluted from the column by using 0 to 0.1 M NaCI concentration gradient solution. However, the WT was eluted at 0.058 M NaCI, while the WT-streptag fusion protein was eluted at 0.046 M NaCl. The insertion of linker peptide required a higher ionic strength and was eluted at 0.17 M NaCl (Figure 2). All samples were eluted at the same flow rate and dissolved in the same buffer.

Kinetic Properties of EAP Fusion Proteins. Table 1 lists the EAP fusion proteins that were constructed and the kinetic constants. Replacement of Asp 101 by Ser in EAP has a large effect on k_{cat}. The k_{cat} and K_m of WT EAP streptag fusion protein are similar to the wild-type. The fusion protein D101S-streptag has about a 9- and 11-fold increase of k_{cat} value over the WT and WT-streptag fusion protein, respectively. The insertion of the linker into the D101S-streptag fusion protein resulted in slight increase of k_{cat} value. The k_{cat} of fusion protein D101S-linker-streptag is 15 times higher than the fusion protein WT-streptag. The k_{cat}/K_m ratio for each of the enzymes is almost identical with the corresponding value for the WT enzyme, since the increment in k_{cat} is compensated for by increase of 23- and 40-fold in the K_m of the D101S-streptag and D101S-linker-streptag fusion enzymes, respectively (Table 1). Therefore, despite the higher catalytic activity of the mutant enzymes each is still as effective a catalyst as the WT enzyme.

The D101S-streptag shows about 40-fold K_m increases over the WT. The introduction of a linker led to a 0.6-fold decreased K_m value relative to the nonlinker mutant, whereas it has the highest specific activity value. This result suggests that the D101S-linker-streptag fusion protein has the highest catalytic efficiency and a higher affinity to the substrate comparing with the fusion protein D101S-streptag. The activity assay after immobilization showed that D101S-linker-streptag also developed the highest residual activity. After immobilization (in microtiter plate), the ratio of residue enzyme activities of the D101S-linker-streptag and D101S-streptag was 8.4, but the ratio of the enzyme activities of the same proteins before immobilization is 2.0. Figure 3 showed the enzyme activity of the fusion proteins after immobilization and nonimmobilization with or without the insertion of the linker peptide. The catalytic activities of the fusion proteins in solution were higher than that in immobilized conditions. But enzymes without linker peptide gave a sharply decreased catalytic activity, while

Table 1. Kinetic Parameters of *E. coli* EAP and Fusion Proteins

enzyme	specific activity (U,[a] pH 10.0, 1 M Tris)	K_m (μM, pH 10.0, 1 M Tris)	k_{cat}[b] (s^{-1})	k_{cat}/K_m ($S^{-1}\,\mu M^{-1}$)
WT	53	89	27.5	0.30
WT-streptag	47	86	21.0	0.24
D101S-streptag	1422	3509	243.0	0.07
WT-linker-streptag	87	94	13.6	0.14
D101S-linker-streptag	1799	2080	308.0	0.15

[a] U = μmol of the substrate ρNPP hydrolyzed/mg of protein/min. [b] The k_{cat} values are calculated per active site from the V_{max} using a dimer molecular weight of 94 000 (*11*). The buffer system is 1.0 M Tris-HCI, pH 10.0. The MW of streptag and linker peptide is about 1100, respectively.

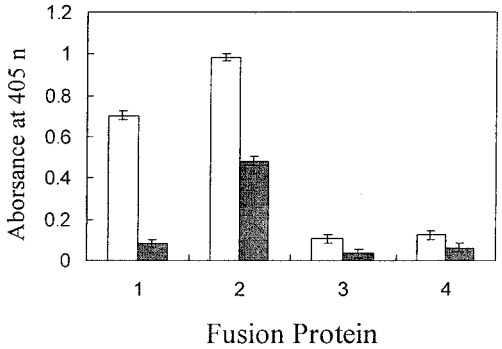

Figure 3. Effect of linker on the degree of residual activity on the polystyrene surface. The fusion proteins were assayed in the absence and presence of linker. Enzyme activity was expressed relative to the activity of the fusion protein in absence of linker. Data represent the mean of three duplicates from one experiment. Key 1, immobilized D101S-linker-streptag (□) and D101S-streptag (■); key 2, nonimmobilized D101S-linker-streptag (□) and D101S-streptag (■); key 3, immobilized WT-linker-streptag (□) and WT-streptag (■); key 4, nonimmobilized WT-linker-streptag (□) and WT-streptag (■).

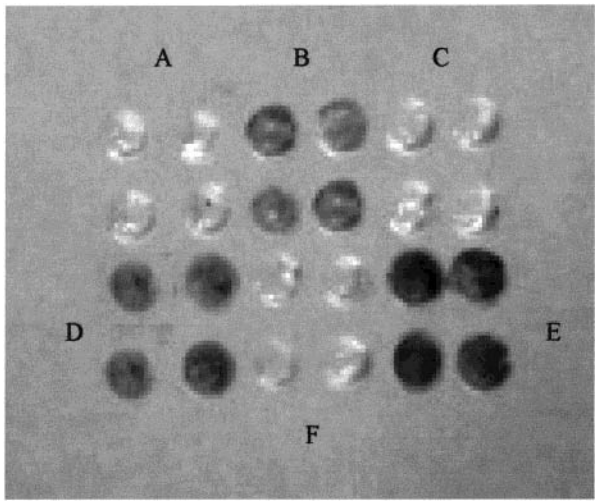

Figure 4. Immobilization of the proteins on glass chip. The positions of the three positive reactions (each loaded four duplicates) and three negative reactions are indicated. Experimental detail is in the text. (A) Denotes the detection of EAP; (B) denotes the detection of EAP-linker-streptag; (C) denotes the detection without substrate; (D) denotes the detection of D101S-streptag; (E) denotes the detection of D101S-linker-streptag; (F) denotes the detection without the streptavidin.

the enzymes with the insertion of linker peptide had a higher recover activity.

Immobilization on Glass Support. Immobilization of the fusion proteins was performed on the surface of a glass slide with four duplicates of each sample. The slide with immobilized proteins was thoroughly washed with distilled water followed by adding the NBT/BCIP and incubated for 10 min. Color then developed. Relative recovery activities of the fusion proteins were evaluated according to the depth of the color spots. As shown in Figure 4, the sequence of depth of the color was D101S-linker-streptag, D101S-streptag, and WT-linker-streptag. Results from the variance analysis and *t*-test also showed that the color among three candidates has extremely notable discrimination, the average margins between arbitrary two of the three candidates (25.75; 35.25; 9.5) are greater than the value of $t_{0.01} \times S_D$ (8.52). No detectable signal was observed when WT, which was used as an experiment control, was spotted on the glass surface by the same procedure.

DISCUSSION

The active sites of enzyme are less rigid and more sensitive to slight changes of conformation during immobilization. General immobilization process, e.g., chemical cross-linking or covalent binding, usually results in alterations in the level of enzyme activity. There are numerous chemical groups on the surface of the enzyme for immobilizing enzyme onto solid supports. For example, there are 40 lysine residues in the EAP structure, most of them are located on the surface of the enzyme with exposure of their amido groups, providing random chemical binding sites. Some of the amido groups are right in the active sites, which may result in poor recovery activity if chemical reagents are used for immobilization. The conception of using EAP-streptag system is to avoid random immobilization as that the C-terminal of the enzyme protein domain, where the streptag fused to, is the unique binding site, leaving the active sites opening toward the bulk solution. The streptag here acts as an anchor. The problem of less activity of the EAP-streptag is overcome by insertion of the linker peptide. This linker peptide is composed of glycine and serine. Glycine is the simplest amino acid, with no ionizable carbon side chain. The absence of a side chain gives the polypeptide backbone at glycine residues much greater conformational flexibility. The side chain of serine is short and hydrophilic due to the presence of a hydroxyl group. The peptide composed of these two amino acids forms a stable α-helix (as viewed by Swiss Protein Data Bank Viewer, SPDBV) in water solution (Figure 5). When the immobilized EAP was secluded away from the support surface by using this long and hydrophilic anchor-chain or spacer arm, it exhibits minimal steric hindrances that could be promoted by the streptag and the proximity of the support surface. The data showed the evidence that catalytic activities of the fusion proteins with linker are much higher than that of the fusion proteins without linker.

Charges on the streptag and the relative position of the peptide and the EAP in aqueous solution affect the elution during ion-exchange chromatography. The streptag peptide contains 10 amino acids (SAWRHPQPGG), of which, only two (R and H) are basic amino acids. The side chain of arginine consists of three hydrophobic

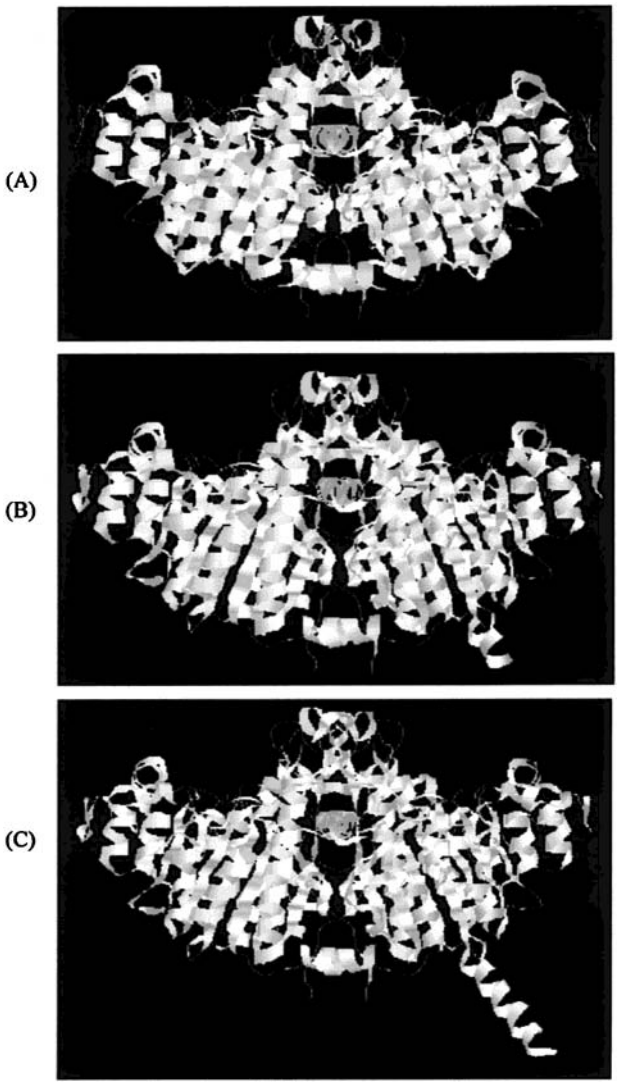

Figure 5. Three-dimensional structure of the EAP (A), EAP-streptag (B) and EAP-linker-streptag (C). The linker peptide shows α-helix at the C-terminal of EAP.

methylene groups and the strong basic δ-guanido group, of which pK'_R is 12.48 and is ionized over almost entire pH range, i.e., it is positively charged in our experimental condition (pH 7.4). Histidine is one of the strongest bases with a pK'_R of 6.20. It is not surprising that EAP-streptag fusion protein needs a lower ionic strength to be eluted from column as the tag has two extra positively amino acids (R and H) than WT. But what is surprising is the large different elution ionic strength between EAP-streptag and EAP-linker-streptag. It is not due to any charge in the linker as the linker is composed of amino acids (G and S) that are neutral at pH 7.4. It is thought that this large difference is due to the linker altering the position of the tag relative to the EAP, the co-effect of the linker, and streptag peptide on the surface of the enzyme, or some unknown interaction between proteins that may lead to charges exposing or covering. That needs to be further verified.

CONCLUSION

We have successfully obtained a higher recover activity by the insertion of a linker peptide between EAP and streptag. The proposed anchor-chain method could serve as a model to build other fusion protein systems and is optimistic to achieve better orientation control of enzyme immobilization, which is potentially useful in high quality construction of biosensors, biochips, and biodevices.

ACKNOWLEDGMENT

This work was supported by Chinese National Nature Science Foundation (no. 39770221) and Joint Project between the Royal Society and the Chinese Academy of Sciences (no. Q174). We thank Dr. Catherine Halliwell for helpful discussions.

LITERATURE CITED

(1) Tischer, W., and Kasche, V. (1999) Immobilized Enzymes: Crystal or Arriers? *Trends Biotechnol. 17* (8), 326−335.
(2) Huang, W., Wang, J., Bhattacharyya, D., and Bachas, L. G. (1997) Improving the Activity of Immobilized Subtilisin by Site-Specific Attachment to Surfaces. *Anal. Chem. 69* (22), 4601−4607.
(3) Bilkova, Z., Mazurova, J., Churacek, J., Horak, D., and Turkova, J. (1999) OrientedImmobilization of Chymotrypsin by Use of Suitable Antibodies Coupled to a Nonporous Solid Support. *J. Chromatogr A. 852* (1), 141−149.
(4) Turkova, J. (1999) Oriented Immobilization of Biologically Active Proteins as aTool for Revealing Protein Interactions and Function. *J. Chromatogr. B 722* (1−2), 11−31.
(5) Nygren, P. A., Stahl, S., and Uhln, M. (1994) Engineering Proteins to FacilitateBioprocessing. *Trends Biotechnol. 12*, 184−188.
(6) Gritsch, S., Neumaier, K., Schmitt, L., and Tampd, R. (1995) Engineered FusionMolecules at Chelator Lipid Interfaces Imaged by Reflection Interference Contrast Microscopy (RICM). *Biosens. Bioelectron. 10*, 805−812.
(7) Hengsakul, M., and Cass, A. E. G. (1996) Protein Patterning with aPhotoactivatable Derivative of Biotin. *Bioconjugate Chem. 7*, 249−254.
(8) Schmidt, T. G. M., Koepke, J., Frank, R., and Skerra, A. (1996) MolecularInteraction between the *strep-tag* Affinity Peptide and its Congate Target Streptavidin. *J. Mol. Biol. 255*, 753−766.
(9) Savage, M. D. (1996) An Introduction to Avidin−Biotin Technology and Options for Biotinylation. *BioMethods*, Vol. 7, p 2, Germany.
(10) Hengsakul, M., and Cass, A. E. G. (1997) Alkaline Phosphatase-Strep Tag Fusion Protein Binding to Streptavidin: Resonant Mirror Studies. *J. Mol. Biol. 266*, 621−632.
(11) Broadshaw, R. A., Cancedda, F., Ericsson, L. H., Newman, P. A., Piccoli, S. P., Schesinger, K., and Walsh, K. A. (1981) Amino Acid Sequence of *Escherichia coli* Alkaline Phosphatase. *Proc. Natl. Acad. Sci. U.S.A. 78*, 3473−3477.
(12) Chang, N. C., Wun-Jing, K., and Ellson, Y. C. (1986) Nucleotide Sequence of theAlkaline Phosphatase Gene of *Escherichia coli. Gene 44*, 121−125.
(13) Kim, E. E., and Wyckoff, H. W. (1991) Reaction Mechanism of AlkalinePhosphatase Based on Crystal Structure, Two-Metal Ion Catalysis. *J. Mol. Biol. 218*, 449−464.
(14) Liqing, C., Neidhart, D., Kohlbrenner, W. M., Mandecki, W., Bell, S., Sowadski, J., and Abad-Zapatero, C. (1992) 3-D Structure of a Mutant (AsplOl→Ser) of *E. coli* Alkaline Phoshatase with Higher Catalytic Activity. *Protein Eng. 5* (7), 605−610.
(15) Brennan, C. A., Christlanson, K., Fleur, M. A. L., and Mandecki, W. (1995) A Molecular Sensor System Based on Genetically Engineered Alkaline Phosphatase. *Biochemistry 92*, 5783−5787.
(16) Brockman, R. W., and Heppel, L. A. (1968) On the Localization of AlkalinePhosphatase and Cyclic Phosphodiesterase in *Escherichia coli. Biochemistry 7*, 2554−2562.

BC000029S

Homogeneous DNA Hybridization Assay by Using Europium Luminescence Energy Transfer

Shinji Sueda, Jingli Yuan, and Kazuko Matsumoto*

Department of Chemistry, Waseda University, 3-4-1 Okubo, Shinjuku-ku, Tokyo 169-8555, Japan. Received March 20, 2000; Revised Manuscript Received September 4, 2000

Homogeneous DNA hybridization assay based on luminescence resonance energy transfer (LRET) from a tetradentate β-diketonate europium chelate, 4,4′-bis(1″,1″,1″,2″,2″,3″,3″-heptafluoro-4″,6″-hexanedion-6″-yl)-chlorosulfo-*o*-terphenyl (BHHCT)-Eu^{3+} (λ_{ex} = 340 nm and λ_{em} = 615 nm), to an organic dye, Cy5 (λ_{ex} = 643 nm and λ_{em} = 669 nm) has been developed, in which two DNA probes whose sequences comprises the whole complementary strand to the target DNA, are used; one probe having a biotin label on the 3′-terminus and the other a Cy5 label on the 5′-terminus. After hybridization, streptavidin labeled with BHHCT-Eu^{3+} was added to the hybridization solution, and in the presence of the target DNA, the sensitized emission of Cy5 was observed when the hybridized complex was irradiated at 340 nm. In the absence of the target DNA, no emission was observed from Cy5.

INTRODUCTION

DNA hybridization assay has been widely used as a research tool for gene expression analysis and diagnosis of infectious and genetic diseases (*1*−*4*). Most of the currently available methods are, however, time-consuming and tedious because the method requires immobilization of the target DNA on a solid support for separation of the unhybridized probe DNA from the hybridized DNA duplex. In this regard homogeneous DNA hybridization assay using fluorescence resonance energy transfer (FRET) is attractive (*5*−*8*), in which two DNA probes, each being complementary to the two different sequences of a target DNA, are used. One probe has a donor dye, while the other an acceptor dye. The target DNA is detected in a homogeneous manner by monitoring the sensitized emission of the acceptor. So far all the systems developed employ organic dye pairs. In such systems, however, substantial background emission is caused both by the donor emission and the directly excited acceptor emission, even though the emission is monitored at the wavelength of the acceptor (*8*).

To circumvent this problem, we have directed our attention to the use of lanthanide chelate (*9*−*14*) as the energy donor. Emission profiles of lanthanide chelates are very sharp usually having fwhm of ca. 10 nm, and the excitation and the emission maximums are far separated. For instance, Eu chelates are excited in the UV region (∼340 nm) and exhibits luminescence at 615 nm. Therefore, the sensitized emission band of the organic acceptor can be easily distinguished from that of the lanthanide chelate donor and also from the excitation light in the UV region. Moreover, the lifetimes of lanthanide chelates are very long (∼1 ms) and as a result, the sensitized emission of the acceptor also becomes long-lived. Thus, by employing time-resolved luminescence measurement, the directly excited emission of the acceptor which is short-lived, can be eliminated (*11*−*14*).

* To whom correspondence should be addressed. Phone: +81-3-5286-3108. Fax: +81-3-5273-3489. E-mail: kmatsu@mn.waseda.ac.jp

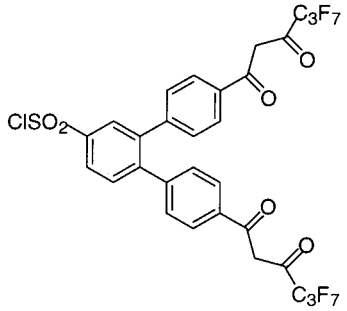

Figure 1. Structure of BHHCT.

Our group has developed a tetradentate β-diketonate europium chelate, 4,4′-bis(1″,1″,1″,2″,2″,3″,3″-heptafluoro-4″,6″-hexanedion-6″-yl)-chlorosulfo-*o*-terphenyl (BHHCT)-Eu^{3+} (Figure 1), which has been successfully used in time-resolved fluoroimmunoassay (*15*−*19*), and also in the detection of DNA immobilized onto a solid support (*20*). In the present study, a homogeneous DNA hybridization assay system based on LRET has been developed by using BHHCT-Eu^{3+} as the donor and an organic dye, Cy5 as the acceptor.

The principle of the method is illustrated in Figure 2, in which two DNA probes, one having a biotin label on the 3′-terminus and the other a Cy5 label on the 5′-terminus, are used. The two probes are complementary to the contiguous regions of a target DNA, such that when hybridized to the target DNA, the two labels come close each other. After hybridization, streptavidin labeled with BHHCT-Eu^{3+} chelate is added to the solution, and when the target DNA is present, the two labels come close and the energy transfer occurs from the Eu^{3+} chelate to Cy5. In the absence of the target DNA such phenomena cannot occur. Therefore, by monitoring the sensitized emission of Cy5, the target DNA can be detected in the homogeneous solution without immobilization and separation steps.

EXPERIMENTAL PROCEDURES

The Labeling of Streptavidin with BHHCT-Eu^{3+} Chelate. All procedures including synthesis of BHHCT

10.1021/bc000030r CCC: $19.00 © 2000 American Chemical Society
Published on Web 10/26/2000

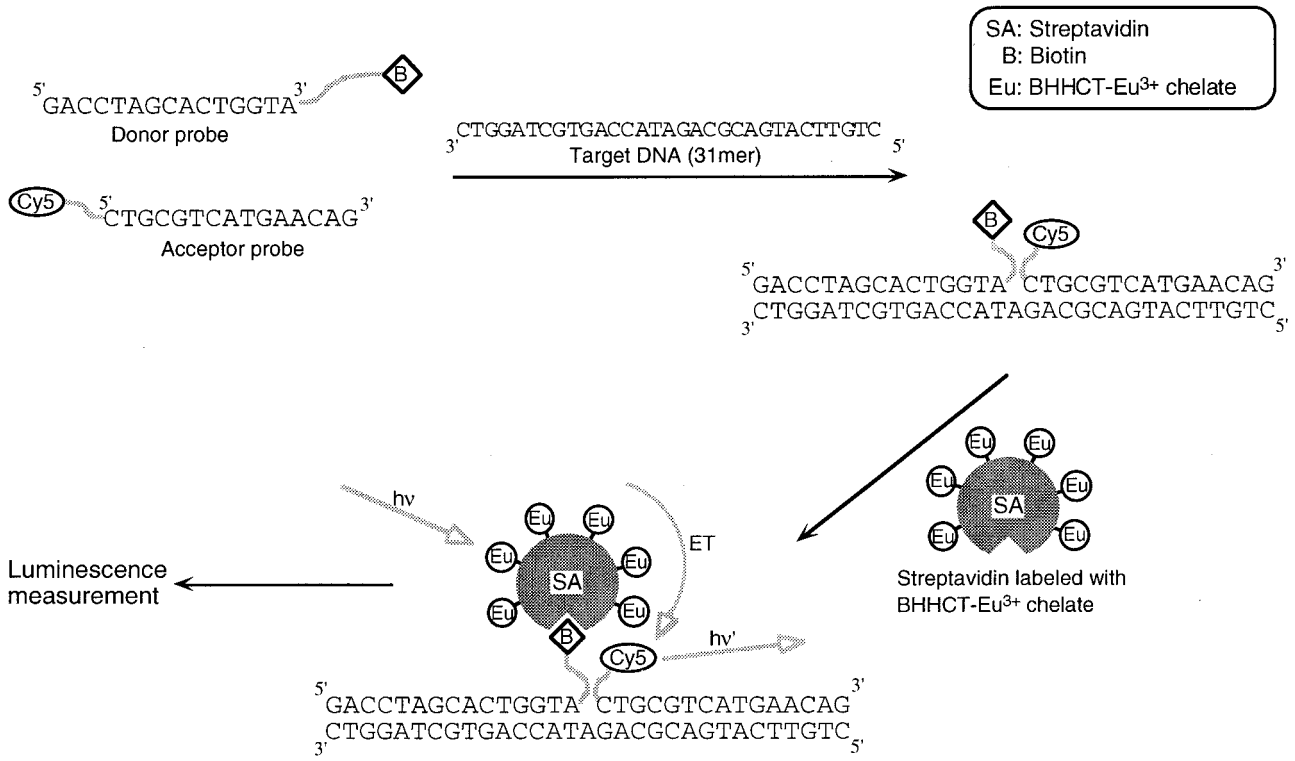

Figure 2. Principle of the homogeneous DNA hybridization assay.

were discussed in the previous paper (*15*). The procedure for labeling of streptavidin (SA) with BHHCT-Eu^{3+} was reported, but is slightly modified in the present study as in the following. To 0.1 M carbonate buffer (pH 9.1) (33 mL) containing 5 mg (8.3×10^{-5} mmol) of SA was added an ethanol solution (0.2 mL) containing 4 mg (4.9×10^{-3} mmol) of BHHCT. After the solution was stirred for 1 h at room temperature, it was dialyzed twice against 4 L of 0.1 M $NaHCO_3$ containing 0.25 g of NaN_3, first for 24 h and then for 7 h. The labeling ratio of BHHCT to SA was determined as $SA(BHHCT)_{20}$ by using the absorbance of the labeled SA solution and the molar extinction coefficient of BHHCT. The complexation with Eu^{3+} was achieved by dilution of the labeled SA solution (1 mL) with 50 mM Tris-HCl buffer (pH 7.8) (24 mL) containing equimolar $EuCl_3$ to BHHCT and incubation for 2 h at 55 °C.

Preparation of the target oligonucleotides (target DNAs) and the modified oligonucleotides (probe DNAs).

Figure 3 shows the target oligonucleotides and modified oligonucleotides used in the present work. All oligonucleotides were prepared on a fully automated DNA synthesizer according to a standard phosphoramide coupling method. Introduction of biotin and Cy5 into the oligonucleotides was achieved by using Biotin TEG CPG and Cy5 Phosphoramidite (GLEN RESEARCH), respectively. The purification of oligonucleotides was carried out with reversed-phase HPLC.

Hybridization Condition. The target oligonucleotides and probe oligonucleotides were mixed at a desired ratio in a buffer containing 10 mM Tris-HCl (pH 7.8) and 0.5 M NaCl. Oligonucleotides were annealed by heating at 50 °C for 15 min and cooling to room temperature.

Luminescence Energy Transfer Measurement. To the solution of the hybridized oligonucleotides was added the solution of BHHCT-Eu^{3+}-labeled SA at a molar ratio of SA to the biotinylated DNA of 1:1. The final concentrations of the probe DNAs and labeled SA were 50 nM. After the solution was incubated for 1 h at room temperature, the luminescence was measured with the excitation at 340 nm. All the luminescence measurement was done on a LS-50B (Perkin-Elmer) fluorometer equipped with a Xenon discharge lamp. A 420 nm cut off filter was employed to eliminate the second-order scattering light. In the time-resolved luminescent measurement, the samples were excited with pulse light of the Xenon lamp, and the spectra were recorded over a gate period of 300-μs after 40-μs delay time.

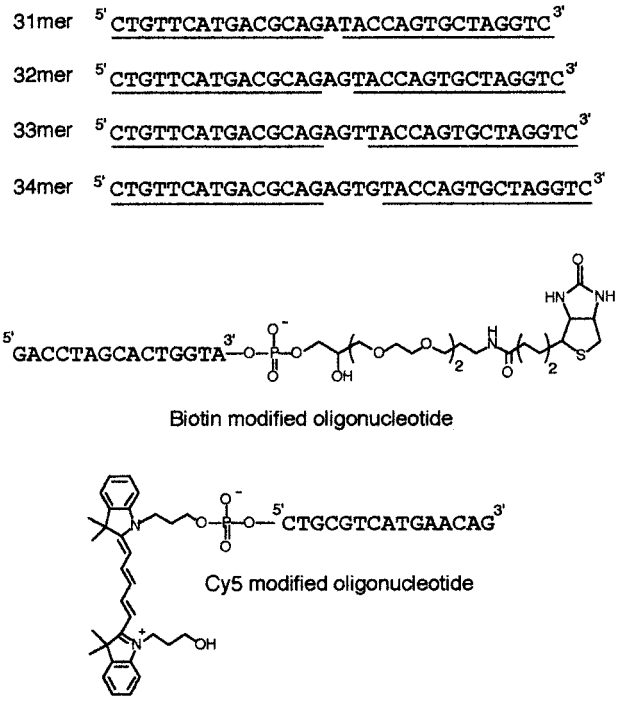

Figure 3. Sequences of the target oligonucleotides (target DNAs) and the modified oligonucleotides (probe DNAs) used in the present study. The binding sites of the probe DNAs on the target DNAs are underlined.

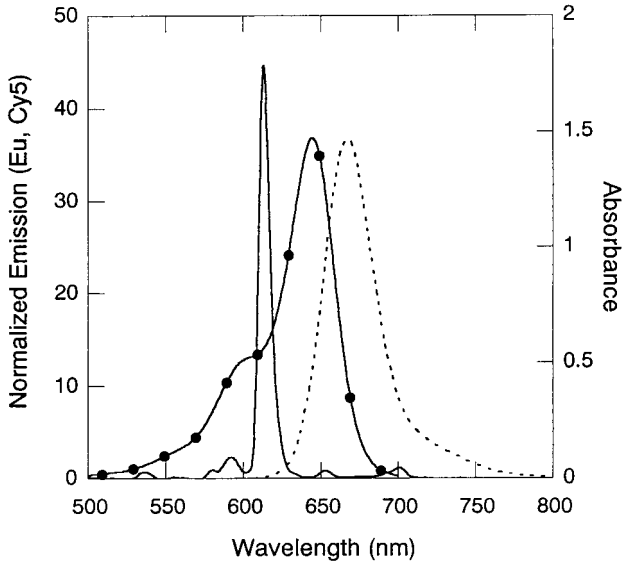

Figure 4. Spectra of BHHCT-Eu^{3+} chelate bound to SA and Cy5 bound to the oligonucleotide. The solid line is the emission spectrum (λ_{ex} = 340 nm) of BHHCT-Eu^{3+} chelate, and the dashed line and solid line with circles are the emission spectrum (λ_{ex} = 643 nm) and absorption spectrum of Cy5, respectively.

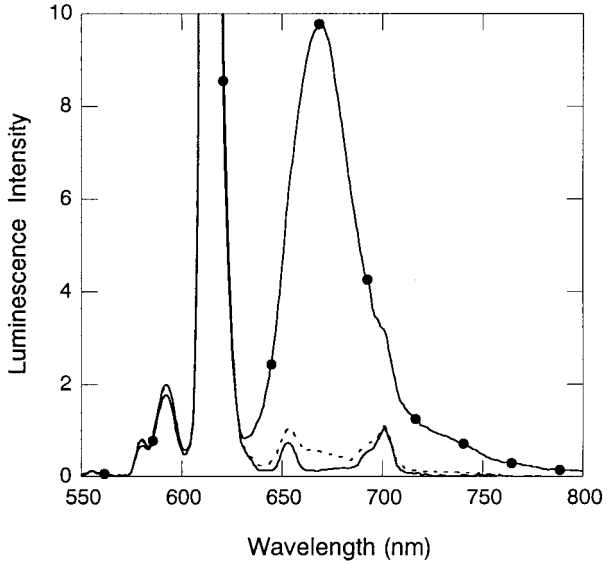

Figure 5. Normal (not time-resolved) emission spectra in the presence (solid line with circles) and absence (dashed line) of the target DNA (31mer). The spectrum of SA labeled with BHHCT-Eu^{3+} chelate alone is also shown (solid line). The concentrations of the probe DNAs, the target DNA, and SA were 50 nM.

RESULTS

Spectral Characteristics of the Donor and Acceptor. Figure 4 shows the emission spectrum of BHHCT-Eu^{3+} chelate bound to SA, and the emission and absorption spectra of Cy5 bound to the oligonucleotide. The emission peak of the Eu^{3+} chelate overlaps on the absorption spectrum of Cy5, satisfying the requirement for luminescence resonance energy transfer. It is also noteworthy that the emission intensity of the Eu^{3+} chelate at the Cy5 emission maximum 669 nm is very weak; the emission intensity of the Eu^{3+} chelate at 669 nm is 280 times lower than that of 615 nm maximum. Such low emission intensity of the donor at the emission wavelength of the acceptor is very important for monitoring the sensitized emission of Cy5.

Energy Transfer Measurements. Figure 5 shows the normal (not time-resolved) emission spectra in the presence and absence of the target DNA, 31mer. As expected, the sensitized emission of Cy5 is observed in the presence of the target DNA, but not in the absence of the target DNA. In Figure 5, the emission spectrum of SA labeled with Eu^{3+} chelate alone (without DNAs) is also shown as the control. Comparison of this spectrum (solid line) with that in the absence of the target DNA (dashed line) shows that slight emission of Cy5 is observed even in the absence of the target DNA. This slight emission is derived from the direct excitation of Cy5 at the wavelength used in this study. However, this emission is very weak compared with that of the sensitized emission of Cy5; as a result, the ratio of the signal to background at 669 nm is very high, approximately 20:1. Such a high signal/background ratio cannot be achieved in the systems using only organic dyes as the donor−acceptor pair.

Similar measurement was carried out with time-resolved mode, and Figure 6 shows the observed time-resolved emission spectra. Similar to the normal luminescence measurement, the sensitized emission of Cy5 was observed by addition of the target DNA. What is different from the normal measurement is that the emission spectrum of the Eu^{3+} chelate alone (solid line) is almost same as the spectrum in the absence of the target DNA (dashed line) with an identical intensity at 669 nm. This means that the directly excited band of Cy5 observed in the normal luminescence measurement can be eliminated by time-resolved measurement. However, the emission intensity of the Eu^{3+} chelate is much stronger in the time-resolved measurement than that of the sensitized emission of Cy5, because the lifetime of the sensitized emission, even though it is increased by FRET, is still shorter than that of the Eu^{3+} chelate. Consequently, the signal/background ratio is somewhat small, 14:1, but the ratio is still superior to those obtained for the organic dyes.

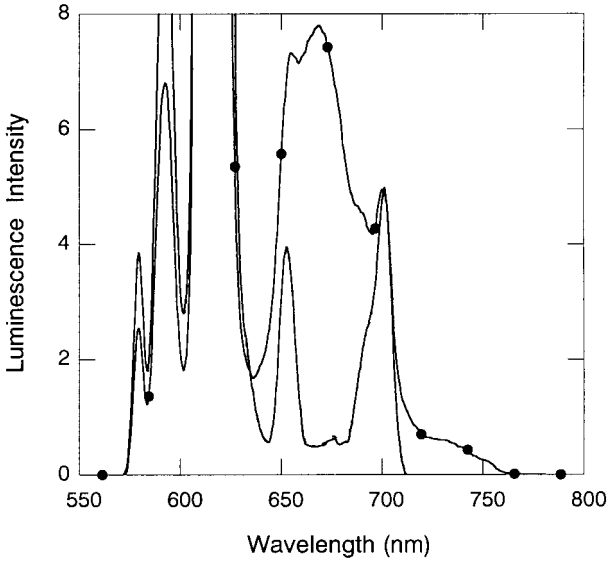

Figure 6. Time-resolved emission spectra in the presence (solid line with circles) and absence (dashed line) of target DNA (31mer) and SA labeled with BHHCT-Eu^{3+} chelate alone (solid line). The spectra were obtained with 40-μs delay time and 300-μs gate time.

Effect of the Unhybridized Spacer Length between the Two Hybridized Sequences on the Target DNA. The effect of the unhybridized spacer length between the two hybridized sequences on the target

Table 1. Relative Intensities of the Sensitized Emission at 669 nm in the Presence of Different Target DNAs[a]

	Relative values of the emission intensity
31mer	1.00
32mer	0.96
33mer	0.95
34mer	0.93

[a] The values are based on the normal luminescence measurement.

DNAs was examined. For this purpose, target DNAs of 31mer, 32mer, 33mer, and 34mer were prepared, each having 1, 2, 3, and 4 inserting bases, respectively, between the hybridized sequences (Figure 3). The luminescence behaviors in the presence of these target DNAs were compared. Table 1 shows the relative intensities of the sensitized emission at 669 nm in the presence of each target DNA. The emission intensity is decreased as the number of the bases between the hybridized sequences is increased. However, the difference is smaller than expected for the well-known dependence of the efficiency of energy transfer on the R^{-6}, where R is the distance between the donor and the acceptor. This may be accounted for by the fact that the distance between donor and acceptor is flexible due to the molecular fluctuation. Biotin is tethered to the oligonucleotide via a long linker of 22 atoms. Moreover, in the present systems, multiple Eu^{3+} chelates labeled to a SA molecule act as the energy donor. From the viewpoint of the practical use, this little dependence of the energy transfer on the distance is advantageous because close contact of the two hybridized sequences are not strictly necessary in order to get effective sensitized emission. That is, wide variety of sequences of the probe DNAs can be employed in the experiment, and this makes the present system more flexible and adaptable to any DNA assay, compared to the previous energy-transfer DNA assays (*8*). In the previous assay, optimum distance between the donor and the acceptor usually exists, and the DNA probes must be designed in a more strict way to obtain the most efficient energy transfer.

Sensitivity of the Detection Method. The sensitivity of the present method was examined by using the 31mer as a target DNA. Figure 7 shows the plot of the Cy5 emission intensity at 669 nm against the concentration of the target DNA. The plot is based on the normal luminescence measurement. Almost the same plot was obtained by the time-resolved luminescence measurement. The detection limit was determined as the concentration corresponding to the twice amount of the background standard deviation. In both measurement modes, detection limit was about 200 pM when 50 nM of the probe DNA was used. By using lower concentrations of the probe DNA, the detection limit would be improved.

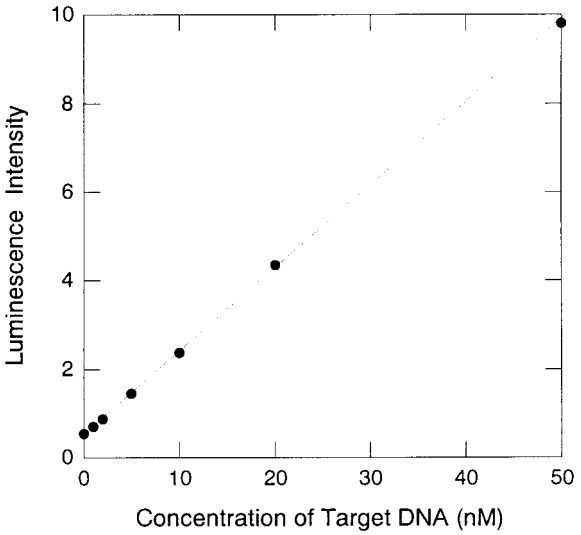

Figure 7. The plot of the Cy5 emission intensity at 669 nm against the concentration of the target DNA (31mer). The data are based on the measurement by normal luminescence mode.

DISCUSSION

In the present work, homogeneous DNA hybridization assay based on energy transfer from BHHCT-Eu^{3+} chelate to Cy5 has been developed. The characteristics of the method are the followings. First, the signal/background ratio at the sensitized emission wavelength is superior to that obtained by using organic dyes as the donor−acceptor pair. This is because the emission intensity of the europium chelate is quite weak at the maximum emission wavelength of Cy5. The other reason is that the Cy5 emission due to the direct excitation is efficiently eliminated by time-resolved luminescence detection. This direct emission of Cy5 is also very effectively suppressed even in the normal luminescence detection, since Cy5 is scarcely excited at the excitation wavelength for the europium chelate, 340 nm (the molar extinction coefficient of Cy5 at 340 nm is about one-seventieth of that at its maximum absorption wavelength, 643 nm). Thus, high signal/background ratio can be achieved even without time-resolved detection, and this shows the great advantage of using Eu chelates as the donor.

Another characteristic of the present method is that the sensitized emission occurs very effectively, since the europium chelate is multiply labeled onto the probe DNA by using the streptavidin−biotin interaction. The multiple europium chelates act as the sensitizer for Cy5, causing strong sensitized emission of Cy5. The intensity of the sensitized emission at 669 nm is about half the magnitude of the intensity observed by direct excitation of Cy5 at its absorption maximum wavelength (643 nm) by using the same instrument equipped with a Xenon lamp. In the most energy transfer experiment reported so far, the ratio of the donor to acceptor is one to one, and the excitation efficiency of the acceptor is not sufficiently high. However, multiple labeling of the conventional donor organic dyes is not useful to enhance the fluorescence of the acceptor, since multiple labeling dose not always increase the donor emission due to self-quenching (*21*). For europium chelates, self-quenching is not a problem, since they have a large Stokes' shift.

In the present method, two detection modes can be employed, one is the normal luminescence mode, and the other is the time-resolved mode. Considering the signal/background ratio alone, the former is better than the latter in the present model systems using synthetic oligonucleotides as the target DNAs. However, in the case of natural DNA samples containing many impurities, the time-resolved detection mode might be more favorable because the background emission caused by the impurities can be effectively eliminated. The effort for clarifying this point and the detailed study concerning the relation of the energy transfer efficiency and the distance between the two probes remain to be made.

ACKNOWLEDGMENT

This work has been supported by CREST (Core Research for Evolutional Science and Technology) of Japan Science and Technology Corporation (JST).

LITERATURE CITED

(1) Schena, M., Shalan, D., Heller, R., Chai, A., Brown, P. O., and Davis, R. W. (1996) Parallel Human Genome Analysis: Microarray-Based Expression Monitoring of 1000 Genes. *Proc. Natl. Acad. Sci. U.S.A. 93*, 10614−10619.

(2) Inoue, S., and Honda, R. (1990) Microplate Hybridization of Amplified Viral DNA Segment. *J. Clin. Microbiol. 28*, 1469−1472.

(3) Sekiya, T., Fushimi, M., Hori, H., Hirohashi, S., Nishimura, S., and Sugimura, T. (1984) Molecular Cloning and the Total Nucleotide Sequence of the Human c-Ha-*ras*-1 Gene Activated in a Melanoma from a Japanese Patient. *Proc. Natl. Acad. Sci. U.S.A. 81*, 4771−4775.

(4) Hsu, I. C., Metcalf, R. A., Sun, T., Welsh, J. A., Wang, N. J., and Harris, C. C. (1991) Mutational Hotspot in the p53 Gene in Human Hepatocellular Carcinomas. *Nature 350*, 427−429.

(5) Heller, M. J., and Morrison, L. E. (1985) Chemiluminescent and Fluorescent Probes for DNA Hybridization Systems. In *Rapid Detection and Identification of Infectious Agents* (D. T. Kingsbury and S. Falkow, Ed.) pp 245−256, Academic Press, New York.

(6) Matthews, J. A., and Kricka, L. J. (1988) Analytical Strategies for the Use of DNA Probes. *Anal. Biochem. 169*, 1−25.

(7) Cardullo, R. A., Agrawal, S., Flores, C., Zamecnik, P. C., and Wolf, D. E. (1988) Detection of Nucleic Acid Hybridization by Nonradiative Fluorescence Resonance Energy Transfer. *Proc. Natl. Acad. Sci. U.S.A. 85*, 8790−8794.

(8) Mergny, J.-L., Boutorine A. S., Garestier, T., Belloc, F., Rougée, M., Bulychev, N. V., Koshikin, A. A., Bourson, J., Lebedev, A. V., Valeur, B., Thuong, N. T., and Hélène, C. (1994) Fluorescence Energy transfer as a probe for Nucleic Acid Structures and Sequences. *Nucleic Acids Res. 22*, 920−928.

(9) Horrocks, W. D., Albin, J. M. (1984) Lanthanide Ion Luminescence in Coordination Chemistry and Biochemistry. *Prog. Inorg. Chem. 31*, 1−104.

(10) Sabbatini, N., Guardigli, M., and Lehn, J.-M. (1993) Luminescence Lanthanide Complexes as Photochemical Supramolecular Devices. *Coord. Chem. Rev. 123*, 201−228.

(11) Prat, O., Lopez, E., and Mathis, G. (1991) Europium(III) Cryptate: A Fluorescent Label for the Detection of DNA Hybrids on Solid Support. *Anal. Biochem. 195*, 283−289.

(12) Seveus, L., Väisälä, M., Syrjanen, S., Sandberg, M., Kuusisto, A., Harju, R., Salo, J., Hemmilä, I., Kojola, H., Soini, E. (1992) Time-Resolved Fluorescence Imaging of Europium Chelate Label in Immunohistochemistry and In Situ Hybridization. *Cytometry 13*, 329−338.

(13) Mathis, G. (1993) Rare Earth Cryptate and Homogeneous Fluoroimmunoassays with Human Sera. *Clin. Chem. 39*, 1953−1959.

(14) Selvin, P. R., and Hearst, J. E. (1994) Luminescence Energy Transfer Using a Terbium Chelate: Improvements on Fluorescence Energy Transfer. *Proc. Natl. Acad. Sci. U.S.A. 91*, 10024−10028.

(15) Yuan, J., and Matsumoto, K. (1998) A New Tetradentate β-Diketonate-Europium Chelate That Can Be Covalently Bound to Proteins for Time-Resolved Fluoroimmunoassay. *Anal. Chem. 70*, 596−601.

(16) Yuan, J., Wang, G., Kimura, H., and Matsumoto, K. (1997) Highly Sensitive Time-Resolved Fluoroimmunoassay of Human Immunoglobulin E by Using a New Europium Fluorescent Chelate as a Label. *Anal. Biochem. 254*, 283−287.

(17) Yuan, J. G., Kimura, H., and Matsumoto, K. (1998) Sensitive Time-Resolved Fluoroimmunoassay of Human Thyroid-Stimulating Hormone by Using a New Europium Fluorescent Chelate as a label. *Anal. Sci. 14*, 421−423.

(18) Kimura, H., Yuan, J., Wang, G., Matsumoto, K., and Mukaida, M. (1999) Highly Sensitive Quantitation of Methamphetamine by Time-Resolved Fluoroimmunoassay Using a New Europium Chelate as a Label. *J. Anal. Toxicol. 23*, 11−16.

(19) Yuan, J. G., Kimura, H., and Matsumoto, K. (1999) Highly Sensitive Detection of Bensulfuron-methyl by Time-Resolved Fluoroimmunoassay Using a Tetradentate β-diketonate Europium Chelate as a label. *Anal. Sci. 15*, 125−128.

(20) Yoshikawa, K., Yuan, J., Matsumoto, K., and Kimura, H. (1999) Time-Resolved Fluorometric Detection of DNA Using a Tetradentate β-Diketonate Europium Chelate as a Label. *Anal. Sci. 15*, 121−124.

(21) Haralambidis, J., Angus, K., Pownall, S., Duncan, L., Chai, M., and Treager, G. W. (1990) The preparation of polyamide-oligonucleotide probes containing multiple nonradioactive labels. *Nucleic Acids Res. 18*, 501−505.

BC000030R

Maleimide-Functionalized Lipids that Anchor Polypeptides to Lipid Bilayers and Membranes

John T. Elliott[†] and Glenn D. Prestwich*

Department of Physiology and Biophysics, The University at Stony Brook, Stony Brook, New York, Department of Medicinal Chemistry, The University of Utah, Salt Lake City, Utah. Received March 27, 2000; Revised Manuscript Received June 13, 2000

Two maleimide-containing diacylglycerol derivatives were synthesized to permit the anchoring of short peptides and longer polypeptides to phospholipid bilayers and membranes. The maleimide was introduced at the site normally occupied by a phospholipid headgroup. The first lipid, the dipalmitoyl ester of 1-maleimido-2,3-propanediol, was developed as a membrane anchor for extracellular domains of transmembrane proteins. The second anchoring lipid, in which the 3-position contained a 6-aminohexanoate, was designed for convenient modification with amine-reactive reporter groups. Specifically, the NBD fluorophore, 7-nitrobenzo-2-oxa-1,3-diazole-aminohexanoic-*N*-hydroxysuccinimide ester, was attached to give an fluorescent anchoring reagent. Next, these reagents were applied to the anchoring of a C-terminally cysteamine-modified 8 kDa polypeptide that comprises the extracellular N-terminal domain of the human thrombin receptor, a transmembrane protease-activated receptor (PAR-1). Gel filtration and fluorescence analysis showed that the fluorescent lipopolypeptide spontaneously inserted into preformed phospholipid vesicles, but it did not insert into whole cell membranes. In contrast, the dipalmitoyl derivative could only be reconstituted into artificial membranes by mixing the lipopolypeptide and phospholipid before vesicle formation. These results suggest that biophysical interactions governing the lipopolypeptide insertion into artificial and cellular membranes may differ. The thiol-reactive lipidating reagents should be valuable materials for studying the structure and function of peptides and polypeptides at phospholipid bilayer surfaces.

INTRODUCTION

Lipid modification of soluble peptides and polypeptides confers amphipathic character to the molecules and typically changes their behavior in aqueous solutions. The amphiphiles have a tendency to aggregate, form micelles and vesicles, and associate with phospholipid bilayers. This property makes it possible to use acylated peptides and polypeptides to investigate biophysical phenomena that occur on cellular membranes. Versatile reagents for the synthesis of lipopeptides are thus an important requirement for the success of such studies. We describe herein two new thiol-reactive lipids and the attachment of these reagents to a thiol-functionalized recombinant 8-kDa polypeptide.

Synthetic lipoconjugates can be used to evaluate the biophysics of protein−membrane interactions. Membrane binding properties of signal transduction and oncogenic proteins that are palmitoylated or myristoylated in vivo have been examined with lipopeptides that represent the native proteins (*1*−*3*). Naturally occurring lipopeptides that function as bacterial cell wall components (*4*), biosurfactants (*5*), or antibiotics (*6*) have been investigated using artificially synthesized analogues under in vitro and in vivo conditions. Lipid conjugates of peptides have also been used to study biologically relevant structural conformations that are induced at phospholipid membrane surfaces (*7*). A lipid modification can significantly increase the lifetime of the membrane-bound complex, thereby improving the data obtained from a structural study. For example, the structural properties of peptide hormones CCK (*8*), gastri (*9*), and yeast α-factor (*10*) were studied in membrane-bound preparations using this approach.

A variety of synthetic methods are available for preparing lipid conjugates of peptides and polypeptides. Acylations can be performed at reactive amino acid side chains (*11*, *12*) or during peptide synthesis on solid-phase resins (*13*−*16*). In the former method, conjugation via a thiol group is convenient because thiol function is often unique in a primary sequence (i.e., Cys). In addition, molecular biology techniques allow site-specific incorporation of cysteine residues when the peptides or polypeptides are produced in cellular systems (*17*). The maleimide group is routinely used as a thiol acceptor, as it exhibits high selectivity and reactivity under essentially neutral aqueous conditions. Several maleimide-based lipidating reagents are commercially available. Two reagents are based on a heterobifunctional four- or six-carbon linker conjugated to the phosphatidylethanolamine headgroup (Avanti Polar Lipids, Alabaster, AL). Another features a 3500 Da poly(ethylene glycol) extending from the phospholipid headgroup (Shearwater Polymers, Huntsville, AL), but the flexible tether introduces considerable uncertainty as to where coupled peptide would reside relative to the membrane surface.

To study the extracellular polypeptide domains of transmembrane membrane proteins, we required a reagent that could anchor a sulfhydryl-containing peptide

* To whom correspondence should be addressed at The University of Utah. Voice: (801) 585-9051; (801) 581-7063. Fax: (801) 585-9053; (801) 581-7087. E-mail: gprestwich@deans.pharm.utah.edu.

[†] The University at Stony Brook. Present address: National Institute of Standards and Technology, Biotechnology Division, 100 Bureau Drive, Gaithersburg, MD 20899.

10.1021/bc000022a CCC: $19.00 © 2000 American Chemical Society
Published on Web 09/12/2000

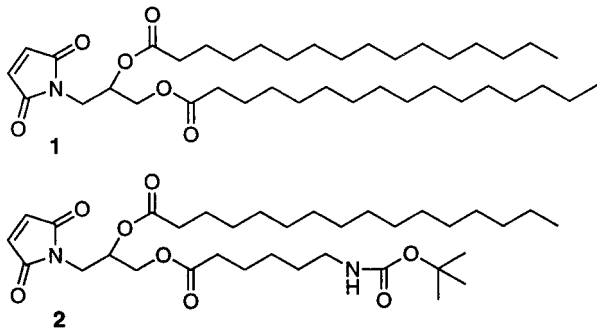

Figure 1. Structures of the maleimido-lipids. Lipid **2** contains a BOC protecting group on the primary acyl chain. Upon BOC removal, the amino-acyl chain can be modified with amine reactive reporter groups.

to a phospholipid bilayer. For our application, it was important that the conjugation site was confined to the region of a phospholipid bilayer normally occupied by the headgroups. Thus, two lipids that contained maleimide functional groups on a diacylglycerol-like backbone were prepared (Figure 1). The first lipid, Pam_2Mal (**1**), was constructed with two palmitoyl chains to serve as a membrane anchor. The second lipid, BOC-AH−PamMal (**2**), was prepared with a palmitoyl and a BOC-protected[1] 6-aminohexanoyl chain. The protected amino-acyl chain was introduced so the lipid could ultimately be modified with amine reactive reporter groups (e.g., fluorophores) to allow facile quantitation and localization of the lipoconjugate (*18*). In this study, the lipid was derivatized to give the fluorescent lipidating reagent 7-nitrobenzo-2-oxa-1,3-diazole-6-aminohexanoyl-AH−PamMal (NBD-PamMal) (**10**).

To evaluate the utility of the lipids, a soluble 8 kDa polypeptide representing the N-terminal extracellular domain of the G protein-coupled human thrombin receptor (PAR-1) (*19*) was selectively derivatized at a C-terminal cysteamine with Pam_2Mal and NBD-PamMal. The lipopolypeptides were assessed for their ability to associate with artificial and cellular membranes by gel filtration and fluorometric assays. The results from this study demonstrate that these new thiol-reactive lipidating reagents will be valuable for preparing lipoconjugates that can be anchored into phospholipid membranes, and can be employed for biological structure and function studies.

EXPERIMENTAL PROCEDURES

Materials and General Methods. NMR spectra were collected on a Varian Gemini 300 instrument. High-resolution FAB-MS was performed at The University of California, Riverside, mass spectrometry facility. MALDI-MS was performed on a Bruker Protein-TOF system using a 3,5-dimethoxy-4-hydroxy-cinnamic acid (sinapinic acid) matrix (CASM, University at Stony Brook, Stony Brook, New York). Uncorrected melting points were determined on a Fisher-Johns apparatus. The purity of the compounds was estimated by TLC, reversed-phase HPLC (RP-HPLC), mass spectrometry and NMR. *N*-Methoxycarbonylmaleimide (NMM) was obtained from Sigma Chemical (St. Louis, MO). Chemical reactions were carried out in HPLC grade solvents and reagent grade solvents were used for silica gel chromatography (flash grade). Phospholipids were purchased from Avanti Polar Lipids (Alabaster, AL). HPLC purifications were performed on an LKB/Bromma 2152 system and the eluate was monitored at 220 or 280 nm. BOC-6-aminohexanoic acid (*20*) and CBZ-(±)-1-amino-2,3-propanediol (*21*) were prepared as previously described.

TLC Stains. Lipid products were identified with 10% phosphomolybdic acid in ethanol (EtOH). Primary amines were detected with 5% ninhydrin in EtOH. Maleimides were identified as previously described (*22*). Fluorescent lipid products were visualized directly under long-wavelength UV illumination (~350 nm).

CBZ-Amino-2,3-dipalmitoyl-propane (4). CBZ-Amino-propanediol **3** (0.45 g, 2.0 mmol) was mixed with palmitic acid (1.22 g, 4.8 mmol) and (dimethylamino)-pyridine (DMAP, 0.49 g, 4.0 mmol) in $CHCl_3$ (20 mL). Diisopropylcarbodiimide (DIC, 790 μL, 5.0 mmol) was added and the mixture was stirred for 16 h at room temperature. The solvent was removed by rotary evaporation and the residual oil was dissolved in methanol (MeOH) (ca. 50 mL) and stored at −20 °C for 1 h. Precipitated material was collected by filtration, redissolved in $CHCl_3$ (1−2 mL) and recrystallized with MeOH. The product was collected by filtration and dried under vacuum. A white solid (0.81 g, 87% yield) was obtained: FAB-MS for $C_{43}H_{75}NO_6$, MH^+ at *m/z* 702.5679 (calcd 702.5673); mp 49−50 °C; ^{1}H NMR (300 MHz, $CDCl_3$) δ 0.83−0.87 (t, 6 H), 1.17−1.23 (m, 48 H), 1.54−1.60 (m, 4 H), 2.24−2.31 (m, 4 H), 3.36−3.48 (m, 2 H), 4.08−4.28 (m, 2 H), 4.96 (b, 1 H), 5.08 (s, 2 H), 7.24−7.34 (m, 5 H). The product was observed on TLC, $R_f = 0.57$ in hexane (Hex):EtOAc (2:1).

CBZ-Amino-3-(BOC-6-aminohexanoyl)-2-propanol (5). CBZ-Amino-propanediol **3** (1.2 g, 5.3 mmol) was mixed with BOC-6-aminohexanoic acid (1.17 g, 5.0 mmol) and DMAP (0.65 g, 5.3 mmol) in $CHCl_3$ (30 mL). The solution was cooled to 0 °C and dicyclohexylcarbodiimide (DCC, 1.65 g, 8.0 mmol) was added. The major product was observed by TLC, $R_f = 0.51$ in EtOAc:Hex (2:1). After 24 h, the urea byproduct was removed by filtration. The solvent was evaporated and the residue was dissolved in a small volume of $CHCl_3$:EtOAc:Hex (3:2:1). The mixture was purified on silica gel by eluting with EtOAc:Hex (2:1). A clear oil was obtained after solvent removal (1.1 g, 45% yield): FAB-MS for $C_{22}H_{34}N_2O_7$, MH^+ at *m/z* 439.2465 (calcd 439.2444); ^{1}H NMR (300 MHz, $CDCl_3$) δ 1.29−1.35 (m, 2 H), 1.41−1.48 (m, 11 H), 1.58−1.65 (m, 2 H), 2.30−2.35 (m, 2 H), 3.07 (br t, 2 H), 3.16−3.47 (m, 2 H), 3.64 (br s, 1 H), 3.93 (m, 1 H), 4.04−4.14 (m, 1 H), 4.64 (br s, 1 H), 5.09 (s, 2 H), 5.43 (br s, 1 H), 7.29−7.33 (m, 5 H).

CBZ-Amino-2-palmitoyl-3-(BOC-6-aminohexanoyl)-propane (6). Secondary alcohol **5** (1.1 g, 2.5 mmol) was mixed with palmitic acid (0.77 g, 3.0 mmol) and DMAP (0.31 g, 2.5 mmol) in $CHCl_3$ (25 mL). DCC (0.64 g, 3.13 mmol) was added and the solution was stirred for 16 h at room temperature. The mixture was cooled (−20 °C) and the urea byproduct was removed by filtration. The

[1] Abbreviations: BOC, di-*tert*-butyl-dicarbonate; CBZ, carbobenzyloxy protecting group; CHRF-288, megakaryoblastic cell-type; DCC, dicyclohexylcarbodiimide; DIC, diisopropylcarbodiimide; DMPC, 1,2-dimyristoyl-*sn*-glycero-3-phosphocholine; DMPG, 1,2-dimyristoyl-*sn*-glycero-3-phosphoglycerol; DTT, dithiothreitol; Hex, hexane; NBD, 7-nitrobenzo-2-oxa-1,3-diazole; NBD-Cl, 4-chloro-NBD; NBD-X-NHS, NBD-6-aminohexanoic-*N*-hydroxysuccinimide ester; NMM, *N*-methoxycarbonyl-maleimide; NTTR, extracellular N-terminal domain of the human thrombin receptor (residues Glu^{30}-Ser^{99}); NTTR-ML, NTTR-dipalmitoyl lipid conjugate; NTTR-(NBD)ML, NTTR-fluorescent lipid conjugate; NTTR-SH, NTTR with a C-terminal sulfhydryl group; PAR-1, protease activated human thrombin receptor; PB, phosphate buffer; POPC, 1-palmitoyl-2-oleoyl-*sn*-glycero-3-phosphocholine; RP-HPLC, reversed-phase HPLC; S2, *Drosophila melangaster* cell-line; TEA, triethylamine; TX-100, Triton X-100.

solvent was removed by rotary evaporation and the remaining residue was dissolved in small volume of $CHCl_3$:EtOAc:Hex (2:1:1), purified on silica gel with EtOAc:Hex (1:1), and concentrated to give a clear oil (1.6 g, 95% yield): FAB-MS for $C_{38}H_{64}N_2O_8$, MNa^+ at *m/z* 699.4590 (calcd 699.4560); ^{1}H NMR (300 MHz, $CDCl_3$) δ 0.82−0.87 (t, 3 H), 1.19−1.68 (m, 41 H), 2.20−2.30 (m, 4 H), 3.04−3.08 (t, 2 H), 3.37−3.44 (m, 2 H), 4.05−4.12 (m, 2 H), 4.23−4.28 (m, 1 H), 5.06 (m, 3 H), 7.27−7.35 (m, 5 H); TLC, $R_f = 0.52$ in Hex:EtOAc (2:1).

1-Amino-2,3-dipalmitoyl-propane (7a). CBZ-protected lipid **4** (2.0 g, 2.8 mmol) was dissolved in warm absolute EtOH (100 mL) containing 5% Pd/C (ca. 500 mg). The solution was saturated with H_2 (ca. 2 atm) and shaken for 6 h at room temperature. $CHCl_3$ (100 mL) was added to the solution, the catalyst was removed by filtration through Celite, and the solvent was removed in vacuo to give a white solid. The product migrated slightly above the origin on TLC in Hex:EtOAc (2:1) and stained positive with ninhydrin.

Pam_2Mal (1). Amino lipid **7a** (300 mg, 0.48 mmol) was mixed with NMM (147 mg, 0.94 mmol) and tetrabutylammonium hydrogen sulfate (150 mg, 0.44 mmol) in $CHCl_3$ (4 mL) on ice. TEA (66 μL, 0.64 mmol) was slowly added over 5 min, and the solution was stirred for an additional 10 min. The solution was removed from the ice and saturated $NaHCO_3$ (8 mL) was added to the organic layer while being vigorously stirred. The maleimido-lipid was observed in the organic layer by TLC, $R_f = 0.83$ in Hex:EtOAc (2:1). After 3 h at room temperature, the phases were separated by low speed centrifugation and the reddish organic layer was concentrated in a rotary evaporator. The residue was dissolved in a small volume of $CHCl_3$:Hex:EtOAc (3:2:1) and the maleimido-lipid was purified on silica gel with a Hex:EtOAc (2:1) and concentrated to give a white crystalline product (211 mg, 69% yield): FAB-MS for $C_{39}H_{69}NO_6$, MNa^+ at *m/z* 670.5005 (calcd 670.5023); mp 62−63 °C; ^{1}H NMR (300 MHz, $CDCl_3$) δ 0.83−0.87 (m, 6 H), 1.16−1.23 (m, 48 H), 1.51−1.61 (m, 4 H), 2.21−2.33 (m, 4 H), 3.68−3.81 (m, 2 H), 4.04−4.25 (m, 2 H), 5.19−5.24 (m, 1 H), 6.69 (s, 2 H). The maleimide proton peaks were observed at 6.69 ppm. The product could be stored as a powder at −20 °C or as a 50 mM solution in $CHCl_3$ at −80 °C for at least one year with less than 5% maleimide hydrolysis.

BOC-AH-PamMal (2). Lipid **2** was prepared using the identical procedure described above for the CBZ removal and maleoylation of dipalmitoyl lipid **4**. The 1-amino-2-palmitoyl-3-(BOC-6-aminohexanoyl)-propane lipid (**7b**) was a clear oil. The maleoylated product (**2**) was observed by TLC ($R_f = 0.5$), developed in Hex:EtOAc (2:1), and purified on silica gel with Hex:EtOAc (2:1). After solvent removal and overnight drying in vacuo, a clear oil was obtained. The oil crystallized into a white waxy solid after standing overnight at −20 °C (277 mg, 69% yield): FAB-MS for $C_{34}H_{58}N_2O_8$, MNa^+ at *m/z* 645.4113 (calcd 645.4091); mp 37−39 °C; ^{1}H NMR (300 MHz, $CDCl_3$) δ 0.82−0.87 (t, 3 H), 1.22−1.67 (m, 41 H), 2.21−2.34 (m, 4 H), 3.07 (br t, 2 H), 3.66−3.81 (m, 2 H), 4.03−4.25 (m, 2 H), 5.18−5.25 (m, 1 H), 6.69 (s, 2 H). The product was stored at −20 °C for at least 5 months without detectable maleimide hydrolysis.

Modified Route to NBD-6-aminohexanoic-NHS Ester (NBD-X-NHS, 9). $NaHCO_3$ (0.63 g, 7.5 mmol) and 6-aminohexanoic acid (0.66 g, 5.0 mmol) were added to H_2O (5 mL). NBD-Cl (0.5 mg, 2.5 mmol) dissolved in MeOH (20 mL) was added and the mixture was stirred at 60 °C for 30 min (*23*). The solution was cooled in ice, acidified to pH 2.0 with concentrated HCl, and the MeOH was removed by rotary evaporation. Excess water (ca. 50 mL) was added and the suspension was homogeneously dispersed by bath sonication. A fine black powder was collected on a 0.45 μm cellulose acetate filter (Fisher Scientific), washed with water, and dried under vacuum. The total yield of crude NBD-6-aminohexanoic acid was 0.6 g (81% yield). Next, the crude NBD-6-aminohexanoic acid (250 mg, 0.85 mmol) and *N*-hydroxysuccinimide (120 mg, 1.02 mmol) were dissolved in acetone (10 mL); DIC (200 μL, 1.28 mmol) was added and the solution was stirred for 16 h at room temperature. The solvent was removed under reduced pressure and the residue was suspended in MeOH (8 mL) in a sonicator bath. The insoluble material was collected by centrifugation (6000*g* for 10 min), washed with MeOH (2 mL), and dried under vacuum. The total yield was 200 mg (57% yield) and the product was greater than 85% pure as determined by RP-HPLC (0−80% CH_3CN/0.1% TFA in 40 min, 1 mL/min, on a C_8 semianalytical column) and NMR (data not shown).

NBD-PamMal (10). The aminohexanoyl chain of lipid **2** (50 mg, 80 μmol) was quantitatively deprotected in $CHCl_3$:TFA (1:1, 1 mL) for 90 min at room temperature. The solvent was evaporated under N_2 and the residue was redissolved in a small amount of $CHCl_3$, and reconcentrated in vacuo to eliminate residual TFA. Next, the deprotected AH−PamMal (**8**) was dissolved in 90%$CHCl_3$/10%MeOH (1 mL), and then NBD-X-NHS **9** (31 mg, 80 μmol) and TEA (27 μL, 200 μmol) were added. The product NBD-PamMal was identified by TLC developed in EtOAc:Hex (2:1, $R_f = 0.09$) or EtOAc ($R_f = 0.32$). The sample was mixed for 60 min at room temperature, concentrated in vacuo to give an orange residue; this oil was dissolved in a small volume of $CHCl_3$:EtOAc:Hex (2:2:1) and purified on silica gel with EtOAc:Hex (2:1) to remove a major fluorescent byproduct, followed by elution with EtOAc. A highly fluorescent product was obtained as an orange oil (64.2 mg, 83% yield). FAB-MS for $C_{41}H_{61}N_6O_{10}$, MNa^+ at *m/z* 821.4428 (calcd 821.4425); ^{1}H NMR (300 MHz, $CDCl_3$) δ 0.83−0.87 (t, 3 H), 1.16−1.84 (m, 38 H), 2.18−2.35 (m, 6 H), 3.21−3.28 (m, 2 H), 3.51−3.53 (m, 2 H), 3.72−3.75 (m, 2 H), 4.02−4.29 (m, 2 H), 5.22−5.25 (m, 1 H), 5.78 (m, 1 H), 6.14−6.17 (d, 1 H), 6.70 (s, 2 H), 8.45−8.48 (d,1 H). Less than 5% of maleimide hydrolysis was detected by ^{1}H NMR. The product was stored at −80 °C as a 50 mM stock solution in $CHCl_3$.

Preparation of the Thrombin Receptor Tether Polypeptide (NTTR-SH). The complete details of the molecular biology and protein purification (*24*) will be published elsewhere. The method is briefly described here. The cDNA encoding the extracellular N-terminal region of the human thrombin receptor (PAR-1) (*19*) Glu^{30}−Ser^{99}, was amplified by PCR and subcloned into the pET-31b polypeptide expression system (Novagen, Milwaukee, WI). After expression, purification and preparative CNBr cleavage, the C-terminal homoserine lactone of the 66 amino acid polypeptide was derivatized with the free-base form of cystamine (*25*) in DMSO essentially as described (*17*). The disulfide containing polypeptide was purified by HPLC, reduced with dithiothreitol (DTT), and again purified by HPLC to generate the 8 kDa polypeptide with a C-terminal cysteamine (called NTTR-SH). The total yield was generally greater than 70% for a 25 mg scale reaction.

Lipid−Polypeptide Conjugation. Either Pam_2Mal **1** or NBD-PamMal **10** (3.0 μmol, 60 μL from 50 mM stock in $CHCl_3$) was mixed with *n*-octyl-glucopyranoside (0.1 mmol, 100 μL from 1 M stock in $CHCl_3$) in a glass test

tube. The solvent was evaporated with a stream of nitrogen, and the residue was dried under vacuum for 2 h. NTTR-SH (5 mg, 0.6 μmol) dissolved in degassed 50 mM phosphate buffer (PB), pH 7.0 (1 mL), was added to the detergent/lipid film. The tube was filled with argon and sealed with Parafilm, and the suspension was homogenized by sonication. After stirring for 2 h at room temperature, the sample was dehydrated in a Speed-Vac. $CHCl_3$ (0.7 mL) was added and the excess lipid, and detergent was extracted with brief bath sonication. The lipopolypeptide was recovered with the addition of MeOH (0.7 mL) and centrifugation (14000*g* for 10 min). The pellet was air-dried and dissolved in 200 μL of DMSO. Water (1 mL) was added and any insoluble material was removed by centrifugation (14000*g*). The supernatant was injected onto a semipreparative C_4 HPLC column (Vydac, 1.0 × 250 mm) and the lipoconjugate was purified with the gradient 20 to 100% B over 60 min at 2 mL/min; mobile phase A, 0% CH_3CN/0.052% TFA; mobile phase B, 90% CH_3CN/0.06% TFA. Product fractions were concentrated in a Speed-Vac, dissolved in water and lyophilized to give polypeptide conjugated to Pam_2Mal **1,** designated NTTR-ML, and the fluorescent lipopolypeptide conjugate from NBD-PamMal **10**, designated NTTR-(NBD)ML. The identity and purity of the products were determined by analytical HPLC, MALDI-MS, UV spectroscopy and fluorometry. Both lipopolypeptides were freely soluble in water and MeOH at concentrations of at least 4 mg/mL.

Reconstitution of Lipopolypeptides into Phospholipid Membranes. Reconstitution experiments were performed with approximately a 200:1 phospholipid to lipopolypeptide molar ratio unless otherwise indicated. 1,2-Dimyristoyl-*sn*-glycero-3-phosphocholine (DMPC) (7 mg, 10 μmol) was transferred into a small round-bottom flask and the solvent was removed under N_2 and then overnight in vacuo. NTTR-ML (23 nmol, 500 μL of a 46 μM stock solution in MeOH) was added to the lipid and homogeneously dispersed by bath sonication. The MeOH was removed by rotary evaporation and the residue was placed under vacuum for 8 h. The lipid film was hydrated with 50 mM PB, pH 7.2 (1 mL), and the contents were transferred to a glass test tube. The tube was filled with argon, sealed with Parafilm, and bath-sonicated (Heat Systems, Farmingdale, NY) for 30 min at 37 °C. Large multi-lamellar vesicles were removed by filtration through a 0.45 μm PVDF membrane (Whatman) and the samples were stored at 37 °C until used (*26*). Lipid loss from filtration was determined by including 0.1 mol % NBD-DMPE in the phospholipid sample and measuring the change in fluorescence after Triton X-100 (TX-100) (2% final concentration) was added to samples corresponding to before and after filtration. The lipid loss varied from 50% for DMPC to 10 for 20% (molar ratio) 1,2-dimyristoyl-*sn*-glycero-3-phosphoglycerol (DMPG)/1,2-dimyristoyl-*sn*-glycero-3-phosphocholine (DMPC) and 1-palmitoyl-2-oleoyl-*sn*-glycero-3-phosphocholine (POPC) vesicle samples. The lipopolypeptide loss from filtration was determined by the fluorescamine assay used in the gel filtration studies described below. The quantity of lipopolypeptide recovered after filtration corresponded to phospholipid recovery (data not shown). The fraction of the lipopolypeptide on the exterior of the vesicles was estimated by comparing the fluorescence intensity of reconstituted vesicle samples treated with fluorescamine before or after solubilizing with 2% TX-100 (*27*).

Spontaneous insertion of NTTR-(NBD)ML into preformed vesicles was achieved by adding NTTR-(NBD)-ML (10 nmol, 10 μL of 10 μM stock in H_2O) directly to a vesicle preparation (ca. 2 mM lipid) and mixing by gentle pipet action. The insertion process could be monitored fluorometrically. NTTR-(NBD)ML (10 nmol) was added to 25 mM PB, pH 7.2 (1 mL), in a fluorescence cuvette. The sample was excited at 475 nm and the emission was monitored at 530 nm. Lipid vesicles (DMPC, 200 μL, from 10 mM stock), prepared as described above without the addition of lipopeptide, were added to the cuvette and the increase in fluorescence was recorded. Similar experiments were also performed with 20% DMPG/DMPC (molar ratio), POPC, and 20% POPG/POPC (molar ratio) vesicles.

Spontaneous insertion of NTTR-(NBD)ML into whole cells was also attempted. Human platelets (outdated, University Blood Bank, The University at Stony Brook), CHRF-288 (R. W. Johnson Pharmaceutical Research Institute) and *Drosophila melangaster* cell-lines (S2) (Invitrogen) were prepared by collecting the cells under low speed centrifugation and resuspending the cells in phosphate-buffered saline, pH 7.4, containing 5 mM EDTA. The final cell density was approximately 10^9 and 10^7 cells/mL for platelets and CHRF-288 or S2 cells, respectively. Cells (100 μL) were added to a NTTR-(NBD)ML sample and changes in fluorescence intensity were monitored at 25 °C. After the fluorescence intensity change had come to equilibrium, POPC vesicles were added determine the quantity of lipopolypeptide that remained in solution and was able to interact with the artificial membranes.

Gel Filtration Analysis of Reconstituted Lipopolypeptides. The extent of lipopolypeptide reconstitution into lipid vesicles or whole cells was determined by incubating the samples at 25 or 37 °C for up to 6 h, followed by separation on CL-6B Sepharose (Pharmacia, 1.5 × 28 cm) with 25 mM PB, pH 7.2. The gravity-driven flow rate was ~0.6 mL/min and 5 min fractions were collected. The 10-nm separation between excitation and emission wavelengths was used to reduce the intensity of scattered light at the detector. Fractions containing vesicles or whole cells could be identified visually as cloudy suspensions or by measuring scattered light intensity (λ_{ex} = 400 nm; λ_{em} = 410 nm) with a fluorometer. Fractions containing the nonfluorescent lipopolypeptide, NTTR-ML, were determined by a fluorescamine assay (*28*): TX-100 (2% final concentration) and TEA (0.1% final concentration) were mixed with an aliquot (1 mL) of each fraction. Fluorescamine (20 μL, 10 mM in dioxane) was added to each sample, and the sample was vortexed for 1 min. Relative concentrations of NTTR-ML in each fraction were determined fluorometrically (λ_{ex} = 395 nm; λ_{em} = 475 nm). Samples containing NTTR-(NBD)ML were determined by adding TX-100 (2% final concentration) to an aliquot (1-mL) of each fraction and measuring the fluorescence intensity of the NBD fluorophore (λ_{ex} = 475 nm; λ_{em} = 535 nm). Control gel filtration experiments were performed with the NTTR polypeptide (unconjugated) preincubated with vesicles and with each lipopolypeptide in the absence of vesicles and whole cells.

RESULTS

Design and Synthesis of the Maleimido-Lipids. Two new maleimide-based lipid reagents were synthesized to permit conjugation with thiol-containing polypeptides and other biomacromolecules (Figure 1). 1-Aminopropanediol was chosen as the glycerol-like backbone for lipid construction. Maleoylation could then be performed at the primary amine to position the conjugation site proximal to the headgroups in a phospholipid membrane

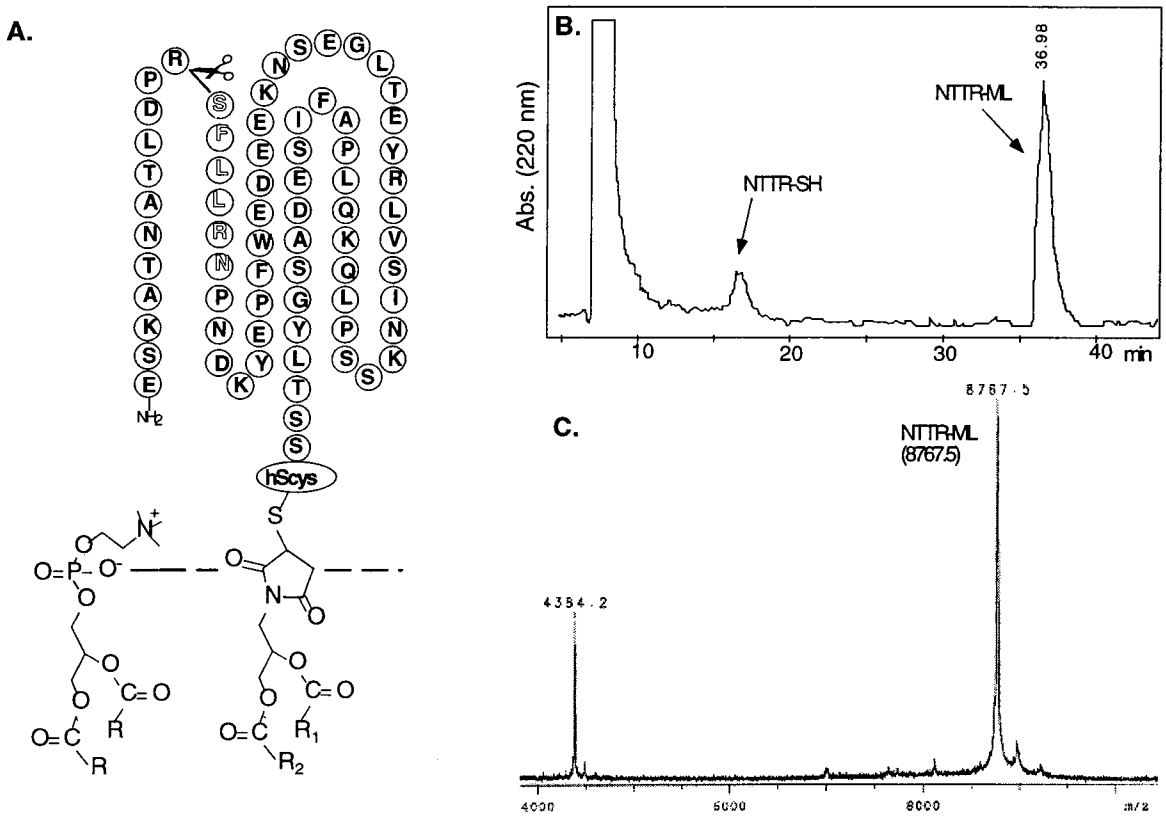

Figure 2. Lipid modification of the N-terminal extracellular domain of the human thrombin receptor. (A) The primary structure of the lipopolypeptide prepared from a maleimide lipid (**1** or **10**) and the 8 kDa polypeptide (NTTR) from the human thrombin receptor (Glu^{30}–Ser^{99}) is shown. The thrombin cleavage site between Arg^{41} and Ser^{42} is indicated by the scissors. The sulfhydryl group at the C-terminal of the thrombin receptor polypeptide (NTTR) is generated with cystamine as described in the text. The maleimide lipid is shown adjacent to a phospholipid to illustrate the expected location of the conjugation site with respect to a phospholipid bilayer. The orientation of the polypeptide does not imply any structural characteristics. R_1 is palmitoyl or NBD-X-aminohexanoyl and R_2 is palmitoyl. (B) HPLC chromatograms after NTTR-SH was coupled to Pam_2Mal (**1**). The hydrophobic modification increased the retention time on a C-4 semipreparative column by 20 min. Similar results were obtained after NTTR-SH was conjugated to NBD-PamMal (**10**). (C) MALDI-MS analysis of the NTTR-ML product. A single product with a mass at 8767.5 Da was observed (calcd 8762.9). The second mass peak is a doubly charged ion.

(see Figure 2A). The dipalmitoyl derivative Pam_2Mal (**1**) was constructed to ensure that the conjugated polypeptide would remain anchored into a phospholipid bilayer. Binding studies have shown that molecules acylated with two long hydrocarbon chains can exhibit long lifetimes in a membrane-bound complex ($t_{1/2}$ exceeding several hours) (*29*). The BOC-protected AH–PamMal reagent (**2**) was constructed to serve as a phospholipid membrane anchor that could be conveniently modified with amine reactive reporter groups. BOC was chosen as the amino acyl protecting group since it could be removed under acidic conditions that would not alter the maleimide group (*22*, *30*).

After CBZ protection, the diol was acylated in the presence of DMAP and a carbodiimide (Scheme 1). Use of *N,N*-diisopropylcarbodiimide during the formation of the dipalmitoyl derivative allowed simultaneous crystallization of **1** and extraction of the urea byproduct with MeOH, thereby eliminating a chromatographic step. Sequential acylation of CBZ-1-amino-propanediol with BOC-6-aminohexanoic acid at the primary alcohol followed by palmitic acid at the secondary alcohol took advantage of the differential reactivity between the primary and secondary alcohols (*31*). Quantitative hydrogenolysis of the CBZ protecting group unmasked the primary amine used for maleoylation.

Maleoylation of Lipids. NMM maleoylates primary amines under mild aqueous conditions (*22*). Maleimide cyclization is dependent on bicarbonate ion; thus, the

Scheme 1. Assembly of Lipid Acyl Chains

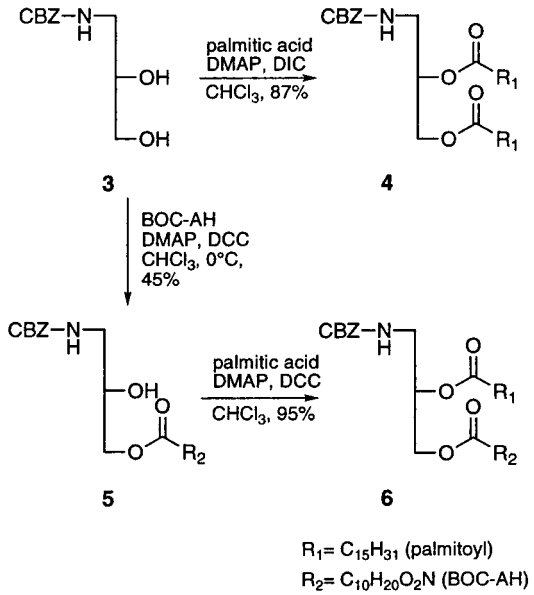

reactants must be partially soluble in aqueous $NaHCO_3$. Since the amino lipids **7a** and **7b** were completely insoluble in aqueous solutions, maleoylation was accomplished in a two-phase system containing a phase transfer catalyst (Scheme 2). An amide–imide intermediate (*22*) was initially formed in the $CHCl_3$ phase and the

Scheme 2. Maleoylation of Lipids

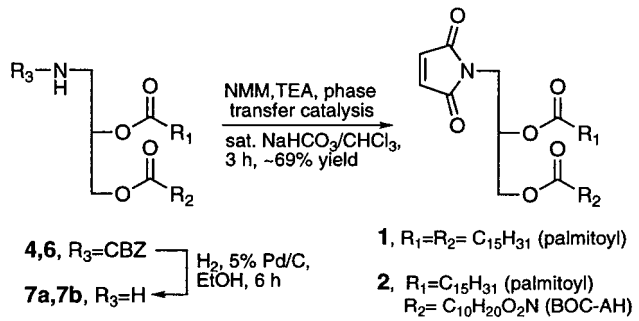

addition of $NaHCO_3$ with vigorous mixing resulted in cyclization to the maleimide. Maleimido-lipids **1** and **2** were recovered in greater than 65% yield with this procedure. The overall reaction rate was approximately 6-fold lower than that reported for the totally aqueous system (*22*). The biphasic system described here should be useful for preparation of other lipid, drug, or fluorophore-conjugating reagents that are not compatible with standard maleimide-forming procedures (*32*−*34*).

Amino Acyl Deprotection and Fluorescent Modification of Lipid 2. BOC protected AH−PamMal (**2**) was designed to improve the experimental versatility of the conjugating reagent. This lipid was found to be very stable upon storage, thus it can be prepared on a semipreparative scale and utilized as required with different amine reactive reporter groups. We chose to modify the lipid with NBD-X-NHS ester, since the derivatization produces a molecule similar to well-characterized fluorescent phospholipids (*35*) and phosphoinositides (*31*, *36*, *37*). In addition, NBD is an environmentally sensitive fluorophore that exhibits a large increase in quantum yield in the presence of hydrophobic environments (*38*).

BOC-AH−PamMal (**2**) was quantitatively deprotected with TFA; no hydrolysis of the maleimide group was observed. Maleimide hydrolysis was undetectable when the deprotected lipid was incubated for 1 h in an organic solvent system (90% $CHCl_3$/10% MeOH with 5 mol equiv of TEA) commonly used for amine acylation with activated reagents. Modification with NBD-X-NHS ester using this solvent system afforded NBD-PamMal (**10**) in 80% yield (Scheme 3). Most activated amine-reactive reporter groups can be used to acylate the amino-acyl lipid under similar conditions. Direct reaction of AH−PamMal (**8**) with NBD-Cl resulted in a number of side products, and the corresponding NBD-lipid could only be purified in a 1% final yield (data not shown).

The synthesis of NBD-6-aminohexanoic-NHS ester (**9**) presented here offers an economical way to prepare large quantities of this reagent. It does not require chromatography and results in a 50−60% overall yield of amine reactive product. The major impurity (less than 15%) is a nonreactive, nonfluorescent hydrolyzed product of NBD-Cl that does not interfere with coupling reactions. This protocol should be applicable to large scale preparations of fluorescent bioconjugates.

Lipid Conjugation to the NTTR Polypeptide. Generation of the thrombin receptor extracellular domain, NTTR, with a C-terminal sulfhydryl group provided the opportunity to conjugate the polypeptide to the maleimido-lipids. Detergent was required to solubilize the lipid and polypeptide, but only *n*-octyl-glucopyranoside, but not SDS or TX-100, resulted in homogeneous suspensions. The lipopolypeptides were easily purified by HPLC on a C_4 column (Figure 2B). MALDI-MS analysis of

Scheme 3. Deprotection and Fluorescent Modification of the Amino-Acyl Chain of Lipid 2

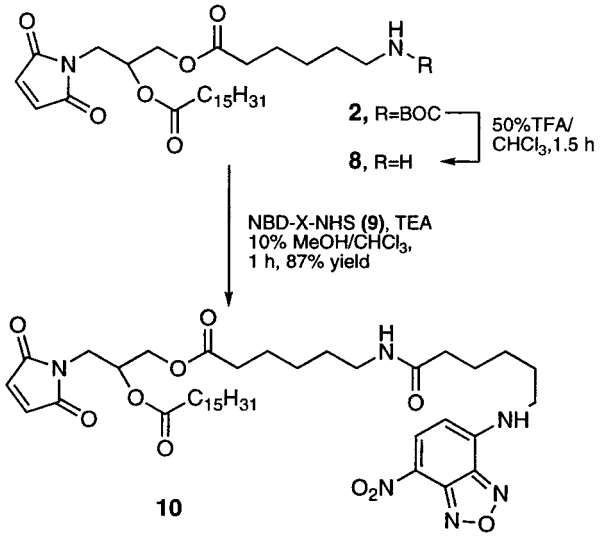

NTTR-ML indicated the formation of a single lipid conjugate with the correct mass (Figure 2C). The observed mass was 8767.5 Da (calcd 8762.9 Da). The fluorescent NTTR-(NBD)ML lipopolypeptide did not generate reproducible MALDI-MS values, but the HPLC chromatogram indicated that only a single new product was created (t_R = 29 min) after the reaction. The conjugation yields were >70% (4 mg) as judged by the preparative HPLC chromatogram (Figure 2B). Lipopolypeptide formation was not observed when the maleimido-lipids were incubated with the NTTR polypeptide that did not contain a free sulfhydryl group.

We attempted to form lipoconjugates by adding NTTR-SH directly to DMPC vesicles containing 2% maleimide lipids. Conjugates could not be detected by HPLC or MALDI-MS suggesting the maleimide group was not available in a sufficiently reactive environment for coupling to occur.

Reconstitution of the Lipopolypeptides into Phospholipid Vesicles. Analysis of the gel filtration chromatograms after application of each lipopolypeptide in the absence of phospholipid vesicles revealed that they elute before the unconjugated 8 kDa NTTR polypeptide (Figure 3A). This suggested that a majority of the lipopolypeptide (>90%) is aggregated in a micellar form at the concentrations (ca. 50−100 nM) used in these experiments. It also indicated that the CMC value for the lipopolypeptides is lower than 50 nM. Analysis of the micelles on a 50 kDa limit size-exclusion gel showed the lipopolypeptides eluted one fraction after the void volume, thereby suggesting the micelles were composed of between 6 and 9 monomers (data not shown).

Both lipoconjugates were tested for the ability to spontaneously insert into phospholipid vesicles. This method of lipopolypeptide incorporation is beneficial in many biochemical applications since it can be performed under gentle in vivo conditions and results in lipoconjugates on the exterior of the membrane surface. Spontaneous insertion of NTTR-ML into DMPC or POPC vesicles after 10 h at 37 °C or 1 h at 50 °C could not be observed using gel filtration analysis (data not shown). The elution profiles of these preparations were identical to NTTR-ML in the absence of vesicles indicating the lipopolypeptide remained in micellar form (Figure 3A). Greater than 90% of NTTR-ML did reconstitute into vesicles when the phospholipids and lipopolypeptide were premixed before

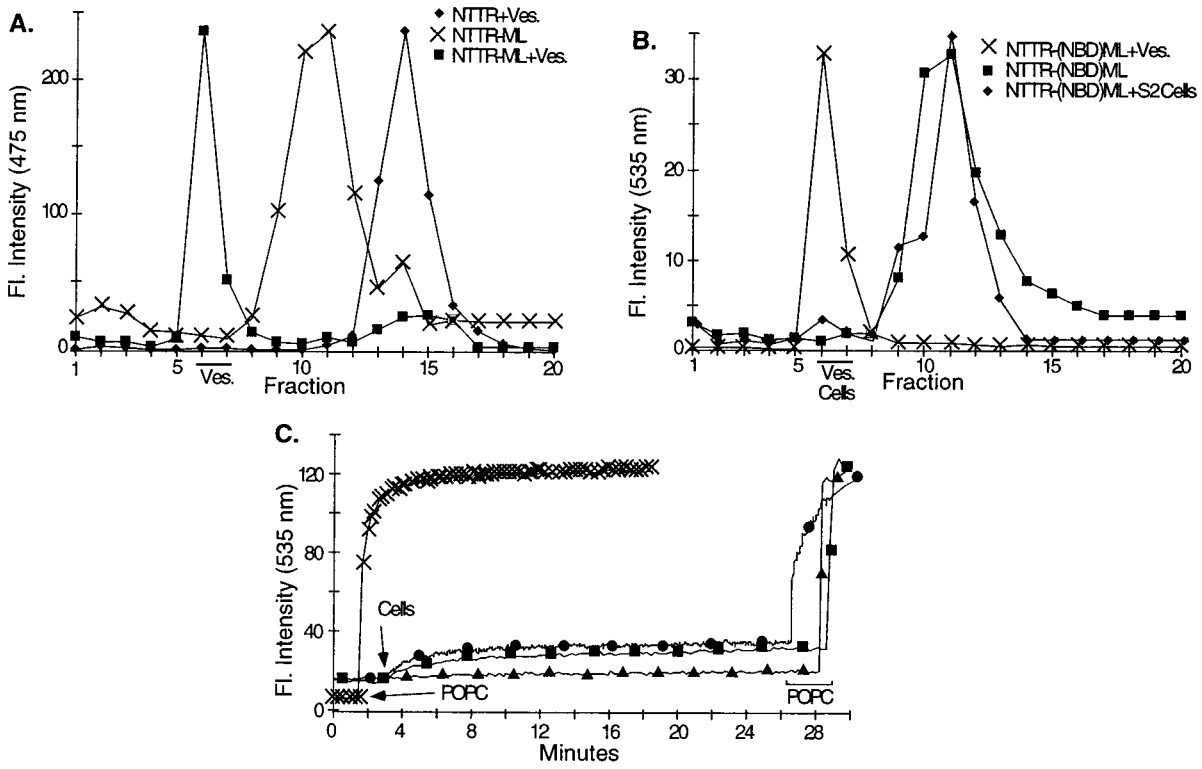

Figure 3. Gel filtration (CL-6B Sepharose) and fluorometric analysis of lipopolypeptide association with phospholipid membranes. (A) Co-mixture of NTTR-ML with DMPC before vesicle formation resulted in greater than 90% incorporation of the lipopolypeptide in vesicles found in the void volume (fractions 6 and 7) (■). The NTTR polypeptide (unconjugated) does not associate with phospholipid membranes (◆). NTTR-ML in the absence of lipid membranes eluted between the vesicle and the free polypeptide fractions indicating the lipopolypeptide is in micellar form (×). A similar chromatogram was observed when NTTR-ML was incubated with preformed DMPC or POPC vesicles (37 °C at 5 h) indicating NTTR-ML does not spontaneously insert into artificial membranes. NTTR-ML concentrations were measured with a fluorescamine assay. (B) NTTR-(NBD)ML was added to DMPC or POPC vesicles and incubated for 5 min before gel filtration analysis. NBD fluorescence was totally associated with the vesicle fractions indicating NTTR-(NBD)-ML spontaneously inserted into the artificial membranes (×). The fluorescent lipopolypeptide in the absence of vesicles eluted with a profile similar to NTTR-ML indicating NTTR-(NBD)ML exists in micellar form (■). Whole cells (results from *Drosophila* S2 cells are shown in the figure) were incubated with NTTR-(NBD)ML before subjecting the cells to gel filtration analysis (◆). Less than 1% of the total fluorescence was recovered in the void volume indicating the lipopolypeptide did not incorporate into whole cell membranes. Similar results were observed with human platelets and CHRF-288 cells. The chromatograms suggested NTTR-(NBD)ML remained in a micellar structure. (C) Spontaneous insertion of NTTR-(NBD)ML into POPC vesicles could be monitored fluorometrically. In micellar form, the NBD fluorophore was quenched [(×) before 2 min]. A 20-fold increase in fluorescence intensity was observed upon the addition of POPC vesicles (×). Addition of human platelet (■), CHRF-288 (▲) or *Drosophila* S2 (●) whole cells induced less than 15% change in fluorescence. Gel filtration results indicated that the increase was not due to spontaneous insertion into the cell membranes. After ca. 25 min, the addition of POPC vesicles to the cell mixtures resulted in the expected fluorescence increase indicating the lipopolypeptide remained in solution (in micellar form) and preferentially interacted with the artificial membranes.

hydration and sonication (Figure 3A). Approximately, 66% (±10%) of the lipopolypeptide was accessible on the outer surface of the vesicles as determined by the fluorescamine assay described in the Experimental Procedures. The unconjugated NTTR polypeptide did not associate with phospholipid vesicles after incubation for several hours at 37 °C (Figure 3A). It eluted approximately four fractions after the lipid derivative indicating that it exists as a smaller molecular weight entity (e.g., monomer) in solution.

NTTR-(NBD)ML did spontaneously insert into preformed vesicles as indicated by complete recovery of the lipopolypeptide in the void volume from the gel filtration column (Figure 3B). Similar results were obtained with 20% DMPG/DMPC and POPC vesicles. Since the quantum yield of the NBD fluorophore is environmentally sensitive, we were able to monitor lipopolypeptide insertion fluorometrically. The fluorescence intensity of NTTR-(NBD)ML reached maximum value (ca. 15-fold increase) within 2 min after vesicle addition suggesting the lipopolypeptide was completely inserted within this period (Figure 3C). This was confirmed by gel filtration, which showed complete lipopolypeptide association with vesicles after only a 5 min incubation (Figure 3B). The increase in quantum yield is likely a result of two environmental changes in the vicinity of the fluorophore. First, the NBD fluorophore becomes positioned into a hydrophobic phospholipid membrane environment. Second, the intermolecular quenching that exists when the lipopolypeptide is in a micellar state is eliminated upon phospholipid membrane association.

Spontaneous insertion of NTTR-(NBD)ML or NTTR-ML into whole cell membranes after 6 h (28 °C for S2 cells, and 37 °C for platelets and CHRF-288 cells) was not observed by gel filtration analysis. Figure 3B shows the results from gel filtration analysis of NTTR-(NBD)-ML incubated with the S2 cells at 28 °C for 6 h. Less than 1% of the NBD fluorescence was recovered in the void volume where the S2 cells were observed by light scattering measurements. Similar results were obtained after gel filtration analysis of NTTR-(NBD)ML preincubated with platelets and CHRF-288 cells (data not shown). The ability of the fluorescent lipopolypeptide to associate with whole cells was also examined fluorometrically. After a 25 min incubation of the fluorescent lipopolypeptide with platelets, CHRF-288 or S2 cells, the fluorescence intensity increased less than 15% when compared to the increase observed upon phospholipid

vesicle addition (Figure 3A). This result suggested that the addition of whole cells could promote an environmental change around the NBD fluorophore, but gel filtration analysis indicated that high-affinity membrane association did not occur. The reasons for the small fluorescent changes are unknown, but the fact that NTTR-(NBD)ML did not spontaneously insert into all three cell-types demonstrated that the behavior was not a cell-specific phenomena. Once the NBD fluorescence reached equilibrium after cell addition (ca. 25 min), the addition of POPC vesicles resulted in an immediate increase in fluorescence to levels that were obtained with only the addition of POPC vesicles (Figure 3C). This suggested that the fluorescent lipopolypeptide remained in solution (in micellar form) and preferentially inserted into the artificial vesicles.

DISCUSSION

Two maleimide-based lipidating reagents were prepared to anchor sulfhydryl-containing peptides and polypeptides into phospholipid membranes. The lipopolypeptide conjugates prepared from each of the lipids were shown to form soluble micellar structures in aqueous solutions. This behavior is consistent with that of lipid-based amphiphiles. Interestingly, the ability of the lipid conjugates to interact with phospholipid membranes appeared to be dependent on the chemical details of the lipid modification and the type of biological membrane. To further understand this phenomenon, it is worth summarizing the properties that govern the interaction between lipid-based amphiphiles and phospholipid membranes.

Two models have been proposed to characterize the interaction between amphiphiles (e.g., lipopeptides) and biological membranes. The first model depicts amphiphile insertion through a monomer intermediate. In this model, the probability of spontaneous insertion is dependent upon the equilibrium between micelle and monomer formation (i.e., CMC value), the rate of monomer escape from the micelle and the rate of monomer insertion into the acceptor membrane (*39*, *40*). The steady-state concentration of free monomer is not necessarily important since studies have shown that spontaneous insertion can occur at amphiphile concentrations that are above their CMC values (*39*, *41*). The dipalmitoyl-based lipopolypeptide, NTTR-ML, appears to be above its CMC value as demonstrated by the gel filtration data. However, the chromatogram also suggests that up to 10% of the conjugate may exist in smaller aggregates or in monomeric form (Figure 3A). This lipopolypeptide did not insert into artificial membranes at room temperature, after 10 h at 37 °C, or 1 h at 50 °C, indicating that it does not exist in a form that allows interaction between the conjugate lipid chains and the membrane surface. In terms of the monomer intermediate model, this suggests that monomer escape and insertion rates were not significantly affected by the increases in temperature. The fluorescent derivative, NTTR-(NBD)ML, did spontaneously insert into POPC, DMPC, and 20% DMPG/DMPC vesicles at room temperature. This indicates that the surface charge and acyl chain composition of the acceptor membrane did not have a significant impact on the NTTR-(NBD)ML insertion process. This lipopolypeptide appears to be above the CMC value at experimental concentrations, although the tailing chromatogram suggests that some portion of NTTR-(NBD)ML may exist as smaller aggregates or monomers (Figure 3B).

The only difference between the dipalmitoyl lipid derivative and the fluorescent lipid derivative is the chemical structure of the primary acyl chain. This indicates the acyl moieties of the lipopolypeptide influences the interaction with artificial membranes. The mechanism by which the fluorescent lipopolypeptide promotes spontaneous insertion is unclear. However, the reduced hydrophobicity of the NBD-labeled acyl chain could influence the monomer escape and insertion rates. It has been shown that an NBD group on a phospholipid acyl chain localizes to the polar headgroup environment, thereby altering the structure of the associated hydrocarbon chain (*35*). The fluorescent lipopolypeptide did not insert into whole cell membranes. This suggests that a property of whole cell membranes that is not exhibited in the artificial membrane systems significantly lowers the fluorescent lipopolypeptide insertion rate.

The second model that has been used to describe an amphiphile insertion process depicts insertion as dependent on a direct interaction between the amphiphile micelle and the phospholipid membrane (*9*, *42*). In this model, collisions between the fluorescent NTTR-(NBD)-ML micelles and the artificial phospholipid vesicles would be responsible for inducing conditions that allow insertion. The same conditions are apparently not achieved when the fluorescent lipopolypeptide micelles collides with whole cell membranes. Two main differences between the artificial and cellular membrane systems exist. First, the sizes of the membrane structures differ. The sonicated vesicles are small in diameter (20−200 nm) (*43*) and the cells used in this experiments are between 2 and 10 μm in diameter. The second difference is that whole cells have a surface richly adorned with glycoproteins and integral proteins. The protein component of the cellular membranes may have prevented NTTR-(NBD)ML association with the cellular surface, but previous reports have shown that various lipidated peptides (*7*, *44*, *45*) and proteins (*46*−*48*) are capable of spontaneous insertion into whole cell membranes. The size of the molecular headgroups, the method of lipid attachment, and the amino acid sequences vary in these studies, thus it is difficult to identify specific factors that prevent the NTTR lipid conjugates from incorporating into cellular membranes. It is possible that the chemical structure of the maleimido-lipids and the specific amino acid sequence of the NTTR polypeptide inhibit insertion into whole cells. Studies of phospholipid transfer from vesicles to whole cell membranes indicate that the transfer rate is dependent on the chemical structure of the acyl chains, backbone, and headgroups of the lipids (*29*, *49*).

The lipid reagents described here were conjugated to an 8 kDa polypeptide (NTTR) from the N-terminal of the human thrombin receptor (protease activated receptor-1, PAR-1) (*19*). These model compounds were prepared to test the ability of the lipids to anchor the polypeptide into phospholipid membranes. The lipoconjugates were also prepared as probes that would be useful for examining structural and biochemical properties of the human thrombin receptor activation mechanism. The G-protein coupled PAR-1 receptor is a seven transmembrane receptor that exhibits an extended extracellular N-terminus. The receptor is activated when thrombin proteolytically cleaves the N-terminus, thereby generating the tethered ligand for the receptor. The NTTR polypeptide is identical to the N-terminal portion of the receptor prior to the first transmembrane segment and includes the thrombin cleavage site (Figure 2A).

The C-terminal lipid modifications used in this study were proposed to mimic the first transmembrane segment of the receptor. Structural features exhibited by the polypeptide while it is anchored into a phospholipid

membrane were considered to be more closely representative of those that may be present in the native receptor (*24*). The NTTR lipid conjugates were also postulated to be useful as biochemical probes for investigating the rate of thrombin receptor cleavage on whole cellular membranes. Specific membrane-associated proteins have been implicated in altering the catalytic activity of thrombin on cellular membrane (*50*). A polypeptide representing the thrombin receptor N-terminus that could be anchored into cellular membranes would aid in characterizing the in vivo elements that influence the rate of thrombin receptor cleavage on a cellular membrane surface. Unfortunately, these studies were prevented by the inability of the NTTR lipopolypeptide to insert into whole cell membranes.

In summary, a general and convenient method for the lipidation of thiol-containing biological molecules was presented. The maleimide-based lipoconjugating reagents Pam_2Mal (**1**) and NBD-PamMal (**10**) are selective for sulfhydryl groups, which can be introduced into proteins, peptides, nucleic acids, or carbohydrates by either chemical or genetic methods. The extracellular N-terminal domain of the human thrombin receptor was derivatized with each lipid as a model system. The lipidated products were formed in high yield and could be reconstituted into artificial phospholipid membranes, although the reconstitution protocols were different for the two conjugates. The lipopolypeptides could not be reconstituted into whole cell membranes for reasons that are not clear. The conjugating reagents will aid in the preparation of acylated peptides and polypeptides for investigating structural and biochemical phenomena that occur at membrane surfaces.

ACKNOWLEDGMENT

We would like to thank Dr. B. S. Coller (The University at Stony Brook, Stony Brook, NY, USB, and Mt. Sinai Medical Center, New York, NY) and Dr. B. E. Maryanoff (R.W. Johnson Pharmaceutical Research Institute, Spring House, PA, RWJPRI) for financial and scientific support. Dr. Q.-M. Gu and Dr. J. F. Marecek (USB) provided valuable insights during development of the synthetic methods. The PAR-1 cDNA was gift from Dr. W. Bahou (USB). Dr. C. Derian (RWJPRI) supplied the CHRF-288 cells and C. Coburn (USB) supplied the *Drosophila* S2 cells.

LITERATURE CITED

(1) Sankaram, M. B. (1994) Membrane interaction of small N-myristoylated peptides: implications for membrane anchoring and protein−protein association. *Biophys. J. 67*, 105−112.

(2) Silvius, J. R., and l'Heureux, F. (1994) Fluorimetric evaluation of the affinities of isoprenylated peptides for lipid bilayers. *Biochemistry 33*, 3014−3022.

(3) Buser, C. A., Sigal, C. T., Resh, M. D., and McLaughlin, S. (1994) Membrane binding of myristylated peptides corresponding to the NH2 terminus of Src. *Biochemistry 33*, 13093−13101.

(4) Muhlradt, P. F., Kiess, M., Meyer, H., Sussmuth, R., and Jung, G. (1997) Isolation, structure elucidation, and synthesis of a macrophage stimulatory lipopeptide from *Mycoplasma fermentans* acting at picomolar concentration. *J. Exp. Med. 185*, 1951−1958.

(5) Maget-Dana, R., and Ptak, M. (1995) Interactions of surfactin with membrane models. *Biophys. J. 68*, 1937−1943.

(6) Stachelhaus, T., Schneider, A., and Marahiel, M. A. (1995) Rational design of peptide antibiotics by targeted replacement of bacterial and fungal domains. *Science 269*, 69−72.

(7) Moroder, L., Romano, R., Guba, W., Mierke, D. F., Kessler, H., Delporte, C., Winand, J., and Christophe, J. (1993) New evidence for a membrane-bound pathway in hormone receptor binding. *Biochemistry 32*, 13551−13559.

(8) Romano, R., Bayerl, T. M., and Moroder, L. (1993) Lipophilic derivatization and its effect on the interaction of cholecystokinin (CCK) nonapeptide with phospholipids. *Biochim. Biophys. Acta 1151*, 111−119.

(9) Romano, R., Musiol, H. J., Weyher, E., Dufresne, M., and Moroder, L. (1992) Peptide hormone-membrane interactions: The aggregational and conformational state of lipogastrin derivatives and their receptor binding affinity. *Biopolymers 32*, 1545−1558.

(10) Jelicks, L. A., Broido, M. S., Becker, J. M., and Naider, F. R. (1989) Interaction of the *Saccharomyces cerevisiae* alpha-factor with phospholipid vesicles as revealed by proton and phosphorus NMR. *Biochemistry 28*, 4233−4240.

(11) Shahinian, S., and Silvius, J. R. (1995) A novel strategy affords high-yield coupling of antibody Fab' fragments to liposomes. *Biochim. Biophys. Acta 1239*, 157−167.

(12) Pecheur, E. I., Hoekstra, D., Sainte-Marie, J., Maurin, L., Bienvenue, A., and Philippot, J. R. (1997) Membrane anchorage brings about fusogenic properties in a short synthetic peptide. *Biochemistry 36*, 3773−3781.

(13) de Bont, H. B. A., van Boom, J. H., and Liskamp, R. M. J. (1992) A convenient synthesis of a lipopeptide containing a diacylglycerol moiety: preparation of a potential inhibitor of protein kinase C. *Recl. Trav. Chim. Pays-Bas 111*, 222−226.

(14) Kung, V. T., and Redemann, C. T. (1986) Synthesis of carboxyacyl derivatives of phosphatidylethanolamine and use as an efficient method for conjugation of protein to liposomes. *Biochim. Biophys. Acta 862*, 435−439.

(15) Winger, T. M., Ludovice, P. J., and Chaikof, E. L. (1996) Lipopeptide conjugates: biomolecular building blocks for receptor activating membrane-mimetic structures. *Biomaterials 17*, 437−441.

(16) Yu, Y., Berndt, P., Tirrell, M., and Fields, G. B. (1996) Self-assembling amphiphiles for construction of protein molecular architecture. *J. Am. Chem. Soc. 118*, 12515−12520.

(17) Kuliopulos, A., and Walsh, C. T. (1994) Production, purification and cleavage of tandem repeats of recombinant peptides. *J. Am. Chem. Soc. 116*, 4599−4607.

(18) Thompson, N. L., Brian, A. A., and McConnell, H. M. (1984) Covalent linkage of a synthetic peptide to a fluorescent phospholipid and its incorporation into supported phospholipid monolayers. *Biochim. Biophys. Acta 772*, 10−19.

(19) Vu, T. H., Hung, D. T., Wheaton, V. I., and Coughlin, S. R. (1991) Molecular cloning of a functional thrombin receptor reveals a novel proteolytic mechanism of receptor activation. *Cell 64*, 1057−1068.

(20) Lee, B. H., Miller, M. J., Prody, C. A., and Neilands, J. B. (1985) Artificial siderophores. 1. Synthesis and microbial iron transport capabilities. *J. Med. Chem. 28*, 317−323.

(21) Canonica, L., Nali, M., and Rindone, B. (1986) New potential immunoenhancing compounds. 1. Syntheses of 1-amino-1-deoxyphosphatidylcholine derivatives. *Gazz. Chim. Ital. 116*, 19−23.

(22) Keller, O., and Rudinger, J. (1975) Preparation and some properties of maleimido acids and maleoyl derivatives of peptides. *Helv. Chim. Acta 58*, 531−541.

(23) Ahnoff, M., Grundevlk, I., Arfwidsson, A., Fonsellus, J., and Persson, B. (1981) Derivatization with 4-chloro-7-nitrobenzofurazan for liquid chromatographic determination of hydroxyproline in collagen hydrolysate. *Anal. Chem. 53*, 485−489.

(24) Elliott, J. T. PhD Dissertation, The University at Stony Brook, Stony Brook, NY, 1999.

(25) Nathan, A. H., and Bogert, M. T. (1941) The synthesis of pyrimidine and purine derivatives of cystamine and of a new type of thiazolidinopyrimidine. *J. Am. Chem. Soc. 63*, 2361−2366.

(26) Signor, G., Mammi, S., Peggion, E., Ringsdorf, H., and Wagenknecht, A. (1994) Interaction of bombolitin III with phospholipid monolayers and liposomes and effect on the activity of phospholipase A2. *Biochemistry 33*, 6659−6670.

(27) Roy, M. T., Gallardo, M., and Estelrich, J. (1997) Bilayer distribution of phosphatidylserine and phosphatidylethanolamine in lipid vesicles. *Bioconjugate Chem. 8*, 941−945.
(28) Udenfriend, S., Stein, S., Bohlen, P., Dairman, W., Leimgruber, W., and Weigele, M. (1972) Fluorescamine: a reagent for assay of amino acids, peptides, proteins and primary amines in the picomole range. *Science 178*, 871−872.
(29) Shahinian, S., and Silvius, J. R. (1995) Doubly lipid-modified protein sequence motifs exhibit long-lived anchorage to lipid bilayer membranes. *Biochemistry 34*, 3813−3822.
(30) Moroder, L., Nyfeler, R., Gemeiner, M., Kalbacher, H., and Wünsch, E. (1983) Immunoassays of peptide hormones and their chemical aspects. *Biopolymers 22*, 481−486.
(31) Chen, J., Profit, A. A., and Prestwich, G. D. (1996) Synthesis of photoactivatable 1,2-*O*-diacyl-*sn*-glycerol derivatives of 1-L-phosphatidyl-D-*myo*-inositol 4,5-bisphosphate (PtdInsP_2) and 3,4,5-trisphosphate (PtdInsP_3). *J. Org. Chem. 61*, 6305−6312.
(32) Kalgutkar, A. S., Crews, B. C., and Marnett, L. J. (1996) Design, synthesis and biochemical evaluation of N-substituted maleimides as inhibitors of prostaglandin endoperoxide synthases. *J. Med. Chem. 39*, 1692−1703.
(33) Nielsen, O., and Buchardt, O. (1991) Facile synthesis of reagents containing a terminal maleimido ligand linked to an active ester. *Synthesis* 819−821.
(34) Tsou, K., Barrnett, R. J., and Seligman, A. M. (1955) Preparation of some N-(1-naphthyl)-maleimides as sulfhydryl group reagents. *J. Am. Chem. Soc. 77*, 4613−4616.
(35) Abrams, F. S., and London, E. (1993) Extension of the parallax analysis of membrane penetration depth to the polar region of model membranes: use of fluorescence quenching by a spin-label attached to the phospholipid polar headgroup. *Biochemistry 32*, 10826−10831.
(36) Prestwich, G. D. (1996) Touching All the Bases: Inositol polyphosphate and phosphoinositide affinity probes from glucose. *Acc. Chem. Res. 29*, 503−513.
(37) Prestwich, G. D., Chaudhary, A., Chen, J., Feng, L., Mehrotra, B., and Peng, J., (1998) Probing Phosphoinositide Polyphosphate Binding to Proteins. In *Phosphoinositides* (K. Bruzik, Ed.) Vol. 818, pp 24−47, American Chemical Society, Washington, DC, 1998.
(38) Chattopadhyay, A., and London, E. (1988) Spectroscopic and ionization properties of N-(7-nitrobenz-2-oxa-1,3-diazol-4-yl)-labeled lipids in model membranes. *Biochim. Biophys. Acta 938*, 24−34.
(39) Kanda, S., Inoue, K., Nojima, S., Utsumi, H., and Wiegandt, H. (1982) Incorporation of a ganglioside and a spin-labeled ganglioside analogue into cell and liposomal membranes. *J. Biochem. 91*, 2095−2098.
(40) Roseman, M. A., and Thompson, T. E. (1980) Mechanism of the spontaneous transfer of phospholipids between bilayers. *Biochemistry 19*, 439−444.
(41) Zalipsky, S., Mullah, N., Harding, J. A., Gittelman, J., Guo, L., and Defrees, S. A. (1997) Poly(ethylene glycol)-grafted liposomes with oligopeptide or oligosaccharide ligands appended to the termini of the polymer chains. *Bioconjugate Chem. 8*, 111−118.
(42) Kremer, J. M., Kops-Werkhoven, M. M., Pathmamanoharan, C., Gijzeman, O. L., and Wiersema, P. H. (1977) Phase diagrams and the kinetics of phospholipid exchange for vesicles of different composition and radius. *Biochim. Biophys. Acta 471*, 177−188.
(43) Woodle, M. C., and Papahadjopoulos, D. (1989) Liposome preparation and size characterization. *Methods Enzymol. 171*, 193−217.
(44) Schroeder, H., Leventis, R., Shahinian, S., Walton, P. A., and Silvius, J. R. (1996) Lipid-modified, cysteinyl-containing peptides of diverse structures are efficiently S-acylated at the plasma membrane of mammalian cells. *J. Cell Biol. 134*, 647−660.
(45) Metzger, J. W., Sawyer, W. H., Wille, B., Biesert, L., Bessler, W. G., and Jung, G. (1993) Interaction of immunologically active lipopeptides with membranes. *Biochim. Biophys. Acta 1149*, 29−39.
(46) James, G., and Olson, E. N. (1990) Fatty acylated proteins as components of intracellular signaling pathways. *Biochemistry 29*, 2623−2634.
(47) Kooyman, D. L., Byrne, G. W., McClellan, S., Nielsen, D., Tone, M., Waldmann, H., Coffman, T. M., McCurry, K. R., Platt, J. L., and Logan, J. S. (1995) In vivo transfer of GPI-linked complement restriction factors from erythrocytes to the endothelium. *Science 269*, 89−92.
(48) Medof, M. E., Nagarajan, S., and Tykocinski, M. L. (1996) Cell-surface engineering with GPI-anchored proteins. *FASEB J. 10*, 574−586.
(49) Homan, R., and Pownall, H. J. (1988) Transbilayer diffusion of phospholipids: dependence on headgroup structure and acyl chain length. *Biochim. Biophys. Acta 938*, 155−166.
(50) Brass, L. F., Pizarro, S., Ahuja, M., Belmonte, E., Blanchard, N., Stadel, J. M., and Hoxie, J. A. (1994) Changes in the structure and function of the human thrombin receptor during receptor activation, internalization, and recycling. *J. Biol. Chem. 269*, 2943−2952.

BC000022A

Experimental Pretargeting Studies of Cancer with a Humanized anti-CEA × Murine anti-[In-DTPA] Bispecific Antibody Construct and a ^{99m}Tc-/^{188}Re-Labeled Peptide

H. Karacay,*,† W. J. McBride,† G. L. Griffiths,† R. M. Sharkey,‡ J. Barbet,§ H. J. Hansen,† and D. M. Goldenberg‡

Immunomedics, Inc., Morris Plains, New Jersey, Garden State Cancer Center, Belleville, New Jersey, and IBC Pharmaceuticals, LLC, Morris Plains, New Jersey. Received April 14, 2000; Revised Manuscript Received August 11, 2000

The aim of this study was to localize ^{99m}Tc and ^{188}Re radionuclides to tumors, using a bispecific antibody (bsMAb) in a two-step approach where the radionuclides are attached to novel peptides incorporating moieties recognized by one arm of the bsMAb. A chemically cross-linked human/murine bsMAb, hMN-14 × 734 (Fab′ × Fab′), anti-carcinoembryonic antigen [CEA] × anti-indium-DTPA was prepared as a prelude to constructing a fully humanized bsMAb for future clinical application. *N*,*N*′-*o*-Phenylenedimaleimide was used to cross-link the Fab′ fragments of the two antibodies at their hinge regions. This construct was shown to be >92% pure and fully reactive with CEA and a divalent (indium)-DTPA-peptide. For pretargeting purposes, a peptide, IMP-192 [Ac-Lys(In-DTPA)-Tyr-Lys(In-DTPA)-Lys(TscG-Cys-)-NH_2 {TscG = 3-thiosemicarbazonylglyoxyl}], with two indium-DTPAs and a chelate for selectively binding ^{99m}Tc or ^{188}Re, was synthesized. IMP-192 was formulated in a "single dose" kit and later radiolabeled with ^{99m}Tc (94−99%) at up to 1836 Ci/mmol and with ^{188}Re (97%) at 459−945 Ci/mmol of peptide. [^{99m}Tc]IMP-192 was shown to be stable by extensive in vitro and in vivo testing and had no specific uptake in the tumor with minimal renal uptake. The biodistribution of the hMN-14 × murine 734 bsMAb was compared alone and in a pretargeting setting to a fully murine anti-CEA (F6) × 734 bsMAb that was reported previously [Gautherot, E., Bouhou, J., LeDoussal, J.-M., Manetti, C., Martin, M., Rouvier, E., and Barbet, J. (1997) Therapy for colon carcinoma xenografts with bispecific antibody-targeted, iodine-131-labeled bivalent hapten. *Cancer 80* (Suppl.), 2618−2623]. Both bsMAbs maintained their integrity and dual binding specificity in vivo, but the hMN-14 × m734 was cleared more rapidly from the blood. This coincided with an increased uptake of the hMN-14 × m734 bsMAb in the liver and spleen, suggesting an active reticuloendothelial cell recognition mechanism of this mixed species construct in naive mice. Animals bearing GW-39 human colonic cancer xenografts were injected with bsMAb (15 μg) and after allowing 24 or 72 h for the bsMAb constructs to clear from the blood (hMN-14 and murine F6 × 734, respectively), [^{188}Re]IMP-192 (7 μCi) or [^{99m}Tc]IMP-192 (10 μCi) was injected at a bsMAb:peptide ratio of 10:1. Tumor uptake of [^{99m}Tc] or [^{188}Re]IMP-192 was 12.6 ± 5.2 and 16.9 ± 5.5% ID/g at 3 h postinjection, respectively. Tumor/nontumor ratios were between 5.6 and 23 to 1 for every major organ, indicating that early imaging with ^{99m}Tc will be possible. Radiation absorbed doses showed a 4.8-, 7.2-, and a 12.6 to 1.0 tumor to blood, kidney, and liver ratios when ^{188}Re was used. Although this new bsMAb pretargeting approach requires further optimization, it already shows very promising targeting results for both radioimmunodetection and radioimmunotherapy of colorectal cancer.

INTRODUCTION

Radioimmunodetection (RAID)[1] and radioimmunotherapy (RAIT) of cancer rely on the selectivity of radiolabeled antibodies directed against tumor-associated antigens binding to and then subsequently being retained in a tumor while clearing from normal tissues. For imaging, radioactivity uptake in a tumor must exceed that of surrounding tissue within a reasonable period of time and with sufficient signal for detection. For RAIT, the amount of radioactivity delivered must be sufficient such that over a period of time the tumor will be exposed to a radiation dose to effect cell killing. The first dose-limiting toxicity for RAIT, in applications to date, has been hematological. This is due to the high radiosensitivity of red marrow and the relatively high amount of radioactivity circulating in the blood; that is a direct consequence of the extended biological half-life of an intact IgG. Thus, increasing tumor/blood ratios while still delivering an adequate absolute amount of radioactivity to a tumor is an important goal for improving RAIT.

* To whom correspondence should be addressed. Phone: (973) 844-7054. Fax: (973) 844-7020. Current address: Garden State Cancer Center, 520 Belleville Ave., Belleville, NJ 07109.

† Immunomedics, Inc.

‡ Garden State Cancer Center.

§ IBC Pharmaceuticals.

[1] Abbreviations: bsMAb, bispecific antibody; CEA, carcinoembryonic antigen; cdr, complementarity-determining region; DMF, dimethylformamide; DTPA, diethylenetriaminepentaacetic acid; HBTU, *O*-benzotriazole-*N*,*N*,*N*′,*N*′-tetramethyl-uronium-hexafluoro-phosphate; HAMA, human anti-murine antibody; HPLC, high-pressure liquid chromatography; HSA, human serum albumin; IACUC, Institutional Animal Care and Use Committee; ID, injected dose; PDM, *N*,*N*′-*o*-phenylenedimaleimide; RAID, radioimmunodetection; RAIT, radioimmunotherapy; RP, reverse phase; SE, size exclusion; TFA, trifluoroacetic acid; TscG, 3-thiosemicarbazonylglyoxylic acid; TscGC, thiosemicarbonylglyoxylcysteinyl group.

10.1021/bc0000379 CCC: $19.00 © 2000 American Chemical Society
Published on Web 11/03/2000

Pretargeting approaches are being investigated as methods proven to be effective for increasing tumor/blood ratios. In a pretargeting method, an antibody conjugate containing a secondary recognition moiety is targeted to tumor, and then allowed to clear from nontarget tissues. Sometime later, a low molecular weight, fast-clearing, radiolabeled ligand recognized by the secondary recognition moiety of the pretargeted antibody conjugate is given. Diverse reagents for antibody-directed pretargeting approaches have been described (Hnatowich et al., 1987; Paganelli et al.,1988; Goodwin et al., 1988; Stickney et al., 1991; Bamias and Epenetos, 1992; Hawkins et al., 1993; Bos et al., 1994). Most have successfully shown improved tumor/nontumor radioactivity ratios as compared to a radiolabeled antibody alone, albeit often at a cost of substantially reduced absolute amounts of radioactivity in the targeted tumor. However, both Axworthy et al. (1994) and Boerman et al. (1999) have reported that the absolute amount of radioactivity delivered to tumors by pretargeting approaches can be comparable to levels achieved with a radiolabeled antibody alone, and could be achieved without sacrificing excellent tumor-to-nontumor ratios.

Two pretargeting methodologies have been reported most prominently, those using avidin−biotin and the other bispecific antibody (bsMAb) reagents. An avidin−biotin approach has the advantage of an exceptionally high binding affinity between the pretargeted antibody conjugate (either a biotin or avidin/streptavidin antibody conjugate) and the radiolabeled ligand (either avidin/streptavidin or biotin) (Rosebrough, 1993; Karacay et al.; Sharkey et al., 1997; Wilbur et al., 1998; Cremonesi et al., 1999). It also has the major disadvantages of the high immunogenicity of the avidins (Chinol et al., 1998), of serum biotinidases that can cleave many biotin conjugates, and the presence of endogenous biotin that can compete for avidin binding sites during pretargeting procedures. Although the alternate bsMAb approach does not engender as high component binding affinities and immunogenicity as the avidin−biotin approach, molecular engineering may be used ultimately to significantly reduce or even eliminate any immunogenicity of the bsMAb construct (Carter and Merchant 1997; Coloma and Morrison, 1997). Also, low molecular weight radiolabeled conjugates (haptens) can be designed that are endogenously unrecognized and are enzymatically resistant. Finally, bsMAb pretargeting results can be improved even more by incorporating radiolabeled bivalent, rather than monovalent, haptens in what has been termed an "affinity enhancement system" (AES) (LeDoussal et al., 1989).

In clinical studies of AES, imaging with an ^{111}In-labeled bivalent peptide hapten [*N*-α(^{111}In/In-DTPA)Tyr-*N*-ϵ(^{111}In/In-DTPA)Lys] given after a pretargeted bsMAb exhibited excellent results in several tumor types (LeDoussal et al., 1990; LeDoussal et al., 1993; Vuillez et al., 1997; Barbet et al., 1998). In these studies, tumors were pretargeted with a murine bsMAb, F6 × 734 (Fab′ × Fab′), anti-carcinoembryonic antigen (CEA) × anti-indium diethylenetriaminepentaacetic acid (DTPA). Although imaging results were impressive, in one study up to 61% of the patients eventually developed a human anti-murine antibody (HAMA) response (Le Doussal et al., 1993). The approach is now being extended to RAIT using the same bsMAb with an ^{131}I-labeled dipeptide (Vuillez et al., 1999). Efforts are currently underway to prepare a fully humanized construct for clinical studies. However, as a prelude to this, a human/murine bsMAb, hMN-14 × 734 (Fab′ × Fab′)(anti-CEA × anti-indium-DTPA) has been prepared and tested in animals. Since a humanized antibody might have different clearance and distribution properties in mice than a fully murine construct, comparisons were made to the murine F6 × murine 734 (Fab′ × Fab′) bsMAb that has been used by the French group.

Unfortunately, the 734 MAb, raised against indium-DTPA, was found to bind too weakly to yttrium-DTPA to enable any progress toward a yttrium-based bsMAb RAIT agent, and thus preclinical RAIT studies have used radioiodinated (I-131) bivalent haptens (Gautherot et al., 1997, 1998, 2000). Although an ^{131}I-based agent may be a highly effective therapeutic, it is important to investigate higher energy nuclides, such as ^{90}Y and ^{188}Re, since these may be more suitable for tumors >1 cm in diameter. The nuclear properties of ^{188}Re [$T_{1/2}$ 16.9 h; 2.12 and 1.96 MeV beta, 71 and 25% abundant; 155 keV imageable gamma, 15% abundant] would make it an ideal therapeutic isotope when bound to a fast-clearing bivalent hapten in the bsMAb approach. Like ^{99m}Tc, ^{188}Re is produced carrier-free (enabling high specific activity labeling of haptens) via a convenient generator system (Knapp et al., 1994). For imaging, ^{99m}Tc has multiple advantages over ^{111}In, including low cost, ready availability, ideal nuclear properties (140 keV γ-emission) for γ cameras, reduced radiation exposure to the patient and a shorter half-life (6 h). Thus, in this report, the initial development and preclinical testing of the human/murine hMN-14 × 734 (Fab′ × Fab′) hybrid bsMAb, and the progression from an [^{111}I]DTPA bivalent hapten to an imaging/therapy ^{99m}Tc/^{188}Re-based bivalent hapten are described.

MATERIALS AND METHODS

Antibodies and Peptides. hMN-14 IgG was prepared as described (Sharkey et al., 1995). The F(ab′)$_2$ of hMN-14 was derived by pepsin digestion and purified by protein A and ion-exchange chromatography. The anti-indium-DTPA antibody 734 F(ab′)$_2$ (Le Doussal et al., 1990) and F6 × 734 (Fab′ × Fab′) bsMAb were supplied by Immunotech (Marseilles, France). A rat anti-idiotypic antibody to hMN-14, termed WI2 (Losman et al., 1994), was used in some of the analytical work with hMN-14-containing MAbs to verify lack of discernible impact on the latter's binding site. The CEA used for immunoreactivity testing was obtained from Scripps (La Jolla, CA).

The hMN-14 × 734 bsMAb was prepared by the chemical coupling of the two reduced Fab′ fragments using *N*,*N*′-*o*-phenylenedimaleimide (PDM) by a published method (Glennie et al., 1987). Briefly, MAbs were reduced separately to their Fab′-SH fragments by incubation with 10 mM 2-mercaptoethylamine at 37° C for 1 h. The 734-Fab′-SH was converted to 734-Fab′-maleimide by reaction with 4 mM PDM at room temperature for 1 h. The Fab′-SH (hMN-14) and Fab′-maleimide (734) intermediates was isolated by centrifuged size-exclusion chromatography (Penefsky, 1979; Meares et al., 1984). The hMN-14 × 734-Fab′ × Fab′ conjugate was produced by reaction of a 1:1 mixture of the two fragments overnight at 4° C. It was purified on a SE (size exclusion) HPLC analytical column (Bio-Sil SEC-250, Bio-Rad, Richmond, CA), equipped with an in-line absorbance detector (Waters 486 or Beckman 167), set at 280 nm. The column was eluted at 1 mL/min with 0.2 M sodium phosphate, pH 6.8, containing 0.02% sodium azide. Only the center portion of the peak corresponding to the bsMAb was collected and used in these studies. The level of monospecific 734-F(ab′)$_2$ in hMN-14-F(ab′)$_2$ bsMAb

IMP-156: Ac-Phe-Lys(DTPA)-Tyr-Lys(DTPA)-NH_2

IMP-192: Ac-Lys(DTPA)-Tyr-Lys(DTPA)-Lys(TscGC)-NH_2, where TscGC is thiosemicarbazonyl-glyoxyl-cysteinyl-

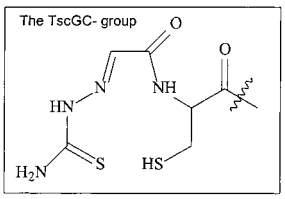

Figure 1. Structures of the peptides IMP-156 and IMP-192, including the $^{99m}Tc/^{188}Re$ chelating thiosemicarbazonyl-glyoxyl-cysteinyl group of IMP-192.

preparations was determined by mixing radiolabeled bsMAb with CEA, followed by SE-HPLC analysis. The level of monospecific hMN-14-F(ab′)$_2$ in hMN-14- × 734-F(ab′)$_2$ bsMAb preparations was determined using a DTPA conjugate of an irrelevant cdr-grafted MAb, hLL2, having the same framework as hMN-14 (Leung et al., 1995). The nonradiolabeled bsMAb and DTPA-hLL2 were mixed and applied to SE-HPLC with in-line UV analysis at 280 nm. In both assays, the percentage of product failing to shift to a higher MW on SE-HPLC was indicative of the levels of monospecific MAbs present in the preparations.

Intermediates for the peptide syntheses were obtained from Advanced ChemTech (Louisville, KY). The chelate-peptide bivalent hapten conjugates shown in Figure 1 (termed IMP-156 and IMP-192) were synthesized using standard solid-phase methods. Briefly, for the IMP-192 peptide, the "Fmoc-based" methodology and Rink amide resin were used. Starting with N^{alpha}-Aloc-Lys($N^{epsilon}$-Fmoc)-OH attached to the resin, N^{alpha}-Fmoc-Cys(Trt)-OH was then added to the side chain of lysine followed by the addition of the 3-thiosemicarbazonylglyoxylic acid (TscG). The latter was prepared by mixing thiosemicarbazone and glyoxylic acid together in a 1:1 ratio in methanol, and evaporating the solvent to generate the desired agent, which was used without further purification. The Aloc group was removed from the lysine using palladium(0)-catalyzed hydrostannolysis (Dangles et al., 1987), the other amino acids were added (N^{alpha}-Fmoc-Tyr(But)-OH, N^{alpha}-Fmoc-Lys($N^{epsilon}$-Aloc)-OH), the N-terminus was acetylated, and the lysine side-chain protecting groups were removed. The two DTPAs were then added to the lysine side chain using a monoactivated DTPA derivative. This was prepared by dissolving DTPA in methanol containing a 300-M excess of a 1.0-M solution of tetrabutylammonium hydroxide. The reaction mixture was rotary evaporated and the residue was dissolved in 100 mL of DMF. The DMF solution was then concentrated under hi-vacuum on the rotary evaporator. This process was repeated two more times to remove methanol. The residue was then dissolved in DMF and reacted with 1 equiv of *O*-benzotriazole-*N*,*N*,*N*′,*N*′-tetramethyl-uronium-hexafluoro-phosphate (HBTU). The reaction, with 6 equiv of the activated DTPA, proceeded overnight, and was repeated until the resin gave a negative ninhydrin test (Kaiser et al., 1970). The peptide was then cleaved from the resin and purified by reversed-phase HPLC. IMP 156 was synthesized in an analogous manner. Structures were confirmed by electrospray mass spectral analysis (IMP-156, MH^+ 1377; IMP-192, MH^+ 1590).

Radiolabeling. ^{125}I and ^{111}In were obtained from NEN Life Science Products (Boston, MA). The bsMAbs were radioiodinated using the chloramine-T method (Greenwood and Hunter, 1963) and purified using centrifuged size-exclusion columns. A typical ^{111}In labeling of IMP-156 is as follows. ^{111}In chloride (1.4 μL, 373 μCi) was mixed with 4.2 μL of 0.5 M sodium acetate, pH 6.1, and IMP-156 (3.3 μL, 4.9×10^{-5} M) in 0.5 M sodium acetate, pH 6.1, was added. After 20 min at room-temperature nonradioactive indium acetate (12.1 μL, 7.5×10^{-5} M in 0.5 M sodium acetate, pH 6.1), was added to bind remaining DTPA moieties.

Fresh sodium [^{99m}Tc] pertechnetate was purchased from Syncor (Kenilworth, NJ) or Mallinckrodt (Pine Brook, NJ). Sodium [^{188}Re] perrhenate was eluted from an in-house $^{188}W/^{188}Re$ generator (Oak Ridge National Laboratory, Oak Ridge, TN) with 0.9% sodium chloride solution. Radiolabeled peptides were analyzed on a Waters 4000 HPLC system having a reversed-phase Waters 8 × 100 mm radial Pak cartridge filled with a C-18 Nova-Pak 4 μm stationary phase. The column was eluted at 3 mL/min with a linear gradient of 100% 0.1% trifluoroacetic acid (TFA) in water to 100% 0.1% TFA in 90% acetonitrile/10% water over 10 min. At 10 min, the flow rate was increased to 5 mL/min and remained at 100% 0.1% TFA in 90% acetonitrile/10% water for 5 min before reequilibration to initial conditions. Both a Waters 486 absorbance detector, set at 220 nm, and an in-line radiation detector (Packard Radiomatic Flo-One or Ludlum) were used for detection.

For subsequent ^{99m}Tc and ^{188}Re radiolabeling, IMP-192 was formulated into lyophilized, single vial, "instant" kits containing excess cold indium. ^{99m}Tc kits contained 78 μg of IMP-192, with 100 μg Sn (II) for pertechnetate reduction, ascorbic acid, and a 6-fold excess of cold indium to peptide, for binding to DTPA. These vials were reconstituted with up to 40 mCi of ^{99m}Tc pertechnetate in 1.5 mL of saline. After 10 min at room temperature, the lead-shielded vials were heated in a boiling water bath for 15 min. For ^{188}Re labeling, kits contained 50 μg of IMP-192, with 660 μg of Sn(II), ascorbic acid, and indium at the same 6:1 indium-to-peptide ratio. These were reconstituted with 17 mCi of freshly eluted ^{188}Re perrhenate in 1.2 mL of saline. For ^{188}Re labeling, vials were heated 1 h in a boiling water bath. In both cases, after cooling, the radiolabeled peptide was diluted in 1.0% human serum albumin (HSA) for animal biodistribution studies.

Purity of the di-indium-DTPA peptides after ^{99m}Tc and ^{188}Re radiolabeling was evaluated by reversed-phase HPLC (as above), as well as ITLC using saturated sodium chloride as eluent. Unbound isotope eluted with the HPLC void volume, and the radiolabeled peptide eluted at 7.2 min. The ability of the radiolabeled peptides to bind to the bsMAbs was evaluated by SE-HPLC. The elution profiles of the radiolabeled bsMAbs and peptides alone were compared to those obtained after mixing the peptides with 734 F(ab)′$_2$, or with hMN-14 × 734-F(ab)′$_2$ bsMAb, at various ratios. Also, radiolabeled peptides were added to preformed mixtures of CEA and bsMAb, prior to similar SE-HPLC analyses, to investigate the ability of the peptides to bind to CEA-bound bsMAbs.

In Vitro Stability and Binding Studies. The in vitro stability of the bsMAb in human serum was tested by incubating the ^{125}I-labeled bsMAb at 37 °C in fresh, sterile-filtered serum taken from a normal donor. Samples were analyzed by SE-HPLC before and after mixing with CEA or WI2. A series of in vitro stability studies were performed on the ^{99m}Tc complex of IMP-192 diluted in 0.9% sodium chloride solution, fresh human serum, 1% HSA (prepared diluted in 0.9% saline from 25% HSA; Alpine Biologics, Blauvelt, NY), and 10 mM cysteine. Aliquots were withdrawn and tested by RP-HPLC at

early (1−2 h) postdilution time points and after overnight incubation.

The ability of components to retain binding to each other was analyzed using radiomatic size-exclusion HPLC and radiolabeled bsMAb and peptides. ^{111}In or ^{99m}Tc/^{188}Re-labeled peptide was injected onto HPLC alone, and immediately after mixing with variable amounts of bsMAb. Incubations were done in the presence of 1% HSA to minimize the possibility of nonspecific binding. When indicated, further incubations of radiolabeled bsMAb, including those radiolabeled by premixing with radiolabeled peptides, were carried out with CEA, WI2 or DTPA-hLL2. Preformed complexes of CEA and bsMAb were treated with radiolabeled peptide to demonstrate binding of the radiolabeled peptide to the antigen−bsMAb complex. In all incubations, components were mixed at room temperature and injected onto HPLC immediately, since component binding was very rapid, and did not change with increasing incubation times or temperatures. The precise mole ratio of these mixtures is given in the Results.

In Vivo Stability and Animal Targeting Studies. All animal experiments were carried out with IACUC-approved protocols. Studies were conducted in 5−8-week-old, female BALB/c or athymic nude mice (CR-Nu-Nu; Taconic, Germantown, NY). Standard lab chow and water were given ad libitum, and water was supplemented with Lugol's iodine solution (1 mL/500 mL) whenever radioiodinated agents were to be administered to animals. The GW-39 human colonic tumor cell line (Goldenberg et al., 1966; Goldenberg and Hansen, 1972) was used to demonstrate targeting to this CEA-producing tumor. It was propagated as serial, subcutaneous xenografts in nude mice, as described elsewhere (Sharkey et al., 1997). All test articles were injected intravenously in the lateral tail vein in 0.1−0.2 mL. At the designated time, groups of animals were anesthetized with sodium pentobarbital, bled by cardiac puncture, and then euthanized by cervical dislocation. Tumors and major organs were removed and weighed. The number of animals per grouping for each study is provided in the Results. The gastrointestinal tissues were counted in toto to include their contents. Whenever possible, urine was removed from the bladder at necropsy, weighed, and counted. Tissues, including weighed blood, were placed in 4-mL vials and counted in a γ-counter using appropriate windows for the isotopes. With paired isotopes, windows were set to eliminate or minimize dual-channel crossover, and figures were corrected for crossover counts, when needed, by reference to empirical measurements of radionuclide standards. In addition, in dual isotope studies, tissues were counted immediately and at a later time, for ^{125}I only, after the short-lived ^{99m}Tc and ^{188}Re nuclides had decayed.

In vivo stability was evaluated in BALB/c mice. ^{125}I-labeled bsMAbs (5 μCi, 15 μg) were administered and necropsies were performed at 1, 2, 4, and 24 h postinjection. Sera were obtained from these animals at these time points. Retention of binding to CEA, and also to [^{111}In]IMP-156, was examined by SE-HPLC analyses of the serum samples before and after mixing them with CEA or [^{111}In]IMP-156, using energy windows set for ^{125}I (0−30 keV) or ^{111}In (80−420 keV), respectively. In the pretargeting experiments, animals received tracer amounts of ^{125}I-labeled bsMAbs (5 μCi, 15 μg/animal), to quantitate tissue uptake of the bsMAb. In each pretargeting study, the amount of peptide given was based on a constant ratio of 10:1 (moles of antibody initially injected to the moles of peptide injected). It is important to emphasize that this ratio was not optimized to provide the best targeting results.

The methodology used to calculate radiation doses in mice has been reported (Sharkey et al., 1990). Radiation dose estimates were determined by first integrating the trapezoidal regions (for tumors) or exponential regions (for normal tissues) defined by the time activity data. For the trapezoidal fit of the tumor, the radioactivity at time zero is assumed to be zero, but for most normal tissues, the μCi/g at time zero is estimated from the exponential decay curve. If there is no exponential decay, the microcurie per gram at time zero is estimated by extrapolating the line described by the first data pair to the *y*-axis (i.e., μCi/g). The resulting integral for each organ is converted to centigray per millicurie with the use of *S* values appropriate for isotope and organ weight by assuming uniformly distributed activity in small unit density spheres (Siegel and Stabin, 1988).

RESULTS

Antibody and Peptide Preparation: Radiolabeling, Immunoreactivity, and In Vitro Stability. On the basis of the starting amount of Fab′, the final yield of the hMN-14 × 734-F(ab′)$_2$ bsMAb after purification was ∼25%. UV analysis at OD$_{280}$ of SE-HPLC profiles showed the product as a single peak. When this product was mixed with a high molecular weight indium−DTPA conjugate (i.e., [In]DTPA-hLL2-IgG), 92−93% of the UV profile shifted to a higher molecular weight, indicating that less than 8% of the product was possibly monospecific hMN-14-F(ab′)$_2$ or nonimmunoreactive bsMAb. Immunoreactivity testing with CEA and the peptides are described below.

The IMP-156 and IMP-192 peptides assayed as single peaks on RP-HPLC and could be stored in bulk for long periods at −20 °C when lyophilized as their TFA salts. When added at a 20-fold molar excess, ^{111}I was quantitatively incorporated in the IMP-156 within 20 min. After radiolabeling was complete, residual DTPA sites on IMP-156 were saturated by addition of a 6-fold molar excess of indium to peptide (approximately 3:1 to available DTPA). The IMP-192 peptide, formulated and lyophilized into single vial kits containing indium-saturated DTPA, was reproducibly labeled with sodium ^{99m}Tc pertechnetate at up to 1836 Ci/mmol in high yield (94−99%), obviating the need for any postlabeling purification. IMP-192, similarly saturated with indium-saturated DTPA, was labeled with ^{188}Re in high yield (96−97%), at a specific activity of 459−945 Ci/mmol of peptide.

A series of SE-HPLC studies were performed to show the binding of the hMN-14 × 734 bsMAb to either IMP-192 or IMP-156 (Figure 2, upper and lower panels, respectively). The radiolabeled peptides eluted around 14 min (Figure 2A). Since the peptides were diluted in HSA, this was a further indication that they would not associate with this serum protein. Furthermore, when mixed with hMN-14 or CEA alone, the peptide continued to elute at its native-size, indicating no nonspecific binding to these proteins (not shown). After incubating with a molar excess of the hMN-14 × 734 bsMAb (unlabeled), all radioactivity from the two peptides shifted to a higher molecular weight, with the main peak at nearly 9.0 min (Figure 2). It should be noted this elution time is earlier than the antibody alone, which elutes at 10.7 min (refer to Figure 4A). This is because the peptides are divalent and capable of binding to 2 bsMAb molecules. When the peptide was added to the bsMAb that had been premixed with a molar excess of CEA, >90% of the peptide

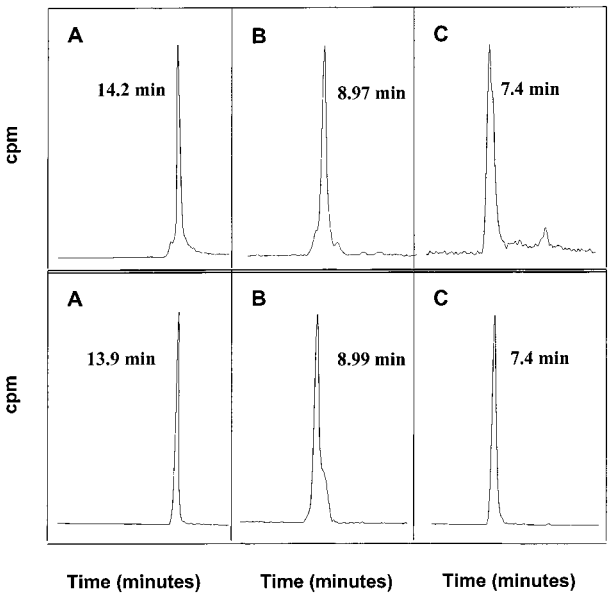

Figure 2. Upper panel. SE-HPLC chromatograms of (A) [^{99m}Tc]IMP-192, (B) [^{99m}Tc]IMP-192 mixed with hMN-14 × 734 bsMAb at 1:47 peptide: bsMAb mole ratio, and (C) [^{99m}Tc]IMP-192 added to hMN-14 × 734 bsMAb premixed with CEA, at 1:7 peptide:bsMAb and 1:10 bsMAb:CEA ratio. Lower panel. SE-HPLC chromatograms showing binding of hMN-14 × 734 to indium-DTPA and CEA. (A) [^{111}In]In-IMP-156, (B) Panel A mixed with hMN-14 × 734 bsMAb at 1:24 peptide:bsMAb mole ratio, (C) [^{111}In]In-IMP-156 added to hMN-14 × 734 bsMAb premixed with CEA. The bsMAb:CEA and peptide:bsMAb mole ratios were 1:10 and 1:24.

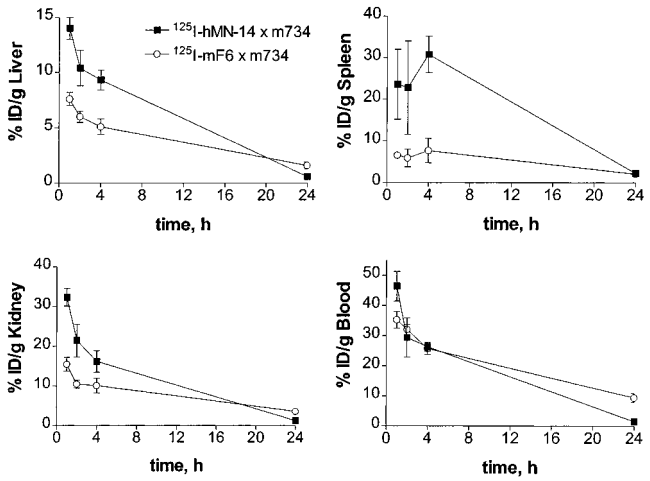

Figure 3. Tissue uptake of [^{125}I]hMN-14 × 734 and [^{125}I]F6 × 734 bsMabs in liver, spleen, kidney, and blood of BALB/c mice, five animals per time point per each bsMAb.

radioactivity migrated to a higher molecular weight, indicating the ability of the 734 arm of the bsMAb to bind to the peptide after first binding to CEA (Figure 2C). The fact that all of the radiolabeled peptides shifted to the higher molecular weight (i.e., to the elution time of a CEA−bsMAb complex rather than the elution time of the bsMAb alone) was further evidence that the bsMAb is essentially free of any cross-linked, immunoreactive 734-F(ab′)$_2$ moiety that theoretically might have formed during preparation of the bsMAb. If this product were present, a portion of the radiolabeled peptide would have eluted at either 10 min (antibody alone) or around 8 min (antibody-antibody complexes formed with the divalent peptide). Indeed, when the radiolabeled peptides were added to a molar excess of the 734 F(ab′)$_2$, all of the radioactivity migrated to the higher molecular weight

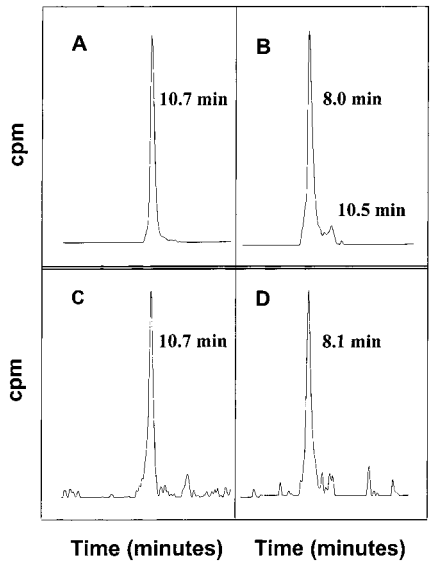

Figure 4. SE-HPLC chromatograms of (A) [^{125}I]hMN-14 × 734 bsMAb, (B) panel A mixed with CEA at 1:10 molar ratio, (C) serum from BALB/c mice 4 h post [^{125}I]hMN-14 × 734 bsMAb injection, and (D) panel C mixed with excess CEA.

fraction, but as expected, when CEA was added, no further shift was seen in the profile because of 734's lack of reactivity with CEA (not shown). Similar studies were carried out with the F6 × 734 bsMAb, which showed identical results (not shown).

To assess the stability of the bsMAb in serum, aliquots of [^{125}I]hMN-14 × 734-F(ab′)$_2$ were incubated at 37 °C in fresh human serum and then examined by SE-HPLC over 3 days. There was no loss of radioiodine from the antibody, but at 72 h, approximately 4−7% of the radioactivity migrated at a higher molecular weight, which suggested the development of a small amount of aggregate. There was no evidence of any product degradation to Fab′ fragments. It is important to note that the UV profile of the native nonradiolabeled product has not shown any tendency to aggregate or dissociate over a period of 12 months. At each time the radiolabeled bsMAb was tested, a portion was also mixed with a molar excess of either CEA or the anti-idiotypic MAb, WI2. Greater than 90% of the freshly prepared ^{125}I-labeled bsMAb migrated to a higher molecular weight, and by 72 h, there was no change, indicating excellent immunoreactivity retention of the radiolabeled bsMAb. Thus, there was no evidence of instability in vitro. Again, similar studies with the F6 × 734 bsMAb, except that CEA was used to illustrate antigen binding, showed identical results (not shown).

In vitro stability studies were also performed with the [^{99m}Tc]IMP-192, using a preparation that showed 99% of ^{99m}Tc bound at time zero. This product was diluted 10-fold in 10 mM cysteine, physiological saline, or human serum (37 °C). Testing at 1, 1.5, and 2.0 h later, respectively, 98−99% of the ^{99m}Tc remained bound to IMP-192. Upon retesting at 19−20 h postdilution, the percentages of ^{99m}Tc remaining bound to the IMP-192 were 89, 96, and 96%, respectively.

In Vivo Stability and Animal Targeting Studies. To assess the stability of the hMN-14 and F6 bsMAbs in vivo, separate groups of BALB/c mice were injected i.v. with 5 μCi (15 μg) of the [^{125}I]bsMAbs. Necropsies were performed at 1, 2, 4, and 24 h after the injection. In addition to quantifying the uptake in the tissues at these times, a portion of the serum was examined by SE-HPLC to assess the molecular integrity of the bsMAb. Signifi-

cant differences were seen in the distribution properties of the hMN-14 and the murine F6 bsMAb constructs (Figure 3). Overall, there was a higher level of the hMN-14 bsMAb in the normal tissues than the murine F6 bsMAb construct at 1 and 4 h. There was nearly a 2-fold higher uptake in the liver and kidneys and almost 4−5-fold higher uptake in the spleen, which also displayed a high variability in uptake. There was less pronounced differences in the blood concentrations at these earlier times, but by 24 h, the level of hMN-14 × 734-F(ab′)$_2$ in the blood was 1.5 ± 0.2% ID/g compared to 9.4 ± 1.5% ID/g for the F6 × 734-F(ab′)$_2$. Analysis of the SE-HPLC elution profiles of the serum revealed no significant degradation of either antibody through 4 h (Figure 4, panels A and C, only hMN-14 bsMAb shown). Adding CEA to bsMAb prior to or after it had been injected into animals made little difference in the HPLC profile of the bsMAb−CEA complexes formed (Figure 4, panels B and D). Identical results were obtained with the F6-based bsMAb. Analysis of the molecular profile of the [^{125}I]hMN-14 bsMAb at 24 h was not possible, due to insufficient radioactivity remaining in the serum. However, analysis of the profile of the F6 bsMAb revealed that it maintained its molecular integrity (not shown). Thus, the bsMAbs in blood are circulating as intact entities, and are capable of binding to both indium−DTPA complexes and to the target antigen. The differences in distribution properties of these two antibodies, especially the enhanced uptake in the spleen, suggest a recognition of the hMN-14 × 734-F(ab′)$_2$ by reticuloendothelial cells, which is different from that of the murine × murine F6 bsMAb construct. This ultimately results in a more rapid blood clearance of the hMN-14 bsMAb.

The bispecific binding specificity of the bsMAbs in serum taken from mice was assessed. Twenty microliters of serum was incubated with a prescribed amount of [^{111}In/In]IMP-156 (0.2 μCi, 4.1 × 10^{-13} mol). The radioactivity profile in the samples was then analyzed by SE-HPLC using an in-line radiation detector with a restricted ^{111}In window. The percentage of [^{111}In/In]IMP-156 that shifted to RT of the bsMAb was 100, 95, and 95 at 1, 2, and 4 h, respectively, for hMN-14 × 734-F(ab′)$_2$. Serum taken at 24 h after the bsMAb injection showed only 10 and 61% of the peptide eluted bound to the hMN-14 × 734-F(ab′)$_2$ and F6 × 734-F(ab′)$_2$, respectively. Retrospective analysis of the amount of bsMAb in the serum, based on the specific activity of the [^{125}I]bsMAb, suggested that this reduction was simply due to an insufficient amount of bsMAb in the serum at 24 h to bind all of the [^{111}In/In]IMP-156 that was added to the serum in vitro. However, the amount of [^{111}In/In]IMP-156 that comigrated to the molecular size of the bsMAb was in agreement with the amount of bsMAb remaining in blood based on the biodistribution data (Figure 3). For example, at 4 and 24 h, there was 26.4 and 1.5% of the [^{125}I]hMN-14 bsMAb in the serum, which corresponded to 7.9 × 10^{-13} and 4.6 × 10^{-14} mol in 20 μL of serum. Since 4.1 × 10^{-13} mol of peptide (containing 8.2 × 10^{-13} mol of DTPA) was added to each serum sample, the maximum portion of the peptide that could be bound was 96 and 11.2% (4 and 24 h), respectively.

The biodistribution of the [^{99m}Tc]IMP-192 alone was also examined. In BALB/c mice, it had an extremely rapid blood clearance, with only 0.3% ID/g remaining in circulation at 1 h postinjection (Table 1). The radioactivity was cleared from the body predominantly by urinary excretion, with 169 ± 95% ID/g in the urine within 1 h (or 6.9 ± 6.8% based on the total urine volume collected). Analysis of urine collected from mice injected with

Table 1. Biodistribution of [^{99m}Tc]IMP-192 Alone in BALB/c Mice[a]

	percent injected dose per gram of tissue (percent injected dose per organ)			
	1 h	2 h	4 h	24 h
liver	0.27 ± 0.18 (0.37 ± 0.21)	0.22 ± 0.16	0.09 ± 0.02	0.04 ± 0.00 (0.048 ± 0.004)
spleen	0.08 ± 0.01 (0.01 ± 0.002)	0.09 ± 0.03	0.05 ± 0.02	0.03 ± 0.01 (0.003 ± 0.000)
kidney	4.16 ± 0.75 (0.60 ± 0.09)	4.05 ± 0.60	3.21 ± 0.99	1.21 ± 0.08 (0.165 ± 0.008)
lungs	0.50 ± 0.23 (0.08 ± 0.02)	0.29 ± 0.08	0.19 ± 0.04	0.05 ± 0.00 (0.046 ± 0.008)
blood	0.30 ± 0.09 (0.41 ± 0.12)	0.21 ± 0.03	0.14 ± 0.04	0.05 ± 0.01 (0.064 ± 0.007)
stomach	0.39 ± 0.18 (0.08 ± 0.04)	0.42 ± 0.18	0.27 ± 0.33	0.02 ± 0.01 (0.011 ± 0.003)
small int.	1.37 ± 0.75 (1.54 ± 0.90)	0.60 ± 0.06	0.21 ± 0.09	0.03 ± 0.01 (0.040 ± 0.015)
large int.	0.41 ± 0.54 (0.29 ± 0.39)	1.53 ± 0.45	1.58 ± 0.70	0.15 ± 0.14 (0.148 ± 0.157)
muscle	0.10 ± 0.06 (ND)	0.05 ± 0.00 (ND)	0.03 ± 0.01	0.00 ± 0.00
urine	169 ± 95 (6.9 ± 6.8)	57 ± 15 (0.011 ± 0.012)	6.30 ± 4.53	0.20 ± 0.02

[a] Values represent the mean with the standard deviation for three animals at each time interval. Values in parenthesis at the 1- and 24-h time intervals indicate the average percentage of [^{99m}Tc]IMP-192 in the total tissue mass (total blood volume estimated to be equal to 7.4% of the body weight).

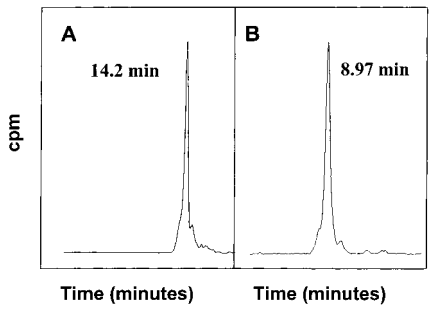

Figure 5. SE-HPLC trace of (A) urine collected from mouse injected with bsMAb and later with [^{99m}Tc]IMP-192 and (B) panel A mixed with excess hMN-14 × 734 bsMAb.

[^{99m}Tc]IMP-192 showed that it contained the intact peptide, since the radioactivity eluting at 14.18 min on SE-HPLC was shifted to a retention time corresponding to that of bsMAb upon addition of hMN-14 × 734-F(ab′)$_2$ (Figure 5). A minor fraction of the [^{99m}Tc]IMP-192 radioactivity was also observed in the small and then the large intestine, suggesting this as another route of excretion. The kidney uptake was about 4% ID/g at 1 h postinjection, but reduced to 1.21 ± 0.08% ID/g by 24 h.

The whole-body clearance of the peptide alone, or if given in a pretargeting setting, was tested in tumor-bearing nude mice (Figure 6). Groups of five mice were given two different amounts of the [^{99m}Tc]IMP-192 peptide, either 1.5 × 10^{-11} mol (28 μCi) or 1.5 × 10^{-10} mol (280 μCi). A separate group of animals was first given the 15 μg of the hMN-14 × 734 bsMAb and then 16 h later, the peptide was given. Animals were placed in a dose calibrator at various times after the peptide injection to determine the residual radioactivity remaining. To correct for radioactivity decay, 28 or 280 μCi of [^{99m}Tc]-IMP-192 were placed in vials and these were read in the dose calibrator before the whole-body readings. The percentage remaining in whole body was calculated from these readings. This study showed >85% of the radioactivity cleared from the animals within 2 to 3 h. This is consistent with the finding in BALB/c mice that the

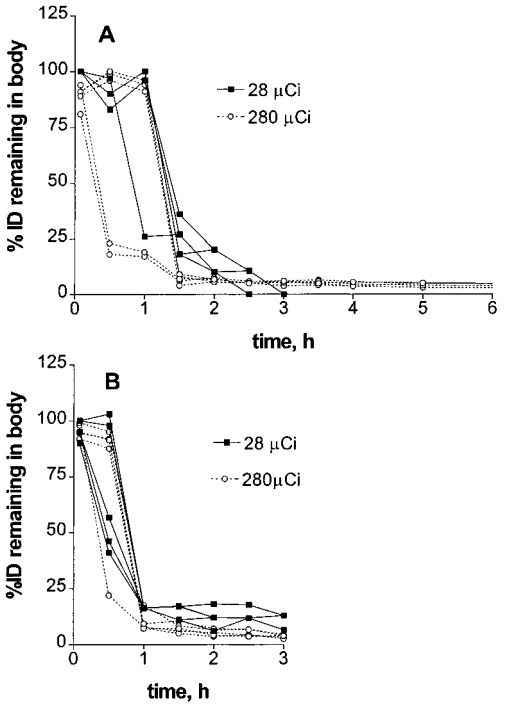

Figure 6. Whole-body clearance (biological) of [^{99m}Tc]IMP-192 (28 μCi, 1.5 $\times$ 10^{-11} mol or 280 μCi, 1.5 $\times$ 10^{-10} mol, (A) alone or (B**)** given 16 h after hMN-14 $\times$ m734 bsMAb was given. Animals were placed in a dose calibrator at 5 and 30 min and then again at 1, 1.5, 2.0, 2.5, 3.0, 4.0, 5.0, and 6 h after the peptide alone, or through 3 h for animals given the bsMAb.

majority of the peptide is cleared from the body through urinary excretion rather than fecal elimination. There was no evidence that increasing the amount of peptide affected the clearance rate, and even animals given the bsMAb 16 h earlier cleared the peptide at a similar rate.

Pretargeting Studies. To examine the targeting ability of the radiolabeled peptide when used in conjunction with the bsMAb, a study was first performed to assess the temporal relationship between the bsMAb and peptide injections. Nude mice bearing GW-39 human colonic cancer xenografts were first given intravenous injections of 150 pmol (15 μg) of the hMN-14 $\times$ 734-F(ab′)$_2$ or the F6 $\times$ 734-F(ab′)$_2$ containing a trace amount of each antibody radiolabeled with ^{125}I. At either 4, 16, 24, or 48 h after the hMN-14 bsMAb, 15 pmol of [^{99m}Tc]IMP-192 was given. A separate group of animals was given the identical amount of [^{99m}Tc]IMP-192 alone. In all groups, the tissue distribution was examined 3 h after the radiolabeled peptide was given. Table 2 shows the results obtained using the hMN-14 bsMAb. An important relationship is the bsMAb and peptide percent uptake in the tumor and blood at each time. When the peptide was injected 4 h after the bsMAb, the concentration of the bsMAb in the blood was too high, and thus a majority of the peptide was bound to the bsMAb in the blood rather than in the tumor. As the bsMAb in the blood cleared, a higher percentage of peptide is found in the tumor, with optimal tumor uptake of the peptide between 16 and 24 h, despite the lower amount of bsMAb in the tumor than at 4 h. Tumor/nontumor ratios continued to improve as the time from the bsMAb injection increased. For example, tumor/blood ratios were 3.6 $\pm$ 1.4 when the peptide was given 24 h after the bsMAb, but this increased to 11.3 $\pm$ 2.2 when an interval of 48 h was given. However, it is noteworthy that the percent uptake per gram of tumor also decreased, and thus, for therapeutic purposes, the earlier addition of the peptide may be preferred. Tumor uptake of the [^{99m}Tc]IMP-192 given alone was only 0.10 $\pm$ 0.02% ID/g, indicating that there is selective uptake of the peptide due to the bsMAb in the tumor. Another noteworthy item was the observation that in the animals given the radiolabeled peptide 4 h after the bsMAb, there was a very high percentage of ^{125}I radioactivity in the stomach. Since the uptake of [^{99m}Tc]-IMP-192 in the stomach was so much lower (i.e., 1.8%), the ^{125}I radioactivity in stomach likely represents a catabolized product. This is very likely since as was seen in Figure 4, there was considerable early accretion of the [^{125}I]hMN-14 bsMAb in the liver and the spleen. Although no significant amount of nonantibody-associated ^{125}I radioactivity was found in the serum at these early times, there is a clear indication that a rapid degradation of the radiolabeled hMN-14 bsMAb is occurring with uptake and excretion of the radioactivity through the GI tract.

On the basis of the previous biodistribution of the ^{125}I-labeled bsMAb alone (Figure 2), there did not appear to be any evidence that the bsMAb's distribution or blood clearance was altered by the addition of the peptide. This was confirmed in a separate study where the bsMAb was given alone or the peptide was given 16 h after the bsMAb. Tumor and blood uptake of [^{125}I]bsMAb alone was 3.7 $\pm$ 1.5 and 1.9 $\pm$ 0.3, respectively, and 2.5 $\pm$ 0.3 and 0.8 $\pm$ 0.08% ID/g at 19 and 27 h, respectively. In the animals given the [^{125}I]bsMAb followed 16 h later with the peptide, tumor and blood uptake was 3.4 $\pm$ 1.1 and 1.7 $\pm$ 0.2% ID/g, respectively, at 19 h, and by 27 h, [^{125}I]-bsMAb uptake was 3.6 $\pm$ 0.9 and 0.8 $\pm$ 0.10% ID/g for tumor and blood, respectively.

By virtue of having the highest tumor uptake and reasonable tumor/nontumor ratios for radiolabeled peptide, 24 h was selected for further evaluation with the hMN-14 bsMAb. Because of the slower blood clearance of the F6 antibody, an interval of 72 h was selected for the following pretargeting studies.

A time course study was designed to assess the distribution of the ^{99m}Tc- and ^{188}Re-labeled IMP-192 over a 24- and 72-h period, respectively. These results are shown in Tables 3−6. By allowing time to let the individual bsMAb clear from the blood, it was evident that even within just 30 min after the [^{99m}Tc]IMP-192 injection, there was a higher uptake of the peptide in the tumor than in any of the normal tissues (Tables 3 and 4). Tumor uptake of the [^{125}I]hMN-14 bsMAb ranged between 5 and 6% ID/g through 3 h after the [^{99m}Tc]IMP-192 injection and was reduced to 3.3 $\pm$ 0.7% ID/g by 24 h (Table 3). During this same time period, the average tumor uptake of the [^{99m}Tc]IMP-192 was between 11 and 14% ID/g, reducing to 8.7 $\pm$ 3.3% ID/g at 24 h. Tumor/blood ratios for the hMN-14 bsMAb pretargeting system were 2.7 $\pm$ 0.7 within 30 min of the [^{99m}Tc]IMP-192 injection and peaked at 16.1 $\pm$ 6.4 at 24 h after injection. The tumor/blood ratio in animals given only the [^{99m}Tc]-IMP-192 was 0.29 $\pm$ 0.14 at 3 h (Table 2) compared to 7.3 $\pm$ 2.3 in the pretargeting system at this same time (Table 3). Even tumor/kidney ratios were >1.0 within 30 min in each bsMAb pretargeting system. In contrast to when the [^{99m}Tc]IMP-192 was given alone, higher concentrations of the peptide were seen in the blood and the other normal tissues in the pretargeting system (e.g., liver, spleen, lungs). This is expected since there was still residual bsMAb remaining in the blood and tissues even at these later times following the bsMAb injection. Thus, the bsMAb-bound peptide would have a delayed clearance in comparison to the peptide alone.

Table 2. Biodistribution of [^{99m}Tc]IMP-192 in Nude Mice Bearing GW-39 Tumors[a]

percent injected dose per gram of tissue
(values in parentheses are the tumor/nontumor ratios for the radiolabeled peptide)

	peptide alone	4 h clearance		16 h clearance		24 h clearance		48 h clearance	
tissue	^{99m}Tc	^{125}I	^{99m}Tc	^{125}I	^{99m}Tc	^{125}I	^{99m}Tc	^{125}I	^{99m}Tc
tumor	0.10 ± 0.02	11.2 ± 3.2	5.5 ± 1.1	5.1 ± 1.1	8.8 ± 3.6	4.8 ± 2.3	14.3 ± 6.9	2.0 ± 0.9	4.8 ± 1.1
liver	0.23 ± 0.01 (0.43 ± 0.09)	5.0 ± 0.6	8.0 ± 0.9 (0.7 ± 0.1)	0.7 ± 0.07	2.5 ± 0.2 (3.5 ± 1.3)	0.6 ± 0.2	1.3 ± 0.2 (11.5 ± 5.5)	0.3 ± 0.1	0.3 ± 0.0 (18.1 ± 3.6)
spleen	0.07 ± 0.01 (1.45 ± 0.27)	12.0 ± 3.7	12.6 ± 4.4 (0.5 ± 0.1)	1.1 ± 0.6	2.6 ± 0.5 (3.4 ± 1.1)	0.6 ± 0.2	0.8 ± 0.3 (21.3 ± 14)	0.3 ± 0.1	0.3 ± 0.1 (15.8 ± 4.3)
kidney	1.87 ± 0.14 (0.05 ± 0.01)	7.5 ± 1.9	12.4 ± 2.8 (0.5 ± 0.1)	1.0 ± 0.1	5.3 ± 1.0 (1.6 ± 0.4)	0.6 ± 0.2	4.5 ± 1.2 (3.4 ± 1.9)	0.4 ± 0.1	3.3 ± 0.7 (1.5 ± 0.2)
lungs	0.14 ± 0.04 (0.72 ± 0.13)	7.7 ± 2.0	9.7 ± 2.8 (0.6 ± 0.1)	1.2 ± 0.1	3.5 ± 0.3 (2.6 ± 1.0)	2.3 ± 1.1	3.1 ± 1.7 (7.1 ± 6.3)	0.3 ± 0.2	0.5 ± 0.2 (11.5 ± 3.3)
blood	0.44 ± 0.35 (0.29 ± 0.14)	15.0 ± 3.8	28.8 ± 7.7 (0.2 ± 0.03)	2.3 ± 0.2	11.9 ± 0.9 (0.7 ± 0.3)	0.9 ± 0.2	3.3 ± 0.5 (4.2 ± 1.8)	0.1 ± 0.01	0.4 ± 0.2 (11.3 ± 2.2)
stomach	0.56 ± 0.16 (0.19 ± 0.08)	48.0 ± 5.3	1.8 ± 0.4 (3.1 ± 0.7)	6.5 ± 0.8	0.8 ± 0.2 (11.2 ± 3.3)	8.7 ± 1.4	1.5 ± 1.5 (14.3 ± 9.5)	0.3 ± 0.2	0.2 ± 0.2 (32.0 ± 18)
small int.	1.29 ± 0.38 (0.08 ± 0.03)	3.3 ± 0.7	8.9 ± 1.0 (0.6 ± 0.1)	0.5 ± 0.02	3.2 ± 1.0 (2.7 ± 0.3)	0.4 ± 0.1	2.7 ± 0.5 (5.0 ± 1.9)	0.1 ± 0.01	0.3 ± 0.1 (20.0 ± 5.5)
large int.	0.65 ± 0.15 (0.15 ± 0.03)	1.7 ± 0.6	1.2 ± 0.7 (5.6 ± 2.9)	0.5 ± 0.07	1.7 ± 0.6 (6.7 ± 5.7)	0.9 ± 0.06	0.3 ± 0.1 (59.0 ± 50.7)	0.2 ± 0.1	1.3 ± 0.2 (3.6 ± 0.6)

[a] Animals were either given the [^{99m}Tc]IMP-192 alone (1.5×10^{-11} mol) or the animals first received [^{125}I]hMN-14 × 734-bsMAb (1.5×10^{-10} mol), and then after 4, 16, 24, and 48 h, they received the radiolabeled peptide. All values were obtained 3 h after the [^{99m}Tc]IMP-192 (1.5×10^{-11} mol), injection and are presented as the mean ± standard deviation with five animals per interval. The average GW-39 weights for each respective group in order shown were 0.113 ± 0.043, 0.102 ± 0.008, 0.120 ± 0.029, 0.404 ± 0.277, and 0.512 ± 0.352 g.

Table 3. Biodistribution of [^{99m}Tc]IMP-192 in Mice Pretargeted with [^{125}I]hMN-14 × m734[a]

percent injected dose per gram of tissue
(values in parentheses are the tumor/nontumor ratios for the radiolabeled peptide)

	30 min		1 h		3 h		24 h	
tissue	^{125}I	^{99m}Tc	^{125}I	^{99m}Tc	^{125}I	^{99m}Tc	^{125}I	^{99m}Tc
tumor	4.9 ± 1.1	11.4 ± 4.8	6.0 ± 2.3	14.3 ± 3.6	5.5 ± 1.1	12.6 ± 5.2	3.3 ± 0.7	8.7 ± 3.3
liver	0.6 ± 0.1	1.4 ± 0.3 (7.9 ± 1.7)	0.5 ± 0.2	0.9 ± 0.2 (15.7 ± 5.4)	0.5 ± 0.1	0.6 ± 0.1 (20.7 ± 7.6)	0.1 ± 0.02	0.4 ± 0.1 (22.3 ± 7.4)
spleen	0.8 ± 0.3	1.2 ± 0.4 (9.4 ± 1.0)	0.7 ± 0.3	0.8 ± 0.2 (19.5 ± 8.6)	0.7 ± 0.2	0.5 ± 0.1 (22.9 ± 7.5)	0.2 ± 0.03	0.4 ± 0.2 (23.8 ± 11.7)
kidney	0.5 ± 0.1	9.9 ± 6.1 (1.2 ± 0.2)	0.5 ± 0.1	4.6 ± 0.7 (3.1 ± 0.6)	0.5 ± 0.1	2.4 ± 0.5 (5.2 ± 1.5)	0.1 ± 0.02	1.2 ± 0.3 (7.3 ± 1.9)
lungs	0.9 ± 0.3	4.2 ± 3.4 (3.7 ± 1.7)	0.8 ± 0.2	3.6 ± 1.9 (5.5 ± 3.6)	0.8 ± 0.3	1.0 ± 0.3 (13.5 ± 7.1)	0.3 ± 0.01	0.3 ± 0.1 (30.8 ± 14.4)
blood	0.9 ± 0.3	4.3 ± 1.2 (2.7 ± 0.7)	1.2 ± 0.4	3.5 ± 0.9 (4.2 ± 1.3)	1.1 ± 0.3	1.7 ± 0.4 (7.3 ± 2.3)	0.2 ± 0.07	0.6 ± 0.2 (16.1 ± 6.4)
stomach	5.0 ± 1.7	3.6 ± 4.8 (17.9 ± 20.9)	6.1 ± 3.3	1.0 ± 1.2 (25.0 ± 14.3)	5.7 ± 3.3	0.5 ± 0.2 (30.7 ± 14.5)	0.8 ± 0.3	0.3 ± 0.2 (42.4 ± 33.3)
small int.	0.4 ± 0.1	1.4 ± 0.3 (8.2 ±3.3)	0.4 ± 0.08	1.4 ± 0.2 (10.3 ± 1.6)	0.5 ± 0.2	1.0 ± 0.5 (14.1 ± 7.6)	0.09 ± 0.02	0.3 ± 0.07 (35.7 ± 11.7)
large int.	0.7 ± 0.4	0.5 ± 0.3 (29.3 ± 12.3)	0.5 ± 0.09	0.3 ± 0.05 (56.3 ± 13.0)	0.8 ± 0.4	0.9 ± 0.3 (14.6 ± 6.7)	0.1 ± 0.03	0.5 ± 0.2 (17.3 ± 8.1)

[a] Nude mice bearing GW-39 human colonic cancer xenografts were given [^{125}I]hMN-14 × m734 (Fab′ × Fab′, 5 μCi, 1.5×10^{-10} mol). Twenty-four hours later, [^{99m}Tc]IMP-192 (10 μCi, 1.6×10^{-11} mol) was injected. All times given in the tables are the means and standard deviations at the hours indicated after the [^{99m}Tc]IMP-192 injection (five animals per time point). The average GW-39 weights for each respective group in order shown were 0.382 ± 0.106, 0.373 ± 0.062, 0.265 ± 0.094, and 0.358 ± 0.110 g.

Interestingly, the percent injected dose per gram of the [^{99m}Tc]IMP-192 in tumors was similar in animals pretargeted with either the F6 bsMAb or the hMN-14 bsMAb, despite the nearly 2-fold higher amount of the F6 bsMAb in the tumor (Table 4). This is most likely explained by the fact that there was also nearly 2-fold more F6 bsMAb than hMN-14 bsMAb in the blood, which would have reduced the amount of [^{99m}Tc]IMP-192 available for tumor binding. As stated earlier, these studies were not conducted under conditions to optimize each targeting system fully.

The pretargeting studies were repeated using [^{188}Re]-IMP-192 in place of [^{99m}Tc]IMP-192, at the same 10:1 bsMAb to IMP-192 ratio (Tables 5 and 6). Because of the longer half-life of ^{188}Re, biodistributions were performed at 3, 24, 48, and 72 h following [^{188}Re]IMP-192 injection. Again, uptake of the [^{188}Re]IMP-192 was higher in the tumor than all the normal tissues as early as 3 h after injection, due to both the rapid clearance of small molecular weight [^{188}Re]IMP-192 and the ready recognition of the radiolabeled peptide by the tumor-localized bsMAb. In contrast to tumor uptake of the [^{188}Re]IMP-192 alone (7 μCi, 1.5×10^{-11} mol of peptide), which at 3 h was 0.36 ± 0.15 (Table 5), [^{188}Re]IMP-192 tumor uptake was 16.9 ± 5.5% ID/g when used with the hMN-14 bsMAb pretargeting system. Overall, no meaningful differences were seen between the ^{99m}Tc- and the ^{188}Re-labeled peptide in either bsMAb pretargeting system at 3 and 24 h, times that were common for the two studies.

Dosimetry. To predict the therapeutic potential of [^{188}Re]IMP-192 in animals pretargeted with hMN-14 734 bsMAb, the biodistribution studies were used to calculate radiation-absorbed doses to the tissues and tumor (Table 7). Even under these conditions which were not fully optimized, the tumor is predicted to receive a radiation dose nearly 12-fold higher than the liver, 7 times higher than the kidneys, and 5-fold higher than the blood. Radiation doses to the gastrointestinal tract, most notably the stomach, were higher than the other organs.

DISCUSSION

Pretargeting is a very attractive modality for the delivery of radionuclides to tumors for both RAID and RAIT, although its complexity requires multiple problems to be solved before it can be applied optimally in a clinical

Table 4. Tissue Uptake of [^{99m}Tc]IMP-192 in Mice Pretargeted with [^{125}I]F6 × m734 bsMAb[a]

percent injected dose per gram of tissue
(values in parentheses are the tumor/nontumor ratios for the radiolabeled peptide)

	30 min		1 h		3 h		24 h	
tissue	^{125}I	^{99m}Tc	^{125}I	^{99m}Tc	^{125}I	^{99m}Tc	^{125}I	^{99m}Tc
tumor	11.1 ± 3.2	11.4 ± 3.9	15.6 ± 3.9	11.1 ± 1.4	11.3 ± 1.5	14.3 ± 6.7	8.1 ± 1.0	10.6 ± 1.4
liver	0.4 ± 0.1	1.7 ± 0.4 (7.0 ± 3.2)	0.4 ± 0.03	1.7 ± 0.5 (6.8 ± 1.4)	0.4 ± 0.1	0.9 ± 0.1 (16.3 ± 5.9)	0.3 ± 0.01	0.6 ± 0.1 (17.4 ± 3.1)
spleen	0.4 ± 0.1	1.9 ± 1.3 (7.5 ± 4.9)	0.4 ± 0.001	1.2 ± 0.1 (9.5 ± 0.2)	0.4 ± 0.1	0.8 ± 0.2 (18.4 ± 8.4)	0.3 ± 0.04	0.5 ± 0.1 (21.9 ± 4.5)
kidney	0.7 ± 0.3	20.8 ± 19.9 (1.1 ± 1.0)	0.6 ± 0.1	7.1 ± 1.0 (1.5 ± 0.03)	0.4 ± 0.1	4.1 ± 0.5 (3.4 ± 1.3)	0.3 ± 0.04	2.3 ± 0.3 (4.6 ± 0.6)
lungs	0.8 ± 0.3	3.1 ± 1.2 (4.4 ± 2.8)	1.0 ± 0.1	3.4 ± 0.9 (3.3 ± 0.5)	0.6 ± 0.2	1.1 ± 0.2 (12.6 ± 4.5)	0.4 ± 0.06	0.5 ± 0.1 (20.7 ± 3.6)
blood	1.6 ± 0.5	8.0 ± 3.2 (1.7 ± 0.9)	1.8 ± 0.3	7.6 ± 1.6 (1.5 ± 0.1)	1.2 ± 0.2	3.4 ± 0.2 (4.2 ± 1.8)	0.8 ± 0.08	1.3 ± 0.2 (8.1 ± 1.5)
stomach	3.8 ± 1.6	0.8 ± 0.6	2.2 ± 0.7	1.2 ± 0.3 (9.2 ± 1.0)	2.3 ± 0.8	0.8 ± 0.6 (23.2 ± 12.6)	1.1 ± 0.2	0.4 ± 0.2 (31.2 ± 10.1)
small int.	0.3 ± 0.1	1.4 ± 0.5 (10.6 ± 4.5)	0.3 ± 0.04	2.1 ± 0.3 (5.4 ± 0.1)	0.2 ± 0.04	1.4 ± 0.5 (10.6 ± 4.5)	0.2 ± 0.02	0.4 ± 0.09 (31.1 ± 5.8)
large int.	0.3 ± 0.2	1.5 ± 0.4 (10.1 ± 4.6)	0.2 ± 0.04	0.8 ± 0.3 (14.4 ± 2.9)	0.2 ± 0.09	1.5 ± 0.4 (10.2 ± 4.6)	0.2 ± 0.04	0.6 ± 0.2 (19.0 ± 7.0)

[a] Nude mice bearing GW-39 human colonic cancer xenografts were given [^{125}I]F6 × m734 (Fab′ × Fab′, 5 μCi, 1.5 × 10^{-10} mol). Three days later, [^{99m}Tc]IMP-192 (10 μCi, 1.6 × 10^{-11} mol) was injected. All times given in the tables are the means and standard deviations at the hours indicated after the [^{99m}Tc]IMP-192 injection (five animals per time point). The average GW-39 weights for each respective group in order shown were 0.902 ± 0.874, 0.342 ± 0.005, 0.588 ± 0.221, and 0.666 ± 0.215 g.

Table 5. Tissue Uptake of [^{188}Re]IMP-192 in Mice Pretargeted with [^{125}I]hMN-14 × m734[a]

percent injected dose per gram of tissue
(values in parentheses are the tumor/nontumor ratios for the radiolabeled peptide)

	peptide alone	3 h		24 h		48 h		72 h	
tissue	^{188}Re	^{125}I	^{188}Re	^{125}I	^{188}Re	^{125}I	^{188}Re	^{125}I	^{188}Re
tumor	0.36 ± 0.15	6.9 ±1.8	16.9 ± 5.5	4.5 ± 0.6	11.1 ± 1.6	2.5 ± 0.5	4.9 ± 1.3	1.7 ± 0.6	3.1 ± 1.4
liver	0.36 ± 0.11	0.4 ± 0.06	0.9 ± 0.2 (17.4 ± 3.8)	0.2 ± 0.04	0.4 ± 0.03 (30.4 ± 6.1)	0.1 ± 0.01	0.2 ± 0.01 (23.9 ± 5.2)	ND	ND
spleen	0.24 ± 0.07	1.4 ± 1.5	1.2 ± 1.0 (20.3 ± 11.3)	0.3 ± 0.05	0.4 ± 0.1 (27.6 ± 6.5)	0.1 ± 0.01	0.3 ± 0.1 (18.8 ± 6.4)	ND	ND
kidney	1.20 ± 0.24	0.5 ± 0.06	2.4 ± 0.3 (6.8 ± 1.8)	0.3 ± 0.04	0.6 ± 0.1 (17.9 ± 5.3)	0.1 ± 0.02	0.3 ± 0.04 (17.3 ± 4.2)	ND	ND
lungs	0.36 ± 0.13	0.8 ± 0.1	1.4 ± 0.3 (11.7 ± 2.8)	0.4 ± 0.06	0.4 ± 0.05 (29.3 ± 7.5)	0.1 ± 0.03	0.1 ± 0.05 (36.5 ± 12.5)	ND	ND
blood	0.75 ± 0.45	1.0 ± 0.1	2.9 ± 0.9 (5.9 ± 2.1)	0.5 ± 0.07	0.8 ± 0.1 (14.7 ± 4.0)	0.2 ± 0.03	0.3 ± 0.1 (16.1 ± 3.1)	ND	ND
stomach	3.62 ± 1.79	4.5 ± 1.4	7.1 ± 1.5 (2.4 ± 0.8)	1.1 ± 0.3	0.3 ± 0.1 (43.2 ± 34.0)	0.2 ± 0.04	0.08 ± 0.03 (67.0 ± 27.8)	ND	ND
small int.	1.38 ± 0.80	0.3 ± 0.08	2.3 ± 0.3 7.2 ± 1.9	0.1 ± 0.01	0.3 ± 0.1 (49.1 ± 26.4)	0.06 ± 0.01	0.07 ± 0.02 (76.4 ± 22.5)	ND	ND
large int.	1.04 ± 0.36	0.3 ± 0.2	0.3 ± 0.2 (94.5 ± 104.7)	0.1 ± 0.03	0.4 ± 0.1 (28.5 ± 17.9)	0.05 ± 0.00	0.08 ± 0.06 (73.8 ± 47.5)	ND	ND

[a] Nude mice bearing GW-39 human colonic cancer xenografts were given [^{125}I]hMN-14 × m734 Fab′ × Fab′ (5 μCi, 1.5 × 10^{-10} mol). Twenty-four hours later, [^{188}Re]IMP-192 (7 μCi, 1.6 × 10^{-11} mol of peptide) was injected. All times given in the tables are the means and standard deviations at the hours indicated after the [^{188}Re]IMP-192 injection (five animals per time point). The data for the [^{188}Re]IMP-192 alone is 3 h after its injection. The average GW-39 weights for each respective group in order shown were 0.098 ± 0.042, 0.160 ± 0.065, 0.136 ± 0.036, and 0.266 ± 0.168. ND, insufficient radioactivity in normal tissue to reliably calculate percent uptake.

setting. Previously, we examined a streptavidin−antibody conjugate/radiolabeled biotin pretargeting approach analogous to the one described by Axworthy et al. (1994). These investigators were able to deliver the same amount of radioactivity to a tumor using radiolabeled biotin as was possible with a radiolabeled antibody conjugate. We also found that excellent tumor/nontumor ratios could be achieved with reasonable absolute tumor uptake using such a system (Sharkey et al., 1997). While animal studies continue to evaluate the therapeutic benefit of the antibody−streptavidin/radiolabeled biotin pretargeting approach in comparison to directly radiolabeled antibody, we continue to have serious concerns with the system, particularly because of the immunogenicity of streptavidin (Chinol et al., 1998). Knowing of the possibilities for future engineering (Carter and Merchant 1997; Coloma and Morrison, 1997) of a humanized agent with minimal, if any, immunogenicity, efforts were undertaken to investigate a bispecific antibody pretargeting approach useful for RAIT.

For these initial studies, we decided to evaluate our humanized antibody to CEA, hMN-14, since this is presently being used in clinical trials. This antibody was paired with the murine antibody specific for [In]DTPA, termed 734, that was used previously by the French investigators with their murine anti-CEA antibody, F6 (Chetanneau et al., 1990). Using established technology (Glennie et al., 1987), a Fab′ fragment of each of these MAbs was coupled site-specifically in their hinge-regions via a thioether linkage to produce a bispecific F(ab′)$_2$. Rigorous SE-HPLC analyses were performed to show bsMAb purity to be greater than 90%, with excellent

Table 6. Tissue Uptake of [^{188}Re]IMP-192 in Mice Pretargeted with [^{125}I]F6 × m734[a]

percent injected dose per gram of tissue
(values in parentheses are the tumor/nontumor ratios for the radiolabeled peptide)

	3 h		24 h		48 h		72 h	
tissue	^{125}I	^{188}Re	^{125}I	^{188}Re	^{125}I	^{188}Re	^{125}I	^{188}Re
tumor	14.7 ± 3.1	19.3 ± 4.2	13.9 ± 4.3	20.3 ± 6.8	6.5 ± 2.0	8.5 ± 2.8	6.2 ± 1.9	6.5 ± 2.6
liver	0.3 ± 0.1	1.3 ± 0.3 (14.9 ± 4.0)	0.2 ± 0.1	0.5 ± 0.2 (40.5 ± 9.1)	0.1 ± 0.02	0.3 ± 0.1 (27.3 ± 10.1)	0.1 ± 0.04	0.3 ± 0.1 (20.0 ± 5.7)
spleen	0.3 ± 0.05	1.0 ± 0.3 (20.7 ± 8.1)	0.2 ± 0.1	0.4 ± 0.1 (57.5 ± 11.3)	0.1 ± 0.02	0.2 ± 0.1 (51.9 ± 18.8)	0.1 ± 0.02	0.2 ± 0.1 (44.0 ± 49)
kidney	0.4 ± 0.05	3.3 ± 0.4 (5.9 ± 0.9)	0.2 ± 0.1	0.7 ± 0.2 (29.9 ± 8.6)	0.1 ± 0.03	0.4 ± 0.1 (24.1 ± 8.7)	0.1 ± 0.03	0.3 ± 0.1 (21.5 ± 6.0)
lungs	0.4 ± 0.1	1.5 ± 0.4 (13.6 ± 5.2)	0.3 ± 0.2	0.4 ± 0.3 (63.8 ± 24.4)	0.1 ± 0.03	0.2 ± 0.1 (60.9 ± 34.4)	0.1 ± 0.01	0.2 ± 0.1 (39.7 ± 18.9)
blood	1.2 ± 0.2	5.1 ± 1.2 (3.9 ± 1.3)	0.6 ± 0.3	1.3 ± 0.8 (16.9 ± 5.1)	0.3 ± 0.1	0.6 ± 0.2 (15.4 ± 6.1)	0.3 ± 0.1	0.5 ± 0.1 (13.4 ± 6.2)
stomach	1.5 ± 0.4	5.9 ± 1.2 (3.3 ± 0.5)	0.8 ± 0.3	0.3 ± 0.1 (84.3 ± 29.5)	0.4 ± 0.2	0.1 ± 0.03 (79.8 ± 23.9)	0.3 ± 0.1	0.05 ± 0.03 (165.3 ± 123.3)
small int.	0.2 ± 0.04	2.0 ± 0.6 (10.0 ± 2.3)	0.1 ± 0.05	0.3 ± 0.1 (82.8 ± 31.8)	0.07 ± 0.01	0.1 ± 0.03 (77.0 ± 24.6)	0.07 ± 0.02	0.09 ± 0.01 (77.2 ± 31.8)
large int.	0.1 ± 0.01	1.2 ± 0.5 (20.5 ± 13.7)	0.1 ± 0.03	0.4 ± 0.2 (40.0 ± 14.9)	0.06 ± 0.01	0.1 ± 0.05 (64.1 ± 23.5)	0.05 ± 0.02	0.10 ± 0.04 (65.2 ± 23.9)

[a] Nude mice bearing GW-39 human colonic cancer xenografts were given [^{125}I]F6 × m734 Fab′ × Fab′ (5 μCi, 1.5 × 10^{-10} mol). Three days later, [^{188}Re]IMP-192 (7 μCi, 1.6 × 10^{-11} mol of peptide) was injected. All times given in the tables are the means and standard deviations at the hours indicated after the [^{188}Re]IMP-192 injection (five animals per time point). The average GW-39 weights for each respective group in order shown were 0.091 ± 0.036, 0.133 ± 0.048, 0.199 ± 0.036, and 0.096 ± 0.028 g.

Table 7. Mean Cumulative Radiation Absorbed Dose Delivered to Tissues Based on Biodistribution of [^{188}Re]IMP-192 in Mice Pretargeted with hMN-14 × 734 bsMAb

tissue	dose (cGy/mCi)
tumor	1954
liver	155
spleen	132
kidney	269
lungs	150
blood	407
stomach	621
small int.	383
large int.	87

retention of binding both to CEA and to [^{111}In/In]DTPA. All of radiolabeled bivalent hapten, [^{111}In/In]IMP-156, could be shifted to a higher molecular weight fraction when combined with bsMAb and CEA, indicating that all of the binding 734 arm was associated with a hMN-14 arm. About 92−93% of the bsMAb migrated to a higher molecular weight by SE-HPLC when combined with [In]DTPA-LL2-IgG, indicating that 7−8% hMN-14 × hMN-14 (Fab′ × Fab′) was likely present. Since it would be preferable to have excess monospecific anti-CEA MAb present rather than excess monospecific anti-DTPA MAb, the 734 Fab′ was selected to be activated with the dimaleimide. In vitro, the hMN-14 × 734 bsMAb was comparable to the previously described all-murine F6 × 734 bsMAb, in that both molecules maintained molecular integrity, as well as capacity for binding to CEA or indium-DTPA.

The murine F6 anti-CEA × 734 construct was used primarily as a positive control to show that substituting the hMN-14 in bsMAb would not affect the quality of the bsMAb. In vitro studies certainly confirmed this, but in vivo, an unexpected rapid blood clearance of the hMN-14 × 734-F(ab′)$_2$ (humanized × murine) compared to the F6 × 734-(Fab′)$_2$ (murine × murine) was found. Thioether-linked F(ab′)$_2$ is not susceptible to reduction and, indeed, was previously shown to have an extended blood circulation time compared to a natural F(ab)$_2$ fragment (Siddiqui et al., 1995), so the linkage chemistry could not explain the rapid clearance seen with the humanized-murine hybrid bsMAb. SE-HPLC was used to assess catabolic products in the serum (e.g., Fab′ fragments or even smaller molecular weight byproducts). Given the amount of radioactivity administered to the animals, the radiolabeled hMN-14 × 734 bsMAb could only be evaluated over 4 h. During this time, there was no evidence of catabolic byproducts to suggest an instability of the bsMAb. Previous studies with hMN-14 F(ab′)$_2$ in mice have shown a similar rapid blood clearance (Leung et al., 1999) in comparison with the corresponding murine F(ab′)$_2$, and we have also noted differences in the clearance properties of murine IgG$_1$ and murine IgG$_{2a}$ and of human IgG$_1$ in nude mice (Sharkey et al., 1991). This observation was ultimately traced to varying amounts of murine IgG$_{2a}$ in different strains of mice (Reddy et al., 1998), but it is uncertain whether a similar mechanism can explain the differences in the clearance of bsMAb fragments, since these molecules lack the Fc-portion of the immunoglobulin molecule that is most frequently associated with its recognition by immune cells. However, an initially high uptake was noted in both the spleen and liver for the hMN-14 bsMAb in comparison to the all murine F6 bsMAb, suggesting that there is a recognition mechanism involved in this enhanced clearance. The elevated uptake of radioiodine in the stomach was a further indication that the hMN-14 bsMAb was likely being catabolized in these organs. The humanized MN-14 × murine 734 bsMAb F(ab′)$_2$ is presently being prepared for clinical use, where it will be possible to reassess its distribution and clearance. However, since clinical studies comparing the murine MN-14 and humanized MN-14 IgG revealed very similar distribution and clearance properties (Sharkey et al., 1995), it is more likely that this preclinical observation is unique to the mouse model. Thus, it might be better to use murine bsMAbs in murine models, as this would maintain the species similarities that will ultimately occur when a fully humanized bsMAb is used clinically.

Despite the observed differences in the clearance rate of the two bsMAbs, the subsequent targeting of both the [^{99m}Tc]- and [^{188}Re]IMP-192 peptides to either conjugate was excellent. Even though a higher tumor uptake was observed with the radioiodinated F6-based bsMAb compared to the hMN-14 bsMAb, initial tumor uptake of the radiolabeled peptide in both pretargeting systems was very similar. This was clearly due to differences in the amount of bsMAb remaining in the blood at the time the peptide was given. This illustrates the importance of fully optimizing the relationship between the amount of bsMAb remaining in the blood at the time the peptide is

given. The best radiolabeled peptide ratios correlated with the highest bsMAb tumor uptakes and the lowest bsMAb blood levels. It is also important to note that there was no evidence that the injection of the radiolabeled peptide affected the blood clearance rate or the organ distribution of the bsMAb. Given the divalent nature of the peptide, it is possible that complexes of 2 bsMAb molecules could form in the blood, and they might be cleared differently or even cause the bound peptide or antibody to distribute differently in the organs. It is possible that at the concentrations of the bsMAb and peptide used in these studies and the times that were examined failed to detect altered kinetics and distribution. This issue should be reexamined once an optimized therapeutic system is developed. Indeed, as shown by Gautherot et al. (1998, 2000), careful optimization is required to achieve superior therapeutic results.

The IMP-156 is not suitable for therapeutic applications with Y-90, because the 734 MAb was unable to bind tightly to the yttrium−DTPA complex. Additionally, [^{90}Y]-DTPA species, wherein one carboxyl group is unavailable due to amide bond formation, are well-known to have poor in vivo stability (Harrison et al., 1991). Although a species containing mixed DOTA and DTPA chelates may be prepared, the similarities of labeling chemistries between yttrium and indium might make selective indium labeling of DTPA and yttrium labeling of DOTA problematic. Another option would be to prepare a new anti-yttrium-DOTA MAb so that a new bsMAb could be used, but this too would restrict the applicability of such a bsMAb to this single system. Instead, we are presently exploring a single peptide-binding MAb that could be used with a peptide that itself could be modified to accommodate multiple binding possibilities. The approach taken here was to work with the 734 antibody, but to construct a new peptide with another binding specificity. Since the chemistries involved in technetium/rhenium radiolabeling are quite distinct from those used in indium chelation, this presented an opportunity to explore the selective radiolabeling of a Tc/Re chelate-peptide that also contained indium−di-DTPA. This peptide, IMP-192, was assembled with a thiosemicarbonylglyoxylcysteinyl group (TscGC), which is a thiol-containing ligand for Tc/Re. It was then formulated with excess nonradioactive indium to saturate DTPA chelate sites and lyophilized into single-vial kits containing stannous ion, for later reconstitution with either ^{99m}Tc or ^{188}Re. ^{99m}Tc-formulated kits were ^{99m}Tc labeled at 1836 Ci/mmol/mmol of peptide (94−99% incorporation), while kits formulated for ^{188}Re were labeled at 459−945 Ci/mmol (96−97%). Successful labeling of both Tc and Re IMP-192 kit formulations indicated that the presence of free and DTPA-bound indium did not interfere with ^{99m}Tc or ^{188}Re labeling of the TscGC chelate. Further studies are planned to determine if higher specific activities can be achieved for therapeutic applications.

Biodistribution studies of [^{99m}Tc]IMP-192 and [^{188}Re]-IMP-192 bivalent haptens alone in normal BALB/c mice showed rapid blood clearance. As with the IMP-156 peptide, the presence of the two DTPAs on the IMP-192 peptide probably aids in rapid renal excretion, and it was gratifying to find that attachment of the TscGC moiety did not materially change the behavior of the IMP-192 di-DTPA peptide. In addition, the in vitro and in vivo studies clearly demonstrate stability of these complexes, with unchanged radiolabeled IMP-192 excreted in urine at early time points postinjection. Unlike radiolabeled biotin (Rusckowski et al., 1996; Sharkey et al., 1997), there was no evidence of selective tumor accretion (i.e., tumor/nontumor ratios > 1.0) of the radiolabeled IMP-192 peptide when administered alone to mice.

Using this pretargeting system, tumor-to-liver, -kidney, -lungs, and -blood ratios were between 3- and 22.9:1 at 1 and 3 h after the [^{99m}Tc]IMP-192 peptide was given, indicating that early imaging will be possible. In comparison, a [^{99m}Tc]Fab′ anti-CEA, prepared by direct labeling of hinge-region thiol groups, and tested in the same preclinical tumor model, gave tumor-to-liver, -kidney, -lungs, and -blood ratios of 1.6-, 0.06-, 1.2-, and 0.9-to-1 at 2 h postinjection (Hansen et al., 1990). With the hMN-14 × 734-F(ab′)$_2$ bsMAb pretargeting method, even the kidney shows a positive tumor-to-nontumor ratio at only 30 min postinjection of [^{99m}Tc]IMP-192. The pretargeted [^{188}Re]IMP-192 peptide gave tumor-to-nontumor ratios between 14.7- and 63.8-to-1 for the major tissues by 24 h postinjection of the ^{188}Re-labeled peptide, and ratios were decidedly positive for each tissue even by 3 h postinjection of the [^{188}Re]IMP-192. For comparison, a ^{188}Re direct-labeled IgG in a similar tumor xenograft model (LS-174T) showed tumor-to-nontumor ratios at 24 h postinjection of 1.8- to 6.1:1, and none of these ratios was positive at 2 h postinjection (Griffiths et al., 1991). Of particular note with these ^{99m}Tc- and ^{188}Re-labeled peptides is the absence of renal retention of the radiometal when compared to radiometal-labeled MAb fragments developed for RAID and RAIT (Behr et al., 1995).

The excellent tumor/nontumor ratios and very reasonable tumor uptakes already suggest that this bsMAb−peptide combination has promising RAID and RAIT applications. RAIT prospects would be improved further if an increase in absolute tumor uptake of radioactivity at these same tumor-to-tissue ratios could be achieved. In the present studies, only small doses of the bsMAb (i.e., 15 μg) were given to each animal, but for RAIT, higher bsMAb protein doses will be used to increase the number of peptide-binding sites localized to the tumor. The use of other bsMAb constructs could also increase the amount of bsMAb localized in the tumor. For instance, use of bsMAb comprising a divalent anti-CEA combined with either a monovalent or even a divalent anti-hapten antibody is of interest. Changing bsMAb valency would increase the size of the bsMAb and likely slow its blood clearance, and then more time would be needed before radiolabeled peptide administration to allow for adequate blood clearance of the bsMAb. Others (Axworthy et al., 1994; Schuhmacher et al., 1995) have used clearing agents to reduce the blood level of nonlocalized pretargeting agents after maximum tumor uptake has been achieved, although clearance mechanisms involving blockade of secondary binding sites can adversely affect subsequent targeting of the low molecular weight RAID/RAIT agent. In this regard, we have an anti-idiotypic MAb (WI2) to the MN-14 anti-CEA arm, which was successfully used for clearance in previous work with MAb-streptavidin studies (Sharkey et al., 1997) and has since been humanized (Losman et al., 1999). We are presently evaluating alternate bsMAb targeting with hMN-14 IgG × 734-Fab′, and hMN-14 F(ab′)$_2$ × 734-Fab′ conjugates, to assess valency and molecular size issues. Ultimately, bsMAbs will be prepared through molecular engineering (Coloma and Morrison, 1997; Merchant and Carter, 1997), at sizes indicated best for either RAID or RAIT application from the current studies. The molecular engineering approach will also provide an opportunity to enhance the productivity and availability of bsMAb constructs, while simultaneously minimizing or eliminating any immunogenicity.

In summary, these studies provide highly promising

preclinical targeting data with human-murine and murine-murine bsMAb $(Fab')_2$. Furthermore, a novel peptide containing metal-selective chelates for indium and for ^{99m}Tc and ^{188}Re radiolabeling allows parallel development for both RAID and RAIT applications. The pretargeting results presented here suggest that early time-point imaging using [^{99m}Tc]IMP-192, with the high tumor-to-tissue ratios versus major internal organs achieved, could provide a new standard for RAID. The data are also very encouraging for therapy with [^{188}Re]IMP-192.

ACKNOWLEDGMENT

We thank Immunotech S. A., Marseilles, France, for providing supplies of the F6 and 734 antibodies. We also thank Ms. H. Spiegelman, L. Reed, and L. Osorio for their assistance with the animal studies and Mr. T. Jackson for radiolabeling. Supported in part by USPHS Grants CA 81760 and CA 37895 from the NIH.

LITERATURE CITED

(1) Axworthy, D. B., Fritzberg, A. R., Hylarides, M. D., Mallett, R. W., Theodore, L. J., Gustavson, L. M., Su, F.-M., Beaumier, P. L., and Reno, J. M. (1994) Preclinical evaluation of an antitumor monoclonal antibody/streptavidin conjugate for pretargeted ^{90}Y radioimmunotherapy in a mouse xenograft model. *J. Immunother. 16*, 158.

(2) Bamias, A., and Epenetos, A. A. (1992) Two-step strategies for the diagnosis and treatment of cancer with bioconjugates. *Antibody, Immunoconjugates, Radiopharm. 5*, 385−395.

(3) Barbet, J., Peltier, P., Bardet, S., Vuillez, J. P., and Chatal, J. F. (1998) Radioimmunodetection of medullary thyroid carcinoma using indium-111 bivalent hapten and anti-CEA × anti-DTPA-indium bispecific antibody. *J. Nucl. Med. 39*, 1172−1178.

(4) Behr, T. M., Sharkey, R. M., Juweid, M. E., Blumenthal, R. D., Dunn, R. M., Griffiths, G. L., Bair, H.-J, Wolf, F. G., Becker, W. S., and Goldenberg, D. M. (1995) Reduction in the renal uptake of radiolabeled monoclonal antibody fragments by cationic amino acids and their derivatives. *Cancer Res. 55*, 3825−3834.

(5) Boerman, O. C., Kranenborg, M. H. G. C., Oosterwijk, E., Griffiths, G. L., McBride, W. J., Oyen, W. J. G., de Weijert, M., Oosterwijk-Wakka, J., Hansen, H. J., and Corstens, F. H. M. (1999) Pretargeting of renal cell carcinoma: improved tumor targeting with a bivalent chelate. *Cancer Res. 59*, 4400−4405.

(6) Bos, E. S., Kuijpers, W. H. A., Meesters-Winters, M., Pham, D. T., deHaan, A. S., van Doormalen, A. M., Kasperson, F. M., van Boeckel, C. A. A., and Gougeon-Bertrand, F. (1994) In vitro evaluation of DNA-DNA hybridization as a two-step approach in radioimmunotherapy of cancer. *Cancer Res. 54*, 3479−3486.

(7) Carter, P., and Merchant, A. M. (1997) Engineering antibodies for imaging and therapy. *Curr. Opin. Biotechnol. 8*, 449−454.

(8) Chetanneau, A., Baum, R. P., Lehur, P. A., Liehn, J. C., Perkins, A. C., Bares, R., Bourguet, P., Herry, J. Y., Saccavini, J. C., and Chatal, J. F. (1990) Multi-centre immunoscintigraphic study using indium-111-labeled CEA-specific and/or 19−9 monoclonal antibody $F(ab')_2$ fragments. *Eur. J. Nucl. Med. 17*, 223−229.

(9) Chinol, M., Casalini, P., Maggiolo, M., Canevari, S., Omodeo, E. S., Caliceti, P., Veronese, F. M., Cremonesi, M., Chiolerio, F., Nardone, E., Siccardi, A. G., and Paganelli, G. (1998) Biochemical modifications of avidin improve pharmacokinetics and biodistribution, and reduce immunogenicity. *Br. J. Cancer 78*, 189−197.

(10) Coloma, M. J., and Morrison, S. L. (1997) Design and production of novel tetravalent bispecific antibodies. *Nat. Biotechnol. 15*, 159−163.

(11) Cremonesi, M., Ferrari, M., Chinol, M. Stabin, M. G., Grana, C., Prisco, G., Robertson, C., Tosi, G., and Paganelli, G. (1999) Three-step radioimmunotherapy with yttrium-90 biotin: dosimetry and pharmacokinetics in cancer patients. *Eur. J. Nucl. Med. 26*, 110−120.

(12) Dangles, O., Guibe F, Balavoine, G., Lavielle, S., and Marquet, A. (1987) Selective cleavage of the allyl and allyloxycarbonyl groups through palladium-catalyzed hydrostannolysis with tributyltin Hydride. Application to the selective protection-deprotection of amino acid derivatives and in peptide synthesis. *J. Org. Chem. 52*, 4984−4993.

(13) DeNardo, S. J., DeNardo, G. L., Brush, J., and Carter, P. (1999) Phage-library-derived human anti-TETA and anti-DOTA scFv for pretargeting RIT. *Hybridoma 18*, 13−21.

(14) Feng, X., Pak, R. H., Kroger, L. A., Moran, J. K., DeNardo, D. G., Meares, C. F., DeNardo, G. L., and DeNardo, S. J. (1998) New anti-Cu-TETA and anti-Y-DOTA monoclonal antibodies for potential use in the pretargeted delivery of radiopharmaceuticals to tumors. *Hybridoma 17*, 125−132.

(15) Gautherot, E. Bouhou, J., LeDoussal, J.-M., Manetti, C., Martin, M., Rouvier, E., and Barbet, J. (1997) Therapy for colon carcinoma xenografts with bispecific antibody-targeted, iodine-131-labeled bivalent hapten. *Cancer 80* (Suppl.), 2618−2623.

(16) Gautherot, E., Le Doussal, J. M., Bouhou, J., Manetti, C., Martin, M., Rouvier, E., Barbet J. (1998) Delivery of therapeutic doses of radioiodine using bispecific antibody-targeted bivalent haptens: a comparative pharmacokinetic and dosimetry study. *J. Nucl. Med. 39*, 1937−1943.

(17) Gautherot, E., Rouvier, E., Daniel, L., Loucif, E., Bouhou, J., Manetti, C., Martin, M., Le Doussal, J. M., and Barbet J. (2000) Pretargeted radioimmunotherapy of human colorectal xenografts with bispecific antibody and ^{131}I-labeled bivalent haptens. *J. Nucl. Med. 41*, 480−487.

(18) Glennie, M. J., McBride, H. M., Worth, A. T., and Stevenson, G. T. (1987) Preparation and performance of bispecific $F(ab'\gamma)_2$ antibody containing thioether-linked $Fab'\gamma$ fragments. *J. Immunol. 139*, 2367−2375.

(19) Goldenberg, D. M., Witte, S., and Elster, K. (1966) GW-39: A new human tumor serially transplantable in the golden hamster. *Transplantation 4*, 760−763.

(20) Goldenberg, D. M., and Hansen, H. J. (1972) Carcinoembryonic antigen present in human colonic neopasms serially propagated in hamsters. *Science 175*, 1117−1118.

(21) Goodwin, D. A., Meares, C. F., McCall, M. J., McTigue, M., and Chaovapong, W. (1988) Pre-targeted immunoscintigraphy of murine tumors with indium-111-labeled bifunctional haptens. *J. Nucl. Med. 29*, 226−234.

(22) Greenwood, F. C., and Hunter, W. M. (1963) The preparation of I-131 labeled human growth hormone of high specific radioactivity. *Biochem. J. 89*, 114−123.

(23) Griffiths, G. L., Goldenberg, D. M., Knapp, F. F., Jr., Callahan, A. P., Chang, C.-H., and Hansen, H. J. (1991) Direct radiolabeling of monoclonal antibodies with generator-produced rhenium-188 for radioimmunotherapy: labeling and animal biodistribution studies. *Cancer Res. 51*, 4594−4602.

(24) Hansen, H. J., Jones, A. L., Sharkey, R. M., Grebenau, R., Blazejewski, N., Kunz, A., Buckley, M. J., Newman, E. S., Ostella, F., and Goldenberg, D. M. (1990). Preclinical evaluation of an "instant" ^{99m}Tc-labeling kit for antibody imaging. *Cancer Res. Suppl. 50*, 794s−798s.

(25) Harrison, A., Walker, C. A., Parker, D., Jankowski, K. J., Cox, J. P., Craig, A. S., Sansom, J. M., Beeley, N. R., Boyce, R. A., Chaplin, L. Eaton, M. A. W., Farnsworth, A. P. H., Millar, K., Millican, A. T., Randall, A. M., Rhind, S. K., Secher, D. S., and Turner, A. (1991) The in vivo release of ^{90}Y from cyclic and acyclic ligand-antibody complexes. *Int. J. Rad. Appl. Instrum. B 18*, 469−476.

(26) Hawkins, G. A., McCabe, R. P., Kim, C.-H., Subramanian, R., Bredehorst, R., McCullers, G. A., Vogel, C.-W., Hanna, M. G., Jr., and Pomata, N. (1993) Delivery of radionuclides to pretargeted monoclonal antibodies using dihydrofolate reductase and methotrexate in an affinity system. *Cancer Res. 53*, 2368−2373.

(27) Hnatowich, D. J., Virzi, F., and Rusckowski, M. (1987) Investigations of avidin and biotin for imaging applications. *J. Nucl. Med. 28*, 1294−1302.

(28) Kaiser, E., Colescott, R.L., Bossinger, C. D., and Cook, P. I. (1970) Color test for detection of free terminal amino groups in the solid-phase synthesis of peptides. *Anal. Biochem. 34*, 595−598.

(29) Karacay, H. Sharkey, R. M., Griffiths, G. L., Govindan, S. V., McBride, W. J., Goldenberg, D. M., and Hansen, H. J. (1997) Development of a streptavidin-anti-carcinoembryonic antigen antibody, radiolabeled biotin pretargeting method for radioimmunotherapy of colorectal cancer: Reagent development. *Bioconjugate Chem. 8*, 585−594.

(30) Knapp, F. F., Jr., Callahan, A. P., Beets, A. L., Mirzadeh, S., and Hsieh, B. (1994) Processing of reactor-produced tungsten-188 for fabrication of clinical scale alumina-based tungsten-188/rhenium-188 generators. *Appl. Radiat. Isot. 45*, 1123−1128.

(31) LeDoussal, J. M., Martin, M., Gautherot, E., Delaage, M., and Barbet, J. (1989) In vitro and in vivo targeting of radiolabeled monovalent and divalent haptens with dual specificity monoclonal antibody conjugates: enhanced divalent hapten affinity for cell-bound antibody conjugate. *J. Nucl. Med. 30*, 1358−1366.

(32) Le Doussal, J.-M., Gruaz-Guyon, A., Martin, M., Gautherot, E., Delaage, M., and Barbet, J. (1990) Targeting of indium-111-labeled bivalent hapten to human melanoma mediated by bispecific monoclonal antibody conjugates: Imaging of tumors hosted in nude mice. *Cancer Res. 50*, 3445−3452.

(33) LeDoussal, J.-M., Chetanneau, A., Gruaz-Guyon, A., Martin, M., Gautherot, E., Lehur, P.-A., Chatal, J.-F., Delaage, M., and Barbet, J. (1993) Bispecific monoclonal antibody-mediated targeting of an indium-111-labeled DTPA dimer to primary colorectal tumors: Pharmacokinetics, biodistribution, scintigraphy and immune response. *J. Nucl. Med. 34*, 1662−1671.

(34) Leung, S. O., Goldenberg, D. M., Dion, A. S., Pellegrini, M. C., Shevitz, J., Shih, L. S., and Hansen, H. J. (1995) Construction and characterization of a humanized, internalizing, B-cell (CD22)-specific, leukemia/lymphoma antibody, LL2. *Mol. Immunol. 32*, 1413−1427.

(35) Leung, S.-O., Qu, Z., Hansen, H. J., Shih, L. B., Wang, J., Losman, M. J., Goldenberg, D. M., and Sharkey, R. M. (1999) The effects of domain deletion, glycosylation, and long IgG_3 hinge on the biodistribution and serum stability properties of a humanized IgG_1 immunoglobulin, hLL2, and its fragments. *Clin. Cancer Res. Suppl. 5*, 3106s−3117s.

(36) Losman, M. J., Novick, K. E., Goldenberg, D. M., and Monestier, M. (1994) Mimicry of a carcinoembryonic antigen epitope by a rat monoclonal anti-idiotype antibody. *Int. J. Cancer 56*, 580−584.

(37) Losman, M. J., Qu, Z., Krishnan, I. S., Wang, J., Hansen, H. J., Goldenberg, D. M., and Leung, S.-O. (1999) Generation and monitoring of cell lines producing humanized antibodies. *Clin. Cancer Res. Suppl. 5*, 3101s−3105s.

(38) Meares, C. F., McCall, M. J., Reardon, D. T., Goodwin, D., A., Diamanti, C. I., and McTigue, M. (1984) Conjugation of antibodies with bifunctional chelating agents: Isothiocyanate and bromoacetamide reagents, methods of analysis, and subsequent addition of metal ions. *Anal. Biochem. 142*, 68−78.

(39) Paganelli, G., Riva, P., Deleide, G., Clivio, A., Chiolerio, F., Scassellati, G. A., Malcovati, M., and Siccardi, A. G. (1988) In vivo labeling of biotinylated monoclonal antibodies by radioactive avidin: a strategy to increase tumor radiolocalization. *Int. J. Cancer Suppl. 2*, 121−125.

(40) Penefsky, H. S. (1979) A centrifuged column procedure for the measurement of ligand binding by beef heart F1. Part G. *Methods Enzymol. 56*, 527−530.

(41) Reddy, N., Ong, G. L., Behr, T. M., Sharkey, R. M., Goldenberg, D. M., and Mattes, M. J. (1998) Rapid blood clearance of mouse IgG2a and human IgG1 in many nude and nu/+ mouse strains is due to low IgG2a serum concentrations. *Cancer Immunol. Immunother. 46*, 25−33.

(42) Rosebrough, S. F. (1993) Pharmacokinetics and biodistribution of radiolabeled avidin, streptavidin and biotin. *Nucl. Med. Biol. 20*, 663−668.

(43) Rusckowski, M., Paganelli, G., Hnatowich, D. J., Magnani, P., Virzi, F., Fogarasi, M., DeLeo, C., Sudati, F., and Fazio, F. (1996) Imaging osteomyelitis with streptavidin and indium-111-labeled biotin. *J. Nucl. Med. 37*, 1655−1662.

(44) Schumacher, J., Klivenyi, G., Matys, R., Stadler, M., Regiert, T., Hauser, H., Doll, J., Maier-Borst, W., and Zoller, M. (1995) Multistep tumor targeting in nude mice using bispecific antibodies and a gallium chelate suitable for immunoscintigraphy with positron emission tomography. *Cancer Res. 55*, 115−123.

(45) Sharkey, R. M., Motta-Hennessy, C., Pawlyk, D., Siegel, J. A., and Goldenberg, D. M. (1990) Biodistribution and radiation dose estimates for yttrium- and iodine-labeled monoclonal antibody IgG and fragments in nude mice bearing human colonic tumor xenografts. *Cancer Res. 50*, 2330−2336.

(46) Sharkey, R. M., Natale, A., Goldenberg, D. M., and M. J. Mattes (1991). Rapid blood clearance of IgG2a and IgG2b in nude mice. *Cancer Res. 51*, 3102−3107.

(47) Sharkey, R. M., Juweid, M., Shevitz, J., Behr, T., Dunn, R., Swayne, L. C., Wong, G. Y., Blumenthal, R. D., Griffiths, G. L., Siegel, J. A., Leung, S., Hansen, H. J., and Goldenberg, D. M. (1995) Evaluation of a complementarity-determining region-grafted (humanized) anti-carcinoembryonic antigen monoclonal antibody in preclinical and clinical studies. *Cancer Res. 55*, 5935s−5945s.

(48) Sharkey, R. M., Karacay, H., Griffiths, G. L., Behr, T. M., Blumenthal, R. D., Mattes, M. J., Hansen, H. J., and Goldenberg, D. M. (1997) Development of a streptavidin-anti-carcinoembryonic antigen antibody, radiolabeled biotin pretargeting method for radioimmunotherapy of colorectal cancer. Studies in a human colon cancer xenograft model. *Bioconjugate Chem. 8*, 595−604.

(49) Siddiqui, A., Quadri, S. M., Griffiths, G. L., Goldenberg, D. M., and Vriesendorp H. M. (1995) Tumor targeting and pharmacokinetics of unmodified and modified $F(ab)_2$ fragments of an anti-CEA murine monoclonal antibody (Immu-14). *Nucl. Med. Biol. 22*, 425−435.

(50) Siegel, J. A., and Stabin, M. G. (1988) Absorbed fractions for electrons and beta particles in small spheres. *J. Nucl. Med. 29*, 803.

(51) Stickney, D. R., Anderson, L. D., Slater, J. B., Ahlem, C. N., Kirk, G. A., Schweighardt, S. A., and Frincke, J. M. (1991) Bifunctional antibody: A binary radiopharmaceutical delivery system for imaging colorectal carcinoma. *Cancer Res. 51*, 6650−6655.

(52) Vuillez, J. P., Moro, D., Brichon, P. Y., Rouvier, E., Brambilla, E., Barbet, J., Peltier, P., Meyer, P., Sarrazin, R., and Brambilla, C. (1997). Two-step radioimmunoscintigraphy for nonsmall cell lung cancer staging using a bispecific anti-CEA/anti-indium-DTPA antibody and an indium-111-labeled DTPA dimer. *J. Nucl. Med. 38*, 507−511.

(53) Vuillez, J. P., Kraeber-Bodere, F., Moro, D., Bardies, M., Douillard, J. Y., Gautherot, E., Rouvier, E., Barbet, J., Garban, F., Moreau, P., and Chatal, J. F. (1999) Radioimmunotherapy of small cell lung carcinoma with the two-step method using a bispecific anti-carcinoembryonic antigen/anti-diethylenetriaminepentaacetic acid (DTPA) antibody and iodine-131 Di-DTPA hapten: results of a Phase I/II trial. *Clin. Cancer Res. 5*, 3259s−3267s.

(54) Wilbur, D. S., Stayton, P. S., To, R., Buhler, K. R., Klumb, L. A., Hamlin, D. K., Stray, J. E., and Vessella, R. L. (1998) Streptavidin in antibody pretargeting. Comparison of a recombinant streptavidin with two streptavidin mutant proteins and two commercially available streptavidin proteins. *Bioconjugate Chem. 9*, 100−107.

BC0000379

Preparation and Evaluation of Tumor-Targeting Peptide−Oligonucleotide Conjugates

Walter Mier,* Ramon Eritja,† Ashour Mohammed, Uwe Haberkorn, and Michael Eisenhut

Department of Nuclear Medicine, Universitätsklinikum Heidelberg, INF 400, 69120 Heidelberg, Germany and European Molecular Biology Laboratory, Meyerhofstrasse 1, 69117 Heidelberg, Germany. Received April 20, 2000; Revised Manuscript Received July 23, 2000

Enormous progress has been made in the development of antisense oligodeoxynucleotides (ODNs) as therapeutic agents inhibiting gene expression. Unfortunately, the therapeutical application of ODNs is still held back because of the low cellular uptake and the lack of specific transport into particular cells. In this paper, we report a drug-targeting system using somatostatin receptors (SSTRs) which are overexpressed in various tumors. Phosphorothioate ODNs were covalently linked to Tyr^3−octreotate, an analogue of somatostatin. The peptide was assembled by solid-phase synthesis, oxidized to form the cyclic disulfide, and subsequently derivatized with a N-terminal maleimido functionality. 5′-Thiol derivatized phosphorothioate-ODNs directed against the protooncogene *bcl-2* were conjugated to this maleimido-modified peptide. Binding studies revealed that the conjugates retain specific binding with nanomolar affinities to SSTRs (IC_{50}-values between 1.83 and 2.52 nM). Furthermore, melting studies with complementary DNA revealed that the terminal conjugation of the ODNs did not significantly affect their hybridization affinity.

INTRODUCTION

Antisense therapy holds great promise for the treatment of gene-related disorders. Still, the major obstacle for an efficient antisense therapy is the low internalization rate into target cells. Even though ODNs[1] are large, negatively charged molecules, they are to some extent transported through the cellular membranes. This uptake is achieved by pinocytosis and processes which are known to be concentration and energy dependent. Depending on the ODN, the cell line and experimental conditions, the uptake rate ranges 1−20%.

Numerous attempts have been made to increase the intracellular bioavailability and to enable specific internalization into selected cell types. A highly efficient and versatile system for uptake enhancement is encapsulation into liposomes. Within liposomes, ODNs are preserved from serum nuclease degradation. Taking advantage from various coating modifications which increase stability and uptake, liposomes have become valuable shuttles for ODNs (*1*). ODNs attached to hydrophobic moieties, such as lipids (*2*), cholesterol (*3*), or geraniol (*4*), show increased antisense effects. However, these effects have always been controversially discussed because of sequence unrelated effects and the lack of a plausible mechanism. Cellular internalization of cationic molecules by adsorptive endocytosis has been exploited by several procedures. For example, cellular import can be increased with ODN−polylysine complexes (*5*) or ODNs conjugated to avidin (*6*). Conjugation of PNA with a monoclonal antibody to the rat transferrin receptor enabled the transport through the blood brain barrier (*7*). This approach led to a 28-fold uptake rate as compared to the unmodified ODN analogue. The complexes formed when mixing ODNs with porphyrin possess enhanced stability and cellular delivery by an unknown mechanism (*8*). The ubiquitously expressed receptors for vitamin B_6 can be addressed with ODNs conjugated to vitamin B_6 (*9*). These conjugates were believed to be taken up by potocytosis. A unique targeting system for liver cells has been developed using the asialo-glycoprotein receptors (*10*). Residues of β-D-galactose within the asialo-glycoprotein mediate the selective uptake of the conjugated ODN into the liver. These findings should stimulate the search for selective targeting vectors which enable enhanced receptor-mediated delivery into other tissues. Peptides which bind to integrins (*11*) and the EGF-receptor family (*12*) represent examples of peptide vectors which have been employed for ODN-transport. These peptides bind to distinct receptors, which upon binding, mediate endocytosis of the peptide−ODN complex. Conjugates of ODNs with penetratins (*13*) or signal peptides (*14*, *15*) acquire increased uptake rates due to the membrane translocation properties of these peptides. Hitherto no targeting system with selectivity for cancer cells and high capacity sufficient for antisense therapy has been found to be effective in vivo.

Somatostatin is a cyclic tetradecapeptide found in the hypothalamus. It is an important regulating peptide which exerts inhibitory effects on the secretion of growth hormones. The SSTRs are known to be overexpressed by a variety of neoplastic tissues such as small cell lung cancers, breast tumors, brain tumors, and many other

* To whom correspondence should be addressed. Phone: 49-6221-567727. Fax: 49-6221-565473. E-mail: walter_mier@med.uni-heidelberg.de.

† European Molecular Biology Laboratory. Present address: Centro de Investigación y Desarrollo C.S.I.C. Jordi Girona 18-26, 08034 Barcelona, Spain.

[1] Abbreviations: Acm, acetamidomethyl; Boc, *tert*-butyloxycarbonyl; BSA, bovine serum albumin; DIPEA, diisopropylethylamine; DTT, dithiothreitol; EDITH, 3-ethoxy-1,2,4-dithiazolin-5-one; Fmoc, 9-fluorenylmethylmethoxycarbonyl; HBTU, 2-(1H-benzotriazol-1-yl)-1,1,3,3-tetramethyluronium hexafluorophosphate; ODN, oligodeoxynucleotide; SPPS, solid-phase peptide synthesis; SSTR, somatostatin receptor; TEAA, triethylammonium acetate; TIS, triisopropylsilane.

10.1021/bc000041k CCC: $19.00 © 2000 American Chemical Society
Published on Web 10/28/2000

(mainly endocrine) tumors. Therefore, the membrane-associated SSTRs represent potential molecular targets for selective delivery into tumor cells. Because of the short biological half-live of the natural somatostatin (<3 min) in vivo, many analogues have been developed. Octreotide, a cyclic octapeptide with an improved specificity and a half-live of about 90 min (*16*) has become the most successful analogue. Recently, it has turned out that octreotate, the carboxylic acid derivative of octreotide, offers improved pharmacological properties and should therefore be an interesting alternative to octreotide (*17*).

A large number of tumor types show aberrant gene expression of the protooncogene *bcl-2*. These abnormalities result in an overexpression of *bcl-2* protein. This protein is known to inhibit apoptosis. Antisense ODNs have been used to inhibit *bcl-2* expression in cellular studies (*18*). The model ODN used in the present studies is a 20-mer that corresponds to a selected part of the coding sequence within the genome of human *bcl-2* cDNA (*19*). Besides their high enzymatic stability, phosphorothioates have been shown to be highly potent in inhibiting *bcl-2* expression (*18*). Therefore, the ODN conjugates were prepared as phosphorothioates.

Even though octreotate contains only eight residues, the synthesis is complicated by several structural features. In particular, cyclization of the disulfide bond does not converge with the introduction of amine- and thiol-reactive groups necessary for conjugation. Hence, a synthetic protocol, which allows the solid-phase formation of the disulfide bond and subsequent attachment of the reactive group has been developed.

In addition to the synthesis, we report herein data on binding specificity to the SSTRs and binding specificity to the corresponding ODNs. These experiments were performed to scrutinize whether the ODN−Tyr^3−octreotate conjugates fulfill the major prerequisites for receptor mediated uptake and antisense effect.

EXPERIMENTAL PROCEDURES

General. The peptides were analyzed and separated by liquid chromatography (HPLC) on a Gyncotech P-580 system (Germering, Germany) equipped with a variable SPD 6-A UV detector and a C-R5A integrator (both Shimadzu, Duisburg, Germany). The columns used were Nucleosil C_{18}, 5 μm, 250 × 4 mm (Macherey & Nagel, Düren, Germany) and LiChrosorb RP-select B 10 μm, 250 × 10 mm (Merck, Darmstadt, Germany). The ODNs were purified on a Waters liquid chromatography system on PRP-1 material 7 μm, 305 × 7 mm (Hamilton, Bondauz, Switzerland). UV measurements as well as the melting studies were performed with a computer interfaced Varian Cary 13 UV−vis spectrophotometer. Mass spectrometry analysis of the peptides and of the oligonucleotides was performed on a matrix-assisted laser desorption ionization time-of-flight mass spectrometer (MALDI-1, Kratos Instruments, England). ^1H and ^{13}C NMR spectra of compound **4** were recorded on a Bruker AM 250 spectrometer and are expressed as δ units relative to CD_3OD (δ = 49.3 for ^{13}C). The peptides were synthesized manually with an in-house manufactured SPPS reactor. The oligodeoxynucleotides were synthesized on an Applied Biosystems model 394 DNA synthesizer or on an PerSeptive Expedite 8900 synthesizer. Lyophilization was performed on a Christ (Osterode, Germany) α1-2 lyophilizator. Membrane-binding experiments were performed using an in-house manufactured filtration apparatus.

Reagents. All standard synthesis reagents were purchased from Merck (Darmstadt, Germany). The chemicals for peptide synthesis were obtained from Novabiochem (Läufelfingen, Switzerland). *N*-Maleimido-6-caproic acid, thallium(III)trifluoroacetate, and TIS were obtained from Fluka (Buchs, Switzerland). The chemicals for the oligonucleotide synthesis were obtained from Perkin-Elmer Applied Biosystems (Norwalk, Connecticut) or PerSeptive Biosystems (Hamburg, Germany). The sulfurization-reagent EDITH was from PerSeptive Biosystems. The thiol linker phosphoroamidite was purchased from Glen research (Sterling, Minnesota). Anhydrous solvents were obtained from Merck, PerSeptive Biosystems, and SDS (Peypin, France). NAP-10 gel filtration columns were from Pharmacia (Uppsala, Sweden). Protein was determined using the Bradford assay (Sigma). Water was purified by a Milli-Q water system from Millipore (Eschborn, Germany). Tyr^3−octreotide was prepared by SPPS. Radioisotope $Na^{125}I$ was purchased from Amersham Pharmacia Biotech (Freiburg, Germany). [^{125}I]Tyr^3−octreotide was prepared by iodination of Tyr^3−octreotide using the chloramine-T method according to the method of Bakker et al. (*20*). The product was purified by HPLC and stored at −80 °C. The complementary unmodified phosphodiester and phosphorothioate ODNs for the melting temperature analysis 5′-GTTCTCCCAGCGTGTGCCAT-3′ (antisense) and 5′-ATGGCACACGCTGGGAGAAC-3′ (sense) were synthesized by standard procedures.

Synthesis of the Maleimido-Peptide 4. The peptide was assembled by Fmoc chemistry on 1 g of Fmoc-Thr-(^{t}Bu)-Wang resin (0.61 mmol/g). N^α-Fmoc amino acids with the following side chain protecting groups were employed: Cys(Acm), Lys(Boc), Thr(^{t}Bu), D-Trp(Boc), and Tyr(^{t}Bu). All couplings were performed in DMF. The peptide chain was constructed manually according to a modified in situ neutralization cycle (*21*). Briefly, this cycle consisted of a 2-fold decoupling (1 and 5 min) with 50% piperidine in DMF and 10 min coupling with 4 equiv of the Fmoc-amino acid (0.4 M in DMF, incubated for 5 min with 3.9 equivof HBTU and 6 equivDIPEA). After completion, the resin (1.75 g dry weight) was treated with piperidine in DMF to deprotect the terminal α-amino-group of the peptide. An aliquot was cleaved and analyzed by HPLC indicating formation of **1** with a yield of >90%. A total of 200 mg of the resin-bound peptide **1** was cyclized at room temperature with a 2-fold molar excess of thallium(III)trifluoroacetate in DMF. As determined by analysis of a small aliquot, formation of **2** was essentially complete within 1 h. After thorough washing, *N*-maleimido-6-caproic acid was coupled as described above, the resin was washed and dried under vacuum overnight. Cleavage was performed with 5 mL of 37:1:1:1 TFA/H_2O/phenol/TIS for 2 h at room temperature. The resin was filtered and washed. The peptide was precipitated by the gradual addition of *tert*-butyl-methyl ether at 4 °C. Purification was accomplished by reversed-phase HPLC on the RP-selectB column using a gradient of 20% B → 50% B in 7.5 min and 50 → 100% B in 5 min (A = H_2O and B = acetonitrile, both containing 0.1% TFA), flow rate = 4 mL/min. Under these conditions, the peptide was eluted at 10.2 min. After lyophilization, 44 mg of **4** (43.6% overall yield) was obtained as a fluffy powder. The purified peptide was characterized by mass spectrometry. Anal. calcd for $C_{59}H_{75}N_{11}O_{15}S_2$ $[M + H]^+$: *m/z* 1243.4. Found: 1244.2. ^{13}C NMR (CD_3OD) δ = 20.02 (q), 20.58 (q), 22.89 (t), 26.28 (t), 27.14 (t), 27.70 (2 C) (t), 29.24 (t), 31.42 (t), 36.75 (t), 38.40 (t), 39.34 (t), 40.19 (t), 40.65 (t), 46.45 (t), 46.52 (t), 53.86 (d), 54.16 (d), 54.43 (d), 55.18 (d), 56.42 (d), 57.68 (d), 59.68 (d), 60.55 (d), 68.55 (d), 69.09 (d), 110.41 (s), 112.33 (d), 116.23 (2 C)

(d), 119.53 (d), 120.05 (d), 122.57 (d), 124.83 (d), 127.74 (d), 128.66 (s), 128.91 (s), 129.34 (2 C) (d), 130.66 (2 C) (d), 131.54 (2 C) (d), 135.32 (2 C) (d), 137.99 (s), 138.56 (s), 157.35 (s), 171.26 (s), 172.11 (s), 172.60 (2 C) (s), 172.74 (s), 173.26 (s), 173.57 (s), 174.20 (s), 174.35 (s), 175.00 (s), 175.36 (s).

Synthesis and Purification of the 5′-Thiol ODNs. The all-phosphorothioate ODNs, 5′-GTTCTCCCAGCGTGTGCCAT-3′ (antisense), 5′-ATGGCACACGCTGGGAGAAC-3′ (sense), and 5′-TACCGTGTGCGACCCTCTTG-3′ (nonsense), were synthesized using β-cyanoethyl phosphoramidite chemistry at the 1 μmol scale. Acetylation was performed by 0.1 M acetic anhydride/tetrahydrofuran (THF) and 0.1 M imidazole/THF. Sulfurization was affected by using the EDITH reagent. The commercially available six-carbon thiol linker phosphoroamidite (1-*O*-dimethoxytrityl-hexyl-disulfide-1′-[(2-cyanoethyl)−(*N*,*N*-diisopropyl)]-phosphoramidite (Glen Research) was coupled to the 5′ end. The final coupling was followed by an acetonitrile wash. The resin was dried under a stream of argon and treated with concentrated ammonia containing 0.1 M DTT at 55 °C for 12 h to simultaneously affect deprotection of the thiol protection as well as cleavage from the resin (*22*). The resin was removed by filtration and rinsed with concentrated ammonia. Rotary evaporation of the resultant solution afforded a clear residue which was dissolved in sterile water. To remove excess DTT, the solution was passed through a NAP-10 gel filtration column. The fractions containing the ODN were immediately used for conjugation to the peptide.

Synthesis of the Tyr³−Octreotate−Oligodeoxynucleotide Conjugates. The 5′-thiol-ODNs in eluent buffer were added to a the maleimido-peptide **4** (5-fold excess) in aqueous 0.1 M TEAA, pH 6.5, containing 20% DMF. The pH was adjusted by adding 1 M TEAA, pH 6.5. The mixture was incubated at room temperature for 4 h after which time analytical HPLC indicated complete conjugation. Buffers A, 5% acetonitrile in 0.1 M TEAA, pH 6.5, and B, 70% acetonitrile in 0.1 M TEAA, pH 6.5, were employed for purification of the conjugates by RP-HPLC. A linear gradient of 0 to 100% B (2 mL/min) in 30 min was used. The conjugates eluting at 22.3 min were collected and lyophilized. Yields were between 34 and 42% (based on the amount of the starting 5′-thiol-ODNs). The conjugates were characterized by MALDI-TOF-analysis using 3-hydroxy-picolinic acid as matrix and a sample preparation essentially as described by Langley et al. (*23*): **5**, m/z = 7822.9 $[M + H]^+$ ($C_{258}H_{335}N_{79}O_{120}P_{20}S_{23}$ calcd, 7819.96 g/mol); **6**, m/z = 7936.8 $[M + H]^+$ ($C_{260}H_{331}N_{95}O_{112}P_{20}S_{23}$, calcd, 7936.07 g/mol); and **7**, m/z = 7823.1 $[M + H]^+$ ($C_{258}H_{335}N_{79}O_{120}P_{20}S_{23}$, calcd 7819.96 g/mol).

Melting Temperature Analysis of Hybridization. Melting studies were performed in stoppered quartz cells (1 cm path length) at 260 nm. Samples were prepared as 0.5 OD solutions of the two complementary oligomers in 1 mL of buffer. The buffer was 50 mM Tris/HCl, pH 7.5, containing 0.15 M NaCl. The melting curves were measured using a temperature gradient from 30 to 90 °C with a ramp rate of 0.5 °C/min. Prior to analysis, all samples were annealed by heating to 90 °C for 5 min and subsequently cooled slowly to room temperature. Analysis was carried out using the Varian thermal software. All T_m values were calculated from the first derivative of the melting curve and represent the average (±standard deviation) of several analyses. Uncertainty in the T_m data is estimated at ±0.5 °C based on repetitions of experiments.

Scheme 1. Preparation of the Tyr³−Octreotate−ODN Conjugates

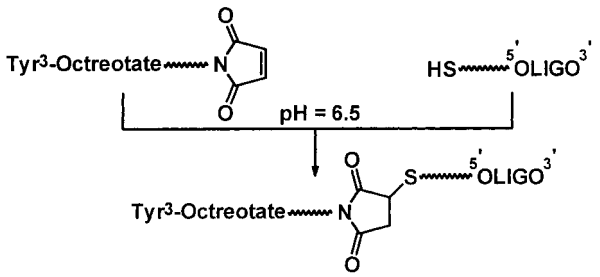

SSTR Binding Assays. The concentration of the conjugates was determined using an estimated extinction coefficient. The extinction coefficient of the conjugate was assumed to be the sum of ϵ_{ODN} and $\epsilon_{peptide}$: $\epsilon_{260nm} = \sum$-[(nA × 15.4 + nC × 7.3 + nG × 11.7 + nT × 8.8) × 0.9] + (nTrp × 3.8 + nTyr × 0.5 + nPhe × 0.2). Using this equation, the following ϵ-values were obtained: **5** = 1.8 × 10^5, **6** = 2.1 × 10^5, and **7** = 1.8 × 10^5. For the binding assays, rat cortex membranes were resuspended at a protein concentration of 500 μg/mL in incubation buffer. Per assay, 100 μg of protein were employed. The incubation buffer was 10 mM HEPES, pH 7.6, containing 5% BSA fraction V, $MgCl_2$ (10 mM), and bacitracin (20 μg/mL). The cell membranes (200 μL) were mixed with 30 μL of incubation buffer containing increasing concentrations of the competitor (conjugates **5**−**7**) (10^{-5}−10^{-10} mol/L). Approximately 20.000 cpm [^{125}I]Tyr³−octreotide (ca. 20 pM) in 70 μL of incubation buffer was added. After 1 h at room temperature, the incubation was stopped by quick filtration trough Whatman GF/B glass fiber filters prewetted with buffer containing 1% BSA. The filters were washed with ice-cold buffer (10 mM Tris, 150 mM NaCl), and the bound radioactivity was counted in a γ counter. Nonspecific binding, as determined by measuring binding in the presence of excess unlabeled octreotide (10^{-6} mol/L), was approximately 10−20% of the total binding. Specific binding was defined as total binding minus nonspecific binding. Results are expressed as specific binding obtained from triplicate experiments.

RESULTS

Synthesis Strategy. To obtain targeted analogues of ODNs, conjugation to the SSTR affine Tyr³−octreotate was performed. Therefore, the peptide was functionalized with a maleimido group and the ODNs were modified with a sulfhydryl group. Upon reaction, a stable thioether bond is formed (Scheme 1).

According to the Merrifield strategy, Tyr³−octreotate was synthesized on a solid support (Scheme 2). The tyrosine was introduced to enable radioactive labeling with iodine. Conjugation of the maleimido moiety to the peptide prohibited subsequent cyclization of the disulfide. Therefore, the success of this peptide synthesis was mainly depending on the elaboration of a protocol for on-resin cyclization.

Attempts to synthesize **2** using trityl protecting groups for cystein were impeded by incomplete couplings. This failure was probably due to the nonpolar aggregations of the lipophilic trityl groups. Using the smaller and polar Acm-protecting group, these problems could be circumvented. As determined by deprotection and HPLC-analysis of an aliquot, **1** was formed in SPPS in more than 90% yield. The deprotection/oxidation was attempted by different protocols [$AgBF_4$ followed by DMSO/HCl (*24*), I_2 (*25*), and $Tl(TFA)_3$ (*26*)]. The oxidation with

Scheme 2. Preparation of the Maleimido Modified Tyr^3−Octreotate[a]

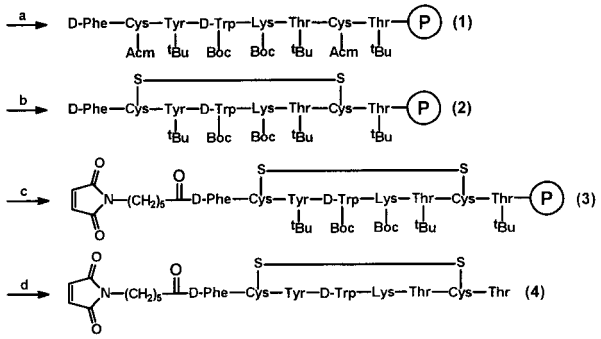

[a] (a) Stepwise elongation, (b) $Tl(TFA)_3$, (c) Mal-$(CH_2)_5$COOH, HBTU, DIPEA, (d) TFA, H_2O, phenol, TIS.

$Tl(TFA)_3$ using a 2-fold molar excess proved to produce the highest yields. The Trp-residue is known be susceptible to modifications during disulfide bond formations. Boc-protection of the D-Trp-moiety was found to be inevitable to obtain **2** in high yields.

Edwards et al. (*26*) have observed severe problems with the on-resin cyclization of octreotide. To definitely confirm the integrity of **4**, NMR analysis was performed. Both the ^{13}C NMR spectrum as well as the ^1H NMR spectrum (data not shown) were in accordance with the structure of **4**, no byproducts could be observed.

Upon oxidation, the ^{13}C NMR resonance of the β-carbon atoms of cystein is shifted considerably downfield (e.g., from $\delta = 25.5$ to $\delta = 38.9$ for cystein in glutathione). Consequently, this chemical shift can be used to determine the oxidation status of disulfide bridged peptides. The ^{13}C NMR signals of the two C_β of cystein in compound **4** appeared at 46.4 and 46.5 ppm, indicating formation of the disulfide bond. The chemical shift of carbons attached to disulfides is sensitive to changes in solvent and pH (*26*), to which this particular high shift can be attributed.

Three 20-mer phosphorothioate ODN sequences complementary to *bcl-2* (sense, antisense, and nonsense sequence) were synthesized on solid support. The six-carbon thiol linker (1-*O*-dimethoxytrityl-hexyl-disulfide-1′-[(2-cyanoethyl)-(*N*,*N*-diisopropyl)]-phosphoramidite was attached to the 5′end. Cleavage was performed in aqueous NH_3 containing 0.1 M DDT at 55 °C overnight. Under these conditions, deprotection of the disulfide protection of the thiol-linker as well as cleavage from the resin was simultaneously achieved. Excess DTT was removed by gel filtration using double-distilled water as eluent. To prevent dimer-formation, the thiol ODNs were immediately conjugated to the maleimido-peptide. Failure to do that led to strongly varying coupling yields. In addition to the thiolated compound, the formation of an ODN byproduct which was not reactive to the maleimido peptide (probably the dimer) was observed and could not be suppressed.

Purification of this ODN and incubation with DTT resulted in slow conversion to the reactive ODN. Attempts to substitute DTT by tris(2-carboxyethyl)phosphine (*27*) led to complex mixtures containing little or no product. Large excess of DTT was found to afford the lowest rate of dimer formation, resulting in reliable good coupling yields.

The conjugation reaction was performed on the basis of the synthesis technique previously described (*28*). Thus, the thiol modified ODNs were added to a solution of **4** in buffer containing DMF at pH 6.5. After 4 h, conjugation had reached completeness, as determined by HPLC. The chromatogram of the crude product mixture showed four peaks. These peaks corresponded to the truncated sequences and the unthiolated oligonucleotide at 16.8 min, the ODN-dimer byproduct at 19.2 min, the conjugate at 21.1 min, and excess maleimido peptide at 24.8 min (Figure 1). Due to the significant differences in size and polarity, the conjugates could be easily separated by HPLC from the side products and excess **4**.

Melting Temperature Analysis. Melting temperature analysis was utilized to determine influences of the peptide moiety on the hybridization efficiency of the antisense ODN−peptide conjugate for its complementary strand. The dissociation of duplexes formed from equimolar concentrations of the ODN conjugates and an unmodified 20-mer ODN target was examined. Measurements were carried out in triplicate. The T_m of the parent unmodified 20-mer phosphodiester sequence was found to be 73.1 ± 0.2 °C. As compared to this, the T_m values of the conjugates **5** (65.0 ± 0.0 °C) and **6** (63.8 ± 0.5 °C) appeared to be relatively low. The T_m of a phosphorothioate ODN is known to be decreased by about 0.5 °C per nucleotide as compared to a corresponding phosphodiester ODN (*29*). Therefore, the T_m curves were typical of those obtained with unmodified ODNs. To prove this, the analogous unmodified phosphorothioate ODNs were prepared. The resulting T_m values of the antisense (64.8 ± 0.5 °C) and the sense strand (66.2 ± 0.5 °C) confirmed that the prediction was correct. In Figure 2 the T_m curves of the duplex containing the conjugates **5**, **6**, the unmodified phosphorothioate ODNs, and the unmodified duplex are compared. These results indicate that the peptide moiety at the 5′-terminus of the 20-mer ODN does not interfere with the hybridization efficiency.

Receptor Binding. To allow examination of competitive displacement, the concentrations of the conjugates were determined accurately using their extinction coefficients. Figure 3 shows the progressive displacement of

Scheme 3. Chemical Structure of the Tyr^3−Octreotate−ODN Hybrid Molecules

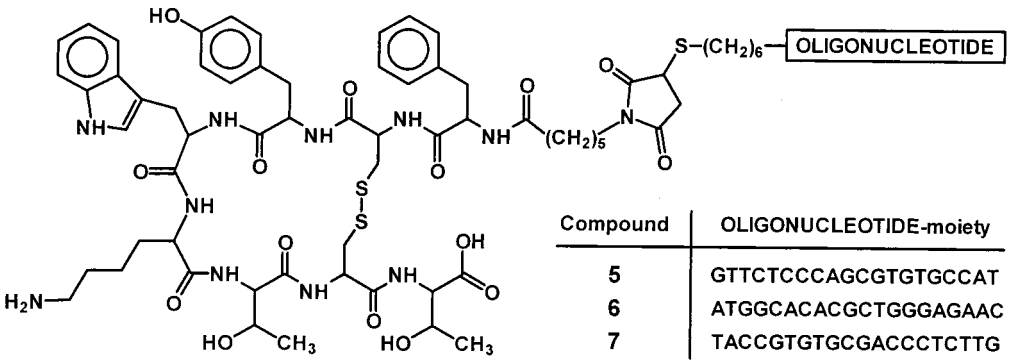

Compound	OLIGONUCLEOTIDE-moiety
5	GTTCTCCCAGCGTGTGCCAT
6	ATGGCACACGCTGGGAGAAC
7	TACCGTGTGCGACCCTCTTG

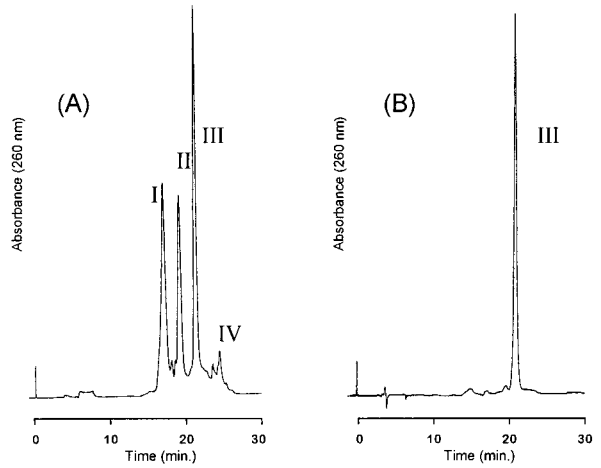

Figure 1. Reversed-phase HPLC chromatogram: Conjugation of a thiol-modified oligonucleotide with maleimido-peptide **4**. (A) Reaction mixture after 4 h. (I) Truncated sequences and the unthiolated oligonucleotide; (II) ODN-dimer byproduct, (III) conjugate, and (IV) excess maleimido peptide. (B) Purified conjugate **6**.

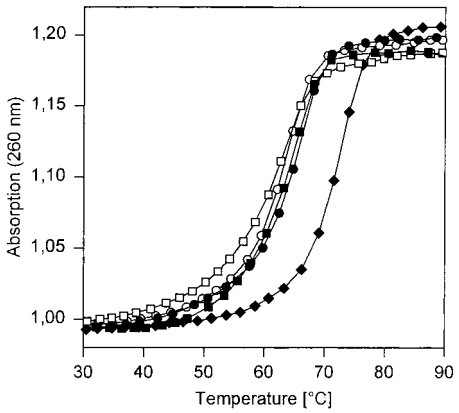

Figure 2. Melting curves of modified and unmodified 20-mer ODNs in 50 mM Tris/HCl (pH 7.5) and 0.15 M NaCl. Duplexes prepared from complementary phosphorodiester strands with antisense*bcl-2* phosphorothioate (○), sense *bcl-2* phosphorothioate (●), ODN conjugate **5** (□), ODN conjugate **6** (■), and control-strand antisense *bcl-2* phosphorodiester (◆). For clarity only every tenth point is plotted.

[^{125}I]Tyr^3–octreotide from rat cortex membranes. The three conjugates investigated bound with high affinity in the low nanomolar range. The IC_{50} values of **5**, **6**, and **7** were 1.83 ± 0.17, 2.52 ± 0.43, and 1.88 ± 0.47 nM, respectively. The similar affinities suggest that the sequence of the ODN does not significantly affect the receptor affinities.

DISCUSSION

The receptors of the hormone somatostatin are known to be overexpressed in various tumors. The ODN conjugates reported herein were designed to be targeted to these plasma membrane receptors. The SSTRs exhibit a high capacity as transport vehicles, e.g., for cargos as big as gold particles (*30*). Furthermore, they show high specificity, as known from octreoscan ([^{111}In]-DTPA-D-Phe^1-octreotide), a radiopharmaceutical for tumor scintigraphy (*31*). Therefore, analogues of somatostatin are ideal transport vehicles for the targeting of tumor cells. These assumptions have very recently been supported by the successful conjugation of cytotoxic compounds to somatostatin derivatives (*32*, *33*). Using a postsynthetic approach, the conjugation of disulfide-bridged peptides

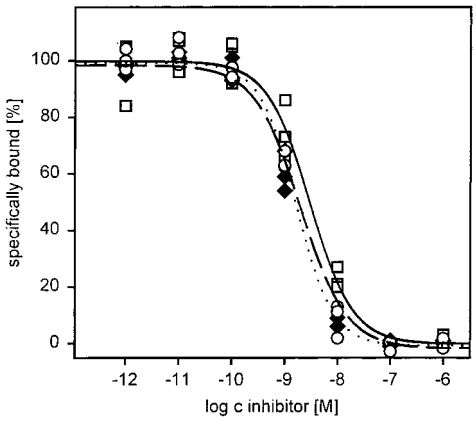

Figure 3. Displacement of [^{125}I]Tyr^3–octreotide from rat cortex membranes (triplicate measurements). The ordinate represents the percent specific binding which is total binding minus binding in the presence of the ODN conjugates **5** (□, straight line), **6** (○, dotted line), and **7** (◆, dashed line).

such as octreotide is complicated. This problem could be solved by coupling of thiol modified ODNs with a maleimido-derivatized peptide. To our knowledge this is the first report of a synthesis which enables the production of stable conjugates of ODNs with disulfide-bridged peptides.

The major targets of conjugates targeted to SSTRs are the receptor subtypes 2 and 5, which are predominantly expressed in SSTR-positive tumors. The feasibility of the ODN conjugates to target SSTRs was demonstrated by receptor binding studies with rat cortex membranes, which mainly express SSTR2. The IC_{50} values of the conjugates were in the low nanomolar range, thus, demonstrating high affinity binding to SSTRs. Investigation of the hybridization properties revealed that the peptide at the 5′-terminus of the 20-mer ODN does not influence the binding to complementary ODNs. These results provide a basis for the improvement of selective uptake of ODNs into tumors and therefore hold promise for further development and application of antisense therapy. Further development of these conjugates investigating their biodistribution, stability, and bioactivity in vivo is in progress.

ACKNOWLEDGMENT

This project was supported by a grant from the Deutsche Forschungsgemeinschaft (Ei 130/15-3). The authors would like to thank D. Keane and M. Wiersma for skilful assistance in ODN synthesis. Essential support for the establishment of receptor binding assays from Dr. Barbara Stolz, Novartis Pharma AG, Switzerland, is gratefully acknowledged.

LITERATURE CITED

(1) Kronenwett, R., Steidl, U., Kirsch, M., Sczakiel, G., and Haas, R. (1998) Oligodeoxyribonucleotide uptake in primary human hematopoietic cells is enhanced by cationic lipids and depends on the hematopoietic cell subset. *Blood 91*, 852–862.

(2) Shea, R. G., Marsters, J. C., and Bischofberger, N. (1990) Synthesis, hybridization properties and antiviral activity of lipid-oligodeoxynucleotide conjugates. *Nucleic Acids Res. 18*, 3777–3783.

(3) Letsinger, R. L., and Chaturvedi, S. (1998) Tailored hydrophobic cavities in oligonucleotide-steroid conjugates. *Bioconjugate Chem. 9*, 826–830.

(4) Shoji, Y., Ishige, H., Tamura, N., Iwatani, W., Norimatsu, M., Shimada, J., and Mizushima, Y. (1998) Enhancement of

anti-herpetic activity of antisense phosphorothioate oligonucleotides 5′ end modified with geraniol. *Drug Target. 5*, 261−273.
(5) Leonetti, J.-P., Degols, G., and Lebleu, B. (1990) Biological activity of oligonucleotide-poly (l-lysine) conjugates: mechanism of cell uptake. *Bioconjugate Chem. 1*, 149−153.
(6) Pardridge, W. M., and Boado, R. J. (1991) Enhanced cellular uptake of biotinylated antisense oligonucleotide or peptide mediated by avidin, a cationic protein. *FEBS Lett. 288*, 30−32.
(7) Pardridge, W. M., Boado, R. J., and Kang, Y. S. (1995) Vector-mediated delivery of a polyamide ("peptide") nucleic acid analogue through the blood-brain barrier in vivo. *Proc. Natl. Acad. Sci. U.S.A. 92*, 5592−5596.
(8) Benimetskaya, L., Takle, G. B., Vilenchik, M., Lebedeva, I., Miller, P., and Stein, C. A. (1998) Cationic porphyrins: novel delivery vehicles for antisense oligodeoxynucleotides. *Nucleic Acids Res. 26*, 5310−5317.
(9) Zhu, T., and Stein, S. (1994) Preparation of vitamin B6-conjugated peptides at the amino terminus and of vitamin B6-peptide−oligonucleotide conjugates. *Bioconjugate Chem. 5*, 312−315.
(10) Lu, X. M., Fischman, A. J., Jyawook, S. L., Hendricks, K., Tompkins, R. G., and Yarmush, M. L. (1994) Antisense DNA delivery in vivo: liver targeting by receptor-mediated uptake. *J. Nucl. Med. 35*, 269−275.
(11) Cooper, R. G., Harbottle R. P., Schneider, H., Coutelle, C., and Miller, A. D. (1999) Peptide mini-vectors for gene delivery. *Angew. Chem., Int. Ed. 38*, 1949−1952.
(12) Deshpande, D., Toledo-Velasquez, D., Thakkar, D., Liang, W., and Rojanasakul, Y. (1996) Enhanced cellular uptake of oligonucleotides by EGF receptor-mediated endocytosis in A549 cells. *Pharm. Res. 13*, 57−61.
(13) Derossi, D., Chassaing, G., and Prochiantz, A. (1998) Trojan peptides: the penetratin system for intracellular delivery. *Trends Cell Biol. 8*, 84−87.
(14) Dokka, S., Toledo-Velasquez, D., Shi, X., Wang, L., and Rojanasakul, Y. (1997) Cellular delivery of oligonucleotides by synthetic import peptide carrier. *Pharm. Res. 14*, 1759−1764.
(15) Chaloin, L., Vidal, P., Lory, P., Mery, J., Lautredou, N., Divita, G., and Heitz, F. (1998) Design of carrier peptide−oligonucleotide conjugates with rapid membrane translocation and nuclear localization properties. *Biochem. Biophys. Res. Commun. 243*, 601−608.
(16) Bauer, W., Briner, U., Doepfner, W., Haller, R., Huguenin, R., Petcher, T. J., and Press, J. (1982) SMS 201−995: A very potent and selective octapeptide analogue of somatostatin with prolonged action. *Life Sci. 31*, 1133−1140.
(17) De Jong, M., Breeman, W. A., Bakker, W. H., Kooij, P. P., Bernard, B. F., Hofland, L. J., Visser, T. J., Srinivasan, A., Schmidt, M. A., Erion, J. L, Bugaj, J. E., Macke, H. R., and Krenning, E. P. (1998) Comparison of (111)In-labeled somatostatin analogues for tumor scintigraphy and radionuclide therapy. *Cancer Res. 58*, 437−441.
(18) Reed, J. C., Stein, C., Subasinghe, C., Haldar, S., Croce, C. M., Yum, S., and Cohen, J. (1990) Antisense-mediated inhibition of BCL2 protooncogene expression and leukemic cell growth and survival: comparisons of phosphodiester and phosphorothioate oligodeoxynucleotides. *Cancer Res. 50*, 6565−6570.
(19) Cotter, F. E., Johnson, P., Hall, P., Pocock, C., al Mahdi, N., Cowell, J. K., and Morgan, G. (1994) Antisense oligonucleotides suppress B-cell lymphoma growth in a SCID-hu mouse model. *Oncogene 10*, 3049−55.
(20) Bakker, W. H., Krenning, E. P., Breeman, W. A., Koper, J. W., Kooij, P. P., Reubi, J. C., Klijn, J. G., Visser, T. J. Docter, R., and Lamberts, S. W. (1990) Receptor scintigraphy with a radioiodinated somatostatin analogue: radiolabeling, purification, biologic activity, and in vivo application in animals. *J. Nucl. Med. 9*, 1501−1509.
(21) Schnölzer, M., Alewood, P., Jones, A., Alewood, D., and Kent, S. B. H. (1992) In situ neutralization in Boc-chemistry solid-phase peptide synthesis. *Int. J. Pept. Protein Res. 40*, 180−193.
(22) Gottschling, D., Seliger, H., Tarrasón, G., Piulats, J., and Eritja, R. (1998) Synthesis of oligonucleotide containing N^4-mercaptoethylcytosine and their use in the preparation of oligonucleotide−peptide conjugates carrying c-myc tag-sequence. *Bioconjugate Chem. 9*, 831−837.
(23) Langley, G. J., Herniman, J. M., Davies, N. L., and Brown, T. (1999) Simplified sample preparation for the analysis of oligonucleotides by matrix-assisted laser desorption/ionisation time-of-flight mass spectrometry. *Rapid Commun. Mass Spectrom. 13*, 1717−1723.
(24) Hunter, M. J., and Komives, E. A. (1995) Deprotection of S-acetamidomethyl cysteine-containing peptides by silver trifluoromethanesulfonate avoids the oxidation of methionines. *Anal. Biochem. 228*, 173−177.
(25) Albericio, F., Hammer, R. P., Garcia-Echeverria, C., Molins, M. A., Chang, J. L., Munson, M. C., Pons, M., Giralt, E., and Barany, G. (1991) Cyclization of disulfide-containing peptides in solid-phase synthesis. *Int. J. Pept. Protein Res. 37*, 402−413.
(26) Edwards, W. B., Fields, C. G., Anderson, C. J., Pajeau, T. S., Welch, M. J., and Fields, G. B. (1994) Generally applicable, convenient solid-phase synthesis and receptor affinities of octreotide analogs. *J. Med. Chem. 37*, 3749−3757.
(27) Han, J. C., and Han, G. Y. (1994) A procedure for quantitative determination of tris(2-carboxyethyl)phosphine, an odorless reducing agent more stable and effective than dithiothreitol. *Anal. Biochem. 220*, 5−10.
(28) Eritja, R., Pons, A., Escarceller, M., Giralt, E., and Albericio, F. (1991) Synthesis of defined peptide−oligonucleotide hybrids containing a nuclear transport signal sequence. *Tetrahedron 47*, 4113−4120.
(29) Freier, M. (1993) Hybridization considerations affecting antisense drugs. In *Antisense Research and Applications* (S. T. Crooke and B. Lebleu, Eds.) 67−82, CRC Press, Boca Raton, FL.
(30) Segond von Banchet, G., Schindler, M., Hervieu, G. J., Beckmann, B., Emson, P. C., and Heppelmann, B. (1999) Distribution of somatostatin receptor subtypes in rat lumbar spinal cord examined with gold-labeled somatostatin and anti-receptor antibodies. *Brain Res. 816*, 254−257.
(31) Krenning, E. P., Kwekkeboom, D. J., Bakker, W. H., Breeman, W. A., Kooij, P. P., Oei, H. Y., van Hagen, M., Postema, P. T., de Jong, M., Reubi, J. C., Visser, T. J., Reijs, A. E. M., Hofland, L. J., Kooper, J. W., and Lamberts, S. W. J. (1993) Somatostatin receptor scintigraphy with [111In-DTPA-D-Phe1]- and [123I-Tyr^3]-octreotide: the Rotterdam experience with more than 1000 patients. *Eur. J. Nucl. Med. 20*, 716−731.
(32) Nagy, A., Schally, A. V., Halmos, G., Armatis, P., Cai, R. Z., Csernus, V., Kovacs, M., Koppan, M., Szepeshazi, K., and Kahan, Z. (1998) Synthesis and biological evaluation of cytotoxic analogues of somatostatin containing doxorubicin or its intensely potent derivative, 2-pyrrolinodoxorubicin. *Proc. Natl. Acad. Sci. U.S.A. 95*, 1794−1799.
(33) Polonowski, A., Schally, A. V., Nagy, A., Sun, B., and Szepeshazi, K. (1999) Inhibition of PC-3 human androgen-independent prostate cancer and its metastases by cytotoxic somatostatin analogue AN-238. *Cancer Res. 59*, 1947−1953.

BC000041K

Concerted Intercalation and Minor Groove Recognition of DNA by a Homodimeric Thiazole Orange Dye

Jakob Bunkenborg,[†] Nikolai I. Gadjev,[‡] Todor Deligeorgiev,[‡] and Jens Peter Jacobsen*,[†]

Department of Chemistry, University of Southern Denmark, Odense University, Odense M, DK-5230 Denmark, and Faculty of Chemistry, University of Sofia, 1126 Sofia, Bulgaria. Received April 28, 2000; Revised Manuscript Received September 15, 2000

The thiazole orange dye TOTO binds to double-stranded DNA (dsDNA) by a sequence selective bis-intercalation. Each chromophore is sandwiched between two base pairs in a (5′-CpT-3′):(5′-ApG-3′) site, and the linker spans two base pairs in the minor groove. We have used one- and two-dimensional NMR spectroscopy to examine the dsDNA binding of an analogue of TOTO in which the linker has been modified to contain a bipyridyl group (viologen) that has minor groove binding properties. We have investigated the binding of this analogue, called TOTOBIPY, to three different dsDNA sequences containing a 5′-CTAG-3′, a 5′-CTTAG-3′, and a 5′-CTATAG-3′ sites, respectively, demonstrating that TOTOBIPY prefers to span three base pairs. The many intermolecular NOE connectivities between TOTOBIPY and the d(CGCTTAGCG):d(CGCTAAGCG) oligonucleotide in the complex shows that the bipyridyl-containing linker is positioned in the minor groove and spans three base pairs. Consequently, we have succeeded in designing and synthesizing a ligand that recognizes an extended recognition sequence of dsDNA as the result of a concerted intercalation and minor groove binding mode.

INTRODUCTION

The study of molecular recognition and in particular the chemical requisites for the formation of specific drug−DNA[1] complexes has been an active research area (Johnson and Boger, 1996). The goal is to rationally design novel molecules, capable of sequence-specific DNA-recognition, by exploiting a combination of both steric and hydrogen bond donor−acceptor complementarity. The very high affinity for DNA exhibited by bis-intercalating agents make them interesting candidates for the design of bimodal DNA-binding molecules by combining this high affinity with the sequence selectivity exhibited by minor groove binding agents.

Recent work in our laboratory has focused on ^{1}H NMR studies of the binding-mode and sequence selectivity of *N*,*N*,*N*′,*N*′-tetramethyl-*N*,*N*′-bis-{3-[4-[(3-methyl-2(*3H*)-benzothiazolilyden)methyl]quinolinium-1-yl]propyl}-1,3-propandiammonium tetraiodide (TOTO, Scheme 1) with various dsDNA oligonucleotides (Bondensgaard and Jacobsen, 1999; Petersen et al., 1999; Bunkenborg et al., 1999; Jensen et al., 1998; Johansen and Jacobsen, 1998; Petersen and Jacobsen, 1998; Faridi et al., 1997; Stærk et al., 1997; Hansen et al., 1996; Spielmann et al., 1995; Jacobsen et al., 1995). We have shown that TOTO binds sequence selectively to double-stranded DNA (dsDNA) by bis-intercalation. Each chromophore is sandwiched between two base pairs in a d(5′-py-*p*-py-3′):d(5′-pu-*p*-pu-3′) site, and the linker spans two base pairs in the minor groove. We have examined the binding of TOTO to various dsDNA oligonucleotides and found that the 5′-CTAG-3′ sequence (or analogues of that) is the most favorable binding motif (Bunkenborg et al., 1999).

Scheme 1. Chemical Structure of TOTO and TOTOBIPY with Numbering Schemes

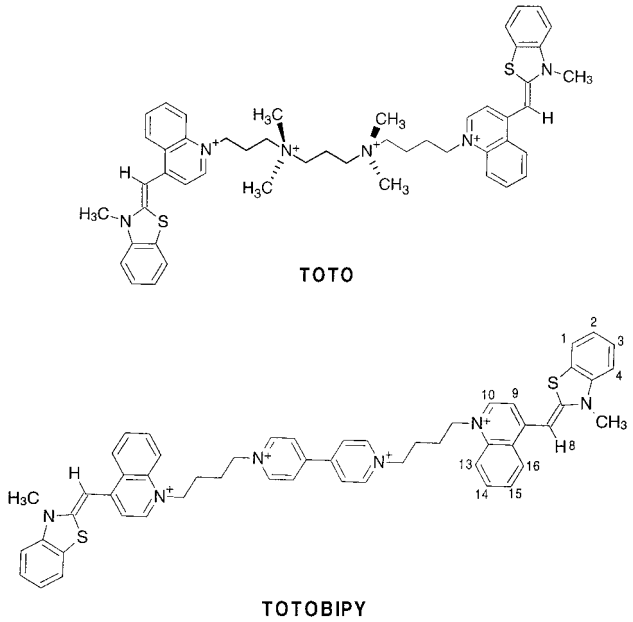

* To whom correspondence should be addressed. E-mail: jpj@chem.sdu.dk.
† University of Southern Denmark.
‡ University of Sofia.

[1] Abbreviations: BIPY, 4,4′-bipyridyl; DNA, deoxyribose nucleic acid; DMSO, dimethyl sulfoxide; dsDNA, double-stranded DNA; DSS, 2,2-dimethyl-2-silapentane-5-sulfonate; DQF-COSY, double quantum filtered correlation spectroscopy; EDTA, ethylenediaminetetraacetic acid; HSQC, heteronuclear single quantum coherence; NMR, nuclear magnetic resonance; NOE, nuclear Overhauser effect; NOESY, nuclear Overhauser effect spectroscopy; RMD, restrained molecular dynamics; TOCSY, total correlation spectroscopy; TOTO, *N*,*N*,*N*′,*N*′-tetramethyl-*N*,*N*′-bis-{3-[4-[(3-methyl-2(*3H*)benzothiazolilyden)methyl]quinolinium-1-yl]propyl}-1,3-propandiammonium tetraiodide; TOTOBIPY, *N*,*N*′-bis-{3-[4-[(3-methyl-2(*3H*)benzothiazolilyden)methyl]-quinolinium-1-yl]butyl}-4,4′-bipyridinium tetraiodide.

10.1021/bc000042c CCC: $19.00 © 2000 American Chemical Society
Published on Web 10/28/2000

The thiazole orange chromophore of TOTO has been shown to prefer to intercalate at a d(5′-C*p*T-3′):d(5′-A*p*G-3′) base pair step. The bis-intercalation of TOTO obeys the nearest neighbor exclusion principle with the linker spanning two bases in the minor groove. The short positively charged polyamine linker of TOTO contributes to the d(5′-T*p*A-3′):d(5′-A*p*T-3′) minor groove preference due to the favorable negative electrostatic potential in the AT-step minor groove (Bunkenborg et al., 1999). Earlier we have synthesized derivatives of TOTO with extended methylene linkers between the quinolinium ring and the quaternary ammonium nitrogen. One of these derivatives was found to predominantly bis-intercalate in the 5′-CTGAG-3′ site (Stærk et al., 1997), but a longer polyamine linker than the one in TOTO reduces the sequence selectivity (Bunkenborg et al., 1999).

How do we avoid the reduction in sequence selectivity when trying to extend the recognition sequence for new TOTO analogues? A rather obvious suggestion is to replace the flexible linker with a more rigid element endowed with some of the typical minor groove binding characteristics. The 4,4′-bipyridyl (viologen) element is well suited for this purpose because it forms a rigid positively charged aromatic linker. Viologen has been shown to endow bis-intercalators with a preference for AT base pairs by serving as a minor groove binder (Takenaka et al., 1997). Consequently, we have synthesized (Deligeorgiev et al., 2000) and investigated the DNA-binding properties of a TOTO analogue with the polyamine linker substituted by a 4,4′-bipyridyl containing linker: *N*,*N*′-bis-{3-[4-[(3-methyl-2(*3H*)benzothiazolilyden)methyl]quinolinium-1-yl]butyl}-4,4′-bipyridinium tetraiodide (TOTOBIPY, Scheme 1). In this paper, we present the results of one- and two-dimensional ^{1}H NMR studies of complexes between dsDNA and TOTOBIPY. We have investigated the binding of TOTOBIPY to three different dsDNA sequences containing the 5′-CTAG-3′, the 5′-CTTAG-3′ and the 5′-CTATAG-3′ sites, respectively. All these sequences contain two d(5′-C*p*T-3′):d(5′-A*p*G-3′) base pair steps as preferred by the thiazole orange chromophore of TOTO, but separated with a different number of base pairs. Thus, we were able to show that TOTOBIPY preferentially spans three base pair steps as the result of a concerted intercalation and minor groove binding mode. The many intermolecular NOEs of the TOTOBIPY−CTTAG complex demonstrates that the BIPY-element is situated in the minor groove as expected.

EXPERIMENTAL PROCEDURES

Materials. Purified DNA oligonucleotides were purchased from DNA Technology (Aarhus, Denmark) and used without further purification. The non-self-complementary single-stranded DNA oligomers were added to an equivalent amount of the complementary strand and duplexes formed by annealing from 80 °C to room temperature over 2 h. In this work, three different oligonucleotides have been used (Scheme 2).

TOTOBIPY was synthesized as described earlier (Deligeorgiev et al., 2000). A stock solution of TOTOBIPY in DMSO-d_6 was used for complex formation with the dsDNA oligonucleotides by the procedure described earlier (Jacobsen et al., 1995). A phosphate buffer containing ethylenediaminetetraacetic acid (EDTA) to complex paramagnetic ions, 2,2-dimethyl-2-silapentane-5-sulfonate (DSS) as a chemical shift reference and NaN_3 as antibacterial agent was added, giving a final concentration in the NMR sample of 10 mM P_i (pD = 7.0), 0.025 mM EDTA, 0.1 mM DSS, and 0.01 mM NaN_3. The complexes were redissolved in 500 μL of 99.96% D_2O (from Cambridge Isotope Laboratories) to yield a concentration of 2 mM. For experiments in H_2O, a mixture of 90% H_2O/10% D_2O (500 μL) was used. The samples remained stable for months.

Scheme 2. Numbering Schemes for the Three dsDNA Duplexes Used

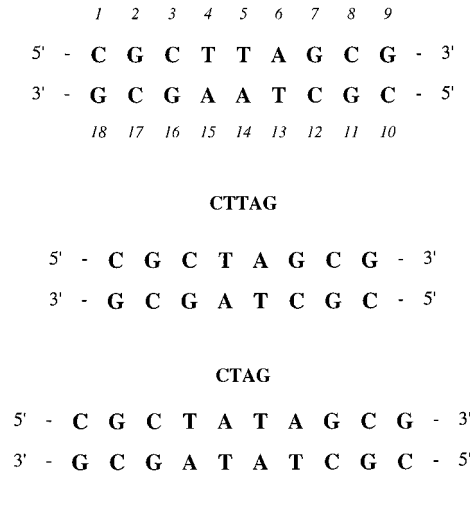

NMR Experiments. All NMR experiments on the DNA−dye complexes were performed on a Varian Unity 500 MHz NMR spectrometer and a Varian INOVA 750 MHz NMR spectrometer. NOESY spectra in D_2O were acquired with a mixing time of 200 ms using 2048 complex points in t_2 and a spectral width of 5000 Hz for a total of 512 t_1-experiments with 64 scans each at 298 K. For the CTTAG−TOTOBIPY complex, an additional NOESY spectrum in D_2O was acquired at 750 MHz with a mixing time of 200 ms using 4096 complex points in t_2 and a spectral width of 7500 Hz for a total of 600 t_1-experiments with 48 scans each at 298 K. NOESY spectra in H_2O were acquired using 2048 complex points and a spectral width of 10 000 Hz using a NOESY pulse sequence where the last 90° pulse was replaced by a pulse containing a notch to suppress the water signal (Stein et al., 1995). This ensured suppression of the water signal together with a linear excitation profile over the whole spectral width.

TOCSY experiments in D_2O were acquired with mixing times of 90 ms using 2048 complex points in t_2 and a spectral width of 5000 Hz with total of 512 t_1 experiments with 64 scans each. DQF-COSY experiments in D_2O were acquired using 2048 complex points in t_2 and a spectral width of 5000 Hz with total of 1024 t_1 experiments with 64 scans each.

The acquired data were processed using FELIX (version 97.2, Biosym/MSI, San Diego, CA). The spectra were assigned in the conventional way as described in the literature (Wijmenga and van Buuren, 1998).

Molecular Modeling. A model structure of the CTTAG−TOTOBIPY complex was obtained by restrained molecular dynamics (RMD) calculations using the *Discover* program (MSI, San Diego, ver. 2.9.7) with a modified AMBER force field. Modifications were made to take the thiazole sulfur atoms and the bipyridyl group into account. Graphical displays were obtained by the *Insight*II program (MSI, SanDiego, ver. 97.2).

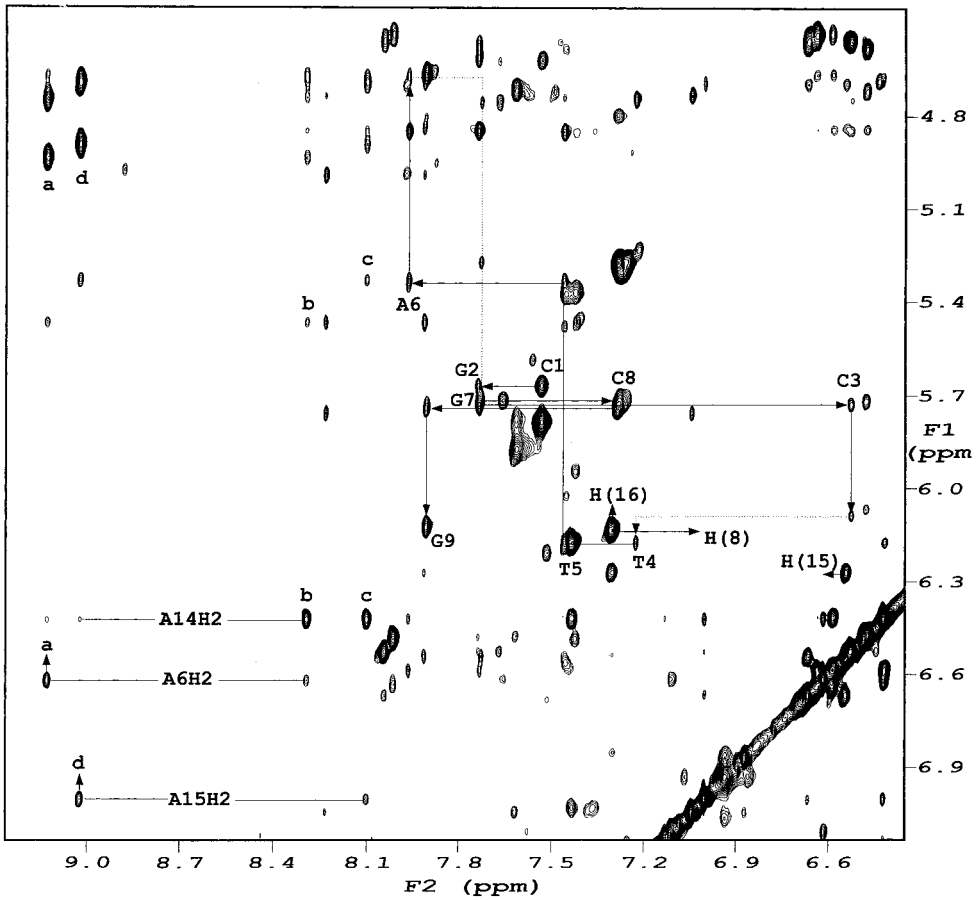

Figure 1. The aromatic to H1′ region of a 750 MHz NOESY spectrum (mixing time of 200 ms) of the CTTAG-TOTOBIPY complex at 25 °C. The sequential $H1'_{(n-1)}$-$H6/H8_{(n)}$-$H1'_{(n)}$ connectivity pattern is shown with solid lines for the 5′-CGCTTAGCG-3′-strand. Interruptions at the 5′-C3pT4-3′ and the 5′-A5pG6-3′ binding sites are indicated with broken lines. A few crucial cross-peaks between TOTOBIPY and the DNA are indicated and in the asymmetric complex there are four distinct bipyridyl proton resonances (Figure 2). Intramolecular cross-peak of the chromophore in TOTOBIPY are also indicated.

The dsDNA strands were built in *InsightII*, and the TOTOBIPY ligand was docked manually into the binding site. Restraints between hydrogens on the DNA and the ligand were obtained from the 200 ms NOESY spectrum using the isolated spin pair approximation. The restraints were divided into classes of weak, medium, and strong connectivities. The three base pairs at each end of the dsDNA were fixed in the B-DNA form by generic restraints. Twenty structures were calculated using the following RMD protocol: initially 100 and 1000 cycles of steepest descent and conjugate gradient energy minimizations, respectively. This was followed by 28 ps of RMD (steps of 1 fs) with the following temperature profile: 600 K for 4 ps and then cooled to 200 K in 50 K steps of 3 ps each. Force constants of 50 kJ/mol were used. Finally, the structures were energy minimized using conjugate gradient until the derivative was less than 0.01 Å.

RESULTS

d(CGCTTAGCG):d(CGTAAGCG) (CTTAG) Oligonucleotide. The mixture of CTTAG + TOTOBIPY yields a spectrum with sharp lines from a single major form (~90%). The NOESY spectrum of this CTTAG−TOTOBIPY complex exhibits the characteristic features of dsDNA sequential connectivities from aromatic H6/H8 protons to both intra- and interresidue H1′ and H2′/H2″. However, the sequential connectivities are interrupted at the 5′-C3*p*T4-3′, 5′-C12*p*T13-3′, 5′-A6*p*G7-3′, and 5′-A15*p*G16-3′ base pair steps. This is clear evidence of bis-intercalation. Interruption of the sequential NOE connectivities is also observed in the cross-peak pattern of the methyl group of T4 and T13 for which the peak to C3 H6 and C12 H6, respectively, are missing. The NOESY spectrum of the complex in H_2O shows the normal Watson−Crick NOE connectivity pattern (Wüthrich, 1986).

The internal NOE connectivities in the chromophore of TOTOBIPY are a distinct feature of the NOESY spectra of the complex. Cross-peak patterns connect H16-H15-H14-H13, H8-$CH_3$6-H4-H3-H2-H1, and H9-H10, respectively. A very strong cross-peak between H8 and H16 and a cross-peak pattern connecting H9-H10-H13 establish the assignments of the individual protons and the conformation of the TOTOBIPY ligand. Resonances in the linker of TOTOBIPY were assigned by combined use of TOCSY and NOESY cross-peaks. On the basis of the cross-peak pattern in the NOESY spectrum, we conclude that the relative conformation of the two ring systems in each chromophore is that indicated in Scheme 1.

A large number of cross-peaks between TOTOBIPY protons and protons on the oligonucleotide was observed. A few of them are indicated in Figure 1 and further illustrated in Figure 2. These intermolecular cross-peaks clearly show that TOTOBIPY bis-intercalates in the (5′-CTTAG-3′):(5′-CTAAG-3′) site. In detail, sequential connectivities for the 5′-T4A5A6-3′ and 5′-T13T14A15-3′ sequences show that no intercalation takes place in this part of the oligonucleotide, proving that the linker spans

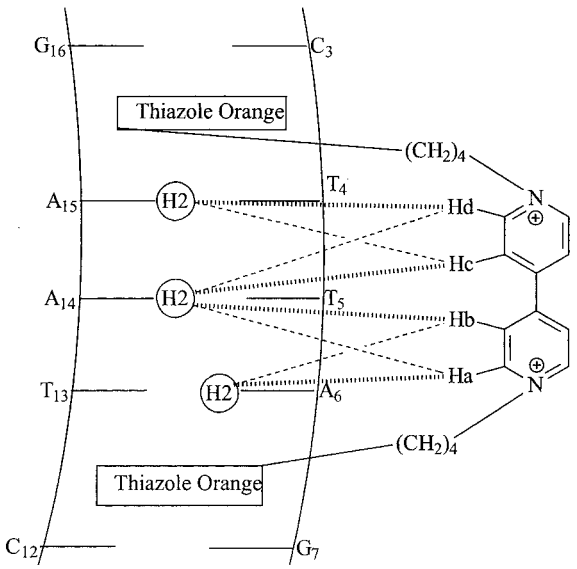

Figure 2. A few of the observed intermolecular NOE connectivities observed between the bipyridyl protons of the linker and the H2 on the adenines. Strong connectivities (| | |) and medium connectivities are both indicated (- - -).

three base pairs. Interruptions in the sequential $H1'_{(n-1)}$-$H6/H8_{(n)}$-$H1'_{(n)}$ pattern confirm the binding site. The aromatic protons on A6 and G7 have cross-peaks to H15 and/or H14 on one of the chromophores while the aromatic protons on A15 an G16 have cross-peaks to H15 and H14 on the other chromophore. Furthermore, an upfield shift of approximately 0.8 ppm of the methyl group proton resonances of T4 and T13 is observed while the methyl resonance of T5 is unchanged. All together, this establishes bis-intercalation in the 5′-C|*TTA*|G-3′ binding site with the linker spanning the three central bases. Cross-peaks in the NOESY spectrum unambiguously show that the linker is positioned in the minor groove. This is demonstrated by a large number of cross-peaks of which some are illustrated in Figure 2.

A remarkable feature of the complex of CTTAG−TOTOBIPY is the occurrence of only four resonances from the 4,4′-bipyridyl moiety. This suggests that the bipyridyl is undergoing rapid rotation within the NMR time scale.

On the basis of the observed NOE connectivities between TOTOBIPY protons and protons on the oligonucleotide, a model of the CTTAG−TOTOBIPY complex was calculated by restrained molecular dynamics. A picture of the model is shown in Figure 3. The model was obtained by using 22 intermolecular restraints to position the TOTO chromophores and 11 restraints to position the bipyridyl ring system in the minor groove. These constraints did not embrace the equivalence of the protons at the bipyridyl group due to the dynamic rotation. Consequently, the model obtained must not be mistaken for a representation of the structure of the complex. The model correctly positions the chromophores at the intercalations sites and the linker in the minor groove, but it does not claim to include detailed structural and dynamic properties of the complex.

d(CGCTAGCG)$_2$ (CTAG) Oligonucleotide. TOTOBIPY forms more than one complex with the CTAG oligonucleotide. Consequently, the 1D NMR spectrum had broad lines due to exchange between the complexes. Severe overlap in the 2D NMR spectra prevented conclusive evidence that would allow identification of the binding sites of TOTOBIPY, but the methyl group resonances suggest that there are two major forms present in almost equal amounts. One is a symmetric complex with single methyl resonance upfield shifted 0.8 ppm. Such an upfield shift is normally observed in binding sites containing a thymidine (Jacobsen et al., 1995; Hansen et al., 1996) and indicates normal bis-intercalation in the (5′-C|*TA*|G-3′)$_2$ binding site. The other major form has one downfield shifted methyl resonance and one ordinary methyl resonance suggesting an asymmetric complex with nonnearest neighbor bis-intercalation in the (5′-C|*TAG*|C-3′)$_2$ site.

d(CGCTATAGCG)$_2$ (CTATAG) Oligonucleotide. The mixture of CTATAG + TOTOBIPY yields two or more complexes with one major asymmetric form. This complex was established as containing a bis-intercalated TOTOBIPY in the 5′-T|*ATA*|G-3′ binding site with the linker spanning three central bases. Once again the linker suits a three base pair step. Basically, there are two identical such binding sites in the palindromic sequence, the other one being the 5′-C|*TAT*|A-3′ site. The line broadening is due to exchange between these two sites.

DISCUSSION

The sequence selectivity and the binding mode of the TOTOBIPY analogue to the three dsDNA oligonucleotides examined in this work is very similar to the one of TOTO. In the CTAG oligonucleotide, both TOTO and TOTOBIPY bind to the 5′-CTAG-3′ site, but in the case of TOTOBIPY, there also exists another major component in which the ligand is bis-intercalated in isolated intercalation sites: (5′-C|*TAG*|C-3′)$_2$. This demonstrates that the partiality of the TOTO chromophore for the (5′-C*p*T-3′):(5′-A*p*G-3′) site competes with the preference of the linker to span three base pairs. An equivalent situation is observed in the CTATAG duplex where more than one complex is formed with TOTOBIPY but still with a three base step spanning major form.

The model of the TOTOBIPY−CTTAG complex summarizes the major structural features. The thiazole orange chromophores are situated in their favorite positions in the two (5′-C*p*T-3′):(5′-A*p*G-3′) sites with the benzothiazole ring systems sandwiched between the purines. All these features are in good accordance with our earlier thiazole orange studies, and thus, the introduction of a new linker has not perturbed the positioning of the chromophores. As evidenced by a number of linker−DNA NOE connectivities, the linker is positioned in the minor groove, but the occurrence of only four resonances from the bipyridyl moiety suggest a dynamical averaging due to a fast rotation on the NMR time scale. This rapid rotation may be considered as an indication of the lifetime of the complex or as an indication of the wide space in the minor groove that allows rotation of the linker while bound to the dsDNA. However, there are no exchange cross-peaks between resonances of the two chromophores indication that the exchange is slow on the NMR time scale. Furthermore, the structure of dsDNA is dynamic and flexible. Consequently, the rotation of the linker might be coupled to the dynamic motions of the duplex without requiring a particular wide minor groove.

Earlier, we have shown (Stærk et al., 1997) that approximately three methylene groups from the chromophore are required to position the middle part of the linker correctly in the minor groove. A model of the TOTOBIPY ligand shows that this middle part of the linker in this dye has a length of approximately 10.5 Å. This length is suited for spanning about three base steps

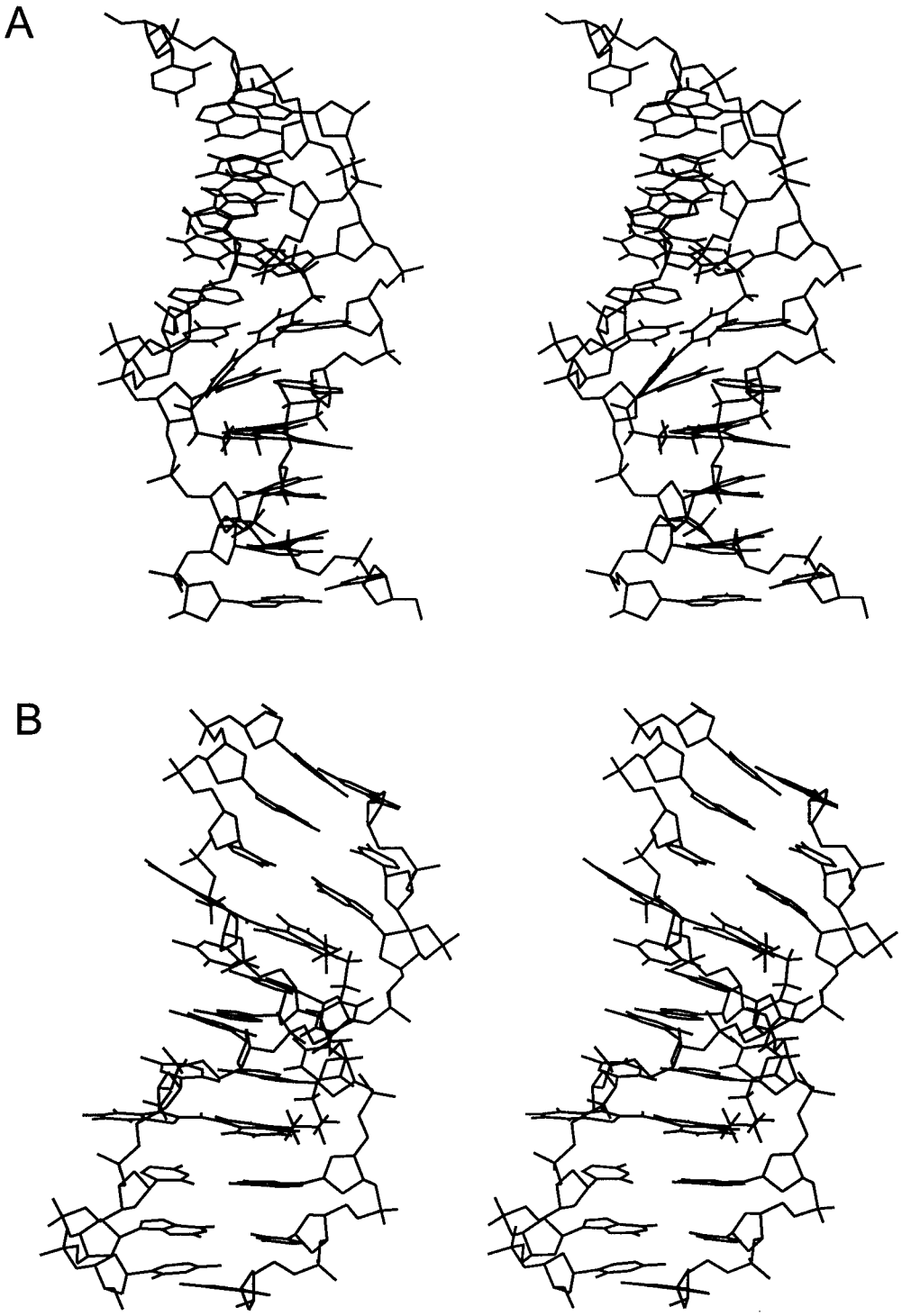

Figure 3. Stereoview of the model of the CTTAG-TOTOBIPY complex obtained by restrained molecular dynamics calculations. The model at the bottom is viewed into the minor groove. The model at the top is turned 90°.

but too short for spanning four. In the CTTAG duplex, TOTOBIPY was observed to give nonnearest neighbor bis-intercalation in oligonucleotides with isolated (5′-CpT-3′):(5′-ApG-3′) base pairs separated by three base pairs. This sequence contains the preferred intercalation sites separated by three base pairs and does thus fulfill both binding requirements of TOTOBIPY. Consequently, we have succeeded in designing and synthesizing a ligand that recognizes DNA in a concerted intercalation and minor groove binding mode that extends the recognition sequence.

In our earlier attempts to elongate the binding sequence, we have tried adding additional methylene groups to the flexible polyamine linker (Bondensgaard and Jacobsen, 1999; Stærk et al., 1997). Although the TOTO13 with the longest linker was capable of spanning three base steps there was a loss of selectivity, e.g., TOTO13 formed more than one complex with the 5′-CTTAG-3′ sequence (Stærk et al., 1997) with a major form in the 5′-C|*TTA*|G-3′ site. The rigid TOTOBIPY only forms one complex and thus the rigid linker seems to hold the chromophores in place. Shedding flexibility and enhancing affinity by introducing rigid elements seems to be a general trend. The importance of the linker has been extensively investigated (Assa-Munt et al., 1985a,b) for acridine bis-intercalators. It was found that while

uncharged polymethylene linkers lead to rapid exchange of the bis-intercalator between different intercalation sites in a $d(AT)_5$:$d(AT)_5$ duplex, the introduction of positively charged spermine linker stabilized the complex due to a retarding of the migration of the intercalator between different binding sites. A further loss of flexibility with a concomitant enhancement in binding affinity was gained by introducing a rigid pyrazole linker. Likewise, a significant improvement in DNA affinity was noted on exchanging a polymethylene linker with a diphenyl-ether (Cory et al., 1985). The affinity gain seems mainly to stem from van der Waals contacts with the walls of minor groove and loss of motional freedom—both of these necessitating steric complementarity between the linker and the target sequence. The bipyridyl linker is probably more sequence selective than the flexible polyamine linker, because the rigid linker will sterically clash with the guanine amino-group protruding into the minor groove while the polyamine linker can adapt more easily. The linear geometry of bipyridyl is probably not optimal for minor groove binding as can be surmised from the family of crescent-shaped minor groove binders (e.g., berenil, distamycin etc). However, the unwinding caused by the intercalating chromophores seems to make this isoconcavity demand less severe.

Thiazole orange (TOTO) and oxazole yellow (YOYO) homodimer polyamine dyes bind avidly to dsDNA by bis-intercalation with a high fluorescence enhancement upon binding (Rye et al., 1992; Glazer and Rye, 1992). The enhancement is attributed to the loss of rotational freedom between the thiazole and quinolinium moieties of the chromophores when inserted between the DNA nucleobases (Larsson et al., 1994). The unaltered chromophore positioning indicates that the new linker does not interfere with the fluorescence properties. Both TOTO and YOYO have been found to cause photocleavage of DNA, though the mechanism depends of the dye:DNA ratio (Åkerman and Tuite, 1996). At high dye:DNA ratios, externally bound dye cleaves in an oxygen-dependent manner, and this mechanism is more efficient than the oxygen-independent cleavage by bis-intercalated dye occurring at lower dye:DNA ratios. Earlier studies have shown that an electron transfer from intercalated ethidium to externally bound methyl-viologen can be photoinduced (Fromherz and Rieger, 1986) and that the one-electron reduced viologen reacts with oxygen leading to cleavage of DNA. A viologen linker containing acridine bis-intercalator has been shown to photocleavage dsDNA (Takenaka et al., 1992). The sequence-selective binding of TOTO-TOTOBIPY combined with its potential photocleaving properties makes it an interesting molecule for further studies.

ACKNOWLEDGMENT

We thank The Instrument Centre for NMR-Spectroscopy of Biological Macromolecules at The Carlsberg Laboratory, Copenhagen granted by The Danish Natural Science Research Council for providing spectrometer time at the 750 MHZ spectrometer. Finally, The Danish Natural Science Research Council and The Technical Research Council are acknowledged for financial support.

LITERATURE CITED

(1) Assa-Munt, N., Denny, W. A., Leupin, W., and Kearns, D. R. (1985a) ^{1}H NMR Study of the Binding of Bis(acridines) to $d(AT)_5$: $d(AT)_5$. 1. Mode of Binding. *Biochemistry 24*, 1441−1449.

(2) Assa-Munt, N., Leupin, W., Denny, W. A., and Kearns, D. R. (1985b) ^{1}H NMR Study of the Binding of Bis(acridines) to $d(AT)_5d(AT)_5$. 2. Dynamic Aspects. *Biochemistry 24*, 1449−1460.

(3) Bondensgaard, K., and Jacobsen, J. P. (1999) Solution Structure and Energy Calculation of Bis-Intercalation of Homodimeric Thiazole Orange Dye Derivatives in DNA: Effects of Modifying the Linker. *Bioconjugate Chem. 10*, 735−744.

(4) Bunkenborg, J., Stidsen, M. M., and Jacobsen, J. P. (1999) On the Sequence Selective Bis-Intercalation of a Homodimeric Thiazole Orange Dye in DNA. *Bioconjugate Chem. 10*, 824−831.

(5) Cory, M., McKee, D. D., Kagan, J., Henry, D. W., and Miller, J. A. (1985) Design, Synthesis, and DNA Binding Properties of Bifunctional Intercalators. Comparison of Polymethylene and Diphenyl Ether Chains Connecting Phenanthridine. *J. Am. Chem. Soc. 107*, 2528−2536.

(6) Deligeorgiev, T. G., Gadjev, N. I., Timtcheva, I. I., Maximova, V. A., Katerinopoulos, H. E., and Foukaraki, E. (2000) Synthesis of Homodimeric Monomethine Cyanine Dyes as Noncovalent Nucleic Acid Labels and Their Absorption and Fluorescence Spectral Characteristics. *Dyes Pigments 44*, 131−136.

(7) Faridi, J., Nielsen, K. E., Stein, P. C., and Jacobsen, J. P. (1997) Dynamic Bis-Intercalation of a Homodimeric Thiazole Orange Dye in DNA: Evidence of Intercalator Creeping. *J. Biomol. Struct. Dyn. 15*, 321−332.

(8) Fromherz, P., and Rieger, B. (1986) Photoinduced Electron Transfer in DNA Matrix from Intercalated Ethidium to Condensed Methyl viologen. *J. Am. Chem. Soc. 108*, 5361−5362.

(9) Glazer, A. N., and Rye, H. S. (1992) Stable dye-DNA intercalation complexes as reagents for high-sensitivity fluorescence detection. *Nature 359*, 859−861.

(10) Hansen, L. F., Jensen, L. K., and Jacobsen, J. P. (1996) Bis-Intercalation of a Homodimeric Thiazole Orange Dye in DNA in Symmetrical Pyrimidine-Pyrimidine-Purine-Purine Oligonucleotides. *Nucleic Acids Res. 24*, 859−867.

(11) Jacobsen, J. P., Pedersen, J. B., Hansen, L. F., and Wemmer, D. E. (1995) Site Selective Bis-Intercalation of a Homodimeric Thiazole Orange Dye in DNA Oligonucleotides. *Nucleic Acids Res. 23*, 753−760.

(12) Jensen, L. K., Gotfredsen, C. H., Bondensgaard, K., and Jacobsen, J. P. (1998) Bis-Intercalation of Homodimeric Thiazole Orange Dyes in Selective Binding Sites of DNA Studied by ^{1}H NMR Spectroscopy. *Acta Chem. Scand. 52*, 641−650.

(13) Johansen, F., and Jacobsen, J. P. (1998) ^{1}H NMR Studies of Bis-Intercalation of a Homodimeric Oxazole Yellow dye in DNA Oligonucleotides. *J. Biomol. Struct. Dyn. 16*, 205−222.

(14) Johnson, D. S., and Boger, D. L. (1996) Supramolecular Reactivity and Transport: Bioorganic Systems. Chapter 3: DNA binding Agents. In *Comprehensive Supramolecular Chemistry* (J. E. D. Davis, J. L. Atwood, D. D. Macnicol, F. Vögtler, and Y. Murakami, Eds.) Vol. 4, pp 73−176, Pergamon.

(15) Larsson, A., Carlsson, C., Jonsson, M., and Albinsson, B. (1994) Characterization of the Binding of the Fluorescent Dyes YO and YOYO to DNA by Polarized Light Spectroscopy. *J. Am. Chem. Soc. 116*, 8459−8465.

(16) Petersen, M., Hamed, A. A., Pedersen, E. B., and Jacobsen, J. P. (1999) Bis-Intercalation of Homodimeric Thiazole Orange Dye Derivatives in DNA. *Bioconjugate Chem. 10*, 66−74.

(17) Petersen, M., and Jacobsen, J. P. (1998) Solution Structure of a DNA Complex with the Fluorescent Bis-Intercalator TOTO Modified on the Benzothizole Ring. *Bioconjugate Chem. 9*, 331−340.

(18) Rye, H. S., Yue, S., Wemmer, D. E., Quesada, M. A., Haugland, R. P., Mathies, R. A., and Glazer, A. N. (1992) Stable Fluorescent Complexes of Double-Stranded DNA with Bis-Intervalating Asymmetric Cyanine Dyes: Properties and Applications. *Nucleic Acids Res. 20*, 2803−2812.

(19) Spielmann, H. P., Wemmer, D. E., and Jacobsen, J. P. (1995) The Solution Structure of a DNA Complex with the

Fluorescent Bis-Intercalator TOTO Determined by NMR Spectroscopy. *Biochemistry 34*, 8542−8553.
(20) Stein, P. C., Jacobsen, J. P., and Spielmann, H. P. (1995) Design and Implementation of a Simple Shaped Notch Filter. *J. Magn. Res., Ser. B 109*, 93−96.
(21) Stærk, D., Hamed, A. A., Pedersen, E. B., and Jacobsen, J. P. (1997) Bis-Intercalation of Homodimeric Thiazole Orange Dyes in DNA: Effect of Modifying the Linker. *Bioconjugate Chem. 8*, 869−877.
(22) Takenaka, S., Ihara, T., and Takagi, M. (1992) Light-Induced DNA Cleavage by Bis-9-acridinyl Viologen Derivative. *Chem. Lett.* 1−4.
(23) Takenaka, S., Sato, H., Ihara, T., and Takagi, M. (1997) Synthesis and DNA Binding Properties of Bis-9-acridinyl Derivatives Containing Mono-, Di- and Tetra-viologen Units as a Connector of Bis-intercalators. *J. Heterocycl. Chem. 34*, 123−127.
(24) Wijmenga, S. S., and van Buuren, B. N. M. (1998) The Use of NMR Methods for Conformational Studies of Nucleic Acids. *Prog. NMR Spectrosc. 32*, 287−387.
(25) Wüthrich, K. (1986) *NMR of Proteins and Nucleic Acids*, John Wiley & Sons, New York.
(26) Åkerman, B., and Tuite, E. (1996) Single- and Double-Strand Photocleavage of DNA by YO, YOYO and TOTO. *Nucleic Acids Res. 24*, 1080−1090.

BC000042C

Radiolabeled Guanine Derivatives for the in Vivo Mapping of O^6-Alkylguanine-DNA Alkyltransferase: 6-(4-[^{18}F]Fluoro-benzyloxy)-9*H*-purin-2-ylamine and 6-(3-[^{131}I]Iodo-benzyloxy)-9*H*-purin-2-ylamine

Ganesan Vaidyanathan,*[,†] Donna J. Affleck,[†] Christina M. Cavazos,[‡] Stewart P. Johnson,[§] Sriram Shankar,[†] Henry S. Friedman,[||,⊥] Michael O. Colvin,[||] and Michael R. Zalutsky[†]

Departments of Radiology, Pediatrics, Surgery and Medicine, and School of Medicine, Duke University Medical Center, Durham, North Carolina 27710. Received May 4, 2000; Revised Manuscript Received August 10, 2000

Two radiolabeled analogues of 6-benzyloxy-9*H*-purin-2-ylamine (O^6-benzylguanine; BG) potentially useful in the in vivo mapping of O^6-alkylguanine-DNA alkyltransferase (AGT) were synthesized. Fluorine-18 labeling of the known 6-(4-fluoro-benzyloxy)-9*H*-purin-2-ylamine (FBG; **6**) was accomplished by the condensation of 4-[^{18}F]fluorobenzyl alcohol with 2-aminopurin-6-yltrimethylammonium chloride (**4**) or 2-amino-6-chloropurine in average decay-corrected radiochemical yields of 40 and 25%, respectively. Unlabeled 6-(3-iodo-benzyloxy)-9*H*-purin-2-ylamine (IBG; **7**) was prepared from **4** and 3-iodobenzyl alcohol. Radioiodination of **9**, prepared from **7** in two steps, and subsequent deprotection gave [^{131}I]**7** in about 70% overall radiochemical yield. The IC_{50} values for the inactivation of AGT from CHO cells transfected with pCMV-AGT were 15 nM for IBG and 50 nM for FBG. The binding of [^{18}F]**6** and [^{131}I]**7** to purified AGT was specific and saturable with both exhibiting similar IC_{50} values (5−6 μM).

INTRODUCTION

A number of alkylating agents such as 1,3-bis(2-chloroethyl)-1-nitrosourea (BCNU), 1-(2-chloroethyl)-3-cyclohexyl-1-nitrosourea (CCNU), 5-(dimethyltriazeno)-imidazole-4-carboxamide (DTIC), and Temozolomide are used in the chemotherapy of various cancers (*1*). The cytotoxicity of these and related alkylating agents stems from their ability to alkylate DNA guanine residues at their O^6-position. Nitrogen mustard alkylating agents such as cyclophosphamide were thought to produce their cytotoxicity through the alkylation of the N^7-position of guanine (*2*); however, it has been recently demonstrated that a significant part of the cytotoxicity of this agent also is mediated by the O^6-alkylation of guanine residues (*3*).

The DNA repair protein O^6-alkylguanine-DNA alkyltransferase (AGT) reverts alkylator cytotoxicity by transferring the O^6-alkyl group from the modified DNA guanine to cysteine-145 in its active site, thereby restoring a normal guanine at the site of the modified base (*4*). However, the resultant alkylated AGT is inactivated for subsequent dealkylations. Because of this, the ability of tumor cells to be resistant to the toxic effects of alkylating agents is dependent on cellular AGT levels; the higher the AGT content, the less effective will be the tumor killing by alkylator therapy. Elevated levels of AGT are known to result in resistance of human gliomas to nitrosoureas (*5*). Indeed, inactivation of AGT by administration of its substrates such as O^6-methylguanine and O^6-benzylguanine (BG) has been shown to increase the cytotoxicity of alkylators such as CCNU and BCNU in human tumor cell lines (*6*, *7*) and xenografts (*8*).

Levels of AGT in human tumors vary considerably among different tumor types as well as patients with a particular malignancy (*9*, *10*). Thus, prior knowledge of AGT levels in individual tumors could greatly facilitate the process of optimizing the efficacy of chemotherapy. Although a few in vitro techniques to quantify AGT levels in tumor tissue have been described (*11*−*13*), none of these are suitable for use in humans. Our objective was to develop radiolabeled BG analogues which bind selectively to AGT with the goal of mapping AGT levels in cancer patients in a noninvasive fashion by external scintigraphy. Potential applications of this technique include the selection of patients most likely to benefit from alkylator therapy, monitoring the effect of these drugs on AGT levels during the therapeutic course, correlating therapeutic success with endogenous AGT, and evaluating the clinical effectiveness of AGT-inactivating agents such as BG.

Positron emission tomography (PET) is a functional imaging modality that can probe altered biochemical pathways and in some cases be used to assess metabolic levels quantitatively (*14*). Fluoroine-18 has a 1.8 h half-life and is the most commonly used radionuclide for PET. To be useful for imaging AGT levels, the radiolabel needs to reside within the alkyl group attached to the O^6-position of the guanine because this group is the one that is transferred to the protein. This criterion is reinforced by the results of a study evaluating a ^{18}F-labeled guanine derivative with the ^{18}F attached at the N^9 position as a fluoroethyl group (*15*). It was hoped that, once dealkylated, the guanine residue attaches to the protein in a noncovalent fashion. However, as we would predict, this

* To whom correspondence should be addressed. Phone: (919) 684-7811. Fax: (919) 684-7122. E-mail: ganesan.v@duke.edu.
† Department of Radiology.
‡ School of Medicine.
§ Department of Pediatrics.
|| Department of Medicine.
⊥ Department of Surgery.

10.1021/bc0000435 CCC: $19.00 © 2000 American Chemical Society
Published on Web 10/25/2000

derivative was not useful for AGT imaging. Fortunately, 6-(4-fluoro-benzyloxy)-9*H*-purin-2-ylamine (O^6-4-fluorobenzylguanine, FBG) is among the purine and pyrimidine derivatives that have been shown to be AGT inactivators (*16*−*20*). The ability of FBG to inactivate AGT in HT29 cell-free extracts and intact cells was shown to be similar to that of BG itself (*16*). Thus, if an appropriate synthesis could be devised, [^{18}F]FBG could be a valuable tool for assessing the AGT levels by PET.

Iodine has a spectrum of radionuclides with different physical properties that are appropriate for external imaging. For example, ^{123}I ($t_{1/2}$ = 13 h) is an excellent radionuclide for use in single photon emission tomography (SPECT). Iodine-124 ($t_{1/2}$ = 4.2 d) has been used for PET. For this reason, the development of radioiodinated analogues of BG also is important. The preparation of radioiodinated guanosine derivatives has been described (*21*); however, their AGT binding properties were not reported. While O^6-4-chlorobenzylguanine (CBG) and O^6-4-bromobenzylguanine (BBG) have been prepared and shown to be good analogues of BG (*17*), to our knowledge, the synthesis and biological activity of 6-(iodo-benzyloxy)-9*H*-purin-2-ylamine (O^6-iodobenzylguanines; IBG) have not been reported. Because a variety of substituents are tolerated in the benzene ring of BG (*16*), an iodinated derivative is expected to be a good analogue of BG as well.

In this study, we have developed methods for the preparation of 3-IBG, and the labeled compounds [^{18}F]FBG and 3-[^{131}I]IBG. In CHO cells transfected with pCMV-AGT, 3-IBG was shown to be more potent than FBG in inactivating AGT. In vitro studies using purified AGT demonstrated specific binding of [^{18}F]FBG and 3-[^{131}I]IBG to AGT.

EXPERIMENTAL SECTION

General. All chemicals were purchased from Aldrich Chemical Co. except as noted. FBG (unlabeled) was obtained as a gift from Dr. Robert Moschel of National Cancer Institute-Frederick Cancer Research and Development Center, Frederick, MD. Sodium [^{131}I]iodide in 0.1 N NaOH was supplied by DuPont-New England Nuclear (North Billerica, MA). [^{18}F]Fluoride activity was produced on the Duke University Medical Center CS-30 cyclotron via the ^{18}O(p,n)^{18}F reaction by irradiating [^{18}O]H_2O in a small volume (300 μL) silver target. The activity was delivered to a solution of Kryptofix (10 mg in 1 mL of CH_3CN) and potassium carbonate (1 mg in 5 μL of water) in a glass tube and then evaporated with argon in an oil bath at 80 °C. The dried activity was resolubilized in 50−100 μL of dry DMSO.

Melting points were determined on a Haake Buchler apparatus and were uncorrected. High-pressure liquid chromatography (HPLC) was performed using one of three systems: (1) two LKB model 2150 pumps, an LKB model 2152 control system, an LKB model 2138 fixed-wavelength UV detector, and a Beckman model 170 radioisotope detector; data were acquired using CIO-DAS08/JR internal and CIO-MINI137 external boards and Labtech DataLab/WIN software (www.computerboards.com); (2) a Beckman System Gold HPLC equipped with a model 126 programable solvent module, a model 168 diode array detector, a model 170 radioisotope detector, and a model 406 analogue interface module; or (3) a Perkin-Elmer Series 4 Liquid Chromatograph connected to a Perkin-Elmer LC-95 UV−vis spectrophotometer detector and a Perkin-Elmer LCI-100 Laboratory Computing Integrator. Methods were programmed using a Perkin-Elmer 6312 display terminal. For reversed-phase chromatography, a Waters μBondapak C18 (10 μm, 3.9 × 300 mm) column or a 3.9 × 300 mm Bondclone 10 (10 μm) C-18 column (Phenomenex, Torrance, CA) was used. Normal-phase HPLC was performed using a 4.6 × 250 mm Partisil (10 μm) column (Alltech, Deerfield, IL). Analytical TLC was performed on aluminum-backed sheets (Silica gel 60 F_{254}), and normal-phase column chromatography was performed using Silica gel 60, both obtained from EM Science (Gibbstown, NJ). Column chromatographic fractions were collected using a Gilson model 203 micro fraction collector (Middleton, WI) or a ISCO Foxy 200 fraction collector (Lincoln, NE), and products identified by TLC. In some cases, an ISCO UA-6 UV−vis detector was placed between the column outlet and the fraction collector to identify fractions. Preparative thick layer chromatography was performed using 20 × 20 cm, 1000 μm plates (Whatman, Clifton, NJ). Before applying the sample, the plates were run in ethyl acetate to clean the plates of any adsorbed impurities. Radio-TLC was initially analyzed using a System 200 Imaging Scanner (BioScan, Washington, DC.) and then cut into strips and counted using an automatic gamma counter (LKB 1282, Wallac, Finland). NMR spectra (^{1}H-300 MHz and ^{13}C-75 MHz) were obtained on a Varian Mercury 300 spectrometer. Chemical shifts are reported in δ units; solvent peaks were referenced appropriately. Mass spectra were obtained on a Hewlett-Packard GC/MS/DS model HP-5988A instrument or on JEOL SX-102 high-resolution mass spectrometer. Elemental analyses were provided by Galbraith Laboratories (Knoxville, TN).

6-(4-[^{18}F]Fluoro-benzyloxy)-9*H*-purin-2-ylamine ([^{18}F]FBG). *p*-[^{18}F]Fluorobenzaldehyde was prepared following previously described procedures (*22*). Briefly, 50−100 mCi of [^{18}F]fluoride was resolubilized in DMSO (50−100 μL), added to 1−2 mg of 4-formyl-(*N*,*N*,*N*-trimethyl)anilinium trifluoromethane sulfonate in a 5-mL Reacti vial, and the mixture was heated in an oil bath at 150 °C for 10 min. The cooled reaction mixture was diluted with water and passed through an activated C18 solid-phase cartridge (Waters). The cartridge was further washed with water (5−10 mL), and 4-[^{18}F]fluorobenzaldehyde was finally eluted with methylene chloride (1−2 mL). The methylene chloride solution was dried with sodium sulfate and passed through a silica cartridge to remove any polar byproducts. Methylene chloride was removed using a rotary evaporator[1] until a volume of about 0.1 mL was reached and the residual solution was transferred to a 1-dram vial.

DIBAL (0.1 mL, 1 M solution in methylene chloride) was added to the above activity and the capped vial was left at room temperature for 10 min. After evaporating the methylene chloride, 1 mL of water was added carefully to the residual activity followed by 50−100 μL of concentrated HCl. The resultant 4-[^{18}F]fluorobenzyl alcohol was extracted from this solution with 3 × 1 mL of ethyl acetate. The combined ethyl acetate fractions were dried with sodium sulfate and concentrated on the rotary evaporator.

The above solution was transferred to a 1-mL Reacti vial and evaporated to dryness. To this dried activity, potassium *tert*-butoxide (50 μL; 1 M in THF) was added and THF was evaporated under an argon flow. The residue was resolubilized in dry DMSO (Pierce, Rockford, IL; 50 μL) and the capped vial was heated at 100 °C for 5 min. The quaternary salt **4** (ref *23*; 1−2 mg) was added

[1] Use of argon to evaporate methylene chloride results in substantial loss of activity. Even with a rotary evaporator, it is important that the evaporation is stopped before the mixture dries.

to the above solution and the mixture was heated for an additional 10 min at 100 °C. [^{18}F]FBG ([^{18}F]**6**; t_R = 18−20 min) was isolated from this reaction mixture by reversed-phase HPLC (system 1) using the Bondaclone column eluted with 0.1% TFA in 15:85 acetonitrile:water at a flow rate of 1 mL/min. The HPLC fractions containing [^{18}F]**6** were evaporated with argon to remove most of the acetonitrile, diluted with water, and passed through a solid-phase cartridge (tC18 ENV Sep Pak; Waters) activated with ethanol and water. The cartridge was washed with 5 mL of 0.9% saline, and the activity was eluted with 0.25 mL portions of ethanol. Most of the activity elutes in fractions 3−5. These pooled ethanol fractions were concentrated, and for in vitro assays, the activity was reconstituted in Tris-buffer.

6-(3-Iodo-benzyloxy)-9*H*-purin-2-ylamine (3-IBG). Sodium hydride (60% in mineral oil; 80 mg, 2 mmol) was added to a solution of 3-iodobenzyl alcohol (498 mg, 2.13 mmol) in dry DMSO (0.5 mL), and the resultant yellow solution was stirred at room temperature for 1 h. The quaternary salt **4** (229 mg, 1 mmol) was added to the mixture and the stirring continued for another 2 h. Acetic acid (170 μL) was added to the clear, homogeneous reaction mixture which was then added with vigorous stirring to about 30 mL of ether. The resultant precipitate was filtered, washed with ether and subsequently with water, and dried over P_2O_5 under vacuum to give 218 mg (60%) of **7**: mp 118−120 °C. HPLC (system 3): Bondapak column was eluted with 0.1% TFA in 30:70 acetonitrile:water at 1 mL/min; t_R = 6.0 min as compared to 8−9 min for 3-iodobenzyl alcohol; ^{1}H NMR (DMSO-d_6) 5.46 (s, 2H, benzylic), 6.28 (br s, 2H, NH_2), 7.21 (t, 1H, *m*-ArH; J_{H-H} = 8.5), 7.52 (d, 1H, *o*-ArH; J_{H-H} = 8.5), 7.72 (d, 1H, *p*-ArH; J_{H-H} = 8.5), 7.84 (s, 1H, *o*′-ArH), 7.87 (s, 1H, H-8), 12.45 (br s, 1 H, NH); ^{13}C NMR (CD_3OD) 67.77 (benzylic), 97.40 (ArC-I), 128.37 (guanine C-5 and *o*-ArCH), 131.19 (*o*′-ArCH and *p*-ArCH), 137.99 (*m*-ArCH and *ipso*-ArC), 138.07 (guanine CH-8 and C-6), 140.34 (guanine C-2 and C-4); MS (FAB$^+$) *m/z*: 368 (MH^+). HRMS calcd for $C_{12}H_{11}IN_5O$ (MH^+) *m/z*: 368.0008. Found: 368.0013 ± 0.0009. Anal. calcd for $C_{12}H_{10}IN_5O$: C, 39.26; H, 2.75; N, 19.08. Found: C, 39.03; H, 2.87; N, 18.17.

6-(3-Iodo-benzyloxy)-9-(2-trimethylsilanyl-ethoxymethyl)-9*H*-purin-2-ylamine (SEM-3-IBG). THF was evaporated from a 1 M solution of potassium *tert*-butoxide in THF (0.83 mL, 830 mmol).[2] To the residue was added **7** (300 mg, 0.82 mmol) followed by DMF (silylation grade; Pierce, 4.2 mL). The mixture was stirred at room temperature under argon for 1 h and cooled to 0 °C, and SEM-chloride (138 mg, 0.83 mmol) was added dropwise. The reaction was allowed to proceed overnight and worked up by partitioning between ethyl acetate and water. Silica gel chromatography using 40:60 ethyl acetate:hexane afforded 105 mg (26%) of **8** as an oil/low melting solid: ^{1}H NMR ($CDCl_3$) −0.02 (s, 9H, −$SiMe_3$), 0.93 (m, 2H, −Si-CH_2−), 3.58 (m, 2H, −Si-CH_2-CH_2-O−), 4.83 (br s, 2H, NH_2), 5.44 (s, 2H, benzylic), 5.50 (s, 2H, −N-CH_2-O−), 7.09 (t, 1H, *m*-ArH; J_{H-H} = 7.7), 7.48 (d, 1H, *o*-ArH; J_{H-H} = 7.5), 7.65 (d, 1H, *p*-ArH; J_{H-H} = 7.8), 7.74 (s, 1H, H-8), 7.86 (s, 1H, *o*′-ArH); ^{13}C NMR ($CDCl_3$); −2.05 (−$SiMe_3$), 17.06 (−CH_2-$SiMe_3$), 66.17 (−Si-CH_2-CH_2-O−), 66.28 (benzylic), 71.14 (−N-CH_2-O−), 93.41 (C-I), 114.48 (guanine C-5), 126.57 (*o*-ArCH), 129.29 (*m*-ArCH), 136.20 (*o*′- and *p*-ArCH), 137.86 (ArCH-*ipso*), 138.72 (guanine CH-8), 153.66 (guanine C-6), 158.52 (guanine C-2), 159.87 (guanine C-4). HRMS (FAB$^+$) calcd for $C_{18}H_{25}IN_5O_2Si$ (MH^+): *m/z* 498.0822. Found: 498.0820 ± 0.0018. Anal. calcd for $C_{18}H_{24}IN_5O_2Si$: C, 43.46; H, 4.86; N, 14.08. Found: C, 43.56; H, 4.69; N, 13.84.

9-(2-Trimethylsilanyl-ethoxymethyl)-6-(3-trimethylstannanyl-benzyloxy)-9H-purin-2-ylamine. A mixture of **8** (50 mg, 0.1 mmol), hexamethylditin (210 mg, 0.64 mmol), and dichlorobis(triphenylphospine)palladium(II) (35 mg, 0.05 mmol) in 3 mL of dioxane was heated at reflux under argon for 1 h. Dioxane was removed from the dark reaction mixture and the residue was resuspended in ethyl acetate. The suspension was filtered through a bed of Celite, and the bed was washed thoroughly with ethyl acetate. The filtrate was concentrated to obtain an oil. This oil was applied to a bed of silica gel and very nonpolar impurities were removed by eluting with hexane. The required product and other byproducts were isolated from the silica gel bed by eluting with ethyl acetate. Ethyl acetate was removed from this solution and the residual oil was subjected to preparative TLC using 40:60 ethyl acetate:hexane to obtain 39 mg (73%) of **9** as a white solid: mp 135−136 °C; ^{1}H NMR ($CDCl_3$) −0.03 (s, 9H, −$SiMe_3$), 0.29 (s, 9H, −$SnMe_3$), 0.92 (m, 2H, -CH_2-$SiMe_3$), 3.57 (m, 2H, −Si-CH_2-CH_2-O−), 4.87 (br s, NH_2), 5.43 (s, 2H, benzylic), 5.55 (s, 2H, −N-CH_2-O−), 7.31−7.61 (m, 4H, ArH), 7.72 (s, 1H, H-8); ^{13}C NMR ($CDCl_3$) −9.37 (−$SiMe_3$), −1.32 (−$SnMe_3$) 17.80 (−CH_2-$SiMe_3$), 66.87 (−Si-CH_2-CH_2-O−), 68.47 (benzylic), 71.84 (−N-CH_2-O−), 127.90 (guanine C-5), 128.28 (*o*-ArCH), 128.56 (*m*-ArCH), 129.24 (*o*′- and *p*-ArCH), 135.47 (ArCH-*ipso*), 135.60 (C−Sn), 135.94 (guanine CH-8), 139.27 (guanine C-6), 154.28 (guanine C-2), 159.31 (guanine C-4); MS (FAB$^+$) *m/z* cluster peaks at 536 (MH^+). HRMS (FAB$^+$) calcd for $C_{21}H_{33}N_5O_2Si^{120}Sn$ (M^+): *m/z* 535.1429. Found: 535.1429 ± 0.0001. Anal. calcd for $C_{21}H_{33}N_5O_2SiSn$: C, 47.21; H, 6.23; N, 13.11. Found: C, 47.35; H, 6.09; N, 12.89.

6-(3-[^{131}I]Iodo-benzyloxy)-9*H*-purin-2-ylamine (3-[^{131}I]IBG). *A. Two-Step Approach.* To a $^1/_2$-dram vial containing 0.2 mg of **9** was added 1−2 μL of ^{131}I in 0.1 N NaOH (about 1 mCi) followed by 10 μL of a 3:1 (v/v) solution of acetic acid:30%H_2O_2. The mixture was sonicated for about 30 s, injected onto a normal-phase HPLC column and eluted with 0.2% acetic acid in 50:50 ethyl acetate:hexane at a flow rate of 1 mL/min. The required product [^{131}I]**8** (t_R = ∼13 min) was isolated in more than 90% radiochemical yield.

Solvents from HPLC fractions containing [^{131}I]**8** were evaporated to a small volume, transferred to a $^1/_2$-dram vial, and the solvents were again evaporated to dryness. The residual radioactivity was treated with trifluoroacetic acid (50 μL) for 5 min at room temperature. Most of the trifluoroacetic acid was evaporated with an argon flow and triturated with 50 μL of ethyl acetate twice to ensure its complete removal. Methanolic ammonia (50 μL) was added to the vial, the vial vortexed, and methanol and ammonia were evaporated off under a flow of argon. The radioactivity was reconstituted in methanol and injected onto a normal-phase HPLC column eluted with 0.1% acetic acid in ethyl acetate at a flow rate of 1 mL/min. The desired [^{131}I]**7** (t_R = ∼13 min) was isolated in 55−60% radiochemical yield. Under these HPLC conditions, both 3-iodobenzyl alcohol and **8** were not retained in the column. To ensure the authenticity of the final product a TLC of it was performed in 5% (v/v) methanol in ethyl acetate along with the unlabeled standard. The retention factor for **7** was 0.3 while that for 3-iodobenzyl alcohol and **8** were 0.8 and 0.9, respectively.

[2] Alternatively, an equivalent amount of sodium hydride was used with similar results.

Alternatively, the deprotection of [^{131}I]**8** to [^{131}I]**7** has also been accomplished with tetra-butylammonium fluoride (TBAF) in THF. For this, TBAF (50 μL, 1 M in THF) was added to a vial containing the residue of [^{131}I]**8**, and the capped vial was heated at 65−70 °C for 25 min. THF was evaporated, and the activity was reconstituted in a mixture of 25 μL of methanol and 5 μL of acetic acid and injected on to a normal-phase HPLC as described above. The radiochemical yield was 85−90%.

B. Single-Step Approach. After radioiodination of **8**, solvents were removed by coevaporating twice with a few microliters of benzene. The residual activity was heated with 50 μL of TBAF in THF for 25 min at 65−70 °C. After evaporating THF, the activity was processed as above and [^{131}I]**7** was isolated by normal-phase HPLC in 70% radiochemical yield.

Cell Culture and Transfection. CHO−K1 cells were maintained in α-MEN (Gibco, Grand Island, NY) containing 10% fetal bovine serum. CHO cells were transfected with a plasmid expressing human AGT (*24*) using FuGENE (Roche Molecular Biochemicals) according to the manufacturer's protocol for transfection of adherent cells. After 48 h, Geneticin (Gibco) was added at a concentration of 500 μg/mL. Clones were isolated from individual cell foci.

AGT Activity Assays. Inactivation of cellular AGT was measured by adding varying concentrations of FBG or IBG to cell cultures that had reached 80−90% confluence. After 4 h of drug treatment, cell extracts were prepared and the AGT activity was measured by assaying the loss of [^{3}H]-O^6-methylguanine from a [^{3}H] methylated calf thymus DNA substrate as described (*6*). The results are expressed as the percentage of the AGT activity present in cell cultures that were not treated with FBG or IBG. For each concentration, the assay was performed in duplicates.

In Vitro Binding of FBG or IBG by AGT. Purified human AGT with a $(His)_6$ tag (*25*) was generously provided by Dr. Anthony E. Pegg of Hershey Medical Center, Pennsylvania State University. About 50 000 counts of [^{18}F]FBG or [^{131}I]IBG were added in the presence or absence of increasing amounts of cold FBG or IBG, respectively, to 10 μg of AGT or to control for nonspecific binding, BSA. The incubation was done in 0.1 mL of 50 mM Tris-Cl, pH 7.5, 5 mM DTT, and 0.1 mM EDTA in the presence of 10 μg of calf thymus DNA. After incubation for 30 min at 37°, the protein was precipitated by the addition of 200 μg of carrier BSA and 1 mL of cold 12% TCA. The precipitated proteins were collected on GF-C (Whatman) filters which were washed extensively with 5% TCA. The results are expressed as the percentage of input activity retained on the filter. For each concentration, the assay was performed in triplicates. The assay was performed twice for both [^{18}F]FBG and [^{131}I]IBG.

RESULTS AND DISCUSSION

Chemistry. It is highly desirable that radiochemical syntheses be performed with the least number of steps possible, particularly for short half-life radionuclides such as ^{18}F (110 min). A prerequisite for insertion of ^{18}F onto a benzene ring by nucleophilic substitution is that the ring contains a suitable leaving group, such as $-NO_2$ or a quaternary ammonium triflate, that is positioned ortho or para to a strongly electron-withdrawing group such as a NO_2 (*26*, *27*). It may be possible to prepare a FBG precursor, such as the one with a $-NO_2$ or a quaternary ammonium group in the place of fluorine, from which [^{18}F]FBG may be produced in a single step. However, this chemistry will not be facile due to the lack of a suitably placed electron-withdrawing group in the molecule. To circumvent this, it was necessary to first prepare ^{18}F-labeled **3** and couple it to the guanine skeleton (Scheme 1). Although the chemistry of [^{18}F]**3** has been reported (*28*, *29*), a slightly different set of conditions was used for its preparation. *p*-[^{18}F]Fluorobenzaldehyde, [^{18}F]**2**, was prepared as reported (*22*). Reduction of [^{18}F]**2** was initially accomplished with $NaBH_4$ in ethanol at 80 °C. However, this involved removal of the initial solvent methylene chloride from a solution of [^{18}F]**2** and reconstitution of [^{18}F]**2** in ethanol. In addition to the extra time needed, this process resulted in a considerable loss of activity due to the very volatile nature of [^{18}F]**2**. It was found that a commercially available solution of DIBAL in methylene chloride was very effective in converting [^{18}F]**2** to [^{18}F]**3** at room temperature. It should be pointed out that the development of a technique to prepare [^{18}F]**3** by on-column reduction of [^{18}F]**2** using $NaBH_4$ has been reported very recently (*30*). Using our procedure, preparation of [^{18}F]**3** from [^{18}F]fluoride could be accomplished in about an hour in an overall decay-corrected radiochemical yield of 50%.

Scheme 1[a]

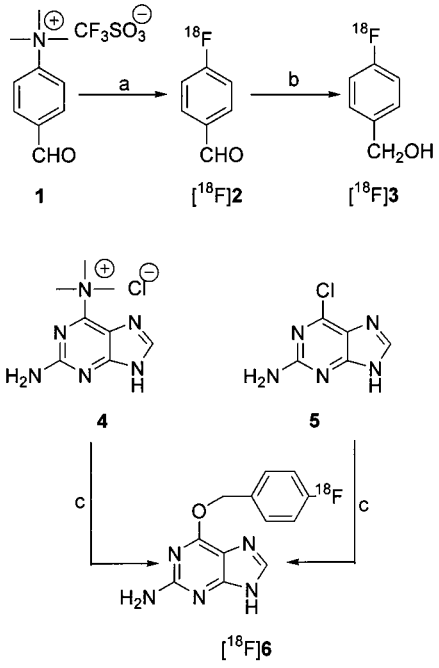

[a] (a) [^{18}F]Fluoride, DMSO. (b) DIBAL, CH_2Cl_2. (c) **3**, Pot. *tert*-butoxide, DMSO.

Unlabeled FBG was originally prepared by the treatment of 2-amino-6-chloropurine (ACP) at 100−130 °C for over 24 h with an excess of the sodium salt of 4-fluorobenzyl alcohol in 4-fluorobenzyl alcohol as solvent (*16*). These conditions are not adaptable to ^{18}F labeling. Even if one started with curie quantities of [^{18}F]**3** and microgram amounts of ACP, the concentration of **3** would be substantially substoichiometric. In addition, the long reaction time is not suitable with ^{18}F. We initially attempted this chemistry by conducting the reaction in a solvent such as THF or DME without success. A number of O^6-hetarylguanines have been prepared in excellent yields based on an earlier report (*31*) using **4** (*23*), instead of ACP, as the starting material (*20*). These reactions proceeded under mild conditions and involved easy workup. The procedure essentially involves the treatment of **4** with the preformed sodium alcoholate (2 equiv of sodium hydride and 5.6 equiv of desired alcohol)

Chart 1

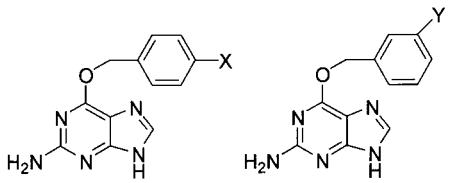

X = F (**6**); Br (**10**); $SnMe_3$ (**11**); I (**12**)

Y = I (**7**); $SnMe_3$ (**13**)

in DMSO at room temperature for 1 h. We have shown that treatment of the preformed sodium salt of 4-fluorobenzyl alcohol (using sodium hydride) with equimolar quantity of **4** in DMSO at room temperature resulted in the formation of **6** in more than 80% yield (HPLC) in 30 min. Subsequently, it was also possible to convert ACP to **6** by doing the reaction in DMSO, albeit at a higher temperature. Treatment of ACP with 2 equiv of the potassium salt of 4-fluorobenzyl alcohol (using potassium *tert*-butoxide) in DMSO at room temperature did not result in the formation of **6**. However, heating the reaction mixture at 130−140 °C for 30 min resulted in about 40% conversion of ACP to **6** as determined by HPLC (details of these reactions not given in the Experimental Section). To augment the rate of the radiochemical reaction of [^{18}F]**3** with **4**, a higher reaction temperature was used. Typically, [^{18}F]**3** was heated with a base in DMSO for 5 min at 100 °C (to ensure deprotonation), and heated again for 10 min after the addition of **4**. Sodium hydride was initially used as a base, but owing to cumbersome handling of sodium hydride, a readily available and easily measurable solution of potassium *tert*-butoxide in THF was used subsequently, giving equally good results. Although in some cases decay-corrected radiochemical yields of about 70% have been obtained for this coupling reaction, the yield generally was around 40%.[3] Little or no radioactivity corresponding to [^{18}F]**3** eluted in reversed-phase HPLC. The remainder of the radioactivity was retained in the column, suggesting the possibility of a highly nonpolar byproduct(s). About 7−9 mCi of [^{18}F]**6** was obtained starting from 100 mCi of resolubilized [^{18}F]fluoride in about 2 h. Although the specific activity of the final product has not been determined systematically, no coeluting carrier peak was generally observed on HPLC. Nonetheless, unlike receptor-based radiopharmaceuticals, very high specific activity is not necessary for O^6-alkyl guanine derivatives and may even be counterproductive because transfer of alkyl groups by AGT follows a second-order kinetics (*32*, *33*).

One of the most commonly used techniques for the preparation of radioiodinated compounds is the radioiododestannylation of the corresponding tin precursor. Initially, we envisaged the preparation of **11** (Chart 1) from the reported compound **10** (*17*). It may be possible to prepare **12** or its radioiodinated analogue by the halodestannylation of **11**; however, attempts to convert **10** to **11** by treatment with hexamethylditin and bistriphenylphosphine palladium dichloride in dioxane were unsuccessful. This was probably due to the insolubility of **10** in dioxane.

Guanine chemistry is often challenging due to the amphoteric nature of guanine derivatives (*34*). Chemical manipulations can be made more facile if the starting compound can be converted to a nonpolar derivative by the introduction of a protecting group. For example, such a strategy has simplified the preparation of polar guanidines (*35*). Guanine derivatives modified with different moieties at the N^9-position have been reported (*36*−*38*). These derivatives have sufficient nonpolar nature to permit purification by silica gel chromatography. Although some of these N^9-substituents (*36*, *38*) may be potentially used as protecting groups, the reported work was not done with that objective. While protecting group methodology has been applied to adenine chemistry (*39*), to our knowledge, such a strategy has not been reported for guanine derivatives themselves. We prepared several ACP surrogates with protecting groups such as trimethylsilylethyl, trimethylsilylethyoxymethyl (SEM), *tert*-butyloxymethyl, and pivaloyloxymethyl at the N^9-position, and converted some of these to their O^6-(substituted)benzyl derivates.[4] For the present work, we used the SEM protecting group. Recently, SEM and *p*-methoxyphenylmethyl (MPM) protecting groups were used to facilitate the coupling of 6-halopurine to glycosylamines (*40*).

Scheme 2[a]

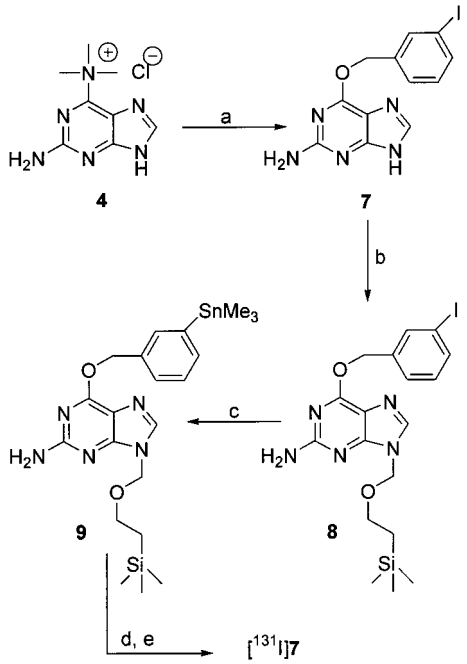

[a] (a) 3-Iodobenzyl alcohol, NaH, DMSO. (b) Pot. *tert*-butoxide, SEM-Cl, DMSO. (c) Hexamethylditin, $(Ph_3P)_2PdCl_2$, dioxane. (d) I-131. H_2O_2, HOAc, sonication. (e) TFA or TBAF.

Although it should have been possible to convert N^9-SEM-ACP to **8** (vide supra), we used an alternative approach as shown in Scheme 2. Compound **7** was prepared from **4** and commercially available 3-iodobenzyl alcohol in 60%[5] isolated yield and converted to **8** by treatment with sodium hydride or potassium *tert*-butoxide and SEM-Cl. The unoptimized isolated yield of **8** from this reaction was only 26%. In contrast, yields of 50−85% have been reported for modification of amines with a SEM group (*41*−*43*). The N^7-regioisomer is a byproduct in the *N*-alkylation of guanines; however, the N^9/N^7 ratio generally is very high (*37*). We did not attempt to isolate the N^7-regioisomer of **8** if any was formed. Compound **8** was smoothly converted to **9** using the palladium-catalyzed stannylation.

Radioiodination of **9** to [^{131}I]**8** was performed easily by sonication for 30 s with ^{131}I and a mixture of acetic acid

[3] In a few reactions, ACP was substituted for **4**; however, the decay-corrected radiochemical yield was only about 25%.

[4] Details will be reported elsewhere

[5] The yields reported in this paper for unlabeled compounds are from one or two trials and are not optimized.

and hydrogen peroxide. The radiochemical yield was more than 90%. Tetrabutylammonium fluoride (TBAF) and TFA are among reagents that have been used for the removal of the SEM group. We initially used TFA for converting [^{131}I]**8** to [^{131}I]**7** based on preliminary results for the deprotection of N^9-(trimethylsilylethyl)-ACP (TMSE-ACP) to ACP. TMSE-ACP was treated with TBAF in DMF or DMSO at room temperature and at 60 °C. TMSE-ACP remained intact at room temperature up to 1 h tested. Analysis of the reaction mixtures left at room temperature for 20 h and those heated at 60 °C for 5 min by HPLC showed several byproduct peaks. On the other hand, a single product peak corresponding to ACP was observed when TMSE-ACP was treated with TFA for 5 min at RT. Treatment of [^{131}I]**8** with TFA at room temperature for 5 min gave 55−60% radiochemical yield of [^{131}I]**7**; 15−20% of unreacted [^{131}I]**8** was recovered. Conducting the reaction for a longer time did not improve the radiochemical yield. A combination of radio-TLC and normal-phase and reversed-phase HPLC was used to verify that the final product was indeed IBG and not the 3-iodobenzyl alcohol. Very little if any of 3-iodobenzyl alcohol was detected in the reaction mixture. In addition, the final product bound to AGT specifically (vide infra) which further supports its authenticity. It was surprising that TFA treatment did not cleave the ethereal linkage between guanine and the benzyl moieties because the instability of BG to acidic conditions has been reported (*44*). This may be due to the lack of water in the reaction mixture or a rate factor may be involved. It should be pointed out that both IBG and FBG were stable during reversed-phase chromatography involving 0.1% TFA in water (pH 2) as a cosolvent.

No deprotection was observed when [^{131}I]**8** was treated with a 1 M solution of TBAF in THF at room temperature up to 30 min, and [^{131}I]**8** was recovered quantitatively. Increasing the reaction temperature to 70 °C resulted in the formation of [^{131}I]**7** in a time-dependent fashion. A maximum radiochemical yield of 85% was obtained after about 25 min, at which time essentially only one radioactive peak corresponding to IBG was seen on HPLC. This is contrary to the results described above for the deprotection of TMSE-ACP with TBAF at macro molar levels. The possible reasons for this are the presence of a better leaving group at the O^6-position in TMSE-ACP and the difference in reaction rates at macro molar and tracer levels.

The above procedures involve two normal-phase HPLC separations. Although it was possible to perform the two steps in the same pot consecutively, there was an unlabeled peak coeluting with the desired radioactive peak when the final mixture was subjected to normal-phase HPLC. This was presumably **13** (Chart 1) because the same peak was seen when **9** was treated with TBAF and injected onto the HPLC. Use of reversed-phase HPLC may be necessary to separate **7** and **13**. However, isolating [^{131}I]**7** from reversed-phase HPLC fractions involves a solid-phase extraction and removal of a solvent such as ethanol or methanol. Because it is much easier to evaporate ethyl acetate, the two normal-phase HPLC procedure is preferred.

Inactivation of AGT Activity by FBG and IBG. Because IBG is a new compound, its ability to inactivate AGT was determined using CHO cells transfected with pCMV-AGT to express AGT. In parallel, the ability of FBG to inactivate AGT under the same conditions also was measured. As shown in Figure 1, IBG inactivated AGT from these cells to a degree higher than that inactivated by FBG. The effective dose of FBG required

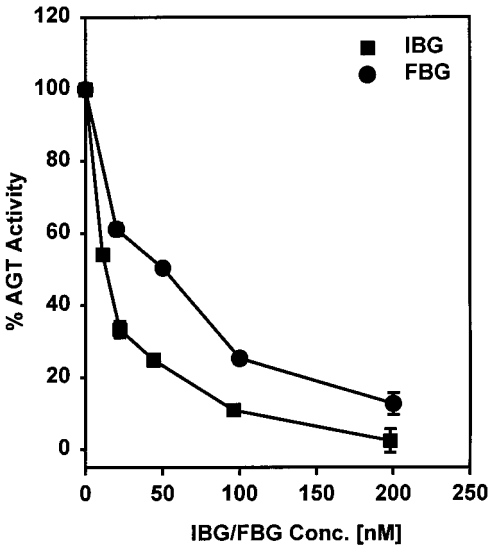

Figure 1. Inactivation of cellular AGT activity by unlabeled FBG and IBG. CHO cells transfected with pCMV-AGT were incubated with varying concentrations of IBG (■) or FBG (●) for 4h and the AGT activity associated with the cells was determined. The results are expressed as the percentage of the AGT activity present in cell cultures that were not treated with FBG or IBG.

to produce 50% inactivation of AGT (IC_{50}) was 50 nM, a value similar to that reported for FBG in HT29 human colon tumor cells (*16*). On the other hand, IBG had an IC_{50} of 15 nM, suggesting that it is more potent than FBG in inactivating AGT. These results demonstrate that introduction of an iodine at the meta-position of the benzyl group in BG did not result in a loss of AGT-inactivating ability.

Binding of Radiolabeled FBG and IBG to Purified AGT. To investigate whether AGT recognizes radiolabeled FBG and IBG as substrates, the efficacy of transfer of their radiolabeled benzyl groups to AGT was determined using the purified protein. For [^{18}F]FBG, the percent of input activity that bound to AGT increased with increasing concentrations of unlabeled FBG reaching a maximum of about 90% at 0.5 μM of FBG (Figure 2). At concentrations higher than 2 μM, saturation was observed. An IC_{50} of 5 μM was calculated. About 60% of radiolabeled IBG bound to AGT over a wide range of concentrations (Figure 3) with saturation noticed at concentrations higher than 3 μM. The IC_{50} for IBG was about 6 μM. These relatively high IC_{50} values further suggest that higher specific activity will not be a requirement for these radiopharmaceuticals. In both cases, the binding was specific as demonstrated by the fact that very little radioactivity was bound to the nonspecific protein BSA with maximum observed AGT to BSA binding ratios of 661 and 35 for [^{18}F]FBG and [^{131}I]IBG, respectively. These results are qualitatively similar to that obtained with O^6-(*p*-hydroxy[^{3}H]methylbenzyl)-guanine, the only other BG derivative labeled at the benzyl part of the molecule (*45*).[6]

Although IBG inactivates AGT from cells to a greater degree than FBG, [^{18}F]FBG had a higher binding to the purified protein than [^{131}I]IBG. This may be due to differential transmembrane transport of the two compounds as a result of differences in their lipophilicity. The lipophilicities of IBG and FBG were not determined per

[6] The preparation of ^{13}C- and ^{14}C-labeled O^6-benzylguanosines has been reported (*46*).

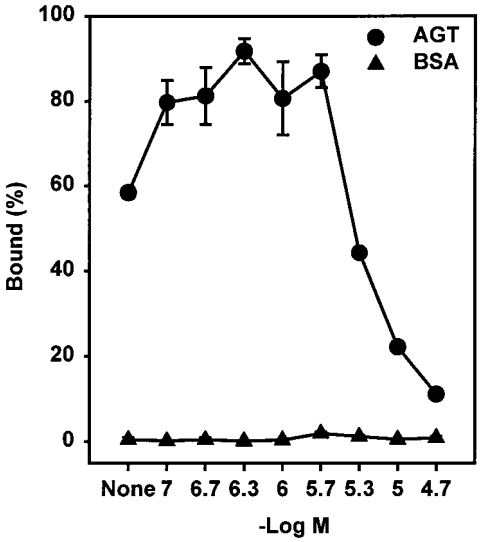

Figure 2. Binding of [^{18}F]FBG to purified AGT as a function of unlabeled FBG concentration. [^{18}F]FBG was incubated for 30 min at 37 °C, in the presence or absence of increasing amounts of unlabeled FBG, with 10 μg of AGT (●), or to control for nonspecific binding, 10 μg of BSA (▲) in a Tris-buffer. The protein associated activity was determined by TCA precipitation.

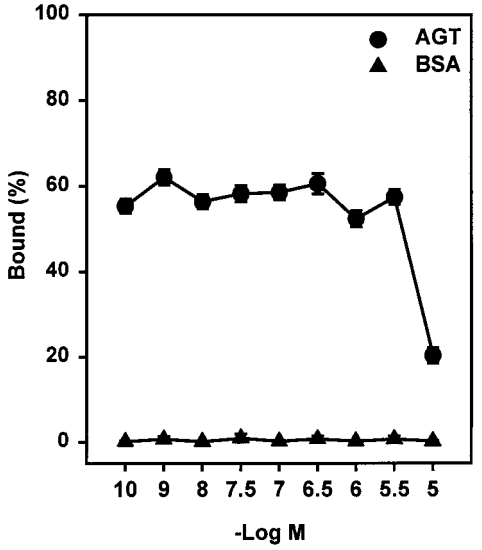

Figure 3. Binding of [^{131}I]IBG to purified AGT as a function of unlabeled IBG concentration. The assay was performed as detailed under Figure 2 by incubating [^{131}I]IBG with AGT (●) or BSA (▲).

se. Intuitively, IBG is expected to be more lipophilic. Reversed-phase HPLC has been used to determine lipophilicities (*47*). In comparison to FBG, a higher percentage of acetonitrile was needed to elute IBG from a reversed-phase column, suggesting that IBG is more lipophilic. However, it should be pointed out that the more nonpolar 4-fluorobenzyl alcohol elutes earlier (t_R = 10−11 min) than FBG (t_R = 18−20 min) under identical reversed-phase HPLC conditions.

CONCLUSION

A new iodine-substituted BG derivative has been prepared and shown to be potent in inactivating AGT activity in CHO cells transfected with AGT. Methods have been developed for the efficient syntheses of [^{18}F]FBG and [^{131}I]IBG, both of which bound specifically to purified AGT. These two radiolabeled BG analogues could be potential agents for the in vivo mapping of AGT. The iodinated derivative may also be a convenient laboratory tool for investigation of action and inactivation of AGT. We are currently working on other BG derivatives, especially fluoromethylbenzylguanine, a ^{18}F-labeled analogue of which could be prepared in a single radiochemical step.

ACKNOWLEDGMENT

This work was supported by Grants CA74817 and CA42324 from National Institutes of Health. Generous gifts of unlabeled FBG from Dr. Robert Moschel of National Cancer Institute and purified AGT from Dr. Anthony Pegg of Pennsylvania State University are gratefully acknowledged. The authors want to thank Marc Silvey and Bent Schoultz for their excellent technical assistance.

LITERATURE CITED

(1) Colvin, O. M. (1997) Alkylating agents and platinum antitumor compounds. In *Cancer Medicine* (J. F. Holland, R. C. Bast, Jr., D. L. Morton, E. Frei, III, D. W. Kufe, and R. R. Weichselbaum, Eds.) Vol. 1, 4th ed., pp 949−975, William and Wilkins, Baltimore, MD.

(2) Benson, A. J., Martin, C. N., and Garner, R. C. (1988) N−(2-Hydroxyethyl)-N-[2-(7-guaninyl)ethyl]amine, the putative major DNA adduct of cyclophosphamide in vitro and in vivo in the rat. *Biochem. Pharmacol. 37*, 2979−2985.

(3) Friedman, H. S., Pegg, A. E., Johnson, S. P., Loktionova, N. A., Dolan, M. E., Modrich, P., Moschel, R. C., Struck, R., Brent, T. P., Ludeman, S., Bullock, N., Kiborn, C., Keir, S., Dong, Q., Bigner, D. D., and Colvin, O. M. (1999) Modulation of cyclophosphamide activity by O^6-alkylguanine-DNA alkyltransferase. *Cancer Chemother. Pharmacol. 43*, 80−85.

(4) Pegg, A. E. (1990) Mammalian O^6-alkylguanine-DNA alkyltransferase: regulation and importance in response to alkylating carcinogenic and therapeutic agents. *Cancer Res. 50*, 6119−6129.

(5) Felker, G. M., Friedman, H. S., Dolan, M. E., Moschel, R. C., and Schold, C. (1993) Treatment of subcutaneous and intracranial brain tumor xenografts with O^6-benzylguanine and 1,2-bis(2-chloroethyl)-1-nitrosourea. *Cancer Chemother. Pharmacol. 32*, 471−476.

(6) Dolan, M. E., Moschel, R. C., and Pegg, A. E. (1990) Depletion of O^6-alkylguanine-DNA alkyltransferase activity by O^6-benzylguanine provides a means to evaluate the role of this protein in protection against carcinogenic and therapeutic alkylating agents. *Proc. Natl. Acad. Sci. U.S.A. 87*, 5368−5372.

(7) Friedman, H. S., Dolan, M. E., Moschel, R. C., Pegg, A. E., Felker, M., Rich, J., Bigner, D. D., and Schold, S. C., Jr. (1992) Enhancement of nitrosourea activity in medulloblastoma and glioblastoma multiforme. *J. Natl. Cancer Inst. 84*, 1926−1931.

(8) Mitchell, R. B., Moschel, R. C., and Dolan, M. E. (1992) Effect of O^6-benzylguanine on the sensitivity of human tumor xenografts to 1,3-bis(2-chloroethyl)-1-nitrosourea on DNA interstrand cross-link formation. *Cancer Res. 52*, 1171−1175.

(9) Lee, S.-M., Harris, M., Rennison, J., McGown, A., Bromley, M., Elder, R. H., Rafferty, J. A., Crowther, D., and Margison, G. P. (1993) Expression of O^6-alkylguanine-DNA-alkyltransferase in situ in ovarian and Hodgkin's tumors. *Eur. J. Cancer. 29A*, 1306−1312.

(10) Hotta, T., Saito, Y., Fujita, H., Mikami, T., Kurisu, K., Kiya, K., Uozumi, T., Isowa, G., Ishizaki, K., and Ikenaga, M. (1994) O^6-Alkylguanine-DNA alkyltransferase activity of human malignant glioma and its clinical implications. *J. Neuro-Oncol. 21*, 135−140.

(11) Lee, S. M., Reid, H., Elder, R. H., Thatcher, N., and Margison, G. P. (1996) Inter- and intracellular heterogeneity of O^6-alkylguanine-DNA alkyltransferase expression in human brain tumors: possible significance in nitrosourea therapy. *Carcinogenesis 17*, 637−641.

(12) Belanich, M., Ayi, T. C., Li, B. F., Kibitel, J. T., Grob, D. W., Randall, T., White, A. B., Citron, M. L., and Yarosh, D.

B. (1994) Analysis of O^6-methylguanine-DNA methyltransferase in individual human cells by quantitative immunofluorescence microscopy. *Oncol. Res. 6*, 129−137.

(13) Li, B. F. (1999) Methods of assaying DNA-repairing enzymes and their alkylated derivatives. U.S. Patent 5,879,-899.

(14) Council on Scientific Affairs (1988) Cyclotrons and radiopharmaceuticals in positron emission tomography. *J. Am. Med. Assoc. 37*, 765−775.

(15) Nesseler, E., Schirrmacher, R., Hamkens, W., and Rösch, F. (1999) Synthesis of 2-amino-6-benzyloxy-9-[^{18}F]fluoroethylpurine, a possible candidate to determine the status of O^6-methylguanine-DNA-methyltransferase (MGMT) of tumor tissue. *J. Labelled Compd. Radiopharm. 42* (Suppl.), S198−S200.

(16) Moschel, R. C., McDougall, M. G., Dolan, M. E., Stine, L., and Pegg, A. E. (1992) Structural features of substituted purine derivatives compatible with depletion of human O^6-alkylguanine-DNA alkyltransferase. *J. Med. Chem. 35*, 4486-4491.

(17) Chae, M.-Y., McDougall, M. G., Dolan, M. E., Swenn, K., Pegg, A. E., and Moschel, R. C. (1994) Substituted O^6-benzylguanine derivatives and their inactivation of human O^6-alkylguanine-DNA alkyltransferase. *J. Med. Chem. 37*, 342−347.

(18) Chae, M.-Y., Swenn, K., Kanugula, S., Dolan, M. E., Pegg, A. E., and Moschel, R. C. (1995) 8-Substituted O^6-benzylguanine, substituted 6(4)−(benzyloxy)pyrimidine, and related derivatives as inactivators of human O^6-alkylguanine-DNA alkyltransferase. *J. Med. Chem. 38*, 359−365.

(19) Terashima, I., and Kohda, K. (1998) Inhibition of human O^6-alkylguanine alkyltransferase and potentiation of the cytotoxicity of chloroethylnitrosourea by 4(6)−(benzyloxy)-2,6(4)-diamino-5-(nitro or nitroso)pyrimidine derivatives and analogues. *J. Med. Chem. 41*, 503−508.

(20) McElhinney, R. S., Donnelly, D. J., McCormick, J. E., Kelly, J., Watson, A. J., Rafferty, J. A., Elder, R. H., Middleton, M. R., Willington, M. A., McMurray, T. B. H., and Margison, G. P. (1998) Inactivation of O^6-alkylguanine-DNA alkyltransferase. 1. Novel O^6-(hetarylmethyl)guanines having basic rings in the side chain. *J. Med. Chem. 41*, 5265−5271.

(21) Mounetou, E., Cussac, C., Mathieu, F., Maurizis, J.-C., Labarre, P., Moreau, M.-F., Veyre, A., and Madelmont, J.-C. (1995) Synthesis of three no-carrier-added O^6-4-[^{125}I] iodobenzylguanine derivatives, new reagents for the assay of O^6-alkylguanine-DNA alkyltransferase activity. *J. Labelled Compd. Radiopharm. 36*, 1215−1225.

(22) Vaidyanathan, G., and Zalutsky, M. R. (1994) Improved synthesis of *N*-succinimidyl 4-[^{18}F]fluorobenzoate and its application to the labeling of a monoclonal antibody fragment. *Bioconjug. Chem. 5*, 352−356.

(23) Kiburis, J., and Lister, J. H. (1971) Nucleophilic displacement of the trimethylammonio-group as a new route to fluoropurine. *J. Chem. Soc. C*, 3942−3947.

(24) Loktionova, N. A., and Pegg, A. E. (1996) Point mutations in human O^6-alkylguanine-DNA alkyltransferase prevent the sensitization by O^6-benzylguanine to killing by *N*,*N*′-bis(2-chloroethyl)-*N*-nitrosourea. *Cancer Res. 56*, 1578−1583.

(25) Edara, S., Kanugula, S., Goodtzova, K., and Pegg, A. E. (1996) Resistance of the human O^6-alkylguanine-DNA alkyltransferase containing arginine at codon 160 to inactivation by O^6-benzylguanine. *Cancer Res. 56*, 5571−5575.

(26) Attinà, M., Gacace, F., and Wolf, A. P. (1983) Labeled aryl fluorides from the nucleophilic displacement of activated nitro groups by $^{18}F-F^-$. *J. Labelled Compd. Radiopharm. 20*, 501−514.

(27) Haka, M. S., Kilbourn, M. R., Watkins, L., and Toorongian, S. A. (1989) Aryltrimethylammonium trifluoromethanesulfonates as precursors to aryl [^{18}F]fluorides: improved synthesis of [^{18}F]GBR-13119. *J. Labelled Compd. Radiopharm. 27*, 823−833.

(28) Hatano, K., Ido, T., and Iwata, R. (1991) The synthesis of o-and p-[^{18}F]fluorobenzylbromides and their application to the preparation of labeled neuroleptics. *J. Labelled Compd. Radiopharm. 29*, 373−380.

(29) Najafi, A., Peterson, A., Buchsbaum, M., O'Dell, S., and Weihmuller, F. (1993) Preparation and preliminary evaluation of [^{18}F]NQ115: a new selective reversible dopamine D2 receptor ligand. *Nucl. Med. Biol. 20*, 549−555.

(30) Iwata, R., Pascali, C., Bogni, A., Horwath, G., Kovács, Yanai, K., and Ido, T. (2000) A new, convenient method for the preparation of 4-[^{18}F]fluorobenzyl halides. *Appl. Radiat. Isot. 52*, 87−92.

(31) McCoss, M., Chen, A., and Tolman, R. L. (1985) Synthesis of the chiral acyclonucleoside antiherpetic agent (s)-9-(2, 3-dihydroxy-1-propoxymethyl)guanine. *Tetrahedron Lett. 26*, 1815−1818.

(32) Spratt, T. E., and Campbell, C. R. (1994) Synthesis of oligodeoxynucleotides containing analogues of O^6-alkylguanine-DNA alkyltransferase. *Biochemistry 33*, 11364−11371.

(33) Spratt, T. E., and de los Santos, H. (1992) Reaction of O^6-alkylguanin-DNA alkyltransferase with O^6-methylguanine analogues: evidence that oxygen of O^6-methylguanine is protonated by the protein to effect methyl transfer. *Biochemistry 31*, 3688−3694.

(34) Zou, R., and Robins, M. J. (1987) High-yield regioselective synthesis of 9-glycosyl guanine nucleosides and analogues via coupling with 2-*N*-acetyl-6-*O*-diphenylcarbamoylguanine. *Can. J. Chem. 65*, 1436−1437.

(35) Vaidyanathan, G., and Zalutsky, M. R. (1997) A new route to guanidines from bromoalkanes. *J. Org. Chem. 62*, 4867−4869.

(36) Ozerov, A. A., and Brel', A. K. (1993) Synthesis of a new potential antiviral agent − 9-allyloxymethylguanine. *Chem. Heterocycl. Compd. 29*, 945−948.

(37) Norman, T. C., Gray, N. S., Koh, J. T., and Schultz, P. G. (1996) A structure-based library approach to kinase inhibitors. *J. Am. Chem. Soc. 118*, 7430−7431.

(38) Dolan, M. E., Roy, S. K., Garbiras, B. J., Helft, P., Paras, P., Chae, M.-Y., Moschel, R. C., and Pegg, A. E. (1998) O^6-Alkylguanine-DNA alkyltransferase inactivation by ester prodrugs of O^6-benzylguanine derivatives and their rate of hydrolysis by cellular esterases. *Biochem. Pharmacol. 55*, 1701−1709.

(39) Magnin, G. C., Dauvergne, J., Burger, A., and Biellmann, J.-F. (1996) *t*-Butyldimethylsilyloxymethyl group, a versatile protecting group of adenine. *Tetrahedron Lett. 43*, 7833−7836.

(40) Chida, N., Suzuki, T., Tanaka, S., and Yamada, I. (1999) Pd-catalyzed coupling reaction of glycosylamines with 6-chloropurines: synthesis of 6-(*β*-D-mannopyranosylamino)-9*H*-purine and its *β*-D-gluco isomer, *N*-glycoside models for spicamycin and septacidin. *Tetrahedron Lett. 40*, 2573−2576.

(41) Zeng, Z., and Zimmerman, S. C. (1988) Convenient synthesis of 9-alkyl and 9-arylacridines form [2-(trimethylsilyl)-ethoxy]methyl (SEM) protected acridone. *Tetrahedron Lett. 29*, 5123−5124.

(42) Lipshutz, B. H., Vaccaro, W., and Huff, B. (1986) Protection of imidazoles as their *β*-trimethylsilylethoxymethyl (SEM) derivatives. *Tetrahedron Lett. 27*, 4095−4098.

(43) Whitten, J. P., Matthews, D. P., and McCarthy, J. R. (1986) [2-(Trimethylsilyl)ethoxy]methyl (SEM) as a novel and effective imidazole and fused aromatic imidazole protecting group. *J. Org. Chem. 51*, 1891−1894.

(44) Safadi, M., Bindra, D. S., Williams, T., Moschel, R. C., and Stella, V. (1993) Kinetics and mechanism of the acid-catalyzed hydrolysis of O^6-benzylguanine. *Int. J. Pharm. 90*, 239−246.

(45) Ciocco, G. M., Moschel, R. C., Chae, M.-Y., McLaughlin, P. J., Zagon, I. S., and Pegg, A. E. (1995) Specific labeling of O^6-alkylguanine-DNA alkyltransferase by reaction with O^6-(*p*-hydroxy[^{3}H]methylbenzyl)guanine. *Cancer Res. 55*, 4085−4091.

(46) Madelmont, J. C., Cussa, C., Dupuy, J. M., Rapp, M., Labarre, P., Chabard, J. L., Maurizis, J. C., Sauzieres, J., Baudry, J. P., Godeneche, D., and Veyre, A. (1992) Marquage par ^{14}C et ^{13}C de la N acetyl O^6 benzyl guanosine. *J. Labelled Compd. Radiopharm. 31*, 793−800.

(47) McCall, J. M. (1975) Liquid−liquid partition coefficients by high-pressure liquid chromatography. *J. Med. Chem. 18*, 549−552.

BC0000435

Dimethyl Suberimidate Cross-Linking of Oligo(dT) to DNA-Binding Proteins

Mark S. Dodson*

Department of Biochemistry and Molecular Biophysics, University of Arizona, Tucson, Arizona 85721-0088.
Received May 9, 2000; Revised Manuscript Received September 2, 2000

Dimethyl suberimidate is a bifunctional reagent that is used for cross-linking the protein components of oligomeric macromolecules. In this report, dimethyl suberimidate is shown to specifically cross-link oligo(dT) of varying lengths to the DNA-binding subunits of a multimeric helicase-primase encoded by herpes simplex virus type 1. This result indicates that dimethyl suberimidate and other imidoester cross-linking reagents may be useful for characterizing the interaction of oligo(dT) with proteins that bind single-stranded DNA.

INTRODUCTION

Chemical cross-linking reagents are commonly used to stabilize nucleoprotein complexes for analysis by a variety of experimental techniques (*1*−*9*). Most cross-linking reagents function to covalently join reactive groups on the polypeptide moieties of a nucleoprotein complex. Covalent joining of proteins to the nucleic acid component of nucleoprotein complexes is generally less efficient since the necessary reactive groups are fewer in number and may not be exposed. Currently only a few reagents, such as aldehydes, methylene blue, and difluorodinitrobenzene, have been used to directly cross-link protein to DNA (*9*−*11*). Thus, additional reagents that cross-link protein to DNA would be useful.

Herpes simplex virus type 1 (HSV-1) encodes a DNA helicase-primase that consists of three different polypeptides, UL5, UL52, and UL8 (*12*). Sequence homology and mutagenesis studies indicate that UL5 and UL52 confer the helicase and primase activities, respectively (*13*−*15*). The UL8 subunit does not bind DNA (*16*). A heterodimeric subassembly consisting of UL5 and UL52 (UL5/52) exhibits all of the activities associated with the holoenzyme, including an ATPase activity that is potently activated by oligo(dT) (*17*−*19*). The minimal length of oligo(dT) that effectively binds to UL5/52 and activates its intrinsic ATPase activity is about 16 nucleotides (*19*). Here it is reported that the bifunctional protein cross-linking reagent dimethyl suberimidate (DMS) can specifically cross-link oligo(dT) to the UL5 and UL52, but not to the UL8, subunits of the HSV-1 helicase primase. This result indicates that imidoesters may serve as useful reagents for characterizing the interaction of DNA-binding proteins with single-stranded DNA ligands.

MATERIALS AND METHODS

Reagents. The UL5/52 subassembly and UL8 were purified as described (*18*, *19*). Deoxythymidine oligonucleotides were obtained from Midland Certified Reagent Co. (Midland, TX). [γ-^{32}P]ATP at 6000 Ci/mmol, bis-acrylamide, ammonium persulfate, and *N*,*N*,*N*′,*N*′-tetramethylenediamine (TEMED) were from Amersham Life Sciences (Piscataway, NJ). T4 polynucleotide kinase and acrylamide were from Life Technologies (Gaithersburg, MD). High-range molecular weight protein standards consisting of myosin, β-galactosidase, phosphorylase b, bovine serum albumin (BSA), and ovalbumin were from Bio-Rad (Hercules, CA). Triethanolamine and dimethyl sulfoxide (DMSO) were from Sigma (St. Louis, MO). DMS was from Pierce (Rockford, IL).

Cross-Linking Assays. Reaction mixtures (10 μL) contained 25 mM *N*-(2-hydroxyethyl)piperazine-*N*′-(3-ethanesulfonic acid) (HEPES), pH 7.5, 3.5 mM $MgCl_2$, 75 mM NaCl, 10% glycerol, 2 mM dithiothreitol (DTT), and the indicated amounts of end-labeled oligo(dT), UL5/52 subassembly, and UL8. The mixtures were incubated for 20 min at 22 °C followed by the addition of 1.5 μL of freshly prepared 180 mM DMS dissolved in either DMSO or 0.5 M triethanolamine buffer, pH 8.5. The mixtures were incubated for 15 min, and another 1.5 μL of DMS solution was added followed by an additional 15 min of incubation. The mixtures were then precipitated by the addition of trichloroacetic acid to a concentration of 10% followed by centrifugation at 12000 × g at 4 °C. The protein pellets were washed with 100 μL of acetone, dissolved in 12 μL of loading buffer consisting of 200 mM Tris-HCl, 10% (v/v) glycerol, 20 mM DTT, and 0.6% SDS, and the cross-linked products were then separated on a denaturing SDS−7.5% polyacrylamide gel. The gels were autoradiographed using an intensifying screen for 12 h at −80 °C followed by staining with Coomassie Brilliant Blue. A Molecular Dynamics PhosphorImager was used to quantitate the results.

RESULTS

Cross-Linking of Oligo(dT) to the HSV-1 Helicase−Primase. In this study, mixtures containing UL5/52 were incubated with radiolabeled oligo(dT)$_{16}$, treated either with DMSO solvent alone or with DMSO containing DMS, and the products were then separated by SDS−PAGE. The gel was then subjected to autoradiography followed by staining with Coomassie Blue to visualize the UL5 and UL52 subunits (Figure 1). No difference was observed in the Coomassie-stained bands between the untreated control and the DMS cross-linked sample (Figure 1A, lanes 1 and 2, respectively). This result indicated that DMS did not cross-link UL5 and UL52

* To whom correspondence should be addressed. Phone: (520) 621-6123. Fax: (520) 621-9288. E-mail: dodson@biosci.arizona.edu.

10.1021/bc000049u CCC: $19.00 © 2000 American Chemical Society
Published on Web 10/21/2000

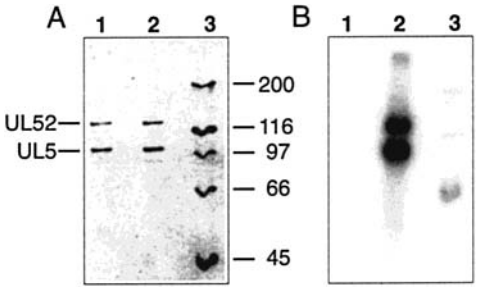

Figure 1. DMS cross-links oligo(dT)$_{16}$ to both UL5 and UL52. Mixtures containing 1.1 μM ^{32}P-labeled oligo(dT)$_{16}$ and 1.4 μM UL5/52 or molecular weight protein standards were assembled and cross-linked with DMS and then separated by SDS−PAGE as described under Materials and Methods. (A) Coomassie-stained gel. Lanes: 1, UL5/52, no DMS; 2, UL5/52 plus DMS; 3, molecular weight standards plus DMS. Molecular weights of the standards are indicated. (B) Autoradiograph of the same gel.

Table 1. Relative Extents of DMS Cross-Linking of Oligo(dT)$_{16}$ to Proteins

polypeptide	relative fraction cross-linked[b]
UL5	1.00
UL52	0.64
myosin (200 kDa)	0.08
β-galactosidase (116 kDa)	0.05
phosphorylase (97 kDa)	0.03
BSA (66 kDa)	0.14
ovalbumin (45 kDa)	0.02

[a] The cross-linked products shown in lanes 2 and 3 of Figure lB were quantitated using a Phosphorlmager. [b] The fraction of probe that was cross-linked to each protein relative to the amount of probe that was cross-linked to UL5 is shown.

together under the conditions used. However, in the autoradiograph, two prominent bands were observed in the lane containing the DMS-treated sample that were not observed in the lane containing the untreated sample (Figure 1B, lanes 1 and 2). The mobilities of these two bands corresponded to the mobilities of UL5 (99 kDa) and UL52 (114 kDa). This result indicates that the oligo(dT)$_{16}$ probe was cross-linked to UL5 and UL52. Quantitation of the cross-linked products indicated that 0.14 and 0.09% of the probe were cross-linked to UL5 and UL52, respectively. Similar results were also obtained using labeled oligo(dT)$_{20}$ as the probe and triethanolamine as the solvent for DMS (data not shown). The amount of probe that was cross-linked to UL5 was consistently higher than the amount that was cross-linked to UL52, with the ratio being 1.43 ± 0.08 to 1.

DMS Cross-Linking of Oligo(dT)$_{16}$ to UL5 and UL52 Is Specific. The specificity of DMS cross-linking of oligo(dT)$_{16}$ to UL5 and UL52 was assessed in the above experiment by comparing the ability of DMS to cross-link the DNA to the control proteins used for molecular weight standards (Figure 1A, lane 3). Only faint traces of the probe were cross-linked to the molecular weight standards (Figure lB, lane 3). The extent of cross-linking to UL5, UL52, and the control proteins was quantitated and compared (Table 1). Cross-linking of the DNA to the control proteins ranged from 5-fold (BSA) to 50-fold (ovalbumin) less than that observed for UL5 and UL52.

Effect of the Length of Oligo(dT) on DMS Cross-Linking of UL5/52. The DMS cross-linking of oligo(dT) to UL5/52 was repeated in the presence and absence of a 3-fold molar excess of UL8 using oligo(dT) species ranging from 12 to 28 nucleotides in length. An excess of UL8 was used to ensure that the heterotrimeric

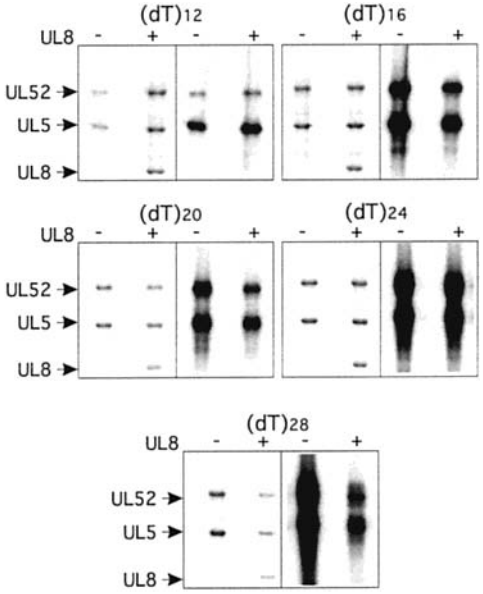

Figure 2. Effect of oligo(dT) length and of UL8 on cross-linking of DNA to UL5/52. Mixtures containing 0.8 μM ^{32}P-labeled oligo-(dT) of the indicated length and 0.6 μM UL5/52 were cross-linked with DMS in the presence or absence of 1.8 μM UL8, and then separated by SDS−7.5% PAGE as described in the Materials and Methods. The left two lanes of each panel show a Coomassie-stained gel containing UL5/52 alone or UL5/52 and UL8. The right two lanes of each panel show the autoradiogram of the gel. The mobilities of the subunits are indicated on the first panel.

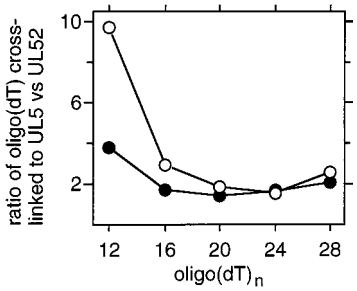

Figure 3. Relative extents of cross-linking of oligo(dT) of varying lengths to UL5 and UL52 in the presence and absence of UL8. The data from Figure 2 were quantitated using a PhosphorImager. The ratio of DNA cross-linked to UL5 versus UL52 is plotted for oligo(dT)s of the indicated lengths. Data are the averages of two separate experiments. Filled symbols, UL8 absent; open symbols, UL8 present.

holoenzyme would be stably formed (*20*). Again, cross-linked products that corresponded to the mobilities of UL5 and UL52 were observed for all lengths of oligo(dT) that were used (Figure 2). No species that correlated to cross-linking of the DNA to UL8 were observed. The relative extents of cross-linking of the oligonucleotides to UL5 and UL52 were quantitated by determining the ratio of the amount of UL5-cross-linked DNA to UL52-cross-linked DNA (Figure 3). This ratio is unaffected by variations in the specific activities of the labeled probes or by variations in the amount of sample loaded on the gel. For oligo(dT)s of 16 or more nucleotides in length, about twice as much DNA was cross-linked to UL5 as was cross-linked to UL52. UL8 had little effect on this ratio. However, this ratio was changed substantially when oligo(dT)$_{12}$ was used as the ligand. In the absence of UL8, about four times as much DNA was cross-linked to UL5 as to UL52. In the presence of UL8 this ratio increased to about 10 to 1.

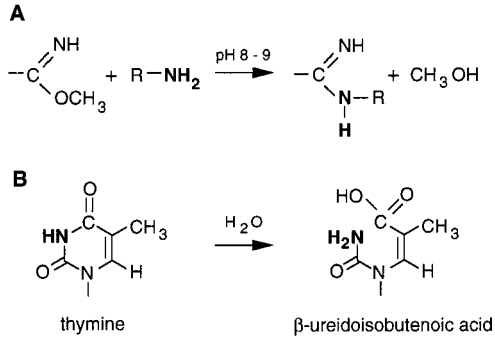

Figure 4. Proposed mechanism for DMS cross-linking of oligo(dT) to protein. (A) The imidoester reaction scheme; (B) hypothesized opening of the thymine ring to yield a primary amine that can participate in the imidoester reaction.

DISCUSSION

Because of its lack of secondary structure, oligo(dT) is frequently used for characterizing the interactions of helicases with DNA ligands (*1*, *8*, *19*, *21*−*23*). We had originally intended to use DMS as a reagent for determining if oligo(dT) induces oligomerization of the HSV-1 helicase-primase. Under the conditions used for DMS cross-linking, we were unable to detect the formation of oligo(dT)-induced oligomers of the HSV-1 helicase-primase. However, we observed that the DNA became covalently cross-linked to UL5 and UL52. This result was unexpected since oligo(dT) lacks the functional groups that are necessary to react with imidoester-based cross-linking reagents. The studies presented in this report indicate that DMS-mediated cross-linking of oligo(dT) to UL5 and UL52 is specific since several non-DNA-binding proteins are cross-linked far less effectively to oligo(dT). The modest amount of cross-linking of oligo(dT) to BSA can be accounted for by a previous observation that BSA weakly binds DNA (*24*). The specificity of cross-linking of oligo(dT) to UL5 and to UL52 is further demonstrated by the failure of DMS to cross-link oligo(dT) to the non-DNA-binding UL8 subunit of the holoenzyme. This covalent cross-linking of oligo(dT) to protein by DMS is a novel result that has not been previously observed.

To demonstrate the utility of DMS as a tool for characterizing nucleoprotein complexes, we used DMS cross-linking to compare the ability of UL5 and UL52 to bind oligo(dT) ligands of varying lengths. For oligo(dT) ligands longer than 16 nucleotides, the ratio of the amount of DNA that is cross-linked to UL5 and UL52 is fairly constant, even in the presence of UL8. Shorter ligands are not cross-linked to either protein as efficiently as the longer DNA species. In the presence of UL8, the amount of oligo(dT)$_{12}$ that is cross-linked to UL5 is 10-fold greater than for UL52. The poor cross-linking of oligo(dT)$_{12}$ to UL5/52 agrees with previous nitrocellulose filter binding and enzymatic activation studies which showed that oligo(dT) ligands shorter than 16 nucleotides are poorly bound by UL5/52 and are also poor activators of the DNA-dependent ATPase activity of UL5/52 (*19*). Our cross-linking results demonstrate that the minimal length of the DNA-binding site in UL5 is shorter than in UL52 and that the UL8 subunit affects the interaction of short oligonucleotides with the UL5/52 subassembly.

DMS cross-links primary amines on proteins by an imidoester reaction (Figure 4A) (*25*). Since there are no primary amines on deoxythymidine, the observation that DMS cross-links oligo(dT) to UL5 and UL52 is puzzling. One explanation could be that the oligonucleotides become trapped by a "caging" effect in which the DNA becomes pinned beneath cross bars of DMS that link some of the residues which form the DNA-binding sites. However, these caged structures would be expected to dissociate when denatured in the SDS−PAGE loading buffer. Alternatively, upon binding of oligo(dT) to UL5 or UL52, some thymine residues may be rendered partially susceptible to hydrolysis or damage at the 3 and 4 positions of the pyrimidine ring. This could yield a β−ureidoisobutenoic acid moiety containing a primary amino group that could participate in the imidoester cross-linking reaction (Figure 4B).

The total fraction of labeled oligo(dT) that was cross-linked to protein in our study was about 0.25%. This figure is roughly comparable to the extent of halogenated oligo(dT) that can be cross-linked to UL5 and UL52 by brief exposure to long wave UV light (*23*).

It is often necessary to test several methods in order to identify one that can be successfully used for cross-linking a specific set of macromolecules. Few methods are available for covalently cross-linking proteins to DNA. Here we have shown that imidoester cross-linking reagents such as DMS offer an alternative to these other methods. In contrast to methylene blue (*10*), DMS can effectively cross-link single-stranded nucleic acids to protein, and, in contrast to aldehyde-based cross-linkers, DMS can yield cross-linked species that retain enzymatic activity (*1*). In addition, DMS may be more appropriate than UV light for cross-linking DNA to proteins in the presence of nucleotides or other UV-absorbing compounds. Thus, the observation that imidoesters such as DMS can covalently cross-link protein to DNA expands the limited repertoire of methods that are available for studying the interaction of DNA with DNA-binding proteins.

ACKNOWLEDGMENT

This research was supported in part by Grant RPG9705601NP from the American Cancer Society. The author thanks Dr. Lauren Murata and Nicoleta Constantin for helpful discussions, critical reading of the manuscript, and assistance with production of the figures.

LITERATURE CITED

(1) Chao, K., and Lohman, T. M. (1991) DNA-induced dimerization of the *Escherichia coli* Rep helicase. *J. Mol. Biol. 221*, 1165−1181.

(2) Dean, F. B., Borowiec, J. A., Eki, T., and Hurwitz, J. (1992) The simian virus-40 T-antigen double hexamer assembles around the DNA at the replication origin. *J. Biol. Chem. 267*, 14129−14137.

(3) Dodson, M., Roberts, J., McMacken, R., and Echols, H. (1985) Specialized nucleoprotein structures at the origin of replication of bacteriophage λ: Complexes with λ O protein and with λ O, λ P, and *Escherichia coli* DnaB proteins. *Proc. Natl. Acad. Sci. U.S.A. 82*, 4678−4682.

(4) Heichman, K. A., and Johnson, R. C. (1990) The hin invertasome: protein-mediated joining of distant recombination sites at the enhancer. *Science 249*, 511−517.

(5) Fouts, E. T., Yu, X., Egelman, E. H., and Botchan, M. R. (1999) Biochemical and electron microscopic image analysis of the hexameric El helicase. *J. Biol. Chem. 274*, 4447−4458.

(6) Levin, M. K., and Patel, S. S. (1999) The helicase from hepatitis C virus is active as an oligomer. *J. Biol. Chem. 274*, 31839−31846.

(7) Dong, F., Gogol, E. P., and von Hippel, P. H. (1995) The phage T4-coded DNA replication helicase (gp41) forms a hexamer upon activation by nucleoside triphosphate. *J. Biol. Chem. 270*, 7462−7473.

(8) Patel, S. S., and Hingorani, M. M. (1993) Oligomeric structure of bacteriophage T7 primase/helicase proteins. *J. Biol. Chem. 268*, 10668−10675.
(9) Simonsson, S., Samulesson, T., and Elias, P. (1998) The herpes simplex virus type 1 origin binding protein. Specific recognition of phosphates and methyl groups defines the interacting surface for a monomeric DNA binding domain in the major groove of DNA. *J. Biol. Chem. 273*, 24633−24639.
(10) Lalwani, R., Maiti, S., and Mukherji, S. (1990) Visible light induced DNA-protein cross-linking in DNA-histone complex and sarcoma-180 chromatin in the presence of methylene blue. *Photochem. Photobiol., B 7*, 57−73.
(11) Toth, J., and Biggin, M. D. (2000) The specificity of protein-DNA cross-linking by formaldehyde: in vitro and in drosophila embryos. *Nucleic Acids Res. 28*, e4.
(12) Crute, J. J., Tsurumi, T., Zhu, L., Weller, S. K., Olivo, P. D., Challberg, M. D., Mocarski, E. S., and Lehman, I. R. (1989) Herpes simplex virus 1 helicase-primase: a complex of three herpes encoded gene products. *Proc. Natl. Acad. Sci. U.S.A. 86*, 2186−2189.
(13) Klinedinst, D. K., and Challberg, M. D. (1994) Helicase-primase complex of herpes simplex type 1: a mutation in the UL52 subunit abolishes primase activity. *J. Virol. 68*, 3693−3701.
(14) Dracheva, S., Koonin, E. V., and Crute, J. J. (1995) Identification of the primase active site of the herpes simplex virus type 1 helicase-primase. *J. Biol. Chem. 270*, 14148−14153.
(15) Graves-Woodward, K. L., Gottlieb, J., Challberg, M. D., and Weller, S. K. (1997) Biochemical analyses of mutations in the HSV-1 helicase-primase that alter ATP hydrolysis, DNA unwinding, and coupling between hydrolysis and unwinding. *J. Biol. Chem. 272*, 4623−4630.
(16) Parry, M. E., Stow, N. D., and Marsden, H. S. (1993) Purification and properties of the herpes simplex virus type-1 UL8 protein. *J. Gen. Virol. 74*, 607−612.
(17) Calder, J. M., and Stow, N. D. (1990). Herpes simplex virus helicase-primase: the UL8 protein is not required for DNA-dependent ATPase and DNA helicase activities. *Nucleic Acids Res. 18*, 3573−3578.
(18) Dodson, M. S., and Lehman, I. R. (1991) Association of DNA helicase and primase activities with a subassembly of the herpes simplex virus 1 helicase-primase composed of the UL5 and UL52 gene products. *Proc. Natl. Acad. Sci. U.S.A. 88*, 1105−1109.
(19) Healy, S., You, X., and Dodson, M. (1997) Interactions of a subassembly of the herpes simplex virus type 1 helicase-primase with DNA. *J. Biol. Chem. 272*, 3411−3415.
(20) Tenney, D. J., Hurlburt, W. W., Micheletti, P. A., Bifano, M., and Hamatake, R. K. (1994) The UL8 component of the herpes-simplex virus helicase-primase complex stimulates primer synthesis by a subassembly of the UL5 and UL52 components. *J. Biol. Chem. 269*, 5030−5035.
(21) Wong, I., Chao, K. L., Bujalowski, W., and Lohman, T. M. (1992) DNA-induced dimerization of the *Escherichia coli* Rep helicase. Allosteric effects of single-stranded and duplex DNA. *J. Biol. Chem. 267*, 7596−7610.
(22) Dodson, M. S., and Lehman, I. R. (1993) The herpes simplex virus type-1 origin binding protein. DNA-dependent nucleoside triphosphatase activity. *J. Biol. Chem. 268*, 1213−1219.
(23) Biswas, N., and Weller, S. K. (1999) A mutation in the C-terminal putative Zn^{2+} finger motif of UL52 severely affects the biochemical activities of the HSV-1 helicase-primase subcomplex. *J. Biol. Chem. 274*, 8068−8076.
(24) Braun, A., and Merrick, B. (1975) Properties of the ultraviolet-light-mediated binding of bovine serum albumin to DNA. *Photochem. Photobiol. 21*, 243−247.
(25) Davies, G. E., and Stark, G. R. (1970) Use of dimethyl suberimidate, a cross-linking reagent, in studying the subunit structure of oligomeric proteins. *Proc. Natl. Acad. Sci. U.S.A. 66*, 651−656.

BC000049U

Preliminary Characterization of Novel Amino Acid Based Polymeric Vesicles as Gene and Drug Delivery Agents

M. D. Brown,[†,‡] A. Schätzlein,[‡] A. Brownlie,[†] V. Jack,[†] W. Wang, L. Tetley,[§] A. I. Gray,[†] and I. F. Uchegbu*[,†]

Department of Pharmaceutical Sciences, University of Strathclyde, CRC Department of Medical Oncology, University of Glasgow, and Department of Infection and Immunity, University of Glasgow, Glasgow G4 0NR, United Kingdom. Received May 10, 2000; Revised Manuscript Received August 10, 2000

The amino acid homopolymers, poly-L-lysine and poly-L-ornithine, have been modified by the covalent attachment of palmitoyl and methoxypoly(ethylene glycol) (mPEG) residues to produce a new class of amphiphilic polymers—PLP and POP, respectively. These amphiphilic amino acid based polymers have been found to assemble into polymeric vesicles in the presence of cholesterol. Representatives of this new class of polymeric vesicles have been evaluated in vitro as nonviral gene delivery systems with a view to finding delivery systems that combine effective gene expression with low toxicity in vivo. In addition, the drug-carrying capacity of these polymeric vesicles was evaluated with the model drug doxorubicin. Chemical characterization of the modified polymers was carried out using ^{1}H NMR spectroscopy and the trinitrobenzene sulfonic acid (TNBS) assay for amino groups. The amphiphilic polymers were found to have an unreacted amino acid, palmitoyl, mPEG ratio of 11:5:1, and polymeric vesicle formation was confirmed by freeze-fracture electron microscopy and drug encapsulation studies. The resulting polymeric vesicles, by virtue of the mPEG groups, bear a near neutral ζ-potential. In vitro biological testing revealed that POP and PLP vesicle−DNA complexes are about one to 2 orders of magnitude less cytotoxic than the parent polymer−DNA complexes although more haemolytic than the parent polymer−DNA complexes. The polymeric vesicles condense DNA at a polymer:DNA weight ratio of 5:1 or greater and the polymeric vesicle−DNA complexes improved gene transfer to human tumor cell lines in comparison to the parent homopolymers despite the absence of receptor specific ligands and lysosomotropic agents such as chloroquine.

INTRODUCTION

Self-assembled systems such as those arising in aqueous media from phospholipids (liposomes) (*1*) and synthetic surfactants (niosomes) (*2*) have been used as drug (*3*, *4*) and gene (*5*) delivery systems. Our studies are concerned with a new class of polymeric vesicles for drug and gene delivery. Previously, drug delivery polymeric vesicles have been prepared from an amphiphilic derivative of the carbohydrate glycol chitosan (*6*). However, the current polymeric vesicles have been prepared from amino acid based polymers and are being evaluated as gene and possibly drug delivery systems.

For gene therapy to become a reality, there is a need for the development of innovative delivery systems which produce clinically significant expression levels in vivo while still remaining nontoxic and nonimmunogenic (*7*). These materials also have to be produced in large quantities and to pharmaceutical standards. Many of the systems that are currently being utilized, both viral and nonviral, are unable to fulfill these requirements, and hence, there are a large number of new gene delivery systems being investigated in the hope that a few will show promise.

Viral systems (*8*) have been studied extensively and include a wide variety of viral types such as retroviruses, adenoviruses, adeno-associated viruses, herpes simplex virus, and the HIV-based lentivirus. All have various inherent disadvantages (*9*) such as safety concerns and scale-up difficulties.

A vast range of nonviral systems has been developed in an attempt to overcome some of the shortfalls of viral systems. These are mainly cationic liposomes (lipoplex) (*7*, *10*), cationic polymers (polyplex) (*11*−*13*) or a combination of cationic liposomes and cationic polymers (lipopolyplex) (*14*).

Gene targeting in vivo requires that the carriers avoid early uptake by the reticuloendothelial system (RES) as well as nonspecific uptake due to electrostatic interactions. The excess positive surface charge of many cationic lipid complexes promotes nonspecific interaction with cells (*15*) which seriously hampers any targeting efforts (*16*). Additionally, the excess positive charge may also reduce the stability of the complex (*17*) and consequently enhance the degradation of DNA[1] in vivo. Hence one of the desirable attributes of a nonviral gene delivery system would be a neutral surface charge. The incorporation of targeting ligands, however, is necessary to achieve more specific targeting of carriers (*18*). Current cationic liposomal vectors largely resist targeting, as they tend to transfect the first capillary bed they arrive at after

* To whom correspondence should be addressed. E-mail: I.F.Uchegbu@strath.ac.uk.
† Department of Pharmaceutical Sciences.
‡ CRC Department of Medical Oncology.
§ Department of Infection and Immunity.

[1] Abbreviations: EthBr, ethidium bromide; DOPE, dioleylphosphatidyl-ethanolamine; FFEM; freeze-fracture electron microscopy; NMR, nuclear magnetic resonance; DNA, deoxyribonucleic acid; PEG, poly(ethylene glycol); mPEG, methoxypoly(ethylene glycol); PLL, poly-L-lysine; PO, poly-L-ornithine; PLP, poly(ethylene glycol)−poly-L-lysine−palmitoyl; POP, poly(ethylene glycol)−poly-L-ornithine−palmitoyl; TNBS, 2,4,6-trinitrobenzenesulfonic acid.

10.1021/bc000052d CCC: $19.00 © 2000 American Chemical Society
Published on Web 10/25/2000

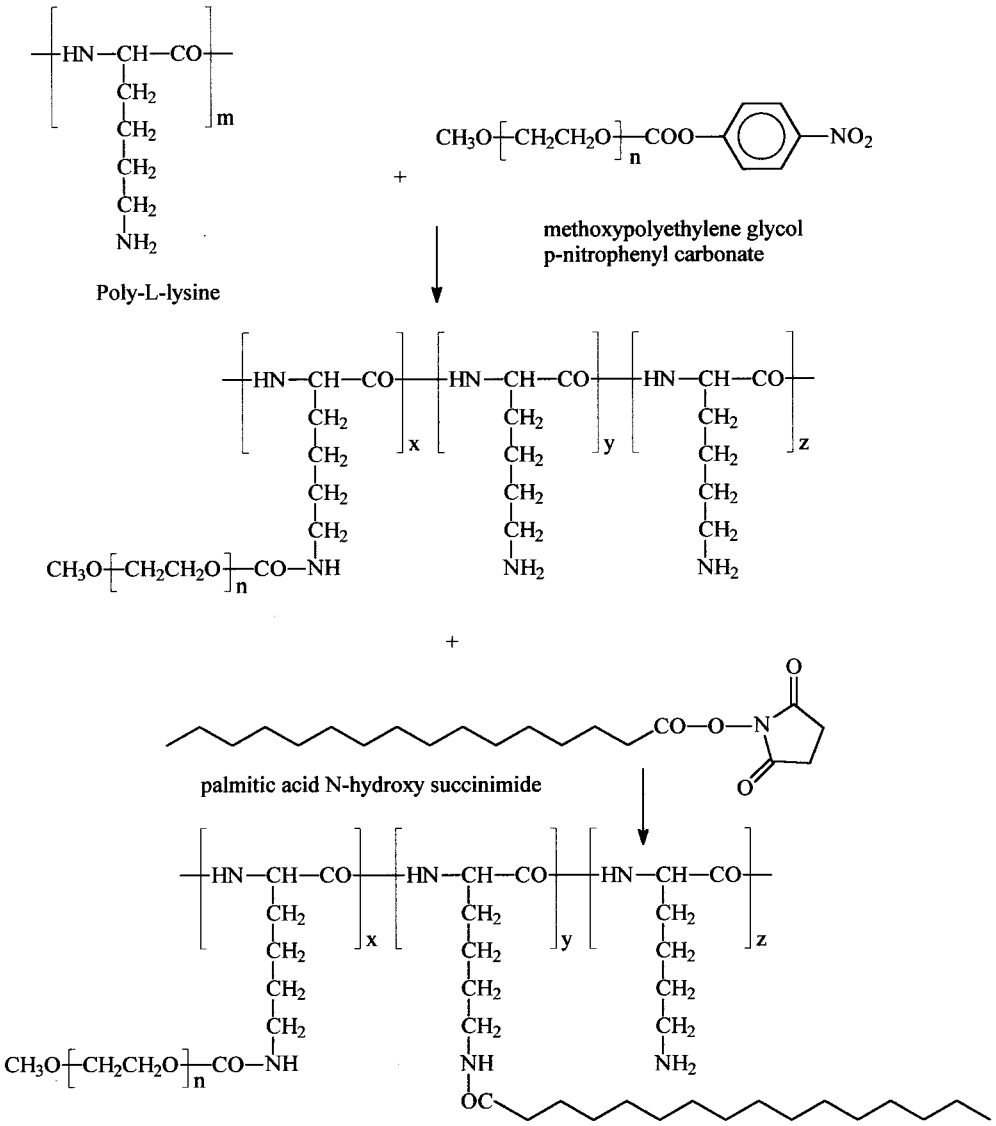

Figure 1. Synthesis of amphiphilic amino acid based polymers as exemplified by the synthesis of a poly-L-lysine based amphiphilic polymer using activated mPEG (mPEG Mw = 5000) and activated palmitoyl compounds, $n = 123$, $m \approx 114$.

intravenous administration—namely the lung endothelium (*19*). While a degree of gene targeting may be achieved with cationic polymers bearing targeting ligands, success has been limited and protein expression is low and transient due probably to the degradation of cationic polymer complexes in the blood and body fluids (*18*). The degradation of liposome complexes in vivo, for example, may be modulated by a poly(ethylene glycol) (PEG) surface (*20*), which may also improve transfection in vivo (*20*). The PEG surface, apart from limiting DNA degradation, will also equip gene carriers with a "stealth" facility and should allow prolonged circulation on intravenous administration (*21*) with possibly a more sustained biological effect. Hence, a PEG-coated surface is also a desirable attribute of a gene delivery system.

The present work describes the synthesis and characterization of amphiphilic amino acid based polymers, their assembly into polymeric vesicles bearing a near neutral surface charge, and their biological characterization as possible gene and drug delivery systems.

MATERIALS AND METHODS

Materials. Poly-L-lysine hydrochloride (PLL, MW 15000−30000), poly-L-ornithine hydrochloride (PO, MW 15000−30000), sodium tetraborate decahydrate, methoxypoly(ethylene glycol) (mPEG)-*p*-nitrophenyl carbonate, palmitic acid *N*-hydroxysuccinimide, phosphate buffered saline (PBS) tablets, and deuterated solvents were obtained from Sigma−Aldrich Co., U.K. Other organic solvents were obtained from Merck, U.K. Sodium hydrogen carbonate was supplied by Fluka, U.K. Plasmids (pCMVsport β-gal) were obtained from Life Sciences, U.K., and tissue culture media from GibcoBRL, U.K.

Synthesis of Modified Poly-L-Amino Acid Polymers. Synthesis was carried out as depicted in Figure 1. The conjugation of methoxypoly(ethylene glycol) (mPEG) to the amino acid homopolymers was carried out according to a modification of the method of Monfardini and others (*22*). PLL or PO (400 mg) was dissolved in sodium tetraborate (0.08 M, 240 mL) and methoxypoly(ethylene glycol)-*p*-nitrophenyl carbonate (mPEG Mw = 5000, 800 mg for PO and 720 mg for the PLL synthesis reaction) added over a 3 h period. The mixture was stirred for a total of 15 h at room temperature protected from light and the product subjected to exhaustive dialysis (Visking tubing, Molecular weight cut off = 12000−14000) against 5 L of water for 24 h with six changes. The conjugation of the palmitic acid groups to the mPEG-poly-L-amino

acid polymers was derived from a method described previously for the synthesis of palmitoyl glycol chitosan (*6*). Sodium hydrogen carbonate (1 g) was dissolved in the dialysate and a solution of palmitic acid *N*-hydroxysuccinimide (260 mg) in absolute ethanol (320 mL for PO or 312 mL for PLL synthesis reaction) was added dropwise. The reaction mixture was then stirred for 72 h and protected from light, and the product was again dialyzed exhaustively against water as described above. The dialysate was freeze-dried, and the freeze-dried material dissolved in chloroform (400 mL). The chloroform solution was filtered to remove unreacted PLL and the filtrate evaporated under reduced pressure at 30−40 °C until the volume had been reduced to about 20 mL. This solution was then added dropwise to diethyl ether (500 mL), and the precipitate collected by filtration. Thus, contaminating palmitic acid, which dissolves in diethyl ether, was removed. To obtain a dry powder, the precipitate was freeze-dried. The poly-L-lysine based amphiphilic polymer (PLP) and the poly-L-ornithine-based amphiphilic polymer (POP) were presented as off-white powders.

^{1}H NMR. ^{1}H NMR (with integration) and ^{1}H correlation spectroscopy experiments (Bruker AMX 400 MHz spectrometer, Bruker Instruments, U.K) were performed on solutions of POP and PLP in $CDCl_3$, palmitic acid N-hydroxysuccinimide in $CDCl_3$, PLL and PO in D_2O and methoxy-polyethylene-glycol-*p*-nitrophenyl carbonate in D_2O. ^{1}H NMR of PLP samples was performed at elevated temperature (48 °C), but all other samples were analyzed at ambient temperatures (25 °C).

Assay for Free Amino Groups. The proportion of free amino groups in the modified polymers may be measured by a comparative titration of the free amino groups in both the unmodified and modified polymers using trinitrobenzene sulfonic acid (TNBS) (*23*). The TNBS assay was carried out by dissolving POP/PLP (5 mg) in methanol (10 mL); 3 mL of this solution was diluted to 10 mL with sodium tetraborate (0.1 M). To a 3 mL aliquot of this methanolic sodium tetraborate solution was then added TNBS solution (75 μL, 0.03 M). The resulting solution was mixed thoroughly and incubated at room temperature for 30 min. The absorbance was read at 420 nm (Unicam UV-1, Unicam Ltd, U.K.), and the weight percent of unmodified polymer was computed from a standard curve prepared using the unmodified polymers, poly-L-lysine and poly-L-ornithine, as appropriate. This experiment was carried out in triplicate.

Gel Permeation Chromatography−Laser Light Scattering. GPC/LLS with refractive index detection was carried out on polymer samples to ensure complete removal of low molecular weight and polymeric (unreacted mPEG-*p*-nitrophenol carbonate and mPEG carboxylic acid) impurities. Poly-L-lysine hydrobromide, mPEG-*p*-nitrophenyl carbonate, and mPEG grafted poly-L-lysine solutions, each dissolved in acetate buffer (0.3 M CH_3COONa/0.2 M CH_3COOH, pH 4.4), were analyzed on a PSS Hema-Bio 300 column (300 × 8 mm, particle size = 10 μm, exclusion limit for dextran = 500 000) and a PSS Hema-Bio 40 column (300 × 8 mm, particle size = 10 μm, exclusion limit for dextran = 3 000 000). The mobile phase was acetate buffer (pH 4.4). Detection was via a Waters 2410 refractive index (RI) detector at 850 nm (Waters Instruments, U.K.) and a Wyatt Mini Dawn static laser light scattering detector equipped with a 20 mV semiconductor diode laser (vertically polarized, λ = 690 nm) at three angles (45, 90, and 135°), Optokem Instruments, U.K. PLP and palmitic acid *N*-hydroxysuccinimide ester samples dissolved in chloroform were analyzed on a Waters Styragel HR 4E column (300 × 7.8 mm, mixed bed pore size, exclusion limit for polystyrene = 50−100000) and a Waters Styragel HR 5E column (300 H 7.8 mm, mixed bed pore size, exclusion limit for polystyrene = 2000−4000000). The mobile phase was chloroform. All the sample solutions were injected at a loading concentration of 1−3 mg/mL (200 μL each injection) using a Waters 717 plus Autosampler, and all the measurements were carried out at room temperature.

Polymeric Vesicle Preparation. POP/PLP vesicles were prepared by sonication of POP/PLP (5 mg) and cholesterol (chol, 2 mg) in phosphate-buffered saline (1 mL, pH 4.0 or 7.0) for 15 min, using a probe sonicator (Soniprobe instruments, U.K.). To prepare doxorubicin-loaded vesicles, POP (5 mg), chol (2 mg), and a solution of doxorubicin (2 mL, 1 mg mL^{-1}) in PBS (pH 4) were probe sonicated (2 × 2 min) and then filtered (0.45 μm), or alternatively PLP (10 mg), cholesterol (4 mg), and a solution of doxorubicin (4 mL, 1 mg mL^{-1}) in PBS (pH 4) were probe sonicated and filtered as described above. To separate unentrapped doxorubicin, the dispersion was ultracentrifuged (150000*g* × 1 h) and the supernatant removed. The pellet was reconstituted in PBS (2 mL, pH 4).

Polymeric Vesicle Sizing and ζ-Potential Measurements. The sizes and ζ-potential (in PBS, pH 7.4) were measured using a Malvern Zetasizer 1000 (size measurements only) or a Malvern Zetasizer 4 (ζ-potential measurements), both from Malvern Instruments, U.K. All measurements were performed at 25 °C. Before the start of each measurement, standards (polystyrene latex beads, 300 nm, Sigma Co., U.K., and Malvern Zetasizer standard, Malvern Instruments) were analyzed. All *z*-average mean and ζ-potential data obtained from the standards agreed with that stated by the manufacturer. The viscosity of the disperse phase was 0.893Cp and the dielectric constant for the ζ-potential measurements was 79.

Doxorubicin Quantification. The doxorubicin loaded vesicles (0.1 mL) were disrupted by dilution with 2-propanol (1 mL) and then diluted with PBS (pH 4). The amount of doxorubicin released form the disrupted vesicles was measured fluorimetrically ($\lambda_{excitation}$ = 480 nm, $\lambda_{emission}$ = 560 nm, Perkin-Elmer LS-50B spectrofluorimeter, Perkin-Elmer, U.K). The doxorubicin standard curve was linear over the range 0.2−10 μg mL^{-1}. This experiment was carried out in triplicate.

Freeze-Fracture Electron Microscopy. Freeze-fracture electron microscopy was used to visualize the polymeric vesicles. Specimens were fast frozen by being plunged into liquid propane/isopentane at −180 °C and transferred cold into a high vacuum freeze-fracture system. Specimens were fractured with a BalTec complementary replica device at −100 °C, and the exposed faces replicated with platinum carbon at 45 °C and backed by carbon at 90°. Replicas were cleaned in acetone/alcohol, rinsed in distilled water, dried on Formvar-coated grids, and finally imaged using a LEO (Zeiss) 902 energy-filtering electron microscope.

Polymeric Vesicle Interaction with DNA. Plasmid (pCMVsport β-gal, Life Technologies, Paisley, U.K) was grown in *Escherichia coli* and plasmid purification was carried out using a QIAGEN Endo-toxin free Giga Plasmid Kit (QIAGEN, Hilden, Germany) according to the manufacturer's instructions. Purity was confirmed by agarose gel electrophoresis (*24*).

The reduced fluorescence of ethidium bromide (EthBr) was used to probe for DNA condensation by the polymeric vesicles. EthBr fluorescence increases significantly (factor

40 compared to unbound EthBr) on intercalation with double-stranded DNA (*25*). The electrostatic interaction between the anionic DNA and cationic groups of the carrier on formation of the DNA−vesicle complex reduces the number of EthBr binding sites, a process termed condensation, ultimately reducing the fluorescence intensity of the EthBr solution.

Complexes of POP and PLP vesicles with DNA were prepared at polymer:DNA ratios of 20:1, 10:1, 5:1, 2.5:1, 1.25:1, 0.625:1, and at various time points the fluorescence intensity ($\lambda_{excitation}$ = 526 nm, $\lambda_{emission}$ = 592 nm) of the complexes determined in the presence of EthBr (40 μg mL^{-1}). The DNA concentration in the cuvette was kept constant (100 μg mL^{-1}), and the polymeric vesicle dispersion medium PBS (pH 4) and a solution of DNA in PBS (pH 4) served as controls.

Haemocompatibility. Approximately 5 mL of human blood was centrifuged (1000*g* × 10 min). The erythrocyte pellet was isolated, washed twice with PBS (pH 7.4) at 4 °C by resuspending the pellet in PBS (pH 7.4), followed by centrifugation (1000*g* × 10 min). The pellet was weighed and a 3% w/w dispersion of the erythrocytes prepared in PBS (pH 7.4). Varying concentrations of the polymeric vesicle−DNA formulations (100 μL) were added to the erythrocyte suspension (100 μL) in 96-well microtiter plates. PBS and Triton X-100 (1% w/v) served as negative and positive controls, respectively. After incubation for 4 h, the microtiter plate was centrifuged (1000*g* × 10 min), the supernatant (100 μL) transferred to a new microtiter plate, and the absorbance measured at 570 nm. Values were corrected for background readings obtained for polymeric vesicles only. The haemolysis given by the Triton-X solution was considered to be 100% while the haemolysis given for the PBS solution was taken as 0%. The results were thus expressed as percentage haemolysis.

Cytotoxicity. A human lung carcinoma cell line (A549, ATCC CCL-185) and a human epidermoid carcinoma cell line (A431, ATCC CRL-1555) were both maintained in Dulbecco's minimum essential medium (DMEM) supplemented with 10% foetal calf serum (FCS) and 2 mM glutamine (GibcoBRL, U.K.) at 10% CO_2 and 37 °C.

The cytotoxicity was assessed by the measurement of the IC_{50} value in a standard MTT (3-[4,5-dimethylthiazol-2-yl]-2,5-diphenyltetrazolium bromide thiazolyl blue indicator dye) assay (*26*). Briefly, 96-well microtiter plates were seeded with 700 cells/well and incubated for 72 h. Dilutions of the polymeric vesicle−DNA formulations (100 μL) in tissue culture medium (Opti-Mem) were incubated with the cells for 4 h. The samples were then replaced with fresh DMEM daily and incubated for 72 h. After this period, the indicator dye (50 μL, 50 mg mL^{-1}) was added to each well and incubated with the cells for 4 h in the dark. The medium and indicator dye were then removed and the cells lysed with dimethylsulfoxide (200 μL). After addition of Sorensen's glycine buffer (25 μL), the absorption was measured at 570 nm. Values were expressed as a percentage of the control to which no vesicles were added.

Transfection Experiments. Cells were seeded in 96-well microtiter plates at 1 × 10^4 cells/well and incubated overnight in a humidified, 10% CO_2 atmosphere at 37 °C. From preliminary transfection experiments (data not shown) and the EthBr assay, the optimal vesicle:DNA ratio was established.

Equal volumes of polymeric vesicle suspensions and plasmid DNA (pCMVsport-β-gal) solutions (100 μg mL^{-1}) were mixed and incubated at room temperature for 30−45 min. The cell incubation medium was replaced by Opti-MEM (100 μL) and the appropriate dilution of the polymeric vesicle−DNA complex (100 μL). Hence, each well received either 2.5 or 1.25 μg of DNA applied at a concentration of 25 or 12.5 μg mL^{-1}. After incubation for 4 h (10% CO_2, 37 °C), the mixture was replaced by DMEM (200 μL) supplemented with FCS (10% v/v), glutamine (2 mM), penicillin (100 IU mL^{-1}), and streptomycin (100 μg mL^{-1}).

The β-galactosidase activity was determined 48 h post-transfection by measuring *o*-nitrophenyl β-D-galactopyranoside (ONPG) cleavage using a photometric assay. After washing with PBS (pH 7.4), cells were lysed by the addition of lysis buffer (0.1% w/v Triton-X, 0.25 M Tris base, pH 8, 70 μL/well) and three freeze−thaw cycles. PBS (pH 7.4, 50 μL) and a solution of ONPG (1.5 mg mL^{-1}, 150 μL) in buffer (sodium dibasic phosphate, 60 mM; magnesium chloride, 1 mM; potassium chloride, 10 mM; β-mercaptoethanol, 50 mM, pH 8) were added to each well. After incubation at 37 °C for 30 min, absorbance at 405 nm was determined in a plate reader and compared to the on-plate β-galactosidase standard curve.

Statistics. Statistical significance was assessed using one way analysis of variance (ANOVA) via the statistical software package Minitab 10.5 for Windows.

RESULTS

Polymer Synthesis and Characterization. Two dialysis steps combined with dissolution of the product in chloroform, the filtration of undissolved material and the final precipitation of the product in diethyl ether, were sufficient for the purification of the modified polymers. The absence of low molecular weight contaminants in the modified polymers was verified by gel permeation chromatography−refractive index output as exemplified for PLP in Figure 2. The reactants palmitic acid *N*-hydroxysuccinimide (retention volume, Rv = 19.5 mL) and unreacted mPEG (Rv = 17.5 mL) were not detected, and the main polymer peak eluted with a Rv = 16.5 mL (Figure 2). After the synthesis of mPEG−poly-L-lysine, unreacted mPEG is detected as a shoulder to the right of the main peak in the light scattering and refractive index detector plots. This shoulder disappears after dialysis.

From the NMR data, the proton assignments of POP were found to be δ 0.88 ppm = CH_3 (palmitoyl), δ 1.25 ppm = CH_2 (palmitoyl), δ 1.60 ppm = CH_2 (palmitoyl, β to carbonyl), δ 2.16 = CH_2 (palmitoyl, α to carbonyl), δ 3.38 ppm = CH_3 (methoxy PEG), δ 3.45−3.82 ppm = CH_2 (PEG) and for PLP at elevated temperature, δ 0.88 ppm = CH_3 (palmitoyl), δ 1.26 ppm = CH_2 (palmitoyl), δ 1.4−1.6 CH_2 (δ protons on lysine and β protons on palmitoyl) δ 2.1−2.6 ppm = CH_2 (α proton on palmitoyl and β and γ protons on lysine) δ 3.15 ppm = CH_2 (ϵ proton on lysine) δ 3.38 ppm = OCH_3 (mPEG), δ 3.45−3.83 ppm = CH_2 (mPEG), δ 4.22pm = CH (α proton on lysine), δ 6.35−6.61 ppm = NH_2 (lysine) δ 7.15 ppm = NH (lysine), δ 7.2 ppm = CH (chloroform). From the ratio of palmitoyl CH_3 and mPEG OCH_3 for each polymer, the ratio of palmitoyl groups to mPEG groups was calculated as 5:1 POP and 4.9:1 for PLP. Originally, the NMR spectra of POP and PLP did not show peaks for the amino acid backbone, indicative of a limited mobility of the modified polymer backbone. This limited mobility of the polymer backbone was confirmed by recording the ^{1}H NMR spectra of PLP at elevated temperature (48 °C), and peaks for the main-chain groups were then observed. The proton assignments for the unmodified polymers are as follows: poly-L-ornithine, δ 1.8 ppm = CH_2 (β and γ protons on

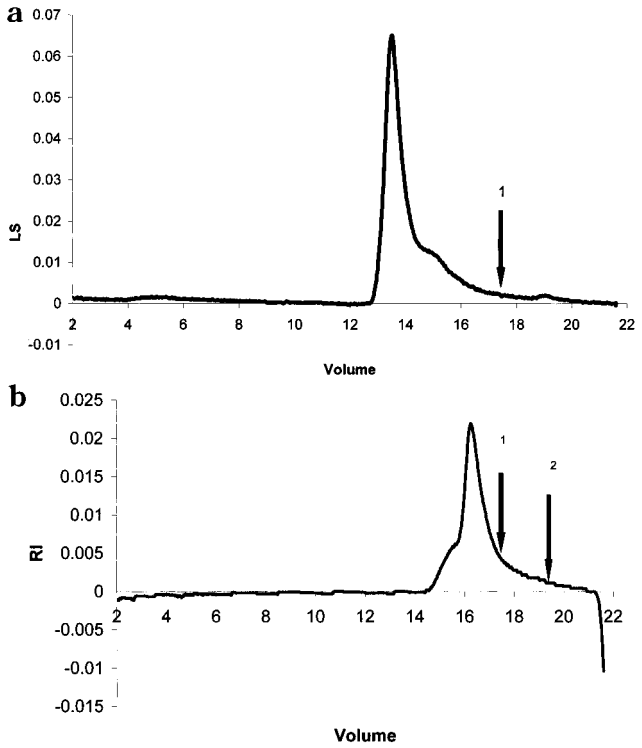

Figure 2. Gel Permeation with (a) multiangle laser light scattering detection and (b) refractive index detection chromatographs of PLP. See Materials and Methods for chromatography conditions. LS = light scattering detector output, RI = refractive index detector output, 1 = point of peak elution of unreacted mPEG, detectable by the light scattering and refractive index detectors as a distinct shoulder, 2 = point of peak elution of the unreacted PNS, detectable by the refractive index detector only.

ornithine), δ 3.0 ppm = CH_2 (δ proton on ornithine) δ 4.3 ppm CH (α carbon on ornithine) and poly-L-lysine δ 1.5 ppm = CH_2 (δ proton on lysine), δ 1.8 = CH_2 (β and γ protons on lysine), δ 3.1 = CH_2 (ϵ proton on lysine), δ 4.4 ppm CH (α proton on lysine).

The TNBS assay (*23*) was used to evaluate the degree of modification of poly-L-ornithine and poly-L-lysine. The amount of accessible amino groups was found to be 1.30 ± 0.04 mmol g^{-1} (n = 3) for POP and 1.32 ± 0.18 mmol g^{-1} (n = 3) for PLP. Clear solutions of PLP and POP in a methanol−aqueous mixture were analyzed. Complete dissolution of PLP and POP is essential if all the unreacted amino groups are to be accessible to the TNBS reagent. The ratio of amino, palmitoyl, and mPEG groups may be assessed if the ratio of palmitoyl to mPEG groups is known using eqs 1−3, which exemplify the calculations for PLP:

$$x + y + z = \mathrm{DP} \tag{1}$$

$$\frac{y}{x} = 5 \tag{2}$$

$$\frac{128z}{5127x + 367y + 128z} \times 100 = 16.9 \tag{3}$$

where x = the number of mPEG groups, y = the number of palmitoyl groups, and z = the number of unreacted lysine groups, DP = the degree of polymerization, 16.9 = the weight percent of unreacted poly-L-lysine, and 5 = the ratio of palmitoyl groups to mPEG groups. Solving for x, y, and z, yields a ratio of free lysine, palmitoyl lysine, mPEGylated lysine of 10.9:5:1. The equivalent ratio for POP is 10.7:5:1. Hence, each PLP chain with a manufacturer's stated degree of polymerization for poly-L-lysine of 123 has on average 7 mPEG groups, 36 palmitoyl groups, and 80 free amine groups, while each POP chain with a manufacturer's stated degree of polymerization for poly-L-ornithine of 97 has on average 6 mPEG groups, 29 palmitoyl groups and 62 free amine groups.

Table 1. Size of PLP and POP Vesicles with DNA, Mean of at Least Three Measurements

sample	size (nm)	polydispersity
POP/CHOL, DNA 20:1 (freshly complexed)	476	0.06
POP/CHOL, DNA 20:1 (6.5 h old)	593	0.47
PLP/CHOL, DNA 20:1 (freshly complexed)	375	0.43
PLP/CHOL, DNA 20:1 (6.5 h old)	426	0.06

Polymeric Vesicle Characterization. Polymeric vesicles prepared from this new class of amphiphilic polymer and cholesterol were visualized by freeze-fracture electron microscopy. Although images of filtered samples are shown in Figure 3, there was no difference in the vesicle morphology when unfiltered samples were imaged. The vesicles diameter measured by photon correlation spectroscopy was 400−600 nm and remained stable for more than 9 months at 4 °C (Figure 2). The vesicles encapsulated doxorubicin at levels of 11.7 ± 1.5 mg g^{-1} PLP and 14 ± 4.2 mg g^{-1} POP, respectively (mean ± sd, n = 3).

Both POP and PLP vesicles condense DNA at polymer to DNA weight ratios of 5:1 or greater. Complexation occurred almost instantaneously and was found to be stable for up to 46 h (Figure 3). These results were also confirmed by agarose gel electrophoresis DNA retardation studies (data not shown). Complexation of the vesicles with DNA did not result in a large change in size (Table 1) and vesicles were present after complexation of the polymeric vesicles with DNA (Figure 3, panels c and d).

The results of the TNBS assay reveal that 5 g of PLP or POP contain 6.5 mmol of free amino groups and since 1 g of DNA contains 3 mmol of phosphate groups, a polymer, DNA weight ratio of 20:1, as used for biological testing, results in a positive to negative charge ratio of 8.7:1. A poly-L-lysine, DNA weight ratio of 5:1, as used for biological testing, would give a positive to negative charge ratio of 10.2:1, and a poly-L-ornithine, DNA weight ratio of 5:1 gives a positive to negative charge ratio of 11.3. The weight ratios used for biological testing were chosen based on the results of the ethidium bromide assay.

The ζ-potential of the polymeric vesicles and polymeric vesicle DNA complexes was seen to become more positive as the level of polymer increased although in essence the ζ-potential was near neutral at the polymer, DNA ratios (20:1) used for the transfection study (see below and Table 2). This is due to the shielding of the positively charged amino groups by the mPEG chains on the outside of the vesicles. The ζ-potential of the unmodified polymer, DNA complexes was extremely positive at the weight ratios (5:1) used for the transfection studies (Table 2).

Haemocompatibility. The haemolytic activity of PLP vesicle−DNA complexes is significantly higher than that of the parent compound (Figure 5), which is not surprising given the amphiphilic character of these new vesicle forming polymers. The haemolytic activity of POP vesicle

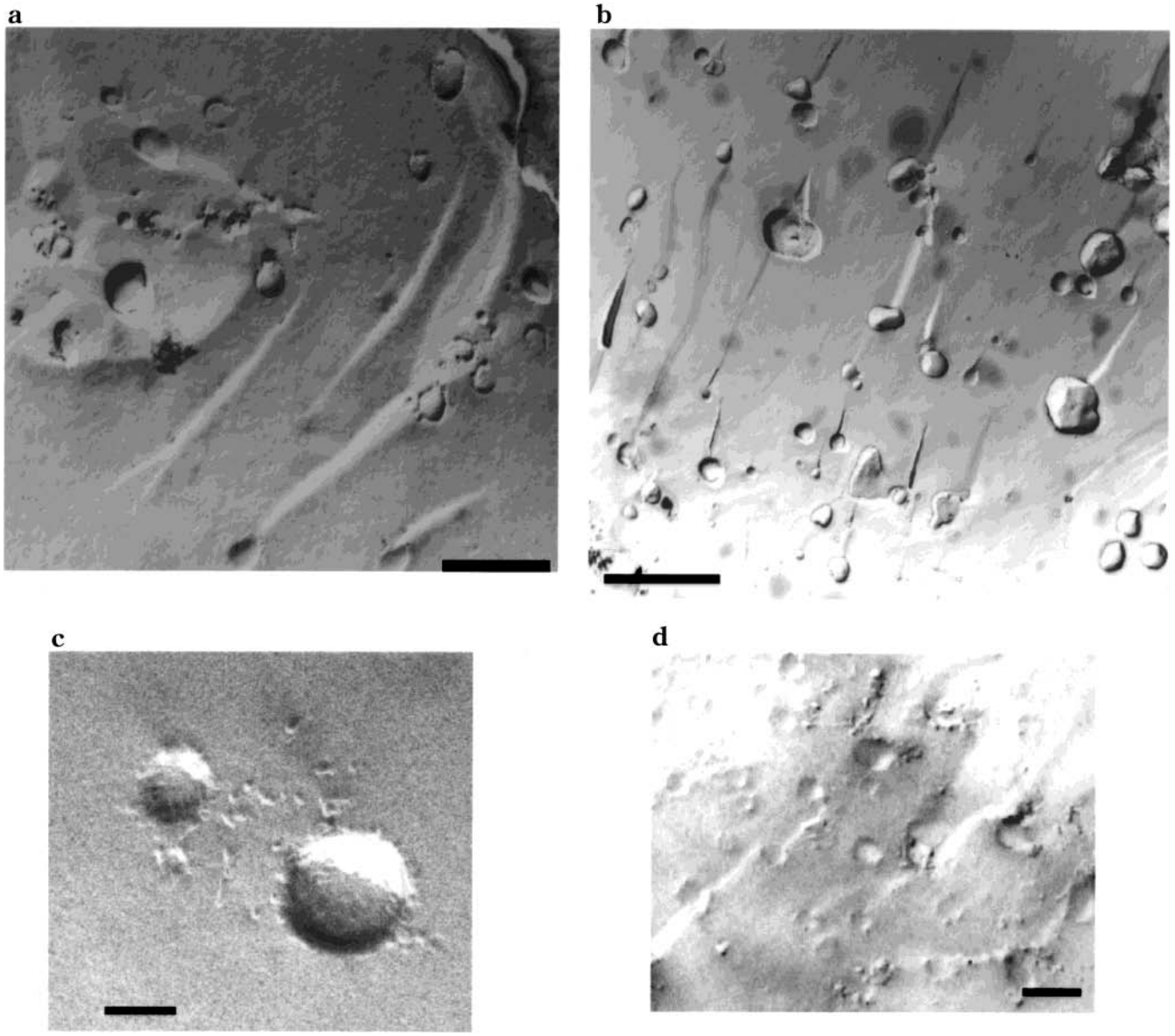

Figure 3. Freeze-fracture electron micrographs (FFEM) of polymeric vesicles. (a) Prepared by sonicating a dispersion of the amphiphilic polymer POP (10 mg) and cholesterol (4 mg) in PBS, pH 4.0 and filtered (0.45 mm), (b) prepared by sonicating a dispersion of PLP (10 mg) and cholesterol (4 mg) in PBS, pH 4.0, filtered (0.45 mm) and stored for 9 months at refrigeration temperatures. Bar = 600 nm. (c) FFEM of POP, cholesterol (5:2) or (d) PLP, cholesterol (5:2) vesicles (unfiltered) complexed with DNA at a polymer DNA ratio of 20:1. Bar for panels c and d = 400 nm.

Table 2. ζ-Potential Measurements of POP/PLP Vesicles and Poly-L-lysine and Poly-L-ornithine, Data = Mean of at Least Three Measurements

sample	polymer:DNA weight ratio	ζ-potential (mV)
PLP, cholesterol (5:1) vesicles	1:0	+2.5
	2.5:1	−21.1
	5:1	−4.2
	10:1	+1.6
	20:1	+ 4.7
POP, cholesterol (5:1) vesicles	1:0	+1.6
	2.5:1	−22.6
	5:1	−11.1
	10:1	−6.7
	20:1	−4.2
poly-L-lysine	5:1	+18.2
poly-L-ornithine	5:1	+10.3

DNA complexes is also increased with respect to the parent polymer at the highest concentration tested only.

Cytotoxicity Results. Vesicles based on the modified polymers POP and PLP were found to be about 1 order of magnitude less toxic than the unmodified polymers in the A549 and A431 cell lines. IC_{50} values of 0.075 mg mL^{-1} (POP), 0.074 mg mL^{-1} (PLP), 0.007 mg mL^{-1} (PLL), and 0.004 mg mL^{-1} (PO) were found in the A431 cell lines, and IC_{50} values of 0.051 mg mL^{-1} (POP), 0.063 mg mL^{-1} (PLP), 0.007 mg mL^{-1} (PLL), and 0.005 mg mL^{-1} (PO) were found in the A549 cell lines (Figure 6, panels a and b). Complexing the polymeric vesicles with DNA still resulted in a 1−2 orders of magnitude improvement in toxicity when compared to the parent polymers. IC_{50} values of 0.028 mg mL^{-1} (POP), 0.083 mg mL^{-1} (PLP), 0.005 mg mL^{-1} (PLL), and 0.004 mg mL^{-1} (PO) were found in the A431 cell lines, and IC_{50} values of 0.912 mg mL^{-1} (POP), 0.396 mg mL^{-1} (PLP), 0.005 mg mL^{-1} (PLL), and 0.005 mg mL^{-1} (PO) were found in the A549 cell lines (Figure 6, panels c and d).

Transfection Results. POP and PLP vesicles were able to transfect both A549 and A431 cells at a polymer, DNA weight ratio of 20:1 (Figure 7). The use of receptor specific ligands such as folate (*27*), transferrin (*28*), or

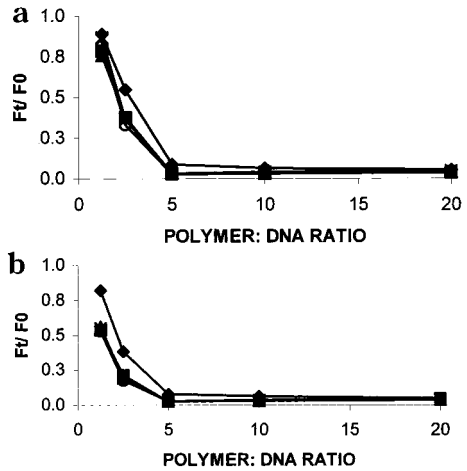

Figure 4. Condensation of DNA by poly-L-amino acid based vesicles. (a) Poly-L-ornithine-based vesicles (POP: chol, 5:2 weight ratio, pH 4). (b) Poly-L-lysine-based vesicles (PLP: chol, 5:2 weight ratio, pH 4) as probed using the reduced fluorescence of an eithidium bromide solution, Ft = EthBr fluorescence in the presence of the polymeric vesicle, DNA complex at time t, F0 = EthBr fluorescence in the presence of DNA; (◆) 0 h, (■) 0.5 h, (▲) 1 h, (□) 6 h, (○) 24 h, (×) 46 h.

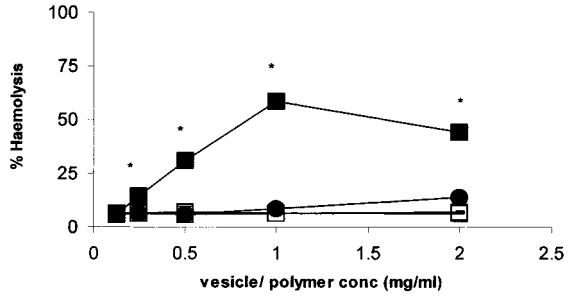

Figure 5. Hemolytic activity of poly-L-amino acid based polymeric vesicle−DNA complexes ($n = 3 \pm$ sd) at varying polymer concentrations. Polymer, DNA weight ratio = 20:1 for polymeric vesicles and 5:1 for unmodified polymers. (+/−) Charge ratio = 9:1 for polymeric vesicles and 10.5:1 for unmodified polymers. (●) POP, chol vesicles (5:1); (■) PLP, chol vesicles (5:1); (○) PO; (□) PLL. (*) Statistically significant difference ($p < 0.05$).

galactose (*29*) or lysomotropic agents such as histidyl residues (*30*) or chloroquine (*31*) was not necessary. DNA was used at a high (25 μg mL^{-1}) and a low (12.5 μg mL^{-1}) concentration level, and the unmodified polymers were no superior to DNA alone in every case. In the A431 cell line (Figure 7a), PLP vesicles were significantly better than all other formulations at the lower (12.5 μg mL^{-1}) DNA concentration level being 7.8 times as efficient as poly-L-lysine and 4.9 times as efficient as DNA alone. Also in the A431 cell line, PLP vesicles were significantly better than the unmodified polymer and DNA at the higher (25 μg mL^{-1}) concentration level being 2.4 times as efficient as poly-L-lysine and 2.1 times as efficient as DNA alone.

In the A549 cell line, all formulations were indistinguishable at the lower DNA concentration level. However, at the higher DNA concentration level POP vesicles were significantly better than DNA alone or the parent polymer PO, being 4.5 times better than DNA and 2.3X better than PO, respectively. Also in the A549 cell line at the higher DNA concentration level, PLP vesicles were significantly better than DNA alone and the parent polymer PLL, being 3.5 times better than DNA alone and 2.3 times better than the unmodified polymer PLL, respectively.

This data demonstrates that the polymeric vesicle formulations are able to improve the transfection efficiency of the poly-L-amino acid polymers significantly with increases of up to 8-fold in some cases.

DISCUSSION

We report here the formation of polymeric vesicles prepared from a new class of amphiphilic polymer. The arrangement of the polymer in the bilayer is most probably as depicted in Figure 8. We have shown previously that hydrophobic modification of hydrophilic carbohydrate polymers is an elegant method for the preparation of polymeric vesicles (*6*). Such polymeric vesicles show good stability on storage and have been tested as drug delivery systems (*32*). The vesicles based on these new amphiphilic polymers PLP and POP were also able to encapsulate drugs such as doxorubicin HCl (MW 543.5) with a capacity of more than 10 mg/g of polymer and hence could potentially serve as drug carriers.

The polymeric vesicles efficiently condense DNA (Figure 4) and may thus be anticipated to confer some protection from nucleases in vivo. They are less cytotoxic than the parent polymers (Figure 6) and transfection competent in vitro with an efficacy better than that of the parent linear polymer in most cases (Figure 7). However, due to the amphiphilic nature of PLP, polymeric vesicles are more haemolytic than the parent homopolymer PLL. POP vesicles are no more haemolytic than the parent polymer PO except at the highest concentration. It remains to be seen whether haemolytic activity observed in vitro will preclude their use by the intravenous route in vivo. Preliminary animal experiments to be reported in a subsequent communication revealed no gross toxic effects when CD1 mice were administered 0.5 mg of PLP via the intravenous route while animals administered 0.25 mg of PLL suffered fatalities within hours.

Although the PLP- and POP-based systems may be useful for drug delivery, they were primarily designed as gene delivery systems that combine a number of properties, which have emerged as being potentially important for in vivo gene delivery and which only exist in disparate systems to date.

Modification of the Poly-L-amino Acid Homopolymer. The conjugation of residues such as galactose (*29*), transferrin (*28*), or asialofetuin (*33*) to poly-L-lysine has been used to facilitate receptor-mediated uptake and targeting of polyplexes. The hydrophilic substitution of poly-L-lysine ϵ-amino groups has also been shown to improve the transfection efficiency in vitro (*34*). A 30−50% modification through coupling of δ-gluconolactone reduced the number of amino groups available for interaction with the DNA. The improved dissociation of the polyplex has been suggested as a possible reason for the higher transfection efficiency. This effect may also be involved in the improvements that we observed after the modification of PLL and PO with both lipophilic and hydrophilic moieties. From ^{1}H NMR and TNBS data the degree of substitution in both the POP and PLP polymer can be estimated to be in the order of 33mole%. Polymeric vesicles interacted strongly with plasmid DNA despite this reduction in charged groups available for binding. The reduction in ethidium bromide fluorescence at a polymer, DNA weight ratio of ≥5:1 (a charge ratio of ≥2:1) indicated that DNA was efficiently condensed by the polymeric vesicles. The 2:1 amino-to-phosphate ratio required for DNA condensation is not surprising consid-

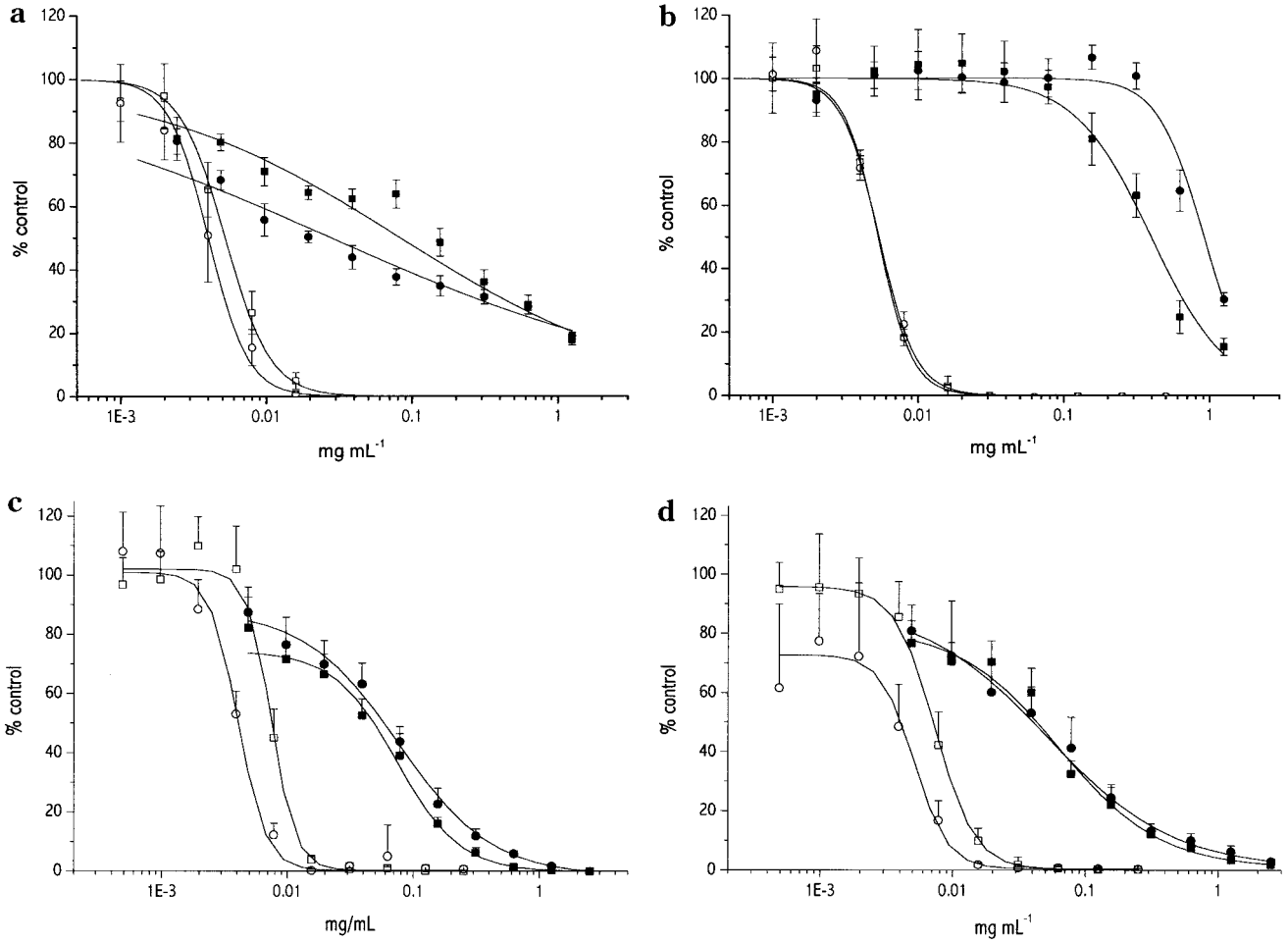

Figure 6. Cytotoxicity in (a) A431 cells and (b) A549 cells after incubation with POP and PLP vesicles−DNA complexes (polymer, DNA = 20:1; (+/−) charge ratio = 9:1) and PLL and PO−DNA complexes (polymer DNA = 5:1, (+/−) charge ratio = 10.5:1) for 4 h and (c) A549 cells and (d) A431 cells after incubation with POP and PLP vesicles and PLL and PO polymers for 4 h ($n = 3 \pm$ sd). (■) PLP, chol (5:1) vesicles, (●) POP, chol (5:1) vesicles, (○) PO, (□) PLL.

ering that some of the positive charges are located in the inner leaflet of the polymeric vesicle (Figure 8). However, the exact ultrastructure the polymeric vesicle:DNA complex remains unclear and although intact vesicles are still visible on electron micrographs of the complexes, some additional discrete much smaller units (10−50 nm) were also observed. There was no evidence that DNA was embedded into multilamellar structures as has been reported for cationic lipids (*35*).

Grafting of liposome membranes with 5−10 mol % PEG (MW 2000−5000) dramatically reduces the binding of plasma protein to particulate drug carriers which in turn prevents the rapid vesicle clearance by the reticuloendothelial system, thus reducing blood clearance and extending circulation times (*14*, *36*). Poly-L-lysine−DNA complexes are also rapidly cleared from the systemic circulation with a plasma half-life of 5 min (*37*). Consequently, attempts have been made to utilize the stabilizing properties of PEG chains by synthesizing PLL-PEG block copolymers (*38*, *39*), thus reducing the interaction with serum proteins and attempting to improve the stability of the polyplexes in vivo.

The conjugation of mPEG groups to the amino acid homopolymers reported here, apart from contributing to the amphiphilic nature of the polymer, also serves to shield the positive charges on the surface of these polymeric vesicles, rendering the vesicles with an essentially neutral ζ-potential (−4.16 to +4.65 mV, Table 1). This compares favorably with the ζ-potentials reported by others (*37*) for PLL, DNA complexes at an amine-to-phosphate ratio of 2:1, +30 mV for such mass ratios of greater than 4:1 (*13*), and our data which gives a value of +10 and +18 mV for PO−DNA (5:1 weight ration) and PLL−DNA (5:1 weight ratio), respectively. All measurements performed in our laboratories were performed in PBS (pH 7.4), and hence, any shielding of the charges by the presence of dissolved salts affected all formulations in equal measure. This electroneutrality also suggests that large proportions of the mPEG chains are exposed on the outside of the polymeric vesicle−DNA complex. The formation of a complex with DNA by these electrically neutral polymeric vesicles is possible because of the fluidity of the mPEG chains, which will allow the negatively charged DNA short periods of access to the positively charged amino groups. Most protocols for the formulation of transfection competent lipoplexes or polyplexes require the use of an excess positive charge for the efficient condensation of the plasmid DNA (*15*). Such complexes carry a net positive charge, which is reflected in their extremely positive ζ-potential (>10 mV). The electrostatic interaction between the negatively charged cells and the positively charged complexes facilitates nonspecific binding and subsequent endosomal uptake (*15*). This is advantageous in vitro but poses a problem for the targeted delivery of such carriers and/or delivery in vivo (*40*). It is also one of the main reasons for the frequently observed accumulation of complexes in the first capillary bed that they encounter after injection, i.e.,

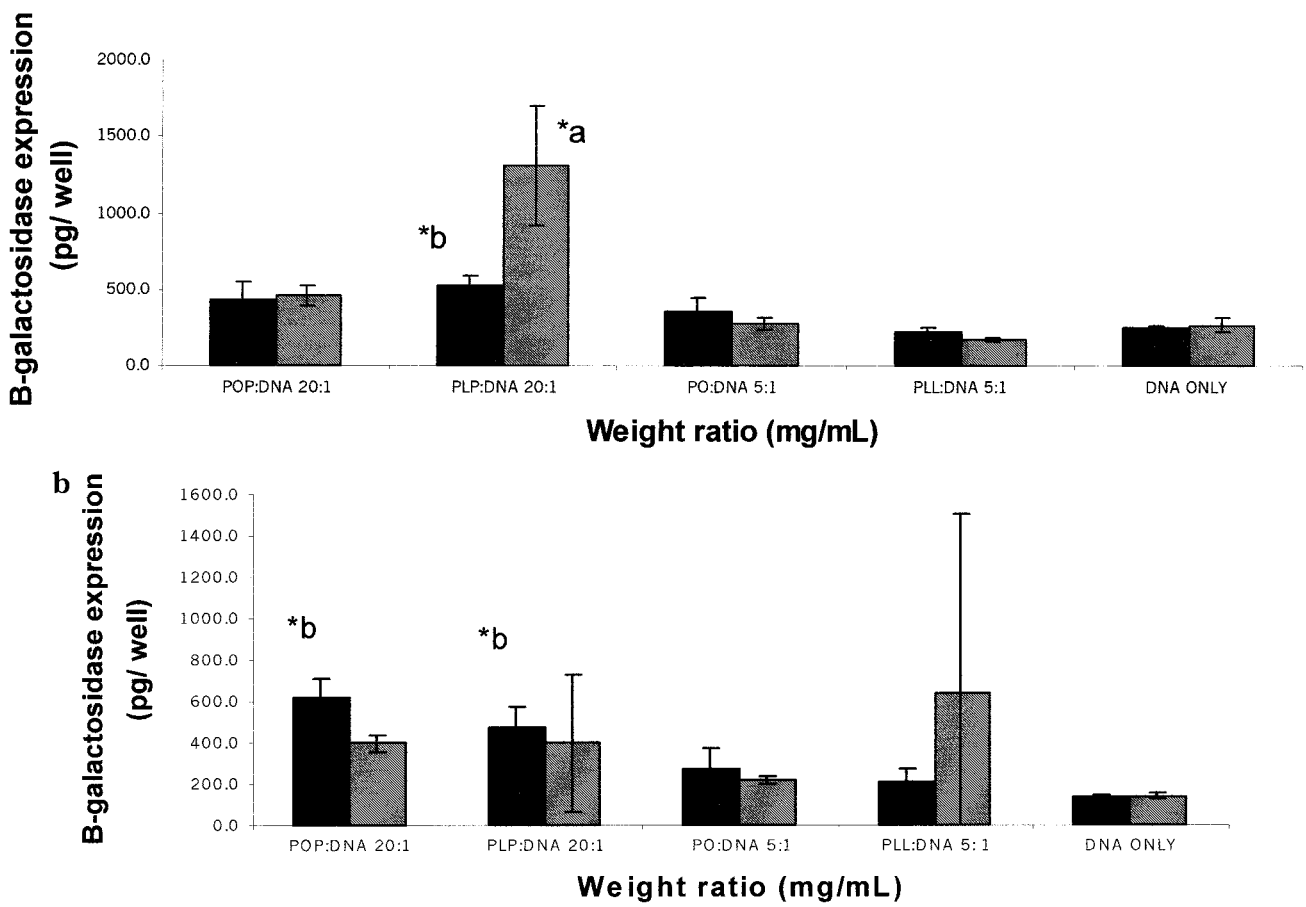

Figure 7. Transfection of pCMVsport-b-gal in (a) the A431 cell line and (b) the A549 cell line with polymeric vesicle formulations, ($n = 3 \pm$ sd), solid bars = 25 μg mL^{-1} DNA and hatched bars = 12.5 μg mL^{-1} DNA, (*a) statistically significant difference ($p < 0.05$) between PLP, chol (5:1) vesicle−DNA formulations and all other formulations and (*b) = statistically significant difference ($p < 0.05$) between polymeric vesicles and parent homopolymers.

the lung (*19*). Targeting of nonviral vectors, i.e., via ligands that bind to specific receptors, is hampered by the presence of excess positive and negative charges (*16*).

The incorporation of PEG in conventional liposomes involves the conjugation of PEG chains to diacyl or dialkyl groups. The properties of such carriers may change, however, with time, as the intermembrane transfer of such conjugates can be quite substantial (*41*). In fact the exchange is rapid enough to allow the "PEGylation" of preformed vesicles within minutes to hours (*42*). Such events will be minimized with the use of polymers bearing pendant PEG groups such as PLP and POP. The complexation of these macromolecules with DNA provides further noncovalent anchorage of PEG groups and is likely to increase the long-term stability of these particulates further.

The polymeric POP and PLP vesicles represent a hybrid system with a unique mixture of polymeric and vesicular properties. The conjugation of lipophilic elements has been used in the past to modify the properties of PLL (*43*). This "lipopoylysine" was based on a low molecular weight poly-L-lysine (MW 3000) to which an average of two dialkylphosphatidyl ethanolamine groups per molecule were conjugated which improved the transfection efficiency by a factor of 100 compared to the unmodified PLL. (*43*). More recently, Kim and others coupled stearyl fatty acid chains to PLL and used this conjugate in conjunction with low-density lipoprotein (LDL) to form complexes of 100 nm which were transfection competent (*44*). However, there have been no reports detailing the attachment of both hydrophobic and hydrophilic elements to amino acid homopolymers. The attachment of palmitoyl groups as well as mPEG groups provided the present polymer with the amphiphilic character required for assembly into vesicles.

Cholesterol. Helper lipids such as DOPE are popular constituents of lipoplexes (*45*). DOPE is generally considered to be one of the most potent helper lipids in vitro (*46*). It acts presumably by facilitating the endosomal escape of the lipoplex (*47*). A number of groups have, however, reported its limitations in vivo and suggested cholesterol as a superior alternative (*20*, *48*). We have therefore chosen cholesterol as the second constituent of our polymeric vesicle system. The inclusion of cholesterol in the systems has also been aimed at increasing the bilayer stability. Neutral gene delivery systems that contain cholesterol have improved half-lives in the bloodstream of mice (*49*). Cholesterol incorporation in the bilayer plus the polymeric nature of the vesicles should provide a more stable complex by preventing serum proteins inserting into the bilayer (*49*), which is thought to be important in the rapid clearance of complexes from the bloodstream (*37*). It is not clear at this time whether the effects of cholesterol in vivo are based on the improved stability or its effects as helper lipid, i.e., improving the intracellular trafficking of the complex.

Cytotoxicity and Haemocompatibility. The amphiphilic derivatives are about 1−2 orders of magnitude less cytotoxic than the respective parent homopolymers (Figure 6). However, the amphiphilic nature of the polymers also means that they interact more strongly with biological membranes. The interaction with eryth-

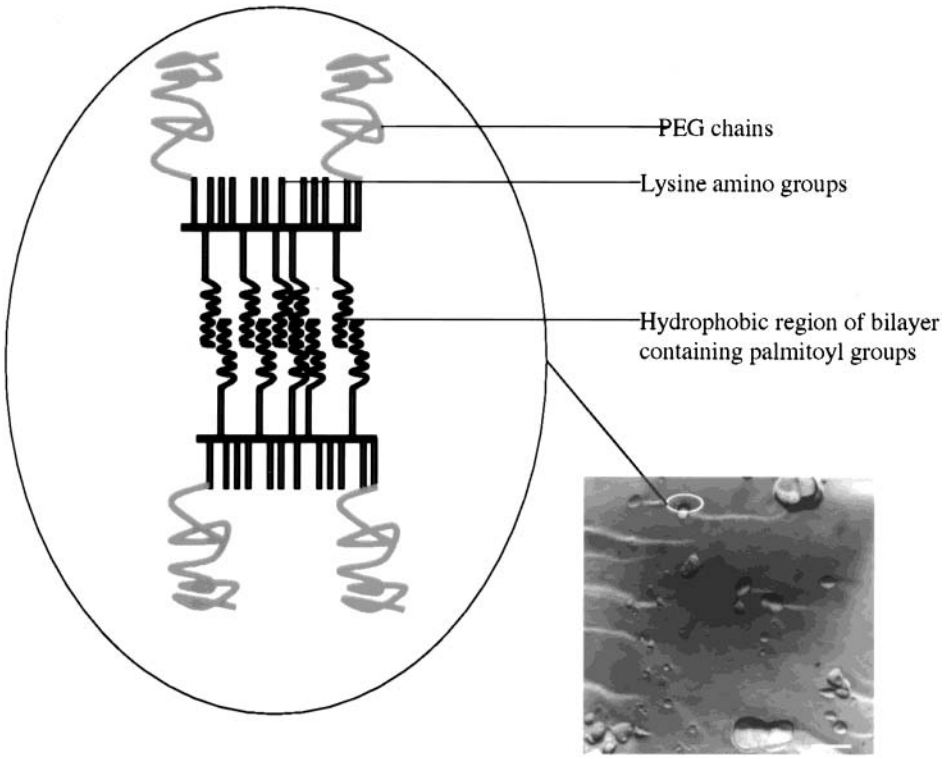

Figure 8. Schematic representation of the organization of the amphiphilic amino acid based polymer in the bilayer.

rocyte membranes and their subsequent lysis has been observed after the administration of cationic lipids and could limit the use of these carriers (*50*), and although the complexation of the cationic lipids to DNA reduces the haemolytic potential (*51*), this may still present a problem for the use of high doses of DNA in humans (*52*). The PLP vesicles show more haemolytic activity than the nonamphiphilic parent polymer−PLL (Figure 6). This could limit their further development as gene delivery systems.

Transfection. The modifications that we have introduced into the homopolymers PLL and PO were designed with the specific problems of in vivo gene delivery in mind. The properties that define a good carrier for in vivo application differ considerably from those, which have been shown to give rise to efficient transfection in vitro. It is not surprising then that the correlation of transfection ability in vitro and in vivo has frequently been shown to be poor (*53*).

Nevertheless, we have studied the ability of our POP- and PLP-based polymeric vesicles in two types of carcinoma cell lines as a preliminary screen. Both types of vesicles transfected both A549 and A431 cells (Figure 7). Transfection efficiency was more than doubled compared to the original polymeric systems and in one case was found to be eight times better. At the higher PLP−DNA concentration in the A431 cell line, transfection efficiency is compromised by the cytotoxicity of the carrier (Figure 7), as the IC_{50} in this cell line for PLP-DNA complexes is 0.083 mg mL^{-1}, but a concentration of 0.5 mg mL^{-1} PLP was applied when DNA concentrations of 25 μg mL^{-1} were used. Higher cell densities were used in the transfection experiments in order to make meaningful observations. With the A549 cell lines a similar polymeric vesicle−DNA concentration of 0.5 mg mL^{-1} and 25 μg mL^{-1}, respectively, did result in an improvement in transfection efficiency when compared to the parent polymers or DNA alone. This is due to the fact that the IC_{50} of POP−DNA and PLP−DNA complexes was higher in this cell line at 0.912 and 0.396 mg mL^{-1}, respectively. This variability in in vitro response underlines the limitations of in vitro assays. While in vitro assays can serve as a crude pointer to efficacy, the results are probably unconnected to the potential of the POP and PLP polymeric vesicles for in vivo gene delivery. The present POP/PLP−DNA complexes bear a neutral surface charge which would probably reduce nonspecific binding to the cells and subsequent uptake (*15, 54*) in vitro. Yet this neutral surface charge would allow specific targeting in vivo once the complexes are conjugated with targeting ligands.

We are currently developing ligand-carrying POP- and PLP-based systems that should allow specific uptake by receptor expressing cells. We are also studying the influence of the modification we have described in this paper on the in vivo transfection efficiency of these systems.

CONCLUSION

Poly-L-amino acids on modification by the attachment of hydrophilic mPEG groups and hydrophobic palmitoyl groups yield a new class of amphiphilic polymers. These polymers form polymeric vesicles in the presence of cholesterol and have been designed with the ultimate aim of producing effective gene transfection levels in vivo, while remaining safe. Such polymeric vesicles are less cytotoxic but more haemolytic than the parent homopolymers. It remains to be seen whether this haemolytic activity will preclude their use via the intravenous route and limit their use to other parenteral routes. The transfer of DNA into live mammalian cells is improved by the use of these polymeric vesicles when compared to the parent homopolymers. This new class of polymeric vesicles bears all the attributes that have been recognized as being favorable for efficient gene delivery in vivo, i.e., the presence of cholesterol, a neutral surface charge and a mPEG surface. They can also support the attachment of targeting ligands for gene targeting.

ACKNOWLEDGMENT

The authors would like to acknowledge Ms. Soryia Siddique who was involved in the early part of this work and Dr. Jane Plumb for useful discussions on the tissue culture experiments.

LITERATURE CITED

(1) New, R. R. C. (1990) Introduction. In *Liposomes a practical approach* (R. R. C. New Ed.) pp 1−32, Oxford University Press, Oxford.

(2) Uchegbu, I. F., Ed. (1999) In *Synthetic surfactant vesicles - an introduction to niosomes and other nonphospholipid systems* (A. T. Florence, G. Gregoriadis, Eds.) Drug Targeting and Delivery Series, 1st ed., Vol. 11, Harwood Academic Publishers, Amsterdam.

(3) Gregoriadis, G. (1995) Engineering liposomes for drug delivery: progress and problems. *Trends Biotechnol. 13*, 527−536.

(4) Uchegbu, I. F., and Vyas, S. P. (1998) Nonionic surfactant vesicles (niosomes) in drug delivery. *Int. J. Pharm. 172*, 33−70.

(5) Porteous, D. J., Dorin, J. R., McLachlan, G., DavidsonSmith, H., Davidson, H., Stevenson, B. J., Carothers, A. D., Wallace, W. A. H., Moralee, S., Hoenes, C., Kallmeyer, G., Michaelis, U., Naujoks, K., Ho, L. P., Samways, J. M., Imrie, M., Greening, A. P., and Innes, J. A. (1997) Evidence for safety and efficacy of DOTAP cationic liposome mediated CFTR gene transfer to the nasal epithelium of patients with cystic fibrosis. *Gene Ther. 4*, 210−218.

(6) Uchegbu, I. F., Schätzlein, A. G., Tetley, L., Gray, A. I., Sludden, J., Siddique, S., and Mosha, E. (1998) Polymeric chitosan-based vesicles for drug delivery. *J. Pharm. Pharmacol. 50*, 453−458.

(7) Gao, X., and Huang, L. (1995) Cationic liposome-mediated gene transfer. *Gene Ther. 2*, 710−722.

(8) Verma, I. M., and Somia, N. (1997) Gene therapy − promises, problems and prospects. *Nature 389*, 239−242.

(9) Jolly, D. (1996) Viral vector systems for gene therapy. In *The Internet book of gene therapy* (R. E. Sobol and K. J. Scanlon, Eds.) pp 3−25, Appleton & Lange, Boston.

(10) Lee, R. J., and Huang, L. (1997) Lipidic vector systems for gene transfer. *Crit. Rev. Ther. Drug Carr. Syst. 14*, 173−206.

(11) Behr, J. P., Demeneix, B., Loeffler, J. P., and Mutul, J. P. (1989) Efficient gene-transfer into mammalian primary endocrine-cells with lipopolyamine-coated DNA. *Proc. Natl. Acad. Sci. U.S.A. 86*, 6982−6986.

(12) Wolfert, M. A., Schacht, E. H., Toncheva, V., Ulbrich, K., Nazarova, O., and Seymour, L. W. (1996) Characterization of vectors for gene therapy formed by self- assembly of DNA with synthetic block copolymers. *Hum. Gene Ther. 7*, 2123−2133.

(13) Pouton, C. W., Lucas, P., Thomas, B. J., Uduehi, A. N., Milroy, D. A., and Moss, S. H. (1998) Polycation−DNA complexes for gene delivery: a comparison of the biopharmaceutical properties of cationic polypeptides and cationic lipids. *J. Controlled Release 53*, 289−299.

(14) Hong, K., Zheng, W., Baker, A., and Papahadjopoulos, D. (1997) Stabilization of cationic liposome-plasmid DNA complexes by polyamines and poly(ethylene glycol)-phospholipid conjugates for efficient in vivo gene delivery. *FEBS Lett. 400*, 233−237.

(15) Mislick, K. A., and Baldeschwieler, J. D. (1996) Evidence for the role of proteoglycans in cation-mediated gene transfer. *Proc. Natl. Acad. Sci. U.S.A. 93*, 12349−12354.

(16) Lee, R. J., and Huang, L. (1998) Folate-targeted, Anionic Liposome-entrapped Polylysine-condensed DNA for Tumor Cell-specific Gene Transfer. *J. Biol. Chem. 271*, 8481−8487.

(17) Plank, C., Mechtler, K., Szoka, F. C., Jr., and Wagner, E. (1996) Activation of the complement system by synthetic DNA complexes: A potential barrier for intravenous gene delivery. *Hum. Gene Ther. 7*, 1437−1446.

(18) Zauner, W., Ogris, M., and Wagner, E. (1998) Polylysine-based transfection systems utilizing receptor-mediated delivery. *Adv. Drug Del. Rev. 30*, 97−113.

(19) Liu, F., Qi, H., Huang, L., and Liu, D. (1997) Factors controlling the efficiency of cationic lipid mediated transfection in vivo via intravenous administration. *Gene Ther. 4*, 517−523.

(20) Hong, K., Zheng, W., Baker, A., and Papahadjopoulos, D. (1997) Stabilization of cationic liposome-plasmid DNA complexes by polyamines and poly(ethylene glycol)-phospholipid conjugates for efficient in vivo gene delivery. *FEBS Lett. 400*, 233−237.

(21) Blume, G., and Cevc, G. (1990) Liposomes for sustained drug release in vivo. *Biochim. Biophys. Acta 1029*, 91−97.

(22) Monfardini, C., Schiavon, O., Caliceti, P., Morpurgo, M., Harris, J. M., and Veronese, F. (1995) A branched monomethoxypoly(ethylene glycol) for protein modification. *Bioconjugate Chem. 6*, 62−69.

(23) Snyder, S., and Sobocinski, P. (1975) An improved 2,4,6-trinitrobenzenesulfonic acid method for the determination of amines. *Anal. Biochem. 64*, 284−288.

(24) Ausubel, F., Brent, R., Kingston, E., Moore, D., Seidman, J., Smith, J., Struhl, K., Eds. (1998) *Current Protocols In Molecular Biology*, John Wiley & Sons, New York.

(25) Pecq, J.-B. L. (1971) Use of ethidium bromide for spearation and determination of nucleic acids of various conformational forms and measurement of their associated enzymes. *Methods Biochem. Anal. 20*, 41−86.

(26) Freshney, R. I. (1994) *Culture of animal cells: a manual of basic technique*, 3rd ed., Wiley-Liss, New York.

(27) Mislick, K. A., Baldeschwieler, J. D., Kayyem, J. F., and Meade, T. J. (1995) Transfection of folate-polylysine DNA complexes: evidence for lysosomal delivery. *Bioconjugate Chem. 6*, 512−515.

(28) Wagner, E., Curiel, D., and Cotten, M. (1994) Delivery of Drugs, Proteins and Genes Into Cells Using Transferrin As a Ligand For Receptor-Mediated Endocytosis. *Adv. Drug Del. Rev. 14*, 113−135.

(29) Erbacher, P., Roche, A. C., Monsigny, M., and Midoux, P. (1995) Glycosylated Polylysine Dna Complexes: Gene-Transfer Efficiency in Relation With the Size and the Sugar Substitution Level of Glycosylated Polylysines and With the Plasmid Size. *Bioconjugate Chem. 6*, 401−410.

(30) Midoux, P., and Monsigny, M. (1998) Efficient gene transfer by histidylated polylysine/pDNA complexes. *Bioconjugate Chem. 10*, 406−411.

(31) Midoux, P., Mendes, C., Legrand, A., Raimond, J., Mayer, R., Monsigny, M., and Roche, A. C. (1993) Specific gene transfer mediated by lactosylated poly-L-lysine into hepatoma cells. *Nucleic Acids Res. 21*, 871−878.

(32) Sludden, J., Uchegbu, I., and Schätzlein, A. (2000) The encapsulation of bleomycin within chitosan based polymeric vesicles does not alter its biodistribution. *J. Pharm. Pharmacol. 52*, 377−382.

(33) Wu, J., Liu, P., Zhu, J. L., Maddukuri, S., and Zern, M. A. (1998) Increased liver uptake of liposomes and improved targeting efficacy by labeling with asialofetuin in rodents. *Hepatology 27*, 772−778.

(34) Erbacher, P., Roche, A. C., Monsigny, M., and Midoux, P. (1997) The reduction of the positive charges of polylysine by partial gluconoylation increases the transfection efficiency of polylysine/DNA complexes. *Biochim. Biophys. Acta 1324*, 27−36.

(35) Radler, J. O., Koltover, I., Salditt, T., and Safinya, C. R. (1997) Structure of DNA-cationic liposome complexes: DNA intercalation in multilamellar membranes in distinct interhelical packing regimes. *Science 275*, 810−814.

(36) Blume, G., and Cevc, G. (1990) Liposomes for the sustained drug release in vivo. *Biochim. Biophys. Acta 1029*, 91−97.

(37) Dash, P., Read, M., Barrett, L., Wolfert, M., and Seymour, L. (1999) Factors affecting blood clearance and in vivo distribution of polyelectrolyte complexes for gene delivery. *Gene Ther. 6*, 643−650.

(38) Toncheva, V., Wolfert, M. A., Dash, P. R., Oupicky, D., Ulbrich, K., Seymour, L. W., and Schacht, E. H. (1998) Novel vectors for gene delivery formed by self-assembly of DNA with poly(L-lysine) grafted with hydrophilic polymers. *Biochim. Biophys. Acta 1380*, 354−368.

(39) Choi, J. S., Lee, E. J., Choi, Y. H., Jeong, Y. J., and Park, J. S. (1999) Poly(ethylene glycol)-*block*-poly(L-lysine) dendrimer: Novel linear polymer/dendrimer block coplymer forming a spherical water-soluble polyionic complex with DNA. *Bioconjugate Chem. 10*, 62−65.
(40) Schaffer, D. V., and Lauffenburger, D. A. (1998) Optimization of cell surface binding enhances efficiency and specificity of molecular conjugate gene delivery [In Process Citation]. *J. Biol. Chem. 273*, 28004−28009.
(41) Silvius, J. R., and Zuckermann, M. J. (1993) Interbilayer transfer of phospholipid-anchored macromolecules via monomer diffusion. *Biochemistry 32*, 3153−3161.
(42) Uster, P. S., Allen, T. M., Daniel, B. E., Mendez, C. J., Newman, M. S., and Zhu, G. Z. (1996) Insertion of poly-(ethylene glycol) derivatized phospholipid into preformed liposomes results in prolonged in vivo circulation time. *FEBS Lett. 386*, 243−246.
(43) Zhou, X. H., Klibanov, A. L., and Huang, L. (1991) Lipophilic polylysines mediate efficient DNA transfection in mammalian-cells. *Biochim. Biophys. Acta 1065*, 8−14.
(44) Kim, J. S., Kim, B. I., Maruyama, A., Akaike, T., and Kim, S. W. (1998) A new nonviral DNA delivery vector: the terplex system. *J. Controlled Release 53*, 175−182.
(45) Felgner, P. L., Barenholz, Y., Behr, J. P., Cheng, S. H., Cullis, P., Huang, L., Jessee, J. A., Seymour, L., Szoka, F., Thierry, A. R., Wagner, E., and Wu, G. (1997) Nomenclature for synthetic gene delivery systems. *Hum. Gene Ther. 8*, 511−512.
(46) Zhou, X. H., and Huang, L. (1994) DNA transfection mediated by cationic liposomes containing lipopolylysine: characterization and mechanism of action. *Biochim. Biophys. Acta 1189*, 195−203.
(47) Mok, K. W., and Cullis, P. R. (1997) Structural and fusogenic properties of cationic liposomes in the presence of plasmid DNA. *Biophys. J. 73*, 2534−2545.
(48) Liu, Y., Mounkes, L. C., Liggitt, H. D., Brown, C. S., Solodin, I., Heath, T. D., and Debs, R. J. (1997) Factors influencing the efficiency of cationic liposome-mediated intravenous gene delivery. *Nat. Biotech. 15*, 167−173.
(49) Semple, S. C., Chonn, A., and Cullis, P. R. (1996) Influence of cholesterol on the association of plasma proteins with liposomes. *Biochemistry 35*, 2521−2525.
(50) Senior, J. H., Trimble, K. R., and Maskiewicz, R. (1991) Interaction of positively charged liposomes with blood: implications for their application in vivo. *Biochim. Biophys. Acta 1070*, 173−179.
(51) Schreier, H., Gagne, L., Bock, T., Erdos, G. W., Druzgala, P., Conary, J. T., and Muller, B. W. (1997) Physicochemical properties and in vitro toxicity of cationic liposome cDNA complexes. *Pharm. Acta Helv. 72*, 215−223.
(52) Templeton, N. S., Lasic, D. D., Frederik, P. M., Strey, H. H., Roberts, D. D., and Pavlakis, G. N. (1997) Improved DNA: Liposome complexes for increased systemic delivery and gene expression. *Nat. Biotech. 15*, 647−652.
(53) Ledley, F. D. (1995) Nonviral gene therapy: the promise of genes as pharmaceutical products. *Hum. Gene Ther. 6*, 1129−1144.
(54) Miller, C. R., Bondurant, B., McLean, S. D., McGovern, K. A., and Obrien, D. F. (1998) Liposome-cell interactions in vitro: Effect of liposome surface charge on the binding and endocytosis of conventional and sterically stabilized liposomes. *Biochemistry 37*, 12875−12883.

BC000052D

Targeting the DNA Cleavage Activity of Copper Phenanthroline and Clip-Phen to A·T Tracts via Linkage to a Poly-*N*-methylpyrrole

Marguerite Pitié,[†] J. David Van Horn,[‡] Denis Brion,[‡] Cynthia J. Burrows,*[,‡] and Bernard Meunier*[,†]

Laboratoire de Chimie de Coordination du CNRS, 205 route de Narbonne, 31 077 Toulouse Cedex 4, France, and Department of Chemistry, University of Utah, 315 South 1400 East, Salt Lake City, Utah 84112.
Received May 19, 2000; Revised Manuscript Received September 18, 2000

To target DNA A·T tracts, a three-ring polyamide containing an *N*-methylpyrrole amino acid has been linked, on solid support, to carboxylic derivatives of phenanthroline and dimers of phenanthroline: 2-Clip-Phen, 3-Clip-Phen, or 2-Clip-Phen containing a long tether. After metalation by $CuCl_2$, the DNA cleavage activities of the different conjugates were compared on a restriction fragment. Cleavage patterns showed that the polyamide moiety of conjugates directs the cleavage activity in the vicinity of A·T tracts but the precise cleavage selectivity of these conjugates was dependent on the type of phenanthroline residue linked to the poly-*N*-methylpyrrole entity.

INTRODUCTION

Molecules able to irreversibly modify nucleic acids have received considerable interest because of their potential application as biological tools or as drugs. In addition, compounds that cleave nucleic acids in a sequence-specific manner are useful as reagents for accessing structural and genetic information (*1*−*3*).

1,10-Phenanthroline is a versatile ligand able to chelate copper to give mono-Phen or bis-Phen complexes at the oxidation state + I or + II (*4*). The $(Phen)_2Cu^{I}$ complex in the presence of hydrogen peroxide efficiently cleaves double-stranded DNA by oxidative attack on deoxyribose units from DNA's minor groove (*5*, *6*), while the Phen-Cu^{I} complex is less efficient (*7*). DNA cleavage products include 5′- and 3′-monophosphate ester termini, free bases, 5-methylenefuranone, and a small amount of 3′-phosphoglycolate (*8*−*10*). Hydrogen peroxide can be generated close to the DNA by $(Phen)_2Cu^{II}$ itself in the presence of a reductant and molecular oxygen. Since these Phen complexes have poor sequence selectivity, different conjugates between phenanthroline and targeting DNA ligands (oligonucleotides, Hoescht-33258, DNA binding protein, ...) have been prepared in order to enhance the cleavage specificity (*11*−*17*). However, these chimeric compounds contain only one phenanthroline unit, which is not the best situation for DNA cleavage since the highest cleavage activies have been observed with a Phen:Cu ratio of 2:1.

We have recently prepared 2- and 3-Clip-Phen derivatives containing two Phen ligands linked at the 2′- or 3′-position by a serinol bridge in order to favor the 2:1 Phen:Cu stoichiometry (*18*, *19*). The oxidative nuclease activity of the copper complexes of these new ligands was found to be higher than with Phen itself, by a factor 2 for 2-Clip-Phen but by a factor 60 for 3-Clip-Phen. Conjugates of 2-Clip-Phen with the natural polyamine spermine (a minor groove binder) (*20*) or intercalators such as acridine derivatives (*21*) have shown an enhanced nuclease activity. Analyses of the cleavage pattern of 2-Clip-Phen or its spermine conjugate have revealed, however, that this ligand cleaves DNA practically without sequence selectivity (*20*).

The DNA cleavage selectivity of Clip-Phen derivatives was expected to be enhanced by covalent attachment to specific DNA recognition elements. While there are several potentially suitable DNA binding compounds, we chose to attach Clip-Phen to a well-characterized distamycin-like binder (see ref *22* and references therein). Distamycin is a tri-*N*-methylpyrrole derivative that tightly binds to the minor groove of DNA through a combination of electrostatic interactions, hydrogen bonds, and van der Waals contacts. While this natural product preferentially binds five successive A·T base pairs, several modifications have recently been reported which allow the targeting of multiple sites. In addition, new methods for the preparation of such compounds on a solid support provide the basis for further flexible control of sequence specificity by hybrid nucleases (*23*, *24*).

Since several factors contribute to the specificity of chimeric reagents prepared with 1,10-phenanthroline, we describe here the preparation of four new conjugates. The distamycin analogue linked to a solid support was attached to Phen, 2- and 3-Clip-Phen or to 2-Clip-Phen-hexyl derivatives (see Figure 1). Their DNA cleavage activity has been compared in the same experimental conditions on a restriction fragment.

MATERIALS AND METHODS

Materials. Boc-*β*-alanine-4-carbonylaminomethyl)-benzyl-ester-copoly(styrene-divinylbenzene)resin (Boc-*β*-Pam-resin, 0.5 mmol/g) was from Advanced Chem. Tech. Chloroform was dried on basic aluminum oxide. Other commercially available reagents and all other solvents were purchased from standard chemical suppliers and used without further purification.

1,2,3-Benzotriazol-1-yl-4-[(*tert*-butoxycarbonyl)amino]-1-methylpyrrole-2-carboxylate (*23*), 2-succinoyl-amino-1,3-bis(1′,10′-phenanthrolin-2′-yloxy)propane [2-Clip-Phen-COOH] (*20*), 2-succinoyl-amino,1-(1′,10′)phenanthrolin-2′-yloxy)ethane [2-Phen-COOH] (*20*), 3-Clip-Phen (*19*), and 2-Clip-Phen-hexylamine (*21*) have been prepared as previously described. Boc-Py-Py-Py-*β*-Pam resin precursor was synthesized by manual solid-phase synthesis method (*23*) on Boc-*β*-Pam-resin (0.5 mmol/g).

[†] Laboratoire de Chimie de Coordination du CNRS.
[‡] University of Utah.

10.1021/bc000050t CCC: $19.00 © 2000 American Chemical Society
Published on Web 10/28/2000

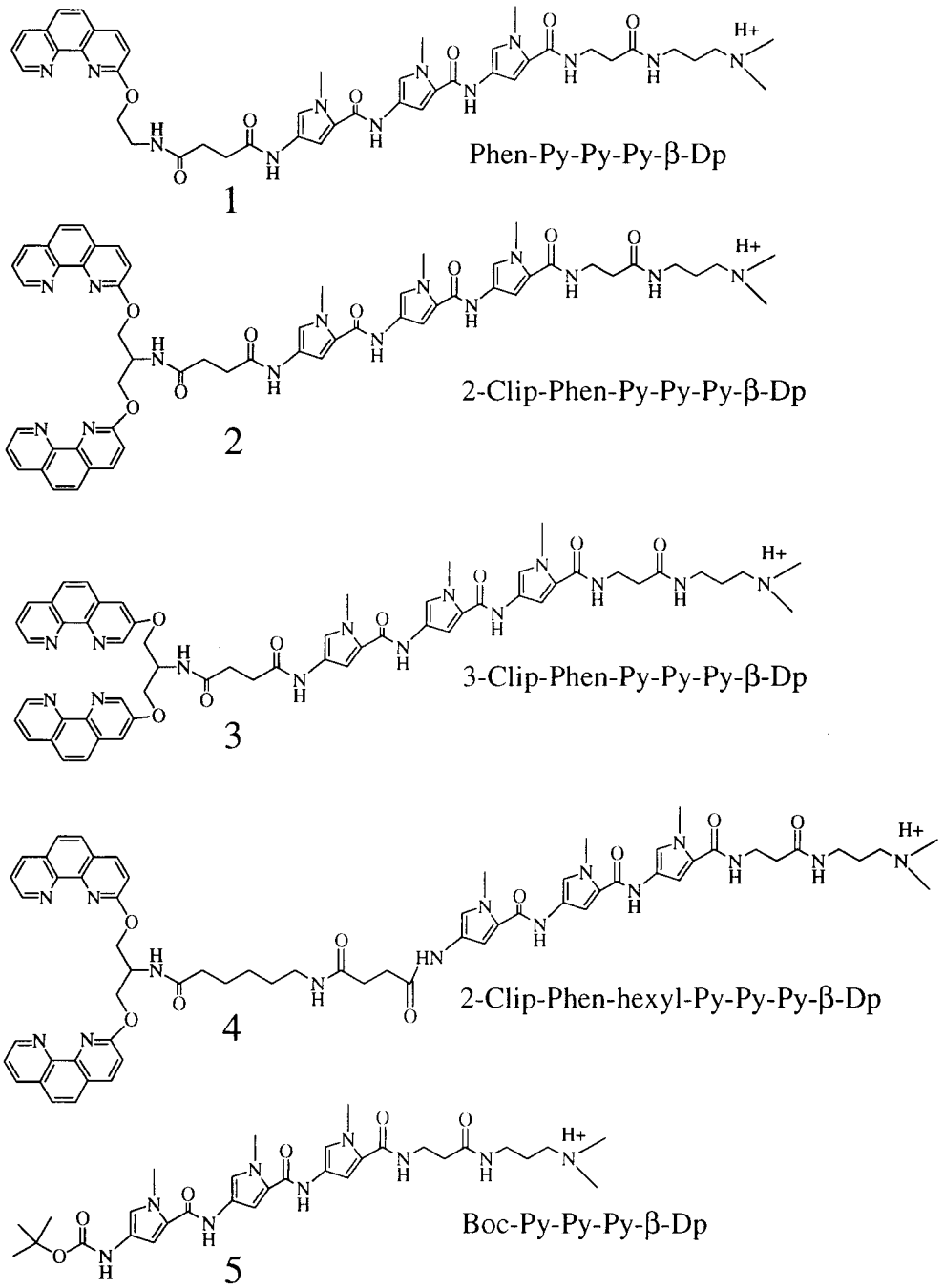

Figure 1. Structures of poly-*N*-methylpyrrole-Clip-Phen (or Phen) conjugates.

HPLC analyses were performed on a reversed-phase Alltima C18 100A 10 μm column (250 × 4.6 mm) from Alltech in 0.1% (v/v) TFA with acetonitrile eluant at a flow rate of 1 mL/min, gradient elution 1.5% acetonitrile/min; the chromatograms were monitored at 255 nm. Preparative HPLC was carried out on a reversed-phase Alphabond C18 10 μm preparative column (150 × 22.5 mm) from Alltech, 0.1% TFA, 1.5% acetonitrile/min, 5 mL/min, or on a reversed-phase Nucleosyl C18 10 μm semipreparative column (250 × 6.2 mm) from Interchim, 0.1% TFA, with 21−28% acetonitrile in 30 min linear gradient, 3 mL/min.

2-Succinoyl-amino-1,3-bis(1′,10′-phenanthrolin-3′-yloxy)propane (3-Clip-Phen-COOH). To a solution of 3-Clip-Phen (59 mg, 0.13 mmol) in 6 mL of dry $CHCl_3$ was added succinic anhydride (30 mg, 0.36 mmol), and the mixture was heated at reflux for 1 h. The product was precipitated after cooling by addition of diethyl ether and centrifuged at 3000 rpm. The pellet was then redissolved in 2 mL of a solution of $CHCl_3/CH_3OH$ (9/1) then precipitated again by diethyl ether to give 3-Clip-Phen-COOH as a pale brown powder (48 mg, 66%). ^{1}H NMR ($CDCl_3$, 250 MHz): δ 9.10 (dd, 2 H, J = 4.5 and 2.0 Hz), 8.85 (d, 2 H, J = 3.0 Hz), 8.47 (d, 1 H, J = 8.0 Hz), 8.17 (dd, 2 H, J = 8.0 and 2.0 Hz), 7.68 and 7.53 (AB, 2 × 2 H, J = 9.0 Hz), 7.55 (dd, 2 H, J = 8.0 and 4.5 Hz), 7.29 (d, 2 H, J = 3.0 Hz), 4.95 (m, 1 H), 4.21 (m, 4 H), 2.84 (m, 4 H). MS (FAB, positive mode, MNBA) m/z 548 (M + H). UV−vis (CH_3OH): 238 nm (ϵ = 75 200 M^{-1} cm^{-1}), 272 nm (ϵ = 54 400 M^{-1} cm^{-1}), 294 nm (sh, ϵ = 29 300 M^{-1} cm^{-1}), 314 nm (sh, ϵ = 10 000 M^{-1} cm^{-1}), 328 nm (ϵ = 7000 M^{-1} cm^{-1}), 348 nm (ϵ = 4700 M^{-1} cm^{-1}).

2-Clip-Phen-hexyl-COOH. To a solution of 2-Clip-Phen-hexyamine (200 mg, 0.35 mmol) in 40 mL of $CHCl_3$, succinic anhydride (100 mg, 0.96 mmol) was added and the mixture was heated at reflux for 1 h. After evapora-

tion of the solvent, the crude product was redissolved in hot methanol, precipitated at −20 ° C and filtered to give 2-Clip-Phen-hexy-COOH as a white powder (133 mg, 56%). ^{1}H NMR (CD_2Cl_2, 500 MHz): δ 9.15 (dd, 2 H, J = 4.0 and 1.5 Hz), 8.42 (d, 1 H, J = 6.5 Hz), 8.30 (dd, 2 H, J = 8.0 and 1.5 Hz), 8.09 (d, 2 H, J = 9.0 Hz), 7.73 and 7.67 (AB, 2 × 2 H, J = 8.5 Hz), 7.65 (dd, 2 H, J = 8.0 and 4.0 Hz), 7.13 (m, 1 H), 7.12 (d, 2 H, J = 9.0 Hz), 5.06 (m, 2 H), 4.86 (m, 3 H), 3.12 (m, 2 H), 2.55 (t, 2 H, J = 7.0 Hz), 2.43 (t, 2 H, J = 7.0 Hz), 2.22 (t, 2 H, J = 7.0 Hz), 1.49 (m, 2 H), 1.35 (m, 2 H), 1.19 (m, 2 H). MS (FAB, positive mode, MNBA) m/z 661 (M + H). UV−vis (CH_3-OH): 226 nm (ϵ = 96 500 M^{-1} cm^{-1}), 276 nm (ϵ = 63 800 M^{-1} cm^{-1}), 296 nm (sh, ϵ = 20 300 M^{-1} cm^{-1}), 322 nm (ϵ = 4000 M^{-1} cm^{-1}), 346 nm (ϵ = 2200 M^{-1} cm^{-1}).

General Protocol of Conjugate Synthesis. Boc-Py-Py-Py-β-Pam resin (ca 0.05 or 0.15 mmol, estimated from initial resin substitution) was placed in a glass peptide synthesis vessel and the Boc group was removed just before use with a 80% TFA/CH_2Cl_2/0.5 M thiophenol solution as previously described (*23*). The resin was then washed with DMF (1×) and CH_2Cl_2 (2×). The carboxylic acid derivative of phenanthroline (40 mM) was activated with 3 equiv of HOBT (1-hydroxybenzotriazole) and 1.7 equiv of DCC in DMF/DIEA (diisopropylethylamine) (2/1) for 5 min; then this mixture was added to the resin and agitated (20 h, room temperature). The synthesis was monitored by analytical HPLC with an aliquot of resin heated in DMAPA [3-(dimethylamino)-1-propylamine] 5 min at 90 ° C (disappearance of the Py-Py-Py-β-Dp peak at 22 min associated to the formation of the conjugate-product peak at 25, 26, or 27 min for conjugates **1**, **2** and **3**, and **4**, respectively). Resin was then isolated by filtration and washed sequencially with an excess of DMF (1×) and CH_2Cl_2 (2×) before being heated in DMAPA for 15 h at 55 ° C. The reaction was then filtered to remove the resin.

Phen-Py-Py-Py-β-Dp (1). Phen-COOH (123 mg, 0.36 mmol) was activated by DCC/HOBT and added to the Py-Py-Py-β-Pam-resin (ca 0.15 mmol). The crude product was obtained in 3 mL of DMAPA then diluted with H_2O and purified by preparative HPLC. Since the isolated product was contaminated by DMAPA, 50% of the material was repurified by preparative HPLC to give, after lyophilization, Phen-Py-Py-Py-β-Dp (**1**) as a yellow powder (22 mg, 25% recovery).^{1}H NMR (DMSO-d_6, 500 MHz): δ 9.90 (s, 2 H), 9.88 (s, 1 H), 9.37 (br s, 1 H), 9.24 (br s, 1 H), 8.90 (br s, 1 H), 8.51 (d, 1 H, J = 8.5 Hz), 8. 47 (br s, 1 H), 8.13 (br s, 1 H), 8.06 (m, 3 H), 7.36 (d, 1 H, J = 8.5 Hz), 7.22 (s, 1H), 7.17 (s, 1 H), 7.15 (s, 1 H), 7.05 (s, 1 H), 6.88 (m, 2 H), 4.67 (m, 2 H), 3.84 (s, 3 H), 3.82 (s, 3 H), 3.81 (s, 3 H), 3.61 (m, 2 H), 3.39 (m, 2 H), 3.12 (m, 2 H), 3.03 (m, 2 H), 2.75 (d, 6 H, J = 4.5 Hz), 2.36 (t, 2 H, J = 7.0 Hz), 1.75 (m, 2H). MS (ES, positive mode, in CH_3CN/H_2O [1/1] with 0.1% TFA) m/z 861.6 (862 calcd for M + H), 431.6 (z = 2, M + 2 H). UV−vis (H_2O): 222 nm (ϵ = 53 400 M^{-1} cm^{-1}), 280 nm (ϵ = 42 600 M^{-1} cm^{-1}), 310 nm (sh, ϵ = 29 200 M^{-1} cm^1). t_R(analytical HPLC): 25 min.

2-Clip-Phen-Py-Py-Py-β-Dp (2). 2-Clip-Phen-COOH (172 mg, 0.32 mmol) was activated by DCC/HOBT and added to the Py-Py-Py-β-Pam-resin (ca 0.15 mmol). The crude product was obtained in 3 mL of DMAPA then precipitated by addition of diethyl ether. The pellet was redissolved in water acidified with formic acid and purified by preparative or semipreparative HPLC. The conjugate was obtained after lyophilization as a yellow powder (24 mg, 11% recovery). ^{1}H NMR (DMSO-d_6, 500 MHz): δ 9.93 (s, 1 H), 9.89 (s, 2 H), 9.31 (br s, 1 H), 9.16 (d, 2 H, J = 3.5 Hz), 8.82 (dd, 2 H, J = 4.5 and 1.2 Hz), 8.82 (1 H), 8. 39 (d, 2 H, J = 9.0 Hz), 8.05 (m, 2 H), 8.00 and 7.93 (AB, 2 × 2 H, J = 8.5 Hz), 7.93 (1 H), 7.33 (d, 2 H, J = 9.0 Hz), 7.21 (d, 1 H, J = 1.5 Hz), 7.16 (s, 2 H), 7. 05 (d, 1 H, J = 2.0 Hz), 6.88 (d, 1 H, J = 1.5 Hz), 6.87 (d, 1 H, J = 2.0 Hz), 4.92 (m, 3 H), 4. 83 (m, 2 H), 3.84 (s, 3 H), 3.81 (s, 3 H), 3.80 (s, 3 H), 3.38 (m, 2 H), 3.11 (m, 2 H), 3.01 (m, 2 H), 2.75 (d, 6 H, J = 4.5 Hz), 2.63 (m, 4 H), 2.35 (t, 2 H, J = 7.0 Hz), 1.74 (m, 2 H). MS (ES, positive mode, in CH_3CN/H_2O [1/1] with 0.1% TFA) m/z 1069.9 (1070 calcd for M + H), 535.7 (z = 2, M + 2 H). UV−vis (H_2O): 218 nm (ϵ = 75 300 M^{-1} cm^{-1}), 276 nm (ϵ = 51 700 M^{-1} cm^{-1}), 316 nm (sh, ϵ = 28 400 M^{-1} cm^{-1}). t_R (analytical HPLC): 26 min.

After DMAPA/diethyl ether precipitation, the conjugate could also be redissolved in DMSO and precipitated by addition of water to give the unprotonated conjugate (17% of recovery). ^{1}H NMR (DMSO-d_6, 250 MHz): δ 9.93 (br s, 2 H), 9.91 (s, 1 H), 9.21 (dd, 2 H, J = 4.2 and 1.5 Hz), 8.85 (d, 1 H, J = 6.5 Hz), 8.56 (dd, 2 H, J = 8.1 and 1.5 Hz), 8.47 (d, 2 H, J = 8.7 Hz), 8.03 and 7.95 (AB, 2 × 2 H, J = 8.6 Hz), 8.02 (m, 1 H), 7. 95 (m, 1 H), 7.83 (dd, 2 H, J = 8.1 and 4.2 Hz), 7.36 (d, 2 H, J = 8.7 Hz), 7.32 (d, 1 H, J = 1.5 Hz), 7.29 (d, 1 H, J = 1.5 Hz), 7.24 (d, 1 H, J = 1.5 Hz), 7.14 (d, 1 H, J = 1.5 Hz), 6.99 (d, 1 H, J = 1.5 Hz), 6.95 (d, 1 H, J = 1.5 Hz), 4.92 (m, 5 H), 3.96 (s, 3 H), 3.93 (br s, 6 H), 3.52 (m, 2 H), 3.19 (m, 2 H), 2.70 (m, 4 H), 2.45 (t, 2 H, J = 7.0 Hz), 2.42 (t, 2 H, J = 7.0 Hz), 2.25 (s, 6 H), 1.65 (m, 2 H). UV−vis (CH_3OH): 230 nm (ϵ = 114 600 M^{-1} cm^{-1}), 276 nm (ϵ = 85 000 M^{-1} cm^{-1}), 292 nm (sh, ϵ = 23 500 M^{-1} cm^{-1}).

3-Clip-Phen-Py-Py-Py-β-Dp (3). 3-Clip-Phen-COOH (48 mg, 0.09 mmol) was activated by DCC/HOBT and added to the Py-Py-Py-β-Pam-resin (ca 0.05 mmol). The crude product was obtained in 1 mL of DMAPA then precipitated by addition of diethyl ether. The pellet was redissolved in water acidified with formic acid and purified by preparative or semipreparative HPLC. The conjugate was obtained after lyophilization as an orange powder (7 mg, 10% recovery). ^{1}H NMR (DMSO-d_6, 500 MHz): δ 9.92 (s, 1 H), 9.89 (s, 1 H), 9.88 (s, 1 H), 9.45 (br s, 1H), 9.13 (d, 2 H, J = 4.0 Hz), 8.96 (d, 2 H, J = 2.0 Hz), 8.85 (m, 2 H), 8.57 (d, 1 H, J = 7.0 Hz), 8.23 (d, 2 H, J = 2.0 Hz), 8.07 (m, 5 H), 7.98 (m, 2 H), 7.19 (s, 1H), 7.17 (s, 1 H), 7.15 (s, 1 H), 7.03 (s, 1 H), 6.88 (s, 1 H), 6.84 (s, 1 H), 4.73 (m, 1 H), 4.52 (m, 4 H), 3.84 (s, 3 H), 3.81 (s, 3 H), 3.79 (s, 3 H), 3.39 (m, 2 H), 3.12 (m, 2 H), 3.02 (m, 2 H), 2.75 (d, 6 H, J = 4.5 Hz), 2.56 (m, 4 H), 2.35 (t, 2 H, J = 7.0 Hz), 1.75 (m, 2H). MS (ES, positive mode, in CH_3CN/H_2O [1/1] with 0.1% TFA) m/z 535.6 (z = 2, 535.5 calcd for M + 2 H), 357.5 (z = 3, M + 3 H). UV−vis (H_2O): 234 nm (ϵ = 69 400 M^{-1} cm^{-1}), 278 nm (ϵ = 48 600 M^{-1} cm^{-1}), 298 nm (sh, ϵ = 41 500 M^{-1} cm^{-1}). t_R (analytical HPLC): 26 min.

2-Clip-Phen-(hexyl)-Py-Py-Py-β-Dp (4). 2-Clip-Phen-hexyl-COOH (59 mg, 0.09 mmol) was activated by DCC/HOBT and added to the Py-Py-Py-β-Pam-resin (ca 0.05 mmol). The crude product was obtained in 1 mL of DMAPA then precipitated by addition of diethyl ether. The pellet was redissolved in water acidified with formic acid and purified by preparative HPLC. The conjugate was obtained after lyophilization as a yellow powder (5 mg, 7% recovery). ^{1}H NMR (DMSO-d_6, 500 MHz): δ 9.89 (s, 2 H), 9.85 (s, 1 H), 9.30 (br s, 1 H), 9.15 (d, 2 H, J = 4.5 Hz), 8.80 (br s, 2 H), 8.63 (d, 1 H, J = 6.5 Hz), 8. 40 (d, 2 H, J = 9.0 Hz), 8.05 (m, 2 H), 8.00 and 7.93 (AB, 2 × 2 H, J = 8.5 Hz), 7.96 (m, 1 H), 7.83 (t, 1 H, J = 7.0 Hz), 7.33 (d, 2 H, J = 9.0 Hz), 7.20 (s, 1 H), 7.16 (s, 1 H), 7. 14 (s, 1 H), 7. 05 (s, 1 H), 6.88 (s, 1 H), 6.85 (d, 1 H),

4.87 (m, 5 H), 3.84 (s, 3 H), 3.81 (s, 3 H), 3.80 (s, 3 H), 3.38 (m, 2 H), 3.11 (m, 2 H), 2.99 (m, 4 H), 2.75 (d, 6 H, $J = 4.5$ Hz), 2.46 (m, 2 H), 2.35 (m, 4 H), 2.25 (t, 2 H, $J = 7.5$ Hz), 1. 74 (m, 2 H), 1.54 (m, 2 H), 1.35 (m, 2 H), 1. 23 (m, 2 H). MS (ES, positive mode, in CH_3CN/H_2O [1/1] with 0.1% TFA) m/z 592.0 ($z = 2$, 592.0 calcd for M + 2 H), 497.1 ($z = 2$, M + 2 H − 197), 395.2 ($z = 3$, M + 3 H). UV−vis (H_2O): 222 nm ($\epsilon = 73\,800\ M^{-1}\ cm^{-1}$), 276 nm ($\epsilon = 51\,500\ M^{-1}\ cm^{-1}$), 308 nm (sh, $\epsilon = 33\,200\ M^{-1}\ cm^{-1}$). t_R (analytical HPLC): 27 min.

Boc-Py-Py-Py-*β*-Dp (5). Boc-Py-Py-Py-β-Pam-resin (ca 0.03 mmol) was heated in 0.5 mL of DMAPA 15 h at 55 ° C. The resin was removed by filtration and the crude product was precipitated by addition of diethyl ether. The pellet was washed with diethyl ether and dried under vacuum before being redissolved in CH_2Cl_2 and precipitated by addition of diethyl ether. The pellet was dissolved in water acidified with trifluoroacetic acid and purified on semipreparative HPLC ($t_R = 20$ min) and lyophilized to give Boc-Py-Py-Py-β-Dp as a white powder (9 mg, 40% recovery). ^{1}H NMR (D_2O, 250 MHz): δ 6.75 (m, 2 H), 6.56 (br s, 1 H), 6.46 (d, 1 H, $J = 1.5$ Hz), 6.40 (d, 1 H, $J = 1.5$ Hz), 6.29 (br s, 1 H), 3.54 (s, 6 H), 3.53 (s, 3 H), 3.42 (t, 2 H, $J = 6.6$ Hz), 3.20 (t, 2 H, $J = 6.6$ Hz), 3.00 (m, 2 H), 2.72 (s, 6H), 2.41 (t, 2 H, $J = 6.5$ Hz), 1.83 (m, 2 H), 1.38 (s, 9 H). MS (ES, positive mode, in CH_3CN/H_2O [1/1] with 0.1% TFA) m/z 640.4 (640.77 calcd for M + H). UV−vis (H_2O): 226 nm ($\epsilon = 21\,500\ M^{-1}\ cm^{-1}$), 306 nm ($\epsilon = 25\,800\ M^{-1}\ cm^{-1}$). t_R (analytical HPLC): 35 min.

Cleavage of 5′-^{32}P-End-Labeled DNA. End-labeled restriction fragment was prepared by sequential digestion of supercoiled pBR322 plasmid DNA with *Eco*RI restriction endonuclease, alkaline phosphatase, [γ-^{32}P]ATP and T4 polynucleotide kinase and then *Rsa*I restriction endonuclease (*25*). The ^{32}P-end-labeled 167 base pair fragment was purified by 8% preparative nondenaturing gel electrophoresis and isolated.

Metalations of the different ligands used in DNA cleavage experiments were carried out using a 1.25 mM $CuCl_2$ concentration with 1 equiv of ligand in water for 1 h at room temperature before dilution of the complex with water to 125 or 25 μM.

Cleavage reactions were carried out in 50 μL total volume containing calf thymus DNA (86 μM nucleotide concentration) and 10^4 cpm of the ^{32}P-end-labeled restriction fragment in 10 mM sodium phosphate buffer (pH 7.2), 100 mM NaCl. After preincubation with complex (1 or 5 μM) for 30 min at room temperature, DNA cleavage was initiated by addition of an aqueous solution of ascorbate (2 μL, 2.5 mM) and samples were incubated for 1 h at 37 °C. 2 μL of a 0.1 M EDTA solution and 8 μL of sodium acetate buffer (3 M, pH 5.2) were then added and samples were precipitated with 120 μL of ethanol. Pellets were rinsed with ethanol and lyophilized. One part of the samples was redissolved in 50 μL of piperidine 0.2 M and heated for 30 min at 90 °C before being lyophilized. Fragments of DNA were analyzed by denaturing 8% polyacrylamide gel electrophoresis. The gels were dried under vacuum and then analyzed using phosphorimagery (Molecular Dynamics). Fragments were identified with respect to Maxam-Gilbert G-sequencing (*26*).

RESULTS AND DISCUSSION

To increase the sequence selectivity of DNA cleavage by Clip-Phen derivatives on a succession of A·T base pairs, four conjugates with the distamycin analogue Py-Py-Py-β-Dp have been prepared (Figure 1). Conjugate **1**, having a less voluminous and sterically constrained nuclease part with only one phenanthroline, has been synthesized for comparison with the efficacy of the two phenanthrolines of Clip-phen derivatives in the cleavage pattern of the conjugates. Conjugates **2** and **3**, with, respectively, 2- and 3-Clip-Phen, allowed analysis of the effect of the bridge position between the two phenanthroline entities of Clip-Phen on the cleavage pattern.

The aliphatic linker between Clip-Phen and poly-*N*-methyl-pyrroles is relatively short (only four single bonds) in conjugates **2** and **3**. Previous reports have been shown that the length of the junction influences both cleavage efficiency and cleavage pattern. Since significant increases in specificity have been obtained in different laboratories for conjugates of poly-*N*-methyl-pyrroles including longer aliphatic linkers (see ref *21* and references therein), conjugate **4** (with 10 single bonds in the spacer) has been prepared for comparison with conjugate **2**. We chose a long 5-methylene spacer in order to increase the flexibility of the linker.

Synthesis Strategy (Figure 2). Phenanthroline amine derivatives were transformed in carboxylic acids by reaction with succinic anhydride. The poly-*N*-methyl-pyrrole portion was synthesized manually on solid support in seven sequential steps from Boc-β-Pam-resin and the Boc-*N*-methyl-pyrrole-OBt synthon (obtained in eight steps from pyrrole) according to Dervan methodology (*23*).

It is known that poly-*N*-methyl-pyrroles are unstable when their N-terminal amine function is unprotected, so we chose to attach the phenanthroline part on this fragile amine in order to protect it without any other modification of conjugates (*23*). This synthetic strategy allowed us to realize the coupling reaction with phenanthroline derivatives on the solid support. This method also provided facile purification (excess of reagents being easily removed and washed by filtration) and avoided isolation of the unstable peptide with the unprotected N-terminal primary amine.

Optimization of the coupling conditions was conducted with the 2-Clip-Phen-COOH derivative. Various attempts to obtain a corresponding activated ester in pure form failed. They included activation of small quantities of 2-Clip-Phen-COOH (less than 0.2 mmol) with DCC/HOBT (1-hydroxybenzotriazole), BOP [(benzotriazol-1-yloxy)tris(dimethylamino)phosphonium]/HOBT or DCC/NHS (*N*-hydroxysuccinimide). In the end, 2 equiv of the carboxylic acid were activated by DCC/HOBT in a DMF/DIEA (diisopropylethylamine) solution, and the crude activation mixture was directly injected into the reaction vessel containing the resin supporting the poly-*N*-methylpyrrole which had been deprotected just before use. After a washing step, the conjugate was cleaved from the support by aminolysis of the resin ester linkage in hot (55 °C) DMAPA [3-(dimethylamino)-1-propylamine] (*23*).

We tried to purify the different conjugates by diluting the crude mixture dissolved in DMAPA with 4 vol of water followed by separation of the product by HPLC on a C18 reversed-phase column. This strategy was tested for purification of conjugate **1**, but it appeared that, at the end of the purification, the conjugate was contaminated with DMAPA and usual small quantity of TFA used in the elution solvant (0.1%; v/v) was unable to neutralize all the amine. Thus, another step of HPLC purification was necessary to remove residual DMAPA from the conjugate. Since alkalinization can damage the C18 column, and conjugates with 2- or 3-Clip-Phen are insoluble in a DMAPA/water mixture, the conjugate dissolved in DMAPA was instead precipitated by addition

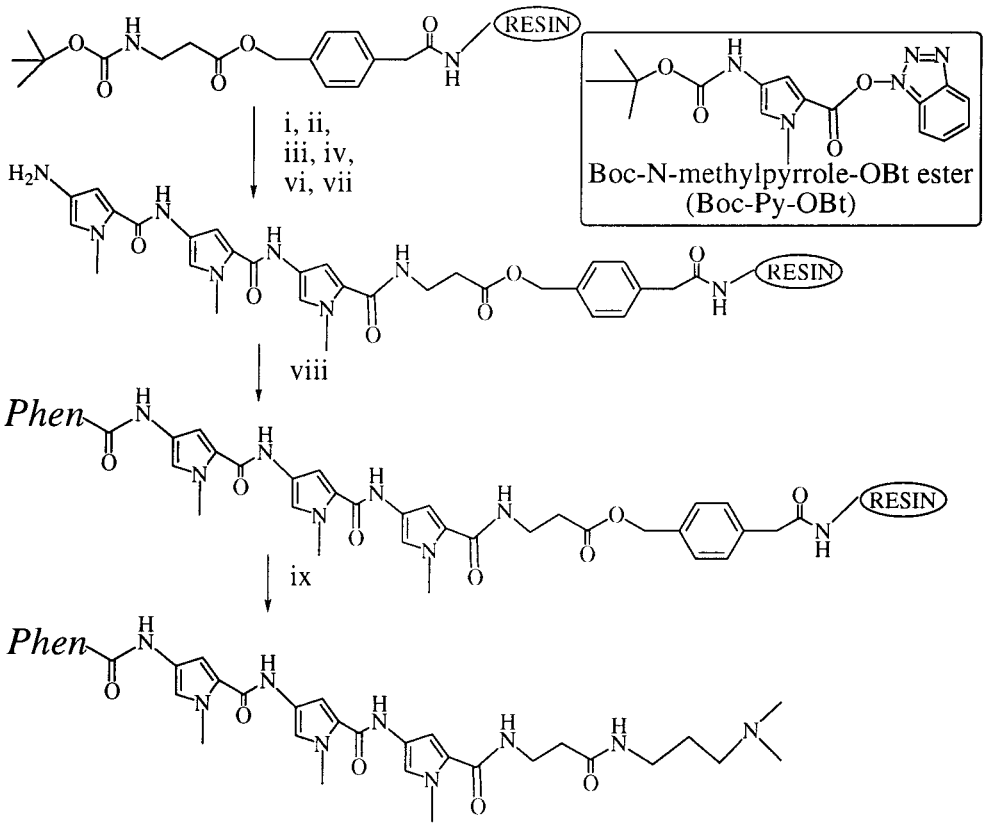

Figure 2. Solid-phase synthetic scheme for poly-*N*-methylpyrrole-Clip-Phen (or Phen) conjugates: (i) 80% TFA/CH_2Cl_2, 0.4 M PhSH; (ii) Boc-Py-OBt, DIEA, DMF; (iii) 80% TFA/CH_2Cl_2, 0.4 M PhSH; (iv) Boc-Py-OBt, DIEA, DMF; (v) 80% TFA/CH_2Cl_2, 0.4 M PhSH; (vi) Boc-Py-OBt, DIEA, DMF; (vii) 80% TFA/CH_2Cl_2, 0.4 M PhSH; (viii) *Phen*-COOH, DCC, HOBT, DIEA, DMF; (ix) DMAPA, 55 °C. (Box) Boc-*N*-methylpyrrole-OBt ester (Boc-Py-OBt) used for peptide synthesis. *Phen*-COOH: 2-Phen-COOH, 2-Clip-Phen-COOH, 3-Clip-Phen-COOH, or 2-Clip-Phen-hexy-COOH.

of diethyl ether in order to remove the major part of the excess amine. The crude product was then dissolved in acidified water and purified by HPLC to give a water-soluble protonated conjugate in a global yield ranging from 7 to 25%. Modifications of the reaction times between the phenanthroline derivative and the peptide, the use of increased equivalents of phenanthroline derivative and activators, or activation of the carboxylic acid group with BOP/HOBT or HBTU [*O*-(benzotriazol-1-yl)-*N*,*N*,*N*′,*N*′-tetramethyluronium hexafluorophosphate] led to similar yields.

Only the global recovery yield of the nine successive steps of the conjugate synthesis can be estimated from the manufacturer's information about the resin substitution. The yield of the coupling reaction between the phenanthroline derivative and the peptide was difficult to determine: (i) The coupling reaction between the phenanthroline derivative and the peptide was monitored by HPLC on aliquots of resin heated in DMAPA by observing the appearance of the conjugate and the disappearance of the unreacted peptide during the reaction. However, various attempts to isolate the unprotected peptide from the resin failed. Only degradated product has been isolated after addition of TFA on the resin in order to remove Boc residues followed by cleavage with DMAPA. Thus, the quantity of unreacted peptide might be underestimated during HPLC monitoring. (ii) Peptide **5** (protected on the N-terminal amine for stability reason), corresponding to the last step before reaction with the phenanthroline derivative, was purified under the same conditions of the conjugates **1**−**4**. During the HPLC purification step, the synthesis seemed efficient since only traces of aborted peptide sequence were

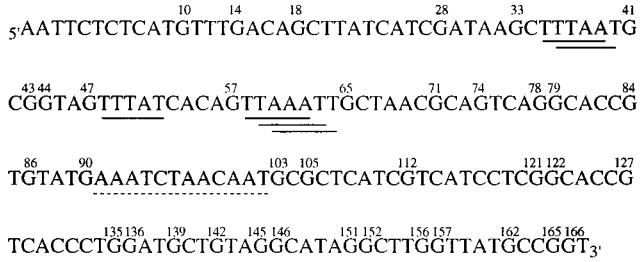

Figure 3. Sequence of the *Eco*RI−*Rsa*I restriction fragment. Preferential binding sites for the distamycin analogue (5 succesive A·T base pairs) are underlined. A secondary binding site observed during cleavage is shown (dashed underline).

observed but only 40% of peptide was recovered. This means that the theoretical peptide quantity can be overestimated in the coupling with the phenanthroline derivative. (iii) During HPLC purification, conjugates were eluted as very broad peaks difficult to collect without loss of material. The peak resolution was better for compound **5** compared to that of conjugate **1**, the worse being for conjugate **4**. Yields were in good correlation with the difficulty of purification.

To reduce the loss of product during the HPLC step, another purification method was optimized in the case of conjugate **2**. After diethyl ether precipitation, the crude product was redissolved in DMSO and precipitated with water. In this case, the conjugate was obtained in the unprotonated form with a better yield (17% versus 11% for HPLC purification).

DNA Cleavage Activity. Conjugates **1**−**4** were metalated with 1 equiv of $CuCl_2$, and their DNA cleavage activities were studied. Comparison of the DNA cleavage

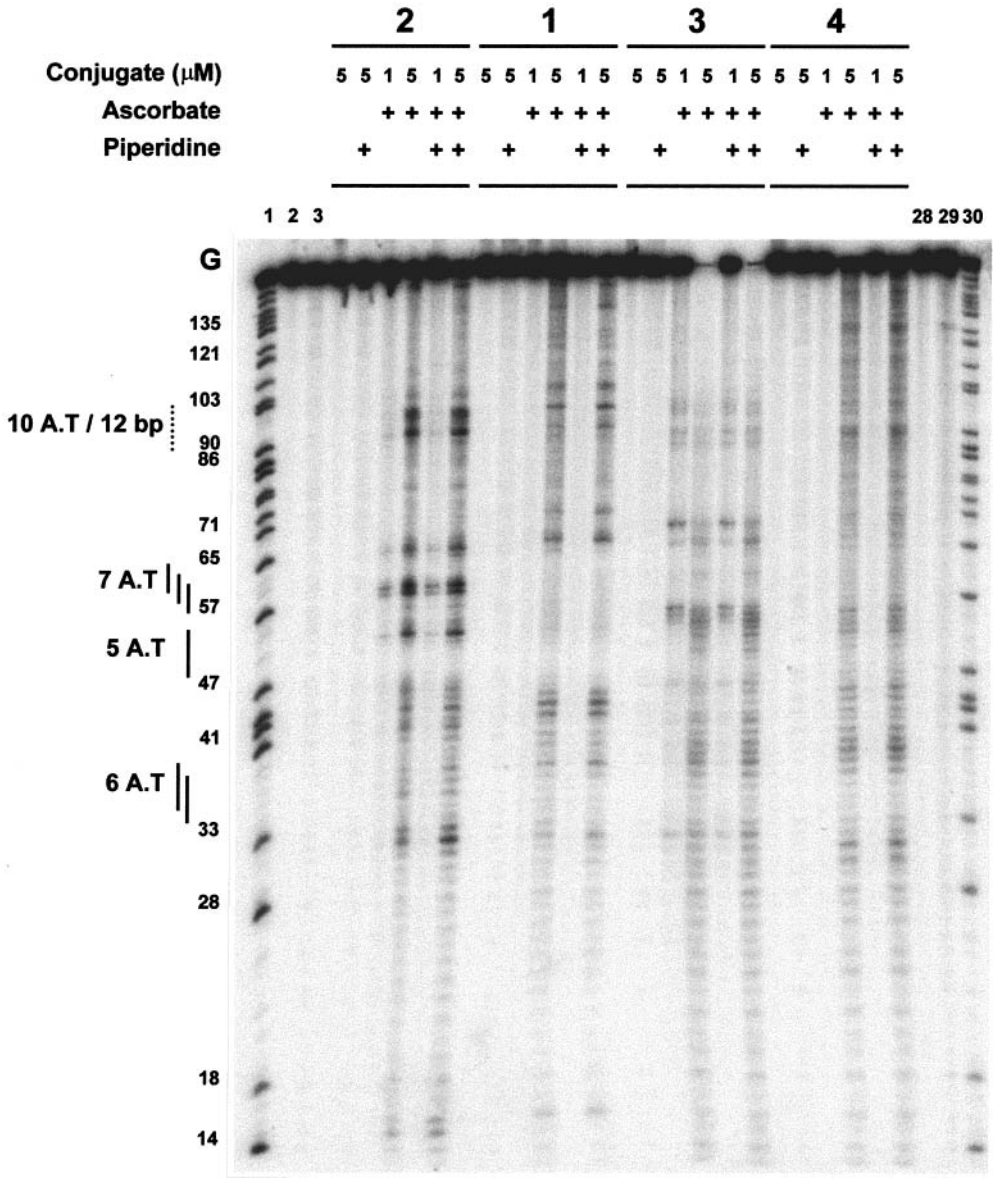

Figure 4. Cleavage of the *Eco*RI-*Rsa*I restriction fragment (10^4 cpm in the presence of 86 μM of random DNA) by conjugates **1**, **2**, **3**, and **4** (1 or 5 μM). The cleavage reaction proceeded for 1 h at 37 °C in the presence of 100 μM ascorbate in 10 mM sodium phosphate buffer (pH 7.2) with 100 mM NaCl. The final concentration of conjugate and piperidine treatment (0.2 M, 30 min at 90 °C) are indicated on the top of the gel. Control experiments were performed with 5 μM of conjugate without ascorbate. Lanes 1 and 30: Maxam−Gilbert G. Lane 2: control DNA. Lane 3: control DNA with piperidine treatment. Lane 28: control ascorbate. Lane 29: control ascorbate with piperidine treatment.

selectivity of these complexes was carried out with the *Eco*RI/*Rsa*I restriction fragment of 167 base pairs from the plasmid pBR322 that was 5′-end labeled with ^{32}P (Figure 3). This restriction fragment contains three sites of high affinity for the distamycin analogue with five, six, and seven successive A·T base pairs, respectively. This sequence has been previously tested for DNA cleavage with (2-Clip-Phen)$CuCl_2$ (results not shown) and with the copper complex of a 2-Clip-Phen-spermine conjugate (*20*), and in both cases, no cleavage specificity was observed.

The DNA target (10^4 cpm) was incubated in the presence of random double-stranded calf thymus DNA (86 μM in nucleotide) with different concentrations of conjugates, and results obtained for 1 and 5 μM of complexes are shown Figure 4. Initiation of the redox activity of these copper complexes was realized by addition of 100 μM ascorbate in the presence of air. The resulting samples were analyzed by PAGE before and after piperidine treatment. Such treatment was performed to reveal all damage mediated by conjugates on their DNA target [direct cleavages (*1*, *27*) and alkali-labile oxidations including base damage (*28*)]. Cleavage sites were determined by comparison with a Maxam−Gilbert G-sequencing lane (*26*).

The four conjugates induced a nonrandom cleavage pattern as confirmed by phosphorimager scanning (Figure 5). Cleavages were confined to localized sites around the three regions containing the successive A·T base pairs highlighted. A secondary binding site was also observed at another A·T rich sequence in which 10 out of 12 base pairs are A·T. This region is also known to be a binding site for distamycin since cleavages at this sequence have been previously observed with the iron complex of EDTA−distamycin conjugate (*29*). No modification of the cleavage pattern was observed after piperidine treatment, indicating that these conjugates performed direct DNA breaks, probably due to deoxyribose oxidation, as is precedented for copper complexes of phenanthroline (*1*).

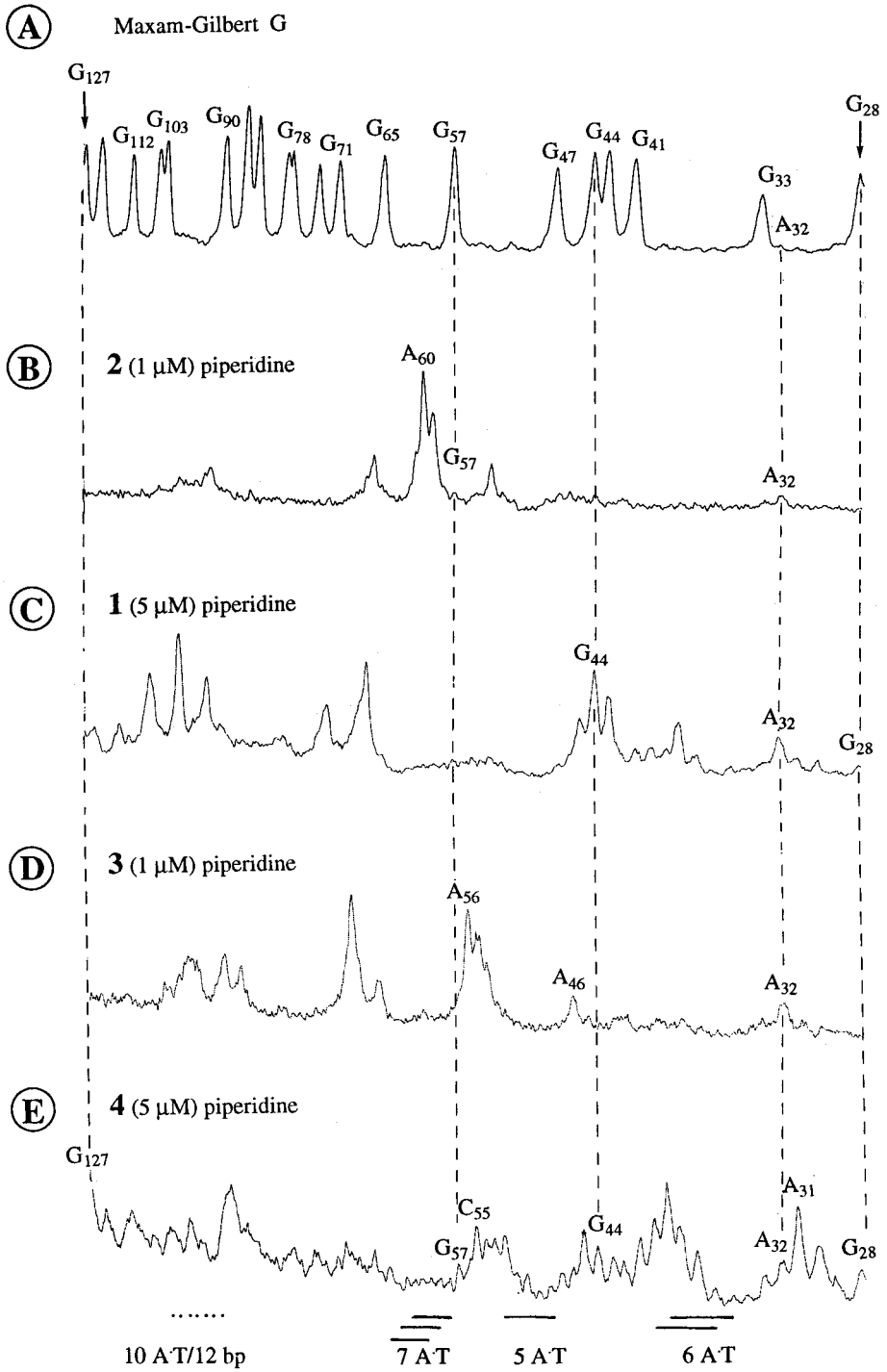

Figure 5. Phosphorimager scanning between G_{28} and G_{127} of the cleavage patterns of the *Eco*RI−*Rsa*I restriction fragment by copper complexes of conjugates **1**, **2**, **3**, and **4** then piperidine treatment. Lane A: Maxam−Gilbert G. Lane B: 1 μM of **2**. Lane C: 5 μM of **1**. Lane D: 1 μM of **3**. Lane E: 5 μM of **4**.

Differences have been observed in the cleavage pattern of each conjugate. As expected, conjugate **3**, with 3-Clip-Phen, was the more active; with 5 μM of the hybrid molecule, nearly all the target was cleaved (compare the residual full-length target in lanes 19 and 21 with other cleavage patterns, Figure 4). At this concentration of **3**, the cleavage pattern was less selective and quantity of small fragments increased dramatically in comparison with cleavage pattern observed for 1 μM of **3** (lanes 18 and 20, Figure 4). This was probably due to multiple cleavages of fragments generated from the target by initial oxidation damage because, for 1 μM of complex, breaks were selectively located around the poly-*N*-methylpyrrole binding sites (see also lane D, Figure 5). Conjugates **1** and **4** were less active DNA cleavers since breaks were only observed with 5 μM complex (lanes 13 and 15 for **1** and lanes 25 and 27 for **4**, Figure 4). The poor DNA cleavage activity of **1** can be explained by the presence of only one phenanthroline unit in the conjugate, complexes of (Clip-Phen)$CuCl_2$ or with two 1,10-phenanthrolines for one copper being known to be more active. The lower cleavage efficiency observed with conjugate **4** indicates that the increase of the tether length between the two parts of conjugate has a negative effect on the cleavage activity. The cleavage pattern obtained with conjugate **4** also showed more diffuse

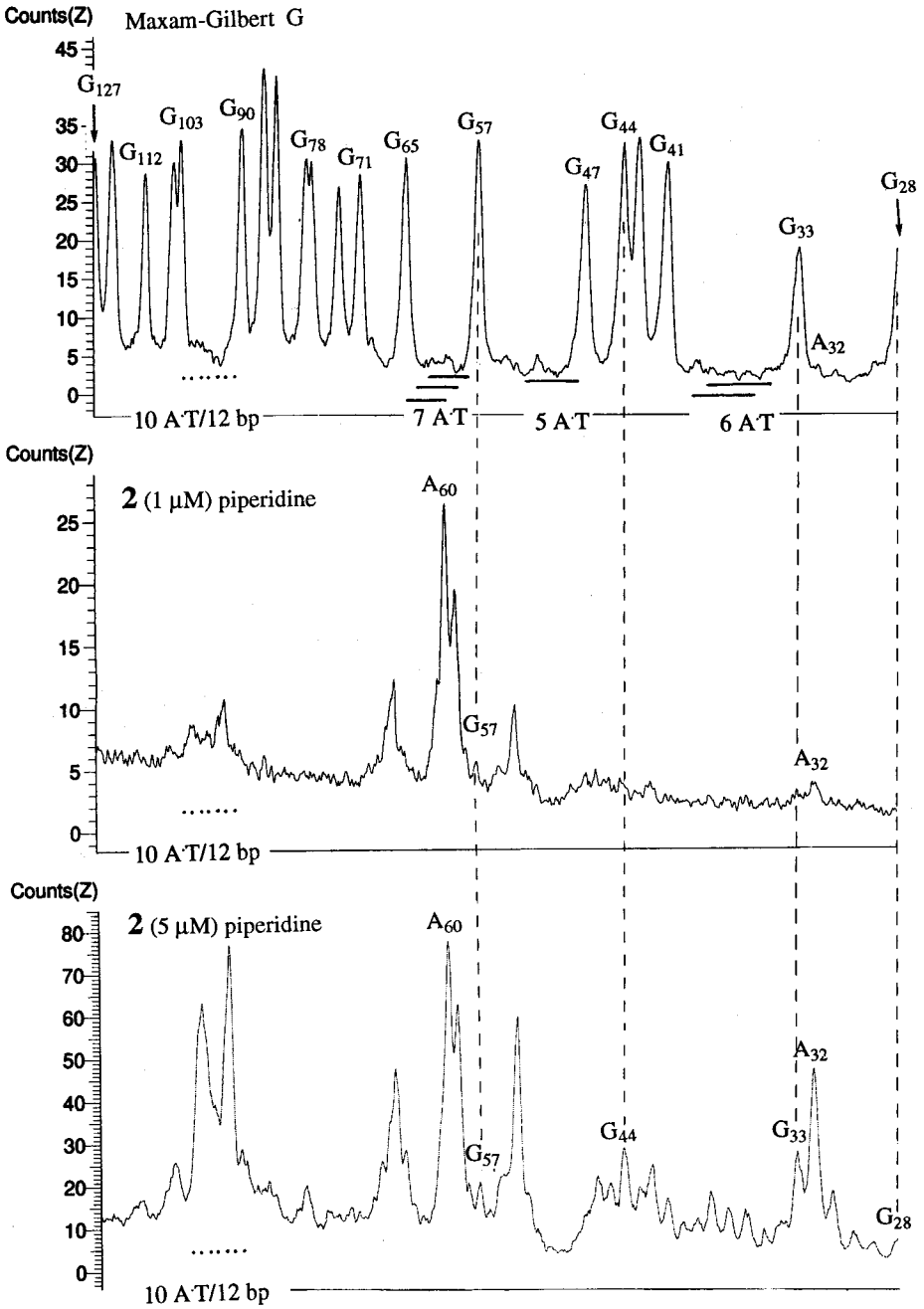

Figure 6. Phosphorimager scanning between G_{28} and G_{127} of the cleavage patterns of the *Eco*RI−*Rsa*I restriction fragment by 1 and 5 μM of copper complex of conjugate **2** then piperidine treatment.

breaks (lanes 25 and 27 Figure 4 and lane E Figure 5). This fact can be attributed to the tether being too long, which allowed the nuclease entity of the conjugate to oxidize a large number of nucleotides around the binding site. A loss of specificity was also observed with **4**.

Major cleavages were observed in the G_{33} to G_{71} region which includes the higher affinity binding site with seven successive A·T base pairs (three overlapping primary binding sites for the poly-*N*-methylpyrrole entity of the conjugates) in the vicinity of other primary binding sites of five and six successive A·T base pairs (Figures 4 and 5). Cleavages were essentially observed on nucleosides on the 5′- and 3′-sides of the higher affinity binding site with a nucleoside preference specific to each conjugate.

In the case of conjugate **2**, cleavage was also observed inside the A·T box (lanes 6−9, Figure 4, and lane B, Figure 5). A comparison of the phosphorimager scanning of the cleavage patterns obtained for 1 and 5 μM of **2** (Figure 6) showed that the cleavage inside the seven A·T base pairs box was preferential for 1 μM of **2**, the quantity of cleavage on the 5′- and 3′-sides of this higher affinity site, the five and six A·T boxes or in the secondary binding site (where 10 out of 12 base pairs are A·T) increasing dramatically for higher concentration of **2** (5 μM).

A comparison of cleavage patterns obtained with copper complexes of **2** and **3** has been done for different experimental conditions including the variation of the concentration of copper complexes, the nature of the buffer (phosphate or Tris), salts (NaCl and $MgCl_2$), and reductant (ascorbate or mercaptopropionic acid), in the presence or not of random double-stranded calf thymus DNA. As it can be observed in Figures 4 and 5, copper complex of **3** (the conjugate with 3-Clip-Phen) cleaved always on the 5′- and 3′-sides of the seven A·T base pairs box when the preferential cleavage site for the copper

complex of **2** (the conjugate with 2-Clip-Phen) was inside this seven A·T box (results not shown).

Another difference in the cleavage pattern was also observed in the case of conjugate **1** (with only one phenanthroline) which was unable to cleave efficiently the sequence between the seven and the five A·T boxes (lanes 13 and 15, Figure 4, and lane C, Figure 5).

These results show that when the peptide part of the conjugates can orient the cleavage around a binding site, a fine specificity of cleavage can be modulated by the position of the bridge joining C2 or C3 of the phenanthroline units of Clip-Phen or by the choice of a system with only one phenanthroline.

CONCLUSION

This work shows that Clip-Phen copper complexes are versatile DNA cleavers which can be easily targeted on a particular DNA sequence by linkage to a specific DNA binder like a poly-*N*-methylpyrrole. The fine-tuning of the cleavage is due to the type of Clip-Phen used in these conjugates and to the tether length. It must be noted that the conjugate based on the 3-Clip-Phen was the most efficient one, indicating that the position of the serinol bridge between the two Phen units has a key role in the redox activity of the ligated copper. Our next goal will be to study if the conjugation of Clip-Phen derivatives also has an influence on the DNA cleavage chemistry of these artificial nucleases.

ACKNOWLEDGMENT

A collaborative CNRS-NSF grant is gratefully acknowledged. We thank Rachel Jameton for her technical assistance during PAGE experiments.

LITERATURE CITED

(1) Sigman, D. S., Mazumder, A., and Perrin, D. M. (1993) Chemical nucleases. *Chem. Rev. 93*, 2295−2316.

(2) Dervan, P. B. (1986) Design of sequence-specific DNA-binding molecules. *Science 232*, 464−471.

(3) Meunier, B., Ed. (1996) *DNA and RNA Cleavers and Chemotherapy of Cancer and Viral Diseases*, Kluwer, Dordrecht.

(4) James, B. R., and Williams, R. J. P. (1961) The oxidation−reduction potentials of some copper complexes. *J. Chem. Soc.* 2007−2019.

(5) Marshall, L. E., Graham, D. R., Reich, K. A., and Sigman, D. S. (1981) Cleavage of deoxyribonucleic acid by the 1,10-phenanthroline-cuprous complex. Hydrogen peroxide requirement and primary and secondary structure specificity. *Biochemistry 20*, 244−250.

(6) Veal, J. M., Merchant, K., and Rill, R. L. (1991) Noncovalent DNA binding of bis(1,10-phenanthroline)copper(I) and related compounds. *Biochemistry 30*, 1132−1140.

(7) Veal, J. M., Merchant, K., and Rill, R. L. (1991) The influence of reducing agent and 1,10-phenanthroline concentration on DNA cleavage by phenanthroline + copper. *Nucleic Acids Res. 19*, 3383−3388.

(8) Kuwabara, M., Yoon, C., Goyne, T. E., Thederahn, T., and Sigman, D. S. (1986) Nuclease activity of 1,10-phenanthroline-copper ion: reaction with CGCGAATTCGCG and its complexes with netropsin and *Eco*RI. *Biochemistry 25*, 7401−7408.

(9) Goyne, T. E., and Sigman, D. S. (1987) Nuclease activity of 1,10-phenanthroline-copper ion. Chemistry of deoxyribose oxidation. *J. Am. Chem. Soc. 109*, 2846−2848.

(10) Zelenko, O., Gallagher, J., and Sigman, D. S. (1997) Scission of DNA with bis(1,10-phenanthroline)copper without intramolecular hydrogen migration. *Angew. Chem., Int. Ed. Engl. 36*, 2776−2778.

(11) Sigman, D. S., Bruice, T. W., Mazumder, A., and Sutton, C. L. (1993) Targeted chemical nucleases. *Acc. Chem. Res. 26*, 98−104.

(12) Gallagher, J., Chen, C. B., Pan, C. Q., Perrin, M., Cho, Y. M., and Sigman, D. S. (1996) Optimizing the targeted chemical nuclease activity of 1,10-phenthroline-copper by ligand modification. *Bioconjugate Chem. 7*, 413−420.

(13) François, J. F., Saison-Behmoaras, T., Chassignol, M., Thuong, N. T., and Helene, C. (1989) Sequence targeted cleavage of single-stranded DNA by oligothymidilates covalently linked to 1,10-phenanthroline. *J. Biol. Chem. 264*, 5891−5898.

(14) Chen, C. B., Mazumder, A., Constant, J. F., and Sigman, D. S. (1993) Nuclease activity of 1,10-phenanthroline-copper: New conjugates with low molecular weight targeting ligands. *Bioconjugate Chem. 4*, 69−77.

(15) Sutton, C., Mazumder, A., Chen, C. B., and Sigman, D. S. (1993) Transforming the *Escherichia coli* Trp repressor into site-specific nuclease. *Biochemistry 32*, 4225−4230.

(16) Pendergrast, P. S., Ebright, Y. W., and Ebright, R. H. (1994) High-specificity DNA cleavage agent: design and application to kilobase and megabase DNA substrates. *Science 265*, 959−962.

(17) Pan, C. Q., Feng, J., Finkel, S. E., Landgraf, R., Johnson, R., and Sigman, D. S. (1994) Structure of the *Escherichia coli* Fis-DNA complex probed by protein conjugated with 1,10-phenanthroline copper(I) complex. *Proc. Natl. Acad. Sci. U.S.A. 91*, 1721−1725.

(18) Pitié, M., Donnadieu, B., and Meunier, B. (1998) Preparation of the new bis(phenanthroline)ligand "Clip-Phen" and evaluation of the nuclease activity of the corresponding copper complex. *Inorg. Chem. 37*, 3486-3489.

(19) Pitié, M., Sudres, B., and Meunier, B. (1998) Dramatic increase of the DNA cleavage activity of Cu(Clip-phen) by fixing the bridging linker on the C^3 position of the phenanthroline units. *Chem. Commun.* 2597−2598.

(20) Pitié, M., and Meunier, B. (1998) Preparation of a spermine conjugate of the bis-phenanthroline ligand "Clip-Phen" and evaluation of the corresponding copper complex. *Bioconjugate Chem. 9*, 604−611.

(21) Ross, S. A., Pitié, M., and Meunier, B. (1999) Synthesis of two acridine conjugates of the bis(phenanthroline) ligand "Clip-Phen" and evaluation of the nuclease activity of the corresponding copper complexes. *Eur. J. Inorg. Chem.* 557−563.

(22) Bailly, C., and Chaires, C. B. (1998) Sequence specific DNA minor groove binders. Design and synthesis of netropsin and distamycin analogues. *Bioconjugate Chem. 9*, 513−538.

(23) Baird, E. E., and Dervan, P. B. (1996) Solid-phase synthesis of polyamides containing imidazole and pyrrole amino acids. *J. Am. Chem. Soc. 118*, 6141−6146.

(24) White, S., Szewczyk, J. W., Turner, J. M., Baird, E. E., and Dervan, P. B. (1998) Recognition of the four Watson−Crick base pairs in the DNA minor groove by synthetic ligands. *Nature 391*, 468−471.

(25) Sambrook, J., Fritsch, E. F., and Maniatis, T. (1989) *Molecular Cloning*; Cold Spring Harbor Laboratory: Cold Spring Harbor, NY.

(26) Maxam, A. M., and Gilbert, W. (1980) Sequencing end-labeled DNA with base specific chemical cleavages. *Methods Enzymol. 65*, 499−599.

(27) Pratviel, G., Bernadou, J., and Meunier, B. (1995) Carbon−hydrogen bonds of DNA sugar units as targets for chemical nucleases and drugs. *Angew. Chem., Int. Ed. Engl. 34*, 746−769.

(28) Burrows, J. C., and Muller, J. G. (1998) Oxidative nucleobase modifications leading to strand scission. *Chem. Rev. 98*, 1109−1151.

(29) Schultz, P. G., Taylor, J. S., and Dervan, P. B. (1982) Design and synthesis of a sequence-specific DNA cleaving molecule. (Distamycin−EDTA)iron (II). *J. Am. Chem. Soc. 104*, 6861−6863.

BC000050T

Low Molecular Weight Disulfide Cross-Linking Peptides as Nonviral Gene Delivery Carriers

Donald L. McKenzie,[†] Elizabeth Smiley,[‡] Kai Y. Kwok,[‡] and Kevin G. Rice*[,†,‡]

Divisions of Medicinal Chemistry and Pharmaceutics, College of Pharmacy University of Michigan, Ann Arbor, Michigan 48109-165. Received May 26, 2000; Revised Manuscript Received August 31, 2000

Cross-linking peptides have been developed by inserting multiple Cys residues into a 20 amino acid condensing peptide that polymerizes through disulfide bond formation when bound to DNA resulting in small, highly stable DNA condensates that mediate efficient in vitro gene transfer [McKenzie et al. (2000) *J. Biol. Chem. 275*, 9970−9977]. In the present study, a minimal peptide of four Lys and two terminal Cys residues was found to substitute for Cys-Trp-$(Lys)_{17}$-Cys, resulting in DNA condensates with similar particle size and gene expression in HepG2 cells. Substitution of His for Lys residues resulted in an optimal peptide of Cys-His-$(Lys)_6$-His-Cys that, in addition to the attributes described above, also provided buffering capacity to enhance in vitro gene expression in the absence of chloroquine. The reported structure−activity relationships systematically explore peptides with combinations of Lys, Cys, and His residues resulting in low molecular weight peptides with improved gene transfer properties.

INTRODUCTION

The size and homogeneity of carrier molecules play a critical role in the success of a nonviral gene delivery system. These two parameters impact the toxicity, antigenicity, and the ability to systematically optimize gene delivery carriers for in vivo applications. A variety of Lys-containing polypeptides (*1*−*5*), dendrimers (*6*, *7*), and polymers such as polyethylenimine (PEI)[1] (*8*, *9*) have been tested for in vitro and in vivo gene delivery. The molecular weight of polylysine or polyethylenimine typically used for gene delivery ranges from 25 000 to over 300 000 amu (*4*, *8*). The high molecular weight (HMW) and heterogeneity of these polymers (*9*, *10*) significantly complicates the ability to develop chemically well-defined conjugates and develop structure activity relationships to optimize gene expression.

Low molecular weight (LMW) carriers could circumvent these problems, provided that they mediate in vitro and in vivo gene transfer as efficiently as their HMW counterparts. Peptides as short as 20 amino acids are able to form small DNA condensates that mediate efficient in vitro gene transfer (*11*−*13*); however, these fail as carriers when tested in vivo due to their lower affinity for DNA, prompting attempts to stabilize LMW carriers bound to DNA to increase their in vivo gene expression (*14*). Trubetskoy et al. inserted stable cross-links onto preformed peptide DNA condensates with heterobifunctional agents resulting in condensates that were active in transfecting cells in culture (*15*, *16*). Adami et al. used glutaraldehyde to cross-link peptide DNA condensates but found an inverse relationship between cross-linking level and in vitro gene expression (*17*). Blessing et al. and Ouyang et al. both incorporated a single sulfhydryl into cationic detergents that underwent dimerization after binding to DNA to form lipids that increased gene expression (*18*, *19*). Recently, LMW peptides possessing multiple Cys residues were introduced as gene delivery agents that form multiple interpeptide disulfide bonds when bound to DNA (*20*). After internalization by the cell, reduction of the cross-linked peptide DNA condensate yielded enhanced levels of gene expression.

In addition to stabilizing peptide DNA condensates, the delivery system needs to facilitate the escape from lysosomal trafficking and delivery of DNA to the cytosol. Several groups have reported methods to facilitate endosomal escape of DNA condensates in vitro by the addition of chloroquine or fusogenic peptides to the transfecting media (*21*−*23*). While these effectively enhance gene transfer in vitro, only recently have fusogenic peptides proven effective for in vivo gene delivery (*23*).

PEI and dendrimers contain secondary and tertiary amines that apparently serve to buffer the endosomal compartment, resulting in osmotic lysis (*24*). Midoux and Monsigny have extended this concept by conjugating His to the side chain of polylysine resulting in a polypeptide that buffers endosomes and enhances gene transfer (*25*).

In the present study, a panel of peptides containing two to eight Lys, one to five His, and either two or three Cys residues was synthesized and evaluated for DNA binding and gene transfer efficiency, in an attempt to further decrease the size of cross-linking peptide carriers and to incorporate endosomal buffering capacity. The results demonstrate that it is possible to substitute short cross-linking peptides for longer sequences, further advancing the concept of LMW cross-linking peptides as novel gene transfer agents.

* To whom correspondence should be addressed. Phone: (734) 763-1032. Fax: (734) 763-2022. E-mail: krice@umich.edu.

[†] Division of Medicinal Chemistry.

[‡] Division of Pharmaceutics.

[1] Abbreviations: Fmoc, N^{α}-9-fluorenylmethyloxycarbonyl; LMW, low molecular weight; HMW, high molecular weight; HBM, Hepes-buffered mannitol; TFA, trifluoroacetic acid; RP-HPLC, reversed-phase high-performance liquid chromatography; MEM, minimal essential media; TCEP, Tris(2-carboxyethyl)-phosphine hydrochloride; EDT, ethane dithiol; QELS, quasi-elastic light scattering; pCMVL, plasmid cytomegalovirus luciferase; RLU, relative light units; LC-MS, liquid chromatography mass spectrometry.

10.1021/bc000056i CCC: $19.00 © 2000 American Chemical Society
Published on Web 11/02/2000

Table 1. Identity and Mass Spectral Analysis of DNA Condensing Peptides

no.	sequence	mass (obs/calc[a])
1	Alk-S-Cys-Trp-$(Lys)_{18}$	2672.5/2672.5
2	Alk-S-Cys-Trp-$(Lys)_8$	1390.7/1390.8
3	Cys-Trp-$(Lys)_{17}$-Cys	2588.9/2589.6
4	Cys-$(Lys)_2$-Cys	480.2/480.7
5	Cys-$(Lys)_4$-Cys	736.4/736.4
6	Cys-$(Lys)_6$-Cys	993.5/993.6
7	Cys-$(Lys)_8$-Cys	1249.2/1249.7
8	Cys-Lys-Cys-Lys-Cys	583.3/583.9
9	Cys-$(Lys)_2$-Cys-$(Lys)_2$-Cys	839.4/839.4
10	Cys-$(Lys)_3$-Cys-$(Lys)_3$-Cys	1096.3/1096.6
11	Cys-$(Lys)_4$-Cys-$(Lys)_4$-Cys	1352.4/1352.9
12	Cys-$(Lys)_4$-His-$(Lys)_3$-Cys	1257.7/1257.7
13	Cys-His-$(Lys)_6$-His-Cys	1266.6/1267.6
14	Cys-His-$(Lys)_3$-His-$(Lys)_2$-His-Cys	1275.6/1275.6
15	Cys-$(His\text{-}Lys)_4$-Cys	1284.6/1284.1
16	Cys-His-Lys-His-Lys-$(His)_2$-Lys-His-Cys	1293.5/1294.5

[a] Masses are calculated as the average mass of the free base.

MATERIALS AND METHODS

N-Terminal Fmoc-protected amino acids, 9-hydroxybenzotriazole (HOBt), diisopropylcarbodiimide (DIC), and diisopropylethylamine were obtained from Advanced ChemTech (Lexington, KY). Substituted Wang resin for peptide synthesis was obtained from ChemImpex (Wood Dale, IL). *N*,*N*-Dimethyformamide, trifluoracetic acid (TFA), acetic acid, acetonitrile, piperidine, and acetic anhydride were purchased from Fisher Scientific (Pittsburgh, PA). LB media, LB agar, D-luciferin, and luciferase from *Photinus pyralis* (EC 1.13.12.7) were obtained from Boehringer Mannheim (Indianapolis, IN). HepG2, COS 7, and CHO cells were from the American Type Culture Collection (Rockville, MD). Inactivated "qualified" fetal bovine serum (FBS) was from Gibco BRL (Grand Island, NY). Bradford reagent was purchased from Bio-Rad (Hercules, CA), and thiazole orange was a gift from Beckton Dickinson Immunocytometry Systems (San Jose, CA). SYBR-Gold was purchased from Molecular Probes, Inc. (Eugene, OR). The 5.6 kb plasmid pCMVL encoding the reporter gene luciferase under the control of the cytomegalovirus promoter was a gift from Dr. M. A. Hickman at the University of California, Davis (*26*). Endotoxin free plasmids were purified from *Escherichia coli* on a Qiagen ultrapure column used according to the manufacturer's instructions, yielding plasmid DNA that was 50:50 supercoiled and open circular as determined by agarose gel electrophoresis. Peptide synthesis was performed on a computer interfaced model 90 Advanced ChemTech solid-phase peptide synthesizer (Lexington, KY). Peptide purification was performed using a semipreparative (10 μm) C_{18} RP-HPLC column from Vydac (Hesperia, CA) on a computer-interfaced HPLC and fraction collector from ISCO (Lincoln, NE). Electrospray mass spectrometry (ES-MS) was performed using a Finnigan LCQ mass spectrometer (San Jose, CA) interfaced with an analytical HPLC from Hitachi (San Jose, CA) using an analytical C18 (5 μm) reversed-phase column from Vydac.

Peptide Synthesis and Characterization. Peptides **1**−**3** (Table 1) were synthesized as previously described (*11*, *20*). All other peptides were synthesized using standard Fmoc procedures with HOBt and DIC double couplings followed by N-capping with acetic anhydride to avoid deletion sequences. The trityl group was used to protect the side-chains of both Cys and His while the Lys side chain was protected with *tert*-butoxycarbonyl. Peptides were cleaved from the resin, and side-chain protecting groups were simultaneously removed by reaction with TFA/EDT/water (95:2.5:2.5 v/v/v) for 1 h at RT.

Peptides were purified to homogeneity using RP-HPLC by injecting up to 6 μmol onto a Vydac C_{18} semipreparative column (2 × 25 cm) eluted isocratically at 10 mL/min with 0.05 v/v% TFA and 2% acetonitrile while monitoring the UV absorbance at 220 nm. The major peak eluting near 20 min was pooled from multiple runs, concentrated by rotary evaporation, lyophilized, and stored dry at −20 °C. Purified peptides were reconstituted in 0.1% TFA (degassed with nitrogen) and characterized by LC-MS by injecting 5 nmol onto a Vydac C18 reversed-phase HPLC column (0.47 × 25 cm) eluted at 1 mL/min with 0.1 v/v% acetic acid containing 0.02 v/v% TFA and an acetonitrile gradient of 0 to 5% over 15 min. The RP-HPLC eluent was directly infused into the electrospray ionization source of a Finnigan LCQ mass spectrometer and mass spectral data was obtained in the positive mode. The amino acid sequence was verified by data dependent ms/ms analysis (*27*, *28*).

The concentration of each purified peptide was determined by fluorescamine analysis using peptide **2** as a standard (*29*). The concentration of each peptide was further verified by ^{1}H NMR using acetone as an internal calibrant. The final purified yield of each peptide was approximately 30%.

The mean pK_a for His residues in peptides **12**−**16** was determined by ^{1}H NMR (*30*−*32*). Each peptide (1 μmol) was prepared in 500 μL of 90:10% v/v of H_2O:D_2O with 0.02% v/v acetone as an internal standard. ^{1}H NMR spectra were obtained on a Bruker 500 MHz spectrometer operated at 23 °C. The pH was measured over the range of 2.5−9.5 using a microelectrode following the addition of 10 μL aliquots of 10 mM sodium hydroxide. The chemical shift of the H2′ proton (8.5−7.6 ppm) was determined at each pH. The mean pK_a was calculated by plotting pH versus the chemical shift as described previously (*30*).

The buffering capacity of peptides **7** and **12**−**16** (Table 1) were compared by dissolving 100 nmol of the acetate salt form of each peptide into 1 mL of 150 mM sodium chloride. The initial pH of 5.5 was titrated down by adding 5 μL aliquots of 5 mM hydrochloric acid while measuring pH using a microelectrode.

Peptide DNA Condensation. Peptide−DNA condensates were prepared by combining 50 μg of DNA in 500 μL of Hepes-buffered mannitol (HBM) (5% w/v mannitol, 5 mM Hepes, pH 7.5) with 0.1−6.5 nmol of peptide in 500 μL of HBM while vortexing to form peptide−DNA condensates with a calculated primary amine to phosphate charge ratio between 0.25 and 8.0 (NH_4^+:PO_4^-). The condensates were allowed to cross-link for 30 min prior to performing physical measurements. The binding of each peptide to DNA was assayed by combining peptide DNA condensates (50 μL) with 950 μL of HBM containing 0.1 μM thiazole orange. The fluorescence of the intercalated dye was measured using an LS50B fluorometer (Perkin-Elmer, U.K.) by exciting at 500 nm while monitoring emission at 530 nm with the slit width set at 15 and 20 nm, respectively. Fluorescence blanks were subtracted from all values before data analysis.

The kinetics of disulfide bond formation of peptides bound to DNA was analyzed indirectly by monitoring the displacement of SYBR-Gold from DNA condensates. Peptide−DNA condensates were formed by combining 20 μg of DNA in 500 μL of HBM containing 1 × SYBR-Gold with 500 μL (26−52 nmol) of peptide in HBM containing 1 × SYBR-Gold to achieve a charge ratio of 4:1 (NH_4^+:PO_4^-). The fluorescence intensity (λ_{ex} 495 nm, λ_{em}

600 nm) was continuously monitored for 30 min to determine the kinetics of cross-linking.

The particle size and ζ potential of peptide DNA condensates were determined by quasielastic light scattering (QELS) using a Brookhaven ZetaPlus. Particle size analysis was performed in triplicate at a DNA concentration of 50 μg/mL in HBM at a charge ratio of 4:1 and a scattering angle of 90°. Data analysis utilized a multimodal volume distribution option included with the instrument. ζ Potential was also determined using 50 μg/mL peptide DNA condensates prepared at a 4:1 charge ratio in HBM. The reported ζ potential was averaged from 10 determinations.

Shear Stress Stability. The relative stability of peptide DNA condensates were examined using a salt sonication assay (*17*). Peptide DNA condensates (200 μL of 50 μg/mL) were formed as described above, incubated at RT for 30 min and then combined with 0−200 μL of 5 M sodium chloride and normalized to 400 μL with HBM to achieve a final sodium chloride concentration of 0, 0.2, 0.4, 0.8, 1.0, 1.5, 2.0, and 2.5 M. Each sample was sonicated for 30 s with a 100 W Microson XL-2000 ultrasonic probe homogenizer (Kontes, Vineland NJ) with a vibrational amplitude of 5 to fragment uncondensed DNA. DNA condensates were digested with 30 μg of trypsin for 12 h at 37 °C, electrophoresed on a 1% agarose gel electrophoresed in TEA buffer for 2 h, then visualized by ethidium bromide staining and destaining prior to photography on a transilluminator.

In Vitro Gene Expression. HepG2 cells (1.5×10^5) were plated on 6 × 35 mm wells and grown to 50% confluency in MEM supplemented with 10% FBS, penicillin, and streptomycin (100 units/mL), sodium pyruvate (100 mM), and L-glutamine (2 mM). Transfections were performed in MEM (2 mL/35 mm well) with 2% FBS with and without 80 μM chloroquine. Peptide DNA condensates (10 μg of DNA in 0.2 mL HBM) were added dropwise to triplicate wells. After a 5 h incubation at 37 °C, the medium was replaced with MEM supplemented with 10% FBS. After 24 h, cells were washed twice with ice-cold phosphate-buffered saline (calcium and magnesium free) and then treated with 0.5 mL of ice-cold lysis buffer (25 mM Tris chloride, pH 7.8, 1 mM EDTA, 8 mM magnesium chloride, 1% Triton X-100, and 1 mM DTT) for 10 min. The cell lysates were scraped, transferred to 1.5 mL microcentrifuge tube, and centrifuged for 7 min at 13000*g* at 4 °C to pellet cellular debris.

Lysis buffer (300 μL), sodium-ATP (4 μL of a 180 mM solution, pH 7, 4 °C), and cell lysate (100 μL, 4 °C) were combined in a test tube, briefly mixed, and immediately placed in the luminometer. Luciferase relative light units (RLU) were recorded on a Lumat LB 9501 (Berthold Systems, Germany) with 10 s integration after automatic injection of 100 μL of 0.5 mM D-luciferin (prepared fresh in lysis buffer without DTT). The RLUs were converted into fmol using a standard curve generated by adding a known amount of luciferase (0.01−100 fmol with specific activity of 2.5 nanounits/fmol) to 35 mm wells containing 50% confluent cells and lysis buffer. Protein concentrations were measured by Bradford assay using bovine serum albumin as a standard (*33*) which determined statistically equivalent ($p > 0.1$) amounts of protein when transfecting with each peptide DNA condensate. The amount of luciferase recovered in each sample was normalized to milligrams of protein and reported as the mean and standard deviation obtained from triplicate transfections.

LipofectAce (Gibco BRL, 1:2.5 w/w dimethyl dioctadecylammonium bromide and dioleoyl phosphatidylethanolamine) was used to mediate gene transfection according to the manufacturer's instructions. The ratio of DNA to LipofectAce was optimized for HepG2 cells. An optimal DNA/LipofectAce ratio was achieved by dissolving 10 μg of DNA in 100 μL of serum free media (SFM) followed by adding 60 μL of LipofectAce prepared in 140 μL of SFM. The LipofectAce DNA complex was then diluted with 1.7 mL of SFM and used to transfect HepG2 cells for 5 h followed by replacing the transfecting media with media supplemented with 10% FBS. The cells were incubated for a total of 24 h, harvested, and analyzed for luciferase as described above.

COS 7 cells (72 000) were plated in 35 mm wells and grown for 24 h to 50% confluency in DMEM (Gibco BRL) supplemented with penicillin and streptomycin (100 U/ml), L-glutamine (4 mM), and 10% FBS. The cells were transfected as described for HepG2 cells. CHO cells (72 000) were grown for 48 h as described above in Ham's F12 media supplemented with penicillin (100 units/mL), streptomycin (100 μg/mL), and 10% FBS then transfected as described above.

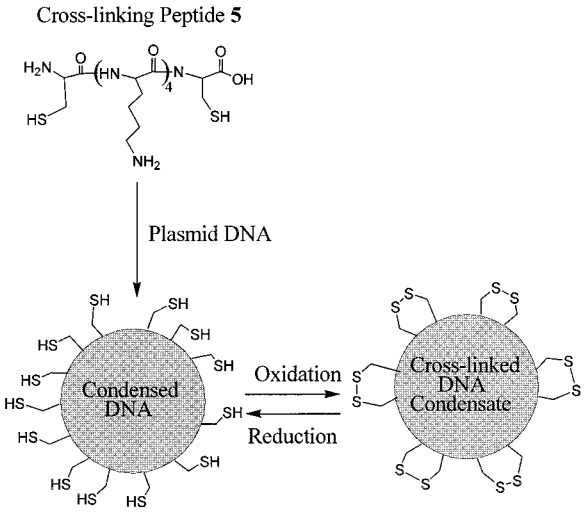

Figure 1. Formation of peptide DNA condensates. Short polylysine peptides containing multiple Cys residues bind to plasmid DNA and spontaneously polymerize through disulfide bond formation resulting in stable peptide DNA condensates.

RESULTS

The number of Lys residues in a DNA condensing peptide can influence the particle size, stability, and gene transfer efficiency of peptide DNA condensates (*11*). Peptides with fewer than 13 Lys residues form increasing larger DNA condensates that dissociate from DNA below a physiological salt concentration (0.15 M) (*11*, *34*). Peptide **1** possesses 18 Lys residues and forms small DNA condensates that are stable in 0.4 M sodium chloride and mediate efficient in vitro gene transfer. However, substitution of an additional Cys residue into this sequence results in cross-linking peptide **3** that significantly increases both the stability of DNA condensates and the in vitro gene transfer efficiency (*20*). Cross-linking peptides function by forming interpeptide disulfide bonds between adjacent peptides bound to DNA resulting in covalent linkages that revert once exposed to the reducing environment of the cell (Figure 1). Here we hypothesize that cross-linking peptides may be further decreased in size while retaining their ability to form small, stable DNA condensates with enhanced gene transfer efficiency. To investigate this, tetra, hexa, octa, and deca peptides **4**−**7** were prepared by systematically

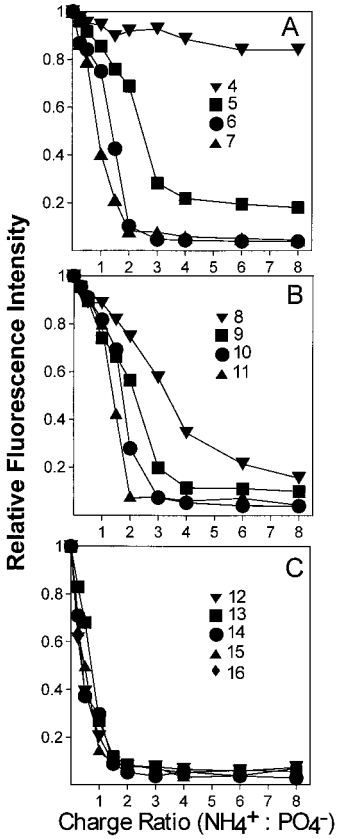

Figure 2. Binding of peptides to DNA. Thiazole orange was used as a displaceable intercalator dye in a peptide titration assay to determine the charge ratio needed to form DNA condensates. Panel A illustrates condensates formed with peptides **4**−**7**, panel B, represents condensates formed with peptides **8**−**11** and panel C shows condensates formed with peptides **12**−**16**. See Table 1 for peptide structures.

increasing the number of Lys residues while keeping the C- and N-terminal Cys residues constant (Table 1). Similarly, penta-, septa-, nona-, and undecapeptides **8**−**11** were prepared by increasing the number of Lys residues while keeping three constant Cys residues (Table 1).

Each peptide was synthesized and purified to homogeneity by RP-HPLC resulting in a purified yield of approximately 30%. LC-MS analysis identified a single peak with molecular weight corresponding to the predicted sequence (Table 1). LC-MS/MS analysis also established y and b fragment ions corresponding to the sequence of the fully reduced peptide. Peptides were maintained in the fully reduced form at pH 2 in deoxygenated 0.1% TFA. However, at neutral pH, and in the absence of a DNA template, cross-linking peptides rapidly oxidized to form disulfide bonds yielding a mixture of cyclic products (data not shown).

To establish the peptide to DNA stoichiometry needed to form DNA condensates, the displacement of thiazole orange from DNA was measured by a decrease in fluorescence intensity as a function of increasing peptide concentration. Titration of DNA with peptides **4**−**7** across charge ratios of 0.25−8:1 (NH_4^+:PO_4^-) resulted in a decrease in the thiazole orange fluorescence that reached a minimum for fully formed peptide DNA condensates (Figure 2A). Peptides **6** and **7** were equivalent at displacing thiazole orange resulting in a maximal inflection at a charge ratio of 2:1. Peptide **5** was less efficient, requiring a charge ratio of 3:1 to condense DNA whereas peptide **4** was even less effective at displacing thiazole

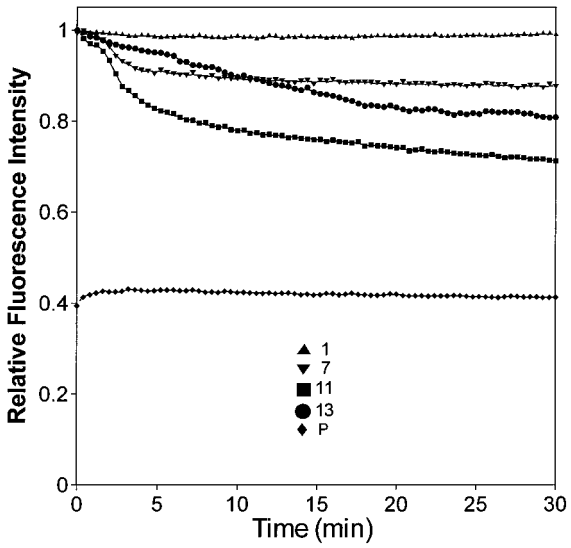

Figure 3. Kinetics of peptide cross-linking on DNA. SYBR-Gold fluorescence intensity was continuously monitored to determine the kinetics of peptide cross-linking on DNA. Representative plots illustrating the kinetics of cross-linking using peptide **7**, **11**, and **13** are compared to the constant fluorescence resulting from non-cross-linking peptide **1** or polylysine$_{1007}$ (**P**) binding to DNA.

orange and apparently failed to form DNA condensates even at a charge ratio of 8. Similar results were obtained for peptides **8**−**11**, establishing that peptide **8** was only able to weakly condense DNA at a charge ratio of 6−8:1 whereas peptides **9**−**11** efficiently displaced thiazole orange resulting in a fluorescence minimum at a charge ratios of 2−4 (Figure 2B). On the basis of these results, subsequent studies utilized a peptide to DNA charge ratio of 4:1 to compare DNA condensates prepared with peptides **5**−**7** and **9**−**11**.

The kinetics of peptide cross-linking on DNA was evaluated using SYBR-Gold as an intercalator dye which, unlike thiazole orange, retains a significant degree of DNA binding and fluorescence intensity even at high peptide:DNA stoichiometry (*20*). Instantaneous formation of peptide DNA condensates using peptides incapable of cross-linking such as **1** or polylysine$_{1007}$, results in a constant SYBR-Gold intensity over time with magnitude inversely related to the affinity of the peptide for DNA (Figure 3). Alternatively, a time-dependent decrease in SYBR-Gold fluorescence intensity results from displacement of fluorophore due to peptide cross-linking on DNA (Figure 3). The results illustrated for peptides **7** and **11** are representative of **4**−**7** and **8**−**11**, respectively, each of which caused a decrease in the SYBR-Gold fluorescence intensity over time reaching an asymptote in 30 min or less indicating reaction completion (Figure 3). Even though cross-linking peptides generate long polymers that form stable DNA condensates as discussed below, the rapid condensation of DNA within seconds followed by the slower process of sulfhydryl cross-linking over 30 min, is apparently less efficient at displacing SYBR-Gold. This leads to a difference in the relative fluorescence intensity at equilibrium for DNA condensates prepared using cross-linking peptides versus polylysine$_{1007}$.

Direct evidence of peptide cross-linking on DNA was determined by measuring the stability of peptide DNA condensates using a salt sonication assay (*17*). Peptide **1** protected DNA from fragmentation up to a sodium chloride concentration of 0.4 M, above which, higher salt concentrations led to dissociation of the peptide and

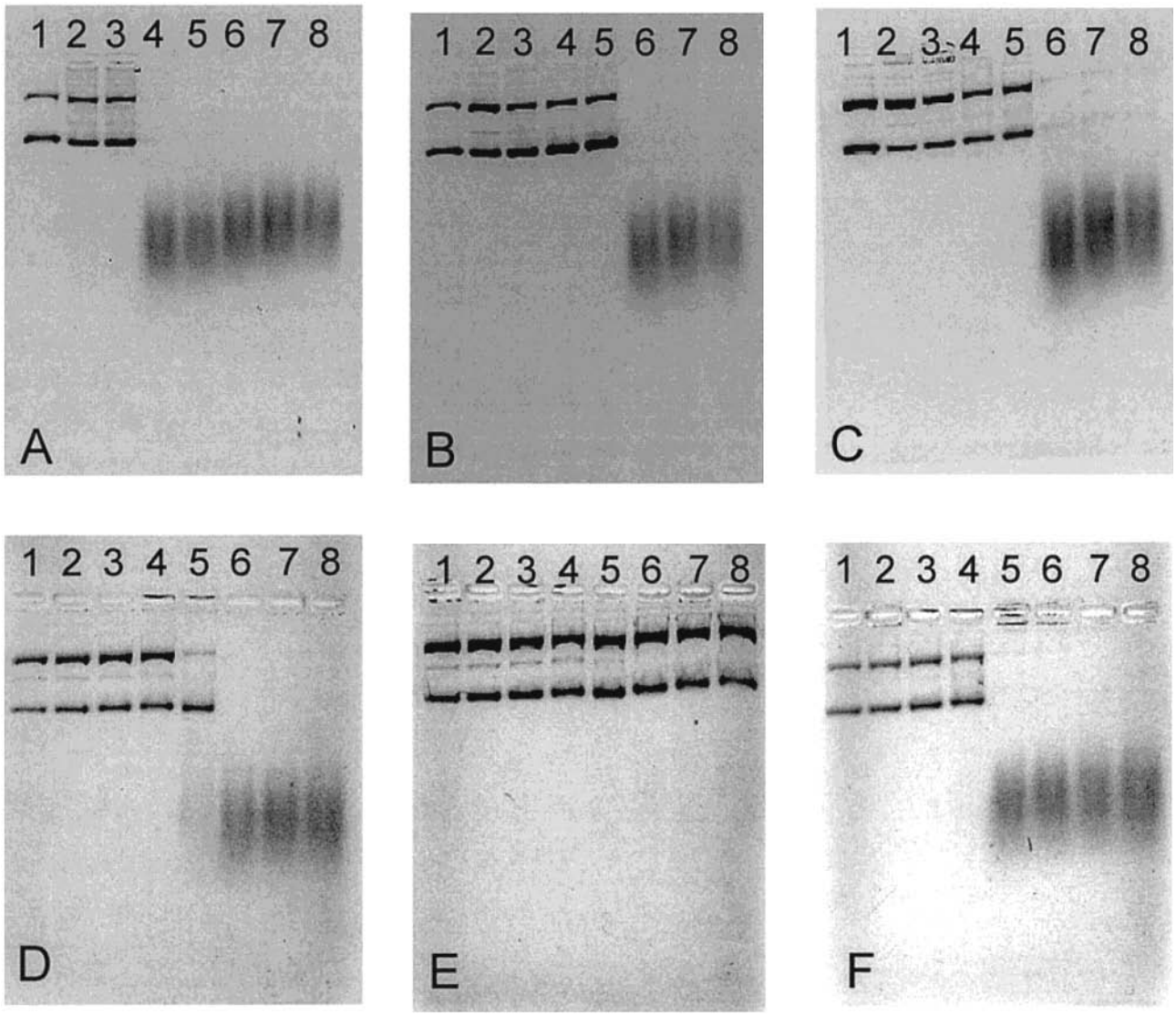

Figure 4. Shear stress stability of peptide DNA condensates. The stability of peptide DNA condensates were analyzed by gel electrophoresis following 30 s sonication in the presence of increasing concentrations of sodium chloride. DNA condensates were formed using peptide **1** (A), **3** (B), polylysine$_{1007}$ (C), **7** (D), **11** (E), and **12** (F). Lanes 1−8 represent sodium chloride concentrations of 0, 0.2, 0.4, 0.8, 1.0, 1.5, 2.0, and 2.5 M sodium chloride, respectively. The results establish DNA condensates prepared with peptides **3**, **7**, and **12** are nearly as stable polylysine$_{1007}$ DNA condensates whereas peptide **11** DNA condensates are completely stable in 2.5 M sodium chloride.

sonicative induced fragmentation of the DNA (Figure 4A). Polylysine$_{1007}$ DNA condensates were found to dissociate above 1 M sodium chloride establishing their greater stability (Figure 4B). Although peptide **3** possesses a similar number of Lys residues as **1**, peptide **3** DNA condensates were also stable in sodium chloride concentrations up to 1 M before dissociation led to sonicative degradation of the DNA (Figure 4C). The enhanced stability of peptide **3** DNA condensates is due to disulfide bond formation since preoxidation of **3**, or reduction of peptide **3** DNA condensates with TCEP, reverted the stability to that of peptide **1** DNA condensates as demonstrated previously (*20*). By comparison, peptide **7** DNA condensates dissociate between 0.8 and 1 M sodium chloride indicating that they are nearly as stable as peptide **3** and polylysine$_{1007}$ DNA condensates (Figure 4D). This result is in contrast to peptide **2** DNA condensates which dissociate below 0.1 M sodium chloride due to the inability to undergo sulfhydryl cross-linking (*34*). Peptides **5** and **6** produced DNA condensates that were somewhat less stable (0.4−0.6 M, not shown) than those produced by peptide **7**, but were still much more stable than peptide **2** DNA condensates (*34*). The stability of peptide **11** DNA condensates established that the addition of a third Cys residue resulted in complete resistance to dissociation up to 2.5 M sodium chloride (Figure 4E). Likewise, peptide **9** DNA condensates resisted dissociation up to 1.5 M sodium chloride, and peptide **10** DNA condensates were stable up to 2.5 M sodium chloride (not shown).

The particle size and ζ potential of each peptide DNA condensate were compared at a charge ratio of 4:1 and a cross-linking time of 30 min. As indicated above, peptide **4** failed to appreciably bind to DNA and could not form DNA condensates detected by QELS. The mean diameter of DNA condensates formed with peptide **5**−**7** was less than 55 nm and compared favorably to DNA condensates prepared using peptide **1** (Table 2). However, the mean diameter of DNA condensates prepared with peptides **9**−**11** were significantly larger (738−1668 nm), most likely resulting from interparticle cross-linking of the internal Cys due to the high molar concentration (163−325 nmol/mL) required to form peptide **9**−**11** DNA condensates (Table 2). In each case, peptides **1**−**3**, **6**, **7**,

Table 2. QELS Particle Size Analysis[a] of Peptide DNA Condensates

no.	particle size (nm)[b]	ζ potential[c] (mV)
1	64 ± 11	26 ± 1
2	159 ± 76	18 ± 2
3	53 ± 16	28 ± 9
4	*d*	*d*
5	38 ± 10	*e*
6	52 ± 4	37 ± 1
7	53 ± 16	26 ± 2
8	*d*	*d*
9	1668 ± 154	*e*
10	1375 ± 324	34 ± 2
11	738 ± 154	31 ± 3
12	87 ± 20	30 ± 2
13	97 ± 40	31 ± 1
14	183 ± 64	20 ± 2
15	205 ± 104	23 ± 1
16	320 ± 169	23 ± 1

[a] Deconvolution of quasielastic light scattering data assumes spherical particles of identical density. [b] Mean diameter determined from the multimodal volume distribution. Average and standard deviation of three determinations. [c] ζ Potential determined from the average and standard deviation of 10 determinations. [d] No particles formed. [e] Peptide concentration at 4:1 charge ratio was too high for stable signal.

10, and **11** DNA condensates prepared at a charge ratio of 4 had a positive ζ potential ranging from +18−37 mV (Table 2).

The in vitro gene transfer efficiency of peptide **1**, **3**, **5**−**7**, and **9**−**11** DNA condensates prepared at a charge ratio of 4:1 were directly compared in three different cell lines (Figure 5). In each cell line tested, peptide **3** enhanced gene expression by 10−40-fold over peptide **1** DNA condensates (Figure 5). Comparison of peptide **3** to that of peptide **5**, **6**, and **7** DNA condensates indicated that the gene expression in HepG2 cells was maintained when decreasing peptide length by eliminating Lys residues (Figure 5A). This is in contrast to published results on peptide **2** which only forms large DNA condensates of 2.4 μm diameter that transfect HepG2 cells with 4-orders of magnitude-less efficiency relative to peptide **1** (*11*). The gene expression in COS 7 cells was inexplicably 5-fold lower for peptide **7** relative to peptide **3**, **5**, and **6** DNA condensates despite otherwise identical physical properties (Figure 5B). The finding that peptide **5** mediated 3-orders of magnitude lower gene expression in CHO cells relative to peptide **3**, **6**, and **7** (Figure 5C) might be due to the decreased reducing capacity of CHO cells (*35*−*37*). Since peptide **5** DNA condensates theoretically possess twice as many disulfide bonds as peptide **7** DNA condensates, CHO cells that produce lower levels of cytosolic glutathione (*35*−*37*) may be less efficient at reducing endocytosed peptide **5** DNA condensates resulting in lower gene expression.

DNA condensates formed with peptide **9**, **10**, and **11** yielded overall lower levels of gene expression in each cell line relative to peptide **7** DNA condensates (Figure 5). This is most likely related to the large particle size (Table 2) which appeared to be inversely related to gene expression in all three cell lines (Figure 5)

The gene expression mediated by peptide DNA condensates is enhanced approximately 10-fold due to the presence of 80 μM chloroquine in the transfecting media which serves as a lysotropic agent (*24*). Midoux and Monsigny have demonstrated that derivatization of polylysine with His produced DNA condensates that buffer the endosomal compartment and thereby substitute for chloroquine in enhancing peptide mediated gene

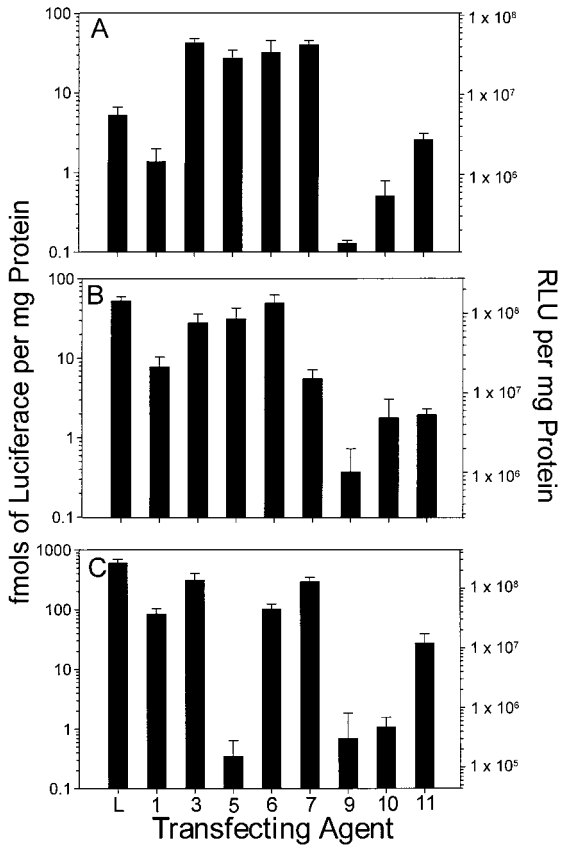

Figure 5. Luciferace expression in HepG2, COS 7, and CHO Cells. The luciferace reporter gene expression for each peptide DNA condensate was measured in HepG2 (A), COS 7 (B), and CHO (C) cells using 80 μM chloroquine during the transfection. Each result represents the mean and standard deviation of three determinations. See Table 1 for peptide structures. L represents LipofectAce.

delivery (*25*). To determine if a similar approach could be applied to enhance the gene transfer of LMW cross-linking peptides, one to five His residues were substituted for Lys residues in **7** to prepare peptides **12**−**16** (Table 1). For this experiment, substitutions were made into **7** as opposed to **6** to allow up to five His residues to be installed while still retaining three Lys residues to mediate binding of the peptide to DNA.

Titration of peptides **12**−**16** with plasmid DNA demonstrated each was equally effective at displacing thiazole orange from DNA, resulting in fully condensed DNA at a charge ratio of 2:1 (Figure 2C). Likewise, analysis of the cross-linking kinetics of peptides **12**−**16** while bound to DNA established reaction completion in approximately 30 min as illustrated by the results for peptide **13** (Figure 3). In each case, a slower cross-linking distinguished His peptides **12**−**16** from that determined for peptides **5**−**11** which may relate to an altered conformational state when **12**−**16** are bound to DNA. Application of the salt sonication assay demonstrated that, like peptide **7**, peptides **12**−**16** formed stable DNA condensates that dissociated above 0.8 M sodium chloride as illustrated using peptide **12** DNA condensates (Figure 4F). In contrast to the similarities between peptide **7** and **12**−**16** described above, particle size analysis revealed that DNA condensates formed with peptides **12**−**16** possessed mean diameters ranging from 87 to 320 nm that increased in proportion to the number of His residues, compared to DNA condensates formed with peptide **7** that had a mean diameter of 53 nm. Despite the larger particle size, peptides **12**−**16** DNA condensates prepared at a charge

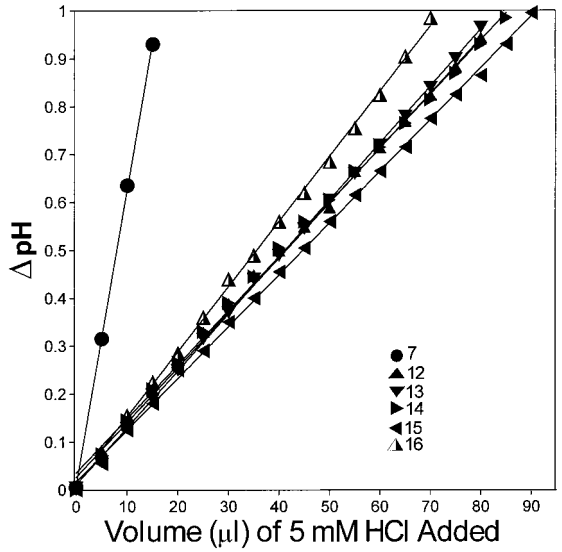

Figure 6. Peptide buffering capacity. The change in pH was monitored for peptides **7** and **12**−**16** by titrating 5 μL aliquots of 5 mM hydrochloric acid into 100 μL of a 0.5 mM peptide solution in 150 mM sodium chloride.

ratio of 4 each had a positive ζ potential ranging from +20−31 mV (Table 2).

The pK_a of cationic polymers such as PEI or dendrimers that buffer endosomes is generally between 5.5 and 7.5 (*24*). To determine if the His residue(s) in peptides **12**−**16** buffer in a similar range, an NMR-based titration established the immidazole side chain in each peptide had a pK_a between 5.5 and 6.0.

Peptides **12**−**16** were compared to peptide **7** in a pH titration experiment to determine if the number of His residues in **12**−**16** would correlate with increasing buffering capacity (Figure 6). Although there was no correlation between and the apparent buffering capacity and the number of His residues in peptides **12**−**16**, each His containing peptide did buffer more efficiently than peptide **7**.

The gene transfer efficiency of peptide **12**−**16** DNA condensates were compared to condensates prepared with peptide **1** and **7** in three cell lines (Figure 7). In the absence (−) of chloroquine, peptide **1** DNA condensates mediated 10−15-fold lower gene expression relative to in the presence (+) of 80 μM chloroquine in each cell line (Figure 7). Peptide **12**− DNA condensates possessing 10% His content mediated 3-fold higher gene expression compared to peptide **7**− DNA condensates in HepG2 cells (Figure 7A). Increasing the His content to 20 or 30% in peptides **13**− and **14**− resulted in a 4-fold enhancement in gene transfection relative to peptide **7**− DNA condensates in HepG2 cells (Figure 7A). The combined contribution of cross-linking and His resulted in gene expression levels for peptide **13**− and **14**− DNA condensates that were equivalent to peptide **1**+ DNA condensates in HepG2 cells (Figure 7A). Peptide **15**− and **16**− DNA condensates were progressively less effective in mediating gene transfer in HepG2 cells despite possessing His content of 40 and 50%, respectively (Figure 7A), presumably the result of an increase in particle size (Table 2). In contrast to the results in HepG2 cells, peptide **12**−**14**− failed to enhance gene expression in COS 7 cells relative to peptide **7**− DNA condensates (Figure 7B). Likewise, the gene expression of peptide **14**− and **15**− DNA condensates were also significantly less in COS 7 cells relative to condensates prepared with peptide **12**− and **13**−. The same comparison in CHO cells established

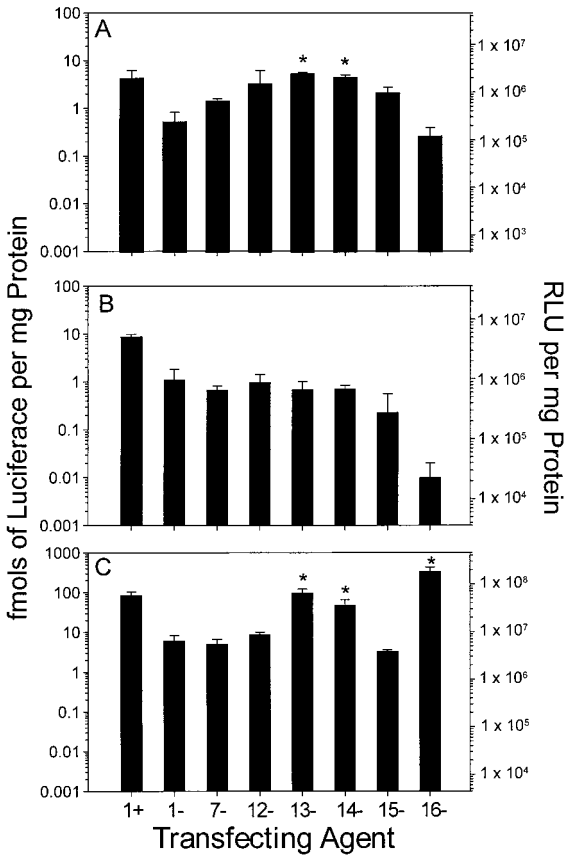

Figure 7. Luciferace expression of endosomal buffered DNA condensates. The luciferace reporter gene expression for peptide DNA condensates in the presence (+) or absence of chloroquine (−) were compared in HepG2 (A), COS 7 (B), and CHO cells (C). Each experimental result represents the mean and standard deviation of three determinations. (*) $p < 0.05$ relative to peptide **7**−. See Table 1 for peptide structures.

that peptide **13**−, **14**−, and **16**− DNA condensates mediated a 10−15-fold enhancement in gene expression relative to peptide **7**− DNA condensates (Figure 7C). The enhanced gene expression of peptide **16**− DNA condensates in CHO cells is an inexplicable result that has been reproduced several times and appears to be contradictory to the trends observed in HepG2 and COS 7 cells.

DISCUSSION

The high molecular weight and polydispersity (*4*, *7*, *9*, *10*) inherent to many nonviral gene transfer agents complicates regiospecific derivatization, characterization, and formulation with DNA. The design of LMW gene transfer agents is an attractive alternative since these can be systematically optimized and may present fewer side effects when used clinically.

In previous studies, we determined peptide **1**, possessing 18 Lys residues, was a minimal peptide to form small (<80 nm) DNA condensates that are stable in 0.4 M saline and transfect cells in culture as efficiently as higher molecular weight polylysine peptides (*11*). Decreasing the number of Lys residues to further shorten chain length such as in peptide **2**, not only led to an increase in the particle size and a three-order of magnitude decrease in the in vitro gene expression level, but also to a loss of stability in normal saline (0.15 M) due to a decrease in DNA binding affinity (*11*, *34*).

The stability of LMW peptide DNA condensates directly relates to in vivo efficacy. Without the aid of a cross-linking strategy, i.v. dosed peptide **1** DNA conden-

sates lack stability in the circulation and are rapidly metabolized without mediating gene expression (*14*). Glutaraldehyde cross-linking provides a means to stabilize LMW DNA condensates for in vivo use but still requires the use of a 20 amino acid peptide to form small condensates.

LMW peptides possessing multiple Cys residues have been proposed as novel gene transfer agents that temporarily form HMW peptides following polymerization on DNA (*20*). Peptide **3** DNA condensates have been shown to form small particles that are comparable in stability to polylysine$_{1007}$ DNA condensates (*20)* (Figure 4). A proposed mechanism involves subsequent reduction in the cell, resulting in the release of DNA and enhanced gene expression relative to peptide **1** DNA condensates. On the basis of these results, we hypothesized that cross-linking peptides could potentially overcome the stability, particle size, and gene transfer limitations described above for very short polylysine peptides. To test this hypothesis, peptides **4**−**11** were compared for their ability to bind, condense, and stabilize DNA and mediate in vitro gene expression.

The results demonstrate peptide **5** as a minimal structure possessing four Lys and two terminal Cys residues that rapidly cross-links on DNA to form small condensates that are stable in 0.4 M salt and mediate gene expression equivalent to peptide **3** DNA condensates in two of the three cell lines tested (Figures 2−5). Peptide **4**, with only two Lys residues, lacked appreciable affinity for DNA and had a greater propensity to undergo internal disulfide bond formation versus template polymerization and was thereby unable to condense DNA.

As anticipated, decreasing the overall length of the peptide from 20 down to 10 residues had little effect on the stability of the cross-linking peptide DNA condensates. Peptide **7** DNA condensates, consisting of eight Lys and two terminal Cys residues, possess the same stability as peptide **3** and polylysine$_{1007}$ DNA condensates (Figure 4). As demonstrated previously, adding an internal Cys to peptide **3** allows for interpeptide cross-linking in addition to linear polymerization which further increases the stability of DNA condensates to above 2.5 M sodium chloride (*20*). Similarly, peptide **9**−**11** DNA condensates were found to be improved in stability although the particle size was much larger. This cannot be the result of too few Lys residues since the particle size of DNA condensates prepared with peptide **5** possessing four Lys residues was 10-fold smaller than that determined for those prepared with peptide **11** possessing eight Lys residues. It is more likely that the internal Cys in peptides **9**−**11** contributes both to interpeptide as well as interparticle cross-linking which occurs rapidly since the particle size determined for peptide **7** or **11** DNA condensates did not change appreciably between 30 min and 24 h. Taken collectively, the data suggest that a small DNA condensate particle size can be achieved with a short, 6−10 amino acid peptide, possessing two terminal Cys residues. Within this size range, additional Cys residues improve stability but significantly increase particle size and thereby decrease in vitro gene expression. Including multiple Cys residues into a 20 amino acid peptide circumvents the problem of increasing particle size (*20*). Although this information is fundamental to the design of a variety of gene delivery systems, when applied to the design of i.v. dosed targeted gene delivery systems, the relationships described for LMW cross-linking peptides binding to DNA will likely change when these are derivatized with poly(ethylene glycol) and targeting moieties such as *N*-glycans (*38*, *39*).

Peptide **7** was selected to determine if substitution of one to five His residues could further enhance expression. The results establish that peptide **13**− and **14**− DNA condensates possessed 4−10-fold enhanced gene expression relative to peptide **7**−, dependent on cell type (Figure 7). Likewise, the gene expression mediated by peptide **1**+ or **13**− DNA condensate in HepG2 and CHO cells were equivalent (Figure 7). These results are in agreement with a previously established mechanism of endosomal buffering for His derivatized polylysine peptides (*25*) and extend this concept by demonstrating that LMW cross-linking peptides can also serve to buffer endosomes and enhance gene expression.

In conclusion, we have extended the concept of LMW cross-linking peptides by identifying the minimal Cys and Lys peptide that polymerizes while bound to DNA leading to enhanced gene expression. The concept of endosomal buffering has been extended by determining the number of His residues in a LMW cross-linking peptide needed to enhance gene expression. Further work is necessary to determine if LMW cross-linking peptides can be used to systematically increase the level of gene expression in vivo.

ACKNOWLEDGMENT

The authors acknowledge financial support provided by NIH Grants GM48049 and DE13004 and support from Selective Genetics, Inc.

LITERATURE CITED

(1) Wagner, E., Zenke, M., Cotton, M., Beug, H., and Birnstiel, M. L. (1990) Transferrin-polycation conjugates as carriers for DNA uptake into cells. *Proc. Natl. Acad. Sci. U.S.A. 87*, 3410−3414.

(2) Wyman, T. B., Nicol, F., Zelphati, O., Scaria, P. V., Plank, C., and Szoka, F. C. (1997) Design, Synthesis, and characterization of a cationic peptide that binds to nucleic acids and permeabilizes bilayers. *Biochemistry 36*, 3008−3017.

(3) Morris, M. C., Vidal, P., Chaloin, L., Heitz, F., and Divita, G. (1997) A new peptide vector for efficient delivery of oligonucleotides into mammalian cells. *Nucleic Acids Res. 25*, 2730−2736.

(4) Toncheva, V., Wolfert, M. A., Dash, P. R., Oupicky, D., Ulbrich, K., Seymour, L. W., and Schacht, E. H. (1998) Novel vectors for gene delivery formed by self-assembly of DNA with poly(L-lysine) grafted with hydrophilic polymers. *Biochim. Biophy. Acta 1380*, 354−368.

(5) McKee, T. D., DeRome, M. E., Wu, G. Y., and Findeis, M. A. (1994) Preparation of asialoorosomucoid-polylysine conjugates. *Bioconjugate Chem. 5*, 306−311.

(6) Tang, M. X., Redemann, C. T., and Szoka, F. C. (1996) In vitro gene delivery be degraded polyamidoamine dendrimers. *Bioconjugate Chem. 7*, 703−714.

(7) Page, D., and Roy, R. (1997) Synthesis and biological properties of mannosylated starburst poly(amidoamine) dendrimers. *Bioconjugate Chem. 8*, 714−723.

(8) Boussif, O., Lezoualc'h, F., Zanta, M. A., Mergny, M. D., Scherman, D., Demeneix, B., and Behr, J. (1995) A versatile vector for gene and oligonucleotide transfer into cells in culture and in vivo: Polyethylenimine. *Proc. Natl. Acad. Sci. U.S.A.* 92, 7297−7301.

(9) Godbey, W. T., Wu, K. K., Hirasake, G. J., and Mikos, A. G. (1999) Improved packing of poly(ethylenimine)/DNA complexes increases transfection efficiency. *Gene Ther. 6*, 1380−1388.

(10) McKenzie, D. L., Collard, W. T., and Rice, K. G. (1999) Comparative gene transfer efficiency of low molecular weight polylysine DNA-condensing peptides. *J. Pept. Res. 54*, 311−318.

(11) Wadhwa, M. S., Collard, W. T., Adami, R. C., McKenzie, D. L., and Rice, K. G. (1997) Peptide-mediated gene deliv-

ery: Influence of peptide structure on gene expression. *Bioconjugate Chem. 8*, 81−88.
(12) Niidome, T., Takaji, K., Urakawa, M., Ohmori, N., Wada, A., Hirayama, T., and Aoyagi, H. (1999) Chain length of cationic α-helical peptide sufficient for gene delivery into cells. *Bioconjugate Chem. 10*, 773−780.
(13) Niidome, T., Ohmori, N., Ichinose, A., Wada, A., Mihara, H., Hirayama, T., and Aoyagi, H. (1997) Binding of cationic α-helical peptides to plasmid DNA and their gene transfer abilities into cells. *J. Biol. Chem. 24*, 15307−15312.
(14) Collard, W. T., Yang, Y., Kwok, K. Y., and Rice, K. G. (2000) Biodistribution, metabolism, and in vitro gene expression of glycopeptide poly(ethylene glycol) DNA co-condensates. *J. Pharm. Sci., 89*, 499−512.
(15) Trubetskoy, V. S., Loomis, A., Slattum, P. M., Hagstrom, J. E., Budker, V. G., and Wolff, J. A. (1999) Caged DNA does not aggregate in high ionic strength solutions. *Bioconjugate Chem. 10*, 624−628.
(16) Trubetskoy, V. S., Budker, V. G., Hanson, L. J., Slattum, P. M., Wolff, J. A., and Hagstrom, J. E. (1998) Self-assembly of DNA-polymer complexes using template polymerization. *Nucleic Acids Res. 26*, 4178−4185.
(17) Adami, R. C., and Rice, K. G. (1999) Metabolic stability of glutaraldehyde cross-linked peptide DNA condensates. *J. Pharm. Sci. 8*, 739−746.
(18) Blessing. T., Remy, J., and Behr, J. (1998) Monomolecular collapse of plasmid DNA into stable virus-like particles. *Proc. Natl. Acad. Sci. U.S.A. 95*, 1427−1431.
(19) Ouyang, M., Remy, J., and Szoka, F. C. (2000) Controlled template-assisted assembly of plasmid DNA into nanometric particles with high DNA concentration. *Bioconjugate Chem. 11*, 104−112.
(20) McKenzie, D. L., Kwok, K. Y., and Rice, K. G. (2000) A potent new class of reductively activated peptide gene delivery agents. *J. Biol. Chem. 275*, 9970−9977.
(21) Wagner, E. (1998) Effects of membrane-active agents in gene delivery. *J. Controlled Release 53*, 155−158.
(22) Midoux, P., Kichler, A., Boutin, V., Maurizot, J., and Monsigny, M. (1998) Membrane permeabilization and efficient gene transfer by a peptide containing several histidines. *Bioconjugate Chem. 9*, 260−267.
(23) Nishikawa, M., Yamauchi, M., Morimoto, K., Ishida, E., Takakura, Y., and Hashida, M. (2000) Heptocyte-targeted in vivo gene expression by intraveneous injection of plasmid DNA complexed with synthetic multi-functional gene delivery system. *Gene Ther. 7*, 548−555.
(24) Pouton, C. W., and Seymour, L. W. (1998) Key issues in nonviral gene delivery. *Adv. Drug Delivery 34*, 3−19.
(25) Midoux, P., and Monsigny, M. (1999) Efficient gene transfer by histidylated polylysine/pDNA complexes. *Bioconjugate Chem. 10*, 406−411.
(26) Hickmann, M. A., Malone, R. W., Lehmann-Bruinsma, K., Sih, T. R., Knoell, K., Szoka, F. C., Walzem, R., Carlson, D. M., and Powell, J. S. (1994) Gene expression following direct injection of DNA into liver. *Hum. Gene Ther. 5*, 1477−1483.
(27) Smith, R. D., Loo, J. A., Edmonds, C. G., Barinaga, C. J., and Udseth, H. R. (1990) New developments in biochemical mass spectrometry: Electrospray ionization. *Anal. Chem. 62*, 882−899.
(28) Arnott, D., Shabanowitz, J., and Hunt, D. F. (1993) Mass spectrometry of proteins and peptides: Sensitive and accurate mass measurement and sequence analysis. *Clin. Chem. 39*, 2005−2010.
(29) Weigele, M., DeBernardo, S. L., Tengi, J. P., and Leimgruber, W. (1972) A novel reagent for the fluorometric assay of primary amines. *J. Am. Chem. Soc. 94*, 5927−5928.
(30) Gasparovic, C., Barba, I., Born, S., Barton, S., Arlis, C., and Mann, P. (1998) A study of imidazole-based nuclear magnetic resonance probes of cellular pH. *Anal. Biochem. 261*, 64−72.
(31) Markley, S. L. (1975) Observation of histidine residues in proteins by means of nuclear magnetic resonance spectroscopy. *Acc. Chem. Res. 8*, 70−80.
(32) Rabenstein, D. L., and Sayer, T. L. (1976) Determination of microscopic acid dissociation constants by nuclear magnetic resonance spectrometry. *Anal. Chem. 48*, 1141−1146.
(33) Bradford, M. M. (1976) A rapid and sensitive method for the quantitation of microgram quantities of protein utilizing the principle of protein-dye binding. *Anal. Biochem. 72*, 248−254.
(34) Adami, R. C., Collard, W. T., Gupta, S. A., Kwok, K. Y., Bonadio, J., and Rice, K. G. (1998) Stability of peptide-condensed plasmid DNA formulations. *J. Pharm. Sci. 87*, 678−683.
(35) Merkel, B. J., Mandel, R., Ryser, H. J.-P., and McCoy, K. L. (1995) Characterization of fibroblasts with a unique defect in processing antigens with disulfide bonds. *J. Immunol. 154*, 128−136.
(36) Shorts, S., Merkel, B. J., Caffrey, R., and McCoy, K. L. (1996) Defective antigen processing correlates with a low level of intracellular glutathione. *Eur. J. Immunol. 26*, 3015−3020.
(37) Mandel, R., Ryser, H. J.-P., Niaki, B., Ghani, F., and Shen, W.-C. (1991) Isolation of variants of chinese hampster ovary cells with abnormally low levels of GSH: Decrease ability to cleave endocytosed disulfide bonds. *J. Cell Physiol. 149*, 60−65.
(38) Kwok, K. Y., McKenzie, D. L., Evers, D. L., and Rice, K. G. (1999) Formulation of highly soluble poly(ethylene glycol)-peptide DNA condensates. *J. Pharm. Sci. 88*, 996−1003.
(39) Collard, W. T., Evers, D. L., McKenzie, D. L., and Rice, K. G. (2000) Synthesis of homogeneous glycopeptides and their utility as DNA condensing agents. *Carbohydr. Res. 323*, 176−184.

BC000056I

Synthesis of Polyamidoamine Dendrimers Having Poly(ethylene glycol) Grafts and Their Ability To Encapsulate Anticancer Drugs

Chie Kojima,[†] Kenji Kono,*[,†,‡] Kazuo Maruyama,[§] and Toru Takagishi[†,‡]

Department of Applied Materials Science, Graduate School of Engineering, Osaka Prefecture University, 1-1 Gakuen-cho, Sakai, Osaka 599-8531, Japan, and Department of Applied Bioscience, Research Institute for Advanced Science and Technology, Osaka Prefecture University, 1-2 Gakuen-cho, Sakai, Osaka 599-8570, Japan, and Faculty of Pharmaceutical Sciences, Teikyo University, Sagamiko, Tsukui-gun, Kanagawa 199-0195, Japan

Polyamidoamine dendrimers having poly(ethylene glycol) grafts were designed as a novel drug carrier which possesses an interior for the encapsulation of drugs and a biocompatible surface. Poly(ethylene glycol) monomethyl ether with the average molecular weight of 550 or 2000 was combined to essentially every chain end of the dendrimer of the third or fourth generation via urethane bond. The poly(ethylene glycol)-attached dendrimers encapsulating anticancer drugs, adriamycin and methotrexate, were prepared by extraction with chloroform from mixtures of the poly(ethylene glycol)-attached dendrimers and varying amounts of the drugs. Their ability to encapsulate these drugs increased with increasing dendrimer generation and chain length of poly(ethylene glycol) grafts. Among the poly(ethylene glycol)-attached dendrimers prepared, the highest ability was achieved by the dendrimer of the fourth generation having the poly(ethylene glycol) grafts with the average molecular weight of 2000, which could retain 6.5 adriamycin molecules or 26 methotrexate molecules/dendrimer molecule. The methotrexate-loaded poly(ethylene glycol)-attached dendrimers released the drug slowly in an aqueous solution of low ionic strength. However, in isotonic solutions, methotrexate and adriamycin were readily released from the poly(ethylene glycol)-attached dendrimers.

INTRODUCTION

Dendrimers are unique synthetic macromolecules with highly branched structure and globular shape (*1*−*3*). Because molecular size and generation of dendrimers are increased stepwise via the repetition of a reaction sequence, their size and structure are highly controllable and their molecular weight distribution is generally very narrow (*3*−*5*). In addition, their interior has been shown to be capable of encapsulating various molecules (*6*−*8*). Therefore, application of dendrimers to drug delivery systems has been of great interest, although their use in this field has remained largely unexplored (*9*).

Several attempts have been made to design dendrimers as drug carriers. It has been shown that drug molecules can be combined to dendrimers through covalent bond. For example, Zhuo et al. prepared polyamidoamine (PAMAM)[1] dendrimers with a cyclic core and attached an anticancer drug 5-fluorouracil to the dendrimers (*10*). Also, methotrexate (MTX) was conjugated to the chain ends of hydrazide terminated poly(aryl ether) dendrimers (*11*). Because dendrimers have a large number of terminal groups to which drug molecules can be conjugated, they can carry drugs at a high density.

Another strategy to the design of dendrimers for drug delivery is their use as a container which encapsulates drug molecules. It has been shown that dendrimers with a hydrophobic interior and hydrophilic chain ends are able to solubilize hydrophobic compounds in aqueous solutions (*12*−*14*). Also, small guest molecules can be physically entrapped in the interior of dendrimers with rigid shells, as reported by Meijer and co-workers (*6*, *15*). These studies indicate that dendrimers can act as an unimolecular nanocapsules for small guest molecules.

Considering the use of dendrimers for drug delivery, it is necessary that they are nontoxic and biocompatible. However, it has been demonstrated that widely used dendrimers, such as PAMAM dendrimers and poly(propylene imine) dendrimers bearing primary amino group termini, are quite cytotoxic, and also these dendrimers were cleared rapidly from the circulation when administered intravenously (*16*, *17*).

It has been shown that covalent attachment of poly(ethylene glycol), which is a nontoxic and nonimmunogenic water-soluble polymer, to proteins decreases their immunogenicity and increases their circulation time (*18*, *19*). In addition, a number of studies have demonstrated that poly(ethylene glycol) chains grafted to surfaces of polymer micelles and liposomes suppress their interaction with plasma proteins and cells and prolong their circulation time in the blood (*20*−*24*). Margerum et al. reported that the incorporation of several poly(ethylene glycol) chains to PAMAM dendrimer-based macromolecular polychelates, which were prepared as contrast

* To whom correspondence should be addressed. Phone: +81-722-54-9330. Fax: +81-722-54-9913. E-mail: kono@ams.osakafu-u.ac.jp.

[†] Department of Applied Materials Science, Osaka Prefecture University.

[‡] Department of Applied Bioscience, Osaka Prefecture University.

[§] Teikyo University.

[1] Abbreviations: PAMAM, polyamidoamine; M-PEG(550), poly(ethylene glycol) monomethyl ether with the number average molecular weight of 550; M-PEG(2000), poly(ethylene glycol) monomethyl ether with the number average molecular weight of 2000; ADR, adriamycin; MTX, methotrexate; Tris, tris(hydroxymethyl)aminomethane; THF, tetrahydrofuran; PBS, phosphate-buffered saline; GPC, gel permeation chromatography; Mn, number average molecular weight; Mw, weight average molecular weight.

10.1021/bc0000583 CCC: $19.00 © 2000 American Chemical Society
Published on Web 11/01/2000

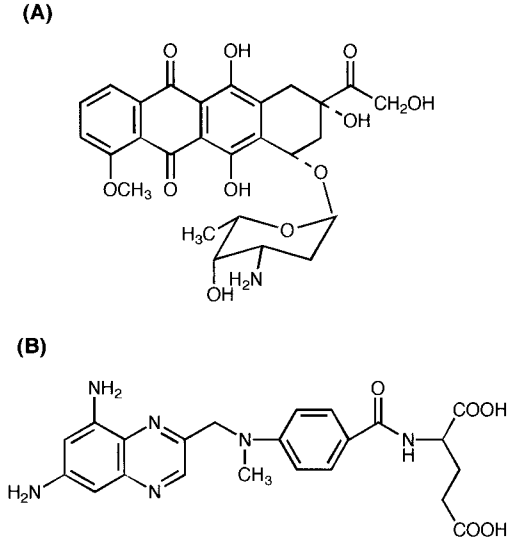

Figure 1. Structures of ADR (A) and MTX (B).

agents for magnetic resonance imaging, could increase their blood elimination half-lives (*25*). On the basis of these findings, it seems that dendrimers covered with poly(ethylene glycol) grafts are attractive compounds as drug carriers in vivo. Such molecules are expected to encapsulate drugs in their dendrimer moiety and reveal biocompatibility due to their hydrophilic shell consisting of poly(ethylene glycol) grafts. In earlier studies, several novel polyether dendrimers having poly(ethylene glycol) grafts have been synthesized by collaboration with Fréchet et al. (*26*, *27*). Also, recently, oligoethylene glycol-terminated dendrimers have been synthesized by other groups and some of them have been shown to encapsulate guest molecules in aqueous solutions (*17*, *28*, *29*).

In this study, we designed PAMAM dendrimers having poly(ethylene glycol) grafts as a novel drug carrier having an interior for encapsulation of drugs and a biocompatible surface. The PAMAM dendrimers were chosen because these dendrimers are widely used and well characterized among dendrimers prepared so far. Poly(ethylene glycol) monomethyl ether (M-PEG), with the average molecular weight of 550 or 2000, was attached to chain ends of PAMAM dendrimers of the third or fourth generation. Their ability to encapsulate anticancer drugs, adriamycin (ADR) and MTX (Figure 1), was investigated. Influences of the dendrimer generation and the M-PEG molecular weight on their encapsulation ability have been described.

EXPERIMENTAL PROCEDURES

General Methods. PAMAM (Starburst) dendrimers of the third and the fourth generations and M-PEGs with the number average molecular weights of 550 [M-PEG(550)] and 2000 [M-PEG(2000)] were purchased from Aldrich Chemical (Milwaukee, WI). 4-Nitrophenyl chloroformate was obtained from Tokyo Kasei Kogyo (Tokyo, Japan). Tris(hydroxymethyl)aminomethane (Tris), tetrahydrofuran (THF), dimethyl sulfoxide, and *N*,*N*-dimethyl formamide were supplied from Kishida Chemical (Osaka, Japan). ADR-HCl was kindly donated by Kyowa Hakko Kogyo (Tokyo, Japan). MTX was purchased from Sigma (St. Louis, MO). THF was purified by distillation. Dimethyl sulfoxide was distilled under vacuum. ^{1}H and ^{13}C NMR spectra were recorded on a JEOL JNM-LA 400 instrument. The proton chemical shifts (δ) are given relative to internal $CHCl_3$ for $CDCl_3$ solutions and to internal HOD for D_2O solutions. Carbon chemical shifts are given relative to internal sodium 3-(trimethylsilyl)-propionate-2,2,3,3-d_4 for D_2O solutions and to $CDCl_3$ for $CDCl_3$ solutions. The number average molecular weight (Mn) and the weight average molecular weight (Mw) of dendrimers were estimated by gel permeation chromatography (GPC) on a system equipped with a series of two columns (Showa Denko Shodex KD805L and KD803) with differential refractive index detection (Jasco RI-930) using *N*,*N*-dimethylformamide as the eluent. Poly(ethylene glycol) was used as the standard for calibration.

Synthesis of M-PEG 4-Nitrophenyl Carbonate. M-PEG 4-nitrophenyl carbonate was prepared via the reaction of M-PEG with 4-nitrophenyl chloroformate (Scheme 1). M-PEG(550) (3.6 mmol) was dissolved in THF (100 mL). To the solution were added 4-nitrophenyl chloroformate (7.2 mmol) and triethylamine (7.2 mmol), followed by stirring for 24 h at room temperature. M-PEG 4-nitrophenyl carbonate was recovered by evaporation of the reaction mixture and purified using a Sephadex LH-20 column (Pharmacia, ϕ 3.5 cm $\times$ 120 cm) with methanol as the eluent. Yield: 63%. The M-PEG(2000) 4-nitrophenyl carbonate was prepared via the same procedure except for the volume of THF (360 mL) and the reaction time (2 days). The crude product (10 g) was purified by recrystallization from chloroform-diethyl ether (15:1, 320 mL). Yield: 78%. ^{1}H NMR ($CDCl_3$) δ 3.38 (s, OCH_3), δ 3.34−3.80 (m, CH_2CH_2O), δ 4.42 (m, $OCOOCH_2$), δ 7.37 (d, aromatic), δ 8.26 (d, aromatic). ^{13}C NMR ($CDCl_3$): δ 58.97 (OCH_3), δ 68.25, 68.54, 70.25, 70.63, 70.73, and 71.85 (OCH_2CH_2), δ 121.72, 125.23, 145.30, and 152.41 (aromatic), δ 155.42 (OCOO).

Synthesis of M-PEG-Attached PAMAM Dendrimers. The M-PEG-attached PAMAM dendrimers were synthesized via the procedure shown in Scheme 1. To a solution of the third generation (G3) PAMAM dendrimer (14 μmol) in dimethyl sulfoxide (10 mL), M-PEG 4-nitrophenyl carbonate (0.9 mmol) was added and the solution was stirred for 5 days at room temperature. The solution was diluted with distilled water and dialyzed using a dialysis bag (molecular weight 12000−14000 cut off) against distilled water for 24 h. The crude compound was lyophilized and then purified either by a Sephadex G-75 column (Pharmacia, ϕ 4 cm $\times$ 45 cm) using water as the eluent in the case in which M-PEG(2000) was used, or by a Sephadex LH-20 column using methanol as the eluent in the case in which M-PEG(550) was used. M-PEG-attached PAMAM dendrimers with the fourth generation (G4) was prepared by the same procedure except for the amount of the dendrimer (7 μmol). In addition, the acetylated G3 PAMAM dendrimer was prepared by the reaction of the G3 dendrimer (8 mg) and acetic anhydride (4 mL) at 40 °C for 2 h and subsequent dialysis against water. The acetylated G3 dendrimer was recovered by lyophilization. Yields of M-PEG(550)-attached G3, M-PEG(2000)-attached G3, M-PEG(550)-attached G4, M-PEG(2000)-attached G4, and acetylated G3 dendrimers were 77, 32, 79, 39, and 69%, respectively. ^{1}H NMR for M-PEG-attached dendrimers (D_2O) δ 2.28 (br, Hc), δ_{PAMAM} 2.51 (br, He), δ_{PAMAM} 2.70 (br, Hd), δ_{PAMAM} 3.09−3.14 (m, Ha,Hb, Hf), δ_{M-PEG} 3.23 (s, OCH_3), δ_{M-PEG} 3.46−3.72 (m, CH_2CH_2O), δ_{M-PEG} 4.05 (br, $NHCOOCH_2$). ^{13}C NMR for M-PEG-attached dendrimers (D_2O): δ_{PAMAM} 35.3 (Cc), δ_{PAMAM} 39.4 (Cf), δ_{PAMAM} 41.8 (Cb), δ_{PAMAM} 42.5 (Ca), δ_{PAMAM} 51.9 (Cd), δ_{PAMAM} 54.1 (Ce), δ_{PAMAM} 177.1 and 177.5 (CONH); δ_{M-PEG} 60.8 (OCH_3), δ_{M-PEG} 66.9, 61.7, 72.2, 72.4, and 73.8 (OCH_2CH_2), δ_{M-PEG} 161.0 (NHCOO). (See Figure 2).

Scheme 1. Synthesis of M-PEG-Attached PAMAM Dendrimers

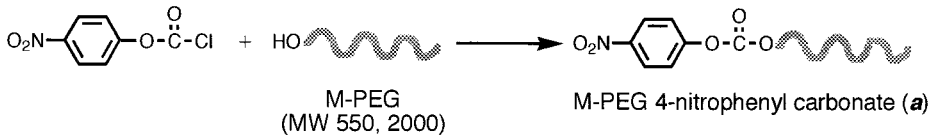

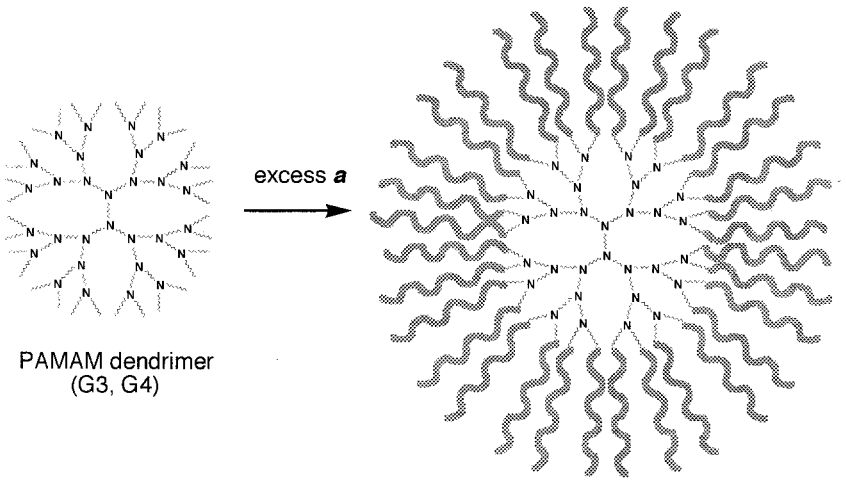

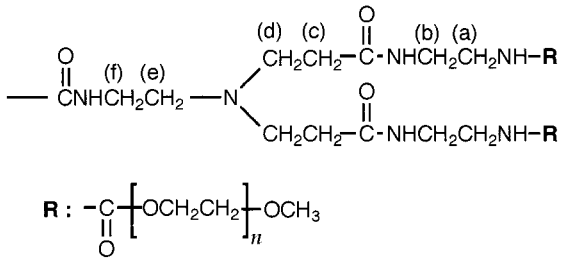

Figure 2. Structure of a part of M-PEG dendrimer.

Encapsulation of Drugs by M-PEG-Attached PAMAM Dendrimers. For the evaluation of encapsulation of ADR by the M-PEG-attached PAMAM dendrimers, a given volume of an ADR-HCl in *N*,*N*-dimethylformamide solution (0.5 mg/mL) was added to the M-PEG-attached PAMAM dendrimer (10 mg) and stirred for 24 h at room temperature in the dark. The solution was evaporated and the residue was further dried under vacuum. Chloroform (2 mL) was added to the dry mixture of the M-PEG-attached dendrimer and ADR and stirred for 6 h to extract a M-PEG-attached dendrimer−ADR complex. The solution was centrifuged at 15 000 rpm for 10 min and the supernatant (1 mL) was evaporated to dryness under vacuum. The dry residue was dissolved in 10 mM acetate-buffered solution of pH 4.5 (1 mL) and the absorbance at 481 nm was measured to determine the amount of ADR. For the encapsulation of MTX by the dendrimers, a given volume of an aqueous MTX solution (1.0 mg/mL) was added to the M-PEG-attached dendrimers (5 mg), stirred for 24 h at room temperature in the dark, and then the mixed solution was lyophilized. Chloroform (1 mL) was added to the residue and stirred overnight in the dark. The chloroform solution of the dendrimer−MTX complex was filtered through a poly(tetrafluoroethylene) membrane (pore size, 200 nm). The filtrate was evaporated, and the residue was dried under vacuum. The obtained dry dendrimer−MTX complex was dissolved in 0.01 M NaOH (2 mL). An aliquot (100 μL) of the solution was added to an aqueous 0.1 M Tris-HCl solution (pH 8.0, 900 μL), and the absorbance at 372 nm was measured to determine the amount of MTX.

Release of Drugs from M-PEG-Attached PAMAM Dendrimers. The release of ADR and MTX from the M-PEG-attached dendrimers was estimated as previously reported (*26*). The M-PEG-attached PAMAM dendrimer containing ADR was prepared by adding 3 equiv of ADR-HCl to 1 equiv of dendrimer via the above procedure. The ADR-containing dendrimer was dissolved in phosphate-buffered saline (PBS) (pH 7.4, 1.0 mL) and transferred to a dialysis bag (molecular weight 12000−14000 cut off). The dialysis bag was immediately placed in 20 mL of PBS and the fluorescence intensity of ADR in the outer phase was monitored using a spectrofluorometer (Shimadzu RF-5000). The excitation and monitoring wavelengths were 471 and 554 nm, respectively. For the evaluation of the MTX release from the M-PEG-attached PAMAM dendrimers, the MTX-loaded dendrimer was prepared by adding 24 equiv of MTX to 1 equiv of the dendrimer and dissolved in 1 mM Tris-HCl-buffered solution (pH 7.4, 2.0 mL) either containing or not containing 150 mM NaCl. The solution was transferred to a dialysis bag, placed in 20 mL of the same Tris-HCl-buffered solution, and the absorbance of MTX at 372 nm in the outer phase was followed using a spectrophotometer (Jasco V-520).

RESULTS AND DISCUSSION

Synthesis and Characterization of M-PEG-Attached PAMAM Dendrimers. We examined conjugation of poly(ethylene glycol) chains to amino groups at chain ends of the PAMAM dendrimers through urethane bonds (Scheme 1). Thus, M-PEGs with the molecular weights of 550 and 2000 were reacted with 4-nitrophenyl chloroformate to obtain M-PEG 4-nitrophenyl carbonate. Two equivalents of the reactive M-PEG were added to 1 equiv of the terminal amino group of the G3 or G4 PAMAM dendrimer. Figure 3 shows the ^{1}H NMR spectra for the PAMAM G3 dendrimers (A) and M-PEG(550) used

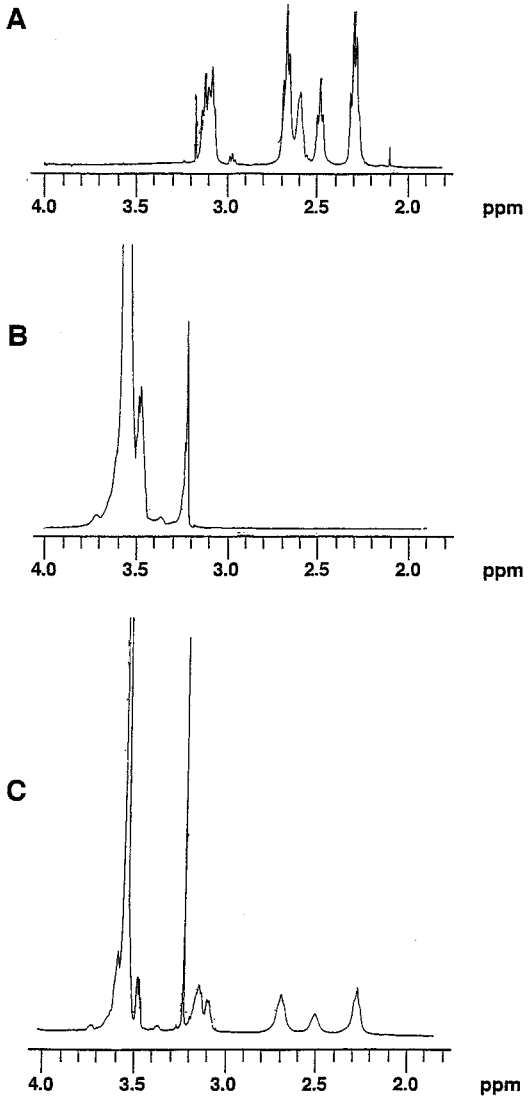

Figure 3. ^{1}H NMR spectra for PAMAM G3 dendrimer (A), M-PEG(550) (B), and M-PEG(550)-G3 dendrimer (C) in D_2O.

for the synthesis (B), and the resultant M-PEG(550)-G3 dendrimer (C). It is apparent that the spectrum of the M-PEG(550)-G3 dendrimer contains signals originating from both the PAMAM G3 dendrimer and M-PEG(550). From the integral ratio of the signal at 2.2−2.3 ppm, which corresponds to the protons of methylenes next to carbonyl groups of the dendrimer, to the signal at 3.23, which corresponds to the protons of the terminal methyl group of M-PEG(550), the average number of M-PEG-(550) chains in the M-PEG(550)-attached G3 dendrimer was estimated to be 33, which agrees with the number of terminal amino groups of the dendrimer. This result implies that an M-PEG chain is combined to every chain end of the dendrimer.

The attachment of M-PEG chain to the chain end of the dendrimer was further confirmed by ^{13}C NMR spectra for these dendrimers (Figure 4). The PAMAM G3 dendrimer showed peaks at 43.7, which corresponds to the carbons next to the terminal amino groups (Figure 4A). However, in the spectrum of the M-PEG-attached dendrimer (Figure 4B), the peak at 43.7 ppm completely disappeared and, instead, a new peak appeared at 42.5 ppm, indicating that every terminal amino group was combined to an M-PEG chain.

The average number of M-PEG chains in the M-PEG-attached PAMAM dendrimers prepared was evaluated

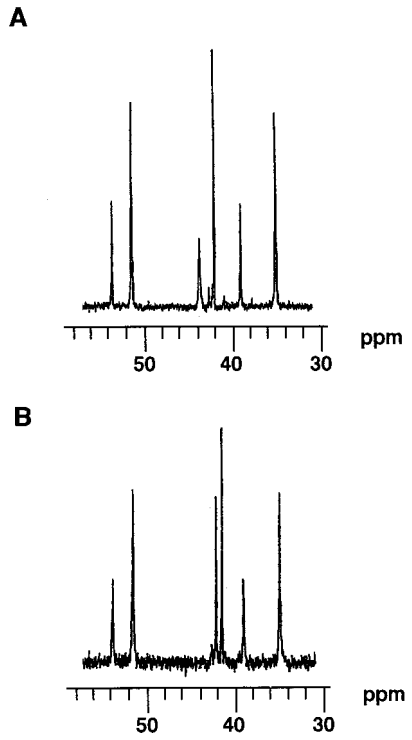

Figure 4. ^{13}C NMR spectra for PAMAM G3 dendrimer (A) and M-PEG(550)-G3 (B) dendrimer (C) in D_2O.

Table 1. Synthesis of M-PEG-Attached Dendrimers

dendrimer	no. of terminal amino group (mol/mol)	no. of M-PEG/dendrimer (mol/mol)	
		in feed	attached
acetylated G3	32	excess	30
M-PEG(550)-G3	32	64	33
M-PEG(2000)-G3	32	64	35
M-PEG(550)-G4	64	128	65
M-PEG(2000)-G4	64	128	63

from their ^{1}H NMR spectra and listed in Table 1. The average number of M-PEG chains attached to the G3 and G4 dendrimers were 33−35 and 63−65, respectively, and are in close agreement with the number of terminal amino groups of the corresponding dendrimers. These results indicate that essentially every terminal amino group combined with an M-PEG chain.

The molecular weights of the M-PEG-attached PAMAM dendrimers were evaluated by GPC analysis. Typical chromatograms for samples of the M-PEG(550)-G4 and the M-PEG(2000)-G4 dendrimers as well as M-PEGs used for the preparation of these modified dendrimers were shown in Figure 5. Peaks of free M-PEG(550) and free M-PEG(2000), which appear at the retention volume of ca. 21 and ca. 20 mL, respectively, were not seen in the chromatograms of these M-PEG-attached dendrimers, indicating that these samples did not contain free M-PEGs. These M-PEG-attached dendrimers showed a sharp peak at ca. 15 or ca. 16 mL, suggesting that their molecular weight distribution is very narrow. However, these sharp peaks were accompanied by small shoulder peaks corresponding to species with higher molecular weights. It is known that commercially available M-PEG is frequently contaminated with telechelic PEG diol. The PEG diol contained in the starting material may have become derivatized with two 4-nitrophenyl carbonate groups on both terminals of its chain by the reaction with 4-nitrophenyl chloroformate. This molecule could cross-link PAMAM dendrimers. Formation of cross-linked

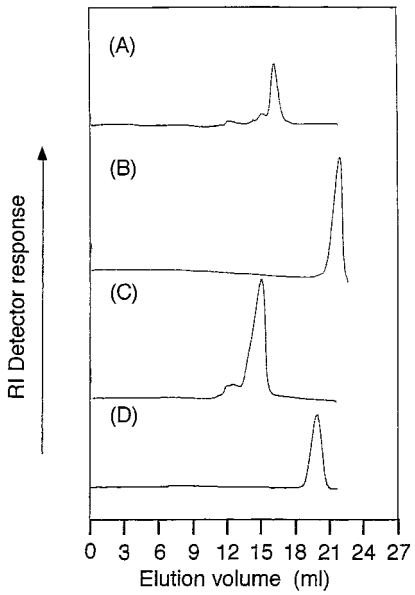

Figure 5. Typical chromatograms for M-PEG(550)-G4 dendrimer (A), M-PEG(550) (B), M-PEG(2000)-G4 dendrimer (C), and M-PEG(2000) (D).

Table 2. Molecular Weight of Dendrimers

	molecular weight			
		GPC data		
dendrimer	nominal[a]	Mn	Mw	Mw/Mn
acetylated G3	8253	3621	3905	1.08
M-PEG(550)-G3	25 341	9581	9872	1.03
M-PEG(2000)-G3	71 741	31 807	34 742	1.09
M-PEG(550)-G4	51 079	15 014	15 527	1.03
M-PEG(2000)-G4	143 879	42 465	44 652	1.05

[a] Calculated by assuming that molecular weights of M-PEG(550) and M-PEG(2000) are 550 and 2000, respectively.

product due to the contamination of PEG diol of the commercially available M-PEG has been observed previously (*26*).

The weight average molecular weight (Mn), the number average molecular weight (Mw) and the polydispersity index (Mw/Mn) for the M-PEG-attached PAMAM dendrimers and the acetylated G3 PAMAM dendrimer were estimated from the peak of the chromatogram and listed in Table 2. As mentioned above, the Mw/Mn ratios for these modified dendrimers were generally close to 1, indicating that their molecular weight distribution is very narrow. However, these molecular weights of the modified dendrimers estimated by GPC were much lower than their nominal molecular weights, indicating that these molecules are very compact as was previously observed in the case of the starburst dendrimers and other types of dendrimers (*1*, *30*).

Tomalia et al. (*1*) have reported that the hydrodynamic diameters of PAMAM dendrimers can be estimated by using a size-exclusion chromatography column calibrated with poly(ethylene glycol) standards and applying an equation developed by Hester and Mitchell (*31*). According to the method of Tomalia et al., the hydrodynamic diameters of the acetylated G3, the M-PEG(550)-G3, and the M-PEG(2000)-G3 dendrimers were estimated to be approximately 3.5, 6.4, and 12.5 nm, respectively, in *N*,*N*-dimethylformamide on the basis of their number average molecular weights. Also, the hydrodynamic diameters of poly(ethylene glycol)s with molecular weights of 550 and 2000 were estimated to be ca. 1.5 and 2.7 nm in the same solvent, using the equation of Hester and Mitchell (*31*) and the relationship between the intrinsic viscosity and the molecular weight of poly(ethylene glycol) reported by Ritscher and Elias (*32*).

In comparison of the hydrodynamic diameters of these modified G3 dendrimers, it is found that difference in the hydrodynamic diameters between the M-PEG(550)-G3 and the acetylated G3 dendrimers is 2.9 nm, which is about twice the hydrodynamic diameter of PEG(550). Thus, it may be considered that the poly(ethylene glycol) chains exist outside of the PAMAM dendrimer and cover its surface. Similarly, difference in the hydrodynamic diameters between the M-PEG(2000)-G3 and the acetylated G3 dendrimers was calculated to be 9 nm. This value is much larger than twice the hydrodynamic diameter of PEG(2000). Therefore, it may be considered that M-PEG chains attached to the dendrimer surface take on an extended conformation. Although these M-PEG-attached G3 dendrimers have the same number of the grafted M-PEG chains, the polymer segment density around the dendrimer surface might be higher for the M-PEG(2000)-G3 dendrimer than the M-PEG(550)-G3 dendrimer. Therefore, the longer M-PEG chain might take on an extended conformation due to repulsion between the neighboring chains. The hydrodynamic diameters of PEG(550)-G4 and PEG(2000)-G4 dendrimers were estimated by the same method to be 8.2 and 14.7 nm, respectively.

Encapsulation of Drugs by M-PEG-Attached PAMAM Dendrimers. Since the PAMAM dendrimer has a basic and hydrophobic interior, we expected that the M-PEG-attached PAMAM dendrimers could encapsulate and retain drugs with a hydrophobic or acidic character by their PAMAM dendrimer moieties in aqueous environments. Thus, we first examined the preparation of the M-PEG-attached dendrimers encapsulating ADR, because ADR is one of the most effective and widely used anticancer drug with a hydrophobic nature.

The M-PEG-attached PAMAM dendrimers were mixed with varying amounts of ADR-HCl and extracted with chloroform. ADR-HCl is essentially insoluble in chloroform. When the primary amino group of ADR is deprotonated, it becomes soluble in chloroform (*33*). However, it has been shown that the amino group of ADR becomes protonated below pH 7 (*34*, *35*), whereas protonation of tertiary amino groups of PAMAM dendrimers occurs below 3.7 (*1*), showing that basicity of the ADR amino group is much higher than that of the dendrimer tertiary amino groups. Therefore, it is unlikely that deprotonation of the ADR amino group is induced in the presence of M-PEG-attached PAMAM dendrimers. Thus, ADR transferred to the chloroform phase is considered to be in the form of a complex with the M-PEG-attached dendrimer.

Figure 6 represents the number of ADR molecules per M-PEG-attached dendrimer in the chloroform phase after the extraction. As the amount of ADR supplied to the modified dendrimer increased, the number of ADR associated with the dendrimer increased and then reached a constant, maximum value. The maximum numbers of ADR molecules per dendrimer for the M-PEG(550)-G3, the M-PEG(2000)-G3, the M-PEG(550)-G4, and the M-PEG(2000)-G4 dendrimers are ca. 1.2, 2.3, 1.6, and 6.5, respectively.

We expected that the M-PEG-attached dendrimers having the larger PAMAM dendrimer moiety would reveal a higher encapsulation ability. In fact, the M-PEG-(2000)-G4 dendrimer showed the highest ability among these M-PEG-attached dendrimers. However, the encapsulation ability of the modified dendrimer depends not

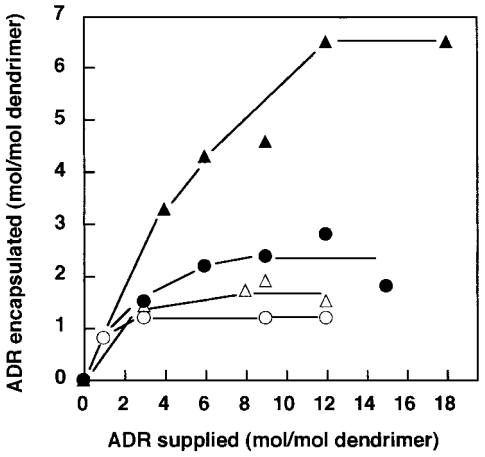

Figure 6. Encapsulation of ADR by M-PEG(550)-attached (open symbols) or M-PEG(2000)-attached (closed symbols) PAMAM G3 (○, ●) and G4 (△, ▲) dendrimers. The number of ADR encapsulated per dendrimer was shown as a function of the ADR/dendrimer molar ratio in feed.

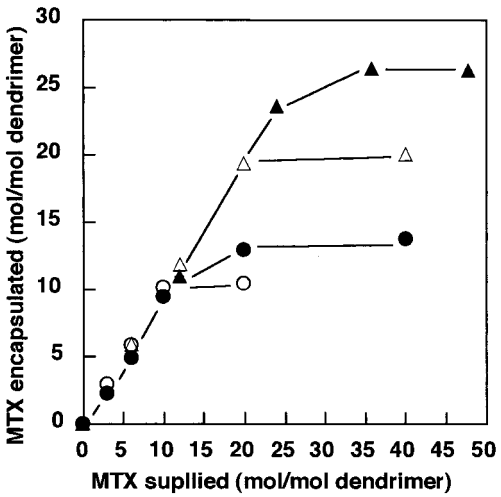

Figure 7. Encapsulation of MTX by M-PEG(550)-attached (open symbols) or M-PEG(2000)-attached (closed symbols) PAMAM G3 (○, ●) and G4 (△, ▲) dendrimers. The number of MTX encapsulated per dendrimer was shown as a function of the MTX/dendrimer molar ratio in feed.

only on the size of the PAMAM dendrimer moiety but also on the chain length of the M-PEG attached to the dendrimer moiety: although the M-PEG(550)-G4 and the M-PEG(2000)-G4 dendrimers have the same PAMAM dendrimer moiety, the former revealed much lower ability than the latter. This fact indicates contribution of the M-PEG layer for the encapsulation of ADR. M-PEG(550) chain may be too short to cover and stabilize the ADR-bound dendrimer moiety. It is also possible that the attachment of long M-PEG chains to the dendrimer chain ends changed conformation of the dendrimer chain, making inner space of the dendrimer larger. Another possibility may be that the M-PEG-rich region of the dendrimer surface solubilized ADR molecules. We observed that ADR was not extracted with chloroform containing the same amount of free M-PEG. However, when concentration of the free M-PEG was further increased, ADR could be transferred to chloroform phase. The amount of transferred ADR increased with increasing the M-PEG concentration in the chloroform phase. This fact may support the possibility of ADR molecules being solubilized in the surface M-PEG layer. It seems that ADR molecules may distribute in both the interior and the M-PEG layer of the dendrimers surface. However, the location of ADR in the M-PEG-attached dendrimers remains to be elucidated at present.

As already mentioned, the PAMAM dendrimer has a basic interior. Therefore, the M-PEG-attached PAMAM dendrimers are expected to exhibit a greater encapsulation ability against acidic drugs than ADR. Thus, next we investigated encapsulation of MTX, which has two carboxyl groups (Figure 1) and has been used for the treatment of various malignant diseases (*36*). The M-PEG-attached dendrimer−MTX complexes were obtained via the extraction with chloroform from mixtures of the modified dendrimers and varying amounts of MTX. The number of MTX molecules associated with one dendrimer molecule as a function of the MTX/dendrimer ratio in feed was shown in Figure 7. As was observed in the case of the encapsulation of ADR, the number of MTX molecules associated with the modified dendrimer increased with increasing amount of MTX supplied and finally reached a constant and maximum value. The maximum numbers of MTX molecules associated with the M-PEG(550)-G3, the M-PEG(2000)-G3, the M-PEG(550)-G4, and the M-PEG(2000)-G4 dendrimers are approximately 10, 13, 20, and 26 mol/mol of dendrimer, respectively. Apparently, the number of the encapsulated drugs by the modified dendrimers increased when MTX was used, compared to the case of ADR. Since these drugs have similar molecular weights, this result suggests that the electrostatic interaction resulted from the acid−base reaction between the dendrimer and MTX is effective for the encapsulation of MTX by the dendrimers. It has already been reported that the PAMAM dendrimers exhibit a high affinity against various acidic compounds (*14*, *37*). As was the case of ADR encapsulation, the number of MTX encapsulated by the dendrimer was affected both by generation of the PAMAM dendrimer moiety and by chain length of the M-PEG graft.

Release of Drugs from M-PEG-Attached PAMAM Dendrimers. To obtain information about the release of ADR from the M-PEG-attached dendrimers, the drug-loaded M-PEG(2000)-G4 dendrimer was dissolved in PBS and dialyzed against PBS. The increase in the ADR concentration in the outer phase was followed and compared with the case of dialysis of free ADR. We observed that the concentration of ADR in the outer phase increased at about the same rate in both cases (data not shown). A similar result was obtained for the dialysis of ADR-loaded M-PEG(2000)-G3 dendrimer (data not shown). These facts suggest that ADR was readily released from the modified dendrimers in PBS. Probably, hydrophobic interaction between ADR and the dendrimer is not strong enough to retain the drug in the interior of the PAMAM dendrimer moiety.

The release of MTX from the M-PEG-attached dendrimers was also investigated by the same method. The MTX-loaded M-PEG(2000)-G4 PAMAM dendrimer was dissolved in 1 mM Tris-HCl-buffered solution of pH 7.4 and dialyzed against the same solution. The time course of MTX concentration in the outer phase during the dialysis was shown in Figure 8. Apparently, the MTX concentration of the outer phase increased more slowly in the case of MTX encapsulated in the M-PEG-attached dendrimer than the case of free MTX, indicating that MTX was gradually released from the modified dendrimer. As mentioned above, MTX was tightly bound to the dendrimer by the electrostatic interaction with the interior of the PAMAM dendrimer and, hence, dissociation of MTX from the dendrimer was suppressed to some

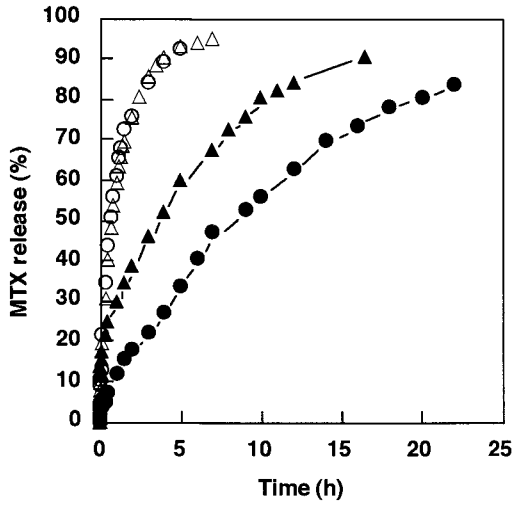

Figure 8. Release of MTX from the M-PEG(2000)-attached G4 dendrimer. The MTX-loaded M-PEG(2000)-G4 dendrimer (○, ●) or free MTX (△, ▲) dissolved in 1 mM Tris-HCl-buffered solution (pH 7.4) containing (open symbols) or not containing (closed symbols) 150 mM NaCl and dialyzed against the same solution. The time course of MTX concentration in the outer phase during the dialysis was shown in the figure.

extent. However, when the dialysis was performed in the presence of 150 mM NaCl, no difference in the release rate was observed between MTX encapsulated in the M-PEG-attached dendrimer and free MTX. Because the electrostatic interaction is weakened by the shielding effect of Na^+ and Cl^-, MTX can dissociate readily from the dendrimer under this condition.

In conclusion, we designed PAMAM dendrimers having M-PEG grafts as a novel drug carrier and showed that M-PEGs with the molecular weights of 550 and 2000 were combined to essentially every chain end of the dendrimer with the generation 3 or 4 via the urethane bond. Also, we prepared the M-PEG-attached dendrimers encapsulating anticancer drugs, ADR and MTX. While the encapsulation ability of the M-PEG-attached PAMAM dendrimers was found to vary, depending on both the molecular weight of M-PEG and the generation of the dendrimer, up to 6.5 ADR molecules and up to 26 MTX molecules could be loaded in the M-PEG(2000)-attached G4 dendrimer, which exhibited the highest ability among the dendrimers prepared in this study. Unfortunately, these drugs were released readily from the M-PEG-attached PAMAM dendrimers in isotonic solutions, probably because the affinity of the dendrimer to these drugs is not strong enough to retain these drugs in their interior. However, it is expected that the M-PEG-attached dendrimers may show higher retention ability for more hydrophobic drugs. Also, introduction of hydrophobic groups into the dendrimers would improve their ability to retain drugs. Thus, findings obtained in this study should provide an important information for the design of dendrimers as drug carriers. We are currently attempting to prepare M-PEG-attached dendrimers with enhanced ability for encapsulation and retention of drugs as well as M-PEG-attached dendrimers having targeting ligands.

ACKNOWLEDGMENT

This work was partly supported by the Grant-in-Aid from Japanese Ministry of Education, Science, and Culture (no. 12680839, 2000) and by Shorai Foundation for Science and Technology.

LITERATURE CITED

(1) Tomalia, D. A., Naylor, A. M., and Goddard, W. A., III (1990) Starburst dendrimers: molecular-level control of size, shape, surface chemistry, topology, and flexibility from atoms to macroscopic matter. *Angew. Chem., Int. Ed. Engl. 29*, 138−175.

(2) Newkome, G. R., Moorefield, C. N., and Vögtle, F. (1996) *Dendritic molecules: concepts, syntheses, perspectives*, VCH, Weinheim.

(3) Fréchet, J. M. J. (1994) Functional polymers and dendrimers: reactivity, molecular architecture, and interfacial energy. *Science 263*, 1710−1715.

(4) Tomalia, D. A., Baker, H., Dewald, Hall, M., Kallos, G., Martin, S., Roeck, J., Ryder, J., and Smith, P. (1985) *Polym. J. 17*, 117−132.

(5) Hawker, C. J., and Fréchet, J. M. J. (1992) Unusual macromolecular architectures: the convergent growth approach to dendritic polyesters and novel block copolymers. *J. Am. Chem. Soc. 4*, 8405−8413.

(6) Jansen, J. F. G. A., de Brabander-van den Berg, E. M. M., and Meijer, E. W. (1994) Encapsulation of guest molecules into a dendritic box. *Science 266*, 1226−1229.

(7) Newkome, G. R., Moorefield, C. N., Baker, G. R., Saunders, M. J., and Grossman, S. H. (1991) Unimolecular micelles. *Angew. Chem., Int Ed. Engl. 30*, 1178−1180.

(8) Pistolis, G., Malliaris, A., Tsiourvas, D., and Paleos, C. M. (1999) Poly(propylene imine) dendrimers as pH-sensitive controlled release systems. *Chem. Eur. J. 5*, 1440−1444.

(9) Liu, M., and Fréchet, J. M. J. (1999) Designing dendrimers for drug delivery. *Pharm. Sci. Technol. Today 2*, 393−401.

(10) Zhuo, R. X., Du, B., and Lu, Z. R. (1999) In vitro release of 5-fluorouracil with cyclic core dendritic polymer. *J. Controlled Release 57*, 249−257.

(11) Kono, K., Liu, M., and Fréchet, J. M. J. (1999) Design of dendritic macromolecules containing folate or methotrexate residues. *Bioconjugate Chem. 10*, 1115−1121.

(12) Newkome, G. R., Moorefield, C. N., Baker, G. R., Saunders, M. J., and Grossman, S. H. (1991) *Angew. Chem., Int. Ed. Engl. 30*, 1176−1178.

(13) Hawker, C. J., Wooley, K. L., and Fréchet, J. M. J. (1993) Unimolecular micelles and globular amphiphiles: dendritic macromolecules as novel recyclable solubilization agents. *J. Chem. Soc., Perkin Trans. 1*, 1287−1297.

(14) Twyman, L. J., Beezer, A. E., Esfand, R., Hardy, M. J., and Mitchell, J. C. (1999) The synthesis of water soluble dendrimers, and their application as possible drug delivery systems. *Tetrahedron Lett. 40*, 1743−1746.

(15) Jansen, J. F. G. A., and Meijer, E. W. (1995) The dendritic box: shape-selective liberation of encapsulated guests. *J. Am. Chem. Soc. 117*, 4417−4418.

(16) Roberts, J. C., Bhalgat, M. K., and Zera, R. T. (1996) Preliminary biological evaluation of polyamidoamine (PAMAM) Starburst dendrimers, *J. Biomed. Mater. Res. 30*, 53−65.

(17) Malik, N., Wiwattanapatapee, R., Klopsch, R., Lorenz, K., Frey, H., Weener, J. W., Meijer, E. W., Paulus, W., and Duncan, R. (2000) Dendrimers: relationship between structure and biocompatibility in vitro, and preliminary studies on the biodistribution of ^{125}I-labeled polyamidoamine dendrimers in vivo. *J. Controlled Release. 65*, 133−148.

(18) Abuchowski, A., van Es, T., Palczuk, N. C., and Davis, F. F. (1977) Alteration of immunological properties of bovine serum albumin by covalent attachment of poly(ethylene glycol). *J. Biol. Chem. 252*, 3578−3581.

(19) Abuchowski, A., McCoy, J. R., Palczuk, N. C., van Es, T., and Davis, F. F. (1977) Effect of covalent attachment of poly(ethylene glycol) on immunogenicity and circulating life of bovine liver catalase. *J. Biol. Chem. 252*, 3582−3586.

(20) Yokoyama, M., Okano, T., Sakurai, Y., Ekimoto, H., Shibazaki, C., and Kataoka, K. (1991) Toxicity and antitumor activity against solid tumors of micelle-forming polymeric anticancer drug and its extremely long circulation in blood. *Cancer Res. 51*, 3229−3236.

(21) Klibanov, A., Maruyama, K., Torchilin, V. P., and Huang, L. (1990) Amphipathic poly(ethylene glycol)s effectively prolong the circulation time of liposomes. *FEBS Lett. 268*, 235−237.
(22) Blume, B., and Cevc, G. (1990) Liposomes for the sustained drug release in vivo. *Biochim. Biophys. Acta 1029*, 91−97.
(23) Woodle, M. C., and Lasic, D. D. (1992) Sterically stabilized liposomes. *Biochim. Biophys. Acta 1113*, 171−199.
(24) Lasic, D. D., and Needham, D. (1995) The stealth liposome: a prototypical biomaterial. *Chem. Rev. 95*, 2601−2628.
(25) Margerum, L. D., Campion, B. K., Koo, M., Shargill, N., Lai, J.-J., Marumoto, A., and Sontum, P. C. (1997) Gadolinium (III) DO3A macrocycles and poly(ethylene glycol) coupled to dendrimers. Effect of molecular weight on physical and biological properties of macromolecular magnetic resonance imaging contrast agents. *J. Alloys Compd. 249*, 185−190.
(26) Liu, M., Kono, K., and Fréchet, J. M. J (2000) Water-soluble dendritic unimolecular micelles: their potential as drug delivery agents. *J. Controlled Release 65*, 121−131.
(27) Liu, M., Kono, K., and Fréchet, J. M. J. (1999) Water-soluble dendrimer-poly(ethylene glycol) starlike conjugates as potential drug carriers. *J. Polym. Sci. Part A: Polym. Chem. Ed. 37*, 3492−3503.
(28) Pan, Y., and Ford, W. T. (1999) Dendrimers with both hydrophilic and hydrophobic chains at every end. *Macromolecules 32*, 5468−5470.
(29) Baars, M. W., Kleppinger, R., Koch, M. H. J., Yeu, S.-L., and Meijer, E. W. (2000) The localization of guests in water-soluble oligoethyleneoxy-modified poly(propylene imine) dendrimers. *Angew. Chem., Int. Ed. 39*, 1285−1288.
(30) Hawker, C. J., and Fréchet, J. M. J. (1990) Preparation of polymers with controlled molecular architecture. A new convergent approach to dendritic macromolecules. *J. Am. Chem. Soc. 112*, 7638−7647.
(31) Hester, R. D., and Mitchell, P. H. (1980) A new universal GPC calibration method. *J. Polym. Sci. Chem. Ed. 18*, 1727−1738.
(32) Ritscher, V. T. A., and Elias, H.-G. (1959) Das problem der membran bei osmotischen messungen an hochpolymeren. III. *Makromol. Chem. 30*, 48−80.
(33) Kwon, G., Naito, M., Yokoyama, M., Okano, T., Sakurai, Y., and Kataoka, K. (1997) Block copolymer micelles for drug delivery: loading and release of doxorubicin. *J. Controlled Release 48*, 195−201.
(34) Eksborg, S. (1978) Extraction of daunorubicin and doxorubicin and their hydroxyl metabolites: self-association in aqueous solution. *J. Pharm. Sci. 67*, 782−785.
(35) Kataoka, K., Matsumoto, T., Yokoyama, M., Okano, T., Sakurai, Y., Fukushima, S., Okamoto, K., and Kwon, G. S. (2000) *J. Controlled Release 64*, 143−153.
(36) Olsen, E. A. (1991) The pharmacology of methotrexate. *J Am. Acad. Dermatol. 25*, 306−318.
(37) Naylor, A. M., Goddard, W. A., III, Kiefer, G. E., and Tomalia, D. A. (1989) Starburst dendrimers. 5. Molecular shape control. *J. Am. Chem. Soc. 111*, 2339−2341.

BC0000583

Development and Characterization of Annexin V Mutants with Endogenous Chelation Sites for ^{99m}Tc

Jonathan F. Tait,*[,†,‡] David S. Brown,[†] Donald F. Gibson,[†] Francis G. Blankenberg,[§] and H. William Strauss[§]

Departments of Laboratory Medicine, Medicine (Medical Genetics) and Pathology, University of Washington, Seattle, Washington 98195-7110, and Department of Radiology, Stanford University, Stanford, California 94305.
Received June 1, 2000; Revised Manuscript Received August 10, 2000

[^{99m}Tc]Annexin V can be used to image organs undergoing cell death during cancer chemotherapy and organ transplant rejection. To simplify the preparation and labeling of annexin V for nuclear-medicine studies, we have investigated the addition of peptide sequences that will directly form endogenous chelation sites for ^{99m}Tc. Three mutant molecules of annexin V, called annexin V-116, -117, and -118, were constructed with N-terminal extensions of seven amino acids containing either one or two cysteine residues. These molecules were expressed cytoplasmically in *Escherichia coli* and purified to homogeneity with a final yield of 10 mg of protein/L of culture. Analysis in a competitive binding assay showed that all three proteins retained full binding affinity for erythrocyte membranes with exposed phosphatidylserine. Using $SnCl_2$ as reducing agent and glucoheptonate as exchange agent, all three proteins could be labeled with ^{99m}Tc to specific activities of at least 50−100 μCi/μg. The proteins retained membrane binding activity after the radiolabeling procedure, and quantitative analysis indicated a dissociation constant (K_d) of 7 nmol/L for the annexin V-117 mutant. The labeling reaction was rapid, reaching a maximum after 40 min at room temperature. The radiolabeled proteins were stable when incubated with phosphate-buffered saline or serum in vitro. Proteins labeled to a specific activity of 25−100 μCi/μg were injected intravenously in mice at a dose of 100 μg/kg, and biodistribution of radioactivity was determined at 60 min after injection. Uptake of radioactivity was highest in kidney and liver, consistent with previous results obtained with wild-type annexin V. Cyclophosphamide-induced apoptosis in vivo could be imaged with [^{99m}Tc]annexin V-117. In conclusion, annexin V can be modified near its N-terminus to incorporate sequences that form specific chelation sites for ^{99m}Tc without altering its high affinity for cell membranes. These annexin V derivatives may be useful for in vivo imaging of cell death.

INTRODUCTION

Membrane phospholipids are distributed asymmetrically in most cells (*1*, *2*). Phosphatidylserine (PS)[1] is normally retained on the intracellular face of the plasma membrane, but this distribution is altered in some physiological and pathological states. PS exposure is part of the normal platelet procoagulant response, and it also occurs during apoptosis, where it may serve as a signal to promote phagocytosis of apoptotic cells and their fragments (*3*). We have recently used annexin V to detect PS exposure in vivo. Annexin V labeled with radioiodine and ^{99m}Tc was used to detect thrombus formation in experimental animals (*4*, *5*). [^{99m}Tc]Annexin V was used to detect cell death in vivo in animal models (*6*−*10*). Because of the clinical applicability of this work in monitoring cancer chemotherapy and rejection of transplanted organs, there is interest in developing new annexin V derivatives with improved imaging properties or greater ease of use.

Some naturally occurring proteins have been labeled directly with technetium, which presumably chelates with favorably disposed atoms from the peptide backbone and/or amino acid side chains. However, this approach lacks generality, and the results are unpredictable for any particular protein. More recently, specific peptide sequences, modeled after short peptides such as mercaptoacetyltriglycine (*11*−*14*), have been introduced into recombinant proteins in order to create endogenous chelation sites for technetium. For example, George et al. (*15*) attached the sequence GGGGC to the C-terminus of two recombinant single-chain Fv antibody proteins. They showed that these proteins could be labeled with ^{99m}Tc to high specific activity. Bogdanov et al. (*16*) showed specific Tc chelation to a construct of green fluorescent protein with the added C-terminal sequence LGGGGC-GGGCGI. In another approach, Waibel et al. (*17*) showed Tc chelation to a recombinant protein containing five or six histidine residues at the C-terminus. Pietersz et al. (*18*) prepared a hybrid protein consisting of metallothionein fused to a single-chain Fv molecule, which was labeled with Tc by transchelation from a precursor protein containing Zn.

It would be advantageous to label annexin V directly with ^{99m}Tc, without requiring attachment of exogenous chelation groups. The N-terminal region of annexin V is

* To whom correspondence should be addressed. Phone (206) 598-6131. Fax: (206) 598-6189. E-mail:tait@u.washington.edu.
† Department of Laboratory Medicine.
‡ Department of Medicine (Medical Genetics) and Pathology.
§ Department of Radiology.

[1] Abbreviations: DTPA, diethylenetriaminepentaacetic acid; HYNIC, 6-hydrazinopyridine-3-carboxylate; IC_{50}, inhibitory concentration 50%; ID, injected dose; ITLC, instant thin-layer chromatography; PBS, phosphate-buffered saline; ROI, region of interest; SDS−PAGE, sodium dodecyl sulfate−polyacrylamide gel electrophoresis.

10.1021/bc000059v CCC: $19.00 © 2000 American Chemical Society
Published on Web 10/21/2000

Table 1. Oligonucleotides Used for Construction of Vectors

oligonucleotide ame	vector	oligonucleotide sequence (5′ to 3′)
JT-289	pJ116	TATGGCATGTGGCGGTGGCCA
JT-290	pJ116	TATGGCCACCGCCACATGCCA
JT-295	pJ117	TATGGCAGGTGGCTGTGGCCA
JT-296	pJ117	TATGGCCACAGCCACCTGCCA
JT-297	pJ118	TATGGCATGTGGCTGCGGTCA
JT-298	pJ118	TATGACCGCAGCCACATGCCA

a suitable site for attachment of additional peptide sequence, since previous work has shown that attachment of small (*19*) and large (*20*) sequences does not alter membrane binding affinity, nor does it affect expression or folding of the recombinant protein in *Escherichia coli*. The three-dimensional structure of annexin V also shows that the N-terminal region is located on the opposite side of the molecule from the membrane binding site (*21*).

In this study, we have prepared three novel derivatives of annexin V that contain N-terminal extensions of seven amino acids that are specifically designed to chelate technetium. One derivative is predicted to form an N_2S_2 chelation site, and two are predicted to form an N_3S site. These derivatives can be produced in high yield by expression in *E. coli*, and they can be labeled to high specific activity with technetium.

MATERIALS AND METHODS

Materials. Recombinant annexin V was produced in *E. coli* as described (*22*). Fluorescein-annexin V was prepared as described (*23*). Sodium glucoheptonate was from Sigma. $SnCl_2{\cdot}2H_2O$ was from Aldrich. Annexin V was derivatized with succinimidyl 6-hydrazinopyridine-3-carboxylate (abbreviated HYNIC) as described (*6*). Erythrocytes with exposed PS (4CPlus Normal Control, part number 7546923) were from Beckman-Coulter (Miami, FL).

Construction and Verification of Plasmids. Several plasmids were constructed to express mutant forms of annexin V in *E. coli* under control of the phage T7 promoter. The parent expression vector was pET12a, available from Novagen Corporation (Madison, WI).

Construction of Vector pJ115, Encoding Annexin V-115 with Cys-316→Ser Mutation. A 232-bp *Bst*BI−*Bam*HI restriction fragment was first isolated from plasmid pANXVC-S-N6 (*19*), also known as pJ110, which encodes a modified annexin V with the Cys-316 → Ser mutation. The same restriction fragment was then removed from plasmid pET12a-PAP1 (*22*), which encodes wild-type annexin V, and the mutated *Bst*BI−*Bam*HI fragment was inserted to form plasmid pJ115. This plasmid was subjected to DNA sequence analysis to verify that the intended mutation had been correctly introduced.

Construction of vectors pJ116, pJ117, and pJ118, encoding the mutant molecules annexin V-116, annexin V-117, and annexin V-118.

For each vector to be constructed, sense and antisense oligonucleotides (with sequences given in Table 1) were designed to encode the desired peptide sequence and to have *Nde*I restriction sites at both ends. Equimolar amounts of sense and antisense oligonucleotide were phosphorylated and annealed to form a double-stranded cassette with *Nde*I-compatible single-stranded ends. The double-stranded oligonucleotide (3.8 ng) was ligated with plasmid pJ115 (0.42 μg) that had been previously digested with *Nde*I and dephosphorylated. The ligation mixture was transformed into *E. coli* strain DH5α. Plasmid DNA was prepared from ampicillin-resistant colonies and screened by PCR for the presence of the desired insert. DNA sequence analysis was then performed on positive clones to verify the presence of the desired insertion and the absence of other adventitious mutations.

Expression and Purification of Proteins. Plasmids pJ116, pJ117, and pJ118 were each transformed into *E. coli* strain BL21(DE3) for cytoplasmic expression. Each clone was grown overnight to saturation at 37 °C with shaking in Terrific Broth containing carbenicillin (50 μg/mL). The cells were separated from culture medium by centrifugation for 10 min at 2560*g* and washed in ice-cold buffer (50 mmol/L TrisHCl, 150 mmol/L NaCl pH 8.0). Bacteria were disrupted by sonication in ice-cold 50 mmol/L Tris·HCl, pH 7.2, 10 mmol/L $CaCl_2$, 1 mmol/L β-mercaptoethanol, and then centrifuged for 20 min at 22530*g*. The supernatant was discarded and the annexin V bound to bacterial membranes was released by resuspending the pellet in 50 mmol/L Tris·HCl, pH 7.2, 20 mmol/L EDTA, 1 mmol/L β-mercaptoethanol. Bacterial membranes were removed by centrifugation for 20 min at 22530*g* and the supernatant containing the annexin V was dialyzed against 20 mmol/L Tris·HCl, pH 8.0, 1 mmol/L β-mercaptoethanol. The dialysand was applied to a Mono Q HR 16/10 column (Pharmacia, Piscataway, NJ) and eluted with a gradient of 0 to 1 mol/L NaCl in the same buffer. The annexin V mutants all eluted at approximately 0.22 mol/L NaCl. The purified protein was concentrated by ultrafiltration to approximately 5 mg/mL, dialyzed against 20 mmol/L HEPES, pH 7.4, 100 mmol/L NaCl, and stored in aliquots at −70 °C. The final yield was approximately 10 mg/L of bacterial culture, with a purity of ∼98% as judged by SDS−PAGE.

Labeling of Proteins with ^{99m}Tc. Unless noted otherwise, mutant proteins were labeled with ^{99m}Tc as follows. A 1-mg aliquot of protein was incubated with 1 mmol/L dithiothreitol for 15 min at 37 °C. This material was then purified on a Sephadex G-25 column (0.9 × 2.8 cm) previously equilibrated with deoxygenated 20 mmol/L sodium citrate, pH 5.2, 100 mmol/L NaCl. This material was stored in glass vials at −20 °C in aliquots of 100 μg in 100 μL of the same buffer. For Tc labeling, glucoheptonate was used as the exchange agent. A solution containing 20 mmol/L sodium glucoheptonate and 10 mmol/L sodium HEPES was adjusted to pH 6.6 and deoxygenated with argon. $SnCl_2{\cdot}2H_2O$ was added to 128 μg/mL, and 1-mL aliquots were dispensed into borosilicate glass vials, lyophilized, capped with Teflon-lined screw caps under argon, and stored at −20 °C. For radiolabeling, 100 μL of $^{99m}TcO_4$ in 0.9% NaCl was added to 200 μL of tin/glucoheptonate (from a lyophilized aliquot freshly reconstituted with 1 mL of deoxygenated H_2O). To this was added 100 μg (100 μL) of reduced protein. The reaction was incubated for 60 min at room temperature.

For labeling of HYNIC−annexin V, tricine was used as the exchange agent. The tin/tricine reduction/exchange reagent was prepared as previously described (*24*); the final composition of the reagent was 200 mmol/L tricine, pH 7.1, 128 μg/mL $SnCl_2.2H_2O$. This reagent was dispensed in 1-mL aliquots into borosilicate glass vials, lyophilized, capped with Teflon-lined screw caps under an argon atmosphere, and stored at −20 °C. For radiolabeling, a 100-μg lyophilized aliquot of HYNIC−annexin V was reconstituted with 100 μL of H_2O, and 100 μL of $^{99m}TcO_4$ in 0.9% NaCl was added. Freshly reconstituted tin/tricine reagent (200 μL) was then added and the reaction mixture was incubated for 15 min at room temperature.

Radiolabeled proteins prepared by either method were purified by applying the reaction mixture (400 μL) to a Sephadex G-25 column (0.9 × 2.8 cm) previously equilibrated with PBS and eluting the column with 1000 μL of PBS. Percent protein-bound radioactivity was determined by ITLC on oven-dried silica gel plates with PBS as solvent. For studies of radiolabel stability in serum, percent protein-bound radioactivity was determined by centrifugal ultrafiltration (3 min at 1860*g*) through a membrane with a 10 000-Da cutoff (Centricon-10 filter, Amicon, Danvers, MA). Radiolabel stability was also assessed by gel filtration on a Superose-12 column (1 × 30 cm) connected to an FPLC system. The column was equilibrated with PBS and eluted at a flow rate of 0.5 mL/min at room temperature.

Cell Binding Assays. The affinity of nonradioactive proteins for cell membranes was determined by their ability to compete with fluorescein-annexin V for binding to erythrocytes with exposed phosphatidylserine (*20*). Mutant proteins were added at various concentrations to 1 mL of a solution containing 5 nmol/L fluorescein-annexin V and 8.3 × 10^6 erythrocytes in a buffer consisting of 10 mmol/L HEPES−Na, pH 7.4, 136 mmol/L NaCl, 2.7 mmol/L KCl, 5 mmol/L glucose, 1 mg/mL BSA (buffer HNKGB) plus 2.5 mmol/L $CaCl_2$. The sample was incubated for 15 min at room temperature. The cells were centrifuged for 3 min at 8300*g*, the supernatant removed, and the fluorescein-annexin V bound to the pelleted cells was released by resuspension in 950 μL of HNKGB buffer containing 5 mmol/L EDTA. The sample was centrifuged again, the supernatant removed, and the concentration of fluorescein-annexin V in the supernatant determined by fluorometry. The results of this assay are summarized as the concentration of competitor protein that inhibits 50% of the binding of fluorescein-annexin V, abbreviated IC_{50}.

The ability of radiolabeled proteins to bind to cell membranes was determined with a similar procedure. Radiolabeled protein at 10 nmol/L final concentration was added to duplicate tubes containing a final volume of 1 mL of buffer HNKGB plus 2.5 mmol/L $CaCl_2$. One tube then received 4.2 × 10^8 erythrocytes. After a 15-min incubation at room temperature, both tubes were centrifuged for 3 min at 8320*g*. Radioactivity was measured in 800 μL of the supernatants. The percentage of radioactivity bound to the cells was calculated from 100 × [1 − (supernatant counts in the presence of cells)/(supernatant counts in absence of cells)].

Quantitative titrations were performed to determine the dissociation constant for protein-membrane interaction as previously described (*25*). Radiolabeled protein (3−150 nmol/L) was added to 1 × 10^7 erythrocytes in buffer HNKGB plus 2.5 mmol/L $CaCl_2$. After a 15-min incubation at room temperature, bound and free ligand were separated by centrifugation through a silicone-oil barrier, and the radioactivity bound to the pelleted cells was determined by scintillation counting; this was converted to number of molecules bound per cell by dividing by the known specific activity. The concentration of free ligand was determined by measuring the radioactivity remaining in the supernatant, corrected for the fraction of nonbindable tracer. The dissociation constant was determined by using nonlinear least-squares analysis to fit the data to a model of noncooperative binding to homogeneous sites.

Biodistribution and Imaging Studies. Each annexin V mutant protein (100 μg) was labeled with ^{99m}Tc (10 mCi) using the glucoheptonate procedure as described above and purified on a Sephadex G-25 column (1.5 × 5 cm) eluted with PBS. The eluate appearing between 2 and 4 mL was pooled. For biodistribution studies, 50 μL (=1.5 μg, 40−150 μCi) of this eluate was injected via the tail vein into 8−10 week old Balb/c mice (Veterinary Services, Department of Comparative Medicine, Stanford University) weighing between 20 and 25 g. Organs and other targets of interest were harvested from groups of 5−7 mice at 60 min after injection; the sample tissues were weighed and then underwent scintillation counting. Samples were counted in a Packard Cobra II gamma counter (Packard, Meriden, CT) with energy windows set between 120 and 170 keV. Scintillation well data were expressed as the percentage of injected dose (%ID) and %ID per gram of tissue (%ID/g) for each sample. Scintillation counting data were adjusted for tail vein infiltration, decay, and background as described previously (*6*).

116: NH_2Ala-Cys-Gly-Gly-Gly-His-Met-Annexin V

117: NH_2Ala-Gly-Gly-Cys-Gly-His-Met-Annexin V

118: NH_2Ala-Cys-Gly-Cys-Gly-His-Met-Annexin V

Figure 1. Primary structures of annexin V mutants. Each mutant protein contains the indicated N-terminal extension of seven amino acids, followed by amino acids 2−320 of human annexin V (*29*). The naturally occurring Cys residue at position 316 has also been mutated to Ser in all three proteins. The initiator methionine residue is not shown because it is removed posttranslationally (*30*). For convenience, the mutant molecules are given arbitrary numerical designations.

For imaging studies, young male (150−200 g, 8−10 week old) Sprague−Dawley rats (Simonsens, Gilroy, CA) were housed and treated in a humane manner in accordance to institutional animal subjects guidelines. Animals were treated with 150 mg/kg of cyclophosphamide (Sigma) reconstituted in 1 mL of PBS and injected intraperitoneally. All animals were then imaged at either 0 or 24 h after cyclophosphamide treatment, followed by sacrifice and well counting of selected tissues. Animals were injected via tail vein with 0.5−1 mCi (37 MBq, 20−40 μg protein/kg) of radiolabeled annexin V 1 h prior to radionuclide imaging and sacrifice. At the time of imaging, rats were sedated with a mixture of 80 mg/kg acepromazine and 40 mg/kg ketamine injected intramuscularly. A Technicare 420 mobile scintillation camera (Technicare; Solon, OH) equipped with a low energy, high resolution parallel hole collimator was used to record the [^{99m}Tc]annexin V distribution. Data were recorded using a 20% window centered on the 140 keV photopeak of ^{99m}Tc into a 256 × 256 matrix of a dedicated computer system for digital display and analysis (ICON; Siemens, Hoffman Estates, IL). All images were recorded for a preset time of 10 min. Region of interest (ROI) image analysis was performed to determine relative counts in one femur (corrected for background in the adjacent soft tissue of the thigh) in comparison to that of the whole body. The result was expressed as the percent of the whole body activity. *P*-Values were calculated using the student *t*-test with a one-tail test for significance assuming equal variances of test and control groups. *P*-values of 0.05 or less were considered significant. Average values are presented along with their associated standard deviations.

RESULTS

Protein Production and Characterization. Three mutant proteins were designed to have N-terminal sequences potentially suitable for chelation of Tc (Figure 1). Annexin V-116 and annexin V-117 were predicted to form an N_3S chelate, while annexin V-118 was predicted

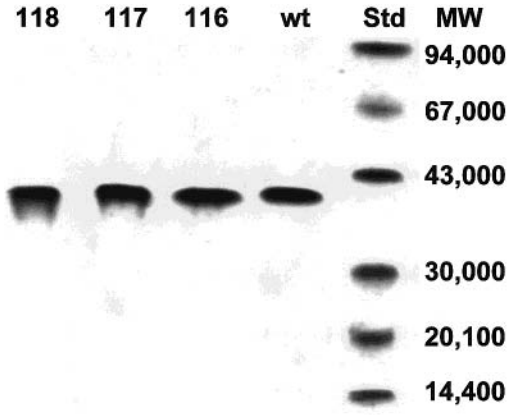

Figure 2. SDS−PAGE analysis of mutant proteins. Recombinant wild-type annexin V and the three mutant annexin V molecules were reduced with β-mercaptoethanol, analyzed on a 10 to 15% gradient gel on a Pharmacia PHAST system, and stained with Coomassie Brilliant Blue.

Table 2. Membrane Binding Activity of Mutant Proteins[a]

protein	IC_{50} (nmol/L)
annexin V	6.8 ± 0.7
annexin V-116	9.3 ± 0.4
annexin V-117	10.3 ± 2.5
annexin V-118	10.0 ± 2.8
HYNIC-annexin V	10.1 ± 2.0

[a] IC_{50} values were determined for unlabeled proteins by competition assay as described in the Materials and Methods. Results are given as mean ± SD with $n = 9$ for annexin V and HYNIC-annexin V and $n = 2$ for mutants 116, 117, and 118.

Table 3. Radiochemical Yield, Purity, and Bioactivity of Labeled Proteins

protein	% radiochemical yield[a]	% radiochemical purity[a,b]	% radioactivity bound to erythrocytes[c]
annexin V	3.9 ± 1.6	not applicable	not applicable
annexin V-116	89.5 ± 5.7	94.4 ± 2.0	77.5 ± 3.5
annexin V-117	88.8 ± 2.0	92.2 ± 1.2	78.1 ± 3.8
annexin V-118	89.9 ± 1.9	94.2 ± 0.6	78.7 ± 3.6
HYNIC-annexin V	97.0%	99.0%	83.9 ± 2.5

[a] Results are given as mean ± SD with $n = 2$ for annexin V, $n = 4$ for mutants 116, 117, and 118, and $n = 1$ for HYNIC-annexin V. [2] % Radiochemical purity was determined by ITLC after purification by gel filtration. [3] Results are given as mean ± SD with $n = 4$ for mutants 116, 117, and 118, and $n = 7$ for HYNIC-annexin V.

to form an N_2S_2 chelate. The single cysteine residue present at position 316 of native annexin V was also mutated to serine to eliminate the possibility that this residue might form a weak binding site for technetium. The structures of all constructs were verified by DNA sequencing. All three proteins could be expressed cytoplasmically in *E. coli* and purified in high yield (10 mg pure protein per liter of bacterial culture) under conditions similar to those used to produce wild-type annexin V (*22*, *26*). SDS−PAGE analysis (Figure 2) showed that all three mutants could be produced in highly pure form. As expected, all three mutant proteins (326 amino acids in length) also migrated with the same apparent molecular weight as wild-type annexin V (319 amino acids).

The bioactivity of the mutant proteins was verified by measuring their ability to compete with wild-type annexin V for binding to erythrocyte membranes with exposed PS (Table 2). All three proteins displaced fluorescein-annexin V with nearly the same relative affinity as wild-type annexin V, indicating that attachment of the N-terminal heptapeptide did not interfere with membrane binding either directly or indirectly. The mutant proteins also had the same IC_{50} values as HYNIC−annexin V, which has been previously used to detect PS exposure in vivo.

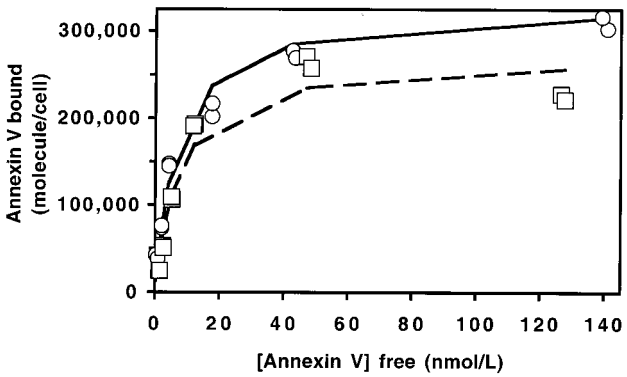

Figure 3. Quantitative cell binding curve. Red blood cells with exposed PS were incubated with varying amounts of [^{99m}Tc]-annexin V-117 (squares) or [^{99m}Tc]HYNIC−annexin V (circles); bound and free ligand were then separated as described in the Materials and Methods and the amount of cell-bound and unbound radioactivity was determined by scintillation counting. The data were fit to a model of noncooperative binding to homogeneous sites. The calculated binding parameters for annexin V-117 were $K_d = 7.3$ nmol/L, $B_{max} = 272\,000$ sites/cell; corresponding values for HYNIC−annexin V were 6.9 nmol/L and 330 000 sites/cell.

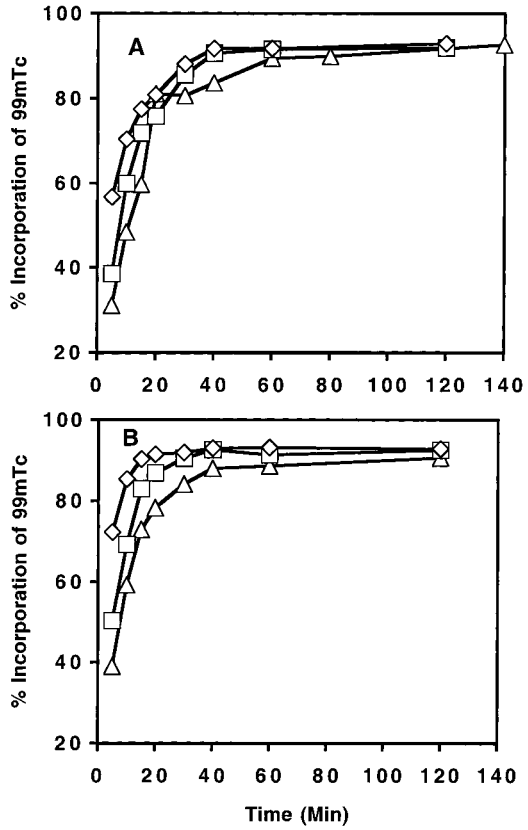

Figure 4. Time course of radiolabeling. Protein (50 μg) was reacted with $^{99m}TcO_4$ (100 μCi), and ITLC was performed on aliquots taken from the reaction mixtures at the indicated times. (A) Labeling at room temperature (22 °C); (B) Labeling at 37 °C. (△) Annexin V-116, (□) annexin V-117, (◇) annexin V-118.

Radiolabeling with ^{99m}Tc. The three mutant proteins were tested for their ability to chelate technetium. As

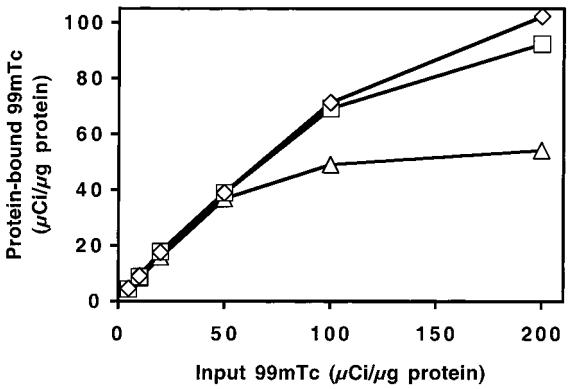

Figure 5. Radiolabeling as a function of technetium/protein ratio. Protein (5−20 μg) was added to technetium (100−500 μCi) to achieve the indicated ratio of technetium to protein. After 60 min at room temperature, ITLC was performed on the reaction mixture to determine percent incorporation of radioactivity into protein. The specific activity was then calculated from the input ratio of technetium to protein multiplied by the percent incorporation of radioactivity into protein. Symbols: as in Figure 4.

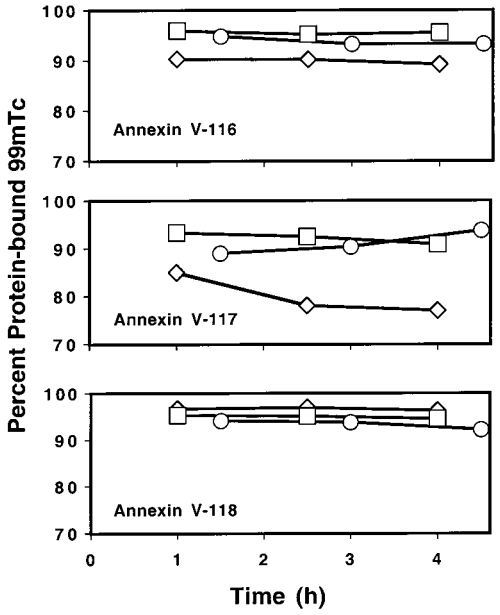

Figure 6. Stability of radiolabeled proteins in vitro. Protein was radiolabeled to a specific activity of 1−2 μCi/μg and purified by gel filtration chromatography as described in the Materials and Methods. Radiolabeled protein was then incubated at a concentration of 250 μg/mL at room temperature in either PBS (diamonds), PBS + 5 mmol/L DTPA (squares), or a 1:1 mixture of PBS and human serum (circles). Aliquots were taken at the indicated times and percent protein-bound ^{99m}Tc was determined.

shown in Table 3, all three proteins incorporated most of the added pertechnetate, as measured by ITLC of the reaction mixture. The percent incorporation was comparable to the value obtained for HYNIC−annexin V under the same conditions. In contrast, there was almost no labeling of wild-type annexin V, indicating that the observed radiolabeling was specifically due to the added N-terminal sequences in the mutant molecules. The radiolabel remained attached to protein after removal of labeling reagents by gel filtration chromatography, as indicated by the high radiochemical purity of gel-filtered proteins.

To verify that the radiolabeled proteins retained membrane binding activity, radiolabeled proteins were incubated with erythrocytes in the presence of calcium,

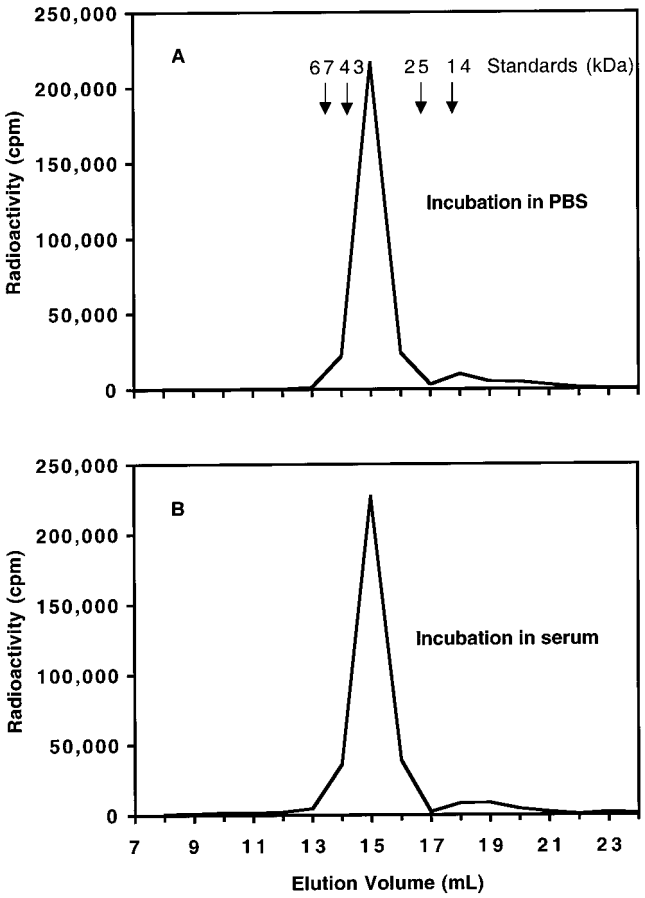

Figure 7. Gel filtration analysis of [^{99m}Tc]annexin V-117. (A) [^{99m}Tc]Annexin V-117 (50 μg in 600 μL of PBS) was incubated for 2 h at room temperature and then analyzed on a Superose-12 column as described in the Materials and Methods. Radioactivity was determined in 1-mL column fractions. The *arrows* indicate the elution positions of globular protein standards with the indicated molecular masses. B. [^{99m}Tc]Annexin V-117 (50 μg in 300 μL of PBS) was mixed with 300 μL of human serum, incubated for 2 h at room temperature, and then analyzed on a Superose-12 column.

and the percentage of radioactivity bound to cells was measured (Table 3). All three proteins showed comparable levels of binding, and this level was comparable to the binding of [^{99m}Tc]HYNIC−annexin V tested under the same conditions.

Quantitative titrations were performed to determine the affinity of the radiolabeled protein for cell membranes with exposed PS. As shown in Figure 3, [^{99m}Tc]annexin V-117 showed high-affinity saturable binding to erythrocytes with exposed PS; the binding curve was essentially identical to that obtained with [^{99m}Tc]HYNIC−annexin V. The measured dissociation constant was 7 nmol/L, consistent with previous results obtained for binding of [^{125}I]annexin V to platelets and erythrocytes (*25, 27*).

Optimization of Labeling Conditions. The time course of labeling was rapid for all three mutants. As shown in Figure 4A, incorporation of ^{99m}Tc occurred rapidly at room temperature, reaching a maximum at 40 min for annexin V-117. The reaction was slightly faster at 37 °C, reaching a maximum at 30 min for annexin V-117 (Figure 4B). For convenience, a 60-min reaction at room temperature was chosen for most subsequent experiments.

To determine if proteins could be labeled to high specific activity, the technetium/protein was varied. As shown in Figure 5, the incorporation of ^{99m}Tc into protein

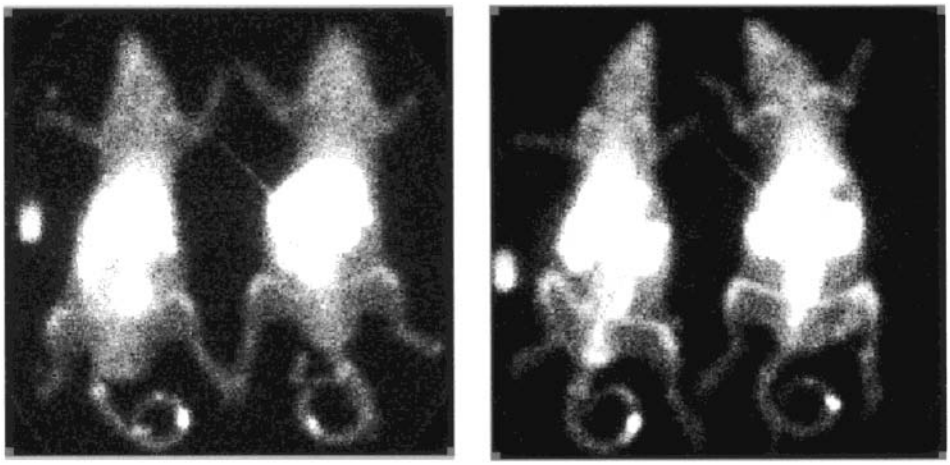

Figure 8. Imaging of apoptosis in bone marrow and spleen. Rats received either no treatment (control) or 150 mg/kg cyclophosphamide (+ cyclophosphamide). After 24 h, they received 0.5 mCi of [^{99m}Tc]annexin V-117 injected via the tail vein. One hour later, images were recorded for 10 min from animals in the supine position.

increased with increasing amounts of added $^{99m}TcO_4$; specific activities of ~100 μCi/μg were readily obtainable for annexin V-117 and annexin V-118.

Stability of Radiolabeled Proteins in Vitro. The stability of the radiolabeled protein in vitro was determined after challenge with phosphate-buffered saline, DTPA (5 mmol/L), and serum (Figure 6). ITLC analysis showed that all three mutant proteins retained the radiolabel over a period of several hours, indicating that the Tc−protein chelate was of high affinity.

These results were confirmed by gel filtration chromatography of [^{99m}Tc]annexin V-117 (Figure 7A). After incubation of [^{99m}Tc]annexin V-117 with PBS for 2 h, almost all of the radioactivity eluted in the same position as monomeric annexin V-117 (M_r 36 000); there was no evidence for multimeric protein aggregates. Similarly, gel filtration chromatography of [^{99m}Tc]annexin V-117 after a 2-h incubation with human serum showed that the radioactivity still eluted in the same position as monomeric annexin V (Figure 7B). Thus, there was no evidence for transchelation of ^{99m}Tc to other serum proteins over a time period consistent with the normal blood clearance time of annexin V (see Discussion).

Biodistribution of Radiolabeled Proteins in Mice. Labeled proteins were injected intravenously in mice and biodistribution was determined 60 min later (Table 4). Uptake was highest in kidney and liver. The overall pattern of uptake was similar to results obtained with [^{99m}Tc]HYNIC−annexin V, indicating that the N-terminal additions to the three mutant molecules had not drastically altered their biodistribution.

Annexin V-117 Imaging of Cyclophosphamide-Treated Rats. To verify that annexin V-117 would be suitable to detect apoptosis in vivo, we used a model of cyclophosphamide-induced apoptosis in rats. Imaging of cyclophosphamide-treated rats clearly showed increased uptake of annexin V-117 in the femurs and spleen compared to control animals (Figure 8), consistent with our earlier studies with HYNIC−annexin V (*6*). Cyclophosphamide-treated rats (N = 5) demonstrated a 56% increase in femoral uptake determined by ROI analyses 24 h after treatment compared with controls (N = 4) (0.325 ± 0.084% versus 0.209 ± 0.056% whole body uptake, respectively; p = 0.0262). Well counting of excised femurs revealed a borderline (p = 0.065) increase of annexin V-117 uptake in treated as compared with control animals (0.239 ± 0.079% ID/g versus 0.167 ± 0.028% ID/g, respectively). Well counting of excised spleens showed a significant 59% increase (p = 0.0303) in splenic uptake in treated animals compared with control (3.27 ± 1.04% ID/g versus 2.06 ± 0.332% ID/g, respectively).

Table 4. Biodistribution of Mutant Molecules in Mice[a]

	% injected dose per organ			
organ	annexin V-116	annexin V-117	annexin V-118	HYNIC−annexin V
carcass	31.94	23.05	21.73	32.64
kidney	17.96	6.17	5.99	39.16
liver	11.24	5.97	10.36	16.59
small intestine	3.50	4.18	6.20	3.31
stomach	3.35	1.69	4.20	0.88
large intestine	1.79	1.15	3.22	0.88
tail	0.79	0.72	0.48	0.71
lung	0.83	0.40	0.60	0.61
blood	0.24	0.36	0.49	0.39
spleen	0.56	0.28	0.42	0.88
bone	0.19	0.14	0.15	0.18
heart	0.11	0.07	0.07	0.14
thymus	0.05	0.04	0.03	0.05
skeletal muscle	0.03	0.03	0.03	0.03
brain	0.02	0.02	0.02	0.01

[a] Results are mean values for n = 5 to 7 animals.

DISCUSSION

We have successfully produced mutant forms of annexin V that have endogenous chelation sites for ^{99m}Tc. These mutant molecules retain bioactivity, as measured by their ability to bind with high affinity to cell membranes with exposed PS. Membrane-binding activity is preserved both before and after labeling with ^{99m}Tc. Labeling of these molecules with ^{99m}Tc is very simple and rapid, and high specific activities can be achieved. Presence of endogenous chelation sites on these proteins greatly simplifies production of material suitable for ^{99m}Tc labeling: the recombinant proteins can be used directly, without the need for complex and time-consuming procedures for attachment of organic Tc chelation groups. The annexin V mutants are also chemically homogeneous, in contrast to the heterogeneous labeling that usually occurs with amine-directed bifunctional organic-labeling reagents.

The mutant annexins show good radiolabel stability in vitro. They are stable to challenge by PBS and serum in vitro for at least several hours, and there is no evidence for transchelation of ^{99m}Tc to other serum proteins during in vitro incubation (Figures 6 and 7). It should be noted that annexin V is very rapidly cleared from the blood; less than 5% of initial radioactivity is present 2.5 h after intravenous injection (*4*, *5*). Annexin V also does not bind to normal erythrocytes, leukocytes, or platelets in whole blood (*28*). These results imply that radiolabeled annexins will be confined to the plasma fraction of blood in vivo, and they will be stable in this compartment until they have been cleared into other body compartments.

The mutant annexins also showed good in vivo radiostability, as judged by the relatively low excretion of ^{99m}Tc in the stomach. Annexin V-117 showed the greatest radiostability in vivo, as judged by the lowest level of ^{99m}Tc present in the stomach (Table 4). This was somewhat surprising, since the N_2S_2 structure in annexin V-118 might be expected to chelate technetium more tightly than the N_3S structure present in annexin V-117. Given its overall combination of properties, annexin V-117 seems the most promising derivative for further development as an in vivo imaging agent.

The biodistribution of annexin V-117 may have several advantages for clinical imaging compared to HYNIC−annexin V. In normal animals, there is only 16% as much uptake in the kidney and 36% as much uptake in the liver, which reduces radiation dose to those organs and may allow the imaging of renal transplant rejection. Bone marrow uptake is also lower in normal control animals, without compromising the relative increase in uptake in the marrow seen in response to cyclophosphamide-induced apoptosis. There is also less uptake in the carcass (probably due to increased excretion in the urine), which will improve target-to-background ratio for most imaging studies. The only comparative disadvantage of annexin V-117 is moderately increased excretion in the stomach and intestines compared to HYNIC−annexin V.

The peptide sequences described in this study (Figure 1) also provide new alternatives for introduction of chelation sites into other proteins. It appears that the sequences described here are comparable to the sequences previously used to label other recombinant proteins in the degree of ^{99m}Tc incorporation and the stability of the label (*15*, *16*). Although we used an N-terminal location for these peptides because that is optimal for annexin V, they would also be likely to work in either an internal or a C-terminal location.

ACKNOWLEDGMENT

We thank Dr. Allan Green for helpful advice and support. This work was partially supported by a grant from Theseus Medical Imaging, Inc., and by NIH Grant HL-61717.

LITERATURE CITED

(1) Zwaal, R. F., and Schroit, A. J. (1997) Pathophysiologic implications of membrane phospholipid asymmetry in blood cells. *Blood 89*, 1121−32.

(2) Bevers, E. M., Comfurius, P., Dekkers, D. W., and Zwaal, R. F. (1999) Lipid translocation across the plasma membrane of mammalian cells. *Biochim. Biophys. Acta 1439*, 317−30.

(3) Fadok, V. A., Voelker, D. R., Campbell, P. A., Cohen, J. J., Bratton, D. L., and Henson, P. M. (1992) Exposure of phosphatidylserine on the surface of apoptotic lymphocytes triggers specific recognition and removal by macrophages. *J. Immunol. 148*, 2207−16.

(4) Tait, J. F., Cerqueira, M. D., Dewhurst, T. A., Fujikawa, K., Ritchie, J. L., and Stratton, J. R. (1994) Evaluation of annexin V as a platelet-directed thrombus targeting agent. *Thromb. Res. 75*, 491−501.

(5) Stratton, J. R., Dewhurst, T. A., Kasina, S., Reno, J. M., Cerqueira, M. D., Baskin, D. G., and Tait, J. F. (1995) Selective uptake of radiolabeled annexin V on acute porcine left atrial thrombi. *Circulation 92*, 3113−21.

(6) Blankenberg, F. G., Katsikis, P. D., Tait, J. F., Davis, R. E., Naumovski, L., Ohtsuki, K., Kopiwoda, S., Abrams, M. J., Darkes, M., Robbins, R. C., Maecker, H. T., and Strauss, H. W. (1998) In vivo detection and imaging of phosphatidylserine expression during programmed cell death. *Proc. Natl. Acad. Sci. U. S. A. 95*, 6349−54.

(7) Blankenberg, F. G., Katsikis, P. D., Tait, J. F., Davis, R. E., Naumovski, L., Ohtsuki, K., Kopiwoda, S., Abrams, M. J., and Strauss, H. W. (1999) Imaging of apoptosis (programmed cell death) with 99mTc annexin V. *J. Nucl. Med. 40*, 184−91.

(8) Vriens, P. W., Blankenberg, F. G., Stoot, J. H., Ohtsuki, K., Berry, G. J., Tait, J. F., Strauss, H. W., and Robbins, R. C. (1998) The use of technetium Tc 99m annexin V for in vivo imaging of apoptosis during cardiac allograft rejection. *J. Thorac. Cardiovasc. Surg. 116*, 844−53.

(9) Blankenberg, F. G., Robbins, R. C., Stoot, J. H., Vriens, P. W., Berry, G. J., Tait, J. F., and Strauss, H. W. (2000) Radionuclide imaging of acute lung transplant rejection with annexin V. *Chest 117*, 834−40.

(10) Ogura, Y., Krams, S. M., Martinez, O. M., Kopiwoda, S., Higgins, J. P., Esquivel, C. O., Strauss, H. W., Tait, J. F., and Blankenberg, F. G. (2000) Radiolabeled annexin V imaging: diagnosis of allograft rejection in an experimental rodent model of liver transplantation. *Radiology 214*, 795−800.

(11) Fritzberg, A. R., Kasina, S., Eshima, D., and Johnson, D. L. (1986) Synthesis and biological evaluation of technetium-99m MAG3 as a hippuran replacement. *J. Nucl. Med. 27*, 111−6.

(12) Fritzberg, A. R., Abrams, P. G., Beaumier, P. L., Kasina, S., Morgan, A. C., Rao, T. N., Reno, J. M., Sanderson, J. A., Srinivasan, A., Wilbur, D. S., and et al. (1988) Specific and stable labeling of antibodies with technetium-99m with a diamide dithiolate chelating agent. *Proc. Natl. Acad. Sci. U.S.A. 85*, 4025−9.

(13) Giblin, M. F., Jurisson, S. S., and Quinn, T. P. (1997) Synthesis and characterization of rhenium-complexed alpha-melanotropin analogues. *Bioconjug. Chem. 8*, 347−53.

(14) Stalteri, M. A., Bansal, S., Hider, R., and Mather, S. J. (1999) Comparison of the stability of technetium-labeled peptides to challenge with cysteine. *Bioconjug. Chem. 10*, 130−6.

(15) George, A. J., Jamar, F., Tai, M. S., Heelan, B. T., Adams, G. P., McCartney, J. E., Houston, L. L., Weiner, L. M., Oppermann, H., and Peters, A. M. (1995) Radiometal labeling of recombinant proteins by a genetically engineered minimal chelation site: technetium-99m coordination by single-chain Fv antibody fusion proteins through a C-terminal cysteinyl peptide [published erratum appears in *Proc. Natl. Acad. Sci U.S.A.* (1996) *93* (18), 9991]. *Proc. Natl. Acad. Sci. U.S.A. 92*, 8358−62.

(16) Bogdanov, A., Jr., Simonova, M., and Weissleder, R. (1998) Design of metal-binding green fluorescent protein variants. *Biochim. Biophys. Acta 1397*, 56−64.

(17) Waibel, R., Alberto, R., Willuda, J., Finnern, R., Schibli, R., Stichelberger, A., Egli, A., Abram, U., Mach, J. P., Pluckthun, A., and Schubiger, P. A. (1999) Stable one-step technetium-99m labeling of his-tagged recombinant proteins with a novel Tc(I)-carbonyl complex. *Nat. Biotechnol. 17*, 897−901.

(18) Pietersz, G. A., Patrick, M. R., and Chester, K. A. (1998) Preclinical characterization and in vivo imaging studies of an engineered recombinant technetium-99m-labeled metallothionein-containing anti-carcinoembryonic antigen single-chain antibody. *J. Nucl. Med. 39*, 47−56.

(19) Tanaka, K., Einaga, K., Tsuchiyama, H., Tait, J. F., and Fujikawa, K. (1996) Preparation and characterization of a

disulfide-linked bioconjugate of annexin V with the B-chain of urokinase: an improved fibrinolytic agent targeted to phospholipid-containing thrombi. *Biochemistry 35*, 922−9.
(20) Tait, J. F., Engelhardt, S., Smith, C., and Fujikawa, K. (1995) Prourokinase-annexin V chimeras. Construction, expression, and characterization of recombinant proteins. *J. Biol. Chem. 270*, 21594−9.
(21) Huber, R., Berendes, R., Burger, A., Schneider, M., Karshikov, A., Luecke, H., Romisch, J., and Paques, E. (1992) Crystal and molecular structure of human annexin V after refinement. Implications for structure, membrane binding and ion channel formation of the annexin family of proteins. *J. Mol. Biol. 223*, 683−704.
(22) Wood, B. L., Gibson, D. F., and Tait, J. F. (1996) Increased erythrocyte phosphatidylserine exposure in sickle cell disease: flow-cytometric measurement and clinical associations. *Blood 88*, 1873−80.
(23) Tait, J. F., Gibson, D., and Fujikawa, K. (1989) Phospholipid binding properties of human placental anticoagulant protein-I, a member of the lipocortin family. *J. Biol. Chem. 264*, 7944−9.
(24) Larsen, S. K., Solomon, H. F., Caldwell, G., and Abrams, M. J. (1995) [99mTc]tricine: a useful precursor complex for the radiolabeling of hydrazinonicotinate protein conjugates. *Bioconjug. Chem. 6*, 635−8.
(25) Tait, J. F., and Gibson, D. (1994) Measurement of membrane phospholipid asymmetry in normal and sickle- cell erythrocytes by means of annexin V binding. *J. Lab. Clin. Med. 123*, 741−8.
(26) Tait, J. F., and Smith, C. (1991) Site-specific mutagenesis of annexin V: role of residues from Arg-200 to Lys-207 in phospholipid binding. *Arch. Biochem. Biophys. 288*, 141−4.
(27) Thiagarajan, P., and Tait, J. F. (1990) Binding of annexin V/placental anticoagulant protein I to platelets. Evidence for phosphatidylserine exposure in the procoagulant response of activated platelets. *J. Biol. Chem. 265*, 17420−3.
(28) Tait, J. F., Smith, C., and Wood, B. L. (1999) Measurement of phosphatidylserine exposure in leukocytes and platelets by whole-blood flow cytometry with annexin V. *Blood Cells Mol. Dis. 25*, 271−8.
(29) Funakoshi, T., Hendrickson, L. E., McMullen, B. A., and Fujikawa, K. (1987) Primary structure of human placental anticoagulant protein. *Biochemistry 26*, 8087−92.
(30) Maurer-Fogy, I., Reutelingsperger, C. P., Pieters, J., Bodo, G., Stratowa, C., and Hauptmann, R. (1988) Cloning and expression of cDNA for human vascular anticoagulant, a Ca2+-dependent phospholipid-binding protein. *Eur. J. Biochem. 174*, 585−92.

BC000059V

A Nonviral DNA Delivery System Based on Surface Modified Silica-Nanoparticles Can Efficiently Transfect Cells in Vitro

Carsten Kneuer,[†] Mohammad Sameti,[†,‡] Udo Bakowsky,[§] Thomas Schiestel,[‡] Hermann Schirra,[‡] Helmut Schmidt,[‡] and Claus-Michael Lehr*[,†]

Department of Biopharmaceutics and Pharmaceutical Technology, Saarland University, 66041 Saarbrücken, Germany, Institute for New Materials gemGmbH, Im Stadtwald, 66123 Saarbrücken, Germany, and Department of Physiological Chemistry, University of Groningen, Groningen, The Netherlands.
Received June 1, 2000; Revised Manuscript Received September 18, 2000

Diverse polycationic polymers have been used as nonviral transfection agents. Here we report the ability of colloidal silica particles with covalently attached cationic surface modifications to transfect plasmid DNA in vitro and make an attempt to describe the structure of the resulting transfection complexes. In analogy to the terms lipoplex and polyplex, we propose to describe the nanoparticle−DNA complexes by the term "nanoplex". Three batches, Si10E, Si100E, and Si26H, sized between 10 and 100 nm and with ζ potentials ranging from +7 to +31 mV at pH 7.4 were evaluated. The galactosidase expression plasmid DNA pCMVβ was immobilized on the particle surface and efficiently transfected Cos-1 cells. The transfection activity was accompanied by very low cytotoxicity, with LD_{50} values in the milligrams per milliliter range. The most active batch, Si26H, was produced by modification of commercially available silica particles with *N*-(6-aminohexyl)-3-aminopropyltrimethoxysilane, yielding spherical nanoparticles with a mean diameter of 26 nm and a ζ potential of +31 mV at pH 7.4. Complexes of Si26H and pCMVβ plasmid DNA formed at w/w ratios of 10 were most effective in promoting transfection of Cos-1 cells in the absence of serum. At this ratio, >90% of the DNA was associated with the particles, yielding nanoplexes with a net negative surface charge. When the transfection medium was supplemented with 10% serum, maximum gene expression was observed at a w/w ratio of 30, at which the resulting particle−DNA complexes possessed a positive surface charge. Transfection was strongly increased in the presence of 100 μM chloroquine in the incubation medium and reached approximately 30% of the efficiency of a 60 kDa polyethylenimine. In contrast to polyethylenimine, no toxicity was observed at the concentrations required. Atomic force microscopy of Si26H−DNA complexes revealed a spaghetti-meatball-like structure. The surface of complexes prepared at a w/w ratio of 30 was dominated by particles half-spheres. Complex sizes correlated well with those determined previously by dynamic light scattering.

INTRODUCTION

The past decade has witnessed the arrival of a range of new synthetic transfection agents, including cationic peptides, dendrimers, polyethylenimine, and novel lipids (*1*−*5*). The efficiency of nonviral transfection systems has improved several orders of magnitude. However, this is not due to the discovery of new transfection reagents per se, but also a product of the grown understanding of the biological processes that take place during transfection and the rational manipulation of these. Milestones include the concept of receptor targeting (*6*) and endosomal escape (chloroquine, endosomolytic peptides and viruses, proton sponges) (*3*, *7*−*9*). Currently, research groups are seeking ways to facilitate the nuclear transfer of transfected DNA after it has entered the cytoplasm (*10*, *11*) or to circumvent this problem by cytoplasmic gene expression (*12*). Exhaustive reviews on these topics have been published recently (*13*−*15*). Along with the more detailed understanding of transfection, the most advanced transfections agents are getting increasingly complex and might already be termed transfection "systems". These will carry a number of functional components that can be more or less integrated: (1) a plasmid or other suitable form of DNA, (2) a DNA carrier, (3) one or more receptor ligand, (4) an endosomolytic factor, (5) a nuclear localization signal, (6) a biocompatible shell and structures to link these functions. With the rising number of necessary components it is becoming increasingly difficult to tightly control the synthesis of such complexes. Wagner and colleagues have successfully employed a system that, in its most complex form, consists of DNA, polylysine or polyethylenimine, a streptavidin−biotin linker, inactivated adenovirus, and transferrin (*16*).

In an attempt to provide alternative DNA carriers for the assembly of such gene transfer systems, we have evaluated the potential of cationically modified silica nanoparticles as a transfection reagent. The ability of these particles to bind and to protect plasmid DNA was shown recently (*17*).

Many polycationic transfection agents are limited in their in vitro transfection efficiency by a pronounced reduction in cell viability. Frequently, the peak in transgene expression is paralleled by the onset of cytotoxicity (*2*, *3*, *18*, *19*). Although some mechanistic studies have

* To whom correspondence should be addressed. Phone: +49 (0)681 302 2039. Fax: +49 (0)681 302 4677. E-mail: lehr@rz.uni-sb.de.
[†] Saarland University.
[‡] Institute for New Materials gemGmbH, Im Stadtwald.
[§] University of Groningen.

10.1021/bc0000637 CCC: $19.00 © 2000 American Chemical Society
Published on Web 11/03/2000

shown the immobilization of membrane patches (*20*), lipid redistribution (*21*), or the thermodynamic stabilization of lipid bilayers by polycations (*22*), the processes that mediate the in vitro toxicity of polycations such as polylysine or polyethyleneimine is not understood. Recent approaches to reduce the toxicity of polymer-based transfection systems include the optimization of formulation parameters (*19*) or the modification of the polymer side chains by glycolylation (*23*). Attention was therefore also paid to the effect of the newly synthesized DNA delivery vehicles on the viability of the exposed cell cultures.

EXPERIMENTAL PROCEDURES

Synthesis of Cationic Silica Nanoparticles. Silica particles surface modified with aminoalkylsilanes were produced as reported previously (*17*). Briefly, batches Si10E and Si26H were synthesized by modification of commercially available silica particles (IPAST, NISSAN Chemical Industries, Tokio, Japan) with *N*-(2-aminoethyl)-3-aminopropyltrimethoxysilane (AEAPS) or *N*-(6-aminohexyl)-3-aminopropyltrimethoxysilane (AHAPS). Twenty grams of particle suspension (corresponding to 6 g of particle dry weight), 20 g of water, and 12 mL of concentrated acetic acid were stirred for 16 h at 80 °C with 7.2 g of AEAPS (Si10E) or 6 g of AHAPS (Si26H). The product was chilled, mixed with 25 mL of ethylene glycol, rotated for 2 h under vacuum at 50 °C, and dialyzed five times for 24 h against 20 L of deionized water. For the synthesis of Si100E, silica particles were generated by the method of Stoeber (*31*) and subsequently modified with one weight equivalent of AEAPS. A mixture of 8 g of triethoxysilane (TEOS) and 13 g of ammonium in 250 mL of ethanol was subjected to a controlled hydrolysis and condensation reaction for 16 h at room temperature. The particles were collected by centrifugation, washed five times and modified with 4.36 g of AEAPS as described above. AEAPS, AHAPS, and TEOS were purchased from ABCR (Karlsruhe, Germany).

Degree of Modification of Si26H. The relative carbon content of unmodified and modified silica particle was measured on a C/H-analyzer, RC-412 (Leco, St. Joseph), using 100−200 mg of particle dry weight. The increase in carbon content was then related to the molecular weight of the hydrolyzed modificator (AHAPS) of 209 g/mol. This allowed the calculation of the degree of cationic modification of the base particle in moles of nitrogen per gram of particle dry weight.

Light Scattering Measurements of ζ Potential and Particle Size. ζ Potential titration curves were obtained using a Malvern Zetasizer 4 (Malvern, U.K.). The instrument was calibrated routinely with a −55 mV standard. Particle size was determined by photon correlation spectroscopy on a ALV 5000 (Laser Vertriebsgesellschaft mbH, Langen, Germany) at a scattering angle of 90° (sampling time 300 s).

Atomic Force Microscopy (AFM). Si26H−DNA complexes were mixed at a w/w ratio of 30 in distilled water, adsorbed to the surface of silicium wafers and the wet surface was examined by atomic force microscopy on a Nanoscope IIIa in tapping mode using a Si_3N_4 cantilever with a spring constant of 34 N/m. Scanning was performed at a scan speed of 2 Hz with a resolution of 512 × 512 pixels. The tip loading force was minimized to avoid structural changes to the sample.

Ethidium Bromide Exclusion Test. For the measurement of ethidium bromide exclusion, DNA was diluted in 50 mM Hepes (pH 7.4) to yield a final concentration of 10 μg/mL, mixed with the desired amount of particle suspension or polymer solution and incubated for 3 min. The final reaction volume was 2 mL in all cases. One milliliter of ethidium bromide (800 ng/mL), or water for the detection of background fluorescence, was added to one-half of the sample and the fluorescence was measured at λ_{ex} = 366 nm and λ_{em} = 590 nm in a F-2000 fluorescence spectrophotometer (HITACHI, Japan).

Table 1. Physicochemical Characteristics of Si10E, Si100E, and Si26H

particle	size (nm) (range)	IEP (pH)	$\zeta_{pH7.4}$ (mV) ($\zeta_{max,}$ fitted)	mol of N/ g of SiNP	spacer in amino-alkylsilane
Si10E	10 (8−12)	8.1	+17 (+44)	nd	ethyl
Si100E	145 (70−220)	7.7	+7 (+56)	nd	ethyl
Si26H	26 (16−50)	8.6	+31 (+57)	0.000 48	hexyl

Agarosegel Electrophoresis. Nanoparticle−DNA complexes were prepared by mixing in 200 μL of 25 mM Hepes (pH 7.4) at a plasmid concentration of 20 μg/mL and electrophoresed on agarose gel (0.7%, ethidium bromide included for visualization) for 2 h at 70 V. Images were taken using a UV transilluminator and a Geldoc2000 gel documentation system (Bio-Rad, Munich, Germany). Band integration and background correction was performed using Molecular Analyst, version 1.1 software (Bio-Rad).

Cosedimentation Analysis. To measure the removal of DNA from the solution, nanoparticle−DNA complexes were prepared as described above and subjected to centrifugation at 21.000*g* for 15 min at room temperature. The concentration of soluble DNA in the supernatant was determined with Hoechst 33 258 dye (*24*).

Cell Culture. Cos-1 cells were obtained from DSMZ (Braunschweig, Germany) and maintained in Dulbecco's modified eagle's medium (DMEM), supplemented with 10% fetal calf serum (Gibco BRL). Cells were incubated at 37 °C with 5% CO_2 in air and subcultured every three to four days using trypsin/EDTA.

Transfections and Cytotoxicity Assay. For transfection, Cos-1 cells were plated in 96-well plates or 16-well chamber slides (Greiner) at a density of 10.000 cells/well and allowed to adhere overnight. Nanoparticle−DNA complexes were prepared by adding the desired amount of particle suspension to 20 μg/mL (final concentration) plasmid DNA in water. After 15 min equillibration at room temperature, the complexes were diluted with one volume of 2xDMEM with or without 20% FCS and 200 μM chloroquine. The semiconfluent monolayers were washed once with PBS and incubated with 100 μL of the test suspension for 4 h at 37 °C with 5% CO_2 in air. The cells were washed once with PBS and incubated for a further 48 h in DMEM + 10% FCS. Cytotoxicity of NP and NP−DNA complexes was determined in a separate set of experiments using the WST-1 assay (Boehringer Mannheim, Germany) according to the manufacturer's instructions. All assays were performed in six replicates.

***β*-Galactosidase Detection.** To assay the average cellular expression of β-galactosidase, cells were washed once with PBS and lysed with 100 μL of 0.2% Triton X-100 (SIGMA) in PBS per well for 30 min at 4 °C. Fifty microliters of lysate was mixed with 50 μL of fresh reaction solution (5 mM 4-methyl-umbeliferryl-β-D-galactoside, 100 mM D-galactose, and 2 mM $MgCl_2$ in PBS, pH 7.4) and incubated for 4 h at 37 °C. The reaction was stopped by the addition of 100 μL 0.2 M glycine-NaOH

(pH 10.3) and the fluorescence (λ_{ex} = 360 nm and λ_{em} = 460 nm) was measured in a Cytofluor II microplate fluorescence reader (Perseptive Biosystems, Bedford, MA). Purified recombinant β-galactosidase (SIGMA, Deisenhofen, Germany) was used as standard. Total protein content was determined from 25 μL of lysate using the BCA assay (Pierce).

For X-Gal staining, cells were fixed with 4% paraformaldehyde for 5 min at room temperature and stained with 1 mg/mL X-Gal (peqlab, Erlangen, Germany) in PBS for 4 h or overnight.

DNA. The β-galactosidase expression plasmid pCMVβ was purchased from ATCC (Manassas, VA) and transformed into *Escherichia coli DH5*α. A Gigaprep from 2500 mL of overnight culture was performed according to the manufacturers instructions (QIAGEN, Hilden, Germany). The DNA was precipitated in 70% ethanol and reconstituted in water to 1 mg/ml.

Other Chemicals. Polyethylenimine with an average molecular weight of 60 kDa according to the manufacturer's information was purchased from SIGMA (Deisenhofen, Germany).

RESULTS

Transfection Activity of NP−DNA Complexes. The ability of Si10E, Si100E, and Si26H to transfect the pCMVβ reporter gene plasmid at a fixed concentration of 10 μg/mL into Cos-1 cells was tested in serum-free and serum-containing medium in the absence and presence of 100 μM chloroquine. As shown in Figure 1A, all tested SiNPs were able to promote transfection. The efficiency was influenced by a number of parameters including the w/w ratio of SiNP:DNA, presence of FCS and presence of chloroquine. The pattern of transfection activity in response to the variables was similar for all nanoparticles.

Presence of 100 μM chloroquine in the transfection medium generally enhanced transfection by all nanoparticles, although there was substantial variation in magnitude. The effect of chloroquine was especially pronounced in the presence of serum, where it could enhance transfection by more than 10-fold for all nanoparticles.

There was also an optimum for the w/w ratio of particle to DNA. In the absence of serum but presence of chloroquine, this was 20, 10, and 10 for Si10E, Si100E, and Si26H, respectively. Above this optimum, a slight but constant decrease in galactosidase activity was observed. This, however, was not accompanied by a reduction in cellular protein content (not shown).

Addition of serum did not affect or improve the efficiency of transfection by all SiNPs. While this effect was relatively small or in some cases only marginal when Si10E or Si100E were used, the improvement of transfection by Si26H complexes prepared at a ratio of 30 was more than 10-fold. The addition of chloroquine and serum in combination improved galactosidase expression by 2 orders of magnitude, reaching approximately 30% of the levels achieved with polyethylenimine−DNA polyplexes prepared at a N/P ratio of 7.5 (w/w = 1). At this ratio, pEI-DNA polyplexes showed the highest level of galactosidase expression in Cos-1 cells in our lab. However, maximum transfection activity coincided with 50% reduction in cellular protein levels when pEI was used as transfection agent.

Figure 1, panels B and C, show the influence of the SiNP to DNA ratio on the resulting galactosidase expression levels in more detail. Low but significant enzyme levels were detectable at w/w ratios of 3. In both cases,

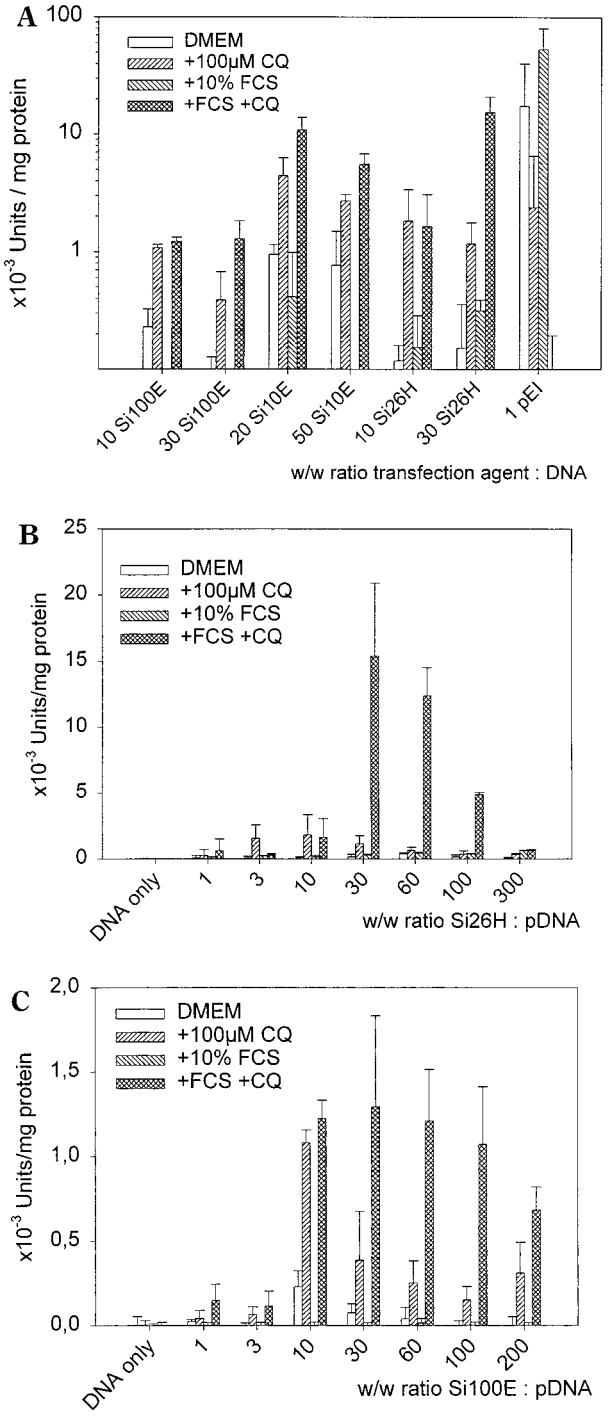

Figure 1. Transfection with pEI, Si10E, Si100E, and Si26H. Semiconfluent Cos-1 cells were incubated with transfection complexes as described in the Materials and Methods. Expression of β-galactosidase was determined using the fluorogenic substrate 4-methyl-umbelliferryl-β-D-galactoside. A total of 10^{-3} enzyme units corresponds to approximately 2 ng of enzyme, and the detection limit was 10 pg of enzyme/well.

transfection in the absence of serum peaked at a ratio of 10. When more particles were added, the activity slowly declined. Supplementation of the transfection medium with 10% of fetal calf serum shifted the curve to higher SiNP:DNA ratios with a maximum at a w/w ratio of 30. Gene expression in experiments performed without the addition of 100 μM chloroquine was at a 2−10-fold lower level but paralleled this course.

Incubation with naked DNA did not result in measurable levels of galactosidase expression in this experimen-

Table 2. In vitro Cytotoxicity of All Transfection Agents Used[a]

transfection agent	LD_{50} (Cos-1 cells) DMEM	DMEM + 10% FCS
pEI	20 μg/mL	40 μg/mL
Si10E	>1 mg/mL	>1 mg/mL
Si100E	>1 mg/mL	>1 mg/mL
Si26H	2.5 mg/mL	>6 mg/mL
pCMVβ	>1 mg/mL	>1 mg/mL
chloroquine	7.5 mM	9.5 mM

[a] Semiconfluent Cos-1 cells grown on 96-well plates were incubated for 4 h with increasing concentrations of the transfection agent in DMEM or DMEM + 10% fcs, supplied with fresh medium and assayed for viability (WST-1 assay) after a further 48 h of growth in DMEM supplemented with 10% fcs.

tal setup. The transfection activity of SiNP−DNA complexes based on 10 and 30 weight equivalents of Si100E and Si26H was confirmed by histochemical staining with X-Gal (not shown).

In Vitro Cytotoxicity of the Transfection Reagents. All transfection reagents were characterized with regard to their effect on the viability of Cos-1 cell monolayers under the same conditions as used for transfection experiments. The LD_{50} values are summarized in Table 2. Only polyethylenimine significantly reduced the viability at concentrations required for efficient transfection. All nanoparticles tested displayed a 50% lethal concentration well above 1 mg/ml. Panels A and B of Figure 2 compare the cytotoxicity of polyethylenimine, the nanoparticle Si26H, and their complexes with plasmid DNA. When applied in concentrations used for transfection, pEI and pEI−DNA complexes reduced viability by up to 50%, while no significant toxicity could be detected for Si26H and its complexes with DNA. In the absence of serum, the factor between the Si26H concentration required for optimum transfection and the LD_{50} of the corresponding complexes was approximately 25. Addition of serum further reduced the cytotoxicity (Figure 2B).

AFM. Atomic force microscopy of Si26H−DNA complexes revealed a structure that can be described with the spaghetti-meatball model. Figure 3 shows a typical example at high resolution. The surface was dominated by Si26H nanoparticles, while DNA strands were not visible and appeared to be localized in the interior. Although the DNA strands could not be resolved within the complex, it can be concluded from the absence of submicron aggregates in DNA-free samples that DNA is wound around and sandwiched by multiple nanoparticles to become physically condensed and covered by these. The size of the resulting complexes was found to be in the range between 100 and 200 nm.

Correlation of Physicochemical Parameters. There was a strong correlation between the nanoparticle-induced decrease in ethidium bromide intercalation, the electrophoretic immobilization of DNA and its removal from solution by centrifugation (Figure 5). All three parameters show significant binding of plasmid DNA at w/w ratios Si26H:DNA above 1, reaching 50% at ratios between 4 and 5. At ratios above 10, >90% of the plasmid was bound to the particle surface as determined by agarosegel electrophoresis (Figure 4). Cosedimentation analysis predicted only 80% binding at this ratio. Upon addition of more Si26H, the DNA binding reached 100%. The exclusion of ethidium bromide from the complex, however, never exceeded 90%.

Si26H−pCMVβ complexes with w/w ratios of 10, 30, 100, and 300 were analyzed for their surface charge by ζ potential measurement (Figure 5). Addition of 10 weight equivalents of Si26H increased the ζ potential from approximately −70 mV for free plasmid DNA to −34 ± 5 mV. At a ratio of 30, the complexes displayed a ζ potential of +25 ± 5 mV, which did not increase further upon addition of more Si26H (28 ± 5 mV at 100:1 and 24 ± 5 mV at 300:1).

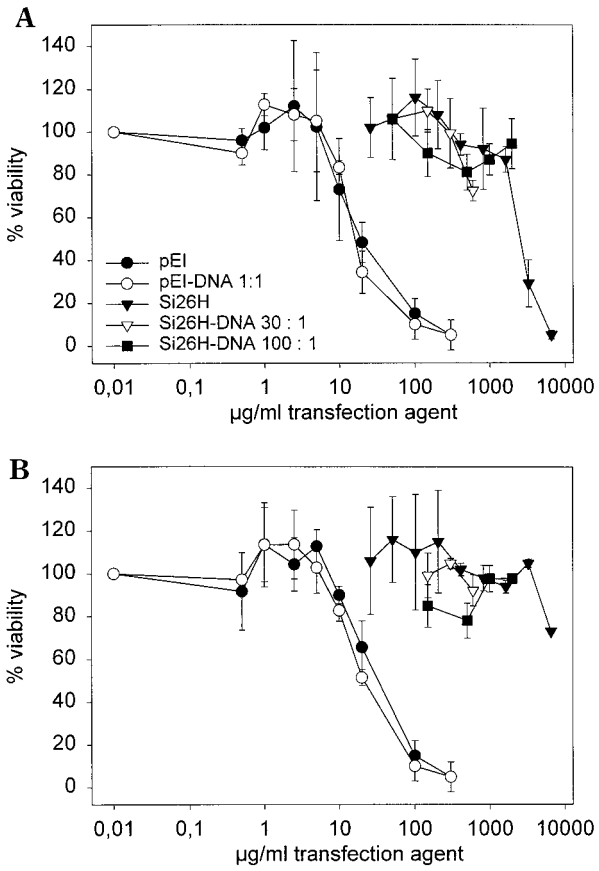

Figure 2. Comparative in vitro cytotoxicity of polyethylenimine and Si26H and their complexes with DNA. Semiconfluent Cos-1 cells grown on 96-well plates were incubated for 4 h with increasing concentrations of pEI, Si26H, or transfection complex in (A) DMEM or (B) DMEM + 10% fcs, supplied with fresh medium and assayed for viability (WST-1) after a further 48 h of growth in DMEM supplemented with 10% fcs. Concentrations always relate to pEI or Si26H.

To relate the w/w ratio Si26H/DNA to the balance of positive and negative charges, the average content of the charge carriers nitrogen and phosphate per gram of Si26H and plasmid DNA, respectively, was calculated. On the basis of the carbon analysis of the unmodified base particle (IPAST) and Si26H, the degree of modfication could be estimated for Si26H as 0.000 48 mol of nitrogen/g of particle dry weight (Table 1). The phosphate content of DNA can be calculated as 0.003 mol of phosphate/g of DNA, assuming an average molecular weight of 330 g/mol of nucleotide. Hence, the w/w ratios Si26H/DNA of 1, 10, and 30 correspond to N/P ratios of 0.16, 1.6, and 4.8, respectively (Table 3).

DISCUSSION

For the purpose of gene transfer, DNA has successfully been complexed with a range of materials including polycationic polymers and cationic liposomes or included in chitosan micro- and nanoparticles. Attempts have also been made to adsorb DNA onto the surface of colloidal particles. So far, dendrimers which are typically smaller than 10 nm and organic nanoparticles that are around

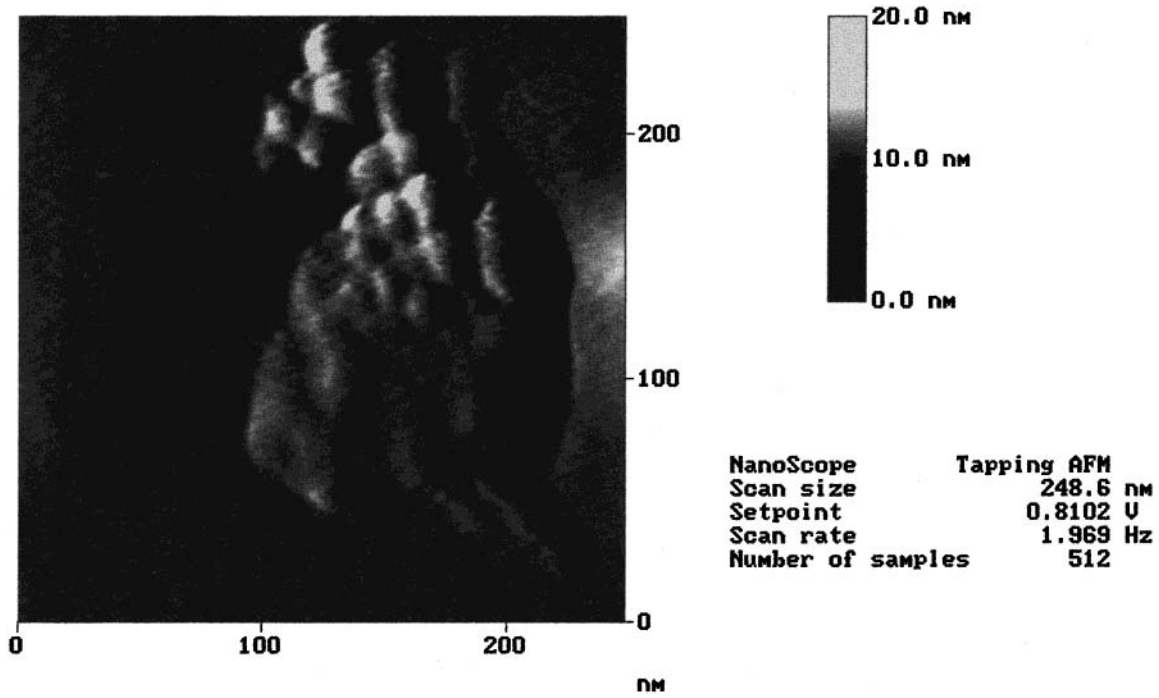

Figure 3. Atomic force microscopy of Si26H−DNA complexes. A suspension of Si26H was added to plasmid DNA to give final concentrations of 20 μg/mL DNA and 600 μg/mL Si26H. The sample was applied to silicium wafers and allowed to adsorb for 30 min at room temperature. Imaging was performed in tapping mode on a Nanoscope IIIa using a Si_3N_4 cantilever with a spring constant of 34 N/m.

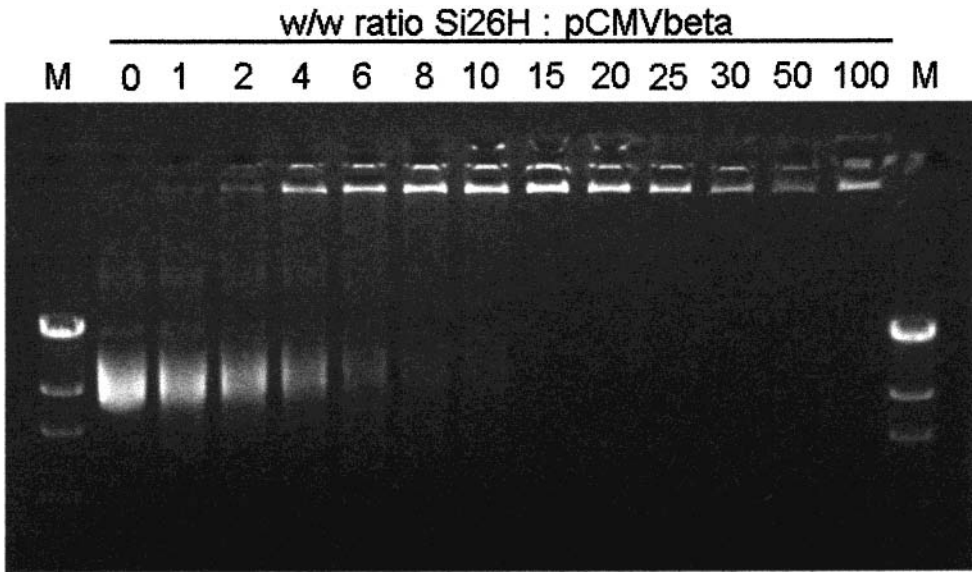

Figure 4. Agarosegel electrophoresis of Si26H-pDNA complexes. Lanes M show DNA marker IV, other lanes correspond to Si26H−pCMVβ complexes prepared at the w/w ratio given on top. The DNA was visualized by ethidium bromide staining and UV transillumination.

300 nm have been evaluated (*3*, *25*). We have synthesized cationically modified silica nanoparticles with sizes of 10−100 nm, that can adsorb DNA, resulting in complexes typically between 100 and 300 nm that should be suitable for cellular uptake. It could now be demonstrated that these particles are also able to efficiently transfect plasmid DNA into cultured cells.

All of the three particle batches tested resulted in measurable and significant galactosidase activity, while DNA alone was inactive. The ratio of particle:DNA optimal for transfection correlated well with the DNA-binding behavior. As shown by agarosegel electrophoresis and cosedimentation analysis, 10 equiv of Si26H were sufficient to bind >90% of the plasmid DNA. The transfection efficiency in the absence of serum peaked at the same ratio. Interestingly, the resulting complexes still displayed a negative surface charge as shown by ζ potential measurements. This confronts with the paradigm that either a high positive charge or specific cellular recognition is necessary for transfection. The addition of fetal calf serum further improved gene expression after transfection with these complexes. This effect was especially pronounced for Si26H−DNA complexes prepared at ratios above 10, which did also display a positive surface charge. This is surprising, as most polyplexes are either not or negatively affected by serum (*26*). On the underlying mechanism can only be speculated. Both a

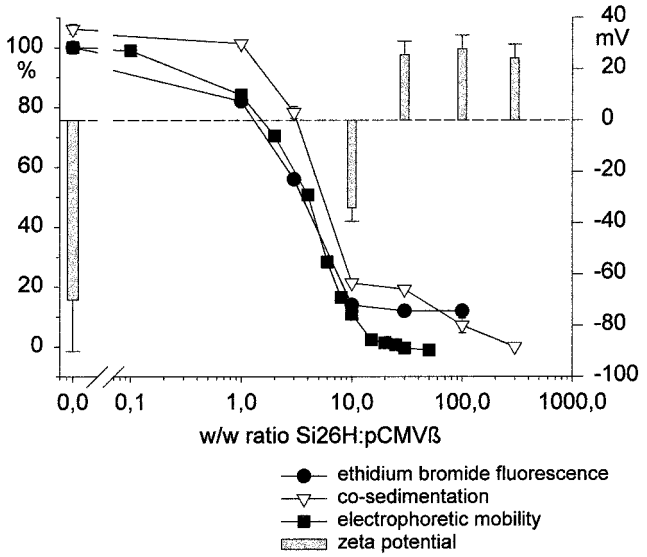

Figure 5. Physicochemical characterization of Si26H−DNA complex formation. Plasmid DNA was incubated with increasing amounts of Si26H at pH 7.4 in 50 mM HEPES for 10 min. Ethidium bromide exclusion from Si26H−DNA complexes, immobilization of DNA in the agarosegel by Si26H, removal of soluble DNA from solution by Si26H, and subsequent centrifugation and the ζ potential of the formed complexes were determined as described in Experimental Procedures.

Table 3. Conversion of w/w Ratios into N/P Ratios for Si26H−DNA Complexes

w/w ratio	N/P ratio[a]
1	0.16
3	0.48
10	1.6
30	4.8

[a] Assuming 0.00048 mol of N/g of particle and average 300 g/mol nucleotide.

physical stabilization or enhancement of cell binding by either specific or unspecific mechanisms would appear feasible.

Another feature of all investigated NP−DNA complexes is that transfection was strongly enhanced by the presence of chloroquine in the transfection medium. As chloroquine is thought to act either via inducing endosomolysis or delaying the endosomal decomposition (*8*), this would suggest that the complexes are internalized by endocytosis and routed to the endosomal/lysosomal compartment. This is not surprising as this pathway is thought to be used by most polyplexes (*9*, *14*, *27*, *28*). However, there is still no agreement on the mode of action of chloroquine, and induction of complex dissociation is discussed as an alternative mechanism to endosomolysis (*29*). Some of the polymers used for transfection, e.g., polyethyleneimine, possess an intrinsic endosomolytic activity, which has been associated with the buffering effect during endosomal acidification. Such polymers require higher nitrogen/phosphate (N/P) ratios of at least 6 for DNA complexation at neutral pH than nonendosomolytic polymers such as poly-L-lysine. Polylysine complexes are usually most effective in the presence of chloroquine and at N/P ratios between 2 and 4 (*30*). For Si26H−DNA complexes, we calculated a conversion factor w/w ratio to N/P ratio of 0.16 based on the carbon analysis of Si26H and an average molecular weight of 330 g/mol nucleotide. This correlates well with the negative ζ potential at w/w = 10 (N/P = 1.6) when it is taken into account that the immobilized imino and amino groups are not fully protonated under these conditions. It would also suggest, that Si26H should, in regard to endosomolysis, rather behave like polylysine than polyethyleneimine. Increasing the buffering capacity of these cationically modified silica nanoparticles might therefore represent a rational approach to improve their potential as transfection agent.

There are a few unique features that make the surface-modified silica nanoparticles described here appear as a promising DNA carrier for transfection systems. Although there are concerns that SiO_2 can exert adverse effects by the induction of NFκB (*31*), colloidal silica is biologically inert and showed much lower cytotoxicity than polyethylenimine. Silica is widely used in cosmetics and pharmaceuticals, for instance as highly disperse SiO_2 (Aerosil) as an excipient for solid oral dosage forms. Furthermore, existing technology could be applied to link ligand molecules via remaining functional groups onto the surface of SiNP−DNA complexes to mediate specific interactions. At least at a sufficient ratio SiNP:DNA, the complex surface is dominated by particle half-spheres, as shown by atomic force microscopy. It does not seem unreasonable to assume, that these half-spheres are not directly involved in DNA binding and carry functional groups that will allow further chemical modification without disturbing the structure of the complex. The facts that lyophilizing and autoclaving SiNP should, in principle, be possible, are further aspects that might make them an attractive addition to the existing repertoire of DNA vectors.

ACKNOWLEDGMENT

This work is part of the interdisciplinary research program "Biologically composed materials and systems" sponsored by the Department of Education, Culture and Science of the Saarland. We thank the "Fonds der Chemischen Industrie" for financial support. U.B. wishes to thank "Stiftung Deutscher Naturforscher Leopoldina" (BMBF/LPD-9901/8-6). Mrs. N. Zghoul is thanked for critical proof-reading of the manuscript.

ABBREVIATIONS

Abbreviations used: CQ, chloroquine; fcs, fetal calf serum; pEI, polyethylenimine; pLL, poly-L-lysine; SiNP, silica nanoparticles; w/w, weight/weight ratio.

LITERATURE CITED

(1) Zelphati, O., Nguyen, C., Ferrari, M., Felgner, J., Tsai, Y., and Felgner, P. L. (1998) Stable and monodisperse lipoplex formulations for gene delivery. *Gene Ther. 5*, 1272−1282.

(2) Boussif, O., Lezoualc'h, F., Zanta, M. A., Mergny, M. D., Scherman, D., Demeneix, B., and Behr, J. P. (1995) A versatile vector for gene and oligonucleotide transfer into cells in culture and in vivo: Polyethylenimine. *Proc. Natl. Acad. Sci. U.S.A. 92*, 7297−7301.

(3) Haensler, J., and Szoka, F. C., Jr. (1993) Polyamidoamine Cascade Polymers Mediate Efficient transfection of Cells in Culture. *Bioconjugate Chem. 4*, 372−379.

(4) Gottschalk, S., Sparrow, J. T., Hauer, J., Mims, M. P., Leland, F. E., Woo, S. L. C., and Smith, L. C. (1996) A novel DNA-peptide complex for efficient gene transfer and expression in mammalian cells. *Gene Ther. 3*, 448−457.

(5) Blessing, T., Remy, J. S., and Behr, J. P. (1998) Monomolecular collapse of plasmid DNA into stable virus-like particles. *Proc. Natl. Acad. Sci. U.S.A. 95*, 1427−1431.

(6) Wagner, E., Zenke, M., Cotten, M., Beug, H., and Birnstiel, M. L. (1990) Transferrin-polycation conjugates as carriers for DNA uptake into cells. *Proc. Natl. Acad. Sci. U.S.A. 87*, 3410−14.

(7) Wagner, E., Plank, C., Zatloukal, K., Cotten, M., and Birnstiel, M. L. (1992) Influenza virus hemagglutinin HA-2

N-terminal fusiogenic peptides augment gene transfer by transferrin-polylysine-DNA complexes: toward a synthetic virus-like gene-transfer vehicle. *Proc. Natl. Acad. Sci. U.S.A. 89*, 7934−7938.

(8) Luthman, H., and Magusson G. (1983) High efficiency polyoma DNA transfection of chloroquine treated cells. *Nucleic Acids Res. 11*, 1295−1308.

(9) Wagner, E., Zatloukai, K., Cotten, M., Kirlappos, H., Mechtler, K., Curiel, D. T., and Birnstiel, M. L. (1992) Coupling of adenovirus to transferrin-polylysin/DNA complexes greatly enhances receptor-mediated gene delivery and expression of transfected genes. *Proc. Natl. Acad. Sci. U.S.A. 89*, 6099−6103.

(10) Zanta, M. A., Belguise-Valladier, P., and Behr, J. P. (1999) Gene delivery: a single nuclear localization signal peptide is sufficient to carry DNA to the cell nucleus. *Proc. Natl. Acad. Sci. U.S.A. 96*, 91−96.

(11) Pouton, C. W. (1998) Nuclear import of polypeptides, polynucleotides and supramolecular complexes. *Adv. Drug Delivery Rev. 34*, 51−64.

(12) Mizuguchi, H., Nakagawa, T., Morioka, Y., Imazu, S., Nakanishi, M., Kondo, T., Hayakawa, T., and Mayumi, T. (1997) Cytoplasmic gene expression system enhances the efficiency of cationic liposome-mediated in vivo gene transfer into mouse brain. *Biochem. Biophys. Res. Commun. 234*, 15−18.

(13) Pouton, C. W., and Seymour, L. W. (1998) Key issues in nonviral gene delivery. *Adv. Drug Delivery Rev. 34*, 3−20.

(14) Plank, C., Zauner, W., and Wagner, E. (1998) Application of membrane-active peptides for drug and gene delivery across cellular membranes. *Adv. Drug Delivery Rev. 34*, 21−36.

(15) Mönkkönen, J., and Urtti, A. (1998) Lipid fusion in oligonucleotide and gene delivery with cationic lipids. *Adv. Drug Delivery Rev. 34*, 37−50.

(16) Cotten, M. (1994) Adenovirus-Augmented, Receptor-Mediated Gene Delivery and some Solutions to the Common Toxicity Problems. In *The Molecular Repertoire of Adenoviruses III - Biology and Pathogenesis. Current Topics in Microbiology and Immunology 199* (W. Doerfler and P. Möhm, Eds.) pp 283−295, Springer-Verlag, Berlin.

(17) Kneuer, C., Sameti, M., Haltner, E. G., Schiestel, T., Schirra, H., Schmidt, H., and Lehr, C. M. (2000) Silica nanoparticles modified with aminosilanes as carriers for plasmid DNA. *Int. J. Pharm.* (In press).

(18) Cherng, J. Y., van de Wetering, P., Talsma, H., Crommelin, D. J. A., and Hennink, W. E. (1996) Effect of Size and serum Proteins on Transfection Efficiency of Poly((2-dimethylamino)ethyl Methacrylate)-Plasmid Nanoparticles. *Pharm. Res. 13*, 1038−1042.

(19) Godbey, W. T., Wu, K. K., Hirasaki, G. J., and Mikos, A. G. (1999) Improved packing of poly(ethylenimine)/DNA complexes increases transfection efficiency. *Gene Ther. 6*, 1380−1388.

(20) Wu, Y. L., Jiang, C., and Ku, K. Y. (1993) The effects of polylysine on the aggregation of surface and on the cleavage furrow of Rana amurensis eggs. *Shih Yen Sheng Wu Hsueh Pao 16*, 51−64.

(21) Yaroslavov, A. A., Kulkov, V. E., Polinsky, A. S., Baibakov, B. A., and Kabanov, V. A. (1994) A polycation causes migration of negatively charged phospholipids from the inner to outer leaflet of the liposomal membrane. *FEBS Lett. 340*, 121−123.

(22) Takahashi, H., Matuoka, S., Kato, S., Ohki, K., and Hatta, I. (1992) Effects of poly(L-lysine) on the structural and thermotropic properties of dipalmitoylphosphatidylglycerol bilayers. *Biochim. Biophys. Acta 1110*, 29−36.

(23) Boussif, O., Delair, T., Brua, C., Veron, L., Pavirani, A. and Kolbe, H. V. (1999) Synthesis of polyallylamine derivatives and their use as gene transfer vectors in vitro. *Bioconjugate Chem. 10*, 877−883.

(24) Araki, T., Yamamoto, A., and Yamada, M. (1987) Accurate determination of DNA content in single cell nuclei stained with Hoechst 33258 fluorochrome at high salt concentration. *Histochemistry 87* (4), 331−338.

(25) Maruyama, A., Ishihara, T., Kim, J. S., Kim, S. W., and Akaike, T. (1997) Nanoparticle DNA Carrier with Poly(L-lysine) Grafted Polysaccharide Coplolymer and Poly(D,L-lactic acid). *Bioconjugate Chem. 8*, 735−742.

(26) Dash, P. R., Read, M. L., Barrett, L. B., Wolfert, M. A., and Seymour, L. W. (1999) Factors affecting blood clearance and in vivo distribution of polyelectrolyte complexes for gene delivery. *Gene Ther. 6*, 643−650.

(27) Coonrod, A., Li, F. Q., and Horwitz, M. (1997) On the mechanism of DNA transfection: efficient gene transfer without viruses. *Gene Ther. 4*, 1313−1321.

(28) Wolfert, M. A., and Seymour, L. W. (1998) Chloroquine and amphipathic peptide helices show synergistic transfection in vitro. *Gene Ther. 5*, 409−414.

(29) Erbacher, P., Roche, A. C., Monsigny, M., and Midoux, P. (1996) Putative Role of Chloroquine in Gene Transfer into a Human Hepatoma Cell Line by DNA/Lactosylated Polylysine Complexes. *Exp. Cell. Res. 225*, 186−194.

(30) Tang, M. X., and Szoka, F. C. (1999) The influence of polymer structure on the interactions of cationic polymers with DNA and morphology of the resulting complexes. *Gene Ther. 4*, 823−832.

(31) Chen, F., Lu, Y., Kuhn, D. C., Maki, M., Shi, X., Sun, S. C., and Demers, L. M. (1997) Calpain Contributes to Silica-Induced IκB-α Degradation and Nuclear factor-κB Activation. *Arch. Biochem. Biophys. 342* (2), 383−388.

BC0000637

Nucleosides and Nucleotides. 204. Synthesis of Oligodeoxynucleotides Containing 6′α-[*N*-(Aminoalkyl)carbamoyloxy]-carbocyclic-thymidines and the Thermal Stability of the Duplexes and Their Nuclease-Resistance Properties†

Yoshihito Ueno, Naoko Karino, and Akira Matsuda*

Graduate School of Pharmaceutical Sciences, Hokkaido University, Kita-12, Nishi-6, Kita-ku, Sapporo 060-0812, Japan. Received June 13, 2000; Revised Manuscript Received August 28, 2000

To construct the nuclease-resistant oligodeoxynucleotides (ODNs) with natural phosphodiester linkages, we synthesized ODNs that contain 6′α-[*N*-(aminoalkyl)carbamoyloxy]-carbocyclic-thymidines (**4**, **5**, and **6**). The stability of these ODNs to nuclease hydrolysis was examined by using snake venom phosphodiesterase (3′-exonuclease) and nuclease S1 (endonuclease). It was found that the ODNs containing **4**, **5**, or **6** were more resistant to both the enzymes than the unmodified ODN. These nuclease-resistant properties are noteworthy, since they have natural phosphodiester linkages. Next, the thermal stabilities of duplexes consisting of these ODNs and either the complementary DNA or RNA were studied by thermal denaturation. The ODNs that contain **4** were found to enhance the thermal stability of the duplexes with the complementary DNA, while those containing **5** or **6** decreased the thermal stability of the ODN−DNA duplexes. On the other hand, all ODNs that contained **4**, **5**, or **6** decreased the thermal stability of the ODN−RNA duplexes.

INTRODUCTION

Oligodeoxynucleotides (ODNs)[1] that are capable of inhibiting cellular processes at the translational level by base pairing with mRNA are known as antisense ODNs (*1*−*4*). Since unmodified ODNs with natural phosphodiester linkages are rapidly hydrolyzed by nucleases found in cell culture media and inside cells, many types of backbone-modified ODNs have been synthesized and used for antisense studies (*5*). Phosphorothioate ODNs, in which one nonbridging phosphate oxygen is replaced by sulfur, are some of the most widely used backbone-modified antisense ODNs. Phosphorothioate ODNs are markedly more resistant to hydrolysis by nucleases than unmodified ODNs and activate RNase H that selectively cleaves the RNA-strand of a DNA−RNA duplex (*2*). However, it is known that their binding affinity for RNA is lower than that of an unmodified ODN (*6*). Furthermore, phosphorothioate ODNs sometimes exhibit non-sequence-specific activity (*7*−*9*).

On the basis of this background information, we have developed new antisense ODNs which have natural phosphodiester linkages and which are also resistant to nucleases. We hypothesized that the natural phosphodiester ODNs carrying basic amino alkyl chains near their phosphodiester moieties might be resistant to nucleases. Since nucleases hydrolyze phosphodiester linkages by a general acid−base catalysis mechanism, including acidic and/or basic amino acid residues at their active sites, the presence of a basic amino group near the phosphodiester moiety of ODNs may prevent nucleolytic hydrolysis by forming an ionic bond with the acidic phosphodiester moiety of ODNs. It is also possible that the amino group attached to ODNs interrupts the catalytic system of nucleases by bonding with an acidic amino residue or by repulsing a basic amino acid residue at the enzyme active sites.

Indeed, we found that ODNs containing a 2′-deoxyuridine analogue **1** which carries an aminoalkyl-linker at the 1′-position (Figure 1) were more resistant to nucleolytic hydrolysis by both snake venom phosphodiesterase (a 3′-exonuclease) and nuclease P1 (an endonuclease) than unmodified ODNs (*10*). We also synthesized ODNs containing a 2′-deoxyuridine analogue **2** which carries an aminohexyl-linker at the 5-position of uracil (*11*−*13*). These ODNs were more resistant to nucleolytic hydrolysis by both snake venom phosphodiesterase and nuclease S1 (an endonuclease) than unmodified ODNs, and were very stable in a medium containing 10% fetal calf serum (*12*, *13*). Furthermore, we found that the ODNs containing a thymidine analogue **3** which carries an aminoethyl-linker at the 4′-position were significantly resistant to nucleolytic hydrolysis by both snake venom phosphodiesterase and DNase I (an endonuclease) and were very stable in PBS containing 50% human serum (*14*). These results indicate that ODNs that have been suitably modified by aminoalkyl-linkers are resistant not only to exonucleases but also to endonucleases, even when they have natural phosphodiester linkages.

† For Part 203 in this series, see M. Sukeda, S. Shuto, I. Sugimoto, S. Ichikawa, and A. Matsuda, submitted for publication.

* To whom correspondence should be addressed. Phone: +81-11-706-3228. Fax: +81-11-706-4980. E-mail: matuda@pharm.hokudai.ac.jp.

[1] Abbreviations: ODN, oligodeoxynucleotide; CPG, controlled pore glass; HPLC, high-performance liquid chromatography; T_m, melting temperature; Bn, benzyl; DMAP, 4-(dimethylamino)-pyridine; DMTr, 4,4′-dimethoxytrityl; TBAF, tetrabutylammonium fluoride; TEAA, triethylammonium acetate; TIPS, triisopropylsilyl.

10.1021/bc0000684 CCC: $19.00 © 2000 American Chemical Society
Published on Web 10/28/2000

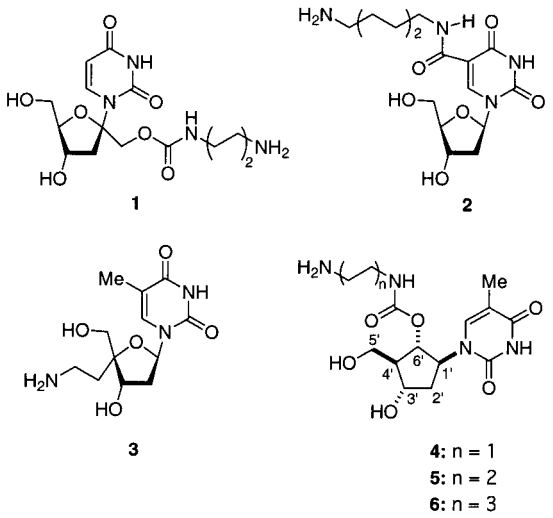

Figure 1. Structures of the modified nucleoside analogues and an atom-numbering system for 6′α-substituted-carbocyclic-thymidines.

On the other hand, it has been reported that ODNs containing a carbocyclic-thymidine, where the furanose ring oxygen is replaced by a CH_2 group, increase thermal stabilities of ODN−RNA duplexes, but nuclease stability against snake venom phosphodiesterase is inadequate for biological applications (*15*, *16*). More recently, Altmann et al. reported that ODNs containing 6′α-aminobutoxy-carbocyclic-thymidine are stable enough in 10% heat-inactivated fetal calf serum although stability against endonuclease was not examined; however, they decrease thermal stabilities of ODN−RNA duplexes (*17*).

It is well-known that naturally occurring polyamines, such as spermidine and spermine, bind strongly to DNAs (*18*−*20*) and stabilize duplex (*21*, *22*) and triplex formation (*23*−*25*). The enhanced thermal stability of duplexes and triplexes is explained by the reduction of the anionic electrostatic repulsion between the phosphate moieties and the cationic amino groups. From these findings, we envisioned introducing an aminoalkyl-linker with a suitable length at the 6′α-position of a carbocyclic-nucleoside. If successful, we would then be able to synthesize the ODNs that enhance the thermal stability of ODN−RNA duplexes and that are also resistant to both exo- and endonucleases by the effect of the aminoalkyl-linker.

In this paper, we report the synthesis of ODNs that contain 6′α-[*N*-(aminoalkyl)carbamoyloxy]-carbocyclic-thymidines (**4**, **5**, and **6**). Stability of these ODNs to nucleolytic hydrolysis by snake venom phosphodiesterase and nuclease S1, and the thermal stability of duplexes of these ODNs with either the complementary DNA or RNA, were studied.

RESULTS AND DISCUSSION

Synthesis. The synthesis of ODNs containing **4**, **5**, or **6** was accomplished in a DNA synthesizer by using a suitably protected 6′α-[*N*-(2-aminoethyl)carbamoyloxy]-carbocyclic-thymidine (**14a**), 6′α-[*N*-(4-aminobutyl)carbamoyloxy]-carbocyclic-thymidine (**14b**), or 6′α-[*N*-(6-aminohexyl)carbamoyloxy]-carbocyclic-thymidine phosphoramidite (**14c**). The synthesis of the 3′-phosphoramidite derivatives **14a**, **14b**, and **14c** is shown in Scheme 1. The hydroxyl group of the epoxide **7**, which was prepared according to the literature procedure (*26*), was silylated using TIPSCl to give the triisopropylsilanyloxy derivative **8** in 90% yield. Treatment of **8** with thymine and NaH in DMF at 145 °C afforded the desired epoxide-opened product **9** in 45% yield with a recovery of **8** in 27% yield. Hydrogenolysis of the benzyl group of **9** gave the diol derivative **10** in 82% yield. Then, the primary hydroxyl group of **10** was protected with a DMTr group to yield **11** in 90% yield. Compound **11** was converted into the carbonylimidazolide, which was reacted with 1,2-diaminoethane, 1,4-diaminobutane, or 1,6-diaminohexane. Without purifying the products, the amino groups were protected with a trifluoroacetyl group to give **12a**, **12b**, and **12c** in 84, 93, and 73% yields, respectively. After desilylation of **12a**, **12b**, and **12c** by TBAF, **13a**, **13b**, and **13c** were then phosphitylated by a standard procedure (*27*) to give the corresponding nucleoside 3′-phosphoramidites **14a**, **14b**, and **14c**.

An unmodified DNA octadecamer (control) and octadecamers containing **4**, **5**, or **6** were synthesized in a DNA synthesizer. The average coupling yields of **14a**, **14b**, and **14c** were 98, 96, and 98%, respectively, using a 0.12 M

Scheme 1[a]

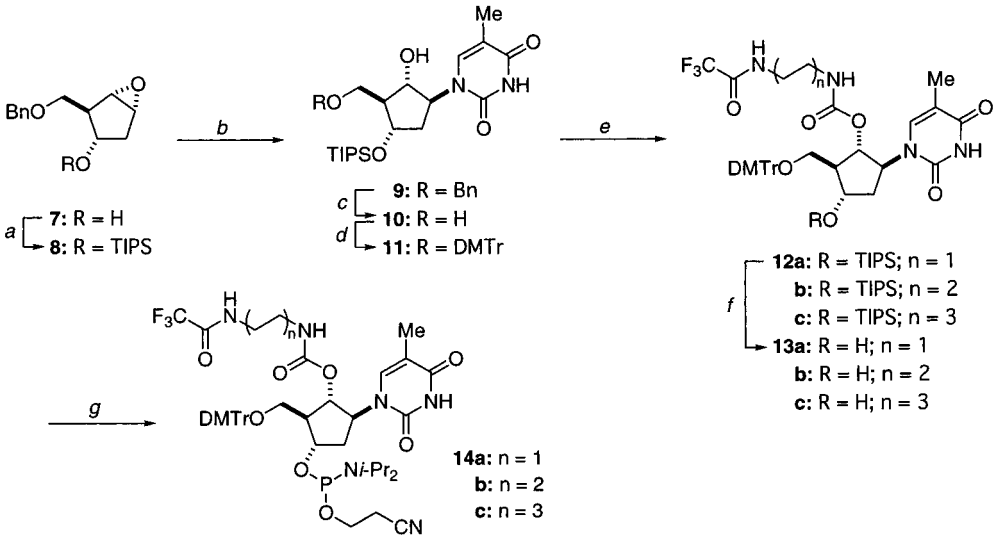

[a] (a) TIPSCl, imidazole, DMF, room temperature; (b) thymine, NaH, DMF, 145 °C; (c) H_2, 10% Pd−C, EtOH, room temperature; (d) DMTrCl, pyridine, room temperature; (e) (1) *N*,*N*′-carbonyldiimidazole, DMAP, pyridine, room temperature; (2) $H_2N(CH_2)_nNH_2$ (n = 2, 4, or 6), pyridine, room temperature; (3) $EtOCOCF_3$, Et_3N, pyridine, room temperature; (f) TBAF, THF, room temperature; (g) 2-cyanoethyl *N*,*N*-diisopropylchlorophosphoramidite, *N*,*N*-diisopropylethylamine, CH_2Cl_2, room temperature.

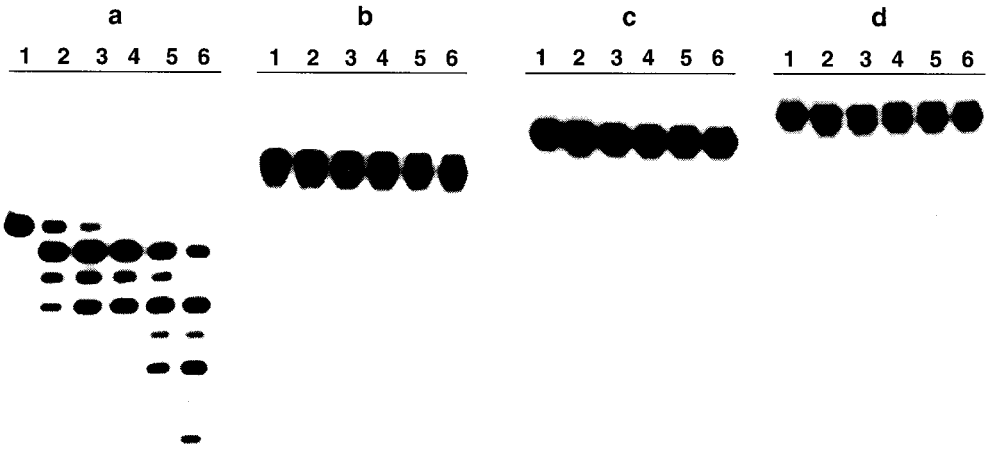

Figure 2. Polyacrylamide gel electrophoresis of 5′-^{32}P-labeled ODNs hydrolyzed by snake venom phosphodiesterase (a) **15**; (b) **21-E**; (c) **21-B**; (d) **21-H**. ODNs were incubated with snake venom phosphodiesterase for 0 min (lane 1), 10 min (lane 2), 20 min (lane 3), 30 min (lane 4), 60 min (lane 5), and 120 min (lane 6). Experimental conditions are described in the Experimental Section.

Table 1. Sequences of ODNs[a]

ODNs	
15	5′-d$(MT)_9$-3′(control)
16-E, **B**, or **H**	5′-d[(M**T**$(MT)_8$]-3′
17-E, **B**, or **H**	5′-d$[(MT)_7$M**T**MT]-3′
18-E, **B**, or **H**	5′-d$[(MT)_4$M**T**$(MT)_4$]-3′
19-E, **B**, or **H**	5′-d$[(MT)_2$M**T**$(MT)_3$M**T**$(MT)_2$]-3′
20-E, **B**, or **H**	5′-d[M**T**$(MT)_3$M**T**$(MT)_2$M**T**MT]-3′
21-E, **B**, or **H**	5′-d[M**T**MTM**T**$(MT)_2$M**T**MTM**T**MT]-3′
22	5′-d[TGGAGAGAGAGAGAGAGAGAGGGT]-3′
23	5′-r[AGAGAGAGAGAGAGAGAGA]-3′

[a] **E** = (**T** = **4**); **B** = (**T** = **5**); **H** = (**T** = **6**); M = 5-methyl-2′-deoxycytidine.

solution of the amidite derivatives in CH_3CN and 600 s for the coupling time. The fully protected ODNs (each 1 μmol scale) linked to the solid supports were treated with concentrated NH_4OH at 55 °C for 12 h. This was followed by C-18 column chromatography. Detritylation gave ODNs **15**−**21** (Table 1). Each ODN in this preparation showed a single peak by reversed-phase HPLC analysis. ODNs **18-E**, **18-B**, **18-H**, **21-E**, **21-B**, and **21-H** were analyzed by matrix-assisted laser desorption/ionization time-of-flight mass spectrometry (MALDI-TOF/MS), and the observed molecular weights supported their structures.

Partial Digestion of ODNs with Snake Venom Phosphodiesterase and Nuclease S1. Since resistance to nucleolytic hydrolysis by nucleases is an important factor in antisense studies, the stability of ODNs containing **4**, **5**, or **6** to nucleolytic digestion was examined. Two kinds of nucleases, snake venom phosphodiesterase (a 3′-exonuclease) and nuclease S1 (an endonuclease), were used in this study. ODNs **21-E**, **21-B**, and **21-H** containing four molecules of **4**, **5**, or **6** were labeled at their 5′-end with ^{32}P and incubated with an appropriate nuclease, and the reactions were then analyzed by polyacrylamide gel electrophoresis under denaturing conditions (*28*).

When snake venom phosphodiesterase was used in the reactions, the control ODN **15** was hydrolyzed randomly by the enzyme after 120 min of the incubation (Figure 2a). In contrast, the phosphodiester linkages at the 5′-sides of **4**, **5**, and **6** were highly resistant to the enzyme (Figure 2, panels b, c, and d). Altmann et al. also reported that ODNs containing 6′α-aminobutoxy-carbocyclic-thymidine are stable in 10% heat-inactivated fetal calf (*17*). Several studies have demonstrated that 3′-exonuclease activities are the major cause of the degradation of unmodified ODNs in serum (*1*). Thus, our data is consistent with the result reported by Altmann et al.

Next, the ODNs were treated with nuclease S1. The phosphodiester linkages around **4**, **5**, and **6** were more resistant to enzymatic hydrolysis than those beside thymidine (Figure 3). The half-lives of ODN **15**, **21-E**, **21-B**, and **21-H** were 13, 37, 32, and 30 min, respectively. In our previous paper, we reported that the heptadecanucleotide containing four molecules of **2** was four times more stable to hydrolysis by nuclease S1 than an unmodified ODN. Also, the ODN containing **3** was about 90 times more stable to hydrolysis by DNase I. Therefore, it was found that the ODNs containing **4**, **5**, or **6** are as resistant to nuclease S1 (an endonuclease) as the ODN containing **2**.

UV Melting Studies of Duplexes. The stability of the duplexes composed of the octadecamers **15**−**21** and a complementary DNA, 5′-d[TGG AGA GAG AGA GAG AGA GAG GT]-3′ (**22**), was next studied by thermal denaturation in a buffer of 0.01 M sodium cacodylate (pH 7.0) containing 0.01 M NaCl. One transition was observed in the melting profile of each duplex. Melting temperatures (T_ms) and the ΔT_m^1 values [T_m(each ODN) − T_m(the control ODN **15**)] are listed in Table 2. The T_m values for the duplexes containing the nucleoside analogue **4** were greater than those of the control duplex (T_m = 51.6 °C), except for the duplex comprised of ODN **16-E** ($\Delta T_m^1 = -0.3$), but all of the T_m values for the duplexes containing analogue **5** or **6** were smaller than those of the control duplex. The stability of the duplexes was dependent on the number of the nucleoside analogues. The duplexes became more stable as the number of **4** increased, while the duplexes became less stable as the number of **5** or **6** increased. The duplexes consisting of ODNs **18-E** containing one molecule of **4** at the center ($\Delta T_m^1 = +2.0$) were more stable than those composed of ODNs **16-E** or **17-E** containing **4** near either the 5′- or 3′-end (ΔT_m^1s = −0.3 and +1.2, respectively). A 4.5 °C increase in T_m was observed for ODNs **21-E** containing four molecules of **4**.

The enhanced thermal stability of the duplexes containing **4** was thought to be due to a reduction of the electrostatic repulsion between phosphate moieties by the ammonium ion at the end of the *N*-(2-aminoethyl)-carbamoyloxy linker. To confirm the effects of the *N*-(aminoalkyl)carbamoyloxy linkers on the thermal stabilities of the duplexes, thermal denaturation was also performed under higher ionic strength (0.1 M NaCl). The

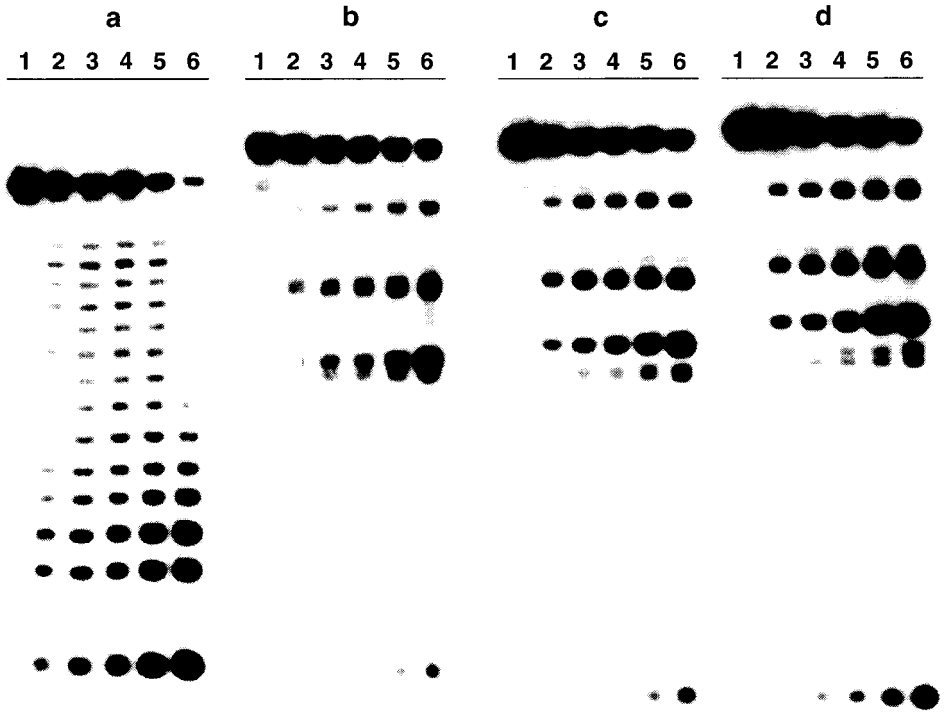

Figure 3. Polyacrylamide gel electrophoresis of 5′-^{32}P-labeled ODNs hydrolyzed by nuclease S1: (a) **15**; (b) **21-E**; (c) **21-B**; (d) **21-H**. ODNs were incubated with nuclease S1 for 0 min (lane 1), 10 min (lane 2), 20 min (lane 3), 30 min (lane 4), 60 min (lane 5), and 120 min (lane 6). Experimental conditions are described in the Experimental Section.

Table 2. Hybridization Data[a]

	ODN/DN[b]				ODN/RN[c]	
ODN	0.01 M NaCl T_m (°C)	ΔT_m^1 [d] (°C)	0.1 M NaCl T_m (°C)	ΔT_m^2 [e] (°C)	0.1 M NaCl T_m (°C)	ΔT_m^1 [d] (°C)
15	51.6		66.1	+14.5	64.0	
16-E	51.3	−0.3	64.7	+13.4		
17-E	52.8	+1.2	65.5	+12.7		
18-E	53.6	+2.0	65.9	+12.3	61.2	−2.8
19-E	54.5	+2.9	66.6	+12.1	59.1	−4.9
20-E	54.2	+2.6	67.0	+12.8	58.7	−5.3
21-E	56.1	+4.5	67.4	+11.3	56.6	−7.4
16-B	51.3	−0.3	64.9	+13.6		
17-B	49.8	−1.8	63.3	+13.5		
18-B	50.3	−1.3	63.9	+13.6	60.3	−3.7
19-B	48.8	−2.8	62.1	+13.3	58.4	−5.6
20-B	48.3	−3.3	61.4	+13.1	57.9	−6.1
21-B	47.8	−3.8	60.2	+12.4	55.3	−8.7
16-H	51.4	−0.2	65.9	+14.5		
17-H	50.7	−0.9	64.6	+13.9		
18-H	50.7	−0.9	64.0	+13.3	61.2	−2.8
19-H	49.4	−2.2	61.8	+12.4	58.0	−6.0
20-H	48.6	−3.0	61.5	+12.9	57.9	−6.1
21-H	48.1	−3.5	60.5	+12.4	55.5	−8.5

[a] Experimental conditions are described in the Experimental Section. [b] The complementary DNA, **22**. [c] The complementary RNA, **23**. [d] ΔT_m^1 = [T_m(each ODN) − T_m(the control ODN **15**)]. [e] ΔT_m^2 = [T_m(0.1 M NaCl) − T_m(0.01 M NaCl)].

ΔT_m^2 values obtained [T_m(0.1 M NaCl) − T_m(0.01 M NaCl)] were compared, as shown in Table 2. The ΔT_m^2 values for the duplexes containing **4** were smaller than those for the control duplex (ΔT_m^2 = +14.5). Furthermore, the ΔT_m^2 values for the duplexes containing **4** seemed to decrease as the number of **4** increased. These results suggest that the terminal ammonium ions in **4** effectively neutralize the phosphate negative charges. On the other hand, the ΔT_m^2 values for the duplexes containing **5** and **6** were also smaller than those for the control duplex, although the values were greater than those for the duplexes containing **4**. This result implies that the terminal ammonium ions in **5** and **6** also contribute to neutralize the phosphate negative charges.

When the ODN analogues containing **4**, **5**, or **6** form duplexes with the complementary DNAs, the *N*-(2-aminoethyl)carbamoyloxy, the *N*-(2-aminobutyl)carbamoyloxy, and the *N*-(2-aminohexyl)carbamoyloxy groups of **4**, **5**, or **6** should be accommodated in the minor grooves, since an O4′ position of a nucleoside is in the minor groove. The minor groove of a DNA−DNA duplex is known to be narrow and deep (*29*). Thus, the *N*-(2-aminobutyl)carbamoyloxy and the *N*-(2-aminohexyl)carbamoyloxy groups of **5** and **6** may not be well accommodated in the minor groove of ODN−DNA duplex. This steric hindrance may offset the favorable electrostatic interactions of the aminoalkyl linkers of **5** and **6**. On the other hand, in the central portion of the minor groove in

the native B-DNA dodecamer duplex, a spine of hydration was found to link with the nitrogen and oxygen atoms of some base moieties (*30*−*32*). Thus, another interpretation is that the bulky *N*-(aminoalkyl)carbamoyloxy groups of **5** and **6** may disorder the spine of hydration in the minor groove, while the small *N*-(aminoethyl)carbamoyloxy group of **4** may be well accommodated in the minor groove without disordering the spine of hydration.

Duplex formation of the octadecamers with the complementary RNA, 5′−r[AGA GAG AGA GAG AGA GAG A]-3′ (**23**) was next studied by thermal denaturation in a buffer containing 0.1 M NaCl. As shown in Table 2, all of the T_m values for the duplexes that contain the nucleoside analogues **4**, **5**, or **6** were smaller than those of the control duplex (T_m = 64.0 °C). The stability of the duplexes was dependent on the number of nucleoside analogues. The duplexes became less stable as the numbers of **4**, **5**, and **6** increased.

The 6′α-substituents of the carbocyclic-thymidines could be readily accommodated within a standard A-type DNA−RNA because the minor groove of A-type duplexes is shallow and flat (*29*). Thus, the results seem to be at least not based on simple steric reasons for the aminoalkyl-linkers. It has been reported that ODNs containing stretches of contiguous 6′α-methyl-carbocyclic-thymidine slightly decrease the thermal stability of the duplexes with complementary RNAs, while those containing stretches of contiguous 6′α-hydroxy-carbocyclic-thymidine increase the thermal stability of ODN−RNA duplexes (*32*, *33*). Thus, the duplex destabilization by the aminoalkyl-linkers might also be related to the release of water molecules from the minor grooves.

CONCLUSION

In this paper, we have reported the synthesis of ODNs containing 6′α-[*N*-(aminoalkyl)carbamoyloxy]-carbocyclic-thymidines (**4**, **5**, and **6**). Resistance of these ODNs to nuclease hydrolysis was examined by using snake venom phosphodiesterase (3′-exonuclease) and nuclease S1 (endonuclease). The ODNs that contain **4**, **5**, or **6** were more resistant to nucleolytic hydrolysis by both the enzymes than the unmodified ODNs. These nuclease-resistant properties are noteworthy, since they have natural phosphodiester linkages. The thermal stability of duplexes consisting of these ODNs and either the complementary DNA or RNA were studied by thermal denaturation. The ODNs that contain **4** were found to enhance the thermal stability of the duplexes with the complementary DNA, while those containing **5** or **6** decreased the thermal stability of the ODN−DNA duplexes. On the other hand, contrary to our expectation, it was found that all ODNs that contain **4**, **5**, or **6** decrease the thermal stability of the ODN−RNA duplexes. However, we believe that these results will serve as fundamental data for developing new antisense molecules.

EXPERIMENTAL PROCEDURES

General Remarks. NMR spectra were recorded at 270 MHz (^{1}H) and at 202 MHz (^{31}P) and are reported in parts per million downfield from TMS or 85% H_3PO_4. *J* values are given in hertz. Mass spectra were obtained by fast-atom bombardment (FAB) method. Thin-layer chromatography was done on Merck coated plates $60F_{254}$. The silica gel or the neutralized silica gel used for column chromatography was Merck silica gel 5715 or ICN silica 60A, respectively.

(1*S*,2*S*,3*S*,5*R*)-2-(Benzyloxymethyl)-3-(triisopropylsilanyloxy)-6-oxabicyclo[3,1,0]hexane (8). A mixture of (1*S*,2*S*,3*S*,5*R*)-2-(benzyloxymethyl)-6-oxabicyclo-[3,1,0]hexan-3-ol (*26*) (1.28 g, 5.80 mmol), TIPSCl (3.72 mL, 17.4 mmol), and imidazole (2.37 g, 34.8 mmol) in DMF (60 mL) was stirred at room temperature. After 16 and 25 h, further amounts of TIPSCl (1.24 mL, 5.80 mmol) and imidazole (0.79 g, 11.6 mmol) were added to the mixture. After 63 h, EtOH (2 mL) was added to the mixture, and the whole was stirred for 10 min. The mixture was concentrated in vacuo and was taken in EtOAc, which was washed with aqueous $NaHCO_3$ (saturated) and brine, dried (Na_2SO_4), and concentrated. The residue was purified by column chromatography (SiO_2, 50% EtOAc in hexane) to give **8** (1.87 g, 85% as an oil): FAB-MS *m*/*z* 377 (MH^+); ^{1}H NMR (270 MHz, $CDCl_3$) δ 7.35−7.28 (m, 5H), 4.50 (dd, *J* = 16.7, 12.1, 2H), 4.26 (d, *J* = 7.4, 1H), 3.52−3.40 (m, 4H), 2.39 (t, *J* = 5.5, 1H), 2.12 (ddd, *J* = 14.8, 7.4, 1.7, 1H), 1.96 (dd, *J* = 14.8, 1.6, 1H), 1.05 (s, 3H), 1.02 (s, 18H). HRMS (FAB) calcd for $C_{22}H_{37}O_3Si$: 377.2510. Found: 377.2495.

(1*S*,2*S*,3*S*,4*S*)-1-[3-(Benzyloxymethyl)-2-(hydroxy)-4-(triisopropylsilanyloxy)cyclopentyl]thymine (9). Thymine (4.04 g, 32.0 mmol) was added to a suspension of sodium hydride (60% oil dispersion, 213 mg, 5.33 mmol) in DMF (40 mL), and the mixture was stirred at room temperature. After 2 h, a solution of **8** (4.31 g, 10.7 mmol) in DMF (4 mL) was added to the mixture, and the whole was heated at 145 °C for 51 h. After the mixture was cooled, the mixture was partitioned between EtOAc and H_2O. The organic layer was washed with brine, dried (Na_2SO_4), and evaporated under reduced pressure. The residue was purified by column chromatography (SiO_2, 60% EtOAc in hexane) to give **9** (2.42 g, 45% as a pale yellow foam) with a recovery of **8** (1.09 g, 27%): FAB-MS *m*/*z* 503 (MH^+); ^{1}H NMR (270 MHz, $CDCl_3$) δ 8.42 (br s, 1H), 7.35−7.29 (m, 5H), 7.00 (s, 1H), 4.64 (dd, *J* = 17.7, 9.2, 1H), 4.53 (m, 2H), 4.31−4.19 (m, 2H), 3.79 (dd, *J* = 9.0, 4.3, 1H), 3.62 (dd, *J* = 9.0, 6.9, 1H), 2.95 (d, *J* = 2.5, 1H), 2.30−2.00 (m, 3H), 1.87 (s, 3H), 1.03 (s, 21H). Anal. calcd for $C_{27}H_{42}N_2O_5Si$: C, 64.51; H, 8.42; N, 5.57. Found: C, 64.37; H, 8.35; N, 5.45.

(1*S*,2*S*,3*S*,4*S*)-1-[2-(Hydroxy)-3-(hydroxymethyl)-4-(triisopropylsilanyloxy)cyclopentyl]thymine (10). A mixture of **9** (1.53 g, 3.04 mmol) and Pd-C (10%, 2.02 g) in EtOH (180 mL) was stirred under atmospheric pressure of H_2 at room temperature. After 10 h, the catalyst was filtered off with a Celite pad, and the filtrate was evaporated under reduced pressure. The residue was purified by column chromatography (SiO, 5% EtOH in EtOAc) to give **10** (1.03 g, 82% as a white powder): FAB-MS *m*/*z* 413 (MH^+); ^{1}H NMR (270 MHz, $CDCl_3$) δ 10.63 (br s, 1H), 7.05 (s, 1H), 4.68 (m, 1H), 4.56 (m, 1H), 4.41 (m, 1H), 4.13 (m, 1H), 3.98 (d, *J* = 11.2, 1H), 3.80 (m, 1H), 3.54 (br s, 1H), 2.60 (m, 1H), 1.98−1.94 (m, 2H), 1.82 (s, 3H), 1.06 (m, 21H). Anal. calcd for $C_{20}H_{36}N_2O_5Si$: C, 58.22; H, 8.79; N, 6.79. Found: C, 58.21; H, 8.67; N, 6.72.

(1*S*,2*S*,3*S*,4*S*)-1-[3-(4,4′-Dimethoxytrityloxymethyl)-2-(hydroxy)-4-(triisopropylsilanyloxy)cyclopentyl]-thymine (11). A mixture of **10** (400 mg, 0.969 mmol) and DMTrCl (394 mg, 1.16 mmol) in pyridine (10 mL) was stirred at room temperature. After 18 h, DMTrCl (98 mg, 0.291 mmol) was added further, and the mixture was stirred at room temperature for 1 h. EtOH (2 mL) was added to the mixture, and the whole was stirred for 10 min. The mixture was concentrated in vacuo and was taken in EtOAc, which was washed with aqueous $NaHCO_3$ (saturated) and brine, dried (Na_2SO_4), and concentrated. The residue was purified by column chromatography (SiO_2, 50% EtOAc in hexane) to give **11** (622 mg, 90% as a white foam): FAB-MS *m*/*z* 714 (M^+); ^{1}H NMR

(270 MHz, $CDCl_3$) δ 8.01 (s, 1H), 7.39−7.24 (m, 9H), 6.99 (d, 1H), 6.84 (s, 2H), 6.81 (s, 2H), 4.56 (dd, J = 17.7, 9.0, 1H), 4.20 (td, J = 9.0, 2.7, 1H), 4.11 (dd, J = 11.1, 6.7, 1H), 3.79 (s, 6H), 3.60 (dd, J = 9.0, 4.3, 1H), 3.19 (m, 1H), 3.13 (d, J = 2.7, 1H), 2.30−2.04 (m, 3H), 1.91 (s, 3H), 0.95−0.94 (m, 21H). HRMS (FAB) calcd for $C_{41}H_{54}N_2O_7Si$: 714.3696. Found: 714.3677. Anal. calcd for $C_{41}H_{54}N_2O_7Si$: C, 68.88; H, 7.61; N, 3.92. Found: C, 68.79; H, 7.69; N, 3.87.

(1*S*,2*S*,3*S*,4*S*)-1-[3-(4,4′-Dimethoxytrityloxymethyl)-2-[*N*-[2-(trifluoroacetamido)ethyl]carbamoyloxy]-4-(triisopropylsilanyloxy)cyclopentyl]thymine (12a). *N*,*N*′-Carbonyldiimidazole (272 mg, 1.68 mmol) and DMAP (68 mg, 0.559 mmol) were added to a solution of **11** (600 mg, 0.839 mmol) in pyridine (15 mL), and the mixture was stirred at room temperature. After 3 h, 1,2-diaminoethane (280 μL, 4.20 mmol) was added to the mixture, which was stirred at room temperature. After 14 h, ethyl trifluoroacetate (3.01 mL, 25.2 mmol) and Et_3N (3.51 mL, 25.2 mmol) were added to the mixture, and the whole was stirred at room temperature. After 24 h, the mixture was concentrated in vacuo and was taken in EtOAc, which was washed with H_2O and brine, dried (Na_2SO_4), and concentrated. The residue was purified by column chromatography (SiO_2, 50% EtOAc in hexane) to give **12a** (629 mg, 84% as a white foam): FAB-MS *m*/*z* 896 (M^+); ^{1}H NMR (270 MHz, $CDCl_3$) δ 8.92 (br s, 1H), 7.90 (br s, 1H), 7.42−7.19, 6.84, 6.81 (m, 13H), 7.02 (s, 1H), 5.32 (m, 1H), 5.12 (m, 2H), 4.23 (br s, 1H), 3.79 (s, 3H), 3.78 (s, 3H), 3.51−3.20 (m, 6H), 2.21−2.01 (m, 3H), 1.82 (s, 3H), 0.98 (m, 21H). HRMS (FAB) calcd for $C_{46}H_{59}F_3N_4O_9Si$: 896.4003. Found: 896.3978. Anal. calcd for $C_{46}H_{59}F_3N_4O_9Si$: C, 61.59; H, 6.63; N, 6.25. Found: C, 61.34; H, 6.63; N, 6.15.

(1*S*,2*S*,3*S*,4*S*)-1-[3-(4,4′-Dimethoxytrityloxymethyl)-2-[*N*-[4-(trifluoroacetamido)butyl]carbamoyloxy]-4-(triisopropylsilanyloxy)cyclopentyl]thymine (12b). Compound **11** (425 mg, 0.594 mmol) was aminobutylcarbamoylated by using 1,4-diaminobutane (298 μL, 2.97 mmol) as described in the preparation of **12a** to give **12b** (512 mg, 93% as a white foam): FAB-MS *m*/*z* 924 (M^+); ^{1}H NMR (270 MHz, $CDCl_3$) δ 8.44 (br s, 1H), 7.42−7.21, 6.84, 6.80 (m, 13 H), 7.04 (s, 1H), 5.27−5.21 (m, 2H), 4.77 (m, 1H), 4.25 (m, 1H), 3.79 (s, 3H), 3.78 (s, 3H), 3.34 (m, 4H), 3.25 (m, 1H), 3.06 (m, 1H), 2.20 (m, 1H), 2.14−2.08 (m, 2H), 1.84 (s, 3H), 1.57 (m, 4H), 0.97 (m, 21H). HRMS (FAB) calcd for $C_{48}H_{63}F_3N_4O_9Si$: 924.4312. Found: 924.4331. Anal. calcd for $C_{48}H_{63}F_3N_4O_9Si$: C, 62.32; H, 6.86; N, 6.06. Found: C, 62.20; H, 6.98; N, 5.88.

(1*S*,2*S*,3*S*,4*S*)-1-[3-(4,4′-Dimethoxytrityloxymethyl)-2-[*N*-[6-(trifluoroacetamido)hexyl]carbamoyloxy]-4-(triisopropylsilanyloxy)cyclopentyl]thymine (12c). Compound **11** (600 mg, 0.839 mmol) was aminohexylcarbamoylated by using 1,6-diaminohexane (488 mg, 4.20 mmol) as described in the preparation of **12a** to give **12c** (584 mg, 73% as a white foam): FAB-MS *m*/*z* 952 (M^+); ^{1}H NMR (270 MHz, $CDCl_3$) δ 8.18 (m, 1H), 7.43−7.21, 6.84, 6.80 (m, 13H), 7.07 (s, 1H), 5.32 (m, 1H), 5.22 (m, 1H), 4.74 (m, 1H), 4.20 (m, 1H), 3.79 (s, 6H), 3.40−3.26 (m, 4H), 3.21 (m, 1H), 3.02 (m, 1H), 2.18 (m, 1H), 2.14−2.00 (m, 2H), 1.87 (s, 3H), 1.54−1.23 (m, 8H), 0.97−0.95 (m, 21H). HRMS (FAB) calcd for $C_{50}H_{67}F_3N_4O_9Si$: 952.4625. Found: 952.4617. Anal. calcd for $C_{50}H_{67}F_3N_4O_9Si$: C, 63.00; H, 7.08; N, 5.88. Found: C, 63.03; H, 7.05; N, 5.72.

(1*S*,2*S*,3*R*,4*S*)-1-[3-(4,4′-Dimethoxytrityloxymethyl)-4-(hydroxy)-2-[*N*-[2-(trifluoroacetamido)ethyl]carbamoyloxy]cyclopentyl]thymine (13). A mixture of **12a** (617 mg, 0.688 mmol) and TBAF (1 M in THF, 2.06 mL, 2.06 mmol) in THF (6 mL) was stirred at room temperature for 4 h. The mixture was partitioned between EtOAc and H_2O. The organic layer was washed with brine, dried (Na_2SO_4), and evaporated under reduced pressure. The residue was purified by column chromatography (SiO_2, 90% AcOEt in hexane) to give **13a** (476 mg, 93% as a white foam): FAB-MS *m*/*z* 741 (MH^+); ^{1}H NMR (270 MHz, $CDCl_3$) δ 9.28 (br s, 1H), 7.89 (br s, 1H), 7.40−7.20, 6.85, 6.82 (m, 13H), 6.97 (s, 1H), 5.34 (br s, 1H), 5.26 (dd, J = 17.5, 8.9, 1H), 4.90 (t, J = 7.6, 1H), 4.29 (br s, 1H), 3.79 (s, 6H), 3.52−3.16 (m, 6H), 2.84 (br s, 1H), 2.29 (m, 1H), 2.23−2.17 (m, 2H), 1.79 (s, 3H). HRMS (FAB) calcd for $C_{37}H_{40}F_3N_4O_9$: 741.2745. Found: 741.2752.

(1*S*,2*S*,3*R*,4*S*)-1-[3-(4,4′-Dimethoxytrityloxymethyl)-4-(hydroxy)-2-[*N*-[4-(trifluoroacetamido)butyl]carbamoyloxy]cyclopentyl]thymine (13b). Compound **12b** (512 mg, 0.553 mmol) was desilylated as described in the preparation of **13a** to give **13b** (411 mg, 97% as a white foam): FAB-MS *m*/*z* 769 (MH^+); ^{1}H NMR (270 MHz, $CDCl_3$) δ 8.80 (s, 1H), 7.41−7.20, 6.85, 6.82 (m, 13H), 6.97 (s, 1H), 5.18 (dd, J = 17.5, 9.1, 1H), 4.97 (m, 1H), 4.90 (m, 1H), 4.29 (m, 1H), 3.79 (s, 6H), 3.46 (dd, J = 9.4, 4.0, 1H), 3.32−3.20 (m, 4H), 3.02 (m, 1H), 2.63 (br s, 1H), 2.28 (m, 1H), 2.19 (m, 2H), 1.81 (s, 3H), 1.57−1.40 (m, 4H). HRMS (FAB) calcd for $C_{39}H_{44}F_3N_4O_9$: 769.3057. Found: 769.3078. Anal. calcd for $C_{39}H_{43}F_3N_4O_9$: C, 60.93; H, 5.64; N, 7.29. Found: C, 60.92; H, 5.53; N, 7.13.

(1*S*,2*S*,3*R*,4*S*)-1-[3-(4,4′-Dimethoxytrityloxymethyl)-4-(hydroxy)-2-[*N*-[6-(trifluoroacetamido)hexyl]carbamoyloxy]cyclopentyl]thymine (13c). Compound **12c** (590 mg, 0.619 mmol) was desilylated as described in the preparation of **13a** to give **13c** (468 mg, 95% as a white foam): FAB-MS *m*/*z* 797 (MH^+); ^{1}H NMR (270 MHz, $CDCl_3$) δ 8.70 (br s, 1H), 7.41−7.19, 6.85, 6.82 (m, 13H), 6.98 (s, 1H), 5.12−5.02 (m, 2H), 4.85 (t, J = 5.9, 1H), 4.26 (m, 1H), 3.79 (s, 6H), 3.45 (dd, J = 9.2, 4.0, 1H), 3.33−2.94 (m, 5H), 2.57 (br s, 1H), 2.24 (m, 1H), 2.16 (m, 2H), 1.84 (s, 3H), 1.51 (m, 2H), 1.41 (m, 2H), 1.27 (m, 4H). HRMS (FAB) calcd for $C_{41}H_{48}F_3N_4O_9$: 797.3370. Found: 797.3378. Anal. calcd for $C_{41}H_{47}F_3N_4O_9$: C, 61.80; H, 5.94; N, 7.03. Found: C, 61.93; H, 5.94; N, 6.94.

(1*S*,2*S*,3*S*,4*S*)-1-[4-(2-Cyanoethoxy-*N*,*N*-diisopropylaminophosphinyl)-3-(4,4′-dimethoxytrityloxymethyl)-2-[*N*-[2-(trifluoroacetamido)ethyl]carbamoyloxy]cyclopentyl]thymine (14a). Compound **13a** (291 mg, 0.393 mmol) was dissolved in CH_2Cl_2 (4 mL) containing *N*,*N*-diisopropylethylamine (137 μL, 0.786 mmol). Chloro(2-cyanoethoxy)(*N*,*N*-diisopropylamino)-phosphine (132 μL, 0.590 mmol) was added to the solution, and the reaction mixture was stirred at room temperature for 1 h. Aqueous $NaHCO_3$ (saturated) and $CHCl_3$ were added to the mixture, and the separated organic layer was washed with aqueous $NaHCO_3$ (saturated) and brine, dried (Na_2SO_4), and concentrated. The residue was purified by column chromatography (a neutralized SiO_2, 60% AcOEt in hexane) to give **14a** (300 mg, 81% as a white foam): FAB-MS *m*/*z* 941 (MH^+); ^{31}P NMR δ 148.47, 148.06. HRMS (FAB) calcd for $C_{46}H_{57}F_3N_6O_{10}P$: 941.3822. Found: 941.3819.

(1*S*,2*S*,3*S*,4*S*)-1-[4-(2-Cyanoethoxy-*N*,*N*-diisopropylaminophosphinyl)-3-(4,4′-dimethoxytrityloxymethyl)-2-[*N*-[4-(trifluoroacetamido)butyl]carbamoyloxy]cyclopentyl]thymine (14b). Compound **13b** (410 mg, 0.533 mmol) was phosphitylated as described in the preparation of **14a** to give **14b** (463 mg, 90% as a white foam): FAB-MS *m*/*z* 969 (MH^+); ^{31}P NMR δ 148.65,

148.42. HRMS (FAB) calcd for $C_{48}H_{61}F_3N_6O_{10}P$: 969.4135. Found: 969.4123.

(1*S*,2*S*,3*S*,4*S*)-1-[4-(2-Cyanoethoxy-*N*,*N*-diisopropylaminophosphinyl)-3-(4,4′-dimethoxytrityloxymethyl)-2-[*N*-[6-(trifluoroacetamido)hexyl]carbamoyloxy]cyclopentyl]thymine (14c). Compound **13c** (437 mg, 0.548 mmol) was phosphitylated as described in the preparation of **14a** to give **14c** (443 mg, 81% as a white foam): FAB-MS *m*/*z* 997 (MH^+); ^{31}P NMR δ 148.74, 148.66. HRMS (FAB) calcd for $C_{50}H_{65}F_3N_6O_{10}P$: 997.4448. Found: 997.4431.

Synthesis of ODNs. ODNs were synthesized on a DNA synthesizer (Applied Biosystem model 381A) by the phosphoramidite method. The fully protected ODNs were then deblocked and purified by the same procedure as for the purification of normal ODNs. That is, each ODN linked to the resin was treated with concentrated NH_4-OH at 55 °C for 12 h, and the released ODN protected by a DMTr group at the 5′-end was chromatographed on a C-18 silica gel column (1 × 10 cm, Waters) with a linear gradient of MeCN from 0 to 30% in 0.1 M TEAA buffer (pH 7.0). The fractions were concentrated, and the residue was treated with aqueous 80% AcOH at room temperature for 20 min, then the solution was concentrated, and the residue was coevaporated with H_2O. The residue was dissolved in H_2O and the solution was washed with Et_2O, then the H_2O layer was concentrated to give a deprotected ODN **16-E** (49), **17-E** (55), **18-E** (51), **19-E** (46), **20-E** (49), **21-E** (38), **16-B** (54), **17-B** (53), **18-B** (55), **19-B** (45), **20-B** (42), **21-B** (46), **16-H** (50), **17-H** (49), **18-H** (54), **19-H** (35), **20-H** (52), and **21-H** (43). The yields are indicated in parentheses as OD units at 260 nm starting from 1 μmol scale.

Matrix-Assisted Laser Desorption/Ionization Time-of-Flight Mass Spectrometry. Spectra were obtained on a Voyager Elite reflection time-of-flight mass spectrometry (PerSeptive Biosystems, Inc., Framingham, MA) equipped with a nitrogen laser (337 nm, 3-ns pulse). 3-Hydroxypicolinic acid (HPA), dissolved in H_2O to give a saturated solution at room temperature, was used as the matrix. Time-to-mass conversion was achieved by calibration by using the peak representing the C^+ cation of the charged derivative to be analyzed. ODN **18-E**: calcd mass, 5505; obsd mass, 5501. ODN **18-B**: calcd mass, 5533; obsd mass, 5529. ODN **18-H**: calcd mass, 5561; obsd mass, 5557. ODN **21-E**: calcd mass, 5805; obsd mass, 5801. ODN **21-B**: calcd mass, 5917; obsd mass, 5913. ODN **21-H**: calcd mass, 6030; obsd mass, 6027.

Partial Hydrolysis of ODNs with Snake Venom Phosphodiesterase. Each ODN labeled with ^{32}P at the 5′-end (10 pmol) was incubated with snake venom phosphodiesterase (0.4 μg) in the presence of Torula RNA (0.15 OD_{260} units) in a buffer containing 37.5 mM Tris-HCl (pH 8.0) and 7.5 mM $MgCl_2$ (total 20 μL) at 37 °C. At appropriate periods, aliquots of the reaction mixture were separated and added to a solution of EDTA (5 mM, 10 μL), then the mixture was heated at 100 °C for 5 min. The solutions were analyzed by electrophoresis on 20% polyacrylamide gel containing 7 M urea (*28*). Densities of radioactivity of the gel were visualized by a Bioimaging Analyzer (Bas 2000, Fuji, Co. Ltd.).

Partial Hydrolysis of ODNs with Nuclease S1. Each ODN labeled with ^{32}P at the 5′-end (10 pmol) was incubated with nuclease S1 (0.2 units) in the presence of Torula RNA (0.54 OD_{260} units) in a buffer containing 30 mM sodium acetate (pH 4.6), 1 mM $ZnSO_4$, and 280 mM NaCl (total 20 μL) at 37 °C. At appropriate periods, aliquots of the reaction mixture were separated and added to a solution of EDTA (5 mM, 10 μL), then the solutions were heated for 5 min at 100 °C. The solutions were analyzed by gel electrophoresis as described above.

Thermal Denaturation. Each solution contains each ODN (3 μM) and the complementary DNA **22** (3 μM) or RNA **23**(3 μM) in an appropriate buffer. The solution containing each ODN was heated at 90 °C for 5 min, then cooled gradually to an appropriate temperature, and used for the thermal denaturation studies. Thermal-induced transitions of each mixture were monitored at 260 nm on a Perkin-Elmer Lambda2S. Sample temperature was increased 0.5 °C/min.

ACKNOWLEDGMENT

This work was supported in part by a Grant-in-Aid for Encouragement of Young Scientists from the Ministry of Education, Science, Sports, and Culture of Japan and a Grant from "Research for the Future" Program of the Japan Society for the Promotion of Science (JSPS-RFTF97I00301).

LITERATURE CITED

(1) Uhlmann, E., and Peyman, A. (1990) Antisense oligonucleotides: a new therapeutic principle. *Chem. Rev. 90*, 544−584.
(2) Milligan, J. F., Matteucci, M. D., and Martin, J. C. (1993) Current concepts in antisense drug design. *J. Med. Chem. 36*, 1923−1937.
(3) Branch, A. D. (1998) A good antisense molecule is hard to find. *Trends Biochem. Sci. 23*, 45−50.
(4) Stein, C. A. (1999) Keeping the biotechnology of antisense in context. *Nat. Biotechnol. 17*, 209.
(5) Mesmaeker, A. D., Altmann K.-H., Waldner, A., and Wendeborn, S. (1995) Backbone modifications in oligonucleotides and peptides nucleic acid systems. *Curr. Opin. Struct. Biol. 5*, 343−355, and references therein.
(6) Kibler-Herzog, L., Zon, G., Uznanski, B., Whittier, G., and Wilson, M. D. (1991) Duplex stabilities of phosphorthioate, methylphosphonate, and RNA analogues of two DNA 14-mers. *Nucleic Acids Res. 19*, 2979−2986.
(7) Guvakova, M. A., Yakubov, L. A., Vlodavsky, I., Tonkinson, J. L., and Stein C. A. (1995) Phosphorothioate oligodeoxynucleotides bind to basic fibroblast growth factor, inhibit its binding to cell surface receptors, and remove it from low affinity binding sites on extracelluar matrix. *J. Biol. Chem. 270*, 2620−2627.
(8) Rockwell, P., O'Connor, W. J., King, K., Goldstein, N. I., Zhang, L. M., and Stein, C. A. (1997) Cell-surface perturbations of the epidermal growth factor and vascular endothelial growth factor receptors by phosphorothioate oligodeoxynucleotides. *Proc. Natl. Acad. Sci. U.S.A. 94*, 6523−6528.
(9) Agrawal, S., and Zhao, Q. (1998) Antisense therapeutics. *Curr. Opin. Chem. Biol. 2*, 519−528.
(10) Ono, A., Dan, A., and Matsuda, A. (1993) Synthesis of oligonucleotides carrying linker groups at the 1′-position of sugar residues. *Bioconjugate Chem. 4*, 499−508.
(11) Ono, A., Haginoya, N., Kiyokawa, M., Minakawa, N., and Matsuda, A. (1994) A novel and convenient postsynthetic modification method for the synthesis of oligodeoxyribonucleotides carrying amino linkers at the 5-position of 2′-deoxyuridine. *Bioorg. Med. Chem. Lett. 4*, 361−366.
(12) Haginoya, N., Ono, A., Nomura, Y., Ueno, Y., and Matsuda, A. (1997) Synthesis of oligodeoxyribonucleotides containing 5-(*N*-aminoalkyl)carbamoyl-2′-deoxyuridines by a new postsynthetic modification method and theri thermal stability and nuclease-resistance properties. *Bioconjugate Chem. 8*, 271−280.
(13) Ueno, Y., Kumagai, I., Haginoya, N., and Matsuda, A. (1997) Effects of 5-(*N*-aminohexyl)carbamoyl-2′-deoxyuridine on endonuclease stability and an ability of oligodeoxynucleotide to activate RNase H. *Nucleic Acids Res. 25*, 3777−3782.
(14) Kanazaki, M., Ueno, Y., Shuto, S., and Matsuda, A. (2000) Highly nuclease-resistant phosphodiester-type oligodeoxynucleotides containing 4′α-*C*-aminoalkylthymidines form ther-

mally stable duplexes with DNA and RNA. A candidate for potent antisense molecules. *J. Am. Chem. Soc. 122*, 2422−2432.
(15) Perbost, M., Lucas, M., Chavis, C., Pompon, A., Baumgartner, H., Rayner, B., Griengl, H., and Imbach, J.-L. (1989) Sugar modified oligonucleotides I. Carbo-oligodeoxynucleotides as potential antisense agents. *Biochem. Biophys. Res. Commun. 165*, 742−747.
(16) Sági, J., Szemzõ, A., Szécsi, J., and Ötvös, L. (1990) Biochemical properties of oligo[(+)-carbocyclic-thymidylates] and their complexes. *Nucleic Acids Res. 18*, 2133−2140.
(17) Altmann, K.-H., Bévierre, M.-O., Mesmaeker, A. D., and Moser, H. E. (1995) The evaluation of 2′- and 6′-substituted carbocyclic nucleosides as building blocks for antisense oligonucleotides. *Bioorg. Med. Chem. Lett. 5*, 431−436.
(18) Tabor, C. W., and Tabor, H. (1976) 1,4-Diaminobutane (putrescine), spermidine, and spermine. *Annu. Rev. Biochem. 45*, 285−306.
(19) Tabor, C. W., and Tabor, H. (1984) Polyamines. *Annu. Rev. Biochem. 53*, 749−790.
(20) Etter, M. C. (1990) Encoding and decoding hydrogen-bond patterns of organic compounds. *Acc. Chem. Res. 23*, 120−126.
(21) Tabor, H. (1962) Protective effect of spermine and other polyamines against heat denaturation of deoxyribonucleic acid. *Biochemistry 1*, 496−501.
(22) Thomas, T. J., and Bloomfield, V. A. (1984) Ionic and structural effects on the thermal helix-coil transition of DNA complexed with natural and synthetic polyamines. *Biopolymers 23*, 1295−1306.
(23) Hampel, K. J., Crosson, P., and Lee, J. S. (1991) Polyamines favor DNA triplex formation at neutral pH. *Biochemistry 30*, 4455−4459.
(24) Thomas, T., and Thomas, T. J. (1993) Selectivity of polyamines in triplex DNA stabilization. *Biochemistry 32*, 14068−14074.
(25) Musso, M., and Van Dyke, M. W. (1995) Polyamine effects on purine-purine-pyrimidine triple helix formation by phosphodiester and phosphorothioate oligodeoxyribonucleotides. *Nucleic Acids Res. 23*, 2320−2327.
(26) Biggadike, K., Borthwick, A. D., Evans, D., Exall, A. M., Kirk, B. A., Roberts, S. M., Stephenson, L., and Youds, P. (1988) Use of diethylaminosulphur trifluoride (DAST) in the preparation of synthons of carbocyclic nucleosides. *J. Chem. Soc., Perkin Trans. 1*, 549−554.
(27) Gait, M. J., Ed. (1984) *Oligonucleotides synthesis: a practical approach*. IRL Press, Oxford, U.K.
(28) Maniatis, T., Fritsch, E. F., and Sambrook, J. (1982) *Molecular cloning: a laboratory manual*, Cold Spring Harbor University Press, Plainview, NY.
(29) Saenger, W. (1984) *Principle of nucleic acid structure*, Springer-Verlag, New York.
(30) Drew, H. R., and Dickerson, R. E. (1981) Structure of a B-DNA dodecamer. III. Geometry of hydration. *J. Mol. Biol. 151*, 535−556.
(31) Kopka, M. L., Fratini, A. V., Drew, H. R., and Dickerson, R. E. (1983) Ordered water structure around a B-DNA dodecamer. A quantitative study. *J. Mol. Biol. 163*, 129−146.
(32) Portmann, S., Altmann, K.-H., Reynes, N., and Egli, M. (1997) Crystal structure of oligodeoxyribonucleotides containing 6′-α-methyl and 6′-α-hydroxy carbocyclic thymidines. *J. Am. Chem. Soc. 119*, 2396−2403.
(33) Altmann, K.-H., Kesselring, R., and Pieles, U. (1996) 6′-Carbon-substituted carbocyclic analogues of 2′-deoxyribonucleosides − Synthesis and effect on DNA/RNA duplex stability. *Tetrahedron 52*, 12699−12722.

BC0000684

Improvement of MRI Probes To Allow Efficient Detection of Gene Expression

Dagmar Högemann, Lee Josephson, Ralph Weissleder, and James P. Basilion*

Center for Molecular Imaging Research, Massachusetts General Hospital, Charlestown, Massachusetts. Received July 7, 2000; Revised Manuscript Received September 18, 2000

Recently, it has been demonstrated that magnetic resonance imaging (MRI) utilizing monocrystalline iron oxide nanoparticles (MIONs) targeted to an engineered transferrin receptor enables imaging of gene expression. However, the relatively high doses of iron oxides used indicated the need for improved MR imaging probes to monitor changes in gene expression in vivo. Using alternative conjugation chemistries to link targeting ligands and iron oxide nanoparticles, we present the development and characterization as well as improved receptor binding and MRI detection of a novel imaging probe. Iron oxide nanoparticles with a cross-linked dextran coat were conjugated to transferrin (Tf) through the linker molecule *N*-succinimidyl 3-(2-pyridyldithio)propionate (SPDP) to yield Tf-S-S-CLIO. The characteristics of this conjugate were evaluated in comparison to Tf-MION and Tf-CLIO generated by oxidative activation of the dextran-coat with subsequent reduction of Schiff's base. SPDP conjugation allowed approximately a 4-fold increase in the number of Tf molecules attached per iron oxide nanoparticle and resulted in a more than 10-fold improvement of binding and uptake by cells. This translated into an imaging probe that was 16 times better for imaging gene expression in a cellular MRI assay. This novel probe for MRI may substantially increase the sensitivity for the detection of endogenous or genetically induced transferrin receptor expression in small numbers of cells and may significantly reduce the imaging dose from over 100 mg/kg to doses of iron oxides that are currently used in clinical imaging.

INTRODUCTION

Real-time noninvasive imaging of gene expression in vivo is a major goal in molecular imaging research. The development of such technology would dramatically alter the way studies are performed. This technology would enable temporal monitoring of gene expression in single living animals during the development of disease or during administration of transgenes for gene therapy and eliminate the need for animal-intensive and labor-intensive studies. Several different imaging modalities have been exploited to image gene expression in vivo; however, none have the high spatial resolution achievable using magnetic resonance imaging (MRI). We have recently capitalized on the high spatial resolution of this technology demonstrating the utility of MRI for imaging gene expression in vivo and its utility for microscopically mapping transgene expression in tumor sections (*1*). To image gene expression in vivo, we previously employed an oxidative strategy of conjugating superparamagnetic monocrystalline iron oxide nanoparticles (MION) to transferrin (Tf). This resulted in targeting of the Tf-MION conjugate to tumors overexpressing engineered human transferrin receptor (ETR, a cell-surface internalizing receptor), cellular accumulation, and detection by MRI (*1*). However, the high doses of Tf-MION contrast agent needed for these studies emphasized the relatively low sensitivity of MRI for probe detection (*1*) and demonstrated the need to develop improved MR contrast agents for imaging gene expression.

In this report, we conjugate Tf to iron oxide particles using the cross-linking reagent *N*-succinimidyl 3-(2-pyridyldithio)propionate (SPDP) to generate a new MR probe and compare its properties with two conjugates prepared by the previously employed oxidative conjugation strategy. We found that the disulfide cross-linked Tf iron oxide conjugates (Tf-S-S-CLIO) had more Tf proteins per iron oxide particle, a higher affinity for the Tf receptor, and altered MR signal intensity in cellular uptake assays at 16-fold lower concentrations.

* To whom correspondence should be addressed. Phone: (617) 726-5788. Fax: (617) 726-5708. E-mail: basilion@helix.mgh.harvard.edu.

EXPERIMENTAL PROCEDURES

Synthesis of Iron Oxide Particles: MION, CLIO, CLIO-NH_2. MION-46 was prepared by reaction of iron salts with ammonium hydroxide in the presence of T10 dextran (*3*). Also, the preparation of cross-linked iron oxide nanoparticles, now defined as CLIO-10, has been described before (*4*). Briefly, a dextran-coated monodispersed iron oxide preparation was prepared and then cross-linked with epichlorohydrin and purified (*4*). To utilize SPDP as the linking reagent, it was necessary to add primary amines to the CLIO. To maintain a chemically defined dextran coat, amidation was performed on CLIO rather than MION particles. To produce iron oxide amine, CLIO-NH_2, CLIO was treated with ammonia and then dialyzed as described (*4*, *5*).

Synthesis of Tf-MION and Tf-CLIO (Figure 1, reactions A and B). To ensure conjugation of high affinity Tf to iron oxide particles, the integrity of holo-Tf (Sigma, St. Louis, MO) was confirmed photometrically prior to conjugation as described (*6*). Reaction of MION or CLIO with Tf was accomplished by partial oxidation of dextrans, reaction with Tf, and subsequent reduction of Schiff's bases as previously described (*2*) and as modified here. MION or CLIO was dialyzed against sodium acetate buffer (10 mM sodium acetate and 0.15

10.1021/bc000079x CCC: $19.00 © 2000 American Chemical Society
Published on Web 11/02/2000

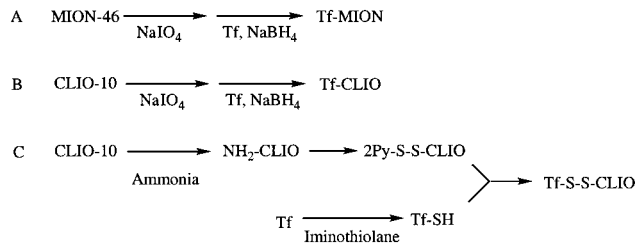

Figure 1. Synthetic scheme of the conjugation of Tf-MION, Tf-CLIO, and Tf-S-S-CLIO.

M NaCl, pH 6). Following dialysis, MION or CLIO was oxidized with sodium periodate (4 mg/mg iron) for 40 min, dialyzed against 0.15 M NaCl for 1 h and dialyzed against sodium bicarbonate buffer (20 mM sodium bicarbonate and 0.15 M NaCl, pH 8.7) for another 40 min. To conjugate MION or CLIO with human diferric Tf, Tf was added at a ratio of 1.7 mg/mg iron. After 3 h of incubation, Schiff's bases were reduced by addition of 15.9 mM sodium cyanoborohydrate and incubation overnight at 4 °C. Magnetic separation columns (Macs separation columns, Miltenyi Biotec, CA) were used to separate nonconjugated Tf from iron oxide particles. To calculate the number of Tf molecules per particle, the protein (BCA, Pierce, Rockford, IL) and iron concentrations of purified material were determined (*2, 7*). Results were expressed as the number of Tf molecules per particle assuming an average of 2064 Fe atoms/particle (*7*). The conjugates were stored in phosphate buffered saline (PBS), pH 8 at 4 °C.

Synthesis of Tf-S-S-CLIO (Figure 1, reaction C). *Derivatization of CLIO with 2-Pyridyl Disulfide.* CLIO-NH_2 was used to prepare 2-pyridyl disulfide derivatized CLIO. One milliliter of CLIO-NH_2 (26 mg of Fe; in 5 mM citrate buffer), 0.67 mL of PBS (pH 8), and 1.3 mL of 3.4×10^{-2} M (in DMSO) *N*-succinimidyl 3-(2-pyridyldithio)-propionate (SPDP; Molecular Biosciences, Boulder, CO) were incubated for 2 h at room temperature. Low molecular impurities were removed by filtration through Sephadex G25F columns equilibrated with PBS, pH 8. The pooled void volume had an iron concentration of 4.5 mg of Fe/mL.

To measure the number of 2-pyridyl disulfide groups attached, 50 μL of the solution were added to 75 μL of DTT (2×10^{-2} M) in PBS, pH 7.4. After 30 min at room temperature, a microconcentrator with a 30 kDa cutoff (Amicon, Beverly, MA) was used to separate the product of the reduction, pyridine-2-thione, from iron. The concentration of pyridine-2-thione was determined using an extinction coefficient of 8100 M^{-1} cm^{-1} at 343 nm. On average, 35 2-pyridyl disulfide groups were introduced per CLIO ($n = 3$). The compound was kept at 4 °C.

Thiolation of Human Diferric Tf (Tf-SH). Equal volumes of diferric Tf (10^{-3} M = 80 mg/mL) and iminothiolane (2.5×10^{-3} M in PBS, 2 mM EDTA, pH 8, degassed) were mixed and incubated for 1 h at room temperature in the dark. Unreacted iminothiolane was removed by filtration through a Sephadex G25F column equilibrated with PBS, 2 mM EDTA, pH 8. The absorption at 280 nm with an extinction coefficient of 1.2×10^5 M^{-1} cm^{-1} (*8*) was used to determine the concentration of Tf. The number of reactive sulfhydryl groups was measured at a wavelength of 412 nm after the addition of Ellman's reagent with an extinction coefficient of 13 600 M^{-1} cm^{-1} (*9, 10*). Under these conditions, a ratio of 0.7:1 sulfhydryl groups/Tf was achieved, and polymerization was not observed.

Synthesis of Tf-S-S-CLIO. Tf-SH (3×10^{-4} M concentration of Tf) and 2Py-S-S-CLIO (1.3×10^{-3} M concentration of 2-pyridyl disulfide groups) were mixed at equal molar ratios of Tf and 2-pyridyl disulfide groups in PBS, pH 8. The mixture was incubated for 18 h at room temperature. Unreacted Tf-SH was separated from Tf-conjugates using magnetic columns and the number of Tf molecules per particle was determined as above. The conjugates were stored in PBS, pH 8, either at 4 °C or shock frozen in liquid nitrogen and kept a −20 °C.

Cell Culture. Rat 9L gliosarcoma cells (Brain Tumor Research Center, San Francisco, CA) (*11*) or rat gliosarcoma cells stably overexpressing an altered form of the human transferrin receptor ETR (9L3.9 cells) (*1, 2*) were grown in Dulbecco's modified Eagle's medium (DMEM, Cellgro, Mediatech, Washington, DC) containing 10% fetal bovine serum (FBS, Cellgro). The medium was changed every 3 days. Transfected cells were periodically passaged with G418 to ensure integrity of the plasmid expression (*2*).

Competition Studies. Human diferric Tf (Sigma, St. Louis, MO) was radiolabeled with $Na^{125}I$ in the presence of IodoGen (Pierce, Rockford, IL). Unbound iodide was removed by centrifugation through Bio-Gel P6 spin-columns (Bio-Rad, Hercules, CA).

Competition studies were performed for the different conjugates in the presence of [^{125}I]Tf and compared to competition curves generated using different concentrations of unlabeled diferric Tf. Cells (9L wild-type or 9L3.9 cells) were plated at a density of 1×10^5 cells/well onto 24 well plates (Falcon, Becton Dickinson, Lincoln Park, NJ). The next day, different concentrations of unlabeled diferric Tf, thiolated Tf, Tf-MION, Tf-CLIO, or Tf-S-S-CLIO (0.25 nM to 2.5 μM in DMEM) were added immediately prior to the addition of [^{125}I]Tf (0.25 nM in DMEM). As a negative control 2Py-S-S-CLIO was mixed with Tf-SH in an amount equal to their respective concentrations in the Tf-S-S-CLIO conjugate and added to cells. After incubation for 1 h at 37 °C the cells were washed three times with Hanks' Balanced Salt Solution (HBSS, Bio-Whittaker, Walkersville, MD) and detached with trypsin (0.05% trypsin, 0.5 mM ethylenediaminetetraacetic acid). Cell-associated radioactivity was counted in a gamma-counter (1282 Compugamma CS, LKB Wallac, Sweden).

SDS−PAGE. Laemmli SDS−PAGE was used to determine the integrity of the different conjugates (*12*). Samples were mixed with SDS sample loading buffer and analyzed by gel electrophoresis using a 4% stacking gel and a 10% separating gel at a thickness of 0.75 mm. Where reducing conditions were required, 5% β-mercaptoethanol was added to the SDS sample buffer and samples were heated at 95 °C for 5 min. Nonreduced samples were not subjected to heating as controls demonstrated that this had no effect on the integrity of the conjugate (data not shown). Two micrograms of protein was loaded per lane. Gels were run at a constant voltage of 120 V and stained with Coomassie Brilliant Blue R-250.

Physical Properties and MR Imaging. The R1 and R2 relaxivities of Tf-MION, Tf-CLIO, and Tf-S-S-CLIO were measured using a 0.47 T tabletop minispec as described (*7*).

For MR imaging, 3.5×10^6 cells (9L wild-type or 3.9 clone) were seeded/10 cm culture dish. The next day, cells were incubated with the conjugates at different concentrations of iron in 2 mL of DMEM. Cells were incubated at 37 °C for 2 h followed by washing with HBSS, trypsinization, washing in DMEM with 10% FBS, and

Table 1. Physical Properties of Superparamagnetic Iron Oxide Conjugates

compd	R_1 (mM × s)$^{-1}$	R_2 (mM × s)$^{-1}$	average Tf-molecule per particle	linker chemistry
Tf-MION	20	62	0.6	nonreversible
Tf-CLIO	26	114	1.2	nonreversible
Tf-S-S-CLIO	32	146	4	reversible

centrifugation. After centrifugation, the cell pellets were resuspended in culture medium and transferred into 250 μL tubes. To form uniform pellets the cells were again centrifuged at 500 rpm for 2 min (Sorvall 7 RT, Kendro Laboratory Products, Newtown, CT). To prevent drying and susceptibility artifacts, the supernatant was not removed. The tubes were placed into a water bath at RT for MR imaging. The phantom allowed the simultaneous imaging of up to 50 different samples. MR imaging was performed with a clinical 1.5 T superconducting magnet (Signa 5.0; GE Medical Systems, Milwaukee, WI) using a 5-in. surface coil. The imaging protocol consisted of a T2 weighted spin−echo sequence (SE, TR 3000 ms, variable TE 16−100 ms). The 1.9 mm imaging slice was carefully placed to avoid partial volume effects. At a field of view of 8 cm^2 and a 256 × 256 imaging matrix each voxel has a size of 0.186 mm^3. Accordingly, in each tube a volume of 9.5 μL accounting for approximately 1.5 × 10^6 cells was imaged. After MR imaging, the viability of the cells was confirmed by trypan blue exclusion and was always greater than 95%. Signal intensity (SI) measurements of cell pellets were obtained by manual placement of regions of interest (ROI) on the cell pellets. ROIs were also placed on the surrounding water to determine the overall homogeneity of the image. Signal intensities plotted against the 10 different TEs showed the differences in T2 decay of each pellet. Curve fitting for exponential decay allowed the calculation of T_2 relaxation times ($SI = Ae^{(-T_E/T_2)} + B$, where SI is the signal intensity, T_E the echo time, A the amplitude, and B the offset for each incubation concentration of conjugate.

RESULTS

Synthesis of Tf-Iron Oxide Conjugates. Previous work demonstrated that the conjugation of Tf to periodate-treated MION decreased the affinity of the conjugated Tf for its receptor (*2*). We hypothesized that the contrast agent could be significantly improved if the affinity of conjugated Tf for transferrin receptor could be increased. To minimize the effects of conjugation on Tf−transferrin receptor binding, we utilized a chemical cross-linking reagent, *N*-succinimidyl 3-(2-pyridyldithio)propionate (SPDP), which has previously been shown to have excellent cross-linking efficiency while maintaining the biological activity of Tf (*10*). The synthesis schemes for all three types of iron oxide conjugates are shown in Figure 1. The use of a chemical cross-linking agent significantly improved the number of Tf molecules conjugated per iron oxide particle. Approximately 4 Tf molecules were bound/iron crystal in Tf-S-S-CLIO compared to 0.6−1.2 Tf/particle in Tf-MION and Tf-CLIO. Physical properties of the different conjugates are summarized in Table 1.

To determine if the conjugation and purification strategies above resulted in successful binding and adequate purity, SDS−PAGE was used to analyze the three different conjugates (Figure 2). A brown color, indicative of iron oxide nanoparticles before staining (upper panel), and a blue color after Coomassie Blue staining (lower panel) showed the co-localization of iron oxide nanoparticles and protein in the gel (lanes 3, 5, and 7). The Tf-MION (lane 3) and to a lesser extent also the Tf-CLIO conjugate (lane 5) contained compounds that migrated through the stacking gel presumably due to Tf bound to iron oxide particles of smaller size. The lack of detection of free Tf or protein degradation products showed that magnetic separation efficiently removed nonconjugated Tf from Tf-MION, Tf-CLIO, and Tf-S-S-CLIO preparations.

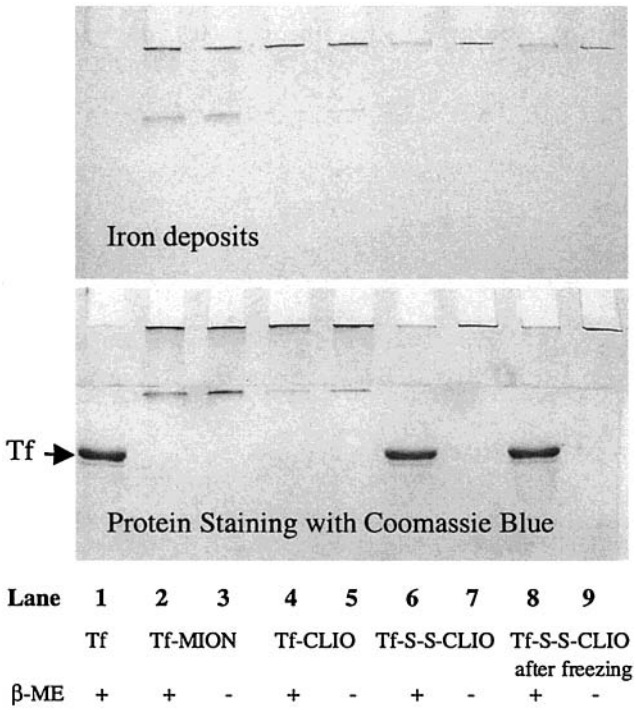

Figure 2. Nonreducing and reducing SDS−PAGE of Tf-MION, Tf-CLIO, and Tf-S-S-CLIO. Two micrograms of nonconjugated Tf (lane 1) or of Tf in each of the conjugates (lanes 2−9) were incubated in SDS-sample buffer with or without β-mercaptoethanol (β-ME), heat treated as indicated in the text and electrophoresed. Upper panel: Gel prior to staining for protein. Lower panel: Gel after Coomassie Blue staining. Arrow indicates migration of authentic Tf standard.

Boiling of Tf-S-S-CLIO in sample buffer containing β-mercaptoethanol, as expected, cleaved the disulfide bond, and no change in the integrity of Tf-S-S-CLIO was observed after prolonged freezing (Figure 2, lanes 6 and 8). In contrast, boiling of Tf-MION and Tf-CLIO in reducing SDS−sample buffer resulted in no release of Coomassie Blue detectable Tf.

Binding and Uptake of Tf, Tf-MION, Tf-CLIO, and Tf-S-S-CLIO. To compare the binding and uptake of the three compounds cells overexpressing a known amount of transferrin receptor, 9L3.9 cells (*1*, *2*) were incubated with a constant amount of [^{125}I]diferric Tf (0.25 nM) in the presence of increasing concentrations of either unlabeled diferric Tf, Tf-S-S-CLIO, Tf-CLIO, Tf-MION, unreacted Tf-SH and 2Py-S-S-CLIO, or 2Py-S-S-CLIO alone (Figure 3A). The concentration for which 50% of the cell associated radioactivity was displaced occurred at 18.7 ± 3.2 nM for diferric Tf and the IC_{50} for Tf-S-S-CLIO was 306.8 ± 21.2 nM. Although it was not possible to generate high enough concentrations of the other conjugates to obtain complete displacement curves, the binding and uptake of Tf-S-S-CLIO was significantly better (greater than 10-fold improved) than either the Tf-MION or the Tf-CLIO conjugates (Figure 3A).

MR Imaging of Tf-MION, Tf-CLIO, and Tf-S-S-CLIO. The next step in these studies was to determine

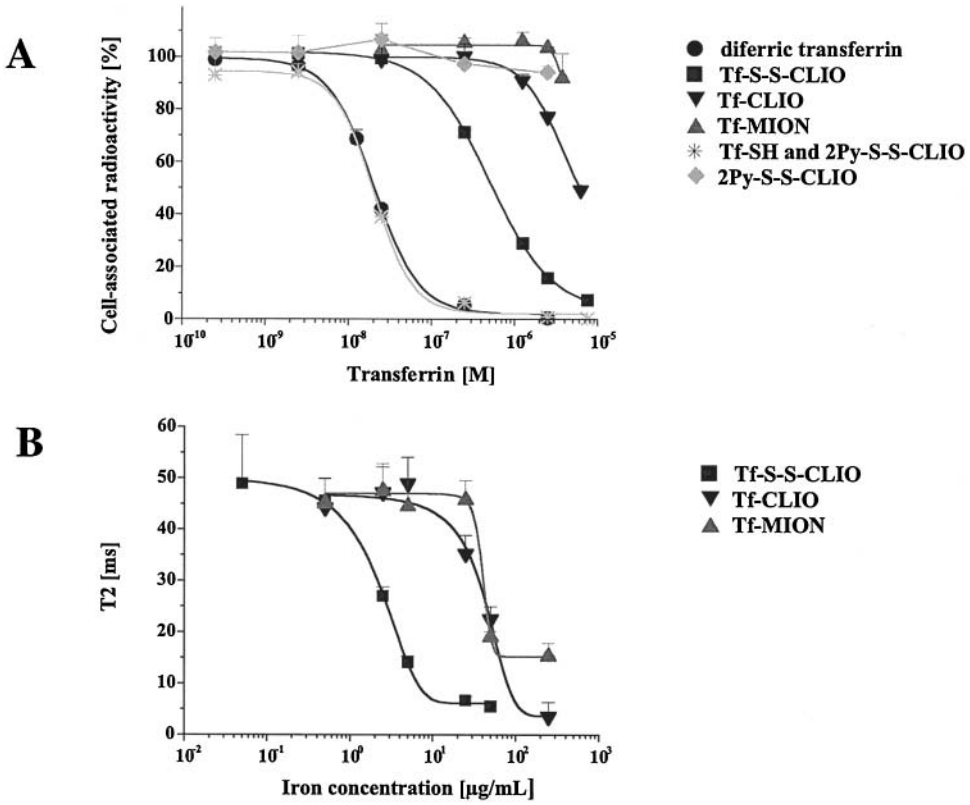

Figure 3. (A) Transferrin receptor competitive binding assay. To compare the relative affinity of the different conjugates and synthesis intermediates for the transferrin receptor a constant amount of [^{125}I]transferrin and increasing amounts of unlabeled diferric Tf, Tf-S-S-CLIO, Tf-CLIO, Tf-MION, Tf-SH freshly mixed with 2Py-S-S-CLIO, and 2Py-S-S-CLIO were co-incubated with cells and total cell associated radioactivity was measured. To account for differences in Tf molecules/particle for the different conjugates the amount of added conjugate was normalized for Tf concentration. 2Py-S-S-CLIO was added in an amount equal to its respective concentration in the Tf-S-S-CLIO conjugate. (B) Transverse relaxivity versus iron concentrations. MR imaging was performed at 10 different echo times (TE 16−100 ms) on the 9L3.9 cell phantoms to allow the calculation of T2 relaxation times. T2 relaxation times were plotted as a function of the concentration of Tf-iron oxide conjugates in the incubation media. The generated curves were used to compare the relative detection of the different imaging probes by MRI.

if changes in Tf-iron oxide binding and uptake would be translated into detectable changes in MR signal intensities. To quantify the changes in signal intensities, we calculated the changes as transverse relaxation times (T2) for each contrast probe at different iron concentrations (see Experimental Procedures). T_2 values were plotted versus the iron concentrations in the incubation media of the cells and used to compare the potency of the different conjugates resulting from binding and intracellular accumulation (Figure 3B). A 50% lower T_2 relaxation time was found after incubation of cells with 16-fold lower concentration of iron for Tf-S-S-CLIO than for Tf-CLIO or Tf-MION (Figure 3B). The changes in signal intensity measured at a single TE for the Tf-MION, Tf-CLIO, and Tf-S-S-CLIO imaging probes are displayed in Figure 4. Signal intensities were dependent on binding and uptake of the conjugates and highly specific for the transferrin receptor. Little to no signal changes were observed after incubation with 250 μg/mL nonconjugated MION or CLIO (data not shown) and a 1000-fold excess of nonconjugated diferric Tf completely inhibited a signal change in comparison to untreated controls.

MR Imaging of Different Levels of Receptor Expression in 9L and 3.9 Cells. Finally, we determined if the improved MRI contrast probe, Tf-S-S-CLIO, was capable of being used to image differences in receptor levels. To assess this, 9L rat glioma cells (9L wild-type) and a derivation of that cell line engineered to overexpress ETR (9L3.9 cells) were incubated with different concentrations of Tf-S-S-CLIO and imaged by MRI. A decrease in signal intensity was observed at much lower concentrations of Tf-S-S-CLIO in 9L3.9 cells compared to wild-type 9L cells (Figure 5). Since receptor-mediated binding for human diferric Tf is identical for both cell types (data not shown), the change in signal intensity most likely resulted from increased binding and uptake of the probe due to an increase in the number of receptors and possibly from changes in relaxivity. Endogenous expression of transferrin receptor could be detected in 9L cells at the highest concentration of contrast probe.

DISCUSSION

We have recently demonstrated that uptake of superparamagnetic monocrystalline iron oxide nanoparticles via the transferrin receptor can be imaged by MRI and correlated to receptor expression (*1*, *2*), while other groups have employed similar strategies to probe for endogenously overexpressed transferrin receptor (*13*) or to load cells with iron oxides (*14*). However, in their current form the targeted iron oxides used to assess transferrin receptor expression in vivo require administration of relatively high doses of Tf-MION (*1*). To improve probe binding and presumably reduce the dose of targeted iron oxide necessary to image transferrin receptor expression we utilized the chemical cross-linking reagent SPDP to generate Tf-S-S-CLIO. The studies presented here show that Tf-S-S-CLIO is an imaging probe that is 16-fold better for MR imaging of transferrin receptor expression and suitable to measure differences in endogenous receptor expression at much lower concentrations of probe.

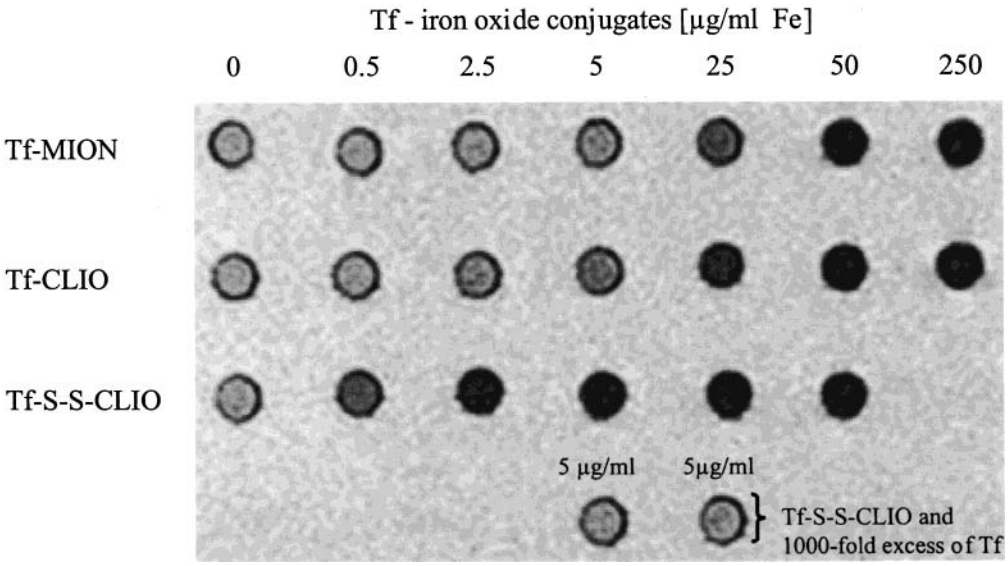

Figure 4. MR imaging of 9L3.9 cell phantoms. 9L3.9 cells, which overexpress TfR, were incubated with the indicated concentrations of Tf-iron oxide conjugates. After the incubation the cells were harvested, washed, pelleted into phantoms and imaged with a T2-weighted MR sequence (GE 1.5 T, Signa 5.0; Spin−Echo Sequence, TR 3000 ms/TE 100 ms). Note that the addition of excess diferric Tf resulted in no change in MR signal compared to untreated controls.

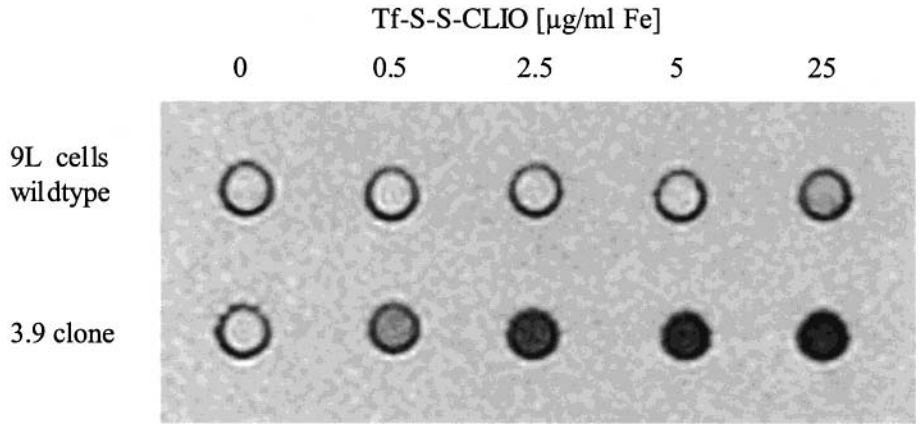

Figure 5. MR imaging of TfR expression. Wild-type 9L cells, expressing relatively low levels of TfR, or 9L3.9 cells, expressing relatively high levels of TfR, were incubated with the indicated concentrations of Tf-S-S-CLIO and imaged as phantoms. The relative difference in TfR expression is clearly visible by T2-weighted MRI (GE 1.5 T, Signa 5.0; Spin−Echo Sequence, TR 3000 ms/TE 50 ms).

The oxidative conjugation strategy that has been used in previous studies produces aldehydes on the dextran coat of the iron oxides. This method can result in multiple direct attachment points between Tf and the polysaccharide of the iron oxides. Therefore, a substantial loss in the biological activity of the protein may result from (1) conjugation to sites that are important for receptor binding or (2) particle interference with receptor binding. To minimize these effects we, sought to bind Tf and iron oxide particles via a linker molecule. We first identified reaction conditions that would produce biologically active Tf bearing a defined number of sulfhydryls (0.7−1.0/Tf) and have determined conditions that yield Tf-SH with binding characteristics indistinguishable from unreacted Tf (Figure 3A and data not shown). The reaction of activated iron oxide nanoparticles, 2Py-S-S-CLIO, with Tf-SH yielded a conjugate, Tf-S-S-CLIO, with approximately 4 Tf- molecules/particle compared to 0.6−1.2 for the oxidative conjugates (Tf-MION and Tf-CLIO). Even after adjustment for the increased number of Tf molecules per particle, the competitive binding assay revealed that Tf-S-S-CLIO has a 10-fold higher affinity for the transferrin receptor than Tf-MION and Tf-CLIO (Figure 3A). Since the difference in biological activity cannot be explained by the increase in particle associated Tf molecules, the improvement in binding of Tf-S-S-CLIO compared to either Tf-MION or Tf-CLIO suggests that the oxidative conjugation chemistry significantly interferes with the binding of the conjugates to the receptor. This may be due to chemical alteration of Tf, cross-linking to a site of Tf directly involved in receptor binding, significant particle-dependent sterical inhibition of Tf-transferrin receptor binding, or a combination of these. While none of these possibilities can be excluded, the binding characteristics of Tf-S-S-CLIO to the transferrin receptor suggest it is likely that sterical inhibition of Tf-MION and Tf-CLIO binding plays a role. Although Tf-S-S-CLIO binds the transferrin receptor much better than Tf-CLIO or Tf-MION, when compared to nonconjugated diferric transferrin Tf-S-S-CLIO is a significantly less effective competitor for [^{125}I]Tf (Figure 3A). Since, there was no detectable difference in the ability of Tf and Tf-SH to compete for [^{125}I]Tf (Figure 3A and data not shown), the difference between Tf and Tf-S-S-CLIO to compete in the displacement assay is likely due to steric hindrance and the overall size of the conjugate rather than being due to thiolation of Tf (i.e., chemical damage or attachment site). These data strongly suggest that

changing the proximity of the iron oxide nanoparticle and Tf can have a significant effect on the interaction of the conjugate with receptor. Furthermore, these data suggest that by lengthening the linker between Tf and the iron oxide it may be possible to synthesize a MR probe with still higher affinity for the transferrin receptor.

It has been reported that the type of disulfide bond formed by conjugation of thiolated Tf and 2Py-S-S-CLIO is relatively stable in plasma with a half-life of 8 h (*15*, *16*) making this a useful coupling chemistry for in vivo probes. The use of this linker chemistry to provide a chemically cleavable linkage between the Tf and CLIO was initially instituted to allow monitoring of the integrity of conjugated Tf following the coupling reaction (Figure 2). However, it is interesting to note that several studies where disulfide bonds have been used to target immunotoxins (*17*−*19*), opioid peptides (*20*) and antibody fragments (*21*) to cells have demonstrated that a labile disulfide bond was necessary for the expression of full activity of these agents. Whether these findings can be transferred to Tf-S-S-CLIO or whether a stable linker is preferable remains to be shown. Further studies to improve this probe in terms of stability, pharmacological profile, bioavailability, relaxation and number of Tf molecules per particle as well as the attachment of other targeting molecules are currently underway.

ACKNOWLEDGMENT

We would like to thank Dr. Anna Moore for her expert advice and help in performing the studies. The work was supported by NIH Grant RO1 CA 85240. Dr. Dagmar Högemann is a recipient of a fellowship from the Deutsche Forschungsgemeinschaft, Germany.

LITERATURE CITED

(1) Weissleder, R., Moore, A., Mahmood, U., Bhorade, R., Benveniste, H., Chiocca E. A., and Basilion, J. P. (2000) In vivo MR imaging of transgene expression. *Nat. Med. 6*, (3), 351−355.

(2) Moore, A., Basilion, J. P., Chiocca, E. A., and Weissleder, R. (1998) Measuring transferrin receptor gene expression by NMR imaging. *Biochim. Biophys. Acta 1402*, 239−249.

(3) Moore, A., Marecos, E., Bogdanov, A., and Weissleder, R., (2000) Tumoral distribution of long-circulating dextran-coated iron oxide nanoparticles in a rodent model. *Radiology 214*, 568−574.

(4) Palmacci, S., and Josephson, L. (1993) Synthesis of polysaccharide covered superparamagnetic oxide colloids. U.S. Patent 5,262,176.

(5) Josephson, L., Tung, C.-H., Moore, A., and Weissleder, R. (1999) High-efficiency intracellular magnetic labeling with novel superparamagnetic-tat peptide conjugates. *Bioconjugate Chem. 10* (2), 186−191.

(6) Klausner, R. D., Van Renswoude, J., Ashwell, G., Kempf, C., Schechter, A. N., Dean, A., and Bridges, K. R. (1983) Receptor-mediated endocytosis of transferrin in K562 cells *J. Biol. Chem. 258* (8), 4715−4724.

(7) Shen, T., Weissleder, R., Papisov, M., Bogdanov, A., and Brady, T. J. (1993) Monocrystalline iron oxide nanocompounds (MION): physicochemical properties. *Magn. Reson. Med. 29*, 599−604.

(8) Wellhöner, H. H., Neville, D. M., Jr., Srinivasachar, K., and Erdmann, G. (1991) Uptake and concentration of bioactive macromolecules by K562 cells via the transferrin cycle utilizing an acid-labile transferrin conjugate. *J. Biol. Chem. 266 (7)*, 4309−4314.

(9) Ellman, G. L. (1959) Tissue sulphydryl groups. *Arch. Biochem. Biophys. 82*, 70−77.

(10) Kratz, F., Beyer, U., Roth, T., Tarasova, N., Collery, P., Lechenault, F., Cayabat, A., Schumacher, P., Unger, C., and Falken, U. (1998) Transferrin conjugates of doxorubicin: synthesis, characterization, cellular uptake, and in vitro efficacy. *J. Pharm. Sci. 87* (3), 338−346.

(11) Jacobs, R., and Fraser, S. (1994) Magnetic resonance microscopy of embryonic cell lineages and movements. *Science 263*, 681−684.

(12) Laemmli, U.K. (1970) Cleavage of structural proteins during the assembly of the head of bacteriophage T4. *Nature 227*, 680−685.

(13) Kresse, M., Wagner, S., Pfefferer, D., Lawaczeck, R., Elste, V., and Semmler, W. (1998) Targeting of ultrasmall superparamagnetic iron oxide (USPIO) particles to tumor cells in vivo by using transferrin receptor pathways. *Magn. Reson. Med. 40*, 236−242.

(14) Bulte, J. W. M., Zhang, S.-C., van Gelderen, P., Herynek, V., Jordan, E. K., Duncan, I. D., and Frank, J. A. (1999) Neurotransplantation of magnetically labeled oligodendrocyte progenitors: magnetic resonance tracking of cell migration and myelination. *Proc. Natl. Acad. Sci. U.S.A. 96* (26), 15256−15261.

(15) Winkler, M. A., Price J. O., Foglesong, P. D., and West, W. H. (1990) Biodistribution and plasma survival in mice of anti-melanoma monoclonal antibody cross-linked to OKT-3. *Cancer Immunol., Immunother. 31* (5), 278−284.

(16) Thorpe, P. E., Wallace, P. M., Knowles, P. P., Relf, M. G., Brown A. N. F., Watson, G. J., Knyba, R. E., Wawrzynczak, E. J., and Blakey, D. C. (1987) New coupling agents for the synthesis of immunotoxins containing a hindered disulfide bond with improved stability in vivo. *Cancer Res. 47*, 5924−5931.

(17) Ramakrishnan, S., Fryxell, D., Mohonraj, D., Olson, M., and Li, B.-Y. (1992) Cytotoxic conjugates containing translational inhibitory proteins. *Annu. Rev. Pharmacol. Toxicol. 32*, 579−621.

(18) Vitetta, E. S., Thorpe, P. E., and Uhr, J. W. (1993) Immunotoxins: magic bullets or misguided missiles? *Immunol. Today 14*, 252−259.

(19) Masuho, Y., Kishida, K., Saito, M., Umemoto, N., and Hara, T. (1982) Importance of the antigen-binding valency and the nature of the cross-linking bond in ricin A-chain conjugates with antibody. *J. Biochem. 91*, 1583−1591.

(20) Bickel, U., Kang, Y.-S., and Pardridge, W. M. (1995) In vivo cleavability of a disulfide-based chimeric opioid peptide in rat brain. *Bioconjugate Chem. 6*, 211−218.

(21) Stein, S., Weiss, A., Adermann, K., Lazarovici, P., Hochman, J., and Wellhöner, H. (1999) A disulfide conjugate between anti-tetanus antibodies and HIV (37−72) Tat neutralizes tetanus toxin inside chromaffin cells. *FEBS Lett. 458* (3), 383−386.

BC000079X

TECHNICAL NOTES

Selective Synthesis of Heterobifunctional Poly(ethylene glycol) Derivatives Containing Both Mercapto and Acetal Terminals

Yoshitsugu Akiyama, Hidenori Otsuka, Yukio Nagasaki,* Masao Kato, and Kazunori Kataoka*

Department of Materials Science & Technology, Science University of Tokyo, 2641 Yamazaki, Noda-shi, Chiba 278-8510, Japan, and Department of Materials Science, Graduate School of Engineering, The University of Tokyo, 7-3-1 Hongo, Bunkyo-ku, Tokyo 113-8656, Japan. Received March 30, 2000; Revised Manuscript Received July 13, 2000

A novel synthetic route to heterobifunctional poly(ethylene glycol) (PEG) derivatives containing both mercapto and acetal terminal groups was established in this study using anionic ring opening polymerization of ethylene oxide (EO) using potassium 3,3-diethoxypropanolate (PDP) as the initiator, followed by the successive conversion of the end-alkoxide group to a methanesulfonic group, and then to an ethyldithiocarbonate moiety. Molecular functionalities of the acetal and the mercapto terminal groups of the heterotelechelic PEG (acetal-PEG-SH) thus prepared were confirmed to 1.00 and 0.85, respectively, indicating that the reaction proceeds almost quantitatively. The obtained acetal-PEG-SH products, including 2-pyridyldithio derivatives, have a promising utility for bioconjugation in the fields of medicine and biology.

PEGylation, which refers to the modification of biomaterials and biomolecules using poly(ethylene glycol) (PEG), has become increasingly important in the fields of pharmaceuticals and biomedical engineering (*1*−*5*), because PEG is a nontoxic, hydrophilic polymer with low interfacial free energy in water and high-chain mobility inducing effective steric stabilization effects (*6*). Furthermore, it is well-documented that exogenous proteins appreciably reduce their antigenicity through PEGylation (*7*, *8*). Several types of PEGylated protein drugs such as adenosine deaminase, asparaginase, and interleukin 2 have been successfully applied in clinical applications (*9*−*11*). In the field of biomedical engineering, construction of tethered PEG brushes on various surfaces through PEGylation has become a major approach to reduce the nonspecific interaction of proteins and cells with biomedical devices. Further, a PEGylated layers may be utilized as a platform for specific molecular recognition and sensing if the free-chain-end of tethered PEG is available for further linking to ligand molecules (*12*). To this end, effective functionalization of the PEG chain-end is of particular importance, facilitating the development of heterotelechelic PEGs possessing different functional groups at each chain end. Indeed, several different approaches were reported for the preparation of heterotelechelic PEG through polymer reactions, starting from hydroxy-terminated homotelechelic PEG (*13*−*15*), yet they often involve many reaction steps with low yields and low selectivities.

The objective of our series of studies on heterotelecheric PEG is to establish novel synthetic routes for various types of heterotelechelic PEGs based on the ring-opening polymerization of ethylene oxide using a metal alkoxide initiator with a protected functional group. In this way, heterotelechelic PEGs possessing functional end-groups such as aldehyde, primary amine, carboxylate, hydroxide, vinyl benzyl, methacryloyl, tosyl, and monosaccharides have been already prepared (*16*−*19*).

We wish to report here the synthesis of a novel heterotelechelic PEG with a high potential utility in the field of bioconjugation: this PEG possesses an acetal group at one end and a mercapto group at the other end. The mercapto end-group is useful for bioconjugation for the following reasons: (1) the mercapto group reacts with several metal surfaces such as gold and silver to provide a reactive PEGylated layer on metal surfaces as a platform material for biosensors and biocatalysis; (2) recombinant DNA technology permits site-specific introduction of the mercapto (cysteine) group at the desired positions in the amino acid sequence of a particular protein. The mercapto-terminated PEG can then be selectively conjugated to the SH-side group of the genetically inserted cysteine residue of the protein, thus obtaining a site-specific PEGylated protein conjugate (*20*). The end-mercapto group of PEG can easily be converted into 2-pyridyldithio-group, which has even more practical value in the PEGylation fields (*21*).

In our strategy to prepare the α-acetal-*ω*-mercapto-PEG, the two-step synthetic method shown in Scheme 1 was employed. According to our previous report (*16*), PEG possessing an acetal group at the α-chain end was prepared by initiating polymerization of ethylene oxide using potassium 3,3-diethoxypropanolate (PDP) as follows: to dry THF (30 mL) in a 100 mL flask with a three-way stopcock under an argon atmosphere were added 3,3-diethoxypropanol (2 mmol) and potassium naphthalene (2 mmol) to form potassium 3,3-diethoxypropanolate (PDP). After stirring for 10 min, liquid EO (140 mmol; cooled below 0 °C) was added via a cooled syringe to the mixture. The mixture was allowed to react for 2 days at

* To whom correspondence should be addressed.

10.1021/bc000034w CCC: $19.00 © 2000 American Chemical Society
Published on Web 10/28/2000

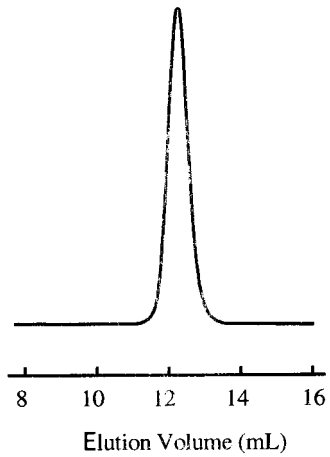

Figure 1. SEC of acetal-PEG-SO_2CH_3 (Instrument; TOSO HLC-8120, detector; RI, column; TOSOH Super HZ 4000+3000+2500, solvent; THF (containing 2 wt % triethylamine), flow rate; 0.35 mL min^{-1}, calibration; standard PEGs).

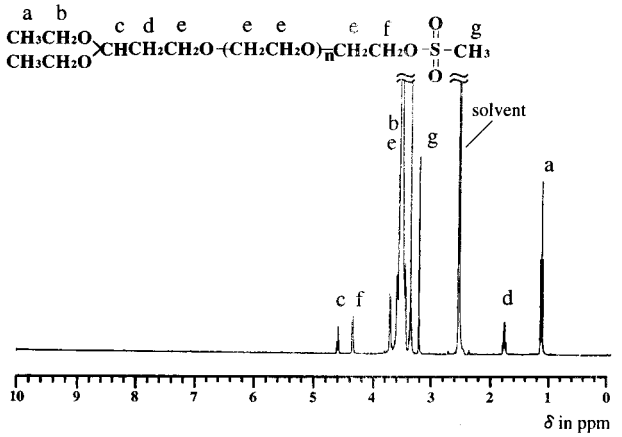

Figure 2. ^1H NMR spectrum of acetal-PEG-SO_2CH_3 in DMSO at room temperature.

Table 1. Characterization of Acetal-PEG-OSO_2CH_3 Prepared Under Several Conditions[a]

run	$[M]_0/[I]_0$	10^3 Mn[b] calcd	10^3 Mn[b] obsd	MWD[b]	yield (%)	ω-end functionality (%)
1	70	3.0	3.1	1.05	92	98
2	80	3.5	3.3	1.02	78	97
3	90	4.0	3.9	1.04	81	98
4	110	5.0	4.7	1.02	84	99

[a] Solvent: THF (30 mL), reaction temperature: 25 °C. [b] Estimated by SEC after polymerization (temperature, 40 °C: eluent THF containing 2 wt % triethylamine.

room temperature. The alkoxide group at the ω-chain end was converted to the methansulfonyl group by the addition of an excess amount of methanesulfonyl chloride as follows: the mixture was added dropwise to a solution of 40 mmol of methanesulfonyl chloride in dry THF (5 mL) using doser at room temperature and stirred for 6 h followed by pouring into 1 L of diethyl ether to obtain the polymer as a white precipitate. The obtained polymer was dried in vacuo and then was analyzed by size-exclusion chromatography (SEC). From the SEC diagram shown in Figure 1, the number-average molecular weight (Mn) and the molecular weight distribution (MWD) were determined to be 3090 and 1.05, respectively. The polymer has a very narrow MWD, and its Mn was close to the calculated value derived from the monomer/initiator ratio, suggesting that the polymerization proceeds without any remarkable side reaction. Figure 2 shows the ^1H NMR spectrum of the obtained α-acetal-ω-methanesulfonyl-PEG. The signals appearing at 3.2 ppm (s, 3H) and 4.3 ppm (t, 2H) were assignable to the methyl and methylene groups adjacent to the sulfonic group, respectively. The clear triad signals based on the acetal methine and methyl protons appear at 4.6 and 1.1 ppm, respectively. The molecular weight of the α-acetal-ω-methanesulfonyl-PEG was then calculated from the intensity ratio of the oxymethylene peak of PEG (3.5 ppm) with the methyl peak in the acetal-moiety assuming the quantitative introduction of an acetal group to the chain end of each polymer molecule (DMSO-d_6, 80 °C). The calculated value of 2880 was in a good agreement with the Mn determined by the SEC analysis (Mn 3090). Furthermore, the ω-end functionality was calculated to be 98% using the ratio of the methyl protons in the methanesulfonic group with methyl protons in the acetal moiety (DMSO-d_6, room temperature). Consequently, NMR and SEC data confirmed that synthesis of the acetal-PEG-SO_2CH_3 was sufficient to proceed. Results of acetal-PEG-SO_2CH_3 synthesis under several conditions are summarized in Table 1. The yield of the polymers was sufficiently high, and their molecular weight can be easily controlled by changing the monomer/initiator ratio.

To convert the methane sulfonyl precursor end-group to the *O*-ethyldithiocarbonate group, the acetal-PEG-SO_2CH_3 was reacted with potassium-*O*-ethyldithiocarbonate in a dry THF/DMF (24:1) cosolvent (25 mL) as follows: to the obtained dry acetal-PEG-SO_2CH_3 (0.10 g), the 20-fold amount of potassium *O*-ethyldithiocarbonate in 25 mL of THF was added and stirred for 3 h at room temperature. The reaction mixture was then mixed with chloroform and washed with a saturated NaCl aqueous solution several times to eliminate impurities from the polymer sample. The organic phase was then concen-

Scheme 1

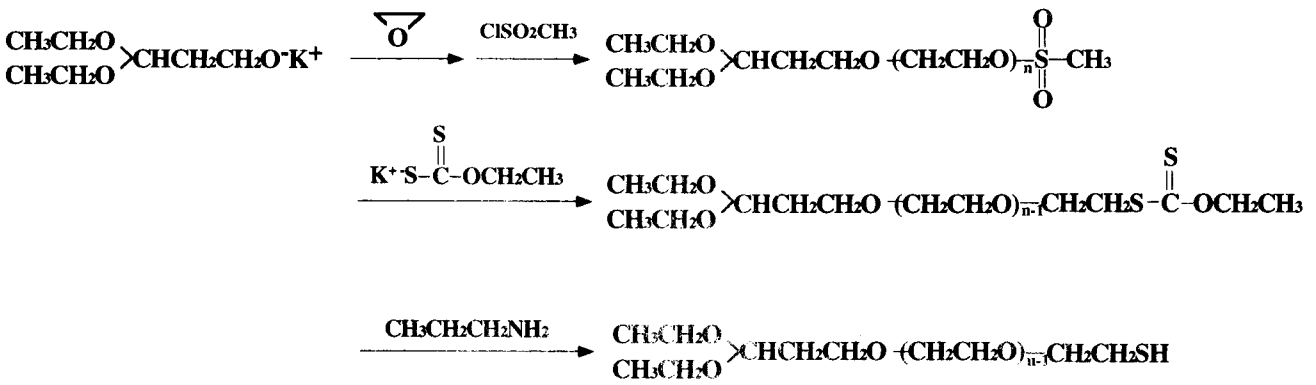

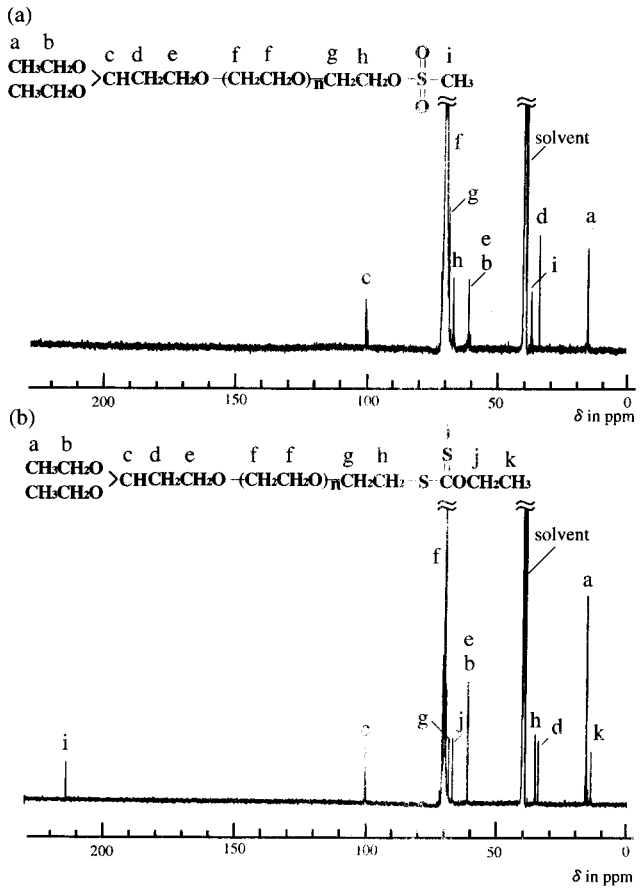

Figure 3. ^{13}C NMR spectra of (a) acetal-PEG-SO_2CH_3 and (b) acetal-PEG-S-C(=S)-OCH_2CH_3 (DMSO, room temperature).

trated by evaporation after drying with sodium sulfate followed by pouring into diethyl ether. The resultant white precipitate was collected and dried in vacuo. Figure 3 shows the ^{13}C NMR spectra of the polymer sample before and after the above reaction. Signals of the methansulfonyl-related carbons such as SO_2CH_3, CH_2-$CH_2OSO_2CH_3$, and $CH_2CH_2OSO_2CH_3$ appearing at 36.9, 68.4 and 66.6 ppm, respectively, completely disappeared in the sample when reacted with potassium *O*-ethyldithiocarbonate (Figure 3b). By contrast, the reacted sample presents new peaks in the ^{13}C NMR spectrum appearing at 214.5, 68.5, and 14.0 ppm, assignable to S-*C*(=S)OCH_2CH_3, S-C(=S)OCH_2CH_3, and S-C(=S)-OCH_2CH_3, respectively. These results clearly indicate quantitative conversion of the ω-methanesulfonyl group to the dithiocarbonate group, which was further confirmed by the ^1H NMR analysis shown in Figure 4. Signals of the methyl and methylene groups adjacent to the sulfonate group completely disappeared, while new peaks appeared at 1.3 (t; 3H) and 4.6 (q; 2H) ppm, assigned to the methyl and methylene groups adjacent to the ethyldithiocarbonate moiety, respectively. The ω-end conversion from methane sulfonate to the ethyldithiocarbonate moiety was again confirmed to be quantitative (97%) based on the ^1H NMR data [CH_2 (4.6 ppm) and CH_3 (1.1 ppm)]. It should be noted that the intensity of the signals derived from the acetal end-groups was unchanged throughout the reaction, indicating that the acetal group at the ω-end remained intact.

It is well-known that the dithiocarbonate group can be easily cleaved by an amine to generate a mercapto group (*12*). Thus, acetal-PEG-S-C(=S)OCH_2CH_3 can be regarded as a precursor of the thiol-ended heterobifunctional PEG. To confirm the generation of mercapto groups

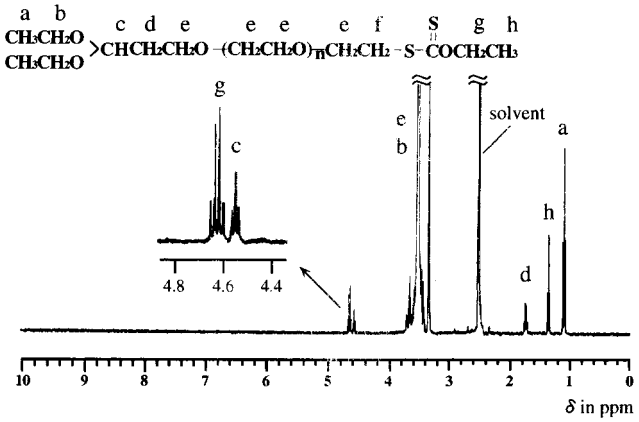

Figure 4. ^1H NMR spectrum of acetal-PEG-S(C=S)-CH_2CH_3 in DMSO at room temperature.

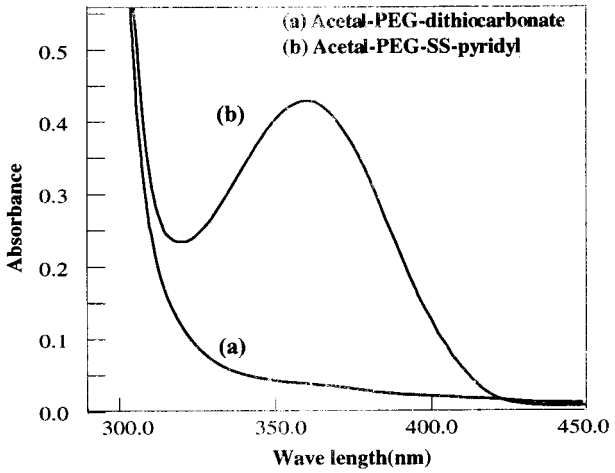

Figure 5. UV absorption spectra of PEG derivatives in MeOH (polymer concentration: 0.1 mM).

through the deprotection of the dithiocarbonate-end-group, acetal-PEG-S-C(=S)OCH_2CH_3 (80 mg) was treated with *n*-propylamine (0.17 mL, 80 times/PEG) in THF (2.0 mL). The mixture was stirred for 3 h at room temperature and then purified in the same manner as described above. The end mercapto group was analyzed by UV spectroscopy using 2-pyridyl disulfide (2-PDS) as a probe molecule: the obtained polymer in MeOH (0.1 mM) was reacted with 5-fold 2-PDS for 2 h at room temperature. The SH group reacts with 2-PDS to release 2-thiopyridon, which is quantified by UV absorbance at 360 nm (ϵ = 5.15×10^3). Figure 5 shows the UV spectra of acetal-PEG-S-C(=S)OCH_2CH_3 (a) and acetal-PEG-S-S-pyridyl (b) clearly demonstrating the existence of the SH-end-group in the sample. Using calibration based on the 2-PDS reaction with 2-mercaptoethanol, the functionality of the SH-end-group per heterotelechelic PEG was calculated to be 0.85. This lowered functionality than 1.0 may be due to the thiol oxidation during the process of purification, although the deprotection reaction itself using *n*-propylamine seems to proceed quantitatively.

In conclusion, the synthesis of a heterobifunctional PEG containing both mercapto and acetal terminal groups (acetal-PEG-SH) was successfully accomplished in this study by EO polymerization with potassium 3,3-diethoxypropanolate and subsequent end-capping with methanesulfonyl chloride. Acetal-PEG-SH was also successfuly converted to the 2-pyridyl derivertive (aceal-PEG-S-S-pyridyl) as follows: freshly deprotected acetal-PEG-SH (0.1 g) solved in dry MeOH (5 mL) was added

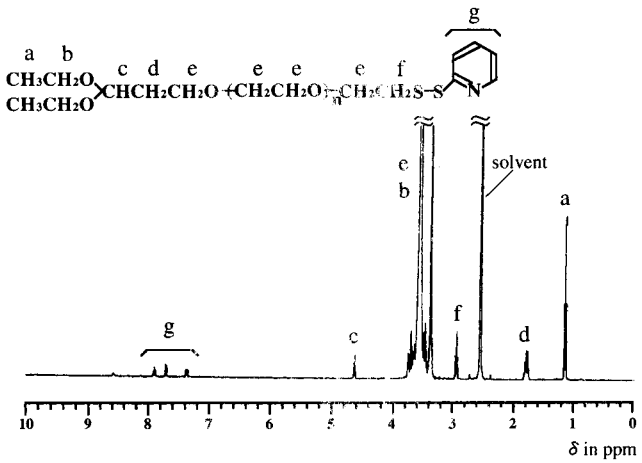

Figure 6. ^{1}H NMR spectrum of acetal-PEG-S−S-pyridyl in DMSO at room temperature.

dropwise to 2-PDS (0.2 g) in dry MeOH (10 mL) and stirred for 2 h at room temperature. The ω-end conversion of PEG from mercapto group to the 2-pyridyldithio group was confirmed to be 68% based on the ^{1}H NMR data shown in Figure 6 [ratio of pyridyl (7.3, 7.6, and 7.8 ppm) to acetal CH_3 (1.1 ppm)]. The obtained heterotelechelic acetal-PEG-SH and acetal-PEG-S-S-pyridyl have potential utility as heterocross-linkers in bioconjugation reactions as well as surface modifiers of metal substrates, including gold and silver, to construct a reactive PEG-brush layer.

LITERATURE CITED

(1) Davis, S., Abuchowski, A., Park, Y. K., and Davis, F. F. (1981) *Clin. Exp. Immunol. 46*, 649.

(2) Harris, J. M., Ed. (1993) *Poly(ethylene glycol) Chemistry, Biotechnical and Biomedical Applications*, Plenum Press, New York.

(3) Harris, J. M., and Zalipsky, S., Ed. (1997) *Poly(ethylene glycol), Chemistry and Biological Applications*, ACS Symposium Series 680, American Chemical Society, Washington, DC.

(4) Cheng, T. L., Wu, P. Y., Wu, M. F., Chern, J. W., and Roffler, S. R. (1999) *Bioconjugate Chem. 10*, 520.

(5) Perez-Luna, V. H., O'Brien, M. J., Opperman, K. A., Hampton, P. D., Lopez, G. P., Klumb, L. A., and Stayton, P. S. (1999) *J. Am. Chem. Soc. 121*, 6469.

(6) Bailey, F. E., Jr., Koleske, J. V., Eds. (1991) *Alkylene Oxide and Their Polymers*, Vol. 35, Marcel Dekker, New York.

(7) Abuchowski, A., van Es, T., Palczuk, N. C., and F. F. (1977) *J. Biol. Chem. 252*, 3582.

(8) Blume, G., Cevc, G., Crommelin, M. D. J. A., Bakker-woudenberg, I. A. J. M., Kluft, C., and Storm, G. (1993) *Biochim. Biophys. Acta 1149*, 180.

(9) Fuertges, F., Abuchowski, A. (1990) *J. Controlled Release 11* (1−3), 139.

(10) Park, Y. K., Abuchowski, A., Davis, S., and Davis, F. (1981) *Anticancer Res. 1* (6), 373.

(11) Ramachandran, R., Katzenstein, D., Winters, M. A., Kundu, S. K., and Merigan, T. C. (1996) *J. Infect. Dis. 173* (4), 1005.

(12) Roberts, C., Chen, C. S., Mrksich, M., Martichonok, V., Ingber, D. E., and Whitesides, G. M. (1998) *J. Am. Chem. Soc. 120*, 6548.

(13) Zalipsky, S. (1995) *Bioconjugate Chem. 6*, 150.

(14) Kaiser, K., Marek, M., Haselgrubler, T., Schindler, H., and Gruber, H. J. (1997) *Bioconjugate Chem. 8*, 545.

(15) Bettinger, T., Remy, J. S., Erbacher, P., and Behr, J. P. (1998) *Bioconjugate Chem. 9*, 842.

(16) Nagasaki, Y., Kutsuna, T., Iijima, M., Kato, M., and Kataoka, K. (1994) *Bioconjugate Chem. 6*, 231.

(17) Nagasaki, Y., Iijima, M., Kato, M., and Kataoka, K. (1995) *Bioconjugate Chem. 6*, 702.

(18) Nakamura, T., Nagasaki, Y., and Kataoka, K. (1998) *Bioconjugate Chem. 9*, 300.

(19) Yokoyama, M., Okano, T., Sakurai, Y., Kikuchi, A., Osako, N., Nagasaki, Y., and Kataoka, K. (1992) *Bioconjugate Chem. 3*, 275.

(20) Stayton, P. S., Shimoboji, T., Long, C., Chilkoti, A., Chen, G., Harris, J. M., and Hoffman, A. S. (1995) *Nature 378*, 472.

(21) Woghiren, C., Sharma, B., and Stein, S. (1993) *Bioconjugate Chem. 4*, 314.

BC000034W